ASM HANDBOOK®

VOLUME 13A

Corrosion: Fundamentals, Testing, and Protection

ASM INTERNATIONAL®

The Materials Information Company

Publication Information and Contributors

Introduction

Corrosion: Fundamentals, Testing, and Protection was published in 2003 as Volume 13A of the *ASM Handbook*. The Volume was prepared under the direction of the ASM Handbook Committee.

Volume Editors

The Volume Editors were Stephen D. Cramer and Bernard S. Covino, Jr.

Authors and Contributors

Thomas A. Adler
Albany Research Center, U.S. Department of Energy
M.K. Adler Flitton
Idaho National Engineering and Environmental Laboratory
Vinod S. Agarwala
Naval Air Systems Command
Tatyana N. Andryushchenko
Intel Corporation
Peggy J. Arps
University of California, Irvine
Denise Aylor
Naval Surface Warfare Center
Robert Baboian
RB Corrosion Service
Christopher C. Berndt
State University of New York, Stony Brook
Marita L. Berndt
Brookhaven National Laboratory
Bennett P. Boffardi
Bennett P. Boffardi and Associates, Inc.
Stuart Bond
TWI Ltd.
Alan Bray
Systems and Materials Research Consultancy
Michiel P.H. Brongers
CC Technologies Laboratories, Inc.
Craig L. Brooks
Analytical Processes/Engineered Solutions, Inc.
Rudolph G. Buchheit
The Ohio State University
Kenneth C. Cadien
Intel Corporation
Richard E. Chinn
Albany Research Center, U.S. Department of Energy
Sean G. Corcoran
Virginia Tech University
Bernard S. Covino, Jr.
Albany Research Center, U.S. Department of Energy

Bruce D. Craig
MetCorr
Stephen D. Cramer
Albany Research Center, U.S. Department of Energy
Chester Dacres
Dacco Sciences Inc.
Marek Danielewski
AGH University of Science and Technology (Krakow)
Guy Davis
Dacco Sciences Inc.
Sheldon Dean
Dean Corrosion Technology
Stephen C. Dexter
University of Delaware
David Dreisinger
University of British Columbia
James C. Earthman
University of California, Irvine
Peter Elliott
Corrosion & Materials Consultancy Inc.
E. Escalante
National Institute of Science and Technology (Retired)
Allen D. Feller
Intel Corporation
Paul B. Fischer
Intel Corporation
Gerald Frankel
The Ohio State University
James Fritz
Technical Marketing Resources
Aleksander Gil
University of Mining & Metallurgy (Krakow)
William A. Glaeser
Battelle Columbus
Richard D. Granata
Florida Atlantic University
Zbigniew Grzesik
The Ohio State University
Harvey Hack
Northrop Grumman Corp.
Harry R. Hanson
Bay Engineering
Christopher Hahin
Illinois Department of Transportation
Robert H. Heidersbach
Dr. Rust, Inc.
Gordon R. Holcomb
Albany Research Center, U.S. Department of Energy
Kyle T. Honeycutt
Analytical Processes/Engineered Solutions, Inc.
Francois Huet
Université Pierre et Marie Curie
Anthony E. Hughes
Commonwealth Scientific & Industrial Research Organisation

Iwao Iwasaki
University of Minnesota
Vijay K. Jain
Indian Institute of Technology
Barnie P. Jones
Oregon Department of Transportation
Russell Jones
Battelle Pacific Northwest Laboratories
Robert M. Kain
Consultant
Russell D. Kane
InterCorr International Incorporated
Farida Kasumzade
Progress Casting Group, Inc.
Robert G. Kelly
University of Virginia
Robert J. Klassen
Royal Military College of Canada
Gerhardus H. Koch
CC Technologies Laboratories, Inc.
David Kolman
Los Alamos National Laboratory
Lorrie Krebs
Dacco Sciences Inc.
Jerome Kruger
Johns Hopkins University
Kyei-Sing Kwong
Albany Research Center, U.S. Department of Energy
Tom Langill
American Galvanizers Association
Ralph W. Leonard
GalvoInfo Center
Brenda J. Little
Naval Research laboratory
Carl E. Locke, Jr.
University of Kansas
Florian Mansfeld
University of Southern California
Philippe Marcus
Ecole Nationale Supérieure de Chimie de Paris
Richard Martin
BJ Unichem Chemical Services
Steven A. Matthes
Albany Research Center, U.S. Department of Energy
Thomas B. Mills
Analytical Processes/Engineered Solutions, Inc.
Anne E. Miller
Intel Corporation
Ted Mooney
Finishing.com. Inc.
Kevin M. Moore
Energetics, Inc.
James Moran
Alcoa Technical Center

Makoto Nishimura
Oak (Nippon) Co., Ltd.
Paul M. Natishan
Naval Research Laboratory
James Noel
University of Western Ontario
Ricardo P. Nogueira
Université Pierre et Marie Curie
Bernard Normand
Université Pierre et Marie Curie
Kevin Ogle
Usinor Research
Joe H. Payer
Case Western Reserve University
Ignacio Perez
Navair
Bopinder S. Phull
Consultant
Jimmy D. Poindexter
BJ Unichem Chemical Services
Scott A. Prost-Domasky
Analytical Processes/Engineered Solutions, Inc.
Elie Protopopoff
Ecole Nationale Supérieure de Chimie de Paris
Robert A. Rapp
The Ohio State University
Vilupanur A. Ravi
California Polytechnic Institute
James C. Rawers
Albany Research Center, U.S. Department of Energy
Raúl B. Rebak
Lawrence Livermore National Laboratory
Izumi N. Reed
Wayne Reitz
North Dakota State University
Anne Robbins
Pierre R. Roberge
Royal Military College of Canada
John R. Scully
University of Virginia
A.J. Sedriks
Office of Naval Research
E. Bud Senkowski
KTA-Tator Inc.
Sadiq Shah
Western Illinois University
Barbara Shaw
Pennsylvania State University
David Shifler
Naval Surface Warfare Center
David W. Shoesmith
University of Western Ontario
David C. Silverman
Argentum Solutions, Inc.

Raymund Singleton
Singleton Corporation
Susan Smialowska
The Ohio State University
Jack Snodgrass
Alcoa Technical Center
Narasi Sridhar
Southwest Research Institute
Kurt H. Stern
Naval Research Laboratory
James Stott
CAPCIS Ltd.
Hideaki Takahashi
Hokkaido University
Hisasi Takenouti
Université Pierre et Marie Curie
Kenneth B. Tator
KTA-Tator Inc.
Neil G. Thompson
CC Technologies Laboratories, Inc.
Garth R. Tingey
Jack Tinnea
Tinnea Associates
Peter F. Tortorelli
Oak Ridge National Laboratory
Joseph H. Tylczak
Albany Research Center, U.S. Department of Energy
Kunigahalli Vasanth
Naval Surface Warfare Center
Lucien Veleva
CINVESTAB-IPN
Y. Paul Virmani
Federal Highway Administration
Mark C. Williams
National Energy Technology Laboratory, U.S. Department of Energy
Charles F. Windisch
Pacific Northwest National Laboratory
Michael Wolpers
Henkel KgaA
Ian Wright
Oak Ridge National Laboratories
Lietai Yang
Southwest Research Institute
Te-Lin Yau
Te-Lin Yau Consultancy
Steven Y. Yu
3M
Małgorzata Ziomek-Moroz
Albany Research Center, U.S. Department of Energy

Reviewers

Robert S. Alwitt
Boundary Technologies, Inc.

David E. Alman
Albany Research Center, U.S. Dept. of Energy
S.V. Babu
Clarkson University
Sean Brossia
Southwest Research Institute
Monica M. Chauviere
ExxonMobil Research and Engineering
Lichun Leigh Chen
Engineered Materials Solutions
O.V. Chetty
Indian Institute of Technology
T.C. Chevrot
TotalFinaElf
Gustavo Cragnolino
Southwestern Research Institute
Jim Crum
Special Metals Corporation
Craig V. Darragh
The Timken Company
Larry DeLashmit
Blair Rubber
Jim Divine
ChemMet, Ltd.
Barry Dugan
Zinc Corp. of America
Henry E. Fairman
Cincinnati Metallurgical Consultants
Robert Frankenthal
Benjamin Fultz
Bechtel Corp.
Martin Gagne
Noranda, Inc.
Edward Ghali
Laval University
Brian Gleeson
Iowa State University
Larry D. Hanke
Materials Evaluation & Engineering Incorporated
Jeffrey A. Hawk
Albany Research Center, U.S. Dept. of Energy
Krista Heidersbach
ChevronTexaco
Dennis D. Huffman
The Timken Company
Fred Ienna
Shell Global Solutions
Tom Jack
Nova Research and Technology Center
Dwight Janoff
FMC Technologies
Mark Jaworoski
United Technologies Research Center
Kent. L. Johnson

Engineering Systems Incorporated
Joanne Jones-Meehan
U.S. Naval Research Laboratory
Dwaine L. Klarstrom
Haynes International Inc.
R. Komanduri
Oklahoma State University
Paul J. Kovach
Stress Engineering Services Incorporated
Virginia M. Lesser
Oregon State University
Donald R. Lesuer
Lawrence Livermore National Laboratory
George J. Licina
Structural Integrity Assoc.
Eugene L. Liening
Dow Chemical Company
McIntyre R. Louthan
Savannah River Tech Center
Kenneth C. Ludema
University of Michigan
Stan P. Lynch
Aeronautical and Maritime Research Laboratory (Australia)
Gregory Makar
Westvaco
William L. Mankins
Metallurgical Services Incorporated
Ron E. Marrelli
Conoco Phillips
George Matzkanin
TRI/NTIAC
Stephen Maxwell
Commercial Microbiology
Gerald H. Meier
University of Pittsburgh
Bert Moniz
DuPont Company
Neville R. Moody
Sandia Corporation
John J. Moore
Colorado School of Mines
Bill Mullins
U.S. Army
John N. Murray
Murray's et al.
Robert M. O'Brien
University of Oregon
Tom O'Keefe
University of Missouri (Rolla)
Sankara Papavinasam
CANMET
Antoine Pourbaix
Cebelcor
Srinivasan Raghavan

University of Arizona
Srikanth K. Raghunathan
Nanomat Incorporated
Robert A. Rapp
The Ohio State University
Anthony P. Reynolds
University of South Carolina
Joseph L. Rose
Pennsylvania State University
Brian J. Saldanha
DuPont Company
John R. Scully
University of Virginia
Ken-ichi Shimizu
Keio University
John A. Shreifels
George Mason University
Robert Silberstein
Northrop Grumman Integrated Systems
Theresa C. Simpson
Bethlehem Steel Corp.
Ron Skabo
CH2M Hill
Karl P. Staudhammer
Los Alamos National Laboratory
Jean Stockard
University of Oregon
Glenn Stoner
University of Virginia
James Strathman
Portland State University
S.R. Taylor
University of Virginia
Herman Terryn
Vrije Universiteit Brussel
Wen-Ta Tsai
National Cheng Kung University
Vilayanur V. Viswanathan
Pacific Northwest National laboratory
J. von Fraunhofer
University of Maryland
Robert Woods
Zaclon, Inc.
John F. Young
J.F. Young International Inc.
Gregory Ke Zhang
Teck Cominco Metals

Foreword

ASM International is pleased to publish *ASM Handbook,* Volume 13A, *Corrosion: Fundamentals, Testing, and Protection,* the first book in a two-volume revision of the landmark 1987 *Metals Handbook,* 9th Edition volume on corrosion. *ASM Handbook,* Volume 13A has been completely revised and updated to address the needs of ASM International members and the global technical community for current and comprehensive information on

corrosion principles, evaluation techniques, and protection methods. Advances in material science and corrosion technologies since the 1987 *Corrosion* volume was published have lessened some of the costs and degradation caused by corrosion. However, the systems that society relies on have increased in complexity during this time, so corrosion can have more far-reaching effects. Corrosion remains a multibillion-dollar problem that confronts nearly every engineer in every industry.

ASM International is indebted to the Co-Chairs and Editors of this Handbook, Stephen D. Cramer and Bernard S. Covino, Jr., who had the vision and the drive to undertake the huge effort to update and revise the 1987 *Corrosion* volume. *ASM Handbook,* Volume 13A is the first fruit of their efforts; they are also leading the project to complete *ASM Handbook,* Volume 13B, *Corrosion: Materials, Environments, and Industries,* scheduled to publish in 2005. The Editors have done an outstanding job in organizing the project, in recruiting renowned experts to oversee sections and to write or revise articles, and in reviewing every manuscript. We are pleased with their vision to recruit authors from Canada, Mexico, France, Germany, United Kingdom, Poland, Japan, India, and Australia, as well as from the United States. This diverse community of volunteers, sharing their knowledge and experience, make this Volume truly an *international* effort.

We thank the authors and reviewers of the 1987 *Corrosion* volume, which at the time was the largest, most comprehensive volume on a single topic ever published by ASM. This new edition builds upon that groundbreaking project. Thanks also go to the ASM Handbook Committee for their oversight and involvement, and to the ASM editorial staff for their tireless efforts.

We are especially grateful to the nearly 200 authors and reviewers listed in the next several pages. Their willingness to invest their time and effort and to share their knowledge and experience by writing, rewriting, and reviewing articles has made this Handbook an outstanding source of information.

Donald R. Muzyka, President, ASM International

Stanley C. Theobald, Managing Director, ASM International

Preface

The direct cost of corrosion in the United States was estimated to be $276 billion annually for 1998, or 3.1% of the 1998 U.S. gross domestic product of $8.79 trillion Ref 1. Of the industry sectors analyzed, utilities and transportation experienced the largest costs. The largest investment in corrosion control and protection strategies was in protective organic coatings. Indirect costs of corrosion, including lost productivity and corrosion-related overhead and taxes, when averaged over industry sectors, were roughly equal to or greater than the direct costs. In some cases they were substantially greater. For example, indirect corrosion costs related to the U.S. bridge infrastructure were estimated to be more than 10 times the $8.3 billion direct cost from bridge corrosion damage. Additional information is available in the article "Direct Costs of Corrosion in the United States" in this Volume.

ASM Handbook, Volume 13A, *Corrosion: Fundamentals, Testing, and Protection,* is the first volume in a two-volume update, revision, and expansion of *Corrosion,* Volume 13 of the ninth edition *Metals Handbook,* published in 1987. The second volume—*ASM Handbook,* Volume 13B, *Corrosion: Materials, Environments, and Industries*—is to be published in 2005. The purpose of these two volumes is to represent the current state of knowledge in the field of corrosion and to provide a perspective on future trends in the field. Metals remain the major focus of the Handbook, but nonmetallic materials occupy a more prominent position that reflects their wide and effective use to solve problems of corrosion. Wet or aqueous corrosion remains the major focus, but dry or gaseous corrosion is discussed more fully, reflecting the increased importance of processes at elevated and high temperatures.

ASM Handbook, Volume 13A recognizes the global nature of corrosion research and practice and the international level of corrosion activities and interactions required to provide cost-effective, safe, and environmentally sound solutions to materials problems in chemically aggressive environments. Twenty percent of the articles in Volume 13A did not appear in the 1987 Handbook. Authors from more than ten countries have contributed to Volume 13A. The table of contents has been translated into Spanish, French, Russian, Japanese, and Chinese to make the Handbook accessible to a diverse audience. Extensive references provide a road map to the corrosion literature and are augmented by Selected References that are a source of additional information.

Information technology has changed dramatically since 1987, and the most significant occurrence has been the development of the Internet as an information resource. In response, ASM International has made the contents of this Handbook and others in the *ASM Handbook* series available on the Web. This Handbook also provides a

list, current at the time of publication, of significant data sources and of major national, international, academic, and government corrosion organizations and institutions that are accessible on the Web.

Corrosion is described by well-known laws of thermodynamics, kinetics, and electrochemistry. The many variables that influence the behavior of a material in its environment can lead to a wide and complex range of performance, from the benign to the catastrophic. Understanding and avoiding detrimental corrosion is an interdisciplinary effort requiring knowledge of chemistry, electrochemistry, materials, engineering, and structures. All applications of engineered materials pivot on the fulcrum between environmental degradation, of which corrosion is a major element, and service or service life, with cost determining the point of balance. Costs are determined not in the spare confines of a material and its environment but in a complex landscape defined by technical, economic, social, environmental, health, safety, legal, and consumer constraints. This is illustrated by the experience of a Portland, OR Water Bureau engineer working to make way for a new light rail line along city streets Ref 2:

…Construction conflicts are anticipated…, but day-to-day construction also alters the original design and corrosion control scheme of existing installations. As development occurs and utilities weave and cross, coatings are damaged, pipes are shorted, wires are cut, and test stations always seem to disappear…Work had to be sequenced and paced to minimize traffic interference… Environmental regulators were classifying the pavement as an engineered cap for brownfield and other contaminated areas…Utilities responded by characterizing the roadway as a constantly opening and closing zipper because we continually construct there… Corrosion control methods for urban areas must be designed for installation and operation in a congested environment that is constantly changing.

This Handbook is organized into six major sections addressing corrosion fundamentals, testing, and protection.

The first Section, "Fundamentals of Corrosion," covers the theory of aqueous and gaseous corrosion from the thermodynamic and kinetic perspectives. It presents the principles of electrochemistry, the mechanisms of corrosion processes, and the methods for measuring corrosion rates in aqueous, molten salt, liquid metals, and gaseous environments. It introduces geochemical modeling as a means for characterizing and understanding corrosion in complex environments. While corrosion is usually associated with the environmental degradation of a material, this Section also describes ways in which corrosion is used for constructive or beneficial purposes.

The second Section, "Forms of Corrosion," describes how to recognize the different types of corrosion and the forces that influence them. It addresses uniform corrosion, localized corrosion, metallurgically influenced corrosion, mechanically assisted corrosion, environmentally induced cracking, and microbiologically influenced corrosion. The Section introduces the complex processes of wear-corrosion interactions that accelerate material deterioration at rates greater than those resulting from wear processes or corrosion processes alone.

The third Section, "Corrosion Testing and Evaluation," describes the planning of corrosion tests, evaluation of test results, laboratory corrosion testing, simulated service testing, and in-service techniques for damage detection and monitoring. It concludes by describing standard methods and practices for evaluating the various forms of corrosion.

The fourth Section, "Methods of Corrosion Protection," begins by discussing as a baseline the corrosion resistance of bulk materials. The Section continues with methods of corrosion protection, including surface treatments and conversion coatings, ceramic, glass and oxide coatings, metal coatings, coatings and linings, electrochemical corrosion control methods, and corrosion inhibitors.

The fifth Section, "Designing for Corrosion Control and Prevention," continues the theme of the fourth Section from the perspective of materials selection and equipment design. Corrosion control is an economic process as well as a technical process, and this Section discusses corrosion economic calculations, predictive modeling for structure service life, and a review of corrosion costs in the United States.

The sixth Section, "Tools for the Corrosionist," covers topics that are complementary to corrosion fundamentals, testing, and protection. It is a new addition to the Handbook. The topics include conventions and definitions in corrosion and oxidation, applications of modern analytical instruments in corrosion, materials science, statistics, and information sources and databases.

Other useful Handbook contents include the "Glossary of Terms," containing definitions of corrosion, electrochemistry, and materials terms common to corrosion and defined in the literature of ISO, ASTM, and NACE International. The "Corrosion Rate Conversion" Section includes conversions in both nomograph and tabular form. The metric conversion guide features conversion factors for common units and includes SI

prefixes. Finally, “Abbreviations and Symbols” provides a key to common acronyms, abbreviations, and symbols.

The six Sections in the Handbook are divided into several subsections. These subsections were organized and written under the leadership of the following individuals (listed in alphabetical order):

Chairperson	Subsection Title
Vinod S. Agarwala	In-Service Techniques for Damage Detection and Monitoring
Rudolph G. Buchheit	Surface Treatments and Conversion Coatings
Bernard S. Covino, Jr.	Laboratory Corrosion Testing
Bruce D. Craig	Environmentally Induced Cracking
Stephen D. Cramer	Simulated Service Testing Metal Coatings Corrosion Inhibitors Tools for the Corrosionist
Marek Danielewski	Fundamentals of Gaseous Corrosion
Stephen C. Dexter	Microbiologically Influenced Corrosion
Peter Elliott	Designing for Corrosion Control and Protection
Gerald Frankel	Metallurgically Influenced Corrosion
William A. Glaeser	Mechanically Assisted Degradation
Russell D. Kane	Uniform Corrosion
Carl E. Locke, Jr.	Electrochemical Corrosion Control Methods
Philippe Marcus	Fundamentals of Corrosion Thermodynamics
Paul M. Natishan	Corrosion Resistance of Bulk Materials
Bopinder S. Phull	Evaluating Forms of Corrosion
Vilupanur A. Ravi	Ceramic, Glass, and Oxide Coatings
Pierre R. Roberge	Planning Corrosion Tests and Evaluating Results
John R. Scully	Fundamentals of Aqueous Corrosion Kinetics
Susan Smialowska	Localized Corrosion
Kenneth B. Tator	Coatings and Linings
Peter F. Tortorelli	Fundamentals Applied to Specific Environments
Ian Wright	Mechanically Assisted Degradation
Margaret Ziomek-Moroz	Fundamentals of Corrosion for Constructive Purposes

These talented and dedicated individuals generously devoted considerable time to the preparation of this Handbook. They were joined in this effort by more than 120 authors who contributed their expertise and creativity in a collaborative venture to write or revise the articles and by more than 200 reviewers and 5 translators. These volunteers built on the contributions of earlier Handbook authors and reviewers who provided the solid foundation on which the present Handbook rests.

For articles revised from the previous edition, the contribution of these authors is acknowledged at the end of articles. This location in no way diminishes their contribution or our gratitude. Those responsible for the current revision are named after the title. The variation in the amount of revision is broad. The many completely new articles presented no challenge for attribution, but assigning fair credit for revised articles was more problematic. The choice of presenting authors' names without comment or with the qualifier “Revised by” is solely the responsibility of the ASM staff.

We thank ASM International and the ASM staff for their skilled support and valued expertise in the production of this Handbook. In particular, we thank Charles Moosbrugger, Gayle Anton, and Scott Henry for their encouragement, tactful diplomacy, and many discussions, plus, we should add, their wistful forbearance as deadlines came and went. The Albany Research Center, U.S. Department of Energy, gave us support and flexibility in our assignments to participate in this project and we are most grateful. In particular, we thank our supervisors Jeffrey A. Hawk and Cynthia P. Doğan, who were most gracious and generous with their encouragement throughout the project.

We close with these thoughtful words from T.R.B. (Tom) Watson, president of NACE International, 1964–65, author of *Why Metals Corrode,* and corrosion leader. (Ref 3)

Mighty ships upon the ocean, suffer from severe corrosion.
Even those that stay at dockside, are rapidly becoming oxide.
Alas, that piling in the sea is mostly Fe_2O_3.
And where the ocean meets the shore, you'll find there's Fe_3O_4.
'Cause when the wind is salt and gusty, things are getting awfully rusty.
We can measure it, we can test it, we can halt it or arrest it;
We can scrape it and weigh it; we can coat it or spray it;
We can examine and dissect it; we can cathodically protect it.
We can pick it up and drop it, but heaven knows we'll never stop it.
So here's to rust, no doubt about it; most of us would starve without it.

That said, given the thermodynamic, kinetic, and economic principles at work in our world, corrosion will not stop. This Handbook helps show us how to live with it.

Stephen D. Cramer
Bernard S. Covino, Jr.
U.S. Department of Energy, Albany Research Center

References

1. G. H. Koch, M. P. H. Brongers, N. G. Thompson, Y. P. Virmani, and J. H. Payer, *Corrosion Cost and Preventive Strategies in the United States*, FHWA-RD-01–156, Federal Highway Administration, U.S. Department of Transportation, Washington D.C., 773 pp., March 2002.

2. Stu Greenberger, Underground Water Utilities – Crowded and Complex, *Mater. Perform.,* Vol. 41, No. 7, July 2002, p. 8.

3. “Rust's a Must,” by T.R.B. Watson, poem reprinted by permission of Jean Watson; also reprinted in *The Boatowner's Guide to Corrosion*, by Everett Collier, Ragged Mountain Press, Camden ME, 2001. One line of the poem was modified for the purposes of this publication.

Officers and Trustees of ASM International (2002–2003)

Donald R. Muzyka
President and Trustee
Special Metals Corporation (retired)
Robert C. Tucker, Jr.
Vice President and Trustee
The Tucker Group, LLC
Gordon H. Geiger
Immediate Past President and Trustee
University of Arizona
John W. Pridgeon
Treasurer
Allvac
Stanley C. Theobald
Secretary and Managing Director
ASM International
Trustees
Reza Abbaschian
University of Florida
Kathleen B. Alexander
Los Alamos National Laboratory
Rodney R. Boyer

Boeing Commercial Airplane Group
Subi Dinda
DaimlerChrysler Corporation
R.G. (Gil) Gilliland
Oak Ridge National Laboratory
Andrew R. Nicoll
Sulzer Metco (US) Inc.
Richard D. Sisson, Jr.
Worcester Polytechnic Institute
George F. Vander Voort
Buehler Ltd.
Lawrence C. Wagner
Texas Instruments Inc.

Members of the ASM Handbook Committee (2002–2003)

Henry E. Fairman
(Chair 2002–; Member 1993–)
Cincinnati Metallurgical Consultants
Jeffrey A. Hawk
(Vice Chair 2002–; Member 1997–)
U.S. Department of Energy
David E. Alman (2002–)
U.S. Department of Energy
Bruce P. Bardes (1993–)
Cincinnati Metallurgical Consultants
Lichun Leigh Chen (2002–)
Engineered Materials Solutions
Craig V. Darragh (1989–)
The Timken Company
Larry D. Hanke (1994–)
Materials Evaluation and Engineering Inc.
Dennis D. Huffman (1982–)
The Timken Company (retired)
Dwight Janoff (1995–)
FMC Corporation
Kent L. Johnson (1999–)
Engineering Systems Inc.
Paul J. Kovach (1995–)
Stress Engineering Services Inc.
Donald R. Lesuer (1999–)
Lawrence Livermore National Laboratory
Huimin Liu (1999–)
Ford Motor Company
William L. Mankins (1989–)
Metallurgical Services Inc.
Srikanth Raghunathan (1999–)
Nanomat Inc.
Karl P. Staudhammer (1997–)
Los Alamos National Laboratory
Kenneth B. Tator (1991–)
KTA-Tator Inc.
George F. Vander Voort (1997–)
Buehler Ltd.

George A. Wildridge (2000–)
Borg Warner Morse TEC Corporation

Previous Chairs of the ASM Handbook Committee

R.J. Austin
(1992–1994) (Member 1984–)
L.B. Case
(1931–1933) (Member 1927–1933)
T.D. Cooper
(1984–1986) (Member 1981–1986)
C.V. Darragh
(1999–2002) (Member 1989–)
E.O. Dixon
(1952–1954) (Member 1947–1955)
R.L. Dowdell
(1938–1939) (Member 1935–1939)
M.M. Gauthier
(1997–1998) (Member 1990–)
J.P. Gill
(1937) (Member 1934–1937)
J.D. Graham
(1966–1968) (Member 1961–1970)
J.F. Harper
(1923–1926) (Member 1923–1926)
C.H. Herty, Jr.
(1934–1936) (Member 1930–1936)
D.D. Huffman
(1986–1990) (Member 1982–)
J.B. Johnson
(1948–1951) (Member 1944–1951)
L.J. Korb
(1983) (Member 1978–1983)
R.W.E. Leiter
(1962–1963) (Member 1955–1958, 1960–1964)
G.V. Luerssen
(1943–1947) (Member 1942–1947)
G.N. Maniar
(1979–1980) (Member 1974–1980)
W.L. Mankins
(1994–1997) (Member 1989–)
J.L. McCall
(1982) (Member 1977–1982)
W.J. Merten
(1927–1930) (Member 1923–1933)
D.L. Olson
(1990–1992) (Member 1982–1988, 1989–1992)
N.E. Promisel
(1955–1961) (Member 1954–1963)
G.J. Shubat
(1973–1975) (Member 1966–1975)
W.A. Stadtler
(1969–1972) (Member 1962–1972)
R. Ward

(1976–1978) (Member 1972–1978)
M.G.H. Wells
(1981) (Member 1976–1981)
D.J. Wright
(1964–1965) (Member 1959–1967)

Staff

ASM International staff who contributed to the development of the Volume included Charles Moosbrugger, Project Editor; Bonnie R. Sanders, Manager of Production; Gayle J. Anton, Editorial Assitant; Nancy Hrivnak, Jill Kinson, and Carol Polakowski, Production Editors; and Kathryn Muldoon, Production Assistant. Editorial Assistance was provided by Elizabeth Marquard, Heather Lampman, Mary Jane Riddlebaugh, and Beverly Musgrove. The Volume was prepared under the direction of Scott D. Henry, Assistant Director of Technical Publications and William W. Scott, Jr., Director of Technical Publications.

Preparation of Online Volume

ASM Handbook, Volume 13A, *Corrosion: Fundatmentals, Testing, and Protection*, was converted to electronic files in 2004. The conversion was based on the First printing (2003). No substantive changes were made to the content of the Volume, but some minor corrections and clarifications were made as needed. ASM International staff who oversaw the conversion of the Volume to electronic files were Sally Fahrenholz-Mann, Sue Hess, and Susan Cheek. The electronic version was prepared under the direction of Stanley Theobald, Managing Director.

Copyright Information

Copyright © 2003
by
ASM International®
All rights reserved
No part of this book may be reproduced, stored in a retrieval system, or transmitted, in any form or by any means, electronic, mechanical, photocopying, recording, or otherwise, without the written permission of the copyright owner.
First printing, October 2003
This book is a collective effort involving hundreds of technical specialists. It brings together a wealth of information from worldwide sources to help scientists, engineers, and technicians solve current and long-range problems.
Great care is taken in the compilation and production of this Volume, but it should be made clear that NO WARRANTIES, EXPRESS OR IMPLIED, INCLUDING, WITHOUT LIMITATION, WARRANTIES OF MERCHANTABILITY OR FITNESS FOR A PARTICULAR PURPOSE, ARE GIVEN IN CONNECTION WITH THIS PUBLICATION. Although this information is believed to be accurate by ASM, ASM cannot guarantee that favorable results will be obtained from the use of this publication alone. This publication is intended for use by persons having technical skill, at their sole discretion and risk. Since the conditions of product or material use are outside of ASM's control, ASM assumes no liability or obligation in connection with any use of this information. No claim of any kind, whether as to products or information in this publication, and whether or not based on negligence, shall be greater in amount than the purchase price of this product or publication in respect of which damages are claimed. THE REMEDY HEREBY PROVIDED SHALL BE THE EXCLUSIVE AND SOLE REMEDY OF BUYER, AND IN NO EVENT SHALL EITHER PARTY BE LIABLE FOR SPECIAL, INDIRECT OR CONSEQUENTIAL DAMAGES WHETHER OR NOT CAUSED BY OR RESULTING FROM THE NEGLIGENCE OF SUCH PARTY. As with any material, evaluation of the material under end-use conditions prior to specification is essential. Therefore, specific testing under actual conditions is recommended.
Nothing contained in this book shall be construed as a grant of any right of manufacture, sale, use, or reproduction, in connection with any method, process, apparatus, product, composition, or system, whether or not covered by letters patent, copyright, or trademark, and nothing contained in this book shall be construed as

a defense against any alleged infringement of letters patent, copyright, or trademark, or as a defense against liability for such infringement.

Comments, criticisms, and suggestions are invited, and should be forwarded to ASM International.

Library of Congress Cataloging-in-Publication Data
ASM International
ASM Handbook
Includes bibliographical references and indexes
Contents: v.1. Properties and selection—irons, steels, and high-performance alloys—v.2. Properties and selection—nonferrous alloys and special-purpose materials—[etc.]—v.21. Composites
1. Metals—Handbooks, manuals, etc. 2. Metal-work—Handbooks, manuals, etc. I. ASM International. Handbook Committee. II. Metals Handbook.
TA459.M43 1990 620.1′6 90-115
SAN: 204-7586
ISBN: 0-87170-705-5
ASM International®
Materials Park, OH 44073-0002
www.asminternational.org
Printed in the United States of America
Multiple copy reprints of individual articles are available from Technical Department, ASM International.

P. Marcus, Introduction to the Fundamentals of Corrosion, *Corrosion: Fundamentals, Testing, and Protection,* Vol 13A, *ASM Handbook*, ASM International, 2003, p 3-4

Introduction to the Fundamentals of Corrosion

Philippe Marcus, Ecole Nationale Supérieure de Chimie de Paris, Université Pierre et Marie Curie

Introduction

THE SIGNIFICANT TECHNICAL CHALLENGES and the high cost directly related to corrosion provide strong incentives for engineers and other technical personnel to develop a firm grasp on the fundamental bases of corrosion. Understanding the fundamentals of corrosion is necessary not only for identifying corrosion mechanisms (a significant achievement by itself), but also for preventing corrosion by appropriate corrosion protection means and for predicting the corrosion behavior of metallic materials in service conditions. Understanding the mechanisms of corrosion is the key to the development of a knowledge-based design of corrosion resistant alloys and to the prediction of the long-term behavior of metallic materials in corrosive environments.

Two major areas are usually distinguished in the corrosion of metals and alloys. The first area is where the metal or alloy is exposed to a liquid electrolyte, usually water, and thus typically called aqueous corrosion. The second area is where corrosion takes place in a gaseous environment, often called oxidation, high- temperature oxidation, or high-temperature corrosion, and called gaseous corrosion here. These two areas have been (and still are sometimes) referred to as wet corrosion and dry corrosion. This distinction finds its origin (and its justification) in some fundamental differences in the mechanisms, in particular the electrochemical nature of reactions occurring in aqueous solution (or in a nonaqueous electrolyte), as compared to the formation of thick oxide layers in air or other oxidizing atmospheres, at high temperature with fast transport processes by solid-state diffusion through a growing oxide. The separation between the two areas, however, should not be overemphasized, because there are also similarities and analogies, for example:

- The initial stages of reaction involve the adsorption of chemical species on the metal surface that can be described by the Gibbs equation for both liquid and gaseous environments.
- The nucleation and growth phenomena of oxide layers and other compounds
- The use of surface analytical techniques

The fundamental aspects of aqueous and gaseous corrosion are addressed in this first Section of the Handbook. Corrosion of metallic materials is generally detrimental and must be prevented, but if it is well understood and controlled, it can also be used in a powerful and constructive manner for electrochemical production of fine patterns on metal as well as on semiconductor surfaces. These constructive purposes also include electrochemical machining (down to the micro- or even the nanoscale), electrochemical and chemical-mechanical polishing, and anodes for batteries and fuel cells. These topics are also addressed in this Section.

P. Marcus, Introduction to the Fundamentals of Corrosion, *Corrosion: Fundamentals, Testing, and Protection,* Vol 13A, *ASM Handbook*, ASM International, 2003, p 3-4

Introduction to the Fundamentals of Corrosion

Philippe Marcus, Ecole Nationale Supérieure de Chimie de Paris, Université Pierre et Marie Curie

Thermodynamics

The thermodynamic aspects of corrosion, whether for aqueous corrosion or gaseous corrosion, are discussed first. This approach is logical because the object of thermodynamics is to examine the driving force for corrosion. Thermodynamics sets the framework of what is possible and what is not. It predicts the direction in which the changes of the system can occur. The only reactions that can take place spontaneously are those that will lower the energy of the system. If thermodynamic calculations predict that a reaction cannot occur, the reaction will indeed not occur. However, thermodynamics does not provide any information on the rate at which a reaction will occur; that is the area of kinetics.

Corrosion in aqueous solution is an electrochemical process where the corroding metal is an electrode in contact with an electrolyte. The processes taking place at the metal surface are thus electrode processes, and such processes must be defined. There is also a need to define electrode potentials and the way they can be measured with reference electrodes. These points are covered in three articles in this Section: "Electrode Processes," "Electrode Potentials," and "Potential Measurements with Reference Electrodes."

With these basic notions defined, it is possible to explain the principle of potential-pH (*E*-pH) diagrams in the article "Potential versus pH (Pourbaix) Diagrams." These diagrams allow us to visualize in a practical and easy way the domains of stability of chemical species (solid phases and dissolved species) and to know at a glance what corrosion reactions can occur in a given metal-solution system. In the article on potential-pH diagrams, the diagrams for high temperature water are also presented, as well as an extension of the concept to species adsorbed on metal surfaces. The more specific topic of thermodynamics of corrosion in molten salts is treated in a separate article, "Molten Salt Corrosion Thermodynamics." The interesting contribution of geochemistry in modeling of stable chemical states in complex chemical environments is considered in the last article, "Geochemical Modeling," in this group of articles on corrosion thermodynamics.

It is not superfluous to reemphasize the fact that thermodynamics can only be a first step in the investigation of the corrosion behavior of a given metal/aqueous solution system. Thermodynamics provides the road map. Using it, the possible destinations are clearly known.

P. Marcus, Introduction to the Fundamentals of Corrosion, *Corrosion: Fundamentals, Testing, and Protection,* Vol 13A, *ASM Handbook*, ASM International, 2003, p 3-4

Introduction to the Fundamentals of Corrosion

Philippe Marcus, Ecole Nationale Supérieure de Chimie de Paris, Université Pierre et Marie Curie

---

Kinetics

Once thermodynamics are understood, it becomes necessary to undertake another task, namely to examine which reactions, among those reactions allowed by thermodynamics, will occur and at what rate. This subject is addressed by a group of articles on the fundamentals of aqueous corrosion kinetics.

The first article, "Kinetics of Aqueous Corrosion," examines the relations between the current and the potential associated with each of the two or more electrochemical reactions constituting the mixed system characteristic of corrosion. The current-potential (*I-E*) curves, the corrosion potential, and the corrosion current form the basis of the kinetic approach. Here activation energies of the reactions come into play. The concept of mixed potential is essential. Corrosion occurs if both an anodic and a cathodic reaction take place, each reaction involving chemical species that correspond to a different oxidation-reduction system. Because of this, the corrosion potential is not an equilibrium potential but rather is considered a mixed potential.

On this ground, and without forgetting the framework set by thermodynamics, the mechanisms of corrosion in aqueous solution are discussed in the article "Aqueous Corrosion Reaction Mechanisms." The latest advances in this area, achieved by an intense effort in research worldwide, are reviewed. Inevitably, areas in which the mechanisms are not yet fully elucidated still exist and justify present and future research.

Passivation of metals and alloys, a phenomenon in which a thin protective layer of oxide or oxihydroxide is formed on the surface, is a major aspect of corrosion from the scientific as well as the engineering point of view. This phenomenon—discussed in the article "Passivity" in this Section—is also an area in which huge

progress has been made in recent years. The mechanisms of oxide film growth, the chemical composition and the chemical states, the crystallographic structure, and the semiconductor properties of passive films are now better understood. The acquired knowledge allows more accurate prediction of the long-term behavior of passive films and design of passive layers that are increasingly resistant to corrosion. It is an area where the contribution of surface chemical and structural analysis has been overwhelming.

It is interesting to note that passivity is a good example of a case where potential-pH diagrams must be used with caution. Indeed, whereas the *E*-pH diagrams predict well the formation of passive oxides on copper, they predict the absence of passive film in acid solution on metals such as nickel, iron, and chromium, which are in fact well passivated. This is due to the very low dissolution rate of the oxides of these metals at low pH. Thanks to the formation of passive films rich in chromium oxide, passivation of alloys containing chromium, whether they are nickel-base or iron-base alloys (stainless steels), is a major feature of highly corrosion-resistant alloys.

Finally, to define critical reaction paths, the appropriate experimental methods must be available to measure corrosion rates. These methods are presented in the last article, "Methods for Determining Aqueous Corrosion Reaction Rates," in the group of articles on fundamentals of corrosion kinetics.

P. Marcus, Introduction to the Fundamentals of Corrosion, *Corrosion: Fundamentals, Testing, and Protection,* Vol 13A, *ASM Handbook*, ASM International, 2003, p 3-4

Introduction to the Fundamentals of Corrosion

Philippe Marcus, Ecole Nationale Supérieure de Chimie de Paris, Université Pierre et Marie Curie

---

Gaseous Corrosion

The next group of articles, on fundamentals of gaseous corrosion (often called oxidation in a broad sense, rather than the strict sense of the formation of an oxide), is organized in a similar manner to the group on aqueous corrosion. The group of articles starts with the "Introduction to the Fundamentals of Corrosion in Gases," followed by a review of thermodynamics in the article "Thermodynamics of Gaseous Corrosion." Here the environment is not conductive, and the ionic processes take place only on the metal surface and in or on the corrosion products. Thermodynamics defines and quantifies the driving force of the oxidation reaction; that is, the lowering of the energy level of the metal. The chemical equilibrium between gas phase (e.g., oxygen, water vapor, hydrogen sulfide) and compounds formed on the metal surface (oxide or sulfide in the examples cited earlier) can be represented by diagrams of the partial pressure of formation versus temperature. Such diagrams, called Ellingham diagrams, allow us to quickly visualize the domains of stability of different oxides. Similar diagrams have also been calculated for sulfides.

The kinetics of gaseous corrosion of metals and alloys and the oxidation mechanisms are examined in two articles: "Kinetics of Gaseous Corrosion Processes" and "Gaseous Corrosion Mechanisms." The different oxidation laws (i.e., the mass increase as a function of time) are presented in detail. The oxide layers developed at high temperature are quite thick (up to several micrometers) compared to the layers formed at room temperature because of kinetic limitations associated with diffusion in the solid state. The diffusion mechanisms, in which defects such as cation and anion vacancies play a key role, are discussed. The effect of impurities is also considered. The differences between the lattice constants of the substrate and the oxide lead to the existence of stresses at the interface and in the oxide. Such stresses play a major role in the properties of the oxide layers, and it is important to understand how they are generated. The role of dislocations is also an important aspect in high temperature oxidation.

In some industrial applications, the corrosive environment is complex, and the corrosion products are not protective oxides. The phenomena related to corrosion by hot gases and combustion products are considered in the article "Gaseous Corrosion Mechanisms."

Appropriate experimental methods must be used to measure the kinetics of dry oxidation. Such methods are described in the last article, "Methods for Measuring Gaseous Corrosion Rates," in this group of articles on the fundamentals of gaseous corrosion.

Corrosion in more specific environments— molten salts (the thermodynamics of which has been addressed in a previous article) and liquid metals—is considered in the next group of articles. Molten salts are addressed in two articles, “Corrosion by Molten Salts” and “Corrosion by Molten Nitrates, Nitrites, and Fluorides.” Under certain conditions, which are described in the article “Corrosion by Liquid Metals,” the liquid metal can penetrate into the grain boundaries of the metallic material at rates that are sometimes spectacular. A dangerous consequence is embrittlement of the metal.

At this point, the reader has been provided with all the fundamental bases of thermodynamics and kinetics necessary to understand the mechanisms of corrosion of metals in aqueous solution and the mechanisms of oxidation at high temperature, including the relevant experimental methods.

P. Marcus, Introduction to the Fundamentals of Corrosion, *Corrosion: Fundamentals, Testing, and Protection,* Vol 13A, *ASM Handbook*, ASM International, 2003, p 3-4

Introduction to the Fundamentals of Corrosion

Philippe Marcus, Ecole Nationale Supérieure de Chimie de Paris, Université Pierre et Marie Curie

---

Constructive Uses of Corrosion

The fundamental electrochemical reactions of corrosion, in particular anodic dissolution, can be, if they are well understood and controlled, used in a very powerful way to design and fabricate patterns on metal surfaces. The article “Electrochemical Machining” describes the use of such reactions to produce surface architectures at scales down to the micrometer and now approaching the nanometer scale. The article “Electropolishing” reviews another use of corrosion for constructive purpose, where electrochemical reactions are used to produce finely polished metallic surfaces by controlled dissolution in an appropriate electrolyte. Chemical- mechanical polishing, often called chemical- mechanical planarization (CMP) is rapidly developing under the impetus of important applications in the microelectronic industry; these advances are described in the article “Chemical-Mechanical Planarization for Semiconductors” in this Section. The combination of mechanical abrasion with dissolution of the surface allows the fast planarization of complex structures (e.g., with narrow copper interconnects). For this process to be efficient and industrially applicable, very good control of the attack taking place in the corrosive bath is necessary and requires a detailed understanding of the mechanisms of dissolution and passivation of the metal surfaces subjected to CMP.

There are other areas of importance in classical and modern technologies that rely, from the mechanistic point of view, on controlled corrosion. These are described in the articles “Electrochemical Refining,” “Anodes for Batteries,” and “Fuel Cells,” which are the final articles in this Section of the Handbook.

P. Marcus, Introduction to the Fundamentals of Corrosion, *Corrosion: Fundamentals, Testing, and Protection,* Vol 13A, *ASM Handbook*, ASM International, 2003, p 3-4

Introduction to the Fundamentals of Corrosion

Philippe Marcus, Ecole Nationale Supérieure de Chimie de Paris, Université Pierre et Marie Curie

---

Conclusions

The fundamental aspects of corrosion, discussed in this Section, are indispensable, not only to understand the mechanisms, but also to control corrosion, to design appropriate means of corrosion protection, and to be able to predict the long-term corrosion behavior of metallic materials. The articles of this Section have been written

by leading scientists from the academic and industrial research world, and this Section represents a major review of the fundamentals of corrosion. It opens the way to the articles of the following Sections on the different forms of corrosion, including uniform corrosion, localized corrosion, and stress-corrosion cracking, on corrosion testing and evaluation, and finally on the methods of corrosion protection.

P. Marcus, Introduction to Fundamentals of Corrosion Thermodynamics, *Corrosion: Fundamentals, Testing, and Protection,* Vol 13A, *ASM Handbook*, ASM International, 2003, p 5

Introduction to Fundamentals of Corrosion Thermodynamics

Philippe Marcus, Ecole Nationale Supérieure de Chimie de Paris, Université Pierre et Marie Curie

---

Introduction

THE DRIVING FORCE of corrosion is the lowering of energy associated with the oxidation of a metal. Thermodynamics examines and quantifies this driving force. It predicts if reactions can or cannot occur (i.e., if the metal will corrode or be stable). It does not predict at what rate these changes can or will occur: this is the area of kinetics. However, knowing from thermodynamics what reactions are possible is a necessary step in the attempt to understand, predict, and control corrosion.

P. Marcus, Introduction to Fundamentals of Corrosion Thermodynamics, *Corrosion: Fundamentals, Testing, and Protection,* Vol 13A, *ASM Handbook*, ASM International, 2003, p 5

Introduction to Fundamentals of Corrosion Thermodynamics

Philippe Marcus, Ecole Nationale Supérieure de Chimie de Paris, Université Pierre et Marie Curie

---

Electrochemical Reactions

Corrosion of metals and alloys in aqueous environments or other ionically conducting liquids is almost always electrochemical in nature. It occurs when two or more electrochemical reactions take place on a metal surface. One of these reactions results in the change of the metal or some elements in the metal alloy from a metallic state into a nonmetallic state. The products of corrosion may be dissolved species or solid corrosion products. Because electrochemical reactions are at the origin of corrosion, the corroding metal surface is considered an electrode. The ionically conducting liquid is the electrolyte in which the reactions take place. Different aspects of these reactions are considered in the articles "Electrode Processes," "Electrode Potentials," and "Potential Measurements with Reference Electrodes" in this Section:

- *The structure of the electrode/electrolyte interface:* There is a separation of charges between electrons in the metal and ions in the electrolyte, creating an electrically charged double layer. The ions in the solution interact with water molecules. Adsorption of ions on the electrode surface may also occur.
- *Transport of chemical species:* This takes place through the double layer and in the electrolyte by diffusion.

- *The potential difference across the electrode/ electrolyte interface:* Electrode potentials need to be measured to evaluate the corrosion behavior of a metal (this is true for both the thermodynamics and the kinetics of corrosion). Potential measurements require the use of reference electrodes.
- *The processes governing corrosion:* These are electrode processes, involving oxidation and reduction reactions (or anodic or cathodic reactions). The corroding system does not produce any net charge and, thus, the electrons produced by the electrochemical oxidation of the metal (the anodic reaction) must be consumed by an electrochemical reduction reaction (the cathodic reaction).

Potential-pH (*E*-pH) diagrams (Pourbaix diagrams), based on equilibrium thermodynamics for metal-water systems, show at a glance the regions of stability of the various phases that can exist in the system. Their principle and their construction are presented in the article "Potential versus pH (Pourbaix) Diagrams" for binary metal-water systems and for ternary metal-additive-water systems. Their applications as well as their limitations are also discussed. The *E*-pH diagrams are very useful as a thermodynamic framework for kinetic interpretation, but they do not provide information on corrosion rates.

The prediction of the corrosion behavior of metals in aqueous solutions at high temperatures is also of considerable importance for different technologies (including power generation systems in general and nuclear power systems in particular). Potential pH diagrams for metals in high temperature water are presented.

The principle of *E*-pH diagrams has been extended to the case of adsorbed species on metal surfaces in water. Whereas the solid compounds treated in the classical diagrams are three-dimensional (bulk) compounds (e.g., oxides, hydroxides, sulfides), the formation of more stable two-dimensional adsorbed phases has been considered only recently. Due to the large energy of adsorption, adsorbed layers may form under *E*- pH conditions in which the usual solid compounds are thermodynamically unstable, and these adsorbed layers can induce marked changes in the corrosion behavior of metals. The method of calculation of the equilibrium potentials of species adsorbed on an electrode surface in water is presented, together with examples of applications, in a section on *E*-pH diagrams for adsorbed species.

P. Marcus, Introduction to Fundamentals of Corrosion Thermodynamics, *Corrosion: Fundamentals, Testing, and Protection,* Vol 13A, *ASM Handbook,* ASM International, 2003, p 5

Introduction to Fundamentals of Corrosion Thermodynamics

Philippe Marcus, Ecole Nationale Supérieure de Chimie de Paris, Université Pierre et Marie Curie

---

Molten Salt Corrosion Thermodynamics

Molten salts constitute a special environment of importance in a number of technologies. There is no solvent analogous to water in molten salts. A specific potential scale must be established for each medium, as described in the article "Molten Salt Corrosion Thermodynamics" in this Section. Equilibrium diagrams, analogous to the *E*-pH diagrams for aqueous solutions, have been constructed. In these diagrams, the equilibrium potential, *E*, is plotted as a function of the activity of oxide in the melt, expressed as pO^{2-} = -log O^{2-}. The thermodynamics of molten salt electrochemical cells is treated here.

P. Marcus, Introduction to Fundamentals of Corrosion Thermodynamics, *Corrosion: Fundamentals, Testing, and Protection,* Vol 13A, *ASM Handbook,* ASM International, 2003, p 5

Introduction to Fundamentals of Corrosion Thermodynamics

Philippe Marcus, Ecole Nationale Supérieure de Chimie de Paris, Université Pierre et Marie Curie

---

Geochemical Modeling

The article "Geochemical Modeling" discusses modeling software that has been developed by geochemists to describe the chemical state of local environments, with interesting and important applications in corrosion. These include nuclear waste storage, atmospheric corrosion involving environmental effects on corrosion product stability, and corrosion in elevated and high-temperature aqueous systems.

Electrode Processes

Revised by E. Protopopoff and P. Marcus, Laboratoire de Physico-Chimie des Surfaces, CNRS, Ecole Nationale Supérieure de Chimie de Paris, Université Pierre et Marie Curie

Introduction

ELECTROCHEMICAL, OR ELECTRODE, REACTIONS are reactions that occur with charge transfer between neutral or ionic reactants and a conducting material, called the electrode, acting as an electron source or an electron sink (Ref 1). Electrochemical reactions involve change in valence; that is, oxidation or reduction of the reacting elements. Oxidation and reduction are commonly defined as follows. Oxidation is the removal of electrons from atoms or groups of atoms, resulting in an increase in valence, and reduction is the addition of electrons to atoms or groups of atoms, resulting in a decrease in valence (Ref 2).

References cited in this section

1. J.O'M. Bockris, A.K.N. Reddy, and M. Gamboa-Aldeco, *Modern Electrochemistry,* Kluwer Academic/Plenum Publishers, New York, 2000
2. L. Pauling, *General Chemistry,* W.H. Freeman, 1964, p 338–360

Electrode Processes

Revised by E. Protopopoff and P. Marcus, Laboratoire de Physico-Chimie des Surfaces, CNRS, Ecole Nationale Supérieure de Chimie de Paris, Université Pierre et Marie Curie

Electrode Reactions

Because electrochemical reactions occur in an electrochemical cell with oxidation reactions occurring at one electrode and reduction reactions occurring at the other electrode, they are often further defined as either cathodic reactions or anodic reactions. By definition, cathodic reactions are those types of reactions that result in reduction, such as:

$$M^{2+}(aq) + 2e^- \rightarrow M(s) \qquad \text{(Eq 1)}$$

Anodic reactions are those types of reactions that result in oxidation, such as:

$$M(s) \rightarrow M^{2+}(aq) + 2e^- \qquad \text{(Eq 2)}$$

Because of the production of electrons during oxidation and the consumption of electrons during reduction, oxidation and reduction are coupled events. If the ability to store large amounts of electrons does not exist,

equivalent processes of oxidation and reduction will occur together during the course of normal electrochemical reactions. The oxidized species provide the electrons for the reduced species.

Electrode Processes

Revised by E. Protopopoff and P. Marcus, Laboratoire de Physico-Chimie des Surfaces, CNRS, Ecole Nationale Supérieure de Chimie de Paris, Université Pierre et Marie Curie

---

The Electric Field near the Electrode

The examples stated earlier, like many aqueous corrosion situations, involve the reaction of aqueous metal species at a metal electrode surface. The metal-aqueous solution interface is complex, as is the mechanism by which the reactions take place across the interface. Because the reduction-oxidation reactions involve ionic species in the electrolyte reacting at or near the metal surface, the electrode surface is charged relative to the solution and the reactions are associated with specific electrode potentials.

The charged interface results in an electric field that extends into the solution and has a dramatic effect. A solution that contains water as the primary solvent is affected by the electric field near the metal because of its structure. Water is polar and can be visualized as dipolar molecules that have a positive side (hydrogen atoms) and a negative side (oxygen atoms). In the electric field caused by the charged interface, the water molecules act as small dipoles and align themselves in the direction of the electric field.

Electrode Processes

Revised by E. Protopopoff and P. Marcus, Laboratoire de Physico-Chimie des Surfaces, CNRS, Ecole Nationale Supérieure de Chimie de Paris, Université Pierre et Marie Curie

---

Solvation of Ions

Ions that are present in the solution are charged because of the loss or gain of electrons. The positive charged ions (cations) and negative charged ions (anions) also have an electric field associated with them. The solvent (water) molecules act as small dipoles; therefore, they are also attracted to the charged ions and align themselves in the electric field established by the charge of the ion. Because the electric field is strongest close to the ion, some water molecules reside very close to an ionic species in solution. The attraction is great enough that these water molecules travel with the ion as it moves through the solvent. The tightly bound water molecules are referred to as the primary water sheath of the ion. The electric field is weaker at distances outside the primary water sheath, but it still disturbs the polar water molecules as the ion passes through the solution. The water molecules that are disturbed as the ion passes, but do not move with the ion, are usually referred to as the secondary water sheath. Figure 1 shows a representation of the primary and secondary solvent molecules for a cation in water. Because of their smaller size relative to anions, cations have a stronger electric field close to the ion and more water molecules are associated in their primary water sheath. Anions have few, if any, primary water molecules. A detailed description of the hydration of ions in solution is given in Ref 1.

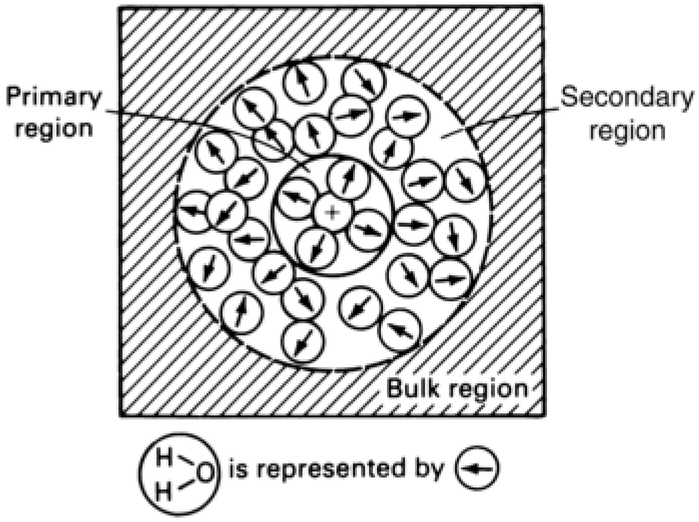

Fig. 1 Schematic of the primary and secondary solvent molecules around a cation in water

Ions and polar water molecules are attracted to the metal-aqueous solution interface of an electrode because of the strong electric field in this region. Water molecules form a first row at the metal surface. This row of water molecules limits the distance to which hydrated ions can approach the interface. Figure 2 shows a schematic diagram of a charged interface and the locations of cations at the surface. Also, the primary water molecules associated with the ionic species limit the distance the cations can approach. The plane of positive charge containing the cations closest to a negatively charged surface is thus at a fixed distance from the metal. This plane of charge is referred to as the outer- Helmholtz plane (OHP).

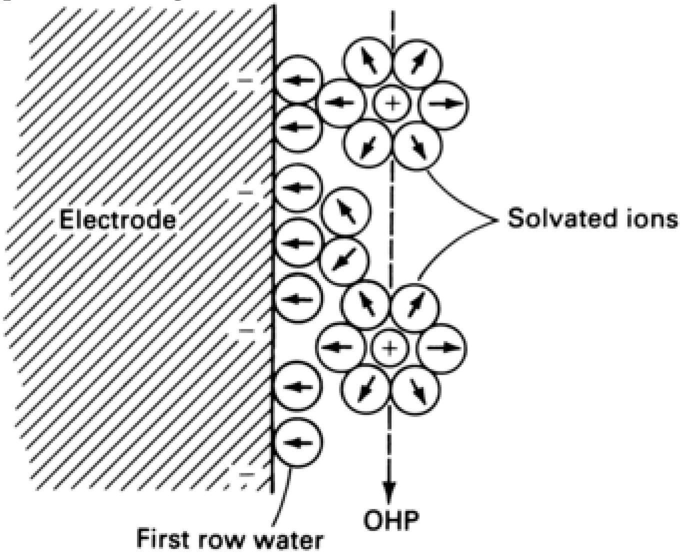

Fig. 2 Schematic of a charged interface and of the locations of cations at the electrode surface. OHP, outer-Helmholtz plane

The region of the interface with charge separation (Fig. 3) is called the electric double layer and can be represented as a charged capacitor (Ref 1). The potential drop across the interface is also often simplified as a linear change in potential from the metal surface to the OHP.

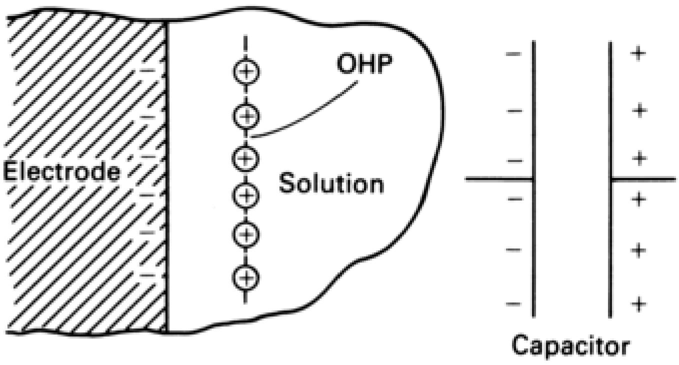

Fig. 3 The simplified electric double layer at a metal-aqueous solution interface and equivalent capacitor. OHP, outer-Helmholtz plane

The electric equivalent of a metal-aqueous solution interface where no reactions with electron transfer occur over a large range of potentials is a simple capacitor (Fig. 3). The electrode is then ideally polarizable. This is the case of mercury in poorly reactive electrolytes (Ref 1). Noble metals like platinum or gold behave as ideal polarizable electrodes within a limited range of potential.
However, on most metals, especially the corrodible ones, reactions with electron transfer across the interface (electrochemical reactions) occur, leading to charge transfer currents, or faradic current. The interface is a barrier to the transfer of electrons from or to the metal; this can be represented by a resistance called the charge-transfer resistance. This resistance is not a simple ohmic resistance, because it varies with the electrode potential. It is constant only in a limited potential range. The electrical circuit equivalent to a metal-electrolyte interface with charge transfer is thus a parallel combination of a double-layer capacitance (C_{DL}) and a charge transfer resistance (R_{CT}) (Fig. 4) (Ref 1). It must be noted that this is the electrical equivalent of a very simple interface; for example, the circuit equivalent to an electrode covered by an oxide film is more complicated (Ref 1).

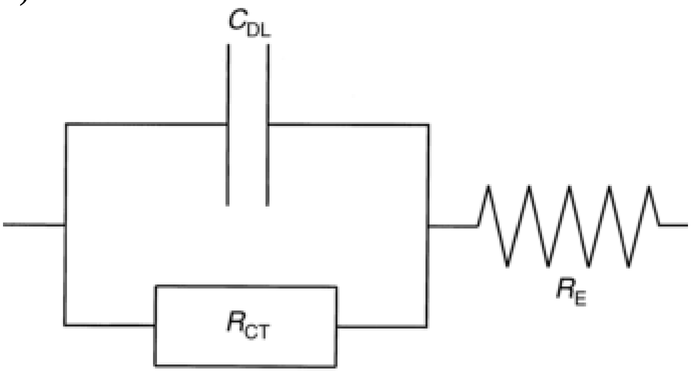

Fig. 4 Electric circuit equivalent to a metal-electrolyte interface showing the double-layer capacitance (C_{DL}) in parallel with the charge transfer resistance (R_{CT}). R_E is the ohmic resistance of the electrolyte (Ref 1).

If there were no difficulty in the transfer of electrons across the interface, the only resistance to the electron flow would be the diffusion of aqueous species to and from the electrode. The electrode would then be ideally nonpolarizable, and its potential would not change until the solution was deficient in electron acceptors and/or donors. This property is sought after for reference electrodes (see the article in this Section, "Potential Measurements with Reference Electrodes").
However, when dealing with the kinetics of electrochemical reactions (see the article "Kinetics of Aqueous Corrosion" in this Volume), the metal-electrolyte interface represents an energy barrier that must be overcome. Thus, reactions at the interface are often dominated by activated processes, and control of activation by polarization plays a significant role in electrochemical kinetics. A key in controlling corrosion consists in minimizing the kinetics of the anodic reaction, that is, dissolution of the metal, or the kinetics of the cathodic reactions.

Reference cited in this section

1. J.O'M. Bockris, A.K.N. Reddy, and M. Gamboa-Aldeco, *Modern Electrochemistry,* Kluwer Academic/Plenum Publishers, New York, 2000

Revised by E. Protopopoff and P. Marcus, Laboratoire de Physico-Chimie des Surfaces, CNRS, Ecole Nationale Supérieure de Chimie de Paris, Université Pierre et Marie Curie

---

Acknowledgment

This article has been adapted from the article by Charles A. Natalie, Electrode Processes, *Corrosion,* Vol 13, *ASM Handbook* (formerly 9th ed. *Metals Handbook*), ASM International, 1987, p 18–19.

Electrode Processes

Revised by E. Protopopoff and P. Marcus, Laboratoire de Physico-Chimie des Surfaces, CNRS, Ecole Nationale Supérieure de Chimie de Paris, Université Pierre et Marie Curie

---

References

1. J.O'M. Bockris, A.K.N. Reddy, and M. Gamboa-Aldeco, *Modern Electrochemistry,* Kluwer Academic/Plenum Publishers, New York, 2000
2. L. Pauling, *General Chemistry,* W.H. Freeman, 1964, p 338–360

E. Protopopoff and P. Marcus, Electrode Potentials, *Corrosion: Fundamentals, Testing, and Protection*, Vol 13A, *ASM Handbook*, ASM International, 2003, p 8–12

Electrode Potentials

E. Protopopoff and P. Marcus, Ecole Nationale Supérieure de Chimie de Paris, Université Pierre et Marie Curie

---

Introduction

ONE OF THE IMPORTANT FEATURES of the electrified interface between the electrode and the electrolyte in the aqueous corrosion of metals is the existence of a potential difference across the double layer, which leads to the definition of the electrode potential. The electrode potential is one of the most important parameters in both the thermodynamics and the kinetics of corrosion. The fundamentals of electrode potentials are discussed in this article. Examples of the calculations of the potential at equilibrium are given in the article "Potential versus pH (Pourbaix) Diagrams" in this Section of the Volume.

E. Protopopoff and P. Marcus, Electrode Potentials, *Corrosion: Fundamentals, Testing, and Protection,* Vol 13A, *ASM Handbook*, ASM International, 2003, p 8–12

Electrode Potentials

E. Protopopoff and P. Marcus, Ecole Nationale Supérieure de Chimie de Paris, Université Pierre et Marie Curie

Thermodynamics of Chemical Equilibria

The object of chemical thermodynamics is to develop a mathematical treatment of the chemical equilibria and the driving forces behind chemical reactions. The desire is to catalog quantitative data concerning known equilibria that later can be used to predict other equilibria.

The driving force for chemical reactions at constant pressure is the Gibbs free energy change, which has been expressed in thermodynamic treatments as the balance between the effects of energy (enthalpy) change and entropy change. The entropy of a system is related to the number of ways in which microscopic particles can be distributed among states accessible to them. The enthalpy (*H*), the entropy (*S*), and the free energy (*G*) are thermodynamic state functions (Ref 1, 2).

Free Energy and Chemical Potential. The Gibbs free energy (*G*) is the result of its enthalpy (*H*) and its entropic factor (*TS*): $G = H - TS$, where *T* is the absolute temperature (in Kelvin) (Ref 2). The partial molar free energy for a substance A is equal to $(\partial G/\partial n_A)_{n_i \neq n_A}, T, P$, where n_A and n_i are the number of moles of A and any other constituent *i* and *P* is the pressure. It is usually called chemical potential (μ_A) and depends not only on the chemical formula of the species involved but also on its activity (a_A) (corrected concentration—see end of this section):

$$(\partial G/\partial n_A)_{n_i \neq n_A, T, P} = \mu_A = \mu_A^0 + RT \ln a_A \quad \text{(Eq 1)}$$

where *R* is the gas constant (8.3143 J/K · mol), and μ_A^0 is the standard chemical potential of A; that is, the chemical potential of A in an arbitrarily selected state. If A is a pure condensed substance, a_A is equal to unity; if A is a species in solution, a_A is equal to the product of the concentration of A (usually molality m_A in number of moles of A per kilogram of solvent) by an activity coefficient (γ_A) representing the deviation from ideal behavior.

The standard state for a gaseous substance is the substance under a pressure such that its fugacity is 1 bar (0.1 MPa), for most gases a pressure of ~1 atm. The standard state for a condensed substance is the pure substance at the given temperature (*T*) and under pressure (*P*). The standard state for a dissolved species is the hypothetical ideal solution of the species with unit molality (mol/kg) at *T* and *P*. The μ_A^0 is dependent on the temperature and, for a condensed substance, also on the pressure (this dependence is small and usually neglected for pressures not too far from 1 bar). The usual convention is to assign the value 0 to the chemical potentials of the elements in their stable form and standard state at 25 °C (77 °F), for example, pure gaseous H_2 and O_2 at fugacity equal to 1 bar, solvated protons at activity unity. Hence, the standard chemical potential of a substance is equal to its standard Gibbs free energy of formation from its elements at 25 °C (77 °F) under 1 bar pressure.

Law of Chemical Equilibria. Consider the following chemical reaction:

$$\Sigma\nu_R R \leftrightarrow \Sigma\nu_P P \quad \text{(Eq 2)}$$

where R and P designate the reactants and products, respectively, and ν_R and ν_P are the associated stoichiometric coefficients.

The molar Gibbs free energy change for this reaction is:

$$\Delta_r G = \Sigma\nu_P\mu_P - \Sigma\nu_R\mu_R \quad \text{(Eq 3)}$$

where μ_P and μ_R are the chemical potentials of the products and reactants, respectively. If the chemical potentials are expressed as in Eq 1, one obtains:

$$\Delta_r G = \left(\Sigma \nu_P \mu_P^o - \Sigma \nu_R \mu_R^o\right) + RT\left(\Sigma \nu_P \ln a_P - \Sigma \nu_R \ln a_R\right) = \Delta_r G^0 + RT \ln\left(\frac{\Pi a_P^{\nu P}}{\Pi a_R^{\nu R}}\right) \quad \text{(Eq 4)}$$

where R is the gas constant, Π is the symbol for multiplying a series of terms, a_P and a_R are the activities of the products and reactants, respectively, and $\Delta_r G^0$ is the standard free energy change for the reaction:

$$\Delta_r G^0 = \Sigma \nu_P \mu_P^o - \Sigma \nu_R \mu_R^o \quad \text{(Eq 5)}$$

When the reaction is in thermodynamic equilibrium (there is no tendency for the reaction to proceed either forward or backward), it has been shown that its molar Gibbs free energy change ($\Delta_r G$) is equal to zero (Ref 2). Then, from Eq. 4 the classic equilibrium law is obtained:

$$\frac{\Pi a^{\nu P}}{\Pi a^{\nu R}} = K_{eq} \quad \text{(Eq 6)}$$

where K_{eq} is the equilibrium constant for the reaction at the temperature T:

$$K_{eq} = \exp\left(-\frac{\Delta_r G^0}{RT}\right) \quad \text{(Eq 7)}$$

The standard chemical potentials, or free energies of formation, of an extensive number of compounds have been cataloged for various temperatures. Typical data sources are listed as the Selected References. This allows the prediction of standard free energy changes and equilibrium constants for reactions over a wide range of conditions.

References cited in this section

1. J.M. Smith and H.C. Van Hess, *Introduction to Chemical Engineering Thermodynamics,* McGraw-Hill, 1975, p 159–162

2. K. Denbigh, *Principles of Chemical Equilibrium,* 2nd ed., Cambridge Press, 1981, p 133–186

E. Protopopoff and P. Marcus, Electrode Potentials, *Corrosion: Fundamentals, Testing, and Protection,* Vol 13A*, ASM Handbook,* ASM International, 2003, p 8–12

Electrode Potentials

E. Protopopoff and P. Marcus, Ecole Nationale Supérieure de Chimie de Paris, Université Pierre et Marie Curie

---

Reactions in Aqueous Solution

Galvanic Cell Reactions. If a strip of metal is placed in water, some metal atoms will be oxidized into hydrated (solvated) ions. Because of the electrons remaining in the metal (called an *electrode*), the positively charged metallic ions will remain very close to the negatively charged metal strip in a double layer, where a very high potential gradient exists, as described in the article “Electrode Processes” in this Volume. Thus, a potential difference will exist between the metal and the solution. This potential difference is not measurable, but it is possible to measure the potential difference between this system and another metal-ion system. If a zinc electrode placed in a solution of zinc ions is linked through an electric circuit including a voltmeter to a copper electrode placed in a solution of copper ions (Fig. 1), a positive potential difference will be measured between the copper electrode and the zinc electrode. This is evidence that copper is a more noble metal than zinc and has

less tendency to oxidize. This can be checked directly by the chemical reaction in Eq 8; if zinc is put into a solution containing copper ions, zinc will dissolve, while copper will deposit from its ions on to the zinc. This metal-displacement reaction is due to the oxidation-reduction reaction between zinc metal and copper ions:

$$Zn(s) + Cu^{2+}(aq) \rightarrow Zn^{2+}(aq) + Cu(s) \qquad \text{(Eq 8)}$$

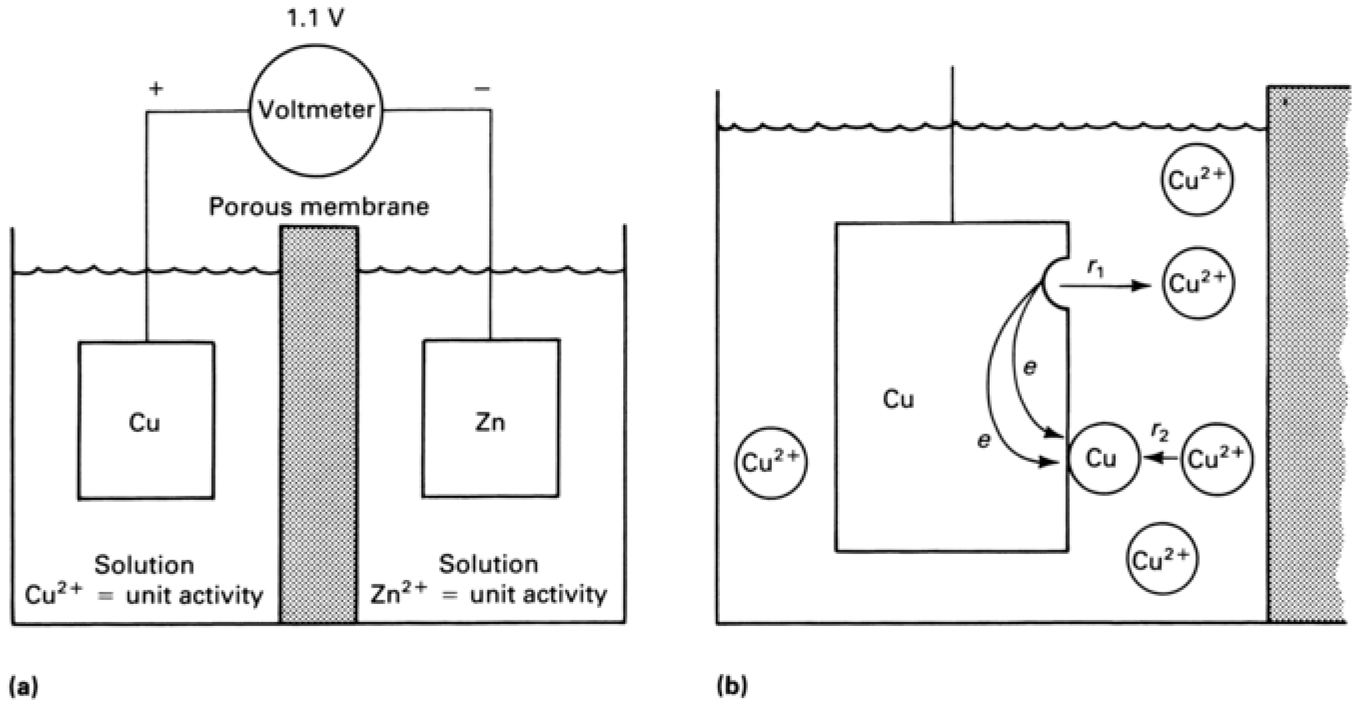

Fig. 1 Typical electrochemical cell (a) used to study the free energy change that accompanies electrochemical or corrosion reactions. In this example, the cell contains copper and zinc electrodes in equilibrium, with their ions separated by a porous membrane to mitigate mixing. For purposes of simplicity, the concentration of metal ions is maintained at unit activity; that is, each solution contains approximately 1 mole of metal ion per liter. The reactions for copper and zinc electrodes in each half-cell are given in Eq 9 and 10. However, at equilibrium, metal dissolution and deposition occur at each electrode at equal rates ($r_1 = r_2$), as shown in (b), which illustrates copper atoms being oxidized to cupric ions and, at other areas, cupric ions being reduced to metallic copper. Source: Ref 3

This reaction takes place spontaneously, because the standard free energy change associated with it ($\Delta_r G^0 = \mu^0_{Zn^{2+}} + \mu^0_{Cu} - \mu^0_{Zn} - \mu^0_{Cu^{2+}}$) is negative. Zinc metal will react with copper ions almost to completion; the reaction will stop only when the concentration of copper ions is very small and such that equilibrium is reached, with $\Delta_r G = \Delta_r G^0 + RT \ln a_{Zn^{2+}}/a_{Cu^{2+}} = 0$. If the reverse procedure is tried, that is, copper metal placed in a solution containing zinc ions, because it is associated with a strongly positive standard free energy change, the reaction will occur to only a very small extent, with the reaction stopping when a certain very small concentration of copper ions has been produced, such that equilibrium is reached.

The same reaction may be studied in an electrochemical cell, such as the one shown and described in Fig. 1(a). An electric circuit links a copper electrode in a solution of copper sulfate to a zinc electrode in a solution of zinc sulfate. If the external conduction path is closed, the oxidation-reduction reaction in Eq 8 will take place but under the form of two spatially separated electron-transfer reactions occurring each at one electrode, which are:

- An oxidation-dissolution reaction involving the extraction of electrons from outer metal atoms to form metallic ions at the zinc electrode, called the anode:

$$Zn(s) \rightarrow Zn^{2+}(aq) + 2e^- \qquad \text{(Eq 9)}$$

- A reduction-deposition reaction involving the addition of electrons to the metallic ions to form metal atoms deposited at the copper electrode, called the cathode:

$$Cu^{2+}(aq) + 2e^{-} \rightarrow Cu(s) \qquad \text{(Eq 10)}$$

Electrons will flow from the zinc anode where they are produced to the copper cathode where they are consumed; the two half-reactions in Eq 9 and 10 naturally combine in the electrochemical cell to form the oxidation-reduction reaction of Eq 8, termed the *chemical cell reaction.* They are referred to as *electrochemical, electrode,* or *half-cell reactions.* The requirement for writing the equation of the overall reaction by combination of the oxidation and reduction half-cell reactions is that the same number of electrons should be produced or consumed at each electrode. At equilibrium, $\Delta_r G = 0$, the electron flow stops, and oxidation and reduction reactions occur at each electrode with equal rates, as shown schematically in Fig. 1(b) for the case of copper dissolution and deposition.

Electrochemical cells in which the electrode reactions take place spontaneously and give rise to an electron flow are called galvanic cells. The chemical energy produced by the cell reaction during the transformation of reactants with high overall free energy into products with low overall free energy can be converted through the electron flow into electrical energy. This principle is used in batteries and fuel cells. The external circuit can be replaced with a direct current (dc) power supply, which will force electrons to go in a direction opposite to the one they tend to go naturally and make the cell reaction proceed in the backward direction to create chemical substances with high overall free energy. This process thus converts electrical into chemical energy and is used in electrolytic cells or battery charging.

Corrosion Reactions. The two types of cell processes described previously are of interest when dealing with corrosion. Corrosion reactions are similar to galvanic cells, with the two electrodes being different parts of the metal. Anodic dissolution takes place on certain zones of the surface of a metal and is coupled to cathodic reactions taking place on other zones. The short circuit provided by the conducting metal leads to a continuous metal dissolution. However, application of external potentials, as in electrolytic cells, can be used to protect metals (see the article “Cathodic Protection” in this Volume).

While the anodic dissolution involves only the metallic phase, the reduction reaction (cathodic reaction) involves the environment. Several different cathodic reactions (consuming electrons) are encountered in metallic corrosion in aqueous systems. The most common are:

- Proton reduction (in acid media):

$$2H^{+}(aq) + 2e^{-} \rightarrow H_2$$

- Water reduction (in neutral or basic media):

$$2H_2O(l) + 2e^{-} \rightarrow H_2 + 2OH^{-}(aq)$$

- Reduction of dissolved oxygen:

$$O_2 + 4H^{+}(aq) + 4e^{-} \rightarrow 2H_2O(l) \quad \text{(in acid media)}$$

$$O_2 + 2H_2O(l) + 4e^{-} \rightarrow 4OH^{-}(aq)$$
$$\text{(in neutral or basic media)}$$

- Metal ion reduction:

$$M^{3+}(aq) + e^{-} \rightarrow M^{2+}(aq)$$

- Metal deposition:

$$M^{2+}(aq) + 2e^- \rightarrow M$$

Proton reduction in acidic media is very common, and oxygen reduction is also often encountered, because aqueous solutions in contact with air contain significant amounts of dissolved oxygen. Metallic ion reduction and metal deposition are less common and are encountered most often in chemical process streams (Ref 4).

References cited in this section

3. M.G. Fontana, *Corrosion Engineering,* 3rd ed., McGraw-Hill, 1986, p 448

4. M.G. Fontana, *Corrosion Engineering,* 2nd ed., McGraw-Hill, 1978, p 251–303

E. Protopopoff and P. Marcus, Electrode Potentials, *Corrosion: Fundamentals, Testing, and Protection,* Vol 13A*, ASM Handbook,* ASM International, 2003, p 8–12

Electrode Potentials

E. Protopopoff and P. Marcus, Ecole Nationale Supérieure de Chimie de Paris, Université Pierre et Marie Curie

---

Thermodynamics of Electrochemical Equilibria

The Electromotive Force of Galvanic Cells. Consider the following two simple half-cell reactions: oxidation at electrode 1:

$$c_1R_1 \rightarrow b_1O_1 + ne^- \qquad \text{(Eq 11)}$$

and reduction at electrode 2:

$$b_2O_2 + ne^- \rightarrow c_2R_2 \qquad \text{(Eq 12)}$$

where R_i represents a reduced species; O_i is an oxidized species; and b_i, c_i are stoichiometric coefficients, and n is an integer.

It is assumed that the spontaneous galvanic cell reaction is the following:

$$b_2O_2 + c_1R_1 \rightarrow b_1O_1 + c_2R_2 \qquad \text{(Eq 13)}$$

If the resistance between the electrodes of the galvanic cell is made very high, so that very little current flows, the extent of reaction being small enough not to change the activities of reactants and products, the potential difference between the two electrodes remains constant and is the maximum cell voltage, called the electromotive force (emf) of the cell. The electrical energy produced is then maximum and equal for the transformation of 1 mole of reactants to the absolute value of the molar free energy of the cell chemical reaction:

$$|\Delta_r G| \approx \text{Charge passed} \times \text{Potential difference}$$

Conversely, if the cell reaction is driven by an outside source of electric power to go against its spontaneous tendency (as in an electrolytic or charging cell), $|\Delta_r G|$ is the minimum energy required to drive the backward reaction. Under ideal thermodynamically reversible conditions, where infinitesimal currents are allowed to flow in one or another direction, the cell reaction is at equilibrium, and the perfect equality holds. A noteworthy property is that, whatever the direction of the cell reaction, the polarity of each electrode remains unchanged (see Fig. 1a, Ref 5). If the cell reaction as written in Eq 13 proceeds spontaneously, the electrons flow into an external circuit from electrode 1 where electrons are produced (Eq 11) to electrode 2 where electrons are consumed (Eq 12). Electrode 2 is a cathode, and its polarity is positive. Electrode 1 is an anode, and its polarity is negative. Conversely, if the cell reaction is driven backward by an outside electric power source, the electrons are forced to flow in the opposite direction (from electrode 2 to 1), and half-reactions 1 and 2 are reversed, so electrode 1 becomes a cathode, and electrode 2 becomes an anode, but the polarities of the two

electrodes are left unchanged. Hence, the magnitude and the sign of the cell voltage at equilibrium (emf) depend only on the couple of half-reactions involved. From the thermodynamic convention, the free energy change of a spontaneous cell reaction, which liberates energy, is negative. If the emf is the potential of electrode 2 minus the potential of electrode 1 ($\Delta E = E_2 - E_1$), and if $\Delta_r G$ designates the free energy of the cell reaction written in the sense of Eq 13, that is, reduction at electrode 2 (Eq 12) and oxidation at electrode 1 (Eq 11), the relation between $\Delta_r G$ and ΔE is:

$$\Delta_r G = -nF\Delta E \qquad \text{(Eq 14)}$$

where n is the number of electrons exchanged in both half-reactions, and F is the Faraday constant (96,487 coulombs) equal to the charge of 1 mole of electrons.

Using Eq 3 and 4, Eq 14 may be rewritten as:

$$\Sigma\nu_P\mu_P - \Sigma\nu_R\mu_R = \left(\Sigma\nu_P\mu_P^0 - \Sigma\nu_R\mu_R^0\right) + RT\ln\left(\frac{\Pi a_P^{\nu P}}{\Pi a_R^{\nu R}}\right) = -nF\Delta E \qquad \text{(Eq 15)}$$

Compared to a chemical equilibrium where, at a given temperature, the ratio $(\Pi a_P^{vP}/\Pi a_R^{vR})$ is equal to a constant K_{eq} (Eq 6), the electrochemical cell at equilibrium is a system with one more degree of freedom, because either the ratio of activities or the cell emf can impose on it.

If the cell reaction occurs under conditions in which the reactants and products are in their standard states, the equation becomes:

$$\Delta_r G^0 = \Sigma\nu_P\mu_P^0 - \Sigma\nu_R\mu_R^0 = -nF\Delta E^0 \qquad \text{(Eq 16)}$$

where ΔE^0 is the standard cell emf.

The Hydrogen Potential Scale. The absolute potential of an electrode, or even the potential difference between a metal electrode and the surrounding solution, cannot be determined experimentally. It is only possible to measure the voltage across an electrochemical cell, that is, the difference of potential between two identical wires connected to two electrodes. A potential scale may be defined by measuring all electrode potentials with respect to an electrode of constant potential, called the reference electrode. The reference electrode arbitrarily chosen to establish a universal potential scale is the standard hydrogen electrode (SHE). It consists of a platinized platinum electrode (wire or sheet) immersed in an aqueous solution of unit activity of protons, saturated with hydrogen gas at a fugacity of 1 bar. The half-cell reaction is the equilibrium:

$$H^+(aq) + e^- \rightleftharpoons \frac{1}{2}H_2(g) \qquad \text{(Eq 17)}$$

The SHE possesses the advantages of achieving its equilibrium potential quickly and reproducibly and maintaining it very stable with time (see comparison with other reference electrodes in the article “Potential Measurements with Reference Electrodes” in this Volume). From the convention, the SHE potential is taken as zero. The potential of any electrode can then be determined with respect to this zero reference and is called the potential of the electrode on the standard hydrogen scale, denoted $E_{(SHE)}$.

The Potential Sign Convention (Reduction Convention). Before establishing tables of standard potentials for various electrodes on the standard hydrogen scale, it is necessary to fix the convention for the sign of a standard potential value (E^0). The potential of any electrode is expressed with respect to the SHE by building (really or virtually) a cell in which the other electrode is a SHE. Consider a typical half-cell reaction with an oxidation-reduction (O/R) couple, where O represents the oxidized species and R the reduced species. The cell is represented as:

$$\text{Pt, } H_2(g)(f = 1 \text{ bar})|H^+(aq)(a = 1) \parallel \text{O/R} \qquad \text{(Eq 18)}$$

Depending on the position of the O/R electrode on the hydrogen scale, the spontaneous single electrode or half-cell reaction will proceed in one direction or the other: R oxidation: $c\text{R} \rightarrow b\text{O} + ne^-$ combined with proton reduction: $H^+(aq) + e^- \rightarrow \frac{1}{2}H_2(g)$; or, O reduction: $b\text{O} + ne^- \rightarrow c\text{R}$ combined with hydrogen oxidation: $\frac{1}{2}H_2(g) \rightarrow H^+(aq) + e^-$.

For example, the coupling of the oxidation/ reduction couple Fe^{2+}/Fe with the H^+/H_2 couple brings about the spontaneous oxidation of iron (the free energy of the cell reaction ΔG_{ox}^{Fe} is negative, the Fe^{2+}/Fe electrode is negative). The situation is entirely different with a Cu^{2+}/Cu system. If coupled with the H^+/H_2 couple, the

reduction of copper ions is spontaneous (ΔG^{Cu}_{red}, negative; ΔG^{Cu}_{ox}, positive, the polarity of the Cu^{2+}/Cu electrode is positive). The difference between these two metal couples in the direction of the spontaneous reaction with respect to the hydrogen couple must be represented by a sign. This sign will allow cataloging cell potentials from single electrode values and hence compute cell emfs. It was shown previously that the polarity of each electrode in an electrochemical cell is invariant, irrespective of whether the electrode reactions proceed in the spontaneous or the reverse direction. The most meaningful convention is to assign to the potential of the O/R electrode the same sign as its experimentally observed polarity in the cell connecting this electrode to the SHE (Eq 18). The potential of the O/R couple on the standard hydrogen scale, in volts, denoted $E_{O/R(SHE)}$, is thus equal to the cell voltage measured as the potential of the O/R electrode minus the potential of the SHE (zero by convention). When the O/R electrode is in equilibrium, the whole cell is also in equilibrium, and the equilibrium electrode potential versus SHE may be obtained by applying Eq 14 to this particular cell:

$$\Delta G_{red} = -nFE_{O/R(SHE)} \qquad \text{(Eq 19)}$$

where ΔG_{red} is the molar free energy change of the balanced reaction of reduction of the oxidized species O by $H_2(g)$:

$$b\mathrm{O} + \frac{n}{2}\mathrm{H}_2(g) \leftrightarrow c\mathrm{R} + n\mathrm{H}^+(\mathrm{aq}) \qquad \text{(Eq 20)}$$

Then:

$$\mathrm{E}_{O/R(SHE)} = -\frac{\Delta G_{red}}{nF} = +\frac{\Delta G_{ox}}{nF} = \frac{b\mu_O - c\mu_R + \frac{n}{2}\mu^0_{H_2}(g) - n\mu^0_{H^+}(aq)}{nF} \qquad \text{(Eq 21)}$$

This *equilibrium potential,* called the *reversible potential,* is the electrode potential measured under zero current (rest potential) when the electrochemical equilibrium between O and R occurs at the electrode-electrolyte interface.

At the International Union of Pure and Applied Chemistry (IUPAC) meeting held in Stockholm in 1953, it was decided that the half-cell reactions should be conventionally written in the reduction direction:

$$b\mathrm{O} + ne^- \leftrightarrow c\mathrm{R} \qquad \text{(Eq 22)}$$

and the corresponding equilibrium potentials referred to the SHE obtained from the relation in Eq 21. The reaction as written in Eq 22 stands implicitly for the overall chemical reaction in Eq 20; the electrode equilibrium potential is conveniently written as:

$$\mathrm{E}_{O/R(SHE)} = \frac{\left(b\mu_O + n\mu^0_{e^-} - c\mu_R\right)}{nF} \qquad \text{(Eq 23)}$$

where $\mu^0_{e^-}$ is the standard chemical potential or Gibbs free energy of a conventional electron, equal to $\mu^0_{H_2}(g) - \mu^0_{H_+}(aq)$. It may be checked that:

$$E^0_{H^+/H_2(SHE)} = \mu^0_{H^+}(aq) + \mu^0_{e^-} - \tfrac{1}{2}\mu^0_{H_2}(g) = 0 \qquad \text{(Eq 24)}$$

The IUPAC convention selects the reduction as the conventional direction for writing electrochemical reactions. This is, of course, not necessarily the spontaneous direction of a reaction, so the corresponding Gibbs free energy change may be positive and the potential negative. As a result of this reduction convention, the potential of the Fe^{2+}/Fe electrode has a negative sign and the one of Cu^{2+}/Cu a positive sign. A negative sign indicates a trend toward corrosion in the presence of H^+ ions; that is, the metallic cations have a greater tendency to exist in aqueous solution than the protons. A positive sign indicates, on the contrary, that the proton is more stable than the metallic cations. It is to be noted that there was another convention, called the American convention, where the equation $\Delta G = -nFE$ is applied to the reactions written in the oxidation direction. This leads to opposite signs for all oxidation/reduction couples. The advantage of the IUPAC convention, now used worldwide, is that the electrode potential signs correspond to the real polarities measured when the electrode of

interest is connected to the standard H^+/H_2 electrode and hence are fixed for a given O/R couple, whether reduction or oxidation is considered.

The Nernst Equation. If the chemical potentials in Eq 23 are developed using Eq 1, the following expression of the equilibrium or reversible potential for half-cell reaction, known as the Nernst equation, is obtained:

$$E_{O/R} = E^0_{O/R} + \frac{RT}{nF} \ln \frac{(a_O)^b}{(a_R)^c} \qquad \text{(Eq 25)}$$

where a_O and a_R are the activities of the oxidized and reduced species, respectively, and $E^0_{O/R}$ is the standard electrode potential referred to the SHE, corresponding to unit activity of both species:

$$E^0_{O/R} = -\frac{\Delta G^0_{red}}{nF} = +\frac{\Delta G^0_{ox}}{nF} = \frac{\left(b\mu^0_O + n\mu^0_{e^-} - c\mu^0_R\right)}{nF} \qquad \text{(Eq 26)}$$

Equation 25 shows that the equilibrium potential increases with the ratio of the activities of the oxidized form to the reduced form.

Reference cited in this section

5. L. Pauling, *General Chemistry,* W.H. Freeman, 1964, p 338–360

E. Protopopoff and P. Marcus, Electrode Potentials, *Corrosion: Fundamentals, Testing, and Protection*, Vol 13A, *ASM Handbook*, ASM International, 2003, p 8–12

Electrode Potentials

E. Protopopoff and P. Marcus, Ecole Nationale Supérieure de Chimie de Paris, Université Pierre et Marie Curie

---

Cell Potentials and the Electromotive Force Series

The standard equilibrium potentials measured at 25 °C (77 °F) relative to the SHE for various metal-ion electrodes can be tabulated in a series, called the emf series, shown in Table 1.

Table 1 Series of standard electrode potentials (electromotive forces)

See also (Fig. 2), which shows a schematic of an electrochemical cell used to determine the potential difference of the zinc electrodes versus SHE.

Electrode reaction	Standard potential at 25 °C (77 °F), volts versus SHE
$Au^{3+} + 3e^- \rightarrow Au$	1.50
$Pd^{2+} + 2e^- \rightarrow Pd$	0.987
$Hg^{2+} + 2e^- \rightarrow Hg$	0.854
$Ag^+ + e^- \rightarrow Ag$	0.800
$Hg_2^{2+} + 2e^- \rightarrow 2Hg$	0.789
$Cu^+ + e^- \rightarrow Cu$	0.521
$Cu^{2+} + 2e^- \rightarrow Cu$	0.337
$2H^+ + 2e^- \rightarrow H_2$	0.000 (Reference)
$Pb^{2+} + 2e^- \rightarrow Pb$	-0.126

$Sn^{2+} + 2e^- \rightarrow Sn$	-0.136
$Ni^{2+} + 2e^- \rightarrow Ni$	-0.250
$Co^{2+} + 2e^- \rightarrow Co$	-0.277
$T1^+ + e^- \rightarrow T1$	-0.336
$In^{3+} + 3e^- \rightarrow In$	-0.342
$Cd^{2+} + 2e^- \rightarrow Cd$	-0.403
$Fe^{2+} + 2e^- \rightarrow Fe$	-0.440
$Ga^{3+} + 3e^- \rightarrow Ga$	-0.53
$Cr^{3+} + 3e^- \rightarrow Cr$	-0.74
$Cr^{2+} + 2e^- \rightarrow Cr$	-0.91
$Zn^{2+} + 2e^- \rightarrow Zn$	-0.763
$Mn^{2+} + 2e^- \rightarrow Mn$	-1.18
$Zr^{4+} + 4e^- \rightarrow Zr$	-1.53
$Ti^{2+} + 2e^- \rightarrow Ti$	-1.63
$Al^{3+} + 3e^- \rightarrow Al$	-1.66
$Hf^{4+} + 4e^- \rightarrow Hf$	-1.70
$U^{3+} + 3e^- \rightarrow U$	-1.80
$Be^{2+} + 2e^- \rightarrow Be$	-1.85
$Mg^{2+} + 2e^- \rightarrow Mg$	-2.37
$Na^+ + e^- \rightarrow Na$	-2.71
$Ca^{2+} + 2e^- \rightarrow Ca$	-2.87
$K^+ + e^- \rightarrow K$	-2.93
$Li^+ + e^- \rightarrow Li$	-3.05

For example, the standard electrode potential for zinc—the accepted value for which is -0.763 V/SHE (Table 1)—is obtained by measuring the emf of a cell made of a SHE and a zinc electrode in a zinc salt solution of unit activity (Fig. 2). As described previously, the emf is a measurement of the maximum potential that exists in the galvanic cell when zero current is flowing between the electrode and the SHE.

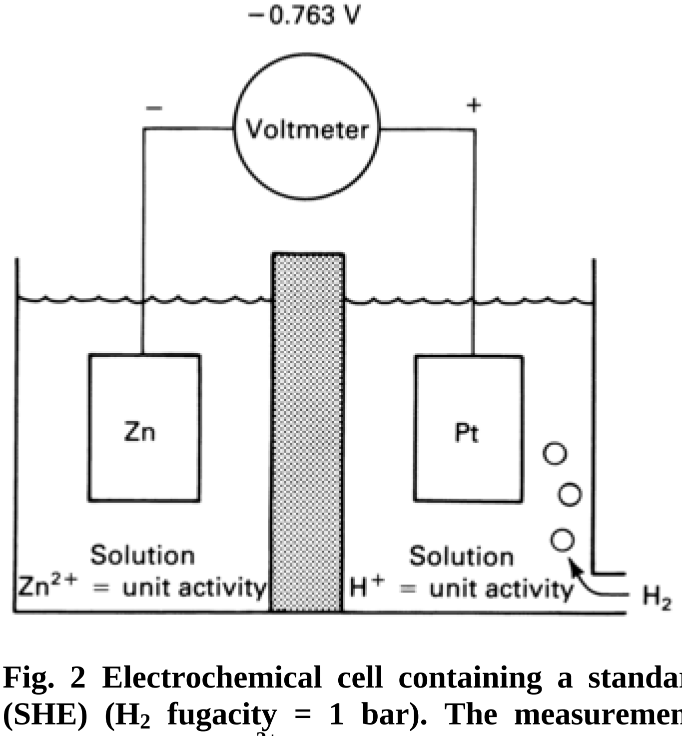

Fig. 2 Electrochemical cell containing a standard zinc electrode and a standard hydrogen electrode (SHE) (H_2 fugacity = 1 bar). The measurement of the cell voltage gives the standard equilibrium potential of the Zn^{2+}/Zn couple versus SHE.

This procedure can be repeated by exchanging the zinc electrode with any other metal, and the surrounding electrolyte by a solution of metal ion, in order to obtain the series of standard half- cell potentials listed in Table 1. The position of a particular metal in the emf series gives an indication of the tendency of the metal to be oxidized. The higher the metal is on the potential scale, the more noble it is and resistant to oxidation; the lower

on the scale it is, the more easily oxidized it is. The metals listed in Table 1 below the H^+/H_2 couple (SHE) are easily oxidized and reduce protons into H_2(g), while the metals listed above the SHE have their metal ions reduced into metal by H_2(g). However, care should be taken when predicting the behavior of a metal from the data in Table 1, because they are given for standard conditions, usually not close to the real corrosion conditions. Changes in concentration (i.e., activity) or temperature will change the electrode potentials according to Eq 25. The comparison between the standard potentials of half-cells from Table 1 is used to predict the abilities of metals to reduce other metal ions from solution. For example, consider the Daniell cell, constituted as follows:

$$Zn \mid Zn^{2+},\ SO_4^{2-} \parallel Cu^{2+},\ SO_4^{2-} \mid Cu \qquad \text{(Eq 27)}$$

The potential of the Cu^{2+}/Cu couple is higher than the potential of the Zn^{2+}/Zn couple. If the electrodes are coupled together in a galvanic cell, electrons will flow from the zinc electrode, which produces electrons via the oxidation reaction, through the external circuit to the copper electrode, which consumes electrons via the reduction reaction. The calculated standard emf for this cell is $\Delta E^0 = E^0(Cu^{+2}/Cu) - E^0(Zn^{+2}/Zn) = +0.337 - (-0.763) = +1.100$ V/SHE. Then, the standard free energy for the cell reaction is (Eq 16) $\Delta_r G^0 = -2F\Delta E^0 = -212.3$ kJ/mol. Its sign indicates that there is a natural tendency for zinc atoms to reduce cupric ions and be oxidized into Zn^{2+} (Eq 8).

It is important to note that the calculated equilibrium potentials are for a very specific condition (standard state) and may not apply to a specific corrosion environment; also, there are thermodynamic quantities that do not take into account the factors that may limit a reaction, such as slow kinetics or protection by corrosion product layers. More complete emf series (Ref 6, 7) and potentials in other environments (Ref 8) are available.

References cited in this section

6. A.J. Bard, R. Parsons, and J. Jordan, *Standard Potentials in Aqueous Solutions,* Marcel Dekker, 1985

7. W.M. Latimer, *Oxidation Potentials,* Prentice-Hall, 1964

8. F.L. La Que, *Corrosion Handbook,* H.H. Uhlig, Ed., John Wiley & Sons, 1948, p 416

E. Protopopoff and P. Marcus, Electrode Potentials, *Corrosion: Fundamentals, Testing, and Protection*, Vol 13A*, ASM Handbook*, ASM International, 2003, p 8–12

Electrode Potentials

E. Protopopoff and P. Marcus, Ecole Nationale Supérieure de Chimie de Paris, Université Pierre et Marie Curie

---

Acknowledgment

Portions of this article have been adapted from C.A. Natalie, Electrode Potentials, *Corrosion,* Vol 13, *Metals Handbook,* 9th ed., ASM International, 1987, p 19–21.

E. Protopopoff and P. Marcus, Electrode Potentials, *Corrosion: Fundamentals, Testing, and Protection*, Vol 13A*, ASM Handbook*, ASM International, 2003, p 8–12

Electrode Potentials

E. Protopopoff and P. Marcus, Ecole Nationale Supérieure de Chimie de Paris, Université Pierre et Marie Curie

---

References

1. J.M. Smith and H.C. Van Hess, *Introduction to Chemical Engineering Thermodynamics,* McGraw-Hill, 1975, p 159–162

2. K. Denbigh, *Principles of Chemical Equilibrium,* 2nd ed., Cambridge Press, 1981, p 133–186

3. M.G. Fontana, *Corrosion Engineering,* 3rd ed., McGraw-Hill, 1986, p 448

4. M.G. Fontana, *Corrosion Engineering,* 2nd ed., McGraw-Hill, 1978, p 251–303

5. L. Pauling, *General Chemistry,* W.H. Freeman, 1964, p 338–360

6. A.J. Bard, R. Parsons, and J. Jordan, *Standard Potentials in Aqueous Solutions,* Marcel Dekker, 1985

7. W.M. Latimer, *Oxidation Potentials,* Prentice-Hall, 1964

8. F.L. La Que, *Corrosion Handbook,* H.H. Uhlig, Ed., John Wiley & Sons, 1948, p 416

E. Protopopoff and P. Marcus, Electrode Potentials, *Corrosion: Fundamentals, Testing, and Protection*, Vol 13A*, ASM Handbook,* ASM International, 2003, p 8–12

Electrode Potentials

E. Protopopoff and P. Marcus, Ecole Nationale Supérieure de Chimie de Paris, Université Pierre et Marie Curie

---

Selected References

- J.W. Cobble, R.C. Murray, Jr., P.J. Turner and K. Chen, High-Temperature Thermodynamic Data for Species in Aqueous Solution, San Diego State University Foundation, Electric Power Research Institute (EPRI) Report NP- 2400, EPRI, May 1982
- K.C. Mills, *Thermodynamic Data for Inorganic Sulfides, Selenides and Tellurides,* Butterworths, 1974
- D.R. Stull and H. Prophet, JANAF Thermochemical Tables, National Bureau of Standards, NSRDS-NBS 37, U.S. Government Printing Office, Washington, D.C., 1971
- D.D. Wagman, W.H. Evans, V.B. Parker, R.H. Schumm, I. Halow, S.M. Bailey, K.L. Churney, and R.L. Nuttall, *J. Phys. Chem. Ref. Data,* Vol 11 (Supplement 2), 1982

E. Protopopoff and P. Marcus, Potential Measurements with Reference Electrodes, *Corrosion: Fundamentals, Testing, and Protection,* Vol 13A, *ASM Handbook*, ASM International, 2003, p 13–-16

Potential Measurements with Reference Electrodes

E. Protopopoff, Laboratoire de Physico-Chimie des Surfaces, CNRS, and P. Marcus, Ecole Nationale Supérieure de Chimie de Paris, Université Pierre et Marie Curie

Introduction

ELECTRODE POTENTIAL MEASUREMENT is an important aspect of corrosion studies and corrosion prevention. It is included in any determination of the corrosion rate of metals and alloys in various environments and in the control of the potential in cathodic and anodic protection. The potential of an electrode can be determined only by measuring the voltage in an electrochemical cell between this electrode and an electrode of constant potential, called the reference electrode. Many errors and problems can be avoided by careful selection of the best reference electrode for a specific case and by knowledge of the electrochemical principles that control the potential measurements in order to obtain meaningful measurements. A reference electrode, once selected, must be properly used, taking into account the stability of its potential and the problem of ohmic (*IR*) drop. Many different reference electrodes are available, and others can be designed by the users themselves for particular situations. Each electrode has its characteristic rest potential value, which is used to convert potential values measured with respect to this reference into values expressed with respect to other references. In particular, the conversion of the potentials from or to the hydrogen scale is frequently required for use of potential- pH diagrams, which are discussed in the article "Potential versus pH (Pourbaix) Diagrams" in this Section of the volume.

E. Protopopoff and P. Marcus, Potential Measurements with Reference Electrodes, *Corrosion: Fundamentals, Testing, and Protection,* Vol 13A, *ASM Handbook*, ASM International, 2003, p 13–-16

Potential Measurements with Reference Electrodes

E. Protopopoff, Laboratoire de Physico-Chimie des Surfaces, CNRS, and P. Marcus, Ecole Nationale Supérieure de Chimie de Paris, Université Pierre et Marie Curie

The Three-Electrode Device

When a system is at rest and no significant current is flowing, the use of only one other electrode as a reference is sufficient to measure the test (or working) electrode potential versus the reference potential. When a current is flowing spontaneously in a galvanic cell or is imposed on an electrolytic cell, reactions at both electrodes are not at equilibrium, and there is consequently an overpotential on each of them. The potential difference measured between the two electrodes then includes the value of the two overpotentials, and it is not possible to determine the potential of the test electrode. To obtain this value, a third electrode, the auxiliary or counterelectrode, must be used (Fig. 1). In this arrangement, current flows only between the test and the auxiliary electrodes. A high-impedance voltmeter placed between the test and the reference electrodes prevents any significant current flow through the reference electrode, which then shows a negligible overpotential and remains very close to its rest potential. Most reference electrodes can be damaged by current flow. The test electrode potential and its changes under electric current flow can then be measured with respect to a fixed reference potential. The three- electrode system is widely used in laboratory and field potential measurement.

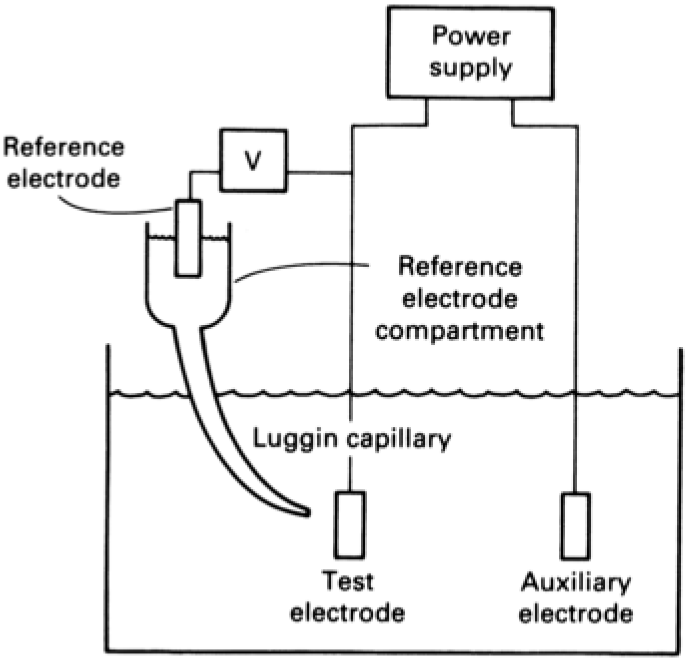

Fig. 1 Three-electrode device. V, voltmeter

E. Protopopoff and P. Marcus, Potential Measurements with Reference Electrodes, *Corrosion: Fundamentals, Testing, and Protection,* Vol 13A, *ASM Handbook,* ASM International, 2003, p 13–-16

Potential Measurements with Reference Electrodes

E. Protopopoff, Laboratoire de Physico-Chimie des Surfaces, CNRS, and P. Marcus, Ecole Nationale Supérieure de Chimie de Paris, Université Pierre et Marie Curie

Electrode Selection Characteristics

A good reference electrode must reach its potential quickly, be reproducible, and remain stable with time. It must have a practically nonpolarizable metal-solution interface; that is, its potential must not depart significantly from the equilibrium value on the passage of a small current across the interface. The potential of the junction between the electrolytes of the reference and test electrodes must be minimized. These criteria are detailed subsequently.

Stable and Reproducible Potential. Electrodes used as references should rapidly achieve a stable and reproducible potential that is free of significant fluctuations. To obtain these characteristics, it is advantageous, whenever possible, to use reversible electrodes, which can easily be made.

The reference electrode arbitrarily chosen to establish a universal potential scale is the standard hydrogen electrode (SHE). It consists of a platinized or black platinum wire or sheet immersed in an aqueous solution of unit activity of protons saturated with hydrogen gas at a fugacity of one bar (14.5 psia). The half-cell reaction is $H^+(aq) + e^- \leftrightarrow \frac{1}{2}H_2(g)$. Any non-standard reversible hydrogen electrode with well-controlled H^+ activity and H_2 fugacity can also be used as a reference. The equilibrium potential (E_{eq}) of a nonstandard reversible hydrogen electrode versus the SHE is, from the Nernst equation (Eq 25 of the article "Electrode Potentials" in this Section of the volume):

$$E_{eq(H^+/H_2)} = E^\circ_{(H^+/H_2)} + \frac{RT}{F}\ln\frac{a_{H^+}}{\sqrt{f_{H_2}}} \quad \text{(Eq 1)}$$

where R is the gas constant, T is the absolute temperature, F is the Faraday constant, a_{H^+} is the proton activity in solution, and f_{H_2} is the H_2 fugacity near the electrode; the SHE potential, $E^o_{(H^+/H_2)}$, is, by convention, equal to zero.

Platinization of a smooth platinum electrode is achieved by electrodeposition from a solution of H_2PtCl_6 of a black platinum layer having a very rough surface and hence a very high specific area. The electrolyte is made up of a mineral acid (HCl or H_2SO_4) with a well-defined activity of H^+. Hydrogen gas is bubbled on the black platinum.

While the hydrogen electrode is the fundamental reference, it has certain disadvantages in real conditions: the electrolyte must be prepared with an accurately known proton activity; the hydrogen gas must be purified, particularly from oxygen; furthermore, the platinum electrode must be frequently replatinized, because it easily gets "poisoned" by the adsorption of impurities present in the solution, which prevents the establishment of the equilibrium potential. For these reasons, practical corrosion measurements are usually not performed with the SHE but with secondary reference electrodes that are easier to construct and handle, less sensitive to impurities, and whose potential is very stable and well- known with respect to the SHE (Ref 1).

The simpler reference electrodes are metal-ion (M^{z+}/M) electrodes, also called metallic electrodes of the first kind. The copper-copper sulfate ($CuSO_4$/Cu) electrode is an excellent example of a good reversible electrode and it is widely used as a reference electrode in the corrosion field. It can easily be made by immersing a copper wire in a glass tube filled with a $CuSO_4$ aqueous solution and terminated by a porous plug (to allow ionic conduction with the cell electrolyte), as shown in Fig. 2.

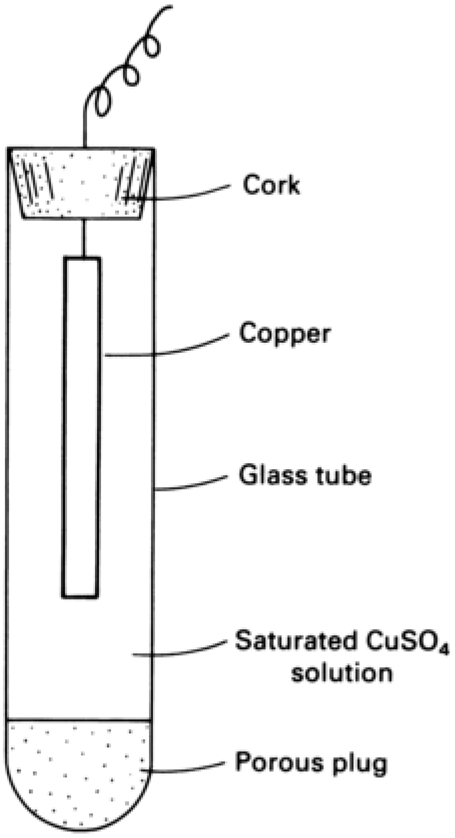

Fig. 2 Schematic of a copper/copper sulfate reference electrode

This electrode is reversible, because a small cathodic current produces the reduction reaction ($Cu^{2+} + 2e^- \rightarrow Cu$), while an anodic current brings about the oxidation reaction ($Cu \rightarrow Cu^{2+} + 2e^-$). Copper is a semi-noble metal and does not dissolve anodically in a solution of protons. In the case of the $CuSO_4$/Cu electrode, the rest potential is equal to the equilibrium potential that can be computed from the Nernst equation:

$$E_{eq(Cu^{2+}/Cu)} = E^0_{(Cu^{2+}/Cu)} + \frac{RT}{2F} \ln a^{2+}_{Cu} \qquad \text{(Eq 2)}$$

where the standard potential $E^o_{(Cu^{2+}/Cu)}$= +0.337 V versus SHE (see Table 1 in the article "Electrode Potentials" in this Volume), and $a_{Cu^{2+}}$ is the activity of Cu^{2+} in the aqueous solution. If a copper solution of

concentration 1.00 mol/L is used (where $a_{Cu^{2+}} < 1$), the equilibrium potential of the $CuSO_4$/Cu electrode takes the value +0.310 V versus SHE at 25 °C (77 °F). This well-defined reversible electrode is reliable and easy to build.

Another common metal-ion electrode is the silver electrode (Ag^+/Ag). The Nernst equation applied to the half-cell reaction $Ag^+ + e^- \leftrightarrow Ag$ gives:

$$E_{eq(Ag^+/Ag)} = E^o_{(Ag^+/Ag)} + \frac{RT}{F}\ln a_{Ag^+} \quad \text{(Eq 3)}$$

where the standard potential $E^o_{(Ag^+/Ag)}$ = 0.800 V versus SHE.

Metallic electrodes of the second kind (also called secondary reference electrodes) are similar electrodes where the potential-determining activity of the metallic ion, $a_{M^{z+}}$, in solution is controlled by putting the metal M in contact with a sparingly soluble M compound (salt, oxide, hydroxide), itself in contact with the solution. Then, $a_{M^{z+}}$ is determined by the solubility product of the salt and the activity of the anion.

For example, if silver chloride (AgCl), only slightly soluble in water, is present on the silver surface, then the following equilibrium holds:

$$AgCl \leftrightarrow Ag^+ + Cl^- \quad \text{(Eq 4)}$$

The equilibrium mass law gives the solubility product as $a_{Ag^+} \cdot a_{Cl^-} = K_{s(AgCl)}$. Expressing a_{Ag^+} from this relation and placing it in Eq 3 leads to the following expression of the equilibrium potential of the Ag^+, Cl^- /AgCl/Ag half-cell:

$$\begin{aligned} E_{(Ag^+,Cl^-/AgCl/Ag)} &= E^0_{(Ag^+/Ag)} + \frac{RT}{F}\ln K_{s(AgCl)} \\ &\quad - \frac{RT}{F}\ln a_{Cl^-} \\ &= E_{(Ag^+,Cl^-/AgCl/Ag)} - \frac{RT}{F}\ln a_{Cl^-} \end{aligned} \quad \text{(Eq 5)}$$

corresponding to the global electrode equilibrium:

$$AgCl + e^- \leftrightarrow Ag + Cl^- \quad \text{(Eq 6)}$$

The standard potential of this reversible silver-silver chloride (Ag/Cl) electrode is $E^o_{(Ag^+,Cl^-/AgCl/Ag)} = E^o_{(Ag^+/Ag)} +$ ln $K_{s(AgCl)}$. At 25 °C, (77 °F), because $E^o_{Ag^+/Ag}$ = 0.800 V/SHE and $K_{s(AgCl)} = 1.78 \cdot 10^{-10}$, $E^o_{(Ag^+,Cl^-/AgCl/Ag)}$ = +0.222 V/SHE (Ref 2). From Eq 5, the potential of this type of reference electrode depends on the activity of the anion in solution (Cl^- here), and this activity is controlled by the addition of a soluble salt of this anion (KCl). If a KCl solution of concentration 1.00 mol/L is used (where $a_{Cl^-} < 1$), the equilibrium potential of the AgCl/Ag electrode takes the value +0.237 V/ SHE at 25 °C (77 °F). In a saturated KCl solution (where $a_{Cl^-} > 1$), it is +0.198 V/SHE (Ref 2).

Figure 3 shows a typical Ag-AgCl electrode. The AgCl coating is made by anodization of the silver wire in a chloride-containing solution. This electrode is easily assembled and can be placed directly into the electrochemical cell. Quite similar are the $Pb/PbSO_4$ and the $Ag\text{-}Ag_2O$ (Ref 1, 2).

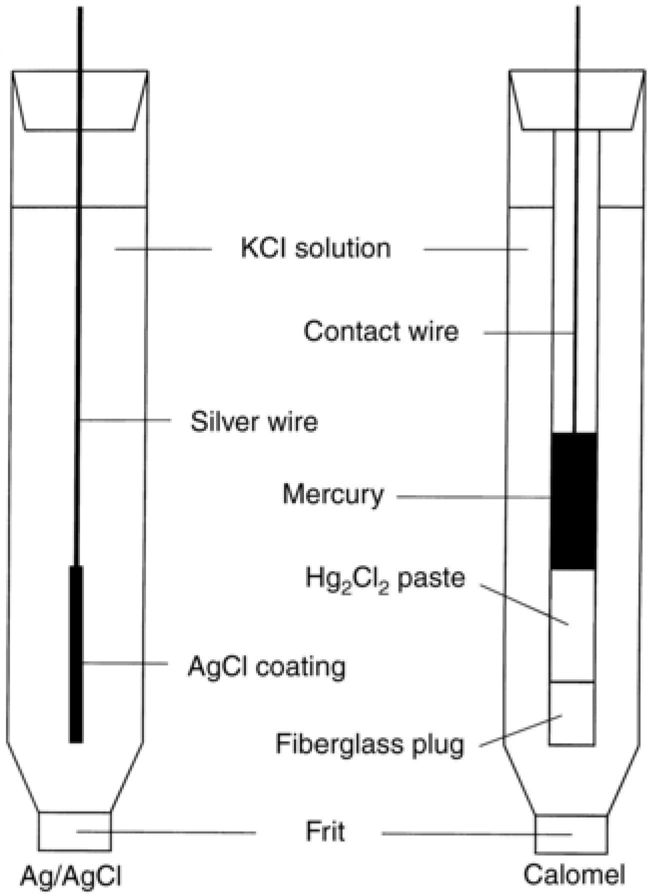

Fig. 3 Schematic of silver-silver chloride and calomel reference electrodes. Source: Ref 12

The most used secondary reference electrode is the calomel electrode ($Hg\text{-}Hg_2Cl_2$). The sparingly soluble salt is, in this case, calomel (Hg_2Cl_2) which floats as a paste on the top of a liquid mercury drop and which, in contact with a KCl solution, dissociates slightly into Hg_2^{2+} and Cl^- ions. Using the same method as for the Ag-AgCl electrode, the following relation is obtained:

$$E_{\left(Hg_2^{2+},Cl^-/Hg_2Cl_2/Hg\right)} = E^\circ_{Hg_2^{2+}/Hg} + \frac{RT}{2F}\ln K_{s(Hg_2Cl_2)} - \frac{RT}{F}\ln a_{Cl^-} = E^\circ_{\left(Hg_2^{2+},Cl^-/Hg_2Cl_2/Hg\right)} - \frac{RT}{F}\ln a_{Cl^-} \quad \text{(Eq 7)}$$

corresponding to the global electrode equilibrium:

$$Hg_2Cl_2 + 2e^- \leftrightarrow 2Hg + 2Cl^- \quad \text{(Eq 8)}$$

Figure 3 shows a typical calomel electrode. A platinum wire connects the electrode to the rest of the circuit. The most usual calomel electrodes are prepared with KCl solutions at a unit molarity of Cl^- (normal calomel electrode or NCE) or saturated calomel electrode or (SCE). At 25 °C (77 °F), $E_{Hg_2^{2+},Cl^-/Hg_2Cl_2/Hg}$ = 0.268 V/SHE, E_{NCE} = 0.281 V, and E_{SCE} = 0.242 V/SHE (Ref 2). The SCE has the advantage of being the easiest to prepare. However, due to the high temperature dependence of the KCl solubility, its potential varies markedly with temperature (~1 mV/°C as compared to 0.1 mV/°C for the NCE) (Ref 2), so its use makes mandatory the accurate monitoring of the temperature of experiment. Moreover, one must be careful when using a calomel electrode that only very low currents pass through the interface, because HgO may form, which irreversibly spoils the electrode.

Similar reference electrodes for measurements in aqueous solutions are the mercurous sulfate electrode (Hg_2^{2+}, $SO_4^{2-}/Hg_2SO_4/Hg$) in a solution of potassium sulfate, and the mercuric oxide electrode (Hg^{2+}, OH^-/HgO/Hg) in a solution of sodium hydroxide. Their potentials at 25 °C (77 °F) may be found in the literature (Ref 1, 2).

All of these secondary reference electrodes are reversible. In some practical cases, nonreversible electrodes such as graphite are used. Although not as good, their potential stability in a particular environment is considered sufficient for certain applications. In the selection of reference electrodes, their durability and price must also be considered.

Low Polarizability. A good reference electrode must have a practically nonpolarizable metal-solution interface; that is, its potential must not depart significantly from the equilibrium value on the passage across it of a small current (even minimized in the three-electrode device, Fig. 1), because the electrode polarization introduces an error in the potential measurement. The potential versus current density response of a good reference electrode, called a polarization curve, should be as flat as possible.

Consider that the electrode equilibrium is bO + ne^- = cR, where O is the oxidized species; R is the reduced species; and n is an integer. The net current density across the interface is proportional to the difference between the anodic and the cathodic rates. If the electrode reaction rate is limited by the electron transfer across the metal-solution interface (electron transfer is slow compared to mass transport of O and R between the bulk solution and the interface), the net current density is simply related to the overpotential $\eta = E - E_{eq}$, where E is the potential, and E_{eq} is the equilibrium potential, by (Ref 3):

$$i = i_0 \exp\left(\frac{-\alpha nF}{RT}\eta\right) - i_0 \exp\left(-\frac{(1-\alpha)nF\eta}{RT}\right) \quad \text{(Eq 9)}$$

where i_0 is the exchange current density of the electrode reaction; and α is the charge transfer coefficient for the anodic reaction ($0 < \alpha < 1$), whose value is close to 0.5 for a single-step reaction (n = 1). (More detailed information on polarization curves can be found in the articles "Kinetics of Aqueous Corrosion" and "Electrochemical Methods of Corrosion Testing" in this Volume).

For potentials close to the equilibrium potential, such as $\eta < RT/F$ (26 mV at room temperature), the relation (Eq 9) can be approximated by a linear i versus η dependence:

$$i = i_0\left(\frac{nF}{RT}\right)\eta \quad \text{(Eq 10)}$$

or

$$\eta = \left(\frac{RT}{nFi_0}\right)i \quad \text{(Eq 11)}$$

The term $RT/nFi_0 = (d\eta/di)_0$ is called the polarization resistance, R_p. A good reference electrode should have a low polarization resistance, which implies high exchange current density. This happens for high rate constants for the anodic and cathodic reactions and high concentrations of reacting species O and R. With regard to this criterion, the SHE that has $i_0 > 10^{-3}$ A/ geometric cm^2 is a particularly good reference electrode (Ref 3).

It is a question of judgment how polarizable the reference electrode can be. The answer depends on the precision required and the impedance of the voltmeter used. A high-impedance voltmeter (10^{12} ohms) may provide acceptable results with a relatively polarizable electrode.

The Liquid Junction Potential. Reference electrodes are usually made of a metal immersed in a well-defined electrolyte. In the case of the $CuSO_4$/Cu electrode, the electrolyte is a saturated $CuSO_4$ aqueous solution; for the SCE, it is a saturated KCl solution. This electrolyte that characterizes the reference electrode must come into contact with the liquid environment of the test electrode to complete the measuring circuit (Fig. 4). There is direct contact between different aqueous media. The difference in chemical composition of the two solutions produces a phenomenon of interdiffusion. In this process, except for a few electrolytes such as KCl, the cations and anions move at different speeds. As an example, in hydrogen chloride (HCl) solution in contact with another medium, the H^+ ions move faster than the Cl^- ions. As a result, a charge separation appears at the limit between the two liquids, the liquid junction. This produces a potential difference called the liquid junction potential, which is included in the measured voltage, V, as expressed in:

$$V = V_T - V_R + V_{LJP} \quad \text{(Eq 12)}$$

where V_T is the test potential to be measured, V_R is the reference electrode potential, and V_{LJP} is the unknown liquid junction potential.

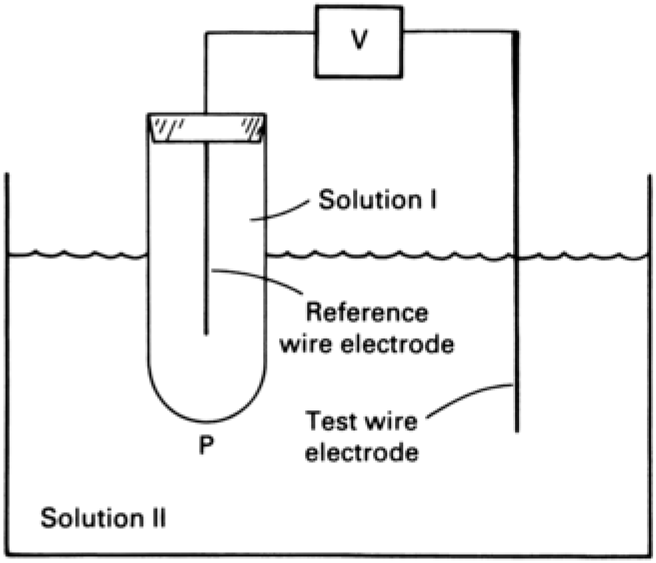

Fig. 4 Schematic of an electrochemical cell with liquid junction potential. P, interface; V, voltmeter

In order to determine V_T, the liquid junction potential must be eliminated or minimized. The best way, when possible, is to design a reference electrode using an electrolyte identical to the solution in which the test electrode is immersed (Fig. 4). However, in most cases this is not possible, and the best approach is to minimize the liquid junction potential by using a reference electrolyte with a chemical composition as close as possible to the corrosion environment. The use of a solution of KCl (such as in the calomel electrode) offers a partial answer. The diffusion rates of potassium (K^+) and chloride (Cl^-) ions are similar. In contact with another electrolyte, a KCl solution does not produce much charge separation and, consequently, no significant liquid junction potential. The ions present in the other solution, however, also diffuse, and they may do so at different rates, thus producing some separation of charge at the interface (P in Fig. 4).

The remaining liquid junction potential, after minimization, constitutes an error that is frequently accepted in electrode potential measurements, especially when compared with results determined under similar experimental conditions. While liquid junction potentials must be minimized as much as possible, there is no general solution for this; each individual case must be well thought out.

References cited in this section

1. D.J.G. Ives and J. Janz, *Reference Electrodes,* Academic Press, 1961

2. C.H. Hamann, A.H. Hamnett, W. Vielstich, *Electrochemistry,* Wiley-VCH, Weinheim, 1998

3. M.G. Fontana, *Corrosion Engineering,* 2nd ed., McGraw-Hill, 1978, p 12

E. Protopopoff and P. Marcus, Potential Measurements with Reference Electrodes, *Corrosion: Fundamentals, Testing, and Protection,* Vol 13A, *ASM Handbook*, ASM International, 2003, p 13–-16

Potential Measurements with Reference Electrodes

E. Protopopoff, Laboratoire de Physico-Chimie des Surfaces, CNRS, and P. Marcus, Ecole Nationale Supérieure de Chimie de Paris, Université Pierre et Marie Curie

Operating Conditions for Reference Electrodes

When a reference electrode has been selected for a particular application, its proper use requires caution and specific measurement conditions. When measuring the potential of a polarized test electrode versus a reference electrode, it is important not to polarize or damage the latter by applying a significant current density. Also, the ohmic (*IR*) drop must be minimized.

Very Low Current Density. It is important to use a reference electrode that operates at its known open-circuit potential and thus avoid applying any significant overpotential to it. This is achieved by using a high-impedance voltmeter that has a negligible input current and, for test electrode polarization measurements, by using an auxiliary electrode in a three-electrode system (Fig. 1).

The value tolerated for the maximum overpotential on the reference electrode, at the condition that it stays under the limit over which the electrode suffers irreversible damages (like the calomel electrode), is a matter of judgment that depends on the accepted magnitude of error in the particular case under investigation. The use of an electrometer or a high-impedance voltmeter (10^{12} ohms) fulfills the usual requirements. When a lower impedance instrument is used, an unacceptable overpotential could result if the electrode is too polarizable.

The *IR* Drop and Its Mitigation. The *IR* drop is an ohmic voltage that results from electric current flow in ionic solutions. Electrolytes have an ohmic resistance; when a current passes through them, an *IR* voltage can be observed between two distinct points. When the reference electrode is immersed at some distance from a working or test electrode, it is in the electric field somewhere along the current path. An electrolyte resistance exists along the path between the test and the reference electrodes. As current flows through that path, an *IR* voltage appears in the potential measurement according to:

$$V = V_T - V_R + IR \qquad \text{(Eq 13)}$$

where V_T is the test potential to be measured, V_R is the reference electrode potential, and *IR* is the ohmic drop. In this case, the liquid junction potential has been neglected. The *IR* drop constitutes a second unknown value in a single equation. It must be eliminated or minimized.

The Luggin capillary is a tube, usually made of glass, that has been narrowed by elongation at one end. The narrow end is placed as close as possible to the test electrode surface (Fig. 1), and the other end of the tube goes to the reference electrode compartment. The Luggin capillary is filled with cell electrolyte, which provides an electric link between the reference and the test electrode. The use of a high-impedance voltmeter prevents significant current flow into the reference electrode and into the capillary tube between the test electrode and the reference electrode compartment (Fig. 1). This absence of current eliminates the *IR* drop, and the measurement of V_T is then possible. A residual *IR* drop may, however, exist between the tip of the Luggin capillary and the test electrode. This is usually negligible, however, especially in high-conductivity media.

The remote electrode technique can be used only for measurement in an electrolyte with very low resistivity, usually in the laboratory. It is applicable, for example, in a molten salt solution, in which the ohmic resistance *R* is very small. In such a case, the reference electrode can be placed a few centimeters away from the test electrode, because the *IR* drop remains negligible. In other electrolytes (for example, in measurements in soils), the ohmic resistance is rather large, and the *IR* drop cannot be eliminated in this manner.

The Current Interruption Technique. In this case, when the current is flowing, the *IR* drop is included in the measurement. A recording of the potential is shown in Fig. 5. At time t_1, the current is interrupted so that $I = 0$ and $IR = 0$.

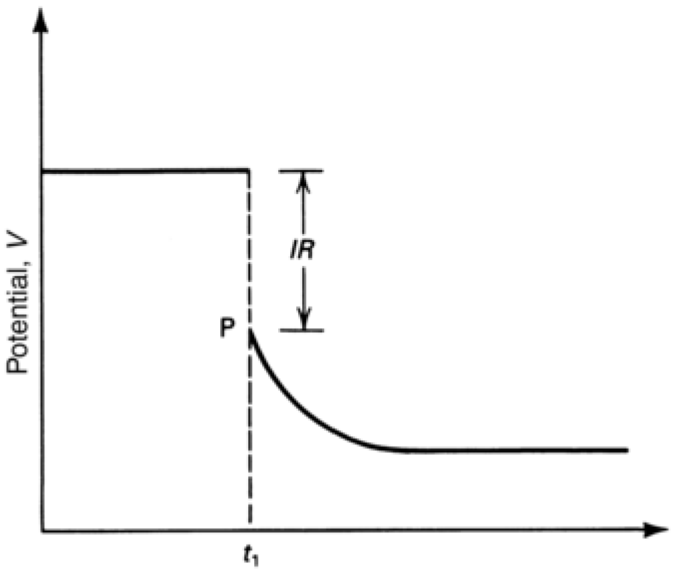

Fig. 5 The potential decay at current interruption. *IR* is the potential drop due to the electrolyte ohmic resistance.

At the moment of the interruption, however, the electrode is still polarized, as can be seen at point P in Fig. 5. The progressive capacitance discharge and depolarization of the test electrode take some time. The potential measured at the instant of interruption then represents the test electrode potential corrected for the *IR* drop. Precise measurements of this potential are obtained with an oscilloscope.
Potential Conversion Between Reference Electrodes. Due to the number of different reference electrodes used, each potential measurement must be accompanied by a clear statement of the reference used. It is often needed to express electrode potentials versus a particular reference, regardless of the actual reference used in the measurement. The procedure is illustrated in the following example. The electrode potential of a buried steel pipe is measured with respect to a $CuSO_4$/Cu electrode, and the value is -650 mV for a pH 4 environment. If that value is mistakenly placed in the iron *E*-pH (Pourbaix) diagram (Fig. 1 in the article “Potential versus pH (Pourbaix) Diagrams” in this Volume), it could be concluded that corrosion will not occur. This conclusion, however, would be incorrect, because the *E*-pH (Pourbaix) diagrams are always computed with respect to the SHE. It is then necessary to express the measured electrode potential with respect to the SHE before consulting the *E*-pH (Pourbaix) diagram. The $CuSO_4$/Cu electrode potential is +310 mV versus SHE, so this value must be added to the measured potential: $E_{SHE} = -650 + 310 = -340$ mV. The principle of this conversion is illustrated in the electrode potential conversion diagram of Fig. 6.

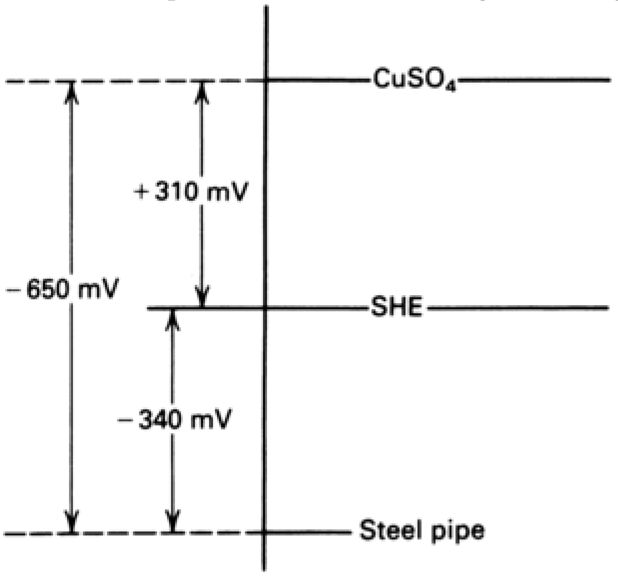

Fig. 6 Diagram of potential conversion between reference electrodes. SHE, standard hydrogen electrode; $CuSO_4$, copper-copper sulfate electrode. SHE, standard hydrogen electrode

The value of -340 mV placed in the *E*-pH Pourbaix diagram at a pH 4 clearly lies in the corrosion region for iron. It would then be definitely necessary to consider the cost benefit of a protection system for the steel pipe.

E. Protopopoff and P. Marcus, Potential Measurements with Reference Electrodes, *Corrosion: Fundamentals, Testing, and Protection,* Vol 13A, *ASM Handbook,* ASM International, 2003, p 13-–16

Potential Measurements with Reference Electrodes

E. Protopopoff, Laboratoire de Physico-Chimie des Surfaces, CNRS, and P. Marcus, Ecole Nationale Supérieure de Chimie de Paris, Université Pierre et Marie Curie

---

Acknowledgment

Portions of this article have been adapted from D.L Piron, Potential Measurements with Reference Electrodes, *Corrosion,* Vol 13, *Metals Handbook,* 9th ed., ASM International, 1987, p 21–24.

E. Protopopoff and P. Marcus, Potential Measurements with Reference Electrodes, *Corrosion: Fundamentals, Testing, and Protection,* Vol 13A, *ASM Handbook,* ASM International, 2003, p 13-–16

Potential Measurements with Reference Electrodes

E. Protopopoff, Laboratoire de Physico-Chimie des Surfaces, CNRS, and P. Marcus, Ecole Nationale Supérieure de Chimie de Paris, Université Pierre et Marie Curie

---

References

1. D.J.G. Ives and J. Janz, *Reference Electrodes,* Academic Press, 1961
2. C.H. Hamann, A.H. Hamnett, W. Vielstich, *Electrochemistry,* Wiley-VCH, Weinheim, 1998
3. M.G. Fontana, *Corrosion Engineering,* 2nd ed., McGraw-Hill, 1978, p 12
4. L. Pauling, *General Chemistry,* W.H. Freeman, 1964, p 338–360

E. Protopopoff and P. Marcus, Potential versus pH (Pourbaix) Diagrams, *Corrosion: Fundamentals, Testing, and Protection*, Vol 13A, *ASM Handbook*, ASM International, 2003, p 17–-30

Potential versus pH (Pourbaix) Diagrams

E. Protopopoff and P. Marcus, CNRS, Ecole Nationale Supérieure de Chimie de Paris, Université Pierre et Marie Curie

Introduction

THE PRINCIPLE OF POTENTIAL-pH DIAGRAMS was established in the 1940s in Belgium by Marcel Pourbaix (Ref 1, 2, 3, 4). A potential- pH diagram is a graphical representation of the relations, derived from the Nernst equation, between the pH and the equilibrium potentials (*E*) of the most probable electrochemical reactions occurring in a solution containing a specific element. The standard equilibrium potentials are computed from thermodynamic data (standard chemical potentials, or Gibbs free energies of formation). The equilibrium relations drawn for a given concentration of the element or for a given ratio of activities of two dissolved species of the element give *E*-pH lines. The representation of the equilibrium pHs for acid-base reactions (independent of the potential) gives vertical lines. All those lines delimit *E*-pH domains of stability for the various species of the element, metal, ions, oxides, and hydroxides. Potential- pH diagrams synthesize many important types of information that are useful in corrosion and in other fields. They make it possible to discern at a glance the stable species for specific conditions of potential and pH (Ref 1, 2, 3, 4).

The principle of *E*-pH diagrams may be simply understood with the case of iron in water. Corrosion in deaerated water is expressed by the electrochemical reaction Fe → Fe^{2+} + 2e^-. The equilibrium potential for the Fe^{2+}/Fe couple can be calculated using the Nernst equation:

$$E_{Fe^{2+}/Fe} = E^{\circ}_{Fe^{2+}/Fe} + \frac{RT}{2F}\ln a_{Fe^{2+}} \qquad \text{(Eq 1)}$$

where $E^{\circ}_{Fe^{2+}/Fe}$ is the standard potential value for the couple, *R* is the gas constant, *T* is the absolute temperature, *F* is the Faraday constant, and $a_{Fe^{2+}}$ is activity for the ferrous ion in solution.

For a given temperature and Fe^{2+} concentration (activity $a_{Fe^{2+}}$), the equilibrium potential is constant and is represented as a horizontal line in a *E*-pH diagram (Fig. 1). This line indicates the potential at which Fe and Fe^{2+} at a given concentration are in equilibrium and can coexist with no net tendency for one to transform into the other. At potentials above the line, iron metal is not stable and tends to dissolve as Fe^{2+}, hence the Fe^{2+} concentration increases until a new equilibrium is reached; this is a domain of stability for Fe^{2+}. At potentials below the equilibrium line, the stability of the metallic iron increases, Fe^{2+} tends to be reduced, and thus its concentration decreases; this is the domain of stability for the metal (Fig. 1).

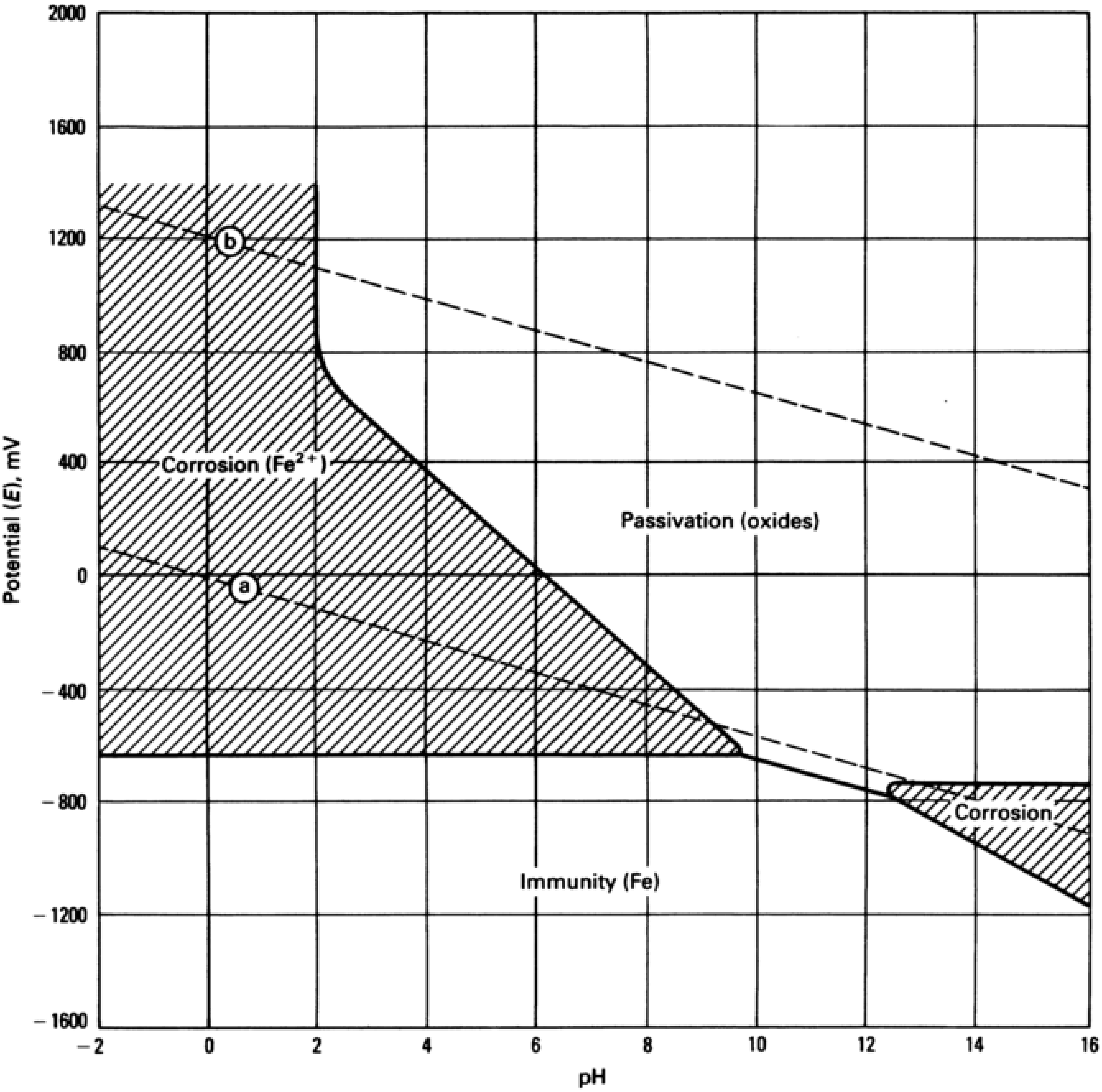

Fig. 1 Iron *E*-pH diagram. Dashed lines a and b are explained in Fig. 7 and in the corresponding text.

The diagrams of all metal-water systems have the same common features; the lower *E*-pH lines give the limit between the domain of stability of the metal and the domain of stability of either the first metallic ion or the first metallic oxide.

For *E*-pH conditions below these lines, the metal is stable, and corrosion cannot take place. This is the immunity region (Fig. 1).

For *E*-pH conditions above the line for the equilibrium between the metal and the first metallic ion, the metal is not stable, and it tends to be oxidized and dissolved into ions. The system is then in the corrosion or activity region of the diagram. Besides the main corrosion region in the stability domains of the metallic ions at low pH (acid corrosion), there is generally also a smaller domain of stability of oxygenated metallic ions at high pHs, leading to alkaline corrosion (Fig. 1).

When the reaction of the metal with water produces an oxide (or hydroxide) that forms a protective layer, the metal is said to be passivated. For *E*-pH conditions above the lines for the metal-oxide and ion-oxide equilibria, the system is in the passivation region (Fig. 1).

Diagrams such as Fig. 1, (Ref 1, 2, 3, 4), have proved to be useful in corrosion as well as in many other fields, such as industrial electrolysis, plating, electrowinning and electrorefining of metals, primary and secondary

electric cells, water treatment, and hydrometallurgy. It is important to emphasize that these diagrams are based on thermodynamic calculations for a number of selected chemical species and the possible equilibria between them. It is possible to predict from a *E*-pH diagram if a metal will tend to corrode or not. It is not possible, however, to determine from these diagrams alone how long a metal will resist corrosion. Pourbaix diagrams offer a framework for kinetic interpretation, but they do not provide information on corrosion rates (Ref 3). They are not a substitute for kinetic studies. Each *E*-pH diagram is computed for selected chemical species corresponding to the possible forms of the element considered in the solution under study. The addition of one or more elements, for example, carbon, sulfur, or chlorine, to a system will introduce new equilibria. Their representation in the *E*-pH diagram will produce a new diagram more complex than the previous one.

References cited in this section

1. M. Pourbaix, Thermodynamique des Solutions Aqueuses Diluées, Potentiel D'oxydo- Réduction (résumé de conférence), *Bull. Soc. Chim. Belgique,* Vol 48, Dec 1938

2. M. Pourbaix, *Thermodynamics of Dilute Aqueous Solutions,* Arnold Publications, 1949

3. R.W. Staehle, Marcel J.N. Pourbaix—Palladium Award Medalist, *J. Eletrochem. Soc.,* Vol 123, 1976, p 23C

4. M. Pourbaix, *Atlas of the Electrochemical Equilibria,* NACE, 1974

E. Protopopoff and P. Marcus, Potential versus pH (Pourbaix) Diagrams, *Corrosion: Fundamentals, Testing, and Protection*, Vol 13A, *ASM Handbook*, ASM International, 2003, p 17–-30

Potential versus pH (Pourbaix) Diagrams

E. Protopopoff and P. Marcus, CNRS, Ecole Nationale Supérieure de Chimie de Paris, Université Pierre et Marie Curie

---

Calculation and Construction of *E*-pH Diagrams

Potential-pH diagrams are based on thermodynamic calculations. The equilibrium lines that set the limits between the various stability domains are calculated for the various electrochemical or chemical equilibria between the chemical species considered. There are three types of reactions to be considered:

- Electrochemical reactions of pure charge (electron) transfer
- Electrochemical reactions involving both electron and solvated proton (H^+) transfer
- Acid-base reactions of pure H^+ transfer (no electrons involved)

Pure Charge Transfer Reactions. These electrochemical reactions involve only a reduced species on one side and an oxidized species and electrons on the other side. They have no solvated protons (H^+) as reacting particles; consequently, they are not influenced by pH. An example of a reaction of this type is the oxidation/ reduction of Ni/Ni^{2+}: $Ni \rightleftharpoons Ni^{2+} + 2e^-$. From the Nernst equation (Eq 1), the equilibrium potential for the couple Ni^{2+}/Ni can be written:

$$E_{Ni^{2+}/Ni} = E^{\circ}_{Ni^{2+}/Ni} + \frac{RT}{2F} \ln a_{Ni^{2+}}$$
$$= E^{\circ}_{Ni^{2+}/Ni} + \frac{RT}{2F} \ln 10 \log a_{Ni^{2+}} \quad \text{(Eq 2)}$$
$$= E^{\circ}_{Ni^{2+}/Ni} + 2.303 \frac{RT}{2F} \log a_{Ni^{2+}}$$

where $E^{o}_{(Ni^{2+}/Ni)}$ is the standard potential for the couple and $a_{Ni^{2+}}$ is the activity of Ni^{2+} in the solution; ***R***, ***T***, and ***F*** are defined in Eq 1; at a temperature of 25 °C (298.15 K), ***RT*** ln 10/***F*** ≈ 0.059 V.

The potential depends on the Ni^{2+} activity but not on H^+ ions. It is then independent of the pH. For a given value of $a_{Ni^{2+}}$, it is represented by a horizontal line in a ***E***-pH diagram.

The standard potential, ***E***^{o}, is:

$$E^{\circ}_{Ni^{2+}/Ni} = \frac{\mu^{0}_{Ni^{2+}} + \mu^{0}_{e^-} - \mu^{0}_{Ni}}{2F} \quad \text{(Eq 3)}$$

By convention, at 25 °C (298.15 K), the standard chemical potentials of a species under elemental form and of the conventional electron are equal to 0. This gives $\mu^{0}_{Ni} = \mu^{0}_{e^-} = 0$ and simplifies the previous equation:

$$E^{\circ}_{Ni^{2+}/Ni}(298.15\ K) = \frac{\mu^{0}_{Ni^{2+}}}{2F}(298.15\ K) \quad \text{(Eq 4)}$$

The values of the standard chemical potentials at 25 °C are found in the *Atlas of Electrochemical Equilibria* (Ref 4) or listed as standard Gibbs free energies of formation in tables of chemical thermodynamic properties (Ref 5) or in specialized papers. They are given for the formation of the substance from its elements in their standard states. The standard state for the dissolved species is the hypothetical ideal solution of the substance at unit molality (number of moles of the species per kilogram of water). At 25 °C, the numerical value of the molality may be approximated by the value of the molarity in number of moles per liter of water.

If the value of $\mu^{0}_{Ni^{2+}}$ at 25 °C is −48.2 kJ/mol (Ref 4), the standard potential is:

$$E^{\circ}_{Ni^{2+}/Ni}(298.15\ K) = \frac{-48{,}200}{2 \times 96{,}487} = -0.25\ V \quad \text{(Eq 5)}$$

This result can be introduced into Eq 2 to give the equilibrium potential for the couple Ni^{2+}/Ni at 25 °C:

$$E_{Ni^{2+}/Ni}(298.15\ K) = -0.25 + 0.030 \log a_{Ni^{2+}} \quad \text{(Eq 6)}$$

As previously stated, this potential depends only on the activity of Ni^{2+}, not on the pH. It is usually assumed in ***E***-pH diagrams that the solution behaves ideally; that is, the activity coefficient of each dissolved species is unity, so the activity of the species is simply equal to the numerical value of its molality (or molarity at 25 °C). This assumption is reasonably accurate for molalities of less than 10^{-3} mol/kg in the pH range 2 to 12. Outside these limits, the Pourbaix diagram is valid only for activities, and molalities must be corrected.

It is customary to select four molalities (molarities at 25 °C): 1 or 10^{0}, 10^{-2}, 10^{-4}, and 10^{-6} mol/kg (mol/L) to show the effect of ion concentration. This will provide four horizontal lines, as shown in Fig. 2:

- At an activity of 10^{o}, $E_{Ni^{2+}/Ni} = E^{o}_{Ni^{2+}/Ni} = -0.25$ V
- With 10^{-2}, $E_{Ni^{2+}/Ni} = -0.25 + 0.030 \log 10^{-2} = -0.31$ V
- With 10^{-4}, $E_{Ni^{2+}/Ni} = -0.37$ V
- With 10^{-6}, $E_{Ni^{2+}/Ni} = -0.43$ V

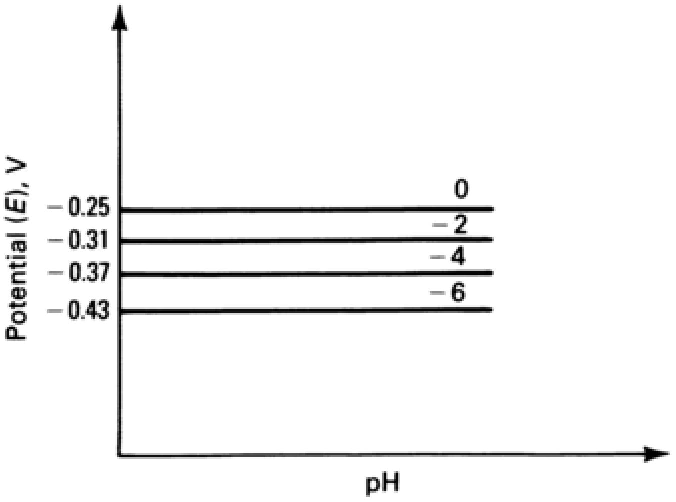

Fig. 2 Partial *E*-pH diagram for the equilibrium Ni^{2+} + 2e^- = Ni for various values of log $a_{Ni^{2+}}$

For any activity of Ni^{2+} in the solution, a horizontal line represents the potential at which nickel ions at the given activity and nickel metal are in equilibrium. Above the line is the region of stability of Ni^{2+} ions at a higher activity; nickel metal at these potentials will tend to corrode (dissolve) and produce Ni^{2+}, the stable species. Below the line, Ni^{2+} ions will tend to be reduced into metallic nickel, and nickel in this condition is stable and will not corrode (dissolve). It is immune to corrosion.

Reactions Involving Both Electron and Proton Transfer. Consider a typical electrochemical reaction with proton transfer in an aqueous electrolyte:

$$b\text{O} + m\text{H}^+ + ne^- \rightleftharpoons c\text{R} + d\text{H}_2\text{O} \qquad \text{(Eq 7)}$$

where O and R are the oxidized and the reduced form of the considered element, respectively; *b*, *m*, *c*, and *d* are stoichiometric coefficients; and *n* is an integer.

From the Nernst equation, the equilibrium potential is equal to:

$$E_{\text{eq(O/R)}} = \frac{\Delta G_{\text{ox}}}{nF} = \frac{\Delta G^{\circ}_{\text{ox}}}{nF} + \frac{RT}{nF}\ln\frac{(a_{\text{O}})^b (a_{\text{H}^+})}{(a_{\text{R}})^c (a_{\text{H}_2\text{O}})} \qquad \text{(Eq 8)}$$

with Δ_{ox} $E^{o}_{(\text{O/R})}$ = $-\Delta G^0_{red}/nF$ = $(b\mu^0_O + m\mu^0_{H+} + n\mu^0_e - c\mu^0_R - d\mu^0_{H_2O})/nF$; where ΔG^0_{red} is the standard Gibbs free energy charge of reduction. The activity of water can be taken equal to unity in not too concentrated aqueous solutions. If O or R is a pure solid phase (oxide, hydroxide, or metal), a_O or a_R is equal to unity. The pH of the solution is pH = -log aH^+. Hence:

$$E_{\text{eq(O/R)}} = E^{\circ}_{\text{eq(O/R)}} + 2.303\frac{RT}{nF}\log\frac{(a_{\text{O}})^b}{(a_{\text{R}})^c} - 2.303\frac{mRT}{nF}\text{pH} \qquad \text{(Eq 9)}$$

This equation shows that the equilibrium potential corresponding to a given ratio $r = (a_O)^b / (a_R)^c$ is a linear function of pH (decreasing if *m* is positive).

As an example, nickel can react with water to form an oxide, according to the electrochemical reaction:

$$\text{Ni} + \text{H}_2\text{O} \rightleftharpoons \text{NiO} + 2\text{H}^+ + 2e^- \qquad \text{(Eq 10)}$$

The Nernst equation can be written as follows:

$$E_{\text{NiO/Ni}^{2+}} = E^{\circ} + 2.303\frac{RT}{zF}\log\frac{a_{\text{NiO}}}{a_{\text{Ni}}} - 2.303\frac{RT}{F}\text{pH} \qquad \text{(Eq 11)}$$

where the standard potential E^o is given by:

$$E^\circ = \frac{\left(\mu^0_{NiO} + 2\mu^0_{H^+} + 2\mu^0_{e^-} - \mu^0_{Ni} - \mu^0_{H_2O}\right)}{2F}$$

From the data in Ref 4:

$$E^\circ(298.15\ K) = \frac{\left(-215{,}940 + 0 + 0 - 0 - (-237{,}190)\right)}{(2 \times 96{,}487)}$$

$$= +0.11\ V$$

The NiO and Ni are solid phases, and they are considered to be pure; their activity is therefore 1. Equation 11 can then be simplified, and the equilibrium potential at 25 °C becomes:

$E_{eq(NiO/Ni)}(298.15\ K) = +0.11 - 0.059\ pH$ (Eq 12)

In this case, the equilibrium potential decreases with an increase in pH, as represented in the partial *E*-pH diagram of Fig. 3. The diagonal line gives the value of the equilibrium potential of the NiO/Ni couple at all pH values. Above the line, NiO is stable, and below it, nickel metal is stable.

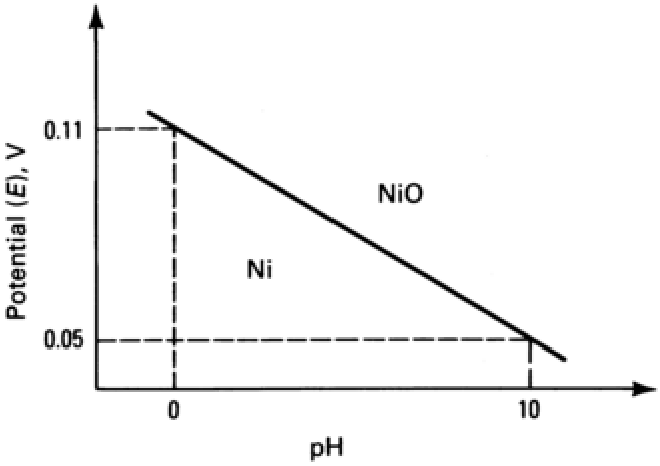

Fig. 3 Partial *E*-pH diagram for the equilibrium Ni + H_2O = NiO + $2H^+$ + 2*e*$^-$

Potential-pH diagrams are very general and can also be applied to electrochemical reactions involving nonmetallic elements. An example involving the reduction of nitrite ion (NO_2^-) to ammonium ion (NH_4^+) is given here. In this case, the metal of the electrode supports the reaction by giving or taking away electrons, as follows:

$$NO_2^- + 8H^+ + 6e^- \rightleftharpoons NH_4^+ + 2H_2O$$

The Nernst equation gives:

$$E = E^\circ + 2.303\left(\frac{RT}{6F}\right)\log\frac{a_{NO_2^-}}{a_{NH_4^+}} - 2.303\frac{8RT}{6F}\,pH \qquad \text{(Eq 13)}$$

where the standard potential is expressed as:

$$E^\circ = \frac{\left(\mu^0_{NO_2^-} + 8\mu^0_{H^+} + 6\mu^0_{e^-} - \mu^0_{NH_4^+} - 2\mu^0_{H_2O}\right)}{6F}$$

From the data in Ref 4:

$$E°(298.15\ \text{K}) = \frac{(-34{,}520 + 0 + 0 - (-79{,}500) - 2(-237{,}190))}{(6 \times 96{,}487)} = +0.90\ \text{V}$$

The equilibrium potential at 25 °C is then given by:

$$E(298.15\ \text{K}) = 0.90 + 0.010 \log \frac{a_{NO_2^-}}{a_{NH_4^+}} - 0.079\ \text{pH} \quad \text{(Eq 14)}$$

This E-pH relation is represented for equal activity in NO_2^- and NH_4^+ by the line drawn in Fig. 4.

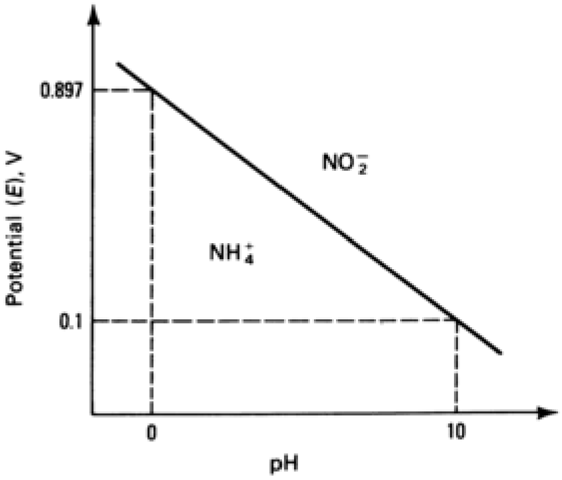

Fig. 4 Partial *E*-pH diagram for the equilibrium NO_2^- + $8H^+$ + $6e^-$ = NH_4^+ + $2H_2O$

Above the line, the ratio $(a_{NO^-{}_2}/a_{NH^+{}_4})$ is higher than unity, so this is a region where $NO_2{}^-$ is predominantly stable. Below the line, the ratio $(a_{NO^-{}_2}/a_{NH^+{}_4})$ is lower than unity, so this is a region where $NH_4{}^+$ is predominantly stable.

Acid-Base Reactions. Consider a typical acid-base chemical reaction in aqueous solution, between the acid form C and the basic form B:

cC + $d$$H_2O$ = bB + $m$$H^+$ (Eq 15)

When the reaction is in thermodynamic equilibrium:

$$\Delta_r G^0 = b\mu_B^0 + m\mu_{H^+}^0 - c\mu_C^0 - d\mu_{H_2O}^0 = -2.303RT \log K_{eq}$$

where $\Delta_r G^0$ is the standard Gibbs free energy change, μ^0 represents the standard chemical potentials of the different substances, and K_{eq} is the equilibrium constant for the reaction: K_{eq} = $(a_B)^b (a_{H^+})^m / (a_C)^c (a_{H_2O})^d$.

The activity of water may be taken equal to unity in not too concentrated aqueous solutions. If B or C is a pure solid phase (metal, oxide, or hydroxide), a_B or a_C is equal to unity. Using pH = $-\log a_{H^+}$, the previous equation may be rearranged as:

$$\log K_{eq} = \log \frac{(a_B)^b}{(a_C)^c} - m\text{pH} = \frac{-\Delta_r G^0}{2.303RT} \quad \text{(Eq 16)}$$

This equation shows that the ratio of the activities of the basic form to the acid form increases with pH. The pH at equilibrium corresponding to a given ratio $r = (a_B)^b/(a_C)^c$ can be determined from:

$$pH_{eq} = \frac{pK_{eq}}{m} + \frac{(\log r)}{m}$$ (Eq 17)

with $pK_{eq} = -\log K_{eq} = \Delta_r G^0/2.303\ RT$.

This equilibrium pH does not depend on the potential and will be represented on the *E*-pH diagram by a vertical line. As an example, in the case of cobalt, Co^{2+} and CoO are involved in an acid-base reaction:

$$Co^{2+} + H_2O \rightleftharpoons CoO + 2H^+$$ (Eq 18)

CoO and H_2O both have activities of 1, so the application of Eq 17 gives:

$$pH_{eq} = \frac{pK_{eq}}{2} - \frac{(\log a_{Co^{2+}})}{2}$$ (Eq 19)

with:

$$pK_{eq} = (\mu^0_{CoO} + 2\mu^0_{H^+} - \mu^0_{Co^{2+}} - \mu^0_{H_2O})/2.303RT.$$

By replacing the standard chemical potentials by their values given in the *Atlas of Electrochemical Equilibria* (Ref 4):

$$pK_{eq}(298.15\text{ K}) = \frac{(-218{,}860 + 0 - (-53{,}560) - (-237{,}190))}{(8.3143 \times 298.15 \times 2.303)} = 12.6$$

and finally:

$$pH_{eq}(298.15\text{ K}) = 6.3 - \frac{(\log a_{Co^{2+}})}{2}$$

Thus, for an activity unity for Co^{2+}, $pH_{eq} = 6.3$. This value can also be obtained by the intersection of two equilibrium *E*-pH lines. As shown previously for nickel, there are electrochemical equilibria between the metal and its first ion (Co^{2+}) and between the metal and its first oxide (CoO). It is possible to determine the equilibrium *E*-pH lines for the couples Co^{2+}/Co and CoO/Co, as shown in Fig. 5. The two lines intersect at point P, and above them are the domains of stability for Co^{2+} and CoO. The boundary between these two domains is a vertical line containing point P and located at pH 6.3 for $a_{Co^{2+}} = 1$ (Fig. 5).

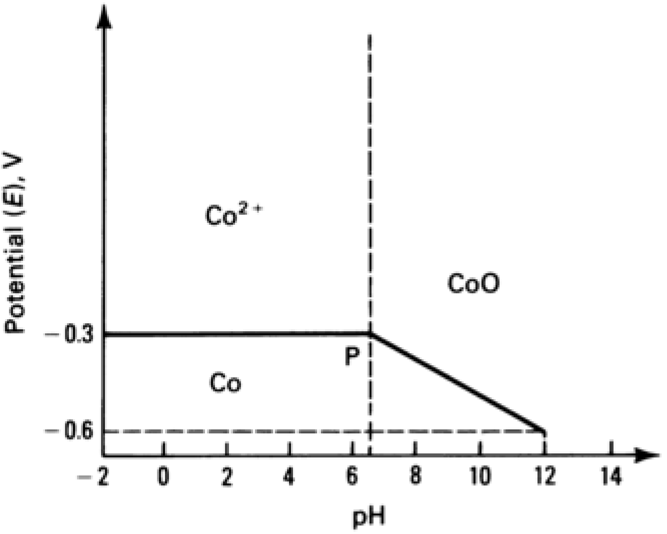

Fig. 5 Partial *E*-pH diagram for the Co^{2+}/Co and CoO/Co couples for $a_{Co^{2+}} = 1$

Figure 6(a) shows a partial *E*-pH diagram for different values of $\log a_{Co^{2+}}$ in which only three chemical species—Co, Co^{2+}, and CoO (or the hydroxide $Co(OH)_2$)—are considered. There are, however, other possible

chemical species, dissolved or solid, that must be considered. This introduces new equilibria that modify the diagram to give Fig. 6(b).

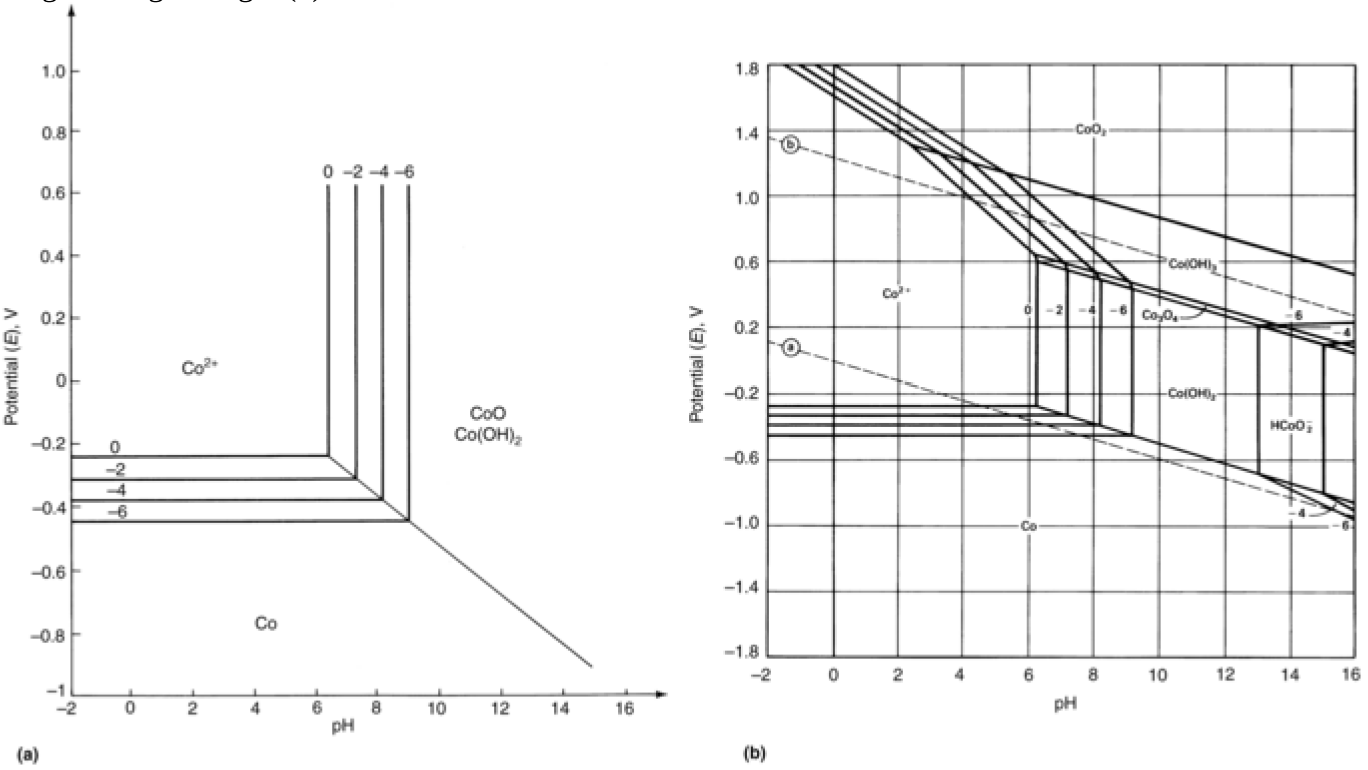

Fig. 6 *E*-pH diagram for the cobalt-water system for various values of log $a_{Co^{2+}}$. (a) Partial *E*-pH diagram. (b) Complete *E*-pH diagram

The Water *E*-pH Diagram. Pourbaix diagrams are traced for equilibrium reactions taking place in water; consequently, the water system must always be considered at the same time as the system under investigation in any *E*-pH diagram. Water can be decomposed into oxygen and hydrogen, according to the following electrode reactions:

$$2H_2O_{(l)} + 2e^- \rightleftharpoons H_{2(g)} + 2OH^-_{(aq)} \qquad \text{(Eq 20)}$$

and

$$H_2O_{(l)} \rightleftharpoons \tfrac{1}{2}O_{2(g)} + 2H^+_{(aq)} + 2e^-$$

Considering the equilibrium of water dissociation/ionization into solvated protons and hydroxide ions:

$$H_2O_{(l)} \rightleftharpoons H^+_{(aq)} + OH^+_{(aq)}$$

equilibria (Eq 20) may also be written as:

$$2H^+_{(aq)} + 2e^- \rightleftharpoons H_{2(g)}$$

and

$$2OH_{(aq)} \rightleftharpoons \tfrac{1}{2}O_{2(g)} + H_2O_{(l)} + 2e^-$$

The equilibrium potentials of these two electrochemical reactions can be determined by using the Nernst equation. For the water/hydrogen or proton/hydrogen couple:

$$E_{H^+/H_2} = E^{\circ}_{H^+/H_2} - \frac{2.303\,RT}{2F}\log f_{H_2} - \frac{2.303\,RT}{F}\text{pH} \qquad \text{(Eq 21)}$$

where f_{H_2} is the fugacity or pressure of hydrogen near the electrode (in fact, dimensionless fugacity is equal to the numerical value of the fugacity expressed in bar). At 25 °C (298.15 K), because, by definition, $E^{o}_{H^+/H_2} = 0$

V/SHE (see the article "Electrode Potentials" in this Section of the Volume), the previous equation can be rewritten as:

$$E_{H^+/H_2}(298.15\ K) = -0.030 \log f_{H_2} - 0.059\ pH \qquad (Eq\ 22)$$

This relation for $f_{H_2} = 1 (p_{H_2} = 1 bar)$ Fig. 6(b) and 7 by line **a**, which decreases with increasing pH.

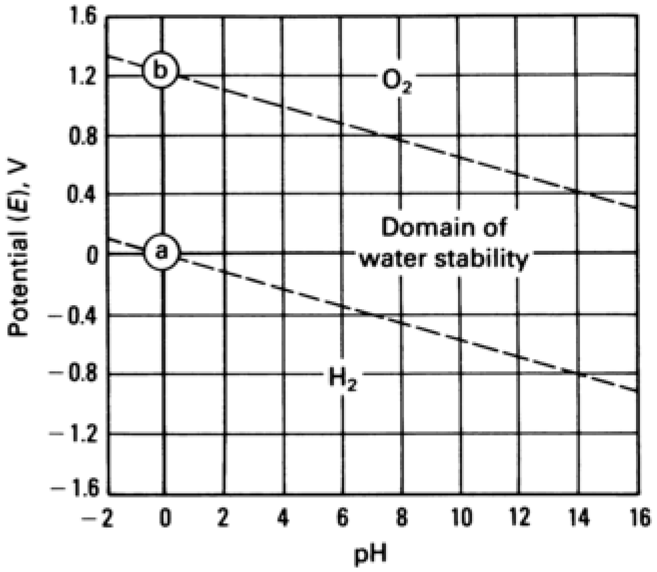

Fig. 7 The water *E*-pH diagram at 25 °C (298.15 K) and 1 bar

For the oxygen/water or oxygen/hydroxide couple:

$$E_{O_2/H_2O} = E^\circ_{O_2/H_2O} + 2.303\frac{RT}{4F}\log f_{O_2} - 2.303\frac{RT}{F}pH \qquad (Eq\ 23)$$

where f_{O_2} is the fugacity of O_2 near the electrode. The water activity is, as usual, assumed to be 1. At 25 °C (298.15 K), the standard potential for O_2/H_2O is 1.23 V SHE (Ref 4), so the equation can be rewritten as:

$$E_{O_2/H_2O}(298.15\ K) = 1.23 + 0.015 \log f_{O_2} - 0.059\ pH \qquad (Eq\ 24)$$

This relation for $f_{O_2} = 1 (p_{O_2} = 1 bar)$ is represented by line **b** in Fig. 6(b) and 7.

It is interesting to note that the pressures of hydrogen and oxygen in the vicinity of the electrode are usually identical and nearly equal to the pressure that exists in the electrochemical cell. To be rigorous, the water vapor pressure should be taken into account, but it is frequently neglected as not being very significant at 25 °C (298.15 K). When the pressure increases, line **b** in Fig. 7 is displaced upward in the diagram, and line **a** is lowered. The result is that the domain of water stability increases with increasing pressure.

The water system is very important for a good understanding of the corrosion behavior of metals; it is represented (usually by dashed lines) in all Pourbaix diagrams (Ref 4).

Conventions for *E*-pH Diagram Construction. In the construction of diagrams for binary (metal-water) systems, the authors follow the original Pourbaix format (Ref 4) and delineate regions within which condensed phases are stable by solid lines, whereas coexistence lines separating the predominance areas for dissolved species are drawn dashed, even in the regions where the condensed species are stable (Fig. 8). Also, it is common to draw the lines of separation between solid compounds and dissolved species for a number of different activities of the latter. The large number of lines may render the diagram difficult to read (Fig. 8). Moreover, the amount of the chemical element considered, when summed over all dissolved species containing this element, should be constant over the diagram. On diagrams calculated on this principle of constant total element concentration, as the activities in the ideal solution model are taken equal to the numerical values of the concentrations

(molalities), the lines corresponding to the limits of the stability domain of a solid species are rounded where two solution species coexist (e.g., the boundaries between domains of Fe^{2+}, Fe^{3+}, and Fe_2O_3 in Fig. 8).

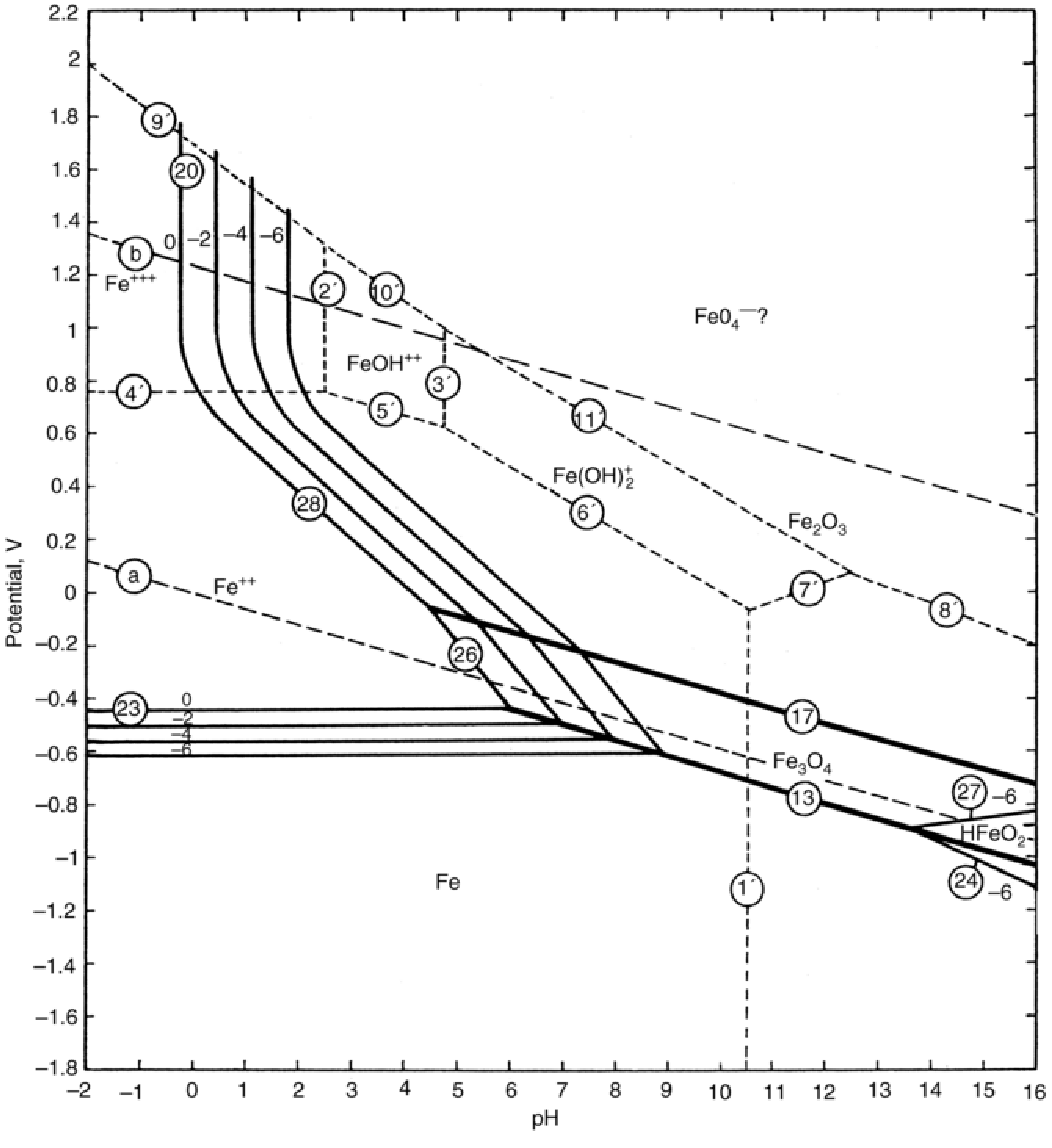

Fig. 8 Original Pourbaix diagram for the iron-water system at 25 °C (298.15 K) (oxides are considered; hydroxides are not). Source: Ref 4

When this principle is adopted rigorously, the diagrams are tedious to compute. Therefore widely adopted convention in calculating the *E*- pH line for the equilibrium between a solid species and a dissolved species is that the dissolved species has simply an activity equal to the molality equal to that it would have if it were the only form present, that is, the selected molality of the element in solution, divided by the number of atoms of the element in a molecule of the species. The effect of this simplifying assumption is that all lines on the diagrams are straight. Figure 9 shows a diagram simplified with respect to the original Pourbaix format (Fig. 8). The diagram (Fig. 9) is further simplified by limiting the pH range from 0 to 14.

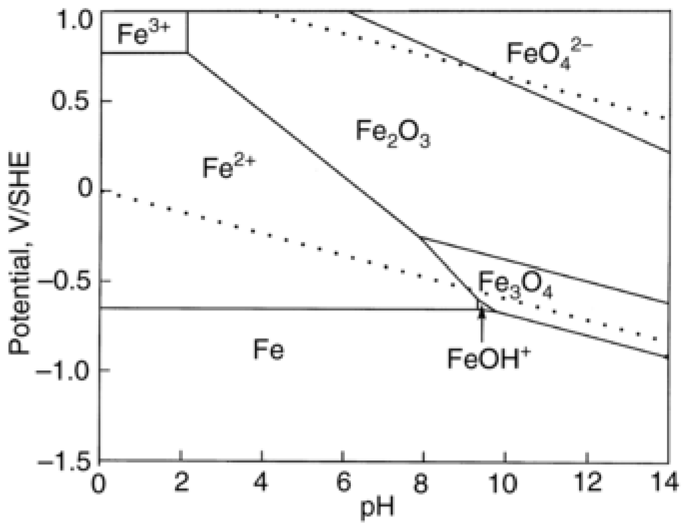

Fig. 9 Simplified *E*-pH diagram for the iron-water system at 25 °C for a molality of dissolved iron equal to 10^{-6} mol/kg. Pressure of hydrogen and oxygen, 1 atm

Consider the consequences of choosing a convention on the element concentration when constructing a diagram. For an equilibrium between two dissolved forms, R and O, of an element. The *E*-pH line calculated for equal concentration of the two forms separates the domains of relative predominance of R and O is calculated from the Nernst equation for equal concentrations of the element under the two forms. When the chemical formulae of the two forms contain the same number of atoms of the element, the concentrations of the two forms are equal, so the logarithmic term with the ratio of activities in the Nernst equation is equal to 0. In this case, the equation of the separation line does not depend on the total concentration of the element (Ref 4, 6, 41). For example, for the reaction:

$$SO_4^{2-} + 10H^+ + 8e^- \rightleftharpoons H_2S_{(aq)} + 4H_2O \qquad \text{(Eq 25)}$$

the equilibrium equation is:

$$E = E^\circ + 2.303\left(\frac{RT}{8F}\right)\log\frac{a_{SO_4^{2-}}}{a_{H_2S}} - 2.303\frac{5RT}{4F}\text{pH} \qquad \text{(Eq 26)}$$

The equation of the limit between the areas of relative predominance of SO_4^{2-} and H_2S(aq) simplifies to:

$$E = E^\circ - 2.303\frac{5RT}{4F}\text{pH} \qquad \text{(Eq 27)}$$

This is not true when the formula of the two dissolved forms do not contain the same number of atoms of the element. For example, for the reaction:

$$S_2O_3^{2-} + 10H^+ + 8e^- \rightleftharpoons 2H_2S + 3H_2O \qquad \text{(Eq 28)}$$

the equilibrium equation is:

$$E = E^\circ + 2.303\frac{RT}{8F}\log\frac{a_{S_2O_3^{2-}}}{\left(a_{H_2S}\right)^2} - 2.303\frac{5RT}{4F}\text{pH} \qquad \text{(Eq 29)}$$

In this case, the equation of the separation line depends on the total concentration of sulfur (molality m_S). If it were considered that the total element amount is constant, the equation of the limit of the areas of relative predominance would correspond to the case where half of sulfur is as H_2S(aq) and the other half as $S_2O_3^{2-}$.

This would be obtained by taking the concentration $m_S/2$ for $H_2S(aq)$ and $m_S/4$ for $S_2O_3^{2-}$ (Ref 4, 6, 41). The equation of the separation line would then be:

$$E = E^\circ + 2.303\frac{RT}{8F}\log\left[\frac{m_S/4}{(m_S/2)^2}\right] - 2.303\frac{5RT}{4F}\text{pH}$$

or

$$E = E^\circ - 2.303\frac{RT}{8F}\log m_S - 2.303\frac{5RT}{4F}\text{pH} \quad \text{(Eq 30)}$$

If the simplifying convention described previously is chosen, the *E*-pH line for equilibrium between two dissolved species is calculated considering that each dissolved species is the only form of the element present in solution; for example, taking the concentration m_S for $H_2S(aq)$ and $m_S/2$ for $S_2O_3^{2-}$. Then, the equation of the separation line is:

$$E = E^\circ + 2.303\left(\frac{RT}{8F}\right)\log\frac{(m_S/2)}{(m_S)^2} - 2.303\frac{5RT}{4F}\text{pH}$$

or

$$E = E^\circ - 2.303\left(\frac{RT}{8F}\right)\log 2 - 2.303\left(\frac{RT}{8F}\right)\log m_S - 2.303\frac{5RT}{4F}\text{pH} \quad \text{(Eq 31)}$$

The simplification with respect to the classic Pourbaix presentation of the diagrams allows a gain of clarity and makes easier the construction of the more complex diagrams for multicomponent systems.

Diagrams for Metastable Species. It is to be noted that the species present in solution in real conditions are not necessarily the more stable ones but may be metastable species that are less stable thermodynamically but, for kinetic reasons, are the ones effectively present in solution for a finite time. A classic example is the sulfur-water system where the oxidized forms of sulfur present in solution are not necessarily the thermodynamically stable species elemental solid sulfur, hydrogenosulfate, HSO_4^-, and sulfate, SO_4^{2-}, ions but can be the metastable dithionates $S_2O_6^{2-}$, hydrosulfites ($HS_2O_4^-$, $S_2O_4^{2-}$) sulfites (H_2SO_3, HSO_3^-, and SO_3^{2-}), tetrathionates ($S_4O_6^{2-}$), or thiosulfates ($HS_2O_3^-$, $S_2O_3^{2-}$) (Ref 4, 6, 7, 41). Possible reactions between the metal and sulfur metastable species are of interest for prediction of corrosion in industrial systems. The *E*-pH diagram for the sulfur-water system showing the thermodynamically stable species is given in Fig. 10 for a sulfur activity (molarity) of 10^{-4} mol/kg. It exhibits a small stability domain of solid sulfur from acid to neutral pHs. The same diagram shows the *E*-pH lines for the case where the thiosulfate species are considered as the only oxidized forms of sulfur (dashed lines). According to the construction conventions, the activity of the dissolved sulfides containing one sulfur atom per molecule or ion is taken as 10^{-4} and the activity of thiosulfate species containing two sulfur atoms per ion as 0.5×10^{-4}.

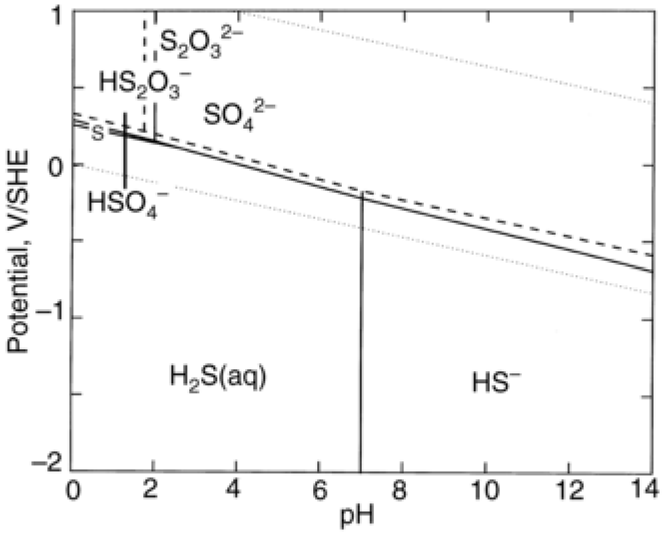

Fig. 10 Simplified *E*-pH diagram for the sulfur-water system at 25 °C. The solid lines represent the stable system. The dashed lines represent the equilibria involving the metastable thiosulfates instead of the stable sulfates. Sulfur molality is 10^{-4} mol/kg. Pressure of hydrogen and oxygen, 1 atm

References cited in this section

4. M. Pourbaix, *Atlas of the Electrochemical Equilibria,* NACE, 1974

5. D.D. Wagman, W.H. Evans, V.B. Parker, R.H. Schumm, I. Halow, S.M. Bailey, K.L. Churney, and R.L. Nuttall, *J. Phys. Chem. Ref. Data,* Vol 11 (Suppl. 2), 1982

6. G. Valensi, "Rapport CEBELCOR-CEFA/ R. 17," 1958; "Rapport Technique CEBELCOR, 121, RT. 207, 1," 1973

7. R.C. Murray, Jr. and D. Cubicciotti, *J. Electrochem. Soc.*, Vol 130, 1983, p 866

41. M. Pourbaix and A. Pourbaix, Rapports Techniques CEBELCOR, 159, RT. 299 (1990)

E. Protopopoff and P. Marcus, Potential versus pH (Pourbaix) Diagrams, *Corrosion: Fundamentals, Testing, and Protection*, Vol 13A, *ASM Handbook*, ASM International, 2003, p 17–-30

Potential versus pH (Pourbaix) Diagrams

E. Protopopoff and P. Marcus, CNRS, Ecole Nationale Supérieure de Chimie de Paris, Université Pierre et Marie Curie

Practical Use of *E*-pH Diagrams

The *E*-pH diagram is an important tool for understanding electrochemical phenomena. It provides useful thermodynamic information in a simple figure. Two cases are presented here to illustrate its practical use in corrosion prediction.

Corrosion of Nickel. A rod of nickel is immersed in an aqueous deaerated acid solution that contains 10^{-4} mol/L of Ni^{2+} ions. The system is at 25 °C (77 °F) under 1 atm pressure. The *E*-pH diagram corresponding to these conditions is shown in Fig. 11.

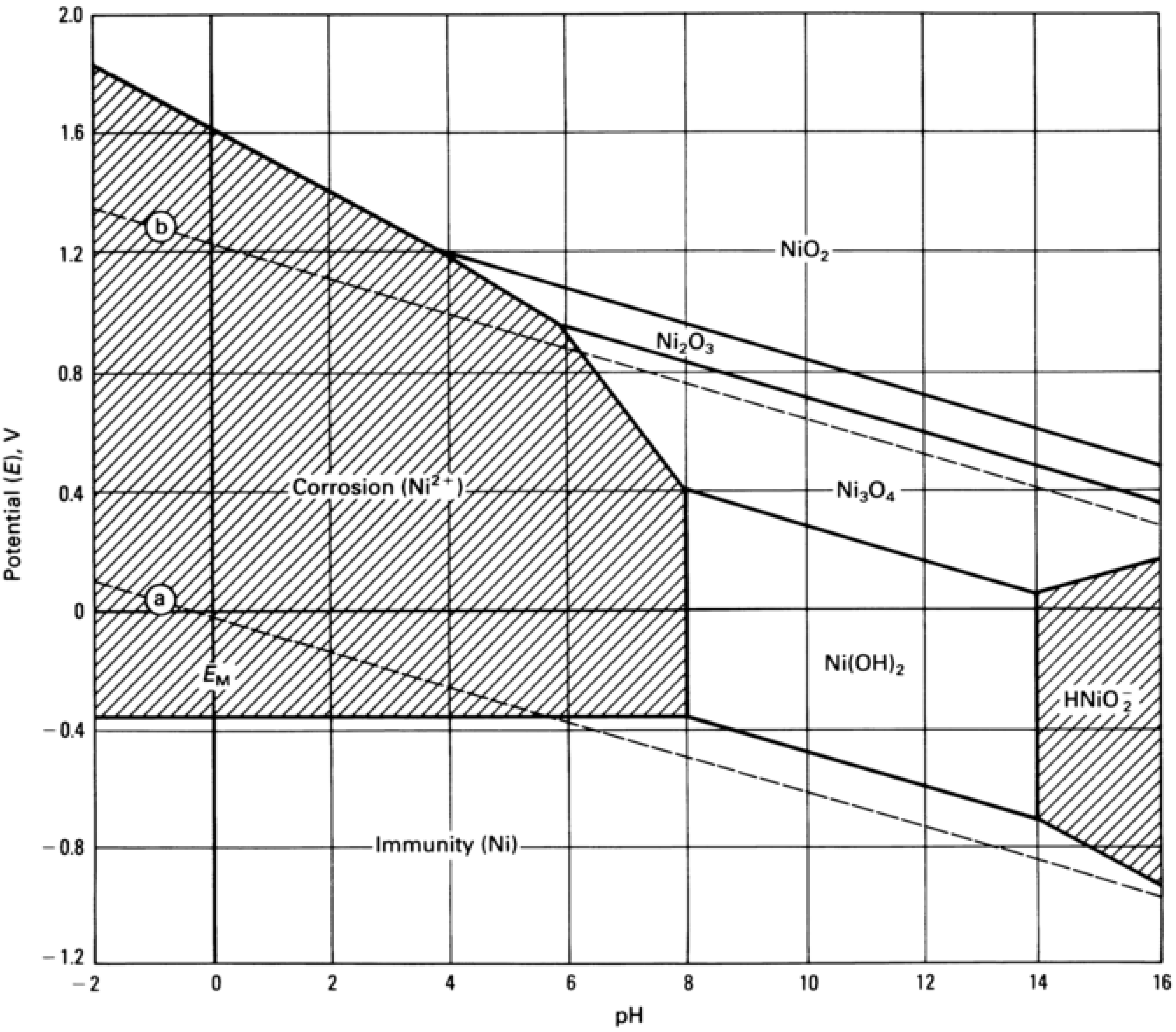

Fig. 11 *E*-pH diagram for nickel for $a_{Ni^{2+}}$= 10^{-4}

At the metal-water interface, two electrochemical reactions are possible:

$Ni \rightleftharpoons Ni^{2+} + 2e^-$ (Eq 32)

and

$2H^+ + 2e^- \rightleftharpoons H_2$ (Eq 33)

The equilibrium potentials of the Ni^{2+}/Ni and the H^+/H_2 electrodes can be computed. From Eq 6, $E_{Ni^{2+}/Ni}$= −0.25 + 0.030 log $a_{Ni^{2+}}$, which, for $a_{Ni^{2+}}$= 10^{-4}, gives $E_{Ni^{2+}/Ni}$≈ −0.37 V (Fig. 2). From Eq 22, E_{H^+/H_2}= −0.059 pH, which, at pH = 1, for example, gives E_{H^+/H_2}≈ −0.06 V. $E_{Ni^{2+}/Ni} < E_{H^+/H_2}$ up to a pH of approximately 6 (Fig. 11). Thus, when connected via an electrical circuit, electrons tend to flow from the more negative nickel electrode, where they are produced by the oxidation reaction, to the less negative hydrogen electrode, where they are consumed by the reduction reaction. In this case, the two electrodes are formed on the surface of the conducting nickel rod. The two reactions will proceed under a common electrode potential or mixed potential, with a value somewhere between the nickel and hydrogen equilibrium potentials. Up to pH ≈ 6, the mixed potential, E_M, is located above the Ni^{2+}/Ni equilibrium potential in the region of Ni^{2+} stability and below the H^+/H_2 equilibrium potential in the region of H_2 stability (Fig. 11). Hence, nickel is not stable at low pH in water, and it tends to oxidize (corrode) into Ni^{2+}, while H^+ is reduced into hydrogen gas (hydrogen evolution).

Thus, the Pourbaix diagram explains the tendency for nickel to corrode in acid solutions. It does not indicate the rate of corrosion, however. This important information has to be obtained from a kinetic experiment, for example, from the recording of current versus potential curve around the corrosion potential.
The Pourbaix diagram also shows that when the pH increases to approximately 6, the difference between the nickel and the hydrogen equilibrium potential decreases in magnitude, and consequently, the corrosion tendency diminishes. For pHs between 6 and 8 (limit of stability of Ni^{2+}), Fig. 11 shows that the hydrogen electrode potential becomes lower than the nickel one. Under these conditions, H^+ can no longer accept the electrons from nickel. The mixed potential of the system is, in this case, below the equilibrium potential of Ni^{2+}/Ni, in the region of metal immunity. Hence, in water at room temperature, nickel does not corrode for pH 6 to 8. No such pH range exists for the iron-water system, where the Fe^{2+}/Fe electrode potential is always lower than the H^+/H_2 electrode potential (Fig. 1, 8, 9). Therefore, iron will always corrode to ferrous ions with evolution of H_2 in acid and neutral solutions. In contrast, the behavior of nickel makes this metal slightly noble (in the small pH range of 6 to 8), and, from the diagram, it is expected to resist corrosion better than iron. Moreover, an increase in hydrogen pressure, according to Eq 22, lowers the equilibrium line of H^+/H_2 while it does not change the equilibrium line of Ni^{2+}/Ni. As a result, an increase in pressure leads to greater corrosion resistance for nickel. For pHs higher than 8, films of NiO (or the hydrated form $Ni(OH)_2$) and Ni_3O_4 can form at the surface at anodic potentials, as can be seen in Fig. 11. These oxides may, in some cases, protect the metal by forming a protective layer that prevents or mitigates further corrosion. This phenomenon is called passivation. It also occurs on iron with the formation of magnetite (Fe_3O_4) or hematite (Fe_2O_3) at anodic potentials (Fig. 8, 9). The presence of species such as chlorine ions may increase the corrosion tendency of metals, because these species may attack the protective layer and then favor corrosion. Figures 1, 8, and 11 illustrate that iron or nickel may corrode (dissolve) in very strong alkaline solutions as $HFeO_2^-$ or $HNiO_2^-$, respectively, or, more likely, as the hydrated forms $Fe(OH)_3^-$ or $Ni(OH)_3^-$.
Corrosion of Copper. Observation of the copper *E*-pH diagram in Fig. 12 immediately reveals that the corrosion of copper immersed in deaerated acid water is not likely to occur. The H^+/H_2 equilibrium potential represented by line **a** is always *lower* than the Cu^{2+}/Cu equilibrium potential. The H^+ ions are stable in contact with copper metal, which cannot corrode (is immune) in water solutions free from oxidizing agents.

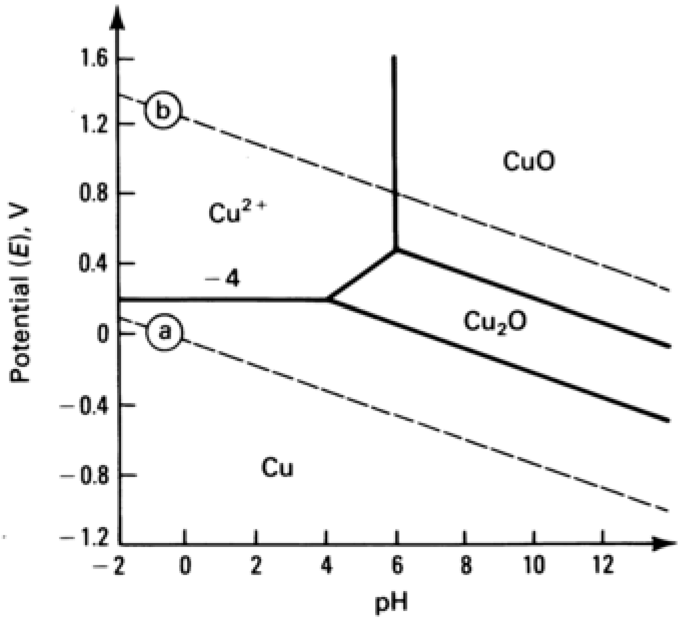

Fig. 12 Partial *E*-pH diagram for copper for $a_{Cu^{2+}}$= 10^{-4}

The presence of dissolved oxygen in nondeaerated solutions introduces another possible reaction: O_2 reduction into H_2O, with an equilibrium potential higher than that of Cu^{2+}/Cu. The O_2/H_2O couple is then a good acceptor for the electrons produced by copper oxidation. The two electrochemical reactions:

$Cu \rightarrow Cu^{2+} + 2e^-$ (Eq 34)

and

$$\frac{1}{2}O_2 + 2H^+ + 2e^- \rightarrow H_2O \qquad \text{(Eq 35)}$$

take place spontaneously in acid solutions at the surface of an immersed piece of copper at a common (mixed) potential. In neutral or alkaline solutions, O_2 reduction will be coupled with copper oxidation into Cu_2O.

E. Protopopoff and P. Marcus, Potential versus pH (Pourbaix) Diagrams, *Corrosion: Fundamentals, Testing, and Protection*, Vol 13A, *ASM Handbook*, ASM International, 2003, p 17-–30

Potential versus pH (Pourbaix) Diagrams

E. Protopopoff and P. Marcus, CNRS, Ecole Nationale Supérieure de Chimie de Paris, Université Pierre et Marie Curie

---

E-pH Diagrams for Ternary Systems

The *E*-pH diagrams for corrosion protection give valuable information if all the substances present in the actual system under investigation (metal or metalloid in aqueous solution) are taken into account when the diagrams are constructed. The previous discussion assumed that the solution did not contain chlorine, sulfur, or other species capable of forming solid compounds or soluble complexes with the metal. In the presence of such elements, other diagrams must be considered that may reveal different metal corrosion behavior. Hence, diagrams for binary metal-water (M-H_2O) systems are of limited usefulness, and diagrams for multicomponent systems must be calculated. For example, the simple diagram of gold in water (Au-H_2O system) does not show any solubility for that metal. The addition of cyanide (CN) ions to the system, however, leads to the formation of a gold complex soluble in water. Hence, gold, which does not corrode in pure water can dissolve in the presence of cyanide. This property is the basis of gold plating and of the hydrometallurgy of that metal. Diagrams for the ternary system Au- CN^--H_2O must then be constructed to show the conditions of stability for the gold complex. A general bibliography of *E*-pH diagrams for multicomponent systems in aqueous solutions is given in Ref 8.

Diagrams for ternary metal-additive-water (M-A-H_2O) systems are frequently used. In most cases, the amount of one element in the dissolved form is substantially greater than that of the other. If so, the reactions involving only the major element will be practically independent of the reactions involving the minor element. Thus, the diagram of the major element alone, drawn with dashed lines, will serve as a background for the diagram for the combined system, drawn with solid lines. The behavior of the minor element may be or may not be independent of that of the major element. It will be independent if the minor element forms no stable solid compound or dissolved complex with the major element; in this case the diagram for the ternary system will just be the diagram of the minor element alone superimposed on the diagram of the major element alone. Otherwise the diagram for the ternary system may be drastically different. Again, the convention is that in the regions of stability of a dissolved species, the latter is considered as the only element form present. When the minor element forms a dissolved complex with the major element, this solution species is considered as a species of the minor element, and hence its concentration is the one of the minor element.

Consider the case where the concentration of additive in the dissolved form is much higher than the tolerated concentration of dissolved metal. First, the *E*-pH diagram for the A-H_2O system must be calculated to determine the areas of predominance for the various species of A. Then, in each area delineated with dashed lines, the *E*-pH equilibria lines for the various reactions between the metal and the predominant A species to form metal compounds or complexes are calculated. A metal-additive dissolved complex is considered as a metal species.

As an example of calculations for a ternary system involving metal-additive solid compounds, consider the following reactions for the iron-sulfur-water system:

- FeS_2/Fe^{2+} equilibrium in sulfide media:

$$FeS_2 + 4H^+ + 2e^- \rightleftharpoons Fe^{2+} + 2H_2S(aq) \qquad \text{(Eq 36)}$$

- or

$$FeS_2 + 2H^+ + 2e^- \rightleftharpoons Fe^{2+} + 2HS^-$$ (Eq 37)

- Fe^{2+}/FeS_2 equilibrium in thiosulfate media:

$$Fe^{2+} + HS_2O_3^- + 5H^+ + 6e^- \rightleftharpoons FeS_2 + 3H_2O$$ (Eq 38)

- or

$$Fe^{2+} + S_2O_3^{2-} + 6H^+ + 6e^- \rightleftharpoons FeS_2 + 3H_2O$$ (Eq 39)

- Fe_2O_3/FeS_2 equilibrium in thiosulfate media:

$$Fe_2O_3 + 2S_2O_3^{2-} + 18H^+ + 14e^- \rightleftharpoons 2FeS_2 + 9H_2O$$ (Eq 40)

At 25 °C (77 °F), the equations for the previously mentioned equilibria are, respectively, if m_S and m_{Fe} are the molalities of sulfur and iron in solution:

$$E = E^\circ - 0.059 \log\left(\frac{m_S}{2}\right) - \frac{0.059}{2} \log m_{Fe} - 2 \times 0.059\ \text{pH}$$ (Eq 41)

or

$$E = E^\circ - 0.059 \log\left(\frac{m_S}{2}\right) - \frac{0.059}{2} \log m_{Fe} - 0.059\ \text{pH}$$ (Eq 42)

$$E = E^\circ + \frac{0.059}{6}\log\left(\frac{m_S}{2}\right) + \frac{0.059}{6}\log m_{Fe} - \frac{5}{6} \times 0.059\ \mathrm{pH} \qquad \text{(Eq 43)}$$

or

$$E = E^\circ + \frac{0.059}{6}\log\left(\frac{m_S}{2}\right) + \frac{0.059}{6}\log m_{Fe} - 0.059\ \mathrm{pH} \qquad \text{(Eq 44)}$$

$$E = E^\circ + \frac{0.059}{7}\log\left(\frac{m_S}{2}\right) - \frac{9}{7} \times 0.059\ \mathrm{pH} \qquad \text{(Eq 45)}$$

Metals may form compounds in dissolved form with sulfur (e.g., $FeSO_4$(aq), $FeSO_4^+$, $CuSO^-_3$). Consider the Cu^{2+}/$CuSO_3^-$ equilibrium in sulfite media in a case where $m_{Cu} \ll m_S$:

$$Cu^{2+} + SO_3^{2-} + e^- \rightleftharpoons CuSO_3^- \qquad \text{(Eq 46)}$$

$$E = E^\circ + 0.059 \log a_{SO_3^{2-}} + 0.059 \log\left(\frac{a_{Cu^{2+}}}{a_{CuSO_3^-}}\right) \qquad \text{(Eq 47)}$$

The equation of the boundary line between the domains of relative predominance of Cu^{2+} and $CuSO_3^-$ would be obtained (if the latter were stable) for $a_{Cu^{2+}} = a_{CuSO_3^-}$ (= m_{Cu}):

$$E = E^o + 0.059 \log m_S \qquad \text{(Eq 48)}$$

An illustration is given for the system iron- sulfur-water in water containing thiosulfates. This case is of technological importance, because thiosulfates dissolved in aqueous solution are known to be detrimental to the corrosion resistance of stainless steels (Ref 9, 10, 11, 12, 13, 14, 15, 16). The concentration of the dissolved sulfur impurity expressed in molality is usually approximately 10^{-4} mol/kg, and the molality of dissolved iron is considered to be 10^{-6} mol/kg. Such a small value allows conservative predictions of corrosion, because it is generally agreed that there is no corrosion when the concentration of metal that can be dissolved in a solution initially free from it is lower or equal to 10^{-6} mol/kg. Thus, the major element here is sulfur, and the binary diagram used as a background is the one of the metastable sulfur-water system (compare with Fig. 10), showing the thermodynamically stable sulfides (H_2S(aq) and HS^-) as reduced forms of sulfur and the metastable thiosulfates ($HS_2O_3^-$ and $S_2O_3^{2-}$) as the only oxidized forms. The ternary diagram for the iron-sulfur-water system is plotted in Fig. 13.

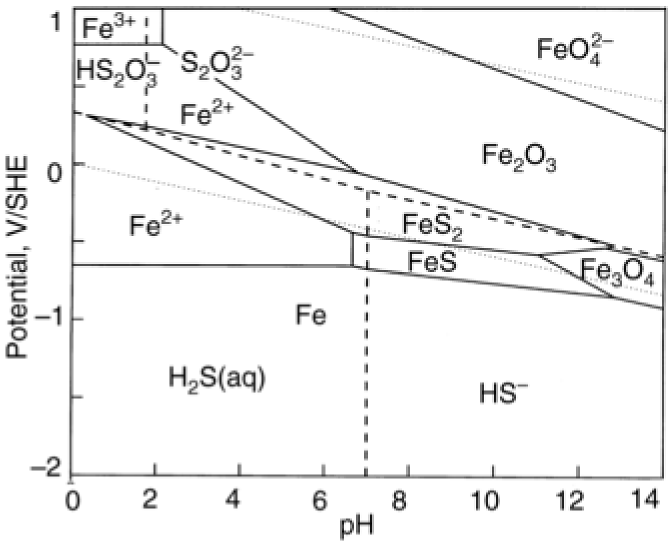

Fig. 13 ***E*-pH diagram for the iron-sulfur-water system at 25 °C (298.15 K) in the case where the metastable thiosulfates are the only oxidized forms of sulfur. The stability domains are limited by the dotted lines for the water system, dashed lines for the sulfur-water system, and solid lines for the iron-sulfur-water system. $m_S = 10^{-4}$ mol/kg. $m_{Fe} = 10^{-6}$ mol/kg**

A comparison with the diagram of the binary iron-water system (Fig. 8, 9) shows that iron interacts with sulfides or thiosulfates in the mid- pH region to form iron sufides (FeS and FeS_2), replacing Fe^{2+} in acid solutions and magnetite (Fe_3O_4) in neutral and alkaline solutions. Because metal sulfides are good ionic conductors, they offer little protection against corrosion. Although the diagram predicts Fe_2O_3 could be formed on the surface under anodic (strongly oxidizing) conditions over a large pH range and protect iron from corrosion, the incompatibility between FeS_2 and Fe_2O_3 actually prevents growth of an adhesive Fe_2O_3 layer (Ref 17). Hence, the diagram predicts that iron passivation will not occur in the presence of sulfides or thiosulfates in solution.

The diagram for the chromium-sulfur-water system is plotted in Fig. 14. There is no range of stability of chromium sulfides (at least for $m_S \leq 10^{-4}$ mol/kg), so the diagram is identical to the binary diagram for the chromium-water system. It shows that chromium sulfides are less stable than the chromic oxide (Cr_2O_3) or hydroxide ($Cr(OH)_3$), which provide the exceptional corrosion resistance of chromium.

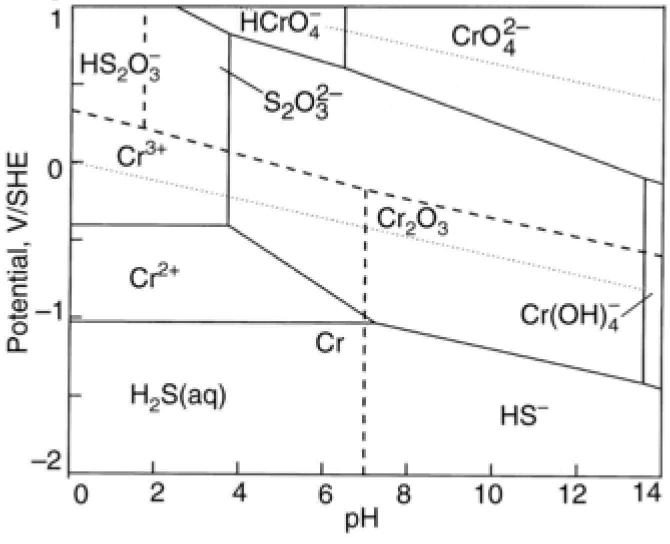

Fig. 14 ***E*-pH diagram for the chromium-sulfur-water system at 25 °C (298.15 K) in the case where the thiosulfates are the only oxidized forms of sulfur. The stability domains are limited by the dotted lines for the water system, dashed lines for the sulfur-water system, and solid lines for the chromium-sulfur-water system. $m_S = 10^{-4}$ mol/kg and $m_{Cr} = 10^{-6}$ mol/kg**

References cited in this section

8. J.V. Muylder, in *Comprehensive Treatise of Electrochemistry,* Vol 4, J. O'M. Bockris, B.E. Conway, E. Yeager, and R.E. White, Ed., Plenum Press, 1981, p 1–96

9. R.C. Newman, H.S. Isaacs, and B. Alman, *Corrosion,* Vol 38, 1982, p 261

10. R.C. Newman K. Sieradski, and H.S. Isaacs, *Metall. Trans. A,* Vol 13, 1982, p 2015

11. R.C. Newman and K. Sieradski, *Corros. Sci.,* Vol 23, 1983, p 363

12. R.C. Newman, *Corrosion,* Vol 41, 1985, p 450

13. D. Tromans and L. Frederick, *Corrosion,* Vol 40, 1984, p 633

14. A. Garner, *Corrosion,* Vol 41, 1985, p 587

15. S.E. Lott and R.C. Alkire, *J. Electrochem. Soc.,* Vol 136, 1989, p 973, 3256

16. C. Duret-Thual, D. Costa, W.P. Yang, and P. Marcus, *Corros. Sci.,* Vol 39, 1997, p 913

17. C.M. Chen, K. Aral, and G.J. Theus, "Computer-Calculated Potential pH Diagrams to 300 °C," EPRI Report NP-3137, Vol 2, Electric Power Research Institute, Babcock & Wilcox Company, June 1983

E. Protopopoff and P. Marcus, Potential versus pH (Pourbaix) Diagrams, *Corrosion: Fundamentals, Testing, and Protection,* Vol 13A, *ASM Handbook*, ASM International, 2003, p 17–-30

Potential versus pH (Pourbaix) Diagrams

E. Protopopoff and P. Marcus, CNRS, Ecole Nationale Supérieure de Chimie de Paris, Université Pierre et Marie Curie

---

E-pH Diagrams for High- Temperature Aqueous Solutions

Prediction of the corrosion behavior of metals in aqueous solutions at high temperatures is of considerable technological interest. Such a situation is steel vessels in contact with pressurized water at 300 °C (573.15 K) in nuclear power reactors. It was necessary to extend the *E*-pH equilibrium diagrams originally established at 25 °C (Ref 4) to higher temperatures. The main problem is that there are few thermodynamic data available for chemical species dissolved in water above 60 °C (333.15 K). The increase in water vapor pressure with temperature in closed cells leads to high pressures. This makes it necessary to carry out experiments in autoclaves, high- strength vessels with special seals (Ref 18). Often, thermodynamic-state functions data at high temperatures are obtained by extrapolation from the data at 25 °C using empirical hypotheses on the influence of temperature on molar heat capacities. In particular, entropy correspondence principles have been established that make possible the calculation of entropies and heat capacities of ions at temperatures up to 300 °C from the entropy values at 25 °C (Ref 19, 20). An alternate treatment of the problem is the calculation of temperature coefficients of standard equilibrium potentials of electrochemical reactions from thermodynamic data at 25 °C (Ref 21). A review of these different methods of estimation is given in Ref 8.

High-temperature Pourbaix diagrams are, by nature, less accurate than those at 25 °C that are based on experimental data, because they are based on estimates. The effects of pressure on the equilibria can be ignored up to 300 °C because the magnitude of the errors introduced is within the uncertainty of the data (Ref 18, 19).

At high temperature, the molar scale for activities must not be used, because, due to water volume changes, the molarity for a given solute quantity (number of moles of solute per liter of water) varies with temperature. One can only use the molality (number of moles of solute per kilogram of water), which is equal to the molarity at 25 °C (77 °F) but is invariant with temperature. The standard state for each dissolved species is the hypothetical ideal solution of the substance at unit molality.

Thermodynamic Conventions for High Temperature. High-temperature thermodynamic calculations for aqueous solutions require one to specify additional conventions, and one must be careful about which convention applies when using a set of high temperature data.

Standard chemical potentials, or Gibbs free energies of formation at a temperature *T*, may be given for the formation of the substance from its elements in their standard states at *T* or at 25 °C (77 °F). Thus, in the first convention, the standard values of elements or diatomic gases are zero at any temperature, whereas, in the second one, they are zero only at 25 °C (77 °F). Using the second convention, values are given in Table 1 for hydrospecies and sulfur species at 25 and 300 °C. Table 2 lists the values for iron and its compounds.

Table 1 Standard Gibbs free energies of formation (chemical potentials) of hydrospecies and sulfur compounds (sulfides and thiosulfates only) at 25 and 300 °C

Species	$\Delta_f G^0$(298.15 K), kJ/mol	$\Delta_f G^0$(573.15 K), kJ/mol	References
H_2(g)	0	-38.786	21
O_2(g)	0	-59.400	21
S(rh,l)	0	-12.678	21
H_2S(g)	-33.282	-93.423	21
H_2O(l)	-237.174	-263.881	22
H^+(aq)	0	0	…
e^-(aq)	0	-19.393	…
H_2S(aq)	-27.861	-78.881	22
HS^-	12.050	13.648	7 22
$HS_2O_3^-$	-532.414	-564.840	7
$S_2O_3^{2-}$	-522.582	-505.260	7

Table 2 Standard Gibbs free energies of formation (chemical potentials) of iron compounds at 25 and 300 °C

Species	$\Delta_f G^0$(298.15 K), kJ/mol	$\Delta_f G^0$(573.15 K), kJ/mol	References
Fe	0	-10.155	17
Fe_3O_4	-1015.457	-1072.468	17
Fe_2O_3	-742.242	-777.906	17
Fe^{2+}	-91.563	-57.497	22
$FeOH^+$	-275.542	-272.542	22
$Fe(OH)_3^-$	-614.989	-629.094[(a)]	17
Fe^{3+}	-17.280	62.718	22
$FeOH^{2+}$	-229.409	-193.548[(a)]	17
$Fe(OH)_2^+$	-438.065	-438.270[(a)]	17
FeO_4^{2-}	-467.290	-375.836[(a)]	17
FeS	-100.754	-124.540	23
FeS_2	-160.168	-181.440	23

(a) Values after correction of the difference in convention for the free energy of formation of H^+(aq) at 300 °C (573.15 K) between this text and Ref 17

Two conventions exist for the potential scale: the "universal" convention and the "alternate" convention. In the universal convention, the electrode potentials are referred to the potential of the standard hydrogen electrode (SHE) at the temperature considered; that is, the potential of the SHE $(p_{H_2} = 1\text{bar}, a_{H^+} = 1)$ is taken equal to 0 V at all temperatures. Hence, the chemical potential (Gibbs free energy) of the conventional electron used in the writing of electrode (half- cell) reactions is, at all temperatures:

$$\left(\mu^0_{e^-}\right)_1 (T) = \tfrac{1}{2}\mu^0_{H_2}(T) - \mu^0_{H^+}(T) \quad \text{(Eq 49)}$$

With this convention, the *E*-pH line for the H^+(aq)/H_2(g) couple passes by the point (*E* = 0, pH = 0) at any *T* (Fig. 13).

In the alternate convention, the potentials are referred to the potential of the SHE at 25 °C (77 °F). Here, the chemical potential of the conventional electron is the same at all temperatures:

$$\left(\mu^{0}_{e^-}\right)_2 = \tfrac{1}{2}\mu^{0}_{H_2}(298.15\ \mathrm{K}) - \mu^{0}_{H^+}(298.15\ \mathrm{K}) = 0 \qquad \text{(Eq 50)}$$

In this convention, the potential of the SHE depends on temperature, and the *E*-pH line for the $H^+(aq)/H_2(g)$ couple intersects the vertical axis for pH = 0 above 0 V for *T* > 25 °C (Fig. 15). The two conventions become identical at 25 °C: $(\mu^{0}_{e^-})_1(298.15\ \mathrm{K}) = (\mu^{0}_{e^-})_2 = 0$.

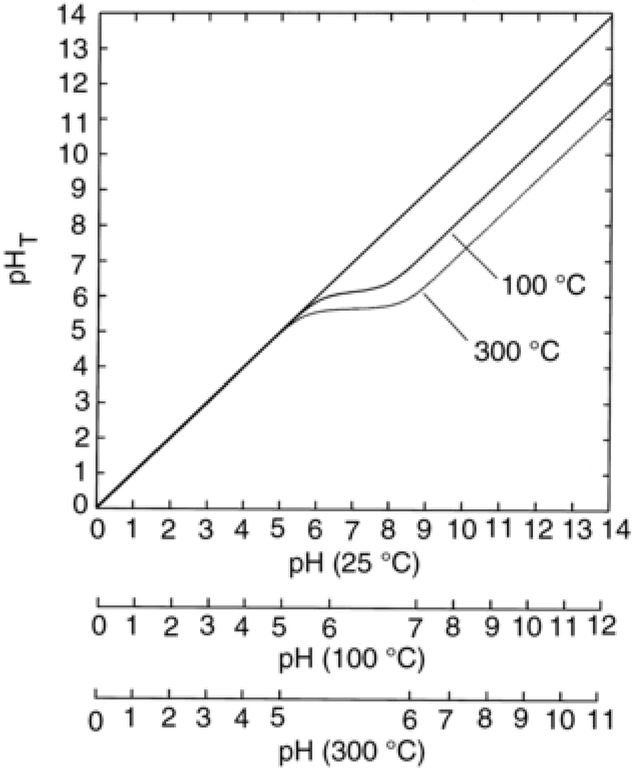

Fig. 15 pH at 100 and 300 °C (373.15 and 573.15 K) versus pH at 25 °C (298.15 K) in an unbuffered solution ($pH_{200} = pH_{300}$). Also, the correspondence between the pH scales at the different temperatures is shown.

Solvated H^+ ($H^+(aq)$) is often considered as a reference substance whose standard chemical potential, or Gibbs free energy of formation, is taken to be zero at all temperatures. Use of the universal convention produces the simple relation $(\mu^{0}_{e^-})_1(T) = \mu^{0}_{H_2}(T)$.

Variation of pH with Temperature. For a correct interpretation of the high-temperature *E*- pH diagrams, the change of pH of the solution with the temperature must be taken into account. The pH of an aqueous solution is determined by:

- The equilibrium constant for water dissociation into solvated protons and hydroxide ions, $H_2O(l) = H^+(aq) + OH^-(aq)$, also called the ionic product of water, $(K_w)_T = a_{H^+} \cdot a_{OH^-}$, which increases with temperature
- The concentrations and dissociation constants of the other constituents of the solution

Because the temperature dependence of dissociation constants is not the same for all acids and bases, it is not possible to calculate the pH scale for a given temperature in a manner that would apply to all aqueous solutions. At least, the temperature effect can be visualized on the *E*-pH diagram at a given temperature by marking by vertical lines the position of three important pH values (Ref 24):

- pH = $-\log_{10}(K_w)_T = 0$, which corresponds to a 1 molal solution of a strong (completely dissociated) acid
- pH = $-\log_{10}(K_w)_T = (pK_w)_T$, which corresponds to a 1 molal solution of a strong base
- pH = $\frac{1}{2}(pK_w)_T$, which corresponds to neutral water. Indeed, in neutral aqueous solutions:

$$\left(a_{H^+}\right)_n = \left(a_{OH^-}\right)_n = \sqrt{\left(K_w\right)_T}$$

Hence, the neutral pH is $pH_n = -\log_{10}(a_{H+})_n = -\frac{1}{2}(\log_{10}(K_w)_T) = \frac{1}{2}(pK_w)_T$.

The pK_w decreases from 14.00 at 25 °C to 12.27 at 100 °C (373.15 K) and 11.30 at 200 and 300 (473.15 and 573.15 K) (Ref 22). Accordingly, the pH of a neutral aqueous solution is 7.00 at 25 °C, whereas it is 6.13 at 100 °C and 5.65 at 200 and 300 °C.

In an unbuffered solution (with completely dissociated acid or base), the proton activity is fixed only by the water ionic product (from here simply denoted K_T), which increases with ***T***. Thus, a solution that has a certain pH at 25 °C will have a lower pH at a higher temperature. In this simple case, the change in pH can be calculated in the following way (Ref 23). Consider the general case of a solution of a certain pH at 25 °C: From the definition of the water ionic product $K_{25} = a^{25}_{H+} \cdot a^{25}_{OH-}$, hence $pK_{25} = pH_{25} + pOH_{25}$. As the temperature is raised, the equilibrium of dissociation of water will be shifted, and equivalent amounts of additional H^+ and OH^- will be generated in solution. Thus:

$$K_T = a^T_{H^+} + a^T_{OH^-} = \left(a^{25}_{H^+} + x\right)\left(a^{25}_{OH^-} + x\right) \qquad \text{(Eq 51)}$$

where *x* is the increase in ion activity as a result of the temperature change from 25 °C to ***T***. This is a quadratic equation in *x*: $x^2 + (a^{25}_{H+} + a^{25}_{OH-})x + (K_{25} - K_T) = 0$, whose physically meaningful solution is:

$$x^+ = \frac{-\left(a^{25}_{H^+} + a^{25}_{OH^-}\right) + \sqrt{\left(a^{25}_{H^+} + a^{25}_{OH^-}\right)^2 + 4\left(K_T - K_{25}\right)}}{2} \qquad \text{(Eq 52)}$$

The pH at *T* is $pH_T = -\log_{10}(a^{25}_{H+} + x^+)$. It takes limiting values:

- $$\begin{aligned} &\text{For low pHs: } pH_{25} < pK_T/2 < 7 \\ &\Rightarrow a^{25}_{H^+} \gg \sqrt{K_T} > \sqrt{K_{25}} \gg a^{25}_{OH^-} \\ &\Rightarrow x^+ \approx \left(K_T - K_{25}\right)/a^{25}_{H^+} \ll a_{H^+_T} \approx a^{25}_{H^+} \\ &\Rightarrow pH_T \approx pH_{25} \end{aligned}$$

- $$\begin{aligned} &\text{For high pHs: } pH_{25} > \left(14 - pK_T/2\right) > 7 \\ &\Rightarrow a^{25}_{H^+} \ll \sqrt{K_{25}} < \sqrt{K_T} \ll a^{25}_{OH^-} \\ &\Rightarrow x^+ \approx \left(K_T - K_{25}\right)\Big/\left(a^{25}_{OH^-}\right)^2 \ll 1 \rightarrow a_{OH^-_T} \approx a^{25}_{OH^-} \\ &\Rightarrow a_{H^+_T} \approx K_T/a^{25}_{OH^-} = a^{25}_{H^+}\, K_T/K_{25} \\ &\Rightarrow pH_T \approx pH_{25} + pK_T \approx pK_{25} \end{aligned}$$

-

$$\text{For neutral pHs: } pH_{25} \approx 7$$
$$\Rightarrow a^{25}_{H^+} \approx a^{25}_{OH^-} \approx \sqrt{K_{25}} \rightarrow K_T$$
$$\approx \left(a^{25}_{H^+} + x^+\right)^2 = \left(a^T_{H^+}\right)^2$$
$$\Rightarrow a^T_{H^+} \approx \sqrt{K_T}$$
$$\Rightarrow pH_T \approx pK_T/2$$

The pH values at 100 and 300 °C are plotted versus the pH at 25 °C 15 in Fig. 15. Also, the correspondence between the pH scales at different temperatures is plotted. (The pH at 200 °C is equal to the pH at 300 °C, because pK_w is practically the same at these two temperatures [Ref 22].) To compare the behavior of an electrode in an unbuffered solution of given pH at 25 °C with the one in the same solution at *T*, the corrected pH must be employed when using the *E*-pH diagram at ***T***.

It must be noted that, in a buffered solution, the pH is fixed by the equilibrium of an acid- base couple, and it is the variation of the acid dissociation constant with temperature that is predominant in fixing the pH variation.

Temperature Effects on the *E*-pH Diagrams for Binary Systems. The diagram for the iron- water system at 300 °C is plotted in Fig. 16. Even after correction of the temperature effect on pH, the net effect of increase of temperature is to shift the diagram to lower values of pH (Ref 17, 23, 24, 25). Comparison of higher-temperature diagrams to the diagram at 25 °C (Fig. 8) gives the following trends for the influence of temperature:

- The domains of stability of the Fe^{2+} and Fe^{3+} cations are contracted to the benefit of condensed species Fe, Fe_3O_4, and Fe_2O_3; that is, the solubility of the latter species in acid solutions is lower at 300 °C than at 25 °C.
- There is an expansion below pH 14 of the domain of stability of the dihypoferrite ion $HFeO_2^-$ (or $Fe(OH)_3^-$) at the expense of Fe, Fe_3O_4, and Fe_2O_3; that is, the solubility of the condensed species in alkaline solutions is substantially greater at 300 °C.

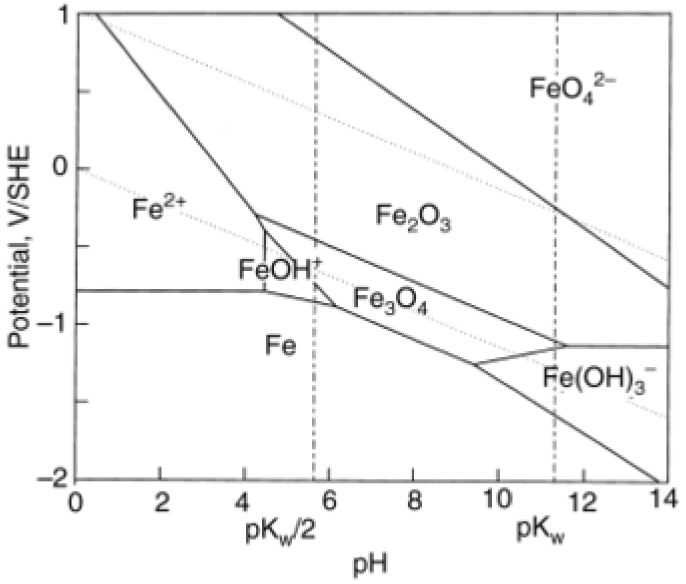

Fig. 16 *E*-pH diagram for the iron-water system at 300 °C (573.15 K). $m_{Fe} = 10^{-6}$ mol/kg

The diagram for the chromium-water system at 300 °C (573.15 K) is plotted in Fig. 17. Compared to the diagram at 25 °C (Fig. 14), $CrOH^{2+}$ replaces Cr^{3+} as the trivalent species at low pH and anodic potentials. Effects of temperature similar to those described for the iron-water system are observed. The Cr_2O_3 (or $Cr(OH)_3$) becomes less soluble (more stable) in acid solution and more soluble (less stable) in alkaline solutions, where CrO_2^- ($Cr(OH)^-_4$) is the stable ion (Ref 17, 26, 27, 28).

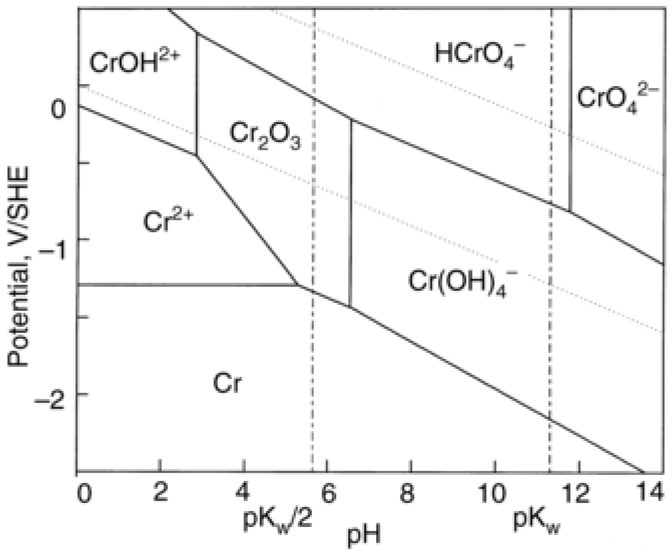

Fig. 17 ***E*-pH diagram for the chromium-water system at 300 °C (573.15 K).** $\mathbf{m_{Cr} = 10^{-6}}$ **mol/kg**

Similar effects are also predicted for various other metals (Ref 17, 18, 26, 27). Thus, the most significant effect of the increase of temperature is an expansion of the domain of corrosion in strong alkaline environment, which was confirmed experimentally (Ref 8, 23).

Temperature Effects on *E*-pH Diagrams for Ternary Systems. Diagrams for multi-component systems in high-temperature aqueous solutions are obviously of great interest for predicting corrosion behavior in numerous industrial conditions. A general bibliography of *E*-pH diagrams for multicomponent systems in high-temperature aqueous solutions is given in Ref 8. As an example, the diagram for the ternary system iron-sulfur-water with thiosulfates at 300 °C (573.15 K), for $a_S = 10^{-4}$ and $a_{Fe} = 10^{-6}$, is shown in Fig. 18. It may be compared to the diagram at 25 °C, presented previously (Fig. 13), to visualize the effects of increasing temperature. Concerning the sulfur-water system, there is an increased stability of the acid forms of dissolved sulfur, H_2S(aq) and $HS_2O_3^-$, at the expense of HS^- and $S_2O_3^{2-}$. At 300 °C, the diagram for the iron-sulfur-water system is identical to the one for the iron-water system (Fig. 16). Besides the effects described previously for the iron-water system (contraction of the domains of stability of Fe^{2+} and Fe^{3+} and expansion of the domain of $Fe(OH)_3^-$), the main effect of temperature rise is that the range of stability of the sulphides FeS and FeS_2 is drastically reduced (Ref 17, 29) and even suppressed for the sulfur activity of the diagram ($a_S = 10^{-4}$).

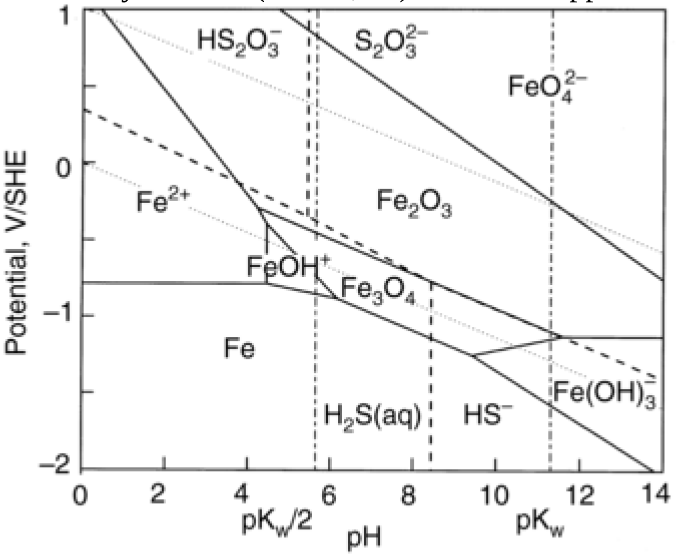

Fig. 18 ***E*-pH diagram for the iron-sulfur-water system at 300 °C (573.15 K) in the case where the thiosulfates are the only oxidized forms of sulfur.** $\mathbf{m_S = 10^{-4}}$ **mol/kg,** $\mathbf{m_{Fe} = 10^{-6}}$ **mol/kg**

Similarly, the diagram for the chromium-sulfur-water system at 300 °C (572 °F) is identical to the diagram for the chromium-water system shown in Fig. 17, because it shows no chromium sulfides.

High-temperature *E*-pH diagrams for various metal-chlorine-water systems, which are very important for the interpretation and prediction of corrosion phenomena in high-salinity brines, can be found in Ref 30. Also, the *E*-pH diagrams for the quaternary system Fe-Cl-S-H_2O up to 250 °C (523.15 K) are of direct interest in the phenomenon of stress cracking in sulfide-containing brines (Ref 31).

References cited in this section

4. M. Pourbaix, *Atlas of the Electrochemical Equilibria,* NACE, 1974

7. R.C. Murray, Jr. and D. Cubicciotti, *J. Electrochem. Soc.,* Vol 130, 1983, p 866

8. J.V. Muylder, in *Comprehensive Treatise of Electrochemistry,* Vol 4, J. O'M. Bockris, B.E. Conway, E. Yeager, and R.E. White, Ed., Plenum Press, 1981, p 1–96

17. C.M. Chen, K. Aral, and G.J. Theus, "Computer-Calculated Potential pH Diagrams to 300 °C," EPRI Report NP-3137, Vol 2, Electric Power Research Institute, Babcock & Wilcox Company, June 1983

18. R.L. Cowan and R.W. Staehle, *J. Electrochem. Soc.,* Vol 118, 1971, p 557

19. C.M. Criss and J.W. Cobble, *J. Am. Chem. Soc.,* Vol 86, 1964, p 5385, 5390, 5394

20. I.L. Khodakovski, B.N. Ryzhenko, and G.B. Naumov, *Geochem. Int.,* Vol 5, 1968, p 1200, translated from *Geokhimia,* No. 12, 1968, p 1486; I.L. Khodakovski, *Geochem. Int.,* Vol 6, 1969, p 29, translated from *Geokhimia,* No. 1, 1969, p 57

21. A.J. de Béthune, T.S. Licht, and N. Swendeman, *J. Electrochem. Soc.,* Vol 106, 1959, p 616; G.R. Salvi and A.J. de Béthune, *J. Electrochem. Soc.,* Vol 108, 1961, p 672

22. J.W. Cobble, R.C. Murray, Jr., P.J. Turner, and K. Chen, "High-Temperature Thermodynamic Data for Species in Aqueous Solution," San Diego State University Foundation, EPRI Report NP-2400, Electric Power Research Institute, May 1982

23. V. Ashworth and P.J. Boden, *Corros. Sci.,* Vol 10, 1970, p 709

24. H.E. Townsend, in *Proceedings of the Fourth International Congress on Metallic Corrosion,* 1969 (Amsterdam), NACE, 1970, p 477

25. H.E. Townsend, *Corros. Sci.,* Vol 10, 1970, p 343

26. P.A. Brook, *Corros. Sci.,* Vol 12, 1972, p 297

27. J.B. Lee, *Corrosion,* Vol 37, 1981, p 467

28. P. Radhakrishnamurty and P. Adaikkalam, *Corros. Sci.,* Vol 22, 1982, p 753

29. R.J. Biernat and R.G. Robins, *Electrochim. Acta,* Vol 17, 1972, p 1261

30. D.D. MacDonald, B.C. Syrett, and S.S. Wing, *Corrosion,* Vol 35, 1979, p 1

31. D.D. MacDonald, "ASTM Sp. Publication 717," ASTM, 1981

E. Protopopoff and P. Marcus, Potential versus pH (Pourbaix) Diagrams, *Corrosion: Fundamentals, Testing, and Protection*, Vol 13A, *ASM Handbook*, ASM International, 2003, p 17–-30

Potential versus pH (Pourbaix) Diagrams

E. Protopopoff and P. Marcus, CNRS, Ecole Nationale Supérieure de Chimie de Paris, Université Pierre et Marie Curie

E-pH Diagrams for Adsorbed Species

The principle of *E*-pH diagrams can be extended to the case of bidimensional layers of species adsorbed on metal surfaces. The solid compounds treated in the usual diagrams are three-dimensional (bulk) compounds (oxides, hydroxides, sulfides, etc.). However, the formation of a three-dimensional solid compound M_xA_y (A may be O, OH, S …) by reaction of gaseous or dissolved forms of A with a metal, M, is often preceded by the formation of a two- dimensional phase of A adsorbed on the metal surface. This surface phase is more stable than the bulk compound (Ref 32). When there is creation of a true chemical bond between A atoms and metal surface atoms (bond energies larger than 200 kJ/mol, at least at low coverage), the adsorption is also called *chemisorption.* Adsorbed (chemisorbed) monolayers may form under *E*-pH conditions where the bulk compounds are thermodynamically unstable, and a classic diagram would predict only the existence of the bare metal. Chemisorption must not be neglected, because the presence of a chemisorbed monolayer can induce marked changes in the reactivity of the metal. For example, it has been shown that a monolayer of sulfur adsorbed on nickel or nickel-iron alloys enhances the anodic dissolution and hinders the formation of the passive film, drastically affecting the corrosion resistance of the metallic material (Ref 33, 34). Therefore, *E*-pH diagrams for adsorbed species are of interest for predicting corrosion risk (Ref 34). The method of calculation of the equilibrium potentials of oxidation-reduction couples involving a species adsorbed on an electrode surface is presented subsequently.

Principle of *E*-pH Diagrams for Adsorbed Species. Consider the case where a species A (which may be an element, H, O, S or a molecular species, OH or H_2O) is adsorbed from solution on a metal surface M in the form of a neutral monolayer [denoted $A_{ads}(M)$]. The adsorption of A from a dissolved species in aqueous solution may result from an electrooxidation or an electroreduction reaction, depending on the valence state of A in the dissolved species (it may then be called electroadsorption). The adsorption of an atom or molecule on a metal surface in water involves the replacement of adsorbed water molecules and a competition with the adsorption of oxygen species (atomic oxygen O or hydroxyl OH) produced by electrooxidation of water or hydroxide (OH^-) ions present in the electrolyte. For simplicity, a Langmuir model for adsorption is taken in which it is assumed that the two-dimensional (surface) phase is an ideal substitutional solution where species adsorb competitively on the same sites without lateral interactions between adsorbed species.

Under these conditions, the chemical potential of each adsorbed species $A_{ads}(M)$ in the surface phase of a metal M can be expressed as follows:

$$\mu_{A_{ads}(M)} = \mu^0_{A_{ads}(M)} + RT \ln\theta_A \qquad \text{(Eq 53)}$$

where θ_A is the relative coverage by adsorbed A ($0 \leq \theta_A \leq 1$; $\theta_A = 1$ for a complete monolayer of A); $\mu^0_{A_{ads}}(M)$ is the standard chemical potential of A, corresponding to the saturation of the surface by $A_{ads}(M)$. The total coverage on the surface is equal to unity; the coverage by water is $\theta_{H_2O} = (1 - \sum\theta_{Ai})$, where θ_{Ai} is the coverage by any other adsorbed species.

As an example of the method of calculation of the *E*-pH relations, consider the adsorption of hydroxyl on a metal surface from adsorbed water:

$$H_2O_{ads}(M) \rightleftharpoons OH_{ads}(M) + H^+ + e^- \qquad \text{(Eq 54)}$$

The equilibrium potential of this half-cell reaction is obtained by applying the Nernst equation, using the expression of the chemical potentials of adsorbed hydroxyl and water, as given in Eq 53:

$$E = E^\circ + 2.303\left(\frac{RT}{F}\right)\log\left[\frac{\theta_{OH}}{\theta_{H_2O}}\right] - 2.303\left(\frac{RT}{F}\right)\text{pH} \quad \text{(Eq 55)}$$

where θ_{OH} and θ_{H_2O} are the relative coverages by adsorbed hydroxyl and water on the M surface.
The standard potential E^o on the SHE scale is given by:

$$E^\circ_{(SHE)} = \frac{\left(\mu^0_{OH_{ads}(M)} + \mu^0_{H^+} + \mu^0_{e^-} - \mu^0_{H_2O_{ads}(M)}\right)}{F} \quad \text{(Eq 56)}$$

The standard chemical potentials, or Gibbs free energies of formation, for adsorbed sulfur oxygen, or hydroxyl are derived from literature thermodynamic data on the reversible chemisorption of these species at the metal-water interface or, if not available, at the metal-gas interface (Ref 35, 36, 37, 38, 39). Adsorbed water is weakly adsorbed on most transition metals, compared to chemisorbed species. In the absence of accurate thermodynamic data, the standard Gibbs free energy of adsorption of water from the liquid state may be neglected; that is, the standard Gibbs free energy of adsorbed water is approximated by the free energy of liquid water. This value and the values for sulfur and oxygen adsorbed on iron, calculated for the formation of the chemisorbed species from S and O_2 in their standard state at 25 °C, are listed in Table 3.

Table 3 Standard Gibbs free energies of formation (chemical potentials) for water, oxygen, and sulfur adsorbed on iron surfaces at 25 and 300 °C

Species	$\Delta_f G^0$(298.15 K), kJ/mol	$\Delta_f G^0$(573.15 K), kJ/mol	References
H_2O_{ads}(Fe)	-237.174[(a)]	-263.881[(a)]	36
O_{ads}(Fe)	-229	-236	36
S_{ads}(Fe)	-176	-188	36

(a) The values taken for H_2O_{ads}(Fe) are the values for H_2O(l). Source: Ref 22

E-pH Equations for Oxygen and Sulfur Adsorbed on Iron. As an example, presented here are the *E*-pH relations for the equilibria between oxygen and sulfur adsorbed on iron and dissolved species in water containing sulfides (H_2S or HS^-) or thiosulfates ($HS_2O_3^-$ or $S_2O_3^{2-}$). It is considered that the ratio of the area of electrode to the volume of solution is small enough so that the activity (molality m_S) of each dissolved sulfur species is independent of the sulfur surface coverage, θ_S. The uncertainty on these equations is relatively high because of the lack of accuracy of the thermodynamic measurements presently available for chemisorbed sulfur and oxygen:

$$S_{ads}(Fe) + H_2O(l) \rightleftharpoons O_{ads}(Fe) + H_2S(aq) \quad \text{(Eq 57)}$$

At 25 °C:

$$\log(\theta_O/\theta_S) = -18.8 - \log m_S \quad \text{(Eq 58)}$$

At 300 °C:

$$\log(\theta_O/\theta_S) = -7.9 - \log m_S \quad \text{(Eq 59)}$$

where θ_O and θ_S are the relative coverages by the adsorbed oxygen and sulfur on the Fe surface.

$$S_{ads}(Fe) + H_2O(l) \rightleftharpoons O_{ads}(Fe) + HS^- + H^+ \quad \text{(Eq 60)}$$

At 25 °C:

$$\log(\theta_O/\theta_S) = \text{pH} - 25.8 - \log m_S \quad \text{(Eq 61)}$$

At 300 °C:

$$\log(\theta_O/\theta_S) = \text{pH} - 16.4 - \log m_S \quad \text{(Eq 62)}$$

$$H_2O_{ads}(Fe) \rightleftharpoons O_{ads}(Fe) + 2H^+ + 2e^- \quad \text{(Eq 63)}$$

$$E^{25} = -0.11 + 0.030\log\left[\theta_O/(1-\theta_S-\theta_O)\right] - 0.059\text{ pH} \quad \text{(Eq 64)}$$

$$E^{300} = -0.22 + 0.057\log\left[\theta_O/(1-\theta_S-\theta_O)\right] - 0.114\text{ pH} \quad \text{(Eq 65)}$$

$$H_2O_{ads}(Fe) + H_2S(aq) \Rightarrow S_{ads}(Fe) + H_2O(l) + 2H^+ + 2e^- \quad \text{(Eq 66)}$$

$$E^{25} = -0.67 - 0.030\log m_S + 0.030\log\left[\theta_S/(1-\theta_S-\theta_O)\right] - 0.059\text{ pH} \quad \text{(Eq 67)}$$

$$E^{300} = -0.67 - 0.057\log m_S + 0.057\log\left[\theta_S/(1-\theta_S-\theta_O)\right] - 0.114\text{ pH} \quad \text{(Eq 68)}$$

$$H_2O_{ads}(Fe) + HS^- \rightleftharpoons S_{ads}(Fe) + H_2O(l) + H^+ + 2e^- \quad \text{(Eq 69)}$$

$$E^{25} = -0.88 - 0.030\log m_S + 0.030\log\left[\theta_S/(1-\theta_S-\theta_O)\right] - 0.030\text{ pH} \quad \text{(Eq 70)}$$

$$E^{300} = -1.15 - 0.057\log m_S + 0.057\log\left[\theta_S/(1-\theta_S-\theta_O)\right] - 0.057\text{ pH} \quad \text{(Eq 71)}$$

$$2S_{ads}(Fe) + 5H_2O(l) \rightleftharpoons 2O_{ads}(Fe) + HS_2O_3^- + 9H^+ + 8e^- \quad \text{(Eq 72)}$$

$$E^{25} = 0.58 - 0.007\log(m_S/2) + 0.015\log(\theta_O/\theta_S) - 0.067\text{ pH} \quad \text{(Eq 73)}$$

$$E^{300} = 0.52 - 0.014\log(m_S/2) + 0.028\log(\theta_O/\theta_S) - 0.128\text{ pH} \quad \text{(Eq 74)}$$

$$2S_{ads}(M) + 5H_2O(l) \rightleftharpoons 2O_{ads}(M) + S_2O_3^{2-} + 10H^+ + 8e^- \quad \text{(Eq 75)}$$

$$E^{25} = 0.60 + 0.007\log(m_S/2) + 0.015\log(\theta_O/\theta_S) - 0.074\text{ pH} \quad \text{(Eq 76)}$$

$$E^{300} = 0.60 + 0.014\log(m_S/2) + 0.028\log(\theta_O/\theta_S) - 0.142\text{ pH} \quad \text{(Eq 77)}$$

Potential-pH Diagrams for Oxygen and Sulfur Adsorbed on Iron. The preceding equations have been used to plot the *E*-pH diagrams for sulfur and oxygen adsorbed on iron in water containing sulfides or thiosulfates (Ref

40). The diagrams at 25 and 300 °C for a molality of dissolved sulfur $m_S = 10^{-4}$ mol/kg are shown in Fig. 19 and 20. The diagrams are superimposed on the iron-sulfur-water diagrams described previously (Fig. 13, 18).

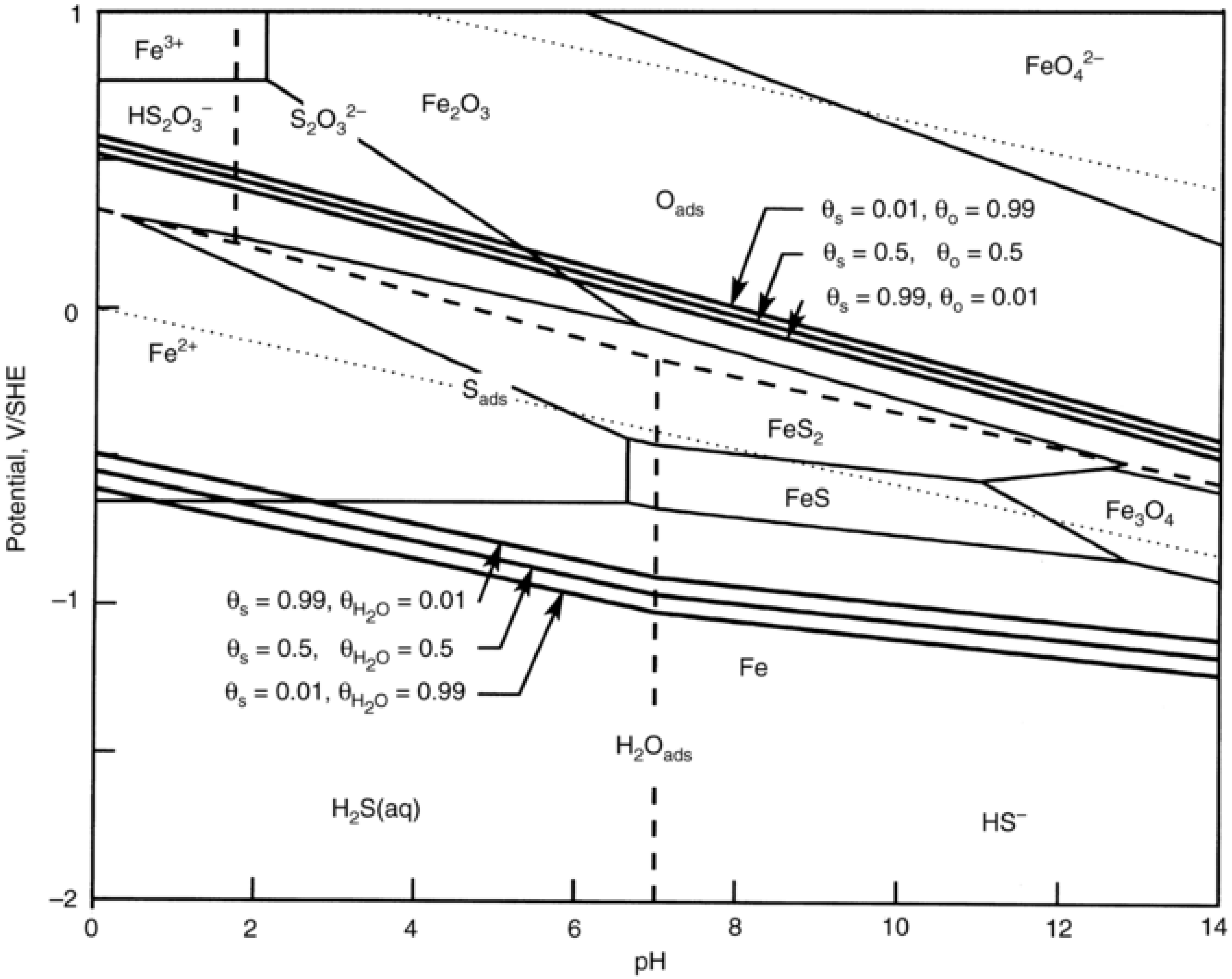

Fig. 19 ***E*-pH diagram for the system of sulfur, oxygen, and water adsorbed on iron at 25 °C (298.15 K) in the case where the thiosulfates are the only oxidized forms of sulfur. The stability domains are limited by the dotted lines for the water system, dashed lines for the sulfur-water system, and thin solid lines for the iron-sulfur-water system and thick solid lines for the adsorbed species system. θ_S and θ_O are the relative surface coverages of adsorbed sulfur and oxygen, respectively. $m_S = 10^{-4}$ mol/kg, $m_{Fe} = 10^{-6}$ mol/kg**

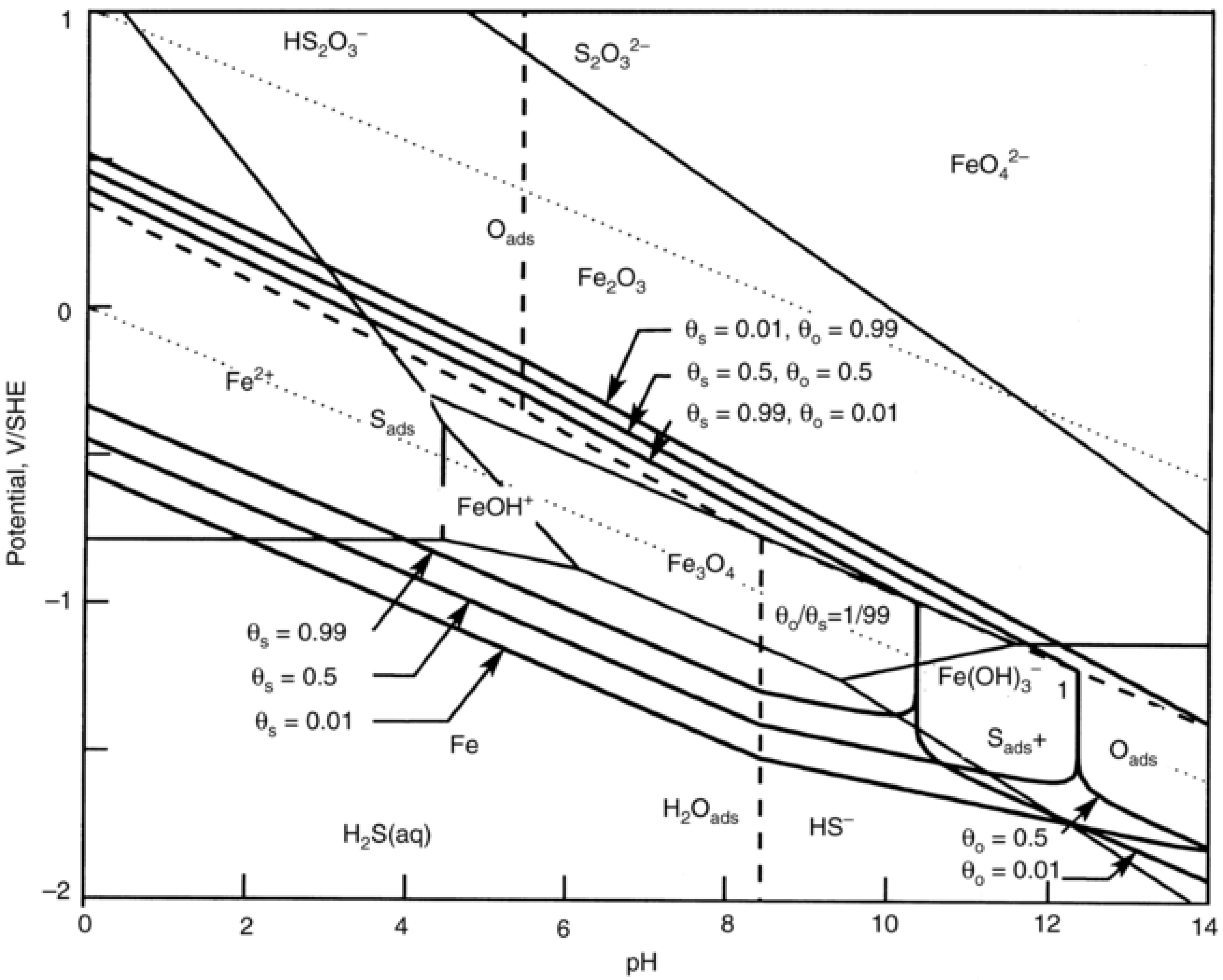

Fig. 20 ***E*-pH diagram for the system of sulfur, oxygen, and water adsorbed on iron at 300 °C (573.15 K) in the case where the thiosulfates are the only oxidized forms of sulfur. The stability domains are limited by the dotted lines for the water system, dashed lines for the sulfur-water system, and thin solid lines for the iron-sulfur-water system and thick solid lines for the adsorbed species system. θ_S and θ_O are the relative surface coverages of adsorbed sulfur and oxygen, respectively. $m_S = 10^{-4}$ mol/kg, $m_{Fe} = 10^{-6}$ mol/kg**

The domains of stability of adsorbed species are limited by lines corresponding to significant values of the surface coverage: $\theta = 0.01$; 0.5; 0.99. For $\theta_S > 0.5$ and a ratio $\theta_O/\theta_S < 0.01$, sulfur is considered as the only adsorbed species in the domain, and θ_O may be neglected in Eq 51, Eq 52, Eq 52, Eq 52, Eq 52. Similarly, for $\theta_O > 0.5$ and a ratio $\theta_O/\theta_S > 100$, oxygen is considered as the only adsorbed species, and θ_S may be neglected in Eq 64 and 65. For $0.01 < \theta_O/\theta_S < 100$, the adsorbed phase is a mixture of coadsorbed sulfur and oxygen, and both terms θ_S and θ_O must be taken into account in the equations.

In the stability domain of H_2S(aq), the ratio θ_O/θ_S is constant (Eq 58, 59). It is negligible at 25 and 300 °C (for $m_S = 10^{-4}$ mol/kg), hence, θ_O can be neglected in Eq 67 and 68, and only sulfur is adsorbed by replacement of water. For a given value of θ_S, the ratio θ_S/θ_{H_2O}($\theta_{H_2O} = 1 - \theta_S - \theta_O$) is fixed, and the *E*-pH relation for sulfur adsorption from H_2S(aq) by replacement of water (Eq 67, 68) gives a straight line (Fig. 19, 20).

In the stability domain of HS^-, the ratio θ_O/θ_S increases with pH, according to Eq 61 and 62. At 25 °C, this ratio is infinitesimal up to pH 14. At 300 °C for $m_S = 10^{-4}$ mol/kg, it becomes significant (>0.01) for a pH value below 14. The pH values corresponding to $\theta_O/\theta_S = 0.01$ (pH = 10.4) and $\theta_O/\theta_S = 1$ (pH = 12.4) are represented by vertical lines in the diagram (Fig. 20). The first vertical line is the left boundary of a domain, where sulfur and oxygen are coadsorbed. In this domain, as the ratio θ_O/θ_S varies with pH, the ratios $\theta_S/(1 - \theta_S - \theta_O)$ and $\theta_O(1 - \theta_S - \theta_O)$ depend both on θ_S (or θ_O) and pH. Therefore, the *E*-pH relations calculated for sulfur adsorption from HS^- (Eq 70, 71) and oxygen adsorption from water (Eq 64, 65), for given values of θ_S and θ_O, give nonstraight

lines (Fig. 20). These lines become vertical at the pH values where the water coverage becomes infinitesimal, that is, the coverage $\theta_S + \theta_O$ reaches unity (full monolayer of coadsorbed sulfur and oxygen). At these pHs, the line for a given sulfur coverage, θ_S, meets the line for the complementary oxygen coverage $\theta_O = 1 - \theta_S$, and they merge with the vertical line plotted for the corresponding ratio θ_O/θ_S (Fig. 20).
In the stability domains of thiosulfates, the *E*- pH relations for the replacement reaction between adsorbed sulfur and oxygen give straight lines for a fixed ratio θ_O/θ_S (Eq 73, 74, 76, 77). A simplification occurs here, because the water coverage $\theta_{H_2O} = 1 - \theta_O - \theta_S$ is negligible in the domain of thiosulfates (that can be checked by associating Eq 58 and 59 or 61 and 62 with 64 and 65 and calculating θ_{H_2O} at the anodic limit of the sulfides domains), so θ_O in Eq 73, 74, 76, and 77 can be approximated by $1 - \theta_S$. Then, straight lines are obtained for given values of θ_S, which delimit the respective stability domains of adsorbed sulfur and oxygen (Fig. 19, 20).
The diagrams (Fig. 19, 20) allow the prediction of the *E*-pH conditions in which sulfur is adsorbed on an iron surface from sulfides or from thiosulfates dissolved in water (Ref 40). The main features are the following: when the potential is increased, adsorbed water molecules are replaced by sulfur atoms adsorbed by electrooxidation of sulfides. Similarly, when the potential is decreased, adsorbed oxygen atoms (or hydroxyl groups) are replaced, totally or partially, by sulfur atoms adsorbed by electroreduction of thiosulfates. The replacement takes place within a very narrow range of potential (~0.06 V at 25 °C; ~0.11 V at 300 °C). At 300 °C, the stability domain of adsorbed sulfur alone is limited at high pH by the domain of coadsorption S_{ads} - O_{ads} (Ref 40).
The two-dimensional reactions involving oxygen (hydroxyl) and sulfur adsorbed on bare iron surfaces are of a different nature than the reactions involving the three-dimensional (bulk) Fe- O(OH) or iron-sulfur compounds. Hence, the diagrams developed here (Fig. 19, 20) are different from the classic *E*-pH diagrams of the iron-sulfur-water system (Fig. 13, 18). However, superimposition of the two types of diagrams is useful to discuss in more detail the possible effects of an adsorbed sulfur layer on the corrosion behavior of iron. At room temperature, the domain of stability of the adsorbed sulfur monolayer includes the stability domains of the bulk metal sulfides and Fe_3O_4 and overlaps the domains of metallic iron (immunity domain) of Fe^{2+} (activity domain), and Fe_2O_3 (Fig. 19). Sulfur adsorption is then expected for *E*-pH conditions where iron sulfides are not thermodynamically stable, which reflects the excess of stability of the two- dimensional chemisorbed species with respect to the three-dimensional compounds. At 300 °C, whereas no region of stability of iron sulfide exists for $m_S = 10^{-4}$ mol/kg, adsorbed sulfur is stable in a large domain, which includes the domain of Fe_3O_4 and overlaps the domains of iron, Fe^{2+}, Fe_2O_3, and $Fe(OH)_3^-$ (Fig. 20).
The prediction of domains of thermodynamic stability of adsorbed sulfur on iron in thiosulfate solutions supports the experimental observation of sulfur adsorption by thiosulfate reduction on iron-chromium alloys, which was invoked to explain the detrimental effect of dissolved thiosulfates on the corrosion resistance of ferritic stainless steels (Ref 16). The diagrams indicate stability of S_{ads} in a large part of the passivity domain. The chemisorption of sulfur on bare iron is a process in competition with the formation of Fe_3O_4 (and Fe_2O_3 in a limited *E*-pH region). The equilibrium *E*-pH diagrams are constructed on a thermodynamic basis and do not indicate which species actually form on a bare iron electrode polarized in the passive domain: the two-dimensional (surface) species S_{ads}(Fe) or a three-dimensional (bulk) oxide. If the kinetics of adsorption of sulfur on bare iron is more rapid than the kinetics of formation of oxide layers on iron, a sulfur monolayer may form on iron and prevent or delay passivation of the iron. Detrimental effects of sulfur on the corrosion resistance of iron are then expected, even under *E*- pH conditions where a classic diagram predicts passivity. The diagrams (Fig. 19, 20) also predict that sulfur is likely to adsorb in part of the domain of anodic dissolution of iron; this is important because dissolution enhanced by adsorbed sulfur is experimentally observed in the activity domains of nickel- and iron-base alloys (Ref 33, 34). Even if the metal is not thermodynamically stable and dissolves, a sulfur monolayer may adsorb on the fresh surface, which is continuously produced, and increase the kinetics of dissolution.
Thus, the *E*-pH diagrams presented here showing the domains of thermodynamic stability of adsorbed layers on metals, provide a basis for assessing the risk of corrosion of metals or alloys induced by species adsorbed from aqueous solutions.

References cited in this section

16. C. Duret-Thual, D. Costa, W.P. Yang, and P. Marcus, *Corros. Sci.,* Vol 39, 1997, p 913

22. J.W. Cobble, R.C. Murray, Jr., P.J. Turner, and K. Chen, "High-Temperature Thermodynamic Data for Species in Aqueous Solution," San Diego State University Foundation, EPRI Report NP-2400, Electric Power Research Institute, May 1982

32. J. Oudar, in *Corrosion Mechanisms in Theory and Practice,* P. Marcus, Ed., Marcel Dekker, Inc., 2002

33. J. Oudar and P. Marcus, *Appl. Surf. Sci.,* Vol 3, 1979, p 48

34. P. Marcus, in *Corrosion Mechanisms in Theory and Practice,* P. Marcus, Ed., Marcel Dekker, Inc., 2002, p 287

35. P. Marcus and E. Protopopoff, *C.R. Acad. Sci. Paris,* Vol 308 (No. II), 1989, p 1685

36. P. Marcus and E. Protopopoff, *J. Electrochem. Soc.,* Vol 137, 1990, p 2709

37. P. Marcus and E. Protopopoff, *J. Electrochem. Soc.,* Vol 140, 1993, 1571

38. P. Marcus and E. Protopopoff, *J. Electrochem. Soc.,* Vol 144, 1997, p 1586

39. P. Marcus and E. Protopopoff, *Corros. Sci.,* Vol 45, 2003, p 1191

40. P. Marcus and E. Protopopoff, *Corros. Sci.,* Vol 39, 1997, p 1741–1752

E. Protopopoff and P. Marcus, Potential versus pH (Pourbaix) Diagrams, *Corrosion: Fundamentals, Testing, and Protection*, Vol 13A, *ASM Handbook*, ASM International, 2003, p 17–-30

Potential versus pH (Pourbaix) Diagrams

E. Protopopoff and P. Marcus, CNRS, Ecole Nationale Supérieure de Chimie de Paris, Université Pierre et Marie Curie

---

Acknowledgment

Portions of this article have been adapted from D.L. Piron, Potential versus pH (Pourbaix) Diagrams, *Corrosion,* Vol 13, *Metals Handbook,* 9th ed., ASM International, 1987, p 24–28.

E. Protopopoff and P. Marcus, Potential versus pH (Pourbaix) Diagrams, *Corrosion: Fundamentals, Testing, and Protection*, Vol 13A, *ASM Handbook*, ASM International, 2003, p 17–-30

Potential versus pH (Pourbaix) Diagrams

E. Protopopoff and P. Marcus, CNRS, Ecole Nationale Supérieure de Chimie de Paris, Université Pierre et Marie Curie

---

References

1. M. Pourbaix, Thermodynamique des Solutions Aqueuses Diluées, Potentiel D'oxydo- Réduction (résumé de conférence), *Bull. Soc. Chim. Belgique,* Vol 48, Dec 1938

2. M. Pourbaix, *Thermodynamics of Dilute Aqueous Solutions,* Arnold Publications, 1949

3. R.W. Staehle, Marcel J.N. Pourbaix—Palladium Award Medalist, *J. Eletrochem. Soc.,* Vol 123, 1976, p 23C

4. M. Pourbaix, *Atlas of the Electrochemical Equilibria,* NACE, 1974

5. D.D. Wagman, W.H. Evans, V.B. Parker, R.H. Schumm, I. Halow, S.M. Bailey, K.L. Churney, and R.L. Nuttall, *J. Phys. Chem. Ref. Data,* Vol 11 (Suppl. 2), 1982

6. G. Valensi, "Rapport CEBELCOR-CEFA/ R. 17," 1958; "Rapport Technique CEBELCOR, 121, RT. 207, 1," 1973

7. R.C. Murray, Jr. and D. Cubicciotti, *J. Electrochem. Soc.,* Vol 130, 1983, p 866

8. J.V. Muylder, in *Comprehensive Treatise of Electrochemistry,* Vol 4, J. O'M. Bockris, B.E. Conway, E. Yeager, and R.E. White, Ed., Plenum Press, 1981, p 1–96

9. R.C. Newman, H.S. Isaacs, and B. Alman, *Corrosion,* Vol 38, 1982, p 261

10. R.C. Newman K. Sieradski, and H.S. Isaacs, *Metall. Trans. A,* Vol 13, 1982, p 2015

11. R.C. Newman and K. Sieradski, *Corros. Sci.,* Vol 23, 1983, p 363

12. R.C. Newman, *Corrosion,* Vol 41, 1985, p 450

13. D. Tromans and L. Frederick, *Corrosion,* Vol 40, 1984, p 633

14. A. Garner, *Corrosion,* Vol 41, 1985, p 587

15. S.E. Lott and R.C. Alkire, *J. Electrochem. Soc.,* Vol 136, 1989, p 973, 3256

16. C. Duret-Thual, D. Costa, W.P. Yang, and P. Marcus, *Corros. Sci.,* Vol 39, 1997, p 913

17. C.M. Chen, K. Aral, and G.J. Theus, "Computer-Calculated Potential pH Diagrams to 300 °C," EPRI Report NP-3137, Vol 2, Electric Power Research Institute, Babcock & Wilcox Company, June 1983

18. R.L. Cowan and R.W. Staehle, *J. Electrochem. Soc.,* Vol 118, 1971, p 557

19. C.M. Criss and J.W. Cobble, *J. Am. Chem. Soc.,* Vol 86, 1964, p 5385, 5390, 5394

20. I.L. Khodakovski, B.N. Ryzhenko, and G.B. Naumov, *Geochem. Int.,* Vol 5, 1968, p 1200, translated from *Geokhimia,* No. 12, 1968, p 1486; I.L. Khodakovski, *Geochem. Int.,* Vol 6, 1969, p 29, translated from *Geokhimia,* No. 1, 1969, p 57

21. A.J. de Béthune, T.S. Licht, and N. Swendeman, *J. Electrochem. Soc.,* Vol 106, 1959, p 616; G.R. Salvi and A.J. de Béthune, *J. Electrochem. Soc.,* Vol 108, 1961, p 672

22. J.W. Cobble, R.C. Murray, Jr., P.J. Turner, and K. Chen, "High-Temperature Thermodynamic Data for Species in Aqueous Solution," San Diego State University Foundation, EPRI Report NP-2400, Electric Power Research Institute, May 1982

23. V. Ashworth and P.J. Boden, *Corros. Sci.,* Vol 10, 1970, p 709

24. H.E. Townsend, in *Proceedings of the Fourth International Congress on Metallic Corrosion,* 1969 (Amsterdam), NACE, 1970, p 477

25. H.E. Townsend, *Corros. Sci.,* Vol 10, 1970, p 343

26. P.A. Brook, *Corros. Sci.,* Vol 12, 1972, p 297

27. J.B. Lee, *Corrosion,* Vol 37, 1981, p 467

28. P. Radhakrishnamurty and P. Adaikkalam, *Corros. Sci.,* Vol 22, 1982, p 753

29. R.J. Biernat and R.G. Robins, *Electrochim. Acta,* Vol 17, 1972, p 1261

30. D.D. MacDonald, B.C. Syrett, and S.S. Wing, *Corrosion,* Vol 35, 1979, p 1

31. D.D. MacDonald, "ASTM Sp. Publication 717," ASTM, 1981

32. J. Oudar, in *Corrosion Mechanisms in Theory and Practice,* P. Marcus, Ed., Marcel Dekker, Inc., 2002

33. J. Oudar and P. Marcus, *Appl. Surf. Sci.,* Vol 3, 1979, p 48

34. P. Marcus, in *Corrosion Mechanisms in Theory and Practice,* P. Marcus, Ed., Marcel Dekker, Inc., 2002, p 287

35. P. Marcus and E. Protopopoff, *C.R. Acad. Sci. Paris,* Vol 308 (No. II), 1989, p 1685

36. P. Marcus and E. Protopopoff, *J. Electrochem. Soc.,* Vol 137, 1990, p 2709

37. P. Marcus and E. Protopopoff, *J. Electrochem. Soc.,* Vol 140, 1993, 1571

38. P. Marcus and E. Protopopoff, *J. Electrochem. Soc.,* Vol 144, 1997, p 1586

39. P. Marcus and E. Protopopoff, *Corros. Sci.,* Vol 45, 2003, p 1191

40. P. Marcus and E. Protopopoff, *Corros. Sci.,* Vol 39, 1997, p 1741–1752

41. M. Pourbaix and A. Pourbaix, Rapports Techniques CEBELCOR, 159, RT. 299 (1990)

E. Protopopoff and P. Marcus, Potential versus pH (Pourbaix) Diagrams, *Corrosion: Fundamentals, Testing, and Protection*, Vol 13A, *ASM Handbook,* ASM International, 2003, p 17–-30

Potential versus pH (Pourbaix) Diagrams

E. Protopopoff and P. Marcus, CNRS, Ecole Nationale Supérieure de Chimie de Paris, Université Pierre et Marie Curie

---

Selected References

- C.M. Chen, K. Aral, and G.J. Theus, “Computer Calculated Potential pH Diagrams to 300 °C,” Vol 1, 2, and 3, EPRI NP-3137, Project 1167-2, Electric Power Research Institute, June 1983
- R.P. Frankenthal and J. Kruger, Ed., Equilibrium Diagrams/Localized Corrosion, *Proceedings of an International Symposium to Honor Marcel Pourbaix on His Eightieth Birthday,* Vol 84–89, The Electrochemical Society, 1984, p 611

K.H. Stern, Molten Salt Corrosion Thermodynamics, *Corrosion: Fundamentals, Testing, and Protection*, Vol 13A, *ASM Handbook*, ASM International, 2003, p 31–33

Molten Salt Corrosion Thermodynamics

Kurt H. Stern, Naval Research Laboratory

Introduction

MOLTEN SALTS—in contrast to aqueous solutions in which an electrolyte (acid, base, salt) is dissolved in a molecular solvent—are essentially completely ionic. Thus the terms *solute* and *solvent* can be defined only in quantitative terms. For example, the terms lose their meaning in a NaCl-AgCl melt where composition can vary continuously from pure NaCl to pure AgCl. This is true even when the electrodes immersed in the melt are reversible only to some of the ions in the melt. For example, in the cell:

$$Ag|AgCl|1NaCl|Cl_2 \qquad \text{(Eq 1)}$$

the chlorine electrode is reversible to Cl^- and the silver electrode is reversible to Ag^+. When this cell is used to obtain thermodynamic data, it is assumed that the cell is stable; that is, its composition does not change with time. However, when the concentration of AgCl is very low, this will not be the case, since the silver electrode will react spontaneously with the melt:

$$Ag + NaCl = AgCl + Na \qquad \text{(Eq 2)}$$

Thus the concentration of AgCl will spontaneously increase in the melt, and the electromotive forces (emf) measured for the preceding cell will not be stable but will change in the direction indicating increasing Ag concentration. The point at which this happens depends on the system.

K.H. Stern, Molten Salt Corrosion Thermodynamics, *Corrosion: Fundamentals, Testing, and Protection*, Vol 13A, *ASM Handbook*, ASM International, 2003, p 31–33

Molten Salt Corrosion Thermodynamics

Kurt H. Stern, Naval Research Laboratory

Thermodynamics of Cells

One major use of electrochemical cells is to obtain thermodynamic data for salts. The basic thermodynamics applicable to galvanic cells for aqueous solutions is discussed elsewhere in this Volume. Only those aspects that are different for molten salts are emphasized in this article. Thus, for the cell given in Eq 1, the cell reactions are:

$Ag = Ag^+ + e^-$ $\quad \frac{1}{2}Cl_2 + e^- = Cl^-$ (Eq 3)

and the result is:

$Ag + \frac{1}{2}Cl_2 = AgCl(a)$ (Eq 4)

where *a* is the activity of AgCl and the cell emf is

$$E = E^\circ - \frac{RT}{F}\ln a \qquad \text{(Eq 5)}$$

It is assumed that when Cl_2 is in its standard state of unit fugacity (nearly equal to unit pressure) and silver is in its standard state (pure metal), E^o is the cell emf for:

$Ag(a = 1) + \frac{1}{2}Cl_2(f = 1) = AgCl(a = 1)$ (Eq 6)

and the only variable in Eq 5 is the activity of AgCl. (It should be emphasized that in any thermodynamic treatment, only neutral components; that is, AgCl, rather than Ag^+ or Cl^-, can appear.) In contrast to aqueous solutions, the activity, *a*, is usually defined on the mole fraction scale. The emf is *E* for the cell reaction shown previously, where:

$\Delta G = -nFE$ (Eq 7)

and

$$\Delta G = \Delta G^\circ + \frac{RT}{F}\ln a \qquad \text{(Eq 8)}$$

The superscript ^{o}(ΔG^o, E^o) refers to the standard state, which in this case is the pure material; that is, AgCl. An activity coefficient, γ, is defined in terms of the activity, *a*, and the mole fraction, *X*:

$$\gamma = a/X$$

Note that γ may be less, equal, or greater than unity. This definition is based on Raoult's law standard state:

$\gamma = 1$ when $a = X$ (Eq 9)

In the case of an electrochemical cell, using Eq 1 as an example, where the cell emf is directly related to the activity of AgCl, the activity of the second component, NaCl, can then be calculated by the Gibbs-Duhem equation, which at constant temperature and pressure is:

$\sum X_i \, d \ln a_i = 0$ (Eq 10)

For the AgCl-NaCl system, the activity of AgCl(a_1) is known from experimental data (Eq 5), and the activity of NaCl(a_2) can then be calculated from Eq 10. The procedure for doing this is discussed in thermodynamic texts such as Ref 1. It generally requires a graphical integration as discussed in standard thermodynamics texts as well as standard free energies of formation (ΔG^o) of the pure components, which can be obtained from reference works like Ref 2. This equation shows that if the composition varies, the chemical potentials of the components do not change independently but instead in a related way.

In contrast to aqueous solutions where the potential of the hydrogen electrode ($\frac{1}{2}H_2 = H^+ + e^-$) is commonly assigned the value “zero” when reactants and products are in their standard states, no such condition exists for molten salts, because there is no solvent analogous to water in molten salts. Thus it is necessary to establish a specific scale for each medium; for example, $\frac{1}{2}Cl_2 + e^- = Cl^-$. It should be noted that while metal electrodes, Ag in the previous example, can be directly immersed in the melt, gas electrodes, like the chlorine electrode, require a solid surface on which the equilibrium $\frac{1}{2}Cl_2 + e^- = Cl^-$ can take place. Graphite has frequently been used for chlorine; platinum is often chosen for other gases, such as oxygen.

References cited in this section

1. G.N. Lewis and M. Randall, revised by K.S. Pitzer and D.F. Brewer, *Thermodynamics,* 2nd ed., McGraw-Hill, 1961, p 552

2. G.J. Janz, *Molten Salt Handbook,* Academic Press, 1967

K.H. Stern, Molten Salt Corrosion Thermodynamics, *Corrosion: Fundamentals, Testing, and Protection,* Vol 13A, *ASM Handbook,* ASM International, 2003, p 31–33

Molten Salt Corrosion Thermodynamics

Kurt H. Stern, Naval Research Laboratory

Electrodes for Molten Salts

The classification of electrodes is similar to that used for aqueous media. There are reference electrodes that maintain a constant potential independent of the melt concentration, and indicator electrodes that are reversible to some ion in the melt and can therefore be used to measure its activity.

Reference Electrodes. Historically, the oldest reference electrodes are those that use a liquid junction (LJ) between the electrode compartment and the melt under study. The Ag/AgCl electrode is of this type, and its half-cell is:

$$\begin{aligned}&\text{Ag/AgCl, NaCl (reference melt)}\\ &\times \text{LJ} \mid \text{(melt under study)}\end{aligned} \qquad \text{(Eq 11)}$$

The melt under study contains the same ions as the reference melt, but its concentration is variable. If the concentrations of the two melts are not too far apart, the LJ potential is probably negligible. One way of forming the junction is to insert an asbestos fiber into a small hole between the compartments. It may also be formed inside a material that is porous and thus can be saturated with the melt but that prevents bulk mixing. Jenkins, Mamantov, and Manning (Ref 3) described a reference for use in molten fluorides based on the Ni/Ni(II) couple, which uses boron nitride as the separator. The boron nitride becomes saturated by the melt and thus serves as an LJ that isolates the reference melt. Porous glass can also be used as a separator, but obviously not in fluoride melts.

Another reference electrode useful in melts that contain oxide ion, usually as Na_2O, was developed by Liang, Bowen, and Elliott (Ref 4). This electrode is:

$$\frac{\text{W, Na}_2\text{S, WS}_2}{11\text{Al}_2\text{O}_3\text{ (beta alumina)}} \qquad \text{(Eq 12)}$$

and operates at an oxide activity fixed by the reaction:

$$\frac{1}{2}\text{W(s)} + \text{Na}_2\text{S} + \frac{1}{2}\text{O}_2 = \frac{1}{2}\text{WS(s)} + \text{Na}_2\text{O} \qquad \text{(Eq 13)}$$

inside a beta alumina membrane, where S is solid. Alternatively, mullite, a ceramic that is also a sodium ion conductor, can also be used as a separator that isolates the reference electrode from the melt under study. This is particularly useful because mullite closed-end tubes are readily available, and the reference electrode and its associated melt are then simply inserted into the tube.

For melts containing dissolved oxides, the oxygen electrode inside a zirconia membrane is a useful reference. The actual electrode is platinum bathed in an environment of O_2 at a fixed partial pressure. Air is usually used as the source of oxygen. The platinum is forced into a zirconia tube stabilized with a divalent oxide, such as CaO, MgO, or Y_2O_3, which acts as an oxide ion conductor. The electrode reaction is:

$$\frac{1}{2}\text{O}_2 + 2e = \text{O}^{2-} \qquad \text{(Eq 14)}$$

Indicator Electrodes. The chief characteristic of indicator electrodes is that their potential varies with the activity of an ionic component, usually in a Nernstian way. The performance of molten salt indicator electrodes does not differ substantially from the performance of other electrodes. For example, the Ag electrode in the melt under study changes its potential with changes in melt composition (Eq 5). However, because of the

technical problems in maintaining an LJ, such as corrosion, most indicator electrodes use solid-state materials that are ionic conductors: stabilized zirconia, which is an oxide-ion conductor; beta-alumina, a sodium-ion conductor; and sulfide-ion conductors, such as Cu_2S. For an example of how the silver reference electrode can be combined with other electrodes to measure oxide ion activity, see Ref 5.

In selecting these materials, the range of temperatures and gas phase composition over which the material is an ionic conductor must be considered. If a substantial fraction of the conductivity is electronic, the response of the electrode will not be Nernstian, and emf measurements will give inaccurate results. For each material there is a diagram that separates the ionic conductivity from the electronic (*n*-type and *p*-type) as a function of pressure and temperature (Ref 6), and it is obviously desirable that most of the conductivity is ionic if the material is to be useful.

Materials based on stabilized zirconia are particularly useful, because they are oxide ion conductors. The electrical properties of these materials have been described in detail (Ref 7). The uses of these materials fall into two categories: equilibrium methods and nonequilibrium methods. Examples of equilibrium methods include:

- Measurement of the O_2 partial pressure in gases (Ref 7)
- Measurement of the O_2 solubility in metals (Ref 7)
- Measurement of the dissociation pressure of solid oxides (Ref 7)
- Measurement of the oxide activity in molten salts (Ref 8, 9, 10) and in glasses (Ref 11)

Nonequilibrium methods include:

- Operation of an oxygen fuel cell (Ref 4)
- Changing the O_2 content of gases (Ref 12, 13)
- Measurement of the diffusivity of O_2 in metals (Ref 14)
- Titration of O_2 into and out of metals (Ref 14) and molten salts (Ref 15)

References cited in this section

3. H.W. Jenkins, G. Mamantov, and D.L. Manning, *J. Electroanal. Chem.,* Vol 19, 1968, p 385
4. W. Liang, H.K. Bowen, and J.F. Elliott, in *Metal-Slag-Gas Reactions and Processes,* A.Z. Foroulis and W.W. Smeltzer, Ed., Electrochemical Society, 1975, p 608
5. K.H. Stern, M.L. Deanhardt, and Rm. Panayappan, *J. Phys. Chem.,* Vol 83, 1979, p 2848
6. W.L. Worrell and J. Hladik, Chapter 17, Vol 1 in *Physics of Electrolytes,* J. Hladik, Ed., Academic Press, 1972
7. T.H. Etsell and S.N. Flengas, *Chem. Revs.,* Vol 70, 1970, p 339
8. R. Combes, J. Vedel, and B. Tremillon, *Anal. Lett.,* Vol 3, 1970, p 523
9. D.R. Flinn and K.H. Stern, *J. Electroanal. Chem.,* Vol 63, 1975, p 39
10. K.H. Stern, Rm. Panayappan, and D.R. Flinn, *J. Electrochem. Soc.,* Vol 124, 1977, p 641
11. G.C. Charette and S.N. Flengas, *Can. Metall.,* Vol 7, 1969, p 191
12. C. Deportes, R. Donneau, and G. Robert, *Bull. Soc. Chim. France,* 1964, p 2221
13. D. Yuan and F.A. Kroger, *J. Electrochem. Soc.,* Vol 116, 1969, p 594
14. R.L. Pastorek and R.A. Rapp, *Trans. Met. Soc. AIME,* Vol 25, 1969, p 1711

15. M.L. Deanhardt and K.H. Stern, *J. Phys. Chem.,* Vol 84, 1980, p 2831

K.H. Stern, Molten Salt Corrosion Thermodynamics, *Corrosion: Fundamentals, Testing, and Protection*, Vol 13A, *ASM Handbook*, ASM International, 2003, p 31–33

Molten Salt Corrosion Thermodynamics

Kurt H. Stern, Naval Research Laboratory

Thermodynamics of Molten Salt Corrosion

Corrosion of metals in aqueous solution has been studied for many years, and the thermodynamic principles have been discussed by Pourbaix (Ref 16, 17). The applicable principles are commonly summarized in Pourbaix diagrams, which contain a great deal of data in a convenient arrangement that allows the prediction of what reactions will occur in a particular system.

A corresponding system for molten salt corrosion has been explicitly described for molten chlorides (Ref 18, 19). In contrast to aqueous solutions where corrosion is always accompanied by oxidation, corrosion in molten salts can be caused by the solubility of the metal in the salt, particularly if the metal dissolves in its own chloride. The more usual case is one in which the metal is oxidized.

Littlewood has used the convention that the free energy of formation of the halide ion from the halogen gas at one atmosphere pressure and unit halide activity is zero at all temperatures. Gibbs energies (ΔG) are converted to potentials by the usual relation $E = -\Delta G/nF$. In Pourbaix diagrams, equilibrium potentials are plotted against pH with a resulting schematic division into regions of stability of different solid phases. For molten salts, Littlewood chose the activity of oxide in the melt, expressed as pO^{2-}(p = -log), and the appropriate diagram is then E versus pO^{2-}. Such diagrams can be constructed for any metal and melt, and Littlewood has described several cases (Ref 20), including those in which there is more than one stable oxide, such as titanium. These diagrams should be as useful for molten salts as Pourbaix diagrams are for aqueous solutions. However, although this work was published about 30 years ago, it does not seem to have been widely used.

Such a diagram that plots potential as a function of pO^{2-} is given in Fig. 1 for the Ti-NaCl system at 800 °C and Fig. 2 for the Ti-$MgCl_2$ system. Note that O^{2-} is the concentration on the mole fraction scale and pO^{2-} is its negative logarithm. On both diagrams, the outer scale, labeled log O_2, refers to the pressure of oxygen gas in each system.

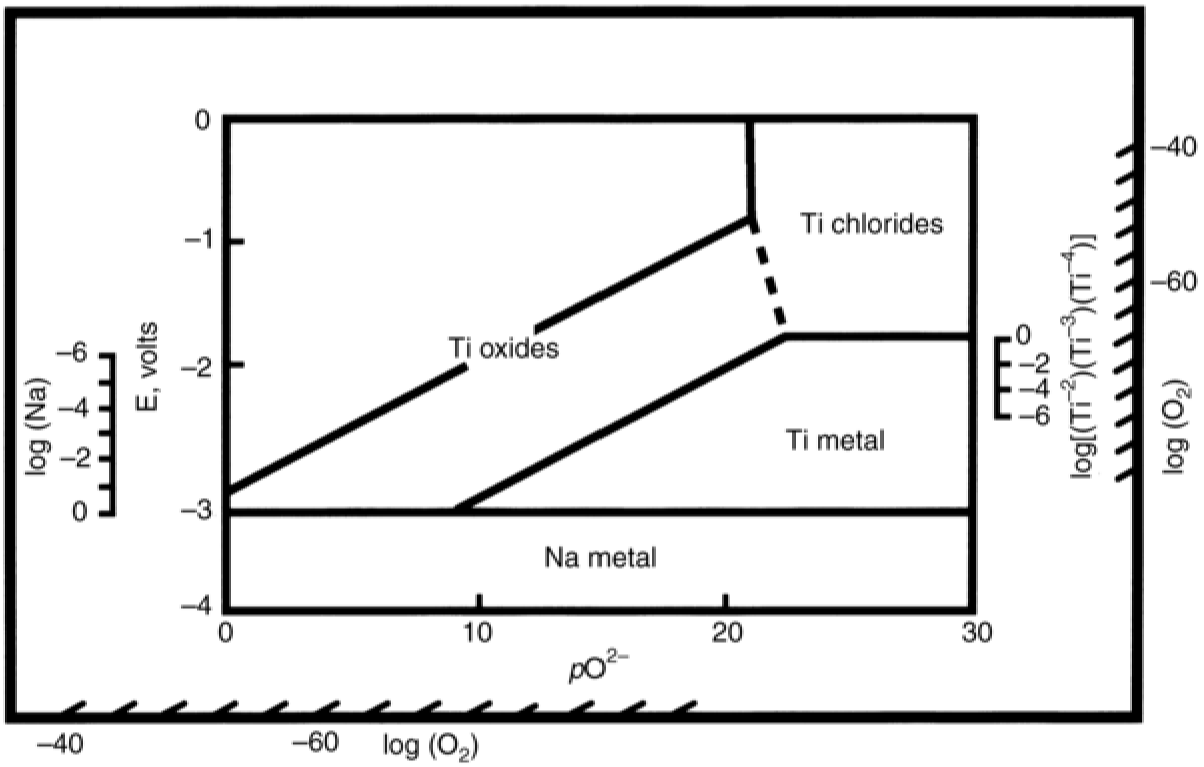

Fig. 1 E-pO^{2-} diagram for Ti-NaCl system at 800 °C (approximate). Source: Ref 20

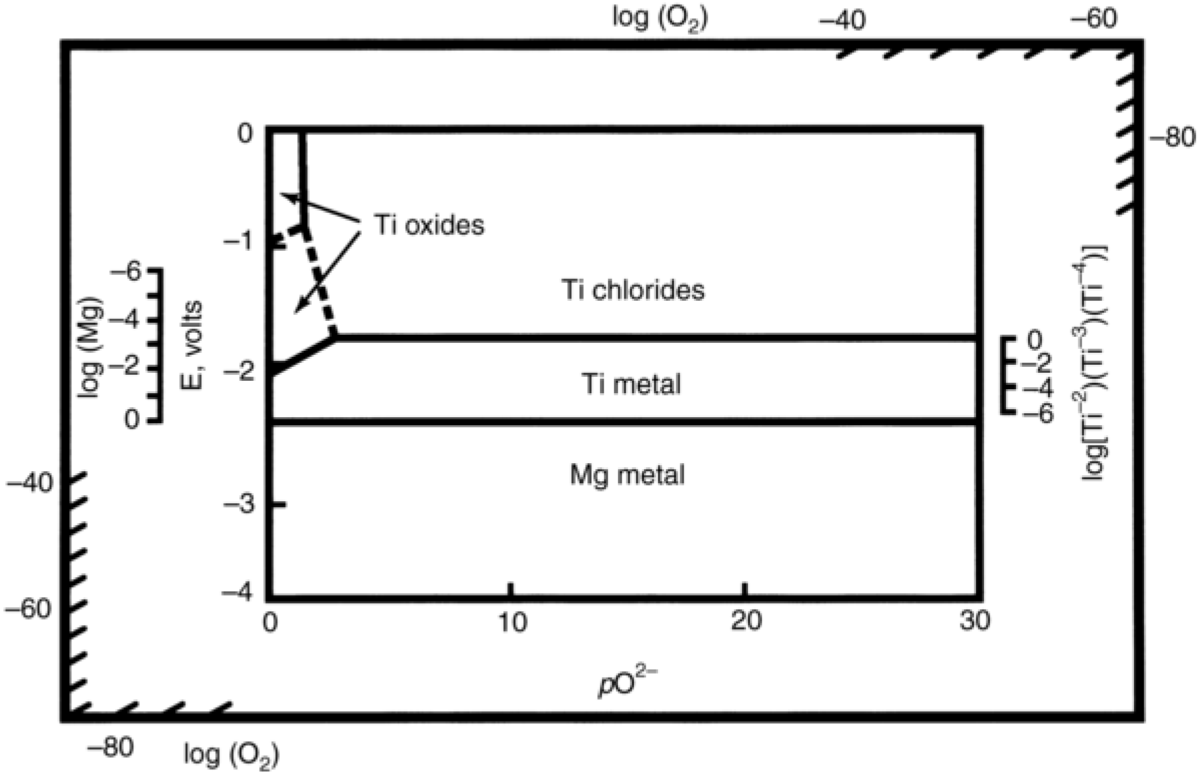

Fig. 2 E-pO^{2-} diagram for Ti-$MgCl_2$ system at 800 °C (approximate). Source: Ref 20

The corrosion of titanium is affected by three factors: the titanium chloride content of the $MgCl_2$ melt, Mg or Na content, and oxygen content of the product. The interplay of the three factors can be readily investigated by a detailed comparison of Fig. 1 and 2. Comparison of the diagrams shows that for a given value of pO^{2-}, the oxygen activity in the titanium metal product would be much lower for magnesium reduction than for sodium reduction. The equilibrium potentials after the reaction has gone to completion will be -3.20V for sodium and -2.47V for magnesium. Suppose, for example, the oxide contamination present in the two cases is sufficient to produce a pO^{2-} value of 20 in the slag and that excess reductant has been used. Figure 1 shows that under these

conditions, the oxygen activity in the titanium metal produced by sodium reduction would be about 10^{-62}, while that produced by magnesium reduction (Fig. 2) would be about 10^{-86}.

References cited in this section

16. M. Pourbaix, *Thermodynamics of Dilute Aqueous Solutions,* Arnold, London, 1949

17. M. Pourbaix, *Atlas of Electrochemical Equilibria in Aqueous Solutions,* NACE International, 1974

18. C. Edeleanu and R. Littlewood, *Electrochim. Acta,* Vol 3, 1960, p 195

19. R. Littlewood and E.J. Argent, *Electrochim. Acta,* Vol 4, 1961, p114, 155

20. R. Littlewood, *J. Electrochem. Soc.,* Vol 109, 1962, p 525

K.H. Stern, Molten Salt Corrosion Thermodynamics, *Corrosion: Fundamentals, Testing, and Protection*, Vol 13A*, ASM Handbook,* ASM International, 2003, p 31–33

Molten Salt Corrosion Thermodynamics

Kurt H. Stern, Naval Research Laboratory

References

1. G.N. Lewis and M. Randall, revised by K.S. Pitzer and D.F. Brewer, *Thermodynamics,* 2nd ed., McGraw-Hill, 1961, p 552

2. G.J. Janz, *Molten Salt Handbook,* Academic Press, 1967

3. H.W. Jenkins, G. Mamantov, and D.L. Manning, *J. Electroanal. Chem.,* Vol 19, 1968, p 385

4. W. Liang, H.K. Bowen, and J.F. Elliott, in *Metal-Slag-Gas Reactions and Processes,* A.Z. Foroulis and W.W. Smeltzer, Ed., Electrochemical Society, 1975, p 608

5. K.H. Stern, M.L. Deanhardt, and Rm. Panayappan, *J. Phys. Chem.,* Vol 83, 1979, p 2848

6. W.L. Worrell and J. Hladik, Chapter 17, Vol 1 in *Physics of Electrolytes,* J. Hladik, Ed., Academic Press, 1972

7. T.H. Etsell and S.N. Flengas, *Chem. Revs.,* Vol 70, 1970, p 339

8. R. Combes, J. Vedel, and B. Tremillon, *Anal. Lett.,* Vol 3, 1970, p 523

9. D.R. Flinn and K.H. Stern, *J. Electroanal. Chem.,* Vol 63, 1975, p 39

10. K.H. Stern, Rm. Panayappan, and D.R. Flinn, *J. Electrochem. Soc.,* Vol 124, 1977, p 641

11. G.C. Charette and S.N. Flengas, *Can. Metall.,* Vol 7, 1969, p 191

12. C. Deportes, R. Donneau, and G. Robert, *Bull. Soc. Chim. France,* 1964, p 2221

13. D. Yuan and F.A. Kroger, *J. Electrochem. Soc.,* Vol 116, 1969, p 594

14. R.L. Pastorek and R.A. Rapp, *Trans. Met. Soc. AIME,* Vol 25, 1969, p 1711

15. M.L. Deanhardt and K.H. Stern, *J. Phys. Chem.,* Vol 84, 1980, p 2831

16. M. Pourbaix, *Thermodynamics of Dilute Aqueous Solutions,* Arnold, London, 1949

17. M. Pourbaix, *Atlas of Electrochemical Equilibria in Aqueous Solutions,* NACE International, 1974

18. C. Edeleanu and R. Littlewood, *Electrochim. Acta,* Vol 3, 1960, p 195

19. R. Littlewood and E.J. Argent, *Electrochim. Acta,* Vol 4, 1961, p114, 155

20. R. Littlewood, *J. Electrochem. Soc.,* Vol 109, 1962, p 525

K.H. Stern, Molten Salt Corrosion Thermodynamics, *Corrosion: Fundamentals, Testing, and Protection*, Vol 13A, *ASM Handbook*, ASM International, 2003, p 31–33

Molten Salt Corrosion Thermodynamics

Kurt H. Stern, Naval Research Laboratory

Selected References

- J. Hladik, Ed., *Physics of Electrolytes,* Vol 1; *Transport Properties in Solid Electrolytes,* Vol 2, *Thermodynamics and Electrode Processes in Solid State Electrolytes,* Academic Press, 1972
- R.W. Laity, D.J.G. Ives, and G. J. Janz, Ed., Reference Electrodes, Chapter 12, *Electrodes in Fused Salt Systems,* Academic Press, 1961

S.A. Matthes, Geochemical Modeling, *Corrosion: Fundamentals, Testing, and Protection*, Vol 13A, *ASM Handbook*, ASM International, 2003, p 34–41

Geochemical Modeling

Steven A. Matthes, U.S. Department of Energy, Albany Research Center

---

Introduction

CORROSION SCIENTISTS AND ENGINEERS frequently need to describe the chemical state of local environments, including mass distribution of aqueous species, and the interaction of these aqueous species with metal surfaces, corrosion films, and gases. In high temperature corrosion, metals may be corroded by nonaqueous fluids or by solids such as slags. These types of interactions are geochemical in nature; that is, the reactions are the same as those found in natural aqueous, high-temperature, or magmatic systems. When

chemical systems are simple with few possible reactions likely to occur, the geochemistry of a local environment may be described through experience and some (usually tedious) hand calculation.

When the geochemistry of an environment is more complex, however, quantitative models of aqueous or solid phase chemistry that are beyond the predictive power of experience and hand calculation are required. The need for a consistent way to evaluate complex geochemical systems has led to a rapid increase in the field of *geochemical modeling.* The rapid growth roughly parallels the rise in power and reduction in cost of computers needed to evaluate the complicated quantitative models of solution chemistry. Geochemical modeling is now being used to understand and predict scaling, susceptibility to corrosion, atmospheric corrosion rates, acid rain, corrosion film solubility, and environmental impacts of aqueous species in runoff.

Geochemical modeling software (GMS) is widely used by scientists and engineers to solve a variety of materials and energy-balance problems. The predictive ability of GMS allows the user to model real situations and to ascertain how materials should behave when subjected to different environments. The advent of inexpensive and powerful desktop computers and a wide variety of both commercial and freeware software tools make this predictive power available to almost every scientist and engineer. As an example, the freeware program PHREEQC is capable of simulating a wide range of aqueous geochemical reactions including the mixing of waters, addition of net irreversible reactions to solution, dissolving and precipitating phases to achieve equilibrium with the aqueous phase, and the effects of changing temperature. The PHREEQC program and commercial software packages such as AquaChem (Fig. 1) now have sophisticated graphical user interfaces for performing geochemical modeling.

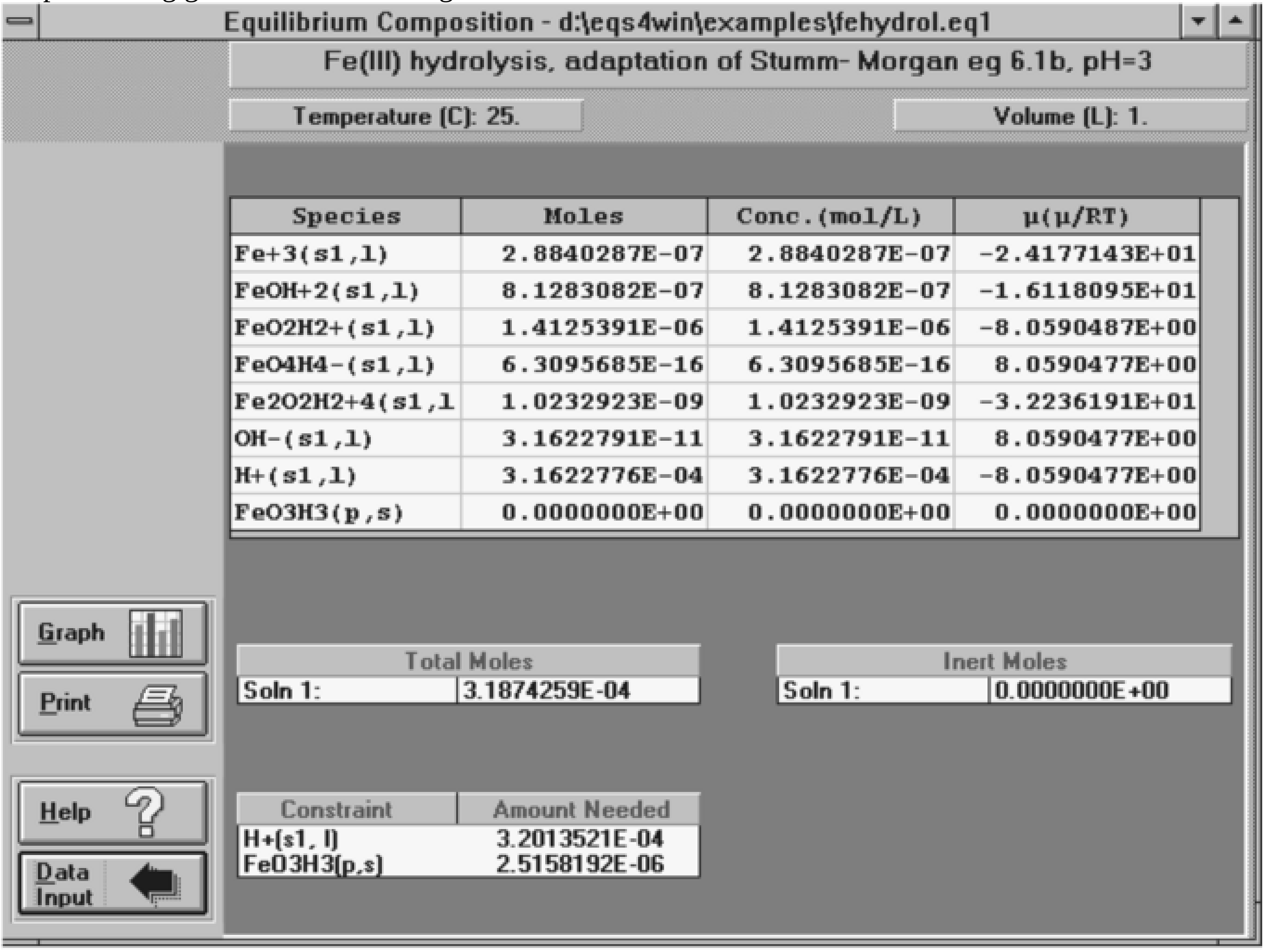

Fig. 1 Determination of equilibrium composition using the geochemical modeling software (GMS) AquaChem

Concentrations of elements, molarities and activities of aqueous species, pH, saturation indices, and the electrochemical oxidation state of the system are calculated with this type of software. Mole transfers of phases to achieve equilibrium can also be calculated as a function of specific reversible and irreversible reactions, provided the necessary thermodynamic data are available.

The electrochemical oxidation state of aqueous systems is usually given as the negative log of the electron activity (*pe*) or the electrochemical oxidation potential (E_H) in geochemical modeling. Just as pH is useful in describing the equilibrium position of all acid/base pairs in a system:

$$(\text{Acid/base}) \qquad \text{HB} = \text{H}^+ + \text{B}^-$$

$$\text{K} = \{\text{H}^+\}\{\text{B}^+\}/\{\text{HB}\} \qquad \text{pH} = -\log\{\text{H}^+\}$$

pe expresses the equilibrium position of all redox pairs in a system. For example, for the Fe^{+3}/ Fe^{+2} redox couple,

$$(\text{Redox}) \qquad \text{Fe}^{+3} + \text{e}^- = \text{Fe}^{+2}$$

$$\text{K} = \{\text{Fe}^{+2}\}/(\{\text{Fe}^{+3}\}\{\text{e}^-\}) \qquad pe = -\log\{\text{e}^-\}$$

Just as pH may be considered the *controlling variable* for the acid/base system, *pe* is the controlling variable for the redox system. Treating the electron like other reactants and products in a system allows redox reactions such as the previous one to be combined directly with other reactions leading to the determination of equilibrium constants for the combined reactions of interest in a system. Although E_H is usually thought of as the measured potential of an aqueous system, it is also related to the *pe* by the equation:

$$E_H = (2.303RT_k/F)pe$$

where R is the gas constant, F is the Faraday constant, and T_k is the absolute temperature.

The environments that GMS best describes, aqueous systems that are open or closed to the atmosphere and that have interactions with one or more solid phases, are precisely the same environments that concern corrosion engineers. Software systems such as The Geochemist's Workbench can easily model aqueous systems in contact with several mineral phases (Fig. 2). Ironically, GMS systems are seldom used by corrosion scientists and engineers, even though geochemical modeling may provide greater insight into the causes and results of corrosion reactions and processes.

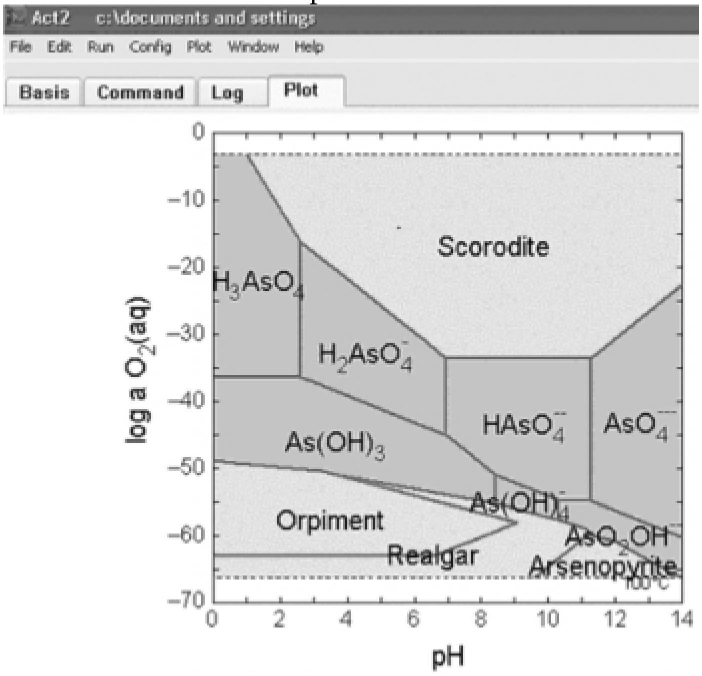

Fig. 2 A plot of log of oxygen activity (log a O_2 (aqueous) versus pH) for arsenic minerals using The Geochemist's Workbench. Log a O_2 is log of oxidation potential.

S.A. Matthes, Geochemical Modeling, *Corrosion: Fundamentals, Testing, and Protection*, Vol 13A, *ASM Handbook*, ASM International, 2003, p 34–41

Geochemical Modeling

Steven A. Matthes, U.S. Department of Energy, Albany Research Center

History of Geochemical Modeling

In 1947, an algorithm for the numerical solution of equilibrium states in a multicomponent system was published (Ref 1). Although intended for a desk calculator, the method was quickly adopted for use with digital computers. The algorithm was based on the evaluation of equations for equilibrium constants.

Garrels and Thompson (Ref 2) calculated (by hand) the composition of seawater in terms of dissociated ions (Na^+, Ca^{++}, HCO_3^-, etc.). This calculation gave rise to a type of geochemical model that predicts species distributions, saturation indices, and gas fugacities from chemical analyses. Equilibrium models of this type have become widely used, largely because of the availability of software such as SOLMNEQ (Ref 3), WATEQ (Ref 4), and MINEQL (Ref 5).

Another type of geochemical model, the reaction path model, was introduced in 1967 (Ref 6) and was used to model the effects of evaporation (gradually increasing concentration) on species distribution. This model extended geochemical modeling from the evaluation of a fixed system to having the ability to simulate a process.

Hegelson (Ref 7) built on previous work by coding the general equations for species distribution and mass transfer into a computer program. The program Path1 (Ref 8) was the first general computer method for modeling reaction paths such as weathering, evaporation, ore deposition, and hydrothermal alteration.

One way of modeling reaction paths is by repeatedly solving for the system equilibrium state algebraically. Karpov and Kaz'min (Ref 9) and Karpov et al. (Ref 10) applied this idea to GMS, allowing an algebraic solution to systems varying in temperature and composition. In 1979, EQ3/EQ6 (Ref 11) was introduced as the first geochemical model to be documented and distributed based on algebraic equations. This greatly simplified the computer code and separated mass and heat transfer calculations from the chemical equilibrium calculations. Parkhurst et al. introduced PHREEQE (Ref 12) (a precursor to PHREEQC) a year later, and most GMS developed since then uses the algebraic method for determination of equilibrium states. A more comprehensive history of GMS can be found in Ref 13.

Today, a large number of sophisticated GMS are available (Table 1) based on the pioneering work conducted in the 1960s and 1970s. These programs owe their existence to the compilation of thermodynamic data on which all geochemical modeling depends (Ref 14). An excellent compilation of thermodynamic and kinetic databases may be found at http://www.nea.fr/html/ science/docs/1996/nsc-doc96-27.html.

Table 1 Sources of geochemical modeling software

Software title	Developer or source
AquaChem	Waterloo Hydrogeologic, Inc. 460 Phillip Street Suite 101 Waterloo, Ontario, Canada N2L 5J2 www.flowpath.com/
ChemSage	GTT-Technologies Kaiserstraβe 100 52134 Herzogenrath, Germany

	gttserv.lth.rwth-aachen.de/gtt/
CHESS	Jan van der Lee School of Mines of Paris 35, rue Saint Honoré 77305 Fontainebleau Cedex, France chess.ensmp.fr
EQ3/EQ6	Thomas J. Wolery, L-631 Lawrence Livermore National Laboratory PO Box 808 Livermore, CA 94550,
EQL/EVP, KINDIS, KIRMAT	Alain Clement CNRS, Centre de Geochémie de la Surface 1 rue Blessig-67084 Strasbourg Cedex France
EQS4WIN	Mathtrek Systems 3-304 Stone Road West, Suite 165 Guelph, Ontario, Canada N1G 4W4 www.mathtrek.com/
FactSage	CRCT Ecole Polytechnique Box 6079, Station Downtown Montreal, Quebec, Canada H3C 3A7 factsage.com/
GEMS	GEMS-PSI C/O D. Kulik Waste Management Laboratory Paul Scherrer Institute CH-5232 Villigen PSI, Switzerland les.web.psi.ch/
GEOCHEM-PC	Dr. David R. Parker

	Dept. Soil and Environmental Sciences University of California Riverside, CA 92521 envisci.ucr.edu/faculty/Parker
The Geochemist's Workbench	Craig Bethke Rockware, Inc. 2221 East St. #1 Golden, CO 80401 www.rockware.com
HARPHRQ	A. Haworth, C.J. Tweed, and S.M. Sharland AEA Decommissioning and Radwaste Harwell Laboratory Oxon OX11 ORA, United Kingdom www.wiz.uni-kassel.de
HSC Chemistry	Outokumpu Research Oy Information Service P.O Box 60 FIN-28101 PORI, Finland www.outokumpu.com/hsc
MINEQL+	Dr. William Schecher Environmental Research Software 16 Middle Street Hallowell, ME 04347 www.mineql.com/
MINTEQA2	Center for Exposure Assessment Modeling U.S. Environmental Protection Agency Environmental Research Laboratory 960 College Station Road Athens, GA 30605-2720 www.epa.gov/ceampubl/mmedia/minteq

Visual MINTEQ	www.lwr.kth.se/english/OurSoftware/Vminteq/
PHREEQC	David Parkhurst U.S. Geological Survey Box 25046, Mail Stop 418 Denver Federal Center Lakewood, CO 80225 wwwbrr.cr.usgs.gov/projects/GWC_coupled/phreeqc
PHRQPITZ	U.S. Geological Survey Hydrologic Analysis Software Support Program 437 National Center Reston, VA 20192 water.usgs.gov/phrqpitz
SOILCHEM	Veronica B. Lanier Sr. Lic. Officer, Physical Sciences Office of Technology Licensing University of California Berkeley, CA 94720-1620 www.cnr.berkeley.edu/~ayang/soilchem
SOLMINEQ	Geochemical Applications & Modelling Software Ltd. Box 51028 Edmonton, Alberta, Canada T5W 5G5 www.telusplanet.net/public/geogams/index
SOLVEQ/CHILLER	Mark H. Reed Department of Geological Sciences 1272 University of Oregon Eugene, OR 97403-1272 mhreed@oregon.uoregon.edu
THERMO	Pyrometallurgy Division, Mintek 200 Hans Strijdom Drive

	Randberg, 2125, South Africa www.mintek.ac.za/Pyromet/Thermo
Thermo-Calc	Thermo_Calc Software Stockholm Technology Park Björnnäsvägen 21 SE-113 47 Stockholm, Sweden www.thermocalc.se
WATEQ4F	U.S. Geological Survey Hydrologic Analysis Software Support Program 437 National Center Reston, VA 20192 water.usgs.gov/software/wateq4f

Many of these sources require a licensing or distribution fee.

References cited in this section

1. S.R. Brinkley, Jr., Calculation of the Equilibrium Composition of Systems of Many Components, *J. Chem. Phys.,* Vol 15, 1947 p 107–110

2. R.M. Garrels, and M.E. Thompson, A Chemical Model for Sea Water at 25° and One Atmosphere Total Pressure, *Am. J. Sci.,* Vol 260, 1962, p 57–66

3. Y.K. Kharaka and I. Barnes, “SOLMNEQ: Solution-Mineral Equilibrium Computations,” Report PB-215-899, U.S. Geological Survey Computer Contributions, 1973

4. A.H. Truesdell and B.F. Jones, WATEQ, A Computer Program for Calculating Chemical Equilibria of Natural Waters, *US Geol. Surv. J. Res.,* Vol 2, 1974, p 233–248

5. J.C. Westall, J.L. Zachary, and F.M.M. Morel, “MINEQL, A Computer Program for the Calculation of Chemical Equilibrium Composition of Aqueous Systems,” Tech. Note 18, Department of Civil Engineering, Massachusetts Institute of Technology, 1976

6. R.M. Garrels, and F.T. Mackenzie, Origin of the Chemical Compositions of Some Springs and Lakes, *Equilibrium Concepts in Natural Waters, Advances in Chemistry Series 67,* American Chemical Society, 1967, p 222–242

7. H.C. Hegelson, Evaluation of Irreversible Reactions in Geochemical Processes Involving Minerals and Aqueous Solutions, I: Thermodynamic Relations, *Geochim. Cosmochim. Acta,* Vol 32, 1968, p 853–877

8. H.C. Hegelson, A Chemical and Thermodynamic Model of Ore Deposition in Hydrothermal Systems, *Miner. Soc. Am. Special Paper,* Vol 3, 1970, p 155–186

9. I.K. Karpov and L.A. Kaz'min, Calculation of Geochemical Equilibria in Heterogeneous Multicomponent Systems, *Geochem. Int.,* Vol 9, 1972, p 252–262

10. I.K. Karpov, L.A. Kaz'min, and S.A. Kashik, Optimal Programming for Computer Calculation of Irreversible Evolution in Geochemical Systems, *Geochem. Int.,* Vol 10, 1973, p 464–470

11. T.J. Wolery, “Calculation of Chemical Equilibrium between Aqueous Solution and Minerals: the EQ3/6 Software Package,” Lawrence Livermore National Laboratory Report UCRL-52658, 1979

12. D.L. Parkhurst, D.C. Thorstenson, and L.N. Plummer, “PHREEQE—A Computer Program for Geochemical Calculations,” U.S. Geological Survey Water-Resources Investigations Report 80-96, 1980

13. C.M. Bethke, *Geochemical Reaction Modeling. Concepts and Applications,* Oxford University Press, 1996, 397 p

14. D.K. Nordstrom, and J.L. Munoz, *Geochemical Thermodynamics,* 2nd ed., Blackwell, 1994

S.A. Matthes, Geochemical Modeling, *Corrosion: Fundamentals, Testing, and Protection*, Vol 13A, *ASM Handbook,* ASM International, 2003, p 34–41

Geochemical Modeling

Steven A. Matthes, U.S. Department of Energy, Albany Research Center

---

Principles of Geochemical Modeling

A *model* is a predictive tool for describing reality in a simplified way. For a model to be successful, it must adequately describe a real system but be simple enough that it can be easily evaluated. The *system* is that portion of the environment one wishes to study. A *closed system* has fixed composition; an *open system* can involve mass transfer into or out of the system. A system has boundaries (extent) that may be as small as a raindrop or as large as an ocean. A general discussion of models can be found in the article “Modeling Corrosion Processes” in this Volume.

Geochemical models are normally based on the equilibrium system containing a liquid and one or more mineral phases with an initial known composition and temperature. This allows the equilibrium state of a system to be determined. In a closed system at known temperature, the model can predict the distribution of mass between mineral phases and aqueous species as well as the species activities, the fugacities of gases that may exist in the system, and the saturation state of the minerals. The constituents of the system remain in chemical equilibrium throughout the calculation. Transfer of mass into or out of the system and variation in temperature drive the system to a series of new equilibria over the course of the reaction path. The composition of a system may be buffered by equilibrium with an external gas reservoir such as the atmosphere (Fig. 3).

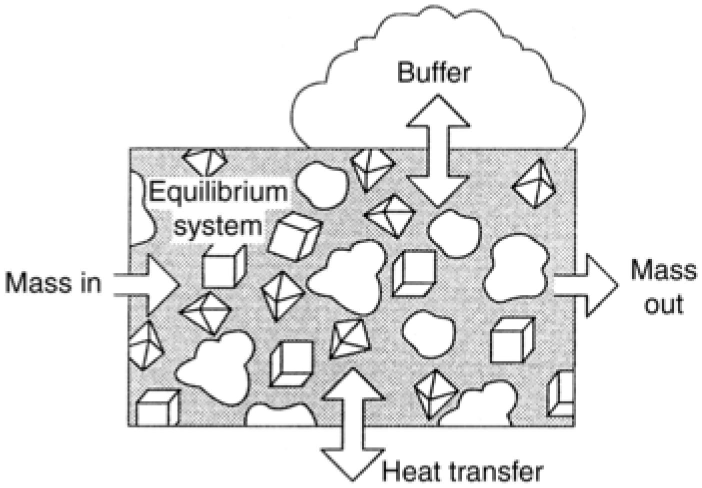

Fig. 3 Schematic diagram of a reaction model. Source: Ref 13

In complicated models, system composition and/or temperature may vary, and so the model must be able to account for transport of mass or heat into or out of the system. The initial equilibrium state is then the starting point for the reaction path to follow.

Because geochemical models deal with equilibrium systems, it is useful to define *equilibrium.* In general a system is in equilibrium when no spontaneous change occurs within the defined boundaries of the system. In this case the system can be said to be in *complete equilibrium,* and all possible chemical reactions are in equilibrium. If one or more possible reactions tend toward equilibrium at an extremely slow rate, the system is in *metastable equilibrium.* In *partial equilibrium,* the liquid phase (fluid) may be in equilibrium but not in equilibrium with one or more mineral phases in contact with it. If a small portion of a system is chosen, this subsystem may be in *local equilibrium.*

A successful geochemical model must at least define:

- Initial conditions of the system (composition and temperature)
- Type of equilibrium to be maintained
- Mass or temperature change occurring in the system during the reaction process to be modeled

The initial system contains by convention 1 kg (2.2 lb) of water, an amount that may be altered by the modeler. Mineral phases may also be included with each mineral in equilibrium with the fluid. In general, the system will be constrained by defining the initial conditions:

- Solvent water mass (1 kg by default)
- Amounts of mineral phases
- Fugacities of any gases at known partial pressure
- Fluid chemistry, amounts of dissolved components as determined by chemical analysis
- Activities of a species such as H^+, HCO_3^-, CO_3^{2-}

Once the initial conditions of a system have been so defined, the modeler can introduce a reactant (*titration model*) to the equilibrium system. The reactant dissolves irreversibly, which may cause mineral phases in the system to dissolve (i.e., the reactant is an acid) or the precipitation of one or more mineral phases that become saturated in relation to the fluid phase. The reaction proceeds until the reactant is exhausted or saturated in the system. In most geochemical systems, the solubility of minerals is very small, so the fluid is likely to reach saturation after only a small amount of mineral has dissolved.

Many corrosion processes occur in liquids in contact with a gaseous phase. The gas (usually the atmosphere in geochemical models) acts to buffer the system chemistry by allowing the fluid to maintain equilibrium with the gas phase. Models of this type are called *fixed-fugacity reaction paths.* Models where the fugacities may vary during the reaction, usually because of a reaction causing the evolution of a gas, are called *sliding-fugacity reaction paths.*

Systems where the activities of the aqueous species may vary during the course of a reaction are called *sliding-activity* models and *fixed-activity* models when the activities remain the same.
In *flow-through reaction path* models, the change in a fluid can be followed as it flows over or through various mineral phases, which may react with the fluid. This type of model may also be used to study changes in equilibrium in a fluid undergoing evaporation.

Reference cited in this section

13. C.M. Bethke, *Geochemical Reaction Modeling. Concepts and Applications,* Oxford University Press, 1996, 397 p

---

S.A. Matthes, Geochemical Modeling, *Corrosion: Fundamentals, Testing, and Protection*, Vol 13A, *ASM Handbook*, ASM International, 2003, p 34–41

Geochemical Modeling

Steven A. Matthes, U.S. Department of Energy, Albany Research Center

---

Limitations in Geochemical Modeling

A geochemical model is only as good as the completeness and accuracy with which the initial system conditions are defined. Usually this requires a chemical analysis, the pH, and/or the oxidation state (the dissolved oxygen content) of liquid samples. The accuracy of pH in particular can be problematic in geochemical systems, as the usually low total dissolved ion content in natural systems makes pH determination difficult. In such cases the use of field pH measurements or isolation of the system from atmospheric CO_2 in transport to the lab is paramount. Accuracy may also be improved by the use of low ionic strength pH standards. Chemical analysis will usually require both atomic spectroscopy for metal cations and ion chromatography or chemometric methods for anions. Liquid samples should not be stabilized by acidification unless the fluid is filtered to remove sediment and/or colloidal solids before acidification.
A model can be successful only if the thermodynamic dataset contains the mineral phases and aqueous species required for the system. Many datasets have limited ranges of pH, and so a dataset that does not contain solubility data for a species above pH 10 will be inadequate for systems at pH greater than 10. In addition, all thermodynamic datasets have errors related to chemical analysis and extrapolation. Many equilibrium constants have been determined for narrow temperature ranges, usually around room temperature, and datasets may contain extrapolated data for temperatures beyond this range.
Accuracy of calculated activity coefficients is another limitation to the model. For solutions of 1 molal or less ionic strength, models that use the Debye-Huckel method are fairly accurate. At higher ionic strengths, however, a model may require “Pitzer equations” to calculate activity coefficients in brines. The program PHREEQPITZ is a GMS designed specifically for systems of this type.
Most importantly, the modeler must make correct assumptions about the kind of equilibrium studied and develop an accurate perception of the reaction process. Does the system defined by the modeler accurately depict the real system? Are the mineral phases the correct ones? Are all the phases present necessary to describe the system? Is the system open or closed?

S.A. Matthes, Geochemical Modeling, *Corrosion: Fundamentals, Testing, and Protection*, Vol 13A, *ASM Handbook*, ASM International, 2003, p 34–41

Geochemical Modeling

Steven A. Matthes, U.S. Department of Energy, Albany Research Center

Describing Equilibrium

A geochemical system for a given bulk composition can be described as the sum total of one or more phases present in the system. *Phases* are separable, distinct, homogeneous regions of space within the system. They are separated from each other by *surfaces,* which are characterized by gross changes in composition and properties between the separated phases.

In most geochemical models, a system will always contain an aqueous phase containing water and dissolved species, and it may also contact mineral and gas phases. If the system has only a fluid phase, it is called *homogeneous.* It is called *heterogeneous* if it contains solid and/or gaseous phases as well. Species are the subcomponents of the phases. A gas phase may contain the species CO_2 or O_2, while the fluid phase may contain the species H^+, Ca^{++}, NO_3^- ,HCO_3^-, CO_3^+, or Cl^-.

Equilibrium is calculated by determining that state (at fixed temperature and pressure) at which the phases, surfaces, and species within the system have reached the minimum value for the Gibb's free energy function. The minimum is determined by evaluating the sum of the chemical potential functions (thermodynamic components) for each of the species in the system being modeled. The problem then becomes how to choose the thermodynamic components that best describe the system.

In a system to be modeled containing (a) water, (b) aqueous species, (c) minerals, and (d) gases, it is first necessary to determine all the possible independent chemical reactions possible between the species. Second, the sum total of the species present must balance the known mass of the system (i.e., if the system starts with 3 millimoles of sodium, it must have 3 millimoles of sodium at the calculated equilibrium). Third, the principle of electroneutrality requires that the ionic species in the fluid remain charge balanced.

Once the distribution of the species in the fluid phase has been determined, satisfying the previously mentioned criteria, the degree of undersaturation or supersaturation of each aqueous species with respect to the mineral phases of the system can be calculated. The *saturation index* is the calculated saturation of a fluid with respect to a mineral phase. Undersaturated minerals have negative saturation indexes. A positive saturation index indicates the mineral is supersaturated and the system is in metastable equilibrium while the system precipitates the supersaturated mineral.

The fugacity of the gases present in the system can also be calculated analogous to the saturation indices. The fugacities calculated are for a gas phase in equilibrium with the system.

Finally, *pe* and E_H, the electrochemical oxidation state of the equilibrium, may be determined. Many natural systems, especially at low temperatures, are not in equilibrium. The calculated values for *pe* and E_H can help ascertain the disequilibrium of a system.

All of the previously described calculations in the geochemical model are subject to Gibb's phase rule, better known as the degrees of freedom of the system. In most geochemical systems the degrees of freedom, or the number of pieces of information needed to describe the state, equals the sum of the number of phases in the system plus the number of aqueous species in the fluid. The number of phases equals each mineral phase plus each gas plus one for the fluid phase in which the aqueous species reside. This supplies the number of independent variables required by thermodynamics to solve each equation of the geochemical model.

Geochemical modeling must also account for changes in the system during the reaction that is modeled. A good example would be the disappearance of a mineral phase that has completely dissolved in the course of the reaction. If such a change to the system takes place, the degrees of freedom for the system change. Also, a mineral surface has been eliminated, the chemical reactions in the system have changed, and the equilibrium constants have altered. The modeling software must be able to compensate for all these changes.

The geochemical model describing a system consists of a set of equations with the principle unknowns typically being the mass of the water, the amount of the mineral phases, and the concentration of the aqueous species.

Although most of the equations in the model are linear, some equations are nonlinear and use the Newton-Raphson iteration method for solving the equations.

S.A. Matthes, Geochemical Modeling, *Corrosion: Fundamentals, Testing, and Protection*, Vol 13A, *ASM Handbook,* ASM International, 2003, p 34–41

Geochemical Modeling

Steven A. Matthes, U.S. Department of Energy, Albany Research Center

---

Applications of Geochemical Modeling to Corrosion

As is true with all geochemical reactions in nature, corrosion is a spontaneous phenomenon. For example, iron is a common component in the crust of the earth. Being a fairly reactive metal, iron is usually found not in the elemental state but as sulfides and oxides. Structures of iron and steel exposed to nature will tend to revert to the compounds (sulfides and oxides) from which the iron was extracted. Like iron, most other metals will corrode to a greater or lesser extent when exposed to air and water in the environment. Geochemical modeling software such as Outokumpu's HSC Chemistry can provide important information on the conditions required for corrosion to occur and ways to limit or prevent corrosion.

One of the earliest applications of GMS to the study of corrosion was in the computer-calculated construction of potential-pH plots, frequently referred to as Pourbaix diagrams (Ref 15). Pourbaix diagrams are a diagnostic tool to thermodynamically determine if a metal will corrode, form a passive film, or remain immune to corrosion when exposed to an aqueous environment (Fig. 4). The Pourbaix diagram consists of a plot of electrochemical potential (E_H) of metallic species in water (for example Fe_3O_4, Fe^{++}, Fe, etc.), versus pH (i.e. the acidity or basicity of water). The plots are constructed by considering which phase is thermodynamically most stable at a given pH, potential, and temperature.

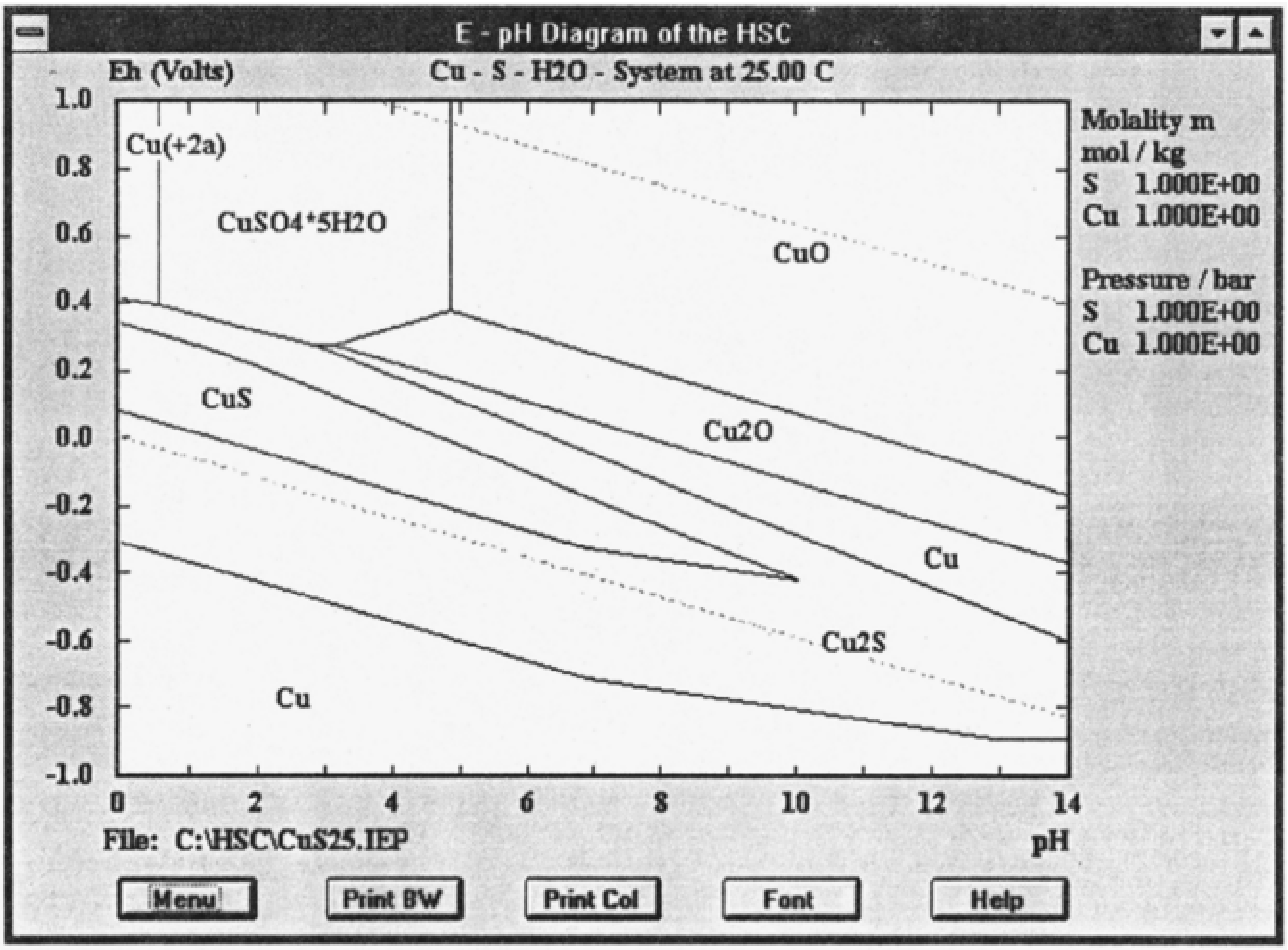

Fig. 4 A Pourbaix diagram (potential versus pH at 25 °C) for the copper, sulfur, water system derived using HSC Chemistry

Using software called POT-pH-TEMP, the Electric Power Research Institute (EPRI) (Ref 16) calculated and published a large number of Pourbaix diagrams for a series of two and three component systems from 25 to 300 °C (75 to 570 °F). Elements studied were, S, Fe, Ni, Cr, C, B, N, Cu, Ti, and Zr. The diagrams were originally applied to corrosion problems in the nuclear power industry but were of such general nature that they have been used on a wide range of corrosion problems. Much GMS will generate the data for producing Pourbaix diagrams or will generate the diagrams themselves (Fig. 4).

One of the more useful features of geochemical modeling software is the ability to predict chemical speciation. In a study on the environmental effects on zinc atmospheric corrosion, Wallinder and Leygraf (Ref 17) were able to model the concentration of zinc species as a function of pH in the runoff water from zinc corrosion films (Fig. 5).

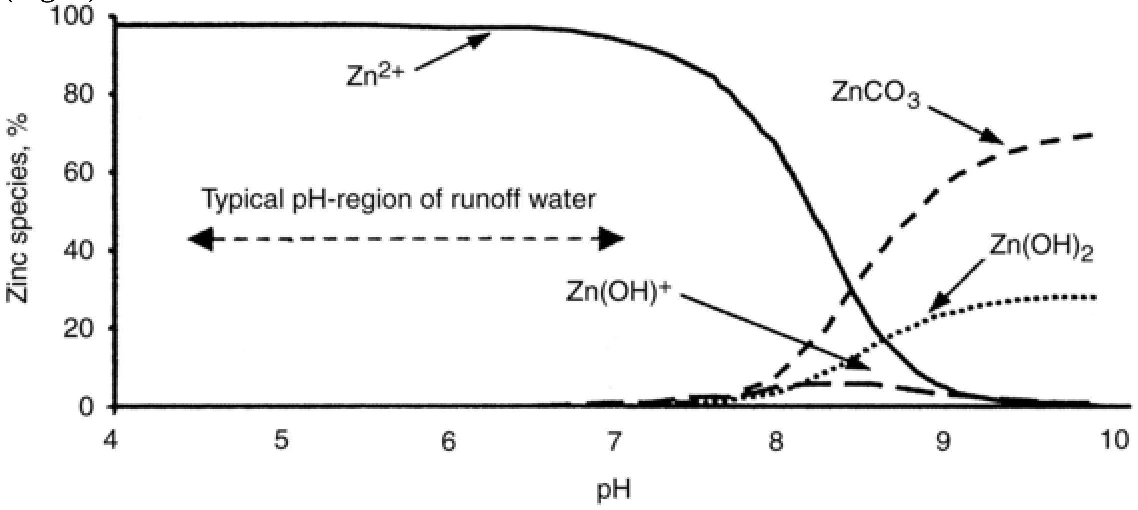

Fig. 5 Chemical speciation of zinc in precipitation runoff as a function of pH predicted by the computer models MINTEQA2 and WHAM. The data are representative of the situation immediately after the runoff is released from zinc sample surfaces exposed in the Stockholm area.

Geochemical modeling software is frequently used in nuclear waste management. A number of articles have been written concerning corrosion of steel canisters and concrete containers or barriers holding nuclear waste. Atkinson et al. (Ref 18) used PHREEQE with additional data on nuclides to model corrosion of iron components and soluble species in concrete. A study of corrosion of metal canisters in a cementitious environment (high pH) using CHEQMATE and PHREEQE was done (Ref 19). The programs EQ3NR and PHREEQE were used to model the solubilities of actinide corrosion products in groundwaters (Ref 20, 21, 22). Interactions between groundwater and cement were studied to assess long-term performance of nuclear waste containment designs. The effect of the corrosion of concrete barriers and the subsequent alkaline plume that resulted were also studied (Ref 23), and others investigated corrosion of cemented waste in salt brines (Ref 24). Sharland et al. (Ref 25) used CHEQMATE and PHREEQE to study changes in E_H of the pore water and the removal of oxygen by the corrosion of metal canisters at a model nuclear repository. The PHREEQE software was also used to calculate variations in E_H in geochemical repositories (Ref 26). The computer model BLT-EC was developed for simulating the release and geochemical transport of contaminants from a subsurface nuclear disposal facility (Ref 27). The leaching behavior of uranium oxide subjected to groundwater corrosion and the resultant speciation was studied (Ref 28). In a later article, a thermodynamic model of the corrosion of uranium dioxide in granitic groundwater was described (Ref 29). The speciation of uranium phases in the weathering zone of the Bangombé U-Deposit using The Geochemist's Workbench (Fig. 6) was also studied (Ref 30).

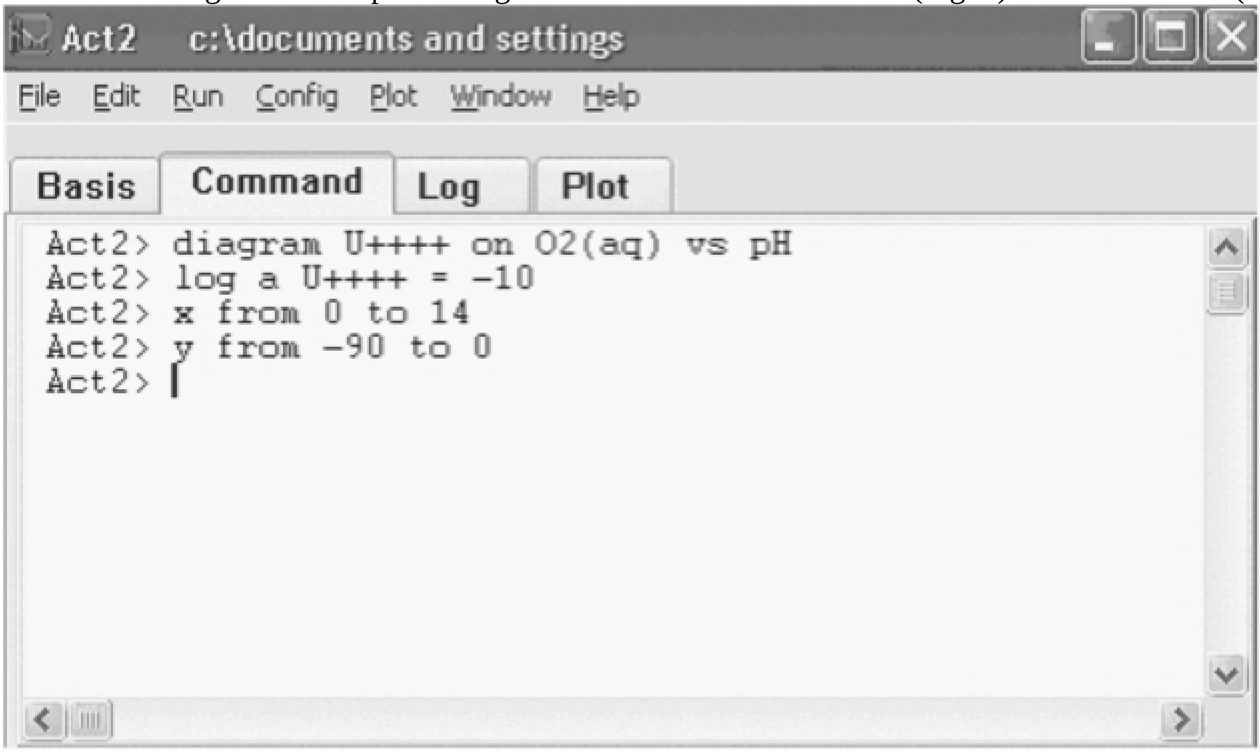

Fig. 6 Programming a U^{4+} stability diagram (log O_2 (aq) versus pH) using The Geochemist's Workbench.

A number of articles have concerned geochemical modeling of the corrosion of vitrified nuclear waste or glass. The programs PHREEQE and GLASSOL were used to examine corrosion of powdered simulated high-level waste glass (Ref 31). The program CONDIMENT was used to model the fluxes of radionuclides released from the corrosion of vitrified waste into the geosphere (Ref 32). Glass corrosion in brines has been investigated using Pitzer equations (Ref 33), and the corrosion of French nuclear glass reference material R717 has also been studied (Ref 34, 35). Lolivier et al. investigated the interaction of the corrosion of R717 with boom clay (Ref 36). Diffusion of radionuclides in compacted bentonite caused by glass corrosion was modeled using PHREEQE (Ref 37). The same program was also used to model the corrosion behavior of powdered glass with or without the presence of oxygen (Ref 38). Aertens and Ghaleb looked at new methods for modeling glass corrosion and investigated two classes of methods for doing this type of modeling. (Ref 39).

In another study, geochemical modeling was used to investigate the effect of sulfate and carbonate mineral-bearing reservoirs on scaling and corrosion damage of production tubing (Ref 40). The software H2OTREAT and MINTEQ were used to evaluate water treatment requirements for aquifer thermal energy storage (Ref 41). The saturation index of calcium carbonate calculated by WATEQ was used to predict corrosion and scaling in water pipe (Ref 42). Geochemical modeling was used for contamination mapping including that caused by secondary pollution from corrosion in another report (Ref 43).

The PHREEQC package has been used to calculate the contributions of acid rain, dry deposition of acid gases, and dissolved CO_2 (Ref 44, 45) to the dissolution of corrosion films from zinc and copper surfaces (Fig. 7). In the same studies and in one by Matthes et al. (Ref 46), PHREEQC was used to calculate solubility curves for a number of known minerals in zinc, copper, and lead corrosion films. The effect of water quality on copper corrosion using MINEQL+ was also studied (Ref 47).

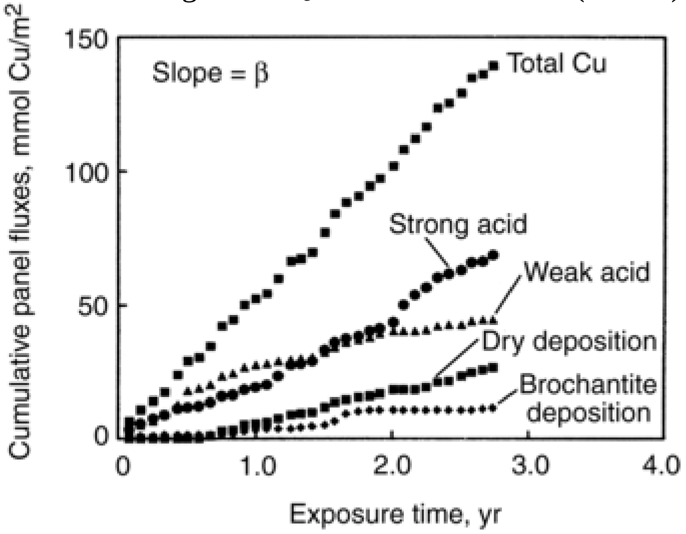

Fig. 7 The contributions of strong acid (acid rain), weak acid (dissolved atmospheric CO_2), and dry deposition (conversion of corrosion film minerals to more soluble species by reaction with acidic gases, SO_2 and HNO_3) to runoff from a copper corrosion film calculated using PHREEQC. The formation of the corrosion film mineral brochantite is also modeled.

References cited in this section

15. M. Pourbaix, *Atlas of Electrochemical Equilibria in Aqueous Solutions,* Pergamon Press, 1966

16. "Computer-Calculated Potential pH Diagrams to 300 °C," prepared by Babcock and Wilcox Company, Electric Power Research Institute NP-3137, Vol 1–3, 1983

17. O.I. Wallinder, and C. Leygraf, Environmental Effects of Metals Induced by Atmospheric Corrosion, *Outdoor Atmospheric Corrosion,* STP 1421, Herb Townsend, Ed., ASTM International, p 185–199

18. A. Atkinson, F.T. Ewart, S.Y.R. Pugh, J.H. Rees, and S.M. Sharland, "Experimental and Modelling Studies of the Near-Field Chemistry for Nirex Repository Concepts, Nuclear Industry Radioactive Waste Executive," Harwell, NSS/R-104CONF- 8711200, 1988, 14 p

19. A. Haworth, S.M. Sharland, C.J. Tweed, W. Lutz, and R.C. Ewing, Modelling of the Degradation of Cement in a Nuclear Waste Repository, *Scientific Basis for Nuclear Waste Management XII,* Materials Research Society, p 447–454

20. M. Snellman, "Solubility of Actinides, Fission and Corrosion Products in Simulated Groundwaters and Sievi Groundwater— PHREEQE and EQ3NR Calculations," Valtion Teknillinen Tutkimukeskus, Otaniemi (FINLAND), YJT-90-05, 1990, 32 p

21. L.J. Criscenti and R.J. Serne, Thermodynamic Modeling of Cement/Groundwater Interaction as a Tool for Long-Term Performance Assessment, *Scientific Basis for Nuclear Waste Management XIII Symposium,* Materials Research Society, p 81–89

22. T. Ohe, J. Ahn, T. Ikeda, T. Kanno, T. Chiba, M. Tsukamoto, S. Nakayama, and S. Nagasaki, Analysis on Evolving Environments of Engineering Barriers of High-Level Radioactive Waste Repositories during the First 1000 Years, *J. At. Energy Soc. Jpn.,* Vol 35 (No. 5), 1993, p 420–437

23. L. Trotignon, H. Peycelon, M. Cranga, and F. Adenot, Modelling of the Interaction between an Engineered Clay Barrier and Concrete Structures in a Deep Storage Vault, *Scientific Basis for Nuclear Waste Management XXII Symposium,* Vol 556, Materials Research Society, 1999, p 607–614

24. B. Kienzler, and P. Vejmelka, “Geochemical Modeling of Corrosion of Cemented Waste Forms in Salt Brines: Experimental Basis, Methods and Results,”Forschungszentrum Karlsruhe GmbH Technik and Umwelt (DE). Inst. Fuer Nukleare Entsorgungstechnik, FZKA-6046, 1998, 40 p

25. S.M. Sharland, P.W. Tasker, and C.J. Tweed, “The Evolution of Eh in the Pore Water of a Model Nuclear Waste Repository,” UKAEA Harwell Lab. (UK), Theoretical Physic Division, AERE-R—12442, 1986, 38 p

26. K. Sasakawa, N. Gennai, J. Nakayama, R. Wada, F. Matsuda, and T. Masuda, Examination of Analysis and Evaluation Method of the Chemical Environment of Geological Repositories by Geochemical Code, *Research and Development, Kobe Steel Engineering Reports,* Vol 41 (No. 2), 1991, p 101–104

27. R.J. MacMinnon, Ecodynamic Reseach Associates, T.M. Sullivan, and R.R. Kinsey, *BLT-EC (Breach, Leach and Transport- Equilibrium Chemistry) Data Input Guide: A Computer Model for Simulating Release and Coupled Geochemical Transport of Contaminants from a Subsurface Disposal Facility,* Nuclear Regulatory Commission, 1997, 363 p

28. P. Trocellier, and J.P. Gallien, Investigation of UO2 Leaching Behavior in Groundwater Using a Nuclear Microprobe: Preliminary Results, *Nucl. Instrum. Methods Phys. Res. B,* Vol. 93 (No. 3), 1994, p 311–315

29. P. Trocellier, C. Cachoir, and S. Guilbert, A Simple Thermodynamical Model to Describe the Control of the Dissolution of Uranium Dioxide in Granitic Groundwater by Secondary Phase Formation, *J. Nucl. Mater.,* Vol 256 (No. 2–3), Elsevier, 1998 p 197–206

30. K.A. Jensen, C.S. Palenik, and R.C. Ewing, U6+ Phases in the Weathering Zone of the Bangombe U-Deposit: Observed and Predicted Mineralogy, *Radiochim. Acta,* Vol 90, 2002, p 1–9

31. J. Patyn, P. Van Iseghem, and W. Timmermans, The Long-Term Corrosion and Modeling of Two Simulated Belgian Reference High-Level Waste Glasses.II, *Scientific Basis for Nuclear Waste Management XIII Symposium,* Materials Research Society, 1990, p 299–307

32. E. Mouche, P. Lovera, and M. Jorda, Near- Field Modeling for the Safety Assessment of French High-Level Waste Repositories, Proc. *First-International Top Meet High Level Radioact. Waste Manage. Part 1,* ASCE, Boston Society of Civil Engineers Sect, 1990, p 691–698

33. B. Grambow, and R. Muller, Chemistry of Glass Corrosion in High Saline Brines, *Scientific Basis for Nuclear Waste Management XIII Symposium,* Materials Research Society, 1990, p 229–240

34. L. Michaux, E. Mouche, J.C. Petit and B. Fritz, Geochemical Modeling of the Long- Term Dissolution Behavior of the French Nuclear Glass R717, *Appl. Geochem.,* 1992, p 41–54

35. E.Y. Vernaz, and J.L. Dussossoy, Current State of Knowledge of Nuclear Waste Glass Corrosion Mechanism, The Case of R717 Glass, *Appl. Geochem.,* 1992, p 13–22

36. P. Lolivier, K. Lemmens, and P. Iseghem, Geochemical Modeling of the Interaction of HLW Glass with Boom Clay Media, *Scientific Basis for Nuclear Waste Management XXI Symposium I,* Materials Research Society, 1998, p 399–406

37. M. Tsukamoto, T. Ohe, T. Fujita, R. Hesbol, and H.P. Hermansson, Diffusion of Radionuclides in Compacted Bentonite: Results from Combined Glass Dissolution and Migration Tests, *Scientific Basis for Nuclear Waste Management XVII Symposium I,* Materials Research Society, 1995, p 291–298

38. Y. Inagaki, H. Furuya, K. Idemitsu, T. Marda, A. Sakai, T. Banba, and S. Muraoka, Corrosion Behavior of a Powdered Simulated Nuclear Waste Glass under Anoxic Condition, *Scientific Basis for Nuclear Waste Management XVII Symposium I,* Materials Research Society, 1995, p 23–30

39. M. Aertens, and D. Ghaleb, New Techniques for Modeling Glass Dissolution, *J. Nuclear Materials,* Vol 298 (No.1–2), 2001, p 37–46

40. D.B. Macgowan, T.L. Dunn, and R.C. Surdam, Geochemical Modeling of Scale Formation and Formation Damage during Production from Sulfate and Carbonate Mineral-Bearing Reservoirs, *Am. Assoc. Petrol. Geolog.,* Vol 75 (No. 3), 1991, p 626

41. L.W. Vail, E.A. Jence, and L.E. Eary, H2OTREAT: An Aid for Evaluating Water Treatment Requirements for Aquifer Thermal Energy Storage, Vol 4, Society of Automotive Engineering, 1992, p 4.131–4.135

42. L.E. Marin, E.P. Santa Anna, and G.V. Oliman, Application of Geochemical Modeling in Hydraulic Engineering, *Ing. Hidraul. Mex.,* Vol 9, 1994, p 63–69

43. T.S. Lee, S.K. Lee, and Y.K. Hong, *Environmental Geophysics and Geochemistry for Contamination Mapping and Monitoring I,* Korea Institute of Geology and Mining and Materials, KR-95-T-3, 1995, 439 p

44. S.D. Cramer, S.A. Matthes, G.R. Holcomb, B.S. Covino Jr., and S.J. Bullard, "Precipitation Runoff and Atmospheric Corrosion," Paper 00452, presented at *Corrosion/2000,* (Houston TX), NACE International, 2000, 15 p

45. S.D. Cramer, S.A. Matthes, B.S. Covino Jr., S.J. Bullard, and G.R. Holcomb, Environmental Factors Affecting the Atmospheric Corrosion of Copper, *Outdoor Atmospheric Corrosion,* STP 1421, H.E. Townsend, Ed., ASTM International, 2002, p 245–264

46. S.A. Matthes, S.D. Cramer, B.S. Covino Jr., S.J. Bullard, and G.R. Holcomb, Precipitation Runoff from Lead, *Outdoor Atmospheric Corrosion,* STP 1421, H.E. Townsend, Ed., ASTM International, 2002, p 265–274

47. S.O. Pehkoen, A. Palit, and X. Zhang, Effect of Specific Water Quality Parameters on Copper Corrosion, *Corrosion,* Vol 58 (No. 2), 2002, p 156–165

S.A. Matthes, Geochemical Modeling, *Corrosion: Fundamentals, Testing, and Protection*, Vol 13A, *ASM Handbook*, ASM International, 2003, p 34–41

Geochemical Modeling

Steven A. Matthes, U.S. Department of Energy, Albany Research Center

Geochemical Modeling Features

Geochemical modeling can perform many useful tasks for the corrosion scientist:

- Construction of E_H vs pH (Pourbaix) diagrams
- Speciation in aqueous and nonaqueous solutions (Fig. 8)
- Construction of solubility curves
- Equilibrium in high-temperature corrosion systems
- Metals complexing
- Calculation of equilibrium concentrations
- Reaction path calculations
- Gas-liquid-solid phase calculations (Fig. 9)
- Surface complexation
- Inverse modeling
- Automatic reaction balancing
- Modeling irreversible reactions

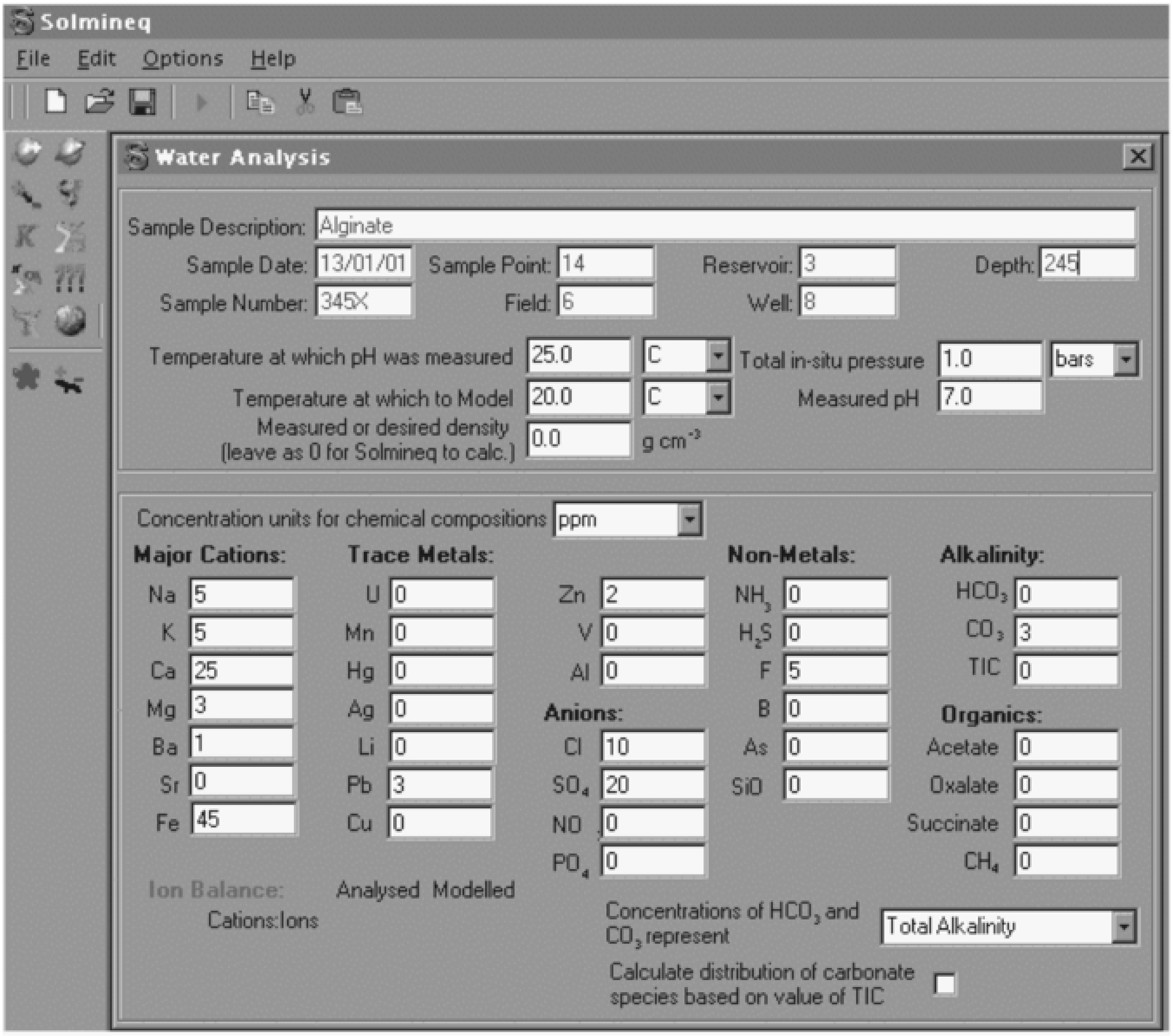

Fig. 8 SOLMINEQ, a geochemical modeling program. Pictured here is the module for aqueous speciation.

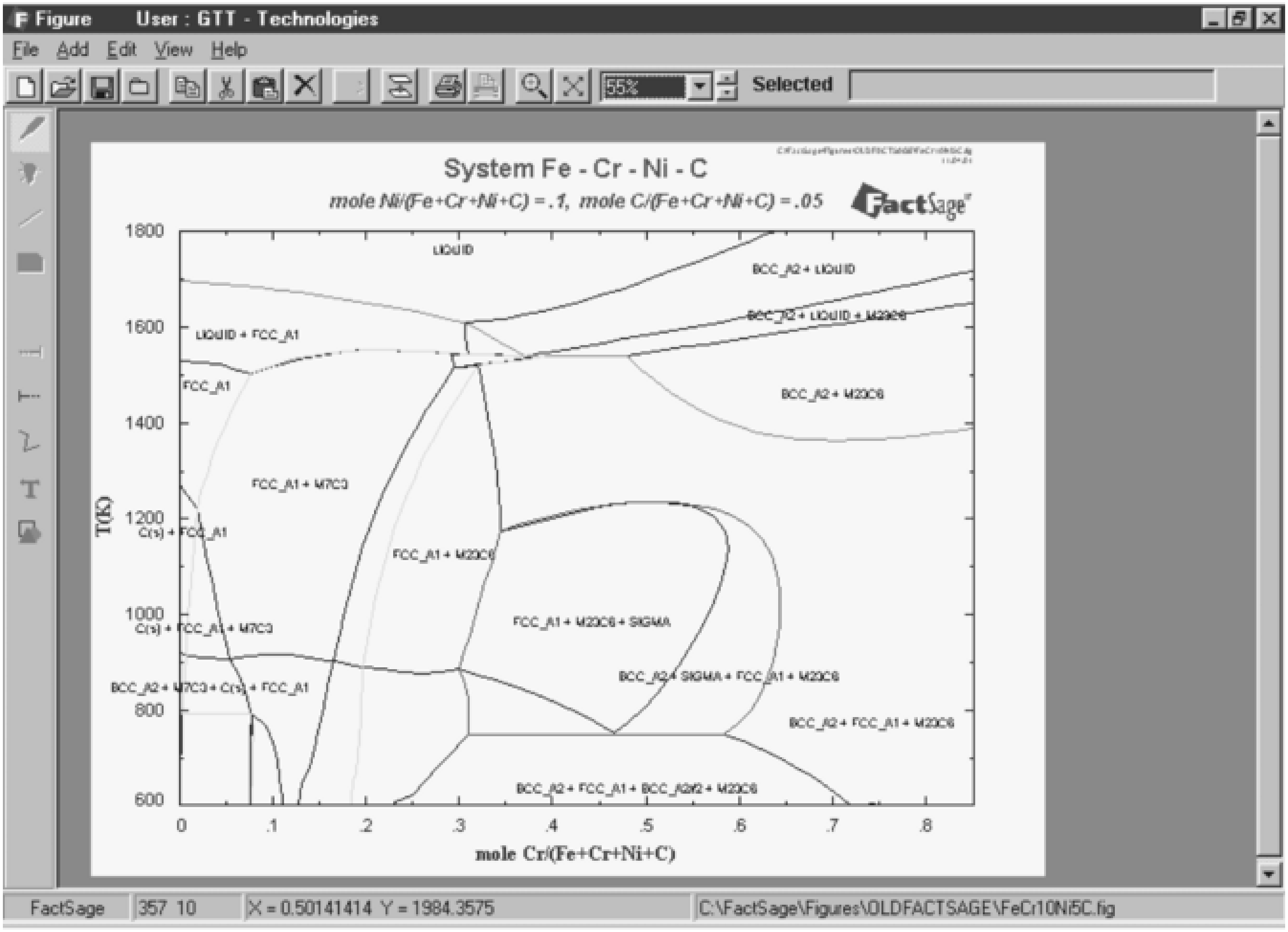

Fig. 9 High-temperature phase diagram for the Fe-Cr-Ni-C system using FactSage (GTT Technologies) geochemical modeling software

These calculations are performed by the use of thermodynamics equations and large databases of thermodynamic data. A number of geochemical modeling software packages that can do these calculations are available, both as commercial and freeware products. Some of these programs are quite complex and have a steep learning curve. Some may require additional user training.

S.A. Matthes, Geochemical Modeling, *Corrosion: Fundamentals, Testing, and Protection*, Vol 13A, *ASM Handbook*, ASM International, 2003, p 34–41

Geochemical Modeling

Steven A. Matthes, U.S. Department of Energy, Albany Research Center

References

1. S.R. Brinkley, Jr., Calculation of the Equilibrium Composition of Systems of Many Components, *J. Chem. Phys.,* Vol 15, 1947 p 107–110

2. R.M. Garrels, and M.E. Thompson, A Chemical Model for Sea Water at 25° and One Atmosphere Total Pressure, *Am. J. Sci.*, Vol 260, 1962, p 57–66

3. Y.K. Kharaka and I. Barnes, “SOLMNEQ: Solution-Mineral Equilibrium Computations,” Report PB-215-899, U.S. Geological Survey Computer Contributions, 1973

4. A.H. Truesdell and B.F. Jones, WATEQ, A Computer Program for Calculating Chemical Equilibria of Natural Waters, *US Geol. Surv. J. Res.,* Vol 2, 1974, p 233–248

5. J.C. Westall, J.L. Zachary, and F.M.M. Morel, “MINEQL, A Computer Program for the Calculation of Chemical Equilibrium Composition of Aqueous Systems,” Tech. Note 18, Department of Civil Engineering, Massachusetts Institute of Technology, 1976

6. R.M. Garrels, and F.T. Mackenzie, Origin of the Chemical Compositions of Some Springs and Lakes, *Equilibrium Concepts in Natural Waters, Advances in Chemistry Series 67,* American Chemical Society, 1967, p 222–242

7. H.C. Hegelson, Evaluation of Irreversible Reactions in Geochemical Processes Involving Minerals and Aqueous Solutions, I: Thermodynamic Relations, *Geochim. Cosmochim. Acta,* Vol 32, 1968, p 853–877

8. H.C. Hegelson, A Chemical and Thermodynamic Model of Ore Deposition in Hydrothermal Systems, *Miner. Soc. Am. Special Paper,* Vol 3, 1970, p 155–186

9. I.K. Karpov and L.A. Kaz'min, Calculation of Geochemical Equilibria in Heterogeneous Multicomponent Systems, *Geochem. Int.,* Vol 9, 1972, p 252–262

10. I.K. Karpov, L.A. Kaz'min, and S.A. Kashik, Optimal Programming for Computer Calculation of Irreversible Evolution in Geochemical Systems, *Geochem. Int.,* Vol 10, 1973, p 464–470

11. T.J. Wolery, “Calculation of Chemical Equilibrium between Aqueous Solution and Minerals: the EQ3/6 Software Package,” Lawrence Livermore National Laboratory Report UCRL-52658, 1979

12. D.L. Parkhurst, D.C. Thorstenson, and L.N. Plummer, “PHREEQE—A Computer Program for Geochemical Calculations,” U.S. Geological Survey Water-Resources Investigations Report 80-96, 1980

13. C.M. Bethke, *Geochemical Reaction Modeling. Concepts and Applications,* Oxford University Press, 1996, 397 p

14. D.K. Nordstrom, and J.L. Munoz, *Geochemical Thermodynamics,* 2nd ed., Blackwell, 1994

15. M. Pourbaix, *Atlas of Electrochemical Equilibria in Aqueous Solutions,* Pergamon Press, 1966

16. “Computer-Calculated Potential pH Diagrams to 300 °C,” prepared by Babcock and Wilcox Company, Electric Power Research Institute NP-3137, Vol 1–3, 1983

17. O.I. Wallinder, and C. Leygraf, Environmental Effects of Metals Induced by Atmospheric Corrosion, *Outdoor Atmospheric Corrosion,* STP 1421, Herb Townsend, Ed., ASTM International, p 185–199

18. A. Atkinson, F.T. Ewart, S.Y.R. Pugh, J.H. Rees, and S.M. Sharland, “Experimental and Modelling Studies of the Near-Field Chemistry for Nirex Repository Concepts, Nuclear Industry Radioactive Waste Executive,” Harwell, NSS/R-104CONF- 8711200, 1988, 14 p

19. A. Haworth, S.M. Sharland, C.J. Tweed, W. Lutz, and R.C. Ewing, Modelling of the Degradation of Cement in a Nuclear Waste Repository, *Scientific Basis for Nuclear Waste Management XII,* Materials Research Society, p 447–454

20. M. Snellman, “Solubility of Actinides, Fission and Corrosion Products in Simulated Groundwaters and Sievi Groundwater— PHREEQE and EQ3NR Calculations,” Valtion Teknillinen Tutkimukeskus, Otaniemi (FINLAND), YJT-90-05, 1990, 32 p

21. L.J. Criscenti and R.J. Serne, Thermodynamic Modeling of Cement/Groundwater Interaction as a Tool for Long-Term Performance Assessment, *Scientific Basis for Nuclear Waste Management XIII Symposium,* Materials Research Society, p 81–89

22. T. Ohe, J. Ahn, T. Ikeda, T. Kanno, T. Chiba, M. Tsukamoto, S. Nakayama, and S. Nagasaki, Analysis on Evolving Environments of Engineering Barriers of High-Level Radioactive Waste Repositories during the First 1000 Years, *J. At. Energy Soc. Jpn.,* Vol 35 (No. 5), 1993, p 420–437

23. L. Trotignon, H. Peycelon, M. Cranga, and F. Adenot, Modelling of the Interaction between an Engineered Clay Barrier and Concrete Structures in a Deep Storage Vault, *Scientific Basis for Nuclear Waste Management XXII Symposium,* Vol 556, Materials Research Society, 1999, p 607–614

24. B. Kienzler, and P. Vejmelka, “Geochemical Modeling of Corrosion of Cemented Waste Forms in Salt Brines: Experimental Basis, Methods and Results,”Forschungszentrum Karlsruhe GmbH Technik and Umwelt (DE). Inst. Fuer Nukleare Entsorgungstechnik, FZKA-6046, 1998, 40 p

25. S.M. Sharland, P.W. Tasker, and C.J. Tweed, “The Evolution of Eh in the Pore Water of a Model Nuclear Waste Repository,” UKAEA Harwell Lab. (UK), Theoretical Physic Division, AERE-R—12442, 1986, 38 p

26. K. Sasakawa, N. Gennai, J. Nakayama, R. Wada, F. Matsuda, and T. Masuda, Examination of Analysis and Evaluation Method of the Chemical Environment of Geological Repositories by Geochemical Code, *Research and Development, Kobe Steel Engineering Reports,* Vol 41 (No. 2), 1991, p 101–104

27. R.J. MacMinnon, Ecodynamic Reseach Associates, T.M. Sullivan, and R.R. Kinsey, *BLT-EC (Breach, Leach and Transport- Equilibrium Chemistry) Data Input Guide: A Computer Model for Simulating Release and Coupled Geochemical Transport of Contaminants from a Subsurface Disposal Facility,* Nuclear Regulatory Commission, 1997, 363 p

28. P. Trocellier, and J.P. Gallien, Investigation of UO2 Leaching Behavior in Groundwater Using a Nuclear Microprobe: Preliminary Results, *Nucl. Instrum. Methods Phys. Res. B,* Vol. 93 (No. 3), 1994, p 311–315

29. P. Trocellier, C. Cachoir, and S. Guilbert, A Simple Thermodynamical Model to Describe the Control of the Dissolution of Uranium Dioxide in Granitic Groundwater by Secondary Phase Formation, *J. Nucl. Mater.,* Vol 256 (No. 2–3), Elsevier, 1998 p 197–206

30. K.A. Jensen, C.S. Palenik, and R.C. Ewing, U6+ Phases in the Weathering Zone of the Bangombe U-Deposit: Observed and Predicted Mineralogy, *Radiochim. Acta,* Vol 90, 2002, p 1–9

31. J. Patyn, P. Van Iseghem, and W. Timmermans, The Long-Term Corrosion and Modeling of Two Simulated Belgian Reference High-Level Waste Glasses.II, *Scientific Basis for Nuclear Waste Management XIII Symposium,* Materials Research Society, 1990, p 299–307

32. E. Mouche, P. Lovera, and M. Jorda, Near- Field Modeling for the Safety Assessment of French High-Level Waste Repositories, Proc. *First-International Top Meet High Level Radioact. Waste Manage. Part 1,* ASCE, Boston Society of Civil Engineers Sect, 1990, p 691–698

33. B. Grambow, and R. Muller, Chemistry of Glass Corrosion in High Saline Brines, *Scientific Basis for Nuclear Waste Management XIII Symposium,* Materials Research Society, 1990, p 229–240

34. L. Michaux, E. Mouche, J.C. Petit and B. Fritz, Geochemical Modeling of the Long- Term Dissolution Behavior of the French Nuclear Glass R717, *Appl. Geochem.,* 1992, p 41–54

35. E.Y. Vernaz, and J.L. Dussossoy, Current State of Knowledge of Nuclear Waste Glass Corrosion Mechanism, The Case of R717 Glass, *Appl. Geochem.,* 1992, p 13–22

36. P. Lolivier, K. Lemmens, and P. Iseghem, Geochemical Modeling of the Interaction of HLW Glass with Boom Clay Media, *Scientific Basis for Nuclear Waste Management XXI Symposium I,* Materials Research Society, 1998, p 399–406

37. M. Tsukamoto, T. Ohe, T. Fujita, R. Hesbol, and H.P. Hermansson, Diffusion of Radionuclides in Compacted Bentonite: Results from Combined Glass Dissolution and Migration Tests, *Scientific Basis for Nuclear Waste Management XVII Symposium I,* Materials Research Society, 1995, p 291–298

38. Y. Inagaki, H. Furuya, K. Idemitsu, T. Marda, A. Sakai, T. Banba, and S. Muraoka, Corrosion Behavior of a Powdered Simulated Nuclear Waste Glass under Anoxic Condition, *Scientific Basis for Nuclear Waste Management XVII Symposium I,* Materials Research Society, 1995, p 23–30

39. M. Aertens, and D. Ghaleb, New Techniques for Modeling Glass Dissolution, *J. Nuclear Materials,* Vol 298 (No.1–2), 2001, p 37–46

40. D.B. Macgowan, T.L. Dunn, and R.C. Surdam, Geochemical Modeling of Scale Formation and Formation Damage during Production from Sulfate and Carbonate Mineral-Bearing Reservoirs, *Am. Assoc. Petrol. Geolog.,* Vol 75 (No. 3), 1991, p 626

41. L.W. Vail, E.A. Jence, and L.E. Eary, H2OTREAT: An Aid for Evaluating Water Treatment Requirements for Aquifer Thermal Energy Storage, Vol 4, Society of Automotive Engineering, 1992, p 4.131–4.135

42. L.E. Marin, E.P. Santa Anna, and G.V. Oliman, Application of Geochemical Modeling in Hydraulic Engineering, *Ing. Hidraul. Mex.,* Vol 9, 1994, p 63–69

43. T.S. Lee, S.K. Lee, and Y.K. Hong, *Environmental Geophysics and Geochemistry for Contamination Mapping and Monitoring I,* Korea Institute of Geology and Mining and Materials, KR-95-T-3, 1995, 439 p

44. S.D. Cramer, S.A. Matthes, G.R. Holcomb, B.S. Covino Jr., and S.J. Bullard, "Precipitation Runoff and Atmospheric Corrosion," Paper 00452, presented at *Corrosion/2000,* (Houston TX), NACE International, 2000, 15 p

45. S.D. Cramer, S.A. Matthes, B.S. Covino Jr., S.J. Bullard, and G.R. Holcomb, Environmental Factors Affecting the Atmospheric Corrosion of Copper, *Outdoor Atmospheric Corrosion,* STP 1421, H.E. Townsend, Ed., ASTM International, 2002, p 245–264

46. S.A. Matthes, S.D. Cramer, B.S. Covino Jr., S.J. Bullard, and G.R. Holcomb, Precipitation Runoff from Lead, *Outdoor Atmospheric Corrosion,* STP 1421, H.E. Townsend, Ed., ASTM International, 2002, p 265–274

47. S.O. Pehkoen, A. Palit, and X. Zhang, Effect of Specific Water Quality Parameters on Copper Corrosion, *Corrosion,* Vol 58 (No. 2), 2002, p 156–165

S.A. Matthes, Geochemical Modeling, *Corrosion: Fundamentals, Testing, and Protection*, Vol 13A, *ASM Handbook*, ASM International, 2003, p 34–41

Geochemical Modeling

Steven A. Matthes, U.S. Department of Energy, Albany Research Center

Selected References

- F. Albaredo, *Introduction to Geochemical Modeling,* Cambridge University Press, April 1996, 563 p
- G.M. Anderson, *Thermodynamics of Natural Systems,* John Wiley & Sons, 1996, 382 p
- G.M. Anderson, and D.A. Crerar, *Thermodynamics in Geochemistry: The Equilibrium Model,* Oxford University Press, 1993, 588 p
- C.A.J. Appelo and D. Postma, *Geochemistry, Groundwater and Pollution,* Balkema, 1994, 536 p
- C.M. Bethke, *Geochemical Reaction Modeling: Concepts and Applications,* Oxford University Press, 1996, 397 p
- K. Denbigh, *The Principles of Chemical Equilibrium,* 4th ed., Cambridge University Press, 1981, 494 p
- J.I. Drever, *The Geochemistry of Natural Waters,* 2nd ed. Prentice Hall, 1988, 437 p
- P. Fletcher, *Chemical Thermodynamics for Earth Scientists,* Longman/Harlow, 1993, 464 p
- D.K. Nordstrom, and J.L. Munoz, *Geochemical Thermodynamics,* 2nd ed., Blackwell Scientific Publications, 1994, 493 p
- J.F. Pankow, *Aquatic Chemistry Concepts,* Lewis Publishers, 1991, 683 p
- K.S. Pitzer, *Thermodynamics,* McGraw-Hill, 1995, 626 p
- W. Stumm, and J.J. Morgan, *Aquatic Chemistry,* 3rd ed., Wiley-Interscience, 1996, 1022 p

D.W. Shoesmith, Kinetics of Aqueous Corrosion, *Corrosion: Fundamentals, Testing, and Protection,* Vol 13A, *ASM Handbook,* ASM International, 2003, p 42–51

Kinetics of Aqueous Corrosion

D.W. Shoesmith, University of Western Ontario

Introduction

THIS ARTICLE gives a general introduction to the kinetics of aqueous corrosion, with an emphasis on electrochemical principles. The concept of a corrosion process as a combination of electrochemical reactions is important, because, for aqueous corrosion processes, electrochemical techniques are the predominant methods used in their study to measure rates as well as in the development of on-line sensors. The primary goal of this article is to introduce the electrochemical concepts. Readers interested in more fundamental details of electrochemistry, electrochemical methods, and their application to corrosion processes will find Ref 1, 2, 3, 4 useful.

References cited in this section

1. J.H. West, *Electrodeposition and Corrosion Processes,* Van Nostrand Reinhold, 1971

2. D. Jones, *Principles and Prevention of Corrosion,* 2nd ed., Prentice Hall, 1996

3. L.L. Shreir, R.A. Jarman, and G.T. Burstein, Ed., Metal/Environment Interactions, *Corrosion,* Vol 1, 3rd ed., Butterworth/Heinemann, 1994

4. L.L. Shreir, R.A. Jarman, and G.T. Burstein, Ed., Corrosion Control, *Corrosion,* Vol 2, 3rd ed., Butterworth/Heinemann, 1994

D.W. Shoesmith, Kinetics of Aqueous Corrosion, *Corrosion: Fundamentals, Testing, and Protection*, Vol 13A, *ASM Handbook*, ASM International, 2003, p 42–51

Kinetics of Aqueous Corrosion

D.W. Shoesmith, University of Western Ontario

Basis of Corrosion Reactions

Aqueous corrosion is an electrochemical process occurring at the interface between a material (commonly, but not exclusively, a metal) and an aqueous solution. For corrosion to occur, an oxidation reaction (generally, metal dissolution and/or metal oxide formation) and a reduction reaction (commonly, proton, water, or dissolved oxygen reduction) must occur simultaneously. In electrochemical terms, an anodic (oxidation, or Ox) reaction:

$$M \rightarrow M^{n+} + ne^- \quad \text{(Eq 1)}$$

where M denotes a metal and M^{n+} a dissolved metal cation, is coupled to a cathodic (reduction, or R) reaction:

$$Ox + ne^- \rightarrow Red \quad \text{(Eq 2)}$$

where Ox denotes a soluble oxidant and Red the reduced form of the oxidant that may or may not be a soluble species. An example of a cathodic reagent that produces a soluble product is oxygen reduction:

$$O_2 + 2H_2O + 4e^- \rightarrow 4OH^- \quad \text{(Eq 3)}$$

An example of a cathodic reaction producing a gaseous product is proton reduction:

$$2H^+ + 2e^- \rightarrow H_2 \quad \text{(Eq 4)}$$

The sum of two electrochemical half-reactions, one anodic (such as Eq 1) and one cathodic (such as Eq 2), is the overall corrosion reaction:

$$M + Ox \rightarrow M^{n+} + Red \quad \text{(Eq 5)}$$

An example is the dissolution of iron in an aerated solution:

$$2Fe + O_2 + 2H_2O \rightarrow 2Fe^{2+} + 4OH^- \quad \text{(Eq 6)}$$

Thus, corrosion is the coupling together of two electrochemical reactions on the same surface. This coupling occurs at a single potential, known as the corrosion potential (E_{corr}). This potential will depend on the relative rates of the coupled anodic and cathodic reactions (see subsequent information), and the oxidation state of the dissolved metal cation may change as E_{corr} changes. Thus, an oxidant capable of driving the corrosion potential to a more positive value could produce a higher oxidation state of the metal (e.g., Fe^{3+} rather than Fe^{2+}). The corroding material-solution combination can be considered a short-circuited galvanic cell in which the energy is dissipated by the consumption of cathodic reagent (oxidant). This situation is illustrated schematically in Fig. 1(a).

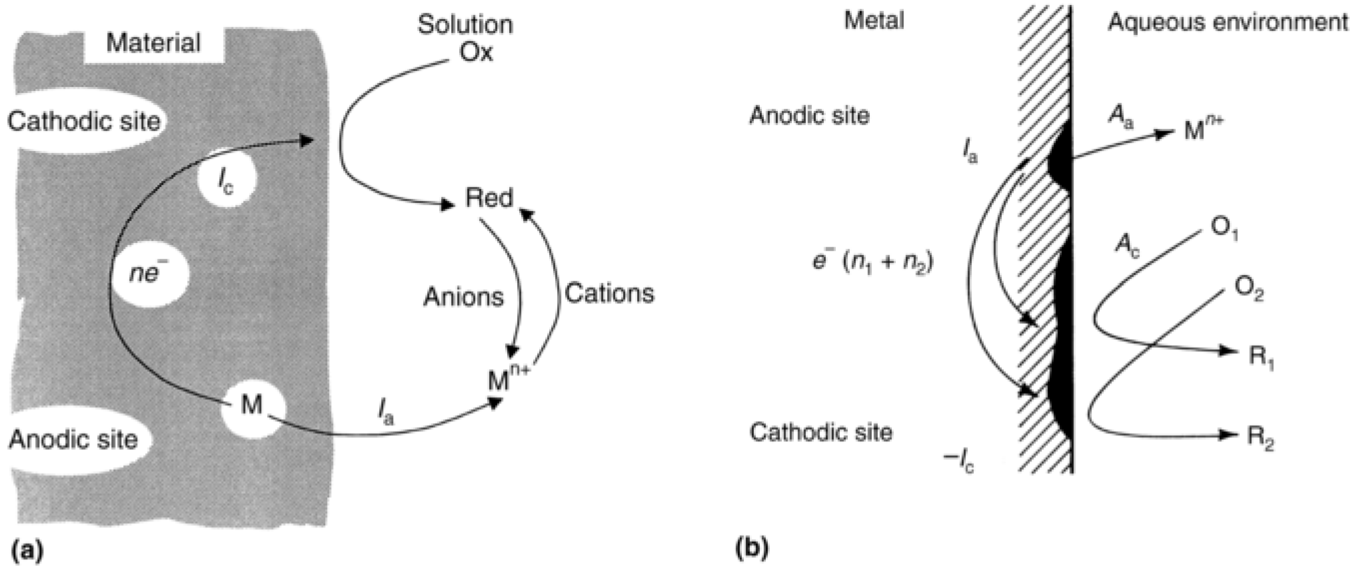

Fig. 1 Galvanic cells. (a) Schematic illustrating the short-circuit galvanic cell that exists during corrosion. (b) The coupling of an anodic reaction with two distinct cathodic reactions. The relative anodic (A_a) and cathodic (A_c) areas of the corroding surface are also illustrated.

To maintain a balance, the amount of cathodic reagent (Ox) consumed must be equal to the amount of corrosion product (M^{n+}) formed. Because electrons are liberated by the anodic reaction and consumed by the cathodic reaction, corrosion can be expressed in terms of an electrochemical current (I). Furthermore, the requirement for mass balance requires that the current flowing into the cathodic reaction must be equal to the current flowing out of the anodic reaction. Clearly, by inspection of Fig. 1(a), these currents are opposite in sign.

By definition, under open-circuit or freely corroding conditions:

$$I_a = |I_c| = I_{corr} \qquad \text{(Eq 7)}$$

where I_a is the anodic current, I_c is the cathodic current, and I_{corr} is the corrosion current. The short-circuited nature of the overall corrosion process means that I_{corr} cannot be directly measured on open circuit. Techniques for its measurement are discussed elsewhere in this Volume. The value of I_{corr} is a measure of the rate of the corrosion process and therefore of the rate of material degradation. The current and the amount of material corroded are related by Faraday's law:

$$I_{corr}t = \frac{nFw}{M} \qquad \text{(Eq 8)}$$

where I_{corr} is expressed in amps; t is the time of exposure to the corrosive environment (seconds); nF is the number of coulombs (C) required to convert 1 mol of material to corrosion product; n is the number of electrons transferred or liberated in the oxidation reaction; F is the Faraday constant (96,480 C/mol); M is the molecular weight of the material in grams (g); and w is the mass of corroded material (g).

It is possible for the anodic reaction to be supported by more than one cathodic reaction (Fig. 1b). For example, in oxygenated acidic solutions, the generic corrosion reaction (Eq 1) could be driven by both proton reduction (Eq 4) and oxygen reduction (Eq 3). When complex alloys are involved, the anodic corrosion reaction may also be the sum of more than one dissolution reaction; that is, the congruent dissolution of a Ni-Cr-Mo alloy would involve the dissolution of each alloy component with partial anodic currents proportional to the atomic fraction of each component in the alloy. The corrosion current (I_{corr}) then equals the sum of the component partial currents:

$$I_{corr} = \sum I_a = -\sum I_c \qquad \text{(Eq 9)}$$

Additionally, the area and location of the anodic and cathodic sites (A_a and A_c, Fig. 1b) may be different. As a consequence, although the total anodic and cathodic currents must be equal, the respective current densities need not be:

$$I_a = -I_c;\ A_a \neq A_c \qquad \text{(Eq 10)}$$

And, therefore:

$$\frac{I_a}{A_a} \neq -\frac{I_c}{A_c} \quad \text{(Eq 11)}$$

The term *I/A* is a current density and will be designated ***i***.

This inequality in current densities can have serious implications. For a smooth, single-component metal surface, the anodic and cathodic sites will be separated, at any one instant, by only a few nanometers. In general terms, the anodic and cathodic sites will shift with time, so that the surface reacts evenly as it undergoes general corrosion. At the atomic scale, however, the surface is not necessarily smooth and is usually considered to comprise surface terraces, ledges, and kinks, as illustrated in Fig. 2. Also, surface defects such as ad-atoms, vacancies, and emergent defects may also exist. Because the coordination number (*N*) of atoms in these various locations differs, that is:

$$N_{terrace} > N_{ledge} > N_{kink} \quad \text{(Eq 12)}$$

there will be a difference in strength of surface bonding, and atoms will be preferentially removed in the order kink, then ledge, then terrace; that is, surface defects represent potential anodic sites.

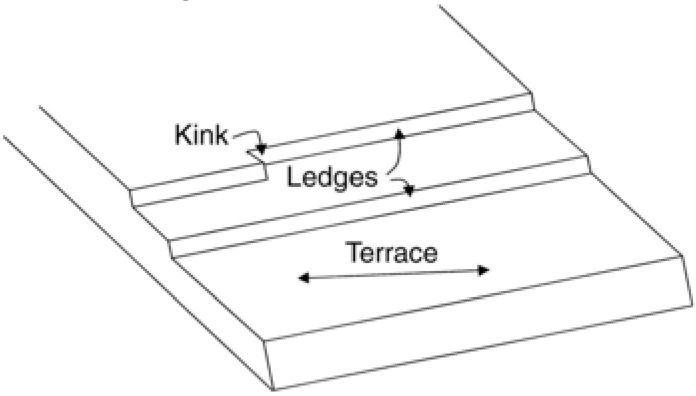

Fig. 2 A metal surface on the atomic scale showing the existence of kinks, ledges, and terraces

The separation of anodes and cathodes induced by these atomic defects is, however, minor compared to the separations induced by other surface features, such as surface asperity, alloy phases, grain boundaries, impurity inclusions, residual stresses due to processes such as cold working, and high-resistance surface oxide films. These features can often lead to the stabilization of discrete anodic and cathodic sites. The specific combination of a small anode area and a large cathode area can lead to large discrepancies in anodic and cathodic current densities, that is, to large anodic current densities at a small number of discrete sites. Such a situation is particularly dangerous when the majority of a metal surface is oxide covered (acting as a cathode) and only a small number of bare metal sites (acting as anodes) are exposed to the solution environment. Such a situation exists during pitting, crevice corrosion, and stress-corrosion cracking, as illustrated for pitting in Fig. 3.

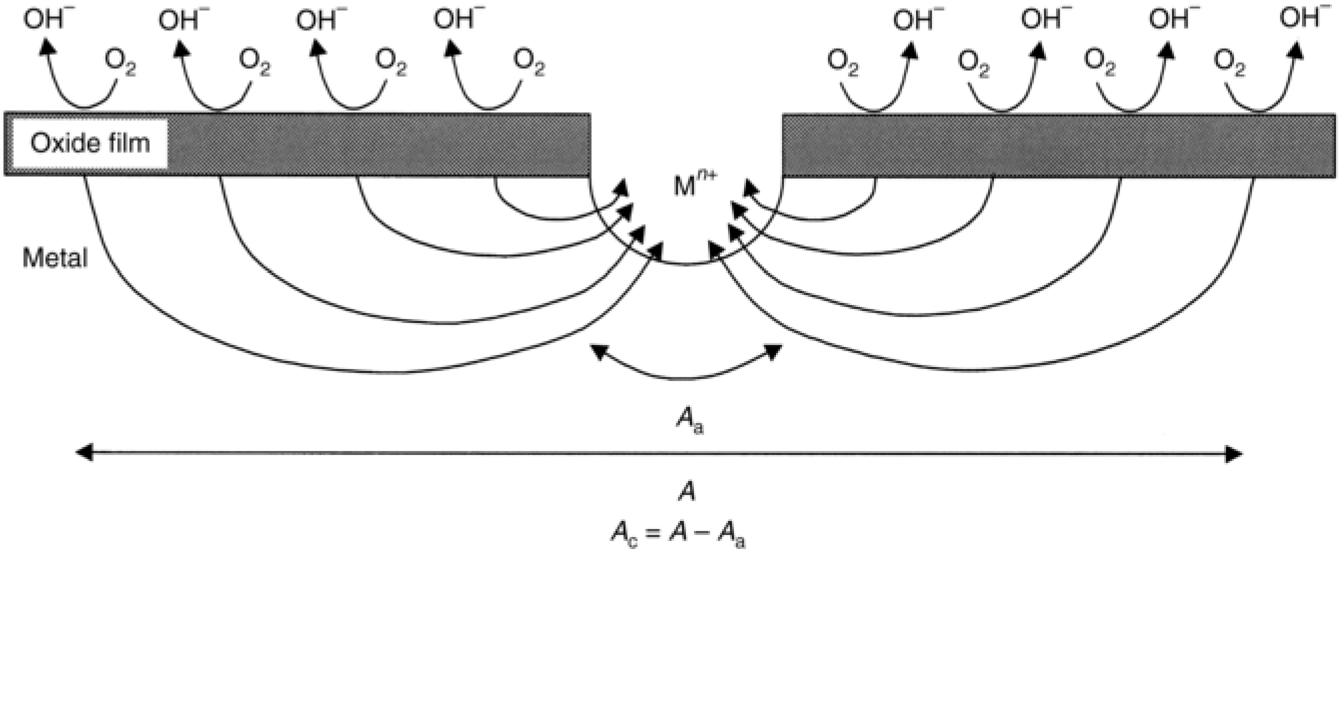

Fig. 3 A small anode/large cathode situation that can exist at a local corrosion site. A_a and A_c are the available anode and cathode areas; M^{n+} is the corrosion product

Thus, it is clear that aqueous corrosion is a complicated process that can occur in a wide variety of forms and is affected by many chemical, electrochemical, and metallurgical variables, including:

- The composition and metallurgical properties of the metal or alloy
- The chemical composition and physical properties of the environment, such as temperature and conductivity
- The presence or absence of surface films
- The properties of the surface films, such as resistivity, thickness, nature of defects, and coherence

---

D.W. Shoesmith, Kinetics of Aqueous Corrosion, *Corrosion: Fundamentals, Testing, and Protection*, Vol 13A, *ASM Handbook*, ASM International, 2003, p 42–51

Kinetics of Aqueous Corrosion

D.W. Shoesmith, University of Western Ontario

Thermodynamic Basis for Corrosion

The thermodynamic feasibility of a particular corrosion reaction is determined by the relative values of the equilibrium potentials, E_e, of the electrochemical reactions involved. These potentials can be determined from the Nernst equation, which, for the two half-reactions, Eq 1 and Eq 2, can be written:

$$(E_e)_{M/M^{n+}} = (E^0)_{M/M^{n+}} + 2.303\frac{RT}{nF}\log\{a_{M^{n+}}\} \quad \text{(Eq 13)}$$

where the activity of the solid, M, is taken as 1, and:

$$(E_e)_{Ox/Red} = (E^0)_{Ox/Red} - 2.303\frac{RT}{nF}\log\left\{\frac{a_{Red}}{a_{Ox}}\right\} \quad \text{(Eq 14)}$$

to yield for the overall corrosion reaction:

$$E_e = \Delta E^0 - \frac{2.303RT\log}{nF}\left\{\frac{a_{M^{n+}}a_{Red}}{a_{Ox}a_M}\right\} \quad \text{(Eq 15)}$$

where ΔE^0 is the difference in standard potentials for the anodic (Eq 1) and cathodic (Eq 2) reactions (available from a table of standard potentials), R is the gas constant equal to 8.314 J/ mol · K, T is absolute temperature, n and F are as defined in Eq 8, and a_i represents the activities of the various species involved. Because the activity of a solid is 1, a_M is eliminated from Eq 15, and it is more common to write the equation in terms of concentration (c):

$$E_e = \Delta E^0 - 2.303\frac{RT\log}{nF}\left\{\frac{c_{M^{n+}}c_{Red}}{c_{Ox}}\right\} \quad \text{(Eq 16)}$$

The thermodynamics of a particular metal- aqueous system can be summarized in a potential-pH, or Pourbaix diagram, as described elsewhere in this Volume. The key feature in determining whether or not a particular corrosion reaction can proceed is the difference in equilibrium potentials (E_e) for the two component electrochemical half-reactions, as illustrated in Fig. 4. That is:

$$(E_e)_{M/M^{n+}} < (E_e)_{Ox/Red} \quad \text{(Eq 17)}$$

Thus, the thermodynamic driving force (ΔE_{therm}) for corrosion is given by:

$$\Delta E_{therm} = (E_e)_{Ox/Red} - (E_e)_{M/M^{n+}} \quad \text{(Eq 18)}$$

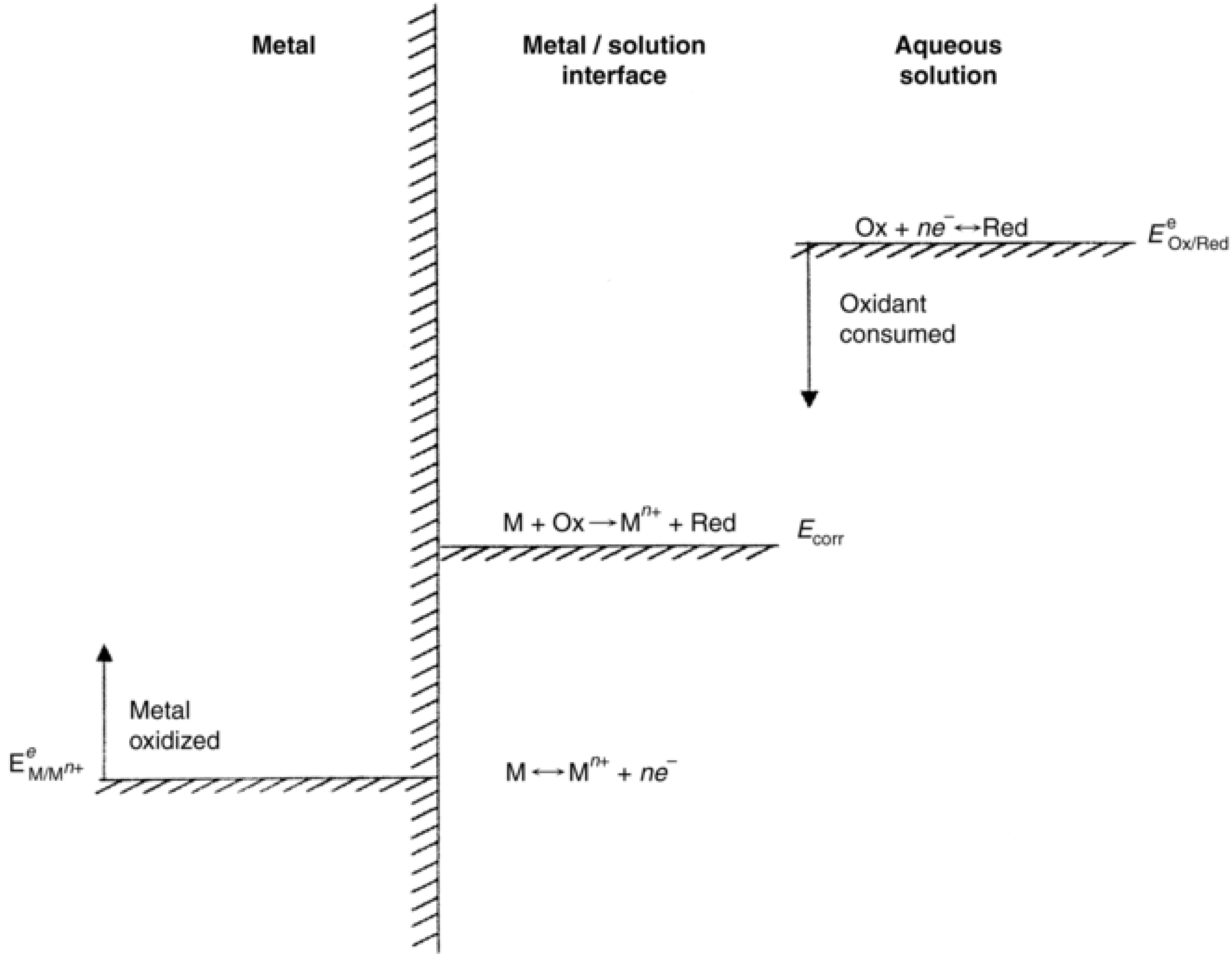

Fig. 4 The thermodynamic driving force for corrosion across a metal/aqueous solution interface in the presence of a soluble oxidant, Ox. The values of the equilibrium potentials are shown schematically.

It is possible that this driving force could increase or decrease with time if either the concentration of available oxidant, c_{Ox}, or the concentration of soluble corrosion product, $c_{M^{n+}}$, change with time, as illustrated in Fig. 4 and discernible by inspection of Eq 16. However, the most important questions for the corrosion engineer are: How fast does the corrosion reaction occur, and can it be prevented or at least slowed to an acceptable rate? To answer these questions and to determine a course of action, it is essential to have some knowledge of the steps involved in the overall corrosion process.

D.W. Shoesmith, Kinetics of Aqueous Corrosion, *Corrosion: Fundamentals, Testing, and Protection*, Vol 13A, *ASM Handbook*, ASM International, 2003, p 42–51

Kinetics of Aqueous Corrosion

D.W. Shoesmith, University of Western Ontario

Kinetics of Aqueous Corrosion Processes

The overall process can be controlled by any one or combination of several reactions depicted in Fig. 5. The interfacial kinetics of either the anodic (step 1) or cathodic (step 2) reactions could be rate controlling. Alternatively, if these reactions are fast and the concentration of cathodic reagent (c_{Ox}) is low, then the rate of transport of the oxidant (Ox) to the cathodic site (step 3 → 2) could be rate limiting. This situation is quite common for corrosion driven by dissolved oxygen that has limited solubility. If the metal dissolution reaction (step 1) is reversible, that is, the reverse metal deposition ($M^{n+} + ne^- \rightarrow M$) can also occur, then the rate of transport of M^{n+} away from the anodic site (step 4) could be rate determining.

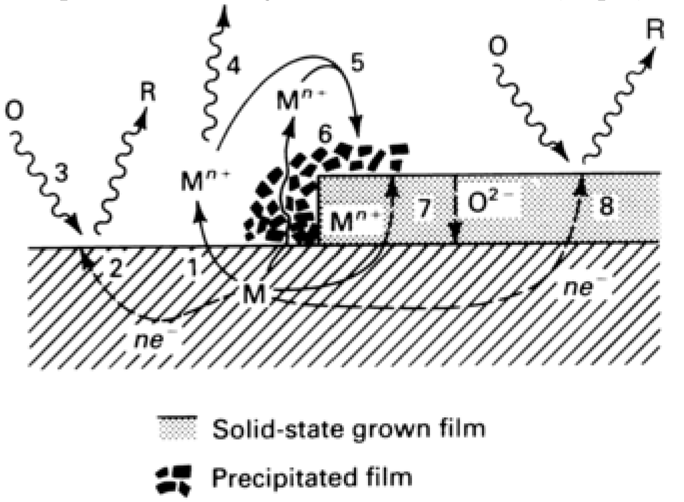

Fig. 5 Various possible reaction steps on a corroding metal surface. Reactions 1 to 8 are defined in the text.

The presence of corrosion films can add many additional complications. If the anodic reaction (step 1) is fast and the transport step (step 4) is slow, then local supersaturation with dissolved corrosion product at the corroding surface:

$$\left(c_{M^{n+}}\right) > \left(c_{M^{n+}}\right)_{sat} \quad \text{(Eq 19)}$$

could lead to the deposition of corrosion product deposits such as oxides, hydroxides, or metal salts. These deposition processes could be accelerated or prevented by local pH changes due to the cathodic reaction (Eq 3) or metal cation hydrolysis equilibria:

$$M^{n+} + yOH^- \leftrightarrow M\left(OH\right)_y^{(n-y)^-} + 2yH^+ \quad \text{(Eq 20)}$$

The local situation at the corroding surface becomes complicated, and the primary parameter governing whether or not corrosion product deposits form, aside from the balance between interfacial kinetics and solution transport, is the deposit solubility and how it varies with pH (Fig. 6). As shown, the solubility tends to be at a minimum at approximately neutral pH and to increase at high and, especially, low pH. At high pH, solubility is increased by the stabilization of hydrolyzed metal cations (i.e., the equilibrium the reaction in Eq 20 is pushed to the right), whereas in acidic solutions, the oxide/hydroxide is destabilized by the increased proton concentration (i.e., the equilibrium in Eq 20 is pushed to the left). This is a very simplified description of oxide/hydroxide solubility, and the reader is referred to Ref. 5 for a more detailed discussion.

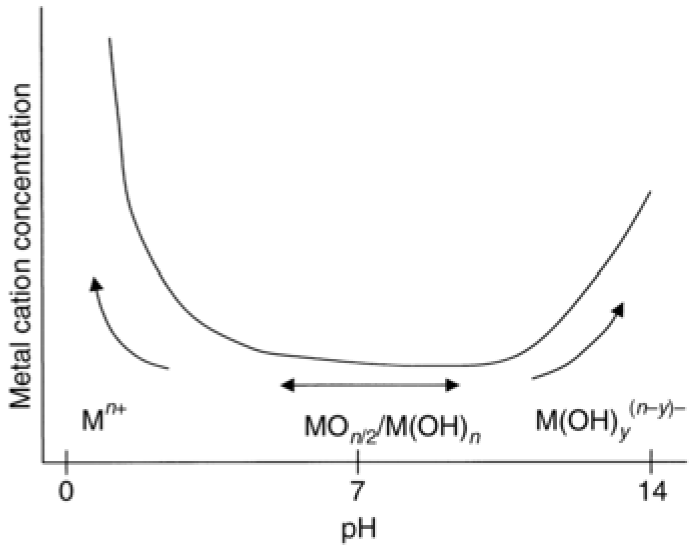

Fig. 6 Solubility of a metal cation as a function of solution pH

Precipitation reactions of this type are likely to produce porous deposits, and corrosion could then become controlled by the transport of M^{n+} or Ox (step 6 in Fig. 5) through these porous deposits. By contrast, when coherent, nonporous oxide films (passive films) form spontaneously on the metal surface by solid state as opposed to precipitation reactions, then ionic or defect transport processes through the oxide (step 7 in Fig. 5) would ensure extremely low corrosion rates. This represents the condition of passivity. The presence of defects in the passive film in the form of pores, grain boundaries, or fractures can lead to localized corrosion. Finally, it is possible for the corrosion process to be controlled by the electronic conductivity of passive films (step 8 in Fig. 5) when the cathodic reaction occurs on the surface of the film. Using this range of possibilities, the remainder of this article discusses some of these processes and the laws that govern them.

Reference cited in this section

5. C.F. Baes and R.E. Mesmer, *The Hydrolysis of Cations,* John Wiley and Sons, 1976.

D.W. Shoesmith, Kinetics of Aqueous Corrosion, *Corrosion: Fundamentals, Testing, and Protection*, Vol 13A, *ASM Handbook*, ASM International, 2003, p 42–51

Kinetics of Aqueous Corrosion

D.W. Shoesmith, University of Western Ontario

Activation Control of Corrosion

Activation control is the term used to describe control of the corrosion process by the electrochemical half-reactions (Eq 1, 2) and step 1 and 2 in Fig. 5 The overall anodic reaction is the transfer of a metal atom from the metal surface to the aqueous solution as the cation M^{n+} or as some hydrolyzed $\left(M(OH)_y^{(ny)+}\right)$ or anion-complexed $\left(MA_y^{(nyx)+}\right)$ form, where complexation is with the anion A^{x-}:

$$M_{surface} \rightarrow M^{+}_{surface} \rightarrow M^{n+}_{surface} \rightarrow M^{n+}_{solution} \quad \text{(Eq 21)}$$

As indicated in Eq 21, various surface intermediates may be involved in the overall anodic dissolution process, although these intermediates may only be detectable in a detailed electrochemical investigation. Thus, the

simplest proposed mechanism for the anodic dissolution of iron under acidic conditions proceeds via the following steps:

$Fe + H_2O \leftrightarrow Fe(OH)_{ads} + H^+ + e$ (Eq 22)

$Fe(OH)_{ads} \leftrightarrow FeOH^+ + e^-$ (Eq 23)

$FeOH^+ + H^+ \leftrightarrow Fe^{2+} + H_2O$ (Eq 24)

Similarly, the cathodic reaction, for example, O_2 reduction, proceeds via a sequence of reaction steps involving intermediates such as hydrogen peroxide:

$O_2 + 2H^+ + 2e^- \rightarrow H_2O_2$ (Eq 25)

$H_2O_2 + 2H^+ + 2e^- \rightarrow 2H_2O$ (Eq 26)

Either the anodic or cathodic reaction can control the overall rate of the corrosion reaction. Electrochemical methods (Ref 6) can be used to disturb these reactions from their equilibrium potentials and hence to determine the relationship between current and potential. An example of the form of this relationship, demonstrating a metal dissolution/deposition reaction, is shown in Fig. 7. This curve follows the Butler-Volmer equation:

$$I = I_0 \left\{ \exp\left(\frac{\alpha F}{RT} \eta \right) - \exp(1-\alpha) \frac{F}{RT} \eta \right\} \quad \text{(Eq 27)}$$

where I is the current; I_0 is the exchange current; F is the Faraday constant; R is the gas constant; T the absolute temperature; and α is the transfer or symmetry coefficient, generally taken to be 0.5. The term η is the overpotential, defined by:

$$\eta = E - (E_e)_{M/M^{n+}} \quad \text{(Eq 28)}$$

where E is the experimentally applied potential, and E_e is given by the Nernst equation (Eq 16), with $\Delta E^0 = E^0_{M/M^{n+}}$. The overpotential is a measure of how far the reaction is from equilibrium.

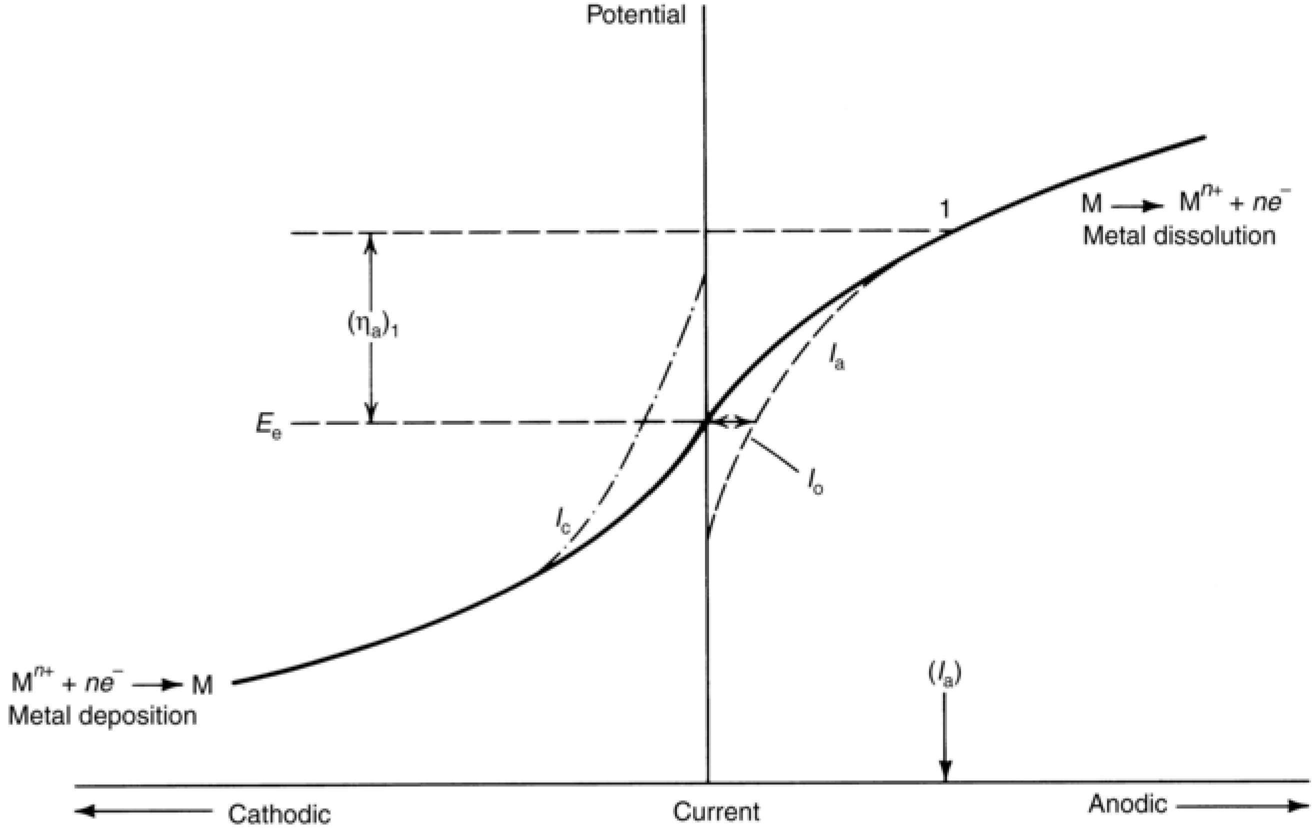

Fig. 7 Current-potential (Butler-Volmer) relationship for a metal dissolution/deposition reaction. The solid line shows the measurable current; the dashed lines (I_a, I_c) show the partial dissolution/deposition

currents; I_o is the exchange current at E_e; (η_a) is the anodic overpotential that would exist if the potential were held at point 1.

At equilibrium (η = 0; $E = E_e$), no measurable current flows, but the equilibrium is dynamic, with the rate of metal dissolution ($M \rightarrow M^{n+} + ne^-$) ($I_a$) equal to the rate of metal cation deposition ($M^{n+} + ne^- \rightarrow M$) ($-I_c$):

$$I_a = -I_c = I_o \quad \text{(Eq 29)}$$

where I_o is termed the exchange current for this electrochemical reaction. The exchange current is the equivalent of an electrochemical rate constant and is therefore a direct measure of the kinetics of the reaction. The dynamic nature of the reaction at $E = E_e$ can be appreciated by consideration of the partial anodic and cathodic currents, plotted as dashed lines in Fig. 7. If the potential is made more positive than the equilibrium potential, then $I_a > |I_c|$ (i.e., the first exponential term in Eq 27 increases in value, and the second one decreases), and the metal dissolution reaction will proceed. Similarly, if E is made more negative than the equilibrium potential, $I_a > |I_c|$, then metal cation deposition proceeds. Over a short potential range, the two reactions oppose each other, but for sufficiently large overpotentials (η_a, anodic; or η_c, cathodic), one reaction occurs at a negligible rate; that is, one or the other of the exponential terms in the Butler-Volmer equation (Eq 27) becomes negligible. In this condition, the overpotential is in the Tafel region (as indicated by point 1 in Fig. 7), and for this positive polarization, the metal dissolution current is given by:

$$I_a = I_o \exp\left\{\frac{\alpha F}{RT}\eta_a\right\} \quad \text{(Eq 30)}$$

or

$$\log I_a = \log I_o + 2.303\frac{\alpha F}{RT}\eta_a \quad \text{(Eq 31)}$$

and a plot of log I_a versus η_a will yield an intercept from which I_o can be obtained and will have a slope with a Tafel coefficient, β_a, given by:

$$\beta_a = 2.303\frac{RT}{\alpha F} \quad \text{(Eq 32)}$$

A similar procedure could be applied for a sufficiently large cathodic overpotential (η_c) to yield an equal value of I_o as well as a value for the cathodic Tafel coefficient, β_c. The values of β_a and β_c contain much information on the mechanism of the dissolution/deposition reaction steps but are commonly used as empirical coefficients in corrosion engineering studies. A similar analysis could be performed for a potential cathodic reaction (Eq 2), and Fig. 8 shows the two current-potential curves on the same plot.

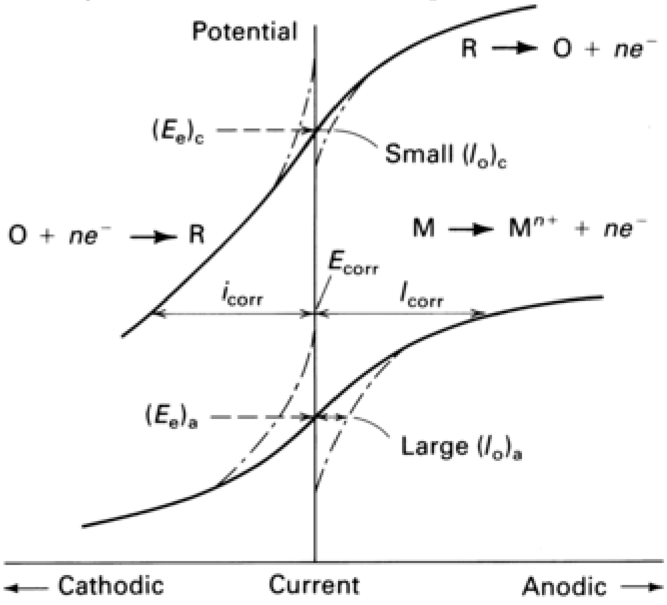

Fig. 8 Current-potential relationships for a metal dissolution/deposition process ($M \leftrightarrow M^{n+} + e^-$) and an oxidant/reductant reaction ($O + ne^- \leftrightarrow R$) showing the coupling together of the anodic component of one

reaction to the cathodic component of the other to yield a corrosion reaction proceeding at the corrosion potential, E_{corr}

The establishment of a corrosion reaction involves the coupling together of the anodic half of one reaction to the cathodic half of another. Which reaction provides which half is determined by the relative values of the equilibrium potentials, that is, condition (Eq 17), as illustrated in Fig. 4. This coupling of half-reactions produces an equation relating the measured current to the corrosion current, which is similar in form to the Butler-Volmer equation (Eq 27):

$$i = i_{corr}\left\{\exp\left(\frac{\alpha_a F\eta}{RT}\right) - \exp\left(\frac{-\alpha_c F\eta}{RT}\right)\right\} \quad \text{(Eq 33)}$$

where i and i_{corr} represent current densities (current/surface area), $\alpha_a \neq \alpha_c$, and there is no reason why $\alpha_a + \alpha_c = 1$, as was the case with the Butler-Volmer equation. Note: From this point on, current densities (i) rather than currents (I) will be used.

Because this coupling of half-reactions produces a short-circuited corrosion reaction on the surface of the metal, the anodic current due to metal dissolution must be equal and opposite in sign to the cathodic current due to oxidant reduction:

$$i_a = -i_c = i_{corr} \quad \text{(Eq 34)}$$

where i_a is given by the first term in Eq 33 and i_c by the second. This coupling together to produce equal anodic and cathodic currents can only occur at a single potential, designated the corrosion potential, E_{corr}, which must lie between the two equilibrium potentials (Fig. 8), thus satisfying the condition in Eq 15:

$$(E_e)_a < E_{corr} < (E_e)_c \quad \text{(Eq 35)}$$

where $(E_e)_a$ is equivalent to $(E_e)_{M/M^{n+}}$ and $(E_e)_c$ to $(E_e)_{Ox/Red}$.

The metal dissolution (anodic) reaction is driven by an anodic activation overpotential:

$$\eta_a^A = E_{corr} - (E_e)_a \quad \text{(Eq 36)}$$

and the oxidant reduction (cathodic) reaction by a cathodic activation overpotential:

$$\eta_c^A = E_{corr} - (E_e)_c \quad \text{(Eq 37)}$$

Obviously, from Eq 18:

$$\Delta E = \eta_a^A + |\eta_c^A| \quad \text{(Eq 38)}$$

Two additional observations can be made with regard to Fig. 8. First, ΔE is sufficiently large that E_{corr} is in the Tafel regions for both the anodic and cathodic half-reaction. This is not necessarily always the case, as discussed subsequently. Second, the two current-potential curves are not necessarily symmetrical and seldom have an identical shape. The shape and symmetry of the curves are determined by the differences in i_o for the coupled anodic and cathodic reactions and the values of the Tafel coefficients, β_a and β_c. In Fig. 8, the metal dissolution/deposition reaction is shown to have a larger i_o than the oxidant/reductant reaction, and the anodic and cathodic branches are shown close to symmetrical (i.e., $\beta_a \sim \beta_c$). The consequence of the large i_o is that the current-potential curve is steep, and only small values of η_a^A are required to achieve large currents. By contrast, the current-potential relationship for the cathodic reaction is shallow, because i_o is small, and the anodic and cathodic branches are not symmetrical (i.e., $\beta_a \neq \beta_c$).

Because both reactions are occurring on different sites on the same surface,Fig. 1, i_{corr} cannot be measured by coupling the metal to an ammeter. However, E_{corr} can be measured against a suitable reference electrode by using a voltmeter with an input impedance high enough to draw insignificant current in the measuring circuit. Figure 8 shows that the value of E_{corr} is determined by the shape of the current-potential relationships for the two reactions; that is, it is a parameter with kinetic but not thermodynamic significance. Because its value is determined by the properties of more than one reaction, the corrosion potential is often termed a mixed potential.

In the literature, diagrams such as the one in Fig. 8 are often plotted in the form log i versus E, and the algebraic sign of the cathodic current is neglected, so that the anodic and cathodic currents can be plotted in the same quadrant (Fig. 9). Such diagrams are termed Evans diagrams. The two linear portions in an Evans diagram are

the Tafel regions, with slopes given by Eq 30 and the equivalent plot for the cathodic reaction. Sometimes, the nonlinearity close to the equilibrium potentials is ignored, and the curves are plotted as totally linear. This approximation acknowledges that, commonly, the two i_o values are orders of magnitude lower than i_{corr} and therefore have a negligible effect on the scale of the Evans diagram. It should be noted that the currents plotted in an Evans diagram are the partial currents for the anodic and cathodic reactions, and that the measurable current is the sum of these two partial currents (taking into account that they are opposite in sign). The value of such diagrams is in their use to illustrate the influence of various parameters on the corrosion process.

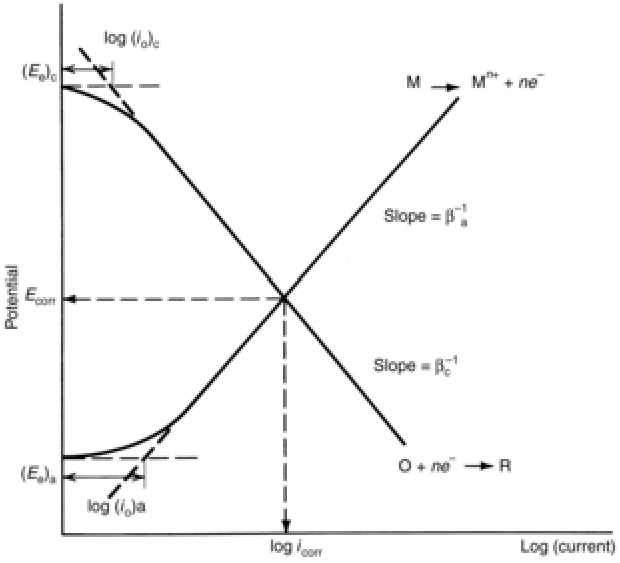

Fig. 9 The current-potential relationships of Fig. 8 plotted in the form of an Evans diagram. Note: The solid lines are partial anodic and cathodic currents, not measurable currents.

Figure 10(a) shows an Evans diagram for the same anodic dissolution process coupled to two different cathodic reactions. Recalling the definition of ΔE_{therm} from Eq 18, the following can be written:

$$\Delta E'_{therm} < \Delta E''_{therm} \quad \text{(Eq 39)}$$

leading to:

$$i'_{corr} < i''_{corr} \quad \text{(Eq 40)}$$

that is, the bigger the difference in equilibrium potentials, the larger the corrosion current. The anodic activation overpotential for the first reaction ($\eta_a^A = E_{corr} - (E_e)_a$) is less than that for the second:

$$\left(\eta_a^A\right)'' > \left(\eta_a^A\right)' \quad \text{(Eq 41)}$$

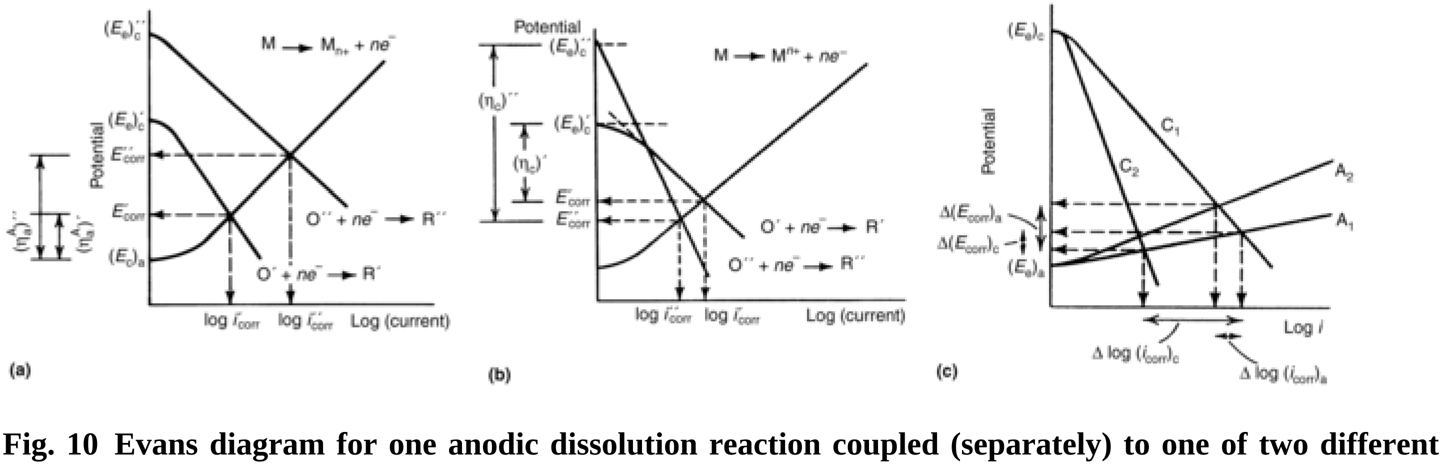

Fig. 10 Evans diagram for one anodic dissolution reaction coupled (separately) to one of two different oxidant reduction reactions. (a) The two oxidant reduction reactions have similar kinetic characteristics (i.e., similar current-potential shapes). (b) The two oxidant reduction reactions have very different kinetic characteristics (i.e., very different current-potential shapes). (c) An anodic dissolution reaction

with a large $(i_{corr})_a$ coupled to an oxidant reduction reaction with a small $(i_{corr})_c$. The currents labeled C_1 and C_2 show the effect on log (i_{corr}) and E_{corr} of changing the concentration of available oxidant.

The value of ΔE_{therm} is not the only parameter controlling the corrosion rate. Figure 10(b) shows the same situation as in Fig. 10(a) , except that the two cathodic reactions possess very different polarization characteristics (i.e., relationships between current and potential). Despite the fact that $(E_e)_c > (E_e)'_c$, the activation overpotential $(\eta_a^A) < (\eta_a^A)'$, and the corrosion couple with the largest thermodynamic driving force produces the lowest corrosion current. Inspection of Fig. 10(b) shows this can be attributed to the differences in exchange currents, i_o, and slopes, hence different Tafel coefficients, β_c, for the two cathodic reactions. This situation is common for active metals in acidic or neutral aerated solutions. Even though the thermodynamic driving force for corrosion is greater in neutral solutions containing dissolved oxygen, corrosion proceeds more rapidly in deaerated acidic solutions. This is due to the slowness of the kinetics for oxygen reduction and can be appreciated by comparing the kinetic characteristics for the two processes on iron. Thus, $(i_o)_{H^+/H_2} = 10^{-3}$ to 10^{-2} A/m^2, and $(\beta_c)_{H^+/H_2} \cong 120$ mV/decade. By comparison, $(i_o)_{O_2/H_2O} \cong 10^{-10}$ A/m^2, and $(\beta_c)_{O_2/H_2O} > 120$ mV/decade.

Rate Control by the Anodic or Cathodic Reaction. The overall rate of corrosion will be controlled by the kinetically slowest reaction, that is, the one with the smallest exchange current and/or largest Tafel coefficient. This can be appreciated from Fig. 10(c) in which $(i_o)_a > (i_o)_c$ and $\beta_a < \beta_c$. This leads to a large difference in activation overpotentials, with:

$$\eta_a^A \ll \eta_a^C \qquad \text{(Eq 42)}$$

This means the cathodic reaction is strongly polarized and must be driven significantly to achieve the corrosion current. By contrast, the anodic reaction remains close to equilibrium, requiring only a small overpotential (anodic) to achieve the same corrosion current.

Under these conditions, the corrosion potential, E_{corr}, lies close to the equilibrium potential for the kinetically fastest reaction. If the cathodic reaction was the fastest, then $E_{corr} \rightarrow (E_e)_C$, and the anodic metal dissolution reaction would be rate controlling. If the kinetics of the two half- reactions were similar (i.e., $(i_o)_a \cong (i_o)_c$ and $\beta_a \cong \beta_c$), then E_{corr} would be approximately equidistant between the two equilibrium potentials, and the corrosion reaction would be under mixed anodic/cathodic control. This is the situation illustrated in Fig. 9. The corrosion of iron in aerated neutral solution can be used to illustrate the point. For the metal dissolution reaction, $(i_o)_{Fe/Fe^{2+}} \cong 10^{-4}$ to 10^{-5} A/m^2 and $(\beta_a)_{Fe/Fe^{2+}} \cong 50$ to 80 mV/decade, whereas for O_2 reduction, $(i_o)_{O_2/H_2O} \cong 10^{-10}$ A/m^2 and $(\beta_c)_{O_2/H_2O} > 120$ mV/decade. Consequently, O_2 reduction should be rate controlling, and E_{corr} would lie close to the equilibrium potential for iron dissolution.

Figure 10(c) also shows the effects of changing the kinetics of the two reactions. Such changes could be caused by increasing the available concentration of cathodic reagent or by increasing the surface area of available metal. Changing the reagent concentration would also lead to a change in $(E_e)_c$, but this is ignored in Fig. 10(c) for the sake of clarity. Changes in the kinetics of the fast anodic reaction are reflected in changes in the value of E_{corr} ($\Delta(E_{corr})_a$ large) but have little effect on i_{corr} ($\Delta\log(i_{corr})_a$ small). However, changes in the kinetics of the slow cathodic reaction have little effect on E_{corr} ($\Delta(E_{corr})_c$ small) but a significant influence on i_{corr} ($\Delta\log(i_{corr})_c$ large). Thus, in this example, the cathodic reaction is the rate-controlling reaction, and the anodic reaction is said to be potential determining. Such changes in E_{corr} can sometimes be used as diagnostic tests for ascertaining the rate-determining step, and the maximum benefit in slowing corrosion can be gained by attending to the rate-determining step. Additionally, a measurement of E_{corr} and its evolution with time provides a simple but only qualitative way of tracking the evolution of a corrosion process with time.

Reference cited in this section

6. A.J. Bard and L.R. Faulkner, *Electrochemical Methods: Fundamentals and Applications*, 2nd ed., John Wiley and Sons, 2001.

D.W. Shoesmith, Kinetics of Aqueous Corrosion, *Corrosion: Fundamentals, Testing, and Protection*, Vol 13A, *ASM Handbook*, ASM International, 2003, p 42–51

Kinetics of Aqueous Corrosion

D.W. Shoesmith, University of Western Ontario

Mass Transport Control

The relationships between current and potential described previously are valid when the overall corrosion process is under activation control, that is, controlled by the interfacial rate of one or the other of the half-reactions (step 1 or 2 in Fig. 5). However, if the cathodic reagent at the corrosion site is in short supply, then mass transport of this reagent could become rate controlling (Eq 3, Fig. 5). Under these conditions, the cathodic charge-transfer process is fast enough to reduce the concentration of the cathodic reagent at the corrosion site to a value less than that in the bulk solution. Because the rate of the cathodic reaction is proportional to the surface concentration of reagent, the reaction rate will be limited (polarized) by this drop in concentration. For a sufficiently fast charge transfer, the surface concentration will fall to 0, and the corrosion process will be totally controlled by flux of oxidant to the corroding surface. In the case of one-dimensional transport, this flux (J) can be calculated from the solution of Fick's first law:

$$J = -D\left(\frac{\partial c_{Ox}}{\partial x}\right)_{x=0} \quad \text{(Eq 43)}$$

at the corroding site ($x = 0$), where D is the diffusion coefficient, and c_O is the reagent concentration at point x. Diffusion gradients evolve with time, according to Fick's second law:

$$\frac{\partial c_O}{\partial t} = D\left(\frac{\partial^2 c}{\partial x^2}\right)_{x,t} \quad \text{(Eq 44)}$$

and, for non-steady-state conditions (i.e., $\partial c/\partial x$ at x varies with time), conditions are complicated.

General corrosion processes, however, generally occur under steady-state conditions, because convective flow of the environment occurs (e.g., flow down a pipe). For this situation, a simple analysis can be achieved by linearizing the concentration-distance profile according to the Nernst diffusion layer treatment (Fig. 11). This linearization yields a demarcation line at a distance, δ, from the surface such that, for $x > \delta$, the bulk concentration is maintained by convection. For $x < \delta$, the oxidant is assumed to be transported to the surface by diffusion only. This solution layer is termed the diffusion layer, and its thickness is determined by the local geometry at the site and the solution velocity (degree of convection). Of course, this is an approximation, because the transition from convective flow to diffusive transport is more gradual and not so strictly demarcated.

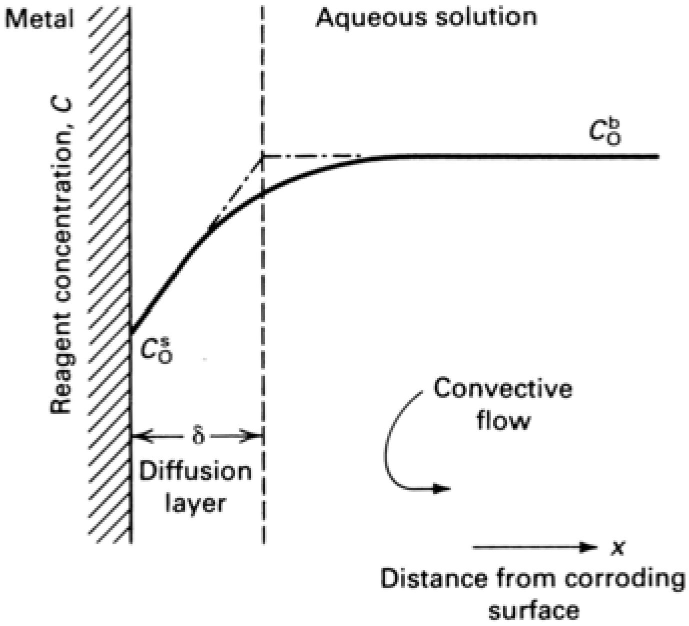

Fig. 11 Illustration showing the concentration-distance profile for oxidant O involved in a corrosion process with a metal in which the overall process is partially controlled by convective-diffusive transport of the oxidant to the corroding surface. The dashed-dotted lines show the concentration profile assumed in the Nernst diffusion layer treatment.

Using this simplified treatment, Eq 43 can be written:

$$J = -\frac{D}{\delta}\left(c_{Ox}^{s} - c_{Ox}^{b}\right) \qquad \text{(Eq 45)}$$

where c_{Ox}^{s} is the oxidant concentration at the corroding surface (x = 0), and c_{O}^{b} is the concentration for $x \geq \delta$. For steady-state conditions, all the oxidant transported down the concentration gradient to the corroding surface must react electrochemically. If it did not, then the concentration at the corroding surface would adjust until it did.

This condition of mass balance means that the cathodic current (expressed in A/cm^2) must be directly proportional to the flux (expressed in mol/cm^2/s). The proportionality constant is given by Faraday's law (Eq 8) and can be written:

$$i_{corr} = i_c = -\frac{nFD_O}{\delta}\left(c_{Ox}^{s} - c_{Ox}^{b}\right) \qquad \text{(Eq 46)}$$

The corrosion current is equal to the cathodic current, because the overall corrosion reaction is controlled by the transport of oxidant to the surface; that is, corrosion can only progress at the rate that oxidant becomes available. Under limiting conditions, $c_{O}^{s} \rightarrow 0$, and a maximum transport-controlled corrosion current is obtained:

$$\left(i_c\right)_{lim} = \left(i_{corr}\right)_{max} = \frac{nFD_{Ox}}{\delta} c_{Ox}^{b} \qquad \text{(Eq 47)}$$

When corrosion is occurring at this limiting rate, the rate can only be increased or decreased by varying either the bulk concentration of oxidant, c_{Ox}^{b}, or the thickness of the diffusion layer, δ.

This limitation on corrosion rate is termed concentration polarization and is illustrated in the Evans diagram in Fig. 12. For a small shift of the potential away from the equilibrium potential (point 1), $c_{Ox}^{s} = c_{Ox}^{b}$, and there is no limitation on reagent supply. The current remains in the Tafel region; that is, charge transfer is still rate controlling, and the overpotential is purely an activation overpotential (η_c^A). For a larger shift of potential from $(E_e)_c$, $c_{Ox}^{s} < c_{Ox}^{b}$ (point 2), and the current is less than expected on the basis of activation control; that is, the current follows the solid line as opposed to the dashed-dotted line. Under these conditions, the current is partly

activation and partly transport controlled, and the total overpotential (η_T) is the sum of an activation (η^A) and a concentration (η^C) overpotential:

$$\eta_T = \eta^A + \eta^C \qquad \text{(Eq 48)}$$

For a sufficiently large polarization from equilibrium, $C^s_{Ox} \rightarrow 0$, the current becomes independent of potential, and the cathodic current is now at the maximum given by Eq 47.

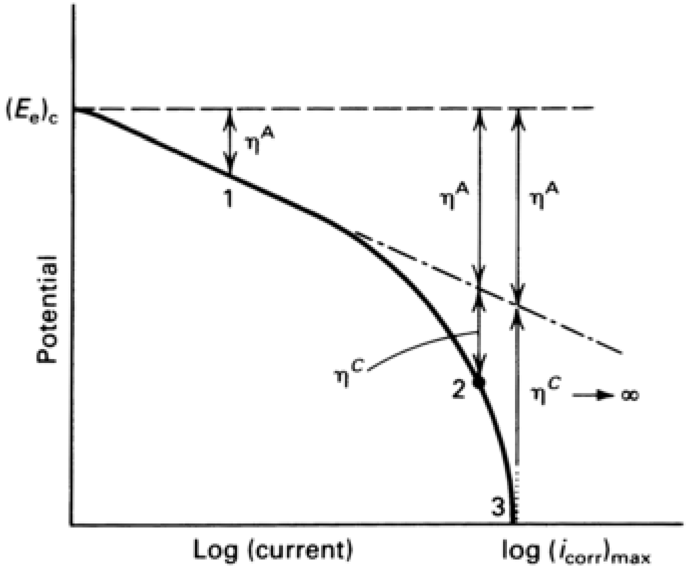

Fig. 12 Partial Evans diagram (i.e., showing only the partial current for the oxidant reduction reaction) for mixed activation-concentration polarization

The effect of a number of corrosion parameters for a corrosion process proceeding under various degrees of activation/mass transport control can be assessed using an Evans diagram, as shown in Fig. 13. Three situations are considered. For cathodic curve 1, corrosion occurs with the anodic reaction totally activation controlled ($\eta^T_a = \eta^A_a$) and the cathodic reaction totally mass transport controlled ($\eta^T_c = \eta^C_c$), that is, $C^s_{Ox} = 0$. If the solution is now made to flow, the thickness of the diffusion layer (δ) will decrease, $(i_c)_{lim}$ (Eq 47) will increase and hence so will the corrosion current. The figure shows that E_{corr} shifts to a more positive value, and:

$$\eta^T_c = (E_e)_c - E_{corr} = \eta^A_c + \eta^C_c \qquad \text{(Eq 49)}$$

decreases due to a decrease in η^C_c. For more vigorous stirring, η^C_c reaches 0, because the flux of oxidant to the corroding surface is now sufficiently large to maintain $C^s_{Ox} = C^b_{Ox}$. Again, E_{corr} shifts to a more positive value to reflect this decrease in η^T_c because $\eta^C_c = 0$. The cathodic reaction is now fully activation controlled ($\eta^T_c = \eta^A_c$), and further increases in fluid velocity will not affect the corrosion rate. Such changes in E_{corr} and i_{corr} with the degree of convection can be used to indicate whether mass transport control is operative. If the anodic, as opposed to the cathodic, reaction was mass transport controlled, then a similar analysis would apply, but E_{corr} would shift to more negative values with increasing degree of convection.

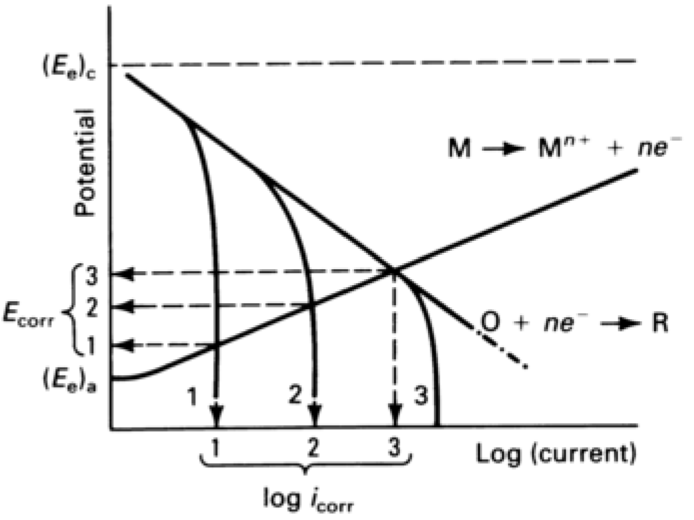

Fig. 13 Evans diagram showing the influence on E_{corr} and log (i_{corr}) of changing the transport rate of oxidant O to the corroding surface

More generally, the term D_O/δ is termed the mass transport coefficient (m_c), and Eq 46 is written in the form:

$$\frac{i_{corr}}{nF} = m_c\left(c^b_{Ox} - c^s_{Ox}\right) \quad \text{(Eq 50)}$$

An equation for the corrosion rate under activation control can also be written in the simplified form:

$$\frac{i_{corr}}{nF} = k_c c^s_{Ox} \quad \text{(Eq 51)}$$

where k_c can be considered a potential-dependent rate constant for the cathodic reaction.

Equation 51 could be considered a restatement of the Butler-Volmer equation, and the reader is referred to standard electrochemical text books for more detailed descriptions (Ref 6). Combining Eq 50 and 51 and eliminating c^s_{Ox} yields:

$$i_{corr} = nFc^b_{Ox}\left\{\frac{m_c k_c}{(m_c + k_c)}\right\} \quad \text{(Eq 52)}$$

where k_c can be considered the activation control parameter and m_c the mass transport control parameter.

Whether activation or mass transport kinetics determine the corrosion rate is straight forwardly appreciated by considering the relative values of m_c and k_c in Eq 52. For $m_c \gg k_c$, the bracketed term reduces to k_c, and the corrosion current is activation controlled. For $m_c \ll k_c$, the term reduces to m_c, and corrosion would be mass transport controlled.

While Eq 52 may define the relative importance of activation and mass transport control, it does not contain any information on the factors that control mass transport and hence determine the value of m_c. The dependence of m_c on solution flow rate can be determined experimentally, and its form varies, depending on the geometry of the system. In general, this dependence takes the form:

$$i_{corr} \propto f^n \quad \text{(Eq 53)}$$

where f is the flow rate, and n is a constant that depends primarily on the geometry of the system. For flow over a flat plate, n is 0.33 for laminar flow (smooth, $Re < 2200$), where Re is the Reynold's number (defined subsequently).

The variation of m_c depends not only on flow rate but also on properties such as the kinematic viscosity of the fluid (ν), the diffusion coefficient of the species (D), as well as the geometry of the system. These effects can be specified using dimensionless parameters such as the Reynold's; Re; and Schmidt, Sc, numbers given by:

$$Re = f\frac{L}{\nu} \quad \text{(Eq 54)}$$

$$Sc = \frac{\nu}{D} \quad \text{(Eq 55)}$$

The Reynolds number is a measure of the ratio of convective to viscous forces in the fluid, and, for laminar flow down a pipe, L is a characteristic length. The Schmidt number quantifies the relationship between hydrodynamic and diffusion boundary layers at the corroding surface. Thus, it can be shown that for flow over a smooth, flat, corroding surface:

$$(i_{corr})_{max} = 0.62nFD_O c_O^b (Re)^{\alpha} (Sc)^{\beta} \quad \text{(Eq 56)}$$

where α and β are numerical constants that depend on the geometry of the system and the convective flow conditions.

Smooth, laminar flow can only be achieved up to a certain Reynold's number or flow rate, *f*, if *L* and ν are constant, beyond which the flow becomes turbulent, and the dependence of i_{corr} on flow rate increases. For still higher rates, activation control can be achieved ($m_c \gg k_c$), and the corrosion rate becomes independent of flow rate. This behavior is illustrated in Fig. 14. The solid line shows the effect of flow rate when the corrosion reaction is fast (k_c large), and a large flow rate is required to achieve activation control ($m_c \gg k_c$). The dotted line shows the behavior expected for a slow corrosion reaction (k_c small), when only a small flow rate is required to achieve activation control.

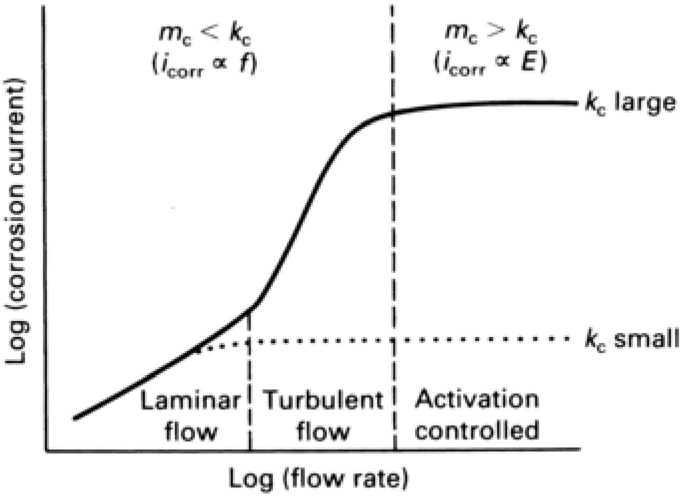

Fig. 14 The influence of solution flow rate on the corrosion rate (expressed as a current) showing the response in different flow regimes

Reference cited in this section

6. A.J. Bard and L.R. Faulkner, *Electrochemical Methods: Fundamentals and Applications,* 2nd ed., John Wiley and Sons, 2001.

D.W. Shoesmith, Kinetics of Aqueous Corrosion, *Corrosion: Fundamentals, Testing, and Protection*, Vol 13A, *ASM Handbook*, ASM International, 2003, p 42–51

Kinetics of Aqueous Corrosion

D.W. Shoesmith, University of Western Ontario

Influence of Corrosion Product Deposits

Thus far in the discussion of transport effects, only the transport of the cathodic reagent (step 3 in Fig. 5) has been considered. The transport of the anodic (metal) dissolution product (step 4 in Fig. 5) also affects the corrosion rate but in a different way. If dissolved metal ions are allowed to build up at the corroding surface, supersaturation of solid oxides/hydroxides can occur, leading to film formation reactions (step 5 in Fig. 5). These corrosion product deposits will form at a rate determined by the rate of the corrosion process and the solubility of the metal cations in the particular exposure environment. Determining their influence on the corrosion rate is not simple. A key feature is the porosity of the deposit (ε), because this determines the area of metal left exposed and also reduces the diffusion coefficient of both the anodic dissolution product and the cathodic reagent by a factor directly proportional to the porosity. The pores are also likely to be nonlinear, and their effective length will be greater than the thickness of the deposit. The diffusion coefficient will, therefore, also be attenuated by a tortuosity (τ) factor. The effective diffusion coefficient (D_{eff}) will be given by:

$$D_{eff} = \varepsilon\tau D_{Ox} \quad \text{(Eq 57)}$$

This situation is illustrated schematically in Fig. 15, and Eq 45 for the corrosion rate could be rewritten to yield:

$$i_{corr} = \frac{nF\varepsilon\tau D_{Ox}}{l}\left(c_{Ox}^{s} - c_{Ox}^{b}\right) \quad \text{(Eq 58)}$$

where corrosion is only occurring on a fraction (ε*A*) of the original exposed metal area, *A*, and *l* is the thickness of the corrosion product deposit. It should be noted that this represents a very simplified discussion of what could be a much more complicated process.

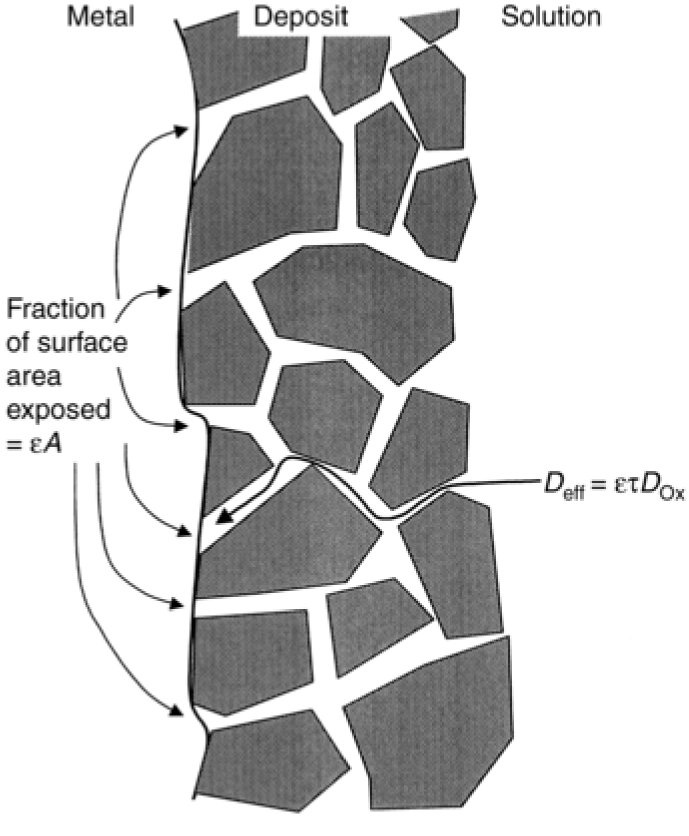

Fig. 15 Schematic illustrating how the presence of a corrosion product deposit influences the corrosion of an underlying metal by limiting both the area of exposed metal and the diffusion of oxidant to the corroding surface. D, diffusion coefficient; ε, porosity; τ, tortuosity factor; *A*, area

D.W. Shoesmith, Kinetics of Aqueous Corrosion, *Corrosion: Fundamentals, Testing, and Protection*, Vol 13A, *ASM Handbook*, ASM International, 2003, p 42–51

Kinetics of Aqueous Corrosion

D.W. Shoesmith, University of Western Ontario

Kinetics of Corrosion of Passive Metals

The formation of a passive film (step 7 in Fig. 5) can have a large influence on the corrosion rate. Passivation becomes thermodynamically possible when the corrosion potential exceeds (becomes more positive than) the potential corresponding to the equilibrium between the metal and one of its oxides/hydroxides:

$$E_{corr} > (E_e)_{M/MO} \quad \text{(Eq 59)}$$

Inspection of the Pourbaix diagram for the metal/ metal oxide/aqueous solution system shows that this condition moves E_{corr} into the oxide stability region, as illustrated in Fig. 16 for the iron/iron oxide/water system. For point 1, $E_{corr} < (E_e)_{M/MO}$, and corrosion of the bare metal is expected, while, for point 2, $E_{corr} > (E_e)_{M/MO}$, and the metal should be oxide covered and passive. It should be noted that experimentally measured primary passive potentials inevitably do not correspond directly with these thermodynamically determined potentials, because kinetic as well as thermodynamic effects are involved in oxide film formation.

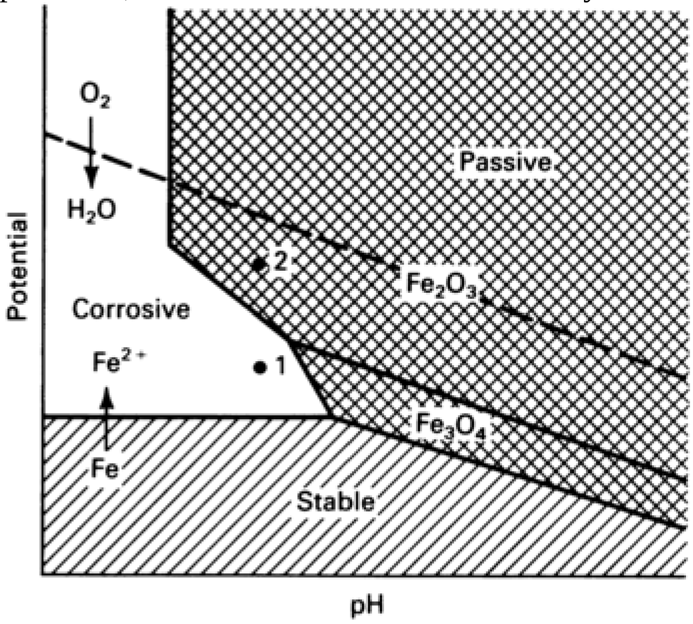

Fig. 16 Simplified Pourbaix (equilibrium potential-pH) diagram for the iron-water system. The upper dashed line shows the potential for H_2O in equilibrium with O_2.

The current-potential or polarization curve for the anodic process is shown in Fig. 17 and can be divided into a number of regions. In region AB, the active region, metal dissolution is unimpeded, because no passive film is present. Because such polarization curves are usually recorded under activation control conditions, local supersaturation leading to the deposition of corrosion products (discussed previously) is generally assumed not to influence the active dissolution of the metal. However, for real corrosion conditions, and especially for reactive metals such as iron, the current in this region could be suppressed by corrosion product deposits, as discussed previously. For the purposes of the present discussion, it is assumed that this does not occur. For active dissolution, therefore, the current should conform to the Tafel relationship (Eq 30), and its extrapolation back to $(E_e)_a$ would yield a value of $(i_o)_a$.

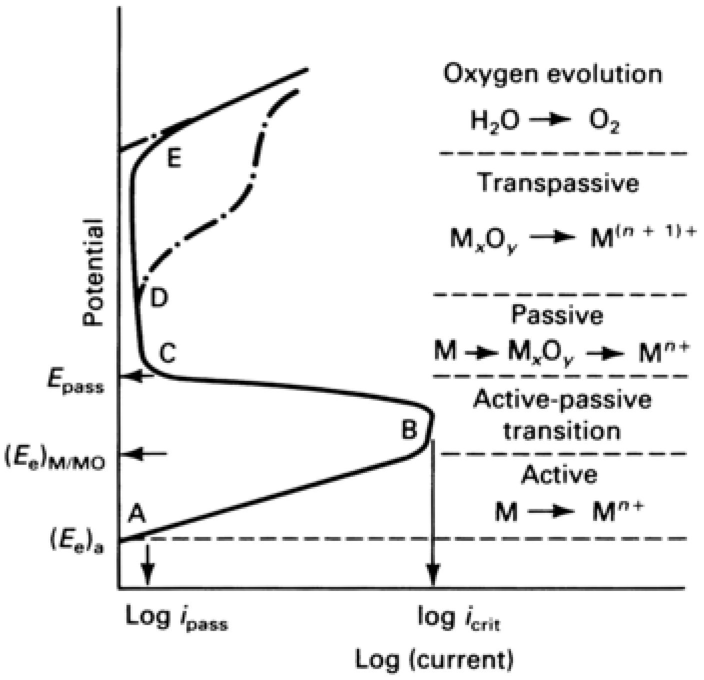

Fig. 17 Polarization curve for a metal that undergoes active-to-passive and passive-to-transpassive transitions

At a potential B, shown in Fig. 17 to coincide with $(E_e)_{M/MO}$ (although, as noted previously, this is rarely the case experimentally), there is a departure from the Tafel relationship, leading eventually to a decrease in current to a low value. The electrode is said to have undergone an active-to-passive transition and, by point C, has become passive. The potential at point B may or may not correspond to the potential $(E_e)_{M/MO}$. Thermodynamics demands only that the condition in Eq 59 be satisfied. The maximum current achieved immediately before the transition is termed the critical passivating current (i_{crit}). The potential at which the current falls to the passive value is called the passivation potential (E_{pass}), and it corresponds to the onset of full passivity. For gold, silver, and platinum, the passivation potential is close to $(E_e)_{M/MO}$, but for most other metals, it is much more positive than this equilibrium value.

For $E > E_{pass}$, the metal is said to be in the passive state, and the current is very low. A comparison of critical currents to passive currents puts the industrial importance of passivity into perspective. Critical passivating currents (expressed as current densities) can be as high as tens of mA/cm^2, while passive currents can be as low as nA/cm^2. Consequently, from the industrial corrosion perspective, the establishment of passivity is an important feature.

A detailed discussion of the properties of passive films is beyond the scope of this article (see the article "Passivity" in this Volume). A number of theories exist to explain the growth kinetics and properties of oxide films, but the discussion of one of them, the point defect model (Ref 7), serves to illustrate the critical features of the current-potential behavior in the passive region. The essential features of this model are shown schematically in Fig. 18. The film is assumed to be composed of an inner barrier layer, whose insulating properties provide the essential corrosion protection, and an outer recrystallized layer that confers little extra corrosion protection and is composed of hydrated metal species. This outer layer may not exist in acidic solutions in which the metal cations are highly soluble (Fig. 6). Considerable experimental evidence exists to support this structure.

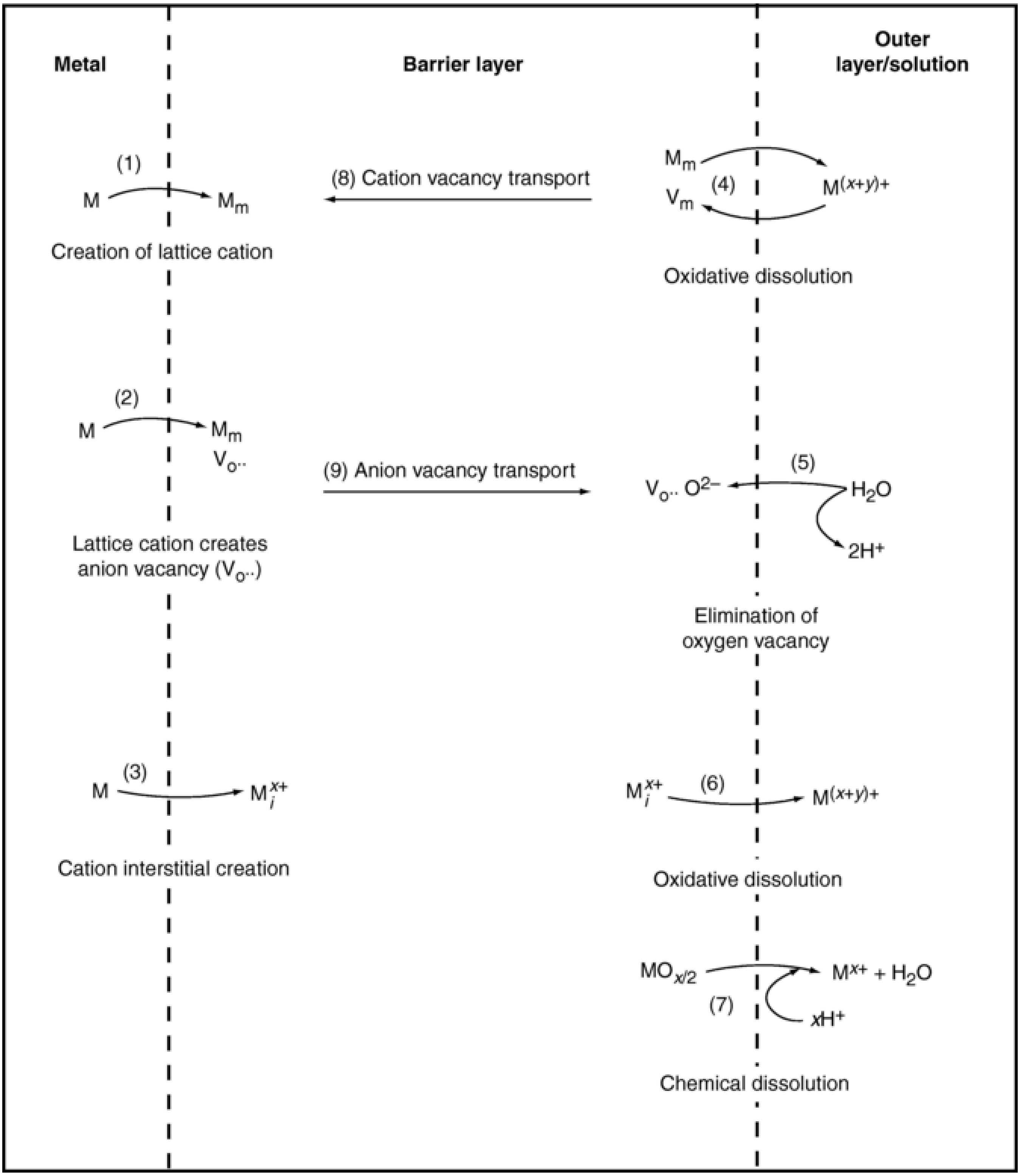

Fig. 18 Schematic description of the point defect model for the growth of a passive oxide film

Oxide growth is assumed to occur by the transport of defects through the film under the influence of the electric field that exists within the oxide. The nature of the defect depends on the metal/alloy and the nature of the growing oxide. However, the key vacancies are anion vacancies $\left(V_{o^{--}}\right)$ created at the metal-oxide interface, cation vacancies (V_m) created at the oxide- solution interface, and cation interstitials created at the metal-oxide interface. The general observation that the current in the passive region is independent of potential can be interpreted in terms of this model. As the potential is increased through the passive region, a progressive thickening of the oxide occurs, such that the electric field within the oxide remains constant. Thus, the steady-state current at each potential is a balance between oxide formation at the metal-oxide interface and

dissolution/recrystallization (to the outer hydrated layer) at the oxide-solution interface. Reference 7 provides more extensive discussions.

For high anodic potentials, the observed behavior depends on the nature of the metal and the properties of the oxide film. For metals that form insulating oxides (e.g., aluminum, titanium, zirconium), the films continue to thicken with increasing potential, and low passive currents are maintained. For other metals, for example, iron, chromium, nickel, and materials such as stainless steels and nickel-chromium alloys, oxygen evolution can occur on the outside of the passive film once the potential exceeds point E (Fig. 17):

$$2H_2O \rightarrow O_2 + 4H^+ + 4e^- \qquad \text{(Eq 60)}$$

For this reaction to occur, the film must be electronically conducting. This is possible because the passive films formed are thin (nanometers) and possess semiconducting properties. The dashed-dotted line in Fig. 17, in the potential region D to E, corresponds to the phenomenon of transpassivity. In this region, the oxide film begins to dissolve oxidatively, generally as a hydrolyzed cation in a higher oxidation state than that which exists in the film. An example would be the dissolution of chromium, present in the passive film on stainless steels as Cr^{III}, as Cr^{VI} in the form of CrO_4^{2-}. While transpassive dissolution, starting at point D, and O_2 evolution, starting at point E, are shown as clearly separated in Fig. 17, they often occur together, and a distinct transpassive region cannot be observed.

When coupled to a cathodic reaction in a corrosion process, a number of criteria must be satisfied if the metal is to be in the passive region and, on normal industrial time scales, free of corrosion:

- The equilibrium potential for the cathodic reaction ($(E_e)_c$) must be greater than the passivation potential (E_{pass}).
- The cathodic reaction must be capable of driving the anodic reaction to a current in excess of the critical passivation current, i_{crit}, in Fig. 17.

Three possible situations are shown in the Evans diagram in Fig. 19. The solid line shows the anodic polarization curve, and lines 1, 2, and 3 show the cathodic polarization curves for three different cathodic half-reactions ($O_n + ne^- \rightarrow R_n$).

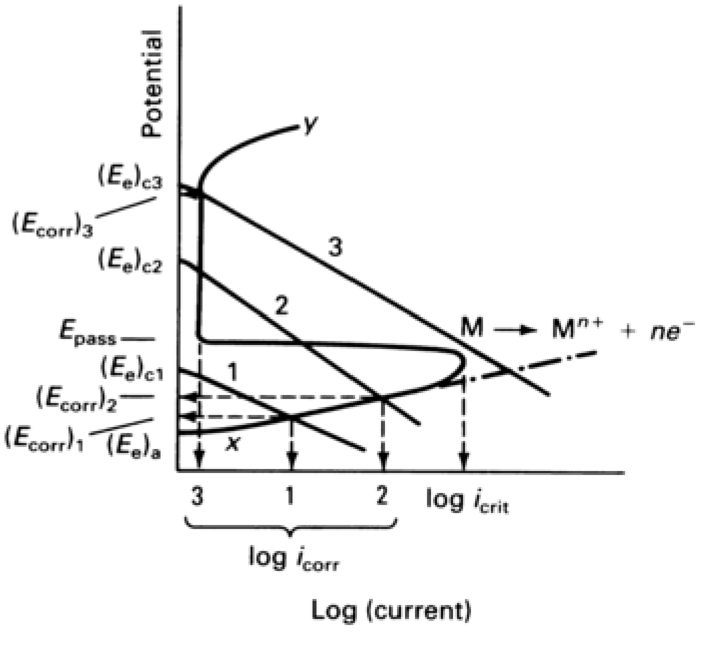

Fig. 19 Effect of various cathodic reactions on the corrosion current and potential for a metal capable of undergoing an active-passive transition

For cathodic reaction 1 (Fig. 19), $(E_e)_{c1} < E_{pass}$. Because the corrosion potential must lie between $(E_e)_a$ and $(E_e)_{c1}$ for the two reactions to form a corrosion couple, the required condition for passivation, $E_{corr} > E_{pass}$, cannot be achieved. Therefore, E_{corr} remains in the active region, and the metal will actively corrode.

For cathodic reaction 2 (Fig. 19), the condition $(E_e)_{c2} > E_{pass}$ is met, but the two polarization curves intersect at an anodic current $<i_{crit}$. Again, $E_{corr} < E_{pass}$, and the metal corrodes in the active region at an even higher current than for cathodic reaction 1.

For cathodic reaction 3 (Fig. 19), the conditions $(E_e)_{c3} > E_{pass}$ and $i > i_{crit}$ are both met. As a consequence, $E_{corr} > E_{pass}$, and the metal passivates, with the corrosion current equal to the passive dissolution current.

It is clear from this discussion that mild oxidizing agents ($\Delta E_{therm} = (E_e)_c - (E_e)_a$ small) could leave the material susceptible to corrosion, and strong oxidizing agents (ΔE_{therm} large) are required to ensure the metal will be in the passive region. However, in the presence of extremely strong oxidizing agents, it is possible for E_{corr} to become sufficiently positive that physical instabilities in the oxide become feasible. These minor film breakdown events can lead to many forms of localized corrosion if allowed to stabilize. A discussion of these processes is beyond the scope of this article, but the danger in fracturing the passive film can be appreciated from a consideration of the extrapolation of the anodic active region, shown by the dashed-dotted line in Fig. 19. If the oxide did not form, then this extrapolation shows that currents at positive potentials would be very large. Thus, breakdown of the passive film at a local site within the passive region would lead to an extremely high local current density and the possibility of deep localized corrosion of the metal.

Reference cited in this section

7. D.D. Macdonald, *Pure Appl. Chem.,* Vol 71, 1999, p 951

D.W. Shoesmith, Kinetics of Aqueous Corrosion, *Corrosion: Fundamentals, Testing, and Protection*, Vol 13A, *ASM Handbook,* ASM International, 2003, p 42–51

Kinetics of Aqueous Corrosion

D.W. Shoesmith, University of Western Ontario

References

1. J.H. West, *Electrodeposition and Corrosion Processes,* Van Nostrand Reinhold, 1971
2. D. Jones, *Principles and Prevention of Corrosion,* 2nd ed., Prentice Hall, 1996
3. L.L. Shreir, R.A. Jarman, and G.T. Burstein, Ed., Metal/Environment Interactions, *Corrosion,* Vol 1, 3rd ed., Butterworth/Heinemann, 1994
4. L.L. Shreir, R.A. Jarman, and G.T. Burstein, Ed., Corrosion Control, *Corrosion,* Vol 2, 3rd ed., Butterworth/Heinemann, 1994
5. C.F. Baes and R.E. Mesmer, *The Hydrolysis of Cations,* John Wiley and Sons, 1976.
6. A.J. Bard and L.R. Faulkner, *Electrochemical Methods: Fundamentals and Applications,* 2nd ed., John Wiley and Sons, 2001.
7. D.D. Macdonald, *Pure Appl. Chem.,* Vol 71, 1999, p 951

F. Huet, R.P. Nogueira, and H. Takenouti, Aqueous Corrosion Reaction Mechanisms, *Corrosion: Fundamentals, Testing, and Protection*, Vol 13A, *ASM Handbook*, ASM International, 2003, p 52–60

Aqueous Corrosion Reaction Mechanisms

François Huet, Ricardo P. Nogueira, Bernard Normand, and Hisasi Takenouti, Université Pierre et Marie Curie and UPR 15 of CNRS, "Laboratoire Interfaces et Systèmes Electrochimiques," Université Pierre et Marie Curie

Introduction

CORROSION OF METALLIC MATERIALS is governed by electrochemical kinetics, so that the general concepts developed for studying electrochemical reaction mechanisms may be applied to corrosion. The processes of charge transfer taking place at the electrode interface within the double layer and of mass transport at the vicinity of the electrode surface are introduced first. Then, the corrosion processes, which involve anodic and cathodic reactions at specific electrode sites, are described briefly. Some reaction mechanisms for cathodic and anodic processes are presented to illustrate the great variety of reaction mechanisms occurring at the electrode interface. Some experimental methods for devising a reliable reaction model are also described. The presentations given here are limited to a survey of each item; readers wishing more detailed information are invited to consult the many books devoted to electrode kinetics and corrosion processes (Ref 1, 2, 3, 4).

References cited in this section

1. H. Kaesche, *Metallic Corrosion, Principles of Physical Chemistry and Current Problems,* NACE International, Houston, TX, 1985

2. F. Mansfeld and U. Bertocci, Ed., *Electrochemical Corrosion Testing,* STP 727, ASTM International, 1981

3. J.C. Scully, Ed., *Treatise on Materials Science and Technology,* Vol 23, *Corrosion: Aqueous Processes and Passive Films,* Academic Press, 1983

4. J.R. Scully, D.C. Silvermann, and M.W. Kendig, Ed., *Electrochemical Impedance: Analysis and Interpretation,* STP 1188, ASTM International, 1994

F. Huet, R.P. Nogueira, and H. Takenouti, Aqueous Corrosion Reaction Mechanisms, *Corrosion: Fundamentals, Testing, and Protection*, Vol 13A, *ASM Handbook*, ASM International, 2003, p 52–60

Aqueous Corrosion Reaction Mechanisms

François Huet, Ricardo P. Nogueira, Bernard Normand, and Hisasi Takenouti, Université Pierre et Marie Curie and UPR 15 of CNRS, "Laboratoire Interfaces et Systèmes Electrochimiques," Université Pierre et Marie Curie

Fundamental Aspects of Electrode Kinetics

Electrochemical reactions may be considered as physical and chemical processes of electric charge transfer between two phases containing different charge carriers: electrons in the metallic phase and ions in the electrolyte. This charge transfer induces an electric current flow and chemical transformations at the interface.

A thorough investigation of an electrochemical process involves the identification of reactants, the separation of elementary interfacial reactions, and the establishment of a reaction mechanism. Analytical methods are generally applied to identify the initial, final, and, sometimes, intermediate species, while kinetic methods are used to identify the links between the elementary reaction steps and assess their rate constant. Kinetic methods differ from other methods by the following points:

- Reactions are localized at the interface so that they concern a tiny volume and a small number of identifiable entities.
- Most in situ surface analytical techniques cannot be applied because of the presence of electrolyte.
- The kinetics are easily characterized by electric signals (the current flowing across the interface and the electrode potential) with more and more sophisticated methods.

The rate of charge transfer reactions governed only by the activation energy is derived first. Then, the case in which mass transport modifies the concentration gradient of the species at the interface and, therefore, changes the overall reaction rate is discussed.

Charge-Transfer Process

Charge transfer may take place as a single step determined by the activation energy or as a multistep transfer involving intermediate species in the reaction.

Single-Step Charge Transfer Reaction Rate. Different macroscopic descriptions allowed the absolute reaction rate, *k*, to be associated with the change in activation energy (Gibbs free energy, or $\Delta G^{\ddagger}$), through the Arrhenius equation:

$$k = C \exp\left(-\frac{\Delta G^{\ddagger}}{RT}\right) \qquad \text{(Eq 1)}$$

where C is a constant, T is the absolute temperature (in K), and R is the gas constant (8.31 J/mol · K). The activation energy change $\Delta G^{\ddagger}$, in electrochemical reactions is not the difference in free energy, ΔG, between the initial and final states of the reactants; it takes into account the height of the energy barrier, as will be explained, and depends on the cell potential E. For a reaction involving the forward and backward single-step transfer of z electrons per molecule of the species considered, the simplest situation, which leads to the empirical Tafel law between the current density and the electrode potential, consists in postulating that a change in potential (ΔE) induces a change in free energy, $\Delta G^{\ddagger}$, according to the following relationship. For the anodic (oxidation) reaction:

$$\Delta G_a^{\ddagger} = \Delta G_{0,a}^{\ddagger} - \alpha z F \Delta E \qquad \text{(Eq 2)}$$

For the cathodic (reduction) reaction:

$$\Delta G_c^{\ddagger} = \Delta G_{0,c}^{\ddagger} + (1-\alpha) z F \Delta E \qquad \text{(Eq 3)}$$

where F is the Faraday constant (96,485 C/mol), α is the charge-transfer coefficient ($0 \leq \alpha \leq 1$). The subscript 0 indicates that all reactants are in a standard state (constant temperature, pressure, potential, activity, etc.). Equations 2 and 3 indicate how the electric energy shift $zF\Delta E$ of the z moles of electrons induced by the electrode potential change (ΔE) is shared between the two partial reactions. This may be illustrated in Fig. 1 that shows the free energy evolution during both the reduction (from left to right) and oxidation reactions (from right to left). The solid lines correspond to the standard conditions for both reactions; in that case ($\Delta E = 0$), $\Delta G_{0,c}^{\ddagger}$ represents the energy required by one mole of oxidized species to reach the activated state, A, from the initial stable state (minimum energy), and be reduced. $\Delta G_{0,a}^{\ddagger}$ represents the energy required by one mole of reduced species to reach the activated state, A, from the initial stable state (minimum energy) and be oxidized. The dashed line corresponds to the activation energy of one mole of oxidized species and z moles of electrons during the reduction reaction after a potential change ΔE. The anodic curve was arbitrarily kept unchanged.

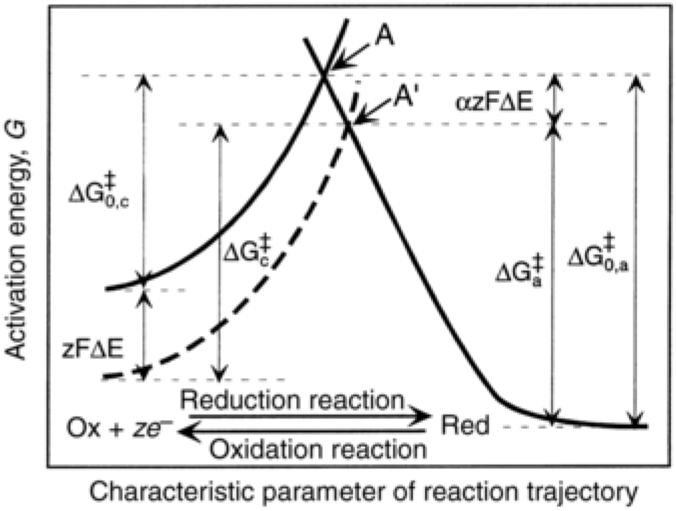

Fig. 1 Schematic representation of the influence of a potential change on the activation energy during charge transfer in an oxidation-reduction reaction

It can be seen graphically that if α represents the fraction of the electric energy $zF\Delta E$ devoted to the activation energy of the oxidation reaction, the height of the energy barrier is decreased by a factor $\alpha zF\Delta E$ for the oxidation reaction (Eq 2) while it is increased by a factor $\Delta G^{\ddagger}_{c} - \Delta G^{\ddagger}_{0,c} = zF\Delta E - \alpha zF\Delta E$ for the reduction reaction (Eq 3). The dependence of the anodic and cathodic rate constants, k_a and k_c, on the electrode potential is obtained as a consequence of Eq 1, Eq 2, Eq 3:

$$k_a = k_{0,a} \exp\left(\frac{\alpha zF}{RT}\Delta E\right) \quad \text{and}$$
$$k_c = k_{0,c} \exp\left(\frac{-(1-\alpha)zF}{RT}\Delta E\right) \qquad \text{(Eq 4)}$$

Current-Potential Relationship. The current provided by the oxidation-reduction reaction is proportional to the net production rate of the oxidized species:

$$i = zF\left\{k_{0,a} C^i_{red} \exp\left(\frac{\alpha zF}{RT}\Delta E\right) - k_{0,c} C^i_{ox} \exp\left(\frac{-(1-\alpha)zF}{RT}\Delta E\right)\right\} \qquad \text{(Eq 5)}$$

where i is the current density, and C^i_{ox}, C^i_{red}(in mol/cm^3) are the concentrations of the oxidized and reduced species at the electrode interface. For a purely charge-transfer controlled reaction, the mass-transport processes are fast so that the concentrations at the interface are equal to the concentrations in the electrolyte bulk and do not depend on the electrode potential. It is convenient to introduce the standard equilibrium potential, E_0, which corresponds to i = 0 for identical concentrations of the oxidized and reduced species in the solution. In that case, since the reaction rates $k_{0,a}$ and $k_{0,c}$ are equal (= k_0, termed *exchange rate constant* of the reaction, in cm/s), i can be expressed as:

$$i = zFk_0\left\{C^i_{red} \exp\left(\frac{\alpha zF}{RT}(E-E_0)\right) - C^i_{ox} \exp\left(\frac{-(1-\alpha)zF}{RT}(E-E_0)\right)\right\} \qquad \text{(Eq 6)}$$

This equation gives the expression (Nernst law) of the equilibrium potential (E_{eq}) in the solution considered ($C^i_{ox} \neq C^i_{red}$):

$$E_{eq} = E_0 + \frac{RT}{zF}\ln\left(\frac{C^i_{ox}}{C^i_{red}}\right) \quad \text{(Eq 7)}$$

from which the overpotential, $\eta = E - E_{eq}$, is defined. Equation 6 gives the Butler-Volmer equation, which is the basis of the electrochemical kinetics (Ref 5, 6):

$$i = i_0\left[\exp\left(\frac{\alpha zF}{RT}\eta\right) - \exp\left(\frac{-(1-\alpha)zF}{RT}\eta\right)\right] \quad \text{(Eq 8)}$$

where the exchange current density (i_0) is defined as:

$$i_0 = zFk_0\left(C^i_{red}\right)^{1-\alpha}\left(C^i_{ox}\right)^{\alpha} \quad \text{(Eq 9)}$$

gives information on the degree of reversibility of the reaction. The Butler-Volmer equation gives the partial anodic and cathodic currents. At sufficiently high anodic overpotentials, the cathodic process becomes negligible. At sufficiently high cathodic overpotentials, the anodic process becomes negligible. The anodic i_a and cathodic i_c current densities are then:

$$i_a = i_0 \exp\left(\frac{\alpha zF}{RT}\eta\right) \quad \text{and}$$

$$i_c = -i_0 \exp\left(\frac{-(1-\alpha)zF}{RT}\eta\right) \quad \text{(Eq 10)}$$

According to the International Union of Pure and Applied Chemistry (IUPAC) recommendation, the cathodic current and its Tafel coefficient, -(1 - α)zF/RT, are expressed by negative values. In these equations (Tafel laws), the logarithm of the current density (in absolute value) is a linear function of the electrode potential. Figure 2 summarizes the current behavior given by Eq 8 and 10.

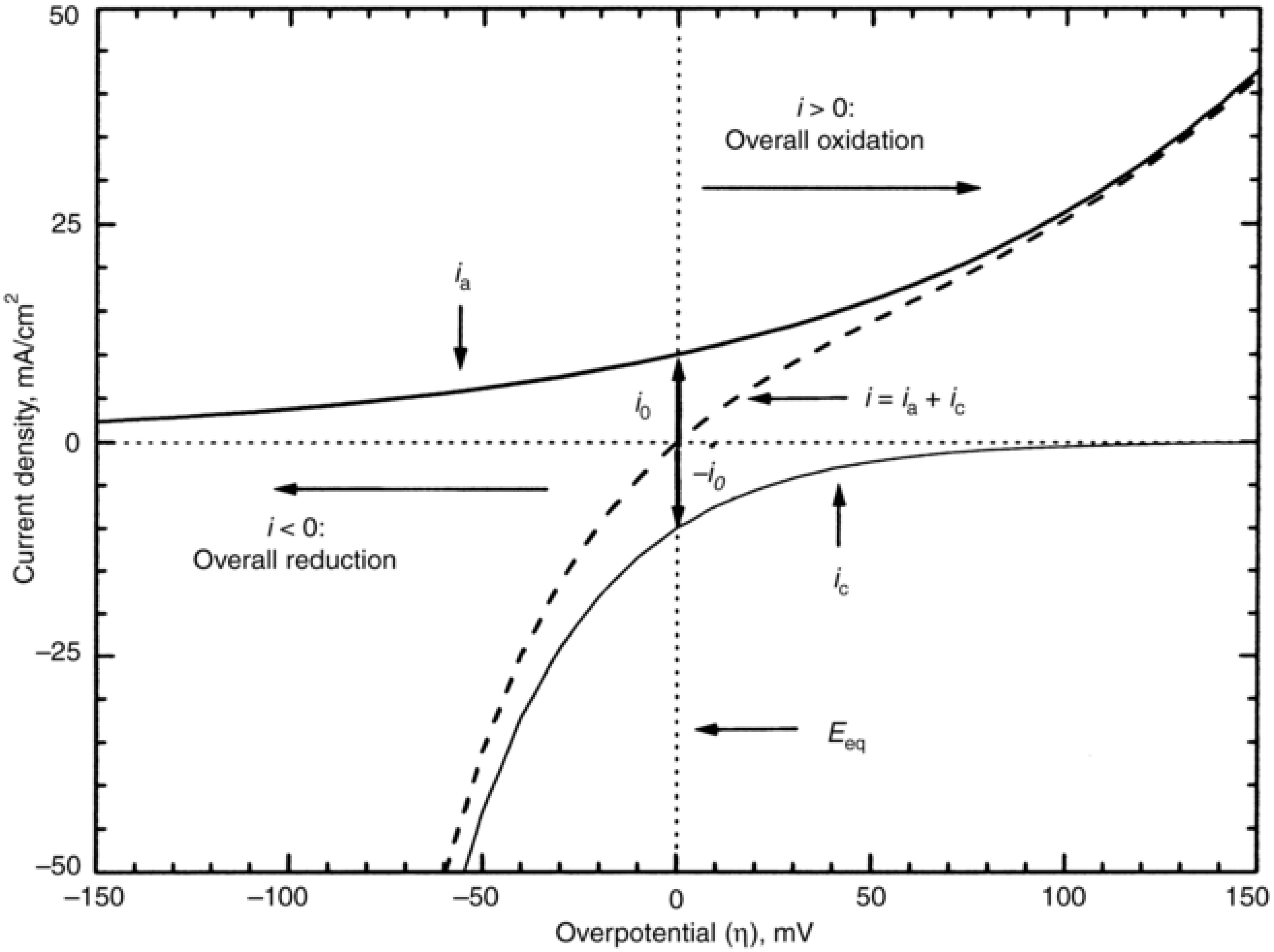

Fig. 2 Butler-Volmer electrode kinetics. i_0 = 10 mA/cm^2, charge transfer coefficient, α = 0.75, charge number, z = 1, T = 298 K

Multistep Charge Transfer. In the single-step charge transfer, z electrons are exchanged simultaneously. However, this requires a much higher activation energy than consecutive elementary reaction steps involving only one electron transfer. As a simple example, consider the situation where two electrons are transferred (z = 2) via two irreversible reactions involving an adsorbed intermediate species, B_{ad}.

$$\mathrm{M} + \mathrm{A}_{sol} \xrightarrow{k_1} \mathrm{B}_{ad} + e^- \qquad \text{(Eq 11)}$$

$$\mathrm{B}_{ad} \xrightarrow{k_2} \mathrm{C}_{sol} + \mathrm{A}_{sol} + e^- \qquad \text{(Eq 12)}$$

M is the metal and A_{sol} and C_{sol} are species in solution. For example, the dissolution of iron in sulfuric acid at low current may be modeled by these reactions with M, A_{sol}, B_{ad}, and C_{sol} representing, respectively, Fe, OH^-, $(FeOH)_{ad}$, and Fe^{2+} in solution (Ref 7). B_{ad} covers a fraction (θ) of the electrode surface area (0 < θ < 1) so that the reaction in Eq 11 takes place only at the fractional area of 1 - θ. If a Langmuir-type adsorption isotherm can be assumed, the superficial concentration (in mol/cm^2) (C_B) of B_{ad} is equal to βθ, where β is the maximum concentration of B_{ad} (in mol/cm^2), while the concentration C_M of atoms M available for the reaction shown in Eq 11 is β(1 - θ). For first-order kinetic reactions, the mass and charge balances can be expressed, respectively, as follows when the concentration of C_{sol} at the interface can be assumed to be constant:

$$\frac{dC_B}{dt} = \beta\frac{d\theta}{dt} = k_1 C_M - k_2 C_B = k_{0,1}\exp(b_1 E)\beta(1-\theta) - k_{0,2}\exp(b_2 E)\beta\theta \qquad \text{(Eq 13)}$$

$$i = F(k_1 C_M + k_2 C_B) = F\left(k_{0,1}\exp(b_1 E)\beta(1-\theta) + k_{0,2}\exp(b_2 E)\beta\theta\right) \qquad \text{(Eq 14)}$$

where b_1 and b_2 are the Tafel coefficients and $k_{0,1}$ and $k_{0,2}$ are the reaction rates, expressed in s^{-1} at the potential E = 0 V, defined with an arbitrary potential reference. In the literature, reaction rates $k'_{0,i} = k_{0,i}\beta$ in mol/cm^2 per s are frequently introduced so that the parameter β appears in Eq 13 only. Often, β values of about 2 to 5 × 10^{-9} mol/cm^2 are used; they correspond to one adsorbed molecule per one surface atom for an electrode with a certain surface roughness. At the steady state (subscript s), there is no time change in the potential, current, and surface coverage; the righthand side of Eq 13 is then equal to zero, which gives the steady-state value of θ:

$$\theta_s = \frac{k'_{0,1}\exp(b_1 E_s)}{\left\{k'_{0,1}\exp(b_1 E_s) + k'_{0,2}\exp(b_2 E_s)\right\}} \qquad \text{(Eq 15)}$$

The equation of the steady-state polarization curve follows, from Eq 14:

$$i = \frac{2F\left\{k'_{0,1}\exp(b_1 E_s)k'_{0,2}\exp(b_2 E_s)\right\}}{\left\{k'_{0,1}\exp(b_1 E_s) + k'_{0,2}\exp(b_2 E_s)\right\}} \qquad \text{(Eq 16)}$$

If $b_1 > b_2$, the current density is determined by the reaction in Eq 11 at low potentials ($k_1 \ll k_2$) and by the reaction in Eq 12 at high potentials ($k_1 \gg k_2$) leading to a Tafel plot [log(i) - E] with two different slopes, b_1 at low potentials and b_2 at high potentials. The surface concentration of the adsorbed intermediate species β · θ or its potential dependence cannot in general be observed experimentally by steady-state methods. In contrast, the impedance technique or other time or frequency resolved methods can track the relaxation of θ induced by a potential change.

Mass Transport Process and Mixed Kinetics

The Butler-Volmer equation is valid for systems under pure charge transfer control; the mass transport is much faster than the charge transfer and ensures the constant supply of reactants at the interface. This is not the case

for fast charge- transfer reactions and differences in the concentration of the reacting species, $C^i_{ox}$and C^i_{red}, at the interface, and C_{ox} and C_{red}, in the bulk of the electrolyte appear. Equation 8 is then rewritten as:

$$i = i_0\left[\frac{C^i_{red}}{C_{red}}\exp\left(\frac{\alpha zF}{RT}\eta\right) - \frac{C^i_{ox}}{C_{ox}}\exp\left(\frac{-(1-\alpha)zF}{RT}\eta\right)\right] \quad \text{(Eq 17)}$$

In this situation, the current density is determined by both the diffusion and activation processes (mixed kinetics). Under the assumption of linear concentrations in the Nernst diffusion layer of thickness δ, the mixed current density (i_{mix}) is:

$$i_{mix} = \frac{zFD_{red}\left(C_{red} - C^i_{red}\right)}{\delta} \quad \text{(Eq 18)}$$

where D_{red} is the diffusion coefficient (cm^2/s) of the reduced species, since the flux of these species consumed in the reaction is balanced by the flux arriving by diffusion. C^i_{red}can be calculated with Fick's law, which gives the full expression of i_{mix}:

$$i_{mix} = i_{act}\frac{D_{red}D_{ox}}{D_{red}D_{ox} + \delta\left(k_c D_{red} + k_a D_{ox}\right)} \quad \text{(Eq 19)}$$

where the pure activation current density (i_{act}) is given by Eq 6:

$$i_{act} = zF(k_a C_{red} - k_c C_{ox}) \quad \text{(Eq 20)}$$

Mass transport of both oxidized and reduced species is supposed here to be controlled by diffusion; if the reaction rate is controlled by diffusion of only one species, the diffusion coefficient of the other species is taken to be infinite.

If the reaction rate is fast enough, the concentration of the species consumed at the interface tends to be zero. The overall reaction is under mass-transport control, and i_{mix} tends to be the diffusion limiting current density (i_{lim}) (given by Eq 18 with $C^i_{red}= 0$), which is independent of the potential. For slower kinetics, the current densities i_{mix}, i_{act}, and i_{lim} are related by the following equation when the reverse reaction is negligible:

$$\frac{1}{i_{mix}} = \frac{1}{i_{lim}} + \frac{1}{i_{act}} \quad \text{(Eq 21)}$$

Figure 3 presents the polarization curves when the overall reaction rate is influenced by the diffusion process. The kinetic constants determining the pure activation current density i_{act} are those used in Fig. 2, while the diffusion limiting current densities are set to 25 mA/cm^2 for both anodic and cathodic reactions. The deviation between the current-density curves ($i_{mix,a}$ and $i_{mix,c}$) for the mixed kinetics and $i_{act,a}$ and $i_{act,c}$ for the pure activation-controlled kinetics can be noted. It should be emphasized that the diffusion effects are already present at the equilibrium potential since the exchange current density (i'_0) is lower in Fig. 3 than i_0 in Fig. 2.

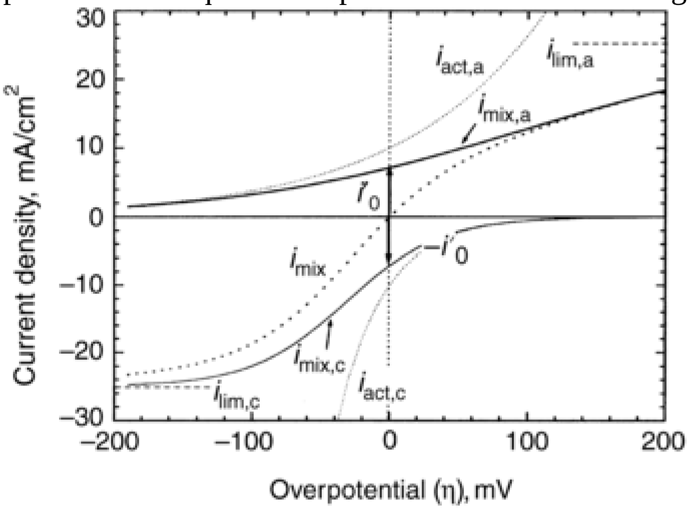

Fig. 3 Polarization curve for mixed kinetics. Same rate constants as for the activation process in Fig. 2. i_{lim} = 25 mA/cm^2 for both reactions

References cited in this section

5. K.J. Vetter, *Electrochemical Kinetics,* Academic Press, 1967
6. A.J. Bard and L.R. Faulkner, *Electrochemical Methods, Fundamentals and Applications,* John Wiley & Sons, Inc., 1980
7. I. Epelboin and M. Keddam, *J. Electrochem. Soc.,* Vol 117, 1970, p 1052

F. Huet, R.P. Nogueira, and H. Takenouti, Aqueous Corrosion Reaction Mechanisms, *Corrosion: Fundamentals, Testing, and Protection,* Vol 13A*, ASM Handbook,* ASM International, 2003, p 52–60

Aqueous Corrosion Reaction Mechanisms

François Huet, Ricardo P. Nogueira, Bernard Normand, and Hisasi Takenouti, Université Pierre et Marie Curie and UPR 15 of CNRS, "Laboratoire Interfaces et Systèmes Electrochimiques," Université Pierre et Marie Curie

---

Electrode Kinetics near the Corrosion Potential

The specifics of electrode kinetics near the zero-overall current are described with respect to the reversible process presented earlier. It is shown that these kinetics may be advantageously analyzed by dynamic techniques such as electrochemical impedance spectroscopy.

Coupling of Anodic and Cathodic Processes. Though corrosion is basically an electrochemical process, no overall current flow is observed during the free corrosion of a metal (M) at the open-circuit potential, because the anodic process that produces electrons and the cathodic process that consumes electrons, which can be written formally:

$$\text{Anodic reaction} \quad M \rightarrow M^{z_a^+} + z_a e^- \tag{Eq 22}$$

$$\text{Cathodic reaction} \quad Ox + z_c e^- \rightarrow \text{Red} \tag{Eq 23}$$

are taking place simultaneously and at the same rate. A more detailed description of these processes is shown later in this article.

The reactions in Eq 22 and 23 are not the forward and backward branches of the same reversible reaction, so that they cannot be referred to the same equilibrium potential. The simplest way to describe the kinetics of both processes is to consider that each reaction obeys the Tafel law (Eq 10), which is often experimentally verified because of the large difference in the equilibrium potentials of the anodic and cathodic processes. The potential must be expressed with respect to the same arbitrarily chosen reference electrode, which gives for the anodic and cathodic current density, respectively, from Eq 6:

$$\begin{aligned} i_a &= z_a F C_M k_{0,a} \exp\left(b_a\left(E - E_{ref}\right)\right) \quad \text{and} \\ i_c &= -z_c F C_{ox}^i k_{0,c} \exp\left(b_c\left(E - E_{ref}\right)\right) \end{aligned} \tag{Eq 24}$$

As stated earlier, free corrosion of metals provides a zero overall current, so that the following relationship at the corrosion potential (E_{corr}) allows the corrosion rate i_{corr} to be derived:

$$\begin{aligned} i_{corr} &= z_a F C_M k_{0,a} \exp\left(b_a\left(E_{corr} - E_{ref}\right)\right) \\ &= z_c F C_{ox}^i k_{0,c} \exp\left(b_c\left(E_{corr} - E_{ref}\right)\right) \end{aligned} \tag{Eq 25}$$

The current density near the corrosion potential is then:

$$i = i_a + i_c = i_{corr}\left\{\exp\left(b_a\left(E - E_{corr}\right)\right) - \exp\left(b_c\left(E - E_{corr}\right)\right)\right\} \quad \text{(Eq 26)}$$

This equation is very similar to Eq. 8, except that the Tafel coefficients b_a and b_c are no longer mutually related by the charge-transfer coefficients (α and 1 - α), and that E_{corr} is a mixed potential and *not* a thermodynamic equilibrium potential. Differentiation of Eq. 26 yields the slope of the polarization curve at the corrosion potential, which is the reciprocal of the polarization resistance (R_p):

$$\frac{di}{dE} = \frac{1}{R_p} = i_{corr}\left(b_a - b_c\right) = 2.303 i_{corr}\frac{\beta_a + \beta_c}{\beta_a\beta_c} \quad \text{(Eq 27)}$$

In this equation, known as the Stern-Geary equation, R_p is given as a function of the Tafel coefficients $b_a(>0)$ and $b_c(<0)$, expressed in V^{-1}, and as a function of the Tafel slopes $\beta_a = 2.303/ b_a$ and $\beta_c = 2.303/|b_c|$, expressed in V/current decade, which are often used in practice. Equation 27 implicitly assumes several hypotheses, namely:

- Both anodic and cathodic processes obey the Tafel law; that is, both reactions are under pure activation control.
- The anodic and cathodic currents are additive but kinetically independent; that is, without any interaction between them.

Since the work of Wagner and Traud in 1938 (Ref 8), it is known that the electrode surface is actually divided into local cells with the particularity that in each cell the anodic and cathodic processes do not simultaneously take place. The spatial distribution of the cathodic and anodic regions is due to local differences in the electrode microstructure, grain boundaries, presence of inclusions, and so forth. If the anodic reaction obeys the Tafel law on the fraction of surface area θ_a where it takes place and if the cathodic reaction obeys the Tafel law on the fraction of surface area θ_c where it takes place, the overall current density can be written:

$$i = i_a + i_c = i_{0,a}\theta_a\exp\left(b_a\left(E - E_{corr}\right)\right) - i_{0,c}\theta_c\exp\left(b_c\left(E - E_{corr}\right)\right) \quad \text{(Eq 28)}$$

where $i_{0,a}$ and $i_{0,c}$ are the mean current densities on the anodic and cathodic regions, respectively, at the corrosion potential. The derivation of Eq 28 at E_{corr} leads to a new expression of the polarization resistance:

$$\frac{1}{R_p} = \frac{di}{dE} = i_{corr}\left(b_a - b_c\right) + i_{0,a}\frac{d\theta_a}{dE} - i_{0,c}\frac{d\theta_c}{dE} \quad \text{(Eq 29)}$$

Comparison of Equations 27 and 29 clearly demonstrates that the Stern-Geary equation is valid only if the fractional surface areas are independent of the potential around E_{corr}. It is important to note that dissolution preferably occurs at crystallographic defects, which are more reactive sites. Moreover, surface coverage is a dynamic feature related to the balance between adsorption/desorption processes. This suggests that changes in the electrode potential are likely to induce changes in the surface coverage of the adsorbed species, which will affect the value of the polarization resistance (Eq 29). Electrochemical impedance spectroscopy (EIS) allows the terms $d\theta_a/dE$ and $d\theta_c/dE$ to be separated from di/dE and, therefore, allows the Stern-Geary equation to be generalized, as shown in the next paragraph.

Brief Review of Electrochemical Impedance Spectroscopy. The current density flowing through the electrode interface may be expressed as a function of the potential (E) and of different parameters (p) of the electrode kinetics, like the surface coverage of adsorbed species, the interfacial concentration of reactants, and so forth:

$$i = f(E, p_1, p_2, p_3 \ldots) \quad \text{(Eq 30)}$$

For simplification, only one parameter (p), which typically may be the surface coverage (θ) by an adsorbed species, is considered in the following. The Taylor expansion of Eq 30 is:

$$di = \left.\frac{\partial i}{\partial E}\right|_p dE + \left.\frac{\partial i}{\partial p}\right|_E dp \quad \text{(Eq 31)}$$

A variation (dE) of potential thus yields a direct change in the current density i (first term in the righthand side of Eq 31) for a constant value of p, and an indirect change (second term) through the variation dp of p. The

change in p generally implies the variation of surface coverage of some species and, therefore, requires a certain time period to occur. Figure 4 schematically presents the i and p changes induced by a small potential jump (ΔE). For simple systems, these changes follow an exponential-like function with the same time constant (τ) that conveys information about the kinetics of the reaction: fast electrochemical systems will show short time constants and slow electrochemical systems will show long time constants.

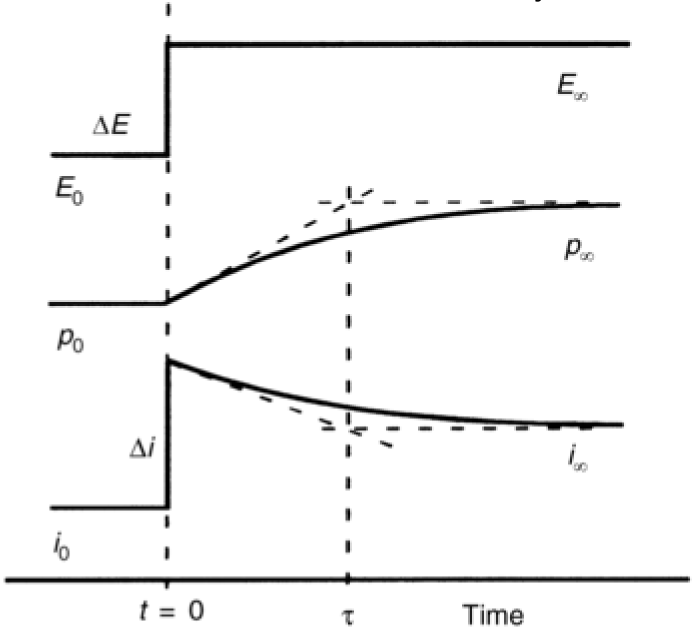

Fig. 4 Schematic representation of a parameter, *p*, and current density, *i*, changes following a potential jump at time *t* = 0

In practice, most electrochemical systems depend on several parameters (p) that have different time constants so that the time behavior of i after a small potential jump ΔE is complex and difficult to interpret. In contrast, valuable kinetic information may be obtained in the frequency domain with EIS, using a small amplitude alternating current (ac) perturbing signal. In the simple case of a single parameter (p) representing the surface coverage (θ) of an intermediate species, Eq 31 gives:

$$\frac{1}{Z_F} = \frac{di}{dE} = \frac{1}{R_t} + \left.\frac{\partial i}{\partial \theta}\right|_E \frac{d\theta}{dE} = \frac{1}{R_t} + \left.\frac{\partial i}{\partial \theta}\right|_E \frac{C}{1 + j\omega\tau} \quad \text{(Eq 32)}$$

where Z_F denotes the faradaic impedance, R_t is the charge-transfer resistance, $\omega = 2\pi f$ is the pulsation and f the frequency (in Hz) of the perturbation signal, and C is constant for a given potential. C is positive if θ increases with increasing E, which corresponds to an adsorption effect for an anodic reaction. C is negative if θ decreases with increasing E, which corresponds to a desorption effect for an anodic reaction. The term $\partial i/\partial\theta|_E$ characterizes the effect of the adsorbed species on the current: i increases if the effect is catalytic while it decreases if the species is an inhibitor or a passivating agent. According to the sign of the last term in Eq 32, an inductive loop ($ImZ_F > 0$) or a capacitive loop ($ImZ_F < 0$) appears in the Nyquist plot of Z_F in the complex plane (ReZ, $-ImZ$) as summarized as follows:

$\partial i/\partial\theta > 0$ (catalyzer)	**$d\theta/dE > 0$ (adsorption)**	**$d\theta/dE < 0$ (desorption)**
	Inductive loop	Capacitive loop
$\partial i/\partial\theta < 0$ (inhibitor/passivating species)	Capacitive loop	Inductive loop

Thus, the adsorption of a catalyzer on the electrode surface and, alternatively, the desorption of an inhibitor lead to an inductive loop in the faradaic impedance. Conversely, the passivation process induces a capacitive behavior.

Equation 32 shows that Z_F is reduced to the charge-transfer resistance (R_t) at high frequency since the term ($1 + j\omega\tau$) tends to infinity. Moreover, from Eq 29, it can be seen that $1/R_t = i_{corr}(b_a - b_c)$ since $d\theta_a/dE$ and $d\theta_c/dE$ vanish at high frequency where di/dE is the inverse of the charge-transfer resistance. In other words, R_t fulfills the Stern-Geary equation when the electrode surface is divided into numerous anodic and cathodic local cells with potential-dependent fractional area, while R_p does not. Thus:

$$i_{corr} = \frac{B}{R_t} \quad \text{with} \quad B = \frac{1}{b_a - b_c} = \frac{1}{2.303} \frac{\beta_a \beta_c}{\beta_a + \beta_c} \qquad \text{(Eq 33)}$$

More generally, if several parameters (*p*) with different associated time constants are involved in the reaction process, several capacitive and/or inductive loops will appear in the impedance diagram. It is worth remembering that the diffusion impedance cannot be represented by a well-defined time constant (τ) as that presented in Eq 32; it shows a more complicated behavior. However, Eq 33 remains valid even when the electrochemical system is partly or completely limited by mass transport (Ref 9).

It is also important to note that Z_F cannot be directly measured. Indeed, the impedance of the metal-electrolyte interface, which is accessible to measure, contains the contributions of the electrolyte (solution) resistance (R_e) and that of the interface capacitance (double-layer capacitance) C_d, in addition to the faradaic component (Z_F). Figure 5(a) presents the electric equivalent circuit of the interface and Fig. 5(b) represents the schematic Nyquist diagram of Z when the product of $\partial i/\partial\theta|_E$ and C in Eq 32 is negative, which gives the capacitive behavior of Z_F.

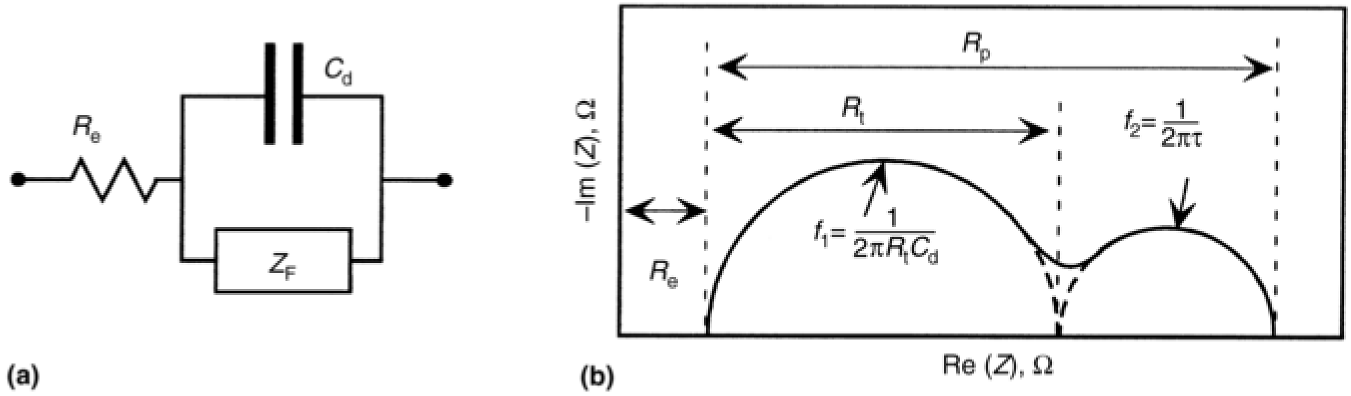

Fig. 5 Impedance models. (a) Equivalent electrical circuit of the interface; (b) Nyquist diagram of Z for a negative product of $\partial i/\partial\theta|_E$ and C in Eq 32

References cited in this section

8. C. Wagner and W. Traud, *Z. Elektrochem.,* Vol 44, 1938, p 391

9. I. Epelboin, C. Gabrielli, M. Keddam, and H. Takenouti, *Electrochemical Corrosion Testing,* F. Mansfeld and U. Bertocci, Ed., STP 727, ASTM International, 1981, p 150–192

F. Huet, R.P. Nogueira, and H. Takenouti, Aqueous Corrosion Reaction Mechanisms, *Corrosion: Fundamentals, Testing, and Protection,* Vol 13A, *ASM Handbook,* ASM International, 2003, p 52–60

Aqueous Corrosion Reaction Mechanisms

François Huet, Ricardo P. Nogueira, Bernard Normand, and Hisasi Takenouti, Université Pierre et Marie Curie and UPR 15 of CNRS, "Laboratoire Interfaces et Systèmes Electrochimiques," Université Pierre et Marie Curie

---

Mechanisms of Cathodic Processes

Cathodic processes are half-cell reactions necessary to allow corrosion reactions to take place. Indeed, the metal-dissolving anodic reaction is forcibly coupled to a cathodic counterpart that consumes the electrons produced by the anodic reaction, so that the overall electronic flux is zero for any free-corroding electrode. In principle, any reduction reaction involving species present in the electrolyte and an equilibrium potential which is higher than that of the metal dissolution can act as the cathodic branch of the overall corrosion reaction (see

Pourbaix, Ref 10, and Evans, Ref 11, diagrams for thermodynamic and kinetic information, respectively). In the case of corrosion in an aqueous medium, the main cathodic processes, which are summarized in the following paragraphs, are easy to identify because of the ubiquitous presence of protons and dissolved oxygen that are active charge acceptors.

Proton Reduction

The main cathodic process in acidic media is proton reduction, or, more precisely, hydronium ion reduction, according to the overall reaction:

$$2H^+ + 2e^- \rightarrow H_2 \qquad \text{(Eq 34)}$$

The final reaction product is dissolved molecular hydrogen that can lead to H_2-bubble evolution over the metallic surface. The reaction in Eq 34 is the overall representation of a multistep reaction mechanism usually referred as the Volmer-Tafel-Heyrovsky route (Ref 5). The first step (Volmer reaction) is the proton discharge at the interface that yields an adsorbed hydrogen atom, H_{ad}, at the metallic surface:

$$H^+ + e^- \rightarrow H_{ad} \qquad \text{(Eq 35)}$$

Then, H_{ad} desorbs in the form of dissolved molecular gas according to two possible pathways. In the Volmer-Heyrovsky route, the hydrogen desorption is an electrochemical reaction involving one proton and one adsorbed H_{ad}:

$$H^+ + H_{ad} + e^- \rightarrow H_2 \qquad \text{(Eq 36)}$$

In contrast, the Volmer-Tafel route is the chemical recombination of two atomic adsorbates without electron transfer:

$$H_{ad} + H_{ad} \rightarrow H_2 \qquad \text{(Eq 37)}$$

The reactions in Eqs 35, 36, 37 are the typical cathodic processes in acidic solutions for most metals (Fe, Zn, Al, etc.) and alloys. Nevertheless, on the basis of the thermodynamic equilibrium analysis (Pourbaix diagram), noble metals, as well as copper, are not expected to corrode with hydrogen evolution, since their dissolution equilibrium potential is higher than that of the proton reduction. However, the presence of complexing agents (for instance, chloride) may act as a reaction catalyst and give rise to copper corrosion with hydrogen evolution.

Oxygen Reduction

Aqueous solutions in contact with air contain different amounts of dissolved oxygen depending on various parameters, such as temperature and electrolyte composition. In practice, most corrosion processes take place in such aerated environments so that dissolved oxygen is almost always available for reduction according to the following overall reactions:

$$O_2 + 2H_2O + 4e^- \rightarrow 4OH^- \quad \text{(neutral and alkaline media)} \qquad \text{(Eq 38)}$$

$$O_2 + 4H^+ + 4e^- \rightarrow 2H_2O \quad \text{(acidic media)} \qquad \text{(Eq 39)}$$

Reactions 38 and 39 represent generic rough simplifications of several possible complex multistep mechanisms that depend on the metal nature and many other parameters. Whatever the specific mechanism, however, aqueous corrosion reactions are often controlled cathodically, which means that the higher the availability of dissolved oxygen in the electrolyte, the higher the corrosion rate. This is why metallic structures in contact with stirred electrolytes or in partially immersed conditions are more prone to severe corrosion attack.

Water Reduction

In some cases, when the electrolyte does not have an excess of protons or dissolved oxygen; that is, in neutral or alkaline deaerated media, the cathodic branch of the corrosion reaction may be the reduction of water itself. The overall reaction is:

$$2H_2O + 2e^- \rightarrow H_2 + 2OH^- \qquad \text{(Eq 40)}$$

which can be split into at least two consecutive steps: water dissociation in H^+ and OH^- that precedes proton reduction (Eq 34). The reactions in Eqs 34 and 40 are alternative descriptions of the same reaction, which is the obvious consequence of the fact that water is a permanent source of protons. In other words, the most adequate description depends on the pH of the solution. From a thermodynamic point of view, the reaction in Eq 40, as well as the reaction in Eq 34, is not supposed to take place as the cathodic counterpart of the corrosion of metal (M) if the dissolution equilibrium potential of $M/M^{z+}{}^{a}$ is higher than that of the H^+/H reaction. For these reasons, copper is not expected to corrode in acidic media or in deaerated media.

References cited in this section

5. K.J. Vetter, *Electrochemical Kinetics,* Academic Press, 1967

10. M. Pourbaix, *Lectures on Electrochemical Corrosion,* Plenum Press, 1973

11. U.R. Evans, *The Corrosion and Oxidation of Metals,* Arnold Publications, Inc., 1960

F. Huet, R.P. Nogueira, and H. Takenouti, Aqueous Corrosion Reaction Mechanisms, *Corrosion: Fundamentals, Testing, and Protection*, Vol 13A*, ASM Handbook*, ASM International, 2003, p 52–60

Aqueous Corrosion Reaction Mechanisms

François Huet, Ricardo P. Nogueira, Bernard Normand, and Hisasi Takenouti, Université Pierre et Marie Curie and UPR 15 of CNRS, "Laboratoire Interfaces et Systèmes Electrochimiques," Université Pierre et Marie Curie

---

Mechanisms of Anodic Processes

Mechanisms of metal dissolution have been widely investigated in the literature and recently reviewed by Keddam (Ref 12). Examples are given below for pure metals (iron, copper) and a binary alloy (Fe-17Cr) corroding in acidic solutions. The emphasis of these examples is on the necessity of coupling the classical experimental techniques (polarization curve, electrochemical impedance) with more advanced techniques (ring-disk electrode, electrochemical quartz-crystal microbalance) in order to collect a large amount of kinetic information to make the proposed reaction mechanism as reliable as possible (Ref 13).

Fe Dissolution in H_2SO_4

The two main dissolution mechanisms reported in the literature, the *catalytic mechanism* by Heusler (Ref 14) and the *consecutive mechanism* by Bockris and others (Ref 15) are summarized first. Then, the effect of an organic inhibitor on the dissolution mechanism of iron in an acidic medium is investigated.

Catalytic Mechanism. In acidic media, iron atoms dissolve and produce ferrous ions in solution (indicated by the subscript sol) according to the overall dissolution reaction:

$$Fe \rightarrow (Fe^{2+})_{sol} + 2e^- \quad \text{(Eq 41)}$$

Heusler proposed the following mechanism for the overall reaction:

$$Fe + OH^- \rightleftarrows Fe(OH)_{ad} + e^- \quad \text{(Eq 42)}$$

$$Fe + Fe(OH)_{ad} \rightarrow Fe(OH)_{ad} + (Fe^{2+})_{sol} + 2e^- \quad \text{(Eq 43)}$$

The adsorbed $Fe(OH)_{ad}$ species formed by the reaction in Eq 42 acts as a catalyzer in the reaction in Eq 43 since it is not consumed. At the steady state, under the assumption that the reaction in Eq 42 is fast (quasi-equilibrium hypothesis), the model predicts a Tafel slope of $(1 + 2\alpha_2)F/RT$ in the polarization curve, where α_2 stands for the

charge-transfer coefficient in the reaction in Eq 43. Heusler postulated a value of 0.5 for α_2; thus this reaction mechanism should exhibit a Tafel slope of 30 mV per decade.

This mechanism is often associated with the presence of crystallographic defects on the electrode surface: for example, $Fe(OH)_{ad}$ would be formed at the kink sites, and $(OH)_{ad}$ would move to its neighbor atom when the reaction in Eq 43 proceeds, because the departure of a kink atom creates a new kink.

Consecutive Mechanism. According to Bockris and others, the dissolution mechanism differs from the previous one on the second step only. The reaction represented by Eq 43 is replaced by:

$$\mathrm{Fe(OH)_{ad}} \rightarrow \mathrm{Fe(OH)^{+}_{sol}} + e^{-} \quad \text{(Eq 44)}$$

$$\mathrm{Fe(OH)^{+}_{sol}} \rightleftarrows \left(\mathrm{Fe^{2+}}\right)_{sol} + \mathrm{OH^{-}} \quad \text{(Eq 45)}$$

$Fe(OH)_{ad}$ plays the role of a reaction intermediate that is consumed. On the basis of similar hypotheses, the reaction in Eq 42 is fast, and the Tafel coefficient of Eq 44 is equal to $\alpha_2 = 0.5$. The Tafel slope $(1 + \alpha_2)F/RT$ of the polarization curve is 40 mV per decade for this mechanism. Hence, under these highly restrictive hypotheses, the mechanism of iron dissolution can be identified by measuring the Tafel slope of the polarization curve.

Later, on the basis of EIS data, Keddam and others pointed out that the hypothesis of fast reversible reaction given in Eq 42 was in contradiction with experimental data (Ref 7). They proposed a reaction mechanism similar to that proposed by Bockris and others but in which the reactions given in Eqs 42 and 44 are irreversible. Good agreement was found between the experimental and theoretical time constants of the relaxation of the surface coverage by $Fe(OH)_{ad}$. The charge-transfer resistance was also in good agreement with that calculated from the Tafel slopes of Eq 42 and 44.

These models with a single intermediate species are able to describe the steady state around the corrosion potential. The nonstationary behavior, however, needs more complex models that take into account three or four species such as those proposed later by Keddam and others (Ref 16).

Effect of Propargylic Alcohol on the Corrosion Mechanism. Propargylic alcohol (PA) is the simplest molecule in the acetylene group and constitutes one of the main compounds for inhibiting corrosion of iron or carbon steel in acidic medium. The inhibiting effect has been examined by Benzekri and others (Ref 17), who coupled EIS and rotating ring-disk electrode (RRDE) experiments, and revisited by Itagaki and others (Ref 18), who used a channel-flow cell described schematically in Fig. 6. The electrolyte flows from the working electrode (WE) to the detector electrode (DE), which are embedded in an insulating material.

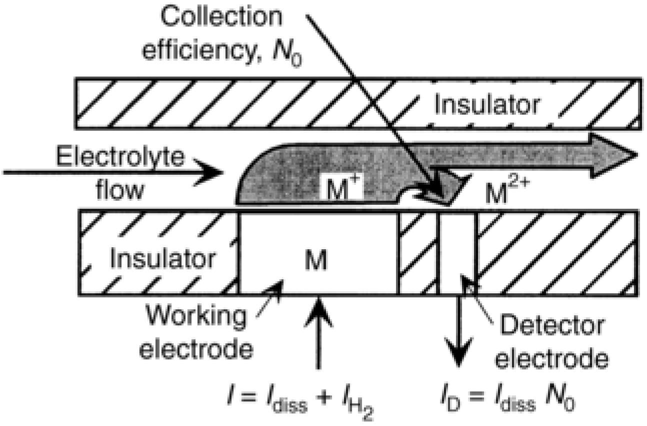

Fig. 6 Schematic representation of the channel-flow cell. Source: Ref 18

At the WE, metal dissolution takes place in parallel with, for instance, hydrogen evolution so that the overall current measured (I) is:

$$I = I_{diss} + I_{H_2} \quad \text{(Eq 46)}$$

where I_{diss} is the dissolution current and I_{H_2} the hydrogen current. A fraction of the metallic ions produced at the WE is oxidized or reduced on the DE, located downstream, according to the potential applied on the DE that is adequately chosen to avoid oxidizing the dissolved hydrogen produced at the WE. The ratio N_0 of the fluxes of ions captured at the DE and produced at the WE, often named *collection efficiency*, is controlled only

by the cell geometry. It can be determined either by calibration experiments or by theoretical calculations. From the currents measured, *I* on the WE and I_D on the DE, the dissolution current $I_{diss} = I_D/N_0$ and the hydrogen current $I_{H_2} = I - I_D/N_0$ on the WE can be evaluated.

Figure 7 presents the results obtained by Itagaki and others (Ref 18) for an iron WE in sulfuric acid with or without the presence of PA. A DE in gold was used to make the influence of dissolved hydrogen oxidation negligible. The potential of the WE was measured against a saturated (mercurous) sulfate electrode (SSE). Figure 7(a) shows that, up to approximately 10 mA/ cm^2, i_{diss} in presence of inhibitor is higher than in its absence. However, this result is not conclusive for the corrosion current since the potential of the electrode was shifted toward more cathodic potentials in the presence of PA that acts essentially to diminish the reduction of hydronium ions. Indeed, weight-loss and impedance measurements have shown that the inhibiting effect of PA essentially decreases the cathodic current at a given potential, so that the overall corrosion process is inhibited (Ref 9).

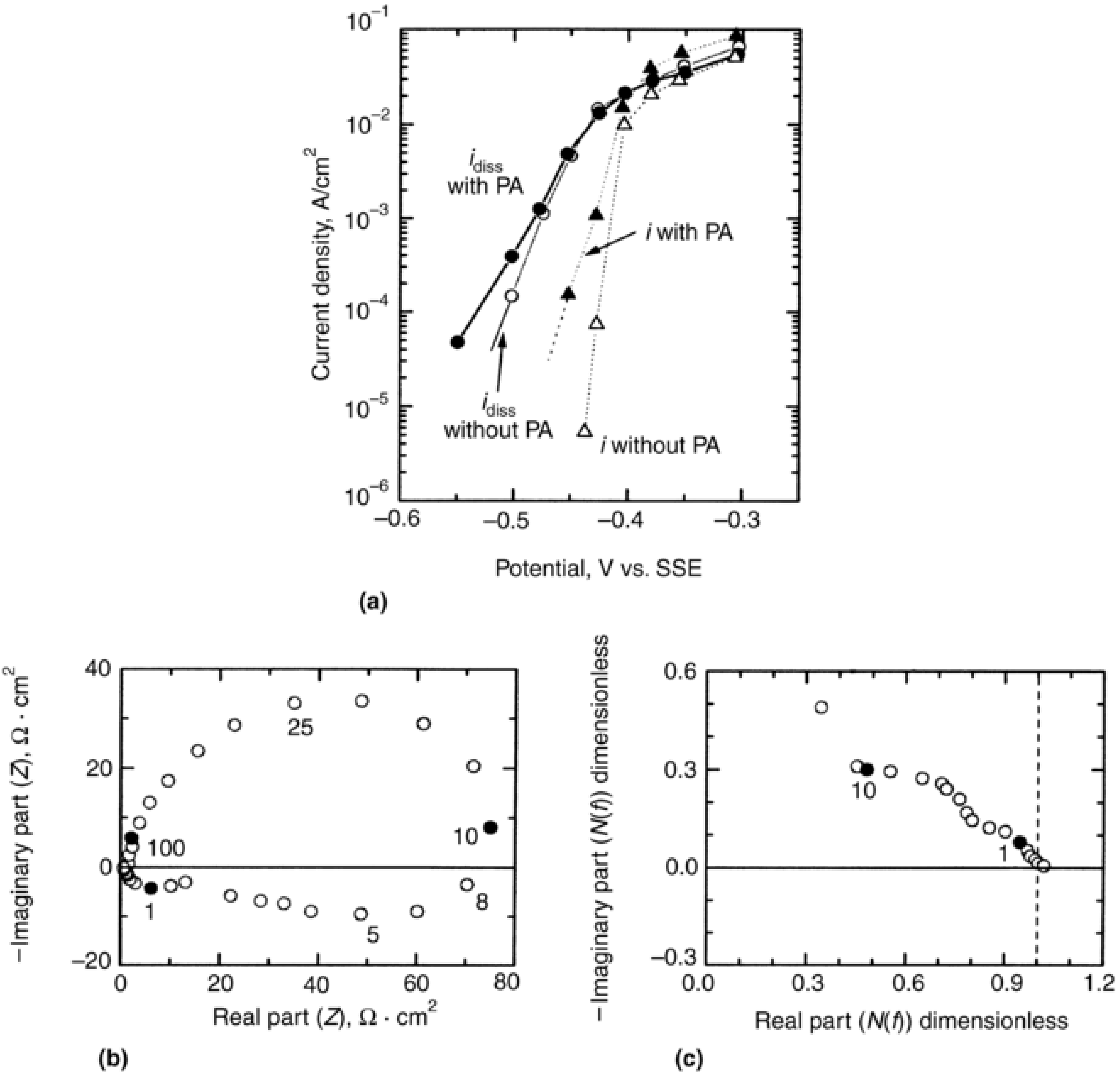

Fig. 7 Dissolution of Fe in Na_2SO_4 + H_2SO_4 (0.5 *M* SO_4^{2-} , pH 1), with or without addition of 50 m*M* propargylic alcohol (PA). (a) *i*: overall working electrode, WE, current density, i_{diss}; Fe dissolution current density. (b) Impedance diagram at 0.5 mA/cm^2 (with PA), (c) emission efficiency $N(f) = \Delta i_{diss}/\Delta i$ (with PA). Source: Ref 18

According to the dissolution models proposed by Heusler and Bockris and others, the reaction mechanism can be determined from the slope of the polarization curve: 30 mV/decade for the catalytic mechanism (Ref 14) and 40 mV per decade for the consecutive dissolution model (Ref 15). However, the slope of the log(i)-E curve in Fig. 7(a) changed from 11 to 25 mV per decade and that of the log(i_{diss})-E curve changed from 32 to 48 mV per decade when the inhibitor was added to the solution. None of these slopes correspond to the reaction mechanisms predicted by Heusler (Ref 14) or Bockris and others (Ref 15). The change in Tafel slope would also suggest that the PA was at the origin of the change in dissolution mechanism whereas it acted mainly on the cathodic reaction, as mentioned previously.

Figure 7(b) presents the electrochemical impedance measured at the overall current density of 0.5 mA/cm^2 in the presence of PA. It is important to mention that the polarization curves in Fig. 7(a) were obtained by a potential sweep method; thus the dynamic behavior investigated in steady-state conditions with the impedance technique was markedly different. The high-frequency capacitive loop, the apex of which was measured at 25 Hz, corresponds to the double- layer capacitance, approximately 80 μF/cm^2, in parallel with the charge-transfer resistance, approximately 80 Ω · cm^2. Two inductive loops can be seen in the low-frequency range (f < 8 Hz). They were attributed to the relaxation of the surface coverages by a dissolution intermediate species (loop around 5 Hz) and by the adsorbed inhibitor (loop around 1 Hz). The impedance spectra at frequencies higher than 2 Hz and the fact that the product $R_t I$ was close to 40 mV suggest that the iron dissolution occurred via the consecutive mechanism proposed by Keddam and others (Ref 7).

The fraction of current consumed to form the dissolving species (here Fe^{2+}) is defined at any frequency (f) by the ratio $N(f) = \Delta I_{diss}/\Delta I$ derived from the ratio $\Delta I_D/\Delta I$, measured under ac regime, divided by the dynamic collection efficiency. Figure 7(c) shows that $N(f)$ was smaller than 1 above 1 Hz, which indicates that a large part of the ac current was not consumed by the dissolution itself but was used in the formation of adsorbed intermediate species. In contrast, the low-frequency limit of $N(f)$ is close to unity, as expected from the Faraday law.

The coupling of advanced experimental techniques offers deeper insight into the reaction mechanism of iron dissolution and also explains how the PA inhibits the corrosion process by decreasing the hydrogen-evolution reaction rate.

Dissolution of Copper in Hydrochloric Acid

Copper and copper alloys are widely used in industrial applications because of their high electrical and thermal conductivity and, also, good corrosion resistance in various media. However, the latter decreases significantly in the presence of chloride ions that lead to copper dissolution as cuprous ions at low anodic potentials and cupric ions at higher potentials (Ref 19). Figure 8 presents results of EIS, ring-disk electrode (RDE), and electrochemical quartz crystal microbalance (EQCM) experiments carried out simultaneously on an electrodeposited copper EQCM electrode surrounded by a thin platinum ring (Ref 20). Since the EQCM electrode could not rotate, an impinging jet cell was employed instead of a RRDE to control the hydrodynamic conditions.

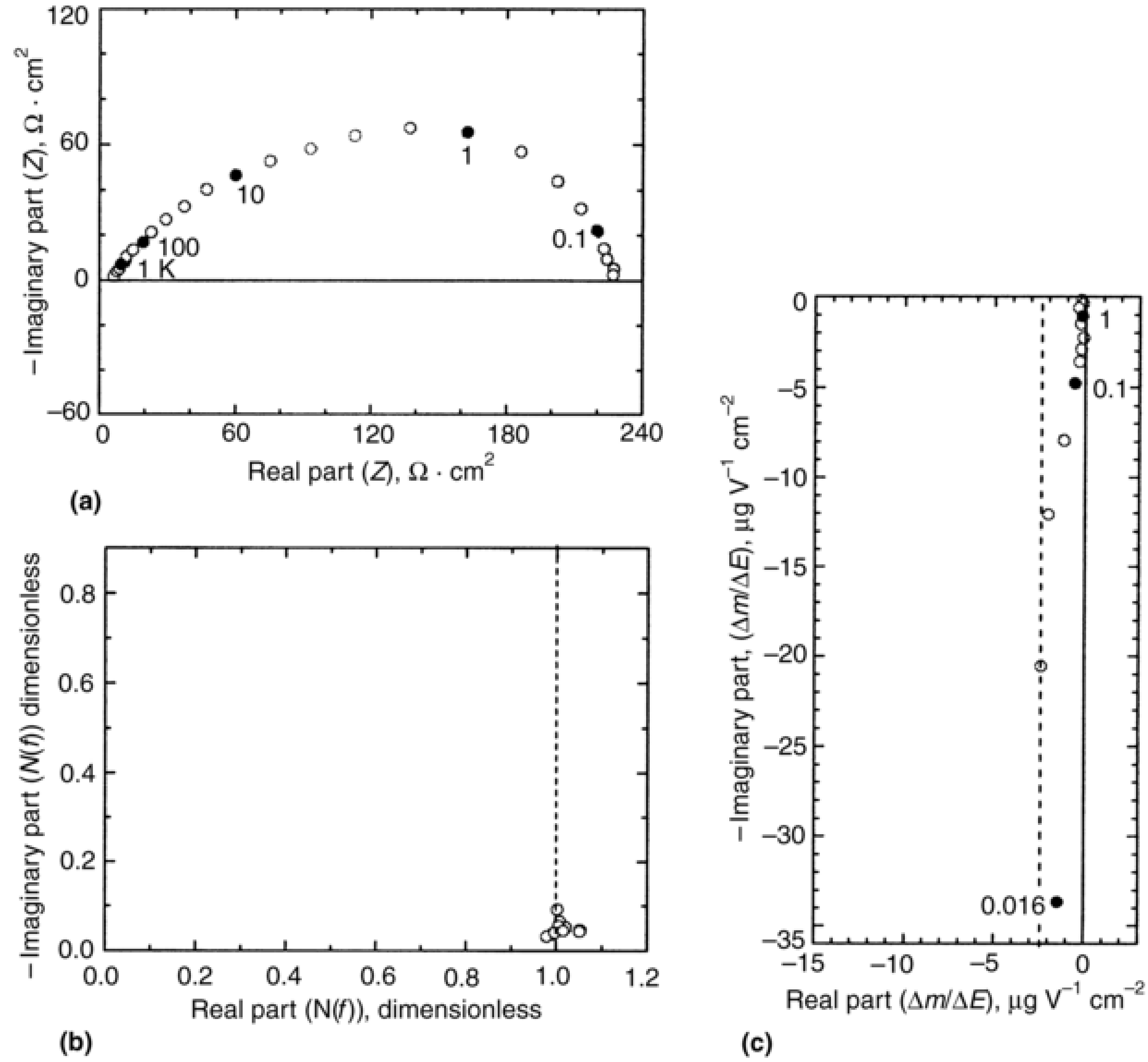

Fig. 8 Dissolution of Cu in 1 *M* NaCl + 0.05 *M* Na_2CO_3, pH 8, *i* = 0.1 mA/cm^2. (a) Impedance diagram; (b) $N(f) = \Delta I_{diss}/\Delta I$; (c) $\Delta m/\Delta E$. Source: Ref 20

The impedance diagram (Fig. 8a) shows two badly separated capacitive loops. The capacitance associated with the high-frequency loop is equal to 50 μF/cm^2 and, therefore, can be attributed to the double-layer capacitance in parallel with the charge-transfer resistance. The low-frequency loop is then related to the faradaic impedance due to the relaxation of the surface coverage by a dissolution intermediate. In contrast with the case of iron presented above, Fig. 8(b) shows an emission efficiency $N(f) = \Delta I_{diss}/\Delta I$ of 1 regardless of the perturbation frequency, indicating that there is no charge transfer in the formation of adsorbed intermediate species; that is, the reaction is purely chemical. The change in mass (Δm) induced by a perturbation in potential ΔE at frequency *f* gives a ratio $\Delta m/\Delta E$ parallel to the imaginary axis in the Nyquist plane (Fig. 8c) at low frequency, with a negative real part, which corresponds actually to electrode dissolution. By coupling EQCM and EIS data, the gram-equivalent (*A*), which represents the change in mass per mole of electrons exchanged ($\Delta Q/F$), can be evaluated as follows:

$$A(\omega) = \frac{\Delta m}{\Delta Q/F} = j\omega F\frac{\Delta m}{\Delta I} = j\omega F\frac{\Delta m}{\Delta E}\frac{\Delta E}{\Delta I} = j\omega F\frac{\Delta m}{\Delta E}(\omega)Z(\omega) \quad \text{(Eq 47)}$$

since $\Delta I = j\omega\Delta Q$ and $Z = \Delta E/\Delta I$. The low- frequency limit of $A(\omega)$, $-2\pi f_0 F\text{Im}(\Delta m/\Delta E)R_p$, can be obtained from the imaginary part of $\Delta m/\ \Delta E = -33.5 \times 10^{-6}$ μg/(V · cm^2) at frequency $f_0 = 16$ mHz. A value of 73.8 g

equivalent, close to the atomic mass of copper (63.5 g) when considering the experimental accuracy, was found, which confirms that copper actually dissolves as a monovalent ion in chloride medium at low anodic potential. The most probable dissolution mechanism consistent with the results of the EIS, RDE, and EQCM techniques is then the following:

$$Cu + Cl^- \rightarrow Cu(Cl^-)_{ad} \quad \text{(Eq 48)}$$

$$Cu(Cl^-)_{ad} \rightarrow (CuCl) + e^- \quad \text{(Eq 49)}$$

The intermediate species, which is likely $Cu(Cl^-)_{ad}$, is adsorbed through a chemical reaction (no charge transfer), as suggested earlier. The subsequent electrochemical desorption of this species is potential dependent and generates the low-frequency capacitive loop in the impedance diagram. These combined EIS, RDE, and EQCM experiments allowed the electric state of the reaction intermediate to be demonstrated unambiguously. This is an important advancement in the understanding of the reaction mechanism.

Anodic Dissolution of a Binary Alloy: Iron-Chromium

Iron-chromium (Fe-Cr) binary alloys constitute a model material for investigating corrosion of stainless steels. This is the reason why the dissolution and passivation mechanisms of iron- chromium alloys have been extensively studied in the literature. The mechanism of Fe-17Cr dissolution in 1*M* H_2SO_4 devised from EIS and RDE experiments (Ref 21) is discussed subsequently. Typical results are presented in Fig. 9. The polarization curve shows that this alloy becomes passive above -0.8 V versus SSE. At the critical potential of approximately -0.88 V versus SSE, the current density was about 3 mA/ cm^2, several orders of magnitude lower than that measured with an iron electrode, indicating that chromium promotes the passivation process substantially.

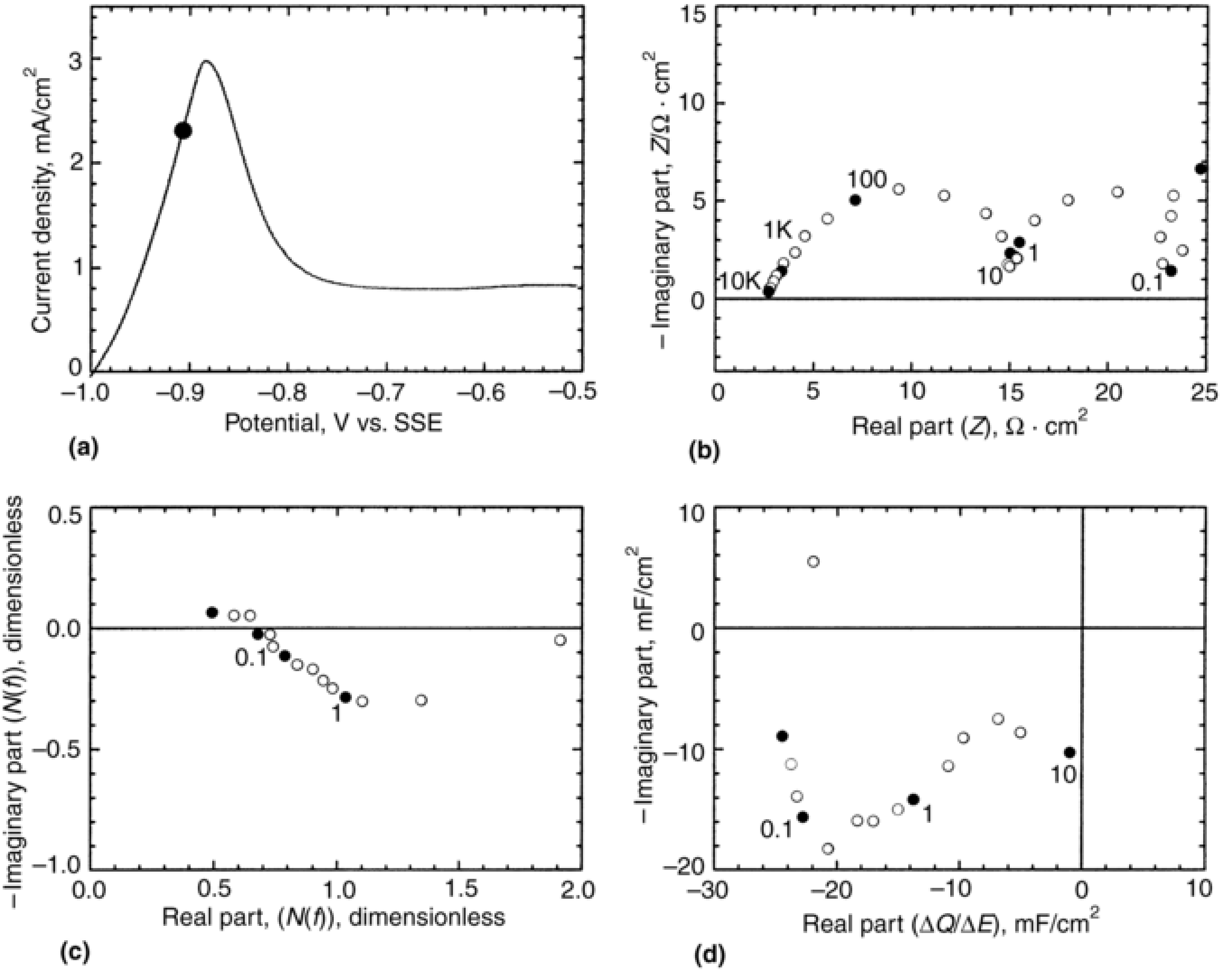

Fig. 9 Dissolution of Fe-17Cr in 1 *M* H_2SO_4. (a) Polarization curve. (b) Impedance diagram at point A. (c) *N*(*f*) at point A. (d) $\Delta Q/\Delta E$ at point A calculated from *N*(*f*) and *Z* data. Source: Ref 22

The impedance diagram, measured at point A of the polarization curve, exhibits four time constants, in addition to the high-frequency time constant related to the charge-transfer resistance in parallel with the double-layer capacitance. The four time constants correspond to the relaxation of the surface coverage by four intermediate species. Figure 9(c) presents the ratio $N(f) = i_{diss}/i$ where i_{diss} is the current density relative to the dissolution of the Fe^{2+} ions collected at the ring and i is the overall current density. Both current densities are the responses to an ac potential perturbation at frequency f. It should be noted that i contains the contribution of both chromium and iron dissolution. A remarkable result is that the modulus of $N(f)$ was greater than unity at frequencies above 1 Hz; that is, the faradaic efficiency of the iron dissolution was surprisingly greater than 100%, indicating that a surplus of charge was supplied to the iron dissolution, as explained later in this article. The ratio $\Delta Q/\Delta E$, where Q denotes the charge stored at the electrode surface calculated according to the algorithm developed for the dissolution of an iron electrode (Ref 17), is given in Fig. 9(d).

To explain the main features of the aforementioned results and of those obtained in the passivation domain for alloys of various Cr content, the simplified reaction mechanism presented in Fig. 10 was devised. Only three reaction intermediates ($Fe(I)_{ad}$, $Fe(II)_{ad}$, and $Cr(III)_{ad}$) were used to avoid a more intricate model that would be difficult to handle. The reactions relative to Cr contained the dissolution in $Cr(II)_{sol}$ species and the formation of a passive species $Cr(III)_{ad}$. The Cr dissolution step is necessary to model the uniformity of the electrode dissolution, which gives a molar ratio of Fe and Cr dissolved in the solution equal to that of the metallic matrix. Otherwise, selective dissolution of iron would give rise to a macroporosity that was not observed experimentally. The effect of the $Cr(III)_{ad}$ passive species was to slow down the iron dissolution rate markedly, as proposed by Frankenthal (Ref 23). The mechanism of Fe dissolution contains the catalytic step (Eq B in Fig. 10) introduced by Heusler, but only two adsorbed species have been considered here instead of four in the mechanism proposed by Keddam and others (Ref 7). This model contains no Fe passivation reaction; the passive behavior observed experimentally was simulated by the Cr passivation that slows down the alloy dissolution by virtue of the uniform dissolution conditions.

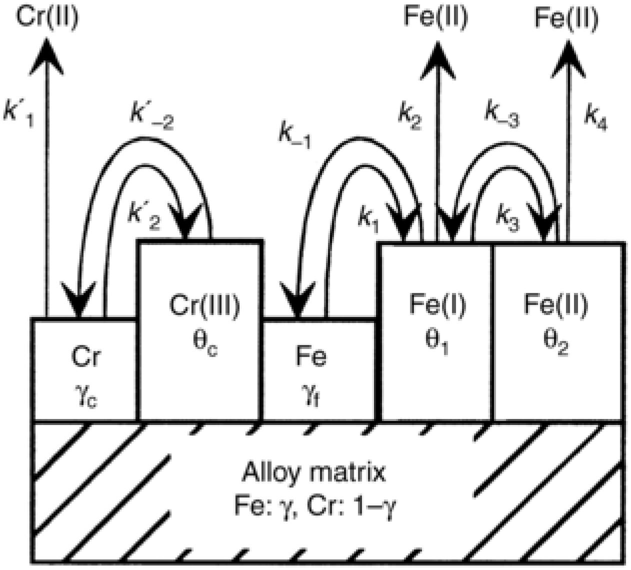

Fe	
$Fe \xleftrightarrow{k_1/k_{-1}} Fe(I)_{ad} + e^-$	(Eq A)
$Fe + Fe(I)_{ad} \xrightarrow{k_2} Fe(I)_{ad} + Fe(II)_{ad} + 2e^-$	(Eq B)
$Fe(I)_{ad} \xleftrightarrow{k_3/k_{-3}} Fe(II)_{ad} + e^-$	(Eq C)
$Fe(II)_{ad} \xrightarrow{k_4} Fe(II)_{sol}$	(Eq D)
Cr	
$Cr \xrightarrow{k_1'} Cr(II)_{sol} + 2e^-$	(Eq E)

$$Cr \xleftrightarrow{k_2'/k_{-2}'} Cr(III)_{ad} + 3e^- \quad \text{(Eq F)}$$

Fig. 10 Schematic representation of the activation-passivation transition mechanism of Fe-Cr alloy in an acidic medium

From the charge and mass balances for the reactions in Fig. 10, the polarization curve, the impedance diagrams, the dynamic emission coefficient $N(f)$ of Fe^{2+}, and the ratio $\Delta Q/\Delta E$ were calculated. Figure 11 presents the results at point A of the polarization curve in Fig. 9(a). The impedance diagram was suitably reproduced except for the low-frequency behavior. This discrepancy is due to the simplifications in the model. The decrease in $N(f)$ with decreasing frequency in Fig. 11(b) was also simulated, but the maximum value was significantly smaller than that obtained experimentally. The extra charge necessary to dissolve the iron beyond the Faraday law, mentioned earlier, was supplied by the surface relaxation of $Cr(III)_{ad}$ species. The $\Delta Q/\Delta E$ curve was also correctly reproduced with two time constants and a negative real part, but the time constant in the simulated high-frequency loop was significantly smaller than the experimental one.

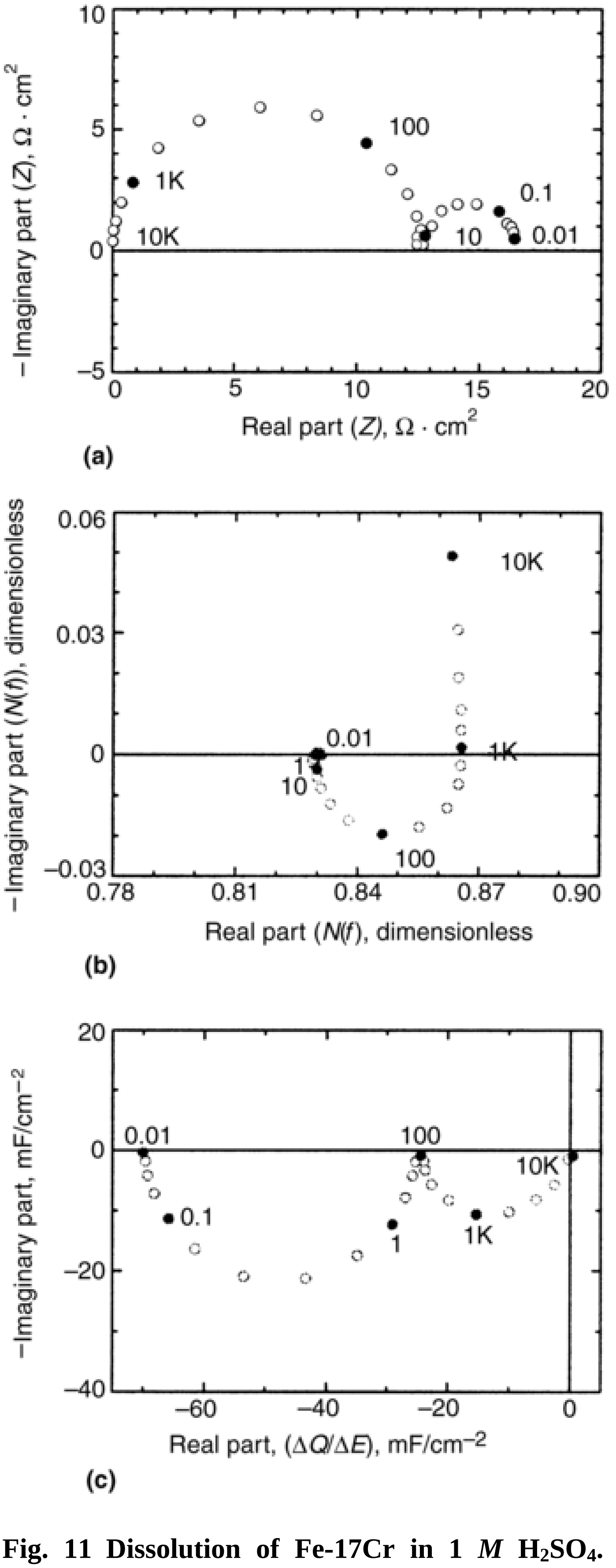

Fig. 11 Dissolution of Fe-17Cr in 1 *M* H_2SO_4. Simulations for the model presented in Fig. 10 at conditions of point A in Fig. 9. (a) Impedance diagram; (b) *N(f)*; (c) $\Delta Q/\Delta E$. Source: Ref 21

The coupling of steady-state polarization, EIS, and RRDE experiments allowed a more reliable model of the reaction mechanism to be proposed. This is a very appropriate method to select the adequate model among all those devised from the single measurement of polarization curves.

References cited in this section

7. I. Epelboin and M. Keddam, *J. Electrochem. Soc.,* Vol 117, 1970, p 1052

9. I. Epelboin, C. Gabrielli, M. Keddam, and H. Takenouti, *Electrochemical Corrosion Testing,* F. Mansfeld and U. Bertocci, Ed., STP 727, ASTM International, 1981, p 150–192

12. M. Keddam, *Corrosion Mechanisms in Theory and Practice,* P. Marcus, Ed., Marcel Dekker Inc, 2002, p 97

13. H. Takenouti, *Electrochemistry,* Vol 67, 1999, p 1063

14. K.E. Heusler, *Z. Elektrochem.,* Vol 62, 1958, p 582

15. J.O'M. Bockris, D. Drazic, and A.R. Despic, *Electrochim. Acta,* Vol 4, 1961, p 325

16. M. Keddam, O. R. Mattos, and H. Takenouti, *J. Electrochem. Soc.,* Vol 128, 1981, p 257, 266

17. N. Benzekri, M. Keddam, and H. Takenouti, *Electrochim. Acta,* Vol 34, 1989, p 1159

18. M. Itagaki, M. Tagaki, K. Watanabe, *Denki Kagaku (Electrochemistry),* Vol 63, 1995, p 425

19. O.E. Barcia, O.R. Mattos, and B. Tribollet, *J. Electrochem. Soc.* Vol 139, 1992, p 446

20. C. Gabrielli, M. Keddam, F. Minouflet-Laurent, and H. Perrot, *Electrochem. Solid-State Letters,* Vol 3, 2000, p 418

21. I. Annergren, M. Keddam, H. Takenouti, and D. Thierry, *Electrochim. Acta,* Vol 41, 1996, p 1121

22. R.P. Frankenthal, *J. Electrochem. Soc.,* Vol 116, 1969, p 580

23. M. Keddam, O.R. Mattos, and H. Takenouti, *Electrochim. Acta,* Vol 31, 1993, p 1158

F. Huet, R.P. Nogueira, and H. Takenouti, Aqueous Corrosion Reaction Mechanisms, *Corrosion: Fundamentals, Testing, and Protection*, Vol 13A, *ASM Handbook*, ASM International, 2003, p 52–60

Aqueous Corrosion Reaction Mechanisms

François Huet, Ricardo P. Nogueira, Bernard Normand, and Hisasi Takenouti, Université Pierre et Marie Curie and UPR 15 of CNRS, "Laboratoire Interfaces et Systèmes Electrochimiques," Université Pierre et Marie Curie

---

References

1. H. Kaesche, *Metallic Corrosion, Principles of Physical Chemistry and Current Problems,* NACE International, Houston, TX, 1985

2. F. Mansfeld and U. Bertocci, Ed., *Electrochemical Corrosion Testing*, STP 727, ASTM International, 1981

3. J.C. Scully, Ed., *Treatise on Materials Science and Technology,* Vol 23, *Corrosion: Aqueous Processes and Passive Films,* Academic Press, 1983

4. J.R. Scully, D.C. Silvermann, and M.W. Kendig, Ed., *Electrochemical Impedance: Analysis and Interpretation,* STP 1188, ASTM International, 1994

5. K.J. Vetter, *Electrochemical Kinetics,* Academic Press, 1967

6. A.J. Bard and L.R. Faulkner, *Electrochemical Methods, Fundamentals and Applications,* John Wiley & Sons, Inc., 1980

7. I. Epelboin and M. Keddam, *J. Electrochem. Soc.,* Vol 117, 1970, p 1052

8. C. Wagner and W. Traud, *Z. Elektrochem.,* Vol 44, 1938, p 391

9. I. Epelboin, C. Gabrielli, M. Keddam, and H. Takenouti, *Electrochemical Corrosion Testing,* F. Mansfeld and U. Bertocci, Ed., STP 727, ASTM International, 1981, p 150–192

10. M. Pourbaix, *Lectures on Electrochemical Corrosion,* Plenum Press, 1973

11. U.R. Evans, *The Corrosion and Oxidation of Metals,* Arnold Publications, Inc., 1960

12. M. Keddam, *Corrosion Mechanisms in Theory and Practice,* P. Marcus, Ed., Marcel Dekker Inc, 2002, p 97

13. H. Takenouti, *Electrochemistry,* Vol 67, 1999, p 1063

14. K.E. Heusler, *Z. Elektrochem.,* Vol 62, 1958, p 582

15. J.O'M. Bockris, D. Drazic, and A.R. Despic, *Electrochim. Acta,* Vol 4, 1961, p 325

16. M. Keddam, O. R. Mattos, and H. Takenouti, *J. Electrochem. Soc.,* Vol 128, 1981, p 257, 266

17. N. Benzekri, M. Keddam, and H. Takenouti, *Electrochim. Acta,* Vol 34, 1989, p 1159

18. M. Itagaki, M. Tagaki, K. Watanabe, *Denki Kagaku (Electrochemistry),* Vol 63, 1995, p 425

19. O.E. Barcia, O.R. Mattos, and B. Tribollet, *J. Electrochem. Soc.* Vol 139, 1992, p 446

20. C. Gabrielli, M. Keddam, F. Minouflet-Laurent, and H. Perrot, *Electrochem. Solid-State Letters,* Vol 3, 2000, p 418

21. I. Annergren, M. Keddam, H. Takenouti, and D. Thierry, *Electrochim. Acta,* Vol 41, 1996, p 1121

22. R.P. Frankenthal, *J. Electrochem. Soc.,* Vol 116, 1969, p 580

23. M. Keddam, O.R. Mattos, and H. Takenouti, *Electrochim. Acta,* Vol 31, 1993, p 1158

F. Huet, R.P. Nogueira, and H. Takenouti, Aqueous Corrosion Reaction Mechanisms, *Corrosion: Fundamentals, Testing, and Protection*, Vol 13A, *ASM Handbook*, ASM International, 2003, p 52–60

Aqueous Corrosion Reaction Mechanisms

François Huet, Ricardo P. Nogueira, Bernard Normand, and Hisasi Takenouti, Université Pierre et Marie Curie and UPR 15 of CNRS, "Laboratoire Interfaces et Systèmes Electrochimiques," Université Pierre et Marie Curie

Selected References

- A.J. Bard and L.R. Faulkner, *Electrochemical Methods, Fundamentals and Applications,* John Wiley & Sons, Inc., 1980
- C. Gabrielli, "Identification of Electrochemical Processes by Frequency Response Analysis," Solartron Instruments, Farnborough, U.K., 1980
- C. Gabrielli, "Use and Applications of Electrochemical Impedance Techniques", Technical Report 24, Solartron Instruments, Farnborough, U.K., 1997
- H. Kaesche, *Metallic Corrosion, Principles of Physical Chemistry and Current Problems,* NACE International, 1985
- M. Keddam, Anodic Dissolution, *Corrosion Mechanisms in Theory and Practice,* P. Marcus, Ed., Marcel Dekker Inc., 2002, p 97

J. Kruger, Passivity, *Corrosion: Fundamentals, Testing, and Protection*, Vol 13A, *ASM Handbook*, ASM International, 2003, p 61–67

Passivity

Jerome Kruger, Johns Hopkins University

Introduction

ALL METALS AND ALLOYS, with the exception of gold, have a thin protective corrosion product film present on their surface resulting from reaction with the environment. If such a film did not exist on metallic materials exposed to the environment, they would revert back to the thermodynamically stable condition of their origin—the ores used to produce them. Some of these films—the passive films—on some, but not all, metals and alloys have special characteristics that enable them to provide superior corrosion- resistant metal surfaces. These protective "passive" films are responsible for the phenomenon of passivity.

The first metal found to exhibit the phenomenon of passivity was iron. Uhlig (Ref 1) has written a review of the history of passivity that lists three 18th century scientists—the Russian Lomonosov in 1738, the German Wenzel in 1782, and the Briton Keir in 1790—who observed that the highly reactive surface of iron became unexpectedly unreactive after immersion in concentrated nitric acid. This effect was first called *passivity* by Schönbein.

This unexpected phenomenon of passivity occupies a central position in controlling corrosion processes, enabling the use of metallic materials in the many technologies of the 21st century. Moreover, it is the breakdown of the passive film that leads to the inability of metals and alloys to perform their assigned functions because of localized corrosion failure modes such as stress corrosion, pitting, crevice corrosion, and corrosion fatigue. Its importance to materials technology transcends, however, corrosion science and corrosion engineering. For example, one of the main reasons silicon replaced germanium in semiconductor device technology was that silicon forms effective passive films and germanium does not (Ref 2).

Early work in the area of passivity that had an enormous impact on providing technology with improved engineering materials is, of course, the development of the stainless steels. This has promoted the continual development of a large number of alloys that exhibit corrosion resistance because of the protection provided by the passive film.

An improved understanding of the role that alloying constituents play in determining the properties of this passive film will lead to guidelines that can be used to develop engineering alloys with improved corrosion resistance. The scope of this article limits the discussion of all of the details on the subject of passivity. Moreover, the passivation behavior of all of the various metals and semiconductors that exhibit passivity is not given. Instead, this article discusses the classic passive metal iron and its alloys as illustrative examples of metals exhibiting passivity. References 3, 4, 5, 6, 7 provide a more extensive treatment of the subject of passivity in general and passivity of other metals and semiconductors in addition to iron.

References cited in this section

1. H.H. Uhlig, *Passivity of Metals,* R.P. Frankenthal and J. Kruger, Ed., Electrochemical Society, 1978, p 1–28

2. A.G. Revesz and J. Kruger, *Passivity of Metals,* R.P. Frankenthal and J. Kruger, Ed., Electrochemical Society, 1978, p 137

3. R.P. Frankenthal and J. Kruger, Ed., *Passivity of Metals,* Electrochemical Society, 1978

4. J. Kruger, *Int. Mater. Rev.,* Vol 33, 1988, p 113–130

5. H. Hasegawa and T. Sugano, Ed., *Passivation of Metals and Semiconductors, Part II, Passivity of Semiconductors,* Pergamon Press, 1990

6. K.E. Heusler, Ed., *Passivation of Metals and Semiconductors,* Materials Science Forum, Vol 185–188, Trans Tech Publications, 1995

7. M.B. Ives, J.L. Luo, and J.R. Rodda, Ed., *Passivity of Metals and Semiconductors,* Proc. Vol 99–42, Electrochemical Society, 2001

J. Kruger, Passivity, *Corrosion: Fundamentals, Testing, and Protection*, Vol 13A, *ASM Handbook*, ASM International, 2003, p 61–67

Passivity

Jerome Kruger, Johns Hopkins University

General Aspects

Importance of Passivity to Corrosion-Control Technology. If the passive film did not exist, most of the technologies that depend on the use of metals could not exist because the phenomenon of passivity is a critical element in controlling corrosion processes. Therefore, the destruction of passivity at local breakdowns leads to a large part of the corrosion failures of metal and alloy structures—localized attack such as pitting, crevice corrosion, stress corrosion, and corrosion fatigue.

The development of the stainless steels in the 1920s is regarded as a major application of the phenomenon of passivity. This development has contributed significantly to modern technology by providing the design engineer with engineering materials such as the large number of iron and nickel-base alloys as well as many other alloy systems that exhibit superior corrosion resistance—this effort continues today.

Types of Passivity. There are two types of passivity:

- *Type 1.* A metal active in the electromotive force (emf) series is passive when its electrochemical behavior in a given environment becomes that of a metal noble in the emf series (low corrosion rate, noble potential).
- *Type 2.* A metal is passive while, still from the standpoint of thermodynamics at an active potential in a given environment, it exhibits a low corrosion rate (low corrosion rate, active potential). This type of passivity can be termed "practical passivity."

Only type 1 passivity is considered here. Examples of metals or alloys exhibiting such passivity are nickel, chromium, titanium, iron in oxidizing environments, stainless steels, and many others. Examples of type 2 passivity are lead in sulfuric acid and iron in an inhibited pickling acid.
A major characteristic of a type 1 passive system is the existence of a polarization curve (*i*, current density, or rate, versus *E*, potential, or driving force), of the sort shown in Fig. 1. It illustrates well a restatement of the definition of type 1 passivity as first proposed by Wagner (Ref 8). He suggested that a metal becomes passive when, upon increasing its potential in the positive or anodic (oxidizing) direction, a potential is reached where the current (rate of anodic dissolution) sharply decreases to a value less than that observed at a less anodic potential. This decrease in anodic dissolution rate, in spite of the fact that the driving force for dissolution is brought to a higher value, is the result of the formation of a passive film.

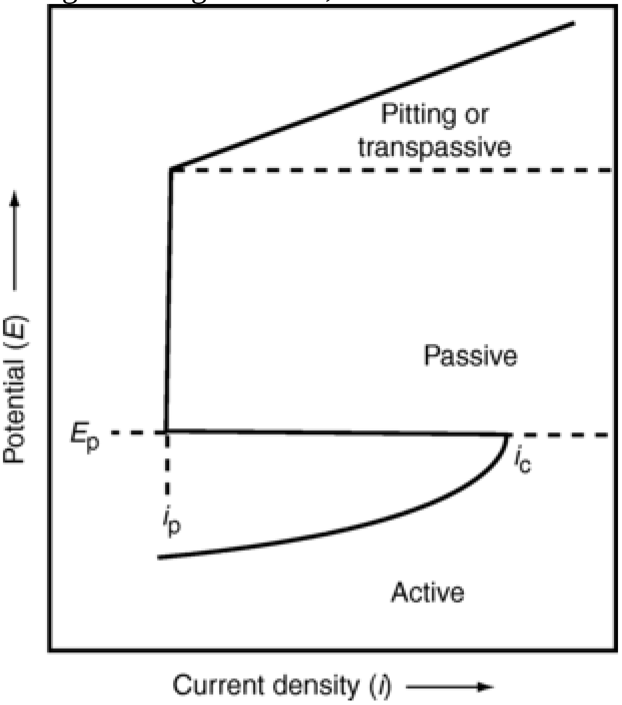

Fig. 1 The idealized anodic polarization curve for an iron-water system exhibiting passivity. Three different potential regions are shown; the active, passive, and pitting or transpassive regions. E_p is potential above which the system becomes passive and exhibits the passive current density i_p. The critical current density for passivation is i_c.

Another more practical definition has been provided by an ASTM standard: "passive—the state of metal surface characterized by low corrosion rates in a potential region that is strongly oxidizing for the metal" (Ref 9).
Employing Passivity to Control Corrosion. Passivity can be used to control corrosion by using methods that bring the potential of the surface to be protected to a value in the passive region. This can be accomplished by the following tactics:

- Using a device called a potentiostat, a current can be applied to the metal to be protected that will set and control the potential at a value greater than the passivating potential, E_p. This method of producing passivity is called anodic protection (Fig. 1).

- For environments containing damaging species such as chloride ions that cause pitting, the potentiostat or other devices that control the potential can be used as in the item above to set the potential to a value in the passive region below the critical potential for pitting, E_{pit}.
- Alloys or metals that spontaneously form a passive film, for example, stainless steels, nickel, or titanium alloys, can be used in applications that require resistance to corrosion. Usually a pretreatment such as that described below is desirable.
- A surface pretreatment can be carried out on an alloy capable of being passivated. The use of such a pretreatment has been a standard practice for stainless steels for many years. The passivating procedure involves immersion of thoroughly degreased stainless steel parts in a nitric acid solution followed by a thorough rinsing in clean, hot water. The most popular solution and conditions of operation for passivating stainless steel is a 30 min immersion in a 20 vol% nitric acid solution at 49 °C (120 °F). However, other solutions and treatments may be used, depending on the type of stainless steel being treated (Ref 10).
- The environment can be modified to produce a passive surface. Oxidizing agents such as chromate and concentrated nitric acid are examples of passivating solutions that maintain a passive state on some metals and alloys.

References cited in this section

8. C. Wagner, *Corros. Sci.,* Vol 5, 1965, p 751–764

9. *Definitions of Terms Relating to Corrosion and Corrosion Testing,* G 13, *Annual Book of ASTM Standards,* ASTM, 1983

10. D. Peckner and I.M. Bernstein, *Handbook of Stainless Steels,* McGraw-Hill, 1977, Ch 24, p 24

J. Kruger, Passivity, *Corrosion: Fundamentals, Testing, and Protection*, Vol 13A, *ASM Handbook*, ASM International, 2003, p 61–67

Passivity

Jerome Kruger, Johns Hopkins University

Thermodynamics of Passivity

Thermodynamics provide a guide to the conditions under which passivation becomes possible. A valuable guide to thermodynamics is the potential-pH diagram, the Pourbaix diagram. Pourbaix's *Atlas of Electrochemical Equilibria in Aqueous Solutions* (Ref 11) describes applications of these potential-pH equilibrium diagrams to corrosion science and engineering. One major application is the establishment of the theoretical domains or conditions for corrosion, immunity, and passivation.

Figure 2 shows a simplified diagram for the iron-water system. The three theoretical domains show on a thermodynamic basis the potential- pH conditions where no corrosion is possible (immunity), where a corrosion-product film forms that may confer protection against corrosion (passivation), and where corrosion is expected (corrosion). (Pourbaix designates the immunity domain as that of "thermodynamic nobility" and the total of the passivation and immunity domains as that of "practical nobility.") Whether the film is passive (protective) or not is a kinetic consideration and not a thermodynamic one (see the section "Nature of the Passive Film" in this article). Such Pourbaix diagrams can identify metals capable of forming films that, depending on their properties, may or may not be protective, and conditions can be determined where there is a transition from passivation to activation. One could call the equilibrium diagrams a "road map of the possible."

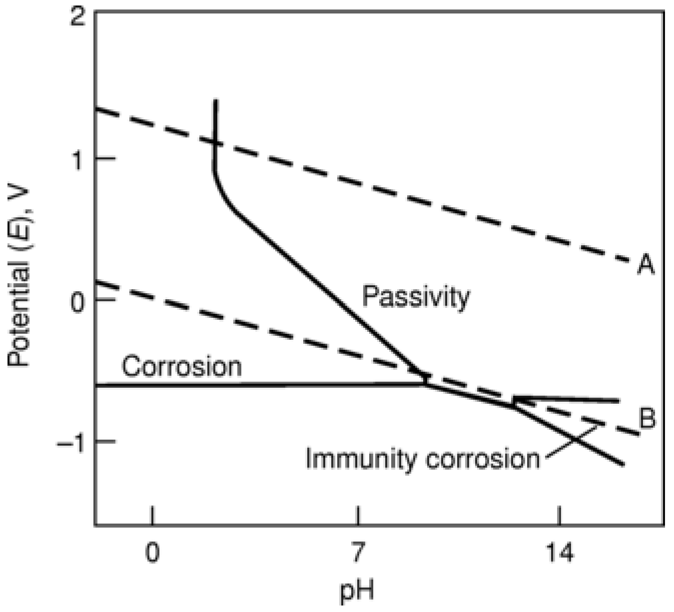

Fig. 2 Simplified potential-pH equilibrium diagram (Pourbaix diagram) for the iron-water system. Above equilibrium line A oxygen is evolved, and below equilibrium line B hydrogen is evolved. Source: Ref 11

The diagrams can, therefore, be used as a basis for identifying the active, passive, and transpassive regions of active-passive polarization curves (see Fig. 1). Thus, potentials above the oxygen-evolution line (the line marked A in Fig. 2) are in the transpassive region. Also, the diagrams can be used to interpret the reasons for loss of the protective nature of the passive film in the transpassive region. For example, the protective layer on stainless steels that contain chromium involves Cr(III); at higher potentials Cr(III) is oxidized to Cr(VI), and the protective Cr_2O_3 becomes the soluble chromate ion, resulting in the loss of corrosion resistance. Usually, the passive regions of the polarization curves correspond to potentials in the equilibrium diagrams where protective solid compounds are stable. However, even though the active regions of the polarization curves usually lie in regions labeled as "corrosion" on the potential-pH diagrams, this is not always the case. For example, iron can passivate in sulfuric acid solutions under conditions where the diagrams would predict corrosion and, hence, an active condition, but the rate of passive-film dissolution is so extremely slow that the film is metastable and thereby prevents metal dissolution.

Reference cited in this section

11. M. Pourbaix, *Atlas of Electrochemical Equilibria in Aqueous Solutions,* 2nd ed., Pergamon Press, 1966

J. Kruger, Passivity, *Corrosion: Fundamentals, Testing, and Protection*, Vol 13A, *ASM Handbook*, ASM International, 2003, p 61–67

Passivity

Jerome Kruger, Johns Hopkins University

Kinetics of Passivity

From the standpoint of the kinetics, passivity can be characterized as the conditions existing on a metal surface because of the presence of a protective film that markedly lowers the rate of corrosion, even though from thermodynamic (corrosion tendency) considerations one would expect active corrosion. Figure 1, which depicts

an idealized anodic polarization curve for a metal surface, can serve as a basis for describing in a general way the kinetics of passivation. Anodic polarization curves obtained from a real system under practical conditions (Ref 12) are shown in Fig. 3. They still include the general features of the ideal curve (Fig. 3). Figure 3 shows a comparison of iron and 304L stainless steel in H_2SO_4. In Fig. 1, where the anodic polarization curve is that of a metal that exhibits an ability to become passive, the current initially increases with an increase in potential, but when the potential reaches the value of the passivating potential, E_p, the critical current density for passivation, i_c, is reached, and a marked drop in current density (corrosion rate) is observed. This is the onset of passivity, and the current density remains low at i_p as the potential is increased to higher values. If the potential is increased to sufficiently high values, the current density begins to rise, and either pitting results or the transpassive region is entered. In the transpassive region, oxygen evolution and possibly increased corrosion takes place.

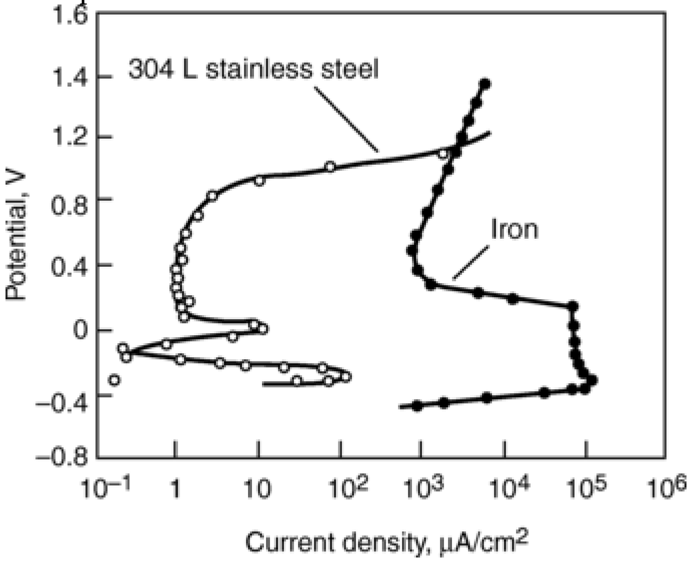

Fig. 3 Comparison of anodic polarization curves for iron and 304L stainless steel in 1 *N* H_2SO_4. Adapted from Ref 12

The corrosion potential of a metal surface is controlled by the intersection of the anodic (potential increases in the positive direction) and cathodic (potential increases in the negative direction) polarization curves where the anodic and cathodic reaction rates are equal. Therefore, even though a metal may be capable of exhibiting passivity, its corrosion rate will depend on where the cathodic polarization curve intersects the passive metal anodic curve of the type shown in Fig. 1. Figure 4 shows three possible cases. If the cathodic reaction produces a polarization curve such as A, which is indicative of oxidizing conditions, the corrosion potential will be located in the passive region, and the system can exhibit a low corrosion rate. If the cathodic reaction produces curve C, which is indicative of reducing conditions, the corrosion potential will be in the active region, and the corrosion rate can be high. Curve B represents an intermediate case where passivity, if it exists at all, will be unstable, and the surface will oscillate between active and passive states.

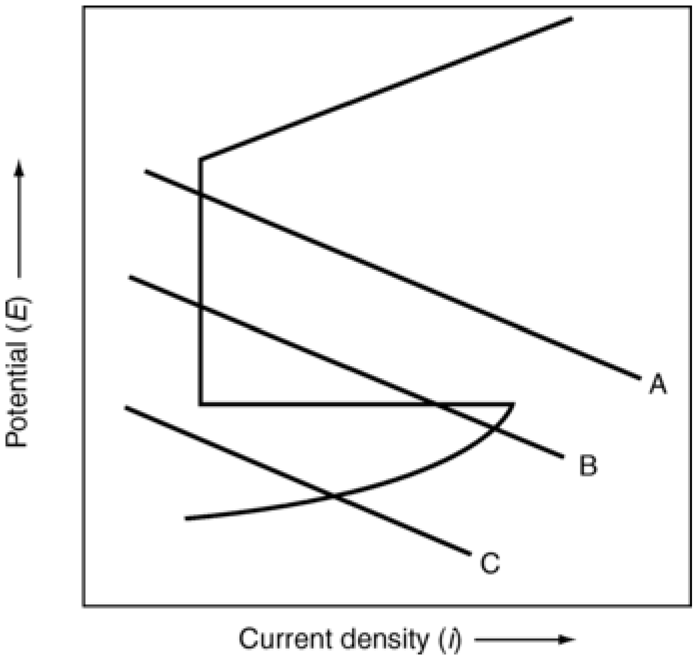

Fig. 4 Intersections of three possible cathodic polarization curves (straight lines A, B, C) with an anodic polarization curve for a system capable of exhibiting passivity. The corrosion rate depends on the current density at the intersection. Curve A produces a passive system, curve C an active system, and curve B an unstable system.

Reference cited in this section

12. M.G. Fontana and N.D. Greene, *Corrosion Engineering,* McGraw-Hill, 1967, p 336–337

J. Kruger, Passivity, *Corrosion: Fundamentals, Testing, and Protection*, Vol 13A, *ASM Handbook*, ASM International, 2003, p 61–67

Passivity

Jerome Kruger, Johns Hopkins University

Nature of the Passive Film

It is now widely believed that a film is responsible for the condition of passivity—one of the major accomplishments of past research. The understanding of the nature of passive films has been greatly enhanced in recent years, resulting in the development of many models of the passive film by the application of a whole array of in situ and ex situ techniques developed over the past 25 to 30 years. Two examples of collections of such models (Fig. 5) have been given by Sato (Ref 13) and Cohen (Ref 14). This section discusses five of the properties of passive films: the thickness, the composition, the structure, and the electronic and mechanical properties. These five aspects are discussed using, for the purpose of illustration, the films on iron and iron alloys. Since all of the properties that determine the nature of the passive film are interrelated, the discussion of each is artificially limited.

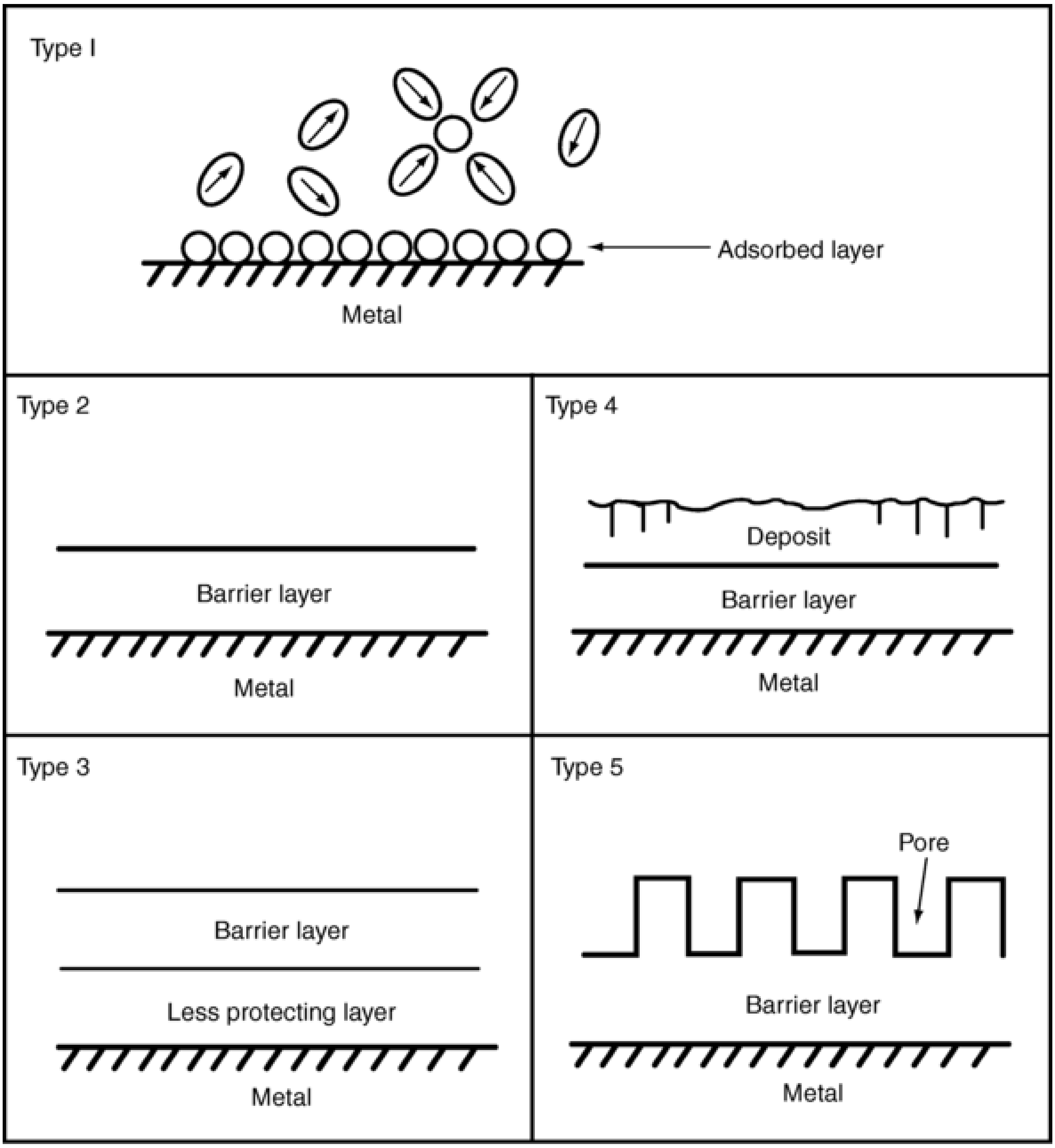
Type I
Adsorbed layer
Metal
Type 2
Barrier layer
Metal
Type 4
Deposit
Barrier layer
Metal
Type 3
Barrier layer
Less protecting layer
Metal
Type 5
Pore
Barrier layer
Metal

(a)

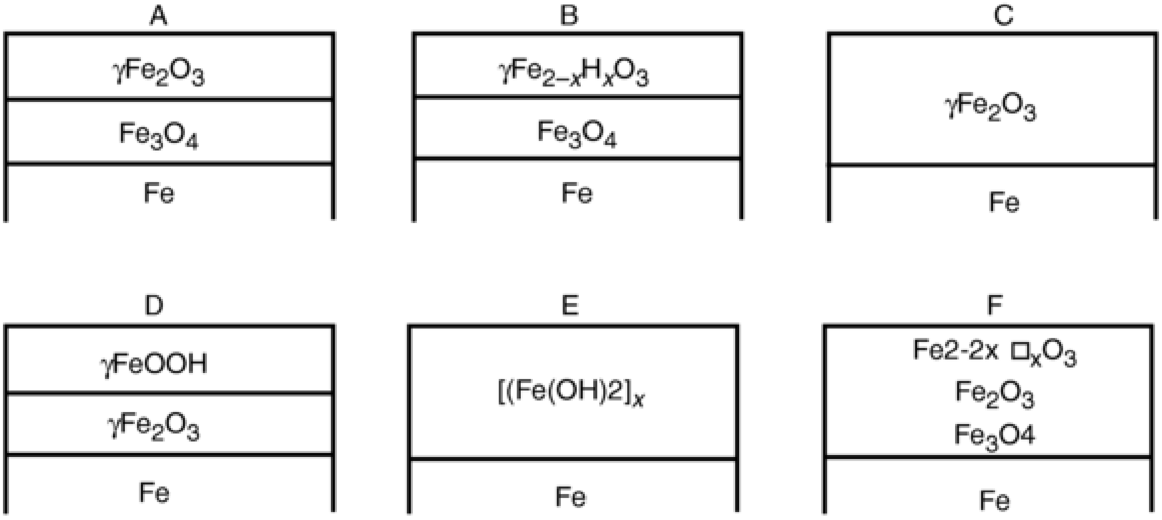
A
γFe_2O_3
Fe_3O_4
Fe
B
$\gamma Fe_{2-x}H_xO_3$
Fe_3O_4
Fe
C
γFe_2O_3
Fe
D
$\gamma FeOOH$
γFe_2O_3
Fe
E
$[(Fe(OH)2]_x$
Fe
F
Fe2-2x $\square_x O_3$
Fe_2O_3
Fe_3O4
Fe

(b)

Fig. 5 Proposed models of the passive film. (a) General models include monolayers and multiple layers. Source: Ref 13. (b) Detailed proposed models for iron having single or double layers containing combinations of oxides, hydroxides, and oxyhydroxides. Source: Ref 14

Thickness. Ever since passivity was discovered, the thickness of the passive film has been a source of great controversy between those who proposed a two-dimensional film (Ref 15), in which an adsorbed monolayer or less than a monolayer of oxygen retards surface reaction rates, and those who proposed a three-dimensional film (Ref 16), in which a phase oxide that had a thickness greater than one unit cell could serve as a barrier to the diffusion of metal cations into the solution. The application of numerous techniques appear to have resolved this issue because, depending on conditions, it has been shown by a number of studies that the passive film can be either two- or three-dimensional.

Some of these studies establishing the three- dimensional picture (thickness > monolayer) have been:

- In situ ellipsometric (Ref 17, 18) measurements of the thickness of the passive film as it formed
- Cathodic reduction (coulometric) measurements of thickness (Ref 19, 20)

For confirming passive-film thicknesses of less than a monolayer, coulometric electrochemical techniques have been employed (Ref 21, 22, 23). One of these studies by Frankenthal (Ref 22) have actually provided a link between two- and three-dimensional films. He found that at low potentials in the passive region (-0.4 to -0.1 V(SHE)) for iron in a nearly neutral borate-buffer solution, the film measured was less than a unit cell for Fe_3O_4 or γFe_2O_3 (around 0.84 nm). This film may be considered to be adsorbed oxygen. Above these potentials, he measured thicknesses greater than the unit cell for the phase oxide with Fe(III), for example, γFe_2O_3. Ellipsometric studies (Ref 24) on easily passivated metals such as chromium also show a quite wide potential region (as much as 1000 mV wide) where passive films exhibit thicknesses less than one unit cell of a phase oxide both in neutral and acidic solutions.

Chemical composition is, perhaps, the major property controlling the nature of passive films. For the passive film on iron, many studies have resulted in a confusing array of chemical compositions.

A good summary of some of the ideas that have come out of these investigations is the collection of some of the proposed models shown in Fig. 5(b) (Ref 14). These models involve either single or double layers that contain different combinations and arrangements of the following oxides, hydroxides, or oxyhydroxides: Fe_3O_4, γFe_2O_3, FeOOH, a polymeric layered $Fe(OH)_2$ (Ref 25), a nonstoichiometric cation-deficient γFe_2O_3 containing varying amounts of protons ($Fe_{2-x}H_xO_3$) (Ref 26), and a cation-deficient Fe_2O_3 ($Fe_{2-2x}G_xO_3$) (Ref 14). In addition to this list from the two models shown in Fig. 5(b) is a later model from Cahan and Chen (Ref 27), who characterize the chemical composition loosely as "a highly protonated, trivalent iron oxyhydroxide capable of existing over a relatively wide range of stoichiometry."

The models for iron shown in Fig. 5(b) have led to a number of issues concerning the chemical compositions of passive films:

- The number of layers in a passive film (Ref 20, 25, 26, 28, 29, 30, 31, 32, 33)
- The presence of hydrogen in some passive films (Ref 30, 34, 35, 36, 37, 38, 39, 40) (where in situ techniques are necessary)
- The existence, nature, and binding states of alloying elements with oxygen in the passive films on alloys (Ref 31, 33, 41, 42, 43)

Structure. Because chemical composition determines structure, these two aspects of the nature of the passive film are tied closely together, making much of the discussion on chemical composition relevant to structure. A major emphasis of many of the structural investigations of the structure of the passive film has been on the issue of crystallinity. Depending on the metal or alloy bearing the passive layer, ex situ studies (Ref 29, 32, 44, 45)—some researchers have found (Ref 32, 34) that structural changes may take place upon the transfer of a passivated specimen from an aqueous solution to the vacuum used in an ex situ technique—and in situ studies (Ref 30, 34, 39, 45, 46) found passive films with either crystalline or noncrystalline structures.

Some studies (Ref 47, 48, 49, 50) have contended that for some systems, for example, high-chromium stainless steels or passive films formed on iron by passivation in chromate solutions, the film is noncrystalline and that this noncrystallinity is promoted by certain alloying elements such as chromium and by the presence of

hydrogen in the structure of the film (Ref 2). There is also a large body of literature suggesting that the crystallization of the oxide layers on titanium alloys adversely affects the properties that enhance the passivity of the film (Ref 51, 52, 53, 54). Other studies (Ref 55, 56) have, however, found that superior passive films are crystalline and become more so upon aging (Ref 57).

Electronic Properties. This aspect of the nature of the passive film is an important factor in controlling the mechanisms of film formation, breakdown, and the rate of metal dissolution. This is so because dissolution, film formation, and breakdown all involve the movement of electrons and ions from the metal surface through the passive film or from the solution into the film. Moreover, electron-transfer reactions that occur on surfaces with passive films depend strongly on the electronic properties of such films.

Iron—like other metals exhibiting type 1 passivity but unlike electronic valve metals such as aluminum, titanium, and tantalum—forms a very thin, passive layer (less than 10 nm). The valve metals, however, whose films are good insulators, can support large electric fields and by so doing form quite thick films (hundreds of nanometers). Oxygen cannot be evolved from valve metals. Iron, when high potentials are applied, evolves oxygen instead of continuing to grow a thicker film. It is for this reason that many workers have suggested that the passive film on iron is a good electronic conductor, or at least a semiconductor (Ref 58). Many ideas on the role of electronic properties of electron-transfer reactions at the passive-film surface have suggested films with different electronic characteristics, namely a semiconducting film (Ref 58, 59, 60, 61, 62, 63) or a film with low electronic conductivity that is an insulator or partially an insulator to support the large fields required if the proposed mechanism of film growth is field-assisted ionic migration (Ref 19, 50, 64, 65).

Cahan and Chen (Ref 27) attempted to reconcile these opposing findings, proposing that the passive film on iron is neither a semiconductor nor an insulator, but a combination of both, that is, a “chemi-conductor,” which they define as “a material whose stoichiometry can be varied by oxidative and/or reductive valency state changes. This nonstoichiometry can then modify the local electronic (and/or ionic) conductivity of the film.”

The mechanical properties of passive films can be an important factor in the breakdown of passivity. Even though the determination of the mechanical properties of passive films is difficult, a few attempts have been made to measure these properties for a number of metals (Ref 66, 67, 68). These studies have shown that applied potentials (Ref 68) and alloying (Ref 66, 67) can control the ductility of some passive layers. It has been suggested (Ref 2) that the effect of alloying may be a consequence of the passive film, for example, on a chromium alloy being more noncrystalline than that on iron. An ex situ study of the passive layers formed in nitric acid solutions on stainless steels (Ref 52) found these films to be crystalline, epitaxial, and composite. This suggested that the mechanical properties of such films may be anisotropic and brittle with a high degree of adherence stress at the metal/film interface.

References cited in this section

2. A.G. Revesz and J. Kruger, *Passivity of Metals,* R.P. Frankenthal and J. Kruger, Ed., Electrochemical Society, 1978, p 137

13. N. Sato, *Passivity of Metals,* R.P. Frankenthal and J. Kruger, Ed., Electrochemical Society, 1978, p 29–58

14. M. Cohen, *Passivity of Metals,* R.P. Frankenthal and J. Kruger, Ed., Electrochemical Society, 1978, p 521–545

15. H.H. Uhlig, *Z. Elektrochem.,* Vol 62, 1958, p 626–632

16. U.R. Evans, *J. Chem. Soc.,* Vol 1927, 1927, p 1020–1040

17. J. Kruger, *J. Electrochem. Soc.,* Vol 110, 1963, p 654–663

18. J. Kruger and J.P. Calvert, *J. Electrochem. Soc.,* Vol 114, 1967, p 43–49

19. P.M.G. Draper, *Corros. Sci.,* Vol 7, 1967, p 91–101

20. M. Nagayama and M. Cohen, *J. Electrochem. Soc.,* Vol 109, 1962, p 781–790

21. K. Kubanov, R. Burstein, and A. Frumkin, *Disc. Faraday Soc.,* Vol 1, 1947, p 259–269

22. R.P. Frankenthal, *Electrochim. Acta,* Vol 16, 1971, p 1845–1857

23. R.P. Frankenthal, *J. Electrochem. Soc.,* Vol 114, 1967, p 542–547

24. K.E. Heusler, *Passivity of Metals,* R.P. Frankenthal and J. Kruger, Ed., Electrochemical Society, 1978, p 771–801

25. R.W. Revie, B.G. Baker, and J.O'M. Bockris, *J. Electrochem. Soc.,* Vol 122, 1975, p 1460–1466

26. M.C Bloom and M. Goldenberg, *Corros. Sci.,* Vol 5, 1965, p 623–630

27. B.D. Cahan and C.-T. Chen, *J. Electrochem. Soc.,* Vol 129, 1982, p 921–925

28. K.S. Vetter, *Z. Elektrochem.,* Vol 62, 1958, p 642–648

29. C.L. Foley, J. Kruger, and C.J. Bechtoldt, *J. Electrochem. Soc.,* Vol 114, 1967, p 944–1001

30. H.T. Yolken, J. Kruger, and J.P. Calvert, *Corros. Sci.,* Vol 8, 1968, p 103–108

31. K. Asami, K. Hashimoto, T. Musumoto, and S. Shimodaira, *Corros. Sci.,* Vol 16, 1976, p 909–914

32. K. Kuroda, B.D. Cahan, Ch. Nazri, E. Yeager, and T.E. Mitchell, *J. Electrochem. Soc.,* Vol 129, 1982, p 2163–2169

33. L.J. Jablonsky, M.P. Ryan, and H.S. Isaacs, *J. Electrochem. Soc.,* Vol 145, 1998, p 1922–1932

34. W.E. O'Grady, *J. Electrochem. Soc.,* Vol 127, 1980, p 555–563

35. G. Okamoto and T. Shibata, *Nature,* Vol 206, 1965, p 1350

36. G.G. Long, J. Kruger, D.R. Black, and M. Kuriyama, *J. Electrochem. Soc.,* Vol 130, 1983, p 240–242

37. M. Kekar, J. Robinson, and A.J. Forty, *Faraday Discuss. Chem. Soc.,* Vol 89, 1990, p 31–40

38. A.J. Davenport, and M. Sansone, *J. Electrochem. Soc.,* Vol 142, 1995, p 727–730

39. J. Kruger, L.A. Krebs, G.G. Long, J.F. Anker, and C.F. Majkrzak, *Passivation of Metals and Semiconductors,* K.E. Heusler, Ed., Materials Science Forum, Vol 185–188, Trans Tech Publications, 1995, p 367–376

40. C.R. Clayton, K. Doss, and J.B. Warren, *Passivity of Metals and Semiconductors,* M. Froment, Ed., 1983, p 585–590

41. A.J. Davenport, H.S. Isaacs, J.A. Bardwell, B. MacDougall, G.S. Frankel, and A.G. Schrott, *Corros. Sci.,* Vol 35, 1993, p 19–25

42. A.J. Davenport, M. Sansone, J.A. Bardwell, A.J. Andlykiewicz, M. Taube, and C.M. Vitus *J. Electrochem. Soc.,* Vol 141, 1994, p L6–8

43. J. Eldrige, M.E. Kordesch, and R.W. Hoffman, *J. Vac. Sci. Technol.,* Vol 20, 1982, p 934–938

44. G.G. Long, J. Kruger, D.R. Black, and M. Kuriyama, *J. Electroanal. Chem.,* Vol 150, 1983, p 603–610

45. L.J. Oblonsky, A.J. Davenport, M.P. Ryan, and M.F. Toney, *Passivity of Metals and Semiconductors,* M.B. Ives, J.L. Luo, and J.R. Rodda, Ed., Proc. Vol 99-42, Electrochemical Society, 2001, p 173–177

46. A.J. Davenport, R.C. Newman, and P. Ernst, *Passivity of Metals and Semiconductors,* M.B. Ives, J.L. Luo, and J.R. Rodda, Ed., Proc. Vol 99-42, Electrochemical Society, 2001, p 65–71

47. T.P. Hoar, *J. Electrochem. Soc.,* Vol 117, 1970, p 17C–22C

48. M.P. Ryan, R.C. Newman, and G.E. Thompson, *Philos. Mag. B,* Vol 70, 1994, p 241–251

49. M.P. Ryan, S. Fugimoto, G.E. Thompson, and R.C. Newman, *Passivation of Metals and Semiconductors,* K.E. Heusler, Ed., Materials Science Forum, Vol 185–188, Trans Tech Publications, 1995, p 233–240

50. G.G. Long, J. Kruger, M. Kuriyama, D.R. Black, E. Farabaugh, D.M. Saunders, and A.I. Goldman, *Proc. Ninth Int. Congress on Metallic Corrosion,* Proc. Vol 3, National Research Council, Ottawa, Canada, 1984, p 419–422

51. T. Shibata and Y.-C. Zhu, *Corros. Sci.,* Vol 36, 1994, p 153–163

52. M. Pankuch, R. Bell, and C.A. Melendres, *Electrochim. Acta,* Vol 38, 1993, p 2777–2779

53. K.E. Healy and P. Ducheyne, *Mater. Sci.,* Vol 4, 1993, p117–126

54. J.S.L. Leach and B.R. Pearson, *Corros. Sci.,* Vol 28, 1988, p 43–56

55. P. Marcus and V. Maurice, *Passivity of Metals and Semiconductors,* M.B. Ives, J.L. Luo, and J.R. Rodda, Ed., Proc. Vol 99-42, Electrochemical Society, 2001, p 30–54

56. V. Vignal, J.M. Olive, and J.C. Roux, *Passivity of Metals and Semiconductors,* M.B. Ives, J.L. Luo, and J.R. Rodda, Ed., Proc. Vol 99-42, Electrochemical Society, 2001, p 208–213

57. W. Yang, D. Costa, and P. Marcus, *J. Electrochem. Soc.,* Vol 141, 1994, p 2669–2676

58. K.J. Vetter, *J. Electrochem. Soc.,* Vol 110, 1963, p 597–605

59. F.M. Delnick and N. Hackerman, *Passivity of Metals,* R.P. Frankenthal and J. Kruger, Ed., Electrochemical Society, 1978, p 116–133

60. E.K. Oshe, I.L. Rosenfeld, and V.C. Doizoskenko *Dokl. Akad. Nauk SSSR,* Vol 194, 1970, p 612–614

61. M. Bojinov, T. Laitinen, K. Mäkelä, T. Saario, T. Sirkiä, and G. Fabricius, *Passivity of Metals and Semiconductors,* M.B. Ives, J.L. Luo, and J.R. Rodda, Ed., Proc. Vol 99-42, Electrochemical Society, 2001, p 201–207

62. W. Schmickler, *Passivity of Metals,* R.P. Frankenthal and J. Kruger, Ed., Electrochemical Society, 1978, p 102–115

63. W. Schultze and U. Stimming, *Z. Phys. Chem., NF,* Vol 98, 1975, p 285–302

64. J. Ord and D.J. DeSmet, *J. Electrochem. Soc.,* Vol 113, 1966, p 1258–1262

65. R.V. Moshtev, *Electrochim. Acta.,* Vol 16, 1971, p 2039–2048

66. S.F. Bubar and D.A. Vermilyea, *J. Electrochem. Soc.,* Vol 113, 1966, p 892–895

67. S.F. Bubar and D.A. Vermilyea, *J. Electrochem. Soc.,* Vol 114, 1967, p 882–885

68. J.S.L. Leach and P. Neufeld, *Corros. Sci.,* Vol 9, 1969, p 225–244

J. Kruger, Passivity, *Corrosion: Fundamentals, Testing, and Protection*, Vol 13A, *ASM Handbook*, ASM International, 2003, p 61–67

Passivity

Jerome Kruger, Johns Hopkins University

Passive-Film Formation and Dissolution

Processes. Passivity results from bringing a metal surface into the passivity region of a system exhibiting a passive polarization curve (Fig. 1) and thereby forming "the passive film." Sato and Okamoto (Ref 69) have pointed out that there are three possible processes that can produce passive films. The three passivation processes defined below describe possible ways in which the imposition of an electrochemical current can result in the formation of a passive film.

Direct film formation involves the reaction of a metal surface with an aqueous solution to form either a chemisorbed oxygen film or a compact three-dimensional (more than one atomic layer) film, usually an oxide or oxyhydroxide represented by:

$$M + H_2O = MO_{ads} + 2H^+ + 2e^- \quad \text{(Eq 1)}$$

or

$$M + H_2O = MO(\text{oxide}) + 2H^+ + 2e^- \quad \text{(Eq 2)}$$

Dissolution precipitation produces a passive layer by the formation of an oxide, oxyhydroxide, or hydroxide film by the precipitation of dissolved metal ions as described by the two-step process:

$$M = M^{z+} + ze^- \quad \text{(Eq 3)}$$

$$M^{z+} + zH_2O = M(OH)_z + zH^+ \quad \text{(Eq 4)}$$

The anodic oxidation of metal ions in solution forms an oxide film containing the metal ion in a higher oxidation state as shown by:

$$M = M^{z+} + ze^- \quad \text{(Eq 5)}$$

$$2M^{z+} + (z + x)H_2O = M_2O_{(z+x)} + 2(z + x)H^+ + 2xe^- \quad \text{(Eq 6)}$$

Rate Laws of Passive-Film Formation. As a result of the passivation processes described previously, it is possible to develop various expressions for the rate of passive-film formation by applying either of two electrochemical methods to form the passive film; these methods are described below.

Galvanostatic anodic oxidation or passivation applies a constant current and measures the change in potential as a function of time. When the potential for that surface, with respect to a reference electrode, is observed as a function of time, it is found that the potential rises initially during an induction time, τ_p, until it reaches a relatively constant value, E_p, the passivation potential, as shown in Fig. 1. The relationship between τ_p and the critical current density for passivation, i_c, is given by Sato and Okamoto (Ref 69) as $\tau_p = k(i - i_c)^n$, where k and n are constants with n having been found to be -1 for iron by Frank (Ref 70).

Potentiostatic anodic oxidation or passivation sets the potential of the metallic surface at a constant value and observes the variation of the current with time. It has been proposed (Ref 71) that potentiostatic passivation involves a competition between metal dissolution and film formation with the total current density, which is the reaction rate for the passivation process given by the expression $i = (i_{diss} + i_{film})(1 - \theta)$, where i_{diss} is the current density for film dissolution, i_{film} is the current density for film formation, and θ is the fraction of the surface covered by the passive film.

Mechanism of Formation. A review of the mechanisms of passive-film formation has been given by Fromhold (Ref 72). He has pointed out that it has been shown experimentally that the relationship between the electric field *E* across the passive film (potential difference across the film divided by the film thickness, usually several millions volts per centimeter) and the current density, *i*, can be given by:

$$E - E^o = A \log i \qquad \text{(Eq 7)}$$

where E^o and *A* are constants. A number of the proposed mechanisms for the growth of the passive film in the limiting thickness region (where film growth levels off) are some form of a field- assisted ion conduction mechanism based on the oxidation theory developed by Cabrera and Mott (Ref 73) such as the hopping (Ref 74), induced space charge (Ref 75), and point defect (Ref 76) mechanisms. A major problem in deciding which of the field-assisted ion conduction mechanisms is operative for iron in neutral solutions is that the kinetics of passive-film growth follow equally well either inverse logarithmic or direct logarithmic rate laws. Figure 6 shows the extent of this problem for iron in a neutral borate buffer solution. The inverse logarithmic law indicates a field-assisted ion conduction mechanism; the direct logarithmic law can be expected from a place-exchange mechanism. In addition, there are the models that do not depend on field-assisted ion conduction. These include the chemisorption of oxygen model (Ref 15, 77), the place-exchange mechanism (Ref 78), and the bipolar fixed charge induced passivity mechanism (Ref 79). Fromhold (Ref 72) has found that no mechanism can adequately explain all aspects of the film-formation process.

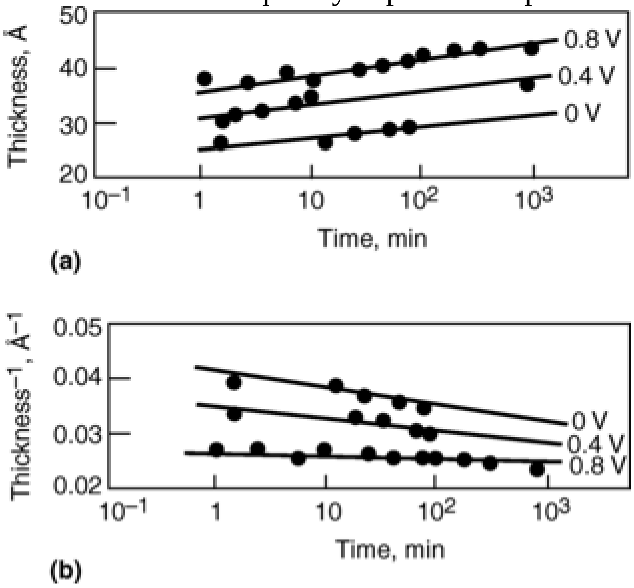

Fig. 6 Logarithmic plots of the growth of passive film on iron by potentiostatic anodic polarization at different potentials in pH 8.4 borate-buffer solution (a) Direct. (b) Inverse. Source: Ref 70

Dissolution. The process of passive-film dissolution is as important as that of film formation in controlling corrosion. Attention has mainly been placed on the dissolution of passive films in acid solutions (Ref 80) that involve either galvanostatic or steady-state open circuit conditions (Ref 58). An important aspect of passive-film dissolution is the existence of a potential, the Flade potential, that delineates the transition from the passive to the active state. It was first observed by Flade (Ref 81) when he found that the open-circuit potential of a passive metal surface decreased continuously and then ceased to change momentarily and arrested, before decaying to more active values that signaled the onset of the active state. Uhlig and King (Ref 82) have given a number of examples of this transition through the Flade potential during the decay of passivity. Other studies (Ref 33, 42, 83, 84) focused on the examination of the reduction and dissolution of individual species in passive films in mildly acidic and basic solutions. Finally, an investigation (Ref 85) that studied passive-film

dissolution in nearly neutral solutions was able to distinguish between the field and chemical effects that result in passive-film thinning.

References cited in this section

15. H.H. Uhlig, *Z. Elektrochem.,* Vol 62, 1958, p 626–632

33. L.J. Jablonsky, M.P. Ryan, and H.S. Isaacs, *J. Electrochem. Soc.,* Vol 145, 1998, p 1922–1932

42. A.J. Davenport, M. Sansone, J.A. Bardwell, A.J. Andlykiewicz, M. Taube, and C.M. Vitus *J. Electrochem. Soc.,* Vol 141, 1994, p L6–8

58. K.J. Vetter, *J. Electrochem. Soc.,* Vol 110, 1963, p 597–605

69. N. Sato and G. Okamoto, *Comprehensive Treatise of Electrochemistry,* J.O'M. Bockris et al., Ed., Vol 4, Plenum Press, 1981, p 193–306

70. U.F. Frank, *Z. Naturforsch.,* Vol 4A, 1949, p 378–391

71. U. Ebersbach, K. Schwabe, and K. Ritter, *Electrochim. Acta,* Vol 12, 1967, p 927–938

72. A.T. Fromhold, *Passivity of Metals,* R.P. Frankenthal and J. Kruger, Ed., Electrochemical Society, 1978, p 59–81

73. N. Cabrera and N. Mott, *Rep. Prog. Phys.,* Vol 12, 1949, p 163–184

74. J. Kruger and J.P. Calvert, *J. Electrochem. Soc.,* Vol 114, 1967, p 43–49

75. A.T. Fromhold, Jr., and J. Kruger, *J. Electrochem. Soc.,* Vol 120, 1973, p 722–729

76. C.Y. Chao, L.F. Lin, and D.D. Macdonald, *J. Electrochem. Soc.,* Vol 128, 1981, p 1187–1194

77. Ya.M. Kolotyrkin and V.M. Knyazheva, *Passivity of Metals,* R.P. Frankenthal and J. Kruger, Ed., Electrochemical Society, 1978, p 678–698

78. N. Sato and M. Cohen, *J. Electrochem. Soc.,* Vol 111, 1964, p 513–519

79. M. Sakashita and N. Sato, *Passivity of Metals,* R.P. Frankenthal and J. Kruger, Ed., Electrochemical Society, 1978, p 479–483

80. K.J. Vetter and F. Gorn, *Electrochim. Acta,* Vol 18, 1973, p 321–326

81. F. Flade, *Z. Phys. Chem.,* Vol 76, 1911, p 513–559

82. H.H. Uhlig and P.F. King, *J. Electrochem. Soc.,* Vol 106, 1959, p 1–7

83. A.J. Davenport, H.S. Isaacs, J.A. Bardwell, B. MacDougall, G.S. Frankel, and A.J. Schrott, *Corros. Sci.,* Vol 35, 1993, p 19–25

84. L.J. Oblonsky, *Passivity of Metals and Semiconductors,* M.B. Ives, J.L. Luo, and J.R. Rodda, Ed., Proc. Vol 99-42, Electrochemical Society, 2001, p 253–257

85. J. Kruger, *Proc. Corrosion and Corrosion Protection,* R.P. Frankenthal and F. Mansfeld, Ed., Vol 81-8, Electrochemical Society, 1981, p 66–76

J. Kruger, Passivity, *Corrosion: Fundamentals, Testing, and Protection*, Vol 13A, *ASM Handbook*, ASM International, 2003, p 61–67

Passivity

Jerome Kruger, Johns Hopkins University

Breakdown of the Passive Film

When a fourth cathodic curve is added above line A in Fig. 4, a line that intersects the anodic passive curve at a point where the current density is increasing sharply, breakdown of the passive film results, leading to the most damaging kinds of corrosion—the localized forms of corrosion, pitting, crevice corrosion, intergranular attack, and stress corrosion. A number of reviews of breakdown or pitting that deal with breakdown as the initiation step of pitting exist (Ref 86, 87, 88, 89, 90).

Mechanisms. Many theories or models have been proposed to describe the events leading to pitting or crevice-corrosion initiation. Successful models must, of course, explain the phenomenology of breakdown. The following phenomena are usually considered to be associated with chemical breakdown that leads to localized attack (Ref 86):

- A certain critical potential for breakdown must be exceeded.
- Damaging species (examples are chloride ions or the higher atomic weight halides) are needed to initiate and propagate breakdown.
- An induction time exists that starts with the initiation of the breakdown process by the introduction of conditions conducive to breakdown and ends with the completion of the process when breakdown commences.
- Highly localized sites exist at which breakdown occurs.

In order to develop a better understanding of breakdowns that can lead to an improved resistance to localized corrosion, three groups of models for passive-film breakdown have been proposed; these groups are described below.

Adsorbed Ion Displacement Model (Ref 91, 92). The passive film is considered by this model to be an adsorbed oxygen film (probably a monolayer). Breakdown occurs when a more strongly adsorbing damaging anion, for example, a chloride ion, displaces the oxygen forming the passive film. After the chloride ion is adsorbed on the surface, the breakdown process is initiated because the bonding of the metal ions to the metal lattice is weakened.

In ion migration or penetration models, damaging anions move through the passive film; the breakdown process is complete when an anion reaches the metal/film interface. All of these models consider the passive film to be three dimensional. They differ widely in their proposed mode of penetration. At one extreme is a model assuming the existence of pores in the passive film (Ref 93, 94). The other type of penetration models are those involving migration of the damaging anion through a lattice, via defects or via some sort of ion-exchange process. Ion migration in a lattice can occur in a variety of ways (Ref 95, 96, 97, 98). Some of these models postulate that the penetrating chloride ions occupy sites in the lattice, and recent x-ray absorption spectroscopic studies find that evidence for the existence of chloride in the lattice of the passive film (Ref 99, 100).

Breakdown repair or film-tearing models involve many dynamic breakdown-repassivation events during which chemically or electrochemically induced mechanical disruption of the passive film is followed by repair of the break. This dynamic process will then lead to the breakdown of passivity (Ref 101, 102). More recent studies (Ref 99, 103) have shown that metastable pitting events—breakdown-repair processes that occur below the critical potential for breakdown, E_{crit}—may be involved in breakdown. One of these studies (Ref 99) proposes a mechanism that describes the events of metastable pitting that lead to stable pit growth as follows:

- Anion (e.g., chloride-ion) movement through the passive film at local sites under an electric field
- Formation of metal chloride at discrete sites at the passive-film/metal interface

- Initiation of pitting upon rupture of the film at metal-chloride sites
- Pit growth at exposed sites sustained when chloride ions under diffusion control can prevent repassivation

It has been pointed out (Ref 91), however, that stable pitting (occurs above E_{crit}), rather than metastable pitting (observed below E_{crit}), is from an engineering standpoint the real corrosion risk.

Effect of Alloy Composition and Structure. Alloy composition has been found to affect breakdown phenomenologically by shifting E_{crit} in the noble direction (Ref 104). This shift has been explained by the production of a passive film that is more difficult to penetrate because it provides fewer diffusion paths (Ref 47, 105), by alloying elements affecting repassivation kinetics (Ref 106), or by the formation of complexes with, for example, molybdenum, an alloy component that increases resistance to pitting by reducing the flux of cation vacancies in the passive film toward the film/metal interface and thereby increasing the induction time for breakdown (Ref 107). Another example has been found for amorphous and partially nanocrystalline alloys of aluminum that exhibit increased pit-growth potentials, reduced pit-propagation rates, and increased repassivation rates when compared to polycrystalline high-purity aluminum (Ref 108). This is an effect of both adding alloy elements and changing the alloy structure.

Alloy structure determines the sites on a surface where the breakdown of the passive film is initiated. These sites have been shown to be related to the defect structure of the underlying metal (Ref 90, 91), with the density of sites in many instances depending on the crystallographic orientation of a particular grain (Ref 109). Another important factor leading to the production of breakdown sites is the presence of nonmetallic inclusions, especially the manganese sulfide inclusions found in stainless steels (Ref 90, 91). Finally, intermetallic phase particles acting as local cathodes (Ref 110, 111) as, for example, the $FeAl_3$ in iron-contaminated aluminum alloys, raise the pH of the local environment and cause alkaline dissolution (Ref 91) of the matrix at its boundary with the particle and thereby initiate breakdown.

References cited in this section

47. T.P. Hoar, *J. Electrochem. Soc.,* Vol 117, 1970, p 17C–22C

86. J. Kruger and K. Rhyne, *Nucl. Chem. Waste Manage.,* Vol 3, 1982, p 205–227

87. J.R. Galvele, *Passivity of Metals,* R.P. Frankenthal and J. Kruger, Ed., Electrochemical Society, 1978, p 285–327

88. M. Janik-Czachor, *J. Electrochem. Soc.,* Vol 128,

J. Kruger, Passivity, *Corrosion: Fundamentals, Testing, and Protection*, Vol 13A, *ASM Handbook*, ASM International, 2003, p 61–67

Passivity

Jerome Kruger, Johns Hopkins University

References

1. H.H. Uhlig, *Passivity of Metals,* R.P. Frankenthal and J. Kruger, Ed., Electrochemical Society, 1978, p 1–28

2. A.G. Revesz and J. Kruger, *Passivity of Metals,* R.P. Frankenthal and J. Kruger, Ed., Electrochemical Society, 1978, p 137

3. R.P. Frankenthal and J. Kruger, Ed., *Passivity of Metals,* Electrochemical Society, 1978

4. J. Kruger, *Int. Mater. Rev.,* Vol 33, 1988, p 113–130

5. H. Hasegawa and T. Sugano, Ed., *Passivation of Metals and Semiconductors, Part II, Passivity of Semiconductors,* Pergamon Press, 1990

6. K.E. Heusler, Ed., *Passivation of Metals and Semiconductors,* Materials Science Forum, Vol 185–188, Trans Tech Publications, 1995

7. M.B. Ives, J.L. Luo, and J.R. Rodda, Ed., *Passivity of Metals and Semiconductors,* Proc. Vol 99–42, Electrochemical Society, 2001

8. C. Wagner, *Corros. Sci.,* Vol 5, 1965, p 751–764

9. *Definitions of Terms Relating to Corrosion and Corrosion Testing,* G 13, *Annual Book of ASTM Standards,* ASTM, 1983

10. D. Peckner and I.M. Bernstein, *Handbook of Stainless Steels,* McGraw-Hill, 1977, Ch 24, p 24

11. M. Pourbaix, *Atlas of Electrochemical Equilibria in Aqueous Solutions,* 2nd ed., Pergamon Press, 1966

12. M.G. Fontana and N.D. Greene, *Corrosion Engineering,* McGraw-Hill, 1967, p 336–337

13. N. Sato, *Passivity of Metals,* R.P. Frankenthal and J. Kruger, Ed., Electrochemical Society, 1978, p 29–58

14. M. Cohen, *Passivity of Metals,* R.P. Frankenthal and J. Kruger, Ed., Electrochemical Society, 1978, p 521–545

15. H.H. Uhlig, *Z. Elektrochem.,* Vol 62, 1958, p 626–632

16. U.R. Evans, *J. Chem. Soc.,* Vol 1927, 1927, p 1020–1040

17. J. Kruger, *J. Electrochem. Soc.,* Vol 110, 1963, p 654–663

18. J. Kruger and J.P. Calvert, *J. Electrochem. Soc.,* Vol 114, 1967, p 43–49

19. P.M.G. Draper, *Corros. Sci.,* Vol 7, 1967, p 91–101

20. M. Nagayama and M. Cohen, *J. Electrochem. Soc.,* Vol 109, 1962, p 781–790

21. K. Kubanov, R. Burstein, and A. Frumkin, *Disc. Faraday Soc.,* Vol 1, 1947, p 259–269

22. R.P. Frankenthal, *Electrochim. Acta,* Vol 16, 1971, p 1845–1857

23. R.P. Frankenthal, *J. Electrochem. Soc.,* Vol 114, 1967, p 542–547

24. K.E. Heusler, *Passivity of Metals,* R.P. Frankenthal and J. Kruger, Ed., Electrochemical Society, 1978, p 771–801

25. R.W. Revie, B.G. Baker, and J.O'M. Bockris, *J. Electrochem. Soc.,* Vol 122, 1975, p 1460–1466

26. M.C Bloom and M. Goldenberg, *Corros. Sci.,* Vol 5, 1965, p 623–630

27. B.D. Cahan and C.-T. Chen, *J. Electrochem. Soc.,* Vol 129, 1982, p 921–925

28. K.S. Vetter, *Z. Elektrochem.,* Vol 62, 1958, p 642–648

29. C.L. Foley, J. Kruger, and C.J. Bechtoldt, *J. Electrochem. Soc.,* Vol 114, 1967, p 944–1001

30. H.T. Yolken, J. Kruger, and J.P. Calvert, *Corros. Sci.,* Vol 8, 1968, p 103–108

31. K. Asami, K. Hashimoto, T. Musumoto, and S. Shimodaira, *Corros. Sci.,* Vol 16, 1976, p 909–914

32. K. Kuroda, B.D. Cahan, Ch. Nazri, E. Yeager, and T.E. Mitchell, *J. Electrochem. Soc.,* Vol 129, 1982, p 2163–2169

33. L.J. Jablonsky, M.P. Ryan, and H.S. Isaacs, *J. Electrochem. Soc.,* Vol 145, 1998, p 1922–1932

34. W.E. O'Grady, *J. Electrochem. Soc.,* Vol 127, 1980, p 555–563

35. G. Okamoto and T. Shibata, *Nature,* Vol 206, 1965, p 1350

36. G.G. Long, J. Kruger, D.R. Black, and M. Kuriyama, *J. Electrochem. Soc.,* Vol 130, 1983, p 240–242

37. M. Kekar, J. Robinson, and A.J. Forty, *Faraday Discuss. Chem. Soc.,* Vol 89, 1990, p 31–40

38. A.J. Davenport, and M. Sansone, *J. Electrochem. Soc.,* Vol 142, 1995, p 727–730

39. J. Kruger, L.A. Krebs, G.G. Long, J.F. Anker, and C.F. Majkrzak, *Passivation of Metals and Semiconductors,* K.E. Heusler, Ed., Materials Science Forum, Vol 185–188, Trans Tech Publications, 1995, p 367–376

40. C.R. Clayton, K. Doss, and J.B. Warren, *Passivity of Metals and Semiconductors,* M. Froment, Ed., 1983, p 585–590

41. A.J. Davenport, H.S. Isaacs, J.A. Bardwell, B. MacDougall, G.S. Frankel, and A.G. Schrott, *Corros. Sci.,* Vol 35, 1993, p 19–25

42. A.J. Davenport, M. Sansone, J.A. Bardwell, A.J. Andlykiewicz, M. Taube, and C.M. Vitus *J. Electrochem. Soc.,* Vol 141, 1994, p L6–8

43. J. Eldrige, M.E. Kordesch, and R.W. Hoffman, *J. Vac. Sci. Technol.,* Vol 20, 1982, p 934–938

44. G.G. Long, J. Kruger, D.R. Black, and M. Kuriyama, *J. Electroanal. Chem.,* Vol 150, 1983, p 603–610

45. L.J. Oblonsky, A.J. Davenport, M.P. Ryan, and M.F. Toney, *Passivity of Metals and Semiconductors,* M.B. Ives, J.L. Luo, and J.R. Rodda, Ed., Proc. Vol 99-42, Electrochemical Society, 2001, p 173–177

46. A.J. Davenport, R.C. Newman, and P. Ernst, *Passivity of Metals and Semiconductors,* M.B. Ives, J.L. Luo, and J.R. Rodda, Ed., Proc. Vol 99-42, Electrochemical Society, 2001, p 65–71

47. T.P. Hoar, *J. Electrochem. Soc.,* Vol 117, 1970, p 17C–22C

48. M.P. Ryan, R.C. Newman, and G.E. Thompson, *Philos. Mag. B,* Vol 70, 1994, p 241–251

49. M.P. Ryan, S. Fugimoto, G.E. Thompson, and R.C. Newman, *Passivation of Metals and Semiconductors,* K.E. Heusler, Ed., Materials Science Forum, Vol 185–188, Trans Tech Publications, 1995, p 233–240

50. G.G. Long, J. Kruger, M. Kuriyama, D.R. Black, E. Farabaugh, D.M. Saunders, and A.I. Goldman, *Proc. Ninth Int. Congress on Metallic Corrosion,* Proc. Vol 3, National Research Council, Ottawa, Canada, 1984, p 419–422

51. T. Shibata and Y.-C. Zhu, *Corros. Sci.,* Vol 36, 1994, p 153–163

52. M. Pankuch, R. Bell, and C.A. Melendres, *Electrochim. Acta,* Vol 38, 1993, p 2777–2779

53. K.E. Healy and P. Ducheyne, *Mater. Sci.,* Vol 4, 1993, p117–126

54. J.S.L. Leach and B.R. Pearson, *Corros. Sci.,* Vol 28, 1988, p 43–56

55. P. Marcus and V. Maurice, *Passivity of Metals and Semiconductors,* M.B. Ives, J.L. Luo, and J.R. Rodda, Ed., Proc. Vol 99-42, Electrochemical Society, 2001, p 30–54

56. V. Vignal, J.M. Olive, and J.C. Roux, *Passivity of Metals and Semiconductors,* M.B. Ives, J.L. Luo, and J.R. Rodda, Ed., Proc. Vol 99-42, Electrochemical Society, 2001, p 208–213

57. W. Yang, D. Costa, and P. Marcus, *J. Electrochem. Soc.,* Vol 141, 1994, p 2669–2676

58. K.J. Vetter, *J. Electrochem. Soc.,* Vol 110, 1963, p 597–605

59. F.M. Delnick and N. Hackerman, *Passivity of Metals,* R.P. Frankenthal and J. Kruger, Ed., Electrochemical Society, 1978, p 116–133

60. E.K. Oshe, I.L. Rosenfeld, and V.C. Doizoskenko *Dokl. Akad. Nauk SSSR,* Vol 194, 1970, p 612–614

61. M. Bojinov, T. Laitinen, K. Mäkelä, T. Saario, T. Sirkiä, and G. Fabricius, *Passivity of Metals and Semiconductors,* M.B. Ives, J.L. Luo, and J.R. Rodda, Ed., Proc. Vol 99-42, Electrochemical Society, 2001, p 201–207

62. W. Schmickler, *Passivity of Metals,* R.P. Frankenthal and J. Kruger, Ed., Electrochemical Society, 1978, p 102–115

63. W. Schultze and U. Stimming, *Z. Phys. Chem., NF,* Vol 98, 1975, p 285–302

64. J. Ord and D.J. DeSmet, *J. Electrochem. Soc.,* Vol 113, 1966, p 1258–1262

65. R.V. Moshtev, *Electrochim. Acta.,* Vol 16, 1971, p 2039–2048

66. S.F. Bubar and D.A. Vermilyea, *J. Electrochem. Soc.,* Vol 113, 1966, p 892–895

67. S.F. Bubar and D.A. Vermilyea, *J. Electrochem. Soc.,* Vol 114, 1967, p 882–885

68. J.S.L. Leach and P. Neufeld, *Corros. Sci.,* Vol 9, 1969, p 225–244

69. N. Sato and G. Okamoto, *Comprehensive Treatise of Electrochemistry,* J.O'M. Bockris et al., Ed., Vol 4, Plenum Press, 1981, p 193–306

70. U.F. Frank, *Z. Naturforsch.,* Vol 4A, 1949, p 378–391

71. U. Ebersbach, K. Schwabe, and K. Ritter, *Electrochim. Acta,* Vol 12, 1967, p 927–938

72. A.T. Fromhold, *Passivity of Metals,* R.P. Frankenthal and J. Kruger, Ed., Electrochemical Society, 1978, p 59–81

73. N. Cabrera and N. Mott, *Rep. Prog. Phys.,* Vol 12, 1949, p 163–184

74. J. Kruger and J.P. Calvert, *J. Electrochem. Soc.,* Vol 114, 1967, p 43–49

75. A.T. Fromhold, Jr., and J. Kruger, *J. Electrochem. Soc.,* Vol 120, 1973, p 722–729

76. C.Y. Chao, L.F. Lin, and D.D. Macdonald, *J. Electrochem. Soc.,* Vol 128, 1981, p 1187–1194

77. Ya.M. Kolotyrkin and V.M. Knyazheva, *Passivity of Metals,* R.P. Frankenthal and J. Kruger, Ed., Electrochemical Society, 1978, p 678–698

78. N. Sato and M. Cohen, *J. Electrochem. Soc.,* Vol 111, 1964, p 513–519

79. M. Sakashita and N. Sato, *Passivity of Metals,* R.P. Frankenthal and J. Kruger, Ed., Electrochemical Society, 1978, p 479–483

80. K.J. Vetter and F. Gorn, *Electrochim. Acta,* Vol 18, 1973, p 321–326

81. F. Flade, *Z. Phys. Chem.,* Vol 76, 1911, p 513–559

82. H.H. Uhlig and P.F. King, *J. Electrochem. Soc.,* Vol 106, 1959, p 1–7

83. A.J. Davenport, H.S. Isaacs, J.A. Bardwell, B. MacDougall, G.S. Frankel, and A.J. Schrott, *Corros. Sci.,* Vol 35, 1993, p 19–25

84. L.J. Oblonsky, *Passivity of Metals and Semiconductors,* M.B. Ives, J.L. Luo, and J.R. Rodda, Ed., Proc. Vol 99-42, Electrochemical Society, 2001, p 253–257

85. J. Kruger, *Proc. Corrosion and Corrosion Protection,* R.P. Frankenthal and F. Mansfeld, Ed., Vol 81-8, Electrochemical Society, 1981, p 66–76

86. J. Kruger and K. Rhyne, *Nucl. Chem. Waste Manage.,* Vol 3, 1982, p 205–227

87. J.R. Galvele, *Passivity of Metals,* R.P. Frankenthal and J. Kruger, Ed., Electrochemical Society, 1978, p 285–327

88. M. Janik-Czachor, *J. Electrochem. Soc.,* Vol 128, 1981, p 513C–519C

89. Z. Szlarska-Smialowska, *Pitting Corrosion of Metals,* National Association of Corrosion Engineers, 1986

90. H. Böhni, *Uhlig's Corrosion Handbook,* R.W. Revie, Ed., 2nd ed., John Wiley, 2000, p 173–190

91. Ya.M. Kolotyrkin, *J. Electrochem. Soc.,* Vol 108, 1961, p 209–216

92. H.P. Leckie and H.H. Uhlig, *J. Electrochem. Soc.,* Vol 113, 1966, p 1262–1267

93. U.R. Evans, L.C. Bannister, and S.C. Britton, *Proc. R. Soc.,* Vol 131A, 1931, p 367–376

94. J.A. Richardson and G.C. Wood, *Corros. Sci.,* Vol 10, 1970, p 313–323

95. M.A. Heine, D.S. Keir, and M.I. Pryor, *J. Electrochem. Soc.,* Vol 112, 1965, p 24–32

96. C.L. McBee and J. Kruger, *Localized Corrosion,* R.W. Staehle, B.F. Brown, J. Kruger, and A. Agrawal, Ed., National Association of Corrosion Engineers, 1974, p 252–260

97. L.F. Lin, C.Y. Chao, and D.D. Macdonald, *J. Electrochem. Soc.,* Vol 128, 1981, p 1194–1198

98. K.E. Heusler and L. Fischer, *Werkst. Korros.,* Vol 27, 1976, p 551–558

99. G.T. Burstein, G.O. Ilevbare, C. Liu, and R.M. Souto, *Passivity of Metals and Semiconductors,* M.B. Ives, J.L. Luo, and J.R. Rodda, Ed., Proc. Vol 99-42, Electrochemical Society, 2001, p 499–504

100. L.A. Krebs and J. Kruger, *Passivity of Metals and Semiconductors,* M.B. Ives, J.L. Luo, and J.R. Rodda, Ed., Proc. Vol 99-42, Electrochemical Society, 2001, p 561–566

101. J. Kruger, *Passivity and Its Breakdown on Iron and Iron Base Alloys,* R.W. Staehle and H. Okada, Ed., National Association of Corrosion Engineers, 1976, p 91–98

102. N. Sato, *Electrochim. Acta,* Vol 16, 1971, p 1683–1692

103. G.S. Frankel, *Passivity of Metals and Semiconductors*, M.B. Ives, J.L. Luo, and J.R. Rodda, Ed., Proc. Vol 99-42, Electrochemical Society, 2001, p 445–476

104. Ya.M. Kolotyrkin, *Corrosion,* Vol 19, 1963, p 261t–270t

105. C.L. McBee and J. Kruger, *Passivity and Its Breakdown on Iron and Iron Base Alloys,* R.W. Staehle and H. Okada, Ed., National Association of Corrosion Engineers, 1976, p 131–132

106. T. Kodama and J.R. Ambrose, *Corrosion,* Vol 33, 1977, p 155–161

107. M. Urguidi and D.D. Macdonald, *J. Electrochem. Soc.,* Vol 132, 1985, p 555–558

108. J.E. Sweitzer, J.R. Scully, R.A. Bley, and J.W.P. Hsu, *Electrochem. Solid-State Lett.,* Vol 2, 1999, p 267–270

109. J. Kruger, *J. Electrochem. Soc.,* Vol 106, 1959, p 736

110. G.A.W. Murray, H.J. Lamb, and H.P. Godard, *Brit. Corros. J.,* Vol 2, 1967, p 216–218

111. J.O. Park, C.H. Paik, and R.C. Alkire, *Critical Factors in Localized Corrosion II,* P.M. Natishan, R.J. Kelly, G.S. Frankel, and R.C. Newman, Ed., Electrochemical Society, 1995, p 218–225

J.R. Scully and R.G. Kelly, Methods for Determining Aqueous Corrosion Reaction Rates, *Corrosion: Fundamentals, Testing, and Protection*, Vol 13A, *ASM Handbook*, ASM International, 2003, p 68–86

Methods for Determining Aqueous Corrosion Reaction Rates

John R. Scully and Robert G. Kelly, University of Virginia

Introduction

CORROSION OF MATERIALS IN AQUEOUS SOLUTIONS is often thermodynamically possible but kinetically limited. Therefore, it is important to determine the rates of corrosion processes. Corrosion rate determination can serve many engineering and scientific purposes. For example, it can be used to:

- Screen available materials to find the most resistant material for a given application.
- Determine operating conditions where corrosion rates are low versus those where rates are high, by varying conditions.
- Determine probable service lifetimes of materials forming components, equipment, and processes.
- Evaluate new alloys or treatments or existing alloys in new environments.
- Evaluate lots, heats, or treatments of materials to ensure that specified quality is achieved before release, shipment, or acceptance.
- Evaluate environmental conditions such as new chemical species, inhibitors, or plant- operation conditions such as temperature excursions.
- Determine the most economical means of reducing corrosion through use of inhibitors, pretreatments, coatings, or cathodic protection.
- Determine the relative corrosivity of one environment compared to another.
- Study corrosion mechanisms.

Methods for determination of corrosion rates can be differentiated between those that measure the cumulative results of corrosion over some period of time and those that provide instantaneous rate information. Corrosion rates do not often increase monotonically with environmental conditions but exhibit sharp thresholds that distinguish regions of low corrosion rates from other regions where corrosion rates are dangerously high. It is sometimes of greater interest to define these thresholds than it is to determine the rates in the regions where corrosion rates are high. Examples of the latter are pitting or crevice corrosion where passive films are broken down and local corrosion rates can be extremely high. This article addresses electrochemical methods for instantaneous rate determination and threshold determination as well as nonelectrochemical methods that can determine incremental or cumulative rates of corrosion.

J.R. Scully and R.G. Kelly, Methods for Determining Aqueous Corrosion Reaction Rates, *Corrosion: Fundamentals, Testing, and Protection*, Vol 13A, *ASM Handbook*, ASM International, 2003, p 68–86

Methods for Determining Aqueous Corrosion Reaction Rates

John R. Scully and Robert G. Kelly, University of Virginia

Electrochemical Methods

Several textbooks and symposia proceedings cover the application of electrochemical methods that can be used for corrosion testing (Ref 1, 2, 3, 4, 5, 6, 7, 8, 9, 10, 11, 12, 13, 14, 15, 16). This article highlights many of the commonly used laboratory methods used to determine instantaneous corrosion rates as well as methods that characterize corrosion thresholds that signal conditions for high rates of corrosion. Techniques discussed include Tafel extrapolation, polarization resistance, electrochemical impedance spectroscopy, electrochemical noise resistance, use of rotating disks and cylinders to study aspects of corrosion affected by solution flow, polarization methods for assessing susceptibility to localized corrosion, scratch repassivation, potential-step repassivation, electrochemical noise applied to pitting, potentiodynamic repassivation techniques for assessing sensitization, and methods for determining underpaint corrosion rates associated with corrosion under organic coatings on metals.

References cited in this section

1. J.O'M. Bockris and A.K.N. Reddy, *Modern Electrochemistry-2,* Plenum Press, 1970
2. E. Gileadi, *Electrode Kinetics for Chemists, Chemical Engineers and Materials Scientists,* VCH Publishers, 1993
3. N.D. Tomashov, *Theory of Corrosion and Protection of Metals,* Macmillan Publishing, 1966
4. D.A. Jones, *Principles and Prevention of Corrosion,* 2nd ed., Macmillan Publishing, 1996
5. M.G. Fontana and N.D. Greene, *Corrosion Engineering,* McGraw-Hill, 1978
6. J. Newman, *Electrochemical Systems,* Prentice-Hall, 1973
7. H.H. Uhlig and R.W. Revie, *Corrosion and Corrosion Control,* John Wiley & Sons, 1985
8. J.O'M. Bockris, B.E. Conway, E. Yeager, and R.E. White, Ed., *Electrochemical Materials Science,* Vol 4, *Comprehensive Treatise of Electrochemistry,* Plenum Press, 1981
9. R. Baboian, Ed., *Electrochemical Techniques for Corrosion,* National Association of Corrosion Engineers, 1977
10. U. Bertocci and F. Mansfeld, Ed., *Electrochemical Corrosion Testing,* STP 727, American Society for Testing and Materials, 1979
11. *Laboratory Corrosion Tests and Standards,* STP 866, G. Haynes and R. Baboian, Ed., American Society for Testing and Materials, 1985
12. *Corrosion Monitoring in Industrial Plants Using Nondestructive Testing and Electrochemical Methods,* STP 908, G.C. Moran and P. Labine, Ed., American Society for Testing and Materials, 1986

13. R. Baboian, Ed., *Electrochemical Techniques for Corrosion Engineers,* National Association of Corrosion Engineers, 1986

14. R. Baboian, W.D. France, Jr., L.C. Rowe, and J.F. Rynewicz, Ed., *Galvanic and Pitting Corrosion-Field and Laboratory Studies,* STP 576, American Society for Testing and Materials, 1974

15. B. Poulson, *Corros. Sci.,* Vol 23 (No. 4), 1983, p 391–430

16. D.D. MacDonald, *Transient Techniques in Electrochemistry,* Plenum Press, 1977

J.R. Scully and R.G. Kelly, Methods for Determining Aqueous Corrosion Reaction Rates, *Corrosion: Fundamentals, Testing, and Protection*, Vol 13A, *ASM Handbook*, ASM International, 2003, p 68–86

Methods for Determining Aqueous Corrosion Reaction Rates

John R. Scully and Robert G. Kelly, University of Virginia

Electrode Reaction Thermodynamics and Kinetics in Corrosion

Metallic corrosion is usually an electrochemical process. Electrochemical processes require anodes and cathodes in electrical contact as well as an ionic conduction path through an electrolyte. The electron flow between the anodic and cathodic areas quantifies the rates of the oxidation and reduction reactions. When anodes are physically separated from cathodes, the current can be readily measured by replacing direct electrical contact with a zero-resistance ammeter (ZRA), The conversion of the reaction rate per unit area, *J*, from units of $mol/cm^2 \cdot s$ to electrical current density, (A/cm^2), is accomplished with Faraday's constant, *F*, and knowledge of the number of electrons, *n*, transferred to complete the electrochemical reaction a single time:

$$i = I/A = nFJ \qquad \text{(Eq 1)}$$

where *I* is the current resulting from an electrochemical reaction over a known electrode surface area, *n* is the number of electrons transferred (equivalents/mol), *F* is Faraday's constant (96,484.6 Coulombs/equivalent), and *A* is the electrode surface area.

Monitoring this current provides the means for assessing the kinetics of the corrosion process, not just the thermodynamic tendencies for corrosion or merely the mass of metal loss registered after the test.

Typical corrosion processes occurring under freely corroding conditions involve at least one cathodic and one anodic reaction. The thermodynamics discussed previously dictate the circumstances where these reactions will proceed spontaneously. The current measured during a polarization experiment, i_{app}, involving a single- charge-transfer-controlled oxidation reaction and single charge-transfer-controlled reduction reaction is:

$$i_{app} = i_{corr}\left[\exp\left(\frac{\alpha_a F(E-E_{corr})}{RT}\right) - \exp\left(-\frac{\alpha_c F(E-E_{corr})}{RT}\right)\right] \qquad \text{(Eq 2)}$$

where i_{corr} is the corrosion current density, *E* is the applied potential, *R* is the ideal gas constant, *T* is the temperature, and α is the transfer coefficient.

The corrosion potential, E_{corr}, is a kinetically and thermodynamically determined “mixed” potential given by the interception of the lines describing the total anodic and cathodic reaction rates. At E_{corr}, $i_{ox} = i_{red}$ and i_{corr} is described by the magnitude of i_{ox} at E_{corr} as shown in Fig. 1. Either reaction rate may become mass-transport limited under certain circumstances, in which case Eq. 2 does not apply.

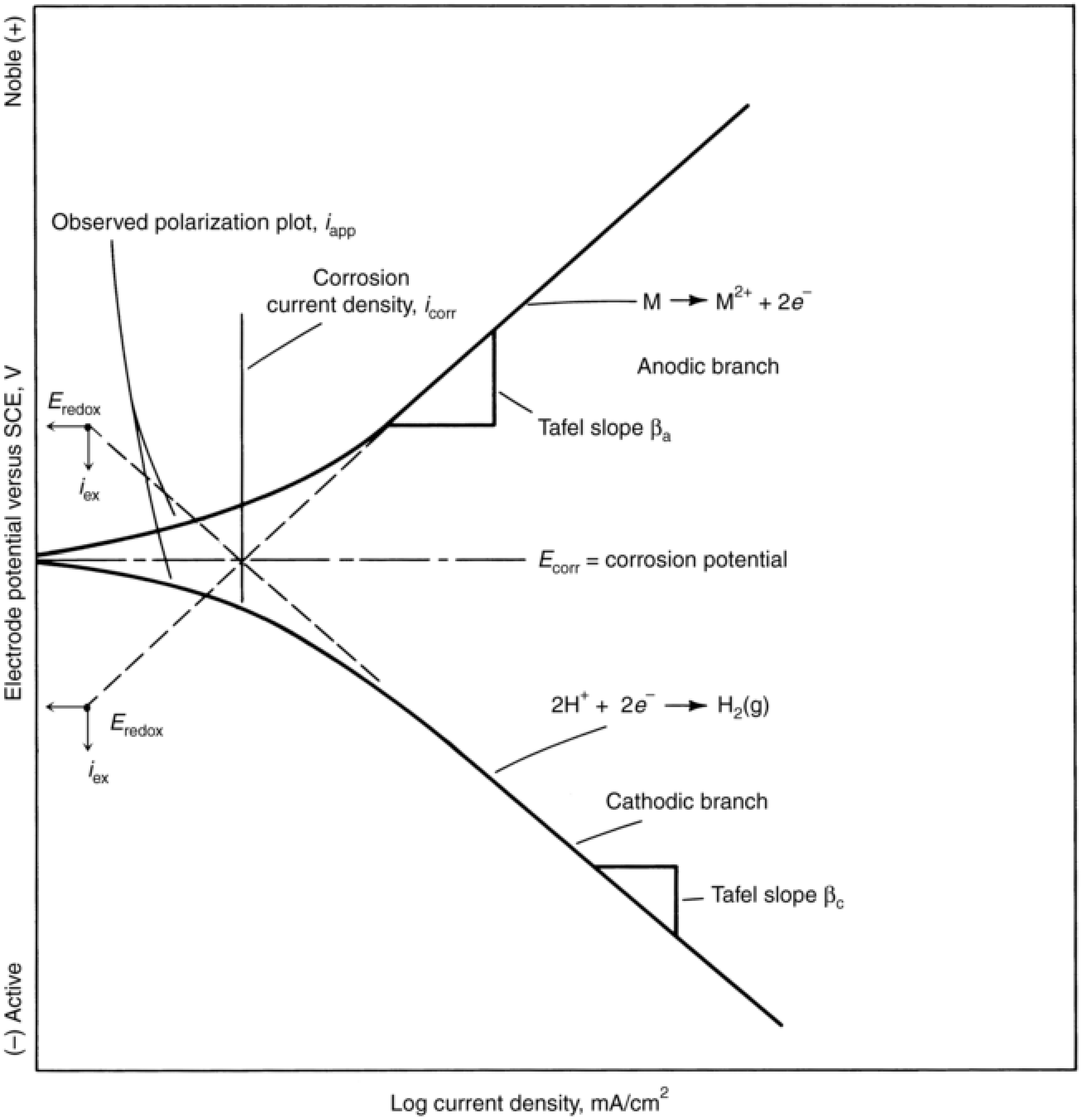

Fig. 1 Application of mixed-potential theory showing the electrochemical potential-current relationship for a corroding system consisting of a single charge-transfer-controlled cathodic reaction and charge-transfer-controlled anodic electrochemical reaction. β_c and β_a are Tafel slopes. Source: Ref 17

Obtaining Corrosion Rates from Electrochemical Kinetic Data. According to mixed- potential theory, any overall electrochemical reaction can be algebraically divided into half-cell oxidation and reduction reactions in which there can be no net electrical charge accumulation (Ref 17). For open-circuit corrosion in the absence of an applied potential, the oxidation of the metal and the reduction of some specie in solution occur simultaneously at the metal/electrolyte interface as described by Eq 2. Under these circumstances, the net measurable current density, i_{app}, is zero. However, a finite rate of corrosion defined by i_{corr} occurs at local anodic sites on the metal surface as indicated in Fig. 1. When the corrosion potential, E_{corr}, is located at a potential that is distinctly different from the reversible electrode potentials (E_{redox}) of either the corroding metal or the species in solution that is cathodically reduced, the oxidation of cathodic reactants or the reduction of any metallic ions in solution becomes negligible. Because the magnitude of i_{ox} at E_{corr} is the quantity of interest in the corroding system, this parameter must be determined independently of the oxidation reaction rates of other adsorbed or dissolved reactants.

The information obtained in a polarization experiment is i_{app} as a function of the potential, E, as shown by the thick solid line in Fig. 1, where $i_{app} = i_{ox} - i_{red}$. To obtain i_{app} as a function of E, the applied potential between the reference electrode and working electrode is controlled and scanned at constant rate (potentiodynamic), instantaneously increased a fixed amount, or stepped at various times (potentiostaircase) (Ref 18). The applied current, I_{app}, is measured and normalized with respect to the surface area (i.e., $i_{app} = I_{app}/A$). Conversely, i_{app} can be supplied between the working and counterelectrodes under galvanostatic or galvanostaircase control, and the resulting potential between the working and reference electrodes is monitored. Several ASTM standards discuss methods for performing these experiments (Ref 19, Ref 20, 21). Several approaches are available to determine i_{corr} from such experimental information. These methods are discussed in the sections that follow.
Conversion of Corrosion Rates to Mass Loss and Penetration Rate. Determination of I_{ox} at open-circuit potential or other potential of interest, where $I_{ox} = i_{ox} \times$ area, over a known period of time leads to direct determination of the mass loss:

$$M = \frac{I_{ox}t(AW)}{nF} \quad \text{(Eq 3)}$$

where M is the mass loss (g), $I_{ox}t$ is the product of current and time (coulombs), and AW is the atomic weight of the electroactive species (g/ mol).
This relation is known as Faraday's First Law. Rearrangement of Eq 3 leads to a straightforward determination of the corrosion penetration rate (applicable only when i_{ox}, μA/cm^2, is uniformly distributed over the entire wetted surface area or where the localized actively corroding area, A, is known), as follows:

$$CR = \frac{K_1 i_{ox}(EW)}{\rho} \quad \text{(Eq 4)}$$

where CR is the corrosion penetration rate (in mm/yr, EW is the equivalent weight (considered dimensionless in this calculation because the units of equivalents/mol are included in K_1), and ρ is the metal or alloy density, g/cm^3.
The constant $K_1 = 3.27 \times 10^{-3}$ when i_{ox} is expressed as μA/cm^2. K_1 has units of mm · g/ μA · cm · yr when CR is desired in mm/yr. ASTM G 102 gives other values for this constant when CR is expressed in other units (Ref 22). Expressions are also available to calculate mass- loss rate per unit area, MR, from knowledge of electrochemical corrosion rate. For instance:

$$MR = K_2 i_{ox}(EW) \quad \text{(Eq 5)}$$

where $K_2 = 8.954 \times 10^{-3}$ g · cm^2/μA · m^2 · d when MR is expressed as g/m^2 · day. For alloys, the equivalent weight EW should be calculated as outlined in ASTM G 102 (Ref 22):

$$EW = \frac{1}{\sum\left(\frac{n_i f_i}{AW_i}\right)} \quad \text{(Eq 6)}$$

where f_i is the mass fraction of the ith component of the alloy (-), AW_i is the atomic weight of the ith component element (g/mol), n_i is the number of electrons transferred or lost when oxidizing the ith component element under the conditions of the corrosion process (equivalents/mol), and i is the number of component elements in the alloy.
n is usually equal to the stable valence of the elements oxidized from the metallic state or must be determined from either a Pourbaix (potential- pH) diagram or experimentally from an analysis of the corroding solution. This expression assumes that all the component elements oxidize when the alloy corrodes and that they are all oxidizing at essentially a uniform rate. In some situations, these assumptions are not valid; in these cases, the calculated corrosion rate will be in error. For example, if an alloy is composed of two or more phases and one phase preferentially corrodes, the calculation must take this into consideration.

References cited in this section

17. C. Wagner and W. Traud, *Z. Electrochem.,* Vol 44, 1938, p 391

18. W.D. France, Jr., Controlled Potential Corrosion Tests: Their Application and Limitations, *Mater. Res. Standard.,* Vol 9 (No. 8), 1969, p 21

19. "Standard Practice for Conventions Applicable to Electrochemical Measurements in Corrosion Testing," G 3, *Wear and Erosion; Metal Corrosion,* Vol 03.02, *Annual Book of ASTM Standards,* ASTM

20. "Standard Reference Test Method for Making Potentiostatic and Potentiodynamic Anodic Polarization Measurements," G 5, *Wear and Erosion; Metal Corrosion,* Vol 03.02, *Annual Book of ASTM Standards,* ASTM

21. "Practice for Conducting Potentiodynamic Polarization Resistance Measurements," G 59, *Wear and Erosion; Metal Corrosion,* Vol 03.02, *Annual Book of ASTM Standards,* ASTM

22. "Practice for Calculation of Corrosion Rates and Related Information from Electrochemical Measurements," G 102, *Wear and Erosion; Metal Corrosion,* Vol 03.02, *Annual Book of ASTM Standards,* ASTM

J.R. Scully and R.G. Kelly, Methods for Determining Aqueous Corrosion Reaction Rates, *Corrosion: Fundamentals, Testing, and Protection,* Vol 13A, *ASM Handbook,* ASM International, 2003, p 68–86

Methods for Determining Aqueous Corrosion Reaction Rates

John R. Scully and Robert G. Kelly, University of Virginia

Electrochemical Methods for the Study of Uniform Corrosion: Polarization Methods

One method for examining the corrosion behavior of a metal is to determine the E-i_{app} relationship by conducting a polarization experiment. The following E-i_{app} relationship is often experimentally observed between applied current and potential. The expression is applicable to charge-transfer-controlled corrosion processes regardless of the exact number of charge-transfer-controlled reactions or reaction steps. It provides the basis for the electrochemical polarization technique (Ref 1, 2, 17, 18, 23):

$$i_{app} = i_{corr}\left[\left(\exp\left\{\frac{2.303(E - E_{corr})}{\beta_a}\right\}\right) - \exp\left\{-\frac{2.303(E - E_{corr})}{\beta_c}\right\}\right] + C\frac{\partial E}{\partial t} \quad \text{(Eq 7)}$$

where C is the interfacial capacitance associated with the electrochemical double layer (Ref 1, 2), and β_a and β_c are the apparent anodic and cathodic Tafel slopes ($\partial E/\partial \log i_{app}$) = $2.303RT/\alpha F$ given by the slopes of the polarization curves in the anodic and cathodic Tafel regimes, respectively, and $\partial E/\partial t$ is the time rate of change in applied potential; that is, the voltage scan rate.

The second term of the expression ($C\partial E/\partial t$) approaches 0 at low voltage scan rates dE/dt. This is desirable since the goal is to obtain i_{corr} at E_{corr}. Note that i_{app} becomes approximately equal to either i_{ox} or i_{red} at large η, where $\eta = (E - E_{corr})$. At very large anodic or cathodic overpotentials, Eq 7 can be rearranged in the form of the Tafel expression (Ref 1, 2, 3, 5, 7, 19, 23):

$$\eta_a = \beta_a \log\left(\frac{i_{app}}{i_{corr}}\right) \quad \text{(Eq 8a)}$$

$$\eta_c = -\beta_c \log\left(\frac{i_{app}}{i_{corr}}\right) \quad \text{(Eq 8b)}$$

where η_a and η_c are the anodic and cathodic overpotentials, respectively.

Equations 8a and (b) are only strictly valid for a single anodic or cathodic reaction, respectively, although approximately linear behavior can be observed despite several reactions. The linear portion of the solid line describing E-i_{app} in Fig. 1 above the E_{corr} describes a single anodic reaction that can be described by Eq 8a.

Tafel Extrapolation to Determine Corrosion Rate. In cases where Eq 8a and (b) are valid, η can be plotted versus log(i_{app}) over a sufficient range to obtain a linear relationship between the logarithm of current density and potential (Ref 1, 5, 7, 23), i_{corr} is determined from extrapolation of i_{app} from either the anodic or the cathodic Tafel region to the open-circuit or corrosion potential (i.e., zero overpotential). Figure 1 illustrates this method. The method is potentially damaging to the corroding metal since a large overpotential must be applied. This is particularly true in the case of anodic polarization, in which the surface is changing because of corrosion and/or passivation of the metal. No ASTM standard currently exists for this method.

Complications with the Polarization Method Involving Solution Resistance. Tafel extrapolation as well as other polarization techniques can be complicated by several factors. One such factor, ohmic resistance, arises from the resistivity of the solution, cell geometry, location of the reference electrode, and magnitude of applied current (Ref 2, 6). Ohmic resistance can contribute a voltage error to the measured potential. This error is summed algebraically with the true interfacial overpotential across the electrochemical interface (the potential usually sought in electrochemical measurements) measured with respect to a reference electrode. Placement of the reference electrode near the working electrode with a Luggin-Haber capillary is used to minimize the solution resistance error, which can be estimated from the product of the applied current density, the solution resistivity, and the perpendicular distance from the Luggin probe to the specimen surface in a planar electrode geometry. The error contributes to the measured overpotential:

$$\eta_{app} = \eta_{true\ interfacial} + i_{app}R_s \quad \text{(Eq 9)}$$

R_s($\Omega \cdot cm^2$) is the uncompensated solution resistance between the working electrode and the position where the reference electrode senses the potential in solution (at the tip of the Luggin- Haber capillary). Thus, $\eta_{app} > \eta_{true}$ at a high anodic or cathodic applied current density, $E_{app} > E_{true}$ and the Tafel slope desired from a fit of Eq 7 or 8a to E versus i_{app} data is not obtained. When the dominant term in Eq 9 is the second term, a linear relationship between η and i_{app} is obtained instead of the semilogarithmic relationship discussed previously. The true scan rate in the potentiodynamic technique may also be altered by ohmic resistance since the applied potential that contains the ohmic component is controlled during the scan, not the true overpotential. Several excellent reviews are available on the subject of the voltage error introduced from solution resistance (Ref 24, 25, 26, 27).

Complications Involving Concentration Polarization Effects. The Tafel relationship established through Eq 7 and 8a is dependent on pure activation control, or charge-transfer control. An additional consideration involves the concept of concentration polarization. In this case, the reaction rate is fast enough that the reacting specie is depleted (reduction reaction) or concentrated (oxidation) at the reacting surface. In order to maintain the reaction rate, diffusion through the electrolyte becomes the kinetic limitation. The reaction becomes diffusion controlled at the limiting current density, i_L. The deviation from activation control in the case of a cathodic reaction can result in an additional overpotential known as a mass-transport overpotential, η_{conc}. This overpotential is described by (Ref 4, 5):

$$\eta_{conc} = \left[\frac{2.303RT}{nF}\right]\log\left[1 - \frac{i_{app}}{i_L}\right] \quad \text{(Eq 10)}$$

where i_L is the mass transfer limiting current density defined by Fick's first law at steady state.

As i_{app} approaches i_L, the concentration overpotential, η_{conc}, becomes very large. The cathodic reaction may be under mixed charge-transfer/mass-transport or mass-transport control for many corrosion situations, particularly if the cathodic reaction is O_2 reduction (Ref 5). The cathodic polarization behavior associated with "mixed" charge-transfer/mass-transfer control can be described mathematically by the algebraic sum of Eq 8a and 10. Tafel extrapolation of cathodic data becomes difficult under these conditions because the Tafel region is not extensive.

For a completely mass-transport-limited corrosion process, the concentration of the cathodic reacting specie C_b approaches 0 at the electrode interface and $i_{corr} = i_L$ (Fig. 2) (Ref 2). The diffusional boundary layer thickness, δ, is decreased by increasing solution stirring or rotation rate, Ω(rad/s), in the case of a rotating cylinder or disk electrode (Ref 1). The limiting current density i_L is a linear function of concentration gradient (Ref 15). The concentration gradient (C_b/δ) increases as a function of $\Omega^{0.5}$ or $\Omega^{0.7}$ for the rotating disk and cylinder, respectively (Ref 2, 15). For a mass-transport-controlled cathodic reaction, i_{corr} is increased with flow as shown in Fig. 2. The governing equation for the rotating cylinder electrode is (Ref 15):

$$i_L = 0.079nFC_bD^{0.64}\nu^{-0.34}\Omega^{0.7}r^{0.4} \quad \text{(Eq 11)}$$

and for the rotating-disk electrode is (Ref 2, 15):

$$i_L = 0.621nFC_bD^{0.67}\nu^{-0.167}\Omega^{0.5} \quad \text{(Eq 12)}$$

where C_b is the reacting species concentration in the bulk solution (moles/cm^3), D is the diffusion coefficient for the reacting specie (cm^2/s), ν is the kinematic viscosity of the solution (cm^2/s), and r is the cylinder or disk radius (cm).

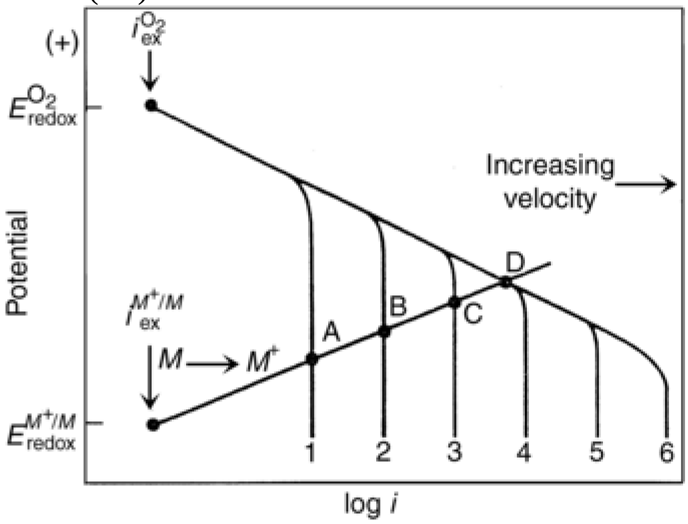

Fig. 2 Application of mixed-potential theory showing the electrochemical potential-current relationship for a corroding system consisting of a mass-transport-controlled cathodic reaction and a charge-transfer-controlled anodic reaction. As the fluid velocity increases from 1 to 4, the corrosion rate increases from A to D.

Corrosion engineers often favor the rotating cylinder to simulate flow in turbulent piping systems since this flow regime is readily obtained (Ref 15). In contrast, the rotating-disk electrode operates in the laminar flow regime even at high rotation rates and does not accurately represent many corrosion situations (Ref 15). No ASTM methods currently exist to examine mass-transport-controlled corrosion kinetics.

References cited in this section

1. J.O'M. Bockris and A.K.N. Reddy, *Modern Electrochemistry-2,* Plenum Press, 1970
2. E. Gileadi, *Electrode Kinetics for Chemists, Chemical Engineers and Materials Scientists,* VCH Publishers, 1993
3. N.D. Tomashov, *Theory of Corrosion and Protection of Metals,* Macmillan Publishing, 1966
4. D.A. Jones, *Principles and Prevention of Corrosion,* 2nd ed., Macmillan Publishing, 1996
5. M.G. Fontana and N.D. Greene, *Corrosion Engineering,* McGraw-Hill, 1978
6. J. Newman, *Electrochemical Systems,* Prentice-Hall, 1973

7. H.H. Uhlig and R.W. Revie, *Corrosion and Corrosion Control,* John Wiley & Sons, 1985

15. B. Poulson, *Corros. Sci.,* Vol 23 (No. 4), 1983, p 391–430

17. C. Wagner and W. Traud, *Z. Electrochem.,* Vol 44, 1938, p 391

18. W.D. France, Jr., Controlled Potential Corrosion Tests: Their Application and Limitations, *Mater. Res. Standard.,* Vol 9 (No. 8), 1969, p 21

19. "Standard Practice for Conventions Applicable to Electrochemical Measurements in Corrosion Testing," G 3, *Wear and Erosion; Metal Corrosion,* Vol 03.02, *Annual Book of ASTM Standards,* ASTM

23. Z. Tafel, *Phys. Chem.,* Vol 50, 1904, p 641

24. D. Britz, *J. Electroanal. Chem.,* Vol 88, 1978, p 309

25. M. Hayes and J. Kuhn, *J. Power Sources,* Vol 2, 1977–1978, p 121

26. F. Mansfeld, *Corrosion,* Vol 38 (No. 10), 1982, p 556

27. L.L. Scribner and S.R. Taylor, Ed., *The Measurement and Correction of Electrolyte Resistance in Electrochemical Tests,* STP 1056, American Society for Testing and Materials, 1990

J.R. Scully and R.G. Kelly, Methods for Determining Aqueous Corrosion Reaction Rates, *Corrosion: Fundamentals, Testing, and Protection*, Vol 13A, *ASM Handbook*, ASM International, 2003, p 68–86

Methods for Determining Aqueous Corrosion Reaction Rates

John R. Scully and Robert G. Kelly, University of Virginia

Polarization Resistance Methods

Stern and Geary simplified the kinetic expression describing charge-transfer-controlled reaction kinetics (Eq 7) for the case of small overpotentials with respect to E_{corr} (Ref 28, 29). Equation 7 can be linearized when $\eta/\beta < 0.1$. This simplified relationship has the following form if the second term describing the capacitive current, $C(\partial E/\partial t)$, is negligible:

$$i_{corr} = \left(\frac{\Delta i_{app}}{2.3\Delta E}\right)\left(\frac{\beta_a\beta_c}{(\beta_a + \beta_c)}\right) \quad \text{(Eq 13)}$$

rearranging:

$$i_{corr} = \left(\frac{1}{2.3R_p}\right)\left(\frac{\beta_a\beta_c}{(\beta_a + \beta_c)}\right) \quad \text{(Eq 14)}$$

where R_p is the polarization resistance ($\Omega \cdot cm^2$) given by $\partial E/\partial i$ at $t = \infty$ and $\Delta E = 0$.
i_{app} is often approximately linear with potential within ±5 to 10 mV of E_{corr} as shown for AISI 430 stainless steel in H_2SO_4 (Fig. 3). The slope of this plot, $\Delta E/\Delta i$, when determined at E_{corr} as shown in Fig. 3 defines the polarization resistance, which is inversely proportional to corrosion rate (Ref 30, 31). The surface area of the working electrode must be known. Knowledge of R_p, β_a, and β_c permit direct determination of the corrosion rate

at any instant in time using Eq 14 (Ref 28, 29, 31, 32). The ASTM standards G 59 (Ref 21) and G 96 (Ref 33) describe standard procedures for conducting polarization resistance measurements.

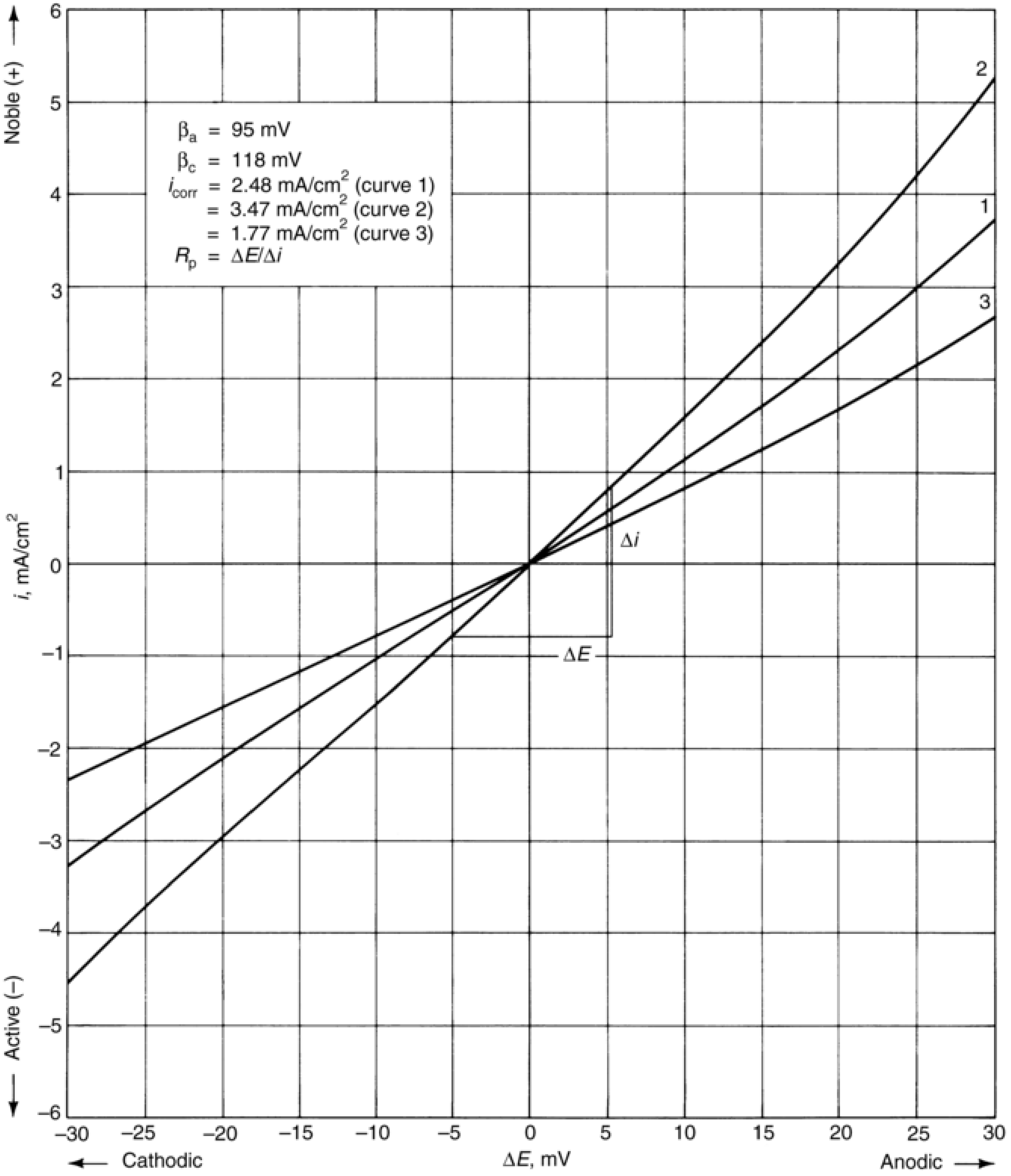

Fig. 3 ASTM G 59 polarization curves for polarization resistance measurements based on the results from eight independent laboratories for type 430 stainless steel in 1 *N* H_2SO_4. Curve 1 is the mean result, with curves 2 and 3 showing the 95% confidence limits. Source: Ref 21

This review focuses on corroding systems with different cathodic and anodic half-cell reactions. However, the concept of polarization resistance applies equally well to reduction-oxidation systems involving a single half-cell reaction. Here, the exchange current density, i_0, may be calculated from the polarization resistance, where R is the ideal gas constant, F is Faraday's constant, T is the temperature, and α_a and α_c are the anodic and cathodic multistep electron-transfer coefficients, respectively, for the reduction-oxidation process.

$$R_n\left(\Omega\cdot \mathrm{cm}^2\right)=\left[\frac{\Delta E}{\Delta i}\right]_{(E-E_{rev})\to 0}$$
$$=\left(\frac{RT}{i_0 F\left(\alpha_a+\alpha_c\right)}\right)$$

Other techniques exploit nonlinearity at larger overpotentials that invalidate the approximation given by Eq 13 (Ref 34). The Oldham-Mansfeld method calculates i_{corr} from nonlinear E versus i_{app} data obtained usually within ±30 mV of E_{corr} using tangent slopes and intercepts to calculate corrosion rate without high overpotential determination of β_a and β_c (Ref 35). Computerized curve fitting can exploit nonlinearity to calculate β_a, and β_c from low overpotential data, avoiding the destructive nature of large overpotentials. The Mansfeld technique substitutes Eq 14 into Eq 7 eliminating i_{corr} (Ref 36). β_a and β_c are determined from the best fit of the resulting expression containing β_a and β_c as unknowns to a nonlinear plot of η versus $2.3 i_{app} R_p$. η versus i_{app} data are obtained within ±30 mV of E_{corr}. R_p is determined from the linear slope of E versus i_{app} within ±5 mV of E_{corr}. i_{corr} is subsequently determined from Eq 13 using the computed values of R_p, β_a, and β_c.

Complications with polarization resistance measurements, and possible remedies are reported in the literature (Ref 34, 35, 36, 37, 38, 39, 40). Three of the most common errors involve: (a) invalidation of the results through oxidation of some other electroactive species besides the corroding metal in question, (b) a change in the open-circuit or corrosion potential during the time taken to perform the measurement, and (c) use of a large η, invalidating the assumption of a linear relationship between i_{app} and E required by Eq 13 and 14.

Another source of error involves cases in which both the anodic and cathodic reactions are not charge-transfer-controlled processes, as required for the derivation of Eq 13. Modifications to Eq 7 exist for cases in which pure activation control is not maintained, such as in the case of partial diffusion control or passivation (Ref 41). Other researchers have attempted to calibrate the polarization resistance method with gravimetrically determined mass loss (Ref 42). In fact, polarization resistance data for a number of alloy- electrolyte systems have been compared to the observed average corrosion currents determined from mass loss via Faraday's law (Ref 32). A linear correspondence was obtained over six orders of magnitude in corrosion rates.

Two other frequently encountered complications are the need to correct polarization data for errors that arise from the contribution of solution resistance, R_s, and the addition of capacitive current, CdE/dt, which occurs with increasing scan rate (Ref 16). Capacitive current gives rise to hysteresis in current-potential plots (Ref 43). Solution resistance contributes to a voltage error as discussed previously, as well as a scan-rate error. Since the applied potential is increased by an ohmic voltage component, an apparent value of polarization resistance R'_P is obtained that overestimates R_p by an amount equal to R_s. Consequently, the corrosion rate is underestimated. Hysteresis in the current density-applied potential plot is brought about for combinations of high voltage scan rate and large interfacial capacitances as well as large polarization resistances. Attempting to determine R_p at too fast of a scan rate underestimates its true value, leading to an overestimation of corrosion rate. This error can be minimized by determining the polarization resistance at a slow scan rate or by extrapolating the results at several slow scan rates to zero scan rate. Alternatively, one may take two or more current-density measurements from potentiostatic data after long time periods near E_{corr} to minimize fast-scan-rate effects. These complications and others have been reviewed elsewhere (Ref 44).

Many treatments of this subject have used an electrical equivalent circuit model to simulate the corroding metal/electrolyte interface (Ref 1, 44, 45). The simplest form of such a model is shown in Fig. 4. The three parameters discussed previously (R_p, R_s, and C) that approximate a corroding electrochemical interface are shown. The algebraic sum of R_s and R_p is measured when a direct-current measurement is performed. The impedance associated with a capacitor approaches infinity as the voltage scan rate approaches 0, and parallel circuit elements are always dominated by the element with the smallest impedance. Therefore, the sum of R_s and R_p is measured. The true corrosion rate will be underestimated when R_s is appreciable. Conversely, any experiment conducted at a fast voltage scan rate causes the algebraic sum of the ohmic resistance and the resultant impedance of the parallel resistive-capacitive network to be measured. This value will be lower than the sum of R_p and R_s determined at an infinitely slow scan rate, as current leaks through the parallel capacitive element at higher scan rate due to its low impedance at high frequency. This will usually result in an overestimation of the true corrosion rate. These complications can be overcome by using the electrochemical impedance method.

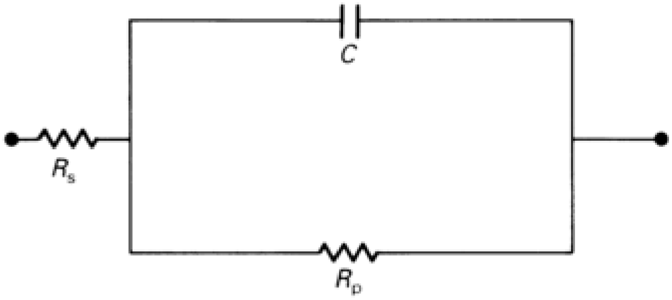

Fig. 4 Electrical equivalent circuit model simulating a simple corroding metal/electrolyte interface. See also Fig. 5. R_s is the solution resistance. R_p is the polarization resistance. *C* is the double-layer capacitance.

References cited in this section

1. J.O'M. Bockris and A.K.N. Reddy, *Modern Electrochemistry-2,* Plenum Press, 1970

16. D.D. MacDonald, *Transient Techniques in Electrochemistry,* Plenum Press, 1977

21. "Practice for Conducting Potentiodynamic Polarization Resistance Measurements," G 59, *Wear and Erosion; Metal Corrosion,* Vol 03.02, *Annual Book of ASTM Standards,* ASTM

28. M. Stern and A.L. Geary, *J. Electrochem. Soc.,* Vol 104, 1957, p 56

29. S. Evans and E.L. Koehler, *J. Electrochem. Soc.,* Vol 108, 1961, p 509

30. M. Stern and R.M. Roth, *J. Electrochem. Soc.,* Vol l04, 1957, p 390

31. M. Stern and A.L. Geary, *J. Electrochem. Soc.,* Vol 105, 1958, p 638

32. M. Stern and E.D. Weisert, Experimental Observations on the Relation between Polarization Resistance and Corrosion Rate, *Proc. ASTM,* Vol 59, 1959, p 1280

33. "Standard Guide for On-Line Monitoring of Corrosion in Plant Equipment (Electrical and Electrochemical Methods)," G 96, *Wear and Erosion; Metal Corrosion,* Vol 03.02, *Annual Book of ASTM Standards,* ASTM

34. S. Barnartt, *Electrochim. Acta,* Vol 15, 1970, p 1313

35. K.B. Oldham and F. Mansfeld, *Corros. Sci.,* Vol 13, 1973, p 813

36. F. Mansfeld, *J. Electrochem. Soc.,* Vol 120, 1973, p 515

37. F. Mansfeld and M. Kendig, *Corrosion,* Vol 37 (No. 9), 1981, p 556

38. R. Bandy and D.A. Jones, *Corrosion,* Vol 32, 1976, p 126

39. M.J. Danielson, *Corrosion,* Vol 36 (No. 4), 1980, p 174

40. J.C. Reeve and G. Bech-Nielsen, *Corros. Sci.,* Vol 13, 1973, p 351

41. I. Epelboin, C. Gabrielli, M. Keddam, and H. Takenouti, *Electrochemical Corrosion Testing,* STP 727, F. Mansfeld and U. Bertocci, Ed., American Society for Testing and Materials, 1981, p 150

42. A.C. Makrides, *Corrosion,* Vol 29 (No. 9), 1973, p 148

43. D.D. MacDonald and M.C.H. McKubre, *Electrochemical Corrosion Testing,* STP 727, F. Mansfeld and U. Bertocci, Ed., American Society for Testing and Materials, 1981, p 110

44. J.R. Scully, *Corrosion,* Vol 56 (No. 2), 2000, p 199–218

45. A.J. Bard and L.R. Faulkner, *Electrochemical Methods: Fundamentals and Applications,* 2nd ed., John Wiley & Sons, 2001

J.R. Scully and R.G. Kelly, Methods for Determining Aqueous Corrosion Reaction Rates, *Corrosion: Fundamentals, Testing, and Protection*, Vol 13A, *ASM Handbook*, ASM International, 2003, p 68–86

Methods for Determining Aqueous Corrosion Reaction Rates

John R. Scully and Robert G. Kelly, University of Virginia

Electrochemical Impedance Methods

One approach for determining the polarization resistance of a metal involves the electrochemical impedance (sometimes known as alternating current, or ac, impedance) method (Ref 2, 43, 44, 45, 46, 47). ASTM G 106, "Practice for Verification of Algorithm and Equipment for Electrochemical Impedance Measurements," contains an appendix reviewing the technique. In this technique, typically a small-amplitude sinusoidal potential perturbation is applied to the working electrode at a number of discrete frequencies, ω. ω is the angular velocity in rad/s, $\omega = 2\pi f$, where f is frequency in Hz. At each one of the discrete frequencies, the resulting current waveform will exhibit a sinusoidal response that is out of phase with the applied potential signal by a certain amount (Φ) and has a current amplitude that is inversely proportional to the impedance of the interface. The electrochemical impedance, $Z(\omega)$, is the frequency-dependent proportionality factor that acts as a transfer function by establishing a relationship between the excitation voltage signal and the current response of the system:

$$Z(\omega) = V(\omega)/i(\omega) \qquad \text{(Eq 15)}$$

where V is the time varying voltage across the circuit [$V = V_0 \sin(\omega t)$], i is the time varying current density through the circuit [$i = i_0 \sin(\omega t + \Phi)$], $Z(\omega)$ is the impedance ($\Omega \cdot cm^2$), and t is time (s),
$Z(\omega)$ is a complex-valued vector quantity with real and imaginary components whose values are frequency-dependent:

$$Z(\omega) = Z'(\omega) + jZ''(\omega) \qquad \text{(Eq 16)}$$

where $Z'(\omega)$ is the real component of impedance [$Z'(\omega) = |Z(\omega)| \cos(\Phi)$], $Z''(\omega)$ is the imaginary component of impedance [$Z''(\omega) = |Z(\omega)| \sin(\Phi)$], j is the imaginary number $\sqrt{-1}$, $|Z(\omega)|$ is the impedance magnitude, where $|Z(\omega)| = (Z'(\omega)^2 + Z''(\omega)^2)^{1/2}$.
The electrochemical impedance is a fundamental characteristic of the electrochemical system it describes. Knowledge of the frequency dependence of impedance for a corroding system allows a determination of an appropriate equivalent electrical circuit describing that system. Table 1 shows the transfer functions for resistors, capacitors, and inductors.

Table 1 Linear circuit elements commonly used in electrochemical impedance

Circuit element	Impedance[(a)]
Resistor	$Z(\omega) = R$
Capacitor	$Z(\omega) = -j/\omega C$
Inductor	$Z(\omega) = j\omega L$

(a) ω is the frequency; $j = \sqrt{-1}$

Figure 4 illustrates the equivalent electrical circuit model for a simple case of an actively corroding metal. The impedance for that system can be described by:

$$Z(\omega) = R_s + \frac{R_p}{1+\omega^2 R_p^2 C^2} - \frac{j\omega C R_p^2}{1+\omega^2 R_p^2 C^2} \qquad \text{(Eq 17)}$$

where ω is the frequency of the applied signal where $\omega = 2\pi f$(rad/s), f is the frequency of the applied signal [Hz(cycles/s)], C is the interfacial capacitance (F/cm^2). R_s is the solution resistance, and R_p is the polarization resistance.

The Bode magnitude and phase information of Fig. 5 and Eq 17 show that at very low frequencies:

$$Z_{\omega\to 0}(\omega) = R_s + R_p \qquad \text{(Eq 18)}$$

while at very high frequencies:

$$Z_{\omega\to\infty}(\omega) = R_s \qquad \text{(Eq 19)}$$

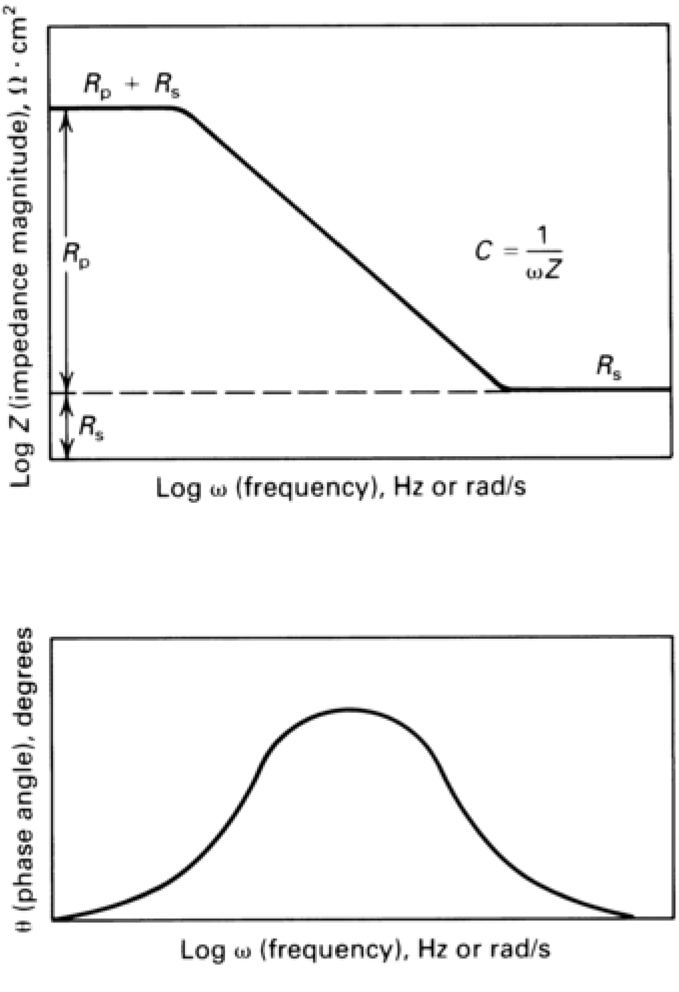

Fig. 5 Bode phase angle and magnitude plots demonstrating the frequency dependence of electrochemical impedance for the circuit model shown in Fig. 4

Determination of R_p is attainable in media of high resistivity because R_p can be mathematically separated from R_s by taking the difference between $Z(\omega)$ obtained at low and high ω($R_p = Z(\omega) \to 0 - Z(\omega) \to \infty$).

Determination of the corrosion rate using Eq 13 also requires knowledge of β_a, β_c and electrode area, *A*, which are not obtained in the impedance experiment (Ref 48). The minimum applied frequency required to obtain $R_s + R_p$ can be approximated by:

$$f_{min} < f_{bp} = \frac{1}{2\pi C\left(R_s + R_p\right)} \qquad \text{(Eq 20)}$$

where f_{bp} is the lower breakpoint frequency (Hz) is approximated by the point on the log|$Z(\omega)$| versus log f plot where the low-frequency plateau dominated by $R_s + R_p$ and the slope -1 region dominated by capacitance produce equal values of $Z(\omega)$, and f_{min} is the minimum test frequency (Hz) required according to Eq 20.

Since the magnitudes of C, R_s, and R_p are not known explicitly a priori, prudence dictates that f_{min} be selected as 0.1 to 0.5 of the estimated f_{bp}. Thus, large values of C, R_s, or R_p dictate that a low f_{min} is required to accurately obtain $R_p + R_s$ at $Z(\omega) \rightarrow 0$. One mHz is typically chosen as a reasonable initial choice of f_{min}, but it is obvious from Eq 20 that either a lower frequency may be required or a higher frequency permitted, depending on circumstances.

Either the anodic or cathodic half-cell reaction can become mass-transport limited and restrict the rate of corrosion at E_{corr}. The presence of diffusion-controlled corrosion processes does not invalidate the electrochemical impedance method but does require extra precaution and a modification to the circuit model of Fig. 4. In this case, the finite diffusional impedance is added in series with the usual charge-transfer parallel resistance shown in Fig. 4. The transfer function for the frequency-dependent finite diffusional impedance, $Z_D(\omega)$, has been described (Ref 49):

$$Z_D(\omega) = R_D\left[\frac{\tanh\sqrt{(j\omega s)}}{\sqrt{(j\omega s)}}\right] \qquad \text{(Eq 21)}$$

where $s = l_{eff}^2/D$ where l_{eff} is the actual finite diffusion length and D is the diffusivity of the diffusing species that limits the interfacial reaction. The value of $Z_D(\omega)$ approaches the real component of diffusional resistance, R_D, as $\omega \rightarrow 0$. The frequency required to obtain R_D depends on the value of s. The larger the value of s, such as when l_{eff} is large or D is small, the lower the frequency required. R_p, defined as $[\partial E/\partial i_{app}]$ as $\omega \rightarrow 0$, is the sum of the charge-transfer-controlled, R_{ct} and diffusion-controlled, R_D, contributions to the polarization resistance assuming that $R_D + R_{ct} \gg R_s$; that is:

$$R_p = R_{ct} + R_D \qquad \text{(Eq 22)}$$

A very low frequency or scan rate may be required to obtain R_p defined by Eq 22 under circumstances where reactions are mass-transport limited as indicated by Eq 21. For instance, in the case where l_{eff} = 0.1 cm and D = 10^{-5} cm^2/ s a frequency below 0.1 mHz is required to obtain R_p from $|Z(\omega)|$ at the zero-frequency limit. Hence, a common experimental problem in the case of diffusion-controlled electrochemical reactions is that extremely low frequencies (or scan rates) are required to complete the measurement of R_p. In the case where R_p is dominated by contributions from mass transport such that Eq 22 applies, the Stern approximation of Eq 13 and 14 must be modified to account for a Tafel slope for either the anodic or cathodic reaction under diffusion-controlled conditions (i.e., β_a or $\beta_c = \infty$). In fact, Eq 7 becomes invalid.

Similarly, a frequency above f_{max} must be applied to obtain R_s:

$$f > f_{max} = \frac{1}{2\pi C R_s} \qquad \text{(Eq 23)}$$

where f_{max} is the frequency required such that $Z(\omega)$ is dominated by R_s.

Typically, f must be in the kHz range to determine R_s. These issues equally plague time as well as frequency domain methods for obtaining R_p since in the time domain measurement, the triangle waveform is simply the Fourier synthesis of a series of sinusoidal signal functions.

The capacitance is also determined from the impedance technique. In many corroding systems, an interfacial capacitance associated with the electrified double-layer scales linearly with the true electrochemical surface area. An electrochemically based estimate of the surface area may be obtained if the area-specific capacitance is known or determined from a plot of C versus surface area (Ref 48).

A common issue in the use of impedance-derived capacitance concerns the use of constant- phase elements (CPE). The impedance associated with a CPE has been given by (Ref 50):

$$Z_{CPE}(\omega) = \left(\frac{1}{Y_0 (j\omega)^n} \right) \quad \text{(Eq 24)}$$

Y_0 is the constant-phase-element parameter. (In the case of the impedance due to capacitance, the value of the capacitance *C*, is the parameter used; that is, $Y_0 = C$, in this expression, and $n = 1$). Y_0 and n are usually assumed to be frequency- independent parameters. The units for Y_0 are s^n/Ω, while those for capacitance (*C*) are s/Ω. Hence, in the case of an ideal capacitor or resistor then $n = 1$ or 0, respectively, and either the magnitude of Y_0 equals the magnitude of *C* with the dimensions s/Ω or $1/Y_0 = R(\Omega)$. In the case of $n = 0.5$, an infinite diffusional impedance best describes the constant-phase element. At issue is the task of extracting physically meaningful parameters conveyed by the capacitance in the case of impedance data that are best represented in an electrical circuit model by a constant-phase element. Examples of such parameters extracted from ideal interfacial capacitance include electrode area in the case of a double- layer capacitance, surface coverage in the case of an adsorption pseudocapacitance, and dielectric constant or dielectric layer thickness in the case of a coating or oxide with dielectric properties. Other parameters may be extracted from capacitance associated with solid-state impedance experiments, but these are beyond the scope of this article. In the case where $n = 0.8$ to 0.99, the CPE is often treated as a nonideal capacitance value and attempts are made to extract physically meaningful parameters from the CPE data. One equation proposed to convert Y_0 into *C* is (Ref 51):

$$C = Y_0 \left(\omega''_{max} \right)^{n-1} \quad \text{(Eq 25)}$$

where ω_{max} is the frequency where the imaginary component of impedance, *Z″*, is maximized. This frequency is independent of *n*. In an earlier approach, $C = Y_0(\omega)^{n-1}/\sin(n\pi/2)$ was suggested as a method for extracting capacitance, *C*, from Y_0 where ω was taken as the frequency where the phase angle was maximized (Ref 52). This method has the disadvantage that the exact value of ω associated with the phase angle maximum changes with the value of *n*.

References cited in this section

2. E. Gileadi, *Electrode Kinetics for Chemists, Chemical Engineers and Materials Scientists,* VCH Publishers, 1993

43. D.D. MacDonald and M.C.H. McKubre, *Electrochemical Corrosion Testing,* STP 727, F. Mansfeld and U. Bertocci, Ed., American Society for Testing and Materials, 1981, p 110

44. J.R. Scully, *Corrosion,* Vol 56 (No. 2), 2000, p 199–218

45. A.J. Bard and L.R. Faulkner, *Electrochemical Methods: Fundamentals and Applications,* 2nd ed., John Wiley & Sons, 2001

46. F. Mansfeld, *Corrosion,* Vol 36 (No. 5), 1981, p 301

47. "Practice for Verification of Algorithm and Equipment for Electrochemical Impedance Measurements," G 106, *Wear and Erosion; Metal Corrosion,* Vol 03.02, *Annual Book of ASTM Standards,* ASTM

48. J.N. Murray, P.J. Moran, and E. Gileadi, *Corrosion,* Vol 44 (No. 8), 1988, p 533

49. D.R. Franceschetti and J.R. Macdonald, *J. Electroanal. Chem.,* Vol 101, 1979, p 307

50. B.A. Boukamp, *Solid State Ionics,* Vol 20, 1986, p 31–44

51. C.H. Hsu and F. Mansfeld, *Corrosion,* Vol 57, 2001, p 747

52. S.F. Mertens, C. Xhoffer, B.C. De Cooman, and E. Temmerman, *Corrosion,* Vol 53, 1997, p 381

J.R. Scully and R.G. Kelly, Methods for Determining Aqueous Corrosion Reaction Rates, *Corrosion: Fundamentals, Testing, and Protection*, Vol 13A*, ASM Handbook*, ASM International, 2003, p 68–86

Methods for Determining Aqueous Corrosion Reaction Rates

John R. Scully and Robert G. Kelly, University of Virginia

Frequency Modulation Methods

Both harmonic and electrochemical frequency modulation (EFM) methods take advantage of nonlinearity in the voltage-current (*E-I*) response of electrochemical interfaces to determine corrosion rate (Ref 53, 54, 55, 56). A special application of harmonic methods involves harmonic impedance spectroscopy (Ref 57). The EFM method uses one or more ac voltage perturbations in order to extract corrosion rate. The electrochemical frequency modulation method has recently been reviewed (Ref 58). In the most often used EFM method, a potential perturbation by two sine waves of different frequencies is applied across a corroding metal interface. The *E-I* behavior of corroding interfaces is typically nonlinear such that a potential perturbation in the form of a sine wave at one or more frequencies can result in a current response at the same and at other frequencies. The result of such a potential perturbation is various ac current responses at various frequencies such as zero, harmonic, and intermodulation. The magnitude of these current responses can be used to extract information on the corrosion rate of the electrochemical interface or conversely the reduction-oxidation rate of an interface dominated by redox reactions as well as the Tafel parameters. This is an advantage over linear polarization resistance and EIS methods, which can provide the $Z(\omega)$ and the polarization resistance of the corroding interface at $\omega = 0$, but do not uniquely determine Tafel parameters in the same set of data. Separate experiments must be used to define Tafel parameters. A special extension of the method involves harmonic impedance spectroscopy where the harmonic currents are converted to harmonic impedance values at various frequencies through knowledge of the magnitude of the ac perturbation.

In the EFM method, an ac voltage perturbation is applied at two frequencies, ω_1 and ω_2. As an example the voltage perturbation could be given as:

$$\eta = V_0[\sin(\omega_1 t) + \sin(\omega_2 t)] \qquad \text{(Eq 26)}$$

where $\eta = E - E_{corr}$ and V_0 is the magnitude of the voltage amplitude applied.

Harmonic current responses occur at ω_1, $2\omega_1$, $3\omega_1$, as well as at ω_2, $2\omega_2$, and $3\omega_2$, and so forth. Additionally, a current response can be seen at various intermodulation frequencies such as $2\omega_1 \pm \omega_2$ and $2\omega_2 \pm \omega_1$. Consider the application of this method to a charge-transfer-controlled corrosion process with an *E-I* response that behaves according to Eq 7. Under the assumption that $\omega_2 > \omega_1$ and $\beta_a < \beta_c$, the corrosion current density, i_{corr}, and Tafel parameters, b_a (where $b_a = \beta_a/\ln 10$) and b_c, can be determined from the equations summarized in Table 2. The current components at the angular frequency ω_1 or ω_2 can be measured at ω_1 or ω_2. The intermodulation components $\omega_1 \pm \omega_2$ can be determined from the signal response at $\omega_1 + \omega_2$ or $\omega_1 - \omega_2$ and so forth. The method is one of the few that enable extraction of corrosion rate and Tafel parameters directly from a single measurement (also see Ref 34 and 35). Currently, there are no ASTM standards for this technique.

Table 2 Governing equations for extraction of i_{corr}, as well as b_a and b_c from harmonic and intermodulation frequency data

Reaction type	Governing equation	Determination of i_{corr}	Determination of Tafel parameters
Charge-transfer-controlled Tafel behavior	$i_{app} = i_{corr}\left[\left(\exp\left\{\frac{2.303(E - E_{corr})}{\beta_a}\right\}\right) - \exp\left\{-\frac{2.303(E - E_{corr})}{\beta_c}\right\}\right]$	$i_{corr} = \frac{{i_{\omega_1\omega_2}}^2}{2\sqrt{8 i_{\omega_1\omega_2} i_{2\omega_2\pm\omega_1} - 3 i^2_{\omega_2\pm\omega_1}}}$	$b_a = \frac{i_{\omega_1\omega_2} V_0}{i_{\omega_2\pm\omega_1} + \sqrt{8 i_{\omega_1\omega_2} i_{2\omega_2\pm\omega_1} - 3 i^2_{\omega_2\pm\omega_1}}}$

Passive or anodic mass-transport control	$i = i_{corr}\left[1 - \exp\left(\frac{-\eta}{b_c}\right)\right]$	$i_{corr} = \frac{i_{\omega_1,\omega_2}^{\ 2}}{2i_{\omega_2\pm\omega_1}}$	$b_c = \frac{i_{\omega_1,\omega_2}}{2i_{\omega_2\pm\omega_1}}V_0$
Cathodic mass-transport control	$i = i_{corr}\left[\exp\left(\frac{\eta}{b_a}\right) - 1\right]$	$i_{corr} = \frac{i_{\omega_1,\omega_2}^{\ 2}}{2i_{\omega_2\pm\omega_1}}$	$b_a = \frac{i_{\omega_1,\omega_2}}{2i_{\omega_2\pm\omega_1}}V_0$

Note that $b_a = \beta_a/\ln 10$, and $b_c = \beta_c/\ln 10$. Also, $i_{2\omega_1\omega_2}$ can be evaluated at $i_{2\omega_1+\omega_2}$ or $i_{2\omega_1-\omega_2}$; $i_{\omega_1\omega_2}$ can be evaluated at $i_{\omega_1+\omega_2}$ or $i_{\omega_1-\omega_2}$; i_{ω_1}, and i_{ω_2} can be evaluated at i_{ω_2} or i_{ω_2}. Source: Ref 58

References cited in this section

34. S. Barnartt, *Electrochim. Acta,* Vol 15, 1970, p 1313

35. K.B. Oldham and F. Mansfeld, *Corros. Sci.,* Vol 13, 1973, p 813

53. J. Devay and L. Meszaros, *Acta Chim. Acad. Sci. Hung.,* Vol 100, 1979, p 183

54. J.S. Gill, M. Callow, and J.D. Scantlebury, *Corrosion,* Vol 39, 1983, p 61

55. G.P. Rao and A.K. Mishra, *J. Electroanal. Chem.,* Vol 77, 1977, p 121

56. L. Meszaros and J. Devay, *Acta Chim. Acad. Sci. Hung.,* Vol 105, 1980, p 1

57. M.C.H. McKubre and B.C. Syrett, *Corrosion Monitoring in Industrial Plants Using Nondestructive Methods,* STP 908, G.C. Moran and P. Labine, Ed., American Society for Testing and Materials, 1986, p 433

58. R.W. Bosch, J. Hubrecht, W.F. Bogaerts, and B.C. Syrett, *Corrosion,* Vol 57, 2001, p 60–70

J.R. Scully and R.G. Kelly, Methods for Determining Aqueous Corrosion Reaction Rates, *Corrosion: Fundamentals, Testing, and Protection*, Vol 13A, *ASM Handbook*, ASM International, 2003, p 68–86

Methods for Determining Aqueous Corrosion Reaction Rates

John R. Scully and Robert G. Kelly, University of Virginia

Electrochemical Noise Resistance

Electrochemical noise analysis can provide a parameter called the electrochemical noise resistance, R_n (Ref 59, 60, 61, 62, 63, 64, 65). This parameter should be used in a manner analogous to polarization resistance. One electrode configuration that enables such a measurement involves connecting a zero-resistance ammeter (ZRA) between two nominally identical corroding electrodes immersed in the same solution. A third, nominally identical electrode can be immersed in solution and connected to the first two using a high-impedance voltmeter. This electrode serves as a “noisy” pseudoreference electrode. This approach is attractive in field applications due to the more rugged nature of the metallic electrode compared to laboratory electrodes but complicates the analysis because two uncorrelated potential sources (i.e., from the couple and the

pseudoreference) are measured in the collection of potential noise, V_n. Since $V_{n(meas)} = (V^2_{n(couple)} + V^2_{n(pseudoref)})^{1/2}$, $V_{n(meas)}$ must be divided by $\sqrt{2}$(Ref 66), to yield $V_{n(couple)}$. Another alternative is a four-electrode arrangement where the first pair is coupled through a zero-resistance ammeter to monitor current and the second pair is connected with a high-impedance voltmeter to sample an uncorrelated $V_{n(couple)}$. Alternatively, a less noisy, conventional reference electrode may be utilized in the three-electrode arrangement. In this case, $V_{n(meas)}$ and $I_{n(meas)}$ are correlated. The reference electrode noise can be separately defined as the electrochemical voltage noise between two nominally identical reference electrodes (Ref 67). If the reference electrode noise is low, then the $\sqrt{2}$correction factor is not needed. In either case, the third electrode (reference electrode) is connected to the first two via a high-impedance voltmeter.

These arrangements enable simultaneous recording of the galvanic current with time and the galvanic couple potential versus time. The standard deviation of the voltage noise divided by the standard deviation of the current noise has been proposed to yield a statistical parameter called the noise resistance R_n (Ref 59, 60, 61, 62, 63, 64, 65, 66, 68). Analysis of simulated noise data has led to the conclusion that the ratio of the standard deviations of the current and voltage noises measured between two identical electrodes can be normalized by surface area by multiplying by $\sqrt{A_v A_i}$(Ref 65):

$$R_n\left(\text{ohm}\cdot\text{cm}^2\right) = \left[\frac{\sigma_{V(\text{meas})}}{\sigma_{I(\text{meas})}}\right]\sqrt{A_V A_I} \qquad \text{(Eq 27)}$$

where $\sigma_{V(meas)}$ is the standard deviation of the voltage noise, $\sigma_{I(meas)}$ is the standard deviation of the current noise, and A_v and A_I are the surface areas of the corroding electrodes used for voltage and current measurement, respectively. Correlations between this parameter and conventionally determined polarization resistance as well as mass-loss-based corrosion rates have been obtained (Ref 60, 66). Unfortunately, experimental confirmation of the area normalization factor has not been extensively performed. Recall that in the case of a polarization resistance determined from E-i_{app} data or EIS data at the zero-frequency limit, measured resistance can be multiplied by electrode area and will yield the same area-normalized polarization resistance over a broad range of electrode areas.

Moreover, the correlation has lacked a rigorous fundamental foundation for correlating R_n with corrosion rate despite the intuitive connection between σ_V and σ_I given by the proportionality factor R_n. The surface of one freely corroding electrode could be divided into area patches that experience fluctuations in interfacial resistance that produce changes in anodic and cathodic half-cell reaction rates in any one. The electrode potential must then change in each patch to drive the half-cell reactions such that the sum of all the anodic half-cell currents from all patches equals the sum of all cathodic half-cell currents, regardless of whether the source of cathodic half-cell current is from capacitive discharge or electrochemical reaction (Ref 64). Some global change in potential also occurs on the electrode. If the first electrode is now connected to a second electrode whose interfacial properties and global electrode potential do not change on their own at the same instant in time and by the same degree as on the first electrode, then a galvanic cell is momentarily created that induces a further difference in anodic and cathodic half-cell currents on the first electrode. Current now flows between the first and second electrode such that the sum of anodic and cathodic half-cell currents over all patches on both electrodes is equal. When the interfacial resistances return to normal values over all patches, the potential difference between the two electrodes is eliminated and so is the measurable current between the two electrodes. Bertocci argued that the external current fluctuation measured between two identical electrodes is identical to the fluctuation in one electrode (Ref 64, 65). Others have argued using concepts of mixed-potential theory that, at worst, the current sampled is only one-half of the total for equal-size electrodes.

Theoretical relationships establishing the connection between R_n and R_p have been sought by several researchers (Ref 65, 69, 70, 71, 72), but their validity has been questioned. A great concern has been that the largest current peaks would occur during the most rapid voltage fluctuations since the electrode interface contains a capacitance through which current can be shorted (Ref 64, 65). Thus, when voltage fluctuations are rapid, the measured noise current will be shorted through the interfacial capacitance assuming a simple electrical equivalent circuit model consisting of two parallel resistor-capacitor networks describing the interface for each electrode connected in series through R_s. This situation would lead to the lowest impedance between the two electrodes during the most rapid voltage fluctuations that, in turn, produce the greatest current fluctuations. The theoretical maximum measured current would be given by the voltage fluctuation divided by

R_s. The outcome would be a statistical noise-resistance parameter that is proportional to, or heavily influenced by, higher- frequency data. Indeed, R_n was found to equal an absolute impedance at some frequency that depended on the frequency of the voltage fluctuations and the RC time constant of the electrode interface in one study of simulated noise (Ref 64). Unfortunately, a R_n value obtained at high frequency would be smaller in magnitude than the R_p obtained at the zero-frequency limit. Hence, it would not represent the desired zero-frequency limit interfacial resistance, R_p. Indeed, such underestimations in the true value of R_p have been observed experimentally (Ref 66, 68).

Recently, a more rigorous theoretical and experimental analysis has been made comparing the spectral noise resistance obtained at each frequency with both the polarization resistance obtained from the zero-frequency limit of impedance magnitude data, $|Z(\omega = 0)|$, as well as the frequency-dependent impedance of two electrodes (Ref 73, 74, 75, 76, 77). The spectral noise resistance $R_{sn}(\omega)$ was determined by taking the square root of power spectral density of the voltage noise $(V^2/Hz)^{1/2}$ and dividing it by the square root of power spectral density of the current noise $(A^2/ Hz)^{1/2}$ at each frequency using the same two- electrode arrangement as discussed previously (Ref 76, 77):

$$R_{sn}(\omega) = \frac{\sqrt{(V_{PSD})}}{\sqrt{(I_{PSD})}} \quad \text{(Eq 28)}$$

$R_{sn}(\omega)$ is proportional to the magnitude of the cell impedance, $|Z(\omega)|$ in the two-electrode arrangement (Ref 76, 77). The proportionality factor is unity in the case of identically sized electrodes in a two-electrode cell with identical impedances and a noiseless reference electrode (Ref 76, 77). Therefore, the spectral noise resistance at the zero-frequency limit could equal the interfacial impedance at the zero-frequency limit $|Z(\omega = 0)|$ in the theoretical case of identical electrode impedances with negligible R_s. Figure 6 gives data for identical iron electrodes in 1 *M* Na_2SO_4 with an iron reference electrode. Here $R_{sn}(\omega) = \sqrt{3}|Z(\omega)|$ due to the noisy reference electrode. Thus $2|Z(\omega)|$ and $R_{sn}(\omega)$ appear to be similar. It is well known that in many instances $|Z(\omega = 0)|$ equals R_p. Even R_n may equal $R_{sn}(\omega = 0) = |Z(\omega = 0)| = R_p$ if $|Z(\omega)|$ equals R_p in the frequency regime dominating the R_n value. The frequency range dominating the R_n value is determined by several factors, but this statement is more likely to be true if $|Z(\omega)|$ and $R_{sn}(\omega)$ both exhibit long low-frequency plateaus over a broad frequency range that encompasses the f_{min} and f_s utilized in the R_n measurement. Here f_{min} is given by the total sampling time, T, where $f_{min} = 1/T$ and f_s equals the data sampling rate. R_n typically varies with f_s and underestimates $|Z(\omega = 0)|$. Unfortunately, $R_{sn}(\omega \rightarrow 0)$ does not equal R_p in the zero-frequency limit under many other conditions, such as when $\log(R_s/R_p) > 0$ or in the case of very noisy reference electrodes (Ref 76, 77). Moreover, $R_{sn}(\omega)$ can be dominated by the properties of the high-impedance electrode in the case of dissimilar electrode impedances that are equally noisy, but this is not always the case. For instance, the low-impedance electrode in a two- electrode cell with a third reference electrode can be sensed by $R_{sn}(\omega)$ if the higher impedance electrode is much noisier than the low-impedance electrode (Ref 76, 77). Recent attempts have been made to address circumstances where $R_{sn}(\omega)$ lies in between $|Z(\omega)|_1$ and $|Z(\omega)|_2$ representing the high- and low-impedance electrodes. Methods have been suggested for sensing the current fluctuations on both electrodes (Ref 72). The reader is referred to these articles for more information.

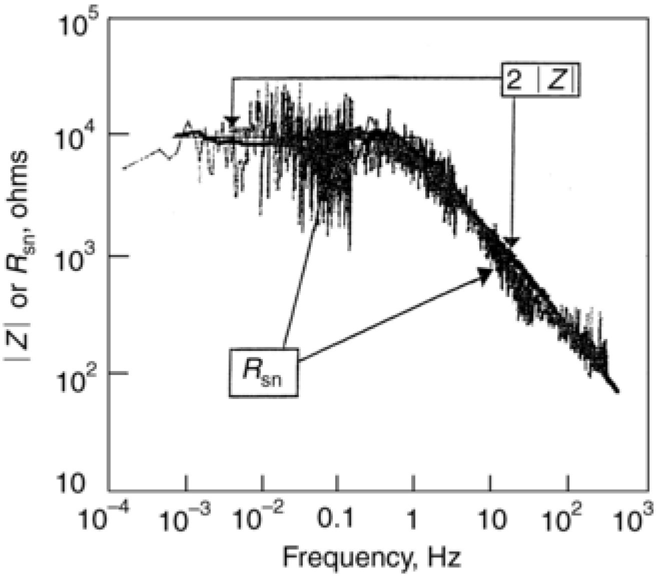

Fig. 6 **$R_{sn}(\omega)$ versus frequency compared to two times the impedance $|Z(\omega)|$ versus frequency for iron in 1 *M* Na_2SO_4 at pH 4 with a "noisy" iron reference electrode. Impedance measurements performed in a two-electrode cell with two iron electrodes produced $2|Z(\omega)|$. $R_{sn}(\omega)$ calculated to equal $\sqrt{3}|Z(\omega)|$ for the case of two iron electrodes coupled through a zero-resistance ammeter and a third iron electrode as reference electrode. Source: Ref 77**

References cited in this section

59. D.A. Eden, A.N. Rothwell, and J.L. Dawson, Paper 444, Proc. Corrosion Conference, 1991, National Association of Corrosion Engineers, 1991

60. J.L. Dawson, *Electrochemical Noise Measurement for Corrosion Applications,* STP 1277, J. Kearns, J.R. Scully, P.R. Roberge, D.L. Reichert, and J.L. Dawson, Ed., American Society of Testing and Materials, 1996, p 3–35

61. D.A. Eden, K. Hladky, D.G. John, and J.L. Dawson, Paper 276, Proc. Corrosion Conference, 1986, National Association of Corrosion Engineers, 1986

62. D.A. Eden and A.N. Rothwell, Paper 292, Proc. Corrosion Conference, 1992, National Association of Corrosion Engineers, 1992

63. A.N. Rothwell and D.A. Eden, Paper 223, Proc. Corrosion Conference, 1992, National Association of Corrosion Engineers, 1992

64. U. Bertocci, *Electrochemical Noise Measurement for Corrosion Applications,* STP 1277, J. Kearns, J.R. Scully, P.R. Roberge, D.L. Reichert, and J.L. Dawson, Ed., American Society of Testing and Materials, 1996, p 39–58

65. U. Bertocci and F. Huet, *Corrosion,* Vol 51, 1995, p 131

66. D.L. Reichert, *Electrochemical Noise Measurement for Corrosion Applications,* STP 1277, J. Kearns, J.R. Scully, P.R. Roberge, D.L. Reichert, and J.L. Dawson, Ed., American Society of Testing and Materials, 1996, p 79–89

67. P.C. Searson and J.L. Dawson, *J. Electrochem. Soc.,* Vol 135 (No. 8), 1988, p 1908

68. F. Mansfeld and H. Xiao, *Electrochemical Noise Measurement for Corrosion Applications,* STP 1277, J. Kearns, J.R. Scully, P.R. Roberge, D.L. Reichert, and J.L. Dawson, Ed., American Society of Testing and Materials, 1996, p 59–78

69. G.P. Bierwagen, *J. Electrochem. Soc.,* Vol 141, 1994, p L155

70. F. Mansfeld and H. Xiao, *J. Electrochem. Soc.,* Vol 141, 1994, p 1403

71. F. Huet, *J. Electrochem. Soc.,* Vol 142, 1995, p 2861

72. J.F. Chen and W.F. Bogaerts, *Corros. Sci.,* Vol 37, 1995, p 1839

73. H. Xiao and F. Mansfeld, *J. Electrochem. Soc.,* Vol 141, 1994, p 2332

74. F. Mansfeld and H. Xiao, *J. Electrochem. Soc.,* Vol 140, 1993, p 2205

75. F. Mansfeld, L.T. Han, and C.C. Lee, *J. Electrochem. Soc.,* Vol 143, 1996, p L286

76. U. Bertocci, C. Gabrielli, F. Huet, and M. Keddam, *J. Electrochem. Soc.,* Vol 144, 1997, p 31

77. U. Bertocci, C. Gabrielli, F. Huet, and M. Keddam, *J. Electrochem. Soc.,* Vol 144, 1997, p 37

J.R. Scully and R.G. Kelly, Methods for Determining Aqueous Corrosion Reaction Rates, *Corrosion: Fundamentals, Testing, and Protection*, Vol 13A, *ASM Handbook*, ASM International, 2003, p 68–86

Methods for Determining Aqueous Corrosion Reaction Rates

John R. Scully and Robert G. Kelly, University of Virginia

Electrochemical Methods for the Study of Galvanic Corrosion Rates

Methods Based on Mixed-Potential Theory. The thermodynamic tendency for galvanic corrosion may be determined from the electromotive series (Ref 4, 5) or from the construction of a galvanic series (Ref 79), as discussed in ASTM G 82, "Guide for Development and Use of a Galvanic Series for Predicting Galvanic Corrosion Performance." Galvanic corrosion rates can also be determined from mixed-potential theory as shown in Fig. 7. In the case of bimetal or multimetal galvanic attack in which two or more metals are electrically in contact with one another, there is in theory a minimum of two cathodic and two anodic reactions. One of each of these reactions is occurring on each metal. In this case, the more noble of the two metals is cathodically polarized, and its anodic reaction rate will thus be suppressed. Conversely, the less noble or anodic material is anodically polarized, and the anodic reaction rate is accelerated. The mixed potential (the galvanic couple potential, E_{couple}) of the galvanic couple and the resulting galvanic current can be uniquely determined from the sums of all of the individual anodic and cathodic currents obtained for each material at each potential when:

$$\Sigma i_a A_a = \Sigma i_c A_c \text{ at } E_{couple} \quad \text{(Eq 29)}$$

where i_a and i_c are the anodic and cathodic current densities ($\mu A/cm^2$), respectively, and A_a and A_c are the anodic and cathodic areas (cm^2).

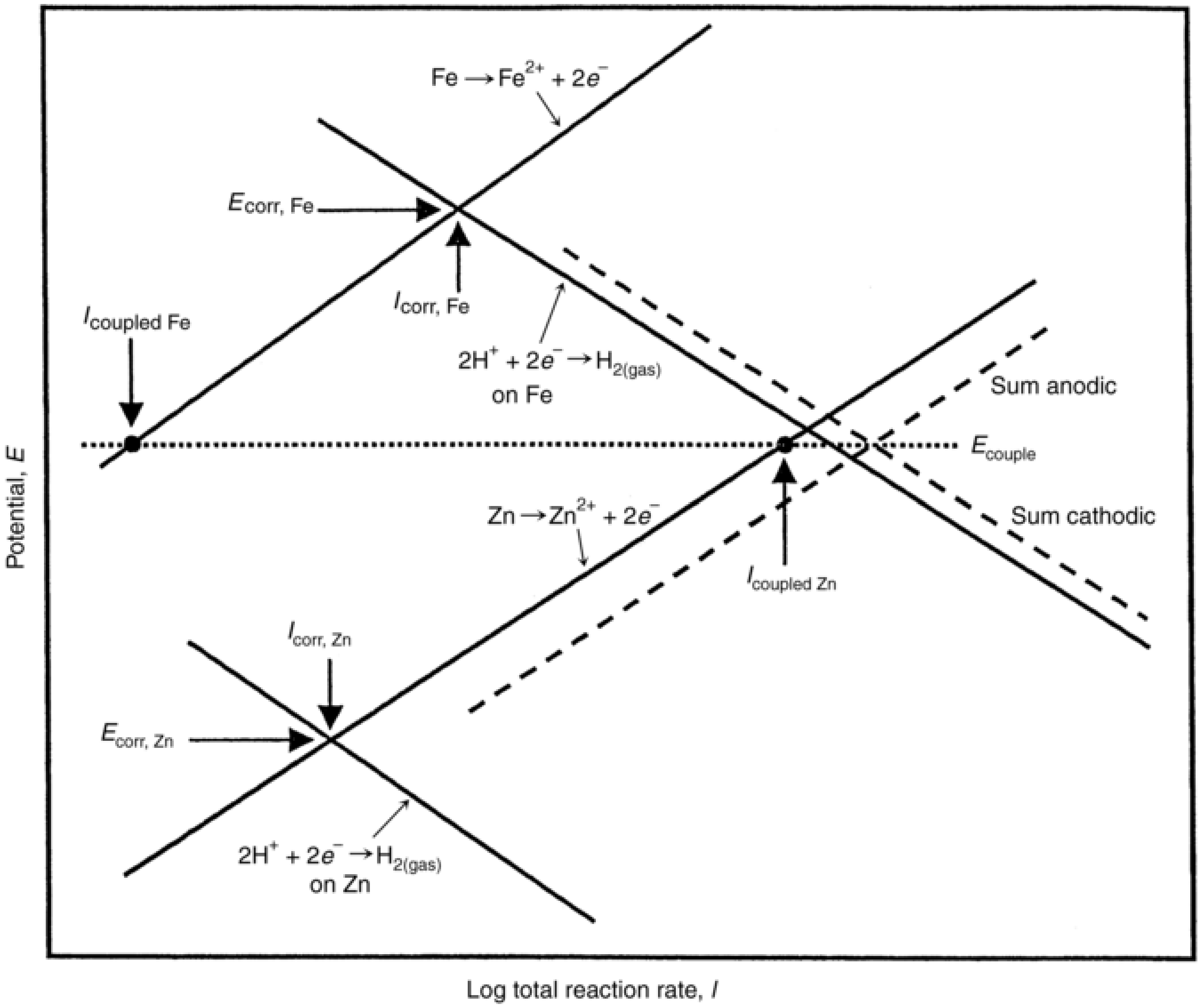

Fig. 7 Potential-current relationships for the case of a galvanic couple between two corroding metals. Iron is the more noble metal; zinc is less noble metal.

The galvanic couple potential is defined by the potential where the sum of the anodic currents equals the sum of the cathodic currents for all of the reactions on all of the metals in the couple. The galvanic couple potential can be determined either by direct measurement with a reference electrode or from polarization data if: (1) polarization data are available for each material in the galvanic couple, (2) the area of each metal is known, and (3) the current distribution is uniform. Once E_{couple} is determined, the galvanic corrosion rate may be estimated for the metal of interest in the couple if a relationship such as given in Eq 7 is known for that metal. In simple bimetal cases, direct superposition of polarization data (corrected for wetted surface area) yields E_{couple} and the galvanic corrosion rate (Ref 79). However, because applied currents instead of true anodic or cathodic currents are measured in any polarization experiment, the E-log(I) superposition technique will introduce the least error when the cathodic reduction reaction rate on the anode is negligible and the anodic oxidation reaction rate on the cathode is negligible at the galvanic couple potential. Obviously, when the open circuit potential OCPs of the anode and cathode are similar, error is more likely. Fortunately, galvanic corrosion may be less significant in these cases. In addition, special care must be taken in the procedures used to develop the polarization data (Ref 79), especially if time effects are to be taken into consideration when evaluating long-term galvanic corrosion behavior.

Direct Measurement of Galvanic Corrosion Rates. A more straightforward procedure involves immersing the two dissimilar metals in an electrolyte and electrically connecting the materials together using a zero-resistance ammeter to measure the additional galvanic current (Ref 9, 80, 81). In this method, the galvanic current is directly determined as a function of time. The galvanic corrosion rate so determined is the additional corrosion

created with the couple and will not equal the true corrosion rate. This is given by the sum of the galvanic corrosion rate and the corrosion rate under freely corroding conditions unless the latter is negligible. Recall that the corrosion rate of the uncoupled anode is undetermined by this method since an equal cathodic reaction rate is occurring on the same surface. A reference electrode connected to the galvanic couple can be used to determine the galvanic couple potential. ASTM standards do not exist for direct, mixed-potential theory, or scanning potential probe methods.

Potential probe methods may be used to determine and map the local ionic currents associated with galvanic corrosion cells between dissimilar metals or heterogeneities on complex alloy surfaces (Ref 82, 83, 84, 85). In the most straightforward application, the local potential is mapped over a planar electrode oriented in the *x-y* plane to give an indication of local current. The basic concept is that the ionic current density in three dimensions can be mapped by either scanning an array of reference electrodes or by vibrating a single electrode. The orthogonal ionic current flow can be expressed in terms of solution conductivity and the gradient in potential in the solution above the galvanic couple:

$$i = -\kappa(\nabla E) \quad \text{(Eq 30)}$$

where κ is the solution conductivity and $\nabla E = \delta_1 dE/dx + \delta_2 dE/dy + \delta_3 dE/dz$ where *x, y,* and *z* define axes in a coordinate system and δ_1, δ_2, and δ_3 are unity vectors. The advantage of the vibrating technique is that minor differences between the reference potential of separate electrodes is eliminated by using a single vibrating reference electrode. The ionic current density so recorded is the component of current density flowing perpendicular to isopotential lines in solution established due to the galvanic couple and the established potential gradient. Therefore, a map of local current can be constructed by scanning over a planar electrode in the *x-y* plane, where *z* is the vertical distance in the solution above the electrode. Locations of high local current imply significant galvanic interactions.

References cited in this section

4. D.A. Jones, *Principles and Prevention of Corrosion,* 2nd ed., Macmillan Publishing, 1996

5. M.G. Fontana and N.D. Greene, *Corrosion Engineering,* McGraw-Hill, 1978

9. R. Baboian, Ed., *Electrochemical Techniques for Corrosion,* National Association of Corrosion Engineers, 1977

79. H. Hack and J.R. Scully, *Corrosion,* Vol 42 (No. 2), 1986, p 79

80. R. Baboian, *Galvanic and Pitting Corrosion-Field and Laboratory Studies,* STP 576, R. Baboian et al., Ed., American Society for Testing and Materials, 1974, p 5

81. F. Mansfeld and J.V. Kenkel, *Galvanic and Pitting Corrosion-Field and Laboratory Studies,* STP 576, R. Baboian et al., Ed., American Society for Testing and Materials, 1974, p 20

82. R.G. Kasper and C.R. Crowe, Comparison of Localized Ionic Currents as Measured from 1-D and 3-D Vibrating Probes, *Galvanic Corrosion,* STP 978, H.P. Hack, Ed., American Society for Testing and Materials, 1988, p 118

83. R.G. Kasper and C.R. Crowe, Comparison of Localized Ionic Currents as Measured from 1-D and 3-D Vibrating Probes, *J. Electrochem. Soc.,* Vol 33, 1986, p 879

84. H.S. Isaacs, The Measurement of Galvanic Corrosion of Soldered Copper Using the Scanning Vibrating Electrode Technique, *Corros. Sci.,* Vol 28, 1988, p 547

85. V.S. Voruganti, H.B. Huft, D. Degeer, and S.A. Bradford, Scanning Reference Electrode Technique for the Investigation of Preferential Corrosion of Weldments in Offshore Applications, *Corrosion,* Vol 47, 1991, p 343

J.R. Scully and R.G. Kelly, Methods for Determining Aqueous Corrosion Reaction Rates, *Corrosion: Fundamentals, Testing, and Protection*, Vol 13A*, ASM Handbook*, ASM International, 2003, p 68–86

Methods for Determining Aqueous Corrosion Reaction Rates

John R. Scully and Robert G. Kelly, University of Virginia

Electrochemical Methods for the Definition of Conditions Where Corrosion Rates Are High

Pitting and crevice corrosion are associated with the local breakdown of passivity, often in halide-containing solutions (Ref 86). Passive corrosion rates are often very low and are not discussed further. Localized corrosion occurs at rates an order of magnitude greater than the rates during passive dissolution. Therefore, it is often of great interest to determine the conditions under which localized corrosion occur instead of the exact propagation rates, which are usually intolerable. Electrochemical tests for evaluating the susceptibility of a material to pitting and to crevice corrosion include potentiodynamic, potentiostatic, scratch potentiostatic, potentiostaircase, tribo-ellipsometric methods, pit-propagation rate curves, galvanostatic, and electrochemical noise measurements (Ref 87, 88). These methods identify critical potential, temperature, and environmental conditions associated with the thresholds between low rates (e.g., passive dissolution at 1 $\mu A/cm^2$ or less than 1 mpy depending on alloy) and high rates of corrosion (e.g., locally as high as 1 A/cm^2). Two critical potentials of significant importance are the breakdown (E_{bd}) and protection (E_{prot}) or repassivation potential. The former is the potential at which pits or crevices develop or become stabilized. The latter is often defined as the least noble potentials at which pits, once formed, will propagate. Below this potential, pits repassivate. A simple potential-based criterion for local corrosion is the comparison of E_{corr} with such a threshold potential associated with breakdown of passive films. A useful concept for safety against the transition to local corrosion is that E_{corr} « E_{bd} and E_{prot} where E_{bd} is often associated with stabilization of local corrosion and E_{prot} is associated with repassivation. When this situation exists, the chance of local high-rate corrosion processes is often low. Therefore, it is important to determine these two potentials.

Cyclic Potentiodynamic Polarization Methods to Determine E_{bd} and E_{prot}. ASTM G 61 (Ref 89) describes a procedure for conducting cyclic potentiodynamic polarization measurements to determine relative susceptibility to localized corrosion. The method is designed for use with iron- or nickel-base alloys in chloride environments. In this test, a cyclic anodic polarization scan is performed at a fixed voltage scan rate. Figure 8(a) shows the cyclic potentiodynamic method. Particular attention is focused on two features of cyclic polarization behavior (Fig. 8a). The first is the potential at which the anodic current increases significantly with applied potential (the breakdown potential, E_{bd}). In general, the more noble this potential, obtained at a fixed scan rate in this test, the less susceptible the alloy is to the initiation of localized attack. The second feature of great interest is the potential at which the hysteresis loop is completed during reverse polarization scan after localized corrosion propagation. This potential is often taken as the repassivation potential or protection potential, E_{prot}. In general, once initiated, localized corrosion sites can propagate only at some potential more positive than the potential at which the hysteresis loop is completed (when determined at a fixed scan rate). In other words, repassivation will occur at more negative potentials even after localized corrosion initiation. Therefore, the more positive the potential at which the hysteresis loop is completed, the less likely that localized corrosion will propagate. ASTM G 61 (Ref 89) discusses cyclic polarization behavior for Hastelloy C-276 and 304 stainless steel in 3.5% sodium chloride solution. Based on this criterion, it is evident that Hastelloy C-276 is more resistant to localized corrosion in this environment than AISI 304 stainless steel.

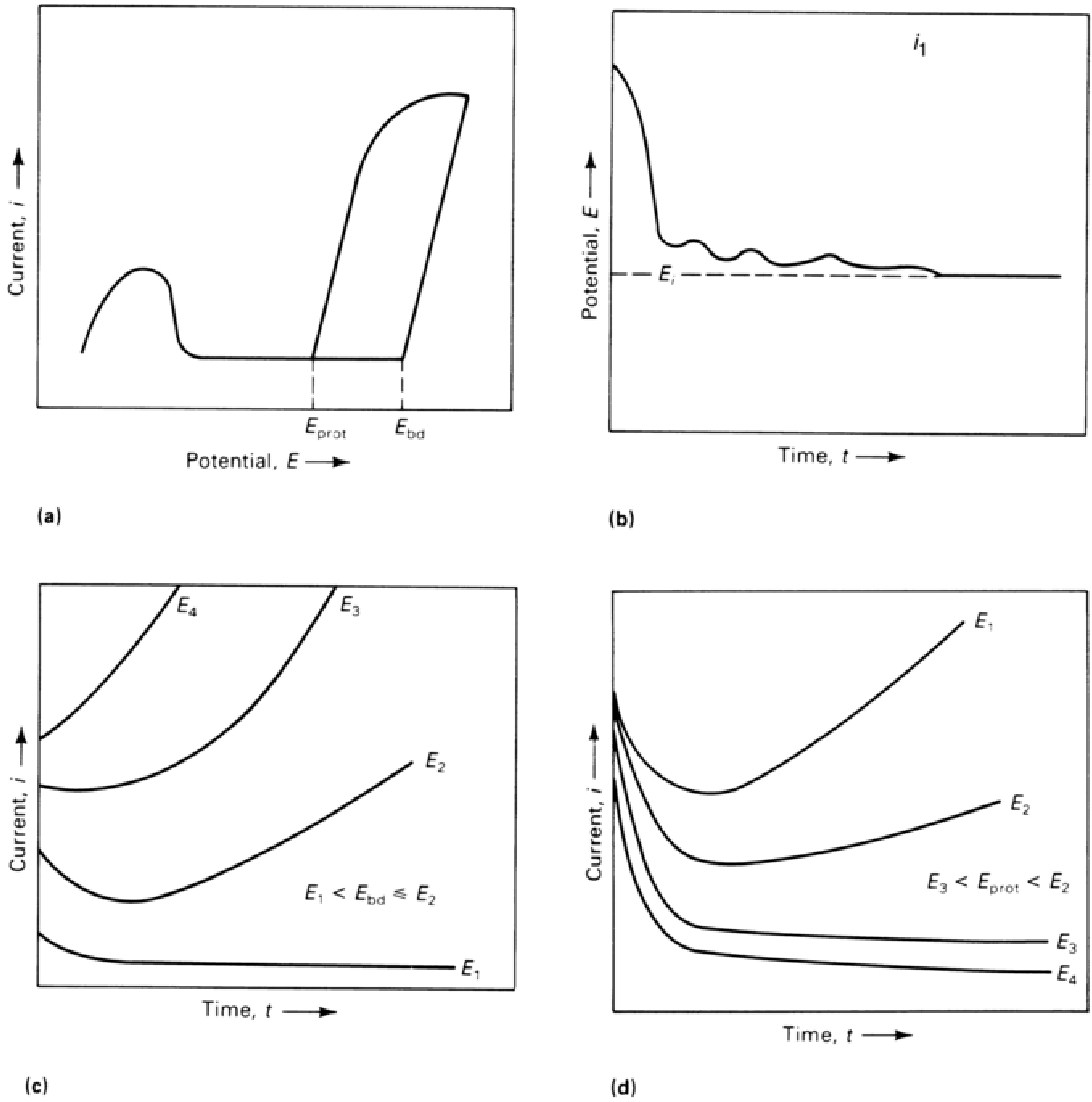

Fig. 8 (a) Cyclic potentiodynamic polarization curve. (b) Galvanostatic potential-time curve for a material. (c) Potentiostatic current-time curve for a previously passivated surface which pits at $E_1 < E_{BD} < E_2$. (d) Potentiostatic current-time curve for active surface. The protection potential is found as $E_3 < E_{prot} < E_2$. Source: Ref 86

Complications with Cyclic Potentiodynamic Polarization Methods. Although the cyclic method is a reasonable method for screening variations in alloy composition and environments for pitting susceptibility, the cyclic potentiodynamic polarization method has been found to have a number of shortcomings (Ref 87, 88, 89, 90, 91, 92). One major problem concerns the effect of the potential scan rate. The values of both E_{bd} and E_{prot} are a strong function of the manner in which the tests are performed, particularly the potential scan rate employed. Experimental values of E_{bd} are linked to the induction time required for pitting. Another complication arises from allowing too much pitting propagation to occur before reversing the scan direction. This either alters the localized chemistry in pits, affects pit depth, or both. Pit depth alters the diffusion length associated with the dilution of pit chemistry necessary for repassivation. This factor affects the polarization behavior after the reversal in the direction of scanning and influences E_{prot}. From an engineering standpoint, metal surfaces held at potentials below the repassivation potential of the deepest pits should be safe against stable pit propagation.

That is to say, stable pits should not propagate. It has been found that E_{bd} observed after potentiostatic holds or the slowest scan rates approaches the protection potential found after minimal pit growth (Ref 92). This suggests the existence of a single critical potential for pit growth in the absence of crevices or other occluded sites (Ref 92).

Potentiostatic and Galvanostatic Methods for Localized Corrosion. The shortcomings of the cyclic potentiodynamic polarization method have become the basis for several other electrochemical techniques. Other methods are shown in Fig. 8. In the galvanostatic or galvanostaircase technique (Fig. 8b), potential is measured versus time at various constant applied currents that are incrementally increased in steps, then reversed, and decreased. In the case of passive materials, a potential rise during galvanostatic testing indicates passive film growth, while a decline indicates breakdown and growth of local corrosion sites. In the galvanostaircase technique, the current is step increased. Potential measurements are made until the time rate of change in potential approaches 0. These forward and reverse potential-current density data are extrapolated to the zero current density to obtain E_{bd} and E_{prot}. The technique is described by ASTM G 100 "Standard Test Method for Conducting Cyclic Galvanostaircase Polarization Tests" (Ref 93) as a test method for aluminum alloys. Potentiostatic methods can overcome the inherent problems involving scan rate. A more conservative estimate of E_{bd} can be obtained by polarizing individual samples for long periods of time at potentials above and below the values of E_{prot} and E_{bd} previously determined from the potentiodynamic method (Fig. 8c). Eventual initiation is indicated by a current increase. In another approach (Fig. 8d), initiation of pits is intentionally induced by applying a "stimulation" potential well above E_{bd} and then quickly shifting to a preselected potential below that value. If this second applied potential is above E_{prot}, propagation of the existing pits will continue and the current will increase. However, at potentials less than E_{prot} the pits will eventually repassivate and the current will subsequently decrease with time. The critical potential for pitting is defined as the most noble potential at which pits repassivate after the stimulation step. This approach is covered in ASTM F 746 "Test Method for Pitting or Crevice Corrosion of Metallic Surgical Implant Materials" (Ref 94).

Determination of E_{prot} by Potential Step- Down or Scan-Down Methods. As stated previously, E_{bd} and E_{prot} often depend strongly on the method by which they are determined and, therefore, do not uniquely define intrinsic material properties. The E_{prot} values determined from the scanning method can be complicated by scan rate, pit size or depth, vertex potential/ current, polarization curve shape, and specimen geometry (Ref 95, 96). Some investigators have found more consistent E_{prot} values after a critical charge has passed, while others report a single critical potential (Ref 92). Often this potential is difficult to determine and has been taken at various points of the polarization curve (Ref 98).

What is needed is a method for determination of E_{prot} that defines a conservative value of this potential that likely reflects a true pit or crevice repassivation potential. Tsujikawa has developed a method for determination of E_{prot} from previously grown pits and crevices (Ref 99, 100). This method and its variations have been successfully used by several research groups and associates the critical potential for repassivation E_{prot} with the need to grow local corrosion sites to a critical minimum size (Ref 101). The method is an enhancement of the determination of E_{prot} from potentiodynamic *E-I* scans that involve scan reversal to the point where pits are repassivated. In the potential step-down method, the potential is first set at a high enough value to induce and grow stable pits to the specified size. The potential can then be stepped down or scanned downward while the pit propagation current is recorded. Subsequently, the potential may be held after initiating a pit in order to determine the time until repassivation (Ref 102). Moreover, long potential holds at selected applied potentials enables confirmation of a true repassivation potential often indicated by an abrupt decrease in current density at the time when the chemical conditions favoring pit stability (often expressed as some fraction of the salt-saturation concentration) are no longer maintained. Abrupt transitions in finite repassivation time toward infinity with increasing hold potential may indicate that conditions favorable to pit growth are sustained. Another benefit of determining E_{prot} from controlled growth of pits and crevices is that the repassivation potential can be determined from pits of preselected sizes that can be controlled by the duration of the potential holds. The method has been successfully applied to nickel-base alloys, stainless steels, and aluminum-base alloys. This method is being standardized by the committee for Japanese Industrial Standards. When a one-dimensional pit or pencil electrode is tested, the pit propagation kinetics can be recorded from a single pit (Ref 103). Whether pit growth is ohmic, mass transport, or charge-transfer controlled may also be determined. Moreover, the effects of various material and solution parameters (e.g., flow rate, conductivity, and solution composition) on pit propagation can be determined.

The Scratch-Repassivation Method for Localized Corrosion. One additional potentiostatic technique to be mentioned in the area of localized corrosion involves the scratch method (Ref 96). In this method, the alloy surface is scratched at a constant potential and the current is measured as a function of time. The potential dependencies of the induction time and the repassivation time are determined by monitoring the current change over a range of different potentials. This is shown in Fig. 9. From this information the critical pitting potential, thought to be less than E_{bd} determined by potentiodynamic scan, can be found. Other methods of studying localized corrosion are also available (Ref 86).

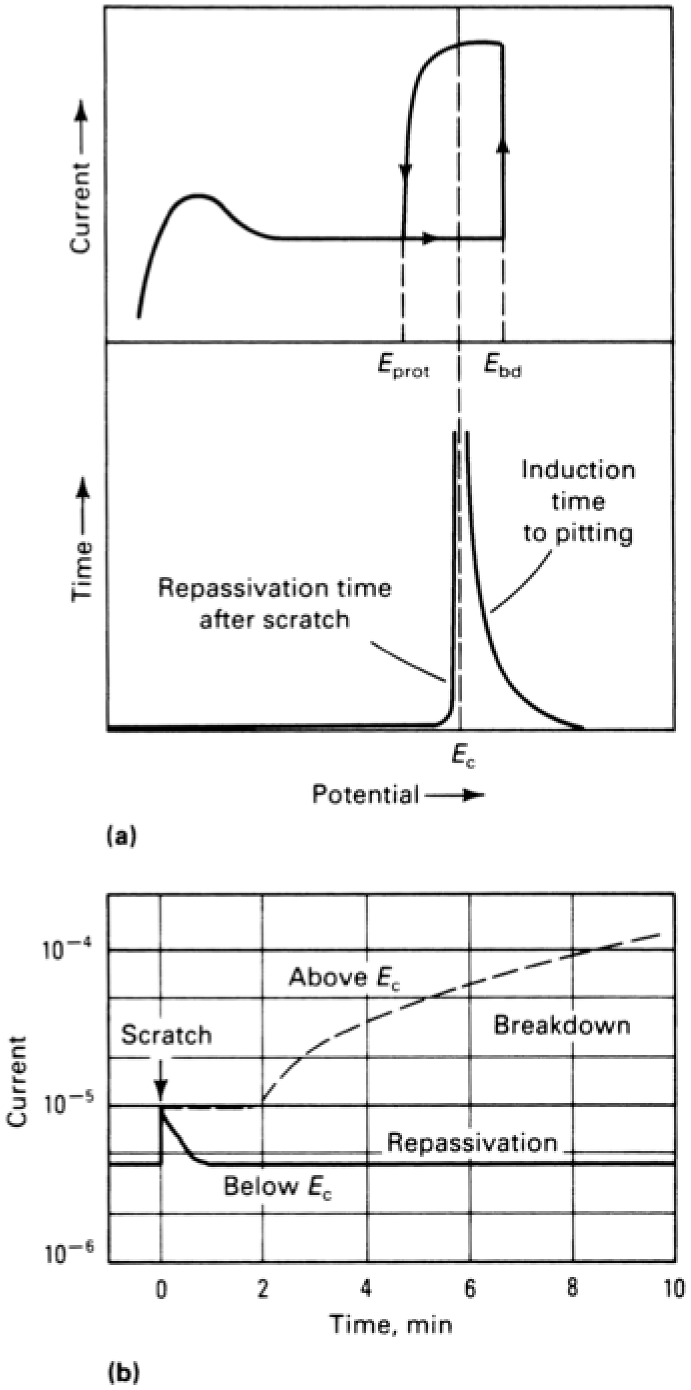

Fig. 9 Potential versus time plot of scratch test illustrating a possible location of the critical potential, E_c, as it relates to the induction time and the repassivation time. Source: Ref 86

Statistical Distributions in Critical Potentials. E_{bd} is typically observed to be a significantly "statistically distributed" property compared to the repassivation potential. This is often observed when critical potentials are determined by potentiodynamic scanning, but can be observed during potentiostatic tests where the pit incubation time and subsequent survival probabilities are also seen to be distributed. E_{prot} distributions are often attributed to distributions in pit size. However, E_{prot} is not distributed when pits are uniformly large (Ref 97)

and may not depend on the depth of corrosion damage at all during crevice corrosion when a crevice former controls mass transport (Ref 104). Statistical distributions in pitting potentials have been observed for AISI 304 (Ref 105), Fe-Cr-X (where X = niobium, molybdenum, or titanium) alloys (Ref 106), AISI 316 (Ref 107), titanium (Ref 108), high-purity aluminum (Ref 109), 2024-T3 (Ref 110), and amorphous aluminum-base alloys (Ref 111). This means that significant variations are seen when a number of specimens are tested under identical conditions. These distributions have been attributed to the stochastic nature of pitting (Ref 107), distributions in oxide-film cation vacancy transport properties (Ref 112), the effects of potential on the nature of the eligible sites for the metastable pit nucleation process (Ref 105), and the population of fatal flaws or pit initiating defects on an electrode surface (Ref 113). The possibility that oxide defects at densities exceeding millions of sites/cm^3 produces specimen-to-specimen variations appears unlikely for specimens with surface areas of the order of a few cm^2. It appears to be more reasonable to expect that sample-to-sample variations are, instead, associated with distributions in the population of micrometer-scale defects such as sulfide inclusions in stainless steel (Ref 114) and constituent particles in aluminum alloys (Ref 112) that control pit nucleation intensity and produce micropit-to-micropit variations in growth rates and transport characteristics (e.g., D_{eff}, pit shape) for a large population of metastable pits grown at a single potential. A statistical distribution of peak I_{pit}/r_{pit} ratios (where I_{pit} is the peak pit current and r_{pit} is pit radius) was observed for a large population of pits at a fixed potential in high-purity aluminum (Ref 109). Although not rigorously proven, it is reasonable to argue that a slightly lower D_{eff} or slightly larger I_{pit}/r_{pit} ratio for a given pit might lead to pit stabilization at differing applied potentials on an electrode with its own unique population of metastable pits. Moreover, such behavior is likely controlled by micrometer- scale defects spaced at tens of micrometer lateral separation distances across planar electrode surfaces. Investigators who seek information on critical potentials for engineering use should consider appropriate specimen sizes relative to critical defect densities and spacings. There are no ASTM standards that address these issues. However, the size of test specimens recommended in many ASTM standards is conservatively large, leading to conservative values of E_{bd}.

Electrochemical noise (EN) methods are used increasingly as a nondestructive tool for evaluating susceptibility to localized corrosion as well as stress-corrosion cracking (SCC), particularly in field or process plant applications (Ref 115, 116, 117, 118, 119, 120). Electrochemical noise methods are appealing because they may be conducted at open circuit without perturbing the corroding system. However, no consensus currently exists as to the most appropriate test procedure or analysis method, or how well results correlate with coupon exposures. The transient development of bare metal at newly formed pit or cracking sites as a result of temporary propagation and repassivation can result in potential noise (open-circuit EN), current noise (potentiostatic EN), or both. In the latter case, the current noise is measured with a zero-resistance ammeter (ZRA) used to monitor a galvanic couple consisting of two identical electrodes while the potential noise comes from the reference electrode (or third metallic electrode) monitoring the couple potential. The noise signal, hereafter referred to as a potential or current time record, is caused by the galvanic couple formed between the very small anode sites corroding at current densities approaching 10 A/cm^2 in pitting corrosion and the much larger remaining cathode surface operating at lower cathodic current densities (e.g., 10 μA/ cm^2). Regarding pitting phenomena, a negative shift in measured potential is observed (OCP and galvanic couple EN), an increase in current is observed for potentiostatic EN, and current fluctuations of either polarity are observed for galvanic couple EN.

Several analysis methods exist including electrochemical (Ref 121), statistical (Ref 119, 120), spectral (Ref 115, 116, 117, 118, 119, 120, 121), and autocorrelation (Ref 117). Some of the approaches for determination of spectral noise resistance during uniform corrosion are discussed in the section on polarization resistance. Electrochemical analysis may also enable the determination of pit sizes from the charge associated with each pitting event (Ref 109) or from attempting to determine pit current densities. Statistical analyses include determining the root mean square (rms), variance, and standard deviations of the EN voltage or current time records, as well as a noise resistance, R_{EN}, taken as the ratio of the rms or standard deviation of the potential and current time records acquired over various periods of time (Ref 105). Spectral analysis consists of Fourier transformation of EN data acquired in the time domain to create a power spectral density plot (Ref 117, 118, 120, 122). Qualitative assessment of the benefits of inhibitors or the effects of process stream variations are made possible by comparing statistical or spectral results. Quantitative analysis and predictive capability still require further development.

Use of Shot Noise Methods During Pitting. In the prepitting stage, multiple subcritical pitting events are often observed. The current time record shows exponential decaying or rising transients associated with discrete

pitting events. In many systems, these prepitting events occur at potentials far more negative than E_{bd} and sometimes E_{prot}. Numerous investigators have proposed that the ratio of peak pit current to pit radius during metastable pitting or product of pit current density times pit radius (I_{pit}/r_{pit} or $i_{pit} \cdot r_{pit}$) provides an insightful parameter that can be used to characterize the risk of stable pit propagation based on the critical acidified chemistry theory of Galvele (Ref 123).

When anodic current is monitored near the pitting potential, multiple overlapping metastable pitting events are often detected as current spikes at potentials just below E_{bd}. Electrochemical noise analysis provides one method for extracting information on pitting from such complicated current time records. That is, the power spectrum for a population of spikes of similar amplitude and duration is the sum of the spectra for each spike and should have the same shape as an individual spike. It has been proposed to use shot noise analysis to calculate the pit charge from power spectral density (PSD) obtained from a current-time record (Ref 124, 125, 126). According to this approach, pit charge, q_{pit}, and through Faraday's Law the pit radius, r_{pit}, for the pit events that dominate the current time record, can be determined from the PSD of a pitting current noise spectrum. The PSD of current fluctuations for the case of randomly occurring, exponentially decaying current spikes associated with metastable pitting events during the prepitting stage can be described by (Ref 123):

$$\frac{I^2}{\Delta f} = \left[\frac{2q_{pit}I_{mean}}{1+(2\pi f\tau)^2}\right] \quad \text{(Eq 31)}$$

where f is the spectrum frequency, Δf is the frequency resolution given by the data acquisition frequency divided by the number of data points collected, q_{pit} is the pit charge, I_{mean} is the mean current from a *I-t* record containing multiple current fluctuations associated with pit events after subtraction of any background passive current, I is the amplitude of pit current fluctuations, and τ is the time constant for individual exponentially decaying current transients that comprise the current fluctuations. Hence, the low-frequency limit of a log $I^2/\Delta f$ versus log f plot provides information on q_{pit} for known I_{mean}. The frequency of the intercept (or breakpoint frequency) of the sloping part of the high- frequency PSD with the low-frequency plateau, f_{bpt}, provides information on the time constant for exponentially decaying pitting events, τ; $f_{bpt} = \frac{1}{2\pi\tau}$. Therefore, q_{pit} and τ_{pit} may be extracted from current PSD plots constructed from current-time data containing many overlapping metastable pitting events. This has been successfully done for aluminum alloys (Ref 127, 128). Unfortunately, the approach has its shortcomings. The parameters recovered are heavily biased toward smaller, more numerous pitting events that dominate the current time record. The biggest and/or fastest growing pits that might readily form stable propagating pits may not be detected. However, the method does enable determination of pit sizes at various potentials and allows the comparison of one environment, temperature, or set of plant conditions to another. No ASTM standard currently exists on this topic.

References cited in this section

86. Z. Szklarska-Smialowska, *Pitting Corrosion of Metals,* National Association of Corrosion Engineers, 1986

87. B.E. Wilde, *Corrosion,* Vol 28, 1972, p 283

88. B.C. Syrett, *Corrosion,* Vol 33, 1977, p 221

89. "Test Method for Conducting Cyclic Potentiodynamic Polarization Measurements for Localized Corrosion Susceptibility of Iron-, Nickel-, of Cobalt-Based Alloys," G 61, *Wear and Erosion; Metal Corrosion,* Vol 03.02, *Annual Book of ASTM Standards,* ASTM

90. N. Pessall and C. Liu, *Electrochim. Acta,* Vol 16, 1971, p 1987

91. B.E. Wilde and E. Williams, *J. Electrochem. Soc.,* Vol 118, 1971, p 1057

92. N.G. Thompson and B.C. Syrett, *Corrosion,* Vol 48 (No. 8), 1992, p 649

93. “Standard Method for Conducting Cyclic Galvanostaircase Polarization,” G 100, *Wear and Erosion; Metal Corrosion,* Vol 03.02, *Annual Book of ASTM Standards,* ASTM

94. “Test Method for Pitting or Crevice Corrosion of Metallic Surgical Implant Materials,” F 746, *Annual Book of ASTM Standards,* ASTM

95. B.E. Wilde and E. Williams, *Electrochem. Acta,* Vol 16, 1971, p 1671

96. K.K. Starr, E.D. Verink, Jr., and M. Pourbaix, *Corrosion,* Vol 2, 1976, p 47

97. N. Sridhar and G.A. Cragnolino, *Corrosion,* Vol 49, 1993, p 885

98. M. Yasuda, F. Weinburg, and D. Tromans, *J. Electrochem. Soc.,* Vol 137, 1990, p 3708

99. S. Tsujikawa, T. Hasamatsu, and G. Boshoku, *Corros. Eng.,* Vol 29, 1980, p 37

100. T. Shinohara, S. Tsujikawa, and G. Boshoku, *Corros. Eng.,* Vol 39, 1990, p 238

101. S. Tsujikawa, Z. Heng, Y. Hisamatsu, and G. Boshoku, *Corros. Eng.,* Vol 32, 1983, p 149

102. D. Dunn and N. Sridhar, Critical Factors in Localized Corrosion II, *Proc. Electrochemical Society 95-15,* P.M. Natishan, R.G. Kelly, G.S. Frankel, R.C. Newman, Ed., 1996, p 79–90

103. G.T. Gaudet, W.T. Mo, T.A. Hatton, J.W. Tester, J. Tilly, H.S. Isaacs, and R.C. Newman, *Am. Inst., Chem. Eng. J.,* Vol 32 (No. 60), 1986, p 949

104. B.A. Kehler, G.O. Ilevbare, and J.R. Scully, *Corrosion,* Vol 57 (No. 12), 2001, p 1042–1065

105. P.C. Pistorius and G.T. Burstein, *Philos. Trans. R. Soc. London,* Vol 341, 1992, p 531

106. T. Shibata, *Trans. ISIJ,* Vol 23, 1983, p 785

107. T. Shibata and T. Takeyama, *Corrosion,* Vol 33, 1977, p 243

108. T. Shibata and Y.-C. Zhu, *Corros. Sci.,* Vol 36 (No. 1), 1994, p 153–163

109. S.T. Pride, J.R. Scully, and J.L. Hudson, *J. Electrochem. Soc.,* Vol 141, 1994, p 3028

110. G.O. Ilevbare, J.R. Scully, J. Yuan, and R.G. Kelly, *Corrosion,* Vol 56 (No. 3), 2000, p 227–242

111. J.E. Sweitzer, G.J. Shiflet, and J.R. Scully, *Tri-Service Military Corrosion Conf. Proc.,* 2002

112. D.D. Macdonald, Critical Factors in Localized Corrosion, *The Electrochemical Society Proceedings Series,* PV 92-9, G.S.Frankel and R.C. Newman, Ed., 1992, p 144

113. T. Suter and R.C. Alkire, *J. Electrochem. Soc.,* Vol 148 (No. 1), 2001, p B36–B42

114. G.T. Burstein and G.O. Ilevbare, *Corros. Sci.,* Vol 38, 1996, p 2257–2265

115. K. Hladky and J.L. Dawson, *Corros. Sci.,* Vol 22, 1982, p 231–237

116. K. Hladky and J.L. Dawson, *Corros. Sci.,* Vol 21, 1982, p 317–322

117. H.S. Bertocci, *Proc. Second International Conf. Localized Corrosion,* NACE-9, H. Isaacs, U. Bertocci, J. Kruger, and S. Smialowska, Ed., National Association of Corrosion Engineers, 1990

118. H.S. Bertocci and J. and Kruger, *Surf. Sci.,* Vol 101, 1980, p 608–618

119. D.A. Eden and A.N. Rothwell, "Electrochemical Noise Data: Analysis and Interpretation," Paper 92, Proc. Corrosion Conference, 1992, National Association of Corrosion Engineers, 1992

120. P.C. Searson and J.L. Dawson, *J. Electrochem. Soc.,* Vol 135, 1988, p 1908–1915

121. D.E. Williams, J. Stewart, and B.H. Balkwill, *Proc. Symposium on Critical Factors in Localized Corrosion,* Vol 92-9, G.S. Frankel and R.C. Newman, Ed., Electrochemical Society, 1992, p 36

122. S.T. Pride, J.R. Scully, and J.L. Hudson, *Electrochemical Noise Measurement for Corrosion Applications,* STP 1277, J.R. Kearns and J.R. Scully, et al., Ed., American Society for Testing and Materials, 1996, p 307

123. J.R. Galvele, *J. Electrochem. Soc.,* Vol 123, 1976, p 464

124. S. Turgoose and R.A. Cottis, "Corrosion Testing Made Easy, Electrochemical Impedance and Noise" (Houston, TX), NACE International, 2000

125. R.A. Cottis, *Corrosion,* Vol 57, 2001, p 265

126. C. Gabrielli, F. Huet, M. Keddam, and R. Oltra, Localized Corrosion as a Stochastic Process, *NACE—9 Advances in Localized Corrosion,* H. Isaacs, U. Bertocci, J. Kruger, and S. Smialowska, Ed., National Association of Corrosion Engineers, 1990, p 93–108

127. J.R. Scully, S.T. Pride, H.S. Scully, and J.L. Hudson, Critical Factors in Local Corrosion II, *Proc. Electrochemical Society,* Vol 95-15, R.G. Kelly et al., Ed., 1996, p 15

128. R.A. Cottis and S. Turgoose, *Mater. Sci. Forum,* Vol 2, 1995, p 192–194

J.R. Scully and R.G. Kelly, Methods for Determining Aqueous Corrosion Reaction Rates, *Corrosion: Fundamentals, Testing, and Protection*, Vol 13A, *ASM Handbook*, ASM International, 2003, p 68–86

Methods for Determining Aqueous Corrosion Reaction Rates

John R. Scully and Robert G. Kelly, University of Virginia

Evaluation of Intergranular Corrosion Rates

Most methods of evaluating intergranular corrosion test for susceptibility as opposed to intergranular corrosion rate. There are many acid-exposure-type tests that rely on visual and metallographic examination to evaluate susceptibility. One example of an electrochemical test that examines susceptibility is described in this section. Stainless steel alloys that exhibit susceptibility can be expected to experience high rates of intergranular corrosion in certain service environments.

Evaluation of Alloy Sensitization. Measurement of the coulombs generated during the electrochemical polarization of a material from the passive range to the active corrosion potential can be used to quantify the susceptibility to intergranular attack associated with the precipitation of chromium carbides and chromium

nitrides at grain boundaries (Ref 129, 130, 131). The method is described by ASTM G 108 (Ref 132). A modification of this procedure, called the double-loop electrokinetic repassivation test (Ref 133, 134), involves a potentiodynamic polarization of the metal surface initially from the open-circuit potential in the active region to a potential in the passive range. This is immediately followed by a reverse polarization in the opposite direction back to the open-circuit potential. The second method is less dependent on surface finish and precise knowledge of the grain size. Both variations of the method are shown in Fig. 10. In the latter method, the degree of sensitization is determined by the ratio, (I_r/I_a), of the maximum current generated in the reactivation, I_r, or reverse scan compared to that generated in the initial anodic scan, I_a. The procedure is contingent on the presence of anodic current during the reactivation scan that results mainly from incomplete passivation of the zone adjacent to the grain boundaries that is depleted of chromium due to carbide precipitation at grain boundaries. For nonsensitized material, the passive film remains essentially intact during the reverse scan and the magnitude of the reactivation polarization peak remains small. For the same reasons, the charge Q (obtained from integration of current versus potential for a known voltage scan rate) in the single-loop method is small for nonsensitized material. As a refinement to the method the charge is normalized by the grain- boundary area (GBA) because this is the area from which most of the current arises in the single reactivation scan (Ref 131):

$$P = Q/GBA \quad \text{(Eq 32)}$$

$$GBA = A_s\left[5.09544\times10^{-3} \times\exp\left(0.34696\times GS\right)\right] \quad \text{(Eq 33)}$$

where P is the reaction charge density associated with the sensitized area (coulombs/cm^2), A_s is the wetted specimen surface area, GBA is the grain-boundary area, and GS is the ASTM grain size in accordance with ASTM E 112, "Test Methods for Determining the Average Grain Size."

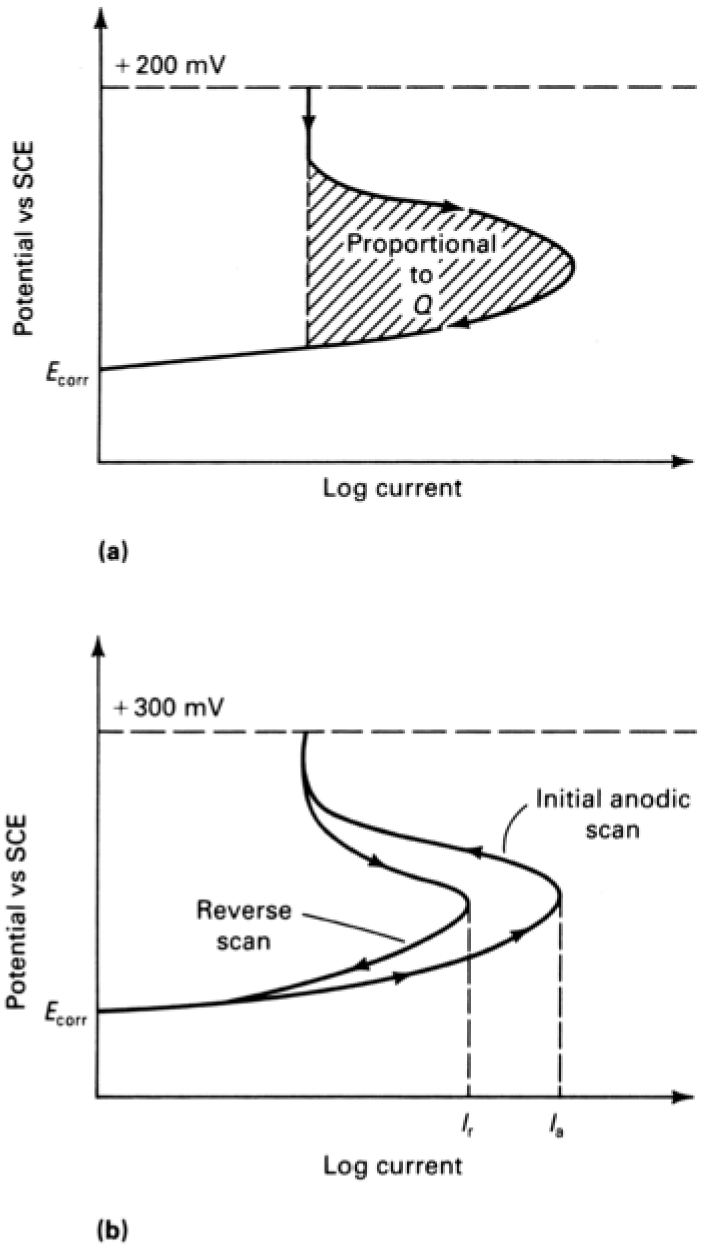

Fig. 10 Two procedures for anodic reactivation polarization testing. (a) Clarke method. (b) Akashi method. Source: Ref 133, 134

The same procedure can be used to normalize the ratio I_r/I_a (Ref 134). The current peak, I_r, for the reactivation scan is normalized for the grain- boundary area, while the initial anodic current peak remains normalized to A_s.

$$\frac{i_r}{i_a} = \left[\frac{I_r}{I_a \times \left[5.09544 \times 10^{-3} \exp\left(0.34696 \times GS\right)\right]}\right] \quad \text{(Eq 34)}$$

i_r/i_a ratios approaching 1 imply sensitization. A number of investigators have correlated this electrochemically derived ratio with optical metallographic evaluations of the degree of material sensitization such as those outlined in ASTM A 262 (Ref 135). This has been accomplished for several different Fe-Ni-Cr alloys (Ref 136, 137, 138). The technique is nondestructive to the underlying metal and can be applied in the field.

Few methods exist for determination of intergranular corrosion rates. Serial metallographic sectioning and the foil-penetration method are the most prominent. In the foil-penetration rate, intergranular penetration is sensed using a foil held at open circuit or under potentiostatic control. The method can be repeated at several foil

thicknesses to determine whether rates are linear or not. In this way, the rate of penetration on the fastest intergranular path can be determined (Ref 139, 140).

References cited in this section

129. P. Novak, R. Stefec, and F. Franz, *Corrosion,* Vol 31 (No. 10), 1975, p 344

130. W.L. Clarke, V.M. Romero, and J.C. Danko, Paper (preprint 180), Proc. Corrosion Conference, 1977, National Association of Corrosion Engineers, 1977

131. W.L. Clarke, R.L. Cowan, and W.L. Walker, *Intergranular Corrosion of Stainless Alloys,* STP 656, R.F. Steigerwald, Ed., American Society for Testing and Materials, 1978, p 99

132. "Test Method for Electrochemical Reactivation (EPR) Test Method for Detecting Sensitization of AISI Type 304 and 304L Stainless Steels," G 108, *Wear and Erosion; Metal Corrosion,* Vol 03.02, *Annual Book of ASTM Standards,* ASTM

133. M. Akashi, T. Kawamoto, and F. Umemura, *Corros. Eng.,* Vol 29, 1980, p 163

134. A.P. Majidi and M.A. Streicher, *Corrosion,* Vol 40 (No. 11), 1984, p 584

135. "Practice for Detecting Susceptibility to Intergranular Attack in Wrought Nickel- Rich, Chromium Bearing Alloys," A 262, *Steel—Plate, Sheet, Strip, Wire; Stainless Steel Bar,* Vol. 01.03, *Annual Book of ASTM Standards,* ASTM

136. J.B. Lee, *Corrosion,* Vol 42 (No. 2), 1986, p 67

137. A. Roelandt and J. Vereecken, *Corrosion,* Vol 42 (No. 5), 1986, p 289

138. J.R. Scully and R. Kelly, *Corrosion,* Vol 42 (No. 9), 1986, p 537

139. F. Hunkeler and H. Bohni, *Corrosion,* Vol 37, 1981, p 645

140. A. Rota and H. Bohni, *Werkst. Korros,* Vol 40, 1989, p 219

J.R. Scully and R.G. Kelly, Methods for Determining Aqueous Corrosion Reaction Rates, *Corrosion: Fundamentals, Testing, and Protection*, Vol 13A, *ASM Handbook*, ASM International, 2003, p 68–86

Methods for Determining Aqueous Corrosion Reaction Rates

John R. Scully and Robert G. Kelly, University of Virginia

Electrochemical Methods for Evaluation of Corrosion Rates under Paints

Electrochemical impedance spectroscopy (EIS) techniques offer an advanced method of evaluating the performance of metallic-based coatings (passive film forming and/or conversion coatings) and the barrier properties of organic coatings and corrosion rates under paints (Ref 141, 142, 143, 144, 145, 146, 147, 148, 149, 150, 151). The method does not accelerate the corrosion reaction and is nondestructive. The technique is quite sensitive to changes in the resistive-capacitive nature of coatings as well as the electrochemical interface. It is possible to monitor the polarization resistance of the corroding interface with this technique. In this respect,

the electrochemical impedance technique offers several advantages over direct current (dc) electrochemical techniques in that resistances related to the corrosion rate can be separated from the high dc resistance of the dielectric coating. This is not possible with the dc methods. Because a large frequency bandwidth is used for the applied signal (usually from the mHz range to the kHz range), the electrochemical impedance technique is "spectroscopic" and surpasses the capabilities of single-frequency impedance methods. The reason for this lies in the capability of the electrochemical impedance technique to discriminate between the resistive properties of the coating because of its ionic and/or electronic conductivity, the capacitive nature of the coating due to its dielectric constant, area, and thickness and the RC time constant of the electrified interface. Although impedance circuit models for coatings (Fig. 11) contain more elements than the model shown in Fig. 4, frequency regimes in which impedance information is primarily due to the coating capacitance or coating resistance can be separated from one another and analyzed independently by using a broad frequency bandwidth. The barrier properties of the coating can be followed as a function of exposure time. Large decreases signify permeation of ionic species through the coating or the presence of defects in the coating (Ref 148, 149). However, this is not the main focus of this article, which addresses methods to determine corrosion rates. The polarization resistance may be determined from the low-frequency time constant as shown in Fig. 11. However, recall that conversion of R_p to corrosion rate requires that the area specific polarization resistance be known as discussed previously. Thus, a major problem is knowledge of the corroding area.

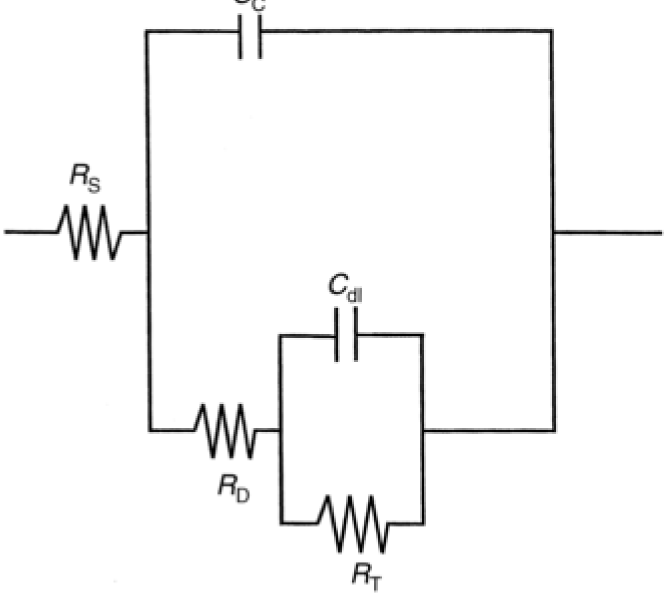

Fig. 11 Electrical equivalent circuit to simulate a coated steel panel with a defect. R_D is the coating defect resistance, R_T is a charge-transfer resistance (similar to R_p) at the metal interface where water has penetrated. C_{dl} is the double-layer capacitance; C_c is the coating capacitance. Source: Ref 144, 145, 147

There are at least two situations that need to be discussed. These are cases where the coating is defect free but acts as an electrolyte allowing underpaint corrosion and the case where there are discrete defects and corrosion only occurs at these sites. Consider the case of an excellent barrier coating with isolated defects. One of the key difficulties in determining the rates of corrosion under paints is assessment of the defect area that is actively corroding. There are several ways to determine active area. Extraction of capacitance from EIS data is possible from equivalent circuit model fitting for sufficiently degraded defective coatings, as shown in Fig. 12. However, conversion of capacitance to area requires knowledge of the area-specific capacitance at the interface between electrolyte and metal. Such area-specific capacitance values have been developed for only a few corroding situations (Ref 48). For instance, area-specific capacitance has been developed for steel in soil, but has not been developed for coatings (Ref 48). The breakpoint frequency is a useful method for estimating the area fraction of physical defects in an organic coating (Ref 147, 148, 149, 150). The dependency between the high-frequency breakpoint frequency and defect area can be described by:

$$f_{bpt} = \left(\frac{1}{2\pi\varepsilon\varepsilon_0\rho}\right)\left(\frac{A_d}{A}\right) \quad \text{(Eq 35)}$$

where A_d is the defect area where electrochemical reactions operate, A is the total painted surface area, and ρ is the resistivity of the coating at the defect.

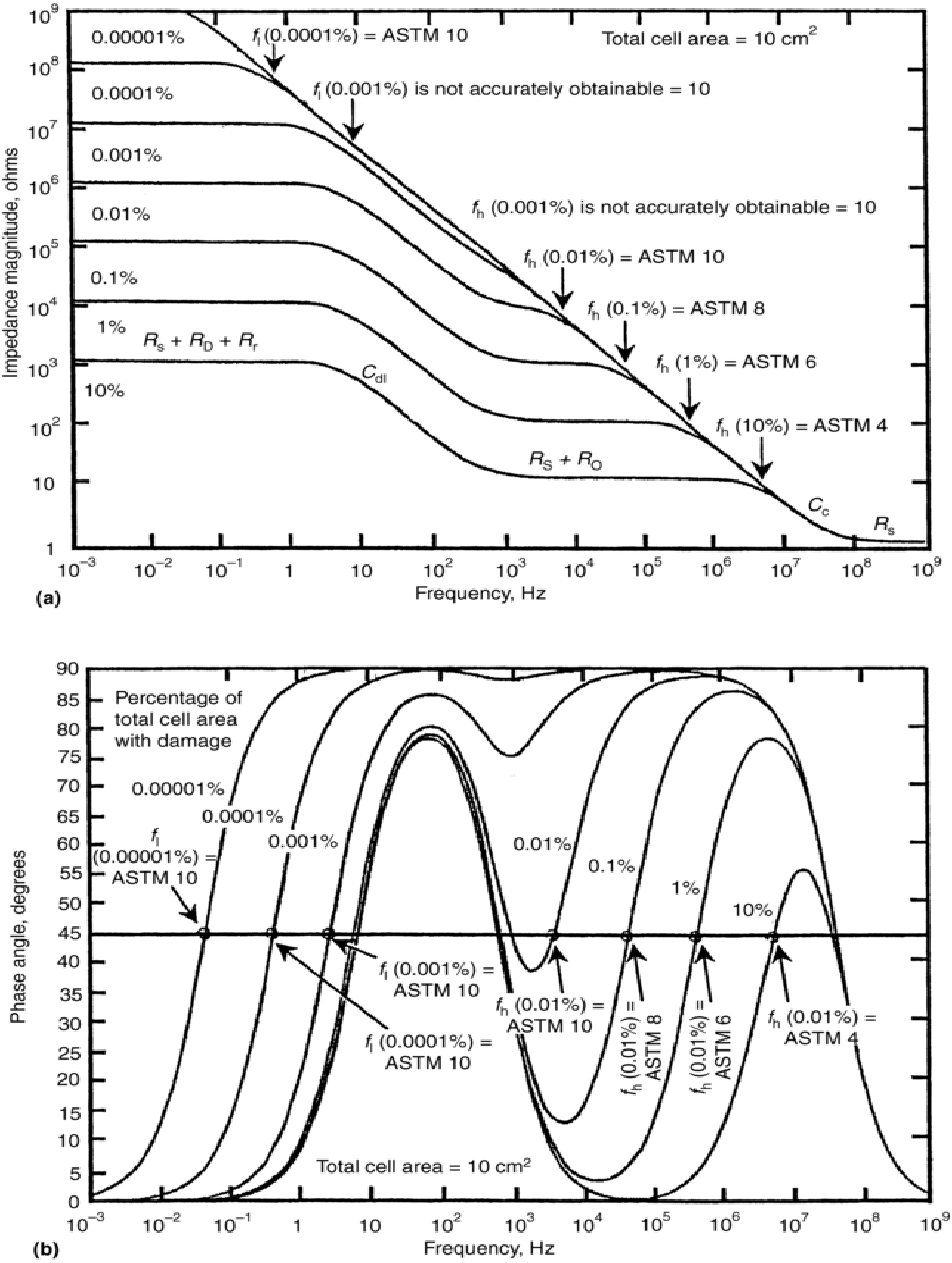

Fig. 12 Theoretical Bode magnitude and phase-angle plots for various known electrochemically active defect areas for a coating containing a cylindrical defect penetrating the metal substrate and no delaminated regions. (a) Bode magnitude. (b) Bode phase angle. ASTM visual ratings according to standards D 610 and D 714 are included for comparison. Source: Ref 150

Equation 35 provides a rough measure of the estimated change in defect area. Increases in f_{bpt} occur mainly as a function of the increases in the defective area. However, circumstances may exist where small increases in ε and very large decreases in ρ occur simultaneously so that f_{bpt} does not relate linearly to defect area. Moreover, bare metal under delaminated coating regions may not be detected under all circumstances especially if the coating resistivity over the delaminated area and dielectric constant are identical to those in regions where the coating is not delaminated. The hypothetical relationship between f_{bpt} and open defect area over a range of pore dimensions is shown in Fig. 12 (Ref 150). From knowledge of defect area, the corrosion rate could be determined at the pore sites.

Electrochemical Noise Methods for Organic Coating Evaluation. Electrochemical noise methods have also been explored as a method to analyze the degradation of polymer- coated metals (Ref 151, 152, 153, 154). A variety of methods have been used. A common method involves the use of a cell with two identical working electrodes connected through a ZRA. The entire galvanic couple is coupled through a high-impedance voltmeter to an ideally noiseless reference electrode. Two samples often experience drastically different behavior; for instance, if one electrode has a coating defect and the other does not then asymmetrical electrode behavior results. The spectral noise impedance obtained is equivalent to the geometric mean of the moduli of individual electrode impedances. Instrument noise should be carefully considered when this approach is used to analyze high-resistance coatings. In principle, a noise-resistance value equivalent to the polarization resistance can be obtained. Knowledge of the corroding area enables calculation of the corrosion rate in the areas where corrosion occurs. Methods have not been developed and consensus has not been reached on approaches for determining corrosion rates under paints using EN methods.

References cited in this section

48. J.N. Murray, P.J. Moran, and E. Gileadi, *Corrosion,* Vol 44 (No. 8), 1988, p 533

141. J.D. Scantlebury, K.N. Ho, and D.A. Eden, *Electrochemical Corrosion Testing,* STP 727, F. Mansfeld and U. Bertocci, Ed., American Society for Testing and Materials, 1981, p 187

142. S. Narian, N. Bonanos, and M.G. Hocking, *J. Oil Colour Chem. Assoc.,* Vol 66 (No. 2), 1983, p 48

143. T.A. Strivens and C.C. Taylor, *Mater. Chem.,* Vol 7, 1982, p 199

144. F. Mansfeld, M.W. Kendig, and S. Tsao, *Corrosion,* Vol 38 (No. 9), 1982, p 478

145. M. Kendig, F. Mansfeld, and S. Tsai, *Corros. Sci.,* Vol 23 (No. 4), 1983, p 317

146. R. Touhsaent and H. Leidheiser, *Corrosion,* Vol 28 (No. 12), 1982, p 435

147. S. Haruyama, M. Asari, and T. Tsuru, Corrosion Protection by Organic Coatings, *The Electrochemical Society Proceedings Series,* M. Kendig and H. Leidheiser, Jr., Ed., 1980, p 197

148. J.R. Scully, *J. Electrochem. Soc.,* Vol 136 (No. 4), 1989, p 979

149. M.W. Kendig and J.R. Scully, *Corrosion,* Vol 46 (No. 1), 1990, p 22

150. H.P. Hack and J.R. Scully, *J. Electrochem. Soc.,* Vol 138 (No. 1), 1991, p 33–40

151. F. Mansfeld and C.C. Lee, *J. Electrochem. Soc.,* Vol 144, 1997, p 2068–2071

152. F. Mansfeld, L.T. Han, C.C. Lee, C. Chen., G. Zhang, and H. Xiao, *Corros. Sci.,* Vol 39, 1997, p 255–279

153. D.E. Tallman and G.P. Bierwagen, Paper No. 380, Proc. Corrosion Conference 1998, National Association of Corrosion Engineers, 1998

154. A. Aballe, A. Bautista, U. Bertocci, and F. Huet, *Corrosion,* Vol 57, 2001, p 35

J.R. Scully and R.G. Kelly, Methods for Determining Aqueous Corrosion Reaction Rates, *Corrosion: Fundamentals, Testing, and Protection*, Vol 13A, *ASM Handbook*, ASM International, 2003, p 68–86

Methods for Determining Aqueous Corrosion Reaction Rates

John R. Scully and Robert G. Kelly, University of Virginia

Nonelectrochemical Methods That Determine Cumulative Mass Loss

Corrosion Rate Determination through Gravimetric Determination of Mass Loss. Corrosion rates are often determined from gravimetric measurement of mass loss in the laboratory either under conditions that mimic those in the field or under conditions that are accelerated. The latter is often achieved by raising the temperature or concentrating corrodents in the aqueous solutions used for testing. Field exposure is also simulated by various lab cabinet methods such as salt spray, prohesion, and Q-fog methods that introduce various weathering cycles including full immersion. The typical wisdom is that the accelerated test protocol produces the same form of corrosion, accelerates the mechanism of corrosion that is operative in the field, and correlates in some manner with field lifetimes or rates. Often the latter is not achieved in accelerated lab tests. In these cases, a relative ranking of materials or treatments is gained from corrosion rate determination by mass loss. It is desired that the same ranking is obtained in field testing. Mass-loss methods can be attractive for use in weathering-type environments that involve wetting and drying. Under these conditions, electrochemical methods may not be suitable.

ASTM standards cover many important procedural factors such as surface finish, and postexposure cleaning required for successful determination of mass loss. For instance, postcleaning exposure can introduce errors if cleaning methods remove additional metal besides the corrosion products. Conversely, nonremoval corrosion products or other deposits can produce mass gain that either partially or completely offsets small mass losses. Ideally, posttest cleaning methods rapidly remove corrosion products, but corrode underlying metal only a negligible amount. It follows that it can be difficult to determine the corrosion rates of passive metals by mass-loss methods because only very small mass changes occur over substantial time periods. In order to obtain measurable mass loss after exposure of a specimen, a rule used is that the exposure period must equal or exceed the ratio 2000/mpy = the number of exposure hours necessary (Ref 4).

Instantaneous corrosion rate determination is not possible from mass loss because the time period of corrosion is uncertain and may not equal the exposure time period. Consequently, corrosion rate determination from a single mass-loss measurement represents an average over the period of exposure. The average corrosion rate can be obtained simply from standard relationships based on Faraday's law given a known mass loss measured after specimen cleaning (Ref 4, 155):

$$\text{Average corrosion rate} = \left(\frac{KW}{AT\rho}\right) \qquad \text{(Eq 36)}$$

where K is a constant (see Table 3), T is the time of exposure (hours), A is the area (cm^2), W is mass loss (grams), and ρ is material density in g/cm^3.

Table 3 Constants *K* used in Eq 36 for desired penetration law units and mass-loss rate units

Corrosion rate units desired	Constant *K* in corrosion rate equation
Mils per year (mpy)	3.45×10^6
Inches per year (ipy)	3.45×10^3
Inches per month (ipm)	2.87×10^2
Millimeters per year (mm/yr)	8.76×10^4
Micrometers per year (μm/yr)	8.76×10^7
Picometers per second (pm/s)	2.78×10^6
Grams per square meter per hour ($g/m^2 \cdot h$)	$1.00 \times 10^4 \times \rho$
Milligrams per square decimeter per day (mdd)	$2.40 \times 10^6 \times \rho$
Micrograms per square meter per second ($\mu g/m^2 \cdot s$)	$2.78 \times 10^6 \times \rho$

Note: ρ is the density in g/cm^3. Source: Ref 155

Many different units are used to express corrosion rates. Using various values of *K*, mass- loss rate in different units can be produced (Ref 155). Appropriate modification of Eq 36 can be used to produce mass-loss rates per unit area (Table 3).

Corrosion usually does not occur at a constant rate during the entire period of exposure. Procedures exist to ascertain whether or not the corrosion rate is increasing, decreasing, or constant with time. Removal at unit time periods in the beginning or end of a total exposure period or at prescribed time intervals can be used to ascertain this information (Ref 4, 5). Periodic determination of mass loss can be converted to mass-loss rate and penetration rate, assuming uniform attack. Mass-loss information can be obtained from full immersion in aqueous environments, alternate immersion, splash and spray, or gaseous corrosion exposure. Moreover, mass-loss methods may be useful in extremely low conductivity environments where electrochemical methods find difficulty. Corrosion rate determination by mass-loss methods can be misleading when corrosion occurs in a highly localized manner. In these cases, a depth gage, calipers, microscopic methods, and metallographic cross sections are preferred.

Corrosion Rate Determination via Electrical-Resistance Methods. The electrical-resistance test method operates on the principle that the electrical resistance of the corrosion measuring element depends on the electrical resistance of the metallic cross section. Resistance is given by:

$$R = (\rho)\left(\frac{l}{A}\right) \quad \text{(Eq 37)}$$

where *R* is resistance of sensing element, ρ is resistivity of sensing element (temperature-dependent material property), l is length of sensing element, and *A* is cross-sectional area.

The resistance of the sensing element increases as the cross-sectional area of the sensing element decreases. Thus, the resistance increase is proportional to the reduction in cross-sectional area of the resistance-sensing element and corrosion can be detected (Ref 156, 157). Clearly, this method is only suitable in cases of uniform corrosion since high aspect ratio pits may not decrease the resistance of the sensing element in proportion to locally high corrosion rates. In practice, a resistance-measuring element constructed of the same material as the material of interest is exposed in the test environment. One shortcoming is when the component of interest cannot be matched exactly in the choice of sensing element. Often a second sensing element protected from the corrosive environment is measured simultaneously. The ratio of the resistances changes is determined. This compensates for any effects of exposure temperature on resistivity. The measurement taken gives the cumulative metal loss at the time of the measurement. The first derivative of measurements taken over time can be used to determine the rate of change of cross-sectional area *A* and, consequently, mass-loss rate. In other words, the slope of the mass-loss curve versus time can yield the mass loss per unit area per unit time. The slope at any time gives the corrosion rate at that time. The method can be used in atmospheric, gaseous, nonaqueous, or other environments where electrochemical methods may be compromised.

Corrosion Rate Determination Using Magnetic Methods. A magnetic field is created by current flow through a wire coil. The magnetic induction whose magnitude is the magnetic flux density can be enhanced by placing a ferromagnetic material in the center of such a wire coil. The saturation flux or magnetic induction reaches a saturation value upon application of a sufficient magnetic field. This saturation flux is proportional to the mass of the ferromagnetic material and its relative permeability. Mass loss by uniform corrosion can be detected by a

decrease in the saturation value upon application of a magnetic field strength that saturates after corrosion has occurred and mass has been lost.

Thus, the change in magnetic saturation induction of a ferromagnetic material can be used to determine the loss in mass of the test object. As in the case of the electrical-resistance methods, localized corrosion will not provide a change in magnetic field strength proportional to very localized depth of attack. A series of measurements on a single electrode provides a means to determine the rate of mass loss and corrosion rate. This method has been applied to coated metals and is capable of determining corrosion rates under painted cobalt (Ref 158, 159).

An additional means of using magnetic effects to measure corrosion rates has been pursued using superconducting quantum interference devices (SQUIDs) to measure the electrical currents within metals resulting from corrosion activity on the metal surface. Magnetic fields are generated perpendicular to the metal surface with an intensity that scales with the corrosion rate. The SQUID acts as a sort of noninvasive ammeter, measuring the electron movement associated with corrosion activity. Early work by Bellingham, et al. (Ref 160, 161) demonstrated that corrosion activity did cause detectable magnetic signals. More recently, Abedi (Ref 162) has shown that a correlation exists between the temporal summation of the spatially integrated magnetic activity (referred to as TSSIMA) and the mass loss due to uniform corrosion for aluminum alloy 7075-T6 (UNS A97075-T6) in 0.1 *M* NaOH. More recent work has shown a correlation between corrosion activity and TSSIMA for crevice corrosion as shown in Fig. 13. The spatial distribution of the damage on surface (Fig. 13) corresponds to the distribution of magnetic activity observed over the 190 h of exposure.

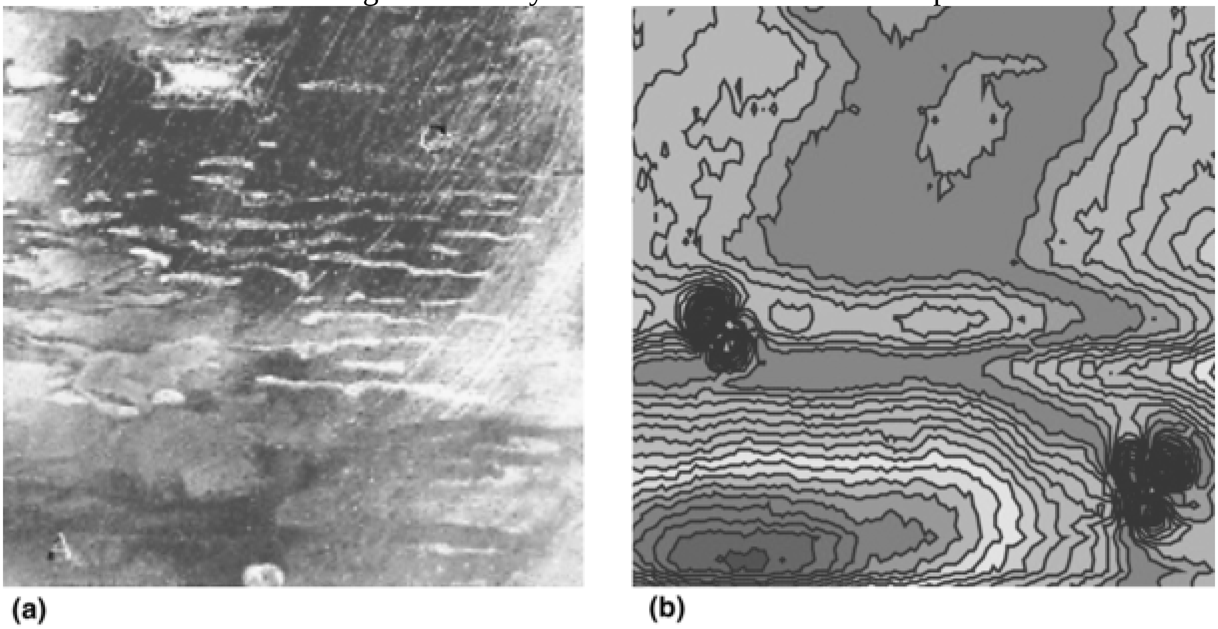

Fig. 13 Noninvasive detection of hidden corrosion. (a) Micrograph of the lower (hidden) surface on a planar 2024-T3 sample that was exposed to a corrosive solution typical of an aircraft lap joint. The dark gray area in the upper center of the image corresponds to noncorroded aluminum. (b) The cumulative magnetic activity of the sample showing the more active regions in white and less active ones in dark gray. Source: Ref 163

The potential advantages of SQUID measurements include their high sensitivity, their noninvasive nature, and thus their ability to probe corrosion activity within occluded regions for which direct electrochemical measurements are not possible (Ref 164). Quantitative interpretation of the signals in terms of metal dissolution still requires development of a stronger theoretical underpinning. In the absence of such, the measurement of corrosion rate requires extensive calibration studies and a control of specimen geometry and corrosion mode.

Corrosion Rate Determination Using the Quartz Crystal Microbalance. The quartz crystal microbalance offers a method for determining the mass loss or gain on an electrode material (m) (Ref 45, 165). In this case, the electrode material must first be deposited on a substrate with piezoelectric properties such as a slice of quartz crystal. Hence, the corrosion rate of the material deposited can be determined. The quartz crystal will oscillate at a frequency, f_0, given by its geometry when a sinusoidal electrical signal is applied at this frequency. The

frequency of oscillation is sensitive to the mass change on the crystal surface as expressed by the Sauerbrey equation (Ref 165):

$$\Delta f = \left(\frac{-2 f_0^2 mn}{(\rho\mu)^{1/2}} \right) = -C_f m \quad \text{(Eq 38)}$$

where Δf is the frequency change given by the addition or subtraction of mass per unit area of quartz crystal, n is the harmonic number of oscillation, μ is the shear modulus of quartz, and ρ is the density of quartz. When these constants are considered together, a single constant known as the sensitivity factor, C_f, is produced such that the mass change is directly proportional to the frequency change. This method can be used to determine mass loss or gain over time in gas- phase, thin-layer, or solution-phase corrosion.

Unfortunately, the behavior of the crystal depends on the medium in which a crystal is operating. Therefore, a coating, film, and/or aqueous solution change the values of f_0 and C_f because such a medium effectively couples to the crystal surface and creates additional resistance to the shear-wave oscillation used to detect a mass change. The method is quite sensitive to mass change. For instance, almost 0.01 μg/cm^2 mass change can be detected by a 1 Hz change in frequency.

The measurement taken gives the cumulative metal loss at the time of the measurement. The first derivative of many measurements taken over time can be used to determine the rate of change of mass and, consequently, the corrosion rate over a known area. This method has been used in several corrosion studies (Ref 166, 167). The method has the advantage of being useful for corrosion-rate determination in the gas phase, in nonaqueous environments, or when other electrochemical reactions may occur at equal or greater rates as the metal dissolution rate. However, the method has the disadvantage of being unable to detect and properly ascertain the rate of localized corrosion when only highly localized changes in mass occur. The resulting frequency change will not reflect the locally high amounts of mass loss.

Solution Analysis Methods. Another nonelectrochemical means of assessing corrosion rate is the analysis of solution composition (Ref 168). As a metallic material corrodes, the metal cations are released into solution. If they can be quantitatively captured and accurately analyzed, the total dissolution of the material can be calculated directly. The challenge in such measurements is related to distribution of the metal-dissolution products. To the extent that cations precipitate as corrosion products, the measured solution concentration will be lowered. However, recent work using solution analysis methods to monitor corrosivity of secondary waters in a nuclear power plant toward the steel piping (Ref 169) has demonstrated that measurement of highly soluble alloying elements may provide an alternative approach. The concentration of soluble manganese was monitored online by ion chromatography and shown to correlate to the amount of solid iron corrosion products collected. Although the manganese was present at substantially less than 1 wt% in the steel, its high solubility in the near-neutral pH of the secondary water allowed it to be monitored whereas the iron precipitated.

Metrological methods, to some degree, represent the most direct approach to measuring corrosion rate. Establishing the extent of material thinning can be done using several approaches including x-ray measurements of thickness, optical measurements of surface topography, and scanning probe microscopies. X-ray radiography measures the material density as a function of position. Calibration standards allow the radiograph to be converted to a thickness map. In the case of optical metrology measurements, a number of commercial methods allow high-resolution measurements of surface topography. Confocal laser scanning microscopy (CLSM), white light interferometry, and scanning laser profilometry systems all have advantages and disadvantages with respect to speed, lateral and depth resolution, field of view, dynamic range, and cost (Ref 170, 171, 172). The scanning probe microscopies (STM, AFM, and NSOM) have been used to measure extremely low corrosion rates (Ref 173).

Assuming the availability of a datum, that is, a position of known thickness (or a calibration curve in the case of radiography), these methods allow quantitative measurements of the material lost due to corrosion. It must be noted that with the exception of painstaking serial, cross-sectional metallography, all metrology methods are line-of-sight for the radiation used. This situation leads to the need to assume that all damage intersects the surface. Undercutting attack, as seen in some pitting systems, can go undetected so the corrosion rate is underestimated. However, corrosion under organic paint can be observed since thin paint layers are transparent to laser radiation (Ref 174).

Thin-layer activation involves the production of a radioactive layer of material on the surface of the structure of interest. Typically, this layer is made via the exposure of a small section to a beam of high-energy charged

particles. Gamma radiation is emitted from the sample as the isotope decays and is detected. As the surface corrodes, less radiation is emitted as the total mass is decreased. In this way, the corrosion rate of the structure can be monitored. The levels of radiation emitted are very small, but the existence of high-sensitivity radiation detectors makes this method highly sensitive. Low corrosion rates can be monitored in situ, and the effects of corrective actions determined quickly (Ref 175).

References cited in this section

4. D.A. Jones, *Principles and Prevention of Corrosion,* 2nd ed., Macmillan Publishing, 1996

5. M.G. Fontana and N.D. Greene, *Corrosion Engineering,* McGraw-Hill, 1978

45. A.J. Bard and L.R. Faulkner, *Electrochemical Methods: Fundamentals and Applications,* 2nd ed., John Wiley & Sons, 2001

155. “Standard Practice for Preparing, Cleaning and Evaluating Corrosion Tests Specimens,” G 1, *Wear and Erosion; Metal Corrosion,* Vol. 03.02, *Annual Book of Standards,* ASTM

156. “Standard Guide for On-line Monitoring of Corrosion in Plant Equipment (Electrical and Electrochemical Methods),” G 96, *Wear and Erosion; Metal Corrosion,* Vol. 03.02, *Annual Book of Standards,* ASTM

157. G. Cooper, *Sensing Probes and Instruments for Electrochemical and Electrical Resistance Corrosion Monitoring,* STP 908, ASTM

158. D.B. Mitton, Ph.D. thesis, University of Manchester Institute of Science and Technology, Manchester, U.K., 1989

159. N.J. Cantini, D.B. Mitton, N. Eliaz, G. Leisk, S.L. Wallace, F. Bellcuci, G.E. Thompson, and R.M. Latanision, *Electrochem. Solid State Lett.,* Vol 396, 2000, p 275–278

160. J.G. Bellingham, M.L.A. MacVicar, M. Nisenoff, and P.C. Searson, *J. Electrochem. Soc.,* Vol 133, 1986, p 1753

161. J.G. Bellingham, M.L.A. MacVicar, and M. Nisenoff, *IEEE Trans. Magn.,* Vol 23, 1987, p 477

162. A. Abedi, Ph.D. Disseration, Vanderbilt University, 2000

163. A. Abedi, J.J. Fellenstein, A.J. Lucas, and J.P. Wikswo, Jr., *Rev. Sci. Instrum.,* Vol 70 (No. 12) , 1999, p 4640–4651

164. G. Skennerton, A. Abedi, R.G. Kelly, and J.P. Wikswo, Jr., *J. Corros. Sci. Eng.,* Vol 3, Paper 2, 2000

165. G. Sauerbrey, *Z. Phys.,* Vol 155, 1959, p 206

166. R. Schumacher, A. Muller, and W. Stockel, *J. Electroanal. Chem.,* Vol 219, 19876, p 311

167. D. Jope, J. Sell, H.W. Pickering, and K.G. Weil, *J. Electrochem. Soc.,* Vol 142, 1995, p 2170

168. C.S. Brossia and R.G. Kelly, *Corrosion,* Vol 54, 1998, p 145–154

169. D. Bostic, G. Burns, and S. Harvey, *J. Chromatogr.,* Vol 602, 1992, p 163

170. M.A. Alodan and W.H. Smyrl, *J. Electrochem. Soc.,* Vol 145, 1998, p 1571

171. J.B. Pawley, Ed., *Handbook of Biological Confocal Microscopy,* 2nd ed., Plenum Press, 1995

172. N. Llorca-Isern, M. Puig, and M. Español, *J. Therm. Spray Technol.,* Vol 8, 1999, p 73

173. L.F. Garfias-Mesias and W.H. Smyrl, *J. Electrochem. Soc.,* Vol 146, 1999, p 2495

174. O. Schneider, G.O. Ilevbare, J.R. Scully, and R.G. Kelly, *Electrochem. Solid State Sci. Lett.,* Vol 4, 2001, p B35

175. D.E. Williams and J. Asher, *Corros. Sci.,* Vol 24, 1984, p 185

J.R. Scully and R.G. Kelly, Methods for Determining Aqueous Corrosion Reaction Rates, *Corrosion: Fundamentals, Testing, and Protection*, Vol 13A, *ASM Handbook*, ASM International, 2003, p 68–86

Methods for Determining Aqueous Corrosion Reaction Rates

John R. Scully and Robert G. Kelly, University of Virginia

References

1. J.O'M. Bockris and A.K.N. Reddy, *Modern Electrochemistry-2,* Plenum Press, 1970

2. E. Gileadi, *Electrode Kinetics for Chemists, Chemical Engineers and Materials Scientists,* VCH Publishers, 1993

3. N.D. Tomashov, *Theory of Corrosion and Protection of Metals,* Macmillan Publishing, 1966

4. D.A. Jones, *Principles and Prevention of Corrosion,* 2nd ed., Macmillan Publishing, 1996

5. M.G. Fontana and N.D. Greene, *Corrosion Engineering,* McGraw-Hill, 1978

6. J. Newman, *Electrochemical Systems,* Prentice-Hall, 1973

7. H.H. Uhlig and R.W. Revie, *Corrosion and Corrosion Control,* John Wiley & Sons, 1985

8. J.O'M. Bockris, B.E. Conway, E. Yeager, and R.E. White, Ed., *Electrochemical Materials Science,* Vol 4, *Comprehensive Treatise of Electrochemistry,* Plenum Press, 1981

9. R. Baboian, Ed., *Electrochemical Techniques for Corrosion,* National Association of Corrosion Engineers, 1977

10. U. Bertocci and F. Mansfeld, Ed., *Electrochemical Corrosion Testing,* STP 727, American Society for Testing and Materials, 1979

11. *Laboratory Corrosion Tests and Standards,* STP 866, G. Haynes and R. Baboian, Ed., American Society for Testing and Materials, 1985

12. *Corrosion Monitoring in Industrial Plants Using Nondestructive Testing and Electrochemical Methods,* STP 908, G.C. Moran and P. Labine, Ed., American Society for Testing and Materials, 1986

13. R. Baboian, Ed., *Electrochemical Techniques for Corrosion Engineers,* National Association of Corrosion Engineers, 1986

14. R. Baboian, W.D. France, Jr., L.C. Rowe, and J.F. Rynewicz, Ed., *Galvanic and Pitting Corrosion-Field and Laboratory Studies,* STP 576, American Society for Testing and Materials, 1974

15. B. Poulson, *Corros. Sci.,* Vol 23 (No. 4), 1983, p 391–430

16. D.D. MacDonald, *Transient Techniques in Electrochemistry,* Plenum Press, 1977

17. C. Wagner and W. Traud, *Z. Electrochem.,* Vol 44, 1938, p 391

18. W.D. France, Jr., Controlled Potential Corrosion Tests: Their Application and Limitations, *Mater. Res. Standard.,* Vol 9 (No. 8), 1969, p 21

19. “Standard Practice for Conventions Applicable to Electrochemical Measurements in Corrosion Testing,” G 3, *Wear and Erosion; Metal Corrosion,* Vol 03.02, *Annual Book of ASTM Standards,* ASTM

20. “Standard Reference Test Method for Making Potentiostatic and Potentiodynamic Anodic Polarization Measurements,” G 5, *Wear and Erosion; Metal Corrosion,* Vol 03.02, *Annual Book of ASTM Standards,* ASTM

21. “Practice for Conducting Potentiodynamic Polarization Resistance Measurements,” G 59, *Wear and Erosion; Metal Corrosion,* Vol 03.02, *Annual Book of ASTM Standards,* ASTM

22. “Practice for Calculation of Corrosion Rates and Related Information from Electrochemical Measurements,” G 102, *Wear and Erosion; Metal Corrosion,* Vol 03.02, *Annual Book of ASTM Standards,* ASTM

23. Z. Tafel, *Phys. Chem.,* Vol 50, 1904, p 641

24. D. Britz, *J. Electroanal. Chem.,* Vol 88, 1978, p 309

25. M. Hayes and J. Kuhn, *J. Power Sources,* Vol 2, 1977–1978, p 121

26. F. Mansfeld, *Corrosion,* Vol 38 (No. 10), 1982, p 556

27. L.L. Scribner and S.R. Taylor, Ed., *The Measurement and Correction of Electrolyte Resistance in Electrochemical Tests,* STP 1056, American Society for Testing and Materials, 1990

28. M. Stern and A.L. Geary, *J. Electrochem. Soc.,* Vol 104, 1957, p 56

29. S. Evans and E.L. Koehler, *J. Electrochem. Soc.,* Vol 108, 1961, p 509

30. M. Stern and R.M. Roth, *J. Electrochem. Soc.,* Vol l04, 1957, p 390

31. M. Stern and A.L. Geary, *J. Electrochem. Soc.,* Vol 105, 1958, p 638

32. M. Stern and E.D. Weisert, Experimental Observations on the Relation between Polarization Resistance and Corrosion Rate, *Proc. ASTM,* Vol 59, 1959, p 1280

33. "Standard Guide for On-Line Monitoring of Corrosion in Plant Equipment (Electrical and Electrochemical Methods)," G 96, *Wear and Erosion; Metal Corrosion,* Vol 03.02, *Annual Book of ASTM Standards,* ASTM

34. S. Barnartt, *Electrochim. Acta,* Vol 15, 1970, p 1313

35. K.B. Oldham and F. Mansfeld, *Corros. Sci.,* Vol 13, 1973, p 813

36. F. Mansfeld, *J. Electrochem. Soc.,* Vol 120, 1973, p 515

37. F. Mansfeld and M. Kendig, *Corrosion,* Vol 37 (No. 9), 1981, p 556

38. R. Bandy and D.A. Jones, *Corrosion,* Vol 32, 1976, p 126

39. M.J. Danielson, *Corrosion,* Vol 36 (No. 4), 1980, p 174

40. J.C. Reeve and G. Bech-Nielsen, *Corros. Sci.,* Vol 13, 1973, p 351

41. I. Epelboin, C. Gabrielli, M. Keddam, and H. Takenouti, *Electrochemical Corrosion Testing,* STP 727, F. Mansfeld and U. Bertocci, Ed., American Society for Testing and Materials, 1981, p 150

42. A.C. Makrides, *Corrosion,* Vol 29 (No. 9), 1973, p 148

43. D.D. MacDonald and M.C.H. McKubre, *Electrochemical Corrosion Testing,* STP 727, F. Mansfeld and U. Bertocci, Ed., American Society for Testing and Materials, 1981, p 110

44. J.R. Scully, *Corrosion,* Vol 56 (No. 2), 2000, p 199–218

45. A.J. Bard and L.R. Faulkner, *Electrochemical Methods: Fundamentals and Applications,* 2nd ed., John Wiley & Sons, 2001

46. F. Mansfeld, *Corrosion,* Vol 36 (No. 5), 1981, p 301

47. "Practice for Verification of Algorithm and Equipment for Electrochemical Impedance Measurements," G 106, *Wear and Erosion; Metal Corrosion,* Vol 03.02, *Annual Book of ASTM Standards,* ASTM

48. J.N. Murray, P.J. Moran, and E. Gileadi, *Corrosion,* Vol 44 (No. 8), 1988, p 533

49. D.R. Franceschetti and J.R. Macdonald, *J. Electroanal. Chem.,* Vol 101, 1979, p 307

50. B.A. Boukamp, *Solid State Ionics,* Vol 20, 1986, p 31–44

51. C.H. Hsu and F. Mansfeld, *Corrosion,* Vol 57, 2001, p 747

52. S.F. Mertens, C. Xhoffer, B.C. De Cooman, and E. Temmerman, *Corrosion,* Vol 53, 1997, p 381

53. J. Devay and L. Meszaros, *Acta Chim. Acad. Sci. Hung.,* Vol 100, 1979, p 183

54. J.S. Gill, M. Callow, and J.D. Scantlebury, *Corrosion,* Vol 39, 1983, p 61

55. G.P. Rao and A.K. Mishra, *J. Electroanal. Chem.,* Vol 77, 1977, p 121

56. L. Meszaros and J. Devay, *Acta Chim. Acad. Sci. Hung.,* Vol 105, 1980, p 1

57. M.C.H. McKubre and B.C. Syrett, *Corrosion Monitoring in Industrial Plants Using Nondestructive Methods,* STP 908, G.C. Moran and P. Labine, Ed., American Society for Testing and Materials, 1986, p 433

58. R.W. Bosch, J. Hubrecht, W.F. Bogaerts, and B.C. Syrett, *Corrosion,* Vol 57, 2001, p 60–70

59. D.A. Eden, A.N. Rothwell, and J.L. Dawson, Paper 444, Proc. Corrosion Conference, 1991, National Association of Corrosion Engineers, 1991

60. J.L. Dawson, *Electrochemical Noise Measurement for Corrosion Applications,* STP 1277, J. Kearns, J.R. Scully, P.R. Roberge, D.L. Reichert, and J.L. Dawson, Ed., American Society of Testing and Materials, 1996, p 3–35

61. D.A. Eden, K. Hladky, D.G. John, and J.L. Dawson, Paper 276, Proc. Corrosion Conference, 1986, National Association of Corrosion Engineers, 1986

62. D.A. Eden and A.N. Rothwell, Paper 292, Proc. Corrosion Conference, 1992, National Association of Corrosion Engineers, 1992

63. A.N. Rothwell and D.A. Eden, Paper 223, Proc. Corrosion Conference, 1992, National Association of Corrosion Engineers, 1992

64. U. Bertocci, *Electrochemical Noise Measurement for Corrosion Applications,* STP 1277, J. Kearns, J.R. Scully, P.R. Roberge, D.L. Reichert, and J.L. Dawson, Ed., American Society of Testing and Materials, 1996, p 39–58

65. U. Bertocci and F. Huet, *Corrosion,* Vol 51, 1995, p 131

66. D.L. Reichert, *Electrochemical Noise Measurement for Corrosion Applications,* STP 1277, J. Kearns, J.R. Scully, P.R. Roberge, D.L. Reichert, and J.L. Dawson, Ed., American Society of Testing and Materials, 1996, p 79–89

67. P.C. Searson and J.L. Dawson, *J. Electrochem. Soc.,* Vol 135 (No. 8), 1988, p 1908

68. F. Mansfeld and H. Xiao, *Electrochemical Noise Measurement for Corrosion Applications,* STP 1277, J. Kearns, J.R. Scully, P.R. Roberge, D.L. Reichert, and J.L. Dawson, Ed., American Society of Testing and Materials, 1996, p 59–78

69. G.P. Bierwagen, *J. Electrochem. Soc.,* Vol 141, 1994, p L155

70. F. Mansfeld and H. Xiao, *J. Electrochem. Soc.,* Vol 141, 1994, p 1403

71. F. Huet, *J. Electrochem. Soc.,* Vol 142, 1995, p 2861

72. J.F. Chen and W.F. Bogaerts, *Corros. Sci.,* Vol 37, 1995, p 1839

73. H. Xiao and F. Mansfeld, *J. Electrochem. Soc.,* Vol 141, 1994, p 2332

74. F. Mansfeld and H. Xiao, *J. Electrochem. Soc.,* Vol 140, 1993, p 2205

75. F. Mansfeld, L.T. Han, and C.C. Lee, *J. Electrochem. Soc.,* Vol 143, 1996, p L286

76. U. Bertocci, C. Gabrielli, F. Huet, and M. Keddam, *J. Electrochem. Soc.,* Vol 144, 1997, p 31

77. U. Bertocci, C. Gabrielli, F. Huet, and M. Keddam, *J. Electrochem. Soc.,* Vol 144, 1997, p 37

78. A. Bautista and F. Huet, *J. Electrochem. Soc.,* Vol 146, 1999, p 1730–1736

79. H. Hack and J.R. Scully, *Corrosion,* Vol 42 (No. 2), 1986, p 79

80. R. Baboian, *Galvanic and Pitting Corrosion-Field and Laboratory Studies,* STP 576, R. Baboian et al., Ed., American Society for Testing and Materials, 1974, p 5

81. F. Mansfeld and J.V. Kenkel, *Galvanic and Pitting Corrosion-Field and Laboratory Studies,* STP 576, R. Baboian et al., Ed., American Society for Testing and Materials, 1974, p 20

82. R.G. Kasper and C.R. Crowe, Comparison of Localized Ionic Currents as Measured from 1-D and 3-D Vibrating Probes, *Galvanic Corrosion,* STP 978, H.P. Hack, Ed., American Society for Testing and Materials, 1988, p 118

83. R.G. Kasper and C.R. Crowe, Comparison of Localized Ionic Currents as Measured from 1-D and 3-D Vibrating Probes, *J. Electrochem. Soc.,* Vol 33, 1986, p 879

84. H.S. Isaacs, The Measurement of Galvanic Corrosion of Soldered Copper Using the Scanning Vibrating Electrode Technique, *Corros. Sci.,* Vol 28, 1988, p 547

85. V.S. Voruganti, H.B. Huft, D. Degeer, and S.A. Bradford, Scanning Reference Electrode Technique for the Investigation of Preferential Corrosion of Weldments in Offshore Applications, *Corrosion,* Vol 47, 1991, p 343

86. Z. Szklarska-Smialowska, *Pitting Corrosion of Metals,* National Association of Corrosion Engineers, 1986

87. B.E. Wilde, *Corrosion,* Vol 28, 1972, p 283

88. B.C. Syrett, *Corrosion,* Vol 33, 1977, p 221

89. "Test Method for Conducting Cyclic Potentiodynamic Polarization Measurements for Localized Corrosion Susceptibility of Iron-, Nickel-, of Cobalt-Based Alloys," G 61, *Wear and Erosion; Metal Corrosion,* Vol 03.02, *Annual Book of ASTM Standards,* ASTM

90. N. Pessall and C. Liu, *Electrochim. Acta,* Vol 16, 1971, p 1987

91. B.E. Wilde and E. Williams, *J. Electrochem. Soc.,* Vol 118, 1971, p 1057

92. N.G. Thompson and B.C. Syrett, *Corrosion,* Vol 48 (No. 8), 1992, p 649

93. "Standard Method for Conducting Cyclic Galvanostaircase Polarization," G 100, *Wear and Erosion; Metal Corrosion,* Vol 03.02, *Annual Book of ASTM Standards,* ASTM

94. "Test Method for Pitting or Crevice Corrosion of Metallic Surgical Implant Materials," F 746, *Annual Book of ASTM Standards,* ASTM

95. B.E. Wilde and E. Williams, *Electrochem. Acta,* Vol 16, 1971, p 1671

96. K.K. Starr, E.D. Verink, Jr., and M. Pourbaix, *Corrosion,* Vol 2, 1976, p 47

97. N. Sridhar and G.A. Cragnolino, *Corrosion,* Vol 49, 1993, p 885

98. M. Yasuda, F. Weinburg, and D. Tromans, *J. Electrochem. Soc.,* Vol 137, 1990, p 3708

99. S. Tsujikawa, T. Hasamatsu, and G. Boshoku, *Corros. Eng.,* Vol 29, 1980, p 37

100. T. Shinohara, S. Tsujikawa, and G. Boshoku, *Corros. Eng.,* Vol 39, 1990, p 238

101. S. Tsujikawa, Z. Heng, Y. Hisamatsu, and G. Boshoku, *Corros. Eng.,* Vol 32, 1983, p 149

102. D. Dunn and N. Sridhar, Critical Factors in Localized Corrosion II, *Proc. Electrochemical Society 95-15,* P.M. Natishan, R.G. Kelly, G.S. Frankel, R.C. Newman, Ed., 1996, p 79–90

103. G.T. Gaudet, W.T. Mo, T.A. Hatton, J.W. Tester, J. Tilly, H.S. Isaacs, and R.C. Newman, *Am. Inst., Chem. Eng. J.,* Vol 32 (No. 60), 1986, p 949

104. B.A. Kehler, G.O. Ilevbare, and J.R. Scully, *Corrosion,* Vol 57 (No. 12), 2001, p 1042–1065

105. P.C. Pistorius and G.T. Burstein, *Philos. Trans. R. Soc. London,* Vol 341, 1992, p 531

106. T. Shibata, *Trans. ISIJ,* Vol 23, 1983, p 785

107. T. Shibata and T. Takeyama, *Corrosion,* Vol 33, 1977, p 243

108. T. Shibata and Y.-C. Zhu, *Corros. Sci.,* Vol 36 (No. 1), 1994, p 153–163

109. S.T. Pride, J.R. Scully, and J.L. Hudson, *J. Electrochem. Soc.,* Vol 141, 1994, p 3028

110. G.O. Ilevbare, J.R. Scully, J. Yuan, and R.G. Kelly, *Corrosion,* Vol 56 (No. 3), 2000, p 227–242

111. J.E. Sweitzer, G.J. Shiflet, and J.R. Scully, *Tri-Service Military Corrosion Conf. Proc.,* 2002

112. D.D. Macdonald, Critical Factors in Localized Corrosion, *The Electrochemical Society Proceedings Series,* PV 92-9, G.S.Frankel and R.C. Newman, Ed., 1992, p 144

113. T. Suter and R.C. Alkire, *J. Electrochem. Soc.,* Vol 148 (No. 1), 2001, p B36–B42

114. G.T. Burstein and G.O. Ilevbare, *Corros. Sci.,* Vol 38, 1996, p 2257–2265

115. K. Hladky and J.L. Dawson, *Corros. Sci.,* Vol 22, 1982, p 231–237

116. K. Hladky and J.L. Dawson, *Corros. Sci.,* Vol 21, 1982, p 317–322

117. H.S. Bertocci, *Proc. Second International Conf. Localized Corrosion,* NACE-9, H. Isaacs, U. Bertocci, J. Kruger, and S. Smialowska, Ed., National Association of Corrosion Engineers, 1990

118. H.S. Bertocci and J. and Kruger, *Surf. Sci.,* Vol 101, 1980, p 608–618

119. D.A. Eden and A.N. Rothwell, "Electrochemical Noise Data: Analysis and Interpretation," Paper 92, Proc. Corrosion Conference, 1992, National Association of Corrosion Engineers, 1992

120. P.C. Searson and J.L. Dawson, *J. Electrochem. Soc.,* Vol 135, 1988, p 1908–1915

121. D.E. Williams, J. Stewart, and B.H. Balkwill, *Proc. Symposium on Critical Factors in Localized Corrosion,* Vol 92-9, G.S. Frankel and R.C. Newman, Ed., Electrochemical Society, 1992, p 36

122. S.T. Pride, J.R. Scully, and J.L. Hudson, *Electrochemical Noise Measurement for Corrosion Applications,* STP 1277, J.R. Kearns and J.R. Scully, et al., Ed., American Society for Testing and Materials, 1996, p 307

123. J.R. Galvele, *J. Electrochem. Soc.,* Vol 123, 1976, p 464

124. S. Turgoose and R.A. Cottis, "Corrosion Testing Made Easy, Electrochemical Impedance and Noise" (Houston, TX), NACE International, 2000

125. R.A. Cottis, *Corrosion,* Vol 57, 2001, p 265

126. C. Gabrielli, F. Huet, M. Keddam, and R. Oltra, Localized Corrosion as a Stochastic Process, *NACE—9 Advances in Localized Corrosion,* H. Isaacs, U. Bertocci, J. Kruger, and S. Smialowska, Ed., National Association of Corrosion Engineers, 1990, p 93–108

127. J.R. Scully, S.T. Pride, H.S. Scully, and J.L. Hudson, Critical Factors in Local Corrosion II, *Proc. Electrochemical Society,* Vol 95-15, R.G. Kelly et al., Ed., 1996, p 15

128. R.A. Cottis and S. Turgoose, *Mater. Sci. Forum,* Vol 2, 1995, p 192–194

129. P. Novak, R. Stefec, and F. Franz, *Corrosion,* Vol 31 (No. 10), 1975, p 344

130. W.L. Clarke, V.M. Romero, and J.C. Danko, Paper (preprint 180), Proc. Corrosion Conference, 1977, National Association of Corrosion Engineers, 1977

131. W.L. Clarke, R.L. Cowan, and W.L. Walker, *Intergranular Corrosion of Stainless Alloys,* STP 656, R.F. Steigerwald, Ed., American Society for Testing and Materials, 1978, p 99

132. "Test Method for Electrochemical Reactivation (EPR) Test Method for Detecting Sensitization of AISI Type 304 and 304L Stainless Steels," G 108, *Wear and Erosion; Metal Corrosion,* Vol 03.02, *Annual Book of ASTM Standards,* ASTM

133. M. Akashi, T. Kawamoto, and F. Umemura, *Corros. Eng.,* Vol 29, 1980, p 163

134. A.P. Majidi and M.A. Streicher, *Corrosion,* Vol 40 (No. 11), 1984, p 584

135. "Practice for Detecting Susceptibility to Intergranular Attack in Wrought Nickel- Rich, Chromium Bearing Alloys," A 262, *Steel—Plate, Sheet, Strip, Wire; Stainless Steel Bar,* Vol. 01.03, *Annual Book of ASTM Standards,* ASTM

136. J.B. Lee, *Corrosion,* Vol 42 (No. 2), 1986, p 67

137. A. Roelandt and J. Vereecken, *Corrosion,* Vol 42 (No. 5), 1986, p 289

138. J.R. Scully and R. Kelly, *Corrosion,* Vol 42 (No. 9), 1986, p 537

139. F. Hunkeler and H. Bohni, *Corrosion,* Vol 37, 1981, p 645

140. A. Rota and H. Bohni, *Werkst. Korros,* Vol 40, 1989, p 219

141. J.D. Scantlebury, K.N. Ho, and D.A. Eden, *Electrochemical Corrosion Testing,* STP 727, F. Mansfeld and U. Bertocci, Ed., American Society for Testing and Materials, 1981, p 187

142. S. Narian, N. Bonanos, and M.G. Hocking, *J. Oil Colour Chem. Assoc.,* Vol 66 (No. 2), 1983, p 48

143. T.A. Strivens and C.C. Taylor, *Mater. Chem.,* Vol 7, 1982, p 199

144. F. Mansfeld, M.W. Kendig, and S. Tsao, *Corrosion,* Vol 38 (No. 9), 1982, p 478

145. M. Kendig, F. Mansfeld, and S. Tsai, *Corros. Sci.,* Vol 23 (No. 4), 1983, p 317

146. R. Touhsaent and H. Leidheiser, *Corrosion,* Vol 28 (No. 12), 1982, p 435

147. S. Haruyama, M. Asari, and T. Tsuru, Corrosion Protection by Organic Coatings, *The Electrochemical Society Proceedings Series,* M. Kendig and H. Leidheiser, Jr., Ed., 1980, p 197

148. J.R. Scully, *J. Electrochem. Soc.,* Vol 136 (No. 4), 1989, p 979

149. M.W. Kendig and J.R. Scully, *Corrosion,* Vol 46 (No. 1), 1990, p 22

150. H.P. Hack and J.R. Scully, *J. Electrochem. Soc.,* Vol 138 (No. 1), 1991, p 33–40

151. F. Mansfeld and C.C. Lee, *J. Electrochem. Soc.,* Vol 144, 1997, p 2068–2071

152. F. Mansfeld, L.T. Han, C.C. Lee, C. Chen., G. Zhang, and H. Xiao, *Corros. Sci.,* Vol 39, 1997, p 255–279

153. D.E. Tallman and G.P. Bierwagen, Paper No. 380, Proc. Corrosion Conference 1998, National Association of Corrosion Engineers, 1998

154. A. Aballe, A. Bautista, U. Bertocci, and F. Huet, *Corrosion,* Vol 57, 2001, p 35

155. "Standard Practice for Preparing, Cleaning and Evaluating Corrosion Tests Specimens," G 1, *Wear and Erosion; Metal Corrosion,* Vol. 03.02, *Annual Book of Standards,* ASTM

156. "Standard Guide for On-line Monitoring of Corrosion in Plant Equipment (Electrical and Electrochemical Methods)," G 96, *Wear and Erosion; Metal Corrosion,* Vol. 03.02, *Annual Book of Standards,* ASTM

157. G. Cooper, *Sensing Probes and Instruments for Electrochemical and Electrical Resistance Corrosion Monitoring,* STP 908, ASTM

158. D.B. Mitton, Ph.D. thesis, University of Manchester Institute of Science and Technology, Manchester, U.K., 1989

159. N.J. Cantini, D.B. Mitton, N. Eliaz, G. Leisk, S.L. Wallace, F. Bellcuci, G.E. Thompson, and R.M. Latanision, *Electrochem. Solid State Lett.,* Vol 396, 2000, p 275–278

160. J.G. Bellingham, M.L.A. MacVicar, M. Nisenoff, and P.C. Searson, *J. Electrochem. Soc.,* Vol 133, 1986, p 1753

161. J.G. Bellingham, M.L.A. MacVicar, and M. Nisenoff, *IEEE Trans. Magn.,* Vol 23, 1987, p 477

162. A. Abedi, Ph.D. Disseration, Vanderbilt University, 2000

163. A. Abedi, J.J. Fellenstein, A.J. Lucas, and J.P. Wikswo, Jr., *Rev. Sci. Instrum.,* Vol 70 (No. 12) , 1999, p 4640–4651

164. G. Skennerton, A. Abedi, R.G. Kelly, and J.P. Wikswo, Jr., *J. Corros. Sci. Eng.,* Vol 3, Paper 2, 2000

165. G. Sauerbrey, *Z. Phys.,* Vol 155, 1959, p 206

166. R. Schumacher, A. Muller, and W. Stockel, *J. Electroanal. Chem.,* Vol 219, 19876, p 311

167. D. Jope, J. Sell, H.W. Pickering, and K.G. Weil, *J. Electrochem. Soc.,* Vol 142, 1995, p 2170

168. C.S. Brossia and R.G. Kelly, *Corrosion,* Vol 54, 1998, p 145–154

169. D. Bostic, G. Burns, and S. Harvey, *J. Chromatogr.,* Vol 602, 1992, p 163

170. M.A. Alodan and W.H. Smyrl, *J. Electrochem. Soc.,* Vol 145, 1998, p 1571

171. J.B. Pawley, Ed., *Handbook of Biological Confocal Microscopy,* 2nd ed., Plenum Press, 1995

172. N. Llorca-Isern, M. Puig, and M. Español, *J. Therm. Spray Technol.,* Vol 8, 1999, p 73

173. L.F. Garfias-Mesias and W.H. Smyrl, *J. Electrochem. Soc.,* Vol 146, 1999, p 2495

174. O. Schneider, G.O. Ilevbare, J.R. Scully, and R.G. Kelly, *Electrochem. Solid State Sci. Lett.,* Vol 4, 2001, p B35

175. D.E. Williams and J. Asher, *Corros. Sci.,* Vol 24, 1984, p 185

M. Danielewski, Introduction to Fundamentals of Corrosion in Gases, *Corrosion: Fundamentals, Testing, and Protection*, Vol 13A, *ASM Handbook*, ASM International, 2003, p 87–89

Introduction to Fundamentals of Corrosion in Gases

Revised by Marek Danielewski, AGH University of Science and Technology, Cracow, Poland

Introduction

ENGINEERING MATERIALS are subject to deterioration when exposed to high-temperature environments. Whether they survive or not in technological applications depends on how fast they react. The rate of corrosion varies widely; some intermetallics (β-NiAl) react extremely slowly. Some metals (Fe) oxidize very rapidly, whereas other metals (Cr, Co) react relatively slowly. From the chemical point of view, the gas- metal reactions represent a broad class of heterogeneous reactions. The composition and structure of the scales produced on metals are a key factor in their behavior in technical applications.

Historically, corrosion in gases has been primarily a problem in combustion systems. Thus, the gas-metal reactions are usually referred to as oxidation in its broad chemical sense, whether the reaction is with pure oxygen, water, sulfur dioxide (SO_2), or whatever the gas might be. The corrosion product (oxide layer) is termed *scale.* Being the corrosion product, the protective properties of scale decrease the reaction rate. The concepts and methods developed to understand gas-metal reactions can be used to describe any arbitrary gas-

solid reaction at high temperature; for example, oxidation of the silicone carbide. The high temperature corrosion is a highly technical challenge; the reason for this is that the efficiency of thermal processes and engines increases with operating temperature. Such high- temperature service is especially damaging to most metals because of the exponential increase of reaction rate with temperature. In most cases, corrosion resistance at high temperatures does not accompany the good mechanical properties of structural materials; therefore, protective coatings must be applied.

Electrochemical principles are insufficient to understand the mechanism of oxidation. For gaseous reactions, a basic understanding of the diffusion processes is much more profitable. The first results of a high-temperature corrosion study (not yet defined as corrosion and even diffusion) were published in 1684 by Boyle in *Experiments and Considerations about the Porosity of Bodies in Two Essays.* In studying reactive diffusion in the Cu-S system, Boyle reported the observation of interaction between copper and sulfur through examination of metallographic cross sections. Electrochemistry and aqueous corrosion principles were developed at the beginning of the 19th century. In 1855 Fick formulated the basic principles of diffusion in solids. The systematic study of high-temperature oxidation began in the 1920s. In 1933 Wagner published his pioneering paper on gas corrosion of metals. The first journal devoted to corrosion in gases, *Oxidation of Metals,* was published in the 1960s.

The following articles introduce the subject of gas corrosion to professional engineers and students. A brief summary of thermodynamic concepts is followed by an explanation of the defect structure of solid oxides and the effect of these defects on the rate of mass transport. Commonly observed kinetics of oxidation are described and related to the observed corrosion mechanisms, as illustrated in Fig. 1 of the next article, “Thermodynamics of Gaseous Corrosion.”

In high temperature gaseous corrosion, the oxidant first adsorbs on the metal surface in molecular (physical adsorption) and ionic form (chemical adsorption), and it may also dissolve in metal. Oxide nucleates at favorable sites and most commonly grows laterally, due to surface diffusion, to form a complete thin film (scale). As the scale thickens, it provides a protective barrier to shield the metal from the gas. For scale growth, electrons must move through the film to reach the oxidant atoms adsorbed on the surface, and oxidant ions and/or metal ions must move through the scale barrier. Diffusion of the oxidant into the metal may result in internal oxidation.

Growth and thermal stresses in the oxide scale may create microcracks and/or delaminate scale from the underlying metal. Stresses affect the diffusion process and modify the oxidation mechanism and very often cause scale spallation. Improved oxidation resistance can be achieved by developing better alloys, by applying protective coatings, and by altering the composition of the gas phase.

M. Danielewski, Introduction to Fundamentals of Corrosion in Gases, *Corrosion: Fundamentals, Testing, and Protection*, Vol 13A, *ASM Handbook*, ASM International, 2003, p 87–89

Introduction to Fundamentals of Corrosion in Gases

Revised by Marek Danielewski, AGH University of Science and Technology, Cracow, Poland

---

Fundamental Data

Essential to an understanding of gaseous corrosion are the crystal structure and the density (molar volume) of the oxide and of the metal on which the oxide builds. Both may affect growth stresses in the oxide. For high-temperature service, the melting points of the oxide and metal, their structure, and thermal expansion coefficients, which affect oxide adherence during heating and cooling, are all important to know. These data for pure metals can be found in Table 1 here and in Table 1 of next article, “Thermodynamics of Gaseous Corrosion.” Likewise, data for oxides are shown in Table 2 and in Table 2 of the next article.

Table 1 Properties of pure metals

Metal	Type	Density, g/cm^3	Coefficient of linear thermal expansion (CTE) at 1000 °C	
			10^{-6} °C	**10^{-6} °F**
Aluminum (Al)	…	2.6989	…	…
Antimony (Sb)	…	6.618	…	…
Arsenic (As)	…	5.72	…	…
Barium (Ba)	…	3.66	…	…
Beryllium (Be)	IF-1 foil grade	1.844	18.4	33.12
Bismuth (Bi)	…	9.8	…	…
Cadmium (Cd)	…	8.64	…	…
Calcium (Ca)	Rolled	1.54	22[a]	39.6[a]
Cerium (Ce)	…	6.7	…	…
Cesium (Cs)	…	1.89	…	…
Chromium (Cr)	As-swaged	7.19	…	…
Cobalt (Co)	…	8.8	…	…
Copper (Cu)	Annealed	8.96	24.8	44.64
Gallium (Ga)	…	5.91	…	…
Germanium (Ge)	…	5.3234	…	…
Gold (Au)	…	19.32	16.7	30.06
Hafnium (Hf)	Rod	13.31	…	…
Indium (In)	…	7.31	…	…
Iridium (Ir)	Cold-drawn	22.65	…	…
Iron (Fe)	…	7.87	24	43.2
Lanthanum (La)	…	6.166	…	…
Lead (Pb)	…	11.34	…	…
Lithium (Li)	…	53	…	…
Magnesium (Mg)	Sand cast	1.74	…	…
Manganese (Mn)	…	7.44	45.7	82.26
Molybdenum (Mo)	Annealed	10.22	6.5	11.7
Neodymium (Nd)	…	7	…	…
Nickel (Ni)	Typical	8.88	…	…
Niobium (Nb)	Annealed Sample	8.6	8.52	15.33
Osmium (Os)	Annealed	22.5	…	…
Palladium (Pd)	…	12.02	13.9	25.02
Platinum (Pt)	CP grade, annealed	21.45	…	…
Potassium (K)	…	86	…	…
Rhenium (Re)	Annealed	21.03	6.65	11.97
Rhodium (Rh)	Annealed	12.4	…	…
Ruthenium (Ru)	Annealed	12.3	…	…
Selenium (Se)	…	4.81	…	…
Silicon (Si)	…	2.329	4.44	7.99
Silver (Ag)	…	10.491	19[a]	34.2[a]
Sodium (Na)	…	971	…	…
Strontium (Sr)	…	2.6	…	…
Tantalum (Ta)	Cold worked	16.65	6.96	12.53
Thorium (Th)	…	11.3	14.9	26.82
Thulium (Tm)	…	9.33	…	…
Tin-alpha (Sn)	…	5.765	…	…
Tin-gamma (Sn)	…	6.45	…	…
Tin-beta (Sn)	…	7.29	…	…

Titanium (Ti)	…	4.5	10.1	18.18
Tungsten (W)	…	19.3	…	…
Uranium (U)	Cast	19.07	…	…
Vanadium (V)	Cold rolled	6.11	10.9	19.62
Yttrium (Y)	…	4.472	…	…
Zinc (Zn)	…	7.1	…	…
Zirconium (Zr)	…	6.53	…	…

(a) CTE at 100 °C (212 °F). Source: Ref 2, 3, 4, 5, 6, 7

Table 2 Structures and properties of oxides

Oxide	Mineral	Density, g/cm^3	Decomposition temperature		Crystal structure
			°C	°F	
Aluminium oxide (Al_2O_3)	…	3.96	…	…	Rhombohedral
Barium oxide (BaO)	…	5.72	…	…	Cubic or Hexagonal
Barium peroxide (BaO_2)	…	4.96	Max 450	Max 842	Tetragonal
Beryllium oxide (BeO)	Bromellite	3.01	…	…	Hexagonal
Bismuth oxide (Bi_2O_3)	…	8.9	…	…	Monoclinic
Bismuth tetraoxide (Bi_2O_4)	…	5.6	…	…	…
Calcium oxide (CaO)	…	3.34	…	…	Cubic
Calcium peroxide (CaO_2)	…	2.9	200	392	…
Cerium (III) oxide (Ce_2O_3)	…	6.2	…	…	Cubic
Cerium (IV) oxide (CeO_2)	Cerianite	7.65	…	…	Cubic
Cesium oxide (Cs_2O)	…	4.65	…	…	Hexagonal
Cesium superoxide ($CsO2_2$)	…	3.77	…	…	Tetragonal
Chromium (II, III) oxide (Cr_3O_4)	…	6.1	…	…	Cubic
Chromium (III) oxide (Cr_2O_3)	Eskolaite	5.22	…	…	Hexagonal—rhomohedral
Chromium (IV) oxide (CrO_2)	…	4.89	400	752	Tetragonal
Chromium (VI) oxide (CrO_3)	…	2.7	250	482	Orthorhombic
Cobalt (II) oxide (CoO)	…	6.44	…	…	Cubic
Cobalt (II, III) oxide (Co_3O_4)	…	6.11	900	1652	Cubic
Cobalt (III) oxide (Co_2O_3)	…	5.18	895	1643	…
Copper (I) oxide (Cu_2O)	Cuprite	6	1800	3272	Cubic
Copper (II) oxide (CuO)	Tenorite	6.31	…	…	Monoclinic
Gallium (III) oxide (Ga_2O_3)	…	6	…	…	Rhombic
Gallium suboxide (Ga_2O)	…	4.77	Min 800	Min 1472	…
Gold (III) oxide (Au_2O_3)	…	…	…	…	…
Hafnium (II) oxide (HfO_2)	Hafnia	…	…	…	Monoclinic
Hafnium oxide (HfO_2)	…	9.68	…	…	Cubic
Indium (III) oxide (In_2O_3)	…	7.18	…	…	Cubic
Iridium (III) oxide (Ir_2O_3)	…	…	1000	1832	…
Iridium (IV) oxide (IrO_2)	…	11.7	1100	2012	Tetragonal
Iron (II) oxide (FeO)	…	6	…	…	Cubic
Iron (II, III) oxide (Fe_3O_4)	Magnetite	5.17	…	…	Cubic
Iron (III) oxide (Fe_2O_3)	Hematite	5.25	…	…	Hexagonal—rhombohedral

Oxide	Mineral	Density, g/cm^3	Decomposition temperature		Crystal structure
			°C	°F	
Iron (III) oxide (Fe_2O_3)	Maghemite	4.88	…	…	Cubic
Lanthanum oxide (La_2O_3)	…	6.51	…	…	…
Lead (II) oxide (PbO)	…	9.64	…	…	Orthorombic
Lead (II,III,IV) oxide (Pb_3O_4)	…	8.92	…	…	Tetragonal
Lead (II,IV) oxide (Pb_2O_3)	…	10.05	…	…	Monoclinic
Lead (IV) oxide (PbO_2)	…	9.64	…	…	Tetragonal
Magnesium oxide (MgO)	Periclase	3.6	…	…	Cubic
Manganese (II) oxide (MnO)	Manganosite	5.37	…	…	Cubic
Manganese (II, III) oxide (Mn_3O_4)	Hausmannite	4.84	…	…	Tetragonal
Manganese (III) oxide (Mn_2O_3)	…	5	…	…	Cubic
Manganese (IV) oxide (MnO_2)	Pyrolusite	5.08	535	995	Tetragonal
Molybdenum (III) oxide (Mo_2O_3)	…	…	…	…	…
Molybdenum (IV) oxide (MoO_2)	…	6.47	1100	2012	Tetragonal
Molybdenum (VI) oxide (MoO_3)	…	4.7	…	…	Rhombohedral
Neodymium oxide (Nd_2O_3)	…	7.24	…	…	Hexagonal
Nickel (II) oxide (NiO)	Bunsenite	6.72	…	…	Cubic
Nickel (III) oxide (Ni_2O_3)	…	…	600	1112	Cubic
Niobium (II) oxide (NbO)	…	7.3	…	…	Cubic
Niobium (IV) oxide (NbO_2)	…	5.9	…	…	Tetragonal
Niobium (V) oxide (Nb_2O_5)	…	4.6	…	…	Orthorhombic
Rhenium (IV) oxide (ReO_2)	…	11.4	900	1652	Orthorhombic
Rhenium (V) oxide (Re_2O_5)	…	7	…	…	Tetragonal
Rhenium (VI) oxide (ReO_3)	…	6.9	400	752	Cubic
Rhenium (VII) oxide (Re_2O_7)	…	6.1	…	…	…
Silver (I) oxide (Ag_2O)	…	7.2	200	392	Cubic
Silver (II) oxide (AgO)	…	7.5	Min 100	Min 212	Monoclinic
Titanium (II) oxide (TiO)	…	4.95	…	…	Cubic
Titanium (III) oxide (Ti_2O_3)	…	4.486	…	…	Hexagonal—rhomohedral
Titanium (III,V) oxide (Ti_3O_5)	…	4.24	…	…	Monoclinic
Titanium dioxide (TiO_2)	Rutile	4.25	…	…	Tetragonal
Titanium dioxide (TiO_2)	Anatase	3.89	…	…	Tetragonal
Titanium dioxide (TiO_2)	Brookite	4.14	…	…	Orthorhombic
Tungsten (IV) oxide (WO_2)	…	10.8	1500–1700	2732–3092	Monoclinic
Tungsten (VI) oxide (WO_3)	…	7.2	…	…	…
Vanadium (II) oxide (VO)	…	5.758	…	…	…
Vanadium (III) oxide (V_2O_3)	Karelianite	4.87	…	…	…

Oxide	Mineral	Density, g/cm^3	Decomposition temperature		Crystal structure
			°C	°F	
Vanadium (IV) oxide (VO_2)	…	4.339	…	…	…
Vanadium (V) oxide (V_2O_5)	…	3.35	1800	3272	Orthorhombic
Yttrium oxide (Y_2O_3)	…	5.03	…	…	Cubic
Zinc oxide (ZnO)	…	5.66	…	…	Hexagonal
Zinc peroxide (ZnO_2)	…	1.57	Min 150	Min 302	…
Zirconium oxide (ZrO_2)	Zirconia	5.68	…	…	Monoclinic

Source: Ref 2, 6

References cited in this section

2. *CRC Handbook of Chemistry and Physics,* R.C. Weast, Ed., 62nd ed., CRC Press, 1981

3. R.B. Ross, *Metallic Materials Specification Handbook,* 4th ed., R.B. Ross, Chapman & Hall, 1992

4. *Properties and Selection: Nonferrous Alloys and Special-Purpose Materials,* Vol 2, *ASM Handbook,* ASM International, 10th ed., 1990

5. *The Metals Databook,* Alok Nayer, McGraw- Hill, New York, 1997

6. *CRC Handbook of Chemistry and Physics,* D.R. Lide, Ed., 79th ed., CRC Press, 1998

7. *ASM Ready Reference: Thermal Properties of Metals,* ASM International, 2002

M. Danielewski, Introduction to Fundamentals of Corrosion in Gases, *Corrosion: Fundamentals, Testing, and Protection*, Vol 13A, *ASM Handbook*, ASM International, 2003, p 87–89

Introduction to Fundamentals of Corrosion in Gases

Revised by Marek Danielewski, AGH University of Science and Technology, Cracow, Poland

References

1. P. Kofstad, Oxidation Mechanisms for Pure Metals in Single Oxidant Gases, *High Temperature Corrosion,* R.A. Rapp, Ed., NACE International, 1983, p 123–138

2. *CRC Handbook of Chemistry and Physics,* R.C. Weast, Ed., 62nd ed., CRC Press, 1981

3. R.B. Ross, *Metallic Materials Specification Handbook,* 4th ed., R.B. Ross, Chapman & Hall, 1992

4. *Properties and Selection: Nonferrous Alloys and Special-Purpose Materials,* Vol 2, *ASM Handbook,* ASM International, 10th ed., 1990

5. *The Metals Databook,* Alok Nayer, McGraw- Hill, New York, 1997

6. *CRC Handbook of Chemistry and Physics,* D.R. Lide, Ed., 79th ed., CRC Press, 1998

7. *ASM Ready Reference: Thermal Properties of Metals,* ASM International, 2002

Z. Grzesik, Thermodynamics of Gaseous Corrosion, *Corrosion: Fundamentals, Testing, and Protection*, Vol 13A, *ASM Handbook*, ASM International, 2003, p 90–96

Thermodynamics of Gaseous Corrosion

Zbigniew Grzesik, University of Mining and Metallurgy (Krakow, Poland)

Introduction

METALS can react chemically when exposed to air or to other more aggressive gases. The reaction rate of some metals is so slow that they are virtually unattacked, but for others, the reaction can be violent. As with most chemical processes, elevated-temperature service is more severe because of the exponential increase in reaction rate with temperature.

The most common reactant is oxygen in the air; therefore, all gas-metal reactions are usually referred to as oxidation, using the term in its broad chemical sense whether the reaction is with oxygen, water vapor, hydrogen sulfide (H_2S), or whatever the gas might be. Throughout this article, the process is called oxidation, and the corrosion product is termed an oxide.

Corrosion in gases differs from aqueous corrosion in that electrochemical principles do not help greatly in understanding the mechanism of oxidation. For gaseous reactions, a fundamental knowledge of the diffusion processes involved is much more useful. The principles of high-temperature oxidation began to be understood in the 1920s, whereas electrochemistry and aqueous corrosion principles were developed approximately 100 years earlier. The first journal devoted to corrosion in gases, *Oxidation of Metals,* began publication in 1970. This article addresses thermodynamic concepts; the commonly observed kinetics of oxidation are described in the article "Kinetics of Gaseous Corrosion Processes" in this Volume.

The mechanisms of oxidation are shown schematically in Fig. 1. The gas is first adsorbed on the metal surface as atomic oxygen. Oxide nucleates at favorable sites and most commonly grows laterally to form a complete thin film. As the layer thickens, it provides a protective scale barrier to shield the metal from the gas. For scale growth, electrons must move through the oxide to reach the oxygen atoms adsorbed on the surface, and oxygen ions, metal ions, or both must move through the oxide barrier. Oxygen may also diffuse into the metal.

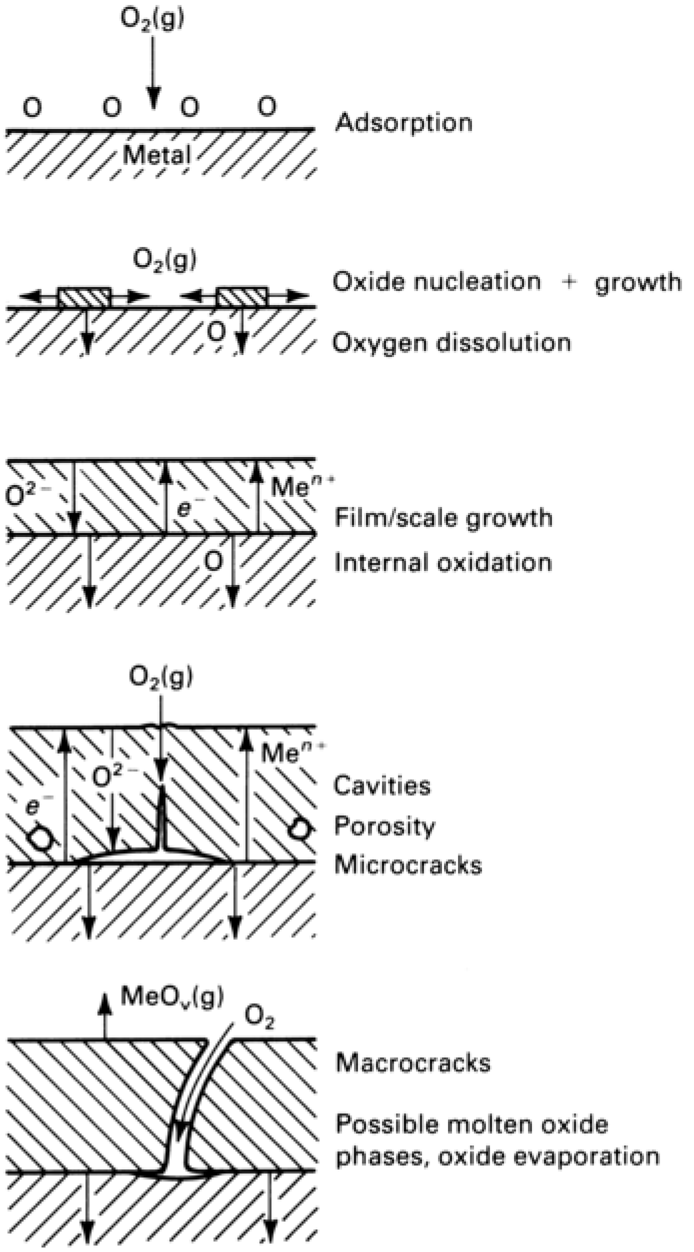

Fig. 1 Schematic of the principal phenomena taking place during the reaction of metals with oxygen. Source: Ref 1

Growth stresses in the scale may create cavities and microcracks in the scale, modifying the oxidation mechanism or even causing the oxide to fail to protect the metal from the gas. Improved oxidation resistance can be achieved by selection of suitable alloys for the given environment and by application of protective coatings.

Reference cited in this section

1. P. Kofstad, Oxidation Mechanisms for Pure Metals in Single Oxidant Gases, *High Temperature Corrosion,* R.A. Rapp, Ed., NACE International, 1983, p 123–138

Z. Grzesik, Thermodynamics of Gaseous Corrosion, *Corrosion: Fundamentals, Testing, and Protection*, Vol 13A, *ASM Handbook*, ASM International, 2003, p 90–96

Thermodynamics of Gaseous Corrosion

Zbigniew Grzesik, University of Mining and Metallurgy (Krakow, Poland)

Fundamental Data

Essential to an understanding of the gaseous corrosion of a metal are the crystal structure and the molar volume of the metal on which the oxide builds, both of which may affect growth stresses in the oxide. For high-temperature service, the melting point of the metal and the structural changes that take place during heating and cooling, which affect oxide adherence, must be known. These data are presented in Table 1 for pure metals. For the oxides, structures, melting and boiling points, molar volume, and oxide/ metal volume ratio (Pilling-Bedworth ratio) are shown in Table 2.

Table 1 Structures and thermal properties of pure metals

Metal	Structure[a]	Transformation temperature		Volume change on cooling[b], %	Melting point		Molar volume[c]	
		°C	°F	°C	°F	cm^3	$in.^3$	
Aluminum	fcc	…	…	…	660.4	1220.7	10.00	0.610
Antimony	rhom	…	…	…	630.7	1167.3	18.18	1.109
Arsenic	rhom	…	…	…	Sublimation 615	1139	12.97	0.791
Barium	bcc	…	…	…	729	1344	39	2.380
Beryllium	(α) hcp	1250	2282	…	…	…	4.88	0.298
	(β) bcc	…	…	-2.2	1290	2354	4.99	0.304
Bismuth	rhom	…	…	…	271.4	520.5	21.31	1.300
Cadmium	hcp	…	…	…	321.1	610	13.01	0.793
Calcium	(α) fcc	448	838	…	…	…	25.9	1.581
	(β) bcc	…	…	-0.4	839	1542	…	…
Cerium	(γ) fcc	726	1339	…	…	…	20.70	1.263
	(δ) bcc	…	…	…	798	1468	…	…
Cesium	bcc	…	…	…	28.64	83.55	70.25	4.287
Chromium	bcc	…	…	…	1875	3407	7.23	0.441
Cobalt	(α) hcp	417	783	…	…	…	6.67	0.407
	(β) fcc	…	…	-0.3	1495	2723	6.70	0.408
Copper	fcc	…	…	…	1084.88	1984.78	7.12	0.434
Dysprosium	(α) hcp	1381	2518	…	…	…	19.00	1.159
	(β) bcc	…	…	-0.1	1412	2573	18.98	1.158
Erbium	hcp	…	…	…	1529	2784	18.45	1.126
Europium	bcc	…	…	…	822	1512	28.98	1.768
Gadolinium	(α) hcp	1235	2255	…	…	…	19.90	1.214
	(β) bcc	…	…	-1.3	1312	2394	20.16	1.230
Gallium	ortho	…	…	…	29.78	85.60	11.80	0.720
Germanium	diamond fcc	…	…	…	937.4	1719.3	13.63	0.832
Gold	fcc	…	…	…	1064.43	1947.97	10.20	0.622
Hafnium	(α) hcp	1742	3168	…	…	…	13.41	0.818
	(β) bcc	…	…	…	2231	4048	…	…

Metal	Structure[a]	Transformation temperature		Volume change on cooling[b], %	Melting point		Molar volume[c]	
		°C	°F	°C	°F	cm^3	$in.^3$	
Holmium	hcp	…	…	…	1474	2685	18.75	1.144
Indium	tetr	…	…	…	156.63	313.93	15.76	0.962
Iridium	fcc	…	…	…	2447	4437	8.57	0.523
Iron	(α) bcc	912	1674	…	…	…	7.10	0.433
	(γ) fcc	1394	2541	1.0	…	…	7.26	0.443
	(δ) bcc	…	…	-0.52	1538	2800	7.54	0.460
Lanthanum	(α) hex	330	626	…	…	…	22.60	1.379
	(β) fcc	865	…	0.5	…	…	22.44	1.369
	(γ) bcc	…	…	-1.3	918	1684	23.27	1.420
Lead	fcc	…	…	…	327.4	621.3	18.35	1.119
Lithium	(β) bcc	-193	-315	…	180.7	357.3	12.99	0.793
Lutetium	hcp	…	…	…	1663	3025	17.78	1.085
Magnesium	hcp	…	…	…	650	1202	13.99	0.854
Manganese	(α) cubic	710	1310	…	…	…	7.35	0.449
	(β) cubic	1079	1974	-3.0	…	…	7.63	0.466
	(γ) tetr	…	…	-0.0	1244	2271	7.62	0.465
Mercury	rhom	…	…	…	-38.87	-37.97	14.81	0.904
Molybdenum	bcc	…	…	…	2610	4730	9.39	0.573
Neodymium	(α) hex	863	1585	…	…	…	20.58	1.256
	(β) bcc	…	…	-0.1	1021	1870	21.21	1.294
Nickel	fcc	…	…	…	1453	2647	6.59	0.402
Niobium	bcc	…	…	…	2648	4474	10.84	0.661
Osmium	hcp	…	…	…	~2700	~4890	8.42	0.514
Palladium	fcc	…	…	…	1552	2826	8.85	0.540
Platinum	fcc	…	…	…	1769	3216	9.10	0.555
Plutonium	α, β, γ	120, 210, 315	248, 410, 599	…	…	…	α 12.04	α 0.735
	δ, δ′, ε	452, 480	846, 896	…	640	1184	ε 14.48	ε 0.884
Potassium	bcc	…	…	…	63.2	145.8	45.72	2.790
Praseodymium	(α) hex	795	1463	…	…	…	20.80	1.269
	(β) bcc	…	…	-0.5	931	1708	21.22	1.295
Rhenium	hcp	…	…	…	3180	5756	8.85	0.540
Rhodium	fcc	…	…	…	1963	3565	8.29	0.506
Rubidium	bcc	…	…	…	38.89	102	55.79	3.405
Ruthenium	hcp	…	…	…	2310	4190	8.17	0.499
Samarium	(α) rhom	734	1353	…	…	…	20.00	1.220
	(β) hcp	922	1692	…	…	…	20.46	1.249
	(γ) bcc	…	…	…	1074	1965	20.32	1.240
Scandium	(α) hcp	1337	2439	…	…	…	15.04	0.918
	(β) bcc	…	…	…	1541	2806	…	…
Selenium	(γ) hex	209	408	…	217	423	16.42	1.002
Silicon	diamond fcc	…	…	…	1410	2570	12.05	0.735
Silver	fcc	…	…	…	961.9	1763.4	10.28	0.627
Sodium	(β) bcc	-237	-395	…	97.82	208.08	23.76	1.450
Strontium	(α) fcc	557	1035	…	…	…	34	2.075
	(β) bcc	…	…	…	768	1414	34.4	2.099

Metal	Structure[a]	Transformation temperature		Volume change on cooling[b], %	Melting point		Molar volume[c]	
		°C	°F	°C	°F	cm^3	$in.^3$	
Tantalum	bcc	…	…	…	2996	5425	10.9	0.665
Tellurium	hex	…	…	…	449.5	841.1	20.46	1.249
Terbium	(α) hcp	1289	2352	…	…	…	19.31	1.178
	(β) bcc	…	…	…	1356	2472.8	19.57	1.194
Thallium	(α) hcp	230	446	…	…	…	17.21	1.050
	(β) bcc	…	…	…	303	577	…	…
Thorium	(α) fcc	1345	2453	…	…	…	19.80	1.208
	(β) bcc	…	…	…	1755	3191	21.31	1.300
Thulium	hcp	…	…	…	1545	2813	18.12	1.106
Tin	(β) bct	13.2	55.8	27	231.9	449.4	16.56	1.011
Titanium	(α) hcp	882.5	1621	…	…	…	10.63	0.649
	(β) bcc	…	…	…	1668	3034	11.01	0.672
Tungsten	bcc	…	…	…	3410	6170	9.55	0.583
Uranium	(α) ortho	661	1222	…	…	…	12.50	0.763
	(β) complex tetr	769	1416	-1.0	…	…	13.00	0.793
	(γ) bcc	…	…	-0.6	1900	3452	8.34	0.509
Vanadium	bcc	1910	3470	…	…	…	…	…
Ytterbium	(β) fcc	7	45	0.1	819	1506	24.84	1.516
Yttrium	(α) hcp	1478	2692	…	…	…	19.89	1.214
	(β) bcc	…	…	…	1522	2772	20.76	1.267
Zinc	hcp	…	…	…	420	788	9.17	0.559
Zirconium	(α) hcp	862	1584	…	…	…	14.02	0.856
	(β) bcc	…	…	…	1852	3366	15.09	0.921

(a) fcc, face-centered cubic; rhom, rhombohedral; bcc, body-centered cubic; hcp, hexagonal close-packed; ortho, orthorhombic; tetr, tetragonal; hex, hexagonal; bct, body-centered tetragonal.
(b) Volume change on cooling through crystallographic transformation.
(c) Molar volume at 25 °C (77 °F) or at transition temperature for structures not stable at 25 °C (77 °F). Source: Ref 2

Table 2 Structures and thermal properties of selected oxides

Oxide	Structure	Melting point		Boiling or decomposition (d)		Molar volume[a]		Volume ratio
		°C	°F	°C	°F	cm^3	$in.^3$	
α-Al_2O_3	*D*5_1 (corundum)	2015	3659	2980	5396	25.7	1.568	1.28
γ-Al_2O_3	(defect-spinel)	γ → α	…	…	…	26.1	1.593	1.31
BaO	*B*1 (NaCl)	1923	3493	~2000	~3632	26.8	1.635	0.69
BaO_2	Tetragonal (CaC_2)	450	842	d.800	d.1472	34.1	2.081	0.87
BeO	*B*4 (ZnS)	2530	4586	~3900	~7052	8.3	0.506	1.70
CaO	*B*1 (NaCl)	2580	4676	2850	5162	16.6	1.013	0.64
CaO_2	*C*11 (CaC_2)	…	…	d.275	d.527	24.7	1.507	0.95
CdO	*B*1 (NaCl)	~1400	~2552	d.900	d.1652	18.5	1.129	1.42
Ce_2O_3	*D*5_2 (La_2O_3)	1692	3078	…	…	47.8	2.917	1.15
CeO_2	*C*1 (CaF_2)	~2600	~4712	…	…	24.1	1.471	1.17
CoO	*B*1 (NaCl)	1935	3515	…	…	11.6	0.708	1.74
Co_2O_3	Hexagonal	…	…	d.895	d.1643	32.0	1.953	2.40
Co_3O_4	*H*1_1 (spinel)	→CoO	…	…	…	39.7	2.423	1.98

Oxide	Structure	Melting point		Boiling or decomposition (d)		Molar volume [a]		Volume ratio
		°C	°F	°C	°F	cm^3	$in.^3$	
Cr_2O_3	*D*5_1 (αAl_2O_3)	2435	4415	4000	7232	29.2	1.782	2.02
Cs_2O	Hexagonal ($CdCl_2$)	…	…	d.400	d.752	66.3	4.046	0.47
Cs_2O_3	Cubic (Th_3P_4)	400	752	650	1202	70.1	4.278	0.50
CuO	*B*26 monoclinic	1326	2419	…	…	12.3	0.751	1.72
Cu_2O	*C*3 cubic	1235	2255	d.1800	d.3272	23.8	1.452	1.67
Dy_2O_3	Cubic (Tl_2O_3)	2340	4244	…	…	47.8	2.917	1.26
Er_2O_3	Cubic (Tl_2O_3)	…	…	…	…	44.3	2.703	1.20
FeO	*B*1 (NaCl)	1420	2588	…	…	12.6	0.769	1.78 on α-iron
α-Fe_2O_3	*D*5_1 (hematite)	1565	2849	…	…	30.5	1.861	2.15 on α-iron
	…	…	…	…	…	…	…	1.02 on Fe_3O_4
γ-Fe_2O_3	*D*5_7 cubic	1457	2655	…	…	31.5	1.922	2.22 on α-iron
Fe_3O_4	*H*1_1 (spinel)	…	…	d.1538	d.2800	44.7	2.728	2.10 on α-iron
	…	…	…	…	…	…	…	~1.2 on FeO
Ga_2O_3	Monoclinic	1900	3452	…	…	31.9	1.947	1.35
HfO_2	Cubic	2812	5094	~5400	~9752	21.7	1.324	1.62
HgO	Defect *B*10(SnO)	…	…	d.500	d.932	19.5	1.190	1.32
In_2O_3	*D*5_3(Sc_2O_3)	…	…	d.850	d.1562	38.7	2.362	1.23
IrO_2	*C*4(TiO_2)	…	…	d.1100	d.2012	19.1	1.166	2.23
K_2O	*C*1(CaF_2)	…	…	d.350	d.662	40.6	2.478	0.45
La_2O_3	*D*5_2 hexagonal	2315	4199	4200	7592	50.0	3.051	1.10
Li_2O	*C*1 (CaF_2)	~1700	~3092	1200	2192	14.8	0.903	0.57
MgO	*B*1 (NaCl)	2800	5072	3600	6512	11.3	0.690	0.80
MnO	*B*1(NaCl)	…	…	…	…	13.0	0.793	1.77
MnO_2	*C*4 (TiO_2)	…	…	d.535	d.995	17.3	1.056	2.37
Mn_2O_3	*D*5_3 (Sc_2O_3)	…	…	d.1080	d.1976	35.1	2.142	2.40
α-Mn_3O_4	*H*1_1 (spinel)	1705	1301	…	…	47.1	2.874	2.14
MoO_3	Orthorhombic	795	1463	…	…	30.7	1.873	3.27
Na_2O	*C*1 (CaF_2)	Sublimation 1275	2327	…	…	27.3	1.666	0.57
Nb_2O_5	Monoclinic	1460	2660	…	…	59.5	3.631	2.74
Nd_2O_3	Hexagonal	~1900	~3452	…	…	46.5	2.838	1.13
NiO	*B*1 (NaCl)	1990	3614	…	…	11.2	0.683	1.70
OsO_2	*C*4 (TiO_2)	…	…	d.350	d.662	28.8	1.757	3.42
PbO	*B*10 tetragonal	888	1630	…	…	23.4	1.428	1.28
Pb_3O_4	Tetragonal	…	…	d.500	d.932	75.3	4.595	1.37
PdO	*B*17 tetragonal	870	1598	…	…	14.1	0.860	1.59
PtO	*B*17 (PdO)	…	…	d.550	d.1022	14.2	0.867	1.56
Rb_2O_3	(Th_3P_4)	489	912	…	…	62.0	3.783	0.56
ReO_2	Monoclinic	…	…	d.1000	d.1832	19.1	1.166	2.16
Rh_2O_3	*D*5_1 (α-Al_2O_3)	…	…	d.1100	d.2012	31.0	1.892	1.87

Oxide	Structure	Melting point		Boiling or decomposition (d)		Molar volume [(a)]		Volume ratio
		°C	°F	°C	°F	cm^3	$in.^3$	
SiO	Cubic	~1700	~3092	1880	3416	20.7	1.263	1.72
SiO_2	β cristobalite *C*9	1713	3115	2230	4046	25.9	1.581	2.15
SnO	*B*10 (PbO)	…	…	d.1080	d.1976	20.9	1.275	1.26
SnO_2	*C*4 (TiO_2)	1127	2061	…	…	21.7	1.324	1.31
SrO	*B*1 (NaCl)	2430	4406	~3000	~5432	22.0	1.343	0.65
Ta_2O_5	Triclinic	1800	3272	…	…	53.9	3.289	2.47
TeO_2	*C*4 (TiO_2)	733	1351	1245	2273	28.1	1.715	1.38
ThO_2	*C*1 (CaF_2)	3050	5522	4400	7952	26.8	1.635	1.35
TiO	*B*1 (NaCl)	1750	3182	~3000	~5432	13.0	0.793	1.22
TiO_2	*C*4 (rutile)	1830	3326	~2700	~4892	18.8	1.147	1.76
Ti_2O_3	*D*5_1 (α-Al_2O_3)	…	…	d.2130	d.3866	31.3	1.910	1.47
Tl_2O_3	*D*5_3 (Sc_2O_3)	717	1323	d.875	d.1607	44.8	2.734	1.30
UO_2	*C*1 (CaF_2)	2500	4532	…	…	24.6	1.501	1.97
U_3O_8	Hexagonal	…	…	d.1300	d.2372	101.5	6.194	2.71
VO_2	*C*4 (TiO_2)	1967	3573	…	…	19.1	1.166	2.29
V_2O_3	*D*5_1 (α-Al_2O_3)	1970	3578	…	…	30.8	1.879	1.85
V_2O_5	*D*8_7 orthorhombic	690	1274	d.1750	d.3182	54.2	3.307	3.25
WO_2	*C*4 (TiO_2)	~1550	~2822	~1430	~2606	17.8	1.086	1.87
β-WO_3	Orthorhombic	1473	…	…	…	32.4	1.977	3.39
W_2O_5	Triclinic	Sublimation, ~850	~1562	~1530	~2786	29.8	1.819	3.12
Y_2O_3	*D*5_3 (Sc_2O_3)	2410	4370	…	…	45.1	2.752	1.13
ZnO	*B*4 (wurtzite)	1975	3587	…	…	14.5	0.885	1.58
ZrO_2	*C*43 monoclinic	2715	4919	…	…	22.0	1.343	1.57

(a) Molar volume at 25 °C (77 °F) or at transition temperature for structures not stable at 25 °C (77 °F). Source: Ref 3

Thermodynamics plays a very important role in studying the gaseous corrosion of metallic materials. It is possible to determine several critical parameters of the oxidation reaction on the basis of thermodynamic data, namely, the temperature and oxidizing gas pressure in which particular chemical compounds can be formed, the phase sequence in the multilayered scale growing on metal, the equilibrium composition of the gas mixture, and partial pressures of volatile oxidation products. In spite of its name, thermodynamics does not inform on the reaction rate; it does not describe “the dynamics” of the systems. Thermodynamics determines the equilibrium state. The Gibbs energy change, which is the driving force of any chemical reaction, is not related to the reaction rate. Reaction rate is a kinetic problem and depends on the mechanism of the slowest step of the overall reaction process. On the other hand, the thermodynamic considerations of metal-oxidant equilibria and phase diagrams are invaluable tools for the interpretation of the oxidation mechanisms and processes. Some typical examples of such considerations are described in the following section of this article.

References cited in this section

2. Properties of Pure Metals, *Properties and Selection: Nonferrous Alloys and Pure Metals,* Vol 2, 9th ed., *Metals Handbook,* American Society for Metals, 1979, p 714–831

3. R.C. Weast, Ed., Physical Constants of Inorganic Compounds, *Handbook of Chemistry and Physics,* 65th ed., The Chemical Rubber Company, 1984, p B68–B161

Z. Grzesik, Thermodynamics of Gaseous Corrosion, *Corrosion: Fundamentals, Testing, and Protection*, Vol 13A, *ASM Handbook*, ASM International, 2003, p 90–96

Thermodynamics of Gaseous Corrosion

Zbigniew Grzesik, University of Mining and Metallurgy (Krakow, Poland)

Free Energy of Reaction

The chemical reaction describing the oxidation process of a pure divalent metal, M, by an oxidizing gas, X_2 (oxygen, sulfur, and others), may be written as:

$$aM + \frac{b}{2}X_2 = M_aX_b \quad \text{(Eq 1)}$$

where M_aX_b is the reaction product (oxide, sulfide, etc.). The fundamental criterion, which allows for the evaluation of whether, at a given temperature and oxidant gas pressure, the oxidation process of a determined metal may occur, is the sign of the Gibbs energy change, ΔG (Ref 4, 5). The Second Law of Thermodynamics describes ΔG as:

$$\Delta G = \Delta H - T\Delta S \quad \text{(Eq 2)}$$

where ΔH denotes the enthalpy of reaction, T is the absolute temperature, and ΔS is the entropy change. For a spontaneous reaction at constant pressure and temperature, ΔG is negative ($\Delta G < 0$). In the case of nonspontaneous reactions, ΔG is positive ($\Delta G > 0$), and if $\Delta G = 0$, the system is at equilibrium. The Gibbs energy change of the chemical reaction given by Eq 1 equals the sum of the chemical potentials, μ, of all components present in the system (M, X_2, M_aX_b):

$$\Delta G = \mu_{M_aX_b} - a\mu_M - \frac{b}{2}\mu_{X_2} \quad \text{(Eq 3)}$$

The chemical potential, μ_i, and the activity, a_i, of a given i-component are interrelated, as follows:

$$\mu_i = \mu_i^0 + RT \ln a_i \quad \text{(Eq 4)}$$

where R is the gas constant, and μ_i^0 is the chemical potential of a given i-component in the standard state. Generally, the activities of pure solid components (such as metals and oxides) are equal to unity, and therefore $\mu_M = \mu_M^0$ and $\mu_{M_aX_b} = \mu_{M_aX_b}^0$. The activity of gaseous component X_2 can be approximated by its pressure:

$$\mu_{X_2} = \mu_{X_2}^0 + RT \ln p_{X_2} \quad \text{(Eq 5)}$$

Thus, Eq 3 may be presented in the following form:

$$\Delta G = \mu_{M_aX_b}^0 - a\mu_M^0 - \frac{b}{2}\mu_{X_2}^0 - \frac{b}{2}RT \ln p_{X_2} \quad \text{(Eq 6)}$$

Because the sum of the standard chemical potentials is the standard Gibbs energy change, ΔG^0, then the previous equation may be written as:

$$\Delta G = \Delta G^0 - \frac{b}{2}RT \ln p_{X_2} \quad \text{(Eq 7)}$$

At equilibrium, where $\Delta G = 0$, Eq 7 can be presented in the form:

$$\Delta G^0 = \frac{b}{2}RT \ln p_{X_2}^{eq} \quad \text{(Eq 8)}$$

In the previous equation, $p_{X_2}^{eq}$ denotes the dissociation pressure of the M_aX_b compound and may be calculated from the following relation:

$$p_{X_2}^{eq} = \exp\left(\frac{2\Delta G^0}{bRT}\right) \quad \text{(Eq 9)}$$

Thermodynamically, if the oxidant pressure is lower than the calculated value of the equilibrium dissociation pressure of the M_aX_b compound, then the metal, M, is not oxidized. In the opposite case, the spontaneous oxidation reaction may occur. It should be emphasized that the calculated value of dissociation pressure of a given compound is related to the equilibrium state. In practice, thermodynamically unstable oxides can be formed during high-temperature oxidation of metals by gases. An example of such unstable oxides is Wustite (FeO), which is unstable in air unless the temperature is higher than 570 °C (1060 °F). In fact, Wustite is a major component of the scale formed on steel beyond this temperature, and after rapid cooling to room temperature, it remains in the scale as a result of the extremely slow decomposition kinetics of FeO. See the Fe-O binary phase diagram (Fig. 2); the diagram shows that other scale components are Fe_2O_3 and Fe_3O_4.

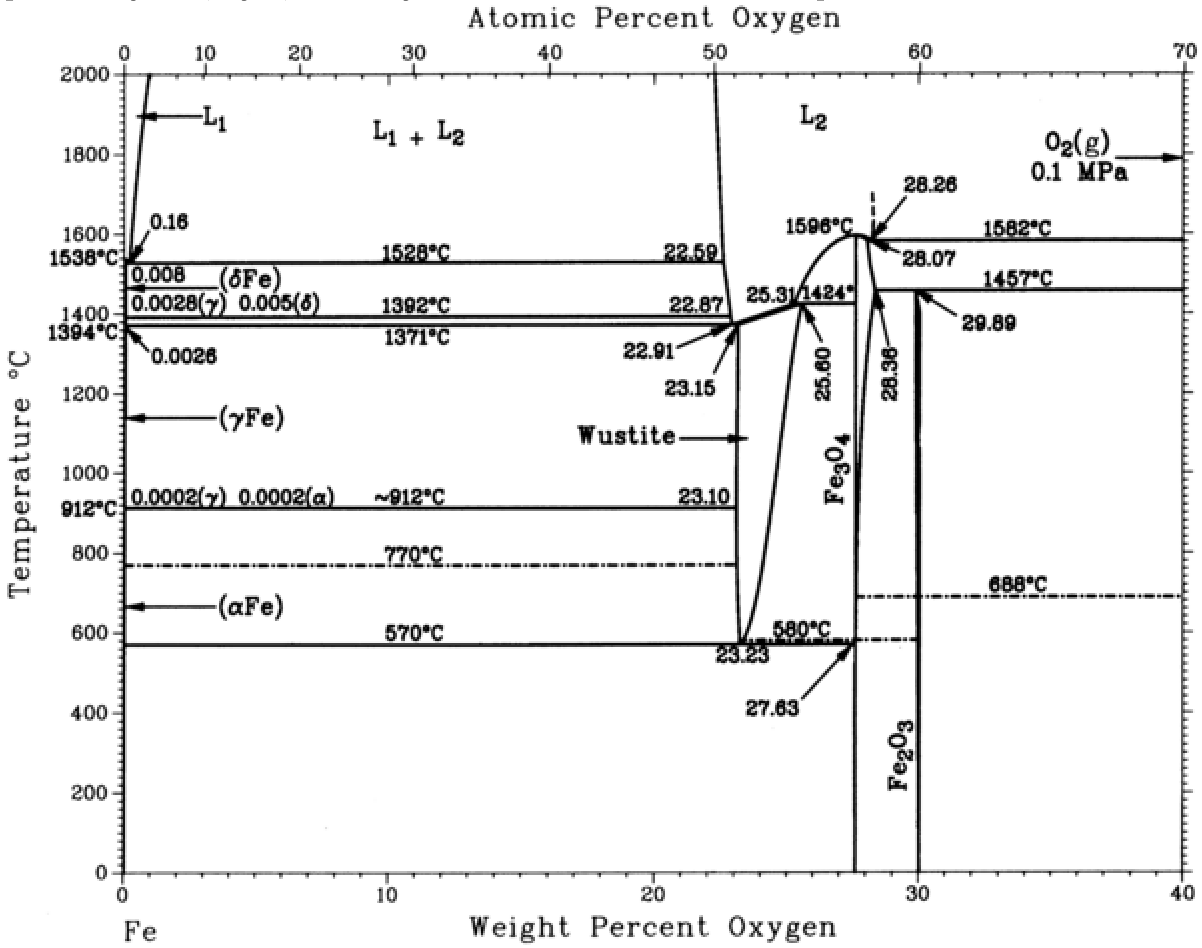

Fig. 2 Iron-oxygen phase diagram

References cited in this section

4. O. Kubaschewski and B.E. Hopkins, *Oxidation of Metals and Alloys,* Butterworths, 1962

5. I. Barin, O. Knacke, and O. Kubaschewski, *Thermochemical Properties of Inorganic Substances,* Springer, 1977

Z. Grzesik, Thermodynamics of Gaseous Corrosion, *Corrosion: Fundamentals, Testing, and Protection*, Vol 13A, *ASM Handbook*, ASM International, 2003, p 90–96

Thermodynamics of Gaseous Corrosion

Zbigniew Grzesik, University of Mining and Metallurgy (Krakow, Poland)

Richardson-Jeffes Diagrams

The determination of the standard Gibbs energy change of formation of oxides as well as the corresponding dissociation pressures of the oxides as a function of temperature—without any calculations—is very convenient when using Richardson-Jeffes diagrams (Gibbs energy-temperature diagrams) (Ref 6). Such a diagram, Fig. 3, is a plot of the standard Gibbs energies of formation of the oxides per mole of oxygen, O_2 (e.g., $2Ni + O_2 = 2NiO$, or $\frac{4}{3}Al + O_2 = \frac{2}{3}Al_2O_3$), versus temperature. Auxiliary outer scales in the upper, right, and bottom part of the plot are used for determination of conditions in which a given metal is oxidized by pure oxygen gas or oxidizing gas mixtures, CO/CO_2 and H_2/H_2O. The standard Gibbs energy change of formation of any oxide at a given temperature can be read directly on the ΔG^0 scale, for example, the Gibbs energy of formation of SiO_2 at 1200 °C (2190 °F) equals approximately -600 kJ for one mole of SiO_2

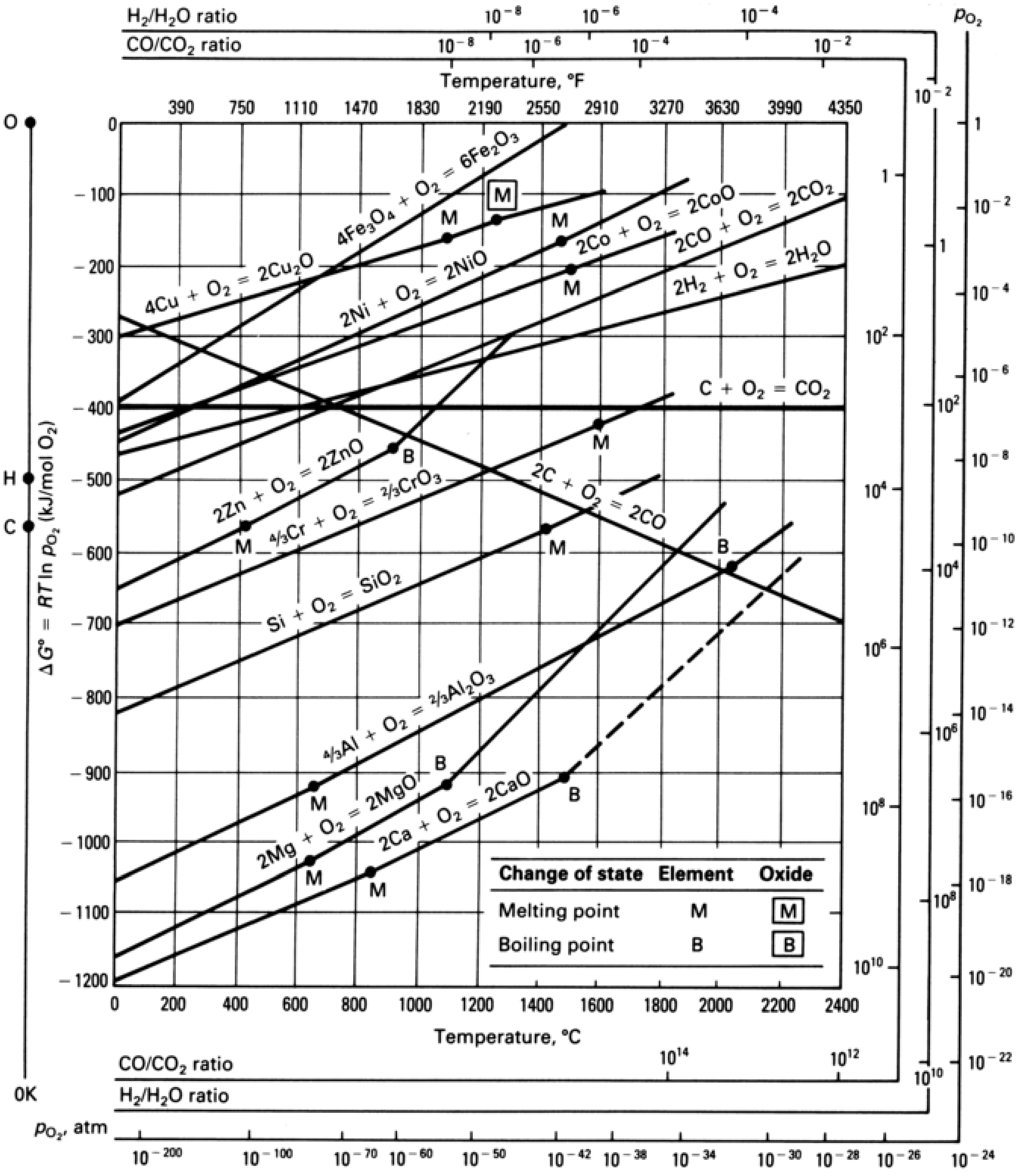

Fig. 3 Richardson-Jeffes diagram showing standard Gibbs free energy of formation as a function of temperature for metal oxide systems. Source: Ref 7

The dissociation pressure of a given oxide at constant temperature can be read on the partial pressure of oxygen, p_{O_2}, scale from the intersection of this scale with a straight line, drawn from index point labeled "O" at the upper left corner of the diagram through the appropriate temperature point on the line, related to the formation of a corresponding oxide. By way of example, the dissociation pressure of SiO_2 is approximately 10^{-20} atm O_2 at 1200 °C (2190 °F). Thus, silicon is not oxidized to SiO_2 at partial pressures lower than 10^{-20} atm at this temperature. On the other hand, from a thermodynamical point of view, SiO_2 can be formed from silicon at any pressure of oxygen greater than 10^{-20} atm at 1200 °C (2190 °F). The determination of the dissociation pressures of oxides is of considerable practical consequence in predicting which metallic materials are oxidized

at given conditions and, as a consequence, how a low partial pressure of oxygen should be used to prevent oxidation. However, very low partial pressures of oxygen in ambient gases ($p_{O_2} < 10^{-6}$ atm) are, in practice, seldom realized by means of vacuum systems or by oxygen-purified noble gases (such as argon or helium). Generally, to obtain very low partial pressure of oxygen, oxidizing gas mixtures are used in which oxygen is one of the components, for example, CO_2-CO-O_2 or H_2O-H_2-O_2. The essential chemical reactions for these gas mixtures can be written as follows:

$$CO_2 = CO + \frac{1}{2}O_2 \quad \text{(Eq 10)}$$

$$H_2O = H_2 + \frac{1}{2}O_2 \quad \text{(Eq 11)}$$

The corresponding equilibrium partial pressures of oxygen, p_{O_2}, established at equilibrium state may be expressed as:

$$p_{O_2} = \left(\frac{p_{CO_2}}{p_{CO}}\right)^2 \exp\left(-\frac{2\Delta G_{10}^0}{RT}\right) \quad \text{(Eq 12)}$$

$$p_{O_2} = \left(\frac{p_{H_2O}}{p_{H_2}}\right)^2 \exp\left(-\frac{2\Delta G_{11}^0}{RT}\right) \quad \text{(Eq 13)}$$

where ΔG_{10}^0 and ΔG_{11}^0 are the standard Gibbs energy changes of the reactions in Eq 10 and 11, respectively. As can be seen from Eq 12 and 13, for constant ratios of p_{CO}/p_{CO_2} or p_{H_2}/p_{H_2O}, the partial pressure of oxygen is also constant and does not depend significantly on the total pressure of the system. In other words, at a given temperature, p_{O_2} can be easily controlled by controlling the ratio of p_{CO}/p_{CO_2} or p_{H_2}/p_{H_2O}. Consequently, it is possible to choose such a ratio of corresponding gases that the partial pressure of oxygen reaches the value of the dissociation pressure of a given oxide. Such an equilibrium ratio can be read off the Richardson-Jeffes diagrams. For instance, to find a p_{CO}/p_{CO_2} ratio for which the Si-SiO_2-O_2 system is at equilibrium at 1000 °C (1830 °F), a straight line should be drawn from the index point labeled “C” at the left-hand scale through the 1000 °C (1830 °F) point on the line related to the formation of SiO_2. The equilibrium p_{CO}/p_{CO_2} ratio can be read from the intersection of this line with the p_{CO}/p_{CO_2} scale and equals 10^6. In the same way, appropriate equilibrium ratios of p_{H_2}/p_{H_2O} can be read using the index point labeled “H” on the left- hand scale and the p_{H_2}/p_{H_2O} scale.

The Richardson-Jeffes diagrams, although very convenient, cannot be used to obtain more precise values of dissociation pressures. In such cases, rather detailed thermodynamic calculations, described at the beginning of this section, should be performed. Diagrams similar to Fig. 3 are available for formation of sulfides, nitrides, carbides, and halides (Ref 8).

References cited in this section

6. F. Richardson and J. Jeffes, *J. Iron Steel Inst.,* Vol 171, 1952, p 167
7. N. Birks and G.H. Meier, *Introduction to High Temperature Oxidation of Metals,* Edward Arnold, 1983
8. G.Y. Lai, *High-Temperature Corrosion of Engineering Materials,* ASM International, 1990

Z. Grzesik, Thermodynamics of Gaseous Corrosion, *Corrosion: Fundamentals, Testing, and Protection*, Vol 13A, *ASM Handbook*, ASM International, 2003, p 90–96

Thermodynamics of Gaseous Corrosion

Zbigniew Grzesik, University of Mining and Metallurgy (Krakow, Poland)

Phase Sequence in the Multilayered Scale

Thermodynamic data can be used to predict the local equilibria in the sequence of phases for multilayered oxide scales. In general, if a metal can form several oxides, the sequence of oxides in the scale growing on this metal can be predicted, with the most oxygen-deficient oxide contacting the metal and the most oxygen-rich oxide next to the gas phase. However, not all oxides are stable at a given temperature and so may not be present in the scale. This is the reason why thermodynamic analysis should be used to determine the phase sequence in the multilayered scale. As an example, referring to the Fe-O phase diagram (Fig. 2) and the oxide layer sequence in the scale growing on iron, the following chemical reactions should be considered:

$$Fe + \frac{1}{2}O_2 = FeO \qquad \text{(Eq 14)}$$

$$3Fe + 2O_2 = Fe_3O_4 \qquad \text{(Eq 15)}$$

$$2Fe + \frac{3}{2}O_2 = Fe_2O_3 \qquad \text{(Eq 16)}$$

For the previous chemical reactions, the dissociation pressure of each oxide can be calculated according to the detailed description given in the first part of this article. At a given temperature, the oxide whose oxygen dissociation pressure is the lowest will form on iron, for example, FeO above 570 °C (1060 °F). To determine whether Fe_3O_4 or Fe_2O_3 forms on FeO, the following reaction and corresponding thermodynamic equilibria should be considered:

$$3FeO + \frac{1}{2}O_2 = Fe_3O_4 \qquad \text{(Eq 17)}$$

$$2FeO + \frac{1}{2}O_2 = Fe_2O_3 \qquad \text{(Eq 18)}$$

The FeO remains at equilibrium with the oxide whose dissociation pressure is lower (Fe_3O_4). As a consequence, during oxidation by oxygen at temperatures higher than 570 °C (1060 °F), the following phase sequence can be expected on the iron substrate: FeO-Fe_3O_4-Fe_2O_3 (Ref 9).

Reference cited in this section

9. P. Kofstad, *High Temperature Corrosion,* Elsevier, 1988, p 8

Z. Grzesik, Thermodynamics of Gaseous Corrosion, *Corrosion: Fundamentals, Testing, and Protection*, Vol 13A, *ASM Handbook*, ASM International, 2003, p 90–96

Thermodynamics of Gaseous Corrosion

Zbigniew Grzesik, University of Mining and Metallurgy (Krakow, Poland)

Kellogg Diagrams

To show a stability range in more complicated multioxidant systems, it is convenient to fix the temperature and plot the other variables, such as gas pressure or alloy composition. These diagrams are called isothermal stability diagrams and show the stability range of particular phases of the system. For the situation of one pure metal and several oxidants, the thermodynamic phase stabilities are shown on log-log plots of the two principal gaseous components, as shown in Fig. 4 for an Fe-O-S system at 727 °C (1341 °F). Such diagrams are constructed on the basis of the chemical potentials of all elements and their compounds that are present in the system. These plots assume that the gas phase is in internal equilibrium with respect to every gaseous species. To plot such a diagram, the equilibria between particular phases of a system should be considered by drawing boundaries, which represent equilibrium between specific oxides or sulfides.

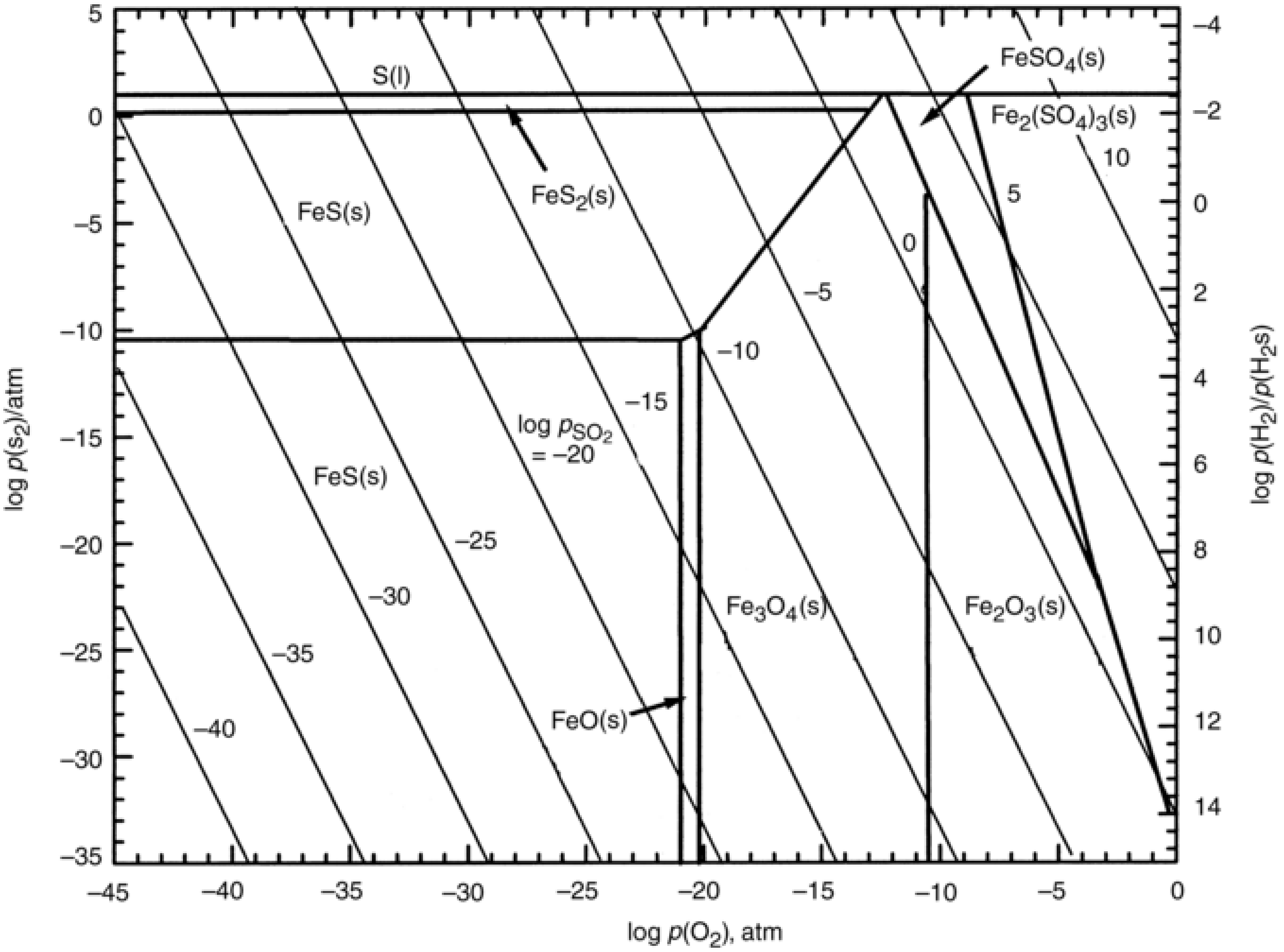

Fig. 4 The thermodynamic phase stabilities in the Fe-O-S system at 727 °C (1341 °F). s, solid; l, liquid

For example, the boundary between Fe(s) and FeO(s) phase (Fig. 4) represents the following equilibrium:

$$Fe + \frac{1}{2}O_2 = FeO \qquad \text{(Eq 19)}$$

The dissociation pressure of FeO equals 2.3 × 10^{-22} atm at 727 °C (1341 °F). Next, the boundary between the appropriate oxide (FeO) and sulfide phase (FeS) is constructed from the following equilibrium:

$$FeO + \frac{1}{2}S_2 = FeS + \frac{1}{2}O_2 \quad \text{(Eq 20)}$$

Z. Grzesik, Thermodynamics of Gaseous Corrosion, *Corrosion: Fundamentals, Testing, and Protection*, Vol 13A, *ASM Handbook*, ASM International, 2003, p 90–96

Thermodynamics of Gaseous Corrosion

Zbigniew Grzesik, University of Mining and Metallurgy (Krakow, Poland)

Determination of Partial Pressures of Gas Mixtures

Because the corrosive action of oxygen, hydrogen, or sulfur and their compounds is very common in many essential branches of modern industry, Kellogg diagrams often present auxiliary scales for $p_{SO_2}, p_{H_2}/p_{H_2S}, p_{H_2O}/p_{H_2}$, and so on. However, the composition of a given gas mixture (e.g., SO_2 and O_2) is a function of temperature. For example, if an iron sample is placed into a container of a SO_2-O_2 gas mixture with defined composition at room temperature, and then the container is heated to a higher temperature, the values of initial partial pressures of SO_2 and O_2 cannot be used to determine the presence of oxidation products on iron. If a composition of a gas mixture is known at a given temperature, it is possible to calculate the partial pressures of particular gases at any temperature. To determine the composition of a gas mixture containing S_2 and O_2 at high temperature, the following equilibria should be considered:

$$S_2 + \frac{1}{2}O_2 = S_2O \quad \text{(Eq 21)}$$

$$S_2O + \frac{1}{2}O_2 = 2SO \quad \text{(Eq 22)}$$

$$SO + \frac{1}{2}O_2 = SO_2 \quad \text{(Eq 23)}$$

$$SO_2 + \frac{1}{2}O_2 = SO_3 \quad \text{(Eq 24)}$$

For the previous chemical reactions, the corresponding oxygen partial pressures can be calculated:

$$p_{O_2} = \left(\frac{p_{S_2O}}{p_{S_2}}\right)^2 \exp\left(\frac{2\Delta G^0_{21}}{RT}\right) \quad \text{(Eq 25)}$$

$$p_{O_2} = \left(\frac{p^2_{SO}}{p_{S_2O}}\right)^2 \exp\left(\frac{2\Delta G^0_{22}}{RT}\right) \quad \text{(Eq 26)}$$

$$p_{O_2} = \left(\frac{p_{SO_2}}{p_{SO}}\right)^2 \exp\left(\frac{2\Delta G^0_{23}}{RT}\right) \quad \text{(Eq 27)}$$

$$p_{O_2} = \left(\frac{p_{SO_3}}{p_{SO_2}}\right)^2 \exp\left(\frac{2\Delta G^0_{24}}{RT}\right) \quad \text{(Eq 28)}$$

Additionally, a mass balance for oxygen and sulfur should be considered:

$$N_S = 2n_{S_2} + 2n_{S_2O} + n_{SO} + n_{SO_2} + n_{SO_3} \quad \text{(Eq 29)}$$

$$N_{O_2} = \frac{1}{2}n_{S_2O} + \frac{1}{2}n_{SO} + n_{SO_2} + \frac{3}{2}n_{SO_3} + n_{O_2} \quad \text{(Eq 30)}$$

where N_S and N_{O_2} denote total amounts of sulfur and oxygen presented in the system (in moles), and $n_{S_2}, n_{S_2O}, n_{SO}, n_{SO_2}, n_{SO_3}$, and n_{O_2} denote the number of moles of a particular gas present at equilibrium in the system at specified temperature. The partial pressure of any gaseous species, p_i, can be written as:

$$p_i = \frac{n_i}{\sum_{i=1}^{m} n_i} p_{tot} \quad \text{(Eq 31)}$$

where n_i is a number of moles of the i-gaseous species, m is the total number of species in the gas mixture, and p_{tot} denotes the total gas pressure (total gas pressure is usually known). Equations 25, 26, 27, 28, 29, 30, 31 can be solved numerically, and the partial pressures of particular gases in the gas mixture can be determined.

Z. Grzesik, Thermodynamics of Gaseous Corrosion, *Corrosion: Fundamentals, Testing, and Protection*, Vol 13A, *ASM Handbook*, ASM International, 2003, p 90–96

Thermodynamics of Gaseous Corrosion

Zbigniew Grzesik, University of Mining and Metallurgy (Krakow, Poland)

Partial Pressures of Volatile Oxidation Products

The oxidation reaction product of a given metal may be volatile, liquid, or solid. Even the solid or liquid product could have a high total vapor pressure involving several species. If the oxidation product is volatile, it is useful to determine its partial vapor pressure as a function of oxygen pressure at a given temperature. In the chromium-oxygen system, three volatile oxides can be formed—CrO(g), CrO_2(g), CrO_3(g)—in which solid chromium, Cr(s), can also sublime to form gaseous chromium, Cr(g). The only stable oxide in the chromium-oxygen system is Cr_2O_3(s). The partial pressures of particular volatile species in the chromium-oxygen system for oxygen pressure less than the dissociation pressure of Cr_2O_3 can be determined from the following equilibria:

$$\mathrm{Cr(s)} + \frac{1}{2}\mathrm{O_2} = \mathrm{CrO(g)} \quad \text{(Eq 32)}$$

$$\mathrm{Cr(s)} + \mathrm{O_2} = \mathrm{CrO_2(g)} \quad \text{(Eq 33)}$$

$$\mathrm{Cr(s)} + \frac{3}{2}\mathrm{O_2} = \mathrm{CrO_3(g)} \quad \text{(Eq 34)}$$

$$\mathrm{Cr(s)} = \mathrm{Cr(g)} \quad \text{(Eq 35)}$$

In the case of oxygen partial pressure higher than the dissociation pressure of Cr_2O_3, the partial pressures of the volatile oxides and gaseous chromium can be determined from the appropriate chemical reaction:

$$\mathrm{Cr_2O_3(s)} = 2\mathrm{CrO(g)} + \frac{1}{2}\mathrm{O_2} \quad \text{(Eq 36)}$$

$$\mathrm{Cr_2O_3(s)} = 2\mathrm{CrO_2(g)} - \frac{1}{2}\mathrm{O_2} \quad \text{(Eq 37)}$$

$$Cr_2O_3(s) = 2CrO_3(g) - \frac{3}{2}O_2 \quad \text{(Eq 38)}$$

$$Cr_2O_3(s) = 2Cr(g) + \frac{3}{2}O_2 \quad \text{(Eq 39)}$$

The results of such calculations are presented in Fig. 5. From a practical point of view, it is very important that the partial pressures of volatile CrO_2 and CrO_3 increase with increasing oxygen pressure and temperature. At temperatures higher than 1000 °C (1830 °F), the weight loss of pure chromium- or chromia (Cr_2O_3)-forming alloys in air, due to the loss of the volatile CrO_2 and CrO_3, can be significant. The Cr_2O_3 layer loses its good protective properties. The reaction kinetics are described by a scaling evaporation mechanism provided in Ref 10.

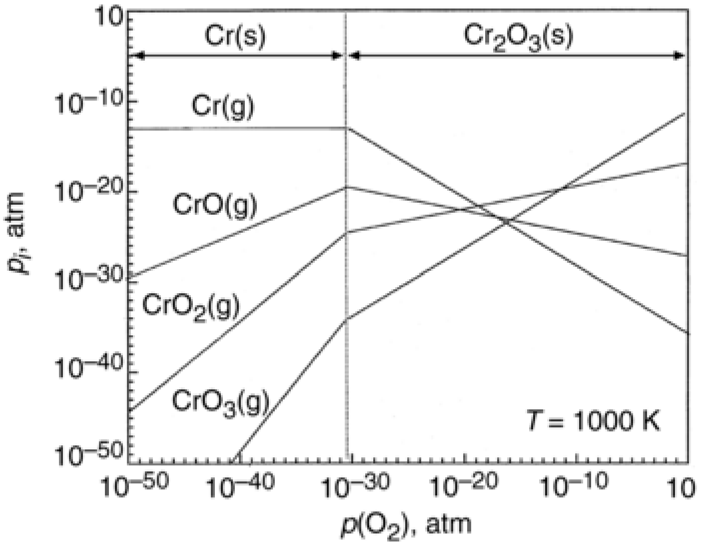

Fig. 5 The diagram of partial pressures of volatile species in the chromium-oxygen system as a function of oxygen pressure at 727 °C (1341 °F). s, solid; g, gas

Theoretical considerations presented in this chapter show that thermodynamics has a fundamental significance in studying the processes occurring in the high-temperature corrosion of metallic materials. Rather simple calculations made on the basis of thermodynamic data determine conditions of temperature, composition, and pressure of reacting gas mixture in which particular reaction products can be formed. As a consequence, thermodynamic considerations may help to optimize the composition of reacting atmosphere and/or alloy and are often the first step in the development of the corrosion resistant materials.

Reference cited in this section

10. C. Tedmon, *J. Electrochem. Soc.,* Vol 113, 1966, p 766

Z. Grzesik, Thermodynamics of Gaseous Corrosion, *Corrosion: Fundamentals, Testing, and Protection*, Vol 13A, *ASM Handbook*, ASM International, 2003, p 90–96

Thermodynamics of Gaseous Corrosion

Zbigniew Grzesik, University of Mining and Metallurgy (Krakow, Poland)

References

1. P. Kofstad, Oxidation Mechanisms for Pure Metals in Single Oxidant Gases, *High Temperature Corrosion,* R.A. Rapp, Ed., NACE International, 1983, p 123–138
2. Properties of Pure Metals, *Properties and Selection: Nonferrous Alloys and Pure Metals,* Vol 2, 9th ed., *Metals Handbook,* American Society for Metals, 1979, p 714–831
3. R.C. Weast, Ed., Physical Constants of Inorganic Compounds, *Handbook of Chemistry and Physics,* 65th ed., The Chemical Rubber Company, 1984, p B68–B161
4. O. Kubaschewski and B.E. Hopkins, *Oxidation of Metals and Alloys,* Butterworths, 1962
5. I. Barin, O. Knacke, and O. Kubaschewski, *Thermochemical Properties of Inorganic Substances,* Springer, 1977
6. F. Richardson and J. Jeffes, *J. Iron Steel Inst.,* Vol 171, 1952, p 167
7. N. Birks and G.H. Meier, *Introduction to High Temperature Oxidation of Metals,* Edward Arnold, 1983
8. G.Y. Lai, *High-Temperature Corrosion of Engineering Materials,* ASM International, 1990
9. P. Kofstad, *High Temperature Corrosion,* Elsevier, 1988, p 8
10. C. Tedmon, *J. Electrochem. Soc.,* Vol 113, 1966, p 766

Z. Grzesik, Thermodynamics of Gaseous Corrosion, *Corrosion: Fundamentals, Testing, and Protection,* Vol 13A, *ASM Handbook,* ASM International, 2003, p 90–96

Thermodynamics of Gaseous Corrosion

Zbigniew Grzesik, University of Mining and Metallurgy (Krakow, Poland)

Selected References

- N. de Nevers, *Physical and Chemical Equilibrium for Chemical Engineers,* John Wiley & Sons, Inc., 2002
- R.E. Sonntag, C. Borgnakke, and G.J. Van Wylen, *Fundamentals of Thermodynamics,* John Wiley & Sons, 1998
- W. Greiner, *Thermodynamics and Statistical Mechanics,* Springer, 1995
- D.E. Winterbone, *Advanced Thermodynamics for Engineers,* Arnold, 1997
- K. Wark, Jr., *Advanced Thermodynamics for Engineers,* McGraw-Hill, 1995
- D.V. Ragone, *Thermodynamics of Materials,* John Wiley & Sons, 1995
- M. Saad, *Thermodynamics: Principles and Practice,* Prentice Hall, 1997
- P.W. Atkins, *The Elements of Physical Chemistry,* Oxford University Press, 1996

M. Danielewski, Kinetics of Gaseous Corrosion Processes, *Corrosion: Fundamentals, Testing, and Protection*, Vol 13A, *ASM Handbook*, ASM International, 2003, p 97–105

Kinetics of Gaseous Corrosion Processes

Marek Danielewski, AGH University of Science and Technology, Cracow, Poland

Introduction

IN 1923, N.B. Pilling and R.E. Bedworth classified metals into two groups: those that form protective oxide scales and those that do not (Ref 1). They suggested that unprotective scales are formed if the volume of the oxide layer is less than the volume of metal reacted. For example, in the oxidation of aluminum:

$$2Al + \frac{3}{2}O_2 = Al_2O_3 \quad \text{(Eq 1)}$$

the Pilling-Bedworth molar volume ratio is:

$$\frac{\text{Volume of 1 mol of } Al_2O_3}{\text{Volume of 2 mol of Al}} = 1.287 \quad \text{(Eq 2)}$$

where the volumes are calculated from molecular and atomic weights and the densities of the phases.

If the ratio is less than 1, the oxide scales are usually nonprotective. Scales on metals such as magnesium, potassium, sodium, and calcium are porous or crack due to tensile stresses and provide no efficient barrier to penetration of the gas to the metal surface. If the ratio is more than 1, the protective scale may develop and protect the metal or alloy from the gas so that oxidation can proceed only by solid-state diffusion, which is slow even at high temperatures (iron, nickel, cobalt, chromium, silicon, and aluminum and their alloys). If the ratio is over 2, as is the case with tungsten and niobium, during the scale growth large compressive stresses often develop in the oxide that may cause the scale to crack and/or spall off, leaving the metal unprotected.

Exceptions to the Pilling-Bedworth classification are numerous. The assumption that metal oxides grow by diffusion of oxygen inward through the oxide layer to the metal is seldom valid. The texture, the direction(s) of scale growth, and the possibility of plastic flow by the oxide or metal were not considered. Nevertheless, historically, Pilling and Bedworth took the first step in understanding of the processes by which metals react with gases. Although there may be exceptions, the volume ratio, as a rough rule-of-thumb, is usually correct. The Pilling- Bedworth volume ratios for many common oxides are listed in Table 2 of the article “Thermodynamics of Gaseous Corrosion” in this Volume.

Reference cited in this section

1. N.B. Pilling and R.E. Bedworth, The Oxidation of Metals at High Temperatures, *J. Inst. Met.,* Vol 29, 1923, p 529–582

M. Danielewski, Kinetics of Gaseous Corrosion Processes, *Corrosion: Fundamentals, Testing, and Protection*, Vol 13A, *ASM Handbook*, ASM International, 2003, p 97–105

Kinetics of Gaseous Corrosion Processes

Marek Danielewski, AGH University of Science and Technology, Cracow, Poland

Defect Structure of Oxides

The basic defect structures of solids were first published by Frenkel (in metals and oxides), Schottky (simple oxides), and Wagner (spinels). Schottky and Wagner started the new discipline, which is now called solid-state chemistry. Point- defect chemistry is the part of it that deals with defect reactions and their equilibria in solids. Such reactions can be written according to Krö ger-Vink notation and must obey the usual rules of electrochemical equations (mass and charge conservancy). The key difference is an additional conservation law, the "rule of the lattice conservancy," which states that only a stoichiometric number of the cationic and anionic lattice elements can be formed/consumed as a result of a reaction. The meaning of symbols used in the chemistry of point defects can be found in general textbooks or monographs on high-temperature corrosion (Ref 2, 3, 4).

Ionic compounds can have appreciable quantities of intrinsic defects (giving rise to ionic conductivity at stoichiometric composition) due to Schottky and/or Frenkel defects (Fig. 1). Schottky defects are combinations of cation vacancies, anion vacancies, and electronic defects:

$$O = V_X + V_{Me} \quad \text{(Eq 3)}$$

where V_X and V_{Me} denote the vacancy in anionic sublattice and cationic sublattice, respectively (Fig. 1a). Schottky defects are formed and annihilate at interfaces, and they seldom dominate in oxides that provide protective scales. At high temperatures, ionic defects are ionized and electronic defects are formed in the proper ratio necessary to maintain electrical neutrality: $0 = e^- + h^\cdot$ where e^- denotes the electron (free or localized) and $h^\cdot$ is the electron hole. During oxidation, when the metal is protected by a layer of oxide, electrons migrate from the metal, through the oxide, to adsorbed oxygen at the oxide/gas interface and accelerate the rate of reaction.

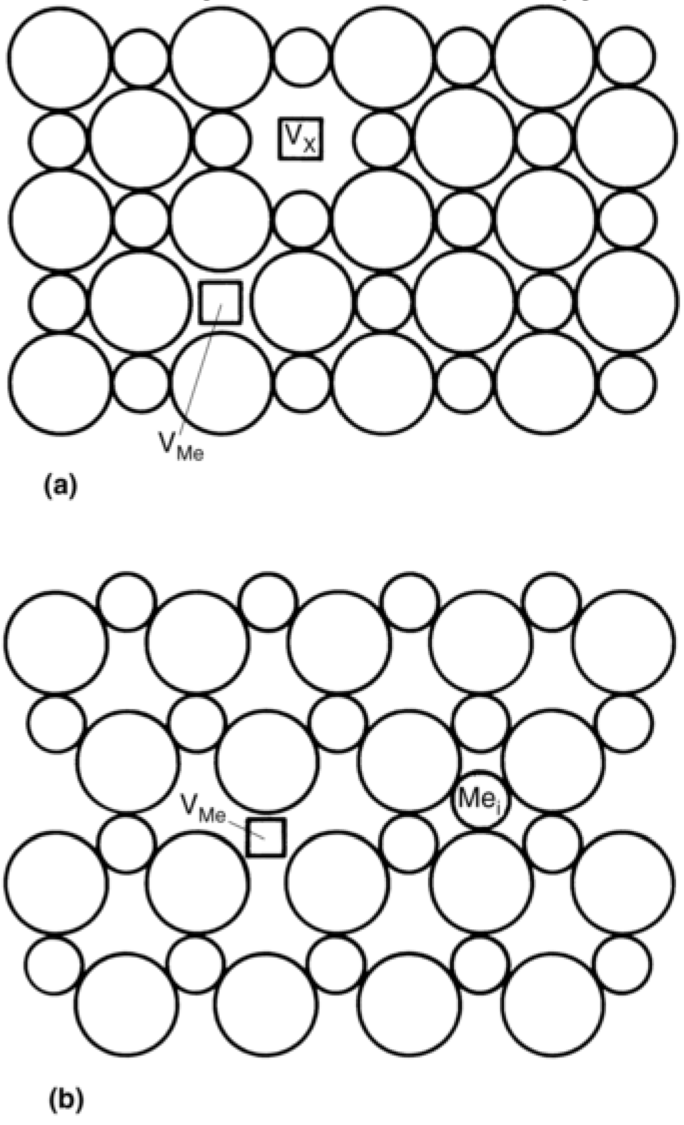

Fig. 1 Defects in ionic crystals. (a) Schottky defect. (b) Frenkel defect. Vacancies (V_X, V_{Me}) are indicated by open squares. Interstitial ion (Me_i) is shown as shaded circle.

Frenkel defects are combinations of cation vacancies, interstitial cations, and electronic defects. The reaction of their formation can be written in the form $Me_{Me} = Me_i + V_{Me}$ (Fig. 1b). Frenkel defects are formed/annihilated within the oxide, are the result of "inner sublimation," and are present in the majority of oxides that protect steels and alloys. Metal cations are generally much smaller than an oxygen anion. Consequently interstitial cations are mobile, showing high diffusivity (mobility). Ionic electrical conductivity is possible in such crystals by the diffusion of interstitial cations and by the diffusion of vacancies. Metallic oxides may have a stoichiometric composition only at specific temperature and pressure conditions. Some oxides always show a certain degree of nonstoichiometry, such as wustite ($Fe_{1-y}O$). This nonstoichiometry usually implies higher concentrations of defects. The higher-defect concentration leads to the formation of a less-protective scale. A typical example is iron, which can be used at temperatures below 570 °C (1060 °F). At $T > 570$ °C, the highly defected wustite is formed ($Fe_{1-y}O$ where $\sim 0.05 < y < 0.18$), accelerating the oxidation rate by two orders of magnitude.

An example of oxides grown to provide protective scales are electronic semiconductors that allow mass transport of ions through the scale layer. They may be categorized as *p*-type, *n*-type, and amphoteric semiconductors (Table 1). They always have the other minority defects that contribute to the diffusivity (ionic conductivity).

Table 1 Classification of electrical conductors: oxides, sulfides, and nitrides

Metallic conductors are in parentheses.

Metal-excess semiconductors (*n*-type)
BeO, MgO, CaO, SrO, BaO, BaS, ScN, CeO_2, ThO_2, UO_3, U_3O_8, TiO_2, TiS_2, (Ti_2S_3), TiN, ZrO_2, V_2O_5, (V_2S_3), VN, Nb_2O_5, Ta_2O_5, Cu_2O, Cr_2S_3, MoO_3, WO_3, WS_2, MnO_2, Fe_2O_3, $MgFe_2O_4$, $NiFe_2O_4$, $ZnFe_2O_4$, $ZnCo_2O_4$, ($CuFeS_2$), ZnO, CdO, CdS, HgS(red), Al_2O_3, $MgAl_2O_4$, $ZnAl_2O_4$, Tl_2O_3, (In_2O_3), SiO_2, SnO_2, PbO_2, and at low oxidant pressures Cr_2O_3, PbS, and MnS
Metal-deficit semiconductors (*p*-type)
UO_2, (VS), (CrS), Cr_2O_3, (<1250 °C, or 2280 °F), $MgCr_2O_4$, $FeCr_2O_4$, $CoCr_2O_4$, $ZnCr_2O_4$, (WO_2), MoS_2, MnO, Mn_3O_4, Mn_2O_3, ReS_2, FeO, FeS, NiO, NiS, CoO, (Co_3O_4), PdO, Cu_2O, Cu_2S, Ag_2O, $CoAl_2O_4$, $NiAl_2O_4$, (Tl_2O), Tl_2S, (GeO), SnS, (PbO), (Sb_2S_3), (Bi_2S_3), and at high oxidant pressures only: Cr_2O_3, PbS, and MnS
Amphoteric conductors
(TiO), (Ti_2O_3), (VO), Cr_2O_3 (>1250 °C, or 2280 °F), MoO_2, FeS_2, (OsS_2), (IrO_2), RuO_2, Cr_2O_3, PbS, and MnS

Source: Ref 5

The *p*-type metal-deficit oxides are nonstoichiometric compounds with cation vacancies being the dominating defects. A typical example is $Ni_{1-y}O$ (Fig. 2), a cation-deficient oxide that provides the additional electrons needed for ionic bonding and electrical neutrality by donating electrons from the 3*d* subshells of a fraction of the nickel ions (i.e., forms electron holes as electronic defects). The reaction of defects in NiO can be written as $\frac{1}{2}O_2(g) = O_O + V_{Ni}'' + 2h^{\cdot}$. In this way, for every cation vacancy present in the oxide, two nickelic ions (Ni^{3+}) will be present. Each Ni^{3+} has a low-energy positively charged electron hole that electrons from other nickelous ions (Ni^{2+}) can easily move into. The positive or *p*-type semiconductors carry most of their current by means of these positive holes.

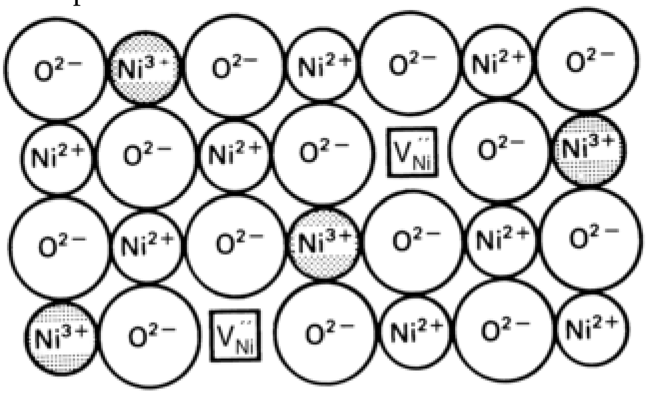

Fig. 2 Ionic arrangement in *p*-type NiO scale. Cation vacancies are indicated as open squares. The Ni^{3+} cations (i.e., the electron holes, h) are shaded, the Ni^{2+} cations are nickel ions in their lattice positions, Ni_{Ni}. Vacancies are open squares.

Cations diffuse through the scale from the Ni/ NiO interface where the nickel atoms enter the oxide: Ni(metallic) + V_{Ni}= Ni_{Ni} + 2e^-. They diffuse by cation vacancies ($J_c = -J_V$) to the NiO/gas interface where they react with adsorbed oxygen: Ni_{Ni} + O^{2-} = V_{Ni}+ Ni_{Ni} + O_O or traditionally Ni_{2+} + O^{2-} = NiO. Electrons migrate from the metal surface, by electron holes, to the adsorbed oxygen atoms, which then become chemisorbed oxygen anions: O(adsorbed) + 2e^- = O^{2-}. In this way, while cations and electrons move outward through the scale toward the gas, cation vacancies, and electron holes move inward toward the metal. Consequently, as the scale thickens, the cation vacancies may accumulate to form voids at the Ni/ NiO interface and "destroy" an otherwise compact scale.

The *n*-type semiconductor oxides have free electrons as the major charge carriers. They may be either cation excess ($Me_{a+y}X_b$) or anion deficient (Me_aX_{b-y}). Beryllium oxide ($Be_{1+y}O$), a cation-excess oxide, is shown in Fig. 3. Oxygen in the gas adsorbs on the $Be_{1+y}O$ surface and picks up free electrons from the oxide to become chemisorbed O^{2-} ions, which then react with excess metal cations at BeO external interface: $Be_i^{\cdot\cdot}$ + O^{2-} = Be_{Be} + O_O (or Be^{2+} + O^{2-} = BeO). The cations diffuse interstitially from the underlying beryllium metal. The free electrons migrate from the metal surface where the beryllium enters the oxide and ionizes: Be(metallic) = $Be_i^{\cdot\cdot}$ + 2e^-. As with *p*-type oxides, the cation-excess *n*-type oxides grow at the oxide/gas interface.

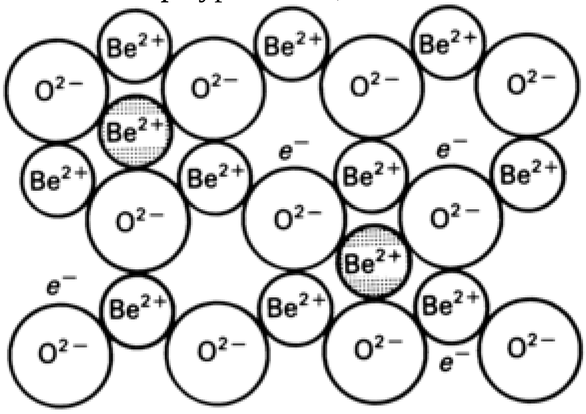

Fig. 3 Ionic arrangement in *n*-type cation-excess BeO. Interstitial cations Be_i are shaded; free electrons are indicated as e^-.

Another group of *n*-type semiconductors oxides is anion deficient, as exemplified by zirconium dioxide (ZrO_{2-y}). In this case, although most of the cations contribute four electrons to the ionic bonding, a small fraction of the zirconium cations contribute only two electrons to become the zirconium ion Zr^{2+}. Therefore, to maintain electrical neutrality, an equal number of anion vacancies must be present in the oxide. This arrangement is shown in Fig. 4. The oxide grows at the metal/oxide interface by inward diffusion of O^{2-} through the anion vacancies in the oxide:

$$J_O = -J_V \quad \text{(Eq 4)}$$

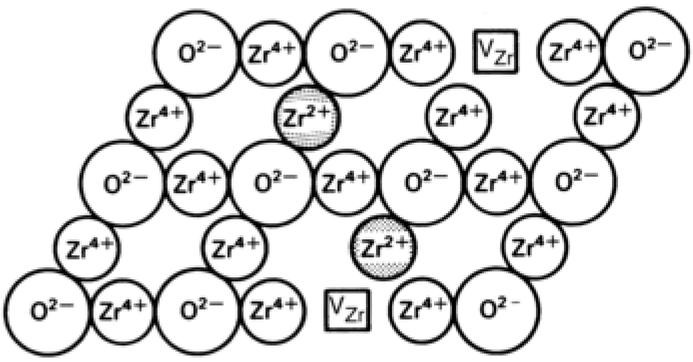

Fig. 4 Ionic arrangement in *n*-type anion-deficient ZrO_2. Anion vacancies, V_{Zr} are indicated as open squares; Zr^{2+} ions are shaded.

Amphoteric Oxides. A number of compounds show nonstoichiometry with either a deficiency of cations or a deficiency of anions. An important example is chromia ($Cr_{2\pm y}O_3$) (Ref 3) and lead sulfide ($Pb_{1\pm y}S$). Both compounds have a minimum in electrical conductivity at the stoichiometric composition and are metal deficient (*p*-type semiconductors) at the high-oxidant activities and metal excess (*n*-type) at low pressures.

Chromium oxide is a cation-excess oxide at low oxygen pressures and a cation-deficient oxide at high oxygen activities. The mechanism of mass transport in the growing chromia scale depends on the oxygen activity. The oxygen pressure may be low enough to keep the whole chromia layer below the stoichiometric composition (in the *n*-type range). In such a case, the chromia scale grows in a manner already discussed for *n*-type semiconductor oxides. At higher oxygen activities the mechanism of diffusion is more complex. Somewhere within the scale there is a transition layer (near-stoichiometric chromia) dividing the oxide into the two “parts,” the *n*-type semiconductor (from the chromium/chromia interface to near-stoichiometric chromia) and the *p*-type semiconductor (from the near-stoichiometric chromia to the chromia/gas interface). The mechanism of diffusion and reactions at interfaces depends on the type of oxide that stays in contact with this interface. Oxygen in the gas adsorbs on the chromia surface and picks up free electrons from the chromia to become a chemisorbed O^{2-} ion: O(adsorbed) + $2e^-$ = O^{2-}. At low oxygen partial pressures, this oxygen ion reacts with chromium interstitial ions that are diffusing interstitially from the chromium metal: $2Cr_i^{\cdot\cdot\cdot} + 3O^{2-} = 2Cr_{Cr} + 3O_O$ (or $2Cr^{3+} + 3O^{2-} = Cr_2O_3$). The free electrons come from the metal surface as the chromium enters chromia and ionizes (Cr(metallic) = $Cr_i^{\cdot\cdot\cdot}$) + $3e^-$). They can travel through vacant high-energy levels, that is, diffuse by the counterflow of the electron holes: $J_e = -J_h$. As with *p*-type oxides, the cation-excess *n*-type chromia grows at the oxide/gas interface as cations diffuse outward through the scale. At high oxygen pressures, chromia in contact with gaseous oxygen is a *p*-type oxide. Thus, the reaction at the external interface is: $2Cr_{Cr} + 3O^{2-} = 2V'''_{Cr} + 2Cr_{Cr} + 3O_O$ (or $2Cr^{3+} + 3O^{2-} = Cr_2O_3$). Somewhere within the growing chromia there is an intermediate layer where the properties of this oxide change from *n*-type to *p*-type. Consequently, outward flow of the interstitial cations converts to the inward vacancy flow (note that this transition of the dominating defects does not affect the direction of the cation flow). Mass transport in amphoteric oxides is not well known; the transition processes may generate stresses and other effects. Grain boundaries and dislocations affect the rate of the transport process.

References cited in this section

2. N. Birks and G.H. Meier, *Introduction to High Temperature Oxidation of Metals,* Edward Arnold, 1983

3. P. Kofstad, *High Temperature Corrosion,* Elsevier Applied Science, 1988

4. M. Schutze, *Corrosion and Environmental Degradation,* Vol 1, *Materials Science and Technology, A Comprehensive Treatment,* R.W. Cahn, P. Haasen, and E.J. Kramer, Ed., Wiley-VCH, 1993

5. O. Kubashewski and B.E. Hopkins, *Oxidation of Metals and Alloys,* 2nd ed., Butterworths, 1962

M. Danielewski, Kinetics of Gaseous Corrosion Processes, *Corrosion: Fundamentals, Testing, and Protection,* Vol 13A, *ASM Handbook,* ASM International, 2003, p 97–105

Kinetics of Gaseous Corrosion Processes

Marek Danielewski, AGH University of Science and Technology, Cracow, Poland

---

Solid-State Diffusion

Diffusion processes in solids play a key role in the oxidation of metals. As already stated, the oxidation reaction may be the result of the outward diffusion of metal ions from the metal surface through the oxide layer to the adsorbed oxygen anions at the oxide/gas interface (e.g., *p*-type NiO), the result of the diffusion of anions inward through the oxide to the metal (e.g., *p*- type ZrO_2) or the result of both processes. The diffusion of atomic oxygen into the metal from the oxide (e.g., into titanium) can also be involved.

Within an alloy, interdiffusion plays a key role, for example, the outward diffusion of the reacting metal atoms during their selective oxidation forces the simultaneous inward diffusion of all other alloy elements.

Diffusion Mechanisms. Atoms or ions move (diffuse) through solids by many mechanisms. The most common is the vacancy mechanism of diffusion. An atom or ion oscillating (“sitting”) on a regular lattice site can move to a vacant site nearby (diffuse by jumping) (Fig. 5a). In many metal systems, vacancies are the dominating defects, while ionic oxides often show a more complex defect structure. They contain Schottky and Frenkel defects that also involve vacancies and electronic defects. For metal atoms, this is relatively easy because the jump distances are short. For ionic crystals, the jump distances are much longer because cation sites are surrounded by anion sites, and vice versa.

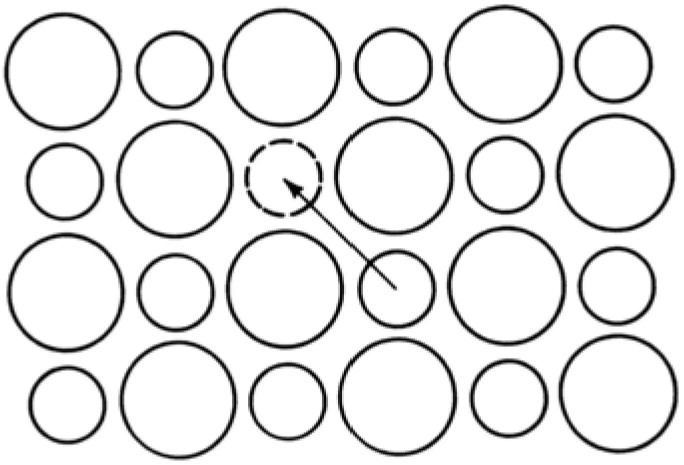

(a)

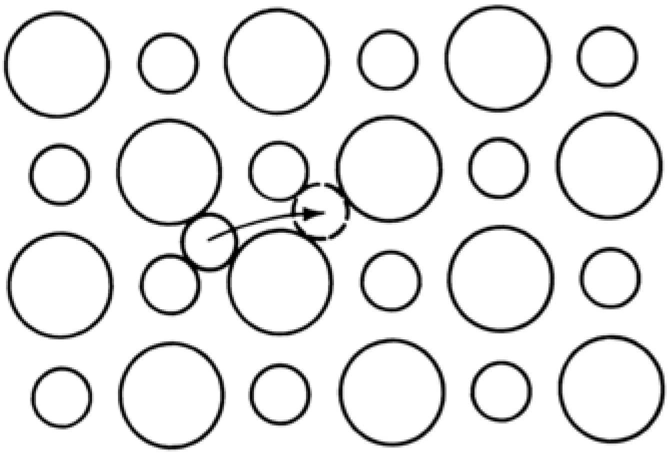

(b)

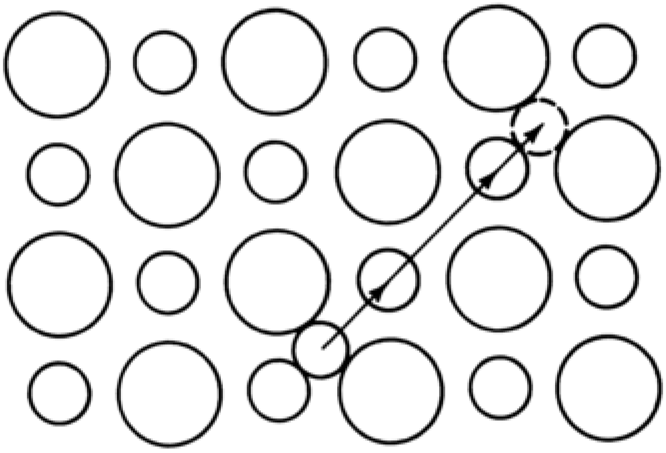

(c)

Fig. 5 Diffusion mechanisms. (a) Vacancy diffusion. (b) Interstitial diffusion. (c) Interstitial diffusion with displacement

Small interstitial atoms diffuse readily from one interstitial position to another. In ionic oxides, the cations may diffuse interstitially (Fig. 5b), but anions are usually not small enough to do so. In ionic crystals, an interstitial ion often moves into a regular lattice site, knocking another ion into a different interstitial position or to the next

lattice site. This chain effect may extend for several atomic spacings in a line or in different direction. Figure 5(c) shows such interstitial diffusion with displacement.

Fick's Law. In 1855, Fick formulated his two laws of diffusion for the simplest sort of diffusion system: a binary system at constant temperature and pressure, with net movement of atoms in only one direction. This is the basic situation for diffusion through an oxide growing on a pure metal.

Fick's first law states that the rate of mass transfer is proportional to the concentration gradient of the diffusing element:

$$\mathbf{J}_i = -D_i \nabla C_i \qquad \text{(Eq 5)}$$

where $\mathbf{J}_i$ is the flux of the i-th specie (i.e., net mass transported per second through a unit surface area perpendicular to the direction of flow), ∇C_i is the concentration gradient (in one-dimensional, planar systems it becomes:) $\nabla C_i = \mathbf{i}(\partial C_i / \partial x)$, and D_i is the proper diffusion coefficient, cm^2/s.

The term "proper" means the necessity of the careful examination of the process (experiment) and model of mass transport before using diffusivity data. To model the oxidation processes (i.e., the reactive diffusion), the chemical diffusion coefficients and/or self-diffusion coefficients are useful. To analyze the interdiffusion, the intrinsic and/or self-diffusion coefficients must be known. The ideal Fickian diffusion (Eq 5) is a tracer diffusion, such as an iron isotope in iron.

Diffusivity (D) is proportional to effective jump frequency (number of jumps per second when an atom changes position, f) and the square of the jump distance (λ) $D = \frac{1}{6} f \lambda^2$. More precisely, it depends on the type of diffusing atoms, the chemical bonding, the crystallographic structure of the alloy or oxide, the temperature, and many other factors. When gas oxidation is analyzed in solids, the diffusivities change many orders of magnitude, $D \in (10^{-18}$ to 10^{-6}, $cm^2/s)$. Other flux formula were proposed by Nernst- Planck, Onsager, Darken, and others.

The Nernst-Planck flux formula is common in electrochemistry and was used by Wagner to analyze the mass transport during the oxidation of the pure metal:

$$\mathbf{J}_i = -B_i C_i \mathbf{F} \qquad \text{(Eq 6)}$$

where B_i is the mobility and $\mathbf{F}$ is the local force acting on the ith element.

The Darken flux formula is common in interdiffusion studies. It was used by Wagner to analyze the reaction of the selective oxidation of the alloy:

$$\mathbf{J}_i = -\mathbf{J}_i^{diff} + C_i v \qquad \text{(Eq 7)}$$

where J_i^{diff} denotes the diffusion flux (given, e.g., by Eq 5 or 6) and v is the drift or convection velocity.

Conservation of Mass. The governing law of diffusion, and the mass transport in general, is the law of mass conservation. Its general form is accepted in all instances of mass transport:

$$\frac{\partial c_i}{\partial t} = -\nabla \mathbf{J}_i + A_i \qquad \text{(Eq 8)}$$

where the terms on the right-hand side are the local divergence ∇ of the flux of the ith element; A_i is the local source/sink of mass, for example, as a result of chemical reactions. This equation reads: the local change of concentration is the effect of the difference between the local inflow and outflow of mass and a result of chemical reactions. The chemical reactions, the last term, can usually be neglected in solids.

In most cases, planar (one-dimensional) systems are analyzed. Thus, the law of mass conservation (or the continuity equation) is:

$$\frac{\partial c_i}{\partial t} = -\frac{\partial \mathbf{J}}{\partial x} \qquad \text{(Eq 9)}$$

When the mass transport is due to the diffusion only, Fick's first law is the proper flux formula, and the diffusivity does not depend on concentration, then Eq 8 reduces to the Fick's 1855 formula. The equation of mass conservation (Eq 9) reduces to Fick's second law:

$$\frac{\partial c_i}{\partial t} = -D_i \frac{\partial^2 C_i}{\partial x^2} \qquad \text{(Eq 10)}$$

As an example of the Fickian diffusion, the diffusion of oxygen into a metal can be analyzed. When internal oxidation does not occur, the concentration of oxygen changes with time according to the Fick's second law (Eq

10). Solution of the problem depends on the initial and the boundary conditions. When oxygen atoms diffuse inwardly from the surface of an infinite plate, with a constant diffusivity D and at the constant interfacial concentration C', the solution has a relatively simple form. The concentration of oxygen is a function of distance from the metal surface and of the time [$C = C(t, x)$]. It is expressed by:

$$\frac{C' - C}{C' - C^0} = \mathrm{erf}\left(\frac{x}{2\sqrt{Dt}}\right) \quad \text{(Eq 11)}$$

where C_0 is a constant, the initial (t = 0) concentration of the oxygen in the plate. The error function, erf, is tabulated in books on diffusion and probability.

Figure 6 shows the oxygen concentration as a function of distance from external interface for an arbitrary time (t > 0). During the whole diffusion process, C^0 and C' are constant. One may now ask how fast an arbitrary concentration of oxygen (C'' = constant < C') changes its "position," that is, how fast the oxygen penetrates the plate. For the fixed value of oxygen concentration, C'', Eq 11 reduces to:

$$x(C'') \propto \sqrt{Dt} \quad \text{(Eq 12)}$$

This means the penetration rate is a parabolic function of time.

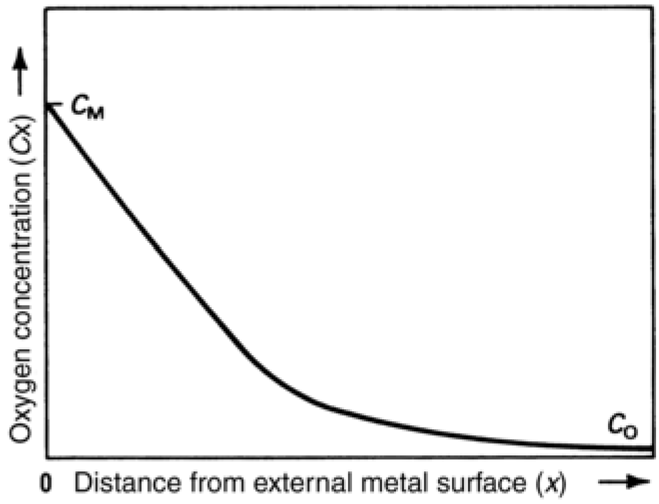

Fig. 6 Non-steady-state diffusion. Oxygen distribution during its diffusion into the semi-infinite plate. C_M, concentration at metal/oxide interface; C_0, initial concentration

The Diffusion Coefficient. Diffusivity is proportional to the defect concentration. All defects in a given sublattice contribute to mass transport; for example, the self-diffusion coefficient of metal, D^*_{Me}, in an oxide is given by:

$$D^*_{Me} = \sum_{i=1}^{n} N_i D^*_i \quad \text{(Eq 13)}$$

where D^*_i denotes the self-diffusion coefficient of the i-th defect and N_i is the molar ratio of defects in Me sublattice.

The diffusion coefficient may also depend on crystal orientation (in hexagonal crystals). It implies anisotropic transport properties, and in such a case diffusivity cannot be expressed as a scalar quantity. For oxides that grow epitaxially and/or have a preferred orientation, the diffusivity can differ by orders of magnitude from that of a random polycrystalline oxide.

Temperature has a major effect on the diffusion coefficient. In the temperature range where a single mechanism of diffusion dominates and where this mechanism is a thermally activated process, the well-known Arrhenius relation holds. According to the Arrhenius equation, diffusivity increases exponentially with temperature:

$$D = D_0 \exp\left(\frac{-Q_a}{RT}\right) \quad \text{(Eq 14)}$$

where D_0 is a constant that depends on frequency of effective jumps, Q_a denotes activation energy for diffusion, R is the gas constant, and T the absolute temperature.

Activation energies for interstitial diffusion are lower than those for vacancy diffusion. The activation energy has a major impact on the temperature dependence of a diffusion process. High values of Q_a mean that the diffusion proceeds much more rapidly at high temperatures, but might be much slower at low temperatures. If the diffusivity D is plotted on a natural logarithm scale as a function of $1/T$, the slope of the resulting straight line is $-Q_a/R$. If the graph shows two intersecting lines, it indicates that the diffusion mechanism that dominates at low temperatures—for example, the grain-boundary diffusion—differs from the one operating at high temperatures (the volume diffusion). Typical values of D_0 and Q_a for diffusion in oxides are listed in Table 2, (Ref 6).

Table 2 Selected diffusion data in metal oxides

Metal oxide	Temperature		Frequency factor (D_0), cm^2/s	Activation energy for diffusion (Q_a)	
	°C	**°F**		**kJ/mol**	**BTU/mol**
Copper in Cu_2O	800–1050	1470–1920	0.12	151.0	143
Nickel in NiO	740–1400	1365–2550	0.017	234	222
Oxygen in Fe_2O_3	1150–1250	2100–2280	10^{11}	610	578
Iron in Fe_3O_4	750–1000	1380–1830	5.2	230	218
Iron in $Fe_{0.92}O$	690–1010	1275–1850	0.014	126.4	120
Chromium in Cr_2O_3	1000–1350	1830–2460	4000	420	398
Oxygen in UO_2	450–600	840–1110	2.6×10^{-5}	124	118
Magnesium in MgO	1400–1600	2550–2910	0.25	330	313

Source: Ref 6

Effect of Impurities. All oxides contain certain substitutional cations (impurities) from the oxidized alloy (present before the oxidation) and/or from the gas phase during oxidation. Although the solubility limit for foreign ions is low, they can have a great effect on the oxide transport properties, and consequently on the oxidation rate.

In *p*-type oxides, such as NiO, the substitutional cations have a valence greater than the Ni^{2+} ions that are replaced, increasing the concentration of cation vacancies. Two aluminum ions (Al^{3+}) replacing two Ni^{2+} ions in the cationic sublattice supply two extra free electrons. Consequently, to maintain the local electrical neutrality condition, an additional cation vacancy must be formed. The increase of concentration of cation vacancies in NiO increases the nickel diffusivity in this oxide. On the other side, substitutional cations with a valence lower than +2 reduce diffusion in NiO by reducing the number of cation vacancies. Divalent cations have little effect on diffusion when substituting for Ni^{2+} ions. For *n*-type oxides, the effect is reversed; if Al^{3+} substitutes some titanium ions (Ti^{4+}) in titanium dioxide (TiO_2), more anion vacancies will be formed in the oxide. Diffusivity of oxygen then increases because of the increase in anion vacancy concentration. Higher- valence impurity ions would decrease oxygen diffusion in *n*-type oxides. The impurity effect is especially important for diffusion at low temperatures at which the native defect concentration is low, and the activation energy is associated with the movement of ions only. At high temperatures, the activation energy increases because it involves formation of defects as well as their motion.

Fast Diffusion Paths. The activation energies for diffusion along line and surface defects in solids are much lower than those for volume diffusion. Dislocations, grain boundaries, porosity networks, and interfaces form rapid diffusion paths. At low temperatures, below the Tammann temperature ($T_T \cong \frac{2}{3} T_m$, where T_m is the melting temperature), volume diffusion is virtually stopped in oxides. In metals, diffusion along dislocations is more important than volume diffusion below about one-half of the absolute melting point, T_m. Above the Tammann temperature, the volume diffusion predominates in both metals and oxides.

Reference cited in this section

6. T. Rosenqvist, Phase Equilibria in Pyrometallurgy of Sulfide Ores, *Metall. Trans. B,* Vol 9b, 1978, p 337–351

M. Danielewski, Kinetics of Gaseous Corrosion Processes, *Corrosion: Fundamentals, Testing, and Protection*, Vol 13A, *ASM Handbook*, ASM International, 2003, p 97–105

Kinetics of Gaseous Corrosion Processes

Marek Danielewski, AGH University of Science and Technology, Cracow, Poland

---

Oxide Texture

Amorphous Oxides. In the very early stages of oxidation and especially at low and intermediate temperatures ($T < T_T$), some oxides appear to grow with an amorphous structure. In general, the oxides in which the molar ratio of oxygen to metal is higher than one form glasses. They contain more oxygen than metal in their formulas so that oxygen triangles or tetrahedra are formed around each of the metal ions. The random network ring structures that result allow large anions or molecular oxygen to move through them more readily than the smaller cations do. Amorphous oxides tend to crystallize as they age. Examples are silicon dioxide (SiO_2), tantalum pentoxide (Ta_2O_5), and niobium pentoxide (Nb_2O_5). In contrast, oxides with M_2O and MO formulas have structures in which the small cations can move readily. They are apparently always crystalline. Examples are NiO, cuprous oxide (Cu_2O), and zinc oxide (ZnO).

In general the amorphous and nanostructure form of oxides increases mobility and is desirable in coatings and alloys that form protective scale as a result of selective oxidation. In such a case, the stability of the oxide layer depends on continuous supply of oxidized metal; that is, it depends on the interdiffusion rate within an alloy.

Epitaxy. As a crystalline oxide grows on a metal surface, it often aligns its crystal structure to be compatible with the structure of the metal substrate. This epitaxial growth results in the best fit between the two different crystal structures. For example, either (111) or (001) planes of Cu_2O grow parallel to the Cu (001) plane with the • 110• directions of Cu_2O parallel to the • 110• of copper (Ref 7).

Stress develops in an epitaxial oxide layer as it grows because of the slight misfit between the oxide and metal crystals. Such stress is likely to produce dislocation arrays within the oxide that eventually become fast diffusion paths and accelerate mass transport through the film. A mosaic structure may develop in the oxide because of the growth stresses. The mosaic structure consists of small crystallites with orientations very slightly tilted or twisted with respect to each other. The boundaries between the crystallites are dislocation arrays that again serve as fast diffusion paths.

Stresses in epitaxial layers increase as the films grow thicker until a point is reached when the bulk scale tends to become polycrystalline and epitaxy is gradually lost. Epitaxy may last up to about 50 nm in many cases, but it seldom exceeds 100 nm.

Preferred Orientation. Above the Tammann temperature the oxide grain size (diameter) increases with the scale thickness. Crystals that are favorably oriented can grow at the expense of their neighboring grains until the oxide surface consists of a few large grains with similar orientation. Below the Tammann temperature, fine-grained scales are formed. The variation in growth rate of different oxide grains produces roughening of the scale surface and is commonly observed (Ref 2, 3, 4).

References cited in this section

2. N. Birks and G.H. Meier, *Introduction to High Temperature Oxidation of Metals,* Edward Arnold, 1983
3. P. Kofstad, *High Temperature Corrosion,* Elsevier Applied Science, 1988

4. M. Schutze, *Corrosion and Environmental Degradation,* Vol 1, *Materials Science and Technology, A Comprehensive Treatment,* R.W. Cahn, P. Haasen, and E.J. Kramer, Ed., Wiley-VCH, 1993

7. K.R. Lawless and A.T. Gwathmey, The Structure of Oxide Films on Different Faces of a Single Crystal of Copper, *Acta Metall.,* Vol 4, 1956, p 153–163

M. Danielewski, Kinetics of Gaseous Corrosion Processes, *Corrosion: Fundamentals, Testing, and Protection*, Vol 13A, *ASM Handbook*, ASM International, 2003, p 97–105

Kinetics of Gaseous Corrosion Processes

Marek Danielewski, AGH University of Science and Technology, Cracow, Poland

---

Oxidation Kinetics

Linear Oxidation Reaction Rates. If the metal surface is not protected by an oxide barrier layer, then the oxidation rate usually remains constant with time. In such a case, the surface processes and/or reactions are the rate-controlling steps. This situation occurs in many cases:

- The Pilling-Bedworth ratio is less than one.
- The oxide is volatile.
- Oxide forms molten eutectic with the underlying metal.
- The scale spalls off or cracks due to internal stresses.
- A porous, unprotective oxide forms on the metals.

The linear oxidation rate is:

$$\frac{dX}{dt} = k_L \qquad \text{(Eq 15)}$$

where X is the mass (or thickness) of the oxide formed, t is the time of oxidation, and k_L is the linear rate constant. Upon integration and when the initial (at $t = 0$) scale thickness equals 0, the linear oxidation equation is:

$$X = k_L t \qquad \text{(Eq 16)}$$

The oxidation never slows down; after a short time at high temperature, the metal will be completely destroyed. Figure 7 shows the relationship between oxide mass and time for linear oxidation.

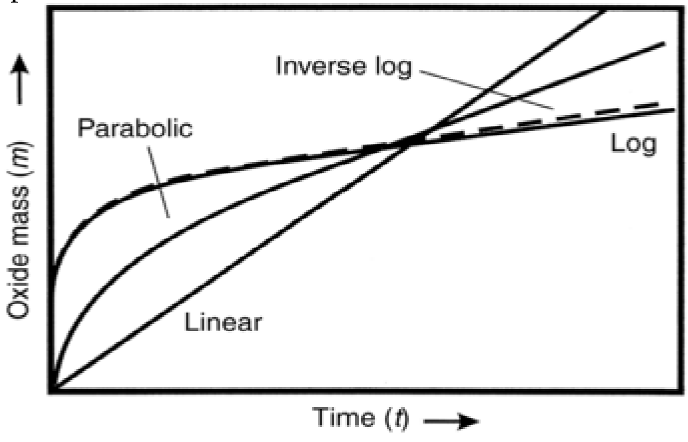

Fig. 7 Types of the oxidation kinetics: linear, logarithmic, inverse logarithmic, and parabolic oxidation kinetics

Logarithmic and Inverse Logarithmic Reaction Rates. At low temperatures when only a thin film of oxide is formed (for example, under 100 nm), the oxidation is usually observed to follow either logarithmic or inverse logarithmic kinetics. Transport processes across the film are rate controlling, with the driving force being electric fields across the film. The logarithmic equation is:

$$X = k_e \log(at + 1) \qquad \text{(Eq 17)}$$

where k_e and a are constants.
The inverse logarithmic equation is:

$$\frac{1}{X} = b - k_i \log t \qquad \text{(Eq 18)}$$

where b and k_i are constants. Under the difficult experimental conditions involved in making measurements in the thin-film range, it is difficult to distinguish between logarithmic and inverse logarithmic oxidation. Both Eq 17 and 18 have two constants that can be adjusted to fit the data quite well. Metals oxidizing with logarithmic or inverse log kinetics reach a limiting film thickness at which oxidation apparently stops. Figure 7 shows the curves for both logarithmic and inverse logarithmic kinetics.

Parabolic Kinetics. When the rate-controlling step in the oxidation process is the diffusion of ions through a compact barrier layer of oxide, with the chemical potential gradient as the driving force, the parabolic rate law is usually observed. As the oxide grows thicker, the diffusion distance increases and the oxidation rate slows down. The rate is inversely proportional to the oxide thickness:

$$\frac{dX}{dt} = \frac{k'}{X} \qquad \text{(Eq 19)}$$

where k' is the parabolic rate constant. Upon separating the variables and integrating Eq 19 with the initial condition that at time $t = 0$ the oxide thickness $X = 0$, the integral form of the parabolic equation results:

$$X^2 = k't \qquad \text{(Eq 20)}$$

Figure 7 shows the parabolic oxidation curve.

Other Reaction Rate Equations. A number of other kinetics equations have been fitted to the experimental data, but it is believed that they describe a combination of the mechanisms described previously, rather than any new basic process. A cubic relationship:

$$X^3 = k't \qquad \text{(Eq 21)}$$

has been reported for very long oxidation periods (t > 10,000 h). It can be shown mathematically to be an intermediate stage between logarithmic and parabolic kinetics.

Initial Oxidation Processes: Adsorption and Nucleation. To begin oxidation, oxygen gas is chemisorbed on the metal surface until a complete two-dimensional oxygen layer is formed. Some atomic oxygen also dissolves into the metal at the same time. After the monolayer forms, discrete nuclei of three-dimensional oxide appear on the surface and begin expanding laterally at an ever-increasing rate. The nuclei may originate at structural defects, such as grain boundaries, impurity particles, and dislocations. The concentration of nuclei depends primarily on the crystal orientation of the metal, with more nuclei forming at high pressures and low temperatures.

These oxide islands grow outward rapidly by surface diffusion of adsorbed oxygen until a complete film three or four monolayers thick covers the metal. The oxidation rate then drops abruptly. If chemisorption were still the rate-controlling (slow) step in oxidation after the thin film is completed, a logarithmic rate law should be observed. The logarithmic rate law is the result of a strong electric field across the film that affects the oxidation rate.

M. Danielewski, Kinetics of Gaseous Corrosion Processes, *Corrosion: Fundamentals, Testing, and Protection*, Vol 13A, *ASM Handbook*, ASM International, 2003, p 97–105

Kinetics of Gaseous Corrosion Processes

Marek Danielewski, AGH University of Science and Technology, Cracow, Poland

Thin-Film Mechanisms

Many theories have been proposed to explain the oxidation mechanism at low temperatures or in the early stages of high-temperature oxidation where logarithmic kinetics are commonly observed. None of the theories are completely accepted yet, and perhaps none is completely correct, but they have common threads of agreement that indicate reasonably well what is happening. Some of the most important theories are briefly described in this Section.

The Cabrera-Mott theory, probably the best established theory of thin-film oxidation, applies to films up to about 10 nm thick (Ref 8). It proposes that electrons from the metal easily pass through the thin film by tunneling to reach adsorbed oxygen at the oxide/gas surface and form oxygen anions. A potential of approximately 1 V is set up between the external oxide surface and the metal. For a film 1 nm thick, the field strength would be 10^7 V/cm, powerful enough to pull cations from the metal and through the film. The rate-controlling step is the transfer of cations (or anions) into the oxide or the movement of the ions through the oxide. The electric field reduces this barrier. The structure of the oxide determines whether cations or anions migrate through the oxide. As the film grows thicker, the field strength decreases until it has so little effect on the ions that the rate-controlling mechanism changes.

Cabrera and Mott developed an inverse logarithmic kinetic equation to describe the mechanism. A logarithmic equation is more commonly observed, but it can be derived from the Cabrera- Mott mechanism if the activation energy for ionic migration is a function of film thickness. Such a situation would exist if the oxide film were initially amorphous and became more crystalline with aging, giving a constant field strength through the film instead of a constant voltage.

The Hauffe-Ilschner theory, a modification of Mott's original concept of a space charge developed across the oxide film, proposes that quantum-mechanical tunneling of electrons is the rate-controlling step (Ref 9). After the film thickness reaches about 10 nm, tunneling becomes increasingly difficult, and the observed reaction rate decreases greatly. For film thickness up to perhaps 20 nm, a logarithmic equation results. For films from 20 to 200 nm thick, the inverse logarithmic relationship holds. Potentials across thin films have been measured; a change in sign of the potential is interpreted as a change from electronic transport control to ionic transport control.

The Grimley-Trapnell theory (Ref 10). Grimley and Trapnell used the Cabrera-Mott model, but assumed a constant electric field instead of a constant potential. They assumed that the adsorbed oxygen layer would always be complete, even at high temperatures and low pressure. The adsorbed oxygen would take electrons from cations in the oxide, not from the metal, so that a space charge would develop at the MO/O-ads interface (O-ads being the adsorbed oxygen layer) and be independent of the oxide thickness. If the rate-controlling step is diffusion of cations through vacancies, logarithmic kinetics should be observed. If some other process is rate controlling, linear kinetics is most likely.

The Uhlig theory, developed by Uhlig and extended by Fromhold, also predicts logarithmic kinetics at temperatures up to 600 K (Ref 11). The rate-controlling step is the thermal emission of electrons from the metal into the oxide (or electron holes from the adsorbed oxygen ions to the oxide) under the combined effects of induced potential and applied field. The field is created by the diffusing ions. Because growth of the film depends on the electronic work function of the metal, the theory explains oxidation rate changes at crystal and magnetic transformations; most other theories do not.

The Wagner Theory of Oxidation. During the oxidation process the two reactants are separated by an oxide layer. Thus, it is necessary to postulate that mass transport (volume diffusion in simple cases) occurs through such growing oxide scale. Before presenting Wagner's derivation of the parabolic rate equation for scale growth

on a metal in which diffusion of ions or electrons is rate-controlling step, a simplified treatment is given to emphasize the main features of diffusion-controlled oxidation.

One can assume that a pure metal reacts with an oxidant and the growth of a dense, planar and single-phase oxide occurs. Moreover, the following conditions regarding this phase are necessary for which the theory is valid:

- One type of defect dominates in the oxide.
- The thermodynamic equilibria are established on both Me/scale and scale/oxidant interfaces.
- The oxide scale shows small deviation from stoichiometry.
- The oxidant solubility in the metal, the oxide evaporation, and any other processes at interfaces are negligible.
- The scale is thick compared with distances over which space charge effects occur (electrical double layer).

From the assumption of low nonstoichiometry it follows that the metal and oxidant concentrations in the growing scale do not depend on position and are constant. Consequently, when the metal (e.g., interstitial cations Me_i) diffusion dominates, Fick's second law (Eq 10) reduces to:

$$\frac{\partial}{\partial x}\mathbf{J}_{Me_i} = 0 \qquad \text{(Eq 22)}$$

from which it follows that the flux of metal does not depend on position in the scale and depends on time only. The rate of growth of the oxide scale, dX/dt, is then proportional to the flux of metal ions $\mathbf{J}_{Me}$ by Fick's first law (Eq 5):

$$\mathbf{J}_{Me} = \mathbf{J}_{Me_i} = -D_{Me_i}\frac{\partial C_{Me_i}}{\partial x} \qquad \text{(Eq 23)}$$

When the diffusion coefficient does not depend on defect concentration, then from Eq 22 and 23 it follows that the gradient of metal concentration in the growing scale is constant. It allows further simplification of the flux formulas:

$$\mathbf{J}_{Me} = -D_{Me_i}\frac{\Delta C_{Me_i}}{X} \qquad \text{(Eq 24)}$$

where both flux and the scale thickness, X, are unknown. The last necessary equation relates the flux of metal at the external interface to the rate of scale formation. It is the mass balance at the scale/oxidant interface and is often called the Stefan condition:

$$\mathbf{J}_{Me} = C_{Me}\frac{dX}{dt} \qquad \text{(Eq 25)}$$

On combining Eq 24 and 25, the differential form of the parabolic rate law follows:

$$\frac{dX}{dt} = \left(D_{Me_i}\frac{\Delta C_{Me_i}}{C_{Me}}\right)\frac{1}{X} = \frac{k'}{X} \qquad \text{(Eq 26)}$$

where the parabolic rate constant (term in the brackets) depends on diffusivity of defects and their concentrations. Integrating with the limit that at time $t = 0$ the oxide thickness $X = 0$, the integral form of the parabolic equation is:

$$X^2 = k't \qquad \text{(Eq 27)}$$

The Wagner Derivation. Figure 8 gives the reaction scheme for which the theory is valid. Two additional assumptions form the foundation of Wagner's theory of metal oxidation: (1) the migration (diffusion) of ions and electrons across the scale is the rate-controlling process, and (2) it is postulated that thermodynamic equilibrium is established locally through the growing scale. From the first postulate it follows that the more general Nernst-Planck flux formula must be used (instead of Fick's first law), which states that the flow of ions and electrons through a growing oxide layer depends on their concentration, mobility, and the driving force for migration (diffusion):

$$\mathbf{J}_i = C_i B_i \mathbf{F} \quad \text{(Eq 28)}$$

where B_i denotes the mobility of diffusing specie i and **F** is the sum of all forces acting on it.

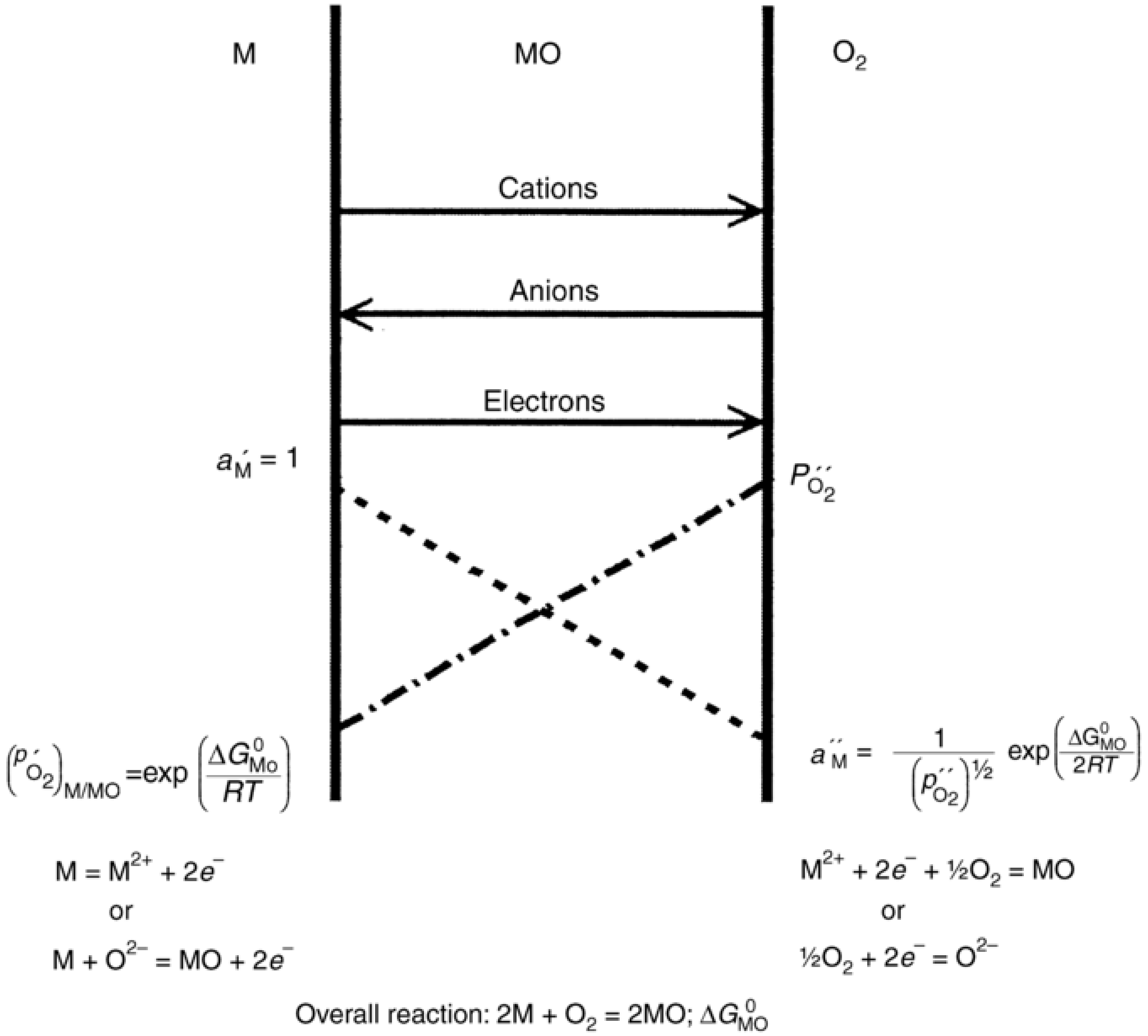

Fig. 8 Diagram of the scale formation according to the Wagner's model

A charged ion (valence z_i) moving through the oxide is acted upon by two forces: the chemical force (chemical potential gradient, $\partial\mu_i/\partial x$) and an electric potential gradient, $\partial\varphi/\partial x$. The flux is then:

$$\mathbf{J}_i = -C_i B_i \frac{1}{N_a}\left(\frac{\partial \mu_i}{\partial x} + z_i \mathbf{F}\frac{\partial \phi}{\partial x}\right) \quad \text{(Eq 29)}$$

where N_a is Avogadro's number, φ an electrical potential, and **F** is Faraday's constant. The mobility and self-diffusion coefficients are related by the Nernst-Einstein relation: $D_i = B_i kT$. Thus, all of the fluxes in Eq 29 can be written as:

$$\mathbf{J}_c = -C_c D_c \frac{1}{RT}\left(\frac{\partial \mu_c}{\partial x} + z_c \mathbf{F}\frac{\partial \phi}{\partial x}\right) \quad \text{(Eq 30)}$$

$$\mathbf{J}_a = -C_a D_a \frac{1}{RT}\left(\frac{\partial \mu_a}{\partial x} + z_a \mathbf{F}\frac{\partial \phi}{\partial x}\right) \quad \text{(Eq 31)}$$

$$\mathbf{J}_e = -C_e D_e \frac{1}{RT}\left(\frac{\partial \mu_e}{\partial x} + \mathbf{F}\frac{\partial \phi}{\partial x}\right) \quad \text{(Eq 32)}$$

where R is the gas constant, $N_a k = R$. These flux expressions introduce a new unknown variable. Consequently, an additional equation is necessary. As the oxide forms, the flow of ions through the scale must be balanced by the flow of electrons to maintain a local charge balance:

$$z_c\mathbf{J}_c + z_a\mathbf{J}_a - \mathbf{J}_e = 0 \quad \text{(Eq 33)}$$

where the subscripts a, c, and e refer to anions, cations, and electrons, respectively. Substituting Eq 30, Eq 31, and 32 into 33 yields:

$$\frac{\partial \phi}{\partial x} = \frac{1}{F}\frac{-C_c D_c z_c \frac{\partial \mu_c}{\partial x} - C_a D_a z_a \frac{\partial \mu_a}{\partial x} + C_e D_e \frac{\partial \mu_e}{\partial x}}{z_c^2 C_c D_c + z_a^2 C_a D_a + C_e D_e} \quad \text{(Eq 34)}$$

The postulate of the local thermodynamical equilibrium allows the assumption that everywhere through the oxide, the equilibria:

$$\mathrm{Me} = \mathrm{Me}^{z_c+} + z_c e \quad \text{(Eq 35)}$$

$$X = X^{z_a+} - |z_a|\, e \quad \text{(Eq 36)}$$

are established during the whole process and it follows that:

$$\mu_{Me} = \mu_c + z_c\mu_e \quad \text{(Eq 37)}$$

$$\mu_X = \mu_a - |z_a|\mu_e \quad \text{(Eq 38)}$$

Moreover, for such isothermal and isobaric process the Gibbs-Duhem relation holds:

$$N_{Me} d\mu_{Me} + N_X d\mu_X = 0 \quad \text{(Eq 39)}$$

Upon taking into account that oxides have near- stoichiometric composition, the ratio of molar concentrations may be expressed as:

$$\frac{N_{Me}}{N_X} = \frac{|z_a|}{z_c} \quad \text{(Eq 40)}$$

and Eq 39 becomes

$$|z_a| d\mu_{Me} + z_c d\mu_X = 0 \quad \text{(Eq 41)}$$

From Eq 37, Eq 38, Eq 39, the electrical potential gradient can be expressed by:

$$\frac{\partial \phi}{\partial x} = \frac{1}{z_c\mathbf{F}} \times \left(-\frac{\partial \mu_c}{\partial x} + \frac{C_e D_e}{z_c^2 C_c D + z_a^2 C_a D_a + C_e D_e}\frac{\partial \mu_{Me}}{\partial x}\right) \quad \text{(Eq 42)}$$

Eq 42 reduces to a simple relation:

$$\frac{\partial \phi}{\partial x} = \frac{1}{z_c\mathbf{F}}\left(-\frac{\partial \mu_c}{\partial x} + \frac{\partial \mu_{Me}}{\partial x}\right) = \frac{1}{\mathbf{F}}\frac{\partial \mu_e}{\partial x} \quad \text{(Eq 43)}$$

Introducing Eq 43 into the flux formulas (Eq 30 and 31) and taking into account relations Eq 37 and 38:

$$J_c = -C_c D_c \frac{1}{RT}\frac{\partial \mu_{Me}}{\partial x} \quad \text{(Eq 44)}$$

$$J_a = -C_a D_a \frac{1}{RT}\frac{\partial \mu_X}{\partial x} \quad \text{(Eq 45)}$$

The scale growth is a result of cation and anion fluxes, $dX = dX_c + dX_a$. Thus, from the mass balances at both interfaces (Eq 35):

$$\frac{dX}{dt} = \frac{dX_c}{dt} - \frac{dX_a}{dt} = \frac{J_{Me}}{C_{Me}} - \frac{J_X}{C_X} \qquad \text{(Eq 46)}$$

Introducing Eq 44 and 45, and the Gibbs-Duhem relation (Eq 41), one gets:

$$\frac{dX}{dt} = -\frac{1}{RT}\left(\frac{|z_a|}{z_c}\frac{C_a D_a}{C_X} + \frac{C_c D_c}{C_{Me}}\right)\frac{\partial \mu_{Me}}{\partial x} \qquad \text{(Eq 47)}$$

The defect diffusion coefficient and self-diffusion coefficients are related through:

$$D^*_{Me} = N_c D_c \qquad \text{(Eq 48)}$$

Thus, Eq 47 becomes:

$$\frac{dX}{dt} = -\frac{1}{RT}\left(\frac{|z_a|}{z_c}D^*_a + D^*_c\right)\frac{\partial \mu_{Me}}{\partial x} \qquad \text{(Eq 49)}$$

The arguments (compare Eq 22, Eq 23, Eq 24, Eq 25, Eq 26 and Eq 49) are valid in the Wagner model. Thus, one can express the right-hand side of Eq 49 using average values. Upon integrating Eq 49 over the entire scale thickness *X*, from the inner surface (metal/oxide interface), at which the metal chemical potential is μ'_{Me}, to μ''_{Me} at the outer (oxide/gas interface) Eq 49 becomes:

$$\frac{dX}{dt} = -\frac{1}{X}\frac{1}{RT}\int_{\mu'_{Me}}^{\mu''_{Me}}\left(\frac{|z_a|}{z_c}D^*_a + D^*_c\right)d\mu_{Me} \qquad \text{(Eq 50)}$$

where

$$k'_p = \frac{1}{RT}\int_{\mu''_{Me}}^{\mu'_{Me}}\left(\frac{|z_a|}{z_c}D^*_a + D^*_c\right)d\mu_{Me} \qquad \text{(Eq 51)}$$

is called the parabolic rate constant. Substituting the Gibbs-Duhem equation:

$$d\mu_{Me} = -\frac{z_c}{|z_a|}d\mu_X = -\frac{1}{2}\frac{z_c}{|z_a|}RT\,d\ln p_{O_2} \qquad \text{(Eq 52)}$$

the result is:

$$k'_p = \frac{1}{RT}\int_{p'_{O_2}}^{p''_{O_2}}\left(D^*_a + \frac{z_c}{|z_a|}D^*_c\right)d\ln p_{O_2} \qquad \text{(Eq 53)}$$

The good agreement between parabolic rate constants calculated from conductivity or diffusivity data and the rate constants measured in oxidation experiments indicates that Wagner's assumptions are generally valid (Ref 2, 3). If the Wagner's principal assumptions about the scale are valid:

- The oxide scale is completely compact and adherent.
- The migration of ions through the scale is the rate-controlling process.
- Thermodynamic equilibrium exists at both the metal/oxide and oxide/gas interfaces.
- Thermodynamic equilibrium exists locally throughout the scale.
- The oxide deviates only slightly from stoichiometry.

Then, the Wagner model allows one to understand or use the model as a starting point for more complex reactions, such as the oxidation of alloys.

Effects of Temperature and Pressure. When kinetics of the oxidation are controlled by diffusion in the growing scale, the parabolic oxidation rate constant (Eq 19) increases exponentially with temperature, following the Arrhenius equation:

$$k'_p = k_0 \exp\left(-\frac{Q_a}{RT}\right) \qquad \text{(Eq 54)}$$

where k_0 is a constant dependent on the oxide composition and the gas pressure. According to Wagner's theory, for cation-deficient or cation- excess oxides where D_c » D_a, the activation energy Q_a for oxide growth is the

same as the activation energy for diffusion of cations in the oxide. For anion-deficient oxides, such as ZrO_2, where D_a » D_c, the activation energy for oxide growth is the same as that for anion diffusion, verifying that ionic diffusion is the rate-controlling process.
To calculate the effect of pressure on the oxidation rate, Eq 53 can be used. For a cation- deficient *p*-type oxide, such as $Ni_{1-y}O$, growth occurs at the oxide/gas interface where:

$$\frac{1}{2}O_2(g) + Ni = NiO$$

Using the Kröger-Vink notation, the formation of the nondefect oxide ($NiO = Ni_{Ni} + O_o$) is given by $\frac{1}{2}O_2(g) + Ni = O_o + Ni_{Ni}$ where Ni_{Ni} and O_o indicate that Ni and O occupy the regular positions in the cationic and ionic sublattice. The formation of defects in this notation can be written as:

$$\tfrac{1}{2}O_2(g) = O_o + V''_{Ni} + 2h^{\cdot} \qquad \text{(Eq 55)}$$

where symbol V_{Ni} stands for a doubly charged cation vacancy, and $h^{\cdot}$ represents an electron hole. Thermodynamic equilibrium is established at the $Ni/O_2(g)$ interface so that at any time the equilibrium constant *K* for the reaction of the oxide formation (Eq 55) is:

$$K = \left[V''_{Ni}\right]\left[h^{\cdot}\right]^2 p_{O_2}^{-1/2} \qquad \text{(Eq 56)}$$

where p_{O_2} is the oxygen partial pressure and the brackets indicate the concentration of the species enclosed; for example, $[V_{Ni}]$ denotes the concentration of cation vacancies. The oxygen concentration at both interfaces is constant. Thus, the local thermodynamic equilibrium conditions imply that locally there must be two electron holes for every cation vacancy, or $[h^{\cdot}] = 2\,[V_{Ni}]$, then:

$$\left[V''_{Ni}\right] = (K/4)^{1/3}\, p_{O_2}^{1/6} \qquad \text{(Eq 57)}$$

The nickel diffusivity is proportional to the vacancy concentration (Eq 13), so that:

$$D^*_{Ni} = D_0 p_{O_2}^{1/6} \qquad \text{(Eq 58)}$$

where D_0 denotes here the cation diffusivity for oxygen pressure equal one.
It may be shown that for an oxide with simple defect structure (where only one type of defect dominates in a cationic or anionic sublattice) Eq 58 takes the form:

$$D^*_{Ni} = D_0 p_{O_2}^{\pm 1/n} \qquad \text{(Eq 59)}$$

where, theoretically, both the sign and *n* (generally a number between 2 and 8) depend on the type of dominating defect.
Substituting Eq 58 into Eq 53, the oxidation rate is:

$$k'_p = \frac{1}{2} D_0 \int_{p'_{O_2}}^{p''_{O_2}} \left(p_{O_2}^{1/6}\right) d\ln p_{O_2} \qquad \text{(Eq 60)}$$

which upon integration becomes:

$$k'_p = 3D_0\left[\left(p''_{O_2}\right)^{1/6} - \left(p'_{O_2}\right)^{1/6}\right] \qquad \text{(Eq 61)}$$

In most cases, the ambient oxygen pressure p_{O_2} is much greater than the nickel oxide dissociation pressure p'_{O_2} so that:

$$k'_p = 3D_0\left(p''_{O_2}\right)^{1/6} \qquad \text{(Eq 62)}$$

Equation 62 explains both the Arrhenius-type temperature dependence and the pressure dependence of the oxidation rate. For an oxide with a simple defect structure and where the concentration of defects at the $Me/O_2(g)$ interface is higher than at the oxide/Me interface, Eq 62 has the form:

$$k'_p = \frac{n}{2} D_0 \left(p''_{O_2} \right)^{\pm 1/n} \quad \text{(Eq 63)}$$

For oxides with a simple defect structure and when the concentration of defects at the Me/ O_2(*g*) interface is lower than at oxide/Me interface—for example, Cu_2O—the oxidation rate is practically independent of the ambient oxygen pressure.

References cited in this section

2. N. Birks and G.H. Meier, *Introduction to High Temperature Oxidation of Metals,* Edward Arnold, 1983

3. P. Kofstad, *High Temperature Corrosion,* Elsevier Applied Science, 1988

8. N. Cabrera and N.F. Mott, Theory of Oxidation of Metals, *Rep. Prog. Phys.,* Vol 12, 1948–1949, p 163–184

9. K. Hauffe and B. Ilschner, Defective-Array States and Transport Processes in Ionic Crystals, *Z. Electrochem.,* Vol 58, 1954, p 467–477

10. T.B. Grimley and B.M.W. Trapnell, The Gas/Oxide Interface and the Oxidation of Metals, *Proc. R. Soc. (London) A,* Vol A234, 1956, p 405–418

11. H.H. Uhlig, Initial Oxidation Rate of Metals and the Logarithmic Equation, *Acta Metall.,* Vol 4, 1956, p 541–554

M. Danielewski, Kinetics of Gaseous Corrosion Processes, *Corrosion: Fundamentals, Testing, and Protection*, Vol 13A*, ASM Handbook,* ASM International, 2003, p 97–105

Kinetics of Gaseous Corrosion Processes

Marek Danielewski, AGH University of Science and Technology, Cracow, Poland

---

Acknowledgment

Portions of this article have been adapted from S.A. Bradford, Fundamentals of Corrosion in Gases, *Corrosion,* Vol 13, *ASM Handbook* (formerly 9th ed. *Metals Handbook*), ASM International, 1987, p 61–76.

M. Danielewski, Kinetics of Gaseous Corrosion Processes, *Corrosion: Fundamentals, Testing, and Protection*, Vol 13A*, ASM Handbook,* ASM International, 2003, p 97–105

Kinetics of Gaseous Corrosion Processes

Marek Danielewski, AGH University of Science and Technology, Cracow, Poland

---

References

1. N.B. Pilling and R.E. Bedworth, The Oxidation of Metals at High Temperatures, *J. Inst. Met.,* Vol 29, 1923, p 529–582

2. N. Birks and G.H. Meier, *Introduction to High Temperature Oxidation of Metals,* Edward Arnold, 1983

3. P. Kofstad, *High Temperature Corrosion,* Elsevier Applied Science, 1988

4. M. Schutze, *Corrosion and Environmental Degradation,* Vol 1, *Materials Science and Technology, A Comprehensive Treatment,* R.W. Cahn, P. Haasen, and E.J. Kramer, Ed., Wiley-VCH, 1993

5. O. Kubashewski and B.E. Hopkins, *Oxidation of Metals and Alloys,* 2nd ed., Butterworths, 1962

6. T. Rosenqvist, Phase Equilibria in Pyrometallurgy of Sulfide Ores, *Metall. Trans. B,* Vol 9b, 1978, p 337–351

7. K.R. Lawless and A.T. Gwathmey, The Structure of Oxide Films on Different Faces of a Single Crystal of Copper, *Acta Metall.,* Vol 4, 1956, p 153–163

8. N. Cabrera and N.F. Mott, Theory of Oxidation of Metals, *Rep. Prog. Phys.,* Vol 12, 1948–1949, p 163–184

9. K. Hauffe and B. Ilschner, Defective-Array States and Transport Processes in Ionic Crystals, *Z. Electrochem.,* Vol 58, 1954, p 467–477

10. T.B. Grimley and B.M.W. Trapnell, The Gas/Oxide Interface and the Oxidation of Metals, *Proc. R. Soc. (London) A,* Vol A234, 1956, p 405–418

11. H.H. Uhlig, Initial Oxidation Rate of Metals and the Logarithmic Equation, *Acta Metall.,* Vol 4, 1956, p 541–554

12. C. Wagner, Contributions to the Theory of the Tarnishing Process, *Z. Phys. Chem.,* Vol B21, 1933, p 25–41

13. R.C. Weast, Ed., *CRC Handbook of Chemistry and Physics,* 62nd ed., CRC Press, 1981

14. R.B. Ross, Ed., *Metallic Materials Specification Handbook,* 4th ed., Chapman & Hall, London, 1992

15. *Properties and Selection: Nonferrous Alloys and Special-Purpose Materials,* Vol 2, *ASM Handbook,* ASM International, 1990

16. A. Nayer, Ed., *The Metals Databook,* McGraw-Hill, 1997

17. D.R. Lide, Ed., *CRC Handbook of Chemistry and Physics,* 79th ed., CRC Press, 1998

M. Danielewski, Kinetics of Gaseous Corrosion Processes, *Corrosion: Fundamentals, Testing, and Protection*, Vol 13A, *ASM Handbook*, ASM International, 2003, p 97–105

Kinetics of Gaseous Corrosion Processes

Marek Danielewski, AGH University of Science and Technology, Cracow, Poland

Selected References

- N. Birks and G.H. Meier, *Introduction to High Temperature Oxidation of Metals,* Edward Arnold, 1983
- A.T. Frumhold, Jr., *Theory of Metal Oxidation, Vol 1—Fundamentals,* North Holland Publishing, 1976
- A.S. Khanna, *Introduction to High Temperature Oxidation and Corrosion,* ASM International, 2002
- P. Kofstad, *High Temperature Corrosion,* Elsevier Applied Science, 1988
- H. Schmalzried, *Chemical Kinetics of Solids,* VCH, 1995
- M. Shutze, *Corrosion and Environmental Degradation,* Vol 1, *Materials Science and Technology, A Comprehensive Treatment,* R.W. Cahn, P. Haasen, E.J. Kramer, Ed., Wiley-VCH, 1993

M. Danielewski, Gaseous Corrosion Mechanisms, *Corrosion: Fundamentals, Testing, and Protection*, Vol 13A, *ASM Handbook*, ASM International, 2003, p 106–114

Gaseous Corrosion Mechanisms

Revised by Marek Danielewski, AGH University of Science and Technology, Cracow, Poland

Introduction

THE CHARACTERISTICS AND BEHAVIOR of scale produced by various types of oxidation are examined in this article. The basic models, concepts, processes and open questions for high-temperature gaseous corrosion are presented.

M. Danielewski, Gaseous Corrosion Mechanisms, *Corrosion: Fundamentals, Testing, and Protection*, Vol 13A, *ASM Handbook*, ASM International, 2003, p 106–114

Gaseous Corrosion Mechanisms

Revised by Marek Danielewski, AGH University of Science and Technology, Cracow, Poland

Properties of Scales

Multiple Scale Layers. A pure metal that can be oxidized to more than one valence state can form a series of oxides in the form of separate layers. For example, iron forms highly defected wustite (FeO), magnetite (Fe_3O_4), and (at high oxygen pressure) hematite (Fe_2O_3) scale layers. The layers will be arranged with the most metal- rich oxide next to the metal and the most oxygen-rich layer on the outside. At temperatures above 583

°C (1081 °F), wustite is stable, and the sequence of oxides in the scale shows the following pattern: $Fe|FeO|Fe_3O_4|Fe_2O_3|O_2(g)$.

At temperatures below 583 °C (1081 °F), rapidly growing wustite is not stable, and consequently, iron shows satisfactory resistance to oxidation. The corrosion-resistant scale formed below 583 °C (1081 °F) on iron consists of magnetite and hematite: $Fe|Fe_3O_4|Fe_2O_3|O_2(g)$. A concentration gradient exists within each layer, with higher metal ion concentration closest to the metal. Another example is the copper-oxygen system, which may form the following sequence of oxides: $Cu|Cu_2O|CuO|O_2(g)$.

If the oxygen partial pressure in the gas is below the dissociation pressures of the outer oxygen-rich oxides, then only the thermodynamically stable, inner oxide(s) will form. In general, the lowest valence, inner oxide will usually show the defects in a cationic sublattice only (vacancies in wustite: $Fe_{1-y}O$, but interstitial cations in $Cr_{2+y}O_3$ and $Cu_{2+y}O$). The highest-valence oxide will usually show the vacancies in cationic and/or defects in anionic sublattices. The nonstoichiometry of such oxides (e.g., Fe_2O_3) is very low and often nonmeasurable. Consequently, the defect structure and transport properties of many technically important oxides are not very well known (e.g., Al_2O_3). A scale consisting of an inner layer with cations diffusing outward and an outer layer with anions diffusing inward will grow at the oxide-oxide interface.

Relative Thickness. When diffusion is the rate-controlling process and no porosity develops in the oxide layers, their relative thickness is proportional to the relative diffusion rates. For compact layers growing by a single diffusion mechanism, the ratio of thicknesses should be related to the ratio of the parabolic rate constants by:

$$\frac{X_1}{X_2} = \left(\frac{k'_{p1}}{k'_{p2}}\right)^{1/2} \quad \text{(Eq 1)}$$

where subscripts 1 and 2 refer to layers 1 and 2. The thickness ratio, consequently, is a constant and does not change with time. Because the ions diffusing through the various layers are likely to be different, and because the crystal structures of the layers are certainly different, the thickness ratio is commonly found to be quite far from unity. One layer is usually much thicker than the others.

When diffusion controls the growth of each layer, the entire scale will appear to follow the parabolic oxidation equation, with an effective parabolic rate constant k'_p. However, this effective parabolic rate constant does not need to follow the Arrhenius equation (Eq. 54 in the article "Kinetics of Gaseous Corrosion Processes" in this Volume) unless the thickness ratios remain far from unity throughout the temperature range, that is, unless one layer predominates in the analyzed temperature range. If an inner scale predominates, its growth is independent of oxygen pressure, but if the outermost scale is the major part of the scale, the rate constant will vary with oxygen pressure.

Paralinear Oxidation. With some metals, the oxidation growth is parabolic at the beginning, but the protective scale gradually changes (as a whole layer or only partially) to a nonprotective layer. If the inner protective layer remains at a constant thickness, then the diffusion through this layer results in a linear rate of oxidation. The outer layer may become nonprotective by sublimation, transformation to a porous layer, fracture, and so on. This type of oxidation behavior that is initially parabolic and gradually transforms to linear is termed paralinear oxidation (Fig. 1).

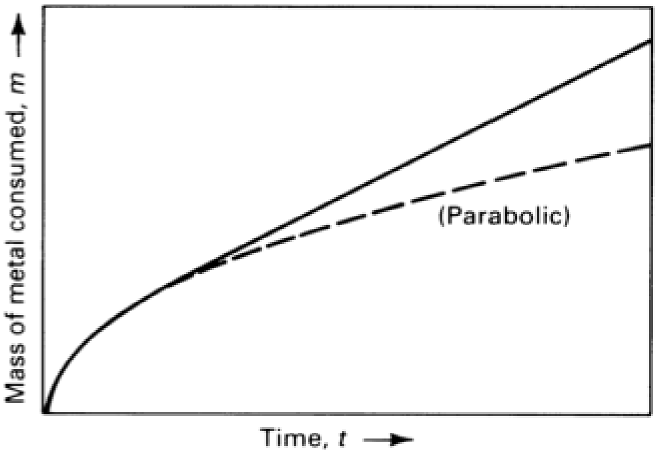

Fig. 1 Paralinear oxidation. Scale growth (mass) is initially parabolic and becomes linear with time.

Oxide Evaporation. At high temperatures, the evaporation of a protective oxide may limit its protective qualities or remove the oxide entirely, because the evaporation rate increases exponentially with temperature. Platinum alloys and refractory metals in particular tend to have volatile oxides. Suboxides and unusual valences are also often found at high temperatures; chromium, for example, forms only one stable solid oxide, Cr_2O_3, but vaporizes as CrO_3 at temperatures above 1173 K (1652 °F). Reactive evaporation in the chromium-oxygen system was measured experimentally and explained theoretically (Ref 1).
Evaporation may be much more intense in gases containing water or halide vapor if volatile hydroxides (hydrated oxides) or oxyhalides form. Theoretically, at low pressures when evaporating molecules do not return to the surface (do not resublimate), the evaporation rate is directly proportional to the sublimation vapor pressure of the oxide. In practical conditions, the total pressure often exceeds 1 atm, while the low oxygen partial pressure creates conditions for oxide evaporation. In such conditions at gas pressures above 10^{-3} to 10^{-4} atm and when the velocity of gas is low (laminar flow), a gaseous stagnant boundary layer slows the escape of the evaporated oxide molecules (stimulates resublimation). The boundary layer becomes thinner at higher gas velocities, leading to higher evaporation losses.
Reactive diffusion provides parabolic oxide growth. The rate of the scale growth decreases (Eq. 53 in the article "Kinetics of Gaseous Corrosion Processes" in this Volume), while the evaporation removes material from the oxide layer at a constant rate (time-independent process). The rate of diffusion through the oxide decreases until the two rates finally become equal. The oxide thickness then remains constant, and the metal oxidizes linearly; that is, the metal consumption shows linear time dependence. If more than one oxide layer protects the metal, the higher-valent, outermost oxide usually has the higher vapor pressure and is more volatile. A detailed analysis of evaporation processes and their impact on oxidation is presented in Ref 2.

References cited in this section

1. K.P. Lillerud and P. Kofstad, *J. Electrochem. Soc.*, Vol 127, 1980, p 2397
2. N. Birks and G.H. Meier, *Introduction to High Temperature Oxidation of Metals,* Edward Arnold, 1983

M. Danielewski, Gaseous Corrosion Mechanisms, *Corrosion: Fundamentals, Testing, and Protection*, Vol 13A, *ASM Handbook*, ASM International, 2003, p 106–114

Gaseous Corrosion Mechanisms

Revised by Marek Danielewski, AGH University of Science and Technology, Cracow, Poland

---

Stresses in Scales

Stress development is inherently coupled with scale growth processes and is often the key factor limiting the protective properties of the scale. During scale growth, recrystallization may occur in either the alloy or the oxide, altering the stresses radically. Changes in temperature usually have a great effect on the stress state for metals in such service. Numerous analyses of practical damage cases have shown that the failure of components is often initiated by stresses resulting from either the oxidation process itself or from operation of the oxidized element. In the past, stress development and relief were often neglected in laboratory investigations; today, the role of stress is well recognized (Ref 2, 3, 4).
There are generally three types of stress that have to be considered:

- External stresses, σ_{ext}, resulting from operation
- Thermally induced stresses, σ_{therm}, due to temperature changes of the system
- Growth stresses, σ_{ox}, resulting from the oxidation/corrosion process itself

The sum of all stresses determines mechanical scale failure. If the sum reaches or exceeds a certain critical value, σ_c, cracking or spalling of the protective oxide follows:

$$\sigma_{tot} = \sigma_{ext} + \sigma_{therm} + \sigma_{ox} \geq \sigma_c \qquad \text{(Eq 2)}$$

Stresses can be measured by different experimental techniques and also predicted from model calculations to assess whether scale failure is likely (Ref 4).

Growth Stresses. The Pilling-Bedworth ratio, first published in 1925, was considered as a major factor for determining the magnitude of growth stress. The Pilling-Bedworth ratio is the ratio of the oxide volume per mole of the metal in the oxide to the metal volume per mole of metal in the metal or alloy. Numerous observations have shown that each step of the scale growth process can generate stress:

- Sometimes crystalline oxides grow on a metal substrate with an epitaxial relationship. As a result of the different lattice parameters, the stresses that develop often limit the epitaxy to several nanometers of scale.
- Polycrystalline oxides develop stresses along their grain boundaries as a consequence of growth of grains in the direction perpendicular to or different from the direction of the scale growth.
- Grain-boundary diffusion, diffusion along oxide grain boundaries, may lead to oxide formation within the growing scale at the boundaries and create compressive stresses.
- Any second phases or foreign inclusions in a metal may oxidize at a rate different from that of the parent metal and create high stresses within the oxide.
- Local changes in composition of the growing scale (due to large deviations from stoichiometry) may result in tensile stress; wustite is an important example, varying from $Fe_{0.95}O$ in equilibrium with the metal to as little as $Fe_{0.84}O$ in equilibrium with Fe_3O_4 at 1370 °C (2500 °F).
- Interdiffusion in a reacting alloy can generate stresses (i.e., Kirkendall effect) when alloy components have different mobilities.
- Diffusion of oxygen into the metal from the oxide creates compressive stresses in the metal, such as in the titanium-oxygen system.
- Surface geometry contributes an additional effect to the growth stresses in an adherent oxide, depending on the surface profile.

Figure 2 shows the four possibilities for changes in stress state in an oxide scale as it grows, assuming that the original growth stresses are compressive (Ref 5).

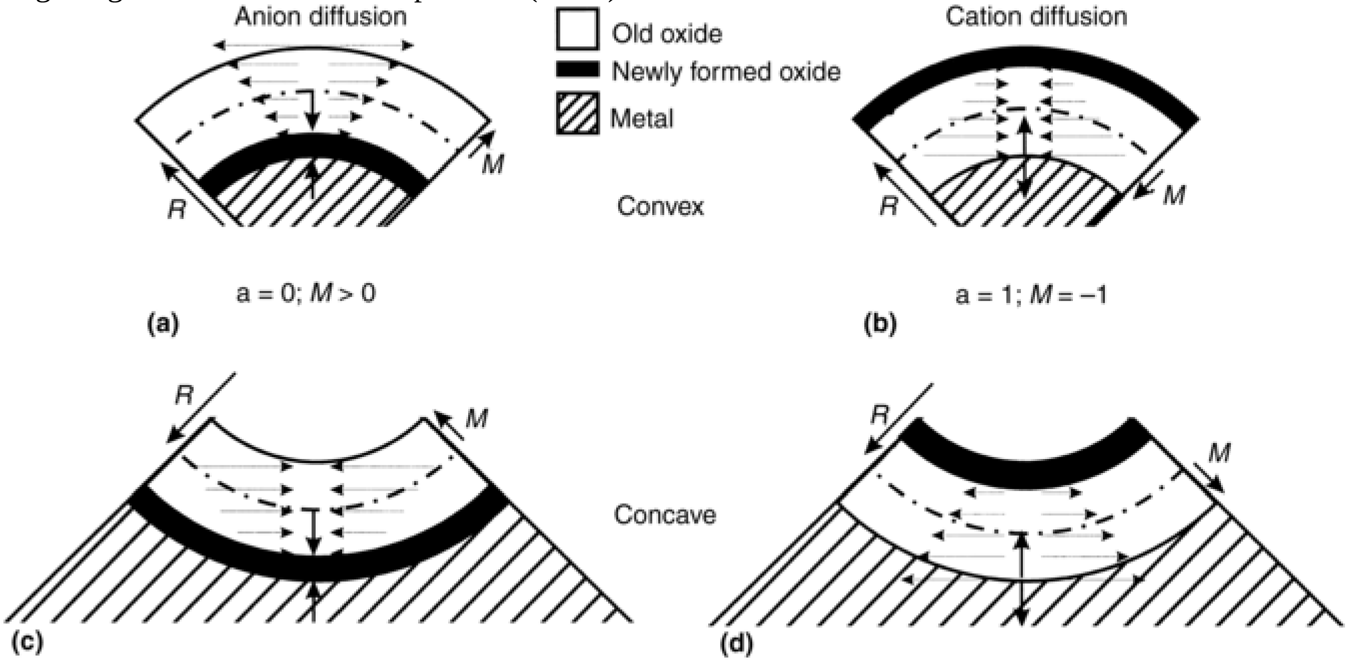

Fig. 2 The development of geometrically induced growth stresses (horizontal arrows) in oxide scales for four combinations of curved surfaces (convex and concave), and growth by anion (left) and by cation (right) diffusion. *R*, radius of curvature; *M*, oxide displacement vector; *a*, volume fraction of oxide formed at the interface. Details of (a) to (d) can be found in the text. Source: Ref 5

For a convex surface on which oxide grows at the oxide-gas interface by cation diffusion outward through the scale (Fig. 2b), the metal surface (M) will gradually recede, increasing the compressive stresses at the metal-oxide interface as long as adhesion is maintained. Figure 2(a) shows oxidation of a convex surface on which the oxide grows at the metal-oxide interface by anion diffusion inward and generates compressive stresses at the metal-oxide interface.

For concave surfaces (Fig. 2d), oxide grows at the oxide-gas interface by outward diffusion of cations. As the metal surface recedes, the compressive growth stresses are reduced and may eventually even become tensile if oxidation continues long enough. Figure 2(c) shows growth on a concave surface by anion diffusion inward for reaction at the metal-oxide interface. Very high compressive stresses develop during growth, until they exceed the cohesive strength of the oxide.

Two major types of growth stresses are distinguished. The first type is the geometrically induced growth stresses that are due to the surface curvature or components (Fig. 2), and the second type is the intrinsic growth stresses. As can often be seen in oxidation experiments on flat samples, the oxide scales crack at the edges of the specimens, for example, during tungsten oxidation. This type of growth stress has been analyzed (Ref 6).

With the help of models, the tangential and radial stresses can be calculated for the ideal case of curved surfaces with a constant radius of curvature. The oxidation increases the strain in the circumferential direction (tangential strain, ϵ^{t}_{ox}) at the rate:

$$\frac{d\varepsilon'_{ox}}{dt} = \frac{M}{R_s}\frac{dh}{dt} = \frac{M}{R_s R_{PB}}\frac{dX}{dt} \quad \text{(Eq 3)}$$

where R_s denotes the radius of curvature of the surface (concave, $R_s < 0$; convex, $R_s > 0$), h is the metal recession, X denotes scale thickness, and R_{PB} is the Pilling-Bedworth ratio. The oxide displacement vector, M, can be calculated from the following expression:

$$M = R_{PB}(1 - a) - (1 - V) \quad \text{(Eq 4)}$$

where a is the volume fraction of oxide formed at the oxide-gas interface and $(1 - a)$ at the metal-oxide interface, and V and $(1 - V)$ denote, respectively, the volume fraction of the metal consumed as a result of the injection of vacancies into the oxidized metal and its volume fraction consumed during oxide formation at the metal-oxide interface.

The scale thickness and metal recession are related:

$$X = R_{PB}h \quad \text{(Eq 5)}$$

Equation 3 allows one to calculate the tangential stresses, σ^{t}_{ox}, when linear elastic behavior can be assumed. The magnitude of the maximum radial stresses, σ^{r}_{ox}, is given by:

$$\sigma^{r}_{ox} = \frac{R_{PB}h}{R_s}\sigma^{t}_{ox} \quad \text{(Eq 6)}$$

The signs of the tangential and radial strains and stresses in the scale and at the metal-oxide interface are given by:

$$\text{sign}\,\varepsilon^{t}_{ox} = \text{sign}\left(-\varepsilon^{r}_{ox}R_s\right) \quad \text{(Eq 7)}$$

$$\text{sign}\,\sigma^{t}_{ox} = \text{sign}\left(-\sigma^{r}_{ox}R_s\right) \quad \text{(Eq 8)}$$

where "+" and "-" denote tensile and compressive stresses, respectively, and R_s is "+" if convex and "-" if concave.

At present, a relatively limited understanding of the mechanisms leading to intrinsic growth stresses has been achieved. The growth stresses were computed for alumina formers (FeCrAl and FeCrAlY alloys) and chromia formers (chromium, NiCr, and FeNiCr stainless steel); oxidation of pure nickel cannot be accurately predicted using model calculations (Ref 4).

Mechanical scale failure takes place when a critical stress level, σ_c, reached. This critical stress level can be converted into a critical strain, ε_c, by dividing the stress by the oxide Young's modulus, E_{ox}, if it is assumed that elastic behavior dominates in scale failure. Strain values are more easily accessible than stress values, because they can be determined by experiments.

Generally, two modes of failure dominate, depending on the stress distribution in the scale: the failure due to tensile stresses and the failure due to compressive stresses. For tensile failure, a mechanical model has been developed describing the critical strain, ε_c:

$$\varepsilon_c = \frac{K_{Ic}}{f E_{ox} \sqrt{\pi c}} \quad \text{(Eq 9)}$$

where K_{Ic} denotes the fracture toughness of the scale, f is a geometrical factor, and c denotes the radius of the defect (pore, crack, precipitate, etc.). Applying this equation, a researcher computed the critical strains for some common oxides (Ref 4).

Transformation Stresses. Preferential oxidation of one component in an alloy may alter the alloy composition to the point that a crystallographic phase transformation occurs. A change in temperature could also cause crystallographic transformation of either the metal or the oxide. The volume change accompanying a transformation creates severe stresses in both the metal and the oxide. Some oxides initially form an amorphous/nanocrystalline structure and gradually crystallize as the film grows thicker. The tensile stress created by volume contraction may partially counteract the compressive growth stresses usually present.

Thermal Stresses. A common cause of failure of oxide protective scales is the stress created by cooling from the reaction temperature. The stress generated in the oxide is directly proportional to the difference in coefficients of linear expansion between the oxide and the metal. Coefficients are listed in Table 1 for a few important metal-oxide systems. In most cases, the thermal expansion of the oxide is less than that of the metal; therefore, compressive stress develops in the oxide during cooling. Multilayered scales will develop additional stresses at the oxide-oxide interface.

Table 1 Coefficients of linear thermal expansion (CTE) of metals and oxides

System	Oxide coefficient		Metal coefficient		Temperature range	
	10^{-6}/K	**10^{-6}/°F**	**10^{-6}/K**	**10^{-6}/°F**	**°C**	**°F**
Fe/FeO	12.2	6.78	15.3	8.50	100–900	212–1650
Fe/Fe_2O_3	14.9	8.28	15.3	8.50	20–900	70–1650
Ni/NiO	17.1	9.50	17.6	9.78	20–1000	70–1830
Co/CoO	15.0	8.3	14.0	7.8	25–350	75–660
Cr/Cr_2O_3	7.3	4.1	9.5	5.3	100–1000	212–1830
Cu/Cu_2O	4.3	2.4	18.6	10.3	20–750	70–1380
Cu/CuO	9.3	5.2	18.6	10.3	20–600	70–1110

Source: Ref 7

References cited in this section

2. N. Birks and G.H. Meier, *Introduction to High Temperature Oxidation of Metals,* Edward Arnold, 1983

3. P. Kofstad, *High Temperature Corrosion,* Elsevier Applied Science, 1988

4. M. Schütze, in *Corrosion and Environmental Degradation,* Vol 1, *Materials Science and Technology, A Comprehensive Treatment,* R.W. Cahn, P. Haasen, and E.J. Kramer, Ed., Wiley-VCH, 1993

5. M.I. Manning, *Corros. Sci.,* Vol 21, 1981, p 301

6. W. Christl, A. Rahmel, and M. Schütze, *Oxid. Met.,* Vol 31, 1989, p 1

7. P. Hancock and R.C. Hurst, The Mechanical Properties and Breakdown of Surface Films at Elevated Temperatures, *Advances in Corrosion Science and Technology,* Vol 4, R.W. Staehle and M.G. Fontona, Ed., Plenum Press, 1974, p 1–84

M. Danielewski, Gaseous Corrosion Mechanisms, *Corrosion: Fundamentals, Testing, and Protection*, Vol 13A, *ASM Handbook*, ASM International, 2003, p 106–114

Gaseous Corrosion Mechanisms

Revised by Marek Danielewski, AGH University of Science and Technology, Cracow, Poland

Stress Relief

The oxide may develop porosity as it grows and relieves stress. If temperatures are high, the stress may reach the yield strength of either the metal or the oxide, so that plastic deformation relieves the stress. A brittle oxide may crack. A strong oxide may remain intact until the internal stresses exceed the adhesive forces between metal and oxide, so that the oxide pulls loose from the metal. These ways in which stresses can be relieved are discussed subsequently.

Porosity. For oxides that grow by cation diffusion outward through cation vacancies (*p*-type oxides, such as NiO), vacancies are created at the oxide-gas interface and diffuse inward through the scale as they exchange places with an equal number of outward-diffusing cations. The vacancies are annihilated within the oxide, at the metal-oxide interface, or within the metal, depending on the system. In some oxides, the vacancies collect together within the oxide to form approximately spherical cavities. The preferred sites for cavity formation are along paths of rapid diffusion, such as grain boundaries and dislocation lines.

Vacancies that are annihilated at the metal-oxide interface may cause detachment of the scale, because voids that form there reduce adhesion of oxide to metal. If detachment is only partial, the oxidation rate slows down, because the cross- sectional area available for diffusion decreases.

Plastic Flow of Oxide. Dislocations are formed in the oxide as it grows epitaxially on the metal because of the crystallographic lattice mismatch between oxide and metal. As the growth continues, these glissile slip dislocations move out into the oxide by the process of glide. Once out in the oxide, they become sessile growth dislocations.

Although dislocations are present in the oxide, slip is not an important process in relieving growth stress (Ref 8). Plastic deformation of the oxide occurs only at high temperatures, at which creep mechanisms become operative. The three important creep mechanisms in oxides are grain- boundary sliding, Herring-Nabarro creep, and climb. Grain-boundary sliding allows relative motion along the inherently weak boundaries. Herring-Nabarro creep allows grain elongation by diffusion of ions away from grain-boundary areas in compression over to boundaries in tension. Within the grains, dislocation climb is controlled by diffusion of the slower-moving ions. The creep rate increases with the amount of porosity in the oxide.

Cracking of Oxide. Tensile cracks relieve growth stresses in the oxide scale. As shown in Fig. 2, tensile stresses may eventually develop in an oxide growing on curved surfaces and cause fracture. In the case of anion diffusion inward on convex surfaces, if oxygen diffuses into the metal, the tensile stresses near the oxide-gas interface develop much more quickly.

Shear cracks can form in an oxide having high compressive stresses near the metal surface, if the scale cohesion is weak and adhesion to the metal is strong. If the metal-oxide interface is planar, a shear crack initiating at the interface can extend rapidly across the surface. However, if the interface is rough because oxidation has concentrated at the grain boundaries of the metal and keyed the oxide into the metal, rapid crack extension may be prevented and scale adherence may be improved.

Periodic cracking of a protective oxide results in the parabolic oxidation being interrupted by a sudden increase in rate when the gas can react directly with the bare metal surface. As oxide begins to cover the metal surface again, parabolic oxidation is resumed. A typical oxidation curve for this repeated process is shown in Fig. 3(a). The time periods between successive parabolic steps are sometimes fairly uniform, because a critical scale thickness is reached that causes cracks to be initiated. The overall oxidation of the metal approaches a slow linear process.

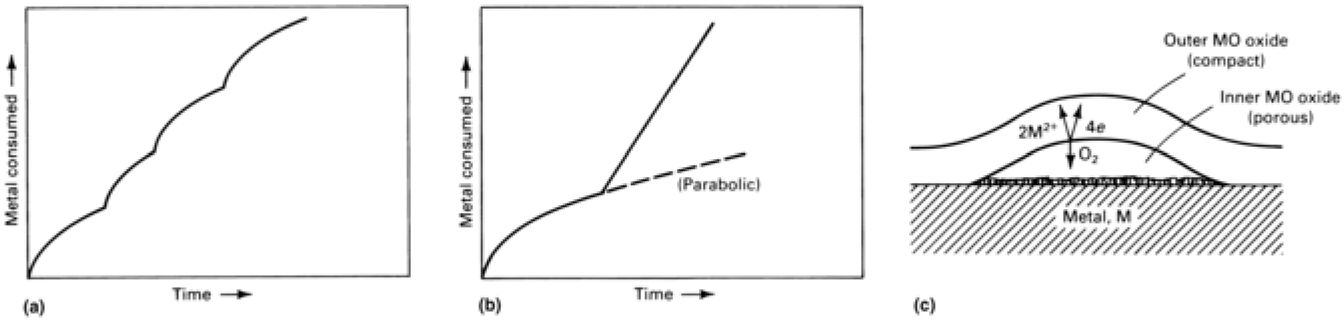

Fig. 3 Cracking of oxide. (a) Periodic cracking of the scale. (b) Breakaway oxidation. (c) Morphology of the single-phase double-layer scale

Occasionally, a metal oxidizes parabolically until the scale cracks or spalls off, and from that time on, the oxidation is linear. The oxide, originally protective, completely loses its protective properties. The breakaway oxidation commonly occurs if many cracks form continuously and extend quickly through the oxide. It can also occur for alloys that have had one component selectively oxidized. When the protective scale spalls off, the metal surface is so depleted in the component that the same protective scale cannot re- form. Breakaway oxidation (Fig. 3b) leaves bare metal continually exposed, unlike paralinear oxidation (Fig. 1), in which an inner protective scale always remains.

Decohesion and Double-Layer Formation. For scale growth by cation diffusion, a protective scale may eventually reach a thickness at which it can no longer deform plastically to conform to the receding metal surface. At this point, decohesion begins at some places along the metal- oxide interface. However, oxidation continues at the oxide-gas interface because cations continue to diffuse outward through the detached scale, driven by the chemical potential gradient across the scale.

At the inner scale surface, the cation concentration decreases, thus locally increasing the oxygen chemical potential. The increased chemical potential results in an increased pressure of O_2 gas that will form in the space between the scale and the metal. The O_2 is then transported to the metal surface by means of surface diffusion and/ or gas phase migration. Because its pressure is greater than the dissociation pressure of oxide in equilibrium with metal, an inner layer of oxide begins to form on the metal. This mechanism is called the dissociation mechanism of the scale growth (Ref 9).

The inner oxide layer forms a porous, fine- grained structure and has essentially the same composition as the compact outer layer. Initially, it starts forming at the nucleation sites of bare metal. The diffusion of O_2 from the outer layer to the inner layer is rate controlling, so that the inner layer grows mainly at its high points and forms a porous scale (Ref 9). Figure 3(c) shows the mechanism of the double-layer scale growth.

For the oxidation of pure chromium, it has been found that at temperatures above 1000 °C (1800 °F), the scale cracks periodically when the intrinsic growth stresses exceed a critical value (Ref 1). Several parabolic partial steps exist in the kinetics curve, which are due to cracking after each of these steps and exposure of the bare metal surface under a detached and cracked oxide scale to the surrounding atmosphere. Thus, the fast, initial oxidation period starts again, leading to a new parabolic partial oxidation curve if the temperature is increased to 1200 °C (2200 °F); the intervals for cracking become so short that they can no longer be resolved in the curve, and a fast, linear curve results. This shows that permanent cracking of the scale by intrinsic growth stresses allows no protection, and therefore, the initial surface oxidation steps are always rate determining. The buckling and cracking of oxide scales due to intrinsic growth stresses can be suppressed by the addition of active-elements to the alloy. There are several possible explanations for the active-element effect, which helps to improve adhesion of the scale and which has been proven for a number of different materials. The major mechanisms are changes of the transport properties in the scale; that is, metal cation diffusion in the outward direction can be suppressed by the presence of certain active elements so that only oxygen-inward transport occurs, leading to scale formation solely at the metal interface and reducing the growth stresses. Numerous mechanisms to explain the reactive- element effect were proposed (Ref 10):

- A change in the transport properties of the oxide; for example, suppression of cation diffusion results in a decreased oxidation rate, and the oxygen-inward diffusion becomes the dominating mode of transport

in the growing scale. As a result of the oxide formation at the metal-oxide interface, the growth stresses are reduced.

- An increase of the density of the nucleation sites at the metal surface results in fine- grained scale, leading to a more plastic scale.
- Highly reactive elements react with sulfur impurities in the metal substrate, thus impeding the segregation of sulfur to the metal-oxide interface, which would otherwise reduce the adhesion of the scale.
- The formation of oxide pegs in the metal (at the metal-oxide interface, for example, at the metal grain boundaries) leads to the keying of the oxide to the metal.
- Reducing the number of physical defects, such as pores in the oxide, decreases the susceptibility of the scale to cracking or detachment.
- The precipitation of oxides containing reactive elements reduces the fast diffusion along the grain boundaries.

Advanced materials and coatings used at temperatures near 1000 °C (1800 °F) benefit from the effect of active-element additions. The active element plays the key role in providing long- term oxidation protection of the protective coatings on gas turbine materials. The most common active elements are yttrium, cerium, rhenium, hafnium, and zirconium.

Deformation of Metal. Foils and thin-wall tubes are often observed to deform during oxidation, thus relieving the oxide growth stresses. At high temperatures, slip and creep mechanisms can be operative in metals while the temperature is still too low for plastic deformation of the oxide. The deformation processes are facilitated by accumulation of porosity in the metal, which is caused by outward cation diffusion (e.g., accumulation/injection of vacancies) and by the selective oxidation of one component of an alloy (e.g., Kirkendall effect in the alloy near the metal-oxide interface).

Catastrophic Oxidation. Although many oxidation failures can be described as catastrophes, the term *catastrophic oxidation* was originally reserved for the special situation in which a liquid phase is formed in the oxidation process. This can occur either when the metal is exposed to the vapors of a low-melting oxide or during oxidation of an alloy having a component that forms a low-melting oxide or sulfide (see Table 2 in the article “Thermodynamics of Gaseous Corrosion” in this Volume). The mechanisms of catastrophic oxidation vary, but the evidence shows that it occurs at the metal-oxide interface. A liquid phase seems to be essential. The liquid usually forms at the oxide-gas surface and penetrates the scale along grain boundaries or pores to reach the metal. The penetration paths can also serve as paths for rapid diffusion of reacting ions. Once at the metal-oxide interface, the liquid spreads out by capillary action, destroying adherence of the solid scale. In the case of alloys, the liquid can penetrate along the grain boundaries and cause intergranular corrosion. When diffusion and/or flow of the oxidant in the gas phase is the rate-limiting process, then oxidation in the absence of a protective scale proceeds linearly. In a case of fast reactions, the metal and corrosion products heat up from the exothermic reaction, and the oxidation process can be even more rapid.

Internal Oxidation/Sulfidation. Internal oxidation (sulfidation) is the term used to describe the formation of fine oxide or sulfide precipitates within an alloy. The oxidant dissolves in the alloy at the metal-oxide interface or at the bare metal surface if the gas pressure is below the dissociation pressure of the metal oxides. Subsequently, it diffuses into the metal and forms the most stable oxide that it can. This is usually the oxide of the most reactive component of the alloy. Internal oxides can form if the reactive element diffuses outward more slowly than the oxygen diffuses inward; otherwise, the surface scale would form. The transport (diffusion) of internally oxidized metal is controlled by the interdiffusion in the alloy. Oxygen transport in an alloy can be treated as Fickian diffusion (Eq 5 and 8 in the article “Kinetics of Gaseous Corrosion Processes” in this Volume). Because the diffusion coefficients of oxidized metal and oxidant vary exponentially with temperature, and because their activation energies are different, it is possible that internal oxidation will occur in an alloy only in a certain temperature range. Because diffusion of oxygen is usually the rate-controlling process in internal oxidation, parabolic behavior is often observed. Based on the assumption that interdiffusion of reactive metal B atoms is negligible and that oxygen has a very low solubility limit in the alloy, the simple quasi- stationary model of the process was formulated. A simple parabolic equation was derived that allows an estimation of the rate of the process (Ref 11):

$$X = \left(\frac{2N_o^S D_o t}{\nu N_B^i} \right)^{1/2} = k_p t^{1/2} \quad \text{(Eq 10)}$$

where N_o^S is the mole fraction of oxygen in the alloy at its surface, N_B^i is the initial mole fraction of reactive metal B in the alloy, D_o is the diffusion coefficient of oxygen in the alloy, v is the ratio of oxygen atoms to metal atoms in the reaction product, and X is the thickness of the internal oxidation zone (i.e., the subscale).

The real processes encountered in practice are more complex. In a binary alloy, a mixed (A,B)O oxide may form as the internal oxide. This will occur if AO and BO have considerable mutual solubility so that the free energy of the system is lowered by precipitation of the mixed oxide. For example, the internal oxide that forms in unalloyed steels is (Fe,Mn)O (Ref 12).

When a cast 25Cr-20Ni-Fe alloy with silicon added is oxidized at 1000 °C (1800 °F), the chromia protective layer is formed on the metal, with the most external layer being a manganese- iron spinel, $(MnFe)Cr_2O_4$. The silica is thermodynamically more stable than chromia. Moreover, the chromia dissociation pressure at the alloy-Cr_2O_3 interface is higher than the Cr-Cr_2O_4 equilibrium. Thus, the amount of oxygen dissolved in the alloy subsurface zone is sufficient to form an internal oxidation subscale (silica precipitation zone).

Internal oxidation of chromium often affects the mechanical properties of alloys; for example, it results in a carbide-free zone. It is a result of the chromium consumption during internal oxidation and of the decomposition of less stable chromium carbides, $Cr_{23}C_6$ (Ref 13). In practice, the protective scales often have cracks, open porosity, or other macrodefects. Moreover, an oxidizing atmosphere can be complex, containing oxygen and sulfur compounds. The cracks are fast diffusion paths for inward transport of oxidant into the underlying steel alloy, and in such a case, the internal sulfidation by the sulfur-bearing molecules is often observed (Ref 14).

Alloy Oxidation: The Doping Principle (Ref 2, 3, 4). For oxides that form according to the mechanism outlined in Ref 12 and that contain impurity cations that are soluble in the oxide, the impurities alter the defect concentration of the scale. Consequently, the oxide growth rate may also be altered by the alloy impurities. Whether the oxidation rate increases or decreases depends on the relative valences of the cations and on the type of oxide.

In a *p*-type semiconducting oxide (NiO, CoO, MnS), the oxidation rate is controlled by cation diffusion through cation vacancies. If the number of cation vacancies can be decreased, the oxidation is slowed. If a few cations with a higher valence are substituted for the regular cations in an oxide, the vacancy concentration is increased. Adding lower-valent cations, such as lithium ions (Li^+), to NiO will reduce the cation vacancy concentration. Substituting ions with the same valence as the rest of the cations in the oxide does not result in a doping effect.

The *n*-type semiconducting oxides behave opposite to the *p*-type oxides. For the oxides that grow by anion diffusion through anion vacancies (typified by ZrO_2), the anion vacancies exist because some cations have a lower-than-normal valence and contribute fewer electrons to the oxygen than required by the structural arrangement. Consequently, anion vacancies are present. If additional low-valent cations replace the regular higher-valent cations, the oxidation rate increases.

The doping principle is not very helpful in developing oxidation-resistant alloys, because the concentration of foreign cations that can be put into solid solution in the oxide is restricted by solubility limits, and the number of foreign ions that could be used is extremely limited by their valence. Moreover, many technically important oxides, nitrides, or sulfides are ionic conductors.

Selective Oxidation. An alloy is selectively oxidized if one component, usually the most reactive one, is preferentially oxidized. Otherwise, when two or more alloy elements react, the process is called concurrent oxidation. The simplest case would be a binary alloy with a uniform scale composed entirely of only the oxide that one of the components can form. An obvious example of selective oxidation would be scale formation on alloy A-B, where A is so noble that AO is not thermodynamically stable at the environmental pressure and temperature. That is, the oxygen partial pressure in the gas is less than the equilibrium (dissociation) pressure of AO oxide. Only BO scale can form.

For situations in which both A and B can react with oxygen at the temperature and gas pressure involved, but A is somewhat more noble than B, the alloy composition determines which oxide forms. The scheme of selective oxidation of a binary alloy is shown in Fig. 4. The *x*-axis is position and the *y*-axis is the concentration. Alloying element A becomes depleted as it reacts at the metal-oxide interface. This creates a concentration gradient of A, causing A to diffuse from the interior of the alloy toward the surface. At the same time, depleting

A near the metal surface increases the concentration of B so that B should diffuse inward. If the diffusivities (J) of A and B in the alloy are similar to the diffusivity of A in the oxide, the element A will not be seriously depleted at the metal-oxide interface, and AO continues to form. However, the diffusion through the alloy is usually much slower than through the oxide; consequently, the concentration of B will increase at the alloy surface until it reaches N_B^*, the critical concentration at which formation of BO is thermodynamically favorable. At that time, BO will form along with AO.

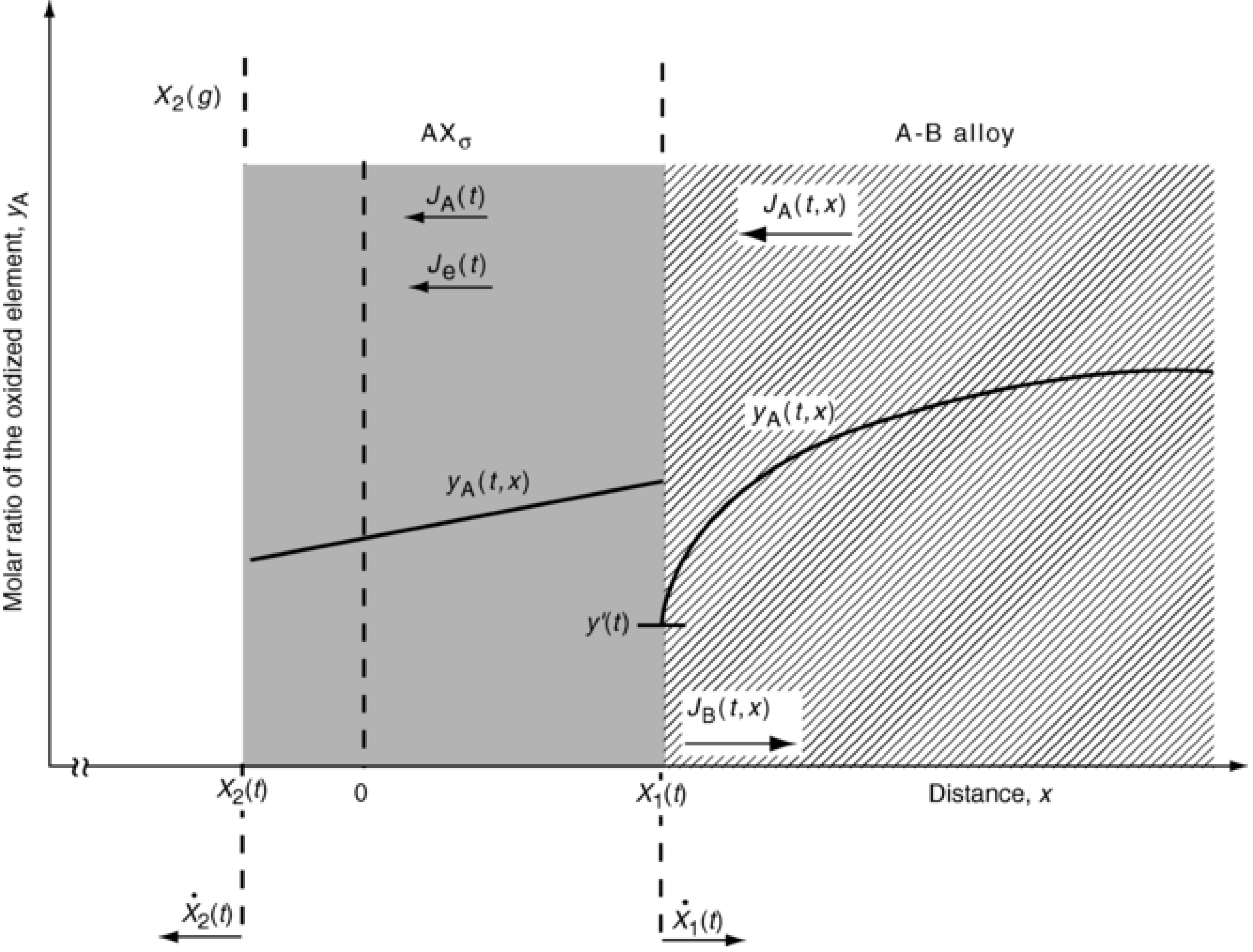

Fig. 4 Schematic showing the mass flow and scale growth during the selective oxidation of a binary alloy. Location is plotted on *x*-axis and the concentration of component A(y_A) is plotted on *y*-axis. The initial surface of A-B alloy (at $t = 0$) is at $x = 0$. $X_1(t)$ and $X_2(t)$ are the positions of the oxide/alloy and oxidant/oxide interface, respectively. $\dot{X}_1(t)$ and $\dot{X}_2(t)$ are their velocities. *J* is the diffusivity flux.

Reducing Oxidation Rates. The oxidation rate of a reactive metal cannot be markedly reduced by alloying it with a noble metal. If the concentration of the reactive element is far greater than the critical concentration needed to form an external scale, that is, if $N_B \gg N_B^*$, alloying with a noble metal will have very little effect on the oxidation rate.

The model of parabolic, selective oxidation of a binary A-B alloy was proposed by Wagner for a binary nickel-platinum alloy (Ref 15). Wagner combined his theory of metal oxidation with the Darken model of interdiffusion in binary alloys (Ref 16), and obtained an analytical solution for the kinetics of oxidation of nickel-platinum-type alloys. His theory later became a starting point for examination of interdiffusion in *p*-type oxide solid solutions for non-steady-state conditions (Ref 17, 18). During selective oxidation of a binary nickel-platinum alloy, the following reaction takes place at the alloy-oxide interface:

$$\text{Ni(alloy)} + \frac{1}{2}O_2(g) = \text{NiO(s)} \qquad \text{(Eq 11)}$$

When diffusivity of the oxidant in the oxide is negligible and a single type of defect dominates in the metal sublattice, then the parabolic rate constant for nickel oxidation is expressed by:

$$k'_p(t) = 3D_o\left[\left(p''_{O_2}\right)^{1/6} - \left(p'_{O_2}(t)\right)^{1/6}\right] \qquad \text{(Eq 12)}$$

where p_{O_2} and $p'_{O_2}(t)$ denote the equilibrium oxygen partial pressure in gas atmosphere and at the NiO-alloy interface.

As a result of nickel depletion at the NiO-Ni interface, the nickel concentration in the alloy decreases. Consequently, the dissociation pressure of NiO in equilibrium with the alloy increases. Thus, $p'_{O_2}(t)$ is an unknown variable depending on time, and the parabolic rate is not a constant but depends on time. When the alloy is an ideal solid solution, that is, $a_{Ni} = y_{Ni}$, the dissociation pressure of NiO for reaction (Eq 11) can be written in the form:

$$p'_{O_2}(t) = K^{-1/2} a_{Ni}(t)^{-1/2} \approx K^{-1/2} y_{Ni}(t)^{1/2} \qquad \text{(Eq 13)}$$

One can relate the parabolic rate constant to the flux (J) of reacting nickel at (Ni-Pt)|NiO interface (compare Table 2 and Fig. 4). The resulting mass balance at this interface (Stefan condition) takes the form:

$$-J_{Ni}(t, X_1(t)) = D_{NiPt} \left.\frac{\partial y_{Ni}}{\partial x}\right|_{x=X_1(t)} = c\frac{dX_1(t)}{dt} \qquad \text{(Eq 14)}$$

where D_{NiPt} is the interdiffusion coefficient in the alloy at the (Ni-Pt)|NiO interface.

Table 2 Basic assumptions by different authors for modeling selective oxidation of alloys

Assumption	Author		
	C. Wagner (Ref 15)	**F. Gesmundo (Ref 17)**	**Danielewski et al. (Ref 18)**
Mass transport in AX_δ **layer**			
An AX_δ layer is a single phase, compact, and adheres well to the alloy.	X	X	X
Local equilibrium in the growing AX_δ layer is postulated. Thus, the mass action law describes the defect structure of the growing scale.	X	X	X
Defects in cationic sublattice dominate; the nonstoichiometry of AX_δ is low.	X	X	X
Diffusion of ionic and electronic defects is a dominating mode of mass transport.	X	X	X
Interdiffusion in a binary alloy (Darken model)			
Oxidized alloy is an ideal solid solution, i.e., $y_i = a_i$	X	X	X
An alloy molar volume does not depend on composition.	X	X	X
Mass transport in an alloy is controlled by interdiffusion.	X	X	X
The Darken model governs the process. Intrinsic diffusivities are equal and do not depend on composition: $D_A = D_B = D_{AB}$ = constant.	X	X	…
Interdiffusion in multicomponent alloys			
Intrinsic diffusion coefficients of all elements in the system are different.	…	…	X
Interfaces			
The local equilibrium at alloy-AX_δ and AX_δ-X_2(g) interfaces prevails. Thus, it follows that a_A (AX_δ) = a_A (alloy).	X	X	X
The model considers *stationary solution* only.	X	…	…
The *nonstationary reaction period,* during which the concentration of the reacting element at the alloy-AX_δ	…	X	X

interface depends on time, is allowed.

On applying Eq 11, Eq 12, Eq 13, Eq 14, one can express the flux at the Ni|NiO interface as a function of the concentration of the diffusing nickel at this interface. Wagner has shown both theoretically and experimentally that alloying nickel with a small amount of platinum will have very little effect on the oxidation. Oxide growth will be markedly slower only when enough platinum is added to make nickel an extremely low concentration of the alloy. The oxidation rate is then no longer controlled by diffusion of nickel through the oxide but rather by interdiffusion of both nickel and platinum in the alloy.

The practical importance of a model of selective oxidation is that it predict the ability of an alloy and/or coating to support formation of a protective scale.

Composite External Scales. Wagner has shown that for an A-B alloy that is forming both AO and BO oxides, the mole fraction of B at the alloy surface must not exceed:

$$N_B^i \le \left(1 - N_A^*\right) = \frac{V}{z_B M_O}\left(\frac{\pi k_p'}{D_B}\right)^{1/2} \qquad \text{(Eq 15)}$$

where N_A^* is the minimum concentration of A necessary to form AO, V is the molar volume of the alloy, z_B is the valence of B, M_O is the atomic weight of oxygen, k_p' is the parabolic rate constant for growth of BO, and D_B is the diffusion coefficient of B in the alloy. The previous formula does not take into account any complications, such as porosity and internal oxidation. If the concentration of B lies anywhere between N_B^* and (1 − N_A^*), thermodynamics predicts that both AO and BO are formed.

Concurrent Oxidation. When oxides of both metals form, their relative positions and distribution depend on the thermodynamic properties of the oxides and the alloy, the diffusion processes, and the reaction mechanisms. There are two common situations: both metals in a binary alloy oxidize to form two separate oxide phases, or mixed oxides, such as spinels, form.

The first situation involves immiscible oxides, with the more stable oxide growing slowly. With both AO and BO stable but with rapid growth of AO and slow growth of BO, the more stable BO may nucleate first but gradually becomes overwhelmed and surrounded by fast-growing AO (Fig. 5a, b). If diffusion in the alloy is rapid, the oxidation proceeds to form an AO scale with BO islands scattered through it. However, if diffusion in the alloy is slow, the metal becomes depleted of A near the metal-oxide interface, while the growth of BO continues until it forms a complete layer, undercutting the AO (Fig. 5c). Pockets of AO at the metal-oxide interface will gradually be eliminated by the displacement reaction, AO + $B_{(alloy)}$ → BO + $A_{(alloy)}$. Because BO is thermodynamically more stable than AO, this reaction will not go in the opposite direction. Such displacement reaction continues even if the oxygen supply is cut off.

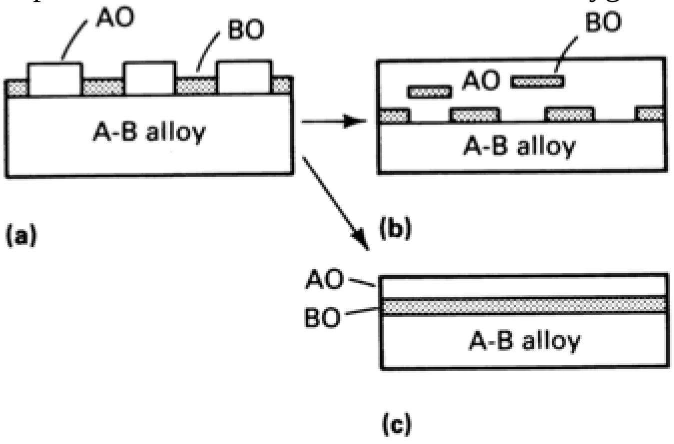

Fig. 5 Simultaneous growth of competing oxides. BO is more stable, but AO grows faster. (a) Early stage with nucleation of both oxides. (b) Later stage if diffusion in alloy is rapid. (c) Final stage if diffusion in alloy is slow

The second situation involves two oxides that are partially miscible. For alloys rich in A, an AO scale will form, with some B ions dissolved substitutionally in the AO structure. If the solubility limit is exceeded when B ions continue to diffuse into the scale, BO precipitates as small islands throughout the AO layer. Even if the

solubility limit is not reached, the more stable BO may nucleate within the AO scale and precipitate. For alloys rich in B, a BO layer first forms. If B ions diffuse through the scale faster than A ions do, the concentration of A ultimately builds up in the scale close to the metal-oxide interface. An AO layer then forms underneath the BO.

Double Oxides. A great deal of research has been directed toward developing alloys that form slow-growing complex oxides. The silicates are particularly important because they can form glassy structures that severely limit diffusion of ions. Therefore, silicide coatings on metals have been successfully used at high temperatures.

Spinels often have extremely low diffusion rates. Spinels are double oxides of a metal with +2 valence and a metal with +3 valence, having the general formula $MO \cdot Me_2O_3$ and also having the crystal structure of the mineral spinel ($MgO \cdot Al_2O_3$). The iron oxide, Fe_3O_4, has an inverse spinel structure. For iron-chromium alloys, the spinel phase can be either stoichiometric $FeO \cdot Cr_2O_3$ or the solid solution $Fe_{3-x}Cr_xO_4$. Although many ternary oxides tend to be brittle, much research has been devoted to minor alloy additions to improve the high-temperature mechanical properties of those ternary scales that are extremely protective.

Corrosion in Complex Atmospheres. High- temperature corrosion has a wide potential for research and development, because new technologies and new materials have led to new challenges with regard to high-temperature corrosion performance. Higher operation temperatures are desired, because they result in higher efficiencies of engines and process plants. The need to operate within more aggressive environments results from the growing demand to dispose of municipal and industrial wastes and residues.

References cited in this section

1. K.P. Lillerud and P. Kofstad, *J. Electrochem. Soc.,* Vol 127, 1980, p 2397

2. N. Birks and G.H. Meier, *Introduction to High Temperature Oxidation of Metals,* Edward Arnold, 1983

3. P. Kofstad, *High Temperature Corrosion,* Elsevier Applied Science, 1988

4. M. Schütze, in *Corrosion and Environmental Degradation,* Vol 1, *Materials Science and Technology, A Comprehensive Treatment,* R.W. Cahn, P. Haasen, and E.J. Kramer, Ed., Wiley-VCH, 1993

8. A. Nayer, *The Metals Databook,* McGraw- Hill, 1997

9. S. Mrowec and T. Werber, *Gas Corrosion of Metals,* National Center for Scientific, Technical and Economic Information, 1978

10. A. Rahmel and M. Schütze, *Oxid. Met.,* Vol 38, 1992, p 255

11. C. Wagner, Types of Reaction in the Oxidation of Alloys, *Z. Elektrochem.,* Vol 63, 1959, p 772–782

12. S.A. Bradford, Formation and Composition of Internal Oxides in Dilute Iron Alloys, *Trans. AIME,* Vol 230, 1964, p 1400–1405

13. H.W. Grünling, S. Leistikov, A. Rahmel, and F. Schubert, in *Aufbau von Oxidschichten auf Hochtemperaturwerkstoffen und ihre technische Bedeutung,* A. Rahmel, Ed., Deutsche Gesellschaft für Metallkunde, 1982, p 7

14. H.J. Grabke, J.F. Norton, and F.G. Castells, in *High Temperature Alloys for Gas Turbines and Other Applications,* W. Betz, R. Brunetaud, et al., Ed., Reidel, 1986, p 245

15. C. Wagner, *J. Electrochem. Soc.,* Vol 99, 1952, p 369

16. L.S. Darken, *Trans. AIME,* Vol 174, 1948, p 184

17. F. Gesmundo and M. Pereira, *Oxid. Met.,* Vol 47, 1997, p 507

18. M. Danielewski, R. Filipek, and A. Milewska, *Solid State Phen.*, Vol 72, 2000, p 23

M. Danielewski, Gaseous Corrosion Mechanisms, *Corrosion: Fundamentals, Testing, and Protection*, Vol 13A, *ASM Handbook*, ASM International, 2003, p 106–114

Gaseous Corrosion Mechanisms

Revised by Marek Danielewski, AGH University of Science and Technology, Cracow, Poland

Sulfidation

In distillation and gasification processes, high amounts of sulfur may be present in the form of H_2S, while, at the same time, the oxygen partial pressures are extremely low. As a result, on conventional materials, sulfide scales are formed instead of oxides. Due to their high defect concentration, the sulfide scales show extremely high growth rates on these materials (Fig. 6), which is contrary to the protective effect that most of the oxide scales exhibit on these materials (Ref 19). For this reason, the use of conventional steels is basically limited to temperatures of 450 to 550 °C (840 to 1020 °F) when sulfidation occurs. To find materials solutions, intensive studies have been performed with a large number of conventional materials and with new groups of materials, such as the aluminides and the silicides. The application of coatings based on these compounds on the low-cost conventional steels seems to be feasible. The highest resistance under these conditions was by $MoSi_2$. However, $MoSi_2$ failed as a coating due to spalling attributed to the difference in thermal expansion of $MoSi_2$ and conventional steels. Iron aluminides are attractive on the basis of cost. However, again, their coefficients of thermal expansion do not match that of low-alloy, high-temperature steels, and they are sensitive to hydrogen embrittlement. Titanium aluminide (TiAl), which is applied as plasma spray coating by different techniques or in the form of a diffusion coating by codiffusion, is used for operating temperatures to 700 °C (1300 °F) in sulfidizing atmospheres.

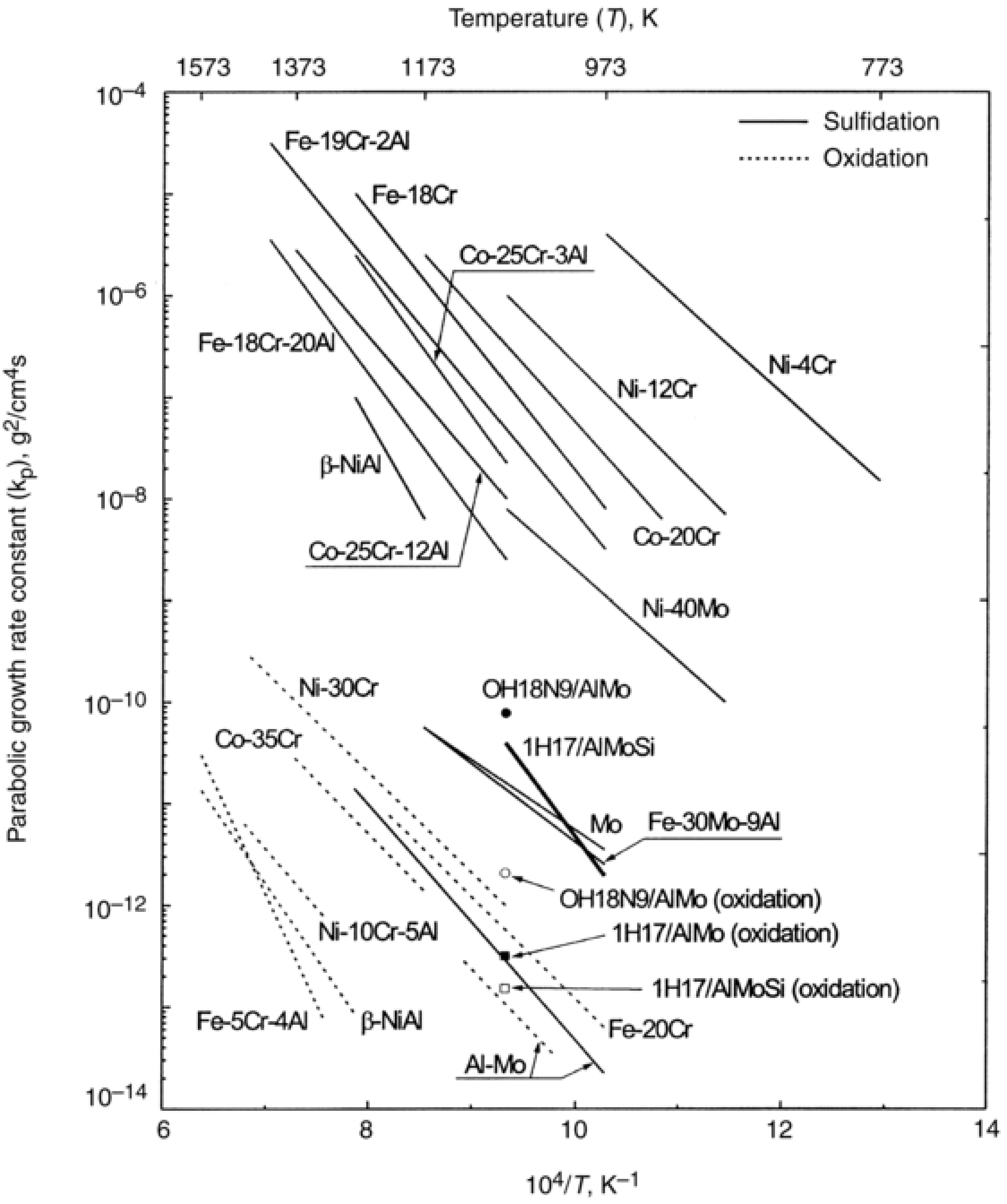

Fig. 6 Collective plot of the temperature dependence of the sulfidation and oxidation rate of binary and ternary alloys and coatings. Source: Ref 19

Reference cited in this section

19. H. Habazaki, K. Takahiro, S.Y. Yamaguchi, K. Hashimoto, J. Dabek, S. Mrowec, and M. Danielewski, *Mater. Sci. Eng. A*, Vol 181/ 182, 1994, p 1099

M. Danielewski, Gaseous Corrosion Mechanisms, *Corrosion: Fundamentals, Testing, and Protection*, Vol 13A, *ASM Handbook*, ASM International, 2003, p 106–114

Gaseous Corrosion Mechanisms

Revised by Marek Danielewski, AGH University of Science and Technology, Cracow, Poland

Metal Dusting

Metal dusting occurs in atmospheres with very low oxygen partial pressures and carbon activities greater than 1. The mechanisms of this process are well understood (Ref 20). During metal dusting, the material disintegrates into a powder of nanosize metal particles and graphite (graphite wool). This process is a catastrophic form of high-temperature corrosion. The incubation period for metal dusting attack in the case of high-alloy materials may last up to more than 10,000 h. The depletion of chromium in the metal subsurface zone of these materials may play a significant role in the initiation of dusting attack. In this case, the use of protective coatings is a solution. These protective coatings could contain a much higher level of the scale-forming elements. Commercial coatings are based on enriching the subsurface of steels by the diffusion of aluminum. Recent investigations show that TiAl coatings and SiAl coatings can further improve the resistance of steels under such conditions (Ref 21).

References cited in this section

20. H.J. Grabke, *Mater. Corros.*, Vol 49, 1998, p 303

21. F. Dettenwanger, C. Rosado, and M. Schü tze, *Proc. Int. Workshop on Metal Dusting*, K. Natesan, Ed., Argonne National Laboratory, 2002

M. Danielewski, Gaseous Corrosion Mechanisms, *Corrosion: Fundamentals, Testing, and Protection*, Vol 13A, *ASM Handbook*, ASM International, 2003, p 106–114

Gaseous Corrosion Mechanisms

Revised by Marek Danielewski, AGH University of Science and Technology, Cracow, Poland

Chlorine Corrosion

A chlorine corrosion knowledge base was created in the 1950s. The mechanisms are well understood, but the use of the metals is still limited up to 650 °C (1200 °F) for environments with low oxygen partial pressures and up to 800 °C (1470 °F) for conventional materials in oxidizing environments. The main problem when chlorine corrosion occurs is the formation of volatile metal chlorides. These metal chlorides develop partial pressures above the critical value of ~10^{-4} atm. Thermodynamic analysis shows that the resistant base alloy should consist of nickel with high amounts of chromium and molybdenum, because their evaporation rates would be low. However, such alloy compositions are sensitive to the presence of oxygen, because highly volatile chromium oxychlorides and molybdenum oxychlorides will be formed. Thus, the development of new materials is an important target for such environments. The existing database on the corrosion resistance under oxidizing/chloridizing environments shows that a high aluminum reservoir in the metal subsurface zone seems to be the only way to offer sufficient corrosion protection at high operating temperatures.

M. Danielewski, Gaseous Corrosion Mechanisms, *Corrosion: Fundamentals, Testing, and Protection*, Vol 13A, *ASM Handbook*, ASM International, 2003, p 106–114

Gaseous Corrosion Mechanisms

Revised by Marek Danielewski, AGH University of Science and Technology, Cracow, Poland

Summary Outline of Alloy Oxidation

A schematic diagram has been constructed to show the complexity of morphologies of scale growth on binary alloys (Ref 22) (Fig. 7). The diagram illustrates some types of structures that are known to form; it does not pretend to present those that would be theoretically possible.

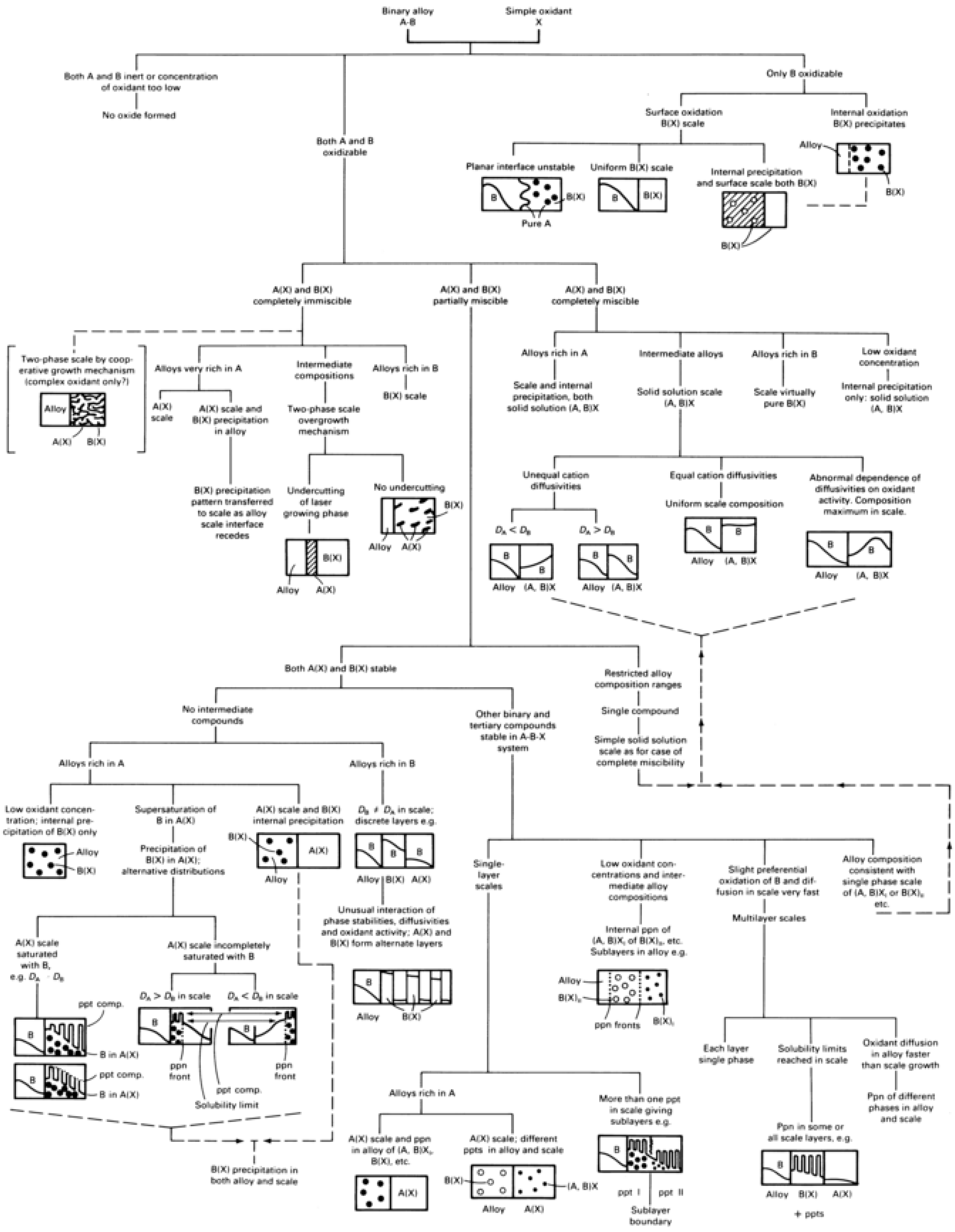

Fig. 7 Schematic showing the relationships between scale morphologies on binary alloys. ppn, precipitation; ppt, precipitate. Source: Ref 22

The demand for an increase in process temperatures requires new structural materials and coatings. There is still a significant potential for theoretical studies. The progress in fundamental studies may significantly speed the development of the new materials and coatings.

Reference cited in this section

22. B.D. Bastow, G.C. Wood, and D.P. Whittle, Morphologies of Uniform Adherent Scales on Binary Alloys, *Oxid. Met.,* Vol 16, 1981, p 1–28

M. Danielewski, Gaseous Corrosion Mechanisms, *Corrosion: Fundamentals, Testing, and Protection*, Vol 13A*, ASM Handbook*, ASM International, 2003, p 106–114

Gaseous Corrosion Mechanisms

Revised by Marek Danielewski, AGH University of Science and Technology, Cracow, Poland

---

Acknowledgment

Portions of this article have been adapted from S.A. Bradford, Fundamentals of Corrosion in Gases, *Corrosion,* Vol 13, *ASM Handbook* (formerly *Metals Handbook*, 9th ed.), ASM International, 1987, p 61–76.

M. Danielewski, Gaseous Corrosion Mechanisms, *Corrosion: Fundamentals, Testing, and Protection*, Vol 13A*, ASM Handbook*, ASM International, 2003, p 106–114

Gaseous Corrosion Mechanisms

Revised by Marek Danielewski, AGH University of Science and Technology, Cracow, Poland

---

References

1. K.P. Lillerud and P. Kofstad, *J. Electrochem. Soc.,* Vol 127, 1980, p 2397
2. N. Birks and G.H. Meier, *Introduction to High Temperature Oxidation of Metals,* Edward Arnold, 1983
3. P. Kofstad, *High Temperature Corrosion,* Elsevier Applied Science, 1988
4. M. Schütze, in *Corrosion and Environmental Degradation,* Vol 1, *Materials Science and Technology, A Comprehensive Treatment,* R.W. Cahn, P. Haasen, and E.J. Kramer, Ed., Wiley-VCH, 1993
5. M.I. Manning, *Corros. Sci.,* Vol 21, 1981, p 301
6. W. Christl, A. Rahmel, and M. Schütze, *Oxid. Met.,* Vol 31, 1989, p 1
7. P. Hancock and R.C. Hurst, The Mechanical Properties and Breakdown of Surface Films at Elevated Temperatures, *Advances in Corrosion Science and Technology,* Vol 4, R.W. Staehle and M.G. Fontona, Ed., Plenum Press, 1974, p 1–84
8. A. Nayer, *The Metals Databook,* McGraw- Hill, 1997
9. S. Mrowec and T. Werber, *Gas Corrosion of Metals,* National Center for Scientific, Technical and Economic Information, 1978

10. A. Rahmel and M. Schütze, *Oxid. Met.,* Vol 38, 1992, p 255

11. C. Wagner, Types of Reaction in the Oxidation of Alloys, *Z. Elektrochem.,* Vol 63, 1959, p 772–782

12. S.A. Bradford, Formation and Composition of Internal Oxides in Dilute Iron Alloys, *Trans. AIME,* Vol 230, 1964, p 1400–1405

13. H.W. Grünling, S. Leistikov, A. Rahmel, and F. Schubert, in *Aufbau von Oxidschichten auf Hochtemperaturwerkstoffen und ihre technische Bedeutung,* A. Rahmel, Ed., Deutsche Gesellschaft für Metallkunde, 1982, p 7

14. H.J. Grabke, J.F. Norton, and F.G. Castells, in *High Temperature Alloys for Gas Turbines and Other Applications,* W. Betz, R. Brunetaud, et al., Ed., Reidel, 1986, p 245

15. C. Wagner, *J. Electrochem. Soc.,* Vol 99, 1952, p 369

16. L.S. Darken, *Trans. AIME,* Vol 174, 1948, p 184

17. F. Gesmundo and M. Pereira, *Oxid. Met.,* Vol 47, 1997, p 507

18. M. Danielewski, R. Filipek, and A. Milewska, *Solid State Phen.,* Vol 72, 2000, p 23

19. H. Habazaki, K. Takahiro, S.Y. Yamaguchi, K. Hashimoto, J. Dabek, S. Mrowec, and M. Danielewski, *Mater. Sci. Eng. A,* Vol 181/ 182, 1994, p 1099

20. H.J. Grabke, *Mater. Corros.,* Vol 49, 1998, p 303

21. F. Dettenwanger, C. Rosado, and M. Schü tze, *Proc. Int. Workshop on Metal Dusting,* K. Natesan, Ed., Argonne National Laboratory, 2002

22. B.D. Bastow, G.C. Wood, and D.P. Whittle, Morphologies of Uniform Adherent Scales on Binary Alloys, *Oxid. Met.,* Vol 16, 1981, p 1–28

A. Gil, Methods for Measuring Gaseous Corrosion Rates, *Corrosion: Fundamentals, Testing, and Protection*, Vol 13A, *ASM Handbook*, ASM International, 2003, p 115–116

Methods for Measuring Gaseous Corrosion Rates

Aleksander Gil, University of Mining and Metallurgy, Cracow, Poland

Introduction

CORROSION RATES of metal alloy test specimens having identical masses but different shapes (e.g., flat circular, cylindrical, or spherical), or identical shapes but different sizes, are not necessarily the same. It has been shown that the best reproducibility of results is obtained with flat samples (Ref 1). Therefore, corrosion studies usually use rectangular- or circular- shaped flat specimens, with thicknesses not exceeding 1 mm (0.04 in.) and total surface area of a few square centimeters (approximately 1 in.^{2}). To eliminate the effect of edges and corners on the corrosion process, these sample parts can be rounded. The corrosion process is additionally

influenced by surface finish (grinding, mechanical or electrolytic polishing, etc.). It is advised to use 600-grit emery paper and ultrasound cleaning when preparing test specimens (Ref 2).

References cited in this section

1. J. Romański, *Corros. Sci.,* Vol 8, 1968, p 67s–89s
2. H.J. Grabke, W. Auer, M.J. Bennett, F. Bregani, F. Gesmundo, D.J. Hall, D.B. Meadowcroft, S. Mrowec, J.F. Norton, W.J. Quadakkers, S.R.J. Saunders, and Z. Zurek, *Werkst. Korros.,* Vol 44, 1993, p 345

A. Gil, Methods for Measuring Gaseous Corrosion Rates, *Corrosion: Fundamentals, Testing, and Protection,* Vol 13A, *ASM Handbook,* ASM International, 2003, p 115–116

Methods for Measuring Gaseous Corrosion Rates

Aleksander Gil, University of Mining and Metallurgy, Cracow, Poland

---

Discontinuous Methods

Most metals react with oxidizing gases (oxygen, nitrogen, sulfur, chlorine) to yield solid products such as scale. These scales are generally adherent to the metallic substrate in a wide temperature range. In such cases, any direct and continuous records of weight losses are impossible. The corrosion rate data can be obtained indirectly by measuring:

- Scale thickness
- Scale weight per unit surface area
- Loss of metal thickness
- Loss of material weight per unit surface area
- Weight change of oxidant bonded in the scale per unit surface area as a function of time

Thickness or weight of the scale or the uncorroded material can be measured in a discontinuous manner at room temperature. Specimens with identical starting dimensions can be exposed to a controlled environment and then removed and measured at differing exposure times. This series of experiments and samples provides the time dependence of the corrosion process.

Scale thickness is measured on the metallographic cross sections. The procedure is simple when the scale is homogeneous, has the same composition on the whole surface, and when internal oxidation does not occur in the metallic core. The dependence of scale thickness on time can be used for the determination of a kinetic law for the oxidation rate. In the case when the rate-controlling step in the oxidation process is the diffusion of ions through a compact barrier layer of oxide with the chemical potential gradient as the driving force, the parabolic rate law is usually observed. As the oxide grows thicker, the diffusion distance increases, and the oxidation rate slows down. The rate (dx/dt) is inversely proportional to the oxide thickness (x) or:

$$\frac{dx}{dt} = \frac{k_p}{x}$$

On integration, the parabolic equation is obtained:

$$x^2 = 2k_pt$$

and the parabolic rate constant, k_p, can be determined from the experiment in units of cm^2/s or similar length squared per time units.

To measure the weight of the scale or the uncorroded metal, it is necessary to remove the corrosion product, which is a rather troublesome task. There are standard practices for removing these corrosion products, however (Ref 3). The discontinuous methods for examining uncorroded base metals are rarely used in studying high-temperature corrosion. However, it should be stressed that the discontinuous methods have certain advantages. Discontinuous methods allow for examination of specimens after different lapse times, so it is possible to follow changes in scale and alloy structure at different stages of the corrosion process.

Reference cited in this section

3. "Preparing, Cleaning, and Evaluating Corrosion Test Specimens," G 1, ASTM International

---

A. Gil, Methods for Measuring Gaseous Corrosion Rates, *Corrosion: Fundamentals, Testing, and Protection*, Vol 13A, *ASM Handbook*, ASM International, 2003, p 115–116

Methods for Measuring Gaseous Corrosion Rates

Aleksander Gil, University of Mining and Metallurgy, Cracow, Poland

---

Continuous Methods

Direct measurements of weight or thickness loss during the corrosion process are possible only in the case when the corrosion product is volatile. Metals that form volatile oxides are not numerous. For example, tungsten, molybdenum, and platinum belong to this group. In such cases, the rate of corrosion can be determined continuously on the basis of thickness or weight changes in time. Thickness can be measured during the corrosion experiment by means of a cathetometer.

The weight of an oxidant bonded by a unit surface area, $\Delta m/A$, in units of g/cm^2, can be measured continuously, and in such a case, oxidation of a single sample provides information for determining the rate of corrosion. Again, if the kinetic law of this process is parabolic, the weight-based parabolic rate constant, k_p, can be calculated in units of $g^2/cm^4 \cdot s$. The three principal methods are volumetric, manometric, and thermogravimetric.

The volumetric method is based on measuring the volume of gaseous oxidant consumed by the corroding material under isobaric conditions (Ref 4). This method is highly sensitive but has some limitations. Oxidation cannot be performed in gas mixtures, and gaseous products cannot be formed, because they would disable accurate measurements of oxidant volume.

The manometric method consists of measuring the pressure variations in the reaction zone brought about by the oxidation process (Ref 5). The manometric method is as sensitive as the volumetric one and has similar limitations. An additional problem is that it does not allow maintaining strictly isobaric conditions during the oxidation test.

Thermogravimetric Analysis (TGA). This method is most frequently used in oxidation rate measurements. It is experimentally simple and does not impose any limitations as far as the gas phase composition is concerned. Thermogravimetry consists of measuring the weight changes of the oxidized sample placed in the reaction zone (Fig. 1a). The precision of new thermobalances is such that mass changes as low as 0.1 μg can be measured. This enables determining very small parabolic rate constants, on the order of 10^{-14} $g^2/cm^4 \cdot s$. Gaseous reaction products do not affect the accuracy of measurements, although the rate of reaction calculated from experimental curves may differ from the "real" rate.

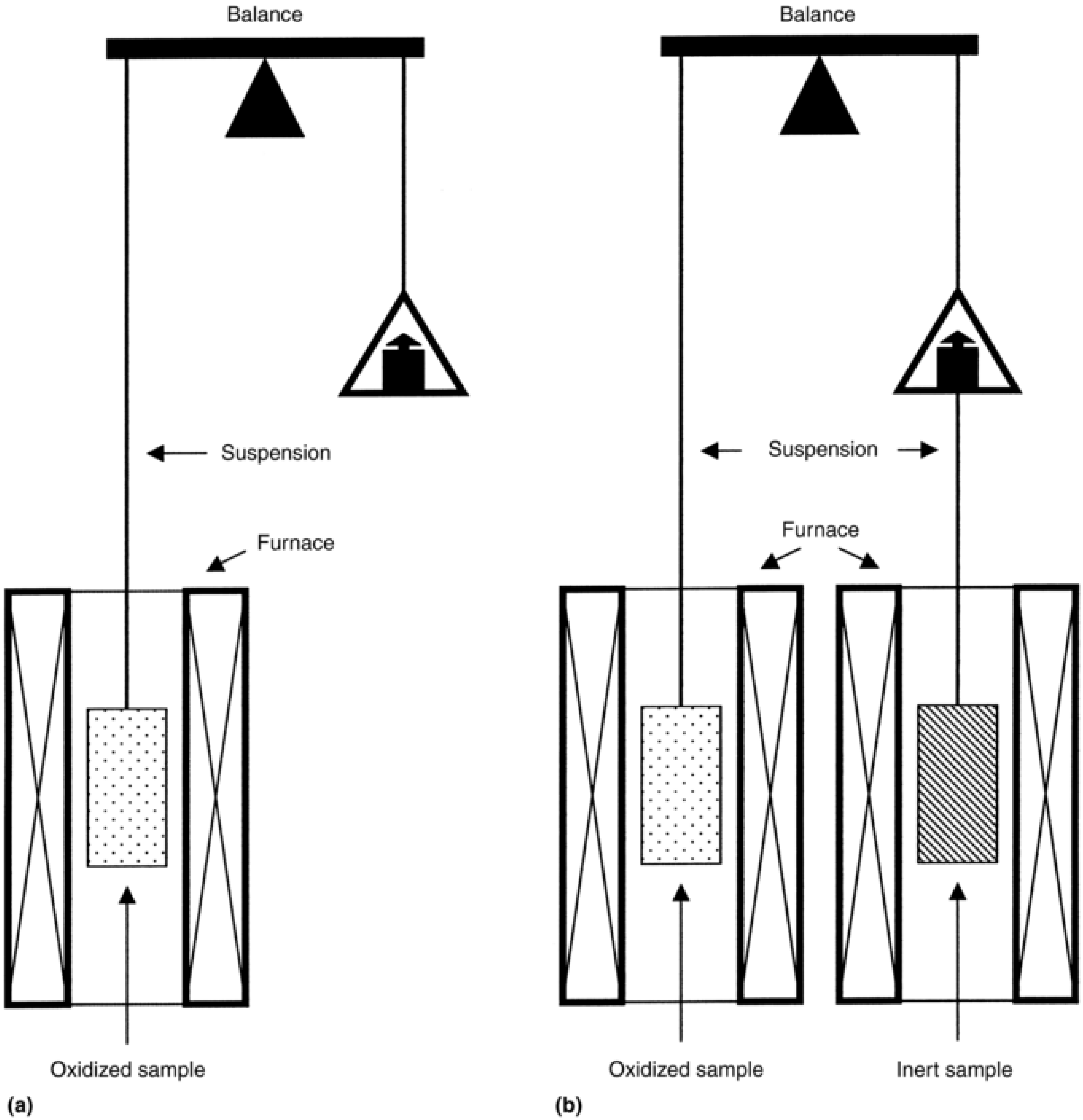

Fig. 1 Schematic drawing of thermobalances for thermogravimetric analysis. (a) Tube furnace and microbalance without compensation for hydrostatic lift. (b) With compensation for hydrostatic lift

The gaseous components may appear as a result of direct reaction between metal and oxidant, but they may also appear as products of secondary reaction between the primary product and the oxidant. In both cases, the weight change taken from the TGA measurement, $\Delta m(t)$, is a difference between the weight of the oxidant taking part in the reaction with the metal, $\Delta m_{ox}(t)$, and the weight of a volatile component of the corrosion product, $\Delta m_{vol}(t)$:

$$\Delta m(t) = \Delta m_{ox}(t) - \Delta m_{vol}(t)$$

The real corrosion rate in such a case is higher than that resulting from the analysis of the TGA curve. This situation arises in chromia formers when the oxidation temperature exceeds approximately 900 °C (1650 °F). Chromium (III) oxide, Cr_2O_3, oxidizes to a volatile CrO_3, and in the presence of water vapor, other volatile compounds are formed, such as $CrO_2(OH)_2$ (Ref 6).

An important source of measuring errors in the TGA method, especially when the weight gains are small, may come from the weight changes of the fixture that supports the sample. The suspensions are usually made of thin

platinum or platinum-rhodium wires, quartz fibers, or preoxidized Fe-Cr-Al wires covered with a protective film of alumina. High temperatures (over 1000 °C, or 1830 °F) and at high partial pressures of oxygen combined with prolonged test times (thousands of hours) would cause a volatile PtO_2 to form. Platinum wires should be avoided. At low partial pressures of oxygen and high temperatures, using quartz suspensions is not recommended because of possible formation of a volatile oxide, SiO. However, by weighing the suspension fixture before and after the experiment, it can be checked whether or not the weight change of the fixture due to corrosion is negligible.

In TGA measurements of oxidation rate, it should be realized that the measured weight of the sample also includes that of gases that are dissolved in the metallic phase without taking part in the oxidation process. One metal with high solubility for oxygen is titanium. Its high- temperature variety, α-Ti, can dissolve as much as 30 at.% oxygen. In the TiAl alloys under the protective alumina scale, there appears a *Z*- phase, $Ti_5Al_3O_2$ (Ref 7), which may bond similar amounts of oxygen as the protective scale. The interpretation of thermogravimetric curves is easier when scale morphologies and cross sections are also examined. This is particularly important when the scale has varying composition on the metal surface and when the internal oxidation zone appears in the metal substrate.

When the specimen is inserted from room temperature into the hot zone of the furnace, it should be realized that its weight slightly increases as a result of hydrostatic lift. The density of gas is inversely proportional to temperature. The hydrostatic lift should be taken into consideration in a situation when the total weight gain of the sample is expected to be small. The effect can be eliminated by means of a thermobalance where the second arm is loaded with a sample having the same dimensions as the investigated one but made of an inert material, for example, Al_2O_3 (Fig. 1b). Both samples are heated to the same temperature. Thermogravimetric curves obtained for the same material in different laboratories exhibit a significant scatter caused by differences in measuring instrument design and experimental conditions. The discrepancies may be due to different gas flow rates in the reaction zone of the furnace, variations in the atmospheric pressure, different air humidity in the case of open systems, or slight differences in temperature or temperature fluctuations in the furnace.

Because of simplicity and high accuracy of measurements, the TGA method is the one most often encountered in corrosion studies. However, other methods can also be used successfully to suit some cases. The thickness of very thin, transparent oxide films is determined by measuring the light interference or polarization changes. It is also possible to determine the rate of corrosion on the basis of measured electrical conductivity of the corrosion product.

References cited in this section

4. J. Engell, K. Hauffe, and B. Ilschner, *Z. Elektrochem.,* Vol 58, 1954, p 478
5. W. Cambell and W. Thomas, *J. Electrochem. Soc.,* Vol 91, 1939, p 623
6. C.A. Stearns, F.K. Kohl, and G.C. Fryburg, *J. Electrochem. Soc.,* Vol 121, 1974, p 89
7. N. Zheng, W. Fischer, H. Gruebmeir, V. Shemet, and W.J. Quadakkers, *Scr. Metall. Mater.,* Vol 33, 1995, p 47

A. Gil, Methods for Measuring Gaseous Corrosion Rates, *Corrosion: Fundamentals, Testing, and Protection*, Vol 13A, *ASM Handbook*, ASM International, 2003, p 115–116

Methods for Measuring Gaseous Corrosion Rates

Aleksander Gil, University of Mining and Metallurgy, Cracow, Poland

---

References

1. J. Romański, *Corros. Sci.*, Vol 8, 1968, p 67s–89s
2. H.J. Grabke, W. Auer, M.J. Bennett, F. Bregani, F. Gesmundo, D.J. Hall, D.B. Meadowcroft, S. Mrowec, J.F. Norton, W.J. Quadakkers, S.R.J. Saunders, and Z. Zurek, *Werkst. Korros.*, Vol 44, 1993, p 345
3. "Preparing, Cleaning, and Evaluating Corrosion Test Specimens," G 1, ASTM International
4. J. Engell, K. Hauffe, and B. Ilschner, *Z. Elektrochem.*, Vol 58, 1954, p 478
5. W. Cambell and W. Thomas, *J. Electrochem. Soc.*, Vol 91, 1939, p 623
6. C.A. Stearns, F.K. Kohl, and G.C. Fryburg, *J. Electrochem. Soc.*, Vol 121, 1974, p 89
7. N. Zheng, W. Fischer, H. Gruebmeir, V. Shemet, and W.J. Quadakkers, *Scr. Metall. Mater.*, Vol 33, 1995, p 47

R.A. Rapp, Corrosion by Molten Salts, *Corrosion: Fundamentals, Testing, and Protection,*, Vol 13A, *ASM Handbook*, ASM International, 2003, p 117–123

Corrosion by Molten Salts

Robert A. Rapp, The Ohio State University

Introduction

THE OPERATION of high-temperature engineering systems, despite their associated materials problems, is inherent to advanced technologies that strive to gain an advantage in thermodynamic driving force or in reaction kinetics or both. Certain high-temperature systems involve the contact of materials with a large quantity, or significant depth, of a salt solution above its liquidus temperature. Such systems include the molten carbonate fuel cell (MCFC), molten chloride baths to melt used aluminum beverage cans, the Hall-Heroult aluminum electrowinning cell with a fluoride (cryolite)-base electrolyte, nitrate/nitrite heat-exchange salts, and fused salt descaling or heat treatment baths. In other important engineering systems, the accelerated corrosion of materials results from the contact of materials with thin films of deposited fused salts. This important corrosion mode, analogous in certain aspects to aqueous atmospheric corrosion near room temperature, is called *hot corrosion.*

Gas turbines, steam generators, incinerators, and various petrochemical process vessels operate at high temperatures (600 to 1100 °C, or 1100 to 2000 °F) and involve metallic or ceramic materials in contact with combustion product gases containing inorganic impurities. As these gases are cooled below their dewpoint, fused alkali sulfate-base salt films may condense on the hardware to generate an aggressive hot corrosion condition. Sometimes, the salt is deposited directly as liquid droplets from the gas stream, sometimes as solid salt particles shed from an upstream filter or compressor for a marine gas turbine. Both in understanding and testing for corrosion by molten salts at high temperatures, the relevant salt depth and the gaseous atmosphere must be respected.

The chemistry and corrosion have been studied for many fused salt systems: chlorides, fluorides, carbonates, sulfates, hydroxides, oxides, and nitrate/nitrite. In analog to aqueous solutions, each of these melts is a dominant ionic conductor of electricity (an electrolyte), and each melt exhibits both an oxidation potential and an acid/base character, which depend on the salt composition and its surrounding environment. Because of their high thermodynamic stability, fused alkali sulfates are frequently formed from the combustion of fossil fuels,

because impurities from both the fuel and the combustion air (perhaps containing a sea salt aerosol) react to form a product based on fused sodium sulfate. Besides its specific engineering significance, fundamental studies of the sodium sulfate system are available in the greatest depth, so this system is chosen to illustrate the important aspects of fused salt corrosion in this article. However, comments pointing out particular aspects of other salt systems are also made. Reference 1 provides a description of further engineering aspects of fused salt corrosion.

Reference cited in this section

1. G.Y. Lai, *High-Temperature Corrosion of Engineering Alloys*, ASM International, 1990

R.A. Rapp, Corrosion by Molten Salts, *Corrosion: Fundamentals, Testing, and Protection,*, Vol 13A, *ASM Handbook*, ASM International, 2003, p 117–123

Corrosion by Molten Salts

Robert A. Rapp, The Ohio State University

Phase Stability and Salt Chemistry

In many respects, the corrosion of materials by fused salts at high temperature has many common aspects with aqueous corrosion near room temperature. Because of its high thermodynamic stability, fused sodium sulfate is frequently the aggressive salt film in combustion product gases that causes hot corrosion. At 1200 K (1700 °F) for the equilibrium:

$$Na_2SO_4 = Na_2O + SO_3(g) \quad \text{(Eq 1)}$$

$$\log a_{Na_2O} + \log P_{SO_3} = -16.7(\text{at } 1200\ K) \quad \text{(Eq 2)}$$

where a_{Na_2O} is the thermodynamic activity for Na_2O, and P is the partial pressure of SO_3. According to Ref 2, one can define the basicity of a sodium-sulfate-base melt as log a_{Na_2O} and its acidity as log P_{SO_3}.

In analog to the Pourbaix approach to the study of aqueous corrosion, Fig. 1 presents a phase stability diagram for the Na-S-O system at 1173 K (1652 °F), where the ordinate is the oxidizing potential and the abscissa is a quantitative measure of the melt basicity/acidity (Ref 3). Figure 1 is calculated from known values of the standard Gibbs formation energies for the phases indicated, and the dotted lines partition the field of Na_2SO_4 stability according to the dominant minority solute species in the Na_2SO_4 solvent. In contrast to aqueous solutions, molecular oxygen has a very low solubility in fused Na_2SO_4, and dissolved SO_3 $(S_2O_7^{2-})$ is the primary oxidizing solute (Ref 4). Oxygen molecules are also almost insoluble in other fused salts. Therefore, in contrast to aqueous solutions, the hydrogen ion has little presence or importance in most fused salts; instead, the electrochemical reduction of oxyanion species is usually important, and the alkali oxide activity is the key indication of melt basicity.

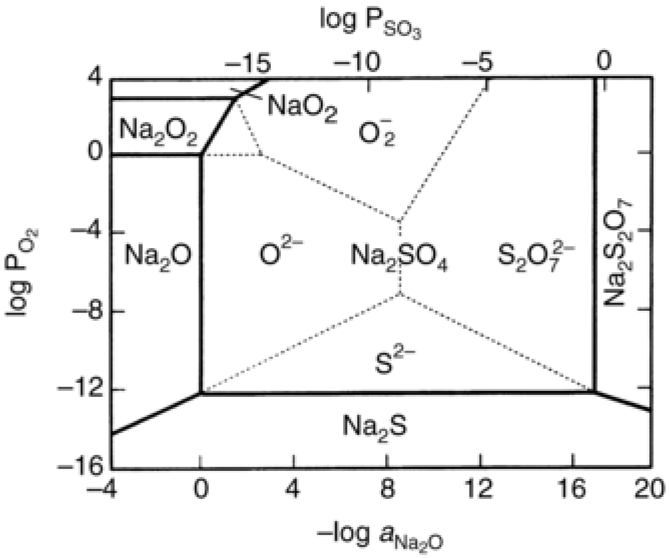

Fig. 1 Na-S-O phase stability diagram for 1173 K (1652 °F). Source: Ref 3

Following the early authors of fused salt stability diagrams, the abscissa for Fig. 1 increases to the right with increasing melt acidity, the opposite to the Pourbaix formalism for aqueous solutions. The basicity and acidity, respectively, of other fused salt systems can be described analogously, so long as only one cation is involved: Na_2CO_3 (log a_{Na_2O}, log P_{CO_2}); NaOH (log a_{Na_2O}, log P_{H_2O}); and $NaNO_3$ (log a_{Na_2O}, log P_{NO_2}). Similar Pourbaix-style phase stability diagrams can be calculated for the other salt systems; today, readily available software will provide such plots.

Electrochemical probes have been developed for the individual measurement of the thermodynamic activities of oxygen and sodium in fused sodium-sulfate-base melts (Fig. 2). These probes involve Na^+- and O^{2-}-conducting solid electrolytes in combination with reference electrodes of known, fixed activities for sodium and oxygen (Ref 3, 5, 6). By the combined use of these two sensors, the thermodynamic activity of Na_2O can be determined, providing a quantitative measure of the melt basicity (abscissa scale in Fig. 1) equivalent to the use of the pH electrode for aqueous solutions. The oxygen sensor alone provides the measurement of the oxygen potential, corresponding to the redox ordinate scale of Fig. 1. When only sodium cations are involved, with sulfate or several other anions, these probes can accurately provide a measure of melt basicity defined as log $a_{Na_2O}$and the oxidation potential (log P_{O_2}). Analogous sensors have been used with fused carbonate melts, fused chloride melts, and for oxyfluoride melts (Ref 7), and they could be developed for other fused salt systems.

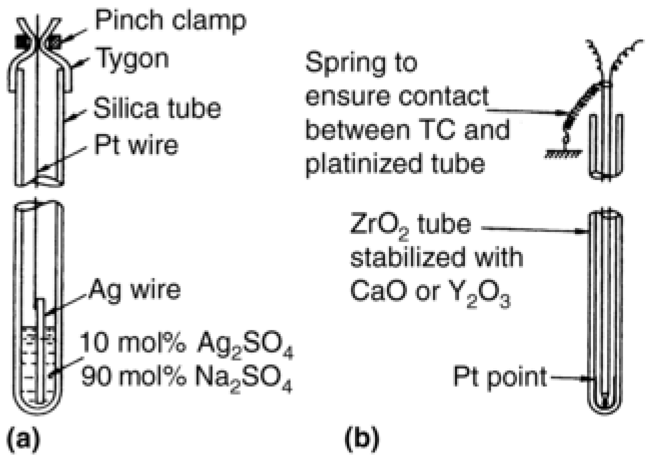

Fig. 2 Experimental electrochemical reference electrodes to simultaneously measure sodium and oxygen activities and thereby, melt basicity. (a) Ag/Ag^+ electrode. (b) ZrO_2 electrode. Source: Ref 3, 5, 6

Because of the high temperatures involved, the usual highly oxidized state of the aggressive fused salts, and the thermodynamic incompatibility of the oxidizing salt and the reducing metal, the hope for corrosion immunity

for materials cannot be realized. Rather, to achieve passivity, the stability and solubility of a protective oxide in contact with the corrosive medium are of great importance, as is the consequence of a localized failure/penetration of the protective oxide. In this context, a protective oxide refers to one obeying diffusion-limited growth kinetics. Thus, the engineer must choose materials and modify processes or environments to achieve an adherent protective oxide with minimal solubility in the fused salt.

Following the Pourbaix approach, the solubility of a (protective) oxide in a (corrosive) solvent is understood by the superposition of a phase stability diagram for that oxide over that for the solvent, for example, Fig. 1 for the Na_2SO_4 salt. Thus, quaternary phase stability diagrams have been generated for many M-Na-S-O systems for the metals of interest, as illustrated by the Cr- Na-S-O stability diagram of Fig. 3 (Ref 8). As for aqueous Pourbaix diagrams, within the field of Cr_2O_3 stability, dashed lines indicate the calculated concentrations for each solute (assuming an ideal solution). The ratio between the actual measured solubilities and the calculated solubilities provides a value for the activity coefficient for the particular solute. Implicit to Fig. 3 is the absence of any field for the stability of chromium metal, either pure or in an alloy. Thus, anytime the fused Na_2SO_4 salt would contact chromium or an alloy containing chromium, a reaction must be expected, most usually to form a sulfide product phase. This behavior is also common to the other important base-metal components, iron, nickel, cobalt, aluminum, and so on (Ref 6). The most important aspect of alloy protection is to prevent contact of the alloy and the salt, for example, by an adherent protective oxide with minimal solubility.

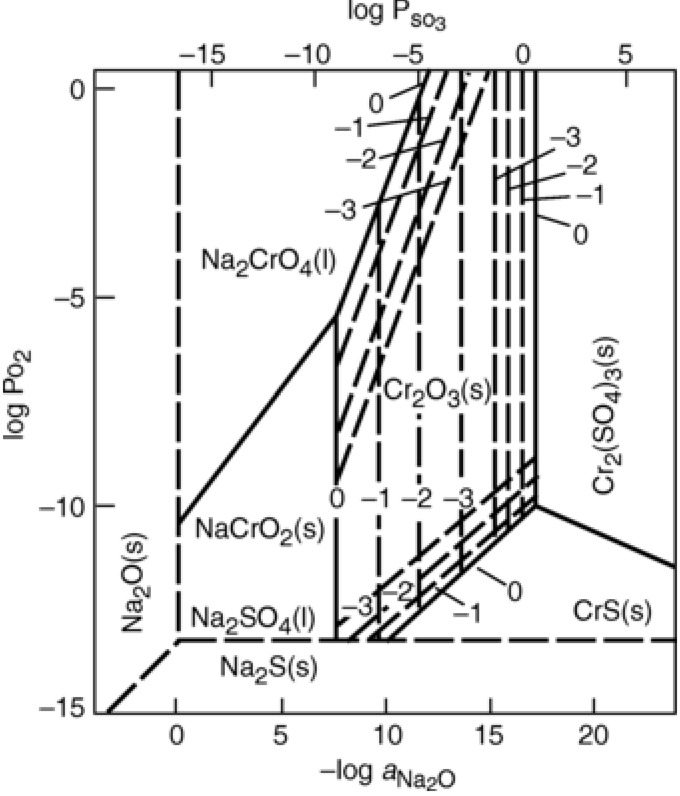

Fig. 3 Na-Cr-S-O phase stability diagram for 1200 K (1700 °F). Source: Ref 8

The Cr-Na-S-O system of Fig. 3 is rather complicated, because Cr_2O_3 can form two acidic ($Cr_2(SO_4)_3$ and CrS) and two basic (Na_2CrO_4 and $NaCrO_2$) solutes. The experimentally measured Cr_2O_3 solubility at 1200 K (1700 °F) and 1 atm O_2 and the relevant dissolution reactions with the predicted slopes are presented in Fig. 4 (Ref 8). In this range of dilute solutions, the expected dependencies for each of the three solutes are closely followed, consistent with Fig. 3. Additional experiments at lower P_{O_2} showed that $NaCrO_2$ becomes the dominant basic solute instead of Na_2CrO_4. Whenever a given cation from an oxide changes its valence on dissolution, for example, forming CrO_4^{2+} from Cr_2O_3 dissolution, the resulting solubility depends on both the basicity and the oxygen activity. In this instance, the solubility of Cr_2O_3 is higher at high oxygen activity and lower at low oxygen activity, for a given basicity. The experimental results of Fig. 4 are in complete agreement with those expected by the Pourbaix thermodynamic approach of Fig. 3, except that at such a high temperature, the oxide solubility can actually be measured and applied to a corrosion model.

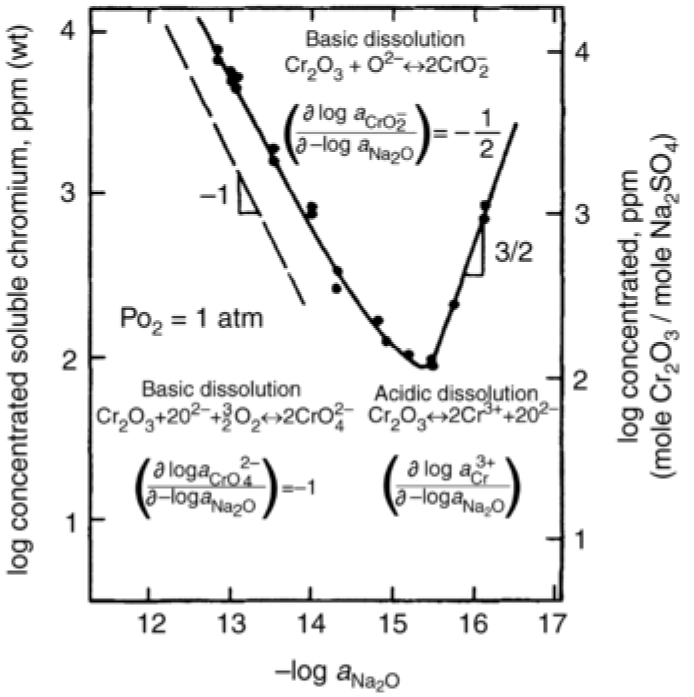

Fig. 4 Experimentally measured solubilities for chromium oxide in fused Na_2SO_4 at 1200 K (1700 °F) and 1 atm oxygen. Source: Ref 8

Figure 5 presents a compilation of such experimentally established solubility plots for 1200 K (1700 °F) and 1 atm O_2 (Ref 5, 6). From these plots, the oxides for nickel and cobalt are the most basic, and the oxides of chromium and aluminum are the most acidic, with approximately six decades of basicity separating their respective solubility minima. For every oxide except SiO_2, the solubility curves comprise the individual contributions from simple (uncomplexed) acidic and basic solutes, with readily predicted slopes. Each plot (except SiO_2) then is comprised of a leg plotting the basic solubility (left side) and another leg plotting the acidic solubility (right side). For basic solubility:

$$MO_x + O^{2-} = MO_{x+1}^{2-}$$
$$d\log\left[MO_{x+1}^{2-}\right]/d\left(-\log a_{Na_2O}\right) = -1 \qquad \text{(Eq 3)}$$

for acidic solubility:

$$MO_x = M^{2x+} + xO^{2-}$$
$$d\log\left[M^{2x+}\right]/d\left(-\log a_{Na_2O}\right) = +x \qquad \text{(Eq 4)}$$

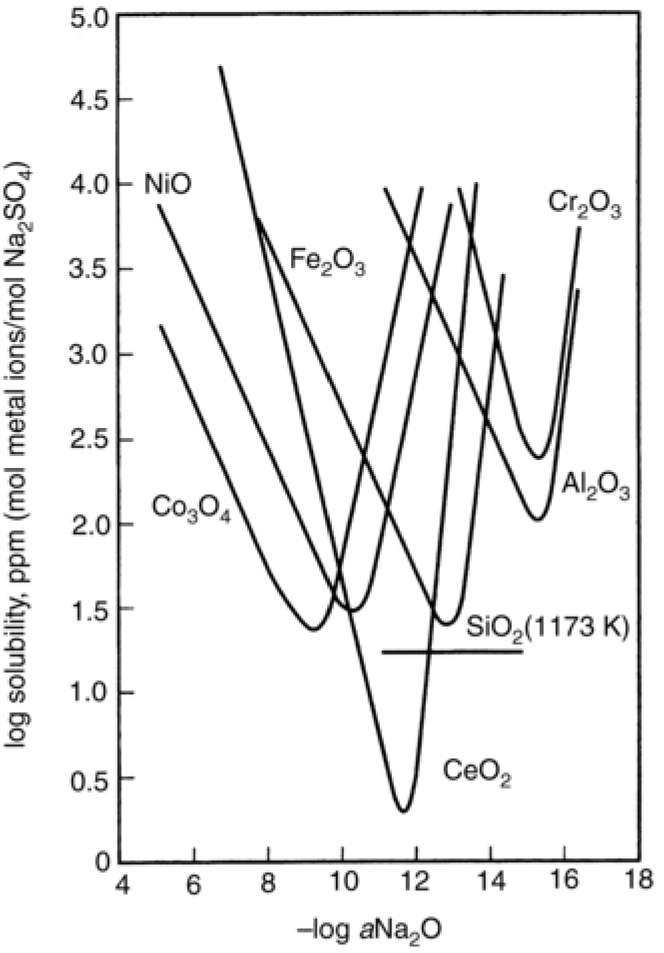

Fig. 5 Compilation of measured solubilities for several oxides in fused pure Na_2SO_4 at 1200 K (1700 °F). Source: Ref 5, 6

Silica, in the indicated (acidic) experimental range, produces only a molecular (no ionic) solute, so no basicity dependence was found. (However, a basic solute does form for silica in more basic solutions.)

The solubility plots of Fig. 5 offer some insight concerning the selection of materials for specific applications. As the first cut, one should choose a material whose slow-growing, adherent oxide scale is close to its solubility minimum for the local conditions in an application, as determined by calculation or measurement. Accordingly, a silica protective film is known to be very resistant to acidic salts, for example, on SiC or Si_3N_4 materials in high-sulfur coal environments (Ref 9). In contact with a quite basic salt, for example, alkali carbonate, silica is readily attacked to form a soluble Na_2SiO_3 product. So, perhaps counter to intuition, combustion product gases in a high-sulfur (acidic) coal-burning facility are less corrosive to a silica-protected material than in an environment with low sulfur but high alkali content. In gas turbine practice, coatings based on Cr_2O_3 and Al_2O_3 have proven effective, because the very acid service condition resulting from sulfur in the fuel and sulfate from seawater corresponds to the minima for their solubility plots. While these protective oxides are the best for this application, any penetration of the oxide provides the condition needed to form sulfides for all of the superalloy components. For this reason, the trace reactive-element additions, such as yttrium, cerium, and lanthanum, which are added to high-temperature alloys to improve scale adherence, also contribute to protection from hot corrosion.

References cited in this section

2. D. Inman and D.M. Wrench, *Br. Corros. J.,* Vol 1, 1966, p 246
3. C.O. Park and R.A. Rapp, *J. Electrochem. Soc.,* Vol 133, 1986, p 1636
4. R. Andresen, *J. Electrochem. Soc.,* Vol 126, 1979, p 328

5. R.A. Rapp, *Corrosion,* Vol 42, 1986, p 568
6. Y.S. Zhang and R.A. Rapp, *J. Met.,* Vol 46, 1994, p 47
7. Y.S. Zhang, X. Wu, and R.A. Rapp, *Metall. Mater. Trans. B,* Vol 34, 2003, p 235
8. Y.S. Zhang, *J. Electrochem. Soc.,* Vol 133, 1986, p 655
9. N.S. Jacobson, *J. Am. Ceram. Soc.,* Vol 76, 1993, p 33

R.A. Rapp, Corrosion by Molten Salts, *Corrosion: Fundamentals, Testing, and Protection,*, Vol 13A*, ASM Handbook*, ASM International, 2003, p 117–123

Corrosion by Molten Salts

Robert A. Rapp, The Ohio State University

Electrochemistry and Fused Salt Corrosion

The electrochemical tests that have proven so important to understanding aqueous corrosion, as reviewed elsewhere in this Volume, also apply directly to corrosion by fused salts. However, fused salt experimentation is probably made more difficult and complicated by the myriad salts of interest. Again, it is important to differentiate between a deep melt and a surface film, because certain important differences in mechanistic interpretation apply. Likewise, because the acid/base and oxidizing potential of a fused salt may be decided by an equilibrium with an ambient gas phase, it is important to match the experimental environment with the service conditions, to the extent possible. For this reason, sulfur-free air should not be substituted in the laboratory testing of hot corrosion for sulfur- laden combustion product gases. Relative to the laboratory electrochemical methods, all the traditional and more advanced techniques can be used for deep melts (crucible tests), for example, three-electrode polarization scanning to establish the kinetics for cathodic and anodic half-cell reactions, chronopotentiometric and chronoamperometric scans, cyclic voltammetry, impedance spectroscopy, electrochemical noise analysis, and so on. Likewise, potentiometric monitoring of the corrosion potential can be done, even for thin fused salt films. Details for such methodologies are beyond the scope of this article, but example studies that establish the electrochemical reactions are available for pure Na_2SO_4 (Ref 3, 10, 11). The Cr-Na-S-O system (Ref 12) and the Mo-Na-S-O system (Ref 13) have been studied in detail.

The mechanistic information that can be gleaned for these electrochemical studies, at least for fused sulfate corrosion of metals, points out the special importance of the cathodic reduction reaction. As shown in Fig. 6, on deep cathodic polarization for a platinum working electrode in fused Na_2SO_4, the reduction of the dissolved oxidant $S_2O_7^{2-}$ (in an acidic melt) becomes quickly limited by diffusion of the ion to the cathode. A resulting sharp drop in the oxidizing potential of the platinum then causes the reduction of the sulfate ion (Ref 3):

$$SO_4^{2-} + 8e^- = S^{2-} + 4O^{2-} \quad \text{(Eq 5)}$$

although this reaction probably occurs over several intermediate steps. Potentiometric reference electrodes, as shown in Fig. 2, have established that when the oxidizing potential dropped rapidly, sulfide ions were formed, and the melt in contact with this cathode greatly shifted in a basic direction.

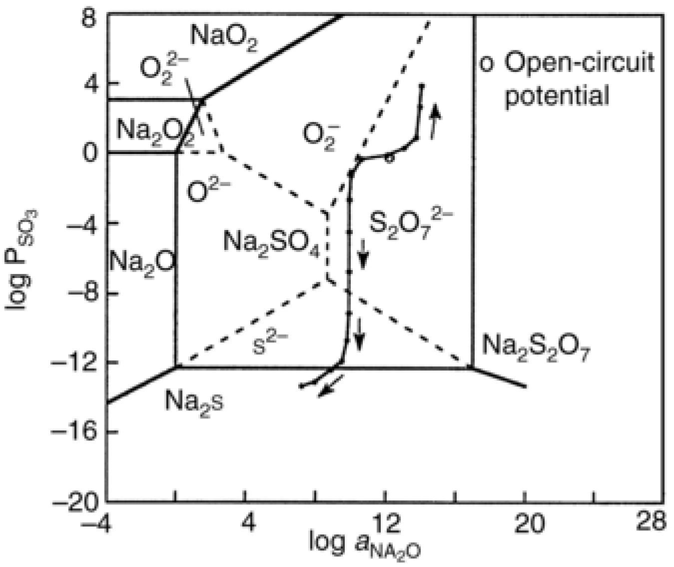

Fig. 6 Trace of basicity and oxygen activity measured on polarization of a platinum working electrode in 0.1% SO_2-O_2 gas at 900 °C (1650 °F). Scan rate, 0.1 mV/s. Source: Ref 3

The relevance of this laboratory experiment on platinum to the corrosive attack of a base metal is apparent. A bare engineering alloy (Fe- Ni-Cr-Al) at high temperatures constitutes a highly reducing condition, equivalent to a deep cathodic polarization driven electrically at the platinum working electrode. If the reactive salt should come into contact with the bare alloy, then immediate sulfidation must be expected, and the salt would locally become very basic. With eutectic temperature in the nickel-sulfur system at 645 °C (1195 °F), perhaps a liquid sulfide product would be formed. This is known to wet and progress along grain boundaries of the alloy. In contact with fused Na_2SO_4, because both chromium and aluminum form thermodynamically more stable sulfides than nickel or iron, these more reactive alloying elements could be removed from the alloy by precipitation of internal sulfides. However, because chromium and aluminum are usually intended to grow and maintain the protective oxide scale, their reaction to form sulfides would eliminate this protection.

Because fused salts are known to readily wet surfaces and interfaces, local ingress of the salt through flaws in the protective scale may also lead to detachment of the scale. Finally, the site of such local sulfide formation would become much more basic than the bulk melt (or salt film), and thus, a gradient in the solubility for the protective oxide in the salt should be established. The significance of the local basicity shift is detailed later. The extreme consequences of a sulfate melt contacting the bare alloy suggests some important aspects for experimental corrosion testing. First, one can never simply immerse a bare base-metal specimen into a bath of hot sulfate salt. An immediate reaction must occur (the metal and the salt are thermodynamically incompatible), so no eventual protection can be expected. Both in experimentation and in engineering applications, some intentionally formed protective oxide should be provided by some preoxidation (in the absence of sulfur). The resistance to fused salt corrosion would then be measured by the initiation time required for the salt to selectively attack some chemical or physical flaw in the protective scale, which would lead to the salt contacting the alloy substrate. For many salt and alloy combinations, rapid attack leading to a failure must be expected after the initiation time.

Of course, different salts pose different types and levels of attack. Consider a nickel-base containment vessel for a fused nitrate/nitrite or carbonate salt. Because nickel does not form a stable nitride or carbide corrosion product, a severe reaction equivalent to sulfide formation in sulfate corrosion is not experienced. However, metal-salt contact would still provide an electrochemical reduction of the oxidizing salt, with a corresponding increase in local melt basicity. If instead, a nickel-chromium or iron-chromium alloy were involved, a nitride or carbide of chromium could result on salt-metal contact. When chloride salts, or complex salts containing chloride, contact a metal, having breached the protective oxide, volatile species are often formed and lost from the alloy. The alloy components iron and chromium often suffer evaporation attack via loss of volatile chlorides, which requires a porous scale in order for the vapors to escape. Sometimes, after volatile species have left the alloy reaction site, the metal component of the vapor species may be reoxidized away from this interface, reforming chlorine (or HCl) vapor to return the substrate to repeat the reaction and continue the cycle.

Such a problem is experienced in incinerator gases and chloride-containing fly ash deposits from coal combustion (Ref 14).

References cited in this section

3. C.O. Park and R.A. Rapp, *J. Electrochem. Soc.,* Vol 133, 1986, p 1636

10. W.C. Fang and R.A. Rapp, *J. Electrochem. Soc.,* Vol 130, 1983, p 2335

11. Y.M. Wu and R.A. Rapp, *J. Electrochem. Soc.,* Vol 138, 1991, p 2683

12. D.Z. Shi and R.A. Rapp, *Werkst. Korros.,* Vol 41, 1990, p 215

13. J. Kupper and R.A. Rapp, *Werkst. Korros.,* Vol 38, 1987, p 187

14. M. Spiegel, *Mater. High Temp.,* Vol 14, 1998, p 221

R.A. Rapp, Corrosion by Molten Salts, *Corrosion: Fundamentals, Testing, and Protection,*, Vol 13A, *ASM Handbook,* ASM International, 2003, p 117–123

Corrosion by Molten Salts

Robert A. Rapp, The Ohio State University

Scale Fluxing: A Hot Corrosion Mechanism

Such a detailed knowledge of oxide solubilities in fused Na_2SO_4, as shown in Fig. 5, leads to the idea that sustained fused salt corrosion could result upon dissolution of the protective oxide and reprecipitation of that solute elsewhere in the salt at a site of lower solubility. The dissolution attack of a protective oxide would reduce its thickness and ultimately lead to its localized attack and scale penetration. A reprecipitation of the solute to form separate oxide particles in the salt would not contribute to any protection. This scale fluxing mechanism is consistent with observed corroded microstructures (porous oxide in a salt matrix) and is applicable to either a deep salt melt or a thin salt film hot corrosion. This scale fluxing mechanism is illustrated for a thin salt film in Fig. 7 (Ref 15) and is denoted as the negative solubility gradient criterion. The decrease in solubility for the oxide across the salt film could be maintained by a combination of gradients in the local salt basicity and its oxygen activity. Probably, such gradients would be more extreme for a salt film (hot corrosion) than for a deep melt. (Remember that the oxidant that is soluble in fused sodium sulfate is dissolved SO_3 [$S_2O_7^{2-}$ ions] and not molecular O_2, as for aqueous solutions.)

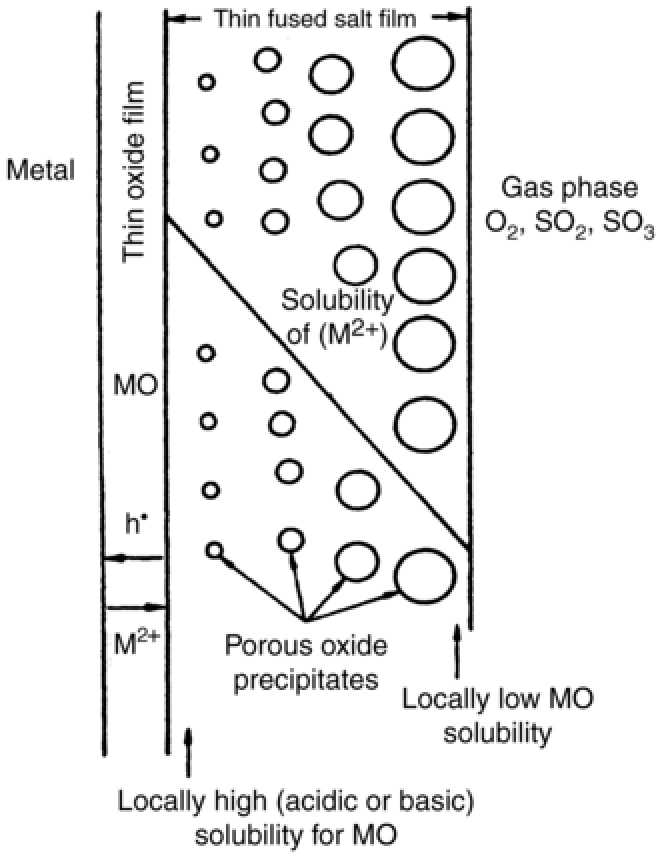

Fig. 7 Reprecipitation of porous MO oxide supported by a negative solubility gradient in the fused salt film. Source: Ref 15

Figure 8 illustrates several conditions leading to a negative solubility gradient on the basis of an idealized solubility curve for the protective oxide (Ref 15). In case A, sustained basic fluxing and reprecipitation is favored, because a dominant basic solute has a higher solubility at the oxide-salt interface than at the salt-gas interface. In case C, an acidic solute satisfies these conditions. In case B, a negative solubility gradient is realized whenever the local conditions cause the corresponding interfacial solubilities to straddle a minimum. Other factors leading to concentration (and solubility) gradients in the salt film include preferential evaporation of some component from the salt-gas interface, such as oxide or oxychloride vapors of refractory metals: vanadium, molybdenum, tungsten, and so on. Reactions, for example, sulfidation, between the salt and the metal lead to high basicity at the metal- salt interface. Likewise, the basicity at the site of the electrochemical reduction reaction is always increased. However, as detailed in Ref 5 and 15, the cathodic reduction reaction might occur at either side of the salt film, depending on several factors, for example, the presence of multivalent transition metal ions in solution. A temperature gradient in the salt at the interface would also contribute to a solubility gradient. Certainly, the solubility of any oxide in any salt would decrease with decreasing temperature. The several sorts of reactions and a thermal gradient all generally lead to some gradient in the solubility of the protective oxide scale. The magnitude of the problem would be greater for a thin salt film than for a deep melt. Accordingly, laboratory studies to test or clarify hot corrosion should not be conducted in a deep melt. The most representative, but expensive, testing for hot corrosion is provided by burner rigs supporting salt injection, where the fuel has the representative sulfur content.

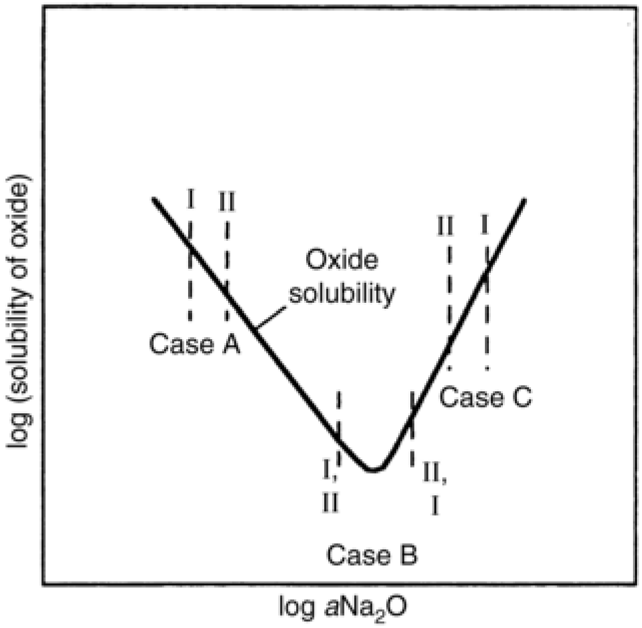

Fig. 8 Types of sustained hot corrosion of a pure metal. Site I is the oxide-salt interface, and site II is the salt-gas interface. Source: Ref 15

Historically, it has been demonstrated (Ref 16) that a condensed fused salt film is required for severe hot corrosion attack, and that Na_2SO_4 vapor in air is innocuous. Researchers (Ref 17, 18, 19) showed that the attack does not necessarily depend on an alloy sulfidation-oxidation sequence but rather on a destructive dissolution (fluxing) of the normally protective oxide in dependence on the presence of Na_2O in the fused salt film. Thin coatings of Na_2CO_3 and $NaNO_3$ on the alloys produced accelerated attack similar to Na_2SO_4, although sulfur was absent from the system. Finally, while pure nickel reacts rapidly with Na_2SO_4, because a sulfide phase is formed, a Na_2CO_3 film does not produce such rapid attack of nickel, because no carbide is formed. In total, these studies illustrated qualitatively that salt-alloy reactions can (but might not) shift the acid/base character of a fused salt film, thereby effecting a fluxing of the protective scale.

During nominally the same time period, researchers (Ref 20) studied the attack of pure nickel and nickel-base alloys beneath a fused Na_2SO_4 film at 1000 °C (1830 °F) and suggested a scale fluxing mechanism consistent with Fig. 7. A basic fluxing of the protective NiO scale and subsequent oxide reprecipitation resulted from the following reaction:

$$4Ni + Na_2SO_4 = Na_2O + 3NiO + NiS \quad \text{(Eq 6)}$$

According to this reaction, nickel metal reacts with fused Na_2SO_4 (not a gas phase reactant) to form NiO and thereby reduces the oxygen activity until the sulfur activity of the salt contacting the metal is sufficient to form liquid nickel sulfide. As sulfur is removed from the salt by reaction with nickel, the local salt basicity (sodium oxide activity) increases, such that the normally protective NiO scale is dissolved/fluxed to form a basic solute, proposed to be nickelate ions. As part of the characteristic morphology for a corroded nickel specimen, nickel sulfide was seen in the metal, and nonprotective NiO particles were found precipitated within the external salt film. These results supported what is today known as a basic fluxing reaction, that is, corrosive attack by forming a basic solute of the protective scale.

Researchers (Ref 21) showed that Al_2O_3- forming nickel-base alloys containing the refractory elements molybdenum, tungsten, or vanadium can suffer Na_2SO_4-induced catastrophic attack, with the formation of stable solute ions involving oxide ions (MoO_4^{2-}, WO_4^{2-}, or VO_3^- ions, respectively). Again, the precipitation of a nonprotective oxide (Al_2O_3) in the salt film correlated to a local reduction in the Al_2O_3 solubility as MoO_3 and WO_3evaporation occurred at the salt-gas interface. Later, researchers (Ref 22) showed that the acidic solubility of any oxide (except SiO_2) would be increased by the presence of strongly acidic components in the salt. This type of accelerated attack associated with refractory metal oxide solutes has become known as acidic fluxing. Researchers (Ref 23) also demonstrated acidic fluxing in the attack of superalloys containing refractory-metal elements.

Besides the designations of basic and acidic scale fluxing, the subject of hot corrosion is otherwise classified into type I high-temperature hot corrosion (HTHC) and type II low-temperature hot corrosion (LTHC). For type I HTHC, the salt film is considered to be the relatively pure solvent, and the temperature must nominally exceed its melting point. For type II LTHC, the liquidus temperature for the salt film could be significantly lower than the melting point for the pure solvent because of a significant dissolution of some corrosion product. The dissolution reactions previously discussed here generally refer to type I HTHC. Researchers (Ref 24) showed that the corrosion kinetics of Na_2SO_4-coated coupons of Ni-30Cr and Co-30Cr alloys suffered maximum rates at approximately 650 and 750 °C (1200 and 1380 °F), respectively, that is, well below the 884 °C (1623 °F) melting point for the pure Na_2SO_4 The reaction product morphologies were characterized by a nonuniform attack in the form of pits, with only minor sulfide formation and little depletion of chromium or aluminum in the alloy substrate. On correlation of the experimentally determined compositions of the final salt films to the calculated phase stability diagrams, the researchers showed that these contaminated salt films were indeed above their liquidus temperatures. Type II hot corrosion was treated in greater detail (Ref 25, 26). Although the details of attack for LTHC differ from those for HTHC, the mechanism for LTCH can also be rationalized in terms of a scale fluxing driven by a negative solubility gradient, as illustrated in Fig. 7.

References cited in this section

5. R.A. Rapp, *Corrosion,* Vol 42, 1986, p 568

15. R.A. Rapp and K.S. Goto, The Hot Corrosion of Metals by Molten Salts, *Molten Salts II,* R. Selman and J. Braunstein, Ed., The Electrochemical Society, 1979, p 159

16. M.A. DeCrescente and N.S. Bornstein, *Corrosion,* Vol 24, 1968, p 127

17. N.S. Bornstein and M.A. DeCrescente, *Trans. Metall. Soc. (AIME),* Vol 245, 1969, p 1947

18. N.S. Bornstein and M.A. DeCrescente, *Corrosion,* Vol 26, 1970, p 209

19. N.S. Bornstein and M.A. DeCrescente, *Metall. Trans.,* Vol 2, 1971, p 2875

20. J.A. Goebel and F.S. Pettit, *Metall. Trans.,* Vol 1, 1970, p 1943

21. J.A. Goebel, F.S. Pettit, and G.W. Goward, *Metall. Trans.,* Vol 4, 1973, p 261

22. Y.S. Zhang and R.A. Rapp, *Corrosion,* Vol 43, 1987, p 348

23. G.C. Fryman, F.J. Kohl, and C.A. Stearns, *J. Electrochem. Soc.,* Vol 131, 1984, p 2985

24. K.L. Luthra and D.A. Shores, *J. Electrochem. Soc.,* Vol 127, 1980, p 2002

25. K.L. Luthra, *Metall. Trans. A,* Vol 13, 1982, p 1647, 1843, 1853

26. K.L. Luthra, *J. Electrochem. Soc.,* Vol 132, 1985, p 1293

R.A. Rapp, Corrosion by Molten Salts, *Corrosion: Fundamentals, Testing, and Protection,*, Vol 13A, *ASM Handbook*, ASM International, 2003, p 117–123

Corrosion by Molten Salts

Robert A. Rapp, The Ohio State University

Consequences of Salt Chemistry on Corrosion

With the understanding that oxide solubilities in fused salts take on the general behavior exhibited in Fig. 5, that is, at least when simple uncomplexed solutes are involved, a number of concepts helpful to controlling corrosion by fused salts can be understood. In general, the analyses that follow apply to both corrosion in deep melts as well as thin films, although, as stated previously, steeper gradients are expected for hot corrosion involving thin salt films.

Negative Solubility Gradient Criterion. Regarding the model for continuing scale dissolution and reprecipitation presented by Fig. 7 and 8, one can inquire whether specific experimental evidence has supported this mechanism. In fact, during the hot corrosion of preoxidized nickel by a fused film of Na_2SO_4, researchers (Ref 27) used potentiometric probes to trace the local changes in P_{O_2} and log a_{Na_2O} as a function of corrosion time. The experiments were done to respond to a question raised (Ref 28) as to how a NiO scale could be subject to sulfidation and basic fluxing when the typical gas turbine combustion product gases are far to the acid side of the NiO solubility minimum shown in Fig. 5. In equilibrium with an acidic gas, a positive solubility gradient should not lead to NiO dissolution/reprecipitation. The researchers found that for certain (inadequate) preoxidation conditions, the NiO oxide was rapidly attacked by the salt film. Consistent with the model for basic fluxing of Eq 6, the penetration of the salt through the NiO scale to contact the nickel substrate led to a large decrease in local P_{O_2}. Simultaneously, sulfidation of the nickel occurred with such a significant increase in the salt film basicity that the negative solubility gradient criterion was indeed satisfied, even for a quite acidic surrounding gas phase. Similar experiments for improved preoxidation conditions (higher nickel purity or thicker scale) showed that the NiO scale was not penetrated, sulfidation and a large shift in basicity did not occur, and the coupon therefore suffered little corrosion attack. These experiments showed the severe consequences of direct salt- metal contact, which causes the local chemistry of the salt film to differ greatly from that in equilibrium with the gas phase. In general, one can conclude that unless the metal is well passivated by a protective oxide, the salt chemistry will be dominated by the reaction at the metal-salt interface.

Synergistic Corrosion. On examining the solubility plots for various oxides in Fig. 5, the great displacement in solubilities for the various oxides is apparent. The common base metals for engineering alloys, nickel, cobalt, and iron, form the most basic oxides (subject to acidic dissolution), while the most common protective oxides, chromia and Al_2O_3, are the most acidic oxides, (subject to basic dissolution). Because the oxidation of an alloy, for example, an iron-chromium alloy (or nickel-chromium, cobalt-chromium, and so on, also involving aluminum) should lead to the presence of both basic and acidic oxides in the protective scale, this situation represents a potential hazard in the presence of a fused salt with a local basicity value between the solubility minima for the two oxides. Therefore, the potential for synergistic dissolution of the protective scale on an iron-chromium alloy was studied (Ref 29) according to the following coupled reactions:

$$Fe_2O_3 = 2Fe^{3+} + 3O^{2-} \quad \text{(acidic dissolution of } Fe_2O_3\text{)} \qquad \text{(Eq 7)}$$

$$Cr_2O_3 + 2O^{2-} + \tfrac{3}{2}O_2(g) = 2CrO_4^{2-} \quad \text{(basic dissolution of } Cr_2O_3\text{)} \qquad \text{(Eq 8)}$$

According to these equations, the product O^{2-} ions for the acidic dissolution of Fe_2O_3 should serve as a reactant for the basic dissolution of Cr_2O_3. For fused Na_2SO_4 salt with a basicity of approximately -13.9 pH (between the relevant minima in Fig. 5), the kinetics of dissolution were measured for powders of Fe_2O_3 and Cr_2O_3, both individually and in the presence of the second oxide. In each case, the mixed oxides dissolved very much faster

than the single oxides. These results show that a mixed oxide protective scale may be subject to accelerated attack by a fused salt. Accordingly, researchers (Ref 24, 25, 26) showed the beneficial effect of high chromium content in nickel-chromium and cobalt-chromium alloys in excluding the oxidation of nickel and cobalt, thereby minimizing type II LTHC. Researchers (Ref 30) showed that cobalt-chromium coatings with more than 37.5% Cr and a small reactive-element addition provide excellent LTHC resistance.

Strongly Acidic Oxides. High-temperature engineering alloys frequently contain the alloying elements chromium, tungsten, and molybdenum, while vanadium is often an impurity in low-grade fuels. The oxides of these elements have the tendency to complex with oxide ions in solutions to form chromate, tungstate, molybdate, and vanadate anions. All of these compounds contribute to a reduction in the liquidus temperature in their solutions with sodium sulfate. A lower liquidus temperature means that the potential for hot corrosion by a thin fused salt film is extended to lower temperatures or farther downstream in a combustion system. In addition, the complexing behavior of these oxides introduces an important influence on the acid/base chemistry of the salt and thereby on the scale fluxing mechanism. A phase stability diagram describing the stable vanadate solutes for a sodium sulfate/vanadate solution containing 30 mol% V species at 1173 K (1652 °F) is presented in Fig. 9(a) (Ref 31). Because of their common axes, Fig. 9(a) for the Na-V-S-O system represents a superposition of the Na-V-O phase stabilities onto Fig. 1 for Na_2SO_4, as was also done in Fig. 3 for the Na-Cr-S-O system. The fields of dominance for the solutes Na_3VO_4 (orthovanadate), $NaVO_3$ (metavanadate), and V_2O_5 (vanadium pentoxide) are apparent in Fig. 9(a), and, under the assumption of an ideal solution, the concentrations of these solutes are plotted in Fig. 9(b) for a sodium sulfate/vanadate solution containing 30 mol% V.

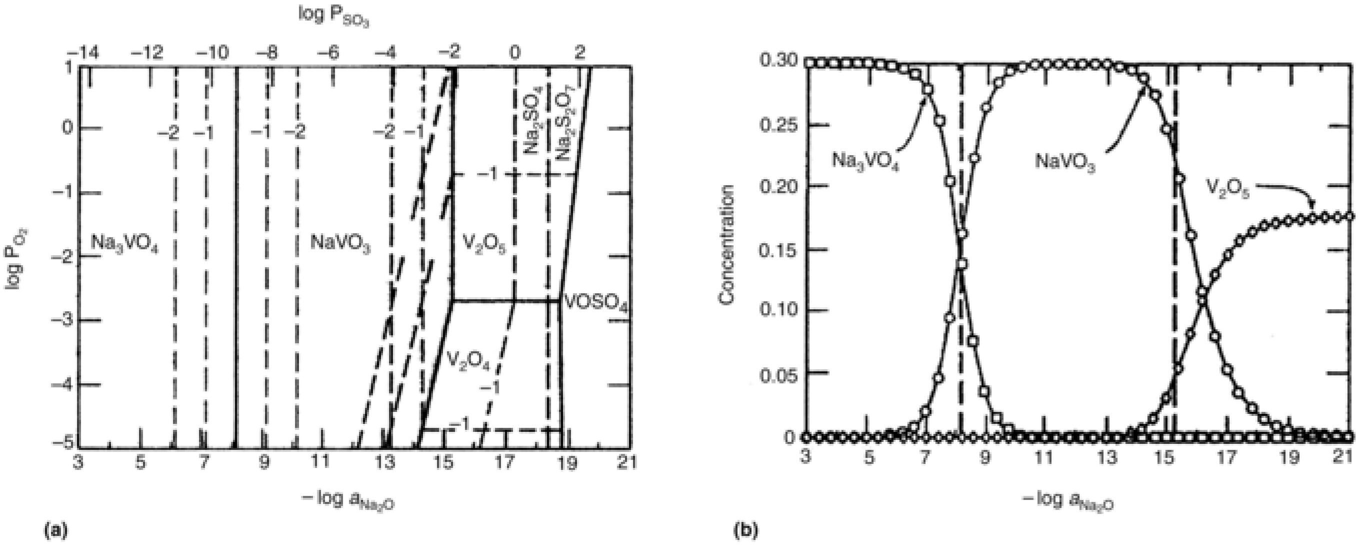

Fig. 9 The Na-V-S-O system. (a) Phase stability diagram at 1173 K (1652 °F). (b) Equilibrium concentrations for Na_3VO_4, $NaVO_3$, and V_2O_5 in a sodium sulfate/vanadate solution containing 30 mol% V at 1173 K (1652 °F)

The solubilities of the oxides CeO_2, HfO_2, and Y_2O_3 were measured as a function of salt basicity at 1173K (1652 °F) and 1 atm O_2 (Ref 22). The results were initially very surprising, because the magnitudes for their solubilities were quite high (approximately 100 ppm at their minima), and the solubility curves seem to be shifted toward a relatively basic value. To clarify these apparent discrepancies, the solubility of CeO_2 in pure Na_2SO_4 was measured for comparison. The plot of Fig. 10 shows that the presence of the vanadate component led to a very large increase in the acidic solubility for CeO_2, which, accordingly, shifted the solubility minimum to a more basic value (Ref 22). The slopes for the acidic dissolution of CeO_2 are in perfect agreement with the reactions:

$$CeO_2 + 2Na_2SO_4 = Ce(SO_4)_2 + 2Na_2O \quad \text{(in pure } Na_2SO_4\text{)} \qquad \text{(Eq 9)}$$

$$3CeO_2 + 4NaVO_3 = Ce_3(VO_4)_4 \quad \text{(in } NaVO_3\text{-}Na_2SO_4 \text{ solution)} \qquad \text{(Eq 10)}$$

Because the oxide CeO_2 has no special properties, the effect of the strong acid $NaVO_3$, and even more so V_2O_5, in increasing the acidic solubility and thereby shifting the melt chemistry must be considered a general occurrence expected for all oxides. The magnitudes of these changes would significantly affect the attack of a metal or alloy through the negative solubility gradient mechanism. Other strongly acidic salts would similarly tend to complex with oxide ions to form, for example, molybdate, tungstate, and chromate ions. The salt AlF_3 is also strongly acidic and complexes with oxide ions, for example, in fused chloride or fluoride solutions, to form three different oxyfluoride complexes.

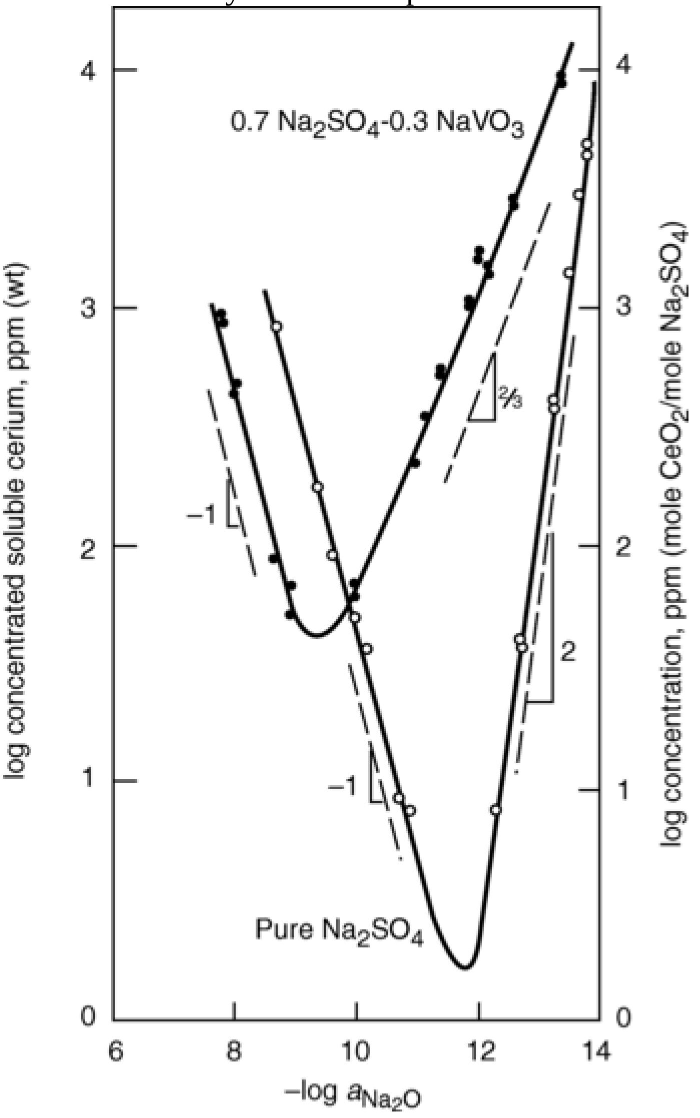

Fig. 10 Measured solubilities of CeO_2 in pure Na_2SO_4 and in 0.7 Na_2SO_4-0.3$NaVO_3$ at 1173 K (1652 °F) and 1 atm O_2

Protective Behavior of Chromium. Finally, one needs to understand why chromium is the most effective alloying element to combat corrosion by sodium sulfate. As illustrated in Fig. 11, the answer seems to lie in the oxygen pressure dependence for the basic dissolution of Cr_2O_3 (Ref 27). Because the valence of chromium is increased from +3 to +6 on Cr_2O_3 dissolution to form CrO_4^{2-} ions, the basic solubility of Cr_2O_3:

$$Cr_2O_3 + 2Na_2O + \frac{3}{2}O_2(g) = 2Na_2CrO_4$$

$$\left(\frac{d\log[Na_2CrO_4]}{d\log P_{O_2}}\right) = +\frac{3}{4} \qquad \text{(Eq 11)}$$

increases with increasing oxygen activity. Figure 11 illustrates the hot corrosion of a Cr_2O_3-protected alloy threatened by penetration of the salt at some grain boundaries or other defect. Because any thin salt film will be more reducing at the oxide-salt interface (certainly at a metal-salt interface) than farther away from this interface (toward the oxidizing gas), the chromate solute will experience a positive solubility gradient, and

therefore, consumptive reprecipitation of oxide in the salt film will not occur. Rather, the chromate ion will reprecipitate the oxide, satisfying a reduction in its solubility, at the most reduced sites, for example, the flaws or grain boundaries of the scale. In this way, the chromium serves as a protective component to plug flaws in the scale. In aqueous solutions, where chromatic inhibitors have been popular (but are now avoided for environmental reasons), the protective mechanism is believed to be the same.

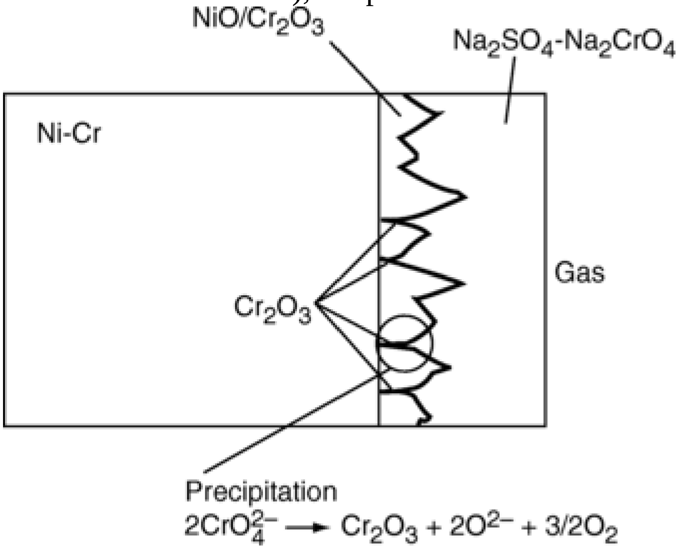

Fig. 11 The role of chromium in inhibiting hot corrosion attack

References cited in this section

22. Y.S. Zhang and R.A. Rapp, *Corrosion,* Vol 43, 1987, p 348

24. K.L. Luthra and D.A. Shores, *J. Electrochem. Soc.,* Vol 127, 1980, p 2002

25. K.L. Luthra, *Metall. Trans. A,* Vol 13, 1982, p 1647, 1843, 1853

26. K.L. Luthra, *J. Electrochem. Soc.,* Vol 132, 1985, p 1293

27. N. Otsuka and R.A. Rapp, *J. Electrochem. Soc.,* Vol 137, 1990, p 46, 53

28. D.A. Shores, in *High-Temperature Corrosion NACE-6,* R.A. Rapp, Ed., NACE, 1983, p 493

29. Y.S. Hwang and R.A. Rapp, *J. Electrochem. Soc.,* Vol 137, 1990, p 1276

30. K.L. Luthra and J.H. Wood, *Thin Solid Films,* Vol 119, 1984, p 217

31. Y.S. Hwang and R.A. Rapp, *Corrosion,* Vol 45, 1989, p 993

R.A. Rapp, Corrosion by Molten Salts, *Corrosion: Fundamentals, Testing, and Protection,*, Vol 13A, *ASM Handbook,* ASM International, 2003, p 117–123

Corrosion by Molten Salts

Robert A. Rapp, The Ohio State University

Conclusions

In this article, the importance of the acid/base and oxidizing character of a fused salt to the corrosion mechanism has been emphasized. In many regards, corrosion by a fused salt shares common characteristics with aqueous corrosion. Corrosion by fused sodium sulfate, also including additions of vanadates, has been emphasized for two reasons: this salt system probably has the greatest practical importance, because it relates to corrosion in combustion product gases; and the fundamental data and models have been better developed for this salt system. For many combinations of fused salt contacting an alloy or other material, the condition leading to failure may be represented by penetration of the salt to contact the reducing substrate, because the salt and the substrate are often thermodynamically incompatible. Consequently, the best protection from fused salt corrosion is then the formation and retention of a dense, adherent protective oxide scale. Because of possible synergistic dissolution, a pure, one-phase protective oxide is preferred. Because of the special solubility dependence for Cr_2O_3 on oxygen activity, chromium serves as the best protective alloy component to resist attack by an acidic salt. In general, where such knowledge is available, a protective scale should be chosen, such that the minimum in its solubility matches the relevant salt condition. In corrosion testing, care should be given so that the salt and gas compositions and the relevant salt thickness are chosen to match the problem. Provision of an initial protective scale by preoxidation is also useful.

R.A. Rapp, Corrosion by Molten Salts, *Corrosion: Fundamentals, Testing, and Protection,*, Vol 13A*, ASM Handbook*, ASM International, 2003, p 117–123

Corrosion by Molten Salts

Robert A. Rapp, The Ohio State University

References

1. G.Y. Lai, *High-Temperature Corrosion of Engineering Alloys,* ASM International, 1990
2. D. Inman and D.M. Wrench, *Br. Corros. J.,* Vol 1, 1966, p 246
3. C.O. Park and R.A. Rapp, *J. Electrochem. Soc.,* Vol 133, 1986, p 1636
4. R. Andresen, *J. Electrochem. Soc.,* Vol 126, 1979, p 328
5. R.A. Rapp, *Corrosion,* Vol 42, 1986, p 568
6. Y.S. Zhang and R.A. Rapp, *J. Met.,* Vol 46, 1994, p 47
7. Y.S. Zhang, X. Wu, and R.A. Rapp, *Metall. Mater. Trans. B,* Vol 34, 2003, p 235
8. Y.S. Zhang, *J. Electrochem. Soc.,* Vol 133, 1986, p 655
9. N.S. Jacobson, *J. Am. Ceram. Soc.,* Vol 76, 1993, p 33
10. W.C. Fang and R.A. Rapp, *J. Electrochem. Soc.,* Vol 130, 1983, p 2335
11. Y.M. Wu and R.A. Rapp, *J. Electrochem. Soc.,* Vol 138, 1991, p 2683
12. D.Z. Shi and R.A. Rapp, *Werkst. Korros.,* Vol 41, 1990, p 215

13. J. Kupper and R.A. Rapp, *Werkst. Korros.,* Vol 38, 1987, p 187

14. M. Spiegel, *Mater. High Temp.,* Vol 14, 1998, p 221

15. R.A. Rapp and K.S. Goto, The Hot Corrosion of Metals by Molten Salts, *Molten Salts II,* R. Selman and J. Braunstein, Ed., The Electrochemical Society, 1979, p 159

16. M.A. DeCrescente and N.S. Bornstein, *Corrosion,* Vol 24, 1968, p 127

17. N.S. Bornstein and M.A. DeCrescente, *Trans. Metall. Soc. (AIME),* Vol 245, 1969, p 1947

18. N.S. Bornstein and M.A. DeCrescente, *Corrosion,* Vol 26, 1970, p 209

19. N.S. Bornstein and M.A. DeCrescente, *Metall. Trans.,* Vol 2, 1971, p 2875

20. J.A. Goebel and F.S. Pettit, *Metall. Trans.,* Vol 1, 1970, p 1943

21. J.A. Goebel, F.S. Pettit, and G.W. Goward, *Metall. Trans.,* Vol 4, 1973, p 261

22. Y.S. Zhang and R.A. Rapp, *Corrosion,* Vol 43, 1987, p 348

23. G.C. Fryman, F.J. Kohl, and C.A. Stearns, *J. Electrochem. Soc.,* Vol 131, 1984, p 2985

24. K.L. Luthra and D.A. Shores, *J. Electrochem. Soc.,* Vol 127, 1980, p 2002

25. K.L. Luthra, *Metall. Trans. A,* Vol 13, 1982, p 1647, 1843, 1853

26. K.L. Luthra, *J. Electrochem. Soc.,* Vol 132, 1985, p 1293

27. N. Otsuka and R.A. Rapp, *J. Electrochem. Soc.,* Vol 137, 1990, p 46, 53

28. D.A. Shores, in *High-Temperature Corrosion NACE-6,* R.A. Rapp, Ed., NACE, 1983, p 493

29. Y.S. Hwang and R.A. Rapp, *J. Electrochem. Soc.,* Vol 137, 1990, p 1276

30. K.L. Luthra and J.H. Wood, *Thin Solid Films,* Vol 119, 1984, p 217

31. Y.S. Hwang and R.A. Rapp, *Corrosion,* Vol 45, 1989, p 993

Corrosion by Molten Nitrates, Nitrites, and Fluorides, *Corrosion: Fundamentals, Testing, and Protection*, Vol 13A, *ASM Handbook*, ASM International, 2003, p 124–128

Corrosion by Molten Nitrates, Nitrites, and Fluorides

Introduction

MOLTEN SALTS, often called fused salts, are used in many engineering systems. They can cause corrosion by the solution of constituents of the container material, selective attack, pitting, electrochemical reactions, mass transport due to thermal gradients, reaction of constituents of the molten salt with the container material, reaction of impurities in the molten salt with the container material, and reaction of impurities in the molten salt with the alloy. Many hundreds of molten salt/metal corrosion studies have been documented, yet predictions of corrosion are difficult if not impossible.

The most prevalent molten salts in use are nitrates and halides. Other molten salts that have been extensively studied but are not widely used include carbonates, sulfates, hydroxides, and oxides.

Corrosion by Molten Nitrates, Nitrites, and Fluorides, *Corrosion: Fundamentals, Testing, and Protection*, Vol 13A, *ASM Handbook*, ASM International, 2003, p 124–128

Test Methods

A number of kinetic and thermodynamic studies of corrosion by molten salts have been carried out in capsule-type containers. These studies can determine the nature of the corroding species and the corrosion products under static isothermal conditions and do provide some much- needed information. However, to provide the information needed for an actual flowing system, corrosion studies must be conducted in thermal convection loops or forced convection loops, which will include the effects of thermal gradients, flow, chemistry changes, and surface area. These loops can also include electrochemical probes and gas monitors. An example of the types of information gained from thermal convection loops during an intensive study of the corrosion of various alloys by molten salts is given subsequently. A thermal convection loop is shown in Fig. 1.

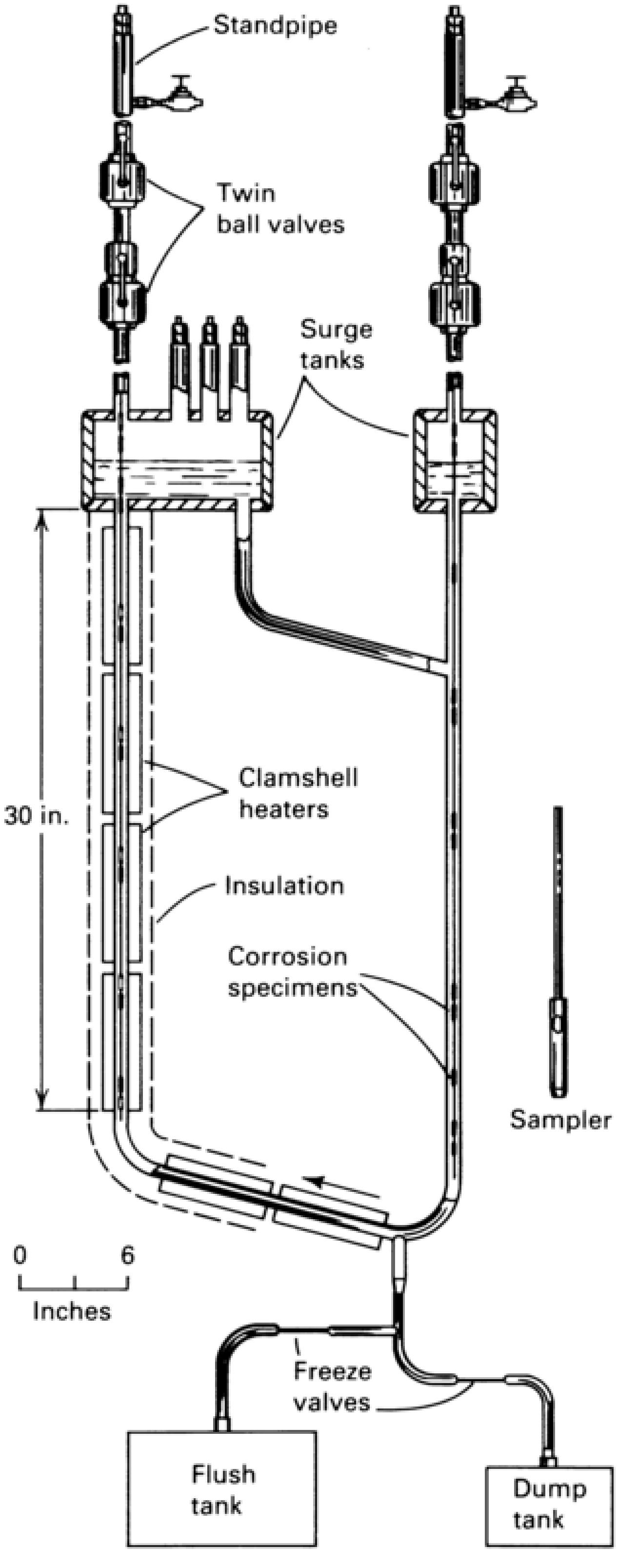

Fig. 1 Natural circulation loop and salt sampler

Purification

Molten salts, whether used for experimental purposes or in actual systems, must be kept free of contaminants. Maintaining purity, which involves initial makeup, transfer, and operation, is specific for each type of molten salt. For example, even though the constituents of the molten fluoride salts used in the Oak Ridge molten salt reactor experiment were available in very pure grades, purification by a hydrogen/hydrogen fluoride (H_2/HF) gas purge for 20 h was necessary (Ref 1). For nitrates with a melting point of approximately 220 °C (430 °F), purging with argon flowing above and through the salt at 250 to 300 °C (480 to 570 °F) removes significant amounts of water vapor (Ref 2). Another purification method used for this same type of salt consisted of bubbling pure dry oxygen gas through the 350 °C (660 °F) melt for 2 h and then bubbling pure dry nitrogen for 30 min to remove the oxygen (Ref 3). All metals that contact the molten salt during purification must be carefully selected to avoid contamination from transfer tubes, thermocouple wells, the makeup vessel, and the container itself. This selection process may be an experiment in itself.

References cited in this section

1. J.W. Koger, Report ORNL-TM-4286, Oak Ridge National Laboratory, Dec 1972
2. P.F. Tortorelli and J.H. DeVan, Report ORNL-TM-8298, Oak Ridge National Laboratory, Dec 1982
3. A. Baraka, A.I. Abdel-Rohman, and A.A. El Hosary, *Br. Corros. J.*, Vol 11, 1976, p 44

Corrosion by Molten Nitrates, Nitrites, and Fluorides, *Corrosion: Fundamentals, Testing, and Protection*, Vol 13A, *ASM Handbook*, ASM International, 2003, p 124–128

Corrosion by Molten Nitrates, Nitrites, and Fluorides

Nitrates/Nitrites

Nitrate mixtures have probably been studied and used more than any other molten salt group. This is perhaps because of the low operating temperatures possible (200 to 400 °C, or 390 to 750 °F). Steels of varying types are generally chosen to contain these systems, because, in general, the basicity of the melt prevents iron corrosion. Protection by passive films is less reliable, because oxide ion discharge may break down the passive film.

Electropolished iron spontaneously passivates in molten sodium nitrate/potassium nitrite ($NaNO_3$-KNO_2) in the temperature range of 230 to 310 °C (445 to 590 °F) at certain potentials (Ref 4). A magnetite (Fe_3O_4) film is formed, along with a reduction of nitrite or any trace of oxygen gas dissolved in the melt. At higher potentials, all reactions occur on the passivated iron. Above the passivation potentials, dissolution occurs, with ferric ion dissolving in the melt. At even higher potentials, nitrogen oxides are evolved, and nitrate ions dissolve in the nitrite melt. At higher currents, hematite (Fe_2O_3) is formed as a suspension, and NO_2 is detected. Carbon steel in molten sodium nitrate/potassium nitrate ($NaNO_3$-KNO_3) at temperatures ranging from 250 to 450 °C (480 to 840 °F) forms a passivating film consisting mainly of Fe_3O_4 (Ref 3).

Iron anodes in molten alkali nitrates and nitrites at temperatures ranging from 240 to 320 °C (465 to 610 °F) acquire a passive state in both melts. In nitrate melts, the protective Fe_3O_4 oxidizes to Fe_2O_3 and the gaseous products differ for each melt (Ref 5).

An interesting study was conducted on the corrosion characteristics of several eutectic molten salt mixtures on such materials as carbon steel, stainless steel, and Inconel in the temperature range of 250 to 400 °C (480 to 750 °F) in a nonflowing system (Ref 6). The salt mixtures and corrosion rates for carbon steel and stainless steel are given in Table 1. As expected, the corrosion rate was much higher for carbon steel than for stainless steel in the same mixture. Low corrosion rates were found for both steels in mixtures containing large amounts of alkaline nitrate. The nitrate ions had a passivating effect.

Table 1   Corrosion rates of iron-base alloys in eutectic molten salt mixtures

Salt mixture	Corrosion rate			
	Carbon steel		**Stainless steel**	
	μm/yr	**mils/yr**	**μm/yr**	**mils/yr**
$NaNO_3$-NaCl-Na_2SO_4 (86.3,8.4,5.3 mol%, respectively)	15	0.6	1	0.03
KNO_3-KCl (94.6 mol%, respectively)	23	0.9	7.5	0.3
LiCl-KCl (58.42 mol%, respectively)	63	2.5	20	0.8

Electrochemical studies showed high resistance to corrosion by Inconel. Again, the sulfate- containing mixture caused less corrosion because of the passivating property of the nitrate as well as the preferential adsorption of sulfate ions.

Surface analysis by Auger electron spectroscopy indicated varying thicknesses of iron oxide, nickel, and chromium layers. The Auger analysis showed that an annealed and air-cooled stainless steel specimen exposed to molten lithium chloride (LiCl)/potassium chloride (KCl) salt had corrosion to a depth five times greater than that of an unannealed stainless steel specimen. Chromium carbide precipitation developed during slow cooling and was responsible for the increased corrosion. The mechanism of corrosion of iron and steel by these molten eutectic salts can be described by the following reactions:

$Fe \leftrightarrow Fe^{2+} + 2e^-$ (Eq 1)

$LiCl + H_2O \leftrightarrow LiOH + HCl$ (Eq 2)

$H^+e^- \leftrightarrow \frac{1}{2}H_2,\ H_2O + 2e^- \rightleftharpoons O^{2-} + H_2$ (Eq 3)

$\frac{1}{2}O_2 + 2e^- \leftrightarrow O^{2-}$ (Eq 4)

$Fe^{3+} + e \leftrightarrow Fe^{2+}$ (Eq 5)

$Fe^{2+} + O^{2-} \leftrightarrow FeO$ (Eq 6)

$3FeO + O^{2-} \leftrightarrow Fe_3O_4 + 2e^-$ (Eq 7)

$2Fe_3O_4 + O^{2-} \leftrightarrow 3Fe_2O_3 + 2e^-$ (Eq 8)

Carbon or chromium-molybdenum steels have been used in an actual flowing and operating system of KNO_3-NaO_2-NaO_3 (53, 40, and 7 mol%, respectively) at temperatures to 450 °C (840 °F) (Ref 7). For higher temperatures and longer times, nickel or austenitic stainless steels are used. Weld joints are still a problem in both cases.

Alloy 800 (UNS N08800) and types 304 (UNS S30400), 304L (UNS S30403), and 316 (UNS S31600) stainless steels were exposed to thermally convective $NaNO_3$-KNO_3 salt (draw salt) under argon at 375 to 600 °C (705 to 1110 °F) for more than 4500 h (Ref 2). The exposure resulted in the growth of thin oxide films on all alloys and the dissolution of chromium by the salt. The weight change data for the alloys indicated that the metal in the oxide film constituted most of the metal loss, that the corrosion rate, in general, increased with temperature, and that, although the greatest metal loss corresponded to a penetration rate of 25 μm/yr (1 mil/ yr), the rate was less than 13 μm/yr (0.5 mil/yr) in most cases. These latter rates are somewhat smaller than those reported for similar loops operated with the salt exposed to the atmosphere (Ref 8, 9) but are within a factor of 2 to 5. Spalling had a significant effect on metal loss at intermediate temperatures in the type 304L stainless steel loop.

Metallographic examinations showed no evidence of intergranular attack or of significant cold-leg deposits. Weight change data further confirmed the absence of thermal gradient mass transport processes in these draw salt systems.

Raising the maximum temperature of the type 316 stainless steel loop from 595 to 620 °C (1105 to 1150 °F) dramatically increased the corrosion rate (Ref 8, 9). Thus, 600 °C (1110 °F) may be the limiting temperature for use of such alloys in draw salt.

References cited in this section

2. P.F. Tortorelli and J.H. DeVan, Report ORNL-TM-8298, Oak Ridge National Laboratory, Dec 1982

3. A. Baraka, A.I. Abdel-Rohman, and A.A. El Hosary, *Br. Corros. J.*, Vol 11, 1976, p 44

4. A.J. Arvia, J.J. Podesta, and R.C.V. Piatti, *Electrochim. Acta*, Vol 16, 1971, p 1797

5. A.J. Arvia, J.J. Podesta, and R.C.V. Piatti, *Electrochim. Acta*, Vol 17, 1972, p 33

6. H.V. Venkatasetty and D.J. Saathoff, *International Symposium on Molten Salts*, 1976, p 329

7. Yu. I. Sorokin and Kh. L. Tseitlin, *Khim. Prom.*, Vol 41, 1965, p 64

8. R.W. Bradshaw, "Corrosion of 304 Stainless Steel by Molten $NaNO_3$-KNO_3 in a Thermal Convection Loop," SAND-80-8856, Sandia National Laboratory, Dec 1980

9. R.W. Bradshaw, "Thermal Convection Loop Corrosion Tests of 316 Stainless Steel and IN800 in Molten Nitrate Salts," SAND-81-8210, Sandia National Laboratory, Feb 1982

Corrosion by Molten Nitrates, Nitrites, and Fluorides, *Corrosion: Fundamentals, Testing, and Protection*, Vol 13A, *ASM Handbook*, ASM International, 2003, p 124–128

Corrosion by Molten Nitrates, Nitrites, and Fluorides

Fluorides

Because of the Oak Ridge molten salt reactor experiment, a large amount of work was done on corrosion by molten fluoride salts (Ref 1). Because these molten salts were to be used as heat- transfer media, temperature gradient mass transfer was very important. Very small amounts of corrosion can result in large deposits, given that the solubility of the corrosion product changes drastically in the temperature range in question. Many other variables can also cause this phenomenon. Thus, a corrosion rate in itself does not provide complete information about corrosion.

Because the products of oxidation of metals by fluoride melts are quite soluble in the corroding media, passivation is precluded, and the corrosion rate depends on other factors, including the thermodynamic driving force of the corrosion reactions. The design of a practicable system using molten fluoride salts, therefore, demands the selection of salt constituents, such as lithium fluoride (LiF), beryllium fluoride (BeF_2), uranium tetrafluoride (UF_4), and thorium fluoride (ThF_4), that are not appreciably reduced by available structural metals and alloys whose components (iron, nickel, and chromium) can be in near-thermodynamic equilibrium with the salt.

A continuing program of experimentation over many years has been devoted to defining the thermodynamic properties of many corrosion product species in molten LiF-BeF_2 solutions. Much of the data has been obtained by direct measurement of equilibrium pressures for such reactions as:

$H_2(g) + FeF_2(d) \leftrightarrow Fe(c) + 2HF(g)$ (Eq 9)

and

$2HF(g) + BeO(c) \leftrightarrow BeF_2(l) + H_2O(g)$ (Eq 10)

where g, c, and d represent gas, crystalline solid, and solute, respectively, using the molten fluoride (denoted 1 for liquid) as the reaction medium. All of these studies have been reviewed, and the combination of these data with those of other studies has yielded tabulated thermodynamic data for many species in molten LiF-BeF_2 (Table 2). From these data, one can assess the extent to which a uranium trifluoride (UF_3)-bearing melt will disproportionate according to the reaction:

$4UF_3(d) \leftrightarrow 3UF_4(d) + U(d)$ (Eq 11)

Table 2 Standard Gibbs free energies (ΔG^f) of formation for species in molten 2LiF-BeF_2.

Temperature range: 733–1000 K

Material[(a)]	$-\Delta G^f = c - dT$[(b)] where:		$-\Delta G^f$ at 1000 K, kcal/mol
	c	***d***	
LiF(l)	141.8	0.0166	125.2
BeF_2(l)	243.9	0.0300	106.9
UF_3(d)	338.0	0.0403	99.3
UF_4(d)	445.9	0.0579	97.0
ThF_4(d)	491.2	0.0624	107.2
ZrF_4(d)	453.0	0.0651	97.0
NiF_2(d)	146.9	0.0363	55.3
FeF_2(d)	154.7	0.0218	66.5
CrF_2(d)	171.8	0.0214	75.2
MoF_6(g)	370.9	0.0696	50.2

(a) The standard state for LiF and BeF_2 is the molten 2LiF-BeF_2 liquid. That for MoF_6(g) is the gas at 1 atm. That for all species with *d* is that hypothetical solution with the solute at unit mole fraction and with the activity coefficient it would have at infinite dilution.

(b) Formula gives $-\Delta G^f$ in kcal/mol for temperature (T) in K in the range 733–1000 K. Source: Ref 10

For the case in which the total uranium content of the salt is 0.9 mol%, as in the Oak Ridge Molten Salt Reactor Experiment, the activity of metallic uranium (referred to as the pure metal) is near 10^{-15} with 1% of the UF_4 converted to UF_3 and is near 2×10^{-10} with 20% of the UF_4 so converted (Ref 11). Operation of the reactor with a small fraction (usually 2%) of the uranium present as UF_3 is advantageous insofar as corrosion and the consequences of fission are concerned. Such operation with some UF_3 present should result in the formation of an extremely dilute (and experimentally undetectable) alloy of uranium with the surface of the container metal. Operation with 50% of the uranium as UF_3 would lead to much more concentrated (and highly deleterious) alloying and to formation of uranium carbides. All evidence to date demonstrates that operation with relatively little UF_3 is completely satisfactory.

The data gathered to date reveal clearly that in reactions with structural metals, M:

$2UF_4(d) + M(c) \leftrightarrow 2UF_3(d) + MF_2(d)$ (Eq 12)

chromium is much more readily attacked than iron, nickel, or molybdenum (Ref 11, 12).

Nickel-base alloys, more specifically, Hastelloy N (Ni-6.5Mo-6.9Cr-4.5Fe) and its modifications, are considered the most promising for use in molten salts and have received the most attention. Stainless steels, having more chromium than Hastelloy N, are more susceptible to corrosion by fluoride melts but can be considered for some applications.

Oxidation and selective attack may also result from impurities in the melt:

$M + NiF_2 \leftrightarrow MF_2 + Ni$ (Eq 13)

$M + 2HF \leftrightarrow MF_2 + H_2$ (Eq 14)

or oxide films on the metal:

$NiO + BeF_2 \leftrightarrow NiF_2 + BeO$ (Eq 15)

followed by reaction of nickel fluoride (NiF_2) with M.

The reactions given in Eq 13, 14, and 15 will proceed essentially to completion at all temperatures. Accordingly, such reactions can lead (if the system is poorly cleaned) to a rapid initial corrosion rate. However, these reactions do not give a sustained corrosive attack.

On the other hand, the reaction involving UF_4 (Eq 12) may have an equilibrium constant that is strongly temperature dependent; therefore, when the salt is forced to circulate through a temperature gradient, a possible mechanism exists for mass transfer and continued attack. Equation 12 is of significance mainly in the case of alloys containing relatively large amounts of chromium.

If nickel, iron, and molybdenum are assumed to form regular or ideal solid solutions with chromium (as is approximately true), and if the circulation rate is very rapid, the corrosion process for alloys in fluoride salts can be simply described. At high flow rates, uniform concentrations of UF_3 and chromium fluoride (CrF_2) are maintained throughout the fluid circuit. Under these conditions, there exists some temperature (intermediate between the maximum and minimum temperatures of the circuit) at which the initial chromium concentration of the structural metal is at equilibrium with the fused salt. This temperature, T_{BP}, is called the balance point.

Because the equilibrium constant for the chemical reaction with chromium increases with temperature, the chromium concentration in the alloy surface tends to decrease at temperatures higher than T_{BP} and tends to increase at temperatures lower than T_{BP}. At some point, the dissolution process will be controlled by the solid-state diffusion rate of chromium from the matrix to the surface of the alloy.

In some melts (NaF-LiF-KF-UF_4, for example), the equilibrium constant for Eq 12 with chromium changes sufficiently as a function of temperature to cause the formation of dendritic chromium crystals in the cold zone. For LiF- BeF_2-UF_4-type mixtures, the temperature dependence of the mass transfer reaction is small, and the equilibrium is satisfied at reactor temperature conditions without the formation of crystalline chromium. Thus, the rate of chromium removal from the salt stream by deposition at cold-fluid regions is controlled by the rate at which chromium diffuses into the cold-fluid wall; the chromium concentration gradient tends to be small, and the resulting corrosion is well within tolerable limits. A schematic of the temperature gradient mass transfer process is shown in Fig. 2.

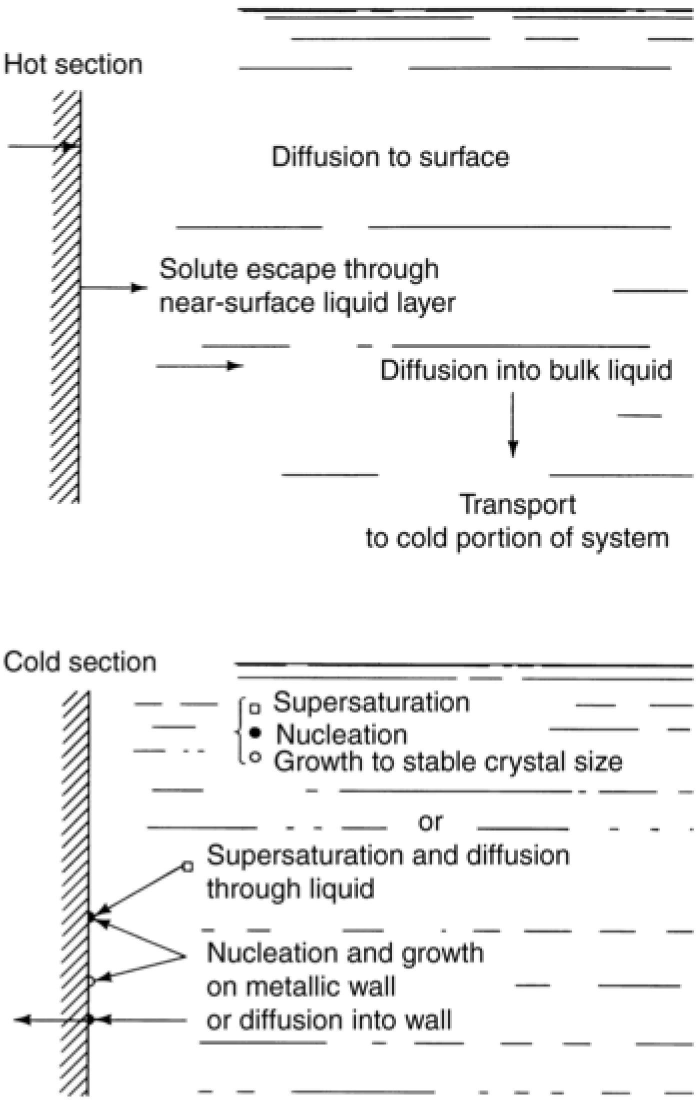

Fig. 2 Temperature-gradient mass transfer

Lithium fluoride/beryllium fluoride salts containing UF_4 or ThF_4 and tested in thermal convection loops showed temperature gradient mass transfer, as noted by weight losses in the hot leg and weight gains in the cold leg (Fig. 3). Hastelloy N was developed for use in molten fluorides and has proved to be quite compatible. The weight changes of corrosion specimens increased with temperature and time (Fig. 4, 5).

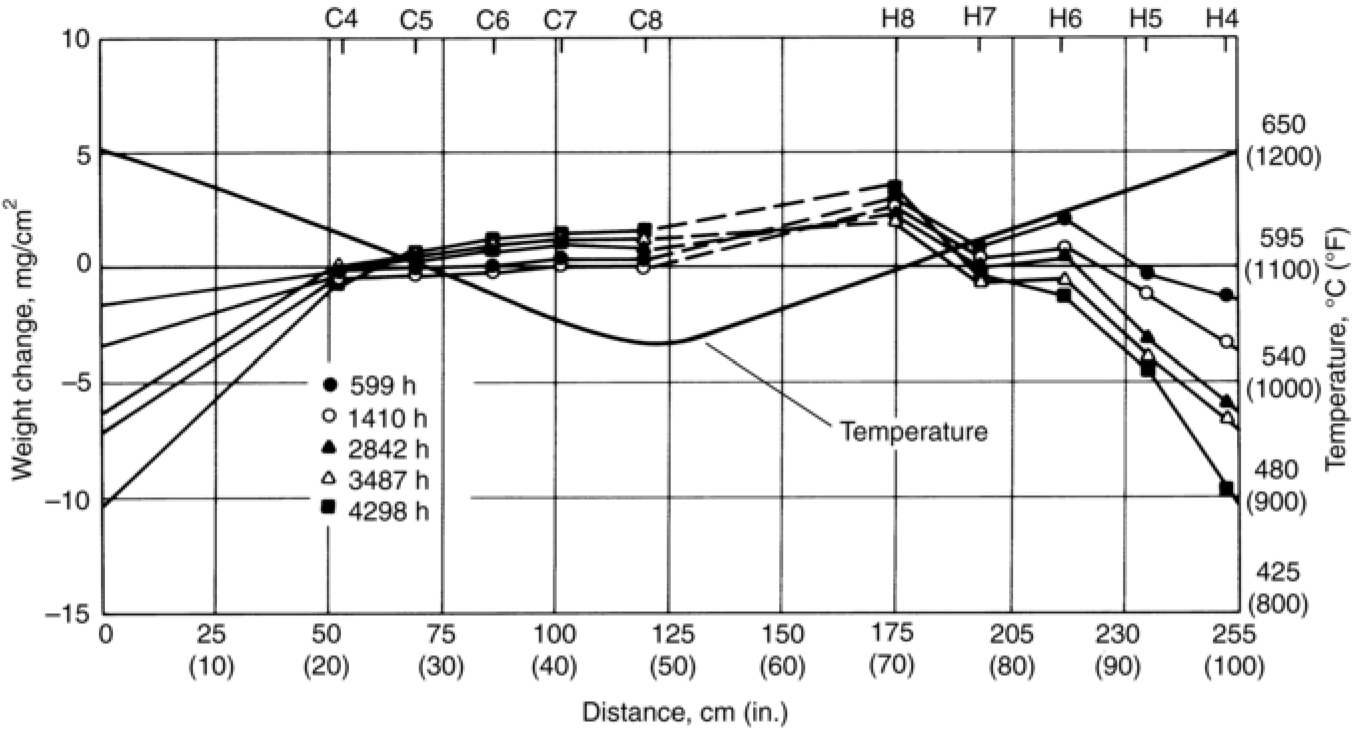

Fig. 3 Weight changes of type 316 stainless steel specimens exposed to LiF-BeF$_2$-ThF$_4$-UF$_4$ (68, 20, 11.7, and 0.3 mol%, respectively) as a function of position (C's, cold leg; H's, hot leg) and temperature

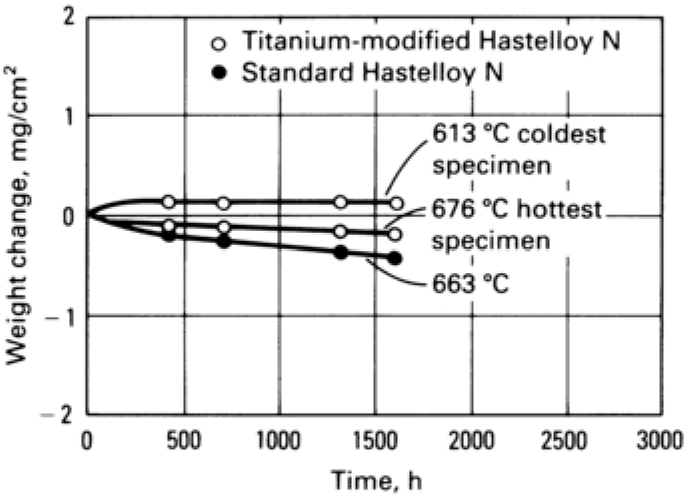

Fig. 4 Weight changes of Hastelloy N specimens versus time of operation in LiF-BeF$_2$-ThF$_4$ (73, 2, and 25 mol%, respectively)

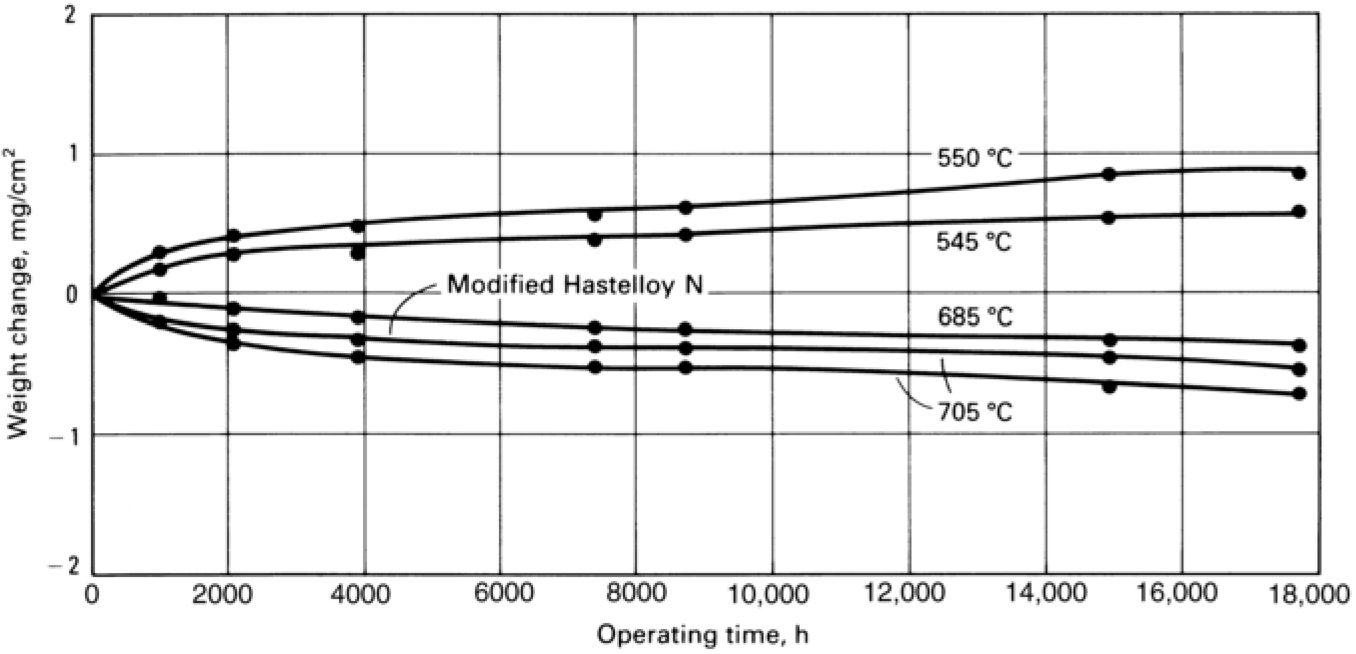

Fig. 5 Weight changes of Hastelloy N exposed to LiF-BeF$_2$-ThF$_4$-UF$_4$ (68, 20, 11.7, and 0.3 mol%, respectively) for various times

A type 304L stainless steel exposed to a fuel salt for 9.5 years (Fig. 6) in a type 304L stainless steel loop showed a maximum uniform corrosion rate of 22 μm/yr (0.86 mil/yr). Voids extended into the matrix for 250 μm (10 mils), and chromium depletion was found (Fig. 7) to extend to a depth of 28 μm (1.1 mil).

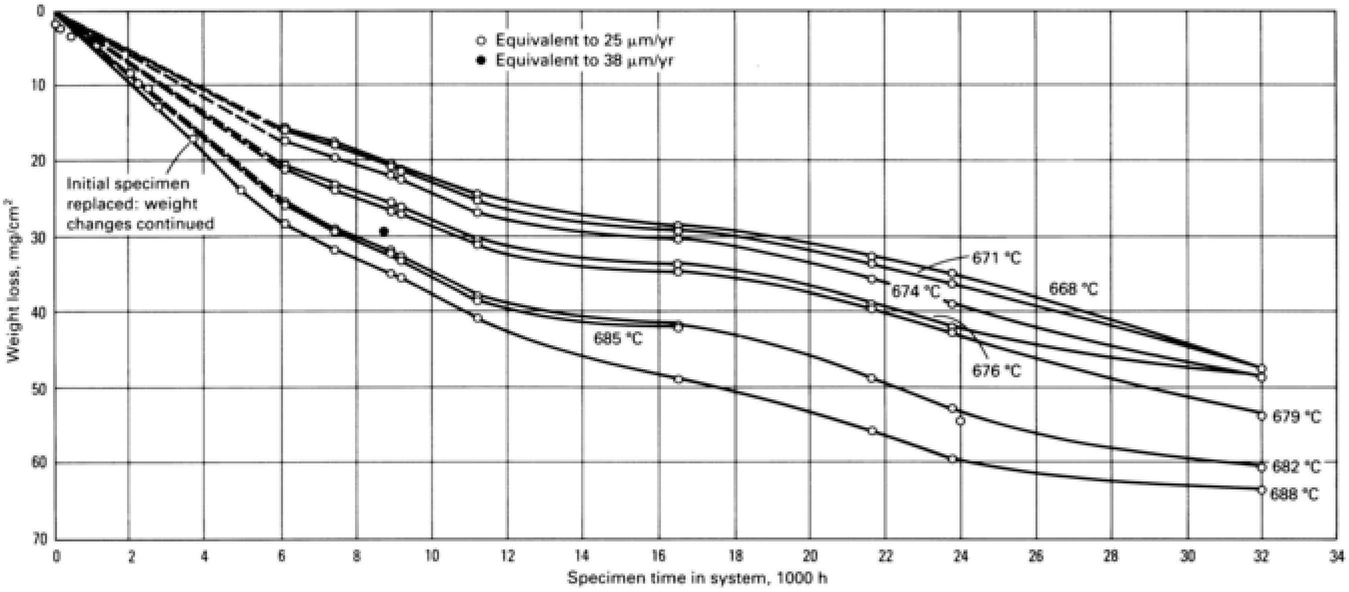

Fig. 6 Weight changes of type 304L stainless steel specimens exposed to LiF-BeF$_2$-ZrF$_4$-ThF$_4$-UF$_4$ (70, 23, 5, 1, and 1 mol%, respectively) for various times and temperatures

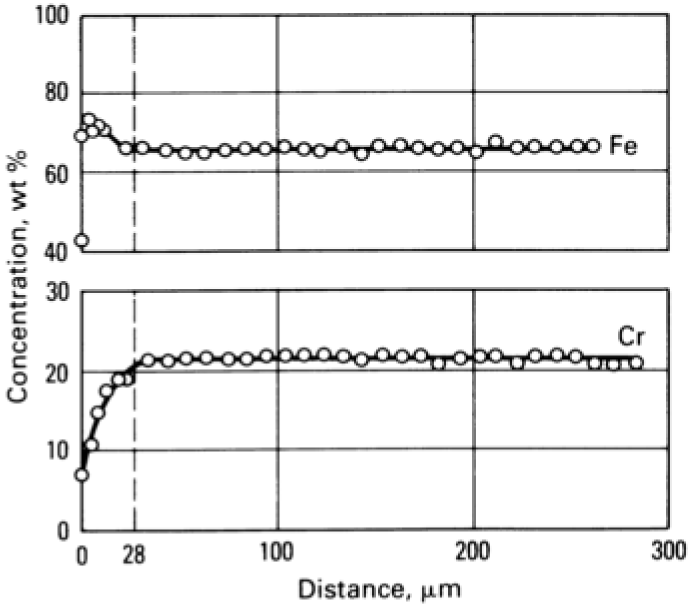

Fig. 7 Chromium and iron concentration gradient in a type 304L stainless steel specimen exposed to LiF-BeF_2-ZrF_4-ThF_4-UF_4 (70, 23, 5, 1, and 1 mol%, respectively) for 5700 h at 688 °C (1270 °F)

The corrosion resistance of a maraging steel (Fe-12Ni-5Cr-3Mo) at 662 °C (1224 °F) was better than that of type 304L stainless steel but was worse than that of a Hastelloy N under equivalent conditions. As shown in Table 3, the average uniform corrosion rate for the maraging steel was 14 µm/yr (0.55 mil/yr). Voids were seen in the microstructure of the specimens after 5700 h, and electron microprobe analysis disclosed a definite depletion of chromium and iron.

Table 3 Comparison of weight losses of alloys at approximately 663 °C (1225 °F) in similar flow fuel salts in a temperature gradient system

Alloy	Weight loss, mg/cm^2		Average corrosion	
	2490 h	**3730 h**	**µm/yr**	**mils/yr**
Maraging steel	3.0	4.8	14	0.55
Type 304 stainless steel	6.5	10.0	28	1.1
Hastelloy N	0.4	0.6	1.5	0.06

Type 316 stainless steel exposed to a fuel salt in a type 316 stainless steel loop showed a maximum uniform corrosion rate of 25 µm/yr (1 mil/ yr) for 4298 h. Mass transfer did occur in the system.

For selected nickel- and iron-base alloys, a direct correlation was found between corrosion resistance in molten fluoride salt and chromium and iron content of an alloy. The more chromium and iron in the alloy, the less the corrosion resistance.

References cited in this section

1. J.W. Koger, Report ORNL-TM-4286, Oak Ridge National Laboratory, Dec 1972

10. C.F. Baes, Jr., “The Chemistry and Thermodynamics of Molten Salt Reactor Fuels,” Paper presented at the AIME Nuclear Fuel Reprocessing Symposium, (Ames, IA), American Institute of Mining, Metallurgical, and Petroleum Engineers, Aug 1969; see also *1969 Nuclear Metallurgy Symposium*, Vol 15, United States Atomic Energy Commission Division of Technical Information Extension

11. G. Long, “Reactor Chemical Division Annual Program Report,” ORNL-3789, Oak Ridge National Laboratory, Jan 1965, p 65

12. J.W. Koger, “MSR Program Semiannual Progress Report,” ORNL-4622, Oak Ridge National Laboratory, Aug 1970, p 170

Corrosion by Molten Nitrates, Nitrites, and Fluorides, *Corrosion: Fundamentals, Testing, and Protection*, Vol 13A, *ASM Handbook*, ASM International, 2003, p 124–128

Corrosion by Molten Nitrates, Nitrites, and Fluorides

Conclusions

In order to study the corrosion of molten salts or to determine what materials are compatible with a certain molten salt, the following questions must be answered. What is the purpose of the investigation? Is the researcher interested in basic studies, or is this work for information or work preliminary to assessment for a real system? For basic studies, capsule experiments or information from capsules is sufficient. Otherwise, flow systems or information from flow systems will be needed at some point to assess temperature gradient mass transfer. Salts to be used in either case need to be purified, and the same purity must be used in each experiment, unless this factor is a variable. Analytical facilities must be used for the chemistry of the salt, including impurity content and surface analysis of the metals in question.

Useful information can be obtained from capsule and flow experiments. It is hoped that the preceding information on specific systems provides an appreciation of the challenges involved and the materials information that can be obtained from various experiments.

Corrosion by Molten Nitrates, Nitrites, and Fluorides, *Corrosion: Fundamentals, Testing, and Protection*, Vol 13A, *ASM Handbook*, ASM International, 2003, p 124–128

Corrosion by Molten Nitrates, Nitrites, and Fluorides

Acknowledgment

Portions of this article were adapted from J.W. Koger, Fundamentals of High-Temperature Corrosion in Molten Salts, *Corrosion,* Vol 13, *ASM Handbook* (formerly *Metals Handbook,* 9th ed.), ASM International, 1987, p 50–55.

Corrosion by Molten Nitrates, Nitrites, and Fluorides, *Corrosion: Fundamentals, Testing, and Protection*, Vol 13A, *ASM Handbook*, ASM International, 2003, p 124–128

Corrosion by Molten Nitrates, Nitrites, and Fluorides

References

1. J.W. Koger, Report ORNL-TM-4286, Oak Ridge National Laboratory, Dec 1972
2. P.F. Tortorelli and J.H. DeVan, Report ORNL-TM-8298, Oak Ridge National Laboratory, Dec 1982

3. A. Baraka, A.I. Abdel-Rohman, and A.A. El Hosary, *Br. Corros. J.*, Vol 11, 1976, p 44

4. A.J. Arvia, J.J. Podesta, and R.C.V. Piatti, *Electrochim. Acta,* Vol 16, 1971, p 1797

5. A.J. Arvia, J.J. Podesta, and R.C.V. Piatti, *Electrochim. Acta,* Vol 17, 1972, p 33

6. H.V. Venkatasetty and D.J. Saathoff, *International Symposium on Molten Salts,* 1976, p 329

7. Yu. I. Sorokin and Kh. L. Tseitlin, *Khim. Prom.,* Vol 41, 1965, p 64

8. R.W. Bradshaw, "Corrosion of 304 Stainless Steel by Molten $NaNO_3$-KNO_3 in a Thermal Convection Loop," SAND-80-8856, Sandia National Laboratory, Dec 1980

9. R.W. Bradshaw, "Thermal Convection Loop Corrosion Tests of 316 Stainless Steel and IN800 in Molten Nitrate Salts," SAND-81-8210, Sandia National Laboratory, Feb 1982

10. C.F. Baes, Jr., "The Chemistry and Thermodynamics of Molten Salt Reactor Fuels," Paper presented at the AIME Nuclear Fuel Reprocessing Symposium, (Ames, IA), American Institute of Mining, Metallurgical, and Petroleum Engineers, Aug 1969; see also *1969 Nuclear Metallurgy Symposium,* Vol 15, United States Atomic Energy Commission Division of Technical Information Extension

11. G. Long, "Reactor Chemical Division Annual Program Report," ORNL-3789, Oak Ridge National Laboratory, Jan 1965, p 65

12. J.W. Koger, "MSR Program Semiannual Progress Report," ORNL-4622, Oak Ridge National Laboratory, Aug 1970, p 170

Corrosion by Molten Nitrates, Nitrites, and Fluorides, *Corrosion: Fundamentals, Testing, and Protection*, Vol 13A*, ASM Handbook,* ASM International, 2003, p 124–128

Corrosion by Molten Nitrates, Nitrites, and Fluorides

Selected References

- C.B. Allen and G.T. Janz, *J. Hazard. Mater.*, Vol 4, 1980, p 145
- R.W. Bradshaw and S.H. Goods, Corrosion Resistance of Stainless Steels during Thermal Cycling in Alkali Nitrate Molten Salts, "Sandia Report, SAND2001-8518," Sept. 2001, 36 p
- R.J. Gale and D.G. Lovering, in *Molten Salt Techniques,* Vol 2, Plenum Press, 1984, p 1
- D. Inman and D.G. Lovering, in *Comprehensive Treatise of Electrochemistry,* Vol 7, Plenum Publishing, 1983
- G.J. Janz and R.P.T. Tompkins, in *Corrosion,* Vol 35, NACE International, 1979, p 485
- C.A.C. Sequeira, *Electrochemistry of Corrosion in Molten Salts,* Trans Tech Publications, Inc., 2003
- C.A.C. Sequeira, High Temperature Corrosion in Molten Salts, *Molten Salt Forum,* Vol 7-7, Trans Tech Publications, Inc., 2003
- Tz. Tzvetkoff, *Mechanism of Growth, Composition and Structure of Passive Films Formed and Their Alloys in Molten Salt Electrolytes,* Trans Tech Publications, Inc., 2003

P.F. Tortorelli and S.J. Pawel, Corrosion by Liquid Metals, *Corrosion: Fundamentals, Testing, and Protection*, Vol 13A, *ASM Handbook*, ASM International, 2003, p 129–134

Corrosion by Liquid Metals

P.F. Tortorelli and S.J. Pawel, Oak Ridge National Laboratory

Introduction

CONCERN ABOUT CORROSION of solids exposed to liquid metal environments, that is, liquid metal corrosion, dates from the earliest days of metals processing, when it became necessary to handle and contain molten metals. Corrosion considerations also arise when liquid metals are used in applications that exploit their chemical or physical properties.

Liquid metals serve as high-temperature reducing agents in the production of metals (such as the use of molten magnesium to produce titanium), and, because of their excellent heat- transfer properties, liquid metals have been used or considered as coolants in a variety of power- producing systems. Examples of such applications include molten sodium for liquid metal fast breeder reactors and central receiver solar stations as well as liquid lithium for fusion and space nuclear reactors.

In addition, tritium breeding in deuterium-tritium fusion reactors necessitates the exposure of lithium atoms to fusion neutrons. Breeding fluids of lithium or lead-lithium are attractive for this purpose. Molten lead or bismuth can serve as neutron multipliers to raise the tritium breeding yield if other types of lithium-containing breeding materials are used. More recently, in the United States, liquid mercury has been selected as the target for the spallation neutron source (SNS) at Oak Ridge National Laboratory. In the SNS scheme, 1 to 2 GeV protons will impinge on flowing mercury to generate an intense source of spallation neutrons. (Several other planned neutron sources worldwide may also use mercury for this application.) Liquid metals can also be used as two-phase working fluids in Rankine cycle power conversion devices (molten cesium or potassium) and in heat pipes (potassium, lithium, sodium, sodium-potassium). Because of their high thermal conductivities, sodium-potassium alloys, which can be any of a wide range of sodium-potassium combinations that are molten at or near room temperature, have also been used as static heat sinks in automotive and aircraft valves.

Whenever the handling of liquid metals is required, whether in specific uses as discussed previously or as melts during processing, a compatible containment material must be selected. At low temperatures, liquid metal corrosion is often insignificant, but in more demanding applications, corrosion considerations can be important in selecting the appropriate containment material and operating parameters. Thus, liquid metal corrosion studies in support of heat pipe technology and aircraft, space, and fast breeder reactor programs date back many years and, more recently, are being conducted worldwide as part of the fusion energy and spallation neutron programs. In this article, the principal corrosion reactions and important parameters that control such processes are briefly reviewed for materials (principally metals) exposed to liquid metal environments. Only corrosion phenomena are covered, and the discussion is limited to corrosion under single-phase (liquid) conditions.

P.F. Tortorelli and S.J. Pawel, Corrosion by Liquid Metals, *Corrosion: Fundamentals, Testing, and Protection*, Vol 13A, *ASM Handbook*, ASM International, 2003, p 129–134

Corrosion by Liquid Metals

P.F. Tortorelli and S.J. Pawel, Oak Ridge National Laboratory

Corrosion Reactions in Liquid Metal Environments

Liquid metal corrosion can manifest itself in various ways. In the most general sense, the following categories can be used to classify relevant corrosion phenomena:

- Dissolution
- Impurity and interstitial reactions
- Alloying
- Compound reduction

Definitions and descriptions of these types of reactions are given subsequently. However, it is important to note that this classification is somewhat arbitrary, and, as will become clear during the following discussion, the individual categories are not necessarily independent of one another.

All of these reactions require the wetting of the solid by the liquid metal. This can be inherently problematic in certain systems or in cases when a solid that would normally be wet by the liquid metal has a surface film that prevents such wetting.

Dissolution

The simplest corrosion reaction that can occur in a liquid metal environment is direct dissolution. Direct dissolution is the release of atoms of the containment material into the melt in the absence of any impurity effects. Such a reaction is a simple solution process and therefore is governed by the elemental solubilities in the liquid metal and the kinetics of the rate-controlling step of the dissolution reaction. The net rate, J, at which an elemental species enters solution, can be described as:

$$J = k(C_0 - C) \qquad \text{(Eq 1)}$$

where J is the rate of mass loss of an element due to dissolution, C_0 is the solubility of that element in the liquid metal, C is its actual concentration in the bulk of the liquid, and k is the effective solution rate constant. Each constituent of the condensed phase is separately governed by Eq 1. Because J is proportional to ($C_0 - C$), high solubilities do not necessarily translate into high dissolution rates, because the driving force for dissolution depends on the actual concentration of the solute in the liquid metal as well as C_0. This forms the crucial differentiation between isothermal liquid metal systems and nonisothermal dynamic ones regarding the stability of a material with respect to dissolution and mass transfer (see the following discusion).

Under isothermal conditions, the rate of this dissolution reaction would decrease with time as C increases. After a period of time, the actual elemental concentration becomes equal to the solubility, and the dissolution rate is then 0. Therefore, in view of Eq 1, corrosion by the direct dissolution process can be minimized by selecting a containment material whose elements have low solubilities in the liquid metal of interest and/or by saturating the melt before actual exposure. However, if the dissolution kinetics are relatively slow, that is, for low values of k, corrosion may be acceptable for short-term exposures. The functional dependence and magnitude of the solution rate constant, k, depend on the rate-controlling step, which, in the simplest cases, can be a transport across the liquid-phase boundary layer, diffusion in the solid, or a reaction at the phase boundary. Measurements of mass changes as a function of time for a fixed $C_0 - C$ (see subsequent discussion) yield the kinetic information necessary for determination of the rate-controlling mechanism.

Corrosion resulting from dissolution in a nonisothermal liquid metal system is more complicated than the isothermal case. Both solvation and solute deposition are normally occurring, and there is essentially a time-invariant ($C_0 - C$) driving force for dissolution at a given temperature. This is because, after a short transient period, C is constant as the flow of the liquid metal quickly establishes a systemwide steady state. Specifically, the value of C is set by the dissolution and deposition rates, the temperature profile, and the functional dependence of C_0 on temperature. As such, C does not vary around a flowing liquid metal system and, at steady state, is constant with time. Unlike the isothermal case, J is only dependent on time through its dependence on k (Eq 1).

The flux description illustrated by Eq 1 applies equally well to deposition when $C > C_0$. Therefore, at temperatures where the solubility (C_0) is greater than the bulk concentration (C), dissolution of an element into the liquid metal will occur, but at lower temperatures in the circuit where $C_0 < C$, a particular element will tend to come out of solution and be deposited on the containment material (or remain as suspended particles). A schematic of such a mass-transfer process is shown in Fig. 1. Such mass-transfer processes under nonisothermal conditions can be of prime importance when, in the absence of dissimilar-metal effects (see subsequent

discussion), forced circulation (pumping) of liquid metals used as heat-transfer media exacerbates the transport of materials from hotter to cooler parts of the liquid metal circuit.

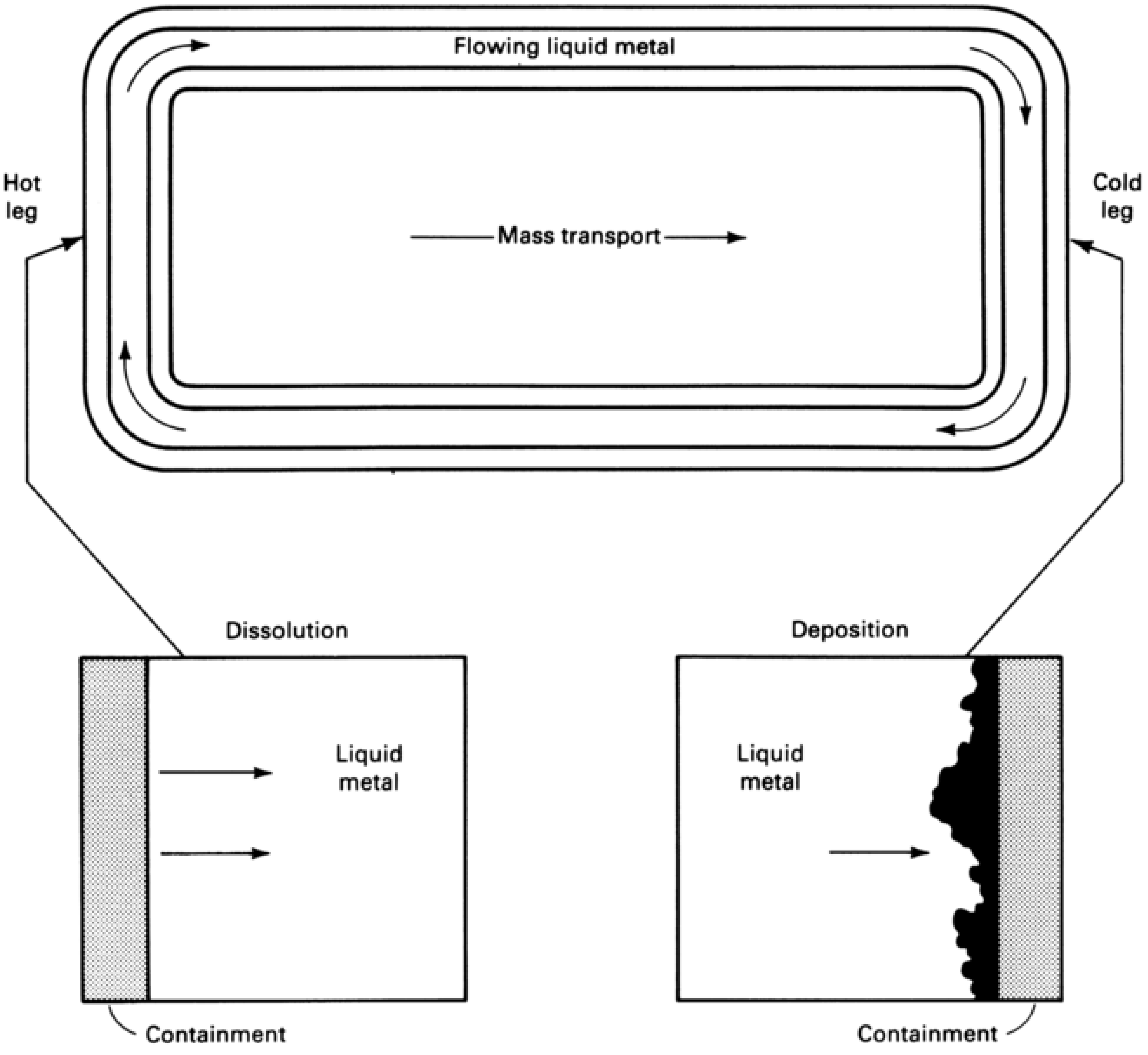

Fig. 1 Schematic of thermal gradient mass transfer in a liquid metal circuit. Source: Ref 1

If the dissolution and deposition behaviors are controlled by the respective forms of Eq 1, measurements of mass change as a function of loop position (x) should yield data resembling the schematic depiction shown in Fig. 2. Using the appropriate analysis methods and simplifying assumptions, measurements of the mass or, for alloys/compounds, composition change as a function of loop position (and, therefore temperature) can provide further data regarding kinetics and the rate-controlling mechanism of mass transport associated with a given material/liquid metal system. This can be computed for any element in a closed tubular liquid metal system where deposition occurs over an area A_p and dissolution over A_s, using the following equation:

$$G = \int A_s J_s \cdot 2\pi r dx - \int A_p J_p \cdot 2\pi r dx \qquad \text{(Eq 2)}$$

where G is the net increase of an element in the circuit per unit time, r is the inside tube radius, J_s is as defined in Eq 1 for dissolution, and J_p is of the same functional form but applies to deposition of an element from the liquid metal with a rate constant k_p. Typically, $G \approx 0$ at steady state, so, using Eq 1 with Eq 2:

$$\int A_s k_s (C_0 - C) \cdot 2\pi r dx = \int A_p k_p (C_0 - C) \cdot 2\pi r dx \qquad \text{(Eq 3)}$$

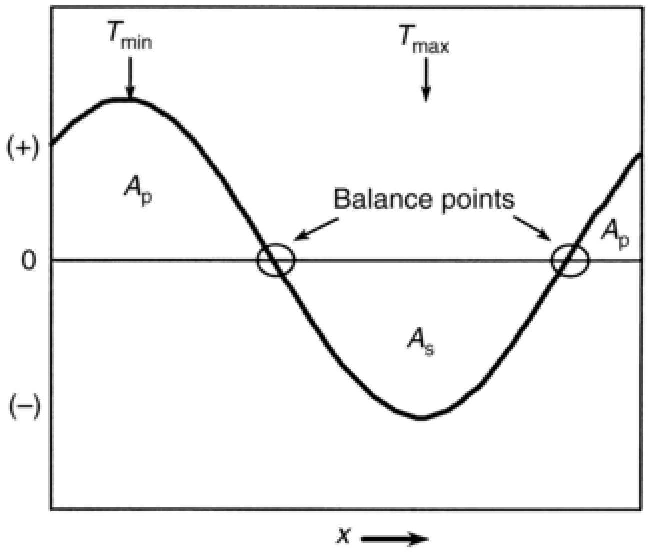

Fig. 2 Schematic depiction of idealized profile of mass change per unit surface area for a liquid metal circuit. T_{max} and T_{min} are maximum and minimum loop temperatures, respectively; x is loop position; A_p is deposition area; and A_s is dissolution area.

The respective areas of dissolution and deposition, A_s and A_p, are delimited by two balance points, which are the values of x at which $J = 0$ (Fig. 2). These balance points are experimentally accessible using an appropriately configured nonisothermal liquid metal loop and are important in determining the relative areas of dissolution and deposition and in modeling the relevant mass-transfer processes. Assuming a linear dependence of C_0 over the relatively small temperature range of most loop experiments, the mass balance represented by Eq 3 indicates that the ratio of the area measurements for dissolution and deposition is inversely proportional to the ratio of their respective rate constants:

$$A_s/A_p \propto k_p/k_s \quad \text{(Eq 4)}$$

Thus, determination of mass change or surface composition profiles around a loop yields insight into the kinetics of the solution process relative to deposition for a given material/liquid metal system. Another use of mass or compositional profiles is to determine estimates of the activation energy for dissolution using reasonable assumptions about the temperature dependence of the solubility. Because the respective activation energies characteristic of the most important rate-controlling processes (surface reaction, liquid-phase diffusion through boundary layer, and solid-state diffusion) are significantly different from each other, such analyses can yield mechanistic information regarding dissolution processes.

Although the mass-transfer analysis described previously is somewhat simplified, experimental measurements of mass or composition changes around a nonisothermal liquid metal loop often yield results that can be described in this way. Figure 3 is an example of an experimentally determined mass-change profile consistent with the schematic one shown in Fig. 2. Sometimes, however, more elaborate analyses based on Eq 1 are required to describe nonisothermal mass transfer precisely. Such treatments must take into account the differences in k around the circuit as well as the possibility that the rate constant for dissolution (or deposition) may not vary monotonically with temperature because of changes in the rate-controlling step within the temperature range of dissolution (deposition). The presence of more than one elemental species in the containment material further complicates the analysis; the transfer of each element typically has to be handled with its own set of thermodynamic and kinetic parameters. Although a thermal gradient increases the amount of dissolution, plugging of coolant pipes by nonuniform deposition of dissolved species in cold zones often represents a more serious design problem than metal loss from dissolution (which sometimes may be handled by corrosion allowances). The most direct way to control deposition, however, is usually to minimize dissolution in the hot zone by use of more corrosion-resistant materials and/or inhibition techniques.

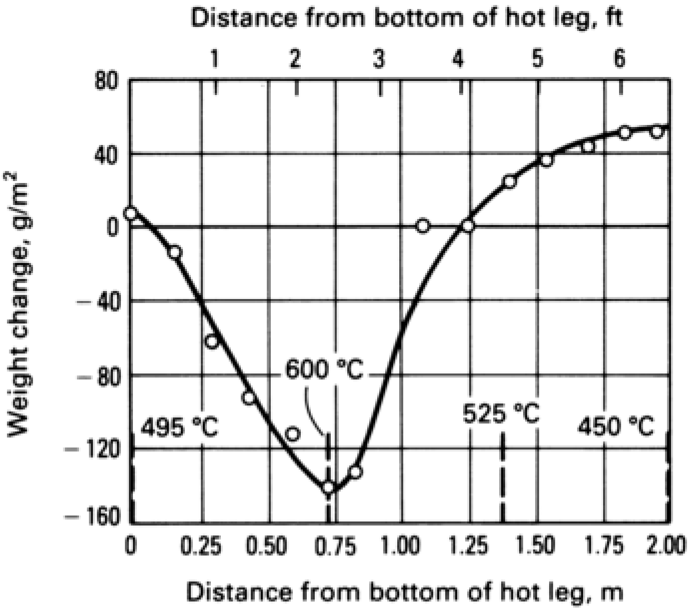

Fig. 3 Mass transfer as characterized by the weight changes of type 316 stainless steel coupons exposed around a nonisothermal liquid lithium type 316 stainless steel circuit for 9000 h. Source: Ref 2

Mass transfer may occur even under isothermal conditions if an activity gradient based on composition differences of solids in contact with the same liquid metal exists in the system. Under the appropriate conditions, dissolution and deposition will act to equilibrate the activities of the various elements in contact with the liquid metal. Normally, such a process is chiefly limited to interstitial element transfer between dissimilar metals, but transport of substitutional elements can also occur. Elimination (or avoidance) of concentration (activity) gradients across a liquid metal system is the obvious and, most often, the simplest solution to any problems arising from this type of mass-transport process.

Under certain conditions, dissolution of metallic alloys by liquid metals can lead to irregular attack (Fig. 4). Although such localized corrosive attack can often be linked to impurity effects (see subsequent discussion) and/or compositional inhomogeneities in the solid, destabilization of a planar surface can occur when there is preferential dissolution of one or more elements of an alloy exposed to a liquid metal. Indeed, the type of attack illustrated in Fig. 4 is thought to be caused by the preferential dissolution of nickel from an Fe-17Cr-11Ni (wt%) alloy (type 316 stainless steel). As such, this process resembles the dealloying phenomenon sometimes observed in aqueous environments. This type of attack has often been observed for austenitic stainless steels in molten lithium, sodium, lead, and other liquid metals when preferential dissolution of nickel occurs. In contrast, an Fe-12Cr- 1MoVW steel did not experience preferential loss of any of its elements and corroded uniformly (Fig. 5) when exposed under the same environment conditions that led to the irregular attack shown in Fig. 4. In cases where preferential dissolution and nonuniform corrosion occur (Fig. 4), the altered near-surface zone has diminished load-bearing capacity, and the section thickness of sound material remaining will be less than what would be calculated based on converting measured mass losses to a surface recession distance.

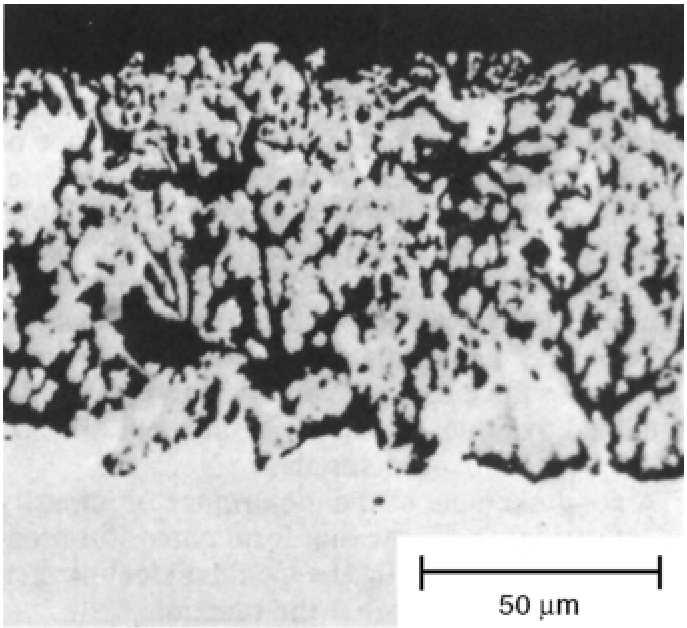

Fig. 4 Polished cross section of type 316 stainless steel exposed to thermally convective Pb-17at.%Li at 500 °C (930 °F) for 2472 h. Source: Ref 3

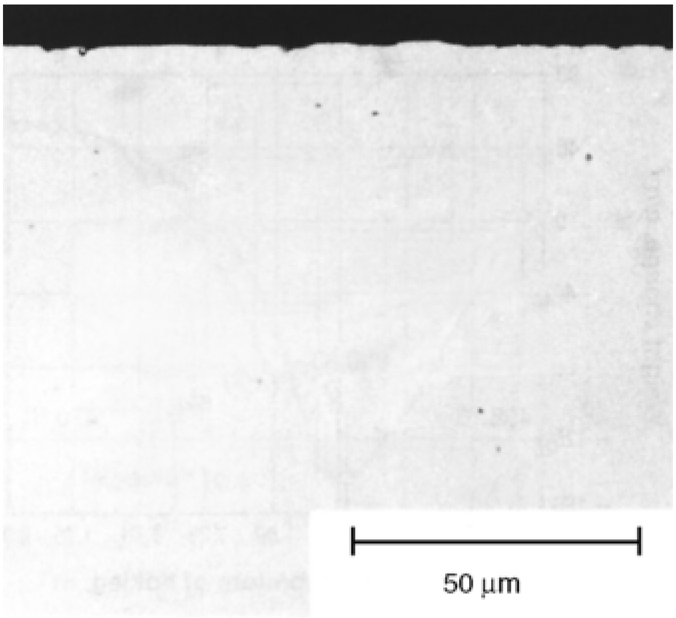

Fig. 5 Polished cross section of Fe-12Cr-1MoVW steel exposed to thermally convective Pb-17at.%Li at 500 °C (930 °F) for 2000 h. Source: Ref 3

Apart from possible effects on morphological development, the changes in surface composition due to preferential elemental dissolution from an alloy into a liquid metal are important in themselves. For example, in austenitic stainless steels, the preferential dissolution of nickel causes a phase transformation to a ferritic structure in the surface region. In many cases, an equilibrium surface composition is achieved, such that the net elemental fluxes into the liquid metal are in the same proportion as the starting concentrations of these elements in the alloy. Such a phenomenon has been rigorously treated and characterized for sodium-steel systems.

Impurity and Interstitial Reactions

For this discussion, impurity or interstitial reactions refer to the interaction of light elements present in the containment material (interstitials) or the liquid metal (impurities). Examples of such reactions include the decarburization of steel in lithium and the oxidation of steel in sodium or lead of high oxygen activity. In many cases, when the principal elements of the containment material have low solubilities in liquid metals (for

example, refractory metals in sodium, lithium, and lead), reactions involving light elements such as oxygen, carbon, and nitrogen dominate the corrosion process. Impurity or interstitial reactions can be generally classified into two types: corrosion product formation and elemental transfer of such species.

Corrosion Product Formation. The general form of a corrosion product reaction is:

$$xL + yM + zI = L_xM_yI_z \quad \text{(Eq 5)}$$

where L is the chemical symbol for a liquid metal atom, M is one species of the containment material, and I represents an interstitial or impurity atom in the solid or liquid (x, y, $z > 0$). The $L_xM_yI_z$ corrosion product that forms by such a reaction may be soluble or insoluble in the liquid metal. If it is soluble, the I species would cause greater dissolution weight losses and would result in an apparently higher solubility of M in L (Eq 1). This is a frequent cause of erroneous solubility measurements and is a good illustration of how dissolution and impurity reactions can be interrelated. Furthermore, if a soluble corrosion product forms at selected sites on the surface of the solid, localized attack will result. Under conditions in which a corrosion product is insoluble, a partial or complete surface layer will form. This can either have a detrimental effect on corrosion resistance or, if the product is continuous and protective (see subsequent discussion), limit further reaction. However, formation of a surface product does not necessarily mean that it can be observed. The product may be unstable outside the liquid metal environment or may dissolve in the cleaning agent used to remove the solidified residue of liquid metal from the exposed containment material.

A good example of the importance of impurity or interstitial reactions that form corrosion products can be found in the sodium-steel-oxygen system. It is thought that the reaction:

$$3Na_2O(l) + Fe(s) = (Na_2O)_2 \cdot FeO(s) + 2Na(l) \quad \text{(Eq 6)}$$

increases the apparent solubility of iron in sodium at higher oxygen activities, while the interaction of oxygen, sodium, and chromium can lead to the formation of surface corrosion products, for example:

$$2Na_2O(l) + Cr(s) = NaCrO_2(s) + 3Na(l) \quad \text{(Eq 7)}$$

This second type of reaction (Eq 7) is of primary importance in the corrosion of chromium-containing steels by liquid sodium. It can be controlled by reducing the oxygen concentration of the sodium to less than approximately 3 ppm and/or by modifying the composition of the alloy through reduction of the chromium concentration of the steel.

Such corrosion product reactions can also be observed in lithium-steel systems, in which nitrogen can increase the corrosiveness of the liquid metal environment. In particular, the reaction:

$$5Li_3N(\text{in } l) + Cr(s) = Li_9CrN_5(s) + 6Li(l) \quad \text{(Eq 8)}$$

or an equivalent one with iron, can play an important role in corrosion by liquid lithium. The Li_9CrN_5 corrosion product tends to be localized at the grain boundaries of exposed steels. Such reaction products can probably also be formed when there is sufficient nitrogen in the solid; experimental observations have indicated that nitrogen can increase corrosion by lithium, whether it is in the liquid metal or in the steel.

Corrosion product formation is also important when certain refractory metals are exposed to molten lithium. Despite their low solubilities in lithium, niobium and tantalum can be severely attacked when exposed to lithium if the oxygen activities of these metals are not low. At temperatures below approximately 900 °C (1650 °F), the lithium reacts rapidly with the oxygen and niobium or tantalum (and their oxides and suboxides) to form a ternary oxide corrosion product. Such reactions result in localized penetration along grain boundaries and selected crystallographic planes. This form of corrosive attack can be eliminated, however, by minimizing the oxygen concentration of these refractory metals (Fig. 6) and by using alloying additions that form oxides that do not react with the lithium and that minimize the amount of uncombined oxygen in the material (1 to 2 at.% Zr in niobium and hafnium in tantalum).

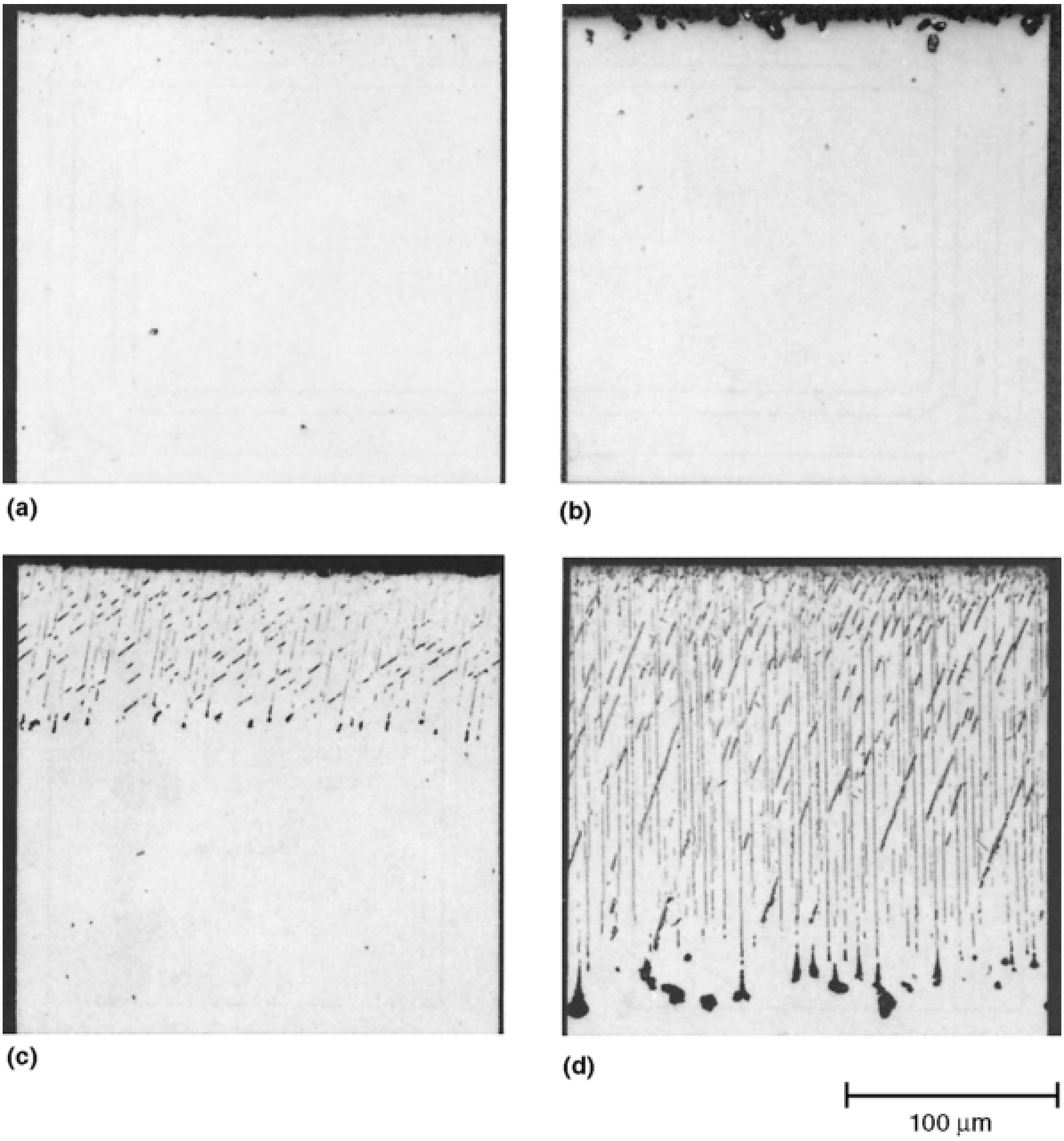

Fig. 6 Effect on initial oxygen concentration (150 to 1700 ppm) in niobium on the depth of reaction with lithium to form a corrosion product. Polished and etched cross sections of niobium exposed to isothermal lithium at 816 °C (1500 °F) for 100 h. (a) 150 ppm. (b) 500 ppm. (c) 1000 ppm. (d) 1700 ppm. Etched with HF-HNO_3-H_2SO_4-H_2O. Source: Ref 4

A final example of a corrosion product reaction that can occur in a liquid metal environment is the oxidation of a solid metal or alloy exposed to molten lead somewhat enriched in oxygen. In some cases, this reaction may actually be beneficial by providing a protective barrier against the highly aggressive lead. This barrier can act in a manner analogous to the behavior observed for the protective oxides formed in high-temperature oxidizing gases. However, this surface product will form and then heal only when the oxygen activity of the melt is maintained at a high level or when oxide formers, such as aluminum or silicon, have been added to the containment alloy to promote protection by the formation of alumina- or silica-containing surface products. Furthermore, reactions of additives to the melt with nitrogen in steel to form nitride surface films are thought to be the cause of reduced corrosion in lead and lead-bismuth systems.

Elemental Transfer of Impurities and Interstitials. The second general type of impurity or interstitial reaction is that of elemental transfer. In contrast to what is defined as corrosion product formation, elemental transfer manifests itself as a net transfer of interstitials or impurities to, from, or across a liquid metal. Although compounds may form or dissolve as a result of such transfer, the liquid metal atoms do not participate in the formation of stable products by reaction with the containment material. For example, because lithium is such a

strong thermodynamic sink for oxygen, exposure of oxygen-containing metals and alloys to this liquid often results in the transfer of oxygen to the melt. Indeed, for oxygen-contaminated niobium and tantalum, high-temperature lithium exposures result in the rapid movement of oxygen into the lithium.

The thermodynamic driving force for light element transfer between solid and liquid metals is normally expressed in terms of a distribution (or partitioning) coefficient. This distribution coefficient is the equilibrium ratio of the concentration of an element, such as oxygen, nitrogen, carbon, or hydrogen, in the solid metal or alloy to that in the liquid. Such coefficients can be calculated from knowledge or estimates of free energies of formation and activities based on equilibrium between a species in the solid and liquid. An example of this approach is its application to decarburization/carburization phenomena in a liquid metal environment. Carbon transfer to or from the liquid metal can cause decarburization of iron-chromium-molybdenum steels, particularly lower-chromium steels, and carburization of refractory metals and higher-chromium alloys. There have been many studies of such reactions for sodium-steel systems. Although less work has been done in the area of lithium-steel carbon transfer, the same considerations apply. Specifically, the equilibrium partitioning of the carbon between the iron-chromium-molybdenum steel and the lithium can be described as:

$$\frac{C_C(\mathrm{s})}{C_C(\mathrm{Li})} = (a_{\mathrm{Cr}})^{x/y} \left[\frac{C_C^{\circ}(\mathrm{s})}{C_C^{\circ}(\mathrm{Li})} \right] e^{\mathrm{f}} \cdot e^{\mathrm{g}} \qquad \text{(Eq 9)}$$

where $C_c(s)$, $C_c(Li)$ is the concentration of carbon in the steel and lithium, respectively; a_{Cr} is the chromium activity of the steel; $C°_C(s)$, $C°_C(Li)$ represent the equilibrium solubilities of carbon in the steel and lithium, respectively; x, y is the stoichiometry of the chromium carbide; and:

$$\mathrm{f} = +\Delta F_{(1/2)\mathrm{Li_2C_2}} / RT$$

$$\mathrm{g} = -\Delta F_{(1/y)\mathrm{Cr_xC_y}} / RT$$

where ΔF represents the free energies of formation of the indicated compounds, R is the gas constant, and T is the absolute temperature.

Equation 9 indicates that in order to decrease the tendency for decarburization of an alloy— that is, to increase the partitioning coefficient, $C_c(s)/C_c(Li)$—the chromium activity of the alloy must be increased or a more thermodynamically stable carbide dispersion must be developed (by alloy manipulation or thermal treatment). Experiments in lithium and sodium have shown that these factors have the desired effect. Tempering of iron-chromium-molybdenum steels to yield more stable starting carbides can significantly reduce decarburization by these two liquid metals. With very unstable microstructures, the steel can be severely corroded because of rapid lithium attack of the existing carbides. Furthermore, alloying additions, such as niobium, form very stable carbides and can dramatically reduce decarburization. In addition, as shown by Eq 9, increasing the chromium level of a steel effectively decreases the tendency for carbon loss. With higher-chromium steels, for example, austenitic stainless steels, carburization can then become a problem. If two dissimilar steels of significantly differing chromium activities and/or microstructures are exposed to the same liquid metal, the melt can act as a conduit for the relatively rapid redistribution of carbon between the two solids. Similar considerations would apply for any light element transfer across a liquid metal in contact with dissimilar materials; this can be further complicated by concentration (activity) gradient mass transfer of substitutional elements, as discussed previously.

Alloying

Reactions between atoms of the liquid metal and those of the constituents of the containment material may lead to the formation of a stable product on the solid without the participation of impurity or interstitial elements:

$$x\mathrm{M} + y\mathrm{L} = \mathrm{M}_x\mathrm{L}_y \qquad \text{(Eq 10)}$$

This is not a common form of liquid metal corrosion, particularly with the molten alkali metals, but it can lead to detrimental consequences if it is not understood or anticipated. Alloying reactions, however, can be used to inhibit corrosion by adding an element to the liquid metal to form a corrosion-resistant layer by reaction of this species with the contaminant material. An example is the addition of aluminum to a lithium melt contained by steel. A more dissolution-resistant aluminide surface layer forms, and corrosion is reduced.

Compound Reduction

Attack of ceramics exposed to liquid metals can occur because of reduction of the solid by the melt. In very aggressive situations, such as when most oxides are exposed to molten lithium, the effective result of such exposure is the loss of structural integrity by reduction-induced removal of the nonmetallic element from the solid. The tendency for reaction under such conditions can be qualitatively evaluated by consideration of the free energy of formation of the solid oxide relative to the oxygen/oxide stability in the liquid metal. Similar considerations apply to the evaluation of potential reactions between other nonmetallic compounds (nitrides, carbides, and so on) and liquid metals.

References cited in this section

1. J.E. Selle and D.L. Olson, in *Materials Considerations in Liquid Metal Systems in Power Generation*, National Association of Corrosion Engineers, 1978, p 15–22

2. P.F. Tortorelli and J.H. DeVan, *J. Nucl. Mater.*, Vol 85 and 86, 1979, p 289–293

3. P.F. Tortorelli and J.H. DeVan, *J. Nucl. Mater.*, Vol 141–143, 1986, p 592–598

4. J.R. DiStefano and E.E. Hoffman, Corrosion Mechanisms in Refractory Metal-Alkali Metal Systems, *At. Energy Rev.*, Vol 2, 1964, p 3–33

P.F. Tortorelli and S.J. Pawel, Corrosion by Liquid Metals, *Corrosion: Fundamentals, Testing, and Protection*, Vol 13A, *ASM Handbook*, ASM International, 2003, p 129–134

Corrosion by Liquid Metals

P.F. Tortorelli and S.J. Pawel, Oak Ridge National Laboratory

---

Considerations in Materials Selection

The previously mentioned types of corrosion reactions must be considered in materials selection for liquid metal containment. In many cases, particularly at low temperature or with less aggressive liquids (such as molten steel), liquid metal corrosion is not an important factor, and many materials, both metals and ceramics, would suffice. Under more severe conditions, however, an understanding of the various types of liquid metal corrosion is necessary to select or develop a compatible containment material. For example, for applications in high-temperature molten lithium, most oxides would be unstable with respect to this liquid metal, low-chromium steels would decarburize, and alloys containing large amounts of nickel or manganese would suffer extensive preferential dissolution and irregular attack. Materials selection would then be limited to higher-chromium ferritic/martensitic steels or high-purity refractory metals and alloys.

A general summary of the types of the most common corrosion reactions and guidelines for materials selection and/or development is given in Table 1, which also includes typical examples for each category. Because two or more concurrent corrosion reactions are possible, and because consideration of all of the applicable materials consequences may lead to opposite strategies, materials selection for liquid metal environments can become quite complex and may require optimization of several factors rather than minimization of any particular one. In addition, an assessment of the suitability of a given material for liquid metal service must be based on the knowledge of its total corrosion response. As in many corrosive environments, a simple numerical rate is not an accurate measurement of the susceptibility of a material when reaction with the liquid metal results in more than one of the modes of attack shown in Fig. 7 and discussed previously. Under such circumstances, a

measurement reflecting total corrosion damage is much more appropriate for judging the ability of a material to resist corrosion by a particular liquid metal.

Table 1 Guidelines for materials selection and/or alloy development based on liquid metal corrosion reactions

Corrosion reaction	Guidelines	Example
Direct dissolution	Lower activity of key elements.	Reduce nickel for lithium, lead, or sodium systems.
Corrosion product formation	Lower activity of reacting elements.	Reduce chromium and nitrogen in lithium systems.
	In case of protective oxide, add elements to promote formation.	Add aluminum or silicon to steel exposed to lead.
Elemental transfer	Increase (or add) elements to decrease transfer tendency.	Increase chromium content in steels exposed to sodium or lithium.
	Minimize element being transferred.	Reduce oxygen content in metals exposed to lithium.
Alloying	Avoid systems that form stable compounds.	Do not expose nickel to molten aluminum.
	Promote formation of corrosion-resistant layers by alloying.	Add aluminum to lithium to form surface aluminides.
Compound reduction	Eliminate solids that can be reduced by liquid metal.	Avoid bulk oxide-lithium couples.

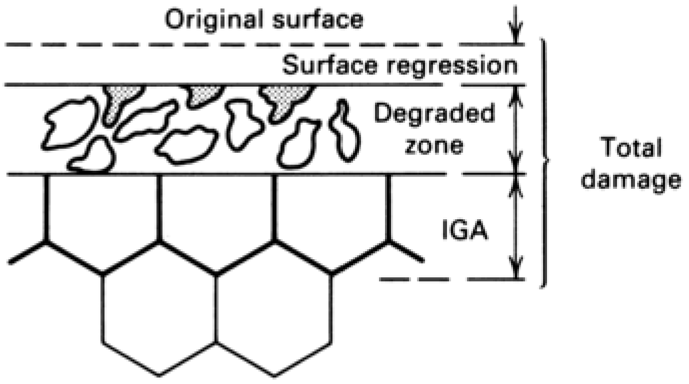

Fig. 7 Representative modes of surface damage in liquid metal environments. IGA, intergranular attack. Source: Ref 5

Reference cited in this section

5. J.H. DeVan and C. Bagnall, in *Proceedings of the International Conference on Liquid Metal Engineering and Technology*, Vol 3, The British Nuclear Energy Society, 1985, p 65–72

P.F. Tortorelli and S.J. Pawel, Corrosion by Liquid Metals, *Corrosion: Fundamentals, Testing, and Protection*, Vol 13A, *ASM Handbook*, ASM International, 2003, p 129–134

Corrosion by Liquid Metals

P.F. Tortorelli and S.J. Pawel, Oak Ridge National Laboratory

Acknowledgment

Research sponsored by the U.S. Department of Energy under contract DE-AC05-00OR22725 with UT-Battelle, LLC.

P.F. Tortorelli and S.J. Pawel, Corrosion by Liquid Metals, *Corrosion: Fundamentals, Testing, and Protection*, Vol 13A, *ASM Handbook*, ASM International, 2003, p 129–134

Corrosion by Liquid Metals

P.F. Tortorelli and S.J. Pawel, Oak Ridge National Laboratory

---

References

1. J.E. Selle and D.L. Olson, in *Materials Considerations in Liquid Metal Systems in Power Generation,* National Association of Corrosion Engineers, 1978, p 15–22
2. P.F. Tortorelli and J.H. DeVan, *J. Nucl. Mater.,* Vol 85 and 86, 1979, p 289–293
3. P.F. Tortorelli and J.H. DeVan, *J. Nucl. Mater.,* Vol 141–143, 1986, p 592–598
4. J.R. DiStefano and E.E. Hoffman, Corrosion Mechanisms in Refractory Metal-Alkali Metal Systems, *At. Energy Rev.,* Vol 2, 1964, p 3–33
5. J.H. DeVan and C. Bagnall, in *Proceedings of the International Conference on Liquid Metal Engineering and Technology,* Vol 3, The British Nuclear Energy Society, 1985, p 65–72

P.F. Tortorelli and S.J. Pawel, Corrosion by Liquid Metals, *Corrosion: Fundamentals, Testing, and Protection*, Vol 13A, *ASM Handbook*, ASM International, 2003, p 129–134

Corrosion by Liquid Metals

P.F. Tortorelli and S.J. Pawel, Oak Ridge National Laboratory

---

Selected References

- T.L. Anderson and G.R. Edwards, The Corrosion Susceptibility of $2\frac{1}{4}$ Cr-1 Mo Steel in a Lithium-17.6 Wt Pct Lead Liquid, *J. Mater. Energy Syst.,* Vol 2, 1981, p 16–25
- R.C. Asher, D. Davis, and S.A. Beetham, Some Observations on the Compatibility of Structural Materials with Molten Lead, *Corros. Sci.,* Vol 17, 1977, p 545–547
- M.G. Barker, S.A. Frankham, and N.J. Moon, The Reactivity of Dissolved Carbon and Nitrogen in Liquid Lithium, *Proceedings of the Third International Conference on Liquid Metal Engineering and Technology,* Vol 2, The British Nuclear Energy Society, 1984, p 77–83
- M.G. Barker, P. Hubberstey, A.T. Dadd, and S.A. Frankham, The Interaction of Chromium with Nitrogen Dissolved in Liquid Lithium, *J. Nucl. Mater.,* Vol 114, 1983, p 143–149

- G.E. Bell, M.A. Abdou, and P.F. Tortorelli, Experimental and Analytical Investigations of Mass Transport Processes of 12Cr- 1MoVW Steel in Thermally Convected Lithium Systems, *Fusion Eng. Des.,* Vol 8, 1989, p 421–427
- N.M. Beskorovainyi, V.K. Ivanov, and M.T. Zuev, Behavior of Carbon in Systems of the Metal-Molten Lithium-Carbon Type, *High- Purity Metals and Alloys,* V.S. Emel'yanov and A.I. Evstyukhin, Ed., Consultants Bureau, 1967, p 107–119
- N.M. Beskorovainyi and V.K. Ivanov, Mechanism Underlying the Corrosion of Carbon Steels in Lithium, *High-Purity Metals and Alloys,* V.S. Emel'yanov and A.I. Evstyukhin, Ed., Consultants Bureau, 1967, p 120–129
- O.K. Chopra, K. Natesan, and T.F. Kassner, Carbon and Nitrogen Transfer in Fe-9Cr-Mo Ferritic Steels Exposed to a Sodium Environment, *J. Nucl. Mater.,* Vol 96, 1981, p 269–284
- O.K. Chopra and P.F. Tortorelli, Compatibility of Materials for Use in Liquid-Metal Blankets of Fusion Reactors, *J. Nucl. Mater.,* Vol 122 and 123, 1984, p 1201–1212
- L.F. Epstein, Static and Dynamic Corrosion and Mass Transfer in Liquid Metal Systems, *Liquid Metals Technology—Part I,* Vol 53 (No. 20), Chemical Engineering Progress Symposium Series, American Institute of Chemical Engineers, 1957, p 67–81
- T. Flament, P.F. Tortorelli, V. Coen, and H.U. Borgstedt, Compatibility of Materials in Fusion First Wall and Blanket Structures Cooled by Liquid Metals, *J. Nucl. Mater.,* Vol 191–194, 1992, p 132–138
- J.D. Harrison and C. Wagner, The Attack of Solid Alloys by Liquid Metals and Salt Melts, *Acta Metall.,* Vol 1, 1959, p 722–735
- E.E. Hoffman, “Corrosion of Materials by Lithium at Elevated Temperatures,” ORNL- 2674, Oak Ridge National Laboratory, March 1959
- A.R. Keeton and C. Bagnall, Factors That Affect Corrosion in Sodium, *Proceedings of the Second International Conference on Liquid Metal Technology in Energy Production,* CONF-800401-P1, J.M. Dahlke, Ed., U.S. Department of Energy, 1980, p 7–18 to 7–25
- B.H. Kolster, The Influence of Sodium Conditions on the Rate for Dissolution and Metal/ Oxygen Reaction of AISI 316 in Liquid Sodium, *Proceedings of the Second International Conference on Liquid Metal Technology in Energy Production,* CONF- 800401-P1, J.M. Dahlke, Ed., U.S. Department of Energy, 1980, p 7–53 to 7–61
- J. Konys and H.U. Borgstedt, The Product of the Reaction of Alumina with Lithium Metal, *J. Nucl. Mater.,* Vol 131, 1985, p 158–161
- K. Natesan, Influence of Nonmetallic Elements on the Compatibility of Structural Materials with Liquid Alkali Metals, *J. Nucl. Mater.,* Vol 115, 1983, p 251–262
- D.L. Olson, P.A. Steinmeyer, D.K. Matlock, and G.R. Edwards, Corrosion Phenomena in Molten Lithium, *Rev. Coatings Corros./Int. Q. Rev.,* Vol IV, 1981, p 349–434
- S.J. Pawel, J.R. DeStefano, and E.T. Manneschmidt, Thermal Gradient Mass Transfer of Type 316L Stainless Steel and Alloy 718 in Flowing Mercury, *J. Nucl. Mater.,* Vol 296, 2001, p 210–218
- B.A. Pint, L.D. Chitwood, and J.R. DiStefano, Long-Term Stability of Ceramics in Liquid Lithium, *J. Nucl. Mater.,* Vol 289, 2001, p 52–56
- A.J. Romano, C.J. Klamut, and D.H. Gurinsky, “The Investigation of Container Materials for Bi and Pb Alloys, Part I: Thermal Convection Loops,” BNL-811, Brookhaven National Laboratory, July 1963
- E. Ruedl, V. Coen, T. Sasaki, and H. Kolbe, Intergranular Lithium Penetration of Low-Ni, Cr-Mn Austenitic Stainless Steels, *J. Nucl. Mater.,* Vol 110, 1982, p 28–36
- J. Sannier and G. Santarini, Etude de la Corrosion de Deux Aciers Ferritiques par le Plomb Liquide Circulant dans un Thermosiphon; Recherche d'un Modele, *J. Nucl. Mater.,* Vol 107, 1982, p 196–217
- C.E. Sessions and J.H. DeVan, Thermal Convection Loop Tests of Nb-1%Zr Alloy in Lithium at 1200 and 1300 °C, *Nucl. Appl. Technol.,* Vol 9, 1970, p 250–259
- S.A Shields and C. Bagnall, Nitrogen Transfer in Austenitic Sodium Heat Transport Systems, *Material Behavior and Physical Chemistry in Liquid Metal Systems,* H.U. Borgstedt, Ed., Plenum Press, 1982, p 493–501
- S.A. Shields, C. Bagnall, and S.L. Schrock, Carbon Equilibrium Relationships for Austenitic Stainless Steel in a Sodium Environment, *Nucl. Technol.,* Vol 23, 1974, p 273–283
- R.N. Singh, Compatibility of Ceramics with Liquid Na and Li, *J. Am. Ceram. Soc.,* Vol 59, 1976, p 112–115

- D.L. Smith and K. Natesan, Influence of Nonmetallic Impurity Elements on the Compatibility of Liquid Lithium with Potential CTR Containment Materials, *Nucl. Technol.*, Vol 22, 1974, p 392–404
- A.W. Thorley, Corrosion and Mass Transfer Behaviour of Steel Materials in Liquid Sodium, *Proceedings of the Third International Conference on Liquid Metal Engineering and Technology,* Vol 3, The British Nuclear Energy Society, 1985, p 31–41
- P.F. Tortorelli, Corrosion of Ferritic Steels by Molten Lithium: Influence of Competing Thermal Gradient Mass Transfer and Surface Product Reactions, *J. Nucl. Mater.,* Vol 155–157, 1988, p 722–727
- P.F. Tortorelli and J.H. DeVan, Effects of a Flowing Lithium Environment on the Surface Morphology and Composition of Austenitic Stainless Steel, *Microstruct. Sci.,* Vol 12, 1985, p 213–226
- P.F. Tortorelli and J.H. DeVan, Mass Transfer Kinetics in Lithium-Stainless Steel Systems, *Proceedings of the Third International Conference on Liquid Metal Engineering and Technology,* Vol 3, The British Nuclear Energy Society, 1985, p 81–88
- J.R. Weeks and H.S. Isaacs, Corrosion and Deposition of Steels and Nickel-Base Alloys in Liquid Sodium, *Adv. Corros. Sci. Technol.,* Vol 3, 1973, p 1–66

M. Ziomek-Moroz, Introduction to Corrosion for Constructive Purposes, *Corrosion: Fundamentals, Testing, and Protection*, Vol 13A, *ASM Handbook*, ASM International, 2003, p 135–138

Introduction to Corrosion for Constructive Purposes

Małgorzata Ziomek-Moroz, Albany Research Center, U.S. Department of Energy

Introduction

PRINCIPLES OF METALLIC CORROSION play a fundamental role in developing industrial processes that employ corrosion for constructive purposes. These processes range from the spontaneous processes in galvanic cells, such as batteries and fuel cells, that convert energy for external applications, to electrolytic cell processes, such as electropolishing, electrochemical machining, and electrochemical refining, that consume energy from external sources. Each of these processes consists of an electrochemical cell with an anode, cathode, and conductive medium or electrolyte. Each of these processes involves electrochemical oxidation and reduction reactions.

The purpose of this introduction is to show the similarities that exist between galvanic and electrolytic cells, while noting that the net or overall reaction for each type of cell leads us to label the electrodes and processes differently. For this purpose, a relatively simple electrochemical system has been chosen, and the changes in kinetics that occur with differentially small potential changes around the equilibrium electrode potentials of two reversible electrodes, Cu and Ag, are examined. In doing this, it should be clear that while differences in the kinetics of the spontaneous galvanic cell and the electrolytic cell can themselves be made differentially small, the industrial processes that are born out of these processes are quite different.

The two reversible electrode systems chosen were a copper electrode immersed in a copper sulfate solution at unit activity of Cu^{2+} and a silver electrode immersed in a silver nitrate solution at unit activity of Ag^{+}. The choice of these electrodes (or half-cells) avoids the complexity that arises with many electrodes of commercial interest where oxides or other stable corrosion products form on the surface. It also avoids the complexity that arises with reactions involving chemical species from different redox systems, such as zinc in an aqueous solution where the reduction reaction can be the evolution of hydrogen or the reduction of dissolved oxygen. The solutions are connected by a porous barrier and are at an ambient temperature of 25 °C (77 °F).

The electrochemical reactions at each electrode are (for copper electrode):

$$Cu^{2+} + 2e^- \underset{I_{a,Cu}}{\overset{I_{c,Cu}}{\rightleftarrows}} Cu \qquad \text{(Eq 1)}$$

(for silver electrode):

$$Ag^{+} + e^- \underset{I_{a,Ag}}{\overset{I_{c,Ag}}{\rightleftarrows}} Ag \qquad \text{(Eq 2)}$$

where I_a and I_c are now just labels indicating that some charges are moving.

M. Ziomek-Moroz, Introduction to Corrosion for Constructive Purposes, *Corrosion: Fundamentals, Testing, and Protection*, Vol 13A, *ASM Handbook*, ASM International, 2003, p 135–138

Introduction to Corrosion for Constructive Purposes

Małgorzata Ziomek-Moroz, Albany Research Center, U.S. Department of Energy

---

Reversible Cell Potential

At equilibrium, the following conditions exist at each electrode:

copper electrode $I_{a,Cu} = I_{c,Cu} = I_{o,Cu}$

silver electrode $I_{a,Ag} = I_{c,Ag} = I_{o,Ag}$

where I_0 is the exchange current for the copper and silver electrochemical reactions, respectively. There is a characteristic electrostatic difference at these electrodes called the *electrode potential difference* that can be measured with respect to the standard hydrogen electrode (SHE).

$$E^{\circ}_{Cu^{2+}/Cu} = 0.340\ V_{SHE}$$

$$E^{\circ}_{Ag^{+}/Ag} = 0.799\ V_{SHE}$$

At equilibrium there is a zero net reaction or current at each electrode.

When the electrodes are connected through a high-impedance device such as an electrometer and the electrolytes are connected via a porous barrier to form the electrochemical cell:

$$Cu\,|\,Cu^{2+}\left(aq,\ a_{Cu(II)} = 1,\ 25^{\circ}C\right)|$$

$$|\,Ag^{+}\left(aq,\ a_{Ag(I)} = 1,\ 25^{\circ}C\right)|\,Ag$$

the net current in the external circuit is zero; that is, the cell current $I_{cell} = 0$. The copper electrode is more active or negative to the more noble or positive silver electrode (Fig. 1). The reversible cell potential ($e_{cell,rev}$) is determined by the electrode potentials:

$$e_{cell,rev} = E^{\circ}_{Ag^{+}/Ag} - E^{\circ}_{Cu^{2+}/Cu}$$

$$= 0.799\ V_{SHE} - 0.340\ V_{SHE} = 0.459\ V$$

This potential could be measured with a high- impedance electrometer between the two electrodes (Fig. 2). The cell is reversible because the electrode potentials remain at their equilibrium potential when perturbed by incrementally small shifts in the cell reactions to produce reversibly small net reactions in one direction or the other. It should be noted that unit activity is not a necessary condition of this example. The reversible electrode potential, E_{rev}, at any other activity of the metal ion, a, is given by the Nernst equation:

$$E_{rev} = E^{o} - (2.303RT/nF) \log a \qquad \text{(Eq 3)}$$

where R is gas constant; F is the Faraday constant, 96,500 C/gram-equivalent; T is the absolute temperature, K; and n is the number of electrons involved in the electrode reaction.

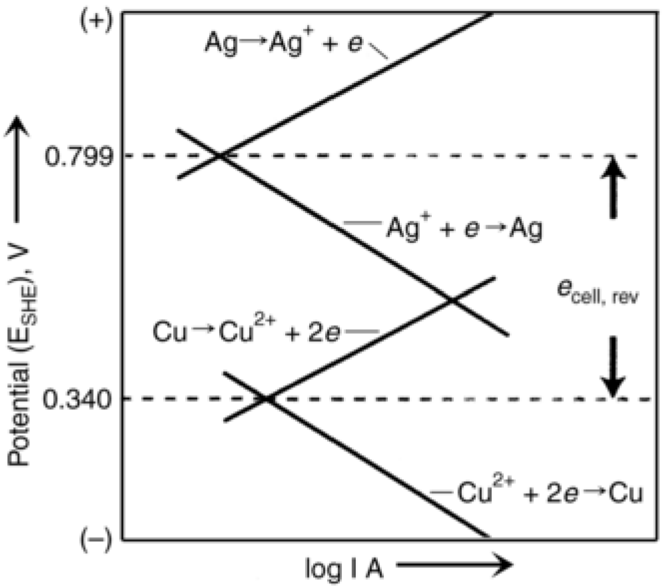

Fig. 1 Potential versus log current plot for reversible cell with copper and silver electrodes

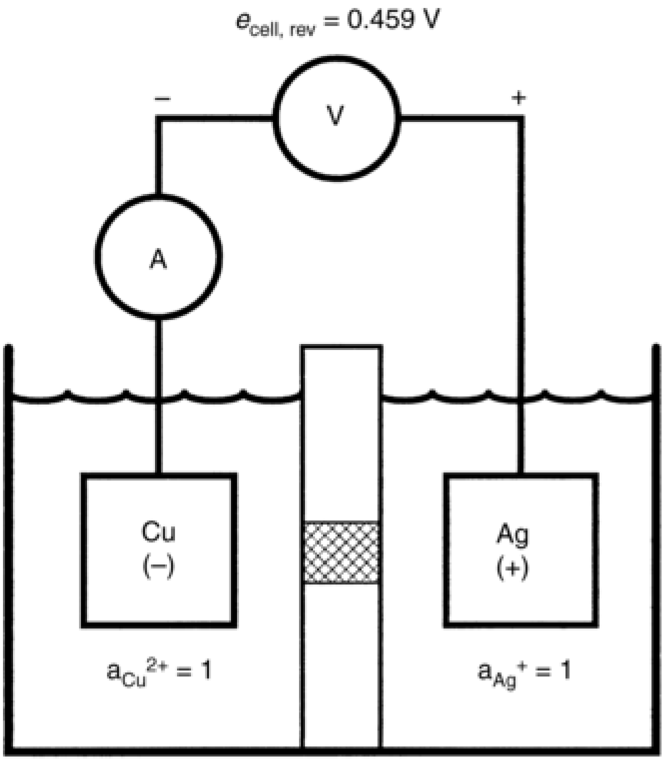

Fig. 2 Reversible cell with copper and silver electrodes. Voltage is measured with a high-resistance electrometer (V), and current is measured with a zero resistance ammeter, (A).

M. Ziomek-Moroz, Introduction to Corrosion for Constructive Purposes, *Corrosion: Fundamentals, Testing, and Protection*, Vol 13A, *ASM Handbook*, ASM International, 2003, p 135–138

Introduction to Corrosion for Constructive Purposes

Małgorzata Ziomek-Moroz, Albany Research Center, U.S. Department of Energy

Irreversible Cell Potential

An electrode becomes irreversible when the electrode reactions are displaced from equilibrium and the electrode potential is no longer at the equilibrium potential. This happens in spontaneous processes when the cell is converting energy for external applications. It happens in electrolytic cells when energy from an external source is doing work on the electrodes. It happens in corrosion because the anodic and cathodic processes are coupled (or shorted) at a mixed or corrosion potential defining the kinetics of the corrosion reaction.
Galvanic Cells. The example of the copper and silver electrodes functions as a galvanic cell when there is a net flow of electrons through an external circuit from the copper electrode to the silver electrode. When this occurs the following conditions exist at the electrodes:

$$\text{copper electrode} \quad I_{a,Cu} > I_{c,Cu}$$

$$\text{silver electrode} \quad I_{a,Ag} < I_{c,Ag}$$

and the electrode potentials, *E*, shift to values between those of the initial equilbrium values and are no longer reversible:

$$E_{Cu^{2+}/Cu} > E^{\circ}_{Cu^{2+}/Cu}$$

$$E_{Ag^{+}/Ag} < E^{\circ}_{Ag^{+}/Ag}$$

The shift in potential, known as electrode polarization, is measured by the overpotential, η, which is the value by which the electrode potential has shifted from its equilibrium or reversible value (Fig. 3):

$$\eta = E - E_{rev}$$

The effect of overpotential on the rate of the electrode reactions controlled by activation polarization is given by the Butler-Volmer equation. This corresponds to the straight lines in Fig. 1 and 4 that describe the anode and cathode reaction rates as a function of potential (or overpotential).

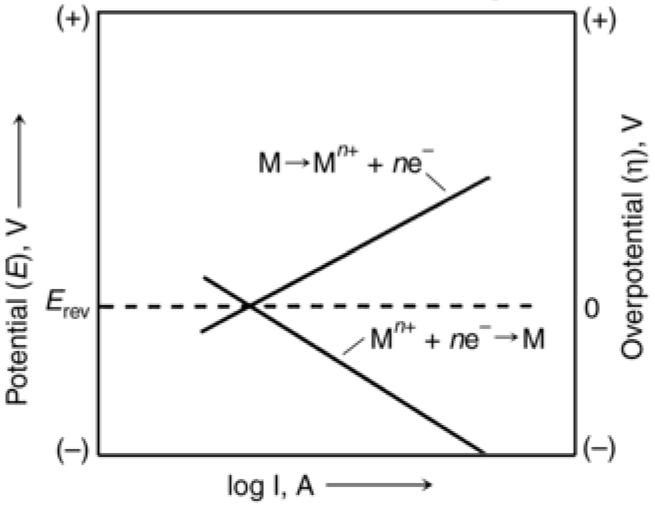

Fig. 3 Potential versus log current plot relating overpotential to potential scale for anodic and cathodic reactions. M is a metal, and *n* is a positive integer.

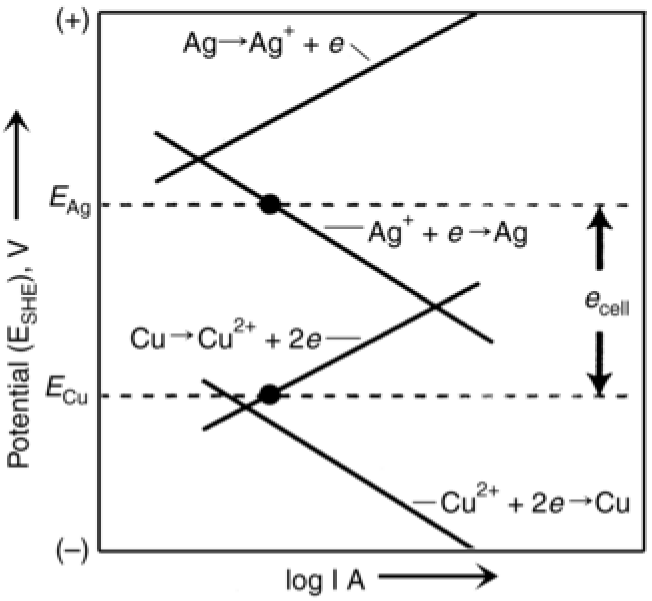

Fig. 4 Potential versus log current plot for galvanic cell with copper and silver electrodes

The set of lines in Fig. 4 allows us to conveniently describe anodic and cathodic reaction rates at the copper and silver electrodes as a function of potential. The shift in electrode potentials for the galvanic cell gives a cell potential, e_{cell}, that is less than the reversible cell potential of Fig. 1:

$$e_{cell} = E^{\circ}_{Ag^+/Ag} - \eta_{Ag,c} - \left(E^{\circ}_{Cu^{2+}/Cu} + \eta_{Cu,a}\right)$$
$$= e_{cell,rev} - \left(\eta_{Ag,c} + \eta_{Cu,a}\right)$$
$$e_{cell} < e_{cell,rev}$$

where the η-values are the overpotentials for the individual anodic and cathodic electrode reactions.
Figure 5 is a circuit that allows the cell potential to be varied in a controlled manner from the reversible cell potential. By reducing the potential between direct current (dc) below $e_{cell,rev}$, the spontaneous galvanic reaction is allowed to proceed. Since the anode reaction is larger than the cathode reaction at the copper electrode, the net reaction is:

$$Cu \rightarrow Cu^{2+} + 2e^-$$

The cathode reaction is larger than the anode reaction at the silver electrode, and the net reaction is:

$$Ag^+ + e^- \rightarrow Ag$$

The overall cell reaction that spontaneously occurs then is:

$$Cu + 2Ag^+ \rightarrow Cu^{2+} + 2Ag$$

and the cell current, $I_{cell} \neq 0$. The galvanic cell can be described as a constructive galvanic cell when $e_{cell} > 0$ and the call is delivering energy to an external device such as an electronic circuit, motor, or light.

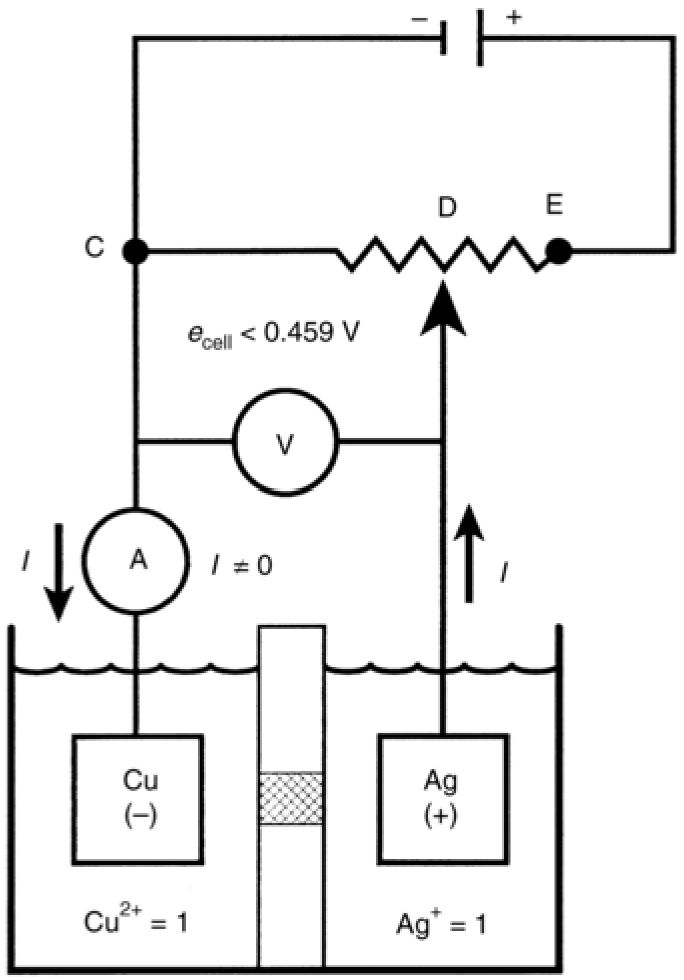

Fig. 5 Galvanic cell with copper and silver electrodes is connected to an external power supply through a voltage divider. The potential, $V_{C\text{-}D}$, can be varied. Voltage, V, is measured with a high resistance electrometer; current, A, is measured with a zero resistance ammeter.

Following the 1953 International Union of Pure and Applied Chemistry (IUPAC) convention, since oxidation occurs at the copper electrode, it is the anode. Reduction occurs at the silver electrode, and it is the cathode. In terms of polarity, the copper electrode is the negative or more active electrode; the silver electrode is the positive or more noble electrode. The flow of current (positive charge) in the external circuit is from the silver electrode to the copper electrode; the electron flow is in the opposite direction, from the copper electrode to the silver electrode.

Electrolytic Cells. The overall electrolytic cell process is not spontaneous because external work must be done on the system to produce the desired reaction. In the case of the copper and silver electrodes, this work is the deposition of copper instead of silver. There is a net flow of electrons through an external circuit from the silver electrode to the copper electrode. When this occurs, the following conditions exist at the electrodes:

$$\text{copper electrode} \quad I_{a,Cu} < I_{c,Cu}$$

$$\text{silver electrode} \quad I_{a,Ag} > I_{c,Ag}$$

and the electrode potentials, E, shift to values outside the range of the initial equilibrium values and are no longer reversible:

$$E_{Cu^{2+}/Cu} < E^{\circ}_{Cu^{2+}/Cu}$$

$$E_{Ag^{+}/Ag} > E^{\circ}_{Ag^{+}/Ag}$$

This shift in electrode potentials for the electrolytic cell gives a cell potential, e_{cell}, that is greater than the reversible cell potential:

$$e_{cell} = E^{\circ}_{Ag^+/Ag} + \eta_{Ag,a} - \left(E^{\circ}_{Cu^{2+}/Cu} + \eta_{Cu,c}\right)$$
$$= e_{cell,rev} + \left(\eta_{Ag,a} + \eta_{Cu,c}\right)$$
$$e_{cell} > e_{cell,rev}$$

as in Fig. 6 compared to Fig. 1. Since the cathode reaction is larger than the anode reaction at the copper electrode, the net reaction is:

$$Cu^{2+} + 2e^- \rightarrow Cu$$

The anode reaction is larger than the cathode reaction at the silver electrode, and the net reaction is:

$$Ag \rightarrow Ag^+ + e^-$$

The overall cell reaction that occurs by the input of external energy is:

$$Cu^{2+} + 2Ag \rightarrow Cu + 2Ag^+$$

and the cell current, $I_{cell} \neq 0$. By increasing the potential between points D and C in Fig. 5 above $e_{cell,rev}$, the nonspontaneous electrolytic reaction proceeds in a controlled way, with the current now in the opposite direction from that of the galvanic cell and the cell potential greater than the reversible cell potential. Since oxidation occurs at the silver electrode, it is now the anode. Reduction occurs at the copper electrode, and it is the cathode. In terms of polarity, the copper electrode is still the negative or more active electrode, the silver electrode is still the positive or more noble electrode. The flow of current (positive charge) in the external circuit is from the copper electrode to the silver electrode; the electron flow is in the opposite direction, from the silver electrode to the copper electrode.

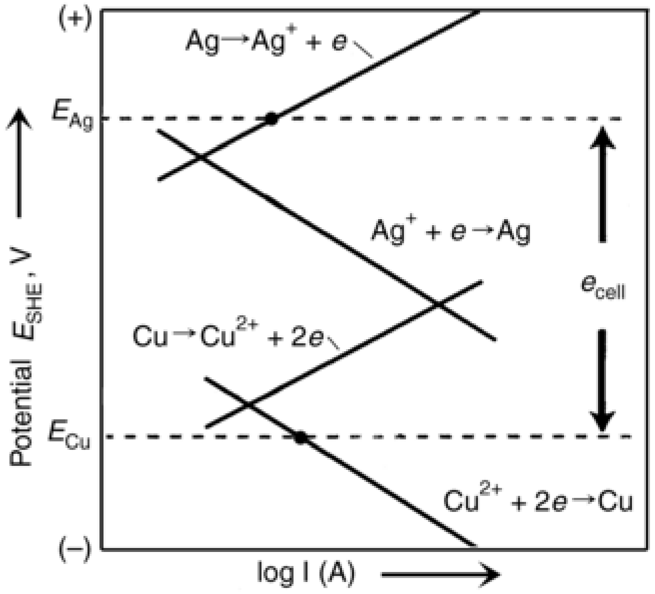

Fig. 6 Potential versus log current plot for electrolytic cell with copper and silver electrodes. The impressed potential difference is e_{cell}.

Corrosion Cells. The corrosion cell is a special case of a galvanic cell. The two electrodes are shorted together in a spontaneous process with both electrodes at the same potential, a mixed potential known as the corrosion potential (E_{corr}). Corrosion cells differ from constructive galvanic cells in that no electrical energy is produced for external application. While there is a net flow of electrons through the circuit from the copper electrode to the silver electrode, this flow produces no useful external work. The following conditions exist at the electrodes:

copper electrode $I_{a,Cu} > I_{c,Cu}$

silver electrode $I_{a,Ag} < I_{c,Ag}$

and the electrode potentials, E, shift to values between those of the initial equilbrium values. They are no longer reversible; that is;

$$E_{Cu^{2+}/Cu} > E^{\circ}_{Cu^{2+}/Cu}$$

$$E_{Ag^{+}/Ag} < E^{\circ}_{Ag^{+}/Ag}$$

In fact, they shift to the corrosion potential (E_{corr}) where:

$$E_{Cu^{2+}/Cu} = E_{Ag^{+}/Ag} = E_{corr}$$

The cell potential (Fig. 7) is:

$$e_{cell} = E_{Ag^{+}/Ag} - E_{Cu^{2+}/Cu} = 0$$

Since the anode reaction is larger than the cathode reaction at the copper electrode, the net reaction is:

$$Cu \rightarrow Cu^{2+} + 2e^{-}$$

The cathode reaction is larger than the anode reaction at the silver electrode, and the net reaction is:

$$Ag^{+} + e^{-} \rightarrow Ag$$

The overall cell reaction that spontaneously occurs is:

$$Cu + 2Ag^{+} \rightarrow Cu^{2+} + 2Ag$$

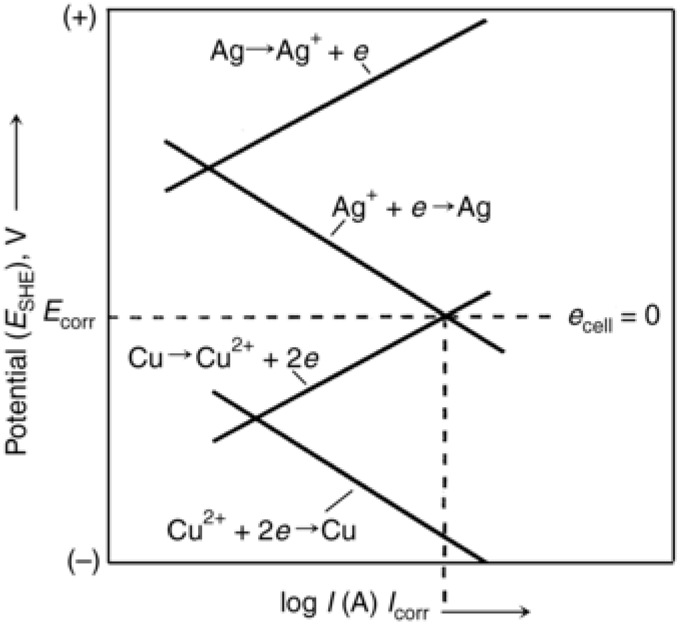

Fig. 7 Potential versus log current plot for corrosion cell with copper and silver electrodes

The cell current (I_{cell}), when measured by a zero resistance ammeter, is equivalent to the corrosion current, I_{corr}. Since oxidation occurs at the copper electrode, it is the anode. Reduction occurs at the silver electrode, and it is the cathode. While both electrodes are at the same potential, the copper electrode is the more active electrode and the silver electrode is the more noble electrode. The flow of current (positive charge) in the external circuit is from the silver electrode to the copper electrode; the electron flow is in the opposite direction, from the copper electrode to the silver electrode.

Table 1 summarizes the conditions that exist at the Cu and Ag electrodes in our example for the different types of cells: reversible, galvanic, electrolytic, and corrosion.

Table 1 Conditions at each electrode in example

Cell type	Electrode reactions		Cell potential	Electrode potentials, E_{SHE}	
	Cu	**Ag**		**Cu^{2+}/Cu**	**Ag^{+}/Ag**
Reversible	$I_a = I_c = I_0$	$I_a = I_c = I_0$	$e_{cell,rev}$ = 0.459 V	E^o = 0.340	E^o = 0.799
Galvanic	$I_a > I_c$	$I_a < I_c$	$e_{cell} < e_{cell,rev}$	$E > E^o$	$E < E^o$
Electrolytic	$I_a < I_c$	$I_a > I_c$	$e_{cell} > e_{cell,rev}$	$E < E^o$	$E > E^o$
Corrosion	$I_a > I_c$	$I_a < I_c$	$e_{cell} = 0$	$E > E^o$	$E < E^o$

Table 2 summarizes the conditions that exist for commercial and industrial electrochemical processes that employ corrosion for constructive purposes, as well as the conditions for corrosion.

Table 2 Cell conditions for commercial and industrial electrode processes

Cell type	Cell potential	Net current	Polarity		Process
			Anode	**Cathode**	
Reversible	$e_{cell,rev}$	$I = 0$	-	+	…
Galvanic	$e_{cell} < e_{cell,rev}$	$I \neq 0$ (spontaneous)	-	+	Batteries, fuel cells
Electrolytic	$e_{cell} > e_{cell,rev}$	$I \neq 0$ (impressed current or impressed potential)	+	-	Electrolytic polishing, electrochemical machining, electrochemical refining
Corrosion	$e_{cell} = 0$	I_{corr} (spontaneous)	-	+	Corrosion, chemical-mechanical planarization

---

M. Ziomek-Moroz, Electropolishing, *Corrosion: Fundamentals, Testing, and Protection,*, Vol 13A*, ASM Handbook,* ASM International, 2003, p 139–142

Electropolishing

M. Ziomek-Moroz, U.S. Department of Energy, Albany Research Center

---

Introduction

ELECTROLYTIC POLISHING, also known as electropolishing, is an electrochemical process that involves anodic dissolution of a metal specimen (anode electrode) in an electrolytic cell. An electrochemical cell is a combination of an anode (an electronic conductor), an electrolyte (an ionic conductor), and a cathode (an electronic conductor); electrochemical processes occur with the passage of electric current in the cell (Ref 1). Irregularities on the anode surface are dissolved preferentially so that the surface becomes smooth and bright (Ref 2). Due to requirements for surface quality, electropolishing is a specific case of anodic dissolution and is essentially the reverse of electroplating. Electropolishing is widely used in many branches of science for purposes such as specimen preparation for corrosion studies. Commercial applications include improving appearance and reflectivity, improving corrosion resistance, removing edge burrs produced by mechanical cutting tools, removing the stressed and disturbed layer of metal caused by mechanical action (mechanical cutting), improving surfaces of medical tools, and removing radioactive contamination from surfaces (Ref 3, 4, 5).

References cited in this section

1. G. Wranglén, *An Introduction to Corrosion and Protection,* Chapman & Hall, 1985

2. “Metallography Principles and Procedures,” Leco Corporation

3. *45th Metal Finishing for Guide Book and Directory,* Metals and Plastics Publications, Inc., 1977

4. K.P. Rajurkar, J. Kozak, and A. Chatterjee, Nonabrasive Finishing Methods *Surface Engineering,* Vol 5, *ASM Handbook,* ASM International, 1994, p 110–117

5. J.R. Davis, Surface Engineering of Carbon and Alloy Steels, *Surface Engineering,* Vol 5, *ASM Handbook,* ASM International, 1994, p 710

M. Ziomek-Moroz, Electropolishing, *Corrosion: Fundamentals, Testing, and Protection,*, Vol 13A, *ASM Handbook*, ASM International, 2003, p 139–142

Electropolishing

M. Ziomek-Moroz, U.S. Department of Energy, Albany Research Center

---

Electrical Circuits

Electropolishing can be carried out in two- electrode and three-electrode systems. A two- electrode laboratory setup is shown in Fig. 1. A workpiece or working electrode (WE), the anode, is connected to the positive terminal of a direct current (dc) power supply. The counterelectrode (CE), the cathode, is attached to the negative terminal. The variable resistor provides control of the current, which is monitored by the ammeter. In commercial use, a pulsed dc may be used.

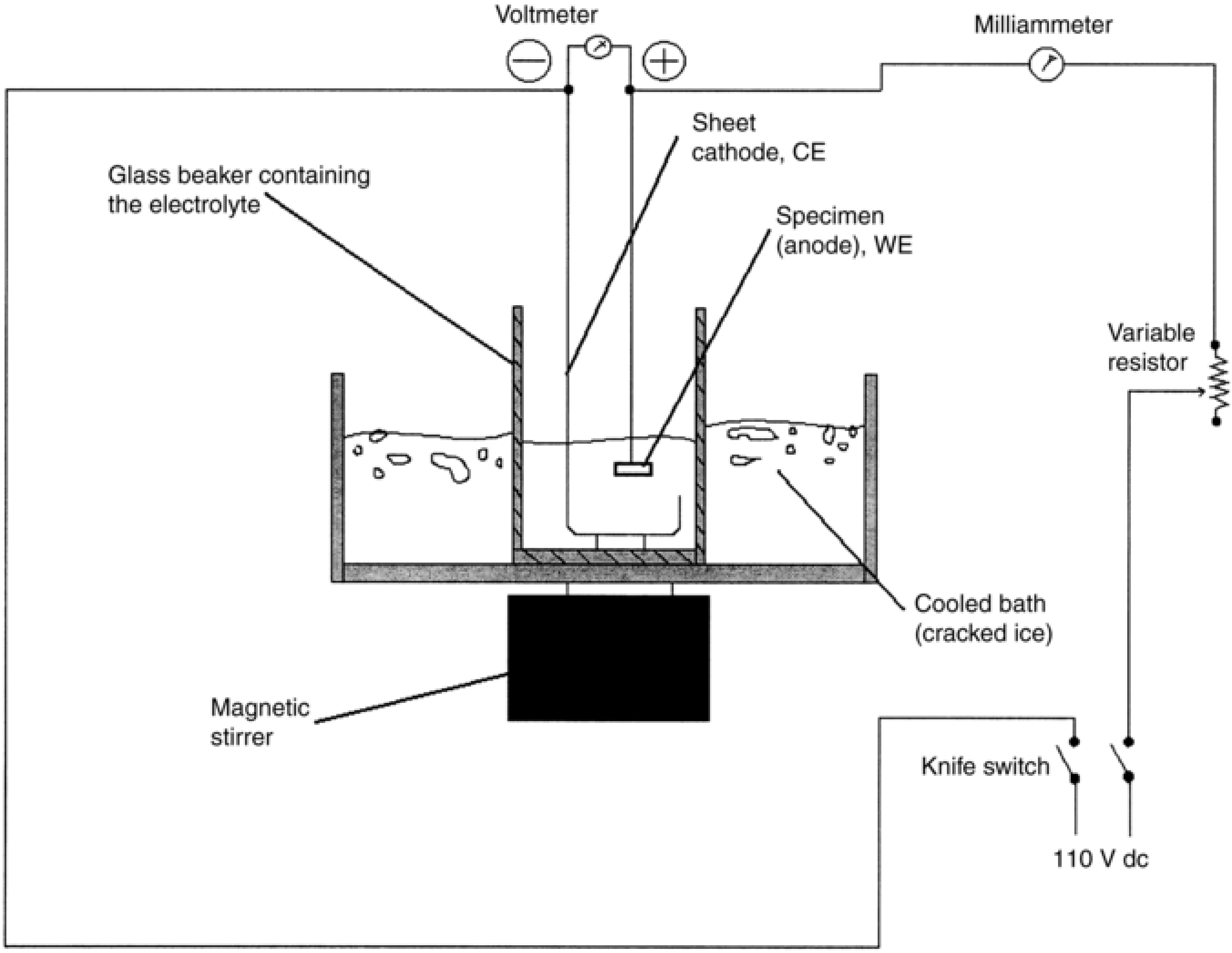

Fig. 1 Two-electrode laboratory setup for electropolishing. WE, working electrode; CE, counterelectrode; dc, direct current

In a three-electrode system (Fig. 2), a potentiostat regulates the dc power to the specimen (WE) and counterelectrode (CE) and receives information on the potential from the reference electrode (RE). The anode workpiece is connected to the working electrode terminal, and the cathode made of platinum or graphite is connected to the counterelectrode terminal. Finally a reference electrode, such as a saturated calomel electrode (SCE), is connected to the reference- electrode terminal to measure the potential of the workpiece.

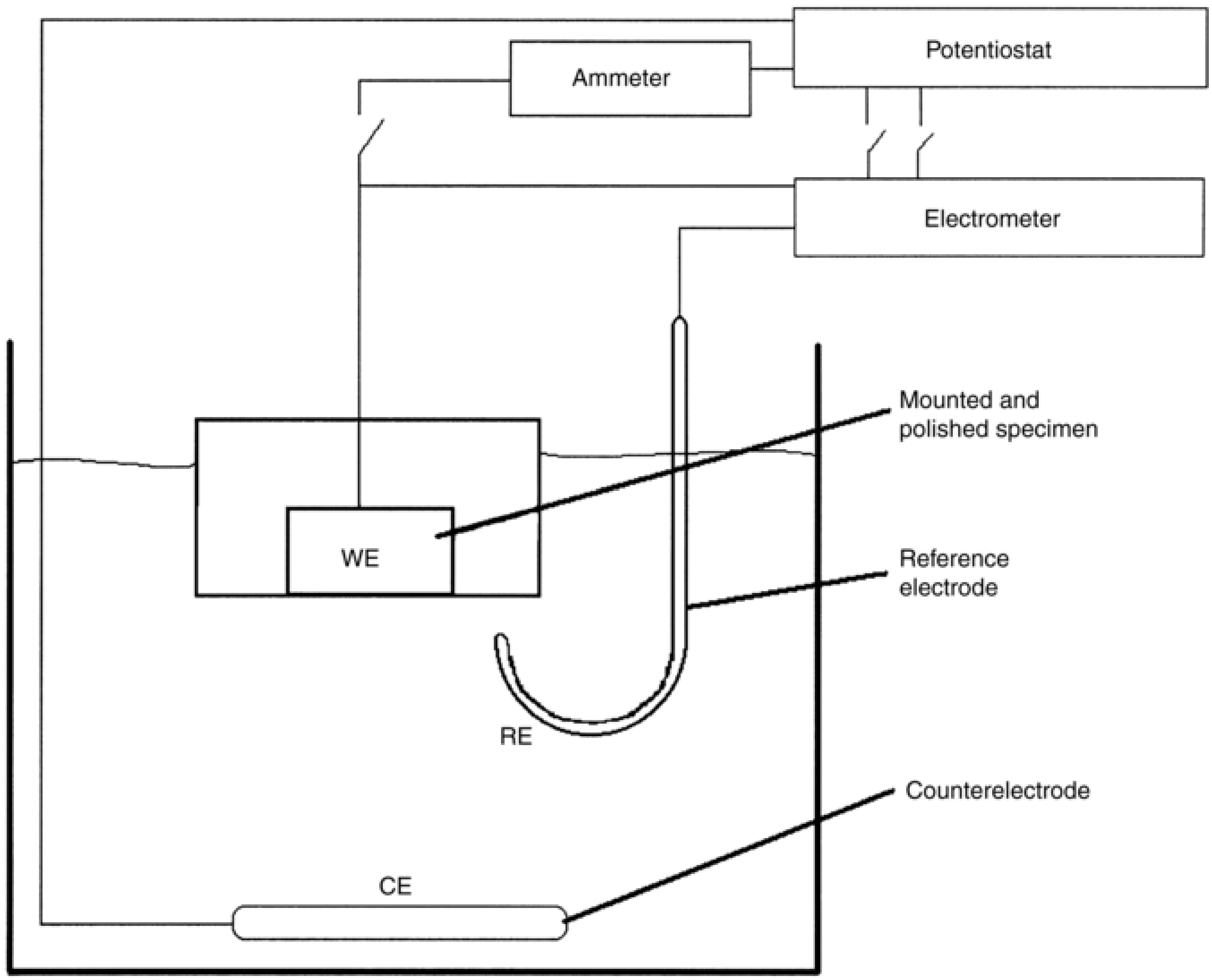

Fig. 2 Three-electrode laboratory setup for electropolishing. WE, working electrode; CE, counterelectrode; RE, reference electrode

The electrical potential of the power supply or potentiostat causes electronic conduction to the WE and CE and ionic conduction in the electrolyte. This may result in controlled anodic dissolution of the anode material and cathodic deposition on the CE of some species present in the electrolyte. During the electrolytic process, the products of the anodic metal dissolution react with the electrolyte to form a film at the surface of the metal as shown in Fig. 3.

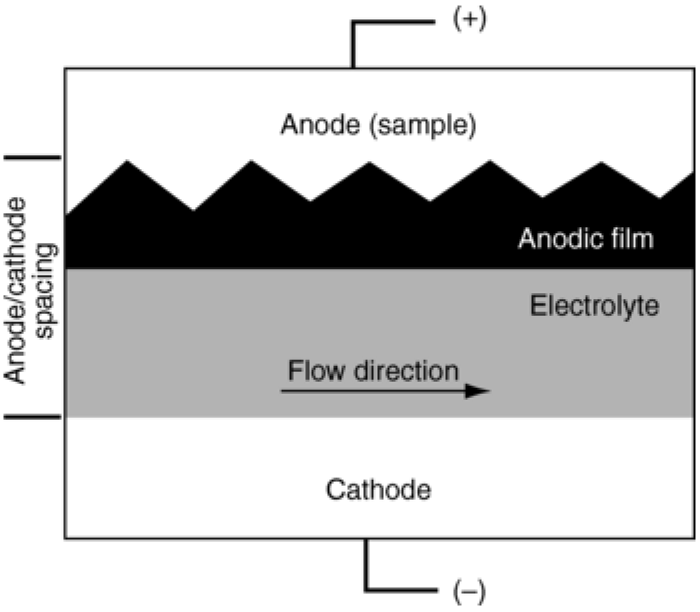

Fig. 3 Formation of anodic film during electropolishing

M. Ziomek-Moroz, Electropolishing, *Corrosion: Fundamentals, Testing, and Protection,*, Vol 13A, *ASM Handbook*, ASM International, 2003, p 139–142

Electropolishing

M. Ziomek-Moroz, U.S. Department of Energy, Albany Research Center

Anodic Processes

Anodic dissolution processes are complex. Depending on the nature of the dissolving metal (M), the electrolyte composition, and the current density, the following anodic (oxidation) reactions may occur:

- Transfer of metal ions into the electrolyte:

$$Me \rightarrow Me^{2+} + 2e^- \quad \text{(Eq 1)}$$

- Formation of oxide layers:

$$Me + 2OH^- \rightarrow MeO + H_2O + 2e^- \quad \text{(Eq 2)}$$

- Evolution of oxygen:

$$4OH^- \rightarrow O_2 + 2H_2O + 4e^- \quad \text{(Eq 3)}$$

During electrolytic polishing, a voltage is applied between the anode and cathode, which are immersed in the electrolyte, through an external electrical circuit as shown in Fig. 1 and 2. If the current is monitored as a function of the cell voltage, polarization curves or current-voltage curves can be generated. Figure 4 shows an idealized anodic polarization curve with regions of cell voltage within which the reactions shown in Eq 1, 2, and 3 may occur.

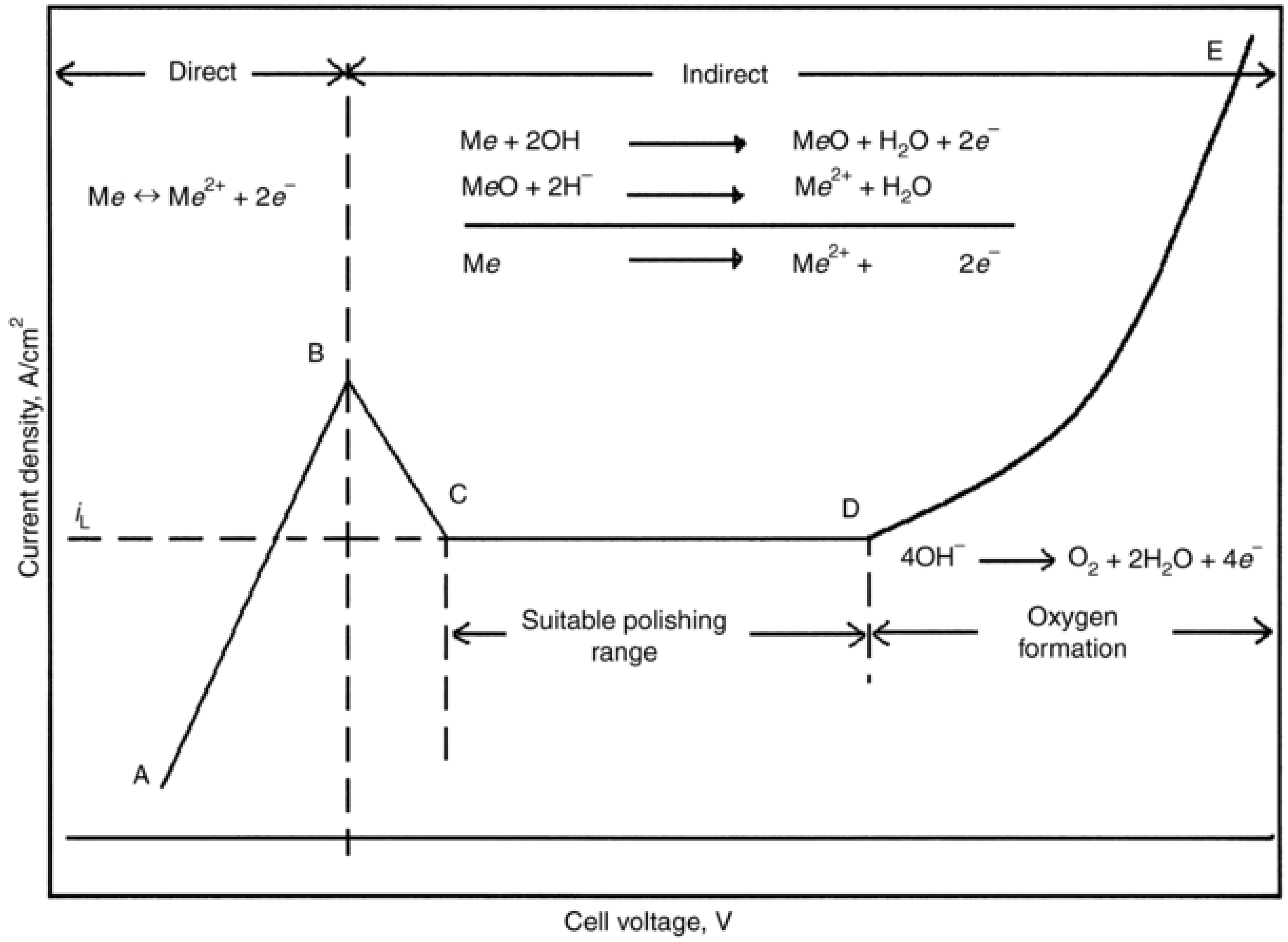

Fig. 4 Idealized anodic polarization curve useful for electropolishing of materials showing active-passive behavior

During electrolytic polishing, positive metal ions (cations) leave the specimen surface and diffuse into the electrolyte, and current increases with increasing applied voltage. In voltage region A-B, active dissolution or a direct etching takes place (the reaction represented by Eq 1). In the B-C voltage region, current decreases with increasing voltage, indicating unstable conditions on the metal surface. This represents active-passive behavior. Constant current with increasing voltage is observed in the C-D range when the anodic film is formed (the reaction shown in Eq 2). This represents passive behavior. At higher voltages (in the D-E range), current increases and the evolution of O_2 takes place (the reaction shown in Eq 3), which resembles transpassive behavior. This type of curve, showing active, active-passive, passive, and transpassive regions, is obtained for copper electropolished in orthophosphoric acid. Electropolishing is achieved by operating at the mass-transfer-limited rate of dissolution in the C-D region. The mass-transfer rate is represented by the limiting current density, i_L, which depends on electrolyte concentration, viscosity, density, and stirring of the electrolyte, as well as the diffusivity of the ionic species present.

Figure 5 is a polarization curve with two distinctive regions, namely: (a) film formation at low voltage and low current and (b) electrolytic polishing at higher voltage and current. Aluminum electropolished in perchloric acid exhibits this type of behavior. The difference in the shapes of the polarization curves for aluminum and copper indicate different electropolishing mechanisms.

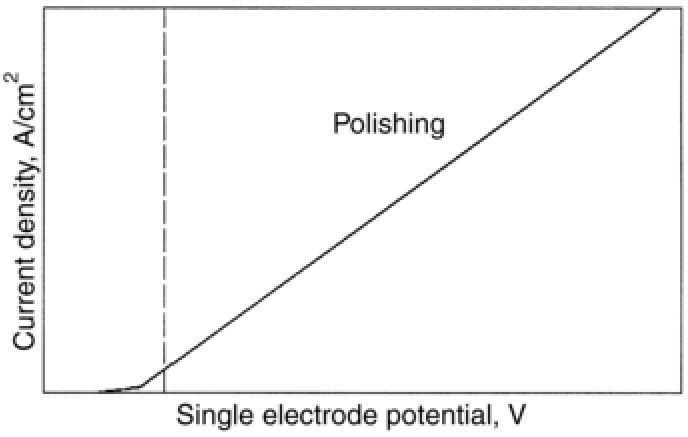

Fig. 5 Idealized anodic polarization curve for electropolishing of materials in oxidizing electrolytes

---

M. Ziomek-Moroz, Electropolishing, *Corrosion: Fundamentals, Testing, and Protection,*, Vol 13A*, ASM Handbook,* ASM International, 2003, p 139–142

Electropolishing

M. Ziomek-Moroz, U.S. Department of Energy, Albany Research Center

---

Selection of Electrolytes

Anodic dissolution of a metal depends on its chemical and physical properties, surface state, the composition of an electrolyte, and process conditions such as temperature, stirring, and current density (Ref 6). For materials that exhibit active-passive behavior, the most suitable polishing range is the passive region (C-D of Fig. 4). During etching, metal dissolves into the electrolyte while during anodic oxidation, the oxide film is not dissolved. The thickness of the anodic film or passivating layer may change, depending on current and electrolyte composition. The ideal electrolyte for electropolishing (Ref 7) must:

- Provide high quality polishing at low voltages and current densities
- Have the ability to function over a large range of current densities and temperatures
- Offer stability and long service life
- Not dissolve the metal when no current is flowing; that is, no spontaneous corrosion occurs
- Be inexpensive, readily available, and safe
- Be recyclable
- Have an ohmic resistance (IR drop) that is sufficiently low to obtain the desired current density at low voltage
- Provide good throwing power; that is, a sample with complex geometry should dissolve uniformly over the entire surface

References cited in this section

6. P.V. Shigoev, *Electrolytic and Chemical Polishing,* Freund Publishing House, Ltd.

7. J. Flis, *Corrosion of Metals and Hydrogen- Related Phenomena,* Institute of Physical Chemistry, Polish Academy of Sciences, Warsaw, 1979

M. Ziomek-Moroz, Electropolishing, *Corrosion: Fundamentals, Testing, and Protection,,* Vol 13A, *ASM Handbook,* ASM International, 2003, p 139–142

Electropolishing

M. Ziomek-Moroz, U.S. Department of Energy, Albany Research Center

Kinetics of Electropolishing

The kinetics of electropolishing is influenced by polishing current, temperature of electrolyte, polishing time, surface preparation, and agitation or stirring of electrolyte, which removes products and bubbles from the anode. The cathode area must be larger than the anode area in order to obtain an optimal polishing rate. Since the electropolishing process is a diffusion-controlled process, stirring or rotating the specimen significantly increases the rate of reaction. Under steady-state conditions, anodic reaction products accumulate on the surface and may interfere with the polishing process (Ref 4). Stirring or the use of a rotating disk electrode maintains a stable temperature and homogeneous composition of the electrolyte and prevents the buildup of corrosion products on the surface of the workpiece. The hydrodynamics of the electrolyte play a critical role in the diffusion control process characteristic of electropolishing as the transfer of reactants to the bulk solution is the rate-determining step in the electropolishing process (Ref 7).

Mechanism of Electropolishing. Surface roughness during electropolishing can vary significantly depending on the stability of the film formed during the passivation stage. Cavities and crevices on the metal surface (Ref 6) require much higher current densities to obtain a uniform polished surface. During electropolishing, a corrosion-product layer forms on the metal surface that has a higher viscosity than the bulk fluid (Ref 8). The thickness of this layer varies over the anode surface area and is greater in crevices. Greater thickness is a result of higher current density.

The leveling of the peaks and crevices of a rough surface follow a sequence where most peaks are dissolved in all directions while crevices are dissolved preferentially in one direction. The diffusion process during electropolishing is faster at the peaks than in the crevices. Unwanted selective etching, once a uniform surface is achieved, can be avoided by optimizing the electropolishing process conditions.

Defects in Electropolishing. Pitting can occur during electropolishing as a result of incorrect electrolyte composition or due to the formation of oxygen bubbles that attack the surface being polished. Blemishes can occur due to intermetallic compounds or inherent defect on the metal surface. Scratches may remain on the electropolished face after inadequate surface preparation (Ref 6, 9).

Hydrodynamic effects, kinematic viscosity, and concentration of electrolyte are the main variables that affect the removal rate during planarization. A rotating disk electrode is useful in the study of the hydrodynamic effects on an electrode. Rotational velocity is limited, so laminar flow is maintained. Generally, the rotating disk electrode is superior to static systems for study of the kinetics of heterogeneous reactions.

For electrolytes in a diffusion controlled process where a stationary condition exists and the process is dependent on mass transfer of solute in a liquid, the following equation governs the process:

$$\mathrm{V} \cdot \nabla C = D \Delta C \qquad \text{(Eq 4)}$$

where D is diffusivity; ΔC is concentration gradient; and V is liquid velocity.

The diffusion layer is also controlled by removal of solute due to the electrochemical reaction and the boundary layer due to the changing velocity of the electrolyte.

The following equations proposed by Levich describe the system in a flow pattern (laminar flow) using a rotating disk electrode (Ref 7):

$$J = D\left(\frac{dC}{dt}\right)_{x=0} = D\frac{(C_0 - C_1)}{\delta} \qquad \text{(Eq 5)}$$

and

$$\delta = 1.61 D^{1/3} \nu^{1/6} \omega^{-1/2} \qquad \text{(Eq 6)}$$

where δ is diffusion layer thickness; J is the magnitude of diffusion flux; D is diffusion coefficient of a reactant, C_0; C_0 is concentration at the disk surface; C_1 is concentration in bulk; ν is kinematics viscosity; and ω is angular velocity of disk.

If the rate of reactant transport is slower than the rate of the chemical reaction, then $C_1 = 0$ and the reaction occurs under diffusion controlled conditions. In the case where reaction rate is slower than the rate of transport, $C_1 = C_0$ and the process is under activation control where corrosion film is not present and the metal continuously corrodes.

For a smooth disk in a laminar flow regime, the rotating disk electrode Reynolds numbers may be calculated by (Ref 7, 10) using the following equation:

$$Re = r^2\omega/\nu \qquad \text{(Eq 7)}$$

where r is the radius of the disk.

In a diffusion process, where $C_1 = 0$, the rate of transfer of any reactant is greatly lower than the chemical change at interface. Combining Eq 5 and 6, one obtains:

$$J = 0.62C_0D^{2/3}\nu^{-1/6}\omega^{1/2} \qquad \text{(Eq 8)}$$

If one multiplies Eq 8 by a number of electrons participating in the reaction (n) and Faraday's constant (F), the removal rate current (I) in the electropolishing process can be obtained with:

$$I = 0.62nFC_0D^{2/3}\nu^{-1/6}\omega^{1/2} \qquad \text{(Eq 9)}$$

Physical properties of the electrolyte such as viscosity, density, concentration of solute and diffusivity play an important role in electrolytic polishing. The removal current density, ($i = I$/ area) is a linear relationship with the square root of angular speed of rotating electrode, ω.

References cited in this section

4. K.P. Rajurkar, J. Kozak, and A. Chatterjee, Nonabrasive Finishing Methods *Surface Engineering,* Vol 5, *ASM Handbook,* ASM International, 1994, p 110–117

6. P.V. Shigoev, *Electrolytic and Chemical Polishing,* Freund Publishing House, Ltd.

7. J. Flis, *Corrosion of Metals and Hydrogen- Related Phenomena,* Institute of Physical Chemistry, Polish Academy of Sciences, Warsaw, 1979

8. H.F. Walton, *J. Electrochem. Soc.,* 1950, p 219–226

9. J.C. Scully, *The Fundamentals of Corrosion,* 3rd ed., The University of Leeds, United Kingdom, Pergamon Press, 1990, p 107–120

10. M.G. Foud., F.N. Zein. and M.L. Ismail, *Electrochim. Acta,* Vol 16, 1971, p 1477–1487

M. Ziomek-Moroz, Electropolishing, *Corrosion: Fundamentals, Testing, and Protection,*, Vol 13A, *ASM Handbook*, ASM International, 2003, p 139–142

Electropolishing

M. Ziomek-Moroz, U.S. Department of Energy, Albany Research Center

---

Properties of Electropolished Surfaces

The physical, corrosion, and mechanical properties of a polished metal surface depend on the nature and the surface state of the metal (Ref 6). The main variables are physical characteristics (crystalline lattice structure, stresses, strains), chemical nature, and surface geometry (distribution of peaks and crevices). Mechanically polished surfaces may have an amorphous or mechanically deformed layer that influences its corrosion behavior. However, this layer is gradually removed to the crystalline structure during electropolishing. Monitoring the chemical composition of the surface using scanning electron microscopy is a way to analyze surface heterogeneity and its effect on electropolishing.

Effect of Electropolishing on Properties of Metals. In general, some of the mechanical properties of electropolished surfaces, such as hardness and Young's modulus, are increased. In some materials, such as stainless steel, no change is observed in static strength parameters (Ref 6). An effect on the fatigue behavior of metals is difficult to determine (Ref 6, 8) due to the complex nature of failure involving stress concentration, cracks, and surface defects. Mechanical polishing produces a cold-worked surface layer that generally enhances the fatigue life of metals. Fatigue life may be reduced when this layer is removed by electropolishing. On the other hand, surface roughness of the metal is reduced, which may increase the fatigue life of steel (Ref 6). Stress concentrations are also reduced.

Magnetic properties of steel alloys are altered when the cold-worked layer is removed by electropolishing. Surface conductance is improved. The effect of electrolytic polishing on the corrosion properties of metals depends on the post- polished oxide that forms and how porous the protective film is. Resistance to uniform corrosion is generally improved following polishing (Ref 7). In the case of aluminum, the protective oxide film that is formed has proven to be beneficial.

References cited in this section

6. P.V. Shigoev, *Electrolytic and Chemical Polishing,* Freund Publishing House, Ltd.

7. J. Flis, *Corrosion of Metals and Hydrogen- Related Phenomena,* Institute of Physical Chemistry, Polish Academy of Sciences, Warsaw, 1979

8. H.F. Walton, *J. Electrochem. Soc.,* 1950, p 219–226

M. Ziomek-Moroz, Electropolishing, *Corrosion: Fundamentals, Testing, and Protection,*, Vol 13A, *ASM Handbook,* ASM International, 2003, p 139–142

Electropolishing

M. Ziomek-Moroz, U.S. Department of Energy, Albany Research Center

---

References

1. G. Wranglén, *An Introduction to Corrosion and Protection,* Chapman & Hall, 1985

2. “Metallography Principles and Procedures,” Leco Corporation

3. *45th Metal Finishing for Guide Book and Directory,* Metals and Plastics Publications, Inc., 1977

4. K.P. Rajurkar, J. Kozak, and A. Chatterjee, Nonabrasive Finishing Methods *Surface Engineering,* Vol 5, *ASM Handbook,* ASM International, 1994, p 110–117

5. J.R. Davis, Surface Engineering of Carbon and Alloy Steels, *Surface Engineering,* Vol 5, *ASM Handbook,* ASM International, 1994, p 710

6. P.V. Shigoev, *Electrolytic and Chemical Polishing,* Freund Publishing House, Ltd.

7. J. Flis, *Corrosion of Metals and Hydrogen- Related Phenomena,* Institute of Physical Chemistry, Polish Academy of Sciences, Warsaw, 1979

8. H.F. Walton, *J. Electrochem. Soc.,* 1950, p 219–226

9. J.C. Scully, *The Fundamentals of Corrosion,* 3rd ed., The University of Leeds, United Kingdom, Pergamon Press, 1990, p 107–120

10. M.G. Foud., F.N. Zein. and M.L. Ismail, *Electrochim. Acta,* Vol 16, 1971, p 1477–1487

M. Ziomek-Moroz, Electropolishing, *Corrosion: Fundamentals, Testing, and Protection,*, Vol 13A, *ASM Handbook*, ASM International, 2003, p 139–142

Electropolishing

M. Ziomek-Moroz, U.S. Department of Energy, Albany Research Center

Selected References

- R. Contolini, S. Mayer, M. Ziomek-Moroz, and E. Patton, Electropolishing Study for ULSI Planarization, *Electrochemical Science and Technology of Copper,* P. Vanysek, M. Alodan, J. Lipkowski, and O.M. Mangussen, Ed., Proc. vol PV 2000-30, Electrochemical Society, Pennington, 2002
- J. Edwards, The Mechanism of Electropolishing of Copper in Phosphoric Acid Solution, *J. Electrochem. Soc.,* 1953, p 223C
- O. Piotrowski, C. Madore, and D. Landolt, The Mechanism of Electropolishing of Titanium in Methanol-Sulfuric Acid Electrolytes, *J. Electrochem. Soc.,* 1998, Vol 145, p 2302
- Machining Methods, Electrochemical, *Encyclopedia of Chemical Technology,* p 608
- H.F. Walton, The Anode Layer in the Electrolytic Polishing of Copper, *J. Electrochem. Soc.,* 1950, p 219

V.K. Jain, Electrochemical Machining, *Corrosion: Fundamentals, Testing, and Protection*, Vol 13A, *ASM Handbook*, ASM International, 2003, p 143–152

Electrochemical Machining

V.K. Jain, Indian Institute of Technology at Kanpur (India)

Introduction

SALT SOLUTIONS (ELECTROLYTES)— unlike metallic conduction where only electrons are the charge carriers—conduct electrical charge by migration of ions in the medium. A feature of electrolysis is that electrical energy is used to produce an electrochemical reaction. The machining process based on this principle is known as electrochemical machining (ECM). In ECM, a small direct current electric potential (5 to 30 V) is applied across two electrodes, the cathode (tool) and anode (workpiece), immersed in an electrolyte. The

transfer of electrons between ions and electrodes completes the electrical circuit. Metal is detached, atom by atom, from the anode surface and appears in the electrolyte as positive ions, which react with hydroxyl ions to form metal hydroxides. During the process, H_2 gas is evolved at the cathode (Fig. 1a). When the workpiece is steel, the reactions are:

$$Fe + 2H_2O \rightarrow Fe(OH)_2 + H_2\uparrow \quad \text{(Eq 1)}$$

$$2H_2O + Fe(OH)_2 + O_2 \rightarrow Fe(OH)_3 \quad \text{(Eq 2)}$$

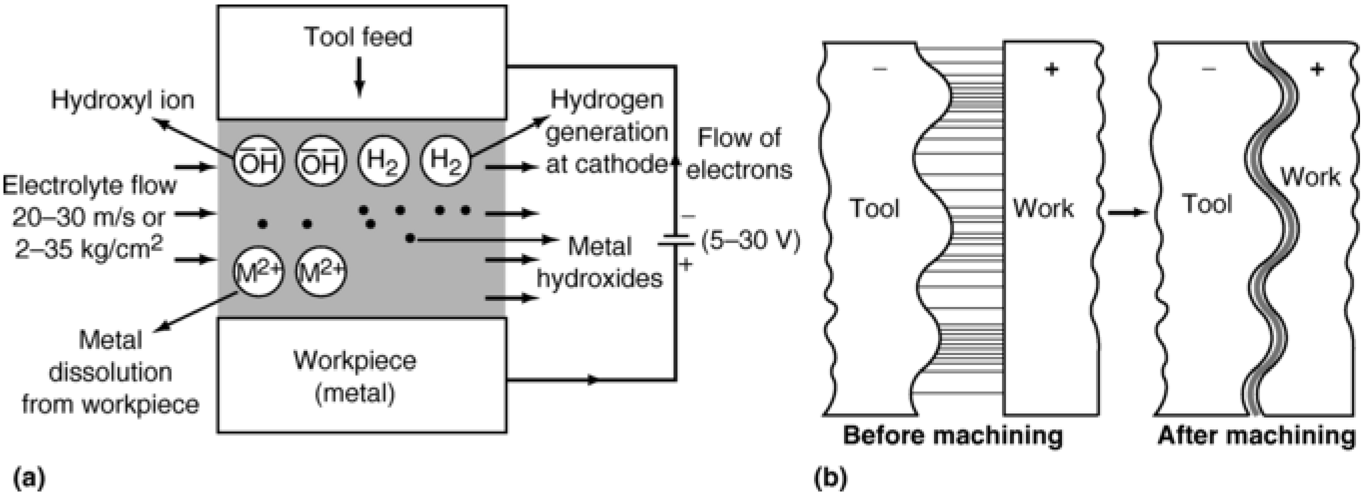

Fig. 1 Elements of electrochemical machining (ECM). (a) Diagram showing dynamics. (b) Tool and work before ECM and after ECM. The density of parallel lines indicates current density.

The smaller the interelectrode gap (IEG)— that is, the gap between anode and cathode—the greater the current flow (Fig. 1b) and the greater the metal-removal rate (MRR). The reaction products (metal hydroxides and gas bubbles) act as a barrier to the flow of electrolytic current. Their effect is minimized by supplying the electrolyte at a pressure varying in the range 2 to 35 kg/cm^2 (30 to 500 psi), leading to the electrolyte flow velocity of 20 to 60 m/s (65 to 195 ft/s). The optimal pressure and the resulting electrolyte flow velocity will depend on the size of the tool and workpiece and the IEG. Electrolyte flowing at high velocity dilutes electrochemical reaction products and removes them from the IEG. It dissipates heat and limits the concentration of ions at the electrode surface to give higher machining rates. The electrolyte conductivity, the voltage across IEG, the gap itself, and tool shape are controlled to define the final anode (workpiece) profile. The electrolyte electrical conductivity depends on composition, concentration, and temperature. Electrolyte temperature can be controlled (within ±1° C) by heating or cooling the electrolyte in the tank. Feed to the tool should be provided at the same rate at which the workpiece surface is descending, so that the IEG remains almost constant during the process. This is known as machining under equilibrium conditions.

Electrochemical machining principles have been used to perform a variety of machining operations (Ref 1), for example, turning, drilling, deburring, wire cutting, deep-hole drilling, and grinding. Electrochemical machining can be used to machine difficult-to-machine electrically conductive materials having complex shapes, deep holes with very high aspect ratio (up to 300:1), and three-dimensional profiles such as turbine blades. It is used in aerospace, automobile, and die-making industries.

Reference cited in this section

1. V.K. Jain, *Advanced Machining Processes,* Allied Publishers, Delhi, India, 2002

V.K. Jain, Electrochemical Machining, *Corrosion: Fundamentals, Testing, and Protection*, Vol 13A, *ASM Handbook*, ASM International, 2003, p 143–152

Electrochemical Machining

V.K. Jain, Indian Institute of Technology at Kanpur (India)

Electrochemical Machining System

An ECM system consists mainly of four subsystems: power source, electrolyte cleaning and supply system, tool and tool-feed system, and workpiece and workpiece-holding system (Fig. 2).

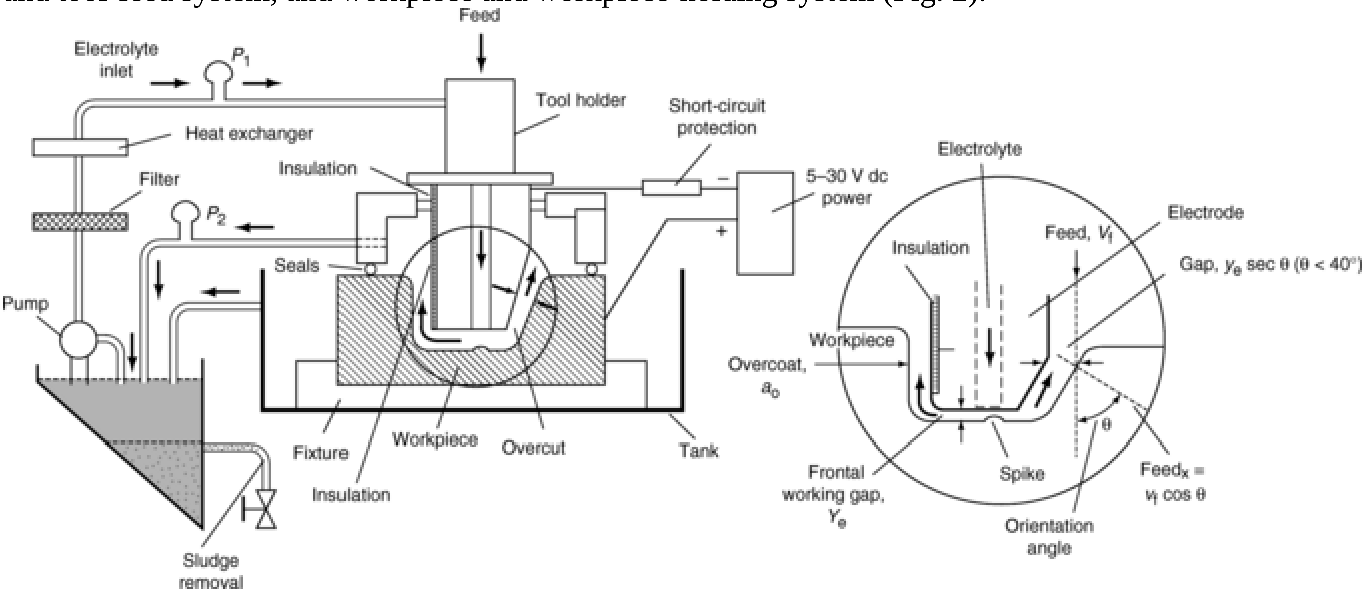

Fig. 2 Diagram of electrochemical machining systems

The power supply provides direct current as high as 40,000 A at low electric potential. Silicon-controlled rectifiers (SCR) are used for control because of their rapid response to the load and their compactness. Power is cut off within 10 μs in the event of sparking to avoid any damage to the tool and workpiece.

The electrolyte supply and cleaning system consists of a pump, filters, piping, control valves, heating or cooling coils, pressure gages, and one or more storage tanks. Electrolyte supply ports can be made in the tool, work, or fixture, depending on the requirements of the electrolyte flow. Electrolyte is cleaned by filters made of noncorroding materials such as Monel and stainless steel to avoid any blockage of the IEG, which is typically 0.3 to 1.0 mm (0.012 to 0.04 in.) by particles carried in the recycled electrolyte. Metallic piping should be grounded to prevent damage by corrosion. Tables and fixtures should also be grounded or should carry a cathodic potential to prevent corrosion. Further, ECM machines must be designed to withstand the hydraulic pressure of the electrolyte, which tends to separate tooling from the workpiece.

Tools and fixtures are made of materials resistant to the very corrosive environment of the system. High thermal and electrical conductivity is needed for tool material. Easy machining of tool material is equally important because dimensional accuracy and surface finish of the tool directly affects the workpiece accuracy and surface finish. Even a small defect on the surface of the tool may leave marks, scratches, nicks, burrs, or lines on the machined surface due to the disturbed flow of electrolyte and altered current density at such irregularities. Aluminum, brass, bronze, copper, and carbon are used. Titanium is used as a tool material when machining with an acid electrolyte that anodizes the cathode. To remove the plated deposits from the tool, the current is reversed periodically. Table 1 gives relative properties of metals used for making tools in ECM. Due to high thermal conductivity, copper and brass will be damaged less than stainless steel and titanium by short circuits. Copper tungsten is highly resistant to damage from short circuits because of its high melting point.

Table 1 Ranking of properties of commonly used tool materials

Property	Tool (electrode) material			
	Copper	**Brass**	**Stainless steel**	**Titanium**
Electrical resistivity	1	4	53	48
Stiffness	1.1	1	1.9	1.1
Machinability	6.0	8.0	2.5	1.0
Thermal conductivity	25	7.5	1.0	2.6

Source: Ref 2

There are three types of tools used in ECM— bare tool, coated tool, and bit-type of tool (Ref 3). Bare tools are usually not recommended, especially in cases of electrochemical drilling where straight-sided deep holes are needed. Areas on the tool where ECM action is not required should be insulated; however, due to the difficulties associated with achieving effective coatings, bit type of tools (Ref 3) are used (Fig. 3). As there is no wear and tear of the tool under normal ECM, theoretically tool life is infinite.

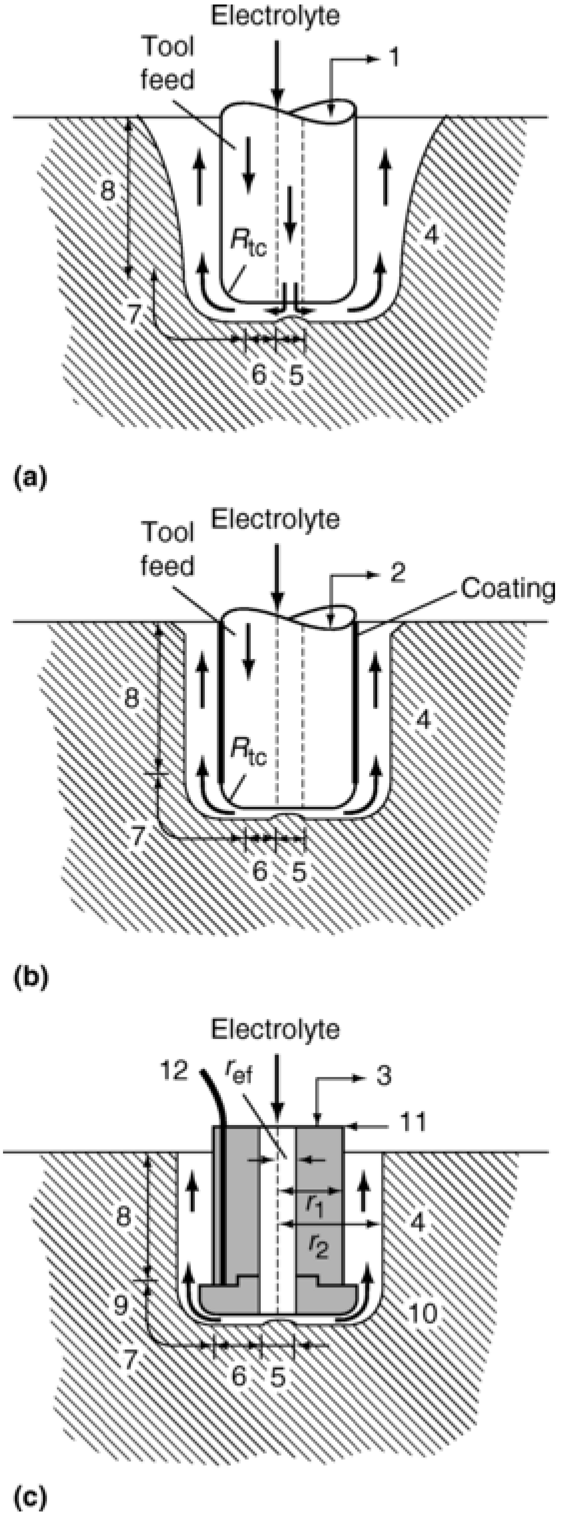

Fig. 3 Anode profile during EC drilling and EC bit drilling processes using (a) bare tool, (b) coated tool, (c) bare bit tool. 1, bare tool; 2, coated tool; 3, bit-type tool; 4, work; 5, stagnation zone; 6, front zone; 7, transition zone; 8, side zone; 9, tapered side for bit-type tool; 10, tool bit; 11, Perspex tool bit holder; 12, electric current conducting wire. R_{tc}, tool corner radius; r_{ef}, electrolyte flow hole radius

Tool feed is controlled either by a stepper motor or a servosystem. Simple machines have manual control, while advanced machines have multiaxis computer control of feed and process parameters.

Workpiece. Electrochemical machining can only be used on electrically conductive workpiece materials. Proper cleaning of the workpiece is essential after ECM to prevent residue from hardening on it. A clean water rinse for corrosion-resistant metals and alkaline cleaning of corrosive materials (steel, cast iron, etc.) is recommended. The workpiece is cleaned with a mild hydrochloric acid solution before a clean water rinse. During ECM, hydrogen is evolved at the tool (cathode); therefore, the probability of hydrogen embrittlement of the workpiece (anode) is minimal. There is no effect of ECM on ductility, yield strength, ultimate strength, and microhardness of the machined component. However, the fatigue strength of conventionally premachined components is reduced after ECM because of the removal of layers having compressive residual stresses. Little information is available about the effect of microstructure on the performance of ECM process. However, grain size and insoluble inclusions also affect surface roughness. Insoluble inclusions can stall the ECM process. Intergranular attack and other defects (pitting, selective etching) induced during ECM seem to be secondary reasons for the reduction in fatigue strength. Intergranular attack can be controlled by appropriate selection of electrolyte and ECM parameters. No effect of hardness of the workpiece material on the process performance has been reported.

Workpiece-holding devices are made of electrically nonconducting materials—such as glass fiber reinforced plastics, plastics, and Perspex— having good thermal stability and low moisture absorption properties.

References cited in this section

2. T.L. Lievestro, Electrochemical Machining, *Machining,* Vol 16, *Metals Handbook,* 9th ed., ASM International, 1989, p 533–541

3. V.K. Jain and P.C. Pandey, Investigations into the Use of Bits as a Cathode in ECM, *Int. J. Mach. Tools Des. Res.,* Vol 22 (No. 4), 1982, p 341–352

V.K. Jain, Electrochemical Machining, *Corrosion: Fundamentals, Testing, and Protection,* Vol 13A, *ASM Handbook,* ASM International, 2003, p 143–152

Electrochemical Machining

V.K. Jain, Indian Institute of Technology at Kanpur (India)

Theory of ECM

Electrochemical machining differs from other industrial processes based on Faraday's laws of electrolysis, such as electroplating. In ECM, the shape and size of the workpiece is changed in a controlled manner, and the minimum current density employed is higher than 8 A/mm^2.

Faraday's law of electrolysis is:

$$m = \frac{I(EW)t}{F} \quad \text{(Eq 3)}$$

where *m* is mass (grams) removed in time *t*, *I* is current, *t* is time (seconds), *EW* is gram equivalent weight of workpiece metal ($EW = A_w/z$; A_w = atomic weight, *z* = valency of dissolution), and *F* is Faraday's constant (96,500 coulombs/gram equivalent, or ampere-seconds/gram equivalent).

Equation 3 does not account for the effects of some of the significant process variables, that is, overpotential, presence of passive film, variation in the electrical conductivity of the electrolyte due to temperature and void concentration along the electrolyte flow path and valence changes during electrochemical dissolution. Regarding the latter, dissolution of iron in NaCl solution depends on the machining conditions and may be either in the form of ferrous hydroxide (Fe^{2+}) or ferric hydroxide (Fe^{3+}) ions.

The mode of dissolution during alloy machining is still more difficult to identify (Ref 1). Since the workpiece is usually an alloy rather than a single element, the evaluation of *m* becomes difficult because electrochemical equivalent of an alloy (EW_a) is generally not well defined. However, two methods have been proposed (Ref 4) to solve this problem.

Method 1 is the percentage by weight method. The value of EW_a is calculated by multiplying the chemical equivalent of individual element (EW_i) by their respective proportion by weight percent (X_i), and then summing them up as given by:

$$EW_a = \frac{1}{100}\sum_{i=1}^{n}(EW_i)X_i \qquad \text{(Eq 4)}$$

where *n* is number of the constituent elements in the alloy.

Method 2 is the superposition of charge method. The amount of electrical charge required to dissolve the mass contribution of individual element of the alloy is calculated and then EW_a is evaluated as:

$$EW_a = \frac{100}{\sum_{i=1}^{n}(X_i/EW_i)} \qquad \text{(Eq 5)}$$

These two methods do not give exactly the same value of EW_a.

The total current (*I*) is not used in dissolving material from the workpiece. Actual MRR depends on the current efficiency (η), which ranges from 75 to 100%.

References cited in this section

1. V.K. Jain, *Advanced Machining Processes,* Allied Publishers, Delhi, India, 2002

4. J.A. McGeough, *Principles of Electrochemical Machining,* Chapman and Hall, London, 1974

V.K. Jain, Electrochemical Machining, *Corrosion: Fundamentals, Testing, and Protection*, Vol 13A*, ASM Handbook*, ASM International, 2003, p 143–152

Electrochemical Machining

V.K. Jain, Indian Institute of Technology at Kanpur (India)

Metal-Removal Rate

It is desirable to have minimum possible IEG (≤0.5 mm) for accurate reproduction of tool shape on the workpiece. The analysis (Ref 1, 5) given in this section is based on the following assumptions:

- Electrical conductivity of electrolyte during the process remains constant.
- The surfaces of anode and cathode are considered to be equipotential.
- Effective voltage (V - ΔV) across the electrodes remains constant.

- The anode dissolves at one fixed valency of dissolution.

In the above assumptions, V is constant potential difference applied across the electrodes, and ΔV is sum of electrode overpotentials including reversible potential. The difference between the equilibrium and working values of the potentials is known as overpotential. This overpotential includes activation, concentration, and resistance overpotentials (Ref 4).

In the case of ECM with plane parallel electrodes, MRR (in gram MRR_g, in volume MRR_v) can be calculated as:

$$MRR_g = \frac{\eta I (EW)}{F} \quad \text{(Eq 6)}$$

$$MRR_v = \frac{\eta I (EW)}{F \rho_a} \quad \text{(Eq 7)}$$

where ρ_a is density of anode (workpiece).

Table 2 gives theoretical material-removal rate for different metals (Ref 4), assuming current efficiency as 100%. The MRR depends on the valence of dissolution and atomic weight of the material. Theoretical MRR ranges from 11 to 84 mm^3/s (2.4 to 18.5 $in.^3/h$).

Table 2 Theoretical metal-removal rate (MRR) for current of 1000 A

Metal	Atomic weight (A_w)		Density (ρ)		Valence, z	Metal-removal rate (MRR_g)		Metal-removal rate (MRR_v)	
	g	**lb**	**g/cm^3**	**$lb/in.^3$**		**g/s**	**lb/h**	**mm^3/s**	**$in.^3/h$**
Aluminum	26.97	0.595	2.67	0.0965	3	0.093	0.74	35	7.7
Beryllium	9.0	0.198	1.85	0.0668	2	0.047	0.37	25	5.5
Chromium	51.99	0.115	7.19	0.2598	2	0.269	2.14	38	8.4
					3	0.180	1.43	25	5.5
					6	0.090	0.71	13	2.9
Cobalt	58.93	0.130	8.85	0.3197	2	0.306	2.43	35	7.7
					3	0.204	1.62	23	5.1
Copper	63.57	0.140	8.96	0.3237	1	0.660	5.24	74	16.3
					2	0.329	2.61	37	8.1
Iron	55.85	0.123	7.86	0.2840	2	0.289	2.29	37	8.1
					3	0.193	1.53	25	5.5
Magnesium	24.31	0.054	1.74	0.0629	2	0.126	1.00	72	15.8
Manganese	54.94	0.121	7.43	0.2684	2	0.285	2.26	38	8.4
					4	0.142	1.13	19	4.2
					6	0.095	0.75	13	2.9
					7	0.081	0.64	11	2.4
Molybdenum	95.94	0.212	10.22	0.3692	3	0.331	2.63	32	7.0
					4	0.248	1.97	24	5.3
					6	0.166	1.32	16	3.5
Nickel	58.71	0.129	8.90	0.3215	2	0.304	2.41	34	7.5
					3	0.203	1.61	23	5.1
Niobium	92.91	0.205	9.57	0.3457	3	0.321	0.04	34	7.5
					4	0.241	1.91	25	5.5
					5	0.193	1.53	20	4.4
Silicon	28.09	0.062	2.33	0.0842	4	0.073	0.58	31	6.8
Tin	118.69	0.262	7.30	0.2637	2	0.615	4.88	84	18.5
					4	0.307	2.44	42	9.2
Titanium	47.9	0.106	4.51	0.1629	3	0.165	1.31	37	8.1
					4	0.124	0.98	28	6.2

Tungsten	183.85	0.405	19.3	0.6973	6	0.317	2.52	16	3.5
					8	0.238	1.89	12	2.6
Uranium	238.03	0.525	19.1	0.6900	4	0.618	4.90	32	7.0
					6	0.412	3.27	22	4.8
Zinc	65.37	0.114	7.13	0.2576	2	0.339	2.69	48	10.6

Source: Ref 4

Linear metal-removal rate (or penetration rate, MRR_l) is given by:

$$MRR_l = \frac{\eta J (EW)}{F \rho_a} \quad \text{(Eq 8)}$$

where J is current density.

The current density in the IEG is a function of shapes of the electrodes, the distance separating the electrodes (y), and effective voltage between them:

$$J = \frac{I}{A} = (V - \Delta V) k / y \quad \text{(Eq 9)}$$

where k is electrical conductivity of electrolyte, y is IEG, and A is workpiece area under the tool.

The voltage applied across the IEG is a controllable parameter and greatly influences ECM performance. For a constant voltage power supply, the magnitude of current flow is controlled by the dynamics of IEG, y.

References cited in this section

1. V.K. Jain, *Advanced Machining Processes,* Allied Publishers, Delhi, India, 2002

4. J.A. McGeough, *Principles of Electrochemical Machining,* Chapman and Hall, London, 1974

5. H. Tipton, The Dynamics of Electrochemical Machining, *Advances in Machine Tool Design and Research,* Pergamon Press, Birmingham, 1964, p 509–522

V.K. Jain, Electrochemical Machining, *Corrosion: Fundamentals, Testing, and Protection*, Vol 13A, *ASM Handbook*, ASM International, 2003, p 143–152

Electrochemical Machining

V.K. Jain, Indian Institute of Technology at Kanpur (India)

Interelectrode Gap

During ECM, the tool moves toward the workpiece at the feed rate (f), but at the same time, work surface moves away from the tool at a rate equal to the penetration rate (MRR_l). Therefore, the effective rate of change of IEG is given by:

$$\frac{dy}{dt} = \frac{J (EW) \eta}{\rho_a F} - f \quad \text{(Eq 10)}$$

Under equilibrium conditions ($dy/dt = 0$, IEG = y_e), the equilibrium gap distance (y_e) and the feed rate have the relationship:

$$f = \frac{(V - \Delta V) k}{y_e} \frac{(EW) \eta}{\rho_a F} \quad \text{(Eq 11)}$$

Knowing the feed rate, the equilibrium gap (y_e) can be calculated from Eq 11. Equation 10 can be rewritten (assuming efficiency as 100%) as:

$$\frac{dy}{dt} = \frac{c}{y} - f \qquad \text{(Eq 12)}$$

where $c = (EW)(V - \Delta V)k/F\rho_a$; c is assumed to remain constant for a given workpiece and electrolyte combination only if $(V - \Delta V)$ and k remain constant during the process. In practice, two cases arise for which Eq 12 can be solved, that is, zero feed rate ($f = 0$) and finite feed rate ($f \neq 0$). In case of zero feed rate, the solution (Ref 5) of Eq 12 is given by Eq 13 for the initial condition, $y = y_0$ at $t = 0$.

$$y = \left(2ct + y_0^2\right)^{1/2} \qquad \text{(Eq 13)}$$

For finite feed rate, the IEG attempts to attain the equilibrium gap. The solution (Ref 4, 5) of Eq 12 is given by:

$$t = \frac{1}{f}\left[y_0 - y_t + y_e \ln\left\{\frac{y_0 - y_e}{y_t - y_e}\right\}\right] \qquad \text{(Eq 14)}$$

where y_t is IEG at any time t.

Generalized equation for IEG. Equation 13 predicts an infinite gap at $t = \infty$. Equation 14 is an implicit equation that is solved for y_t only by iterative process. Hence, Eq 14 is not especially convenient to handle in those cases where numerical methods such as finite-element methods, finite-difference methods, or boundary-element methods are applied to analyze the ECM process. A single equation has been derived (Ref 6) for numerical methods analysis. It is applicable simultaneously to both the cases, that is, for $f = 0$ and $f \neq 0$. Equation 10 can be written in the following form:

$$dy = \left(\frac{(EW)J\eta}{F\rho_a} - f\right)dt \qquad \text{(Eq 15)}$$

All the factors except J on the right-hand side of this equation can be treated as constant during ECM. The domain of interest in numerical methods is then divided into elements whose size is quite small; therefore, within an element J can be assumed to remain constant over a small interval of time dt. Therefore, Eq 15 can be written as:

$$dy = (c - f)dt \qquad \text{(Eq 16)}$$

where $c = \{[(EW)\eta]/F\rho_a\}$ and is assumed to be constant. After integration, Eq 16 can be written (for $y = y_0$ at $t = 0$) as:

$$y = y_0 + (c - f)t \qquad \text{(Eq 17)}$$

Equation 17 is valid only for a small interval of time ($t = \Delta t$). Hence, it can be written:

$$y = y_0 + (c - f)\Delta t \qquad \text{(Eq 18)}$$

Equation 18 is valid for both the cases for feed rate (Ref 7), and the total computer time is reduced.

References cited in this section

4. J.A. McGeough, *Principles of Electrochemical Machining,* Chapman and Hall, London, 1974

5. H. Tipton, The Dynamics of Electrochemical Machining, *Advances in Machine Tool Design and Research,* Pergamon Press, Birmingham, 1964, p 509–522

6. V.K. Jain and P.C. Pandey, Tooling Design for ECM: A Finite Element Approach, *J. Eng. Ind. (Trans. ASME),* Vol 103, 1981, p 183–191

7. V.K. Jain and P.C. Pandey, Tooling Design for ECM, *Prec. Eng.,* Vol 2, 1980, p 195–206

V.K. Jain, Electrochemical Machining, *Corrosion: Fundamentals, Testing, and Protection*, Vol 13A, *ASM Handbook*, ASM International, 2003, p 143–152

Electrochemical Machining

V.K. Jain, Indian Institute of Technology at Kanpur (India)

Electrolyte Conductivity

Electrolyte electrical conductivity is a function of local temperature (*T*) and presence of sludge and gas bubbles (hydrogen, oxygen, vapor, and other gas bubbles) in the IEG. As a result, the IEG gets tapered along the electrolyte flow direction. For precision machining, temperature of the electrolyte should be controlled within ±1 °C (±1.8 °F). This may require heating or cooling the electrolyte. In the analysis given below, only the effects of temperature and hydrogen gas bubbles are taken into account.

Using the law of conservation of heat, the temperature gradient (dT/dx) along the path of electrolyte flow (x-direction) can be derived (Ref 8) as follows:

$$\frac{dT}{dx} = \frac{(V - \Delta V)^2}{U \rho_e C_e \bar{y}^2} \cdot k = \bar{A}k \qquad \text{(Eq 19)}$$

where the density (ρ_e) and specific heat (C_e) of the electrolyte are assumed to remain constant in the IEG. Average values of IEG ($\bar{y}$) and electrolyte flow velocity ($\bar{U}$) are also assumed to remain unchanged. Thus,

$$\bar{A} = \frac{(V - \Delta V)^2}{U \rho_e C_e (\bar{y})^2}$$

can be treated as constant.

Electrical conductivity (k) of the electrolyte varies linearly with temperature as:

$$k = k_0(1 + \alpha \cdot \Delta T) \qquad \text{(Eq 20)}$$

where α is a temperature coefficient of specific conductance [$\alpha = dk/(k_0 dT)$]. Solving after substituting Eq 20 in Eq 19 gives:

$$(T - T_0) = \frac{1}{\alpha}\left[\exp(\alpha \bar{A} k_0 x) - 1\right] \qquad \text{(Eq 21)}$$

It can also be shown that:

$$J = \frac{(V - \Delta V)}{y} k_0 \left[\exp(\alpha \bar{A} k_0 x)\right] \qquad \text{(Eq 22)}$$

To incorporate the effect of temperature as well as hydrogen gas bubbles on electrolyte conductivity, the following equation has been suggested (Ref 9, 10):

$$k = k_0\{(1 + \alpha \cdot \Delta T)(1 - \alpha_v)^n\} \qquad \text{(Eq 23)}$$

A value of exponent n between 1.5 to 2.0 has been used (Ref 9, 10, 11). This equation, however, does not account for the effect of size and distribution of H_2 bubbles. Effect of change in temperature and concentration of NaCl and HCl on their conductivity is shown in Fig. 4.

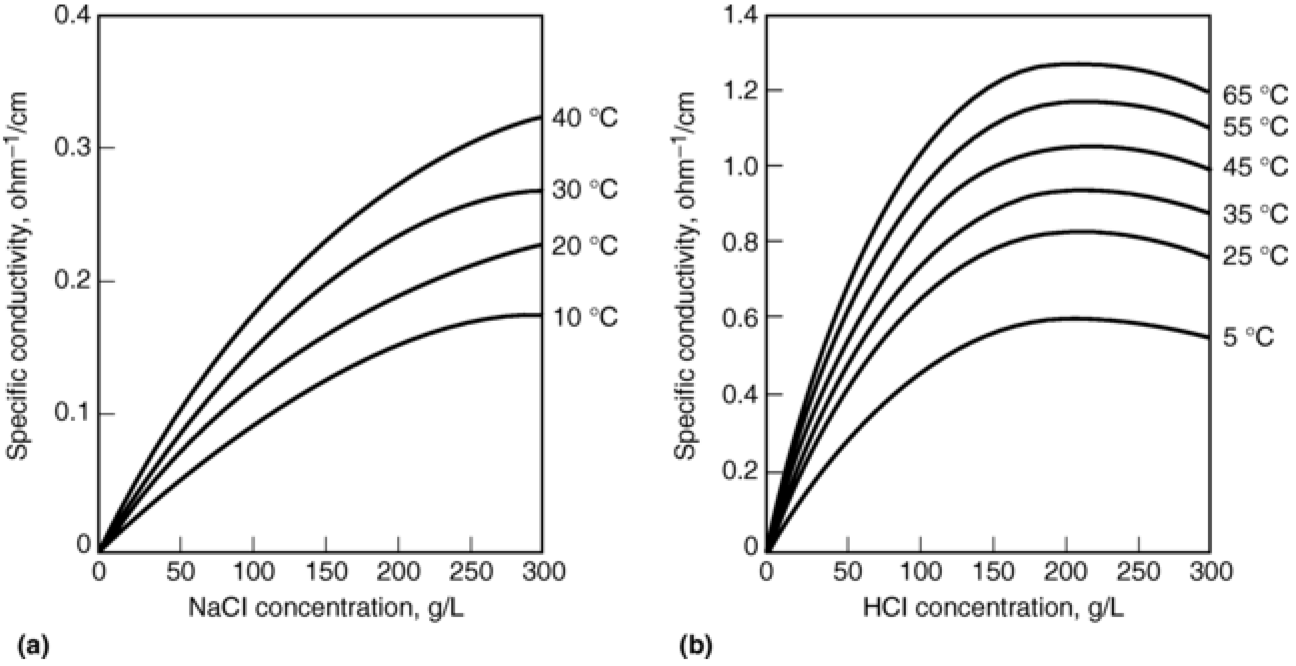

Fig. 4 Electrical conductivity of electrolyte as a function of temperature and concentration of (a) NaCl, (b) HCl. Source: Ref 12

References cited in this section

8. P.C. Pandey and H.S. Shan, *Modern Machining Processes,* Tata McGraw Hill, Delhi, India, 1980

9. J.F. Thorpe and R.D. Zerkle, Analytical Determination of the Equilibrium Gap in Electrochemical Machining, *Int. J. Mach. Tools Des. Res.,* Vol 9, 1969, p 131–144

10. J. Hopenfeld and R.R. Cole, Prediction of the Dimensional Equilibrium Cutting Gap in Electrochemical Machining, *J. Eng. Ind. (Trans. ASME),* Vol 91, 1969, p 75–765

11. V.K. Jain, P.G. Yogindra, and S. Murugan, Prediction of Anode Profile in ECBD and ECD Operations, *Int. J. Mach. Tools Manuf.,* Vol 27 (No. 1), 1987, p 113–134

12. A.E. DeBarr and D.A. Oliver, Ed., *Electrochemical Machining,* Macdonald and Co. Ltd, 1975

V.K. Jain, Electrochemical Machining, *Corrosion: Fundamentals, Testing, and Protection*, Vol 13A, *ASM Handbook,* ASM International, 2003, p 143–152

Electrochemical Machining

V.K. Jain, Indian Institute of Technology at Kanpur (India)

Process Control

Electrochemical machining has a unique self- regulating feature. Under the equilibrium condition ($f = MRR_l$), machining takes place at a constant IEG (that is, equal to y_e). If this were not true at all times during ECM, either $f < MRR_l$ or $f > MRR_l$.

If $f < MRR_l$, initially IEG will increase and it will attain a value greater than the equilibrium gap value ($y > y_e$). Because of this, the current density will also decrease as compared to J_e (current density under equilibrium condition) and the MRR_l will also decrease. In other words, the difference between f and MRR_l will decrease, or the process will move toward the equilibrium gap condition.
If $f > MRR_l$, the reverse argument will be true, and again the IEG will converge to the equilibrium gap (or $MRR_l = f$). The self-regulating convergence is shown in the Fig. 5, where the IEG always attempts to reach the equilibrium gap value, y_e.

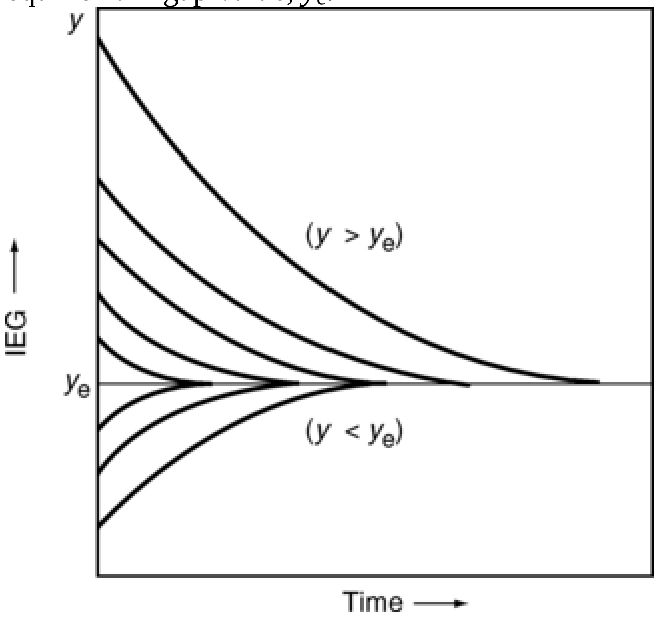

Fig. 5 The interelectrode gap (IEG) as a function of time the self-regulating feature of ECM is shown, as gaps with different initial values (y) converge to the equilibrium gap (y_e).

V.K. Jain, Electrochemical Machining, *Corrosion: Fundamentals, Testing, and Protection*, Vol 13A, *ASM Handbook*, ASM International, 2003, p 143–152

Electrochemical Machining

V.K. Jain, Indian Institute of Technology at Kanpur (India)

Electrolytes

A good electrolyte for ECM must have high electrical conductivity, high specific heat, good chemical and electrochemical stability, controllable passivating effect, low viscosity, and low toxicity and corrosivity (Ref 2, 12). Electrolyte in the IEG conducts current between anode and cathode, removes reaction products, and dissipates heat produced during the process. The electrolytes perform better when the crystal structure of the workpiece is fine grained, and its constituents (in case of an alloy) dissolve at uniform rate. Electrolytes used in ECM are classified in three categories: neutral salt, alkaline, and acidic. Each type has its own merits.
Sludging electrolytes produce hydroxide sludges that must be removed before recycling. Sodium chloride (NaCl) solutions are the most commonly used electrolytes in ECM. During ECM, water is depleted, producing H_2 gas and hydroxides (Eq 1 and 2), which are insoluble in water. NaCl electrolyte is corrosive in nature and produces large amounts of sludge. The ratio of the amount of sludge formed to the amount of metal dissolved ranges between 6 and 8 for NaCl electrolyte. There is no universal electrolyte that can be employed for every type of metal and alloy. Table 3 (Ref 12) recommends some electrolytes for a limited range of metals and alloys. Under certain circumstances, mixtures of electrolytes, such as $NaNO_3$ and NaCl or NaCl and HCl, are used. For instance, $NaNO_3$ is passivating and more expensive, but gives smoother surfaces in certain cases.

Table 3 Electrolytes for the electrochemical machining of metals

Workpiece metal	Electrolyte			Removal rate	
	Major constituent	**Concentration (max)**			
		kg/L of H_2O	**lb/gal of H_2O**	**$mm^3 \times 10^3$/min per 1000 A**	**$in.^3$/min per 1000 A**
Steel; iron- nickel-, and cobalt-base alloys	NaCl or KCl	0.30	2.5	2.1	0.13
	$NaNO_3$	0.60	5	2.1	0.13
Steel; hardened tool steel	$NaClO_3$	0.78	6.5	2.0	0.12
Gray iron	NaCl	0.30	2.5	2.0[(a)(b)]	0.12[(a)(b)]
	$NaNO_3$	0.60	5	2.0[(a)(b)]	0.12[(a)(b)]
White cast iron	$NaNO_3$	0.60	5	1.6[(c)]	0.10[(c)]
Aluminum and aluminum alloys[(d)]	$NaNO_3$	0.60	5	2.1	0.13
	NaCl or KCl	0.30	2.5	2.1	0.13
Titanium alloys	NaCl or KCl[(e)]	0.12	1	1.6	0.10
Tungsten	NaOH[(f)]	0.18[(g)]	1.5[(g)]	1.0	0.06
Molybdenum	NaOH[(h)]	0.18	1.5	1.0	0.06
	NaCl or KCl	0.30	2.5	1.0	0.06
Copper and copper alloys[(d)]	NaCl or KCl	0.30	2.5	4.4	0.27
	$NaNO_3$	0.60	5	3.3	0.20
Zirconium	NaCl or KCl	0.30	2.5	2.1	0.13

(a) Feed rates limited by graphite particle size.
(b) Maximum; can vary widely.
(c) Rough surface finish.
(d) $NaNO_3$ electrolyte provides better surface finish.
(e) Voltage must be greater than.
(f) NaOH used up in process and must be replenished.
(g) Minimum of 9 kg/L (0.75 lb/gal.)
(h) pH of electrolyte decreases with use; maintain pH by adding NaOH or KOH. Source: Ref 2

Nonsludging electrolyte such as NaOH solutions are used in ECM of heavy metals such as tungsten and molybdenum and their alloys. The electrolyte becomes depleted during ECM due to the formation of compounds such as sodium tungstate ($Na_2WO_4 \cdot 2H_2O$) and sodium molybdate ($Na_2MoO_4 \cdot 2H_2O$) while machining tungsten and molybdenum, respectively. These compounds are soluble in water (hence, no sludge), but these heavy metals tend to plate out onto the cathode, which is undesirable. However, a periodic voltage polarity reversal will keep the tool cathode surfaces clean.

Filtration. Effective filtration of sludge-forming electrolyte is very essential to maintain the performance of the ECM process. In no case should the electrolyte contain more than 2 wt% sludge when in use. Presence of sludge particles in the IEG can lead to short circuits. Filtering, centrifuging, and settling are used to remove sludge.

Electrolyte flow rate, controlled by pressure, in the IEG affects electrolyte conductivity by changing its temperature and the hydrogen gas bubble size and distribution in the IEG. Electrolyte flow rate must be high enough to remove machining by-products as quickly as possible. Electrolyte flow rate influences surface finish R_a value (centerline average value of surface finish is abbreviated as R_a) and current efficiency, η, as well as MRR. A high ratio of electrolyte flow rate to the current across the IEG is desirable, but the cost of pumping increases. A rule of thumb is approximately 1 L/min for each 100 A for machining steel with NaCl. High flow rate usually reduces the value of R_a and minimizes the formation of deposits on the cathode. Excessive flow rate can lead to local erosion of tool/ workpiece and sticking of precipitates on to the workpiece. To produce a smooth, uniform surface on the workpiece, the tool must be designed so there is uniform flow over the entire machining area. This is difficult at high flow velocities of 30 to 60 m/s (100 to 200 ft/s). The design of tools for complex-shaped workpieces requires an understanding of multiphase fluid flow (involving liquid, gas, and solid phases), electrical and electrochemical principles, as well as experience and ingenuity.

Back Pressure. Attempts have been made (Ref 2) to study the effect of back pressure in the IEG. Increased back pressure in ECM reduces imprints of flow lines on the workpiece and increase drilled-hole diameter, but results

in higher hydraulic forces and tooling cost. Hole diameter and current at constant voltage are increased with increase in back pressure because the resulting hydrogen bubbles are smaller, leading to increased conductivity (Fig. 6).

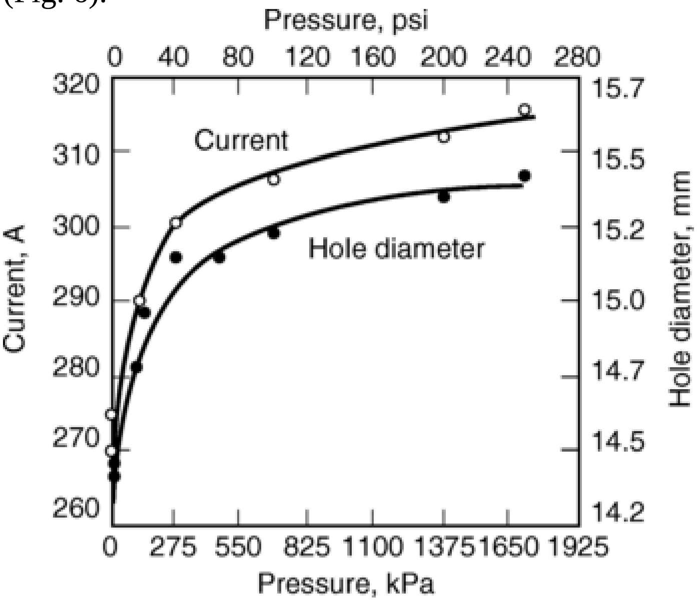

Fig. 6 Effect of electrolyte back pressure on hole size and current at constant voltage. Source: Ref 2

Safety precautions are important in ECM. Dry oxidizing salts such as sodium nitrate and sodium chlorate are hazardous. Mists, vapors, and dusts of alkaline electrolyte can damage body tissues. Appropriate ventilation of the work area and use of protective gloves, face shields, and masks are required. To prevent hydrogen explosion, hydrogen evolved during ECM must be vented from the work area. Proper storage, handling, and disposal of the electrolytes used in machining of heavy metals are also very important.

References cited in this section

2. T.L. Lievestro, Electrochemical Machining, *Machining,* Vol 16, *Metals Handbook,* 9th ed., ASM International, 1989, p 533–541

12. A.E. DeBarr and D.A. Oliver, Ed., *Electrochemical Machining,* Macdonald and Co. Ltd, 1975

V.K. Jain, Electrochemical Machining, *Corrosion: Fundamentals, Testing, and Protection*, Vol 13A, *ASM Handbook*, ASM International, 2003, p 143–152

Electrochemical Machining

V.K. Jain, Indian Institute of Technology at Kanpur (India)

Workpiece Shape Prediction

Analytical and computational models (Fig. 7) for workpiece shape prediction have been developed (Ref 13, 14, 15, 16, 17, 18, 19, 20, 21, 22, 23, 24, 25, 26, 27, 28), ranging from the simple "cos θ" principle to those based on approximate numerical techniques. These models have been used to predict work profile in different zones of electrochemically drilled blind holes, that is, side, transition, front, and stagnation zones (Fig. 8). The ability to predict variations in IEG in different zones for any given tool and operating conditions is a prerequisite for proper design of ECM tools and anode shape prediction (Ref 13, 14, 15, 16, 17, 18, 19, 20, 21, 22, 23, 24, 25, 26, 27, 28).

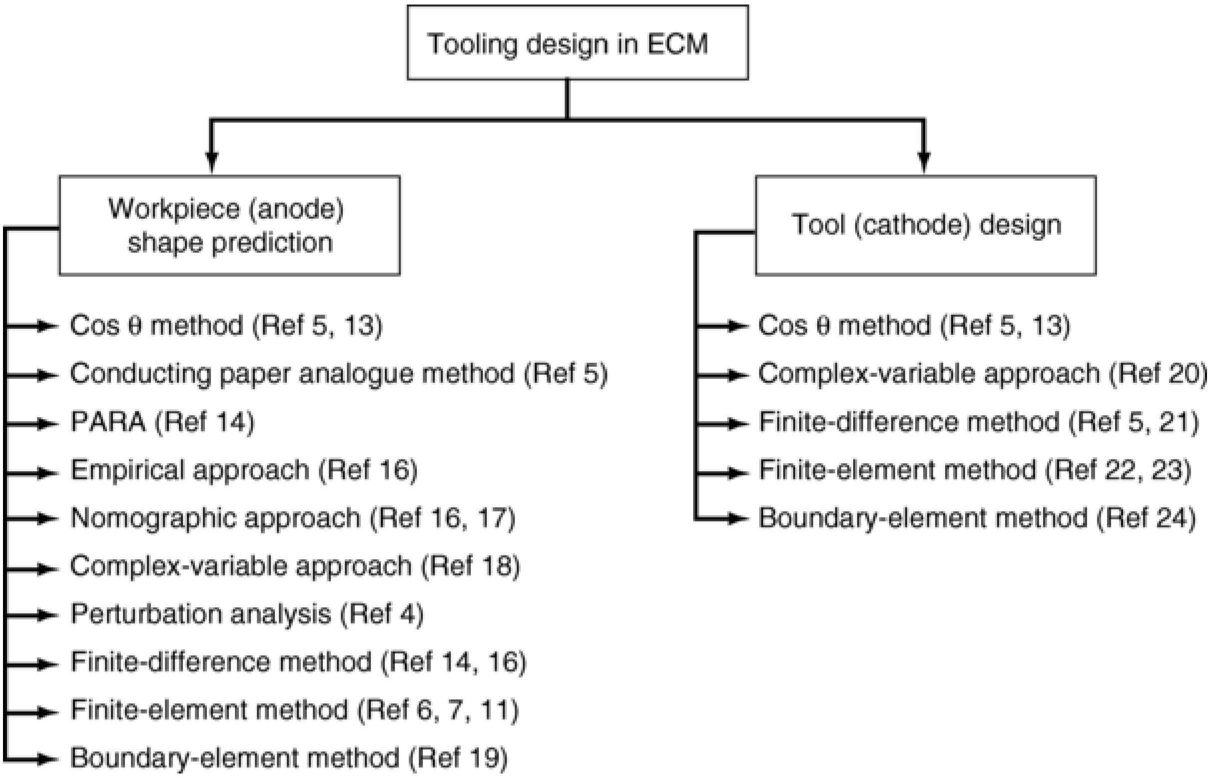

Fig. 7 Various proposed models for anode shape prediction and tool design in ECM

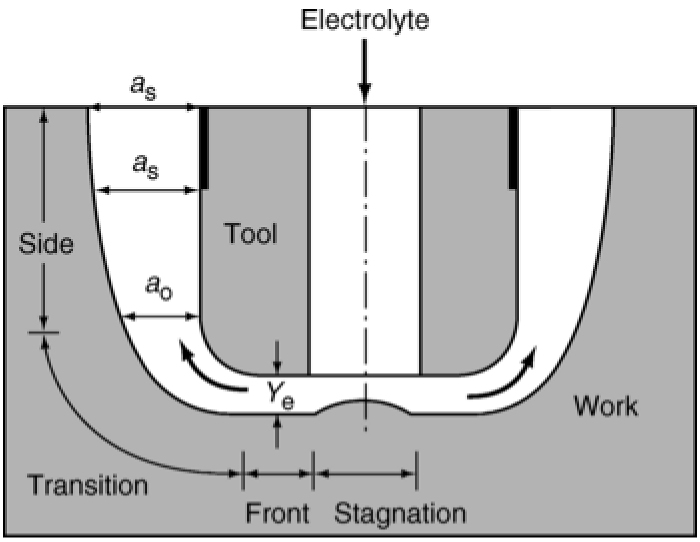

Fig. 8 Diagram of electrochemical drilling with outward mode of electrolyte flow showing various zones. a_s, side gap

Techniques for workpiece shape prediction require the use of high-speed computers. In cos θ method (Ref 5), equilibrium shape is computed corresponding to a tool whose profile is approximated by a large number of planar sections inclined at different angles. If the feed direction is inclined at an angle θ normal to the tool face, the equilibrium gap is equal to (y_e/cos θ). This approach is based on many simplified assumptions and is not recommended for complex- shaped workpieces (Ref 6).

Empirical methods attempt to derive equations based on the experimental observations of IEG in the transition and side zones to predict a complete anode profile. Various models (Ref 15, 16, 29) have been proposed in terms of equilibrium gap, tool corner radius (r_c), and bare length of the tool (b_b). Nomographic methods have been proposed (Ref 17, 29) for the evaluation of side gap for the known values of y_e, r_c, and b_b. Such methods have proved useful in planning an ECM operation. However, the empirical and nomographic methods cannot be generalized and are valid only for the specified machining conditions, tool and work material combination, and type of electrolyte.

More complicated problems may require Laplace's equation to be solved to determine the operating potential, *V*, by numerical methods such as finite-difference method (Ref 14), finite- element method (Ref 11), or boundary-element method (Ref 19). The procedure followed to solve such problems is:

- The electric field potential at different points is calculated by solving Laplace equation using one of the numerical methods.
- Using the field-distribution data, current density is calculated.
- With the help of Eq 21, temperature distribution in the IEG is evaluated, and it is used to modify the electrolyte conductivity.
- The interelectrode gap is computed using Eq 18 at different points in the domain of interest to predict the anode shape.

References cited in this section

5. H. Tipton, The Dynamics of Electrochemical Machining, *Advances in Machine Tool Design and Research,* Pergamon Press, Birmingham, 1964, p 509–522

6. V.K. Jain and P.C. Pandey, Tooling Design for ECM: A Finite Element Approach, *J. Eng. Ind. (Trans. ASME),* Vol 103, 1981, p 183–191

11. V.K. Jain, P.G. Yogindra, and S. Murugan, Prediction of Anode Profile in ECBD and ECD Operations, *Int. J. Mach. Tools Manuf.,* Vol 27 (No. 1), 1987, p 113–134

13. H. Tipton, The Determination of Tool Shape for Electrochemical Machining, *Mach. Prod. Eng.,* 1968, p 325–328

14. Report No. 145, Production Engineering Research Association, Melton Mowbray, 1968

15. V.K. Jain, Vinod K. Jain, and P.C. Pandey, Corner Reproduction Accuracy in Electrochemical Drilling of Blind Holes, *J. Eng. Ind. (Trans. ASME),* Vol 106, 1984, p 55–61

16. W. König and H.J. Hümb, Mathematical Model for the Calculation of the Contour of the Anode in Electrochemical Machining, *Ann. CIRP,* Vol 25, 1977, p 83–87

17. H. Heitmann, Surface Roughness Formation and Determination of Optimum Working Conditions in Electrochemical Die Sinking, *Proc. Second AIMTDR Conf.,* 1968, p 41–47

18. Y.G. Tsuei, C.H. Yen, and R.H. Nilson, Theoretical and Experimental Study of Workpiece Geometry in Electrochemical Machining, *ASME,* Paper 76-WA/Prod, presented in WAM, 1977, p 1–5

19. O.H. Narayanan, S. Hinduja, and C.F. Noble, The Prediction of Workpiece Shape During Electrochemical Machining by the Boundary Element Method, *Int. J. Mach. Tools Des. Res.,* Vol 26 (No. 3), 1986, p 323–338

20. R.H. Nilson and Y.G. Tsuei, Free Boundary Problem for the Laplace Equation with Application to ECM Tool Design, *J. Eng. Ind. (Trans. ASME),* Vol 98, 1976, p 54–58

21. P. Lawrence, Computer Aided Design for ECM Electrodes, *Int. J. Mach. Tools Des. Res.,* Vol 21, 1981, p 379–385

22. M.S. Reddy, V.K. Jain, and G.K. Lal, Tool Design for ECM: Correction Factor Method, *J. Eng. Ind. (Trans. ASME),* Vol 110, 1988, p 111–118

23. V.K. Jain, K. Ravi, G.K. Lal, and K.P. Rajurkar, Investigations into Tool Design for Electrochemical Drilling, *Process. Adv. Mater.,* Vol 1 (No. 1), 1991, p 105–121

24. O.H. Narayanan, S. Hinduja, and C.F. Noble, Design of Tools for Electrochemical Machining by the Boundary Element Method, *Proc. Inst. Mech. Eng.,* Vol 200 (C3), 1986, p 195–205

25. V.K. Jain and K.P. Rajurkar, An Integrated Approach for Tool Design in ECM, *Prec. Eng.,* Vol 13 (No. 2), 1991, p 111–124

26. M.B. Nanyakkara and C.N. Larsson, Computation and Verification of Workpiece Shape in Electrochemical Machining, *20th Int. Machine Tool Design and Research Conf.,* UMIST, U.K., 1976, p 617–624

27. H. Tipton, Calculation of Tool Shape for ECM, *Electrochemical Machining,* C.L. Faust, Ed., Electrochem. Soc., 1971, p 87–102

28. V.K. Jain and P.C. Pandey, On the Reproduction of Corner Anode Profile During Electrochemical Drilling of Blind Holes, *J. Eng. Ind. (Trans. ASME),* Vol 106 (No. 1), 1984, p 55–61

29. W. König and D. Pahl, Accuracy and Optimal Working Conditions in ECM, *Ann. CIRP,* Vol 8 (No. 2), 1970, p 223–230

V.K. Jain, Electrochemical Machining, *Corrosion: Fundamentals, Testing, and Protection*, Vol 13A, *ASM Handbook*, ASM International, 2003, p 143–152

Electrochemical Machining

V.K. Jain, Indian Institute of Technology at Kanpur (India)

Tool Design

Electrochemical machining tools used to be produced by experienced and skilled toolmakers using mostly hand finishing. Nowadays, computer-controlled machine tools can produce ECM tools more accurately while reducing time and cost.

Tool design involves the computation of tool shape and size, which would produce a workpiece having the desired shape, size, and accuracy when machined under the specified machining conditions (Ref 2, 12, 13, 14). Tool-design problems are still difficult to solve. Cumbersome and expensive, “trial-and-error” philosophy is often exercised on the shop floor. Several attempts have been made to develop a useful tool- design model (Fig. 7) (Ref 13, 20, 21, 22, 23, 24, 25, 27). The cos θ (Ref 13) method has been developed for designing cathode shape, but it has many limitations. The complex variable technique (Ref 20) is applicable only for simple shapes and is unable to tackle discontinuities of work and tool surfaces. The boundary-element method (Ref 24) has also been employed for the solution of tool-design problems.

A correction-factor method using finite-element analysis has been proposed (Ref 22, 23) for one- and two-dimensional tool-design problems. The concept of correction factor has been applied to modify the tool shape in each cycle of computation. The tool-shape-modification process continues until the difference between the work shape obtainable by the designed tool and the desired work shape is well within the specified tolerances.

The tool-design procedure involves five major steps:

1. Using the anode shape prediction model (based on finite-element analysis), the anode profile is estimated for an assumed (or modified) tool shape and specified machining conditions. The initial tool shape is assumed to be complementary to the workpiece shape.

2. The computed and the desired work shapes are compared, and the difference between the two is evaluated as an error.
3. If the error is more than the specified tolerance value, a correction factor is calculated.
4. The tool shape is modified by applying the correction factor.
5. Steps 1 to 4 are repeated until the desired tool shape is achieved.

This concept of correction factor can be applied to other tool-design models employing finite-difference or boundary-element technique.
Figure 9 shows the computed work shape and the work shape obtained experimentally for a bit- type tool. The difference between the experimental and the computed work shapes at the top of the drilled hole is due to the effect of stray- current attack and was not incorporated in the present model. The difference between the designed tool shape and the used tool shape is attributed to inaccuracy in the anode shape prediction model and the measurement of overcut in the transition zone. Obtainable anode shapes indicate that to achieve taper-free cavities, either insulated or a bit-type tool should be used. Overcut and taper are governed by the bare part of the tool (b_b).

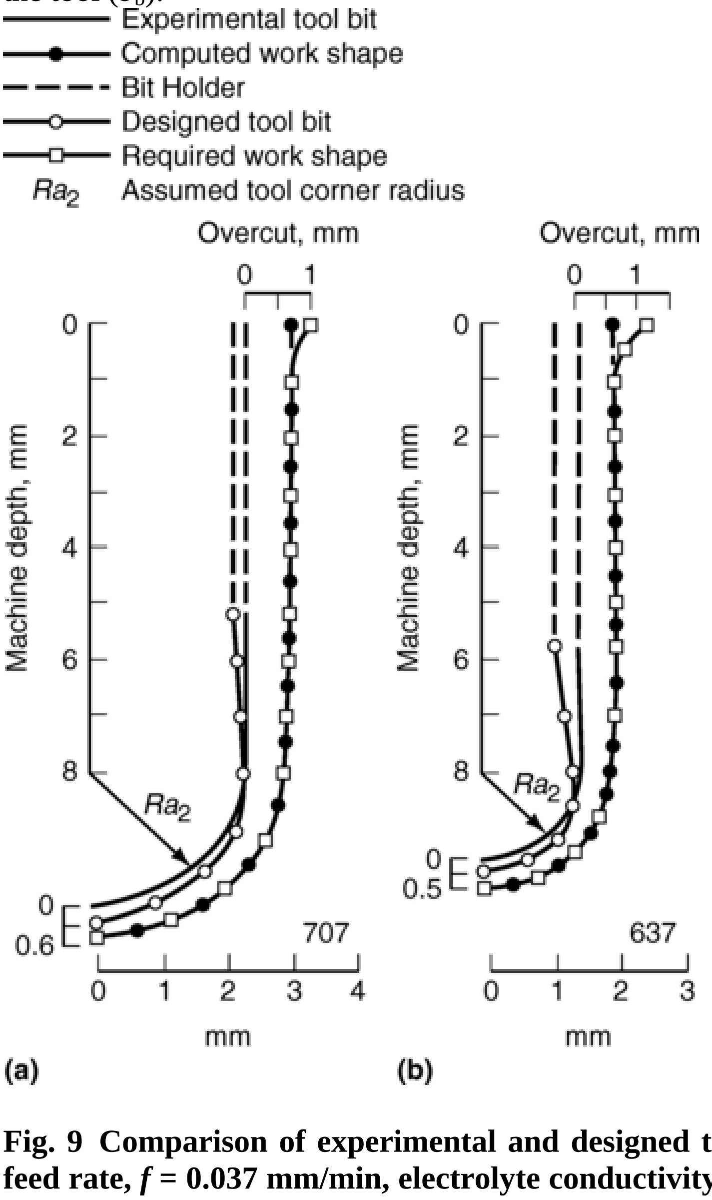

Fig. 9 Comparison of experimental and designed tool profiles used during electrochemical bit drilling, feed rate, f = 0.037 mm/min, electrolyte conductivity, k = 0.0007 Ω^{-1}/mm. (a) E_v = 6.54 V, r_t = 6.03 mm, r_{tc} = 2.39 mm, b_b = 5.22 mm. (b) E_v = 7.64 V, r_t = 5.50 mm, r_{tc} = 1.50 mm, b_b = 3.80 mm. Source: Ref 22

Different modes of electrolyte flow are shown in Fig. 10. Sudden changes in flow direction may lead to stagnation resulting in striations, ridges, or protuberances on the workpiece. This predicament can be resolved by having more than one hole (or slot) in the tool to deliver electrolyte to the IEG, but sometimes it is necessary to conduct an additional ECM operation to get rid of these irregularities.

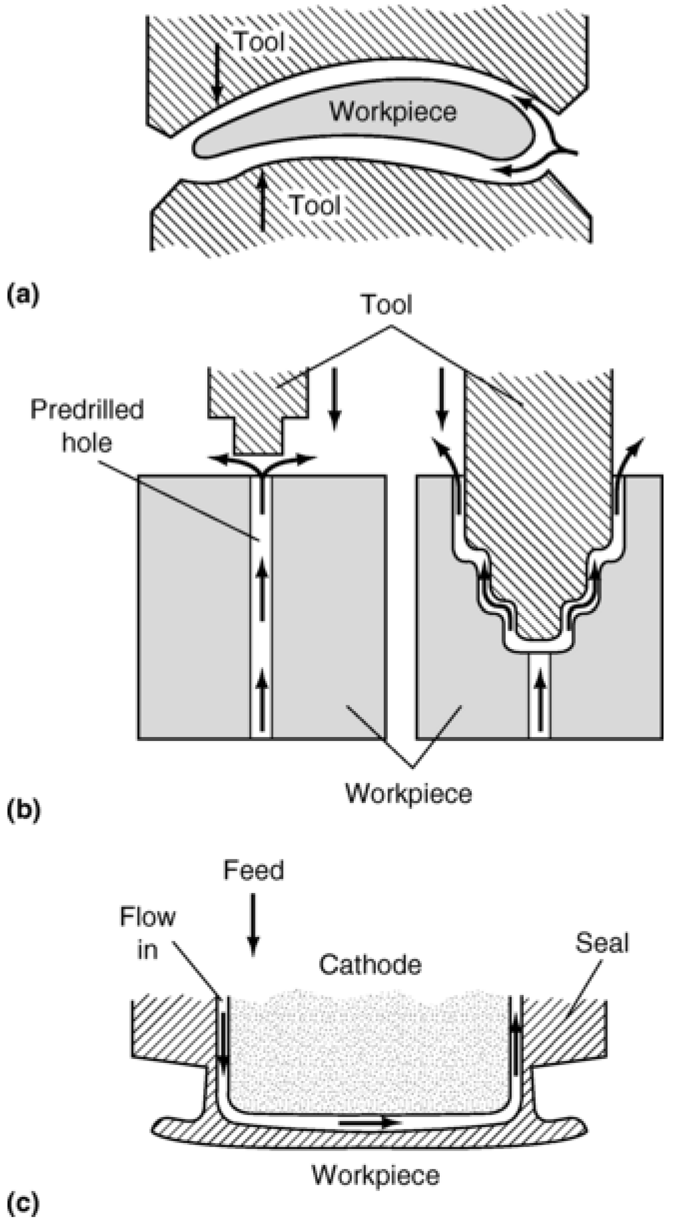

Fig. 10 Tools for electrochemical machining. (a) Dual external-cutting tool for a turbine blade, cross-flow type. Special fixtures are to confine electrolyte flow. (b) Tool for sinking a stepped-through hole with electrolyte entering through predrilled hole in the workpiece. (c) Cross-flow tool used to generate ribs on a surface without leaving flow lines on the part. Electrolyte is fed down one side, across the face, and up the second side. Source: Ref 2

Insulation is important to control the electric current. The insulating material should have high electrical resistivity, low (or no) water absorption, chemical resistance to the electrolyte, wear resistance, and resistance to heat at high working temperatures (200 °C, or 400 °F). It should be smooth and uniform in thickness (≥0.05 mm, or 0.002 in.). Preformed insulation can be shrink fitted with adhesives. At low electrolyte flow rates and low current density, materials like Teflon, epoxy, urethane, phenolic, and powder coating work satisfactorily. Tools with such insulation have enough life if the tool has a lip to protect the insulation from the flow force of the electrolyte. Sprayed or dipped epoxy resins are among the most effective insulating materials. Nylon, acetal, and fiberglass reinforced epoxy give better insulation.

References cited in this section

2. T.L. Lievestro, Electrochemical Machining, *Machining,* Vol 16, *Metals Handbook,* 9th ed., ASM International, 1989, p 533–541

12. A.E. DeBarr and D.A. Oliver, Ed., *Electrochemical Machining,* Macdonald and Co. Ltd, 1975

13. H. Tipton, The Determination of Tool Shape for Electrochemical Machining, *Mach. Prod. Eng.,* 1968, p 325–328

14. Report No. 145, Production Engineering Research Association, Melton Mowbray, 1968

20. R.H. Nilson and Y.G. Tsuei, Free Boundary Problem for the Laplace Equation with Application to ECM Tool Design, *J. Eng. Ind. (Trans. ASME),* Vol 98, 1976, p 54–58

21. P. Lawrence, Computer Aided Design for ECM Electrodes, *Int. J. Mach. Tools Des. Res.,* Vol 21, 1981, p 379–385

22. M.S. Reddy, V.K. Jain, and G.K. Lal, Tool Design for ECM: Correction Factor Method, *J. Eng. Ind. (Trans. ASME),* Vol 110, 1988, p 111–118

23. V.K. Jain, K. Ravi, G.K. Lal, and K.P. Rajurkar, Investigations into Tool Design for Electrochemical Drilling, *Process. Adv. Mater.,* Vol 1 (No. 1), 1991, p 105–121

24. O.H. Narayanan, S. Hinduja, and C.F. Noble, Design of Tools for Electrochemical Machining by the Boundary Element Method, *Proc. Inst. Mech. Eng.,* Vol 200 (C3), 1986, p 195–205

25. V.K. Jain and K.P. Rajurkar, An Integrated Approach for Tool Design in ECM, *Prec. Eng.,* Vol 13 (No. 2), 1991, p 111–124

27. H. Tipton, Calculation of Tool Shape for ECM, *Electrochemical Machining,* C.L. Faust, Ed., Electrochem. Soc., 1971, p 87–102

V.K. Jain, Electrochemical Machining, *Corrosion: Fundamentals, Testing, and Protection*, Vol 13A, *ASM Handbook*, ASM International, 2003, p 143–152

Electrochemical Machining

V.K. Jain, Indian Institute of Technology at Kanpur (India)

Integrated Approach for Tool Design in ECM

The present status of tool design in ECM results in low productivity, high response time to the product changes, high lead and delivery times, and high overall cost. In the future, ECM activities will be integrated by employing the capabilities of high-speed computers. This would result in integration of computer-aided design (CAD) with process planning, including computer simulation and its testing, and finally computer-aided manufacturing (CAM). An attempt for such integration would lead to enhanced productivity, higher material and equipment utilization, and better consistency and quality.

When machining complicated components, it is not always possible to complete the machining process from raw material to the finished component in a single step (Ref 30). When a large amount of material is to be removed, or very high accuracy is required, the machining should be planned in two or more stages, rough and finish machining, as is done in conventional machining. The rules must be developed for the quantity of material left for finish machining so that the desired accuracy can be achieved with minimal cost (Ref 31). Sometimes machining may involve different types of ECM operations, such as die sinking, grinding, or wire cutting. Some components may need electric-discharge machining or conventional machining. The proper

sequence of these operations is important. Figure 11(a) shows high-velocity electrolyte impinging on a previously machined surface that could result in corrosion and product rejection. Figure 11(b) shows ECM in proper sequence of the same component (Ref 30).

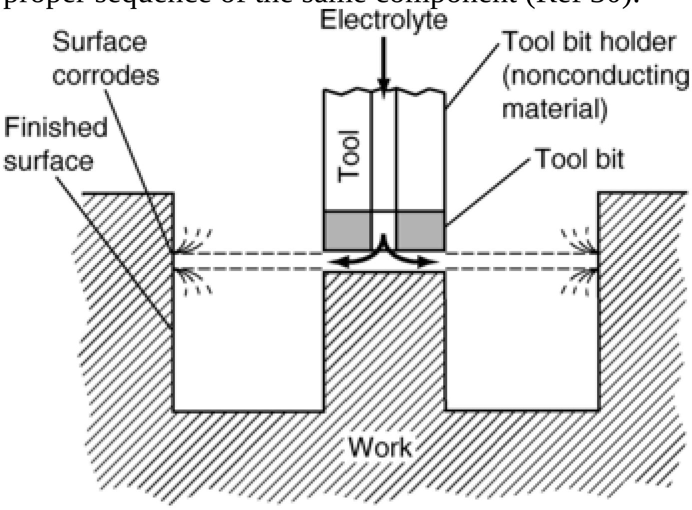

(a)

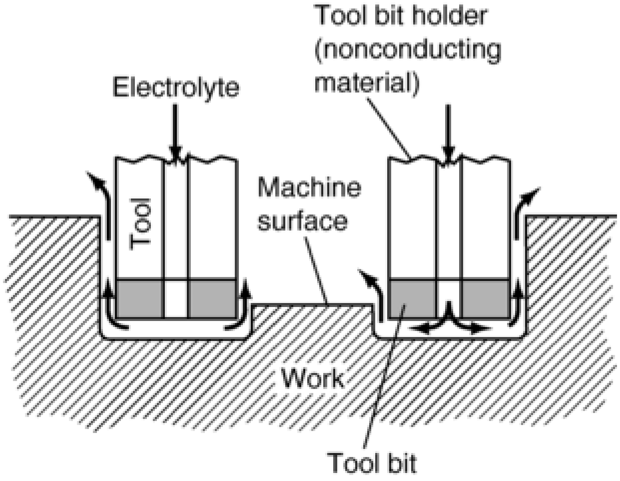

(b)

Fig. 11 Sequence of operations. (a) Improper sequencing would result in unwanted corrosion. (b) Proper sequencing where the center was machined first. Source: Ref 30

The integrated ECM process planning (Ref 31) scheme has three components: system input, optimization, and process simulation.

System input provides all the relevant data and initial information necessary to design the tool, validate the designed tool, and plan the machining of components.

Optimization of machining parameters (electrolyte flow velocity, voltage, and feed rate) must be established. This can be done by multicriteria optimization (Ref 32) rather than by single-objective optimization. In multicriteria optimization of ECM process, a linear goal programming technique is employed using geometrical accuracy, material-removal rate, and tool life as objective functions. Temperature, passivation, and choking are used as constraints. Voltage, feed rate, and electrolyte flow velocity are considered design variables. According to rough or finish machining, objective functions are assigned priorities and weights. For example, in finish machining, accuracy would have first priority and metal-removal rate second. This would be reversed for rough machining.

Process simulation can be used to evaluate alternative process plans and trade-offs. Process simulation is used to reduce lead time, lower cost, increase product quality, and provide a better understanding of the process (Ref 33). Simulation of the ECM process will significantly reduce and, in some cases, eliminate the iterative process of full-scale testing of tools before releasing them for actual production by the machine shop (Fig. 12).

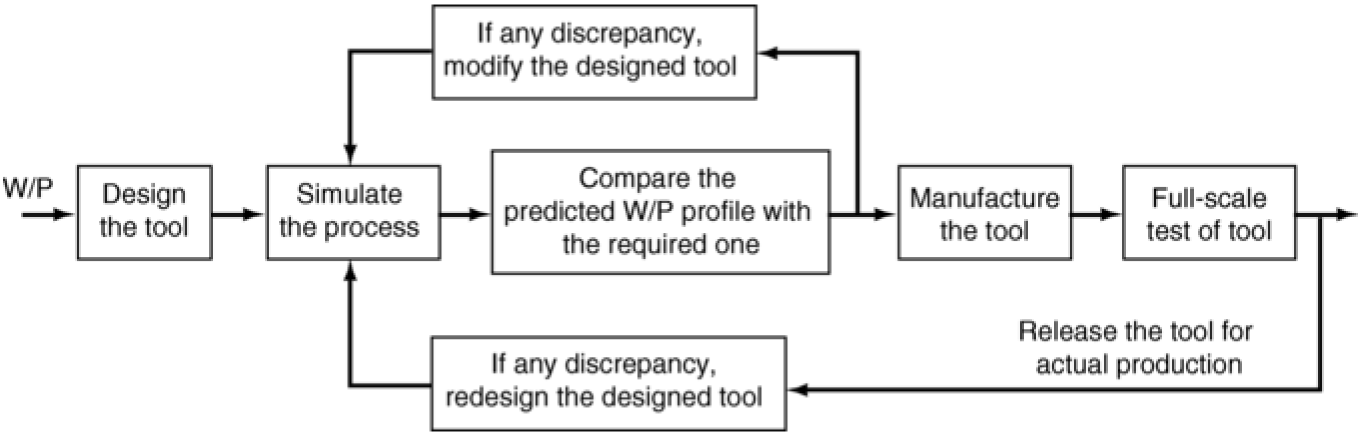

Fig. 12 Proposed procedure for designing and testing a tool for ECM. Workpiece (W/P). Source: Ref 25

A finite-element simulator for the ECM process generates an element mesh from the stored graphic description of the part. The finite-element nodes, elements, and boundary conditions are submitted to the simulation analysis program. A postprocessor or graphic output display of the results exhibits the expected and desired workpiece profile and the designed tool profile. The process plan displays the machining parameters, electrolyte and its concentration, the code of the selected machine tool, and the names and sequence of operations. Figure 13 shows a typical ECM process-simulation plan.

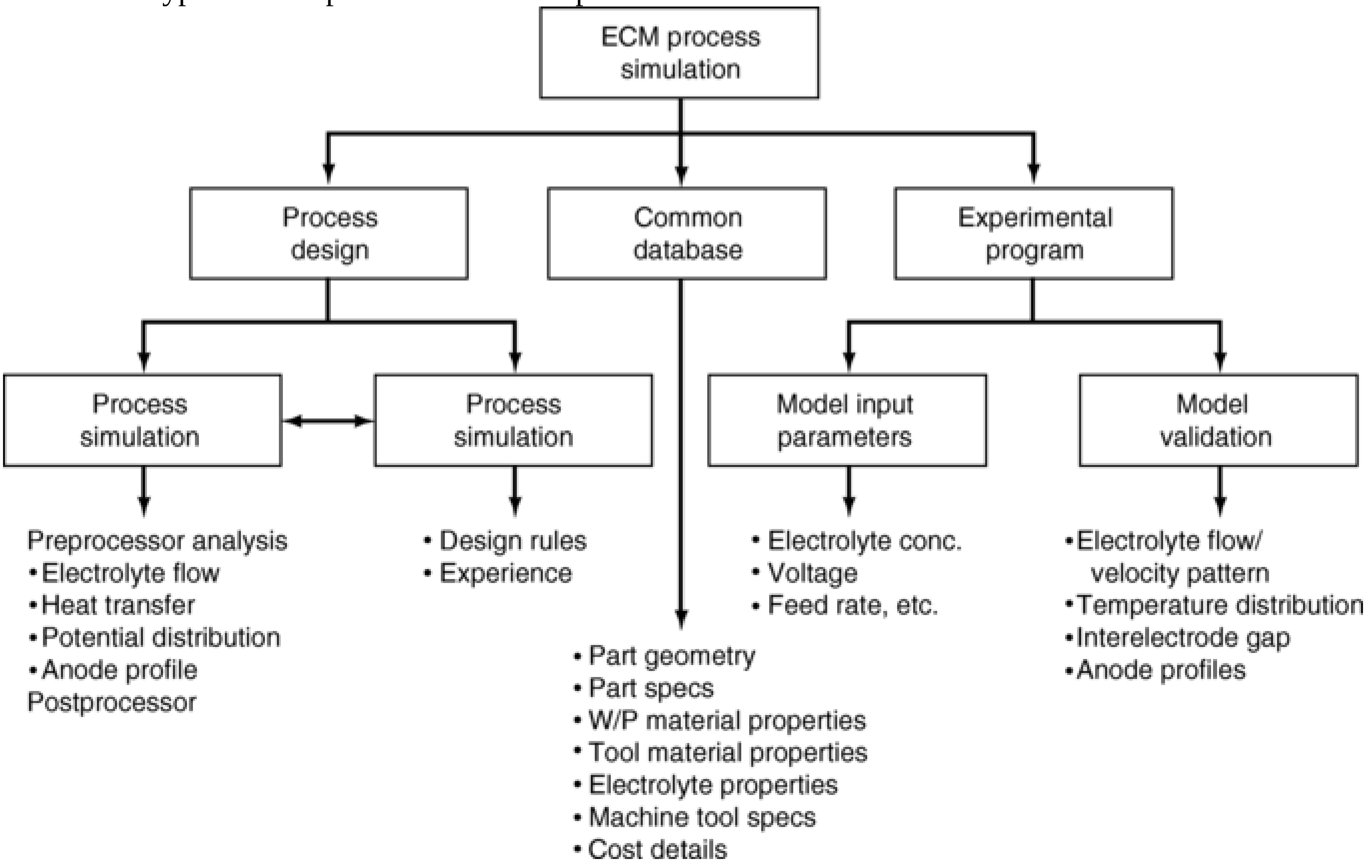

Fig. 13 Simulation program for ECM. Source: Ref 25

References cited in this section

25. V.K. Jain and K.P. Rajurkar, An Integrated Approach for Tool Design in ECM, *Prec. Eng.,* Vol 13 (No. 2), 1991, p 111–124

30. J.F. Wilson, *Practice and Theory of Electrochemical Machining,* Wiley Interscience, 1971

31. Gurusaran, J.L. Batra, and V.K. Jain, Computer Aided Process Planning for ECM, *Tenth Int. Conf. Production Research,* Nottingham, U.K., 1989, p 780–789

32. B.G. Acharya, V.K. Jain, and J.L. Batra, Multi Objective Optimization of ECM Process, *Prec. Eng.*, Vol 8 (No. 2), 1986, p 88–96

33. K.C. Maddux and S.C. Jain, CAE for the Manufacturing Engineer: The Role of Process Simulation in Concurrent Engineering, *Proc. ASME Symp. Manufacturing Simulation and Processes,* A.P. Tseng, D.R. Durham, and R. Komanduri, Ed., PED 20, 1986, p 1–16

V.K. Jain, Electrochemical Machining, *Corrosion: Fundamentals, Testing, and Protection*, Vol 13A, *ASM Handbook*, ASM International, 2003, p 143–152

Electrochemical Machining

V.K. Jain, Indian Institute of Technology at Kanpur (India)

Process Capabilities and Limitations

Electrochemical machining can machine highly complicated and curved shapes in a single pass. Tool life is very high so a large number of pieces can be machined by the same tool. Machinability of work materials is independent of physical and mechanical properties. Machined surfaces are stress and burr free with good surface finish. Scrap production and overall machining times are reduced.

Electrochemical machining also has limitations. Accuracy of the machined component depends on tool design, degree of process control imposed, and complexity in the shapes produced. Machining of materials containing hard spots, inclusions, sand, and scale present some practical difficulties. Electrochemical machining cannot produce sharp corners and edges.

The roughness of the machined surface is controlled mainly by local current density. High current density in the front gap produces low values of surface roughness. The best surface roughness varies between 0.1 and 1.0 μm (0.004 and 0.04 mil), while low value of current density in the side gap results in the high values of surface roughness (may be as rough as 5 μm or more). Variables affecting local current density ultimately affect surface roughness.

The usual accuracy achievable in ECM is approximately ±0.013 mm (±0.0005 in. 0.005 in.) and ±0.25 mm (±0.010 in.) in front and side gaps, respectively. The best tolerance that can be achieved is ±0.025 mm (±0.001 in.), internal radius as 0.8 mm (0.030 in.), external radius as 0.5 mm (0.020 in.), 0.001 mm/mm (0.001 in./in.) as taper, and 0.05 mm (0.020 in.) as overcut.

V.K. Jain, Electrochemical Machining, *Corrosion: Fundamentals, Testing, and Protection*, Vol 13A, *ASM Handbook*, ASM International, 2003, p 143–152

Electrochemical Machining

V.K. Jain, Indian Institute of Technology at Kanpur (India)

Application Examples

It has been reported (Ref 12) that cost advantage of the ECM process over conventional machining varies from 4 to 1 to 9 to 1.

Example 1: ECM of a Stainless Steel Nozzle. A nozzle (Fig. 14a) is made from a 316 stainless steel tube using a machine that could provide maximum current of 500 A, voltage ≤ 24 V. A copper tool was fed into one end of the tube to make conical-shaped hole. The initial current was 20 A (voltage = 17 V) and ended with the current as 310 A. Electrolyte used was NaCl (0.12 kg/L, or 1 lb/gal, of water) at 27 °C (80 °F) and 550 kPa (80 psi) pressure. Feed rate of 5.8 mm/min (0.25 in./min) took a total of 7.6 min to produce the nozzle with a surface roughness of 0.125 to 0.250 μm (5 to 10 μin.) (Ref 2).

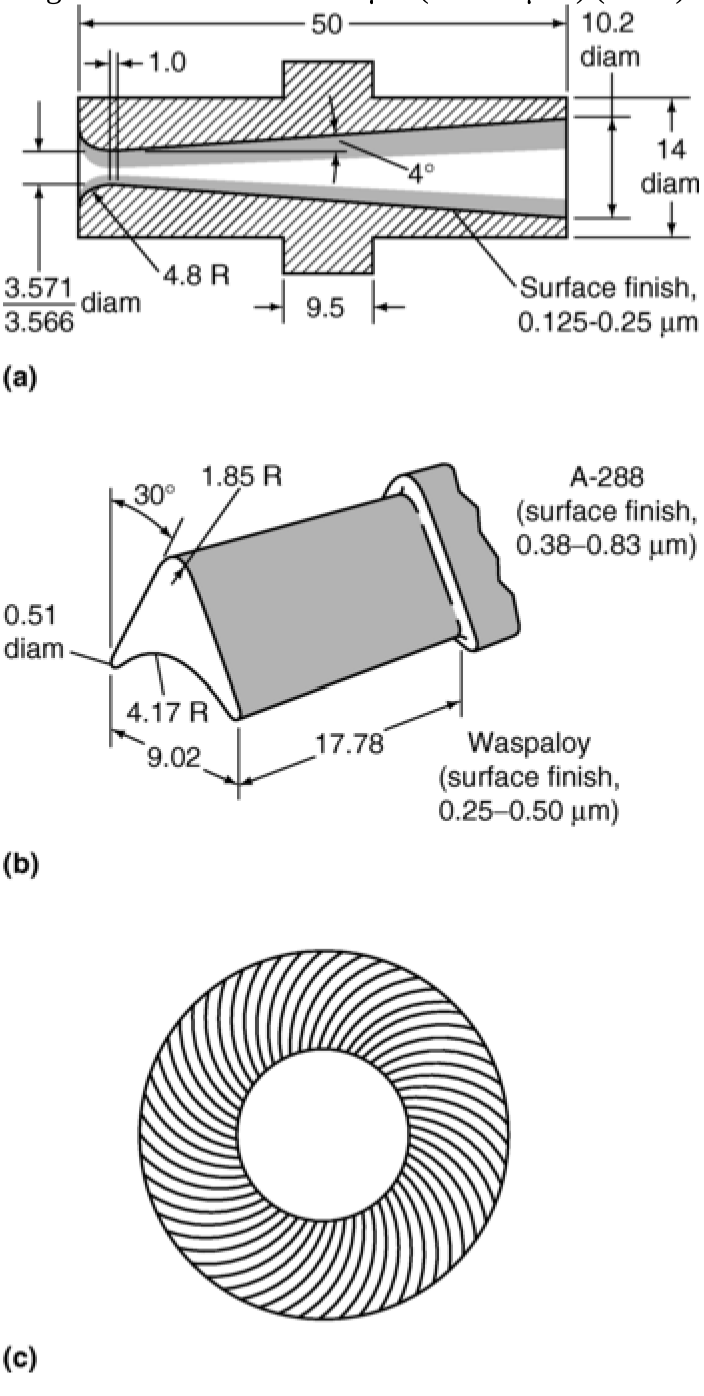

Fig. 14 Examples of applications. (a) Finishing a conical hole in a nozzle. (b) Contouring a turbine blade surface. (c) Cutting spiral grooves in a friction plate. Source: Ref 2

Another copper tool was used to machine the radius at the other end of the hole. Parameters used were: current varied from 20 to 220 A, f = 2.5 mm/min (0.100 in./min), total machining time = 2.00 min, penetration depth = 4.95 mm (0.19 in.), and internal finish obtained = 0.125 to 0.25 μm (5 to 10 μin.) (Ref 2).

Example 2: ECM of a Turbine Blade. The turbine blade (Fig. 14b) made of heat-resistant alloy (A-286 alloy) was machined by ECM that could provide maximum current of 5000 A at 2 to 20 V dc. A tool was made of

copper-tungsten alloy. The $NaNO_3$ electrolyte (0.26 kg/L, 2.2 lb/ gal of water) at 43 °C (110 °F) was employed. Other parameters were:

- Current = 100 to 170 A
- Pressure = 900 to 1400 kPa (130 to 205 psi)
- Flow rate = 7.6 L/min (2 gal/min)
- f = 7.6 mm/min (0.3 in./min)

The surface roughness achieved was 0.38 to 0.63 μm (15 to 25 μin.) (Ref 2).
Example 3: ECM of Spiral Grooves in a Friction Disk. Seventy-two equally spaced spiral grooves (Fig. 14c), 0.38 mm (0.015 in.) deep and 1.0 mm (0.040 in.) wide were made in a friction disk (1020 steel, 60 to 75 HRB) using ECM machine, which could provide maximum current, $I \approx$ 600 to 650 A, voltage = 20 V, electrolyte → NaCl (0.15 kg/L, or 1.25 gal/lb of water), T = 30 to 32 °C (85 to 90 °F), P = 690 kPa (100 psi), electrolyte flow rate = 40 L/min (10 gal/min), f = 1.3 mm/min (0.050 in./min).

References cited in this section

2. T.L. Lievestro, Electrochemical Machining, *Machining,* Vol 16, *Metals Handbook,* 9th ed., ASM International, 1989, p 533–541

12. A.E. DeBarr and D.A. Oliver, Ed., *Electrochemical Machining,* Macdonald and Co. Ltd, 1975

V.K. Jain, Electrochemical Machining, *Corrosion: Fundamentals, Testing, and Protection*, Vol 13A, *ASM Handbook,* ASM International, 2003, p 143–152

Electrochemical Machining

V.K. Jain, Indian Institute of Technology at Kanpur (India)

Acknowledgment

The author wishes to acknowledge the suggestions of Mr. Syadwad Jain of Ohio State University, Columbus, OH, and help of Ms. Lalitha and Ms. Shaifali Mehrotra of I.I.T. Kanpur, India, in the preparation of this manuscript.

V.K. Jain, Electrochemical Machining, *Corrosion: Fundamentals, Testing, and Protection*, Vol 13A, *ASM Handbook,* ASM International, 2003, p 143–152

Electrochemical Machining

V.K. Jain, Indian Institute of Technology at Kanpur (India)

References

1. V.K. Jain, *Advanced Machining Processes,* Allied Publishers, Delhi, India, 2002

2. T.L. Lievestro, Electrochemical Machining, *Machining,* Vol 16, *Metals Handbook,* 9th ed., ASM International, 1989, p 533–541

3. V.K. Jain and P.C. Pandey, Investigations into the Use of Bits as a Cathode in ECM, *Int. J. Mach. Tools Des. Res.,* Vol 22 (No. 4), 1982, p 341–352

4. J.A. McGeough, *Principles of Electrochemical Machining,* Chapman and Hall, London, 1974

5. H. Tipton, The Dynamics of Electrochemical Machining, *Advances in Machine Tool Design and Research,* Pergamon Press, Birmingham, 1964, p 509–522

6. V.K. Jain and P.C. Pandey, Tooling Design for ECM: A Finite Element Approach, *J. Eng. Ind. (Trans. ASME),* Vol 103, 1981, p 183–191

7. V.K. Jain and P.C. Pandey, Tooling Design for ECM, *Prec. Eng.,* Vol 2, 1980, p 195–206

8. P.C. Pandey and H.S. Shan, *Modern Machining Processes,* Tata McGraw Hill, Delhi, India, 1980

9. J.F. Thorpe and R.D. Zerkle, Analytical Determination of the Equilibrium Gap in Electrochemical Machining, *Int. J. Mach. Tools Des. Res.,* Vol 9, 1969, p 131–144

10. J. Hopenfeld and R.R. Cole, Prediction of the Dimensional Equilibrium Cutting Gap in Electrochemical Machining, *J. Eng. Ind. (Trans. ASME),* Vol 91, 1969, p 75–765

11. V.K. Jain, P.G. Yogindra, and S. Murugan, Prediction of Anode Profile in ECBD and ECD Operations, *Int. J. Mach. Tools Manuf.,* Vol 27 (No. 1), 1987, p 113–134

12. A.E. DeBarr and D.A. Oliver, Ed., *Electrochemical Machining,* Macdonald and Co. Ltd, 1975

13. H. Tipton, The Determination of Tool Shape for Electrochemical Machining, *Mach. Prod. Eng.,* 1968, p 325–328

14. Report No. 145, Production Engineering Research Association, Melton Mowbray, 1968

15. V.K. Jain, Vinod K. Jain, and P.C. Pandey, Corner Reproduction Accuracy in Electrochemical Drilling of Blind Holes, *J. Eng. Ind. (Trans. ASME),* Vol 106, 1984, p 55–61

16. W. König and H.J. Hümb, Mathematical Model for the Calculation of the Contour of the Anode in Electrochemical Machining, *Ann. CIRP,* Vol 25, 1977, p 83–87

17. H. Heitmann, Surface Roughness Formation and Determination of Optimum Working Conditions in Electrochemical Die Sinking, *Proc. Second AIMTDR Conf.,* 1968, p 41–47

18. Y.G. Tsuei, C.H. Yen, and R.H. Nilson, Theoretical and Experimental Study of Workpiece Geometry in Electrochemical Machining, *ASME,* Paper 76-WA/Prod, presented in WAM, 1977, p 1–5

19. O.H. Narayanan, S. Hinduja, and C.F. Noble, The Prediction of Workpiece Shape During Electrochemical Machining by the Boundary Element Method, *Int. J. Mach. Tools Des. Res.,* Vol 26 (No. 3), 1986, p 323–338

20. R.H. Nilson and Y.G. Tsuei, Free Boundary Problem for the Laplace Equation with Application to ECM Tool Design, *J. Eng. Ind. (Trans. ASME),* Vol 98, 1976, p 54–58

21. P. Lawrence, Computer Aided Design for ECM Electrodes, *Int. J. Mach. Tools Des. Res.,* Vol 21, 1981, p 379–385

22. M.S. Reddy, V.K. Jain, and G.K. Lal, Tool Design for ECM: Correction Factor Method, *J. Eng. Ind. (Trans. ASME),* Vol 110, 1988, p 111–118

23. V.K. Jain, K. Ravi, G.K. Lal, and K.P. Rajurkar, Investigations into Tool Design for Electrochemical Drilling, *Process. Adv. Mater.,* Vol 1 (No. 1), 1991, p 105–121

24. O.H. Narayanan, S. Hinduja, and C.F. Noble, Design of Tools for Electrochemical Machining by the Boundary Element Method, *Proc. Inst. Mech. Eng.,* Vol 200 (C3), 1986, p 195–205

25. V.K. Jain and K.P. Rajurkar, An Integrated Approach for Tool Design in ECM, *Prec. Eng.,* Vol 13 (No. 2), 1991, p 111–124

26. M.B. Nanyakkara and C.N. Larsson, Computation and Verification of Workpiece Shape in Electrochemical Machining, *20th Int. Machine Tool Design and Research Conf.,* UMIST, U.K., 1976, p 617–624

27. H. Tipton, Calculation of Tool Shape for ECM, *Electrochemical Machining,* C.L. Faust, Ed., Electrochem. Soc., 1971, p 87–102

28. V.K. Jain and P.C. Pandey, On the Reproduction of Corner Anode Profile During Electrochemical Drilling of Blind Holes, *J. Eng. Ind. (Trans. ASME),* Vol 106 (No. 1), 1984, p 55–61

29. W. König and D. Pahl, Accuracy and Optimal Working Conditions in ECM, *Ann. CIRP,* Vol 8 (No. 2), 1970, p 223–230

30. J.F. Wilson, *Practice and Theory of Electrochemical Machining,* Wiley Interscience, 1971

31. Gurusaran, J.L. Batra, and V.K. Jain, Computer Aided Process Planning for ECM, *Tenth Int. Conf. Production Research,* Nottingham, U.K., 1989, p 780–789

32. B.G. Acharya, V.K. Jain, and J.L. Batra, Multi Objective Optimization of ECM Process, *Prec. Eng.,* Vol 8 (No. 2), 1986, p 88–96

33. K.C. Maddux and S.C. Jain, CAE for the Manufacturing Engineer: The Role of Process Simulation in Concurrent Engineering, *Proc. ASME Symp. Manufacturing Simulation and Processes,* A.P. Tseng, D.R. Durham, and R. Komanduri, Ed., PED 20, 1986, p 1–16

34. J.L. Bennett, *Building Decision Support System,* Addison Wesley, 1983

35. L. Kops, Effect of Pattern of Grain Boundary Network on Metal Removal Rate in Electrochemical Machining Process, *J. Eng. Ind. (Trans. ASME),* Vol 98, 1976, p 360–368

V.K. Jain, Electrochemical Machining, *Corrosion: Fundamentals, Testing, and Protection*, Vol 13A, *ASM Handbook*, ASM International, 2003, p 143–152

Electrochemical Machining

V.K. Jain, Indian Institute of Technology at Kanpur (India)

Selected References

- G.F. Benedict, *Nontraditional Manufacturing Processes,* Marcel Dekker, 1987

- D.T. Chin, Anodic Film and ECM Dimensional Control: A Study of Steel Electrodes in Solutions Containing Na_2SO_4 and $NaClO_4$, *J. Electrochem. Soc.,* Vol 121 (No. 12), 1974, p 1592–1595
- W.G. Clark and J.A. McGeough, Temperature Distribution in the Gap in the Electrochemical Machining, *J. Appl. Electrochem.,* Vol 7, 1977, p 277–286
- A.K.M. DeSilva and J.A. McGough, Computer Application in Unconventional Machining, *J. Mater. Process. Technol.,* Vol 107, 2000, p 276–282
- J. Kozak, M. Chuchro, A. Ruszaj, and K. Karbowski, The Computer Aided Simulation of Electrochemical Process with Universal Spherical Electrodes When Machining Sculptured Surfaces, *J. Mater. Process. Technol.,* Vol 107, 2000, p 283–287
- J. Kozak, K.P. Rajkumar, and R. Balkrishna, Study of Electrochemical Jet Machining Process, *J. Manuf. Sci. Eng. (Trans. ASME),* Vol 1996, p 490–498
- M.E. Merchant, Newer Methods for the Precision Working of Metals: Research and Present Status, *Proc. Int. Conf. on Production Research (ASME),* 1962, p 93–107
- K.P. Rajurkar, C.L. Schnacker, and R.P. Lindsay, Some Aspects of ECM Performance, *Ann. CIRP,* Vol 37 (No. 1), 1988, p 183–186
- K.P. Rajurkar and D. Zhu, Improvement of Electrochemical Machining Accuracy by Using Orbital Electrode Movement, *Ann. CIRP,* Vol 48 (No. 1), 1999, p 139–142
- A. Ruszaj, Investgation Aiming to Increase Electrochemical Machining Accuracy, *Prec. Eng.,* Vol 12 (No. 1), 1999, p 43–48
- K. Seimiya, An Approximate Method for Predicting Gap Profile in Electrochemical Machining, *Proc. Fifth Int. Conf. Prod. Eng.* (Tokyo, Japan), 1984, p 389–394
- S.M. Trendler, ECM and Ultrasonic Machining for Faster Die Machining, *Die Cast. Eng.,* Jan/Feb 1985, p 66–67
- F. Zawistowski, New System of Electrochemical Form Machining Using Universal Rotating Tool, *Int. J. Mach. Tools Manuf.,* Vol 30 (No. 3), 1990, p 475–483
- M. Zybura Skrabalak and A. Ruszaj, The Influence of Electrode Surface Geometrical Surface on Electrochemical Soothing Process, *J. Mater. Process. Technol.,* Vol 107, 2000, p 288–292

V.K. Jain, Electrochemical Allied Processes, *Corrosion: Fundamentals, Testing, and Protection,* Vol 13A, *ASM Handbook,* ASM International, 2003, p 153–156

Electrochemical Allied Processes

V.K. Jain, Indian Institute of Technology Kanpur

Introduction

SPECIFIC MACHINING PROCESSES that employ electrochemical machining (ECM) technology include deburring, and deep-hole drilling. The principles of electrochemical machining are presented in the article “Electrochemical Machining” in this Volume. This article shows the applications of ECM to specific processes and discusses a variation of the steady-state process, pulse machining.

V.K. Jain, Electrochemical Allied Processes, *Corrosion: Fundamentals, Testing, and Protection*, Vol 13A, *ASM Handbook*, ASM International, 2003, p 153–156

Electrochemical Allied Processes

V.K. Jain, Indian Institute of Technology Kanpur

Electrochemical Deburring

A designer usually considers aspects of a component such as material, form, dimensional accuracy, surface texture, and heat treatment, but perhaps not the surface integrity and edge quality (Ref 1). These last two factors are important aspects for the performance and life of a product, however.

When a component is processed by a conventional machining method, it is usually left with burrs along intersecting surfaces. Such burrs are unwanted and could be a hazard when handling the component, but they can be removed by one of several deburring processes.

In modern industrial technology, the deburring process has attained considerable importance because of stringent quality standards. Presence of burrs on a component affects its functional, physiological, and aesthetic requirements (Ref 2). Burrs create a hindrance in assembly, they may degrade corrosion preventive or aesthetic coatings, and loosened burrs may result in excessive wear of the sliding or rolling surfaces. Different types of burrs are listed in Table 1 (Ref 3).

Table 1 Types of burrs formed during different manufacturing methods

Type of burr	Schematic	Remarks
Compressive burr	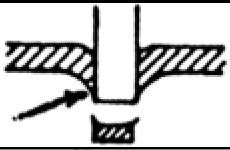	The burr produced in blanking and piercing operations in which slug separates from the parent material under compressive stress
Cutting-off burr	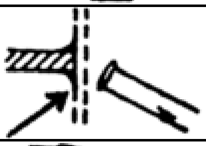	A projection of material left when the workpiece falls from the stock
Corner burr		Intersection of three or more surfaces
Edge burr	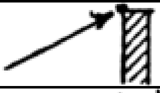	Intersection of two surfaces
Entrance burr	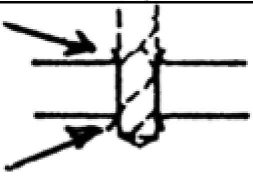	Cutting tool enters in the workpiece
Exit burr		Cutting tool exits the workpiece
Feather burr		Fine or thin burr

Flash burr		Portion of flash remaining on the part after trimming
Hanging burr		Loose burr not firmly attached to the workpiece
Rollover burr	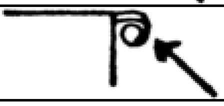	Burr formed when it exits over a surface and allows the chips to be rolled away

Source: Ref 3

Deburring processes can be mechanical, abrasive, thermal, chemical, and electrochemical. Mechanical deburring using brushes or scrapers is unreliable and is a burr-minimizing process, which does not meet the requirements of high edge quality. The abrasive deburring processes (tumbling, sand blasting, or vibratory) have low reliability, poor uniformity, low metal removal rate, and tend to charge the workpiece with grit. In thermal deburring, the deburring chamber temperature is about 3500 °C (6330 °F), which burns out burrs and sharp edges on the component. In chemical deburring, burrs are dissolved in a chemical medium. In electrochemical deburring (ECD), the principle of anodic dissolution is applied to dissolve the burrs.

Electrochemical deburring works on the same principle as ECM. The tool is either insulated on all surfaces except the part that is adjacent to the burrs, or a bit type of tool is used (Ref 4). The tool tip (or bit) should overlap the area to be deburred by about 1.5 to 2.0 mm (0.06 to 0.08 in.). Electrochemical deburring is useful for burrs located in inaccessible areas where other deburring processes are not effective (Ref 5, 6). In ECD, the magnitude of current and electrolyte flow rate are lower than ECM. Secondly, the tool is stationary (Fig. 1). The current magnitude and its duration of flow to suit a particular component are determined by trial. The commonly used electrolytes are NaCl and $NaNO_3$. The interelectrode gap (IEG) is usually in the range of 0.1 to 0.3 mm (0.004 to 0.012 in.). A deburred steel component shows a localized deposit (Fe_3O_4— dark gray and ≤1 μm, or 4×10^{-6} in., thick) that is a reaction product of the process. This deposit is conductive and disappears during heat treatment of the components.

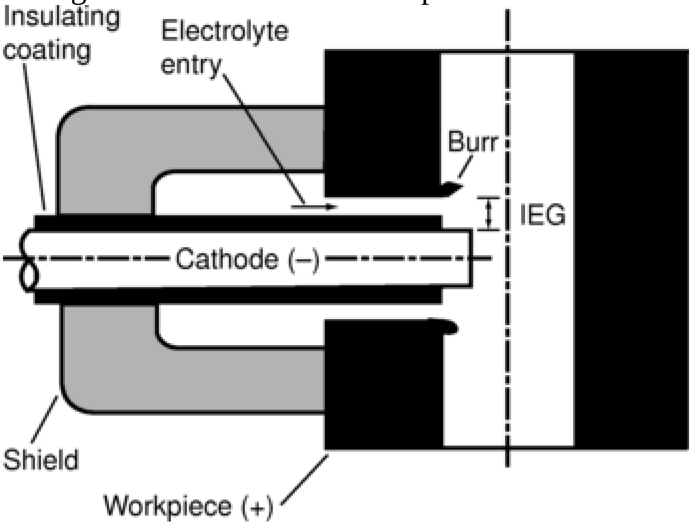

Fig. 1 Electrochemical deburring at the intersection of two holes

Machine tools for ECD are usually designed with multiple work stations served from a single power supply. Their elements and functions are the same as those of ECM tools except for the tool-feed system. Before applying ECD for a particular type of job, the thickness, shape, and repeatability of the burrs on the parts must be known. The more uniform the shape and size of the burrs, the more efficient the burr-removal operation. Further, the tool head that dissolves the burrs should be shaped as a replica of the contour of the work. Portable ECD units equipped with 50 A power supplies (Ref 4) are also available and are useful to deburr tubes and pipes of varying configuration, length, and cross- sectional area.

Applications in consumer appliances, biomedical, aerospace, and automobile industries include gears, splines, drilled holes, milled components, fuel supply and hydraulic system components, and intersecting holes in crankshafts (Ref 2).

Apart from economics, ECD gives higher reliability, reduced operation time, more uniformity, and it can be easily automated. Deburring components takes about 45 to 60 s cycle time on a 500 A machine. The hydroxides

removed during ECD can be safely used as a raw material for the lapping paste. The components should be thoroughly washed before deburring, and properly cleaned after deburring (Ref 2).

References cited in this section

1. K. Takazawa, The Challenge of Burr Technology and Its Worldwide Trends, *Bull. JSPE,* Vol 22 (No. 3), 1988, p 165–170

2. M.G.J. Naidu, Electrochemical Deburring for Quality Production, *Proc. Winter School on AMT,* V.K. Jain and S.K. Choudhury, Ed., IIT Kanpur (India), 1991

3. V.K. Jain, *Advanced Machining Processes,* Allied Publishers, New Delhi, 2002

4. V.K. Jain and P.C. Pandey, Investigations into the Use of Bits as a Cathode in ECM, *Int. J. Mach. Tools Des. Res.,* Vol 22 (No. 4), 1982, p 341–352

5. G.F. Benedict, *Non-traditional Manufacturing Processes,* Marcel Dekker, 1987

6. E. Rumyantsev and A. Davydev, *Electrochemical Machining of Metals,* Mir Publishers, Moscow, 1989

V.K. Jain, Electrochemical Allied Processes, *Corrosion: Fundamentals, Testing, and Protection*, Vol 13A, *ASM Handbook*, ASM International, 2003, p 153–156

Electrochemical Allied Processes

V.K. Jain, Indian Institute of Technology Kanpur

Electrochemical Deep-Hole Drilling

Deep small holes are required in many applications, such as turbine rotor and stator assembly for cooling, crankshaft oil holes, holes in fuel- injection nozzles, and holes in spinnerets. The principle of anodic dissolution has been applied for making such small-diameter deep holes in hard-to-machine materials. This process is also known as shaped-tube electrolytic machining (Ref 7). This process basically differs from conventional ECM in two aspects: either a mixture (neutral salt and acidic electrolyte) or acidic electrolyte is used, and a coated tubular cathode is used. The mixture or acidic electrolyte is added to circumvent the production of insoluble precipitate (sludge) during conventional ECM, which inhibits machining process by obstructing the flow path of the electrolyte. The coated tubular cathode controls the magnitude of overcut. Certain minimum overcut is desirable to serve as a return path for the electrolyte (Ref 8). If acid (HCl, H_2SO_4, or HNO_3) is used as electrolyte, then periodic reversal of the polarity for a very short duration of time (5–10 s) is essential to remove any film built up on the cathode.

Such reversal is usually not required if a mixture of the electrolytes is used (Ref 7, 8, 9). Simultaneous drilling of many holes is possible (Ref 7, 9). A modern air-pressure turbine rotor and stator assembly may have 20,000 cooling holes having diameters ranging from 1 to 4 mm (0.04 to 0.16 in.) and aspect ratios of 40 to 200. The rotor blades are subjected to high stresses, very high temperature and vibration, and are made of difficult-to-machine superalloys. Analysis of the data in Table 2 (Ref 8) indicates that laser-beam machining and electron-beam machining cannot be used because of upper limit of thickness of the workpiece (only 18 mm, or 0.7 in., or so) that can be drilled. Electrical discharge machining (EDM) suffers in comparison with electrochemical deep-hole drilling due to relatively lower aspect ratio, shallower depths, poorer surface finish, and surface integrity.

Table 2 Comparison of process capabilities of the advanced methods of deep-hole drilling

Parameter	Process				
	EDM	**STEM**	**ESD**	**LBM**	**EBM**
Hole diameter, mm (in.)	0.125–6.25 (0.005–0.25)	0.75–2.5 (0.03–0.1)	0.125–0.875 (0.005–0.034)	0.125–1.25 (0.005–0.5)	0.025–1.0 (0.001–0.04)
Hole depth, mm (in.)					
Common Max	3.125 (0.123)	125 (4.9)	18.75 (0.74)	5.0 (0.2)	2.5 (0.1)
Ultimate	62.5 (2.5)	900 (35.4)	25 (1.0)	17.5 (0.7)	7.5 (0.3)
Aspect ratio					
Typical	10:1	16:1	16:1	16:1	6:1
Maximum	20:1	300:1	40:1	75:1	100:1
Cutting rate, mm/s (in./s)	0.0125 (0.0005)	0.025 (0.001)	0.025 (0.001)	<1 (<0.04)	0.25 (0.01)
Finish, µm (µin.)	1.6–3.2 (63–125)	0.8–3.2 (32–125)	0.25–1.6 (10–63)	0.8–6.35 (32–250)	0.8–6.35 (32–250)
Operating voltage	30–100 V	5–25 V	150–850 V	…	150 kV
Surface integrity	Heat-affected surface, no burrs	No residual stress, no burrs	No residual stress, no burrs	Heat-affected surface	Heat-affected surface

EDM, electric discharge machining; STEM, shaped-tube electrolytic machining; ESD, electrostream drilling; LBM, laser beam machining; EBM, electron beam machining. Source: Ref 8

Other applications of deep-hole drilling include: oil passages in bearings where EDM will cause microcracks, fuel nozzles, and starting holes (depth ≥100 mm, or 4 in.,) for wire EDM. One of the major problems of deep-hole drilling is loss of electrolyte pressure upon breakthrough of the bottom of the workpiece. This problem has been successfully resolved by the use of thin, dummy workpieces at the bottom. Use of dummy workpiece (Fig. 2) at the top surface of the workpiece overcomes the problem of nonuniform diameter at the tool entry side due to stray cutting.

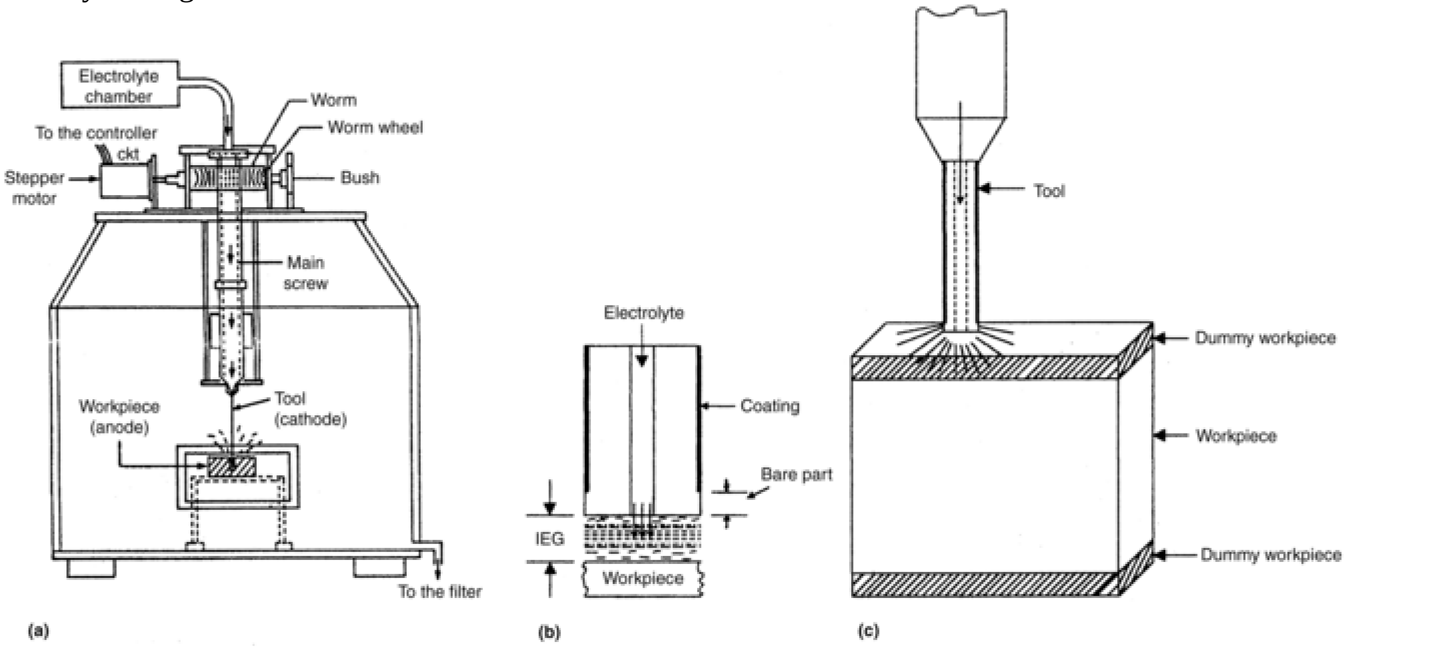

Fig. 2 System for electrochemical deep-hole drilling. (a) Equipment. (b) Enlarged view of tool and workpiece. (c) Dummy workpiece and tool. Source: Ref 8

The electrochemical deep-hole drilling system shown in Fig. 2 includes four subsystems: power supply, tool and tool feed, electrolyte cleaning and supply, and workholding and machining chamber.

The power supply subsystem gives comparatively low direct current at 5 to 20 V (between electrodes). The available current will limit the number of holes being drilled simultaneously; typically, 40 A/hole is required.

The cathode is tubular and is made of the same materials used in ECM tools. It has an insulation coating throughout its length except a small bare part (Fig. 2). Increase in the length of the bare part of the tool will

increase overcut, which will reduce the required pressure to pump electrolyte through the side gap. Pure titanium tubes coated with an appropriate resin are commonly used. The bare part of the cathode tip should have a slightly larger diameter than the diameter of the coated cathode for increased tool life.

The straightness of the tool is most critical, and it should be checked periodically. Cathode guides should also be provided to minimize tool wandering. Feed rate to the tool varies over a wide range: 0.76 to 2.00 mm/min (0.03 to 0.08 in./min) depending on the machining conditions and electrolyte conductivity in IEG.

The electrolyte system consists of a pump capable of supplying electrolyte in IEG at a pressure of 60 to 300 kPa (8.7 to 43.5 psi) and quantity 20 to 150 cm^3/min (1.2 to 9.2 $in.^3$/min). It also consists of filters and heat exchanger. The machining chamber should be well closed to eliminate spattering of the electrolyte. It should also have an exhaust fan to remove hydrogen gas from the machining and nearby area.

The workpiece holding fixture is usually made of electrically nonconducting materials such as acrylic plastics. The workpiece is a conducting material and is connected to the direct-current (dc) power supply.

Process capabilities. Hole diameter usually lies between 0.5 to 2.5 mm (0.02 to 0.1 in). Highest aspect ratio claimed is 300 to 1 (hole tolerance in diameter ±5%), and surface roughness may lie in the range of 0.8 to 3.2 μm (32 to 125 μin.). The machined component is stress- as well as burr-free. The hole wander ranges from 0.001 to 0.003 mm/mm. The axes of the holes drilled by this process need not be vertical to the workpiece surface and can have inclination as high as 20°.

References cited in this section

7. N.M. Anthony, Shaped Tube Electrolytic Machining, *Machining,* Vol 16, 9th ed., *Metals Handbook,* 1989, p 554–556

8. S. Sharma, V.K. Jain, and R. Shekar, Electrochemical Drilling of Inconel Superalloy with Acidified NaCl Electrolyte, *Advanced Manufacturing Technology,* 2002, p 492–500

9. Shape Tube Electrolytic Machining— STEM, *Machining Data Handbook,* Vol 2, 3rd ed., Machinability Data Center, Metcut Research Assoc. Inc., Cincinnati, OH, 1980, p 17–71 to 17–75

V.K. Jain, Electrochemical Allied Processes, *Corrosion: Fundamentals, Testing, and Protection*, Vol 13A, *ASM Handbook*, ASM International, 2003, p 153–156

Electrochemical Allied Processes

V.K. Jain, Indian Institute of Technology Kanpur

Pulse Electrochemical Machining

During ECM, anodic dissolution takes place continuously throughout the process. As a result, a large amount of heat and gas bubbles are generated that should be dissipated from the interelectrode gap as fast as possible. For this purpose, a high-pressure pumping system is required so that the electrolyte flows at very high velocity in IEG. In turn, a heavy machine-tool structure is essential to maintain the rigidity against high hydraulic forces.

To moderate the aforementioned requirements associated with high-velocity electrolyte flow, researchers (Ref 10), have suggested the use of pulsed direct current in ECM, shown in Fig. 3(a). The period of the pulse (t_p) consists of an on- time (t_{on}) with high instantaneous current density and an off-time (t_{off}) when the system dissipates heat and pumps out the by-products produced during on-time. During pulse ECM, the IEG is usually less than or equal to 0.1 mm (0.004 in.), which yields better accuracy of the machined component than if the IEG were larger. In pulse ECM, the IEG distribution in the direction of electrolyte flow is more uniform. Further, the gradients of temperature, gas concentration, and conductivity along the electrolyte flow direction

are smaller than those in continuous ECM. This is true particularly when shorter on-time pulses are used, which also give better accuracy and higher metal-removal rate (MRR).

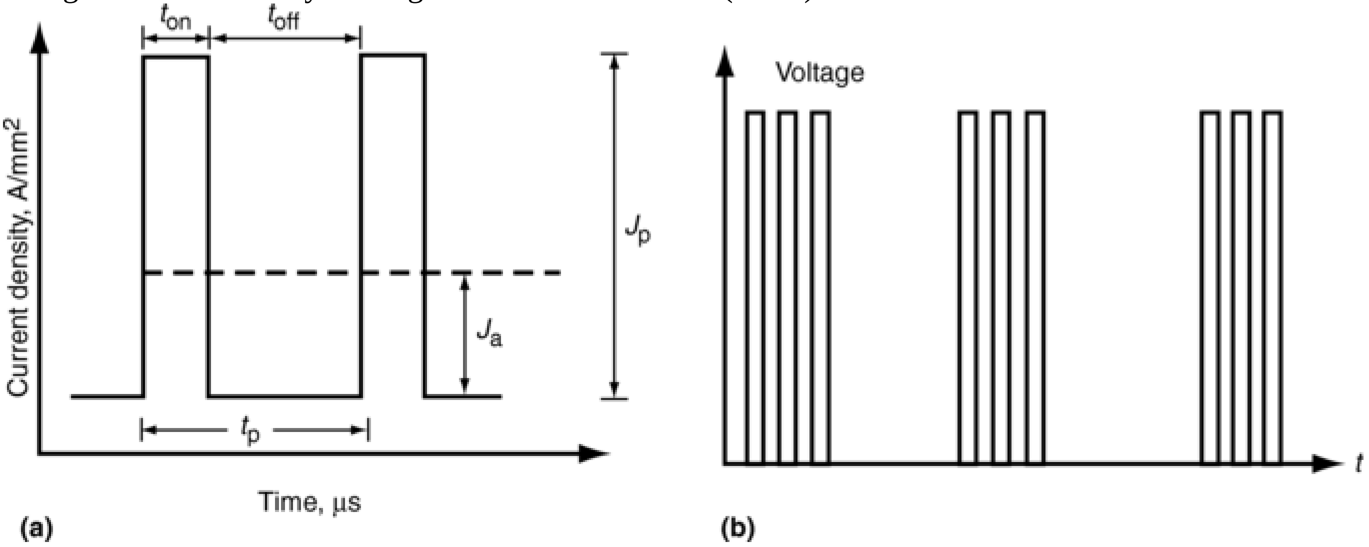

Fig. 3 Power input for pulse ECM system. (a) Current pulses. (b) Group of voltage pulses

The voltage pulses may be either in the form of single pulse (Fig. 3a) or groups of pulses (Fig. 3b) depending on the pulse-generator design. The effects of electrolytic flushing may be increased by retracting the tool from the workpiece during the pulse off-time, thus enlarging IEG while the system is at rest (Ref 11).

The peak current density (J_p) (Fig. 3a) and the duty cycle (t_{on}/t_p) can be independently controlled for regulating process performance. The average current density (J_a) is:

$$J_a = J_p(t_{on}/t_p) \quad \text{(Eq 1)}$$

where $t_p = t_{on} + t_{off}$.

Electrolyte heating takes place during on-time and results in the instantaneous temperature change (ΔT_p) and average temperature change (ΔT_a). If only ohmic heating is considered, ΔT_p can be calculated as:

$$\Delta T_p = J_p^2 t_p \big/ \left(k\rho_e C_p\right) \quad \left(\text{for } t_p \ll L/u\right) \quad \text{(Eq 2)}$$

where k, ρ_e, and C_p are specific conductivity, density, and specific heat of electrolyte, respectively. L is electrode length, and u is electrolyte flow velocity. To remove all of the heated electrolyte from IEG between the consecutive pulses, t_{off} should be greater than L/u. Then:

$$\Delta T_a = J_a^2 L \big/ \left(k\rho_e C_p u\right) = J_p^2 \left(t_{on}/t_p\right)^2 L \big/ \left(k\rho_e C_p u\right) \quad \text{(Eq 3)}$$

The pulse generator used has voltage as high as 100 V, current pulse of 100 A, frequency 0.5 to 5 kHz, and low duty cycle.

It has been reported (Ref 10) that during pulse ECM, metals can be dissolved at very high instantaneous current density (300 A/cm^2) with good surface finish and high metal dissolution efficiency (~100%) with comparatively low electrolyte flow velocity. The average current density is very low (3 A/cm^2), too small for industrial shaping operations but good enough for finishing operations. At low electrolyte flow velocity, electrolyte heating may lead to sparking due to the presence of large gas bubbles.

Theoretically, it has been found that the IEG variation during pulse ECM is more uniform than that in continuous ECM. For better performance of the ECM, small gap size should be accompanied by shorter pulse on-time.

The pulse ECM system has applications in automobile, aerospace, and die-making industries.

References cited in this section

10. M. Datta and D. Landolt, Electrochemical Machining under Pulsed Current Conditions, *Electrochem. Acta*, Vol 26 (No. 7), 1981, p 899–907

11. J. Kozak, K.P. Rajurkar, and B. Wei, Modeling and Analysis of Pulse Electrochemical Machining (PECM), *J. Eng. Ind. (Trans. ASME),* Vol 116, 1994, p 316–323

V.K. Jain, Electrochemical Allied Processes, *Corrosion: Fundamentals, Testing, and Protection*, Vol 13A, *ASM Handbook*, ASM International, 2003, p 153–156

Electrochemical Allied Processes

V.K. Jain, Indian Institute of Technology Kanpur

Acknowledgment

Author acknowledges the suggestions of Mr. Syadwad Jain of Ohio State University, (Columbus) and the help of Ms. Lalitha of I.I.T. Kanpur (India) in the preparation of this manuscript.

V.K. Jain, Electrochemical Allied Processes, *Corrosion: Fundamentals, Testing, and Protection*, Vol 13A, *ASM Handbook*, ASM International, 2003, p 153–156

Electrochemical Allied Processes

V.K. Jain, Indian Institute of Technology Kanpur

References

1. K. Takazawa, The Challenge of Burr Technology and Its Worldwide Trends, *Bull. JSPE,* Vol 22 (No. 3), 1988, p 165–170
2. M.G.J. Naidu, Electrochemical Deburring for Quality Production, *Proc. Winter School on AMT,* V.K. Jain and S.K. Choudhury, Ed., IIT Kanpur (India), 1991
3. V.K. Jain, *Advanced Machining Processes,* Allied Publishers, New Delhi, 2002
4. V.K. Jain and P.C. Pandey, Investigations into the Use of Bits as a Cathode in ECM, *Int. J. Mach. Tools Des. Res.,* Vol 22 (No. 4), 1982, p 341–352
5. G.F. Benedict, *Non-traditional Manufacturing Processes,* Marcel Dekker, 1987
6. E. Rumyantsev and A. Davydev, *Electrochemical Machining of Metals,* Mir Publishers, Moscow, 1989
7. N.M. Anthony, Shaped Tube Electrolytic Machining, *Machining,* Vol 16, 9th ed., *Metals Handbook,* 1989, p 554–556
8. S. Sharma, V.K. Jain, and R. Shekar, Electrochemical Drilling of Inconel Superalloy with Acidified NaCl Electrolyte, *Advanced Manufacturing Technology,* 2002, p 492–500
9. Shape Tube Electrolytic Machining— STEM, *Machining Data Handbook,* Vol 2, 3rd ed., Machinability Data Center, Metcut Research Assoc. Inc., Cincinnati, OH, 1980, p 17–71 to 17–75

10. M. Datta and D. Landolt, Electrochemical Machining under Pulsed Current Conditions, *Electrochem. Acta,* Vol 26 (No. 7), 1981, p 899–907

11. J. Kozak, K.P. Rajurkar, and B. Wei, Modeling and Analysis of Pulse Electrochemical Machining (PECM), *J. Eng. Ind. (Trans. ASME),* Vol 116, 1994, p 316–323

V.K. Jain, Electrochemical Hybrid Processes, *Corrosion: Fundamentals, Testing, and Protection*, Vol 13A, *ASM Handbook*, ASM International, 2003, p 157–159

Electrochemical Hybrid Processes

V.K. Jain, Indian Institute of Technology at Kanpur (India)

Introduction

HYBRID PROCESSES are those in which two or more machining processes are combined to take advantage of the worthiness of each. For example, conventional grinding produces components with good surface finish and dimensional tolerances, but such components may have burrs, comparatively large heat-affected zones, and thermal residual stresses. Such weaknesses are not found in electrochemically machined (ECM) components. Hence, a hybrid process, electrochemical grinding (ECG), was developed, in which about 10% of the total material is removed by mechanical abrasive action while the remaining 90% is removed by anodic dissolution. In the same way, other processes like electrochemical spark machining (ECSM) (for electrically nonconducting materials), electrochemical arc machining (ECAM), and electrochemical spark grinding (ECSG), have been developed to achieve the end products with the desired dimensional and surface characteristics. Here, only ECG is discussed.

V.K. Jain, Electrochemical Hybrid Processes, *Corrosion: Fundamentals, Testing, and Protection*, Vol 13A, *ASM Handbook*, ASM International, 2003, p 157–159

Electrochemical Hybrid Processes

V.K. Jain, Indian Institute of Technology at Kanpur (India)

Electrochemical Grinding

As in other anodic dissolution processes, the workpiece is electrically conductive. The workpiece is usually made of a difficult-to-machine alloy, heat treated hard (≥60 HRC) material, or thermosensitive material. Electrochemical grinding gives stress- and burr-free components with smooth surface finish. The working principle of ECG is illustrated in Fig. 1 in which the grinding wheel (cathode) is similar to a conventional grinding wheel, except that the bonding (or matrix) material is electrically conductive (metal). Electrolyte is supplied through an interelectrode gap (IEG) between the wheel and the workpiece. Electrolyte is recirculated, so an effective supply and filtration system is needed. The commonly used electrolytes are sodium chloride (NaCl) and sodium nitrate ($NaNO_3$).

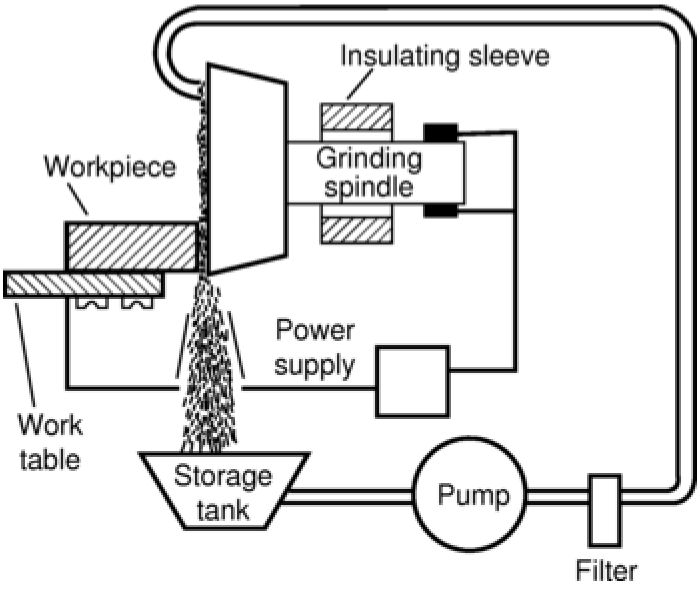

Fig. 1 Schematic of electrochemical grinding components

Abrasive particles protruding from the bonding material in the wheel help maintain a constant IEG as the particles act as spacers. The service life of the ECG wheel is about ten times that of the conventional grinding wheel because only 10% of the total removal is by abrasive action, and length of the contact arc is small.

Surface speed of the wheel ranges from 1200 to 1800 m/min (3900 to 5900 ft/min). The depth of cut is usually less than 2.5 mm (0.1 in.) and is limited by the wheel contact arc length, which should never exceed 19 mm (0.75 in.); otherwise, the electrolyte becomes ineffective because of higher concentration of H_2 gas bubbles and sludge (Ref 1).

In ECG, the area in which machining takes place can be divided into three zones (Fig. 2). In zone I, material removal is due to electrochemical dissolution that occurs at the leading edge of the ECG wheel. Rotation of the ECG wheel helps draw electrolyte into the IEG. As a result of electrochemical reaction in zone I, reaction products (including gases) contaminate electrolyte and change its conductivity. The presence of sludge, to some extent, increases conductivity of electrolyte (Ref 2), while the presence of gases decreases it. The net result is usually a decrease in the conductivity of the electrolyte in the direction of flow, resulting in a smaller IEG. As a result, abrasive particles touch the workpiece surface and start removing material by abrasive action. Thus, part of the material removed is in the form of chips. Further, electrolyte is trapped between the abrasive particles and the workpiece surface, and it forms a tiny electrolytic cell as shown in Fig. 2. In each electrolytic cell, a small amount of material from the workpiece is electrochemically dissolved.

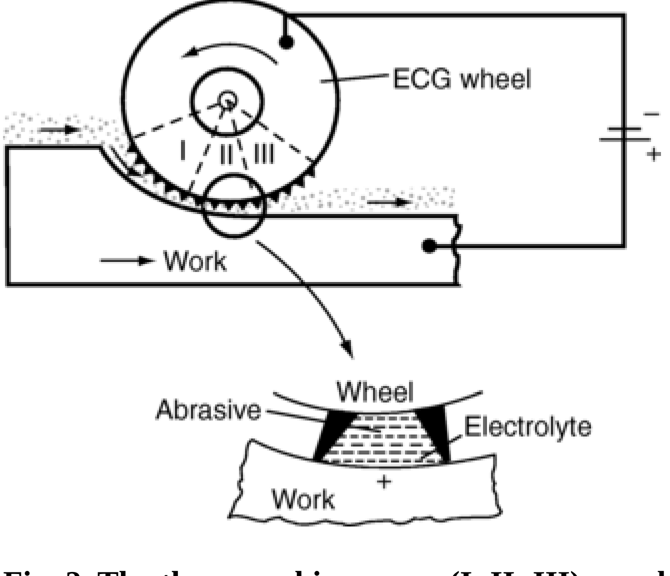

Fig. 2 The three working zones (I, II, III) are shown. Mechanism at work in each is detailed in the text. Tiny electrochemical cell formation in ECG is shown in the insert.

The electrolyte is forced into the IEG in zone II by rotational motion of the ECG wheel. Local electrolyte pressure increases, which suppresses formation of gas bubbles in the gap, yielding a higher metal-removal rate. Chemical or electrochemical reaction may result in the formation of a passive layer on the workpiece surface. In zone II, abrasive grains remove metal and the nonreactive oxide layer. Most of the metal oxides formed are insoluble in water and electrically nonconductive. Removal of the nonreactive oxide layer by protruding abrasive particles helps in electrolytic dissolution, exposing fresh metal for further electrolytic action. Hence, this process is also called mechanical assisted electrochemical grinding (Ref 3).

In zone III, material removal is totally by electrochemical dissolution. Zone III starts at the point where the ECG wheel lifts off the work surface. Pressure is released slowly. In this zone, scratches or burrs that might have formed on the workpiece in zone II are removed.

Five different kinds of ECG operations can be performed: (a) electrochemical (EC) cylindrical grinding, (b) EC form grinding, (c) EC surface grinding, (d) EC face grinding, and (e) EC internal grinding. Electrochemical cylindrical grinding is the slowest process because of the limited contact area between the wheel and the workpiece. Electrochemical face grinding is the fastest process, as it has the largest contact area between the anode and the cathode. In EC surface grinding, the workpiece reciprocates, which controls uneven wear on the wheel. Electrochemical internal grinding and EC form-grinding operations are similar to the conventional internal and form-grinding operations.

References cited in this section

1. G.F. Benedict, *Non-traditional Manufacturing Processes,* Marcel Dekker Inc., 1987, London

2. V.K. Jain, S. Tandon, and P. Kumar, Experimental Investigation into Electrochemical Spark Machining of Composites, *Trans. ASME, J. Eng. Industry,* Vol 12, 1990, p 194–197

3. A. Bhattacharyya, *New Technol.,* The Institution of Engineers (I), Calcutta, 1973

V.K. Jain, Electrochemical Hybrid Processes, *Corrosion: Fundamentals, Testing, and Protection*, Vol 13A, *ASM Handbook*, ASM International, 2003, p 157–159

Electrochemical Hybrid Processes

V.K. Jain, Indian Institute of Technology at Kanpur (India)

The ECG Machine Tool

The ECG system is very similar to a conventional grinder. Machine tools for ECG may be either vertical- or horizontal-spindle types. Such machines can be used for internal as well as external EC grinding. Table feeds should be designed so that there is no slip-stick effect on the table or sliding when the motion is slow. The basic elements of the ECG machine tool are power supply, EC grinding wheel, feed system, cleaning system, and workpiece.

Power supply for ECG is usually 0 to 25 V (but the system usually operates below maximum levels 15 V to avoid sparkover). Current levels are up to 1000 A (with upper limit of 3000 A). It is advantageous to minimize current ripples.

The probability of short circuiting during ECG is very low because of the presence of the protruding abrasives, which create a positive IEG. There is less need to have short circuit cut- off devices in this system.

Wheels for ECG are made of abrasive particles, such as Al_2O_3 or diamond, a bonding agent (usually resin), and a conductive medium like copper. The particle size of the abrasive varies over a wide range (60 to 320 mesh number). The diamond wheel, with either metal bond or resin bond, is used for grinding heat treated steels with

hardness ≥60 HRC, carbides, and stellite. It is sometimes recommended that the diamond grit (Ref 4) should be blocky, to burnish the oxide residue from the workpiece, rather than sharp, to abrade.

Formed wheels are also used in ECG. Such wheels can be dressed by a single point diamond dresser or by reversing the wheel polarity. Since physical abrasion of the workpiece material is less, the ECG wheel retains its form for a much longer period than a conventional formed grinding wheel (4 to 8 hr before dressing). During dressing, not more than 0.025 mm (0.001 in.) per pass of material is removed with a cross feed of 300 to 380 mm/min (12 to 15 in./min. The wheel spindle must be electrically insulated from the rest of the machine (Ref 5).

The protruding abrasive grains on the wheel serve three important functions: (a) for abrasive action; (b) for tiny cell formation; and (c) as a spacer between electrodes. The electrolyte nozzle must ride against the wheel and be angled to break the air layer and allow the electrolyte to be absorbed into the cavities that exist around the grit.

In ECG, the rotating grinding wheel is only partially immersed in the electrolyte. It is important in ECG that the electrolyte reaches the interface of wheel and workpiece. The rotation of the wheel helps carry sufficient electrolyte into the area of contact between the workpiece and the wheel. The point at which electrolyte is applied to the wheel should be as close as practicable to the machining area. The grinding wheel speed should be such that there is neither a scarcity of fresh electrolyte nor throw from the wheel by excessive centrifugal force. The electrolyte supply should begin prior to starting the wheel rotating.

Declogging of the grinding wheel can be done by reversing its polarity (making the tool an anode) for a short period. It may, however, result in a longer machining time and degeneration of the wheel shape. During ECG, wheel-workpiece force is usually low (140 to 1400 kPa, or 0.02 to 0.20 ksi) and it depends on contact area.

Electrolytes used in ECG should be capable of forming oxide films on the workpiece to protect the surrounding metal from corrosion. This oxide film formed on the surface being machined is constantly removed by the abrasive particles to expose the nascent work surface for EC dissolution. There is no electrolyte that can be used for all workpiece materials. For ECG of tungsten, alkaline electolytes such as Na_2CO_3 or NaOH are used. Electrolytes for ECG usually have additives to provide corrosion inhibition.

References cited in this section

4. R.E. Phillips, Electrochemical Grinding, *Machining,* Vol 16, *ASM Handbook*, 10th ed., 1989, p 542–547
5. A. Buttner and D.A. Lindenback, Electrolytic Dressing of Diamond Wheels for use in Steel Grinding, *Ind. Diamond Rev.,* 1969, p 450–454

V.K. Jain, Electrochemical Hybrid Processes, *Corrosion: Fundamentals, Testing, and Protection*, Vol 13A, *ASM Handbook*, ASM International, 2003, p 157–159

Electrochemical Hybrid Processes

V.K. Jain, Indian Institute of Technology at Kanpur (India)

Process Characteristics

Performance of ECG processes depends on various parameters such as wheel speed, workpiece feed, electrolyte type, electrolyte concentration, current density, and wheel pressure. By adjusting these parameters, the metal-removal rate (MRR) and surface finish can be varied (Ref 6).

Current Density. With higher current density, both MRR and surface finish improve. If the applied voltage is too high, it may deteriorate surface finish of the workpiece and damage the grinding wheel. The presence of such high voltage results in spark formation at the front of the wheel.

Feed Rate. If the feed rate is too high, the abrasive particles will prematurely detach from the wheel, leading to excessive wheel wear. If it is too low, a large overcut, poor tolerance, and poor surface finish will be produced. The feed rate should maintain the IEG at approximately 0.25 mm (10 mils) when a freshly dressed wheel is used. Optimal feed rate depends on current density, wheel speed, and wheel parameters. Typical parameters are feed-rate 1.9 mm/min, MRR = 1600 mm^3/min, current, I = 1000 A and current density, J = 1.2 A/mm^2.

Magnetism. The effect of magnetic fields on electrolytic grinding using diamond, SiC, and Al_2O_3 wheels has been studied (Ref 7). In the case of a diamond wheel, process performance was improved, but the same is untrue for the Al_2O_3 wheel. In the case of a SiC wheel, the improvement obtained is marginal. The magnetic field interacts with the moving charged particles and may affect the rates of both mass transport and charge transfer processes (Ref 8). The magneto-hydrodynamic force leads to stirring of electrolyte, particularly in the neighborhood of electrodes; enhanced mobility; and an increased rate of electrochemical reactions.

Temperature. ECG is a cold process (with bulk temperature <100 °C, or 212 °F), thus preventing structural damage and grinding cracks. However, electrochemically ground specimens show relatively poor fatigue strength, possibly due to stray current attack on the surface, which leaves a series of pits that would act as sites for fatigue crack initiation (Ref 9).

References cited in this section

6. G. Kuppuswamy, Electrochemical Grinding: An Investigation of the Metal Removal Rate, *Proc. 7th AIMTDR Conf.*, (Coimbatore, India), 1976, p 337–340

7. G. Kuppuswamy and V.C. Venkatesh, Wheel Parameters and Effect of Magnetic Field on Electrolytic Grinding, *J. Inst. Eng. (I) Part ME(I)*, Vol 60, 1979, p 17–20

8. J. Dash and W.W. King, Electrothinning and Electrodeposition of Metals in Magnetic Fields, *J. Electrochem. Soc.*, Vol 119, 1972, p 51–56

9. A.E. DeBarr and D.A. Oliver, *Electrochemical Machining*, MacDonald, London, 1968

V.K. Jain, Electrochemical Hybrid Processes, *Corrosion: Fundamentals, Testing, and Protection*, Vol 13A, *ASM Handbook*, ASM International, 2003, p 157–159

Electrochemical Hybrid Processes

V.K. Jain, Indian Institute of Technology at Kanpur (India)

Process Capabilities

Metal removal achieved during ECG may be 10 times greater than for conventional grinding on hard materials (hardness ≥65 HRC). Abrasive particles maintain the electrical insulation between cathode and anode, and determine an effective gap that may be as low as 0.025 mm (1 mil). Metal removal in ECG depends on current density, abrasive type, size, electrolyte concentration, wheel speed, and metallurgical properties of the workpiece. In spite of more initial investment, the cost of EC grinding is lower than that of conventional grinding due to much higher MRR during ECG. Gedam and Noble (Ref 10) concluded that fine grits and low-concentration wheels show a tendency to draw more current and thereby achieve greater MRR than coarse grits and high concentration wheels.

For materials easily machined by conventional methods, ECG gives lower MMRs than the conventional method provides.

Surface finish obtained by ECG ranges from 0.12 to 0.80 μm. The surface produced by ECG is free of grinding scratches and burrs. Surface finish on nonhomogeneous materials during ECG is better than that produced

during conventional grinding. The surface finish generated in ECG also depends on the crystalline structure of the workpiece. The finer the crystalline structure, the finer is the surface finish. This process generates a surface that has the topography of a crystalline structure instead of the tool marks. Generally, the finished surface has gray to black matte finish, while in some cases it is bright.

To improve surface finish, a finish pass at low voltage and high feed rate should be made. The surface metal is burnished, with the crests of the hills being pushed into the valleys of the crystalline structure, thereby generating a smoother finish also known as sparkout pass. In this pass, selection of a proper ECG wheel with appropriate grit size and type is important because it determines the end-finish quality. Wheels of 200 to 320 grit size have been successful in finishing surgical instruments and industrial knives. Risk of thermal damage is also reduced.

Accuracy of the electrochemically ground surfaces depends on the current density, electrolyte flow rate, and metallurgical aspects of the workpiece material itself. Highly reactive metals such as alloys with high chromium content require mild electrolyte to produce low overcuts. The state of electrolyte conductivity should be monitored for good results. Achievable tolerance in ECG varies from ±0.010 to 0.025 mm (±0.4 to 1 mil) under well-controlled conditions. Achievable inside and outside corner radii during ECG have been in the range of 0.25 to 0.40 mm (10 to 16 mils) and 0.1 to 0.2 mm (4 to 8 mils), respectively. Finer grit wheels produce sharper corners but require more frequent wheel dressing because of more rapid wheel wear and form breakdown.

Workpieces have shown no evidence of hydrogen embrittlement due to H_2 evolved at the cathode. ECG produces workpieces without work hardening and grind burns.

Reference cited in this section

10. A. Gedam and C.F. Noble, An Assessment of the Influence of Some Wheel Variables in Peripheral Electrochemical Grinding, *Int. J. Mach. Tool Des. Res.*, Vol 11, 1971, p 1–12

V.K. Jain, Electrochemical Hybrid Processes, *Corrosion: Fundamentals, Testing, and Protection*, Vol 13A, *ASM Handbook*, ASM International, 2003, p 157–159

Electrochemical Hybrid Processes

V.K. Jain, Indian Institute of Technology at Kanpur (India)

Applications

Electrochemical grinding is economical for grinding carbide cutting-tool inserts. Microscopic study of electrochemically ground surfaces of the cemented carbide does not reveal microcracks or any other defects or damage to the microstructure. This process is also used to reprofile worn locomotive traction motor gears. Usually, wear marks from the gear tooth surfaces are removed by removing as much as 0.38 mm (15 mils) thickness of material. Electrochemical grinding does not affect gear hardness and does not impose residual stresses. The process is also used for burr-free sharpening of hypodermic needles, grinding of superalloy turbine blades, and form grinding of fragile aerospace honeycomb metals.

Electrochemical grinding of WC-Co has been reported (Ref 11). The initial specific etching rate of cobalt phase is higher than that of the WC phase. In addition to the direct dissolution of material, the electrolysis process in ECG weakens the cermet material by selective removal of cobalt. When the in-feed rate during ECG is less than the initial specific etching rate of the cobalt phase, selective etching of cobalt occurs that reduces mechanical power requirements for machining. At higher in-feed rates, the reduction in mechanical power requirement is marginal. Study of surface roughness produced during ECG clearly indicates that there is selective electrochemical etching of the metal phase (cobalt). It weakens the composite material and thereby reduces the forces required for mechanical grinding.

Reference cited in this section

11. R. Levinger and S. Malkin, Electrochemical Grinding of WC-Co Cemented Carbides, ASME Paper 78-WA/PROD-26, Winter Annual Meeting, San Francisco, 1979, p 1–10

V.K. Jain, Electrochemical Hybrid Processes, *Corrosion: Fundamentals, Testing, and Protection*, Vol 13A, *ASM Handbook*, ASM International, 2003, p 157–159

Electrochemical Hybrid Processes

V.K. Jain, Indian Institute of Technology at Kanpur (India)

Acknowledgment

Author acknowledges the suggestions of Mr. Syadwad Jain of Ohio State University, Columbus (USA) and the help of Ms. Lalitha of I.I.T. Kanpur (India) in the preparation of this manuscript.

V.K. Jain, Electrochemical Hybrid Processes, *Corrosion: Fundamentals, Testing, and Protection*, Vol 13A, *ASM Handbook*, ASM International, 2003, p 157–159

Electrochemical Hybrid Processes

V.K. Jain, Indian Institute of Technology at Kanpur (India)

References

1. G.F. Benedict, *Non-traditional Manufacturing Processes,* Marcel Dekker Inc., 1987, London
2. V.K. Jain, S. Tandon, and P. Kumar, Experimental Investigation into Electrochemical Spark Machining of Composites, *Trans. ASME, J. Eng. Industry,* Vol 12, 1990, p 194–197
3. A. Bhattacharyya, *New Technol.,* The Institution of Engineers (I), Calcutta, 1973
4. R.E. Phillips, Electrochemical Grinding, *Machining,* Vol 16, *ASM Handbook,* 10th ed., 1989, p 542–547
5. A. Buttner and D.A. Lindenback, Electrolytic Dressing of Diamond Wheels for use in Steel Grinding, *Ind. Diamond Rev.,* 1969, p 450–454
6. G. Kuppuswamy, Electrochemical Grinding: An Investigation of the Metal Removal Rate, *Proc. 7th AIMTDR Conf.,* (Coimbatore, India), 1976, p 337–340
7. G. Kuppuswamy and V.C. Venkatesh, Wheel Parameters and Effect of Magnetic Field on Electrolytic Grinding, *J. Inst. Eng. (I) Part ME(I),* Vol 60, 1979, p 17–20
8. J. Dash and W.W. King, Electrothinning and Electrodeposition of Metals in Magnetic Fields, *J. Electrochem. Soc.,* Vol 119, 1972, p 51–56

9. A.E. DeBarr and D.A. Oliver, *Electrochemical Machining,* MacDonald, London, 1968

10. A. Gedam and C.F. Noble, An Assessment of the Influence of Some Wheel Variables in Peripheral Electrochemical Grinding, *Int. J. Mach. Tool Des. Res.,* Vol 11, 1971, p 1–12

11. R. Levinger and S. Malkin, Electrochemical Grinding of WC-Co Cemented Carbides, ASME Paper 78-WA/PROD-26, Winter Annual Meeting, San Francisco, 1979, p 1–10

D. Dreisinger and Z. Zheng, Electrochemical Refining, *Corrosion: Fundamentals, Testing, and Protection*, Vol 13A, *ASM Handbook*, ASM International, 2003, p 160–163

Electrochemical Refining

D. Dreisinger and Zhimin Zheng, University of British Columbia

---

Introduction

ELECTROCHEMICAL REFINING is the purification process for producing commercially pure metals from crude metals. The process is carried out in an electrochemical cell with an external power supply where the anodic dissolution and cathodic deposition processes occur simultaneously. The objective of the electrochemical refining is to purify the crude metals, from thermally processed ores or scrap, and produce high- purity metals. This production is most efficient by maintaining precisely spaced, flat vertical anodes and cathodes. The cathodes are supplied with a warm, low-impurity electrolyte with a high concentration of metal ions. Careful process control of the supply of leveling and grain-refining agents, current density, and temperature is essential.

D. Dreisinger and Z. Zheng, Electrochemical Refining, *Corrosion: Fundamentals, Testing, and Protection*, Vol 13A, *ASM Handbook*, ASM International, 2003, p 160–163

Electrochemical Refining

D. Dreisinger and Zhimin Zheng, University of British Columbia

---

Electrochemical Cell

Both electrodes are immersed in suitable electrolytic solutions. The anode participates actively in the electrochemical refining reaction. The crude metal oxidizes at the metal-electrolyte interface, releases electrons, and dissolves as a metal ion into the aqueous solution. To maintain charge balance, the released electrons are transported to the cathode via an external circuit. At the cathode, the dissolved metal is deposited as a refined metals species. To refine effectively the impure metal, the impurities contained in the crude metal must be rejected from the final refined metal cathode. The principle of the process is that the impurities are either not dissolved and form “slimes” on the anode surface, or, if the impurities do dissolve, they are not redeposited on the cathode. Typical impurity distribution in the refining cell is summarized in Table 1.

Table 1 Distribution of impurities in some refining processes

Refining process	Impurities														
	PM	**Au**	**Ag**	**Se**	**Te**	**S**	**Cu**	**Sb**	**As**	**Bi**	**Ni**	**Co**	**Fe**	**Pb**	**Zn**
Au	E	…	S	…	…	…	E	…	…	…	…	…	…	S	…
Ag	Se	S	…	…	S	…	E	…	…	S	…	…	…	sE	…
Cu	S	S	S	S	S	S	…	S	sE	SE	sE	…	E	S	E
Ni	S	S	S	…	…	S	sE	…	E	…	…	E	E	Se	…
Pb	S	S	S	…	S	…	S	Se	S	S	E	E	E	…	E

PM, platinum group metals; S, the impurity is in the anode slime; E, the impurity is in the electrolyte; sE, impurity is mostly in the electrolyte; and Se, the impurity is mostly in the slime. Source: Ref 4

Reference cited in this section

4. Roskill Reports on Metals and Minerals, www.roskill.co.uk

D. Dreisinger and Z. Zheng, Electrochemical Refining, *Corrosion: Fundamentals, Testing, and Protection*, Vol 13A, *ASM Handbook*, ASM International, 2003, p 160–163

Electrochemical Refining

D. Dreisinger and Zhimin Zheng, University of British Columbia

Metals Purified

The electrochemical refining process is applied for the metal purifications of copper, nickel, silver, gold, tin, and lead (Ref 2). In the year 2000, approximately 1.04×10^7 tonnes (2.30×10^{10} lb) of copper were produced from electrochemical refining (Ref 3); about 1.23×10^6 tonnes (2.87×10^9 lb) of nickel were produced (Ref 2); and electrolytic tin production was 2.55×10^5 tonnes (5.62×10^8 lb) (Ref 4). Tonnes are metric tons equal to 10^3 kg. The purities of the refined electrolytic metals typically range from 99.99 to 99.999%.

From Table 1, it can be seen that in the gold, silver, copper, and lead refining processes, the impurities more noble than the refined metals remain undissolved in the anode slimes. Consequently, these impurities cannot plate and contaminate the cathodes. In nickel refining, on the other hand, some noble impurities partially dissolve in the electrolyte and will plate on the cathode if it is immersed in the same electrolyte. This is the main reason why nickel refining cells have porous diaphragms separating the catholyte (solution surrounding the cathode) from the anolyte (solution surrounding the anode). Anolyte solution is withdrawn from the refining cell and purified for noble metal impurities before being reintroduced into the catholyte compartment of the cell.

References cited in this section

2. C.H. Hamann, A. Hamnett, and W. Vielstich, Ed., *Electrochemistry*, Wiley-VCH, New York, 1998, p 315–317
3. J.W. Weidner and M. Doyle, *J. Electrochem. Soc.*, Vol 148 (No. 11), 2000, p K1–K41
4. Roskill Reports on Metals and Minerals, www.roskill.co.uk

D. Dreisinger and Z. Zheng, Electrochemical Refining, *Corrosion: Fundamentals, Testing, and Protection*, Vol 13A, *ASM Handbook*, ASM International, 2003, p 160–163

Electrochemical Refining

D. Dreisinger and Zhimin Zheng, University of British Columbia

---

Principles of the Electrochemical Reactions

Electrochemical reactions are heterogeneous chemical reactions that occur via the transfer of charge across the interface between an electrode and an electrolyte. The features of electrode reactions in the refining process can be expressed as follows:

Anodic reaction: $M^{0}_{(s),\text{impure}} \rightarrow M^{n+}_{(aq)} + ne^{-}$ (Eq 1)

Cathodic reaction: $M^{n+}_{(aq)} + ne^{-} \rightarrow M^{0}_{(s),\text{pure}}$ (Eq 2)

Overall reaction (cell reaction):

$M^{0}_{(s),\text{impure}} \rightarrow M^{0}_{(s),\text{pure}}$ (Eq 3)

In contrast to a galvanic cell, the cell for the electrochemical refining is an electrolytic cell that requires an input of electrical energy to produce chemical transformations. Thus, the cell has a negative equilibrium cell potential and a positive value of the Gibbs free energy change. While the cell is under refining current load, the cell voltage increases and can be expressed as:

$E_I = E_0 + \eta_{tc} - \eta_{ta} - IR_{int}$ (Eq 4)

where

$\eta_{ta} = \eta_a + \eta_{conc,a}$ (Eq 5)

$\eta_{tc} = \eta_c + \eta_{conc,c}$ (Eq 6)

where E_I is the cell voltage; E_0 is the open-circuit cell voltage; I is the current; R_{int} is the internal resistance of the electrochemical cell; η_c and η_a are the cathode and anode polarization overpotentials; $\eta_{conc,c}$ and $\eta_{conc,a}$ are the cathode and anode concentration overpotentials; and η_{tc} and η_{ta} are the total overpotentials at the cathode and anode, respectively.

If impurities collect as a physical slime barrier on the surface of the dissolving anode, then the anode overpotential can be written as:

$\eta_{ta} = \eta_a + \eta_{conc,a} + \eta_{sl}$ (Eq 7)

and the internal resistance of the cell can be written:

$R_{int} = R_{al} + R_{cl} + R_{sp}$ (Eq 8)

where η_{sl} is the potential drop across the slime layer, R_{al} is the resistance of anolyte, R_{cl} is the resistance of catholyte, and R_{sp} is the resistance of the separator if required.

D. Dreisinger and Z. Zheng, Electrochemical Refining, *Corrosion: Fundamentals, Testing, and Protection*, Vol 13A, *ASM Handbook*, ASM International, 2003, p 160–163

Electrochemical Refining

D. Dreisinger and Zhimin Zheng, University of British Columbia

Physical Properties of Electrochemical Cells

The basic components required for the electrochemical refining cell are an electrochemically soluble anode, a cathode, ionic contact between the electrodes (via an electrolytic solution), and an electronic power supply connected to the anode and cathode. Monopolar cells are used in electrochemical refining. In this system, anodes and cathodes are placed alternately in the cell and are electrically connected in parallel. With this arrangement, alternate electrodes in the cell dissolve metal (anodes), and deposit refined metal (cathodes). This arrangement is shown in Fig. 1.

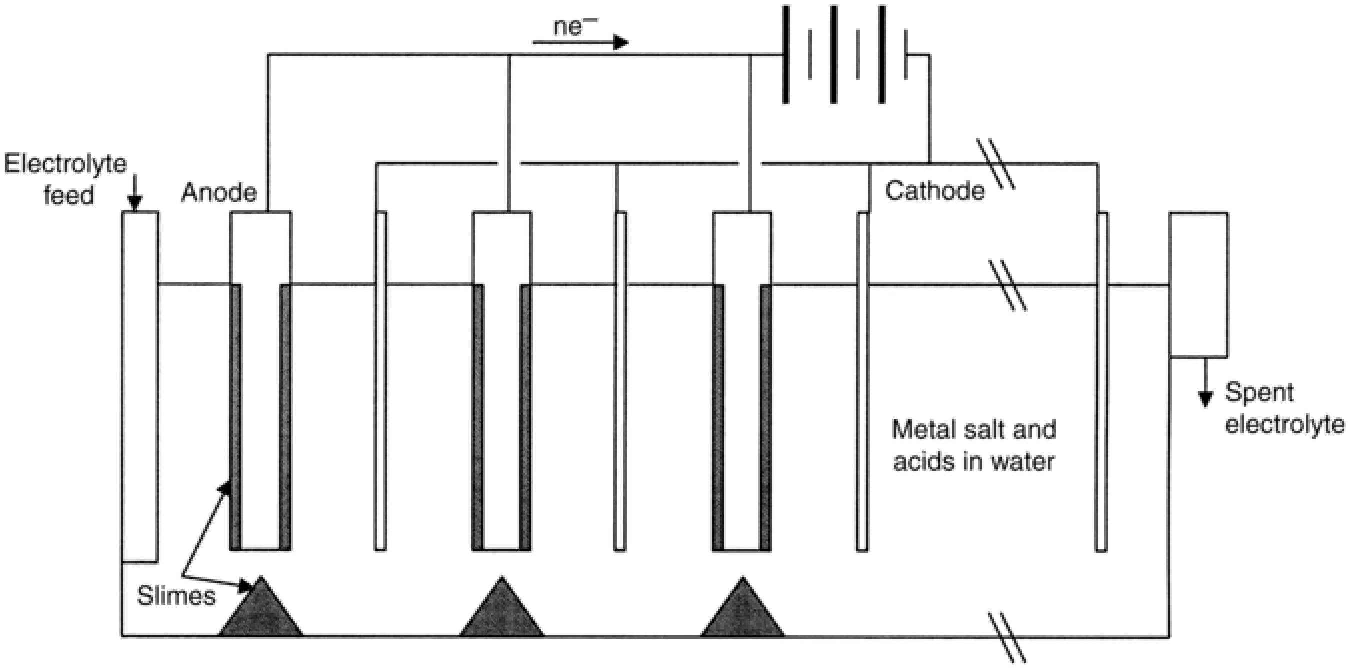

Fig. 1 Schematic of an electrochemical cell without separators for metal refining

A combination of diffusion and natural convection enhances the electrical transport of metal ions from the anode surface into the bulk electrolyte and, from there, onto the cathode surface. The concentration of metal ions near the anode is higher than in the bulk electrolyte, while near the cathode, the metal concentration is lower than in the bulk. These concentration gradients at the electrode surfaces cause the electrolyte near both electrodes to have a different specific gravity than the bulk electrolyte. The specific gravity differences induce a slow flow within the electrode diffusion layers-downward flow at the anode and upward flow at the cathode. This is shown schematically in Fig. 2. Note the presence of an anode slime layer, which adds an additional diffusion barrier to the movement of metal ions from the anode surface to the bulk electrolyte.

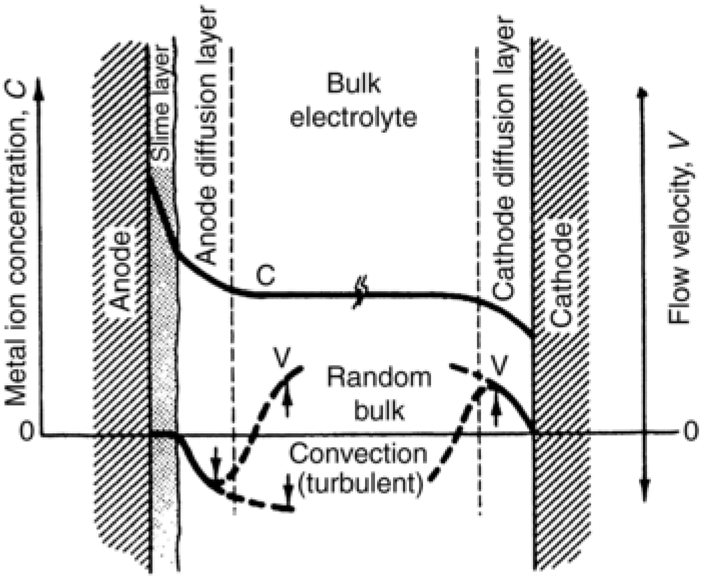

Fig. 2 Natural convection and concentration profiles in the metal refining electrolyte

The electrolytic solutions contain ions, which are atoms or groups of atoms that have lost or gained electrons and, as a result, are positively or negatively charged, respectively. Refining solutions are formed by dissolving metal salts and acid in water. These compounds may then be completely or partially dissociated into ions. Salts, such as copper sulfate ($CuSO_4$) and nickel sulfate ($NiSO_4$), and acids, such as sulfuric acid (H_2SO_4), hydrochloric acid (HCl), and hydrofluosilicic acid (H_2SiF_6), are often used in refining cells (Table 2).

Table 2 Electrolytes used in metal electrochemical refining

Electrolyte	Refining process					
	Cu	**Ni**	**Pb**	**Sn**	**Au**	**Ag**
Metal salt	$CuSO_4$	$NiSO_4$	$PbSiF_6$	$SnSO_4$	$AuCl_4$	$AgNO_3$
Acid	H_2SO_4	HCl, H_2SO_4	H_2SiF_6	H_2SO_4, $HOC_6H_4SO_3H$	HCl	HNO_3

Source: Ref 2

In electrochemical refining systems, supporting electrolytes are added to increase the solution conductivity, thereby decreasing the ohmic potential drop between electrodes. This makes the current density distribution more uniform in reactors with larger electrodes. For charged electroactive species, the mass transport limited current will be lower in the presence of a supporting electrolyte, since increasing the electrode potential does not then enhance the migrational component of the transport rate of electroactive species, as more of the current is being carried in the bulk solution by the supporting electrolyte. At the electrode, the net flux of all species is zero except for that of the reactant so that in the diffusion layer, the supporting electrolyte ions and the reactant counter ions have zero net velocity, adopting concentration distributions under the forces of migration and diffusion. Beyond the boundary layer, Ohm's law applies in a well- stirred bulk electrolyte. Generally, convection decreases the importance of the migrational flux of the supporting electrolyte and augments that of the reactant, as in the case of copper refining (Fig. 2).

The electrical circuit in the refining cell can be classified into two parts. Within the cell, current flows electronically within the structures of anode and cathode, and ionically in the electrolyte between them. In the external circuit, the current flows in the direction from cathode to anode that a positive charge would flow. The flow of electrons is shown in Fig. 1.

The separator, if present, serves as a barrier to lessen the mixing of anodic and cathodic solution species. Plastic meshes or filter cloths are used as separators. Separators also prevent interelectrode contact and may promote turbulence next to the electrodes in order to enhance mass transport of electroactive species.

Reference cited in this section

2. C.H. Hamann, A. Hamnett, and W. Vielstich, Ed., *Electrochemistry*, Wiley-VCH, New York, 1998, p 315–317

D. Dreisinger and Z. Zheng, Electrochemical Refining, *Corrosion: Fundamentals, Testing, and Protection*, Vol 13A, *ASM Handbook*, ASM International, 2003, p 160–163

Electrochemical Refining

D. Dreisinger and Zhimin Zheng, University of British Columbia

Engineering Considerations in the Refining Process

It is desirable to operate at the maximum current density in order to deposit metal in the shortest time. The maximum current density for refining is determined by the mass transfer processes at the surface of the cathode or anode. The mass transfer processes are controlled by the thickness of the Nernst boundary layer at the surface of the electrode. The boundary layer can be decreased by increasing flow velocity of the electrolyte. In industrial practice, the current density is fixed at a value at which the deposit on the cathode is satisfactory in smoothness and brightness.

To minimize the energy consumption for the electrochemical cell, it is necessary to lower the electrolyte resistance and minimize the values of the respective overpotentials at the anode and cathode. Minimizing the distance between electrodes decreases the electrolyte resistance. Raising the temperature and increasing the concentration of dissolved metal salt can decrease the absolute values of the overpotentials. Typical refining conditions are summarized in Table 3.

Table 3 Operating parameters in metal electrochemical refining

Refining processes	Operating parameters						
	Current density		**Temperature**		**Cell voltage, V**	**Current efficiency, %**	**Energy consumption, kW·h/kg**
	A/m^2	**A/in.^{2}**	**°C**	**°F**			
Cu	250–300	0.16–0.20	60–70	140–160	~0.28	~97	0.3–0.4
Ni	~200	~0.13	~60	~140	~1.9	~96	1.9
Pb	160–200	0.10–0.13	30–40	86–104	0.35–0.65	~95	~0.13
Sn	~95	~0.06	~40	~104	~0.3	~85	~0.22
Au	~1200	~0.77	~75	~167	…	…	…
Ag	~300	~0.20	~35	~95	…	…	…

Source: Ref 2, 5

The general technological processes involved in electrochemical refining include:

- Continuous supply of fresh electrolyte to an individual cell
- Continuous withdrawal of the spent stream from the electrolyte circuit system
- Periodic removal of “finished” cathodes
- Supply of new cathodes
- Periodic removal of spent anodes
- Supply of soluble anodes
- Periodic removal of anode slimes

These principles are similar in the operations of all metal refining systems. The theoretical and technological principles are illustrated in detail in the individual example of metal refining processes.

Copper Electrochemical Refining Industrial Practice. Copper refining process serves two purposes (Ref 3). First, it produces copper essentially free of deleterious impurities; second, it separates valuable impurities from the copper for subsequent recovery as by-products. This process is the basis of purification of pyrometallurgical copper, which is used as the anode. The impure copper is cast in the shape of anodes approximately 1.0 × 1.0 × 0.05 m (40 × 40 × 2 in.) weighing 300 to 400 kg (660 to 880 lb). These anodes are cast with lugs that support the anodes off the walls of the cell. The lugs are used to make external electrical connection to the cell bus bars.

The starting cathodes can be pure copper sheets made by electrodeposition on smooth starting blanks of stainless steel or titanium. Many copper refineries have now adopted stainless steel sheets or blanks in place of the copper sheets. When using stainless steel sheets, the final copper product is stripped and the stainless steel cathode blank is returned to the cell. The electrode spacing from anode center to cathode center is approximately 5 cm (2 in.). The current density is about 250 to 300 A/m^2 (0.16 to 0.20 A/in.^{2}).

The anodes are consumed and replaced at regular intervals of 10 to 28 days. Up to two successive cathodes are harvested during the same period. The electrolytic solution contains approximately 40 to 50 g/L of copper as copper sulfate and about 160 to 200 g/L of sulfuric acid. The temperature is maintained at 65 to 70 °C (150 to 160 °F) to lower the resistance of the electrolytic solutions that are circulated through the cells. The lead or plastic-lined tanks of wood or concrete hold about 20 to 50 anodes and one more cathode than anode.

When a copper anode and a copper cathode are immersed in the acidified copper sulfate solution and the current is applied, copper will dissolve at the anode and be deposited at the cathode. Only those impurities in the copper anode with normal potentials negative of the working potential of anode, such as iron, nickel, and lead, will dissolve as ions. More noble metals, such as gold and silver, remain behind in finely divided metallic form and collect under the anode as anode "slime" or anode "sludge." These slimes are processed further for the recovery of the valuable metals. However, at the working potential of the cathode, only copper will deposit; the metals less noble than copper do not deposit but accumulate in the solutions. This process requires periodic purification of the electrolytic solution.

In copper refining practice, it is found that three main factors influence the purity of copper cathodes:

- The physical arrangement of the anodes and cathodes in the cells
- Chemical conditions for refining
- Operating conditions

The physical arrangement in the cell is very important in a well-run refinery. Attention is paid to casting flat and identical weight anodes, pressing anodes and cathodes flat, machining the anode support lugs so the anodes hang vertically, and spacing the anodes and cathodes precisely in racks before loading them in the cells (Ref. 6). Bent anodes or starting sheets are not introduced into the refining system so the possibility of short circuits is minimized.

Optimizing chemical conditions for refining are maintaining constant and high concentration of copper ions over the faces of the cathodes; maintaining appropriate concentrations of leveling, and grain-refining agents over the faces of the cathodes; removing slime particles in the electrolyte; and lowering concentrations of dissolved impurities in the electrolyte. The common additive agents include:

Agent	Amount	
	kg per metric ton of cathode	**wt%**
Bone glue	0.03–0.2	0.003–0.02
Thiourea	0.03–0.15	0.003–0.015
Avitone (Du Pont)	0–0.06	0–0.006
Hydrochloride	0.035–0.08	0.0035–0.008

The removing of slime particles and the lowering of concentrations of impurities in the electrolyte can be achieved by continuously purifying an electrolyte bleed stream. About 0.1 to 0.2 m^3 of electrolyte bleed is purified per tonne of product cathode. (About 0.012 to 0.024 gal/lb. of product cathode).

Several factors impact the quality of electrolytic metals and the cost of metal production. Optimal operating conditions are obtained by maintaining high temperature, choosing appropriate cathode current density, and maximizing current efficiency. Although heating the electrolyte requires considerable energy, it increases electrolyte conductivity, decreases electrolyte density and viscosity, and increases the solubility of copper sulfate. These changes lead to decreased electrical energy consumption, minimizing the formation of floating slimes (precipitates of impurities), minimizing the contamination of cathodes, and preventing the precipitation

of copper sulfate. A high current density gives a high rate of copper deposition but also tends to cause dendritic growth and anode passivation. Furthermore, it tends to cause entrapment of electrolyte and slimes on the cathode and lowers cathode purity. Each refinery must balance these competing economic factors. Anode-to-cathode short circuits, stray current to ground, and reoxidation of cathode copper mainly cause a decrease in current efficiency (Ref 7). Short circuits can be minimized by improving physical arrangement and including additives. Stray current losses are due largely to current flow to ground via spilled electrolyte. Thus, avoiding spills can minimize the losses. Oxygen absorption in the electrolyte can result in the reoxidation of cathode copper. It is important, therefore, to keep the electrolyte flow quiescent to minimize the occurrence of reoxidation.

Nickel Electrochemical Refining Industrial Practice (Ref 8 and 9). The refining process of nickel metal anode serves two purposes. First, it produces nickel essentially free of deleterious impurities (such as iron, cobalt, lead, arsenic, and copper). Second, it separates valuable impurities (such as gold, silver, and platinum group metals) from the nickel for subsequent recovery as by-products. Nickel refining is carried out in sulfate and chloride electrolytes. This latter electrolyte system has two major advantages over the sulfate system. It has higher conductivity, which results in a lower cell voltage, and it permits the use of chlorine for electrolyte purification (Ref 9). To obtain the high purity nickel cathodes, the cathode is enclosed in a separate compartment formed by a modacrylic cloth diaphragm stretched over a wooden box frame. A hydrostatic head of electrolyte can be built up relative to the anolyte through the diaphragm. This hydrostatic head forces nickel-depleted electrolyte through the diaphragm, from the cathode compartment into the anolyte, at a rate sufficient to prevent the ingress of either anolyte itself, or impurity ions, by diffusion into the cathode compartment. Thus, the soluble impurities can be kept in the anolyte and removed through a solution purification process.

The nickel cathode starting sheets are made by deposition onto titanium or stainless steel blanks. After two days the nickel starting sheets are peeled from the inert blanks. These starting sheets are used as cathodes, and electrolytic nickel is built up for about 10 days in the refining cell. The final nickel metal that is obtained has a purity exceeding 99.9 wt%.

The purified electrolytic solutions, a mixed sulfuric acid and hydrochloride acid solution, are pumped continuously through the cathode compartment. The electrorefining process also facilitates the recovery of precious metals and other metals of value from anode slimes.

Lead Electrochemical Refining Industrial Practice. Most lead electrochemical refining is carried out in fluosilicic acid and lead fluosilicate electrolyte, which produces a lead cathode exceeding 99.99% purity. This electrolyte system has a major advantage over a sulfate system, as it has a higher solubility, which results in a lower cell voltage. In the refining process, more noble metals (gold, silver, and platinum) remain undissolved and accumulate in the anode slimes. The slime adheres on the anode and retains its initial form so that cells do not need to be cleaned and deslimed regularly. The cell voltage rises with the increasing thickness of the slime coating and may reach up to twice the initial voltage. Thus, the energy consumption imposes an economic limitation.

Metals with lower potential than lead, iron, nickel, and zinc dissolve into electrolyte. Since the lead bullion anode contains very low levels of the impurities, the enrichment of them in the electrolyte takes longer periods of time than it does in other types of metal refining. A small amount of electrolyte is lost because of fluosilicic acid decomposition (Ref 10).

References cited in this section

2. C.H. Hamann, A. Hamnett, and W. Vielstich, Ed., *Electrochemistry,* Wiley-VCH, New York, 1998, p 315–317

3. J.W. Weidner and M. Doyle, *J. Electrochem. Soc.,* Vol 148 (No. 11), 2000, p K1–K41

5. A.K. Biswas and W.G. Davenport, Ed., *Extractive Metallurgy of Copper,* Pergamon Press, 1994, p 324–354

6. J. Bosscher and W. Berends, *Electrometallurgical Plant Practice,* L.P. Clessens and G.B. Harris, Ed., Pergamon Press, New York, p 271–279

7. M. Landau and H. Traulsen, Hydrometallurgy and Electrometallurgy, *Copper/Cobre 91,* Vol III, W.C. Cooper, D.J. Kemp, G.E. Lagos, and K.G. Tan, Ed., Pergamon Press, New York, 1991, p 517–527

8. A.R. Burkin, Ed., *Extractive Metallurgy of Nickel,* Wiley Press, 1987, p 56

9. F. Habashi, Ed., *Handbook of Extractive Metallurgy,* Vol II, Wiley-VCH, 1997, p 746–750

10. F. Habashi, Ed., *Handbook of Extractive Metallurgy,* Vol II, Wiley-VCH, 1997, p 581–640

D. Dreisinger and Z. Zheng, Electrochemical Refining, *Corrosion: Fundamentals, Testing, and Protection*, Vol 13A, *ASM Handbook*, ASM International, 2003, p 160–163

Electrochemical Refining

D. Dreisinger and Zhimin Zheng, University of British Columbia

---

References

1. J.O. Bockris, B.E. Conway, E. Yeager, and R.E. White, Ed., *Comprehensive Treatise of Electrochemistry,* Plenum Press, 1980, p 327–377

2. C.H. Hamann, A. Hamnett, and W. Vielstich, Ed., *Electrochemistry,* Wiley-VCH, New York, 1998, p 315–317

3. J.W. Weidner and M. Doyle, *J. Electrochem. Soc.,* Vol 148 (No. 11), 2000, p K1–K41

4. Roskill Reports on Metals and Minerals, www.roskill.co.uk

5. A.K. Biswas and W.G. Davenport, Ed., *Extractive Metallurgy of Copper,* Pergamon Press, 1994, p 324–354

6. J. Bosscher and W. Berends, *Electrometallurgical Plant Practice,* L.P. Clessens and G.B. Harris, Ed., Pergamon Press, New York, p 271–279

7. M. Landau and H. Traulsen, Hydrometallurgy and Electrometallurgy, *Copper/Cobre 91,* Vol III, W.C. Cooper, D.J. Kemp, G.E. Lagos, and K.G. Tan, Ed., Pergamon Press, New York, 1991, p 517–527

8. A.R. Burkin, Ed., *Extractive Metallurgy of Nickel,* Wiley Press, 1987, p 56

9. F. Habashi, Ed., *Handbook of Extractive Metallurgy,* Vol II, Wiley-VCH, 1997, p 746–750

10. F. Habashi, Ed., *Handbook of Extractive Metallurgy,* Vol II, Wiley-VCH, 1997, p 581–640

A.E. Miller, P.B. Fischer, A.D. Feller, T.N. Andryushchenko, and K.C. Cadien, Chemical-Mechanical Planarization for Semiconductors, *Corrosion: Fundamentals, Testing, and Protection*, Vol 13A, *ASM Handbook*, ASM International, 2003, p 164–169

Chemical-Mechanical Planarization for Semiconductors

Anne E. Miller, Paul B. Fischer, Allen D. Feller, Tatyana N. Andryushchenko, and Kenneth C. Cadien, Intel Corporation

Introduction

CHEMICAL-MECHANICAL PLANARIZATION (CMP) of metals has been described in the literature as (a) mechanically accelerated corrosion, (b) erosion corrosion, or (c) metallic corrosion enhanced by wear, during which the reaction products on the metal surface are removed by continuous abrasion. As a form of controlled corrosion, CMP has enabled significant advancements in the ultralarge-scale integration (ULSI) processes of the semiconductor industry. The history, process, chemistry, electrochemistry, and defect issues for CMP are reviewed in this article.

A.E. Miller, P.B. Fischer, A.D. Feller, T.N. Andryushchenko, and K.C. Cadien, Chemical-Mechanical Planarization for Semiconductors, *Corrosion: Fundamentals, Testing, and Protection*, Vol 13A, *ASM Handbook*, ASM International, 2003, p 164–169

Chemical-Mechanical Planarization for Semiconductors

Anne E. Miller, Paul B. Fischer, Allen D. Feller, Tatyana N. Andryushchenko, and Kenneth C. Cadien, Intel Corporation

History

Chemical-mechanical planarization was first introduced as an integrated circuit (IC) manufacturing technology in early 1990. The first application for CMP was to planarize (or flatten) the topography in the interlayer dielectric (ILD), typically SiO_2, from underlying metal lines. Chemical-mechanical planarization prevented the topography of the lower metal layers from affecting upper metal layers and thereby had the beneficial effect of enabling the extension of optical lithography to the submicron regime by using deep ultraviolet (UV) wavelengths. It is now typical for leading edge devices to have more than seven layers of metals. Scanning electron microscopy cross-sectional micrographs are shown in Fig. 1, indicating the topography prior to the advent of CMP (a) and the planar surfaces available due to CMP (b).

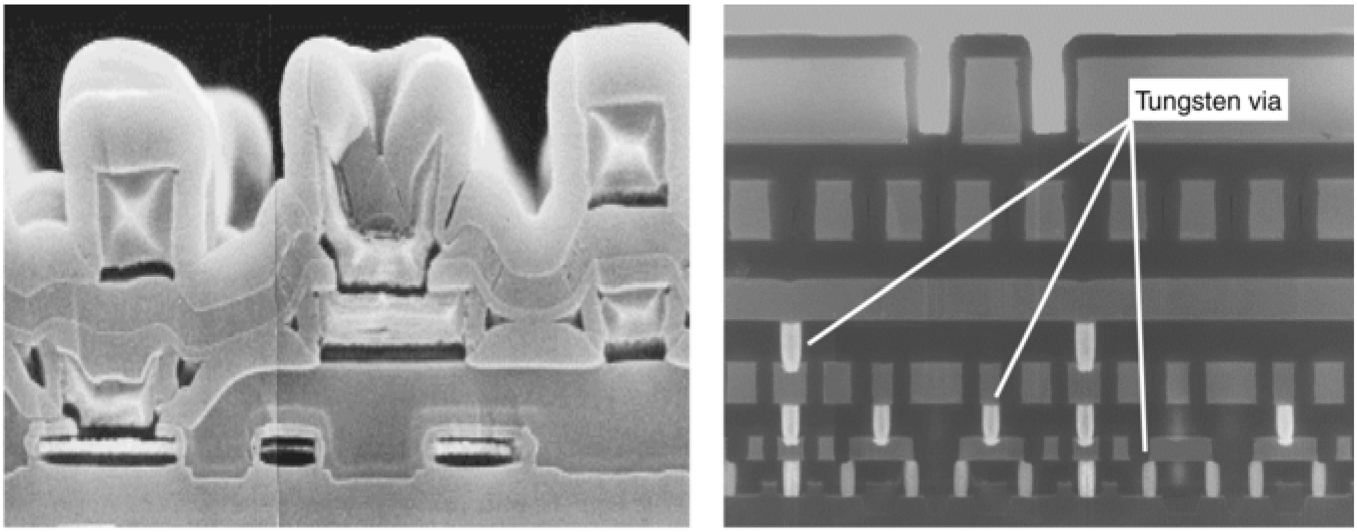

(a) (b)

Fig. 1 Micrographs of semiconductor device cross sections. (a) 1.0 µm technology; two metal layers made before the advent of chemical-mechanical planarization (CMP). (b) 0.25 µm technology; five metal layers, using CMP technology. Tungsten vias provide electrical connection between layers.

Other applications of CMP for smoothing and/ or polishing followed. These included polycrystalline silicon polishing for polysilicon gate devices and shallow trench isolation polishing where SiO_2 overburden (excess material to ensure proper fill) is removed. The polishing stops on a Si_3N_4 layer, leaving behind a SiO_2-filled trench. These types of polishing primarily involved mechanical removal of the silicon or SiO_2 layers. Slurries with high pH (10 to 11) were used to soften the substrate surface to enhance removal rates.

In addition to ILD polishing, thin-film metal polishing emerged as the next major application for CMP technology. Metal polishing in the IC industry originated with tungsten (W). Metal CMP involves redox reactions and controlled corrosion of the metal in order to achieve a high removal rate with good selectivity or a low removal rate on the underlying ILD. Tungsten, in conjunction with a thin titanium nitride adhesion layer, is used in IC manufacturing to form vias, metal lines that interconnect metal layers. Vias are the bright, vertical cylinders in Fig. 1(b). Tungsten is deposited by chemical vapor deposition, forming a film that is conformal. The film is deposited uniformly and thus retains the existing topography. Prior to the advent of CMP, the tungsten overburden was removed by a plasma etchback process that left a large recess in the via. Tungsten polishing was found to remove tungsten uniformly and quickly while giving very small via recesses. A comparison of wafer surfaces after tungsten CMP and tungsten etchback is shown in Fig. 2(a) and (b). The figure shows atomic force micrographs of 10 by 10 micron square regions of the wafer surface. The scale orthogonal to the wafer surface is 250 nm per division in the *Z*-direction as indicated on the figure. This shows that not only is the post-tungsten CMP via recess less, but also the surface of the ILD is much smoother than with plasma etchback.

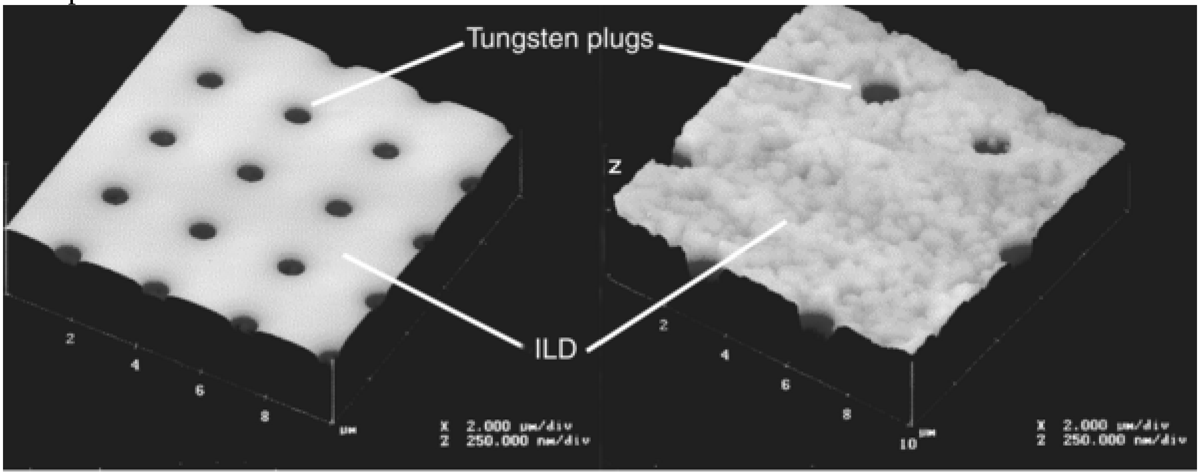

(a) (b)

Fig. 2 Atomic force micrographs of the surface of an integrated circuit wafer after (a) tungsten polishing and (b) tungsten plasma etchback. ILD, interlayer dielectric

Near the end of the 1990s, the delay in sending signals down metal interconnects became the limiter for device performance. This delay is related to the resistance of the metal as well as the capacitance between metal lines. This capacitance is a function of the dielectric constant of the ILD as well as the spacing between the metal lines. It became clear that the resistivity of aluminum was too high and it should be replaced by copper. In addition, the ILD, which traditionally had been SiO_2, would need to be replaced by low-dielectric-constant materials. Copper was first introduced in 1999 by IBM Corporation, using a novel patterning technique called damascene or inlaid copper. Unlike aluminum, copper is not easily plasma etched. The damascene process required first etching trenches and vias in the ILD where the metal lines are wanted. Next, the trenches were filled with a copper diffusion barrier layer of tantalum and/or tantalum nitride, a copper electroplate seed layer, and a thick copper electroplate layer. Finally, the copper and barrier layer overburden is then polished back to leave the copper damascene structure, as shown in Fig. 3.

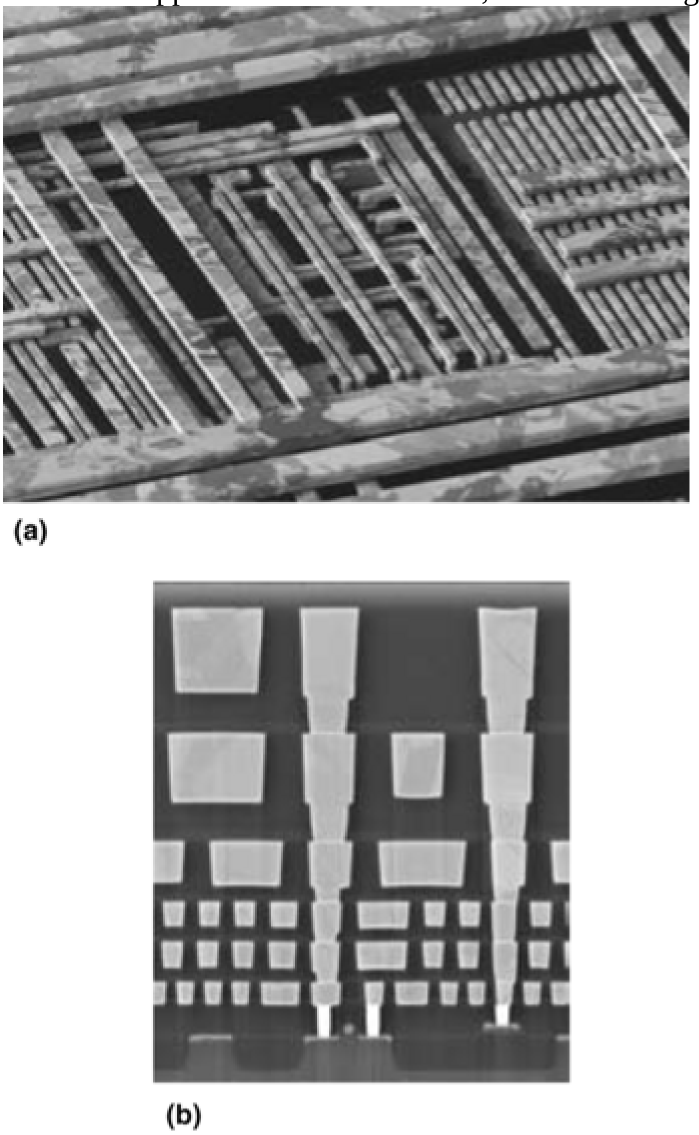

Fig. 3 Damascene structure of 0.13 µm copper interconnects after copper chemical-mechanical planarization. (a) View from above. (b) Cross section.

A.E. Miller, P.B. Fischer, A.D. Feller, T.N. Andryushchenko, and K.C. Cadien, Chemical-Mechanical Planarization for Semiconductors, *Corrosion: Fundamentals, Testing, and Protection*, Vol 13A, *ASM Handbook*, ASM International, 2003, p 164–169

Chemical-Mechanical Planarization for Semiconductors

Anne E. Miller, Paul B. Fischer, Allen D. Feller, Tatyana N. Andryushchenko, and Kenneth C. Cadien, Intel Corporation

Chemical-Mechanical Planarization Overview

A schematic of CMP process equipment is shown in Fig. 4. During CMP, a wafer is pressed down into a polyurethane polishing pad that is glued to a rotating base plate. Slurry is pumped onto the polishing pad and is distributed over the pad surface by centripetal force. Grooves in the pad aid the slurry flow. Chemical-mechanical planarization tools also have endpoint systems that can detect when a layer has been cleared. Commercial high-volume CMP tools have many variations on the basic configurations shown in Fig. 4. These include through-the-pad slurry delivery, linear pad motion, and integrated cleaning units. Discussion of these variations is beyond the scope of this article.

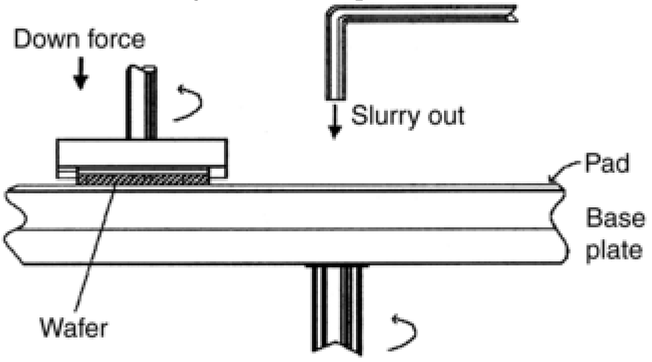

Fig. 4 Schematic of chemical-mechanical planarization setup

By definition, CMP consists of both mechanical and chemical components. The mechanical wafer environment during CMP consists of the pad, temperature, normal forces, shear forces, relative velocity of the wafer with respect to the pad, and slurry abrasive. The mechanical response of the polishing rate is typically described by the Preston equation, which states that the polishing rate is equal to the product of a process-dependent constant, the Preston coefficient, the polishing pressure, and the relative velocity between the polishing pad and the wafer (Ref 1).

The slurry also provides the wafer chemical environment. For metal CMP, it is the slurry that determines the redox potential and controls the beneficial corrosion of the wafer. The electrochemistry of metal CMP is discussed subsequently.

Reference cited in this section

1. F. Preston, The Theory and Design of Plate Glass Polishing Machines, *J. Soc. Glass Tech.*, Vol 11, 1927, p 214–256

A.E. Miller, P.B. Fischer, A.D. Feller, T.N. Andryushchenko, and K.C. Cadien, Chemical-Mechanical Planarization for Semiconductors, *Corrosion: Fundamentals, Testing, and Protection*, Vol 13A, *ASM Handbook*, ASM International, 2003, p 164–169

Chemical-Mechanical Planarization for Semiconductors

Anne E. Miller, Paul B. Fischer, Allen D. Feller, Tatyana N. Andryushchenko, and Kenneth C. Cadien, Intel Corporation

Chemistry of Metal CMP

In addition to an abrasive, a metal slurry may consist of an oxidizer, a corrosion inhibitor, a polishing rate accelerator, and a surfactant to modify the abrasives and metal surface. The reduction-potential difference between the metal and the oxidizer in the slurry is the thermodynamic driving force for the electrochemical reactions in metal polishing. The other nonoxidizing slurry components, such as accelerators and corrosion inhibitors, modify the electrochemical response and resulting polishing performance. The applications of CMP to tungsten and copper alloys are of prime interest in the semiconductor industry and are discussed in more detail.

Copper CMP. The formation of a corrosion product is a result of metallic oxidation occurring simultaneously with the reduction of the other available reactants. For example, the corrosion of copper during CMP can be expressed as an anodic reaction, where copper metal is oxidized:

$$Cu \rightarrow Cu^{+} + e^{-} \qquad \text{(Eq 1)}$$

$$Cu^{+} \rightarrow Cu^{2+} + e^{-} \qquad \text{(Eq 2)}$$

For film formation, the oxidation of copper to Cu_2O in aqueous solutions with dissolved oxygen is expressed as:

$$4Cu + 2H_2O \rightarrow 2Cu_2O + 4H^{+} + 4e^{-} \qquad \text{(Eq 3)}$$

More typically in slurries, the oxidation is driven by reduction of an oxidizer (Ref 2). For the reduction of H_2O_2, the net reaction is:

$$2Cu + H_2O_2 \rightarrow Cu_2O + H_2O \qquad \text{(Eq 4)}$$

The choice of oxidizer is dependent not only on the electrochemical reduction potential of the metal ion and oxidizer but also on the pH and other slurry additives, which can modify the thermodynamic regions of corrosion, passivation, and immunity that are typically described by the Pourbaix diagram (Ref 3). For CMP, it is advantageous to operate in a passivating region. For the copper-water system, this happens at intermediate pH range, where oxide film formation (as described by Eq. 3) occurs.

Copper readily corrodes in oxidizing solutions. In addition, under the right chemical conditions, copper forms an oxide film, but it is of poor quality. Copper is also a very soft metal, so high polishing pressures cannot be used to achieve high polishing rates, because copper smears.

To address these issues with copper, CMP slurries for copper are chemically complex. In addition to an oxidizer, a corrosion inhibitor is required to passivate the surface. The use of benzotriazole (BTA) as an inhibitor of copper corrosion was documented as early as 1947 (Ref 4). It is clear that BTA bonds to the copper oxide on the surface of copper and reinforces the protective nature of the copper oxide (Ref 5, 6). It has been proposed that BTA be used in copper slurries as an answer to the incomplete oxide passivation (Ref 7). A typical model of the copper-BTA polymer structure is shown in Fig. 5.

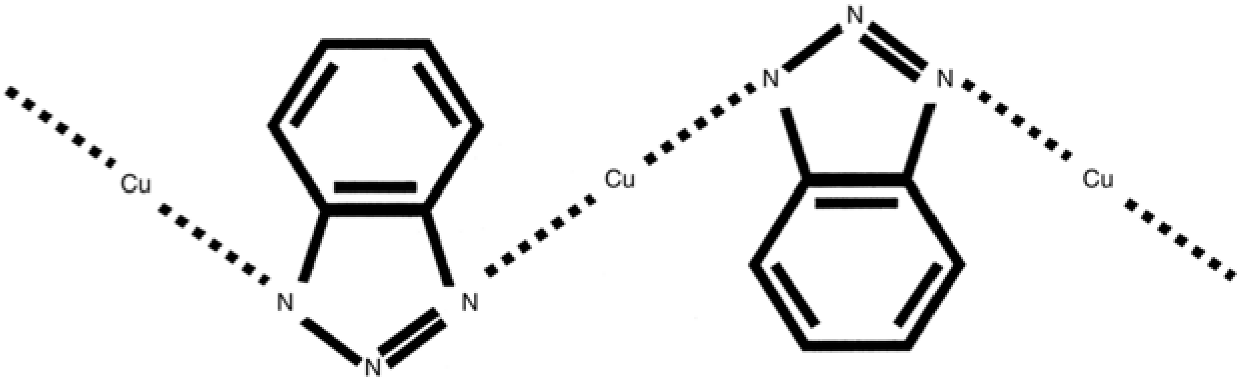

Fig. 5 Copper-BTA passive film structure

A corrosion inhibitor protects low-lying recessed areas while the high points in the topography are flattened (Ref 7, 8). The addition of the inhibitor tends to form a stable film that increases the pH range for passivation described by the Pourbaix diagrams (Ref 9).

For copper polishing, additives that improve solubility by complexing copper, such as ammonia (Ref 10) or glycine (Ref 11), have been used. Some of these additives, glycine in particular, have been shown to not only improve solubility of copper ions and thus reduce the pH range for passivation described by the Pourbaix diagram, but also aid in the reduction of peroxide oxidizer due to the catalytic effect of the glycine- copper complex (Ref 11). Surfactant additives have been used to enhance polish rate selectivity of the metal to underlying barrier or ILD layer and to ensure abrasive particles remain in suspension.

An abrasive such as silica or alumina is then used to remove the oxide-BTA film, exposing fresh copper and thus achieving a removal rate of 300 to 700 nm/min.

Tungsten CMP. The CMP of tungsten tends to require simpler chemistries than copper CMP. Kaufman and others (Ref 8) first proposed that tungsten be polished to form vias. They described a model of a tungsten slurry containing an etchant, a passivating agent (corrosion inhibitor), and an abrasive. In this model, elevated tungsten features contacting the polishing pad remove any passivation, thus exposing the metal to the etchant. Meanwhile, the passivation protects lower metal areas, thereby allowing the polishing process to planarize the tungsten film. Once the film is flat, polishing proceeds by subsequent steps of passivation, removal of the passivated layer by the polishing pad, etching, and then passivation. The process is repeated until the overburden is removed. The passivation also reduces via recess by protecting the via once it is recessed below the surface of the ILD.

The oxidizing agent, ferricyanide ($Fe(CN)_6^{3-}$), was first used as a metal etchant for tungsten (Ref 12). However, when ferricyanide reacts with tungsten, the product formed is either the stable passivating film (WO_3) or the soluble ion (WO_4^{2-}), as seen in the following equations:

$$W + 6Fe(CN)_6^{3-} + 3H_2O \rightarrow WO_3 + 6Fe(CN)_6^{4-} + 6H^+ \quad \text{(Eq 5)}$$

$$W + 6Fe(CN)_6^{3-} + 4H_2O \rightarrow WO_4^{2-} + 6Fe(CN)_6^{4-} + 8H^+ \quad \text{(Eq 6)}$$

The role of pH in these reactions has been studied (Ref 13). It was found that by lowering the pH below 4 and buffering the polishing slurry to the desired pH of 3, passivation of the tungsten surface was the predominant reaction, and any localized drop in pH during the polishing process was reduced. The selection of a pH range that allowed passivation of the tungsten surface was based on the Pourbaix diagram (Ref 3). Adjustment of abrasives such as silica or alumina, polishing pads, and mechanical parameters, such as downforce, rotational speed, and fluid flow, all contributed to the polishing performance, but the chemical control of corrosion was the key to tungsten polishing planarity.

Alternate slurries using the same pH range, 2 to 4, and the same abrasives, but using hydrogen peroxide (H_2O_2) or the Fe^{3+} in ferric nitrate ($Fe(NO_3)_3$) as the oxidizing agent, have been developed:

$$W + 3H_2O_2 + 3H_2O + 6H^+ \rightarrow WO_3 + 6H^+ + 6H_2O \quad \text{(Eq 7)}$$

$$W + 3H_2O + 2Fe^{3+} \rightarrow WO_3 + 6H^+ + 2Fe \quad \text{(Eq 8)}$$

Because slurries using $Fe(NO_3)_3$ as the oxidizing agent actually have a pH of 1.5 to 1.8, corrosion of the manufacturing equipment and deposits of hydrolyzed iron are significant issues for tool reliability. Slurries based on ferricynanide at a pH of 3 avoid these issues.

A simple model for the the role of the abrasive during metal polishing is that abrasive particles impart the mechanical momentum that enables removal of the passive film. However, various metal oxide abrasive materials have been studied, showing that the abrasive surface is more chemically active when the abrasive surface charge is close to zero at its isoelectric point (IEP) (Ref 14). In neutral pH ranges, CeO_2 with an IEP of approximately 7 has been found to have high oxide polishing rates due to a high number of surface sites that form and break bonds during the polishing process. For tantalum barrier layers, polishing rates also depend on the abrasive hardness in addition to the availability of reactive surface sites (Ref 15). Additives such as H_2O_2 and $Fe(NO_3)_3$ reduce the tantalum polishing rate due to the relatively hard, passivating oxide(s) formed.

References cited in this section

2. J.M. Steigerwald, S.P. Murarka, and R.J. Gutman, *Chemical Mechanical Planarization of Microelectronic Materials,* John Wiley & Sons, Inc., 1996

3. M. Pourbaix, *Atlas of Electrochemical Equilibria in Aqueous Solutions,* Pergamon Press, 1966

4. Proctor and Gamble, Ltd., British Patent 652,339, Dec 1947

5. H. Leidheiser, Jr. and R.E. Krieger, Ed., *The Corrosion of Copper, Tin and Their Alloys,* Robert E. Kreiger Publishing Co., 1979, p 120

6. V. Brusic, M.A. Frisch, B.N. Eldridge, F.P. Novak, F.B. Kaufman, B.M. Rush, and G.S. Frankel, Copper Corrosion With and Without Inhibitors, *J. Electrochem. Soc.,* Vol 138, 1991, p 2253–2259

7. Q. Luo, D.R. Campbell, and S.V. Babu, Chemical-Mechanical Polishing of Copper in Acidic Media, *CMP-MIC Conference, 96,* IMIC, Feb 1996, p 145–151

8. F.B. Kaufman, D.B. Thompson, R.E. Broadie, M.A. Jaso, W.L. Guthrie, D.J. Pearson, and M.B. Small, Chemical-Mechanical Polishing for Fabricating Patterned W Metal Features as Chip Interconnects, *J. Electrochem. Soc.,* Vol 138, 1990, p 3460–3464

9. D. Tromans, Aqueous Potential-pH Equilibria in Copper-Benzotriazole Systems, *J. Electrochem. Soc.,* Vol 145, 1998, p L42s–L45s

10. J.M. Steigerwald, D.J. Duquette, S.P. Murarka, and R.J. Gutmann, Electrochemical Potential Measurements During the Chemical Mechanical Polishing of Copper Thin Films, *J. Electrochem. Soc.,* Vol 142, 1995, p 2379–2385

11. M. Hariharaputhiran, J. Zhang, S. Ramarajan, J.J. Keleher, Y. Li, and S.V. Babu, Hydroxyl Radical Formation in H_2O_2-Amino Acid Mixtures and Chemical Mechanical Polishing of Copper, *J. Electrochem. Soc.,* Vol 147, 2000, p 3820–3826

12. T.A. Sankoff and E.A. Chandross, High Resolution Tungsten Patterning Using Buffered, Mildly Basic Etching Solutions, *J. Electrochem. Soc.,* Vol 122 , 1975, p 294

13. Intel Corp., U.S. Patent 5,340,370, Aug 1994

14. L.M. Cook, Chemical Processes in Glass Polishing, *J. Non-Cryst. Solids,* Vol 120, 1990, p 152–171

15. Y. Li, M. Hariharaputhiran, and S.V. Babu, Chemical-Mechanical Polishing of Copper and Tantalum with Silica Abrasives, *J. Mater. Res.*, Vol 16, 2001, p 1066–1073

A.E. Miller, P.B. Fischer, A.D. Feller, T.N. Andryushchenko, and K.C. Cadien, Chemical-Mechanical Planarization for Semiconductors, *Corrosion: Fundamentals, Testing, and Protection*, Vol 13A, *ASM Handbook*, ASM International, 2003, p 164–169

Chemical-Mechanical Planarization for Semiconductors

Anne E. Miller, Paul B. Fischer, Allen D. Feller, Tatyana N. Andryushchenko, and Kenneth C. Cadien, Intel Corporation

Electrochemical Theories and Methods in CMP

Electrochemical theories, such as the mixed- potential theory, are discussed elsewhere in this Volume. Analytical techniques, such as direct current (dc) potentiodynamic polarization and alternating current (ac) impedance measurements, may be applied to analyze the polishing mechanism during CMP.

The metallic polishing process is a corrosion- erosion process that involves a transfer of charge. The rate of chemical change is proportional to a flow of charge, so the polishing rate can be correlated with a reaction current or current density. As in typical potentiodynamic analysis, there is an exponential relationship between the current density and the overpotential or the potential difference between the applied and equilibrium potentials. Some electrochemical techniques used for studying corrosion phenomena for bulk materials are also applicable to CMP of the thin films used in ULSI fabrication processes.

In order to evaluate the corrosion rate by the electrochemical techniques, such as potentiodynamic measurements, the oxidation-reduction reactions are accelerated either in cathodic or anodic directions by the application of an external potential, and the net current is measured. At the intersection of the anodic and cathodic slopes, a mixed potential termed the *corrosion potential,* E_c, and the corresponding corrosion current, i_c, occurs. The corrosion current can be used to estimate the removal rate of metallic species from the surface in the absence of polishing.

The corrosion potential and corrosion current depend on several factors, including whether the reactions are controlled by Tafel kinetics or concentration polarization. Under Tafel kinetics, charge transfer is rate controlling and the current density increases proportionally to the overpotential. Concentration polarization means the rate-limiting step is mass transfer to or from the surface, and the current density increases very slowly with the overpotential. For example, in dc potentiodynamic polarization measurements, the potential is scanned within a relatively wide potential range around the corrosion potential. The dc polarization curves display the kinetics of the anodic and cathodic reactions, the corrosion rates, the dissolution mechanisms, and the ability of the metal to passivate itself (Ref 16).

It is known from the Pourbaix diagram for the copper-water system (Ref 3) that copper can be passivated in the pH range between 6.5 and 12.5, depending on the potential of the metal-liquid interface. Figure 6 shows that in the presence of a complexing agent, in this case, citrate ions, the active-passive polarization behavior of copper is not observed at pH 8.5 but is observed at pH 12. This indicates that the low pH boundary of the passivation region for the copper Pourbaix diagram is shifted to a higher pH.

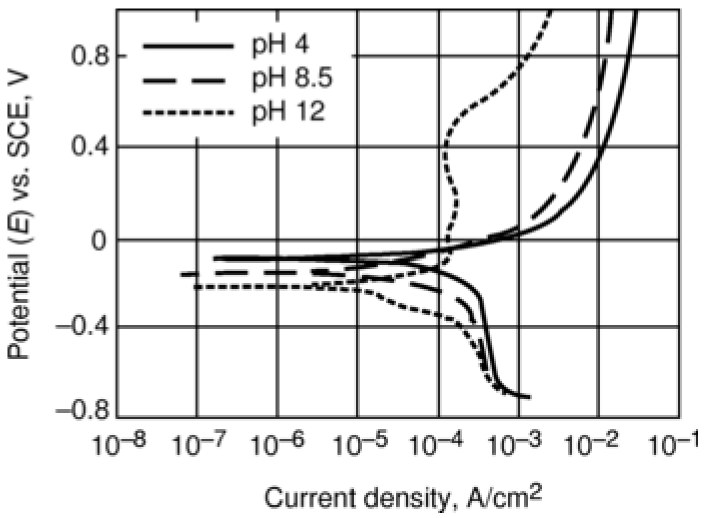

Fig. 6 Effect of pH on polarization behavior of copper in 0.01 *M* citrate solutions. SCE, saturated calomel electrode reference

With additions of hydrogen peroxide to the pH 4.5 solutions containing citrate ions, the driving force for copper oxidation increases, and the corrosion potential shifts in the noble direction (Fig. 7). Small concentrations of H_2O_2, up to 1%, increase the corrosion current and copper dissolution rate (or static etch rate) of copper. At higher concentrations of H_2O_2, the copper dissolution rate is suppressed, and passivation is observed at this lower pH. The copper polishing rate shows the same trend that was confirmed experimentally on the wafer scale.

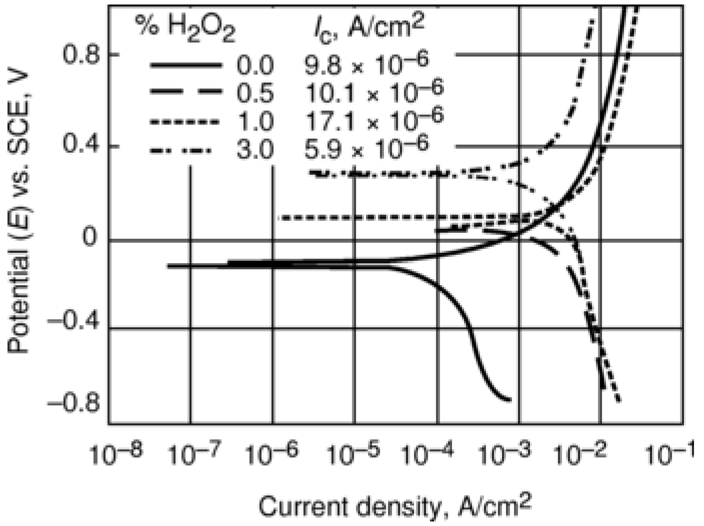

Fig. 7 Effect of H_2O_2 additions on polarization behavior of copper in 0.01 *M* citrate solutions. I_c, corrosion current density. SCE, saturated calomel electrode reference

Several investigators have reported the use of dc potentiodynamic polarization measurements performed with rotating disk electrodes made from bulk metals, without and with continuous abrasion of the electrode, which allows the simulation of the CMP process and relates the corrosion rate to the polishing rate (Ref 2, 17, 18, 19, 20).

Direct current potentiodynamic measurements have been used to predict CMP performance of the oxidizing/etching reagents for tungsten (Ref 17). The corrosion potential has been shown to decrease (become more active) and the corrosion current density to increase with abrasion of the surface. This indicates that the passivating layer is being removed by the abrasion process. Researchers have shown that the potentiodynamic curves of copper in 5% HNO_3 show only a very small difference between the corrosion potentials of the abraded and unabraded surfaces as well as a low Tafel slope in the anodic range (Ref 20). This indicates that there is no copper surface passivation in HNO_3. The dissolution of copper is the dominating reaction, and mechanical abrasion does not enhance the corrosion rate.

It is clear from these studies that the magnitudes of the differences in corrosion potential and corrosion current with and without abrasion, as well as the Tafel slope for anodic polarization, indicate the presence or absence of the passivating layer.

A method was introduced of studying the electrochemistry of CMP by measuring the electrochemical mixed potential of copper during polishing. These measurements explained the polishing performance in several ammonia- based slurries (Ref 10). Once polishing began, the concentration of dissolved oxygen decreased, providing the cathodic half-cell reaction for copper dissolution. After the initial drop, the potential rose steadily in the NH_4OH and the NH_4NO_3 slurries during the polishing as copper ions built up, while the potential for the NH_4Cl slurry remained nearly constant. The polishing rate was shown to correlate with the change in potential during polishing. The greatest change in potential for the NH_4OH slurry corresponded to the highest polishing rate. Complexing of copper ions with dissolved ammonia increases the dissolution rate of the abraded material and therefore increases the polishing rate. Increases in mixed potential in the noble direction indicate relative increases in copper ion concentration and may also be used to predict polishing rate behavior (Ref 7).

Cyclic voltammetry was used to investigate the electrochemical behavior of copper in 1 *M* sodium acetate (NaAc) solution at pH 5.8, with and without the presence of BTA (Ref 21). The researchers found that the initial step in the inhibition is the adsorption of BTA onto the copper surface. The copper oxide film is not modified at the early stage of adsorption, and its cathodic reduction occurs at the same potential, regardless of the presence of BTA. At prolonged immersion and higher BTA concentrations, the cathodic current peak during reduction shifted toward more negative potentials, suggesting structural changes in the film. When Cu(I)-BTA complex is formed, ionic movement through the film becomes rate determining. The Cu(I)-BTA thickness and protection against corrosion increase by increasing the BTA concentration and immersion time.

The slurry composition is an important factor in the CMP step. Basic electrochemical theories may be very useful in the fundamental characterization and formulation of CMP slurries as well as in overall CMP process development. What follows are processes that can adversely affect CMP.

References cited in this section

2. J.M. Steigerwald, S.P. Murarka, and R.J. Gutman, *Chemical Mechanical Planarization of Microelectronic Materials,* John Wiley & Sons, Inc., 1996

3. M. Pourbaix, *Atlas of Electrochemical Equilibria in Aqueous Solutions,* Pergamon Press, 1966

7. Q. Luo, D.R. Campbell, and S.V. Babu, Chemical-Mechanical Polishing of Copper in Acidic Media, *CMP-MIC Conference, 96,* IMIC, Feb 1996, p 145–151

10. J.M. Steigerwald, D.J. Duquette, S.P. Murarka, and R.J. Gutmann, Electrochemical Potential Measurements During the Chemical Mechanical Polishing of Copper Thin Films, *J. Electrochem. Soc.,* Vol 142, 1995, p 2379–2385

16. V. Brusic, G. Frankel, C.-K. Hu, M. Plechaty, and G. Schwartz, Corrosion and Protection of Thin-Line Conductors in VLSI Structures, *IBM J. Res. Devel.,* Vol 37 (No. 2), March 1993, p 173–188

17. J. Farkas, R. Carpio, R. Bajaj, C. Galanakis, R. Jairath, B. Jones, and S.-M. Tzeng, Oxidation and Etching of Tungsten in CMP Slurries, *Conference Proceedings ULSI-X,* Materials Research Society, 1995, p 25–32

18. V. Brusic, D. Scherber, F. Kaufman, R. Kistler, and C. Streinz, Electrochemical Approach to Au and Cu CMP Process Development, *Electrochemical Society Proceedings,* Vol 96-22, 1997, p 176–185

19. E. Kneer, C. Raghunath, V. Mathew, and S. Raghavan, Electrochemical Measurements During the Chemical Mechanical Polishing of Tungsten Thin Films, *J. Electrochem. Soc.,* Vol 144, 1997, p 3041–3049

20. R. Carpio, J. Farkas, and R. Jairath, Initial Study on Copper CMP Slurry Chemistries, *Thin Solid Films,* Vol 266, 1995, p 238–244

21. M. Metikos-Hukovic, R. Babic, and A. Marinovic, Spectrochemical Characterization of Benzotriazole on Copper, *J. Electrochem. Soc.,* Vol 145, 1998, p 4045–4051

A.E. Miller, P.B. Fischer, A.D. Feller, T.N. Andryushchenko, and K.C. Cadien, Chemical-Mechanical Planarization for Semiconductors, *Corrosion: Fundamentals, Testing, and Protection*, Vol 13A, *ASM Handbook*, ASM International, 2003, p 164–169

Chemical-Mechanical Planarization for Semiconductors

Anne E. Miller, Paul B. Fischer, Allen D. Feller, Tatyana N. Andryushchenko, and Kenneth C. Cadien, Intel Corporation

Uncontrolled Corrosion— Chemically Induced Defects

One of the challenges of CMP of thin-film metals is to minimize the localized, uncontrolled corrosion effects that cause defects. These critical defects derive from classical corrosion processes, such as pitting corrosion, galvanic corrosion, and excess etching. While changes in process conditions and post-polish buffing can assist in defect reduction, the most significant method of controlling these defects is in selection of the chemistry (Ref 22), as is discussed subsequently.

Pitting Corrosion. Classically, pitting corrosion occurs when an isolated region of the metal is exposed to an increasingly more aggressive corrosion environment than the bulk of the metal (Ref 23). For thin films as well as bulk materials, pitting corrosion initiates at impurities or local surface topography changes. Post-CMP, it is difficult to differentiate between pitting and crevice corrosion as the source of a defect.

For thin-film and bulk copper, the critical reaction for propagation of pits is the oxidation of copper to Cu_2O and a cathodic reaction, such as reduction of oxygen or other oxidizing species, in the slurry. While Cl^- is the classic metal-pitting agent, for copper, SO_4^{2-}, PO_4^{3-}, NO_3^-, and HCO_3^- are also known pitting agents (Ref 24, 25, 26). Figure 8 shows an example of pitting defects for a wafer polished with a peroxide-based copper slurry in the presence of 900 ppm of halide. For this slurry, there is no pH drop, because there is no net change in the number of hydrogen ions when the copper is oxidized by peroxide (Eq 4) (Ref 22). When used as an oxidant, ammonium persulfate has also been shown to induce deep pits through an entire 400 nm copper film thickness, due to formation of sulfate ions as a byproduct of the reduction of persulfate ($S_2O_8^{2-}$ + 2e^- → $2SO_4^{2-}$). Unlike peroxide reduction, the persulfate reaction does not consume H^+ ions, and a substantial net drop in pH occurs when persulfate oxidizes copper, enhancing the corrosion and pitting rate (Ref 22). While the addition of corrosion inhibitors and pitting agent getters serves to minimize pitting, the key to prevention is eliminating the presence of the pitting agent.

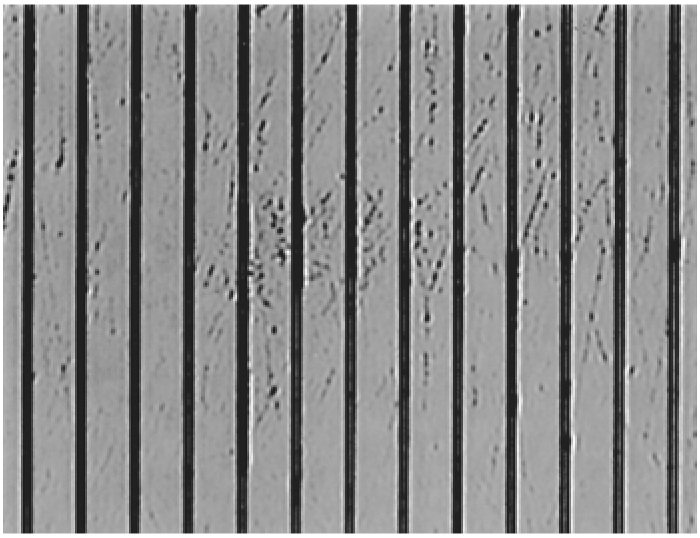

Fig. 8 An example of pitting corrosion induced by 900 ppm of halide. Source: Ref 22

Galvanic Corrosion. When two dissimilar metals are in contact with an electrolyte, oxidation occurs at one metal and reduction at the other, leading to etching of the first metal and redeposition of the second metal. For the copper damascene pattern with a titanium barrier, this causes recessing of the titanium barrier relative to the copper damascene line (Ref 2). For tantalum, another typical barrier, the galvanic couple is:

$$2Ta + 5H_2O \rightarrow Ta_2O_5 + 10H^+ + 10e^- \qquad \text{(Eq 9)}$$

$$Cu^{2+} + 2e^- \rightarrow Cu \qquad \text{(Eq 10)}$$

Galvanic corrosion resulting in reprecipitation of copper nodules has been observed for both titanium (Ref 2) and tantalum (Ref 22).

Chemical Etching. When high slurry dissolution rates or static etch rates are measured in the absence of polishing, it can lead to enhanced surface texturing. This is shown in Fig. 9 for a patterned wafer exposed to a peroxide-based copper slurry formulation and a static etch rate of 400 A/min. Texturing occurs in the center of wide structures conformally coated during copper electroplating. The center of these structures etches faster than the pad planarizes. In the presence of Cu^{2+} ions and complexing agents such as glycine (Ref 11), the activity of peroxide is significantly increased. Sixfold static etch rate increases have been observed (Ref 22), further contributing to the overall etch rate. Increased pH and inhibitors such as BTA can be used to control static etch rates. Polisher design, operating conditions, and consumable choices dictate mass-transport properties.

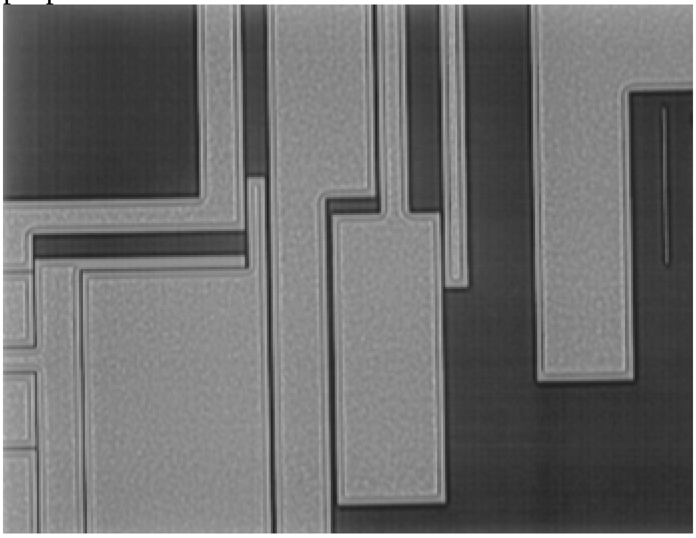

Fig. 9 Texturing defect induced by a high-static-etch slurry. Source: Ref 22

Chemical effects are a significant consideration in CMP processes. During CMP, the wafers that are polished are exposed to a slurry consisting of particles and combinations of chemistries. The wafers need to be cleaned then dried prior to subsequent processing. Many commercial CMP tools include integrated cleaning and drying tools. This significantly reduces the time that post-CMP wafers are wet. It should be noted that deionized water is very corrosive.

Post-CMP cleaning systems typically consist of water rinses, cleaning in megasonic ultrasonic chemical baths, and/or dual-sided scrubbing. It is has been found that the mechanical action of scrubbing is required to return wafers to pristine condition post-CMP.

A detailed description of the subject of CMP cleaning is beyond the scope of this section. However, it is important to note that remarkable photoelectric effects have been observed during the cleaning phase of post-copper CMP. The CMP cleaning processes typically involve one or more aqueous scrub steps, followed by a spin- rinse-dry where the drying is expedited by a heat lamp. During these cleaning steps, light-induced copper dendritic growth has been observed. Figure 10 shows an example of copper dendrite growth occurring on the surface of a patterned copper wafer during the post-CMP cleaning step.

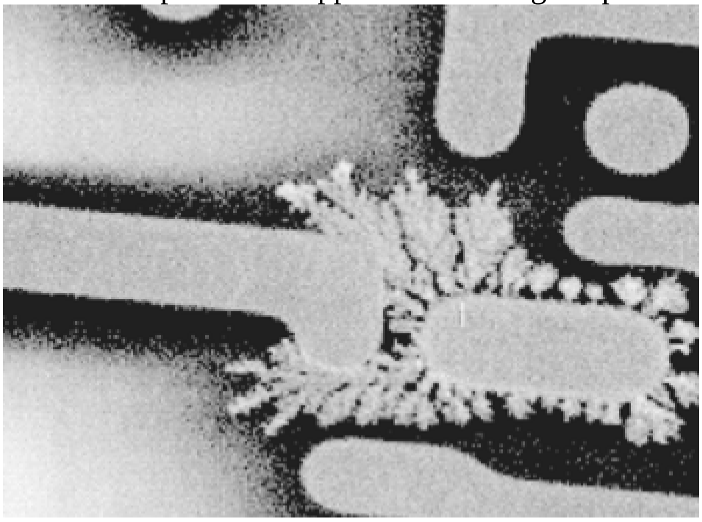

Fig. 10 Light-induced copper dendrite growth during post-CMP cleaning

The dendrite growth emanates from a copper pad connected to an *n*-type well that serves as the cathode. Incident photons excite electron- hole pairs in *p-n* junctions, as in photovoltaic cells. Electric fields within the *p-n* junction sweep the electrons toward the *n*-type material and the holes toward the *p*-type material. Copper connected to the *p*-type and *n*-type material forms the anode and cathode, respectively. Copper is oxidized at the anode (with the electrons being canceled by photo-induced holes), $Cu \rightarrow Cu^{2+} + 2e^-$. Copper is reduced at the cathode by the photo-induced electrons, $Cu^{2+} + 2e^- \rightarrow Cu$. The dendrite defect effect occurs primarily at lower metal layers and can be controlled by avoiding incident illumination during wet cleaning.

References cited in this section

2. J.M. Steigerwald, S.P. Murarka, and R.J. Gutman, *Chemical Mechanical Planarization of Microelectronic Materials,* John Wiley & Sons, Inc., 1996

11. M. Hariharaputhiran, J. Zhang, S. Ramarajan, J.J. Keleher, Y. Li, and S.V. Babu, Hydroxyl Radical Formation in H_2O_2-Amino Acid Mixtures and Chemical Mechanical Polishing of Copper, *J. Electrochem. Soc.,* Vol 147, 2000, p 3820–3826

22. A.E. Miller, P.B. Fischer, A.D. Feller, and K.C. Cadien, Chemically Induced Defects During Copper Polish, *Interconnect Technology Conference 2001,* Proceedings of the IEEE 2001 International, 2001, p 143–145

23. R. Walker, Benzotriazole, a Corrosion Inhibitor for Antiques, *J. Chem. Edu.,* Vol 57, 1980, p 789

24. N.W. Polan, F.J. Ansuini, C.W. Dralle, F. King, W.W. Kirk, T.S. Lee, H. Leidheiser, Jr., R.O. Lewis, and G.P. Sheldon, Corrosion of Copper and Copper Alloys, *Corrosion,* Vol 13, *Metals Handbook,* 9th ed., ASM International, 1987, p 610–640

25. J.-P. Duthil, G. Mankowski, and A. Giusti, The Synergetic Effect of Chloride and Sulfate on Pitting Corrosion of Copper, *Corros. Sci.,* Vol 38, 1996, p 1839–1849

26. M. Edwards, J. Rehring, and T. Meyer, Inorganic Anions and Copper Pitting, *Corrosion,* Vol 50, 1994, p 366–372

A.E. Miller, P.B. Fischer, A.D. Feller, T.N. Andryushchenko, and K.C. Cadien, Chemical-Mechanical Planarization for Semiconductors, *Corrosion: Fundamentals, Testing, and Protection,* Vol 13A, *ASM Handbook,* ASM International, 2003, p 164–169

Chemical-Mechanical Planarization for Semiconductors

Anne E. Miller, Paul B. Fischer, Allen D. Feller, Tatyana N. Andryushchenko, and Kenneth C. Cadien, Intel Corporation

---

Conclusions

The beneficial effect of controlled corrosion during CMP of thin-film ICs has led to a significant decrease in topography variations and has enabled the required deep ultraviolet lithography methodology for multilayer ULSI metallization. In addition to a significant mechanically induced erosion or wearing process, the chemical and electrochemical corrosion effects are critical in controlling CMP of metals. Maintaining a balance between controlled and uncontrolled corrosion is responsible for the appreciable removal rates, low topography, and low surface defects on polished metallic interconnects.

A.E. Miller, P.B. Fischer, A.D. Feller, T.N. Andryushchenko, and K.C. Cadien, Chemical-Mechanical Planarization for Semiconductors, *Corrosion: Fundamentals, Testing, and Protection,* Vol 13A, *ASM Handbook,* ASM International, 2003, p 164–169

Chemical-Mechanical Planarization for Semiconductors

Anne E. Miller, Paul B. Fischer, Allen D. Feller, Tatyana N. Andryushchenko, and Kenneth C. Cadien, Intel Corporation

---

References

1. F. Preston, The Theory and Design of Plate Glass Polishing Machines, *J. Soc. Glass Tech.,* Vol 11, 1927, p 214–256

2. J.M. Steigerwald, S.P. Murarka, and R.J. Gutman, *Chemical Mechanical Planarization of Microelectronic Materials,* John Wiley & Sons, Inc., 1996

3. M. Pourbaix, *Atlas of Electrochemical Equilibria in Aqueous Solutions,* Pergamon Press, 1966

4. Proctor and Gamble, Ltd., British Patent 652,339, Dec 1947

5. H. Leidheiser, Jr. and R.E. Krieger, Ed., *The Corrosion of Copper, Tin and Their Alloys,* Robert E. Kreiger Publishing Co., 1979, p 120

6. V. Brusic, M.A. Frisch, B.N. Eldridge, F.P. Novak, F.B. Kaufman, B.M. Rush, and G.S. Frankel, Copper Corrosion With and Without Inhibitors, *J. Electrochem. Soc.,* Vol 138, 1991, p 2253–2259

7. Q. Luo, D.R. Campbell, and S.V. Babu, Chemical-Mechanical Polishing of Copper in Acidic Media, *CMP-MIC Conference, 96,* IMIC, Feb 1996, p 145–151

8. F.B. Kaufman, D.B. Thompson, R.E. Broadie, M.A. Jaso, W.L. Guthrie, D.J. Pearson, and M.B. Small, Chemical-Mechanical Polishing for Fabricating Patterned W Metal Features as Chip Interconnects, *J. Electrochem. Soc.,* Vol 138, 1990, p 3460–3464

9. D. Tromans, Aqueous Potential-pH Equilibria in Copper-Benzotriazole Systems, *J. Electrochem. Soc.,* Vol 145, 1998, p L42s–L45s

10. J.M. Steigerwald, D.J. Duquette, S.P. Murarka, and R.J. Gutmann, Electrochemical Potential Measurements During the Chemical Mechanical Polishing of Copper Thin Films, *J. Electrochem. Soc.,* Vol 142, 1995, p 2379–2385

11. M. Hariharaputhiran, J. Zhang, S. Ramarajan, J.J. Keleher, Y. Li, and S.V. Babu, Hydroxyl Radical Formation in H_2O_2-Amino Acid Mixtures and Chemical Mechanical Polishing of Copper, *J. Electrochem. Soc.,* Vol 147, 2000, p 3820–3826

12. T.A. Sankoff and E.A. Chandross, High Resolution Tungsten Patterning Using Buffered, Mildly Basic Etching Solutions, *J. Electrochem. Soc.,* Vol 122 , 1975, p 294

13. Intel Corp., U.S. Patent 5,340,370, Aug 1994

14. L.M. Cook, Chemical Processes in Glass Polishing, *J. Non-Cryst. Solids,* Vol 120, 1990, p 152–171

15. Y. Li, M. Hariharaputhiran, and S.V. Babu, Chemical-Mechanical Polishing of Copper and Tantalum with Silica Abrasives, *J. Mater. Res.,* Vol 16, 2001, p 1066–1073

16. V. Brusic, G. Frankel, C.-K. Hu, M. Plechaty, and G. Schwartz, Corrosion and Protection of Thin-Line Conductors in VLSI Structures, *IBM J. Res. Devel.,* Vol 37 (No. 2), March 1993, p 173–188

17. J. Farkas, R. Carpio, R. Bajaj, C. Galanakis, R. Jairath, B. Jones, and S.-M. Tzeng, Oxidation and Etching of Tungsten in CMP Slurries, *Conference Proceedings ULSI-X,* Materials Research Society, 1995, p 25–32

18. V. Brusic, D. Scherber, F. Kaufman, R. Kistler, and C. Streinz, Electrochemical Approach to Au and Cu CMP Process Development, *Electrochemical Society Proceedings,* Vol 96-22, 1997, p 176–185

19. E. Kneer, C. Raghunath, V. Mathew, and S. Raghavan, Electrochemical Measurements During the Chemical Mechanical Polishing of Tungsten Thin Films, *J. Electrochem. Soc.,* Vol 144, 1997, p 3041–3049

20. R. Carpio, J. Farkas, and R. Jairath, Initial Study on Copper CMP Slurry Chemistries, *Thin Solid Films,* Vol 266, 1995, p 238–244

21. M. Metikos-Hukovic, R. Babic, and A. Marinovic, Spectrochemical Characterization of Benzotriazole on Copper, *J. Electrochem. Soc.,* Vol 145, 1998, p 4045–4051

22. A.E. Miller, P.B. Fischer, A.D. Feller, and K.C. Cadien, Chemically Induced Defects During Copper Polish, *Interconnect Technology Conference 2001*, Proceedings of the IEEE 2001 International, 2001, p 143–145

23. R. Walker, Benzotriazole, a Corrosion Inhibitor for Antiques, *J. Chem. Edu.,* Vol 57, 1980, p 789

24. N.W. Polan, F.J. Ansuini, C.W. Dralle, F. King, W.W. Kirk, T.S. Lee, H. Leidheiser, Jr., R.O. Lewis, and G.P. Sheldon, Corrosion of Copper and Copper Alloys, *Corrosion,* Vol 13, *Metals Handbook,* 9th ed., ASM International, 1987, p 610–640

25. J.-P. Duthil, G. Mankowski, and A. Giusti, The Synergetic Effect of Chloride and Sulfate on Pitting Corrosion of Copper, *Corros. Sci.,* Vol 38, 1996, p 1839–1849

26. M. Edwards, J. Rehring, and T. Meyer, Inorganic Anions and Copper Pitting, *Corrosion,* Vol 50, 1994, p 366–372

A.E. Miller, P.B. Fischer, A.D. Feller, T.N. Andryushchenko, and K.C. Cadien, Chemical-Mechanical Planarization for Semiconductors, *Corrosion: Fundamentals, Testing, and Protection*, Vol 13A, *ASM Handbook*, ASM International, 2003, p 164–169

Chemical-Mechanical Planarization for Semiconductors

Anne E. Miller, Paul B. Fischer, Allen D. Feller, Tatyana N. Andryushchenko, and Kenneth C. Cadien, Intel Corporation

Selected References

- S.V. Babu, K.C. Cadien, and H. Yano, Ed., *Chemical-Mechanical Polishing 2001—Advances and Future Challenges,* Materials Research Society Symposium Proceedings, April 2001, p 671
- P.V. Zant, *Microchip Fabrication: A Practical Guide to Semiconductor Processing,* 4th ed., McGraw Hill Professional, April 2000

C.F. Windisch, Jr., Anodes for Batteries, *Corrosion: Fundamentals, Testing, and Protection*, Vol 13A, *ASM Handbook*, ASM International, 2003, p 170–177

Anodes for Batteries

Charles F. Windisch, Jr., Pacific Northwest National Laboratory

Introduction

THIS ARTICLE examines constructive corrosion as it occurs in power-generating devices, specifically batteries. Because corrosion in batteries (as in many other systems) can take several forms, the distinction between constructive and destructive processes is first discussed. This distinction provides a framework for the subsequent discussion on the criteria used to select viable anodes for batteries. These criteria are based on measurements of the same fundamental thermodynamic and kinetic properties of metals that are germane to

destructive corrosion, but, in the case of batteries and other systems where constructive corrosion occurs, the objectives are completely opposite. The reason is obvious: instead of minimizing corrosion in these systems, the objective is generally to promote it.

Following a discussion of the thermodynamic principles of constructive corrosion in batteries, including a summary of parameters commonly used to rank performance based on these principles, the kinetic aspects of constructive corrosion in batteries is discussed. Several examples are provided to illustrate how the kinetics of the corrosion process varies among different battery systems. Another aspect of constructive corrosion in batteries is then described, specifically, situations where corrosion is promoted in battery manufacturing for the purpose of preparing electrochemically active material. Finally, a discussion is provided on a few important cases where destructive corrosion occurs in batteries. While other articles in this Volume focus on destructive corrosion, the discussion presented here is meant to emphasize how constructive and destructive processes in batteries can be very similar, both energetically and mechanistically, and how subtle variations in battery conditions can strongly influence which of the two competing processes occurs.

C.F. Windisch, Jr., Anodes for Batteries, *Corrosion: Fundamentals, Testing, and Protection*, Vol 13A, *ASM Handbook*, ASM International, 2003, p 170–177

Anodes for Batteries

Charles F. Windisch, Jr., Pacific Northwest National Laboratory

---

Constructive versus Destructive Corrosion in Batteries

There are three roles that corrosion, or oxidation of a metal, may play at anodes in batteries. Two of these are constructive and hence desirable. The third is destructive and therefore undesirable.

Two Constructive Roles. "A battery is a device that converts the chemical energy contained in its active materials directly into electrical energy by means of an electrochemical oxidation- reduction (redox) reaction" (Ref 1). The active material at the anode of a battery is the "fuel" that undergoes oxidation. When this anode material or fuel is a metal, the oxidation process consists of corrosion. In the general case, the anodic or corrosion reaction may be represented by the equations:

$$M(s) \rightarrow M^{n+}(dis) + ne^- \quad \text{(Eq 1)}$$

or

$$mM(s) + nX^{m-}(dis) \rightarrow M_mX_n(s) + (n \cdot m)e^- \quad \text{(Eq 2)}$$

where M(s) is the solid metal anode, X^{m-}(dis) is a complexing anion dissolved in the electrolyte, and *m* and *n* are integers. Equation 1 represents anode reactions where the metal is oxidized and dissolves. Complexation of the dissolved cations usually occurs, but the reaction products remain soluble. Such soluble metal complexes are included in the designation M^{n+}(dis). Equation 2 consists of oxidation reactions in which an insoluble reaction product is formed through complexation and precipitation. In aqueous electrolytes, the product is usually an oxide or hydroxide, and the reactants often include H_2O.

The previously mentioned form of corrosion in batteries is constructive, because it is part of the battery reaction that generates the desired electrical energy. Another type of constructive corrosion in batteries is oxidation of metals during battery manufacturing. This consists of purposeful oxidation of a metal to form an oxide that eventually serves as the active mass (usually for the positive electrode). The best example of this type of corrosion is in the manufacturing of the lead-acid battery, as described subsequently. Once the oxide or positive active mass (PAM) is formed, the metal at the electrode simply acts as a current source or collector while the electrochemical reactions involve the oxide.

A Destructive Role. Destructive corrosion in batteries can also occur. It usually consists of oxidation of the metal anode during storage; however, destructive corrosion can also occur in parallel with constructive corrosion while the battery is operating. In general, destructive corrosion involves the direct reaction of the metal anode with the electrolyte (Fig. 1). This corrosion results in loss of active material and is reflected in

shortening of shelf life and/or lowering of capacity. In addition, corrosion products from the direct reaction can include solid precipitates and gases. The former are problematic, because they can create barriers to the transport of electroactive species and increase internal resistance. The higher internal resistance causes undesirable voltage drops in the cell under load. Gases that are sometimes generated by direct reaction of the anode metal include hydrogen, whose presence poses an obvious safety hazard. Finally, metal anodes may undergo passivation by direct reaction with the electrolyte. While highly desirable in most instances for thermodynamically active metals, passivation at a battery anode is usually deleterious.

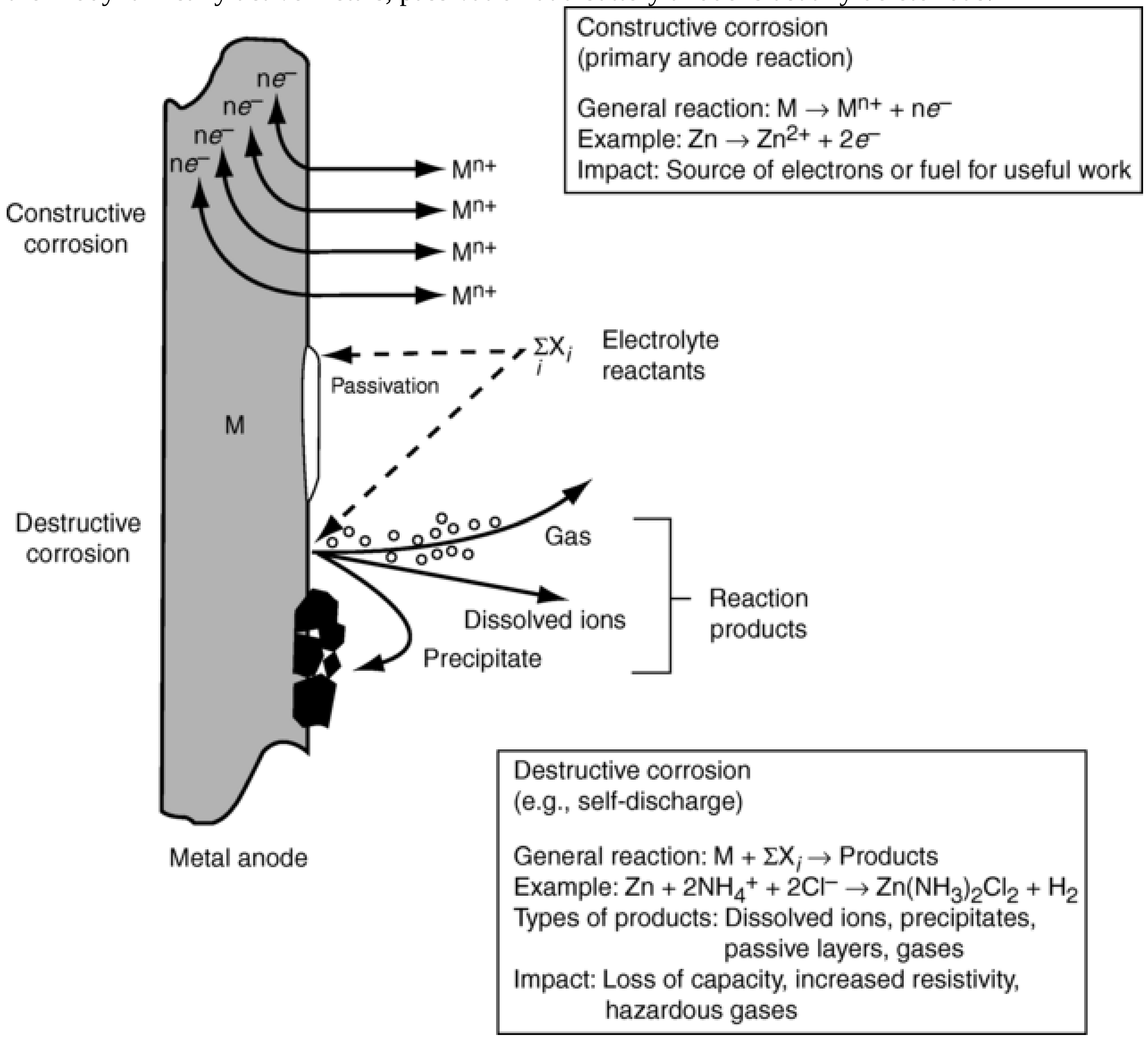

Fig. 1 Illustration of constructive and destructive corrosion reactions for a battery anode

By their nature, passive films inhibit the transport of ionic species. This is the reason why these films, once formed, reduce the corrosion rate of metals. Unfortunately, charge transport at battery anodes involves the metal ions that are the primary products of the constructive corrosion process. Passivation slows down the transport of these constructive ions even more effectively than precipitated films, increasing resistance dramatically and thereby adversely affecting battery performance. This is the reason why passivation-prone metals such as aluminum and titanium, which are highly active and have very large free-energy changes associated with their oxidation reactions in water and other electrolytes, are sparingly, if ever, used as anodes in battery systems.

The key to making sure that only constructive corrosion of the anode occurs is to select compositions of the electrodes and electrolyte, as well as an optimal design of cell geometry, that disfavors the formation of cathodes on the anode metal and minimizes the potential for direct reaction of metal with the electrolyte. Strategies for minimizing this type of corrosion usually involve alloying of the anode with metals that polarize

it and thus lower corrosion rates under open-circuit conditions, removing impurities in the metal that may act as depolarizers, and modifying the electrolyte with corrosion inhibitors.

Several examples of the two types of constructive corrosion in batteries are provided here, with a discussion of how thermodynamic and kinetic aspects of the corrosion processes influence the performance of the batteries. The discussion is not meant to be a comprehensive treatment of batteries. Its purpose is to illustrate the way in which techniques and concepts in corrosion science are relevant to batteries and where, in these particular instances, the focus is on making the corrosion reactions as favorable and as facile as possible, rather than on attempting to minimize their effects, as is usually the case in corrosion studies. In addition to the discussion of the constructive types of corrosion in batteries, some instances of the destructive type of corrosion are also given. The reason for including examples of the destructive form is to highlight their chemical similarity to the constructive types and to illustrate the endeavors of battery manufacturers to design systems that promote one type of corrosion over the other.

Reference cited in this section

1. D. Lindon, Ed., *Handbook of Batteries,* 2nd ed., McGraw-Hill, Inc., 1995

C.F. Windisch, Jr., Anodes for Batteries, *Corrosion: Fundamentals, Testing, and Protection*, Vol 13A, *ASM Handbook*, ASM International, 2003, p 170–177

Anodes for Batteries

Charles F. Windisch, Jr., Pacific Northwest National Laboratory

Constructive Corrosion as Part of Power Generation

Batteries that use metals as anodes that oxidize or corrode during discharge according to the reactions in Eq 1 or 2 are plentiful. The reason for this is that metals are easily fabricated, often inexpensive, and usually, as pure elements, chemically very simple materials. Most importantly, however, most metals are in a thermodynamically unstable state, typically able to oxidize in gaseous and especially aqueous environments under ambient conditions. This makes them good fuels for chemical reactions. Additionally, their high electrical conductivities make them excellent candidates for sources of electrochemical energy as well, specifically as anodes in many battery systems. In batteries, they are one of the two phases in an “electrode (anode or half-cell) of the first kind” (Ref 2), where the second phase is the electrolyte containing cations of the metal.

The tendency of metals to oxidize during battery discharge is reflected in the usually substantial negative Gibbs free-energy change for the reactions in Eq 1 or 2. Metals that oxide more readily have more negative Gibbs free-energy changes, and one might conclude that these metals should make better anodes for batteries. However, battery performance (even from a strictly thermodynamic viewpoint) depends not only on this free-energy change but on how much of this energy can be extracted from a given mass of metal. Batteries are often used as power supplies where size and weight are design constraints, so a quantity called the specific capacity or maximum electrical storage density is commonly used to compare the potential performance. The specific capacity is the maximum amount of charge that can be extracted from 1 kg of metal, assuming a certain number of moles of electrons (n) are transferred during oxidation of 1 mole of metal (Ref 3). Defined in units of Ah/kg, the specific capacity is:

$$\text{Specific capacity} = x[n \times F]/[3600 \times m] \quad \text{(Eq 3)}$$

where F is the Faraday constant, 96,500 C/gram equivalent; m is the mass of the cell or half-cell; and x is the theoretical number of moles of reaction accompanying the complete discharge of the cell. Commonly, specific capacities are compared per unit mass of anode material, so, in this case, m is set equal to M, the atomic weight of the metal in kg/mol, and x is taken as unity:

Specific capacity (per unit anode mass) = $[n \times F]/[3600 \times M]$ (Eq 4)

The specific capacities for metals found in several common batteries, calculated using Eq 4, are listed in Table 1 (Ref 1, 3).

Table 1 Metals in common batteries

Metal	Reaction	Battery designation	Standard potential (E^0), V	Specific capacity, Ah/kg	Specific energy density, kWh/kg
Li	$Li \rightarrow Li^+ + e^-$	Lithium sulfur	-3.05	3860	11.76
Na	$Na \rightarrow Na^+ + e^-$	Sodium sulfur	-2.71	1170	3.17
Mg	$Mg \rightarrow Mg^{2+} + 2e^-$	Magnesium	-2.36	2210	5.22
Zn	$Zn \rightarrow Zn^{2+} + 2e^-$	Leclanche	-0.763	820	0.63
Cd	$Cd \rightarrow Cd^{2+} + 2e^-$	Nickel cadmium	-0.403	477	0.19
Pb	$Pb \rightarrow Pb^{2+} + 2e^-$	Lead acid	-0.126	259	0.03

In addition to specific capacity, two other properties of anodes, metals or otherwise, are useful in comparing battery performance. These are the specific energy (in kWh/kg) and the specific power (in kW/kg). Similar to specific capacity, the specific energy has a theoretical and practical value, with the theoretical value for complete discharged equal to:

Specific energy = $x[n \times F \times E_{cell}]/[3.6 \times 10^6 \times m]$ = [Specific capacity] $\times E_{cell}/1000$ (Eq 5)

where E_{cell} is the reversible electrode cell potential (Ref 1, 3). As in the case of the specific capacity, anodes can be compared by taking the E_{cell} as the standard half-cell potential for the oxidation reaction ($-E^0$ in Table 1, where E^0 is defined as the standard reduction potential, per common convention) and assuming m is then equal to M, the atomic weight of the electrode material (the metal). (Note that this is the same as coupling the anode reaction to the normal hydrogen electrode.) Specific energies for some important battery systems are given in Table 1.

The previously mentioned two parameters for rating battery performance, specific capacity and specific energy, are an indication of how well a metal can act as a vessel loaded with realizable electricity. They are maximum or theoretical values derived from summing up the total number of electrons available (Eq 3 or 4) and considering the reversible available Gibbs free energy embodied in E_{cell} (Eq 5). The extent to which these quantities are realized depends on many factors (Ref 2). Other factors affecting battery performance are:

- A consideration of the cathode reaction and its energetics. The total cell potential depends on the cathode reaction as well as the anode reaction. A given metal anode may show great potential (have a large theoretical specific energy), but difficulties in finding a compatible cathode with a moderately large half- cell potential (assuring a large cell potential) may limit the utility of this metal as an anode material.
- The mass, m, in Eq 3, Eq 4, Eq 5 was taken as the mass of the metal anode. In reality, performance (electricity produced per mass) is determined by the total mass of the battery, including grids, containers, electrolyte, and electrical connections.
- The potential in Eq 5 is a reversible thermodynamic potential that is lessened by the presence of ohmic drops in the cell and any overpotentials arising from activation, diffusion and other transport barriers, concentration gradients, undesirable chemical reactions and precipitate formation, refinement or changes in morphology at the anodes on prolonged cycling, as well as other kinetic factors.

Actual or practical specific energies of batteries are usually significantly less than the maximum values, as illustrated in Table 2 (Ref 1, 2, 3, 4). In fact, only approximately 25% of theoretical capacity is typically

attained under most conditions as a result of design and discharge requirement (Ref 1). Some of the electrochemical factors that contribute to these losses are discussed subsequently.

Table 2 Comparison of theoretical and practical specific energies for common batteries

Battery	Cell reaction [(a)]	E^0_{cell}, V	Specific energy, kWh/kg [(b)]	Practical specific energy, kWh/kg [(b)]
Lithium iodine	$Li(s) + 1/2I_2(s) \rightarrow LiI(s)$	2.80 (25 C)	1.9[(c)]	1.1[(c)]
Li-TiS$_2$	$xLi(s) + TiS_2(s) \rightarrow Li_xTiS_2(s)$	2.15	0.484	0.05–0.12
Lithium sulfur oxide	$2Li(s) + 2SO_2(g) \rightarrow Li_2S_2O_4(s)$	3.1	1.17	0.26
Sodium sulfur	$2Na(l) + 5S(l) \rightarrow Na_2S_5(l)$[(d)]	2.08 (350 C)	0.790	0.10
Magnesium	$Mg(s) + 2MnO_2(s) + H_2O(l) \rightarrow Mn_2O_3(s) + Mg(OH)_2(s)$	2.8	0.76	0.100
Zinc-silver oxide	$Zn(s) + AgO(s) + H_2O(l) \rightarrow Zn(OH)_2(s) + 2Ag(s)$	1.81	0.510	0.120
Air cell	$Zn(s) + 1/2O_2(g) \rightarrow ZnO(s)$	1.65 (65 C)	1.090	0.34
Alkaline zinc	$Zn(s) + MnO_2(s) + 1/2H_2O(l) \rightarrow MnOOH(s) + ZnO(s)$	1.5	0.336	0.038–0.125
Leclanche cell	$Zn(s) + 2MnO_2(s) + 2NH_4Cl(aq) \rightarrow 2MnOOH(s) + Zn(NH_3)_2Cl_2(s)$[(f)]	1.5–1.7 (20 C)	0.14[(e)]	0.085[(e)]
Nickel cadmium	$2NiOOH(s) + Cd(s) + 2H_2O \rightarrow 2Ni(OH)_2(s) + Cd(OH)_2$	1.35	0.244	0.020–0.035
Lead acid	$Pb(s) + PbO_2(s) + 2H_2SO_4(l) \rightarrow 2PbSO_4(s) + 2H_2O(l)$	2.1	0.252	0.035

(a) The state of the reactants is s, solid; g, gas; l, liquid; aq, aqueous solution.
(b) Includes mass of anode plus cathode materials only, unless noted. Practical values are obtained under typically specified conditions for these batteries and include a range spanned by different designs, e.g., button and cylinder.
(c) Units are Wh/cm^3.
(d) Initial cell reaction. As discharge progresses, cell reaction changes with the observed decrease in specific energy.
(e) Includes mass of all cell components.
(f) One of a number of reactions proposed for this complicated chemical process

The various kinetic factors alluded to in the last of the previous three bulleted items, which reduce the cell potential and limit battery performance, depend on current density. For a given current density at which it is desired to provide electricity, the various kinetic factors that reduce the cell potential should be as low as possible. Because the potential and current density cannot be varied indiscriminately, the selection of battery components, including the metal anode, becomes a complex process and relies on many electrochemical kinetics techniques that relate current and potential, similar to approaches used in corrosion science but with different objectives.

Because of the need to consider both potential and current at a specified external load, a useful parameter for comparing battery performance is the specific power (W/kg):

$$\text{Specific power} = [I \times E]/m \quad \text{(Eq 6)}$$

where I is the current (in amperes) (Ref 1, 2), and E is the actual cell potential (in volts). Because E depends on current, the specific power may be a complex function of current, with the relationship depending on the collection of kinetic factors that diminish the cell potential from its maximum reversible value. The specific power parameter, therefore, captures the overall kinetic aspects of battery performance and is used to select battery systems where energy needs to be supplied at a given rate. A battery may have a large capacity for

storing energy (large energy density), for example, but if it has a low specific power, it would only be used where the energy is required at a very slow rate of delivery.

The typical relationship between power and current during battery discharge is illustrated in Fig. 2. Curve A is a typical polarization curve that shows how the voltage of the cell usually changes during discharge. There are three regions: (I) initially, there is a rapid fall in voltage at low current because of electrode polarization involving one or both electrodes; (II) next, there is an almost-linear region with a usually small slope dominated by the internal ohmic resistance of the cell; and (III) finally, at high current, the depletion of electrode material at the electrode surfaces causes a limiting current effect where the slope becomes very large. It should be cautioned that the curves in this figure are idealized and that there are often more complicated behaviors and usually a time dependency associated with the buildup or depletion of reaction products or subsequent morphologies. For this reason, discharge curves are also often shown in terms of how potential varies with time or fraction of discharge completed under fixed-load or fixed-current conditions. Curve B in Fig. 2 shows how the power varies for a cell with discharge characteristics shown in curve A. The power curve exhibits a maximum. At low-current draw, where the voltage of the cell is maximum (as is the efficiency), the power is low because current is low (Eq 6). At intermediate currents, where voltage decreases but current increases, the power increases due to the unusually small slope of the ohmic-dominated region II. It is important to remember that when the power is maximum (when energy is delivered most rapidly), the voltage (and efficiency) of the cell is not optimal. As current is increased further into region III, both power and voltage fall to 0.

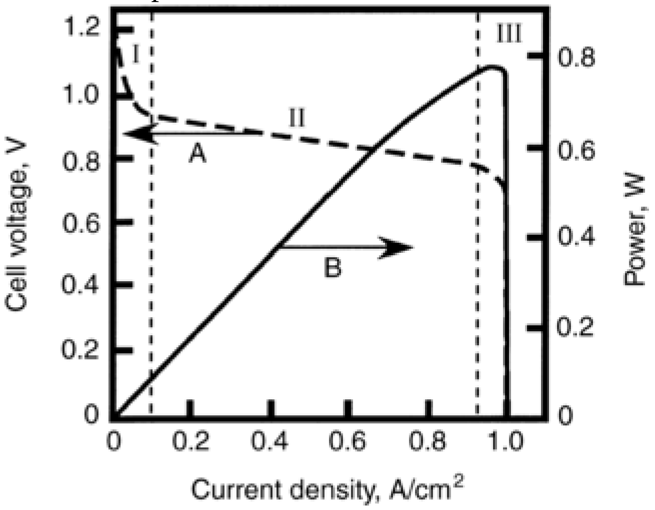

Fig. 2 Typical relationship between cell voltage, power, and current density for a battery. Conditions are divided into three regions: I, low current; II, linear midrange; III, high current. A, typical polarization curve; B, curve showing how power varies for a cell with discharge characteristics of curve A. Source: Ref 2

The curves in Fig. 2 illustrate changes in battery performance that are partly impacted by the kinetics of oxidation of the anode material. When the anode is a metal, the curves are influenced by the same types of activation and mass transport barriers that are commonly studied for controlling the corrosion of structural and electronic metal-based structures. In the case of batteries, however, the emphasis is usually on lowering these barriers to facilitate oxidation of the metal and thus maintain the anode potential as high as possible. Two important caveats are worth mentioning, however. First, the emphasis on lowering activation barriers relates to the primary anode discharge reaction only. Parasitic corrosion reactions involving the anode material often occur in batteries during normal use or storage, and the focus here is on eliminating or inhibiting these reactions (often with chemical inhibitors), much like the focus in other corrosion-related studies. Secondly, metal anodes in secondary batteries are unlike most metallic systems undergoing corrosion in that they are recycled many times so as to regenerate the metal. This recycling causes continued refinement of the metallic microstructure and composition, the extent of which depends on many factors, including discharging and charging rates, depth of discharge, temperature, and so on. To understand the effects of these changes, discharge curves are often obtained over many battery charge/discharge cycles. Application of other electrochemical techniques, including transient electrochemical measurements and impedance studies, is also helpful.

Because the focus here is corrosion or oxidation of metallic electrodes, further discussion of overall battery performance is limited. Rather, two battery systems are selected, and specific issues related to anode oxidation

in these batteries during discharge are briefly discussed. The purpose of this discussion is twofold: to show how the constructive corrosion reaction (primary discharge reaction) at the anode is typically monitored by electrochemical methods and to illustrate how various aspects of this corrosion reaction influence battery performance. The anodes selected for discussion are the zinc anode in the mercury battery (Zn/HgO) and the lithium metal anode in a rechargeable lithium battery.

Zinc Anode in the Mercury Battery. The mercury battery, often fabricated in the form of a button, is used in a wide range of applications where a miniature power source with a relatively constant voltage is required throughout long discharge periods (Ref 1, 2). As shown in the cross section in Fig. 3, the battery has an amalgamated zinc anode, a concentrated aqueous potassium hydroxide electrolyte that is saturated with zincate ions with ZnO, and a mercuric oxide/ graphitic carbon (HgO(s)/C) cathode. The anode is usually in the form of a porous, compressed cylindrical pellet or button of amalgamated zinc powder and gelled electrolyte. Alternatively, a spiral of corrugated zinc foil spaced with an absorbent paper layer is used in a wound configuration.

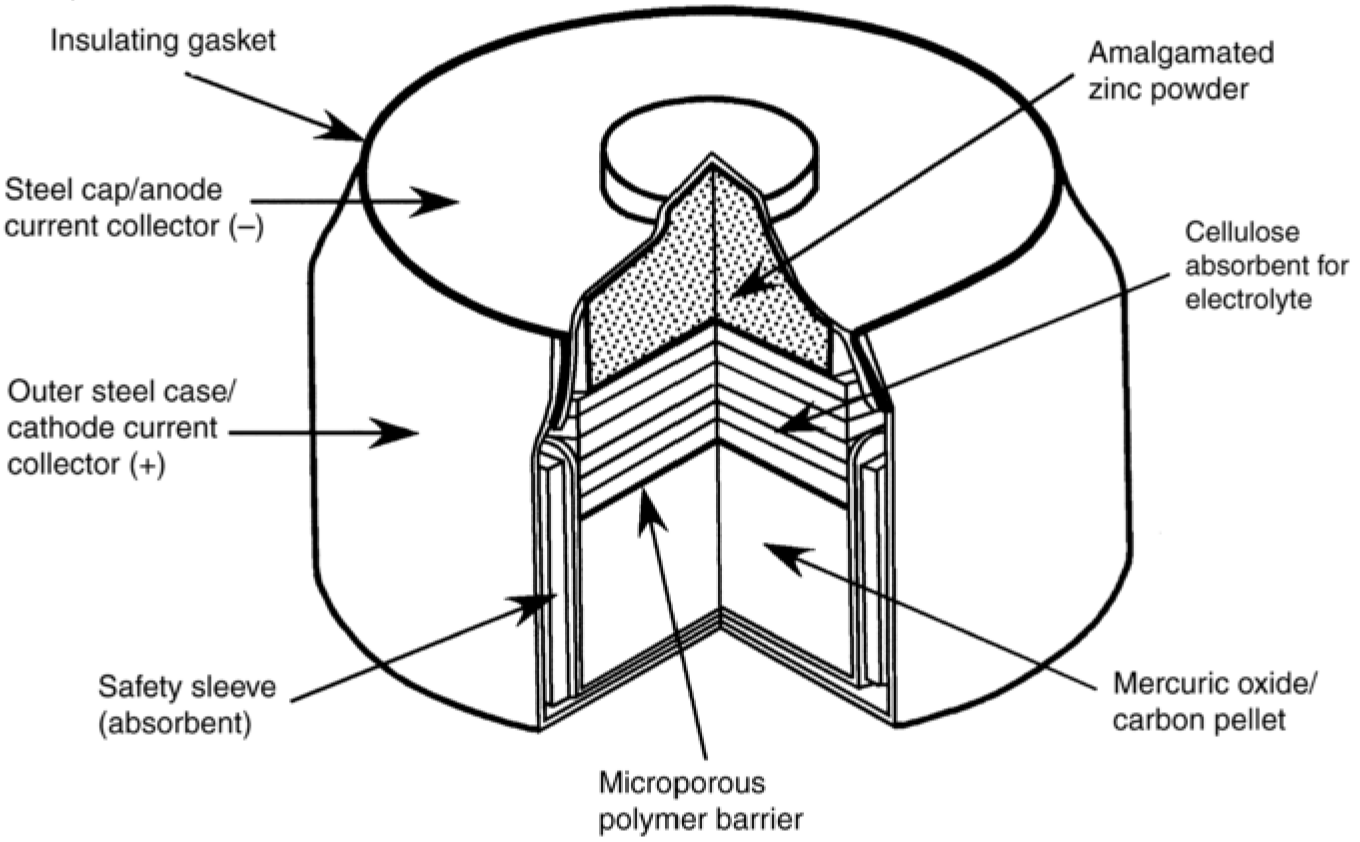

Fig. 3 Cross section of a typical mercury button cell. Source: Ref 2

The anode reaction (negative electrode) is:

$$Zn(s) + OH^-(aq) \rightarrow Zn(OH)_4^{2-}(aq) + 2e^- \quad \text{(Eq 7a)}$$

$$Zn(OH)_4^{2-}(aq) \rightarrow ZnO(s) + 2OH^-(aq) + H_2O(l) \quad \text{(Eq 7b)}$$

and the cathode reaction (positive electrode) is:

$$HgO(s) + H_2O(l) + 2e^- \rightarrow Hg(l) + 2OH^-(aq) \quad \text{(Eq 8)}$$

so that the overall reaction is:

$$Zn(s) + HgO(s) \rightarrow ZnO(s) + Hg(l) \quad \text{(Eq 9)}$$

In these reactions and those that follow, the state of the reactants is given: s, solid; l, liquid; aq, in aqueous solution; and g, gas.

Note that the sum of Eq 7a(a) and (b) is the half-cell corrosion reaction for zinc. It includes the oxidative dissolution of zinc metal, with the crystallization of ZnO from the electrolyte. How efficiently this reaction occurs, as well as how facile it is, partly determines the performance characteristics of this battery. The battery has a nominal cell voltage of 1.35 V and a typical practical specific energy of 0.100 kWh/kg at 20 °C (70 °F)

under favorable discharge conditions. The latter compares with a theoretical specific energy of 0.255 kWh/kg. Typical discharge curves (Ref 4) are shown in Fig. 4. Note that they have a particularly flat region II, extending to almost full cell capacity at low current drains, under constant discharge conditions. This behavior makes these batteries very stable voltage sources and explains why they are commonly used as reference standards in regulated power supplies and other devices.

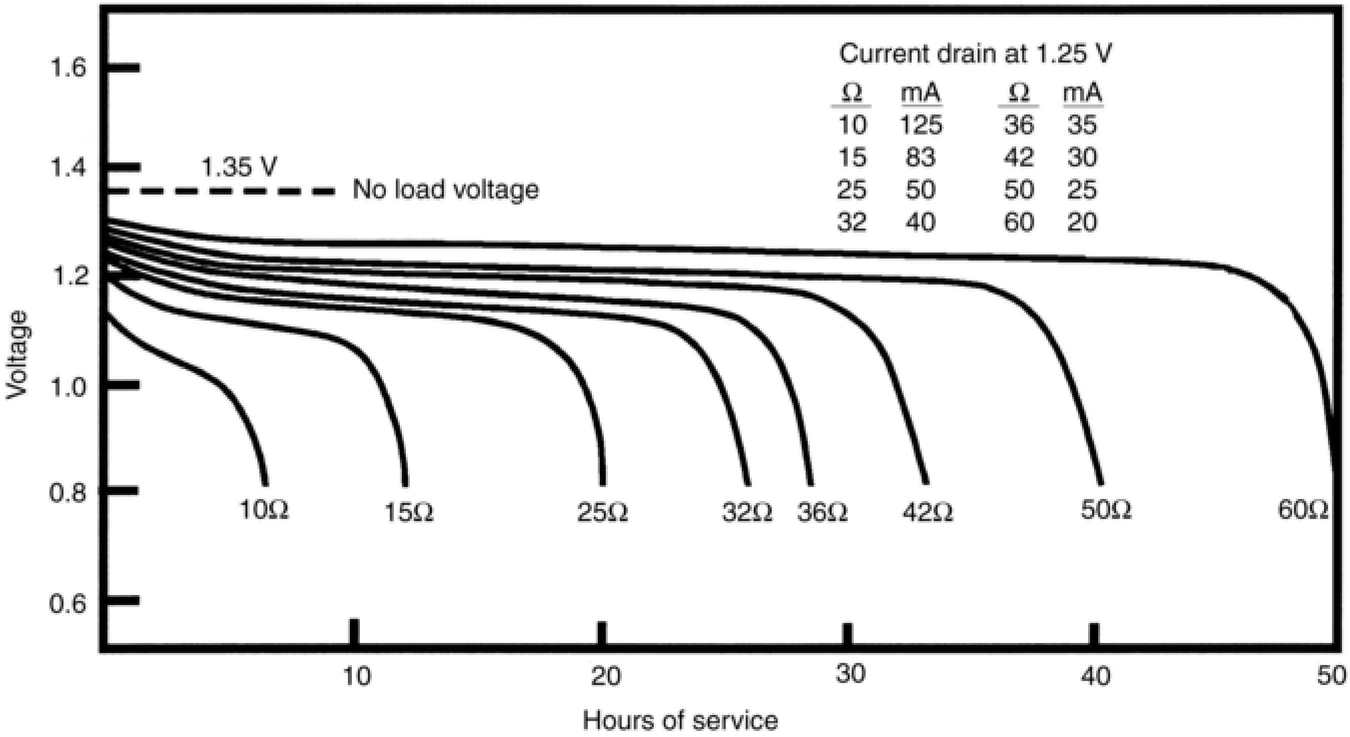

Fig. 4 Discharge curves for a typical Zn-HgO battery under various loads. Source: Ref 4

The mercury battery has some shortcomings, however. Low-temperature performance is not particularly favorable, especially when the current demands are low or intermittent. As shown in Fig. 5, there is a decrease in the capacity of the battery, similar, but to a different extent, for different configurations, when operated below room temperature (Ref 4). The behavior indicates a decreased rate of ion discharge of the zinc, which has been attributed to the growth of deposited ZnO on the anode. Low temperatures apparently favor precipitation of excessive ZnO, which functions as a resistive barrier and lowers the cell potential under constant current conditions. Again, note the focus here is on avoiding conditions where a resistive layer forms rather than on promoting their formation. Formation of protective films on battery metal anodes is favorable only when the films limit undesirable parasitic reactions, as discussed subsequently. If the films interfere in a negative way (by increasing overvoltage or limiting capacity) with the principal battery discharge reaction, they are undesirable. Over the years, much research in battery science has been devoted to controlling the growth of anode reaction products that adversely affect battery performance.

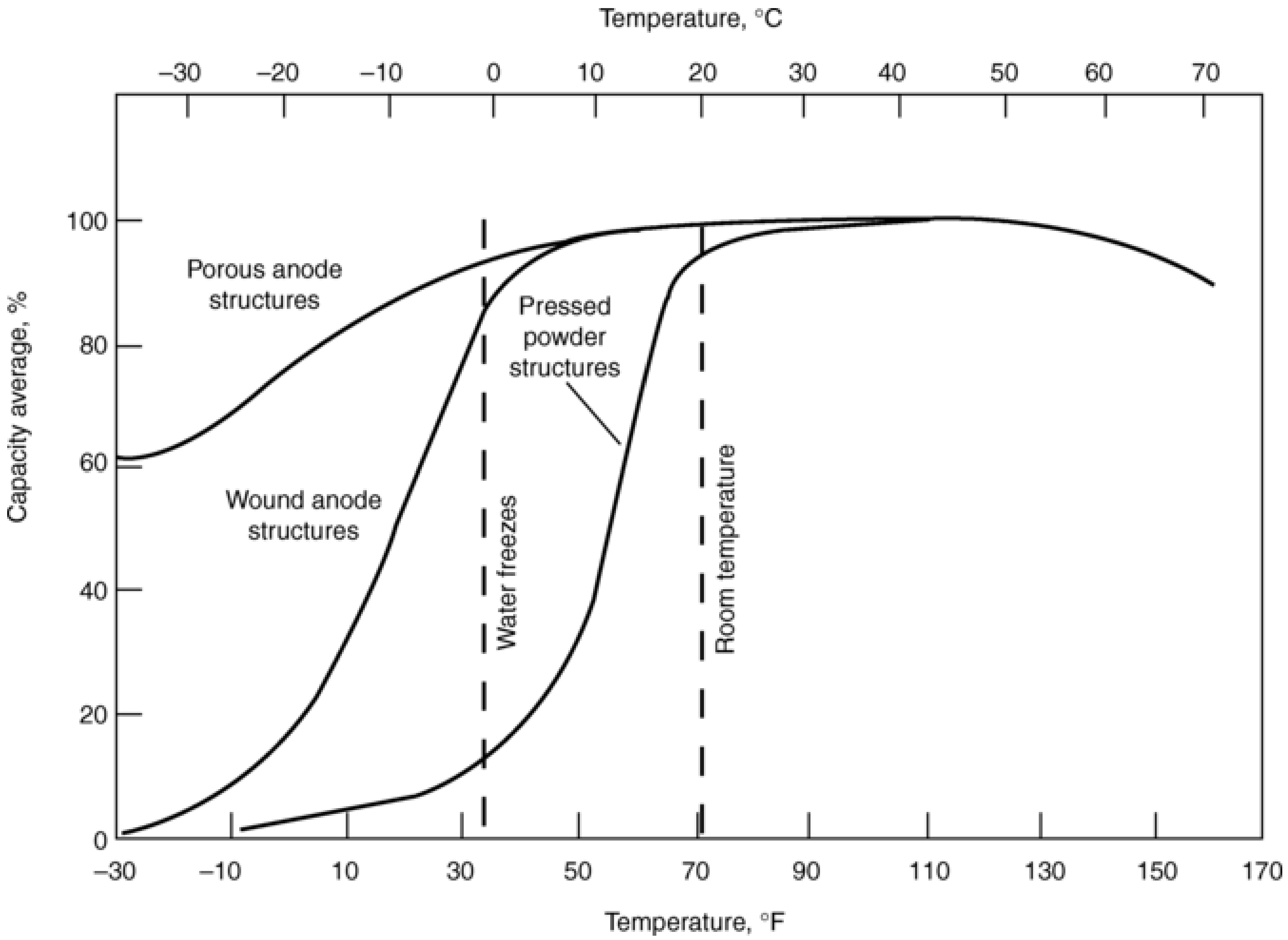

Fig. 5 Effect of temperature on the capacity of a Zn-HgO battery. The loss of capacity at lower temperatures due to ZnO formation is demonstrated, as is the sensitivity to anode morphology. Source: Ref 4

Another anode-related problem in the mercury battery system is the potential for hydrogen gas production. Usually, excess cathode material is incorporated in the battery to keep the battery reactions zinc-limited, (Ref 2), lessening the possibility that excess zinc in an exhausted battery could react directly with the electrolyte and liberate hydrogen. Even for a charged battery, however, the potential for hydrogen production is present, unless the overpotential for hydrogen is increased on the zinc anode. This is usually done by adding mercury or, preferably, another gassing inhibitor to the anode as an amalgam. Great attention is also paid to controlling impurities in the zinc, because minor amounts of these impurities can act as local cathodes on the zinc, promoting hydrogen generation.

Lithium Anode in the Rechargeable Lithium Battery. Primary batteries containing lithium-metal anodes have been available for some time and use a number of configurations employing several types of cathode materials, including both gases (SO_2) and solids (MnO_2, V_2O_5, FeS_2, and CuO). A cross-sectional view of a Li/MnO_2 coin cell is shown in Fig. 6. Secondary (rechargeable) versions of this battery system have been more problematic, however, largely because of safety issues related to hydrogen production and thermal runaway. These shortcomings, coupled with a continuous improvement in the performance of lithium-ion batteries, has largely halted further development of lithium-metal-based batteries in favor of their lithium-ion counterparts. This is unfortunate, because the highest energy densities available for lithium batteries are achieved using lithium metal as anodes. Batteries with lithium metal are also more likely to be cheaper than lithium-ion batteries containing composite anodes. More recently, developments involving new electrolyte systems (polyethylene oxide and its derivatives, and other organic electrolytes that polymerize or react to shut down the battery during runaway conditions) have shown promise in reducing some of the safety concerns and have caused somewhat of a revival in lithium-metal anode systems.

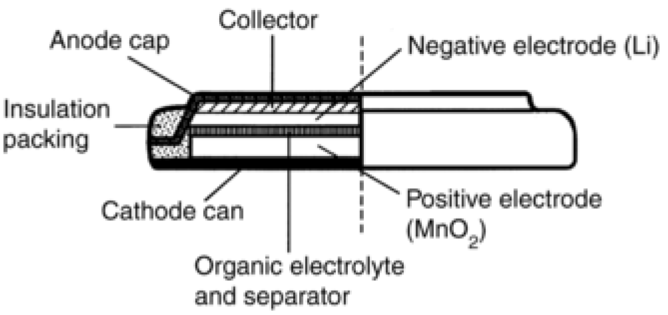

Fig. 6 Cross section of a Li/MnO_2 coin cell. Courtesy of Duracell, Inc.

A recent design for a rechargeable battery using a Li_xMnO_2 cathode was developed during the early 1990s (Ref 5). In this battery, the anode reaction (negative electrode) is the corrosion reaction for lithium:

$$Li(s) \rightarrow Li^+(dis) + e^- \quad \text{(Eq 10)}$$

while the cathode reaction (positive electrode) involves intercalation of the Li^+ ions, similar to the electrode processes in the lithium-ion battery systems. Early versions of this battery exhibited capacities greater than 190 Ah/kg but also required slow charging rates in order to realize hundreds of cycles from them. Consequently, some of the focus of recent work on these batteries is in understanding the changes associated with the lithium-metal anode that occur during charging and how these changes influence the charging capacity. The results of these studies prove to be an interesting example of how the morphology of the lithium metal deposited during charging is influenced by the charging conditions and how this morphology, in turn, influences the oxidation or (desired) corrosion reactions that occur during discharge.

As shown in Fig. 7, the cycle life of the Li- Li_xMnO_2 cell is significantly reduced at charging current densities above 0.3 mA/cm^2, although the drop-off in capacity levels off at approximately 100 cycles. This dramatic decrease has been associated with a decrease in the available active electrode area and an increase in the cell impedance (Ref 6). Careful analysis of lithium- metal electrodes cycled at different charging rates showed very different morphologies. Low charging rates favored the formation of larger lithium grains, while higher rates of charging gave very small grains. Moreover, the grain size was similarly smaller when the charging rate exceeded the value where the capacity leveled off in Fig. 7, indicating a direct correlation between grain size and cycle life. The implications on battery performance are clear. As the grains of lithium formed during charging become smaller, the amount of active surface area increases. While a larger surface area might be expected to favor the anode half-cell reaction, they also make the anode more reactive toward solution species. Higher reactivity causes more depletion of electrolyte during cycling, the formation of lithium- electrolyte reaction products (confirmed by analysis), and eventually, cell failure due to an increase in battery impedance.

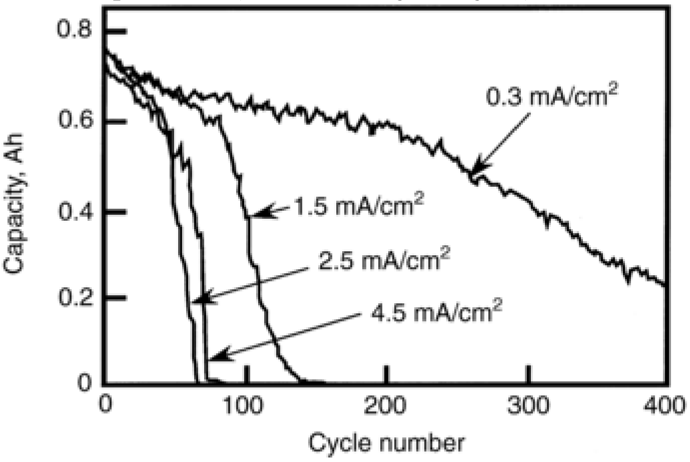

Fig. 7 Cycle life plots of Li-Li_xMnO_2 batteries discharged at 1.25 mA/cm^2 and different charging rates. Source: Ref 5

References cited in this section

1. D. Lindon, Ed., *Handbook of Batteries*, 2nd ed., McGraw-Hill, Inc., 1995

2. C. Vincent and B. Scrosati, *Modern Batteries: An Introduction to Electrochemical Power Sources,* 2nd ed., John Wiley and Sons, Inc., 1997

3. J.O'M. Bockris and A.K.N. Reddy, *Modern Electrochemistry,* Vol 2, Plenum Press, 1970

4. J.O'M. Bockris, B.E. Conway, E. Yeager, and R.E. White, Ed., *Comprehensive Treatise of Electrochemistry,* Vol 3, Plenum Press, 1981

5. P. Dan, E. Mengeritsky, Y. Geronov, D. Aurbach, and I. Weissman, *J. Power Sources,* Vol 54, 1995, p 143

6. D. Aurbach, E. Zinigrad, H. Teller, and P. Dan, *J. Electrochem. Soc.,* Vol 147, 2000, p 1274

C.F. Windisch, Jr., Anodes for Batteries, *Corrosion: Fundamentals, Testing, and Protection*, Vol 13A, *ASM Handbook*, ASM International, 2003, p 170–177

Anodes for Batteries

Charles F. Windisch, Jr., Pacific Northwest National Laboratory

---

Constructive Corrosion as Part of Battery Manufacturing

In addition to corrosion reactions playing the constructive central role as one of the half-cell reactions during the operation (discharge) of batteries with metal anodes, corrosion processes sometimes are employed during battery manufacturing to generate the active mass for electrodes. An example of this secondary constructive role of corrosion is in the preparation of the oxide pastes used to make the positive plates (specifically, the positive active mass, or PAM, on these plates) of the lead-acid battery.

Oxide Paste Fabrication in the Lead-Acid Battery. Despite on-going efforts to develop smaller and lighter alternatives, the lead-acid battery has continued to serve as one of the most successful power sources in automotive and allied applications for combined vehicle starting, vehicle lighting, and engine ignition. It has been in commercial use for more than a century. Its key advantages include low cost, excellent rechargeability, high cell voltage (2.2 V), good high-rate performance, and lower sensitivity to temperature than other batteries (Ref 2, 7).

The anode reaction (negative electrode) is:

$$Pb(s) \rightarrow Pb^{2+}(aq) + 2e^- \quad \text{(Eq 11a)}$$

$$Pb^{2+}(aq) + SO_4^{2+}(aq) \rightarrow PbSO_4(s) \quad \text{(Eq 11b)}$$

and the cathode reaction (positive electrode) is:

$$PbO_2(s) + 4H^+(aq) + 2e^- \rightarrow Pb^{2+}(aq) + H_2O(l) \quad \text{(Eq 12a)}$$

$$Pb^{2+}(aq) + SO_4^{2-}(aq) \rightarrow PbSO_4(s) \quad \text{(Eq 12b)}$$

The overall cell reaction is:

$$Pb(s) + PbO_2(s) + 2H_2SO_4(l) \rightarrow 2PbSO_4(s) + 2H_2O(l) \quad \text{(Eq 13)}$$

The formation of barely soluble lead sulfate at both the anode and cathode is one of the unique characteristics of this battery and leads to the overall process being called double sulfatation. The anode reaction involves oxidation (constructive corrosion) of the lead. Because the battery is rechargeable, the lead-metal microstructure evolves during subsequent discharging and charging cycles, leading to surface area/microstructure effects on oxidation similar to those discussed previously for lithium-metal batteries. In

particular, much research has focused on the prevention of anode passivation using chemical additives that promote more desirable polymorphs of lead sulfate.

The constructive corrosion of lead plays another important role in the lead-acid battery, however. This role involves the fabrication of the PAM for the cathode (positive electrode). The cathode reaction in the lead-acid battery involves the reduction of PbO_2(s) in the form of a paste that is in electrical contact with a lead-metal grid (Ref 1, 2, 7). The PbO_2(s) paste must be prepared according to specific procedures, developed after years of testing by the battery industry, in order to meet performance targets for the batteries. These procedures involve oxidizing (corroding) highly refined (usually virgin or primary) lead metal using either a Barton pot or a ball mill. In the Barton pot process, molten lead, sprayed into droplets, is heated in a pot-shaped vessel where it reacts with air. This produces solid particles of lead metal coated with a lead oxide (PbO). The amount of free lead left over is between 15 and 30%. In ball milling, lead-metal pieces are put into a rotary mechanical mill, resulting in the formation of small flakes that are then oxidized by a stream of air. The resulting oxides contain 15 to 30% free lead in the shape of flattened platelets coated by oxide.

The PbO/Pb feedstock described previously is often mixed with additional oxide, red lead (Pb_3O_4), and then converted to a plastic, doughy material by mixing with water and sulfuric acid in a pony mixer. The resulting paste is used to coat the lead grids. Once the grids are coated, the paste is cured in air. Later, after battery assembly is completed, an additional formation step converts the paste to a fully charged active mass. During the curing process, at temperatures ranging between 25 and 90 °C (77 and 195 °F), depending on humidity, the balance of the metallic lead is oxidized (corroded). Proper curing conditions have been another area of extensive study by the industry. Different combinations of lead oxides and sulfates, with different degrees of hydration, are obtained under various conditions of temperature, airflow, and humidity. Clearly, corrosion of the residual free lead during curing partly determines the composition and structure of the final mixture of lead oxides that makes up the PAM, one of the most important determinants of lead-acid battery performance.

References cited in this section

1. D. Lindon, Ed., *Handbook of Batteries,* 2nd ed., McGraw-Hill, Inc., 1995

2. C. Vincent and B. Scrosati, *Modern Batteries: An Introduction to Electrochemical Power Sources,* 2nd ed., John Wiley and Sons, Inc., 1997

7. D. Pavlov, Power Sources for Electric Vehicles, *Studies in Electrical and Electronic Engineering 11,* B.D. McNicol and D.A.J. Rand, Ed., Elsevier, 1984, p 111–511

C.F. Windisch, Jr., Anodes for Batteries, *Corrosion: Fundamentals, Testing, and Protection*, Vol 13A, *ASM Handbook*, ASM International, 2003, p 170–177

Anodes for Batteries

Charles F. Windisch, Jr., Pacific Northwest National Laboratory

---

Destructive Corrosion

There are also a number of important examples of corrosion specific to batteries that are destructive and undesirable, and these have been the focus of extensive study by the battery industry. It would seem incomplete, therefore, if some discussion of at least one or two cases of this type of corrosion was not included here. These corrosion processes involve parasitic reactions that destroy electrode materials, with consequences including loss of active mass, pollution of the electrolyte, passivation or precipitate formation that increases internal resistance or interferes with the normal charging process, and the generation of gases, with associated safety risks.

Shelf Reactions in Zinc-Carbon Batteries. Shelf reactions in batteries are reactions that occur during storage or when the battery is not in use. One of the most important types of shelf reactions is corrosion of metallic electrodes, both anodes and cathodes. In zinc-carbon batteries, corrosion problems involve the zinc anode. Other components in this cell include a manganese dioxide cathode and an electrolyte of ammonium chloride and/or zinc chloride dissolved in water. When only zinc chloride is used, the battery is called a zinc chloride battery to distinguish it from the Leclanche cell, where ammonium chloride is the primary electrolyte component.

There is more than one proper discharge reaction for zinc-carbon cells, depending on the magnitude of discharge and the type of electrolyte (Ref 1). In all cases, the anode reaction involves the oxidation of zinc metal:

$$Zn(s) \rightarrow Zn^{2+}(aq) + 2e^- \qquad \text{(Eq 14)}$$

with the Zn^{2+} ions then undergoing various complexation reactions with hydroxide, chloride, and ammonia.

When undesirable corrosion of the zinc anode occurs during storage, the zinc reacts directly with the electrolyte according to three mechanisms (Ref 2). These reactions rob fuel from the battery and generate corrosion products that degrade battery performance and/or raise safety concerns. When oxygen is present:

$$Zn(s) + 2NH_4^+(aq) + Cl^-(aq) + 1/2O_2(g) \rightarrow Zn(NH_3)_2Cl_2(s) + H_2O(l) \qquad \text{(Eq 15)}$$

Obviously, this reaction can be minimized by proper sealing of the battery container.

In the absence of oxygen, however, corrosion can still occur according to the following reaction:

$$Zn(s) + 2NH_4^+(aq) + Cl^-(aq) \rightarrow Zn(NH_3)_2Cl_2(s) + H_2(g) \qquad \text{(Eq 16)}$$

This corrosion reaction is normally slow, because there is a significant overvoltage for H_2 generation on zinc under cell storage conditions. However, the presence of minor impurities in the metal (such as nickel, iron, and copper) can reduce this overvoltage significantly, allowing the reaction in Eq 16 to occur and H_2 to be generated. Interestingly, the metallic impurities can be generated by Ni^{2+}, Fe^{2+}, and Cu^{2+} ions in the electrolyte according to the following type of reaction, which is also the third mechanism for corrosion of the zinc anode:

$$Zn(s) + Fe^{2+}(aq) \rightarrow Zn^{2+}(aq) + Fe(s) \qquad \text{(Eq 17)}$$

The reaction in Eq 17 can also involve Ni^{2+} and Cu^{2+} ions in the electrolyte and usually occurs at local sites on the anode, as shown in Fig. 8. These local cells can generate large amounts of H_2 as well as the metallic impurities that promote additional corrosion according to the reaction in Eq 16. Furthermore, the reaction products may be generated in the form of large dendrites that result in short circuiting of the cells.

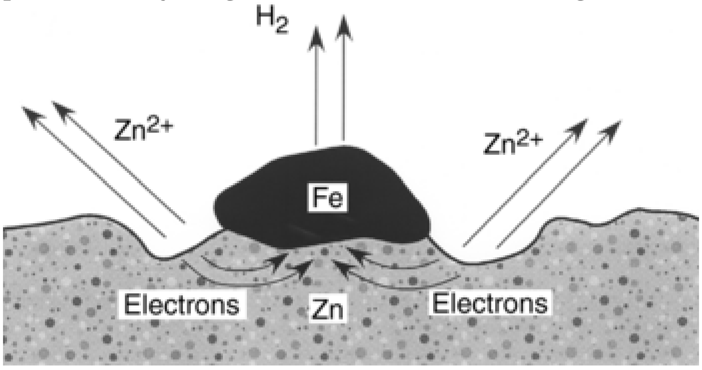

Fig. 8 Schematic showing zinc dissolution due to local corrosion of a zinc anode in a zinc-carbon battery. Source: Ref 2

Inhibition of the last two types of corrosion (i.e., occurring with or without oxygen) is usually accomplished by appropriately modifying the morphology and composition of the anode and the composition of the electrolyte. Amalgamation of the zinc with mercury, using a mercury salt added to the electrolyte, for example, results in an increase in overvoltage for hydrogen production and fosters the dissolution of surface impurities, lessening the possibility that they will form local electrochemical couples with the zinc. The mercury also promotes a more desirable smooth surface on the zinc that disfavors the occurrence of corrosion sites. Recent concerns about safety, however, have necessitated replacements for mercury. Current versions of zinc-carbon cells use higher-purity zinc anodes and electrolyte to lessen the role of the reactions in Eq 16 and 17, as well as tighter cell

casings to reduce air contamination. Other corrosion inhibitors are also used, including chromates, organic surfactants, and chelating agents.

Lead Grid Corrosion in the Lead-Acid Battery. The lead grids used in the lead-acid battery are subject to corrosion reactions during battery storage similar to the zinc anodes in the zinc- carbon battery. For the lead-acid battery, however, corrosion reactions can also occur and cause problems at the positive electrode (cathode), because both electrodes use a lead grid as part of the electrode assembly. Moreover, they can occur during battery operation. Premature capacity loss, an important mode of performance failure in lead-acid batteries, is sometimes attributed to the formation or changes of corrosion layers at the positive electrode during battery operation (Ref 8, 9, 10).

The corrosion reactions at the positive electrode (cathode) during battery operation usually involve the reaction of the lead in the grid with oxygen that diffuses through the oxide layers on the grid or by self-discharge, where lead reacts directly with PbO_2. The composition of these oxide layers is very complicated and has been the subject of much study by the lead-acid battery industry. In general, the oxide next to the grid is a corrosion layer, initially formed during one or more steps in the battery manufacture, and is composed of two parts (Ref 10), as shown in Fig. 9. Closer to the lead metal there is a thin, dense corrosion layer of oxide with the lead ions in a reduced state, nominally PbO, that can protect the grid from corrosion but can also add a resistive component to the circuit. A second, outer layer is porous and nominally composed of PbO_2. It should be recognized that both oxide layers are actually nonstoichiometric and vary through their thickness. Understanding the composition of these layers and how they are influenced by metal composition and treatment conditions is an area of major interest to the lead-acid battery industry. On top of the corrosion layer is the PAM, composed of mostly PbO_2, although, here again, the chemistry is more complicated, involving differing polymorphs of PbO_2 and distributions based on manufacturing conditions. Battery performance, of course, depends on many of these varying parameters, involving both the corrosion layers and the PAM.

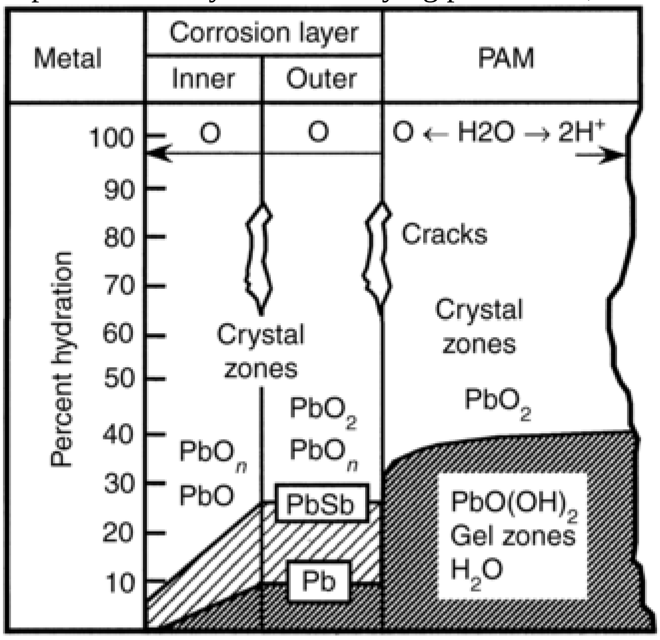

Fig. 9 Schematic of corrosion layers on Pb and Pb-Sb grids in the positive electrode in a lead-acid battery as proposed by Pavlov. The structural elements are positioned along the abscissa. The interface between the metal and the inner corrosion sublayer is used as the ordinate, where the percent of hydration of the separate structural elements of the plate are presented. In general, the outer corrosion sublayer is hydrated in the form of a gel. The degree of hydration is approximately 10% in pure Pb electrodes, whereas it varies between 15 and 25% in Pb-Sb electrodes. There is 30 to 35% hydration of the positive active mass (PAM). Percent hydration refers to percentage contributed by $Pb(OH)_2$, gel zones, and H_2O. Source: Ref 9

Corrosion of the positive electrode (cathode) during battery operation involves diffusion of oxygen through the corrosion layers. As it diffuses and before it reaches the metal grid, the oxygen also reacts with the various substoichiometric oxides that make up the corrosion layer:

$Pb + O \rightarrow PbO$ (Eq 18)

$PbO + (n - 1)O \rightarrow PbO_n$ $(1 < n < 2)$ (Eq 19)

$PbO_n + (2 - n)O \rightarrow PbO_2$ (Eq 20)

Depending on the rates of the various reactions in Eq 18, Eq 19, Eq 20, corrosion layers of varying composition and properties are formed. If the reaction in Eq 18 is rapid, mostly PbO forms, and the corrosion layer evolves into a thin, highly resistive, passive layer. In other words, formation of the inner corrosion layer is favored. Alternatively, if the reactions in Eq 19 and 20 are favored, the corrosion products become more loaded with electrochemically active PbO_2. This more porous structure has lower ohmic resistance but, in the absence of an inner corrosion layer, offers little protection to the lead grid for further corrosion. Understanding how battery operating conditions and compositional parameters influence the various rates of the reactions in Eq 18, Eq 19, Eq 20, therefore, becomes important. Achieving an inner corrosion layer with good conductivity and adequate passivating quality, while at the same time affording an outer corrosion layer with good electrochemical activity and contact with the PAM, requires tailoring conditions to obtain appropriate reaction rates that favor PbO_n in the inner layer. Antimony, tin, and bismuth grid-alloy additives are commonly used for this purpose (Fig. 10).

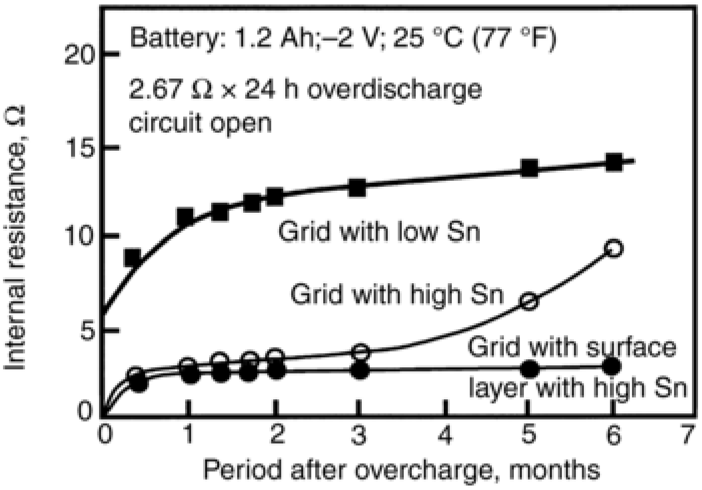

Fig. 10 Effect of tin on internal resistance of lead alloys or lead grids with a tin-rich coating during overcharge conditions in a lead-acid battery. Source: Ref 10

References cited in this section

1. D. Lindon, Ed., *Handbook of Batteries,* 2nd ed., McGraw-Hill, Inc., 1995

2. C. Vincent and B. Scrosati, *Modern Batteries: An Introduction to Electrochemical Power Sources,* 2nd ed., John Wiley and Sons, Inc., 1997

8. D. Pavlov, *J. Power Sources,* Vol 46, 1993, p 171

9. D. Pavlov, *J. Power Sources,* Vol 48, 1994, p 179

10. D. Pavlov, *J. Power Sources,* Vol 53, 1995, p 9

C.F. Windisch, Jr., Anodes for Batteries, *Corrosion: Fundamentals, Testing, and Protection,* Vol 13A, *ASM Handbook,* ASM International, 2003, p 170–177

Anodes for Batteries

Charles F. Windisch, Jr., Pacific Northwest National Laboratory

Conclusions

The previous discussion is a brief overview of how corrosion in batteries occurs, with both constructive and destructive results. Factors related to its constructive roles, both thermodynamic and kinetic, are virtually identical to those related to destructive roles, both in batteries and elsewhere. These factors include Gibbs free-energy considerations, the magnitude of overpotentials, and the presence and mechanisms of competing reactions. However, what scientists and engineers seek to do with these factors is completely opposite for the two cases. When corrosion is constructive, that is, metal anode oxidation during normal battery operation, the emphasis is on obtaining the most negative free- energy change and reducing overpotentials for the primary anode reaction. When corrosion is destructive, that is, self-discharge during storage or parallel corrosion reactions during operation, the focus is on the most positive free-energy change and finding ways to increase the overpotentials for these undesirable reactions.

C.F. Windisch, Jr., Anodes for Batteries, *Corrosion: Fundamentals, Testing, and Protection*, Vol 13A, *ASM Handbook,* ASM International, 2003, p 170–177

Anodes for Batteries

Charles F. Windisch, Jr., Pacific Northwest National Laboratory

References

1. D. Lindon, Ed., *Handbook of Batteries,* 2nd ed., McGraw-Hill, Inc., 1995
2. C. Vincent and B. Scrosati, *Modern Batteries: An Introduction to Electrochemical Power Sources,* 2nd ed., John Wiley and Sons, Inc., 1997
3. J.O'M. Bockris and A.K.N. Reddy, *Modern Electrochemistry,* Vol 2, Plenum Press, 1970
4. J.O'M. Bockris, B.E. Conway, E. Yeager, and R.E. White, Ed., *Comprehensive Treatise of Electrochemistry,* Vol 3, Plenum Press, 1981
5. P. Dan, E. Mengeritsky, Y. Geronov, D. Aurbach, and I. Weissman, *J. Power Sources,* Vol 54, 1995, p 143
6. D. Aurbach, E. Zinigrad, H. Teller, and P. Dan, *J. Electrochem. Soc.,* Vol 147, 2000, p 1274
7. D. Pavlov, Power Sources for Electric Vehicles, *Studies in Electrical and Electronic Engineering 11,* B.D. McNicol and D.A.J. Rand, Ed., Elsevier, 1984, p 111–511
8. D. Pavlov, *J. Power Sources,* Vol 46, 1993, p 171

9. D. Pavlov, *J. Power Sources,* Vol 48, 1994, p 179

10. D. Pavlov, *J. Power Sources,* Vol 53, 1995, p 9

M.C. Williams, Fuel Cells, *Corrosion: Fundamentals, Testing, and Protection*, Vol 13A, *ASM Handbook*, ASM International, 2003, p 178–186

Fuel Cells

Mark C. Williams, U.S. Department of Energy, National Energy Technology Laboratory

Introduction

FUEL CELLS are electrochemical devices that convert the chemical energy of a reaction directly into electrical energy, water, and heat. In principle, a fuel cell operates like a battery, but does not run down or require recharging as long as hydrogen-rich fuel is supplied. The basic physical structure or building block of most fuel cells consists of an electrolyte layer in contact with porous anode and cathode electrodes on either side. Figure 1 is a simplified diagram that demonstrates how a fuel cell works.

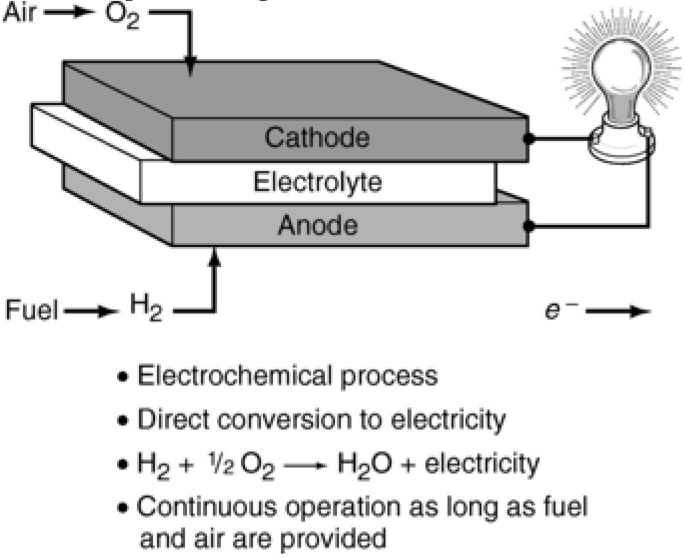

Fig. 1 Schematic of a fuel cell

In a typical fuel cell, gaseous fuels are fed continuously to the anode (negative electrode) compartment, and an oxidant, such as oxygen from air, is fed continuously to the cathode (positive electrode) compartment. Encouraged by a catalyst, the hydrogen atom oxidizes into a proton (H^+) and an electron (e^-) that take different paths to the cathode. The proton passes through the electrolyte. The electrons create a separate current that can be utilized before they return to the cathode to form O^{2-}. The oxygen ion then reunites with the proton to form a molecule of water.

A fuel-cell system that includes a fuel reformer can utilize the hydrogen from any hydrocarbon fuel, from natural gas to methanol, and even gasoline. Gaseous hydrogen has become the fuel of choice for most applications, because of its high reactivity when suitable catalysts are used, its ability to be produced from hydrocarbons for terrestrial applications, and its high energy density when stored cryogenically for closed-environment applications, such as in space. Similarly, the most common oxidant is gaseous oxygen, which is readily and economically available from air for terrestrial applications and is also easily stored in a closed environment. Since the fuel cell relies on chemistry and not combustion, emissions from this type of system would still be much smaller than emissions from the cleanest fuel-combustion processes.

In reality, degradation primarily from corrosion limits the practical operating life of fuel cells. Components must meet certain general requirements in order to be useful. No components may exhibit any significant changes in volume between room temperature and the fabrication temperature. The components must be chemically stable in order to limit chemical interactions with other cell components. They must have similar thermal expansion in order to minimize thermal stresses that may cause cracking and delamination during thermal cycling or fabrication. It is also desirable that fuel-cell components have high strength and durability, are easy to fabricate, and are relatively inexpensive.

M.C. Williams, Fuel Cells, *Corrosion: Fundamentals, Testing, and Protection*, Vol 13A, *ASM Handbook*, ASM International, 2003, p 178–186

Fuel Cells

Mark C. Williams, U.S. Department of Energy, National Energy Technology Laboratory

---

Performance

The ideal performance of a fuel cell depends on the electrochemical reactions that occur between different fuels and oxygen. Low-temperature fuel cells—polymer electrolyte (PEFC), alkaline (AFC), and phosphoric acid (PAFC)— require noble metal electrocatalysts to achieve practical reaction rates at the anode and cathode, and H_2 is the only acceptable fuel. With high- temperature fuel cells—molten carbonate (MCFC) and solid oxide (SOFC), for example— the requirements for catalysis are relaxed, and the number of potential fuels expands. (Other types of fuel cells are not addressed in this article.) For example, carbon monoxide “poisons” a noble metal anode catalyst such as platinum in low-temperature fuel cells, but it competes with H_2 as a reactant in high-temperature fuel cells where nonnoble metal catalysts such as nickel can be used. Table 1 shows the types and associated electrochemical reactions that occur in fuel cells.

Table 1 Electrochemical reactions in fuel cells

Fuel cell	Anode reaction	Cathode reaction
Polymer electrolyte (PEFC)	$H_2 \rightarrow 2H^+ + 2e^-$	$\frac{1}{2}O_2 + 2H^+ + 2e^- \rightarrow H_2O$
Phosphoric acid (PAFC)	$H_2 \rightarrow 2H^+ + 2e^-$	$\frac{1}{2}O_2 + 2H^+ + 2e^- \rightarrow H_2O$
Alkaline (AFC)	$H_2 + 2(OH)^- \rightarrow 2H_2O + 2e^-$	$\frac{1}{2}O_2 + H_2O + 2e^- \rightarrow 2(OH)^-$
Molten carbonate (MCFC)	$H_2 + CO_3^{2-} \rightarrow H_2O + CO_2 + 2e^-$ $CO + CO_3^{2-} \rightarrow 2CO_2 + 2e^-$	$\frac{1}{2}O_2 + CO_2 + 2e^- \rightarrow CO_3^{2-}$
Solid oxide (SOFC)	$H_2 + O^{2-} \rightarrow H_2O + 2e^-$ $CO + O^{2-} \rightarrow CO_2 + 2e^-$ $CH_4 + 4O^{2-} \rightarrow 2H_2O + CO_2 + 8e^-$	$\frac{1}{2}O_2 + 2e^- \rightarrow O^{2-}$

In addition to H_2, CO and CH_4 are shown in Table 1 as undergoing oxidation. In actuality, insignificant direct oxidation of the CO and CH_4 may occur. It is common systems-analysis practice to assume that H_2, the more readily oxidized fuel, is produced by CO and CH_4 reacting (at equilibrium) with H_2O through the water-gas shift ($CO + H_2O \rightarrow H_2 + CO_2$) and steam-reforming reactions ($CH_4 + H_2O \rightarrow 3H_2 + CO$), respectively. The H_2 calculated to be produced from CO and CH_4, along with any H_2 in the fuel- supply stream, is referred to as equivalent H_2. The temperature and catalyst of state-of-the-art MCFCs provide the proper environment for the water-gas shift reaction to produce H_2 and CO_2 from CO and H_2O. An MCFC that reacts only with H_2 and CO is known as an external-reforming (ER) MCFC. An internal-reforming (IR) MCFC has a reforming catalyst

placed in proximity to the anode to promote the reforming reaction to produce H_2 and CO_2 from CH_4 and H_2O. The direct oxidation of CO and CH_4 in a high-temperature SOFC is feasible without the catalyst, but again the direct oxidation of these fuels is not as favorable as the water-gas shift of CO to H_2 and reforming of CH_4 to H_2. These are critical arguments in determining the equations to describe the electrical characteristics and the energy balance of the various types of cells. It is fortunate that converting CO and CH_4 to equivalent H_2 then reacting within the cell simplifies the prediction of the electrochemical behavior of the fuel cell.

The actual cell potential is decreased from its equilibrium potential because of irreversible losses. Multiple phenomena contribute to irreversible losses in an actual fuel cell. These losses are called polarization, overpotential, or overvoltage (η), and they originate primarily from three sources: activation polarization (η_{act}), ohmic polarization (η_{ohm}), and concentration polarization (η_{conc}). These losses result in a cell voltage (V_{cell}) that is less than its ideal voltage (E). The summary equation

$$V_{cell} = \Delta E_e - |\eta_{cathode}| - |\eta_{anode}| - iR$$

where $\Delta E_e = E_{cathode} - E_{anode}$, i is the current flowing through the cell, and R is the total cell resistance including electronic, ionic, and contact resistances.

This equation shows that current flow in a fuel cell results in a decrease in the cell voltage because of losses by electrode and ohmic polarizations. The goal of fuel-cell developers is to minimize the polarization so that V_{cell} approaches ΔE_e. This goal is approached by modifications to fuel-cell design (improvement in electrode structures, better electrocatalysts, more conductive electrolyte, thinner cell components, etc.). For a given cell design, it is possible to improve the cell performance by modifying the operating conditions, for example higher gas pressure, higher temperature, or a change in gas composition to lower the gas-impurity concentration. However, for any fuel cell, compromises exist between achieving higher performance by operating at higher temperature or pressure and the problems associated with the stability or durability of cell components encountered under more severe conditions.

As shown in Fig. 2, the activation-polarization loss is dominant at low current density. At this point, electronic barriers must be overcome prior to current and ion flow. Activation losses increase as current increases. Ohmic polarization (loss) varies directly with current, increasing over the entire range of current because cell resistance remains essentially constant. Gas-transport losses (concentration polarization) occur over the entire range of current density, but they become prominent at high limiting currents where it becomes difficult to provide enough reactant flow to the cell-reaction sites.

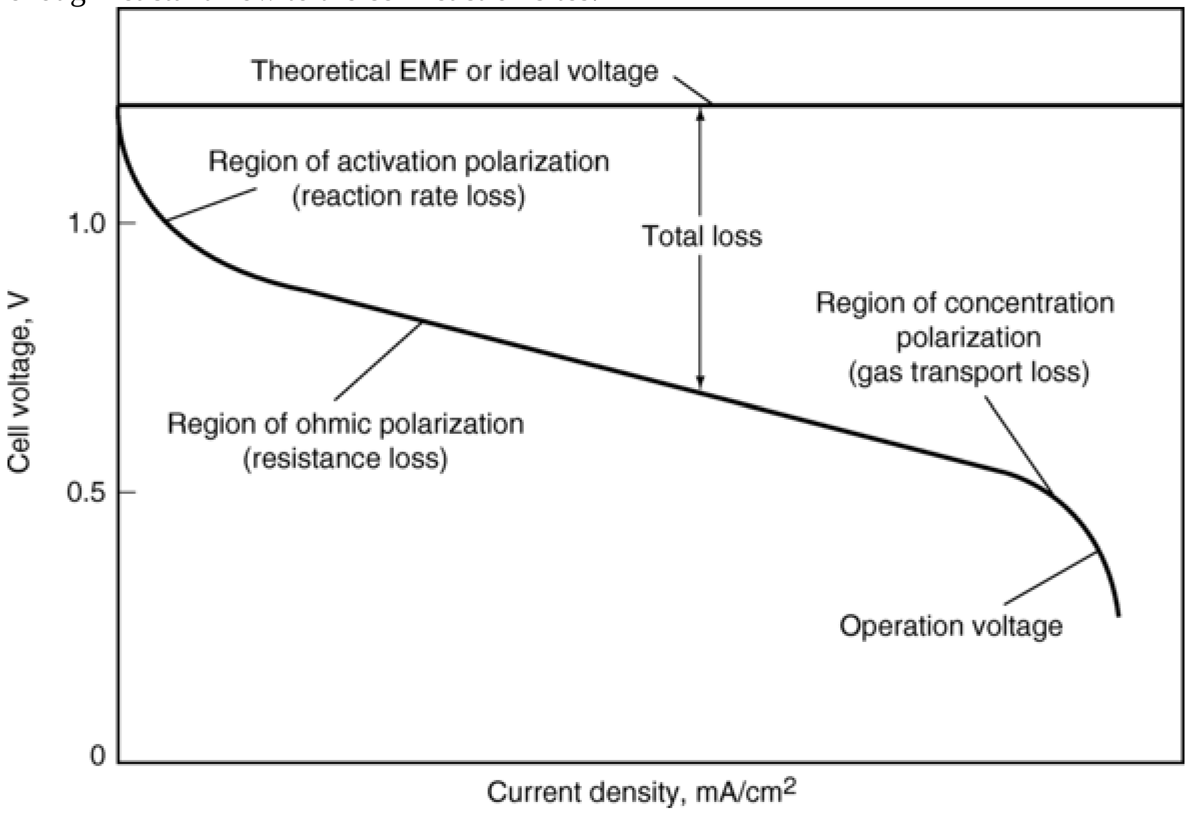

Fig. 2 Ideal and actual fuel-cell voltage versus current density characteristics

Changing the cell-operating parameters (temperature and pressure) can have either a beneficial or a detrimental impact on fuel-cell performance and on the performance of other system components. These effects may be offsetting. Changes in operating conditions may lower the cost of the cell, but increase the cost of the surrounding system. Compromises in the operating parameters are usually necessary to meet the application requirements, obtain lowest system cost, and achieve acceptable cell life. Operating conditions are based on defining specific system requirements, such as power level, voltage, or system weight. From this and through interrelated systems studies, the power, voltage, and current requirements of the fuel-cell stack and individual cells are determined. It is a matter of selecting a cell operating point (cell voltage and related current density) until the design requirements are satisfied (such as lowest cost, lightest unit, highest power density). For example, a design point at high current density will allow a smaller cell size at lower capital cost to be used for the stack, but the result is a lower system efficiency (because of the lower cell voltage) and attendant higher operating cost. This type of operating point would be typified by a vehicle application where light weight and small volume are important drivers for cost effectiveness. Operating at a lower current density, but higher voltage (higher efficiency, lower operating cost) would be more suitable for stationary power- plant operation. It is evident that the selection of the cell design point interacts with the application objectives.

M.C. Williams, Fuel Cells, *Corrosion: Fundamentals, Testing, and Protection*, Vol 13A, *ASM Handbook*, ASM International, 2003, p 178–186

Fuel Cells

Mark C. Williams, U.S. Department of Energy, National Energy Technology Laboratory

---

Fuel-Cell Technology Overview

The most common classification of fuel cells begins with the type of electrolyte used in the cells as listed in the order of approximate operating temperature:

Fuel cell	Approximate operating temperature	
	°C	**°F**
Polymer electrolyte (PEFC)	80	175
Alkaline (AFC)	100	212
Phosphoric acid (PAFC)	200	390
Molten carbonate (MCFC)	650	1200
Solid oxide (SOFC)	600–1000	1110–1830

The operating temperature and useful life of a fuel cell dictate the physicochemical and thermomechanical properties of materials used in the cell components such as electrodes, electrolyte, interconnect, and current collector. Aqueous electrolytes are limited to temperatures of about 200 °C (390 °F) or lower because of their high water vapor pressure and/or rapid degradation at higher temperatures. The operating temperature also plays an important role in dictating the type of fuel that can be used in a fuel cell. The low- temperature fuel cells with aqueous electrolytes are, in most practical applications, restricted to hydrogen as a fuel. In high-temperature fuel cells, CO and even CH_4 can be used because of the inherently rapid electrode kinetics and the lesser need for high catalytic activity at high temperature. However, descriptions later in this section note that the higher-temperature cells can favor the conversion of CO and CH_4 to hydrogen, then use the equivalent hydrogen as the actual fuel. Major differences among the various cells are shown in Table 2. A detailed description of these fuel cells can be found in Ref 1.

Table 2 Summary of major differences of the fuel-cell types

	PEFC	AFC	PAFC	MCFC	SOFC
Electrolyte	Ion-exchange membranes	Mobilized or immobilized potassium hydroxide	Immobilized liquid phosphoric acid	Immobilized liquid molten carbonate	Ceramic
Operating temperature °C (°F)	80 (175)	65–220 (150–430)	205 (400)	650 (1200)	600–1000 (1110–1830)
Charge carrier	H^+	OH^-	H^+	CO_3^{2-}	O^{2-}
External reformer for CH_4	Yes	Yes	Yes	No	No
Prime cell components	Carbon-base	Carbon-base	Graphite-base	Stainless-base	Ceramic
Catalyst	Platinum	Platinum	Platinum	Nickel	Perovskites
Product water management	Evaporative	Evaporative	Evaporative	Gaseous product	Gaseous product
Product heat management	Process gas + independent cooling medium	Process gas + electrolyte calculation	Process gas + independent cooling medium	Internal reforming + process gas	Internal reforming + process gas

Polymer-Electrolyte Fuel Cells. Because of the intrinsic nature of the materials used, the polymer-electrolyte fuel cell, also commonly referred to as proton-exchange membrane (PEM), operates at temperatures less than 100 °C (212 °F), typically in the 60 to 80 °C (140 to 175 °F) range. When compared to other fuel cells, PEFC technology has been capable of very high current densities: while most technologies can operate up to approximately 1 A/cm^2, the polymer-membrane cell has operated at up to 4 A/cm^2 (Ref 2). This ability is due primarily to the membrane used. Other desirable attributes include fast-start capability and rapid response times to load changes. Because of the high power density capability, smaller, lighter-weight stacks are possible. Other beneficial attributes of the cell include no corrosive fluid hazard and lower sensitivity to orientation. As a result, the PEFC is particularly suited for vehicular-power application. Transportation applications suggest that the fuel of choice might be of comparable energy density to gasoline, although hydrogen storage on board in the form of pressurized gas and the partial oxidation of gasoline are being considered. The PEFC is also being considered widely for stationary-power applications, perhaps using natural gas or other hydrogen-rich gases.

The low operating temperature of a PEFC has both advantages and disadvantages. Low-temperature operation is advantageous because the cell can start from ambient conditions quickly, especially when pure hydrogen fuel is available. It is a disadvantage in CO-containing fuel streams, because carbon will attack or poison the platinum catalyst sites, masking the catalytic activity and reducing cell performance. The effect is reversible by flowing a CO-free gas over the electrode. To minimize the CO poisoning, operating temperatures must be greater than 120 °C (250 °F), at which point there is a reduction in chemisorption and electrooxidation. Due to CO affecting the anode, only a few ppm of CO can be tolerated at 80 °C (175 °F). Because reformed and shifted hydrocarbons contain about 1% CO, a mechanism to eliminate CO in the fuel gas is needed. This can be accomplished with preferential oxidation (PROX) that selectively oxidizes CO relative to H_2 using a precious metal catalyst. The low operating temperature also means that little, if any, heat is available from the fuel cell for endothermic reforming (Ref 3).

Recent PEFC development has focused on operation in the 160 °C (320 °F) range using an ion-exchange membrane, polybenzimidazole (PBI). The higher operating temperature eliminates CO poisoning by eliminating CO occlusion of the platinum sites. Also, this operating regime provides higher-quality heat for possible use in stationary combined heat/power (CHP) applications. Because PBI requires significantly lower water content to facilitate proton transport, an additional benefit is that water management is dramatically simplified (Ref 4).

Both temperature and pressure have a significant influence on cell performance. Present cells operate at 80 °C (175 °F) over a gage pressure range of 0.0010 to 1.0 MPa (~0.1 to 150 psig). Nominally, 0.285 MPa (40 psig) is

used for some transportation applications (Ref 5). Using appropriate current collectors and supporting structure, polymer-electrolyte fuel cells and electrolysis cells should be capable of operating at pressures up to 20 MPa (3000 psi) and differential pressures up to 3.5 MPa (500 psi).

The standard electrolyte material in PEFCs belongs to the fully fluorinated Teflon-based family similar to that produced by E.I. DuPont de Nemours & Company, Inc. for space application in the mid-1960s. The membrane is characterized by its equivalent weight (inversely proportional to the ion-exchange capacity). A typical equivalent weight range is 800 to 1100 milliequivalents per dry gram of polymer. The type used most often in the past was Nafion No. 117, a melt-extruded membrane manufactured by DuPont. The perfluorosulfonic acid family of membranes exhibits exceptionally high chemical and thermal stability and is stable against chemical attack in strong bases, strong oxidizing and reducing acids, Cl_2, H_2, and O_2 at temperatures up to 125 °C (257 °F). Nafion consists of a fluoropolymer backbone, similar to Teflon, upon which sulfonic acid groups are chemically bonded (Ref 6). Nafion membranes have exhibited long life in selected operating conditions and electrochemical applications. In selected fuel- cell tests and water-electrolysis systems, lifetimes of more than 50,000 h have been demonstrated. The Dow Chemical Company produced an electrolyte membrane, the XUS 13204.10, that contained a polymeric structure similar to that of Nafion, except that the side chain length was shortened. As a result, the membrane properties were significantly impacted, including a higher degree of water interactions within the membrane. This translated to lower electrical resistance and permitted higher current densities than the Nafion membrane, particularly when used in thinner form (Ref 7). These short side- chain membranes exhibited good performance and stability, but are no longer being supplied by Dow. Furthermore, due to Nafion's present expense and other engineering issues, new alternative membranes are being developed by a number of companies.

The alkaline fuel cell was one of the first modern fuel cells to be developed, beginning in 1960. The application at that time was to provide on-board electric power for the Apollo space vehicle. Desirable attributes of the AFC include excellent performance compared to other candidate fuel cells due to its active O_2 electrode kinetics and flexibility to use a wide range of electrocatalysts. The AFC continues to be used: it now provides on-board power for the Space Shuttle Orbiter. These AFCs operate at relatively high temperature and pressure to meet the requirements for space applications. More recently, a major focus of the technology has been for terrestrial applications in which low-cost components operating at near-ambient temperature and pressure with air as the oxidant are desirable.

The AFC developed for space application was based, in large part, on work initiated by F.T. Bacon in the 1930s. By 1952, construction and performance testing of a 5 kW alkaline fuel cell, operating on H_2 and O_2, were completed. The fuel cell developed by Bacon operated at 200 to 240 °C (390 to 465 °F) with 45% KOH electrolyte. Pressure was maintained at 40 to 55 atm (4 to 5.5 MPa, or 590 to 800 psi) to prevent the electrolyte from boiling. At this relatively high temperature and pressure, performance of the cell was quite good (0.78 V at 800 mA/cm^2). The anode consisted of a dual-porosity nickel electrode (two-layer structure with porous nickel of 16 μm maximum pore diameter on the electrolyte side and 30 μm pore diameter on the gas side). The cathode consisted of a porous structure of lithiated NiO. The three-phase boundary in the porous electrodes was maintained by a differential gas pressure across the electrode, since a wetproofing agent was not available at that time. Polytetrafluoroethylene (PTFE) as a wetproofing material did not exist, and it would not have been stable in the high-temperature alkaline solution (Ref 8).

The unusual economics for remote-power applications—such as space, undersea, and military applications—result in the cell itself not being strongly constrained by cost. The consumer and industrial markets, however, require the development of low-cost components if the AFC is to successfully compete with alternative technologies. Much of the recent interest in AFCs for mobile and stationary terrestrial applications has addressed the development of low-cost cell components. In this regard, carbon-base porous electrodes play a prominent role. It remains to be demonstrated whether alkaline cells will prove commercially viable for the transportation sector (Ref 9).

The state-of-the-art AFC stacks in the Space Shuttle Orbiter are rectangular with a width of 38 cm (15 in.) a length of 114 cm (45 in.), and a height of 35 cm (14 in.). They weigh 118 kg, (260 kg), produce a peak power of 12 kW at a minimum of 27.5 V (end of life), and operate at an average power of 7 kW. They operate in the same pressure range of 4 atm (0.4 MPa, or 60 psi) as the Apollo cells, but at a lower temperature of 85 to 95 °C (185 to 200 °F) and higher current density (0.88 V at 470 mA/cm^2. The fuel cells demonstrate 3.4 W/cm^2 at 0.8 V and 4300 mA/cm^2 (Ref 10). The electrodes contain high loadings of noble metals: 80%Pt-20%Pd anodes are loaded at 10 mg/cm^2 on silver-plated nickel screen; 90%Au-10%Pt cathodes are loaded at 20 mg/cm^2 on silver-

plated nickel screen. Both are bonded with PTFE to achieve high performance at the lower temperature of 85 to 95 °C (185 to 200 °F). A wide variety of materials (e.g., potassium titanate, ceria, asbestos, zirconium phosphate gel) have been used in the microporous separators for AFCs. The electrolyte is 35% KOH and is replenished via a reservoir on the anode side. Gold-plated magnesium is used for the bipolar plates (Ref 11).

The life-limiting event in the present Orbiter cell is KOH corrosion of the cell frame (cell support). Present stack life is 2600 h. The cell stacks have demonstrated capability to reach this life in 110 flights and a total of ~87,000 h in the Orbiter as of July 2002. Present practice is to refurbish the power unit at 2600 h by installing a new stack and cleaning and inspecting the balance of equipment. The stack life is being improved to 5000 h by elongating the path length associated with KOH-induced corrosion of the cell frame. A 10-cell short stack has demonstrated the new 5000 h concept. The concept is now being qualified in a complete power plant (Ref 12).

Electrode development in circulating electrolyte AFCs has concentrated on multilayered structures with porosity characteristics optimized for flow of liquid electrolytes and gases (H_2 and air) and catalyst development. Another area for concern is the instability of PTFE, which causes weeping of the electrodes. Most developers use noble metal catalysts; some use nonnoble catalysts. Spinels and perovskites are being developed in an attempt to lower the cost of the electrodes. Development of low-cost manufacturing processes includes powder mixing and pressing of carbon-base electrodes, sedimentation and spraying, and high-temperature sintering. Other approaches to increasing life and reducing weight and cost include investigating epoxy resins, polysulfone, and acrylonitrile-butadiene-styrene (ABS). Framing techniques under development include injection molding, filter pressing, and welding (Ref 13).

The phosphoric-acid fuel cell (PAFC) was the first fuel-cell technology to be commercialized. There have been only minor changes in cell design in recent years. The major U.S. manufacturer has concentrated on improving cell stability and life and in improving the reliability of system components at reduced cost. Nevertheless, further increases in power density and reduced cost are needed to achieve economic competitiveness with other energy technologies.

The evolution of cell components from 1965 to the present day for PAFCs is summarized in Table 3. A major breakthrough in PAFC technology that occurred in the late 1960s was the development of carbon black and graphite for cell-construction materials (Ref 14, 15). Carbon black and graphite were sufficiently stable to replace the more expensive gold-plated tantalum cell hardware used at the time. The use of high- surface-area graphite to support platinum permitted a dramatic reduction in platinum loading without sacrificing electrode performance. However, carbon corrosion and platinum dissolution become an issue at cell voltages above ~0.8 V.

Table 3 Evolution of cell-component technology for phosphoric-acid fuel cells

Component	Circa 1965	Circa 1975	Current status[(a)]
Anode	PTFE-bonded Pt black	PTFE-bonded Pt/C	PTFE-bonded Pt/C
Anode loading	9 mg Pt/cm^2	0.25 mg Pt/cm^2	0.10 mg Pt/cm^2
Cathode	PTFE-bonded Pt black	PTFE-bonded Pt/C	PTFE-bonded Pt/C
Cathode loading	9 mg Pt/cm^2	0.5 mg Pt/cm^2	0.5 mg Pt/cm^2
Electrode support	Ta mesh screen	Graphite structure	Graphite structure
Electrolyte support	Glass fiber paper	PTFE-bonded SiC	PTFE-bonded SiC
Electrolyte	85% H_3PO_4	95% H_3PO_4	100% H_3PO_4
Electrolyte reservoir	…	Porous graphite plate	Porous graphite plate
Cooler	…	…	1 per ~7 cells; embedded stainless steel tubes in graphite plate

(a) More than 40,000 h component life demonstrated in commercial power plants

In the mid-1960s, the conventional porous electrodes were PTFE—bonded platinum black, and the loadings were about 9 mg Pt/cm^2. During the past two decades, platinum supported on carbon black has replaced platinum black in porous PTFE-bonded electrode structures as the electrocatalyst. A dramatic reduction in

platinum loading has also occurred; the loadings are currently about 0.10 mg Pt/cm^2 in the anode and about 0.50 mg Pt/cm^2 in the cathode.

The operating temperatures and acid concentrations of PAFCs have increased to achieve higher cell performance. Temperatures of about 200 °C (390 °F) and acid concentrations of 100% H_3PO_4 are commonly used today. Although the present practice is to operate at atmospheric pressure, the operating pressure of PAFCs surpassed 8 atm (0.1 MPa, or 120 psi) in the 11 MW electric-utility demonstration plant, confirming an increase in power-plant efficiency. However, a number of issues remain, for example, whether to design and operate PAFC units at atmospheric versus pressurized conditions.

Another important issue, independent of power-unit size, is that pressure promotes-corrosion. Phosphoric-acid (H_3PO_4) electrolyte produces a vapor. This vapor, which forms over the electrolyte, is corrosive to cell locations other than the active cell area. These cell locations are at a mixed voltage (open circuit and cell voltage) that can be more than ~0.8 V/C. That is the limit above which corrosion occurs. An increase in cell total pressure causes the partial pressure of the H_3PO_4 vapor to increase, causing increased corrosion in the cell. Cell temperature must also be increased with pressurized conditions to produce steam for the steam reformer (Ref 16).

A bipolar plate separates the individual cells and electrically connects them in series in a fuel- cell stack. In some designs, the bipolar plate also contains gas channels that feed the reactant gases to the porous electrodes and remove the reaction products and inert gases. Bipolar plates made from graphite resin mixtures that are carbonized at low temperature (~900 °C, or 1650 °F) are not suitable because of their rapid degradation in PAFC operating environments (Ref 17). However, corrosion stability is improved by heat treatment to 2700 °C (4890 °F) (Ref 18). That is, the corrosion current is reduced by two orders of magnitude at 0.8 V in 97% H_3PO_4 at 190 °C (375 °F) and 4.8 atm (0.48 MPa, or 70.5 psi). The all- graphite bipolar plates are sufficiently corrosion resistant for a projected life of 40,000 h in PAFCs, but they are still relatively costly to produce.

Several important technology development efforts include catalyst improvements, advanced gas diffusion electrode development, and tests on materials that offer better carbon-corrosion protection. Transition metal (e.g., iron, cobalt) organic macrocycles from the families of tetramethoxyphenylporphyrins (TMPP), phthalocyanines (PC), tetraazaannulenes (TAA), and tetraphenylporphyrins (TPP) have been evaluated as oxygen-reduction electrocatalysts in PAFCs. One major problem with these organic macrocycles is their limited chemical stability in hot concentrated phosphoric acid. However, after heat treatment of the organic macrocycle, such as CoTAA, CoPC, CoTMPP, FePC, FeTMPP, on carbon at about 500 to 800 °C (930-1470 °F), the pyrolyzed residue exhibits electrocatalytic activity that, in some instances, is comparable to that of platinum and has promising stability, at least up to about 100 °C (212 °F) (Ref 19). Another successful approach for enhancing the electrocatalysis of oxygen reduction is to alloy platinum with transition metals such as titanium, chromium, vanadium, zirconium, and tantalum (Ref 20). The enhancement in electrocatalytic activity has been explained by a correlation between the optimal nearest-neighbor distance of the elements in the alloy and the bond length in oxygen (Ref 21).

Conventional cathode catalysts comprise either platinum or platinum alloys supported on conducting carbon black at 10 wt% Pt. Present platinum loadings on the anode and cathode are 0.1 and 0.5 mg/cm^2, respectively (Ref 22, 23). It has been suggested by researchers that the amount of platinum may have been reduced to the extent that it might be cost effective to increase the amount of platinum loading on the cathode (Ref 24). However, a problem exists in that fuel-cell stack developers have not experienced satisfactory performance improvements when increasing the platinum loading. Johnson Matthey Technology Centre (J-M) presented data that resulted in improved performance in nearly direct proportion to that expected based on the platinum increase (Ref 25). Initial tests by J-M confirmed previous results: using platinum alloy catalyst with a 10 wt% net platinum loading improves performance. Platinum/nickel alloy catalysts yielded a 49 wt% increase in specific activity over pure platinum. This translated into a 39 mV improvement in the air electrode performance at 200 mA/cm^2.

The anode of a phosphoric-acid fuel cell is subject to a reduction in performance when even low amounts of contaminants are preferentially absorbed on the noble catalysts. Yet, hydrogen- rich fuel gases, other than pure hydrogen, are produced with contaminant levels well in excess of the tolerance limit of the anode. Of particular concern are CO, COS, and H_2S in the fuel gas. The fuel stream in a state-of-the-art PAFC anode, operating at approximately 200 °C (390 °F), must contain 1 vol% or less of CO, less than 50 ppm by volume (ppmv) of COS plus H_2S, and less than 20 ppmv of H_2S. Current practice is to place COS and H_2S cleanup systems and CO shift converters prior to the cell (normally in the fuel processor before reforming) to reduce the fuel-stream

contaminant levels to the required amounts. Giner performed experiments to develop a contaminant-tolerant anode catalyst in order to reduce or eliminate the cleanup equipment (Ref 26). An anode catalyst, G87A-17-2, was identified that resulted in only a 24 mV loss from reference when exposed to a 75% H_2, 1% CO, 24% CO_2, 80 ppmv H_2S gas mixture at 190 °C (375 °F), 85% fuel utilization, and 200 mA/ cm^2. A baseline anode experienced a 36 mV loss from the reference at the same conditions. At 9.2 atm (0.92 MPa, or 135 psi) pressure, the anode loss was only 19 mV at 190 °C (375 °) and 17 mV at 210 °C (410 °F) (compared to pure H_2) with a gas of 71% H_2, 5% CO, 24% CO_2, and 200 ppmv H_2S. Economic studies comparing the trade-off between decreased cell performance with increased savings in plant cost showed no advantage when the new anode catalyst was used with gas containing 1% CO/200 ppmv H_2S. A $7/kW increase resulted with the 5% CO gas (compared to a 1% CO gas) at a 50 MW size. Some savings would result by eliminating the low-temperature shift converter. The real value of the catalyst may be its ability to tolerate excessive CO and H_2S concentrations during fuel- processor upsets and to simplify the system by eliminating equipment.

The molten-carbonate fuel cell operates at approximately 650 °C (1200 °F). The high operating temperature is needed to achieve sufficient conductivity of its carbonate electrolyte yet allow the use of low-cost metal-cell components. An effect associated with this high temperature is that noble metal catalysts are not required for the cell electrochemical oxidation and reduction processes. The higher operating temperature of MCFCs provides the opportunity for achieving higher overall system efficiencies (potential for heat rates below 7500 Btu/kWh) and greater flexibility in the use of available fuels. On the other hand, the higher operating temperature places severe demands on the corrosion stability and life of cell components, particularly in the aggressive environment of the molten-carbonate electrolyte. Another difference between PAFCs and MCFCs lies in the method used for electrolyte management in the respective cells. In a PAFC, PTFE serves as a binder and wetproofing agent to maintain the integrity of the electrode structure and to establish a stable electrolyte/gas interface in the porous electrode. The phosphoric acid is retained in a matrix of PTFE and SiC between the anode and cathode. There are no high-temperature, wetproofing materials available for use in MCFCs that are comparable to PTFE. Thus, a different approach is required to establish a stable electrolyte/gas interface in MCFC porous electrodes. The MCFC relies on a balance in capillary pressures to establish the electrolyte interfacial boundaries in the porous electrodes.

Table 4 provides a chronology of the evolution in cell-component technology for MCFCs. In the mid-1960s, electrode materials were, in many cases, precious metals, but the technology soon evolved to the use of nickel-base alloys at the anode and oxides at the cathode. Since the mid- 1970s, the materials for the electrodes and electrolyte structure (molten carbonate/$LiAlO_2$) have remained essentially unchanged. A major development in the 1980s was the evolution in the technology for fabrication of electrolyte structures (Ref 27, 28). Over the past 28 years, the performance of single cells has improved from about 10 to >150 mW/cm^2. During the 1980s, both the performance and endurance of MCFC stacks showed dramatic improvements. Several MCFC stack developers have produced cell stacks with cell areas up to 1 m^2 (10.8 ft^2) cells. Tall, full-scale stacks fabricated to date include several FuelCell Energy (FCE, formerly Energy Research Corporation) 300 plus cell stacks with ~9000 cm^2 (1395 in.^{2}) cell area producing >250 kW.

Table 4 Evolution of cell-component technology for molten-carbonate fuel cells

Component	Circa 1965	Circa 1975	Current status
Anode	Pt, Pd, or Ni	Ni-10Cr	Ni-Cr/Ni-Al/Ni-Al-Cr 3–6 μm (0.12–0.24 mil) pore size 45–70% initial porosity 0.20–1.5 mm (0.008–0.06 in.) thickness 0.1–1 m^2/g
Cathode	Ag_2O or lithiated NiO	Lithiated NiO	Lithiated NiO-MgO 7–15 μm (0.3–0.6 mil) pore size

			70–80% initial porosity 60–65% after lithiation and oxidation 0.5–1 mm (0.02–0.04 in.) thickness 0.5 m^2/g
Electrolyte support	MgO	Mixture of α-, β-, and γ$LiAlO_2$ 10–20 m^2/g 1.8 mm (0.07 in.) thickness	γ$LiAlO_2$, α$LiAlO_2$ 0.1–12 m^2/g 0.5–1 mm (10.02–0.04 in.) thickness
Electrolyte[(a)], wt%	52Li-48Na 43.5Li-31.5Na-25K "Paste"	62Li-38K Hot-press "tile" 1.8 mm (0.07 in.) thickness	62Li-38K 60Li-40Na 51Li-48Na Tape cast 0.5–1 mm (0.02–0.04 in.) thickness

(a) A mole percent of alkali carbonate salt

The conventional process used to fabricate electrolyte structures until about 1980 involved hot pressing (~34 MPa, or 5 ksi) mixtures of $LiAlO_2$ and alkali carbonates (typically >50 vol% in liquid state) at temperatures slightly below the melting point of the carbonate salts (e.g., 490 °C, or 915 °F, for electrolyte containing 62 mol% Li_2CO_3-38 mol% K_2CO_3). These electrolyte structures also called electrolyte tiles, were relatively thick (1 to 2 mm, or 0.04 to 0.08 in.) and difficult to produce in large sizes because large tooling and presses were required. The electrolyte structures produced by hot pressing are often characterized by void spaces (<5% porosity), poor uniformity of microstructure, generally poor mechanical strength, and high ***iR*** drop. To overcome the shortcomings of hot- pressed electrolyte structures, alternative processes such as tape casting (Ref 27) and electrophoretic deposition (Ref 29) for fabricating thin electrolyte structures were developed. The greatest success to date with an alternative process has been reported with tape casting, which is a common processing technique used by the ceramics industry. This process involves dispersing the ceramic powder in a solvent that contains dissolved binders (usually an organic compound), plasticizers, and additives to yield the proper slip rheology. The slip is cast over a moving smooth substrate, and the desired thickness is established with a doctor blade device. After drying the slip, the "green" structure is assembled into the fuel cell where the organic binder is removed by thermal decomposition, and the absorption of alkali carbonate into the ceramic structure occurs during cell startup. The tape casting and electrophoretic deposition processes are amenable to scale-up, and thin electrolyte structures (0.25 to 0.5 mm, or 0.01 to 0.02 in.) can be produced.

The bipolar plates used in MCFC stacks are usually fabricated from thin (~380 μm, or 15 mil) sheets of a corrosion-resistant alloy such as Incoloy 825, 310S, or 316L stainless steel that are coated on one side, the side exposed to fuel gases in the anode compartment with a nickel layer. The nickel layer is stable in the reducing-gas environment of the anode compartment, and it provides a conductive surface coating with low contact resistance. There are approaches to circumvent the problems associated with gas leaks and corrosion of bipolar plates (Ref 30). Corrosion is largely overcome by application of a coating (~50 μm, or 2 mil, thickness) at the vulnerable locations on the bipolar plate. For example, the wet-seal area on the anode side is subject to a high chemical potential gradient because the fuel gas inside the cell and the ambient environment (usually air) on the outside of the cell promote corrosion (about two orders of magnitude greater than in the cathode wet-seal area) (Ref 31). A thin aluminum coating in the wet-seal area of a bipolar plate provides corrosion protection by forming a protective layer of $LiAlO_2$ after reaction of aluminum with Li_2CO_3 (Ref 32). Such a protective layer

would not be useful in areas of the bipolar plate that must permit electronic conduction because $LiAlO_2$ is an insulating material.

A dense and electronically insulating layer of $LiAlO_2$ is not suitable for providing corrosion resistance to the cell current collectors because these components must remain electrically conductive. The typical materials used for this application are type 316 stainless steel and nickel- plated stainless steels. However, materials with better corrosion resistance are required for long- term operation of MCFCs. Research is continuing to understand the corrosion processes of high-temperature alloys in molten-carbonate salts under both fuel-gas and oxidizing-gas environments (Ref 33) and to identify improved alloys for MCFCs. Stainless steels such as type 310 and 446 have demonstrated better corrosion resistance than type 316 (Ref 34).

There is a need to provide better tolerance to sulfur poisoning gases in systems using MCFCs, especially when considering coal operation. Sulfur-tolerant cells could eliminate cleanup equipment that impacts system efficiency. This is especially true if low-temperature cleanup is required, because the system efficiency and capital cost suffer when the fuel-gas temperature is first reduced, then increased to the cell temperature level. Tests are being conducted on ceramic anodes to alleviate the problems, including sulfur poisoning, being experienced by the anodes (Ref 35). Anodes are being tested with undoped $LiFeO_2$ and $LiFeO_2$ doped with manganese and niobium. Preliminary testing, where several parameters were not strictly controlled, showed that the alternative electrodes exhibited poor performance and would not operate over 80 mA/ cm^2. At the present time, no alternative anodes have been identified. Future work will focus on a better understanding of material behavior and developing alternative materials with emphasis on sulfur tolerance.

The solid-oxide fuel cell is viable for generating electricity from hydrocarbon fuels. The high operating temperature, from 700 to 1000 °C (1290 to 1830 °F), allows internal reforming, promotes rapid kinetics with nonprecious materials, and produces high-quality by-product heat for cogeneration or for use in a bottoming cycle. The high temperature of the SOFC, however, places stringent requirements on its materials. The development of suitable low-cost materials and low-cost fabrication of ceramic structures is presently the key technical challenge facing SOFC commercialization.

Two different design configurations are being developed for SOFCs motivated by considerations of how to seal the anode and cathode compartments, ease of manufacturing, and minimizing losses due to electric resistance. The two principal types are tubular and planar, as shown in Fig. 3. The tubular SOFC has undergone development since the late 1950s. Operating between 900 and 1000 °C (1650 and 1830 °F), the long tubes have relatively high electrical resistance but are simple to seal. Some tubular designs eliminate the need for seals and allow for thermal expansion. Several tubular units are presently operating in the field, with tens of thousands of hours of demonstrated operation. In the tubular configuration, bundles of tubes that are closed at one end are arranged in parallel. Air is introduced to the inside of each tube, while fuel flows over the outside of the cells. Oxygen ions migrate through the electrolyte to react with fuel; the flow of ions produces electricity.

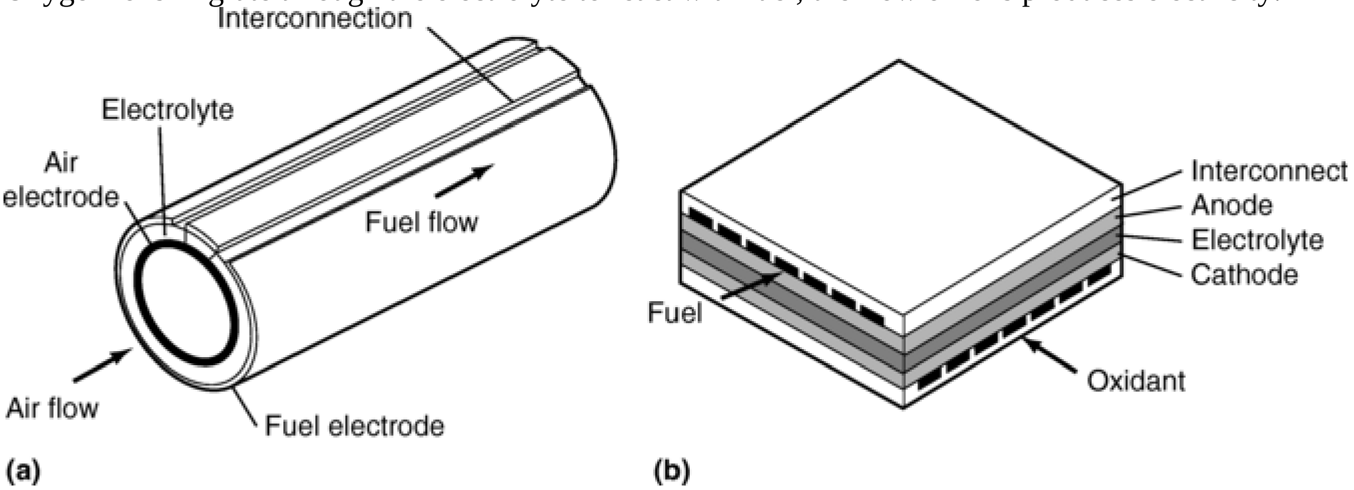

Fig. 3 Solid oxide fuel-cell configurations. (a) Tubular. (b) Planar

The planar solid-oxide fuel cell (PSOFC) is composed of flat, thin ceramic plates. The PSOFC operates at 800 °C (1470 °F) or even less. Ultrathin electrode/electrolyte sheets have low electrical resistance in order to achieve high efficiency. Operation at temperatures lower than the tubular SOFC enables less exotic materials of construction, thus saving on cost. In the planar configuration, the anode, electrolyte, and cathode form thin, flat

layers that are sintered together and then separated by bipolar plates similar to the design of other types of fuel cells. The plates can be rectangular, square, circular, or segmented in series and can be manifolded externally or internally. Many of the PSOFCs use metallic bipolar plates and are operated at a lower temperature than the all-ceramic tubular design.

To limit corrosion on the air side, the operating temperature of the PSOFC must be maintained below 800 °C (1470 °F). However, the conductivity of the electrolyte decreases with falling temperature. There are two options for mitigating decreased performance in this case. The well-established yttria-stabilized zirconia (YSZ) electrolyte can be used at temperatures as low as 700 °C (1290 °F) when the thickness is about 15 μm. To go to even lower temperatures, more conductive electrolytes such as lanthanum gallate, scandium-doped zirconia, or gadolinium-doped ceria (GDC) can be used (Ref 36, 37, 38, 39). At significantly reduced operating temperature, the lanthanum manganite cathode material becomes limited by kinetics to the point that it must be modified or replaced.

With respect to cathode materials, the choice depends on the specific ceramic electrolyte material, the desired operating temperature, the electrochemical cell design, and the specific ceramic fabrication methods. Perovskite-structured lanthanum strontium manganite (LSM) has been the most frequently used material for SOFCs, including both planar and tubular. Another perovskite material with similar properties is lanthanum calcium manganite (LCM). Both of these materials offer an excellent thermal expansion match with zirconia electrolytes and provide good performance above 800 °C (1470 °F). For applications requiring lower-temperature operation—600 to 800 °C (1110 to 1470 °F)—a range of alternative perovskite-structured ceramic electrodes are available. These include lanthanum strontium ferrite (LSF), lanthanum strontium cobalt ferrite (LSCF), lanthanum strontium manganese ferrite (LSMF), praseodymium strontium manganite (PSM), and praseodymium strontium manganese ferrite (PSMF). Improved performance of the cathode can be obtained by blending electrolyte material, such as YSZ, samarium-doped ceria (SDC) or GDC, with the perovskite material, such as LSM or PSMF. The incorporation of electrolyte material into the cathode materials has been shown to improve electrode performance at lower temperatures by increasing the volume of active sites available for electrochemical reactions. The electrolyte concentration is typically 40 vol%.

Based on the above, it can be seen that recent technology development in the PSOFC cell components and materials has been the change to a thinner electrolyte layer, anode-supported cells, the use of metallic interconnect plates, and more conductive materials for electrolytes. A summary of the advantages associated with these advances is presented in Table 5. From the table, it can be seen that the shift to thinner electrolytes has created the opportunity to reduce operating temperature and to use metal interconnects while still increasing power density. Development of higher-conductivity electrolytes will further enhance these benefits. Developers are also evaluating the anode-supported electrolyte layer with YSZ, a proven material. Higher-conductivity electrolytes may allow the use of thicker electrolyte layers at lower temperatures.

Table 5 Recent technology advances on planar cells and potential benefits

	Technology advance	Potential benefit
Design	Electrode (anode)-supported thin electrolyte unit cells	Lower resistance of electrolyte Increased power density
System	Lower temperature of operation	Use of metallic interconnects and manifolding possible
Materials	Metallic interconnect plates	Lower cost Lower resistance interconnect Mechanical solution to thermal expansion of stack
	More conductive electrolyte materials: Sc-Zr oxides Ce-Gd oxides	Reduced voltage drop across electrolyte

The requirements for stack-seal materials are extremely stringent. To avoid stress due to thermal expansion mismatch with adjacent components, the coefficient of thermal expansion (CTE) must be similar to that of the other components, typically in the range of 10 to 13 × 10^{-6}/°C (5.6 to 7.2 × 10^{-6}/°F). Chemical compatibility with the stack components and gaseous constituents of the highly oxidizing and reducing environments is also of primary concern. In addition, the seal should be electrically insulating to prevent shorting within the stack. A principal advantage of glass seals is that the glass composition can be tailored to optimize physical properties such as the CTE. However, several problems remain with regard to the use of glass seals in PSOFCs. The two issues of concern are the brittle nature of glass ceramics, and glasses tend to react with other cell components, such as electrodes, at SOFC operating temperatures.

A possible alternative to glass is the use of compressive, nonbonding seals. This approach permits the individual stack components to freely expand and contract during thermal cycling. However, the use of compressive seals also brings several new challenges to SOFC stack design; a load frame must be included to maintain the desired level of compressive load during operation, and the stack components must be able to withstand the compressive load required for adequate sealing for the lifetime of the stack. Research is in the early stage and has focused on micas (Ref 40), which are composed of sheets of silicate platelets (Ref 41).

Tubular Solid-Oxide Fuel Cells. Table 6 briefly describes the materials now used in various cell components of the tubular SOFC and those that were considered during earlier development. Because of the high operating temperatures of the present tubular SOFCs—900 to 1000 °C (1650 to 1830 °F)—materials used in cell components are limited by chemical stability in oxidizing and reducing environments, chemical stability of contacting materials, conductivity, and thermomechanical compatibility.

Table 6 Evolution of cell-component technology for tubular solid-oxide fuel cells

Component	Circa 1965	Circa 1975	Current status[a]
Anode	Porous Pt	Ni/ZrO_2 cermet	Ni/ZrO_2 cermet Deposit slurry, EVD fixed 12.5 × 10^{-6}/°C CTE ~150 μm (~6 mils) thickness 20–40% porosity
Cathode	Porous Pt	Stabilized ZrO_2 impregnated with praseodymium oxide and covered with SnO doped In_2O_3	Doped lanthanum manganite Extrusion, sintering ~2 mm (~0.08 in.) thickness 11 × 10^{-6}/°C CTE from room temperature to 1000 °C (1830 °F) 30–40% porosity
Electrolyte	Yttria-stabilized ZrO_2 0.5 mm (0.02 in.) thickness	Yttria-stabilized ZrO_2	Yttria-stabilized ZrO_2 (8 mol% Y_2O_3) EVD 10.5 × 10^{-6}/°C CTE from room temperature to 1000 °C (1830 °F) 30–40 μm (1.2–1.6 mils)

			thickness
Cell interconnect	Pt	Mn-doped cobalt chromite	Doped lanthanum chromite Plasma spray 10×10^{-6}/°C CTE ~100 µm (~4 mils) thickness

CTE, coefficient of thermal expansion.
(a) Specification for Siemens Westinghouse SOFC.

To make a tubular SOFC, the cathode tube is fabricated first by extrusion and sintering. As shown in Table 6, it has a porosity of 30 to 40% to permit rapid transport of the reactant and product gases to the cathode/electrolyte interface where the electrochemical reactions occur. The electrolyte is applied to the cathode tubes by electrochemical vapor deposition (EVD), which for many years has been the heart of Siemens Westinghouse technology (Ref 42). In this process, the appropriate metal chloride vapor is introduced on one side of the tube surface, and O_2/ H_2O is introduced on the other side. The gas environments on both sides of the tube act to form a galvanic couple. The net result is the formation of a dense, uniform metal oxide layer in which the deposition rate is controlled by the diffusion rate of ionic species and the concentration of electronic charge carriers. This procedure is used to fabricate the solid YSZ electrolyte.

Present fuel-cell designs make use of thin-film concepts where films of electrode and electrolyte material are deposited on one another and sintered, forming a cell structure. The fabrication techniques differ according to the type of cell configuration and developer. After the electrode has been prepared, the electrode is coated with the electrolyte. The coating may be applied using a variety of techniques, including tape calendering, dip coating, spray coating, electrophoretic deposition, or spin coating. In each case, developers strive for a thin, dense, pinhole-free electrolyte coating.

Alternative material research includes investigating materials that exhibit:

- Polarizable (easily weakened) metal oxygen bonds
- Open, layered structures for greater ion mobility
- Lower coordination numbers for the mobile ions

These are important criteria for high conductivity (Ref 43). This approach to electrolyte development is to stabilize a very conductive oxide by compound formation or by solid-solution formation with more stable oxides. Conductivity of 0.1/Ω · cm has been obtained with zinc-doped $La_{1-x}Bi_xAlO_3$ compared to 1.8×10^{-2}/Ω · cm for YSZ at 700 °C (1290 °F) (Ref 44).

References cited in this section

1. A.J. Appleby and F.R. Foulkes, *Fuel Cell Handbook,* Van Nostrand Reinhold, 1989

2. D.S. Watkins et al., Abstracts, *37th International Power Sources Symposium,* The Electrochemical Society, 1988, p 782

3. M. Krumpelt, R. Kumar, J. Miller, and C. Christianson, *1992 Fuel Cell Seminar Program and Abstracts,* 29 Nov–2 Dec 1992 (Tucson, AZ), The Fuel Cell Seminar Organizing Committee, 1992, p 35

4. W.D. Ernst, PEM Technology Development at Plug Power, *2000 Fuel Cell Seminar Program and Abstracts,* 30 Oct–2 Nov 2000 (Portland OR), Fuel Cell Seminar Organizing Committee

5. J.C. Amphlett, M. Farahani, R.F. Mann, B.A. Peppley, and P.R. Roberge, *Proc. 26th Intersociety Energy Conversion Engineering Conference,* Vol 3, *Conversion Technologies/Electrochemical Conversion,* 4–9 Aug 1991, American Nuclear Society, 1991, p 624

6. T. Ralph, Proton Exchange Membrane Fuel Cells: Progress in Cost Reduction of the Key Components, *Plat. Met. Rev.,* Vol 41, 1997, p 102–113

7. K. Prater, The Renaissance of the Solid Polymer Fuel Cell, *J. Power Sources,* 1990, p 29

8. J.O'M. Bockris and A.J. Appleby, *Energy,* Vol 11, 1986, p 95

9. G.F. McLean, T. Niet, S. Prince-Richard, and N. Djilali, An Assessment of Alkaline Fuel Cell Technology, *Int. J. Hydrogen Energy,* Vol 27, 2002, p 507–526

10. Communication with UTC Fuel Cells, July 2002

11. D.W. Sheibley and R.A. Martin, *Prog. Batteries Solar Cells,* Vol 6, 1987, p 155

12. Meeting with UTC Fuel Cells, June 2002

13. K. Strasser, *J. Electrochem. Soc.,* Vol 127, 1980, p 2173–2177

14. A.J. Appleby, *Proc. Workshop on the Electrochemistry of Carbon,* S. Sarangapani, J.R. Akridge, and B. Schumm, Ed., The Electrochemical Society, 1984, p 251

15. K.V. Kordesch, "Survey of Carbon and Its Role in Phosphoric Acid Fuel Cells," BNL 51418, Brookhaven National Laboratory, Dec 1979

16. Meeting with UTC Fuel Cells, June 2002

17. L. Christner, J. Ahmad, and M. Farooque, *Proc. Symposium on Corrosion in Batteries and Fuel Cells and Corrosion in Solar Energy Systems,* C.J. Johnson and S.L. Pohlman, Ed., The Electrochemical Society, 1983, p 140

18. P.W.T. Lu and L.L. France, *Extended Abstracts,* Fall Meeting of The Electrochemical Society, Vol 84-2, Abstract No. 573, The Electrochemical Society, 1984, p 837

19. J.A.S. Bett, H.R. Kunz, S.W. Smith, and L.L. Van Dine, "Investigation of Alloy Catalysts and Redox Catalysts for Phosphoric Acid Electrochemical Systems," FCR- 7157F, International Fuel Cells for Los Alamos National Laboratory, Contract No. 9- X13-D6271-1, 1985

20. P.N. Ross, "Oxygen Reduction on Supported Pt Alloys and Intermetallic Compounds in Phosphoric Acid," Final Report, EM-1553, Contract 1200-5, Electric Power Research Institute, Sept 1980

21. V. Jalan and J. Giner, *DECHEMA Monographs,* Vol 102, J.W. Schultze, Ed., VCH Verlagsgesellschaft, Weinheim, West Germany, 1986, p 315

22. Communications with IFC, Sept 2000

23. "Advanced Water-Cooled Phosphoric Acid Fuel Cell Development, Final Report," Report No. DE/MC/24221-3130, International Fuel Cells Corp. for U.S. DOE, Contract DE-AC21-88MC24221, Sept 1992

24. T. Ito, K. Kato, S. Kamitomai, and M. Kamiya, Organization of Platinum Loading Amount of Carbon-Supported Alloy Cathode for Advanced Phosphoric Acid Fuel Cell, *Fuel Cell Seminar Abstracts,* 1990 Fuel Cell Seminar, 25–28 Nov 1990 (Phoenix, AZ)

25. J.S. Buchanan, G.A. Hards, L. Keck, and R.J. Potter, Investigation into the Superior Oxygen Reduction Activity of Platinum Alloy Phosphoric Acid Fuel Cell Catalysts, *Fuel Cell Seminar Program and Abstracts,* 29 Nov–2 Dec 1992 (Tucson, AZ)

26. N.D. Kackley, S.A. McCatty, and J.A. Kosek, "Improved Anode Catalysts for Coal Gas-Fueled Phosphoric Acid Fuel Cells," Final Report DOE/MC/25170-2861, prepared for U.S. Department of Energy, Contract DE-AC21-88MC25170, July 1990

27. H.C. Maru, L. Paetsch, and A. Pigeaud, *Proc. Symposium on Molten Carbonate Fuel Cell Technology,* R.J. Selman and T.D. Claar, Ed., The Electrochemical Society, 1984, p 20,

28. R.J. Petri and T.G. Benjamin, *Proc. 21st Intersociety Energy Conversion Engineering Conference,* Vol 2, American Chemical Society, 1986, p 1156

29. C.E. Baumgartner, V.J. DeCarlo, P.G. Glugla, and J.J. Grimaldi, *J. Electrochem. Soc.,* Vol 132, 1985, p 57

30. A. Pigeaud, A.J. Skok, P.S. Patel, and H.C. Maru, *Thin Solid Films,* Vol 83, 1981, p 1449

31. R.A. Donado, L.G. Marianowski, H.C. Maru, and J.R. Selman, *J. Electrochem. Soc.,* Vol 131, 1984, p 2535, 2541

32. R.B. Swaroop, J.W. Sim, and K. Kinoshita, *J. Electrochem. Soc.,* Vol 125, 1978, p 1799

33. M. Farooque, ERC, "Development on Internal Reforming Carbonate Fuel Cell Technology, Final Report," prepared for U.S. DOE/METC, DOE/MC/23274-2941, Oct 1990, p 3–18

34. D.A. Shores and P. Singh, *Proc. Symposium on Molten Carbonate Fuel Cell Technology,* R.J. Selman and T.D. Claar, Ed., The Electrochemical Society, 1984, p 271

35. G. Kucera, K. Myles, A. Brown, M. Roche, D. Chu, and E. Indacochea, ANL's Research and Development of Alternate Components for MCFCs, *Proc. Fourth Annual Fuel Cells Contractors Review Meeting,* U.S. DOE/ METC, July 1992, p 31–41

36. J.B. Goodenough and K. Huang, "Lanthanum Gallate as a New SFOC Electrolyte," Proc. Fuel Cells '97 Review Meeting

37. M.N. Silver, "Recent Advances in SOFC Electrolyte, Cathode, and Anode Ceramic Materials," presented at the 26th Annual International Conference on Advanced Ceramics and Composites, 13–18 Jan 2002 (Cocoa Beach, FL)

38. R.J. Ball and R. Stevens, "Novel Composite Electrolytes for Solid Oxide Fuel Cell Applications," presented at the 26th Annual International Conference on Advanced Ceramics and Composites, 13–18 Jan 2002 (Cocoa Beach, FL)

39. S. Barnett, E. Perry, and D. Kaufmann, "Application of Ceria Layers to Increase Low Temperature SOFC Power Density," Proc. Fuel Cells '97 Review Meeting

40. J. Kim and A. Vikar, *Solid Oxide Fuel Cells—VI,* S. Singhal and M. Dokiya, Ed., Electrochemical Society, PV 99-19, 1999, p 830

41. Product Literature, Amethyst Galleries, Inc., Dublin, OH

42. A.O. Isenberg, *Proc. Symposium on Electrode Materials on Processes for Energy Conversion and Storage*, J.D.E. McIntyre, S. Srinivasan, and F.G. Will, Ed., The Electrochemical Society, 1977, p 682

43. I. Bloom, et al., Electrolyte Development for Intermediate Temperature Solid Oxide Fuel Cells, *Fuel Cell Seminar Program and Abstracts,* 29 Nov–2 Dec 1992 (Tucson, AZ)

44. I. Bloom and M. Krumpelt, “Intermediate Temperature Electrolytes for SOFC,” Proc. Fourth Annual Fuel Cells Contractors Review Meeting, U.S. DOE/METC, July 1992

M.C. Williams, Fuel Cells, *Corrosion: Fundamentals, Testing, and Protection*, Vol 13A, *ASM Handbook*, ASM International, 2003, p 178–186

Fuel Cells

Mark C. Williams, U.S. Department of Energy, National Energy Technology Laboratory

---

Advantages and Limitations of the Types of Fuel Cells

The fuel-cell types addressed in this overview have significantly different operating regimes. As a result, their materials of construction, fabrication techniques, and system requirements differ. These distinctions result in individual advantages and limitations that govern the potential of the various cells to be used for different applications.

Advantages and Limitations of Polymer- Electrolyte Fuel Cells. Polymer-electrolyte fuel cells, such as SOFCs, have a solid electrolyte. As a result, this cell exhibits excellent resistance to gas crossover. In contrast to the SOFC, the cell operates at a low 80 °C (175 °F). This results in a capability to bring the cell to its operating temperature quickly, but the rejected heat cannot be used for cogeneration or additional power. Test results have shown that the cell can operate at very high current densities compared to the other cells. However, heat- and water-management issues may limit the operating power density of a practical system. The PEFC tolerance for CO is in the low ppm level for low-temperature PEFC, but can be in many thousands of ppm for emerging high-temperature PEFC designs.

Advantages and Limitations of Phosphoric- Acid Fuel Cells. The CO_2 in the reformed fuel gas stream and the air does not react with the electrolyte in a phosphoric-acid electrolyte cell, but is a diluent. This attribute and the relatively low temperature of the PAFC made it a prime, early candidate for terrestrial application. Although its cell performance is somewhat lower than the alkaline cell because of the slow oxygen reaction rate of the cathode, and although the cell still requires hydrocarbon fuels to be reformed into a hydrogen-rich gas, the PAFC system efficiency improved because of its higher-temperature environment and less-complex fuel conversion (no membrane and attendant pressure drop). The need for scrubbing CO_2 from the process air is also eliminated. The rejected heat from the cell is high enough in temperature to heat water or air in a system operating at atmospheric pressure. Some steam is available in PAFCs, a key point in expanding cogeneration applications.

Phosphoric-acid fuel-cell systems achieve about 37 to 42% electrical efficiency based on the lower heating value (LHV) of natural gas. This is at the low end of the efficiency goal for fuel-cell power plants. Phosphoric-acid fuel cells use high-cost precious metal catalysts such as platinum. The fuel has to be reformed external to the cell, and CO has to be shifted by a water- gas reaction to below 3 to 5 vol% at the inlet to the fuel-cell anode or it will affect the catalyst. These limitations have prompted development of the alternate, higher-temperature cells, MCFC and SOFC.

Advantages and Limitations of Alkaline Fuel Cells. The AFC was one of the first modern fuel cells to be developed, beginning in 1960. The application at that time was to provide on- board electric power for the Apollo space vehicle. Desirable attributes of the AFC include its excellent performance on H_2 and O_2 compared to other candidate fuel cells due to its active O_2 electrode kinetics and its flexibility to use a wide range of

electrocatalysts, an attribute that provides development flexibility. Once development was in progress for space application, terrestrial applications began to be investigated. Developers recognized that pure hydrogen would be required in the fuel stream, because CO_2 in any reformed fuel reacts with the KOH electrolyte to form a carbonate, reducing the ion mobility of the electrolyte. Pure H_2 could be supplied to the anode by passing a reformed, hydrogen-rich fuel stream by a precious metal (palladium/silver) membrane. The H_2 molecule is able to pass through the membrane by absorption and mass transfer and into the fuel-cell anode. However, a significant pressure differential is required across the membrane and the membrane is prohibitive in cost. Even the small amount of CO_2 in ambient air, the source of O_2 for the reaction, would have to be scrubbed. At the time, U.S. investigations determined that scrubbing of the small amount of CO_2 within the air, coupled with purification of the hydrogen, was not cost effective and that terrestrial application of the AFC could be limited to special applications, such as closed environments, at best. Major research and development on AFC is no longer done in the United States, but recent development in Europe has created renewed interest in this fuel-cell type.

Advantages and Limitations of Molten- Carbonate Fuel Cells. Many of the disadvantages of the lower-temperature as well as higher- temperature cells can be alleviated with the higher operating temperature MCFC, ~650 °C (~1200 °F). This temperature level results in several benefits: the cell can be made of commonly available sheet metals that can be stamped for less costly fabrication, the cell reactions occur with nickel catalysts rather than with expensive precious metal catalysts, reforming can take place within the cell if a reforming catalyst is added (results in a large efficiency gain), CO is a directly usable fuel, and the rejected heat is of sufficiently high temperature to drive a gas turbine and/or produce high-pressure steam for use in a steam turbine or for cogeneration. Another advantage of the MCFC is that it operates efficiently with CO_2-containing fuels such as biofuel-derived gases. This benefit is derived from the cathode-performance enhancement resulting from CO_2 enrichment.

The MCFC has some disadvantages, however: the electrolyte is very corrosive and mobile, and a source of CO_2 is required at the cathode (usually recycled from anode exhaust) to form the carbonate ion. Sulfur tolerance is controlled by the reforming catalyst and is low, which is the same for the reforming catalyst in all cells. Operation requires use of stainless steel as the cell hardware material. The higher temperatures promote material problems, particularly mechanical stability, that impact cell life.

Advantages and Limitations of Solid-Oxide Fuel Cells. The SOFC is the fuel cell with the longest continuous development period, starting in the late 1950s, several years before the AFC. Because the electrolyte is solid, the cell can be cast into flexible shapes, such as tubular, planar, or monolithic. The solid ceramic construction of the cell also alleviates any cell-hardware corrosion problems characterized by the liquid electrolyte cells and has the advantage of being impervious to gas crossover from one electrode to the other. The absence of liquid also eliminates the problem of electrolyte movement or flooding in the electrodes. The kinetics of the cell are fast, and CO is a directly usable fuel as it is in the MCFC. There is no requirement for CO_2 at the cathode as with the MCFC. At the temperature of presently operating SOFCs, ~1000 °C (~1830 °F), fuel can be reformed within the cell. The temperature of an SOFC is significantly higher than that of the MCFC. However, some of the rejected heat from an SOFC is needed for preheating the incoming process air.

The high temperature of the SOFC has its drawbacks. There are thermal expansion mismatches among materials, and sealing between cells is difficult in the flat-plate configurations. The high operating temperature places severe constraints on materials selection and results in difficult fabrication processes. The SOFC also exhibits a high electrical resistivity in the electrolyte, which results in a lower cell performance than the MCFC by approximately 100 mV. Researchers would like to develop cells at a reduced temperature of 650 °C (1200 °F), but the electrical resistivity of the presently used solid electrolyte material would increase substantially.

M.C. Williams, Fuel Cells, *Corrosion: Fundamentals, Testing, and Protection*, Vol 13A, *ASM Handbook*, ASM International, 2003, p 178–186

Fuel Cells

Mark C. Williams, U.S. Department of Energy, National Energy Technology Laboratory

Acknowledgment

This article was adapted from the National Energy Technology Laboratory's (NETL) *Fuel Cell Handbook, Sixth Edition,* October 2002; a free copy of this handbook, in CD-ROM format, may be requested at the website www.netl.doe.gov.

The U.S. Department of Energy (DOE) is the largest funder of fuel-cell technology research and development in the United States. The DOE Office of Fossil Energy (FE) 2002 Budget was more than $50 million for stationary fuel cells, and the DOE Office of Energy Efficiency and Renewable Energy (EE) budget was slightly smaller for transportation fuel cells. The National Energy Technology Laboratory (NETL) manages the FE program that has a future focus based on the Solid State Energy Conversion Alliance (SECA) with goals of $400/kW by 2010, 40–60% efficiency, and coal-fuel hybrid applications by 2015 for FutureGen and Vision 21 power plants (Ref 45). The EE program has a future focus based on FreedomCAR and Hydrogen Fuel with a decision in 2015.

Reference cited in this section

45. W. Surdoval, G. McVay, P. Singh, and M. Williams, "SECA Program Plan: Making Fuel Cells Available to America," U.S. Dept. of Energy, NETL–PNNL, www.seca.doe.gov website, Jan 2002

M.C. Williams, Fuel Cells, *Corrosion: Fundamentals, Testing, and Protection*, Vol 13A, *ASM Handbook*, ASM International, 2003, p 178–186

Fuel Cells

Mark C. Williams, U.S. Department of Energy, National Energy Technology Laboratory

References

1. A.J. Appleby and F.R. Foulkes, *Fuel Cell Handbook,* Van Nostrand Reinhold, 1989
2. D.S. Watkins et al., Abstracts, *37th International Power Sources Symposium,* The Electrochemical Society, 1988, p 782
3. M. Krumpelt, R. Kumar, J. Miller, and C. Christianson, *1992 Fuel Cell Seminar Program and Abstracts,* 29 Nov–2 Dec 1992 (Tucson, AZ), The Fuel Cell Seminar Organizing Committee, 1992, p 35
4. W.D. Ernst, PEM Technology Development at Plug Power, *2000 Fuel Cell Seminar Program and Abstracts,* 30 Oct–2 Nov 2000 (Portland OR), Fuel Cell Seminar Organizing Committee

5. J.C. Amphlett, M. Farahani, R.F. Mann, B.A. Peppley, and P.R. Roberge, *Proc. 26th Intersociety Energy Conversion Engineering Conference,* Vol 3, *Conversion Technologies/Electrochemical Conversion,* 4–9 Aug 1991, American Nuclear Society, 1991, p 624

6. T. Ralph, Proton Exchange Membrane Fuel Cells: Progress in Cost Reduction of the Key Components, *Plat. Met. Rev.,* Vol 41, 1997, p 102–113

7. K. Prater, The Renaissance of the Solid Polymer Fuel Cell, *J. Power Sources,* 1990, p 29

8. J.O'M. Bockris and A.J. Appleby, *Energy,* Vol 11, 1986, p 95

9. G.F. McLean, T. Niet, S. Prince-Richard, and N. Djilali, An Assessment of Alkaline Fuel Cell Technology, *Int. J. Hydrogen Energy,* Vol 27, 2002, p 507–526

10. Communication with UTC Fuel Cells, July 2002

11. D.W. Sheibley and R.A. Martin, *Prog. Batteries Solar Cells,* Vol 6, 1987, p 155

12. Meeting with UTC Fuel Cells, June 2002

13. K. Strasser, *J. Electrochem. Soc.,* Vol 127, 1980, p 2173–2177

14. A.J. Appleby, *Proc. Workshop on the Electrochemistry of Carbon,* S. Sarangapani, J.R. Akridge, and B. Schumm, Ed., The Electrochemical Society, 1984, p 251

15. K.V. Kordesch, “Survey of Carbon and Its Role in Phosphoric Acid Fuel Cells,” BNL 51418, Brookhaven National Laboratory, Dec 1979

16. Meeting with UTC Fuel Cells, June 2002

17. L. Christner, J. Ahmad, and M. Farooque, *Proc. Symposium on Corrosion in Batteries and Fuel Cells and Corrosion in Solar Energy Systems,* C.J. Johnson and S.L. Pohlman, Ed., The Electrochemical Society, 1983, p 140

18. P.W.T. Lu and L.L. France, *Extended Abstracts,* Fall Meeting of The Electrochemical Society, Vol 84-2, Abstract No. 573, The Electrochemical Society, 1984, p 837

19. J.A.S. Bett, H.R. Kunz, S.W. Smith, and L.L. Van Dine, “Investigation of Alloy Catalysts and Redox Catalysts for Phosphoric Acid Electrochemical Systems,” FCR- 7157F, International Fuel Cells for Los Alamos National Laboratory, Contract No. 9- X13-D6271-1, 1985

20. P.N. Ross, “Oxygen Reduction on Supported Pt Alloys and Intermetallic Compounds in Phosphoric Acid,” Final Report, EM-1553, Contract 1200-5, Electric Power Research Institute, Sept 1980

21. V. Jalan and J. Giner, *DECHEMA Monographs,* Vol 102, J.W. Schultze, Ed., VCH Verlagsgesellschaft, Weinheim, West Germany, 1986, p 315

22. Communications with IFC, Sept 2000

23. “Advanced Water-Cooled Phosphoric Acid Fuel Cell Development, Final Report,” Report No. DE/MC/24221-3130, International Fuel Cells Corp. for U.S. DOE, Contract DE-AC21-88MC24221, Sept 1992

24. T. Ito, K. Kato, S. Kamitomai, and M. Kamiya, Organization of Platinum Loading Amount of Carbon-Supported Alloy Cathode for Advanced Phosphoric Acid Fuel Cell, *Fuel Cell Seminar Abstracts,* 1990 Fuel Cell Seminar, 25–28 Nov 1990 (Phoenix, AZ)

25. J.S. Buchanan, G.A. Hards, L. Keck, and R.J. Potter, Investigation into the Superior Oxygen Reduction Activity of Platinum Alloy Phosphoric Acid Fuel Cell Catalysts, *Fuel Cell Seminar Program and Abstracts,* 29 Nov–2 Dec 1992 (Tucson, AZ)

26. N.D. Kackley, S.A. McCatty, and J.A. Kosek, "Improved Anode Catalysts for Coal Gas-Fueled Phosphoric Acid Fuel Cells," Final Report DOE/MC/25170-2861, prepared for U.S. Department of Energy, Contract DE-AC21-88MC25170, July 1990

27. H.C. Maru, L. Paetsch, and A. Pigeaud, *Proc. Symposium on Molten Carbonate Fuel Cell Technology,* R.J. Selman and T.D. Claar, Ed., The Electrochemical Society, 1984, p 20,

28. R.J. Petri and T.G. Benjamin, *Proc. 21st Intersociety Energy Conversion Engineering Conference,* Vol 2, American Chemical Society, 1986, p 1156

29. C.E. Baumgartner, V.J. DeCarlo, P.G. Glugla, and J.J. Grimaldi, *J. Electrochem. Soc.,* Vol 132, 1985, p 57

30. A. Pigeaud, A.J. Skok, P.S. Patel, and H.C. Maru, *Thin Solid Films,* Vol 83, 1981, p 1449

31. R.A. Donado, L.G. Marianowski, H.C. Maru, and J.R. Selman, *J. Electrochem. Soc.,* Vol 131, 1984, p 2535, 2541

32. R.B. Swaroop, J.W. Sim, and K. Kinoshita, *J. Electrochem. Soc.,* Vol 125, 1978, p 1799

33. M. Farooque, ERC, "Development on Internal Reforming Carbonate Fuel Cell Technology, Final Report," prepared for U.S. DOE/METC, DOE/MC/23274-2941, Oct 1990, p 3–18

34. D.A. Shores and P. Singh, *Proc. Symposium on Molten Carbonate Fuel Cell Technology,* R.J. Selman and T.D. Claar, Ed., The Electrochemical Society, 1984, p 271

35. G. Kucera, K. Myles, A. Brown, M. Roche, D. Chu, and E. Indacochea, ANL's Research and Development of Alternate Components for MCFCs, *Proc. Fourth Annual Fuel Cells Contractors Review Meeting,* U.S. DOE/ METC, July 1992, p 31–41

36. J.B. Goodenough and K. Huang, "Lanthanum Gallate as a New SFOC Electrolyte," Proc. Fuel Cells '97 Review Meeting

37. M.N. Silver, "Recent Advances in SOFC Electrolyte, Cathode, and Anode Ceramic Materials," presented at the 26th Annual International Conference on Advanced Ceramics and Composites, 13–18 Jan 2002 (Cocoa Beach, FL)

38. R.J. Ball and R. Stevens, "Novel Composite Electrolytes for Solid Oxide Fuel Cell Applications," presented at the 26th Annual International Conference on Advanced Ceramics and Composites, 13–18 Jan 2002 (Cocoa Beach, FL)

39. S. Barnett, E. Perry, and D. Kaufmann, "Application of Ceria Layers to Increase Low Temperature SOFC Power Density," Proc. Fuel Cells '97 Review Meeting

40. J. Kim and A. Vikar, *Solid Oxide Fuel Cells—VI,* S. Singhal and M. Dokiya, Ed., Electrochemical Society, PV 99-19, 1999, p 830

41. Product Literature, Amethyst Galleries, Inc., Dublin, OH

42. A.O. Isenberg, *Proc. Symposium on Electrode Materials on Processes for Energy Conversion and Storage*, J.D.E. McIntyre, S. Srinivasan, and F.G. Will, Ed., The Electrochemical Society, 1977, p 682

43. I. Bloom, et al., Electrolyte Development for Intermediate Temperature Solid Oxide Fuel Cells, *Fuel Cell Seminar Program and Abstracts,* 29 Nov–2 Dec 1992 (Tucson, AZ)

44. I. Bloom and M. Krumpelt, "Intermediate Temperature Electrolytes for SOFC," Proc. Fourth Annual Fuel Cells Contractors Review Meeting, U.S. DOE/METC, July 1992

45. W. Surdoval, G. McVay, P. Singh, and M. Williams, "SECA Program Plan: Making Fuel Cells Available to America," U.S. Dept. of Energy, NETL–PNNL, www.seca.doe.gov website, Jan 2002

B.S. Covino, Jr. and S.D. Cramer, Introduction to Forms of Corrosion, *Corrosion: Fundamentals, Testing, and Protection*, Vol 13A, *ASM Handbook*, ASM International, 2003, p 189

Introduction to Forms of Corrosion

Bernard S. Covino, Jr. and Stephen D. Cramer, U.S. Department of Energy, Albany Research Center

Introduction

WHILE CORROSION CAN TAKE MANY FORMS, it is most generally defined as a chemical or electrochemical reaction between a material and its environment that produces a deterioration (change) of the material and its properties. Organizing the forms of corrosion has the advantage that corrosion processes with similar mechanisms can be considered together. Categorization of the forms of corrosion has existed in various schemes for many years. A broad view would separate corrosion into two categories: corrosion that is not influenced by any other process and corrosion that is influenced by another process, such as the presence of stresses or erosion. A more focused view would categorize corrosion as uniform or localized, aqueous or gaseous, wet or dry, and so forth.

This Section, “Forms of Corrosion,” contains six subsections. Four of them (“Uniform Corrosion,” “Localized Corrosion,” “Metallurgically Influenced Corrosion,” and “Microbiologically Influenced Corrosion”) fit under the classification of corrosion that is not influenced by any outside process. Two of them (“Mechanically Assisted Degradation” and “Environmentally Induced Cracking”) address corrosion that is influenced by another process.

B.S. Covino, Jr. and S.D. Cramer, Introduction to Forms of Corrosion, *Corrosion: Fundamentals, Testing, and Protection*, Vol 13A, *ASM Handbook*, ASM International, 2003, p 189

Introduction to Forms of Corrosion

Bernard S. Covino, Jr. and Stephen D. Cramer, U.S. Department of Energy, Albany Research Center

Uniform Corrosion

Uniform corrosion processes include many corrosion phenomena that are encountered in the practice of corrosion engineering and corrosion science. The majority of those phenomena deal with either aqueous or gaseous corrosion, although there are concerns about materials for use in molten salt and liquid metal environments. Gaseous corrosion is usually associated with high-temperature environments. Atmospheric corrosion is not considered a part of gaseous corrosion because the corrosion reaction occurs in a thin aqueous layer on the surface of the metal. Galvanic and stray current corrosion are not environment specific but rather can occur in any of the environments mentioned earlier.

B.S. Covino, Jr. and S.D. Cramer, Introduction to Forms of Corrosion, *Corrosion: Fundamentals, Testing, and Protection*, Vol 13A, *ASM Handbook*, ASM International, 2003, p 189

Introduction to Forms of Corrosion

Bernard S. Covino, Jr. and Stephen D. Cramer, U.S. Department of Energy, Albany Research Center

Localized Corrosion

Localized corrosion is described as corrosion that occurs at discrete locations on a material. While this is true and accounts for the naming of this form of corrosion, it is also the localized state of the environment that causes the accelerated attack of materials. Thus the propagation of pits on passive metal surfaces, the aggressive attack where two metals overlap to form a crevice, and the distinctive filiform attack on metal surfaces coated with thin organic layers result from differences in the metallurgy of the alloy and because the localized chemistry of the environment is different from that of the bulk of the environment.

B.S. Covino, Jr. and S.D. Cramer, Introduction to Forms of Corrosion, *Corrosion: Fundamentals, Testing, and Protection*, Vol 13A, *ASM Handbook*, ASM International, 2003, p 189

Introduction to Forms of Corrosion

Bernard S. Covino, Jr. and Stephen D. Cramer, U.S. Department of Energy, Albany Research Center

Metallurgically Influenced Corrosion

To understand “Metallurgically Influenced Corrosion,” it is first important to understand what is meant by *metallurgy*. It has been described as “the art and science of procuring and adapting metals to satisfy human wants” (Ref 1). As such, it includes the recovery of metals from ores (*extractive metallurgy*), the formation of metals into various forms (*mechanical metallurgy*), and the understanding of the interaction of the chemical species, crystal orientations, and dislocations in metals and alloys (*physical metallurgy*). All of these processes can influence the composition, structure, stress level, and impurities in metals and alloys and, thus, their corrosion behavior. Another process, welding, is usually applied after metals are formed and shaped by metallurgical techniques. Welding produces localized changes in the composition, structure, stress level, and impurities in the joined metals and thus also can affect corrosion.

Reference cited in this section

1. A.R. Guy, *Elements of Physical Metallurgy,* 2nd ed., Addison-Wesley Publishing Company, Inc., Reading, MA, 1960, p 1

B.S. Covino, Jr. and S.D. Cramer, Introduction to Forms of Corrosion, *Corrosion: Fundamentals, Testing, and Protection*, Vol 13A, *ASM Handbook*, ASM International, 2003, p 189

Introduction to Forms of Corrosion

Bernard S. Covino, Jr. and Stephen D. Cramer, U.S. Department of Energy, Albany Research Center

Mechanically Assisted Degradation

Mechanically assisted degradation involves processes where external interactions can influence the corrosion rate. Examples are fretting, cavitation, and impingement corrosion, and corrosion fatigue. This subsection includes two new articles on the interaction between wear and corrosion processes in aqueous and gaseous environments. Wear and corrosion can occur separately, but usually there is some synergy between them that requires special tools or procedures to investigate.

B.S. Covino, Jr. and S.D. Cramer, Introduction to Forms of Corrosion, *Corrosion: Fundamentals, Testing, and Protection*, Vol 13A, *ASM Handbook*, ASM International, 2003, p 189

Introduction to Forms of Corrosion

Bernard S. Covino, Jr. and Stephen D. Cramer, U.S. Department of Energy, Albany Research Center

Environmentally Induced Cracking

Environmentally induced cracking is a form of corrosion in which the external influence on the corrosion process is stress. For stress-corrosion cracking, the stress is often externally applied. For hydrogen damage, liquid metal induced embrittlement, and solid metal induced embrittlement, the stress is induced by reactions with the environment.

B.S. Covino, Jr. and S.D. Cramer, Introduction to Forms of Corrosion, *Corrosion: Fundamentals, Testing, and Protection*, Vol 13A, *ASM Handbook*, ASM International, 2003, p 189

Introduction to Forms of Corrosion

Bernard S. Covino, Jr. and Stephen D. Cramer, U.S. Department of Energy, Albany Research Center

Environmentally Induced Cracking

Environmentally induced cracking is a form of corrosion in which the external influence on the corrosion process is stress. For stress-corrosion cracking, the stress is often externally applied. For hydrogen damage, liquid metal induced embrittlement, and solid metal induced embrittlement, the stress is induced by reactions with the environment.

B.S. Covino, Jr. and S.D. Cramer, Introduction to Forms of Corrosion, *Corrosion: Fundamentals, Testing, and Protection*, Vol 13A, *ASM Handbook*, ASM International, 2003, p 189

Introduction to Forms of Corrosion

Bernard S. Covino, Jr. and Stephen D. Cramer, U.S. Department of Energy, Albany Research Center

References

1. A.R. Guy, *Elements of Physical Metallurgy,* 2nd ed., Addison-Wesley Publishing Company, Inc., Reading, MA, 1960, p 1

D.C. Silverman, Aqueous Corrosion, *Corrosion: Fundamentals, Testing, and Protection*, Vol 13A, *ASM Handbook*, ASM International, 2003, p 190–195

Aqueous Corrosion

Revised by David C. Silverman, Argentum Solutions, Inc.

Introduction

CORROSION is a process created by the interaction (reaction) between a material, often a metal or alloy, and its environment that results in degradation of that material. Corrosion is affected by the properties of both the metal or alloy and the environment. In this brief overview focusing on degradation of metals and alloys in aqueous systems, the environment variables shown as follows are addressed:

- pH (acidity)
- Oxidizing power (electrochemical potential)
- Temperature and heat transfer
- Velocity (fluid movement)
- Solution components and their concentration

One point to bear in mind is that corrosion is a process, not a property. That distinction means that the corrosion resistance of a material depends as much on the environmental components and system dynamics to which the material is exposed as it does to the chemical composition and structure of the material itself. The discussion is not meant to be all-inclusive but to provide an overview of the complex effects that environmental variables can have on corrosion and to emphasize some of the more important relationships among them. Often, particular effects can only be deduced from carefully planned experimental testing designed to duplicate the actual system. The more understanding one has of how environmental variables might affect corrosion, the better the chances that the experiment will simulate the actual conditions. The influence of biological organisms on these environmental variables is also an important consideration.

Thermodynamics provides a theoretical framework within which the effects of several environmental variables might be pictured. In aqueous corrosion, the format often used is the potential-pH diagram, or Pourbaix diagram (Ref 1). The expanded portion of the potential-pH diagram of iron at 25 °C (77 °F) shown in Fig. 1 is considered as an example of how this framework might be used (Ref 2). These diagrams are thermodynamic

and show the most stable state of the metal in an aqueous solution. The dependence of iron corrosion on oxidizing power (electromotive force), acidity (pH), temperature, and species concentration is illustrated in Fig. 1. For example, suppose the corrosion potential lies at -0.5 V standard hydrogen electrode (SHE) at a pH of 8. The most stable state of iron is Fe^{2+}, indicating that iron dissolution is possible. If the pH is increased to 10 (the acidity is decreased), the most stable state becomes magnetite (Fe_3O_4), and most likely, the corrosion rate of iron would greatly decrease, its surface becoming oxidized. If the pH is then decreased to approximately 8.5, the most stable state (Fe^{2+} or Fe_3O_4) would depend on the concentration of the dissolved iron species. The concentration of dissolved species could influence the corrosion rate. A change in temperature would alter the entire diagram, changing both the areas of stability and the components within those areas.

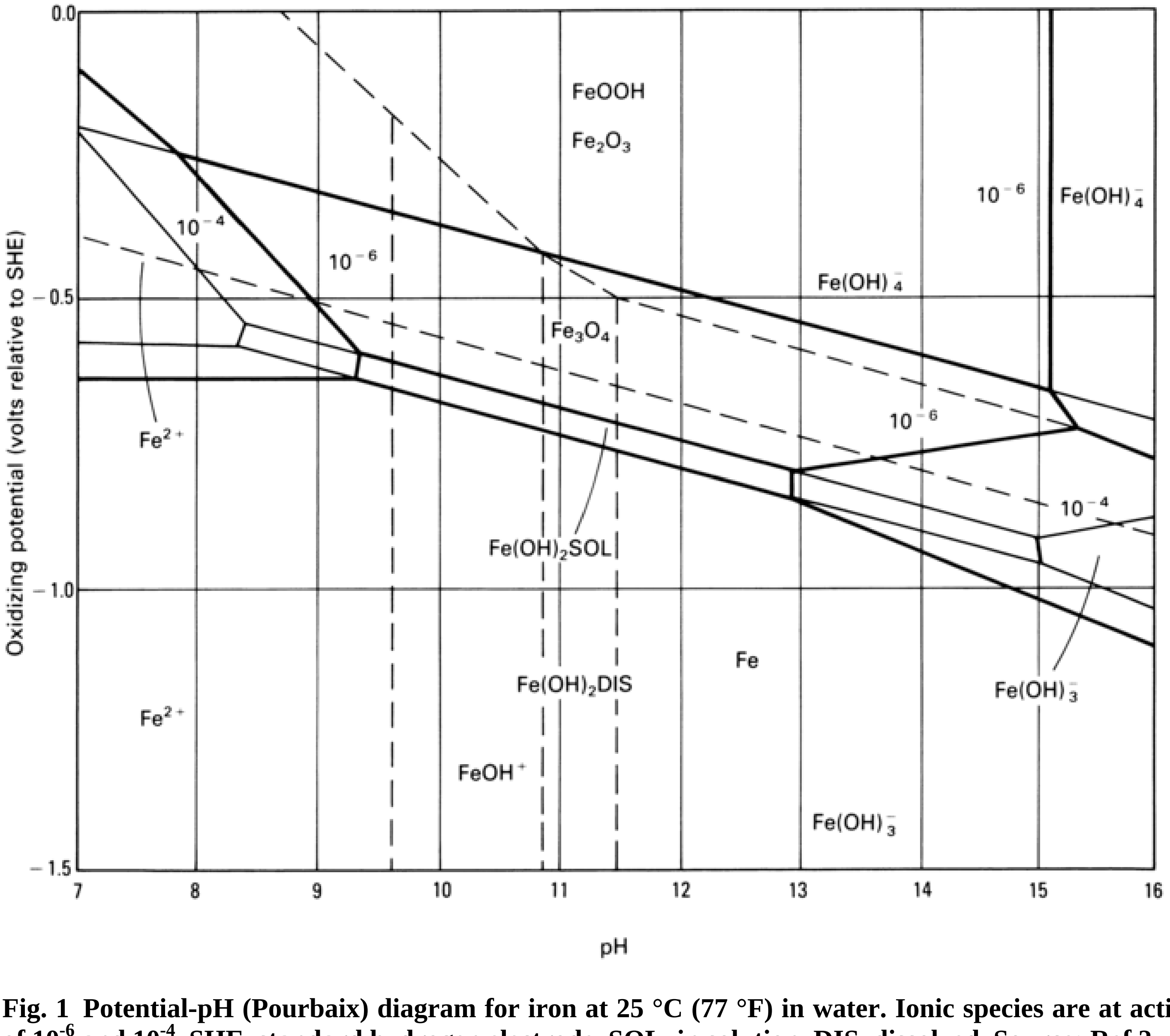

Fig. 1 Potential-pH (Pourbaix) diagram for iron at 25 °C (77 °F) in water. Ionic species are at activities of 10^{-6} and 10^{-4}. SHE, standard hydrogen electrode. SOL, in solution. DIS, dissolved. Source: Ref 2

The simple example of Fig. 1 shows the dominating role that environmental variables can play in corrosion. Complex interrelationships can exist. The combined values of the variables pH, potential, concentration, and temperature not only affect corrosion but also affect the action of each variable. For example, with respect to Fig. 1, the effect of a pH change depends on the concentration of the dissolved species, and vice versa. Although the variables are discussed individually, the important point is to realize that the effect of one variable can be influenced by the magnitude of another. This relationship appears throughout this article.

References cited in this section

1. M. Pourbaix, *Atlas of Electrochemical Equilibria in Aqueous Solutions,* National Association of Corrosion Engineers, 1974

2. D.C. Silverman, Presence of Solid $Fe(OH)_2$ in EMF-pH Diagram for Iron, *Corrosion,* Vol 38 (No. 2), 1982, p 453

D.C. Silverman, Aqueous Corrosion, *Corrosion: Fundamentals, Testing, and Protection*, Vol 13A, *ASM Handbook*, ASM International, 2003, p 190–195

Aqueous Corrosion

Revised by David C. Silverman, Argentum Solutions, Inc.

Effect of pH (Acidity)

The concept of pH is complex. It is related to, but not synonymous with, hydrogen concentration or amount of acid. Before discussing how the magnitude of pH affects corrosion, some fundamentals are required. The pH is defined as the negative of the base ten logarithm of the hydrogen ion activity (Ref 3). This latter quantity is related to the concentration or molality through an activity coefficient. The term is expressed as

$$pH = -\log a_{H^+} = -\log \gamma_{H^+} m_{H^+} \quad \text{(Eq 1)}$$

where a_{H^+} is the hydrogen ion activity, γ_{H^+} is the hydrogen ion activity coefficient, and m_{H^+} is the molality (mol/1000 cm^3 of water). The value of the activity coefficient is a function of everything in the solution (ions, nonionized species, etc.) as well as the environmental variables of temperature and pressure.

The pH is usually measured with a pH meter, which is actually an electrometer. The voltage of a hydrogen ion specific electrode is measured relative to a reference electrode. This voltage is compared to the internally stored calibration obtained from a defined standard to yield the unknown pH. The actual hydrogen ion concentration (acidity level) can be calculated from this measured pH if the activity coefficient is known. The calculated hydrogen ion concentration is at best an estimate (Ref 3, 4), because the test solution usually has constituents that are far different from those of the buffer. The hydrogen ion concentration estimated from the pH as measured by a pH meter and the actual amount of acid as defined by the actual hydrogen ion concentration are related but not necessarily equal.

The importance of the hydrogen ion lies in its ability to interact with an alloy surface. Many alloys of commercial interest form an oxidized surface region, the outermost atomic layer that often contains hydroxide-like species when water is present. The nature of such a structure would tend to depend on hydrogen ion concentration, possibly through a reaction such as Eq 2 that can be one step in the corrosion mechanism (Ref 5):

$$H_2O \leftrightarrow OH_{adsorbed} + H^+ + e^- \quad \text{(Eq 2)}$$

Thus, under certain conditions, the hydrogen ion concentration can influence corrosion through the equilibrium that exists with it, water, and the hydroxide or oxide formed on the alloy surface. The interaction with the surface can, in principle, result in the sequence shown in Eq 3, which tends to be in the direction of increasing passivity of the metal M and increasing thickness of the surface region. The hydroxyl species in the first two steps tend to be derived from the dissociation of water (hydrolysis), in which hydrogen ions tend to be liberated. Water is a by-product created in the last step. The process can stop at any point, depending on the alloy and the environmental variables influencing the reaction (Ref 5):

$$M \rightarrow MOH \rightarrow M(OH)_n \rightarrow MO \quad \text{(Eq 3)}$$

This type of interaction often results in a corrosion rate dependence on hydrogen ion concentration in the form of:

$$r = k\left(C_{H^+}\right)^n \quad \text{(Eq 4)}$$

where *r* is the corrosion rate, *k* is the rate constant, C_{H^+} is the hydrogen ion concentration, and *n* is an exponent. The value and sign of *n* can depend on the hydrogen ion concentration. This type of dependence of

the reaction rate on the hydrogen ion concentration is found in a number of systems, which are discussed subsequently. This discussion is not meant to be all-encompassing but is meant to provide a flavor for how this dependence is observed in practice.

Strongly Acid Conditions (pH < 5). Iron or carbon steel shows a complex dependence of the corrosion rate on pH. At low pH, the corrosion mechanism depends not only on the hydrogen ion concentration but also on the counter-ions present. Thus, all discussion must include the total constituency of the fluid. For example, the corrosion rate of iron in sulfuric acid (H_2SO_4) between a pH of less than 0 and approximately 4 tends to be limited by the diffusion of and saturation concentration of iron sulfate ($FeSO_4$) (Ref 6, 7). In concentrated H_2SO_4, iron can initially form a salt layer of $FeSO_4$. Mass transfer becomes sensitive to fluid velocity, and the corrosion rate itself becomes sensitive to the fluid flow rate. The metal dissolution rate is so high that the corrosion rate is equal to the mass transfer rate of iron from this saturated film of $FeSO_4$ at the metal surface.

Corrosion of iron in hydrochloric acid (HCl) follows a different mechanism, and pH has a different effect on corrosion. The rate of corrosion is rapid at all acidic concentrations of pH < 3. Unlike the sulfate ion in H_2SO_4, the chloride ion seems to participate in and accelerate the corrosion rate (Ref 8). The corrosion rate increases with hydrogen ion concentration (decreasing pH). These effects are reflected in Eq 4, when n is a positive number. This behavior indicates that in HCl, the hydrogen ion directly influences the reaction kinetics. The ion does not influence corrosion through mass transfer.

Corrosion of iron in phosphoric acid (H_3PO_4) solution follows a similar mechanism but with a subtle twist. Again, no passive film exists on the surface; however, the corrosion rate, at least between a pH of 0.75 and 4, seems to be independent of phosphate ion concentration at constant pH (Ref 9).

The important point is that the pH effect on corrosion of carbon steel at low pH is not simple. Knowledge of how pH affects corrosion in one acid does not necessarily translate to knowledge in another acid. Very little fundamental information is available on the effect of acid mixtures on corrosion, so kinetic equations relating corrosion rate to concentration in these systems usually do not exist.

Ferritic iron-chromium alloys have been found to exhibit behavior in concentrated H_2SO_4 reminiscent of the behavior of carbon steel. A strong fluid velocity sensitivity has been noted in 1 *M* H_2SO_4 (5 to 10 wt%) (Ref 10) for those alloys with less than 12 wt% Cr and in the 68 to 93 wt% H_2SO_4 range (Ref 11) for E-Brite 26-1 (26 wt% Cr). The corrosion rate tends to be related to the rate of mass transfer of $FeSO_4$ from a saturated film on the surface. The one difference is that the presence of oxygen may impart a pseudopassivity that can be unstable. The major point is that the presence of chromium in the alloy does not necessarily increase protection in this environment. Both chromium content and H_2SO_4 concentration must be considered simultaneously, especially because an 18 wt% Cr ferritic alloy tends to be under activation control in 1 *M* H_2SO_4 (Ref 10).

The addition of nickel to create austenitic alloys alters this behavior in H_2SO_4 and eliminates, or at least diminishes, this sensitivity to fluid motion, especially in the hydrogen activity range of 10^{-3} to greater than 1 (pH range from approximately 3 to less than 0). At lower pH, the higher acid concentrations may produce a velocity sensitivity (Ref 12). Unfortunately, kinetic data are sparse on the effect of pH on the low corrosion rates expected for many of these alloys in this low pH range of -0.5 to 3. At still lower pH, the behavior is complex, and the particular literature on the alloy should be consulted. Impurities in the H_2SO_4 can significantly alter the corrosion resistance.

The behavior of austenitic alloys in HCl is far different from that in H_2SO_4, even at the same pH or hydrogen ion concentration. The change from sulfate to chloride anion tends to be detrimental. The presence of the chloride ion raises the possibility of localized attack, for example crevice corrosion, pitting, and stress-corrosion cracking (SCC) (Ref 13). Once again, behavior with respect to pH is complex. The literature on the particular alloy should be consulted to determine the actual behavior as a function of pH in acidic solutions.

Non Group VIII base alloys show different types of pH dependencies at low pH. For example, in HCl, titanium is passive to a pH of approximately 0 or slightly lower. Then, a fairly abrupt change in mechanism occurs at still lower pH. There, titanium begins to corrode rather rapidly (Ref 14). The hypothesis is that the titanium valence changes from +4 to +3 and that Ti^{3+} is soluble (Ref 14, 15). The behavior in H_2SO_4 is somewhat different.

Other metals and alloys are affected by acidic pH in different ways. Unfortunately, mechanistic data are less plentiful than for iron-base alloys. A number of metals show a very strong dependence of corrosion on pH. With aluminum, the rate increases exponentially as pH decreases in the acidic region (Ref 16). Indeed, the corrosion rate tends to have a very sharp minimum at a pH of 7 to 9, with sharp corrosion rate increases with both increasing and decreasing pH (Ref 1, 16).

A similar effect of a sharp decrease in corrosion rate with increasing pH for pH < 4 has been noted for both zinc in HCl and lead in nitric acid (HNO_3) (Ref 17). Indeed, this type of behavior would be expected for any metal or alloy whose oxide is soluble in acids, such as zinc, aluminum, lead, tin, and copper.

Near-Neutral Conditions (5 < pH < 9). Corrosion behavior and alloy-environment interactions in the near-neutral pH region differ significantly from those under acidic conditions. In most cases, pH no longer plays a dominant role in corrosion.

Iron (as carbon steel) has been one of the most extensively studied metals in this environment. Under strongly acidic conditions, the oxide or hydroxide layers tend to dissolve. In the higher pH range, however, especially above a pH of approximately 5, these layers tend to remain on the surface. These layers have significant three dimensional structure, which tends to be determined by the anions present in the solution (Ref 18). In addition, the corrosion kinetics become independent of pH, and hydrogen ion reduction is no longer an important reaction (Ref 19). The major reaction governing corrosion in most practical applications tends to be the reduction of oxygen dissolved in solution. Under some conditions, magnetite Fe_3O_4 can be formed, which tends to passivate iron (Ref 18). Thus, pH in this range no longer plays a major direct role in corrosion of iron, although the pH can still affect the solubility and equilibrium of other ions such as sequestering agents and corrosion inhibitors. These other components can play a major role in corrosion in, for example, industrial cooling- water systems.

This characteristic of pH in the range of 5 < pH < 9 no longer playing a dominant role is found with other metals, such as zinc and lead (Ref 17). Aluminum shows a very sharp minimum in corrosion rate at approximately a pH of 7 to 9, with the minimum being somewhat dependent on the counter-ion in solution (Ref 16).

Alloys such as the austenitic iron-base and nickel-base alloys, ferritic alloys, and duplex alloys also tend to have general corrosion rates that are independent of pH in this range. Indeed, in pure water, these alloys would be passive. The presence of other species, such as chloride ions and oxygen, plays a much more dominant role, possibly changing the mechanism from uniform corrosion to localized attack.

Strongly Basic Conditions (pH > 9). Basic conditions offer yet another set of corrosion characteristics. In some cases, corrosion rate increases with pH (decreasing hydrogen ion concentration) or at least remains finite. In other cases, the increase in pH causes corrosion to occur when none was present at lower pH. These two types of behavior seem to encompass most metals and alloys, and representative examples are described subsequently to demonstrate this behavior.

Iron corrosion persists even at high pH. In fact, it can be greater than that under more neutral conditions. This persistence (or increase) is caused by soluble species $Fe(OH)_3^-$ or, at elevated potentials, $Fe(OH)_4^-$ being the most thermodynamically stable corrosion products (Ref 1, 2). Even though a number of iron hydroxide species can be found that can create a porous barrier (Ref 20), corrosion still persists, although usually at a fairly low rate, until very high pH is reached (Ref 17).

At very high pH (e.g., concentrated caustic) and especially at somewhat elevated temperatures, carbon steel can undergo SCC (Ref 21). Some environments that can cause SCC at high pH are sodium hydroxide (NaOH) at very high pH, carbonates and bicarbonates at moderately basic pH values, and possibly amines, although this point is controversial. Steel has been reported to suffer SCC at lower pH, but this behavior is less prevalent. Examples of these environments are hydrogen fluoride (HF) vapors and hydrogen sulfide (H_2S) in water. The mechanism in these cases may be one of hydrogen embrittlement (Ref 22).

A number of metals exhibit a sharp increase in corrosion rate with increasing pH. Among these are aluminum, zinc, and lead (Ref 16, 17). Aluminum corrosion increases very dramatically, changing by almost two orders of magnitude between a pH of 8 and 10. This increase is virtually independent of counter-ion and can be attributed to the formation of soluble aluminum hydroxide products (Ref 1).

Tantalum, which suffers virtually no corrosion under most acidic and neutral pH conditions, shows a significant increase in corrosion rate at high pH (Ref 24). The cause of this corrosion is believed to be a slow dissolution or flaking off of surface layers (Ref 24.) This dissolution is thought to be caused by the formation of soluble tantalum hydroxide corrosion products (Ref 14).

Some metals, such as nickel and zirconium, are very resistant to corrosion at high pH. Nickel and especially zirconium rely on the formation of insoluble oxides for their corrosion protection (Ref 23).

The austenitic and ferritic alloys tend to be immune to corrosion until very high pH or strong basicity is reached. One reason is that chromium, which is included in many of these alloys and which tends to accumulate on the surface, forms a passive oxide. This oxide, for example chromium oxide (Cr_2O_3), is insoluble under

these conditions. Changes in temperature, however, can affect corrosion at high pH. An example is initiation of SCC of type 304 or 316 stainless steel in very hot, concentrated caustic but not in cold caustic.

References cited in this section

1. M. Pourbaix, *Atlas of Electrochemical Equilibria in Aqueous Solutions,* National Association of Corrosion Engineers, 1974

2. D.C. Silverman, Presence of Solid $Fe(OH)_2$ in EMF-pH Diagram for Iron, *Corrosion,* Vol 38 (No. 2), 1982, p 453

3. R.A. Robinson and R.H. Stokes, *Electrolyte Solutions,* 2nd ed., Academic Press, 1959

4. R.G. Bates, *Electrometric pH Determinations,* John Wiley & Sons, 1954

5. P. Lorbeer and W.J. Lorenz, The Kinetics of Iron Dissolution and Passivation in Solutions Containing Oxygen, *Electrochim. Acta,* Vol 25 (No. 4), 1980, p 375

6. B.T. Ellison and W.R. Schmeal, Corrosion of Steel in Concentrated Sulfuric Acid, *J. Electrochem. Soc.,* Vol 125 (No. 4), 1978, p 524

7. T.K. Ross, G.C. Wood, and I.J. Mahmud, The Anodic Behavior of Iron Carbon Alloys in Moving Acid Media, *J. Electrochem. Soc.,* Vol 113, 1966, p 334

8. R.J. Chin and K. Nobe, Electrodissolution Kinetics of Iron in Chloride Solutions, *J. Electrochem. Soc.,* Vol 119 (No. 11), 1972, p 1457

9. A.N. Katrevick, G.M. Florianovich, and Ya.M. Kolotyrkin, Clarification of the Kinetic Parameters of the Reaction of the Active Dissolution of Iron in Phosphate Solutions, *Zashch. Met.,* Vol 10 (No. 4), 1974, p 369

10. B. Alexandre, A. Caprani, J.C. Charbonnier, M. Keddam, and P.H. Morel, The Influence of Chromium on the Mass Transfer Limitation of the Anodic Dissolution of Ferritic Steels Fe-Cr in Molar Sulfuric Acid, *Corros. Sci.,* Vol 21 (No. 11), 1981, p 765

11. D.C. Silverman and M.E. Zerr, Application of Rotating Cylinder Electrode—E-Brite 26-1/Concentrated Sulfuric Acid, *Corrosion,* Vol 42 (No. 11) 1986, p 633

12. "The Corrosion Resistance of Nickel Containing Alloys in Sulfuric Acid and Related Compounds," CEB-1, International Nickel Company, Inc., 1983

13. "Resistance of Nickel and High Nickel Alloys to Corrosion by Hydrochloric Acid, Hydrogen Chloride, and Chlorine," CEB-3, International Nickel Company, Inc., 1974

14. D.C. Silverman, Derivation and Application of EMF-pH Diagrams, *Electrochemical Techniques for Corrosion Engineers,* R. Baboian, Ed., NACE International, 1986

15. A. Alon, M. Frenkel, and M. Schorr, Corrosion and Electrochemical Behavior of Titanium in Acidic, Oxidizing, Aqueous, and Alcoholic Systems, *Proceedings of the Fourth International Congress on Metallic Corrosion,* National Association of Corrosion Engineers, 1969, p 636

16. V. Vujicic and B. Lovrecek, A Study of the Influence of pH on the Corrosion Rate of Aluminum, *Surf. Technol.,* Vol 25, 1985, p 49

17. N.D. Tomashov, *Theory of Corrosion and Protection of Metals,* B.H. Tytell, I. Geld, and H.S. Preiser, Trans., Macmillan, 1966

18. M. Fischer, Possible Models of the Reaction Mechanism and Discussion of the Functions of Passivating Additions During the Chemical Passivation of Iron in Weakly Acidic, Neutral and Basic pH Ranges, *Werkst. Korros.,* Vol 29, 1978, p 188

19. B.J. Andrzejaczek, Influence of Oxygen on the Kinetics of Corrosion Processes on Iron in Water, *Korrosion,* Vol 15 (No. 5), 1984, p 239

20. R.N. Sylva, The Hydrolysis of Iron (III), *Rev. Pure Appl. Chem.,* Vol 22, 1972, p 115

21. W. Frank and L. Graf, Mechanism of Intergranular Corrosion and Intergranular Stress Corrosion Cracking in Mild Steels, *Res. Mech.,* Vol 13, 1985, p 251

22. M.G. Fontana and N.D. Green, *Corrosion Engineering,* 3rd ed., McGraw-Hill, 1986

23. D.R. Knittel, Zirconium: A Corrosion Resistant Material for Industrial Applications, *Chem. Eng.,* Vol 87 (No. 11), 1980, p 98

24. M. Schussler, *Corrosion Data Survey on Tantalum,* Fansteel, Inc., 1972

D.C. Silverman, Aqueous Corrosion, *Corrosion: Fundamentals, Testing, and Protection*, Vol 13A, *ASM Handbook*, ASM International, 2003, p 190–195

Aqueous Corrosion

Revised by David C. Silverman, Argentum Solutions, Inc.

Oxidizing Power (Electrochemical Potential)

Oxidizing power, or potential, relates to the ability to remove or add electrons from the metal so as to oxidize or reduce the surface. This variable is separated from the discussions on solution chemistry because such a potential can be applied by an external voltage source, by galvanic coupling of different metals or alloys, or by other species present in the environment. Practical applications include increasing passivity by altering the surface oxide (anodic protection) or preventing corrosion by supplying electrons to the metal that would normally be yielded by metal corrosion (cathodic protection). The anodic reaction rate is shifted or changed in the protected metal.

The alteration of the surface state to impart passivity is normally accomplished by anodic polarization of the metal or alloy surface to a potential noble to the corrosion potential. If an external voltage source is used to change the voltage, the technique is known as anodic protection (see the article "Anodic Protection" in this Volume or Ref 25). Among the practical examples of using externally applied anodic potentials to mitigate corrosion are mild steel and type 304 or 316 stainless steel in concentrated H_2SO_4, H_3PO_4, and NaOH (Ref 22).

The addition of components to the environment may alter the surface potential to create a passive film. In this case, the species reacts with the metal to form a tenacious metal-oxide compound that passivates the surface. There are several well-known examples of anodic polarization of the surface by changing the environment. For example, the addition of small amounts of ozone to water decreases the corrosion of carbon steel in water (Ref 26). The hypothesis is that the corrosion potential moves in a noble direction, and the ozone reacts with the iron to create a more tenacious oxide. In another example, the addition of small amounts of HNO_3 to H_2SO_4 has

been shown to retard the corrosion of stainless steels. The hypothesis is that the potential is forced in the noble direction, and the surface oxide layer becomes more protective.

Polarization of the surface potential in the active or cathodic direction can also be used to decrease corrosion. When the potential is lowered by means of an external voltage source, the technique is known as cathodic protection (Ref 27). Many practical examples exist, such as the protection of steel at coating defects in underground carbon steel pipelines or the protection of ship hulls in seawater (see the article “Cathodic Protection” in this Volume). The electrons are supplied from either an inert or active counterelectrode.

Direct electrical coupling of a metal to a more active metal is another example of using cathodic potentials to affect corrosion. Coupling zinc to steel to protect the steel is a major example. In this case, zinc corrosion liberates electrons to the steel, and the steel potential moves in a cathodic or active direction (Ref 28).

Oxygen tends to polarize carbon steel in the noble direction and increase its corrosion. The addition of such species as sulfite (SO_3^{2-}) or hydrazine tends to cause a reaction with the oxygen and thus remove it (Ref 28). The effect of SO_3^{2-} tends to be to move the surface potential in the active direction. Such movement of potential may decrease the corrosion of iron (Ref 17). Any change in potential may depend on other components, especially if they can interact with the inhibitor and the metal surface. Also, if the alloy is passive and if this passivity is maintained by the oxygen, this addition could increase corrosion by moving the alloy into an active corrosion region (Ref 17).

References cited in this section

17. N.D. Tomashov, *Theory of Corrosion and Protection of Metals,* B.H. Tytell, I. Geld, and H.S. Preiser, Trans., Macmillan, 1966

22. M.G. Fontana and N.D. Green, *Corrosion Engineering,* 3rd ed., McGraw-Hill, 1986

25. O.L. Riggs, Jr., and C.E. Locke, *Anodic Protection: Theory and Practice in the Prevention of Corrosion,* Plenum Press, 1981

26. H.H. Uhlig, *Corrosion and Corrosion Control,* John Wiley & Sons, 1963

27. J.H. Fitzgerald, Jr., Engineering of Cathodic Protection Systems, Ch. 57, in *Uhlig's Corrosion Handbook,* 2nd ed., R.W. Revie, Ed., John Wiley and Sons, Inc., 2000

28. Bimetallic Corrosion, L.L. Shrier, R.A. Jarman, and G.T. Burstein, Ed., *Corrosion,* Vol 1, p 1:213, Butterworth-Heinemann, Oxford, 1994

D.C. Silverman, Aqueous Corrosion, *Corrosion: Fundamentals, Testing, and Protection*, Vol 13A, *ASM Handbook,* ASM International, 2003, p 190–195

Aqueous Corrosion

Revised by David C. Silverman, Argentum Solutions, Inc.

Temperature and Heat Transfer

Temperature is a complex external variable. Temperature is analogous to potential. A potential difference creates a current flow, the objective of which is to eliminate the potential difference. In a similar manner, a temperature difference creates a heat flow, the objective of which is to eliminate the temperature difference. Both potential and temperature are measures of energy.

Temperature can affect corrosion in a number of ways. If the corrosion rate is governed completely by the elementary process of metal oxidation (called activation control), the corrosion rate increases exponentially with an increase in temperature. This relationship is reflected in the Arrhenius expression:

$$r = A\exp\left(\frac{-E}{RT}\right) \qquad \text{(Eq 5)}$$

where *r* is the corrosion rate, *A* is a pre-exponential factor, *E* is an activation energy, *R* is the gas constant, and *T* is the absolute temperature.

The effect of temperature on corrosion rate is calculated by solving Eq 5 at two temperatures and taking the ratio of the rates:

$$\ln\left(\frac{r_1}{r_2}\right) = \left(\frac{-E}{R}\right)\left(\frac{\Delta T}{T_1T_2}\right) \qquad \text{(Eq 6)}$$

where the subscripts 1 and 2 refer to the two temperatures, and ΔT is the difference in temperature (T_2 - T_1). Equation 6 can be used to evaluate the effect of a temperature change on corrosion rate for this simple rate process. Examples of corrosion that follow this simple rate law are iron in HCl (Ref 29) and iron in sodium sulfate (Na_2SO_4) at a pH of approximately 2 (Ref 30). This situation is most common for corrosion under acidic conditions.

The temperature of the metal and the temperature of the solution often cannot be discussed separately from other variables. If a component in the solution that is important in corrosion has limited solubility, a temperature change can alter the concentration of that component that can be dissolved in a solution. This increased solubility can have a profound effect on corrosion.

One classic example is the corrosion of iron in the presence of oxygen in systems both closed from the atmosphere and open to the atmosphere. The corrosion rate of iron in a system closed to the atmosphere has been shown to increase almost linearly with temperature from approximately 40 to 160 °C (105 to 320 °F). In the open system, the corrosion rate increases up to approximately 80 °C (175 °F) and then decreases (Ref 17). Oxygen mass transfer, which is proportional to the oxygen concentration in the liquid, controls the corrosion rate of steel in water. As temperature increases, oxygen solubility decreases so that the oxygen tends to leave the liquid. In the closed system, the oxygen cannot escape from the vapor space above the liquid. As temperature increases, the water vapor pressure increases, which tends to maintain the oxygen concentration in the liquid. The corrosion rate (mass transfer rate) continues to increase with temperature. In the open systems, oxygen can escape from the immediate vicinity of the liquid. The vapor pressure remains constant. Above a certain temperature, the liquid-phase oxygen concentration in equilibrium with oxygen in the atmosphere has decreased to the extent that the corrosion (mass transfer) rate decreases.

Another point often overlooked is that the ionization constant of water increases with temperature. Pure water with pH of 7 at one temperature has a lower pH at a higher temperature. Thus, an increase in temperature could affect corrosion by moving the pH from a neutral to an acidic value.

Fluid temperature changes can affect the polarity in galvanic corrosion. The corrosion potential of the anode might be more sensitive to temperature than that of the cathode. The anode potential can actually become noble with respect to that of the cathode (Ref 17). An example is the iron-zinc couple, the polarity of which can reverse as temperature increases. Iron actually protects the zinc. The temperature of this reversal is as low as 60 °C (140 °F), but there is some dependence of temperature on constituents.

Solution temperature can also affect the onset of localized attack of passive alloys such as type 304 and 316 stainless steels. The solution usually contains a species, such as chloride ion, that aids in the initiation process (Ref 31). The time to initiation of crevice corrosion has been shown to be a function of temperature. There are indications that such initiation times do not always decrease with increasing temperature (Ref 31). In addition, a critical crevice temperature can be defined for many of these alloys (Ref 32). This critical temperature determines the temperature boundary at which crevice corrosion can initiate. Indeed, the critical crevice temperature has been shown to be a function of the chromium and molybdenum content of austenitic and ferritic alloys.

In practice, elevated or depressed temperatures are often created by heat transfer through a metal wall. Thus, the metal wall can be at a temperature different from that of the bulk fluid. Controversy exists over whether corrosion in the absence of heat transfer is identical to corrosion in the presence of heat transfer, even if the metal temperatures are identical in the two situations (Ref 29).

The effect of a difference between wall and fluid temperatures on corrosion depends on the corrosion mechanism. If the corrosion rate is under activation control and follows Eq 5, the corrosion rate in the presence of heat transfer might be similar to that expected for corrosion at the same wall temperature in the absence of heat transfer. If the corrosion rate is controlled by the diffusion of a species such as oxygen to the surface, then heat transfer may greatly change the corrosion rate. This effect has several possible causes (Ref 33, 34). First, a temperature difference between the wall and bulk solution can affect the solubility and diffusion coefficient of the diffusing species. Second, boiling near or on the wall can increase turbulence and possibly cause cavitation or increased diffusion (mass transfer). Third, heat transfer in the absence of fluid flow, as in stagnant tanks, can cause natural convection currents that can enhance mass transfer. Thus, if heat transfer is present, it must be considered an environmental variable.

References cited in this section

17. N.D. Tomashov, *Theory of Corrosion and Protection of Metals,* B.H. Tytell, I. Geld, and H.S. Preiser, Trans., Macmillan, 1966

29. Ya.M. Kolotyrkin, V.S. Pakhomov, A.G. Parshin, and A.V. Chekhovskii, Effect of Heat Transfer on Corrosion of Metals, *Khim. Neft. Mashinostr.,* Vol 16 (No. 12), 1980, p 20

30. J.W. Oldfield, T.S. Lee, and R.M. Kain, Avoiding Crevice Corrosion of Stainless Steels, *Proceedings of Stainless Steels '84,* Institute of Metals, 1985, p 205

31. R.J. Brigham, The Initiation of Crevice Corrosion on Stainless Steels, *Mater. Perform.,* Vol 24 (No. 12), 1985, p 44

32. J.R. Kearns, Crevice, Corrosion Tests and Standards—Application and Interpretation, R. Baboian, Ed., ASTM International, 1995

33. A.G. Parshin, V.S. Parkhomov, and Ya.M. Kolotyrkin, The Influence of Heat Transfer on the Kinetics of Cathode Processes With Limiting Diffusion Steps, *Corros. Sci.,* Vol 22 (No. 9), 1982, p 845

34. T.K. Ross, Corrosion and Heat Transfer—A Review, *Br. Corros. J.,* Vol 2, 1967, p 131

D.C. Silverman, Aqueous Corrosion, *Corrosion: Fundamentals, Testing, and Protection*, Vol 13A, *ASM Handbook*, ASM International, 2003, p 190–195

Aqueous Corrosion

Revised by David C. Silverman, Argentum Solutions, Inc.

Velocity and Fluid Movement

Fluid flow rate, or fluid velocity, is also a complex variable (Ref 35). Its influence on corrosion depends on the alloy, fluid components, fluid physical properties, geometry in which the fluid is contained, and corrosion mechanism. These relationships are best discussed in terms of specific examples. In a number of instances, the corrosion rate is determined by the rate of transfer of a species between the surface and the fluid. This situation arises when the corrosion reaction itself is very rapid and one of the corrosion reactants or products has low solubility in the bulk fluid. The corrosion rate becomes a function of the concentration gradient and is expressed by:

$r = k(C_W - C_B)$ (Eq 7)

where r is the corrosion rate, k is a mass transfer coefficient, C_W is the concentration of the rate- limiting species at the metal wall, and C_B is the concentration of the rate-limiting species in the bulk fluid. The value of k can often be correlated with the dimensionless quantities Reynolds number (Re) and Schmidt number (Sc). The mass transfer coefficient is expressed in terms of the Sherwood number (Sh). These numbers are related to physical properties of the fluid and geometry by:

$$\mathrm{Re} = \left(\frac{vd}{\nu}\right) \quad \text{(Eq 8a)}$$

$$\mathrm{Sc} = \left(\frac{\nu}{D}\right) \quad \text{(Eq 8b)}$$

$$\mathrm{Sh} = \left(\frac{kd}{D}\right) \quad \text{(Eq 8c)}$$

where v is the fluid velocity, d is a characteristic length (for example, pipe diameter), ν is the kinematic viscosity (absolute viscosity divided by density), k is the mass transfer coefficient, and D is the diffusion coefficient.

For many geometries, these quantities can be related by:

$$\mathrm{Sh} = a\mathrm{Re}^b\mathrm{Sc}^c \quad \text{(Eq 9)}$$

where a, b, and c are constants. Equations 7, 8a, 8b, 8c, 9 indicate that the corrosion rate can be calculated if it depends on the mass transfer rate of a species from or to the bulk fluid. The only information required is the geometry, fluid velocity, and physical properties. There are a number of examples of corrosion that follow this behavior. The corrosion of carbon steel and E-Brite 26- 1 in concentrated H_2SO_4 is governed by the rate of mass transfer of $FeSO_4$ from a saturated layer on the surface (Ref 6, 7, 11). Carbon steel corrosion in water in the near-neutral pH range is usually governed by the rate of mass transfer of dissolved oxygen from the bulk fluid to the surface, even in the presence of a porous oxidized layer on the surface (Ref 36). If such a porous surface hydroxide layer becomes thick enough or dense enough, the mass transfer rate might become limited by diffusion through that porous film. Under these circumstances, the constants a, b, and c could change from those for a smooth surface. The equation itself may change, for example, by incorporating a term for the ratio of the surface roughness dimension to the length dimension.

This effect of velocity has ramifications for localized attack, especially pitting and crevice corrosion. The presence of fluid flow can sometimes be beneficial in preventing or decreasing localized attack. For example, type 316 stainless steel has been shown to pit in quiescent seawater but not in moving seawater (Ref 37). When the seawater is moving, the mass transfer rate of oxygen is high enough to maintain a completely passive surface, but in the absence of flow, the mass transfer of oxygen is too slow, and the surface cannot remain passive (Ref 38). This observation indicates that sometimes, fluid velocity can be beneficial even if the corrosion rate involves the mass transfer of a reactant or product. The propensity for localized attack to occur can sometimes be decreased by maintaining sufficient fluid motion.

Under other circumstances, fluid flow has been reported to cause a type of erosion of a surface through the mechanical force of the fluid itself. This process is called impingement. It involves the removal of loosely adhered corroded surface layers on the metal or alloy by the high wall shear stress created by the flowing fluid. Examples of such erosion occur either where fluid is forced to turn direction, for example, at pipe bends (Ref 22), or where high surface shear stresses can exist, for example on ship hulls (Ref 39).

Controversy surrounds the effect that fluid shear stress at the wall has on corrosion. Earlier work has suggested that a critical wall shear stress can be defined above which impingement of a single-phase fluid causes corrosion and below which such an effect is absent (Ref 39). However, the equations that relate fluid shear stress and mass transfer to Reynolds number are so closely related that differentiation between dependence on mass transfer and dependence on fluid shear stress at the wall becomes difficult (Ref 40). Current thinking leans toward most velocity-sensitive corrosion in single-phase fluids being largely caused by mass transfer between the fluid and the corroding surface and not by a removal of the passive film or oxidized surface layers by momentum transfer between the fluid and the wall (Ref 41). There remains the possibility at extremely high

flow rates or extremely high shear stresses that fluid motion could remove a weakly adsorbed inhibitor, but the evidence for such effects remains cloudy.

When solids are present in the liquid, they can cause wear or solid erosion-corrosion (Ref 42). This wear is caused by the relative movement of the solids with respect to the surface. Again, such wear is more prevalent where fluid is forced to change direction or where high shear stresses occur. The particles must penetrate the laminar sublayer with enough force to remove the passive film on the alloy. Therefore, high shear stresses are often required for this type of erosion to occur. This problem can be significant in systems carrying saltwater and solids (for example, sand or coal) and carbon steel carrying air plus particulates.

References cited in this section

6. B.T. Ellison and W.R. Schmeal, Corrosion of Steel in Concentrated Sulfuric Acid, *J. Electrochem. Soc.,* Vol 125 (No. 4), 1978, p 524

7. T.K. Ross, G.C. Wood, and I.J. Mahmud, The Anodic Behavior of Iron Carbon Alloys in Moving Acid Media, *J. Electrochem. Soc.,* Vol 113, 1966, p 334

11. D.C. Silverman and M.E. Zerr, Application of Rotating Cylinder Electrode—E-Brite 26-1/Concentrated Sulfuric Acid, *Corrosion,* Vol 42 (No. 11) 1986, p 633

22. M.G. Fontana and N.D. Green, *Corrosion Engineering,* 3rd ed., McGraw-Hill, 1986

35. K.D. Efird, Flow-Induced Corrosion, Ch 14, and J. Postlethwaite and S. Nesic, Erosion- Corrosion in Single and Multiphase Flow, Ch 15, in *Uhlig's Corrosion Handbook,* 2nd ed., R.W. Revie, Ed., John Wiley and Sons, Inc., 2000

36. B.K. Mahato, C.Y. Cha, and L.W. Shemilt, Unsteady State Mass Transfer Coefficients Controlling Steel Pipe Corrosion Under Isothermal Flow Conditions, *Corros. Sci.,* Vol 20, 1980, p 421

37. H.R. Copson, Effects of Velocity on Corrosion, *Corrosion,* Vol 16 (No. 2), 1960, p 86t

38. T.R. Beck and S.G. Chan, Experimental Observations and Analysis of Hydrodynamic Effects on Growth of Small Pits, *Corrosion,* Vol 37 (No. 11), 1981, p 665

39. P.A. Lush, S.P. Hutton, J.C. Rowlands, and B. Angell, The Relation Between Impingement Corrosion and Fluid Turbulence Intensity, *Proceedings of the Sixth European Congress on Metallic Corrosion,* 1977, p 137

40. D.C. Silverman, Rotating Cylinder Electrode-Geometry Relationships for Prediction of Velocity Sensitive Corrosion, *Corrosion,* Vol 44, 1988, p 42

41. K.J. Kennelley, R.H. Hausler, and D.C. Silverman, Ed., *Flow-Induced Corrosion: Fundamental Studies and Industrial Experience,* NACE International, 1991

42. B. Vyas, Erosion-Corrosion, *Treatise on Materials Science and Technology,* Vol 16, Academic Press, 1979, p 357

D.C. Silverman, Aqueous Corrosion, *Corrosion: Fundamentals, Testing, and Protection,* Vol 13A*, ASM Handbook,* ASM International, 2003, p 190–195

Aqueous Corrosion

Revised by David C. Silverman, Argentum Solutions, Inc.

Component Concentration and Composition

The concentration and makeup of components within the aqueous-based fluid often influence how the other variables manifest themselves. This brief overview discussion highlights how the concentration of dissolved species works with other variables to influence corrosion behavior.

During the previous discussion, the point was made that pH plays a major role in corrosion. For iron, the corrosion rate is large at very low pH, is independent of pH in the neutral pH range, decreases with increasing pH, and finally increases again at very high pH. Additions of small amounts of other components can change this behavior. For example, addition of chloride to H_2SO_4 increases the corrosion rate of iron. This increase is reported to be proportional to the chloride ion concentration raised to approximately the 0.5 power (Ref 43). A similar effect is reported for chloride ion in HCl (Ref 8). Thus, chloride ion accelerates the corrosion of iron in acidic solutions. However, bromide and iodide ions may inhibit corrosion (Ref 44), although this finding is controversial (Ref 17).

The addition of a second component can influence the effect of an already present component. For example, the dependence of the corrosion rate of iron on chloride ion concentration can significantly decrease in neutral solutions when oxygen is present (Ref 44). In addition, as salt concentration increases, the oxygen solubility decreases, masking the effect of chloride ion. The chloride ion effect depends on the cation in concentrated salt solutions, with the rate increasing in the order lithium chloride (LiCl), sodium chloride (NaCl), and potassium chloride (KCl) partially because of differences in oxygen solubility in the presence of these salts (Ref 17). These results illustrate that the effect of the concentration of one component on corrosion can often be influenced by the other environmental variables.

Small additions of certain inhibitors or passivators have a marked effect on corrosion. For example, as little as 0.0023 mol/L of sodium nitrite ($NaNO_2$) or sodium sulfite (Na_2SO_3) can decrease the pit initiation rate of aluminum. Little improvement is found at higher concentration for this system (Ref 45). This behavior is often found with many types of inhibitors. For example, small concentrations (10 ppm) of $NaNO_2$ (a passivator) can drastically inhibit the corrosion of iron, with little further decrease in corrosion found at higher concentrations (Ref 46). The critical concentration can depend on pH and on the presence of other dissolved ions or molecules. The actual concentration needed for a given system must be determined experimentally. Similarly, many organic inhibitors cause a drastic decrease in corrosion rate at very low concentrations, especially for iron in acidic solutions, with no benefit observed on increasing the inhibitor concentration (Ref 47). Inhibitors tend to interact with the surface in one of three ways: a gettering by a component, such as hydrazine, of a finite amount of impurity, such as oxygen, in the solution; oxidation (passivation) of the surface or incorporation in the three-dimensional oxide (nitrite, phosphate, or chromate); or adsorption on the exposed surface area to block corrosion (many organic inhibitors in acid) (Ref 47, 48). Adding an inhibitor to a fluid, even at low concentrations, has been found to change the sensitivity to fluid motion (Ref 49). Conversely, the amount of inhibitor required has been found to be affected by fluid motion, sometimes even decreasing with the onset of fluid motion.

Although this type of behavior is common even for iron in neutral, aqueous environments, exceptions do exist. Sometimes, corrosion can increase with inhibitor concentration until a maximum is reached, followed by a rapid decrease with still further increases in concentration (Ref 46). An example is chromate ion. Chromate ion is normally considered to be an inhibitor. However, at very low concentrations and in the presence of strong activating ions such as chlorides in acidic media, chromate ion can actually accelerate corrosion until enough chromate is present. Also, synergistic action may be observed in which the efficacy of one inhibitor depends on the presence of another species, for example, oxygen or other oxidizing agents. An example is the synergistic action of zinc ions and hydroxyethane diphosphonic acid (HEDP) to passivate the steel surface (Ref 48). Zinc

ions alone cannot passivate steel, and HEDP alone is only modestly successful. Together, they form a more potent inhibitor system, their action virtually independent of the concentration of dissolved oxygen.
A question often asked is, “What is the amount of chloride that is allowable before localized corrosion (crevice corrosion, pitting, or SCC) can occur in austenitic alloys?” The answer is not straightforward. Work with boiling, saturated magnesium chloride suggests that 42 wt% Ni in the alloy prevents SCC (Ref 22). This rule of thumb, however, does not answer the question. The maximum chloride concentration depends on the pH, other constituents, temperature, and other variables—some environmental, some metallurgical.

References cited in this section

8. R.J. Chin and K. Nobe, Electrodissolution Kinetics of Iron in Chloride Solutions, *J. Electrochem. Soc.*, Vol 119 (No. 11), 1972, p 1457

17. N.D. Tomashov, *Theory of Corrosion and Protection of Metals*, B.H. Tytell, I. Geld, and H.S. Preiser, Trans., Macmillan, 1966

22. M.G. Fontana and N.D. Green, *Corrosion Engineering*, 3rd ed., McGraw-Hill, 1986

43. S.S. Abd. El Rehim, M. Sh. Shalaby, and S.M. Abd. El Halum, Effect of Some Anions on the Anodic Dissolution of Delta-S2 Steel in Sulfuric Acid, *Surf. Technol.*, Vol 24, 1985, p 241

44. E. McCafferty, Electrochemical Behavior of Iron Within Crevices in Nearly Neutral Chloride Solutions, *J. Electrochem. Soc.*, Vol 121 (No. 9), 1974, p 1007

45. H. Boehni, Pitting and Crevice Corrosion, *Corrosion in Power Generating Equipment*, Proceedings of the Eighth International Brown Boveri Symposium, 1984, p 29

46. M. Cohen, Dissolution of Iron, *Corrosion Chemistry*, G.R. Brubaker and P.B.P. Phipps, Ed., ACS Symposium Series, 89, American Chemical Society, 1979, p 126

47. A. Raman and P. Labine, Ed., Reviews on Corrosion Inhibitor Science and Technology, NACE International, 1993

48. Y.I. Kuznetsov, *Organic Inhibitors of Corrosion of Metals*, (A.D. Mercer, Scientific translator and J.G.N. Thomas, Scientific editor), Plenum Press, 1996

49. D.C. Silverman, Corrosion Prediction from Circuit Models-Application to Evaluation of Corrosion Inhibitors, in *Electrochemical Impedance-Analysis and Interpretation*, J.R. Scully, D.C. Silverman, and M.W. Kendig, Ed., STP 1188, ASTM International, 1993

D.C. Silverman, Aqueous Corrosion, *Corrosion: Fundamentals, Testing, and Protection*, Vol 13A, *ASM Handbook*, ASM International, 2003, p 190–195

Aqueous Corrosion

Revised by David C. Silverman, Argentum Solutions, Inc.

Acknowledgment

This article has been adapted from D.C. Silverman and R.B. Puyear, Effects of Environmental Variables on Aqueous Corrosion, in *Corrosion,* Volume 13, *Metals Handbook,* 9th ed., ASM International, 1987.

D.C. Silverman, Aqueous Corrosion, *Corrosion: Fundamentals, Testing, and Protection*, Vol 13A, *ASM Handbook,* ASM International, 2003, p 190–195

Aqueous Corrosion

Revised by David C. Silverman, Argentum Solutions, Inc.

References

1. M. Pourbaix, *Atlas of Electrochemical Equilibria in Aqueous Solutions,* National Association of Corrosion Engineers, 1974
2. D.C. Silverman, Presence of Solid $Fe(OH)_2$ in EMF-pH Diagram for Iron, *Corrosion,* Vol 38 (No. 2), 1982, p 453
3. R.A. Robinson and R.H. Stokes, *Electrolyte Solutions,* 2nd ed., Academic Press, 1959
4. R.G. Bates, *Electrometric pH Determinations,* John Wiley & Sons, 1954
5. P. Lorbeer and W.J. Lorenz, The Kinetics of Iron Dissolution and Passivation in Solutions Containing Oxygen, *Electrochim. Acta,* Vol 25 (No. 4), 1980, p 375
6. B.T. Ellison and W.R. Schmeal, Corrosion of Steel in Concentrated Sulfuric Acid, *J. Electrochem. Soc.,* Vol 125 (No. 4), 1978, p 524
7. T.K. Ross, G.C. Wood, and I.J. Mahmud, The Anodic Behavior of Iron Carbon Alloys in Moving Acid Media, *J. Electrochem. Soc.,* Vol 113, 1966, p 334
8. R.J. Chin and K. Nobe, Electrodissolution Kinetics of Iron in Chloride Solutions, *J. Electrochem. Soc.,* Vol 119 (No. 11), 1972, p 1457
9. A.N. Katrevick, G.M. Florianovich, and Ya.M. Kolotyrkin, Clarification of the Kinetic Parameters of the Reaction of the Active Dissolution of Iron in Phosphate Solutions, *Zashch. Met.,* Vol 10 (No. 4), 1974, p 369
10. B. Alexandre, A. Caprani, J.C. Charbonnier, M. Keddam, and P.H. Morel, The Influence of Chromium on the Mass Transfer Limitation of the Anodic Dissolution of Ferritic Steels Fe-Cr in Molar Sulfuric Acid, *Corros. Sci.,* Vol 21 (No. 11), 1981, p 765
11. D.C. Silverman and M.E. Zerr, Application of Rotating Cylinder Electrode—E-Brite 26-1/Concentrated Sulfuric Acid, *Corrosion,* Vol 42 (No. 11) 1986, p 633
12. "The Corrosion Resistance of Nickel Containing Alloys in Sulfuric Acid and Related Compounds," CEB-1, International Nickel Company, Inc., 1983
13. "Resistance of Nickel and High Nickel Alloys to Corrosion by Hydrochloric Acid, Hydrogen Chloride, and Chlorine," CEB-3, International Nickel Company, Inc., 1974

14. D.C. Silverman, Derivation and Application of EMF-pH Diagrams, *Electrochemical Techniques for Corrosion Engineers,* R. Baboian, Ed., NACE International, 1986

15. A. Alon, M. Frenkel, and M. Schorr, Corrosion and Electrochemical Behavior of Titanium in Acidic, Oxidizing, Aqueous, and Alcoholic Systems, *Proceedings of the Fourth International Congress on Metallic Corrosion,* National Association of Corrosion Engineers, 1969, p 636

16. V. Vujicic and B. Lovrecek, A Study of the Influence of pH on the Corrosion Rate of Aluminum, *Surf. Technol.,* Vol 25, 1985, p 49

17. N.D. Tomashov, *Theory of Corrosion and Protection of Metals,* B.H. Tytell, I. Geld, and H.S. Preiser, Trans., Macmillan, 1966

18. M. Fischer, Possible Models of the Reaction Mechanism and Discussion of the Functions of Passivating Additions During the Chemical Passivation of Iron in Weakly Acidic, Neutral and Basic pH Ranges, *Werkst. Korros.,* Vol 29, 1978, p 188

19. B.J. Andrzejaczek, Influence of Oxygen on the Kinetics of Corrosion Processes on Iron in Water, *Korrosion,* Vol 15 (No. 5), 1984, p 239

20. R.N. Sylva, The Hydrolysis of Iron (III), *Rev. Pure Appl. Chem.,* Vol 22, 1972, p 115

21. W. Frank and L. Graf, Mechanism of Intergranular Corrosion and Intergranular Stress Corrosion Cracking in Mild Steels, *Res. Mech.,* Vol 13, 1985, p 251

22. M.G. Fontana and N.D. Green, *Corrosion Engineering,* 3rd ed., McGraw-Hill, 1986

23. D.R. Knittel, Zirconium: A Corrosion Resistant Material for Industrial Applications, *Chem. Eng.,* Vol 87 (No. 11), 1980, p 98

24. M. Schussler, *Corrosion Data Survey on Tantalum,* Fansteel, Inc., 1972

25. O.L. Riggs, Jr., and C.E. Locke, *Anodic Protection: Theory and Practice in the Prevention of Corrosion,* Plenum Press, 1981

26. H.H. Uhlig, *Corrosion and Corrosion Control,* John Wiley & Sons, 1963

27. J.H. Fitzgerald, Jr., Engineering of Cathodic Protection Systems, Ch. 57, in *Uhlig's Corrosion Handbook,* 2nd ed., R.W. Revie, Ed., John Wiley and Sons, Inc., 2000

28. Bimetallic Corrosion, L.L. Shrier, R.A. Jarman, and G.T. Burstein, Ed., *Corrosion,* Vol 1, p 1:213, Butterworth-Heinemann, Oxford, 1994

29. Ya.M. Kolotyrkin, V.S. Pakhomov, A.G. Parshin, and A.V. Chekhovskii, Effect of Heat Transfer on Corrosion of Metals, *Khim. Neft. Mashinostr.,* Vol 16 (No. 12), 1980, p 20

30. J.W. Oldfield, T.S. Lee, and R.M. Kain, Avoiding Crevice Corrosion of Stainless Steels, *Proceedings of Stainless Steels '84,* Institute of Metals, 1985, p 205

31. R.J. Brigham, The Initiation of Crevice Corrosion on Stainless Steels, *Mater. Perform.,* Vol 24 (No. 12), 1985, p 44

32. J.R. Kearns, Crevice, Corrosion Tests and Standards—Application and Interpretation, R. Baboian, Ed., ASTM International, 1995

33. A.G. Parshin, V.S. Parkhomov, and Ya.M. Kolotyrkin, The Influence of Heat Transfer on the Kinetics of Cathode Processes With Limiting Diffusion Steps, *Corros. Sci.,* Vol 22 (No. 9), 1982, p 845

34. T.K. Ross, Corrosion and Heat Transfer—A Review, *Br. Corros. J.,* Vol 2, 1967, p 131

35. K.D. Efird, Flow-Induced Corrosion, Ch 14, and J. Postlethwaite and S. Nesic, Erosion- Corrosion in Single and Multiphase Flow, Ch 15, in *Uhlig's Corrosion Handbook,* 2nd ed., R.W. Revie, Ed., John Wiley and Sons, Inc., 2000

36. B.K. Mahato, C.Y. Cha, and L.W. Shemilt, Unsteady State Mass Transfer Coefficients Controlling Steel Pipe Corrosion Under Isothermal Flow Conditions, *Corros. Sci.,* Vol 20, 1980, p 421

37. H.R. Copson, Effects of Velocity on Corrosion, *Corrosion,* Vol 16 (No. 2), 1960, p 86t

38. T.R. Beck and S.G. Chan, Experimental Observations and Analysis of Hydrodynamic Effects on Growth of Small Pits, *Corrosion,* Vol 37 (No. 11), 1981, p 665

39. P.A. Lush, S.P. Hutton, J.C. Rowlands, and B. Angell, The Relation Between Impingement Corrosion and Fluid Turbulence Intensity, *Proceedings of the Sixth European Congress on Metallic Corrosion,* 1977, p 137

40. D.C. Silverman, Rotating Cylinder Electrode-Geometry Relationships for Prediction of Velocity Sensitive Corrosion, *Corrosion,* Vol 44, 1988, p 42

41. K.J. Kennelley, R.H. Hausler, and D.C. Silverman, Ed., *Flow-Induced Corrosion: Fundamental Studies and Industrial Experience,* NACE International, 1991

42. B. Vyas, Erosion-Corrosion, *Treatise on Materials Science and Technology,* Vol 16, Academic Press, 1979, p 357

43. S.S. Abd. El Rehim, M. Sh. Shalaby, and S.M. Abd. El Halum, Effect of Some Anions on the Anodic Dissolution of Delta-S2 Steel in Sulfuric Acid, *Surf. Technol.,* Vol 24, 1985, p 241

44. E. McCafferty, Electrochemical Behavior of Iron Within Crevices in Nearly Neutral Chloride Solutions, *J. Electrochem. Soc.,* Vol 121 (No. 9), 1974, p 1007

45. H. Boehni, Pitting and Crevice Corrosion, *Corrosion in Power Generating Equipment,* Proceedings of the Eighth International Brown Boveri Symposium, 1984, p 29

46. M. Cohen, Dissolution of Iron, *Corrosion Chemistry,* G.R. Brubaker and P.B.P. Phipps, Ed., ACS Symposium Series, 89, American Chemical Society, 1979, p 126

47. A. Raman and P. Labine, Ed., Reviews on Corrosion Inhibitor Science and Technology, NACE International, 1993

48. Y.I. Kuznetsov, *Organic Inhibitors of Corrosion of Metals,* (A.D. Mercer, Scientific translator and J.G.N. Thomas, Scientific editor), Plenum Press, 1996

49. D.C. Silverman, Corrosion Prediction from Circuit Models-Application to Evaluation of Corrosion Inhibitors, in *Electrochemical Impedance-Analysis and Interpretation,* J.R. Scully, D.C. Silverman, and M.W. Kendig, Ed., STP 1188, ASTM International, 1993

L. Veleva and R.D. Kane, Atmospheric Corrosion, *Corrosion: Fundamentals, Testing, and Protection*, Vol 13A, *ASM Handbook*, ASM International, 2003, p 196–209

Atmospheric Corrosion

Lucien Veleva, CINVESTAV-IPN, Yucatan, Mexico; Russell D. Kane, InterCorr International, Inc.

Introduction

ATMOSPHERIC CORROSION is the degradation and destruction of metallic materials and their structure and properties due to interaction with the terrestrial atmosphere at its characteristic air temperature, humidity, air chemistry, and climatic values (Ref 1, 2, 3, 4, 5, 6, 7, 8, 9, 10, 11, 12, 13). Atmospheric corrosion is distinguished from the corrosion of metals exposed to high temperatures in an absence of moisture on the metal surface (dry or gaseous corrosion), which does not correspond to the terrestrial atmospheric humidity and temperature. The mechanism of high-temperature corrosion is a chemical corrosion, and it is quite different from atmospheric corrosion. (See the article “High-Temperature Gaseous Corrosion” in this Volume.)

The majority of metal structures and equipment are exposed to terrestrial air conditions to some degree and therefore can suffer from atmospheric corrosion. In some severe cases, the metal can be completely destroyed and converted to corrosion products. With background knowledge of the principal exposure conditions and their influence on metal corrosion, most serious corrosion problems can be prevented. It is recognized that several industries face difficult corrosion problems because of very aggressive atmospheres, including the electrical power transmission and distribution industry, chemical/ petrochemical production plants and equipment, aircraft, automotive manufacture and associated components, transportation infrastructure, offshore structures and equipment, the construction industry, and electronic devices.

Atmospheric corrosion occurs spontaneously but may be slowed, prevented, and controlled but never stopped. The reason is that the commonly used metals are not in a pure state in the earth, except for some noble metals. Metals usually are in ores, chemical compounds that include oxygen, hydrogen, and sulfur. These mineral compounds are the thermodynamic steady state of the metals, in which Gibbs free energy (ΔG) has a minimum value. For the separation of the metals from their ores and for metallurgical and manufacturing processes, energy, in the form of heat, chemical, electrical, or mechanical, elevates the metal to a higher energy level. The metal product is not in its most thermodynamically stable state. This fact drives metals to convert into corrosion products having a chemical composition similar to that of the original ores that are in a more thermodynamically stable state. When metals come in contact with the atmosphere (oxygen) and water (moisture) in the presence of corrosive species such as chlorides or sulfur dioxide, the corrosion process starts, and corrosion products such as oxides, hydroxides, or oxyhydroxides are formed. Table 1 shows the tendency for corrosion of some metals as a function of the energy required for their separation from ores.

Table 1 Position of some metals according to their standard electrode potentials in aqueous solutions at 25 °C (77 °F) in V (versus NHE)(a)

Metal	Standard electrode potential at 25 °C (77 °F), V
Higher excess of free energy **(very high corrosion tendency)**	
Potassium	-2.92
Magnesium	-2.34
Beryllium	-1.70
Aluminum	-1.67
Manganese	-1.05
Zinc	-0.76
Chromium	-0.71
Iron	-0.44

Cadmium	-0.40
Cobalt	-0.34
Nickel	-0.27
Tin	-0.25
Lead	-0.14
Copper	0.34
Silver	0.80
Palladium	0.83
Platinum	1.2
Gold	1.42
Lower excess of free energy **(low tendency for corrosion)**	

Note: The excess of free energy is related to the standard electrode (metal) potential value. (Complete metal electrode potential values can be found in *Tables of Standard Electrode Potentials,* G. Milazzo and S. Caroli, Ed., Wiley-Interscience, 1977.). (a) NHE, normal hydrogen electrode = SHE, standard hydrogen electrode with hydrogen ions at unity activity/concentration (a = 1,aqueous)

References cited in this section

1. L.L. Shreir, R.A. Jarman, and G.T. Burstein, Ed., Corrosion, Vol 1, *Metal/Environment Reactions,* 3rd ed., Butterworth- Heinemann, 1994

2. “Economic Effect of Metallic Corrosion in the United States,” NBS Special Publications 511-1 and 511-2, National Bureau of Standards, May 1978

3. S.C. Cederquist, Cost of Corrosion Studies Underway, *Mater. Perform.,* Vol 38 (No. 5), 1999, p 26–28

4. G.H. Koch, M.P.J. Brongers, N.G. Thompson, Y.P. Virmani, and J.H. Payer, “Corrosion Costs and Preventive Strategies in the United States,” FHWA-RD-01-156, Federal Highway Administration, U.S. Department of Transportation, March 2002

5. B.C. Syrett, J.A. Gorman, M.L. Arey, G.H. Kosch, and G.A. Jacobson, Cost of Corrosion, *Mater. Perform.,* Vol 41 (No. 3), 2002, p 18–22

6. U. Evans, Electrochemical Mechanism for Atmospheric Rusting, *Nature,* Vol 206, June 1965, p 980–982

7. I.L. Rozenfeld, *Atmospheric Corrosion of Metals,* B.H. Tytel, Ed., National Association of Corrosion Engineers, 1973

8. V. Kucera and E. Mattsson, *Atmospheric Corrosion,* W.H. Ailor, Ed., John Wiley & Sons, 1982

9. *Corrosion Basics, An Introduction,* National Association of Corrosion Engineers 1984

10. E. Mattsson, Corrosion: An Electrochemical Problem, *Chem. Technol.,* April 1985, p 234–243

11. P. Marcus and J. Oudar, Ed., *Corrosion Mechanism in Theory and Practice,* Marcel Dekker, Inc., 1995

12. C. Leygraf and T. Graedel, *Atmospheric Corrosion,* Wiley-Interscience, 2000

13. M. Pourbaix, *Atlas of Electrochemical Equilibria in Aqueous Solutions,* NACE- Cebelcor, 1974

L. Veleva and R.D. Kane, Atmospheric Corrosion, *Corrosion: Fundamentals, Testing, and Protection*, Vol 13A, *ASM Handbook*, ASM International, 2003, p 196–209

Atmospheric Corrosion

Lucien Veleva, CINVESTAV-IPN, Yucatan, Mexico; Russell D. Kane, InterCorr International, Inc.

Elements of the Process

Atmospheric corrosion is an aqueous process, and its mechanism is electrochemical. There is not only a transfer of mass during the chemical reaction but also an interchange of charged particles (electrons and ions) at the interface of the metal (an electronic conductor) and the electrolyte (an ionic conductor). The transfer of electrons (flow of electric current) occurs because of the formation of a galvanic corrosion cell on the metal surface. Three elements are necessary for the cell operation: anode and cathode sites, an electrolyte, and an oxidizing agent.

Anode and cathode sites form multiple corrosion cells.

Anodes are the areas on the metal with a higher energy state, due to various factors such as inhomogeneous metal composition, grain boundary, multiple metallurgical phases, local metal defects, and nonuniform metal treatments. The oxidation corrosion reaction is done on the anodic sites:

$$\mathrm{Me} - ne^{-} \bullet \ \mathrm{Me}^{n+} \cdot (m\mathrm{H_2O}) \qquad \text{(Eq 1)}$$

where Me is the metal. The metal is dissolved at the anode to form cations (positively charged ions). These may originally appear as metal hydrated ions ($Me^{n+} \cdot (mH_2O)$ but subsequently convert into oxides and hydroxides, the metal corrosion products. For example, steel atmospheric corrosion products typically include α- and γ-FeOOH as main constituents.

Cathodes are the metal sites with a lower energy state, for example, inert non-metallic inclusions and lower active-metal phases or structures. The cathodic reaction occurs on these sites and involves the reduction of an oxidizing agent, such as air, oxygen, or hydrogen ions.

An electrolyte, such as moisture, comes in contact with the metal surface. The moisture contains dissolved ionic species (atmospheric pollutants) and is a good ionic conductor that can sustain electrochemical reactions.

An oxidizing agent, such as oxygen and hydrogen ions (H^+), is necessary for accepting the electrons emitted from the metal in the anode reaction (Eq 1):

$$\mathrm{Oxy} + e^{-} \bullet \ \mathrm{Red_{form}} \qquad \text{(Eq 2)}$$

$$\frac{1}{2}\mathrm{O_2} + \mathrm{H_2O} + 2e^{-} \bullet \ 2\mathrm{OH^-} \qquad \text{(Eq 3)}$$

$$2\mathrm{H^+} + \mathrm{H_2O} + 2e^{-} \bullet \ \mathrm{H_2} \uparrow \text{(gas)} \qquad \text{(Eq 4)}$$

where Oxy is the oxidizing agent, and Red is the reduced species.

Corrosion Reactions. Figures 1 and 2 illustrate the corrosion reactions (oxidation and reduction) that occur on the metal surface at the metal-electrolyte interface and the movement of electrons from the anodic to cathodic sites. The net electric current is zero, because the electrons liberated during the oxidation of the metal (Eq 1) are accepted by the oxidizing agent in the cathodic (reduction) reaction (Eq 2). In Fig. 2, the oxidizing agent is the H^+ ion (cation), a principal ion in the moisture formed on the metal surface exposed to industrial and urban atmospheres. Typically in these sites, the atmosphere may be contaminated by SO_2, which can be converted to H_2SO_3 and then to H_2SO_4 (sulfuric acid) in the presence of moist air. When this occurs in the atmosphere, acid rain is formed, which is a severe environment for metal structures. The movement of the electrons from anodic to cathodic sites in a metal is a result of the difference in Gibbs free energy between the anode (higher level) and the cathode (lower level). This results in a potential difference between both reaction metal sites, which yields a current flow from the anodic to cathodic sites. Detailed information about the possible corrosion reaction (and their metal potential values) as a function of aqueous electrolyte concentration and pH (acidity or alkalinity) in the presence of certain ions (atmospheric contamination) can be found using Pourbaix diagrams

(Ref 13). These diagrams are a useful tool for any corrosion engineer and scientist in evaluating and understanding the conditions that lead to specific corrosion reactions and their associated corrosion products.

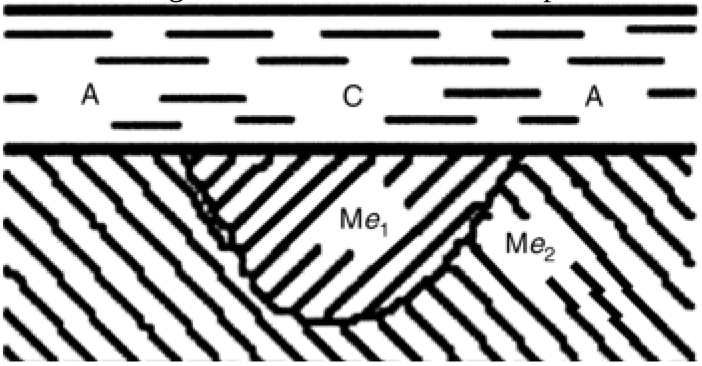

Fig. 1 Schematic presentation of corrosion metal cell formed by anodic (A) and cathodic (C) sites. The A sites (Me_2) have a more negative potential (*E*) relative to that of the C sites (Me_1).

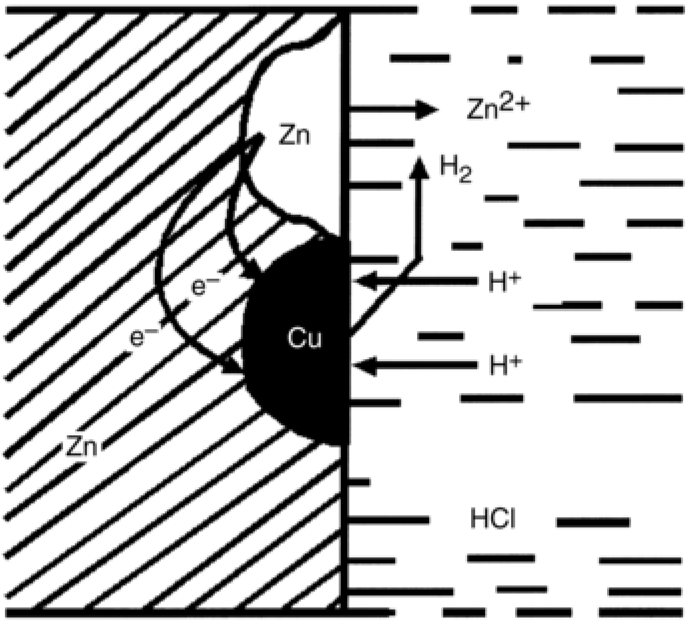

Fig. 2 Schematic presentation of the corrosion galvanic cell created in a zinc-copper alloy in an acid environment. The cathode is the copper-rich phase and the anode is the zinc-rich phase. The corrosion attack is selective to the zinc-rich phase.

Types of Atmospheric Corrosion Attack. Atmospheric corrosion can occur in two basic forms: uniform (general) and non-uniform (localized) attack. Uniform corrosion results at a similar corrosion rate over the metal surface and has the same appearance throughout (Fig. 3a). Uniform attack is typical for atmospheric corrosion of steel and copper. Localized corrosion usually occurs at small and specific locations on the metal surface where the corrosion process is focused, resulting in local acceleration of the corrosion rate (Fig. 3b). This type of corrosion attack is referred to as pitting corrosion and can be observed on aluminum and its alloys, zinc (hot dip zinc or electrodeposited zinc on steel), stainless steels, nickel, and other metals. It is often induced by the presence of chloride ions, which can be found in airborne salinity in marine-coastal environments. Localized attack of some aluminum alloys, such as those containing copper, can take the form of layered corrosion, exfoliation, detachment, and deformation, of thin layers within the metal surface when exposed to coastal environments.

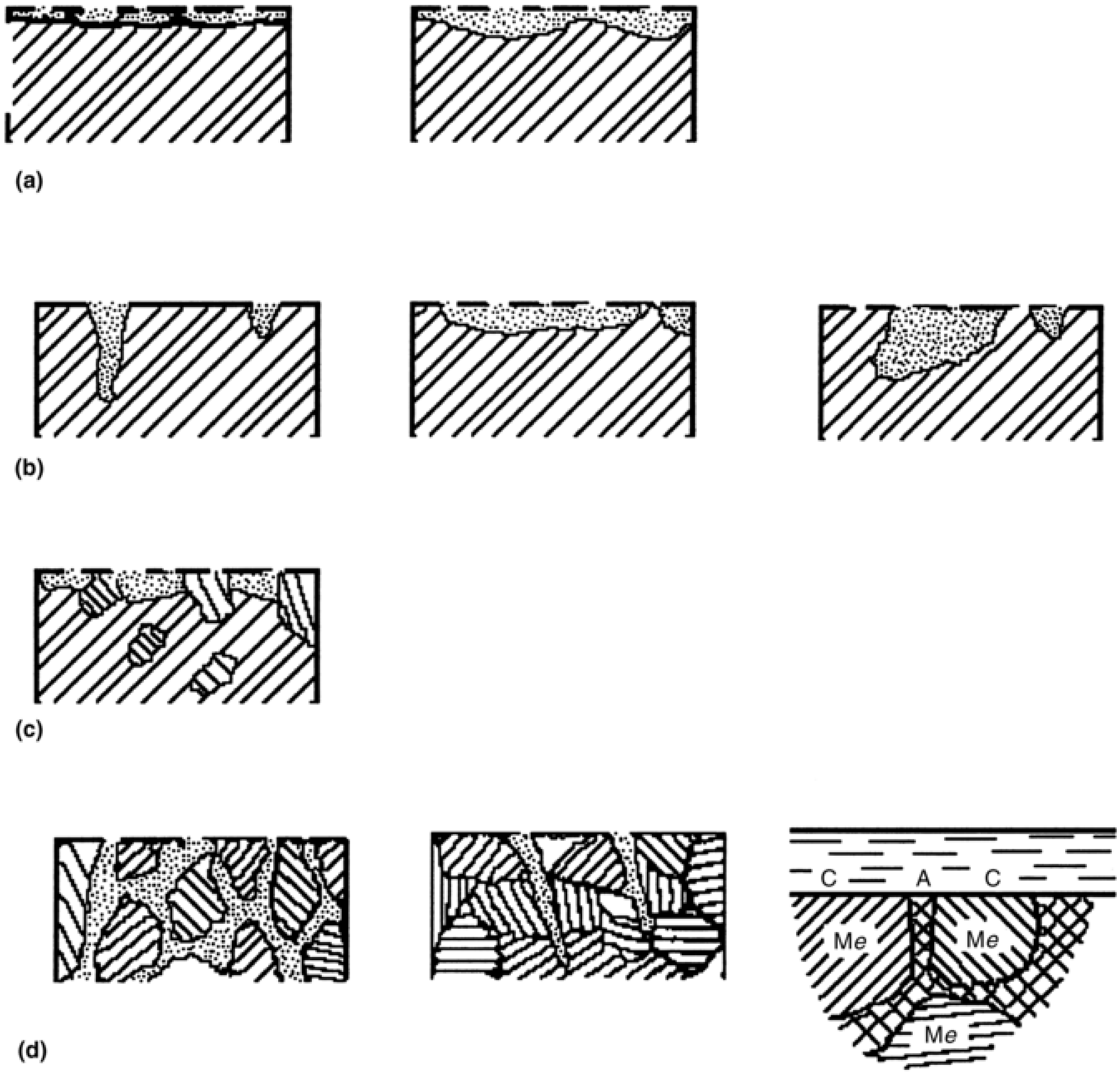

Fig. 3 Schematic presentation of cross sections of several forms of corrosion attacks. (a) Uniform. (b) Nonuniform (localized). (c) Selective. (d) Intergranular. C, cathodic areas (M*e*); A, anodic areas between the metal grains

Localized atmospheric corrosion can also be observed on the surface of brass and copper-zinc alloys due to the reaction of the distinct alloying metals in contact with the environment. In this case, the corrosion is referred to as selective corrosion (Fig. 3c). Some metals or alloys can be susceptible to localized attack that forms at locations of distinct phases on the grain boundaries. This corrosion is recognized as intergranular corrosion (Fig. 3d). An example is the corrosion in cast iron, which occurs around the boundary of the ferritic phase or at carbides in grain boundaries of stainless steels. The atmospheric corrosion process can also be increased when two or more different metals are in direct contact in a structure. This metal coupling allows the formation of a galvanic corrosion cell having different electromotive force (voltage), depending on the potential values of the metals in contact (Table 1) (Fig. 4).

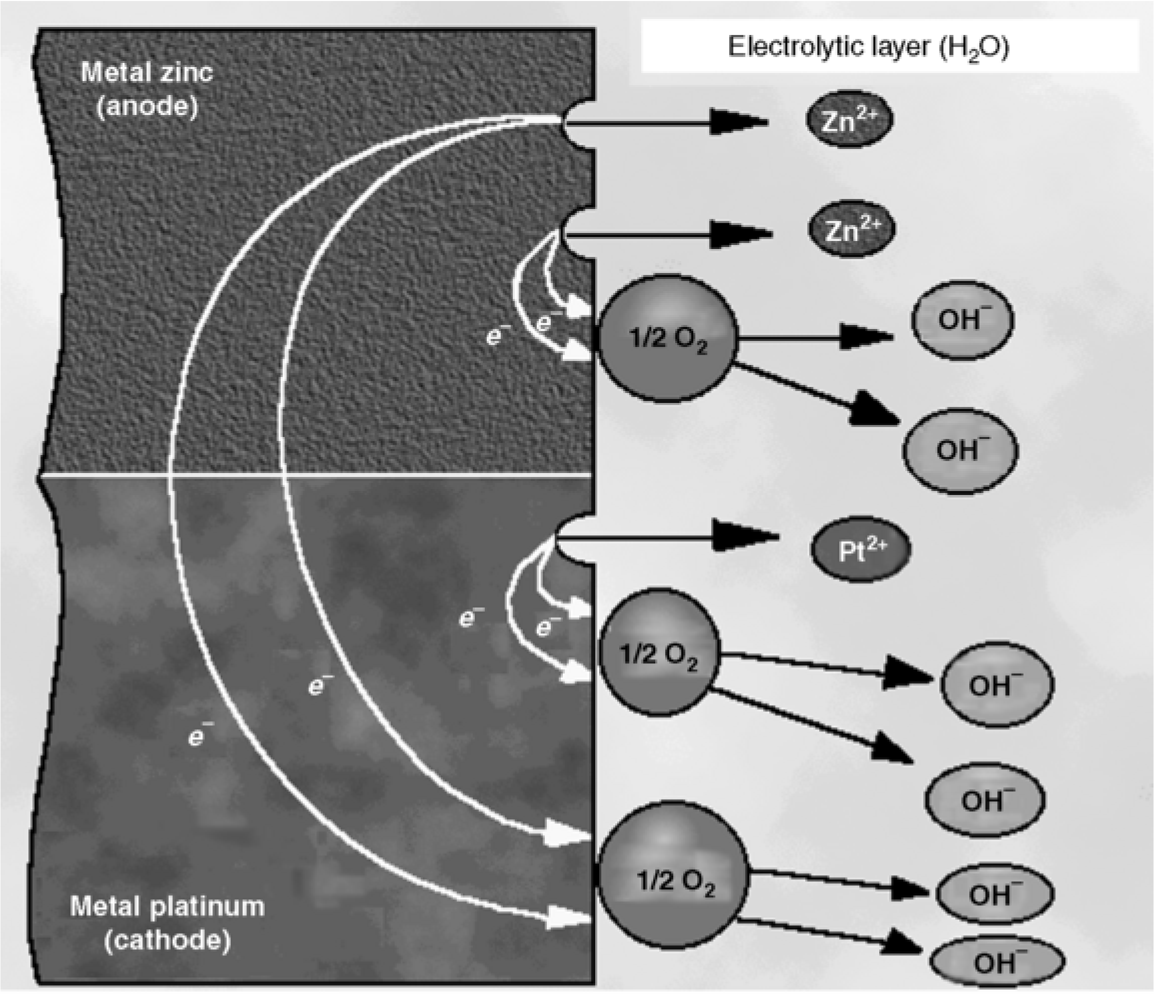

Fig. 4 Schematic presentation of corrosion reaction in galvanic coupling of zinc and platinum

A very dangerous type of atmospheric corrosion attack is metal cracking, which can occur when a metal structure such as a bridge is exposed to a corrosive environment and continuous or cyclic mechanical loading. This combination leads to surface or internal microcrevices, fissures, and cracks that result in stress-corrosion cracking (under relatively constant loads) or fatigue corrosion (under cyclic deformation).

Reference cited in this section

13. M. Pourbaix, *Atlas of Electrochemical Equilibria in Aqueous Solutions,* NACE- Cebelcor, 1974

L. Veleva and R.D. Kane, Atmospheric Corrosion, *Corrosion: Fundamentals, Testing, and Protection,* Vol 13A, *ASM Handbook,* ASM International, 2003, p 196–209

Atmospheric Corrosion

Lucien Veleva, CINVESTAV-IPN, Yucatan, Mexico; Russell D. Kane, InterCorr International, Inc.

Atmospheric Parameters and Their Influence

A variety of atmospheric factors, climatic conditions, and air-chemical pollutants determines the corrosiveness of the atmosphere and contributes to the metal corrosion process in distinct ways (Ref 1, 7, 8, 12, 13, 14, 15, 16, 17, 18, 19, 20, 21, 22, 23, 24, 25, 26, 27, 28, 29, 30, 31, 32, 33).

Climatic characteristics play a major role in the atmospheric corrosion process. To fully understand atmospheric corrosion, it is important to properly describe and characterize the environment that causes metal degradation. Factors and the interaction between them that need to be considered are sun radiation, air temperature, relative humidity, air chemistry, precipitation, winds, and the mechanical and chemical action of natural forces such as sand and rock particles, soil dust, volcanic dust, organic matter, and industrial dust. Also, various physical, chemical, and biological factors, including manipulation of the environment as may occur in many engineering applications, must be considered. Such factors can directly affect the corrosion rate of metals exposed in outdoor or indoor atmospheres. The atmospheric corrosion process can be further complicated and accelerated when micro- and/or macroorganisms are present. In humid tropical and subtropical climates, microbial corrosion or biocorrosion is commonly observed.

When studying the atmospheric corrosion of engineering materials, the most important factors related to the climate and its effect on that material are represented by a combination of:

- Temperature (*T*) and relative humidity (RH), often described as the temperature-humidity complex (THC). Humidity is a measure of the amount of water vapor in air, and relative humidity is the ratio between absolute humidity and its saturation value, expressed in percentage. This percentage is a reverse function of the temperature (*T*); the RH increases while the *T* is decreasing, and vice versa.
- Annual values of pluvial precipitation (PP)
- Time of wetness (TOW), during which moisture exists on the metal surface, and corrosion may occur. This moisture layer on the metal surface can be generated by rain, fog, snow, dew condensation, and capillary condensation.

Standards that are useful in characterizing the environment, as well as atmospheric corrosion test standards, are listed in Table 2.

Table 2 Standards for testing and characterizing atmospheric corrosion

Designation	Title
International Organization of Standardization (ISO), Geneva, Switzerland	
ISO 8565	"Metals and Alloys, Atmospheric Corrosion Testing, General Requirements for Field Tests"
ISO 9223	"Corrosion of Metals and Alloys, Corrosivity of Atmospheres, Classification"
ISO 9225	"Corrosion of Metals and Alloys, Corrosivity of Atmospheres, Measurement of Pollution"
ISO 9226	"Corrosion of Metals and Alloys, Corrosivity of Atmospheres, Method of Determination of Corrosion Rate of Standard Specimens for the Evaluation of Corrosivity"
ISO 8407	"Corrosion of Metals and Alloys, Removal of Corrosion Products from Corrosion Test Specimens"
ISO 11463	"Corrosion of Metals and Alloys, Evaluation of Pitting Corrosion"
ISO 7384	"Corrosion Tests in Artificial Atmospheres, General Requirements"
ISO 9227	"Corrosion Tests in Artificial Atmospheres, Salt Spray Tests"
ASTM International, West Conshohocken, PA, USA	
ASTM G 50	"Standard Practice for Conducting Atmospheric Corrosion Tests on Metals"
ASTM G 4	"Standard Guide for Conducting Corrosion Coupon Tests in Field Applications"
ASTM G 1	"Standard Practice for Preparing, Cleaning, and Evaluating Corrosion Test Specimens"
ASTM G 92	"Standard Practice for Characterization of Atmospheric Test Sites"
ASTM G 84	"Standard Practice for Measurement of Time-of-Wetness on Surfaces Exposed to Wetting Conditions as in Atmospheric Corrosion Testing"
ASTM G 91	"Standard Practice for Monitoring Atmospheric SO_2 Using the Sulphation Plate Technique"
ASTM G 140	"Standard Test Method for Determining Atmospheric Chloride Deposition Rate by Wet Candle Method"
ASTM G 33	"Standard Practice for Recording Data from Atmospheric Corrosion Tests of Metallic-

	Coated Steel Specimens”
ASTM G 107	“Standard Guide for Formats for Collection and Compilation of Corrosion Data for Metals for Computerized Database Input”
ASTM G 135	“Standard Guide for Computerized Exchange of Corrosion Data for Metals”
ASTM G 46	“Standard Guide for Examination and Evaluation of Pitting Corrosion”
ASTM G 101	“Standard Guide for Estimating the Atmospheric Corrosion Resistance of Low-Alloy Steels”
ASTM G 48	“Standard Test Method for Pitting and Crevice Corrosion Resistance of Stainless Steels and Related Alloys by Use of Ferric Chloride Solution”
ASTM G 112	“Standard Guide for Conducting Exfoliation Corrosion Test in Aluminum Alloys”
ASTM G 66	“Standard Test Method for Visual Assessment of Exfoliation Corrosion Susceptibility of 5*xxx* Series Aluminum Alloys (ASSET Test)”
ASTM G 38	“Standard Practice for Making and Using C-Ring Stress-Corrosion Test Specimens”
ASTM G 16	“Standard Guide for Applying Statistics to Analysis of Corrosion Data”
ASTM G 31	“Standard Practice for Laboratory Immersed Corrosion Testing of Metals”
ASTM B 117	“Standard Practice for Operating Salt Spray (Fog) Apparatus”
ASTM G 85	“Standard Practice for Modified Salt Spray (Fog) Testing”
ASTM G 87	“Standard Practice for Conducting Moist SO_2 Tests”
ASTM G 60	“Standard Test Method for Conducting Cyclic Humidity Tests”
ASTM G 3	“Conventions Applicable to Electrochemical Measurements in Corrosion Testing”
ASTM G 102	“Standard Practice for Calculation of Corrosion Rates and Related Information from Electrochemical Measurements”
ASTM G 100	“Standard Test for Conducting Cyclic Galvanostaircase Polarization”
ASTM G 59	“Standard Test Method for Conducting Potentiodynamic Polarization Resistance Measurements”
ASTM G 5	“Standard Reference Test Method for Making Potentiostatic and Potentiodynamic Anodic Polarization Measurements”
ANSI/ASTM G 61[(a)]	“Conducting Cyclic Potentiodynamic Polarization Measurements for Localized Corrosion”
ASTM G 106	“Standard Practice for Verification of Algorithm and Equipment for Electrochemical Impedance Measurements”
ASTM G 61	“Standard Test Method for Conducting Cyclic Potentiodynamic Polarization Measurements for Localized Corrosion Susceptibility of Iron-, Nickel-, or Cobalt-Based Alloys”
ASTM G 96	“Standard Guide for On-Line Monitoring of Corrosion in Plant Equipment (Electrical and Electrochemical Methods)”

(a) ANSI, American National Standards Institute

Time of Metal Wetness. In recent years, this parameter has received special attention, because it is the fundamental parameter that relates to the time during which the metal surface is covered by a thin electrolyte layer containing air contaminants and during which the corrosion cell can operate (Ref 19, 22, 25, 26, 27, 28, 29). The TOW is usually calculated in hours, according to International Organization for Standardization (ISO) 9223, “Corrosion of Metals and Alloys, Corrosivity of Atmospheres, Classification,” and includes the daily temperature/relative humidity (T-RH) complex, using 80% as a critical RH value for $T \geq 0$ °C (32 °F), when the condensation starts on the metal (Ref 1). Above RH 90% and $T < 25$ °C (77 °F), the dewpoint is reached, and the moisture formed on the metal surface is visible. The wet layer is actually thicker than that formed by initial condensation. This change of the moisture layer thickness, in turn, induces an alteration in the metal corrosion rate. The thinner layer of moisture is a minor barrier for the diffusion of molecular oxygen from the environment. The thin aqueous layer can be practically saturated in dissolved oxygen; thus, the corrosion rate of the metal is actually more rapid in the thinner layer formed by first condensation than in the relatively thick layer formed at higher RH.

The rain is a climatic factor that also contributes to moisture formation on a metal surface, but it can have additional effects. These include dilution and washing of the corrosive pollutants deposited on the metal surface. This situation results in a decrease of the corrosion rate, even when the TOW is prolonged. Precipitation can also dissolve some metal corrosion products soluble in water (zinc carbonate and hydroxide,

for example). A fresh metal surface will be in closer contact with the atmosphere, resulting in an increase in the corrosion rate. This situation is in contrast to the compact and well-adhered corrosion product layer, formed on the metal surface, that can act as a physical barrier for oxygen diffusion to cathodic sites and that results in a decrease in the rate of corrosion.

The environmental corrosion aggressiveness category of an atmosphere can be assigned based on the annual TOW value according to ISO 9223. However, this procedure is adequate to use only in an atmosphere free from chloride. In the presence of chlorides, the deposition of hygroscopic contaminants (for example, chloride salts in marine-coastal regions) occurs on the metal surface. This lowers the critical relative humidity value (RH_c), and corrosion can start at RH as low as ~40 to 50% (Ref 1). This fact implies that in a marine-coastal environment, the higher concentration of chlorides can increase the real TOW in a zone even far from the shore (Ref 25). The development of corrosion and TOW has been detected on samples exposed to the open atmosphere in the Antarctic when the temperature is below 0 °C (32 °F). Reduction of the RH_c value can be produced by deposition of ammonium sulfates on the metal surface, which are known to accelerate corrosion and provide sulfate ions. It was confirmed (Ref 29) by measuring TOW, using a copper-gold sensor according to ASTM G 84, that the annual TOW value was as large as 8500 h at a location 20 to 30 km (12 to 18 miles) from the seashore in a marine- coastal atmosphere in a humid tropical climate. This value is twice the value of 4500 to 4800 h for a typical rural-urban environment. This fact can explain the different corrosion rates observed for standard metals (low-carbon steel, copper, zinc) when exposed to these atmospheres. This difference in TOW values is due mainly to specific changes in their daily T-RH complex. Because of this, it is recommended that the daily T-RH complex be used rather than the annual T and RH average.

Figure 5 presents the daily T-RH complex of two atmospheres, marine-coastal and rural-urban, both part of a tropical humid climate. It can be seen that the corrosion cell can work almost all day in the marine-coastal environment at relatively constant T and RH values (due to the sea thermodynamic buffer capacity), while in the rural-urban atmosphere, the corrosion cell is interrupted during the daily hours and starts again when the RH reaches the critical value (≥80%) for formation of moisture on the metal surface. The results (Fig. 5) also indicate that the metal surface exposed in the rural-urban environment experiences wet/dry cycles. Such cycles affect the structure and morphology of corrosion products and promote micro- and macrocracking, as well as the detachment and exfoliation of internal corrosion layers. The difference in the daily T-RH complex of the marine-coastal and rural- urban environments also has another important effect on metal corrosion behavior. Because TOW occurs in different temperature ranges (Fig. 6, 7), this fact determines a distinct corrosion rate. Following the 10° rule, a 10 °C (18 °F) temperature difference can roughly change the corrosion rate by an order of magnitude.

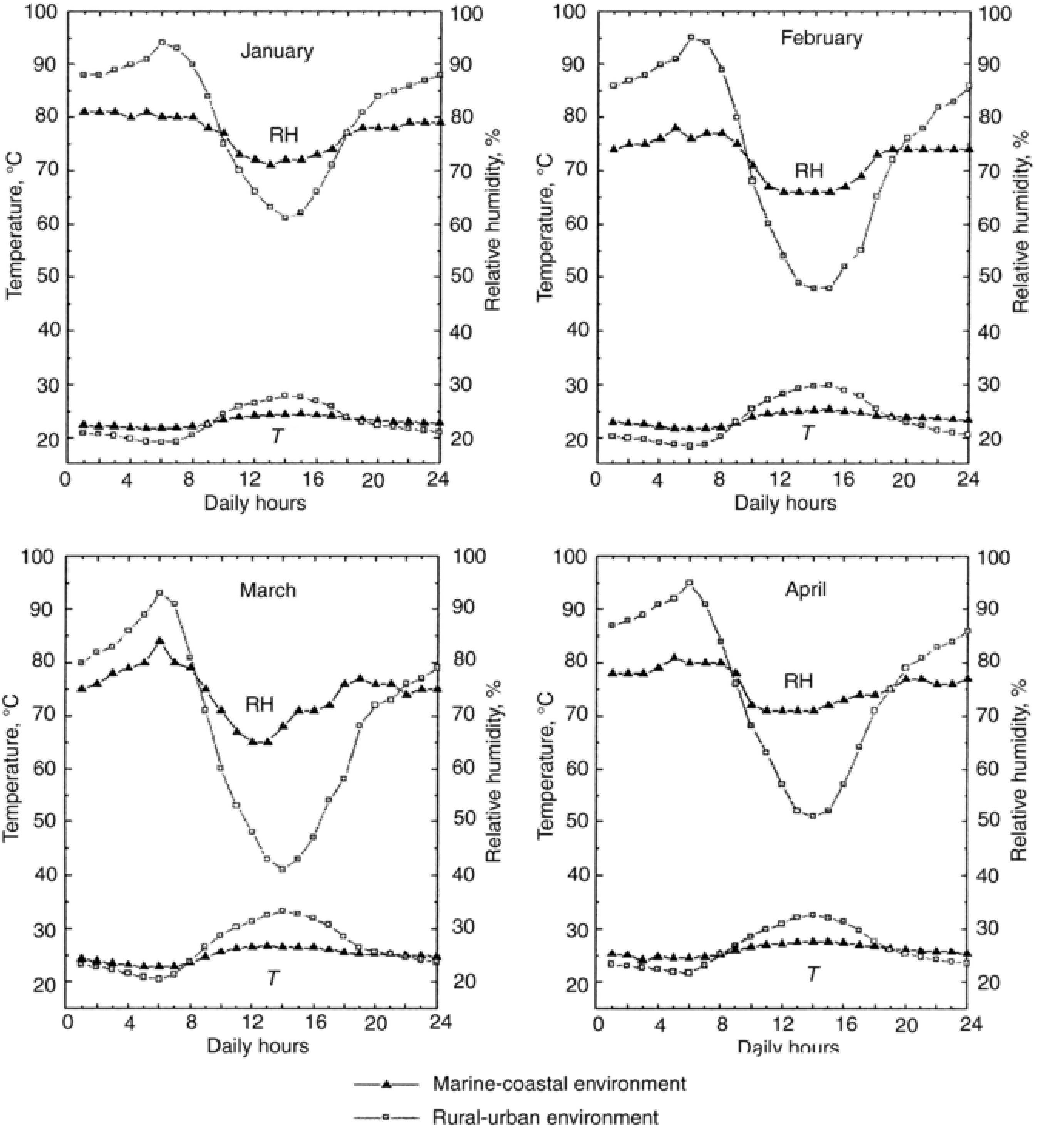

Fig. 5 Variation in temperature (*T*) and relative humidity (RH) during 1998 in marine-coastal and rural-urban environments with tropical humid climate (Gulf of Mexico)

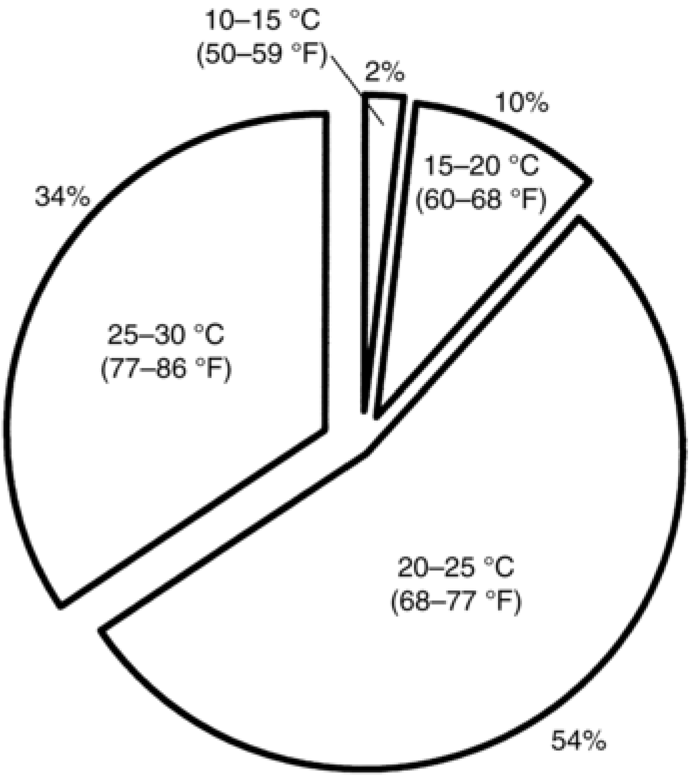

Fig. 6 Distribution of the annual time of wetness (%) in different temperature intervals presented in the rural-urban tropical humid environment of Merida, 30 km (18 miles) from the Gulf of Mexico, in 1998

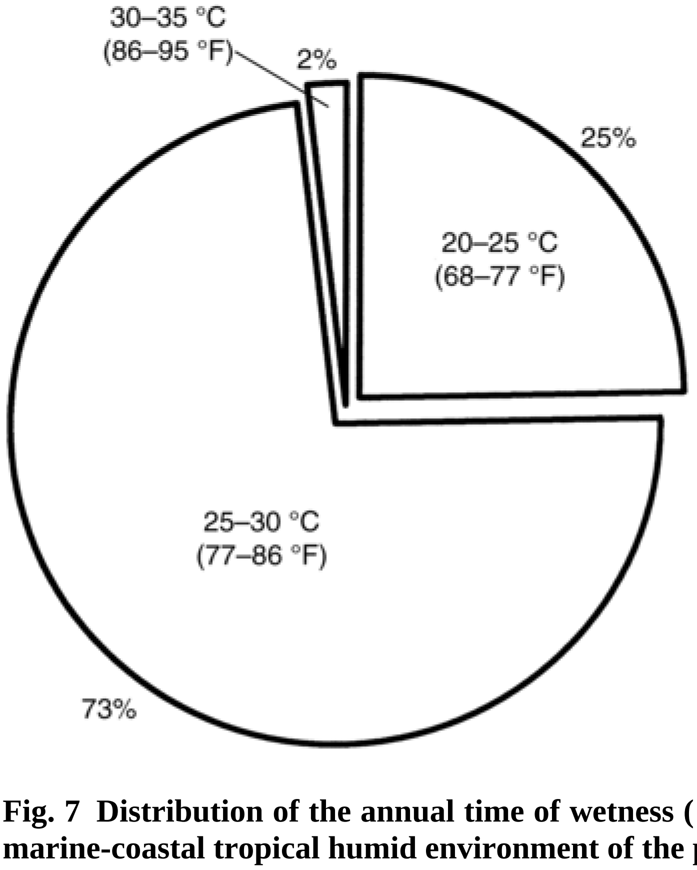

Fig. 7 Distribution of the annual time of wetness (%) in different temperature intervals presented in the marine-coastal tropical humid environment of the port of Progreso (Gulf of Mexico) in 1998

The nature and orientation of the metal surface and its inclination to the horizon or exposure angle also influence the real metal *T* and TOW values, due to the difference in solar absorbance, emissivity, and conductivity of the metal. The surface condition and color of the metal and its corrosion products are factors. These specific characteristics contribute to surface *T* and TOW changes. Exposed metals with corrosion products on the surface can have a higher *T* compared to that of the environment (Fig. 8, 9). In cold regions,

this can result in the appearance of liquid on the metal surface, even when ambient temperature is below 0 °C (32 °F). This explains why metals having a similar TOW period can corrode at different rates when they are exposed in distinctly different climatic areas. Therefore, defining the T-RH complex is of primary importance in completely understanding the corrosion process. Local TOW values can also be extended, due to the porous cavity structure of corrosion products on the metal surface.

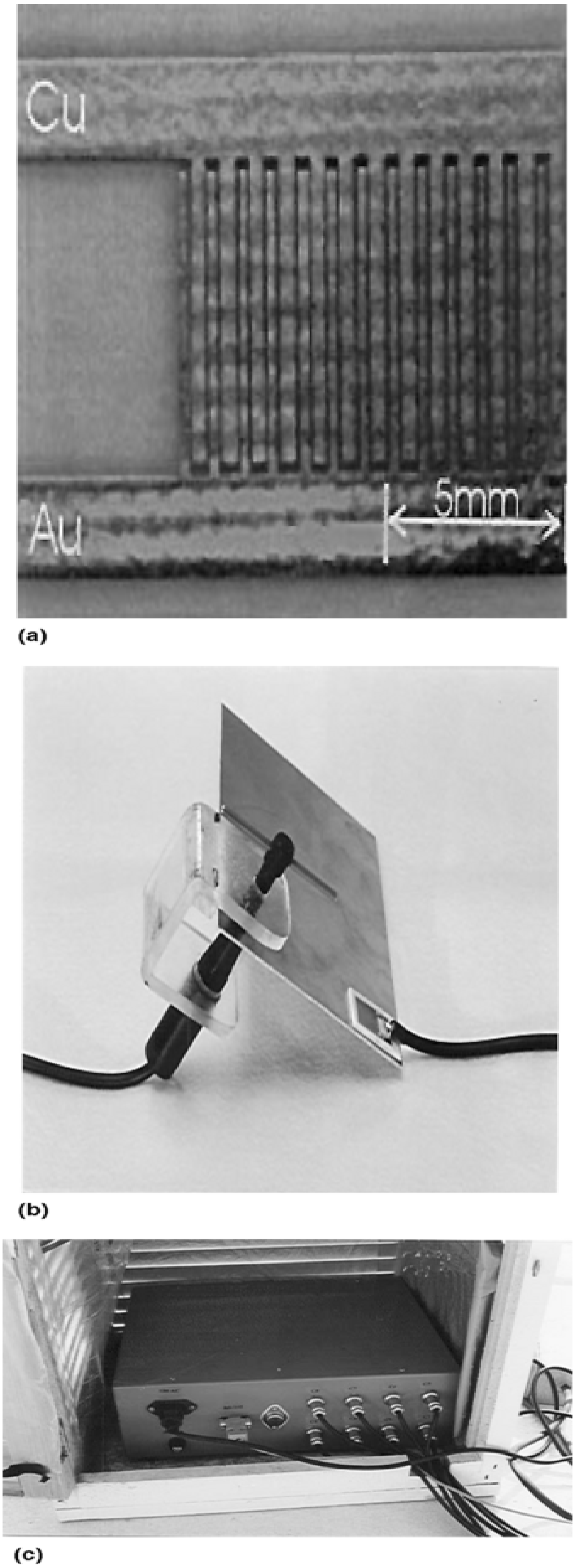

Fig. 8 Sensor system for measurement of time of wetness (TOW). (a) Closeup view of sensor. (b) Sensors for TOW and temperature measurements on the surface of sample. (c) View of the sensor electronic system

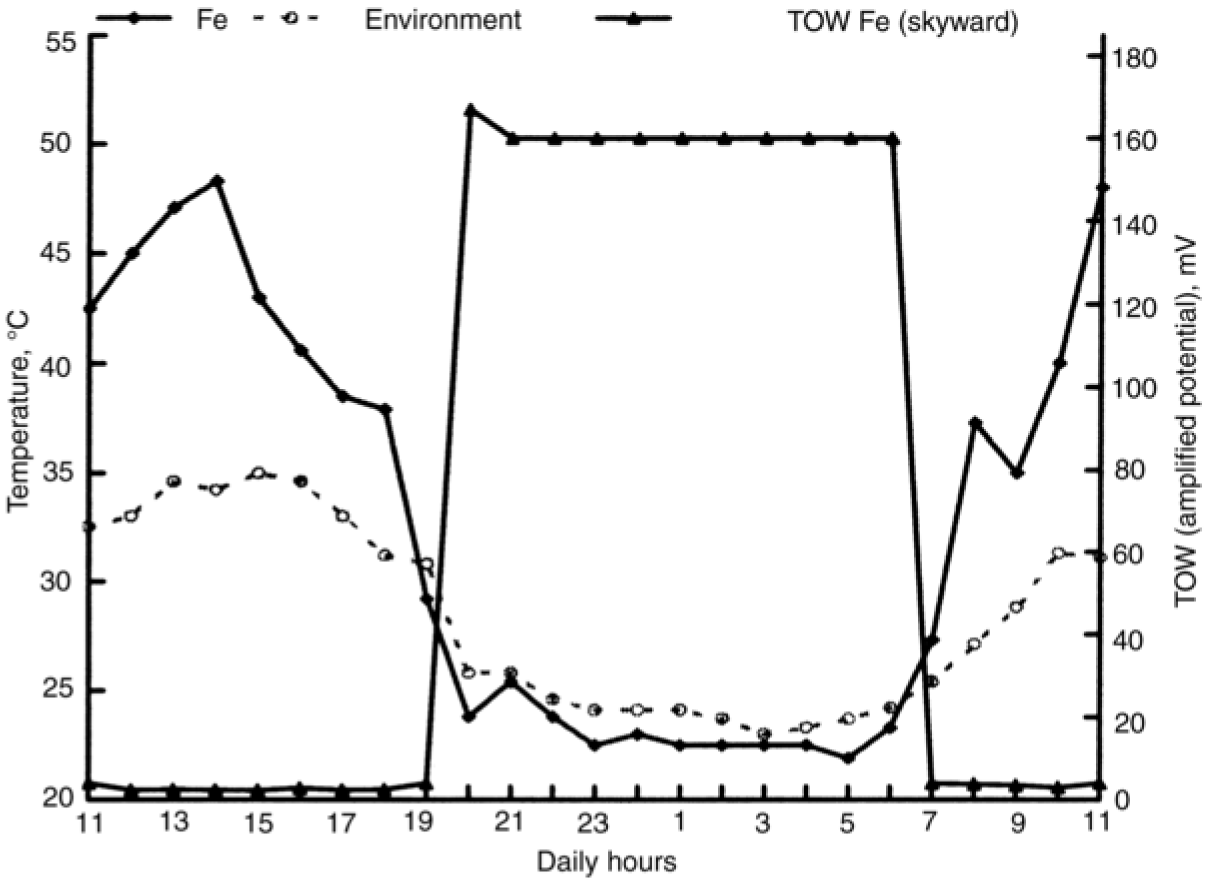

Fig. 9 Variation of environmental and low-carbon steel (Fe) sample temperatures and time of wetness (TOW) measured on the steel surface (an amplified potential of the gold-copper sensor). Registered over two days

Metal temperature and TOW values are influenced by winds and their predominate direction (north or south, continental or onshore). This can change the type and amount of atmospheric pollutants that settle on the metal surface. In some cases, winds can transport sand and other hard particles that provoke accelerated metal erosion or corrosion-erosion effects.

References cited in this section

1. L.L. Shreir, R.A. Jarman, and G.T. Burstein, Ed., Corrosion, Vol 1, *Metal/Environment Reactions,* 3rd ed., Butterworth- Heinemann, 1994

7. I.L. Rozenfeld, *Atmospheric Corrosion of Metals,* B.H. Tytel, Ed., National Association of Corrosion Engineers, 1973

8. V. Kucera and E. Mattsson, *Atmospheric Corrosion,* W.H. Ailor, Ed., John Wiley & Sons, 1982

12. C. Leygraf and T. Graedel, *Atmospheric Corrosion,* Wiley-Interscience, 2000

13. M. Pourbaix, *Atlas of Electrochemical Equilibria in Aqueous Solutions,* NACE- Cebelcor, 1974

14. T.S. Lee and E.A. Baker, Calibration of Atmospheric Corrosion Test Sites, *Atmospheric Corrosion of Metals,* STP 767, S.W. Dean, Jr. and E.C. Rhea, Ed., American Society for Testing and Materials, 1982, p 250–266

15. S.D. Cramer and L.G. McDonald, Atmospheric Factors Affecting the Corrosion of Zinc, Galvanized Steel and Copper, *Corrosion Testing and Evaluation: Silver Anniversary Volume,* STP 1000, R. Baboian and S.W. Dean, Jr., Ed., American Society for Testing and Materials, 1990, p 241–259

16. S. Feliu, M. Morcillo, and S. Feliu, Jr., The Prediction of Atmospheric Corrosion from Meteorological and Pollution Parameters, Part I: Annual Corrosion; Part II: Long- Term Forecasts, *Corros. Sci.,* Vol 34, 1993, p 403–414; 415–422

17. S.K. Roy and K.H. Ho, Corrosion of Steel in Tropical Marine Atmospheres, *Br. Corros. J.,* Vol 29 (No. 4), 1994, p 287–291

18. D.H. Vu, *Atmospheric Corrosion of Metals in Tropics,* Nauka, Moscow, Russia, 1994

19. I.S. Cole, R. Holgate, P. Kao, and W. Ganther, The Rate of Drying of Moisture from a Metal Surface and Its Implication for Time of Wetness, *Corros. Sci.,* Vol 37 (No. 3), 1995, p 455–465

20. A.A. Mikhailov, M.N. Suloeva, and E.G. Vasileva, Environmental Aspects of Atmospheric Corrosion, *Water, Air and Soil Pollution,* Vol 85, 1995, p 2673–2678

21. D. Knotkova, P. Boschek, and K. Kreislova, Results of ISO CORRAG Program: Processing of One-Year Data in Respect to Corrosivity Classification, *Atmospheric Corrosion,* STP 1239, W.W. Kirk and H.H. Lawson, Ed., American Society for Testing and Materials, 1995, p 38–55

22. S.W. Dean and D.B. Reiser, Time of Wetness and Dew Formation: A Model of Atmospheric Heat Transfer, *Atmospheric Corrosion,* STP 1239, W.W. Kirk and H.H. Lawson, Ed., American Society for Testing and Materials, 1995, p 3–10

23. J. Tidblad, A.A. Mikhailov, V. Kucera, Application of a Model for Prediction of Atmospheric Corrosion in Tropical Environments, *Marine Corrosion in Tropical Environments,* STP 1399, S.W. Dean, G. Hernandez-Duque Delgadillo, and J.B. Bushman, Ed., American Society for Testing and Materials, 1995, p 250–285

24. M. Morcillo, J. Simancas, and S. Feliu, Long-Term Atmospheric Corrosion in Spain: Results after 13–16 Years of Exposure and Comparison with Worldwide Data, *Atmospheric Corrosion,* STP 1239, W.W. Kirk and H.H. Lawson, Ed., American Society for Testing and Materials, 1995, p 195–214

25. L. Veleva, G. Pérez, and M. Acosta, Statistical Analysis of the Temperature-Humidity Complex and Time of Wetness of a Tropical Climate in the Yucatan Peninsula in Mexico, *Atmosph. Environ.,* Vol 31 (No. 5), 1997, p 773–776

26. L. Veleva and L. Maldonado, Classification of the Atmosphere Corrosivity in the Humid Tropical Climate, *Br. Corros. J.,* Vol 33 (No. 1), 1998, p 53–57

27. S. Feliu, M. Morcillo, and B. Chico, Effect of Distance from Sea on Atmospheric Corrosion Rate, *Corrosion,* Vol 55 (No. 6), 1999, p 883–891

28. J. Tidblad, A.A. Mikhailov, and V. Kucera, Model for the Prediction of the Time of Wetness from Average Annual Data on Relative Air Humidity and Air Temperature, *Prot. Met. (Russia),* Vol 36 (No. 6), 2000, p 533–540

29. L. Veleva and M.A. Alpuche-Aviles, Time of Wetness (TOW) and Surface Temperature Characteristics of Corroded Metals in Humid Tropical Climate, *Outdoor Atmospheric Corrosion,* STP 1421, H.E. Townsend, Ed., American Society for Testing and Materials, 2002, p 48–58

30. S.W. Dean and D.B. Reiser, Analysis of Long-Term Atmospheric Corrosion Results from ISO CORRAG Program, *Outdoor Atmospheric Corrosion,* STP 1421, H.E. Townsend, Ed., American Society for Testing and Materials, 2002, p 3–18

31. R.D. Klassen, P.R. Roberge, D.R. Lenard, and G.N. Blenkinsop, Corrosivity Patterns Near Sources of Salt Aerosols, *Outdoor Atmospheric Corrosion,* STP 1421, H.E. Townsend, Ed., American Society for Testing and Materials, 2002, p 19–33

32. J. Tidblad, V. Kucera, A. Mihhailov, and D. Knotkova, Improvement of the ISO Classification System Based on Dose-Response Functions Describing the Corrosivity of Outdoor Atmospheres, *Outdoor Atmospheric Corrosion,* STP 1421, H.E. Townsend, Ed., American Society for Testing and Materials, 2002, p 73–87

33. H. Le Thi Lien and P. Thy San, The Effect of Environmental Factors on Carbon Steel Atmospheric Corrosion; The Prediction of Corrosion, *Outdoor Atmospheric Corrosion,* STP 1421, H.E. Townsend, Ed., American Society for Testing and Materials, 2002, p 103–108

L. Veleva and R.D. Kane, Atmospheric Corrosion, *Corrosion: Fundamentals, Testing, and Protection,* Vol 13A, *ASM Handbook,* ASM International, 2003, p 196–209

Atmospheric Corrosion

Lucien Veleva, CINVESTAV-IPN, Yucatan, Mexico; Russell D. Kane, InterCorr International, Inc.

Air Chemistry and Principal Pollutants Inducing Corrosion

Air chemistry is closely related to the corrosion aggressiveness of the atmosphere and this fact needs careful attention (Ref 1, 7, 8, 9, 11, 12). It is recognized that *chlorides* (airborne salinity) and *sulfur dioxide* (SO_2) are the principal pollutants that can accelerate the atmospheric corrosion rate by several orders of magnitude.

The principal source of chlorides is aerosols, which are suspensions of small liquid or solid particles in the atmosphere that come from salt spray and salt fog in the vicinity of the seashore and from the contaminated environment around industrial plants producing hydrogen chloride and sodium hypochloride. Chloride ion (Cl^-) is one of the principal environmental agents that accelerates corrosion and, in particular, pitting attack. Chlorides do damage by penetrating and destroying the normally protective and passive layer of oxides and hydroxides formed under natural conditions. Such protective surface films on metals exposed to atmospheres free of chloride include copper (Cu_2O, copper patina), aluminum (Al_2O_3), and zinc (ZnO and $Zn(OH)_2$).

A second aggressive environmental pollutant for metals is SO_2 gas. It is found in urban and industrial atmospheres and, in the prescence of oxygen, is easily converted to sulfuric acid in the condensed moisture layer on the metal surface. The sulfuric acid dissociates to give H^+ ions ($H_2SO_4 \leftrightarrow 2H^+ + SO_4^{2-}$), which participate as the *oxidizing agent* in the *cathodic corrosion reaction* (Eq 1, 4 and Fig. 2). Due to the presence of H^+ ions, the moisture has a lower pH (often below 4.5). The addition of SO_2 air contamination, acid rain, results in a highly accelerated corrosion rate. Some metals, such as aluminum and zinc, are relatively resistant in pH-neutral atmospheres (pH ≈ 6 to 7.5) but corrode rapidly in an acid environment (Ref 12).

According to ISO 9223, the annual average deposition rate ($mg/m^2/day$) of chlorides (airborne salinity) and sulfur dioxide (SO_2) compounds is used to classify the atmospheric corrosivity. The recommended methods for measurement of chloride and sulfate levels are the wet candle and sulfation plate sampling apparatuses, as cited in ISO 9225, "Corrosion of Metals and Alloys, Corrosivity of Atmospheres, Measurement of Pollution."

Some atmospheric gases, such as carbon dioxide (CO_2), nitrogen dioxide (NO_2), ozone (O_3), ammonia (NH_3), hydrogen sulfide (H_2S), and hydrogen chloride (HCl), and organic acids, such as formic (HCOOH) and acetic (CH_3COOH), are also known to be highly corrosive for several commonly used metals. After being dissolved in

the moisture layer on the metal surface, these gases result in a number of ions and ionic species, such as H^+, CO_3^{2-}, Cl^-, NH_4^+, NO_3^-, SO_4^{2-}, $COOH^-$, and CH_3COO^-, that may have a major influence on the corrosion mechanism process, which increases the corrosion current from electrochemical (galvanic) cells, and the resultant corrosion rate.
Most aerosol particles absorb water, leading to an increase in the TOW period and the corrosive process.

References cited in this section

1. L.L. Shreir, R.A. Jarman, and G.T. Burstein, Ed., Corrosion, Vol 1, *Metal/Environment Reactions,* 3rd ed., Butterworth- Heinemann, 1994

7. I.L. Rozenfeld, *Atmospheric Corrosion of Metals,* B.H. Tytel, Ed., National Association of Corrosion Engineers, 1973

8. V. Kucera and E. Mattsson, *Atmospheric Corrosion,* W.H. Ailor, Ed., John Wiley & Sons, 1982

9. *Corrosion Basics, An Introduction,* National Association of Corrosion Engineers 1984

11. P. Marcus and J. Oudar, Ed., *Corrosion Mechanism in Theory and Practice,* Marcel Dekker, Inc., 1995

12. C. Leygraf and T. Graedel, *Atmospheric Corrosion,* Wiley-Interscience, 2000

L. Veleva and R.D. Kane, Atmospheric Corrosion, *Corrosion: Fundamentals, Testing, and Protection,* Vol 13A*, ASM Handbook,* ASM International, 2003, p 196–209

Atmospheric Corrosion

Lucien Veleva, CINVESTAV-IPN, Yucatan, Mexico; Russell D. Kane, InterCorr International, Inc.

Thermodynamics of Atmospheric Corrosion and Use of Pourbaix Diagrams

When the question is asked, “Under what conditions can corrosion of metals occur in aqueous solutions?”, the answer can usually be found using Pourbaix diagrams, which show regions of metal stability and corrosion on axes of metal electrochemical potential as a function of pH of the electrolyte (Ref 13). It is well known that metals occur in different states, depending mainly on the pH of the environment and their electrochemical potential (e.g., Gibbs free energy, Table 1). Pourbaix diagrams show the forms of the metal that are thermodynamically stable over a range of pH and electrochemical potential.
Atmospheric Corrosion of Iron and Carbon Steels. The most-used metal for construction of structures and equipment is iron, because it is the main constituent of the carbon and alloy steels. The iron Pourbaix diagram (Fig. 10) demonstrates the possibility for multiple states: corrosion (active state), passivity and immunity (Ref 1, 13, 34, 35, 36, 37, 38, 39, 40, 41, 42, 43, 44, 45, 46).

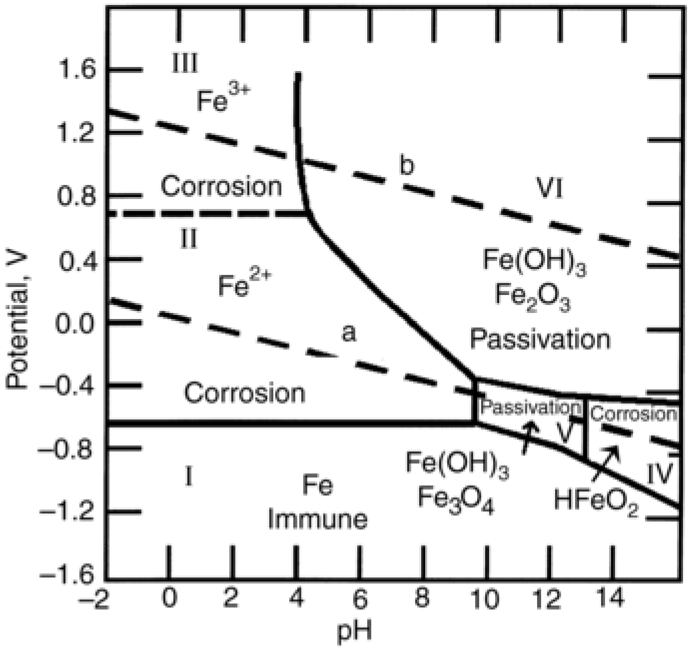

Fig. 10 Pourbaix diagram (metal potential versus pH) for iron in aqueous (water) solution

In the region of potentials and pH values defined by $Fe(OH)_3$ and Fe_2O_3 (the solid compounds thermodynamically stable in these conditions), the initial corrosion process forms a very dense and usually thin and impervious rust layer of iron oxide and oxyhydroxides that acts as an effective physical barrier between the metal and corrosive atmosphere. Due to this physical barrier, oxygen and water molecules cannot easily penetrate and reach the underlying metal surface. Therefore, the corrosion process is effectively stopped, and the metal is in a passive state.

Iron can also be observed in another passive region, that of Fe_3O_4 and $Fe(OH)_2$, when corrosion produces an oxide (magnetite, Fe_3O_4) that is a very thin, dense, and almost transparent rust layer. This layer can also act as an effective physical barrier that stops corrosion. However, for this passive state to exist, the metal needs be exposed to an environment at an alkaline pH higher than 8.5 to 9. This explains the passive carbon steel state when it is embedded in an alkaline (pH > 12 to 13) concrete environment, such as occurs in steel reinforcement. However, any changes of pH (below the pH 8.5 to 9) remove the metal from the passive state, and corrosion can resume. This is what happens in the case of the phenomenon referred to as carbonation of concrete. Reinforcing steel suffers serious and accelerated corrosion due to the lowering of concrete pH as a result of the penetration of CO_2 gas from the atmosphere into the concrete pores. This will cause subsequent dissolution of the steel in the moisture, filling the pores of the concrete.

A very dangerous pollutant for the destruction of the passive oxide layer, even in a favorable alkaline pH medium, is the chloride ion. The chloride ion has a relatively small ionic radius and high mobility in aqueous solutions. It can penetrate the oxide layer, resulting in its destruction, increasing the corrosion rate, and often leading to localized corrosion (pitting). It should be noted that the complete mechanism of chloride-induced corrosion and pit formation on iron alloys is still not well explained, and several models have been proposed (Ref 11).

Figure 10 shows two regions of corrosion (active) metal state, when the metal is corroded either to Fe^{2+} or Fe^{3+} ions, depending on pH and potential values. In natural atmospheric conditions, the standard potential of iron is negative (approximately -0.44 V, Table 1). This situation indicates that in neutral and low-acid industrial environments, the iron carbon steel and low- alloy steel will corrode whenever the pH of the environment is lower than 8.5 to 9. The corrosion attack on iron and steels generally occurs uniformly, extending on all metal surfaces to the same extent.

An interesting case is the immune-metal state, which is not present for all metals but is possible for iron. The corrosion of steel is not possible in the region of pH and potentials where iron is in the thermodynamically stable immune condition, as shown in Fig. 10. An external voltage can be applied to take the iron potential from its standard state (-0.44 V, Table 1) to more negative values (less than -0.6 to -0.7 V). This is the basis for the cathodic protection applied to underground metallic pipeline systems, steel-reinforced concrete bridges, ships, offshore platforms, and other metal structures.

Atmospheric Corrosion of Aluminum. Another widely used metal for construction is aluminum. Thermodynamically, it is very active and immediately corrodes when produced (Table 1, high level of free energy and high negative potential value) (Ref 1, 13, 47, 48, 49, 50, 51, 52, 53). The Pourbaix diagram (Fig. 11) shows three states that are possible for this metal (and its alloys): passivity, immunity, and corrosion (active) (Ref 13). There is a region of pH and potentials where the metal is passivated and well protected from atmospheric corrosion, due to the formation of a very thin, transparent, and adherent low-porosity hydrated oxide layer ($Al_2O_3H_2O$). This layer, however, can be destroyed by the presence of chloride ions in the environment, which will produce pitting. The passive layer provides very good corrosion resistance when exposed to normal atmospheric conditions and lower resistance to corrosion when structures are exposed in marine-coastal environments. Aluminum and its alloys can also exhibit a layered corrosion exfoliation attack.

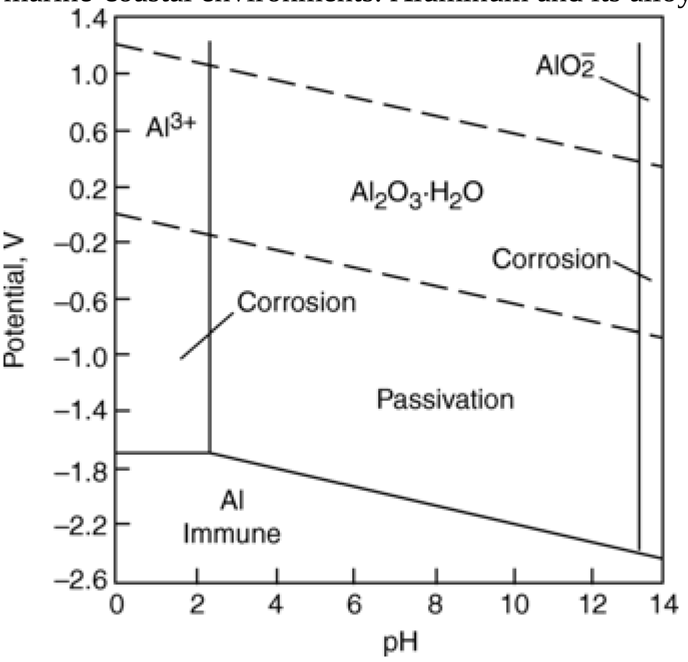

Fig. 11 Pourbaix diagram (potential versus pH) for aluminum in water at 25 °C (77 °F)

In natural conditions, aluminum has a high negative standard potential value (-1.67 V, Table 1), but due to the immediate formation of a passive oxide layer, it can be protected in environments where the pH is in the range of 2 to 14. However, the range of pH from 4 to 9 is the practical range for many applications where stability exists, and the highly passive layer forms and remains protective. This results in generally good corrosion resistance and the wide use of aluminum. The corrosion state is found in very polluted, mainly SO_2, industrial atmospheres, where pH is below 2, and also in alkaline environments over a substantial range of potentials (Fig. 11). In noncontaminated atmospheres, and after a long exposure time, small pits (100 μm, or 4 mil deep) can occur for aluminum in contact with water (high values of TOW). The presence of metal impurities (iron, copper) increases this pitting, which is rate controlled by oxygen cathodic reduction on the surface inclusion, Hence, the growth of the pit depth slows as the pit diameter increases. Galvanic couple corrosion (bimetallic corrosion) occurs when a metal having a less negative standard potential than that of aluminum (Table 1) is brought into contact. Copper is a cathode in the formed pair with aluminum.

The metal potential of aluminum must be shifted to values more negative than -1.7, using an external source of direct current to reach the immune state. Cathodic protection can be carried out but may run into difficulties arising from local pH increases, which could lead to the dissolution of the protective oxide film on the aluminum surface. Corrosion protection for aluminum can be obtained through anodizing, which is achieved by growing a thicker oxide film (approximately 20 μm, or 0.8 mil) under anodic polarization in appropriate electrolytes.

Pure aluminum is seldom used for structures, because its alloys have better mechanical properties. However, alloy corrosion resistance varies from less than that of pure aluminum when alloyed with magnesium and copper to much better when combined with tungsten and tantalum. One of the most widely used aluminum alloys is Duralumin, which contains 4% Cu and a small amount of other metals, such as iron. This alloy corrodes much more readily than pure aluminum. Localized pitting corrosion is usually observed as the failure mode, due to the breakdown of the passive oxide layer.

Atmospheric Corrosion of Copper. Copper is widely used because of its good corrosion resistance in a variety of atmospheres (Ref 1, 13, 54, 55, 56, 57, 58, 59, 60, 61, 62, 63, 64, 65, 66, 67), high electric and thermal conductivities, and attractive mechanical properties when exposed at low, moderate, and high temperatures (Ref 1). Its electrochemical potential value is positive (+0.34 V, Table 1) in natural environments, as compared to values observed for iron and aluminum, and close to the potentials for noble nonreactive metals. Therefore, copper is not very active chemically, and its rate of oxidation, when exposed to the atmosphere, is very low. The corrosion open-circuit potential (OCP) of copper is usually below the standard hydrogen reaction potential value (0.00 V, Table 1), and due to this fact, there is no participation by hydrogen ion (H^+) as an oxidizing agent in the cathodic corrosion reaction (Eq 4) when the atmosphere is very polluted (as in the acid pH range). According to the Pourbaix diagram (Ref 13) for copper (Fig. 12), three thermodynamic states are possible: corrosion, passivity, and immunity. It can be seen that in atmospheres with neutral and alkaline pH, copper is passive (at a standard metal potential of +0.34 V), due to the formation of an oxide layer of Cu_2O (cuprite). Another passive state can be obtained when the metal potential is shifted to more positive values, forming copper oxide (CuO). The immune state requires more negative potential values (using an external electric source), where the metal does not corrode regardless of pH value. The diagram in Fig. 12 shows two regions of the metal corrosion state: one at low (acid) pH and the other at higher (alkaline) pH values, when metal ions (Cu^{2+}) and complex anions (CuO_2^{2-}), respectively, are formed during the anodic corrosion reaction (Eq 1).

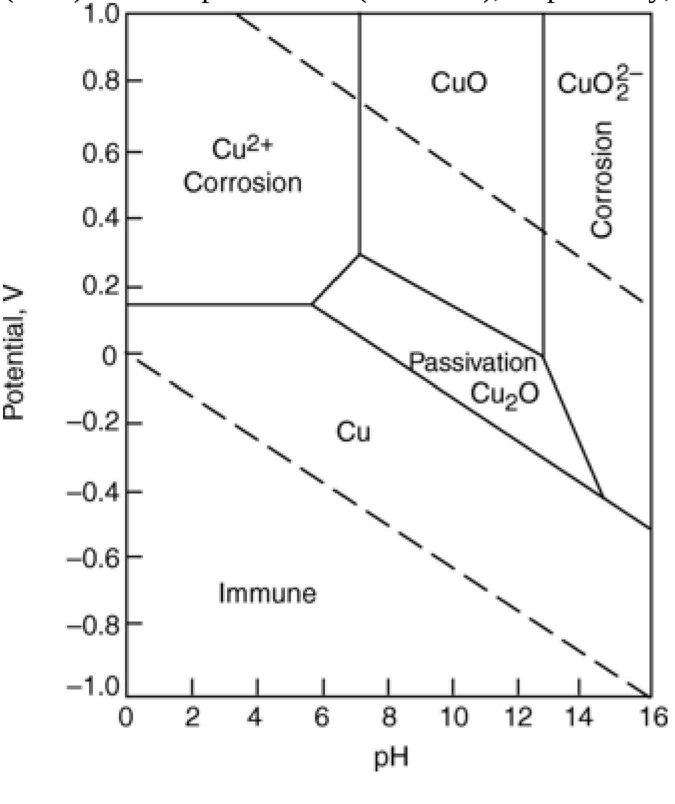

Fig. 12 Pourbaix diagram (potential versus pH) for copper in water at 25 °C (77 °F)

The atmospheric behavior and protection of copper against corrosion is of interest because it is a construction material in monuments, churches, and architectural objects. The oxide passive layer (Cu_2O, cuprite) formed during the initial stages of the copper corrosion process is called the patina, and extensive investigations have been dedicated to this subject, especially for restoration of monuments (Ref 56, 57, 58, 59, 60, 65). The patina layer is transparent (≈30 Å of thickness at the beginning) and changes color from orange to red-brown. The color deepens to dark brown when the thickness of this layer increases. Recent studies have revealed that copper patina consists of Cu_2O/CuO ($Cu(OH)_2$ or $CuO \cdot H_2O$). In marine-coastal and industrial atmospheres, the color of the patina can be superficially changed to a more greenish hue because of the formation of copper basic salts, such as sulfates in urban or rural environments, chlorides in marine atmospheres, nitrates, and carbonates. The knowledge of patina formation and its development in time is also used for the creation of an artificial copper patina. This type of surface treatment can be used to give a more antiquated appearance to copper objects.

Atmospheric Corrosion of Zinc. The ability of zinc to galvanically protect steel, because of its more negative standard electrochemical potential, has given this metal a wide variety of application (Ref 1, 13, 68, 69, 70, 71, 72, 73, 74, 75, 76, 77, 78, 79, 80). Although zinc by itself is available in sheet, plate, strip, and pressure die castings, its principal uses for corrosion control are as a coating on steel and as zinc anodes for cathodic protection of steel on underground pipelines, oil rigs, offshore structures, and bridges.

Because of the low standard negative potential value for zinc (-0.76, Table 1), it is a very active metal and tends to corrode in contact with air and moisture, Figure 13 presents the Pourbaix diagram of zinc and shows that when a moisture layer forms on zinc with a neutral pH (pH ≈ 6 to 7), corrosion occurs, and the main corrosion product is $Zn_5(CO_3)_2(OH)_6$ (hydrozincite). In rural environments, this corrosion layer is dense and adherent; therefore, the metal is relatively well protected. In highly polluted industrial atmospheres, the corrosion rate may increase substantially with time of exposure. Strongly acid or basic environments tend to dissolve the stable corrosion film, leading to significantly higher corrosion rates. In acidic atmospheres, no protective corrosion films form on zinc, leading to very rapid metal dissolution. Certain ionic species, such as chlorides, also promote the dissolution of zinc corrosion products and lead to higher corrosion rates.

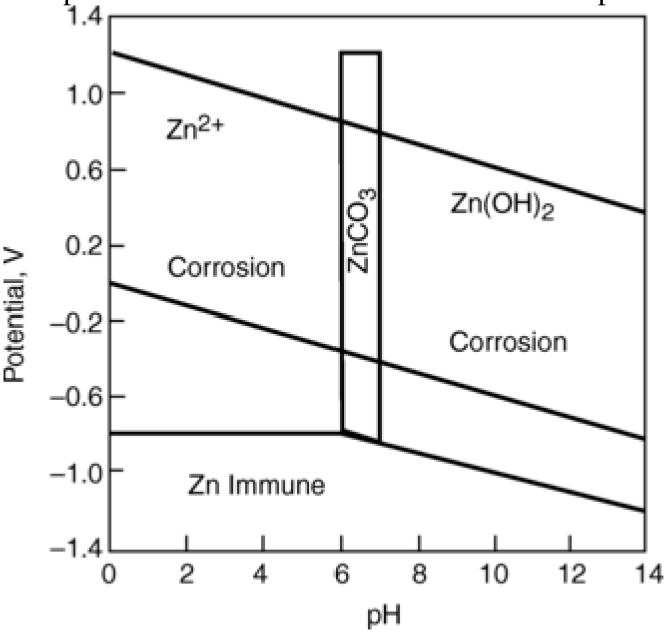

Fig. 13 Pourbaix diagram (potential versus pH) for zinc in water at 25 °C (77 °F)

When zinc is used as a coating on steel, the steel is a cathode, and the zinc coating is the anode. Corrosion protection in this situation is attributed to a combination of the corrosion resistance of zinc and the sacrificial protection that is afforded by zinc to the steel. This cathodic protection is also provided when zinc anodes are electrically connected to a steel structure and both are immersed in the same conductive electrolyte.

Note that Pourbaix diagrams do not give information about the kinetics or rate of the corrosion process. They indicate the thermodynamic conditions for the development of corrosion, the possibility for reaching other oxidation states, and the corrosion product composition. This information, in turn, indicates possible regimes for metal dissolution or protection. Moreover, these diagrams correspond to metals exposed in pure aqueous solutions that do not include other ions, such as SO_4^{2-}, Cl^-, NO_3^-, and CO_3^- contaminants. However, the effects of other species can be taken into account, using more complex Pourbaix diagrams (Ref 13) or through thermodynamic modeling software. For example, the presence of SO_4^{2-}, Cl^-, NO_3^-, and CO_3^- ions as atmospheric contaminants in the metal-moisture system can eliminate the immune copper state (Ref 13), as predicted using the Pourbaix diagram shown in Fig. 12. Therefore, when investigating the influence of service environments, it is necessary to analyze the atmosphere for all its parameters (T-RH complex and air chemistry) and to use the Pourbaix diagrams as a guide to the thermodynamics of the metal dissolution process.

References cited in this section

1. L.L. Shreir, R.A. Jarman, and G.T. Burstein, Ed., Corrosion, Vol 1, *Metal/Environment Reactions,* 3rd ed., Butterworth- Heinemann, 1994

11. P. Marcus and J. Oudar, Ed., *Corrosion Mechanism in Theory and Practice,* Marcel Dekker, Inc., 1995

13. M. Pourbaix, *Atlas of Electrochemical Equilibria in Aqueous Solutions,* NACE- Cebelcor, 1974

34. U.R. Evans, Mechanism of Atmospheric Rusting, *Corros. Sci.,* Vol 12, 1972, p 227–246

35. T. Misava, K. Asami, K. Hashimoto, and S. Shimodaira, The Mechanism of Atmospheric Rusting and the Protective Amorphous Rust on Low Alloy Steels, *Corros. Sci.,* Vol 14, 1974, p 279–289

36. J.B. Johnson, P. Elliott, M.A. Winterbottom, and G.C. Wood, Short-Term Atmospheric Corrosion of Mild Steel at Two Weather and Pollution Monitored Sites, *Corros. Sci.,* Vol 17, 1977, p 691–700

37. E. Mattson, The Atmospheric Corrosion Properties of Some Common Structural Metals: A Comparative Study, *Mater. Perform.,* Vol 21, July 1982, p 9–19

38. E.A. Baker, Long-Term Corrosion Behavior of Materials in the Marine Atmosphere, *Degradation of Metals in the Atmosphere,* STP 965, S.W. Dean and T.S. Lee, Ed., American Society for Testing and Materials, 1988, p 125–144

39. T.E. Graedel and R.P. Frankonthal, Corrosion Mechanism for Iron and Low Alloy Steel Exposed to the Atmosphere, *J. Electrochem. Soc.,* Vol 137 (No. 8), 1990, p 2385–2394

40. J.L. Crolet, Mechanism of Uniform Corrosion Under Corrosion Deposits, *J. Mater. Sci.,* Vol 28, 1993, p 2589–2606

41. S.H. Zhang and S.B. Lyon, The Electrochemistry of Iron, Zinc and Copper in Thin Layer of Electrolytes, *Corros. Sci.,* Vol 35 (N.S. 1–4), 1993, p 713–718

42. J.O'M. Bockris and S.U. Khan, On the Mechanism of the Dissolution of Iron: The Catalytic Mechanism, *Surface Electrochemistry: A Molecular Level Approach,* Plenum Press, 1994, p 756–771

43. A. Cox and S.B. Lyon, An Electrochemical Study of the Atmospheric Corrosion of Mild Steel, Part III: The Effect of Sulfur Dioxide, *Corros. Sci.,* Vol 36 (No. 7), 1994, p 1193–1199

44. S.K. Roy and K.H. Ho, Corrosion of Steel in Tropical Marine Atmospheres, *Br. Corros. J.,* Vol 29 (No. 4), 1994, p 287–291

45. L. Maldonado, L. Veleva, P. Quintana, O.T. Rincon, A. Rincon, C. Corvo and Haces, Electrochemical, Gravimetric and X-Ray Characterization of Low Carbon Steel Corrosion Rate and Products After Atmospheric Exposure in the Caribbean Area, *Corros. Rev.,* Vol 19, 5–6 Nov. 2001

46. L. Veleva, "Phase Transformation of Iron Hydroxide in the Corrosion Products Formed in Humid Tropical Climate," Paper 03602, 58th Annual Conference, Corrosion 2003, NACE, 2003

47. Z. Szklarska-Smialovwska, Review of Literature on Pitting Corrosion Published Since 1960, *Corrosion,* Vol 27 (No. 6), 1971, p 223–233

48. A.M. Beccaria, E.D. Mor, and G. Poggi, Examination of Aluminum Corrosion Products in Marine or Industrial-Marine Atmosphere, *Werkst. Korros.,* Vol 34 (No. 5), 1983, p 236–240

49. R.T. Foley, Localized Corrosion of Aluminum Alloys—A Review, *Corrosion,* Vol 42 (No. 5), 1986, p 227–286

50. J.J. Friel, Atmospheric Corrosion Products on Al, Zn and Al-Zn Metallic Coatings, *Corrosion,* Vol 42 (No. 7), 1986, p 422–426

51. T.E. Graedel, Corrosion Mechanism for Aluminum Exposed to the Atmosphere, *J. Electrochem. Soc.,* Vol 136 (No. 4), 1989, p 204C–211C

52. J.O'M. Bockris and S.U. Khan, Aspect of Aluminum Corrosion, *Surface Electrochemistry: A Molecular Level Approach,* Plenum Press, 1994, p 771–778

53. Z. Szklarska-Smialovwska, Pitting Corrosion of Aluminum, *Corros. Sci.,* Vol 41, 1999, p 1743–1767

54. C.W. Hummer, Jr., Corrosion of Metals in Tropic Environments—Copper and Wrought Copper Alloys, *Mater. Prot.,* Jan 1968, p 41–47

55. E. Mattsson and R. Holm, Atmospheric Corrosion of Copper and Its Alloys, *Atmospheric Corrosion,* W.H. Ailor, Ed., Wiley, Inc., 1982, p 365–381

56. T.E. Graedel, K. Nassau, and J.P. Franey, Copper Patinas Formed in the Atmosphere, Part I: Introduction, *Corros. Sci.,* Vol 27 (No. 7), 1987, p 639–657

57. T.E. Graedel, Copper Patinas Formed in the Atmosphere, Part II: A Qualitative Assessment of Mechanisms, *Corros. Sci.,* Vol 27 (No. 7), 1987, p 721–740

58. R.L. Opila, Copper Patinas: An Investigation by Auger Electron Spectroscopy, *Corros. Sci.,* Vol 27, 1987, p 685–694

59. R. Baboian, E.L. Bellante, and E.B. Cliver, Ed., *The Statue of Liberty Restoration,* NACE, 1990

60. R.A. Livingston, Influence of the Environment on the Patina of the Statue of Liberty, *Environ. Sci. Technol.,* Vol 25 (No. 8), 1991, p 1400–1408

61. P. Eriksson, L.-G. Johansson, and H. Strandberg, Initial Stages of Copper Corrosion in Humid Air Containing SO_2 and NO_2, *J. Electrochem. Soc.,* Vol 140 (No. 1), 1993, p 53–58

62. J.F. Dante and R.G. Kelly, The Evolution of the Adsorbed Solution Layer During Atmospheric Corrosion and Its Effect on the Corrosion Rate of Copper, *J. Electrochem. Soc.,* Vol 140 (No. 7), 1993, p 1890–1897

63. A. Salnick, W. Faubel, H. Klewe-Nebenius, A. Vend, and H.J. Ache, Photothermal Studies of Copper Patina Formed in the Atmosphere, *Corros. Sci.,* Vol 37 (No. 5), 1995, p 741–767

64. A.A. Ambler and A.A.J. Bain, Corrosion of Metals in Tropics, *J. Appl. Chem.,* Sept 1995, p 437–467

65. L. Veleva, P. Quintana, R. Ramanauskas, R. Pomés, and L. Maldonado, Mechanism of Copper Patina Formation in Marine Environments, *Electrochim. Acta,* Vol 41 (No. 10), 1996, p 1641–1646

66. L. Veleva and M. Luja, SEM Characterization of Copper Corrosion Products (Patina) Formed in a Tropical Humid Climate, *Br. Corros. J.,* Vol 34 (No. 1), 1999, p 34–36

67. S.D. Cramer, S.A. Matthes, B.S. Covino, S.J. Bullard, and G.R. Holcomb, Environmental Factors Affecting the Atmospheric Corrosion of Copper, *Outdoor Atmospheric Corrosion,* STP 1421, H.E. Townsend, Ed., American Society for Testing and Materials, 2002, p 245–264

68. C.J. Slunder and W.K. Boyd, *Zinc: Its Corrosion Resistance,* Zinc Institute Inc., 1971

69. C.J. Slunder and W.K. Boyd, *Zinc: Its Corrosion Resistance,* 2nd ed., T.K. Christman and J. Payer, Ed., Int. Lead Zinc Research Org., Inc., 1983

70. I. Suzuki, The Behavior of Corrosion Products on Zinc in Sodium Chloride Solution, *Corros. Sci.,* Vol 25 (No. 11), 1985, p 1029–1034

71. S.D. Cramer, J.P. Carter, P.J. Linstrom, and D.R. Flinn, Environmental Effects in the Atmospheric Corrosion of Zinc, *Degradation of Metals in the Atmosphere,* STP 965, S.W. Dean and T.S. Lee, Ed., American Society for Testing and Materials, 1988, p 229–247

72. F.H. Haynie, Environmental Factors Affecting the Corrosion of Galvanized Steel, *Degradation of Metals in the Atmosphere,* STP 965, S.W. Dean and T.S. Lee, Ed., American Society for Testing and Materials, 1988, p 282–289

73. T.E. Graedel, Corrosion Mechanism for Zinc Exposed to the Atmosphere, *J. Electrochem. Soc.,* Vol 136 (No. 4), 1989, p 193C–203C

74. A. Askey, S.B. Lyon, G.E. Thompson, J.B. Johnson, G.C. Wood, M. Cooke, and P. Sage, The Corrosion of Iron and Zinc by Atmospheric Hydrogen Chloride, *Corros. Sci.,* Vol 34 (No. 2), 1993, p 233–247

75. J.M. Costa and M. Vilarrasa, Effect of Air Pollution on Atmospheric Corrosion of Zinc, *Br. Corros. J.,* Vol 28 (No. 2), 1993, p 117–120

76. J. Svensson and L.G. Johansson, A Laboratory Study of the Initial Stages of the Atmospheric Corrosion of Zinc in the Presence of NaCl; Influence of SO_2 and NO_2, *Corros. Sci.,* Vol 34 (No. 5), 1993, p 721–740

77. X.G. Zhang and H.Q. Tran, Effect of Cycling Wetting and Drying on Corrosion of Zinc and Steel, *Cyclic Cabinet Corrosion Testing,* STP 1238, G.S. Haynes, Ed., American Society for Testing and Materials, 1995, p 125–135

78. P. Quintana, L. Veleva, W. Cauich, R. Pomes, and L. Peña, Study of the Composition and Morphology of Initial Stages of Corrosion Products Formed on Zn Plates Exposed to the Atmosphere of Southeast Mexico, *Appl. Surf. Sci.,* Vol 99, 1996, p 325–334

79. J.W. Spence, F.H. Haynie, F.W. Lipfert, S.D. Cramer, and L.G. McDonald, Atmospheric Corrosion Model for Galvanized Steel Structures, *Corrosion,* Vol 48 (No. 12), 1992, p 1009–1019

80. R.A. Legault and V.P. Pearson, Kinetics of the Atmospheric Corrosion of Galvanized Steel, *Atmospheric Factors Affecting the Corrosion of Engineering Metals,* STP 646, S.K. Coburn, Ed., American Society for Testing and Materials, 1978, p 83–96

L. Veleva and R.D. Kane, Atmospheric Corrosion, *Corrosion: Fundamentals, Testing, and Protection*, Vol 13A, *ASM Handbook*, ASM International, 2003, p 196–209

Atmospheric Corrosion

Lucien Veleva, CINVESTAV-IPN, Yucatan, Mexico; Russell D. Kane, InterCorr International, Inc.

Models for Prediction of Atmospheric Corrosion

Models predicting the corrosion damage of metals exposed to atmosphere have been a recent addition to understanding corrosion in atmospheric environments (Ref 12, 16, 18, 21, 23, 26, 32, 79, 80, 81, 82, 83, 84, 96). They are important and useful in predicting the durability of metallic structures and their degradation due to the corrosion process.

First-year atmospheric corrosion weight loss is a parameter that allows the classification of a given atmosphere into a corrosivity category. ISO 9223 uses the annual corrosion rate (weight loss per year) of four standard metals (low-carbon steel, copper, zinc, and aluminum) exposed according to ISO 9226. For this purpose, flat samples are exposed on racks, usually at 45° in Europe or 30° angle of inclination to the horizon for a period of 1 year. The formed corrosion products on the metal surface are removed from the coupons in accordance with ISO 8407, and the metal weight loss (g/m^2/year) or corrosion penetration (μm/year) is determined. Based on these results, corrosivity categories are assigned. Classification of the atmosphere is the basis for the design of good corrosion protection through material selection. Annual corrosion data are also used for prediction of longer-term service life of metal construction in given environments.

The corrosiveness of atmospheric sites can be determined according to ISO 9223, based on annual deposition rate (ISO 9226) of the principal pollutants, such as SO_2 and Cl^-. However, the evaluation of atmospheric corrosivity is more directly connected to metal performance when the aggressiveness category of a given atmosphere is assigned based on the annual corrosion rates of standard metal samples in combination with the annual deposition rate of the main contaminants.

The corrosion rate (C, in g/m^2) of a given metal after time (t, in years) depends directly on its first-year atmospheric corrosion rate (A, in g/m^2 or μm) and its dependence with the time (n):

$$C = At^n \quad \text{(Eq 5)}$$

where A and exponent n are dependent on the type of metal and climatic parameters. Values of n typically range from 0.5 to 1, with most values being close to unity.

The bilogarithmic model of atmospheric corrosion gives a linear relationship between log C and log t:

$$\log C = A + n \log t \quad \text{(Eq 6)}$$

Parameter A depends on properties of the test site and suggests a correlation with climatic variables and air chemistry (TOW, T-RH complex, and pollution level). For this reason, it is often correlated to the pollutant level of SO_2 and Cl^- and to meteorological parameters, leading to a relationship such as the following:

$$A = a_1 + a_2 \text{TOW} + a_3 C_{SO_2} + a_4 C_{Cl^-} \quad \text{(Eq 7)}$$

where a_1, a_2, a_3, and a_4 are coefficients, and C_{SO_2} and C_{Cl^-} are the deposition rates (mg/m^2/day) of these pollutants, measured according to ISO 9225.

A general model has been proposed that divides the total corrosion attack (K) into three dominating parts:

$$K = f_{dry}(SO_2) + f_{dry}(Cl) + f_{wet}(H^+) \quad \text{(Eq 8)}$$

where $f_{dry}(SO_2)$ is the effect of dry deposition of SO_2, $f_{dry}(Cl)$ is the effect of dry deposition of chlorides, and $f_{wet}(H^+)$ is the effect of wet deposition of H^+ (acid rain), which is not included in ISO 9223.

The terms of SO_2 and chlorides can be expressed as follows:

$$f_{dry}(SO_2) = A(SO_2)^B(TOW)^C \exp\{g(T)\} \quad \text{(Eq 9)}$$

$$f_{dry}(Cl) = D(Cl)^E(TOW)^F \exp\{kT)\} \quad \text{(Eq 10)}$$

where A, B, C, D, E, F, and *k* are constants; TOW is time of wetness; *T* is temperature, and *g*(*T*) is a temperature function.

Many dose/response relationships can be obtained, and the significance of factors can be judged. The results of these efforts are not yet suitable for general use at the international level. The main reason is that the physical-chemical background of the atmospheric corrosion is very complicated, and the interpretation of its kinetics is limited. One serious complication is the phenomenon of runoff on the corroded metal surface, which is difficult to involve in a general dose/response relationship because of its specific particularities of corrosion reactions and product-formation chemistry. For example, in marine-coastal areas or regions with a calcareous soil, dust of calcium compounds is deposited on the metal surface. Sulfur compound pollutants are absorbed in the surface, and a series of additional reactions begin, with gypsum (calcium sulfate) as the end product. Gypsum, which is more soluble than calcium carbonate, is then washed away by rain. An increase of volume and variations in temperatures can take place when calcium carbonate reacts to form gypsum.

Results from a number of atmospheric corrosion testing programs show that the bi-logarithmic model (Eq 6) for atmospheric corrosion is applicable to a number of commonly used metals (carbon steels, low-alloyed steels, galvanized steels, and aluminized steels) in many environments. Wide-ranging atmospheric corrosion tests of standard metals have been conducted to unify operational procedures and to acquire metal corrosion data for modeling and predicting atmospheric corrosion. Based on these efforts, corrosivity maps of atmospheres in a number of countries have been created. The bilogarithmic model is helpful in extrapolating short-term atmospheric corrosion data to longer time. When considering corrosion severity over the long term, changes in the environment may be more significant than deviations from the model.

References cited in this section

12. C. Leygraf and T. Graedel, *Atmospheric Corrosion,* Wiley-Interscience, 2000

16. S. Feliu, M. Morcillo, and S. Feliu, Jr., The Prediction of Atmospheric Corrosion from Meteorological and Pollution Parameters, Part I: Annual Corrosion; Part II: Long- Term Forecasts, *Corros. Sci.,* Vol 34, 1993, p 403–414; 415–422

18. D.H. Vu, *Atmospheric Corrosion of Metals in Tropics,* Nauka, Moscow, Russia, 1994

21. D. Knotkova, P. Boschek, and K. Kreislova, Results of ISO CORRAG Program: Processing of One-Year Data in Respect to Corrosivity Classification, *Atmospheric Corrosion,* STP 1239, W.W. Kirk and H.H. Lawson, Ed., American Society for Testing and Materials, 1995, p 38–55

23. J. Tidblad, A.A. Mikhailov, V. Kucera, Application of a Model for Prediction of Atmospheric Corrosion in Tropical Environments, *Marine Corrosion in Tropical Environments,* STP 1399, S.W. Dean, G. Hernandez-Duque Delgadillo, and J.B. Bushman, Ed., American Society for Testing and Materials, 1995, p 250–285

26. L. Veleva and L. Maldonado, Classification of the Atmosphere Corrosivity in the Humid Tropical Climate, *Br. Corros. J.,* Vol 33 (No. 1), 1998, p 53–57

32. J. Tidblad, V. Kucera, A. Mihhailov, and D. Knotkova, Improvement of the ISO Classification System Based on Dose-Response Functions Describing the Corrosivity of Outdoor Atmospheres, *Outdoor Atmospheric Corrosion,* STP 1421, H.E. Townsend, Ed., American Society for Testing and Materials, 2002, p 73–87

79. J.W. Spence, F.H. Haynie, F.W. Lipfert, S.D. Cramer, and L.G. McDonald, Atmospheric Corrosion Model for Galvanized Steel Structures, *Corrosion,* Vol 48 (No. 12), 1992, p 1009–1019

80. R.A. Legault and V.P. Pearson, Kinetics of the Atmospheric Corrosion of Galvanized Steel, *Atmospheric Factors Affecting the Corrosion of Engineering Metals,* STP 646, S.K. Coburn, Ed., American Society for Testing and Materials, 1978, p 83–96

81. M. Pourbaix, The Linear Bilogarithmic Law for Atmospheric Corrosion, *Atmospheric Corrosion,* W.H. Ailor, Ed., Wiley, Inc., 1982, p 107–121

82. Yu.M. Panchenko and P.V. Strekalov, Correlation between Corrosion Mass Losses and Corrosion Product Quantity Retained on Metals in a Cold, Moderate and Tropical Climate, *Prot. Met. (Russia),* Vol 30 (No. 5), 1994, p 459–467

83. M. Morcillo, S. Feliu, and J. Simancas, Deviation from Bilogarithmic Law for Atmospheric Corrosion of Steel, *Br. Corros. J.,* Vol 28 (No. 1), 1993, p 50–52

84. J.L. Crolet, The Electrochemistry of Corrosion Beneath Corrosion Deposits, *J. Mater. Sci.,* Vol 28, 1993, p 2577–2588

96. S. Matthes, S. Cramer, S. Bullard, B. Covino, and G. Holcomb, "Atmospheric Corrosion and Precipitation Runoff from Zinc and Zinc Alloy Surfaces," Paper 03598, 58th Annual Conference, Corrosion 2003, NACE, 2003

L. Veleva and R.D. Kane, Atmospheric Corrosion, *Corrosion: Fundamentals, Testing, and Protection*, Vol 13A*, ASM Handbook*, ASM International, 2003, p 196–209

Atmospheric Corrosion

Lucien Veleva, CINVESTAV-IPN, Yucatan, Mexico; Russell D. Kane, InterCorr International, Inc.

Atmospheric Corrosion and Precipitation Runoff from Corroded Metals

Atmospheric corrosion of some metal structures, such as zinc and copper sheets commonly used for roofing and drain water systems, zinc anodes for cathodic protection, and zinc and zinc-aluminum coatings, involves the formation of protective oxide/hydroxide corrosion products that act as effective physical barriers between the metal and the aggressive atmosphere. However, due to interaction with the environment, the metal protective film could suffer modification into nonprotective corrosion products. Physical removal from the metal surface through dissolution of soluble corrosion products in precipitation runoff or by spalling could result (Ref 85, 86, 87, 88, 89, 90, 91, 92, 93, 94, 95, 96). Precipitation runoff is water from rain, dew, snow, or fog that drains from a surface and contains air- or waterborne deposited reactants and soluble ions from the metal surface. For that reason, traces of metals such as copper, zinc, lead, and iron are commonly detected in roof runoff water.

The use of copper as a roofing material has a long tradition, and zinc sheets have been used for over 200 years. During the last decade, a concern has been raised by legislators in Europe and the United States on the quantity of metal removed from a roof during precipitation and the potential effect that the released metal may have on the environment. Urban stormwater is recognized as a source of contaminants, including trace metals, and roof runoff is a contributor. It has been reported that galvanized roofs can contribute zinc concentrations of between 1 and 44 g/m^3, whereas tile roofs contribute between 0.01 and 2.6 g/m^3 of zinc in the runoff.

An extensive investigation in the last decade, with parallel field and laboratory exposures, was conducted to establish atmospheric corrosion and metal runoff processes, mainly on copper and zinc used for roofing applications. It has been proven that the runoff rate of zinc is considerably lower than its corrosion rate, varying between a quotient of 50 to 90% for zinc and 20 to 50% for copper during exposure of up to 5 and 2 years, respectively. Detailed studies have been performed to disclose the effect of various parameters on the runoff rate, including surface orientation and inclination, natural patinated copper, patina composition, rain duration and volume, rain pH, and length of dry periods in between rain events. Based on field exposures and literature data, a correlation has been established between runoff rate and the prevailing SO_2 environmental

concentration. The runoff rate of zinc and copper increases with increasing SO_2 level for exposure sites of similar annual precipitation quantities (500 to 1000 mm/year, or 20 to 40 in./year).

High metal concentrations have been found in the initial rain volume flushing the surface—the *first flush,* during which the most easily soluble and poorly adhesive corrosion products are washed off from the surface. The magnitude of first flush depends on the presence and amount of soluble corrosion products and also is associated with the capacity of the corrosion products to absorb and retain water. In turn, this is related with their adherence, morphology, thickness, porosity, and presence of internal micro- and macrocracks and defects.

The precipitation volume is considered as the most important parameter affecting the runoff quantity of copper and zinc. Samples exposed in different environments exhibit large differences in the magnitude of the first flush. For copper and zinc panels preexposed in Swedish urban, rural, and marine environments, yearly runoff rates were 1.2, 0.7, and 1.7 g/m^2/year of copper and 2.6, 1.6, and 3.7 g/m^2/ year of zinc, assuming an annual precipitation of 500 mm/year (20 in./year).

The first-flush effect usually decreases to rather constant metal concentration during the subsequent rains. The metal concentration in runoff increases with rain acidity, decreases with rain intensity, and increases with length of the dry period preceding a rain event. Drizzle (<1 mm/h, or 0.04 in./h), with the longest surface contact period, results in an increased amount of released copper.

It is considered by researchers that the copper runoff is caused by proton- or ligand-induced water dissolution of the noncrystalline cupric sulfate as a part of copper corrosion products formed in environments polluted with SO_2, HCl, and NO_x. The runoff effect is more pronounced for aged copper (≥40 years old). No significant differences have been observed between episodes of light rain (≈8 mm/h, or 0.3 in./h) and moderate rain (≈20 mm/h, or 0.8 in./h).

In the case of copper patina formed in natural environments, a higher wetting capacity and absorption of rainwater have been found on green- patinated copper compared to brown-patinated, which explains a higher magnitude of copper being released during first flush. The total annual runoff rate of copper is significant for green-patinated samples, whereas it is negligible for brown-patinated samples.

Zinc commonly forms voluminous and highly porous atmospheric corrosion products. This may explain why no large differences in runoff rate have been seen between new and aged zinc samples in the reported field investigations. Rather, the reason may be related to a high susceptibility for proton-induced dissolution of zinc corrosion products by rain. During the dry period, neutral zinc salts with high solubility constants are frequently formed, such as $ZnSO_4$ or $Zn(NO_3)_2$. These are easily dissolved during the first-flush release; then, less soluble zinc salts are formed, including zinc hydrosulfates and zinc hydrocarbonates, which govern the dissolution rate during the steady-state runoff.

Lead ions may also be introduced into the environment by the flow of precipitation runoff from the surface of old lead structures, such as gutters, roofs, piping, siding, and sculptures. This metal is of particular concern to the public because of the adverse effect of even very small amounts on human health. The corrosion rate of lead depends on solubility and the physical characteristics of the corrosion products formed. Lead presents a high corrosion resistance in exposure to the atmosphere and to water, due to the formation of insoluble lead salts deposited on its surface. However, in natural and domestic waters, the corrosion rate depends on the degree of water hardness (calcium and magnesium salts content), the content of dissolved oxygen, and the CO_2 concentration. In the absence of passivating substances (such as carbonates), any oxidizing agent can cause lead to corrode. The presence of nitrate and chloride ions interferes with the formation of a protective layer or penetrates it, thus increasing the corrosion. Corrosion film studies indicate that lead in the runoff is primarily from solubility of lead carbonate (cerrusite) and lead hydroxyl carbonate (hydrocerrusite).

While atmospheric corrosion rates of metals usually exhibit a continuous decrease with time, the yearly runoff rates are fairly independent of time. The runoff process can be presented at any time *t* by the mass balance:

$$C(t) = T(t) + R(t) \qquad \text{(Eq 11)}$$

where $C(t)$ is the cumulative corrosion mass loss, $T(t)$ is the protective corrosion mass loss, and $R(t)$ is the cumulative nonprotective corrosion product (runoff effect).

In dry-season exposure of metals in polluted atmospheres (pH below 5), the environment reacts with the metal surface, forming neutral salts (soluble products), but there is little or no runoff. When the precipitation starts, these salts are dissolved in the presence of acid gases as pollutants of the atmosphere. In the absence of spalling or significant accumulation of nonprotective corrosion products, R in Eq 11 represents the cumulative loss of soluble corrosion products in precipitation runoff. The time derivative of Eq 11 shows that the corrosion rate is equal to the rate of protective film growth and the rate of corrosion film loss in precipitation runoff:

$dC/dt = dT/dt + dR/dt$ (Eq 12)

After long exposure, when the corrosion layer is developed and further corrosion film grows at a slower rate, dT/dt approaches 0, and the corrosion rate is equal to the rate of precipitation runoff loss. Recent results suggest that, following an inductive period when the corrosion film is establishing itself on the metal surface, the cumulative runoff from corroding metal surfaces (such as rolled zinc, thermal spray zinc, and zinc- aluminum and aluminum-zinc-indium alloys) is linear to time and precipitation volume and relatively insensitive to seasonal variations in precipitation chemistry, air chemistry, and meteorology.

References cited in this section

85. I. Odnevall, P. Verbiest, W. He, and C. Leygraf, The Influence of Patina Age and Pollutant Levels on the Runoff Rate of Zinc from Roofing Materials, *Corros. Sci.,* Vol 40, 1998, p 1977–1982

86. I. Odnevall, P. Verbiest, W. He, and C. Leygraf, Effect of Exposure Direction and Inclination on the Runoff Rates of Zinc and Copper Roofs, *Corros. Sci.,* Vol 42, 2000, p 1471–1487

87. W. He, I. Odnevall, and C. Leygraf, A Laboratory Study of Copper and Zinc Runoff during First Flush and Steady-State Conditions, *Corros. Sci.,* Vol 43, 2001, p 127–146

88. W. He, I. Odnevall, and C. Leygraf, A Comparison between Corrosion Rates and Runoff Rates from New and Aged Copper and Zinc as Roofing Material, *Water, Air, and Soil Pollution: Focus 1,* 2001, p 67–82

89. X. Zhang, W. He, I. Odnevall, J. Pan, and C. Leygraf, Determination of Instantaneous Corrosion Rates and Runoff of Copper from Naturally Patinated Copper during Continuous Rain Events, *Corros. Sci.,* Vol 44, 2002, p 2131–2151

90. I. Odnevall and C. Leygraf, Environmental Effects of Metals Induced by Atmospheric Corrosion, *Outdoor Atmospheric Corrosion,* STP 1421, H.E. Townsend, Ed., American Society for Testing and Materials, 2002, p 185–199

91. S. Bertling, I. Odnevall, C. Leygraf, and D. Berggren, Environmental Effects of Zinc Runoff from Roofing Materials—A New Multidisciplinary Approach, *Outdoor Atmospheric Corrosion,* STP 1421, H.E. Townsend, Ed., American Society for Testing and Materials, 2002, p 200–215

92. W. He, W. Odnevall, and C. Leygraf, Runoff Rates of Zinc—A Four-Year Field and Laboratory Study, *Outdoor Atmospheric Corrosion,* STP 1421, H.E. Townsend, Ed., American Society for Testing and Materials, 2002, p 216–229

93. I. Odnevall, T. Korpinen, R. Sundberg, and C. Leygraf, Atmospheric Corrosion of Natural and Pre-Patinated Copper Roofs in Singapore and Stockholm—Runoff Rates and Corrosion Products Formed, *Outdoor Atmospheric Corrosion,* STP 1421, H.E. Townsend, Ed., American Society for Testing and Materials, 2002, p 230–244

94. S. Matthes, S. Cramer, B. Covino, S. Bullard, and G. Holcomb, Precipitation Runoff from Lead, *Outdoor Atmospheric Corrosion,* STP 1421, H.E. Townsend, Ed., American Society for Testing and Materials, 2002, p 245–265–274

95. H. Michels, B. Boulanger, and N. Nikolaidis, Environmental Impact of Stormwater Runoff from a Copper Roof, *Mater. Perform.,* Vol 42 (No. 2), 2003, p 70–74

96. S. Matthes, S. Cramer, S. Bullard, B. Covino, and G. Holcomb, "Atmospheric Corrosion and Precipitation Runoff from Zinc and Zinc Alloy Surfaces," Paper 03598, 58th Annual Conference, Corrosion 2003, NACE, 2003

L. Veleva and R.D. Kane, Atmospheric Corrosion, *Corrosion: Fundamentals, Testing, and Protection*, Vol 13A, *ASM Handbook*, ASM International, 2003, p 196–209

Atmospheric Corrosion

Lucien Veleva, CINVESTAV-IPN, Yucatan, Mexico; Russell D. Kane, InterCorr International, Inc.

Biologically Influenced Atmospheric Corrosion

Atmospheric corrosion can be accelerated in the presence of different types of bacteria and, specifically, anaerobic bacteria, which may convert a noncorrosive environment to a very aggressive one. Therefore, microbiologically induced corrosion (MIC) is given serious attention, because MIC failure in plant service systems can also have an ecological impact (Ref 97, 98, 99, 100, 101, 102, 103, 104, 105, 106). Microorganisms have been shown to play an important role in the corrosion of mild steel, austenitic alloys, and copper-base alloys, despite the fact that copper ions are toxic to most organisms. Failures in these materials are generally manifested by pitting, erosion-corrosion, and occasionally by stress-corrosion cracking.

The role of microbes or bacteria in the corrosion of metals is due to their chemical activities (metabolism) associated with microbial growth and reproduction. For example, the MIC of metals by sulfate-reducing bacteria (SRB) is a recognized problem in pipelines. This bacteria is anaerobic and also functions in poorly drained wet soil that has a pH from 6 to 8; contains sulfate ions, organic compounds, and minerals in the absence of oxygen; and has a temperature from 20 to 30 °C (70 to 85 °F). In well-aerated local sites, the anaerobic bacteria cause no problem. For metabolism of the bacteria, oxygen is extracted from the sulfate ions, and this reaction converts the soluble sulfates to sulfide (hydrogen sulfide), which is a pitting activator and attacks the metal surface, forming, for example, iron sulfide (FeS). It has also been suggested that hydrogen sulfide may be subsequently oxidized to thiosulfate, which is an even more aggressive pitting activator. The formed sulfides and other reduced-sulfur compounds can catalyze the anodic dissolution of stainless steels and lower their repassivation and pitting potential, which increases the metal susceptibility to pitting.

The corrosive microbial effect on metals can be attributed to the removal of electrons from the metal and the formation of corrosion products by:

- Direct chemical action of metabolic product, such as sulfuric acid, inorganic or organic sulfides, and chelating agents such as organic acid
- Changes in oxygen content, salt concentration, and pH, thus increasing the possibilities for differential diffusion, concentration gradients, and so on, which establish local electrochemical corrosion cells

One predominant mechanism for mild steel is the bacteria reduction of cathodic hydrogen, resulting in the depolarization of the cathode, which facilitates the cathodic corrosion reaction. The presence of hydrogenase in the SRB allows the use of hydrogen gas as an electron donor in place of carbohydrates as an energy source. In this case, the levels of assimilable carbon (usually organic) and energy sources (nitrogen, sulfate, and phosphate) in the water layer to support the growth and activity of SRB also need to be considered. This mechanism is valid where the cathodic reaction can involve the generation of hydrogen. The other mechanism is the bacterial production of sulfide, leading to the formation of FeS deposits. These deposits are hypothesized to act as large surface areas for the cathodic reaction and also as cathodic areas in a galvanic cell with the steel.

Rate and extent of corrosion are related directly to bacteria growth in contact with the metallic surface. Biofilm bacteria growing on a surface produce extracellular polymeric substances that promote sediment attachment, leading to the development of deposits and colonies of anaerobic bacteria, specifically SRB, which have been

implicated in most MIC failures. Bacteria have been found that are capable of growing on many kinds of coating materials (including hydrocarbons).

Monitoring is particularly important for early effective MIC control, because biofilms can form on metal surfaces very rapidly. Once a mature biofilm is established, the slime layer produced by the microorganisms, along with corrosion products, makes the biofilm extremely resistant to the effects of chemical treatments. The key symptom that usually indicates SRB involvement in the corrosion process of ferrous alloys is localized corrosion filled with black sulfide corrosion products. Tests for SRB include counts of total viable sulfate reducers. Other tests include measurement of the hydrogen uptake of a soil and the time for a soil sample to blacken a medium used to grow sulfate reducers. Chemical analysis of the water layer on the metal is helpful in determining the critical nutrients necessary to support microbiological activity. These tests should be conducted under the direction of a microbiologist who has experience in MIC. Field test kits are currently available that employ an antibody tagging technique to identify and facilitate the determination of the population of microbes.

Microbiologically influenced corrosion can be studied using field survey and different techniques, such as electrochemical polarization curves and polarization resistance, electrochemical impedance spectroscopy, thin-film electrical resistance probe, galvanic current measurement, scanning electron microscopy and energy-dispersive spectroscopy surface analysis, Mössbauer spectroscopy and x-ray diffraction for analysis of corrosion products, and so on. See the articles “Microbiologically Influenced Corrosion” and “Microbiologically Influenced Corrosion Testing” in this volume.

References cited in this section

97. J.G. Stoecker, Guide for the Investigation of Microbiological Induced Corrosion, *Mater. Perform.,* Vol 20 (No. 9), 1981, p 32

98. D.H. Pope, Discussion of Methods for the Detection of Microorganisms Involved in Microbiologically Influenced Corrosion, *Biologically Induced Corrosion—Proceedings of the International Conference,* NACE, 1986, p 275

99. S.W. Borenstein, *Microbiologically Influenced Corrosion Handbook,* (NACE Item 37740) Industrial Press, 1994

100. H.A. Videla, *Manual of Biocorrosion,* (NACE Item 38214) CRC Press Inc., 1996

101. B.J. Little, P.A. Wagner, and F. Mansfeld, *CTME: Microbiologically Influenced Corrosion,* (Item 37546) NACE International, 1997

102. V. Rainha and T. Fonesca, Kinetic Studies on the SRB Influenced Corrosion on Steel: A First Approach, *Corros. Sci.,* Vol 39 (No. 4), 1997, p 807–813

103. H.A. Widela, *A Practical Manual of Biocorrosion and Biofouling for the Industry,* (English, Spanish and Portuguese Editions), (NACE Item 38251) CYTED Research Network XV BIOCORR, 1998

104. C.A.C. Sequeira, Ed., “Microbial Corrosion,” (European Federation of Corrosion Report 29) NACE Item 38331, IOM Communications, Ltd., 2000

105. P. Angell and K. Urbanic, Sulphate-Reducing Bacteria Activity as a Parameter to Predict Localized Corrosion of Stainless Steel, *Corros. Sci.,* Vol 42, 2000, p 897–912

106. T. Rap, T. Sairam, B. Viswanathan, and K. Nair, Carbon Steel Corrosion by Iron Oxidizing and Sulfate Reducing Bacteria in a Freshwater Cooling System, *Corros. Sci.,* Vol 42, 2000, p 1417–1431

L. Veleva and R.D. Kane, Atmospheric Corrosion, *Corrosion: Fundamentals, Testing, and Protection,* Vol 13A*, ASM Handbook*, ASM International, 2003, p 196–209

Atmospheric Corrosion

Lucien Veleva, CINVESTAV-IPN, Yucatan, Mexico; Russell D. Kane, InterCorr International, Inc.

Trends in Atmospheric Corrosion Research and Methods

Atmospheric corrosion processes have been studied by exposure tests, accelerated corrosion testing, as well as electrochemical, surface analytical, and spectroscopic techniques (Ref 107, 108, 109, 110, 111, 112, 113, 114, 115, 116, 117, 118, 119, 120, 121, 122, 123, 124, 125, 126, 127, 128, 129, 130, 131, 132, 133, 134, 135, 136, 137, 138, 139, 140, 141, 142, 143, 144, 145, 146, 147, 148, 149, 150, 151, 152, 153, 154, 155). These methods often give only integral information on corrosion processes (anodic and cathodic) occurring at the solid-liquid interface. The development of local electrochemical techniques, such as scanning vibrating electrode technique, localized electrochemical impedance spectroscopy, and scanning Kelvin probe, with different lateral resolutions and the increased use of various scanning probe microscopes (scanning tunneling microscope, atomic force microscope, electrochemical scanning tunneling microscope, electrochemical force atomic microscope, magnetic force microscope, scanning electrochemical microscope, and scanning near-field optical microscope) in corrosion science allow local processes (in situ) to be studied on an atomic scale.

Combining conventional electrochemical and surface analytical measurements with these local techniques permits the treatment of corrosion as a local phenomenon and contributes to a better understanding of the processes and the effects of the controlling factors. Currently, local atomistic events and effects of surface imperfections of different dimensionality on the interfacial processes can be directly analyzed. Since the development of in situ scanning probe microscopy techniques, the structures, thermodynamics, and kinetics of interfacial processes can be investigated directly in a real-time domain on an atomic scale at the solid-liquid interface. These technical achievements point out a new direction of corrosion research aimed toward elaborate new corrosion models based on the submicroscopic approach to the electrochemistry of corrosion metal processes. While these techniques are currently in the forefront of today's research, they will likely yield large future benefits in terms of better characterization of corrosion phenomena and prediction of corrosive degradation.

References cited in this section

107. J.D. Sinclair, An Instrumental Gravimetric Method for Indexing Materials, Contaminants, and Corrosion Products According to Their Hygroscopicity, *J. Electrochem. Soc.,* Vol 125 (No. 5), 1978, p 734–742

108. R.D. Smith, An Accelerated Atmospheric Corrosion Test (AACT), *Factor Affecting the Corrosion of Engineering Metals,* STP 646, S.K. Coburn, Ed., American Society for Testing and Materials, 1978, p 160–164

109. T.R. Shaw, Corrosion Map of the British Isles, *Factor Affecting the Corrosion of Engineering Metals,* STP 646, S.K. Coburn, Ed., American Society for Testing and Materials, 1978, p 204–215

110. D. Kontkova and K. Barton, Corrosion Aggressivity of Atmospheres (Derivation and Classification), *Atmospheric Corrosion of Metals,* STP 767, S.W. Dean, Jr. and E.C. Rhea, Ed., American Society for Testing and Materials, 1982, p 225–249

111. A.B. Harker, F. Haynie, F. Mansfeld, D.R. Strauss, and D.A. Landis, Measurement of the Sulfur Dioxide and Sulfuric Acid Aerosol Induced Corrosion of Zinc in a Dynamic Flow System, *Atmosph. Environ.,* Vol 1 (No. 11), 1982, p 2691–2702

112. C. Fiaud, M. Safavi, and J. Vedel, Identification of the Corrosion Products Formed on Copper in Sulfur Containing Environments, *Werkst. Korros.,* Vol 35 (No. 8), 1984, p 361–366

113. S.B. Lyon, G.E. Thompson, J.B. Johnson, G.C. Wood, and J.M. Ferguson, Accelerated Atmospheric Corrosion Testing Using a Cyclic Wet/Dry Exposure Test: Aluminum, Galvanized Steel and Steel, *Corrosion,* Vol 43 (No. 12), 1987, p 719–726

114. H. Grange, C. Bieth, H. Boucher, and G. Delapierre, A Capacitive Humidity Sensor with Very Fast Response Time and Very Low Hysteresis, *Sens. Actuators,* No.12, 1987, p 291–296

115. D.M. Drazic and V. Vascic, The Correlation between Accelerated Laboratory Corrosion Tests and Atmospheric Corrosion Station Tests on Steels, *Corros. Sci.,* Vol 29 (No. 10), 1989, p 1197–1204

116. M. Stratmann and H. Streckel, On the Atmospheric Corrosion of Metals Which are Covered with Thin Electrolyte Layers, Part I: Verification of the Experimental Technique; Part II: Experimental Results; Part III: The Measurement of Polarization Curves on Metal Surfaces Which are Covered by Thin Electrolyte Layers, *Corros. Sci.,* Vol 30 (No. 6/7), 1990, p 681–734

117. J.W. Spence, E.O. Edney, F.H. Haynie, C.D. Stiles, E.W. Corse, M.S. Wheeker, and S.F. Cheek, Advanced Laboratory and Field Exposure Systems for Testing Materials, *Corrosion Testing and Evaluation: Silver Anniversary Volume,* STP 1000, R. Baboian and S.W. Dean, Ed., American Society for Testing and Materials, 1900, p 191–207

118. G. Nekoksa, Correlation of Failure Analysis Corrosion Testing, *Corrosion Testing and Evaluation: Silver Anniversary Volume,* STP 1000, R. Baboian and S.W. Dean, Ed., American Society for Testing and Materials, 1900, p 66–79

119. A.M. Beccaria, Zinc Layer Characterization on Galvanized Steel by Chemical Methods, *Corrosion,* Vol 46 (No. 11), 1990, p 906–912

120. R.J. Cordner, Atmospheric Corrosion Survey of New Zealand, *Br. Corros. J.,* Vol 25 (No. 2), 1990, p 115–118

121. J. Scully, Electrochemical Methods for Laboratory Corrosion Testing, *Corrosion Testing and Evaluation: Silver Anniversary Volume,* STP 1000, R. Baboian and S.W. Dean, Ed., American Society for Testing and Materials, 1900, p 351–378

122. W.G. Clark, Jr. and M.J. Metala, The Nondestructive Characterization of Corrosion, *Corrosion Testing and Evaluation: Silver Anniversary Volume,* STP 1000, R. Baboian and S.W. Dean, Ed., American Society for Testing and Materials, 1900, p 39–40

123. G. Haynes, Review of Laboratory Corrosion Tests and Standards, *Corrosion Testing and Evaluation: Silver Anniversary Volume*, STP 1000, R. Baboian and S.W. Dean, Ed., American Society for Testing and Materials, 1900, p 281–288

124. A. Sterling, A. Atrens, and I.O. Smith, Accelerated Atmospheric Corrosion of Copper and Copper Alloys, *Br. Corros. J.,* Vol 25 (No. 4), 1990, p 271–278

125. I. Odnevall and C. Leygraf, A Comparison between Analytical Methods for Zinc Specimens Exposed in a Rural Atmosphere, *J. Electrochem. Soc.*, Vol 138 (No. 7), 1991, p 1923–1928

126. S.B. Lyon, G.E. Thompson, and J.B. Johnson, Materials Evaluation Using Wet-Dry Mixed Salt-Spray Tests, *New Methods for Corrosion Testing of Aluminum Alloys*, STP 1134, V.S. Agarwala and G.M. Ugiansky, Ed., American Society for Testing and Materials, 1992, p 20–31

127. E.M. Rosen and D.C. Silverman, Corrosion Prediction from Polarization Scans Using an Artificial Neural Network Integrated with an Expert System, *Corrosion,* Vol 48 (No. 9), 1992, p 734–744

128. A.Y. Peng, S.B. Lyon, G.E. Thompson, J.B. Johnson, G.C. Wood, and J.M. Ferguson, Comparison of Cross-Sectional Image Analysis with Weight Change Measurements for Assessing Non-Uniform Attack during Corrosion Testing of Aluminum, *Br. Corros. J.,* Vol 28 (No. 2), 1993, p 103–106

129. W.S. Dean, Classifying Atmospheric Corrosivity—A Challenge for ISO, *Mater. Perform.,* Vol 32 (No. 10), 1993, p 53–58

130. D. Persson and C. Leygraf, In Situ Infrared Reflection Absorption Spectroscopy for Studies of Atmospheric Corrosion, *J. Electrochem. Soc.,* Vol 140 (No. 5), 1993, p 1256–1260

131. J. Stringer and A.J. Markworth, Application of Deterministic Chaos Theory to Corrosion, *Corros. Sci.,* Vol 35 (No. 1–4), 1993, p 751–760

132. D.O. Wipf, Initiation and Study of Localized Corrosion by Scanning Electrochemical Microscopy, *Colloids Surf. A: Physicochem. Eng. Aspects,* Vol 93, 1994, p 251–261

133. A. Cox and S.B. Lyon, An Electrochemical Study of the Atmospheric Corrosion of Mild Steel, Part I: Experimental Method, *Corros. Sci.,* Vol 36 (No. 7), 1994, p 1167–1176

134. A. Cox and S.B. Lyon, An Electrochemical Study of the Atmospheric Corrosion of Iron, Part II: Cathodic and Anodic Processes on Uncorroded and Pre-Corroded Iron, *Corros. Sci.,* Vol 36 (No. 7), 1994, p 1177–1192

135. L. Fraigi, S.N. Gwirc, and D. Lupi, A Thick Film Sensor for Atmospheric Corrosion Testing, *Sens. Actuators B,* No. 18–19, 1994, p 558–561

136. S. Motoda, Y. Suzuki, T. Shinohara, Y. Kojima, S. Tsujikawa, W. Oshikawa, S. Itomura, T. Fukushima, and S. Izumo, ACM (Atmospheric Corrosion Monitoring) Type Corrosion Sensor to Evaluate Corrosivity of Marine Atmosphere, *Corros. Eng. (Jpn.),* Vol 43, 1994, p 538–594

137. S. Motoda, Y. Suzuki, T. Shinohara, Y. Kojima, S. Tsujikawa, W. Oshikawa, S. Itomura, T. Fukushima, and S. Izumo, Corrosive Factors of Marine Atmosphere Analyzed by ACM Sensor for 1 Year, *Corros. Eng. (Jpn.),* Vol 44, 1995, p 253–265

138. R. Alkire, and M. Verhoff, Electrochemical Reaction Engineering in Materials Processing, *Chem. Eng. Sci.,* Vol 49 (No. 24A), 1994, p 4085–4093

139. R. Baboian, Ed., *Corrosion Tests and Standards: Application and Interpretation,* ASTM Manual Series, American Society for Testing and Materials, 1995

140. S.B. Lyon, C.W. Wong, and P. Ajiboye, An Approach to the Modeling of Atmospheric Corrosion, *Atmospheric Corrosion,* STP 1239, W.W. Kirk and H.H. Lawson, Ed., American Society for Testing and Materials, 1995, p 26–37

141. P.R. Roberge, What Is Accelerated in Accelerated Testing: A Framework for Definition, *Cyclic Cabinet Corrosion Testing,* STP 1238, G.S. Haynes, Ed., American Society for Testing and Materials, 1995, p 18–36

142. G.A. King, Corrosivity Mapping: A Novel Tool for Materials Selection and Asset Management, *Mater. Perform.,* Vol 34 (No. 1), 1995, p 7–9

143. J. Tidblad and C. Leygraf, Atmospheric Corrosion Effects of SO_2 and NO_2: A Comparison of Laboratory and Field-Exposed Copper, *J. Electrochem. Soc.,* Vol 142 (No. 3), 1995, p 749–756

144. A. Nishikata, Y. Ichihara, and T. Tsuru, An Application of Electrochemical Impedance Spectroscopy to Atmospheric Corrosion Study, *Corros. Sci.,* Vol 37 (No. 6), 1995, p 897–911

145. M. Urqudi and D. Van Voorthis, "Prediction of Single-Phase Erosion-Corrosion in Mild Steel Pipes Using Artificial Neural Networks and a Deterministic Model," Paper 546, Proceedings of NACE'95 Corrosion Congress, NACE, 1995

146. A.O. Salnick and W. Faubel, Photoacoustic FT-IR Spectroscopy of Natural Copper Patina, *Appl. Spectrosc.,* Vol 49, 1995, p 1516–1523

147. L. Veleva, S. Thomas, E. Marrin, A. Cruz- Orea, I. Delgadillo, J. Alvarado-Gil, P. Quintana, R. Pomes, F. Sanchez, H. Vargas, and L. Miranda, On the Use of Photoacoustic Technique for Corrosion Monitoring of Metals: Cu and Zn Oxides Formed, *Corros. Sci.,* Vol 39 (No. 9), 1997, p 1641–1655

148. J.W. Still and D.O. Wipf, Breakdown of the Passive Layer by Use of the Scanning Electrochemical Microscope, *J. Electrochem. Soc.,* Vol 144 (No. 8), 1997, p 2657–2665

149. C. Leygraf and M. Forslund, Quartz Crystal Microbalance for In Situ Outdoor Corrosivity Studies, Paper 238, Proceedings of NACE'98 Corrosion Congress, NACE, 1998

150. A. Garcia-Quiroz, S. Tomás, H. Vargas, A. Cruz-Orea, J. Alvarado, L. Veleva, L. Miranda, Photoacoustic Spectroscopy of Corrosion Products of Copper Formed in Tropical Environments, *Instrum. Sci. Technol.,* Vol 26 (No. 2–3), 1998, p 241–260

151. R. Ramanauskas, L. Muleshkova, L. Maldonado, and P. Dobrovolskis, Characterization of the Corrosion Behavior of Zn and Zn Alloy Electrodeposits: Atmospheric and Accelerated Tests, *Corros. Sci.,* Vol 40 (No. 2–3), 1998, p 401–410

152. E. Kálmán, Trends in Corrosion Research, *Electrochim. Acta,* Vol 46, 2001, p 3607–3609

153. W.T. Stephen, Increase Your Confidence in Corrosion Test Data, *Mater. Perform.,* Vol 40 (No. 3), 2001, p 58–61

154. H. Katayama, M. Yamamoto, and K. Kodama, Atmospheric Corrosion Monitoring Sensor in Outdoor Environment Using AC Impedance Technique, *Outdoor Atmospheric Corrosion,* STP 1421, H.E. Townsend, Ed., American Society for Testing and Materials, 2002, p 171–181

155. J. Repp, Accelerated Corrosion Testing— Truths and Misconceptions, *Mater. Perform.,* Vol 41 (No. 9), 2002, p 60–63

L. Veleva and R.D. Kane, Atmospheric Corrosion, *Corrosion: Fundamentals, Testing, and Protection,* Vol 13A, *ASM Handbook*, ASM International, 2003, p 196–209

Atmospheric Corrosion

Lucien Veleva, CINVESTAV-IPN, Yucatan, Mexico; Russell D. Kane, InterCorr International, Inc.

References

1. L.L. Shreir, R.A. Jarman, and G.T. Burstein, Ed., Corrosion, Vol 1, *Metal/Environment Reactions,* 3rd ed., Butterworth- Heinemann, 1994
2. "Economic Effect of Metallic Corrosion in the United States," NBS Special Publications 511-1 and 511-2, National Bureau of Standards, May 1978
3. S.C. Cederquist, Cost of Corrosion Studies Underway, *Mater. Perform.,* Vol 38 (No. 5), 1999, p 26–28
4. G.H. Koch, M.P.J. Brongers, N.G. Thompson, Y.P. Virmani, and J.H. Payer, "Corrosion Costs and Preventive Strategies in the United States," FHWA-RD-01-156, Federal Highway Administration, U.S. Department of Transportation, March 2002
5. B.C. Syrett, J.A. Gorman, M.L. Arey, G.H. Kosch, and G.A. Jacobson, Cost of Corrosion, *Mater. Perform.,* Vol 41 (No. 3), 2002, p 18–22
6. U. Evans, Electrochemical Mechanism for Atmospheric Rusting, *Nature,* Vol 206, June 1965, p 980–982
7. I.L. Rozenfeld, *Atmospheric Corrosion of Metals,* B.H. Tytel, Ed., National Association of Corrosion Engineers, 1973
8. V. Kucera and E. Mattsson, *Atmospheric Corrosion,* W.H. Ailor, Ed., John Wiley & Sons, 1982
9. *Corrosion Basics, An Introduction,* National Association of Corrosion Engineers 1984
10. E. Mattsson, Corrosion: An Electrochemical Problem, *Chem. Technol.,* April 1985, p 234–243
11. P. Marcus and J. Oudar, Ed., *Corrosion Mechanism in Theory and Practice,* Marcel Dekker, Inc., 1995
12. C. Leygraf and T. Graedel, *Atmospheric Corrosion,* Wiley-Interscience, 2000
13. M. Pourbaix, *Atlas of Electrochemical Equilibria in Aqueous Solutions,* NACE- Cebelcor, 1974
14. T.S. Lee and E.A. Baker, Calibration of Atmospheric Corrosion Test Sites, *Atmospheric Corrosion of Metals,* STP 767, S.W. Dean, Jr. and E.C. Rhea, Ed., American Society for Testing and Materials, 1982, p 250–266
15. S.D. Cramer and L.G. McDonald, Atmospheric Factors Affecting the Corrosion of Zinc, Galvanized Steel and Copper, *Corrosion Testing and Evaluation: Silver Anniversary Volume,* STP 1000, R. Baboian and S.W. Dean, Jr., Ed., American Society for Testing and Materials, 1990, p 241–259

16. S. Feliu, M. Morcillo, and S. Feliu, Jr., The Prediction of Atmospheric Corrosion from Meteorological and Pollution Parameters, Part I: Annual Corrosion; Part II: Long- Term Forecasts, *Corros. Sci.,* Vol 34, 1993, p 403–414; 415–422

17. S.K. Roy and K.H. Ho, Corrosion of Steel in Tropical Marine Atmospheres, *Br. Corros. J.,* Vol 29 (No. 4), 1994, p 287–291

18. D.H. Vu, *Atmospheric Corrosion of Metals in Tropics,* Nauka, Moscow, Russia, 1994

19. I.S. Cole, R. Holgate, P. Kao, and W. Ganther, The Rate of Drying of Moisture from a Metal Surface and Its Implication for Time of Wetness, *Corros. Sci.,* Vol 37 (No. 3), 1995, p 455–465

20. A.A. Mikhailov, M.N. Suloeva, and E.G. Vasileva, Environmental Aspects of Atmospheric Corrosion, *Water, Air and Soil Pollution,* Vol 85, 1995, p 2673–2678

21. D. Knotkova, P. Boschek, and K. Kreislova, Results of ISO CORRAG Program: Processing o

---

R. Baboian, Galvanic Corrosion, *Corrosion: Fundamentals, Testing, and Protection*, Vol 13A, *ASM Handbook*, ASM International, 2003, p 210–213

Galvanic Corrosion

Robert Baboian, RB Corrosion Service

Introduction

GALVANIC CORROSION occurs when a metal or alloy is electrically coupled to another metal or conducting nonmetal in the same electrolyte. The three essential components are:

- Materials possessing different surface potential
- A common electrolyte
- A common electrical path

When dissimilar metals or alloys in a common electrolyte are electrically isolated from each other, they do not experience galvanic corrosion, regardless of the proximity of the metals or their relative potential or size. When dissimilar metals are electrically coupled (i.e., galvanic coupling), corrosion of the less corrosion resistant metal increases, and the surface becomes anodic, while corrosion of the more corrosion resistant metal decreases, and the surface becomes cathodic. The driving force for corrosion or galvanic current flow is the potential developed between the dissimilar metals. The extent of corrosion resulting from galvanic coupling is affected by the following factors:

- The potential difference between the metals or alloys
- The nature of the environment
- The polarization behavior of the metals or alloys
- The geometric relationship of the component metals or alloys

The difference in potential between dissimilar metals or alloys causes electron flow between them when they are electrically coupled in a conductive solution. The direction of electron flow, and therefore the galvanic

behavior, depends on which metal or alloy is more active. The more active metal or alloy becomes anodic, and the more noble metal or alloy becomes cathodic in the couple.

R. Baboian, Galvanic Corrosion, *Corrosion: Fundamentals, Testing, and Protection*, Vol 13A, *ASM Handbook*, ASM International, 2003, p 210–213

Galvanic Corrosion

Robert Baboian, RB Corrosion Service

Galvanic Series

A galvanic series of metals and alloys is useful for predicting galvanic relationships. Such a series is an arrangement of metals and alloys according to their potentials as measured in a specific electrolyte. The galvanic series allows one to determine which metal or alloy in a galvanic couple is more active and which is more noble. In some cases, the separation between the two metals or alloys in the galvanic series gives an indication of the probable magnitude of corrosive effect.

The potential of a metal or alloy is affected by environmental factors. Corrosion product films and other changes in surface composition can occur in some environments; therefore, no one value can be given for a particular metal or alloy. This requires a galvanic series to be measured in each environment of interest. Most commonly, the galvanic series has been constructed from measurements in seawater, as shown in Table 1. With certain exceptions, this series is broadly applicable to other natural waters and in uncontaminated atmospheres.

Table 1 Galvanic series in seawater at 25 °C (77 °F)

Corroded end (anodic, or least noble)
Magnesium
Magnesium alloys
Zinc
Galvanized steel or galvanized wrought iron
Aluminum alloys
5052, 3004, 3003, 1100, 6053, in this order
Cadmium
Aluminum alloys
2117, 2017, 2024, in this order
Low-carbon steel
Wrought iron
Cast iron
Ni-Resist (high-nickel cast iron)
Type 410 stainless steel (active)
50-50 lead-tin solder
Type 304 stainless steel (active)
Type 316 stainless steel (active)
Lead
Tin
Copper alloy C28000 (Muntz metal, 60% Cu)
Copper alloy C67500 (manganese bronze A)
Copper alloys C46400, C46500, C46600, C46700 (naval brass)
Nickel 200 (active)
Inconel alloy 600 (active)

Hastelloy alloy B
Chlorimet 2
Copper alloy C27000 (yellow brass, 65% Cu)
Copper alloys C44300, C44400, C44500 (admiralty brass)
Copper alloys C60800, C61400 (aluminum bronze)
Copper alloy C23000 (red brass, 85% Cu)
Copper C11000 (ETP copper)
Copper alloys C65100, C65500 (silicon bronze)
Copper alloy C71500 (copper nickel, 30% Ni)
Copper alloy C92300, cast (leaded tin bronze G)
Copper alloy C92200, cast (leaded tin bronze M)
Nickel 200 (passive)
Inconel alloy 600 (passive)
Monel alloy 400
Type 410 stainless steel (passive)
Type 304 stainless steel (passive)
Type 316 stainless steel (passive)
Incoloy alloy 825
Inconel alloy 625
Hastelloy alloy C
Chlorimet 3
Silver
Titanium
Graphite
Gold
Platinum
Protected end (cathodic, or most noble)

Note: ETP, electrolytic tough pitch

Because most engineering materials are alloys, the measurement of galvanic corrosion employing actual materials is much more useful than predicting current flow from the electromotive force series. Therefore, tabulations such as Table 1 can be very useful.

R. Baboian, Galvanic Corrosion, *Corrosion: Fundamentals, Testing, and Protection*, Vol 13A, *ASM Handbook*, ASM International, 2003, p 210–213

Galvanic Corrosion

Robert Baboian, RB Corrosion Service

Polarization

As stated previously, electron flow occurs between metals or alloys in a galvanic couple. This current flow between the more active and more noble members causes shifts in potential due to polarization, because the potentials of the metals or alloys tend to approach each other.

The magnitude of the shift depends on the environment, as does the initial potential. If the more noble metal or alloy is more easily polarized, its potential is shifted more toward the more active metal or alloy potential. The shift in potential of the more active metal or alloy in the direction of the cathode is therefore minimized so that accelerated galvanic corrosion is not as great as would otherwise be expected. On the other hand, when the more noble metal or alloy is not readily polarized, the potential of the more active metal shifts further toward

the cathode (that is, in the direction of anodic polarization) such that appreciable accelerated galvanic corrosion occurs.

R. Baboian, Galvanic Corrosion, *Corrosion: Fundamentals, Testing, and Protection*, Vol 13A, *ASM Handbook*, ASM International, 2003, p 210–213

Galvanic Corrosion

Robert Baboian, RB Corrosion Service

Area, Distance, and Geometric Effects

Factors such as area ratios, distance between electrically connected materials, and geometric shapes also affect galvanic-corrosion behavior.

Area effects in galvanic corrosion involve the ratio of the surface area of the more noble to the more active members(s). The area ratio is unfavorable when the surface area of the more noble metal or alloy is large in comparison to the more active member and the galvanic couple is under cathodic control. Under these conditions, the anodic current density on the more active metal or alloy becomes extremely large. The resulting polarization leads to increased corrosion of the active metal. The opposite area ratio—large active member surface, smaller noble member surface—(with the couple under cathodic control) produces only slightly accelerated galvanic effects because of the predominant polarization of the more noble material.

Effect of Distance. Dissimilar metals in a galvanic couple that are in close physical proximity usually suffer greater galvanic effects than those that are further apart. The distance effect is dependent on solution conductivity because the path of current flow is the primary consideration. Thus, if dissimilar pipes are butt welded with the electrolyte flowing through them, the most severe corrosion will occur adjacent to the weld on the anodic member.

Effect of Geometry. The geometry of the circuit also affects galvanic corrosion in that current does not readily flow around corners. This is simply an extension of the principle described previously, in which the current takes the path of least resistance.

R. Baboian, Galvanic Corrosion, *Corrosion: Fundamentals, Testing, and Protection*, Vol 13A, *ASM Handbook*, ASM International, 2003, p 210–213

Galvanic Corrosion

Robert Baboian, RB Corrosion Service

Modes of Attack

Corrosion of the anodic member(s) of a galvanic couple may take the form of general or localized corrosion, depending on the configuration of the couple, the nature of the corrosion film produced, and the nature of the metals or alloys involved. Generally, there are five major categories.

Dissimilar Metals. The combination of dissimilar metals in engineering design by mechanical or other means is quite common—for example, in heating or cooling coils, vessels, heat exchangers, and machinery. Such combinations often lead to galvanic corrosion.

Nonmetallic Conductors. Less frequently recognized is the influence of nonmetallic conductors as cathodes in galvanic couples. Carbon brick in vessels is strongly cathodic to the common structural metals and alloys.

Impervious graphite, especially in heat-exchanger applications, is cathodic to the less noble metals and alloys. Carbon-filled polymers can act as noble metals in a galvanic couple.
Another example is the behavior of conductive corrosion films, such as mill scale (magnetite, or Fe_3O_4) or iron sulfides on steel, or of lead sulfate on lead. Such films can be cathodic to the base metal exposed at breaks or pores in the scale (Fig. 1) or even to such extraneous items as valves or pumps in a piping system.

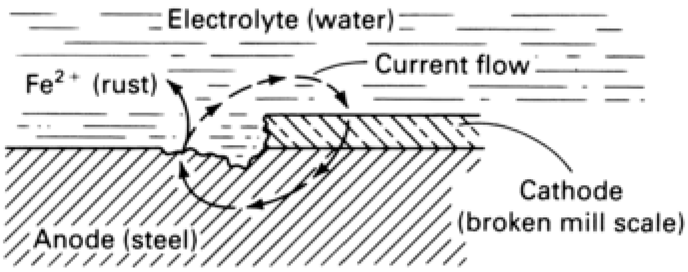

Fig. 1 Schematic showing how breaks in mill scale (Fe_3O_4) can lead to galvanic corrosion of steel

Metallic Coatings. Two types of metallic coatings are used in engineering design: noble metal coatings and sacrificial metal coatings. Noble metal coatings are used as barrier coatings over a more reactive metal. Galvanic corrosion of the substrate can occur at pores, damage sites, and edges in the noble metal coating. Sacrificial metal coatings provide cathodic protection of the more noble base metal, as in the case of galvanized steel or Alclad aluminum.
Cathodic Protection. Magnesium, zinc, and aluminum galvanic (sacrificial) anodes are used in a wide range of cathodic protection applications. The galvanic couple of the more active metal and a more noble structure (usually steel, but sometimes aluminum, as in underground piping) provides galvanic (sacrificial) cathodic protection, while accelerated corrosion of the sacrificial metal anode occurs.
Metal Ion Deposition. Ions of a more noble metal may be reduced on the surface of a more active metal—for example, copper on aluminum or steel, and silver on copper. This process is also known as cementation, especially with regard to aluminum alloys. The resulting metallic deposit provides cathodic sites promoting further galvanic corrosion of the more active metal.

R. Baboian, Galvanic Corrosion, *Corrosion: Fundamentals, Testing, and Protection*, Vol 13A, *ASM Handbook*, ASM International, 2003, p 210–213

Galvanic Corrosion

Robert Baboian, RB Corrosion Service

Predicting Galvanic Corrosion

The most common method of predicting galvanic corrosion is by immersion testing of the galvanic couple in the environment of interest. Although time-consuming, this is the most desirable method of investigating galvanic corrosion. Screening tests are conducted initially to eliminate as many candidate materials as possible. These screening tests consist of one or more of the following three electrochemical techniques: potential measurements, current measurements, and polarization measurements.
Potential measurements are made to construct a galvanic series of metals and alloys, as described previously. As a first approximation, the galvanic series is a useful tool. However, it has serious shortcomings. Metals and alloys that form passive films will exhibit varying potentials with time and are therefore difficult to position in the series with certainty. Also, the galvanic series does not provide information on the polarization characteristics of the materials and so is not helpful in predicting the probable magnitude of galvanic effects.
Measurement of galvanic currents between coupled metals or alloys is based on the use of a zero-resistance milliammeter (ZRA). Zero-resistance electrical continuity between the members of the galvanic couple is maintained electronically, while the resulting current is measured with the ammeter. Use of this technique

should take into account certain limitations. First, when localized corrosion such as pitting or crevice corrosion is possible in the galvanic couple, long induction periods may be required before these effects are observed. Test periods must be of sufficient duration to take this effect into account. Also, the measured galvanic current is not always a true measure of the actual corrosion current, because the galvanic current is the algebraic sum of the currents due to anodic and cathodic reactions. When cathodic currents are appreciable at the mixed potential of the galvanic couple, the measured galvanic current is significantly lower than the true corrosion current. Large differences between the true corrosion rate calculated by mass loss and that obtained by galvanic current measurements have been observed.

Polarization measurements on the members of a galvanic couple can provide precise information concerning their behavior. The polarization curves and the mixed potential for the galvanically coupled metals in a particular environment can be used to determine the magnitude of the galvanic-corrosion effects as well as the type of corrosion.

An important application in the use of polarization measurements in galvanic corrosion is the prediction of localized corrosion. Polarization techniques and critical potentials are used to measure the susceptibility to pitting and crevice corrosion of metals and alloys coupled in chloride solutions. In addition, this technique is valuable in predicting galvanic corrosion among three or more coupled metals or alloys.

R. Baboian, Galvanic Corrosion, *Corrosion: Fundamentals, Testing, and Protection*, Vol 13A, *ASM Handbook*, ASM International, 2003, p 210–213

Galvanic Corrosion

Robert Baboian, RB Corrosion Service

Performance of Alloy Groupings

Light Metals. Magnesium occupies an extremely active position in most galvanic series and is therefore highly susceptible to galvanic corrosion. It is widely used as a sacrificial anode in cathodic protection.

Aluminum and its alloys also occupy active positions in the galvanic series and are subject to failure by galvanic attack (Fig. 2, 3). In chloride-bearing solutions, aluminum alloys are susceptible to galvanically induced localized corrosion, especially in dissimilar-metal crevices. In this type of environment, severe galvanic effects are observed when aluminum alloys are coupled with more noble metals and alloys. Cementation effects are also observed in the presence of dissolved heavy-metal ions such as copper, mercury, or lead. Some aluminum alloys are used for sacrificial anodes in seawater. An active, anodic alloy is used to clad aluminum, protecting it against pitting in some applications.

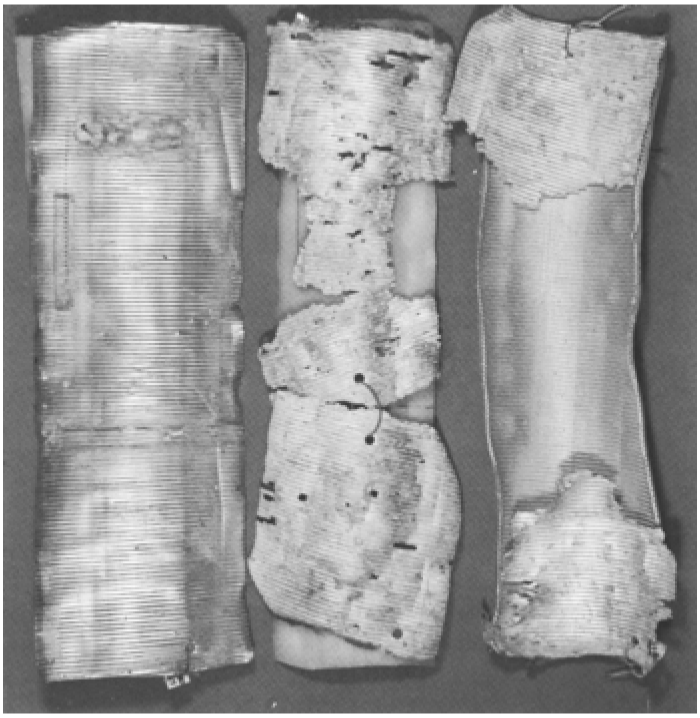

Fig. 2 Galvanic corrosion of aluminum shielding in buried telephone cable coupled to buried copper plates. Courtesy of R. Baboian, Texas Instruments, Inc.

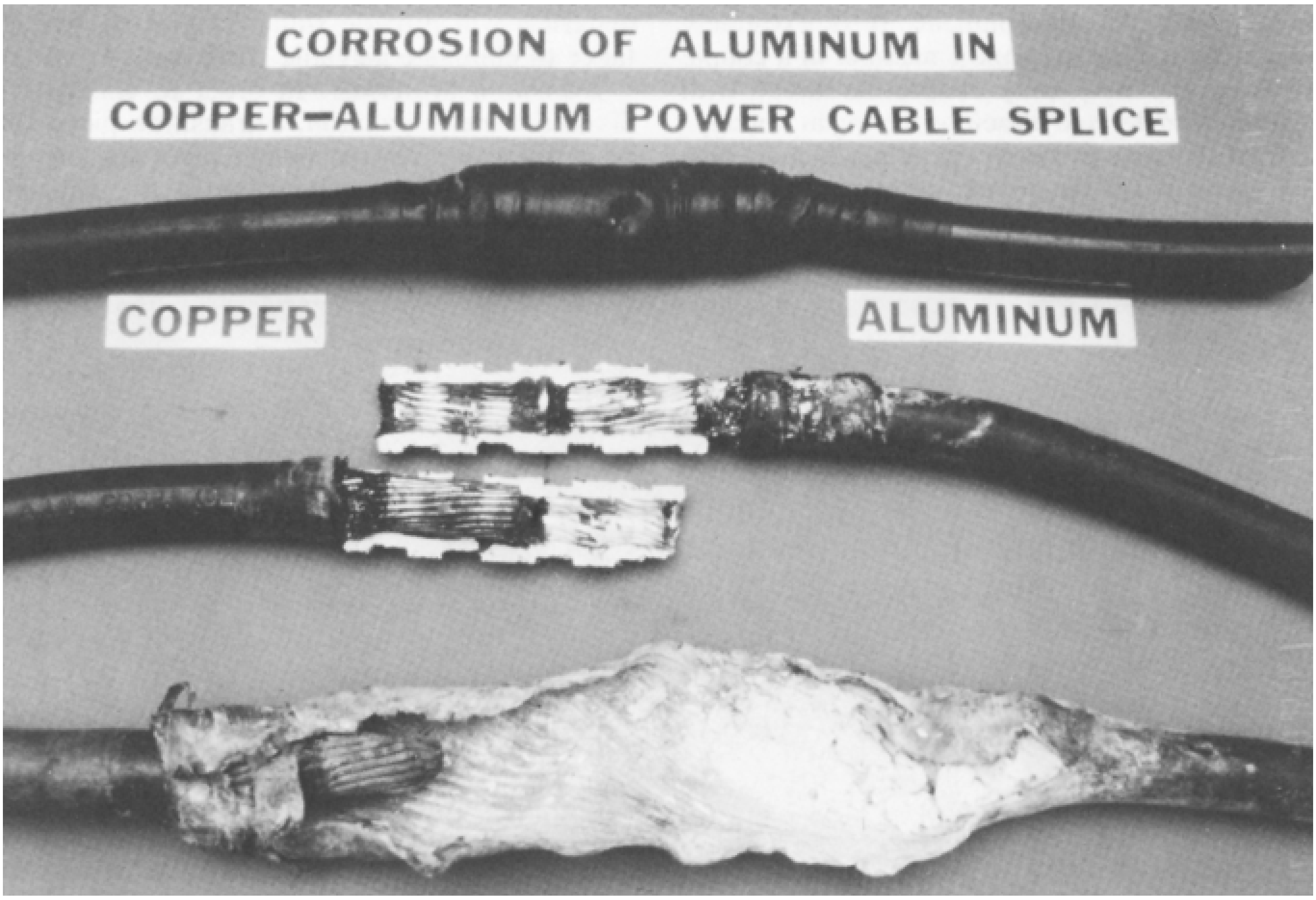

Fig. 3 Galvanic corrosion of aluminum in buried power cable splice (copper to aluminum). Courtesy of R. Baboian, Texas Instruments, Inc.

In the absence of chlorides or when chloride concentrations are low (as in potable water), aluminum and its alloys may be less active because of greater stability of the protective oxide film. Galvanic effects are not as severe under these conditions.
Iron and steel are fairly active materials and require protection against galvanic corrosion by less active, more noble, alloys. They are, however, more noble than aluminum and its alloys in chloride solutions. However, a reversal of potential can occur in low-chloride waters, which causes iron or steel to become more active than aluminum. A similar reversal can occur between iron and zinc in hot waters of a specific type of chemistry. Examples of galvanic corrosion of iron and steel are shown in Fig. 4 and 5.

Fig. 4 Galvanic corrosion of painted steel auto body panel in contact with stainless steel wheel opening molding. Courtesy of R. Baboian, Texas Instruments, Inc.

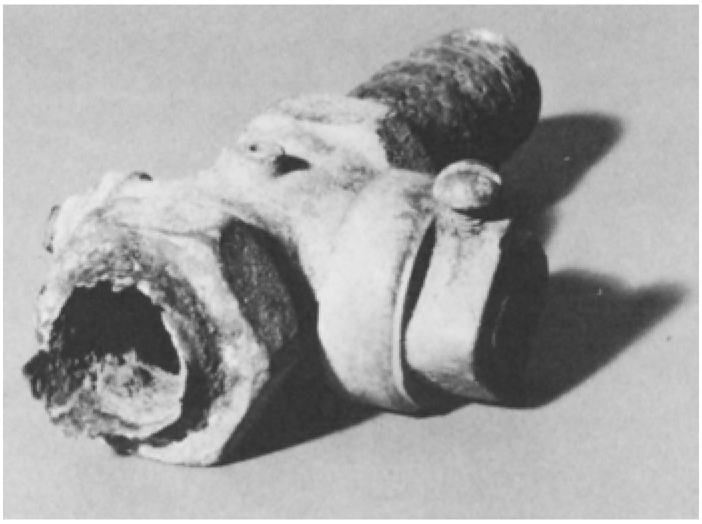

Fig. 5 Galvanic corrosion of steel pipe at brass fitting in humid marine atmosphere. Courtesy of R. Baboian, Texas Instruments, Inc.

Stainless Steels. Galvanic corrosion behavior of stainless steels is difficult to predict because of the influence of passivity. In the common galvanic series, a noble position is assumed by stainless steels in the passive state, while a more active position is assumed in the active state (Table 1). This dual position in galvanic series in chloride-bearing aqueous environments has been the cause of some serious design errors. More precise information on the galvanic behavior of stainless steels can be obtained by using polarization curves, critical potentials, and the mixed potential of the galvanic couple. In chloride-containing environments, galvanically induced localized corrosion of many stainless steels occurs in couples with copper or nickel and their alloys and with other more noble materials. However, couples of stainless and copper alloys are often used with impunity in freshwater cooling systems. Iron and steel tend to protect stainless steel in aqueous environments when galvanically coupled. The passive behavior of stainless steels makes them easy to polarize; thus, galvanic

effects on other metals or alloys tend to be minimized. However, galvanic corrosion of steel can be induced by stainless steels, particularly in aqueous environments and with adverse area ratios.

Lead, Tin, and Zinc. These three materials occupy similar positions in the galvanic series, although zinc is the most active. The oxide films formed on these materials can shift their potentials to more noble values. Thus, in some environments, they may occupy more noble positions than one might otherwise expect. For example, the tin coating in tin cans is anodic to steel under anaerobic conditions in the sealed container but becomes cathodic when the can is opened and exposed to air. Zinc is an active metal. It is susceptible to galvanic corrosion and is widely used for galvanic anodes in cathodic protection as a sacrificial coating (for example, galvanizing or electroplating) and as a metallic pigment in certain paints and coatings.

Copper Alloys. Copper and its alloys occupy an intermediate position in the galvanic series. They are not readily polarized in chloride-bearing aqueous solutions; therefore, they cause severe accelerated corrosion of more active metals, such as aluminum and its alloys and the ferrous metals. Somewhat similar to the nickel alloys, they lie between the active and passive positions for stainless steels (Table 1) and therefore induce localized corrosion of the active alloys.

Nickel Alloys. Nickel and its alloys are not readily polarized and therefore cause accelerated corrosion of more active materials, such as aluminum and ferrous alloys. In chloride-containing solutions, nickel is somewhat more noble than copper, and the cupronickels lie somewhere in between. Nickel and its alloys are similar to copper alloys in their effects on stainless steels. In some environments, the cast structure of a nickel weld may be anodic to the wrought parent metals.

The combination of a passive surface with the inherent corrosion resistance of nickel-chromium alloys, such as Inconel alloy 600 and Hastelloy alloy C-276, places them in more noble positions in the traditional galvanic series. In chloride-bearing solutions, Inconel alloy 600 is reported to occupy two positions because of the existence of active and passive states in a manner similar to stainless steels (Table 1). These alloys are readily polarized, and galvanic effects on other less noble metals and alloys therefore tend to be minimized.

Cobalt-base alloys, most of which are chromium bearing, are resistant to galvanic corrosion because of their noble position in the galvanic series. However, in environments in which their passive film is not stable, they occupy a more active position and can be adversely affected by more noble materials. The fact they they polarize readily tends to reduce their galvanic effects on less noble materials.

Reactive Metals. Titanium, zirconium, and tantalum are extremely noble because of their passive films. In general, these alloys are not susceptible to galvanic corrosion, and their ease of polarization tends to minimize adverse galvanic effects on other metals or alloys. Because of the ease with which they pick up hydrogen in the atomic state, they may themselves become embrittled in galvanic couples. Tantalum repair patches in glass-lined vessels have been destroyed by contact with cooling coils or agitators made of less noble alloys. Tantalum is susceptible to attack by alkalies, such as may form in the vicinity of a cathode in neutral solutions.

Noble Metals. The term *noble metal* is applied to silver-, gold-, and platinum-group metals. This designation in itself describes their position in the galvanic series and their corresponding resistance to galvanic corrosion. However, they do not polarize readily and can therefore have a marked effect in galvanic couples with other metals or alloys. This effect is observed with gold and silver coatings on copper, nickel, aluminum, and their alloys.

R. Baboian, Galvanic Corrosion, *Corrosion: Fundamentals, Testing, and Protection*, Vol 13A, *ASM Handbook*, ASM International, 2003, p 210–213

Galvanic Corrosion

Robert Baboian, RB Corrosion Service

Methods of Control

Materials Selection. Combinations of metals or alloys widely separated in the relevant galvanic series should be avoided unless the more noble material is easily polarized. Metallic coatings can be used to reduce the separation in the galvanic series, as described subsequently.

Environmental Control. In particular cases, it is possible to reduce or eliminate galvanic-corrosion effects between widely dissimilar metals or alloys in a particular environment. The use of corrosion inhibitors is effective in some cases. Elimination of cathodic depolarizers such as oxygen (deaeration of water by thermomechanical means plus oxygen scavengers such as sodium sulfite or hydrazine) is every effective in some aqueous systems.

Barrier coatings of a metallic nature have already been discussed. Inert barrier coatings, organic or vitreous, can effectively isolate the metals from the environment. It is extremely dangerous to coat the anodic member of a couple, because this only reduces its area to the holiday in the coating, with severely accelerated localized attack occurring at the holidays in the otherwise protective coating. If inert barrier coatings are employed, both the anode and cathode must be protected—for example, the heads, tubesheets, and tubes (for a distance of the first 4 to 6 tube diameters on the tube side) of a water- cooled heat exchanger.

Electrochemical techniques are comprised of three alternative methodologies: electrical isolation, use of transition materials, and cathodic protection.

Electrical Isolation. The joint between dissimilar metals can be isolated to break the electrical continuity. Use of nonmetallic inserts, washers, fittings, and coatings at the joint between the materials will provide sufficient electrical resistance to eliminate galvanic corrosion.

Transition Materials. In order to eliminate a dissimilar-metal junction, a transition piece can be introduced. The transition piece consists of the same metals or alloys as in the galvanic couple bonded together in a laminar structure. The transition piece is inserted between the members of the couple such that the similar metals mate with one another. The dissimilar-metal junction then occurs at the bond interface, excluding the electrolyte.

Cathodic Protection. Sacrificial metals, such as magnesium or zinc, may be introduced into the galvanic assembly. The most active member will corrode while providing cathodic protection to the other members in the galvanic assembly (for example, zinc anodes in cast iron waterboxes of copper alloy water-cooled heat exchangers). Impressed-current systems can provide the same effect.

Design. Unfavorable area ratios should be avoided. Metal combinations should be used in which the more active metal or alloy surface is relatively large. Rivets, bolts, and other fasteners should be of a more noble metal than the material to be fastened. Dissimilar-metal crevices, such as at threaded connections, are to be avoided. Crevices should be sealed, preferably by welding or brazing, although putties are sometimes used effectively. Replaceable sections of the more active member should be used at joints, or the corrosion allowance of this section should be increased, or both.

R. Baboian, Galvanic Corrosion, *Corrosion: Fundamentals, Testing, and Protection*, Vol 13A, *ASM Handbook*, ASM International, 2003, p 210–213

Galvanic Corrosion

Robert Baboian, RB Corrosion Service

Acknowledgment

This article is based on one by Robert Baboian and Steven L. Pohlman, Galvanic Corrosion, in *Corrosion,* Volume 13, *Metals Handbook,* 9th ed., ASM International, 1987, pages 83–87. We thank Robert Baboian for reviewing this article for this edition.

R. Baboian, Galvanic Corrosion, *Corrosion: Fundamentals, Testing, and Protection*, Vol 13A, *ASM Handbook*, ASM International, 2003, p 210–213

Galvanic Corrosion

Robert Baboian, RB Corrosion Service

Selected References

- R. Baboian, Ed., *Corrosion Tests and Standards*, ASTM International, 1995
- R. Baboian, Galvanic Corrosion, *Forms of Corrosion-Recognition and Prevention*, C.P. Dillon, Ed., NACE International, 1982
- V. Chaker, Ed., Corrosion Effect of Stray Currents and the Techniques for Evaluating Corrosion of Rebars in Concrete, *Corrosion of Rebars in Concrete*, STP 906, American Society for Testing and Materials, 1984
- H.P. Hack, *Galvanic Corrosion Test Methods*, NACE International, 1993
- X.G. Zhang, Galvanic Corrosion, *Uhlig's Corrosion Handbook*, R.W. Revie, Ed., Wiley, 2000

H.R. Hanson, Stray-Current Corrosion, *Corrosion: Fundamentals, Testing, and Protection*, Vol 13A, *ASM Handbook*, ASM International, 2003, p 214–215

Stray-Current Corrosion

Revised by Harry R. Hanson, Bay Engineering, Inc.

Introduction

STRAY-CURRENT CORROSION is caused by an externally induced electrical current. Examples of this situation are commonly observed in rail transit systems, pipeline systems, and electric distribution systems (Ref 1, 2, 3). Detailed technical presentations of stray current corrosion can be found in the literature (Ref 4, 5, 6).

Stray currents (or interference currents) are defined as those currents that follow paths other than their intended circuit. Unfortunately, nearly all stray current discharges are very local and concentrated, ensuring accelerated corrosion will occur. They leave their intended path because the current finds a path with lower resistance, such as a buried metal pipe, some other metal structure, or an electrolyte with low resistance such as salt water. The current then flows to and from that structure and causes accelerated corrosion whenever it leaves a metallic structure and flows into an electrolyte.

For example, in a pipeline that is cathodically protected, if a foreign pipeline crosses or passes close to the protected pipeline, current from the cathodic protection system can gather onto the foreign pipeline and then be discharged from the foreign line when it crosses *or comes close to* the protected pipeline. This is particularly true in higher resistivity soil. Accelerated corrosion occurs on the foreign line at the point of current discharge. The location of the discharge can be detected because the pipe-to-soil potential is very low at that point.

Likewise in an oil or gas field, where the flowline system or the well casings from several wells are being protected using a centrally located rectifier and ground bed, the path of lowest resistance is usually to the nearest well, down the well casing until a low-resistant formation containing salt water is encountered. The current then travels through the salt-water formation to the other more remote wells in the field where it travels up the well casing to the flowline and then returns to the rectifier. Accelerated corrosion occurs on the well casings of the close wells where current is discharged from the casing to the formation. This corrosion is

extremely difficult to detect and is very expensive to correct. It can cause a blowout in the well to occur because of the corroded casing and can result in a fire or spill.
Insulating flanges can cause corrosion from stray currents. Usually the insulating flange is separating pipes that have different ownership or different levels of cathodic protection. If current collects on the pipeline downstream of the protected pipeline, this current may flow back to the insulated flange, discharge into the earth on one side of the flange, and flow to the other side of the flange that is connected to the protected pipeline. Corrosion occurs where the current discharges from the unprotected, downstream pipeline.

References cited in this section

1. M.J. Szeliga, "Rail Transit Stray Current Control: Then and Now," Paper 592, presented at Corrosion/93 (Houston, TX), NACE International, Inc., March 1993

2. F.A. Perry, "A Review of Stray Current Effects on a Gas Transmission Main in the Boston, Massachusetts Area," Paper 590, presented at Corrosion/94 (Houston, TX), NACE International, Inc., March 1994

3. J. Dabkowski, "A Review of AC Power Line Couponing unto Buried Pipelines," Paper 561, presented at Corrosion/98 (Houston, TX), NACE International, Inc., March 1998

4. M.G. Fontana and N.D. Greene, *Corrosion Engineering,* 2nd ed., McGraw-Hill, 1978

5. J. Morgan, *Cathodic Protection,* 2nd ed., NACE International, Inc., The Corrosion Society, 1993

6. A.W. Peabody, *Control of Pipeline Corrosion,* 2nd ed., NACE International, Inc., The Corrosion Society, 2001

H.R. Hanson, Stray-Current Corrosion, *Corrosion: Fundamentals, Testing, and Protection*, Vol 13A, *ASM Handbook*, ASM International, 2003, p 214–215

Stray-Current Corrosion

Revised by Harry R. Hanson, Bay Engineering, Inc.

Sources of Stray Currents

Almost any electrical systems that use grounds or grounding in their system can create stray direct current (dc) problems. In the past, electric railways were a major source of stray dc. This source became less common with the diminished use of electric rail systems, but modern urban/suburban transit systems still rely on electric light-rail systems. Stray-current control is a factor in the rehabilitation of electrified railways for urban/suburban transit systems (Ref 7) and in the development of improved materials and design techniques for stray-current control of electrified rail systems. Improvements include special insulation methods for rail systems (Ref 8) and the use of special materials and design techniques for the embedment of track in the congested downtown portion of the system to achieve levels of track-to-earth isolation (Ref 9).
In one case, extensive testing was performed on existing water piping in the vicinity of a light- rail transit system to assess the conditions on existing utility piping (Ref 10). Stray-current corrosion can readily be detected by taking pipe- to-soil potentials. Stray-current corrosion can usually be determined by studying the location and size of all the facilities in a system and their proximity to foreign structures.
Other important sources of stray current include cathodic protection systems, electrical welding machines, and other grounded dc electric sources. Stray currents are frequently encountered problems in cathodic-protection

systems. Figure 1(a) shows an arrangement in which stray currents were produced when the owner of a buried tank installed cathodic protection, not knowing of the presence of a nearby pipeline. The pipeline rapidly failed by corrosion because of the stray currents. If the pipeline had been cathodically protected, stray-current attack could have caused the buried tank to fail. The stray-current problem shown in Fig. 1(a) was corrected by electrically connecting the tank and the pipeline by an insulated buss connection and by installing a second anode (Fig. 1b). Thus, both pipe and tank were protected without stray- current effects.

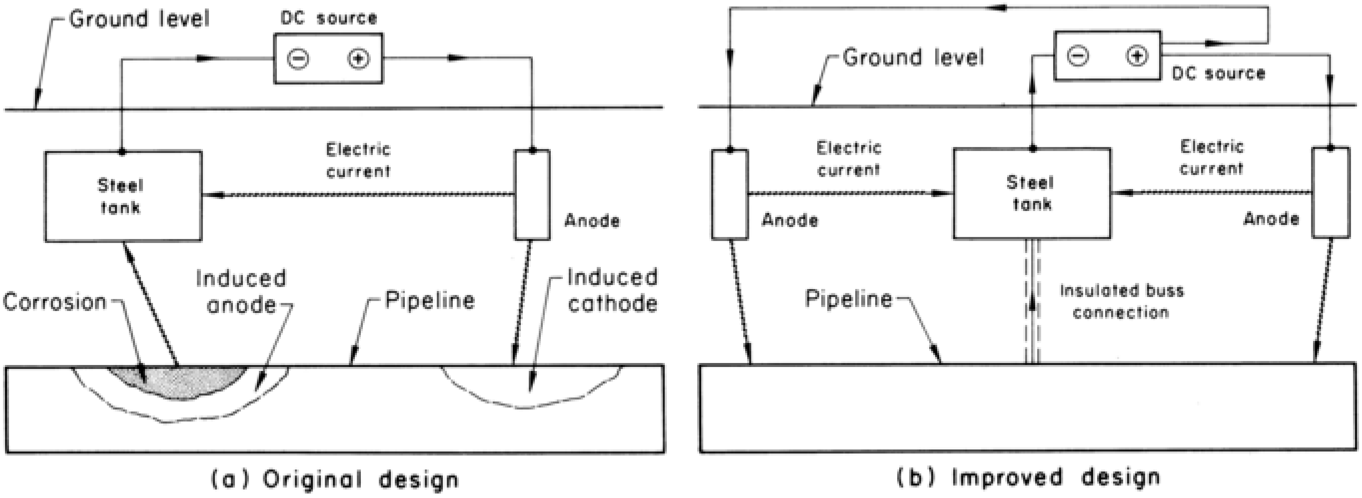

Fig. 1 Cathodic-protection system for a buried steel tank. (a) The original design that caused local failure of a nearby unprotected buried pipeline by stray-current corrosion. (b) Improved design. Installation of a second anode and an insulated buss connection provided protection for both tank and pipeline, preventing stray currents.

In another example, an on-board electric welding machine can create stray currents in a ship and can cause accelerated attack of the hull of the ship as the stray currents generated at the welding electrodes pass out of the hull through the water back to a grounded dc line located on shore. Work boats or construction barges that do welding of structures or pipelines in the water are always careful to ensure that grounds to the vessel make the vessel more negative and are essentially furnishing cathodic protection to the work vessel. If the grounds are not carried to the structure being constructed, it will cause severe stray-current damage to the structure. Another example is a steel-hulled vessel that is moored to a dock facility that is cathodically protected. The cathodic protection system on the dock can cause stray current damage to the vessel.

Stray currents cause accelerated corrosion to occur where they leave the metal structure and enter the surrounding electrolyte. The site where the current enters the structure will become cathodic in nature, while the site where the current leaves the metal will become anodic. These sites may be hundreds of yards apart. Stray current flowing along a pipeline typically will not cause damage inside the pipe, because of the high conductivity of the metal compared to the fluid in the pipe. However, internal corrosion can occur if an insulating flange is placed in the pipeline and the fluid stream (such as salt water) is highly conductive. In this case, the damage occurs at the point where the current enters the electrolyte from within the pipe. If the pipe is carrying a low resistivity fluid and is also buried, corrosion can occur on both the internal and external surface of the pipeline.

Stray currents are usually thought of as being dc currents. However, severe damage can be also caused by alternating currents (ac). Alternating currents are induced onto pipelines that run parallel and close to power lines. Alternating-current corrosion is less severe as the frequency increases. Stray-ac corrosion is also less severe if the pipeline is laid in clay soils containing high ion contents but can be severe if the pipeline is laid in high-resistivity sandy soils. Alternating currents induced in active-passive metals, such as stainless steel, can destroy the passivity of the metal, causing it to lose its corrosion resistance. Alternating reduction and oxidation of the surface layers resulting from the induced ac causes the passive layers to become porous and layered. Unlike dc stray-current corrosion, induced-ac corrosion cannot be mitigated by adjusting the pipe to soil potential of the pipe. It is controlled by removing the ac from the pipeline and flowing the current to earth via ground beds or zinc anodes.

References cited in this section

7. J.H. Fitzgerald III, R. Bosma, and F. Paladines, Building Stray Current Control into the Rehabilitation of an Old Transit Yard and Shop Facility in a Large Urban Area, *CORROSION 98*, NACE International, Inc., 1998, p 558/1-558/13

8. D. Galler and P.L. Todd, Improved Rail-Fastener Insulation for Stray-Current Control, *Corrosion Forms & Control for Infrastructure*, STP 1137, ASTM International, 1992, p 170–182

9. S.R. Farnsworth and N.J. Moriber, Portland's Light Rail System: Control of Stray Currents at the Source, *Mater. Perform.*, Vol 29 (No. 7), July 1990, p 19–25

10. M.J. Szeliga and J Silhan, "New Developments in the Collection of Stray Current Field Data," Paper 582, 1994, p 9

H.R. Hanson, Stray-Current Corrosion, *Corrosion: Fundamentals, Testing, and Protection*, Vol 13A, *ASM Handbook*, ASM International, 2003, p 214–215

Stray-Current Corrosion

Revised by Harry R. Hanson, Bay Engineering, Inc.

Prevention of Stray-Current Corrosion

There are several ways to prevent damage from stray currents. Foremost, the flow or leakage of current from the metal to an electrolyte (the ground) should be stopped. This is done by a method called bonding, which removes the stray current via a separate conductor. Bonding consists of connecting the stray-current conductor to the protected conductor with a wire, thus eliminating the need for the current to leave the metal and enter the soil. If both lines have cathodic protection systems, the bonding of the two lines can be achieved via an adjustable resistor. The amount of current can then be adjusted so that the pipe-to-soil potentials of each line are similar. Often the resistance of the bonding wire is adjusted so that the potential of either line is not changed when the rectifiers are cycled on and off.

Sacrificial anodes can also be used to prevent stray current corrosion. By connecting galvanic anodes to the unprotected pipeline that is being damaged by stray currents, the potential of the unprotected line can be changed and made equal to the protected line at the point of crossing. If the two lines have the same potential, there is no reason for the currents to leave one line for the other, and stray currents are eliminated. Pipe coatings used without cathodic protection are not an effective way to control stray current problems. Coating on lines that also are cathodically protected are beneficial and usually make the problems of stray currents less severe and more easily controlled.

H.R. Hanson, Stray-Current Corrosion, *Corrosion: Fundamentals, Testing, and Protection*, Vol 13A, *ASM Handbook*, ASM International, 2003, p 214–215

Stray-Current Corrosion

Revised by Harry R. Hanson, Bay Engineering, Inc.

Acknowledgment

This article has been adapted from the article by Steven L. Pohlman, Stray-Current Corrosion, *Corrosion,* Vol 13, *ASM Handbook* (formerly 9th ed. *Metals Handbook*), ASM International, 1987, p 87.

H.R. Hanson, Stray-Current Corrosion, *Corrosion: Fundamentals, Testing, and Protection,* Vol 13A, *ASM Handbook,* ASM International, 2003, p 214–215

Stray-Current Corrosion

Revised by Harry R. Hanson, Bay Engineering, Inc.

References

1. M.J. Szeliga, "Rail Transit Stray Current Control: Then and Now," Paper 592, presented at Corrosion/93 (Houston, TX), NACE International, Inc., March 1993
2. F.A. Perry, "A Review of Stray Current Effects on a Gas Transmission Main in the Boston, Massachusetts Area," Paper 590, presented at Corrosion/94 (Houston, TX), NACE International, Inc., March 1994
3. J. Dabkowski, "A Review of AC Power Line Couponing unto Buried Pipelines," Paper 561, presented at Corrosion/98 (Houston, TX), NACE International, Inc., March 1998
4. M.G. Fontana and N.D. Greene, *Corrosion Engineering,* 2nd ed., McGraw-Hill, 1978
5. J. Morgan, *Cathodic Protection,* 2nd ed., NACE International, Inc., The Corrosion Society, 1993
6. A.W. Peabody, *Control of Pipeline Corrosion,* 2nd ed., NACE International, Inc., The Corrosion Society, 2001
7. J.H. Fitzgerald III, R. Bosma, and F. Paladines, Building Stray Current Control into the Rehabilitation of an Old Transit Yard and Shop Facility in a Large Urban Area, *CORROSION 98,* NACE International, Inc., 1998, p 558/1-558/13
8. D. Galler and P.L. Todd, Improved Rail-Fastener Insulation for Stray-Current Control, *Corrosion Forms & Control for Infrastructure,* STP 1137, ASTM International, 1992, p 170–182
9. S.R. Farnsworth and N.J. Moriber, Portland's Light Rail System: Control of Stray Currents at the Source, *Mater. Perform.,* Vol 29 (No. 7), July 1990, p 19–25
10. M.J. Szeliga and J Silhan, "New Developments in the Collection of Stray Current Field Data," Paper 582, 1994, p 9

H.R. Hanson, Stray-Current Corrosion, *Corrosion: Fundamentals, Testing, and Protection*, Vol 13A, *ASM Handbook*, ASM International, 2003, p 214–215

Stray-Current Corrosion

Revised by Harry R. Hanson, Bay Engineering, Inc.

Selected References

- V. Chaker, Ed., Corrosion Effect of Stray Currents and the Techniques for Evaluating Corrosion of Rebars in Concrete, *Corrosion of Rebars in Concrete,* STP 906, ASTM International, 1984
- M.G. Fontana and N.D. Greene, *Corrosion Engineering,* 2nd ed., McGraw-Hill, 1978
- J. Morgan, *Cathodic Protection,* 2nd ed., NACE International, Inc., The Corrosion Society, 1993
- A.W. Peabody, *Control of Pipeline Corrosion,* 2nd ed., NACE International, Inc., The Corrosion Society, 2001

R.D. Kane, Molten Salt Corrosion, *Corrosion: Fundamentals, Testing, and Protection*, Vol 13A, *ASM Handbook*, ASM International, 2003, p 216–219

Molten Salt Corrosion

Revised by Russell D. Kane, InterCorr International, Inc.

Introduction

THE CORROSION of metal containers by molten, or fused, salts has been observed for an extended period of time, but over the last several decades, more effort has been directed toward understanding corrosion phenomena at higher temperatures. Annotated bibliographies of molten salt corrosion for different media and metal combinations have been published and are cited in the Selected References for this article. Additional information on molten salt corrosion can be found in the articles “Molten Salt Corrosion Thermodynamics” and “Corrosion by Molten Salts” in this Volume.

R.D. Kane, Molten Salt Corrosion, *Corrosion: Fundamentals, Testing, and Protection*, Vol 13A, *ASM Handbook*, ASM International, 2003, p 216–219

Molten Salt Corrosion

Revised by Russell D. Kane, InterCorr International, Inc.

Mechanisms of Molten Salt Corrosion

Two general mechanisms of corrosion can exist in molten salts. One is the metal dissolution caused by the solubility of the metal in the melt. This dissolution is similar to that in molten metals but is not common. The second and most common mechanism is the oxidation of the metal to ions, a mechanism similar to aqueous

corrosion. For this reason, molten salt corrosion has been identified as an intermediate form of corrosion between molten metal and aqueous corrosion.

General, or uniform, metal oxidation and dissolution is a common form of molten salt corrosion but is not the only form of corrosion seen. Selective leaching is very common at higher temperatures, as are pitting and crevice corrosion at lower temperatures. All the forms of corrosion observed in aqueous systems, including stress-assisted corrosion, galvanic corrosion, erosion-corrosion, and fretting corrosion, have been seen in fused salts.

Electrochemically, the molten salt/metal surface interface is very similar to the aqueous solution/metal surface interface. Many of the principles that apply to aqueous corrosion, such as anodic reactions leading to metal dissolution and cathodic reduction of an oxidant, also apply to molten salt corrosion. Based on this concept, recent studies have been successful in using electrochemical test methods commonly used in aqueous solutions (e.g., electrochemical noise, linear polarization, and harmonic distortion analysis) to make measurements of corrosion and localization in laboratory studies. This work has even been carried on to use in commercial plant operations to help relate changes in process variables to periodic conditions of accelerated corrosion (Ref 1).

The concept of acid and base behavior of the melt is very similar to that of its aqueous counterpart. The corrosion process is mainly electrochemical in nature because of the excellent ionic conductivity of most molten salts. Some investigators feel that dissolved water enhances the electrochemical corrosion nature of the molten salts.

Even though the corrosion mechanism is similar, there are major differences between molten salt and aqueous corrosion. The differences arise mainly from the fact that molten salts are partially electronic conductors as well as ionic conductors. This fact allows for reduction reactions to take place in the melt as well as at the metal-melt interface. This behavior also allows increase in frequency of cathodic reactions and can therefore lead to a substantial increase in corrosion rate over a similar electrochemically controlled aqueous system, especially if the corrosion media contain very few oxidants. Because of property differences between water and molten salt, the rate-controlling step in most molten metal systems is ion diffusion into the bulk solution, not the charge transfer reaction that is typical of aqueous systems. Molten salt systems operate at higher temperatures than aqueous systems, which leads to different forms of corrosion attack. Electrochemical measurements have highlighted these differences between aqueous and molten salt environments, particularly in terms of characterizing their polarization through the classical Stern-Geary relationship. Values obtained in a molten salt system tend to be much different than those observed in an aqueous system, brought about by the simultaneous presence of many ionic species and the combined ionic and electronic conduction mechanisms in molten salts. However, use of these techniques has resulted in meaningful measurement of corrosion rates that correlate with actual mass losses in system components in combustion environments (Fig. 1, 2).

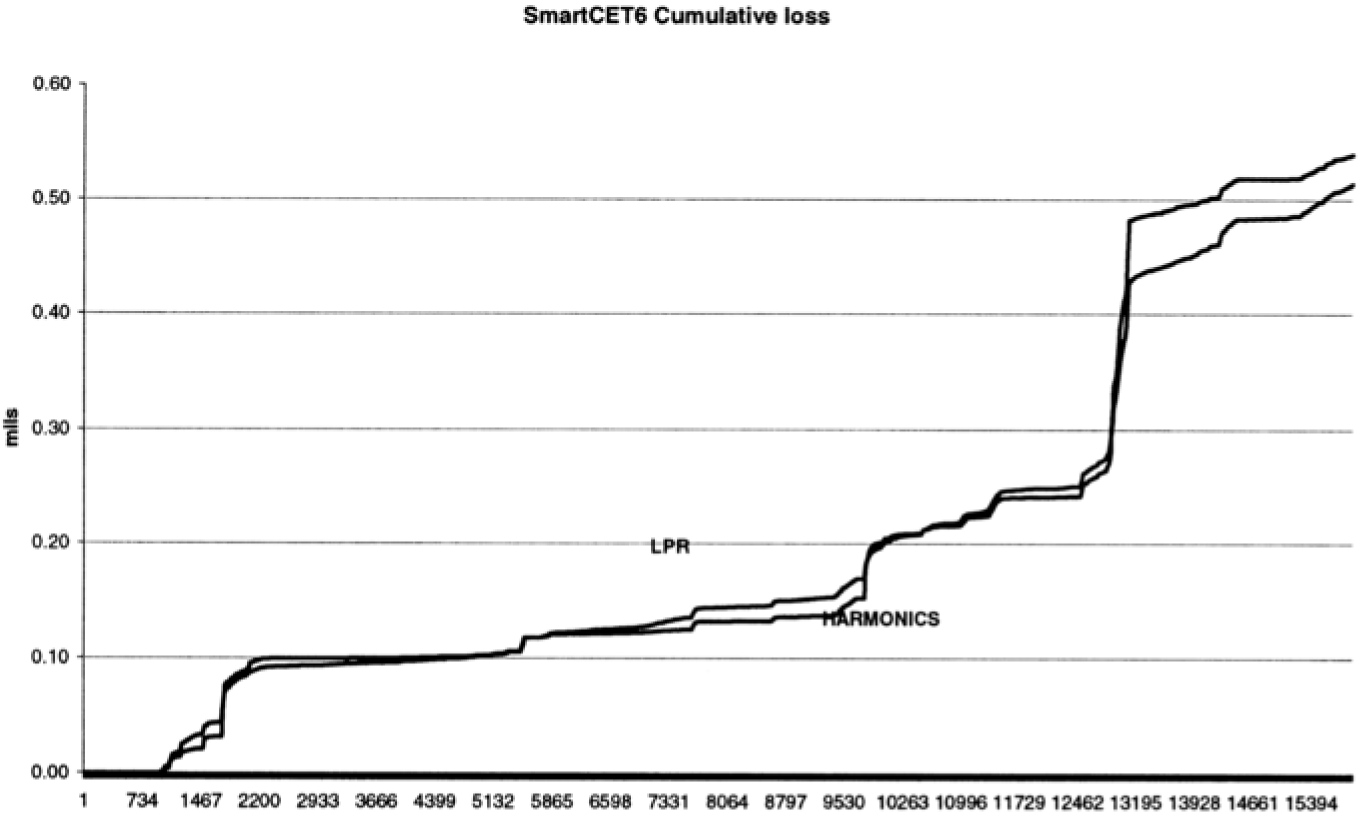

Fig. 1 Cumulative-loss data from electrochemical measurements in molten slag. LPR, linear polarization resistance; harmonics, harmonic distortion analysis (HDA). Source: Ref 1

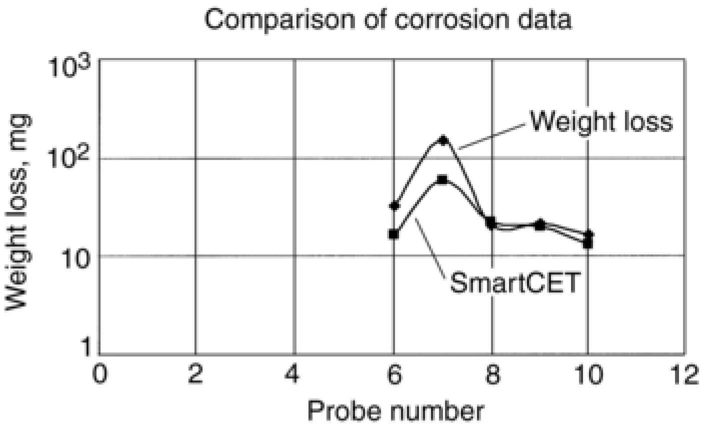

Fig. 2 Comparison of weight-loss data from electrochemical measurements in molten slag. Weight loss is from test coupons. SmartCET is a real-time corrosion-monitoring system (InterCorr International, Inc.). Field measurements were made on the fireside of a coal fueled boiler. Source: Ref 1

In aqueous systems in which specific elements are removed from alloys, such as the dezincification of zinc from brass, it is not clear whether the nobler element is oxidized at some stage in the process and is subsequently plated out or whether the element agglomerates by a surface diffusion mechanism. In both cases, bulk diffusion is unlikely to play a major role. In high-temperature molten salt systems, dissolution of the less noble element is the most probable mechanism and even occurs when the element is present at low concentration. Unlike aqueous systems, the rate of dissolution is therefore related to the bulk diffusion of the selectively leached element.

Because molten salt corrosion reactions are reduction/oxidation controlled, the relative nobilities of the salt melts and the metals are important. The corrosion potential of the melt is often controlled by impurities in the melt or gas phase, which increases the cathodic reaction rate or changes the acidic or basic nature of the melt. The aggressiveness of the salt melts is typically governed by its redox equilibria.

Thermal gradients in the melt can cause dissolution of metal at hot spots and metal deposition at cooler spots. The result is very similar to aqueous galvanic corrosion, and, like aqueous galvanic corrosion, a continuous electrical path is necessary between the hot and cold areas. Crevice corrosion has been observed, and wash-line attack caused by oxygen concentration corrosion is not uncommon at the metal/ molten salt/air interface.

High-temperature corrosion in molten salts often exhibits selective attack and internal oxidation. Chromium depletion in Fe-Cr-Ni alloy systems can occur by the formation of a chromium compound at the surface and by the subsequent removal of chromium from the matrix, leaving a depleted zone. Thus, the selectively removed species move out, while vacancies move inward and eventually form voids. The voids tend to form at grain boundaries in most chromium-containing metals, but in some high- nickel alloys, the voids form in the grains. Specific examples of the types of corrosion expected for the different metal-fused salt systems follow.

Reference cited in this section

1. D.A. Eden, InterCorr International, Inc., private communication, 2001

R.D. Kane, Molten Salt Corrosion, *Corrosion: Fundamentals, Testing, and Protection*, Vol 13A, *ASM Handbook*, ASM International, 2003, p 216–219

Molten Salt Corrosion

Revised by Russell D. Kane, InterCorr International, Inc.

Types of Molten Salts

Molten Fluorides. Fluoride melts are important because of their consideration for nuclear reactor cooling systems. Corrosion in many fluoride molten salt melts is accelerated because protective surface films are not formed. In fact, the fluoride salts act as excellent fluxes and dissolve the various corrosion products.

Typically, nickel-base alloys show better corrosion resistance than iron-base alloys. Studies have also shown that most nickel- and iron-base alloys that contain varying amounts of chromium show void formation to varying depths. In nonisothermal flow systems, the metallic material shows void formation in the hot section and deposits in the cold section. In most alloys that contain chromium, depletion of the chromium accompanies the void formation. Analysis of the attacked metal and salt clearly shows that selective removal and outward diffusion of chromium result from oxidation by the fluoride mixture.

Inconel alloy 600 and certain stainless steels become magnetic after exposure to molten fluoride salt. This magnetism is caused by the selective removal of the chromium and the formation of a magnetic iron-nickel alloy covering the surface. The conditions of the melt need to be controlled to minimize the selective removal of the alloying elements. This control can be done by maintaining the melt in a reducing condition. Addition of beryllium metal to the melt is one way to slow the corrosion rate. Examples of microstructures of nickel-base and stainless steels as a result of exposure to molten salts are shown in Fig. 3.

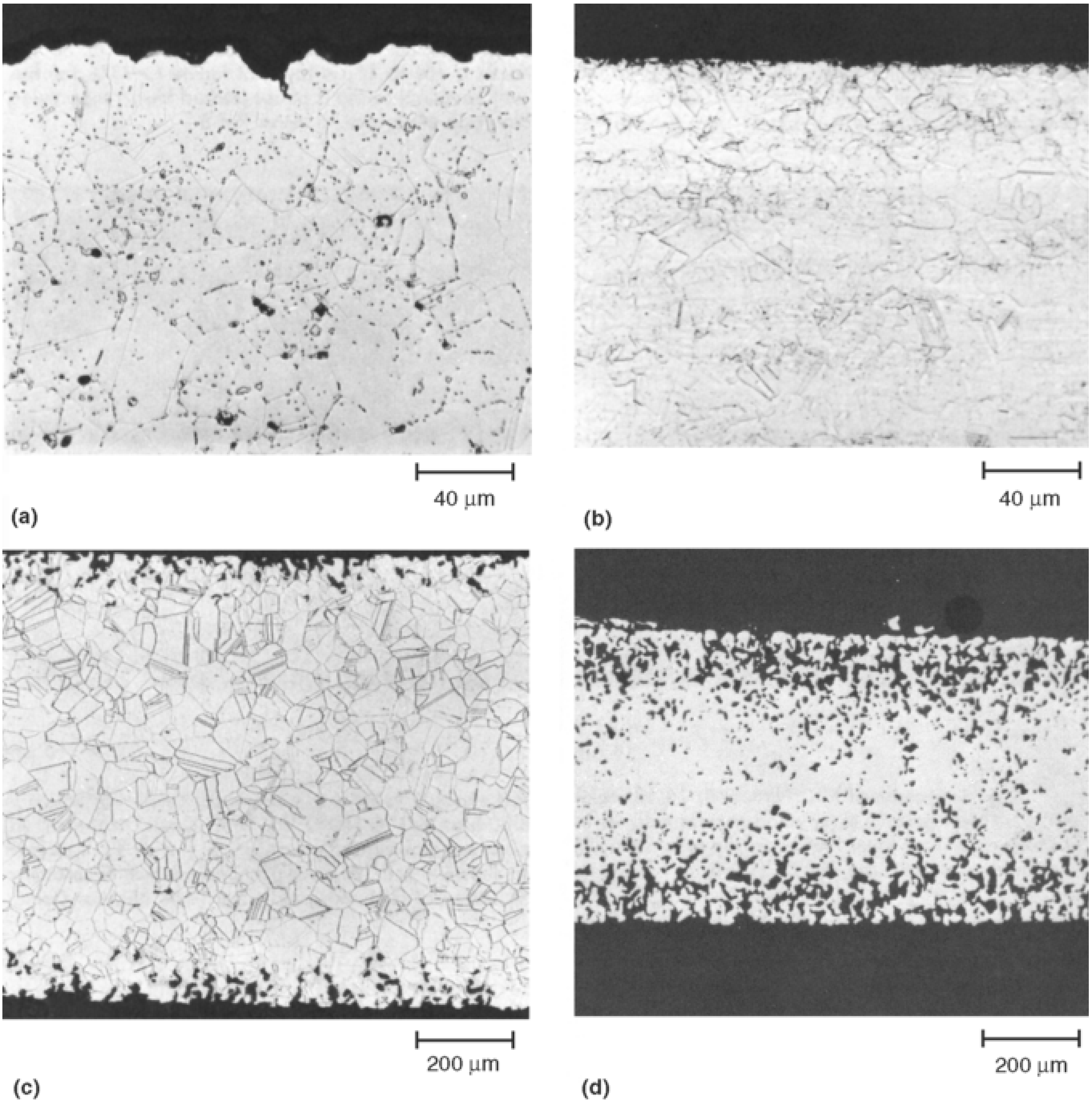

Fig. 3 Effect of molten salt corrosion on nickel-base and stainless steel alloys. In all four examples, chromium depletion (dealloying) was the result of prolonged exposure. Accompanying chromium depletion was the formation of subsurface voids, which did not connect with the surface or with each other. As chromium was leached from the surface of the metal, a concentration (activity) gradient resulted and caused chromium atoms from the underlying region to diffuse toward the surface, leaving behind a zone enriched with vacancies. These vacancies would then agglomerate at suitable sites—primarily at grain boundaries and impurities. The vacancies became visible as voids, which tended to agglomerate and grow with increasing time and temperature. (a) Microstructure of Hastelloy alloy N exposed to LiF-BeF_2-ThF_4-UF_4 (68, 20, 11.7, 0.3 mol%, respectively) for 4741 h at 700 °C (1290 °F). (b) Microstructure of Hastelloy alloy N after 2000 h exposure to LiF-BeF_2-ThF_4 (73, 2, 25 mol%, respectively) at 676 °C (1249 °F). (c) Microstructure of type 304L stainless steel exposed to LiF-BeF_2-ZrF_4-ThF_4-UF_4 (70, 23, 5, 1, 1 mol%, respectively) for 5700 h at 688 °C (1270 °F). (d) Microstructure of type 304L stainless steel exposed to LiF-BeF_2-ZrF_4-ThF_4-UF_4 (70, 23, 5, 1, 1 mol%, respectively) for 5724 h at 685 °C (1265 °F). Courtesy of J.W. Koger, Martin Marietta Energy Systems

Chloride Salts. Molten salts consisting of chlorides are important and commonly used in the heat treating industry and for batteries and fuel cells. However, they have generally been less studied than fluoride systems. Some of the many systems include:

- NaCl-KCl
- KCl-Na_2CO_3
- NaCl-KCl-$BaCl_2$
- NaCl-$BaCl_2$
- NaCl-$BaCl_2$-$CaCl_2$

and many more.

In general, chloride salts attack steels very rapidly, with preferential attack of the carbides. Aluminum coatings on steels are not effective, but the addition of nickel to steel is beneficial. Nickel-base alloys decrease in resistance with increased oxygen partial pressure. In chloride salts, no protective oxide scale is formed on nickel-base alloys. The attack of metal surfaces in pure sodium chloride has been observed at temperatures above 600 °C (1110 °F).

In most cases with Fe-Ni-Cr alloys, corrosion takes the form of intergranular attack (Fig. 4). An increase of chromium in the alloy from 10 to 30% increases the corrosion rate by a factor of 7, while changes in nickel content have no effect. Thus, the intergranular attack is most likely selective with respect to chromium. The chromium removal begins at the grain boundary and continues with diffusion of the chromium from within the grain to the boundary layer, gradually enlarging the cavity in the metal. The gross corrosive attack is probably caused by the free chlorine, which is a highly oxidizing material, attacking the highly active structure-sensitive sites, such as dislocations and grain boundaries.

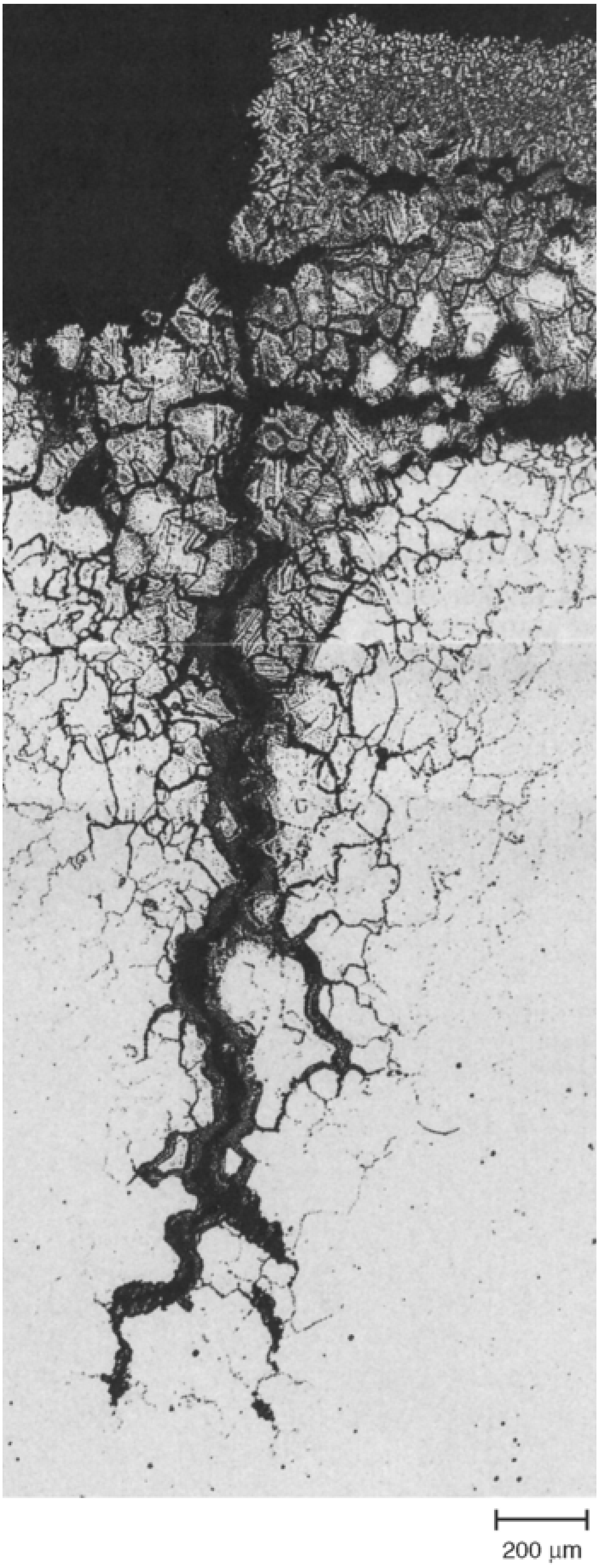

Fig. 4 Intergranular attack of a Ni-Cr-Fe alloy heat treat basket after service for six months. Source: Ref 2

Selective attack of Inconel alloy 600 is observed in molten chloride melts. The resulting attacked region is a layer of porous, spongelike material (Fig. 5). The pores are not interconnected and are typically located at the grain boundaries.

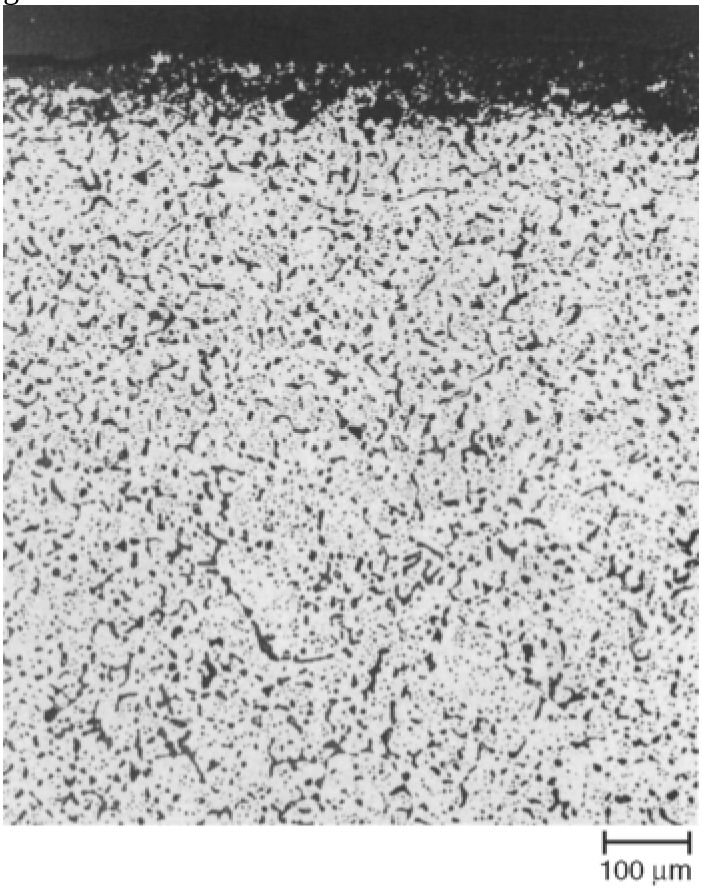

Fig. 5 Corrosion attack in a nickel-base alloy after two months at 870 °C (1600 °F) in a molten $BaCl_2$ salt bath. Source: Ref 2

Intergranular attack and rapid scale growth occur with zirconium alloys over 300 °C (570 °F). Platinum can be protected by the addition of oxide ions to the melt; this addition assists in the formation of a passive film.

Molten nitrates are commonly used for heat treatment baths; therefore, a great deal of material compatibility information exists. Plain carbon and low-alloy steels form protective iron oxide films that effectively protect the metal surface to approximately 500 °C (930 °F). Chromium additions increase the corrosion resistance of the steel, and hydroxide additions to the melt further increase the resistance of chromium-containing steels. Aluminum and aluminum alloys should never be used to contain nitrate melts, because of the danger of explosion.

Molten Sulfates. High-temperature alloys containing chromium perform well in sulfate salts because they form a protective scale. If the chromium content is not sufficient, the alloy suffers severe external corrosion and internal sulfidation. Non-film-forming metals, such as copper and silver, corrode very rapidly.

Hydroxide Melts. Stainless steels perform poorly in hydroxide melts because of selective oxidation of the chromium, which leads to pore formation in the metal. Nickel is more resistant than stainless steels or unalloyed steels.

The peroxide content of the melt controls the corrosion rate. An increase in water vapor and a decrease in oxygen pressure reduce the peroxide content and subsequently reduce the corrosion rate. An exception to this rule occurs with silver, which shows an increase in corrosion rate with increased water vapor. Most glass and silica are rapidly attacked by hydroxide melts, while alumina is more resistant.

Carbonate Melts. Austenitic stainless steels perform well in carbonate melts up to 500 °C (930 °F). If temperatures to 600 °C (1110 °F) are required, nickel-base alloys containing chromium are needed. For temperatures to 700 °C (1290 °F), high-chromium alloys containing at least 50% Cr are required. Above 700 °C (1290 °F), the passive films that form at lower temperatures break down and preclude the use of metals. Aluminum coatings on steel structures perform well to 700 °C (1290 °F). For higher temperatures, alumina is

required. Nickel does not provide adequate protection, because of intergranular attack caused by the formation of nickel oxides.

Reference cited in this section

2. G.Y. Lai, *High-Temperature Corrosion of Engineering Alloys*, ASM International, 1990

R.D. Kane, Molten Salt Corrosion, *Corrosion: Fundamentals, Testing, and Protection*, Vol 13A, *ASM Handbook*, ASM International, 2003, p 216–219

Molten Salt Corrosion

Revised by Russell D. Kane, InterCorr International, Inc.

Prevention of Molten Salt Corrosion

There is a lack of reliable data for molten salts on structural material under industrial conditions, but several general rules should be observed. A material should be selected that will form a passive nonsoluble film in the melt, if possible. Material selection is the key to successful containment. Minimizing the entry of oxidizing species such as oxygen and water into the melt is very important. The oxidizing power of the melt or its redox potential should be kept as low as possible, which can be accomplished by additives. The temperature of the bath should be kept as low as possible. The lower temperature not only decreases the diffusion rates of the ions into the melt but lowers the solubility of potentially passive surface films. Temperature gradients should be eliminated within the melts to decrease the selective dissolution and plating at hot and cold sites.

R.D. Kane, Molten Salt Corrosion, *Corrosion: Fundamentals, Testing, and Protection*, Vol 13A, *ASM Handbook*, ASM International, 2003, p 216–219

Molten Salt Corrosion

Revised by Russell D. Kane, InterCorr International, Inc.

Acknowledgment

This article has been adapted from J.W. Koger and S.L. Pohlman, Molten-Salt Corrosion, *Corrosion*, Volume 13, *Metals Handbook*, 9th ed., ASM International, 1987, p 88–91.

R.D. Kane, Molten Salt Corrosion, *Corrosion: Fundamentals, Testing, and Protection*, Vol 13A, *ASM Handbook*, ASM International, 2003, p 216–219

Molten Salt Corrosion

Revised by Russell D. Kane, InterCorr International, Inc.

References

1. D.A. Eden, InterCorr International, Inc., private communication, 2001
2. G.Y. Lai, *High-Temperature Corrosion of Engineering Alloys,* ASM International, 1990

R.D. Kane, Molten Salt Corrosion, *Corrosion: Fundamentals, Testing, and Protection*, Vol 13A, *ASM Handbook*, ASM International, 2003, p 216–219

Molten Salt Corrosion

Revised by Russell D. Kane, InterCorr International, Inc.

Selected References

- M.G. Fontana and N.D. Greene, *Corrosion Frequency,* McGraw Hill, 1978
- G.J. Janz and R.P.T. Tomkins, *Corrosion,* Vol 35, NACE International, 1979, p 485
- J.W. Koger, *Advances in Corrosion Science and Technology,* Vol 4, Plenum Press, 1974
- D.G. Lovering, Ed., *Molten Salt Technology,* Plenum Press, 1982
- A. Rahmel, Corrosion, *Molten Salt Technology,* Plenum Press, 1982
- L.L. Sheir, Ed., *Corrosion,* Vol 1, Newnes- Butterworths, 1979, p 2.10

R.D. Kane, Liquid Metal Corrosion, *Corrosion: Fundamentals, Testing, and Protection*, Vol 13A, *ASM Handbook*, ASM International, 2003, p 220–227

Liquid Metal Corrosion

Revised by R.D. Kane, InterCorr International, Inc.

Introduction

LIQUID METALS have long been considered for the improvement of efficiency in heat-transfer systems. A recent example, from which many illustrations in this section are drawn (Fig. 1, 2, 3, 4, 5, 6), is the work that has been performed around the world on the sodium-cooled fast breeder reactor. This concept led to large-scale research and development programs that have continued through more than two decades. The result is a vast wealth of knowledge related to sodium corrosion behavior in all its varied aspects. The body of information

greatly overshadows the corrosion data compiled for other liquid metals. This type of reactor was in commercial operation in France and the former Soviet Union for power generation at the time this article was written. Development reactors were operating in the United Kingdom, Germany, Japan, India, and the United States.

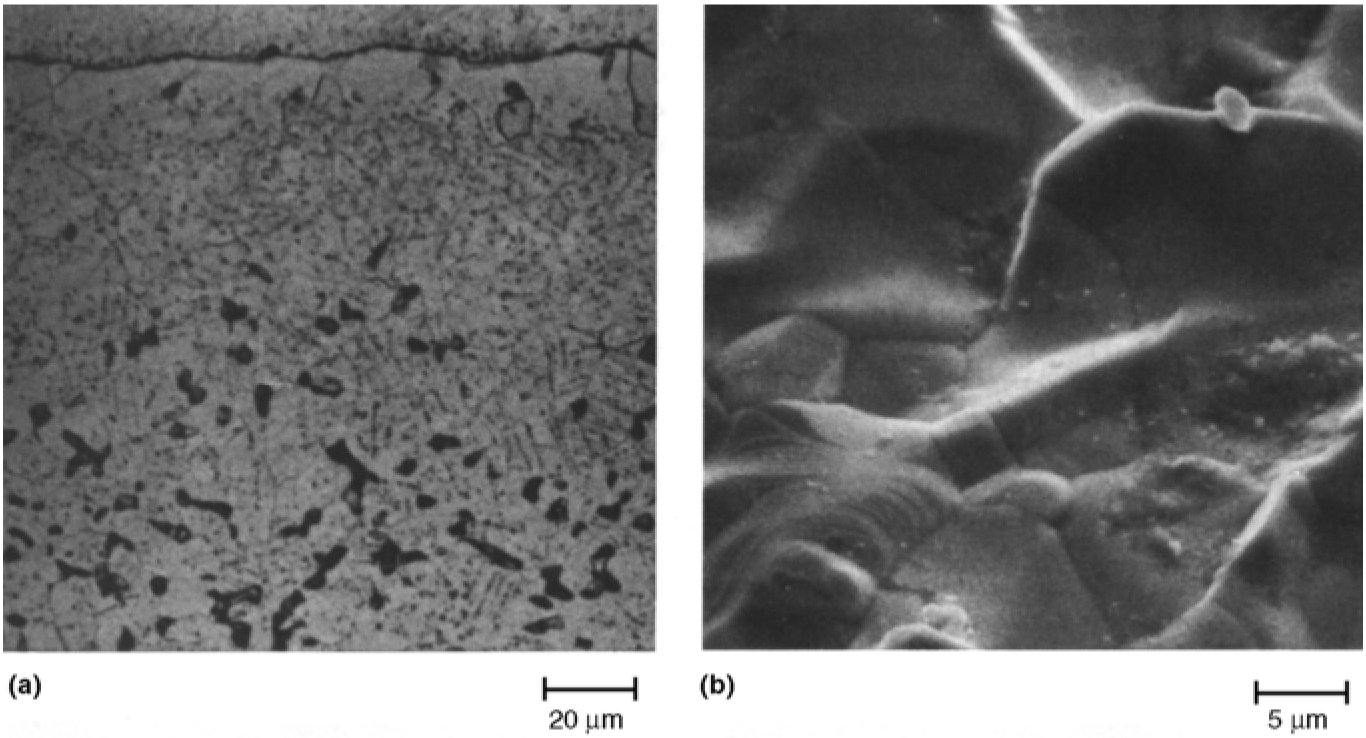

Fig. 1 Corrosion of type 316 stainless steel exposed to liquid sodium for 8000 h at 700 °C (1290 °F); hot leg of circulating system. Surface regression is uniform; a 10 to 15 µm layer of ferrite (>95% Fe) has formed. Total damage depth: 27 µm. (a) Light micrograph of wall section showing σ-phase (etched black) suppressed by composition changes to a depth of ~50 µm. (b) SEM micrograph of surface. Source: Ref 1

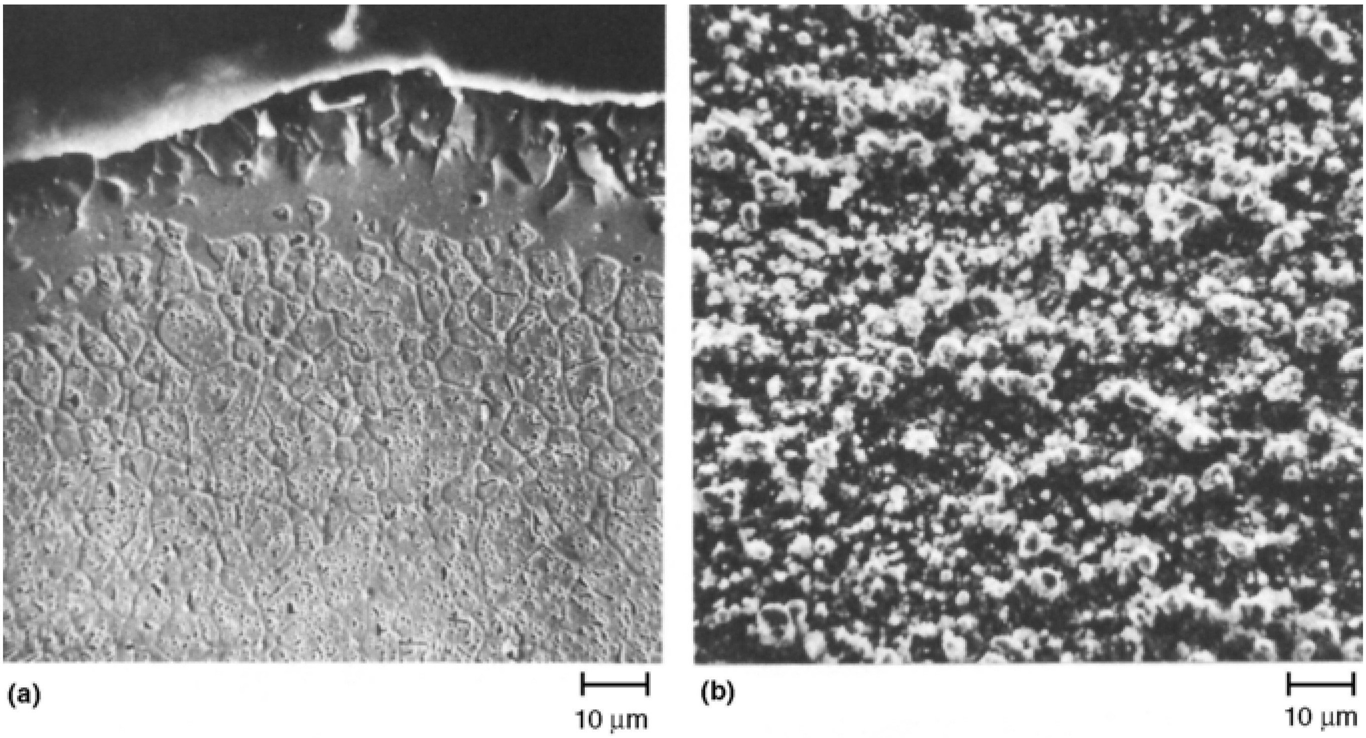

Fig. 2 Corrosion of X8CrNiMoVNb 16 13 stainless steel exposed to flowing sodium. (a) Ferrite formation in the surface layer and grain boundaries after 5000 h at 700 °C (1290 °F). SEM. Oxalic acid etch. (b) SEM of the deposition layer formed on the same steel after exposure to flowing sodium at 590 °C (1095

°F). Specimen taken downstream from the 700 °C (1290 °F) hot leg specimen shown in (a). The dark particles are rich in chromium and oxygen; some of the bright crystals are rich in calcium. Courtesy of H.U. Borgstedt, Karlsruhe Nuclear Center

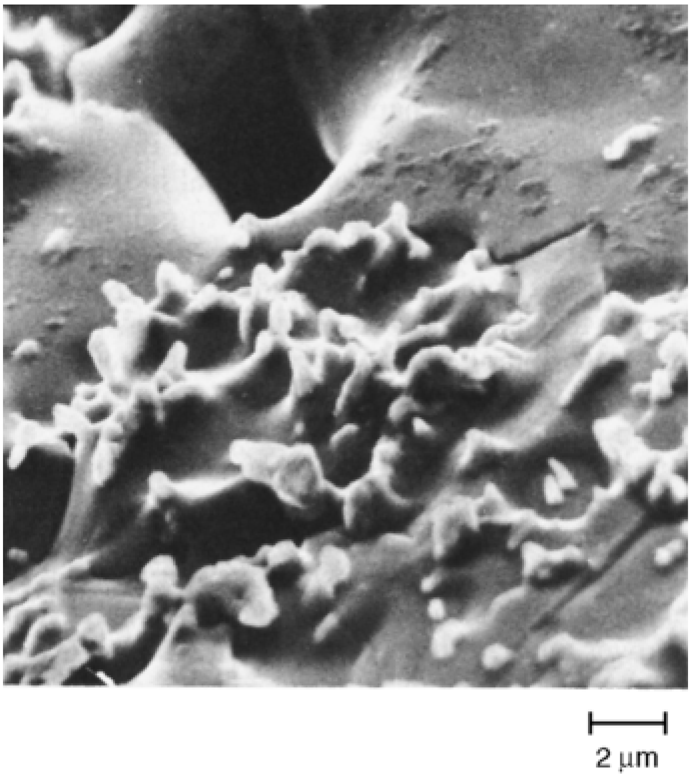

Fig. 3 Typical surface appearance of a stabilized stainless steel (X10CrNiMoTi 15 15) after a 5000 h exposure to flowing sodium at 700 °C (1290 °F). Cavities are formed at the grain corners; corallike particles of a MoFe phase are on the grain surfaces. Courtesy of H.U. Borgstedt, Karlsruhe Nuclear Center

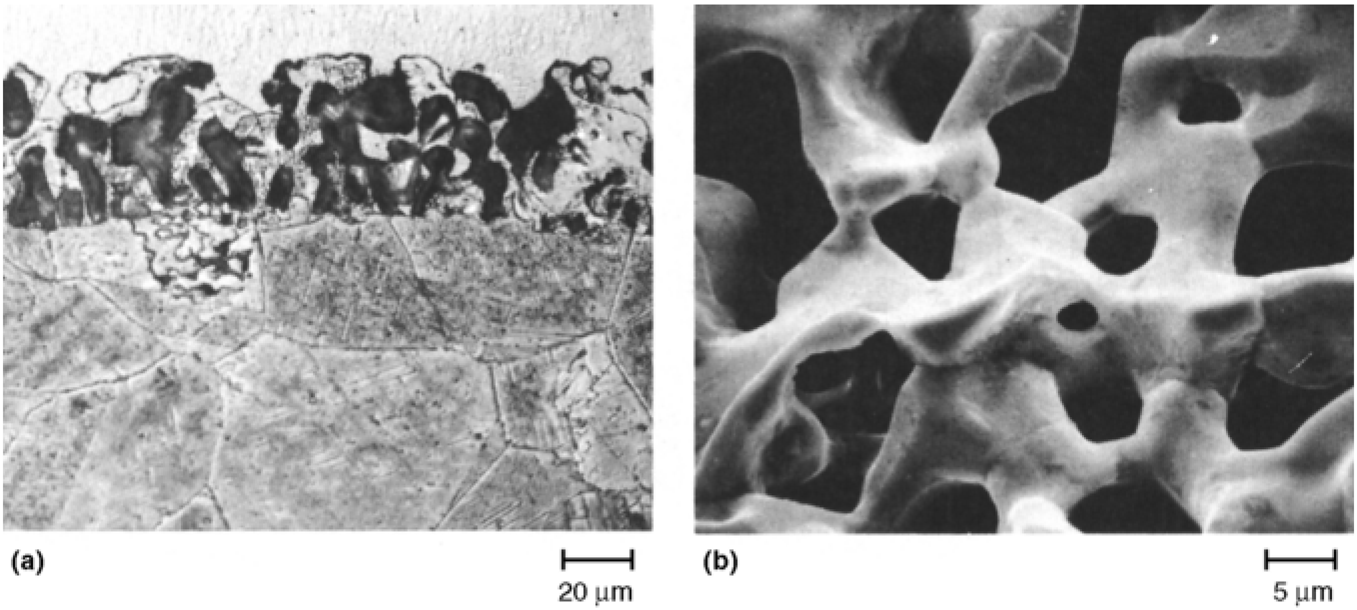

Fig. 4 Corrosion of Inconel alloy 706 exposed to liquid sodium for 8000 h at 700 °C (1290 °F); hot leg of circulating system. A porous surface layer has formed with a composition of ~95% Fe, 2% Cr, and <1% Ni. The majority of the weight loss encountered can be accounted for by this subsurface degradation. Total damage depth: 45 μm. (a) Light micrograph. (b) SEM of the surface of the porous layer. Source: Ref 1

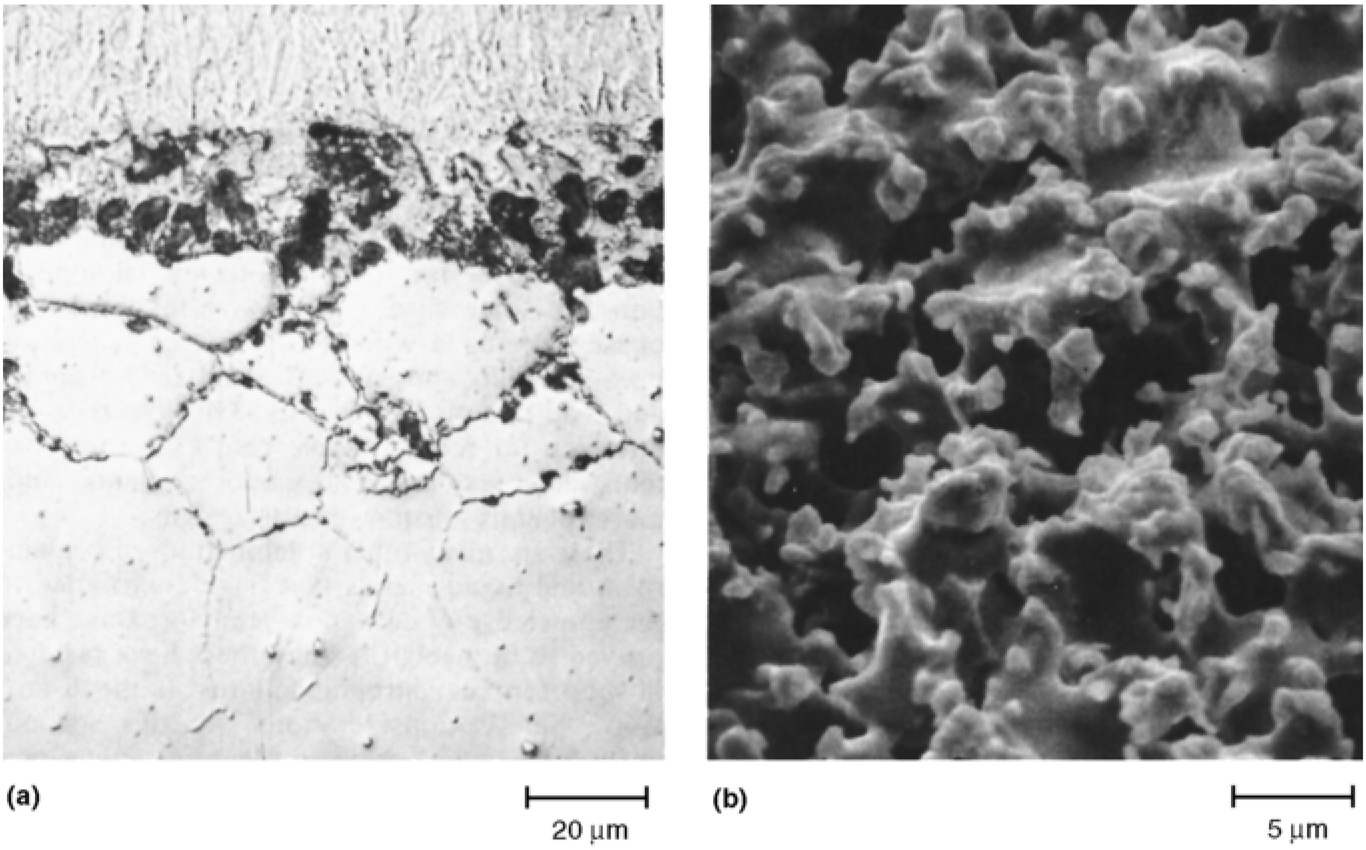

Fig. 5 Corrosion of Nimonic PE 16 exposed to the same conditions described for Fig. 4. A porous corallike surface layer has formed, with a composition similar to that of Inconel alloy 706 but with the addition of corrosion-resistant FeMo particles at the coral tips. Intergranular attack beneath this layer extends to a depth of 75 µm. Total damage depth: 135 µm. (a) Light micrograph. (b) SEM of the surface of the porous layer. Source: Ref 1

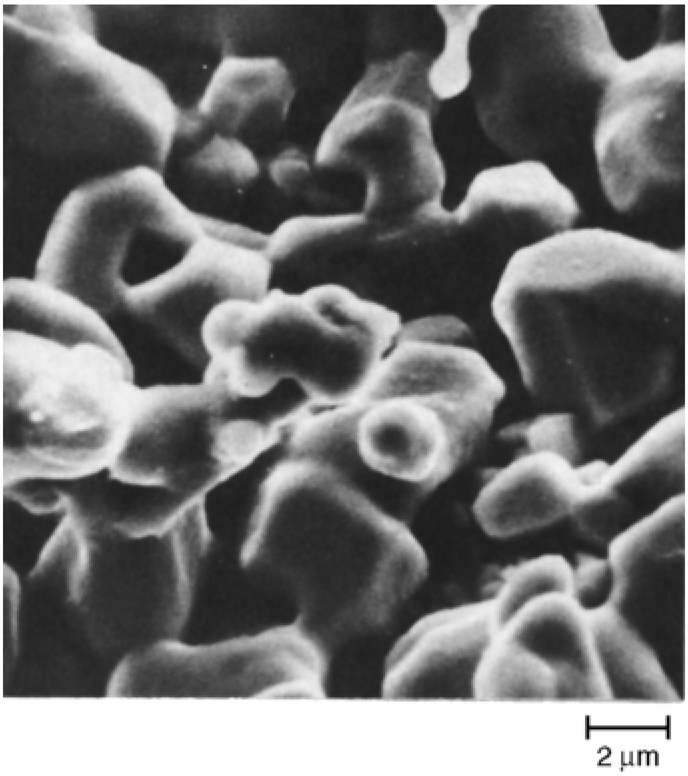

Fig. 6 Deposition of iron-rich crystals on Stellite 6 sheet after ~5000 h in flowing sodium at 600 °C (1110 °F). Courtesy of H.U. Borgstedt, Karlsruhe Nuclear Center

Reference cited in this section

1. C. Bagnall and R.E. Witkowski, "Microstructural and Surface Characterization of Candidate LMFBR Fuel Cladding and Duct Alloys After Exposure to Flowing Sodium at 700 °C," WARD-NA-3045-53, U.S. Energy Research and Development Agency Technical Information Center, June 1978

R.D. Kane, Liquid Metal Corrosion, *Corrosion: Fundamentals, Testing, and Protection*, Vol 13A, *ASM Handbook*, ASM International, 2003, p 220–227

Liquid Metal Corrosion

Revised by R.D. Kane, InterCorr International, Inc.

Experience in Systems Exposed to Liquid Metals

Liquid lithium systems have been designed for two widely different areas: space nuclear power and fusion reactors. These two applications draw on unique properties of this liquid metal and have led to studies with a wide range of containment materials and operating conditions. Space power reactors require low mass; this in turn demands high-temperature operation. Lithium, with its low melting point/high boiling point and high specific heat, is an ideal candidate heat-transfer medium. Refractory metal alloy containment is essential for these reactors, which may have design operating temperatures as high as 1500 °C (2730 °F).

Liquid lithium in fusion reactor concepts is selected because, here, the neutronics allow tritium fuel to be bred from the lithium; this is essential to viable economics of the reactor. Containment temperatures are below 700 °C (1290 °F); therefore, iron-base alloys can be used for construction.

The effects of liquid lithium on stainless steel, nickel, and niobium containment materials are shown in Fig. 7, Fig. 8, Fig. 9, Fig. 10, Fig. 11, Fig. 12, Fig. 13, Fig. 14, Fig. 15, Fig. 16.

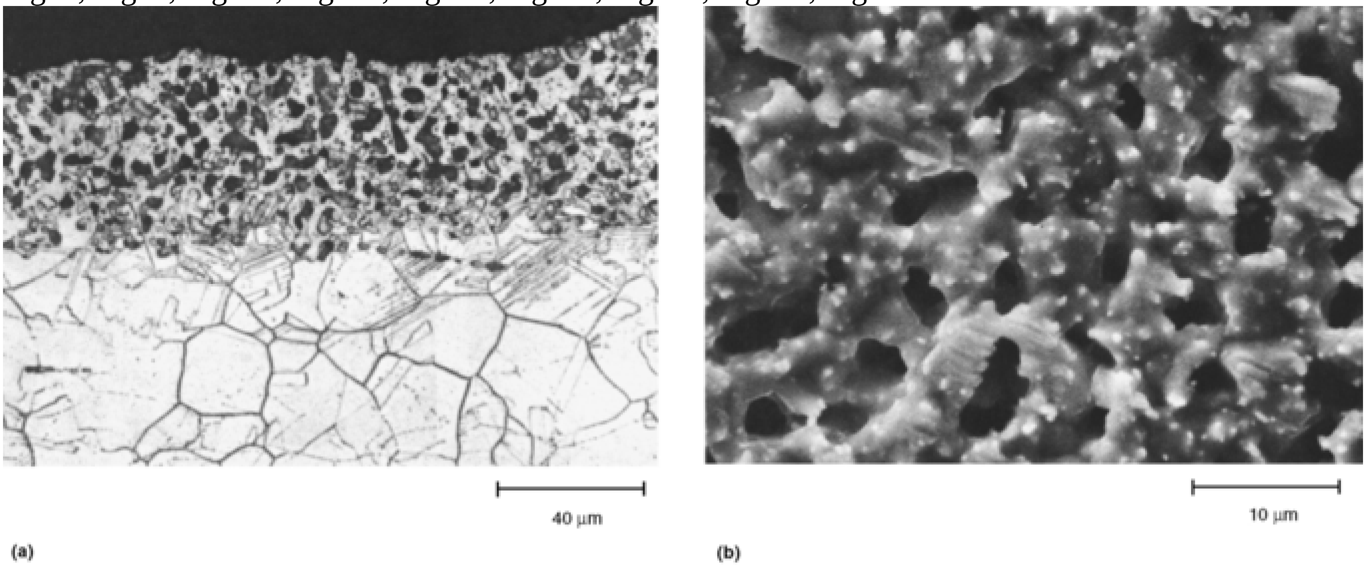

Fig. 7 Corrosion of type 316 stainless steel exposed to thermally convective lithium for 7488 h at the maximum loop temperature of 600 °C (1110 °F). (a) Light micrograph of polished and etched cross section. (b) SEM showing the top view of the porous surface. Source: Ref 2

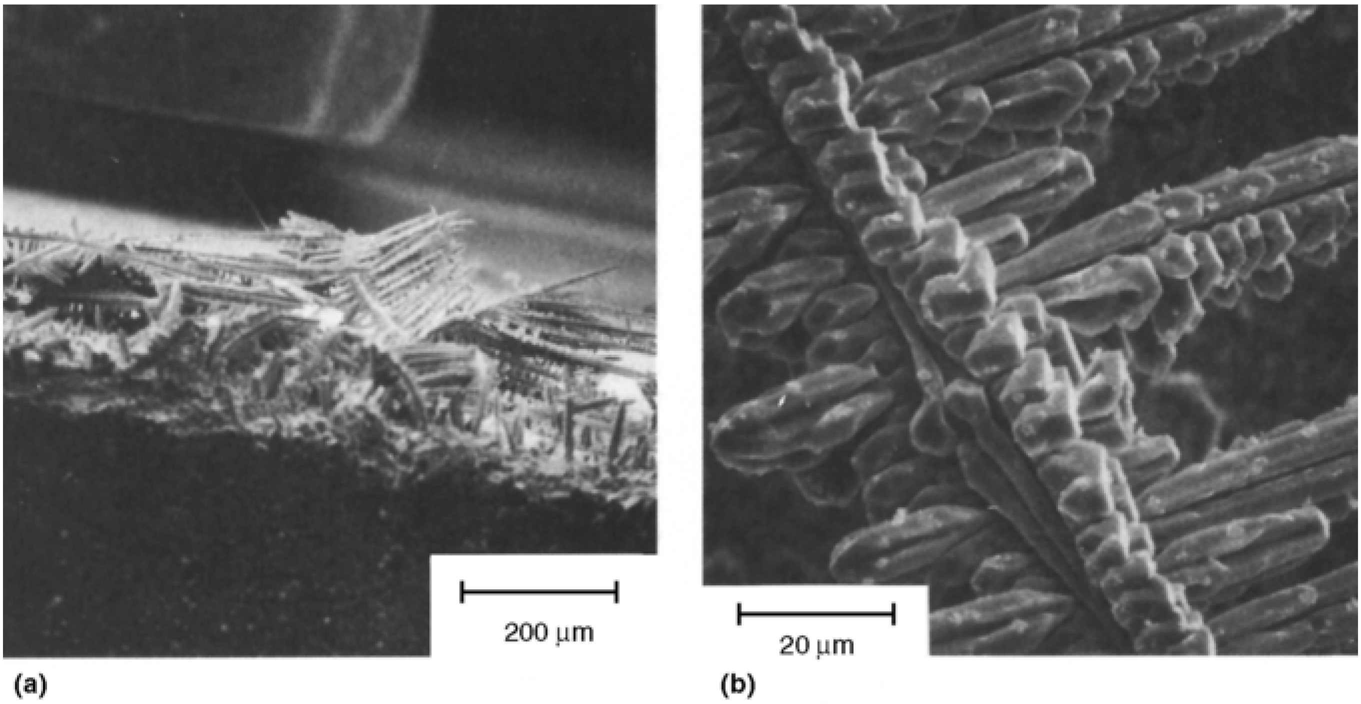

Fig. 8 **SEM micrographs of chromium mass-transfer deposits found at the 460 °C (860 °F) position in the cold leg of a lithium/type 316 stainless steel thermal convection loop after 1700 h. Mass-transfer deposits are often a more serious result of corrosion than wall thinning. (a) Cross section of specimen on which chromium was deposited. (b) Top view of surface. Source: Ref 3**

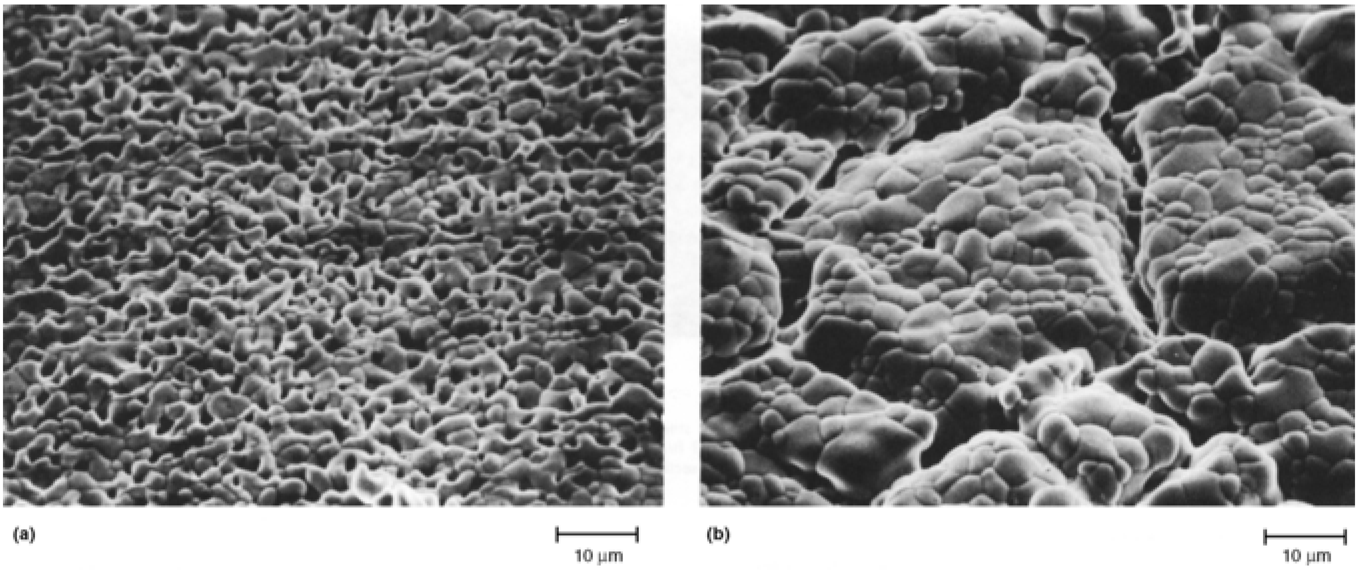

Fig. 9 **Changes in surface morphology along the isothermal hot leg of a type 304 stainless steel pumped lithium system after 2000 h at 538 °C (1000 °F). Composition changes transform the exposed surface from austenite to ferrite, containing approximately 86% Fe, 11% Cr, and 1% Ni. (a) Inlet. (b) 7.7 m (25 ft) downstream. Source: Ref 4**

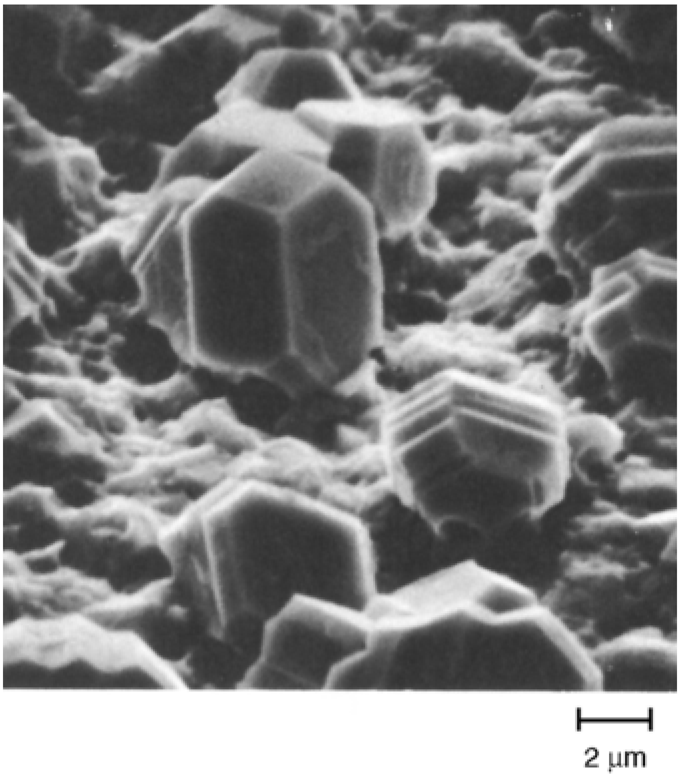

Fig. 10 Mass-transfer deposits on X10CrNiMoTi 15 15 stainless steel after 1000 h exposure in static liquid lithium at 700 °C (1290 °F). Deposits are of the composition of the capsule steel (18Cr-8Ni). Courtesy of H.U. Borgstedt, Karlsruhe Nuclear Center

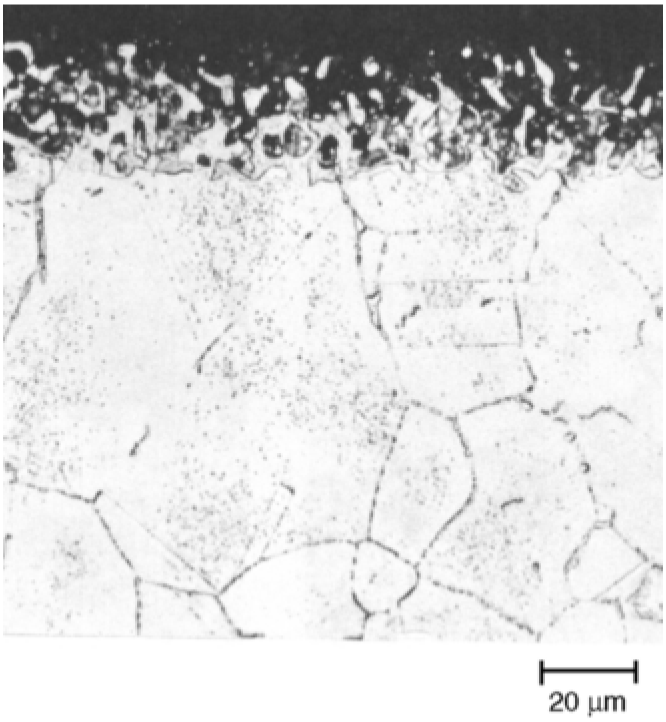

Fig. 11 Corrosion of a capsule wall of 18 10 CrNiMoTi stainless steel by static lithium in the presence of zirconium foil. A porous ferritic surface layer has formed. Source: Ref 5

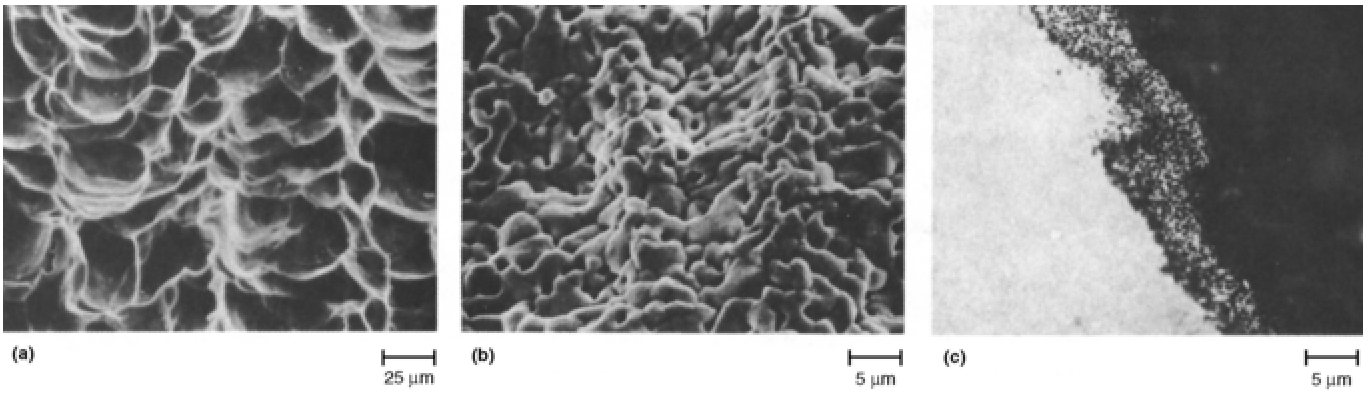

Fig. 12 Effects of flowing lithium on the inside surface of a type 316 stainless steel tubing. (a) Pickled surface before exposure. Composition: 65.8 Fe-18.0Cr-9.2Ni-3.3Mn-2.6Mo-0.9Si. (b) After exposure in flowing lithium (0.3 m/s, or 1 ft/s) for 1250 h at 490 °C (915 °F). Composition: 88.6Fe-7.5Cr-1.7Ni-0.6Mn. (c) After exposure to flowing lithium (1.3 m/s, or 4.3 ft/s) for 3400 h at 440 °C (825 °F). Taper section used to magnify damaged surface zone in metallographic mount. Courtesy of D.G. Bauer and W.E. Stewart, University of Wisconsin

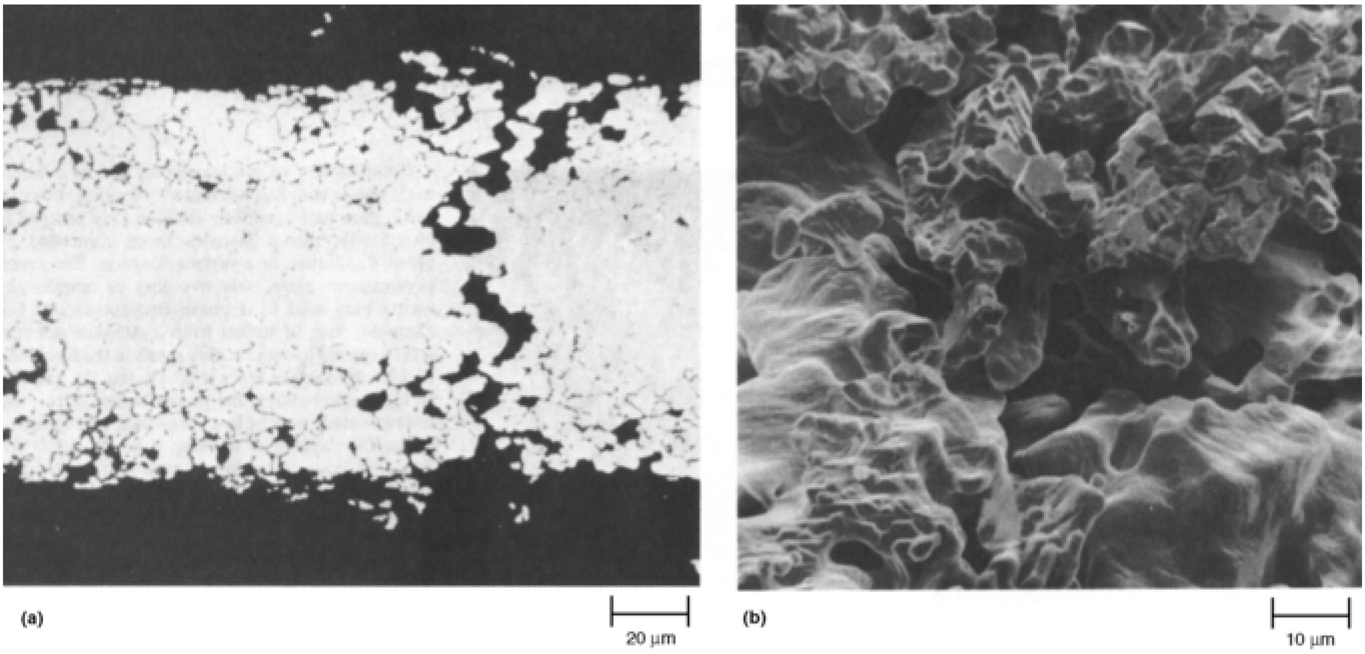

Fig. 13 Corrosion of nickel in static lithium after exposure for 300 h at 700 °C (1290 °F). (a) Light micrograph. (b) SEM micrograph. Source: Ref 6

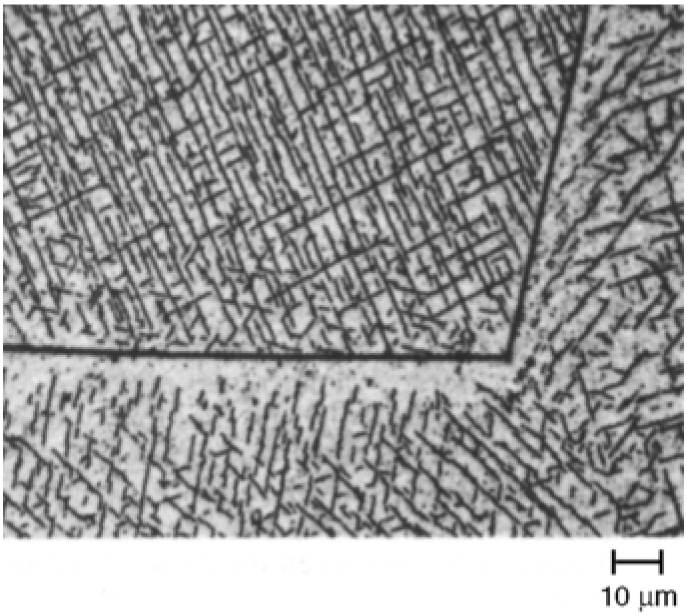

Fig. 14 Light micrograph of the polished and etched cross section of niobium containing 1500 wt ppm of oxygen showing the transcrystalline and grain-boundary penetration that occurred after exposure to isothermal lithium for 100 h at 500 °C (930 °F). Source: Ref 7

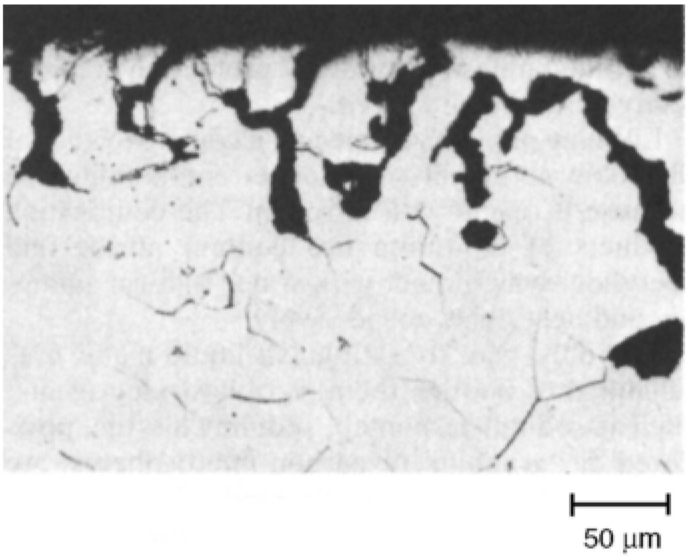

Fig. 15 Intergranular attack of unalloyed niobium exposed to lithium at 1000 °C (1830 °F) for 2 h. Light micrograph. Etched with 25% HF, 12.5 HNO_3, 12.5% H_2SO_4 in water. Source: Ref 8

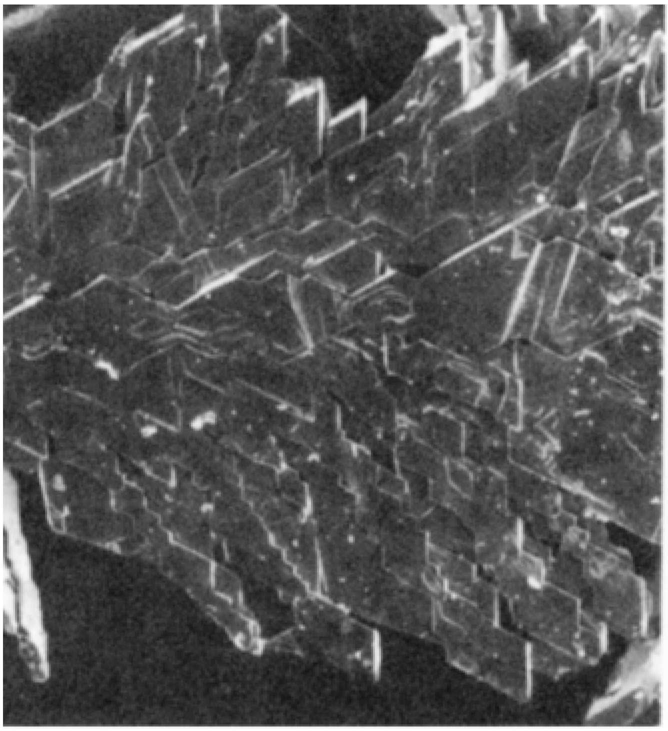

(a)

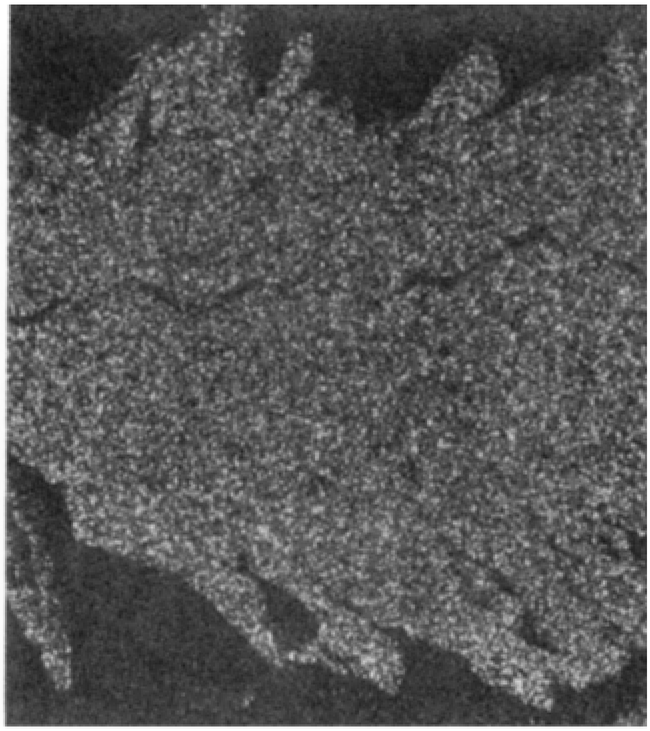

(b)

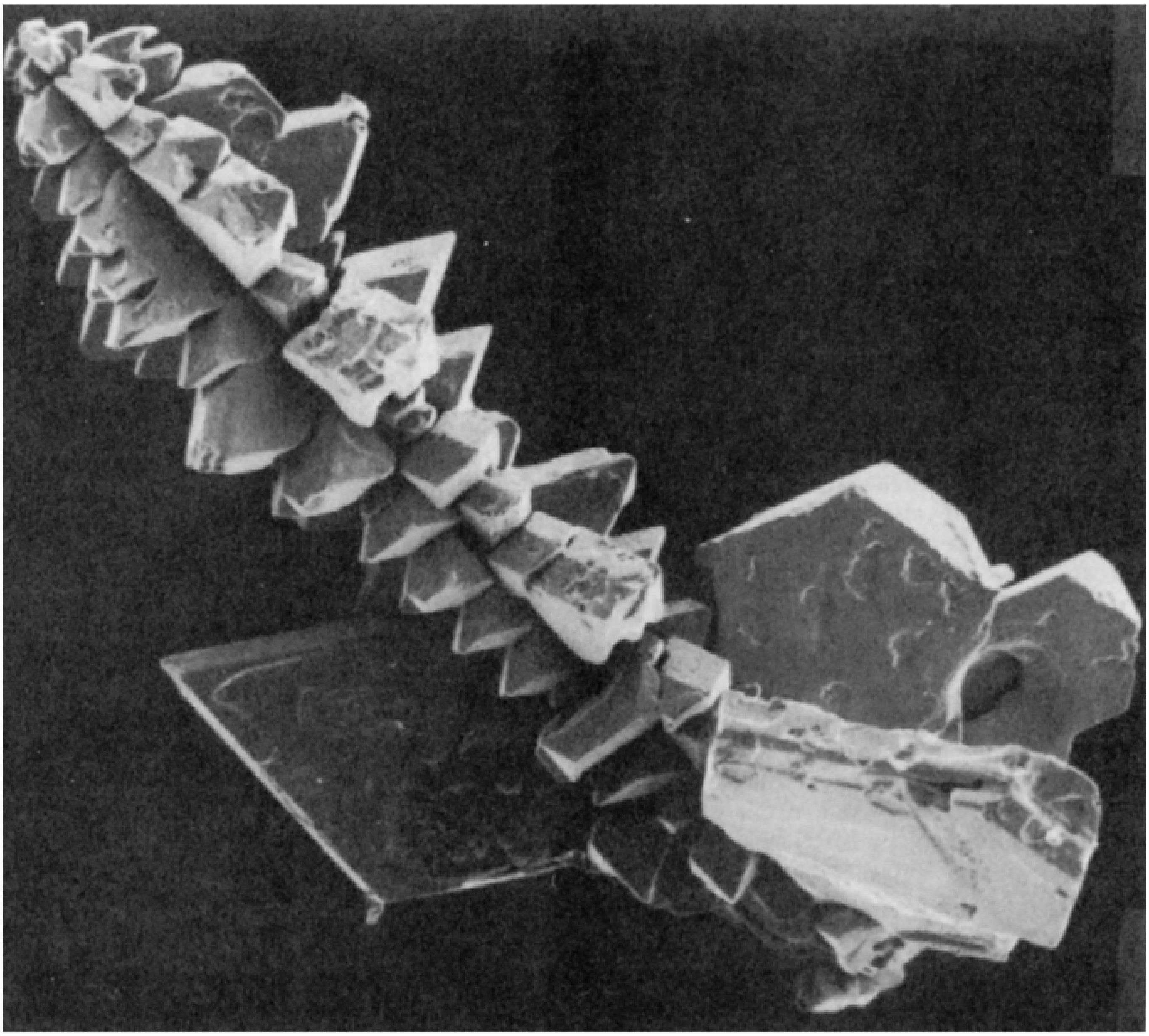

(c)

Fig. 16 Iron crystals found in a plugged region of a failed pump channel of a lithium processing test loop. Multifaceted platelike crystals are ~0.4 mm (0.015 in.) across. Composition: 86 to 93% Fe, 7 to 14% Ni, 0 to 1% Mn. (a) SEM. 70×. (b) Iron x-ray scan. 70×. (c) SEM. 90×. Source: Ref 9

Liquid mercury, potassium, and cesium have also been used for space and terrestrial applications. In some cases, these have involved two- phase systems in which the corrosion consideration became significantly altered. Lead, lead-bismuth, and lead-lithium alloys (Fig. 17) (Ref 10) have received attention for topping cycle heat extraction systems, heat exchangers, reactor coolants, and, more recently, fusion reactor designs.

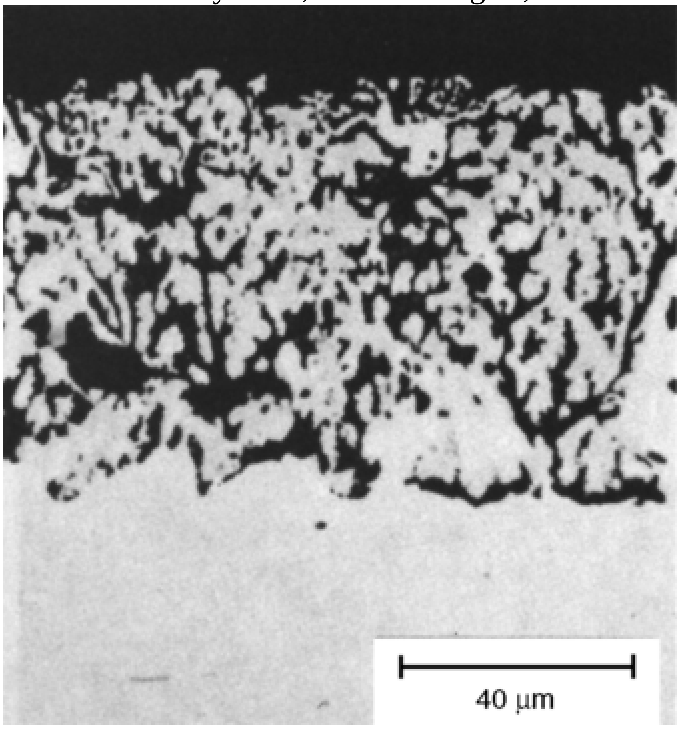

Fig. 17 Light micrograph of the polished cross section of a type 316 stainless steel exposed to thermally convective Pb-17at.% Li at 500 °C (930 °F) for 2472 h. Source: Ref 10

Many other combinations of containment and liquid metals have contributed to the knowledge of corrosion behavior; some have proved to be benign, while others have resulted in short-term catastrophic failures. For example, liquid mercury is also of potential interest, because it is an impurity, process additive, and/or by-product of many commercial industrial processes found in the refining and petrochemical industry. Exposure to liquid mercury can affect containment materials through a number of mechanisms, including amalgamation, galvanic acceleration of aqueous corrosion, and embrittlement.

In the discussion presented in this article, some brief notes are given regarding safety precautions for handling liquid metals, operating circulating systems, dealing with fire and spillage, and cleaning contaminated components.

References cited in this section

2. P.F. Tortorelli and J.H. DeVan, Effects of a Flowing Lithium Environment on the Surface Morphology and Composition of Austenitic Stainless Steel, *Microstruct. Sci.,* Vol 12, 1985, p 213–226

3. P.F. Tortorelli and J.H. DeVan, Mass Transfer Deposits in Lithium-Type 316 Stainless Steel Thermal Convection Loops, *Proceedings of the Second International Conference on Liquid Metal Technology in Energy Production,* CONF-800401, National Technical Information Service, 1980, p 13–56 to 13–62

4. C. Bagnall, A Study of Type 304 Stainless Steel Containment Tubing From a Lithium Test Loop, *J. Nucl. Mater.,* Vol 103 and 104, 1981, p 639–644

5. H.U. Borgstedt, *J. Nucl. Mater.,* Vol 103 and 104, 1981, p 693–698

6. H.U. Borgstedt, *Mater. Chem.,* Vol 5, 1980, p 95–108

7. J.R. DiStefano, "Corrosion of Refractory Metals by Lithium," M.S. thesis, University of Tennessee, 1963

8. W.F. Brehm, "Grain Boundary Penetration of Niobium by Lithium," Ph.D. thesis, Report HYO-3228-11, Cornell University, 1967

9. V.A. Maroni et al.,"Analysis of the October 5, 1979, Lithium Spill and Fire in the Lithium Processing Test Loop," ANL-81-25, Prepared for the U.S. Department of Energy under Contract W-31-109-Eng-38, Argonne National Laboratory, Dec 1981

10. P.F. Tortorelli and J.H. DeVan, Corrosion of Ferrous Alloys Exposed to Thermally Convective Pb-17 at.% Li, *J. Nucl. Mater.,* Vol 141–143, 1986, p 592–598

R.D. Kane, Liquid Metal Corrosion, *Corrosion: Fundamentals, Testing, and Protection*, Vol 13A, *ASM Handbook,* ASM International, 2003, p 220–227

Liquid Metal Corrosion

Revised by R.D. Kane, InterCorr International, Inc.

Forms of Liquid-Metal Corrosion

The forms in which liquid-metal corrosion are manifested can be divided into the following categories:

- Dissolution from a surface by (a) direct dissolution; (b) surface reaction, involving solid metal atom(s), the liquid metal, and an impurity element present in the liquid metal; or (c) intergranular attack
- Impurity and interstitial reactions
- Alloying
- Compound reduction

All the variables present in the system play a part in the form and rate of corrosion established. Several key factors have a major influence on the corrosion of metals and alloys by liquid- metal systems or liquid-vapor metal coolants. These are:

- Composition, impurity content, and stress condition of the metal or alloy
- Exposure temperature and temperature range
- Impurity content of the liquid metal
- Circulating or static inventory
- Heating/cooling conditions
- Single or two-phase coolant
- Liquid metal velocity
- Presence/control of corrosion inhibition elements
- Exposure time
- Monometallic or multialloy system components
- Wear or abrasion on metal surfaces
- Use of surface treatments designed to enhance passive surface films

These factors have a varied influence, depending on the combination of containment material and liquid metal or liquid-metal alloy. In many cases, such as with sodium, the initial period of exposure (of the order of 100 to 1000 h, depending on temperature and liquid metal involved) is a time of rapid corrosion that eventually reaches a much slower steady-state condition as factors related to solubility and activity differences in the system approach a dynamic equilibrium. In some systems, this eventually leads to the development of a similar composition on all exposed corroding surfaces. High-nickel alloys and stainless steel exposed together in the high-temperature region of a sodium system will, for example, all move toward a composition that is more than 95% Fe.

In the case of liquid mercury, its effects on aluminum or stainless alloys (e.g., stainless steels and nickel-base alloys) usually do not proceed automatically from the start of first exposure. The normal passive surface films (oxides) on aluminum and stainless alloys are a natural barrier to liquid-metal attack. It is only where these films are penetrated, mechanically damaged, or chemically attacked by other chemical species in the environment that liquid-metal corrosion proceeds. Mercury exposure of aluminum alloys can lead to at least three forms of attack: (a) amalgamation, a process by which aluminum and mercury form liquid solution (amalgamation does not require moisture); (b) amalgamation corrosion characterized by rapid weight loss, pitting, and possible intergranular corrosion and corrosion product formation in oxidizing environments; and (c) cracking, which involves rapid crack propagation and embrittlement at stresses substantially less than the normal material yield strength (Ref 11).

Compatibility of a liquid metal and its containment material varies widely, as illustrated in Fig. 1, Fig. 2, Fig. 3, Fig. 4, Fig. 5, Fig. 6, Fig. 7, Fig. 8, Fig. 9, Fig. 10, Fig. 11, Fig. 12, Fig. 13, Fig. 14, Fig. 15, Fig. 16, Fig. 17. For a pure metal, surface attrition may proceed in an orderly, planar fashion, being controlled by either dissolution or a surface reaction. For a multicomponent alloy, selective loss of certain elements may lead to a phase transformation. For example, loss of nickel from austenitic stainless steel exposed to liquid sodium may result in the formation of a ferritic surface layer (Fig. 1, 2a, 9, 11). In high-nickel alloys, the planar nature of the corroding surface may be lost altogether, and a porous, spongelike layer may develop (Fig. 4, 5). A more insidious situation can produce intergranular attack; liquid lithium, for example, penetrates deep into refractory metals if precautions are not taken to ensure that the impurity element oxygen is in an oxide form more stable than Li_2O or LiO solutions and is not left free in solid solution. Figure 15 illustrates intergranular attack in niobium.

Three factors—surface attrition, depth of depleted zone (for an alloy), and the presence of intergranular attack—should be evaluated collectively in any liquid-metal system. This evaluation leads to an assessment of total damage, which may be presented either as a rate or as a cumulative allowance that must be made for the exposure of a given material over a given time. A large body of literature exists in which rate relationships for numerous liquid-metal/containment combinations have been established (e.g., see the Selected References).

One vitally important aspect of liquid-metal corrosion that is often overlooked is deposition. Corrosion itself is very often not a factor of major concern, because surface recession rates in regions of maximum attack are often of the order of microns per year. The formation of compounds in the circulating liquid metal and the accumulation of deposits in localized regions where there is a drop in temperature, a change in flow rate or flow direction, or an induced change in surface roughness can, however, be very serious. If these deposits do not succeed in restricting flow channels completely, their nature is often such that they are only loosely adherent to deposition surfaces and may be dislodged by vibrations or thermal shock in the system, thus creating a major coolant flow restriction in a high-temperature region. Most deposits have a very low packing density; therefore, deposit growth can proceed at a rate that outstrips corrosion by several orders of magnitude. Examples of loosely adherent deposits are shown in Fig. 2(b), 6, 8, and 10. Figure 16 shows iron crystals that restricted flow in a pump channel of a lithium processing test loop.

Liquid-metal corrosion, as in other forms of corrosion, involves an appreciation for the source of corrosion in any system and an understanding of how potential sinks operate on the corrosion burden, particularly if the liquid metal is not static but is circulated in a heat-transfer system either by pumping or by thermal convection.

Reference cited in this section

11. R.D. Kane and S.M. Wilhelm, “Combatting Liquid Metal Attack by Mercury in Ethylene and Cryogenic Gas Plants,” Results of Joint Industry-Sponsored Research Program—Final Report, InterCorr International, Inc., Houston, TX, 1992

R.D. Kane, Liquid Metal Corrosion, *Corrosion: Fundamentals, Testing, and Protection*, Vol 13A, *ASM Handbook*, ASM International, 2003, p 220–227

Liquid Metal Corrosion

Revised by R.D. Kane, InterCorr International, Inc.

Safety Considerations

The extensive work with the alkali and liquid metals has shown that such materials can be safely handled and used, provided certain precautions are heeded. The requirements for the safe use of liquid metals are, in essence, those of good industrial or laboratory practice, involving protection from contamination, chemical reactions, exposure to toxic or irritating substances, and protection from high temperatures. More specific information and details on safe operation and handling are available in Ref 12 and 13 and in the Materials Safety Data sheets issued by the Manufacturing Chemists' Association.

Chemical Reactivity. All the liquid metals react with oxygen and moisture to some degree; with the alkali metals, the reaction is vigorous enough to be potentially hazardous, particularly with potassium, rubidium, and cesium. Use of inert gas covers and the exclusion of moisture are the best defenses. Even with the nonalkali metals, where the reactions with water are slow, water, such as that found on equipment that is not completely dry, must not be brought in contact with liquid metals because of the danger of a steam explosion that can scatter liquid metal over a considerable area, damaging equipment and inflicting severe burns on unprotected workers. It goes without saying that workers in the vicinity of liquid-metal systems should wear appropriate protective clothing (Ref 12).

Potassium, rubidium, and cesium form higher oxides than the monoxide when exposed to air; these compounds are powerful oxidizing agents, often shock sensitive, and definitely hazardous in the proximity of organic materials. They form at room temperature in contact with the solid metals. The practical application of this information is the need for extreme caution when handling the metals or compounds of the heavier alkali metals, particularly when they have been stored for extended periods under less-than-ideal conditions or when cleaning spills or fire residues. It is noted that the sodium-potassium eutectic alloy (NaK) forms potassium superoxide when exposed to air or oxygen. Because NaK is liquid at normal room temperature, small leaks at low temperature do not necessarily freeze and self-seal.

Circulating Systems. It is usually convenient to provide a closed circulating system, or loop, in which to perform liquid-metal corrosion experiments. Reference 13 describes a simple system; the principles involved are the same for even very complex specialized devices. The loop provides the means for circulation of the liquid metal; it contains devices for on-line purification (if needed), while the inert cover gas protects against chemical contamination. Insulation and an enclosure protect against high temperatures and the spread of reaction products in case of a containment breach. Such systems provide a safe, convenient environment for handling liquid metals. Detailed operating procedures, involving common-sense principles such as maintaining the inert cover gas at all times and melting frozen metals by directionally heating away from a free surface, must be worked out for each system. The tens of millions of hours of safe operation of such systems, ranging from 1 L capacity test rigs to 4000 MW (thermal) nuclear reactors, validate the concept. References 14 and 15 describe many such test systems and the experiments performed in them.

Recovery from Spills and Accidents. It must be remembered that spills of the nonalkali metals, even though the chemical reactivity hazard may not be great, must be handled with care because of the toxic nature of many of the metals and their vapors. Leaks and spills of the alkali metals, particularly when some of the leaked material has burned, present a special hazard, because the spilled material often contains finely divided unreacted metal mixed with combustion products. Such mixtures can react vigorously with moist air, water, and alcohol. The products of the heavier alkali metals are the most reactive in this respect, but mixtures containing sodium and lithium are certainly not immune to violent reactions if carelessly handled. Cleanup of these residues must be approached with extreme care.

Removal of Residual Metals from Corrosion Specimens. Nonalkali metals often can be removed from corrosion specimens by draining, forming an amalgam or solution with an alkali metal, and then removing the mixture by

a technique discussed subsequently. Alkali metals can be removed from specimens by reaction with water or alcohols; the most vigorous reaction is with water, and the rate decreases as one progresses to heavier-weight alcohols. The reaction becomes more vigorous with increasing atomic weight of the alkali metals. Cesium-water reactions are definitely explosive. Use of ethanol and methanol is generally safe for sodium reaction, but one must remember the flammability hazard with alcohol vapors. The glycol ethers, such as butyl cellosolve, can also be used; they react more slowly than water, present less of a fire hazard than ethanol or methanol, but have toxic liquid and vapors. The water, alcohol, and glycol ether reactions all generate hydrogen; adequate ventilation must be provided to prevent the buildup of the hydrogen and the attendant danger of an explosion.

Anhydrous liquid ammonia forms a true solution with the alkali metals and can be used to remove adherent alkali metals from corrosion specimens. Precautions against the hazards of liquid ammonia must be taken; the alkali metal in solution with ammonia is then usually reacted with water or alcohol before the ammonia mixture is discarded. The conditions must be maintained truly anhydrous in order to avoid hydrogen generation and contamination of the samples. Hydrogen can become implanted in refractory metal samples and embrittle them even at subzero temperatures. If the proper equipment is available, evaporation of the residual metal from the surface can be done with excellent results.

Removal of alkali materials from pipework, if hydrogen generation is not a problem, can be accomplished with alcohol or gycol ether reaction, optionally followed by water rinsing to wash away the reaction products. It must be remembered that these reagents react very slowly, if at all, with oxides of the alkali metals. Another successful method in use is reaction with water vapor/inert gas (argon or nitrogen) mixtures, or water spray in an inert carrier gas, followed by water rinsing. Evaporation has also been successfully used and could be considered where hydrogen generation is not permitted. Ammonia- based systems have also been used for refractory metal pipework where hydrogen generation was prohibited. References 13, 14, and 15 contain more detailed information.

Fire Protection and First Aid. Firefighting and medical treatment should, of course, be left to the professionals. There are, however, several factors to keep in mind. An alkali metal fire does not expand, as does, for example, a petroleum fire. It does produce vast quantities of caustic smoke that react with moisture in or on the body, and this produces severe burns. The smoke must be avoided unless respiratory protection and protective clothing are worn.

Lithium presents a special hazard because of the toxic nature of some of its compounds and because it reacts with nitrogen. The combustion products of a lithium fire contain nitride and acetylide, which react with water to form ammonia and acetylene, respectively.

The only way to extinguish liquid-metal fires reliably is to smother them; various drying agents, such as sodium carbonate, sodium chloride, powdered dry graphite, or carbon microspheres, are effective. The sodium compounds should not be used on a lithium fire because of the chemical displacement reaction producing sodium metal that takes place. Instead, the graphite products should be used for extinguishment. It should be noted that few substances float on lithium; most tend to sink. Reference 16, however, describes the use of a ternary eutectic BaCl-NaCl-KCl salt for effective lithium fire extinguishment.

Inert gas blanketing is also effective for extinguishing fires; argon is preferred to nitrogen because of its higher density. Very effective fire suppression can be achieved by using inert gas blanketing in combination with a catch pan having a perforated floor to let the escaping liquid metal run to a second argon-blanketed chamber underneath the first. Of course, the hazards of oxygen-deficient atmospheres must be recognized and controlled when using inert gas flooding as fire suppression. Reference 17 provides more information about fire suppression in the alkali metals.

Emergency first aid treatment should concentrate on removing the victim from danger (for example, out of the smoke generated by a fire) and then removing the metal or compounds from skin and eyes. Running water is the most effective treatment, because the cooling and flushing effect overcomes any hazard from reaction of a small amount of metal on the skin or clothing. Safety showers and eyewash fountains should be readily available to workers involved with liquid metals; they should not be eliminated because of the presence of the alkali metals. More than one person has been spared serious injury because a safety shower was available to wash away a sodium spill.

References cited in this section

12. O.J. Foust, Ed., *Liquid Metals Handbook, Sodium and NaK Supplement,* U.S. Atomic Energy Commission, 1970

13. C.C. Addison, *The Chemistry of the Liquid Alkali Metals,* John Wiley & Sons, 1984

14. *Proceedings of the Second International Conference on Liquid Metal Technology in Energy Production,* CONF-800401, National Technical Information Service, 1980

15. *Proceedings of the Third International Conference on Liquid Metal Engineering and Technology,* Thomas Telford Ltd., 1985

16. D.W. Jeppson et al., *Lithium Literature Review: Lithium's Properties and Interactions,* HEDL-TME-78-15, National Technical Information Service, 1978

17. L.D. Muhlestein, Liquid Metal Reactions Under Postulated Accident Conditions for Fission and Fusion Reactors, *Proceedings of the Second International Conference on Liquid Metal Technology in Energy Production,* CONF-800401, National Technical Information Service, 1980

R.D. Kane, Liquid Metal Corrosion, *Corrosion: Fundamentals, Testing, and Protection*, Vol 13A, *ASM Handbook,* ASM International, 2003, p 220–227

Liquid Metal Corrosion

Revised by R.D. Kane, InterCorr International, Inc.

Acknowledgment

This article has been adapted from "Corrosion in Liquid Metals," by C. Bagnall and W.F. Brehm, *Corrosion,* Volume 13, *ASM Handbook,* ASM International, 1987.

R.D. Kane, Liquid Metal Corrosion, *Corrosion: Fundamentals, Testing, and Protection*, Vol 13A, *ASM Handbook*, ASM International, 2003, p 220–227

Liquid Metal Corrosion

Revised by R.D. Kane, InterCorr International, Inc.

References

1. C. Bagnall and R.E. Witkowski, "Microstructural and Surface Characterization of Candidate LMFBR Fuel Cladding and Duct Alloys After Exposure to Flowing Sodium at 700 °C," WARD-NA-3045-53, U.S. Energy Research and Development Agency Technical Information Center, June 1978

2. P.F. Tortorelli and J.H. DeVan, Effects of a Flowing Lithium Environment on the Surface Morphology and Composition of Austenitic Stainless Steel, *Microstruct. Sci.,* Vol 12, 1985, p 213–226

3. P.F. Tortorelli and J.H. DeVan, Mass Transfer Deposits in Lithium-Type 316 Stainless Steel Thermal Convection Loops, *Proceedings of the Second International Conference on Liquid Metal Technology in Energy Production,* CONF-800401, National Technical Information Service, 1980, p 13–56 to 13–62

4. C. Bagnall, A Study of Type 304 Stainless Steel Containment Tubing From a Lithium Test Loop, *J. Nucl. Mater.,* Vol 103 and 104, 1981, p 639–644

5. H.U. Borgstedt, *J. Nucl. Mater.,* Vol 103 and 104, 1981, p 693–698

6. H.U. Borgstedt, *Mater. Chem.,* Vol 5, 1980, p 95–108

7. J.R. DiStefano, "Corrosion of Refractory Metals by Lithium," M.S. thesis, University of Tennessee, 1963

8. W.F. Brehm, "Grain Boundary Penetration of Niobium by Lithium," Ph.D. thesis, Report HYO-3228-11, Cornell University, 1967

9. V.A. Maroni et al.,"Analysis of the October 5, 1979, Lithium Spill and Fire in the Lithium Processing Test Loop," ANL-81-25, Prepared for the U.S. Department of Energy under Contract W-31-109-Eng-38, Argonne National Laboratory, Dec 1981

10. P.F. Tortorelli and J.H. DeVan, Corrosion of Ferrous Alloys Exposed to Thermally Convective Pb-17 at.% Li, *J. Nucl. Mater.,* Vol 141–143, 1986, p 592–598

11. R.D. Kane and S.M. Wilhelm, "Combatting Liquid Metal Attack by Mercury in Ethylene and Cryogenic Gas Plants," Results of Joint Industry-Sponsored Research Program—Final Report, InterCorr International, Inc., Houston, TX, 1992

12. O.J. Foust, Ed., *Liquid Metals Handbook, Sodium and NaK Supplement,* U.S. Atomic Energy Commission, 1970

13. C.C. Addison, *The Chemistry of the Liquid Alkali Metals,* John Wiley & Sons, 1984

14. *Proceedings of the Second International Conference on Liquid Metal Technology in Energy Production,* CONF-800401, National Technical Information Service, 1980

15. *Proceedings of the Third International Conference on Liquid Metal Engineering and Technology,* Thomas Telford Ltd., 1985

16. D.W. Jeppson et al., *Lithium Literature Review: Lithium's Properties and Interactions,* HEDL-TME-78-15, National Technical Information Service, 1978

17. L.D. Muhlestein, Liquid Metal Reactions Under Postulated Accident Conditions for Fission and Fusion Reactors, *Proceedings of the Second International Conference on Liquid Metal Technology in Energy Production,* CONF-800401, National Technical Information Service, 1980

R.D. Kane, Liquid Metal Corrosion, *Corrosion: Fundamentals, Testing, and Protection,* Vol 13A, *ASM Handbook,* ASM International, 2003, p 220–227

Liquid Metal Corrosion

Revised by R.D. Kane, InterCorr International, Inc.

Selected References

- C.C. Addison, *The Chemistry of the Liquid Alkali Metals,* John Wiley & Sons, 1984
- *Alkali Metal Coolants,* Symposium Proceedings (Vienna), International Atomic Energy Agency, 1967
- T.L. Anderson and G.R. Edwards, *J. Mater. Energy Syst.,* Vol 2, 1981, p 16–25
- C. Bagnall and D.C. Jacobs, "Relationships for Corrosion of Type 316 Stainless Steel in Sodium," WARD-NA-3045-23, National Technical Information Service, 1974
- W.E. Berry, *Corrosion in Nuclear Applications,* John Wiley & Sons, 1971
- H.U. Borgstedt, Ed., *Proceedings of the Conference on Material Behavior and Physical Chemistry in Liquid Metal Systems,* Plenum Press, 1982
- H.U. Borgstedt and C.M. Matthews, *Applied Chemistry of the Alkali Metals,* Plenum Press, 1986
- W.F. Brehm, "Grain Boundary Penetration of Niobium by Lithium," Ph.D. dissertation, Report HYO-3228-11, Cornell University, 1967
- C.F. Cheng and W.E. Ruther, *Corrosion,* Vol 28 (No. 1), 1972, p 20–22
- M.H. Cooper, Ed., *Proceedings of the International Conference on Liquid Metal Technology in Energy Production,* CONF-760503, P1 and P2, National Technical Information Service, 1977
- J.M. Dahlke, Ed., *Proceedings of the Second International Conference on Liquid Metal Technology in Energy Production,* CONF- 300401-P1 and P2, National Technical Information Service, 1981
- J.F. DeStefano and E.E. Hoffman, *At. Energy Rev.,* Vol 2, 1964, p 3–33
- J.H. DeVan et al., Compatibility of Refractory Alloys with Space Reactor System Coolants and Working Fluids, in CONF-830831D, National Technical Information Service, 1983
- J.E. Draley and J.R. Weeks, Ed., *Corrosion by Liquid Metals,* Plenum Press, 1970
- R.L. Eichelberger and W.F. Brehm, "Effect of Sodium on Breeder Reactor Components," Paper 106, presented at Corrosion/78, National Association of Corrosion Engineers, 1978
- A.H. Fleitman and J.R. Weeks, Mercury as a Nuclear Coolant, *Nucl. Eng. Des.,* Vol 16 (No. 3), 1971
- J.D. Harrison and C. Wagner, *Acta Metall.,* Vol 1, 1959, p 722–735
- S.A. Jannson, Ed., *Chemical Aspects of Corrosion and Mass Transfer in Liquid Metals,* The Metallurgical Society, 1973
- C.J. Klamut, D.G. Schweitzer, J.G.Y. Chow, R.A. Meyer, O.F. Kammerer, J.R. Weeks, and D.H. Gurinsky, Material and Fuel Technology for an LMFR, *Progress in Nuclear Engineering Series IV, V2-Technology Engineering and Safety,* Pergamon Press, 1960
- *Proceedings of the International Conference on Liquid Alkali Metals,* Proceedings of the British Nuclear Energy Society, Thomas Telford Ltd., 1973
- *Proceedings of the International Conference on Sodium Technology and Large Fast Reactor Design,* ANL-7520, Part I, National Technical Information Service, 1969
- *Proceedings of the Third International Conference on Liquid Metal Engineering and Technology,* Proceedings of the British Nuclear Energy Society, Thomas Telford Ltd., 1985
- M.C. Rowland et al.,"Sodium Mass Transfer XV. Behavior of Selected Steels Exposed in Flowing Sodium Test Loops," GEAP-4831, National Technical Information Service, 1965
- P.F. Tortorelli and J.H. DeVan, Corrosion of Fe-Cr-Mn Alloys in Thermally Convective Lithium and Corrosion of Ferrous Alloys Exposed to Thermally Convective Pd-17at.% Li, *J. Nucl. Mater.,* Vol 141–143, *Proceedings of the Second International Conference on Fusion Reactor Materials* (Chicago, April 1976), 1986, p 579–583, 592–598
- J.R. Weeks, *Nucl. Eng. Des.,* Vol 15, 1971, p 363–372
- J.R. Weeks and H.S. Isaacs, *Adv. Corros. Sci. Technol.,* Vol 3, 1973, p 1–65

R.D. Kane, High-Temperature Gaseous Corrosion, *Corrosion: Fundamentals, Testing, and Protection*, Vol 13A, *ASM Handbook*, ASM International, 2003, p 228–235

High-Temperature Gaseous Corrosion

Revised by Russell D. Kane, InterCorr International, Inc.

Introduction

WHEN METAL IS EXPOSED TO AN OXIDIZING GAS at elevated temperature, corrosion can occur by direct reaction with the gas, without the need for the presence of a liquid electrolyte. This type of corrosion is referred to as tarnishing, high-temperature oxidation, scaling, or gaseous corrosion. As shown in Fig. 1 (Ref 1), the rate of attack (in terms of weight gain) increases substantially with temperature for many steels and stainless steel alloys. The surface film typically thickens as a result of reaction at the scale/gas or metal/scale interface due to cation or anion transport through the scale, which behaves as a solid electrolyte. For continuous, nonporous scales, ionic transport through the scale is the rate-controlling process. The thermodynamic stability, the ionic defect structure, and certain morphological features of the scale formed are key factors in determining the resistance of an alloy to a specific environment.

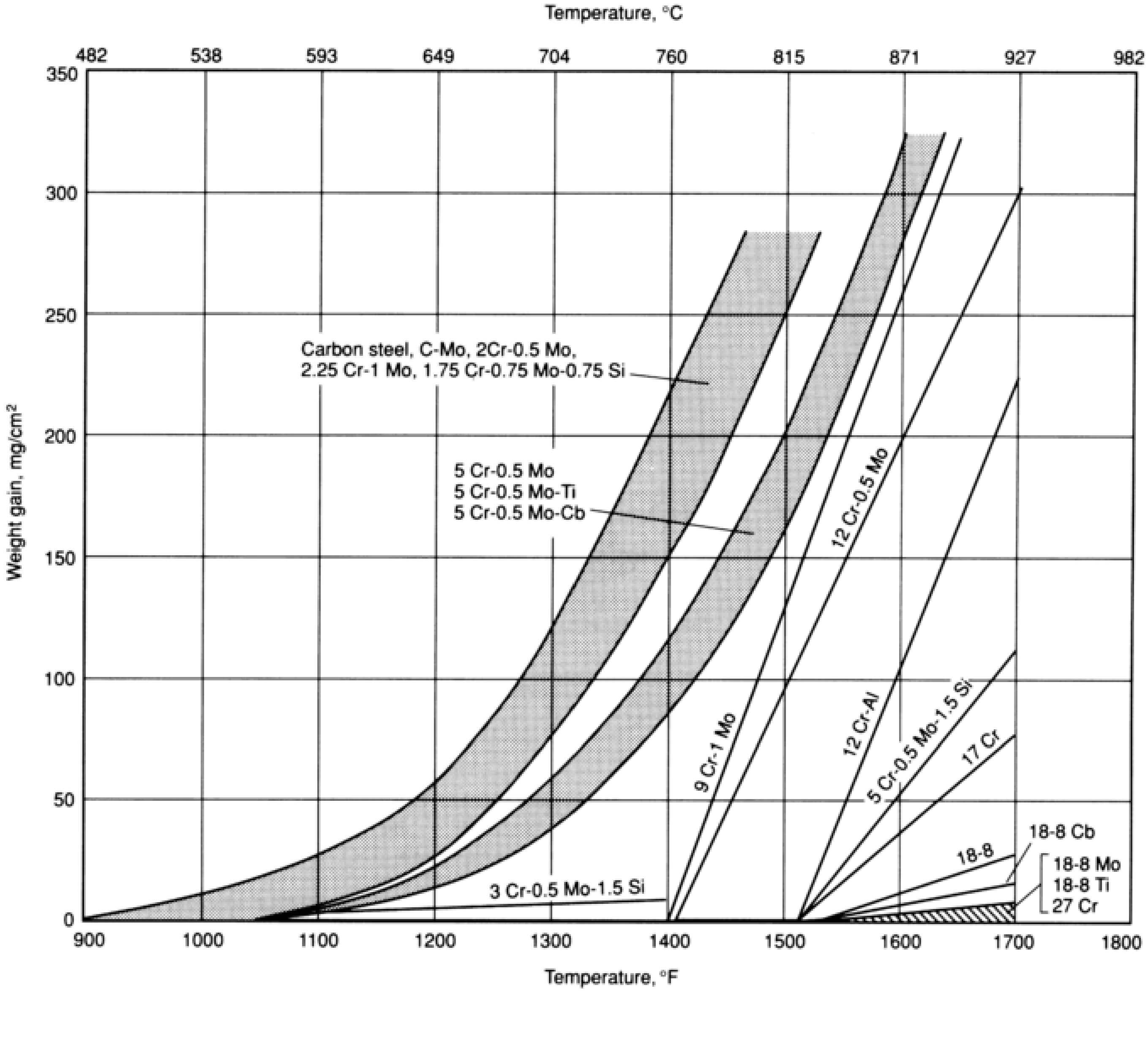

Fig. 1 Oxidation resistance of carbon, low-alloy and stainless steels in air after 100 h at temperatures from 590 to 930 °C (1100 to 1700 °F). Source: Ref 1

Initial film growth is usually very rapid. If the scale is a nonporous solid and completely covers the metal surface, the reaction rate will decrease when the thickness reaches a few thousand angstroms as the transport of reactive species through the film becomes rate controlling. The subsequent corrosion rate depends on the details of this transport mechanism, which may be due to electrical potential or concentration gradients or to migration along preferential paths, and so may correspond to any of several rate laws, as shown in Fig. 2. Where a diffusion process is rate controlling, the kinetics usually follow a parabolic rate law, in which the rate progressively decreases with time (see Fig. 3) (Ref 2). Figure 4(a) illustrates the compact, continuous protective scale of essentially chromium oxide (Cr_2O_3) formed on alloy 800. If the scale is porous (or is formed as a vapor species) or does not completely cover the metal surface, a linear rate is usually experienced.

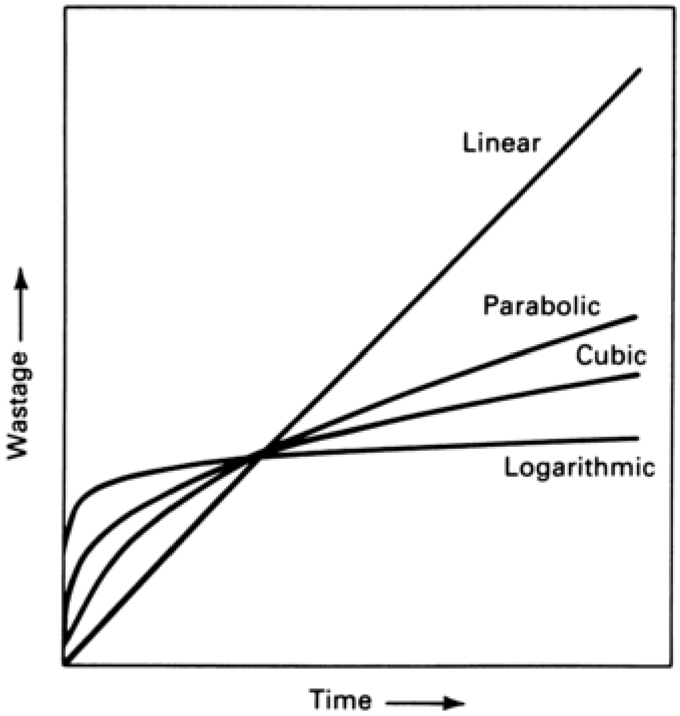

Fig. 2 Forms of kinetic curves that represent various thermal degradation processes

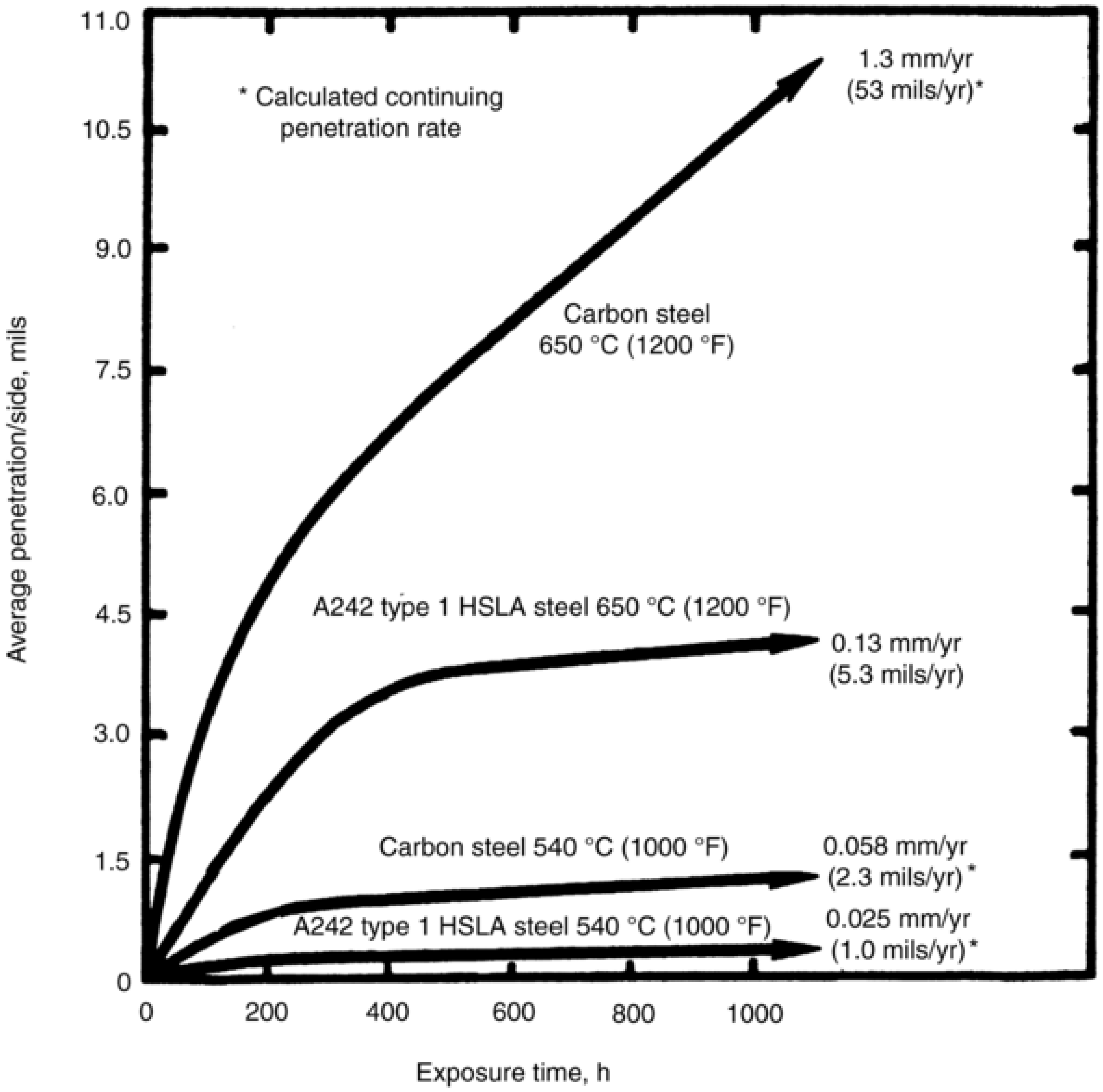

Fig. 3 Oxidation of carbon steel and high-strength low-alloy (HSLA) steel in air. Source: Ref 2

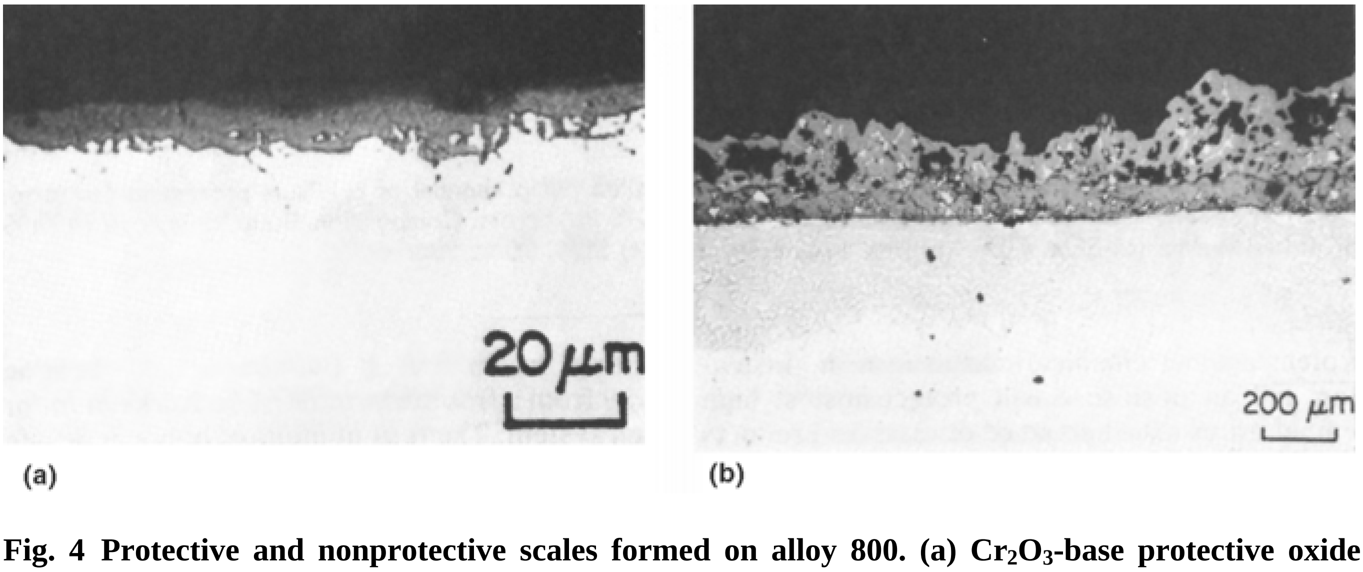

Fig. 4 Protective and nonprotective scales formed on alloy 800. (a) Cr_2O_3-base protective oxide scale formed in sulfur-free oxidizing gas. (b) Sulfide-oxide scale formed in reducing conditions containing hydrogen sulfide. Courtesy of I.G. Wright, Battelle Columbus Division

The latter circumstance can be assessed from the Pilling-Bedworth ratio, which is the ratio of the volumes of oxide produced to that of the metal consumed by oxidation; values of 1.0 or greater result in complete surface coverage by oxide and, usually, protective behavior. This is not a complete or foolproof measure for assessing the likelihood of protective scaling behavior. At high temperatures, the growth of nominally protective oxides may be sufficiently rapid that the compressive stresses resulting from a Pilling- Bedworth ratio greater than 1 become sufficiently great that the scale (or alloy) deforms, resulting in spalling that acts as a stress-relief mechanism; in some cases, the protection offered by such scales may be low at this point, as shown in Fig. 5.

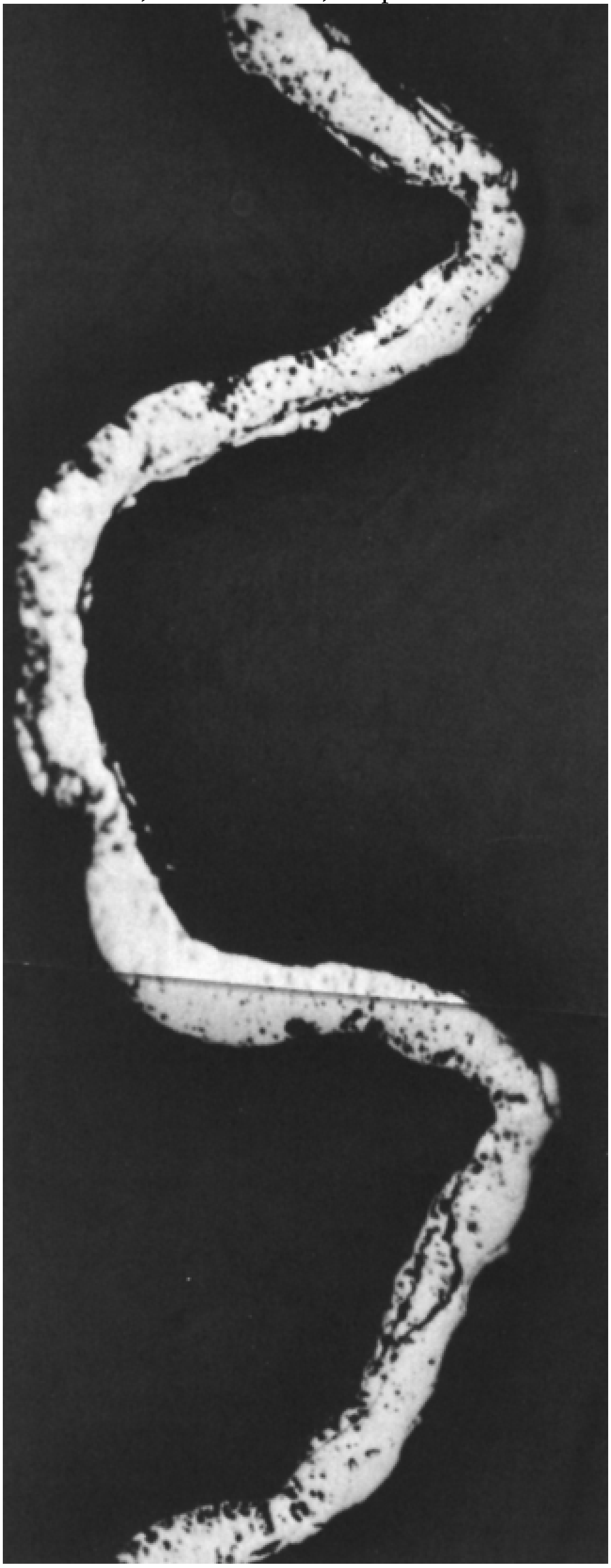

Fig. 5 Cr_2O_3 scale formed on pure chromium at 1100 °C (2012 °F). A Pilling-Bedworth ratio of 2.0 results in high compressive stress in the scale, which is relieved by buckling and spalling. Courtesy of I.G. Wright, Battelle Columbus Division

The desired characteristics for a protective oxide scale include:

- High thermodynamic stability (highly negative Gibbs free energy of formation) so that it forms preferentially to other reaction products possible under the exposure conditions
- Low vapor pressure so that the oxide forms as a solid and does not evaporate into the atmosphere
- Pilling-Bedworth ratio greater than 1.0 so that the oxide completely covers the metal surface
- Low coefficient of diffusion of reactant species (metal cations and corrodent anions) so that the scale has a slow growth rate
- High melting temperature
- Good adherence to the metal substrate, which usually involves a coefficient of thermal expansion close to that of the metal, and sufficient high-temperature plasticity to resist fracture from differential thermal expansion stresses that can result particularly from thermal cycling

High-temperature scales are usually thought of as oxides, but may also be sulfides, possibly carbides, or mixtures of these species. Oxides and sulfides are nonstoichiometric compounds and semiconductors.
There are essentially two types of semiconductors: *p*-type (or positive carrier)—which may have vacancies in its metal lattice or an excess of anions contained interstitially—and *n*-type (or negative carrier)—which may have an excess of metal ions contained interstitially or vacant anion lattice sites. For diffusion-controlled scaling, the rate of scale growth can be altered by modification of the concentration of the particular defects involved. For example, *p*-type oxides exhibit increased cationic transport rates (increased oxidation rates) at increased oxygen pressures, while transport in *n*-type oxides is essentially independent of oxygen pressure. Both types of oxide can be doped by the addition of specific ions to the oxide lattice. For *p*-type metal deficit oxides, for example, the addition of cations of higher valence than the native cations results in an increase in the number of cation vacancies and therefore an increase in the oxidation rate, while lower-valence cation additions have the opposite effect.
Sulfides typically exhibit an intrinsically greater rate of transport of anions and cations than the oxides of the same metal and so provide scales that are significantly less protective than oxides.

References cited in this section

1. H.E. McGarrow, Ed., *Making, Shaping and Treating Steel,* United States Steel Corp., 1971. p 1136

2. R.T. Jones, in *Process Industry Corrosion,* National Association of Corrosion Engineers, 1986, p 373

R.D. Kane, High-Temperature Gaseous Corrosion, *Corrosion: Fundamentals, Testing, and Protection*, Vol 13A*, ASM Handbook*, ASM International, 2003, p 228–235

High-Temperature Gaseous Corrosion

Revised by Russell D. Kane, InterCorr International, Inc.

High-Temperature Oxidation

Alloys intended for high-temperature applications are designed to have the capability of forming protective oxide scales. Alternatively, where the alloy has ultrahigh-temperature- strength capabilities (which is usually synonymous with reduced levels of protective scale- forming elements), it must be protected by a specially

designed coating. Oxides that effectively meet the criteria for protective scales listed previously and can be formed on practical alloys are limited to Cr_2O_3, alumina (Al_2O_3), and possibly silicon dioxide (SiO_2). In the pure state, Al_2O_3 exhibits the slowest transport rates for metal and oxygen ions and so should provide the best oxidation resistance.

Alloying requirements for the production of specific oxide scales have been translated into minimum levels of the scale-forming elements, or combinations of elements, depending on the base alloy composition and the intended service temperature. Figure 6 represents the oxidation rate of iron-chromium alloys (1000 °C, or 1832 °F, in 0.13 atm oxygen) and depicts the types of oxide scale associated with various alloy types in this range of chromium content. Figure 7 illustrates the morphology of a semiprotective scale formed on a cobalt-chromium alloy. Alloys based on these minimum specifications will form the desired protective oxide upon initial exposure, but because of the accompanying depletion of the scale-forming element, they will probably be unable to re-form the protective layer in the event of loss or failure of the initial scale.

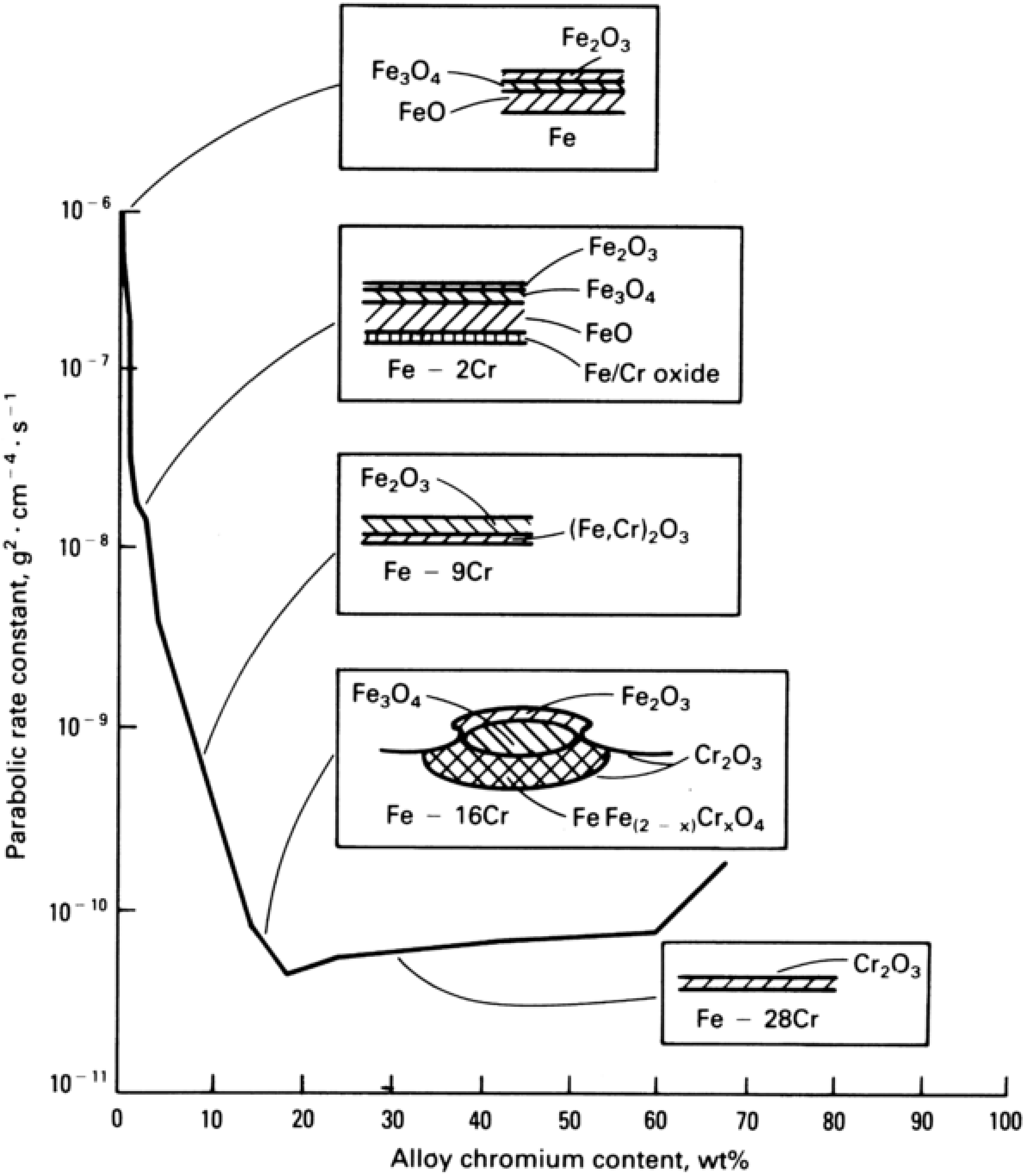

Fig. 6 Variation of the oxidation rate and oxide scale structure with alloy chromium content (based on isothermal studies at 1000 °C, or 1832 °F, in 0.13 atm oxygen)

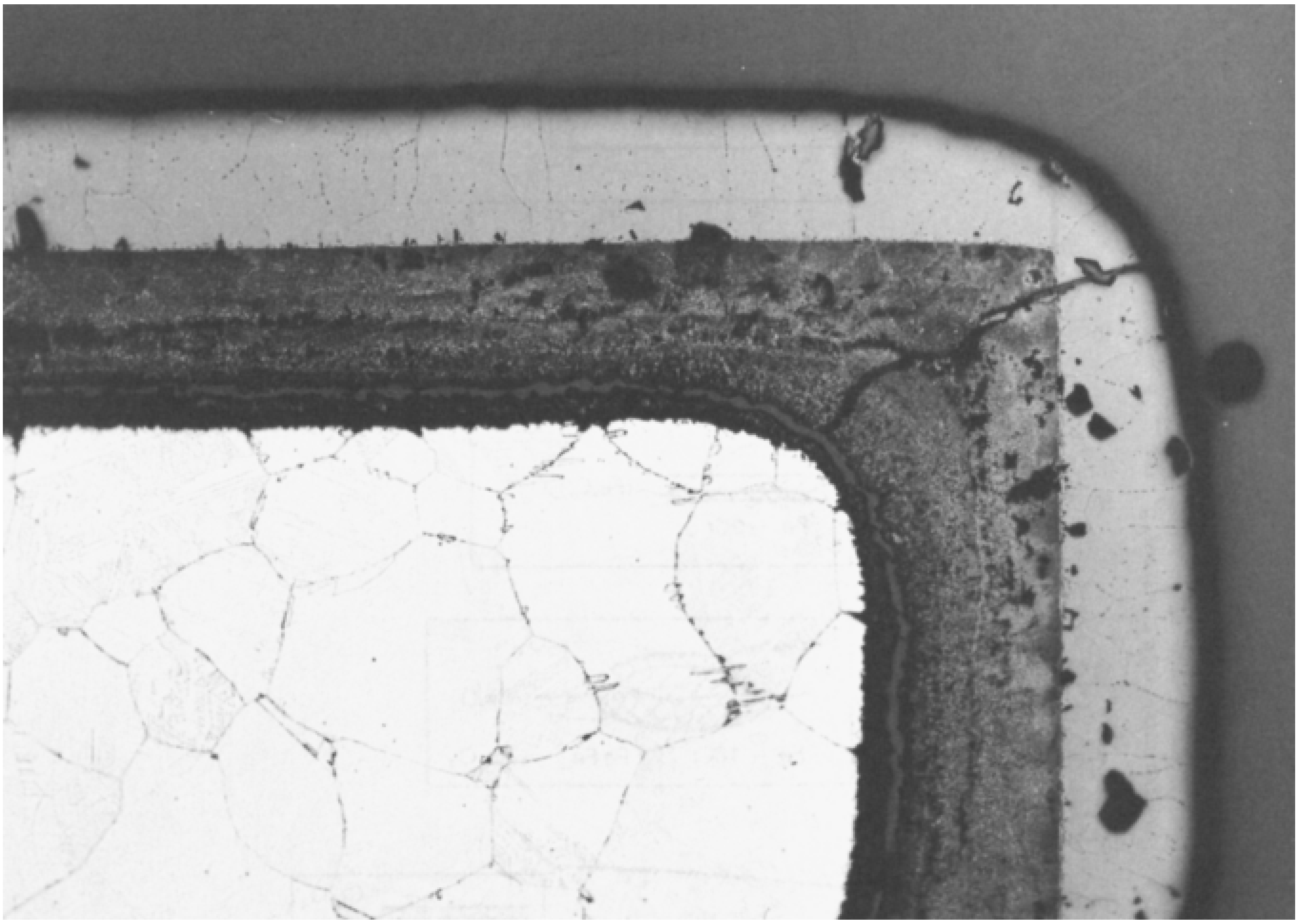

Fig. 7 Multilayer oxide scale formed on Co-10Cr alloy at 1100 °C (2012 °F). Outer layer is CoO; inner (mottled gray) layer is CoO containing dissolved chromium and particles of Co-Cr spinel. The chromium level in this alloy is insufficient to form a fully protective Cr_2O_3 scale. Courtesy of I.G. Wright, Battelle Columbus Division

A useful concept in assessing the potential high-temperature oxidation behavior of an alloy is that of the reservoir of scale-forming element contained by the alloy in excess of the minimum level (around 20 wt% for iron-chromium alloy at 1000 °C, or 1832 °F, according to Fig. 6). The more likely the service conditions are to cause repeated loss of the protective oxide scale through spalling, erosion, wear, or mechanical stresses, the greater the reservoir of scale-forming element required in the alloy for continued protection. Extreme cases of this concept result in chromizing or aluminizing to enrich the surface regions of the alloy or in the provision of an external coating rich in the scale-forming elements.

The breakdown of protective scales based on Cr_2O_3 or Al_2O_3 appears, in the majority of cases, to originate through mechanical means. The most common is spallation as a result of thermal cycling, or loss through erosion or abrasion. Typical scale structures on an Fe-18Cr alloy after thermal cycling are shown in Fig. 8. Cases in which the scales have been destroyed chemically are usually related to reactions occurring beneath deposits, especially where these consist of molten species. An additional mode of degradation of protective Cr_2O_3 scale is through oxidation to the volatile chromium trioxide (CrO_3), which becomes prevalent above about 1010 °C (1850 °F) and is greatly accelerated by high gas flow rates.

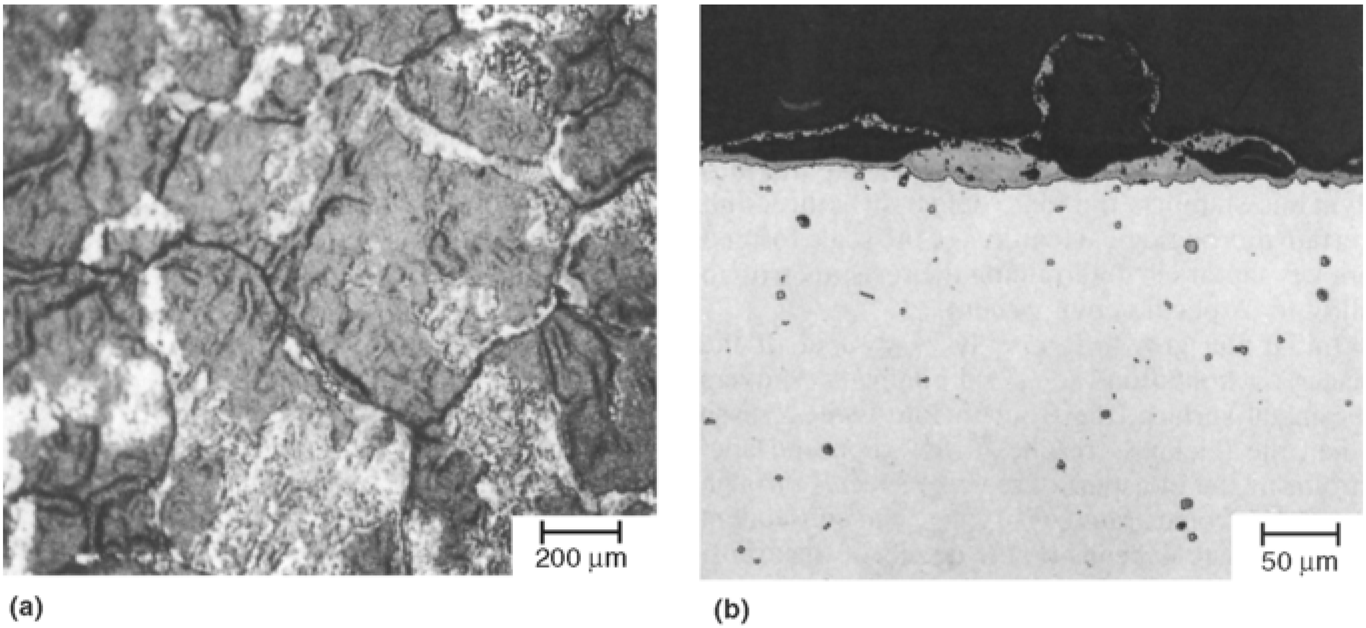

Fig. 8 Topography (a) and cross section (b) of oxide scale formed on Fe-18Cr alloy at 1100 °C (2012 °F). The bright areas on the alloy surface (a) are areas from which scale has spalled. The buckled scale and locally thickened areas (b) are iron-rich oxide. The thin scale layer adjacent to the alloy is Cr_2O_3, which controls the oxidation rate. Courtesy of I.G. Wright, Battelle Columbus Division

Because these protective oxide scales will form wherever the alloy surface is exposed to the ambient environment, they will form at all surface discontinuities; therefore, the possibility exists that notches of oxide will form at occluded angles in the surface, which may eventually serve to initiate or propagate cracks under thermal cycling conditions. The ramifications of stress-assisted oxidation (and of oxidation assisting the applied stress) in the production of failure conditions are not very well understood, but can constitute important considerations in predicting corrosion performance in actual operating systems and be of benefit in practical failure analysis.

R.D. Kane, High-Temperature Gaseous Corrosion, *Corrosion: Fundamentals, Testing, and Protection,* Vol 13A, *ASM Handbook,* ASM International, 2003, p 228–235

High-Temperature Gaseous Corrosion

Revised by Russell D. Kane, InterCorr International, Inc.

Sulfidation

When the sulfur activity (partial pressure, concentration) of the gaseous environment is sufficiently high, sulfide phases, instead of oxide phases, can be formed. The mechanisms of sulfide formation in gaseous environments and beneath molten-salt deposits have been determined in recent years. In the majority of environments encountered in practice by oxidation-resistant alloys, Al_2O_3 or Cr_2O_3 should form in preference to any sulfides, and destructive sulfidation attack occurs mainly at sites where the protective oxide has broken down. The role of sulfur, once it has entered the alloy, appears to be to tie up the chromium and aluminum as sulfides, effectively redistributing the protective scale-forming elements near the alloy surface and thus interfering with the process of formation or re-formation of the protective scale. If sufficient sulfur enters the alloy so that all immediately available chromium or aluminum is converted to sulfides, then the less stable sulfides of the base metal may form because of morphological and kinetic reasons. It is these base metal sulfides that are often responsible for the observed accelerated attack, because they grow much faster than the

oxides or sulfides of chromium or aluminum; in addition, they have relatively low melting points, so that molten slag phases are often possible. Figure 4 compares a protective (oxide) scale and a nonprotective (sulfide) scale formed on alloy 800. It is precisely this effect that provides the requirement for materials with higher alloy content of oxide-forming elements to impart increased sulfidation resistance.

Sulfur can transport across continuous protective scales of Al_2O_3 and Cr_2O_3 under certain conditions, with the result that discrete sulfide precipitates can be observed immediately beneath the scales on alloys that are behaving in a protective manner. For reasons indicated previously, as long as the amount of sulfur present as sulfides is small, there is little danger of accelerated attack. However, if oxidizing conditions exist, once sulfides have formed in the alloy, there is a tendency for the sulfide phases to be preferentially oxidized by the encroaching reaction front and for the sulfur to be displaced inward, forming new sulfides deeper in the alloy, often in grain boundaries or at the sites of other chromium- or aluminum-rich phases, such as carbides. In this way, fingerlike protrusions of oxide/sulfide can be formed from the alloy surface inward, which may act to localize stress or otherwise reduce the load-bearing section. Such attack of an austenitic stainless steel experienced in a coal-gasifier product gas is shown in Fig. 9. The sulfidation behavior of alloy 800 at temperatures and oxygen and sulfur potentials representative of coal-gasification processes is illustrated in Fig. 10, Fig. 11, Fig. 12. Additionally, as the oxygen and sulfur activities may vary in service, the tendencies for sulfidation and oxidation to persist or coexist change as well. Figure 13 (Ref 3) shows a stability diagram for the Cr-S-O system. This indicates how the dominant corrosion mechanism can change from oxidation or sulfidation depending on the availability of sulfur and oxygen. This figure also indicates the predominance of oxidation under all but the highly reducing conditions provided by very low oxygen partial pressure.

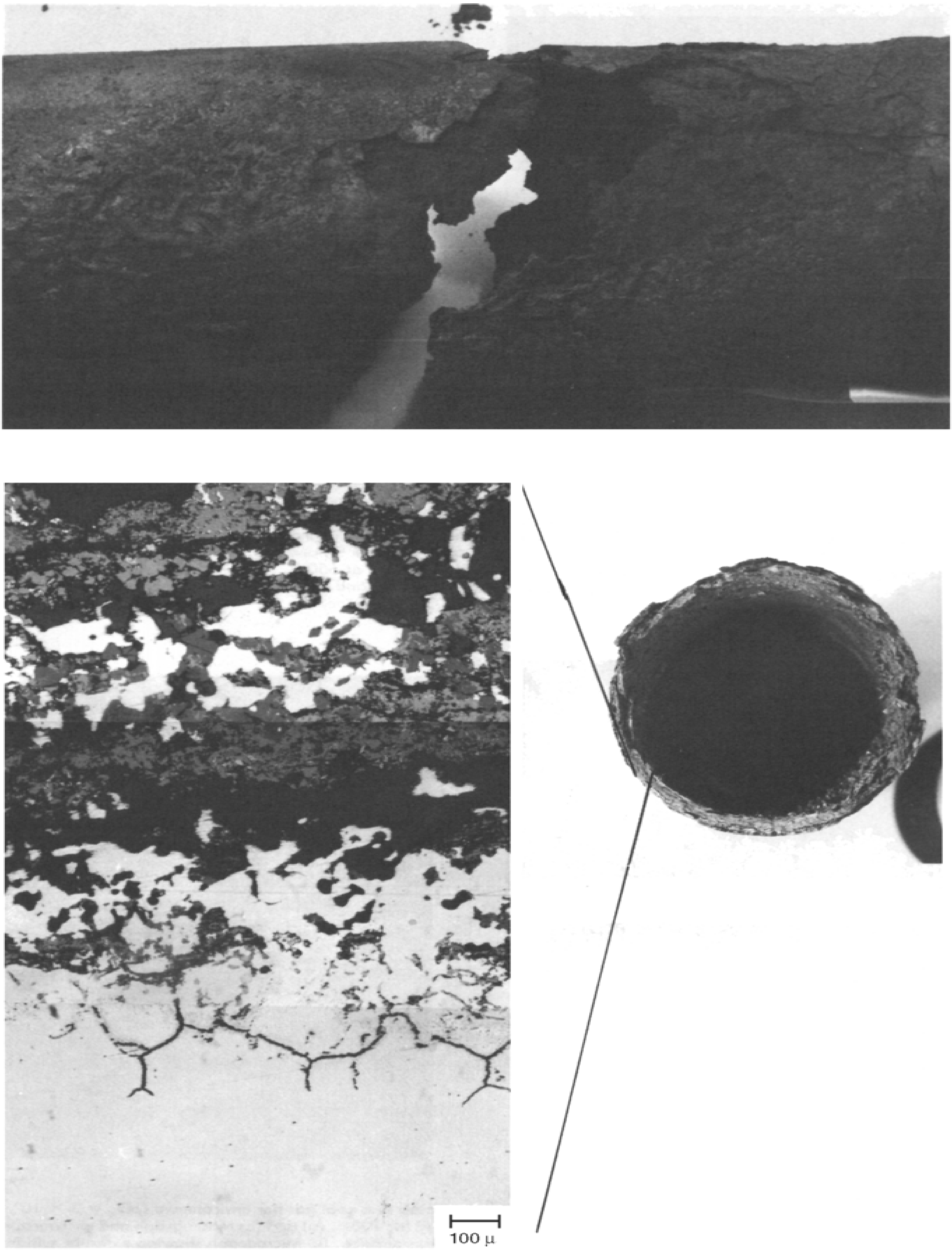

Fig. 9 Example of high-temperature sulfidation attack in a type 310 heat-exchanger tube after ~100 h at 705°C (1300 °F) in coal-gasifier product gas

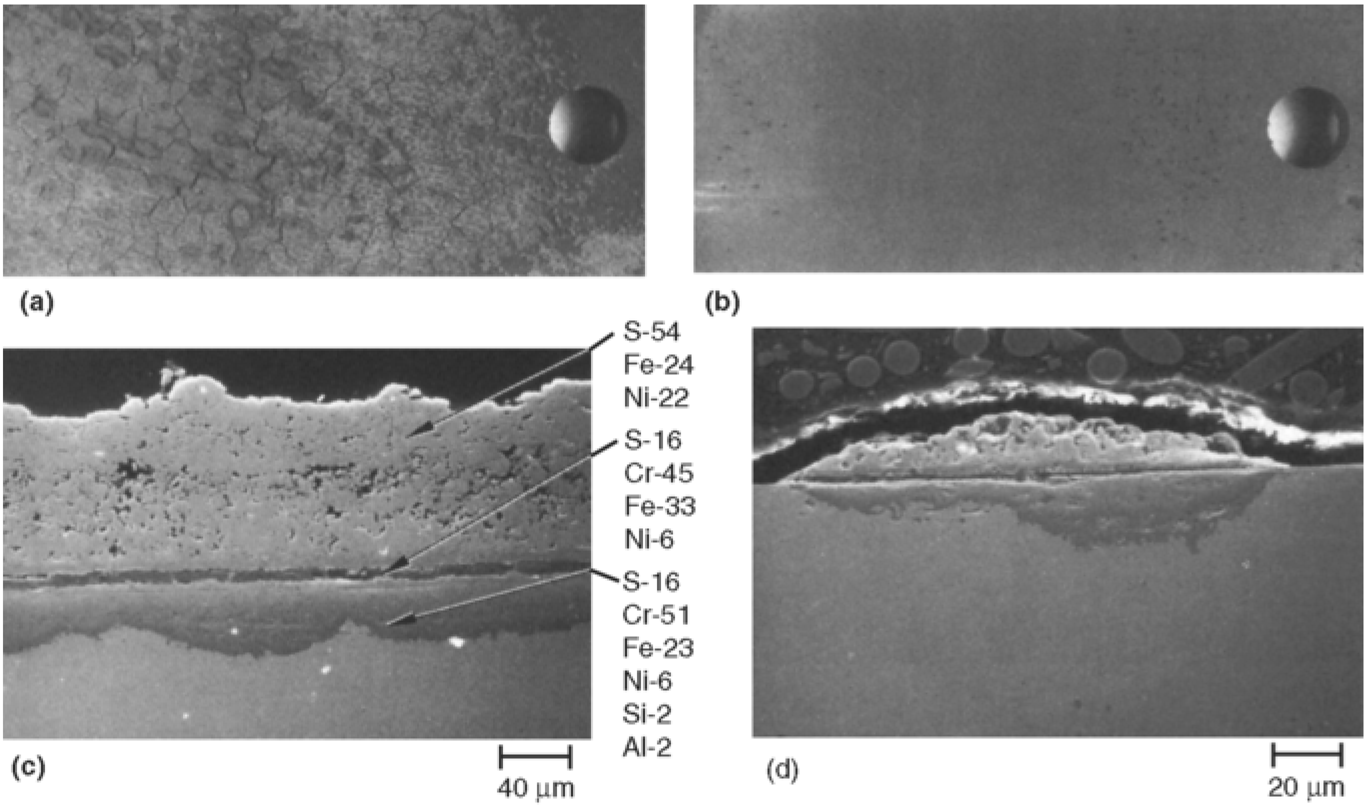

Fig. 10 Alloy 800 test coupons with a 0.254 mm (0.01 in.) diam grain size exposed to a coal-gasifier environment for 100 h. (a) and (c) Tested at 650 °C (1200 °F) and oxygen and sulfur partial pressures of 3 × 10^{-24} atm and 1 × 10^{-8} atm, respectively. (b) and (d) Tested at 650 °C (1200 °F) and p_{O_2}= 3 × 10^{-24} atm and p_{S_2}= 1 × 10^{-9} atm. Scanning electron micrographs show sulfide scale (c) and an external sulfide formation (d). (a) and (b) ~2×. Courtesy of G.R. Smolik and D.V. Miley, E.G. & G. Idaho, Inc.

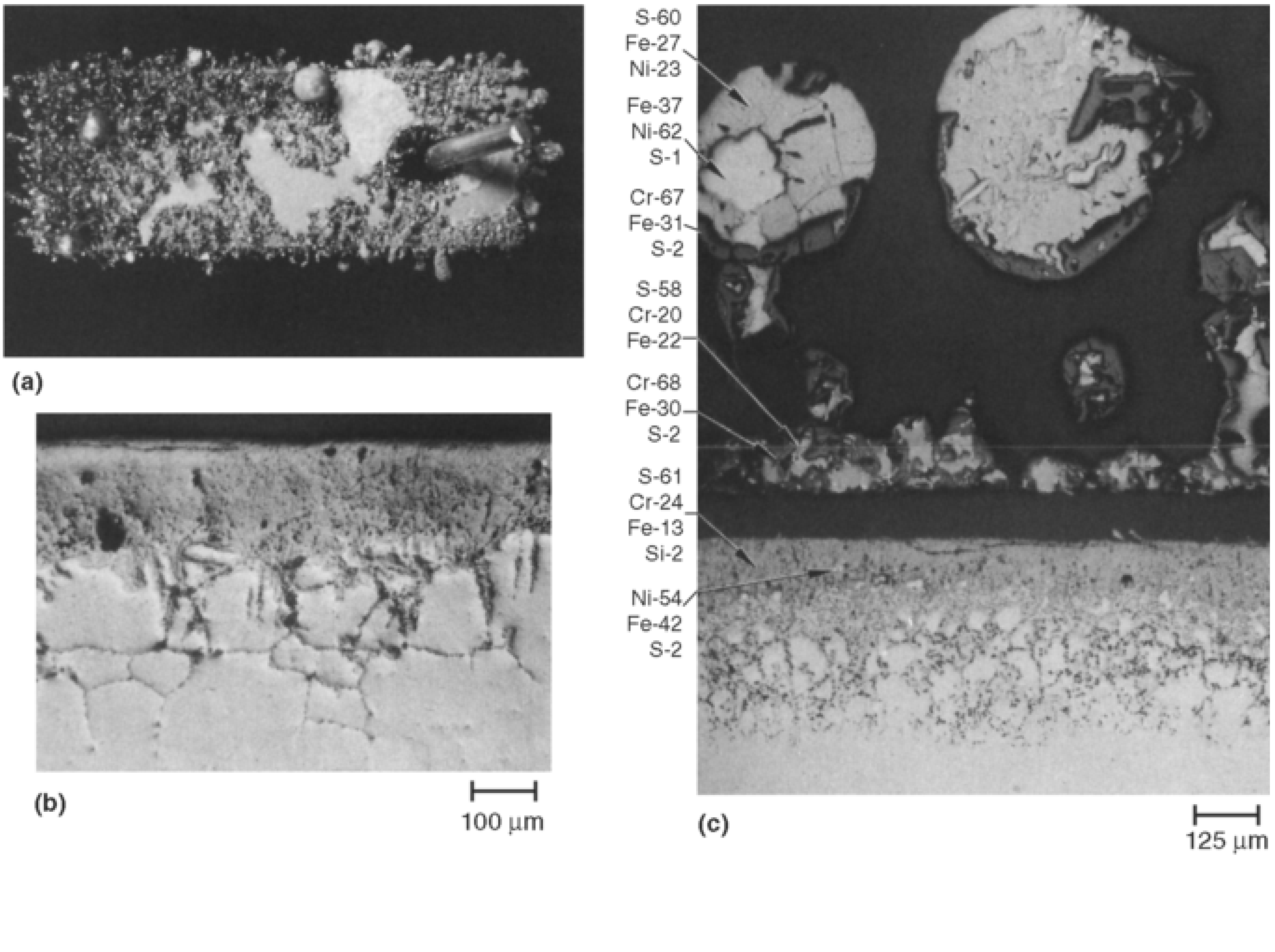

Fig. 11 Sulfidation attack of alloy 800 test coupons exposed to a coal-gasifier environment (p_{O_2} = 3 × 10^{-20} atm and p_{S_2}= 1 × 10^{-7} atm) at 870 °C (1600 °F) for 100 h. (a) and (b) Macrograph and micrograph, respectively, of a test coupon with a 0.254 mm (0.01 in.) diam grain size. (c) Micrograph showing external sulfides, sulfide scale, and intergranular sulfidation of a test coupon with a 0.022 to 0.032 mm (0.0008 to 0.0013 in.) diam grain size. (a) ~1.5×. Courtesy of G.R. Smolik and D.V. Miley, E.G. & G. Idaho, Inc.

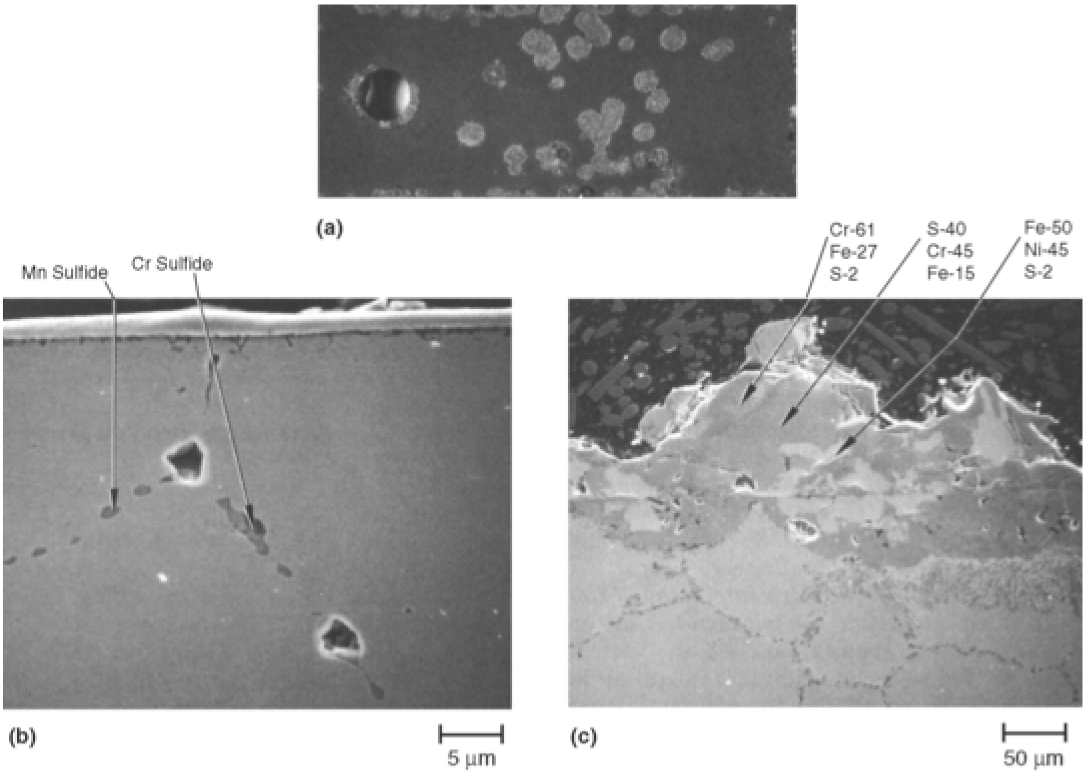

Fig. 12 Macrograph (a) of an alloy 800 test coupon with a 0.254 mm (0.01 in.) diam grain size exposed to a coal-gasifier environment (p_{O_2} = 3 × 10^{-19} atm and p_{S_2}= 1 × 10^{-7} atm) at 870 °C (1600 °F) for 100 h. ~1.5×. Micrographs (b) and (c) show cross sections through the Cr_2O_3 layer and disrupted oxide region having external sulfides. Courtesy of G.R. Smolik and D.V. Miley, E.G. & G. Idaho, Inc.

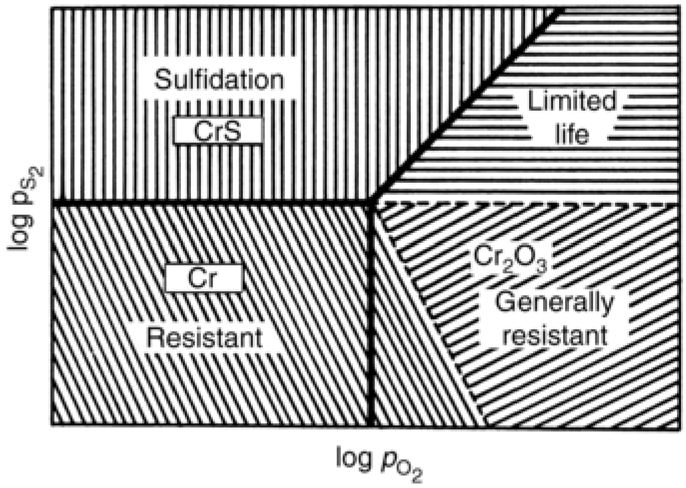

Fig. 13 Stability of the Cr-S-O system Source: Ref 3

Reference cited in this section

3. H.W. Eiselstein and E.N. Skinner, in *Effect of Cyclic Heating and Stressing on Metals at Elevated Temperature,* STP 165, American Society for Testing and Materials, 1954, p 162

R.D. Kane, High-Temperature Gaseous Corrosion, *Corrosion: Fundamentals, Testing, and Protection*, Vol 13A, *ASM Handbook*, ASM International, 2003, p 228–235

High-Temperature Gaseous Corrosion

Revised by Russell D. Kane, InterCorr International, Inc.

Carburization

As in the case of sulfide penetration, carburization of high-temperature alloys is thermodynamically unlikely except at very low oxygen partial pressures, because the protective oxides of chromium and aluminum are generally more likely to form than the carbides. However, carburization can occur kinetically in many carbon-containing environments. Carbon transport across continuous nonporous scales of Al_2O_3 or Cr_2O_3 is very slow, and alloy pretreatments likely to promote such scales, such as initially smooth surfaces or preoxidation, have generally been found to be effective in decreasing carburization attack. In practice, the scales formed on high-temperature alloys often consist of multiple layers of oxides resulting from localized bursts of oxide formation in areas where the original scale was broken or lost. The protection is derived from the innermost layer, which is usually richest in chromium or aluminum. Concentration of gaseous species such as carbon monoxide in the outer porous oxide layers appears to be one means by which sufficiently high-carbon activities can be generated at the alloy surface for carburization to occur in otherwise oxidizing environments. The creation of localized nonoxidizing, microenvironments is also possible under surface deposits that create stagnant conditions not permeable by the ambient gas, resulting in local regions of low oxygen activities where carburization can persist.

Once inside the alloy, the detrimental effects of the carbon depend on the location, composition, and morphology of the carbide formed. Austenitic steels should carburize more readily than ferritic steels because of the high solubility of carbon in austenite. Iron-chromium alloys containing less than about 13% Cr contain various amounts of austenite, depending on temperature, and should be susceptible to carburization, while alloys with 13 to 20% Cr will form austenite as a result of absorption of small amounts of carbon. Iron-chromium alloys containing more than ~20% Cr can absorb considerable amounts of carbon before austenite forms, becoming principally $(CrFe)_{23}C_6$ and ferrite. An example of rapid high-temperature carburization attack of an austenitic stainless steel is shown in Fig. 14.

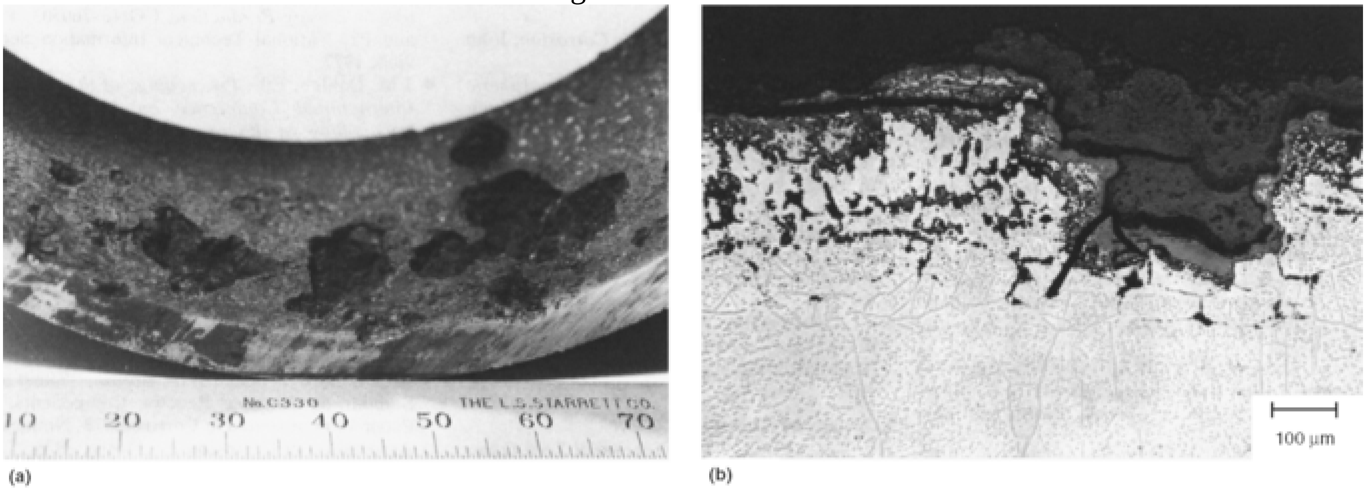

Fig. 14 Example of high-temperature carburization attack pitting in type 310 reactor wall after ~4000 h exposure to coal-gasification product gas. The pits were formed during operation under conditions of high-carbon activity in the gas. (a) Overall view of pitting. (b) Section through a pit. Courtesy of I.G. Wright, Battelle Columbus Division

Alloying elements can exert an influence on the susceptibility to carburization of various alloys. In particular, silicon, niobium, tungsten, titanium, and the rare earths have been noted as promoting resistance to

carburization. The influence of silicon is particularly noteworthy as shown in Fig. 15 (Ref 4). It shows particular benefits in terms of reducing weight gain over the range of 1.5 to 2.5% in the bulk for Fe-Ni- Cr alloys of nominally 24 to 28% Cr and 20% Ni. Minor alloying additions of niobium in Ni- Cr-Fe alloys have been shown to reduce carburization rates by up to 25% over those without niobium additions. Experience with aluminum and manganese has been varied, although aluminum additions and diffusion coatings have shown particular promise in being able to set up a barrier to carbon ingress, thereby increasing resistance to carburization. Studies of alloy ratio of nickel and chromium have shown that alloys based on 50:50 nickel-to-chromium composition have generally better resistance than alloys where this ratio is 0.5 or 0.25. However, the presence of lead, molybdenum, cobalt, zirconium, and boron are considered detrimental to carburization resistance.

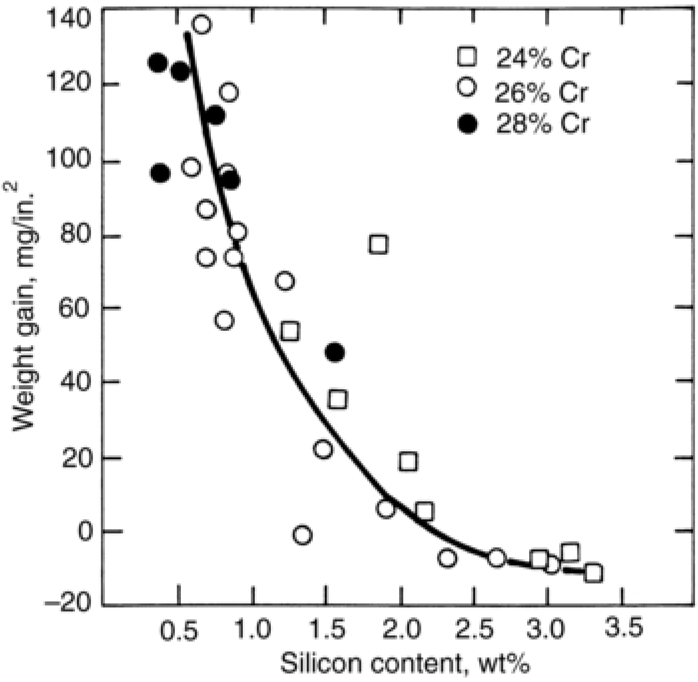

Fig. 15 Effect of silicon on the carburization resistance of cast Fe-20Ni-Cr alloys tested at 1090 °C (2000 °F) for 24 h in wet ethane Source: Ref 4

Reference cited in this section

4. L.H. Wolfe, *Mater. Perform.,* April 1978, p 38

R.D. Kane, High-Temperature Gaseous Corrosion, *Corrosion: Fundamentals, Testing, and Protection,* Vol 13A*, ASM Handbook,* ASM International, 2003, p 228–235

High-Temperature Gaseous Corrosion

Revised by Russell D. Kane, InterCorr International, Inc.

Other Forms of High-Temperature Corrosion

Hydrogen Effects. In hydrogen environments at elevated temperatures and pressures, there is increasing availability of atomic hydrogen that can easily penetrate metal structures and react internally with reducible species. An example is the attack experienced by carbon and low-alloy steels, in which atomic hydrogen reacts with iron carbide to form methane, which then leads to loss of strength from decarburization, formation of voids, and fissuring of the steel. Alloy steels with stable carbides, such as chromium carbides, are less

susceptible to this form of attack due to the greater stability of chromium carbide versus Fe_3C found in carbon steels. However, as the partial pressure of hydrogen and/or the temperature of exposure increases, a greater amount of these alloying additions are required to prevent such attack. One example is 2.25Cr-1Mo, a steel that undergoes some decarburization in high- temperature high-pressure hydrogen, but is less likely to fissure than carbon steel. However, as the conditions increase in severity, higher-alloy steels such as 5Cr-0.5Mo or 9Cr-1Mo may be required. The susceptibility of steels to attack by hydrogen can be judged from the Nelson Curves, which indicate the regions of temperature and pressure in which a variety of steels will suffer attack.

Another alloy susceptible to hydrogen attack is copper containing small amounts of cuprous oxide. This oxide reacts to form steam within the alloy, resulting in significant void formation.

Hot corrosion generally refers to a form of accelerated attack experienced by the hot gas path components of gas turbine engines. Two forms of hot corrosion can be distinguished; most of the corrosion encountered in turbines burning liquid fuels can be described as type I hot corrosion, which occurs primarily in the metal temperature range of 850 to 950 °C (1550 to 1750 °F). This is a sulfidation-based attack on the hot gas path parts involving the formation of condensed salts, which are often molten at the turbine operating temperature. The major components of such salts are sodium sulfate (Na_2SO_4) and/or potassium sulfate (K_2SO_4), apparently formed in the combustion process from sulfur from the fuel and sodium from the fuel or the ingested air. Because potassium salts act very similarly to sodium salts, alkali specifications for fuel or air are usually taken to be the sum total of sodium plus potassium. An example of the corrosion morphology typical of type I hot corrosion is shown in Fig. 16.

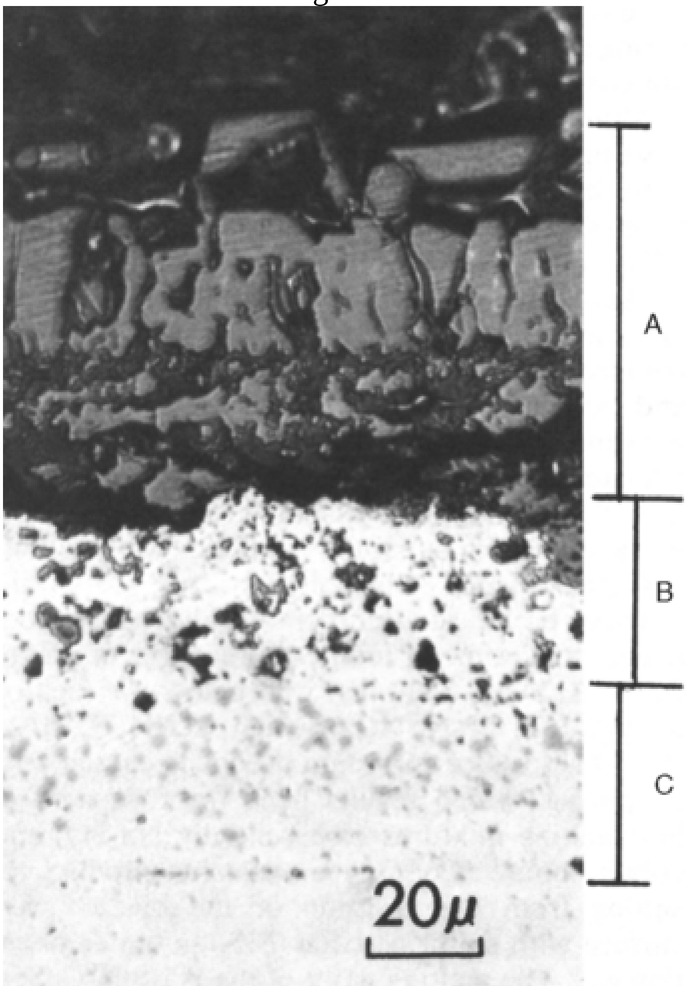

Fig. 16 Ni-20Cr-2ThO$_2$ after simulated type I hot-corrosion exposure (coated with Na$_2$SO$_4$ and oxidized in air at 1000 °C, or 1832 °F). A, nickel-rich scale; B, Cr$_2$O$_3$ subscale; C, chromium sulfides. Courtesy of I.G. Wright, Battelle Columbus Division

Very small amounts of sulfur and sodium or potassium in the fuel and air can produce sufficient Na_2SO_4 in the turbine to cause extensive corrosion problems because of the concentrating effect of turbine pressure ratio. For example, a threshold level has been suggested for sodium in air of 0.008 ppm by weight below which hot corrosion will not occur. Type I hot corrosion, therefore, is possible even when premium fuels are used. Other

fuel (or air) impurities, such as vanadium, phosphorus, lead, and chlorides, may combine with Na_2SO_4 to form mixed salts having reduced melting temperature and thus broaden the range of conditions over which this form of attack can occur. This is one of the major problems in combustion of impure fuels and incineration of municipal wastes. Also, agents such as unburned carbon can promote deleterious interactions in the salt deposits.

Research in the 1970s and 1980s led to greater definition of the relationships among temperature, pressure, salt concentration, and salt vapor- liquid equilibria so that the location and rate of salt deposition in an engine can be predicted. Additionally, it has been demonstrated that a high chromium content is required in an alloy for good resistance to type I hot corrosion. The trend to lower chromium levels with increasing alloy strength has therefore rendered most superalloys inherently susceptible to this type of corrosion. The effects of other alloying additions, such as tungsten, molybdenum, and tantalum, have been documented, and their effects on rendering an alloy more or less susceptible to type I hot corrosion are known and mostly understood.

Although various attempts have been made to develop figures of merit to compare superalloys, these have not been universally accepted. Nonetheless, the near standardization of such alloys as alloy 738 and alloy 939 for first-stage blades/ buckets, and FSX-414 for first-stage vanes/nozzles, implies that these are the accepted best compromises between high-temperature strength and hot-corrosion resistance. It has also been possible to devise coatings with alloying levels adjusted to resist this form of hot corrosion. The use of such coatings is essential for the protection of most modern superalloys intended for duty as first-stage blades or buckets.

Type II, or low-temperature hot corrosion, occurs in the metal temperature range of 650 to 700 °C (1200 to 1300 °F), well below the melting temperature of Na_2SO_4, which is 884 °C (1623 °F). This form of corrosion produces characteristic pitting, which results from the formation of low-melting mixtures of essentially Na_2SO_4 and cobalt sulfate ($CoSO_4$), a corrosion product resulting from the reaction of the blade/bucket surface with sulfur trioxide (SO_3) in the combustion gas. The melting point of the Na_2SO_4-$CoSO_4$ eutectic is 540 °C (1004 °F). Unlike type I hot corrosion, a partial pressure of SO_3 in the gas is critical for the reactions to occur. Knowledge of the SO_3 partial pressure-temperature relationships inside a turbine allows some prediction of where type II hot corrosion can occur. Cobalt- free nickel-base alloys (and coatings) may be more resistant to type II hot corrosion than cobalt-base alloys; it has also been observed that resistance to type II hot corrosion increases with the chromium content of the alloy or coating. Results from corrosion tests over several commercial alloys over a range of temperatures using a mixed-ash composition of Na_2SO_4 and K_2SO_4 is shown in Fig. 17 (Ref 5). It is the role of alloy composition and service temperature to define conditions for acceptable corrosion resistance and alloy use.

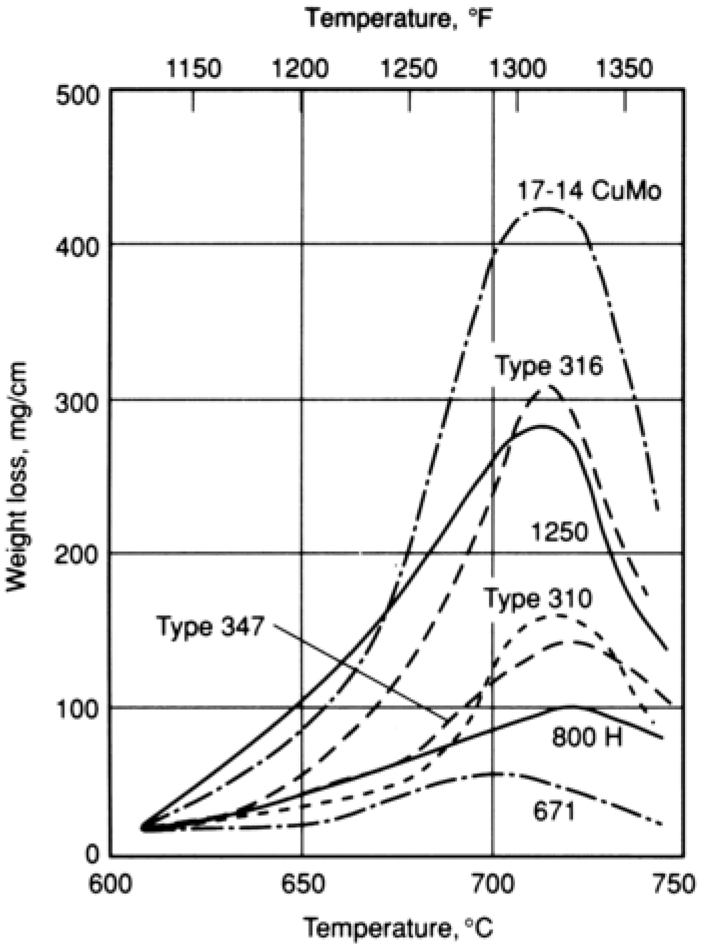

Fig. 17 Results of laboratory tests conducted in synthetic flue gas ($80N_2$-$15CO_2$-$4O_2$-$1SO_2$, saturated with H_2O) with synthetic ash (37.5 mol% Na_2SO_4, and 25 mol% Fe_2O_3) covering samples. Exposure was 50 h. Source: Ref 5

Reference cited in this section

5. J.S. Benjamin, *Metall. Trans.,* Vol 1, 1970, p 2943

R.D. Kane, High-Temperature Gaseous Corrosion, *Corrosion: Fundamentals, Testing, and Protection,* Vol 13A, *ASM Handbook,* ASM International, 2003, p 228–235

High-Temperature Gaseous Corrosion

Revised by Russell D. Kane, InterCorr International, Inc.

Acknowledgment

This article is adapted from Ian G. Wright “High-Temperature Corrosion,” *Corrosion,* Vol 13, 9th edition, *Metals Handbook,* ASM International, 1987, pages 97–101.

R.D. Kane, High-Temperature Gaseous Corrosion, *Corrosion: Fundamentals, Testing, and Protection*, Vol 13A, *ASM Handbook*, ASM International, 2003, p 228–235

High-Temperature Gaseous Corrosion

Revised by Russell D. Kane, InterCorr International, Inc.

References

1. H.E. McGarrow, Ed., *Making, Shaping and Treating Steel,* United States Steel Corp., 1971. p 1136
2. R.T. Jones, in *Process Industry Corrosion,* National Association of Corrosion Engineers, 1986, p 373
3. H.W. Eiselstein and E.N. Skinner, in *Effect of Cyclic Heating and Stressing on Metals at Elevated Temperature,* STP 165, American Society for Testing and Materials, 1954, p 162
4. L.H. Wolfe, *Mater. Perform.,* April 1978, p 38
5. J.S. Benjamin, *Metall. Trans.,* Vol 1, 1970, p 2943

R.D. Kane, High-Temperature Gaseous Corrosion, *Corrosion: Fundamentals, Testing, and Protection*, Vol 13A, *ASM Handbook*, ASM International, 2003, p 228–235

High-Temperature Gaseous Corrosion

Revised by Russell D. Kane, InterCorr International, Inc.

Selected References

- E.F. Bradley, Ed., *Source Book on Materials for Elevated Temperature Applications,* American Society for Metals, 1979
- B.R. Cooper and W.A. Ellingson, Ed., *The Science and Technology of Coal and Coal Utilization,* Plenum Press, 1984
- D.L. Douglass, Ed., *Oxidation of Metals and Alloys,* American Society for Metals, 1971
- U.R. Evans, *The Corrosion and Oxidation of Metals—First Supplementary Volume,* St. Martin's Press, 1968
- A.B. Hart and A.J.B. Cutler, Ed., *Deposition and Corrosion in Gas Turbines,* John Wiley & Sons, 1973
- U.L. Hill and H.L. Black, Ed., *The Properties and Performance of Materials in the Coal Gasification Environment,* Materials/Metalworking Technology Series, American Society for Metals, 1981
- D.R. Holmes and A. Rahmel, Ed., *Materials and Coatings to Resist High-Temperature Corrosion,* Applied Science, 1978
- *Hot Corrosion Problems Associated With Gas Turbines,* STP 421, American Society for Testing and Materials, 1967
- A.S. Khanna, *Introduction to High Temperature Oxidation and Corrosion,* ASM International, 2002
- O. Kubaschewski and B.E. Hopkins, *Oxidation of Metals and Alloys,* 2nd ed., Academic Press, 1962
- G.Y. Lai, *High-Temperature Corrosion of Engineering Alloys,* ASM International, 1990
- D.B. Meadowcroft and M.I. Manning, Ed., *Corrosion-Resistant Materials for Coal Conversion Systems,* Applied Science, 1983

- S. Mrowec and T. Werber, *Gas Corrosion of Metals,* W. Bartoszewski, Trans., Foreign Science Publications, Department of the National Center for Scientific, Technical and Economic Information, available from National Technical Information Service, 1978
- R.A. Rapp, Ed., *High-Temperature Corrosion,* Publication 8, National Association of Corrosion Engineers, 1983
- M.F. Rothman, Ed., *High Temperature Corrosion in Energy Systems,* The Metallurgical Society, 1985
- H. Schmalzried, *Solid State Reactions,* A.D. Pelton, Trans., Academic Press, 1974
- I.G. Wright, Ed., *Corrosion in Fossil Fuel Systems,* Vol 83-5, Conference Proceedings, The Electrochemical Society, 1983

G.S. Frankel, Pitting Corrosion, *Corrosion: Fundamentals, Testing, and Protection*, Vol 13A, *ASM Handbook*, ASM International, 2003, p 236–241

Pitting Corrosion

G.S. Frankel, The Ohio State University

Introduction

MANY ENGINEERING ALLOYS, such as stainless steels and aluminum alloys, are useful only because of passive films, which are thin (nanometer-scale) oxide layers that form naturally on the metal surface and greatly reduce the rate of corrosion of the alloys. Such passive films, however, are often susceptible to localized breakdown, resulting in accelerated dissolution of the underlying metal. If the attack initiates on an open surface, it is called pitting corrosion; at an occluded site, it is called crevice corrosion. These closely related forms of localized corrosion can lead to accelerated failure of structural components by perforation or by acting as an initiation site for cracking. Figure 1 shows an example of deep pits on a metal surface.

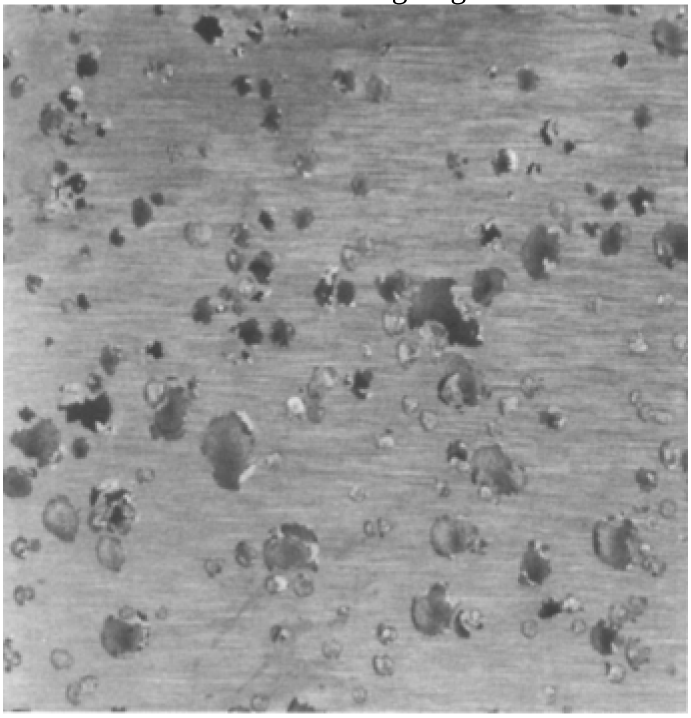

Fig. 1 Deep pits in a metal

It should be noted that, whereas localized dissolution following breakdown of an otherwise protective passive film is the most common and technologically important type of pitting corrosion, pits can form under other conditions as well. For instance, pitting can occur during active dissolution if certain regions of the sample are more susceptible and dissolve faster than the rest of the surface. This section concentrates on the better-known and widely studied phenomenon of pitting corrosion of passive metals.

Pitting corrosion is influenced by many different parameters, including the environment, metal composition, potential, temperature, and surface condition. Important environmental parameters include aggressive ion concentration, pH, and inhibitor concentration. Other phenomenological aspects of localized corrosion include the stochastic nature of the processes and the stages of localized attack, including passive film breakdown, metastable attack, stable growth, and perhaps eventual arrest.

G.S. Frankel, Pitting Corrosion, *Corrosion: Fundamentals, Testing, and Protection*, Vol 13A, *ASM Handbook*, ASM International, 2003, p 236–241

Pitting Corrosion

G.S. Frankel, The Ohio State University

Phenomenology of Pitting Corrosion

Environment and Development of Local Environment. Classical pitting corrosion caused by passive film breakdown will only occur in the presence of aggressive anionic species, and chloride ions are usually, although not always, the cause. The severity of pitting tends to vary with the logarithm of the bulk chloride concentration (Ref 1). The reason for the aggressiveness of chloride has been pondered for some time, and a number of notions have been put forth. Chloride is an anion of a strong acid, and many metal cations exhibit considerable solubility in chloride solutions (Ref 2). Chloride is a relatively small anion with a high diffusivity; it interferes with passivation, and it is ubiquitous as a contaminant.

The presence of oxidizing agents in a chloride-containing environment is usually extremely detrimental and will further enhance localized corrosion. It should be noted that chromate is an oxidizing agent that typically inhibits corrosion by reducing to form Cr^{III} film. Most oxidizing agents enhance the likelihood of pitting corrosion by providing extra cathodic reactants and increasing the local potential. Of course, dissolved oxygen is the most common oxidizing agent. One of the reactions by which oxygen reduction occurs is:

$$O_2 + 2H_2O + 4e^- \rightarrow 4OH^-$$
$$E_{rev} = 1.23 - 0.059\ \text{pH}\ (\text{vs. SHE}) \qquad \text{(Eq 1)}$$

where E_{rev} is reversible potential, and SHE is standard hydrogen electrode.

Removal of oxidizing agents, such as removal of dissolved oxygen by deaeration, is one powerful approach for reducing susceptibility to localized corrosion. The influence of potential on pitting corrosion is described subsequently.

Pitting is considered to be autocatalytic in nature; once a pit starts to grow, the local conditions are altered such that further pit growth is promoted. The anodic and cathodic electrochemical reactions that comprise corrosion separate spatially during pitting (Fig. 2). The local pit environment becomes depleted in cathodic reactant (e.g., oxygen), which shifts most of the cathodic reaction (such as is given by Eq 1) to the boldly exposed surface outside of the pit cavity, where this reactant is more plentiful. The pit environment becomes enriched in metal cations as a result of the dissolution process in the pit (written for a generic metallic element, M):

$$M \rightarrow M^{n+} + ne^- \qquad \text{(Eq 2)}$$

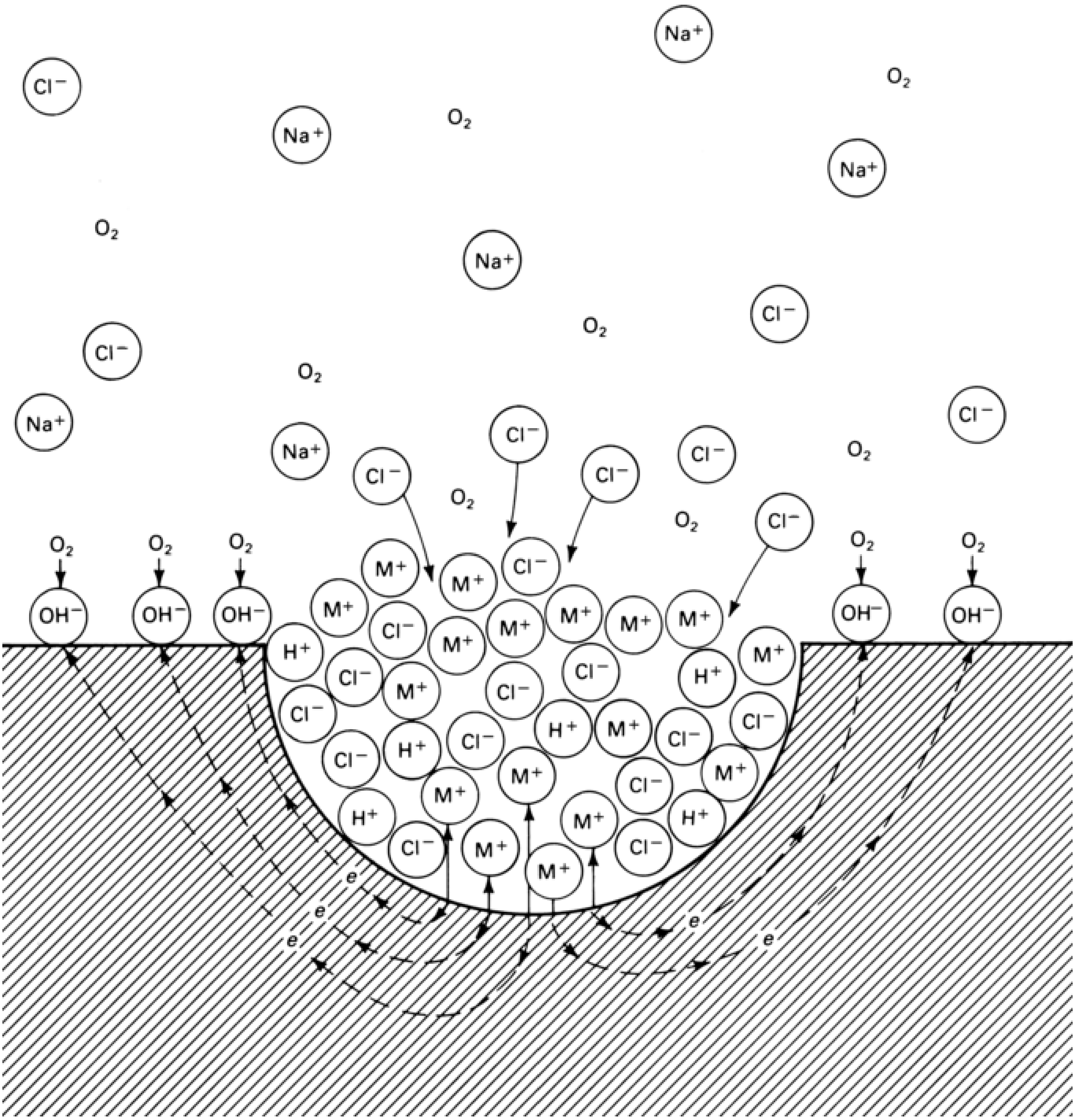

Fig. 2 Autocatalytic process occurring in a corrosion pit. The metal, M, is being pitted by an aerated NaCl solution. Rapid dissolution occurs in the pit, while oxygen reduction takes place on the adjacent metal surfaces.

The concentration of an anionic species such as chloride must also increase within the pit in order to balance the charge associated with the cation concentration and to maintain charge neutrality. This enrichment of anions occurs by electromigration from the bulk solution in response to the potential gradient that develops as a result of the ohmic potential drop along the current path between the inside of the pit and the cathodic sites on the boldly exposed surface. The final aspect of the local pit environment that must be considered is the pH, which decreases, owing to cation hydrolysis:

$$\begin{aligned} Me^{2+} + 2H_2O &\rightarrow Me(OH)^+ + H^+ + H_2O \\ &\rightarrow Me(OH)_2 + 2H^+ \end{aligned} \quad \text{(Eq 3)}$$

The common cathodic reactions that must accompany the dissolution occurring in the pit, such as the oxygen reduction reaction (Eq 1), result in a local increase in the pH at the cathodic sites. The acidity developed in the pit is not neutralized by the cathodic reaction because of the spacial separation of the anodic and cathodic reactions. In summary, the local pit environment is depleted in the cathodic reactant, such as dissolved oxygen; enriched in metal cation and an anionic species, such as chloride; and acidified. This acidic chloride environment is aggressive to most metals and tends to prevent repassivation and promote continued propagation of the pit.

A detailed analysis of the influence of pit chemistry changes on pit growth and stability is provided in Ref 2 and 3. The concentration of various ionic species at the bottom of a model one-dimensional pit geometry was determined as a function of current density based on a material balance that considered generation of cations by dissolution, outward diffusion, and thermodynamic equilibrium of various reactions such as cation hydrolysis (Eq 1). It was found that a critical value of the product $x \cdot i$, where x is pit depth and i is current density, corresponded to a critical pit acidification for sustained pit growth. Current density in a pit is a measure of the corrosion rate within the pit and thus a measure of the pit penetration rate. This $x \cdot i$ value can be used to determine the current density required to initiate or sustain pitting at a defect of a given size.

As the pit current density increases, the ionic concentration in the pit solution increases, often reaching supersaturation conditions. A solid salt film may form on the pit surface, at which point the ionic concentration would drop to the saturation value, which is the value in equilibrium with the salt layer. Under these conditions, the pit growth rate is limited by mass transport out of the pit. Salt films are not required for pit stability (although some have suggested that they are) (Ref 4, 5, 6, 7, 8, 9), but they enhance stability by providing a buffer of ionic species that can dissolve into the pit to reconcentrate the environment in the event of a catastrophic event, such as the sudden loss of a protective pit cover. Under mass- transport-limited growth, pits will be hemispherical with polished surfaces. In the absence of a salt film (at lower potentials), pits may be crystallographically etched or irregularly shaped in some other fashion.

Potential. Electrochemical studies of pitting corrosion have found that characteristic potentials exist. Stable pits form at potentials noble to the pitting potential, E_P, and will grow at potentials noble to the repassivation potential, E_R, which is lower than E_P. The effect of potential on pitting corrosion and the meaning of these characteristic potentials can best be understood with the schematic polarization curve shown in Fig. 3. This figure is a plot of the potential versus the logarithm of the current density. Potential is measured versus a reference electrode, commonly a saturated calomel electrode (SCE), and a potentiostat is used, along with an auxiliary or counter electrode, to make such measurements. As mentioned previously, current density is a measure of the rate of reaction. Common practice for measuring such curves involves potentiodynamic polarization or automatic scanning of the potential from a low value, such as the corrosion potential, to higher values (Ref 10).

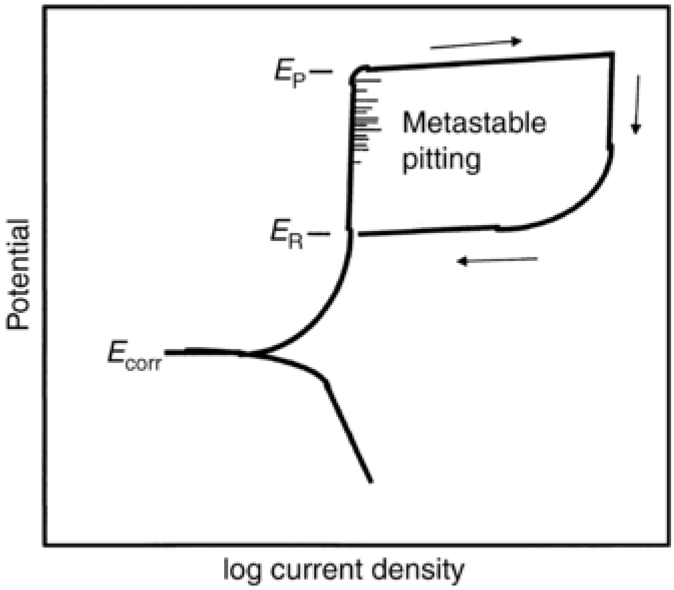

Fig. 3 Schematic of a polarization curve showing critical potentials and metastable pitting region. E_P, pitting potential; E_R, repassivation potential; E_{corr}, corrosion potential. Source: Ref 1

The schematic polarization curve in Fig. 3 shows the case of a spontaneously passive material, meaning that a protective passive film is present on the metal surface at the open circuit or corrosion potential, E_{corr}. During upward scanning, breakdown occurs, and a stable pit starts growing at the pitting potential E_P, where the current increases sharply from the passive current level and, on reversal of the scan direction, repassivates at E_R, where the current drops back to low values representative of passive dissolution. Corrosion experts generally consider that materials exhibiting higher values of E_P and E_R are more resistant to pitting corrosion, and cyclic polarization experiments are commonly used for this purpose. In an oxidizing environment, or for a material that is very susceptible to pitting, the open circuit potential, which is determined by the intersection of the polarization curves associated with the anodic and cathodic partial reactions, will be above E_P, and the material will spontaneously pit at open circuit.

A correlation has been found such that metals with low experimentally determined pitting potentials have a higher tendency to form pits naturally at open circuit (Ref 1). If the E_{corr} is far below the E_P, then there is a low likelihood that the potential will ever go high enough to approach the E_P and initiate a pit. Therefore, the difference between the E_P and E_{corr} in a given environment is the margin of safety and is also used as a measure of the susceptibility to localized corrosion (Ref 11, 12, 13). Because the repassivation potential E_R is typically lower than E_P, the difference between E_R and E_{corr} is a more conservative measure of pitting susceptibility. If the corrosion potential were to always remain below the potential at which pits repassivate, then there is a very low likelihood that pitting will occur at all. A final measure of pitting susceptibility is the difference between E_P and E_R, which is related to the extent of hysteresis in a cyclic potentiodynamic polarization curve. Generally, alloys that are susceptible to pitting corrosion exhibit a large hysteresis.

It should be noted that several other names and subscripts have been used to describe these characteristic potentials. For instance, it is common to use the term *breakdown potential* (E_b) for the initiation potential, because one is not always sure if the form of localized attack is pitting, crevice corrosion, or intergranular corrosion, or if the current increase is the result of general transpassive dissolution. The pitting potential is sometimes referred to as the pit nucleation potential, E_{np}, and the repassivation potential is sometimes called the protection potential, E_{prot}. If creviced samples are used, the potentials might be referred to as crevice potential, E_{crev}, and crevice repassivation potential, $E_{r,crev}$.

The measures of susceptibility described previously are useful for comparing the vulnerability of various alloys to localized corrosion in a given environment or for comparing the relative aggressiveness of different environments. However, there is abundant experimental evidence suggesting that these interpretations of the characteristic potentials are simplistic and insufficient for the development of a fundamental understanding of the mechanism of pitting corrosion. For instance, the potentiodynamically determined pitting potential of many materials exhibits a wide experimental scatter, of the order of hundreds of millivolts. Furthermore, E_P is, in many cases, a function of experimental parameters, such as potential scan rate. As is described subsequently, so-called metastable pits initiate and grow for a period at potentials well below the pitting potential (Ref 14), which provides evidence in contradiction to the definition of the pitting potential as being the potential above which pits initiate. The meaning of the repassivation potential has also been called into question. The E_R of ferritic stainless steel decreases (i.e., moves in the active direction) with increasing values of the current density at which the potential scan direction is reversed (Ref 12, 15). So, deeper pits apparently repassivate at lower potentials. In contrast, the repassivation potential for pits in aluminum seems to be relatively independent of the extent of prior pit growth for a limited number of experiments (Ref 16). A similar lack of dependence of E_R on prior growth has been found for pits in stainless steel and other corrosion-resistant alloys but only after the passage of large charge densities (Ref 17). Furthermore, pits did not initiate at potentials below this limiting E_R, even after very long times (up to 38 months), which validates the use of the repassivation potential as a design criterion (Ref 18).

Alloy composition and microstructure can have strong effects on the tendency for an alloy to pit (Ref 19). Chromium concentration plays the dominant role in conferring passivity to ferrous alloys. The pitting potential was correspondingly found to increase dramatically as the chromium content increased above the critical 13% value needed to create stainless steel (Ref 20). Increasing the concentration of nickel, which stabilizes the austenitic phase, moderately improves the pitting resistance of iron-chromium (Ref 20). Small increases in certain minor alloying elements, such as molybdenum in stainless steels, can greatly reduce pitting susceptibility (Ref 19). Molybdenum is particularly effective but only in the presence of chromium. Small amounts of other elements, such as nitrogen and tungsten, also have a strong influence on the pitting resistance of stainless steels (Ref 21, 22).

Various measures have been developed to describe the beneficial effects of steel composition on resistance to localized corrosion. The pitting resistance equivalent number (PREN) was originally developed as a pitting index for stainless steels (Ref 22):

$$PREN = Cr + 3.3Mo + 16N \text{ (wt\%)} \quad \text{(Eq 4)}$$

The multiplier value for nitrogen could be as high as 30. The PREN has been correlated to various other measures of corrosion resistance for stainless steels, such as the critical pitting temperature, which is described in the next section.

Because aluminum is a very active and reactive metal, the homogeneous addition of almost any metal (except zinc, lead, and magnesium) into aluminum alloys results in an increase in pitting potential (Ref 23, 24, 25, 26, 27, 28). In order for this alloying to be beneficial, it is essential that the structure remain single phase. The pitting potential of binary aluminum-copper alloys increased with copper concentration as long as the copper was in solid solution (Ref 29).

Pits almost always initiate at some chemical or physical heterogeneity at the surface, such as inclusions, second-phase particles, solute-segregated grain boundaries, flaws, mechanical damage, or dislocations (Ref 19). Most engineering alloys have many or all such defects, and pits will tend to form at the most susceptible sites first. Pits in stainless steels are often associated with MnS inclusions, which are found in most commercial steels. The role of MnS inclusions in promoting the breakdown and localized corrosion of stainless steels has been recognized for some time (Ref 30, 31). Recent improvements in alloy production have led to steels with lower sulfur content to improve pitting resistance.

Pits in aluminum alloys are typically associated with intermetallic particles (Ref 32, 33). As described previously, copper additions to aluminum resulted in improvements in pitting resistance when the copper was in solid solution. However, when particles of the intermetallic θ phase (Al_2Cu) formed, the resistance to pitting decreased back to the range of aluminum alloyed with little copper (Ref 29). The decrease in pitting potential with formation of θ phase was explained by the existence of a copper-depleted region near the particles (Ref 29). This region would have a lower pitting potential, so pits would tend to form there first. Another study found that microsegregation of copper and iron impurities at nodes in high-purity aluminum was sufficient to increase the tendency for pitting corrosion at open circuit (Ref 34).

Temperature is also a critical factor in pitting corrosion, because many materials will not pit at a temperature below a certain value, which may be extremely sharp and reproducible (Ref 35, 36, 37, 38, 39, 40, 41). This effect can be seen either by varying the temperature at a range of fixed applied potentials or by varying the potential for a range of constant temperature experiments. Figure 4 is a plot of pitting and repassivation potentials for three different stainless steels in 1 *M* NaCl as a function of solution temperature (Ref 40). At low temperatures, extremely high breakdown potentials are observed, corresponding to transpassive dissolution, not localized corrosion. Just above the critical pitting temperature (CPT), pitting corrosion occurs at a potential that is far below the transpassive breakdown potential. This value of CPT is independent of environmental parameters and applied potential over a wide range and is a measure of the resistance to stable pit propagation (Ref 35). At higher temperatures, the pitting potential decreases with increasing temperature and chloride concentration. The CPT can be used, similar to pitting potential, as a means for ranking susceptibility to pitting corrosion; the higher the CPT, the more resistant the alloy is to pitting (Ref 35). If crevice corrosion is the primary concern, creviced samples can be used to determine a critical crevice temperature (CCT), which is typically lower than the corresponding CPT. Aluminum alloys do not exhibit a CPT in aqueous chloride solutions at temperatures down to 0 °C (32 °F) (Ref 42).

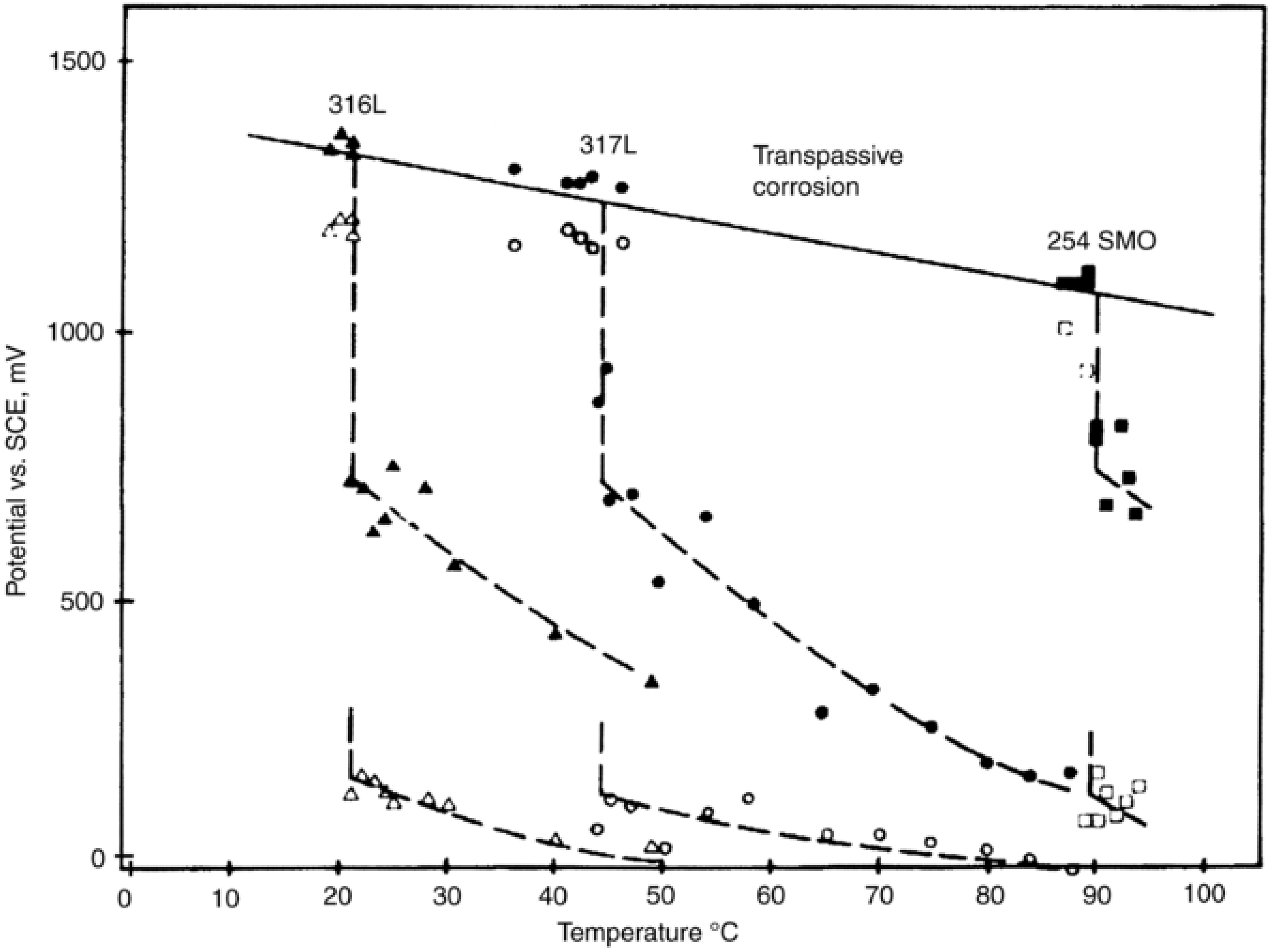

Fig. 4 Pitting (filled symbols) and repassivation (open symbols) in 1 *M* NaCl as a function of temperature for different grades of stainless steel. SCE, saturated calomel electrode. Source: Ref 40

Surface Condition. The exact condition of a surface can have a large influence on the pitting behavior of a material. In general, samples prepared with a rough surface finish are more susceptible to pitting and exhibit a lower pitting potential. For example, the pitting potential of type 302 stainless steel with a 120-grit finish was shown to be approximately 150 mV lower than that for the same material with a 1200-grit finish over a range of chloride concentrations (Ref 43). The effect of surface roughness on pitting is related to the stabilization criteria described subsequently. Rougher surfaces have more occluded sites, which can sustain the conditions required for active dissolution at lower current densities and thus lower potentials because of the longer diffusion path length and slower rate of diffusion.

For stainless steels, heat treatment, grinding, and abrasive blasting have been reported to be detrimental to pitting resistance, whereas pickling in HNO_3 + HF scales or passivation in HNO_3 is beneficial (Ref 22). Heat treatments in air generate a chromium oxide scale and a chromium-depleted region under the scale. The scale is typically removed mechanically, and the chromium-depleted region is removed by pickling (Ref 22). Other common surface defects include heat tint from welding, embedded iron particles from machining, and MnS inclusions. The detrimental effects of these defects are minimized and the overall surface condition improved by passivation in nitric acid, which increases the chromium content of the surface oxide film.

The effects of surface condition on localized corrosion are significant enough that care must be taken to not apply experimental data collected on samples with special preparation to a real application without taking the surface condition into account.

Inhibitors. Pitting can be inhibited by the same approaches that are commonly used to reduce corrosion in general. All of the factors described previously can be used to mitigate pitting corrosion: environment, alloy composition and structure, potential, and temperature. As mentioned previously, oxidizing agents accelerate

pitting by increasing the potential, so removal of oxidizing agents, for instance, by deaeration, reduces the tendency for pitting corrosion.

Various chemicals, when added to corrosive solutions, will inhibit pitting (Ref 19). Common inorganic inhibitors include sulfates, nitrates, chromates, and molybdates. Some, such as sulfate, may act simply by providing supporting electrolyte that reduces the migration of chloride ions into the pit. It was suggested that nitrate might reduce inside pits in aluminum, consuming protons and thereby reducing pH (Ref 44). Others might adsorb at active sites or reduce pit growth kinetics.

High-strength aluminum alloys, which are susceptible to pitting, owing to the influence of copper-containing intermetallic particles, are often protected using a system of coatings. The standard coating system uses a chromate conversion layer covered by organic paint coats. The primer coat might contain chromate pigments for further corrosion protection. The chromate conversion layer is formed by immersion into an acidic bath containing dichromate, fluoride, and ferricyanide. The fluoride destabilizes the aluminum oxide, allowing the following reaction to occur (Ref 45, 46):

$$Cr_2O_7^{2-} + 8H^+ + 2Al \rightarrow 2Al^{3+} + 2Cr(OH)_3 + H_2O \quad \text{(Eq 5)}$$

Chromate conversion layers also contain some amount of unreduced chromate ions as a result of adsorption of chromate onto a $Cr^{III}_x(OH)_y$ backbone (Ref 47). The resulting coating is a Cr^{III}-Cr^{VI} mixed oxide with an approximately 3 to 1 Cr^{III} to Cr^{VI} molar ratio. The chromate retained in the coating is critical for providing a self-healing capability (Ref 45, 46). Chromate- coated samples scratched to the substrate and exposed to a corrosive environment such as a salt spray will usually not exhibit severe corrosion at the scratch. Chromate in the conversion coating can be released into solution, where it is mobile and migrates to exposed areas on the aluminum alloy surface. Even at very dilute concentrations, chromate in solution adsorbs on active sites on the alloy and is reduced to form a monolayer of Cr^{III} species by a reaction similar to the one that occurs when the conversion coating forms (Eq 5). This layer is effective at reducing the activity of both anodic and cathodic sites on the alloy surface. Chromate pigment in primer should act the same way to protect a scratched area. Owing to the carcinogenic nature of chromate, considerable effort has been put into developing an equally effective and environment-friendly replacement system. However, nothing developed to date is as effective as chromate for reducing the corrosion of high-strength aluminum alloys (Ref 48).

Stochastics. Because pitting events are relatively rare and unpredictable, pit initiation may be considered to be random in nature. Stochastic or probabilistic approaches have been developed to handle this randomness and the large scatter typically observed in measurements of pitting potential and induction time (which is the time for a stable pit to form following a sudden increase in potential into the pitting range, or following the injection of chloride into a nonaggressive solution). A large ensemble of pitting potential values follows a normal distribution, suggesting random variation (Ref 49). The probability for pitting (P) can be determined by:

$$P(E) = n/(1 + N) \quad \text{(Eq 6)}$$

where N is the total number of samples studied, and n is the number of samples that had pitted at a potential of E or lower (Ref 49). The potential at P = 0.5 is a representative value for a given material and surface preparation. Induction times at a given potential can also be measured and the survival probability, $P(t)$, determined using Eq 6, except that n is the number of samples that initiate pits by time t after application of the potential. The pit-generation rate, λ, can then be given by (Ref 49):

$$\lambda(t) = -\frac{d}{dt} \ln P(t) \quad \text{(Eq 7)}$$

The value of the pit-generation rate can also be used as a measure of susceptibility to pitting.

References cited in this section

1. H.P. Leckie and H.H. Uhlig, *J. Electrochem. Soc.,* Vol 113, 1966, p 1262
2. J.R. Galvele, *Corros. Sci.,* Vol 21, 1981, p 551
3. J.R. Galvele, *J. Electrochem. Soc.,* Vol 123, 1976, p 464

4. G.T. Burstein and S.P. Mattin, The Nucleation and Early Stages of Growth of Corrosion Pits, *Critical Factors in Localized Corrosion II,* Vol PV 95-15, P.M. Natishan, R.J. Kelly, G.S. Frankel, and R.C. Newman, Ed., The Electrochemical Society, 1995, p 1

5. T.R. Beck and R.C. Alkire, *J. Electrochem. Soc.,* Vol 126, 1979, p 1662

6. T.R. Beck, *J. Electrochem. Soc.,* Vol 129, 1982, p 2413

7. R.C. Alkire and K.P. Wong, *Corros. Sci.,* Vol 28, 1988, p 411

8. R.C. Alkire and M. Feldman, *J. Electrochem. Soc.,* Vol 135, 1988, p 1850

9. K.P. Wong and R.C. Alkire, *J. Electrochem. Soc.,* Vol 137, 1990, p 3010

10. "Conducting Cyclic Potentiodynamic Polarization Measurements for Localized Corrosion Susceptibility of Iron-, Nickel-, or Cobalt-Based Alloys," G 61-86, *Annual Book of ASTM Standards,* ASTM

11. "Conducting Cyclic Potentiodynamic Polarization Measurements for Localized Corrosion Susceptibility of Iron-, Nickel-, or Cobalt-Based Alloys," G 61, *Annual Book of ASTM Standards,* ASTM

12. B.E. Wilde and E. Williams, *Electrochim. Acta,* Vol 16, 1971, p 1971

13. B.E. Wilde and E. Williams, *J. Electrochem Soc.,* Vol 117, 1970, p 775

14. G.S. Frankel, L. Stockert, F. Hunkeler, and H. Boehni, *Corrosion,* Vol 43, 1987, p 429

15. B.E. Wilde, On Pitting and Protection Potentials: Their Use and Possible Misuses for Predicting Localized Corrosion Resistance of Stainless Alloys in Halide Media, *Localized Corrosion,* Vol NACE-3, R.W. Staehle, B.F. Brown, J. Kruger, and A. Agrawal, Ed., NACE, 1974, p 342

16. M. Yasuda, F. Weinberg, and D. Tromans, *J. Electrochem. Soc.,* Vol 137, 1990, p 3708

17. N. Sridhar and G.A. Cragnolino, *Corrosion,* Vol 49, 1993, p 885

18. D.S. Dunn, Y.-M. Pan, and G.A. Cragnolino, "Stress Corrosion Cracking, Passive and Localized Corrosion of Alloy 22 High Level Radioactive Waste Containers," Report Paper 00206, Corrosion2000, NACE, 2000

19. Z. Szklarska-Smialowska, *Pitting Corrosion of Metals,* NACE, 1986

20. J. Horvath and H.H. Uhlig, *J. Electrochem. Soc.,* Vol 115, 1968, p 791

21. A.J. Sedriks, Effects of Alloy Composition and Microstructure on the Localized Corrosion of Stainless Steels, *Advances in Localized Corrosion,* Vol NACE-9, H. Isaacs, U. Bertocci, J. Kruger, and S. Smialowska, Ed., NACE, 1990, p 253

22. A.J. Sedriks, *Corrosion of Stainless Steels,* Wiley-Interscience, 1996

23. G.S. Frankel, M.S. Russak, C.V. Jahnes, M. Mirzamaani, and V.A. Brusic, *J. Electrochem. Soc.,* Vol 136, 1989, p 1243

24. W.C. Moshier, G.D. Davis, J.S. Ahearn, and H.F. Hough, *J. Electrochem. Soc.,* Vol 133, 1986, p 1063

25. W.C. Moshier, G.D. Davis, J.S. Ahearn, and H.F. Hough, *J. Electrochem. Soc.,* Vol 134, 1987, p 2677

26. W.C. Moshier, G.D. Davis, and G.O. Cote, *J. Electrochem. Soc.,* Vol 136, 1989, p 356

27. W.C. Moshier, G.D. Davis, T.L. Fritz, and G.O. Cote, *J. Electrochem. Soc.,* Vol 137, 1990, p 1317

28. R.B. Inturi and Z. Szklarska-Smialowska, *Corros. Sci.,* Vol 34, 1993, p 1201

29. I.L. Muller and J.R. Galvele, *Corros. Sci.,* Vol 17, 1977, p 179

30. G.S. Eklund, *J. Electrochem. Soc.,* Vol 121, 1974, p 467

31. G. Wranglén, *Corros. Sci.,* Vol 14, 1973, p 331

32. K. Kowal, J. DeLuccia, J.Y. Josefowicz, C. Laird, and G.C. Farrington, *J. Electrochem. Soc.,* Vol 143, 1996, p 2471

33. R.M. Rynders, C.-H. Paik, R. Ke, and R.C. Alkire, *J. Electrochem. Soc.,* Vol 141, 1994, p 1439

34. A.P. Bond, G.F. Bolling, and H.A. Domian, *J. Electrochem. Soc.,* Vol 13, 1966, p 773

35. P.E. Arnvig and A.D. Bisgard, "Determining the Potential Independent Critical Pitting Temperature (CPT) By a Potentiostatic Method Using the Avesta Cell," Paper 437, Corrosion 96, NACE, 1996

36. P.E. Arnvig and R.M. Davison, Paper 209, *Proc. 12th International Corrosion Congress,* (Houston, TX), NACE, 1993, p 1477

37. R.J. Brigham and E.W. Tozer, *Corrosion,* Vol 29, 1973, p 33

38. R.J. Brigham and E.W. Tozer, *Corrosion,* Vol 30, 1974, p 161

39. R. Qvarfort, *Corros. Sci.,* Vol 28, 1988, p 135

40. R. Qvarfort, *Corros. Sci.,* Vol 29, 1989, p 987

41. N.J. Laycock, M.H. Moayed, and R.C. Newman, Prediction of Pitting Potentials and Critical Pitting Temperatures, *Critical Factors in Localized Corrosion II,* Vol PV 95-15, P.M. Natishan, R.J. Kelly, G.S. Frankel, and R.C. Newman, Ed., The Electrochemical Society, 1995, p 68

42. R.C. Newman, UMIST, personal communication, 1996

43. N.J. Laycock and R.C. Newman, *Corros. Sci.,* Vol 39, 1997, p 1771

44. S.B. deWexler and J.R. Galvele, *J. Electrochem. Soc.,* Vol 121, 1974, p 1271

45. C. Edeleanu and U.R. Evans, *Trans. Faraday Soc.,* Vol 47, 1951, p 1121

46. M.W. Kendig, A.J. Davenport, and H.S. Isaacs, *Corros. Sci.,* Vol 34, 1993, p 41

47. G.S. Frankel and R.L. McCreery, Inhibition of Al Alloy Corrosion by Chromates, *Interface,* Vol 10, 2002, p. 34–38

48. "Alternatives to Chromium for Metal Finishing," Report 0273RE95, National Center for Manufacturing Sciences, 1995

49. T. Shibata and T. Takeyama, *Corrosion,* Vol 33, 1977, p 243

G.S. Frankel, Pitting Corrosion, *Corrosion: Fundamentals, Testing, and Protection*, Vol 13A, *ASM Handbook*, ASM International, 2003, p 236–241

Pitting Corrosion

G.S. Frankel, The Ohio State University

Stages of Pitting

Pitting can be considered to consist of various stages: passive film breakdown, metastable pitting, pit growth, and pit stifling or death. Any of these stages may be considered to be the most critical. For instance, once the passive film breaks down and a pit initiates, there is a possibility that a stable pit will grow. On the other hand, pits will not initiate if they cannot grow at least for a short while. The passive state is required for pitting to occur, but some researchers believe that details of the passive film composition and structure play a minor role in the pitting process. This view is supported by the fact that many observations of pitting tendency can be fully accounted for by growth considerations. Furthermore, pit growth is critical in practical applications of failure prediction. Finally, the metastable pitting stage may be thought to be the most important, because only pits that survive this stage become stable growing pits. Metastable pits exist on the edge of stability. Studies of metastable pits can therefore provide insight into fundamental aspects of pitting, because both initiation and stability are key factors in metastable pitting.

Pit Initiation and Passive Film Breakdown. The breakdown of the passive film and the details of pit initiation comprise the least understood aspect of the pitting phenomenon. Breakdown is a rare occurrence that happens extremely rapidly on a very small scale, making direct observation extraordinarily difficult. The passive film is often drawn schematically as a simple inert layer covering the underlying metal and blocking access of the environment to the metal. The reality is, of course, much more complicated. Depending on alloy composition, environment, potential, and exposure history, this film can have a range of thickness, structure, composition, and protectiveness. Typical passive films are quite thin and support an extremely high electric field (on the order of 10^6 to 10^7 V/ cm). The passage of a finite passive current density is evidence of continual reaction of the metal, to result in film thickening, dissolution into the environment, or some combination of the two. The view of the passive film as being a dynamic structure, rather than static, is critical to the proposed mechanisms of passive film breakdown and pit initiation.

Theories for passive film breakdown and pit initiation have been categorized into three main mechanisms that focus on passive film penetration, film breaking, or adsorption (Ref 50, 51). As with most such situations, different mechanisms or combinations of these mechanisms may be valid for different metal-environment systems. These mechanisms have been considered in terms of pure metal systems. However, pits in real alloys are most often associated with inclusions or second-phase particles, and these factors must also be taken into consideration.

Metastable Pitting. Metastable pits are pits that initiate and grow for a limited period before repassivating. Large pits can stop growing for a variety of reasons, but metastable pits are typically considered to be those of micron size, at most, with a lifetime on the order of seconds or less. Metastable pits are important to understand because, under certain conditions, they continue to grow to form large pits. Metastable pits can form at potentials far below the pitting potential (which is associated with the initiation of stable pits) and during the induction time before the onset of stable pitting at potentials above the pitting potential. These events are characterized by potential transients in the active direction at open circuit or under an applied anodic current, or anodic current transients under an applied anodic potential. Such transients have been reported in stainless steels (Ref 14, 52, 53, 54, 55, 56, 57, 58) and aluminum (Ref 59, 60) for many years. Individual metastable pit current transients can be analyzed for pit current density, and stochastic approaches can be applied to groups of metastable pits. It has been argued that when stable pits are small, they behave identically to metastable pits and, in fact, are metastable (Ref 14). Stable pits survive the metastable stage and continue to grow, whereas metastable pits repassivate and stop growing, for some reason.

Stable Pitting and Pit Growth. Pits grow at a rate that depends on material composition, pit electrolyte concentration, and pit-bottom potential. The mass-transport characteristics of the pit influence pit growth

kinetics through the pit electrolyte concentration. Pit stability depends on the maintenance of pit electrolyte composition and pit-bottom potential that are at least severe enough to prevent repassivation of the dissolving metal surface at the pit bottom.

In order to understand pit growth and stability, it is essential to ascertain the rate-determining factors. Pit growth can be controlled by the same factors that can limit any electrochemical reaction: charge-transfer processes (activation), ohmic effects, mass transport, or some combination of these factors. Pit growth at low potentials below the range of limiting pit current densities is controlled by a combination of ohmic, charge transfer, and concentration overpotential factors. At high potentials, mass transport may be rate controlling. Ultimately, however, mass transport determines the stability of pits even at lower potentials, because the local environment controls passivation. The rate of pit growth decreases with time for pitting controlled by either ohmic or mass-transport effects. The pit growth rate often varies with t^{-n}, where n is approximately equal to 0.5.

Pits often grow with a porous cover. This cover can make visual detection extremely difficult, so that the awareness of the severity of attack is overlooked and the likelihood of catastrophic failure is enhanced. The pit cover might be a thick, precipitated product layer that forms as the concentrated and acidic pit solution meets the bulk environment, which might be neutral or limited in water, as in the case of atmospheric corrosion. Small pits in stainless steels often have a pit cover that is a remnant of the undermined passive film (Ref 14). Larger pits in stainless steel can be covered by a layer with a considerable thickness of metal that is detached from the rest of the metal sample (Ref 61). These covers make optical detection extremely difficult, because they remain reflective. A short exposure to ultrasonic agitation, however, removes the cover and reveals the whole pit diameter.

Death and Pit Arrest. Despite the autocatalytic nature of pitting, large pits, which would be considered to be stable by any criterion, can stop growing or die. As mentioned previously, if the conditions (environment and potential) at the dissolving wall of a pit are not sufficiently aggressive, the pit will repassivate. The potential at the pit bottom is lower than that at the outer surface as a result of the ohmic potential drop associated with current flow out of the pit. As the pit deepens, the ohmic path length and ohmic resistance increase. This tends to cause an increase in the ohmic potential drop, a decrease in the local potential, and a decrease in the pit current density. The environment tends to be acidic and rich in chloride, owing to hydrolysis of the dissolved metal cations and electrolytic migration of chloride into the pit. The high concentration in the pit is depleted by transport out of the pit but is replenished by continued dissolution at the pit bottom. As the pit deepens, the rate of transport out of the pit decreases, so the pit can be stable with a lower anodic current density replenishing the environment. As mentioned previously, the pit current density tends to decrease with time, owing to an increase in the pit depth and ohmic potential drop. Repassivation might occur if a sudden event, such as loss of a pit cover, caused a sudden enhancement of transport and dilution of the pit environment to the extent that the rate of dissolution at the pit bottom would be insufficient to replenish the lost aggressive environment.

References cited in this section

14. G.S. Frankel, L. Stockert, F. Hunkeler, and H. Boehni, *Corrosion,* Vol 43, 1987, p 429

50. H.-H. Strehblow, *Werkst. Korros.,* Vol 27, 1976, p 792

51. H.-H. Strehblow, Mechanisms of Pitting Corrosion, *Corrosion Mechanisms in Theory and Practice,* P. Marcus and J. Oudar, Ed., Marcel Dekker, 1995, p 201

52. N. Pessall and C. Liu, *Electrochim. Acta,* Vol 16, 1971, p 1987

53. Y. Hisamatsu, T. Yoshii, and Y. Matsumura, Electrochemical and Microscopical Study of Pitting Corrosion of Austenitic Stainless Steel, *Localized Corrosion,* Vol NACE-3, R.W. Staehle, B.F. Brown, J. Kruger, and A. Agrawal, Ed., NACE, 1974

54. D.E. Williams, J. Stewart, and P.H. Balkwill, *Corros. Sci.,* Vol 36, 1994, p 1213

55. H. Ezuber and R.C. Newman, Growth-Rate Distribution of Metastable Pits, *Critical Factors in Localized Corrosion,* Vol PV 92- 9, G.S. Frankel and R.C. Newman, Ed., The Electrochemical Society, 1992, p 120

56. P.C. Pistorius and G.T. Burstein, *Philos. Trans. R. Soc. (London) A,* Vol 341, 1992, p 531

57. P.C. Pistorius and G.T. Burstein, *Corros. Sci.,* Vol 33, 1992, p 1885

58. P.C. Pistorius and G.T. Burstein, *Corros. Sci.,* Vol 36, 1994, p 525

59. G.C. Wood, W.H. Sutton, J.A. Richardson, T.N.K. Riley, and A.G. Malherbe, The Mechanism of Pitting of Aluminum and Its Alloys, *Localized Corrosion,* R.W. Staehle, B.F. Brown, J. Kruger, and A. Agrawal, Ed., NACE, 1974, p 526

60. S.T. Pride, J.R. Scully, and J.L. Hudson, *J. Electrochem. Soc.,* Vol 141, 1994, p 3028

61. B. Baroux, Further Insights on the Pitting Corrosion of Stainless Steels, *Corrosion Mechanisms in Theory and Practice,* P. Marcus and J. Oudar, Ed., Marcel Dekker, 1995, p 265

G.S. Frankel, Pitting Corrosion, *Corrosion: Fundamentals, Testing, and Protection*, Vol 13A, *ASM Handbook*, ASM International, 2003, p 236–241

Pitting Corrosion

G.S. Frankel, The Ohio State University

References

1. H.P. Leckie and H.H. Uhlig, *J. Electrochem. Soc.,* Vol 113, 1966, p 1262

2. J.R. Galvele, *Corros. Sci.,* Vol 21, 1981, p 551

3. J.R. Galvele, *J. Electrochem. Soc.,* Vol 123, 1976, p 464

4. G.T. Burstein and S.P. Mattin, The Nucleation and Early Stages of Growth of Corrosion Pits, *Critical Factors in Localized Corrosion II,* Vol PV 95-15, P.M. Natishan, R.J. Kelly, G.S. Frankel, and R.C. Newman, Ed., The Electrochemical Society, 1995, p 1

5. T.R. Beck and R.C. Alkire, *J. Electrochem. Soc.*, Vol 126, 1979, p 1662

6. T.R. Beck, *J. Electrochem. Soc.,* Vol 129, 1982, p 2413

7. R.C. Alkire and K.P. Wong, *Corros. Sci.,* Vol 28, 1988, p 411

8. R.C. Alkire and M. Feldman, *J. Electrochem. Soc.,* Vol 135, 1988, p 1850

9. K.P. Wong and R.C. Alkire, *J. Electrochem. Soc.,* Vol 137, 1990, p 3010

10. "Conducting Cyclic Potentiodynamic Polarization Measurements for Localized Corrosion Susceptibility of Iron-, Nickel-, or Cobalt-Based Alloys," G 61-86, *Annual Book of ASTM Standards,* ASTM

11. “Conducting Cyclic Potentiodynamic Polarization Measurements for Localized Corrosion Susceptibility of Iron-, Nickel-, or Cobalt-Based Alloys,” G 61, *Annual Book of ASTM Standards,* ASTM

12. B.E. Wilde and E. Williams, *Electrochim. Acta,* Vol 16, 1971, p 1971

13. B.E. Wilde and E. Williams, *J. Electrochem Soc.,* Vol 117, 1970, p 775

14. G.S. Frankel, L. Stockert, F. Hunkeler, and H. Boehni, *Corrosion,* Vol 43, 1987, p 429

15. B.E. Wilde, On Pitting and Protection Potentials: Their Use and Possible Misuses for Predicting Localized Corrosion Resistance of Stainless Alloys in Halide Media, *Localized Corrosion,* Vol NACE-3, R.W. Staehle, B.F. Brown, J. Kruger, and A. Agrawal, Ed., NACE, 1974, p 342

16. M. Yasuda, F. Weinberg, and D. Tromans, *J. Electrochem. Soc.,* Vol 137, 1990, p 3708

17. N. Sridhar and G.A. Cragnolino, *Corrosion,* Vol 49, 1993, p 885

18. D.S. Dunn, Y.-M. Pan, and G.A. Cragnolino, “Stress Corrosion Cracking, Passive and Localized Corrosion of Alloy 22 High Level Radioactive Waste Containers,” Report Paper 00206, Corrosion2000, NACE, 2000

19. Z. Szklarska-Smialowska, *Pitting Corrosion of Metals,* NACE, 1986

20. J. Horvath and H.H. Uhlig, *J. Electrochem. Soc.,* Vol 115, 1968, p 791

21. A.J. Sedriks, Effects of Alloy Composition and Microstructure on the Localized Corrosion of Stainless Steels, *Advances in Localized Corrosion,* Vol NACE-9, H. Isaacs, U. Bertocci, J. Kruger, and S. Smialowska, Ed., NACE, 1990, p 253

22. A.J. Sedriks, *Corrosion of Stainless Steels,* Wiley-Interscience, 1996

23. G.S. Frankel, M.S. Russak, C.V. Jahnes, M. Mirzamaani, and V.A. Brusic, *J. Electrochem. Soc.,* Vol 136, 1989, p 1243

24. W.C. Moshier, G.D. Davis, J.S. Ahearn, and H.F. Hough, *J. Electrochem. Soc.,* Vol 133, 1986, p 1063

25. W.C. Moshier, G.D. Davis, J.S. Ahearn, and H.F. Hough, *J. Electrochem. Soc.,* Vol 134, 1987, p 2677

26. W.C. Moshier, G.D. Davis, and G.O. Cote, *J. Electrochem. Soc.,* Vol 136, 1989, p 356

27. W.C. Moshier, G.D. Davis, T.L. Fritz, and G.O. Cote, *J. Electrochem. Soc.,* Vol 137, 1990, p 1317

28. R.B. Inturi and Z. Szklarska-Smialowska, *Corros. Sci.,* Vol 34, 1993, p 1201

29. I.L. Muller and J.R. Galvele, *Corros. Sci.,* Vol 17, 1977, p 179

30. G.S. Eklund, *J. Electrochem. Soc.,* Vol 121, 1974, p 467

31. G. Wranglén, *Corros. Sci.,* Vol 14, 1973, p 331

32. K. Kowal, J. DeLuccia, J.Y. Josefowicz, C. Laird, and G.C. Farrington, *J. Electrochem. Soc.,* Vol 143, 1996, p 2471

33. R.M. Rynders, C.-H. Paik, R. Ke, and R.C. Alkire, *J. Electrochem. Soc.,* Vol 141, 1994, p 1439

34. A.P. Bond, G.F. Bolling, and H.A. Domian, *J. Electrochem. Soc.,* Vol 13, 1966, p 773

35. P.E. Arnvig and A.D. Bisgard, “Determining the Potential Independent Critical Pitting Temperature (CPT) By a Potentiostatic Method Using the Avesta Cell,” Paper 437, Corrosion 96, NACE, 1996

36. P.E. Arnvig and R.M. Davison, Paper 209, *Proc. 12th International Corrosion Congress,* (Houston, TX), NACE, 1993, p 1477

37. R.J. Brigham and E.W. Tozer, *Corrosion,* Vol 29, 1973, p 33

38. R.J. Brigham and E.W. Tozer, *Corrosion,* Vol 30, 1974, p 161

39. R. Qvarfort, *Corros. Sci.,* Vol 28, 1988, p 135

40. R. Qvarfort, *Corros. Sci.,* Vol 29, 1989, p 987

41. N.J. Laycock, M.H. Moayed, and R.C. Newman, Prediction of Pitting Potentials and Critical Pitting Temperatures, *Critical Factors in Localized Corrosion II,* Vol PV 95-15, P.M. Natishan, R.J. Kelly, G.S. Frankel, and R.C. Newman, Ed., The Electrochemical Society, 1995, p 68

42. R.C. Newman, UMIST, personal communication, 1996

43. N.J. Laycock and R.C. Newman, *Corros. Sci.,* Vol 39, 1997, p 1771

44. S.B. deWexler and J.R. Galvele, *J. Electrochem. Soc.,* Vol 121, 1974, p 1271

45. C. Edeleanu and U.R. Evans, *Trans. Faraday Soc.,* Vol 47, 1951, p 1121

46. M.W. Kendig, A.J. Davenport, and H.S. Isaacs, *Corros. Sci.,* Vol 34, 1993, p 41

47. G.S. Frankel and R.L. McCreery, Inhibition of Al Alloy Corrosion by Chromates, *Interface,* Vol 10, 2002, p. 34–38

48. “Alternatives to Chromium for Metal Finishing,” Report 0273RE95, National Center for Manufacturing Sciences, 1995

49. T. Shibata and T. Takeyama, *Corrosion,* Vol 33, 1977, p 243

50. H.-H. Strehblow, *Werkst. Korros.,* Vol 27, 1976, p 792

51. H.-H. Strehblow, Mechanisms of Pitting Corrosion, *Corrosion Mechanisms in Theory and Practice,* P. Marcus and J. Oudar, Ed., Marcel Dekker, 1995, p 201

52. N. Pessall and C. Liu, *Electrochim. Acta,* Vol 16, 1971, p 1987

53. Y. Hisamatsu, T. Yoshii, and Y. Matsumura, Electrochemical and Microscopical Study of Pitting Corrosion of Austenitic Stainless Steel, *Localized Corrosion,* Vol NACE-3, R.W. Staehle, B.F. Brown, J. Kruger, and A. Agrawal, Ed., NACE, 1974

54. D.E. Williams, J. Stewart, and P.H. Balkwill, *Corros. Sci.,* Vol 36, 1994, p 1213

55. H. Ezuber and R.C. Newman, Growth-Rate Distribution of Metastable Pits, *Critical Factors in Localized Corrosion,* Vol PV 92- 9, G.S. Frankel and R.C. Newman, Ed., The Electrochemical Society, 1992, p 120

56. P.C. Pistorius and G.T. Burstein, *Philos. Trans. R. Soc. (London) A,* Vol 341, 1992, p 531

57. P.C. Pistorius and G.T. Burstein, *Corros. Sci.,* Vol 33, 1992, p 1885

58. P.C. Pistorius and G.T. Burstein, *Corros. Sci.,* Vol 36, 1994, p 525

59. G.C. Wood, W.H. Sutton, J.A. Richardson, T.N.K. Riley, and A.G. Malherbe, The Mechanism of Pitting of Aluminum and Its Alloys, *Localized Corrosion,* R.W. Staehle, B.F. Brown, J. Kruger, and A. Agrawal, Ed., NACE, 1974, p 526

60. S.T. Pride, J.R. Scully, and J.L. Hudson, *J. Electrochem. Soc.,* Vol 141, 1994, p 3028

61. B. Baroux, Further Insights on the Pitting Corrosion of Stainless Steels, *Corrosion Mechanisms in Theory and Practice,* P. Marcus and J. Oudar, Ed., Marcel Dekker, 1995, p 265

G.S. Frankel, Pitting Corrosion, *Corrosion: Fundamentals, Testing, and Protection*, Vol 13A, *ASM Handbook*, ASM International, 2003, p 236–241

Pitting Corrosion

G.S. Frankel, The Ohio State University

Selected References

- B. Baroux, Further Insights on the Pitting Corrosion of Stainless Steels, *Corrosion Mechanisms in Theory and Practice,* 2nd ed., P. Marcus, Ed., Marcel Dekker, 2002, p. 311
- G.S. Frankel, Pitting Corrosion of Metals; A Review of the Critical Factors, *J. Electrochem. Soc.,* Vol 145, 1998, p 2186
- H. Isaacs, U. Bertocci, J. Kruger, and S. Smialowska, Ed., *Advances in Localized Corrosion,* Vol NACE-9, NACE, 1990, p 253
- A.J. Sedriks, *Corrosion of Stainless Steels,* Wiley-Interscience, 1996
- R.W. Staehle, B.F. Brown, J. Kruger, and A. Agrawal, Ed., *Localized Corrosion,* Vol NACE-3, NACE, 1974
- H.-H. Strehblow, Mechanisms of Pitting Corrosion, *Corrosion Mechanisms in Theory and Practice,* 2nd ed., P. Marcus, Ed., Marcel Dekker, 2002, p. 243
- Z. Szklarska-Smialowska, *Pitting Corrosion of Metals,* NACE, 1986

R.G. Kelly, Crevice Corrosion, *Corrosion: Fundamentals, Testing, and Protection*, Vol 13A, *ASM Handbook*, ASM International, 2003, p 242–247

Crevice Corrosion

R.G. Kelly, University of Virginia

Introduction

CREVICE CORROSION, corrosion in occluded regions, is one of the most damaging forms of material degradation. Engineering structures as diverse as lap joints in aircraft, flanged pipes in chemical-processing plants, metal surfaces under initially protective coatings, and environmentally assisted cracks in metallic materials all have an occluded solution. This similitude was originally pointed out by Brown (Ref 1) and has gained general acceptance (Ref 2) due to the striking similarities in the chemical composition and behavior of occluded regions such as crevices, pits, cracks, and exfoliation sites. Thus, one can consider a crevice as a generic occluded system.

Crevice corrosion occurs when a wetted metallic surface is in close proximity to another surface, as shown schematically in Fig. 1. Typically, the average separation (called the gap, *g*) between the two surfaces is between 0.1 and 100 μm. For some material/environment combinations, this geometric arrangement can lead to accelerated attack of the metal surface, as shown in Fig. 2. There are numerous practical cases of geometries that lead to crevice corrosion. In almost any engineered structure there are many instances in which two or more materials are, by design, in close proximity as described previously. If electrolyte can be rigorously excluded from these regions, crevice corrosion is not possible, as one of the requirements for corrosion has been removed. Unfortunately, achieving and maintaining such complete exclusion of electrolyte is often impossible, so an appreciation of crevice corrosion becomes important.

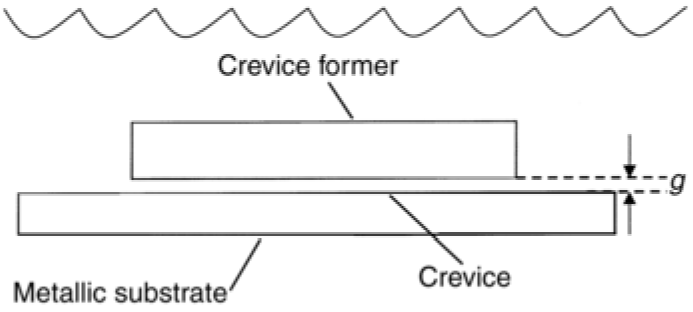

Fig. 1 Geometry of crevice corrosion. The average separation is the gap, *g*.

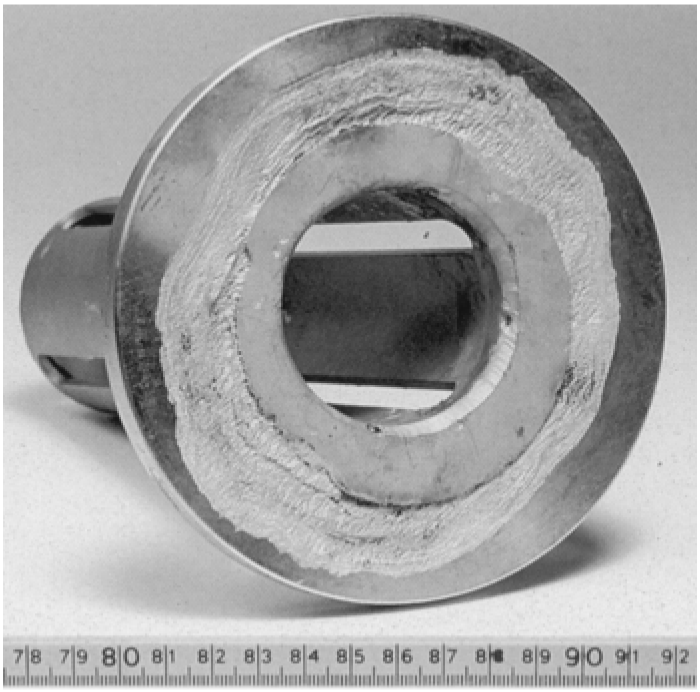

Fig. 2 Crevice corrosion under seal in type 316 stainless steel sieve from steam condenser cooling water system exposed to flowing seawater for two years at less than 40 °C (104 °F). Source: Ref 56

A generic geometry for crevice corrosion can be seen in Fig. 1 in cross section. The substrate is the metallic material of interest. It is separated from the crevice former by a gap, *g*, that, for an ideal crevice, is constant over the length of the crevice, *l*. The fully exposed surface is that area of the substrate outside the crevice former that is fully immersed in the electrolyte. The properties of the substrate can strongly influence the rate of crevice corrosion (Ref 2, 3).

Several examples of the results of crevice corrosion are shown in Fig. 3, Fig. 4, Fig. 5, Fig. 6. The similarities in topography among the examples include the accelerated attack of the substrate under the crevice former and the virtual absence of attack on the fully exposed surface. The accelerated attack within the crevice usually appears as uniform corrosion or pitting. In some cases, it is thought that the attack starts as metastable pits that coalesce into a more uniform attack.

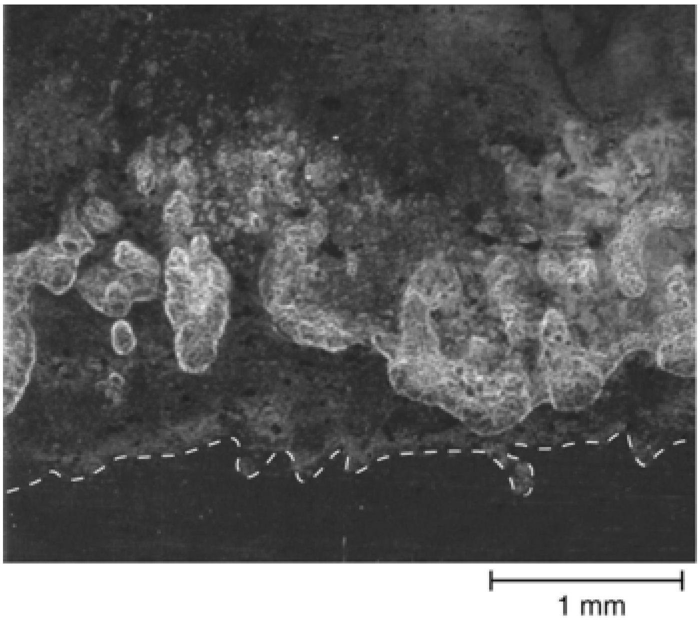

Fig. 3 Crevice corrosion of type 304 stainless steel after polarization at +0.05 V(SCE) in 0.017 *M* NaCl. Mouth of crevice is at the bottom edge of the micrograph. The material boundary is the broken white line. Area of attack is light region above broken line. Source: Ref 4

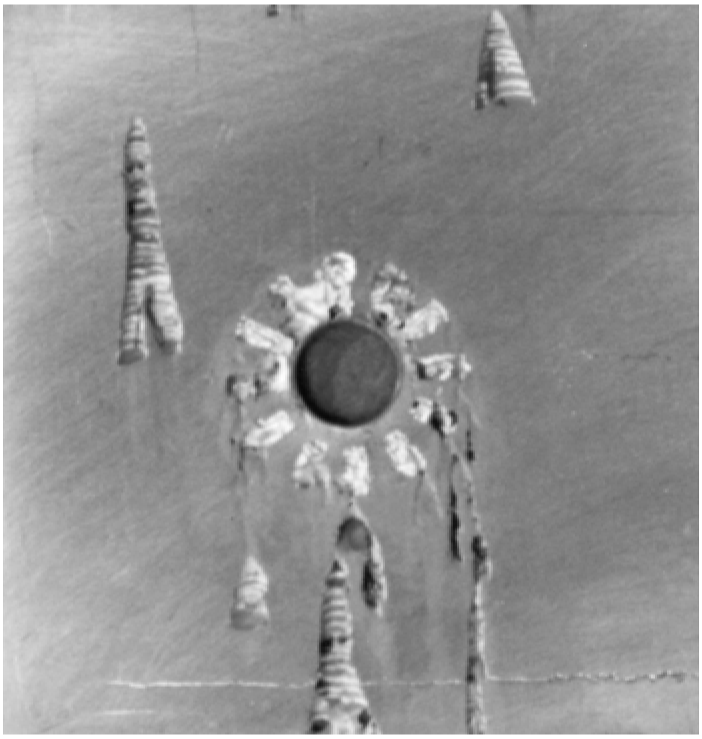

Fig. 4 Example of the results of crevice corrosion. Type 304 stainless steel exposed to 6 wt.% ferric chloride for 48 h at room temperature with castellated crevice washer applied around center hole. Pitting also occurred at several sites outside the crevice. The draining of the occluded solution from the crevice sites (and pits) led to the river pattern of attack outside the initial localized corrosion sites.

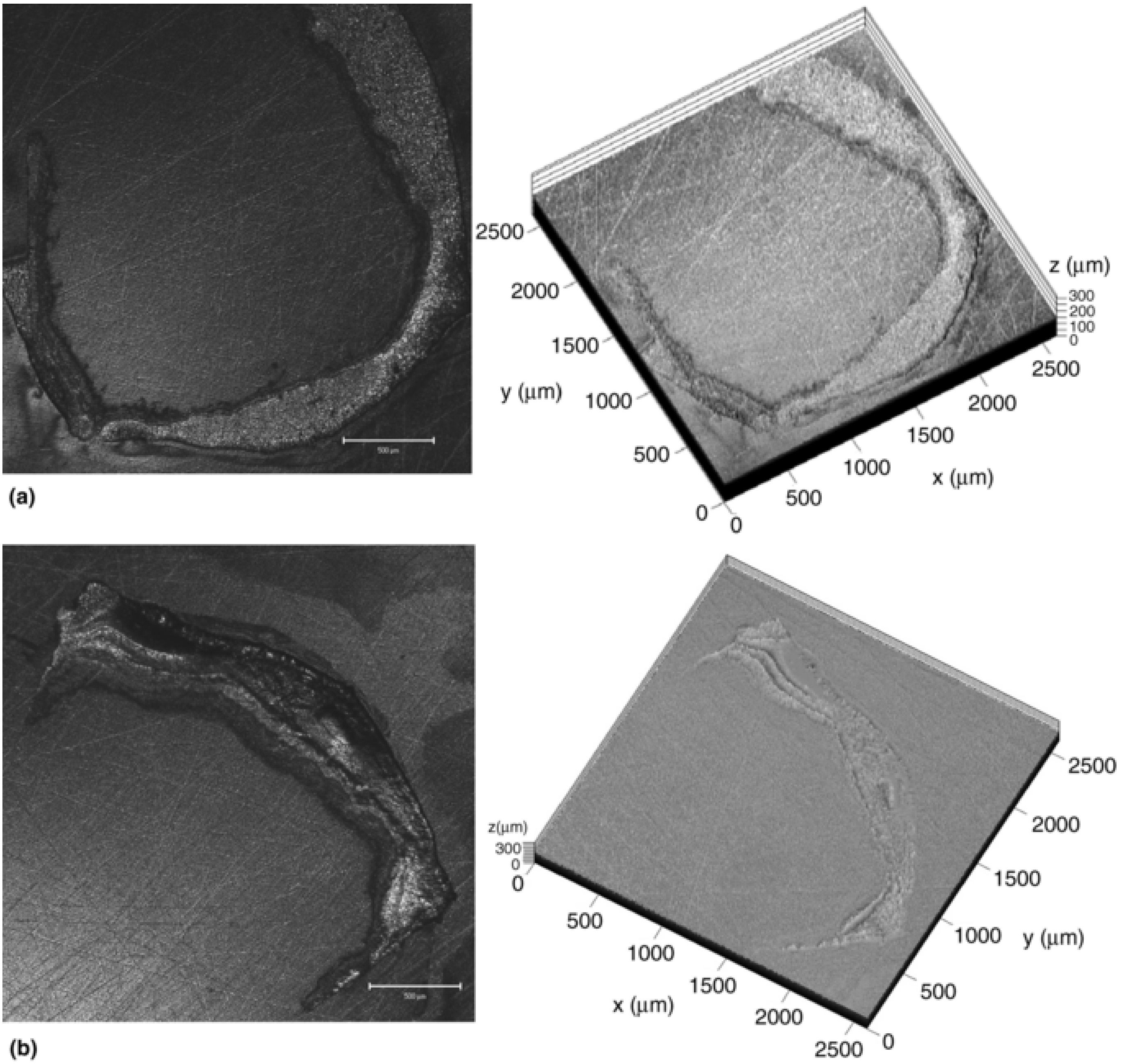

Fig. 5 Confocal laser scanning micrographs of air aged nickel alloys after cyclic potentiodynamic polarization testing with a crevice former in place at 95 °C in pH 7.75 electrolyte for electrolyte having a [Cl^-]:[SO_4^{2-}] of 100:1. The accumulated anodic charge for each alloy was approximately 2.5 C. (a) Alloy 625. (b) Alloy C22. Source: Ref 5

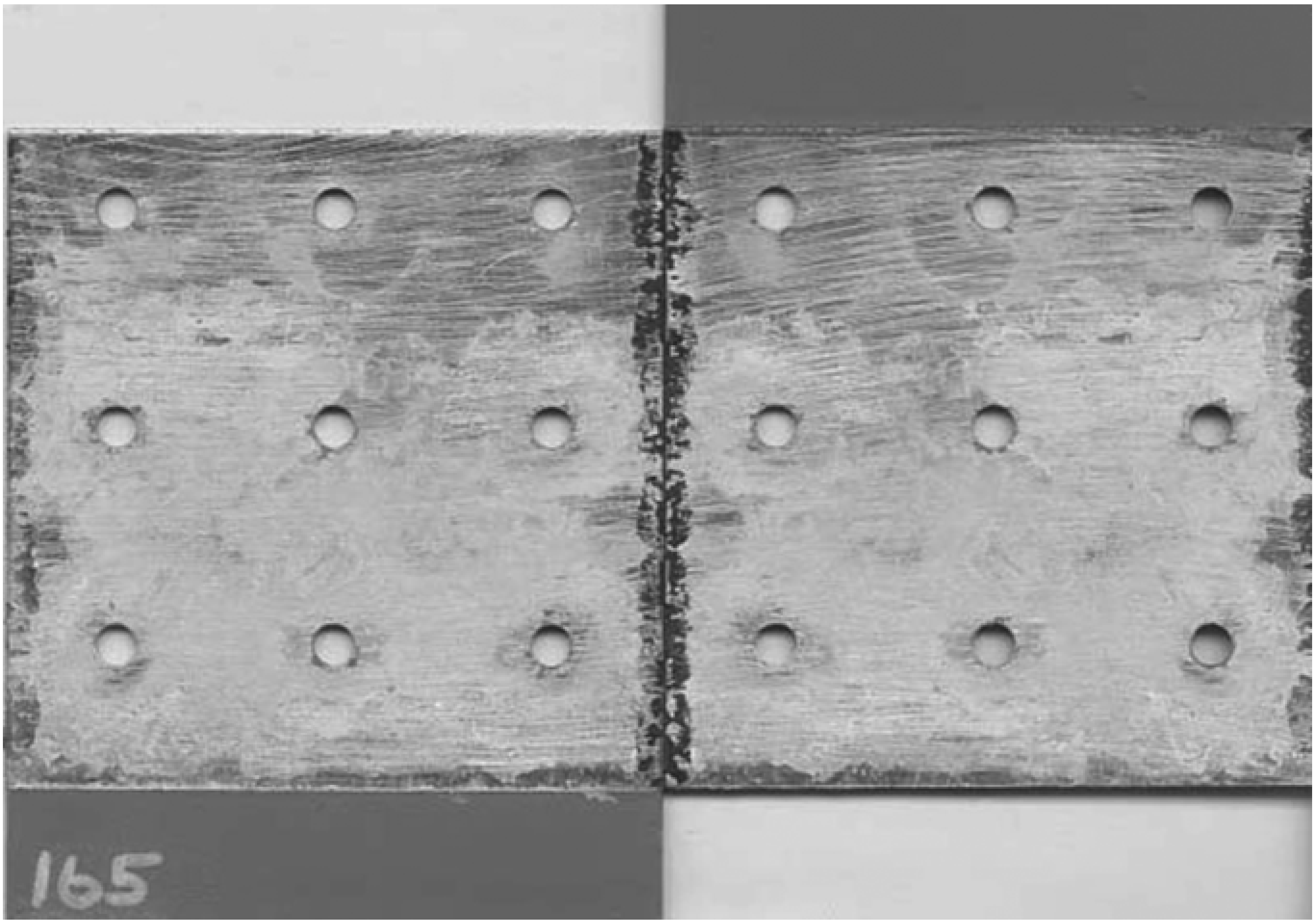

Fig. 6 Crevice corrosion of aluminum, alloy 2024-T3 faying surfaces after three-month exposure to simulated lap-joint solution. Exterior surfaces were painted. Source: Ref 6

References cited in this section

1. B.F. Brown, *Corrosion,* Vol 26, 1970, p 249

2. Z. Szlarska-Smialowska, *Pitting Corrosion of Metals,* National Association of Corrosion Engineers, 1976, p 301

3. T.P. Hoar, *Faraday Soc. Discuss.,* Vol 1, 1947, p 299

4. C.S. Brossia and R.G. Kelly, *Corrosion Sci.,* Vol 40, 1998, p 1851

5. B.A. Kehler, G.O. Ilevbare, and J.R. Scully, *Corrosion,* Vol 57, 2001, p 1042

6. L.B. Simon, J.L. Elster, and R.G. Kelly, *Proc. 2000 ASIP Conference* (San Antonio, TX), U.S. Air Force Research Laboratory and the U.S. Air Force Aeronautical Systems Center, Dec 2000

56. E.D.D. During, Ed., *Corrosion Atlas,* Elsevier, 1988

R.G. Kelly, Crevice Corrosion, *Corrosion: Fundamentals, Testing, and Protection*, Vol 13A, *ASM Handbook*, ASM International, 2003, p 242–247

Crevice Corrosion

R.G. Kelly, University of Virginia

Critical Factors

Crevice corrosion involves three fundamental types of processes: electrochemical reactions, homogeneous chemical reactions, and mass transport. The electrochemical reactions include both dissolution and reduction reactions. The spatial variation of the rates of these reactions determines the development of the attack topography characteristic of crevice corrosion. The important types of homogeneous chemical reactions include hydrolysis, precipitation reactions, and homogeneous oxidation/reduction reactions of dissolved species. These reactions can have substantial effects on the corrosivity of the occluded environment, in particular with regard to the local pH. Mass transport by diffusion and convection generally tends to minimize differences between the occluded region conditions and those on the fully exposed surface. However, the tight geometry inherent in crevices leads to severe restriction of mass transport, allowing large differences in concentration and electrochemical potential to develop and be maintained between the fully exposed surface and the occluded crevice region.

The geometry of a crevice defines the phenomenon. The two dimensions that characterize a crevice, the gap, *g*, and the depth or length, *l*, exert a great deal of control on the initiation and propagation of crevice corrosion. In general, the tighter the crevice (i.e., the smaller the gap) the more severe the crevice attack. Note that the crevice in Fig. 1 is an idealized schematic of a real crevice. The gaps in real crevices are highly variable throughout the occluded region because they are defined by the meeting of asperities on the two surfaces as shown in Fig. 7. An actual crevice has a highly distributed geometry. Conventional methods of preparing occluded geometry samples, such as by pressing serrated polytetrafluoroethylene (PTFE) washers onto polished metal surfaces, do not allow rigorously defined crevices to be made. Conventional polishing does not make truly flat surfaces, but a series of ridges and asperities. Pressing the PTFE washer onto the polished metal surface forms an occluded region with a wide range of crevice gaps including small areas of intimate contact. Although the total crevice volume and nominal crevice gap of the occluded region can be determined with appropriate experiments (Ref 4, 7, 8), the local conditions within the occluded region will vary based on the surface finishes and relative hardness of the contacting surfaces. Variations in time will occur due to creep of the PTFE.

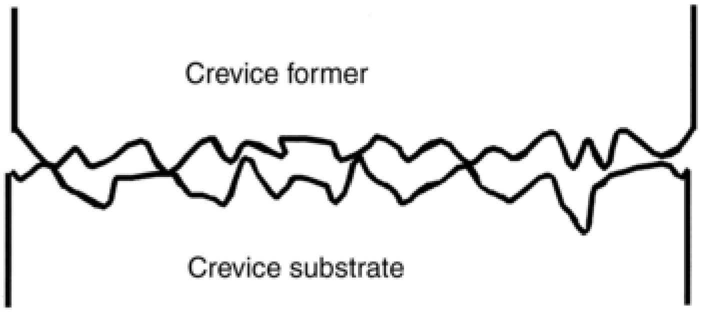

Fig. 7 Cross section of a crevice in which surface asperities cause variations in local gap

As mentioned previously, convection is usually not considered important in crevice corrosion due to the restricted geometry. There are some cases in which this assumption is not valid. Lott and Alkire (Ref 9) have investigated the effects of flow past the mouths of localized corrosion sites (pits). They found that a recirculation motion can develop within a localized corrosion site. Although this flow can mix the occluded solution, there was little mixing between the occluded region solution and the bulk solution. Flow *through* crevices can inhibit the initiation of crevice corrosion by making the development of the aggressive

environment in the occluded region more difficult. There are a variety of “flow-through” crevices, including support plates in heat exchangers in nuclear reactors (Ref 10).

Material. In order for crevice corrosion to occur, the vast majority of the surface must be passive. This is due to both the need to distinguish localized attack within the crevice and the need for the fully exposed surface to serve as a net cathode to support the high rate of anodic activity within the occluded region. Stainless steels are widely recognized as being susceptible to crevice corrosion (Ref 11). Other alloy systems that rely on passivation for corrosion protection—such as nickel-, titanium-, and aluminum- base alloys—can also be susceptible, although conditions for attack may differ. Titanium alloys are the most resistant to crevice corrosion with high temperatures and high chloride concentrations required.

Although stainless steels and nickel alloys are susceptible, alloying can improve the resistance dramatically. Additions of nickel and chromium, along with molybdenum and nitrogen, increase the resistance of the material to crevice corrosion. Chromium, molybdenum, and nitrogen are particularly potent, and there are beneficial synergistic interactions among them (Ref 11).

Copper-base alloys can suffer from a type of crevice corrosion known as metal-ion concentration-cell corrosion. Although there remains some controversy regarding the mechanism, it can be said that crevice-related attack for copper alloys is distinctly different from that for stainless steels. In the case of copper alloys, the most severe corrosion occurs *outside* the crevice, rather than inside. It is generally thought that the concentration of metal ions in the crevice electrolyte renders the crevice area cathodic to the area immediately outside the mouth of the crevice. Corrosion outside of the crevice (anode) progressed because the bulk environment contained a much lower concentration of metal ions (Ref 12).

Environment. The chemical composition of the environment affects crevice corrosion by providing a solution in which the material is passive while also containing anions that can lead to local breakdown (such as chloride ions). These aggressive anions will concentrate over time in the crevice to the point where localized depassivation occurs there. The bulk pH of the solution will tend to influence the time to the initiation of crevice corrosion, with more alkaline pH values tending to increase the initiation time. As with other forms of localized corrosion, more anodic (positive) potentials exacerbate crevice corrosion. This potential can develop due to the presence of oxidizers dissolved in solution, such as oxygen, chlorine, or ozone, or it can be imposed externally. One means of external imposition of potential is galvanic coupling to a more noble material.

Increased temperature is the clearest accelerant for crevice corrosion, and so it is the basis for several accelerated corrosion tests. For titanium alloys, there is a generally accepted lower limit of crevice corrosion of 70 °C (158 °F) (Ref 13).

Stifling of Crevice Corrosion. Crevice corrosion, like many other forms of localized corrosion, typically starts at a high rate and then slows with time. Under steady-state external conditions (i.e., chemical composition, temperature, potential), the rate decays somewhat to one controlled by the interaction between the steady- state conditions within the occluded region (i.e., occluded chemical composition, potential distribution, and dissolution kinetics) and those of the fully exposed surface (i.e., cathodic kinetics that are often diffusion controlled). While this steady state exhibits lower rates than the early transient, the rates can still be in the 25 to 250 μm/yr/ (1 to 10 mil/yr) range.

Relationships with Pitting. Crevice corrosion shares many characteristics and phenomenology with other forms of localized corrosion such as pitting, intergranular attack, environmentally assisted cracking, and dealloying. In all of those cases, the electrochemical and chemical conditions within an occluded region become altered with respect to the conditions on fully exposed surfaces. These variations can lead to rates of attack within the occluded region that are many orders of magnitude higher than those observed on the fully exposed surfaces. Generally, a material/environment combination that leads to pitting can also lead to crevice corrosion. Because of the many commonalities among the various types of localized corrosion, understanding crevice corrosion allows insights to be gained into the factors that influence the other forms of localized corrosion.

References cited in this section

4. C.S. Brossia and R.G. Kelly, *Corrosion Sci.,* Vol 40, 1998, p 1851

7. S.E. Lott and R.C. Alkire, *J. Electrochem. Soc.,* Vol 136, 1989, p 973

8. C.S. Brossia and R.G. Kelly, *Corrosion,* Vol 54, 1998, p 145

9. S.E. Lott and R.C. Alkire, *J. Electrochem. Soc.,* Vol 136, 1989, p 973

10. M.C.H. McKubre and S.C. Leach, in *Proc. Third Int. Symp. Environmental Degradation of Materials in Nuclear Power Systems—Water Reactors,* TMS, 1988, p 217

11. A.J. Sedriks, *Corrosion of Stainless Steels,* 2nd ed., Wiley-Interscience, 1996

12. N. Polan, Corrosion of Copper and Copper Alloys, *Corrosion,* Vol 13, *ASM Handbook,* ASM International, 1987, p 612

13. R.W. Schutz and D.E. Thomas, Corrosion of Titanium and Titanium Alloys, Corrosion, Vol 13, *ASM Handbook,* ASM International, 1987, p 669

R.G. Kelly, Crevice Corrosion, *Corrosion: Fundamentals, Testing, and Protection*, Vol 13A, *ASM Handbook*, ASM International, 2003, p 242–247

Crevice Corrosion

R.G. Kelly, University of Virginia

Selected Examples

Example 1: Crevice Corrosion of Stainless Steel in Aqueous Chloride. The most studied of all alloy systems for crevice corrosion is stainless steel. Since soon after their creation and establishment as "stainless" during exposure to marine atmospheres, iron-chromium-base alloys have been widely used in hopes of taking advantage of their superior inherent corrosion resistance. Unfortunately, that same widespread use has led to their use in environments in which they are susceptible to localized corrosion (Ref 11). Much of what is known about crevice corrosion is based on studies of stainless steels conducted to develop alloys more resistant to localized corrosion and to provide data for appropriate materials selection. The effects of alloy composition (Ref 14, 15), microstructure (Ref 16), crevice geometry (Ref 17), surface finish (Ref 18), and environmental parameters such as solution composition (Ref 19, 20, 21), temperature (Ref 22, 23, 24), and solution velocity (Ref 25) have been extensively studied.

Example 2: Crevice Corrosion of Nickel alloys in Chlorinated Seawater. Nickel-base alloys can be made very resistant to crevice corrosion through the addition of substantial amounts of chromium and molybdenum, along with minor additions of tungsten. Nonetheless, these highly resistant alloys are not immune. For example, alloy 625 tubes (Ni-Cr-Fe-Mo) were found to suffer crevice corrosion under vinyl hoses secured with serrated nylon hose clamps as part of a flow loop containing chlorinated seawater (Ref 26). The chlorine additions were sufficient to raise the potential of the material to the point that crevice corrosion initiated. Several studies have focused on the mechanisms underlying the initiation, demonstrating the need for an extremely aggressive occluded solution and high electrochemical potential (Ref 27, 28, 29).

Example 3: Crevice Corrosion of Aluminum Alloys in Aircraft Lap Joints. Corrosion of structural aluminum alloys can pose limitations on the service life of aircraft. The physical design of aircraft requires the formation of many regions that have an occluded geometry in which water and corrosive species can be trapped. For example, the areas of overlap between the inner and outer skins form an occluded site, referred to as a lap splice joint. During service, moisture is drawn into these sites by capillary action. Pollutant gases, such as SO_2 and NO_x, dissolve in the water, forming a corrosive solution that attacks the protective oxide on the material (Ref 30). Airplane takeoffs and landings near the ocean can lead to Cl^- ingress, acid rain can cause pH effects, and simple maintenance procedures (wash and deicing solutions) may lead to harmful crevice effects over the life of the aircraft.

Analyses of rehydrated corrosion products from lap joints have shown that more than 25 different ions can be present within these aircraft lap joints. These ions are present in low concentrations and have total ionic strength less than 80 mM (Ref 31). In fact, the highest concentration of chloride measured was 19 mM. Certain ions were commonly present in more than 75% of the samples. Although the ionic concentrations were low, Lewis (Ref 32) showed that some ions, even at these levels, had significant impact on the corrosion current density and/or corrosion potential.

The dilute ionic concentration and mildly alkaline pH found in this analysis is a chemical environment that is different than is generally thought to exist in a pit or crevice of aluminum (Ref 33). Pits and crevice sites usually involve acidic solutions because the metal cations formed by alloy dissolution react with water and form metal hydroxides and H^+ ions. For charge neutrality, anions such as chloride then migrate to the site from the bulk solution. Because of the geometry of the site, these ions become trapped and result in increasing concentration and higher rates of dissolution of the alloy. Therefore, the solution within pits and crevices tends to be acidic and highly concentrated.

In contrast, the lap-joint environment becomes neither concentrated nor acidic. This difference is due to the lack of an external cathodic reaction. In traditional pits and crevices, the majority of the cathodic reaction (e.g., $2O_2 + 2H_2O + 4e^- = 4OH^-$) occurs well away from the corrosion site. However, in lap-joint corrosion, the external surface often dries significantly before the occluded region (Ref 6). The lack of electrolyte on the external surface forces the cathodic reaction to occur within the occluded region. The production of OH^- ions in the cathodic reaction competes with the formation of H^+ ions in metal hydrolysis, and the result is a mildly alkaline environment in the case of aluminum (Ref 32).

Example 4: Crevice Corrosion of Titanium Alloys. Titanium alloys are among the most resistant to crevice corrosion. Extensive studies of crevice corrosion of these alloys have shown that these alloys do not suffer from crevice corrosion at temperatures less than 70 °C (158 °F). Ikeda et al. (Ref 34) have shown that by alloying with small amounts of molybdenum, nickel, or palladium, resistance to crevice corrosion is maintained to almost 200 °C (392 °F) in 10 wt.% $FeCl_3$.

References cited in this section

6. L.B. Simon, J.L. Elster, and R.G. Kelly, *Proc. 2000 ASIP Conference* (San Antonio, TX), U.S. Air Force Research Laboratory and the U.S. Air Force Aeronautical Systems Center, Dec 2000

11. A.J. Sedriks, *Corrosion of Stainless Steels,* 2nd ed., Wiley-Interscience, 1996

14. J.W. Oldfield, *Int. Met. Rev.,* Vol. 32, No. 3, 1987, p. 1

15. T. Ujiro et al., in *Proc. Int. Conf. Stainless Steels,* Iron and Steel Institute of Japan, Tokyo, 1991, p 86

16. H.J. Dundas and A.P. Bond, paper 206, Corrosion/85, National Association of Corrosion Engineers, 1985

17. T.S. Lee and R.M. Kain, paper 69, Corrosion/83, National Association of Corrosion Engineers, 1983

18. R.M. Kain, *Mater. Perf.,* Vol 23 (No. 2), 1984, p 24

19. R.M. Kain and J.W. Oldfield, paper 384, Corrosion/84, National Association of Corrosion Engineers, 1984

20. P. Gallagher, R.E. Malpas, and E.B. Shone, *Brit. Corros. J.,* Vol 23 (No. 4), 1988, p 229

21. A. Cigada, G. Rondelli, B. Vincentini, and G. Dallaspezia, in *Proc. 12th Int. Corrosion Congress,* Vol 3B, NACE International, 1993, p 1938

22. T. Hodgkiess, P. Habilomatis, and R. Ramsay, paper 24, Corrosion/84, National Association of Corrosion Engineers, 1984

23. T.S. Lee, *Electrochemical Corrosion Testing,* STP 727, American Society for Testing and Materials, 1981, p 43

24. R.M. Kain, paper 230, Corrosion/79, National Association of Corrosion Engineers, 1979

25. M.H. Peterson, T.J. Lennox, and R.E. Groover, *Mater. Perform.,* Vol 9 (No. 6), 1989, p 16

26. P.A. Klein, R.J. Ferrara, R.M. Kain, Corrosion/89, paper 112, National Association of Corrosion Engineers, 1989

27. R.M. Kain and P.A. Klein, paper 158, Corrosion/90, National Association of Corrosion Engineers, 1990

28. R.S. Lillard, M.J. Jurinski, and J.R. Scully, *Corrosion,* Vol 50, 1994, p 251

29. R.S. Lillard and J.R. Scully, *J. Electrochem. Soc.,* Vol 141, 1994, p 3006

30. S. Szlarska-Smialowska and J. Mankowski, *Corros. Sci.,* Vol 18, 1978, p 953

31. K.S. Lewis, J. Yuan, and R.G. Kelly, *J. Chromatogr. A.,* Vol 850, 1999, p 375

32. K.S. Ferrer and R.G. Kelly, Development of an Aircraft Lap Joint Simulant Environment, *Corrosion,* Vol 58, 2002, p 452–459

33. A.H. Lee, B.F. Brown, and R.T. Foley, *Corrosion,* Vol 36, 1980, p 373

34. B.M. Ikeda, M.G. Bailey, C.F. Clarke, and D.W. Shoesmith, “Crevice Corrosion of Titanium under Nuclear Fuel Waste Conditions,” report AECL-9568, Atomic Energy of Canada Ltd., 1989

R.G. Kelly, Crevice Corrosion, *Corrosion: Fundamentals, Testing, and Protection*, Vol 13A, *ASM Handbook*, ASM International, 2003, p 242–247

Crevice Corrosion

R.G. Kelly, University of Virginia

Testing

An excellent review of testing methods has been presented by Kearns (Ref 35). This section briefly reviews the types of methods that have been developed for differentiating and ranking the resistance of alloys toward crevice corrosion. See also the article “Evaluating Crevice Corrosion” in this Volume.

Standardized Accelerated Tests. A variety of ASTM standards have been developed in which materials are exposed to severe environments for crevice corrosion. For example, the ferric chloride test (Ref 36) employs a high concentration of chloride at a low pH, with the ferric/ferrous ion couple providing an elevated potential. Increased temperature can also be used to accelerate the process.

To further exacerbate the situation, tight crevices can be imposed by using a multiple-crevice assembly (Ref 37) as shown in Fig. 8. The castellated washer provides up to 20 possible sites for crevice corrosion on each side of the coupon. By applying a consistent torque, several replicate samples can be used to develop a statistical basis for comparison of alloy resistance.

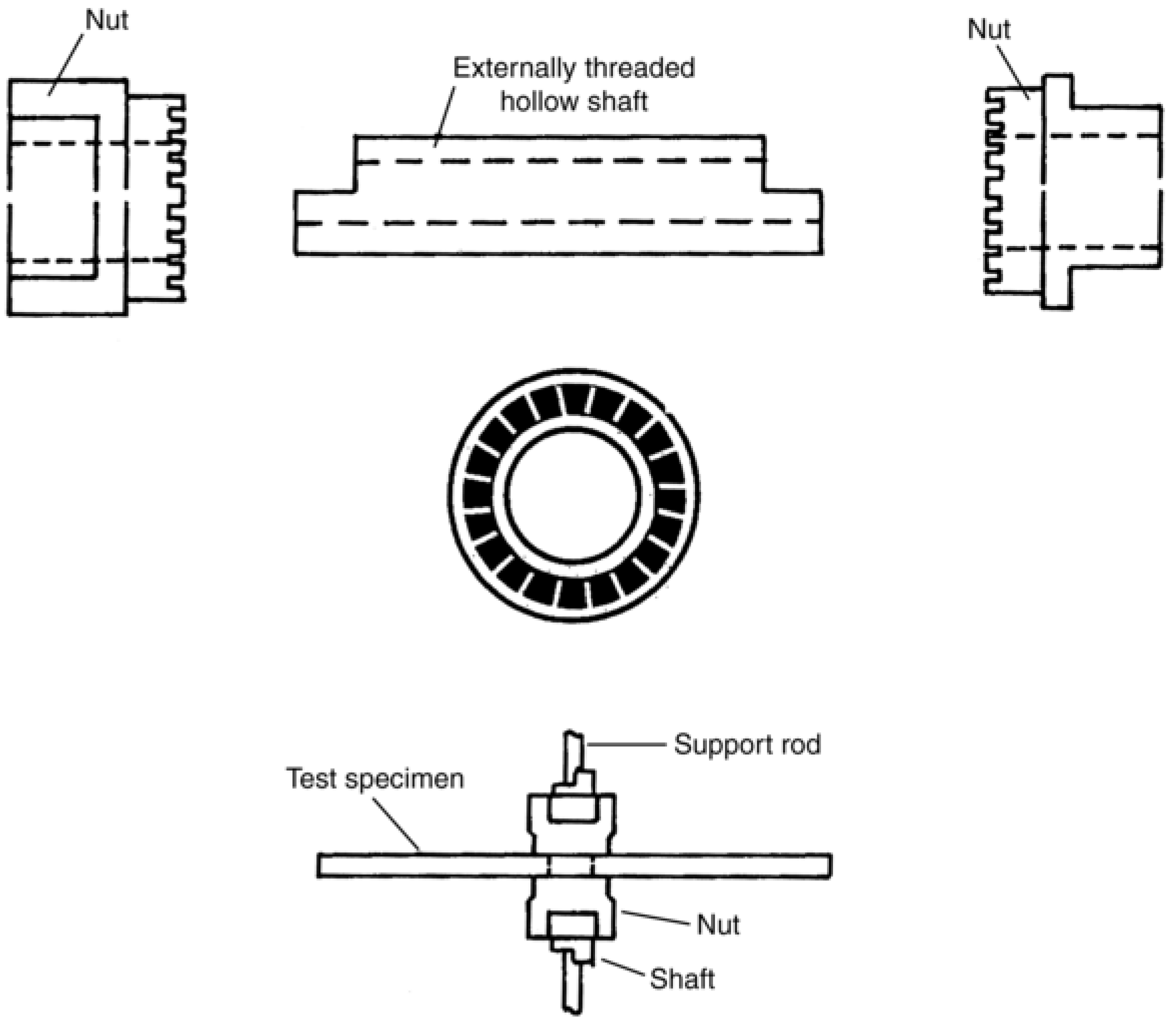

Fig. 8 Various views of the multiple-crevice assembly. Source: Ref 11

Electrochemical Testing. There are a number of tests that combine electrochemical polarization with elevated temperature to determine the critical crevice temperature (CCT). The CCT can then be used to rank the relative crevice-corrosion resistance. Typically, a constant positive potential is applied while a programmed temperature change is imposed. The current necessary to maintain the constant potential is monitored. When the applied potential and temperature combination is sufficient to cause crevice corrosion, the applied current increases dramatically and the CCT is thus determined. It has been found that this transition from passive to crevice corrosion is very sharp and reproducible (Ref 38).

Sridhar and coworkers (Ref 39) followed the work of Tsujikawa and Hisamatsu (Ref 40) by using a modification of ASTM F 746 (Ref 41) to determine the repassivation potential for crevice corrosion. In their approach, crevice corrosion is initiated under controlled conditions using a high applied potential. The ability of the material to resist localized corrosion is quantified by determining the highest applied potential at which the material can repassivate. They have shown that the repassivation potential determined in this way is an excellent measure of the long-term performance of stainless and nickel- base alloys as shown in Fig. 9 (Ref 39). They have demonstrated that a properly measured repassivation potential can be used as an engineering design criterion, not just as a comparative screening parameter. By maintaining the open-circuit potential of the surface of a material below the repassivation potential, significant localized corrosion is completely prevented. Although it has not been proved that absolutely no crevice corrosion initiates, propagation is stifled to the point of insignificance on a large engineering structure. This demonstration provides not only a valuable tool for preliminary design, but also a criterion to ensure that localized corrosion has been stopped once started.

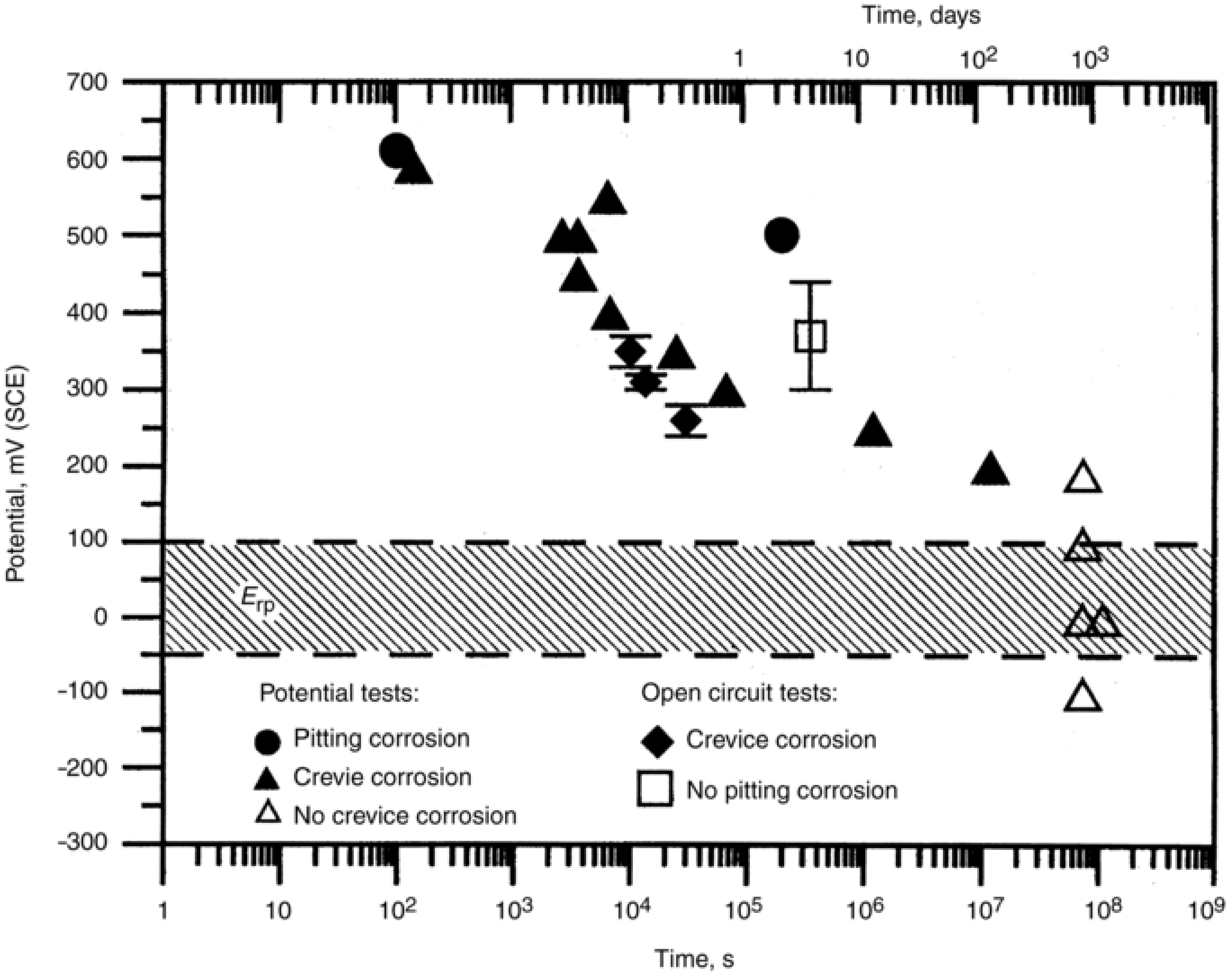

Fig. 9 Effects of applied potential and corrosion potential on the pitting- and crevice-corrosion initiation time for alloy 825 in 1000 ppm Cl^- at 95 °C (203 °F). Note that at and below the repassivation potential, E_{rp} no initiation occurs out to at least three years. Source: Ref 39

References cited in this section

11. A.J. Sedriks, *Corrosion of Stainless Steels,* 2nd ed., Wiley-Interscience, 1996

35. J.R. Kearns, *Corrosion Tests and Standards: Application and Interpretation,* R. Baboian, Ed., Manual 20, American Society for Testing and Materials, 1995, p 175

36. J.W. Oldfield, *Int. Met. Rev.,* Vol 32 (No. 3), 1987, p 153

37. D.B. Anderson, in *Galvanic and Pitting Corrosion—Field and Laboratory Studies,* STP 516, American Society for Testing and Materials, 1976, p 231

38. R. Qvarfort, *Corros. Sci.,* Vol 29, 1989, p 987

39. D.S. Dunn, G.A. Cragnolino, and N. Sridhar, *Corrosion,* Vol 56, 2000, p 90

40. S. Tsujikawa and Y. Hisamatsu, *Improvement of Corrosion Resistance of Structural Materials in Aggressive Media,* Y.M. Kolotyrkin, Ed., Nauka, Moscow, 1984

41. B.C. Syrett, *Corrosion,* Vol 33, 1977, p 221

R.G. Kelly, Crevice Corrosion, *Corrosion: Fundamentals, Testing, and Protection*, Vol 13A, *ASM Handbook*, ASM International, 2003, p 242–247

Crevice Corrosion

R.G. Kelly, University of Virginia

Prevention or Mitigation of Crevice Corrosion

Strategies for the prevention of crevice corrosion or lessening its effects include design awareness, use of inhibitors, and electrochemical control methods.

Design. The primary means of preventing crevice corrosion is careful design. To the extent possible, passive materials should not be placed in crevice arrangements. Unfortunately, in most engineering structures complete avoidance of crevices is not practical; pipe sections must be connected via flanges, vessels are not made from a single sheet of material, and so forth. In these cases, careful design would dictate maximizing the gap and minimizing the length (depth) of any crevices created. By making the geometry less restricted, the development of an aggressive chemistry is more difficult, and the potential drop within the crevice will also be smaller.

Making a crevice so tight as to preclude electrolyte uptake is usually not practical in the long term. Extremely tight crevices that are *not* watertight exhibit tremendous capillary action, drawing in solution over long distances just as a large tree draws moisture from the soil to the top of its canopy. The extremely restricted geometry is perfect for the development of severe crevice corrosion. Even crevices that are initially “too tight for water uptake” will likely loosen with time, leading to electrolyte ingress.

Alkire and coworkers (Ref 42) have demonstrated the effects of flow on the inhibition of pitting. Similar ideas can be applied to crevice corrosion. In both instances, flow would act to inhibit *initiation* of attack to the extent that the flow lines enter the occluded region. For pit initiation, flow at the surface is very successful at delaying or preventing aggressive solution development. In a crevice, the large length-to-gap ratio makes initiation control much less effective than for pits.

Ironically, once a crevice has initiated, the flow of solution across the fully exposed surface generally acts to increase the propagation rate. This effect results from the increased flow on cathodic reactions on the fully exposed surface that are mass-transport controlled, such as oxygen reduction. As the cathodic reaction rate increases, the polarization of the internal, crevice anode increases as well, leading to increased dissolution rates. This effect is mitigated to the extent that the crevice is under ohmic control due to the restricted geometry (Ref 43).

Material selection for crevice-corrosion resistance normally follows that used for pitting resistance. Ratings based on composition have been published for ferrous materials, using the CCT as the figure of merit. There is a strong correlation between the CCT and the pitting resistance equivalence number (PREN) for stainless steels, as might be expected. In both cases, the more chromium, molybdenum, and nitrogen in the alloy, the higher the resistance. Note that the CCT is always lower than the critical pitting temperature (CPT). An example of this phenomenon (Fig. 10) shows the effect of alloyed molybdenum on the resistance of stainless steels.

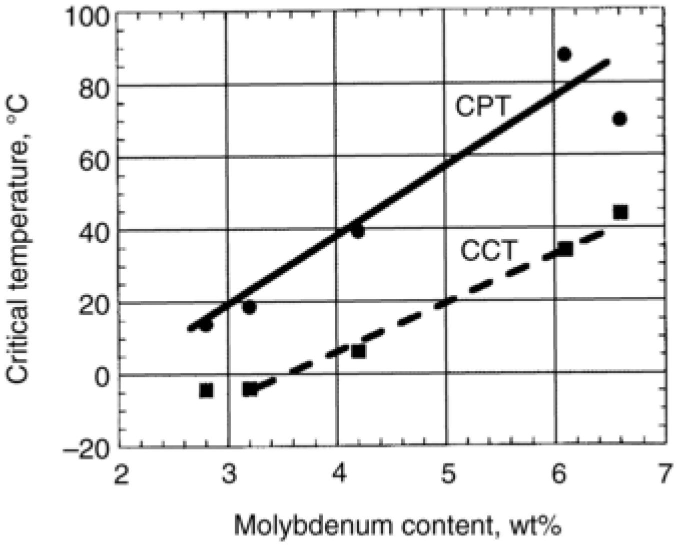

Fig. 10 Critical pitting and crevice temperatures (CPT and CCT, respectively) as a function of molybdenum content for commercial austenitic stainless steels. Source: Ref 35

In general, the lower the passive current density of the material, the smaller its active/passive transition, and the more stable its oxide, the more resistant it is to crevice corrosion. Of particular importance is the dependence of these parameters on the pH and chloride content.

Inhibitors. In addition to alloying, solution- phase inhibition has been shown to reduce the occurrence of crevice corrosion. Again, similarities to inhibitors for pitting have been observed, as expected. Inhibitors tend to be less effective for crevice corrosion than pitting because of the much longer transport lengths required for the inhibitor to move close to the active region. In order to arrive there in sufficient concentration to be effective, the bulk concentration generally needs to exceed the bulk chloride concentration by a factor of five or more (on a molar basis).

Many nonaggressive anions have been investigated as localized corrosion inhibitors in Cl^- solutions, including SO_4^{2-}, ClO_4^-, and NO_3^-(Ref 44). Anions that are not electroactive (e.g., SO_4^{2-} and ClO_4^-) have been suggested to function as inhibitors via a supporting electrolyte effect (Ref 45, 46, 47). A supporting electrolyte effect occurs when a species—for example, sulfate— competitively migrates and adsorbs on the metal surface with Cl^-, thereby slowing or preventing the increase in the Cl^- concentration in the occluded region. Thus, the relative concentration and mobility of the other anion compared to Cl^- are critically important. The presence of SO_4^{2-} would delay the accumulation of Cl^- in the occluded site, but the same occluded-site chemistry would be necessary for initiation to occur. Newman and Ajjawi (Ref 48) proposed that some inhibiting anions form a salt film during the early stages of localized corrosion initiation, under which passivation can occur via inward water diffusion. In the case of NO_3^-, an electroactive anion, Newman et al. (Ref 48, 49) proposed that inhibition occurs via one of three possible mechanisms:

- Electroreduction of NO_3^-, to NH_4^+, which consumes H^+ and produces water
- Electroreduction of NO_3^- to elemental nitrogen, which in turn blocks some proportion of the active kink sites on the surface at which dissolution occurs
- Formation of a redox couple between Fe^{2+} and NO_3^- that consumes H^+ at low pH and assists in the formation of an Fe-OH barrier film at high pH

In the case of crevice corrosion, Lu and Ives (Ref 50) has shown that cerium treatments of fully exposed surface can inhibit crevice corrosion of stainless steels. This effect is presumably by a poisoning of the rate of oxygen reduction (cerium oxides are poor oxygen reduction surfaces), which leads to an inability of the external surface to support the dissolution rate of the occluded region to the extent necessary to produce and maintain an aggressive occluded solution. Insulating coatings (e.g., paints) on the fully exposed surface can also mitigate crevice corrosion in a similar manner by reducing the ability of that surface to consume the electrons generated by the anodic dissolution within the crevice. This decrease in cathode area limits the rates of anodic dissolution

possible within the crevice and thereby can limit crevice corrosion. It should be noted that many corrosion-resistant alloys are notoriously difficult to paint due to poor adherence between the passive film and the organic coating. Loss of adhesion can lead to additional crevice sites.
Potential control can be effective in suppressing the initiation and propagation of crevice corrosion. The electrochemical potential of an interface can be controlled by maintaining the potential of the alloy/solution interface at sufficiently low potential; this has been shown to prevent crevice-corrosion stabilization (Ref 51). As shown in Fig. 11, the repassivation potential for crevice corrosion becomes independent of the amount of charge passed. Kehler *et al.* (Ref 5) have demonstrated the same for alloy 625 and alloy C-22, including the deleterious effects of increased temperature and concentration ratio of [Cl^-]:[other anions].

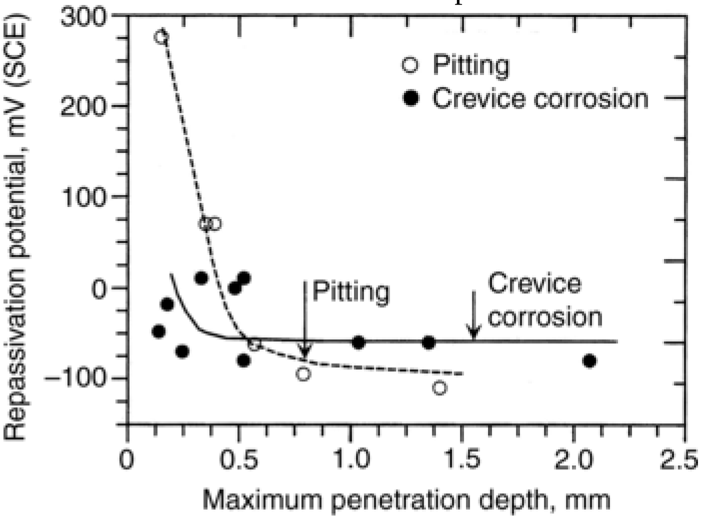

Fig. 11 The repassivation potential of alloy 825 as a function of prior crevice corrosion and pit depth. The results show a bounding value independent of penetration depth. Test conditions: 1000 ppm Cl^- at 95 °C (200 °F); back scan, 5 mV/s. Source: Ref 39

Cathodic protection can be used to combat crevice corrosion (Ref 28, 52), in some cases, with sufficiently low potentials preventing it altogether. It should be noted that anodic protection is generally not effective in preventing crevice corrosion. In fact, anodic polarization generally *increases* the rate of the crevice attack. The only situation for which anodic polarization would be useful in preventing crevice corrosion is for systems that can be completely described by the ohmic drop model and for which no changes occur in either the occluded solution composition or the electrochemical behavior of the material in the occluded region.
More information on mechanisms of crevice corrosion and the controlling factors can be found in reviews on the subject (Ref 43, 53, 54, 55).

References cited in this section

5. B.A. Kehler, G.O. Ilevbare, and J.R. Scully, *Corrosion,* Vol 57, 2001, p 1042

28. R.S. Lillard, M.J. Jurinski, and J.R. Scully, *Corrosion,* Vol 50, 1994, p 251

35. J.R. Kearns, *Corrosion Tests and Standards: Application and Interpretation,* R. Baboian, Ed., Manual 20, American Society for Testing and Materials, 1995, p 175

39. D.S. Dunn, G.A. Cragnolino, and N. Sridhar, *Corrosion,* Vol 56, 2000, p 90

42. R.C. Alkire, D.B. Reiser, and R.L. Sari, *J. Electrochem. Soc.,* Vol 131, 1984, p 2795

43. H.W. Pickering, *Mater. Sci. Eng. A,* Vol 198, 1995, p 213

44. Z. Szklarska-Smialowska, *Pitting Corrosion of Metals,* National Association of Corrosion Engineers, 1986

45. I.L Rosenfeld and V.P. Maksimchuk, *Dokl. Akad. Nauk SSSR,* Vol 131, 1960, p 354

46. M. Prazak, J. Tousek, and W. Spanily, *Zashch. Met.,* Vol 5, 1969, p 371

47. H.P. Leckie and H.H. Uhlig, *J. Electrochem. Soc.,* Vol 113, 1966, p 1261

48. R.C. Newman and M.A.A. Ajjawi, *Corros. Sci.,* Vol 26, 1986, p 1057

49. R.C. Newman and T. Shahrabi, *Corros. Sci.,* Vol 27, 1987, p 827

50. Y.C. Lu and M.B. Ives, *Corros. Sci.,* Vol 37, 1995, p 145

51. N. Sridhar, D.S. Dunn, C.S. Brossia, and G.A. Cragnolino, *Research Topical Symp. Localized Corrosion,* G.S. Frankel and J.R. Scully, Ed., NACE International, 2001, p 1

52. T.S. Lee and A.H. Tuthill, paper 63, Corrosion/82, National Association of Corrosion Engineers, 1982

53. J.W. Oldfield, Ed., Crevice Corrosion: The Science and its Control in Engineering Practice, *Research Topical Symposium,* Corrosion '96, NACE International, 1996

54. A.J. Betts and L.H. Boulton, *Brit. Corros. J.,* Vol 28, 1993, p 279

55. A. Turnbull, in *Advances in Localized Corrosion,* NACE-9, National Association of Corrosion Engineers, 1990, p 359

R.G. Kelly, Crevice Corrosion, *Corrosion: Fundamentals, Testing, and Protection*, Vol 13A, *ASM Handbook*, ASM International, 2003, p 242–247

Crevice Corrosion

R.G. Kelly, University of Virginia

References

1. B.F. Brown, *Corrosion,* Vol 26, 1970, p 249

2. Z. Szlarska-Smialowska, *Pitting Corrosion of Metals,* National Association of Corrosion Engineers, 1976, p 301

3. T.P. Hoar, *Faraday Soc. Discuss.,* Vol 1, 1947, p 299

4. C.S. Brossia and R.G. Kelly, *Corrosion Sci.,* Vol 40, 1998, p 1851

5. B.A. Kehler, G.O. Ilevbare, and J.R. Scully, *Corrosion,* Vol 57, 2001, p 1042

6. L.B. Simon, J.L. Elster, and R.G. Kelly, *Proc. 2000 ASIP Conference* (San Antonio, TX), U.S. Air Force Research Laboratory and the U.S. Air Force Aeronautical Systems Center, Dec 2000

7. S.E. Lott and R.C. Alkire, *J. Electrochem. Soc.,* Vol 136, 1989, p 973

8. C.S. Brossia and R.G. Kelly, *Corrosion,* Vol 54, 1998, p 145

9. S.E. Lott and R.C. Alkire, *J. Electrochem. Soc.,* Vol 136, 1989, p 973

10. M.C.H. McKubre and S.C. Leach, in *Proc. Third Int. Symp. Environmental Degradation of Materials in Nuclear Power Systems—Water Reactors,* TMS, 1988, p 217

11. A.J. Sedriks, *Corrosion of Stainless Steels,* 2nd ed., Wiley-Interscience, 1996

12. N. Polan, Corrosion of Copper and Copper Alloys, *Corrosion,* Vol 13, *ASM Handbook,* ASM International, 1987, p 612

13. R.W. Schutz and D.E. Thomas, Corrosion of Titanium and Titanium Alloys, Corrosion, Vol 13, *ASM Handbook,* ASM International, 1987, p 669

14. J.W. Oldfield, *Int. Met. Rev.,* Vol. 32, No. 3, 1987, p. 1

15. T. Ujiro et al., in *Proc. Int. Conf. Stainless Steels,* Iron and Steel Institute of Japan, Tokyo, 1991, p 86

16. H.J. Dundas and A.P. Bond, paper 206, Corrosion/85, National Association of Corrosion Engineers, 1985

17. T.S. Lee and R.M. Kain, paper 69, Corrosion/83, National Association of Corrosion Engineers, 1983

18. R.M. Kain, *Mater. Perf.,* Vol 23 (No. 2), 1984, p 24

19. R.M. Kain and J.W. Oldfield, paper 384, Corrosion/84, National Association of Corrosion Engineers, 1984

20. P. Gallagher, R.E. Malpas, and E.B. Shone, *Brit. Corros. J.,* Vol 23 (No. 4), 1988, p 229

21. A. Cigada, G. Rondelli, B. Vincentini, and G. Dallaspezia, in *Proc. 12th Int. Corrosion Congress,* Vol 3B, NACE International, 1993, p 1938

22. T. Hodgkiess, P. Habilomatis, and R. Ramsay, paper 24, Corrosion/84, National Association of Corrosion Engineers, 1984

23. T.S. Lee, *Electrochemical Corrosion Testing,* STP 727, American Society for Testing and Materials, 1981, p 43

24. R.M. Kain, paper 230, Corrosion/79, National Association of Corrosion Engineers, 1979

25. M.H. Peterson, T.J. Lennox, and R.E. Groover, *Mater. Perform.,* Vol 9 (No. 6), 1989, p 16

26. P.A. Klein, R.J. Ferrara, R.M. Kain, Corrosion/89, paper 112, National Association of Corrosion Engineers, 1989

27. R.M. Kain and P.A. Klein, paper 158, Corrosion/90, National Association of Corrosion Engineers, 1990

28. R.S. Lillard, M.J. Jurinski, and J.R. Scully, *Corrosion,* Vol 50, 1994, p 251

29. R.S. Lillard and J.R. Scully, *J. Electrochem. Soc.,* Vol 141, 1994, p 3006

30. S. Szlarska-Smialowska and J. Mankowski, *Corros. Sci.,* Vol 18, 1978, p 953

31. K.S. Lewis, J. Yuan, and R.G. Kelly, *J. Chromatogr. A.,* Vol 850, 1999, p 375

32. K.S. Ferrer and R.G. Kelly, Development of an Aircraft Lap Joint Simulant Environment, *Corrosion,* Vol 58, 2002, p 452–459

33. A.H. Lee, B.F. Brown, and R.T. Foley, *Corrosion,* Vol 36, 1980, p 373

34. B.M. Ikeda, M.G. Bailey, C.F. Clarke, and D.W. Shoesmith, "Crevice Corrosion of Titanium under Nuclear Fuel Waste Conditions," report AECL-9568, Atomic Energy of Canada Ltd., 1989

35. J.R. Kearns, *Corrosion Tests and Standards: Application and Interpretation,* R. Baboian, Ed., Manual 20, American Society for Testing and Materials, 1995, p 175

36. J.W. Oldfield, *Int. Met. Rev.,* Vol 32 (No. 3), 1987, p 153

37. D.B. Anderson, in *Galvanic and Pitting Corrosion—Field and Laboratory Studies,* STP 516, American Society for Testing and Materials, 1976, p 231

38. R. Qvarfort, *Corros. Sci.,* Vol 29, 1989, p 987

39. D.S. Dunn, G.A. Cragnolino, and N. Sridhar, *Corrosion,* Vol 56, 2000, p 90

40. S. Tsujikawa and Y. Hisamatsu, *Improvement of Corrosion Resistance of Structural Materials in Aggressive Media,* Y.M. Kolotyrkin, Ed., Nauka, Moscow, 1984

41. B.C. Syrett, *Corrosion,* Vol 33, 1977, p 221

42. R.C. Alkire, D.B. Reiser, and R.L. Sari, *J. Electrochem. Soc.,* Vol 131, 1984, p 2795

43. H.W. Pickering, *Mater. Sci. Eng. A,* Vol 198, 1995, p 213

44. Z. Szklarska-Smialowska, *Pitting Corrosion of Metals,* National Association of Corrosion Engineers, 1986

45. I.L Rosenfeld and V.P. Maksimchuk, *Dokl. Akad. Nauk SSSR,* Vol 131, 1960, p 354

46. M. Prazak, J. Tousek, and W. Spanily, *Zashch. Met.,* Vol 5, 1969, p 371

47. H.P. Leckie and H.H. Uhlig, *J. Electrochem. Soc.,* Vol 113, 1966, p 1261

48. R.C. Newman and M.A.A. Ajjawi, *Corros. Sci.,* Vol 26, 1986, p 1057

49. R.C. Newman and T. Shahrabi, *Corros. Sci.,* Vol 27, 1987, p 827

50. Y.C. Lu and M.B. Ives, *Corros. Sci.,* Vol 37, 1995, p 145

51. N. Sridhar, D.S. Dunn, C.S. Brossia, and G.A. Cragnolino, *Research Topical Symp. Localized Corrosion,* G.S. Frankel and J.R. Scully, Ed., NACE International, 2001, p 1

52. T.S. Lee and A.H. Tuthill, paper 63, Corrosion/82, National Association of Corrosion Engineers, 1982

53. J.W. Oldfield, Ed., Crevice Corrosion: The Science and its Control in Engineering Practice, *Research Topical Symposium,* Corrosion '96, NACE International, 1996

54. A.J. Betts and L.H. Boulton, *Brit. Corros. J.,* Vol 28, 1993, p 279

55. A. Turnbull, in *Advances in Localized Corrosion,* NACE-9, National Association of Corrosion Engineers, 1990, p 359

56. E.D.D. During, Ed., *Corrosion Atlas,* Elsevier, 1988

C. Hahin and R.G. Buchheit, Filiform Corrosion, *Corrosion: Fundamentals, Testing, and Protection,* Vol 13A, *ASM Handbook,* ASM International, 2003, p 248–256

Filiform Corrosion

Christopher Hahin, Illinois Department of Transportation; Rudolph G. Buchheit, Ohio State University

Introduction

FILIFORM CORROSION occurs on metallic surfaces coated with organic films that are typically 0.05 to 0.1 mm (2 to 4 mil) thick. Common objects such as a coated aluminum automobile wheel (Fig. 1) and a lacquered hammerhead (Fig. 2) are susceptible. The pattern of attack is characterized by the appearance of fine filaments emanating in random directions from one or more initiation sites. Filaments may propagate in one direction over relatively long distances. The source of initiation is usually a defect or mechanical scratch in the coating. The filaments are fine tunnels composed of corrosion products underneath a bulged and cracked coating. Filiform tracks are visible at arm's length as small blemishes. On closer examination, they appear as fine striations shaped like tentacles or cobweblike traces (Fig. 3). Though popular literature describes filiforms as “wormlike,” this corrosion is not biological in origin.

Fig. 1 Filiform corrosion on cast aluminum alloy automotive wheels that were lacquered with a clear coat to prevent dulling of the aluminum. Arrows indicate sites of significant activity. Note that each filiform originates at sharp corners where the clear coat is very thin, cracked, or severed.

Fig. 2 Filiform corrosion on a clear-lacquered steel hammerhead exposed to humid conditions. Fine filaments have extended over the entire surface of the hammerhead, with filiforms originating at corners, grind marks, or other sites where the coating varies in thickness.

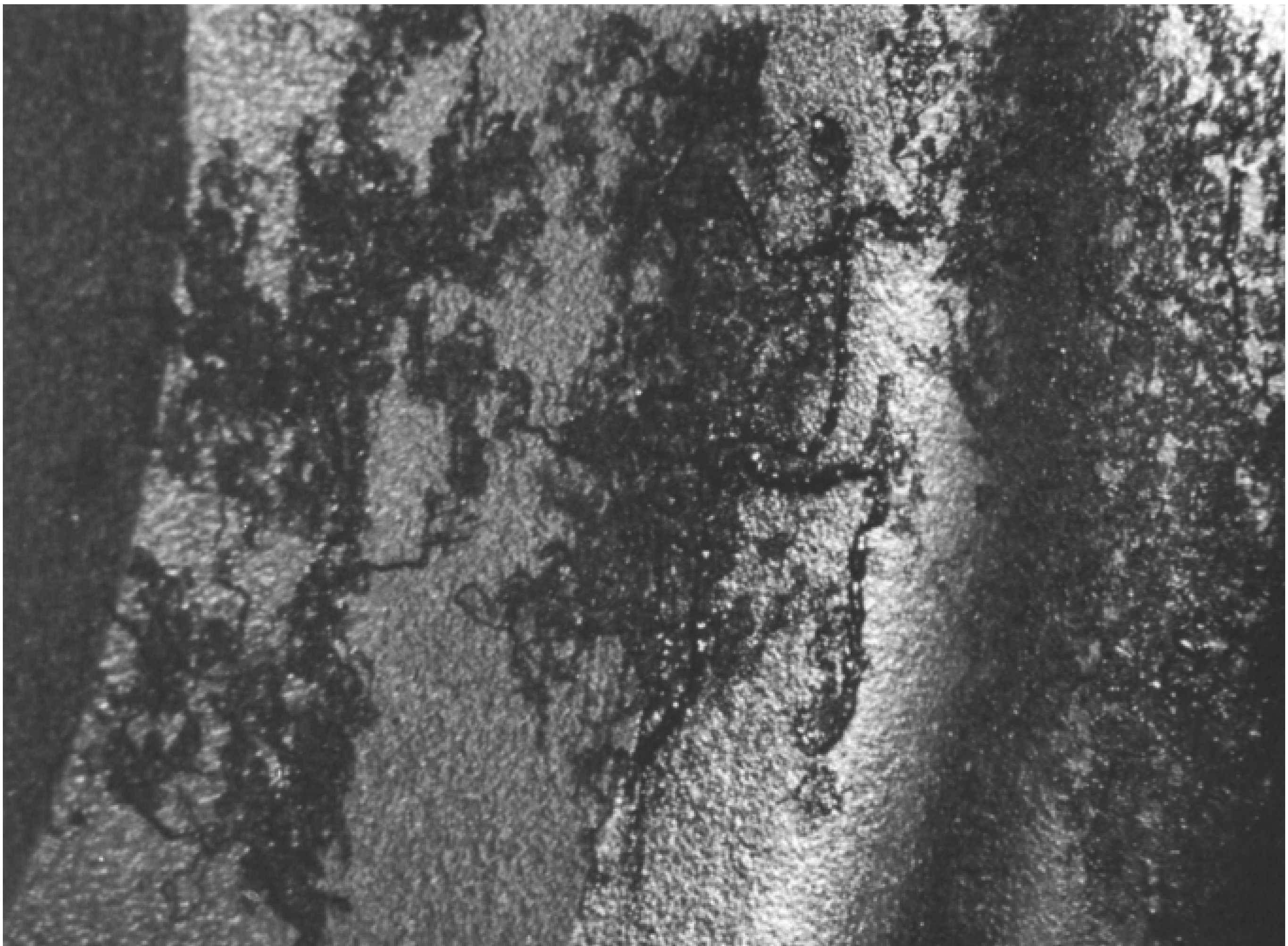

Fig. 3 A lacquered steel can lid exhibiting filiform corrosion showing both large and small filaments partially oriented in the rolling direction of the steel sheet. Without this 10× magnification by a light microscope, the filiforms look like fine striations or minute tentacles.

C. Hahin and R.G. Buchheit, Filiform Corrosion, *Corrosion: Fundamentals, Testing, and Protection*, Vol 13A, *ASM Handbook*, ASM International, 2003, p 248–256

Filiform Corrosion

Christopher Hahin, Illinois Department of Transportation; Rudolph G. Buchheit, Ohio State University

Occurrence of Attack

Filiform corrosion has been observed to occur under a wide range of organic coatings and proceeds with the same general characteristics on steel, aluminum, and magnesium. Filiform corrosion occurs on painted plain-carbon steel and aluminum sheet, coated steel cans, aluminum foil laminated packaging, and other lacquered metallic items placed in areas with high humidity. The susceptibility of a metal to filiform corrosion can be determined by placing coated and scribed samples in a warm humidified chamber. An initiating salt or vapor is used before humidification. If susceptible, filiform tracks will gradually grow outward from the scratches. Many of these filaments will later orient themselves in the rolling direction of the sample substrate.

Filiform attack occurs at ambient or slightly elevated temperatures when the relative humidity (RH) is between 65 and 90%. Blistering is favored over filiform corrosion when the RH approaches 100% (Ref 1). Blistering is believed to result from the fact that at high humidities organic coatings become water saturated and permeable to oxygen, making it difficult to sustain differential aeration and separation of anode and cathode. On the dry side of the humidity range, filiform corrosion of nitrocellulose lacquer coated steel has been reported at RH values as low as 58%. Filiform corrosion at even lower RH has been reported for aluminum in chemically aggressive environments (Ref 2). The average width of a filament varies between 0.05 and 3 mm (2 and 120 mils). Filament width depends on the coating, the ambient RH, and the corrosive environment. Typical filament height is about 20 μm (0.8 mil). The filament growth rate can vary widely, with rates ranging from 0.01 to 0.85 mm/day (0.4 to 35 mils/day). The depth of attack in the filiform tunnels can be as deep as 15 μm (0.6 mil) (Table 1). The fluid in the leading head of a filiform is typically acidic, with a pH from 1 to 4. Oxygen or air and water are needed to sustain filiform corrosion, indicating that filiform corrosion is a special differential-aeration cell.

Table 1 Filiform corrosion growth rates on various coated metals

Coating	Initiating environment	Typical rate		Relative humidity, %	Filament width	
		mm/day	**mils/day**		**mm**	**mils**
Steels						
Varnish	NaCl	0.33–0.53	13–21	65–85	0.1–0.3	4–12
	Acetic acid	0.5	20	86	0.15	6
Copol	NaCl	0.03	1.2	60–94	…	…
Lacquer	Acetic acid	0.85	33.5	…	0.1–0.5	4–20
Linseed oil	NaCl	0.04–0.08	1.6–3.1	…	0.05–0.1	2–4
Alkyds	NaCl	0.50	20	80	0.1–0.5	4–20
	Acetic acid	0.1	4	85	…	…
Alkyd urea	$FeCl_2$	0.26–0.43	10–17	80	0.25	10
Epoxy urea	NaCl/FeCl;i2	0.01–0.46	0.4–18	80	0.25	10
Epoxy	Acetic acid	0.16	6.3	85	…	…
Acrylic	NaCl	0.19–0.86	7.5–34	80	0.25	10
	Acetic acid	0.1	4	85	…	…
Polyurethane	NaCl	0.16–0.50	6.3–20	90	0.1–0.3	4–12
	Acetic acid	0.09	3.5	85	…	…
Polyester	Acetic acid	0.08	3.1	85	…	…
Aluminum alloys						

Alkyds	HCl vapor	0.1	4	85	0.5–1.0	20–40
Acrylic	HCl vapor	0.1	4	85	0.5–1.0	20–40
Polyurethane	HCl vapor	0.1	4	75–85	0.5–1.0	20–40
Polyester	HCl vapor	0.2	4	85	0.5–1.0	20–40
Epoxy	HCl vapor	0.09	3.5	85	0.5–1.0	20–40
Magnesium						
Alkyds	HCl vapor	0.2	8	75	…	…
Acrylic	HCl vapor	0.3	12	75	…	…
Polyurethane	HCl vapor	0.3	12	75	…	…
Polyester	HCl vapor	0.2	8	75	…	…
Epoxy	HCl vapor	0.3	12	75	…	…

References cited in this section

1. B.S. Skerry and C.H. Simpson, *Corrosion,* Vol 49, 1993, p 663

2. R. Preston and B. Sanyal, *J. Appl. Chem.,* Vol 6, 1956, p 26

C. Hahin and R.G. Buchheit, Filiform Corrosion, *Corrosion: Fundamentals, Testing, and Protection,* Vol 13A, *ASM Handbook,* ASM International, 2003, p 248–256

Filiform Corrosion

Christopher Hahin, Illinois Department of Transportation; Rudolph G. Buchheit, Ohio State University

---

Mechanism of Attack

The driving force for filiform corrosion is the voltage generated by differential aeration between its active head, which is deaerated and acidic, and a filamentous tail, which is aerated and alkaline (Fig. 4). Separation of anode and cathode is essential for filiform corrosion to occur. Substantial voltage differences of 0.3 to 0.4 V between head and tail can be measured, depending on conditions and amount of aeration. As the filiform track proceeds, the coating and metal are disbonded and the coating is lifted. The precise mechanism by which disbondment and lifting happens has not been established, but some metal dissolution is involved. Filiform corrosion will occur in environments that contain species aggressive enough to cause corrosion attack of the substrate metal. The presence of oxygen is a requirement for filiform-corrosion tracks to propagate. Oxygen is supplied to the cathodic regions behind the head of the track by diffusion through the corrosion product in the tail or by cracks in the coating uplifted by the passage of the head. A close-up of the head-tail interface is shown in Fig. 5. Filiform corrosion does not directly affect the mechanical integrity of the structure. However, it is aesthetically unpleasing and causes progressive degradation of the protective organic coating, which may lead to the onset of more damaging forms of localized corrosion. In the case of protective foils and packaging, filiform corrosion can lead to breaches in the foil barrier, allowing for vapor transmission, contamination, or slow loss of product.

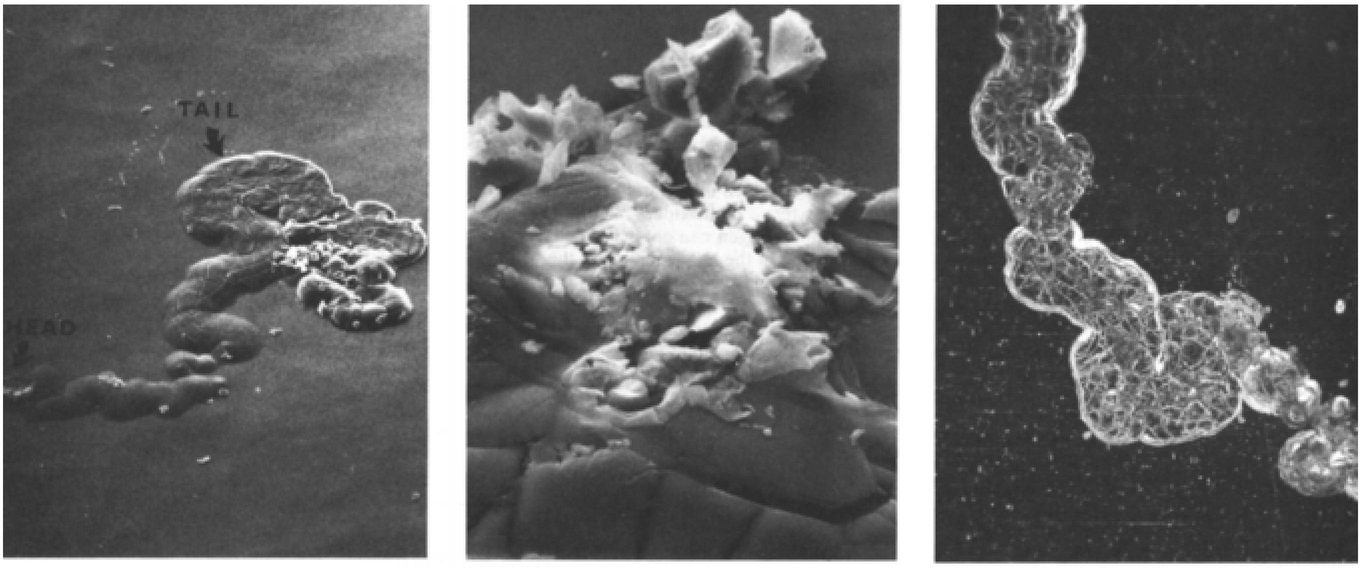

(a) (b) (c)

Fig. 4 Filiform corrosion on PVC-coated aluminum foil. (a) Advancing head and cracked tail section of a filiform cell. Scanning electron microscopy (SEM). 80×. (b) The gelatinous corrosion products of aluminum oozing out of the porous end tail section of a filiform cell. SEM. 830×. (c) Tail region of a filiform cell. Tail appears iridescent due to internal reflection. Light microscopy. 60×

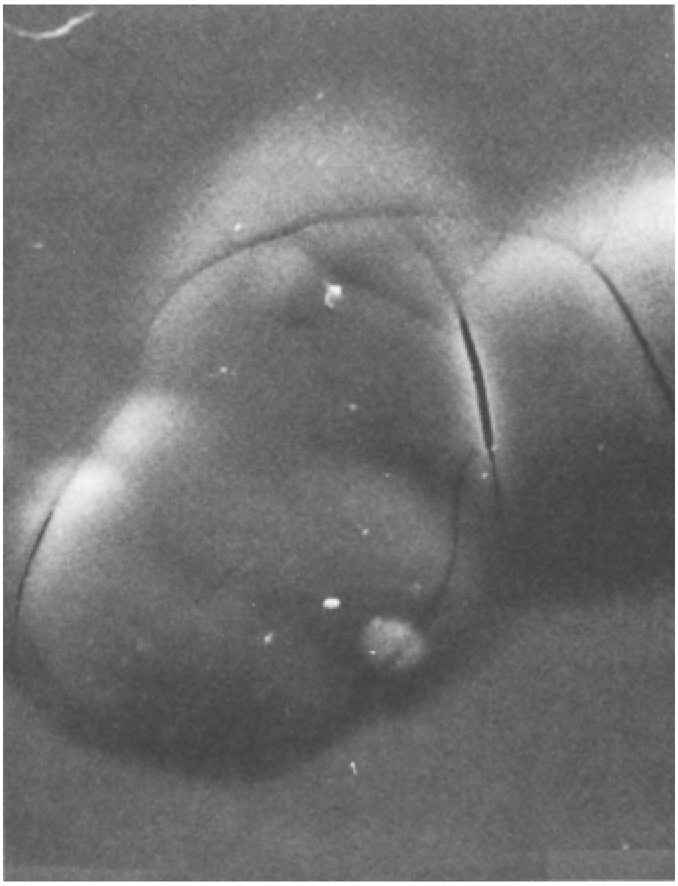

Fig. 5 Close-up of the advancing head shown in Fig. 4(a). Minute cracks can be seen at the head-tail interface of a filiform-corrosion cell. These cracks are entry points for water and air to provide a source of hydroxyl ions and an electrolyte. Intermediate corrosion products are just beginning to form in the head, and they undergo further reaction to form an expanded tail. The tail region is a progressive reaction zone that ultimately forms spent corrosion products. Between the head and porous end, ions gradually react with water and oxygen and are slowly transported in the direction of the tail to form final corrosion products. Scanning electron microscopy. 760×

C. Hahin and R.G. Buchheit, Filiform Corrosion, *Corrosion: Fundamentals, Testing, and Protection*, Vol 13A, *ASM Handbook*, ASM International, 2003, p 248–256

Filiform Corrosion

Christopher Hahin, Illinois Department of Transportation; Rudolph G. Buchheit, Ohio State University

Tests for Filiform Corrosion

There are numerous standard tests for filiform corrosion that involve scoring or scratching the coated specimen exposing it to corrosive fluid or vapor, and then placing it in a warm, humidified atmosphere. To accelerate filiform attack, chlorides are the commonly used corrosive ion, obtained from either from salt spray, fog, concentrated vapor, or dipping.

The standard test in the United States is ASTM D 2803, "Guide for Testing Filiform Corrosion Resistance of Organic Coatings on Metal." Coated metal specimens are scribed to bare metal and subjected to a salt fog atmosphere up to 24 h, rinsed in distilled water, and then placed wet in a closed cabinet at 25 °C (77 °F) and 85% RH. An accelerated alternate test exposes specimens in salt fog at 80% RH at 40 °C (104 °F). Time of exposure typically varies from 100 to 1000 h.

ISO 4623, "Paints and Varnishes—Filiform Corrosion Tests," is the international standard for determination of resistance and has two parts, one for steel (ISO 4623-1) and one for aluminum (ISO 4623-2). The ISO methods apply sodium chloride either by dipping specimens in solution for 60 s or by salt fogging for 24 h. Afterwards, specimens are humidified at 80% RH at 40 °C (104 °F) for a specified time. There are several other accelerated tests for aluminum used in the aircraft and automotive industries. Hydrochloric acid vapor is frequently employed as a filiform initiator.

However, the salt spray and salt fog filiform tests have been criticized as poor predictors of performance of metallic parts in actual environments. Corrosion mechanisms differ when subject to alternating wet-dry conditions rather than high concentrations of salt or continuous fog. Other atmospheres and salts besides the chloride ion can contribute to corrosive conditions (Ref 3).

Testing according to SAE J2334, "Cosmetic Corrosion Lab Test," has shown the best correlation to typical performance of automotive coatings in various locations throughout North America. The SAE J2334 test is an alternating wet-dry cycle, consisting of humidification, dipping in a combination of ionic salts, then drying at 60 °C (140 °F) and 50% RH, and then repeating this cycle up to 80 times or more. This corresponds to approximately 5 years of actual service (Ref 3). For filiforms to develop, the humidification stage should be 80 to 95% RH at 40 to 50 °C (104 to 122 °F). Many manufacturers provide a variety of humidity chambers and cabinets that are either manually operated or can automatically program test cycles for several of these standards. Additional information is provided in the article "Cabinet Testing" in this Volume.

Reference cited in this section

3. H.E. Townsend, "Salt Spray Test is Bogus," Paper presented at SAE World Congress, (Detroit), April 2000

C. Hahin and R.G. Buchheit, Filiform Corrosion, *Corrosion: Fundamentals, Testing, and Protection*, Vol 13A, *ASM Handbook*, ASM International, 2003, p 248–256

Filiform Corrosion

Christopher Hahin, Illinois Department of Transportation; Rudolph G. Buchheit, Ohio State University

Filiform Corrosion of Steels

Most of the early work on filiform-corrosion phenomenology and mechanisms was conducted to account for its occurrence on organically coated steel. However, as more recent research has shown, the understanding developed for filiform corrosion of steels extends with certain modifications to organically coated aluminum and magnesium alloys.

Characteristics of Filiform Corrosion in Coated and Tin-Plated Steels. Filiform corrosion has been noted for a wide range of low-alloy carbon steels and steels plated with tin. The general appearance of filiform cells on coated steels consists of an active head, which is blue, blue- green, or grayish in color, and a brownish, rusty filament-shaped tail. Filament growth tends to be more random when the steel surface has no burnished texture or pronounced rolling direction. Steels and tin-plated steels are routinely coated to provide resistance to atmospheric corrosion, to isolate foodstuffs from their containers, and to provide an adherent surface for ink and paint. Filiform corrosion is an important corrosion problem for these materials. Filiform corrosion of cast irons and high-alloy steels including stainless steels has not been reported.

The corrosion rate of steel itself is fairly low in alkaline environments but increases markedly in acidic environments, especially when the pH is less than 3. Steels can passivate under strongly oxidizing conditions. However, most natural environments are not sufficiently oxidizing to induce passivation in low-carbon steels. As a result, the primary oxidant in these environments, dissolved oxygen, serves to stimulate the corrosion of steel greatly.

Tin plating on steel is very thin, on the order of 1.5 μm (0.06 mil) thick, and is a porous barrier. In terms of corrosion, tin itself is amphoteric; it corrodes in alkaline and acidic solutions. However, it is also a seminoble metal and is not rapidly attacked in certain deaerated acids. In some environments, the porous tin layer is cathodic to the underlying steel. In aggressive environments, the tin plate provides little corrosion protection for the substrate. Steel and tin are both readily corroded by aerated acids, and conditions of low pH, aeration, and high-chloride concentrations are often found to exist in the active heads of filiform-corrosion cells.

Organic coatings are applied to steel and tin- plated steel to shield it from moist or humid environments to prevent rusting. Transparent organic coatings can also be lightly tinted with various dyes to impart a brass, bronze, or bluish cast to improve the appearance of the steel.

Filiform corrosion has been observed on steel and tin-plated steel coated with lacquers, varnish, polyurethane, boiled linseed oil, and various alkyd, urea, and epoxy paints. The coatings are applied by spraying, by direct contact with the rubber rolls, by dipping, or by electrostatic methods. Cured and dried coatings are uneven in thickness, with numerous hills and valleys. Lacquers can contain entrapped solvents if they are insufficiently cured. Scratches or scores in tin-plated cans may lead to filiform corrosion and eventual penetration of the can wall (Ref 4).

In general, organic coatings are flexible, and they tend to soften at higher temperatures. Coatings can separate from the steel substrate due to mechanical action. The ease of separation depends on how well the surface was prepared before it was coated. Organic coatings can be permeable to water and can have numerous flaws caused by inherent porosity, improper application of the coating, poor curing, or solvent entrapment. Coated articles may sustain some minor mechanical abrasions during their curing or storage. Coatings often crack if fast cured by radiant or forced-air heat, which causes shrinkage or uneven cross linking when polymerized. Coatings also crack when blistered by corrosion- product expansion, gas evolution, or water retention. Coatings, therefore, have many potential defect sources at which filiform corrosion can initiate. Heads of filiform cells will continue to remain active as long as the coating keeps expanding and cracking if moisture and oxygen are available.

Conditions Contributing to Filiform Attack. As indicated previously, filiform corrosion generally occurs in coated steels when the RH is between 60 and 95% in a temperature range of 20 to 40 °C (70 to 104 °F), though

the active range of RH differs for different coating systems. Filiform tracks initiate at coating defects such as cut edges, scratches, pinholes, or inclusions. Thin areas may sustain breaks caused by ultraviolet light or chemical degradation. Filiform susceptibility is increased by surface roughness and poor surface cleanliness. In terms of environmental conditions, filiform corrosion appears to occur in environments that would lead to corrosion attack of the unprotected substrate. For steels, filiform corrosion is observed to occur in chloride and sulfate electrolytes as well as in organic acids such as acetic acid.

Mechanism of Filiform Attack on Steel. As indicated previously, organic coatings on steels contain numerous defects where air and aqueous condensate can penetrate to the steel substrate and initiate corrosion. If the condensing atmosphere contains significant concentrations of salts, particularly those containing chlorides or sulfates, the substrate will corrode. Filiform attack may occur if a differential-aeration cell arises in the defect. In this situation, it is likely that the deaerated acidic anodic site is at the periphery of the defect and the aerated alkaline cathodic site is near the center of the defect. An example of such a configuration is a blister in a coating that is punctured near its center.

The solution in the advancing head of a filiform track is usually acidic, with moisture and oxygen entering primarily through the long tail or in cracks in the coating over the tail. The typical pH in the filiform head ranges from 1 to 4. Once established, potential-measurement regions normally indicate a potential difference of up to 0.3 V between the head and tail (Ref 5). Anions such as chloride, sulfide, or sulfate may enter the head from a corrosive atmosphere or by direct deposition on the surface and combine with the condensed water vapor that percolates through the cracked coating. Corrosive agents from the environment may be supplemented by continual leaching of solvents or unreacted constituents of the coating that combine with water. The head is filled with ferrous ions and the tail with ferric hydroxides and hydrated iron oxides, depending on the position in the tail and the age of the filaments.

During filiform propagation, the head moves along the coating metal interface, dissolving some of the substrate and forcing the coating from the steel substrate by corrosion product expansion. If the coating remains wet, adhesion to the substrate continues to decline (Ref 6). Behind the head, the new open space is filled with corrosion products or hydrogen gas from hydrogen reduction in the acidic filiform track head (Ref 7). The constant forward motion of a filament will cease if the tail is not continually aerated and supplied with water-vapor condensate. Interestingly, the advancing head of a filament is deflected or halted when it contacts a tail of another filiform. Why this occurs is not precisely known. The phenomenon may involve disruption of the differential-aeration cell on which filiform propagation depends, or a change in the acidic head chemistry as it encounters a filiform track, which may be more alkaline.

The mechanism of coating-substrate separation in the head region is not yet fully understood. Filiform heads tend to progress predominantly in the forward direction rather than spreading in a uniform radial manner. Microscopic valleys generated by rolling or grinding typically have less oxygenation when filled with the coating, whereas hills would have more aeration, and may be populated with harder, intermetallic cathodic sites. In advanced cases of filiform attack, head tunneling may appear to be more random. Corrosion product expansion and the undercutting of the coating-steel interface in the head are major contributors to filament head bulging (Ref 6). Head and tail solution chemistry may also affect the film strength of the coating and its bonding to the steel substrate. The head is a moving pool of acidic electrolyte, while the tail is alkaline and filled with corrosion products. The alkalinity of the tail region may lead to local saponification in susceptible resins causing cracking and debonding.

The size of a filament is apparently governed by the original defect size and the flexibility of the film. The texture of the rolled surface and the nature of the coating also shape the geometry and the spread rate of filiform attack. The ferrous ions formed in the head are transported toward the tail and further oxidized in the first section of the tail by forming ferric hydroxide.

Water and oxygen can enter the cell at cracks in the coating in the tail region or at the head- tail interface. Water is either consumed by the head electrolyte or can be involved in cathodic reactions. Hydroxyl ions are generated by the oxygen-reduction reaction, which takes place in the tail:

$$O_2 + 2H_2O + 4e^- \leftrightarrow 4OH^- \quad \text{(Eq 1)}$$

There is a general transport of iron ions toward the tail region, where they combine with hydroxyl ions to form ferric hydroxides. Toward the end of the tail, ferric hydroxide may decompose to ferric oxide and water. Other hydrated corrosion products may also form. Because the corrosion products of iron expand considerably, the coating bulges or splits. As the coating further cracks or splits, more oxygen and water can enter the tail, further stimulating filiform corrosion, blistering, or general corrosion of the substrate. In some brittle coatings, the head

may be very small, and cracks may form rapidly. The filiform head is an advancing pool of acidic electrolyte, whereas the tail is a progressive zone of corrosion products and reactants converted to an expanded gel or perceptible iron oxides. A general diagram illustrating the mechanism of filiform corrosion in iron and steel is shown in Fig. 6(a).

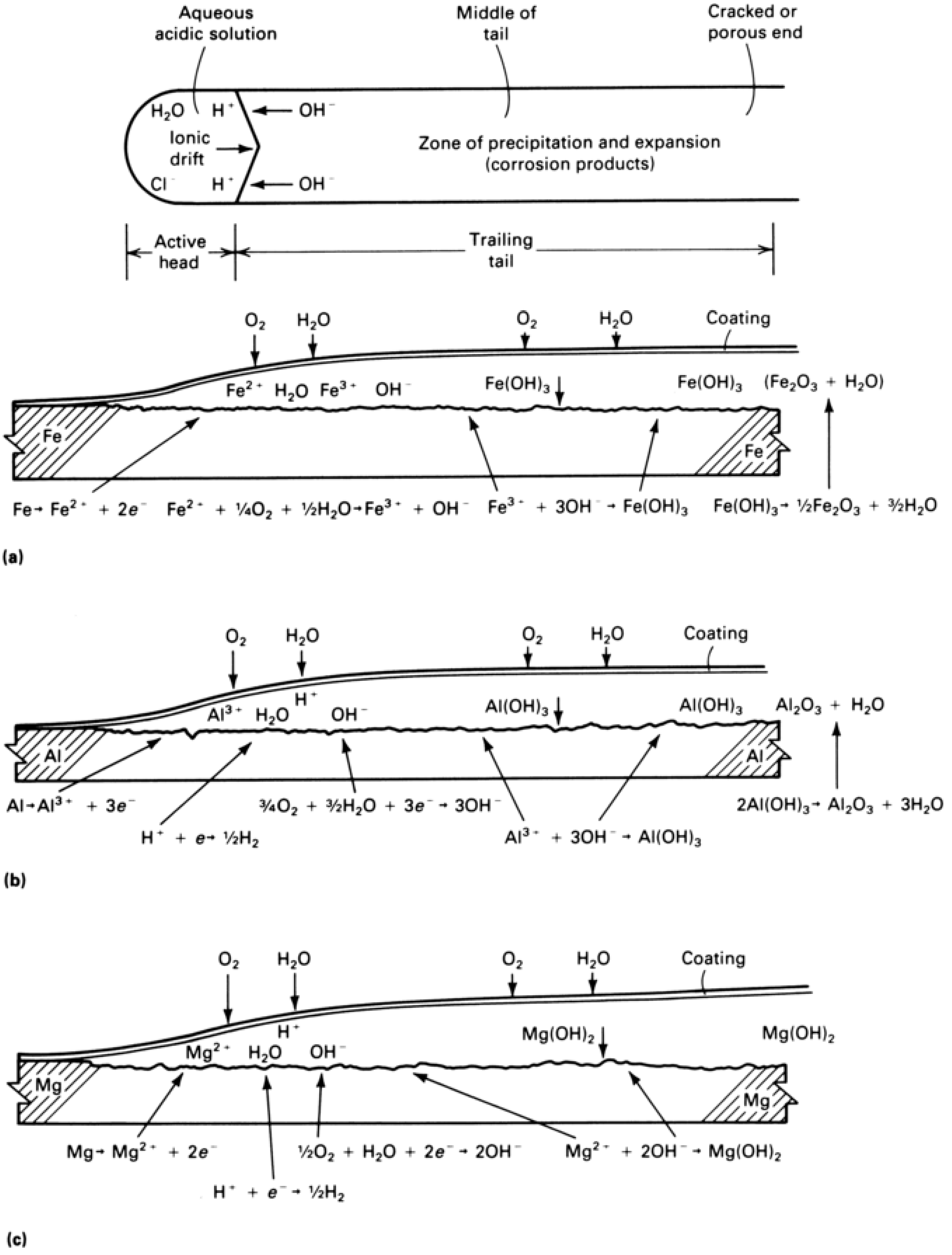

Fig. 6 Diagrams of the filiform-corrosion cell in steel (a), aluminum (b), and magnesium (c). Corrosion products and predominant reactions are labeled. Filiform corrosion is a differential-aeration cell driven by differences in oxygen concentration in the head versus the tail section. Potential differences between the head and tail are of the order of 0.1 to 0.2 V.

Water is required to form an electrolyte and to stimulate hydroxyl production. Water is necessary for the formation of new heads from a central defect source. The corrosivity of the head electrolyte is increased when salts are present on the surface or in the condensed water vapor. High salt concentrations in the head electrolyte decrease oxygen solubility and may further acidify the head solution. Several studies have shown that sealing the cracked tail halts filiform corrosion (Ref 8, 9, 10). By sealing the porous tail with epoxy, oxygen was prevented from entering. Similar effects were achieved by replacing oxygen with nitrogen gas. The driving force of the reaction—differential aeration—was stopped, and the filiform heads ceased to advance.

In the case of tin-coated steels, filiform corrosion is slowed if the tin coating weight is more than 0.35 g/m^2. However, if the coating weight is between 0.1 and 0.35 g/m^2, an acceleration of filiform corrosion is noted (Ref 11). Since heavier weight tin coatings are relatively more uniform than light coatings, the retardation of filiform corrosion is presumably due to polarization of the oxygen-reduction reaction. Stimulation of filiform corrosion by lower-weight coatings was attributed to reinforcement of local galvanic cells by the highly porous, light weight coating of tin.

References cited in this section

4. J.E. Charbonneau, "Investigation of Corrosion and Container Integrity in Metal Food Containers Using SEM and X-Ray Microanalysis," *Scanning,* Vol 23, September

5. W. Schmidt and M. Stratmann, *Corros. Sci.,* Vol 40, 1998, p 1441

6. T. Schauer, A. Joos and E. Praschak, "Supplemental Investigation of Protection Afforded by Selected Coating Systems Against Filiform Corrosion," Research Institute for Pigments and Paints, Stuttgart, Germany, 1996

7. W. Funke, *Prog. Org. Coatings,* Vol 9, 1981, p 29

8. R.T. Ruggeri and T.R. Beck, *Corrosion,* Vol 39, 1983, p 452

9. W. Salbaugh and E. Chan, *J. Paint Technol.,* Vol 38, 1966, p 417

10. W. Salbaugh, W. DeJager, S. Hoover, and L. Hutchinson, *J. Paint Technol.,* Vol 44, 1972, p 76

11. J. Morita and M. Yoshida, *Corrosion,* Vol 50, 1994, p 11

C. Hahin and R.G. Buchheit, Filiform Corrosion, *Corrosion: Fundamentals, Testing, and Protection*, Vol 13A, *ASM Handbook*, ASM International, 2003, p 248–256

Filiform Corrosion

Christopher Hahin, Illinois Department of Transportation; Rudolph G. Buchheit, Ohio State University

Filiform Corrosion of Coated Aluminum and Magnesium

Filiform corrosion is frequently observed on coated aluminum sheet, plate, and foil, and on magnesium sheet and castings and is of interest to the automotive and aircraft industries. The appearance of filiform corrosion in aluminum and magnesium is similar to that of iron and steel, except that the corrosion products are gelatinous and milky in color. When dry, their filaments may take on an iridescent or clear appearance because of internal light reflection. Filament growth rates for aluminum are similar to those of coated steels. Magnesium has somewhat higher growth rates than aluminum. Filiform attack in both aluminum and magnesium is particularly severe in warm coastal and tropical regions where aerosolized salt occurs or in industrial areas where airborne-pollutant concentrations are high.

Aluminum is susceptible to filiform corrosion in RH ranging from 75 to 95%, and at temperatures between 20 and 40 °C (70 and 105 °F). Filiform corrosion at low RH can occur in the presence of HCl vapor (Ref 10). In such situations, filiform propagation has been reported for relative humidities as low as 30%. Filiform tracks grow most rapidly at 85% RH in aluminum. Typical filament growth rates average about 0.1 mm/day (4 mils/day). Filament width varies with increasing relative humidity—from 0.3 to 3 mm (12 to 120 mils). The depth of penetration in aluminum can be as deep as 15 μm (0.6 mil). Numerous coating systems used on aluminum are susceptible to filiform corrosion, including epoxy, polyurethane, alkyd, phenoxy, and vinyls. Condensates containing the chloride, bromide, sulfate, carbonate, and nitrate ions can stimulate filiform growth in coated aluminum alloys. Growth rates for filiform corrosion on aluminum and magnesium coated with lacquers and various slower drying resins are summarized in Table 1.

Tests for Filiform Corrosion of Aluminum Alloys. In addition to the standard ASTM and ISO tests for filiform corrosion on aluminum, several other tests are widely used in the aircraft industry. In DIN 65472, "Filiform Corrosion Test of Coatings on Aluminum" (sometimes referred to as the Lockheed test), the scribed samples are exposed to fuming hydrochloric acid (HCl) for 60 min. In the modified Lockheed test, specimens are immersed in saturated aluminum chloride ($AlCl_3$) solution for 120 min. Afterward, samples are placed in a humidity cabinet at 82% RH for 1000 h at 40 °C (104 °F). Lengths of filiforms are quantified in millimeters for comparison of different coatings and substrate treatments.

NATO endorses the use of British Standard EN 3665, whereby 2024-T4 clad aluminum panels of 100 by 40 by 0.8 mm (approximately 3.9 by 1.6 by 0.031 in.) are chromate pickled, coated, scratched through the clad layer, and then exposed to fuming HCl acid vapors for 1 h at 23 °C (73 °F). Panels are subsequently placed in a humidity chamber at 40 °C and 82% RH for 1500 h. The degree of filiform damage is also evaluated by filament length (Ref 12).

These tests provide for rapid screening and comparison of various coatings and treatments of aluminum-copper alloys. They can also be applied to screening and qualitative evaluations of other aluminum alloys of the 3*xxx*, 5*xxx*, 6*xxx*, 7*xxx* and 8*xxx* series.

Mechanism of Filiform Attack on Aluminum and Magnesium. In many respects, filiform corrosion on aluminum and magnesium is similar to that on steels. Filiform corrosion is driven by the formation of differential-aeration cells at defect sites on coated substrates. The filiform cell consists of an active head and a tail that receives oxygen and condensed water vapor through cracks in the applied coating. In aluminum, the head may be filled with alumina gel. Gas bubbles may be present if the head is very acidic. In magnesium, the head appears blackish because of the etching of the magnesium, but the corrosive fluid is clear when the head is broken. Filiform tails in aluminum and magnesium are whitish in appearance. The corrosion products are hydroxides and oxides of aluminum and magnesium, respectively. Anodic reactions produce Al^{3+} or Mg^{2+} ions, which react to form insoluble precipitates with the hydroxyl ions produced in the oxygen-reduction reaction occurring predominately in the tail.

The mechanism of initiation and activation in aluminum and magnesium are essentially the same as for coated steel, as shown in Fig. 6(b) and (c). The acidified head is a moving pool of electrolyte, but the tail is a region in which aluminum ion transport and gradual reaction with hydroxyl ions take place. The final corrosion products are partially hydrated and fully expanded in the porous tail. The head and middle sections of the tail are corresponding locations for the various initial reactant ions and the intermediate products of corroding aluminum in aqueous media.

In contrast to steel, aluminum and magnesium show a greater tendency to form blisters in acidic media, with hydrogen gas evolved in cathodic reactions in the head region. The corrosion products in the tail are either aluminum trihydroxide ($Al(OH)_3$), a whitish gelatinous precipitate, or magnesium hydroxide ($Mg(OH)_2$), a whitish precipitate.

Surface-Active Layers. A high incidence of filiform-corrosion damage on painted aluminum architectural alloys used in Western Europe triggered a systematic investigation of the origins of the problem in the late 1980s and early 1990s (Ref 13). One of the root causes was determined to be an electrochemically active layer that formed on the surface of hot-rolled aluminum sheet product. Such layers, termed surface-active layers (SALs), and their effect on filiform corrosion were characterized and described in several reports published through the late 1990s (Ref 14, 15, 16, 17, 18).

Surface-active layers have been found on 1*xxx,* 3*xxx,* 8*xxx* Al alloys and may exist on certain 5*xxx* and certain 6*xxx* alloys. These layers form during hot rolling or annealing heat treatments carried out either in air or vacuum. Surface active layers are about 1 μm (0.04 mil) thick and consist of small, submicrometer grains and a dispersion of small noble intermetallic and magnesium oxide particles. The anodic activity of SALs is primarily attributed to the fine grain size and enrichment of alloying and trace elements in the layer, most notably magnesium. Noble intermetallic particles such as Al_3Fe dispersed throughout the layer are believed to be important in triggering electrochemical activity of the layer by forming microgalvanic couples with the surrounding SAL matrix. When noble intermetallic particles are not present in the SAL, electrochemical activity of the layer is decreased, supporting the notion that intermetallic particles play a key role in determining SAL activity. Figure 7 shows an ultramicrotomed cross section of a SAL on Al alloy 8006-O, and Fig. 8 shows the key microstructural characteristics of SALs.

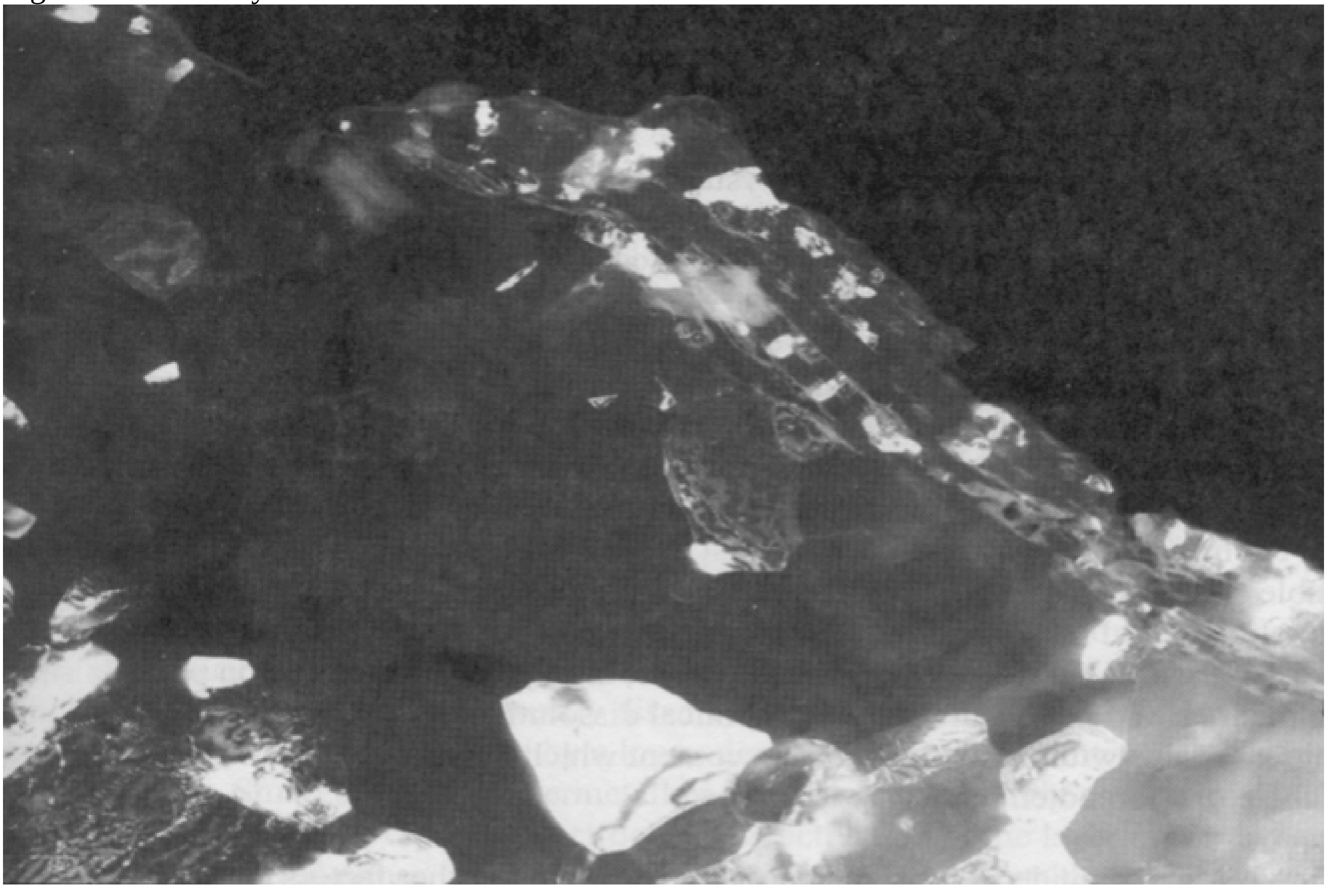

Fig. 7 Dark-field transmission electron micrograph showing a cross section through a surface-active layer on aluminum-iron alloy 8006-O

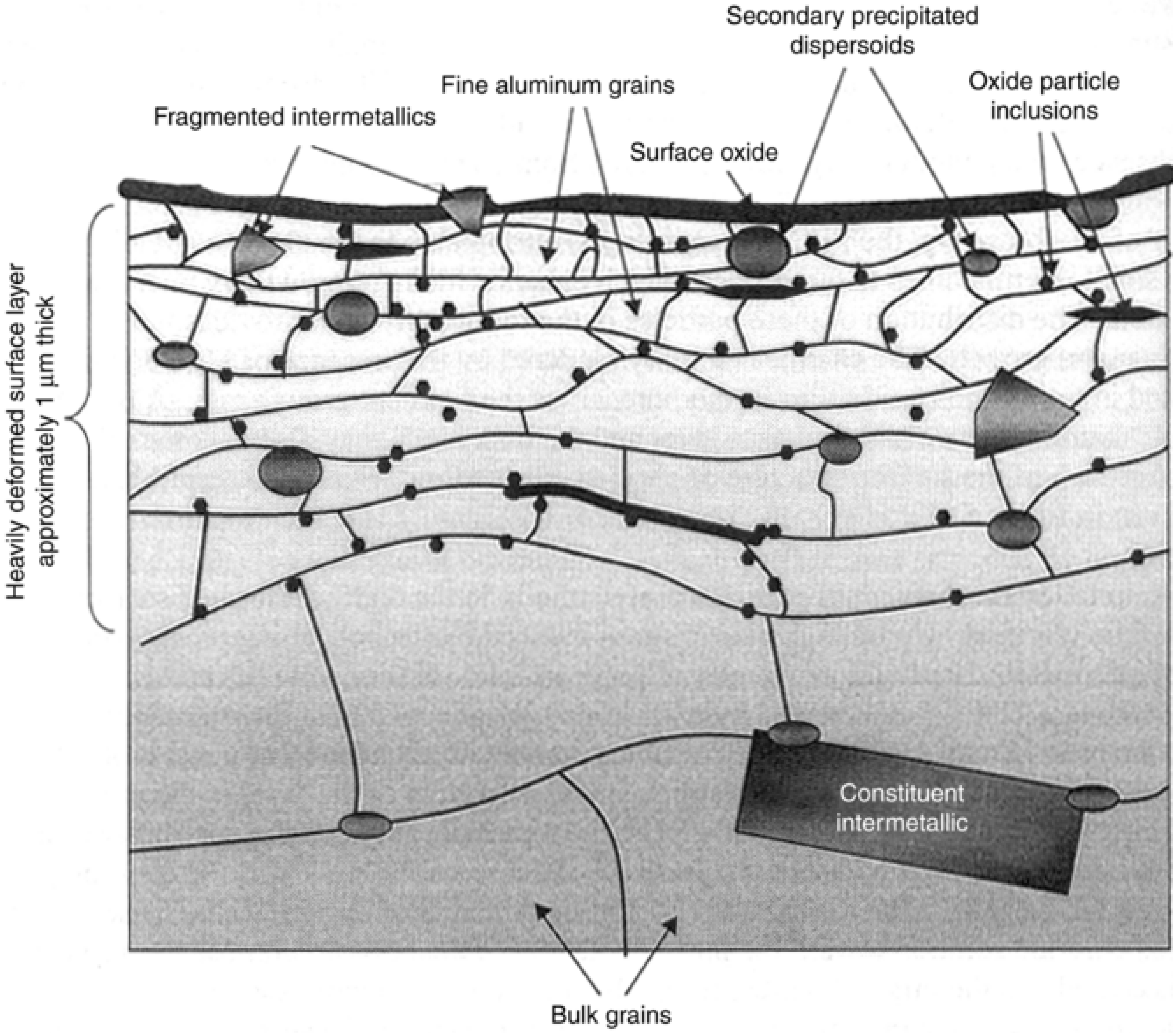

Fig. 8 Schematic of the near-surface microstructure of a rolled aluminum-manganese alloy showing the main microstructural characteristics of surface-active layers

Formation of SALs depends on alloy chemistry, thermal history, and to a lesser extent deformation processing by rolling. It has been observed that alloys with less than 100 ppm Mg develop less-active surface layers than alloys with magnesium contents greater than this threshold value. To activate this magnesium oxide particle-rich layer, noble alloying elements such as iron, copper, and silicon *must* be segregated into intermetallic particles at the surface. Manganese is also normally present in alloys that form active layers, but its role in the electrochemical aspects of the process is difficult to ascertain based on current reports. It is important to emphasize that electrochemical activity has only been observed when both a magnesium-rich oxide layer and noble intermetallic particles are present in the surface layer. Accordingly, the highest-purity aluminum alloys (1*xxx*) do not exhibit surface layers that are active.

In an interesting twist on the issue, it has been suggested that magnesium-oxide-rich layers may confer useful levels of sacrificial cathodic corrosion protection if the noble intermetallic particle population is small. In the thermomechanical processing of sheet product, elevated- temperature processes such as hot rolling and annealing stimulate SAL formation. In particular, elevated-temperature treatments promote segregation of trace elements to external surfaces and the high density of grain boundaries present in fine-grained surface layers. Very active layers have been formed by annealing at 440 °C (824 °F) for 1 to 2 h in air. Elevated-temperature processes may also promote precipitation of certain noble intermetallic particles. Rolling itself does not appear to greatly promote layer activity unless it is carried out at elevated temperature. However, cold rolling does tend to leave rolling marks on the sheet surface that preferentially orient filiform tracks along the rolling direction.

Surface-active layers can be detected by electrochemical corrosion tests, but since the layers are quite thin, transient approaches or experiments that can be completed in the short time before the layer dissolves must be used. Evidence of SALs can be detected in open-circuit potential measurements, where very active potential values are recorded at first. With time, the potential drifts in the noble direction as the layer dissolves away, exposing the underlying alloy substrate. Anodic current transients collected over several minutes during anodic polarization are strongly enhanced by the presence of SALs.

Other factors being equal, filiform-corrosion susceptibility is strongly enhanced when thin organic coatings are applied directly over SALs. Enhanced susceptibility is characterized by an increase in the number density of filiform tracks and an increase in the kinetics of filiform-track propagation. Often, filiform-track growth is strongly oriented in the rolling direction when SALs are affecting the process.

Remediation of filiform susceptibility due to SALs can be accomplished using standard metal-finishing practices. Chemical etching, chemical conversion coating, conversion coating with cerium chloride additions, or anodization can all be used to dissolve away the active layer. However, surface treatment must be sufficient to fully dissolve the SAL. Of these treatments, electropolishing reduced filament length the most. Electropolishing removed SALs and produced a microscopically flat surface (Ref 19).

Filiform Corrosion in Aircraft. Aircraft are routinely painted for corrosion protection, decreased drag resistance, and identification. Aircraft structural components and skins are routinely fastened with bolts and rivets and have numerous exposed faying surfaces where debris and moisture can lodge. These fasteners and other sharp skin edges are common initiation sites for filiform corrosion (Ref 20). Aircraft operating in warm, marine environments sustain considerable corrosion damage. In recent years, filiform corrosion was observed on 2*xxx* and 7*xxx* series aluminum alloys coated with polyurethane and other coatings (Ref 21, 22). Aluminum-copper alloy 2024-T4 is an aircraft material susceptible to filiform corrosion because of the presence of iron-bearing intermetallic compounds. The presence of 0.25% or more iron in 2024 accentuates the formation of long filiform threads (Ref 23). Filiform corrosion increased in severity when chloride concentrations on the metal were high, particularly when the aircraft were frequently flying over ocean waters or based in coastal airfields and hangars. Prepainted surface treatment quality and the choice of primers were also important in controlling filiform corrosion. Two-coat polyurethane and primed two-component epoxy paint systems experience far fewer incidences of filiform corrosion than single-coat systems did (Ref 24). Filiform corrosion rarely occurred when bare aluminum was chromic-acid anodized or primed with chromate or chromate-phosphate conversion coatings. Rougher surfaces also experienced a greater severity of filiform attack. If left unchecked, filiform corrosion may lead to more serious structural damage caused by other forms of corrosion such as pitting and intergranular corrosion.

Filiform Corrosion in Packaging. Aluminum is widely used for cans and other types of packaging. Aluminum foil is routinely laminated to paper, plastic film, or paperboard to form a moisture or vapor barrier. If the aluminum foil is consumed by filiform corrosion, the product may be contaminated, lost, or dried out because of breaks in the vapor barrier. Typical coatings on aluminum foil are nitrocellulose and polyvinyl chloride (PVC), which provide a good intermediate layer for colorful printing inks.

Degradation of the foil-laminated paperboard may occur during its production or its subsequent storage in a moist or humid environment (Figure 9). During the production of foil-laminated paperboard, moisture from the paperboard is released after heating in a continuous-curing oven. Heat curing dries the lacquer on the foil. Filiform corrosion can result as the heated laminate is cut into sheets and stacked on skids, while the board is still releasing stored moisture. As shown in Fig. 10, the hygroscopic paperboard is a good storage area for moisture. Packages later exposed to humidities above 75% in warm areas can also experience filiform attack. Coatings with water-reactive solvents, such as polyvinyl acetate, should not be used. Any solvents entrapped in the coating can weaken the coating, induce pores, or provide an acidic media for further filament propagation. Harsh curing environments can also result in the formation of flaws in the coating due to uneven shrinkage or rapid volatilization of the solvent. Rough handling can induce mechanical rips and tears.

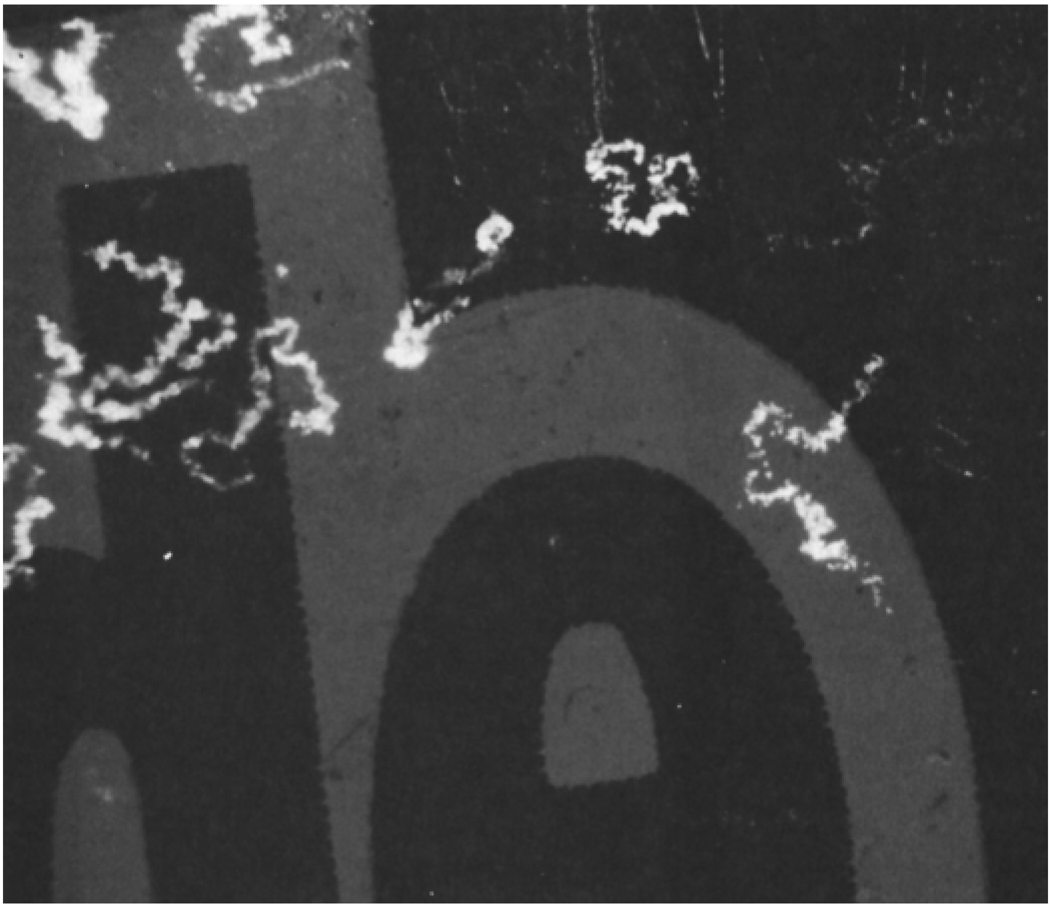

Fig. 9 Penetration of the aluminum foil vapor barrier on laminated packaging. The interior of the package is back illuminated, showing the loss of aluminum foil to filiform attack. Light microscopy. 10×

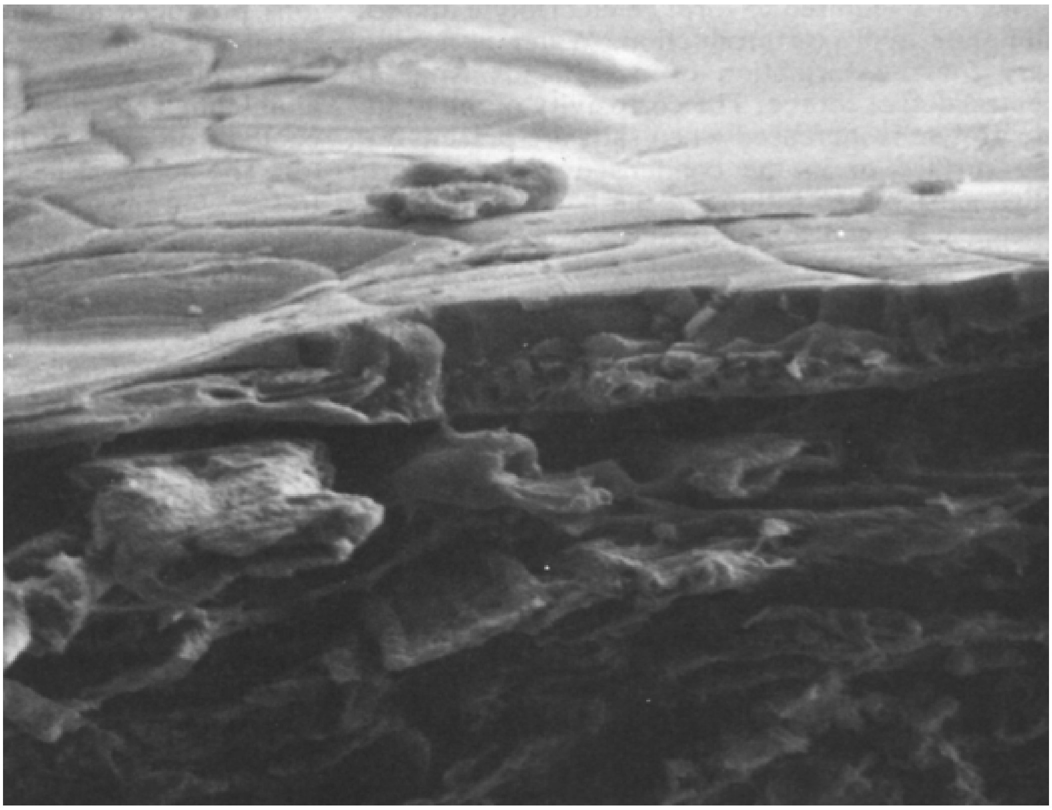

Fig. 10 Cross section of aluminum foil laminated on paperboard showing the expansion of the polyvinyl chloride coating by the corrosion products of filiform corrosion. Note the void spaces between the paperboard fibers that can entrap water. Scanning electron microscopy. 650×

Figure 11 shows typical flaws in PVC coating applied by a chromium-plated gravure. The tendency to follow flaws in the coated foil, such as hills and valleys or mechanical gouges in coating, is demonstrated in the filiform tracks on foil- coated paperboard observed by light microscopy (Fig. 12).

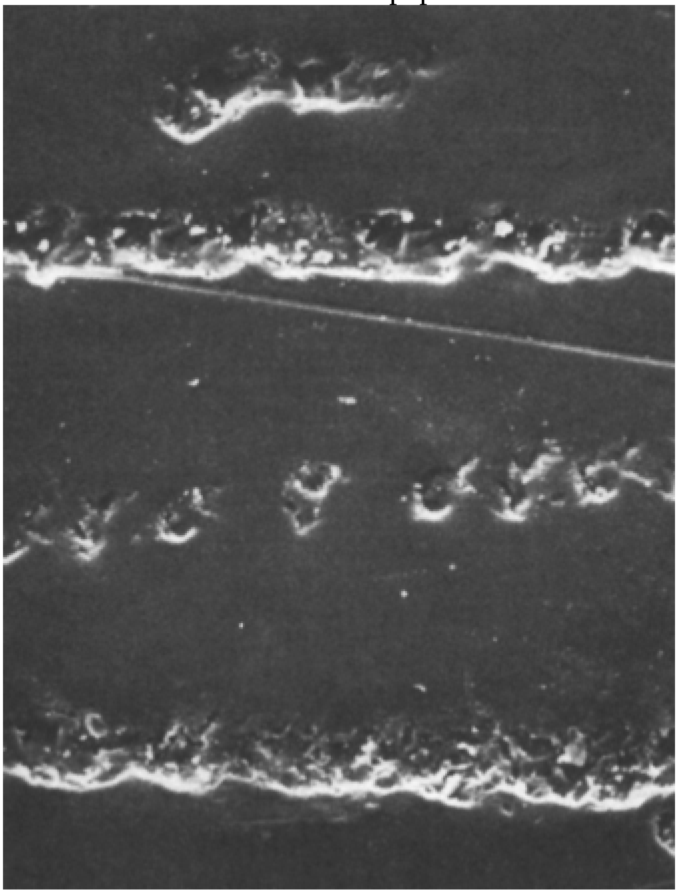

Fig. 11 Scratches in a nitrocellulose coating on aluminum induced by light abrasion. Hills and valleys in the foil are induced by a diamond-imprint gravure roll that applies the nitrocellulose as a lacquer. Scanning electron microscopy. 200×

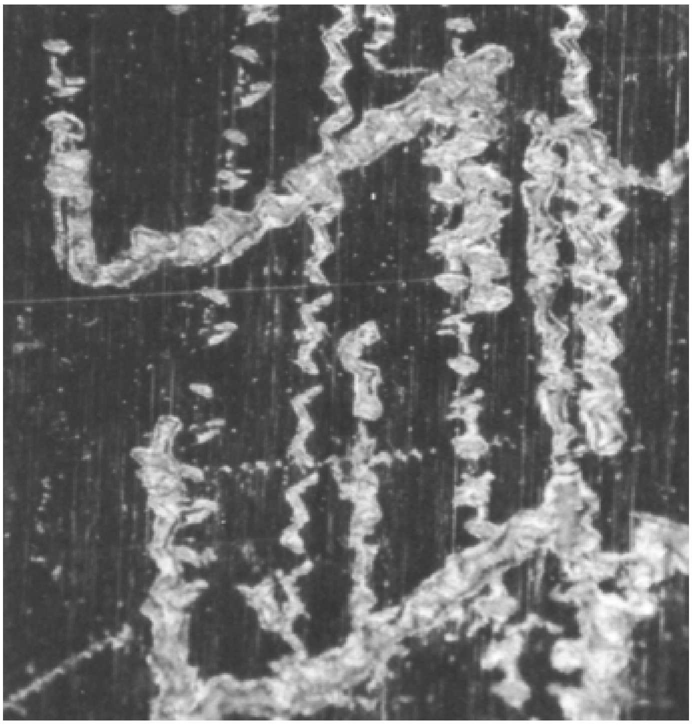

Fig. 12 Filiform in a nitrocellulose-coated aluminum foil laminated to paperboard showing a tendency to follow both the gravure imprint and the rolling direction of the sheet. Light microscopy. 75×

References cited in this section

10. W. Salbaugh, W. DeJager, S. Hoover, and L. Hutchinson, *J. Paint Technol.,* Vol 44, 1972, p 76

12. STANAG No. 4477, "Specification for Paints and Paint Systems Resistant to Chemical Agents and Decontaminants for Protection of Aerospace Military Equipment," NATO Standardization Agreement, 27 Mar 2001, (Internet 4477)

13. H. Leth-Olsen and K. Nisancioglu, *Corrosion,* Vol 53, 1999, p 705

14. H. Leth-Olsen, J.H. Nordlein, and K. Nisancioglu, *J. Electrochem. Soc.,* Vol 144, 1997, p L196

15. H. Leth-Olsen and K. Nisancioglu, *Corros. Sci.,* Vol 40, 1998, p 1179

16. H. Leth-Olsen and K. Nisancioglu, *Corros. Sci.,* Vol 40, 1998, p 1195

17. H. Leth-Olsen and K. Nisancioglu, *Corros. Sci.,* Vol 40, 1998, p 2051

18. K. Nisancioglu, J.H. Nordlein, A. Afseth, and G.M. Scamans, *Mater. Sci. Forum,* Vol 331–337, 2000, p 111

19. A.J. Kayes, M.J. Robinson and S. Impey, "Influence of Cleaning and Surface Treatment on Filiform Corrosion of Aluminum Alloys," *J. Corros. Sci. Technol.,* Vol 2, Sept 1999

20. "Inspection of Aircraft for Validation of Alternatives to Chromate-Containing Primer Coatings," National Defense Center for Environmental Excellence, Johnstown, PA, Nov 2000

21. P. Bijlmer, *Adhesive Bonding of Aluminum Alloys,* Marcel Dekker, 1985, p 21

22. W. Ryan, *Environment, Economics, Energy,* Vol 1, Society for the Advancement of Materials and Process Engineering, 1979, p 638

23. D.A. Little and J.R. Scully, "Role of Substrate Alloy Heterogeneity in Underpaint Corrosion in Aluminum Alloys," USAF Office of Scientific Research, Grant F49620- 96-1-0175, Dayton, OH, 2001

24. MIL-PRF-85582C, "Epoxy Primer Coating," Naval Air Warfare Center, Lakehurst, NJ, May 1994

C. Hahin and R.G. Buchheit, Filiform Corrosion, *Corrosion: Fundamentals, Testing, and Protection*, Vol 13A, *ASM Handbook*, ASM International, 2003, p 248–256

Filiform Corrosion

Christopher Hahin, Illinois Department of Transportation; Rudolph G. Buchheit, Ohio State University

---

Prevention of Filiform Corrosion

Prevention and mitigation of filiform corrosion is accomplished through adjustment of the environment and changes in the substrate and coating systems.

Reduction in Relative Humidity below 60%. Although the most direct method, reducing relative humidity is not practical if the metal is exposed to the elements or is in motion, as is the case for aircraft and automobiles. For

articles in longer-term storage, controlled environments are beneficial—for example, the use of drying fans and humidistats or the addition of desiccants to plastic packaging or to small, confined areas. Structural designs can prevent moisture entrapment by better drainage or by attempting to exclude moisture entry. Reducing the ambient temperature can also be beneficial because it results in a decrease in the amount of moisture the air can hold.

Use of Primers, Anodizing, and Other Preventatives. Filiform corrosion is reduced when the steel substrate is galvanized. Zinc-rich primers, chromated and phosphatized primers, with tough, slow curing intermediate coats of polyurethane and epoxy, have reduced filiform susceptibility on steel substrates. Zinc chromate primers, chromic acid anodizing, and chromate or chromate-phosphate conversion coatings have provided varying degrees of relief from filiform corrosion in aluminum alloys. Water-displacing oils and other penetrating film formers provide only temporary relief from filiform corrosion on aluminum surfaces (Ref 25).

Multiple-Coat Paint Systems and Powder Coatings. Multiple coats on metal surfaces slow down diffusion of moisture and have fewer penetration and defect sites than single-coat paint systems. Multiple-coat systems resist penetration by mechanical abrasion and have fewer hills and valleys. Thicker coatings achieved by layer buildup and slower curing have demonstrated substantially better resistance to filiform corrosion by decreasing oxygen and moisture penetration, decreased solvent entrapment, and fewer initiation sites. Powder coating systems are also beneficial, since they are thermally fused, resulting in tough coatings with better resistance to moisture permeability. Smooth, well-prepared primed metal surfaces generally have better resistance than rougher surfaces.

Use of Less-Active Metal Substrates. Steel, aluminum, and magnesium are all chemically active. Their alloys contain intermetallic compounds, which can be dispersed, precipitated, and agglomerated during hot rolling and annealing. Although these alloys generally have improved mechanical properties, recent work shows that their heterogeneity and presence of SALs increase their susceptibility to filiform corrosion. Careful surface preparation is important in limiting the effects of these detrimental active layers. The substitution of more-resistant materials exposed to the initiating environment, such as copper, austenitic stainless steel, or titanium, may be necessary. Unless a coating is mandatory, a material substitution may eliminate the central part of the problem. Economics and structural considerations, however, will usually dictate whether a material substitution is a practical solution.

Reference cited in this section

25. M. Salagras, P.G. Bushnell, P.N. Trathen, and B.R. Hinton, “Use of Corrosion Prevention Compounds for Arresting the Growth of Corrosion in Aluminum Alloys,” Defence Science & Technology Organisation, Victoria, Australia, Nov 1996

C. Hahin and R.G. Buchheit, Filiform Corrosion, *Corrosion: Fundamentals, Testing, and Protection*, Vol 13A, *ASM Handbook*, ASM International, 2003, p 248–256

Filiform Corrosion

Christopher Hahin, Illinois Department of Transportation; Rudolph G. Buchheit, Ohio State University

---

References

1. B.S. Skerry and C.H. Simpson, *Corrosion,* Vol 49, 1993, p 663
2. R. Preston and B. Sanyal, *J. Appl. Chem.,* Vol 6, 1956, p 26
3. H.E. Townsend, “Salt Spray Test is Bogus,” Paper presented at SAE World Congress, (Detroit), April 2000

4. J.E. Charbonneau, “Investigation of Corrosion and Container Integrity in Metal Food Containers Using SEM and X-Ray Microanalysis,” *Scanning,* Vol 23, September

5. W. Schmidt and M. Stratmann, *Corros. Sci.,* Vol 40, 1998, p 1441

6. T. Schauer, A. Joos and E. Praschak, “Supplemental Investigation of Protection Afforded by Selected Coating Systems Against Filiform Corrosion,” Research Institute for Pigments and Paints, Stuttgart, Germany, 1996

7. W. Funke, *Prog. Org. Coatings,* Vol 9, 1981, p 29

8. R.T. Ruggeri and T.R. Beck, *Corrosion,* Vol 39, 1983, p 452

9. W. Salbaugh and E. Chan, *J. Paint Technol.,* Vol 38, 1966, p 417

10. W. Salbaugh, W. DeJager, S. Hoover, and L. Hutchinson, *J. Paint Technol.,* Vol 44, 1972, p 76

11. J. Morita and M. Yoshida, *Corrosion,* Vol 50, 1994, p 11

12. STANAG No. 4477, “Specification for Paints and Paint Systems Resistant to Chemical Agents and Decontaminants for Protection of Aerospace Military Equipment,” NATO Standardization Agreement, 27 Mar 2001, (Internet 4477)

13. H. Leth-Olsen and K. Nisancioglu, *Corrosion,* Vol 53, 1999, p 705

14. H. Leth-Olsen, J.H. Nordlein, and K. Nisancioglu, *J. Electrochem. Soc.,* Vol 144, 1997, p L196

15. H. Leth-Olsen and K. Nisancioglu, *Corros. Sci.,* Vol 40, 1998, p 1179

16. H. Leth-Olsen and K. Nisancioglu, *Corros. Sci.,* Vol 40, 1998, p 1195

17. H. Leth-Olsen and K. Nisancioglu, *Corros. Sci.,* Vol 40, 1998, p 2051

18. K. Nisancioglu, J.H. Nordlein, A. Afseth, and G.M. Scamans, *Mater. Sci. Forum,* Vol 331–337, 2000, p 111

19. A.J. Kayes, M.J. Robinson and S. Impey, “Influence of Cleaning and Surface Treatment on Filiform Corrosion of Aluminum Alloys,” *J. Corros. Sci. Technol.,* Vol 2, Sept 1999

20. “Inspection of Aircraft for Validation of Alternatives to Chromate-Containing Primer Coatings,” National Defense Center for Environmental Excellence, Johnstown, PA, Nov 2000

21. P. Bijlmer, *Adhesive Bonding of Aluminum Alloys,* Marcel Dekker, 1985, p 21

22. W. Ryan, *Environment, Economics, Energy,* Vol 1, Society for the Advancement of Materials and Process Engineering, 1979, p 638

23. D.A. Little and J.R. Scully, “Role of Substrate Alloy Heterogeneity in Underpaint Corrosion in Aluminum Alloys,” USAF Office of Scientific Research, Grant F49620- 96-1-0175, Dayton, OH, 2001

24. MIL-PRF-85582C, “Epoxy Primer Coating,” Naval Air Warfare Center, Lakehurst, NJ, May 1994

25. M. Salagras, P.G. Bushnell, P.N. Trathen, and B.R. Hinton, "Use of Corrosion Prevention Compounds for Arresting the Growth of Corrosion in Aluminum Alloys," Defence Science & Technology Organisation, Victoria, Australia, Nov 1996

G.S. Frankel, Introduction to Metallurgically Influenced Corrosion, *Corrosion: Fundamentals, Testing, and Protection*, Vol 13A, *ASM Handbook*, ASM International, 2003, p 257

Introduction to Metallurgically Influenced Corrosion

G.S. Frankel, The Ohio State University

Introduction

THE FUNDAMENTAL UNDERSTANDING of electrochemical corrosion kinetics is based on the uniform dissolution of an unfilmed, pure, homogeneous metal that is equally exposed at all locations to a homogeneous environment. Corrosion engineers know that this description does not reflect reality in practical situations. In many engineering structures, dissimilar alloys are connected in a variety of ways, crevices often exist, and the environment is variable and dependent on local flow conditions. Furthermore, metals and alloys are typically covered with a surface layer. Their corrosion behavior is influenced by the surface layer and by a host of metallurgical factors. Even extremely pure single crystals have defects that can affect corrosion, but impurities and alloying elements, grain boundaries, second phases, and inclusions often have a dominant effect. Finally, welded structures almost always corrode first at the welds because of metallurgical heterogeneities that exist in and near welds. In general, the most susceptible site or defect on a metal surface will be the first to be attacked when it is exposed to a corrosive environment. Sometimes such attack simply results in innocuous removal of the susceptible material, leaving a surface with improved corrosion resistance. The most susceptible defects that lead to sustained attack will control the form of corrosion.

The corrosion resistance of stainless steels and nickel-based alloys varies markedly depending on the alloying elements and processing conditions. Under many conditions, stainless steels exhibit localized corrosion, which is greatly affected by the alloy composition and metallurgical factors. Pitting corrosion in stainless steels often initiates at MnS inclusions owing to the reactivity of the sulfides and the effect of the S- containing dissolution products on the nearby passive film. The formation of carbides at grain boundaries can reduce corrosion resistance through the formation of susceptible Cr-depleted zones in the neighboring matrix. A continuous network of such Cr-depleted zones can render stainless steel sensitized, or extremely susceptible to sustained intergranular corrosion or stress corrosion cracking. Other phases, such as sigma and chi phases, can also be detrimental, especially in oxidizing environments. On the other hand, stainless steel does not always corrode by a localized form of attack. When a solutionized low-sulfur stainless steel is exposed to boiling nitric acid, the attack is not local in nature but rather is dominated by the orientation of the grains so that a stepped structure develops with the most susceptible orientations corroding faster.

The corrosion resistance of aluminum alloys is completely dominated by metallurgical factors. High-purity aluminum is rather resistant to corrosion in most neutral pH environments. The passive film is relatively insulating, protective, and noncatalytic. However, commercial aluminum alloys contain alloying elements, impurity elements, precipitated phases and intermetallic constituent particles. The precipitated phases and intermetallic particles can be anodic or cathodic relative to the matrix or can switch between the two with time as a result of selective dissolution. Anodic particles can be initiation sites for pitting corrosion, and cathodic particles can be active cathodes, supporting the cathodic reaction necessary for sustained attack. These phases can form at grain boundaries and result in a sensitized structure if the grain boundary precipitate or neighboring solute-depleted zone is susceptible to sustained attack. Wrought aluminum alloys often have an elongated grain

structure, which can result in susceptibility to exfoliation corrosion or orientation-dependent stress corrosion cracking. Solid solution alloying of aluminum can alter the susceptibility to localized corrosion, either decreasing, as with copper alloying, or increasing the susceptibility as in the case of zinc alloying. Clearly, the metallurgical effects on the corrosion of aluminum alloys are varied and complex.

When an alloy composed of a solid solution of various elements corrodes, it is typical that one or more elements dissolve preferentially, leaving other elements enriched on the surface. This dealloying process depends strongly on nonmetallurgical factors such as environment and potential. However, the dealloyed microstructure is vastly altered, often resulting in a reduction of strength and other properties.

Welded microstructures can be extremely complex and often change drastically over a very short distance. The fusion zone or weld metal is a dendritic structure that solidified from a molten state. Bordering the fusion zone are transition, unmixed and partially-melted zones, and the heat affected zone (HAZ). These zones can be reheated and altered by subsequent weld passes in multipass welding. For alloys with structures that depend strongly on thermal history, such as steels, the final microstructure can be extremely complex. Since welded structures are often quite susceptible to corrosion, over-alloyed filler metals are often used to enhance the weld corrosion resistance. For stainless steels with sufficiently high carbon content, sensitization in the HAZ is another major problem.

Corrosion is a reaction between a metal and its environment, and both are important in the process. The articles presented here focus on the metal side of the corrosion reaction and describe a wide range of metallurgical factors that influence corrosion.

J.J. Noel, Effects of Metallurgical Variables on Aqueous Corrosion, *Corrosion: Fundamentals, Testing, and Protection*, Vol 13A, *ASM Handbook*, ASM International, 2003, p 258–265

Effects of Metallurgical Variables on Aqueous Corrosion

James J. Noël, University of Western Ontario

Introduction

THE CORROSION BEHAVIOR of a metal or alloy is determined by its composition and structural features, the environment and stresses to which it is exposed, and the behavior of any corrosion products generated (e.g., formation of passive films or hydrolysis to produce acidity). This article provides an overview of the ways in which the metallurgical variables, namely composition and structure, influence the corrosion properties of metals and alloys.

J.J. Noel, Effects of Metallurgical Variables on Aqueous Corrosion, *Corrosion: Fundamentals, Testing, and Protection*, Vol 13A, *ASM Handbook*, ASM International, 2003, p 258–265

Effects of Metallurgical Variables on Aqueous Corrosion

James J. Noël, University of Western Ontario

Fundamentals of Pure Metals, Impure Metals, and Alloys

The fundamental nature of pure elements and materials containing alloying elements and impurities provides a starting point for a discussion of the metallurgical influences on corrosion.

Pure Elements. Nominally pure metals are crystalline in the solid state. Except in the very rare applications that make use of individual (single) crystals, masses of pure metal in practical use are polycrystalline; that is, they are made up of a large number of individual, irregular-shaped crystals (commonly called grains), fully joined together at the atomic level.

Usually, the spatial orientations of different grains (as defined by their intrinsic crystallographic planes) are random with respect to each other (Ref 1). This means that there must be a zone of transition over which the crystallographic orientation changes from that found in one grain to that found in its neighbors. This transitional zone is known as a *grain boundary* and is a three-dimensional region of little or no long-range crystallographic order, although some short-range order is usually present. This disorder makes grain boundaries energetically favorable sites of residence for impurities and other imperfections.

Other regions of atomic disarray can be found, even within individual crystals, in the form of *defects*—imperfections arising from a number of sources—the most significant of which are described in the following paragraphs. Defects may be classified according to their spatial dimensionality, which may be 0, 1, or 2.

Point defects (zero-dimensional) are atom- sized imperfections in crystals (Fig. 1). These include interstitial atoms, which are atoms present in the spaces between the lattice positions, vacancies (the absence of one or more atoms from the crystal lattice), and foreign atoms in lattice positions. Point defects may be present in the metal from the time of its solidification or introduced later by heating, plastic deformation, or bombardment with high-energy radiation.

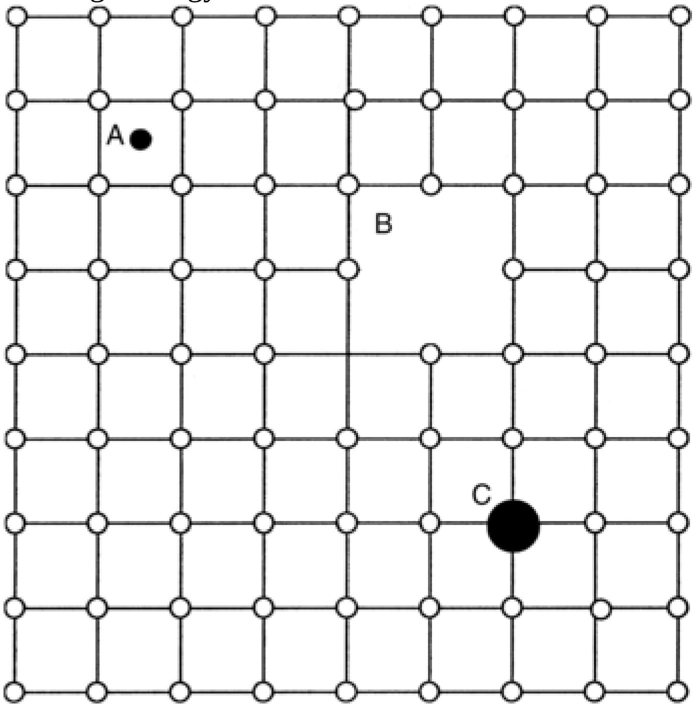

Fig. 1 Point defects. A, interstitial atom; B, vacancy; C, foreign atom in lattice site

Line defects (one-dimensional) are of two types—edge dislocations and screw dislocations. An edge dislocation (Fig. 2) is the region of imperfection that lies along the internal edge of an incomplete plane of atoms within a crystal. In a screw dislocation (Fig. 3), a portion of the crystal is displaced such that the atom planes no longer have a separate existence but rather comprise a single, continuous ribbonlike structure in the form of a helical ramp or screw thread with a pitch of one interplanar spacing per turn. The screw dislocation is the line of distortion that lies along the axis of the ramps perpendicular to the atom planes.

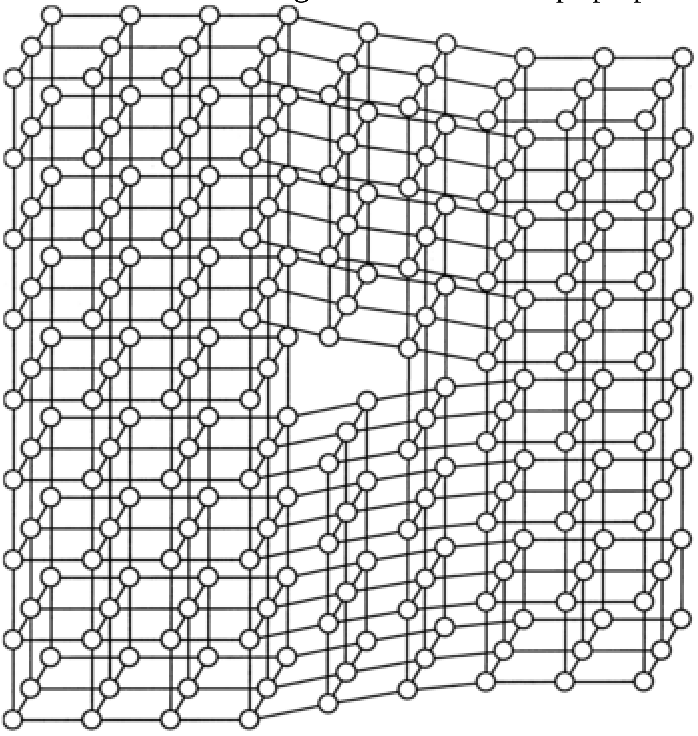

Fig. 2 Edge dislocation

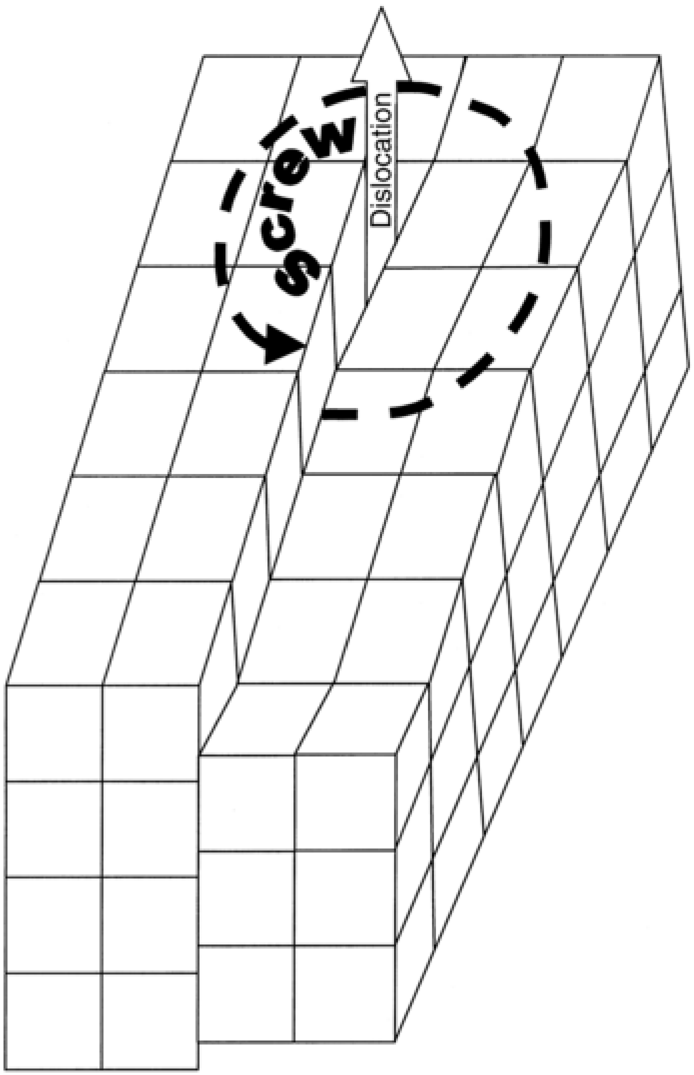

Fig. 3 Screw dislocation

It is geometrically impossible for a dislocation to have a terminus located within a perfect region of a crystal; it must terminate at a free surface, at a grain boundary, on another dislocation, or on itself. In principle, dislocations may lie on any crystallographic plane but are usually found along the planes of most-dense atomic packing. These two features promote the formation of networks of combined screw and edge dislocations, which can be quite extensive within the crystal along the most closely packed crystallographic planes. Dislocations can be created by plastic deformation of a crystal, and their movements are important in determining the deformation properties of a material (Ref 1).

Plane defects-stacking faults (two-dimensional) are imperfect regions of a crystal resulting from errors in the positioning of entire atomic layers. Stacking faults consist of an error in the sequence of crystallographic layering within a crystal that disrupts the expected order of a perfect crystal of that type. Stacking faults can arise during crystal growth or as a consequence of plastic deformation but can only occur along the close-packed planes within a crystal (Ref 1).

For example, both the face-centered cubic (fcc) and hexagonal close-packed (hcp) crystal types are built of stacks of the same type of close-packed atomic layers. The difference between the two lattices is in the registry between each close-packed plane and the ones above and below it. In a fcc crystal, three different alignments of the close-packed planes are required. These are denoted *a*, *b*, and *c*. Thus, a fcc crystal is built of stacks of these layers in the sequence *abcabcabc* and so forth. In a hcp crystal, only two different alignments of the close-packed layers are required, and the sequence is *ababab* and so forth. If, for instance, within a fcc crystal, an error is made in the sequencing of layers such that the order is abcababcabc and so forth, this constitutes a stacking fault. In this case one could consider the underlined portion of the sequence to be a thin slice of hcp crystal positioned within the fcc lattice. Stacking faults can extend across the entire width of a crystal and can

be produced during crystal formation or sometimes during plastic deformation by certain dislocation movements (Ref 1).

Grain boundaries are the transitional zones surrounding each crystal in a solid that mark the interfaces between the crystal and its neighbors. They are often only a few atoms wide and can be considered practically two-dimensional. The atoms in this region assume positions that come as close as possible to satisfying both adjacent lattices simultaneously. Their ability to find such sites depends on the difference in orientation between adjoining grains. Grain boundaries are also subject to the disarray caused by the many dislocations and stacking faults that terminate there. In spite of all this, the overall divergence from the crystalline order must be somewhat limited; otherwise the material would fail easily along the grain boundaries under tension. As at other surfaces, the free energy at grain boundaries is higher than that of the crystals themselves but not as high as at free surfaces. Impurities tend to find these regions to be energetically more favorable sites of residence than sites within the crystal lattice, especially if the impurities are present in concentrations beyond their solubility limits (Ref 1).

Inclusions are three-dimensional defects consisting of insoluble particles of foreign material in the metal and may be either intentionally or accidentally incorporated.

Voids (another type of three-dimensional defect) are empty or gas-filled spaces within the metal. They may be formed, for example, by bubbles of gas that were trapped in the metal on solidification, as a consequence of *shrinkage* (the contraction of the metal as it cools), or by coalescence of a number of vacancies in the metal (Ref 2). Inclusions and voids are normally orders of magnitude larger than single-impurity atoms or vacancies but could be considered to reduce to these point defects, respectively, in the limit of small size (Ref 3).

Impure Metals and Alloys. Pure metals have limited engineering applications due to their cost and frequently poor mechanical properties. Vast improvements in mechanical properties can often be achieved by combining two or more elements to form an alloy. Alloys or metals with significant levels of impurities (unintentional alloys) are usually crystalline like nominally pure metals, but it is sometimes possible to prepare them in amorphous forms (Ref 4, 5, 6, 7).

In crystalline form, alloys are subject to the same types of defects as pure metals. Additionally, crystalline alloys may consist of a solid solution of one or more elements (solutes) in the major (base) component, or they may contain more than one phase. That is, adjacent grains may have slightly or extremely different compositions and be of identical or disparate crystallographic types. Often, there is one predominant phase, known as the matrix, and other secondary phases, called precipitates. The presence of these kinds of inhomogeneities often results in the alloy having radically different mechanical properties and chemical reactivities than the pure constituent elements.

The grain boundaries in alloys and impure metals are preferred sites for accumulation (segregation) of solute atoms, since the latter fit more readily into disordered regions than into the perfect crystals (i.e., they have a higher solubility in the grain boundary regions). Likewise, solute atoms and impurities tend to congregate at defects within the grains as well. Grain boundaries are also the favored precipitation sites for secondary phases formed during solid-state transformations. Consequently, the grain boundaries are often more resistant to mechanical deformation and have different chemical reactivities than the grains themselves (Ref 1).

In amorphous form, alloys lack the long-range order that is characteristic of crystalline materials, although they do retain a short-range order similar to that of liquids and true glasses (thus the name glassy metals) (Ref 1). Traditionally, glassy metals have been formed by very rapid cooling on the order of ~10^6 K/s (2 × 10^6 °F/ s) during the solidification of a melt. This “freezes” the atoms almost instantly in nearly the same positions they occupied in the liquid state. There is insufficient time available during the solidification process for crystals to nucleate and grow or for impurities and alloying elements, which are dispersed uniformly throughout the melt, to segregate. The resultant material is thus chemically and structurally homogeneous and free from one- and two-dimensional defects, secondary phases, and grain boundaries. (In a sense, one could consider a glassy metal to consist entirely of a large three-dimensional defect.)

Alternative methods of preparing glassy metals include vapor deposition and electrodeposition techniques (Ref 1, 4). More recent efforts have generated metallic glasses by mechanical milling of crystalline powders (Ref 6), and certain alloy compositions that form glasses even when cooled from the melt at relatively low rates of less than 10 K/s (18 °F/s) have been discovered (Ref 5, 7). The latter two glass-forming methods have overcome some of the problems of the past (such as the tendency of metastable glassy metals to recrystallize and the requirement that at least one dimension of the glassy product be very thin to permit rapid cooling), thereby allowing production of bulk metallic glasses for use as structural components in engineered structures. New

classes of “nanocrystalline” materials, substances with a high grain- boundary to grain-volume ratio, are also offering novel possibilities in this area (Ref 5).

As a result of the extensive disorder, glassy metals often have physical, chemical, and mechanical properties that differ greatly from those of crystalline alloys of the same elemental compositions. They can be much more corrosion resistant than the compositionally equivalent crystalline alloys, in large part due to the absence of multiple phases, grain boundaries, and other defects.

Phase diagrams are graphical presentations of the ranges of temperatures and compositions over which the different phases and mixtures of phases are thermodynamically stable. This includes the boundaries between the solid and liquid states (i.e., melting points), as well as those between different solid phases. Phase diagrams are termed binary, ternary, or quaternary if they describe two-, three-, or four-element mixtures, respectively. This type of information is invaluable to those who are trying to understand the behavior of metals and alloys, and entire volumes of these data have been published (Ref 8, 9, 10). A phase diagram of a portion of the iron-carbon system (Ref 9) is shown (Fig. 4) as an example.

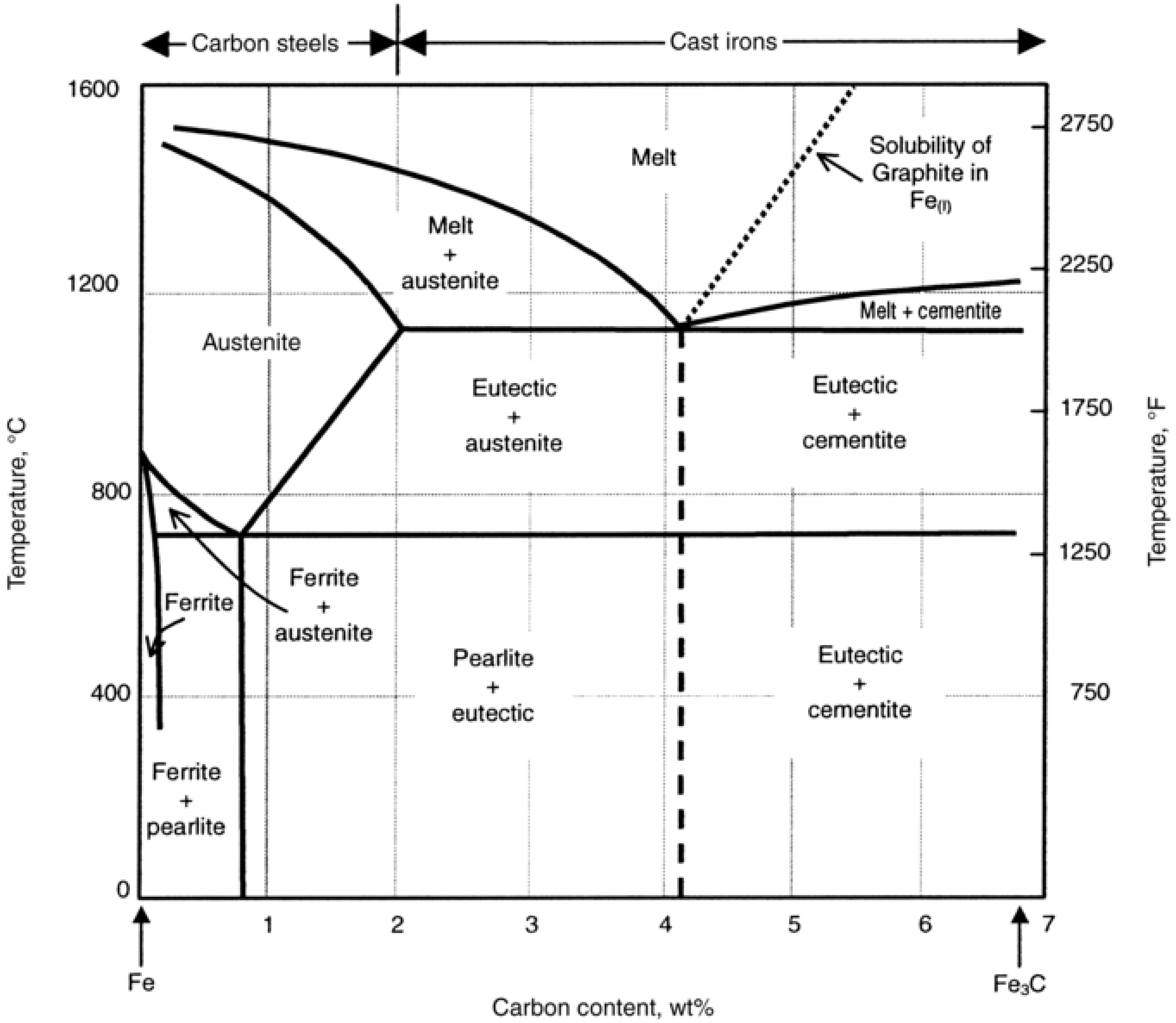

Fig. 4 A portion of the phase diagram for the iron-carbon system showing the many phases possible in steels and cast irons

The phase-temperature-composition relationships shown in phase diagrams are usually intended to represent the state of affairs in a system at true thermodynamic equilibrium; however, the observed phases of real materials may differ somewhat from those predicted by the phase diagram. Many metallic materials are metastable to some degree, and a number of nonequilibrium phase diagrams are also available (Ref 10). There are several possible origins of metastable phases, depending on the situation: “impurity” effects on the phase relationship

(some alloying additions and impurities act to stabilize, at room temperature, phases normally found at higher temperatures); or loss of atomic mobility before equilibrium is reached during solidification of a melt (this is how glassy metals are often prepared), during cooling of the solid to room temperature, or during subsequent heating and cooling events.

The various classes of metallic phases that may be encountered in crystalline alloys include substantially pure elements, solid solutions of one element in another, and *intermetallic compounds* (ionically, covalently, or metallically bonded intermediate phases of specific and relatively simple stoichiometry). All of these may be found in one or more allotropic forms (i.e., the same composition, but with different crystal packing orders), depending on the material. One may also find "metalloid" phases, such as carbides. (In metallurgy, as in this article, metalloid phases are considered to be those containing elements commonly present in simple steel: carbon, manganese, phosphorus, silicon, and sulfur. This differs from the way the term is used in chemistry to describe elements with properties intermediate between those of metals and nonmetals, specifically boron, silicon, germanium, arsenic, antimony, tellurium, and polonium.) Other nonmetallic phases may also be present in some cases, especially in the form of *inclusions,* which are particles of insoluble foreign material in the matrix. Particles composed of various oxides, sulfides, and silicates are common inclusions in metals and alloys (Ref 1); for example, manganese sulfide in stainless steels.

References cited in this section

1. L.E. Samuels, *Metals Engineering: A Technical Guide,* ASM International, 1988, p 5, 6, 238
2. R.A. Higgins, *Engineering Metallurgy, Part 1: Applied Physical Metallurgy,* Robert E. Krieger Publishing Company, 1983, p 69
3. M.H. Richman, *An Introduction to the Science of Metals,* Blaisdell Publishing Company, 1967, p 112, 113
4. Metallic Glasses, in *Handbook of Corrosion Data,* 2nd Ed., ASM International, 1995, p 83, 84
5. A.L. Greer, K.L. Rutherford, and I.M. Hutchings, Wear Resistance of Amorphous Alloys and Related Materials, *International Materials Reviews,* Vol 47 (No. 2), 2002, p 87–112
6. D.J. Li, A.J. Akerman, K.J. Doherty, S.J. Poon, and G.J. Shiflet, Swift Amorphization of a Supersaturated Titanium Solution by Mechanical Milling, *Scr. Mater.,* Vol 38 (No. 4), 1998, p 603–609
7. A. Peker and W.L. Johnson, A Highly Processable Metallic Glass: $Zr_{41.2}Ti_{13.8}Cu_{12.5}Ni_{10.0}Be_{22.5}$, *Appl. Phys. Lett.,* Vol 63 (No. 17), 1993, p 2342–2344
8. W.G. Moffat, *The Handbook of Binary Phase Diagrams,* General Electric, 1978
9. T.B. Massalski, Ed., *Binary Alloy Phase Diagrams,* American Society for Metals, 1986
10. Y. Kawazoe, T. Masumoto, K. Suzuki, A. Inoue, A.P. Tsai, J.Z. Yu, T. Aihara, Jr., and T. Nakanomyo, *Phase Diagrams and Physical Properties of Nonequilibrium Alloys, Subvolume A: Nonequilibrium Phase Diagrams of Ternary Amorphous Alloys,* Y. Kawazoe, Ed., Landolt-Börnstein New Series: Numerical Data and Functional Relationships in Science and Technology, Group III: Condensed Matter, Vol 37, Springer-Verlag, 1997

J.J. Noel, Effects of Metallurgical Variables on Aqueous Corrosion, *Corrosion: Fundamentals, Testing, and Protection*, Vol 13A, *ASM Handbook*, ASM International, 2003, p 258–265

Effects of Metallurgical Variables on Aqueous Corrosion

James J. Noël, University of Western Ontario

Influence on Corrosion

The presence of impurities, alloying constituents, defects, multiple phases, and other metallurgical features, sometimes in very small amounts, can have a profound influence on the corrosion resistance of a material, affecting the susceptibility to, rate, mechanism, and form of corrosion. The exposure of structural and compositional inhomogeneities to corrosive environments invites the possibility of enhanced or preferential (localized) attack. This fact is used to great advantage in metallographic analysis, where chemical etching is frequently used to reveal the microstructural characteristics of a material for the optical microscope, but is usually a negative attribute in materials applications. Some of the corrosion consequences of common metallurgical practices and microstructural features are discussed individually in later sections of this article, but it should be noted that they are often not independent of each other.

Crystallography and Defects. Corrosion results in the removal of atoms from a metal by dissolution or conversion to an oxidized phase, such as an oxide or sulfide. The metal atoms most likely to undergo corrosion are those with the highest free energy. Thus, atoms located within the bulk of the material are much less susceptible to corrosion than those in the outermost layers of the metal surface, and corrosion reactions are generally considered to be surface chemistry.

Not all surface atoms have the same free energy, either. Depending on the orientation of the grains with respect to the metal surface, different crystallographic planes may be exposed to the environment, each one having a different reactivity. Even within a region of the surface having only a single crystallographic orientation, there will be variations in free energy (see Fig. 5). Atoms residing in close-packed planes are strongly coordinated on all but one side and would be at lower energy than atoms located on step edges, which have fewer nearest neighbors. Similarly, removal of atoms located at kink sites would be even more energetically favorable, and “adatoms,” having the minimal degree of attachment to the metal, would be the easiest to detach.

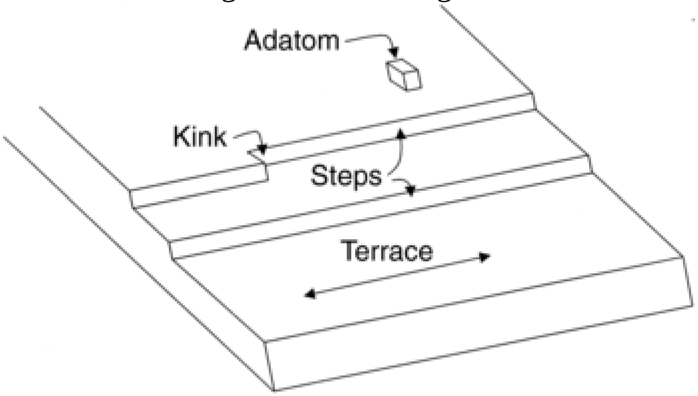

Fig. 5 Schematic depiction of the possible arrangements of residence sites for metal atoms on a surface. Steps are also called ledges

In electrochemical terms, the equilibrium corrosion potentials of these sites would be ordered:

$$E_{e(adatom)} < E_{e(kink)} < E_{e(step)} < E_{e(plane)} \quad \text{(Eq 1)}$$

where $E_{e(plane)}$ would be most noble. Likewise, kinks and other sites of reduced coordination to the underlying metal, such as sites where dislocations intersect the surface or where point defects are exposed, are energetically favorable points of corrosive attack. Since these defects tend to concentrate at grain boundaries, which are in themselves zones of disorder, one can expect that, in electrochemical terms again:

$E_{e(\text{grain boundary})} < E_{e(\text{grain})}$ (Eq 2)

The thermodynamic driving force for the corrosion reaction, ΔE_{therm}, is given by

$\Delta E_{\text{therm}} = E_{e(c)} - E_{e(a)}$ (Eq 3)

where $E_{e(c)}$ and $E_{e(a)}$ are the equilibrium potentials for the cathodic (reduction) and anodic (metal oxidation) reactions, respectively. Thus, on a given corroding metal surface (i.e., with a constant value of $E_{e(c)}$), the driving force for corrosion will be stronger at the grain boundaries than on the grains themselves.

In principle, therefore, preferential attack of the grain boundaries, known as *intergranular corrosion,* is a possible outcome, but in practice little corrosion damage of any consequence can actually be attributed to differences in the energetics of corrosion caused by atomic disorder, independent of compositional differences. The magnitude of electrochemical potential differences that can be generated by defects is, in fact, quite small (Ref 11, 12). The relationship between the free energy stored in defects (ΔG), and the resultant change in electrochemical potential (ΔE) is given by:

$\Delta G = -\text{n}F\Delta E$ (Eq 4)

where n is the change in oxidation number of the metal when it corrodes and F is Faraday's constant. For example, cold working a metal to introduce defects amounting to 100 kJ/kg of stored energy will afford only about 3 mV of potential difference. For an active corrosion process having anodic kinetics with a Tafel slope of 60 mV/ decade, this potential shift would correspond to a corrosion rate change of about 10%. Moreover, a slight initial grain boundary etching will remove many of the highest energy atoms, thereby decreasing the difference in equilibrium corrosion potentials between the grains and grain boundaries even further.

For a passive metal, the corrosion rate is much less dependent on potential, so intergranular corrosion driven by free energy differences arising from disorder in the metal are even less likely. However, on surfaces protected by a passive film, grain boundaries and defects can sometimes promote preferential attack by disrupting the formation of a continuous protective layer (Ref 11, 12). If the presence of defects results in imperfections or discontinuities in the overlying passive film, these sites may not be well protected by the passive film but instead can serve as initiation sites for localized corrosion processes.

The influence of compositional inhomogeneities resulting from impurity segregation and the formation of certain precipitate particles at grain boundaries usually outweighs the effects of any lattice disorder. Most serious cases of intergranular attack arise from compositional dissimilarities rather than structural defects (Ref 11). Conversely, kinetic limitations and compositional differences may completely eliminate preferential corrosion of grain boundaries or make the grain boundaries even more corrosion resistant than the grains.

One form of corrosion in which structural defects do seem to play a role is stress-corrosion cracking (Ref 12). The presence of a large number of stacking faults makes it easier for grains to slip (i.e., facilitates shear displacement of one part of the grain with respect to another). The material then has a greater tendency to creep rather than crack to relieve tensile stresses. In some materials, decreasing the free energy stored in stacking faults can change the nature of stress- corrosion cracking from intergranular to transgranular.

Another structural feature of metals, texture, the degree to which the orientations of different grains in a material deviate from a random distribution in favor of a preferred direction, can also influence material corrosion behavior. Passivation and repassivation tend to be enhanced on densely packed crystallographic planes because there are fewer steps and kinks, so texture can have an impact on the passivation characteristics. The susceptibility to stress-corrosion cracking can also be impacted by material texture, because the bias in grain orientation will favor alignment of stacking faults in different grains along preferred directions, with consequent effects on slip processes and, ultimately, stress-corrosion cracking, depending on the direction of any tensile stresses.

The grain geometry has a significant bearing on the corrosion properties of some metals (Ref 11). For example, rolled or extruded aluminum alloys tend to have flattened, elongated grains that are aligned parallel to each other as a consequence of the fabrication process. Because the material structure consists of sheetlike layers of thin grains, these materials are susceptible to a specific form of intergranular corrosion, called *exfoliation,* in which grain boundary attack strips layer after layer of grains from the surface. The corrosion products, which occupy a larger volume than that of the metal consumed in their formation, exert a wedging pressure between the layers of grains, helping to pry them apart and advance the intergranular attack. The lamellar structure of these materials also facilitates intergranular stress-corrosion cracking by providing aligned grain boundaries

along which the material can be relatively easily "unzipped" by a stress-corrosion process, especially when the stresses are acting in the direction perpendicular to the plane of the layers.

The grain size has been observed to influence crevice corrosion and stress-corrosion cracking processes on metals (Ref 12, 13). Fine-grained materials have more grain boundaries and a higher grain-boundary to grain-volume ratio than metals with larger grains. Crevice corrosion initiates most readily at weak points in the passive oxide film, which are most likely to be located over grain boundaries. Thus, small-grained metals present more susceptible sites for crevice corrosion initiation. In stress-corrosion cracking, for a given stress, the time to failure increases as the grain size decreases (Ref 13) due to an increased resistance to slip. A detailed description of the relationship between grain size and slip has been published (Ref 14).

Alloying. One of the principal reasons for alloying structural metals is, in many cases, to improve corrosion resistance. In alloys designed for specific mechanical properties, such as tensile strength or hardness, further alloying additions are commonly made to enhance the corrosion resistance as well.

Alloying can affect the corrosion resistance in many different ways. Changes in the nobility of the metal, the dissolution kinetics, the performance of a passive film, the phase structure of the material, the ability to catalyze the cathodic half-reaction, and other corrosion-influencing parameters can all result from alloying. Some of these changes help to decrease and others to increase the susceptibility, corrosion rate, and extent of corrosion damage. Some of these effects are described subsequently.

Genuine changes in the thermodynamic properties of the metal can be achieved by alloying. If alloying increases the nobility of a material (i.e., it results in an increase in the equilibrium potential of the anodic half-reaction ($E_{e(a)}$), perhaps by increasing the metal-metal bond energy), then the driving force for corrosion (ΔE_{therm}), will decrease. Thus:

$$E_{e(a)M} < E_{e(a)A} \quad \text{(Eq 5)}$$

where M and A denote metal and alloy, respectively. From Eq 3:

$$[E_{e(c)} - E_{e(a)M}] > [E_{e(c)} - E_{e(a)A}] \quad \text{(Eq 6)}$$

or

$$\Delta E_{therm\ M} > \Delta E_{therm\ A} \quad \text{(Eq 7)}$$

The decrease in thermodynamic driving force for corrosion may result in a corresponding decrease in the corrosion current density (i_{corr}) as illustrated (Fig. 6). Alloy systems ennobled in this fashion are relatively uncommon and often require very system-specific alloying additions, habitually noble metals (e.g., platinum, gold, palladium, etc.). Frequently, ennoblement is achieved only after enrichment of the metal surface in the minor alloy constituent, which occurs via limited selective dissolution of the major component. Subsequent mechanical damage to the thin, enriched surface layer may result in temporary reinitiation of corrosion. The decrease in the anodic dissolution rate of titanium in hydrochloric acid solutions on alloying with Nb or Zr, for example, has been attributed to strong covalent bonding between neighboring Ti, Nb, and Zr atoms through sharing of unpaired d-electrons (Ref 15).

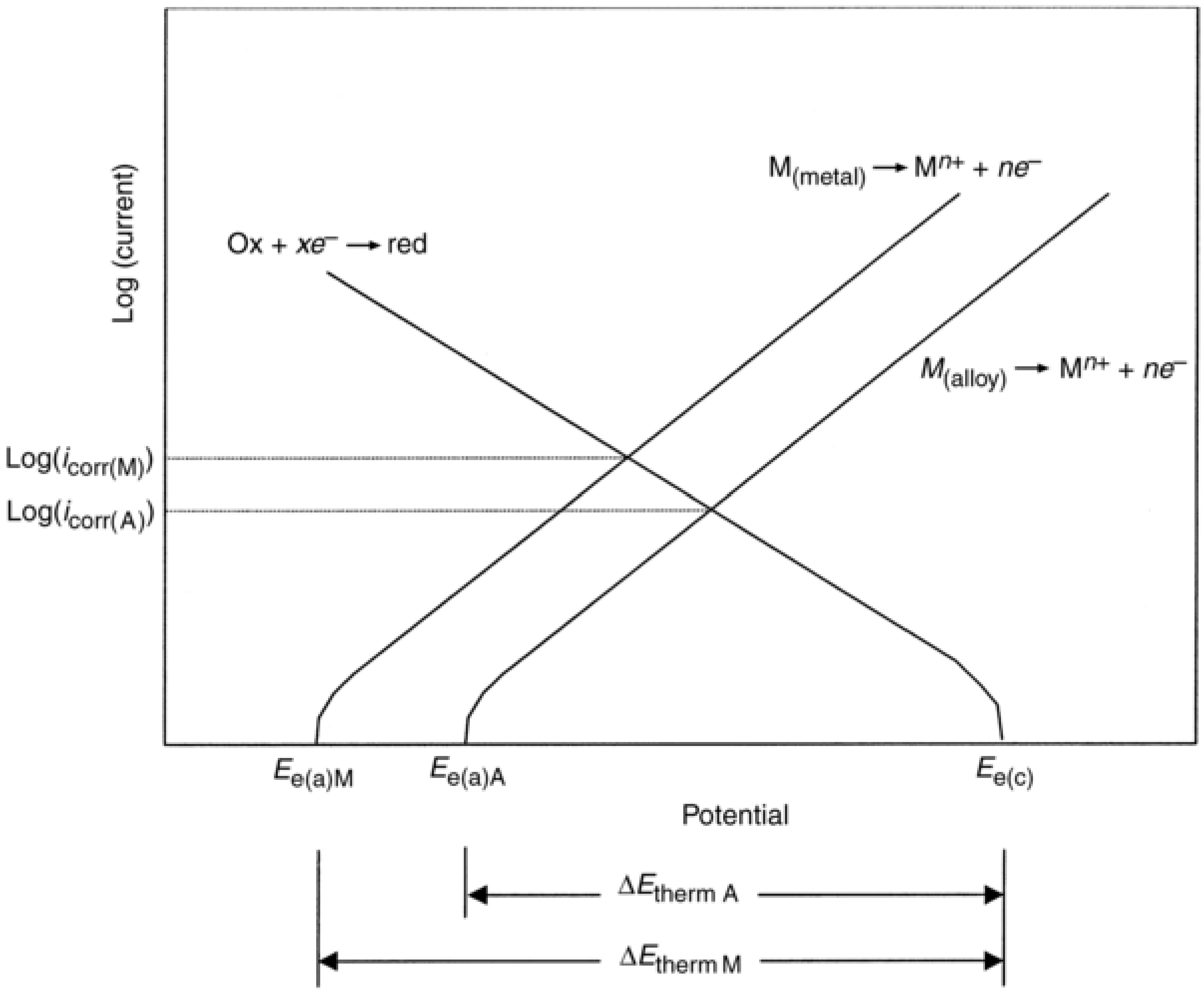

Fig. 6 Effect of increasing the nobility of a material by alloying on the thermodynamic driving force for corrosion (ΔE_{therm}), and on the corrosion rate (as represented by i_{corr})

On passive metals, the addition of controlled amounts of certain alloying elements is often used to improve the performance of the passive film. Such improvements can be effected by a variety of mechanisms, including increases in the thermodynamic stability of the passive film, an enhanced tendency to form a continuous barrier between metal and environment, decreases in the dissolution kinetics, a lower critical current for passivation, greater rates of repassivation, suppression of electron transfer, and superior wear resistance to diminish possibilities for erosion corrosion.

A well-known example of passive film enhancement by alloying is the addition of chromium to iron alloys. The beneficial effects of chromium in the alloy can be attributed to its incorporation into the passive oxide film, where it has a number of effects, (Fig. 7). As the chromium content of the alloy is increased, the solubility of the passive oxide layer decreases, the passivation potential (E_{pass}) and the entire passive potential range move to less noble potentials, the passive dissolution current density (i_{pass}) decreases, and the critical current density for passivation (i_{crit}) decreases. In Fig. 7, only alloy number 3 would spontaneously passivate under the influence of the cathodic half-reaction shown, since only in that case is i_{crit} exceeded by the rate of the cathodic half-reaction at the potential corresponding to the peak of the active-to-passive transition. Spontaneous passivation would occur in this case because the only potential at which the rates of the anodic and cathodic half-reactions are equal, as required for charge balance, lies within the passive region.

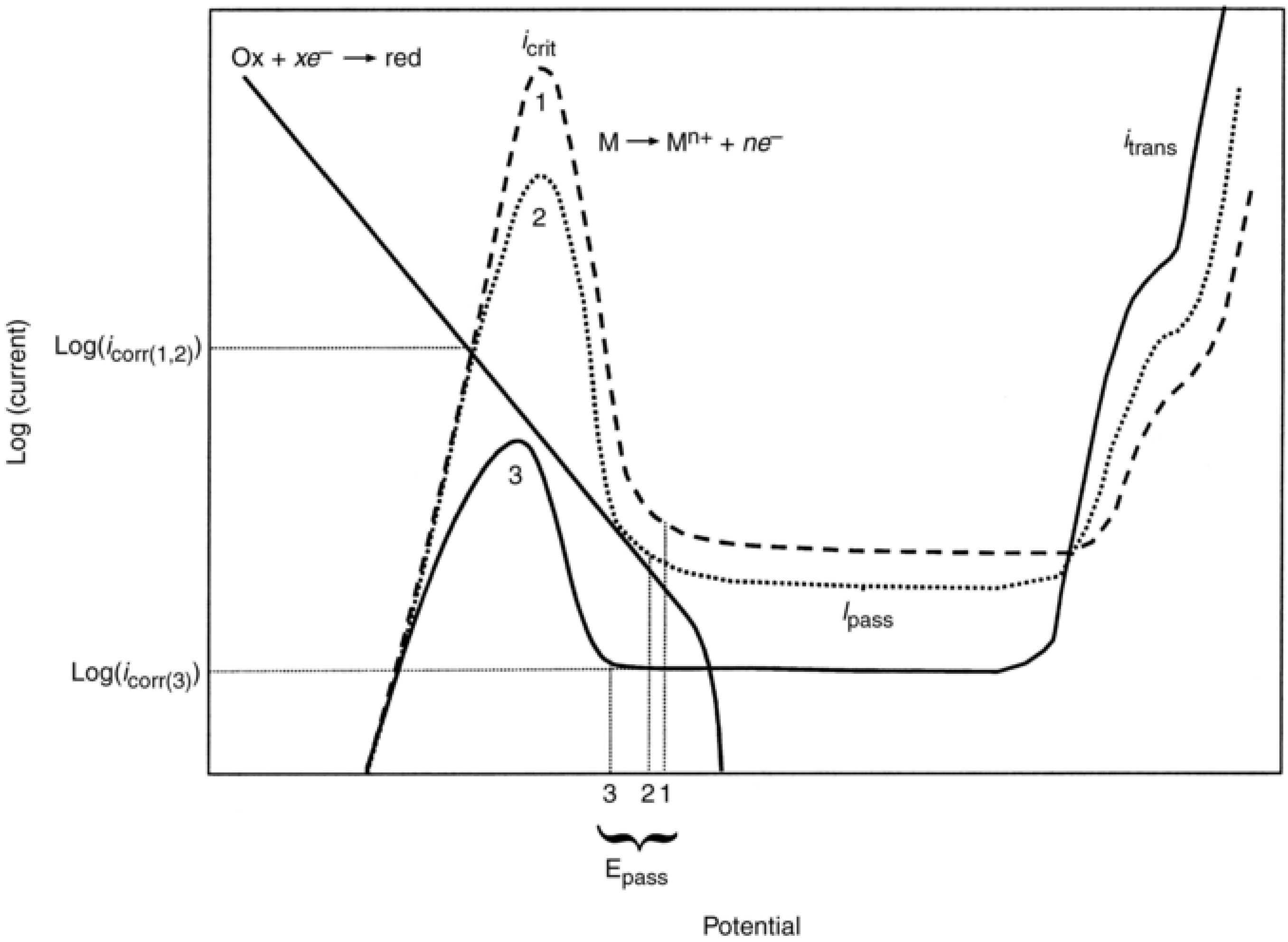

Fig. 7 Log (current) versus potential showing the effects of chromium content on the oxidation current of steels. Curve 1, low chromium content; curve 2, intermediate chromium content, curve 3, high (>12 wt%) chromium content

It has been empirically determined that a minimum of 11 to 12 wt% Cr is required to induce passivity in steels in common industrial environments. Improvements in passivity continue with increasing chromium content up to about 16 to 18 wt%, and the further addition of up to 8 wt% nickel enhances passivity even more and stabilizes the austenitic phase (Ref 16). The widely popular 18-8 stainless steels (Fe-18Cr-8Ni) are designed to take advantage of these effects.

One drawback of increasing the chromium content of these alloys is that it increases the likelihood and severity of transpassive dissolution (i_{trans} in Fig. 7). Transpassive dissolution can happen in metal and alloy systems in which the metal ions in the passive film have available a higher oxidation state that yields more soluble species. The higher oxidation state may be achieved if strong enough oxidizing conditions prevail. In the case of Cr and its alloys, transpassive dissolution can occur when conditions at the passive surface become sufficiently oxidizing that Cr ions in the highly insoluble Cr^{III} oxide are oxidized to the more soluble Cr^{VI} ions, and the material loses its passivity. Because the metal is very strongly polarized in the anodic direction when it loses its passivity, corrosion damage can be rapid and severe.

Many other systems show improved corrosion resistance due to improved passive film properties. Sometimes, even a small concentration of an alloying element has an important effect. Pitting resistance of type 316 stainless steel is improved with the addition of 2 to 3 wt% Mo (Ref 11), and decreased susceptibility to impingement attack is achieved in brass with 2 wt% Al and in cupronickel alloys to which 1 to 2 wt% Fe has been added. Detrimental effects are also possible, such as the reduction in pitting resistance that can result from the presence of small amounts of impurities in aluminum.

Changes in the phase structure of the material induced by alloying are also very common (Fig. 4). These can alter the corrosion properties of the material, often for the worse. For example, in austenitic stainless steels, the

presence of ferrite decreases the pitting resistance, while martensite may increase the susceptibility to hydrogen embrittlement.

One of the most common and insidious effects of the presence of multiple phases is to enable galvanic corrosion effects. The situation is much more serious than simply grains of one phase having a higher corrosion rate than neighboring grains of another phase. In galvanic corrosion of an alloy, the sites of the anodic and cathodic half- reactions become spatially separated and fixed on grains of different phases. The corrosion of the least noble phase is accelerated by the presence of another phase that provides sites for the corresponding cathodic half reaction. The latter phase can potentially increase the rate of corrosion damage to the former by enhancing the cathodic half-reaction in two ways; first, by providing a larger surface area for the cathodic half-reaction, and second, by catalyzing the cathodic half-reaction (i.e., by increasing the cathodic current density). Acute local damage often ensues. Galvanic corrosion resulting in severe intergranular attack may even be promoted simply by segregation of small amounts of impurities to the grain boundaries. Even among corroding grains, there may be variations in corrosion rate; those grains with the highest rates will suffer more corrosion damage.

An example of severe galvanic corrosion that is so common and well known that it has its own name, graphitic corrosion, occurs on gray cast irons. (Graphitic corrosion is often called graphitization, but that term is more appropriately reserved for the high-temperature decomposition of iron carbide to form graphite particles in steels.) Gray cast irons consist of graphitic flakes in a matrix of ferrite or pearlite. When gray cast irons corrode, the graphite flakes are very noble, but the ferritic or pearlitic matrix corrodes readily, with the interconnected network of graphite flakes serving as the cathodic-charge distribution system. The metal matrix can be completely consumed by the anodic half-reaction. This is supported by the cathodic half reaction occurring on the graphite flakes, which offer a large and continually increasing cathode area. The end result is a lump of iron corrosion products held together by a network of graphite flakes. Galvanic effects are not so severe on ductile iron materials, due to differences in the morphology of the graphite particles. In the latter material, the graphite is found in the form of spherical particles, which do not remain electrically connected to each other once the metal between them has been oxidized and therefore do not offer such a large cathodic surface area to drive the anodic reaction (Ref 11).

In certain active-passive systems such as titanium alloys, galvanic effects can actually be used to help prevent corrosion by reinforcing passivity (Ref 16) (see Fig. 8). Based on the results of research on noble metal effects on the corrosion resistance of titanium (Ref 17), an extensive series of titanium alloys containing very small (<1%) concentrations of metals that are known to enhance hydrogen, water, or oxygen reduction (e.g., Pt, Pd, Ru, and even Ni) has been developed specifically to take advantage of this method of enforcing passivity. The exposed catalytic particles increase the rate of the cathodic reaction to such an extent that the magnitude of the cathodic current would be higher than that of the anodic current at any given potential except in the passive region of Ti. Thus, the metal could only adopt spontaneously a potential corresponding to passivation of the Ti, as shown in Fig. 8. On the other hand, alloying additions may also help to inhibit corrosion by suppressing cathodic electron transfer reactions, if the cathodic half-reaction is rate limiting. Such an effect has been observed on Ti alloys containing significant amounts (13 to 50%) of Zr or Nb (Ref 18).

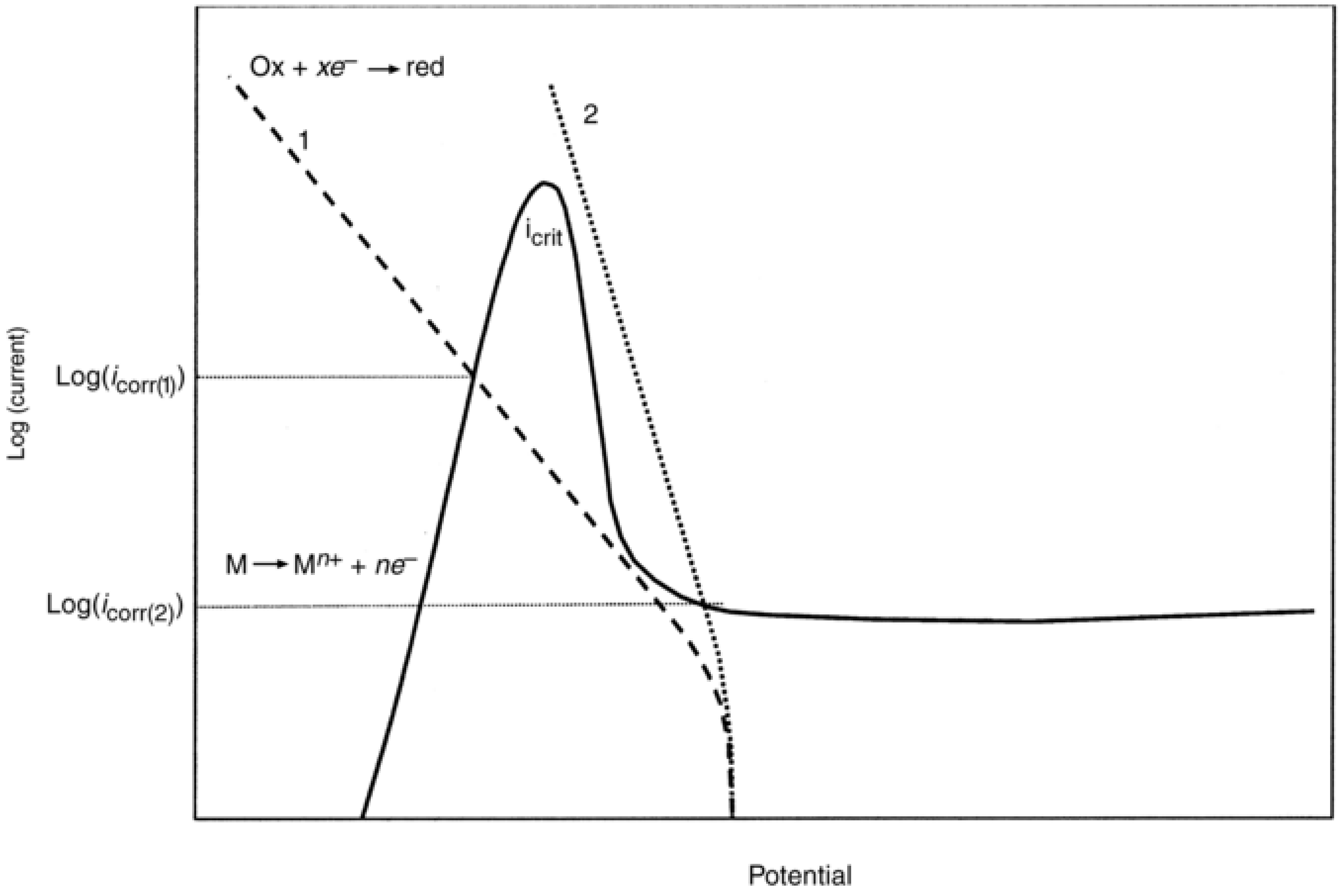

Fig. 8 Log (current) versus potential illustration of the influence of noble metal alloying on the kinetics of the cathodic half-reaction that reinforces spontaneous passivity on dilute titanium alloys. Curve 1, current of cathodic half-reaction on unalloyed titanium; curve 2, current of cathodic half-reaction on titanium with noble metal addition

Inclusions may be present in an alloy either as unintentional contaminants or purposeful additions intended to improve such features as weldability and machinability. Inclusions are not true alloying components but still can have detrimental effects on the corrosion performance of a material, often acting as preferential initiation sites for localized corrosion. The manganese sulfide inclusions commonly found in steels, for instance, are well known initiation sites for pitting corrosion.

Often unnoticed until after a metal component fails, *dealloying,* or *selective leaching,* is an alloying-related form of corrosion. In cases of dealloying, a process that is somewhat similar to galvanic corrosion but at the subgrain level, selective dissolution of one element from a homogeneous, single-phase alloy occurs. Dealloying affects many alloy systems, and the process is known by several very descriptive names that point to specific problems with particular alloying components, such as *decarburization, decobaltification, denickelification,* and *dezincification.*

The classic example of dealloying is the dezincification of alpha brasses (Ref 11). In this case, zinc is preferentially dissolved from the brass, leaving behind the copper in the form of a porous, mechanically weak residue. This can lead to instances of unexpected and sudden failure of brass components because the corrosion damage can appear to be superficial, and little dimensional change is usually observed, even when only a thin remnant of sound metal endures. Dealloying of brass can generally be avoided by maintaining a minimum of 85 wt% Cu in the alloy. Prevention of dealloying has been considered in terms of percolation theory, which is concerned with determining the minimum concentration of a single component that would be required in order to form a continuously interconnected layer within the material, thereby preventing further corrosion by providing an unreactive barrier between the active metal and its environment.

Additional information on dealloying is available in the article “Effects of Metallurgical Variables on Dealloying Corrosion” in this Volume.

Welding, Working, and Heat Treatments. The effects of welding, working, and the heat treatments applied to metals are numerous and frequently interrelated. All three of these actions can result in changes in the number

of defects in the metal, the size and shape of the grains, and the distribution of alloying elements, impurities, and minor phases. These parameters, in turn, have a very large impact on the corrosion properties of the material, as discussed earlier in this article. Thus, welding, working, and heat treatment are considered together in this article.

Welding is a joining method in which the metal parts to be joined are partially melted at the site of the intended joint, then resolidified to form a solid union. Sometimes a filler metal is used to facilitate the bonding. Welding has a number of effects on the metallurgy and corrosion resistance of the metal. Because the melting and resolidification are uncontrolled in terms of temperature and heating and cooling rates, the grain structure and size may be changed in an uncontrolled fashion. Areas adjacent to the weld, though not melted themselves, are heated to temperatures at which grain growth and significant segregation or mixing of alloy components and impurities can occur. The region is known as the *heat-affected zone* (HAZ).

The creation of a HAZ can result in a significant loss of corrosion resistance in alloys. This is especially true of stainless steels. To keep the chromium in these materials uniformly dispersed throughout, they are cooled rapidly from high temperatures (at which the chromium is completely dissolved in the alloy) so that there is insufficient time for the chromium to segregate before it becomes immobilized at lower temperatures. However, heating to temperatures in the range 400 to 800 °C (750 to 1470 °F), which happens in the HAZ, makes the atoms sufficiently mobile that chromium and carbon atoms are able to encounter each other and precipitate as chromium carbide particles. In the process, as chromium atoms from the surrounding matrix participate in the growth of the chromium carbide, the region surrounding each precipitate particle becomes depleted of chromium. When the chromium content of these regions drops below approximately 12 wt%, the local corrosion resistance diminishes dramatically and the material becomes readily susceptible to severe localized corrosion in those areas (Ref 11, 12, 13). This phenomenon is termed *sensitization.* Corrosion of sensitized alloys is exacerbated by the presence of large areas of passive metal surface surrounding the sensitized area. The passive regions can act as cathodic sites and thereby help to accelerate metal oxidation, a result made worse by the large cathodic-to-anodic area ratio. The tendency toward sensitization can be reduced by employing low-carbon stainless steels (such as type 304L) to avoid carbide formation, by adding other elements that strongly bind carbon (such as niobium or titanium), and by avoiding processes (such as welding) that generate temperatures in the 400 to 800 °C (750 to 1470 °F) range within the metal (Ref 11).

Structural and compositional differences between the base metal and the weld are also a source of potential corrosion problems. The weld metal tends to be inferior to the base metal due to inhomogeneities, a dendritic microstructure, and elevated concentrations of impurities. Occasionally, welding-introduced impurities can have beneficial effects too, such as the increase in pitting resistance of types 304 and 316 stainless steel welds on incorporation of nitrogen in the weldment during gas-tungsten arc welding. The type of welding process employed can also influence susceptibility to stress-corrosion cracking (Ref 12).

Certain heat treatments are known to sensitize some materials. In this case, sensitization occurs across the whole sample, not just along a narrow HAZ next to a weld. It is also possible to stabilize sensitized materials using heat treatments. For instance, chromium carbide precipitates in stainless steels can be redissolved by heat treatment above about 1035 °C (1895 °F). Rapid quenching after the homogenizing heat treatment prevents the chromium carbide particles from reforming, leaving the chromium well dispersed in the metal. Heat treatments can also help to anneal out crystal defects, thereby further reducing the impact on corrosion (Ref 12).

The growth of precipitate particles promoted by heat treatments can also lead to galvanic corrosion effects. Such is the case with precipitation-hardened Al-Cu, Al-Mg, and Al-Zn-Mg alloys (Ref 11). In Al-Cu alloys, $CuAl_2$ precipitates are nobler than the matrix, whereas $MgZn_2$ and Mg_2Al_3 are less noble than their Al- Zn-Mg or Al-Mg matrixes, respectively. The heat treatments that are beneficial mechanically, because they improve hardness by causing precipitate formation, are at the same time detrimental to the corrosion resistance because the growth of different phases within the material favors the possibility of galvanic corrosion. The severity of subsequent attack depends on the characteristics of the heat treatments to the extent that they control the size and distribution of intergranular precipitates. Generally, alloys that are heat-treated to peak hardness are most severely attacked by corrosion, while, those that are overaged are somewhat less susceptible (Ref 11).

The application of cold work to a metal may also alter its corrosion properties, but not necessarily by the mechanism that one might first expect. The creation of defects and high-energy atoms in the metal does little to change the corrosion potential (Ref 11, 12) and usually does not lead to serious corrosion damage, as was discussed previously. Instead, is seems to be the effects of cold work on the protectiveness of the passive film

and work-induced sensitization (Ref 12, 13) that more strongly determine the influence of cold work on corrosion properties.

Cold work has been found to lead to precipitation of fine particles of chromium carbide at grain boundaries in stainless steels. These grow coarser with increasing amounts of work, leading to sensitization. They also help increase the rate of sensitization during any subsequent heating events. The protectiveness of the surface oxide on stainless steels has been observed to increase after application of cold work as a result of a work-induced conversion of the single-layer mixed Fe_2O_3/Cr_2O_3 oxide to a double layer consisting of mixed Fe_2O_3/Cr_2O_3 on the outside and $Fe_{2-x}Cr_xO_4$ spinel mixed with Cr_2O_3 on the interior (Ref 12).

Cold work that shapes and orients grains, introduces texture, and changes the stacking fault density of a material can affect the corrosion properties in a variety of ways. The transition from intergranular to transgranular stress-corrosion cracking with increasing cold work, observed in a number of alloys (Ref 12), and the role of cold work in modifying the grain structure of aluminum alloys such that they become susceptible to exfoliation corrosion processes, (Ref 11) are two examples of the consequences of cold work, as described earlier. Cold work can also help in promoting stress-corrosion cracking in susceptible materials by introducing residual stresses. In this case, the influence on corrosion is a mechanical, rather than a chemical, consequence of metallurgical processing.

References cited in this section

11. E.N. Pugh, Corrosion: Metallurgical Aspects, *Encyclopedia of Materials Science and Engineering,* Vol 2, Pergamon Press, 1986, p 889–890

12. P. Rodriguez, Influence of Metallurgical Variables on Corrosion, *10th International Congress on Metallic Corrosion Conf. Proc.,* Vol V, Trans Tech Publications, 1989, p 31–42

13. P. Rodriguez, Influence of Metallurgical Variables on Stress Corrosion Behaviour of Austenitic Stainless Steels, *J. Electrochem. Soc. India,* Vol 44 (No. 3), July 1995, p F43–F50

14. T.L. Johnson and C.E. Feltner, Grain Size Effects in the Strain Hardening of Polycrystals, *Metall. Trans.,* Vol 1, May 1970, p 1161–1167

15. S.Y. Yu, J.R. Scully, and C.M. Vitus, Influence of Niobium and Zirconium Alloying Additions on the Anodic Dissolution Behavior of Activated Titanium in HCl Solutions, *J. Electrochem. Soc.,* Vol 148 (No. 2), 2001, p B68–B78

16. M.G. Fontana, *Corrosion Engineering,* McGraw-Hill, 1986, p 226, 491–499

17. M. Stern and H. Wissenberg, The Influence of Noble Metal Alloying Additions on the Electrochemical and Corrosion Behavior of Titanium, *J. Electrochem. Soc.,* Vol 106 (No. 9), 1959, p 759–764

18. S.Y. Yu and J.R. Scully, Corrosion and Passivity of Ti-13%Nb-13%Zr in Comparison to Other Biomedical Implant Alloys, *Corrosion,* Vol 53 (No. 12), December 1997, p 965–976

J.J. Noel, Effects of Metallurgical Variables on Aqueous Corrosion, *Corrosion: Fundamentals, Testing, and Protection*, Vol 13A, *ASM Handbook*, ASM International, 2003, p 258–265

Effects of Metallurgical Variables on Aqueous Corrosion

James J. Noël, University of Western Ontario

References

1. L.E. Samuels, *Metals Engineering: A Technical Guide,* ASM International, 1988, p 5, 6, 238

2. R.A. Higgins, *Engineering Metallurgy, Part 1: Applied Physical Metallurgy,* Robert E. Krieger Publishing Company, 1983, p 69

3. M.H. Richman, *An Introduction to the Science of Metals,* Blaisdell Publishing Company, 1967, p 112, 113

4. Metallic Glasses, in *Handbook of Corrosion Data,* 2nd Ed., ASM International, 1995, p 83, 84

5. A.L. Greer, K.L. Rutherford, and I.M. Hutchings, Wear Resistance of Amorphous Alloys and Related Materials, *International Materials Reviews,* Vol 47 (No. 2), 2002, p 87–112

6. D.J. Li, A.J. Akerman, K.J. Doherty, S.J. Poon, and G.J. Shiflet, Swift Amorphization of a Supersaturated Titanium Solution by Mechanical Milling, *Scr. Mater.,* Vol 38 (No. 4), 1998, p 603–609

7. A. Peker and W.L. Johnson, A Highly Processable Metallic Glass: $Zr_{41.2}Ti_{13.8}Cu_{12.5}Ni_{10.0}Be_{22.5}$, *Appl. Phys. Lett.,* Vol 63 (No. 17), 1993, p 2342–2344

8. W.G. Moffat, *The Handbook of Binary Phase Diagrams,* General Electric, 1978

9. T.B. Massalski, Ed., *Binary Alloy Phase Diagrams,* American Society for Metals, 1986

10. Y. Kawazoe, T. Masumoto, K. Suzuki, A. Inoue, A.P. Tsai, J.Z. Yu, T. Aihara, Jr., and T. Nakanomyo, *Phase Diagrams and Physical Properties of Nonequilibrium Alloys, Subvolume A: Nonequilibrium Phase Diagrams of Ternary Amorphous Alloys,* Y. Kawazoe, Ed., Landolt-Börnstein New Series: Numerical Data and Functional Relationships in Science and Technology, Group III: Condensed Matter, Vol 37, Springer-Verlag, 1997

11. E.N. Pugh, Corrosion: Metallurgical Aspects, *Encyclopedia of Materials Science an*

J.J. Noel, Effects of Metallurgical Variables on Aqueous Corrosion, *Corrosion: Fundamentals, Testing, and Protection*, Vol 13A, *ASM Handbook*, ASM International, 2003, p 258–265

Effects of Metallurgical Variables on Aqueous Corrosion

James J. Noël, University of Western Ontario

Selected References

- W.D. Callister, Jr., *Materials Science and Engineering: An Introduction,* 4th edition, John Wiley & Sons, 1997
- J.R. Davis, Ed., *Alloying: Understanding the Basics,* ASM International, 2001
- L.S. Van Delinder, Ed., *Corrosion Basics: An Introduction*, NACE International, 1984
- M.G. Fontana, *Corrosion Engineering,* McGraw-Hill, 1986
- L.E. Samuels, *Metals Engineering: A Technical Guide,* ASM International, 1988

J.D. Fritz, Effects of Metallurgical Variables on the Corrosion of Stainless Steels, *Corrosion: Fundamentals, Testing, and Protection*, Vol 13A, *ASM Handbook*, ASM International, 2003, p 266–274

Effects of Metallurgical Variables on the Corrosion of Stainless Steels

James D. Fritz, TMR Stainless

Introduction

METALLURGICAL VARIABLES can influence the corrosion behavior of austenitic, ferritic, duplex, and martensitic stainless steels. The distribution of carbon is probably the most important variable influencing the susceptibility of these alloys to intergranular corrosion, but nitrogen and metallic phases are also important, particularly with the more highly alloyed stainless steel grades. This article describes the effects of important metallurgical and processing variables, on corrosion of stainless steels. Related information is provided in the article "Corrosion Resistance of Stainless Steels and Nickel Alloys" in this Volume.

J.D. Fritz, Effects of Metallurgical Variables on the Corrosion of Stainless Steels, *Corrosion: Fundamentals, Testing, and Protection*, Vol 13A, *ASM Handbook*, ASM International, 2003, p 266–274

Effects of Metallurgical Variables on the Corrosion of Stainless Steels

James D. Fritz, TMR Stainless

Austenitic Stainless Steels

Intergranular Corrosion. At temperatures above approximately 1035 °C (1900 °F), chromium carbides are completely dissolved in austenitic stainless steels. However, when these steels are slowly cooled from these high temperatures or reheated into the range of 425 to 815 °C (800 to 1500 °F), chromium carbides are precipitated at the grain boundaries. These carbides contain more chromium than the matrix does.

The precipitation of the carbides depletes the matrix of chromium adjacent to the grain boundary. The diffusion rate of chromium in austenite is slow at the precipitation temperatures; therefore, the depleted zone persists, and the alloy is sensitized to intergranular corrosion. This sensitization occurs because the depleted zones have higher corrosion rates than the matrix in many environments. Figure 1 illustrates how the chromium content influences the corrosion rate of iron-chromium alloys in boiling 50% H_2SO_4 containing ferric sulfate, $Fe_2(SO_4)_3$. In all cases, the alloys are in the passive state. The wide differences in the corrosion rate are the result of the differences in the chromium content. With the lower-chromium-bearing stainless steels, the passive film is more soluble in the acid, and therefore, more metal must dissolve to repair the film.

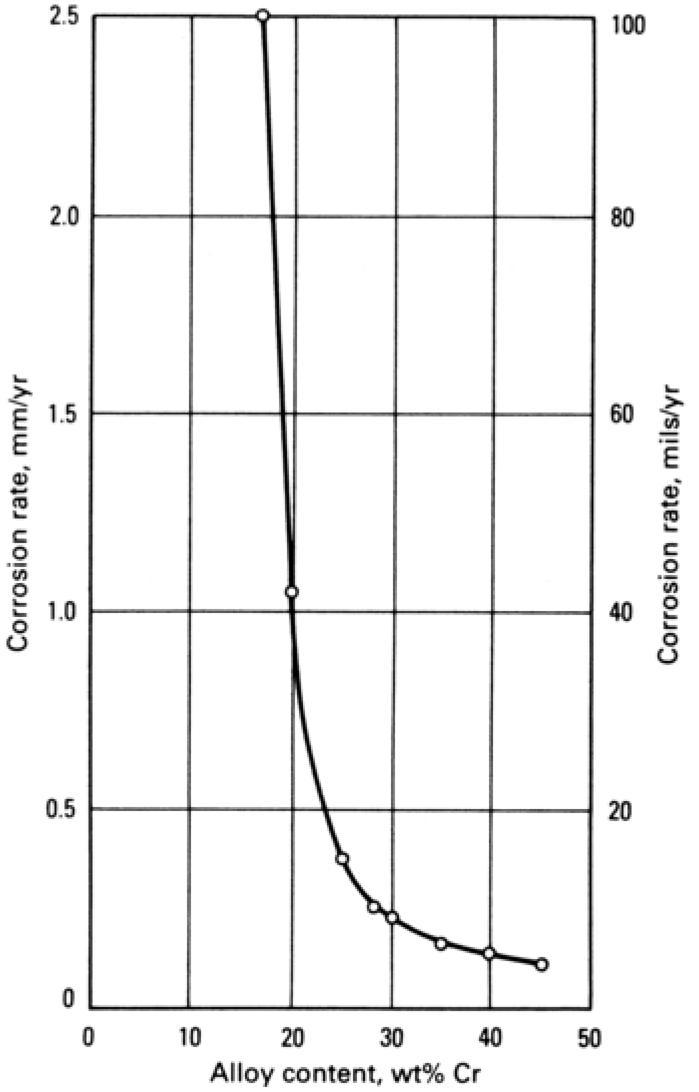

Fig. 1 The effect of chromium content on the corrosion behavior of iron-chromium alloys in boiling 50% H_2SO_4 with $Fe_2(SO_4)_3$. Source: Ref 1

If the austenitic stainless steels are cooled rapidly to below approximately 425 °C (800 °F), the carbides do not precipitate, and the steels are immune to intergranular corrosion. Reheating the alloys to 425 to 815 °C (800 to 1500 °F), as for stress relief, causes carbide precipitation and sensitivity to intergranular corrosion. The maximum rate of carbide precipitation occurs at approximately 675 °C (1250 °F). Because this is a common temperature for the stress relief of carbon and low-alloy steels, care must be exercised in selecting stainless steels to be used in dissimilar-metal joints that are to be stress relieved.

Welding is the common cause of the sensitization of stainless steels to intergranular corrosion. Although the cooling rates in the weld itself and the base metal immediately adjacent to it are sufficiently high to avoid carbide precipitation, the weld thermal cycle brings part of the heat- affected zone (HAZ) into the precipitation

temperature range. Carbides can precipitate, and a zone somewhat removed from the weld becomes susceptible to intergranular corrosion (Fig. 2). Welding does not always sensitize austenitic stainless steels. In thin sections, the thermal cycle may be such that no part of the HAZ is at sensitizing temperatures long enough to cause carbide precipitation. Once the precipitation has occurred, it can be removed by reheating the alloy to above 1035 °C (1895 °F) and cooling it rapidly. This thermal treatment dissolves the chromium carbide precipitates and restores the chromium-depleted zone. This practice is commonly termed solution anneal.

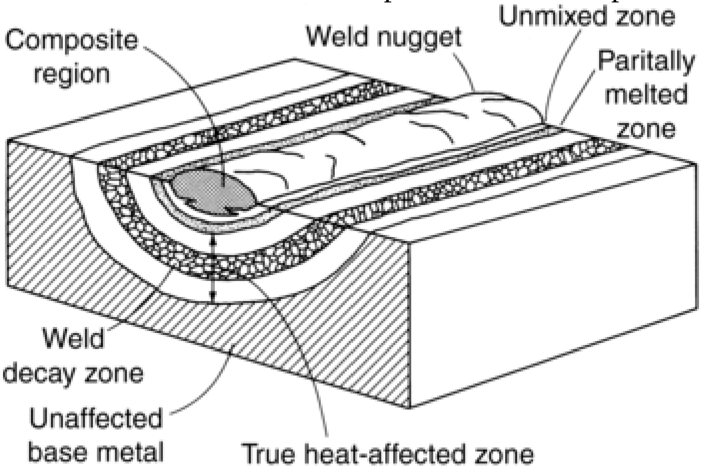

Fig. 2 Schematic diagram of the regions of a weld in austenitic stainless steel. Source: Ref 2

Avoiding Intergranular Corrosion. Susceptibility to intergranular corrosion in austenitic stainless steels can be avoided by limiting their carbon contents or by adding elements whose carbides are more stable than those of chromium. For most austenitic stainless steels, restricting their carbon contents to 0.03% or less prevents sensitization during welding and most heat treatment. This method is not effective for eliminating sensitization that would result from long- term service exposure at 425 to 815 °C (800 to 1500 °F).

At temperatures above 815 °C (1500 °F), titanium and niobium form more stable carbides than chromium and are added to stainless steels to form these stable carbides, which remove carbon from solid solution and prevent precipitation of chromium carbides. The most common of these stabilized grades are types 321 and 347. Type 321 contains minimum titanium content of 5 × (C% + N%), and type 347 a minimum niobium content of 8 × C%. Nitrogen must be considered when titanium is used as a stabilizer, not because the precipitation of chromium nitride is a problem in austenitic steels, but because titanium nitride is very stable. Titanium combines with any available nitrogen; therefore, this reaction must be considered when determining the total amount of titanium required to combine with the carbon.

The stabilized grades are more resistant to sensitization by long-term exposure at 425 to 815 °C (800 to 1500 °F) than the low-carbon grades are, and the stabilized grades are the preferred materials when service involves exposure at these temperatures. For maximum resistance to intergranular corrosion, these grades are given a stabilizing heat treatment at approximately 900 °C (1650 °F). The purpose of the treatment is to remove carbon from solution at temperatures where titanium and niobium carbides are stable, but chromium carbides are not. Such treatments prevent the formation of chromium carbide when the steel is exposed to lower temperatures.

Figure 3 illustrates how both carbon control and stabilization can eliminate intergranular corrosion in as-welded austenitic stainless steels. It also shows that the sensitized zone in these steels is somewhat removed from the weld metal.

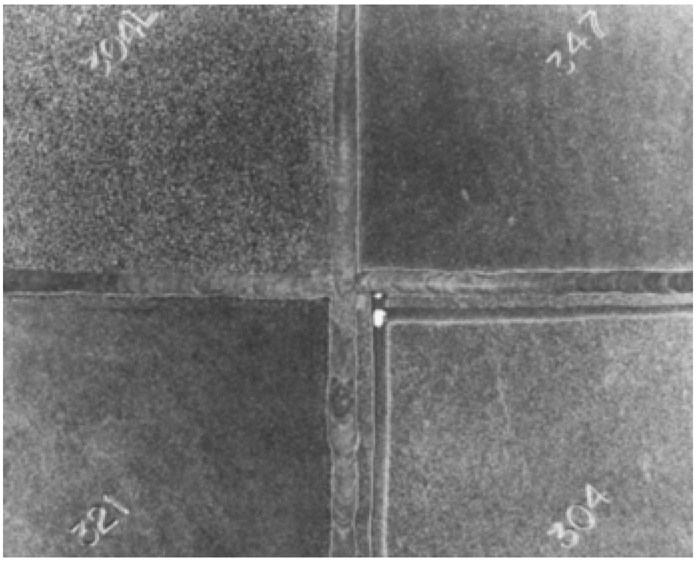

Fig. 3 Weld decay and methods for its prevention. The four different panels were joined by welding and then exposed to a hot solution of HNO_3/HF. Weld decay, such as that shown in the type 304 steel (bottom right), is prevented by reduction of the carbon content (type 304L, top left) or by stabilization with titanium (type 321, bottom left) or niobium (type 347, top right). Source: Ref 3

Knife-Line Attack. Stabilized austenitic stainless steels may become susceptible to a localized form of intergranular corrosion known as knife- line attack or knife-line corrosion. During welding, the base metal immediately adjacent to the fusion line is heated to temperatures high enough to dissolve the stabilizing carbides, but the cooling rate is rapid enough to prevent carbide precipitation. If weldments in stabilized grades are then heated into the sensitizing temperature range of 425 to 815 °C (800 to 1500 °F), for example, during stress-relieving treatments, high-temperature service, or subsequent weld passes, chromium carbide can precipitate. The precipitation of chromium carbide leaves the narrow band adjacent to the fusion line susceptible to intergranular corrosion.

Knife-line attack can be avoided by the proper choice of welding variables and by the use of stabilizing heat treatments.

Testing for Intergranular Corrosion. The common methods of testing austenitic stainless steels for susceptibility to intergranular corrosion are described in ASTM A 262 (Ref 4). There are five acid immersion tests and one etching test. The oxalic acid etch test is used to screen samples to determine the need for further testing. Samples that have acceptable microstructures are considered not to be susceptible to intergranular corrosion and require no further testing. Samples with microstructures indicative of carbide precipitation must be subjected to one of the immersion tests. Tests for intergranular corrosion are summarized in a table in the article "Evaluating Intergranular Corrosion" in this Volume. This table includes ferritic stainless steels and nickel-rich chromium alloys as well as austenitic stainless steels.

Several electrochemical tests based on the polarization behavior of stainless steels susceptible to intergranular corrosion have been proposed (Ref 5, 6, 7, 8, 9, 10, 11). Although the tests have received considerable attention, only the single-loop electrochemical potentiokinetic reactivation (EPR) test has been adopted in a national standard (Ref 12). With this test, a polished stainless steel surface is first held at the corrosion potential (≈-400 mV versus saturated calomel electrode, or SCE) for 1 to 2 min in a test solution of sulfuric acid and potassium thiocyanate (0.5*M* H_2SO_4 + 0.01*M* KSCN) at -1 °C (30 °F). The electrode potential is then raised to a passive potential of +200 mV versus the SCE and held for 2 min. After this passivation step, the potential is decreased to the corrosion potential at a constant potential scan rate of 6 V/h. If the specimen is sensitized, the chromium-depleted regions reactivate during the potential scan back to the corrosion potential, resulting in a well-defined current loop. The charge, *Q,* measured during the reactivation scan can be related to the degree of sensitization. With this technique, the grain size must be measured to approximate the area of attack of chromium-depleted material. The double-loop EPR test (Ref 9, 10, 11, 12) is a refinement of the single-loop technique and avoids the necessity of polishing the test surface and measuring the grain size.

Intergranular Stress-Corrosion Cracking (SCC). Austenitic stainless steels that are susceptible to intergranular corrosion are also subject to intergranular SCC. The problem of the intergranular SCC of sensitized austenitic

stainless steels in boiling high-purity water containing oxygen has received a great deal of study. This seemingly benign environment has led to cracking of sensitized stainless steels in many boiling water nuclear reactors (Ref 44, 45, 46).

Sensitized stainless alloys of all types crack very rapidly in the polythionic acid that forms during the shutdown of desulfurization units in petroleum refineries (Ref 13, 14). Because this service involves long-term exposure of sensitizing temperatures, the stabilized grades should be used.

Effect of Ferrite and Martensite. Phases other than carbides can also influence the corrosion behavior of austenitic stainless steels. Ferrite, which is the result of an intentional balancing of the composition of some stainless steels to obtain greater resistance to hot cracking, appears to reduce pitting resistance as well as the resistance to strong acids. The presence of martensite may render the steels susceptible to hydrogen embrittlement under some conditions. Martensite can be produced by the deformation of unstable austenite. Although this phenomenon can occur in a number of commercial stainless steels, it is most common in the lower-nickel steels such as type 301, in which the transformation is used to increase formability. The presence of strain-induced martensite has been shown to increase the corrosion rate of type 304L in 10% sulfuric acid (Ref 15). This increased corrosion rate is believed to be the result of preferential attack of the martensite phase.

Effect of Sigma Phase. The effect of σ phase on the corrosion behavior of austenitic stainless steel has received considerable attention. This hard, brittle intermetallic phase precipitates in the same temperature range as chromium carbide and may produce susceptibility to intergranular corrosion in some environments.

Because it is hard and brittle, σ phase affects mechanical as well as corrosion properties. Although it is often associated with δ-ferrite, it can form directly from austenite.

The effects of σ phase on the corrosion behavior of austenitic stainless steels are most serious in highly oxidizing environments. With standard grades such as 316L and CF3M, the problem is of practical concern only if the phase is continuous. Although discrete particles of σ phase may be attacked directly, such corrosion does not seem to contribute significantly to the penetration of the steel. With the more highly alloyed stainless steel grades, the precipitation of σ phase can result in a substantial loss in pitting and crevice corrosion resistance. This is discussed in the section “High-Performance Stainless Steels” in this article.

The most important corrosion problem with σ phase in austenitic stainless steels occurs before it is microscopically resolved (Ref 16). When the low-carbon molybdenum-containing austenitic stainless steels (such as type 316L and CF3M) or the stabilized grades (such as type 321 and type 347) are exposed at 675 °C (1245 °F), they may become susceptible to intergranular corrosion in nitric acid (HNO_3) and, in some cases, $Fe_2(SO_4)_3$-H_2SO_4. This susceptibility cannot be explained by carbide precipitation, and σ phase usually cannot be found in the optical microstructure. However, because some of the susceptible steels do exhibit continuous networks of σ phase, it has been assumed that this constituent is the cause of the intergranular corrosion. The hypothesis is that even when σ phase is not visible in the optical microstructure, its effects are felt through some precursor or invisible phase. Invisible σ phase must be considered when testing for susceptibility to intergranular corrosion, but it seems to affect corrosion resistance only in very oxidizing environments, such as HNO_3.

Unsensitized austenitic stainless steels (that is, solution-annealed material containing no carbides or other deleterious phases) are subject to intergranular corrosion in very highly oxidizing environments, such as HNO_3 containing hexavalent chromium (Ref 17). None of the regularly controlled metallurgical variables influences this type of intergranular attack. Additional information on, and micrographs of, σ phase in austenitic stainless steels can be found in the article “Wrought Stainless Steels” in *Metallography and Microstructures,* Volume 9 of *ASM Handbook,* 1985, formerly *Metals Handbook,* 9th edition.

References cited in this section

1. R.F. Steigerwald, *Metall. Trans.,* Vol 5, 1974, p 2265–2269
2. W.F. Savage, *Weld. Des. Eng.,* Dec 1969
3. M.A. Streicher, in *Intergranular Corrosion of Stainless Alloys,* STP 656, R.F. Steigerwald, Ed., American Society for Testing and Materials, 1978, p 3–84

4. “Standard Practices for Detecting Susceptibility to Intergranular Attack in Austenitic Stainless Steels,” A 262, *Annual Book of ASTM Standards,* American Society for Testing and Materials

5. W.L. Clarke, R.L. Cowan, and W.L. Walker, in *Intergranular Corrosion of Stainless Alloys,* STP 656, R.F. Steigerwald, Ed., American Society for Testing and Materials, 1978, p 99–132

6. M. Akashi, T. Kawomoto, and F. Umemura, *Corros. Eng.,* Vol 29, 1980

7. A.P. Majidi and M.A. Steicher, *Corrosion,* Vol 40 (No. 11), 1984, p 584

8. A.P. Majidi and M.A. Steicher, *Electrochemical Techniques for Corrosion Engineering,* R. Baboian, Ed., NACE, 1986, p 217

9. S. Frangini and A. Mignone, *Corrosion,* Vol 48 (No. 9), 1992, p 715

10. J.P. Sydow, D.L. Reichert, and G.E. Stoner, *Mater. Perform.,* Vol 1, 1991, p 68

11. J.F. Grubb and J.D. Fritz, “Comparison of the Double-Loop EPR Test with ASTM A 262 B,” Paper 185, Corrosion 97, NACE International, 1997

12. “Standard Test Method for Electrochemical Reactivation (EPR) for Detecting Sensitization of AISI Type 304 and 304L Stainless Steels,” G 108, *Annual Book of ASTM Standards,* ASTM

13. A. Dravnieks and C.H. Samans, *Proc. API,* Vol 37 (No. 3), 1957, p 100

14. R.C. Scarberry, S.C. Pearman, and J.R. Crum, *Corrosion,* Vol 32, 1976, p 401–406

15. J.D. Fritz and B.W. Parks, Jr., “The Influence of Martensite on the Corrosion Resistance of Austenite Stainless Steels,” Paper 00507, Corrosion 2000, NACE International, 2000

16. D. Warren, *Corrosion,* Vol 15, 1959, p 213t–220t

17. M.A. Streicher, *J. Electrochem. Soc.,* Vol 106, 1959, p 161–180

44. B.M. Gordon, *Mater. Perform.,* Vol 19, 1980, p 29

45. G.S. Was and P.L. Andresen, *J. Met.,* Vol 44 (No. 4), 1992, p 8

46. P.M. Scott, *Corros. Sci.,* Vol 25 (No. 8–9), 1985, p 583

J.D. Fritz, Effects of Metallurgical Variables on the Corrosion of Stainless Steels, *Corrosion: Fundamentals, Testing, and Protection*, Vol 13A, *ASM Handbook*, ASM International, 2003, p 266–274

Effects of Metallurgical Variables on the Corrosion of Stainless Steels

James D. Fritz, TMR Stainless

Ferritic Stainless Steels

Intergranular Corrosion. The mechanism for intergranular corrosion in ferritic stainless steels is largely accepted as being the same as that in austenitic stainless steels. Chromium compounds precipitate at grain boundaries, and this causes chromium depletion in the grains immediately adjacent to the boundaries (Ref 18, 19). This lowering of the chromium content leads to increased corrosion rates in the oxidizing solutions usually used to evaluate intergranular corrosion.

There are several differences between the sensitization of ferritic and austenitic stainless steels to intergranular corrosion. The first is that the solubility of nitrogen in austenite is great enough that chromium nitride precipitation is not a significant cause of intergranular corrosion in austenitic steels. It is, however, a significant cause in ferritic stainless steels. The second is the temperature at which sensitization occurs. Sensitization in austenitic steels is produced by heating between 425 and 815 °C (800 and 1500 °F). In conventional ferritic alloys, sensitization is caused by heating above 925 °C (1700 °F). This difference is the result of the relative solubility of carbon and nitrogen in ferrite and austenite. Because the sensitization temperatures are different for austenitic and ferritic steels, it is not surprising that the welding of susceptible steels produces different zones of intergranular corrosion. In austenitic steels, intergranular corrosion occurs at some distance from the weld, where the peak temperature reached during welding is approximately 675 °C (1250 °F). Because the sensitization of ferritic stainless steels occurs at higher temperatures, the fusion zone and the weld itself are the most likely areas for intergranular corrosion.

The mere presence of chromium carbides and nitrides in ferritic stainless steels does not ensure that they will be subject to intergranular corrosion. On the contrary, the usual annealing treatment for conventional ferritic stainless steels is one that precipitates the carbides and nitrides at temperatures (700 to 925 °C, or 1300 to 1700 °F) at which the chromium can diffuse back into the depleted zones. These same treatments would, of course, sensitize austenitic stainless steels because of the much slower rate of diffusion of chromium in austenite.

Avoiding Intergranular Corrosion. Clearly, the most straightforward method of preventing intergranular attack in ferritic stainless steels is to restrict their interstitial contents. The results shown in Table 1 give an indication of the levels of carbon and nitrogen required to avoid intergranular corrosion of Fe-Cr-Mo alloys in boiling 16% H_2SO_4-copper-copper sulfate ($CuSO_4$) solutions. Evaluation was by bending. The samples that passed had no cracks after bending.

Table 1 Results of ASTM A 763, practice Z, on representative as-welded ferritic stainless steels

Welds were made using the gas tungsten arc welding technique with no filler metal added.

Alloy	Interstitial content, wt%		Result
	C	**N**	
18Cr-2Mo	0.002	0.004	Pass
	0.010	0.004	Fail
	0.002	0.009	Fail
26Cr-1Mo	0.002	0.005	Pass
	0.004	0.010	Partial failure
	0.003	0.016	Fail
	0.013	0.006	Fail

Source: Ref 20

For 18Cr-2Mo alloys to be immune to intergranular corrosion, it appears that the maximum level of carbon plus nitrogen is 60 to 80 ppm; for 26Cr-1Mo steels, this level rises to approximately 150 ppm. The notation of partial failure for the 26Cr-1Mo steel containing 0.004% C and 0.010% N indicates that only a few grain boundaries opened on bending and that it probably represents the limiting composition. Using the 50% H_2SO_4-$Fe_2(SO_4)_3$ test, it was determined that the interstitial limits for the 29Cr-4Mo steel were 0.010% C (max) and 0.020% N (max), with the additional restriction that the combined total not exceed 250 ppm (Ref 19). As their alloy contents increase, the iron-chromium-molybdenum steels seem to grow more tolerant of interstitials with regard to intergranular corrosion.

The levels of carbon and nitrogen that are needed to keep 18Cr-Mo alloys free of intergranular corrosion are such that very low interstitial versions of 18% Cr alloys have received little commercial attention. The 26Cr-1Mo and 29Cr-4Mo steels have been made in considerable quantity with very low interstitials, for example, 20 ppm C and 100 ppm N.

The low-interstitial ferritic stainless steels respond to heat treatment in a manner somewhat similar to that of austenitic stainless steels. As the results for weldments in Table 1 indicate, rapid cooling from high temperature preserves resistance to intergranular corrosion. However, depending on alloy content and interstitial levels, these alloys may be sensitive to a cooling rate from temperatures above approximately 600 °C (1110 °F) (Ref 21, 22). Less pure Fe-Cr-Mo alloys can also be affected by a cooling rate from approximately 800 °C (1470 °F), but at higher temperatures, it is impossible to quench them fast enough to avoid intergranular attack.

Isothermal heat treatments can also produce sensitivity to intergranular corrosion in low-interstitial ferritic stainless steels (Ref 22). For example, the effects of annealing at 620 °C (1150 °F) on the intergranular corrosion of 26% Cr alloys with 0 to 3% Mo were studied (Ref 23). The alloys contained 0.007 to 0.013% C and 0.020 to 0.024% N. As little as 10 min at temperature can lead to intergranular corrosion; however, continuing the treatment for 1 to 2 h can cure the damage (Table 2). Increasing the molybdenum content delays the onset of sensitization and makes it less severe. It does, however, delay recovery.

Table 2 Corrosion rates of 26% Cr ferritic stainless steels containing 0 to 3% Mo that were annealed for 15 min at 900 °C (1650 °F), water quenched, annealed for increasing times at 620 °C (1150 °F), then water quenched

Testing was performed according to recommendations in ASTM A 763, practice X (ferric sulfate/sulfuric acid test).

Alloy	Corrosion rate, mg/dm^2/d						
	900 °C (1650 °F) anneal	**Annealing time at 620 °C (1150 °F)**					
		10 min	**30 min**	**1 h**	**2 h**	**4 h**	**5 h**
26-0	50	15,700	270	62	81	85	43
		15,600	264	50	67	85	43
26-1	43	5950[(a)]	8030[(a)]	990	50	40	53
	37	8220[(a)]	12,400[(a)]	890	50	37	50
26-2	78	15,600	940	138	80	74	270
	77	15,500	500	132	80	70	226
26-3	50	104	214	258	98	102	58
	50	95	160	96	93	97	58

(a) 56 h in test solution. Source: Ref 23

The very low levels of interstitials needed to ensure that ferritic stainless steels are immune to intergranular corrosion suggest that stabilizing elements might offer a means of preventing this type of corrosion without such restrictive limits on the carbon and nitrogen. Both titanium and niobium can be used, and each has its advantages (Ref 24). In general, weld ductility is somewhat better in the titanium-containing alloys, but the toughness of the niobium steels is better. As noted previously, titanium-stabilized alloys are not recommended for service in HNO_3, but the niobium-containing steels can be used in this environment.

Table 3 shows the results of Cu-$CuSO_4$-16% H_2SO_4 tests on 26Cr-1Mo and 18Cr-2Mo steels with additions of either titanium and/or niobium. Inspection of the data suggests that the required amount of titanium cannot be described by a simple ratio as it is in austenitic steels. The amount of titanium or niobium required for ferritic stainless steels to be immune to intergranular corrosion in the $CuSO_4$-16% H_2SO_4 test has been investigated (Ref 25). It has been determined that for 26Cr-1Mo and 18Cr-2Mo alloys, the minimum stabilizer concentration is given by:

$$\mathrm{Ti} + \mathrm{Nb} = 0.2 + 4\,(\mathrm{C} + \mathrm{N}) \quad \text{(Eq 1)}$$

According to Ref 25, this minimum combination is valid for combined carbon and nitrogen contents in the range of 0.02 to 0.05%. It should be emphasized that the limits set in Eq 1 are truly minimal and are needed in the final product if intergranular attack is to be avoided.

Table 3 Results of ASTM A 763, practice Z, tests on as-welded ferritic stainless steels with titanium or niobium

Welds were made using gas tungsten arc welding with no filler metal added.

Alloy	(C + N), wt%	Ti, wt%	Nb, wt%	Ti or Nb/(C + N), %	Result
18Cr-2Mo	0.022	0.16	…	7.3	Fail
	0.028	0.19	…	6.8	Fail
	0.027	0.23	…	8.5	Pass
	0.057	0.37	…	6.5	Pass
	0.079	0.47	…	5.9	Pass
18Cr-2Mo	0.067	…	0.32	4.8	Fail
	0.067	…	0.61	9.1	Pass
	0.030	…	0.19	6.3	Pass
26Cr-1Mo	0.026	0.17	…	6.5	Fail
	0.026	0.22	…	8.5	Fail
	0.026	0.26	…	10.0	Pass
26Cr-1Mo	0.026	…	0.17	6.5	Fail
	0.025	…	0.33	13.2	Pass

Source: Ref 20

This guideline is empirical and cannot be explained on the basis of stoichiometry. The alloys in the study (Ref 25) were fully deoxidized with aluminum before the stabilizing additions were made. Therefore, it is unlikely that excess stabilizer is required for the purpose of reacting with oxygen.

The susceptibility of titanium-stabilized steels to intergranular attack in HNO_3 has been noted earlier. Because there is evidence that titanium carbide can be directly attacked by HNO_3, this mechanism is usually used to explain intergranular corrosion in titanium-containing steels. Another explanation that could be advanced about the intergranular attack of titanium-bearing steels under highly oxidizing conditions is an invisible σ phase such as that encountered in type 316L and discussed previously.

Testing for Intergranular Corrosion. Standardized test methods for detecting the susceptibility of ferritic stainless steels to intergranular corrosion are described in ASTM A 763 (Ref 26). The methods are similar to those described in ASTM A 262 (Ref 4) for austenitic stainless steels in that there is an oxalic acid etch test and three acid immersion tests. The principal difference between the two standards is the use of microscopic examination of samples exposed to the boiling acid solutions. The presence or absence of grain dropping becomes the acceptance criterion for these samples.

Effects of Austenite and Martensite. The austenitic and martensitic phases are discussed together for ferritic stainless steels because they are interrelated; one can occur as the result of the other.

High-purity iron-chromium alloys are ferritic at all temperatures up to the melting point if they contain more than approximately 12% Cr. However, the gamma loop in iron-chromium alloys can be greatly expanded by the addition of carbon and nitrogen. For example, it was found that the ferrite-austenite boundary was extended to 29% Cr in alloys that contained 0.05% C and 0.25% N (Ref 27).

Although the formation of austenite in ferritic stainless steels can be avoided by restricting their interstitial contents or by combining the interstitials with such elements as titanium or niobium, many of the ferritic stainless steels that are produced commercially undergo partial transformation to austenite. Once the austenite is formed, the question is how it is transformed. In one study, for example, the transformation products were dependent on the chromium content and the cooling rate (Ref 28). Slow cooling leads to the transformation of austenite into ferrite and carbides in all of the steels examined, but quenching can either produce martensite or retain the austenite.

The martensite start temperature (M_s) for a 17% Cr steel was measured at 176 °C (349 °F), and it was found that the transformation was 90% complete at 93 °C (199 °F) (Ref 28). The M_s for a 21% Cr steel was -160 °C (-256 °F), and martensite did not form in quenched 25% Cr alloys. Untempered martensite obviously reduces the toughness and ductility of ferritic stainless steels, and its presence is one cause of the poor ductility of welded type 430. In discussing this work (Ref 28), other researchers observed that welded type 430 (17% Cr) had poor ductility but that welded type 442 (21% Cr) had good ductility (Ref 29). These findings were attributed to the

transformation of austenite to martensite in the lower-chromium steel (type 430) but not in the 21% Cr steel (type 442). Both weldments were subject to intergranular corrosion, however.

The austenite retained in the higher-chromium steels is saturated with carbon, and when it is heated into the carbide precipitation region, for example, 760 °C (1400 °F), it loses carbon and becomes unstable enough to transform to martensite on cooling. This transformation product must then be tempered to restore ductility.

Another study found that martensite in type 430 corroded at a higher rate than the surrounding ferrite in boiling 50% H_2SO_4 + $Fe_2(SO_4)_3$ (Ref 19). This difference was attributed to the partitioning of chromium between ferrite and austenite at high temperatures. Because the austenite is lower in chromium, the martensite that forms from it would also be lower in chromium. The 50% H_2SO_4-$Fe_2(SO_4)_3$ test is quite sensitive to changes in chromium content in the 12 to 18% Cr range (Fig. 1). The test is less sensitive at higher chromium contents; therefore, no preferential attack was noted in austenite formed in type 446. This same austenite was preferentially attacked by boiling 5% H_2SO_4, presumably because of its higher interstitial content.

These corrosion experiments help to elucidate the effect of metallurgical factors on the corrosion behavior of ferritic stainless steels. However, these experiments describe situations rarely encountered in practice, because the mechanical properties of steels with such microstructures limit their usefulness.

Effect of Sigma and Related Phases. In contrast to the case of austenitic steels, the occurrence of σ phase in most commercial ferritic stainless steels can be predicted from the iron- chromium phase diagram. Fortunately, the kinetics of σ formation are very sluggish, and σ phase is not normally encountered in the processing of commercial ferritic stainless steels.

The formation of σ phase in the iron-chromium system has been thoroughly researched, and the literature has been well summarized (Ref 30). The phase has the nominal composition of FeCr, but it can dissolve approximately 5% of either iron or chromium. It forms congruently from ferrite at 815 °C (1500 °F). The sluggishness of the reaction makes it difficult to define the low-temperature limits of the σ phase field, but the ferrite/ferrite + σ phase boundary has been estimated at 9.5% Cr at 480 °C (895 °F) (Ref 30). Cold work accelerates the precipitation of σ phase.

There is relatively little information on how σ phase affects the corrosion behavior of ferritic stainless steels; however, continuous networks would be expected to be more troublesome than isolated colonies. Because σ phase contains more chromium than does the ferrite, its presence could also affect the corrosion behavior by either local or general depletion of the chromium content of the matrix.

One study investigated the corrosion behavior of an Fe-47Cr alloy that was heat treated so that it was either entirely ferrite or entirely σ phase (Ref 31). These data are shown in Table 4. The types of environments studied induced reducing (active), oxidizing (passive), and pitting corrosion conditions. The differences were greatest in the oxidizing and pitting environments. These results indicate that σ phase is more likely to corrode than ferrite in many instances and that no chromium depletion mechanism need be invoked to explain how σ phase can reduce the corrosion resistance.

Table 4 The effect of crystal structure on the corrosion behavior of an Fe-47Cr alloy

Solution	Corrosion rate, $g/dm^2/d$		
	Ferrite	**σ phase**	**Ratio**[(a)]
Reducing			
10% HCl boiling	1461	7543	5.2
10% H_2SO_4 boiling	2939	7422	2.5
50% H_2SO_4 boiling	5088	5280	1.04
Oxidizing			
50% H_2SO_4 + $Fe_2(SO_4)_3$ boiling	0.0195	0.196	10
50% H_2SO_4 + $CuSO_4$ boiling	0.0170	0.415	24
65% HNO_3 boiling	0.0205	0.861	42
HNO_3 + HF at 65 °C (150 °F)	0.00	0.06	…
Pitting			
10% $FeCl_3 \cdot 6H_2O$ at room temperature	0.00	2.5	…

(a) Corrosion rate of σ phase ÷ corrosion rate of ferrite. Source: Ref 31

In molybdenum-containing ferritic steels, χ phase, which is closely related to σ phase, can be found (Ref 32). It occurs in the temperature range of 550 to 950 °C (1020 to 1740 °F). It has the nominal composition Fe_2CrMo,

but there are deviations from stoichiometry. In an investigation of the effect of heat treatment on the microstructure of 29Cr-4Mo alloys, both χ and σ phases were found in material held in the 700 to 925 °C (1290 to 1695 °F) range (Ref 33). Long- term aging of the 29Cr-4Mo steel did not render it susceptible to intergranular corrosion in the boiling 50% H_2SO_4 + $Fe_2(SO_4)_3$ solution.

This work also included 29Cr-4Mo-2Ni alloys, and χ and σ phases were seen to form much more quickly in these steels than in nickel-free materials. This observation is consistent with earlier results that nickel additions up to approximately 2% can accelerate the formation of σ phase in iron-chromium alloys (Ref 34). At higher levels, nickel decreases the rate of σ- phase precipitation. Sigma and χ reduce the ductility of the 29Cr-4Mo-2Ni alloys but do not cause it to undergo intergranular corrosion. However, long-term aging at 815 °C (1500 °F) did render them susceptible to crevice corrosion in 10% hydrated ferric chloride ($FeCl_3 \cdot 6H_2O$) at 50 °C (120 °F). In this case, the ferrite was preferentially attacked, perhaps because it was depleted in chromium and molybdenum by precipitation of the second phase.

There is some evidence that the invisible χ or σ phase may affect the properties of stabilized 18Cr-2Mo ferritic stainless steels aged at approximately 620 °C (1150 °F). For example, it was shown that aging for even relatively short times could produce extensive intergranular corrosion in 18Cr-2Mo-Ti steels exposed to boiling 50% H_2SO_4 + $Fe_2(SO_4)_3$ (Ref 35). The steels were not subject to intergranular attack in 10% HNO_3 + 3% hydrofluoric acid (HF) or in boiling 16% H_2SO_4 + 6% $CuSO_4$ + Cu, and both of these solutions are known to produce intergranular attack in improperly stabilized ferritic stainless steels. Similar behavior has been noted in niobium-stabilized 18Cr-2Mo steels (Ref 36). In neither case was χ or σ phase clearly present at the grain boundaries.

References cited in this section

4. "Standard Practices for Detecting Susceptibility to Intergranular Attack in Austenitic Stainless Steels," A 262, *Annual Book of ASTM Standards,* American Society for Testing and Materials

18. A.P. Bond, *Trans. Metall. Soc. AIME,* Vol 245, 1969, p 2127–2134

19. M.A. Streicher, *Corrosion,* Vol 29, 1973, p 337–360

20. R.F. Steigerwald, *Metalloved. Term. Obrab. Met.,* No. 7, 1973, p 16–20

21. D. Van Rooyen, *Corrosion,* Vol 31, 1975, p 327–337

22. R.J. Hodges, *Corrosion,* Vol 27, 1971, p 119–127, 164–167

23. C.R. Rarey and A.H. Aronson, *Corrosion,* Vol 28, 1972, p 255–258

24. A.P. Bond and E.A. Lizlovs, *J. Electrochem. Soc.,* Vol 116, 1969, p 1306–1311

25. H.J. Dundas and A.P. Bond, in *Intergranular Corrosion of Stainless Alloys,* STP 656, R.F. Steigerwald, Ed., American Society for Testing and Materials, 1978, p 154–178

26. "Standard Practices for Detecting Susceptibility to Intergranular Attack in Ferritic Stainless Steels," A 763, *Annual Book of ASTM Standards,* American Society for Testing and Materials

27. E.A. Baelecken, W.A. Fischer, and K. Lorenz, *Stahl Eisen,* Vol 81, 1961, p 768–778

28. A.E. Nehrenberg and P. Lillys, *Trans. ASM,* Vol 46, 1954, p 1176–1213

29. A.J. Lena, R.A. Lula, and G.C. Kiefer, *Trans. ASM,* Vol 46, 1954, p 1203–1205

30. D.C. Ludwigson and H.S. Link, in *Advances in the Technology of Stainless Steels and Related Alloys,* STP 369, American Society for Testing and Materials, 1965, p 249–310

31. R.F. Steigerwald and M.A. Streicher, “Interpretation of Potentiostatic Polarization Curves; Role of Alloy Structure and Solution Composition,” paper presented at the annual meeting, (St. Louis, MO), National Association of Corrosion Engineers, 1967

32. J.G. McMullin, S.F. Reiter, and D.G. Ebeling, *Trans. ASM,* Vol 46, 1954, p 799–811

33. M.A. Streicher, *Corrosion,* Vol 30, 1974, p 115–125

34. A.J. Lena, *Met. Prog.,* Vol 66 (No. 1), 1954, p 86–90

35. E.A. Lizlovs and A.P. Bond, *J. Electrochem. Soc.,* Vol 122, 1975, p 589–593

36. H. Ogawa, Nippon Steel Corporation, unpublished research, 1974

J.D. Fritz, Effects of Metallurgical Variables on the Corrosion of Stainless Steels, *Corrosion: Fundamentals, Testing, and Protection*, Vol 13A, *ASM Handbook*, ASM International, 2003, p 266–274

Effects of Metallurgical Variables on the Corrosion of Stainless Steels

James D. Fritz, TMR Stainless

Duplex Stainless Steels

Duplex stainless steels are those that are composed of a mixture of austenite and ferrite, most typically with each phase in the range of 25 to 75%. The common wrought austenitic stainless steels, such as types 304 and 316, are usually balanced to contain approximately 5% ferrite to facilitate welding, but this level would not be sufficient for the steel to be classified as a duplex stainless steel. The common cast stainless steels, such as CF-8 and CF-8M, are mostly austenite with some ferrite, perhaps 10 to 15% to aid in avoiding hot cracking during solidification, but these steels also would not typically be called duplex stainless steels. These steels are often considered to be simple analogs of wrought alloys with similar compositions; however, they do not always have the same response to heat treatment. The corrosion evaluation of these alloys deserves further study.

Wrought duplex stainless steel may have either a ferrite matrix (type 329) or an austenitic matrix (U50). The most common duplex alloys, such as 2205, typically contain 50 to 60% austenite in a ferrite matrix. The modern alloys are produced with low carbon contents, usually less than 0.03%, and intergranular corrosion resulting from carbide precipitation generally has not been a practical problem.

These alloys are usually high in chromium (22 to 27%) and molybdenum (2 to 4%). As a result, these alloys are prone to the formation of intermetallic phases such as σ and χ if they are not cooled rapidly through the 900 to 700 °C (1650 to 1290 °F) range (Ref 37). Although these intermetallic compounds do degrade the corrosion resistance of the alloys, they have a more drastic effect on the mechanical properties, particularly the impact properties. If a duplex alloy has satisfactory impact properties, it probably will not experience reduced corrosion resistance. In both wrought and cast duplex stainless steel alloys, it appears that the high rate of diffusion of chromium in the ferrite phase generally minimizes depleted zones and, therefore, intergranular corrosion.

Testing for the Presence of σ/χ Phases. Because of the necessity of avoiding detrimental intermetallic phases in duplex stainless steel, standard test methods have been developed to detect their presence in wrought products. The ASTM A 923 specification (Ref 38) covers test procedures for wrought 2205 material (S31803 and S32205) and for 2507 (S32750). This specification includes a sodium hydroxide etch test for rapid screening of material as well as a Charpy impact test and a ferric chloride corrosion test for detecting the presence of σ/χ phase.

References cited in this section

37. H.D. Solomon and T.M. Devine, Paper 8201-089, presented at the ASM Metals Congress, (St. Louis, MO), American Society for Metals, 1982

38. "Standard Test Method for Detecting Detrimental Intermetallic Phase in Wrought Duplex Austenitic/Ferritic Stainless Steels," A 923, *Annual Book of ASTM Standards,* ASTM

J.D. Fritz, Effects of Metallurgical Variables on the Corrosion of Stainless Steels, *Corrosion: Fundamentals, Testing, and Protection*, Vol 13A, *ASM Handbook*, ASM International, 2003, p 266–274

Effects of Metallurgical Variables on the Corrosion of Stainless Steels

James D. Fritz, TMR Stainless

High-Performance Stainless Steels

In the 1980s and 1990s, more highly alloyed grades of austenitic, ferritic, and duplex stainless steel were developed. These grades provide improved corrosion resistance and higher strength levels compared to commodity grades such as type 304 and 316 stainless steels. Although the terms *superaustenitic, superferritic,* and *superduplex* are often used to describe these alloys, there is no universally accepted definition for a "super" stainless steel.

The relative resistance of a stainless steel to chloride pitting and crevice corrosion can be related to an alloy composition by an empirical formula called the pitting resistance equivalent number (PREN). Over the years, various PREN expressions have been presented (Ref 47, 48, 49, 50, 51), but the most commonly used expression is:

$$\text{PREN} = \%\text{Cr} + 3.3[\%\text{Mo} + 0.5\ (\%\text{W})] + x \cdot \%\text{N} \quad \text{(Eq 2)}$$

where x is typically given as either 16 or 30, and composition is weight percent.

The choice of either 16 or 30 for the nitrogen coefficient is generally based on personnel preference. A systematic investigation (Ref 52) of the correlation between various PREN formulas and the critical pitting temperature revealed that all formulas show comparable correlation with a slight tendency towards decreased correlation with the higher nitrogen coefficients.

A grade is generally designated as a super stainless steel if its PREN approaches 40 or more. Some of the more common wrought austenitic, ferritic, and duplex stainless steels that fall into this category are presented in Tables 5, 6, 7, respectively.

Table 5 Chemical compositions of wrought high-performance austenitic stainless steels

Name	UNS number	Composition, wt%							PREN[b]
		C[a]	N	Cr	Ni	Mo	Cu	Other	
20 Mo-6	N08026	0.03	0.10–0.16	22.0–26.0	33.0–37.0	5.0–6.7	2.0–4.0	…	40
Conifer 1925hMo	N08926	0.02	0.15–0.25	19.0–21.0	24.0–26.0	6.0–7.0	0.50–1.50	…	41
Uranus SB8	N08932	0.020	0.17–0.25	24.0–26.0	24.0–26.0	4.7–5.7	1.0–2.0	…	42
254 SMO	S31254	0.02	0.18–0.22	19.5–20.5	17.5–18.5	6.0–6.5	0.50–1.00	…	42
AL-6XN	N08367	0.03	0.18–	20.0–	23.5–	6.0–	0.75	…	43

			0.25	22.0	25.5	7.0			
Nirosta 4565S	S24565	0.03	0.40–0.60	23.0–25.0	16.0–18.0	3.5–5.0	…	Mn 3.5–6.5	41
Nicrofer 3127hMo	N08031	0.02	0.15–0.25	26.0–28.0	30.0–32.0	6.0–7.0	1.0–1.4	…	48
654 SMO	S32654	0.02	0.45–0.55	24.0–26.0	21.0–23.0	7.0–8.0	0.30–0.60	Mn 2.0–4.0	54

UNS, Unified Numbering System; PREN, pitting resistance equivalent number. The Si, P, and S ranges are not presented.
(a) Maximum composition.
(b) Calculated using nominal composition and PREN = %Cr + 3.3 [%Mo + 0.5 (%W)] + 16(%N)

Table 6 Chemical compositions of wrought high-performance ferritic stainless steels

Name	UNS number	Composition, wt%							PREN(b)
		C(a)	**N(a)**	**Cr**	**Ni**	**Mo**	**Cu(a)**	**Other**	
E-Brite 26-1	S44627	0.010	0.015	25.0–27.0	0.50	0.75–1.50	0.20	Nb 0.05–0.2	27
Monit	S44635	0.025	0.035	24.5–26.0	3.5–4.5	3.5–4.5	…	Ti, Nb	36
Sea-cure	S44660	0.030	0.040	25.0–28.0	1.0–3.5	3.0–4.0	…	Ti, Nb	35
AL 29-4C	S44735	0.030	0.045	28.0–30.0	1.00	3.6–4.2	…	Ti	40

UNS, Unified Numbering System; PREN, pitting resistance equivalent number. The Si, P, and S ranges are not presented.
(a) Maximum composition.
(b) Calculated using nominal composition and PREN = %Cr + 3.3 [%Mo + 0.5 (%W)]

Table 7 Chemical compositions of wrought high-performance duplex stainless steels

Name	UNS number	Composition, wt%							PREN(b)
		C(a)	**N**	**Cr**	**Ni**	**Mo**	**Cu**	**Other**	
7-Mo Plus	S32950	0.03	0.15–0.35	26.0–29.0	3.5–5.2	1.0–2.5	…	…	32
DP3	S31260	0.03	0.10–0.30	24.0–26.0	5.5–7.5	2.5–3.5	0.20–0.80	W 0.1–0.5	34
47N	…	0.03	0.14–0.20	24.0–26.0	5.5–7.5	2.5–3.5	…	…	34
255	S32550	0.04	0.10–0.25	24.0–27.0	4.5–6.5	2.9–3.9	1.5–2.5	…	35
DP3W	S39274	0.03	0.24–0.32	24.0–26.0	6.0–8.0	2.5–3.5	0.20–0.80	W 1.5–2.5	36
100	S32760	0.03	0.20–0.30	24.0–26.0	6.0–8.0	3.0–4.0	0.5–1.0	W 0.5–1.0	37
52N+	S32520	0.03	0.20–0.35	24.0–26.0	5.5–8.0	3.0–5.0	0.5–3.0	…	37
2507	S32750	0.03	0.24–0.32	24.0–26.0	6.0–8.0	3.0–5.0	0.50	…	38

UNS, Unified Numbering System; PREN, pitting resistance equivalent number. The Si, P, and S ranges are not presented.
(a) Maximum composition.
(b) Calculated using nominal composition and PREN = %Cr + 3.3 [%Mo + 0.5 (%W)] + 16 (%N)

Although these grades exhibit outstanding corrosion resistance, the high alloying content makes them susceptible to the formation of detrimental secondary phases. Table 8 lists the secondary phases that have been found in high-performance stainless steels. These phases can be classified as carbides, nitrides, or intermetallic compounds. High-performance stainless steels, in general, have low carbon levels, and the ferritic grades are

stabilized with titanium and/or niobium additions. Because of this, chromium carbide sensitization is generally not a concern. The most important phase in terms of its effect on corrosion resistance is σ and, to a lesser extent, the χ phase. These phases form over the same temperature range, approximately 550 to 1050 °C (1020 to 1920 °F), and have similar formation kinetics. Because of this, the precipitation of the χ phase is often concurrent with σ but usually in a much smaller volume fraction. As with σ phase, the formation of χ results in reduced corrosion resistance and loss of ductility and toughness. It is important to note the high solubility of nitrogen in the austenitic and duplex stainless steels. It is the effect of nitrogen delaying the precipitation of intermetallic phases that has allowed these highly alloyed stainless steels to see practical application, including regular use in the as-welded condition in highly corrosive environments.

Table 8 Secondary phases in high-performance stainless steels

Stainless steels[(a)]	Phase	Symbol	Type	Formula	Temperature range[(b)]	
					°C	**°F**
D	Chromium carbide	…	M_7C_3	$(Cr,Fe,Mo)_7C_3$	950–1050	1740–1920
A,D,F	Chromium carbide	…	$M_{23}C_6$	$(Cr,Fe,Mo)_{23}C_6$	600–950	1110–1740
A,D,F	Chromium carbide	…	M_6C	$(Cr,Fe,MoNb)_6C$	700–950	1290–1740
D,F	Chromium nitride	…	M_2N	$(Cr,Fe)_2N$	650–950	1200–1740
D	Chromium nitride	…	MN	CrN	…	…
D	Fe-Mo nitride	…	M_5N	$Fe_7Mo_{13}N_4$	550–600	1020–1110
A	Nb-Cr nitride	Z	MN	(NbCr)N	700–1000	1290–1830
F	Titanium carbonitride	…	MC	Ti(CN)	700 m.p.	1290 m.p.
F	Niobium carbonitride	…	MC	Nb(CN)	700 m.p.	1290 m.p.
A,D,F	Sigma	σ	AB	(Fe,Cr,Mo,Ni)	550–1050	1020–1920
A,D,F	Chi	χ	$A_{48}B_{10}$	$Fe_{36}Cr_{12}Mo_{10}$ $(FeNi)_{36}Cr_{18}(TiMo)_4$	600–900	1110–1650
D,F	Alpha prime	α′	…	CrFe(Cr 61–83%)	350–550	660–1020
A,D,F	Laves	η	A_2B	$(FeCr)_2(Mo,Nb,Ti,Si)$	550–900	1020–1650
D,F	R	R	…	(Fe,Mo,Cr,Ni)	550–650	1020–1200
D	Tau	τ	…	…	550–650	1020–1200

R, R intermetallic phase.
(a) Type code: A = austenitic, D = duplex, F = ferritic.
(b) m.p., melting point. Source: Ref 39

The high-performance ferritic and duplex grades are also vulnerable to alpha-prime (α′) precipitation in the temperature range of 350 to 550 °C (660 to 1020 °F). This chromium-rich phase does not have a large impact on the corrosion resistance, but its formation can result in a substantial loss of toughness. This phenomenon has been termed 475 °C (885 °F) embrittlement.

The kinetics of the σ and χ transformations are dependent on the alloy composition. Higher chromium and molybdenum contents favor higher rates of formation and potentially larger volume fractions. Nitrogen

additions in austenitic and duplex steels retard the transformation reactions. Because of this, the tendency to form these detrimental phases can vary substantially from alloy to alloy as well as within a specific grade, depending on the composition of the alloy. A summary of the isothermal precipitation kinetics of important phases in some specific high-performance austenitic, ferritic, and duplex stainless steels is shown in Fig. 4, 5, and 6, respectively. These time-temperature-precipitation diagrams show that the σ/χ precipitation kinetics can be quite rapid, in the 800 to 900 °C (1475 to 1650 °F) temperature range. Because of this, temperature excursions and cooling rates must be designed to avoid the precipitation of these undesirable phases. If undesirable phases are present, they can be redissolved and the corrosion and toughness properties restored by a solution anneal heat treatment.

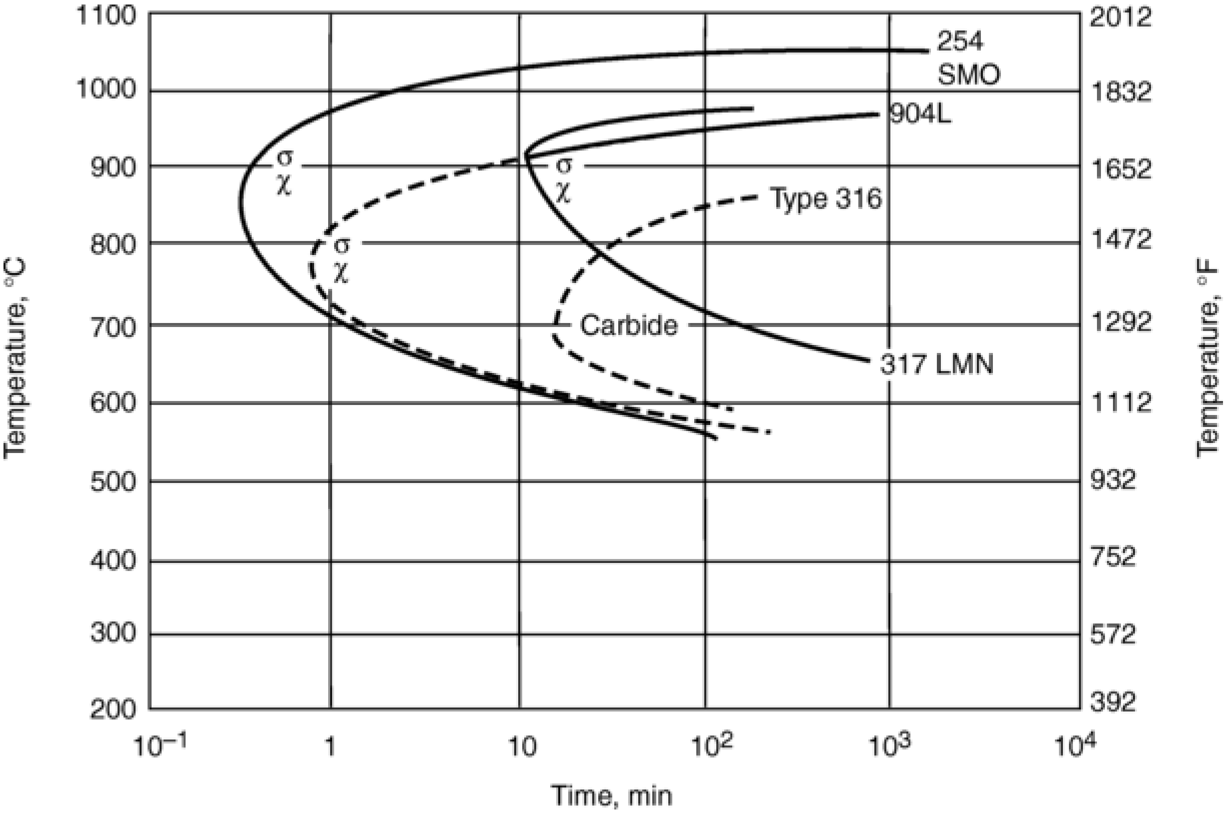

Fig. 4 Isothermal precipitation kinetics for detrimental σ/χ phases for the 254 SMO (S31254), 904L, and 317 LMN alloys. For comparison, the isothermal stability curve for the formation of chromium carbide in type 316 stainless steel is presented. Source: Ref 39

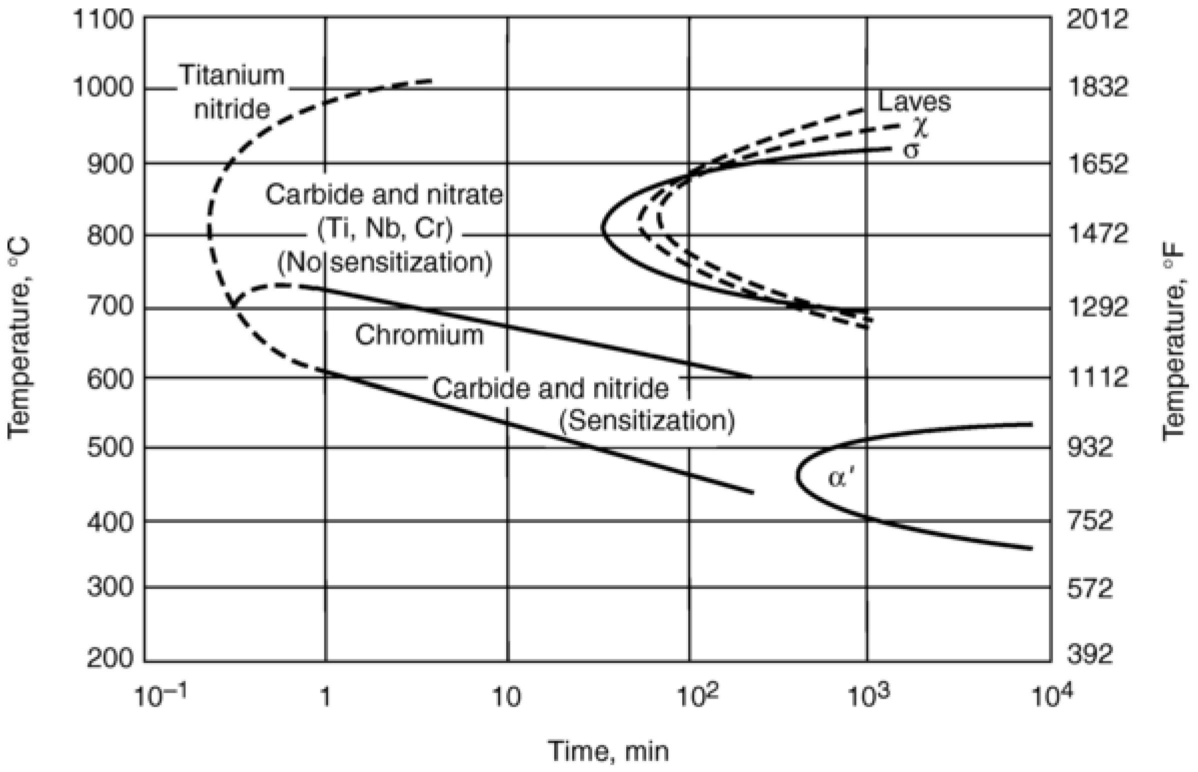

Fig. 5 Isothermal precipitation kinetics for carbides, nitrides, σ/χ, and α′ phases in ferritic alloys containing 26% Cr, 1–4% Mo, and 0–4% Ni. Source: Ref 39

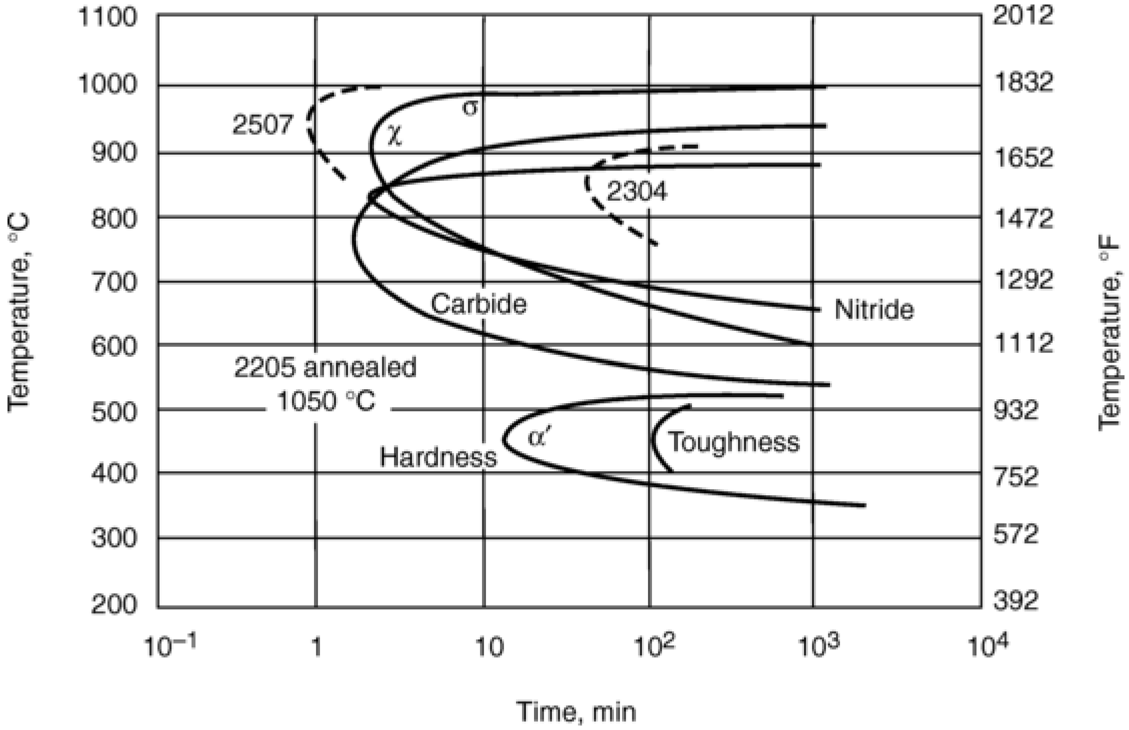

Fig. 6 Isothermal precipitation kinetics of carbides, σ/χ, and α′ phases in 2304, 2205, and 2507 duplex stainless steels. Source: Ref 39

The presence of σ/χ formation can have a strong impact on the resistance of stainless steel to localized chloride attack. The effects of isothermal heat treatments in the temperature range of 550 to 1050 °C (1020 to 1920 °F) on the critical pitting and critical crevice corrosion temperatures of Unified Numbering System (UNS) N08367 alloy have been investigated (Ref 40). The resulting isocritical pitting temperature and isocritical crevice temperature curves are summarized in Fig. 7 and 8, respectively.

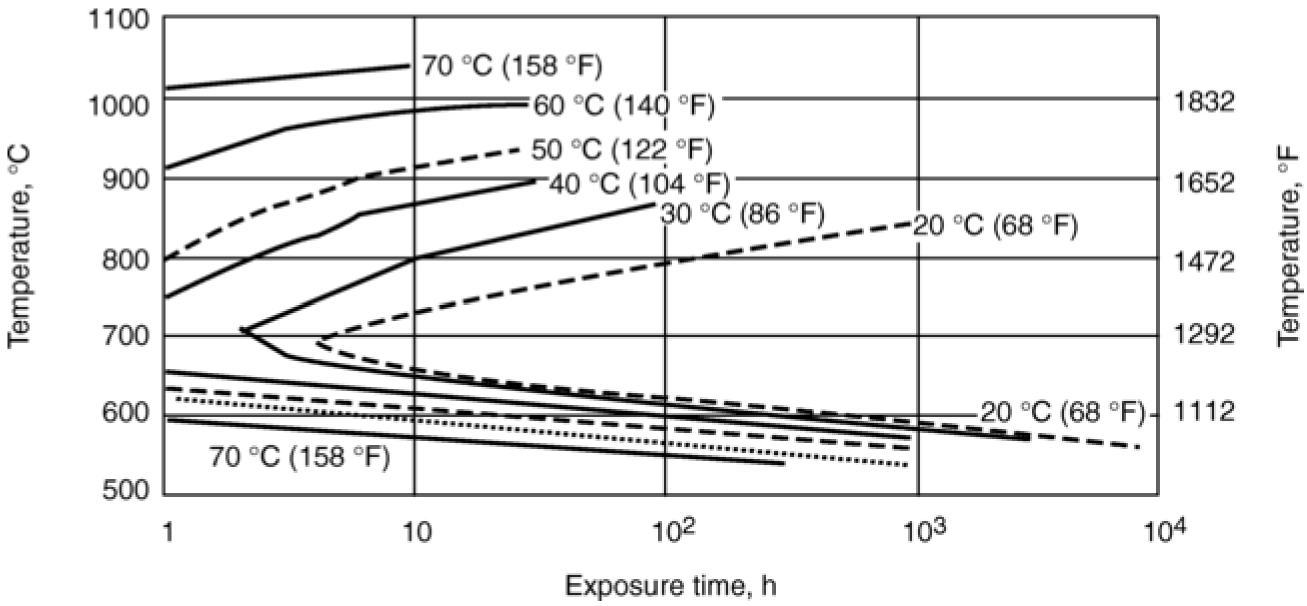

Fig. 7 Isocritical pitting temperature curves measured with the AL-6XN (N08367) alloy in 6% ferric chloride. Source: Ref 40

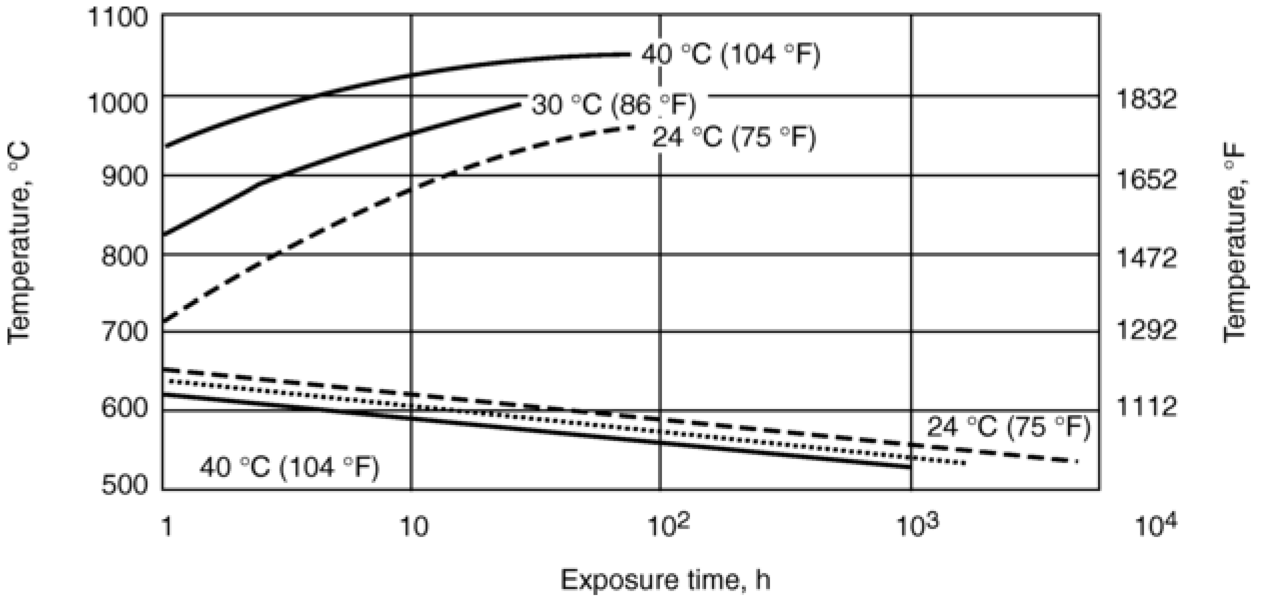

Fig. 8 Isocritical crevice corrosion temperature curves measured with the AL-6XN (N08367) alloy in 6% ferric chloride. Source: Ref 40

Similar drops in the critical pitting and critical crevice corrosion temperatures measured with 25% Cr superduplex stainless steels have been reported (Ref 41, 42). With ferritic stainless steels, the precipitation of σ/χ phase produces a loss of corrosion resistance (Ref 43). However, the loss of corrosion properties with ferritic stainless steels is usually of secondary concern compared to the loss in toughness. The change in the room-temperature impact properties of the UNS S44735 alloy after various isothermal anneals is given in Fig. 9. This plot shows a substantial loss of toughness in the 315 to 538 °C (600 to 1000 °F) range and the 593 to 900 °C (1100 to 1650 °F) range due to the formation of α′ and σ, respectively.

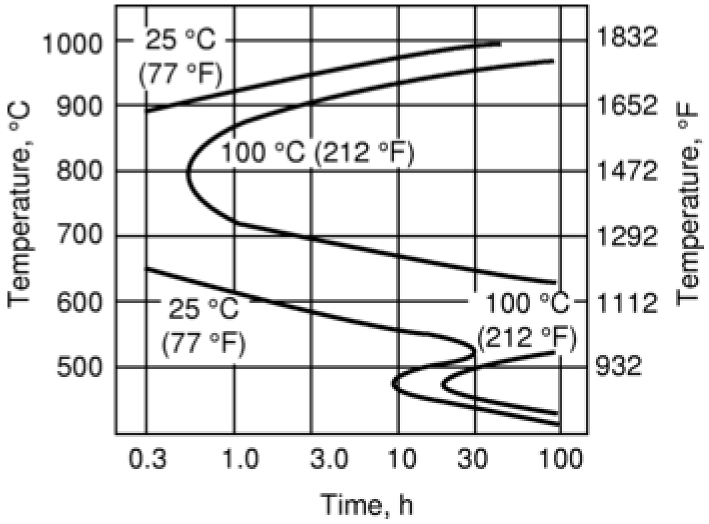

Fig. 9 Impact embrittlement behavior of a 29% Cr-4% Mo ferritic alloy measured at 25 and 100 °C (77 and 212 °F) with Charpy V-notch specimens. Curves indicate where specimens demonstrated a 50% brittle fracture surface. Isofracture appearance transition temperature profiles. Source: Ref 43

References cited in this section

39. *High-Performance Stainless Steels,* Reference Book Series 11 021, Nickel Development Institute

40. J.F. Grubb, High-Temperature Aging of 6% Mo Superaustenitic Stainless Steel, *Proceedings of Stainless Steel 96,* (Dusseldorf), Verein Deutscher Eisenhuttenleute, 1996

41. R.N. Gunn, “Effects of Thermal Cycles on the Properties of 25% Cr Duplex Stainless Steel Plates—Preliminary Studies,” Technology Briefing 505/1995, TWI, April 1995

42. M.E. Wilms, V.J. Gadgh, J.M. Krougman, and F.P. Ijsseling, The Effect of σ-Phase Precipitation at 800 °C on the Corrosion Resistance in Sea-Water of a High Alloyed Duplex Stainless Steel, *Corros. Sci.,* Vol 36 (No. 5), 1994, p 871

43. G. Aggen, H.E. Deverell, and T.T. Nichol, in *Microstructures Versus Properties of 29- 4 Ferritic Stainless Steel,* STP 672, American Society for Testing and Materials, 1979, p 334

47. M. Renner, U. Heubner, M.U. Rockel, and E. Wallis, *Werkst. Korros.*, Vol 37, 1986, p 183–190

48. N. Suutala and M. Kurkela, *Proc. of Stainless Steels '84* (Gothenburg), Chalmers University of Technology and Jernkontoret (Sweden) and The Metals Society (United Kingdom), 1984, p 240–247

49. J.E. Truman, *Proc. of UK Corrosion 1987,* Brighton, 1987, p 111–129

50. T. Kitada, Y. Kobayashi, M. Tsuji, T. Taira, K. Ume, and M. Ito, *Nippon Kokan Tech. Rep.* (Overseas), No. 51, 1987, p 37–45

51. G. Herbsleb, *Werkst. Korros.,* Vol 33, 1982, p 334–340

52. E. Alfonsson and R. Qvarfort, *Avesta Corrosion Management,* ACOM No. 1-92, 1992

J.D. Fritz, Effects of Metallurgical Variables on the Corrosion of Stainless Steels, *Corrosion: Fundamentals, Testing, and Protection*, Vol 13A, *ASM Handbook*, ASM International, 2003, p 266–274

Effects of Metallurgical Variables on the Corrosion of Stainless Steels

James D. Fritz, TMR Stainless

References

1. R.F. Steigerwald, *Metall. Trans.*, Vol 5, 1974, p 2265–2269
2. W.F. Savage, *Weld. Des. Eng.*, Dec 1969
3. M.A. Streicher, in *Intergranular Corrosion of Stainless Alloys*, STP 656, R.F. Steigerwald, Ed., American Society for Testing and Materials, 1978, p 3–84
4. “Standard Practices for Detecting Susceptibility to Intergranular Attack in Austenitic Stainless Steels,” A 262, *Annual Book of ASTM Standards,* American Society for Testing and Materials
5. W.L. Clarke, R.L. Cowan, and W.L. Walker, in *Intergranular Corrosion of Stainless Alloys,* STP 656, R.F. Steigerwald, Ed., American Society for Testing and Materials, 1978, p 99–132
6. M. Akashi, T. Kawomoto, and F. Umemura, *Corros. Eng.,* Vol 29, 1980
7. A.P. Majidi and M.A. Steicher, *Corrosion,* Vol 40 (No. 11), 1984, p 584
8. A.P. Majidi and M.A. Steicher, *Electrochemical Techniques for Corrosion Engineering,* R. Baboian, Ed., NACE, 1986, p 217
9. S. Frangini and A. Mignone, *Corrosion,* Vol 48 (No. 9), 1992, p 715
10. J.P. Sydow, D.L. Reichert, and G.E. Stoner, *Mater. Perform.,* Vol 1, 1991, p 68
11. J.F. Grubb and J.D. Fritz, “Comparison of the Double-Loop EPR Test with ASTM A 262 B,” Paper 185, Corrosion 97, NACE International, 1997
12. “Standard Test Method for Electrochemical Reactivation (EPR) for Detecting Sensitization of AISI Type 304 and 304L Stainless Steels,” G 108, *Annual Book of ASTM Standards,* ASTM
13. A. Dravnieks and C.H. Samans, *Proc. API,* Vol 37 (No. 3), 1957, p 100
14. R.C. Scarberry, S.C. Pearman, and J.R. Crum, *Corrosion,* Vol 32, 1976, p 401–406
15. J.D. Fritz and B.W. Parks, Jr., “The Influence of Martensite on the Corrosion Resistance of Austenite Stainless Steels,” Paper 00507, Corrosion 2000, NACE International, 2000
16. D. Warren, *Corrosion,* Vol 15, 1959, p 213t–220t
17. M.A. Streicher, *J. Electrochem. Soc.,* Vol 106, 1959, p 161–180
18. A.P. Bond, *Trans. Metall. Soc. AIME,* Vol 245, 1969, p 2127–2134

19. M.A. Streicher, *Corrosion,* Vol 29, 1973, p 337–360

20. R.F. Steigerwald, *Metalloved. Term. Obrab. Met.,* No. 7, 1973, p 16–20

21. D. Van Rooyen, *Corrosion,* Vol 31, 1975, p 327–337

22. R.J. Hodges, *Corrosion,* Vol 27, 1971, p 119–127, 164–167

23. C.R. Rarey and A.H. Aronson, *Corrosion,* Vol 28, 1972, p 255–258

24. A.P. Bond and E.A. Lizlovs, *J. Electrochem. Soc.,* Vol 116, 1969, p 1306–1311

25. H.J. Dundas and A.P. Bond, in *Intergranular Corrosion of Stainless Alloys,* STP 656, R.F. Steigerwald, Ed., American Society for Testing and Materials, 1978, p 154–178

26. "Standard Practices for Detecting Susceptibility to Intergranular Attack in Ferritic Stainless Steels," A 763, *Annual Book of ASTM Standards,* American Society for Testing and Materials

27. E.A. Baelecken, W.A. Fischer, and K. Lorenz, *Stahl Eisen,* Vol 81, 1961, p 768–778

28. A.E. Nehrenberg and P. Lillys, *Trans. ASM,* Vol 46, 1954, p 1176–1213

29. A.J. Lena, R.A. Lula, and G.C. Kiefer, *Trans. ASM,* Vol 46, 1954, p 1203–1205

30. D.C. Ludwigson and H.S. Link, in *Advances in the Technology of Stainless Steels and Related Alloys,* STP 369, American Society for Testing and Materials, 1965, p 249–310

31. R.F. Steigerwald and M.A. Streicher, "Interpretation of Potentiostatic Polarization Curves; Role of Alloy Structure and Solution Composition," paper presented at the annual meeting, (St. Louis, MO), National Association of Corrosion Engineers, 1967

32. J.G. McMullin, S.F. Reiter, and D.G. Ebeling, *Trans. ASM,* Vol 46, 1954, p 799–811

33. M.A. Streicher, *Corrosion,* Vol 30, 1974, p 115–125

34. A.J. Lena, *Met. Prog.,* Vol 66 (No. 1), 1954, p 86–90

35. E.A. Lizlovs and A.P. Bond, *J. Electrochem. Soc.,* Vol 122, 1975, p 589–593

36. H. Ogawa, Nippon Steel Corporation, unpublished research, 1974

37. H.D. Solomon and T.M. Devine, Paper 8201-089, presented at the ASM Metals Congress, (St. Louis, MO), American Society for Metals, 1982

38. "Standard Test Method for Detecting Detrimental Intermetallic Phase in Wrought Duplex Austenitic/Ferritic Stainless Steels," A 923, *Annual Book of ASTM Standards,* ASTM

39. *High-Performance Stainless Steels,* Reference Book Series 11 021, Nickel Development Institute

40. J.F. Grubb, High-Temperature Aging of 6% Mo Superaustenitic Stainless Steel, *Proceedings of Stainless Steel 96,* (Dusseldorf), Verein Deutscher Eisenhuttenleute, 1996

41. R.N. Gunn, "Effects of Thermal Cycles on the Properties of 25% Cr Duplex Stainless Steel Plates—Preliminary Studies," Technology Briefing 505/1995, TWI, April 1995

42. M.E. Wilms, V.J. Gadgh, J.M. Krougman, and F.P. Ijsseling, The Effect of σ-Phase Precipitation at 800 °C on the Corrosion Resistance in Sea-Water of a High Alloyed Duplex Stainless Steel, *Corros. Sci.,* Vol 36 (No. 5), 1994, p 871

43. G. Aggen, H.E. Deverell, and T.T. Nichol, in *Microstructures Versus Properties of 29- 4 Ferritic Stainless Steel,* STP 672, American Society for Testing and Materials, 1979, p 334

44. B.M. Gordon, *Mater. Perform.,* Vol 19, 1980, p 29

45. G.S. Was and P.L. Andresen, *J. Met.,* Vol 44 (No. 4), 1992, p 8

46. P.M. Scott, *Corros. Sci.,* Vol 25 (No. 8–9), 1985, p 583

47. M. Renner, U. Heubner, M.U. Rockel, and E. Wallis, *Werkst. Korros.,* Vol 37, 1986, p 183–190

48. N. Suutala and M. Kurkela, *Proc. of Stainless Steels '84* (Gothenburg), Chalmers University of Technology and Jernkontoret (Sweden) and The Metals Society (United Kingdom), 1984, p 240–247

49. J.E. Truman, *Proc. of UK Corrosion 1987,* Brighton, 1987, p 111–129

50. T. Kitada, Y. Kobayashi, M. Tsuji, T. Taira, K. Ume, and M. Ito, *Nippon Kokan Tech. Rep.* (Overseas), No. 51, 1987, p 37–45

51. G. Herbsleb, *Werkst. Korros.,* Vol 33, 1982, p 334–340

52. E. Alfonsson and R. Qvarfort, *Avesta Corrosion Management,* ACOM No. 1-92, 1992

J.D. Fritz, Effects of Metallurgical Variables on the Corrosion of Stainless Steels, *Corrosion: Fundamentals, Testing, and Protection*, Vol 13A, *ASM Handbook*, ASM International, 2003, p 266–274

Effects of Metallurgical Variables on the Corrosion of Stainless Steels

James D. Fritz, TMR Stainless

Selected References

- *High-Performance Stainless Steels,* Reference Book Series No 11 021, Nickel Development Institute
- *Intergranular Corrosion of Stainless Alloys,* STP 656, ASTM, 1978
- R.W. Revie, *Uhlig's Corrosion Handbook, 2nd ed.,* Wiley-Interscience Publication, 2000, p 601–678
- A.J. Sedriks, *Corrosion of Stainless Steels,* 2nd ed., Wiley-Interscience Publication, 1996

J. Moran, Effects of Metallurgical Variables on the Corrosion of Aluminum Alloys, *Corrosion: Fundamentals, Testing, and Protection*, Vol 13A, *ASM Handbook*, ASM International, 2003, p 275–278

Effects of Metallurgical Variables on the Corrosion of Aluminum Alloys

Jim Moran, Alcoa

Introduction

THE METALLURGICAL EFFECTS on corrosion of aluminum can be classified into two categories. In the first category are effects from insoluble, intermetallic constituent particles. These can be formed from trace impurity elements, most notably iron, and/or from purposely added alloying elements such as Al-Cu-Mg constituents in 2*xxx* alloys. In this context the term *insoluble* can refer to "thermodynamically insoluble," as is the case for most Al-Fe-X particles, or to "commercially insoluble," in that the kinetics of dissolution are too sluggish to dissolve the particles during nominal thermal practices in production, as is the case for Al-Cu-Mg constituents in 2*xxx* alloys. The constituent particles play a predominant role in pitting corrosion. In the second general category are effects from precipitation of secondary phases, usually as a result of a controlled thermal process such as age hardening. This includes both intergranular and intragranular precipitation, as well as effects from solute remaining in solid solution.

Also see the article "Corrosion Resistance of Aluminum Alloys" in this Volume.

J. Moran, Effects of Metallurgical Variables on the Corrosion of Aluminum Alloys, *Corrosion: Fundamentals, Testing, and Protection*, Vol 13A, *ASM Handbook*, ASM International, 2003, p 275–278

Effects of Metallurgical Variables on the Corrosion of Aluminum Alloys

Jim Moran, Alcoa

Effect of Constituent Particles on Pitting Corrosion of Aluminum

In the commercial production of aluminum ingot and billet, some trace amount of impurities is incorporated into the alloy (Ref 1, 2, 3). Iron is common. Iron has an exceptionally low solubility in aluminum and precipitates out during ingot solidification in the form of various insoluble intermetallic phases, commonly referred to as constituent particles. These particles are on the order of a few microns to a few tens of microns in size and have various compositions, depending on the iron level and alloying elements. Commonly identified compositions include Al_3Fe, Al_7Cu_2Fe, and various other Al_x(Fe, Cu, Mn) type compounds. Other constituents are alloy specific. For example, alloy 2024 (Al-Cu-Mg) contains relatively large (on the same order of magnitude as the iron-bearing constituent particles) S-phase (Al_2CuMg) particles. Although these particles are thermodynamically soluble during solution heat treatment, the kinetics are insufficient for complete dissolution. Hence, the particles are present even after solution heat treatments, such as for T3 and T4 tempers.

Constituent particles are well known sites for pit initiation, due to galvanic interaction with the surrounding matrix (Ref 4, 5, 6, 7). Depending on initial composition, some constituent particles are cathodic to the matrix, and others are anodic. Some exhibit a changing galvanic effect as the corrosion process ensues. A compilation of the corrosion potentials for a large number of aluminum-based constituent particles is provided in Ref 8. These data can be used to help predict the galvanic polarity in a pit initiation event. The iron and manganese-bearing particles are considered to be cathodic to the matrix. Selective matrix dissolution surrounding the

cathodic particles promotes pit initiation. The severity of pitting is dependent on the degree of clustering of the particles (Ref 7). A region of smaller, isolated particles will promote a mild, shallow pitting attack. In a region with clustered particles, the smaller pits can link up to form larger pits. This clustering can be across the surface, or it can be subsurface, which would promote deeper pitting.

The Al-Cu-Mg particles inherent to 2*xxx* series alloys have been identified as anodic to the matrix (Ref 6). In this case the initial dissolution occurs in the particle, as opposed to the surrounding matrix. The net effect is similar, in that a pit is initiated at the location of galvanic attack. More discussion of the impact of these copper-bearing particles on corrosion performance is included in the section on 2*xxx* alloys.

While the mechanistic specifics can vary by particle type, the result is similar. The particle/ matrix interface is a site of preferential dissolution, resulting in the initiation of a pitting site.

References cited in this section

1. *Corrosion of Aluminum and Aluminum Alloys,* J.R. Davis, Ed., ASM International, 1999

2. *Aluminum: Properties and Physical Metallurgy,* J.E. Hatch, Ed., ASM International, 1984

3. Aluminum and Aluminum Alloys, *Alloying: Understanding the Basics,* J.R. Davis, Ed., ASM International, 2001, p 352–416

4. Z.S. Smialowska, Pitting Corrosion of Aluminum, *Corros. Sci.,* Vol 41, 1999, p 1743–1767

5. J.O. Park, C.H. Paik, Y.H. Huang, and R.C. Alkire, Influence of Fe-Rich Intermetallic Inclusions on Pit Initiation on Aluminum Alloys, *J. Electrochem. Soc.,* Vol 146 (No. 2), 1999, p 517–523

6. R.G. Buchheit, R.P. Grant, P.F. Hlava, B. Mckenzie, and G.L. Zender, Local Dissolution Phenomena Associated with S Phase particles in Alloy 2024, *J. Electrochem. Soc.,* Vol 144 (No. 8), 1997, p 2621–2628

7. C.M. Liao, J.M. Olive, M. Gao, and R.P. Wei, In-Situ Monitoring of Pitting Corrosion in Alloy 2024, *Corrosion,* Vol 54 (No. 6), p 451–453

8. R.G. Buchheit, A Compilation of Corrosion Potentials Reported for Intermetallic Phases in Aluminum Alloys, *J. Electrochem. Soc.,* Vol 142 (No. 11), 1995, p 3994–3996

J. Moran, Effects of Metallurgical Variables on the Corrosion of Aluminum Alloys, *Corrosion: Fundamentals, Testing, and Protection,* Vol 13A, *ASM Handbook,* ASM International, 2003, p 275–278

Effects of Metallurgical Variables on the Corrosion of Aluminum Alloys

Jim Moran, Alcoa

1*xxx* Series Alloys

These alloys are at least 99% pure aluminum. They are relatively corrosion resistant but can be susceptible to pitting, caused by Al-Fe-X constituent particles. However, the pitting severity is not great as in other alloy classes. The degree of pitting susceptibility is greater for the less pure 1*xxx* grades, such as those having greater iron content.

J. Moran, Effects of Metallurgical Variables on the Corrosion of Aluminum Alloys, *Corrosion: Fundamentals, Testing, and Protection*, Vol 13A, *ASM Handbook*, ASM International, 2003, p 275–278

Effects of Metallurgical Variables on the Corrosion of Aluminum Alloys

Jim Moran, Alcoa

2*xxx* Series Alloys

The alloying element common to all 2*xxx* alloys is copper. Several common alloys also contain magnesium and/or manganese. These alloys are precipitation hardened. After final fabrication, the alloys are solution heat treated and quenched. They are then frequently used in the as-quenched and naturally aged (room temperature) condition (T3 or T4 tempers) or artificially aged to increase strength via formation of Al- Cu(-Mg) strengthening precipitates (T6 or T8 tempers).

Similar to all aluminum alloys, constituent particles play a key role in pit initiation. In addition to the Al-Fe-*X* types of particles, 2*xxx* alloys contain Al-Cu and Al-Cu-Mg particles. The Al-Cu-Mg particles have been the subject of active research in recent years (e.g., Ref 6). These particles are initially anodic to the surrounding matrix. However, as a result of dealloying, they can become copper rich and cathodic. In either case, the galvanic interaction at the particle/matrix interface results in pit initiation.

Due to the copper content, 2*xxx* alloys tend to be more susceptible to pitting and general attack than other alloys. During dissolution of Al-Cu- Mg particles, regions of metallic copper are formed on the alloy, thereby promoting accelerated galvanic attack and increasing the pitting severity relative to non-copper-containing alloys (Ref 6). This copper can serve to initiate new pits or can assist in the propagation of already- established pits.

Depending on temper and processing specifics, the intergranular (IG) corrosion and stress- corrosion cracking (SCC) resistance of 2*xxx* alloys can vary significantly. The basic mechanism is galvanic interaction between the grain boundary region and the interior grain matrix (Ref 2, 3). Consider alloy 2024 in the solution heat treated temper (T3 or T4). If quenched too slowly, the alloy can be highly susceptible to IG corrosion. When poorly quenched, large Al- Cu(-Mg) precipitates form along the grain boundary. This produces a copper-depleted-zone along the boundaries, and a galvanic couple is then established. The copper-depleted zone is anodic with respect to the matrix, which still has considerable copper in solid solution. The boundary region is then preferentially attacked, promoting IG corrosion. When properly quenched, eliminating the precipitation of large grain boundary phases, the copper-depleted zone does not develop and IG corrosion susceptibility is low. In either case, fast or slow quench, artificial aging to peak strength greatly reduces the IG corrosion susceptibility. As the aging process ensues, copper is continually removed from solid solution to form Al-Cu(-Mg) precipitates, both intragranularly (these are the primary strengthening precipitates) and intergranularly. Sufficient copper is eventually removed from solid solution in the grain matrix such that the copper content is similar to that of the near-boundary region. Hence, the galvanic driving force is removed, and the IG corrosion susceptibility is greatly reduced.

Even in well-quenched 2024, the IG corrosion rate can be accelerated in underaged tempers. The mechanism is similar. Initially, precipitation can be favored on grain boundaries, and the galvanic process described previously ensues. Continued aging toward peak-aged eliminates this. A similar scenario exists for SCC and exfoliation corrosion. More quantitative information on acceptable quench rates and the effect of quench rate are provided in Ref 1 and 2.

The pitting behavior, on the other hand, is not significantly affected by quench rate and is only moderately affected by aging. The pitting behavior is predominantly determined by the constituent particles, as previously discussed, and these particles are not significantly affected by quench rate or aging time.

Much of the preceding discussion focuses on alloy 2024. The general trends and mechanisms are believed similar for other commercially used 2*xxx* alloys (e.g., 2014, 2008, 2036); however, the severity can differ from alloy to alloy. Pitting susceptibility is related to the copper content. Lower-copper alloys (2036, 2008) exhibit significantly better pitting resistance than higher- copper alloys, such as 2024. The variation in IG corrosion

susceptibility as a function of copper content is less pronounced. Effects of quench rate and aging time, as discussed previously, are more dominant factors in determining IG corrosion susceptibility.

References cited in this section

1. *Corrosion of Aluminum and Aluminum Alloys,* J.R. Davis, Ed., ASM International, 1999

2. *Aluminum: Properties and Physical Metallurgy,* J.E. Hatch, Ed., ASM International, 1984

3. Aluminum and Aluminum Alloys, *Alloying: Understanding the Basics,* J.R. Davis, Ed., ASM International, 2001, p 352–416

6. R.G. Buchheit, R.P. Grant, P.F. Hlava, B. Mckenzie, and G.L. Zender, Local Dissolution Phenomena Associated with S Phase particles in Alloy 2024, *J. Electrochem. Soc.,* Vol 144 (No. 8), 1997, p 2621–2628

J. Moran, Effects of Metallurgical Variables on the Corrosion of Aluminum Alloys, *Corrosion: Fundamentals, Testing, and Protection*, Vol 13A, *ASM Handbook*, ASM International, 2003, p 275–278

Effects of Metallurgical Variables on the Corrosion of Aluminum Alloys

Jim Moran, Alcoa

3*xxx* Series Alloys

The alloys in this series contain primarily manganese (<1.5%). Several also contain magnesium (<1.5%). They are strengthened by work hardening and are produced in extruded, sheet, and plate forms. These alloys offer corrosion characteristics similar to those of 1*xxx* series alloys, with perhaps a slightly better resistance to corrosion. Manganese can be incorporated into the constituent particles, which results in corrosion potential more similar to that of the matrix: hence, less galvanic driving force for pitting. These alloys are generally considered to have excellent corrosion resistance. They commonly find use in beverage and food containers, building products, heat exchanger tubing, and other general uses requiring good corrosion resistance with moderate strength.

J. Moran, Effects of Metallurgical Variables on the Corrosion of Aluminum Alloys, *Corrosion: Fundamentals, Testing, and Protection*, Vol 13A, *ASM Handbook*, ASM International, 2003, p 275–278

Effects of Metallurgical Variables on the Corrosion of Aluminum Alloys

Jim Moran, Alcoa

4*xxx* Series Alloys

The alloys in this series contain primarily silicon (<14%). Because of their low melting point characteristics, these alloys are used primarily for braze and weld filler applications. These alloys are usually produced as sheet or wire, and are found in the as-cast condition following a thermal joining process. Much of the silicon in these alloys precipitates out as elemental silicon. Although elemental silicon is highly cathodic to the aluminum

matrix, the silicon particles are easily polarized to near the potential of the matrix; hence their effect on corrosion susceptibility is minimal. However, when silicon is used in a thermal joining process, there have been cases where it has diffused into the grain boundaries of the materials being joined and caused decreased corrosion resistance.

J. Moran, Effects of Metallurgical Variables on the Corrosion of Aluminum Alloys, *Corrosion: Fundamentals, Testing, and Protection*, Vol 13A, *ASM Handbook*, ASM International, 2003, p 275–278

Effects of Metallurgical Variables on the Corrosion of Aluminum Alloys

Jim Moran, Alcoa

5*xxx* Series Alloys

The alloys in this series contain primarily magnesium (<6%). Several of the alloys also contain manganese. Alloys in this series are strengthened by work hardening and are produced primarily as sheet and plate. In general, 5*xxx* series alloys provide excellent resistance to all forms of corrosion. This accounts for their common use in a variety of applications requiring good corrosion resistance, including building products, chemical processing, and food handling. They are also alloys of choice for marine applications, including boat building. Magnesium additions generally improve the corrosion resistance in seawater.

There is one drawback to the use of 5*xxx* alloys in corrosive environments. Those alloys with greater than approximately 3% magnesium can become sensitized when exposed to moderate temperatures or after long time periods (many years) at room temperature. In this context, sensitization refers to selective precipitation of beta phase, Mg_2Al_3, along grain boundaries. Beta is highly anodic to the aluminum matrix and forms a continuous grain boundary network when exposed to moderately elevated temperatures. Once beta is formed, the material becomes highly susceptible to IG corrosion and, depending on specific alloy and grain structure, can also be rendered susceptible to exfoliation and stress- corrosion cracking (Ref 2). The time required to form a sensitized microstructure is dependent on the magnesium content, alloy temper, exposure temperature, and initial processing (Ref 2, 9). Some 5*xxx* alloys can be thermally processed to remove a significant amount of the magnesium during fabrication, thereby greatly lowering the propensity for sensitization (Ref 2, 9)

References cited in this section

2. *Aluminum: Properties and Physical Metallurgy,* J.E. Hatch, Ed., ASM International, 1984

9. E.H. Dix, W.A. Anderson, and M.B. Shumaker, Influence of Service Temperature on the Resistance of Wrought Al-Mg Alloys to Corrosion, *Corrosion,* Vol 15, 1959, p 55–62

J. Moran, Effects of Metallurgical Variables on the Corrosion of Aluminum Alloys, *Corrosion: Fundamentals, Testing, and Protection*, Vol 13A, *ASM Handbook*, ASM International, 2003, p 275–278

Effects of Metallurgical Variables on the Corrosion of Aluminum Alloys

Jim Moran, Alcoa

6*xxx* Series Alloys

The alloys in this series contain primarily magnesium and silicon, some with additions of copper and/or manganese (<1.2%). These alloys are strengthened by precipitation hardening, with the primary precipitate being Mg_2Si. These alloys generally have good corrosion resistance. Those that contain copper have somewhat poorer corrosion resistance.

Similar to most commercial aluminum alloys, Al-Fe-X constituents play a dominant role in pit initiation. Most 6*xxx* alloys provide excellent resistance to pitting corrosion. Intergranular corrosion resistance can vary. Low copper alloys, such as 6061, the most common 6*xxx* alloy, with a stoichiometric balance of Mg and Si, exhibit good resistance to all forms of corrosion. Alloys with an excess of silicon (that is, more than is needed to form Mg_2Si), tend to be more susceptible to IG corrosion. The silicon segregates to the grain boundaries, producing a silicon-depleted zone along the boundaries, which is anodic to the boundary and the matrix. This produces preferential attack along the grain boundaries, similar to the mechanism discussed for copper-depleted zones in 2*xxx* alloys (Ref 1, 10, 11).

Copper is added to some 6*xxx* alloys to augment strength. Examples include 6013, 6056, and 6111. Although pitting susceptibility is only slightly worse than it is for copper-free 6*xxx* alloys, IG corrosion susceptibility can be significantly worse. The severity is dependent on copper content and temper. The general mechanism is similar to that for 2*xxx,* albeit some of the specifics are still areas of active research. In general, a copper-depleted region develops along the grain boundaries. Whether this is from precipitation of Al-Mg-Si-Cu phases (such as Q-phase) or copper substitution into Mg_2Si, or both, is not fully understood. In any event, the copper-depleted region is preferentially attacked by the copper-rich matrix and copper-containing boundary particles (Ref 12, 13, 14). This mechanism is similar to that considered dominant in 2*xxx* alloys. With sufficient aging, sufficient copper is removed from solid solution in the grain matrix, and the galvanic driving force is removed. Intergranular susceptibility is significantly decreased. Unlike 2*xxx* alloys, where the IG corrosion susceptibility can be decreased by artificial aging to peak strength, 6*xxx* alloys often require overaging beyond peak strength in order to significantly decrease IG corrosion susceptibility.

References cited in this section

1. *Corrosion of Aluminum and Aluminum Alloys,* J.R. Davis, Ed., ASM International, 1999

10. A. Bhattamishra and K. Lal, Influence of Aging on Corrosion Behavior of Al-Mg-Si Alloys in Chloride and Acid Media, *Z. Metallkd.,* Vol 89, 1998, p 793

11. D.O. Sprowls and R.H. Brown, Stress Corrosion Mechanisms for Aluminum Alloys, *Conf. Proc. on Fundamental Aspects of Stress Corrosion Cracking,* R.W. Staehle, Ed., National Association of Corrosion Engineers, 1967, p 466

12. T.D. Burleigh, E. Ludwiczak, and R.A. Petri, Intergranular Corrosion of an Aluminum-Magnesium-Silicon-Copper Alloy, *Corrosion,* Vol 51, 1995, p 50

13. K. Yamaguchi and K. Tohma, Effect of Zn Addition on Intergranular Corrosion Resistance of Al-Mg-Si-Cu Alloys, *Proc. Sixth International Conf. on Aluminum Alloys* (Toyohashi, Japan), Japan Institute of Light Metals, 1998, p 1657

14. T.D. Burleigh, Microscopic Investigation of the Intergranular Corrosion of Alloy 6013- T6, *The Third International Conf. on Aluminum Alloys* (Trondheim, Norway), L. Arnberg et al., Ed., 1992, p 435

J. Moran, Effects of Metallurgical Variables on the Corrosion of Aluminum Alloys, *Corrosion: Fundamentals, Testing, and Protection*, Vol 13A, *ASM Handbook*, ASM International, 2003, p 275–278

Effects of Metallurgical Variables on the Corrosion of Aluminum Alloys

Jim Moran, Alcoa

7*xxx* Series Alloys

The alloys in this series all contain zinc (<9%). In addition, nearly all of these alloys contain magnesium (<4%), and many of them contain copper (<3%). The alloys can be generally divided into two categories. The first category consists of the copper-containing, high- strength alloys (e.g., 7075, 7050, 7055). These alloys are available in various forms (sheet, plate, extrusion) and are used extensively in the aerospace industry. The second category is low- copper alloys (e.g., 7005, 7029). These alloys offer somewhat better resistance to general corrosion and pitting (due to low copper) and are used in structural applications and automotive applications such as bumpers.

The mechanisms of corrosion and environmental fracture of 7*xxx* alloys, particularly the role of the microstructure in corrosion behavior, have been studied for decades and continue to be an area of active research. An in-depth treatment of this topic is beyond the scope of this review section. Several thorough reviews of the mechanisms of environmental fracture of 7*xxx* aluminum alloys are available (Ref 11, 15, 16, 17).

High-strength, copper-containing 7*xxx* alloys are strengthened by a precipitation-hardening sequence, including solution heat treatment and quench, followed by artificial aging. The primary precipitation sequence is complex, with a series of Guinier-Preston (GP) zones and metastable phases, resulting ultimately in the equilibrium phase, M, (or η) ($MgZn_2$), and/or T ($Mg_3Zn_3Al_2$), depending on composition. Copper can also be incorporated into the precipitates (Ref 18, 19).

As in most aluminum alloys, in the 7*xxx* alloys, constituent particles play a dominant role in pit initiation. The severity of pitting is dependent on the copper content. Lower-copper alloys are somewhat less susceptible to pitting corrosion, due to the same basic mechanism previously described in detail for 2*xxx* alloys.

While the basic pitting performance and mechanism are similar to those for other aluminum alloys, the IG corrosion, exfoliation, and stress-corrosion cracking (SCC) susceptibility of this class of alloys is far more complex. The specific metallurgical features controlling the corrosion performance are equally complex. Metallurgical effects on corrosion behavior of these alloys have been studied for decades (Ref 11, 15, 16, 17) and continue to be areas of active research (Ref 19, 20, 21, 22). Much of the work is particularly focused on SCC. However, in many cases the exfoliation and IG corrosion performance will trend similarly with SCC. This is not a universal rule; there are some exceptions for commercial alloys and tempers. Here, however, the general assumption will apply unless specifically stated otherwise.

Key factors in determining the corrosion behavior are temper and copper content. The alloy class can be generalized by these two factors, with some specific deviations outlined below. First, consider the effect(s) of temper. Tempers of commercial significance include W, T6, and various overaged T7X tempers. Detailed definitions of temper designations can be found in Ref 1 and 2. A discussion of the corrosion performance of each is provided in subsequent paragraphs.

W temper refers to a material that has been solution heat treated and quenched but given no artificial aging. Given the low strength and instability of W temper, it is not commercially viable for final product. However, some manufacturing paths exploit its high formability, then age-harden to a commercially viable temper. Hence, 7*xxx* alloys can be shipped, stored, and worked in W temper. W temper can be highly susceptible to IG corrosion, exfoliation, and SCC if quenched slowly. This can occur in thin product, given an inadequate quench, or in thicker plate, where the cooling rate towards the midthickness is slow. The proposed mechanism is similar to 2*xxx* IG corrosion. Preferential precipitation at boundaries of copper-containing precipitates occurs during an inadequate quench. This promotes preferential galvanic attack in the copper-depleted regions near the boundaries.

The T6 temper, often referred to as peak-aged, indicates artificial aging to a peak strength level. Stress-corrosion cracking and exfoliation susceptibility are typically high in this temper.

Overaging to T7X tempers improves SCC and exfoliation resistance. Several T7 tempers are used commercially. T73 is significantly overaged and offers excellent resistance to SCC and exfoliation. However, there is a significant decrease in strength, relative to T6 temper. T76 temper is less overaged than T73. It is nominally defined as having higher strength than T73, good exfoliation resistance, and SCC resistance better than that of T6 but usually not as good as that of T73. The most overaged temper would be T73. The most recent T7X temper developed is T77. Products available in T77 offer good SCC and exfoliation resistance with less of a strength penalty than traditional T76 or T73 tempers. A more thorough review of the effect of temper is provided in Ref 1.

The mechanism by which overaging improves SCC and exfoliation resistance remains an area of active research. In the most general sense, there are two mechanistic categories proposed for SCC (Ref 11, 15, 16, 17). The first is anodic dissolution, which is characterized by one or more galvanic processes at or near the grain boundaries (e.g., similar to that discussed for IG corrosion in the 2*xxx* section). The second is hydrogen-assisted cracking, in which hydrogen, by one or more of several proposed mechanisms, enhances embrittlement at the crack tip, promoting mechanical fracture. There is evidence that more copper becomes incorporated into precipitates, both intragranular and intergranular, as 7*xxx* alloys are aged beyond peak age (Ref 18, 19). The role of increased copper in reducing SCC can be discussed in terms of either general mechanism (Ref 19, 20, 21, 22).

Copper content also plays a role. Consider the comparison of alloys 7075 and 7050, where 7050 has a higher copper content. For W temper, 7050 is more susceptible to IG forms of corrosion (SCC, IGC, exfoliation), than 7075. It is believed that the higher-copper alloy retains more copper in grain boundary precipitates during the quench. In T6 and T7X tempers, 7050 is less susceptible than 7075. A clear mechanism for this effect is still an area of active research. One hypothesis, based on a hydrogen embrittlement model, is that the additional copper content leads to more copper incorporation into precipitates, which in turn provides enhanced trapping of hydrogen, thereby slowing the rate of hydrogen embrittlement (Ref 21).

Low-Copper, 7*xxx* Alloys. Due to the low copper content, these 7*xxx* alloys exhibit excellent resistance to general corrosion and pitting. However, as a group, they are relatively more susceptible to SCC than higher-copper 7*xxx* alloys. Depending on composition and processing specifics, many low-copper 7*xxx* alloys have an unrecrystallized microstructure. This is beneficial to SCC resistance in applications where the dominant stresses are in the longitudinal and long transverse orientations. With proper engineering, such alloys are successfully used in commercial structural applications. Alloys that are recrystallized tend to be more susceptible to SCC. Whereas overaging improves the SCC resistance of copper-containing 7*xxx* alloys, it does not greatly improve the SCC resistance of the low-copper 7*xxx* alloys. For more information on low-copper 7*xxx* alloys, see Ref 1.

References cited in this section

1. *Corrosion of Aluminum and Aluminum Alloys,* J.R. Davis, Ed., ASM International, 1999

2. *Aluminum: Properties and Physical Metallurgy,* J.E. Hatch, Ed., ASM International, 1984

11. D.O. Sprowls and R.H. Brown, Stress Corrosion Mechanisms for Aluminum Alloys, *Conf. Proc. on Fundamental Aspects of Stress Corrosion Cracking,* R.W. Staehle, Ed., National Association of Corrosion Engineers, 1967, p 466

15. N.J.H. Holroyd, Environment-Induced Cracking of High-Strength Aluminum Alloys, *Proc. of the Fifth International Conf. on Environment-Induced Cracking,* R.P. Gangloff and M.B. Ives, Ed., NACE, 1990

16. T.D. Burleigh, Postulated Mechanisms for Stress Corrosion Cracking of Aluminum Alloys: A Review of the Literature, 1980–1989, *Corrosion,* Vol 47, 1991, p 89–98

17. M.O. Speidel and M.V. Hyatt, Stress Corrosion Cracking of High Strength Aluminum Alloys, *Adv. Corros. Sci. Technol.,* Vol 2, M.G. Fontana and R.W. Staehle, Ed., Plenum Press, 1972

18. A. Bigot, F. Danois, P. Auger, D. Blavette, and A. Reeves, Tomographic Atom Probe Study of Age Hardening Precipitation in Alloy 7050, *Mater. Sci. Forum,* Vol 217–222, 1996, p 695–700

19. T. Ramgopal, P.I. Gouma, and G.S. Frankel, Role of Grain Boundary Precipitates and SDZ on the Intergranular Corrosion of Aluminum Alloy AA7150, *Corrosion,* Vol 58, 2002, p 687

20. L.M. Young, "Microstructural Dependence of Aqueous-Environment Assisted Crack Growth and Hydrogen Uptake in Alloy 7050," Ph.D. dissertation, University of Virginia, Aug 1999

21. G.A. Young, "Hydrogen Environment Assisted Cracking of an Al-Zn-Mg(-Cu) Alloy," Ph.D. dissertation, University of Virginia, Aug 1999

22. K.R. Cooper, "Chemistry and Electrochemistry of Environment-Assisted Cracking of an Al-Zn-Mg-Cu Alloy," Ph.D. dissertation, University of Virginia, May 2001

J. Moran, Effects of Metallurgical Variables on the Corrosion of Aluminum Alloys, *Corrosion: Fundamentals, Testing, and Protection*, Vol 13A, *ASM Handbook*, ASM International, 2003, p 275–278

Effects of Metallurgical Variables on the Corrosion of Aluminum Alloys

Jim Moran, Alcoa

References

1. *Corrosion of Aluminum and Aluminum Alloys,* J.R. Davis, Ed., ASM International, 1999

2. *Aluminum: Properties and Physical Metallurgy,* J.E. Hatch, Ed., ASM International, 1984

3. Aluminum and Aluminum Alloys, *Alloying: Understanding the Basics,* J.R. Davis, Ed., ASM International, 2001, p 352–416

4. Z.S. Smialowska, Pitting Corrosion of Aluminum, *Corros. Sci.,* Vol 41, 1999, p 1743–1767

5. J.O. Park, C.H. Paik, Y.H. Huang, and R.C. Alkire, Influence of Fe-Rich Intermetallic Inclusions on Pit Initiation on Aluminum Alloys, *J. Electrochem. Soc.,* Vol 146 (No. 2), 1999, p 517–523

6. R.G. Buchheit, R.P. Grant, P.F. Hlava, B. Mckenzie, and G.L. Zender, Local Dissolution Phenomena Associated with S Phase particles in Alloy 2024, *J. Electrochem. Soc.,* Vol 144 (No. 8), 1997, p 2621–2628

7. C.M. Liao, J.M. Olive, M. Gao, and R.P. Wei, In-Situ Monitoring of Pitting Corrosion in Alloy 2024, *Corrosion,* Vol 54 (No. 6), p 451–453

8. R.G. Buchheit, A Compilation of Corrosion Potentials Reported for Intermetallic Phases in Aluminum Alloys, *J. Electrochem. Soc.,* Vol 142 (No. 11), 1995, p 3994–3996

9. E.H. Dix, W.A. Anderson, and M.B. Shumaker, Influence of Service Temperature on the Resistance of Wrought Al-Mg Alloys to Corrosion, *Corrosion,* Vol 15, 1959, p 55–62

10. A. Bhattamishra and K. Lal, Influence of Aging on Corrosion Behavior of Al-Mg-Si Alloys in Chloride and Acid Media, *Z. Metallkd.,* Vol 89, 1998, p 793

11. D.O. Sprowls and R.H. Brown, Stress Corrosion Mechanisms for Aluminum Alloys, *Conf. Proc. on Fundamental Aspects of Stress Corrosion Cracking,* R.W. Staehle, Ed., National Association of Corrosion Engineers, 1967, p 466

12. T.D. Burleigh, E. Ludwiczak, and R.A. Petri, Intergranular Corrosion of an Aluminum-Magnesium-Silicon-Copper Alloy, *Corrosion,* Vol 51, 1995, p 50

13. K. Yamaguchi and K. Tohma, Effect of Zn Addition on Intergranular Corrosion Resistance of Al-Mg-Si-Cu Alloys, *Proc. Sixth International Conf. on Aluminum Alloys* (Toyohashi, Japan), Japan Institute of Light Metals, 1998, p 1657

14. T.D. Burleigh, Microscopic Investigation of the Intergranular Corrosion of Alloy 6013- T6, *The Third International Conf. on Aluminum Alloys* (Trondheim, Norway), L. Arnberg et al., Ed., 1992, p 435

15. N.J.H. Holroyd, Environment-Induced Cracking of High-Strength Aluminum Alloys, *Proc. of the Fifth International Conf. on Environment-Induced Cracking,* R.P. Gangloff and M.B. Ives, Ed., NACE, 1990

16. T.D. Burleigh, Postulated Mechanisms for Stress Corrosion Cracking of Aluminum Alloys: A Review of the Literature, 1980–1989, *Corrosion,* Vol 47, 1991, p 89–98

17. M.O. Speidel and M.V. Hyatt, Stress Corrosion Cracking of High Strength Aluminum Alloys, *Adv. Corros. Sci. Technol.,* Vol 2, M.G. Fontana and R.W. Staehle, Ed., Plenum Press, 1972

18. A. Bigot, F. Danois, P. Auger, D. Blavette, and A. Reeves, Tomographic Atom Probe Study of Age Hardening Precipitation in Alloy 7050, *Mater. Sci. Forum,* Vol 217–222, 1996, p 695–700

19. T. Ramgopal, P.I. Gouma, and G.S. Frankel, Role of Grain Boundary Precipitates and SDZ on the Intergranular Corrosion of Aluminum Alloy AA7150, *Corrosion,* Vol 58, 2002, p 687

20. L.M. Young, “Microstructural Dependence of Aqueous-Environment Assisted Crack Growth and Hydrogen Uptake in Alloy 7050,” Ph.D. dissertation, University of Virginia, Aug 1999

21. G.A. Young, “Hydrogen Environment Assisted Cracking of an Al-Zn-Mg(-Cu) Alloy,” Ph.D. dissertation, University of Virginia, Aug 1999

22. K.R. Cooper, “Chemistry and Electrochemistry of Environment-Assisted Cracking of an Al-Zn-Mg-Cu Alloy,” Ph.D. dissertation, University of Virginia, May 2001

R.B. Rebak, Effects of Metallurgical Variables on the Corrosion of High-Nickel Alloys, *Corrosion: Fundamentals, Testing, and Protection*, Vol 13A, *ASM Handbook*, ASM International, 2003, p 279–286

Effects of Metallurgical Variables on the Corrosion of High-Nickel Alloys

Raúl B. Rebak, Lawrence Livermore National Laboratory

Introduction

NICKEL-BASE ALLOYS are solid solutions based in the element nickel. Even though nickel base alloys, in general, contain a large proportion of other alloying elements, these alloys maintain the face-centered cubic lattice structure (fcc or gamma) from the nickel-base element. As a consequence of the fcc structure, nickel-base alloys have excellent ductility, malleability, and formability. Nickel alloys are also readily weldable.

There are two large groups of the commercial nickel-base alloys. One group was designed to withstand high-temperature and dry or gaseous corrosion, while the other is mainly dedicated to withstanding low-temperature aqueous corrosion. Nickel-base alloys used for low-temperature aqueous or condensed systems are generally known as corrosion-resistant alloys (CRA), and nickel alloys used for high-temperature applications are known as heat-resistant alloys (HRA), high-temperature alloys (HTA), or superalloys. The practical industrial boundary between high- and low-temperature nickel alloys is approximately 500 °C (or near 1000 °F). Most of the nickel alloys have a clear use either as CRA or HRA; however, a few alloys can be used for both applications (e.g., alloy 625, Unified Numbering Systems, or UNS N06625).

This article is dedicated mostly to the metallurgical effects on the corrosion behavior of CRA. For each specific alloy, a metallurgical effect is considered when the overall composition of the alloy is the same; however, the corrosion performance could change due to the presence of second phases or a weld seam. Before going into detail on the metallurgical effects, a brief introduction on the importance of alloying elements on the corrosion behavior of nickel alloys is presented. Moreover, a brief description is given of the corrosion applications of HRA.

R.B. Rebak, Effects of Metallurgical Variables on the Corrosion of High-Nickel Alloys, *Corrosion: Fundamentals, Testing, and Protection*, Vol 13A, *ASM Handbook*, ASM International, 2003, p 279–286

Effects of Metallurgical Variables on the Corrosion of High-Nickel Alloys

Raúl B. Rebak, Lawrence Livermore National Laboratory

Heat-Resistant Alloys

Unlike CRA, which are mostly selected for their capacity to resist corrosion in a given environment, most HRA need to play a dual role. Namely, besides the capacity to withstand the corrosive aggressiveness of the environment, HRA also need to keep significant strength at high temperatures. Near and above 1000 °C (1830 °F), alloy selection is dominated by how strong the alloy is in this temperature range. Table 1 shows a short compilation of the most common HRA engineering nickel alloys and a brief description of their application.

Table 1 Nominal compositions of selected heat-resistant nickel alloys

UNS	Alloy	Composition, %	Common high-

No.		**Cr**	**Ni**	**Co**	**Mo**	**Nb**	**Ti**	**Al**	**Fe**	**C**	**Other**	temperature applications
N06002	Hastelloy X	22.0	49.0	1.5 max	9.0	…	…	2.0	15.8	0.15	0.6 W	Combustion chambers, heat treatment components
N06075	Nimonic 75	19.5	75.0	…	…	…	0.4	0.15	2.5	0.12	0.25 max Cu	Gas turbines, heat treatment equipment
N06230	Haynes 230	22.0	55.0	5.0 max	2.0	…	…	0.35	3.0 max	0.10	14.0 W, 0.015 max B, 0.02 La	Gas turbines, superheater tubes
N06600	Inconel 600	15.5	76.0	…	…	…	…	…	8.0	0.08	0.25 Cu	Furnace components
N06601	Inconel 601	23.0	60.5	…	…	…	…	1.35	14.1	0.05	0.5 Cu	Furnace and heat treatment components, combustion chambers
N06617	Inconel 617	22.0	55.0	12.5	9.0	…	…	1.0	…	0.07	…	Gas turbine combustion cans, furnace components
N06625	Inconel 625	21.5	61.0	…	9.0	3.6	0.2	0.2	2.5	0.05	…	Aerospace, pollution control equipment
N07214	Haynes 214	16.0	76.5	…	…	…	…	4.5	3.0	0.03	…	Specialized heat treatment equipment, turbine parts
N07718	Inconel 718	19.0	52.5	…	3.0	5.1	0.9	0.5	18.5	0.08 max	0.15 max Cu	Gas turbines, rocket engines, nuclear applications
N07750	Inconel X-750	15.5	73.0	…	…	1.0	2.5	0.7	7.0	0.04	0.25 max Cu	Gas turbine components, pressure vessels, applications in nuclear reactors
N08811	Incoloy 800HT	21.0	32.5	…	…	…	0.4	0.4	46.0	0.08	0.8 Mn, 0.5 Si, 0.4 Cu	Industrial furnaces, carburizing equipment
N12160	Haynes HR-160	28.0	37.0	29.0	…	…	…	…	2.0	0.05	2.75 Si, 0.5 Mn	Thermocouple shields, calciner components
N10242	Haynes 242	8.0	62.5	2.5 max	25.0	…	…	0.5 max	2.0 max	0.10 max	0.006 max B	Turbine seal rings, fasteners

UNS, Unified Numbering System

There are many different industrial high-temperature environments. In general, practical use has divided these environments according to the most common causes of failure of a component in service. The most common failures are associated to the attack by a specific element, such as oxygen (which causes oxidation), carbon (carburization and metal dusting), sulfur (sulfidation), halogen (e.g., chlorination), and nitrogen (nitridation). Other modes of failure, such as molten metal attack and hot corrosion, are less specific. Detailed descriptions of

such modes of attack are given elsewhere is this Volume and in Ref 1 and 2. The most common high-temperature degradation mode is oxidation, and the protection against oxidation, in general, is given by the formation of a chromium oxide scale. The presence of a small amount of aluminum or silicon in the alloy may improve the resistance against oxidation of a chromia-forming alloy (Table 1). Attack by other elements, such as chlorine and sulfur, depends strongly on the partial pressure of oxygen in the environment (Ref 2).

References cited in this section

1. G.Y. Lai, *High-Temperature Corrosion of Engineering Alloys,* ASM International, 1990
2. B. Gleeson, High-Temperature Corrosion of Metallic Alloys and Coatings, *Corrosion and Environmental Degradation,* Vol II, Wiley-VCH, 2000, p 173

R.B. Rebak, Effects of Metallurgical Variables on the Corrosion of High-Nickel Alloys, *Corrosion: Fundamentals, Testing, and Protection*, Vol 13A*, ASM Handbook*, ASM International, 2003, p 279–286

Effects of Metallurgical Variables on the Corrosion of High-Nickel Alloys

Raúl B. Rebak, Lawrence Livermore National Laboratory

Effect of Chemical Composition on the Corrosion Behavior of Nickel Corrosion-Resistant Alloys

Nickel alloys are highly resistant to corrosion, and, in most environments, nickel alloys outperform the most advanced stainless steels. One of the reasons is because nickel can be alloyed more heavily than iron. That is, large amounts of specific elements can be dissolved purposely into nickel to tailor an alloy for a particular environment. In general, industrial environments can be divided into two broad categories: *reducing* and *oxidizing.* These terms refer to the range of electrode potential that the alloy experiences, and it is controlled by the cathodic reaction in the system. Thus, a reducing condition is generally controlled by the discharge of hydrogen from a reducing acid, such as hydrochloric acid. An oxidizing environment has a potential that is higher than the potential for hydrogen discharge. This potential may be established by cathodic reactions, such as reduction of dissolved oxygen (O_2) from the atmosphere, chlorine gas (Cl_2), hydrogen peroxide (H_2O_2), chromates (CrO_4^{2-}), nitrates (NO_3^-), and metallic ions in solution, such as ferric (Fe^{3+}) and cupric (Cu^{2+}). Nickel alloys, the same as other alloys, may suffer two main types of corrosion: *uniform* corrosion and *localized* corrosion. Uniform corrosion may happen under reducing conditions in the active region of potentials and also under oxidizing conditions in the form of a slow, passive corrosion. Localized corrosion, such as pitting and crevice corrosion, generally occurs under oxidizing conditions. Stress-corrosion cracking (SCC) or environmentally assisted cracking (EAC) could occur at any electrochemical potential range. Three conditions are necessary for the occurrence of SCC: a susceptible material composition and microstructure, a specific aggressive environment, and the presence of tensile stresses.

Based on chemical composition, corrosion-resistant nickel-base alloys can be grouped as commercially pure nickel, Ni-Cu alloys, Ni-Mo alloys, Ni-Cr-Mo alloys, and Ni-Cr-Fe alloys. Table 2 gives the composition of the most familiar commercial wrought nickel-base alloys. A brief description of the corrosion behavior of each group of alloys is given subsequently. More extended analyses are given elsewhere (Ref 3, 4).

Table 2 Nominal compositions of selected corrosion-resistant nickel alloys

UNS No.	Alloy name	Composition, %						
		Ni	**Cr**	**Cu**	**Mo**	**Fe**	**W**	**Others**
Commercially pure nickel								
N02200	Ni-200	99.6	…	…	…	0.2	…	0.2 Mn
Nickel-copper alloy								
N04400	Monel 400	67	…	31.5	…	1.2	…	…
Nickel-molybdenum alloys								
N10665	Hastelloy B-2	72	…	…	28	…	…	…
N10675	Hastelloy B-3	68.5	1.5	…	28.5	1.5	…	…
Nickel-chromium-molybdenum alloys								
N10276	Hastelloy C-276	59	16	…	16	5	4	…
N06455	Hastelloy C-4	68	16	…	16	…	…	…
N06022	Hastelloy C-22	59	22	…	13	3	3	…
N06200	Hastelloy C-2000	59	23	1.6	16	…	…	…
N06059	Nicrofer 5923hMo (alloy 59)	59	23	…	16	1	…	…
N06686	Inconel 686	46	21	…	16	5	4	…
Nickel-chromium-iron alloys								
N06600	Inconel 600	76	15.5	…	…	8	…	…
N08825	Incoloy 825	43	21	2.2	3	30	…	1 Ti
N06030	Hastelloy G-30	44	30	2	5	15	2.5	4 Co
R20033	Nicrofer 3033 (alloy 33)	31	33	0.6	1.6	32	…	0.4 N

UNS, Unified Numbering System

Commercially Pure Nickel. The most widely accepted application of commercially pure nickel is in the handling of highly concentrated caustic solutions. Nickel has lower corrosion rates in hot caustic solutions than alloyed nickel due to the preferential dissolution of elements such as chromium and molybdenum. Nickel can also tolerate cold reducing acids well because of the slow discharge of hydrogen on its surface. Hot reducing acids and oxidizing acids corrode pure nickel rapidly (Fig. 1).

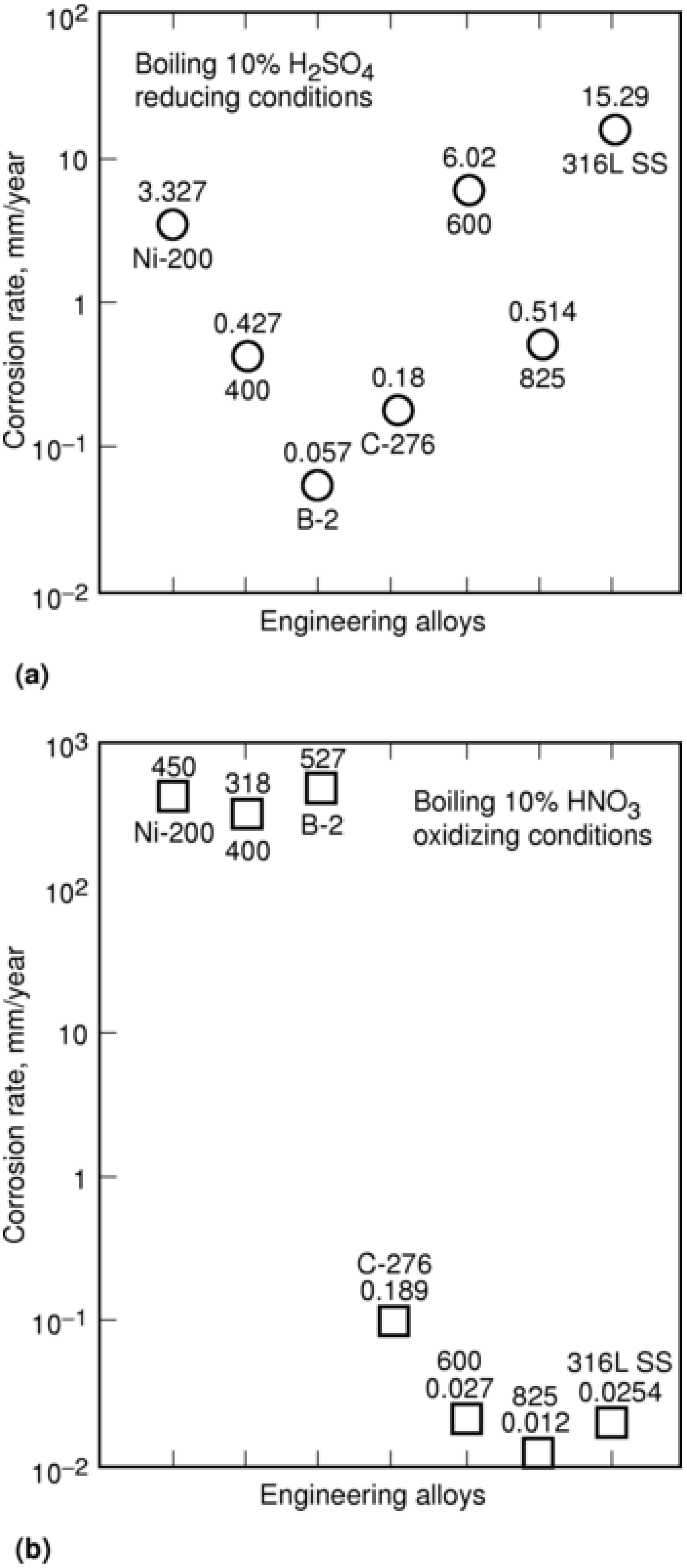

Fig. 1 Corrosion behavior of alloys from five nickel alloy groups compared to that of 316L stainless steel (SS). (a) In boiling 10% sulfuric acid, reducing conditions. (b) In 10% boiling nitric acid, oxidizing conditions. Source: Data from Ref 3

Nickel-Copper. A main application of nickel- copper alloys, alloy 400, K500, and Monel alloys, is in the handling of pure hydrofluoric acid. However, if oxidants such as oxygen are present in hydrofluoric acid, nickel-copper alloys may suffer intergranular attack (Ref 5). Nickel-copper alloys are slightly more resistant to general corrosion than Ni-200 in hot reducing and oxidizing acids, such as sulfuric acid and nitric acid (Fig. 1).

Nickel-molybdenum alloys (commonly known as B-type alloys) were specifically developed to withstand reducing HCl at all concentrations and temperatures. Besides expensive materials such as tantalum, nickel-

molybdenum alloys are the best alloys for hot hydrochloric acid (Ref 3). Nickel-molybdenum alloys are also used in the handling of other corrosive reducing environments, such as sulfuric, acetic, formic, hydrofluoric, and phosphoric acids. Figure 1(a) shows that B-2 has the lowest corrosion rate in boiling 10% sulfuric acid. However, nickel-molybdenum alloys perform poorly in oxidizing acids (Fig. 1b) or, for example, in HCl contaminated with ferric ions (Ref 6).

Nickel-Chromium-Molybdenum. There are many commercially available Ni-Cr-Mo alloys today. All these alloys were derived from the original C-alloy (N10002), which was introduced to the market in cast form in 1932. The more advanced Ni-Cr-Mo alloys are N06686, N06059 (alloy 59), and Hastelloy C-2000. However, the more common Ni-Cr-Mo alloy in industrial applications is alloy C-276 (N10276) which was introduced in the market in the mid- 1960s. Nickel-chromium-molybdenum alloys are the most versatile nickel alloys, because they contain molybdenum, which protects against corrosion under reducing conditions, and chromium, which protects against corrosion under oxidizing conditions (Ref 7). Figure 1 shows that C-276 has low corrosion rates both in reducing conditions (boiling 10% sulfuric acid) and oxidizing conditions (boiling 10% nitric acid). One of the major applications of Ni-Cr-Mo alloys is in the presence of hot chloride-containing solutions. Under these conditions, most of the stainless steels would suffer crevice corrosion, pitting corrosion, and SCC. However, Ni-Cr-Mo alloys are highly resistant, if not immune, to chloride- induced attack in most industrial applications (Ref 3).

Nickel-Chromium-Iron. The last group of nickel-base CRA is the group of Ni-Cr-Fe alloys. These alloys also may contain smaller amounts of molybdenum and/or copper. Nickel-chromium-iron alloys, in general, are less resistant to corrosion than Ni-Cr-Mo alloys; however, they could be less expensive and therefore find a wide range of industrial applications. Figure 1(a) shows that the corrosion rate of alloy 600 in sulfuric acid is higher than the corrosion rate of alloy 825. The latter contains small amounts of molybdenum and copper (Table 2), which are beneficial alloying elements for resistance to sulfuric acid. Also, alloy 825 has a lower corrosion rate in nitric acid (Fig. 1b), because it contains larger amounts of chromium. One of the most common applications of Ni-Cr-Fe alloys, such as alloy 33 and N06030, is in the industrial production of phosphoric acid and in highly oxidizing media such as nitric acid.

References cited in this section

3. R.B. Rebak, Corrosion of Non-Ferrous Alloys, Part I: Nickel-, Cobalt-, Copper-, Zirconium- and Titanium-Base Alloys, *Corrosion and Environmental Degradation,* Vol II, Wiley-VCH, 2000, p 69
4. C.P. Dillon *Corrosion Control in the Chemical Process Industry,* NACE International, 1994
5. R.B. Rebak, J.R. Dillman, P. Crook, and C.V.V. Shawber, *Mater. Corros.,* Vol 52, 2001, p 289–297
6. R.B. Rebak and P. Crook, Paper 00499, Corrosion/2000, NACE International, 2000
7. D.C. Agarwal and J. Kloewer, Paper 01325, Corrosion/01, NACE International, 2001

R.B. Rebak, Effects of Metallurgical Variables on the Corrosion of High-Nickel Alloys, *Corrosion: Fundamentals, Testing, and Protection,* Vol 13A, *ASM Handbook,* ASM International, 2003, p 279–286

Effects of Metallurgical Variables on the Corrosion of High-Nickel Alloys

Raúl B. Rebak, Lawrence Livermore National Laboratory

Factors Affecting the Corrosion Behavior of Nickel-Base Alloys

The corrosion of metal and alloys depends on internal and external factors. Internal factors include chemical composition and microstructure of the alloy, and external factors include electrolyte composition, temperature, and electrode potential. In general, the use of nickel-base alloys in corrosive applications is based on their chemical composition. For example, a nickel-base alloy such as N06030 (Table 2) could be used under highly oxidizing acidic conditions, because it contains a large amount of chromium. Other alloys, such as B-3 (Table 2), are recommended for highly reducing acidic conditions, because they contain a large amount of molybdenum. However, for each alloy of unique chemical composition, the corrosion behavior also depends on the particular microstructural or metallurgical condition of its matrix. A typical example of this is the behavior of autogenously welded pipes in industrial corrosive applications. Both the weld seam and the wrought matrix from which the weld seam was derived have essentially the same overall chemical composition. However, it is commonly observed in specimen returned from the field that the weld seam and the immediately adjacent matrix have lower corrosion resistance than the contiguous unaffected wrought matrix. This dissimilar corrosion behavior is not due to a different chemical composition but to a different microstructure or metallurgical condition of the alloy. The weld seam would have a cast microstructure, which is generally anisotropic, with areas of high concentration of alloying elements, while other areas are impoverished in these same elements. The matrix area immediately adjacent to the weld is called the heat-affected zone (HAZ). The area of the HAZ still retains the overall wrought isotropic structure of the matrix; however, it can suffer solid-state transformations (intergranular precipitation) due to the higher temperature excursion during welding. The area immediately next to the HAZ has the isotropic fcc microstructure of a wrought matrix with equiaxed grains. Therefore, in a narrow region near the weld, there are three areas of equivalent chemical composition but of different microstructure. Each of these areas responds differently to the external corrosive environment.
Another effect of microstructure on the analysis of corrosion behavior is the orientation of the testing coupons. This detail is commonly overlooked. When a testing coupon is prepared from a plate material, there are two main directions in the coupon, that is, parallel to the rolling direction (longitudinal) and perpendicular (or transverse) to the rolling direction (across the thickness of the plate). Even though the coupon is fully mill annealed with isotropic chemical composition, it is not infrequent to observe that the perpendicular direction of the plate behaves in a different manner from the parallel direction, especially in cases where SCC and localized corrosion may be expected. The direction across the thickness of the plate, in general, has lower corrosion resistance than the parallel direction. The presence of nonmetallic inclusions elongated in the longitudinal direction sometimes leads to localized end-grain attack on transverse cut edges.

R.B. Rebak, Effects of Metallurgical Variables on the Corrosion of High-Nickel Alloys, *Corrosion: Fundamentals, Testing, and Protection*, Vol 13A, *ASM Handbook*, ASM International, 2003, p 279–286

Effects of Metallurgical Variables on the Corrosion of High-Nickel Alloys

Raúl B. Rebak, Lawrence Livermore National Laboratory

Changes in Microstructure

This section discusses in detail the corrosion implications of changing the alloy microstructure via three different processes: (a) solid-state transformation or second-phase precipitation, which includes the precipitation of intermetallic phases in a Ni-Cr-Mo alloy and the precipitation of secondary carbides in a Ni-Cr-Fe alloy; (b) cold work in Ni-Mo and Ni-Cr-Mo alloys; and (c) comparison of corrosion behavior between cast and wrought microstructures in Ni-Cr-Mo alloys.

Phase Stability of Nickel-Base Alloys and Corrosion Behavior

Second-Phase Precipitation. In general, Ni- Cr-Mo and Ni-Cr-Fe alloys (Table 2) contain a large amount of alloying elements, which determine their specific corrosion resistance and therefore field applicability. These elements are dissolved into the liquid metal at high temperature, and they remain in solid solution when the

final product is cooled. At ambient temperatures, these alloys remain a single-phase fcc microstructure indefinitely. However, if most of these nickel-base alloys are exposed to temperatures above 500 °C (930 °F) for varying periods of time, they may develop second-phase precipitates, which in turn change the mechanical properties and corrosion resistance of these alloys. In general, the larger the amount of alloying elements, the more unstable the fcc microstructure of the alloy. Currently, there are several commercial Ni-Cr-Mo alloys (Table 2) that are highly alloyed to increase their corrosion resistance; however, this overalloying may adversely impact their phase stability. The effects on corrosion behavior of second-phase formation due to thermal instability is discussed in detail for Hastelloy C-22, but similar behavior may happen in alloys C-276, C-4, 686, and 59. Another type of phase instability is the formation of secondary carbides. In most of today's alloys, this issue is being resolved by keeping a low content of carbon in the alloy. However, since the 1970s, the presence of secondary carbides was an important issue in the resistance of Inconel 600 (Table 2) to SCC in deoxygenated high-temperature water. This issue is also subsequently discussed in detail.

Effect of Intermetallic Phases. Hastelloy C- 22 (UNS N06022) is a Ni-Cr-Mo alloy (Table 2) that contains approximately 22% Cr, 13% Mo, 3% W, and 3% Fe. Due to its high chromium content, this alloy remains passive in most industrial applications and therefore has a very low general corrosion rate. The combination of the alloying elements chromium, molybdenum, and tungsten imparts the alloy with an excellent resistance to pitting corrosion, crevice corrosion, and SCC, especially in halide-containing environments (Ref 8, 9, 10, 11, 12, 13, 14, 15).

Due to its overall resistance to corrosion, this alloy is a candidate material to fabricate the external layer of the high-level nuclear waste containers for the potential repository site that the Department of Energy is characterizing in Yucca Mountain, Nevada. As a result of the heat generated by the radioactive decay of the waste, the containers might experience temperatures as high as 160 °C (320 °F) during their first 1000 years of emplacement. The lifetime design of the containers is 10,000 years, and their maximum allowed temperature is 350 °C (660 °F). Because of concerns that alloy N06022 may suffer phase instability during the long predicted time of emplacement, systematic studies are being carried out to fully characterize the ranges of time and temperature at which the alloy might undergo solid-state phase transformation.

Haynes International started low-temperature aging studies of alloy N06022 and other alloys in 1989. The most recent results were obtained from samples removed after 40,000 h of aging. Laboratory studies of these aged samples have shown that the mechanical and corrosion properties of the alloy did not change after it was aged for up to 40,000 h at 427, 343, or 260 °C (800, 650, or 500 °F) (Ref 9, 10). The next test on these aged samples occurs for a total aging time of 100,000 h (~12 years).

It is known that precipitation of detrimental second phases occurs when alloy N06022 is aged at temperatures above 600 °C (1110 °F) for much shorter periods of time. Therefore, several studies have been carried out to fully characterize the second-phase precipitation in the alloy for shorter periods of time at higher temperatures (Ref 16, 17, 18, 19, 20). The precipitation of these secondary phases affects the corrosion resistance in aggressive acidic solutions and the mechanical properties of wrought and welded alloy N06022 (Ref 21, 22, 23, 24, 25). In the fully annealed condition, alloy N06022 is a metastable fcc solid solution. When the alloy is aged at intermediate temperatures (600 °C, or 1110 °F), it can precipitate several intermetallic phases (Ref 20). Two of the most common phases are μ phase and P phase, which are similar both chemically and crystallographically. Precipitation of the intermetallic detrimental phases, in general, begins at the grain boundaries, and for longer aging times, the precipitation starts growing at twin boundaries and later, inside the grains (Ref 20). Temperature-time-transformation diagrams and micrographs for alloy N06022 have been published (Ref 17, 20, 22). These intermetallic secondary phases tend to be rich in either chromium or molybdenum, which are the elements that give the alloy its excellent corrosion resistance. Therefore, it can be suggested that the formation of the intermetallic phases may leave a narrow adjacent area of the matrix depleted in these beneficial elements (chromium and molybdenum), causing an increase in the corrosion rate of the alloy in aggressive acidic solutions. On the other hand, the corrosion behavior of the aged alloy N06022 microstructure in multiionic underground water was the same as the corrosion behavior of the unaged microstructure (Ref 25). Similarly, the corrosion rate of aged alloy N06022 was the same as the corrosion rate of an unaged alloy when tested in boiling 10% NaOH (caustic solution) (Ref 21).

Changes in the Corrosion Rate of Alloy N06022 as a Consequence of Second-Phase Precipitation. Figures 2(a) and (b) show the corrosion rate of wrought and gas tungsten arc welded (GTAW) alloy N06022, respectively, in ASTM G 28 Method A solution for seven aging temperatures and thirteen different aging times (Ref 26). The ASTM G 28 Method A test involves the immersion of the testing coupon in an oxidizing acidic solution

consisting of boiling 50% sulfuric acid plus 42 g/L of ferric sulfate for 24 h. Details about testing coupon configuration, aging procedures, and corrosion testing are published elsewhere (Ref 26).

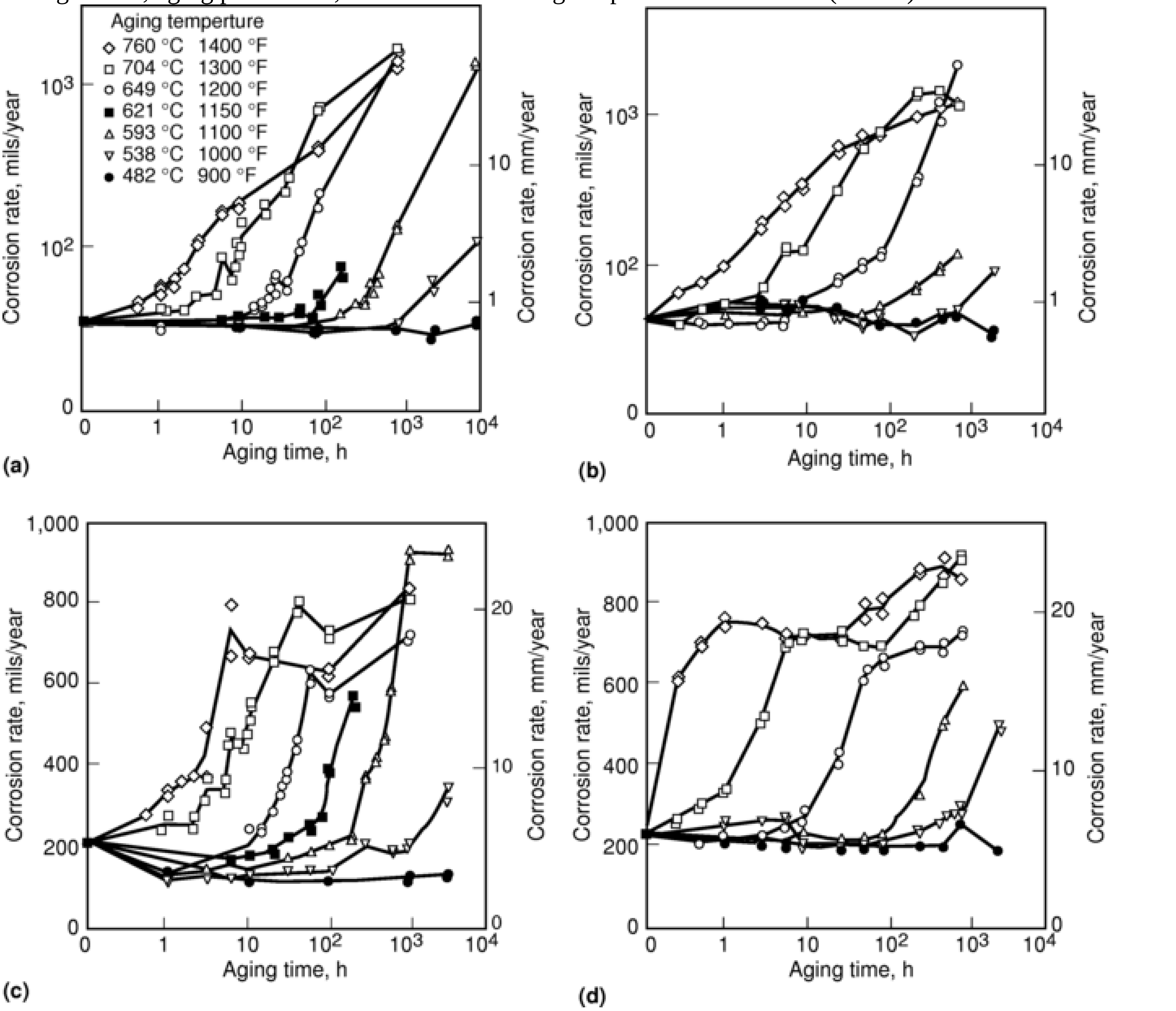

Fig. 2 Corrosion rate as a function of aging time and temperature for alloy C-22 (UNS N06022). (a) Aged wrought alloy in boiling sulfuric acid/ferric sulfate (ASTM G 28 Method A). (b) Gas tungsten arc welded (GTAW) alloy in boiling sulfuric acid/ferric sulfate (ASTM G 28 Method A). (c) Aged wrought alloy in boiling 2.5% HCl. (d) GTAW alloy in boiling 2.5% HCl. Source: Ref 26

The corrosion rate of aged alloy N06022 in this oxidizing solution increases gradually as the aging time and the aging temperature (T) increase, for $T \geq 538$ °C (1000 °F). For samples aged at 482 °C (900 °F), the corrosion rate remains the same, even after aging for 10,000 h (Fig. 2a). Coupons that were aged, for example, at 704 and 760 °C (1300 and 1400 °F) for times longer than 3 h show preferential corrosion at the grain boundaries. At higher aging times, deeper grain-boundary attack is observed, and in certain testing conditions, some grains fell away, because they became completely detached from the samples. Aging increases the susceptibility of attack of the HAZ in ASTM G 28 Method A solution. Figures 2(c) and (d) show the corrosion rate of wrought and GTAW alloy N06022, respectively, in boiling 2.5% HCl solution (Ref 26). For both types of coupons, the corrosion rate increases approximately 3 times after a certain threshold aging time at each temperature. The threshold time increases as the temperature decreases. Figure 2(c) shows that for the wrought coupons, the corrosion rate initially decreases slightly with the aging time. This behavior seems to suggest that a small amount of aging would be beneficial for corrosion resistance under reducing conditions (Ref 26). The reason for this behavior is still not fully understood. For the higher aging temperatures, 760, 704, and 649 °C (1400,

1300, and 1200 °F), the corrosion rate seems to reach a plateau for an intermediate aging time. This behavior is more noticeable for the GTAW coupons (Fig. 2d). For both types of the samples aged at 482 °C (900 °F), the corrosion rate remains the same, even after aging for 3000 h. Observation of the tested coupons in boiling 2.5% HCl solution shows preferential intergranular attack that becomes deeper and wider as the aging time increases. At aging times of 1000 h and higher, preferential corrosion attack at twins inside the grains is observed. For the shorter aging times, there is preferential attack at the HAZ; however, for the longer aging times, the attack becomes more uniform across the testing coupon.

Figure 3 shows the effect of welding on the corrosion rate of alloy N06022. Figure 3(a) shows the corrosion rate in ASTM G 28 Method A for wrought and as-welded coupons at two aging temperatures, 760 and 538 °C (1400 and 1000 °F), as a function of aging time. For all aging times, the corrosion rate of welded coupons is always higher than the corrosion rate of wrought coupons. At the aging temperature of 760 °C (1400 °F) and at the aging time of 10 h, the corrosion rate of the welded coupons is approximately 2 times the corrosion rate of the wrought coupons. Figure 3(b) shows the corrosion rate in boiling 2.5% HCl solution for wrought and as-welded coupons at two aging temperatures, 760 and 538 °C (1400 and 1000 °F), as a function of aging time. For the shorter aging times (up to 3 to 6 h), the corrosion rate of the welded coupons is approximately 3 times the corrosion rate of the wrought coupons; however, for aging times of 6 h and longer, the difference in the corrosion rate is smaller.

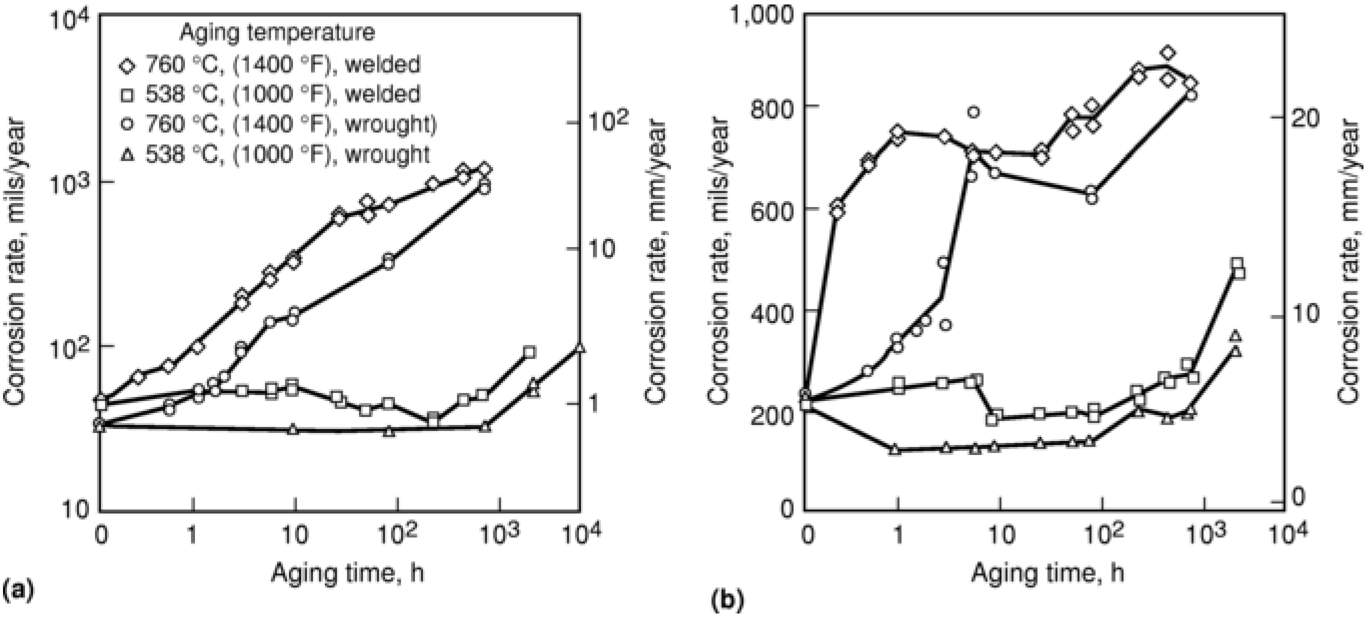

Fig. 3 Corrosion rates for wrought and for gas tungsten arc welded (GTAW) alloy C-22 (UNS N06022). (a) In boiling sulfuric acid/ferric sulfate (ASTM G 28 Method A). (b) In boiling 2.5% HCl solution. Source: Ref 25

The increase in the corrosion rate of high-temperature aged alloy N06022 is pronounced in highly reducing conditions (boiling pure HCl solutions) and highly oxidizing solutions (boiling 50% sulfuric acid plus 42 g/L ferric sulfate). However, at intermediate oxidizing potentials, the aged alloy is still able to maintain passivity. This was corroborated through potentiodynamic anodic polarization (Ref 23) and through corrosion immersion tests in boiling HCl solutions contaminated with different levels of ferric ions (Ref 21).

Secondary Carbide Effect in the Resistance of UNS N06600 to SCC in High-Temperature Water. Inconel 600 (UNS N06600) is a Ni-Cr- Fe alloy (Table 2) that contains approximately 16% Cr and 9% Fe. Because this alloy has excellent resistance to general corrosion in high- temperature water, it was selected for fabrication of the heat exchanger tubes in pressurized water reactor nuclear power plants. However, it was later found that alloy N06600 tubes cracked in service both from the primary and secondary side (Ref 27, 28). Factors that control the susceptibility of the alloy to SCC include grain- boundary microchemistry, thermal treatment or distribution of secondary carbides, presence of cold work, applied stress, temperature, solution pH, electrochemical potential, partial pressure of hydrogen, and so on (Ref 29). The first three factors are metallurgical or internal factors. Of these, only the thermal treatment or second- phase precipitation of carbides is discussed in this section.

The presence of secondary carbides in alloy N06600 plays an important role in its resistance to SCC. It is known that precipitation of secondary carbides occurs when the alloy is exposed to temperatures between 500 and 900 °C (930 and 1650 °F) for varying periods of time (Ref 30). These carbides are generally rich in chromium; therefore, a secondary carbide precipitation is often accompanied by a chromium depletion zone. The formation of a chromium-depleted area is generally called sensitization. It has been suggested that sensitization or chromium depletion in alloy N06600 per se does not play any role in the susceptibility of the alloy to SCC in deoxygenated high-temperature water (Ref 29, 31).

The morphology and distribution of secondary carbides at the grain boundary plays the most important role in the resistance of alloy N06600 to SCC. An alloy exhibiting continuous or semicontinuous grain-boundary carbides has the highest resistance to SCC (Ref 32, 33). A microstructure with mainly intragranular carbides and widely spaced, discrete grain-boundary carbides is very susceptible to SCC in hydrogenated (deoxygenated) solutions Ref 32. This clear influence of carbide distribution on the susceptibility of the alloy to SCC was confirmed several times via laboratory testing and also through removal of tubes with different heat treatment from operating heat exchangers in nuclear power plants (Ref 29). There is no agreement among the corrosion engineers on why the presence of intergranular carbides is beneficial for the resistance to SCC. Some researchers correlated the presence of carbides at the grain boundaries with microdeformation mechanisms at the crack tip (Ref 34). It has been argued that intergranular carbides promote an easy source for dislocations and therefore reduce the crack tip stress state (Ref 34). Other authors explained the beneficial effect of carbides by the difference in electrochemical behavior between the carbides and the adjacent matrix in hydrogenated high-temperature water (Ref 35).

Effect of Cold Work on the Corrosion Resistance

Cold work (CW) is the result of the mechanical plastic deformation of a metal (alloy) at relatively low (ambient) temperatures. With increasing amount of CW, the hardness and strength of the material increases. That is, a CW microstructure has a higher yield stress and lower elongation to failure than a non-CW or annealed microstructure of the same chemical composition. In a CW microstructure, the grains of the metal are deformed, and the density of dislocations is several orders of magnitude higher than in an annealed microstructure.

Cold Work and the General Corrosion of Ni-Mo and Ni-Cr-Mo Alloys. Figures 4 and 5 show the effect of CW on the general corrosion behavior of nickel alloys. Figure 4 shows that the corrosion rate of N10665 (Hastelloy B-2) in boiling 20% HCl is approximately 0.34 mm/year (13 to 14 mils/year) and does not change in the range of CW between 0 and 50%. In this same range of CW, the hardness of alloy B-2 increases from 90 HRB to more than 40 HRC (Fig. 4). A boiling solution of HCl would be reducing and therefore promote a general or uniform corrosion rate in a nickel-molybdenum alloy such as B-2 (Table 2). Figure 5 shows that the corrosion rate of N06455 (Hastelloy C-4) in boiling 10% HCl is approximately 6 to 7 mm/year (250 to 275 mils/year) and does not change in the range of CW between 0 and 50%. Because a Ni-Cr-Mo alloy has a lower amount of molybdenum than a nickel-molybdenum alloy, the corrosion rate of Ni-Cr-Mo alloys in boiling HCl solutions is generally higher than the corrosion rate of nickel- molybdenum alloys in similar solutions (Ref 36). Figure 5 also shows that the corrosion rate of C-4 in ASTM G 28 Method A solution is approximately 3.56 mm/year (140 mils/year) and does not change with the amount of CW between 0 and 50%. For both reducing, 10% HCl, and oxidizing, ASTM G 28 Method A, solutions, the general corrosion rate does not change as the amount of CW is increased in the alloy. Results from Fig. 5 suggest that the higher presence of dislocations in a CW microstructure does not affect considerably the hydrogen evolution reaction under reducing conditions or the passivation characteristics under oxidizing conditions for nickel alloys.

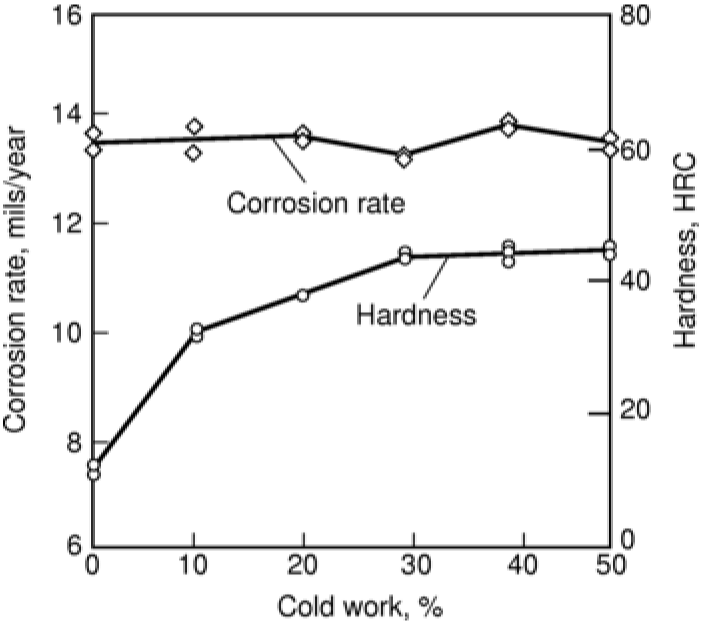

Fig. 4 Effect of cold work on the general corrosion behavior of alloy B-2 (UNS N10665) in boiling 20% HCl

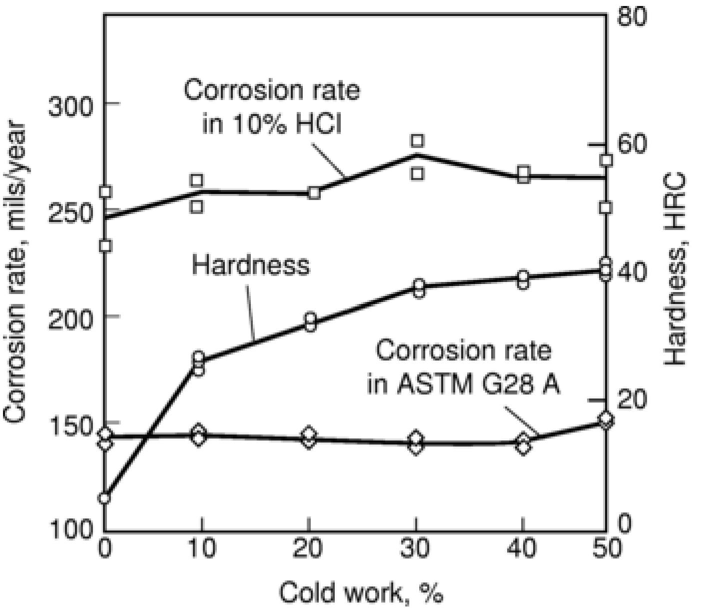

Fig. 5 Effect of cold work on the general corrosion behavior of alloy C-4 (UNS N06455) in boiling acid solutions

Cold Work and SCC of Ni-Cr-Fe Alloys. The SCC susceptibility of alloy N06600 depends, among other factors, on the amount of CW that the microstructure contains. For the same environmental conditions, alloys with similar chemical composition have different susceptibility to SCC, depending on their yield stress and ductility. The yield stress increases with the amount of CW; therefore, it could be inferred that a cold-worked microstructure would be more susceptible to SCC than an annealed microstructure. This is especially true for alloy N06600 in hydrogenated high-temperature water. Most of the failures of steam generator plant tubes occurred in the cold-deformed areas, such as in the expansion transition zone at the tube sheet and at the tightest radii in the U-bend area (Ref 27).

The enhanced susceptibility to SCC of CW tubes from field observations was repeatedly confirmed through laboratory testing. For example, it was reported that annealed alloy N06600 tubing did not suffer SCC using the slow strain-rate test in water at 350 °C (662 °F) even after 408 h of straining (Ref 37). However, after 35% CW was applied to the gage of the alloy specimen, the fracture surface was 65% intergranular after only 60 h of slow strain-rate testing. Another study has shown that the crack growth rate by SCC in alloy N06600 can be

increased 100 times if the alloy is 40% cold worked (Ref 38). Other researchers have shown that there is a monotonic increase in the crack growth rate in the alloy with the amount of applied CW to the specimens, following a power law (Ref 39). Even though it is known that the presence of CW increases the susceptibility of the alloy to SCC in deoxygenated water, there is not yet a fundamental understanding of the reason (Ref 29).

Another effect of microstructure on the susceptibility of alloy N06600 to SCC is the orientation of the test specimen from the original mill-processed plate. The orientation effect could be called a pure microstructural effect, because there is no induced CW or second-phase precipitation. For practical purposes, the etched microstructure of the alloy in the longitudinal direction (parallel to rolling) cannot be differentiated from the microstructure in the transverse direction (across the plate). However, SCC crack growth rates in the transverse direction are larger than in the longitudinal direction (Ref 40).

Cold Work and Environmentally Assisted Cracking (EAC) of Ni-Cr-Mo Alloys. Nickel alloys are used extensively in the oil and gas industry during the drilling of deep and corrosive oil and gas wells. One of the most common nickel alloys for these applications is C-276 (N10276) (Table 2). Other nickel alloys used include Incoloy 825 (N08825), Hastelloy G-3 (N06985) and G-50 (N06950) (Ref 41). These alloys are generally used in the form of tubular products for applications in sour wells; that is, wells containing high amounts of hydrogen sulfide (H_2S) combined with the presence of chlorides (Cl^-) and carbon dioxide (CO_2). Testing for susceptibility of alloys to EAC in oil and gas applications is generally conducted in aqueous solutions containing 5% NaCl + 0.5% acetic acid + saturation with H_2S solution (Ref 42), or in variations of this solution. These nickel alloys are generally used in the cold worked (CW) condition to increase their strength. For C-276, for example, the hardness may increase from 92 HRB in the mill-annealed condition to 41 HRC with a 50% cold reduction. This increase in hardness (or yield stress) of the alloy often manifests as a decrease in resistance to EAC, such as in sulfide cracking (Ref 43). As a consequence, the oil and gas industry prepared standards to limit the hardness of materials for applications in oilfield equipment. For example, according to NACE International standard MR0175-2002, the hardness limit for alloy C-276 (N10276) is 35 HRC (Ref 44).

Corrosion of Cast Forms as Contrasted to Wrought Forms

Versions of many wrought nickel-base alloys are available in cast form. The specifications for the castings are given in the ASTM A 494 standard. Table 3 gives the composition of the most popular cast nickel-base alloys and the approximate equivalent to the wrought versions. The main difference in the chemical composition between the cast alloys (Table 3) and their wrought versions (Table 2) is in the higher amount of impurities, such as carbon and silicon, allowed in the cast alloys. Carbon is naturally present in the melt and cannot be removed without special treatment, such as argon oxygen decarburization (AOD). Silicon is necessary in the melt, because it contributes to fluidity during pouring and filling of the molds.

Table 3 Compositions of selected cast nickel-base alloys

Alloy	Corresponding wrought alloy	Composition, %									
		C	**Si**	**Mn**	**Cu**	**Fe**	**Cr**	**P**	**S**	**Mo**	**Others**
Cast nickel											
CZ-100[(a)]	Ni 200	1.0	2.0	1.5	1.25	3.0	…	0.03	0.03	…	…
Nickel-copper alloy											
M-35-1	Alloy 400	0.35	1.25	1.5	26.0–33.0	3.50 max	…	0.03	0.03	…	…
Nickel-molybdenum alloy											
N-12MV	Alloy B-2	0.12	1.0	1.0	…	4.0–6.0	1.0	0.04	0.03	26.0–30.0	0.20–0.60 V
Nickel-chromium-molybdenum											
CW-12MW	Alloy C-276	0.12	1.0	1.0	…	4.5–7.5	15.5–17.5	0.04	0.03	16.0–18.0	0.20–0.40 V, 3.75–5.25 W
CW-2M	Alloy C-4	0.02	0.8	1.0	…	2.0	15.0–	0.03	0.03	15.0–	0.20–0.60

						max	17.5			17.5	V
CX2MW	Alloy C-22	0.02	0.8	1.0	…	2.0–6.0	20.0–22.5	0.025	0.025	12.5–14.5	2.5–3.5 W, 0.35 V max
Nickel-chromium-iron											
CY-40	Alloy 600	0.40	3.0	1.5	…	11.0 max	14.0–17.0	0.03	0.03	…	…

Note: C and Si are maximum values.

(a) 95% Ni min

The cast versions of the nickel-base alloys do not have the same corrosion resistance as the corresponding wrought products, mainly due to the higher carbon and silicon contents and the anisotropic microstructure of the cast products. Carbon promotes the formation of carbides, and silicon is associated with the precipitation of intermetallic phases, such as μ phase. Secondary- phase compounds are formed during the slow cooling of the cast parts in the molds. After casting, high-temperature solution annealing followed by water quenching is necessary to remove the secondary phases. The specific heat treatment depends on the previous history of the castings, such as silicon content and cooling rate of the mold. A CX-2MW cast containing 0.52% Si requires a 20 min anneal at 1232 °C (2250 °F) followed by water quenching to redissolve most of the original precipitates. The performance of a cast nickel-base alloy is generally based on the microstructural quality, such as the amount of interdendritic segregation, secondary carbides, and intermetallic phases. Failures are commonly attributed to inappropriate casting techniques or heat treatments. Therefore, the corrosion rates of cast alloys vary significantly from one cast to another, even though the overall composition of the cast part is the same. Table 4 gives comparative corrosion rates of several cast alloys as well as the corrosion rates of the corresponding wrought alloys. In general, for all environments, the corrosion rate of the wrought alloys was lower than the corrosion rate of the cast versions. The smallest difference in behavior was given by the CW-2M/C-4 pair. For the other two alloys in Table 4, the corrosion rate of the wrought material was considerably lower than that of the cast version, especially in the oxidizing solutions containing chlorides (ASTM G 28 Method B and boiling 10% $FeCl_3$). The corrosion behavior of cast versus wrought material was inverted for the boiling 65% nitric acid (oxidizing conditions), probably due to the beneficial effect of silicon in the cast alloys.

Table 4 Corrosion rates of selected cast and wrought nickel alloys

Environment	Corrosion rate, mm/year					
	CW-12MW (cast)	**C-276 (wrought)**	**CW-2M (cast)**	**C-4 (wrought)**	**CX-2MW (cast)**	**C-22 (wrought)**
Sulfuric acid/ferric sulfate, boiling (ASTM G 28 Method A)	26.8	6.1	5	4.2	1.8	0.6
Mixed acid-oxidizing salt solution, boiling (ASTM G 28 Method B)	46.5	1.4	54.6	58.3	0.7	0.18
10% HCl, boiling	21.8	7.3	5.9	5.8	17.6	10.2
10% H_2SO_4, boiling	0.4	0.58	0.5	0.79	0.7	0.28
30% H_2SO_4, boiling	2	1.4	1.7	1.8	2.8	1.6
65% HNO_3, boiling	20.5	22.6	11.9	1.35	3	5.5
10% $FeCl_3$, boiling	43.2	0.1	96.6	6.8	4	0.02

Note: The cast alloys were annealed for 20 min at 1230 °C (2250 °F), followed by water quenching. Source: Ref 3

References cited in this section

3. R.B. Rebak, Corrosion of Non-Ferrous Alloys, Part I: Nickel-, Cobalt-, Copper-, Zirconium- and Titanium-Base Alloys, *Corrosion and Environmental Degradation,* Vol II, Wiley-VCH, 2000, p 69

8. P.E. Manning and J.D. Schöbel, *Werkst. Korros.,* Vol 37, 1986, p 137

9. R.B. Rebak, in *Proceedings of the Symposium on Passivity and Its Breakdown,* Vol 97-26, The Electrochemical Society, 1998, p 1001

10. R.B. Rebak and N.E. Koon, Paper 153, Corrosion/98, NACE International, 1998

11. K.A. Gruss, G.A. Cragnolino, D.S. Dunn, and N. Sridhar, Paper 149, Corrosion/98, NACE International, 1998

12. R.B. Rebak and P. Crook, in *Critical Factors in Localized Corrosion III,* Vol PV 98- 17, The Electrochemical Society, 1999, p 289

13. R.B. Rebak, N.E. Koon, J.P. Cotner, and P. Crook, in *Passivity and Localized Corrosion,* Vol PV 99-27, The Electrochemical Society, 1999, p 473

14. D.S. Dunn, G.A. Cragnolino, and N. Sridhar, in *Scientific Basis for Nuclear Waste Management XXII,* Vol 556, Materials Research Society, 1999, p 879

15. B.A. Kehler, G.O. Ilevbare, and J.R. Scully, Paper 182, Corrosion/2000, NACE International, 2000

16. S.J. Matthews, in *Proceedings of the Third International Conference on Superalloys,* Claitor's Publishing Division, 1976, p 215

17. U.L. Heubner, E. Altpeter, M.B. Rockel, and E. Wallis, *Corrosion,* Vol 45, 1989, p 249

18. H.M. Tawancy, *J. Mater. Sci.,* Vol 31, 1996, p 3929

19. T.S. Edgecumbe Summers, M.A. Wall, M. Kumar, S.J. Matthews, and R.B. Rebak, in *Scientific Basis for Nuclear Waste Management XXII,* Vol 556, Materials Research Society, 1999, p 919

20. T.S. Edgecumbe Summers, T. Shen, and R.B. Rebak, in *Aging Studies and Lifetime Extension of Materials,* Kluwer Academic/ Plenum Publisher, 2001, p 507

21. R.B. Rebak, N.E. Koon, J.R. Dillman, P. Crook, and T.S. Edgecumbe Summers, Paper 181, Corrosion/2000, NACE International, 2000

22. R.B. Rebak, T.S. Edgecumbe Summers, and R.M. Carranza, in *Scientific Basis for Nuclear Waste Management XXIII,* Vol 608, Materials Research Society, 2000, p 109

23. R.B. Rebak, N.E. Koon, and P. Crook, in *Electrochemical Approach to Selected Corrosion and Corrosion Control Studies,* No. 28, The Institute of Materials, 2000, p 245

24. T.S. Edgecumbe Summers, R.B. Rebak, T.A. Palmer, and P. Crook, in *Scientific Basis for Nuclear Waste Management XXV,* Materials Research Society, to be published

25. R.B. Rebak, T.S. Edgecumbe Summers, T. Lian, R.M. Carranza, J.R. Dillman, T. Corbin, and P. Crook, Paper 542, Corrosion/ 2002, NACE International, 2002

26. R.B. Rebak and P. Crook, Transportation, Storage and Disposal of Radioactive Materials, *ASME Pressure Vessel and Piping Conference,* 4–8 Aug 2002 (Vancouver, Canada), American Society of Mechanical Engineers, p 111

27. A.R. McIlree, T. Olberg, and J. Nestell, Primary Side Stress- Corrosion Cracking, *Steam Generator Reference Book,* Electric Power Research Institute, 1985, p 7-1 to 7-26

28. J.P.N. Paine, T. Oldberg, R. Marlow, and S. Brown, Tube Intergranular Attack and Stress-Corrosion Cracking on the Secondary Side, *Steam Generator Reference Book,* Electric Power Research Institute, 1985, p 8-1 to 8-64

29. Z. Szklarska-Smialowska and R.B. Rebak, Stress-Corrosion Cracking of Alloy 600 in High-Temperature Aqueous Solutions: Influencing Factors, Mechanisms and Models, *Control of Corrosion on the Secondary Side of Steam Generators,* NACE International, 1996, p 223–257

30. R.C. Scarberry, S.C. Pearman, and J.R. Crum, *Corrosion,* Vol 32, 1976, p 401

31. T. Magnin, J.-M. Boursier, D. Noel, R. Rios, and F. Vaillant, Corrosion Deformation Interaction During Stress-Corrosion Cracking of Alloy 600 in Primary Water, *Proceedings of Sixth International Symposium on Environmental Degradation of Materials in Nuclear Power Systems-Water Reactors,* TMS, 1993, p 669–676

32. G.S. Was, *Corrosion,* Vol 46, 1990, p 319

33. G.S. Was, J.L. Hertzberg, and V. Thaveeprungsriporn, Effect of Grain Boundary Composition and Structure on IGSCC of Alloy 600, *Control of Corrosion on the Secondary Side of Steam Generators,* NACE International, 1996, p 347–400

34. S.M. Bruemmer, L.A. Charlot, and C.H. Henager, Jr., *Corrosion,* Vol 43, 1987, p 782

35. R.B. Rebak, Z. Xia, and Z. Szklarska-Smialowska, *Corrosion,* Vol 49, 1993, p 867

36. R.B. Rebak and P. Crook, Nickel Alloys for Corrosive Environments, *Adv. Mater. Process.,* Vol 157 (No. 2) Feb 2000, p 37–42

37. N. Totsuka, E. Lunarska, G. Cragnolino, and Z. Szklarska-Smialowska, *Corrosion,* Vol 43, 1987, p 505

38. M.O. Speidel and R. Magdowski, Stress- Corrosion Cracking Crack Growth of Nickel-Base Alloys in High-Temperature Water, *Proceedings of Sixth International Symposium on Environmental Degradation of Materials in Nuclear Power Systems-Water Reactors,* TMS, 1993, p 361–371

39. R.B. Rebak, Z. Xia, and Z. Szklarska-Smialowska, *Corrosion,* Vol 51, 1995, p 689

40. W.C. Moshier and C.M. Brown, *Corrosion,* Vol 56, 2000, p 307

41. E.L. Hibner and C.S. Tassen, “Corrosion Resistant OCTGs and Matching Age-Hardenable Bar Products for a Range of Sour Gas Service Conditions,” Paper 01102 (Houston) NACE International, 2001

42. “Laboratory Testing of Metals for Resistance to Sulfide Stress Cracking and Stress Corrosion Cracking in H2S Environments,” Standard TM0177-2002, NACE International, 2002

43. J. Kolts and N. Sridhar, “Environmental Embrittlement of Nickel and Nickel Alloys—An Analogy to Steels and Austenitic Stainless Steels” *Corrosion of Nickel-Base Alloys,* American Society for Metals, 1985, p 199

44. “Sulfide Stress Cracking Resistant Metallic Materials for Oilfield Equipment,” Standard MR0175-2002, NACE International, 2002

R.B. Rebak, Effects of Metallurgical Variables on the Corrosion of High-Nickel Alloys, *Corrosion: Fundamentals, Testing, and Protection*, Vol 13A, *ASM Handbook*, ASM International, 2003, p 279–286

Effects of Metallurgical Variables on the Corrosion of High-Nickel Alloys

Raúl B. Rebak, Lawrence Livermore National Laboratory

Conclusions

In the materials selection process for corrosion applications, the chemical composition of the alloy is generally the most important factor that an engineer considers. However, examples given in this article demonstrate that the metallurgical condition or microstructure of a particular nickel alloy is also a very important factor. For the same overall chemical composition, the corrosion rate of the same alloy can vary several orders of magnitude, depending on its particular microstructure. The most important metallurgical factors that need to be considered are second-phase precipitation by thermal instability and the presence of CW. The latter is especially important in cases where SCC may be expected.

R.B. Rebak, Effects of Metallurgical Variables on the Corrosion of High-Nickel Alloys, *Corrosion: Fundamentals, Testing, and Protection*, Vol 13A, *ASM Handbook*, ASM International, 2003, p 279–286

Effects of Metallurgical Variables on the Corrosion of High-Nickel Alloys

Raúl B. Rebak, Lawrence Livermore National Laboratory

References

1. G.Y. Lai, *High-Temperature Corrosion of Engineering Alloys,* ASM International, 1990
2. B. Gleeson, High-Temperature Corrosion of Metallic Alloys and Coatings, *Corrosion and Environmental Degradation,* Vol II, Wiley-VCH, 2000, p 173
3. R.B. Rebak, Corrosion of Non-Ferrous Alloys, Part I: Nickel-, Cobalt-, Copper-, Zirconium- and Titanium-Base Alloys, *Corrosion and Environmental Degradation,* Vol II, Wiley-VCH, 2000, p 69
4. C.P. Dillon *Corrosion Control in the Chemical Process Industry,* NACE International, 1994
5. R.B. Rebak, J.R. Dillman, P. Crook, and C.V.V. Shawber, *Mater. Corros.,* Vol 52, 2001, p 289–297
6. R.B. Rebak and P. Crook, Paper 00499, Corrosion/2000, NACE International, 2000
7. D.C. Agarwal and J. Kloewer, Paper 01325, Corrosion/01, NACE International, 2001
8. P.E. Manning and J.D. Schöbel, *Werkst. Korros.,* Vol 37, 1986, p 137
9. R.B. Rebak, in *Proceedings of the Symposium on Passivity and Its Breakdown,* Vol 97-26, The Electrochemical Society, 1998, p 1001
10. R.B. Rebak and N.E. Koon, Paper 153, Corrosion/98, NACE International, 1998

11. K.A. Gruss, G.A. Cragnolino, D.S. Dunn, and N. Sridhar, Paper 149, Corrosion/98, NACE International, 1998

12. R.B. Rebak and P. Crook, in *Critical Factors in Localized Corrosion III,* Vol PV 98- 17, The Electrochemical Society, 1999, p 289

13. R.B. Rebak, N.E. Koon, J.P. Cotner, and P. Crook, in *Passivity and Localized Corrosion,* Vol PV 99-27, The Electrochemical Society, 1999, p 473

14. D.S. Dunn, G.A. Cragnolino, and N. Sridhar, in *Scientific Basis for Nuclear Waste Management XXII,* Vol 556, Materials Research Society, 1999, p 879

15. B.A. Kehler, G.O. Ilevbare, and J.R. Scully, Paper 182, Corrosion/2000, NACE International, 2000

16. S.J. Matthews, in *Proceedings of the Third International Conference on Superalloys,* Claitor's Publishing Division, 1976, p 215

17. U.L. Heubner, E. Altpeter, M.B. Rockel, and E. Wallis, *Corrosion,* Vol 45, 1989, p 249

18. H.M. Tawancy, *J. Mater. Sci.,* Vol 31, 1996, p 3929

19. T.S. Edgecumbe Summers, M.A. Wall, M. Kumar, S.J. Matthews, and R.B. Rebak, in *Scientific Basis for Nuclear Waste Management XXII,* Vol 556, Materials Research Society, 1999, p 919

20. T.S. Edgecumbe Summers, T. Shen, and R.B. Rebak, in *Aging Studies and Lifetime Extension of Materials,* Kluwer Academic/ Plenum Publisher, 2001, p 507

21. R.B. Rebak, N.E. Koon, J.R. Dillman, P. Crook, and T.S. Edgecumbe Summers, Paper 181, Corrosion/2000, NACE International, 2000

22. R.B. Rebak, T.S. Edgecumbe Summers, and R.M. Carranza, in *Scientific Basis for Nuclear Waste Management XXIII,* Vol 608, Materials Research Society, 2000, p 109

23. R.B. Rebak, N.E. Koon, and P. Crook, in *Electrochemical Approach to Selected Corrosion and Corrosion Control Studies,* No. 28, The Institute of Materials, 2000, p 245

24. T.S. Edgecumbe Summers, R.B. Rebak, T.A. Palmer, and P. Crook, in *Scientific Basis for Nuclear Waste Management XXV,* Materials Research Society, to be published

25. R.B. Rebak, T.S. Edgecumbe Summers, T. Lian, R.M. Carranza, J.R. Dillman, T. Corbin, and P. Crook, Paper 542, Corrosion/ 2002, NACE International, 2002

26. R.B. Rebak and P. Crook, Transportation, Storage and Disposal of Radioactive Materials, *ASME Pressure Vessel and Piping Conference,* 4–8 Aug 2002 (Vancouver, Canada), American Society of Mechanical Engineers, p 111

27. A.R. McIlree, T. Olberg, and J. Nestell, Primary Side Stress- Corrosion Cracking, *Steam Generator Reference Book,* Electric Power Research Institute, 1985, p 7-1 to 7-26

28. J.P.N. Paine, T. Oldberg, R. Marlow, and S. Brown, Tube Intergranular Attack and Stress-Corrosion Cracking on the Secondary Side, *Steam Generator Reference Book,* Electric Power Research Institute, 1985, p 8-1 to 8-64

29. Z. Szklarska-Smialowska and R.B. Rebak, Stress-Corrosion Cracking of Alloy 600 in High-Temperature Aqueous Solutions: Influencing Factors, Mechanisms and Models, *Control of Corrosion on the Secondary Side of Steam Generators,* NACE International, 1996, p 223–257

30. R.C. Scarberry, S.C. Pearman, and J.R. Crum, *Corrosion,* Vol 32, 1976, p 401

31. T. Magnin, J.-M. Boursier, D. Noel, R. Rios, and F. Vaillant, Corrosion Deformation Interaction During Stress-Corrosion Cracking of Alloy 600 in Primary Water, *Proceedings of Sixth International Symposium on Environmental Degradation of Materials in Nuclear Power Systems-Water Reactors,* TMS, 1993, p 669–676

32. G.S. Was, *Corrosion,* Vol 46, 1990, p 319

33. G.S. Was, J.L. Hertzberg, and V. Thaveeprungsriporn, Effect of Grain Boundary Composition and Structure on IGSCC of Alloy 600, *Control of Corrosion on the Secondary Side of Steam Generators,* NACE International, 1996, p 347–400

34. S.M. Bruemmer, L.A. Charlot, and C.H. Henager, Jr., *Corrosion,* Vol 43, 1987, p 782

35. R.B. Rebak, Z. Xia, and Z. Szklarska-Smialowska, *Corrosion,* Vol 49, 1993, p 867

36. R.B. Rebak and P. Crook, Nickel Alloys for Corrosive Environments, *Adv. Mater. Process.,* Vol 157 (No. 2) Feb 2000, p 37–42

37. N. Totsuka, E. Lunarska, G. Cragnolino, and Z. Szklarska-Smialowska, *Corrosion,* Vol 43, 1987, p 505

38. M.O. Speidel and R. Magdowski, Stress- Corrosion Cracking Crack Growth of Nickel-Base Alloys in High-Temperature Water, *Proceedings of Sixth International Symposium on Environmental Degradation of Materials in Nuclear Power Systems-Water Reactors,* TMS, 1993, p 361–371

39. R.B. Rebak, Z. Xia, and Z. Szklarska-Smialowska, *Corrosion,* Vol 51, 1995, p 689

40. W.C. Moshier and C.M. Brown, *Corrosion,* Vol 56, 2000, p 307

41. E.L. Hibner and C.S. Tassen, “Corrosion Resistant OCTGs and Matching Age-Hardenable Bar Products for a Range of Sour Gas Service Conditions,” Paper 01102 (Houston) NACE International, 2001

42. “Laboratory Testing of Metals for Resistance to Sulfide Stress Cracking and Stress Corrosion Cracking in H2S Environments,” Standard TM0177-2002, NACE International, 2002

43. J. Kolts and N. Sridhar, “Environmental Embrittlement of Nickel and Nickel Alloys—An Analogy to Steels and Austenitic Stainless Steels” *Corrosion of Nickel-Base Alloys,* American Society for Metals, 1985, p 199

44. “Sulfide Stress Cracking Resistant Metallic Materials for Oilfield Equipment,” Standard MR0175-2002, NACE International, 2002

S.G. Corcoran, Effects of Metallurgical Variables on Dealloying Corrosion, *Corrosion: Fundamentals, Testing, and Protection*, Vol 13A, *ASM Handbook*, ASM International, 2003, p 287–293

Effects of Metallurgical Variables on Dealloying Corrosion

Sean G. Corcoran, Virginia Polytechnic Institute and State University

Introduction

DEALLOYING is a corrosion process in which one or more elements are selectively dissolved, leaving behind a porous residue of the remaining element(s). For example, in the silver- gold system, silver can be almost 100% removed in various acid electrolytes, leaving behind porous gold, as shown in Fig. 1. This bicontinuous metal-void structure is highly brittle in nature and has been linked to stress-corrosion cracking in many alloy systems (Ref 1, 2, 3, 4, 5, 6). The seasonal cracking of brass is perhaps the best recognized (Ref 7). Perhaps the first detailed investigation in the scientific literature on alloy corrosion was reported by Calvert and Johnson in 1866 (Ref 8) on copper-zinc alloys. Beyond its direct relevance to stress-corrosion cracking, interest in the dealloying phenomenon extends to the accelerated corrosion in aluminum alloy 2024-T3 (Unified Numbering System, or UNS, A92024) (Ref 9, 10) and the development of high-surface-area electrodes (Ref 11) and catalysts (Ref 12, 13).

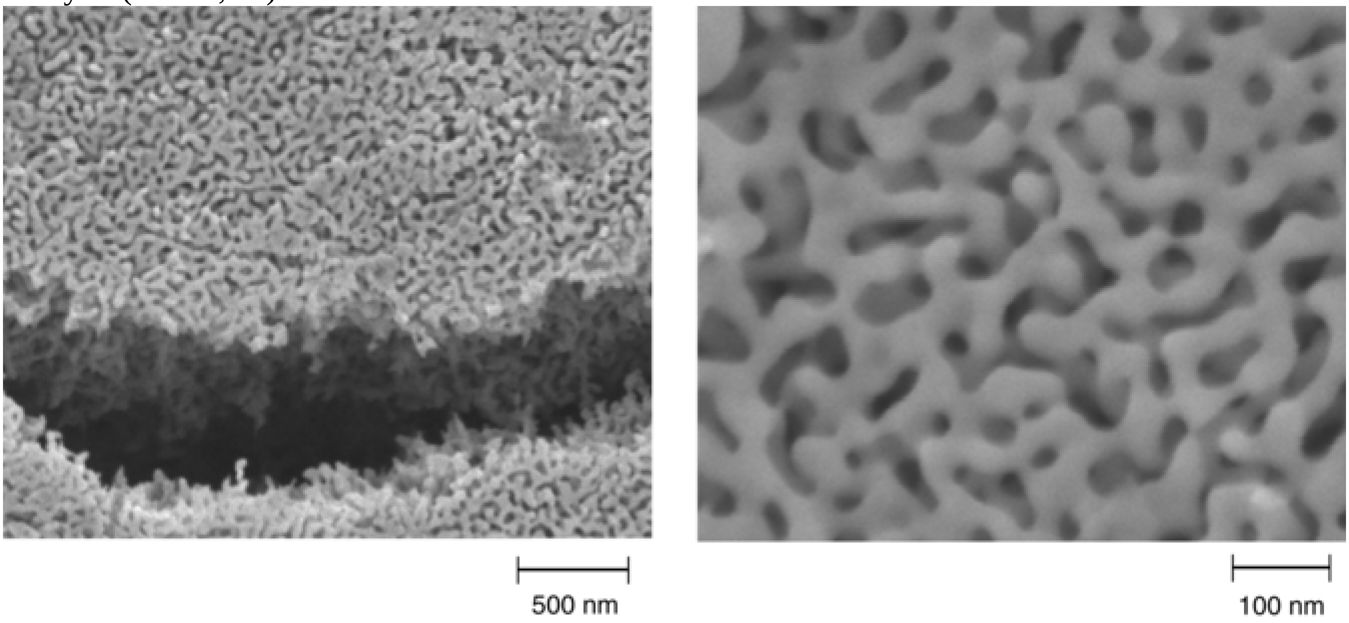

Fig. 1 Two micrographs at different magnifications of porous gold created by dealloying $Ag_{0.75}Au_{0.25}$ in 0.1 *M* $HClO_4$ at 650 mV saturated mercury-mercury sulfate (MSE). The sample was then heat treated at 250 °C (480 °F) for 30 min to coarsen the porosity.

References cited in this section

1. K. Sieradzki and R.C. Newman, Brittle Behavior of Ductile Metals during Stress-Corrosion Cracking, *Philos. Mag. A,* Vol 51, 1985, p 95–132

2. R.C. Newman, R.R. Corderman, and K. Sieradzki, Evidence for Dealloying of Austenitic Stainless Steels in Simulated Stress Corrosion Crack Environments, *Br. Corros. J.,* Vol 24, 1989, p 143–148

3. D.E. Williams, R.C. Newman, Q. Song, and R.G. Kelly, Passivity Breakdown and Pitting Corrosion of Binary-Alloys, *Nature,* Vol 350, 1991, p 216–219

4. H.W. Pickering, Characteristic Features of Alloy Polarization Curves, *Corros. Sci.,* Vol 23, 1983, p 1107–1120

5. J.S. Chen, M. Salmeron, and T.M. Devine, *Corros. Sci.,* Vol 34, 1993, p 2071

6. T.B. Cassagne, W.F. Flanagan, and B.D. Lichter, On the Failure Mechanism of Chemically Embrittled Cu_3Au Single Crystals, *Metall. Trans. A,* Vol 17, 1986, p 703–710

7. H. Moore, S. Beckinsale, and C.E. Mallinson, The Season-Cracking of Brass and Other Copper Alloys, *J. Inst. Met.,* Vol 25, 1921, p 35–153

8. C. Calvert and R. Johnson, Action of Acids upon Metals and Alloys, *J. Chem. Soc.,* Vol 19, p 434–454

9. N. Dimitrov, J.A. Mann, M. Vukmirovic, and K. Sieradzki, Dealloying of Al_2CuMg in Alkaline Media, *J. Electrochem. Soc.,* Vol 147, 2000, p 3283–3285

10. R.G. Buchheit, R.P. Grant, P.F. Hlava, B. McKenzie, and G.L. Zender, Local Dissolution Phenomena Associated with S Phase (Al_2CuMg) Particles in Aluminum Alloy 2024-T3, *J. Electrochem. Soc.,* Vol 144, 1997, p 2621–2628

11. D.V. Pugh, A. Dursun, and S.G. Corcoran, Formation of Nanoporous Platinum by Selective Dissolution of Cu from $Pt_{0.25}Cu_{0.75}$, *J. Electrochem. Soc.,* 2003, in press

12. A.D. Tomsett, H.E. Curry-Hyde, M.S. Wainwright, D.J. Young, and A.J. Bridgewater, Structural Changes during the Leaching of Copper-Based Raney Catalysts, *Appl. Catal.,* Vol 33, 1987, p 119–127

13. A.J. Smith, T. Tran, and M.S. Wainwright, Kinetics and Mechanism of the Preparation of Raney Copper, *J. Appl. Electrochem.,* Vol 29, 1999, p 1085–1094

S.G. Corcoran, Effects of Metallurgical Variables on Dealloying Corrosion, *Corrosion: Fundamentals, Testing, and Protection*, Vol 13A, *ASM Handbook*, ASM International, 2003, p 287–293

Effects of Metallurgical Variables on Dealloying Corrosion

Sean G. Corcoran, Virginia Polytechnic Institute and State University

---

Dealloying in Aqueous Environments

Dealloying has been observed in a number of systems, and a few of these are discussed in this section. The alloy systems discussed here do not represent an exhaustive list but are chosen for their practical or historical significance. In fact, an exhaustive list could not be developed, because it is now known that dealloying can occur in nearly any system in which a large difference in equilibrium potential exists between the alloying components, and the fraction of the less noble constituent(s) is significantly high.

Dezincification. The dezincification of brass is the most well-studied dealloying system, receiving considerable attention after the observation of seasonal cracking of brass cartridge casings (Ref 7). In the 1920s, significant interest focused on the mechanism of brass dealloying with relevance to brass condensor tubes and other components used in seawater applications (Ref 7, 14, 15). Quoting early researchers (Ref 14), "… brass may

behave as an entity when corroded, and that the resulting copper is redeposited … will, in course of time, come to be regarded as correct, in spite of almost universal rejection at the present time." Presently, although the exact role of the redeposition mechanism is not fully understood, it is generally accepted that the dissolution of both copper and zinc and the subsequent redeposition of copper does occur during the corrosion of copper-zinc alloys in many electrolytic solutions. However, it should be pointed out that this condition is not necessary for dezincification to occur, although it surely enhances the rate (see the section "Mechanisms" in this article).

Brasses are immune to dealloying when the zinc compositon is less than approximately 15 at.%. For alloys with greater than 15% Zn, uniform dealloying has been observed in both marine and acidic freshwater environments, while plug (or local) dealloying is typically observed under deposits in seawater environments (Ref 7, 14, 15). Plug dealloying (Fig. 2) occurs spontaneously in 70:30 brass tubes after immersion in seawater at elevated temperatures for a few days and is associated with the formation of a white zinc-salt deposit. Dealloying has also been observed in ammonia-containing solutions (Ref 16, 17, 18), sodium nitrite solutions (Ref 19), and dilute acidic solutions (Ref 14, 15). The dealloying of β-brass (and also two-phase brass alloys) is particularly severe, owing to the high zinc composition of the β phase. In two-phase alloys, the β phase is attacked first, leaving behind a porous copper structure that can act as a cathode, driving the dealloying of the α phase. Dezincification is directly related to the stress-corrosion cracking of copper-zinc alloys (Ref 17).

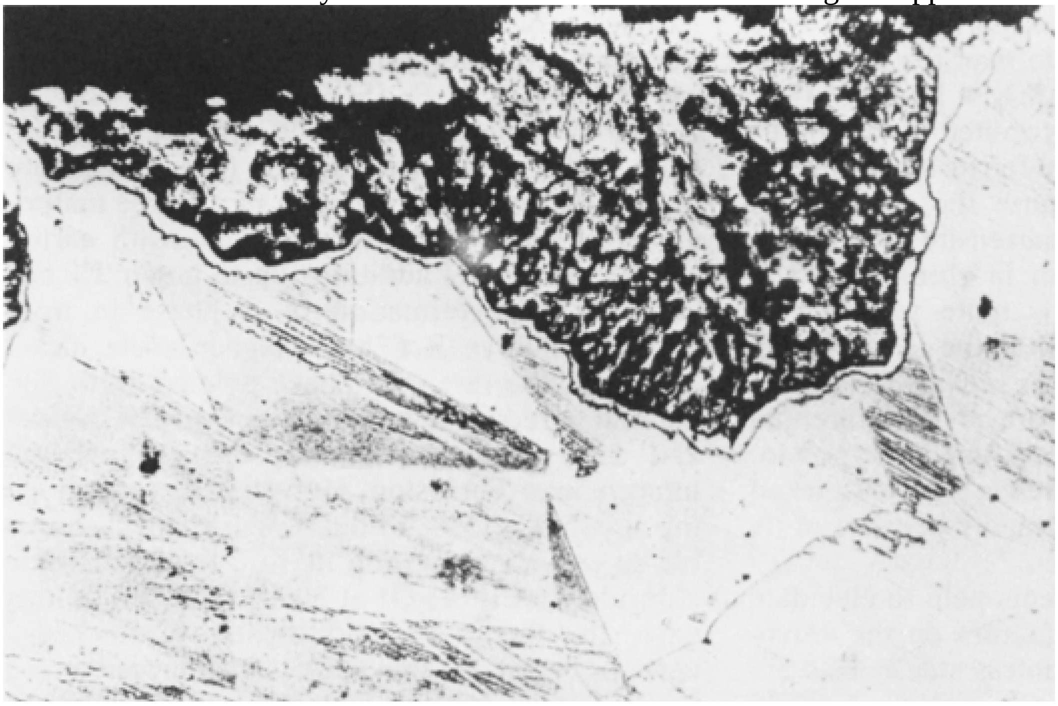

Fig. 2 Plug-type dezincification in an α-brass (70Cu-30Zn) exposed for 79 days in 1 *N* NaCl at room temperature. Note porous structure within the plug. Dark line surrounding the plug is an etching artifact. Total width shown is 0.56 mm (2.2 mils).

Dezincification of α-brass can be minimized by adding 1% Sn, as in admiralty brass (71Cu- 28Zn-1Sn, UNS C44400) and naval brass (60Cu-39Zn-1Sn, UNS C46400), and further inhibited by adding less than 0.1% of arsenic (Ref 20), antimony, or phosphorus. Uniform dealloying in admiralty brass is shown in Fig. 3.

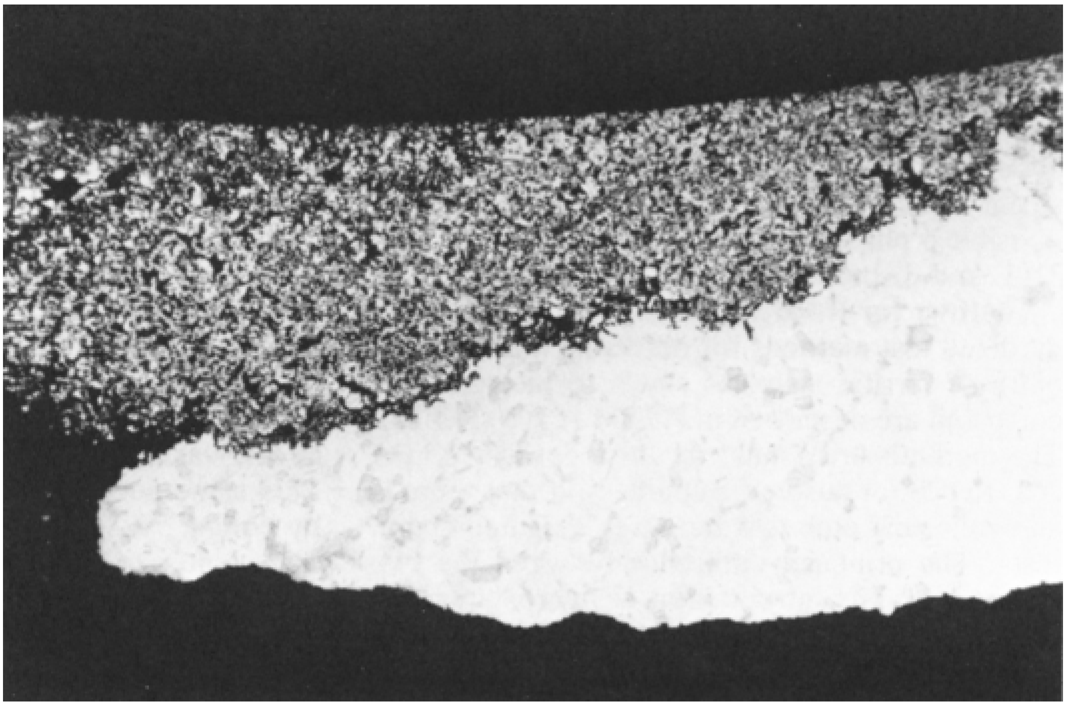

Fig. 3 Uniform-layer dezincification in an admiralty brass 19 mm ($\frac{3}{4}$ in.) diameter heat-exchanger tube. The top layer of the micrograph, which consists of porous, disintegrated particles of copper, was from the inner surface of the tube that was exposed to water at pH 8.0, 31 to 49 °C (87 to 120 °F), and 207 kPa (30 psi). Below the dezincified layer is the bright yellow, intact, admiralty brass outer tube wall. Width of figure is 2.5 mm (0.1 in.). Courtesy of James J. Dillon. Permission granted by Nalco Chemical Company, 1987

Graphitic Corrosion. Another major example of dealloying is graphitic corrosion that occurs in gray cast iron. Gray cast iron has a continuous graphite network in its microstructure that is cathodic to iron and remains behind as a weak, porous network as the iron is selectively removed from the alloy. Graphitic corrosion is observed on buried pipelines after many years of service. Examples of graphitic corrosion are shown in Fig. 4.

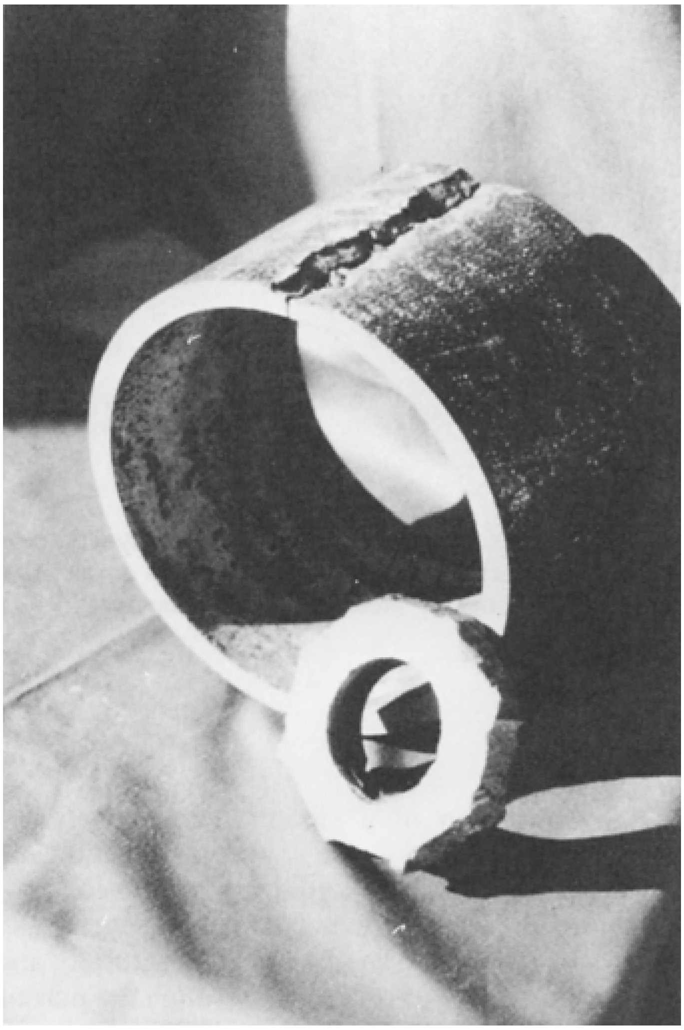

Fig. 4 A 200 mm (8 in.) diameter gray iron pipe that failed because of graphitic corrosion. The pipe was part of a subterranean fire control system. The external surface of the pipe was covered with soil; the internal surface was covered with water. Severe graphitic corrosion occurred along the bottom external surface where the pipe rested on the soil. The small-diameter piece in the foreground is a gray iron pump impeller on which the impeller vanes have disintegrated because of graphitic corrosion. Courtesy of Robert D. Port. Permission granted by Nalco Chemical Company, 1987

Dealuminification. Recent investigations have shown the importance of the dealloying of S-phase (Al_2CuMg) particles on the corrosion of aluminum aircraft alloys, specifically aluminum alloy 2024-T3 (Ref 9, 10). In 2024-T3, the S- phase particles represent approximately 60% of the particle population. These particles are of the order of 1 μm in diameter, with a separation of the order of 5 μm representing an area surface fraction of 3% (Ref 10). The selective removal of aluminum and magnesium from these particles leaves behind a porous copper particle that becomes the preferential site for oxygen reduction (Ref 9). Because the copper particles are small in size and separated over fairly large distances, they behave as microelectrodes and can support much higher oxygen reduction rates than might be expected (as high as 100 $\mu A/cm^2$ or 645 $\mu A/in.^2$) (Ref 9). These sites serve as the cathodes to drive the corrosion of the aluminum matrix, thus releasing more copper on the surface to act as cathodic sites, further driving the corrosion reaction.

Dealloying of Noble Metal Alloys. Dealloying has been observed in the silver-gold (Ref 21, 22, 23, 24, 25, 26, 27, 28), copper-gold (Ref 5, 29, 30, 31, 32, 33), copper-platinum (Ref 11), aluminum-platinum (Ref 34), aluminum-copper (Ref 13, 17, 35, 36, 37, 38), copper- zinc-aluminum (Ref 12, 39), copper-nickel (Ref 40, 41) and manganese-copper systems (Ref 37, 42, 43). The brittle nature of these films is shown in Fig. 5 for porous platinum. The silver-gold and copper-gold systems have been extensively investigated because they represent systems in which the dissolution-redeposition mechanism can be ruled out (see the section "Mechanisms" in this article); that is, gold does not undergo dissolution. The silver-gold system exists as a single-phase random solid solution for all alloy compositions, making this system a particularly well-behaved model system for

dealloying studies. Figures 6, 7, and 8 show one particularly comprehensive set of data for the silver-gold system in acid electrolyte. These results are subsequently discussed further.

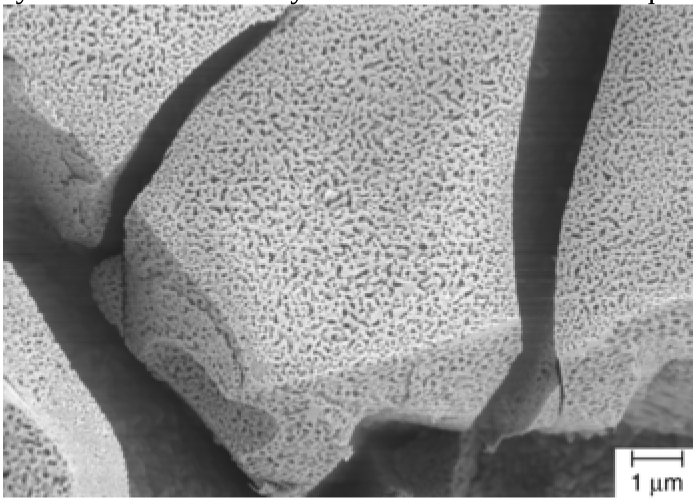

Fig. 5 Dealloyed $Cu_{0.75}Pt_{0.25}$ demonstrating the extreme brittle nature of these materials. The sample was heat treated at 650 °C (1200 °F) for 30 min following the dealloying to coarsen the porosity to a size scale easily observable in the electron microscope. The as-dealloyed structure consists of pores of 3 nm in diameter. Both intergranular and transgranular cracking are common in these materials.

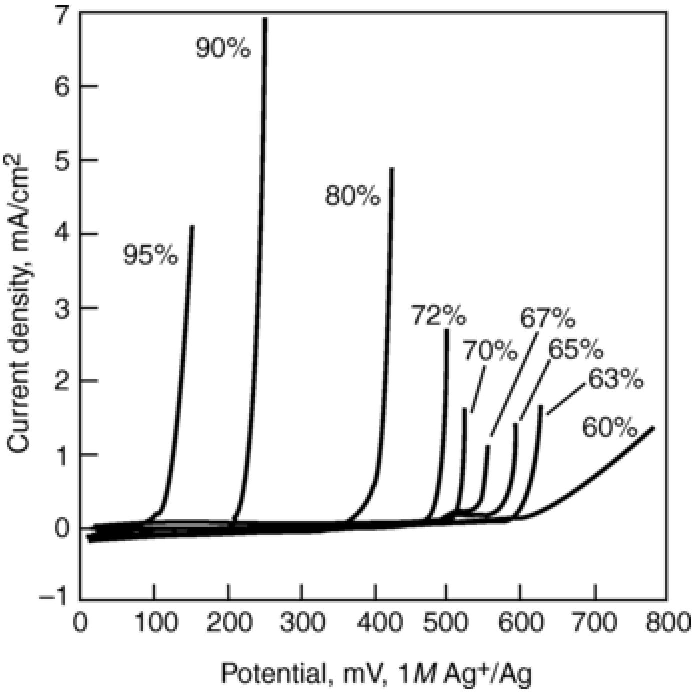

Fig. 6 Current-potential behavior of various silver-gold alloys in the 1 *M* $AgClO_4$ + 1 *M* $HClO_4$ solution. Percent silver is given on curves. No selective dissolution was observed for alloys containing less than 60 at.% Ag. Source: Ref 26

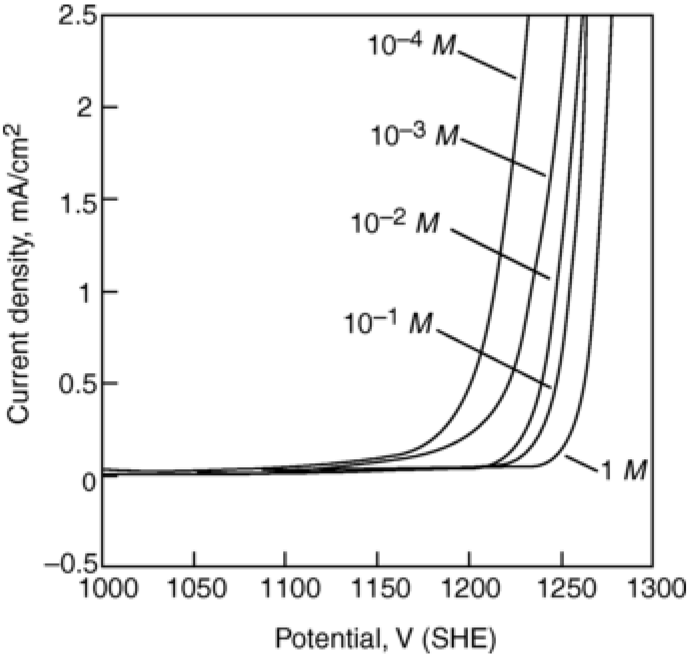

Fig. 7 Current-potential behavior of the $Ag_{0.72}Au_{0.28}$ alloy in various *M* $AgClO_4$ + 1 *M* $HClO_4$. SHE, standard hydrogen electrode. Source: Ref 26

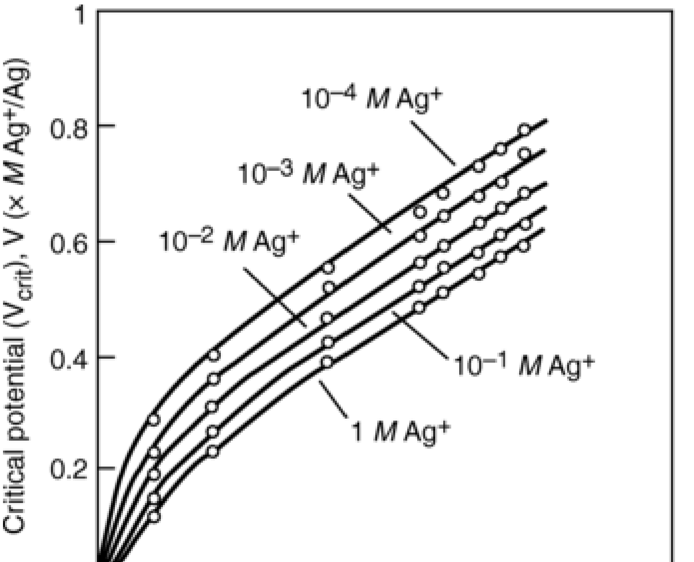

Fig. 8 Summary of critical potentials as a function of the atomic percent of gold in the alloy for all alloys in various *M* $AgClO_4$ + 1 *M* $HClO_4$. The points correspond to the data, and the curves are fits using Eq 3. Source: Ref 26

Other Systems. In general, dealloying can occur in any system where a large difference exists in the equilibrium potentials of the alloy elements. A number of systems have been developed or investigated by various researchers in attempts at better understanding the dealloying process or in an interest to develop various porous metal structures. Of some of the more technologically relevant materials, evidence for dealloying has been reported in austenitic stainless steel and iron-nickel alloys in acidified chloride containing solutions (Ref 2, 46), reduction of titanium dioxide in molten calcium chloride (Ref 44, 45), and dissolution of copper-aluminum, and copper-zinc-aluminum alloy pellets in NaOH solutions to produce Raney (Grace Davison) metal particles (Ref 12, 13).

References cited in this section

2. R.C. Newman, R.R. Corderman, and K. Sieradzki, Evidence for Dealloying of Austenitic Stainless Steels in Simulated Stress Corrosion Crack Environments, *Br. Corros. J.,* Vol 24, 1989, p 143–148

5. J.S. Chen, M. Salmeron, and T.M. Devine, *Corros. Sci.,* Vol 34, 1993, p 2071

7. H. Moore, S. Beckinsale, and C.E. Mallinson, The Season-Cracking of Brass and Other Copper Alloys, *J. Inst. Met.,* Vol 25, 1921, p 35–153

9. N. Dimitrov, J.A. Mann, M. Vukmirovic, and K. Sieradzki, Dealloying of Al_2CuMg in Alkaline Media, *J. Electrochem. Soc.,* Vol 147, 2000, p 3283–3285

10. R.G. Buchheit, R.P. Grant, P.F. Hlava, B. McKenzie, and G.L. Zender, Local Dissolution Phenomena Associated with S Phase (Al_2CuMg) Particles in Aluminum Alloy 2024-T3, *J. Electrochem. Soc.,* Vol 144, 1997, p 2621–2628

11. D.V. Pugh, A. Dursun, and S.G. Corcoran, Formation of Nanoporous Platinum by Selective Dissolution of Cu from $Pt_{0.25}Cu_{0.75}$, *J. Electrochem. Soc.,* 2003, in press

12. A.D. Tomsett, H.E. Curry-Hyde, M.S. Wainwright, D.J. Young, and A.J. Bridgewater, Structural Changes during the Leaching of Copper-Based Raney Catalysts, *Appl. Catal.,* Vol 33, 1987, p 119–127

13. A.J. Smith, T. Tran, and M.S. Wainwright, Kinetics and Mechanism of the Preparation of Raney Copper, *J. Appl. Electrochem.,* Vol 29, 1999, p 1085–1094

14. R.B. Abrams, The Dezincification of Brass, *Trans. Am. Chem. Soc.,* Vol 42, 1922, p 39–55

15. G.D. Bengough, R.M. Jones, and R. Pirret, Fifth Report to the Corrosion Committee of the Institute of Metals, *J. Inst. Met.,* Vol 23, 1920, p 65–158

16. J.A. Beavers and E.N. Pugh, The Propagation of Transgranular Stress-Corrosion Cracks in Admiralty Metal, *Metall. Trans. A,* Vol 11, 1980, p 809–820

17. K. Sieradzki, J.S. Kim, A.T. Cole, and R.C. Newman, The Relationship Between Dealloying and Transgranular Stress-Corrosion Cracking of Cu-Zn and Cu-Al Alloys, *J. Electrochem. Soc.,* Vol 134, 1987, p 1635–1639

18. C. Edeleanu and A.J. Forty, Some Observations on the Stress Corrosion Cracking of Alpha-Brass and Similar Alloys, *Philos. Mag.,* Vol 5, 1960, p 1029–1040

19. A.T. Cole, R.C. Newman, and K. Sieradzki, A Comparison and Evaluation of Bare Surface Electrochemical Techniques for the Investigation of Stress Corrosion Cracking in Alpha Brass, *Corros. Sci.,* Vol 28, 1988, p 109–118

20. M.J. Pryor and G. Kar-Kheng, The Effect of Arsenic on the Dealloying of Alpha-Brass, *J. Electrochem. Soc.,* Vol 129, 1982, p 2157–2163

21. S.G. Corcoran, D.G. Wiesler, and K. Sieradzki, An In Situ Small Angle Neutron Scattering Investigation of $Ag_{0.7}Au_{0.3}$ Dealloying Under Potential Control, *Mater. Res. Soc. Sym. Proc.,* Vol 451, 1997, p 93–98

22. R.G. Kelly, A.J. Frost, T. Shahrabi, and R.C. Newman, Brittle Fracture of an Au/Ag Alloy Induced by a Surface Film, *Metall. Trans. A,* Vol 22, 1991, p 531–541

23. A.J. Forty and P. Durkin, A Micromorphological Study of the Dissolution of Silver- Gold Alloys in Nitric Acid, *Philos. Mag. A,* Vol 42, 1980, p 295

24. P. Durkin and A.J. Forty, Oxide Formation during the Selective Dissolution of Silver from Silver-Gold Alloys in Nitric Acid, *Philos. Mag. A,* Vol 45, 1982, p 95–105

25. J. Erlebacher, M.J. Aziz, A. Karma, N. Dimitrov, and K. Sieradzki, Evolution of Nanoporosity in Dealloying, *Nature,* Vol 410, 2001, p 450–453

26. K. Sieradzki, N. Dimitrov, D. Movrin, C. McCall, N. Vasiljevic, and J. Erlebacher, The Dealloying Critical Potential, *J. Electrochem. Soc.,* Vol 149, 2002, p B370–B377

27. R.C. Newman, S.G. Corcoran, J. Erlebacher, M.J. Aziz, and K. Sieradzki, Alloy Corrosion, *Mater. Res. Soc. Bull.,* Vol 24, 1999, p 24–28

28. G.S. Duffo and J.R. Galvele, *Corros. Sci.,* Vol 30, 1990, p 249

29. B. Bakish and W.D. Robertson, Structure- Dependent Chemical Reaction and Nucleation of Fracture in Cu_3Au Single Crystals, *Acta Metall. Mater.,* Vol 4, 1956, p 342–351

30. T.P. Moffat, F.-R.F. Fan, and A.J. Bard, Electrochemical and Scanning Tunneling Microscopic Study of Dealloying of Cu_3Au, *J. Electrochem. Soc.,* Vol 138, 1991, p 3224–3235

31. J.S. Chen, A. Kadic-Galeb, M. Ferrari, and T.M. Devine, Embrittlement of Nano-scale Structures, *Mech. Res. Commun.,* Vol 19, 1992, p 555–561

32. J.D. Fritz and H.W. Pickering, Selective Anodic Dissolution of Cu-Au Alloys: TEM and Current Transient Study, *J. Electrochem. Soc.,* Vol 138, 1991, p 3209–3218

33. B.G. Ateya, J.D. Fritz, and H.W. Pickering, Kinetics of Dealloying of a Copper-5 Atomic Percent Gold Alloy, *J. Electrochem. Soc.,* Vol 144, 1997, p 2606–2613

34. M.C. Simmonds, H. Kheyrandish, J.S. Colligon, M.L. Hitchman, N. Cade, and J. Iredale, The Observation of a Threshold in the De-Alloying of Sputter-Deposited Pt_xAl_{1-x} Alloy Thin Films, *Corros. Sci.,* Vol 40, 1998, p 43–48

35. J. Szot, D.J. Young, A. Bourdillon, and K.E. Easterling, Cellular Morphologies in a De- Alloying Residue, *Philos. Mag. Lett.,* Vol 55, 1987, p 109–114

36. K. Sieradzki and R.C. Newman, Stress Corrosion Cracking, *J. Phys. Chem. Solids,* Vol 48, 1987, p 1101–1113

37. M.J. Pryor and J.C. Fister, The Mechanism of Dealloying of Copper Solid Solutions and Intermetallic Phases, *J. Electrochem. Soc.,* Vol 131, 1984, p 1230–1235

38. A.D. Tomsett, D.J. Young, M.R. Stammbach, and M.S. Wainwright, Ageing of Dealloyed Copper, *J. Mater. Sci.,* Vol 25, 1990, p 4106–4112

39. M.S. Wainwright and D.L. Trimm, Methanol Synthesis and Water-Gas Shift Reactions on Raney Copper Catalysts, *Catal. Today,* Vol 23, 1995, p 29–42

40. R. Pope, B. Little, and R. Ray, Microscopies, Spectroscopies and Spectrometries Applied to Marine Corrosion of Copper, *Biofouling,* Vol 16, 2000, p 83

41. A.M. Beccaria, G. Poggi, P. Traverso, and M. Ghiazza, A Study of the De-Alloying of 70Cu-30Ni Commercial Alloy in Sulfide Polluted and Unpolluted Sea Water, *Corros. Sci.*, Vol 32, 1991, p 1263–1275

42. D.S. Keir and M.J. Pryor, The Dealloying of Copper-Manganese Alloys, *J. Electrochem. Soc.*, Vol 127, 1980, p 2138–2144

43. U.S. Min and J.C.M. Li, The Microstructure and Dealloying Kinetics of a Cu-Mn Alloy, *J. Mater. Res.*, Vol 9, 1994, p 2878–2883

44. G.Z. Chen, D.J. Fray, and T.W. Farthing, Direct Electrochemical Reduction of Titanium Dioxide to Titanium in Molten Calcium Chloride, *Nature*, Vol 407, 2000

45. D.J. Fray, Electrochemical Method Uses Molten Calcium Chloride to Extract Metals Directly from Their Oxides, *Mater. Res. Soc. Bull.*, Vol 25, 2000, p 11–12

46. R.C. Newman and A. Mehta, An AC impedance Study of the De-Alloying of Fe-Ni Alloys, and Its Relevance to Chloride SCC of Stainless Steels, *Corros. Sci.*, Vol 28, 1988, p 1183–1187

S.G. Corcoran, Effects of Metallurgical Variables on Dealloying Corrosion, *Corrosion: Fundamentals, Testing, and Protection*, Vol 13A, *ASM Handbook*, ASM International, 2003, p 287–293

Effects of Metallurgical Variables on Dealloying Corrosion

Sean G. Corcoran, Virginia Polytechnic Institute and State University

---

The Critical Potential

Figure 9 shows a schematic illustration of the current-potential behavior of a binary alloy undergoing selective dissolution as well as the corresponding dissolution of the individual pure elements. One way in which to quantify the susceptibility of an alloy to dealloying is to define its critical potential (Ref 4). The critical potential is the value of potential associated with the "knee" in the schematic curve of Fig. 9 (above this, potential dealloying proceeds). It is important to recognize that the critical potential is not very well defined; the dashed lines represent the ambiguity in defining the critical potential for this schematic curve. The position of this knee is dependent on the sweep rate, the prior history of the alloy surface, as well as the alloy composition and electrolyte composition.

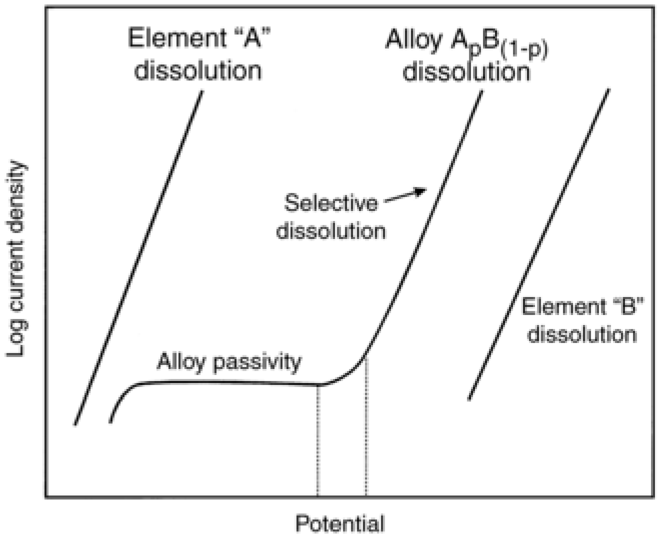

Fig. 9 Schematic illustration of the current-potential behavior of elemental metal "A" and "B" dissolution and the corresponding "$A_pB_{(1-p)}$" alloy dissolution. The critical potential corresponds to that associated with the knee in the curve and is not sharply defined. The shape of the knee is affected by sweep rate as well as alloy and electrolyte composition. The dashed vertical lines indicate typical ambiguity in defining a critical potential.

Reference cited in this section

4. H.W. Pickering, Characteristic Features of Alloy Polarization Curves, *Corros. Sci.,* Vol 23, 1983, p 1107–1120

S.G. Corcoran, Effects of Metallurgical Variables on Dealloying Corrosion, *Corrosion: Fundamentals, Testing, and Protection*, Vol 13A, *ASM Handbook*, ASM International, 2003, p 287–293

Effects of Metallurgical Variables on Dealloying Corrosion

Sean G. Corcoran, Virginia Polytechnic Institute and State University

---

Below the Critical Potential

Small but measurable currents (i) exist below the critical potential. These currents rapidly decay in time (t) following a power-law behavior, $i \propto t^{-m}$, with m in the range of 0.5 to 1.0.

There have been two main opposing views for dealloying below the critical potential (Ref 47, 48) that represent the two limiting cases of the problem. Researchers (Ref 48) consider the evolution of concentration gradients near the surface as surface atoms of "A" that are dissolved into the electrolyte. Continued dissolution results from the diffusion of "A" atoms from the bulk of the alloy driven by the developing concentration gradient. Equating the kinetics of dissolution and diffusion, the researchers have developed analytical equations for the decaying current with time.

Other researchers (Ref 47) argue that, owing to curvature effects, "A" atoms located in terraces do not dissolve below the critical potential, and hence, dissolution initially begins at step edges and at a few large clusters of "A" atoms existing on the surface. The surface morphology evolves through the coalescence and diffusion of surface vacancies and vacancy clusters. Dissolution is supported when vacancy clusters contact "A" atoms in the surface layer or expose large clusters of "A" atoms in the second-layer terrace. The vacancy clusters grow with continued dissolution of "A" atoms, and, as a result, its overall diffusion decreases with time, resulting in a decreasing current. In situ scanning tunneling microscopy (STM) results support the mechanism of vacancy clustering and preferential attack at step edges (Ref 47, 49).

References cited in this section

47. K. Wagner, S.R. Brankovic, N. Dimitrov, and K. Sieradzki, Dealloying Below the Critical Potential, *J. Electrochem. Soc.,* Vol 144, 1997, p 3545–3555

48. B.G. Ateya and H.W. Pickering, The Effects of Potential and Kinetic Parameters on the Formation of Passivating Noble Metal Rich Surface Layers during the Selective Dissolution of Binary Alloys, *Corros. Sci.,* Vol 38, 1996, p 1245–1267

49. J.S. Chen, F. Sanz, D.F. Ogletree, V.M. Hallmark, T.M. Devine, and M. Salmeron, Selective Dissolution of Copper from Au-Rich Cu-Au Alloys—An Electrochemical STM Study, *Surf. Sci.,* Vol 292, 1993, p 289–297

S.G. Corcoran, Effects of Metallurgical Variables on Dealloying Corrosion, *Corrosion: Fundamentals, Testing, and Protection*, Vol 13A, *ASM Handbook*, ASM International, 2003, p 287–293

Effects of Metallurgical Variables on Dealloying Corrosion

Sean G. Corcoran, Virginia Polytechnic Institute and State University

Morphology Above the Critical Potential

Initially, there was some debate on the morphology of porous dealloyed structures. It is now well recognized that these structures consist of bicontinuous metal-void phases, as shown in Fig. 1. The as-dealloyed structure consists of pore spacing on the nanometer scale and can be as small as 2 to 3 nm in, for example, the platinum-copper system (Ref 11). The structure can be coarsened to larger-length scales at elevated temperatures (Ref 50) (Fig. 5). Small-angle neutron scattering has been recently applied to the characterization of porous metals in both in situ and ex situ experiments (Ref 21, 51, 52). The researchers have found a dependence of the morphology on dealloying potential, electrolyte composition, halide additions to the electrolyte, alloy composition, temperature, and time.

References cited in this section

11. D.V. Pugh, A. Dursun, and S.G. Corcoran, Formation of Nanoporous Platinum by Selective Dissolution of Cu from $Pt_{0.25}Cu_{0.75}$, *J. Electrochem. Soc.*, 2003, in press

21. S.G. Corcoran, D.G. Wiesler, and K. Sieradzki, An In Situ Small Angle Neutron Scattering Investigation of $Ag_{0.7}Au_{0.3}$ Dealloying Under Potential Control, *Mater. Res. Soc. Sym. Proc.*, Vol 451, 1997, p 93–98

50. R. Li and K. Sieradzki, Ductile-Brittle Transition in Random Porous Au, *Phys. Rev. Lett.*, Vol 68, 1992, p 1168–1171

51. S.G. Corcoran, K. Sieradzki, and D. Wiesler, in *Proceedings of the Symposium on Scattering for Materials Science II*, D.A. Neumann, T.P. Russell, and B.J. Wuensch, Ed., Materials Research Society, 1994, p 377–382

52. S.G. Corcoran, The Morphology of Alloy Corrosion, *Proceedings of the Symposium on Critical Factors in Localized Corrosion III*, R.G. Kelly, G.S. Frankel, P.M. Natishan, and R.C. Newman, Ed., The Electrochemical Society, 1999, p 500–507

S.G. Corcoran, Effects of Metallurgical Variables on Dealloying Corrosion, *Corrosion: Fundamentals, Testing, and Protection*, Vol 13A, *ASM Handbook*, ASM International, 2003, p 287–293

Effects of Metallurgical Variables on Dealloying Corrosion

Sean G. Corcoran, Virginia Polytechnic Institute and State University

Mechanisms

One of the fundamental questions regarding the formation of porous metals is the mechanism by which the selective dissolution process is maintained over more than a few atomic layers, leading to the three-dimensional porous structures shown in Fig. 1. Four possible mechanisms have been offered for the formation of porous metals:

- *The ionization-redeposition mechanism:* Both elements of the binary alloy dissolve, but the more noble element is redeposited (Ref 14).
- *The surface diffusion mechanism:* Only the less noble element is dissolved, and the remaining more noble element aggregates by surface diffusion (Ref 53).
- *The volume diffusion mechanism:* The less noble element is dissolved, but both atoms move in the solid phase by volume diffusion (Ref 54, 55).
- *The percolation model of selective dissolution:* The surface diffusion model was extended to account for preexisting interconnected paths of like elements in the binary alloy (Ref 56) and was later extended to include curvature effects on the dissolution potential (Ref 26, 57).

Before briefly reviewing the proposed mechanisms, it is useful to consider some features experimentally observed for dealloying systems. Any useful model of the dealloying process must be consistent with the experimentally observed behaviors.
There are common features associated with dealloying systems. They include:

- The electrochemical behavior consists of a dealloying critical potential above which the bicontinuous morphologies shown in Fig. 1 develop. The critical potential is dependent on the applied scan rate (Ref 26), electrolyte composition (Ref 26), presence of halides (Ref 58), temperature, and alloy composition (Ref 26, 58).
- The resultant pore morphologies are bicontinuous (Ref 52) and qualitatively resemble that of spinodally decomposed systems (Ref 52). They do not resemble (negative) dendritelike morphologies, as is expected for aggregation processes (Ref 59).
- The average pore spacing increases as the applied potential is decreased (Ref 21, 52), increases as the dealloying rate is decreased (Ref 60), and increases with an increase in the electrolyte temperature (Ref 60).
- Coarsening of the porosity occurs during the dealloying process and is potential dependent (Ref 52, 61). The pore size increases as $t^{0.25}$, consistent with surface diffusion coarsening (Ref 21, 51).
- Intermixing is observed at alloy surfaces during dealloying, which can result in the formation of low-composition phases or compositional variations in the dealloyed structure (Ref 33).
- An alloy compositional threshold exists, below which dealloying will not occur for a given alloy system (Ref 17, 56).
- Complete selectivity is obtained in certain binary alloy systems; for example, in the gold alloy and platinum alloy systems, only the alloying element is dissolved. For less noble systems, such as copper-zinc, both elements may undergo dissolution.

Ionization-Redeposition Mechanism for Selective Dissolution. One of the first mechanisms proposed for the dezincification of brass was the idea that both the copper and zinc dissolve into the electrolyte, followed by the redeposition of copper at more cathodic sites (Ref 14, 15). This model was thought to be necessary to explain how dealloying could be maintained over macroscopic depths. It is now clear that this mechanism is not a necessary condition for dealloying. For example, in the gold-silver system, only selective removal of silver occurs in 0.1 *M* $HClO_4$, because the gold can only undergo oxidation and not dissolution. This is also true for many other gold- and platinum-base systems. However, in the copper-zinc system, the dissolution of copper and zinc may occur simultaneously, although at different rates. In fact, during the production of Raney copper, researchers (Ref 13) measured a change in corrosion potential consistent with the ionization-redeposition mechanism. When present, this mechanism would result in accelerated dealloying kinetics and would be expected to affect overall pore size.
It is worth pointing out that, owing to curvature effects, the dissolution of copper may occur at values less than the standard equilibrium electrode potential. As the zinc is selectively dissolved, high-curvature copper regions develop. Considering the average initial radius of one of these regions to be of the order of 3 nm, then the

change in the equilibrium potential for copper dissolution can be calculated using a Gibbs- Thomson relationship:

$$\Delta E \cong \frac{\gamma\Omega}{nq}\kappa \quad \text{(Eq 1)}$$

where γ is the surface free energy, Ω is the atomic volume, n is the number of electrons tranferred per atom, q is the charge of an electron, and $\kappa = r^{-1}$, where r is the radius of the initial curvature of the bicontinuous dealloyed structure. For $\gamma = 1$ J/m^2, $\Omega = 1.6 \times 10^{-29}$ m^3, $n = 1$, $q = 1.602 \times 10^{-19}$ C, and $r = 3 \times 10^{-9}$ m, the equilibrium potential is decreased by 33 mV.

Volume Diffusion Model for Selective Dissolution. In this mechanism (Ref 54, 55, 62, 63), the less noble element in the alloy undergoes selective dissolution. The dissolution process is maintained beyond the first few monolayers by volume diffusion of both elements in the solid phase. The inherent problem with this mechanism is that, at room temperature, the rate of transport of the less noble element to the surface is not sufficient to support the dealloying current densities greater than 10 mA/cm^2 (64 mA/in.^{2}) observed experimentally. A mechanism was proposed (Ref 55) in an attempt to account for the requirement of unusually high volume diffusivities that would be necessary to support experimentally observed dealloying currents. The researchers proposed that as the alloy is subjected to the preferential removal of the less noble element, surface vacancies are created. These vacancies can be filled by either atoms on the surface, annihilation at step edges on the surface, coalescence into larger vacancy clusters, or by atoms from the lattice layer below. Taking the best-case scenario and allowing vacancies to only be filled by the lattice layer below, vacancies and divacancies are injected into the crystal volume below the surface. This would result in a buildup of excess vacancies beyond the thermodynamic equilibrium concentration and enhanced diffusion of the less noble element toward the surface and the more noble element away from the surface, owing to compositional gradients created by the selective removal process. This upper-bound calculation, based on a divacancy diffusion mechanism, can support currents as high as 0.2 mA/cm^2 (1.3 mA/in.^{2}), corresponding to a divacancy diffusivity of 10^{-12} cm^2/s (1.6×10^{-13} in.^{2}/s). Researchers (Ref 64) showed that if the dealloying process is rate limited by the volume diffusion of the less noble element to the electrolyte-alloy interface, a roughening instability is predicted. This instability is proposed as a mechanism to explain the highly porous morphologies observed in dealloyed systems.

There are several problems with the volume diffusion mechanism. In calculating an upper bound on the current, the researchers have had to use some extreme assumptions. For example, the mole fraction of divacancies needed to support a current of 0.2 mA/cm^2 (1.3 mA/in.^{2}) is 10^{-2}. This number is approximately 100 times larger than the equilibrium mole fraction of monovacancies at the melting point of a metal. Even with these assumptions, the value of 0.2 mA/cm^2 (1.3 mA/in.^{2}) is 10 to 100 times lower than experimentally measured dealloying currents. Further, the model does not seem to provide any basis for explaining experimentally observed compositional dependences of the dealloying current, critical compositional thresholds for dealloying, and the prediction of a critical potential.

The model also predicts that a surface-roughening instability occurs with the rate-limiting step in the metal phase. This instability is similar to that for aggregation processes (Ref 59) and should therefore lead to the formation of a (negative) dendritelike morphology rather than a bicontinuous structure, which exists for the dealloying process.

Researchers (Ref 37) pointed out that the dealloying rates for copper alloys (copper-aluminum, copper-manganese, and copper-zinc) do not fall in the same order as diffusion rates for the same alloys. For example, copper-manganese displays, by far, the fastest dealloying kinetics but the smallest diffusivity. Further, if one considers varying compositions in the copper-aluminum system, one finds 4 orders of magnitude increase in dealloying kinetics from the β' to θ phase, while the diffusion coefficient actually decreases slightly. The volume diffusion mechanism is also fairly insensitive to alloy composition, while it is observed that the dealloying current densities increase several orders of magnitude as the aluminum composition in copper-aluminum is increased from 30 to 60%.

Surface Diffusion/Structural Rearrangement Model for Selective Dissolution. The surface diffusion model, or the surface disordering-reordering model (Ref 53), proposes that the less noble element is preferentially dissolved. The remaining more noble element is now in a highly disordered state and begins to reorder by surface diffusion and nucleation of islands of almost pure noble metal. The coalescence of these islands continues to expose fresh alloy surface where further dissolution will occur, leading to the formation of tunnels

and pits. Additions to the electrolyte of ions that would influence the surface diffusivity of the more noble metal would be expected to influence the dealloying process. Such observations have been observed experimentally; examples include potential-dependent coarsening of porosity (Ref 21, 61) and changes in the critical dealloying potential, owing to electrolyte impurity additions (Ref 58). However, the most common argument against this model is that the mechanism for sustained three-dimensional porosity development is not clear, and that the model predicts a nearly pure noble-metal dealloyed structure. The model, as originally formulated, would predict an enriching at the surface of the more noble element, eventually bringing an end to further dealloying. Calculations (Ref 53) do predict the formation of pits in the alloy surface but also predict the continual decreasing of the pit radius with time, at which time the dealloying process ceases. Much of these issues has been resolved by recognizing the importance of percolation concepts and curvature in dealloying and coarsening processes, as discussed in the next section.

A structural rearrangement of the more noble element, leaving behind a porous residue for the electrolyte to penetrate into the alloy, was also proposed (Ref 42) as an alternative to selective dissolution by volume diffusion. These researchers also recognized the fact that continuous paths of the less noble solute exist at high alloy concentrations (Ref 37). The solute can be easily removed along these paths, leaving behind the more noble element in high-energy configurations. The subsequent local rearrangement creates clusters and voids in the form of the bicontinuous morphologies. This structure then allows for penetration of electrolyte into the alloy for further dissolution and alleviates the problem of continuing dissolution through bulk transport of the solute to the surface. These ideas are central to the percolation model for selective dissolution developed later (Ref 56).

Percolation Model for Selective Dissolution. In many alloy systems, a sharp critical composition of the less noble element exists, below which dealloying does not occur (Ref 17). For the zinc-copper and aluminum-copper systems, the threshold is 18 ± 2 at.% for zinc and 14 ± 2 at.% for aluminum, respectively. These critical compositions are not consistent with the conventional views for a surface diffusion mechanism of dealloying. Motivated by the fact that these critical thresholds are very close to the site percolation thresholds for the face-centered cubic (fcc) lattice (19.8%) (Ref 65), researchers (Ref 56) developed the percolation model for selective dissolution. This model extends the surface diffusion model to include the importance of the atomic placement of atoms in the randomly packed alloy. The model predicts that, as a minimum requirement, a continuous connected cluster of the less noble atoms must exist in order for the selective dissolution process to be maintained for more than just the first few monolayers of the alloy. This percolating cluster of atoms provides a continuous active pathway for the corrosion process as well as a pathway for the electrolyte to penetrate the solid. As the dealloying process proceeds along these pathways, a highly porous network is created at the atomic scale. The structure immediately begins to coarsen by curvature-driven surface diffusion, which has been confirmed experimentally using impedance spectroscopy (Ref 61) and small-angle neutron experiments (Ref 21, 51, 52). The coarsening process enlarges the diameter of the pores, allowing further electrolyte into the alloy.

More recently, researchers (Ref 56, 57) analyzed the dealloying process in terms of a kinetic roughening instability occurring between curvature-dependent dissolution (roughening) and surface diffusion (smoothening). This analysis provides a basis for understanding critical compositions that do not fall close to the site percolation threshold. For example, the critical composition of silver in silver-gold is approximately 60%, which is substantially elevated from the fcc site percolation threshold of 19.8%. At the present time, this model is the most promising, in that it can qualitatively (and many times, quantitatively) explain the most common features associated with dealloying, including critical composition thresholds for dealloying, compositional dependence of the critical potential, and the formation of a bicontinuous dealloyed morphology.

Taking into account curvature effects, one can show from classical thermodynamics that the chemical-potential difference between a flat surface and a surface of curvature, κ, is given by $\Delta\mu = \gamma\Omega\kappa$, where γ is the isotropic solid-liquid interfacial free energy per unit area, and Ω is the atomic volume. As mentioned, the local equilibrium metal/metal-ion electrode potential is given by:

$$E = \bar{E} - \frac{\gamma\Omega\kappa}{nq} \quad \text{(Eq 2)}$$

where $\bar{E}$ is the electrode potential for a flat surface, and κ is given by $\kappa = -\ddot{y}/(1 + \dot{y}^2)^{3/2}$, where the single dot and double dot represent derivatives with respect to position. Equation 2 demonstrates that as an electrode is

maintained at its equilibrium potential, $\bar{E}$, regions of positive curvature will tend to dissolve, and regions of negative curvature will tend to be deposition sites (ignoring any overpotentials necessary for these reactions).

The significance of the previous discussion is that, in contrast to elemental metal dissolution, regions of negative curvature must be created during alloy dissolution, owing to the selectivity of attack. This represents an additional energy that must be overcome by the dissolution process. The final form for the critical potential, $\eta(p)_{crit}$, following Ref 26, can then be written as:

$$\eta(p)_{crit} = E(p)_{crit} - \bar{E} = \frac{2}{\xi_a}\delta + \frac{2k_B T}{nq} \times \sinh^{-1}\left(\frac{\pi^2\gamma\Omega}{nq\delta}\frac{D_s N_s}{J_o}\frac{1}{\xi_a^2}\right) \quad \text{(Eq 3)}$$

where $\delta = \beta - (\gamma\Omega/nq)$, β is the variation in equilibrium potential of the alloy surface, owing to compositional fluctuations, γ is the solid-liquid interfacial energy, Ω is the atomic volume, n is the number of electrons transferred per atom, and q is the charge of an electron; ξ_a is the compositional length scale in the material, which can be taken as the percolation cluster size, $\xi_a = [(1 + p)a/1 - p]$, p is the fraction of dissolving species "A," and a is the near-neighbor distance in the lattice; $k_B$is the Boltzmann constant; T is the temperature; D_s is the surface diffusivity; N_s is the atom density on the surface; and J_0 is the exchange current density. For the silver-gold system, these variables take the values: $\Omega = 1.685 \times 10^{-29}$ m^3, $q = 1.602 \times 10^{-19}$ C, $n = 1$, $a = 2.880 \times 10^{-10}$ m, $k_B = 1.381 \times 10^{-23}$ J/K, $N_s = 1.395 \times 10^{19}$/m^2 for the [111] surface, $D_s = 2 \times 10^{-13}$ m^2/s, $T = 298$ K, and $\gamma \cong 1$ J/m^2. This leaves δ and J_0 as fitting parameters.

This equation has been tested for a series of silver-gold alloys as a function of alloy composition and electrolyte composition. The alloy composition varies the value of the percolation cluster size, ξ_a, in Eq 3, while the electrolyte composition varies the exchange current density, J_0. Figures 6 and 7 are the experimentally measured current density versus potential relationships as a function of alloy composition and electrolyte composition, respectively. The researchers defined the critical potential as the value of the potential at which the current reaches a value of 1 mA/cm^2 (6.5 mA/in.^{2}). Figure 8 summarizes this data for the electrolyte of various M $AgClO_4$ + 1 M $HClO_4$ and shows the fit to the data using Eq 3. The equation performs remarkably well at fitting the variation of the critical potential over a wide range of experimental variables for the silver-gold system and at generating reasonable values of the fitting parameters δ and J_o.

References cited in this section

13. A.J. Smith, T. Tran, and M.S. Wainwright, Kinetics and Mechanism of the Preparation of Raney Copper, *J. Appl. Electrochem.*, Vol 29, 1999, p 1085–1094

14. R.B. Abrams, The Dezincification of Brass, *Trans. Am. Chem. Soc.*, Vol 42, 1922, p 39–55

15. G.D. Bengough, R.M. Jones, and R. Pirret, Fifth Report to the Corrosion Committee of the Institute of Metals, *J. Inst. Met.*, Vol 23, 1920, p 65–158

17. K. Sieradzki, J.S. Kim, A.T. Cole, and R.C. Newman, The Relationship Between Dealloying and Transgranular Stress-Corrosion Cracking of Cu-Zn and Cu-Al Alloys, *J. Electrochem. Soc.*, Vol 134, 1987, p 1635–1639

21. S.G. Corcoran, D.G. Wiesler, and K. Sieradzki, An In Situ Small Angle Neutron Scattering Investigation of $Ag_{0.7}Au_{0.3}$ Dealloying Under Potential Control, *Mater. Res. Soc. Sym. Proc.*, Vol 451, 1997, p 93–98

26. K. Sieradzki, N. Dimitrov, D. Movrin, C. McCall, N. Vasiljevic, and J. Erlebacher, The Dealloying Critical Potential, *J. Electrochem. Soc.*, Vol 149, 2002, p B370–B377

33. B.G. Ateya, J.D. Fritz, and H.W. Pickering, Kinetics of Dealloying of a Copper-5 Atomic Percent Gold Alloy, *J. Electrochem. Soc.*, Vol 144, 1997, p 2606–2613

37. M.J. Pryor and J.C. Fister, The Mechanism of Dealloying of Copper Solid Solutions and Intermetallic Phases, *J. Electrochem. Soc.,* Vol 131, 1984, p 1230–1235

42. D.S. Keir and M.J. Pryor, The Dealloying of Copper-Manganese Alloys, *J. Electrochem. Soc.,* Vol 127, 1980, p 2138–2144

51. S.G. Corcoran, K. Sieradzki, and D. Wiesler, in *Proceedings of the Symposium on Scattering for Materials Science II,* D.A. Neumann, T.P. Russell, and B.J. Wuensch, Ed., Materials Research Society, 1994, p 377–382

52. S.G. Corcoran, The Morphology of Alloy Corrosion, *Proceedings of the Symposium on Critical Factors in Localized Corrosion III,* R.G. Kelly, G.S. Frankel, P.M. Natishan, and R.C. Newman, Ed., The Electrochemical Society, 1999, p 500–507

53. A.J. Forty and G. Rowlands, A Possible Model for Corrosion Pitting and Tunnelling in Noble-Metal Alloys, *Philos. Mag. A,* Vol 43, 1981, p 171–188

54. H.W. Pickering, Volume Diffusion during Anodic Dissolution of a Binary Alloy, *J. Electrochem. Soc.,* Vol 115, 1968, p 143–147

55. H.W. Pickering and C. Wagner, Electrolytic Dissolution of Binary Alloys Containing a Noble Metal, *J. Electrochem. Soc.,* Vol 114, 1967, p 698–706

56. K. Sieradzki, R.R. Corderman, K. Shukla, and R.C. Newman, Computer Simulations of Corrosion: Selective Dissolution of Binary Alloys, *Philos. Mag. A,* Vol 59, 1989, p 713–746

57. K. Sieradzki, Curvature Effects in Alloy Dissolution, *J. Electrochem. Soc.,* Vol 140, 1993, p 2868–2872

58. A. Dursun, D.V. Pugh, and S.G. Corcoran, Dealloying of Ag-Au Alloys in Halide Containing Electrolytes: Effect on Critical Potential and Pore Size, *J. Electrochem. Soc.,* 2003, in press

59. W.W. Mullins and R.F. Sekerka, Stability of a Planar Interface during Solidification of a Dilute Binary Alloy, *J. Appl. Phys.,* Vol 35, 1964, p 444–451

60. A.D. Tomsett, D.J. Young, and M.S. Wainwright, Pore Development during Selective Leaching, *J. Electrochem. Soc.,* Vol 131, 1984, p 2476–2481

61. R.G. Kelly, A.J. Young, and R.C. Newman, The Characterization of the Coarsening of Dealloyed Layers by EIS and Its Correlation with Stress-Corrosion Cracking, *Electrochemical Impedance: Analysis and Interpretation,* STP 1188, J.R. Scully, D.C. Silverman, and M.W. Kendig, Ed., American Society for Testing and Materials, 1993, p 94–112

62. H.W. Pickering, in *Fundamental Aspects of Stress Corrosion Cracking,* R.W. Staehle, A.J. Forty, and D. van Rooyen, Ed., NACE, Ohio State University, 1967, p 159–177

63. H.W. Pickering, Formation of New Phases during Anodic Dissolution of Zn-Rich Cu- Zn Alloys, *J. Electrochem. Soc.,* Vol 117, 1970, p 8–15

64. J.D. Harrison and C. Wagner, The Attack of Solid Alloys by Liquid Metals and Salt Melts, *Acta Metall. Mater.,* Vol 7, 1959, p 722–735

65. D. Stauffer and A. Harmony, *Introduction to Percolation Theory,* Taylor and Francis, London, 1991

S.G. Corcoran, Effects of Metallurgical Variables on Dealloying Corrosion, *Corrosion: Fundamentals, Testing, and Protection*, Vol 13A, *ASM Handbook*, ASM International, 2003, p 287–293

Effects of Metallurgical Variables on Dealloying Corrosion

Sean G. Corcoran, Virginia Polytechnic Institute and State University

References

1. K. Sieradzki and R.C. Newman, Brittle Behavior of Ductile Metals during Stress-Corrosion Cracking, *Philos. Mag. A,* Vol 51, 1985, p 95–132
2. R.C. Newman, R.R. Corderman, and K. Sieradzki, Evidence for Dealloying of Austenitic Stainless Steels in Simulated Stress Corrosion Crack Environments, *Br. Corros. J.,* Vol 24, 1989, p 143–148
3. D.E. Williams, R.C. Newman, Q. Song, and R.G. Kelly, Passivity Breakdown and Pitting Corrosion of Binary-Alloys, *Nature,* Vol 350, 1991, p 216–219
4. H.W. Pickering, Characteristic Features of Alloy Polarization Curves, *Corros. Sci.,* Vol 23, 1983, p 1107–1120
5. J.S. Chen, M. Salmeron, and T.M. Devine, *Corros. Sci.,* Vol 34, 1993, p 2071
6. T.B. Cassagne, W.F. Flanagan, and B.D. Lichter, On the Failure Mechanism of Chemically Embrittled Cu_3Au Single Crystals, *Metall. Trans. A,* Vol 17, 1986, p 703–710
7. H. Moore, S. Beckinsale, and C.E. Mallinson, The Season-Cracking of Brass and Other Copper Alloys, *J. Inst. Met.,* Vol 25, 1921, p 35–153
8. C. Calvert and R. Johnson, Action of Acids upon Metals and Alloys, *J. Chem. Soc.,* Vol 19, p 434–454
9. N. Dimitrov, J.A. Mann, M. Vukmirovic, and K. Sieradzki, Dealloying of Al_2CuMg in Alkaline Media, *J. Electrochem. Soc.,* Vol 147, 2000, p 3283–3285
10. R.G. Buchheit, R.P. Grant, P.F. Hlava, B. McKenzie, and G.L. Zender, Local Dissolution Phenomena Associated with S Phase (Al_2CuMg) Particles in Aluminum Alloy 2024-T3, *J. Electrochem. Soc.,* Vol 144, 1997, p 2621–2628
11. D.V. Pugh, A. Dursun, and S.G. Corcoran, Formation of Nanoporous Platinum by Selective Dissolution of Cu from $Pt_{0.25}Cu_{0.75}$, *J. Electrochem. Soc.,* 2003, in press
12. A.D. Tomsett, H.E. Curry-Hyde, M.S. Wainwright, D.J. Young, and A.J. Bridgewater, Structural Changes during the Leaching of Copper-Based Raney Catalysts, *Appl. Catal.,* Vol 33, 1987, p 119–127
13. A.J. Smith, T. Tran, and M.S. Wainwright, Kinetics and Mechanism of the Preparation of Raney Copper, *J. Appl. Electrochem.,* Vol 29, 1999, p 1085–1094
14. R.B. Abrams, The Dezincification of Brass, *Trans. Am. Chem. Soc.,* Vol 42, 1922, p 39–55
15. G.D. Bengough, R.M. Jones, and R. Pirret, Fifth Report to the Corrosion Committee of the Institute of Metals, *J. Inst. Met.,* Vol 23, 1920, p 65–158

16. J.A. Beavers and E.N. Pugh, The Propagation of Transgranular Stress-Corrosion Cracks in Admiralty Metal, *Metall. Trans. A,* Vol 11, 1980, p 809–820

17. K. Sieradzki, J.S. Kim, A.T. Cole, and R.C. Newman, The Relationship Between Dealloying and Transgranular Stress-Corrosion Cracking of Cu-Zn and Cu-Al Alloys, *J. Electrochem. Soc.,* Vol 134, 1987, p 1635–1639

18. C. Edeleanu and A.J. Forty, Some Observations on the Stress Corrosion Cracking of Alpha-Brass and Similar Alloys, *Philos. Mag.,* Vol 5, 1960, p 1029–1040

19. A.T. Cole, R.C. Newman, and K. Sieradzki, A Comparison and Evaluation of Bare Surface Electrochemical Techniques for the Investigation of Stress Corrosion Cracking in Alpha Brass, *Corros. Sci.,* Vol 28, 1988, p 109–118

20. M.J. Pryor and G. Kar-Kheng, The Effect of Arsenic on the Dealloying of Alpha-Brass, *J. Electrochem. Soc.,* Vol 129, 1982, p 2157–2163

21. S.G. Corcoran, D.G. Wiesler, and K. Sieradzki, An In Situ Small Angle Neutron Scattering Investigation of $Ag_{0.7}Au_{0.3}$ Dealloying Under Potential Control, *Mater. Res. Soc. Sym. Proc.,* Vol 451, 1997, p 93–98

22. R.G. Kelly, A.J. Frost, T. Shahrabi, and R.C. Newman, Brittle Fracture of an Au/Ag Alloy Induced by a Surface Film, *Metall. Trans. A,* Vol 22, 1991, p 531–541

23. A.J. Forty and P. Durkin, A Micromorphological Study of the Dissolution of Silver- Gold Alloys in Nitric Acid, *Philos. Mag. A,* Vol 42, 1980, p 295

24. P. Durkin and A.J. Forty, Oxide Formation during the Selective Dissolution of Silver from Silver-Gold Alloys in Nitric Acid, *Philos. Mag. A,* Vol 45, 1982, p 95–105

25. J. Erlebacher, M.J. Aziz, A. Karma, N. Dimitrov, and K. Sieradzki, Evolution of Nanoporosity in Dealloying, *Nature,* Vol 410, 2001, p 450–453

26. K. Sieradzki, N. Dimitrov, D. Movrin, C. McCall, N. Vasiljevic, and J. Erlebacher, The Dealloying Critical Potential, *J. Electrochem. Soc.,* Vol 149, 2002, p B370–B377

27. R.C. Newman, S.G. Corcoran, J. Erlebacher, M.J. Aziz, and K. Sieradzki, Alloy Corrosion, *Mater. Res. Soc. Bull.,* Vol 24, 1999, p 24–28

28. G.S. Duffo and J.R. Galvele, *Corros. Sci.,* Vol 30, 1990, p 249

29. B. Bakish and W.D. Robertson, Structure- Dependent Chemical Reaction and Nucleation of Fracture in Cu_3Au Single Crystals, *Acta Metall. Mater.,* Vol 4, 1956, p 342–351

30. T.P. Moffat, F.-R.F. Fan, and A.J. Bard, Electrochemical and Scanning Tunneling Microscopic Study of Dealloying of Cu_3Au, *J. Electrochem. Soc.,* Vol 138, 1991, p 3224–3235

31. J.S. Chen, A. Kadic-Galeb, M. Ferrari, and T.M. Devine, Embrittlement of Nano-scale Structures, *Mech. Res. Commun.,* Vol 19, 1992, p 555–561

32. J.D. Fritz and H.W. Pickering, Selective Anodic Dissolution of Cu-Au Alloys: TEM and Current Transient Study, *J. Electrochem. Soc.,* Vol 138, 1991, p 3209–3218

33. B.G. Ateya, J.D. Fritz, and H.W. Pickering, Kinetics of Dealloying of a Copper-5 Atomic Percent Gold Alloy, *J. Electrochem. Soc.,* Vol 144, 1997, p 2606–2613

34. M.C. Simmonds, H. Kheyrandish, J.S. Colligon, M.L. Hitchman, N. Cade, and J. Iredale, The Observation of a Threshold in the De-Alloying of Sputter-Deposited Pt_xAl_{1-x} Alloy Thin Films, *Corros. Sci.,* Vol 40, 1998, p 43–48

35. J. Szot, D.J. Young, A. Bourdillon, and K.E. Easterling, Cellular Morphologies in a De- Alloying Residue, *Philos. Mag. Lett.,* Vol 55, 1987, p 109–114

36. K. Sieradzki and R.C. Newman, Stress Corrosion Cracking, *J. Phys. Chem. Solids,* Vol 48, 1987, p 1101–1113

37. M.J. Pryor and J.C. Fister, The Mechanism of Dealloying of Copper Solid Solutions and Intermetallic Phases, *J. Electrochem. Soc.,* Vol 131, 1984, p 1230–1235

38. A.D. Tomsett, D.J. Young, M.R. Stammbach, and M.S. Wainwright, Ageing of Dealloyed Copper, *J. Mater. Sci.,* Vol 25, 1990, p 4106–4112

39. M.S. Wainwright and D.L. Trimm, Methanol Synthesis and Water-Gas Shift Reactions on Raney Copper Catalysts, *Catal. Today,* Vol 23, 1995, p 29–42

40. R. Pope, B. Little, and R. Ray, Microscopies, Spectroscopies and Spectrometries Applied to Marine Corrosion of Copper, *Biofouling,* Vol 16, 2000, p 83

41. A.M. Beccaria, G. Poggi, P. Traverso, and M. Ghiazza, A Study of the De-Alloying of 70Cu-30Ni Commercial Alloy in Sulfide Polluted and Unpolluted Sea Water, *Corros. Sci.,* Vol 32, 1991, p 1263–1275

42. D.S. Keir and M.J. Pryor, The Dealloying of Copper-Manganese Alloys, *J. Electrochem. Soc.,* Vol 127, 1980, p 2138–2144

43. U.S. Min and J.C.M. Li, The Microstructure and Dealloying Kinetics of a Cu-Mn Alloy, *J. Mater. Res.,* Vol 9, 1994, p 2878–2883

44. G.Z. Chen, D.J. Fray, and T.W. Farthing, Direct Electrochemical Reduction of Titanium Dioxide to Titanium in Molten Calcium Chloride, *Nature,* Vol 407, 2000

45. D.J. Fray, Electrochemical Method Uses Molten Calcium Chloride to Extract Metals Directly from Their Oxides, *Mater. Res. Soc. Bull.,* Vol 25, 2000, p 11–12

46. R.C. Newman and A. Mehta, An AC impedance Study of the De-Alloying of Fe-Ni Alloys, and Its Relevance to Chloride SCC of Stainless Steels, *Corros. Sci.,* Vol 28, 1988, p 1183–1187

47. K. Wagner, S.R. Brankovic, N. Dimitrov, and K. Sieradzki, Dealloying Below the Critical Potential, *J. Electrochem. Soc.,* Vol 144, 1997, p 3545–3555

48. B.G. Ateya and H.W. Pickering, The Effects of Potential and Kinetic Parameters on the Formation of Passivating Noble Metal Rich Surface Layers during the Selective Dissolution of Binary Alloys, *Corros. Sci.,* Vol 38, 1996, p 1245–1267

49. J.S. Chen, F. Sanz, D.F. Ogletree, V.M. Hallmark, T.M. Devine, and M. Salmeron, Selective Dissolution of Copper from Au-Rich Cu-Au Alloys—An Electrochemical STM Study, *Surf. Sci.,* Vol 292, 1993, p 289–297

50. R. Li and K. Sieradzki, Ductile-Brittle Transition in Random Porous Au, *Phys. Rev. Lett.,* Vol 68, 1992, p 1168–1171

51. S.G. Corcoran, K. Sieradzki, and D. Wiesler, in *Proceedings of the Symposium on Scattering for Materials Science II,* D.A. Neumann, T.P. Russell, and B.J. Wuensch, Ed., Materials Research Society, 1994, p 377–382

52. S.G. Corcoran, The Morphology of Alloy Corrosion, *Proceedings of the Symposium on Critical Factors in Localized Corrosion III,* R.G. Kelly, G.S. Frankel, P.M. Natishan, and R.C. Newman, Ed., The Electrochemical Society, 1999, p 500–507

53. A.J. Forty and G. Rowlands, A Possible Model for Corrosion Pitting and Tunnelling in Noble-Metal Alloys, *Philos. Mag. A,* Vol 43, 1981, p 171–188

54. H.W. Pickering, Volume Diffusion during Anodic Dissolution of a Binary Alloy, *J. Electrochem. Soc.,* Vol 115, 1968, p 143–147

55. H.W. Pickering and C. Wagner, Electrolytic Dissolution of Binary Alloys Containing a Noble Metal, *J. Electrochem. Soc.,* Vol 114, 1967, p 698–706

56. K. Sieradzki, R.R. Corderman, K. Shukla, and R.C. Newman, Computer Simulations of Corrosion: Selective Dissolution of Binary Alloys, *Philos. Mag. A,* Vol 59, 1989, p 713–746

57. K. Sieradzki, Curvature Effects in Alloy Dissolution, *J. Electrochem. Soc.,* Vol 140, 1993, p 2868–2872

58. A. Dursun, D.V. Pugh, and S.G. Corcoran, Dealloying of Ag-Au Alloys in Halide Containing Electrolytes: Effect on Critical Potential and Pore Size, *J. Electrochem. Soc.*, 2003, in press

59. W.W. Mullins and R.F. Sekerka, Stability of a Planar Interface during Solidification of a Dilute Binary Alloy, *J. Appl. Phys.,* Vol 35, 1964, p 444–451

60. A.D. Tomsett, D.J. Young, and M.S. Wainwright, Pore Development during Selective Leaching, *J. Electrochem. Soc.,* Vol 131, 1984, p 2476–2481

61. R.G. Kelly, A.J. Young, and R.C. Newman, The Characterization of the Coarsening of Dealloyed Layers by EIS and Its Correlation with Stress-Corrosion Cracking, *Electrochemical Impedance: Analysis and Interpretation,* STP 1188, J.R. Scully, D.C. Silverman, and M.W. Kendig, Ed., American Society for Testing and Materials, 1993, p 94–112

62. H.W. Pickering, in *Fundamental Aspects of Stress Corrosion Cracking,* R.W. Staehle, A.J. Forty, and D. van Rooyen, Ed., NACE, Ohio State University, 1967, p 159–177

63. H.W. Pickering, Formation of New Phases during Anodic Dissolution of Zn-Rich Cu- Zn Alloys, *J. Electrochem. Soc.,* Vol 117, 1970, p 8–15

64. J.D. Harrison and C. Wagner, The Attack of Solid Alloys by Liquid Metals and Salt Melts, *Acta Metall. Mater.*, Vol 7, 1959, p 722–735

65. D. Stauffer and A. Harmony, *Introduction to Percolation Theory,* Taylor and Francis, London, 1991

S. Bond, Corrosion of Carbon Steel Weldments, *Corrosion: Fundamentals, Testing, and Protection*, Vol 13A, *ASM Handbook*, ASM International, 2003, p 294–300

Corrosion of Carbon Steel Weldments

Revised by Stuart Bond, TWI Ltd., United Kingdom

Introduction

THE CORROSION BEHAVIOR of carbon steel weldments produced by fusion welding is dependent on a number of factors. Corrosion of carbon steel weldments can be due to metallurgical effects, such as preferential corrosion of the heat-affected zone (HAZ) or weld metal, or it can be associated with geometrical aspects, such as stress concentration at the weld toe, or creation of crevices due to joint design. Additionally, specific environmental conditions can induce localized corrosion such as temperature, conductivity of the corrosive fluid, or thickness of the liquid corrosive film in contact with the metal. In some cases, both metallurgical and geometric factors will influence behavior, such as in stress-corrosion cracking. Preferential weldment corrosion of carbon steels has been investigated since the 1950s, commencing with the problems on ice breakers, but the problem continues today in different applications.

This article describes issues related to corrosion of carbon steel weldments and remedial measures that have proven successful in specific cases; however, it is still difficult to predict whether attack will be concentrated on the HAZ, weld metal, or both areas in susceptible conditions. Care is also required in transfer of remedial measures to different applications because of the complexity of interacting factors that may lead to additional problems. Frequently, therefore, corrective measures need to be applied once a problem is identified, but laboratory testing is recommended for applications where preferential attack is anticipated.

S. Bond, Corrosion of Carbon Steel Weldments, *Corrosion: Fundamentals, Testing, and Protection*, Vol 13A, *ASM Handbook*, ASM International, 2003, p 294–300

Corrosion of Carbon Steel Weldments

Revised by Stuart Bond, TWI Ltd., United Kingdom

Influence of Weld Microstructure

Consideration must be given to the compositional effects of the base metal and welding consumable and to the different welding processes used. The base metal experiences temperatures ranging from ambient at a distance away from the weld to the melting point at the fusion boundary during welding. Therefore, metallurgical transformations occur across the weld metal and HAZ, and these microstructures can significantly alter the intrinsic corrosion rate of the steel. Fusion welding produces a weld metal that, due to the high cooling rate, is effectively a chill casting containing a high density of lattice defects and segregation of elements (Ref 1). A wide range of microstructures can be developed in a weldment based on cooling rates, and these microstructures are dependent on energy input, preheat, metal thickness (heat sink effects), weld bead size, and reheating effects due to multipass welding. As a result of their different peak temperatures, chemical compositions, and weld inclusions (oxides and sulfides), weld metal microstructures are usually significantly different from those of the HAZ and base metal. Similarly, corrosion behavior can also vary, but in cases where corrosion mitigation measures are correctly applied, for example, coating or cathodic protection or inhibition, these will normally be adequate to prevent preferential corrosion of carbon steel weldments.

Another important factor to note is that for a given composition, hardness levels will be lowest for high heat inputs, such as those produced by submerged arc weldments, and will be highest for low-energy weldments (with faster cooling rates) made by, for example, the shielded metal arc, gas tungsten arc, and metal inert-gas processes. Note that in comparing the heat input, it is necessary to account for the arc efficiency to compare processes. Depending on the welding conditions, weld metal microstructures generally tend to be fine grained with basic flux and somewhat coarser with acid or rutile (TiO_2) flux compositions.

Reference cited in this section

1. T.G. Gooch, "The Effect of Welding on Material Corrosion Behaviour," NACE International Process Industries Corrosion Seminar, 13–16 Oct 1986, (Houston, TX)

S. Bond, Corrosion of Carbon Steel Weldments, *Corrosion: Fundamentals, Testing, and Protection*, Vol 13A, *ASM Handbook*, ASM International, 2003, p 294–300

Corrosion of Carbon Steel Weldments

Revised by Stuart Bond, TWI Ltd., United Kingdom

Residual Stress

During welding, the base metal, HAZ, and underlying weld passes experience stresses due to thermal expansion and contraction. On solidification, high levels of residual stress, often close to the material yield stress, remain as a result of weld shrinkage. Stress-concentration effects as a result of geometrical discontinuities, such as weld reinforcement (excess weld metal) and lack of full weld penetration (dangerous because of the likelihood of crevice corrosion and the possibility of fatigue cracking), are also important because of the possibility of stress-corrosion cracking (SCC) in some environments.

S. Bond, Corrosion of Carbon Steel Weldments, *Corrosion: Fundamentals, Testing, and Protection*, Vol 13A, *ASM Handbook*, ASM International, 2003, p 294–300

Corrosion of Carbon Steel Weldments

Revised by Stuart Bond, TWI Ltd., United Kingdom

Geometrical Factors

It should be recognized that excess root penetration can interrupt fluid flow close to the wall of a pipe in high-flow-rate operation, leading to impingement corrosion downstream of the weld. Alternatively, in low-velocity oil and gas systems where the water content is entrained in the bulk fluid, such excess penetration can cause flow disruption and water dropout, allowing pooling of water downstream of the weld, which can lead to increased corrosion of the weldment or adjacent base metal (Ref 2).

Reference cited in this section

2. J.S. Smart, Weld Corrosion in Lines Deserves Closer Attention, *Pipeline Gas Ind.*, Vol 79 (No. 6), June 1996, p 33–35

S. Bond, Corrosion of Carbon Steel Weldments, *Corrosion: Fundamentals, Testing, and Protection*, Vol 13A, *ASM Handbook*, ASM International, 2003, p 294–300

Corrosion of Carbon Steel Weldments

Revised by Stuart Bond, TWI Ltd., United Kingdom

Preferential Heat Affected Zone Corrosion

A wide range of HAZ microstructures can be produced because, close to the fusion boundary, the HAZ transformation to austenite on heating will be followed on cooling by transformation to give either a ferrite-carbide microstructure or martensite, depending on material composition, peak temperature, and cooling rate. Farther from the weld, the material will be exposed to a lower peak temperature, so only partial reaustenization occurs, and those areas heated below the ferrite- to-austenite transformation temperature (Ac_1) will not be significantly affected, other than by some carbide coarsening and tempering. Despite these variations, in the majority of applications, there is little influence on the corrosion performance, and preferential HAZ corrosion is relatively rare. Where preferential HAZ attack has been reported, it is more common in carbon and carbon-manganese steels than in higher-alloy grades (Ref 1).

An example of preferential corrosion in the HAZ of a carbon steel weldment is shown in Fig. 1. This phenomenon has been observed in a wide range of aqueous environments, the common link being that the environments are fairly high in conductivity, while attack has usually, but not invariably, occurred at pH values below approximately 7 to 8.

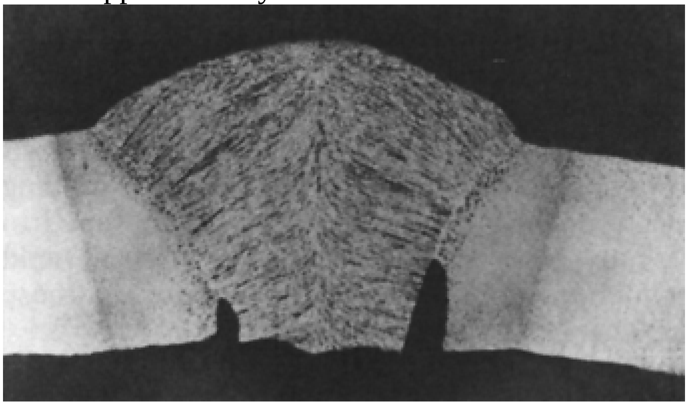

Fig. 1 Preferential corrosion in the heat affected zone of a carbon steel weldment after service in an aqueous environment. 5×. Source: Ref 3

Preferential HAZ corrosion in seawater was reported in the 1960s and attributed to the presence of low-temperature transformation products such as martensite, lower bainite, or retained austenite (Ref 4). Therefore, steel compositions favoring increased hardenability (e.g., increase in manganese content) may lead to increased localized corrosion, but microalloyed steels are not susceptible. *Tramline corrosion* is a term applied to preferential HAZ corrosion concentrated at the fusion boundaries and has been observed in acidic aqueous environments such as acid mine waters.

There is clearly a microstructural dependence, and studies on HAZs show corrosion to be appreciably more severe when the material composition and welding parameters are such that hardened structures are formed. It has been known for many years that hardened steel may corrode more rapidly in acid conditions than fully tempered material, apparently because local microcathodes on the hardened surface stimulate the cathodic hydrogen evolution reaction. The rate of corrosion is usually governed by the cathodic (reduction) rate, when other limiting factors are not present, and therefore, it is a factor in acidic environments but less so in neutral or alkaline conditions. On this basis, it is proposed that water treatments ensuring alkaline conditions should be less likely to induce HAZ corrosion, but even at a pH near 8, hydrogen ion (H^+) reduction can account for approximately 20% of the total corrosion current; pH values substantially above this level would be needed to suppress the effect completely. Furthermore, if such treatments may be useful to control preferential HAZ

corrosion when it has not been anticipated, it is considered to be more reliable to avoid the problem through design. Avoidance through selection of appropriate material or welding procedure, for example, to minimize hardness, is the preferred remedial approach, because postweld heat treatment (PWHT) may necessitate temperatures high enough for normalizing to gain full benefit, which is usually impractical (Ref 1).

In some oil and gas production environments, preferential weldment corrosion may lead to enhanced HAZ attack or weld metal corrosion. In the late 1980s, studies of the problems associated with preferential weldment corrosion in sweet oil and gas production systems were undertaken (Ref 5). In some cases, the HAZ was attacked, while in other cases, the weld metal was preferentially corroded. Where enhanced HAZ corrosion was observed, the composition was more influential than the microstructure; however, hardened transformed microstructures suffered increased corrosion. The postweld heat treatment at 590 °C (1100 °F) for stress relief was beneficial in reducing HAZ attack (Ref 2), despite the previous comments.

HAZ/Fusion Line Corrosion of Welded Line Pipe. There is a particular case of preferential weldment corrosion worth highlighting in respect to electric-resistance-welded/high-frequency-induction-welded (ERW/HFI) pipe, where attack of the seam weld HAZ/fusion line can occur in aqueous environments or when exposed to the water phase in a mixed-phase system due to flow conditions or water dropout at low points. This grooving corrosion has been attributed to inclusions within the pipe material being exposed at the pipe surface and modified by the weld thermal cycle (Ref 4). A normalizing heat treatment can reduce or prevent occurrence. However, the major remedial action is the selection of a cleaner alloyed steel (Ref 6). Corrosion is due to electrochemical potential differences (galvanic corrosion) between the HAZ/fusion line and the parent material, attributed to the unstable MnS inclusions produced during the welding cycle. It is highlighted that the potential difference may only be of the order of perhaps 30 to 70 mV, but the low surface area ratio of anode to cathode results in high corrosion rates (between 1 to 10 mm, or 0.04 to 0.4 in., per year). Mitigation against this form of corrosion was achieved through modified steel composition in the 1970s; the addition of copper plus reduced sulfur to minimize MnS formation and the addition of calcium, nickel, or titanium to stabilize the remaining sulfur eliminates the potential difference. Such corrosion has become less common in recent years, due to awareness of these issues and remedial measures.

References cited in this section

1. T.G. Gooch, “The Effect of Welding on Material Corrosion Behaviour,” NACE International Process Industries Corrosion Seminar, 13–16 Oct 1986, (Houston, TX)

2. J.S. Smart, Weld Corrosion in Lines Deserves Closer Attention, *Pipeline Gas Ind.,* Vol 79 (No. 6), June 1996, p 33–35

3. T.G. Gooch and P.H.M. Hart, “Review of Welding Practices for Carbon Steel Deaerator Vessels,” Paper 303, presented at Corrosion/86, (Houston, TX), National Association of Corrosion Engineers, March 1986

4. J.L. Robinson, Preferential Corrosion of Welds, *The Welding Institute Research Bulletin,* Vol 20, Jan and Feb 1979

5. “Preferential Corrosion of Carbon Steel Weldments in Oil and Gas Production Systems,” Joint Industry Project 5563/28/89, TWI and CAPCIS, 1989

6. R.W. Revie, Ed., *Uhlig's Corrosion Handbook,* 2nd ed., John Wiley & Sons, 2000, p 542

S. Bond, Corrosion of Carbon Steel Weldments, *Corrosion: Fundamentals, Testing, and Protection*, Vol 13A, *ASM Handbook*, ASM International, 2003, p 294–300

Corrosion of Carbon Steel Weldments

Revised by Stuart Bond, TWI Ltd., United Kingdom

Preferential Weld Metal Corrosion

The weld metal in a carbon-manganese steel may suffer preferential corrosion, but again, if quality corrosion mitigation is in place for the main structure, such as coating or cathodic protection, this preferential attack is also normally prevented. However, there are cases where coating failure or inefficient inhibition can then lead to localized corrosion.

It is probable that similar microstructural considerations also apply to the preferential corrosion of weld metal, but in this case, the situation is further complicated by the presence of deoxidation products, their type and number depending largely on the flux system employed. Consumable type plays a major role in determining weld metal corrosion rate, and the highest rates of metal loss are normally associated with shielded metal arc electrodes using a basic coating. In seawater, for example, the corrosion rate for a weld made using a basic-flux-coated consumable may be three times as high as for weld metal from a rutile-flux-coated consumable. Fewer data are available for submerged arc weld metals, but it would appear that they are intermediate between basic and rutile flux shielded metal arc electrodes and that a corrosion rate above that of the base steel can be expected. In many cases, the underlying cause of the problem is the electrochemical potential difference between the weld metal and the adjacent parent steel, as discussed subsequently.

S. Bond, Corrosion of Carbon Steel Weldments, *Corrosion: Fundamentals, Testing, and Protection*, Vol 13A, *ASM Handbook*, ASM International, 2003, p 294–300

Corrosion of Carbon Steel Weldments

Revised by Stuart Bond, TWI Ltd., United Kingdom

Galvanic Corrosion

Some of the earliest problems of weld metal corrosion related to ships in arctic waters, where the action of ice abraded the paint to expose bare steel and damaged the anodes, thus rendering the cathodic protection system ineffective. In these cases, it was observed that enhanced corrosion of the weld metal was due to electrochemical potential differences between the weld metal and the base metal, such that the weld metal is anodic in the galvanic couple. Further detailed studies were undertaken in the late 1980s to assess more modern steels and welding consumables in arctic waters off Canada (Ref 7). Both HAZ and weld metal attack were observed, and the general conclusions were that for steels between 235 and 515 MPa (34 and 75 ksi) minimum yield strength, high manganese content (1.4%) in the parent steel resulted in enhanced preferential HAZ attack, but this could be reduced via increased heat input during welding. Generally, the rate of weld metal attack was dependent on the nickel and copper contents of the welding consumable and was less influenced by parent steel composition, although a steel with copper, nickel, and chromium additions led to a more noble parent steel, hence accelerating weld metal attack. It was noted that parent steel with low silicon content led to increased weld metal corrosion, supporting the earlier findings that silicon $< 0.2\%$ can be detrimental, but the opposite was observed for silicon in the weld metal.

It is highlighted that, as for the autogenous seam weld in ERW/HFI pipe, the difference in corrosion potential for the separated regions (parent steel, HAZ, and weld metal) may be only a few tens of millivolts, but due to

the low surface area ratio of anode to cathode in conductive solutions, the attack on the anodic weld metal or HAZ may be very high. Also, on-going corrosion of the parent steel will continue, and if this rate is unacceptable, mitigation or protection methods are required for the base material in addition to consideration of ways to control the enhanced localized attack at the weldments. Generally, such weld metal attack has occurred in high-conductivity media, and the measures described to ensure the weld metal is cathodic (more noble) relative to the base metal have been successful. However, this may not be successful in different environmental conditions.

Reference cited in this section

7. R.J. Brigham et al., Evaluation of Weld- Zone Corrosion of Shipbuilding Steel Plates for Use in the Arctic Environment, *Can. Metall. Q.,* Vol 27 (No. 4), 1988, p 311–321

S. Bond, Corrosion of Carbon Steel Weldments, *Corrosion: Fundamentals, Testing, and Protection*, Vol 13A, *ASM Handbook*, ASM International, 2003, p 294–300

Corrosion of Carbon Steel Weldments

Revised by Stuart Bond, TWI Ltd., United Kingdom

Mitigation of Preferential Weldment Corrosion

Optimized process selection and welding procedures will assist in achieving good-quality welds, ensuring full weld penetration and minimizing excessive weld reinforcement; postweld dressing by grinding (a costly method) can be effective in minimizing the geometric effects.

A stress-relieving heat treatment may be effective in reducing residual stress (internal weld shrinkage stress) and metal hardness to safe levels in most cases of concern regarding environmentally assisted cracking (stress-corrosion cracking and sulfide stress cracking).

A PWHT stress relief has also been reported to be beneficial in reducing HAZ attack (Ref 1). However, in other cases, avoidance through selection of appropriate material or welding procedure is the preferred remedial approach, because PWHT may necessitate temperatures high enough for normalizing to gain full benefit, which is usually impractical (Ref 1).

Mitigation of preferential weld metal corrosion may be achieved in some cases via alloying additions to make the weld metal cathodic to the adjacent base metal. It must be noted that although the weld becomes cathodic to the base material, accelerated corrosion of the base metal is unlikely, because the anode-to-cathode surface area ratio becomes very high. However, care is required in extrapolating remedial measures proven in one environment, because they may not be efficient in different conditions. For example, the factors influencing such localized corrosion in sweet oil and gas environments are complex, and the use of nickel-containing weld metal for the root, successful in mitigating attack in seawater injection systems, has led to incidents of preferential attack in particular systems operated at temperatures of approximately 70 to 80 °C (160 to 175 °F) (Ref 8).

However, when introducing measures to avoid weld metal corrosion, care must be taken to avoid enhanced corrosion of the adjacent HAZ, due again to galvanic effects, particularly where the environment has relatively low conductivity, such as freshwater (Ref 4).

In summary, preferential weldment corrosion of carbon steels has been observed in diverse applications, from plate steels in the marine industry to pipe and process equipment, piping tankage, pressure vessels (Ref 9), and similar equipment in the oil and gas sectors. Some typical case histories are presented as follows, but mitigation in most cases requires an assessment of the particular environment and materials involved and will likely necessitate some testing to evaluate the performance in service.

References cited in this section

1. T.G. Gooch, "The Effect of Welding on Material Corrosion Behaviour," NACE International Process Industries Corrosion Seminar, 13–16 Oct 1986, (Houston, TX)

4. J.L. Robinson, Preferential Corrosion of Welds, *The Welding Institute Research Bulletin*, Vol 20, Jan and Feb 1979

8. M.B. Kermani and L.M. Smith, Ed., *CO_2 Corrosion Control in Oil and Gas Production*, European Federation of Corrosion Publication 23, The Institute of Materials, London, 1997

9. C.G. Arnold, "Galvanic Corrosion Measurement of Weldments," Paper 71, presented at Corrosion/80, (Chicago, IL), National Association of Corrosion Engineers, March 1980

S. Bond, Corrosion of Carbon Steel Weldments, *Corrosion: Fundamentals, Testing, and Protection*, Vol 13A, *ASM Handbook*, ASM International, 2003, p 294–300

Corrosion of Carbon Steel Weldments

Revised by Stuart Bond, TWI Ltd., United Kingdom

Industrial Case Studies

In one case, premature weld failures were experienced in a 102 mm (4 in.) ASTM A53 pipe that was used to transfer a mixture of chlorinated hydrocarbons and water. During construction, the pipeline was fabricated with E7010-Al welding electrodes (see Table 1 for the compositions of all materials discussed in these examples). Initial weld failures and subsequent tests showed the following welding electrodes to be anodic to the A53, grade B, base metal: E7010-Al, E6010, E6013, E7010-G, and E8018-C2. Two nickel- base electrodes—Inco-Weld A (American Welding Society, or AWS, A5.11, class ENiCrFe-2) and Incoloy welding electrode 135—were tested; they were found to be cathodic to the base metal and to prevent rapid weld corrosion. The corrosion rates of these various galvanic couples are listed in Table 2.

Table 1 Compositions of carbon steel base metals and some filler metals subject to galvanic corrosion. See Tables 3 and 4 for corrosion rates of galvanic couples.

Metal	Composition, wt%						
	C	**Mn**	**Si**	**Cr**	**Ni**	**Fe**	**Others**
Base metals							
ASTM A53, grade B	0.30	1.20	…	…	…	bal	…
ASTM A285, grade C	0.22	0.90	…	…	…	bal	…
Filler metals							
E6010	No specific chemical limits						
E6013	No specific chemical limits						
E7010-Al	0.12	0.60	0.40	…	…	bal	0.4–0.65Mo
E7010-G	…	1.00[a]	0.80[a]	0.30[a]	0.50[a]	bal	0.2Mo, 0.1V
E7016	…	1.25[b]	0.90	0.20[b]	0.30[b]	bal	0.3Mo, 0.08V[b]
E7018	…	1.60[c]	0.75	0.20[c]	0.30[c]	bal	0.3Mo, 0.08V[c]
E8018-C2	0.12	1.20	0.80	…	2.0–2.75	bal	…
ENiCrFe-2 (Inco Weld	0.10	1.0–3.5	1.0	13.0–	bal	12.0	1–3.5Mo, 0.5Cu, 0.5–3(Nb

A)				17.0			+ Ta)
Incoloy welding electrode 135	0.08	1.25–2.50	0.75	26.5–30.5	35.0–40.0	bal	2.75–4.5Mo, 1–2.5Cu

(a) The weld deposit must contain only the minimum of one of these elements.
(b) The total of these elements shall not exceed 1.50%.
(c) The total of these elements shall not exceed 1.75%.
Source: Ref 9

Table 2 Corrosion rates of galvanic couples of ASTM A53, grade B, base metal and various filler metals in a mixture of chlorinated hydrocarbons and water

The areas of the base metal and the deposited weld metal were equal.

Filler metal	Base metal corrosion rate		Filler metal corrosion rate	
	mm/yr	**mils/yr**	**mm/yr**	**mils/yr**
E6010	0.4	15	0.9	35
E6013	0.18	7	0.9	35
E7010-Al	1.3	50	4.3	169
E7010-G	1.7	68	2.8	112
E8018-C2	0.36	14	1.7	66
Inco Weld A	0.48	19	0.013	0.5
Incoloy welding electrode 135	0.36	14	<0.0025	<0.1

Source: Ref 9

Another example is the failure of low-carbon steel welds in seawater service at 25 °C (75 °F). Fabrications involving ASTM A285, grade C, plate welded with E6013 electrodes usually start to fail in the weld after 6 to 18 months in seawater service at this temperature. Welds made with E7010 electrodes do not fail. Tests were conducted in seawater at 50 °C (120 °F) using A285, grade C, plate welded with E6010, E7010-Al, and E7010-G. It was determined that E7010-Al was the best electrode to use in seawater and that E6010 and E7010-G were not acceptable (although they were much better than E6013), because they were both anodic to the base metal. A zero resistance ammeter was used to determine whether the electrodes were anodic or cathodic to the base metal.

In another case, welds made from E7010-Al electrodes to join ASTM A285, grade C, base metal were found to be anodic to the base metal when exposed to raw brine, an alkaline-chloride (pH > 14) stream, and raw river water at 50 °C (120 °F). When E7010-G was exposed to the same environment, it was anodic to the base metal in raw brine and raw river water and was cathodic to ASTM A285, grade C, in the alkaline-chloride stream. When the base metal was changed to ASTM A53, grade B, and A106, grade B, it was found that E7010-Al weld metal was cathodic to both when exposed to raw brine at 50 °C (120 °F).

Finally, routine inspection of a column in which a mixture of hydrocarbons was water washed at 90 °C (195 °F) revealed that E7016 welds used in the original fabrication were corroding more rapidly than the ASTM A285, grade C, base metal. Corroded welds were ground to sound metal, and E7010-Al was used to replace the metal that was removed. Approximately 3 years later, during another routine inspection, it was discovered that the E7010-Al welds were being selectively attacked. Tests were conducted that showed E7010-Al and E7016 weld metals to be anodic to A285, grade C, while E7018 and E8018-C2 would be cathodic. Corrosion rates of these various galvanic couples are given in Table 3.

Table 3 Corrosion rates of galvanic couples of ASTM A285, grade C, base metal and various filler metals at 90 °C (195 °F) in water used to wash a hydrocarbon stream

Filler metal	Base metal corrosion rate		Filler metal corrosion rate	
	mm/yr	**mils/yr**	**mm/yr**	**mils/yr**
E7010-Al	0.69	27	0.81	32
E7016	0.46	18	0.84	33
E7018	1.3	50	1.2	48
E8018-C2	2.2	85	1.04	41

Source: Ref 9

These examples demonstrate the necessity for testing each galvanic couple in the environment for which it is intended. Higher-alloy filler metals can sometimes be used to advantage to prevent rapid preferential weld corrosion.

Reference cited in this section

9. C.G. Arnold, "Galvanic Corrosion Measurement of Weldments," Paper 71, presented at Corrosion/80, (Chicago, IL), National Association of Corrosion Engineers, March 1980

S. Bond, Corrosion of Carbon Steel Weldments, *Corrosion: Fundamentals, Testing, and Protection*, Vol 13A, *ASM Handbook*, ASM International, 2003, p 294–300

Corrosion of Carbon Steel Weldments

Revised by Stuart Bond, TWI Ltd., United Kingdom

Stress-Corrosion Cracking

There is no doubt that residual welding stresses can contribute to SCC in specific environments in which such failure represents a hazard. This is the case for failure by both active path and hydrogen embrittlement mechanisms, and, in the latter case, failure may be especially likely at low-heat-input welds because of the enhanced susceptibility of the hardened structures inevitably formed. Most SCC studies of welds in carbon and carbon-manganese steels have evaluated resistance to hydrogen-induced SCC, especially under sour (H_2S) conditions prevalent to the oil and gas industry, which is commonly referred to as sulfide stress cracking (SSC). Although full definition of the effect of specific microstructural types has not been obtained, an overriding influence of hardness is evident (Fig. 2) and well accepted. The situation regarding active path cracking is less clear, but there are few, if any, cases in which SCC resistance increases at higher strength levels. On this basis, it is probable that soft, transformed microstructures around welds are preferable. In order that hard spots in the HAZ are not overlooked in weld procedure qualification, many standards now require the use of the Vickers hardness testing for welds, using 5 or 10 kg (e.g., ASTM E 92) loads, because the larger indenter used for Rockwell C measurements (often stipulated for parent material) will not identify such critical regions.

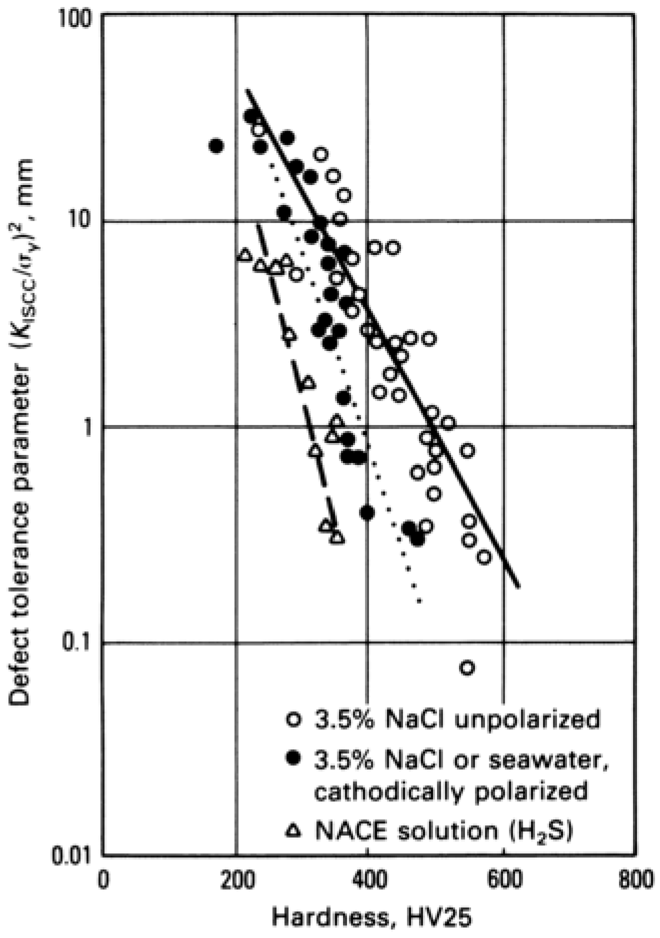

Fig. 2 Stress-corrosion cracking (SCC) defect tolerance parameter (K_{ISCC}/σ_y), where K_{ISCC} is the threshold SCC intensity factor and σ_y is yield stress versus hardness for carbon steel weldments in three environments. Data are derived from published tests on precracked specimens of various types of carbon steel base metals, heat-affected zones, and weld metals. SCC defect tolerance parameter is dependent on crack length; details are available in Ref 3. Source: Ref 3

Carbon and low-alloy steels are also known to fail by SCC when exposed to solutions containing nitrates (NO_3^-). Refrigeration systems using a 30% magnesium nitrate ($Mg(NO_3)_2$) brine solution, for example, are commonly contained in carbon steel. In this case, pH adjustment is important, as is temperature. Failures in the HAZ due to SCC have been reported when brine temperatures have exceeded 30 °C (90 °F) during shutdown periods. To avoid these failures, carbon steel is being replaced with type 304L stainless. Others have stress-relieved welded carbon steel systems and have operated successfully, although elevated-temperature excursions are discouraged.

SCC in Oil Refineries. Monoethanolamine (MEA) is an absorbent used to remove acid gases containing H_2S and CO_2 in oil refining operations. Recent failures in several refineries have shown that cracks can be parallel or normal to welds, depending on the orientation of principal tensile stresses. Cracking has been reported to be both transgranular and intergranular.

Before 1978, postweld stress relief of carbon steel weldments in MEA systems was performed only when the metal temperature of the equipment was expected to exceed 65 °C (150 °F) and the acid gas contained more than 80% CO_2 or when temperatures were expected to exceed 95 °C (200 °F) in any acid gas concentration.

Currently, any equipment containing MEA at any temperature and at any acid gas concentration is being postweld stress relieved. This is the result of surveys conducted by several refineries to define the extent of the SCC problem in this environment. These inspection programs showed that leaks were widespread and were found in vessels that ranged in age from 2 to 25 years. However, there were no reports of cracking in vessels that had been postweld stress relieved. In addition, it was found that all concentrations of MEA were involved and that MEA solutions were usually at relatively low temperatures (below 55 °C, or 130 °F). Equipment found to suffer from cracking included tanks, absorbers, carbon treater drums, skimming drums, and piping. The

following example of a metallurgical investigation conducted by one oil refinery illustrates the problem of SCC of carbon steel in amine service (Ref 10).

Leaking Carbon Steel Weldments in a Sulfur Recovery Unit. In December 1983, two leaks were discovered at a sulfur recovery unit. More specifically, the leaks were at pipe-to-elbow welds in a 152 mm (6 in.) diameter line operating in lean amine service at 50 °C (120 °F) and 2.9 MPa (425 psig). Thickness measurements indicated negligible loss of metal in the affected areas, and the leaks were clamped. In March 1984, 15 additional leaks were discovered, again at pipe-to-elbow welds of lean amine lines leading to two major refining units. The piping had been in service for approximately 8 years.

Investigation. Metallurgical examination of several of the welds revealed that leaking occurred at what appeared to be stress-corrosion cracks originating from the inside surface. Cracks were present in weld metal and base metal approximately 5 mm (0.2 in.) away from the weld, and they passed through the HAZ, as shown in Fig. 3. In other cases, stress-corrosion cracks also originated in the HAZ. The cracks typically ran parallel to the weld (Fig. 4).

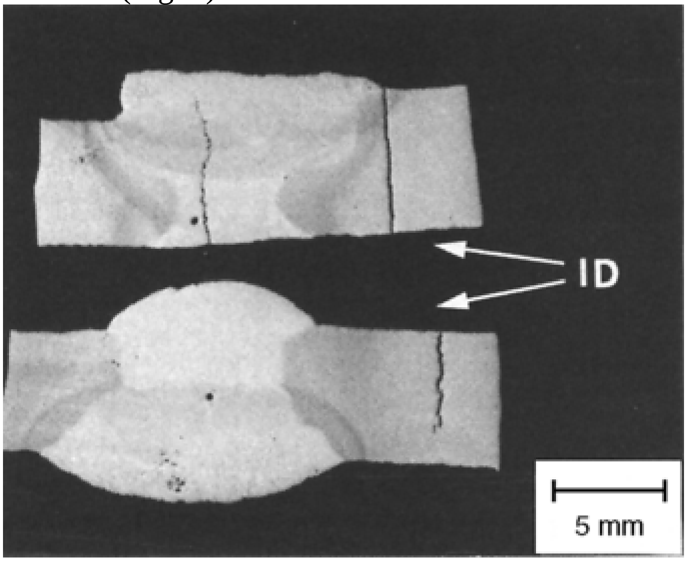

Fig. 3 Cross sections of pipe-to-elbow welds showing stress-corrosion cracks originating from the inside surface of the weld metal and the base metal. ID, inside diameter. Source: Ref 10

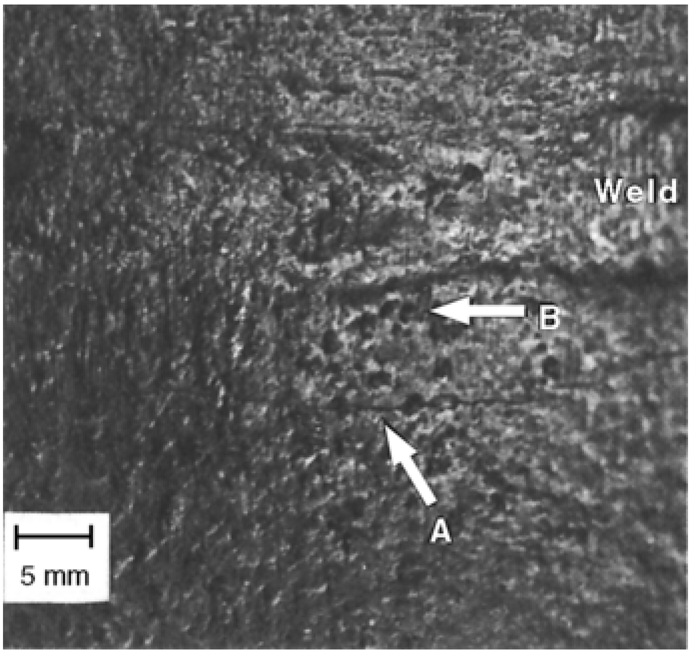

Fig. 4 Photograph of inside surface of a pipe showing 38 mm (1.5 in.) stress-corrosion crack (A) next to and parallel to a circumferential weld. Also shown are shallow corrosion pits (B). Source: Ref 10

Brinell hardness values, obtained by conversion of Knoop microhardness readings, were 133 to 160 (pipe base metal), 160 to 230 (weld metal), 182 to 227 (HAZs), and 117 to 198 (elbow base metal). The pipe base metal had an equiaxed fine-grain microstructure typical of low-carbon steel, and the elbow base metal had a nonequiaxed microstructure typical of hot-finished fittings. Carbon contents ranged from 0.25 to 0.30% by weight. Cracking was intergranular, as shown in Fig. 5 and 6.

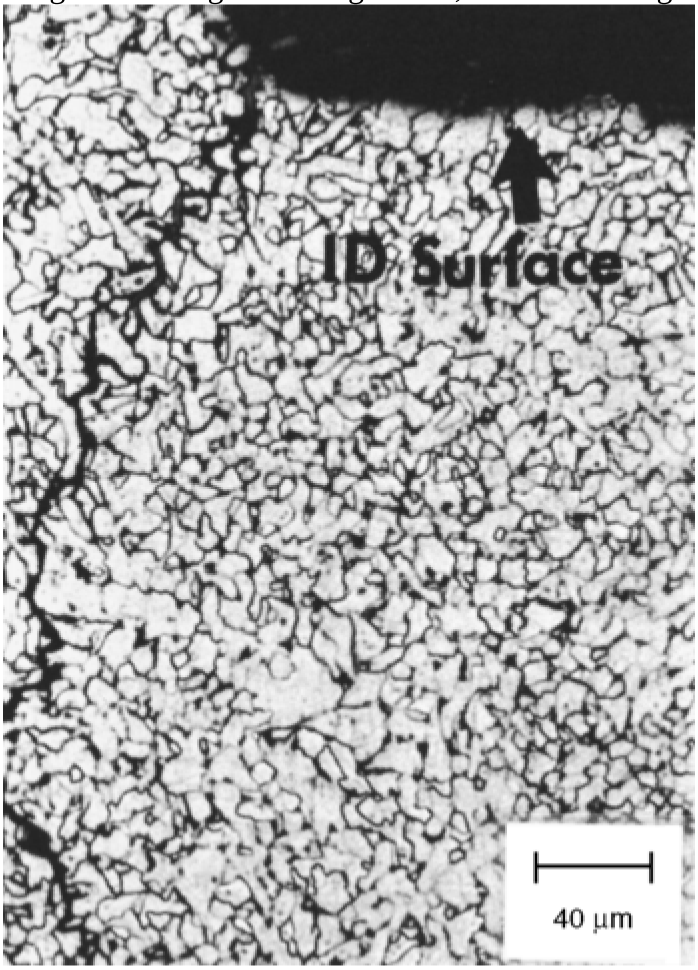

Fig. 5 Micrograph showing tight intergranular stress-corrosion cracking originating at the inside surface of a pipe. ID, inside diameter. Source: Ref 10

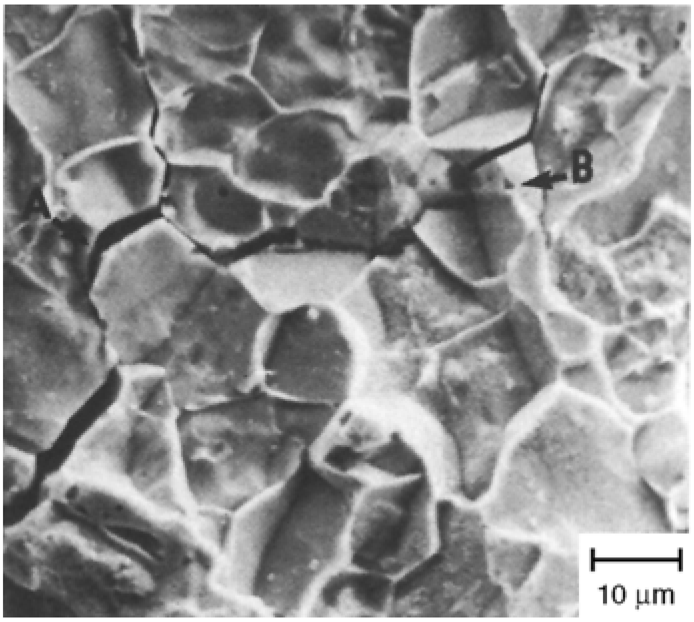

Fig. 6 Scanning electron micrograph showing intergranular stress-corrosion cracking (A) and initiation sites for pitting (B) on the inside surface of a pipe. Source: Ref 10

The refinery operators immediately embarked on a program of visual inspection of all amine lines. As of June 1985, a total of 35 leaks in lean amine piping had been discovered. All leaks were at cracks in or around pipe-to-elbow welds, except for two leaks at welds that connected a tee and reducer, respectively. Piping size ranged from 76 to 305 mm (3 to 12 in.). Service temperature ranged from 40 to 60 °C (100 to 140 °F), with most leaks having occurred in lines carrying lean amine at 55 °C (130 °F). Pressures ranged from atmospheric to 2.9 MPa (425 psig), with most leaks having occurred between 2.8 and 2.9 MPa (400 and 425 psig). All piping had been in service for approximately 8 years, except two leaks at piping welds that had been in service for only 4 years.
As had been generally accepted industry practice, the specifications called for stress relieving or PWHT of piping and vessels in amine service at temperatures above 95 °C (200 °F). Therefore, it was highly unlikely that any of the leaking welds had received PWHT. Further metallurgical examination of leaking welds from various lines conclusively confirmed that the leaking originated at stress-corrosion cracks. No leaks were found in rich amine piping. The characteristics of the mode of fracture suggested that the failure mechanism was a form of caustic SCC.
It is interesting to note that other researchers also have metallographically examined numerous samples of similar cracks; their results can be summarized as follows:

- Cracks were essentially intergranular and were filled with gray oxide scale.
- Hardness of welds and HAZs was less than 200 HB.
- Cause of fracture was believed to be a form of caustic SCC.
- Cracking occurs whether or not MEA solutions contain corrosion inhibitors.

Preventive Measures. As a result of this particular investigation and others, all welds in equipment in MEA service are being inspected. Wet fluorescent magnetic-particle inspection after sandblasting to remove oxides and scale appears to be the most effective technique. Shear- wave ultrasonic (SWU) inspection has also been used for piping, but it does not always distinguish SCC and other defect indications, such as shrinkage cracks, slag inclusions, lack of fusion, or fatigue cracks. Nevertheless, SWU is considered helpful, because these other types of defects also can pose a threat to the structural integrity of the system in question. Inspection frequency is dependent on the critical nature of the particular equipment in question, and, most important, all welds in these systems are now being postweld stress relieved.
Corrosion of Welds in Carbon Steel Deaerator Tanks. Deaerator tanks, the vessels that control free oxygen and other dissolved gases to acceptable levels in boiler feedwater, are subject to a great deal of corrosion and cracking. Several years ago, there were numerous incidences of deaerator tank failures that resulted in injury to personnel and property damage losses. Since that time, organizations such as the National Board of Boiler and Pressure Vessel Inspectors and the Technical Association of the Pulp and Paper Industry have issued warnings to plant operators, and these warnings have resulted in the formation of inspection programs for evaluating the integrity of deaerator tanks. As a result, many operators have discovered serious cracking. The following example illustrates the problem (Ref 11).
Weld Cracking in Oil Refinery Deaerator Vessels. Two deaerator vessels with associated boiler feedwater storage tanks operated in similar service at a refinery. The vertical deaerator vessels were constructed of carbon steel (shell and dished heads), with trays, spray nozzles, and other internal components fabricated of type 410 stainless steel. Boiler feedwater was treated by sand filtration using pressure filters, followed by ion-exchange water softening. Hardness was controlled at less than 0.5 ppm calcium carbonate ($CaCO_3$). A strong cationic primary coagulant (amine) was used to aid the filtering of colloidal material. Treated water was blended with condensate containing 5 ppm of a filming amine corrosion inhibitor. Final chemistry of the feedwater was controlled to the concentration limits given in Table 4. Oxygen scavenging was ensured by the addition of catalyzed sodium bisulfite ($NaHSO_3$) to the storage tanks. Treated water entered the top of the tray section of the deaerators through five or six spray nozzles and was stored in the horizontal tanks below the deaerators.

Table 4 Concentration limits on deaerator feedwater

Control parameter	Concentration limit
Total hardness	<0.5 ppm as $CaCO_3$
Phenolphthalein alkalinity	Trace (max)
Methyl orange alkalinity	14–18 ppm as $CaCO_3$

Chloride	7.6–8.8 ppm
Total dissolved solids	70–125 ppm

Source: Ref 11

Inspection Results. Deaerator vessel and storage tank A were inspected. All tray sections were removed from the deaerator. With the exception of the top head-to-shell weld in the deaerator, all internal welds were ground smooth and magnetic particle inspected. No cracks were found. Corrosion damage was limited to minor pitting of the bottom head in the deaerator vessel.

Inspection of deaerator vessel B revealed cracking at one weld. Tray sections were removed from the deaerator vessel, and shell welds were gritblasted. Except for the top head-to-shell weld in the deaerator, all internal welds in both B units were then ground smooth and magnetic particle inspected. Three transverse cracks were found at the bottom circumferential weld in the deaerator vessel. These were removed by grinding to a depth of 1.5 mm (0.06 in.).

Inspection of storage tank B revealed numerous cracks transverse to welds. With the shell constructed from three rings of plate, the longitudinal ring welds were located just below the water level. These longitudinal welds exhibited no detectable cracking. One circumferential crack was found above the working water level in the vessel. The remaining cracks were located at circumferential welds below the working water level. Numerous cracks transverse to circumferential welds were detected, but only one longitudinal crack was detected. All cracks were removed by grinding to a depth of 2 mm (0.08 in.).

Unlike deaerator vessel A, it was noted that none of the spray nozzles in deaerator vessel B was operational at the time of inspection. In addition, two valves had fallen to the bottom of the deaerator vessel. The bottom section of trays in deaerator vessel B had fallen to the bottom of the storage vessel. Corrosion damage in deaerator vessel B was limited to underdeposit pitting attack at circumferential welds in the bottom.

Metallurgical Analysis. A section was cut from a circumferential weld region in storage tank B. As shown in Fig. 7, the cracking was predominantly transverse to the weld. Chemical analysis was performed on samples cut from weld metal and base metal; the results are given in Table 5. The results show that the steel plate was not aluminum-or silicon-killed but was most likely a rimmed grade. Cross sections were cut perpendicular to both transverse and longitudinal cracks and were examined metallographically.

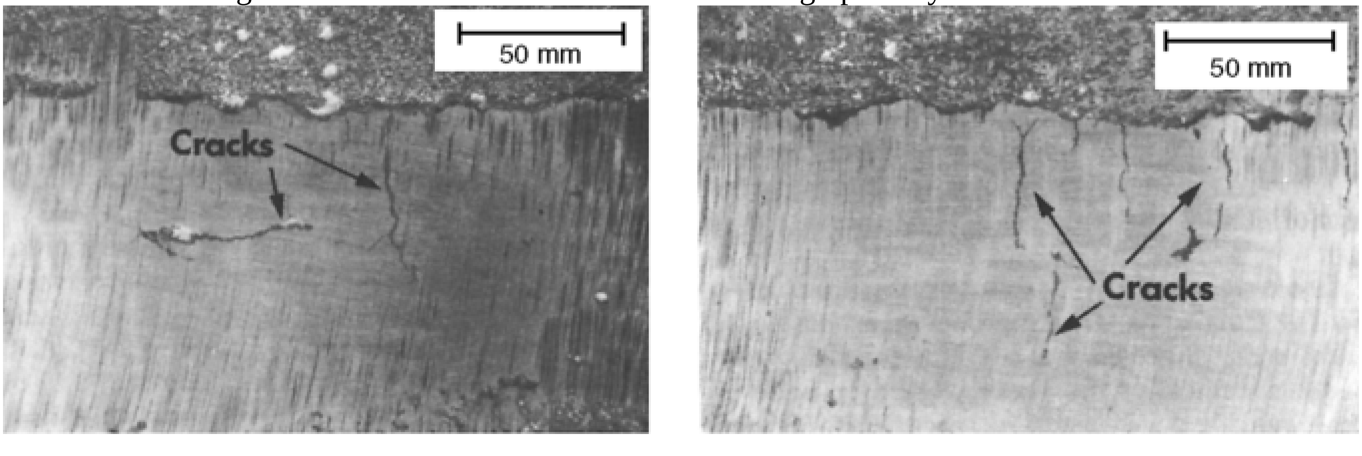

(a) (b)

Fig. 7 Transverse and longitudinal cracks on as-ground weld areas on the inside surface of storage vessel B. (a) Transverse and longitudinal cracks. (b) Transverse cracks. Source: Ref 11

Table 5 Chemical analyses of steels and weld deposit

Sample	Analysis, wt%								
	C	**Mn**	**Si**	**P**	**S**	**Ni**	**Cr**	**Mo**	**Al**	**Fe**
Plate 1	0.25	0.88	<0.05	0.029	0.036	<0.05	<0.05	<0.03	<0.01	bal
Plate 2	0.21	0.83	<0.05	0.03	0.024	<0.05	<0.05	<0.03	<0.01	bal
Weld deposit	0.14	0.53	0.14	0.035	0.031	<0.05	<0.05	<0.03	<0.01	bal

Source: Ref 11

As shown in Fig. 8, metallographic examination of the base metal structures revealed ferrite and lamellar pearlite phases with a nearly equiaxed grain structure. The approximate grain size was ASTM 6 to 7. Figure 9

shows a longitudinal crack in a weld HAZ, with associated grain refinement. Cracking initiated from the bottom of a pit. The oxide associated with the major crack was extensive and contained numerous secondary cracks. Analysis of the oxide deposit within the crack by wavelength-dispersive spectroscopy revealed slightly less oxygen than an Fe_2O_3 standard. Therefore, it was assumed that the oxide deposit was a mixture of Fe_3O_4 and Fe_2O_3.

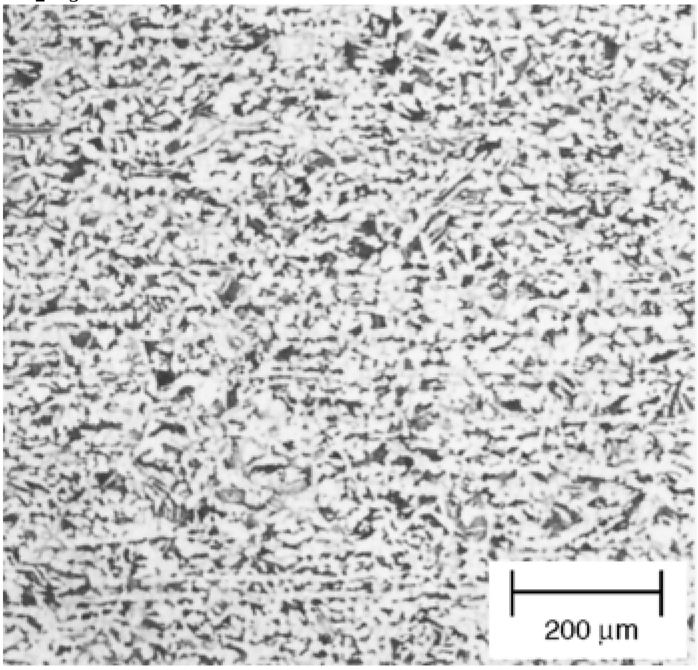

Fig. 8 Micrograph of the typical base metal microstructure of storage vessel B. Etching with nital revealed ferrite (light) and lamellar pearlite (dark). Source: Ref 11

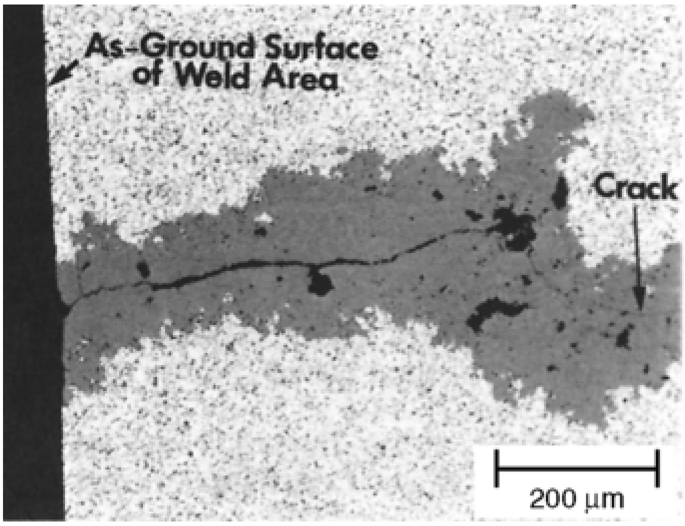

Fig. 9 Micrograph of a longitudinal crack in the heat affected zone of a weld from storage vessel B. Etched with nital. Source: Ref 11

Figure 10 shows a crack extending into base metal, transverse to the weld, with secondary cracking to the periphery of the oxidized region. It was clear that the oxide exhibited extensive internal cracking. Figure 10 also shows the entrainment of lamellar pearlite phase (dark) within the oxide corrosion product. In addition, the crack tips are blunt.

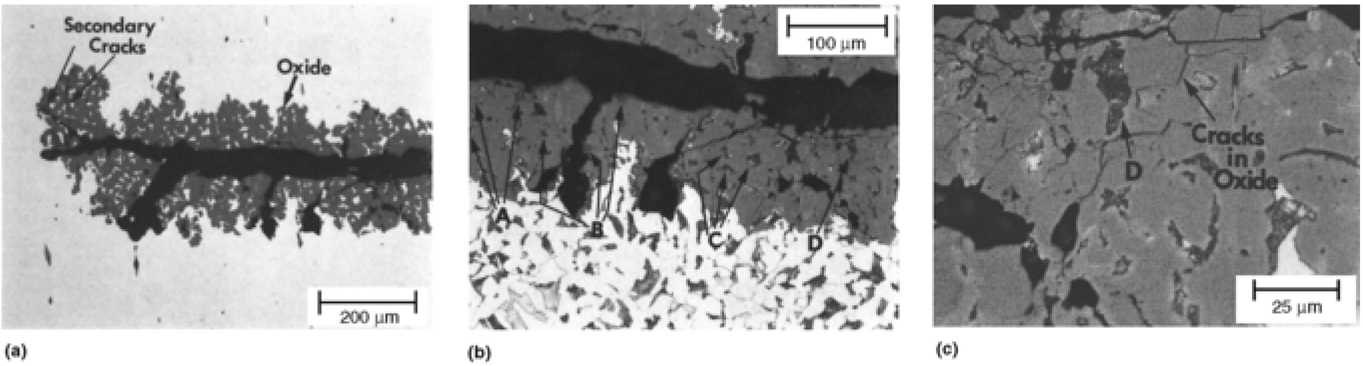

Fig. 10 Micrographs of a transverse crack in storage vessel B. (a) Crack extending into base metal. As-polished. (b) Lamellar pearlite phase (dark) entrained in the oxide corrosion product. (c) Microcracks and entrained pearlite phase in the oxide corrosion product. (b) and (c) Etched with nital. Source: Ref 11

Discussion. The cracks described in this example are very similar to those found in many other investigations, despite a variety of deaerator vessel designs and operating conditions. Cracks typically display the following characteristics:

- Cracks occur most often in welds and HAZs but can also occur in the base metal.
- Cracks are generally transverse to the weld HAZ and occur both parallel and perpendicular to the hoop stress direction.
- The worst cracks appear to be located in circumferential and head-to-shell welds in horizontal vessel designs.
- Cracks are concentrated at, but not solely located within, the working water level in the vessel.
- Cracks are perpendicular to the vessel plate surface.
- Cracks are predominantly transgranular, with minor amounts of branching.
- Cracks are filled with iron oxide. Cracking of the oxide corrosion product is followed by progressive corrosion. The ferrite phase is selectively attacked, with retention of the pearlite phase within the oxide corrosion product.
- Cracks initiate from corrosion pits. Weld defects, however, can also become active sites for crack initiation.
- Crack tips are blunt.

Conclusions. These findings suggest that the failure mechanism is a combination of low-cycle corrosion fatigue and stress-induced corrosion. Extensive oxide formation relative to the depth of cracking is a key feature. The formation of oxide was associated with corrosion attack of the ferrite phase. The lamellar pearlite phase remained relatively intact and was contained within the oxide product. The oxide itself exhibited numerous cracks, allowing aqueous corrosion of fresh metal to occur at the oxide-metal interface. Mechanical or thermal stresses are most likely responsible for this network of cracks within the oxide product. The mechanism appears to be stress-assisted localized corrosion. Sharp, tight cracks were not found in fresh metal beyond the periphery of the oxide corrosion product. It therefore appears reasonable that cracking could have occurred subsequent to corrosion and within the brittle oxide.

Cracking at welds and HAZs suggests that residual weld shrinkage stresses play a major role. Welds in deaerator vessels typically have not been postweld stress relieved. It is not unusual to find residual welding stresses of yield strength magnitude. This problem can be aggravated by vessel design (high localized bending stresses around saddle supports that fluctuate with water level and are accelerated by operational upsets).

No fault was found with the steel plate chemical composition or with welding consumables. There was no evidence of embrittlement or caustic SCC (that is, no branched intergranular cracks).

Recommendations. All welds in deaerator vessels should be postweld stress relieved. Operational upsets should be avoided, and water chemistry must be maintained within acceptable limits. This is especially true with regard to water oxygen levels, which should be kept low to minimize pitting corrosion. Detailed assessment of the influence of welding on the occurrence of such cracking and mitigation methods is provided in Ref 3.

References cited in this section

3. T.G. Gooch and P.H.M. Hart, "Review of Welding Practices for Carbon Steel Deaerator Vessels," Paper 303, presented at Corrosion/86, (Houston, TX), National Association of Corrosion Engineers, March 1986

10. J. Gutzeit and J.M. Johnson, "Stress-Corrosion Cracking of Carbon Steel Welds in Amine Service," Paper 206, presented at Corrosion/86, (Houston, TX), National Association of Corrosion Engineers, March 1986

11. G.E. Kerns, "Deaerator Cracking—A Case History," Paper 310, presented at Corrosion/ 86, (Houston, TX), National Association of Corrosion Engineers, March 1986

S. Bond, Corrosion of Carbon Steel Weldments, *Corrosion: Fundamentals, Testing, and Protection*, Vol 13A, *ASM Handbook*, ASM International, 2003, p 294–300

Corrosion of Carbon Steel Weldments

Revised by Stuart Bond, TWI Ltd., United Kingdom

Acknowledgment

This article has been adapted from a portion of the article "Corrosion of Weldments," in *Corrosion*, Vol 13, *Metals Handbook,* 9th ed., ASM International, 1987, p 362–368.

S. Bond, Corrosion of Carbon Steel Weldments, *Corrosion: Fundamentals, Testing, and Protection*, Vol 13A, *ASM Handbook*, ASM International, 2003, p 294–300

Corrosion of Carbon Steel Weldments

Revised by Stuart Bond, TWI Ltd., United Kingdom

References

1. T.G. Gooch, "The Effect of Welding on Material Corrosion Behaviour," NACE International Process Industries Corrosion Seminar, 13–16 Oct 1986, (Houston, TX)

2. J.S. Smart, Weld Corrosion in Lines Deserves Closer Attention, *Pipeline Gas Ind.,* Vol 79 (No. 6), June 1996, p 33–35

3. T.G. Gooch and P.H.M. Hart, "Review of Welding Practices for Carbon Steel Deaerator Vessels," Paper 303, presented at Corrosion/86, (Houston, TX), National Association of Corrosion Engineers, March 1986

4. J.L. Robinson, Preferential Corrosion of Welds, *The Welding Institute Research Bulletin,* Vol 20, Jan and Feb 1979

5. “Preferential Corrosion of Carbon Steel Weldments in Oil and Gas Production Systems,” Joint Industry Project 5563/28/89, TWI and CAPCIS, 1989

6. R.W. Revie, Ed., *Uhlig's Corrosion Handbook,* 2nd ed., John Wiley & Sons, 2000, p 542

7. R.J. Brigham et al., Evaluation of Weld- Zone Corrosion of Shipbuilding Steel Plates for Use in the Arctic Environment, *Can. Metall. Q.,* Vol 27 (No. 4), 1988, p 311–321

8. M.B. Kermani and L.M. Smith, Ed., *CO_2 Corrosion Control in Oil and Gas Production,* European Federation of Corrosion Publication 23, The Institute of Materials, London, 1997

9. C.G. Arnold, “Galvanic Corrosion Measurement of Weldments,” Paper 71, presented at Corrosion/80, (Chicago, IL), National Association of Corrosion Engineers, March 1980

10. J. Gutzeit and J.M. Johnson, “Stress-Corrosion Cracking of Carbon Steel Welds in Amine Service,” Paper 206, presented at Corrosion/86, (Houston, TX), National Association of Corrosion Engineers, March 1986

11. G.E. Kerns, “Deaerator Cracking—A Case History,” Paper 310, presented at Corrosion/ 86, (Houston, TX), National Association of Corrosion Engineers, March 1986

S. Bond, Corrosion of Carbon Steel Weldments, *Corrosion: Fundamentals, Testing, and Protection*, Vol 13A, *ASM Handbook*, ASM International, 2003, p 294–300

Corrosion of Carbon Steel Weldments

Revised by Stuart Bond, TWI Ltd., United Kingdom

Selected References

- J.R. Davis, Ed., *ASM Specialty Handbook: Carbon and Alloy Steels,* ASM International, 1996
- S. Lampman, Ed., *Weld Integrity and Performance,* ASM International, 1997

Corrosion of Stainless Steel Weldments, *Corrosion: Fundamentals, Testing, and Protection*, Vol 13A, *ASM Handbook*, ASM International, 2003, p 301–316

Corrosion of Stainless Steel Weldments

Introduction

STAINLESS STEELS are iron-base alloys that contain a minimum of approximately 11% Cr, the amount needed to prevent the formation of rust in unpolluted atmospheres (hence the designation *stainless*). Few stainless steels contain more than 30% Cr or less than 50% Fe. They achieve their stainless characteristics through the formation of an invisible and adherent chromium-rich oxide surface film. This oxide forms and heals itself in the presence of oxygen. Other elements added to improve particular characteristics include nickel,

molybdenum, copper, titanium, aluminum, silicon, niobium, nitrogen, sulfur, and selenium. Carbon is normally present in amounts ranging from less than 0.03% to over 1.0% in certain martensitic grades.

Corrosion of Stainless Steel Weldments, *Corrosion: Fundamentals, Testing, and Protection*, Vol 13A*, ASM Handbook,* ASM International, 2003, p 301–316

Corrosion of Stainless Steel Weldments

Metallurgical Factors

Stainless steel base metals and thus the welding filler metals used with them are almost invariably chosen on the basis of adequate corrosion resistance for the intended application. This usually means that the welding filler metal must at least match (and sometimes overmatch) the contents of the base metal in terms of specific alloying elements, such as chromium, nickel, and molybdenum.

The cycle of heating and cooling that occurs during the welding process affects the microstructure and surface composition of welds and adjacent base metal. Consequently, the corrosion resistance of autogenous welds (welds made without the use of filler metals) and welds made with matching filler metal may be inferior to that of properly annealed base metal because of:

- Microsegregation
- Precipitation of secondary phases
- Formation of unmixed zones
- Recrystallization and grain growth in the weld heat-affected zone (HAZ)
- Volatilization of alloying elements from the molten weld pool
- Contamination of the solidifying weld pool

Corrosion resistance can usually be maintained in the welded condition by:

- Balancing alloy compositions to inhibit certain precipitation reactions
- Shielding molten and hot metal surfaces from reactive gases in the weld environment
- Removing chromium-enriched oxides and chromium-depleted base metal from thermally discolored (heat tinted) surfaces
- Choosing the proper welding parameters (Ref 1)

Weld Solidification. During the welding process, a number of important changes occur that can significantly affect the corrosion behavior of the weldment. Heat input and welder technique obviously play important roles. The way in which the weld solidifies is equally important to understanding how weldments may behave in corrosive environments (Ref 2).

A metallographic study has shown that welds solidify into various regions, as shown in Fig. 1. The composite region, or fusion zone, essentially consists of filler metal that has been diluted with material melted from the surrounding base metal. Next to the composite region is the unmixed zone where the base metal is melted and then quickly solidified to produce a composition similar to that of the base metal (Ref 4). For example, when type 304 stainless steel is welded using a filler metal with high chromium-nickel content, steep concentration gradients of chromium and nickel are found in the fusion zone, whereas the unmixed zone has a composition similar to the base metal (Fig. 2). The weld interface is the surface bounding the region within which complete melting occurred during welding, and it is evidenced by the presence of a cast structure. Beyond the weld interface is the partially melted zone, which is a region of the base metal within which the proportion melted ranges from 0 to 100%. Lastly, the true HAZ is that portion of the base metal within which microstructural change has occurred in the absence of melting. Although the various regions of a weldment shown in Fig. 1 are for a single-pass weld, similar solidification patterns and compositional differences can be expected to occur in underlying weld beads during multipass applications.

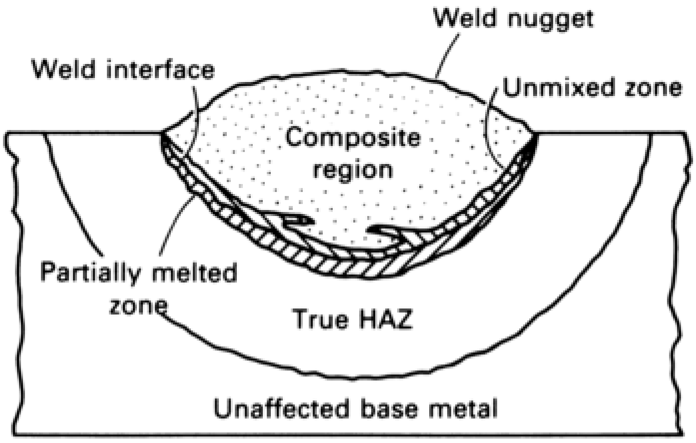

Fig. 1 Weld cross section. Source: Ref 3

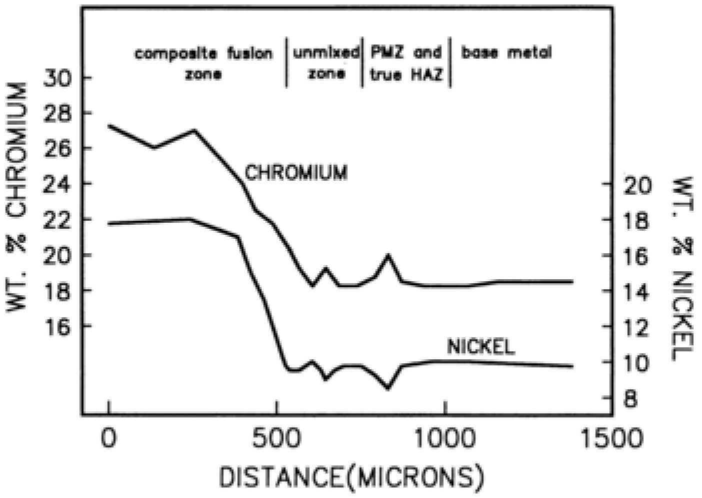

Fig. 2 Concentration profile of chromium and nickel across the weld fusion boundary region of type 304 stainless steel. Source: Ref 4

References cited in this section

1. F.C. Brautigam, Welding Practices That Minimize Corrosion, *Chem. Eng.,* 17 Jan 1977, p 145–147

2. M.A. Streicher, Theory and Application of Evaluation Tests for Detecting Susceptibility to Intergranular Attack in Stainless Steels and Related Alloys—Problems and Opportunities, *Intergranulur Corrosion of Stainless Alloys,* STP 656, American Society for Testing and Materials, 1978, p 70

3. W.F. Savage, New Insight into Weld Cracking and a New Way of Looking at Welds, *Weld. Des. Eng.,* Dec 1969

4. W.A. Baeslack III, J.C. Lippold, and W.F. Savage, Unmixed Zone Formation in Austenitic Stainless Steel Weldments, *Weld. J.,* Vol 58 (No. 6), 1979, p 168s–176s

Corrosion of Stainless Steel Weldments, *Corrosion: Fundamentals, Testing, and Protection*, Vol 13A, *ASM Handbook*, ASM International, 2003, p 301–316

Corrosion of Stainless Steel Weldments

Corrosion of Austenitic Stainless Steel Weldments

The corrosion problems commonly associated with welding of austenitic stainless steels are related to precipitation effects and chemical segregation. These problems can be eliminated or minimized through control of base metal metallurgy, control of the welding practice, and selection of the proper filler metal.

Preferential Attack Associated with Weld Metal Precipitates. In austenitic stainless steels, the principal weld metal precipitates are δ-ferrite, σ-phase, and $M_{23}C_6$ carbides. Small amounts of M_6C carbide may also be present. Sigma phase is often used to describe a range of chromium- and molybdenum-rich precipitates, including χ and laves (η) phases. These phases may precipitate directly from weld metal, but they are most readily formed from weld metal δ- ferrite in molybdenum-containing austenitic stainless steels.

The δ-ferrite transforms into brittle intermetallic phases, such as σ and χ, at temperatures ranging from 500 to 850 °C (930 to 1560 °F) for σ and 650 to 950 °C (1200 to 1740 °F) for χ. The precipitation rate for σ and χ phases increases with the chromium and molybdenum contents. Continuous intergranular networks of a phase reduce the toughness, ductility, and corrosion resistance of austenitic stainless steels.

It is extremely difficult to discriminate between fine particles of σ and χ phases by using conventional optical metallographic techniques; hence the designation σ/χ phase. The use of more sophisticated analytical techniques to identify either phase conclusively is usually not justified when assessing corrosion properties, because the precipitation of either phase depletes the surrounding matrix of crucial alloying elements. Grain-boundary regions that are depleted in chromium and/or molybdenum are likely sites for attack in oxidizing and chlorine-bearing solutions. The damage caused by preferential corrosion of alloy-depleted regions ranges from the loss of entire grains (grain dropping) to shallow pitting at localized sites, depending on the distribution and morphology of the intermetallic precipitate particles at grain boundaries. Figure 3 shows two views of an austenitic stainless steel exhibiting intergranular corrosion. Figure 3(a) shows the surface of the sample. The grain structure is visible due to the attack, and some grains have fallen out (grain dropping). The cross-sectional view (Fig. 3b) shows the depth of penetration of the attack along the grain boundaries.

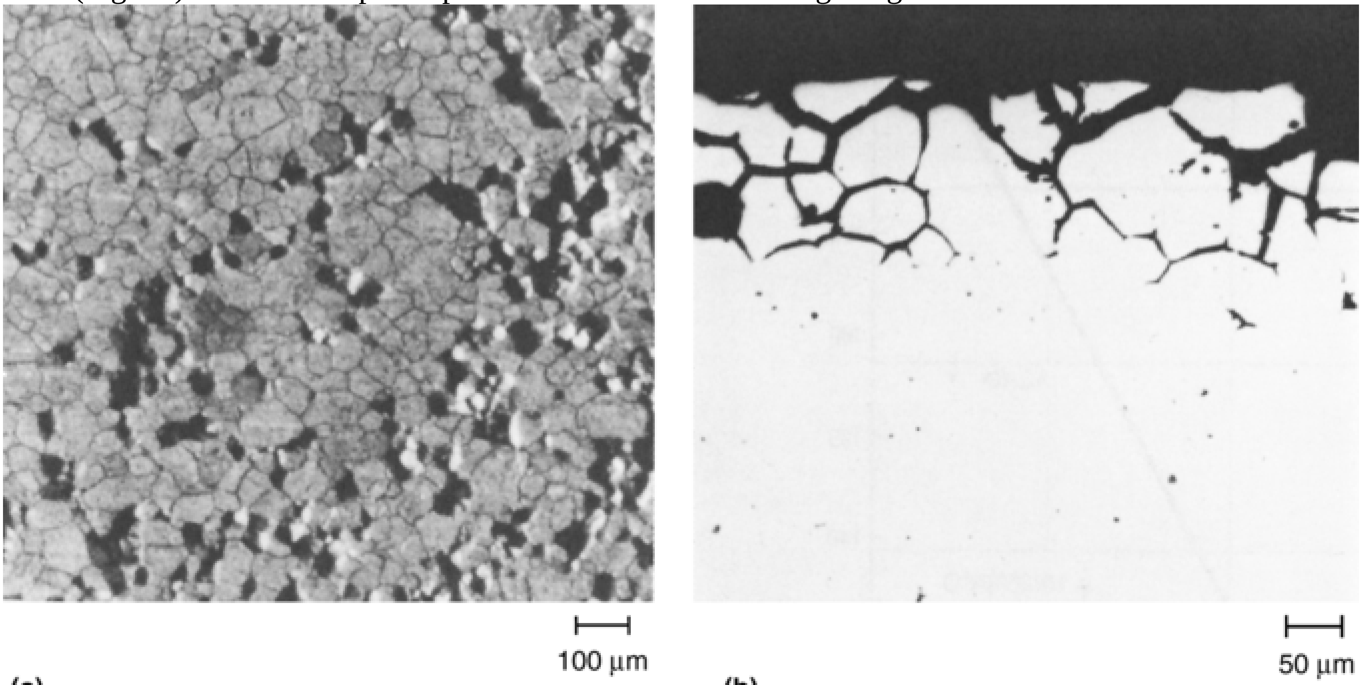

(a) (b)

Fig. 3 Planar (a) and cross-sectional (b) views of intergranular corrosion (grain dropping) in a sensitized austenitic stainless steel. As-polished. (a) 50×. (b) 100×. Courtesy of G.F. Vander Voort, Carpenter Technology Corporation

Because these precipitates are usually chromium- and molybdenum-rich, they are generally more corrosion resistant than the surrounding austenite. However, there are some exceptions to this rule.
Preferential attack associated with δ-ferrite and σ can be a problem when a weldment is being used close to the limit of corrosion resistance in environments represented by three types of acidic media:

- Mildly reducing (e.g., hydrochloric acid, HCl)
- Borderline active-passive (e.g., sulfuric acid, H_2SO_4)
- Highly oxidizing (e.g., nitric acid, HNO_3)

Acid cleaning of type 304 and 316 stainless steel black liquor evaporators in the pulp and paper industry with poorly inhibited HCl can lead to weld metal δ-ferrite attack (Fig. 4, 5). Attack is avoided by adequate inhibition (short cleaning times with sufficient inhibitor at low enough temperature) and by specification of full- finished welded tubing (in which the δ-ferrite networks within the weld metal structure are altered by cold work and a recrystallizing anneal). The latter condition can easily be verified with laboratory HCl testing, and such a test can be specified when ordering welded tubular products.

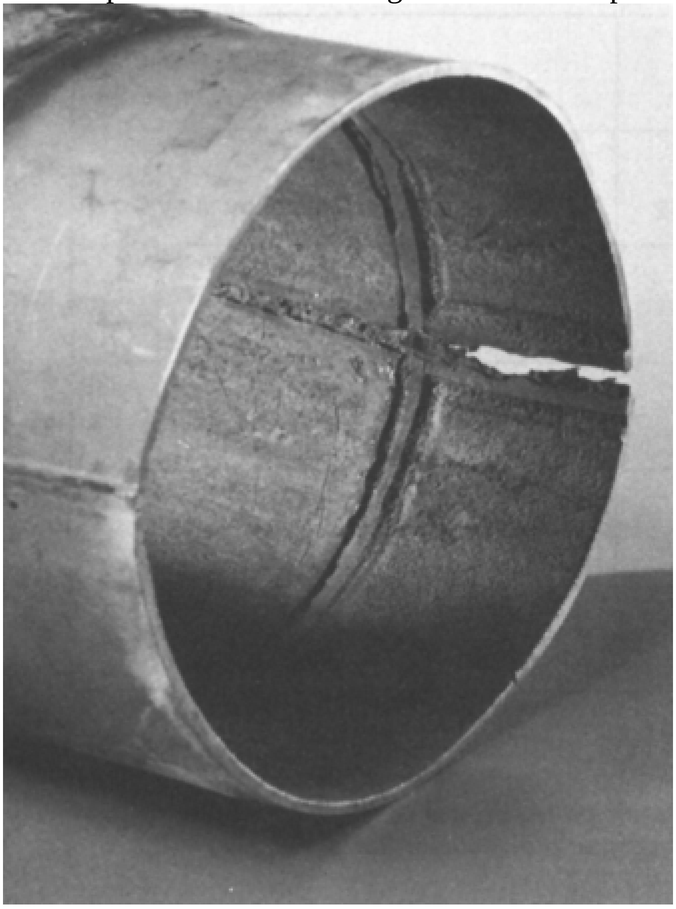

Fig. 4 Corroded type 316 stainless steel pipe from a black liquor evaporator. Two forms of attack are evident: preferential attack of the weld metal ferrite, suffered during HCl acid cleaning, and less severe attack in the sensitized HAZ center. Source: Ref 5

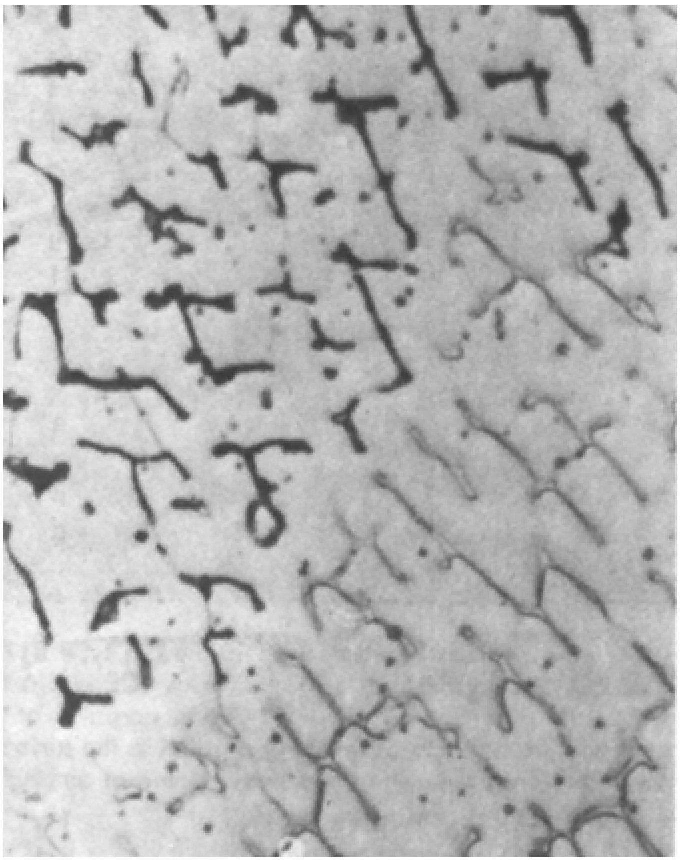

Fig. 5 Preferential corrosion of the vermicular ferrite phase in austenitic stainless steel weld metal. Discrete ferrite pools that are intact can be seen in the lower right; black areas in the upper left are voids where ferrite has been attacked. Electrolytically etched with 10% ammonium persulfate. 500×. Source: Ref 6

Sulfuric acid attack of a phase or of chromium- and molybdenum-depleted regions next to σ-phase precipitates is commonly reported. However, it is difficult to predict because the strong influence of tramp oxidizing agents, such as ferric (Fe^{3+}) or cupric (Cu^{2+}) ions, can inhibit preferential attack. Type 316L weld filler metal has been formulated with higher chromium and lower molybdenum to minimize σ- phase formation, and filler metals for more highly alloyed materials such as 904L (Fe-22Cr- 26Ni-4.5Mo) are balanced to avoid δ-ferrite precipitation and thus minimize σ-phase.

Highly oxidizing environments such as those found in bleach plants could conceivably attack δ-ferrite networks and σ phase. However, this mode of attack is not often a cause of failure, probably because free-corrosion potentials are generally lower (less oxidizing) than that required to initiate attack. Preferential attack of δ-ferrite in type 316L weld metal is most often reported after prolonged HNO_3 exposure, as in nuclear-fuel reprocessing or urea production. For these applications, a low corrosion rate in the Huey test (ASTM A 262, practice C) is specified (Ref 7).

Pitting Corrosion. Under moderately oxidizing conditions, such as a pulp and paper bleach plant, weld metal austenite may suffer preferential pitting in alloy-depleted regions. This attack is independent of any weld metal precipitation and is a consequence of microsegregation or coring in weld metal dendrites. Preferential pitting is more likely:

- In autogenous (no filler) gas-tungsten arc (GTA) welds (Fig. 6)
- In 4 to 6% Mo alloys (Table 1)
- When the recommended filler metal has the same composition as the base metal (Fig. 7)
- When higher-heat-input welding leaves a coarse microstructure with surface-lying dendrites (Fig. 8). Such a microstructure is avoided by use of a suitably alloyed filler metal (Fig. 7)

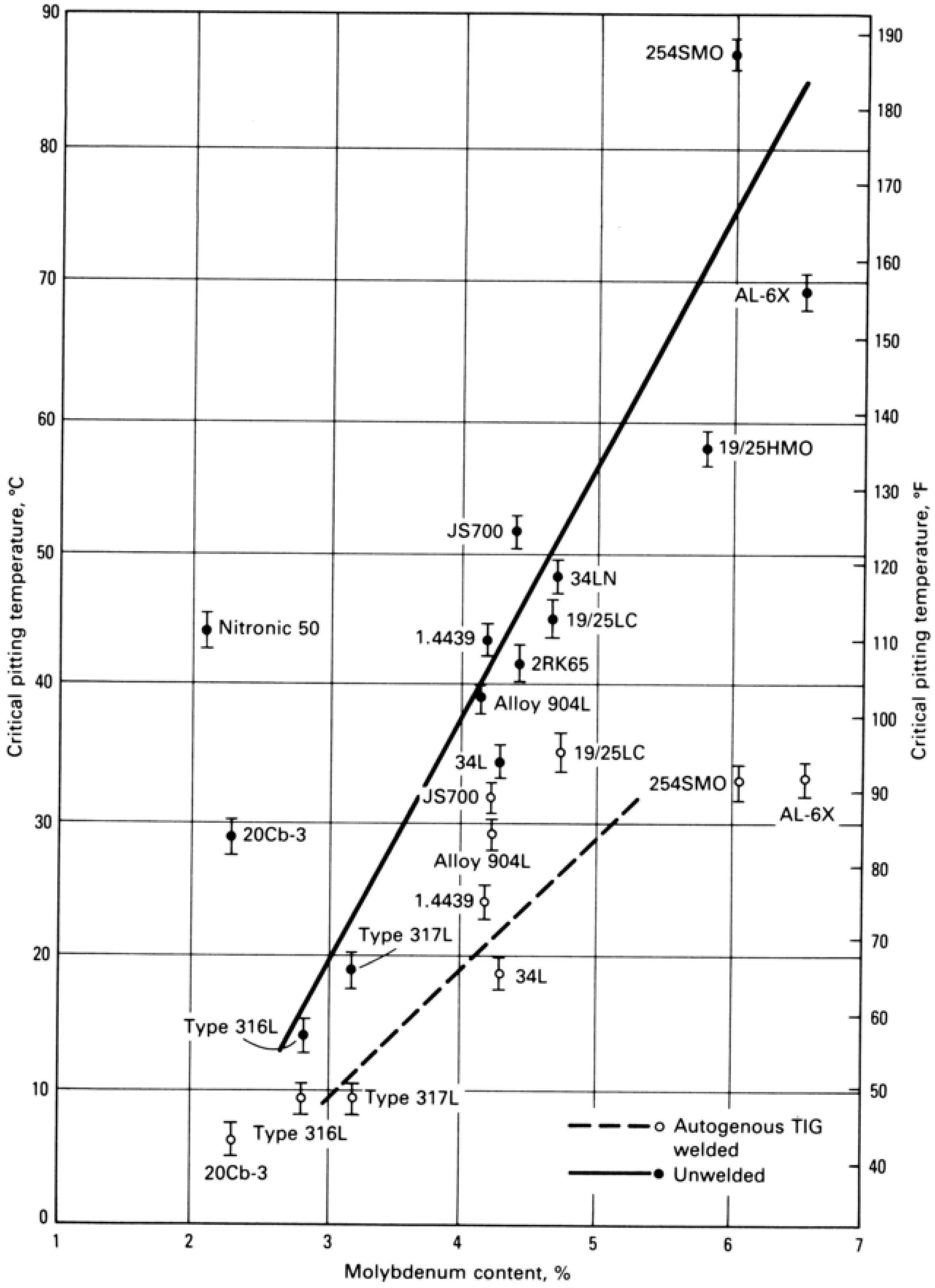

Fig. 6 Critical pitting temperature versus molybdenum content for commercial austenitic stainless steels tested in 10% $FeCl_3$. Resistance to pitting, as measured by the critical pitting temperature, increases with molybdenum content and decreases after autogenous tungsten inert gas welding. Source: Ref 5

Table 1 Amounts of principal alloying elements in stainless steels tested for pitting resistance

Test results are shown in Fig. 6 and 7.

Alloy	Composition, %			
	Cr	**Ni**	**Mo**	**N**
Base metals				
Type 316L	16	13	2.8	…
Type 317L	18	14	3.2	…
34L	17	15	4.3	…
34LN	18	14	4.7	…
1.4439	18	14	4.3	0.13
Nitronic 50	21	14	2.2	0.20
20Cb-3	20	33	2.4	…
Alloy 904L	20	25	4.2	…
2RK65	20	25	4.5	…
JS700	21	25	4.5	…
19/25LC	20	25	4.8	…
AL-6X	20	24	6.6	…
254SMO	20	18	6.1	0.20
19/25HMO	21	25	5.9	0.15
Filler metals				
Type 316L	19	12	2.3	…
Type 317L	19	13	3.8	…
309MoL	23	14	2.5	…
Batox Cu	19	24	4.6	…
254SLX	20	24	5.0	…
SP-281	20	25	4.6	…
Jungo 4500	20	26	4.4	…
Nicro 31/27	28	30	3.5	…
Thermanit 30/40E	28	35	3.4	…
SAN 27.31.4.LCuR	27	31	3.5	…
Incoloy alloy 135	27	31	3.5	…
Hastelloy alloy G	22	38	3.7	…
P 12	21	61	8.6	…
Inconel alloy 112	21	61	8.7	…
Hastelloy alloy C-276	15	58	15.4	…

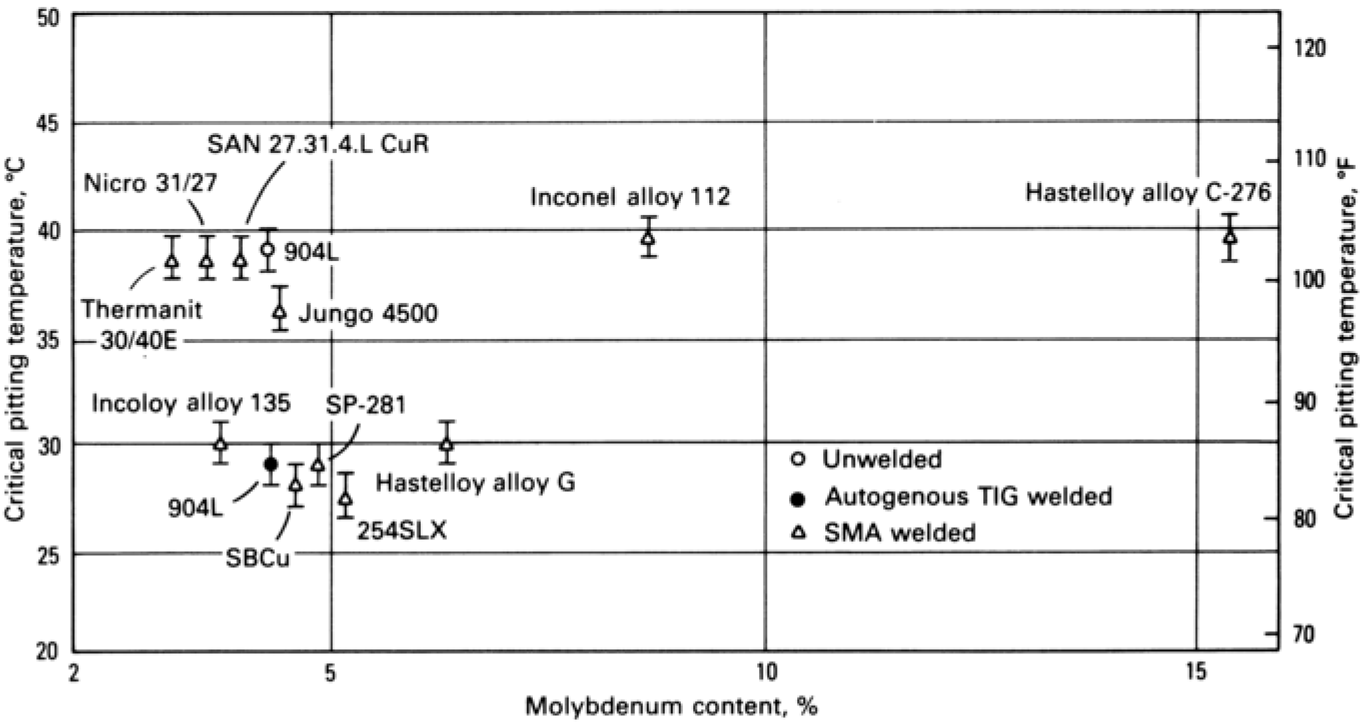

Fig. 7 Effects of various welding techniques and filler metals on the critical pitting temperature of alloy 904L. Data for an unwelded specimen are included for comparison. Source: Ref 5

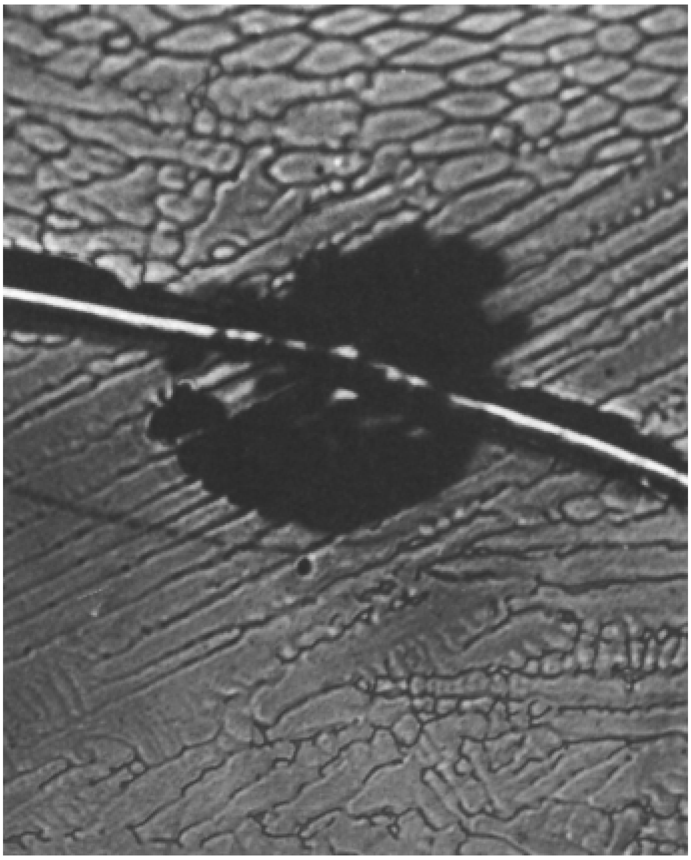

Fig. 8 A scratch-initiated pit formed in type 317L weld metal at 190 mV versus SCE in 0.6 *N* NaCl (pH 3) at 50 °C (120 °F). Pitting occurred at a grain with primary dendrites lying parallel to the surface rather than in grains with dendrites oriented at an angle to the surface.

Filler metals with pitting resistance close to or better than that of corresponding base metals include:

Base metal	Filler metals
Type 316L	316L, 317L, 309MoL
Type 317	317L, 309MoL
Alloy 904	Sandvik 27.31.4.LCuR, Thermanit 30/40 E, Nicro 31/27, Fox CN 20 25 M, IN-112, Avesta P12, Hastelloy alloy C-276
Avesta 254 SMO	Avesta P12, IN-112, Hastelloy alloy C-276

Even when suitable fillers are used, preferential pitting attack can still occur in an unmixed zone of weld metal. High-heat-input welding can leave bands of melted base metal close to the fusion line. The effect of these bands on corrosion resistance can be minimized by welding techniques that bury unmixed zones beneath the surface of the weldment.

When the wrong filler metal is used, pitting corrosion can readily occur in some environments. In the example shown in Fig. 9, the type 316L base metal was welded with a lower-alloy filler metal (type 308L). Tap water was the major environmental constituent contributing to crust formation on the weld joint. The type 316L base metal on either side of the joint was not affected.

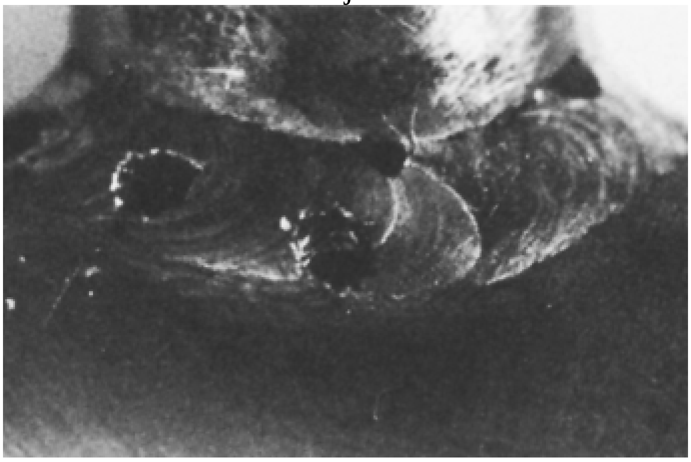

Fig. 9 Pitting of underalloyed (relative to the base metal) type 308L weld metal. The type 316L stainless steel base metal is unaffected. About 2.5×

Crevice Corrosion. Defects such as residual welding flux and microfissures create weld metal crevices that are easily corroded, particularly in chloride-containing environments. Some flux formulations on coated shielded metal arc electrodes produce easily detached slags, and others give slags that are difficult to remove completely, even after grit blasting. Slags from rutile (titania- base) coatings are easily detached and give good bead shape. In contrast, slags from the basic- coated electrodes for out-of-position welding can be difficult to remove; small particles of slag may remain on the surface, providing an easy initiation site for crevice attack (Fig. 10).

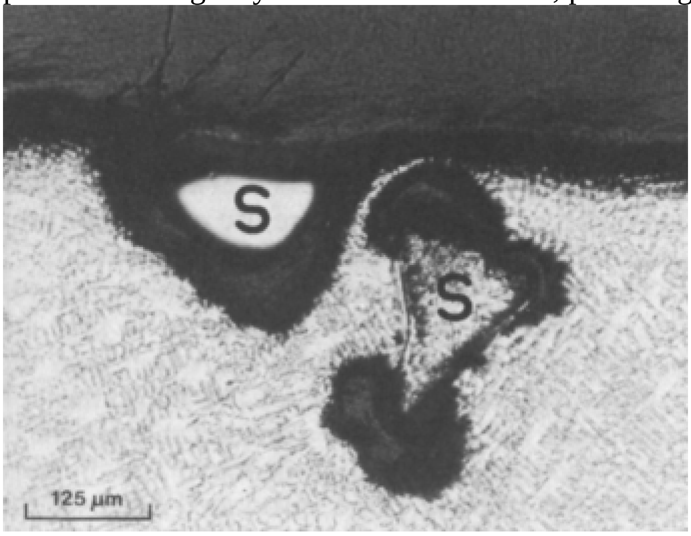

Fig. 10 Crevice corrosion under residual slag (S) in IN-135 weld metal after bleach plant exposure. Etched with glycergia. Source: Ref 5

Microfissures or their larger counterparts, hot cracks, also provide easy initiation sites for crevice attack, which will drastically reduce the corrosion resistance of a weldment in the bleach plant. Microfissures are caused by thermal contraction stresses during weld solidification and are a problem that plagues austenitic stainless steel fabrications. These weld metal cracks are more likely to form when phosphorus and sulfur levels are higher (i.e., >0.015% P and >0.015% S), with high-heat-input welding, and in austenitic weld metal in which the δ-ferrite content is low (<3%).

Small-scale microfissures are often invisible to the naked eye, and their existence can readily explain the unexpectedly poor pitting performance of one of a group of weldments made with filler metals of apparently similar general composition. The microfissure provides a crevice, which is easily corroded because stainless alloys are more susceptible to crevice corrosion than to pitting. However, microfissure-crevice corrosion is often mistakenly interpreted as self-initiated pitting (Fig. 11, 12).

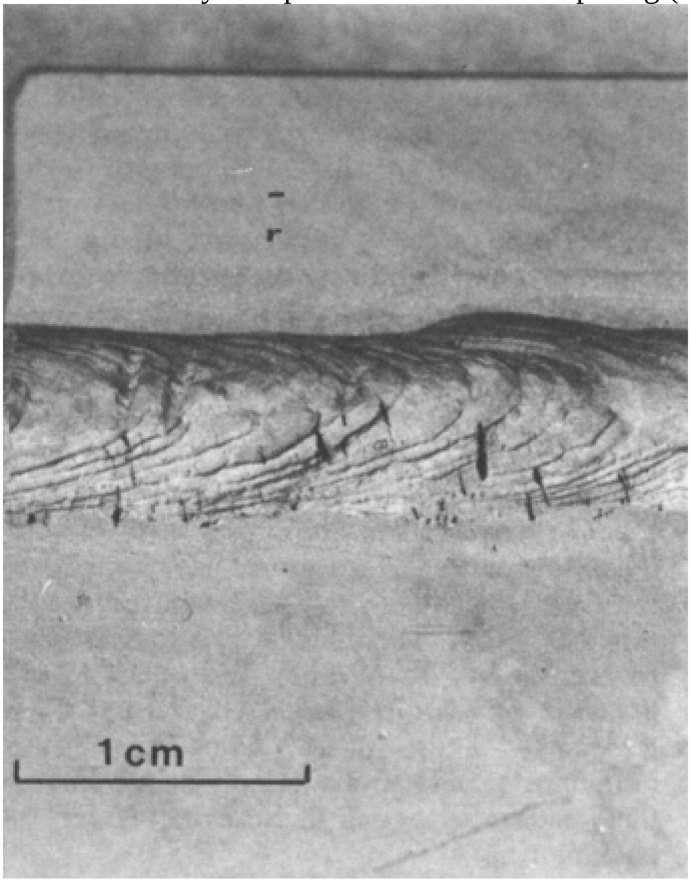

Fig. 11 Microfissure corrosion on IN-135 weld metal on an alloy 904L test coupon after bleach plant exposure. See also Fig. 12. Source: Ref 5

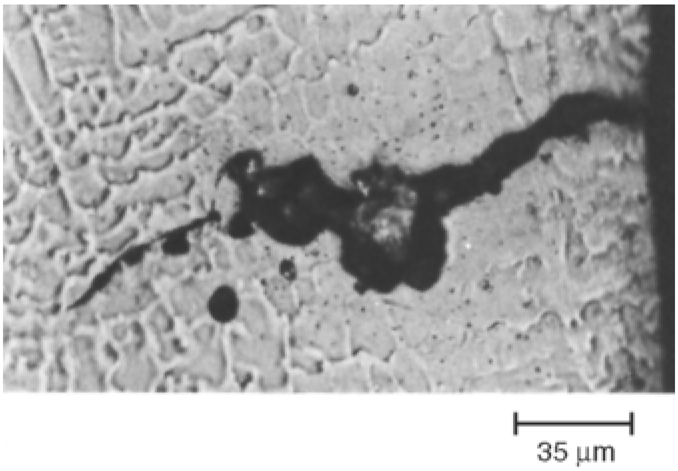

Fig. 12 Section from the bleach plant test coupon in Fig. 11 showing crevice corrosion that has almost obliterated evidence of a microfissure. This form of attack is often mistakenly interpreted as self-initiating pitting; more often, crevice corrosion originates at a microfissure. Etched with glycergia. Source: Ref 5

Crevice corrosion sites can also occur at the beginning or end of weld passes, between weld passes, or under weld spatter areas. Weld spatter is most troublesome when it is loose or poorly adherent. A good example of this type of crevice condition is the type 304 stainless system shown in Fig. 13.

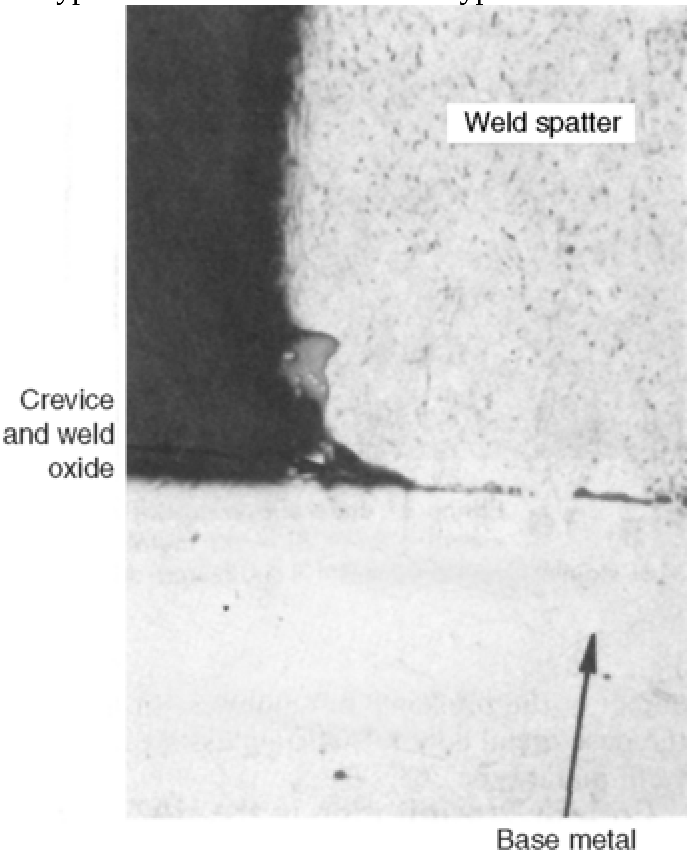

Fig. 13 Cross section of a weldment showing crevice corrosion under weld spatter. Oxides (light gray) have formed on the spatter and in the crevice between spatter and base metal.

Microfissure corrosion in austenitic stainless steel weldments containing 4 to 6% Mo is best avoided with the nickel-base Inconel 625, Inconel 112, or Avesta P12 filler metals, which are very resistant to crevice attack. Some stainless electrodes are suitable for welding 4% Mo steels, but they should be selected with low phosphorus and sulfur to avoid microfissure problems.

Hot tap water is not thought to be particularly aggressive; however, Fig. 14 shows what can happen to a weld that contains a lack-of-fusion defect in the presence of chlorides. In this case, the base metal is type 304 stainless steel, and the weld metal is type 308.

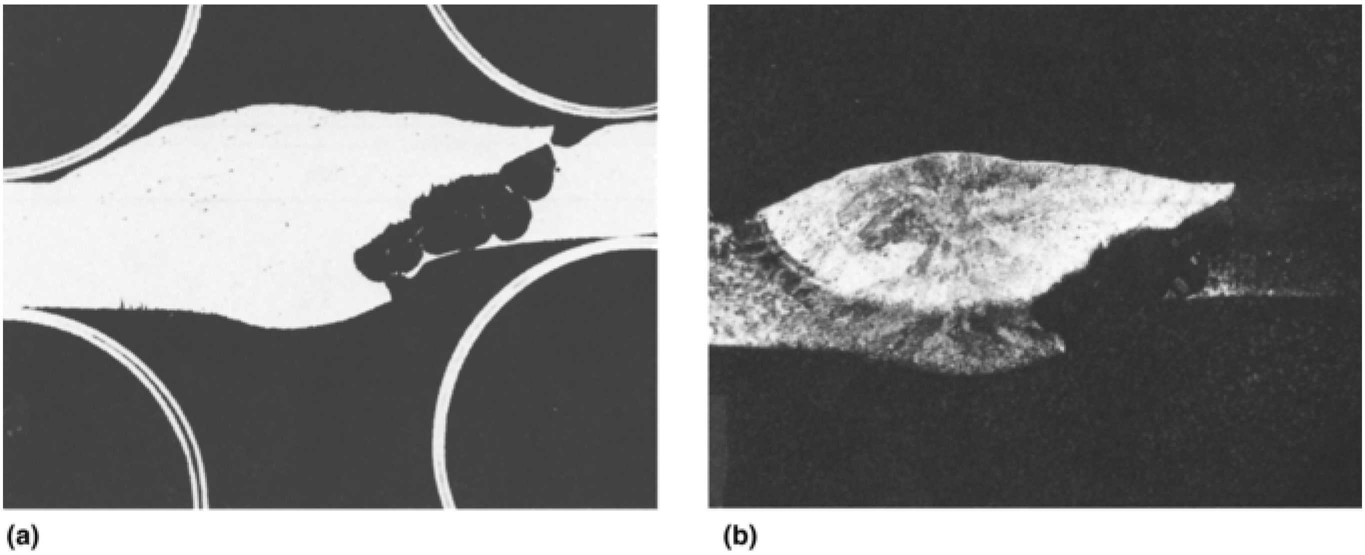

Fig. 14 Unetched (a) and etched (b) cross sections of a type 304 stainless steel weldment showing chloride pitting attack along a crevice by a lack-of-fusion defect. Service environment: hot tap water

Sensitization. The best known weld-related corrosion problem in stainless steels is weld decay (sensitization) caused by carbide precipitation in the weld HAZ. Sensitization occurs in a zone subject to a critical thermal cycle in which chromium-rich carbides precipitate and in which chromium diffusion is much slower than that of carbon. The carbides are precipitated on grain boundaries that are consequently flanked by a thin chromium-depleted layer. This sensitized microstructure is much less corrosion resistant, because the chromium-depleted layer and the precipitate can be subject to preferential attack (Fig. 15, 16). In North America, sensitization is avoided by the use of low-carbon grades such as type 316L (0.03% C max) in place of sensitization-susceptible type 316 (0.08% C max). In Europe, it is more common to use 0.05% C (max) steels, which are still reasonably resistant to sensitization, particularly if they contain molybdenum and nitrogen; these elements appear to raise the tolerable level of carbon and/or heat input. However, low-carbon stainless steels carry a small cost premium and so are not universally specified.

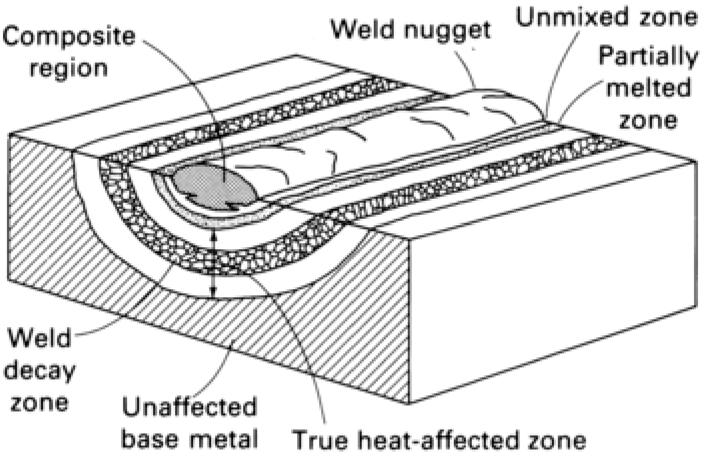

Fig. 15 Diagram of weld decay (sensitization) in an austenitic stainless steel weldment. Source: Ref 3

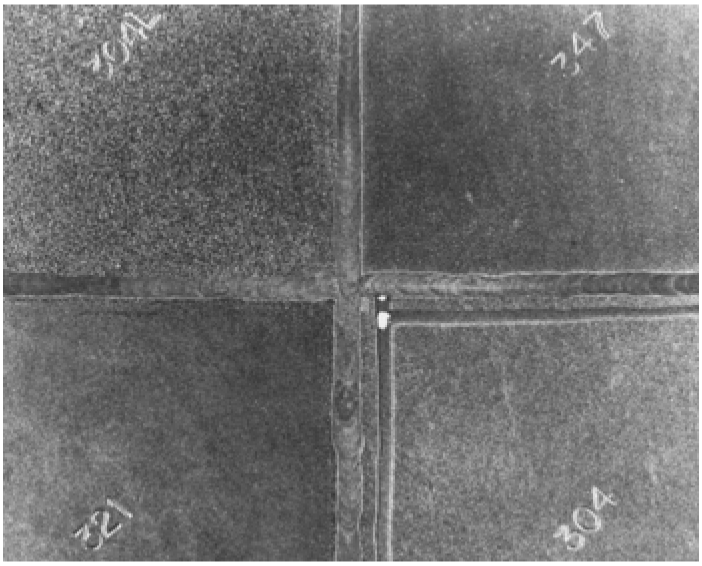

Fig. 16 Weld decay and methods for its prevention. The four different panels were joined by welding and then exposed to a hot solution of HNO_3/HF. Weld decay, such as that shown for the type 304 steel (bottom right), is prevented by reduction of the carbon content (type 304L, top left) or by stabilizing with titanium (type 321, bottom left) or niobium (type 347, top right). Source: Ref 2

Thiosulfate ($S_2O_3^{2-}$) pitting corrosion will readily occur in sensitized HAZs of type 304 weldments in paper machine white-water service (Fig. 17). This form of attack can be controlled by limiting sources of $S_2O_3^{2-}$ contamination; the principal one is the brightening agent sodium hyposulfite ($Na_2S_2O_4$). However, nonsensitized type 304 will also be attacked. Consequently, type 316L is the preferred grade of stainless steel that should be specified for paper machine service.

Fig. 17 Thiosulfate pitting in the HAZ of a type 304 stainless steel welded pipe after paper machine white-water service. Source: Ref 5

At higher solution temperatures, sensitized type 304 and type 316 are particularly susceptible to stress-corrosion cracking (SCC), whether caused by chlorides, sulfur compounds, or caustic. For example, type 304 or 316 kraft black liquor evaporators and white liquor tubing are subject to SCC in sensitized HAZs. In many cases cracking occurs after HCl acid cleaning. Although the initial crack path may be intergranular, subsequent propagation can have the characteristic branched appearance of transgranular chloride SCC. Intergranular SCC caused by sulfur compounds can also occur during the acid cleaning of sensitized stainless steels in kraft liquor systems.

Sigma Precipitation in HAZs. When the higher molybdenum alloys such as 904L, AL- 6XN, and 254SMO were first developed, one of the anticipated corrosion problems was attack of single-phase precipitates in weld HAZs. This form of attack has subsequently proved to be either superficial or nonexistent in most applications, probably because the compositions of the alloys have been skillfully formulated to minimize phase-related hot-rolling problems.

More recently, nitrogen has been added to molybdenum-bearing austenitic stainless steels to retard the precipitation of chromium- and molybdenum-rich intermetallic compounds (σ or χ phases). The incubation time for intermetallic precipitation reactions in Fe-Cr-Ni-Mo stainless alloys is significantly increased by raising the alloy nitrogen content. This has allowed the commercial production of thick plate sections that can be fabricated by multipass welding operations. In addition to suppressing the formation of deleterious phases, nitrogen, in cooperation with chromium and molybdenum, has a beneficial effect on localized corrosion resistance in oxidizing acid-chloride solutions.

Corrosion Associated with Postweld Cleaning. Postweld cleaning is often specified to remove the heat-tinted metal formed during welding. Recent work has shown that cleaning by stainless steel wire brushing can lower the corrosion resistance of a stainless steel weldment (Fig. 18). This is a particular problem in applications in which the base metal has marginal corrosion resistance. The effect may be caused by inadequate heat-tint removal, by the use of lower-alloy stainless steel brushes such as type 410 or 304, or by the redeposition of abraded metal or oxides.

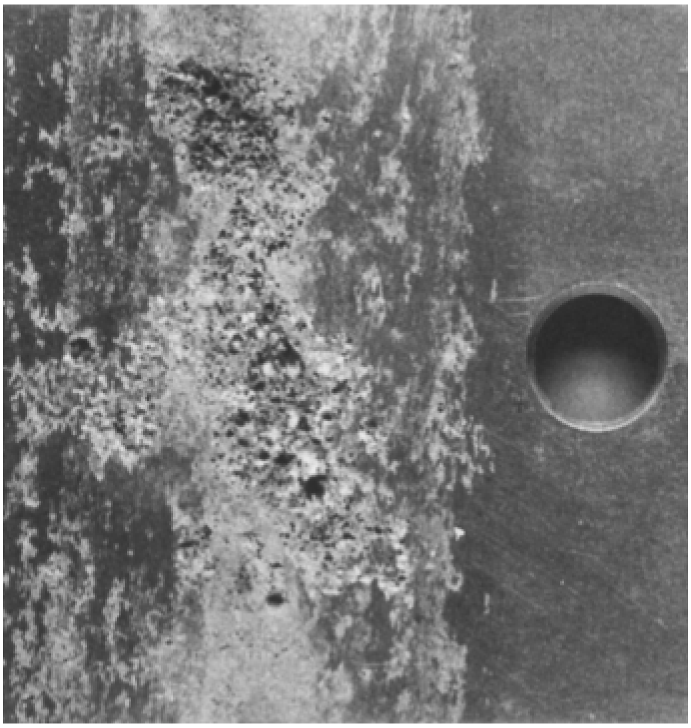

Fig. 18 Pitting corrosion associated with stainless steel wire brush cleaning on the back of a type 316L stainless steel test coupon after bleach plant exposure. Source: Ref 5

Any cleaning method may be impaired by contamination or by lack of control. Results of a study in bleach plants suggest that pickling and glass bead blasting can be more effective than stainless wire brushing and that brushing is more difficult to perform effectively in this case.

Corrosion Associated with Weld Backing Rings. Backing rings are sometimes used when welding pipe. In corrosion applications, it is important that the backing ring insert be consumed during the welding process to avoid a crevice. In the example shown in Fig. 19, the wrong type of backing ring was used, which left a crevice

after welding. The sample was taken from a leaking brine cooling coil used in the production of nitroglycerin. The cooling coils contained calcium chloride ($CaCl_2$) brine inhibited with chromates. Coils were made by butt welding sections of seamless type 304L stainless steel tubing. This failure was unusual because several forms of corrosion had been observed.

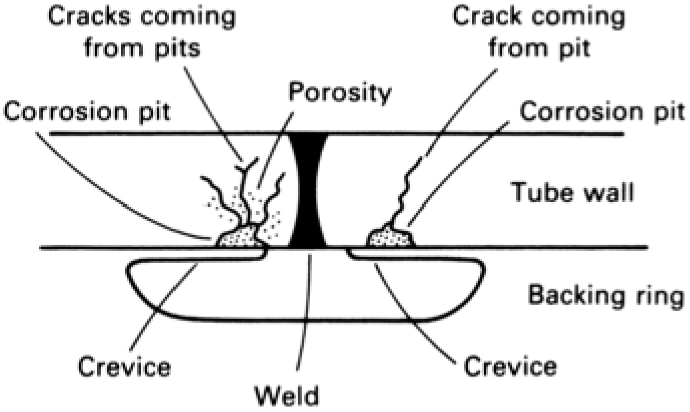

Fig. 19 Stainless steel nitrator cooling coil weld joint. Failure was caused by improper design of the backing ring, which was not consumed during welding and left a crevice. Source: Ref 8

A metallographic examination of a small trepanned sample revealed:

- *Microstructure:* The base metal and weld metal microstructures appeared satisfactory.
- *Pitting:* Irregular corrosion pits were seen on the inside tube surface at crevices formed by the tube and the backing ring adjacent to the tube butt weld. The deepest pits extended 0.1 to 0.2 mm (4 to 8 mils) into the 1.65 mm (0.065 in.) thick tube wall.
- *Cracking:* There were numerous brittle, branching transgranular cracks originating on the inside surface at the crevice under the backing ring.
- *Preferential weld corrosion:* Extensive preferential corrosion of the ferrite phase (vermicular morphology) in the tube weld had occurred and penetrated almost completely through the tube wall. Corrosion originated on the outside surface of the tube.

It was concluded that the preferential weld corrosion from the process side was the most probable cause of the actual leak in the nitrator coil. The preferential corrosion of ferrite in nitrating mixtures of HNO_3 and H_2SO_4 is well known. Whether this corrosion causes a serious problem depends on the amount of ferrite present in the weld. If the amount of ferrite is small and the particles are not interconnected, the overall corrosion rate is not much higher than that of a completely austenitic material. If the particles are interconnected, as in this case, there is a path for fairly rapid corrosion through the weld, causing failure to occur.

To minimize this problem, two possible solutions were considered. The first was to weld the coils with a filler metal that produces a fully austenitic deposit, and the second was to solution anneal at 1065 °C (1950 °F) after welding to dissolve most of the ferrite. It would also help to select stainless steel base metal by composition (e.g., high nickel, low chromium content) to minimize the production of ferrite during welding. Welding with a fully austenitic filler metal was considered to be the best approach.

Cracking on the brine side was caused by chloride SCC. The cracking probably did not happen during operation at 15 °C (60 °F) or lower. It is thought that the cracking most likely occurred while the coil was being decontaminated at 205 to 260 °C (400 to 500 °F) in preparation for weld repairing of the leak. Brine trapped in the crevice between the tube wall and the backing ring was boiled to dryness. Under these conditions, SCC would occur in a short time.

There probably were stress cracks behind all of the backing rings. Because the future life of this coil was questionable, a new coil was recommended.

The pitting corrosion caused by the brine was not considered to be as serious as it first appeared. If this had been the only corrosion (and the sample had been representative of the coil), the coil would not have failed for a considerable length of time. The decontamination process, which evaporated the trapped brine, produced some of the observed corrosion and made the pitting appear worse than it was before decontamination.

Because chromates are anodic inhibitors, they can also greatly increase the corrosion (usually by pitting) in the system if insufficient quantities are used. This might have occurred in the crevices in the nitrator coil butt welds, regardless of the bulk solution concentration. The best solution to this problem was to eliminate the crevices, that is, not to use backing rings.

Effects of GTA Weld Shielding Gas Composition. The chromium in a stainless steel has a strong chemical affinity for oxygen and carbon. Weld pools formed by electric arc processes must be shielded from the atmosphere to prevent slag formation and oxidation (Fig. 20), to maintain a stable arc, and to reduce contamination of the molten metal by the weld environment. Argon or argon plus helium gas mixtures are commonly used in GTA welding processes to create a barrier between the solidifying weld and the atmosphere. In other cases, nitrogen is commonly used as a backing gas to protect the backside of the root pass.

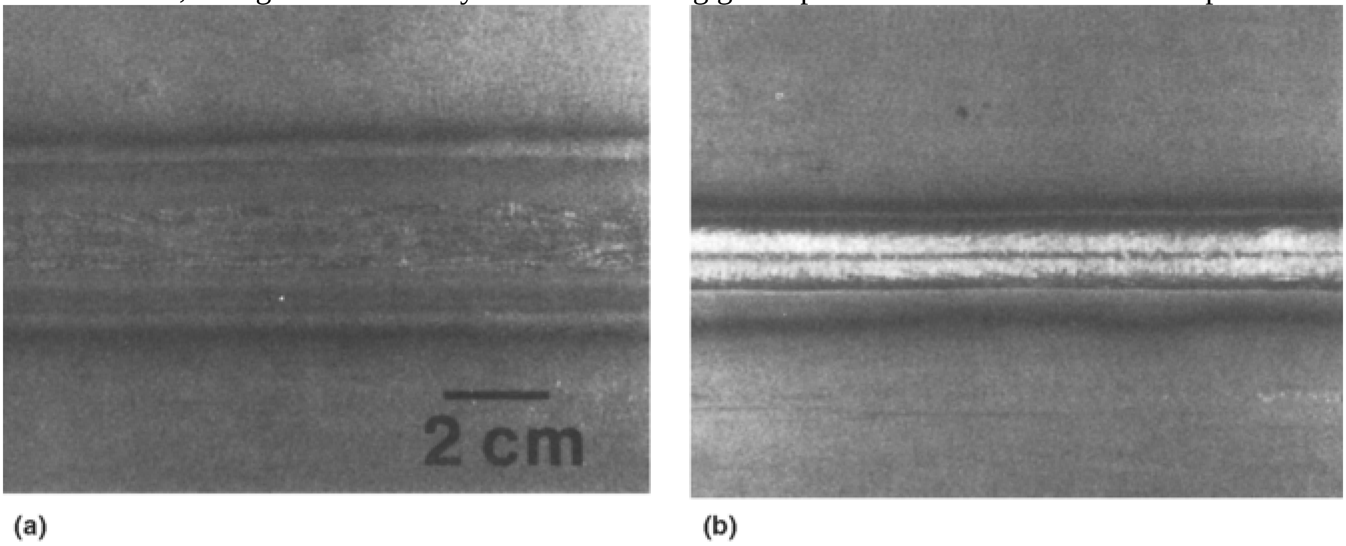

Fig. 20 Examples of properly shielded (a) and poorly shielded (b) autogenous gas tungsten arc welds in type 304 stainless steel strip. Source: Ref 8

The composition of a shielding gas can be modified to improve the microstructure and properties of GTA welds in austenitic stainless steels. More specifically, the use of argon mixed with small volumes of nitrogen (10 vol% N_2 or less) in a GTA welding process enhances the corrosion resistance of Fe-Cr-Ni-Mo-N stainless alloys in oxidizing acid chloride solutions (Fig. 21). In certain nonoxidizing solutions, argon-nitrogen shielding gas reduces the δ-ferrite content of weld metal and influences weld metal solidification behavior.

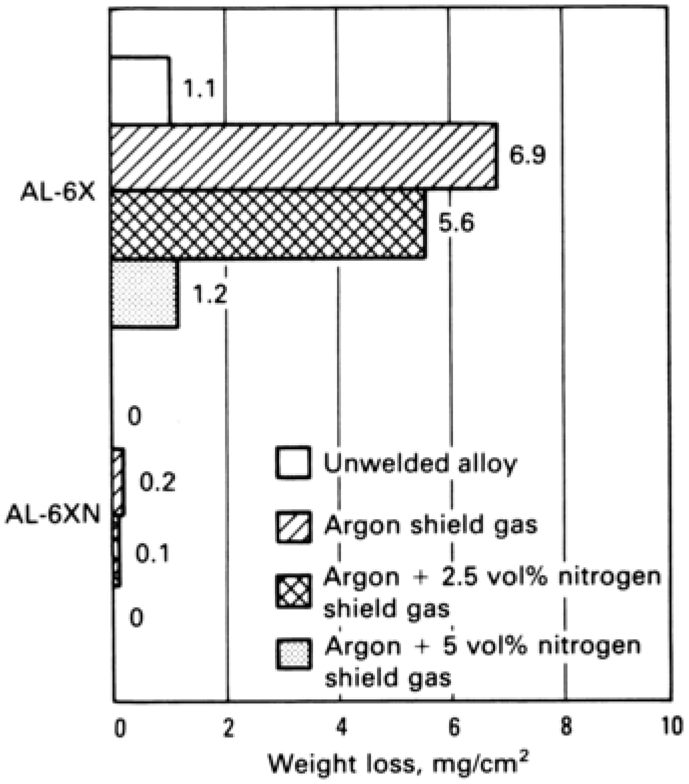

Fig. 21 Effect of gas tungsten arc weld shielding gas composition on the corrosion resistance of two austenitic stainless steels. Welded strip samples were tested according to ASTM G 48; test temperature was 35 °C (95 °F). Source: Ref 8

The nitrogen content of weld metal increases with the partial pressure of nitrogen in the GTA weld shielding gas. The increase in weld metal nitrogen content is greater when nitrogen is mixed with an oxidizing gas, such as carbon dioxide (CO_2), than with either a reducing (hydrogen) or a neutral (argon) gas. Porosity and concavity are observed in austenitic stainless steel weld metals when more than 10 vol% N is added to an argon shielding gas. Although solid-solution additions of nitrogen are not detrimental to the SCC resistance of unwelded molybdenum- containing austenitic stainless steels, an increased weld metal nitrogen content tends to increase susceptibility to SCC.

Effects of Heat-Tint Oxides on Corrosion Resistance. Under certain laboratory conditions, a mechanically stable chromium-enriched oxide layer can be formed on a stainless steel surface that enhances corrosion resistance. In contrast, the conditions created by arc-welding operations produce a scale composed of elements that have been selectively oxidized from the base metal. The region near the surface of an oxidized stainless steel is depleted in one or more of the elements that have reacted with the surrounding atmosphere to form the scale. The rate of oxidation for a stainless steel, and consequently the degree of depletion in the base metal, are independent of the alloy composition. They are controlled by diffusion through the oxide.

The oxidized, or heat-tinted, surface of a welded stainless steel consists of a heterogeneous oxide composed primarily of iron and chromium above a chromium-depleted layer of base metal. The properties of such a surface depend on:

- The time and temperature of the thermal exposure
- The composition of the atmosphere in contact with the hot metal surface
- The chemical composition of the base metal beneath the heat-tint oxide
- The physical condition of the surface (contamination, roughness, thermomechanical history) prior to heat tinting
- The adherence of the heat-tint oxide to the base metal

The defects, internal stresses, and composition of the heat-tint oxide make it a poor barrier to any corrosive media that might initiate localized corrosion in the chromium-depleted layer of base metal.

The severity of localized corrosion at heat- tinted regions exposed to oxidizing chloride solutions is directly related to the temperature of the hot metal surface during welding. A heat-tint oxide on an austenitic stainless steel exposed in air first becomes obvious at approximately 400 °C (750 °F). As the surface temperature is increased, differently colored oxides develop that appear to be superimposed on the oxides formed at lower temperatures. Table 2 shows the relationship between welding conditions and heat- tint color (Ref 9). Dark blue heat-tint oxides are the most susceptible to localized corrosion. Gas- shielded surfaces do not form the same distinctly colored oxides as surfaces exposed to air during welding, but gas-shielded surfaces can also be susceptible to preferential corrosion.

Table 2 Welding conditions and corrosion resistance of heat-tinted UNS S31726 stainless steel plate

Welding conditions[(a)]				Corrosion test results[(b)]		
Heat input		**Welding current, A**	**Centerline heat-tint color**	**Maximum pit depth**		**Number of pits on heat-tinted surface**
kJ/mm	**kJ/in.**			**mm**	**mils**	
0.3	7.525	50	None	0.1	4	2
0.59	15.050	100	Straw	0.7	28	10
0.89	22.576	150	Rose	0.8	31	50
1.19	30.101	200	Blue	0.7	28	>70
1.48	37.626	250	White	0.9	35	>70

(a) Single-pass autogenous bead-on-plate GTA welds were made to heat tint the root surface of 6.4 mm ($\frac{1}{4}$ in.) thick plate samples.
(b) Duplicate coupons, each with one 25 × 51 mm (1 × 2 in.) heat-tinted surface, were exposed to 10% $FeCl_3$ solutions at 50 °C (120 °F). The weld face and edges of each coupon were covered with a protective coating.

Whether a weld heat tint should be removed prior to service depends on the corrosion behavior of the given alloy when exposed to the particular environment in question. Preferential corrosion at heat-tinted regions is most likely to occur on an alloy that performs near the limit of its corrosion resistance in service, but certain solutions do not affect heat-tinted regions. Even when heat-tinted regions are suspected of being susceptible to accelerated corrosion in a particular environment, the following factors should be considered:

- The rate at which pits, once initiated in the chromium-depleted surface layer, will propagate through sound base metal
- The hazards associated with the penetration of a process unit due to localized corrosion
- The cost and effectiveness of an operation intended to repair a heat-tinted stainless steel surface

The corrosion resistance of heat-tinted regions can be restored in three stages. First, the heat- tint oxide and chromium-depleted layer are removed by grinding or wire brushing. Second, the abraded surface is cleaned with an acid solution or a pickling paste (a mixture of HNO_3 and HF suspended in an inert paste or gel) to remove any surface contamination and to promote the reformation of a passive film. Third, after a sufficient contact time, the acid cleaning solution or pickling paste is thoroughly rinsed with water, preferably demineralized or with a low chloride ion (Cl^-) content.

Grinding or wire brushing might not be sufficient to repair a heat-tinted region. Such abrading operations may only smear the heat-tint oxide and embed the residual scale into the surface, expose the chromium-depleted layer beneath the heat-tint oxide, and contaminate the surface with ferrous particles that were picked up by the grinding wheel or wire brush. A stainless steel surface should never be abraded with a wheel or brush that has been used on a carbon or low-alloy steel; wire brushes with bristles that are not made of a stainless steel of similar composition should also be avoided. Conversely, attempting to repair a heat-tinted region with only a pickling paste or acid solution can stain or even corrode the base metal if the solution is overly aggressive or is allowed to contact the surface for an extended time. If the acid is too weak, a chromium-depleted scale residue could remain on a surface, even if the chromium-depleted layer were completely removed by a grinding operation. Mechanically ground surfaces generally have inferior corrosion resistance compared to properly acid-pickled surfaces.

Unmixed Zones. All methods of welding stainless steel with a filler metal produce a weld fusion boundary consisting of base metal that has been melted but not mechanically mixed with filler metal and a partially melted zone in the base metal. The weld fusion boundary lies between a weld composite consisting of filler metal diluted by base metal and an HAZ in the base metal (Fig. 1). The width of the unmixed zone depends on the local thermal conditions along the weld fusion line. For a GTA welding process, the zone is narrowest at the weld face and widest near the middle of the weld thickness.
An unmixed zone has the composition of base metal but the microstructure of an autogenous weld. The microsegregation and precipitation phenomena characteristic of autogenous weldments decrease the corrosion resistance of an unmixed zone relative to the parent metal. Unmixed zones bordering welds made from overalloyed filler metals can be preferentially attacked when exposed on the weldment surface (Fig. 22). The potential for preferential attack of unmixed zones can be reduced by minimizing the heat input to the weld and/or by flowing molten filler metal over the surface of the unmixed zone to form a barrier to the service environment. Care must be taken in this latter operation to avoid cold laps and lack-of-fusion defects. In both cases, preferential attack is avoided as long as the surface of the unmixed zone lies beneath the exposed surface of the weldment.

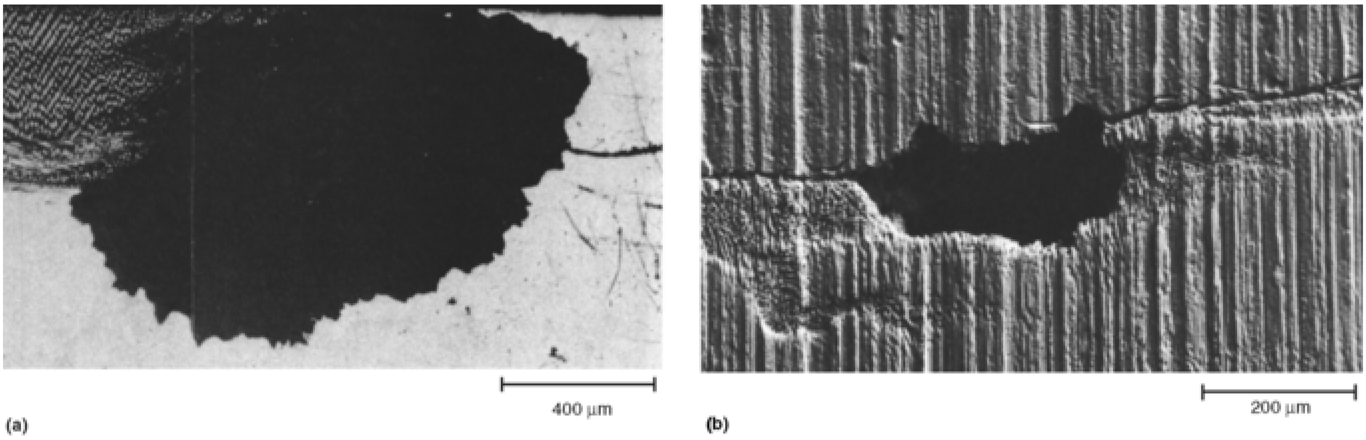

Fig. 22 Optical (a) and scanning electron (b) micrographs of pitting in the unmixed zone of Fe-Cr-Ni-Mo stainless steel plates that were gas tungsten arc welded with an overalloyed filler metal. The unmixed zones were preferentially attacked in an oxidizing acid chloride solution at elevated temperatures.

Chloride SCC. Welds in the 300-series austenitic stainless steels, with the exception of types 310 and 310Mo, contain a small amount of δ-ferrite (usually less than 10%) to prevent hot cracking during weld solidification. In hot, aqueous chloride environments, these duplex weldments generally show a marked resistance to cracking, while their counterparts crack readily (Fig. 23). The generally accepted explanation for this behavior is that the ferrite phase is resistant to chloride SCC and impedes crack propagation through the austenite phase. Electrochemical effects may also play a part; however, under sufficient tensile stress, temperature, and chloride concentration, these duplex weldments will readily crack. An example is shown in Fig. 24.

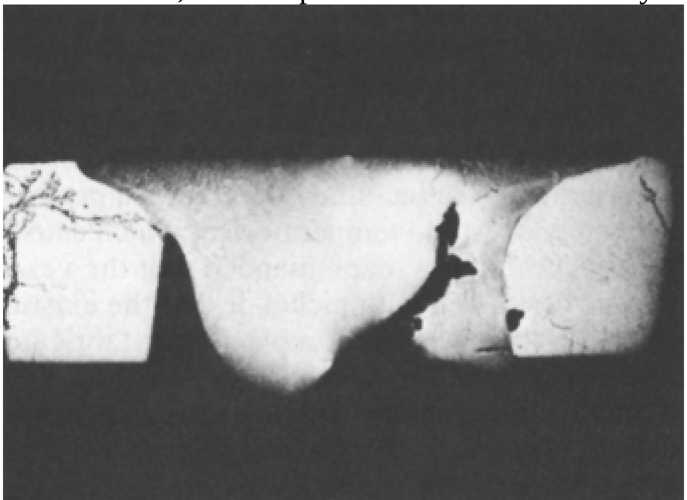

Fig. 23 Selective attack of a type 317L stainless steel weldment and chloride stress-corrosion cracking of the adjacent 317L base metal. The environment was a bleaching solution (7 g/L Cl_2) at 70 °C (160 °F).

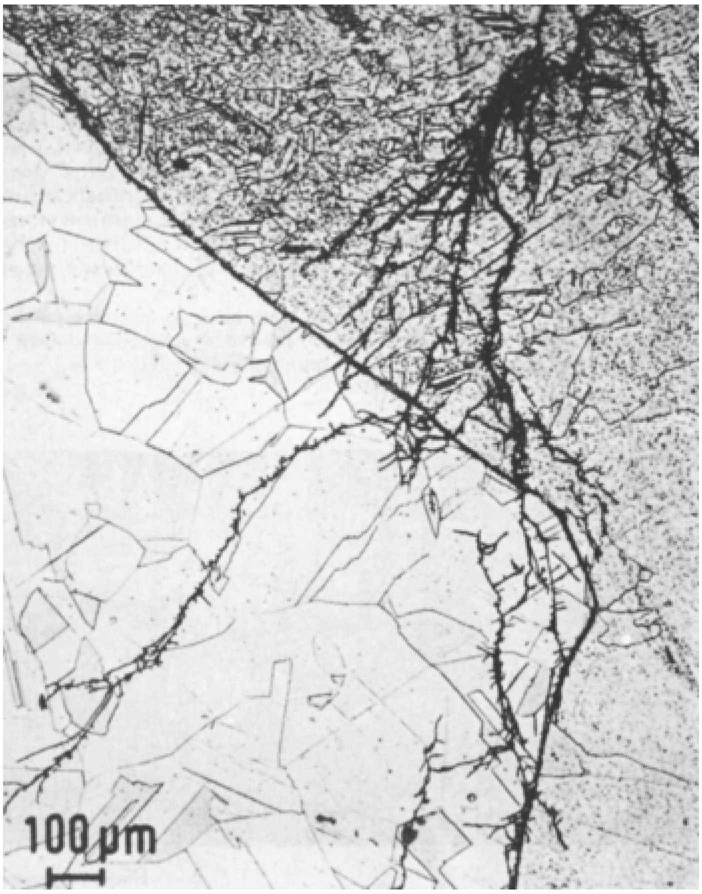

Fig. 24 Chloride stress-corrosion cracking of type 304 stainless steel base metal and type 308 weld metal in an aqueous chloride environment at 95 °C (200 °F). Cracks are branching and intergranular.

Caustic Embrittlement (Caustic SCC). Susceptibility of austenitic stainless steels to this form of corrosion usually becomes a problem when the caustic concentration exceeds approximately 25% and temperatures are above 100 °C (212 °F). Because welding is involved in most fabrications, the weld joint becomes the focus of attention because of potential stress-raiser effects and because of high residual shrinkage stresses. Cracking occurs most often in the weld HAZ.

In one case, a type 316L reactor vessel failed repeatedly by caustic SCC in which the process fluids contained 50% sodium hydroxide (NaOH) at 105 °C (220 °F). Failure was restricted to the weld HAZ adjacent to bracket attachment welds used to hold a steam coil. The stresses caused by the thermal expansion of the Nickel 200 steam coil at 1034 kPa (150 psig) aggravated the problem. Figure 25 shows the cracks in the weld HAZ to be branching and intergranular. Because it was not practical to reduce the operating temperature below the threshold temperature at which caustic SCC occurs, it was recommended that the vessel be weld overlayed with nickel or that the existing vessel be scrapped and a replacement fabricated from Nickel 200.

Fig. 25 Caustic stress-corrosion cracking in the heat-affected zone of a type 316L stainless steel NaOH reactor vessel. Cracks are branching and intergranular.

Microbiologically Influenced Corrosion (MIC). Microbiological corrosion in the process industries is most often found in three areas: cooling water systems, aqueous waste treatment, and groundwater left in new equipment or piping systems after testing. Nearly all confirmed cases of MIC have been accompanied by characteristic deposits. These are usually discrete mounds. Deposit color can also be an indication of the types of microorganisms that are active in the system. For example, iron bacteria deposits on stainless steel, such as those produced by *Gallionella,* are often reddish.

Investigators have shown that in almost all cases the environment causing the damage was a natural, essentially untreated water containing one or more culprit species of microbiological organisms. In the case of austenitic stainless steel weldments, corrosion generated by bacteria takes a distinctive form, that is, subsurface cavities with only minute pinhole penetration at the surface. The following case history illustrates these characteristics (Ref 10).

Example 1: Microbiological Corrosion of Butt Welds in Water Tanks. New production facilities at one plant site required austenitic stainless steels, primarily types 304L and 316L, for resistance to HNO_3 and organic acids and for maintaining product purity. The piping was shop fabricated, field erected, and then hydrostatically tested. All of the large (>190,000 L, or 25,000 gal) flat-bottom storage tanks were field erected and hydrostatically tested. During the early stages of construction, sodium-softened plant well water (also used for drinking) containing 200 ppm of chlorides was used for testing.

No attempts were made to drain the pipelines after testing. Tanks were drained, but then refilled to a depth of approximately 0.5 to 1 m (2 to 3 ft) for ballast because of a hurricane threat. The water was left in the tanks to evaporate.

The problem became evident when water was found dripping from butt welds in type 304L and 316L piping (nominal wall thickness 3.2 mm, or $\frac{1}{8}$in.) approximately 1 and 4 months, respectively, after the hydrotest. Internal inspection showed pits in and adjacent to welds under reddish brown deposits. Tank manways were

uncovered, and similar conditions were found. As shown in Fig. 26, moundlike deposits were strung out along weld seams in the tank bottoms.

Fig. 26 Moundlike microbiological deposits along a weld seam in the bottom of a type 304L stainless steel tank after several months of exposure to well water at ambient temperature. Source: Ref 10

Figure 27 shows a closeup view of a typical deposit still wet with test water. The brilliantly colored deposit was slimy and gelatinous in appearance and to the touch, and it measured 75 to 100 mm (3 to 4 in.) in width. At one point during the investigation, a similar deposit on a weld that was covered with about 150 mm (6 in.) of water was thoroughly dispersed by hand. Twenty-four hours later, the deposit had returned in somewhat diminished form at exactly the same location.

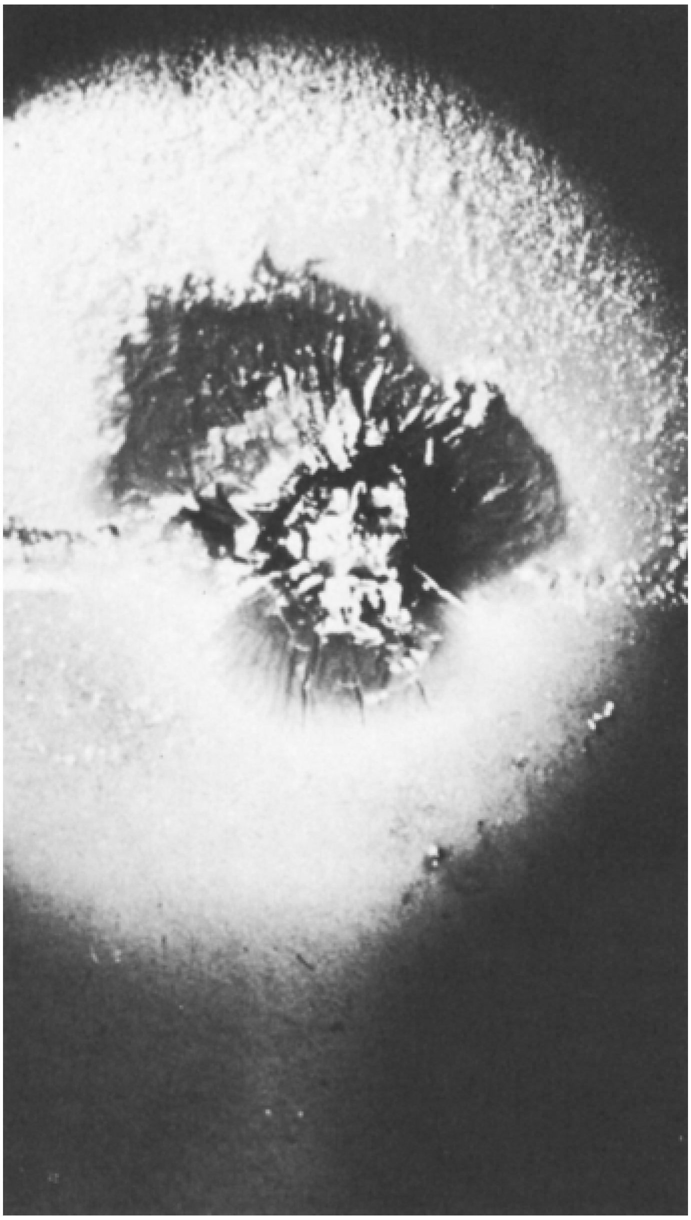

Fig. 27 Close-up of a wet deposit as shown in Fig. 26. Source: Ref 10

Figure 28 shows a nearly dry deposit. After wiping the deposit clean, a dark ring-shape stain outlining the deposit over the weld was noted (Fig. 29). There was, however, no evidence of pitting or other corrosion, even after light sanding with emery. Finally, probing with an icepick revealed a large, deep pit at the edge of the weld, as shown in Fig. 30. Figure 31, a radiograph of this weld seam, shows the large pit that nearly consumed the entire width of the weld bead, as well as several smaller pits. A cross section through a large pit in a 9.5 mm ($\frac{3}{8}$ in.) thick type 304L tank bottom is shown in Fig. 32.

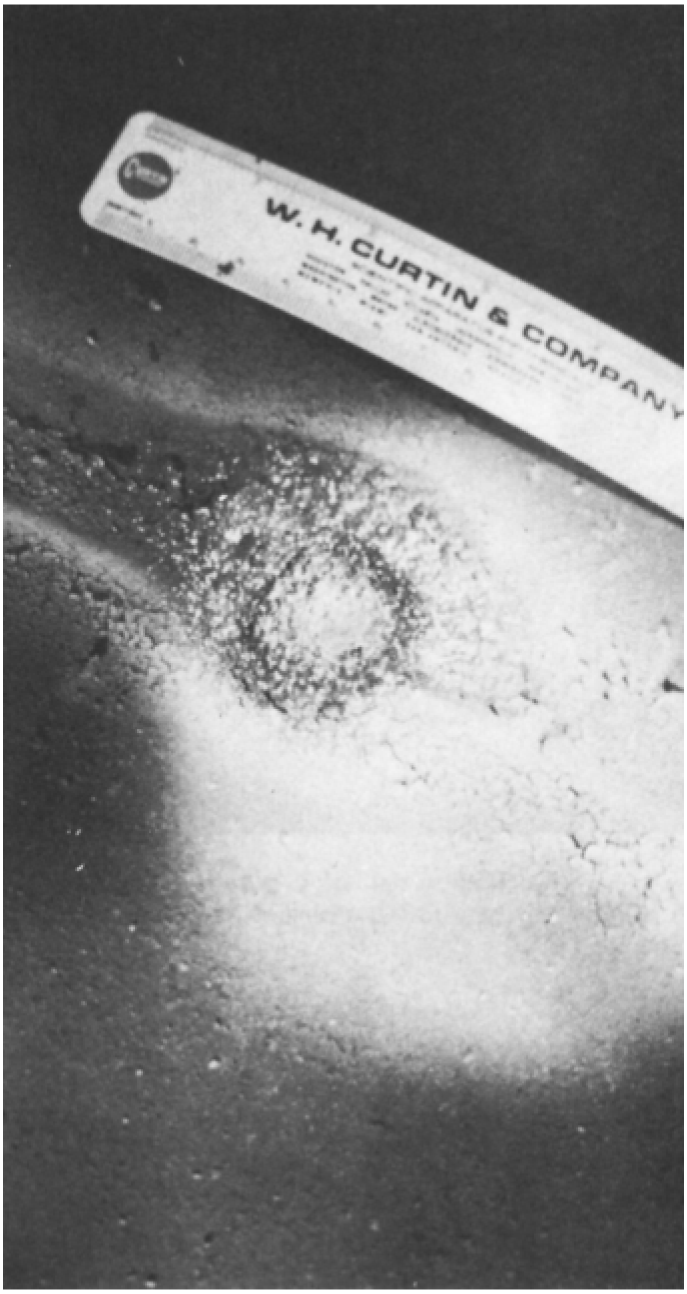

Fig. 28 Close-up of a dry deposit. See also Fig. 26 and 27. Source: Ref 10

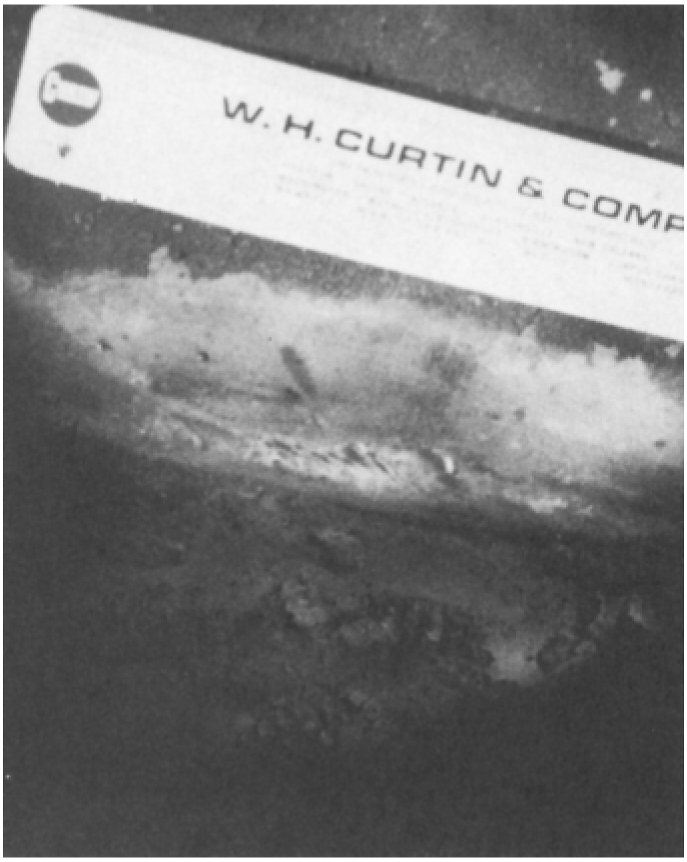

Fig. 29 Ring-shape stain left around a weld after removal of the type of deposit shown in Fig. 26, Fig. 27, Fig. 28. Source: Ref 10

Fig. 30 Large pit (center) at the edge of the weld shown in Fig. 29. The pit was revealed by probing with an ice pick. Source: Ref 10

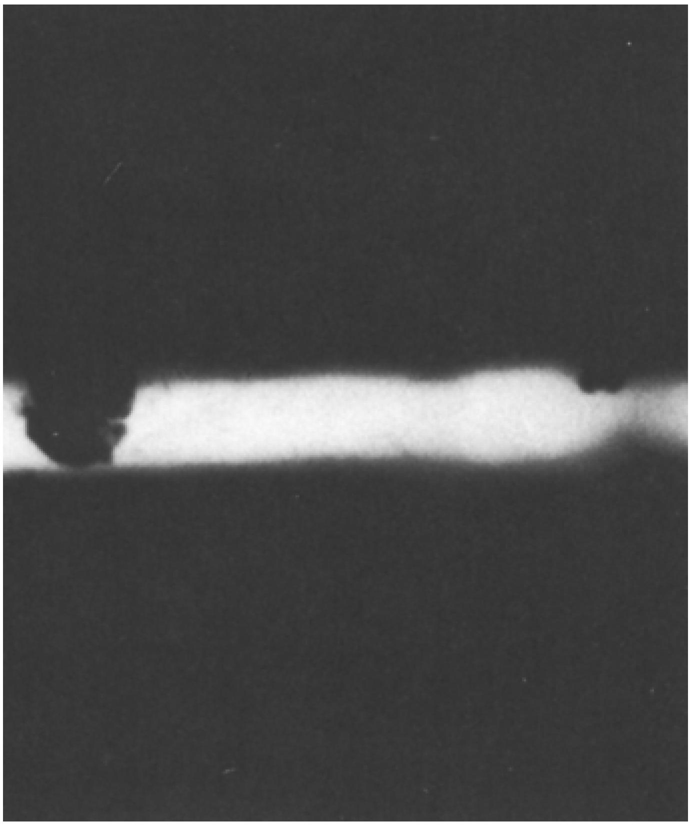

Fig. 31 Radiograph of a pitted weld seam in a type 304L stainless steel tank bottom. Source: Ref 10

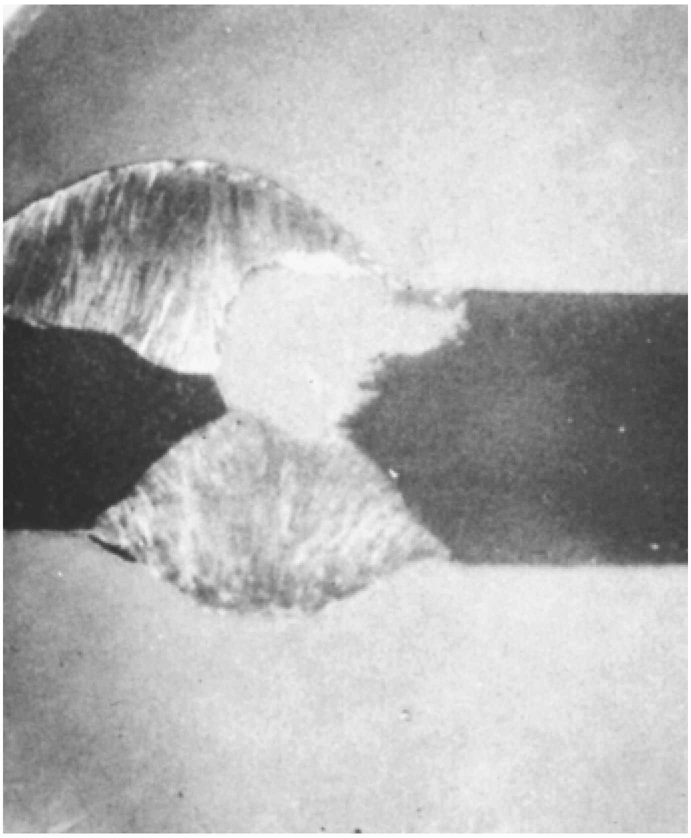

Fig. 32 Cross section through a pitted weld seam from a type 304L tank showing a typical subsurface cavity. Source: Ref 10

The characteristics of this mode of corrosion were a tiny mouth at the surface and a thin shell of metal covering a bottle-shape pit that had consumed both weld and base metal. There was no evidence of intergranular or

interdendritic attack of base or weld metal. However, pitted welds in a type 316L tank showed preferential attack of the δ-ferrite stringers (Fig. 33).

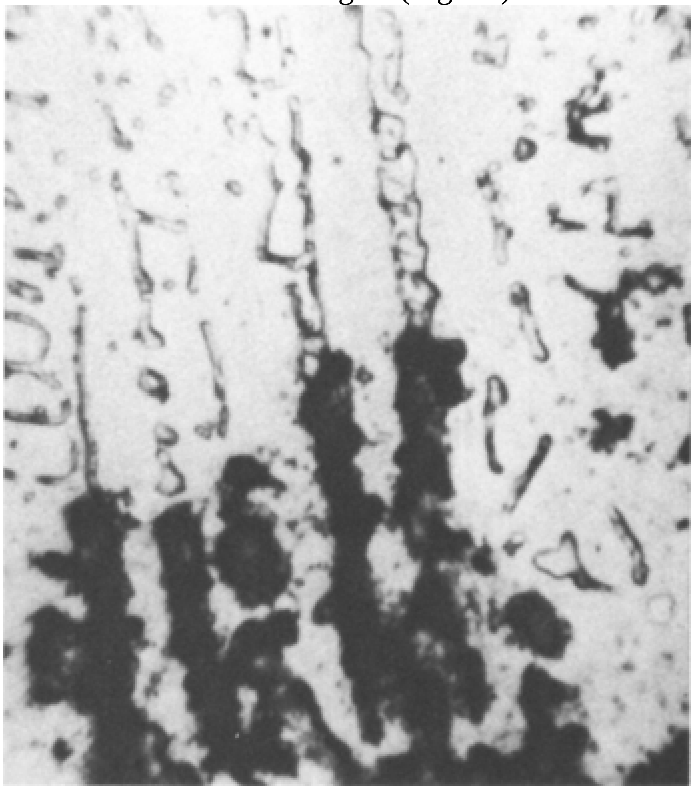

Fig. 33 Micrograph showing preferential attack of δ-ferrite stringers in type 316L stainless steel weld metal. 250×. Source: Ref 10

This type 316L tank was left full of hydrotest water for 1 month before draining. The bottom showed severe pitting under the typical reddish- brown deposits along welds. In addition, vertical rust-colored streaks (Fig. 34) were found above and below the sidewall horizontal welds, with deep pits at the edges of the welds associated with each streak (Fig. 35).

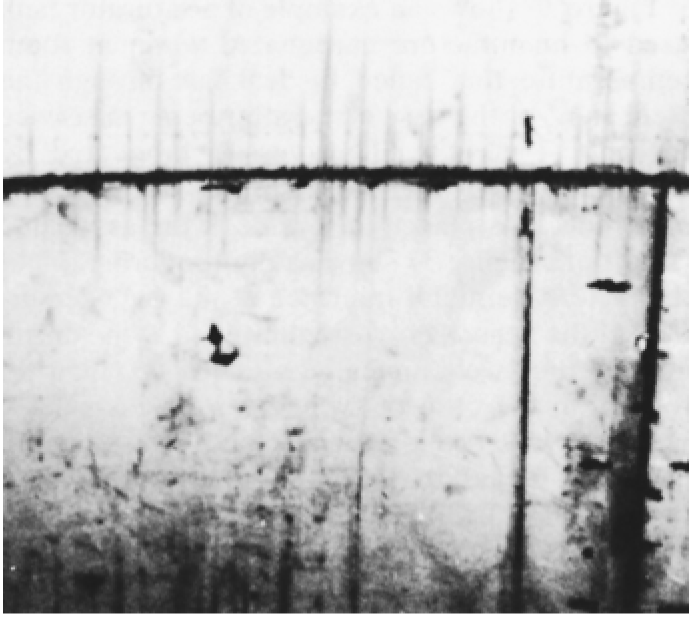

Fig. 34 Rust-colored streaks transverse to horizontal weld seams in the sidewall of a type 316L stainless steel tank. Source: Ref 10

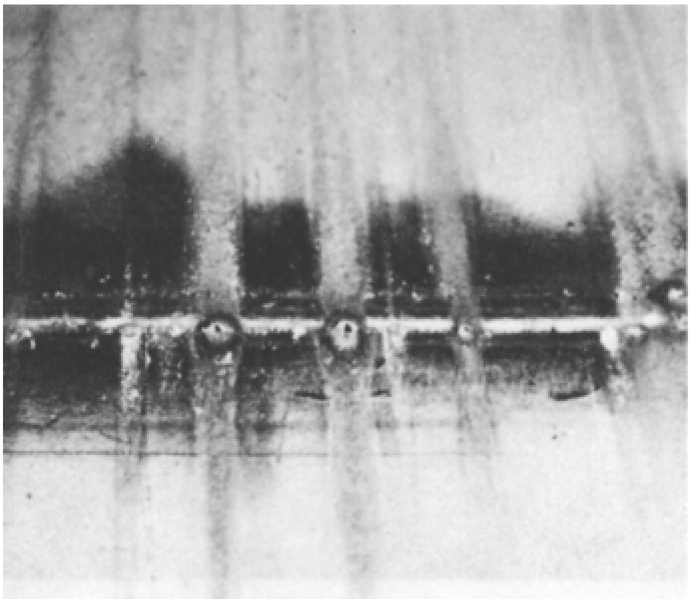

Fig. 35 Close-up of the rust-colored streaks shown in Fig. 34. Source: Ref 10

Analyses of the well water and the deposits showed high counts of iron bacteria (*Gallionella*) and iron-manganese bacteria (*Siderocapsa*). Both sulfate-reducing and sulfur-oxidizing bacteria were absent. The deposits also contained large amounts (thousands of parts per million) of iron, manganese, and chlorides.
As indicated, nearly all biodeposits and pits were found at the edges of, or very close to, weld seams. It is possible that the bacteria in stagnant well water were attracted by an electrochemical phenomenon or surface imperfections (oxide or slag inclusions, porosity, ripples, and so on) typically associated with welds. A sequence of events for the corrosion mechanism in this case might be:

1. Attraction and colonization of iron and iron- manganese bacteria at welds
2. Microbiological concentration of iron and manganese compounds, primarily chlorides, because Cl^- was the predominant anion in the well water
3. Microbiological oxidation to the corresponding ferric and manganic chlorides, which either singly or in combination are severe pitting corrodents of austenitic stainless steel
4. Penetration of the protective oxide films on the stainless steel surfaces that were already weakened by oxygen depletion under the biodeposits

All affected piping was replaced before the new facilities were placed in service. The tanks were repaired by sandblasting to uncover all pits, grinding out each pit to sound metal, and then welding with the appropriate stainless steel filler metal. Piping and tanks have been in corrosive service for about 19 years to date with very few leaks, indicating that the inspection, replacement, and repair program was effective.

References cited in this section

2. M.A. Streicher, Theory and Application of Evaluation Tests for Detecting Susceptibility to Intergranular Attack in Stainless Steels and Related Alloys—Problems and Opportunities, *Intergranulur Corrosion of Stainless Alloys,* STP 656, American Society for Testing and Materials, 1978, p 70

3. W.F. Savage, New Insight into Weld Cracking and a New Way of Looking at Welds, *Weld. Des. Eng.,* Dec 1969

5. A. Garner, How Stainless Steel Welds Corrode, *Met. Prog.,* Vol 127 (No. 5), April 1985, p 31

6. K.F. Krysiak, “Cause and Prevention of Unusual Failures of Materials,” Paper 19, presented at Corrosion/83, Anaheim, CA, National Association of Corrosion Engineers, April 1983

7. "Standard Practices for Detecting Susceptibility to Intergranular Attack in Austenitic Stainless Steels," A 262, *Annual Book of ASTM Standards,* American Society for Testing and Materials

8. J.R. Kearns and H.E. Deverell, "The Use of Nitrogen to Improve Fe-Cr-Ni-Mo Alloys for the Chemical Process Industries," Paper 188, presented at Corrosion/86, Houston, TX, National Association of Corrosion Engineers, March 1986

9. J.R. Kearns, "The Corrosion of Heat Tinted Austenitic Stainless Alloys," Paper 50, presented at Corrosion/85, Boston, MA, National Association of Corrosion Engineers, March 1985

10. G. Kobrin, Corrosion by Microbiological Organisms in Natural Waters, *Mater. Perform.,* Vol 15 (No. 7), 1976

Corrosion of Stainless Steel Weldments, *Corrosion: Fundamentals, Testing, and Protection*, Vol 13A, *ASM Handbook*, ASM International, 2003, p 301–316

Corrosion of Stainless Steel Weldments

Corrosion of Ferritic Stainless Steel Weldments

Conventional 400-series ferritic stainless steels such as types 430, 434, and 446 are susceptible to intergranular corrosion and to embrittlement in the as-welded condition. Corrosion in the weld area generally encompasses both the weld metal and weld HAZ. Early attempts to avoid some of these problems involved the use of austenitic stainless steel filler metals; however, failure by corrosion of the HAZ usually occurred even when exposure was to rather mild media for relatively short periods of time.

Figure 36 shows an example of a saturator tank used to manufacture carbonated water at room temperature that failed by leakage through the weld HAZ of the base metal after only 2 months of service. This vessel, fabricated by welding with a type 308 stainless steel welding electrode, was placed in service in the as-welded condition. Figure 37 shows a micrograph of the weld/base-metal interface at the outside surface of the vessel; corrosion initiated at the inside surface. Postweld annealing—at 785 °C (1450 °F) for 4 h in the case of type 430 stainless steel—restores weld area ductility and resistance to corrosion equal to that of the unwelded base metal.

Fig. 36 As-welded type 430 stainless steel saturator tank used in the manufacture of carbonated water that failed after two months of service. The tank was shielded metal arc welded using type 308 stainless steel filler metal. Source: Ref 11

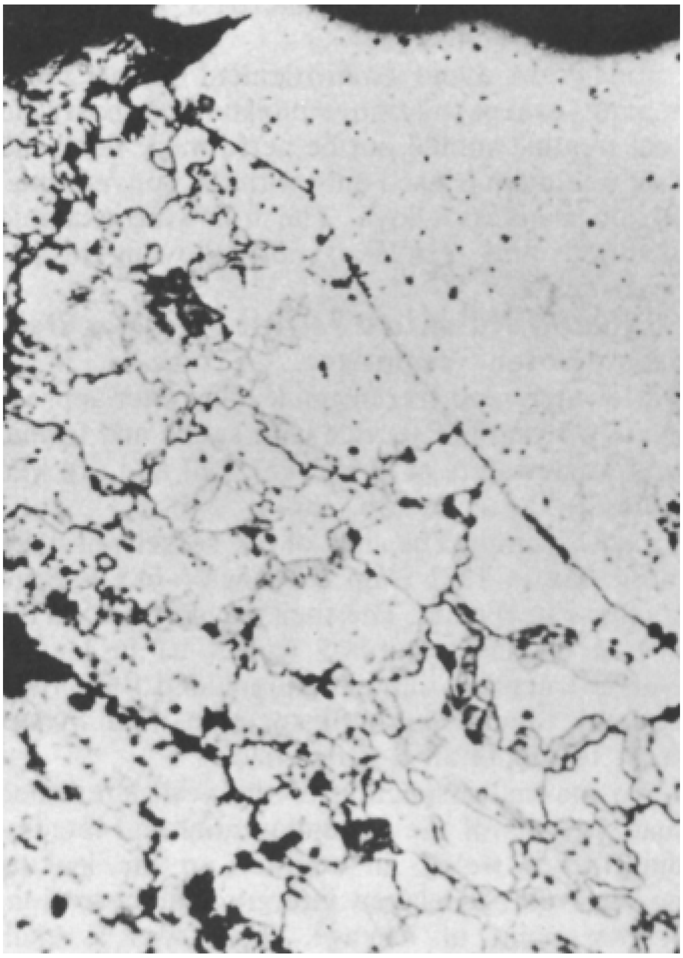

Fig. 37 Micrograph of the outside surface of the saturator tank in Fig. 36 showing intergranular corrosion at the fusion line. Source: Ref 11

To overcome some of these earlier difficulties and to improve weldability, several of the standard grade ferritic stainless steels have been modified. For example, type 405, containing nominally 11% Cr, is made with lower carbon and a small aluminum addition of 0.20% to restrict the formation of austenite at high temperature so that hardening is reduced during welding. For maximum ductility and corrosion resistance, however, postweld annealing is necessary. Recommendations for welding include either a 430- or a 309-type filler metal, the latter being used where increased weld ductility is desired.

Superferritic Stainless Steels. In the late 1960s and early 1970s, researchers recognized that a new generation of high Cr-Mo-Fe ferritic stainless steels, commonly referred to as *superferritics,* possess a desirable combination of good mechanical properties and resistance to general corrosion, pitting, and SCC. These properties make them attractive alternatives to the austenitic stainless steels commonly plagued by chloride SCC.

It was reasoned that the formation of martensite (as well as the need for preheat and postweld heat treatment) could be eliminated by controlling the interstitial element (carbon, oxygen, and nitrogen) content of these new ferritic alloys, either by ultrahigh purity or by stabilization with titanium or niobium. The welds would thus be corrosion resistant, tough, and ductile in the as-welded condition. To achieve these results, electron beam vacuum refining, vacuum and argon-oxygen decarburization, and vacuum induction melting processes were used. From this beginning, two basic ferritic alloy systems evolved:

- *Ultrahigh purity:* The (C + N) interstitial content is less than 150 ppm (Ref 12)
- *Intermediate purity:* The (C + N) interstitial content exceeds 150 ppm (Ref 12)

Chromium contents in these alloys generally range from 25 to 28% with ≥3% Mo (some alloys, however, contain less molybdenum). Nickel additions are also used with a maximum level of 4%. Although not usually mentioned in the alloy chemistry specifications, oxygen and hydrogen are also harmful, and these levels must be carefully restricted.

The unique as-welded properties of the superferritic stainless steels have been made possible by obtaining very low levels of impurities (including carbon, nitrogen, hydrogen, and oxygen, in the case of the alloys described as ultralow interstitials) and by obtaining a careful balance of niobium and/or titanium to match the carbon content in the case of the alloys with intermediate levels of interstitials. For these reasons, every precaution must be taken, and welding procedures that optimize gas shielding and cleanliness must be selected to avoid pickup of carbon, nitrogen, hydrogen, and oxygen.

To achieve maximum corrosion resistance, as well as maximum toughness and ductility, the GTA welding process with a matching filler metal is usually specified; however, dissimilar high-alloy weld metals have also been successfully used. In this case, the choice of dissimilar filler metal must ensure the integrity of the ferritic metal system. Regardless of which of the new generation of ferritic stainless steels is to be welded, the following precautions are considered essential:

- The joint groove and adjacent surfaces must be thoroughly degreased with a solvent, such as acetone, that does not leave a residue. This will prevent pickup of impurities, especially carbon, before welding. The filler metal must also be handled carefully to prevent it from picking up impurities. Solvent cleaning is also recommended. *Caution: Under certain conditions, when using solvents, a fire hazard or health hazard may exist.*
- A welding torch with a large nozzle inside diameter, such as 19 mm ($\frac{3}{4}$ in.), and a gas lens (inert gas calming screen) is necessary. Pure, welding-grade argon with a flow rate of 28 L/min (60 ft^3/h) is required for this size nozzle. In addition, the use of a trailing gas shield is beneficial, especially when welding heavy-gage materials. Use of these devices will drastically limit the pickup of nitrogen and oxygen during welding. Back gas shielding with argon is also essential. *Caution: Procedures for welding austenitic stainless steels often recommend the use of nitrogen backing gas. Nitrogen must not be used when welding ferritic stainless steels. Standard GTA welding procedures used to weld stainless steels are inadequate and therefore must be avoided.*
- Overheating and embrittlement by excessive grain growth in the weld and HAZ should be avoided by minimizing heat input. In multipass welds, overheating and embrittlement should be avoided by keeping the interpass temperature below 95 °C (200 °F).
- To avoid embrittlement further, preheating (except to remove moisture) or postweld heat treating should not be performed. Postweld heat treatment is used only with the conventional (less highly alloyed) ferritic stainless alloys.

The following example illustrates the results of not following proper procedures.

Example 2: Corrosion of Welds in a Ferritic Stainless Steel Wastewater Vaporizer. A nozzle in a wastewater vaporizer began leaking after approximately 3 years of service with acetic and formic acid wastewaters at 105 °C (225 °F) and 414 kPa (60 psig).

Investigation. The shell of the vessel was weld fabricated in 1972 from 6.4 mm ($\frac{1}{4}$ in.) E-Brite (UNS S44627, Fe-26Cr-1Mo+Nb) stainless steel plate. The shell measured 1.5 m (58 in.) in diameter and 8.5 m (28 ft) in length. Nondestructive examination included 100% radiography, dye-penetrant inspection, and hydrostatic testing of all E-Brite welds.

An internal inspection of the vessel revealed that portions of the circumferential and longitudinal seam welds, in addition to the leaking nozzle weld, displayed intergranular corrosion. At the point of leakage, there was a small intergranular crack. Figure 38 shows a typical example of a corroded weld. A transverse cross section through this weld will characteristically display intergranular corrosion with grains dropping out (Fig. 39). It was also noted that the HAZ next to the weld fusion line also experienced intergranular corrosion a couple of grains deep as a result of sensitization (Fig. 40).

Fig. 38 Top view of a longitudinal weld in 6.4 mm ($\frac{1}{4}$ in.) E-Brite ferritic stainless steel plate showing intergranular corrosion. The weld was made with matching filler metal. About 4×

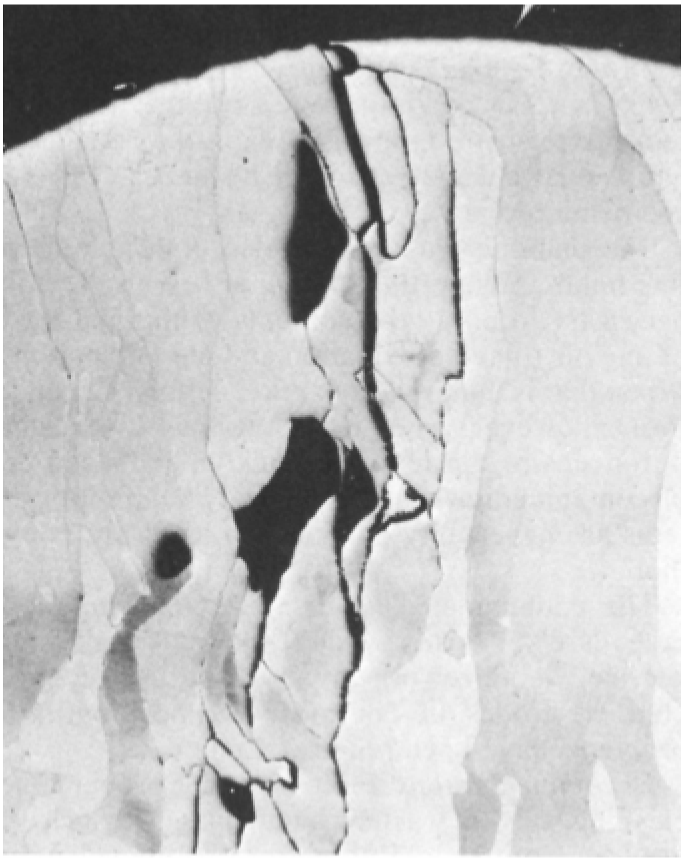

Fig. 39 Intergranular corrosion of a contaminated E-Brite ferritic stainless steel weld. Electrolytically etched with 10% oxalic acid. 200×

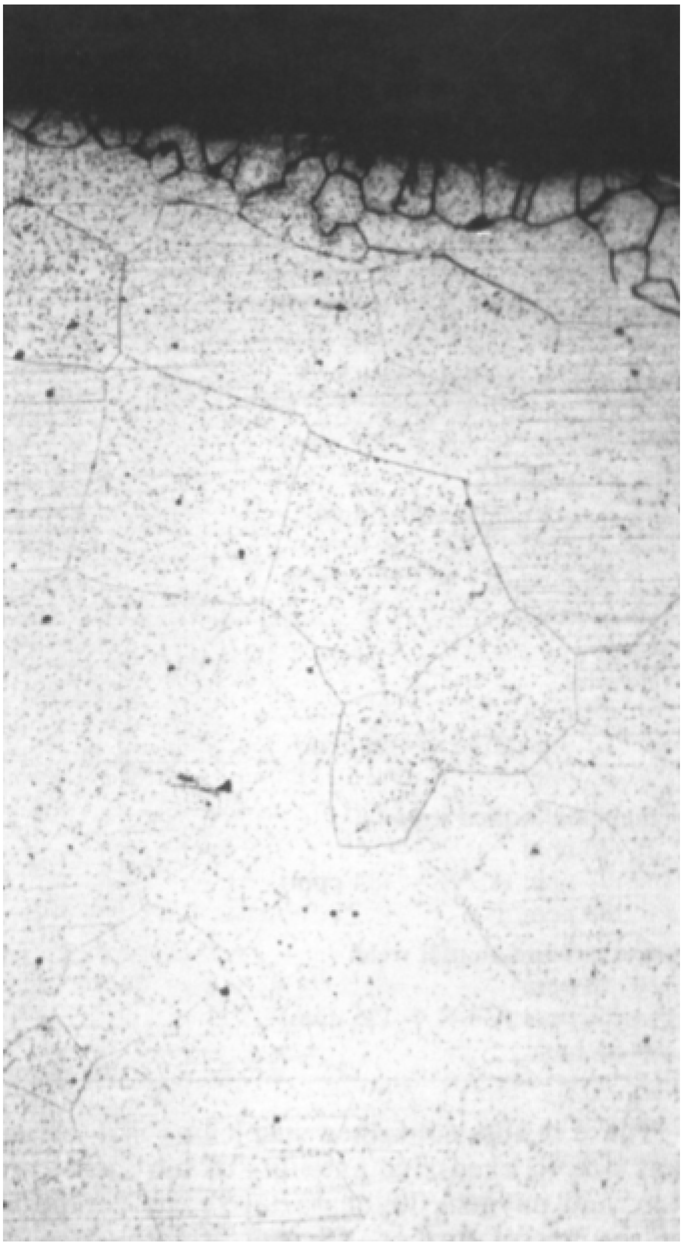

Fig. 40 Intergranular corrosion of the inside surface heat-affected zone of E-Brite stainless steel adjacent to the weld fusion line. Electrolytically etched with 10% oxalic acid. 100×

The evidence indicated weldment contamination; therefore, effort was directed at finding the levels of carbon, nitrogen, and oxygen in the various components present before and after welding. The averaged results were:

Base plate
C = 6 ppm
N = 108 ppm (C + N = 114 ppm)
O = 57 ppm
Corroded longitudinal weld
C = 133 ppm
N = 328 ppm (C + N = 461 ppm)
O = 262 ppm
Corroded circumferential weld
C = 34 ppm
N = 169 ppm (C + N = 203 ppm)

O = 225 ppm
Weld wire
C = 3 ppm
N = 53 ppm (C + N = 56 ppm)
O = 55 ppm
Sound longitudinal weld
C = 10 ppm
N = 124 ppm (C + N = 134 ppm)
O = 188 ppm
Sound circumferential weld
C = 20 ppm
N = 106 ppm (C + N = 126 ppm)
O = 85 ppm

These results confirmed suspicions that failure was due to excessive amounts of nitrogen, carbon, and oxygen. To characterize the condition of the vessel further, Charpy V-notch impact tests were run on the unaffected base metal, the HAZ, and the uncorroded (sound) weld metal. These tests showed the following ductile-to-brittle transition temperatures:

Specimen	Ductile-to-brittle transition temperature	
	°C	**°F**
Base metal	40 ± 3	105 ± 5
HAZ	85 ± 3	180 ± 5
Weld	5 ± 3	40 ± 5

Comparison of the interstitial levels of the corroded welds, sound welds, base metal, and filler wire suggested that insufficient joint preparation (carbon pickup) and faulty gas shielding were probably the main contributing factors that caused this weld corrosion failure. Discussions with the vendor uncovered two discrepancies. First, the welder was using a large, 19 mm ($\frac{3}{4}$ in.) inside diameter ceramic nozzle with a gas lens, but was flowing only 19 L/min (40 ft^3/h) of argon; this was the flow rate previously used with a 13 mm ($\frac{1}{2}$ in.) inside diameter gas lens nozzle. Second, a manifold system was used to distribute pure argon welding gas from a large liquid argon tank to various satellite welding stations in the welding shop. The exact cause for the carbon pickup was not determined.

Conclusions. Failure of the nozzle weld was the result of intergranular corrosion caused by the pickup of interstitial elements and subsequent precipitation of chromium carbides and nitrides. Carbon pickup was believed to have been caused by inadequate joint cleaning prior to welding. The increase in the weld nitrogen level was a direct result of inadequate argon gas shielding of the molten weld pool. Two areas of inadequate shielding were identified: improper gas flow rate for a 19 mm ($\frac{3}{4}$ in.) diam gas lens nozzle and contamination of the manifold gas system.

In order to preserve the structural integrity and corrosion performance of the more highly alloyed ferritic stainless steels, it is important to avoid the pickup of the interstitial elements carbon, nitrogen, oxygen, and hydrogen. In this particular case, the vendor used a flow rate intended for a smaller welding torch nozzle. The metal supplier recommended a flow rate of 23 to 38 L/ min (50 to 60 ft^3/min) of argon for a 19 mm ($\frac{3}{4}$ in.) gas lens nozzle. The gas lens collect body is an important and necessary part of the torch used to weld these alloys. Failure to use a gas lens will result in a flow condition that is turbulent enough to aspire air into the gas stream, thus contaminating the weld and destroying its mechanical and corrosion properties.

The manifold gas system also contributed to this failure. When this system is first used, it is necessary to purge the contents of the manifold of any air to avoid oxidation and contamination. When that is done, the system functions satisfactorily; however, when it is shut down overnight or for repairs, air reinfiltrates, and a source of contamination is reestablished. Manifold systems are never fully purged, and leaks are common.

The contaminated welds were removed, and the vessels were rewelded and put back into service. Some rework involved the use of covered electrodes of dissimilar composition. No problems have been reported to date.

Recommendations:

- To ensure proper joint cleaning, solvent washing and wiping with a clean lint-free cloth should be performed immediately before welding. The filler wire should be wiped with a clean cloth just prior to welding. *Caution: Solvents are generally flammable and can be toxic. Ventilation should be adequate. Cleaning should continue until cloths are free of any residues.*
- When GTA welding, a 19 mm ($\frac{3}{4}$ in.) diam ceramic nozzle with a gas lens collect body is recommended. An argon gas flow rate of 28 L/min (60 ft^3/min) is optimum. Smaller nozzles are not recommended. Argon back gas shielding is mandatory at a slight positive pressure to avoid disrupting the flow of the welding torch.
- The tip of the filler wire should be kept within the torch shielding gas envelope to avoid contamination and pickup of nitrogen and oxygen. (They embrittle the weld.) If the tip becomes contaminated, welding should be stopped, the contaminated weld area should be ground out, and the tip of the filler wire that has been oxidized should be snipped off before proceeding with welding.
- A manifold gas system should not be used to supply shielding and backing gas. Individual argon gas cylinders have been found to provide optimal performance. A weld button spot test should be performed to confirm the integrity of the argon cylinder and all hose connections. In this test, the weld button sample should be absolutely bright and shiny. Any cloudiness is an indication of contamination. It is necessary to check for leaks or to replace the cylinder.
- Corrosion resistance is not the only criterion when evaluating these new ferritic stainless steels. Welds must also be tough and ductile, and these factors must be considered when fabricating welds.

Lastly, dissimilar weld filler metals can be successfully used. To avoid premature failure, the dissimilar combination should be corrosion tested to ensure suitability for the intended service.

References cited in this section

11. R.H. Espy, "How Corrosion and Welding Conditions Affect Corrosion Resistance of Weldments in Type 430 Stainless Steel," Paper 22, presented at Corrosion/68, Houston, TX, National Association of Corrosion Engineers, 1968

12. K.F. Krysiak, Welding Behavior of Ferritic Stainless Steels—An Overview, *Weld. J.,* Vol 65 (No. 4), April 1986, p 37–41

Corrosion of Stainless Steel Weldments, *Corrosion: Fundamentals, Testing, and Protection*, Vol 13A, *ASM Handbook*, ASM International, 2003, p 301–316

Corrosion of Duplex Stainless Steel Weldments

In the wrought condition, duplex stainless steels have microstructures consisting of a fairly even balance of austenite and ferrite. The new generation of duplex alloys, which have a composition centered around Fe-26Cr-6.5Ni-3.0Mo, are now being produced with low carbon and a nitrogen addition. These alloys are useful because of their good resistance to chloride SCC, pitting corrosion, and intergranular corrosion in the as-welded condition.

The distribution of austenite and ferrite in the weld and HAZ is known to affect the corrosion properties and the mechanical properties of duplex stainless steels. Figure 41 shows the effect of the ferrite-austenite balance on the pitting resistance of a duplex stainless steel. To achieve a satisfactory balance in properties, it is essential that both base metal and weld metal be of the proper composition. For example, without nickel enrichment in the filler rod, welds can be produced with ferrite levels in excess of 80%. Such microstructures have very poor

ductility and inferior corrosion resistance. For this reason, autogenous welding (without the addition of filler metal) is not recommended unless postweld solution annealing is performed, which is not always practical. To achieve a balanced weld microstructure, a low carbon content (~0.02%) and the addition of nitrogen (0.1 to 0.2%) should be specified for the base metal. Low carbon helps to minimize the effects of sensitization, and the nitrogen slows the precipitation kinetics associated with the segregation of chromium and molybdenum during the welding operation. Nitrogen also enhances the reformation of austenite in the HAZ and weld metal during cooling.

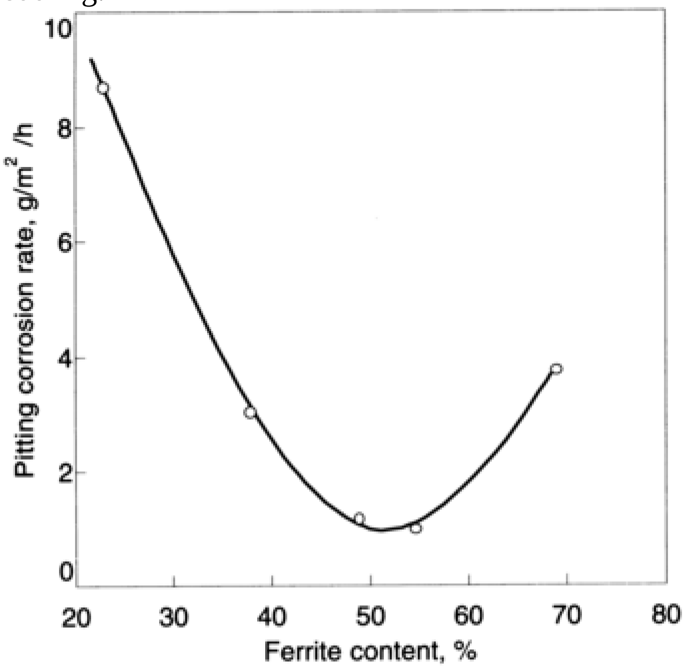

Fig. 41 Effect of ferrite-austenite balance on pitting resistance of Fe-22Cr-5.5Ni-3.0Mo-0.12N gas tungsten arc stainless steel welds. Source: Ref 13

Because these duplex alloys have been used in Europe for many years, guidelines relating to austenite-ferrite phase distribution are available. It has been shown that to ensure resistance to chloride SCC, welds should contain at least 25% ferrite. To maintain a good phase balance for corrosion resistance and mechanical properties (especially ductility and notch toughness) comparable to those of the base metal, the average ferrite content of the weld should not exceed 60%. This means using welding techniques that minimize weld dilution, especially in the root pass. Conditions that encourage mixing of the lower-nickel base metal with the weld metal reduce the overall nickel content. Weld metal with a lower nickel content will have a higher ferrite content, with reduced mechanical and corrosion properties. Once duplex base metal and welding consumables have been selected, it is then necessary to select joint designs and weld parameters that will produce welding heat inputs and cooling rates so as to produce a favorable balance of austenite and ferrite in the weld and HAZ.

Researchers have shown that the high-ferrite microstructures that develop during welding in lean (low-nickel) base metal and weld metal compositions can be altered by adjusting welding heat input and cooling rate. In these cases, a higher heat input that produces a slower cooling rate can be used to advantage by allowing more time for ferrite to transform to austenite. There are, however, some practical aspects to consider before applying higher heat inputs indiscriminately. For example, as heat input is increased, base metal dilution increases. As the amount of lower-nickel base metal in the weld increases, the overall nickel content of the deposit decreases. This increases the potential for more ferrite, with a resultant loss in impact toughness, ductility, and corrosion resistance. This would be another case for using an enriched filler metal containing more nickel than the base metal. Grain growth and the formation of embrittling phases are two other negative effects of high heat inputs. When there is uncertainty regarding the effect that welding conditions will have on corrosion performance and mechanical properties, a corrosion test is advisable.

The influence of different welding conditions on various material properties of alloy 2205 (UNS S31803, Fe-22Cr-5.5Ni-3.0Mo-0.15N) has been studied (Ref 14). Chemical compositions of test materials are given in Table 3, and the results of the investigation are detailed in the following sections.

Table 3 Chemical compositions of alloy 2205 specimens tested and filler metals used in Ref 14

Specimen size and configuration	Element, %									
	C	Si	Mn	P	S	Cr	Ni	Mo	Cu	N
Parent metals										
48.1 mm (1.89 in.) OD, 3.8 mm (0.149 in.) wall tube	0.015	0.37	1.54	0.024	0.003	21.84	5.63	2.95	0.09	0.15
88.9 mm (3.5 in.) OD, 3.6 mm (0.142 in.) wall tube	0.017	0.28	1.51	0.025	0.003	21.90	5.17	2.97	0.09	0.15
110 mm (4.3 in.) OD, 8 mm (0.31 in.) wall tube	0.027	0.34	1.57	0.027	0.003	21.96	5.62	2.98	0.09	0.13
213 mm (8.4 in.) OD, 18 mm (0.7 in.) wall tube	0.017	0.28	1.50	0.026	0.003	21.85	5.77	2.98	0.10	0.15
20 mm ($\frac{3}{4}$ in.) plate	0.019	0.39	1.80	0.032	0.003	22.62	5.81	2.84	…	0.13
Filler metals										
1.2 mm (0.047 in.) diam wire	0.011	0.48	1.61	0.016	0.003	22.50	8.00	2.95	0.07	0.13
1.6 mm (0.063 in.) diam rod	0.011	0.48	1.61	0.016	0.003	22.50	8.00	2.95	0.07	0.13
3.2 mm (0.125 in.) diam wire	0.011	0.48	1.61	0.016	0.003	22.50	8.00	2.95	0.07	0.13
3.25 mm (0.127 in.) diam covered electrode	0.020	1.01	0.82	0.024	0.011	23.1	10.4	3.06	…	0.13
4.0 mm (0.16 in.) diam covered electrode	0.016	0.94	0.78	0.015	0.011	23.0	10.5	3.13	…	0.11

Intergranular Corrosion. Despite the use of very high arc energies (0.5 to 6 kJ/mm, or 13 to 150 kJ/in.) in combination with multipass welding, the Strauss test (ASTM A 262, practice E) (Ref 7) failed to uncover any signs of sensitization after bending through 180°. The results of Huey tests (ASTM A 262, practice C) on submerged-arc welds showed that the corrosion rate increased slightly with arc energy in the studied range of 0.5 to 6.0 kJ/mm (13 to 150 kJ/in.). For comparison, the corrosion rate for parent metal typically varies between 0.15 and 1.0 mm/yr (6 and 40 mils/yr), depending on surface finish and heat treatment cycle.

Similar results were obtained in Huey tests of specimens from bead-on-tube welds produced by GTA welding. In this case, the corrosion rate had a tendency to increase slightly with arc energy up to 3 kJ/mm (75 kJ/in.).

Pitting tests were conducted in 10% ferric chloride ($FeCl_3$) at 25 and 30 °C (75 and 85 °F) in accordance with ASTM G 48 (Ref 15). Results of tests on submerged-arc test welds did not indicate any significant change in pitting resistance when the arc energy was increased from 1.5 to 6 kJ/mm (38 to 150 kJ/in.). Pitting occurred along the boundary between two adjacent weld beads. Attack was caused by slag entrapment in the weld; therefore, removal of slag is important.

Gas tungsten arc weld test specimens (arc energies from 0.5 to 3 kJ/mm, or 13 to 75 kJ/in.) showed a marked improvement in pitting resistance with increasing arc energy. In order for duplicate specimens to pass the $FeCl_3$ test at 30 °C (85 °F), 3 kJ/mm (75 kJ/in.) of arc energy was required. At 25 °C (75 °F), at least 2 kJ/mm (50 kJ/in.) was required to achieve immunity. Welds made autogenously (no nickel enrichment) were somewhat inferior; improvements were achieved by using higher arc energies.

For comparison with a different alloy, Fig. 42 shows the effect of heat input on the corrosion resistance of Ferralium alloy 255 (UNS S32550, Fe-25.5Cr-5.5Ni-3.0Mo-0.17N) welds made autogenously and tested on $FeCl_3$ at 15 °C (60 °F). Preferential corrosion of the ferrite phase is shown in Fig. 43. In a different test, Ferralium alloy 255 was welded autogenously and tested in a neutral chloride solution according to ASTM D 1141 (Ref 17) at 60 to 100 °C (140 to 212 °F). In this case, preferential attack of the austenite phase was observed. An example is shown in Fig. 44. Similar results would be expected for alloy 2205.

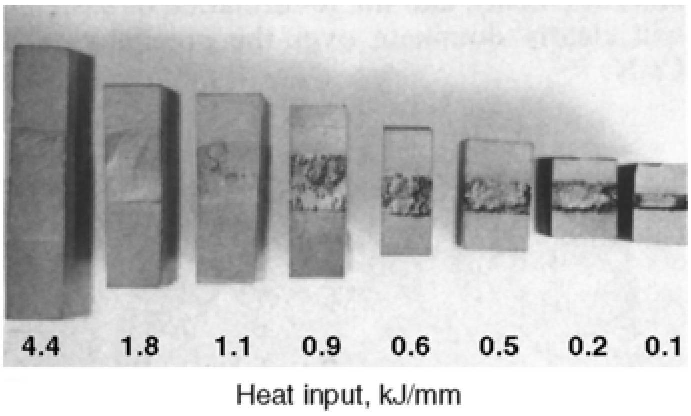

Fig. 42 Effect of welding heat input on the corrosion resistance of autogenous gas tungsten arc welds in Ferralium alloy 255 in 10% $FeCl_3$ at 10 °C (40 °F). The base metal was 25 mm (1 in.) thick. Source: Ref 16

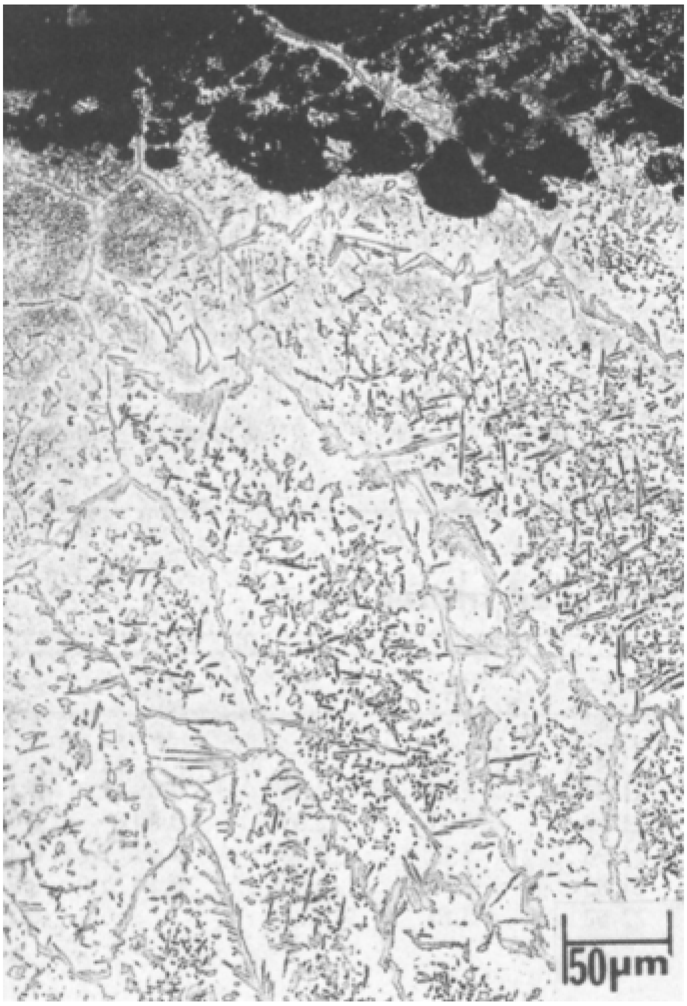

Fig. 43 Preferential corrosion of the ferrite phase in the weld metal of Ferralium alloy 255 gas tungsten arc welds in 10% $FeCl_3$ at room temperature. Base metal was 3.2 mm ($\frac{1}{8}$ in.) thick.

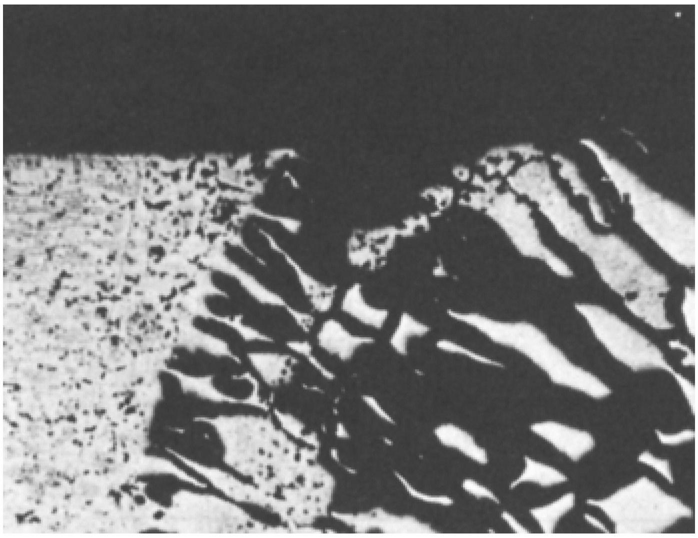

Fig. 44 Preferential attack of the continuous austenite phase in an autogenous gas tungsten arc weld in Ferralium alloy 255. Crevice corrosion test was performed in synthetic seawater according to ASTM D 1141 (Ref 17) at 100 °C (212 °F). Etched with 50% HNO_3. 100×

A study of the alloy 2205 weld microstructures (Ref 14) revealed why high arc energies were found to be beneficial to pitting resistance. Many investigations have indicated that the presence of chromium nitrides in the ferrite phase lowers the resistance to pitting of the weld metal and the HAZ in duplex stainless steels. In this study, both weld metal and HAZ produced by low arc energies contained an appreciable amount of chromium nitride (Cr_2N) (Fig. 45). The nitride precipitation vanished when an arc energy of 3 kJ/mm (75 kJ/in.) was used (Fig. 46).

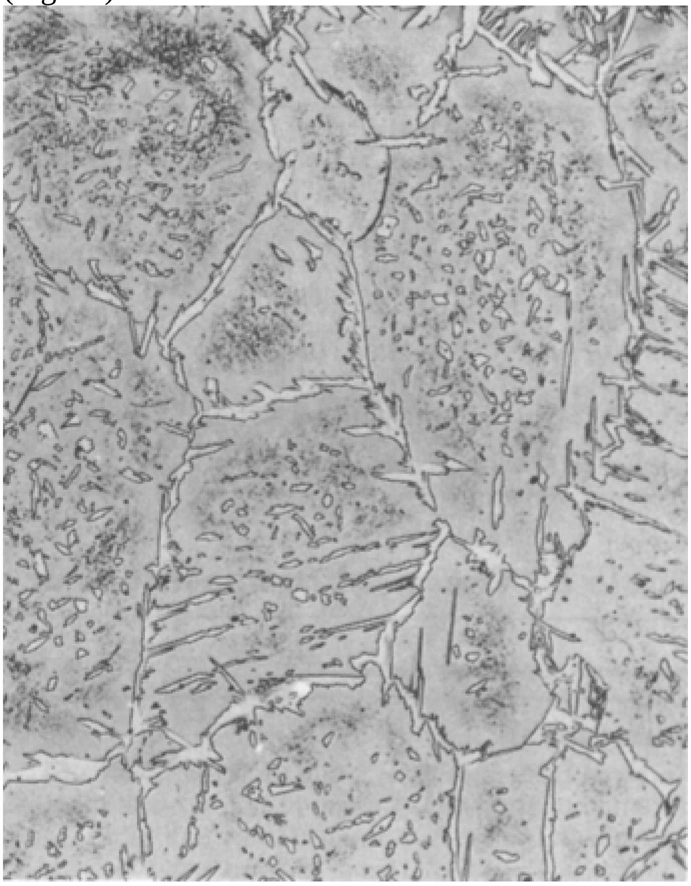

Fig. 45 Microstructure of bead-on-tube weld made by autogenous gas tungsten arc welding with an arc energy of 0.5 kJ/mm (13 kJ/in.). Note the abundance of chromium nitrides in the ferrite phase. See also Fig. 46. 200×. Source: Ref 14

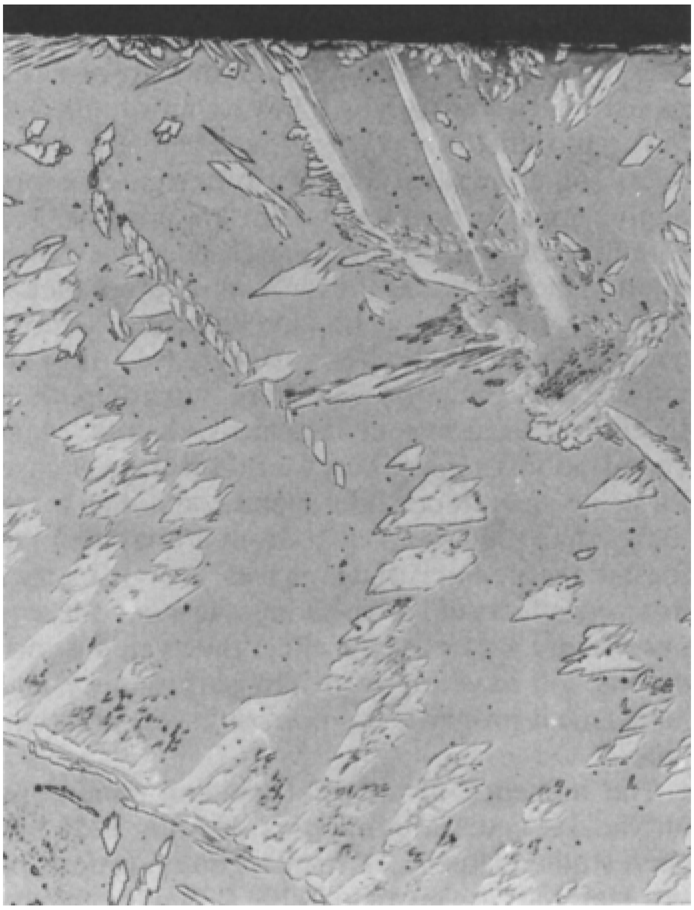

Fig. 46 Microstructure of bead-on-tube weld made by autogenous gas tungsten arc welding with an arc energy of 3 kJ/mm (76 kJ/in.). Virtually no chromium nitrides are present, which results in adequate pitting resistance. 200×. Source: Ref 14

The results of $FeCl_3$ tests on submerged-arc welds showed that all top weld surfaces passed the test at 30 °C (85 °F) without pitting attack, irrespective of arc energy in the range of 2 to 6 kJ/mm (50 to 150 kJ/in.). Surprisingly, the weld metal on the root side, which was the first to be deposited, did not pass the same test temperature.

The deteriorating effect of high arc energies on the pitting resistance of the weld metal on the root side was unexpected. Potentiostatic tests carried out in 3% sodium chloride (NaCl) at 400 mV versus saturated calomel electrode SCE confirmed these findings. Microexamination of the entire joint disclosed the presence of extremely fine austenite precipitates, particularly in the second weld bead (Fig. 47) but also in the first or root side bead. The higher the arc energy, the more austenite of this kind was present in the first two weld beads. Thus, nitrides give rise to negative effects on the pitting resistance, as do fine austenite precipitates that were presumably reformed at as low a temperature as approximately 800 °C (1470 °F).

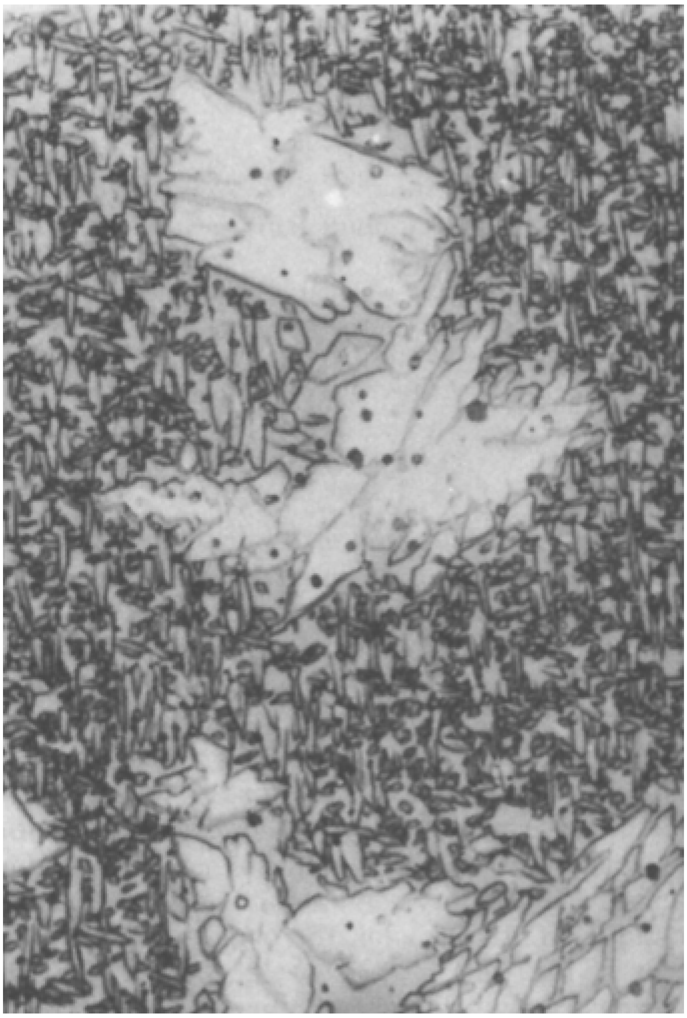

Fig. 47 Microstructure of the second weld bead of a submerged-arc weld joint in 200 mm ($\frac{3}{4}$ in.) duplex stainless steel plate. The extremely fine austenite precipitate was formed as a result of reheating from the subsequent weld pass, which used an arc energy of 6 kJ/mm (150 kJ/in.). 1000×. Source: Ref 14

Therefore, the resistance of alloy 2205 to pitting corrosion is dependent on several factors. First, chromium nitride (Cr_2N) precipitation in the coarse ferrite grains upon rapid cooling from temperatures above about 1200 °C (2190 °F) causes the most severe impairment to pitting resistance. This statement is supported by a great number of $FeCl_3$ tests as well as by potentiostatic pitting tests. Generally, it seems difficult to avoid Cr_2N precipitation in welded joints completely, particularly in the HAZ, the structure of which can be controlled only by the weld thermal cycle. From this point of view, it appears advisable to employ as high an arc energy as practical in each weld pass. In this way, the cooling rate will be slower (but not slow enough to encounter 475 °C, or 885 °F, embrittlement), and the re- formation of austenite will clearly dominate over the precipitation of Cr_2N.

In addition, if there were no restriction on maximum interpass temperature, the heat produced by previous weld passes could be used to decrease the cooling rate further in the critical temperature range above about 1000 °C (1830 °F). Preliminary tests with preheated workpieces have shown the significance of temperature in suppressing Cr_2N precipitation. Currently, the maximum recommended interpass temperature for alloy 2205 is 150 °C (300 °F). This temperature limit does not appear to be critical, and it is suggested that this limit could be increased to 300 °C (570 °F). The maximum recommended interpass temperature for Ferralium alloy 255 is 200 °C (390 °F). Excessive grain growth as a result of too much heat input must also be considered to avoid loss of ductility and impact toughness.

Second, the fine austenite precipitates found in the reheated ferrite when high arc energies and multipass welding were combined are commonly referred to as γ_2 in the literature. The harmful influence of γ_2 on the pitting resistance has been noted with isothermally aged specimens, but as far as is known, it has never been observed in connection with welding. It is felt, however, that γ_2 is less detrimental to pitting than Cr_2N.

Moreover, γ_2 formation is believed to be beneficial to mechanical properties, such as impact strength and ductility.

A third factor that lowers pitting resistance is oxide scale. Where possible, all surface oxides should be removed by mechanical means or, preferably, by pickling. Root surfaces (in pipe), however, are generally inaccessible, and pitting resistance must rely on the protection from the backing gas during GTA welding. It is therefore advisable to follow the current recommendation for stainless steels, which is a maximum of 25 ppm oxygen in the root backing gas.

Stress-Corrosion Cracking. The SCC resistance of alloy 2205 in aerated, concentrated chloride solutions is very good. The effect of welding on the SCC resistance is negligible from a practical point of view. The threshold stress for various welds, as well as for unwelded parent metal in the calcium chloride ($CaCl_2$) test, is as high as 90% of the tensile strength at the testing temperature. This is far above all conceivable design limits.

Also, in environments containing both hydrogen sulfide (H_2S) and chlorides, the resistance of welds is almost as high as for the parent metal. In this type of environment, however, it is important to avoid too high a ferrite content in weld metal and the HAZ. For normal welding of joints, the resulting ferrite contents should not cause any problems. For weld repair situations, however, care should be taken so that extremely high ferrite contents (>75%) are avoided. To preserve the high degree of resistance to SCC, the ferrite content should not be less than 25% (Ref 18).

Another reason to avoid coarse weld microstructures (generated by excessive welding heat) is the resultant nonuniform plastic flow, which can locally increase stresses and induce preferential corrosion and cracking effects.

Use of High-Alloy Filler Metals. In critical pitting or crevice corrosion applications, the pitting resistance of the weld metal can be enhanced by the use of high Ni-Cr-Mo alloy filler metals. The corrosion resistance of such weldments in Ferralium alloy 255 is shown in Table 4. For the same weld technique, it can be seen that using high-alloy fillers does improve corrosion resistance. If high-alloy fillers are used, the weld metal will have better corrosion resistance than the HAZ and the fusion line. Therefore, again, proper selection of welding technique can improve the corrosion resistance of the weldments.

Table 4 Corrosion resistance of Ferralium alloy 255 weldments using various nickel-base alloy fillers and weld techniques

3.2 mm (0.125 in.) plates tested in 10% $FeCl_3$ for 120 h

Filler metal	Critical pitting temperature					
	Gas tungsten arc		**Gas metal arc**		**Submerged arc**	
	°C	**°F**	**°C**	**°F**	**°C**	**°F**
Hastelloy alloy G-3	30–35	85–95[(a)]	30	85[(a)]	30–35	85–95[(b)]
IN-112	30	85[(a)]	…	…	35–40	95–105[(b)]
Hastelloy alloy C-276	…	…	…	…	25–30	75–85[(a)]
Hastelloy alloy C-22	30	85[(a)]	…	…	35–40	95–105[(a)]

(a) Haz.

(b) HAZ plus weld metal

References cited in this section

7. "Standard Practices for Detecting Susceptibility to Intergranular Attack in Austenitic Stainless Steels," A 262, *Annual Book of ASTM Standards,* American Society for Testing and Materials

13. T.G. Gooch, Corrosion Resistance of Welds in Duplex Stainless Steels, *Duplex Stainless Steels '91,* Vol 1, *Les Editions de Physique,* 1991, p 325–346

14. B. Lundquist, P. Norberg, and K. Olsson, "Influence of Different Welding Conditions on Mechanical Properties and Corrosion Resistance of Sandvik SAF 2205 (UNS S31803)," Paper 10, presented at the Duplex Stainless Steels '86 Conference, the Hague, Netherlands, Oct 1986

15. “Standard Test Methods for Pitting and Crevice Corrosion Resistance of Stainless Steels and Related Alloys by the Use of Ferric Chloride Solution,” G 48, *Annual Book of ASTM Standards,* American Society for Testing and Materials

16. N. Sridhar, L.H. Flasche, and J. Kolts, Effect of Welding Parameters on Localized Corrosion of a Duplex Stainless Steel, *Mater. Perform.,* Dec 1984, p 52–55

17. “Standard Specification for Substitute Ocean Water,” D 1141, *Annual Book of ASTM Standards,* American Society for Testing and Materials

18. E. Perteneder, J. Tosch, and G. Rabensteiner, “New Welding Filler Metals for the Welding of Girth Welds on Pipelines of Corrosion-Resistant Cr-Ni-Mo-N-Duplex Steels,” paper presented at the International Conference on Welding in Energy Related Projects, Toronto, Canada, Welding Institute of Canada, Sept 1983

Acknowledgment

The information in this article is largely taken from:

- K.F. Krysiak, et al., Corrosion of Weldments, *Corrosion,* Vol 13, 9th ed., *Metals Handbook,* ASM International, 1987, p 344–367
- D.L. Olson, et al., Corrosion of Weldments, *Welding, Brazing, and Soldering,* Vol 6, *ASM Handbook,* ASM International, 1993, p 1065–1069

Corrosion of Stainless Steel Weldments, *Corrosion: Fundamentals, Testing, and Protection,* Vol 13A, *ASM Handbook,* ASM International, 2003, p 301–316

Corrosion of Stainless Steel Weldments

References

1. F.C. Brautigam, Welding Practices That Minimize Corrosion, *Chem. Eng.,* 17 Jan 1977, p 145–147

2. M.A. Streicher, Theory and Application of Evaluation Tests for Detecting Susceptibility to Intergranular Attack in Stainless Steels and Related Alloys—Problems and Opportunities, *Intergranulur Corrosion of Stainless Alloys,* STP 656, American Society for Testing and Materials, 1978, p 70

3. W.F. Savage, New Insight into Weld Cracking and a New Way of Looking at Welds, *Weld. Des. Eng.,* Dec 1969

4. W.A. Baeslack III, J.C. Lippold, and W.F. Savage, Unmixed Zone Formation in Austenitic Stainless Steel Weldments, *Weld. J.,* Vol 58 (No. 6), 1979, p 168s–176s

5. A. Garner, How Stainless Steel Welds Corrode, *Met. Prog.*, Vol 127 (No. 5), April 1985, p 31

6. K.F. Krysiak, "Cause and Prevention of Unusual Failures of Materials," Paper 19, presented at Corrosion/83, Anaheim, CA, National Association of Corrosion Engineers, April 1983

7. "Standard Practices for Detecting Susceptibility to Intergranular Attack in Austenitic Stainless Steels," A 262, *Annual Book of ASTM Standards,* American Society for Testing and Materials

8. J.R. Kearns and H.E. Deverell, "The Use of Nitrogen to Improve Fe-Cr-Ni-Mo Alloys for the Chemical Process Industries," Paper 188, presented at Corrosion/86, Houston, TX, National Association of Corrosion Engineers, March 1986

9. J.R. Kearns, "The Corrosion of Heat Tinted Austenitic Stainless Alloys," Paper 50, presented at Corrosion/85, Boston, MA, National Association of Corrosion Engineers, March 1985

10. G. Kobrin, Corrosion by Microbiological Organisms in Natural Waters, *Mater. Perform.,* Vol 15 (No. 7), 1976

11. R.H. Espy, "How Corrosion and Welding Conditions Affect Corrosion Resistance of Weldments in Type 430 Stainless Steel," Paper 22, presented at Corrosion/68, Houston, TX, National Association of Corrosion Engineers, 1968

12. K.F. Krysiak, Welding Behavior of Ferritic Stainless Steels—An Overview, *Weld. J.,* Vol 65 (No. 4), April 1986, p 37–41

13. T.G. Gooch, Corrosion Resistance of Welds in Duplex Stainless Steels, *Duplex Stainless Steels '91,* Vol 1, *Les Editions de Physique,* 1991, p 325–346

14. B. Lundquist, P. Norberg, and K. Olsson, "Influence of Different Welding Conditions on Mechanical Properties and Corrosion Resistance of Sandvik SAF 2205 (UNS S31803)," Paper 10, presented at the Duplex Stainless Steels '86 Conference, the Hague, Netherlands, Oct 1986

15. "Standard Test Methods for Pitting and Crevice Corrosion Resistance of Stainless Steels and Related Alloys by the Use of Ferric Chloride Solution," G 48, *Annual Book of ASTM Standards,* American Society for Testing and Materials

16. N. Sridhar, L.H. Flasche, and J. Kolts, Effect of Welding Parameters on Localized Corrosion of a Duplex Stainless Steel, *Mater. Perform.,* Dec 1984, p 52–55

17. "Standard Specification for Substitute Ocean Water," D 1141, *Annual Book of ASTM Standards,* American Society for Testing and Materials

18. E. Perteneder, J. Tosch, and G. Rabensteiner, "New Welding Filler Metals for the Welding of Girth Welds on Pipelines of Corrosion-Resistant Cr-Ni-Mo-N-Duplex Steels," paper presented at the International Conference on Welding in Energy Related Projects, Toronto, Canada, Welding Institute of Canada, Sept 1983

Corrosion of Nonferrous Alloy Weldments, *Corrosion: Fundamentals, Testing, and Protection*, Vol 13A, *ASM Handbook*, ASM International, 2003, p 317–321

Corrosion of Nonferrous Alloy Weldments

Introduction

IT IS NOT UNUSUAL to find that, although the wrought form of a metal or alloy is resistant to corrosion in a particular environment, the welded counterpart is not. Further, welds can be made with or without the addition of filler metal. However, there are also many instances in which the weld exhibits corrosion resistance superior to that of the unwelded base metal. There also are times when the weld behaves in an erratic manner, displaying both resistance and susceptibility to corrosive attack. Corrosion failures of welds occur in spite of the fact that the proper base metal and filler metal have been selected, industry codes and standards have been followed, and welds have been deposited that possess full weld penetration and have proper shape and contour.
It is sometimes difficult to determine why welds corrode; however, one or more of the following factors often are implicated:

- Weldment design
- Fabrication technique
- Welding practice
- Welding sequence
- Moisture contamination
- Organic or inorganic chemical species
- Oxide film and scale
- Weld slag and spatter
- Incomplete weld penetration or fusion
- Porosity
- Cracks (crevices)
- High residual stresses
- Improper choice of filler metal
- Final surface finish

This article describes some of the metallurgical factors that affect corrosion of weldments and then reviews considerations for selected nonferrous alloy systems: aluminum, titanium, tantalum, and nickel.

Metallurgical Factors

The cycle of heating and cooling that occurs during the welding process affects the microstructure and surface composition of welds and adjacent base metal. Consequently, the corrosion resistance of autogenous welds (welds made without the addition of filler metals) and welds made with matching filler metal may be inferior to that of properly annealed base metal because of:

- Microsegregation

- Precipitation of secondary phases
- Formation of unmixed zones
- Recrystallization and grain growth in the weld heat-affected zone (HAZ)
- Volatilization of alloying elements from the molten weld pool
- Contamination of the solidifying weld pool

Corrosion resistance can usually be maintained in the welded condition by balancing alloy compositions to inhibit certain precipitation reactions, by shielding molten and hot metal surfaces from reactive gases in the weld environment, by removing chromium-enriched oxides and chromium-depleted base metal from thermally discolored (heat tinted) surfaces, and by choosing the proper welding parameters (Ref 1).

Weld Solidification. During the welding process, a number of important changes occur that can significantly affect the corrosion behavior of the weldment. Heat input and welder technique obviously play important roles. The way in which the weld solidifies is equally important to understanding how weldments may behave in corrosive environments (Ref 2).

A metallographic study has shown that welds solidify into various regions, as illustrated in Fig. 1. The composite region, or weld nugget, consists of essentially filler metal that has been diluted with material melted from the surrounding base metal. Next to the composite region is the unmixed zone, a zone of base metal that melted and solidified during welding without experiencing mechanical mixing with the filler metal. The weld interface is the surface bounding the region within which complete melting was experienced during welding, and it is evidenced by the presence of a cast structure. Beyond the weld interface is the partially melted zone, which is a region of the base metal within which the proportion melted ranges from 0 to 100%. Lastly, the true HAZ is that portion of the base metal within which microstructural change has occurred in the absence of melting. Although the various regions of a weldment shown in Fig. 1 are for a single-pass weld, similar solidification patterns and compositional differences can be expected to occur in underlying weld beads during multipass applications.

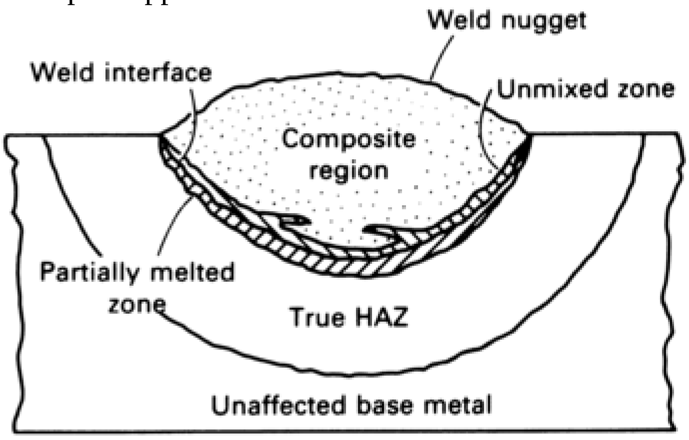

Fig. 1 Schematic of a weld cross section. Source: Ref 3

References cited in this section

1. F.C. Brautigam, Welding Practices That Minimize Corrosion, *Chem. Eng.*, 17 Jan 1977, p 145–147

2. M.A. Streicher, Theory and Application of Evaluation Tests for Detecting Susceptibility to Intergranular Attack in Stainless Steels and Related A

Corrosion of Nonferrous Alloy Weldments, *Corrosion: Fundamentals, Testing, and Protection*, Vol 13A, *ASM Handbook*, ASM International, 2003, p 317–321

Corrosion of Aluminum Alloy Weldments

Variations in microstructure across the weld and HAZ of aluminum weldments are known to produce susceptibility to corrosion in certain environments (Ref 4). These differences can be measured electrochemically and are an indication of the type of corrosion behavior that might be expected. Although some aluminum alloys can be autogenously welded, the use of a filler metal is preferred to avoid cracking during welding and to optimize corrosion resistance.

The variations in corrosion potential (equilibrium potential) across three welds are shown in Fig. 2 for alloys 5456, 2219, and 7039. These differences can lead to localized corrosion, as demonstrated by the corrosion of the HAZ of an as-welded structure of alloy 7005 shown in Fig. 3. In general, the welding procedure that puts the least amount of heat into the metal has the least influence on microstructure and the least chance of reducing the corrosion behavior of aluminum weldments.

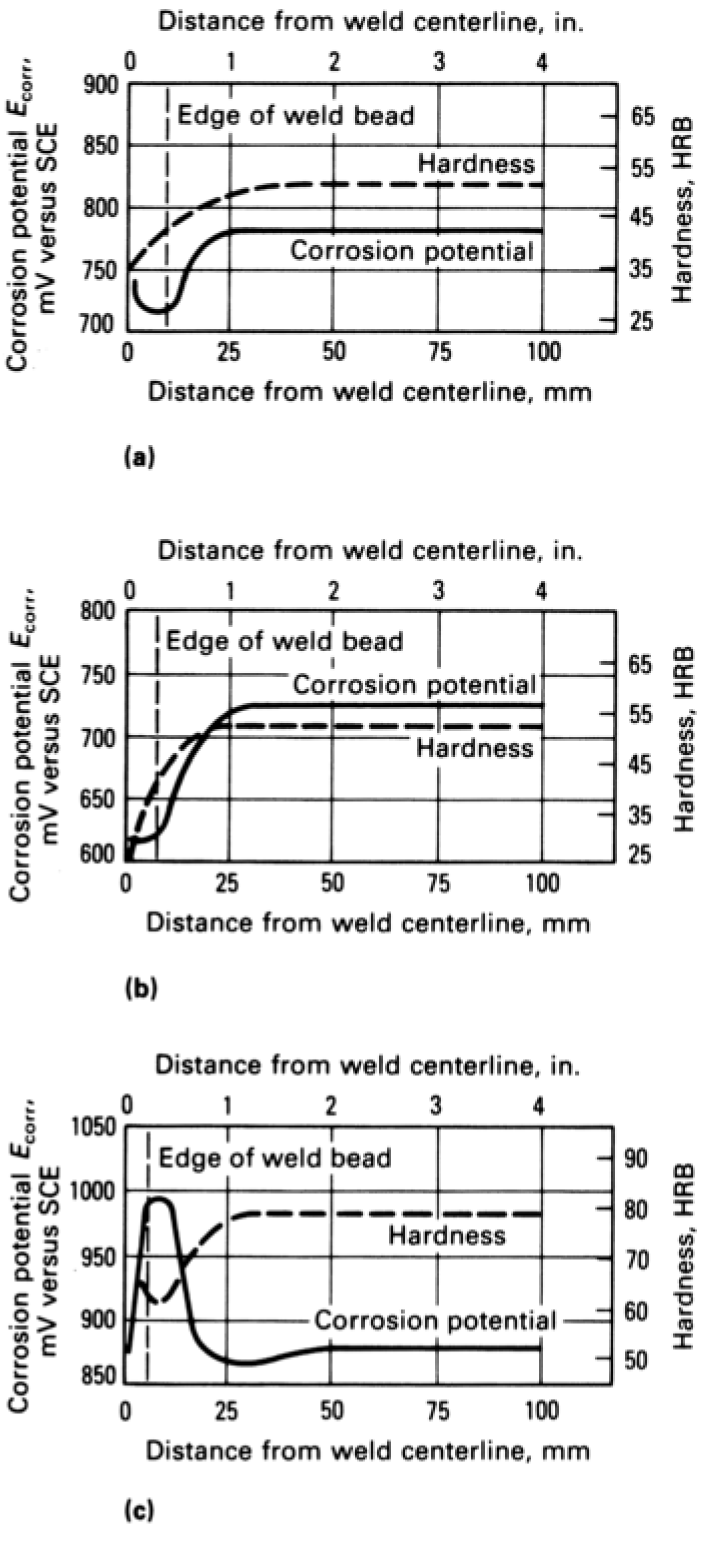

Fig. 2 Effect of the heat of welding on microstructure, hardness, and corrosion potential of welded assemblies of three aluminum alloys. The differences in corrosion potential between the HAZ and the base metal can lead to selective corrosion. (a) Alloy 5456-H321 base metal with alloy 5556 filler; 3-pass metal inert gas weld. (b) Alloy 2219-T87 base metal with alloy 2319 filler; 2-pass tungsten inert gas weld. (c) Alloy 7039-T651 base metal with alloy 5183 filler; 2-pass tungsten inert gas weld. SCE, saturated calomel electrode. Source: Ref 4

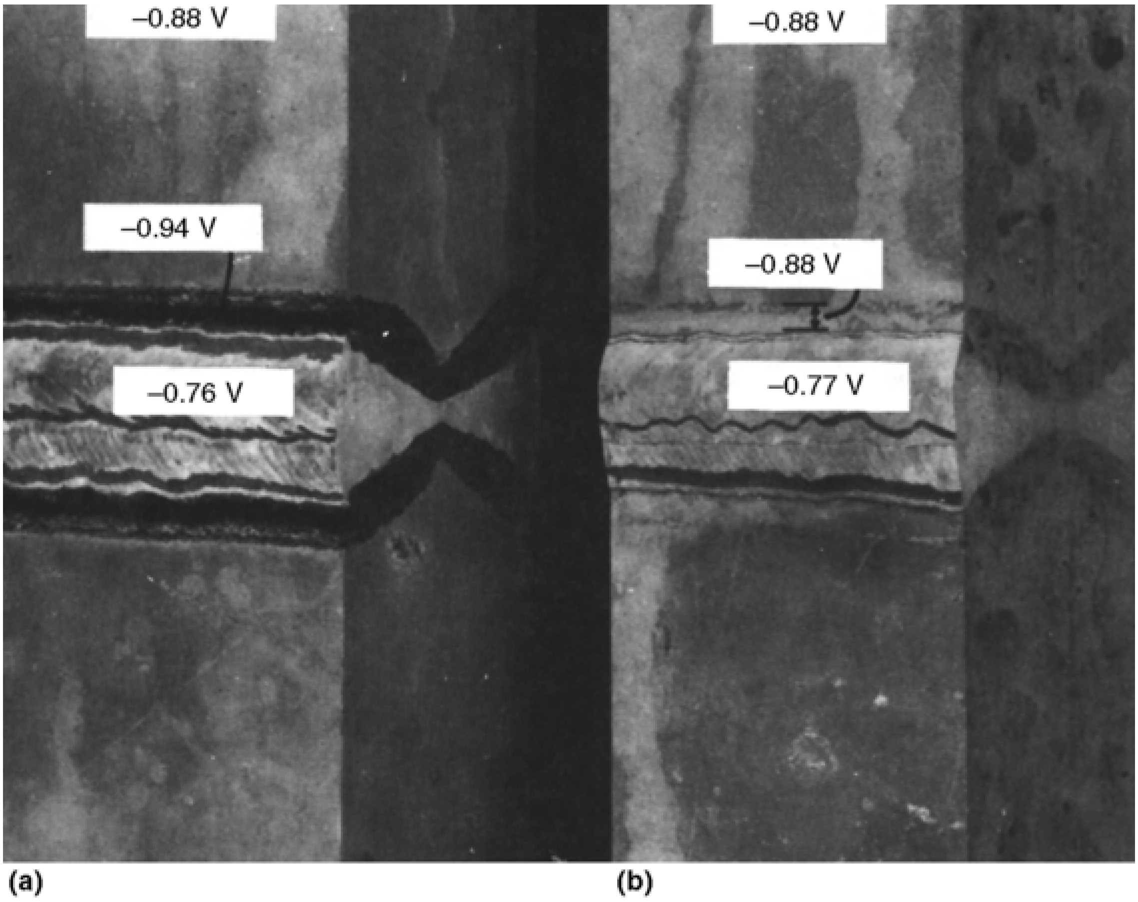

Fig. 3 Welded assemblies of aluminum alloy 7005 with alloy 5356 filler metal after a 1 year exposure to seawater. (a) As-welded assembly shows severe localized corrosion in the HAZ. (b) Specimen showing the beneficial effects of postweld aging. Corrosion potentials of different areas of the weldments are shown where they were measured. Electrochemical measurements performed in 53 g/L NaCl plus 3 g/L H_2O_2 versus a 0.1 *N* calomel reference electrode and recalculated to a saturated calomel electrode. Source: Ref 4

Tables are available in the article "Welding of Aluminum Alloys" in *Welding, Brazing, and Soldering,* Volume 6 of *ASM Handbook,* that summarize filler alloy selection recommended for welding various combinations of base metal alloys to obtain maximum properties, including corrosion resistance. Care must be taken not to extrapolate the corrosion performance ratings indiscriminately. Corrosion behavior ratings generally pertain only to the particular environment tested, usually rated in continuous or alternate immersion in fresh or saltwater. For example, the highest corrosion rating (A) is listed for use of filler alloy 4043 to join 3003 alloy to 6061 alloy. In strong (99%) nitric acid (HNO_3) service, however, a weldment made with 4043 filler alloy would experience more rapid attack than a weldment made using 5556 filler metal. With certain alloys, particularly those of the heat treatable 7*xxx* series, thermal treatment after welding is sometimes used to obtain maximum corrosion resistance (Fig. 3) (Ref 5, 6, 7).

As with many other alloy systems, attention must be given to the threat of crevice corrosion under certain conditions. Strong (99%) HNO_3 is particularly aggressive toward weldments that are not made with full weld penetration. Although all of the welds shown in Fig. 4 appear to be in excellent condition when viewed from the outside surface, the first two welds (Fig. 4a and b), viewed from the inside, are severely corroded. The weld made using standard gas tungsten arc (GTA) welding practices with full weld penetration (Fig. 4c) is in good condition after 2 years of continuous service.

Fig. 4 Corrosion of three aluminum weldments in HNO_3 service. (a) and (b) Gas tungsten arc (GTA) and oxyacetylene welds, respectively, showing crevice corrosion on the inside surface. (c) Standard GTA weld with full penetration is resistant to crevice corrosion.

Researchers have shown that aluminum alloys, both welded and unwelded, have good resistance to uninhibited HNO_3 (both red and white) up to 50 °C (120 °F). Above this temperature, most aluminum alloys exhibit knife-line attack (a very thin region of corrosion) adjacent to the welds. Above 50 °C (120 °F), the depth of knife-line attack increases markedly with temperature. One exception was found in the case of a fusion-welded 1060 alloy in which no knife-line attack was observed even at temperatures as high as 70 °C (160 °F). In inhibited fuming HNO_3 containing at least 0.1% hydrofluoric acid (HF), no knife-line attack was observed for any commercial aluminum alloy or weldment even at 70 °C (160 °F).

More information on the welding of aluminum and aluminum alloys is available in the articles "Welding of Aluminum Alloys" and "Procedure Development and Practice Considerations for Resistance Welding" in *Welding, Brazing, and Soldering,* Volume 6 of *ASM Handbook.*

References cited in this section

4. J.E. Hatch, Ed., *Aluminum: Properties and Physical Metallurgy,* American Society for Metals, 1984, p 283

5. *Welding Aluminum,* American Welding Society—The Aluminum Association, 1972

6. J.G. Young, BWRA Experience in the Welding of Aluminum-Zinc-Magnesium Alloys, *Weld. Res. Suppl.,* Oct 1968

7. "Alcoa Aluminum Alloy 7005," Alcoa Green Letter, Aluminum Company of America, Sept 1974

Corrosion of Nonferrous Alloy Weldments, *Corrosion: Fundamentals, Testing, and Protection,* Vol 13A, *ASM Handbook,* ASM International, 2003, p 317–321

Corrosion of Nonferrous Alloy Weldments

Corrosion of Titanium Alloy Weldments

Although titanium and its alloys are used chiefly for their desirable mechanical properties, among which the most notable is their high strength-to-weight ratio, another important characteristic of titanium and its alloys is their outstanding resistance to corrosion. Commercially pure (CP) titanium offers excellent corrosion resistance in most environments, except those media that contain fluoride ions. Titanium is more corrosion resistant than stainless steel in many industrial environments, and its use in the chemical process industry has been gradually increasing. Titanium exhibits excellent resistance to atmospheric corrosion in both marine and industrial environments.

Successful application of titanium and its alloys can be expected in mildly reducing to highly oxidizing environments in which protective oxide films spontaneously form and remain stable. Titanium and its alloys have been found to be largely immune to corrosion-related failure in most environments, although titanium alloys are generally less resistant to corrosion than CP titanium.

In unalloyed titanium and many titanium alloys, weld zones are just as resistant to corrosion as the base metal is. Other fabrication processes (such as bending or machining) also appear to have no influence on basic corrosion resistance.

Weldments and castings of CP grades and alpha-beta alloys such Ti-6Al-4V generally exhibit corrosion resistance similar to that of their unwelded, wrought counterparts. These titanium alloys contain so little alloy content and second phase that metallurgical instability and thermal response are not significant. Therefore, titanium weldments and associated HAZs generally do not experience corrosion limitations in welded components when normal passive conditions prevail for the base metal. However, under marginal or active conditions, for corrosion rates greater than or equal to 100 μm/year, weldments can experience accelerated corrosion attack relative to the base metal, depending on alloy composition. The increasing impurity (e.g., iron, sulfur, oxygen) content associated with the coarse, transformed beta microstructure of weldments appears to be a factor. Few published data are available concerning the corrosion resistance of titanium alloy weldments and castings other than Ti-6Al-4V, and limited information on other product forms has been reported.

Corrosion of Nonferrous Alloy Weldments, *Corrosion: Fundamentals, Testing, and Protection*, Vol 13A, *ASM Handbook*, ASM International, 2003, p 317–321

Corrosion of Nonferrous Alloy Weldments

Corrosion of Tantalum Alloy Weldments

Examination of equipment fabricated from tantalum that has been used in a wide variety of service conditions and environments generally shows that the weld, HAZ, and base metal display equal resistance to corrosion. This same resistance has also been demonstrated in laboratory corrosion tests conducted in a number of different acids and other environments. However, in applications for tantalum-lined equipment, contamination of the tantalum with iron from underlying backing material, usually carbon steel, can severely impair the corrosion resistance of tantalum. About the only known reagents that rapidly attack tantalum are fluorine; HF and acidic solutions containing fluoride; fuming sulfuric acid (H_2SO_4) (oleum), which contains free sulfur trioxide (SO_3); and alkaline solutions.

Oxygen Tolerance of Tantalum Weldments. Tantalum reacts with oxygen, nitrogen, and hydrogen at elevated temperatures. The absorption of these interstitial elements, often called a gettering reaction, produces a sharp reduction in ductility and can cause embrittlement. This impairment in ductility (and also in notch toughness, as manifested by an increase in ductile-to-brittle transition temperature) can be considered a form of corrosion. The other group Va refractory metals (niobium and vanadium) and the group IVa reactive metals (titanium, zirconium, and hafnium) can also suffer similar attack.

On the basis of chemical composition, the maximum oxygen tolerance for tantalum weldments appears to be approximately 400 to 550 ppm; for Tantaloy 63 (Ta-2.5W-0.15Nb) weldments, it is approximately 350 to 500 ppm. Although commercially pure tantalum exhibits a somewhat higher tolerance for oxygen (and total interstitial contamination) than Tantaloy 63, the latter material appears to have somewhat better resistance to oxidation; this tends to offset the advantage tantalum has of a higher allowable oxygen pickup before embrittlement occurs. It should be noted that these conclusions are based on the assumption that oxygen is distributed relatively uniformly throughout the cross section in all parts of the weldment. A locally high concentration, such as a high surface contamination of oxygen or nitrogen, could result in a severe loss in ductility and could possibly even produce embrittlement. Therefore, all handling, cleaning, and fabrication practices on tantalum and its alloys should avoid producing such surface contamination as well as gross contamination.

Corrosion of Nonferrous Alloy Weldments, *Corrosion: Fundamentals, Testing, and Protection*, Vol 13A, *ASM Handbook,* ASM International, 2003, p 317–321

Corrosion of Nickel and High-Nickel Alloy Weldments

The corrosion resistance of weldments is related to the microstructural and microchemical changes resulting from thermal cycling. The effects of welding on the corrosion resistance of nickel-base alloys are similar to the effects on the corrosion resistance of austenitic stainless steels, as described in the article "Corrosion of Stainless Steel Weldments" in this Volume. For example, sensitization due to carbide precipitation in the HAZ is a potential problem in both classes of alloys. However, in the case of nickel- base alloys, the high content of such alloying elements as chromium, molybdenum, tungsten, and niobium can result in the precipitation of other intermetallic phases, such as μ, σ, and η.

Therefore, this section is concerned with the characteristics of the various nickel-base alloys and the evolution of these alloys. The corrosion resistance of weldments is dictated not only by the HAZ but also by the weld metal itself. The effect of elemental segregation on weld metal corrosion must also be examined. The nickel-base alloys discussed in this section are the solid- solution alloys.

The nickel-molybdenum alloys, represented by Hastelloy alloys B (UNS N10001) and B-2 (UNS N10665), have been primarily used for their resistance to corrosion in nonoxidizing environments such as HCl. Hastelloy alloy B has been used since approximately 1929 and has suffered from one significant limitation: weld decay. The welded structure has shown high susceptibility to knife-line attack adjacent to the weld metal and to HAZ attack at some distance from the weld. The former has been attributed to the precipitation of molybdenum carbide (Mo_2C); the latter, to the formation of M_6C-type carbides. This necessitated postweld annealing, a serious shortcoming when large structures are involved. The knife-line attack on an alloy B weldment is shown in Fig. 5. Many approaches to this problem were attempted, including the addition of carbide-stabilizing elements, such as vanadium, titanium, zirconium, and tantalum, as well as the lowering of carbon.

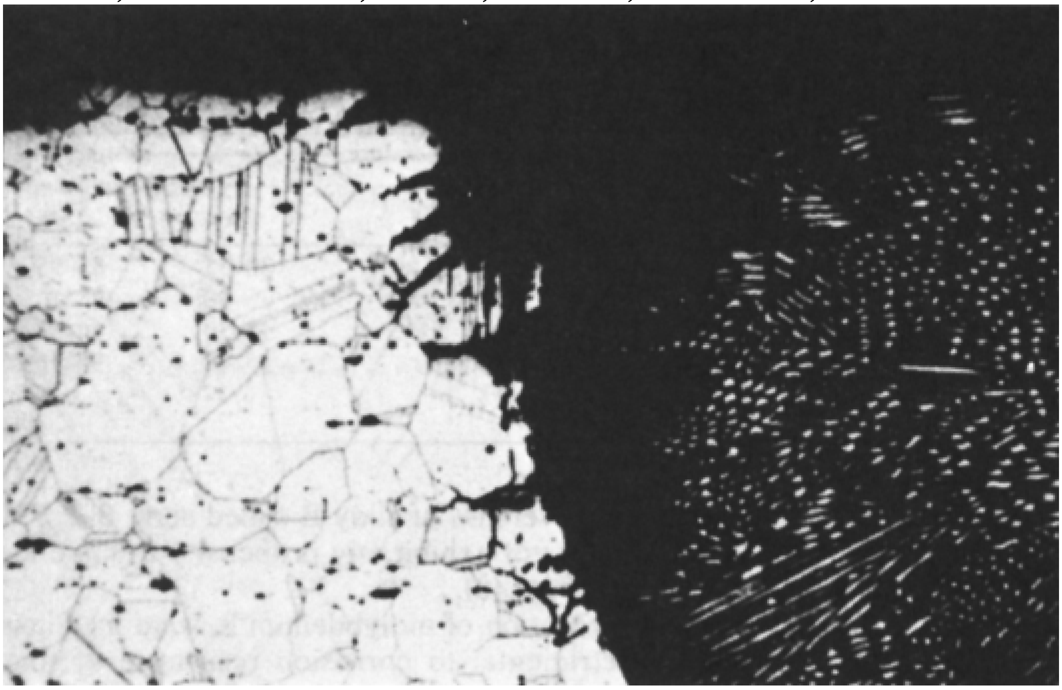

Fig. 5 Cross section of a Hastelloy alloy B weldment corroded after 16 days of exposure in boiling 20% HCl. 80×. Source: Ref 8

The addition of 1% V to an alloy B-type composition was first patented in 1959. The resultant commercial alloys—Corronel 220 and Hastelloy alloy B-282—were found to be superior to alloy B in resisting knife-line attack but were not immune to it. In fact, it was demonstrated that the addition of 2% V decreased the corrosion

resistance of the base metal in HCl solutions. During this time, improvements in melting techniques led to the development of a low-carbon low-iron version of alloy B called alloy B-2. This alloy did not exhibit any propensity to knife-line attack (Fig. 6).

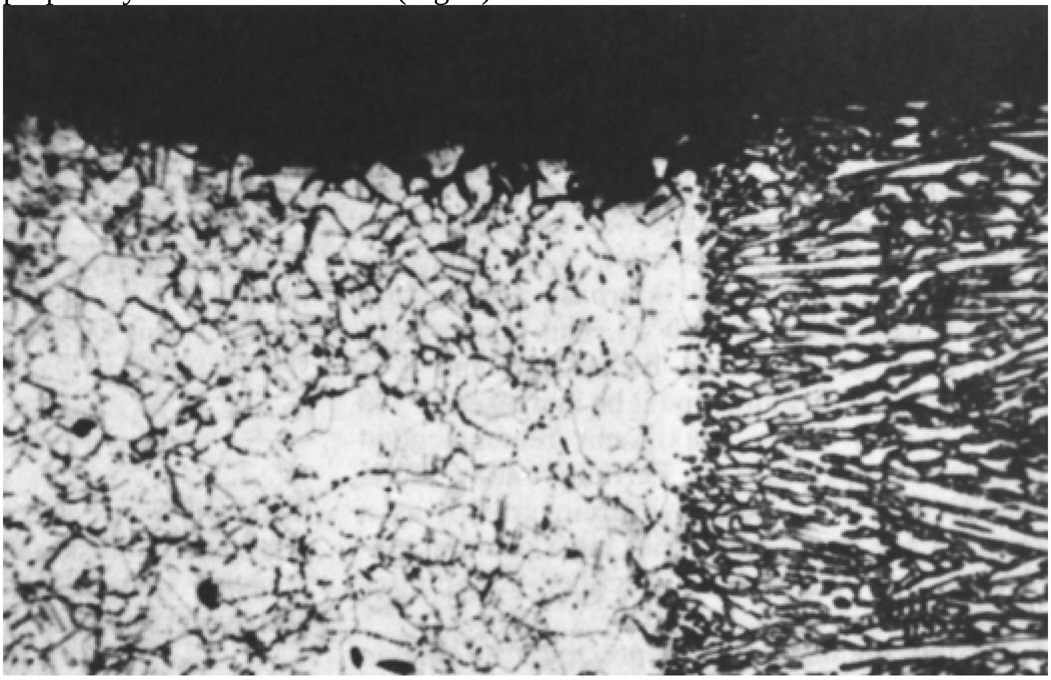

Fig. 6 Cross section of a Hastelloy alloy B-2 weldment after 16 days of exposure to boiling 20% HCl. 80×. Source: Ref 8

Segregation of molybdenum in weld metal can be detrimental to corrosion resistance in some environments. In the case of boiling HCl solutions, the weld metal does not corrode preferentially. However, in H_2SO_4 + HCl and H_2SO_4 + H_3PO_4 acid mixtures, preferential corrosion of as-welded alloy B-2 has been observed (Fig. 7). No knife-line or HAZ attack was noted in these tests. During solidification, the initial solid is poorer in molybdenum and therefore can corrode preferentially. This is shown in Fig. 7 for an autogenous GTA weld in alloy B-2. In such cases, postweld annealing at 1120 °C (2050 °F) is beneficial.

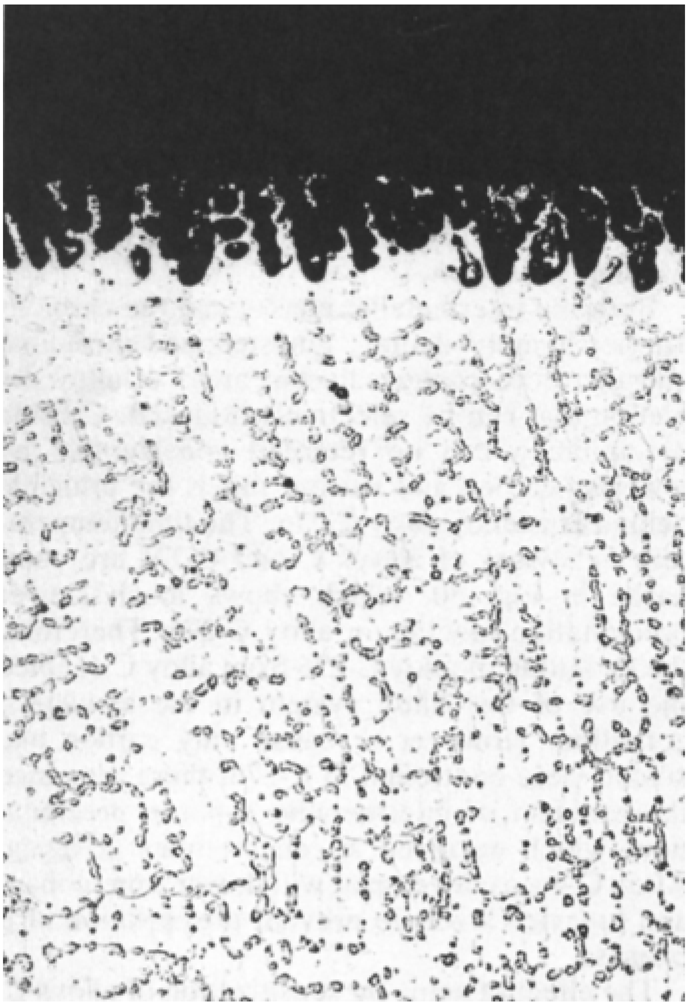

Fig. 7 Preferential corrosion of autogenous gas tungsten arc weld in Hastelloy alloy B-2 exposed to boiling 60% H_2SO_4 + 8% HCl

The nickel-chromium-molybdenum alloys represented by the Hastelloy C family of alloys and by Inconel 625 have also undergone evolution because of the need to improve the corrosion resistance of weldments. Hastelloy alloy C (UNS N10002), containing nominally 16% Cr, 16% Mo, 4% W, 0.04% C, and 0.5% Si, had been in use for some time but had required the use of postweld annealing to prevent preferential weld and HAZ attack. Many investigations were carried out on the nature of precipitates formed in alloy C, and two main types of precipitates were identified. The first is a Ni_7Mo_6 intermetallic phase called μ, and the second consists of carbides of the Mo_6C type. Other carbides of the $M_{23}C_6$ and M_2C were also reported. Another type, an ordered Ni_2Cr-type precipitate, occurs mainly at lower temperatures and after a long aging time; it is not of great concern from a welding viewpoint.

Both the intermetallic phases and the carbides are rich in molybdenum, tungsten, and chromium and therefore create adjacent areas of alloy depletion that can be selectively attacked. Carbide precipitation can be retarded considerably by lowering carbon and silicon; this is the principle behind Hastelloy alloy C-276. The time-temperature behaviors of alloys C and C-276 are compared in Fig. 8, which shows much slower precipitation kinetics in alloy C-276. Therefore, the evolution of alloy C-276 from alloy C enabled the use of this alloy system in the as- welded condition. However, because only carbon and silicon were controlled in C-276, there remained the problem of intermetallic μ-phase precipitation, which occurred at longer times of aging. Alloy C-4 was developed with lower iron, cobalt, and tungsten levels to prevent precipitation of μ phases.

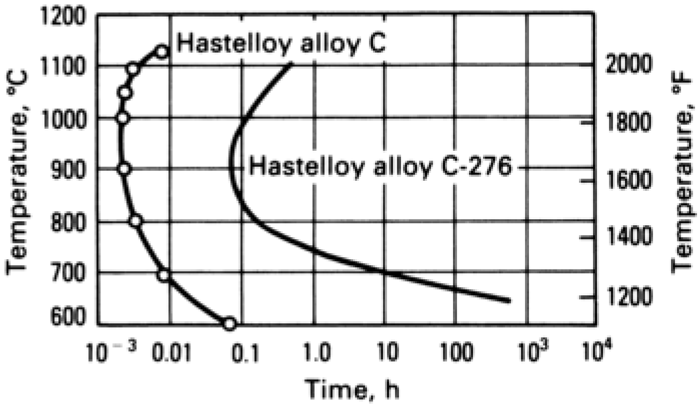

Fig. 8 Time-temperature transformation curves for Hastelloy alloys C and C-276. Intermetallics and carbide phases precipitate in the regions to the right of the curves. Source: Ref 9

The effect of aging on sensitization of alloys C, C-276, and C-4 is shown in Fig. 9. For alloy C, sensitization occurs in two temperature ranges (700 to 800 °C, or 1290 to 1470 °F, and 900 to 1100 °C, or 1650 to 2010 °F) corresponding to carbide and μ-phase precipitation, respectively. For alloy C-276, sensitization occurs essentially in the higher temperature region because of μ- phase precipitation. Also, the μ-phase precipitation kinetics in alloy C-276 are slow enough not to cause sensitization problems in many high-heat-input weldments; however, precipitation can occur in the HAZ of alloy C-276 welds (Fig. 10). Because C-4 has lower tungsten than C-276, it has lower pitting and crevice corrosion resistance, for which tungsten is beneficial. Therefore, an alternate solution to alloy C-4 was needed in which both corrosion resistance and thermal stability are preserved. Hastelloy alloy C-22 has demonstrated improved corrosion resistance and thermal stability.

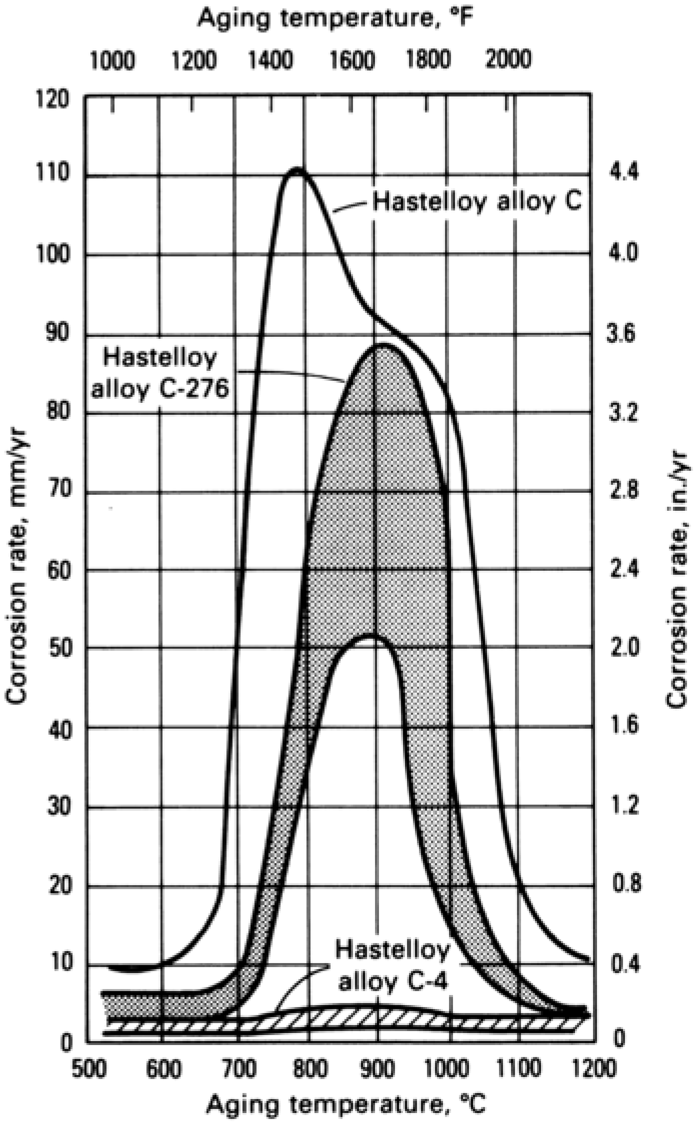

Fig. 9 Effect of 1 h aging treatment on corrosion resistance of three Hastelloy alloys in 50% H_2SO_4 + 42 g/L $Fe_2(SO_4)_3$. Source: Ref 10

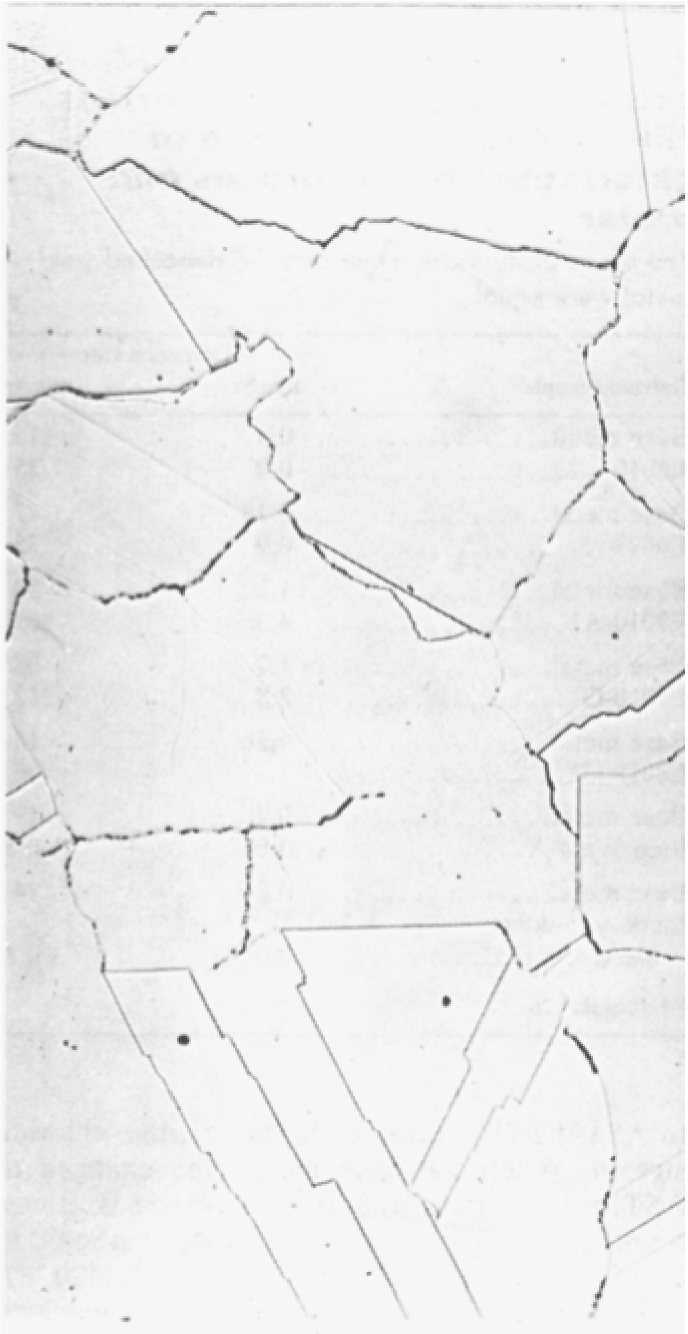

Fig. 10 Typical microstructure of the HAZ of a multipass submerged arc weld in Hastelloy alloy C-276. Source: Ref 11

Because of the low carbon content of alloy C- 22, the precipitation kinetics of carbides were slowed. Because alloy C-22 has lower molybdenum and tungsten levels than alloy C-276, μ- phase precipitation was also retarded.

From a weld HAZ point of view, this difference is reflected in lower grain-boundary precipitation even in a high-heat-input weld (Fig. 11). The HAZ microstructure of alloy C-4 was similar to this. This difference in the sensitization of the HAZ is also illustrated in Fig. 12, which shows that the HAZ and weld metal of alloy C-276 are attacked to a considerable extent in an oxidizing mixture of H_2SO_4 ferric sulfate ($Fe_2(SO_4)_3$), and other chemicals.

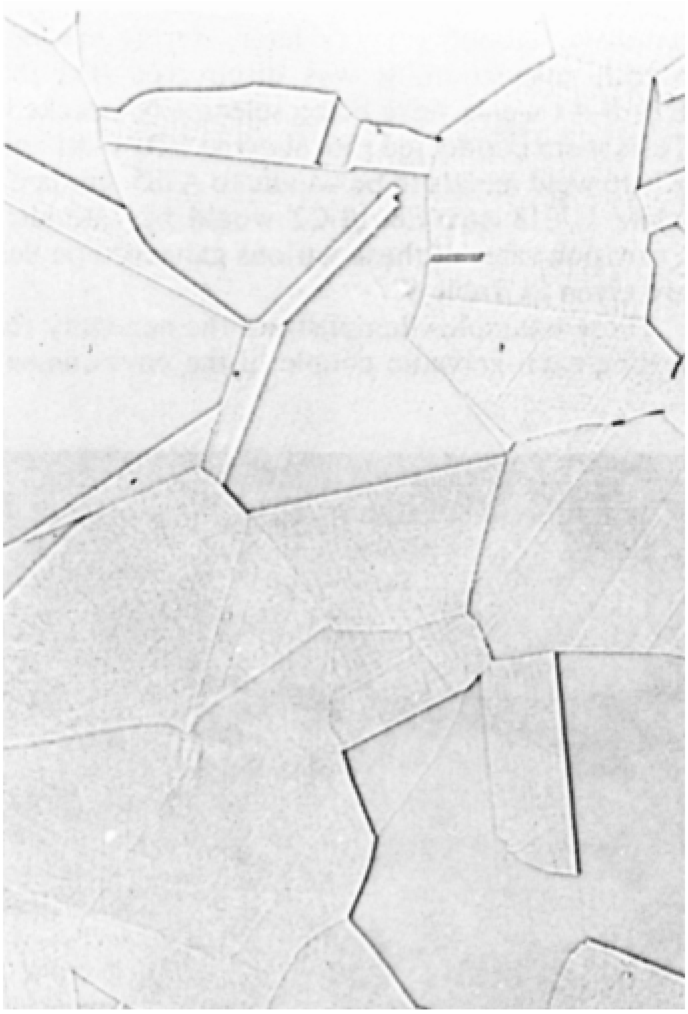

Fig. 11 Typical microstructure of the HAZ of a multipass submerged arc weld in Hastelloy alloy C-22. Matching filler metal was used. Source: Ref 11

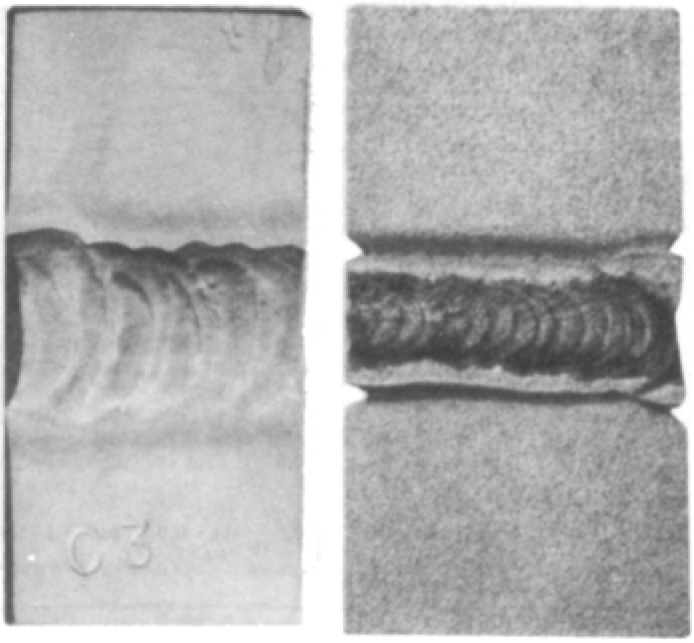

(a) (b)

Fig. 12 Corrosion of the weld metal and the HAZ in Hastelloy alloys (a) C-22 and (b) C-276 in an aerated mixture of 6 vol% H_2SO_4 + 3.9% $Fe_2(SO_4)_3$ + other chemicals at 150 °C (300 °F). Source: Ref 11

References cited in this section

8. F.G. Hodge and R.W. Kirchner, Paper 60, presented at Corrosion/75 (Toronto, Canada), National Association of Corrosion Engineers, April 1975
9. R.B. Leonard, *Corrosion,* Vol 25 (No. 5), 1969, p 222–228
10. F.G. Hodge and R.W. Kirchner, Paper presented at the Fifth European Congress on Corrosion (Paris), Sept 1973
11. P.E. Manning and J.D. Schobel, Paper presented at ACHEMA '85 (Frankfurt, West Germany), 1985; See also *Werkst. Korros.,* March 1986

Corrosion of Nonferrous Alloy Weldments, *Corrosion: Fundamentals, Testing, and Protection*, Vol 13A, *ASM Handbook*, ASM International, 2003, p 317–321

Corrosion of Nonferrous Alloy Weldments

Acknowledgments

This article was adapted from K.F. Krysiak et al., Corrosion of Weldments, *Corrosion,* Vol 13, *Metals Handbook,* 9th ed., ASM International, 1987, p 344–368. The section on titanium alloys was adapted from M.J. Donachie, Jr., *Titanium: A Technical Guide,* 2nd ed., ASM International, 2000, p 123–124.

Corrosion of Nonferrous Alloy Weldments, *Corrosion: Fundamentals, Testing, and Protection*, Vol 13A, *ASM Handbook*, ASM International, 2003, p 317–321

Corrosion of Nonferrous Alloy Weldments

Acknowledgments

This article was adapted from K.F. Krysiak et al., Corrosion of Weldments, *Corrosion,* Vol 13, *Metals Handbook,* 9th ed., ASM International, 1987, p 344–368. The section on titanium alloys was adapted from M.J. Donachie, Jr., *Titanium: A Technical Guide,* 2nd ed., ASM International, 2000, p 123–124.

W. Glaeser and I.G. Wright, Forms of Mechanically Assisted Degradation, *Corrosion: Fundamentals, Testing, and Protection*, Vol 13A, *ASM Handbook*, ASM International, 2003, p 322–330

Forms of Mechanically Assisted Degradation

William Glaeser and Ian G. Wright, Battelle Columbus Laboratories

Introduction

MECHANICALLY ASSISTED DEGRADATION of metals is defined as any type of degradation that involves both a corrosion mechanism and a wear or fatigue mechanism. This article discusses five such forms of degradation: erosion, fretting, fretting fatigue, cavitation and water drop impingement, and corrosion fatigue. Only the mechanisms of these forms of degradation are discussed. The analyses of failures involving these mechanisms, as well as means of failure prevention, are detailed in *Failure Analysis and Prevention,* Volume 11 of *ASM Handbook.*

W. Glaeser and I.G. Wright, Forms of Mechanically Assisted Degradation, *Corrosion: Fundamentals, Testing, and Protection*, Vol 13A, *ASM Handbook*, ASM International, 2003, p 322–330

Forms of Mechanically Assisted Degradation

William Glaeser and Ian G. Wright, Battelle Columbus Laboratories

Erosion

Erosion can be defined as the removal of surface material by the action of numerous individual impacts of solid or liquid particles. Erosive wear should not be confused with abrasive or sliding wear, because the mechanisms of material removal, and therefore the materials selection criteria (though rudimentary), are different. In its mildest form, erosive wear manifests often as a light polishing of the upstream surfaces of components penetrating the flowstream, or of bends or other stream-deflecting structures. This is illustrated in Fig. 1, which shows carbon steel heat-transfer tubes in a fluidized-bed combustor. The tubes have been polished through the action of particles of sand impacting at a velocity of approximately 1.8 m/s (6 ft/s). The black appearance of these tubes is due to the oxide scale, which has been polished (that is, thinned) by the erosive action but not completely removed. In this case, metal wastage is probably a result of high-temperature corrosion assisted by erosion.

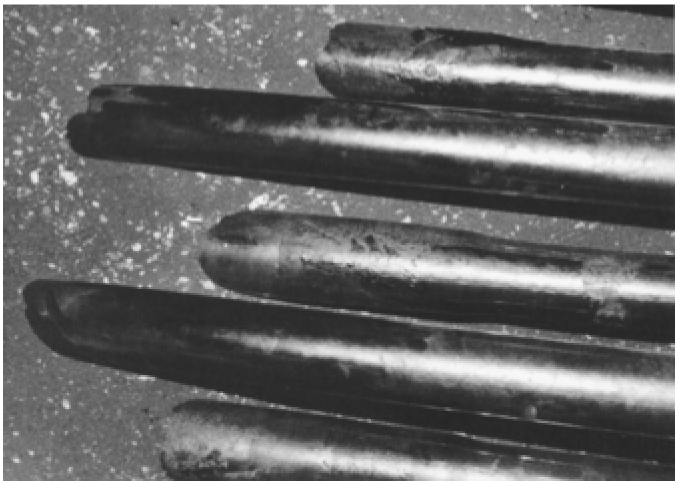

Fig. 1 Polishing of heat-transfer tubes from erosion by sand in a fluidized-bed combustor

Where the erosive action is more severe, any scales or deposits are removed, and the polished, eroded surface is base metal. Such surfaces on low-alloy steels are often very susceptible to rusting; therefore, swabbing the tubes with a damp cloth can give a useful indication of the erosion zones and patterns. Figure 2 shows such rusting on the underside of a tube from a different fluidized-bed combustor. This rusting indicates that erosion occurred in a uniform zone around the bottom of the tube, up to the 9 o'clock position.

Fig. 2 Carbon steel heat-transfer tube from a fluidized bed that was damaged by erosion and subsequent rusting

Erosion attack can be quite localized, as shown by the polished zones on the tube supports from a steam boiler (Fig. 3). Localized fly ash-laden gas flow between the tube rows (supported on the lugs) eroded through the oxide scale and polished the metal surface beneath.

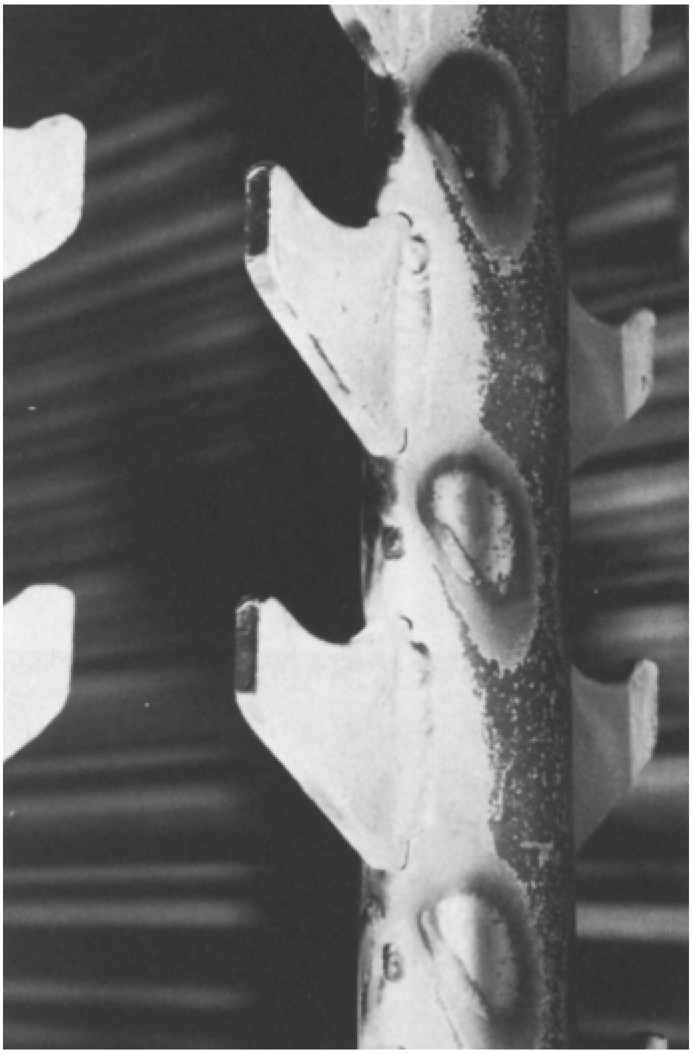

Fig. 3 Erosion of a tube support by ash-laden flue gas

In more severe cases, erosion can result in very rapid attack that quickly leads to thinning and penetration. Conditions that give rise to such rapid erosion usually involve high velocities, large amounts of entrained solid or liquid particles, and abrupt changes in direction of the fluid. These conditions can lead to segregation and concentration of the eroding particles. Examples of such rapid erosion are shown in Fig. 4, 5, 6.

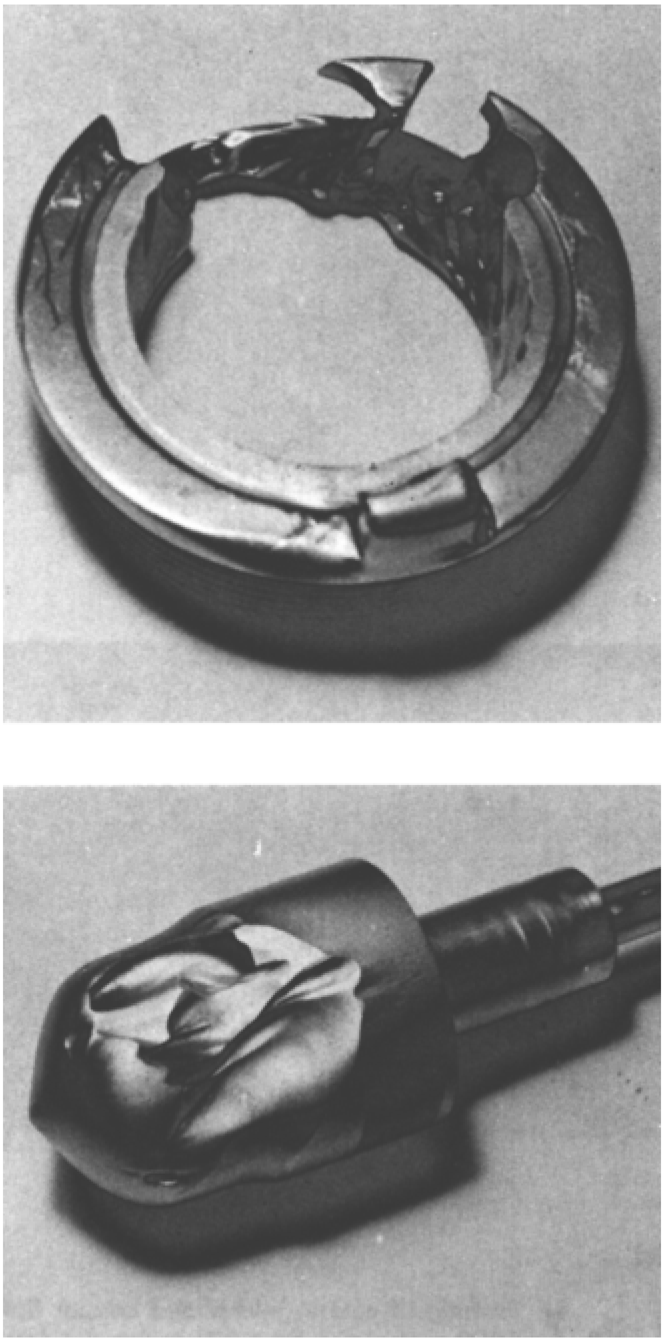

Fig. 4 Hardfaced stainless steel plug and seat, from a slurry flow control valve, that were eroded by high-velocity flow through the narrow orifice created during throttling

Fig. 5 Eroded tube inserts from the inlet end of a fire-tube boiler. The inserts were eroded by particle-laden flue gas, which was forced to turn as it entered the boiler.

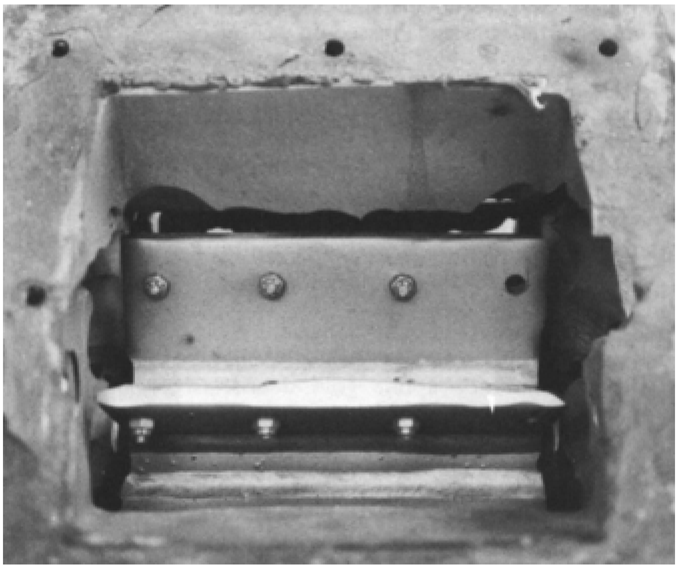

Fig. 6 Erosion of a rotary valve handling dust from a cyclone. The wear plates in the valve show some material loss, but the major damage is to the casing. Gaps between the casing and the valve allowed leakage of high-velocity air with entrained dust.

Erosion is thought typically to involve the action of a dilute dispersion of small solid (or liquid) particles entrained in a fluid jet, and it is from studies in this type of regime that most of the current understanding of erosion phenomena is derived. Strictly controlled laboratory studies of simplified systems or part processes in actual or simulated situations have provided a basis for the analysis of erosion damage produced under quite limiting circumstances: by the impacts of individual particles where particle motion is largely unconstrained in the approach to the target, during impact, and in rebounding from the target. There are many variables that can affect erosion. Important system variables are the relative velocities of the erodent and target; the angle of impact; the mass, size, size distribution, shape, hardness, and composition of the erodent particles; the number density of the particles in the conveying fluid or the frequency of impact; and the density and viscosity of the fluid.

The factors that affect the resistance of materials to erosion are difficult to define. Simple correlations of erosion rate have been attempted with target material hardness, melting temperature, elastic modulus, and so on, with some success for pure elements but less-than-universal application to steels and other alloys or ceramic materials. The relative importance of specific materials properties likely will change, depending on the predominating mechanisms of erosion, which in turn depend on any of the large number of systems variables and on the way in which the target material absorbs the energy of impact. For discrete impacts at a shallow angle to the target surface, it appears that the primary mode of material loss is through the displacement of material in the path of the erodent and the eventual loss of the displaced material by subsequent cutting or by fracture, if the material is embrittled.

This form of erosion can be equated to micromachining. The simple, elegant model discussed in Ref 1 and 2 and its refinements, relating erosion essentially to material hardness, has been found to predict erosion rates of approximately the right magnitude, even if the ability of the model to rank different alloys is sometimes poor. This model can be stated simply as:

$$\frac{\text{Erosion loss}}{\text{Quantity of impacting erodent}} = C \cdot F(\theta)\frac{\rho v^2}{\text{HV}}$$

where C is a system constant, $F(\theta)$ is a function of the angle of impact, ρ is the density of the erodent, v is the erodent velocity, and HV is the hardness of the target.

Other refinements to this model, as well as approaches to sophisticated models, have been proposed and are discussed fully in other reviews (Ref 3, 4, 5). In the later refinements (Ref 2) of this model, the velocity

dependence of erosion is increased from 2 to approximately 2.3. Nevertheless, the general relationship between erosive loss and erodent kinetic energy is not changed.

The functional relationship between erosion loss and the angle of impact is complex. For impacts at larger angles to the target surface, fluid flow considerations indicate that in most practical cases, the erodent particles actually strike the surface at a variety of shallower angles, depending on the size and velocity of the particles and the drag exerted on them by the conveying fluid. For impacts normal to the target surface, therefore, it is likely that only a small fraction of the particles actually impact at 90°. The forms of material loss involve surface displacement and cutting as well as modes that result from normal impacts. For most metallic materials, normal impacts result in indentation and local displacement of the surface by sharp particles, but less angular particles cause deformation and/or eventual fatigue, depending on the rate at which the deformation can be accommodated. Most ceramic materials suffer cracking from normal impacts; the form and extent of the cracking depend on the intensity of the impact (particle size, velocity, and shape) and on the structure of the ceramic.

Erosion models that describe erosion by deformation and fracture are based on elastic-plastic indentation fracture mechanics. The volume of the target surface removed following an individual impact usually is taken to be the volume enclosed by the radial and lateral cracks resulting from the impact. The depth of the lateral cracks can be related to the hardness of the target, while the length of the radial crack is a function of both hardness and toughness. The exact form of the relationship among erosion loss, hardness, and fracture toughness depends on assumed details of the geometry of the damage and mode of material removal. The predicted velocity dependence of erosion is usually approximately 3. Further discussion of these erosion models can be found in Ref 6 and 7.

In practice, erosive conditions cover a wide spectrum. In situations where the concentration of erodent particles is so great that the independent action of individual particles is unlikely, the form of damage may be more similar to scouring from particles embedded in a massive backing than that from discrete particle impacts. Rules derived for abrasive wear (see the article "Abrasive Wear" in *Friction, Lubrication, and Wear Technology,* Volume 18 of *ASM Handbook*) may then be more appropriate. In a large number of systems of practical importance, the density and viscosity of the carrier fluid are significantly different from those associated with airborne dilute phase erosion; therefore, the motion of the erodent particles before, during, and after impact may be quite different from that considered in most erosion models. The actual mechanisms of erosion, as well as the relationships with, for example, nominal angle of impact, may not correspond with those where air is the carrier fluid. Overall, at the present state of development, analytical relationships between systems and materials variables, as well as material loss through erosion, can be used only as a guide to the relative importance of the variables encountered. Testing under conditions that simulate accurately the situation under consideration is probably the best method of forming a basis for decision making. More information on failures caused by erosion is available in the article "Liquid Impact Erosion" in *Failure Analysis and Prevention,* Volume 11 of *ASM Handbook.*

References cited in this section

1. I. Finnie, *Wear,* Vol 3, 1960, p 87
2. I. Finnie and D.H. McFadden, *Wear,* Vol 48, 1978, p 181
3. C.M. Preece and N.H. Macmillan, *Ann. Rev. Mater. Sci.,* Vol 7, 1977, p 95
4. I.G. Wright, C.W. Price, and R.B. Herchenroeder, "High-Temperature Erosion/Corrosion of Alloys," EPRI RP-557, Electric Power Research Institute, 1978
5. W.F. Adler, Ed., *Erosion: Prevention and Useful Applications,* STP 664, American Society for Testing and Materials, 1979
6. C.M. Preece, Ed., Erosion, Vol 16, *Treatise on Materials Science and Technology,* Academic Press, 1979

7. A.G. Evans, M.E. Gulden, and M. Rosenblatt, *Proc. R. Soc. (London)*, Vol A361, 1978, p 343

W. Glaeser and I.G. Wright, Forms of Mechanically Assisted Degradation, *Corrosion: Fundamentals, Testing, and Protection*, Vol 13A, *ASM Handbook*, ASM International, 2003, p 322–330

Forms of Mechanically Assisted Degradation

William Glaeser and Ian G. Wright, Battelle Columbus Laboratories

Fretting Corrosion

Fretting corrosion is a combined wear and corrosion process in which material is removed from contacting surfaces when motion between the surfaces is restricted to very small amplitude oscillation (as low as 3 or 4 nm). Usually, the condition exists in machine components that are considered fixed and not expected to wear. Pressed-on wheels can often fret at the shaft/ wheel hole interface.

Oxidation is the most common element in the fretting process. In oxidizing systems, fine metal particles removed by adhesive wear are oxidized and trapped between the fretting surfaces. The oxides act like an abrasive (such as lapping rouge) and increase the rate of material removal. This type of fretting in ferrous alloys is recognized easily by the red material oozing from between the contacting surfaces.

Fretting can also persist in contacts where no corrosion exists. For example, gold fretting against gold produces fine gold debris. Fretting occurs in the vacuum of outer space.

A serious fretting problem that has injury potential is the loosening of wheels or flywheels from shafts or axles. Railroad car wheels, for example, are shrink fitted onto their axles. If the wheel loosens from running vibrations and comes off during operation of the train, it can cause derailment and has the potential of becoming a loose, rolling missile capable of penetrating nearby buildings.

Electrical connectors for low-current circuits are generally gold or gold-base alloys. Because of the high cost of gold, very thin electroplated gold coatings are used for contacts. Gold plate thicknesses as small as 0.25 μm (0.01 mil) are used. When electric contacts are subjected to vibrations of continual expansion and contraction from periodic thermal excursions, the small relative motion between the contacts produces fretting wear and the eventual removal of the gold plate. As the gold is removed, the substrate is subjected to atmospheric corrosion, and the contact resistance rises to intolerable levels. In addition, fretting debris becomes trapped between the surfaces and causes degraded conductivity. Fretting of electrical contacts is not anticipated in the design, and although it is common, it often comes as a surprise to the user. A typical progression of fretting damage induced between a solid gold rider on cobalt-gold-plated copper is shown in Fig. 7.

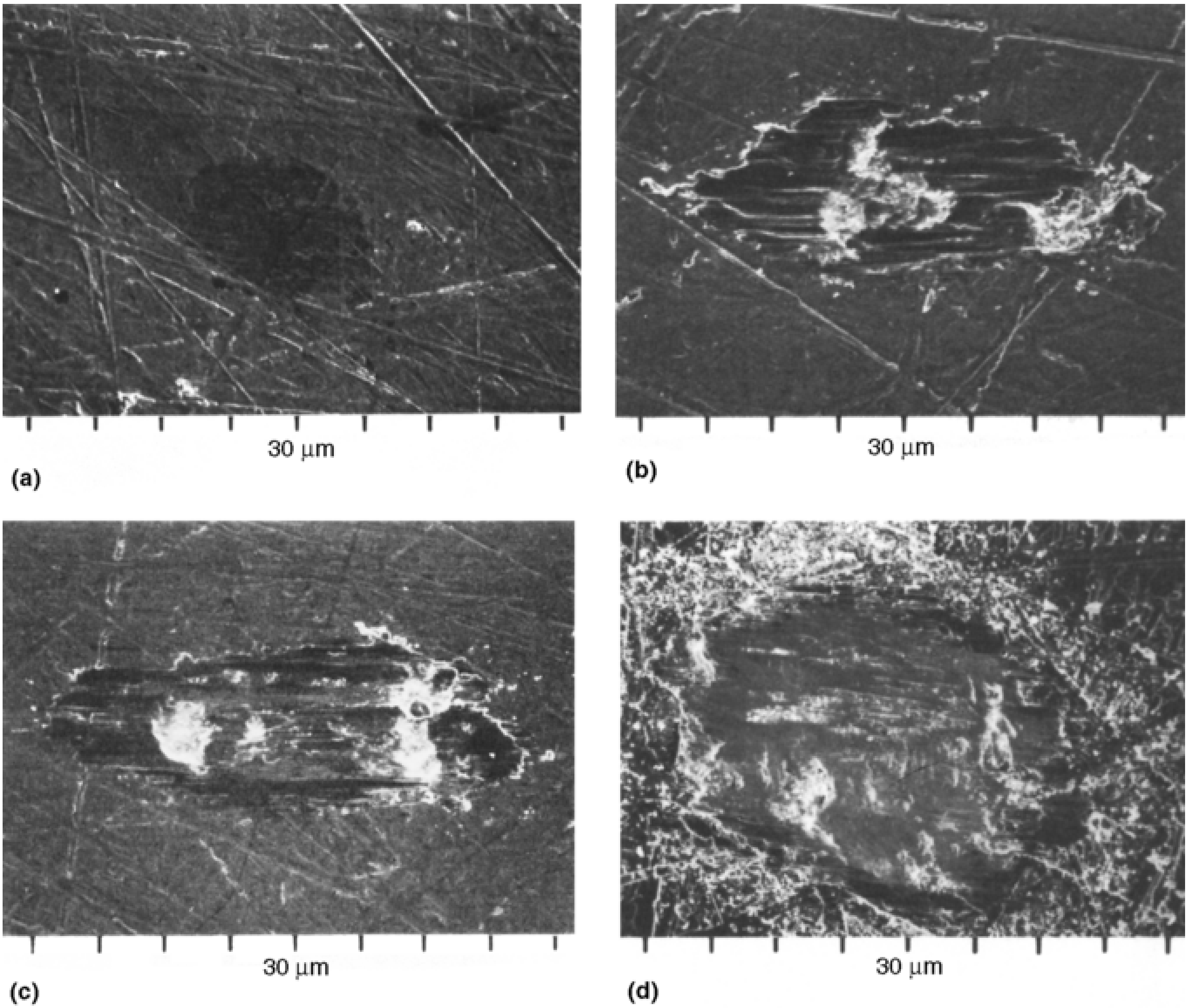

Fig. 7 Fretting of cobalt-gold-plated copper flats in contact with solid gold in an electrical contact. (a) After 1000 cycles. (b) After 10^4 cycles. (c) After 10^5 cycles. (d) After 10^6 cycles. Source: Ref 8

Fretting corrosion has been a continuing problem in nuclear reactors. The condition is found on heat-exchanger tubes and on fuel elements. In both cases, long, flexible tubes are in contact with support surfaces and subjected to vibrations generated by fluid flow as the coolant flows around them. The supports for heat-exchanger tubes and fuel elements cannot be rigid because the tubes must be able to expand or contract under thermal excursions without binding (this is also true for any tube heat-exchanger system). Tube impact fretting caused by flow-induced tube vibrations can reduce wall thickness, requiring eventual replacement. Extensive experimentation has revealed that the interaction of tube support clearance, excitation force, and type of tube motion controls wear rates (Ref 9). Other mechanical parts susceptible to fretting damage include couplings, riveted and pin joints, surgical implants, rolling-contact bearings, and bridge bearings.

Factors Affecting the Severity of Fretting Corrosion

The following factors are known to influence the severity of fretting. If fretting conditions exist, fretting cannot be eliminated completely but can be reduced in severity.

Contact Load. As long as fretting amplitude is not reduced, fretting wear increases linearly with increasing load.

Amplitude. There appears to be no measurable amplitude below which fretting does not occur. However, if the contact conditions are such that deflection is only elastic, it is not likely that fretting damage occurs. Fretting wear loss increases with amplitude. The effect of amplitude can be linear, or there can be a threshold amplitude

above which rapid increase in wear occurs (Ref 10). The transition is not well established and probably depends on the geometry of the contact.

Frequency. When the fretting is measured in volume of material removed per unit sliding distance, there does not appear to be a frequency effect.

Number of Cycles. An incubation period occurs during which fretting wear is negligible (Ref 11). After the incubation period, a steady- state wear rate is observed. Figure 8 shows local cold welding on a fretted steel surface early in the fretting process (500 cycles). As the fretting continues, a more general surface roughening occurs, as shown in Fig. 9.

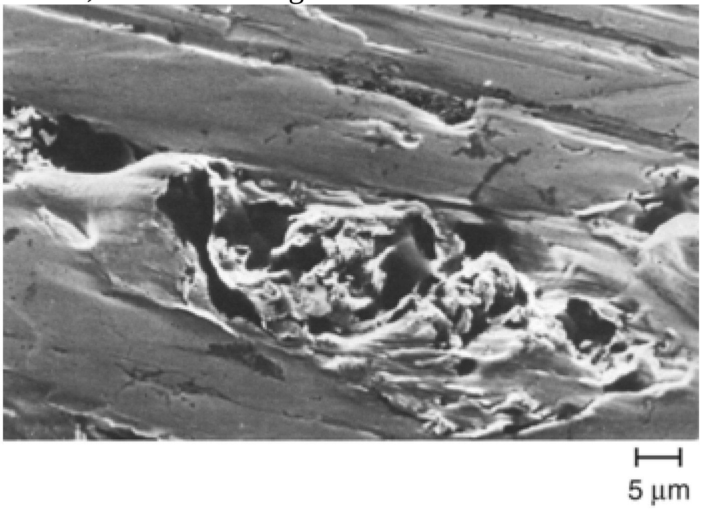

Fig. 8 Local cold welding on the surface of 0.2% C steel after 500 fretting cycles. Courtesy of R.B. Waterhouse, University of Nottingham

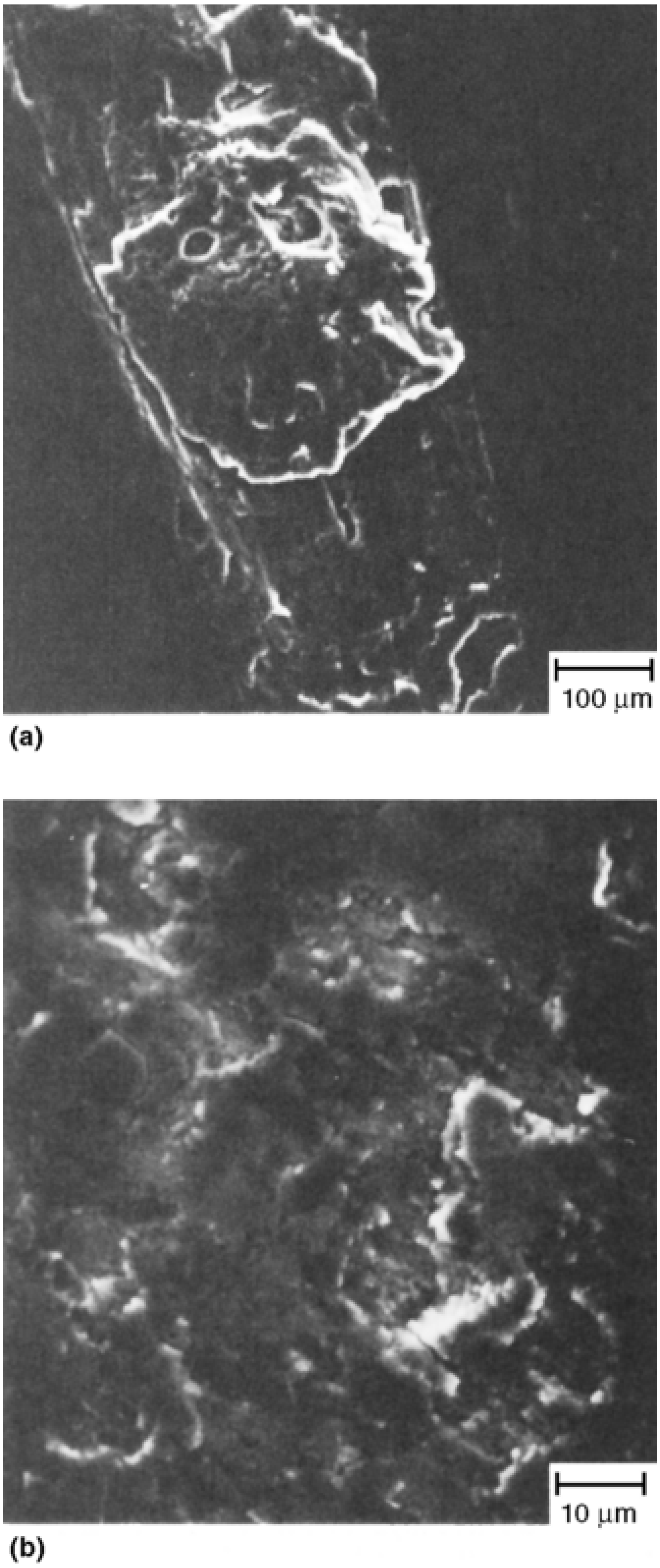

Fig. 9 Damage to Monel alloy after fretting in air at room temperature for (a) 1000 cycles and (b) 5 × 10^4 cycles. Courtesy of R.C. Bill, NASA Lewis Research Center

Relative Humidity. For materials that rust in air, fretting wear is higher in dry air than in saturated air. The effect of humidity is shown in Fig. 10 and 11. In dry air, both the iron and nickel produce debris that remains in the contact region. The debris separates the surfaces and reduces the contacts. As humidity is increased, the debris becomes more mobile, escaping the contact and allowing metal-to-metal contact, as shown in Fig. 10 and 11. Diffraction analysis of the debris from the iron surfaces shows it to be α-F_2O_3 (Ref 12).

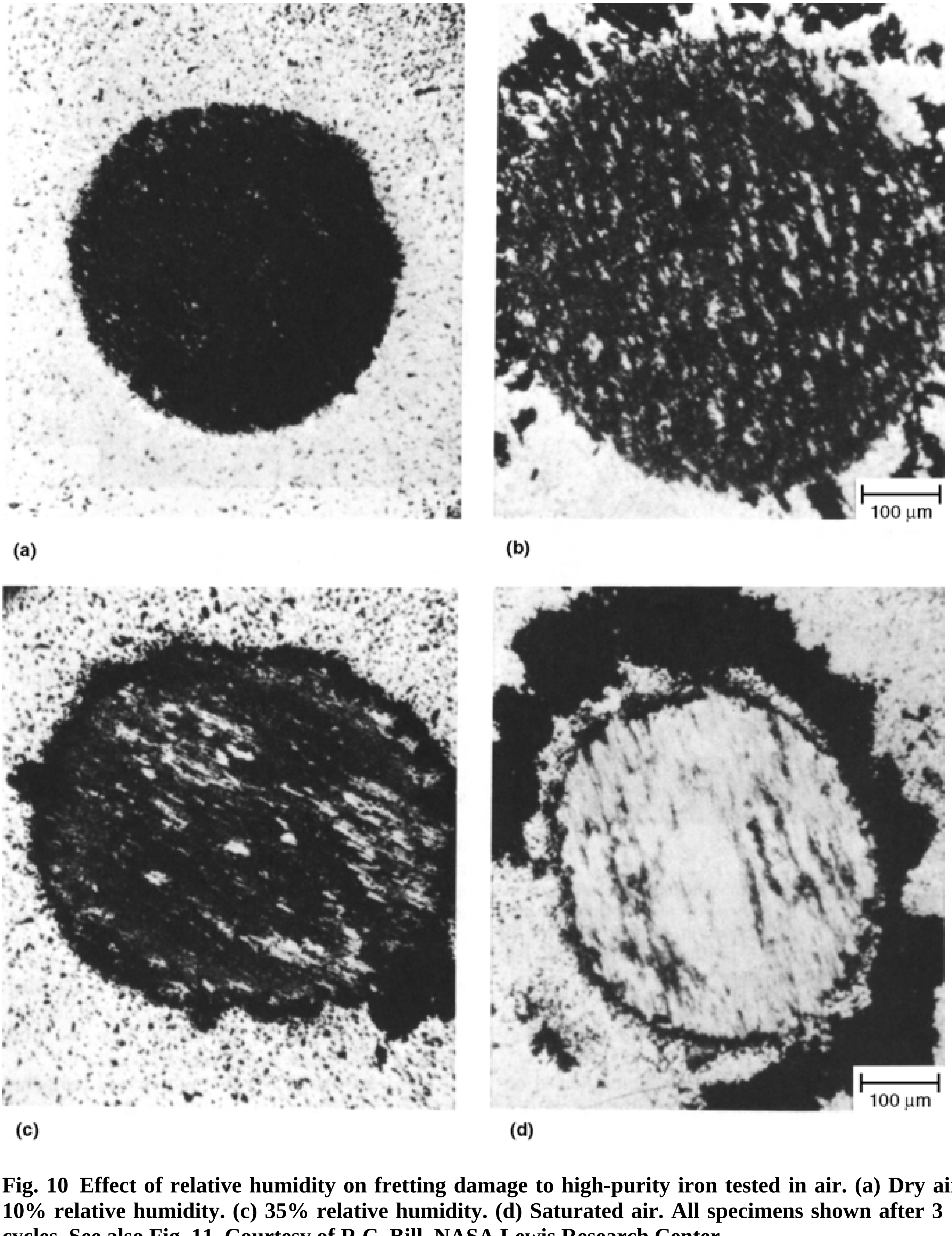

Fig. 10 Effect of relative humidity on fretting damage to high-purity iron tested in air. (a) Dry air. (b) 10% relative humidity. (c) 35% relative humidity. (d) Saturated air. All specimens shown after 3×10^5 cycles. See also Fig. 11. Courtesy of R.C. Bill, NASA Lewis Research Center

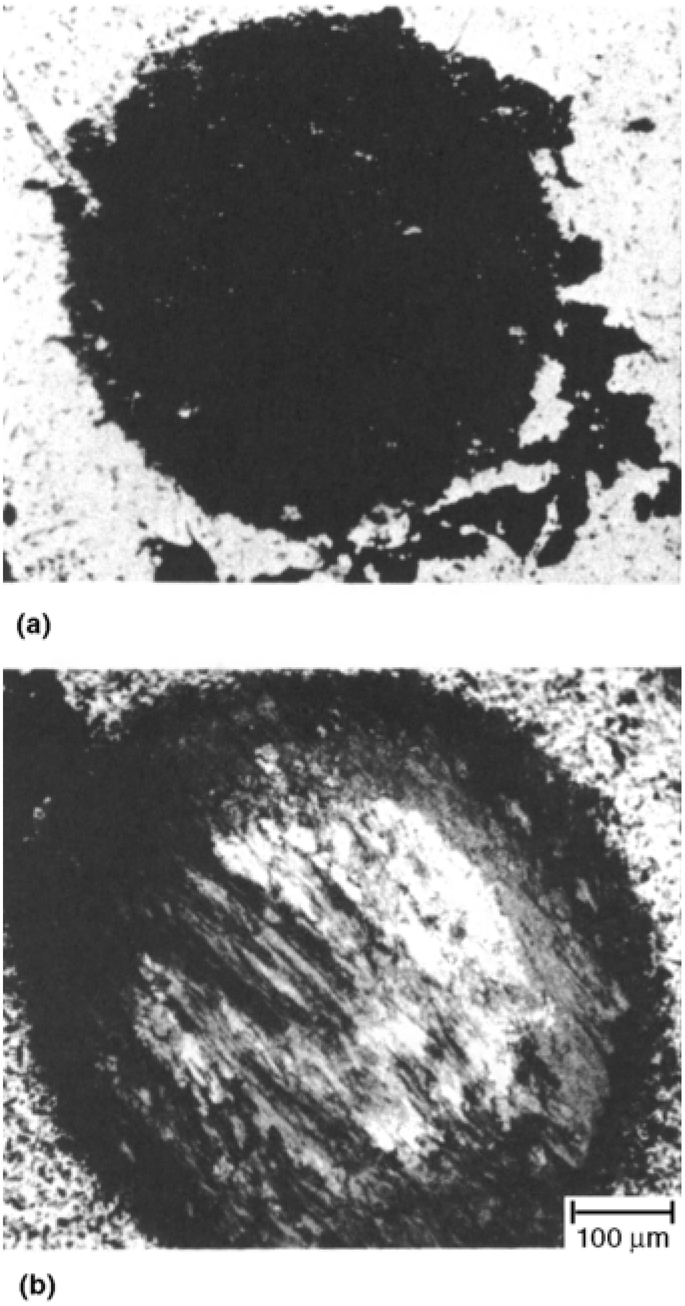

Fig. 11 Effect of relative humidity on fretting damage to high-purity nickel. Damage produced after 3 × 10^5 cycles in (a) dry air and (b) saturated air. See also Fig. 10. Courtesy of R.C. Bill, NASA Lewis Research Center

Temperature. The effect of elevated temperature on fretting depends on the oxidation characteristics of the metals. If increased temperature encourages the growth of a protective, tough oxide layer that prevents metal-to-metal contact, the fretting rate is lower. Low-carbon steel tends to show a sudden decrease in fretting wear rate at approximately 200 °C (390 °F) (Ref 13). For titanium alloys, an increase in wear rate has been observed between 350 and 500 °C (660 and 930 °F), and a rapid decrease in wear has been observed above 550 °C (1020 °F) (Ref 12, 14). Even the difference between room-temperature wear and wear at 650 °C (1200 °F) is significant (Fig. 12, 13). Figure 12 shows the surface damage from room-temperature fretting, illustrating the inadequate protection afforded by the oxide. Figure 13 shows the effect of the tough, thick oxide layer formed at 650 °C (1200 °F), which protects the metal surface. It has been shown that superalloys behave similarly to titanium at elevated temperatures (Ref 15). A glassy layer of compacted oxide particles has been found on the fretted surface after high temperature. This layer reduces the fretting wear considerably. The formation of this glassy oxide layer has been linked to an increase of 130% in fretting fatigue strength of Inconel 718 (Ref 16).

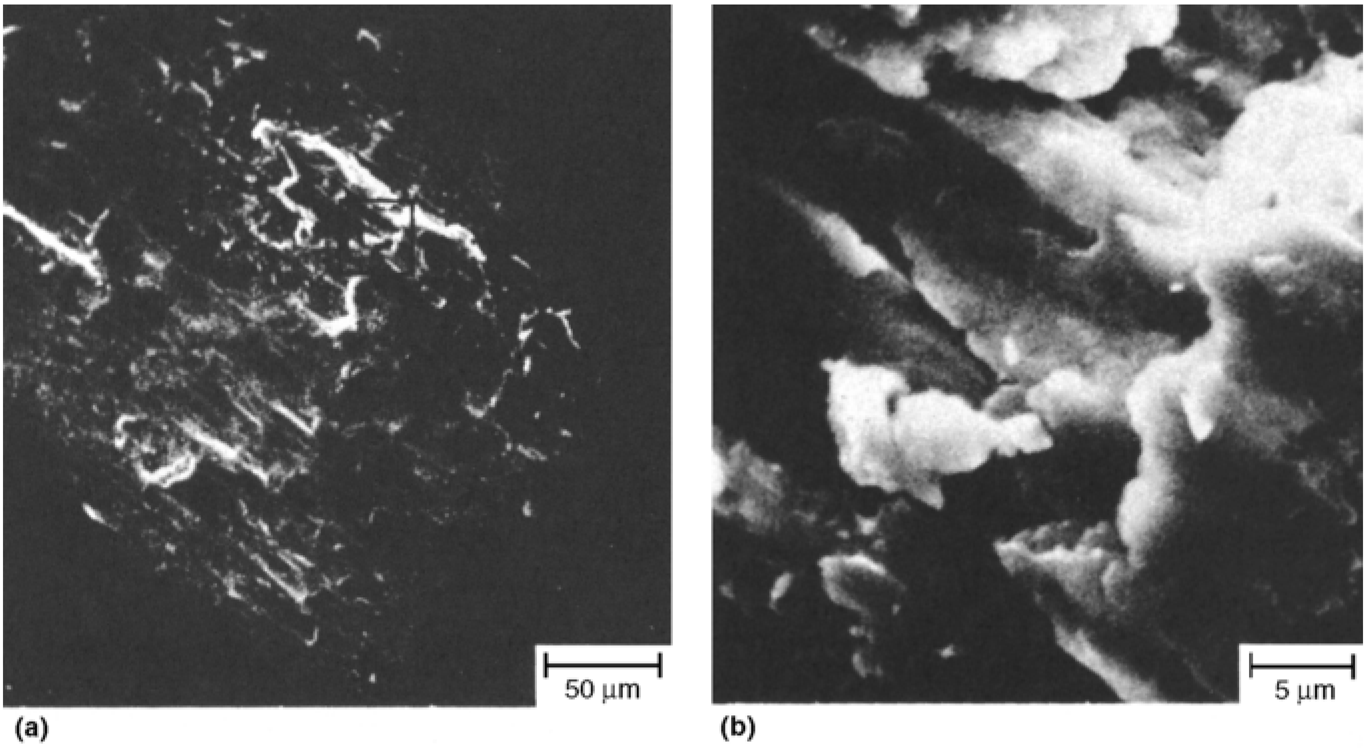

Fig. 12 Scanning electron microscope micrographs of titanium surfaces fretted at room temperature after 1000 cycles. (a) Overall view of damage. (b) Closeup of area in box in (a). Tested in air at fretting frequency of 55.8 Hz, amplitude of 70 µm, and normal load of 1.47 N (0.33 lbf). Compare with Fig. 13. Courtesy of R.C. Bill, NASA Lewis Research Center

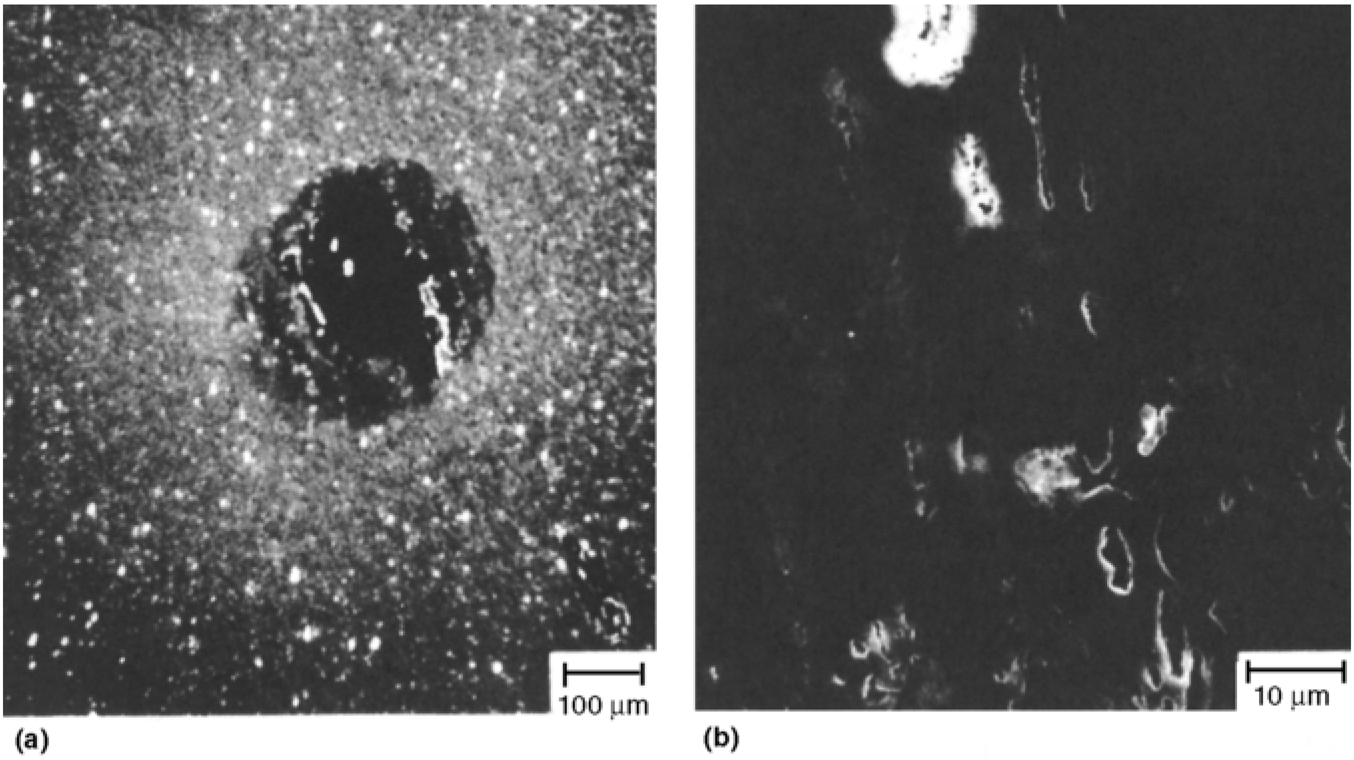

Fig. 13 Titanium surfaces fretted at 650 °C (1200 °F) after 10^5 cycles. The formation of a tough, thick oxide layer at this temperature decreased the amount of damage (compare with Fig. 12). (a) Overall view. (b) Closeup of central region. Courtesy of R.C. Bill, NASA Lewis Research Center

References cited in this section

8. M. Antler and M.H. Drozdowicz, Fretting Corrosion of Gold-Plated Connector Contacts, *Wear,* Vol 74, 1981–1982, p 27–50

9. P.L. Ko, J.H. Tromp, and M.K. Weckworth, Heat Exchanger Tube Fretting Wear: Corrosion of Tube Motion and Wear, *Materials Evaluations Under Fretting Conditions,* STP 780, American Society for Testing and Materials, 1981, p 86–105

10. R.B. Waterhouse, *Fretting Corrosion,* Pergamon Press, 1972, p 111–113

11. D.W. Hoeppner and G.L. Gross, *Wear,* Vol 27, 1974, p 61

12. R.C. Bill, Review of Factors That Influence Fretting Wear, *Materials Evaluations Under Fretting Conditions,* STP 780, American Society for Testing and Materials, 1982, p 176, 178–179

13. P.L. Hurricks, The Fretting Wear of Mild Steel from 200 °C to 500 °C, *Wear,* Vol 30, 1974, p 189

14. R.C. Bill, Technical Note TN D-7570, National Aeronautics and Space Administration, 1974

15. R.B. Waterhouse, The Fretting Wear of Nitrogen-Bearing Austenitic Stainless Steel at Temperatures to 600 °C, *Trans. ASME,* Vol 08, p 359–363

16. D.E. Taylor, Fretting Fatigue in High-Temperature Oxidizing Gases, *Fretting Fatigue,* Applied Science, 1981, p 196–201

W. Glaeser and I.G. Wright, Forms of Mechanically Assisted Degradation, *Corrosion: Fundamentals, Testing, and Protection*, Vol 13A, *ASM Handbook*, ASM International, 2003, p 322–330

Forms of Mechanically Assisted Degradation

William Glaeser and Ian G. Wright, Battelle Columbus Laboratories

---

Fretting Fatigue

Fretting decreases the fatigue life of parts operating under fatigue loading. Gas turbines experience this problem with clamped joints and shrink-fitted parts. These parts are subjected to high-frequency, low-amplitude vibrations, often in combination with bending fatigue stress states (Ref 17). The combined action of fretting and reversing bending stress causes accelerated crack initiation and an increase in the rate of crack propagation. The result is a decrease in the fatigue strength of a given alloy. The effect on 4130 steel is shown in Fig. 14. In this case, the fatigue strength of the alloy is reduced under fretting, and the sensitivity to load is increased. Fretting fatigue begins as a crack in the fretting scar zone. An example of a fretting fatigue crack is shown in Fig. 15. The crack is located at the boundary of the fretting scar. This is one attribute of fretting fatigue that identifies the origin of the fatigue. The fatigue crack, once initiated at the boundary of the fretted zone, propagates into the surface at an angle to the surface (Fig. 16). Other examples of the crack behavior are shown in Fig. 17 and 18. Wire rope can fail by fretting fatigue. As the rope flexes, wire strands rub against each other and produce fretting at the wire-wire contacts. If the fretting occurs in a zone that is also subject to cyclic fatigue stresses, failure occurs. An example of wire rope fretting fatigue is shown in Fig. 19 Note the lip in the detail micrograph in Fig. 20.

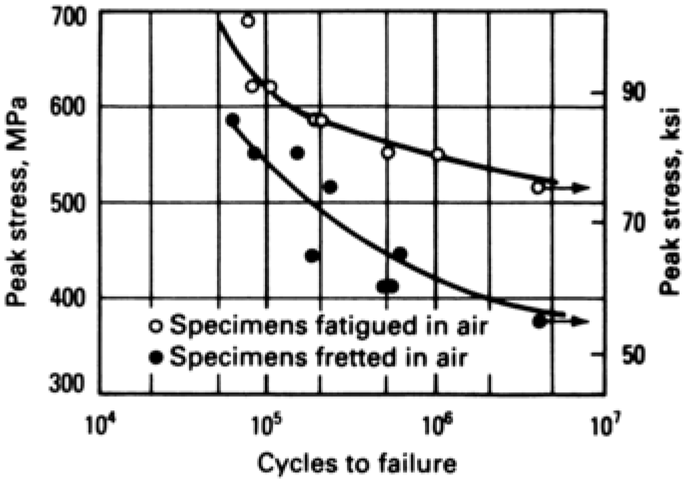

Fig. 14 Comparison of fatigue life for 4130 steel under fretting and nonfretting conditions. Specimens were water quenched from 900 °C (1650 °F), tempered 1 h at 450 °C (840 °F), and tested in tension-tension fatigue. Normal stress was 48.3 MPa (7 ksi); slip amplitude was 30 to 40 μm.

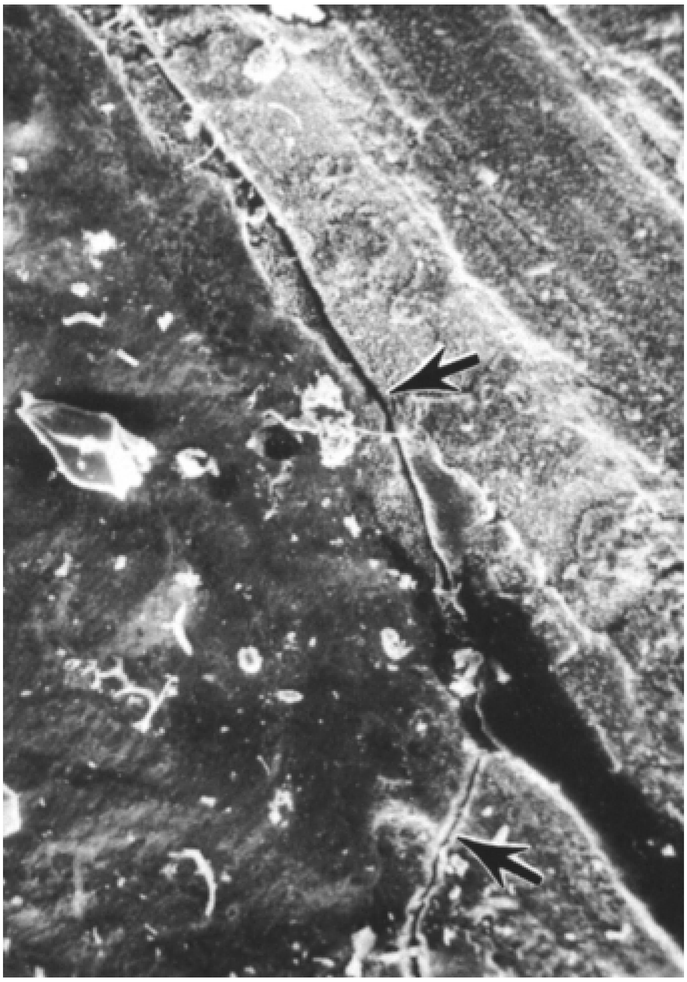

Fig. 15 Fretting scar on fatigued steel specimen showing location of fatigue crack (arrow). Source: Ref 18

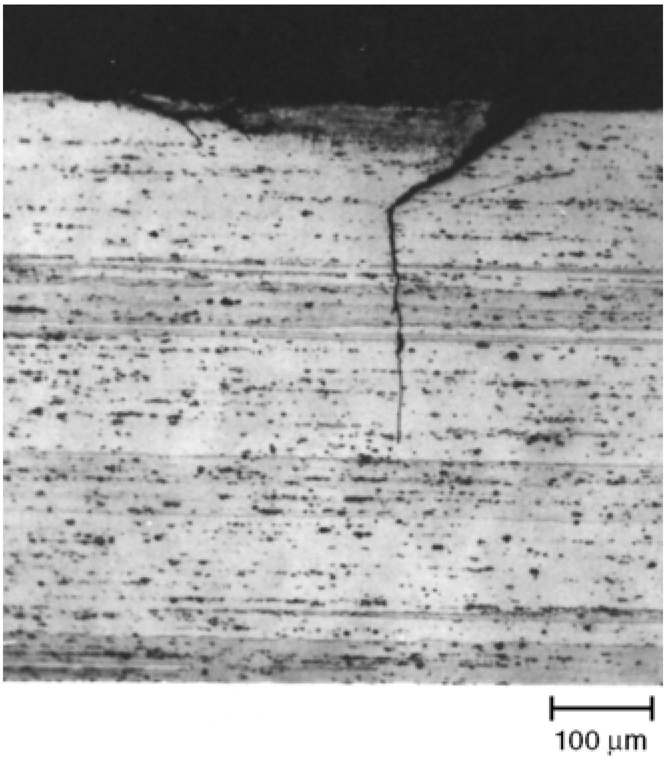

Fig. 16 Section through a bar of aged Al-4Cu alloy showing a crack initiated by fretting fatigue. Courtesy of R.B. Waterhouse, University of Nottingham

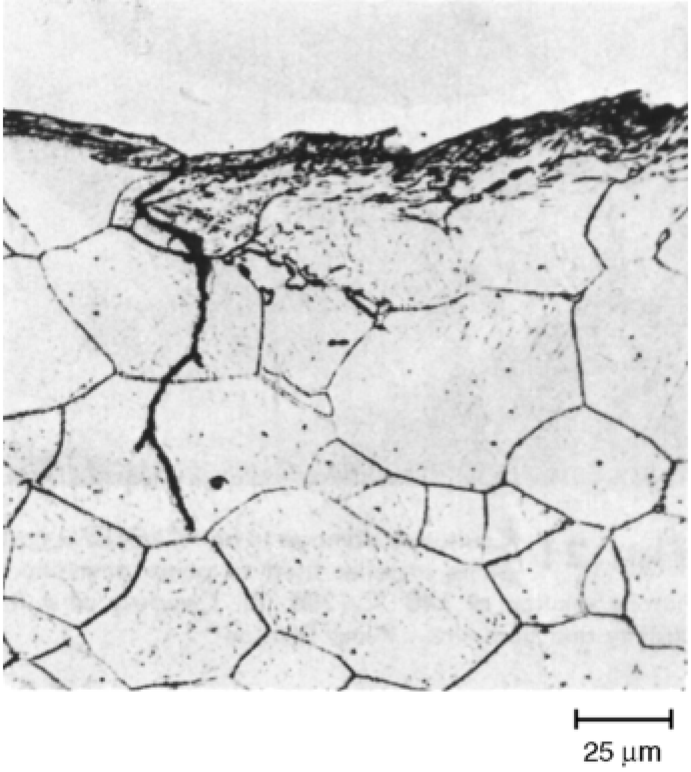

Fig. 17 Section showing fretting damage and fatigue crack initiation in 0.2% C steel. Courtesy of R.B. Waterhouse, University of Nottingham

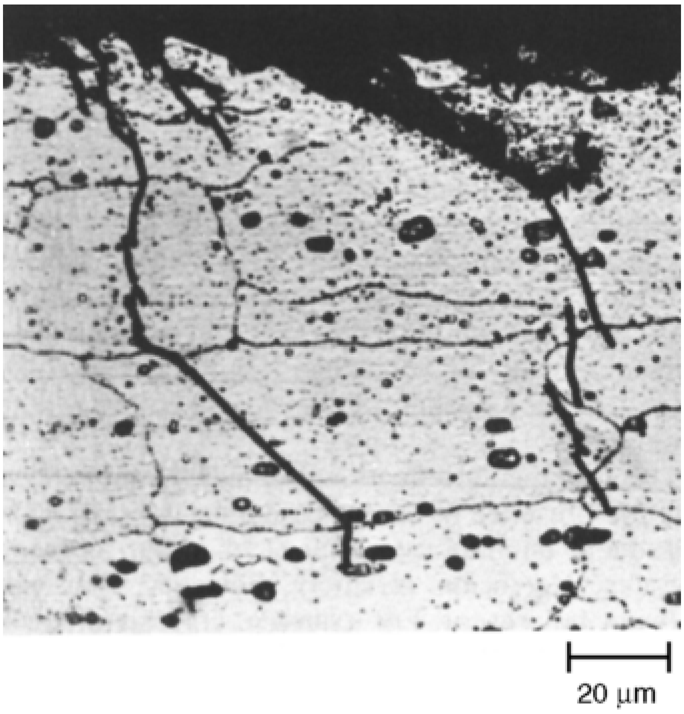

Fig. 18 Section showing fretting damage and fatigue cracks in Al-6Zn-3Mg alloy. Courtesy of R.B. Waterhouse, University of Nottingham

Fig. 19 Fretting fatigue failure of steel wire rope after seawater service. Wire diameter was 1.5 mm (0.06 in.). See also Fig. 20. Courtesy of R.B. Waterhouse, University of Nottingham

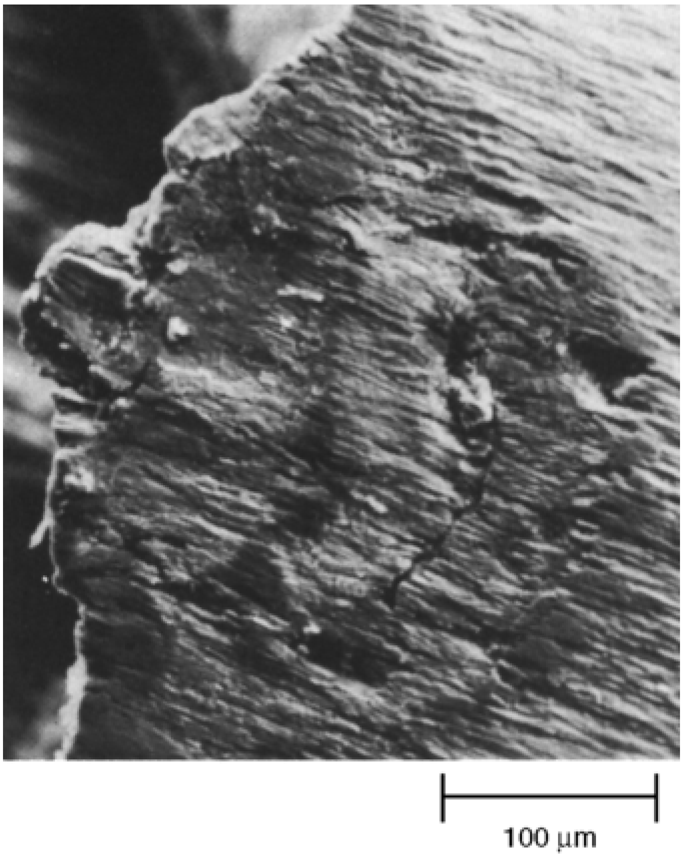

Fig. 20 Higher-magnification view of Fig. 19 showing fretting fatigue crack on the other side of the wear scar in Fig. 19. Courtesy of R.B. Waterhouse, University of Nottingham

Recently, considerable attention has been given to fretting fatigue of aircraft turbine vanes. The fretting occurs in the dovetail joints that hold the vanes in the rotor disks. The problem occurs in the compressor section of the turbine. The vanes and disks are made of titanium alloy Ti-6Al-4V. It has been shown that fretting alone can produce surface cracks in the titanium components (Ref 19). An example of fretting-generated cracks in alloy Ti-6Al-4V is shown in Fig. 21. The figure is a micrograph from a sectioned as-fretted fatigue specimen prior to fatigue testing. Note that there are several cracks oriented at an angle to the surface and that cracks are filled with debris. Some branching crystallographic cracks (shown by the arrows) can be seen. The resulting fracture has a transgranular character. Deeper into the fracture, typical fatigue striations are often found. Fretting significantly reduces the fatigue strength of the blades and disks, requiring more frequent maintenance to ensure blade integrity.

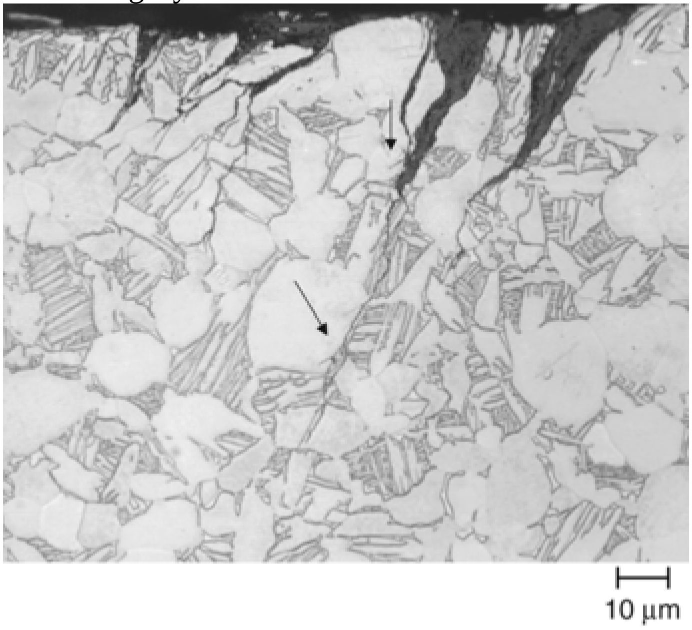

Fig. 21 Micrograph showing cracking of sectioned alloy Ti-6Al-4V fatigue specimen prefretted before fatigue testing. Arrows indicate branching crystallographic cracks.

References cited in this section

17. T.C. Lindley and K.J. Nix, The Role of Fretting in the Initiation and Early Growth of Fatigue Cracks in Turbo-Generator Materials, *Multiaxial Fatigue,* STP 853, American Society for Testing and Materials, 1982, p 340–360

18. R.B. Waterhouse, Theories of Fretting Processes, *Fretting and Fatigue,* Applied Science, 1981, p 207–211

19. W.A. Glaeser and B.H. Lawless, Behavior of Alloy Ti-6Al-4V Under Prefretting and Subsequent Fatigue Conditions, *Wear,* Vol 250, 2001, p 621–630

W. Glaeser and I.G. Wright, Forms of Mechanically Assisted Degradation, *Corrosion: Fundamentals, Testing, and Protection*, Vol 13A, *ASM Handbook*, ASM International, 2003, p 322–330

Forms of Mechanically Assisted Degradation

William Glaeser and Ian G. Wright, Battelle Columbus Laboratories

---

Cavitation Erosion and Water Drop Impingement

Cavitation erosion occurs on metal surfaces in contact with a liquid. Pressure differentials in the fluid generate gas or vapor bubbles in the fluid. When these bubbles encounter a high-pressure zone, they collapse and cause explosive shocks to the surface. These surface shocks cause localized deformation and pitting. Cavitation pits eventually link up and cause a general roughening of the surface and material removal. Cavitation is similar to particle erosion in its damage. However, surface features formed by cavitation are different from those formed by particle erosion. Cavitation produces rounded microcraters in the surface, while particle erosion produces imprints of the impacting particles. Crater formation moves surface material to the edges of the craters, and these extrusions eventually break off, causing loss of material from the surface. The sharp pressure pulses caused by the collapsing bubbles are highly localized and can remove weak or soft portions of microstructural phases (for example, ferrite from pearlite) (Ref 20).

Scattered shallow dimples or depressions are the earliest evidence of cavitation erosion in ductile surfaces. This represents an incubation period before the actual loss of material. Damage is seen first in the weaker elements of the microstructure.

Material removal is different for soft materials and hard materials. Soft materials suffer local plastic deformation and penetration. Babbitt, for example, becomes pitted with steep-sided pits that group together in patterns reflecting the fluid dynamics. Hard materials experience localized microcracking and chipping from the pressure pulses. Brittle materials, such as glass and some plastics, appear to develop surface cracking at minute surface flaws.

In materials that depend on passivating films for corrosion protection, cavitation causes an apparent accelerated attack. In a corrosive medium, the cavitation removes the protective film, and corrosion weakens the material to the mechanical removal process. Figure 22 shows cavitation damage to an Alloy Casting Institute (ACI) CN-7M stainless steel impeller that was used to pump ammonium nitrate solution at 140 °C (280 °F). Hardfacing materials and cemented carbides react differently to cavitation than to abrasion (Ref 21). The carbides are selectively eroded from the Stellite (Stoody Deloro Stellite, Inc.) alloys, while cemented carbides suffer loss of the cobalt or nickel binder. Cavitation occurs in hydraulic equipment, fluid pump impellers, ship propellers, hydrodynamic bearings, fluid seals, inlets to heat-exchanger tubes, diesel engine wet cylinder liners, hydrofoils,

liquid metal power plants, and steam turbines. Cavitation occurs in diesel engine main bearings and wrist pin bearings. Two sources have been identified in diesel bearings (Ref 22) downstream from bearings lubrication grooves and in engines subjected to rapid radial shaft movement. The reference suggests ways to design bearings to prevent cavitation.

Fig. 22 Cavitation damage to an ACI CN-7M stainless steel cast pump impeller used to pump ammonium nitrate solution at 140 °C (280 °F). Courtesy of A.R. Wilfley and Sons, Inc., Pump Division

Water drop impingement erosion is similar to cavitation in that it causes pitting of surfaces and may involve a cavitation mechanism. Two areas are most notable for water drop impingement: steam turbines and helicopter rotor blades. In turbines, condensation of steam produces droplets that are carried into the rotor blades, with consequent surface damage. Raindrop erosion on helicopter blades is the result of elastic compression waves produced by multiple impacts and their interaction; this action generates tensile stresses just below the surface and causes cracking.

Water drop impingement damage can appear to be somewhat different from cavitation damage in ductile materials. The cavities in the surface show a directionality that is related to the angle of attack of the drops.

References cited in this section

20. E.H.R. Wade and C.M. Preece, Cavitation Erosion of Iron and Steel, *Metall. Trans. A,* Vol 9, Sept 1978, p 1299–1310

21. C.J. Heathcock and A. Ball, Cavitation Erosion of Cobalt-Base Stellite Alloys, Cemented Carbides and Surface Treated Low Alloy Steels, *Wear,* Vol 74, 1981–1982, p 11–26

22. D. Brewe, Slider Bearings, *Modern Tribology Handbook,* B. Bhushan, Ed., CRC Press, 2001, p 1022–1026

W. Glaeser and I.G. Wright, Forms of Mechanically Assisted Degradation, *Corrosion: Fundamentals, Testing, and Protection,* Vol 13A, *ASM Handbook*, ASM International, 2003, p 322–330

Forms of Mechanically Assisted Degradation

William Glaeser and Ian G. Wright, Battelle Columbus Laboratories

---

Corrosion Fatigue

Corrosion fatigue occurs in metals as a result of the combined action of a cyclic stress and a corrosive environment. Corrosion fatigue is dependent on the interactions among loading, environmental, and metallurgical factors. For a given material, the fatigue strength (or fatigue life at a given maximum stress value) generally decreases in the presence of an aggressive environment. The effect varies widely, depending primarily on the particular metal-environment combination. The environment may affect the probability of fatigue crack initiation, the fatigue crack growth rate, or both. Figure 23 shows an example of corrosion fatigue failure in a Ti-6Al- 4V alloy.

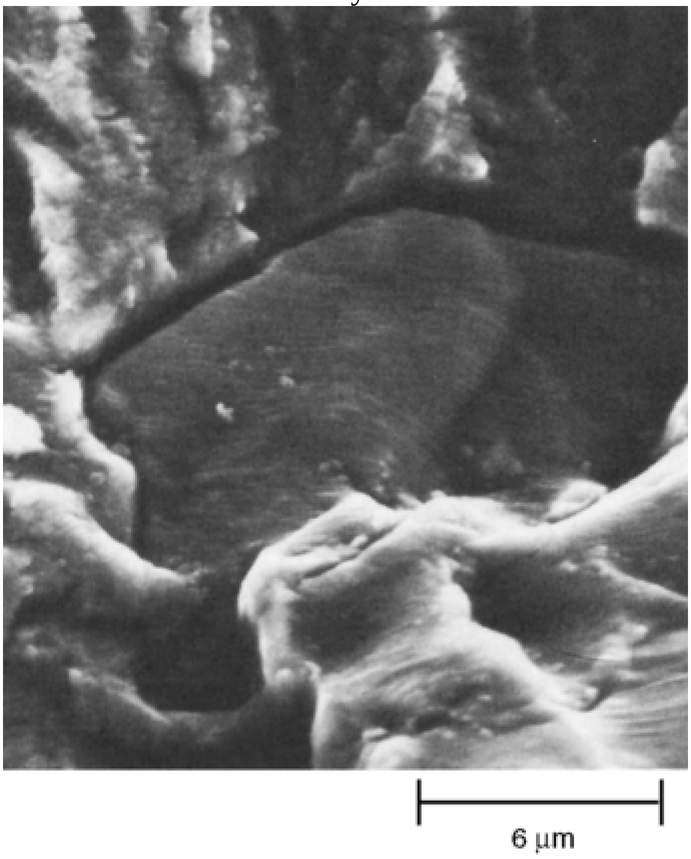

Fig. 23 Corrosion fatigue of a Ti-6Al-4V alloy tested in ambient air. Intergranular cracking and fatigue striations are evident on the fracture surface; the grain appears to have separated from the rest of the microstructure. Source: Ref 21

Corrosion Fatigue Crack Initiation. The influence of an aggressive environment on fatigue crack initiation of a material is illustrated in Fig. 24, which compares the smooth-specimen stress- life (*S-N*) curves obtained from inert and aggressive environments. Because as much as 95% of the structure life is spent on fatigue crack initiation, *S-N* curve comparison provides a good indication of the effect of environment on crack initiation. As shown in Fig. 24, an aggressive environment can promote crack initiation and can shorten the fatigue life of the structure. Corrosion fatigue cracks are always initiated at the surface, unless there are near-surface defects that act as stress concentration sites and facilitate subsurface crack initiation. Surface features at origins of corrosion fatigue cracks vary with the alloy and with specific environmental conditions. In carbon steels, cracks often originate at hemispherical corrosion pits and often contain significant amounts of corrosion products. The cracks are often transgranular and may exhibit a slight amount of branching. Surface pitting is not a prerequisite for corrosion fatigue cracking of carbon steels nor is the transgranular fracture path; corrosion fatigue cracks sometimes occur in the absence of pits and follow grain boundaries or prior-austenite grain boundaries.

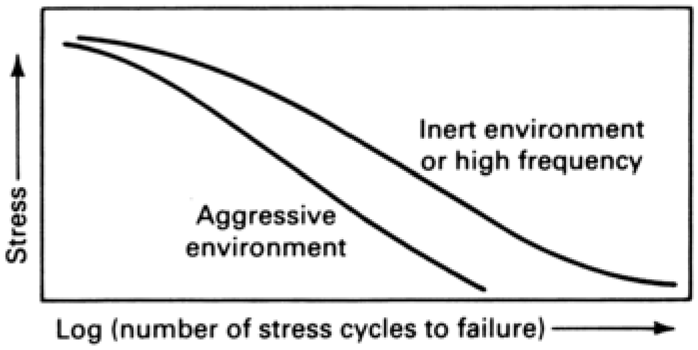

Fig. 24 Comparison of *S-N* curves for a material in an inert environment (top curve) and an aggressive environment (lower curve)

In aluminum alloys exposed to aqueous chloride solutions, corrosion fatigue cracks originate frequently at sites of pitting or intergranular corrosion. Initial crack propagation is normal to the axis of principal stress. This is contrary to the behavior of fatigue cracks initiated in dry air, where initial growth follows crystallographic planes. Initial corrosion fatigue cracking normal to the axis of principal stress also occurs in aluminum alloys exposed to humid air, but pitting is not a requisite for crack initiation.

Corrosion fatigue cracks in copper and various copper alloys initiate and propagate intergranularly. Corrosive environments have little additional effect on the fatigue life of pure copper over that observed in air, although they change the fatigue crack path from transgranular to intergranular. Copper-zinc and copper-aluminum alloys, however, exhibit a marked reduction in fatigue resistance, particularly in aqueous chloride solutions. This type of failure is difficult to distinguish from stress-corrosion cracking (SCC), except that it may occur in environments that normally do not cause failures under static stress, such as sodium chloride or sodium sulfate solutions.

Environmental effects can usually be identified by the presence of corrosion damage or corrosion products on fracture surfaces or within growing cracks. Corrosion products, however, may not always be present. For example, corrosion fatigue cracking of high-strength steel exposed to a hydrogen-producing gas, such as water vapor, may be difficult to differentiate from some other forms of hydrogen damage. At sufficiently high frequencies, the fracture surface features produced by corrosion fatigue crack initiation and propagation do not differ significantly from those produced by fatigue in nonaggressive environments.

Corrosion Fatigue Crack Propagation. Although corrosion fatigue phenomena are diverse, several variables are known to repeatedly influence crack growth rate:

- Stress-intensity range
- Load frequency
- Stress ratio
- Aqueous environment electrode potential
- Environment
- Metallurgical variables

Effects of such variables as temperature, load history and waveform, stress state, and environment composition are unique to specific materials and environments (Ref 23, 24, 25, 26, 27, 28, 29, 30, 31).

Stress-Intensity Range. For embrittling environments, crack growth generally increases with increasing stress intensity (ΔK); the precise dependence, however, varies markedly. Materials that are extremely environment-sensitive, such as ultrahigh-strength steel in distilled water (Fig. 25), are characterized by high growth rates that depend on ΔK to a reduced power. Time-dependent corrosion fatigue crack growth occurs mainly above the threshold stress intensity for static load cracking and is modeled through linear superposition of SCC and inert environment fatigue rates (Ref 31, 32).

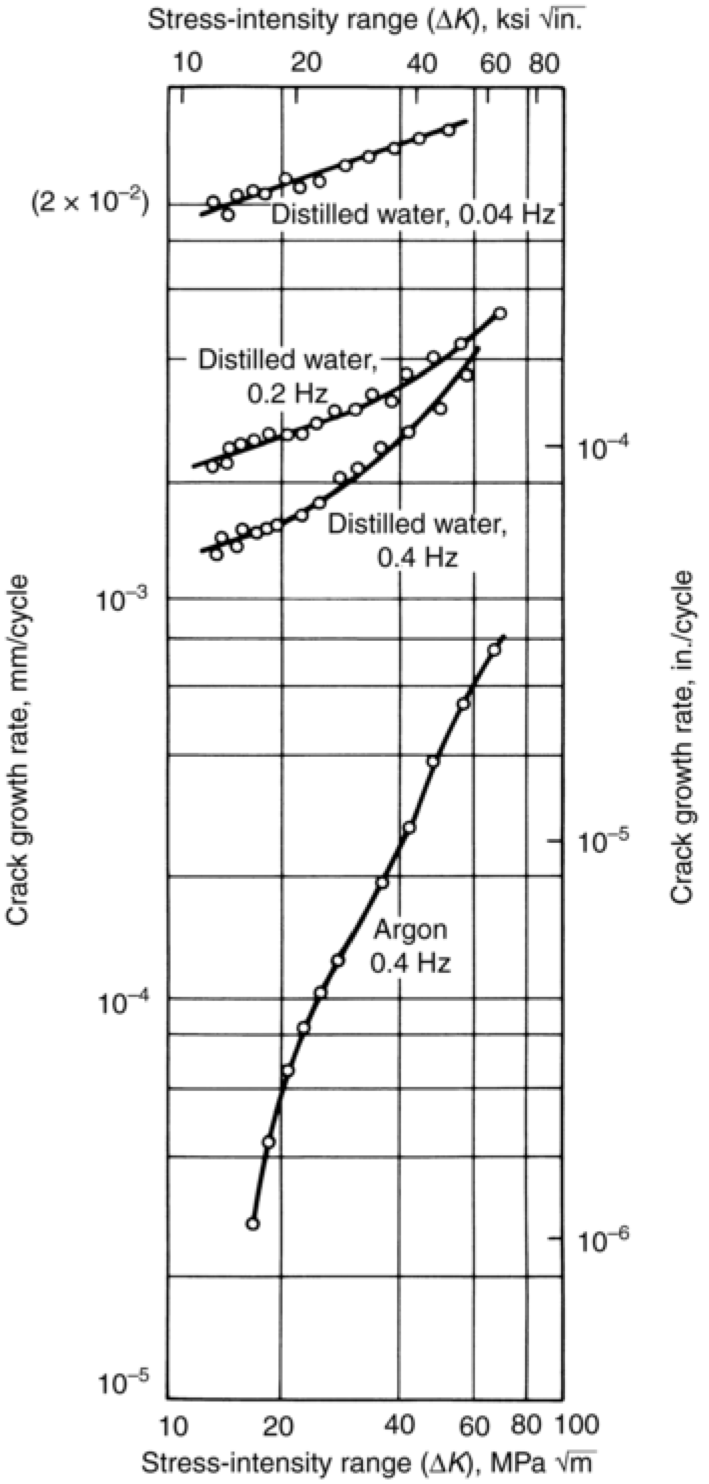

Fig. 25 Effect of stress-intensity range and loading frequency on corrosion fatigue crack growth in ultrahigh-strength 4340 steel exposed to distilled water at 23 °C (73 °F)

Frequency. Cyclic load frequency is the most important variable that influences corrosion fatigue for most material, environment, and stress- intensity conditions. The rate of brittle cracking above that produced in vacuum generally decreases with increasing frequency. Frequencies exist above which corrosion fatigue is eliminated. The dominance of frequency is related directly to the time dependence of the mass transport and chemical reaction steps required for brittle cracking. Basically, insufficient time is available for chemical embrittlement at rapid loading rates; damage is purely mechanical, equivalent to crack growth in vacuum.

Stress Ratio. Rates of corrosion fatigue crack propagation generally are enhanced by increased stress ratio, *R*, which is the ratio of the minimum stress to the maximum stress. Stress ratio has only a slight influence on fatigue crack growth rates in a benign environment.

Electrode potential, similar to loading frequency, strongly influences corrosion fatigue crack propagation rates in aqueous environments. Controlled changes in the potential of a specimen can result in either the complete elimination or the dramatic enhancement of brittle fatigue cracking. The precise influence depends on the mechanism of the environmental effect and on the anodic or cathodic magnitude of the applied potential.

Environment. Increasing the chemical activity of the environment—for example, by lowering the pH of a solution, by increasing the concentration of the corrosion species, or by increasing the pressure of a gaseous environment—generally decreases the resistance of a material to corrosion fatigue. Decreasing the chemical activity of the environment improves resistance to corrosion fatigue.

In aluminum alloys and high-strength steels, for example, corrosion fatigue behavior is related to the relative humidity or partial pressure of water vapor in the air. Corrosion fatigue crack growth rates for these materials generally increase with increasing water vapor pressure until a saturation condition is reached. Figure 26 shows the appearance of the fracture surfaces of an aluminum alloy fatigue tested in argon and in air with water vapor present. Temperature can have a significant effect on corrosion fatigue. The effect is complex and depends on temperature range and the particular material-environment combination in question, among other factors. The general tendency, however, is for fatigue crack growth rates to increase with increasing temperature.

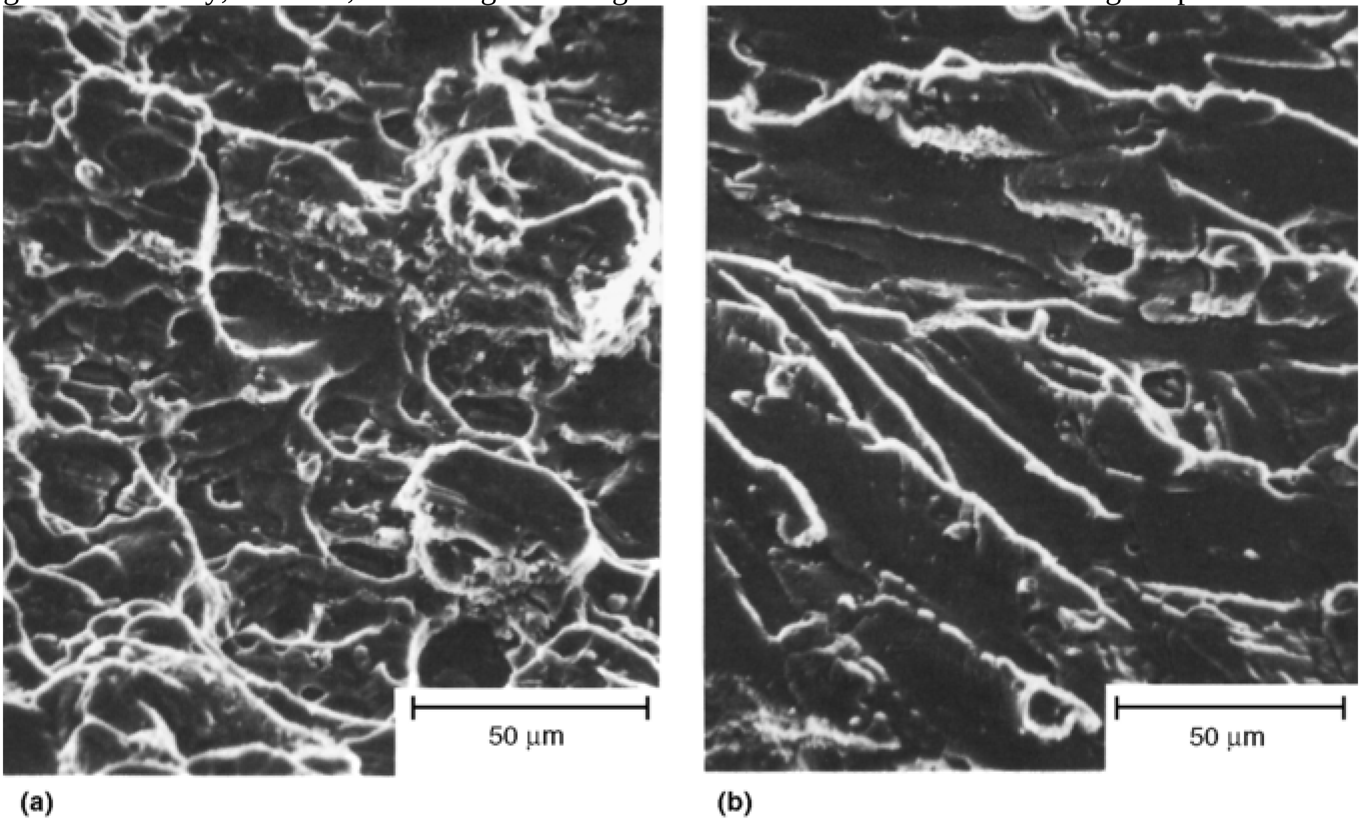

Fig. 26 Effect of water vapor on the fracture surface appearance of aluminum alloy 2219-T851 fatigue tested (a) in 0.101 MPa (1 atm) dry argon and (b) in 27 Pa (0.2 torr) water vapor. Testing conditions were the same except for frequency, which was 20 Hz in (a) and 5 Hz in (b). The magnifications, while too low to resolve fatigue striations clearly, indicate the general change in fracture morphology. Crack propagation was from left to right. Source: Ref 33

Other factors, including the metallurgical condition of the material (such as composition and heat treatment) and the loading mode (such as uniaxial), affect corrosion fatigue crack propagation. The article "Evaluating Corrosion Fatigue" in this Volume contains detailed information on testing methods and the use of fracture mechanics to predict corrosion fatigue behavior.

Relationship Between Corrosion Fatigue and SCC. The relationship between corrosion fatigue and two other environmental cracking mechanisms, SCC and hydrogen embrittlement, is shown in Fig. 27. Many investigations have attempted to link the mechanisms of corrosion fatigue and other environmental cracking processes (especially SCC); examples of these include Ref 35 to 38. There are, however, many unanswered questions about the mechanisms of these phenomena. Experimental evidence relating SCC and corrosion fatigue is presented in the article "Evaluating Corrosion Fatigue" in this Volume.

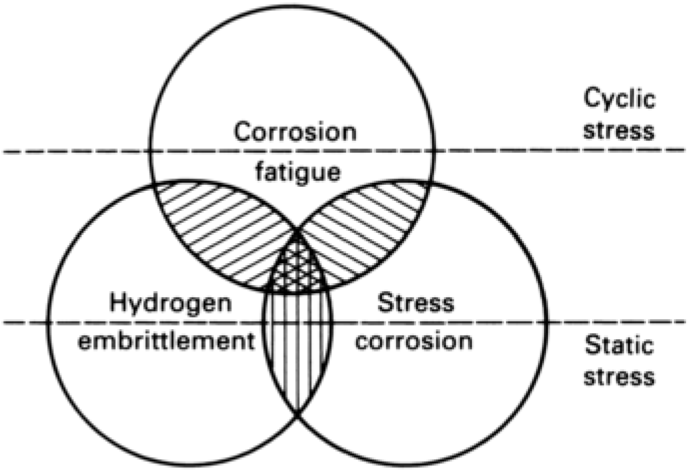

Fig. 27 Schematic showing the relationship among SCC, corrosion fatigue, and hydrogen embrittlement. Source: Ref 34

References cited in this section

21. C.J. Heathcock and A. Ball, Cavitation Erosion of Cobalt-Base Stellite Alloys, Cemented Carbides and Surface Treated Low Alloy Steels, *Wear,* Vol 74, 1981–1982, p 11–26

23. M. Yanishevsky and D.W. Hoeppner, "Corrosion Fatigue Behavior of Ti-6Al-4V in Simulated Body Environments," paper presented at the 16th Annual Technical Meeting of the International Metallographic Society, July 1983 (Calgary, Canada)

24. I.M. Bernstein and A.W. Thompson, Ed., *Hydrogen Effects in Metals,* The Metals Society of the American Institute of Mining, Metallurgical, and Petroleum Engineers, 1981

25. C.E. Jaske, J.H. Payer, and V.S. Balint, "Corrosion Fatigue of Metals in Marine Environments," MCIC Report 81-42, Battelle Columbus Laboratories, 1981

26. S.W. Dean, E.N. Pugh, and G.M. Ugiansky, Ed., *Environment-Sensitive Fracture: Evaluation and Comparison of Test Methods,* STP 821, American Society for Testing and Materials, 1984

27. Z.A. Foroulis, Ed., *Environment-Sensitive Fracture of Engineering Materials,* The Metals Society of the American Institute of Mining, Metallurgical, and Petroleum Engineers, 1978

28. J. Hochmann, J. Slater, R.D. McCright, and R.W. Staehle, Ed., *Stress-Corrosion Cracking and Hydrogen Embrittlement of Iron- Base Alloys,* NACE, 1976

29. T.W. Crooker and B.N. Leis, Ed., *Corrosion Fatigue: Mechanics, Metallurgy, Electrochemistry and Engineering,* STP 801, ASTM, 1984

30. O. Deveraux, A.J. McEvily, and R.W. Staehle, Ed., *Corrosion Fatigue: Chemistry, Mechanics and Microstructure,* NACE, 1973

31. H.L. Craig, Jr., T.W. Crooker, and D.W. Hoeppner, Ed., *Corrosion Fatigue Technology,* STP 642, ASTM, 1978

32. M.H. Kamdar, Ed., *Embrittlement by Liquid and Solid Metals,* The Metallurgical Society, 1984

33. A.J. McEvily and R.P. Wei, Fracture Mechanics and Corrosion Fatigue, *Corrosion Fatigue: Chemistry, Mechanics, and Microstructure,* O. Deveraux, A.J. McEvily, and R.W. Staehle, Ed., NACE, 1973, p 381–395

34. R.P. Wei and G. Shim, Fracture Mechanics and Corrosion Fatigue, *Corrosion Fatigue: Mechanics, Metallurgy, Electrochemistry and Engineering,* STP 801, T.W. Crooker and B.N. Leis, Ed., ASTM, 1984, p 5–25

35. R.P. Wei, P.S. Pao, R.G. Hart, T.W. Weir, and G.W. Simmons, *Metall. Trans. A,* Vol 11, 1980, p 151

38. D.A. Jones, A Unified Mechanism of Stress Corrosion and Corrosion Fatigue, *Metall. Trans. A,* Vol 16, June 1985, p 1133–1141

W. Glaeser and I.G. Wright, Forms of Mechanically Assisted Degradation, *Corrosion: Fundamentals, Testing, and Protection*, Vol 13A, *ASM Handbook*, ASM International, 2003, p 322–330

Forms of Mechanically Assisted Degradation

William Glaeser and Ian G. Wright, Battelle Columbus Laboratories

---

References

1. I. Finnie, *Wear,* Vol 3, 1960, p 87

2. I. Finnie and D.H. McFadden, *Wear,* Vol 48, 1978, p 181

3. C.M. Preece and N.H. Macmillan, *Ann. Rev. Mater. Sci.,* Vol 7, 1977, p 95

4. I.G. Wright, C.W. Price, and R.B. Herchenroeder, "High-Temperature Erosion/Corrosion of Alloys," EPRI RP-557, Electric Power Research Institute, 1978

5. W.F. Adler, Ed., *Erosion: Prevention and Useful Applications,* STP 664, American Society for Testing and Materials, 1979

6. C.M. Preece, Ed., Erosion, Vol 16, *Treatise on Materials Science and Technology,* Academic Press, 1979

7. A.G. Evans, M.E. Gulden, and M. Rosenblatt, *Proc. R. Soc. (London),* Vol A361, 1978, p 343

8. M. Antler and M.H. Drozdowicz, Fretting Corrosion of Gold-Plated Connector Contacts, *Wear,* Vol 74, 1981–1982, p 27–50

9. P.L. Ko, J.H. Tromp, and M.K. Weckworth, Heat Exchanger Tube Fretting Wear: Corrosion of Tube Motion and Wear, *Materials Evaluations Under Fretting Conditions,* STP 780, American Society for Testing and Materials, 1981, p 86–105

10. R.B. Waterhouse, *Fretting Corrosion,* Pergamon Press, 1972, p 111–113

11. D.W. Hoeppner and G.L. Gross, *Wear,* Vol 27, 1974, p 61

12. R.C. Bill, Review of Factors That Influence Fretting Wear, *Materials Evaluations Under Fretting Conditions,* STP 780, American Society for Testing and Materials, 1982, p 176, 178–179

13. P.L. Hurricks, The Fretting Wear of Mild Steel from 200 °C to 500 °C, *Wear,* Vol 30, 1974, p 189

14. R.C. Bill, Technical Note TN D-7570, National Aeronautics and Space Administration, 1974

15. R.B. Waterhouse, The Fretting Wear of Nitrogen-Bearing Austenitic Stainless Steel at Temperatures to 600 °C, *Trans. ASME,* Vol 08, p 359–363

16. D.E. Taylor, Fretting Fatigue in High-Temperature Oxidizing Gases, *Fretting Fatigue,* Applied Science, 1981, p 196–201

17. T.C. Lindley and K.J. Nix, The Role of Fretting in the Initiation and Early Growth of Fatigue Cracks in Turbo-Generator Materials, *Multiaxial Fatigue,* STP 853, American Society for Testing and Materials, 1982, p 340–360

18. R.B. Waterhouse, Theories of Fretting Processes, *Fretting and Fatigue,* Applied Science, 1981, p 207–211

19. W.A. Glaeser and B.H. Lawless, Behavior of Alloy Ti-6Al-4V Under Prefretting and Subsequent Fatigue Conditions, *Wear,* Vol 250, 2001, p 621–630

20. E.H.R. Wade and C.M. Preece, Cavitation Erosion of Iron and Steel, *Metall. Trans. A,* Vol 9, Sept 1978, p 1299–1310

21. C.J. Heathcock and A. Ball, Cavitation Erosion of Cobalt-Base Stellite Alloys, Cemented Carbides and Surface Treated Low Alloy Steels, *Wear,* Vol 74, 1981–1982, p 11–26

22. D. Brewe, Slider Bearings, *Modern Tribology Handbook,* B. Bhushan, Ed., CRC Press, 2001, p 1022–1026

23. M. Yanishevsky and D.W. Hoeppner, "Corrosion Fatigue Behavior of Ti-6Al-4V in Simulated Body Environments," paper presented at the 16th Annual Technical Meeting of the International Metallographic Society, July 1983 (Calgary, Canada)

24. I.M. Bernstein and A.W. Thompson, Ed., *Hydrogen Effects in Metals,* The Metals Society of the American Institute of Mining, Metallurgical, and Petroleum Engineers, 1981

25. C.E. Jaske, J.H. Payer, and V.S. Balint, "Corrosion Fatigue of Metals in Marine Environments," MCIC Report 81-42, Battelle Columbus Laboratories, 1981

26. S.W. Dean, E.N. Pugh, and G.M. Ugiansky, Ed., *Environment-Sensitive Fracture: Evaluation and Comparison of Test Methods,* STP 821, American Society for Testing and Materials, 1984

27. Z.A. Foroulis, Ed., *Environment-Sensitive Fracture of Engineering Materials,* The Metals Society of the American Institute of Mining, Metallurgical, and Petroleum Engineers, 1978

28. J. Hochmann, J. Slater, R.D. McCright, and R.W. Staehle, Ed., *Stress-Corrosion Cracking and Hydrogen Embrittlement of Iron- Base Alloys,* NACE, 1976

29. T.W. Crooker and B.N. Leis, Ed., *Corrosion Fatigue: Mechanics, Metallurgy, Electrochemistry and Engineering,* STP 801, ASTM, 1984

30. O. Deveraux, A.J. McEvily, and R.W. Staehle, Ed., *Corrosion Fatigue: Chemistry, Mechanics and Microstructure,* NACE, 1973

31. H.L. Craig, Jr., T.W. Crooker, and D.W. Hoeppner, Ed., *Corrosion Fatigue Technology,* STP 642, ASTM, 1978

32. M.H. Kamdar, Ed., *Embrittlement by Liquid and Solid Metals,* The Metallurgical Society, 1984

33. A.J. McEvily and R.P. Wei, Fracture Mechanics and Corrosion Fatigue, *Corrosion Fatigue: Chemistry, Mechanics, and Microstructure,* O. Deveraux, A.J. McEvily, and R.W. Staehle, Ed., NACE, 1973, p 381–395

34. R.P. Wei and G. Shim, Fracture Mechanics and Corrosion Fatigue, *Corrosion Fatigue: Mechanics, Metallurgy, Electrochemistry and Engineering,* STP 801, T.W. Crooker and B.N. Leis, Ed., ASTM, 1984, p 5–25

35. R.P. Wei, P.S. Pao, R.G. Hart, T.W. Weir, and G.W. Simmons, *Metall. Trans. A,* Vol 11, 1980, p 151

36. F.P. Ford, Current Understanding of the Mechanism of Stress Corrosion and Corrosion Fatigue, *Environment-Sensitive Fracture: Evaluation and Comparison of Test Methods,* STP 821, S.W. Dean, E.N. Pugh, and G.M. Ugianski, Ed., ASTM, 1984, p 32–51

37. R.P. Gangloff, Ed., Embrittlement by the Localized Crack Environment, *Proceedings of the Symposium on Localized Crack Chemistry and Mechanics in Environment- Assisted Cracking,* Oct 1983 (Philadelphia, PA), The Metallurgical Society, 1984

38. D.A. Jones, A Unified Mechanism of Stress Corrosion and Corrosion Fatigue, *Metall. Trans. A,* Vol 16, June 1985, p 1133–1141

W. Glaeser and I.G. Wright, Forms of Mechanically Assisted Degradation, *Corrosion: Fundamentals, Testing, and Protection*, Vol 13A*, ASM Handbook,* ASM International, 2003, p 322–330

Forms of Mechanically Assisted Degradation

William Glaeser and Ian G. Wright, Battelle Columbus Laboratories

---

Selected References

- Forms of Corrosion: Recognition and Prevention, *Corrosion: Understanding the Basics,* J.R. Davis, Ed., ASM International, 2000, p 99–192
- C.M. Hansson and I.L.H. Hansson, Cavitation Erosion, *Friction, Lubrication, and Wear Technology,* Vol 18, *ASM Handbook,* ASM International, 1992, p 214–220
- H.M. Herro and R.D. Port, Cavitation Damage, *The Nalco Guide to Cooling Water System Failure Analysis,* McGraw-Hill, 1993, p 270–271
- B.W. Madsen, Corrosive Wear, *Friction, Lubrication, and Wear Technology,* Vol 18, *ASM Handbook,* ASM International, 1992, p 271–279
- R.B. Waterhouse, Fretting Wear, *Friction, Lubrication, and Wear Technology,* Vol 18, *ASM Handbook,* ASM International, 1992, p 242–256

I. Iwasaki, Aqueous Corrosion-Wear Interactions, *Corrosion: Fundamentals, Testing, and Protection*, Vol 13A, *ASM Handbook*, ASM International, 2003, p 331–337

Aqueous Corrosion-Wear Interactions

Iwao Iwasaki, University of Minnesota Duluth

Introduction

WEAR AND CORROSION of slurry-handling equipment cause major maintenance problems, constituting a major cost for the mining and mineral processing industries. Wear and corrosion processes are complex—dependent on mechanical, physical, chemical, and electrochemical actions—not only on ferrous materials, but also on the minerals that come in contact with them. Collisions of mineral particles cause erosion of the surface and removal of corrosion resistant films, resulting in accelerated corrosion. Synergistic effects between erosion and corrosion have been extensively studied, leading to the formulation of the ASTM G 119, "Determining Synergism Between Wear and Corrosion" (Ref 1). Electroactive mineral particles, typically sulfide minerals, can galvanically couple with ferrous materials and further accelerate their corrosion. Conversely, the surface properties of mineral particles are altered and their beneficiation behaviors can be adversely affected. Wear is a critical issue in grinding mills and is also pertinent in sand pumps and slurry pipelines.

Grinding precedes concentration processes in the beneficiation of minerals. Rod mills and ball mills are used most widely in the mineral processing industry for grinding. As available mineral deposits become lower in grade, a finer grind for liberation is required. Power consumption per ton of concentrates produced increases, and the wear of balls used in fine grinding is increased in proportion to the increase in power consumption. The cost of grinding media wear often approaches or even exceeds the power cost of grinding (Ref 2, 3). In the United States, 28.5×10^9 kWh of electricity and 1 million tons of grinding media are used each year in grinding minerals, coal, and cement (Ref 4). Therefore, the reduction of wear of grinding media is just as important as the reduction in power consumption.

Within a ball mill, some of the balls are lifted, and falling balls impact among themselves. The rest of the balls are rolling against each other, causing abrasion of their surfaces. Both impact and abrasion lead to the grinding of mineral particles and the wear of grinding balls. The wear of grinding balls in wet grinding mills has been attributed to abrasion, corrosion, and impact, but their contributions to overall wear is not well established. Impact wear is an important problem in large operating mills, but it is not observed in laboratory ball mills. Abrasive wear also is claimed to become more important than corrosive wear in large industrial mills with much larger fall height (Ref 5).

The following three points are addressed from the results observed in laboratory ball mills:

- Relative significance of corrosion and abrasion
- Mechanism by which the galvanic interaction between grinding balls and mineral particles not only accelerates the ball wear but also adversely affects the flotation of minerals
- Guidelines for developing abrasion and corrosion resistant grinding media materials that are cost effective and do not adversely affect the flotation of minerals

References cited in this section

1. "Standard Guide for Determining Synergism between Wear and Corrosion," G 119- 93, *Annual Book of ASTM Standards*, ASTM International, 1993

2. F.D. DeVaney and M.H. Coghill, The Relation of Ball Wear to Power in Grinding, *Eng. Min. J.*, Vol 138, 1937, p 337–340

3. I. Iwasaki, J.J. Moore, and L.A. Lindeke, Effect of Ball Mill Size on Media Wear, *Miner. Metall. Process.,* Vol 4, 1987, p 160–166
4. *Comminution and Energy Consumption,* National Academy of Sciences, Washington, D.C., 1981, p 27
5. J.J. Moore and I. Iwasaki, The Role of Abrasion and Corrosion in Grinding Media Wear, DOE/ID/12441-T1, Vol 1, Office of Scientific and Technical Information, United States Department of Energy, 1986, 137 p

---

I. Iwasaki, Aqueous Corrosion-Wear Interactions, *Corrosion: Fundamentals, Testing, and Protection*, Vol 13A, *ASM Handbook*, ASM International, 2003, p 331–337

Aqueous Corrosion-Wear Interactions

Iwao Iwasaki, University of Minnesota Duluth

Methods of Wear Measurements

Corrosive wear may be estimated from total wear if abrasive wear can be experimentally measured. For measurements of abrasive wear, the following four methods have been considered (Ref 6, 7, 8).

- In dry grinding, corrosion does not occur. However, the grinding mechanism is fundamentally different between dry and wet grinding. Wear in dry grinding cannot be used directly to represent abrasive wear in wet grinding. In wet grinding, ball surfaces are coated with slurries at all times, whereas in dry grinding, mineral particles do not stick to the surface of balls and the grinding proceeds mainly between mill walls and balls. As a result, the grinding efficiency is often quite low. When an ore contains some minerals with hydroxyl radicals, such as amphiboles and pyroxenes, the moisture released by grinding packs mineral particles around balls and the grinding process is in effect halted.
- Corrosion does not occur if an organic liquid with low electrical conductivity is used in place of water. The mechanism of grinding, however, appears to be different from that in water under seemingly identical conditions. Slurry rheology is thought to influence the grinding efficiency and wear.
- Corrosion may be suppressed by using corrosion inhibitors or by raising the pH. However, if the slurry is dispersed or flocculated by the addition of these reagents, ball wear is affected. Slurry rheology markedly influences wear behavior.
- A nitrogen atmosphere suppresses corrosion. As iron is an active metal, corrosion can occur even in a nitrogen atmosphere. However, the influence of corrosion is minimal and slurry rheology is not affected, so this is considered the most suitable method of estimating abrasive wear.

Several idealized methods have been used to investigate the effects of erosion/abrasion and corrosion in the wear of grinding balls, but it is difficult to correlate directly to plant practice. Marked ball wear tests are capable of providing test data close to practice (Ref 9). In this method, a sufficient number of marked balls are mixed with a regular charge of balls in a ball mill, and the weight decrease of the marked balls is measured after a certain time of grinding. In a laboratory scale, a 203 mm (8 in.) diameter porcelain mill charged with 126 balls of 25 mm (1 in.) diameter, of which about a dozen balls are marked, may be used (Ref 10, 11).

Ball wear data after dry and wet grinding using the marked ball wear test, plotted against grinding time, remain a straight line for well over 2 h, indicating that wear rates stayed constant over an extended period of time. The size distributions of the ground minerals, however, show that dry ground minerals are appreciably coarser than wet ground minerals (Ref 6, 7, 11). By determining the surface areas of the ground minerals using an air permeability method, ball wear is plotted against the surface-area increase by grinding (Fig. 1). In the figure, it is evident that wet grinding gives a notably larger surface-area increase than dry grinding. Such an observation

suggests that the mechanisms of dry and wet grinding are fundamentally different, and abrasive wear under dry grinding cannot represent the wear under wet grinding.

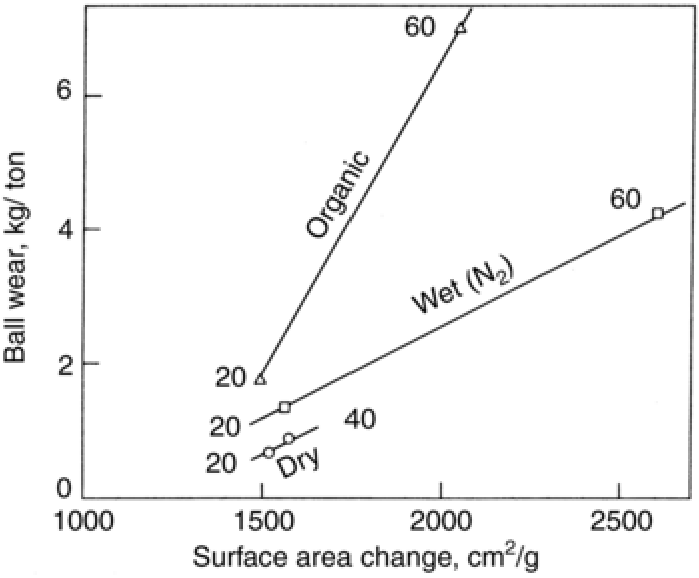

Fig. 1 Mild steel ball wear as a function of surface area change of ground magnetic taconite. On ends of plotted lines are the grinding times in minutes. Source Ref 6, 7, 10.

In Fig. 1, the results for organic liquid indicate that even though the wear rate is notably higher, the sample is not ground as fine as when water is used in grinding (Ref 11). Apparently, this wear behavior reflects the effect of slurry rheology on ball wear.

References cited in this section

6. I. Iwasaki, S.C. Riemer, J.N. Orlich, and K.A. Natarajan, Corrosive and Abrasive Wear in Ore Grinding, *Wear,* Vol 103, 1985, p 253–267

7. I. Iwasaki, R.L. Pozzo, K.A. Natarajan, K. Adam, and J.N. Orlich, Nature of Corrosive and Abrasive Wear in Ball Mill Grinding, *Int. J. Miner. Process.,* Vol 22, 1988, p 345–360

8. R.L. Pozzo and I. Iwasaki, Pyrite-Pyrrhotite-Grinding Media Interactions and Their Effects on Media Wear and Flotation, *J. Electrochem. Soc.,* Vol 136 (No. 6), 1989, p 1734–1740

9. T.E. Norman and C.M. Loeb, Jr., Wear Tests on Grinding Balls, *Trans. AIME,* Vol 176, 1948, p 490–520

10. K.A. Natarajan, S.C. Riemer, and I. Iwasaki, Ball Wear in Magnetic Taconite Grinding, Paper 19-1, *Proc. of 44th Annual Mining Symposium,* Center for Continuation Study, University of Minnesota, 1983

11. R. Perez and J.J. Moore, The Application of the Scanning Electron Microscope in Determining the Interaction of Abrasion and Corrosion in Mineral Grinding Media, *Microstruct. Sci.,* Vol 2, 1983, p 207–234

I. Iwasaki, Aqueous Corrosion-Wear Interactions, *Corrosion: Fundamentals, Testing, and Protection*, Vol 13A, *ASM Handbook*, ASM International, 2003, p 331–337

Aqueous Corrosion-Wear Interactions

Iwao Iwasaki, University of Minnesota Duluth

Model of Corrosive Wear

Corrosion of grinding balls may be classified into two types (Ref 6, 10). One type is called the differential abrasion cell (Fig. 2a), in which freshly abraded areas of the surface become anodes while unabraded areas become cathodes. Thus the corrosion reaction involves dissolution of iron by oxidation at freshly abraded areas and oxygen reduction at unabraded areas. Another type (Fig. 2b), involves galvanic interaction between electroactive minerals and balls. Sulfide minerals with high open circuit potentials become cathodes, while carbon steel balls become anodes. Corrosive wear by this galvanic interaction overshadows the corrosive wear by the differential abrasion cell.

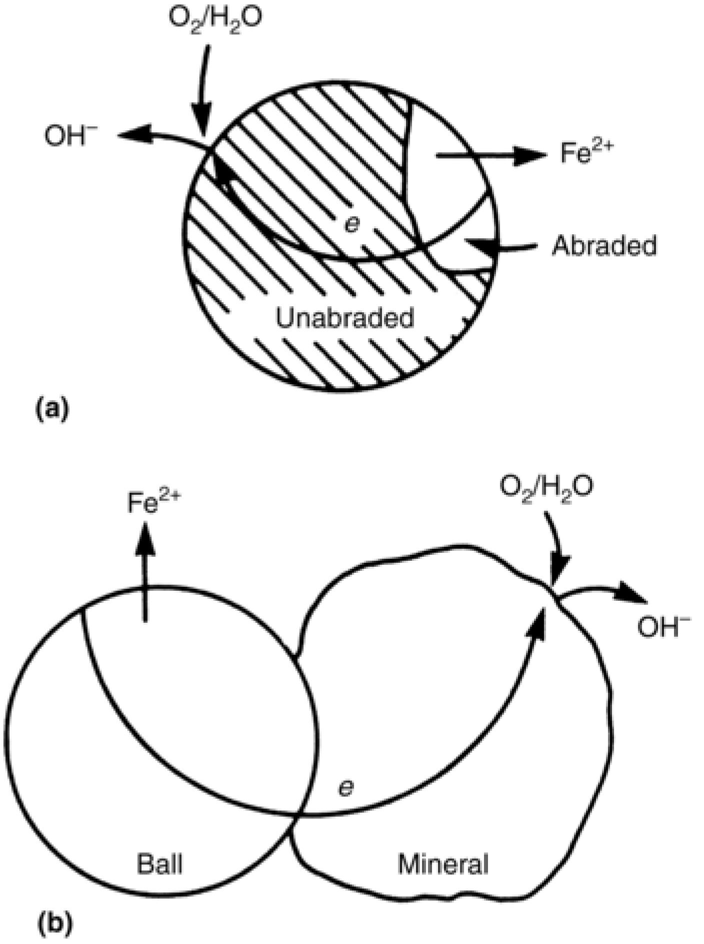

Fig. 2 Corrosion model for grinding balls in ore slurry in aqueous medium. (a) Differential abrasion cell. (b) Galvanic interaction cell. Source: Ref 6, 10

Figure 3 shows the effect of adding pyrrhotite (Fe_nS_{n+1}, typically Fe_7S_8) to a magnetic taconite ore ($\frac{1}{3}$ magnetite (Fe_3O_4), $\frac{2}{3}$siliceous gangue) and of mill atmosphere on ball wear. The results may be summarized as follows (Ref 12).

- In the absence of pyrrhotite, the effect of mill atmosphere is relatively minor.

- In the case of mild steel (MS) and high-carbon low-alloy (HCLA) steel, ball wear markedly increases with the addition of pyrrhotite under an oxygen atmosphere.
- Under a nitrogen atmosphere, ball wear is independent of pyrrhotite addition.
- With austenitic stainless steel (SS-A) balls, ball wear is virtually independent of mill atmosphere and also of the level of pyrrhotite addition.

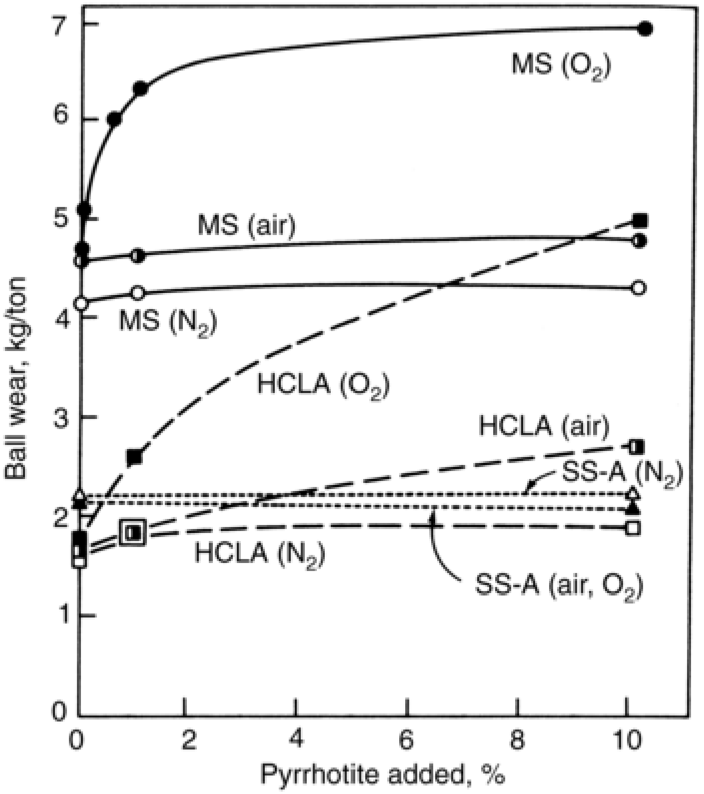

Fig. 3 Wear of mild steel (MS), high-carbon low-alloy steel (HCLA), and austenitic stainless steel (SS-A) balls as a function of pyrrhotite addition under different aeration conditions. Source: Ref 10

It is apparent that the wear of carbon steel balls is strongly influenced by the presence of pyrrhotite, particularly in mill atmospheres containing oxygen. Such an observation suggests that the wear under a nitrogen atmosphere is essentially due to abrasion, and the difference between the wear under an air or oxygen atmosphere and the wear under a nitrogen atmosphere represents corrosive wear.

Evidence in support of such an assumption may be provided by scanning electron microscope observations of the ball surfaces after grinding (Ref 6, 10, 11). Ball surfaces ground under a nitrogen atmosphere show numerous indentations with sharp ridges, suggesting that there is very little corrosion. Under an oxygen atmosphere, ridges become rounded and the appearance of corrosion becomes particularly severe in the presence of pyrrhotite.

References cited in this section

6. I. Iwasaki, S.C. Riemer, J.N. Orlich, and K.A. Natarajan, Corrosive and Abrasive Wear in Ore Grinding, *Wear,* Vol 103, 1985, p 253–267

10. K.A. Natarajan, S.C. Riemer, and I. Iwasaki, Ball Wear in Magnetic Taconite Grinding, Paper 19-1, *Proc. of 44th Annual Mining Symposium,* Center for Continuation Study, University of Minnesota, 1983

11. R. Perez and J.J. Moore, The Application of the Scanning Electron Microscope in Determining the Interaction of Abrasion and Corrosion in Mineral Grinding Media, *Microstruct. Sci.,* Vol 2, 1983, p 207–234

12. K.A. Natarajan, S.C. Riemer, and I. Iwasaki, Influence of Pyrrhotite on the Corrosive Wear of Grinding Balls in Magnetite Ore Grinding, *Int. J. Miner. Process.,* Vol 13, 1984, p 73–81

I. Iwasaki, Aqueous Corrosion-Wear Interactions, *Corrosion: Fundamentals, Testing, and Protection*, Vol 13A, *ASM Handbook*, ASM International, 2003, p 331–337

Aqueous Corrosion-Wear Interactions

Iwao Iwasaki, University of Minnesota Duluth

Polarization Curve Measurements under Abrasion

Whether corrosive wear may be defined as the difference between wear under an air or oxygen atmosphere and wear under a nitrogen atmosphere can be examined by converting the weight losses to corrosion currents using Faraday's law and comparing with the corrosion currents obtained from electrochemical measurements under abrasive conditions in a slurry (Ref 8, 13).

Figure 4 shows an example of polarization curves of pyrrhotite (Fe_nS_{n+1}) and HCLA steel determined in a quartzite (SiO_2) slurry. According to corrosion theory, the intersection of the cathodic polarization curve of pyrrhotite and the anodic polarization curve of HCLA steel is the corrosion current. However, the total corrosion current between ground pyrrhotite and HCLA steel needs to be corrected for their respective surface areas. In this example, the surface area of the ground pyrrhotite was measured, and the polarization curve of pyrrhotite was drawn by taking the cathode/anode area ratio of 26.

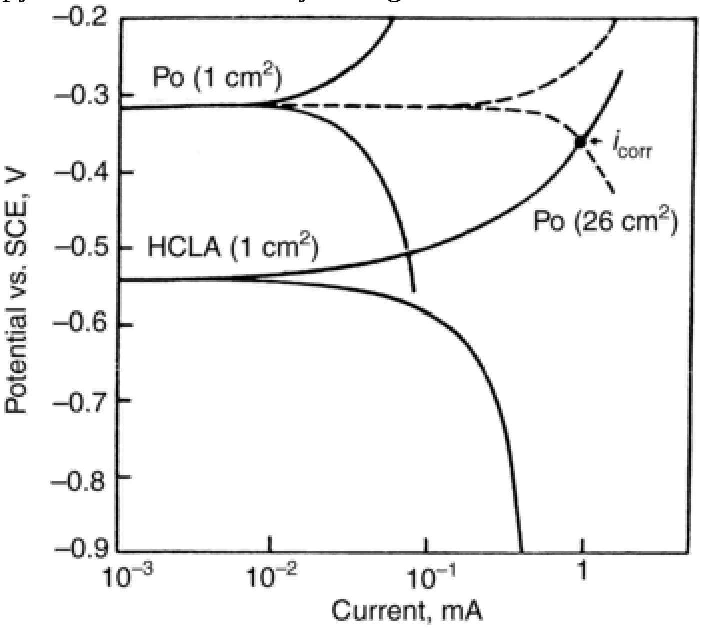

Fig. 4 Polarization curves. Estimation of corrosion current (i_{corr}) for the pyrrhotite (Po)-high-carbon low-alloy (HCLA) steel electrodes under abrasion in a quartzite slurry by adjusting to the surface area ratio of ground pyrrhotite and HCLA steel balls. SCE, saturated calomel electrode. Source: Ref 13

The corrosion current determined in this manner comes out to be 8 A/m^2 (0.74 A/ft^2) of ball surface. The total corrosion current is calculated to be 2.0 A for 126 balls of 25 mm (1 in.) diameter. This value agrees well with a value of 2.1 A estimated from the marked ball wear test data by using Faraday's law. This agreement demonstrates the role played by galvanic interaction in corrosive wear (Ref 8, 13).

References cited in this section

8. R.L. Pozzo and I. Iwasaki, Pyrite-Pyrrhotite-Grinding Media Interactions and Their Effects on Media Wear and Flotation, *J. Electrochem. Soc.*, Vol 136 (No. 6), 1989, p 1734–1740

13. R.L. Pozzo and I. Iwasaki, An Electrochemical Study of Pyrrhotite-Grinding Media Interaction under Abrasive Conditions, *Corrosion*, Vol 43, 1987, p 159–164

I. Iwasaki, Aqueous Corrosion-Wear Interactions, *Corrosion: Fundamentals, Testing, and Protection*, Vol 13A, *ASM Handbook*, ASM International, 2003, p 331–337

Aqueous Corrosion-Wear Interactions

Iwao Iwasaki, University of Minnesota Duluth

Effect of Galvanic Interactions on Flotation

Thus far, the nature of reactions that occur at the surface of steel media in contact with pyrrhotite (Fe_nS_{n+1}) has been discussed. Now the manner in which the surfaces of pyrrhotite in contact with mild steel or stainless steel are affected by galvanic interaction is considered.

Figure 5 shows such an effect on pyrrhotite surfaces as manifested by its flotation behavior. The floatability of pyrrhotite left in air-exposed water in a glass beaker does not change with time. Pyrrhotite left in a stainless steel beaker does not show much change. However, the floatability of pyrrhotite contacted with a low-carbon steel crucible in air-exposed water notably decreases. When oxygen is bubbled into the water, the floatability is seen to decrease by an additional 15%. Conversely, when nitrogen is bubbled into the water, the floatability of pyrrhotite in contact with low-carbon steel is at the same level as pyrrhotite in contact with glass. Therefore, the galvanic interaction by contacting with low-carbon steel in the presence of oxygen adversely affects its floatability (Ref 14).

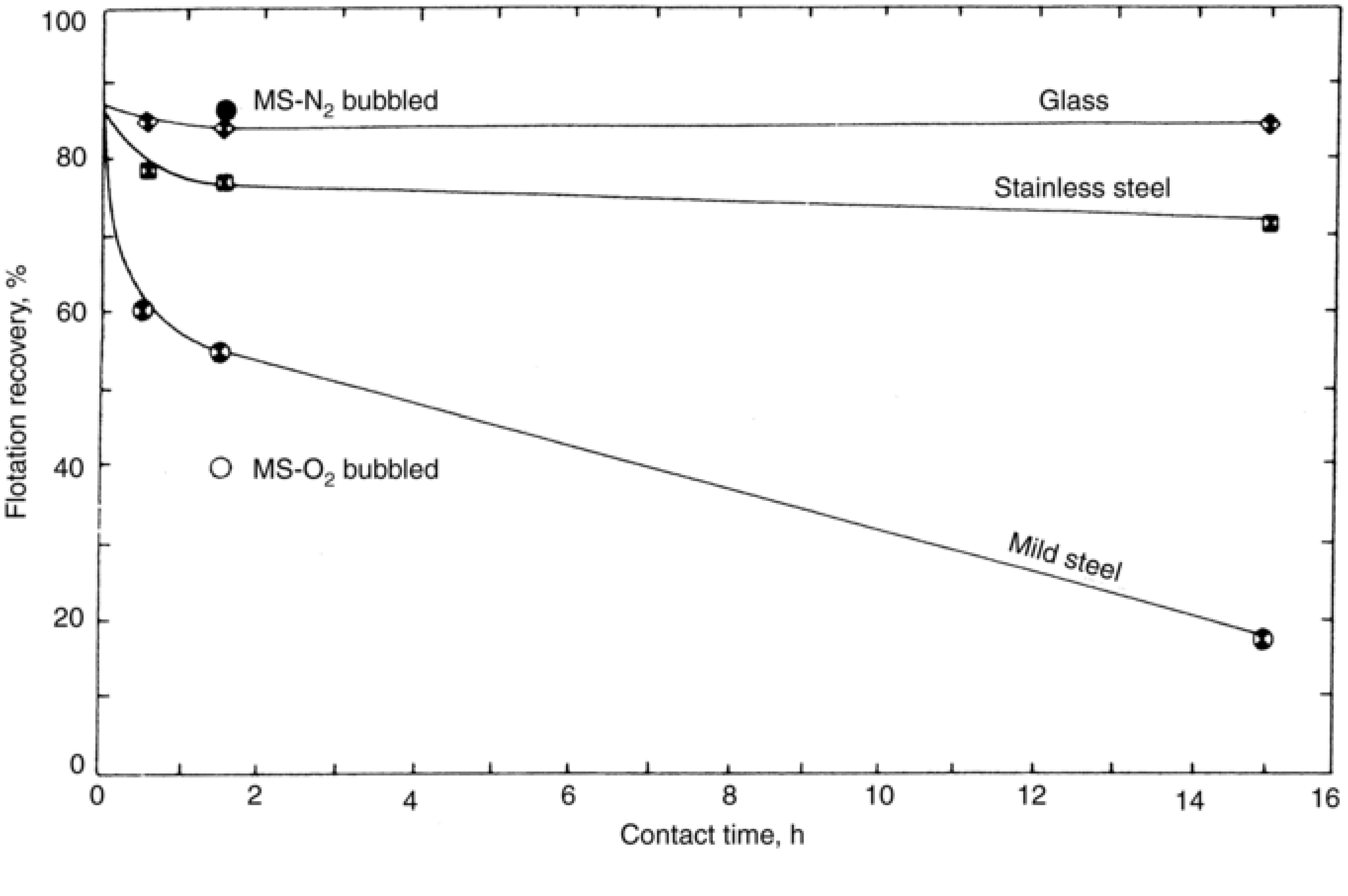

Fig. 5 Flotation of pyrrhotite as a function of contact time with glass, mild steel (MS) and austenitic stainless steel in air-exposed distilled water at natural pH unless indicated otherwise. Comparison of MS in bubbled environment given. Source: Ref 14

Reference cited in this section

14. J.J. Pavlica and I. Iwasaki, Electrochemical and Magnetic Interactions in Pyrrhotite Flotation, *Trans. SME/AIME,* Vol 272, 1982, p 1885–1890

I. Iwasaki, Aqueous Corrosion-Wear Interactions, *Corrosion: Fundamentals, Testing, and Protection,* Vol 13A, *ASM Handbook,* ASM International, 2003, p 331–337

Aqueous Corrosion-Wear Interactions

Iwao Iwasaki, University of Minnesota Duluth

Mechanism of Electrochemical Interaction

Galvanic interaction between pyrrhotite and metallic iron leads to the formation of an iron hydroxide coating on the mineral by the reaction of hydroxyl ions released by the reduction of oxygen at the surface of a pyrrhotite cathode, and Fe^{2+} released from pyrrhotite (abbreviated as FeS). It interferes with the flotation as follows (Ref 14, 15):

$$\frac{1}{2}O_2 + H_2O + 2e^- = 2OH^- \quad \text{(Eq 1)}$$

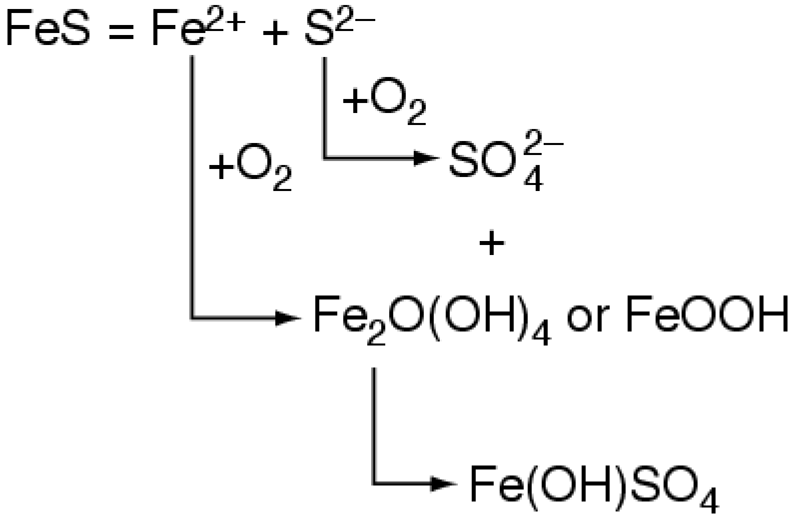

(Eq 2)

At the steel anode, iron is oxidized and Fe^{2+} is released:

$$Fe = Fe^{2+} + 2e^- \quad \text{(Eq 3)}$$

This Fe^{2+} also becomes iron hydroxide, which coats the sulfide mineral surfaces and contributes to the interference with flotation. According to corrosion theory, the rates of oxidation reactions equal the rates of reduction reactions. Corrosive wear, therefore, should increase in proportion to the partial pressure of oxygen, and the hydroxide coating that forms on the pyrrhotite surface becomes heavier and seriously interferes with flotation. The presence of oxygen at the surface of pyrrhotite, a sign of the proposed mechanism, can be detected by Auger electron spectroscopy (Ref 15).

Thus, galvanic interaction affects not only the corrosive wear of grinding balls but also the flotation of pyrrhotite. A similar mechanism is reported on the flotation of galena (PbS) (Ref 16) arsenopyrite (FeAsS) (Ref 17), chalcopyrite ($CuFeS_2$) (Ref 18), and sphalerite (ZnS) (Ref 19).

References cited in this section

14. J.J. Pavlica and I. Iwasaki, Electrochemical and Magnetic Interactions in Pyrrhotite Flotation, *Trans. SME/AIME,* Vol 272, 1982, p 1885–1890

15. K. Adam, K.A. Natarajan, and I. Iwasaki, Grinding Media Wear and Its Effect on the Flotation of Sulfide Minerals, *Int. J. Miner. Process.,* Vol 12, 1984, p 39–54

16. M.E. Learmont and I. Iwasaki, The Effect of Grinding Media on Flotation of Galena, *Miner. Metall. Process.,* Vol 1, 1984, p 136–143

17. I. Iwasaki, H. Nakazawa, A.S. Malicsi, and X. Li, Recovery of Platinum-Group Metals from Gabbroic Rocks, *J. Met.,* Vol 40 (No. 6), 1988, p 36–39

18. M.K. Yellogi Rao and K.A. Natarajan, Effect of Electrochemical Interactions Among Sulfide Minerals and Grinding Medium on Chalcopyrite Flotation, *Miner. Metall. Process.,* Vol 6, 1989, p 146–151

19. Vathsala and K.A. Natarajan, Some Electrochemical Aspects of Grinding Media Corrosion and Sphalerite Flotation, *Int. J. Miner. Process.,* Vol 26, 1989, p 193–203

I. Iwasaki, Aqueous Corrosion-Wear Interactions, *Corrosion: Fundamentals, Testing, and Protection,* Vol 13A, *ASM Handbook,* ASM International, 2003, p 331–337

Aqueous Corrosion-Wear Interactions

Iwao Iwasaki, University of Minnesota Duluth

Relative Significance of Corrosion and Abrasion in Wear

Table 1 shows an example of the results of laboratory marked ball wear tests for three types of steel balls in the wet grinding of magnetic taconite (Ref 6, 7). Ball wear is seen to increase with increasing oxygen partial pressure for mild steel and high-carbon low-alloy (HCLA) steel balls, and the increase is more pronounced when 10% by weight of pyrrhotite is added to the magnetic taconite. Assuming that wear under a nitrogen atmosphere approximates abrasive wear, the differences from wear in air and oxygen atmospheres represent corrosive wear. Table 2 shows percent corrosion in wear estimated in this manner.

Table 1 Grinding media wear in wet grinding of magnetic taconite in the absence and presence of pyrrhotite

	Mill atmosphere	Ball wear, mg per ball/h			
		Mild steel	**HCLA steel**	**Stainless steel**	
	Magnetic taconite	N_2	33.6 ± 0.4	13.0 ± 1.5	19.5 ± 0.1
Air		37.3 ± 0.7	13.8 ± 0.8	18.5 ± 0.1	
O_2		38.1 ± 0.5	14.2 ± 0.8	18.9 ± 0.9	
Magnetic taconite + 10% pyrrhotite	N_2	34.8 ± 0.4	15.1 ± 1.5	19.9 ± 0.3	
	Air	38.6 ± 0.5	21.7 ± 2.3	18.5 ± 1.1	
	O_2	55.5 ± 0.3	40.5 ± 3.5	18.7 ± 0.2	

HCLA, high-carbon low-alloy. Source: Ref 6, 7

Table 2 Corrosion as a percent of total wear loss in taconite grinding

	Change in mill atmosphere	Corrosion in wear, %		
		Mild steel	**HCLA steel**	**Stainless steel**
Magnetic taconite	N_2 to air	10	6	(-5)
	N_2 to O_2	12	8	(-3)
Magnetic taconite +10% pyrrhotite	N_2 to air	10	30	(-7)
	N_2 to O_2	37	63	(-6)

HCLA, high-carbon low-alloy. Source: Ref 6, 7

Corrosion of mild steel and HCLA steel in the grinding of magnetic taconite is about 10%, and, therefore, abrasive wear is about 90%. In the case of stainless steel, the wear under air and oxygen atmospheres even decreases somewhat due to passivation.

When pyrrhotite (Fe_nS_{n+1}) is added to magnetic taconite, the wear of HCLA steel notably increases to approximately 30%. In the case of mild steel, the effect of pyrrhotite is relatively small. This is because mild steel is less abrasion resistant than HCLA steel and more abraded debris is generated. This is magnetically attracted to the surface of pyrrhotite and lowers the open circuit potential of the mineral, thereby lowering the galvanic interaction (Ref 13). Under an oxygen atmosphere, the corrosion of mild steel and high-carbon steel reached approximately 40 to 60%. This is because the metallic iron debris generated is oxidized and the open circuit potential of pyrrhotite increases and helps promote the galvanic interaction. In this case also, the wear of stainless steel decreased under an oxygen atmosphere, which suggests that the corrosion component in an abrasive environment may be controlled by a proper selection of alloy composition.

References cited in this section

6. I. Iwasaki, S.C. Riemer, J.N. Orlich, and K.A. Natarajan, Corrosive and Abrasive Wear in Ore Grinding, *Wear,* Vol 103, 1985, p 253–267

7. I. Iwasaki, R.L. Pozzo, K.A. Natarajan, K. Adam, and J.N. Orlich, Nature of Corrosive and Abrasive Wear in Ball Mill Grinding, *Int. J. Miner. Process.,* Vol 22, 1988, p 345–360

13. R.L. Pozzo and I. Iwasaki, An Electrochemical Study of Pyrrhotite-Grinding Media Interaction under Abrasive Conditions, *Corrosion,* Vol 43, 1987, p 159–164

I. Iwasaki, Aqueous Corrosion-Wear Interactions, *Corrosion: Fundamentals, Testing, and Protection,* Vol 13A, *ASM Handbook,* ASM International, 2003, p 331–337

Aqueous Corrosion-Wear Interactions

Iwao Iwasaki, University of Minnesota Duluth

Galvanic Interactions in Multielectrode Systems

When complex sulfide ores are involved, multielectrode galvanic cells develop between minerals and grinding balls as well as among the minerals themselves. Figure 6 shows combination potentials and galvanic currents of a short- circuited pyrite (FeS_2), pyrrhotite (Fe_nS_{n+1}), and mild steel electrode under abrasion in a quartzite (SiO_2) slurry bubbled with oxygen (Ref 20). Pyrite, with a high open circuit potential, acts as the cathode on which oxygen reduction takes place. Pyrrhotite, with a lower open circuit potential, becomes an anode and dissolves. Such behavior suggests lower corrosion activity for mild steel when in contact with pyrite and pyrrhotite simultaneously than when in contact with pyrite alone.

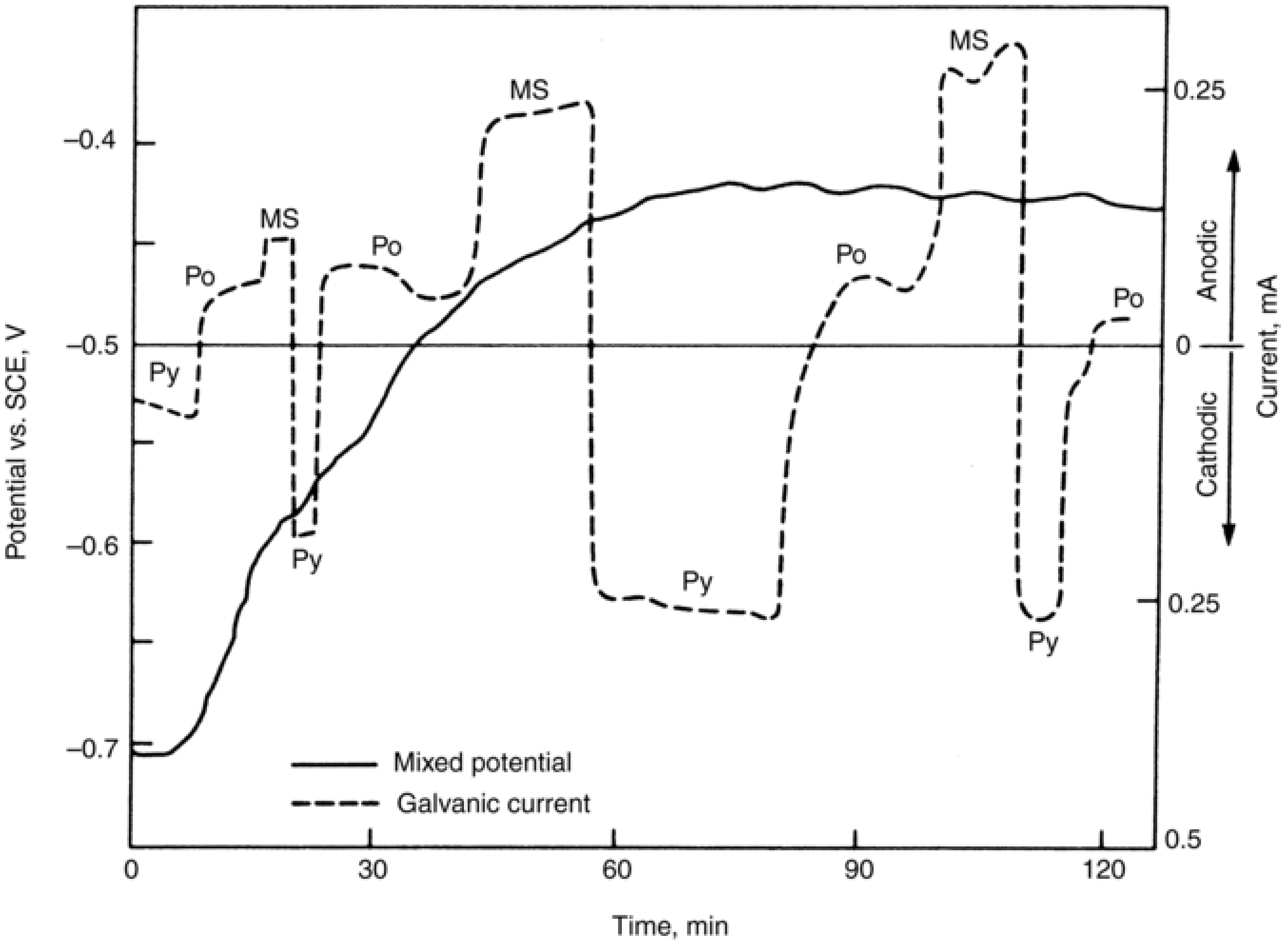

Fig. 6 Combination potentials and galvanic currents of a short-circuited pyrite-pyrrhotite-mild steel (MS) electrode under abrasion in a quartzite slurry in a 0.05 *M* sodium sulfate solution at neutral pH under oxygen atmosphere. Pyrrhotite, Po. Pyrite, Py. Source: Ref 20

Polarization curves of a pyrite, pyrrhotite, and mild steel combination are shown in Fig. 7. Point 1 represents the corrosion current for a pyrite- mild steel combination, and point 2 represents a pyrrhotite-mild steel combination. Point 3 represents a three-electrode combination involving pyrite, pyrrhotite, and mild steel. In Table 3, the results of marked ball wear tests and polarization measurements are compared. The table shows general agreement between the corrosion currents calculated from the marked ball wear tests and the corresponding corrosion currents determined from the polarization curves. Greater corrosion loss in the presence of pyrite with respect to corrosion loss in the presence of pyrrhotite can be understood by the nobler behavior developed by pyrite relative to pyrrhotite. The anodic behavior of the pyrrhotite electrode in the three-electrode system may also be understood by the smaller ball wear due to corrosion when both pyrrhotite and pyrite are present than when pyrite alone is present in the ore charge.

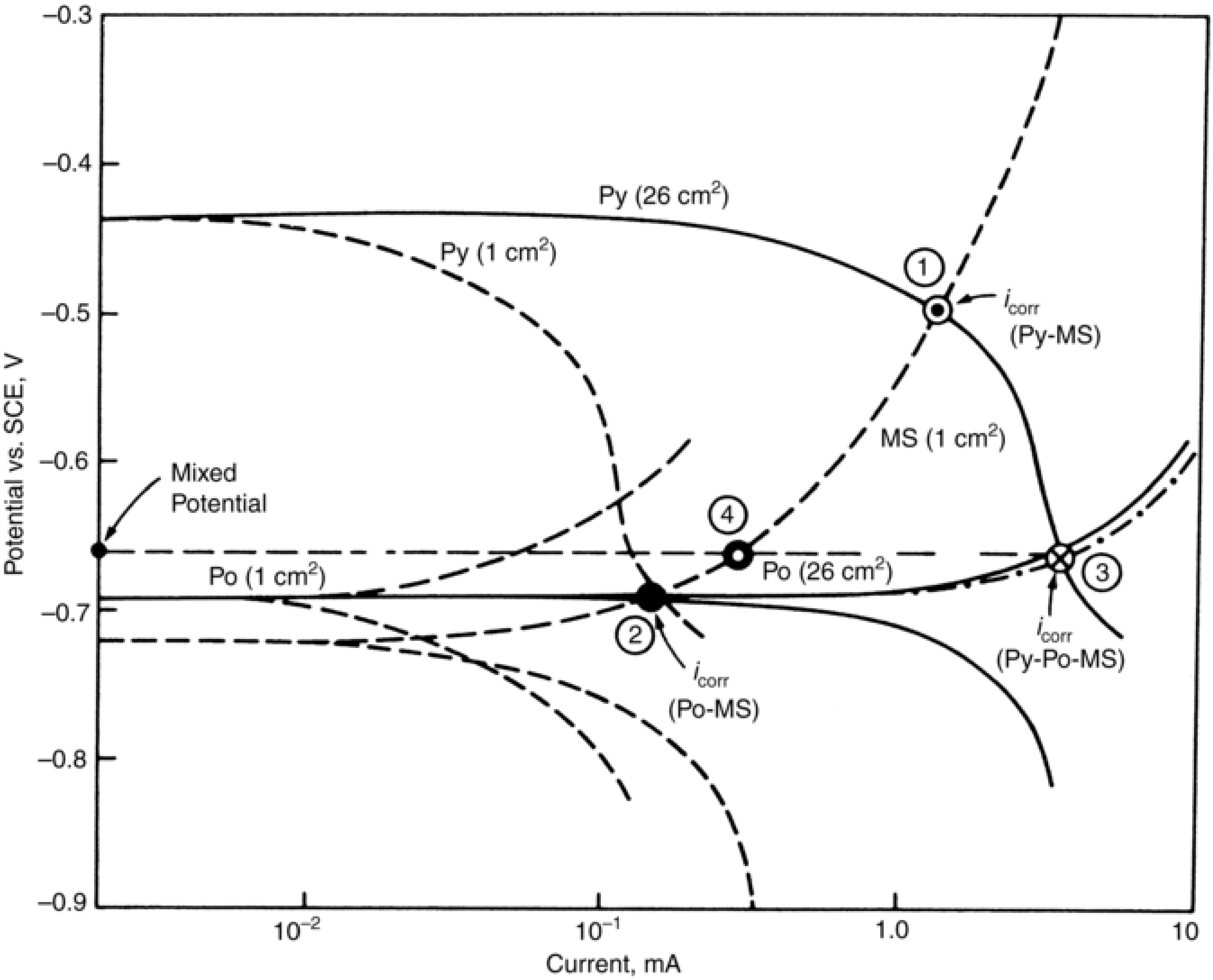

Fig. 7 Polarization curves. Estimation of corrosion currents (i_{corr}) for pyrite (Py)-mild steel (MS), pyrrhotite (Po)-MS, and Py-Po-MS systems under abrasion in a quartzite slurry by adjusting to the surface area ratios of ground minerals and steel balls. Numbered points are discussed in the text. Source: Ref 20

Table 3 Corrosive wear of mild steel balls in wet grinding of quartzite

Conditions	Corrosive wear, g per m^2/h	Corrosion current, A/m^2	
		From MBWT	**From polarization curves**
Qz + 5% Po	5.9 ± 1.1	5.6	1.6
Qz + 5% Py	7.9 ± 1.5	7.5	12.9
Qz + 5% Po + 5% Py	6.4 ± 1.7	5.9	3.1

Conditions are combinations of ores by weight percent. Quartzite, Qz. Pyrrhotite, Po. Pyrite, Py. MBWT, marked ball wear tests. Source: Ref 20

A similar electrochemical behavior is reported on a chalcopyrite ($CuFeS_2$), pyrrhotite (Fe_nS_{n+1}) and mild steel combination, and the results are correlated to their flotation behaviors (Ref 21).

References cited in this section

20. R.L. Pozzo and I. Iwasaki, Effect of Pyrite and Pyrrhotite on the Corrosive Wear of Grinding Media, *Miner. Metall. Process.*, Vol 4, 1987, p 166–171

21. X. Cheng, I. Iwasaki, and K.A. Smith, Electrochemical Study of Multi-Electrode Systems and Their Relevance to the Differential Flotation of Complex Sulfide Ores, *Miner. Metall. Process.,* Vol 16, 1999, p 69–71

I. Iwasaki, Aqueous Corrosion-Wear Interactions, *Corrosion: Fundamentals, Testing, and Protection*, Vol 13A, *ASM Handbook*, ASM International, 2003, p 331–337

Aqueous Corrosion-Wear Interactions

Iwao Iwasaki, University of Minnesota Duluth

Case History on Material Selection for Grinding Balls

To minimize corrosion loss and the adverse effect on flotation, it is necessary to search for materials that form passive films rapidly on grinding ball surfaces.

Figure 8 shows the polarization curves of austenitic stainless steel (SS-A), martensitic stainless steel (SS-M) and HCLA steel under abrasion in a quartzite (SiO_2) slurry, bubbled with oxygen, as a function of rotating speed (Ref 22). Austenitic stainless steel at rest is fully covered with a passive film. As the rotational speed is increased, the current flow increases, indicating that more active surfaces are exposed. The electrode potential shifts toward negative or more active direction. Anode currents increase in the order SS-A, SS-M, and HCLA steel. In fact, the curves of HCLA steel show little dependence on rotational speed, suggesting that the HCLA steel surface forms essentially no effective passive film in a neutral solution.

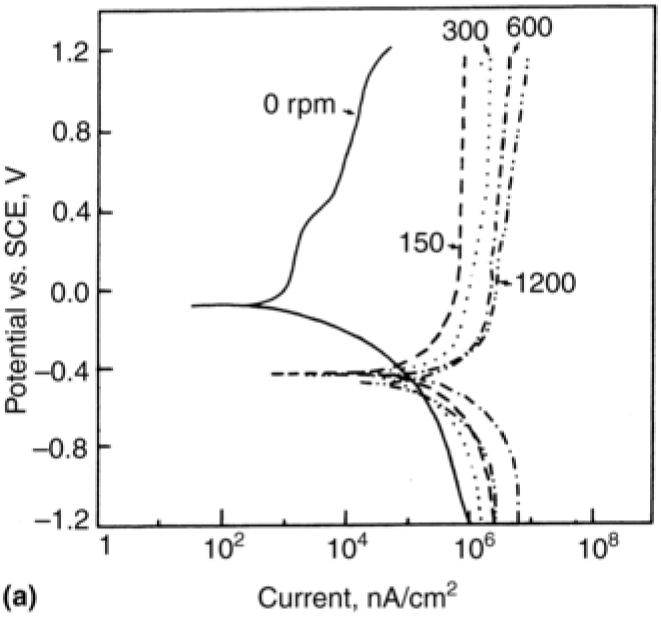
Potential vs. SCE, V
1.2
0.8
0.4
0.0
−0.4
−0.8
−1.2
1
10^2
10^4
10^6
10^8
Current, nA/cm^2
0 rpm
300
600
150
1200
(a)

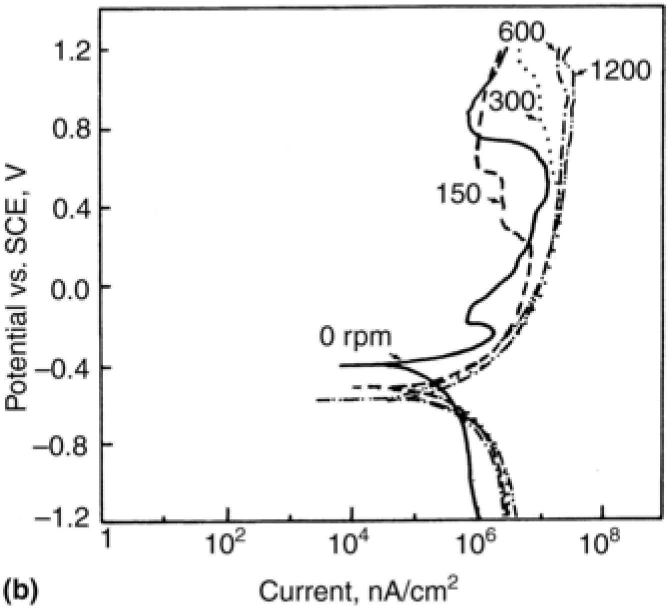
Potential vs. SCE, V
1.2
0.8
0.4
0.0
−0.4
−0.8
−1.2
1
10^2
10^4
10^6
10^8
Current, nA/cm^2
600
1200
300
150
0 rpm
(b)

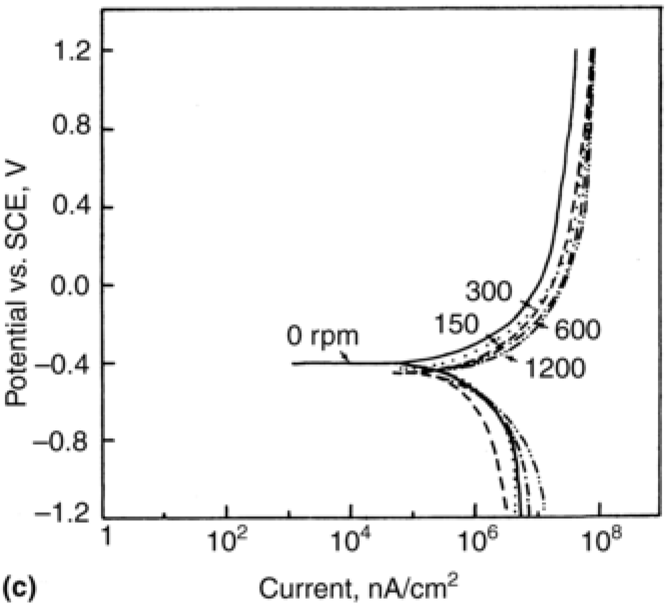
Potential vs. SCE, V
1.2
0.8
0.4
0.0
−0.4
−0.8
−1.2
1
10^2
10^4
10^6
10^8
Current, nA/cm^2
300
0 rpm
150
600
1200
(c)

Fig. 8 Polarization curves of (a) austenitic stainless steel (SS-A), (b) martensitic stainless steel (SS-M) and (c) high-carbon low alloy steel (HCLA) balls under abrasion in oxygenated quartzite slurries at different rotating speeds. Source: Ref 22

The results thus far indicate that HCLA steel is abrasion resistant but not corrosion resistant. Conversely, austenitic stainless steel is corrosion resistant but not abrasion resistant. Therefore, those materials that are as hard as HCLA steel and as corrosion resistant as austenitic stainless steel are desirable for grinding media application. High-chromium cast iron holds a possibility of combining both properties in a material. It is of interest what level of chromium imparts the electrochemical properties similar to those of austenitic stainless steel. Tests using a series of chromium-bearing cast iron balls having a Cr content ranging from 0 to 29% can provide such information. Polarization curves determined on this series of balls by changing the rotational speed under an oxygen atmosphere show that 0% Cr cast iron resembles HCLA steel, while those of 29% Cr cast iron resemble austenitic stainless steel (Ref 23).

Under a nitrogen atmosphere at a constant applied potential, anodic currents of chromium- bearing cast iron electrodes remain virtually independent of rotational speed, which suggests that very few passive films are formed. Hence, by extrapolating the anodic currents (measured as a function of rotational speed at a constant applied potential under an oxygen atmosphere) to that obtained under a nitrogen atmosphere, the anodic currents of fully active surfaces may be estimated. Here, there is no time to form a passive film at that rotational speed. Figure 9 shows the rates of passive film formation estimated from the rotational speed and the diameter of a ball used as the rotating electrode (Ref 24). The figure includes the results obtained on austenitic stainless steel (SS-A) in a similar manner along with those obtained on high-chromium cast iron (HCCl) balls containing 26 and 29% Cr. The rates of passive film formation are about 2 m/s (6.6 ft/s) and increase with increasing anodic potential. The rates of 29% Cr cast iron are similar to those of austenitic stainless steel (SS-A), but the rates of 26% Cr cast iron are somewhat lower. Therefore, high chromium cast iron can combine both hardness and corrosion resistance by rapid passive film formation.

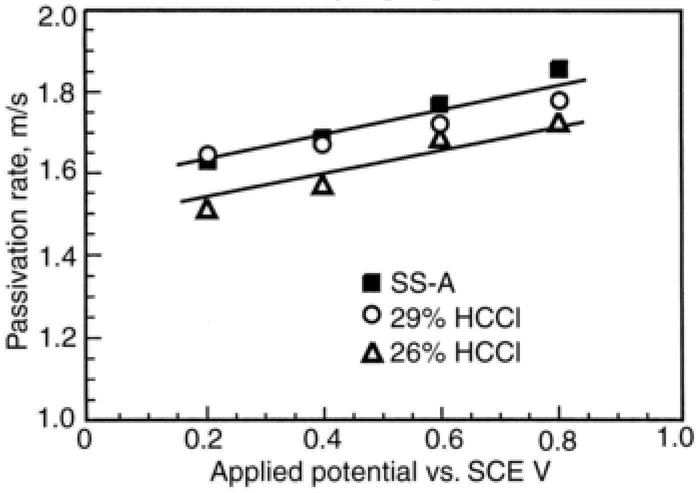

Fig. 9 Rates of passive film formation of austenitic stainless steel (SS-A) and high chromium cast iron (HCCI) balls in an oxygen atmosphere. Source: Ref 23

Wear Characteristics of Chromium-Bearing Cast Iron. Figure 10shows the wear data obtained for various cast iron balls under a nitrogen or oxygen atmosphere using artificial ore samples of quartzite (SiO_2) and quartzite mixed with either pyrrhotite (Fe_nS_{n+1}) or chalcopyrite ($CuFeS_2$). In a nitrogen atmosphere, the ball wear is essentially unaffected by the presence of sulfide minerals (Ref 23). A slight decrease in wear with increasing chromium content may be related to the abrasion resistance, which is governed by ball microstructure and carbide hardness.

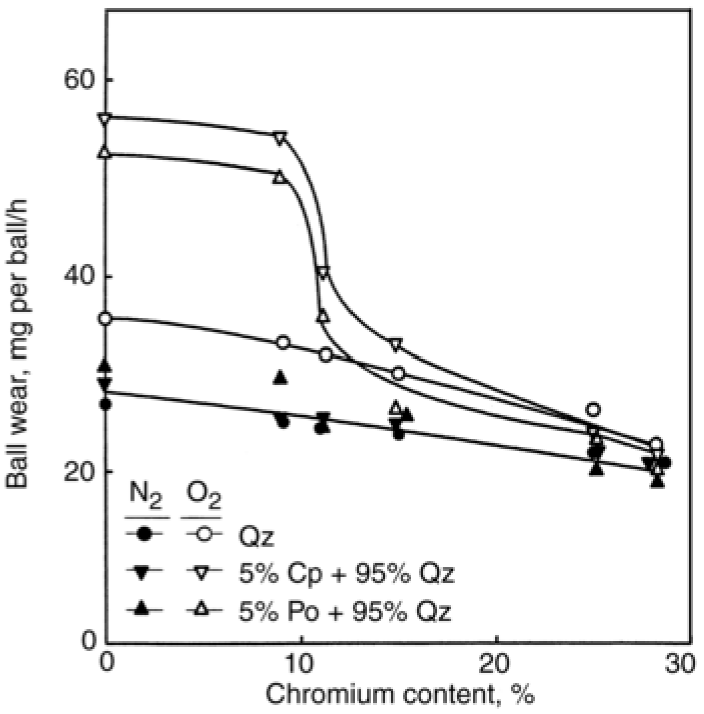

Fig. 10 The effect of chromium contents on the wear of ball materials in wet grinding of quartzite (Qz), quartzite with either 5% pyrrhotite (Po) or 5% chalcopyrite (Cp) slurries in the presence and absence of oxygen. Source: Ref 24

When a quartzite sample is ground in an oxygen atmosphere, ball wear increases. The difference between wear under nitrogen and oxygen atmospheres increases with decreasing chromium level. This difference can be attributed to corrosion due to differential abrasion cell, as discussed previously, and wear increases with a decreasing chromium level. In the presence of pyrrhotite and chalcopyrite, ball wear increases markedly in an oxygen atmosphere when ball chromium levels are below 10%. Apparently, there is a marked change in the nature of the passive film at low- and high-chromium contents. A transition in media wear is observed between 8.5% and 16% Cr.

Flotation of Samples Ground with Chromium-Bearing Cast Iron Balls. Figure 11 shows the flotation recoveries of pyrrhotite from a pyrrhotite-quartzite mixture, ground with various cast iron balls, as a function of collector addition (Ref 23). Potassium ethyl xanthate (KEX) is used as a collector for floating the sulfide mineral. The collector is adsorbed on pyrrhotite but not on quartzite. The collector-coated particles are attached to air bubbles, thereby leading to flotation separation. In a nitrogen atmosphere, the flotation of pyrrhotite, ground with cast iron balls containing less than 11% Cr, is minimal, even when an excessive amount of the collector is used. Although these results appear to contradict the results shown in Fig. 5, this behavior may be attributed to abraded debris generated in grinding. The abraded debris is magnetically attracted to the pyrrhotite surface, thereby lowering the open-circuit potential of pyrrhotite. Apparently, lowering of the potential prevented oxidation of the xanthate collector to dixanthogen, an effective form of the adsorbed collector for flotation.

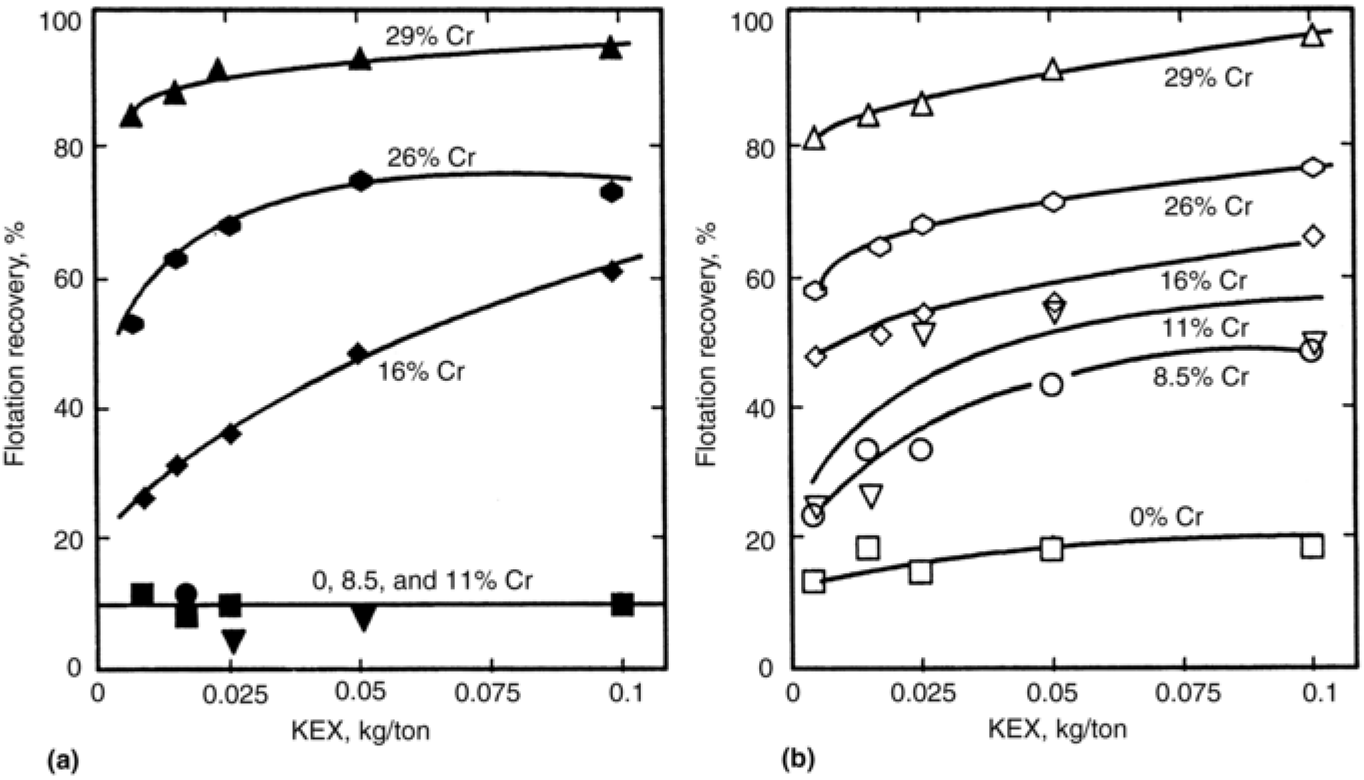

Fig. 11 Batch flotation results using potassium ethyl xanthate (KEX) on a quartzite with 5% pyrrhotite mixture ground with various cast iron ball materials under (a) nitrogen or (b) oxygen atmosphere. Source: Ref 24

Flotation results on the samples ground with 16 and 26% Cr balls show increasingly higher flotation recoveries and become less sensitive to the atmosphere in the grinding mill. Samples ground with 29% Cr balls give nearly full recoveries, even with a minimal addition of the collector. Formation of passive films raises the open circuit potentials of abraded debris, thereby relieving the adverse effect on the flotation of pyrrhotite by restoring its open-circuit potential.

Conclusions. Corrosion of ferrous materials is accelerated under abrasive conditions in slurries by the differential abrasion cell reactions. In the presence of sulfide minerals, corrosion is further accelerated by galvanic interaction. Sulfide mineral surfaces are also altered by contacting with ferrous materials, and their flotation recoveries are adversely affected. Flotation behaviors of pyrrhotite (Fe_nS_{n+1}) are complexly affected by abraded debris generated in grinding, which is magnetically attracted to pyrrhotite surfaces. This abraded debris alters the open circuit potential of pyrrhotite. Its mechanism may be clarified by studying the electrochemical behaviors under abrading conditions in a slurry medium.

Galvanic interaction phenomena play an important role in the wear of rods and balls in grinding, of slurry pipelines, and of sand pumps. In the case of grinding balls, high-chromium cast iron appears to be the material of choice because it is not only wear resistant but also does not adversely affect flotation.

References cited in this section

22. J.W. Jang, I. Iwasaki, and J.J. Moore, Wear Behavior of Martensite and Ferrite in High Chromium Steel Balls in Wet Grinding and Implication to Flotation, *Miner. Metall. Process.*, Vol 6, 1989, p 161–166

23. V. Rajagopal and I. Iwasaki, The Nature of Corrosive and Abrasive Wear of Chromium Bearing Cast Iron Grinding Media, *Corrosion*, Vol 48, 1992, p 132–139

24. V. Rajagopal, A.S. Malicsi, and I. Iwasaki, Effect of Chromium on the Cast-Iron Properties and Performance in Wet Grinding, *Miner. Metall. Process.*, Vol 9, 1992, p 34–40

I. Iwasaki, Aqueous Corrosion-Wear Interactions, *Corrosion: Fundamentals, Testing, and Protection,* Vol 13A, *ASM Handbook*, ASM International, 2003, p 331–337

Aqueous Corrosion-Wear Interactions

Iwao Iwasaki, University of Minnesota Duluth

References

1. "Standard Guide for Determining Synergism between Wear and Corrosion," G 119- 93, *Annual Book of ASTM Standards,* ASTM International, 1993

2. F.D. DeVaney and M.H. Coghill, The Relation of Ball Wear to Power in Grinding, *Eng. Min. J.,* Vol 138, 1937, p 337–340

3. I. Iwasaki, J.J. Moore, and L.A. Lindeke, Effect of Ball Mill Size on Media Wear, *Miner. Metall. Process.,* Vol 4, 1987, p 160–166

4. *Comminution and Energy Consumption,* National Academy of Sciences, Washington, D.C., 1981, p 27

5. J.J. Moore and I. Iwasaki, The Role of Abrasion and Corrosion in Grinding Media Wear, DOE/ID/12441-T1, Vol 1, Office of Scientific and Technical Information, United States Department of Energy, 1986, 137 p

6. I. Iwasaki, S.C. Riemer, J.N. Orlich, and K.A. Natarajan, Corrosive and Abrasive Wear in Ore Grinding, *Wear,* Vol 103, 1985, p 253–267

7. I. Iwasaki, R.L. Pozzo, K.A. Natarajan, K. Adam, and J.N. Orlich, Nature of Corrosive and Abrasive Wear in Ball Mill Grinding, *Int. J. Miner. Process.,* Vol 22, 1988, p 345–360

8. R.L. Pozzo and I. Iwasaki, Pyrite-Pyrrhotite-Grinding Media Interactions and Their Effects on Media Wear and Flotation, *J. Electrochem. Soc.,* Vol 136 (No. 6), 1989, p 1734–1740

9. T.E. Norman and C.M. Loeb, Jr., Wear Tests on Grinding Balls, *Trans. AIME,* Vol 176, 1948, p 490–520

10. K.A. Natarajan, S.C. Riemer, and I. Iwasaki, Ball Wear in Magnetic Taconite Grinding, Paper 19-1, *Proc. of 44th Annual Mining Symposium,* Center for Continuation Study, University of Minnesota, 1983

11. R. Perez and J.J. Moore, The Application of the Scanning Electron Microscope in Determining the Interaction of Abrasion and Corrosion in Mineral Grinding Media, *Microstruct. Sci.,* Vol 2, 1983, p 207–234

12. K.A. Natarajan, S.C. Riemer, and I. Iwasaki, Influence of Pyrrhotite on the Corrosive Wear of Grinding Balls in Magnetite Ore Grinding, *Int. J. Miner. Process.,* Vol 13, 1984, p 73–81

13. R.L. Pozzo and I. Iwasaki, An Electrochemical Study of Pyrrhotite-Grinding Media Interaction under Abrasive Conditions, *Corrosion,* Vol 43, 1987, p 159–164

14. J.J. Pavlica and I. Iwasaki, Electrochemical and Magnetic Interactions in Pyrrhotite Flotation, *Trans. SME/AIME,* Vol 272, 1982, p 1885–1890

15. K. Adam, K.A. Natarajan, and I. Iwasaki, Grinding Media Wear and Its Effect on the Flotation of Sulfide Minerals, *Int. J. Miner. Process.,* Vol 12, 1984, p 39–54

16. M.E. Learmont and I. Iwasaki, The Effect of Grinding Media on Flotation of Galena, *Miner. Metall. Process.,* Vol 1, 1984, p 136–143

17. I. Iwasaki, H. Nakazawa, A.S. Malicsi, and X. Li, Recovery of Platinum-Group Metals from Gabbroic Rocks, *J. Met.,* Vol 40 (No. 6), 1988, p 36–39

18. M.K. Yellogi Rao and K.A. Natarajan, Effect of Electrochemical Interactions Among Sulfide Minerals and Grinding Medium on Chalcopyrite Flotation, *Miner. Metall. Process.,* Vol 6, 1989, p 146–151

19. Vathsala and K.A. Natarajan, Some Electrochemical Aspects of Grinding Media Corrosion and Sphalerite Flotation, *Int. J. Miner. Process.,* Vol 26, 1989, p 193–203

20. R.L. Pozzo and I. Iwasaki, Effect of Pyrite and Pyrrhotite on the Corrosive Wear of Grinding Media, *Miner. Metall. Process.,* Vol 4, 1987, p 166–171

21. X. Cheng, I. Iwasaki, and K.A. Smith, Electrochemical Study of Multi-Electrode Systems and Their Relevance to the Differential Flotation of Complex Sulfide Ores, *Miner. Metall. Process.,* Vol 16, 1999, p 69–71

22. J.W. Jang, I. Iwasaki, and J.J. Moore, Wear Behavior of Martensite and Ferrite in High Chromium Steel Balls in Wet Grinding and Implication to Flotation, *Miner. Metall. Process.,* Vol 6, 1989, p 161–166

23. V. Rajagopal and I. Iwasaki, The Nature of Corrosive and Abrasive Wear of Chromium Bearing Cast Iron Grinding Media, *Corrosion,* Vol 48, 1992, p 132–139

24. V. Rajagopal, A.S. Malicsi, and I. Iwasaki, Effect of Chromium on the Cast-Iron Properties and Performance in Wet Grinding, *Miner. Metall. Process.,* Vol 9, 1992, p 34–40

I. Iwasaki, Aqueous Corrosion-Wear Interactions, *Corrosion: Fundamentals, Testing, and Protection*, Vol 13A, *ASM Handbook*, ASM International, 2003, p 331–337

Aqueous Corrosion-Wear Interactions

Iwao Iwasaki, University of Minnesota Duluth

Selected References

- While this article emphasized the role played by galvanic cell action, synergism between erosion/abrasion and corrosion using such electrochemically inactive solids as Al_2O_3 and SiO_2 pertains to differential cell action, as explained in Fig. 2(a). For more detailed mechanisms of the synergism of erosive-corrosive wear, readers are referred to the following:

- C. Allen and A. Ball, A Review of the Performance of Engineering Materials Under Prevalent Tribological and Wear Situations in South African Industries, *Tribol. Int.,* Vol 29 (No. 2), 1996, p 105–116
- I. Garcia, D. Drees, and J.P. Celis, Corrosion- Wear of Passivating Materials in Sliding Contacts Based on a Concept of Active Wear Track Area, *Wear,* Vol 249, 2001, p 452–460

- J.A. Hawk, B.W. Madsen, and S. Dillich, Tribological Issues in Mining and Minerals Processing, *Proc. of Symposium on Tribology in Manufacturing, ASME/STLE Tribology Conference,* 16–19 Oct 1994, (Lahaina, Maui, HI), Vol 5, 1994, p 1–41
- P. Jemmely, S. Mischler, and D. Landolt, Electrochemical Modeling of Passivation Phenomena in Tribo-Corrosion, *Wear,* Vol 237, 2000, p 63–76
- J. Jiang, M.M. Stack, and A. Neville, Modelling the Tribo-Corrosion Interaction in Aqueous Sliding Conditions, *Tribol. Int.,* Vol 35, 2002, p 669–679
- D. Kotlyar, C.H. Pitt, and M.E. Wadsworth, Simultaneous Corrosion and Abrasion Measurements Under Grinding Conditions, *Corrosion,* Vol 44 (No. 5), 1988, p 221–228
- B.W. Madsen, Measurement of Wear and Corrosion Rates Using a Novel Slurry Wear Test, *Mater. Perform.,* Vol 26 (No. 1), 1987, p 21–28
- B.W. Madsen, Measurement of Erosion-Corrosion Synergism with a Slurry Wear Test Apparatus, *Wear,* Vol 123 (No. 2), 1988, p 127–142
- A. Neville, and X. Hu, Mechanical and Electrochemical Interactions During Liquid-Solid Impingement on High-Alloy Stainless Steels, *Wear,* Vol 251, 2001, p 1284–1294
- C.H. Pitt and Y.M. Chang, Jet Slurry Corrosive Wear of High-Chromium Cast Iron and High-Carbon Steel Grinding Ball Alloys, *Corrosion,* Vol 42 (No. 6), 1986, p 312–317
- W.J. Schumacher, Corrosive Wear Principles, *Mater. Perform.,* Vol 32 (No. 7), 1993, p 50–53
- M.M. Stack, N. Corlett, and S. Turgoose, Some Recent Advances in the Development of Theoretical Approaches for the Construction of Erosion-Corrosion Maps in Aqueous Conditions, *Wear,* Vol 233–235, 1999, p 535–541
- S.W. Watson, F.J. Friedersdorf, B.W. Madsen, and S.D. Cramer, Methods of Measuring Wear-Corrosion Synergism, *Wear,* Vol 181–183, 1995, p 476–484
- R.J.K. Wood and S.P. Hutton, The Synergistic Effect of Erosion and Corrosion: Trends in Published Results, *Wear,* Vol 140, 1990, p 387–394

J.H. Tylczak and T.A. Adler, Gaseous Corrosion-Wear Interactions, *Corrosion: Fundamentals, Testing, and Protection*, Vol 13A, *ASM Handbook*, ASM International, 2003, p 338–344

Gaseous Corrosion-Wear Interactions

Joseph H. Tylczak and Thomas A. Adler, Albany Research Center, U.S. Department of Energy

---

Introduction

WEAR AND CORROSION are not easy to avoid in most industrial or manufacturing processes. Many industrial processes run at elevated temperatures, and pieces of equipment can become heated with use. Unfortunately, increased heat can exacerbate both wear and corrosion. In terms of wear, rising temperatures soften metals and make their surfaces easier to penetrate. A variety of wear mechanisms can operate including adhesive (or sliding), abrasive, erosive, and fretting. In terms of corrosion, thermal kinetics accelerate the chemical reactions that degrade material. Together, wear and corrosion can lead to high economic costs and productivity losses, as worn and/or corroded equipment requires increased repair and maintenance. The interactions between wear and corrosion in dry environments are addressed in this article.

Various industries experience increased maintenance costs as a result of oxidation-wear interactions. The power-generation industry is one such example. In coal-fired plants, the coal is pulverized in a highly abrasive process. Heated air, which accelerates corrosion, carries the coal fines through metal tubes to the burner units. The moving fines erode these metal pipes. At the end of the pipes, the fines are injected into the boiler through nozzles that themselves are eroded by the coal fines and oxidized as a result of the high temperatures. Products of combustion, waste silica, and exhaust gas can erode heat-exchange tubes in a boiler.

Burning biomass (Ref 1, 2) accelerates erosion-corrosion in power plants. Sliding wear can be a challenge on control valves (Ref 3) and hot drag chain conveyors. In coal-burning power plants, both in pulverized-coal and fluidized-bed (Ref 4) systems, high-temperature erosion-corrosion can occur on everything from boiler tubes and reheaters to the economizers.

Other industries also pay a heavy cost for wear-corrosion interactions. Crushing and grinding ores and minerals are sometimes done at elevated temperatures, which can lead to accelerated abrasive wear (Ref 5). Hot forming extrusion dies, hot drag chain conveyors for smelters and heat treaters, and continuous caster rolls can suffer from sliding wear (Ref 5). Cutting and machining metals at high speed can produce temperatures as high as 1000 °C (1800 °F), which leads to abrasive wear, adhesive wear, and corrosion (Ref 6). Cutting wood, particularly particleboard, can generate temperatures estimated as high as 800 to 1000 °C (1500 to 1800 °F) and cause wear and oxidation to the cutting tips (Ref 7). Other applications faced with wear- corrosion problems include: steam turbines, gas turbines, sliding electric contacts, internal combustion engines (cylinder liners, piston rings, valve seats, and valves), compressors, furnace parts, extrusion parts (dies), gas-cooled nuclear reactors, and brake rotors and drums.

A better understanding of how wear and corrosion interact in gaseous environments is necessary because together they can do more damage than either would do alone. The ability to decrease their synergistic impact can reduce significantly maintenance and replacement costs in a variety of manufacturing industries.

References cited in this section

1. S. Collins, Biomass-Fired Plants Face Down Near-Term Challenges, *Power,* Vol 137, 1993, p 51–53

2. M.A. Uusitalo, P.M.J. Vuoristo, and M.A. Mäntylä, Elevated Temperature Erosion- Corrosion of Thermal Sprayed Coatings in Chlorine Containing Environments, *Wear,* Vol 252, 2002, p 586–594

3. B.S. Mann and B. Prakash, High Temperature Friction and Wear Characteristics of Various Coating Materials for Steam Valve Spindle Application, *Wear,* Vol 240, 2000, p 223–230

4. P.M. Rogers, I.M. Hutchings, and J.A. Little, Coatings and Surface Treatments for Protection against Low-Velocity Erosion- Corrosion in Fluidized Beds, *Wear,* Vol 186–187, 1995, p 238–246

5. H. Berns and S. Koch, High Temperature Sliding Abrasion of a Nickel-Base Alloy and Composite, *Wear,* Vol 225–229, 1999, p 154–162

6. S. Dolinšek, B. Šuštaršič, and J. Kopač, Wear Mechanisms of Cutting Tools in High- Speed Cutting Processes, *Wear,* Vol 250, 2001, p 349–356

7. H. Stewart, R. Rapp, M. Padilla, and A. Ried, *Proc Tenth Int. Wood Machining Seminar,* Forest Products Laboratory, University of California, Berkeley, CA, 1985, p 54–71

J.H. Tylczak and T.A. Adler, Gaseous Corrosion-Wear Interactions, *Corrosion: Fundamentals, Testing, and Protection*, Vol 13A, *ASM Handbook*, ASM International, 2003, p 338–344

Gaseous Corrosion-Wear Interactions

Joseph H. Tylczak and Thomas A. Adler, Albany Research Center, U.S. Department of Energy

Introduction

WEAR AND CORROSION are not easy to avoid in most industrial or manufacturing processes. Many industrial processes run at elevated temperatures, and pieces of equipment can become heated with use. Unfortunately, increased heat can exacerbate both wear and corrosion. In terms of wear, rising temperatures soften metals and make their surfaces easier to penetrate. A variety of wear mechanisms can operate including adhesive (or sliding), abrasive, erosive, and fretting. In terms of corrosion, thermal kinetics accelerate the chemical reactions that degrade material. Together, wear and corrosion can lead to high economic costs and productivity losses, as worn and/or corroded equipment requires increased repair and maintenance. The interactions between wear and corrosion in dry environments are addressed in this article.

Various industries experience increased maintenance costs as a result of oxidation-wear interactions. The power-generation industry is one such example. In coal-fired plants, the coal is pulverized in a highly abrasive process. Heated air, which accelerates corrosion, carries the coal fines through metal tubes to the burner units. The moving fines erode these metal pipes. At the end of the pipes, the fines are injected into the boiler through nozzles that themselves are eroded by the coal fines and oxidized as a result of the high temperatures. Products of combustion, waste silica, and exhaust gas can erode heat-exchange tubes in a boiler.

Burning biomass (Ref 1, 2) accelerates erosion-corrosion in power plants. Sliding wear can be a challenge on control valves (Ref 3) and hot drag chain conveyors. In coal-burning power plants, both in pulverized-coal and fluidized-bed (Ref 4) systems, high-temperature erosion-corrosion can occur on everything from boiler tubes and reheaters to the economizers.

Other industries also pay a heavy cost for wear-corrosion interactions. Crushing and grinding ores and minerals are sometimes done at elevated temperatures, which can lead to accelerated abrasive wear (Ref 5). Hot forming extrusion dies, hot drag chain conveyors for smelters and heat treaters, and continuous caster rolls can suffer from sliding wear (Ref 5). Cutting and machining metals at high speed can produce temperatures as high as 1000 °C (1800 °F), which leads to abrasive wear, adhesive wear, and corrosion (Ref 6). Cutting wood, particularly particleboard, can generate temperatures estimated as high as 800 to 1000 °C (1500 to 1800 °F) and cause wear and oxidation to the cutting tips (Ref 7). Other applications faced with wear- corrosion problems include: steam turbines, gas turbines, sliding electric contacts, internal combustion engines (cylinder liners, piston rings, valve seats, and valves), compressors, furnace parts, extrusion parts (dies), gas-cooled nuclear reactors, and brake rotors and drums.

A better understanding of how wear and corrosion interact in gaseous environments is necessary because together they can do more damage than either would do alone. The ability to decrease their synergistic impact can reduce significantly maintenance and replacement costs in a variety of manufacturing industries.

References cited in this section

1. S. Collins, Biomass-Fired Plants Face Down Near-Term Challenges, *Power,* Vol 137, 1993, p 51–53
2. M.A. Uusitalo, P.M.J. Vuoristo, and M.A. Mäntylä, Elevated Temperature Erosion- Corrosion of Thermal Sprayed Coatings in Chlorine Containing Environments, *Wear,* Vol 252, 2002, p 586–594
3. B.S. Mann and B. Prakash, High Temperature Friction and Wear Characteristics of Various Coating Materials for Steam Valve Spindle Application, *Wear,* Vol 240, 2000, p 223–230

4. P.M. Rogers, I.M. Hutchings, and J.A. Little, Coatings and Surface Treatments for Protection against Low-Velocity Erosion- Corrosion in Fluidized Beds, *Wear,* Vol 186–187, 1995, p 238–246

5. H. Berns and S. Koch, High Temperature Sliding Abrasion of a Nickel-Base Alloy and Composite, *Wear,* Vol 225–229, 1999, p 154–162

6. S. Dolinšek, B. Šuštaršič, and J. Kopač, Wear Mechanisms of Cutting Tools in High- Speed Cutting Processes, *Wear,* Vol 250, 2001, p 349–356

7. H. Stewart, R. Rapp, M. Padilla, and A. Ried, *Proc Tenth Int. Wood Machining Seminar,* Forest Products Laboratory, University of California, Berkeley, CA, 1985, p 54–71

J.H. Tylczak and T.A. Adler, Gaseous Corrosion-Wear Interactions, *Corrosion: Fundamentals, Testing, and Protection*, Vol 13A, *ASM Handbook*, ASM International, 2003, p 338–344

Gaseous Corrosion-Wear Interactions

Joseph H. Tylczak and Thomas A. Adler, Albany Research Center, U.S. Department of Energy

---

Mechanisms

The following sections discuss the mechanisms of wear and their interactions with gaseous corrosion. Further information on the mechanisms of gaseous corrosion is available in the article “Gaseous Corrosion Mechanisms” in this Volume.

Abrasive wear is the removal of material due to the relative motion of hard particles or protuberances against another surface. Although most research tends to focus on the wearing surface with the most potential for economic loss or gain, it should be noted that when two surfaces come into contact, wear can take place on both.

The rate at which a given surface abrades is dependent on the properties of the surfaces in contact, the presence of abrasives between them, the speed of contact, and the environmental conditions. In short, loss rates are not an inherent property of a given material. For example, a crusher grinding coal will not wear as quickly as an identical one grinding silicon carbide. A ball mill will see a different wear rate grinding coal than will a ball-and-race mill.

Abrasion is typically categorized according to types of contact and contact environment. Types of contact include two-body wear and three-body wear. Two-body wear occurs when an abrasive interacts with a single surface. Three-body wear occurs when an abrasive interacts with two surfaces or with a single surface and other particles. Two-body systems typically experience 10 to 1000 times as much loss as three-body systems for a given load and path length of wear. Contact environments (Fig. 1) are separated into open (or free) and closed (or constrained) contact. Blickensderfer (Ref 8) showed in several different tests that for a given load and wear path length, the wear rate is about the same for open and closed systems. However, the abrasive loss in closed systems will often appear higher than the abrasive loss in open systems. This can occur because closed systems tend to involve higher loads.

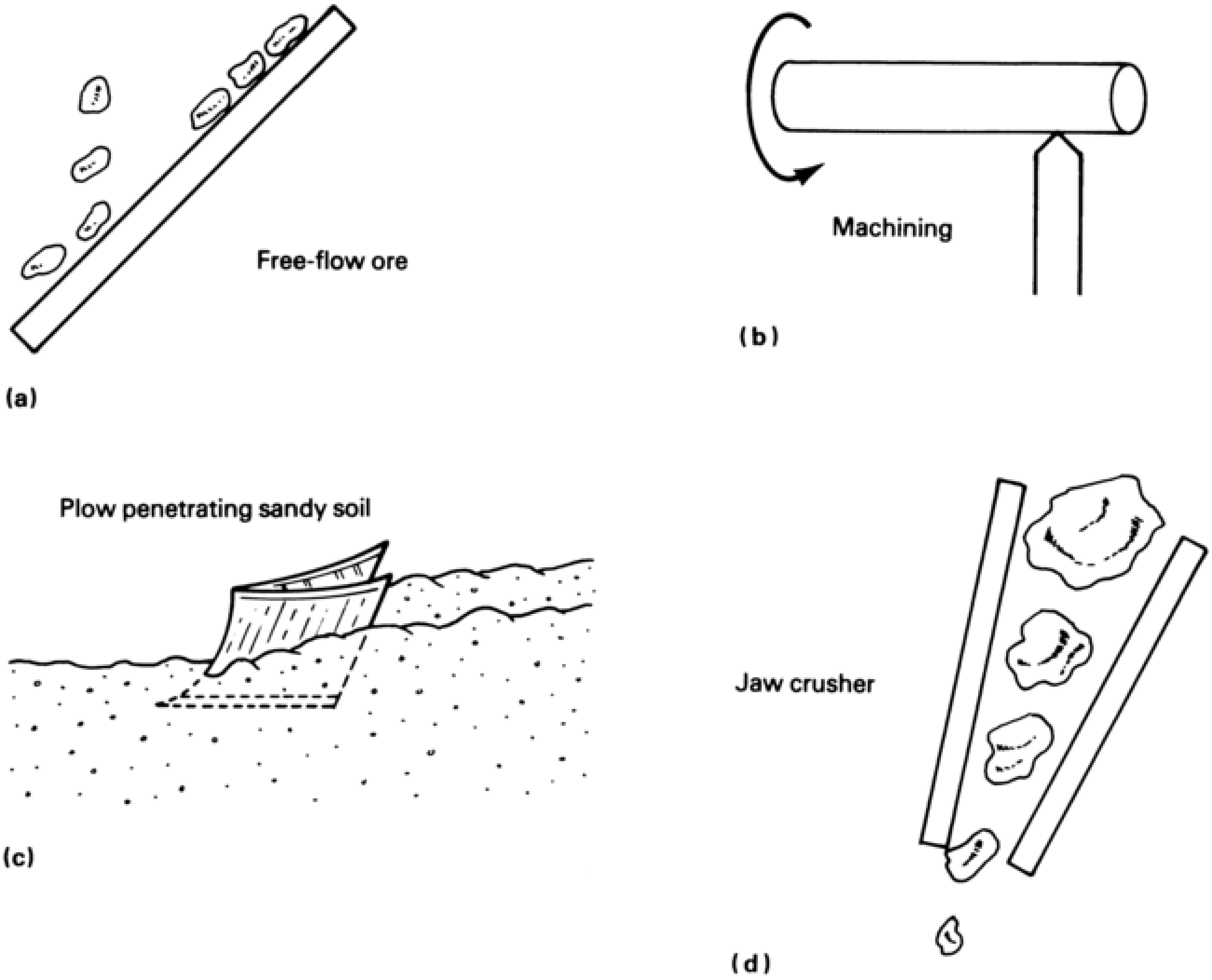

Fig. 1 Types of contact during abrasive wear. (a) Open two-body. (b) Closed two-body. (c) Open three-body. (d) Closed three-body

Abrasion can be divided further into low- stress, high-stress, and gouging classifications. Low-stress abrasion occurs when the abrasive remains relatively intact. High-stress abrasion exists when abrasive particles are being crushed (for example, in a ball mill where both the grinding balls and the abrasive material such as coal are worn down). In gouging, a relatively large abrasive surface cuts pieces off of another surface (for example, ore passing through a jaw crusher).

Several mechanisms have been proposed to explain how material is removed from a surface during abrasion. These mechanisms include fracture, fatigue, and melting. Due to the complexity of abrasion, no one mechanism completely accounts for all of the material loss.

Plowing is the process of displacing material from a groove to the sides. This occurs under light loads and does not result in any real material loss. However, the new surface created as a function of the material relocation is susceptible to loss through microfatigue. When the ratio of shear strength of the contact surface to the shear strength of the bulk rises to a high enough level—0.5 to 1.0—it is possible to develop a wedge on the front of an abrasive tip. In this case, the total amount of material displaced from the groove is greater than the material displaced to the sides. Wedge formation is still a fairly mild form of abrasive wear.

The most severe form of wear for a ductile material is cutting. During the cutting process, the abrasive tip removes chips from the second wear surface. This results mostly in material removal, as there is very little displaced material relative to the size of the groove. For every sharp abrasive particle there exists a critical angle that defines the difference between plowing and cutting. This angle is dependent on the material being abraded. The critical angles range from 45° for copper to 85° for aluminum (Ref 9, 10). Since all angles will be represented during abrasive wear, both cutting and plowing will be observed. Kato (Ref 11) and others have analyzed the effect of a rounded tip pushing through a surface. They found that the degree of penetration is

critical to the transition from plowing and wedge formation to cutting. When the degree of penetration, defined as depth of penetration divided by the contact area, exceeded about 0.2, cutting was the predominant mode of wear.

Archard's equation is commonly used to model abrasive wear (Ref 12):

$$W = k\frac{Ld}{H} \qquad \text{(Eq 1)}$$

This formula was derived for adhesive wear, but has also proven useful in measuring abrasive wear. W is the volume of material removed, k is a constant, L is load, d is distance traveled, and H is hardness of the material.

It is common to describe materials as having either good wear resistance or poor wear resistance. Wear resistance, R, is defined as the reciprocal of the wear volume:

$$R = \frac{1}{W} \qquad \text{(Eq 2)}$$

and the higher the value R, the better the wear resistance.

Brittle materials have an additional mode of abrasive wear, microfracture, which occurs when forces applied by the abrasive grain exceed the fracture toughness of a material. This is often the mode for wear removal of corrosive layers formed on the surface of metals.

Another mechanism of wear loss is thermally related processes such as the melting that can occur during a wear event. Loss via melting requires small, localized areas of strain-induced adiabatic heating. Research indicates that there can be enough temperature rise for dislocation recovery to take place near the abraded surface (Ref 13). The temperature rise can also contribute to the formation of a corrosion product layer.

It has been shown both experimentally and theoretically that the hardness of a material correlates with its abrasion rate. Extensive tests by Khruschov (Ref 14). documented an inverse relationship between abrasion rate and annealed hardness for pure metals (Fig. 2). Khruschov also tested steels of varying hardness and found an inverse linear relationship between wear and hardness, although the slope of the equation was different than that for pure metals.

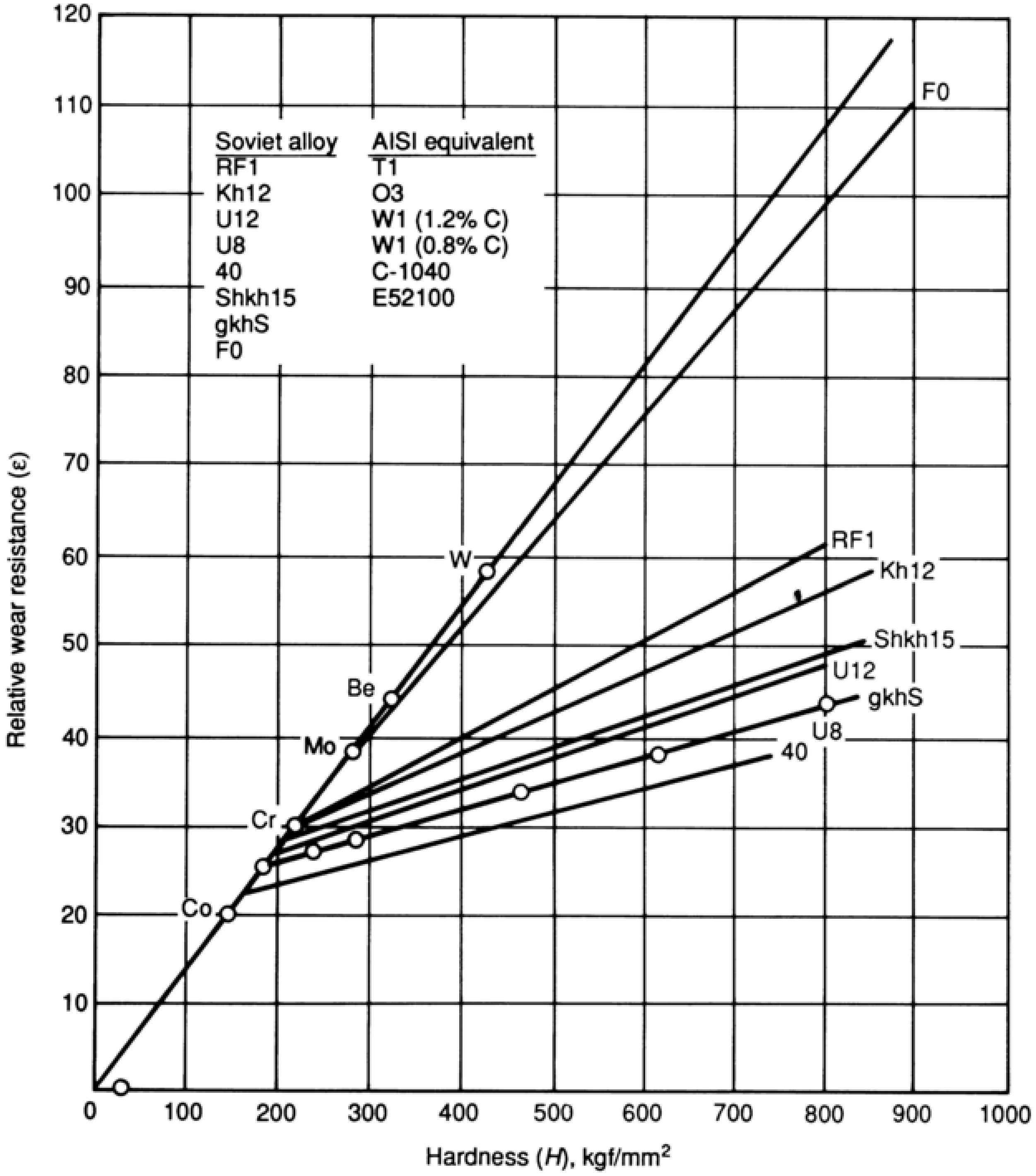

Fig. 2 Wear resistance versus hardness for pure metals and some steel alloys. Source: Ref 14

The hardness of abrasive particles is important to the rate of abrasive wear. As the hardness of the abrasive exceeds that of the wear material, the abrasive wear typically increases, as shown in Fig. 3.

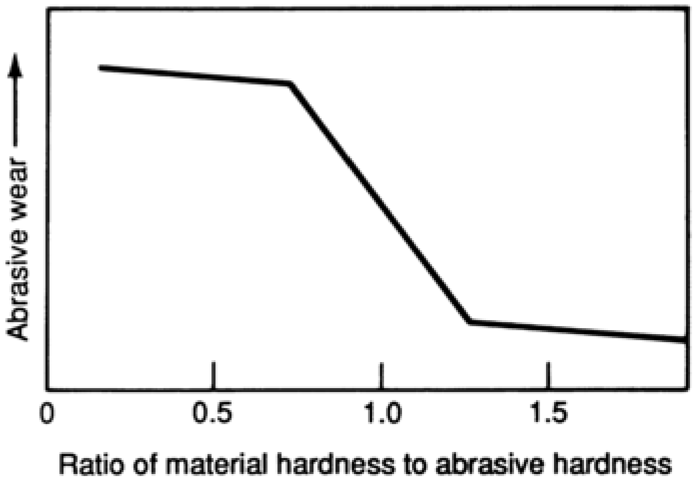

Fig. 3 Effect of abrasive hardness relative to material hardness on abrasive wear, showing the wear transition as wear surface becomes as hard as the abrasive

Elevated-temperature abrasion can produce what seems to be an unexpected result. Consider the case of a three-body abrasive-wear test on pure aluminum and copper (Ref 15). The copper abraded faster as the temperature increased to 400 °C (750 °F). At similar temperatures, the aluminum showed a slight decrease in abrasion. The increase for copper was attributed to an easily removed oxide coating. The decrease for aluminum was caused by a thin protective oxide film and abrasive particles embedded in the surface of the aluminum.

One common method of improving the abrasion resistance of a material is to add or form secondary-phase hard particles. Tungsten-carbide particles, with their high hardness (~2000 HV) and impressive toughness, are commonly added to steels to form materials more resistant to abrasion. In the tungsten-carbide/steel composite, the softer steel matrix is worn away, leaving the hard tungsten-carbide particles to protect the bulk material. This combination works best at temperatures below 700 °C (1300 °F).

Higher temperatures require other additives. Cr_3C_2 carbides are a good wear match for additions to nickel-base alloys. The combination is stable at higher temperatures. Above 800 °C (1500 °F) the carbides can actually work with other wear debris to form a protective glaze. Another hard particle that shows promise at high temperatures is TiC. Berns (Ref 16) has shown that in situ formed TiC particles, which are harder than Cr_3C_2, have promise for applications at 750 °C (1400 °F) in alloys with a NiCrAlSi matrix.

Erosive Wear. The mechanism of pure erosion, although extensively studied, is not fully understood. The impact of gases, liquids, solids, or a combination thereof onto a surface can result in erosive wear. The study of the erosion of ductile metals (Ref 17, 18, 19) is more advanced than that of brittle materials (Ref 20). Kosel (Ref 21) produced a review of solid-particle erosion on both ductile metals and brittle ceramics that includes corrosion effects. Additional sources (Ref 22) have attempted to bring more clarity to the field. Factors such as the rate of erosion, angle of impact, and velocity are all vitally important in predicting and reducing material loss.

In dry, elevated-temperature environments, erosion is usually a function of solid particles propelled by a gas stream. Erosion can be expected whenever there is a stream of entrained solids with a velocity above 1 m/s (2.2 mph). Thinning of the material subject to the gas stream can help identify damage caused by erosion. Other indications of erosion include localized changes in surface finish, or in some cases, the development of ripple patterns.

Erosion damage is sometimes mistaken for that of abrasion. Studying the wear environment is one way to differentiate between the two. Erosion occurs when particles rebound chaotically off of other surfaces; abrasion results from particles sliding along the surface. The wear on a boiler tube, for example, would be erosive due to the constant flow of airborne coal fines. The wear in a fluidized bed could be either abrasive or erosive, depending on the operating conditions.

Erosion in the absence of oxidation can be modeled in terms of three types of variables: material properties, impingement properties (such as flow variables), and particle properties. The material properties usually included in erosion models include strain-rate effects, hardness, and microstructure (Ref 23). Impingement properties include particle velocity (ν), angle of incidence (α), and particle concentration. Particle properties include shape, size, hardness, and resistance to fracture.

Materials are typically described in terms of being brittle or ductile. This is based on the response of the material to the angle of incidence of the flow (Ref 23). Brittle materials such as glass or ceramics exhibit a maximum erosion rate at a 90° angle of incidence; the wear decreases as the angle of incidence decreases. Ductile materials, such as pure metals and low-alloy steels, have a maximum erosion rate at a low angle of incidence, usually 15 to 30°, as shown in Fig. 4).

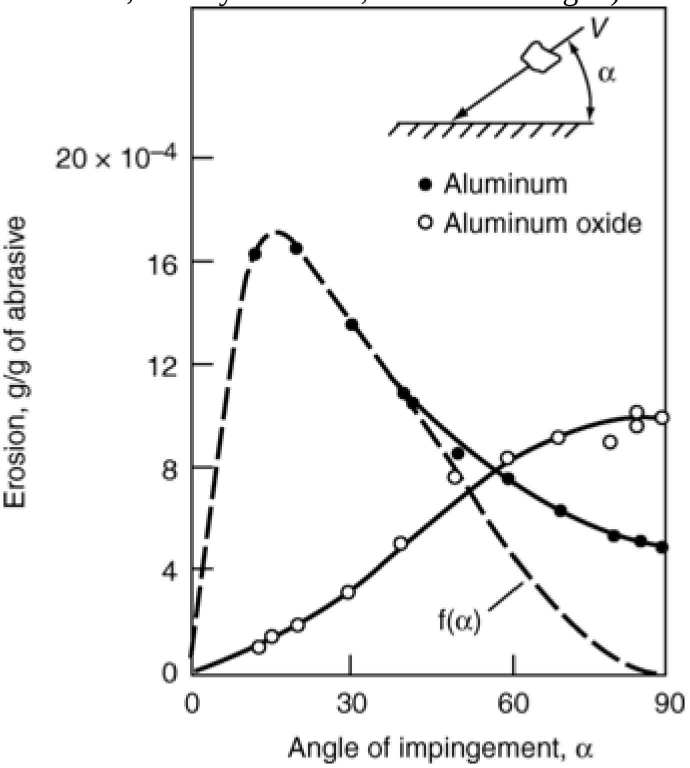

Fig. 4 Effect of angle of impingement on erosion rate for a ductile and brittle material, from Finnie (Ref 22). Note: aluminum oxide (Al_2O_3) data has been multiplied by 10 to better show the results. The line f(α) shows a projected model.

An oxidized metal can exhibit both brittle and ductile properties: the bulk metal can be ductile while its corrosion layer is brittle. In severe erosive conditions, the damage caused by an abrasive may penetrate through the brittle oxide layer and produce wear to the ductile base material. In the case of less-severe erosion conditions, the abrasive may remove the brittle oxide layer while having no impact on the ductile bulk material. In other instances, wear losses can include both the ductile bulk metal and semibrittle oxide layer. In this last case, the maximum erosion rate will be at an intermediate angle of incidence.

A fairly simple power-law model has been developed to equate erosion rate, *E*, with particle velocity:

$$E = kv^n \qquad \text{(Eq 3)}$$

where *k* is a constant and *n* is a velocity exponent that is dependent on material and erosion conditions. The value of *n* typically ranges from 2 to 2.5 for metals and 2.5 to 3 for ceramics.

The size of the abrasive particle seems to have little effect for particles larger that 100 μm. For particle sizes smaller than 100 μm the erosion rate decreases with particle size. There is very little erosion for particle sizes smaller than 5 to 10 μm.

The addition of oxidation to the erosion process leads to damage that is a function not only of material properties, but also of properties of the environment. The "Erosion by Liquid and Solid Impact" conferences have been a leading forum for research into the combined effects of oxidation and erosion (Ref 24, 25). While there may be some initial decrease in erosion as temperatures increase, pure erosion tends to increase as temperatures increase for both metals and ceramics. The combined erosion-corrosion process tends to show further increases in material loss at increasing temperatures. Most high-temperature alloys, designed for service below 850 °C (1560 °F), depend on a chrome oxide layer for protection against rapid oxidation. The ability of materials to resist further oxidation depends on a solid, nonporous adherent layer. Figure 5 shows the effect of erosion on a material forming a nonprotective brittle oxide, in this case Ti-6Al- 4V eroded at 700 °C (1300 °F) using 270 μm SiO_2 at a particle velocity of 20 m/s (45 mph). The dark areas are a thick oxide layer, and the

light areas have a thin oxide nonprotective layer, subject to continued oxidation and erosion. In this case, the erosion accelerates the corrosion by helping remove the brittle, oxidized surface. In contrast, Fig. 6 shows the erosion of a metal that forms a protective oxide layer, in this case type 310 stainless steel (UNS S31000) eroded using the same conditions. In this case, only small chips can be found in the protective layer. The surface also shows mechanical damage, such as small cracks and depressions, where the abrasive impacted the surface.

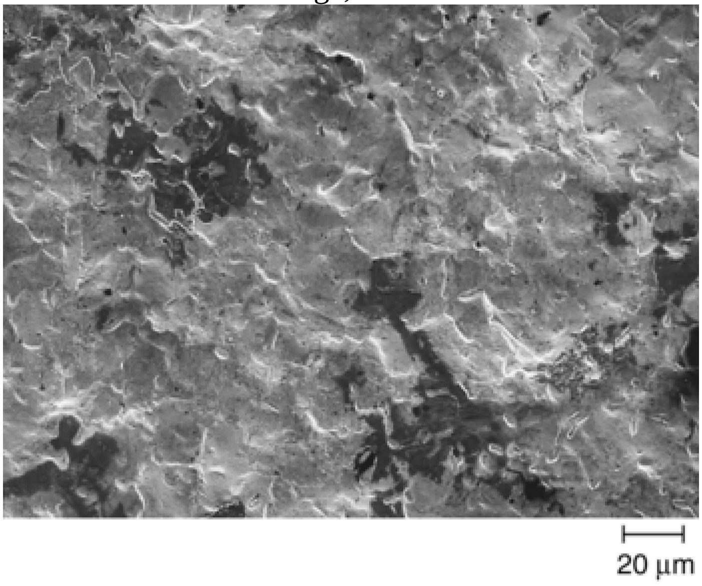

Fig. 5 Erosion on nonprotective oxide layer. Ti-6Al-4V sample eroded at 700 °C (1300 °F) in air using 270 µm SiO_2 abrasive at 20 m/s (45 mph)

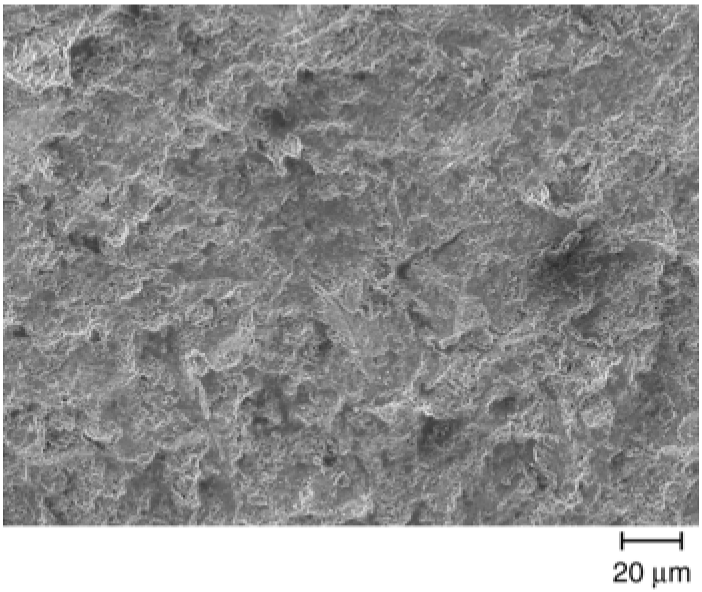

Fig. 6 Erosion on a protective oxide layer. Type 310 stainless steel (UNS S31000) sample eroded at 700 °C (1300 °F) in air using 270 µm SiO_2 abrasive at 20 m/s (45 mph)

Models of oxidation-enhanced erosion typically have several degradation regimes, depending on the temperature and the erodent energy (Ref 26). These can be classified by whether the scale thickness, ζ, maintains a constant thickness, ζ_{ss}, and if the removal rate is constant with respect to time. If the removal of the oxide is due to erosion alone, the removal rate can be represented as:

$$\frac{d\zeta}{dt} = -k' \quad \text{(Eq 4)}$$

The scale thickness, ζ, often grows at a rate proportional to $t^{0.5}$, and this growth rate is called the parabolic rate. The oxide growth rate $d\zeta/dt$ is described by:

$$\frac{d\zeta}{dt} = \frac{k_p}{\zeta} \qquad \text{(Eq 5)}$$

where k_p represents the parabolic rate constant.

If a continuous protective scale remains on the surface of the material during erosion-oxidation, then there is a parabolic rate constant $k_{o,e}$ that is a function of oxidation and erosion conditions. Further, if the oxide removal rate constant is represented by k', then the previous equation can be rewritten as:

$$\frac{d\zeta}{dt} = \frac{k_{o,e}}{\zeta} - k' \qquad \text{(Eq 6)}$$

For the removal of a mix composite layer where the oxide removal rate is much faster than the parabolic rate, $k_{o,e}$, the rate will be dependent on time and the removal rate can be written as:

$$x = -k''t \qquad \text{(Eq 7)}$$

Finally where no oxide layer forms, the loss will only be due to erosion of the metal. This removal rate will be dependent on time and can be written as:

$$x = -k'''t \qquad \text{(Eq 8)}$$

Rishel (Ref 27) has illustrated the different oxidation/erosive regimes in Fig. 7. The regimes include, starting at the top moving by increasing erodent energy:

- Oxidation where the erodent has no effect. In this case if the removal rate constant, $k_{o,e}$, divided by ζ_{ss} is much greater than outer surface removal rate k', so the loss rate is dependent on the oxidation rate.
- Erosion enhanced oxidation, EEO, where the erodent damages the oxide layer and leads to faster oxidation. In this case there are three forms of EEO. In type I, the scaling rate is essentially unaffected by the erosion, so $k_{o,e} = k_p$. For type II, the erosion increases the rate of oxide-scale formation so $k_{o,e} > k_p$. For type III of EEO, the erosion causes spalling of the oxide scale, as seen in Fig. 5.
- The regime of oxidation-modified erosion, where the oxidation enhances the ability of the erodent to remove material. In this case, the total removal is a function of time.
- Bulk erosion, where the erodent energy is able to cut through the surface scale and remove the bulk material below the scale. In this case, the total removal is also just a function of time. Maps of these regimes have been produced to help illustrate the different mechanisms in operation (Ref 28).

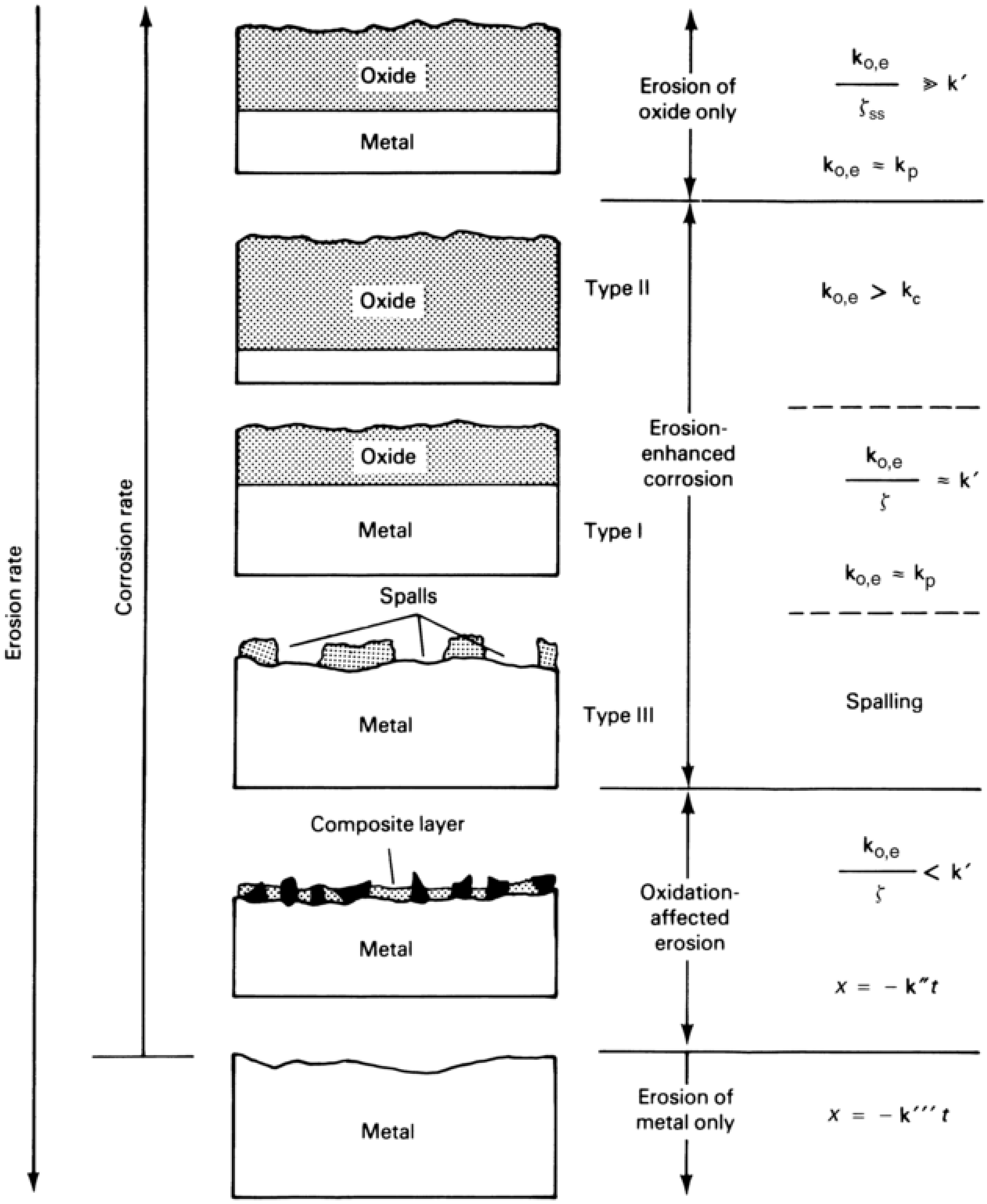

Fig. 7 Erosion-corrosion interaction regimes, in order of increasing corrosion. Source: Ref 27

In a study of stainless steels exposed to a combustion atmosphere from a propane-fired abrasive-jet machine at 975 °C, (1790 °F), Ives (Ref 29) found the velocity dependence of erosion rate, *E*, for a 90° impact of $v^{1.8}$. The tests were conducted using a commercial grade of SiC with the average particle size of ~135 μm. By comparison, the velocity dependence at room temperature was $v^{2.5}$. The results show the thickness loss decreased with increasing chromium content (Table 1). Aluminum additions had a beneficial effect under the conditions of excess fuel at 1000 °C (1800 °F) and a particle velocity of 55 m/s (180 ft/s, or 123 mph).

Table 1 Erosion-corrosion test results, using excess fuel at 1000 °C (1800 °F) and 55 m/s (123 mph) particle velocity of ~135 μm (5 mils) SiC abrasive

Alloy	Major alloying constituents, wt%	Thickness loss, μm/h	
		α = 90°	**α = 45°**
I-671	51Cr, 47Ni	19	31
I-601	22Cr, 61Ni, 1.2Al	29	62
I-800	33Cr, 21Ni, 42Fe	70	80
310	25Cr, 21Ni, 52Fe	73	80
446	25Cr, 72Fe	90	130
316	17Cr, 12Ni, 68Fe, 2.5Mo	150	160
304	19Cr, 10Ni, 68Fe	195	190

α is angle of impingement. Source: Ref 29

Erosion-corrosion maps have been developed in order to show the effects of different variables and to identify different degradation mechanisms (Ref 30). These maps should help the design engineer select materials and understand the mechanisms involved in erosion-corrosion at elevated temperatures (Ref 31).

Fretting Wear. Fretting is a form of wear that occurs between contacting surfaces subjected to cyclic relative motion of extremely small amplitude, usually in the range of 1 to 100 μm. This wear typically occurs on surfaces that are not intended to move in this manner, such as bearing mounts, hubs, and shafts. This is often considered a form of corrosion since usually the debris formed rapidly oxidizes.

The relative motion between the two surfaces causes fretting. The contact creates an abrasive wear on the oxide films on both surfaces, removing the passive layer while leaving oxide debris particles. These debris particles contribute to the wear process, increasing the wear as time passes. The passive layer on a fretting part is continuously restored and destroyed as new material is exposed to the atmosphere and oxidized. The destruction of the layer produces additional wear debris, which goes on to produce more corrosion and wear.

In steels, this debris layer can form a white etch-resistant layer, which is extremely hard and brittle (Fig. 8). This layer has been described as martensite.

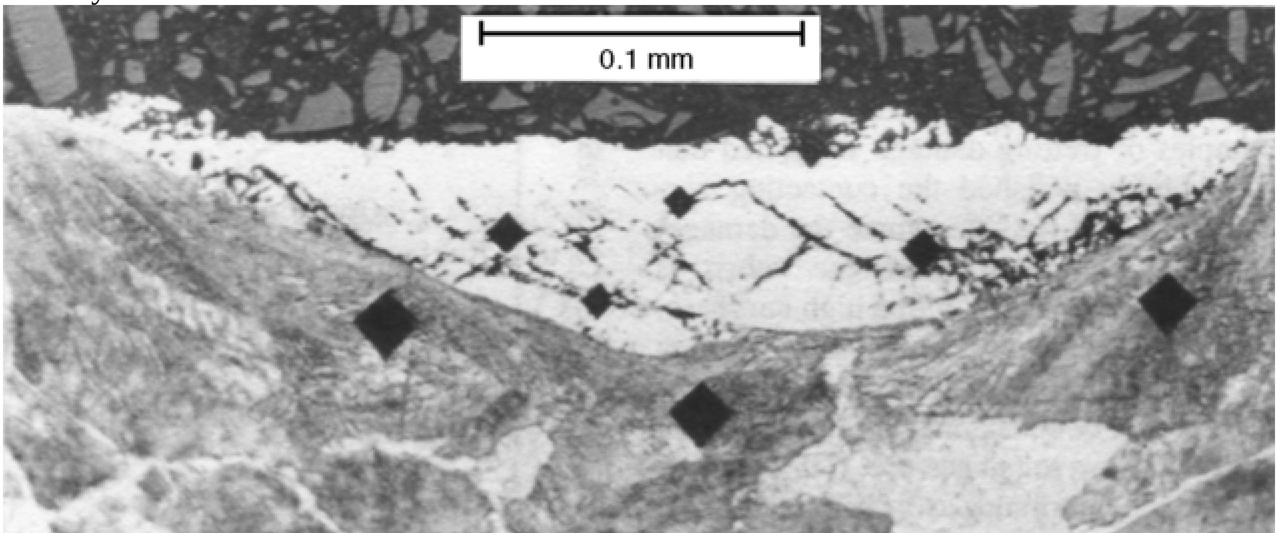

Fig. 8 Cross section of a white layer of martensite produced by fretting, after 105 fretting cycles and a contact stress of 40 MPa (5.8 ksi). Source: Ref 32

While not usually considered a major issue, fretting is known to occur at elevated temperatures. Examples of this are found in gas and steam turbines. Fretting at elevated temperatures can form low friction glazes (Ref 33), which will reduce the loss material.

Sliding Wear. Adhesive, oxidational, and sliding wear refers to the wear that takes place when one surface "slides" over another. This typically occurs in machining, unlubricated machinery, and material-handling operations. Machining is an example of the adhesive-wear process. At the tip of the cutting tool, the chip is separated from the bulk of the part. This chip may strike the tool further back. This can lead to both the dulling of the tip and crater wear further back. During high-speed machining tool temperatures can reach 1000 °C (1800 °F), which can cause oxidation of the tool surface. Typically, the self- formed oxide layer will be less resistant to adhesive wear than the bulk of the tool. As a consequence, wear damage accelerates as competition between the removal of the oxide film and the formation of fresh oxide occurs.

Oxidation has long been considered a fundamental aspect of sliding wear (Ref 34). Oxidation can occur at relatively low sliding velocities, in the range of 0.2 to 1 m/s (8 to 40 in./s) (Ref 35). Oxidation accelerates with increasing temperature and can lead to the formation of a protective layer under many conditions. These layers tend to be in the range of 3 to 4 μm thick and are quite beneficial in unlubricated conditions.

References cited in this section

8. R. Blickensderfer, B.W. Madsen, and J.H. Tylczak, Comparison of Several Types of Abrasive Wear Tests, *Proc. Int. Conf. Wear of Materials* (Vancouver, B.C., Canada), American Society of Mechanical Engineers, 1985, p 313

9. A.J. Sedriks and T.O. Mulhearn, The Effect of Work-Hardening on the Mechanics of Cutting in Simulated Abrasive Processes, *Wear,* Vol 7, 1964, p 451–459

10. T. Sasaki and K. Okamura, The Cutting Mechanism of Abrasive Grain, *Bull. JSME,* Vol 12, 1960, p 547

11. K. Kato, Wear Mode Transitions, *Scr. Metall.,* Vol 24, 1990, p 815–820

12. J.F. Archard, Contact and Rubbing of Flat Surfaces, *J. Appl. Phys.,* Vol 24, 1953, p 981

13. G. Sundararajan, A New Model for Two- Body Abrasive Wear Based on the Localization of Plastic Deformation, *Wear,* Vol 117, 1987, p 1–35

14. M.M. Khruschov, Resistance of Metals to Wear by Abrasion, as Related to Hardness, *Proc. Conf. Lubrication Wear,* Institution of Mechanical Engineers, London, 1957, p 655–659

15. S. Soemantri, A.C. McGee, and I. Finnie, Some Aspects of Abrasive Wear at Elevated Temperatures, *Wear of Materials,* 1985, Proc. Int. Conf. Wear of Materials, American Society of Mechanical Engineers, 1985, p 338–344

16. H. Berns and B Wewers, Development of an Abrasion Resistant Steel Composite with in situ TiC Particles, *Wear,* Vol 251, 2001, p 1386–1395

17. G.P. Tilly, Erosion Caused by Impact of Solid Particles in Wear, *Erosion,* Vol 13, *Treatise of Materials Science and Technology,* Academic Press, 1979

18. A.W. Ruff and S.M. Wielerhorn, Erosion by Solid Particle Impact, *Erosion,* Vol 16, *Treatise on Material Science and Technology,* Academic Press, 1979

19. W.F. Adler, Ed., STP 664, *Erosion: Prevention and Useful Applications,* ASTM, 1979

20. J.E. Ritter, Ed., *Erosion of Ceramic Materials,* Trans. Tech. Publications, Zurich, Switzerland, 1992

21. T.H. Kosel, Solid Particle Erosion, *Friction, Lubrication, and Wear Technology,* Vol 18, *ASM Handbook,* ASM International 1992, p 199–213

22. I. Finnie, Some Reflections on the Past and Future of Erosion, *Wear,* Vol 186–187, 1995, p 1–10

23. G. Sundararajan, The Solid Particle Erosion of Metallic Materials: The Rationalization of the Influence of Material Variables, *Wear,* Vol 186–187, 1995, p 129–144

24. I. Hutchings, and J. Little, Proc. Eighth Int. Conf. Erosion by Liquid and Solid Impact: ELSI VIII, *Wear,* Vol 186–187, 1995

25. J. Little, Proc. Ninth Int. Conf. Erosion by Liquid and Solid Impact: ICEAW I, *Wear,* Vol 233–235, 1999

26. R.H. Barkalow and F.S. Pettit, Corrosion/ Erosion of Materials in Coal Combustion Gas Turbines, *Proc. Conf. Corrosion/Erosion of Cal Conversion System Materials* (Berkeley, CA), 24–26 Jan 1979, National Association of Corrosion Engineers, 1979, p 139–173

27. D.M. Rishel, F.S. Petit, and N. Birks, Some Principal Mechanisms in the Simultaneous Erosion and Corrosion Attack of Metals at High Temperature, paper 16, *Proc. Conf. Corrosion-Erosion-Wear of Materials at Elevated Temperatures* (Berkeley, CA), 31 Jan–2 Feb 1990 A.V. Levy, Ed., NACE/ EPRI/LBL/DOE-FE

28. D.J. Stephenson and J.R. Nicholls, Modelling the Influence of Surface Oxidation on High Temperature Erosion, *Wear,* Vol 186–187, 1995, p 284–290

29. L.K. Ives, Erosion of 310 Stainless Steel at 975 °C in Combustion Gas Atmospheres, *Trans. ASME,* April 1977, p 126–132

30. M.M. Stack and L. Bray, Interpretation of Wastage Mechanisms of Materials Exposed to Elevated Temperature Erosion-Corrosion Using Erosion-Corrosion Maps and Computer Graphics, *Wear,* Vol 186–187, 1995, p 273–283

31. M.M. Stack, Looking Beyond the Millennium: Critical Issues in the Evaluation of Materials Performance for Resistance to Erosive Wear in Corrosive Conditions, *Wear,* Vol 233–235, 1999, p 484–496

32. J. Dobromirski and I.O. Smith, Metallographic Aspects of Surface Damage, Surface Temperature, and Crack Initiation in Fretting Fatigue, *Wear,* Vol 117, 1987, p 347–357

33. M.M. Hamdy and R.B. Waterhouse, The Fretting-Fatigue Behavior of a Nickel- Based Alloy (Inconel 718) at Elevated Temperatures, *Proc Int. Conf Wear of Materials 1979,* American Society of Mechanical Engineers, 1979, p 351–355

34. T.F.J. Quinn, J.L. Sullivan, and D.M. Rowson, Origins and Development of Oxidational Wear at Low Ambient Temperatures, *Wear,* Vol 94, 1984, p 175–191

35. G. Straffelini, D. Trabucco, and A. Molinari, Oxidative Wear of Heat-Treated Steels, *Wear,* Vol 250, 2001, p 485–491

J.H. Tylczak and T.A. Adler, Gaseous Corrosion-Wear Interactions, *Corrosion: Fundamentals, Testing, and Protection*, Vol 13A*, ASM Handbook*, ASM International, 2003, p 338–344

Gaseous Corrosion-Wear Interactions

Joseph H. Tylczak and Thomas A. Adler, Albany Research Center, U.S. Department of Energy

---

Measurement

The techniques of measuring wear and corrosion have resulted in the creation of many standard practices and specialized pieces of equipment. This Volume outlines many of the corrosion-measurement techniques, while

Friction, Wear, and Lubrication, Vol 18, *ASM Handbook,* (Ref 36) outlines many of the wear-measurement techniques. Jet, whirling arm, and slinger tests have all been used successfully in the field of erosion. While the jet test (Ref 37) is most commonly used, there are definite advantages to the whirling-arm test. With the whirling-arm test, the impact velocity is well known, and an entire face of the specimen can be eroded, producing a more uniform surface. The machining test is the most commonly used high-temperature abrasive test, because the process of machining produces an elevated temperature. For slow abrasive elevated-temperature tests one of the most commonly used is a high- temperature ring-on-disk test.

Measurement of the interaction between corrosion and wear modes of damage is more difficult. One standard for measuring these interactions is ASTM G 119 (Ref 38). The scope of this standard is aqueous corrosion and wear, and applies to systems in liquid solutions or slurries. However, aspects of it can be adapted to dry corrosion and wear interactions as well.

The measurement of corrosion, wear, and corrosion/wear interactions is a multistep process. Each component of the interaction must be measured separately. The results may then be combined to create a complete picture of the damage process.

An example of this process is the measurement of the degradation on combustion walls in coal-fired boilers. First, one must fully understand the environment around the combustion walls. This would include knowing the temperature, gas chemistry, velocity of the gases, and the abrasive causing the erosion. After determining these details, the following tests might be used for measurements. First, an oxidation test should be performed in the combustion gas in the boiler. In this case, the gas should include the impurities (such as SO_2 and HCl) as well as the major gases, since they will greatly affect the scales formed. This measurement will show the loss rate due to the gaseous corrosion or oxidation process. An erosion test would be run, using an abrasive similar in both type and size to that found in the ash of the boiler. In the case of a coal-fired boiler, a quartz abrasive would probably best represent the abrasive found in the ash. The erosion test would need to be run in a neutral (nonoxidizing) atmosphere to block the effects of the corrosion. Elevated temperature would be necessary, since temperature alone has been shown to affect erosion rates. Different test velocities for the abrasive may be run to determine the sensitivity of the erosion rate to velocity. Finally, combined wear-corrosion tests would need to be run, fully simulating the boiler conditions. The synergistic effect can then be determined (after converting all the loss rates to a common unit such as surface recession rate in mm/day) by subtracting the individual corrosion and erosion results from the final combined test. The resulting number represents the degree to which oxidation-wear interactions increase the wear:

$$W_s = W_T - W_e - C \quad \text{(Eq 9)}$$

where W_s is the erosion-corrosion synergy or interaction term, W_T is the total loss, W_e is the wear due to erosion, and C is the loss due to corrosion. The loss from erosion-corrosion interaction can then be divided by the total loss to get the percentage loss due to the interaction ($S_{e\text{-}c}$):

$$S_{e\text{-}c} = W_s/W_T \quad \text{(Eq 10)}$$

References cited in this section

36. P.J. Blau, Ed., *Friction, Lubrication, and Wear Technology,* Vol 18, *ASM Handbook,* ASM International, 1992

37. "Standard Test Method for Conducting Erosion Tests by Solid Particle Impingement Using Gas Jets," G 76-02, *Wear and Erosion; Metal Corrosion,* Vol 03.02, *Annual Book of ASTM Standards,* ASTM, 2002

38. "Standard Guide for Determining Synergism Between Wear and Corrosion," G 119- 93, *Wear and Erosion; Metal Corrosion,* Vol 03.02, *Annual Book of ASTM Standards,* ASTM, 1998

J.H. Tylczak and T.A. Adler, Gaseous Corrosion-Wear Interactions, *Corrosion: Fundamentals, Testing, and Protection*, Vol 13A, *ASM Handbook*, ASM International, 2003, p 338–344

Gaseous Corrosion-Wear Interactions

Joseph H. Tylczak and Thomas A. Adler, Albany Research Center, U.S. Department of Energy

Control

There is no definitive answer to the problem of wear, corrosion, and wear-corrosion interactions. In some environments, a trade-off between corrosion and wear can lead to a minimum of material loss. At intermediate temperatures, a corrosive layer can serve to protect the bulk material from wear (Ref 39). At high temperatures, over 800 °C (1500 °F), protective mixed-oxide layers can form, causing a decrease in the total loss rate.

Changing temperatures in manufacturing environments may have the potential to decrease material loss. Some abrasives grow softer with increased temperatures and thus decrease wear. Additional research needs to be done to determine if there are any manufacturing processes where this would be a viable solution.

In certain circumstances, changing the physical environment may offer potential for decreased wear and corrosion. Sulfur reacts with metals to form nonprotective coatings. Decreasing the sulfur compounds in a manufacturing environment, such as using a lower-sulfur coal, can thus reduce the material loss associated with both wear and corrosion.

Efforts have been made to identify advanced materials resistant to wear-corrosion (Ref 40). Coatings, for example, have been shown to offer viable wear-corrosion protection. This enables one to put high-alloy materials on the surface where they are most needed. In some cases, applying coatings to the base material can minimize material loss. There are six common coating techniques used for wear-corrosion control. Physical vapor disposition (PVD) produces a very thin (2–10 μm, or 0.08–0.4 mil) protective layer of a material that is vaporized and deposited. Chemical vapor deposition (CVD), which produces a 5 to 15 μm (0.2 to 0.6 mil) protective layer, is made by a gas-phase decomposition of a material onto a part. Flame spray uses a heated flame to partially melt a thin (0.25–0.6 mm, or 0.01–0.02 in.) coating, commonly a high- chrome alloy, and adhere it to the base material. Diffusion coating involves covering the surface to be treated with a mostly inert material such as alumina, and heating resulting in an interaction that creates a thin (0.25–0.3 mm, or 0.01–0.012 in.) protective layer. Weld overlays consist of a thicker (1–2 mm, or 0.04–0.08 in.) protective layer of higher-alloy metal welded over the base material. Thick (12–20 mm, or 0.47–0.79 in.) refractory coatings, such as silicon carbide base materials, can be bonded to a metallic base. Experience indicates that these all have useful applications, but overlays and refractory coatings may be the most resistant to severe erosion-corrosion.

Different environments require different solutions. In some instances, engineering changes to temperatures, equipment design, flow rates, and so forth, can minimize wear and corrosion. Lubrication, when it can be used, is a partial solution. Selecting advanced materials, such as ceramics or intermetallics, is another possible option. There are three possibilities for reducing erosion-corrosion damage: (a) modify the erodent, (b) change the material, and (c) change the aerodynamics so the particle impacts are less damaging (Ref 41).

The more that is known about wear-corrosion interaction and the environmental specifics of a given manufacturing process, the more likely it is that solutions can be found to the wear-corrosion problem.

References cited in this section

39. A. Levy, J. Yan, and J. Patterson, Elevated Temperature Erosion of Steels, *Wear,* Vol 108, 1986, p 43–60

40. V. Shanov and W. Tabakoff, Erosion Resistance of Coatings for Metal Protection at Elevated Temperatures, *J. Surf. Coat. Technol.,* Vol 86–87, 1997, p 86–93

41. J. Stringer, Practical Experience with Wastage at Elevated Temperatures in Coal Combustion Systems, *Wear,* Vol 186–187, 1995, p 11–27

J.H. Tylczak and T.A. Adler, Gaseous Corrosion-Wear Interactions, *Corrosion: Fundamentals, Testing, and Protection*, Vol 13A, *ASM Handbook*, ASM International, 2003, p 338–344

Gaseous Corrosion-Wear Interactions

Joseph H. Tylczak and Thomas A. Adler, Albany Research Center, U.S. Department of Energy

References

1. S. Collins, Biomass-Fired Plants Face Down Near-Term Challenges, *Power,* Vol 137, 1993, p 51–53

2. M.A. Uusitalo, P.M.J. Vuoristo, and M.A. Mäntylä, Elevated Temperature Erosion- Corrosion of Thermal Sprayed Coatings in Chlorine Containing Environments, *Wear,* Vol 252, 2002, p 586–594

3. B.S. Mann and B. Prakash, High Temperature Friction and Wear Characteristics of Various Coating Materials for Steam Valve Spindle Application, *Wear,* Vol 240, 2000, p 223–230

4. P.M. Rogers, I.M. Hutchings, and J.A. Little, Coatings and Surface Treatments for Protection against Low-Velocity Erosion- Corrosion in Fluidized Beds, *Wear,* Vol 186–187, 1995, p 238–246

5. H. Berns and S. Koch, High Temperature Sliding Abrasion of a Nickel-Base Alloy and Composite, *Wear,* Vol 225–229, 1999, p 154–162

6. S. Dolinšek, B. Šuštaršič, and J. Kopač, Wear Mechanisms of Cutting Tools in High- Speed Cutting Processes, *Wear,* Vol 250, 2001, p 349–356

7. H. Stewart, R. Rapp, M. Padilla, and A. Ried, *Proc Tenth Int. Wood Machining Seminar,* Forest Products Laboratory, University of California, Berkeley, CA, 1985, p 54–71

8. R. Blickensderfer, B.W. Madsen, and J.H. Tylczak, Comparison of Several Types of Abrasive Wear Tests, *Proc. Int. Conf. Wear of Materials* (Vancouver, B.C., Canada), American Society of Mechanical Engineers, 1985, p 313

9. A.J. Sedriks and T.O. Mulhearn, The Effect of Work-Hardening on the Mechanics of Cutting in Simulated Abrasive Processes, *Wear,* Vol 7, 1964, p 451–459

10. T. Sasaki and K. Okamura, The Cutting Mechanism of Abrasive Grain, *Bull. JSME,* Vol 12, 1960, p 547

11. K. Kato, Wear Mode Transitions, *Scr. Metall.,* Vol 24, 1990, p 815–820

12. J.F. Archard, Contact and Rubbing of Flat Surfaces, *J. Appl. Phys.,* Vol 24, 1953, p 981

13. G. Sundararajan, A New Model for Two- Body Abrasive Wear Based on the Localization of Plastic Deformation, *Wear,* Vol 117, 1987, p 1–35

14. M.M. Khruschov, Resistance of Metals to Wear by Abrasion, as Related to Hardness, *Proc. Conf. Lubrication Wear,* Institution of Mechanical Engineers, London, 1957, p 655–659

15. S. Soemantri, A.C. McGee, and I. Finnie, Some Aspects of Abrasive Wear at Elevated Temperatures, *Wear of Materials,* 1985, Proc. Int. Conf. Wear of Materials, American Society of Mechanical Engineers, 1985, p 338–344

16. H. Berns and B Wewers, Development of an Abrasion Resistant Steel Composite with in situ TiC Particles, *Wear,* Vol 251, 2001, p 1386–1395

17. G.P. Tilly, Erosion Caused by Impact of Solid Particles in Wear, *Erosion,* Vol 13, *Treatise of Materials Science and Technology,* Academic Press, 1979

18. A.W. Ruff and S.M. Wielerhorn, Erosion by Solid Particle Impact, *Erosion,* Vol 16, *Treatise on Material Science and Technology,* Academic Press, 1979

19. W.F. Adler, Ed., STP 664, *Erosion: Prevention and Useful Applications,* ASTM, 1979

20. J.E. Ritter, Ed., *Erosion of Ceramic Materials,* Trans. Tech. Publications, Zurich, Switzerland, 1992

21. T.H. Kosel, Solid Particle Erosion, *Friction, Lubrication, and Wear Technology,* Vol 18, *ASM Handbook,* ASM International 1992, p 199–213

22. I. Finnie, Some Reflections on the Past and Future of Erosion, *Wear,* Vol 186–187, 1995, p 1–10

23. G. Sundararajan, The Solid Particle Erosion of Metallic Materials: The Rationalization of the Influence of Material Variables, *Wear,* Vol 186–187, 1995, p 129–144

24. I. Hutchings, and J. Little, Proc. Eighth Int. Conf. Erosion by Liquid and Solid Impact: ELSI VIII, *Wear,* Vol 186–187, 1995

25. J. Little, Proc. Ninth Int. Conf. Erosion by Liquid and Solid Impact: ICEAW I, *Wear,* Vol 233–235, 1999

26. R.H. Barkalow and F.S. Pettit, Corrosion/ Erosion of Materials in Coal Combustion Gas Turbines, *Proc. Conf. Corrosion/Erosion of Cal Conversion System Materials* (Berkeley, CA), 24–26 Jan 1979, National Association of Corrosion Engineers, 1979, p 139–173

27. D.M. Rishel, F.S. Petit, and N. Birks, Some Principal Mechanisms in the Simultaneous Erosion and Corrosion Attack of Metals at High Temperature, paper 16, *Proc. Conf. Corrosion-Erosion-Wear of Materials at Elevated Temperatures* (Berkeley, CA), 31 Jan–2 Feb 1990 A.V. Levy, Ed., NACE/ EPRI/LBL/DOE-FE

28. D.J. Stephenson and J.R. Nicholls, Modelling the Influence of Surface Oxidation on High Temperature Erosion, *Wear,* Vol 186–187, 1995, p 284–290

29. L.K. Ives, Erosion of 310 Stainless Steel at 975 °C in Combustion Gas Atmospheres, *Trans. ASME,* April 1977, p 126–132

30. M.M. Stack and L. Bray, Interpretation of Wastage Mechanisms of Materials Exposed to Elevated Temperature Erosion-Corrosion Using Erosion-Corrosion Maps and Computer Graphics, *Wear,* Vol 186–187, 1995, p 273–283

31. M.M. Stack, Looking Beyond the Millennium: Critical Issues in the Evaluation of Materials Performance for Resistance to Erosive Wear in Corrosive Conditions, *Wear,* Vol 233–235, 1999, p 484–496

32. J. Dobromirski and I.O. Smith, Metallographic Aspects of Surface Damage, Surface Temperature, and Crack Initiation in Fretting Fatigue, *Wear,* Vol 117, 1987, p 347–357

33. M.M. Hamdy and R.B. Waterhouse, The Fretting-Fatigue Behavior of a Nickel- Based Alloy (Inconel 718) at Elevated Temperatures, *Proc Int. Conf Wear of Materials 1979,* American Society of Mechanical Engineers, 1979, p 351–355

34. T.F.J. Quinn, J.L. Sullivan, and D.M. Rowson, Origins and Development of Oxidational Wear at Low Ambient Temperatures, *Wear,* Vol 94, 1984, p 175–191

35. G. Straffelini, D. Trabucco, and A. Molinari, Oxidative Wear of Heat-Treated Steels, *Wear,* Vol 250, 2001, p 485–491

36. P.J. Blau, Ed., *Friction, Lubrication, and Wear Technology,* Vol 18, *ASM Handbook,* ASM International, 1992

37. "Standard Test Method for Conducting Erosion Tests by Solid Particle Impingement Using Gas Jets," G 76-02, *Wear and Erosion; Metal Corrosion,* Vol 03.02, *Annual Book of ASTM Standards,* ASTM, 2002

38. "Standard Guide for Determining Synergism Between Wear and Corrosion," G 119- 93, *Wear and Erosion; Metal Corrosion,* Vol 03.02, *Annual Book of ASTM Standards,* ASTM, 1998

39. A. Levy, J. Yan, and J. Patterson, Elevated Temperature Erosion of Steels, *Wear,* Vol 108, 1986, p 43–60

40. V. Shanov and W. Tabakoff, Erosion Resistance of Coatings for Metal Protection at Elevated Temperatures, *J. Surf. Coat. Technol.,* Vol 86–87, 1997, p 86–93

41. J. Stringer, Practical Experience with Wastage at Elevated Temperatures in Coal Combustion Systems, *Wear,* Vol 186–187, 1995, p 11–27

J.H. Tylczak and T.A. Adler, Gaseous Corrosion-Wear Interactions, *Corrosion: Fundamentals, Testing, and Protection*, Vol 13A, *ASM Handbook*, ASM International, 2003, p 338–344

Gaseous Corrosion-Wear Interactions

Joseph H. Tylczak and Thomas A. Adler, Albany Research Center, U.S. Department of Energy

---

Selected References

- R.L. Deuis, C. Subramanian, and J. M. Yellup, Dry Sliding Wear of Aluminum Composites—A Review, *Compos. Sci. Technol.,* Vol 57, 1997, p 415–435
- S. Hogmark, Å. Hammarsten, and S. Söderberg, On the Combined Effects of Corrosion and Erosion, *Proc. Sixth Int. Conf. on Erosion by Liquid and Solid Impact,* 1983, p 37-1 to 37-8
- S.C. Lim and M.F. Ashby, Wear-Mechanism Maps, *Acta Metall.,* Vol 35, 1987, p 1–24
- F.H. Stott, High-Temperature Sliding Wear of Metals, *Tribol. Int.,* Vol 35, 2002, p 489–495
- F.H. Stott, The Role of Oxidation in the Wear of Alloys, *Tribol. Int.,* Vol 31, 1998, p 61–71
- G. Sundararajan and M. Roy, Solid Particle Erosion Behavior at Room and Elevated Temperatures, *Tribol. Int.,* Vol 30, 1997, p 339–359

B. Craig, Introduction to Environmentally Induced Cracking, *Corrosion: Fundamentals, Testing, and Protection*, Vol 13A, *ASM Handbook*, ASM International, 2003, p 345

Introduction to Environmentally Induced Cracking

Bruce Craig, MetCorr

Introduction

THIS SUBSECTION was developed to introduce the fundamental aspects of environmentally induced cracking. It provides theoretical basis for further discussions on the evaluation, testing, and methods of protection against environmentally induced cracking found in the rest of this Volume. In the time between the publication of the first *ASM Handbook* on corrosion in 1987 and this publication, considerable work has been done in the area of environmentally induced cracking. However, little gain has been made on the theory of the various cracking mechanisms, and certainly the same is true for progress in modeling or quantitative methods to predict cracking induced by the environment. Thus, the information presented in the previous edition remains fresh today and provides a good starting point for a basic understanding of environmentally induced cracking. Where appropriate, the authors and reviewers of this subsection have updated or added information that brings this subsection up to the current state of the art. The efforts of the original authors are acknowledged at the end of each article.

B. Craig, Introduction to Environmentally Induced Cracking, *Corrosion: Fundamentals, Testing, and Protection*, Vol 13A, *ASM Handbook*, ASM International, 2003, p 345

Bruce Craig, MetCorr

Mechanisms That Induce Cracking

This subsection addresses the mechanisms of corrosion that produce cracking of metals and intermetallic compounds as a result of exposure to their environment. This cracking may take the form of relatively slow, stable crack extension with a predictable growth rate or, as is often the case, unpredictable catastrophic fracture. The subsection is divided into four articles (after this brief introduction). Each addresses a specific type of cracking or embrittlement phenomena: stress-corrosion cracking (SCC), hydrogen damage (frequently referred to as hydrogen embrittlement), liquid-metal embrittlement, and solid metal induced embrittlement. In general, these different phenomena show many similarities, and it would at first seem appropriate to propose an all-encompassing mechanism to account for these behaviors. For example, all of these phenomena generally are dependent on yield strength and applied stress. As both of these factors increase, resistance to SCC, hydrogen damage, liquid-metal embrittlement, and solid metal induced embrittlement decreases. However, as presented in the discussion of each of these phenomena, many differences between the various forms of environmentally induced cracking are encountered, and in fact, substantial differences are observed for behavior of metals and alloys within a specific form of cracking.

At this time, the understanding of each of these mechanisms of cracking is largely phenomenological. No satisfactory theory exists for any of these mechanisms that totally explains all behavior observed either under laboratory or field conditions. Although many theories that are specific to the behavior of certain alloy systems or environments, exist, none is universal enough to explain, for example, the diverse behavior of hydrogen

damage for systems that develop hydrides versus alloys of iron that do not form hydrides. There are many of these contradictory factors that impede the development of an all- encompassing theory.

Additionally, there has been a continuing controversy since the 1960s concerning the actual micromechanistic causes of SCC, which some investigators consider to be related to hydrogen damage and not strictly an active-path corrosion phenomenon. Although certain convincing data exist for a role of hydrogen in SCC of certain alloys, sufficient data are not available to generalize this concept.

As the understanding of these forms of cracking increases, the complexity of each also increases. For example, liquid-metal embrittlement has long been a recognized form of cracking induced by liquid metals. However, it has been shown that certain metals can become embrittlers below their melting point and that embrittlement by these metals becomes progressively worse as the temperature approaches the melting point. This behavior, although similar to liquid-metal embrittlement, is sufficiently different to warrant reclassifying it as *solid metal induced embrittlement.* Many of the environmentally induced fractures that were previously termed liquid-metal embrittlement are now considered solid metal induced embrittlement.

Because satisfactory mechanistic models have not been developed for any of these forms of environmental cracking, the prediction of environmentally assisted cracking is essentially nonexistent. However, the need for prediction of these types of failures is most important, because observable and measurable corrosion usually does not occur before or during crack initiation or propagation. When corrosion does occur, it is highly localized such as pitting or crevice attack and may be difficult to detect.

The field of environmentally assisted cracking is one of the most active in corrosion research, and it is continually changing. Therefore, the reader is encouraged to consult the most current literature for more detail on specific theories and alloy behavior. Toward this end, Selected References are given at the end of each article. Additional information also can be found in the articles “Evaluating Stress-Corrosion Cracking” and “Evaluating Hydrogen Embrittlement” in this Volume.

R.H. Jones, Stress-Corrosion Cracking, *Corrosion: Fundamentals, Testing, and Protection*, Vol 13A, *ASM Handbook*, ASM International, 2003, p 346–366

Stress-Corrosion Cracking

R.H. Jones, Battelle Pacific Northwest National Laboratory

Introduction

STRESS-CORROSION CRACKING (SCC) describes service failures in engineering materials that occur by slow environmentally induced crack propagation. The observed crack propagation is the result of the combined and synergistic interaction of mechanical stress and corrosion reactions. This is a simple definition of a complex subject, and, like most simplifications, it fails to identify the boundaries of the subject. As a result, before this problem can be discussed in detail, one must clearly define the type of loading involved, the types of materials involved, the types of environments that cause this type of crack propagation, and the nature of the interactions that result in this phenomenon. The term *stress-corrosion cracking* is used frequently to describe any type of environmentally induced or assisted crack propagation. However, in this discussion, the focus is on the normal usage of the term as defined subsequently.

One frequent misconception is that SCC is the result of stress concentration at corrosion-generated surface flaws (as quantified by the stress- intensity factor, K); when a critical value of stress concentration, K_{crit}, is reached, mechanical fracture results. Although stress concentration does occur at such flaws, these defects do not exceed the critical value required to cause mechanical fracture of the material in an inert environment ($K_{SCC} < K_{crit}$). Precorrosion followed by loading in an inert environment will not result in any observable crack propagation, while simultaneous environmental exposure and application of stress will cause time-dependent subcritical crack propagation. The term *synergy* was used to describe this process because the combined simultaneous interaction of mechanical and chemical forces results in crack propagation where neither factor

acting independently or alternately would result in the same effect. The exact nature of this interaction is the subject of numerous scientific investigations and is covered in the section "Crack Propagation Mechanisms" in this article.

The stresses required to cause SCC are small, usually below the macroscopic yield stress, and are tensile in nature. The stresses can be externally applied, but residual stresses often cause SCC failures. However, compressive residual stresses can be used to prevent this phenomenon. Static loading usually is considered to be responsible for SCC, while environmentally induced crack propagation due to cyclic loading is defined as *corrosion fatigue* (see the section "Corrosion Fatigue" in the article "Forms of Mechanically Assisted Degradation" in this Volume). The boundary between these two classes of phenomena is vague, and corrosion fatigue often is considered to be a subset of SCC. However, because the environments that cause corrosion fatigue and SCC are not always the same, these two should be considered separate phenomena.

The term *stress-corrosion cracking* usually is used to describe failures in metallic alloys. However, other classes of materials also exhibit delayed failure by environmentally induced crack propagation. Ceramics exhibit environmentally induced crack propagation (Ref 1), and polymeric materials frequently exhibit craze cracking as a result of the interaction of applied stress and environmental reactions (Ref 2, 3, 4, 5). Until recently, it was thought that pure metals were immune to SCC; however, it has been shown that pure metals are susceptible to SCC (Ref 6, 7). This discussion focuses on the SCC of metals and their alloys and is not concerned with stress- environment interactions in ceramics and polymers.

Environments that cause SCC are usually aqueous and can be condensed layers of moisture or bulk solutions. Typically, SCC of an alloy is the result of the presence of a specific chemical species in the environment. Thus, the SCC of copper alloys, traditionally referred to as *season cracking*, is virtually always due to the presence of ammonia in the environment, and chloride ions cause or exacerbate cracking in stainless steels and aluminum alloys. Also, an environment that causes SCC in one alloy may not cause SCC in another alloy. Changing the temperature, the degree of aeration, and/or the concentration of ionic species may change an innocuous environment into one that causes SCC failure. Also, an alloy may be immune in one heat treatment and susceptible in another. As a result, the list of all possible alloy-environment combinations that cause SCC is expanding continually, and the possibilities are virtually infinite. A partial listing of some of the more commonly observed alloy-environment combinations that result in SCC is given in Table 1.

Table 1 Alloy-environment systems exhibiting SCC

Alloy	Environment
Carbon steel	Hot nitrate, hydroxide, and carbonate/bicarbonate solutions
High-strength steels	Aqueous electrolytes, particularly when containing H_2S
Austenitic stainless steels	Hot, concentrated chloride solutions; chloride-contaminated steam
High-nickel alloys	High-purity steam
a-brass	Ammoniacal solutions
Aluminum alloys	Aqueous Cl^-, Br^-, and I^- solutions
Titanium alloys	Aqueous Cl^-, Br^-, and I^- solutions; organic liquids; N_2O_4
Magnesium alloys	Aqueous Cl^- solutions
Zirconium alloys	Aqueous Cl^- solutions; organic liquids; I_2 at 350 °C (660 °F)

In general, SCC is observed in alloy-environment combinations that result in the formation of a film on the metal surface. These films may be passivating layers, tarnish films, or dealloyed layers. In many cases, these films reduce the rate of general or uniform corrosion, making the alloy desirable for resistance to uniform corrosion in the environment. As a result, SCC is of greatest concern in the corrosion-resistant alloys exposed to aggressive aqueous environments. The exact role of the film in the SCC process is the subject of current research and is covered in the discussion "Crack Propagation Mechanisms" in this article. Table 2 lists some alloy-environment combinations and the films that may form at the crack tip.

Table 2 Alloy-environment combinations and the resulting films that form at the crack tip

Metal or alloy	Environment	Initiating layer
α-brass, copper-aluminum	Ammonia	Dealloyed layer (Cu)
Gold-copper	$FeCl_3$	Dealloyed layer (Au)
	Acid sulfate	Dealloyed layer (Au)
Iron-chromium nickel	Chloride	Dealloyed layer (Ni)
	Hydroxide	Dealloyed layer or oxide
	High-temperature water	Dealloyed layer or oxide
α-brass	Nitrite	Oxide
Copper	Nitrite	Oxide
	Ammonia (cupric)	Porous dissolution zone
Ferritic steel	High-temperature water	Oxide
	Phosphate	Oxide (?)
	Anhydrated ammonia	Nitride
	$CO/CO_2/H_2O$	Carbide
	CS_2/H_2O	Carbide
Titanium alloys	Chloride	Hydride
Aluminum alloys, steels	Various media	Near-surface hydrogen

References cited in this section

1. T.A. Michalske and S.W. Freiman, *Nature,* Vol 295, 11 Feb 1982, p 511

2. J.F. Fellers and B.F. Kee, *J. Appl. Polymer Sci.,* Vol 18, 1974, p 2355

3. E.H. Andrews, *Developments in Polymer Science,* Applied Science, 1979

4. H.T. Sumison and D.P. Williams, in *Fatigue of Composite Materials,* STP 569, ASTM, 1975, p 226

5. C. Zeben, in *Analysis of the Test Methods for High Modulus Fibers and Composites,* STP 521, ASTM, 1973, p 65

6. K. Sieradski and R.C. Newman, *Philos. Mag. A,* Vol 5 (No. 1), 1985, p 95

7. T. Cassaigne, E.N. Pugh, and J. Kruger, National Bureau of Standards and Johns Hopkins University, unpublished research, 1987

R.H. Jones, Stress-Corrosion Cracking, *Corrosion: Fundamentals, Testing, and Protection*, Vol 13A, *ASM Handbook*, ASM International, 2003, p 346–366

Stress-Corrosion Cracking

R.H. Jones, Battelle Pacific Northwest National Laboratory

The Phenomenon of SCC

Stress-corrosion cracking is a delayed failure process. That is, cracks initiate and propagate at a slow rate from 10^{-9} to 10^{-6} m/s (4×10^{-7} to 4×10^{-4} in./s), until the stresses in the remaining ligament of metal exceed the fracture strength. The sequence of events involved in the SCC process usually is divided into three stages:

- Crack initiation and stage 1 propagation
- Stage 2 or steady-state crack propagation
- Stage 3 crack propagation or final failure

Distinction among these stages is difficult because the transition occurs in a continuous manner and the division is therefore arbitrary. To enhance the understanding of this process, these steps are discussed in the context of typical experimental techniques and results. Stress-corrosion cracking experiments can be classified into three different categories:

- Tests on statically loaded smooth samples
- Tests on statically loaded precracked samples
- Tests using slowly straining samples

More detailed information on these tests can be found in the article "Evaluating Stress-Corrosion Cracking" in this Volume.
Tests on statically loaded smooth samples usually are conducted at various fixed stress levels, and the time to failure of the sample in the environment is measured. Figure 1 illustrates the typical results obtained from this type of test. In Fig. 1, the logarithm of the measured time to failure, t_f, is plotted against the applied stress, $\sigma_{applied}$, and the time to failure can be seen to increase rapidly with decreasing stress; a threshold stress, σ_{th}, is determined where the time to failure approaches infinity. The total time to failure at a given stress consists of the time required for the formation of a crack (the incubation or initiation time, t_{in}, and the time of crack propagation, t_{cp}. These experiments can be used to determine the maximum stress that can be applied to avoid SCC failure, to determine an inspection interval to confirm the absence of SCC crack propagation, or to evaluate the influence of metallurgical and environmental changes on SCC. However, the actual time for the formation or initiation of cracks is strongly dependent on a wide variety of parameters, such as surface finish and prior history. If a cracklike flaw or a crevice is present in the material, then the time to initiate a crack may be reduced dramatically (Ref 8).

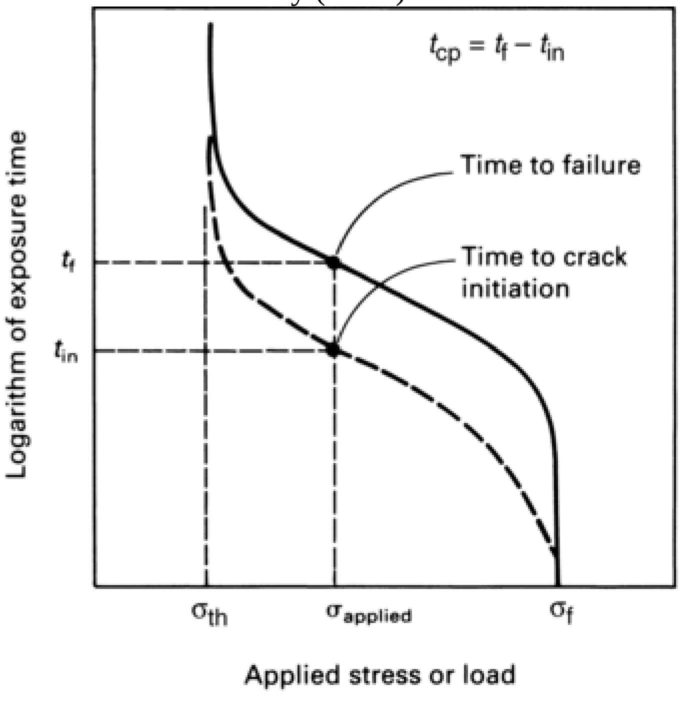

Fig. 1 Schematic of a typical time to failure as a function of initially applied stress for smooth sample stress-corrosion cracking tests

Tests on statically loaded precracked samples usually are conducted with either a constant applied load or with a fixed crack opening displacement, and the actual rate or velocity of crack propagation, *da/dt*, is measured (Ref 9). The magnitude of the stress distribution at the crack tip (the mechanical driving force for crack propagation) is quantified by the stress intensity factor, *K*, for the specific crack and loading geometry. As a result, the crack propagation rate, *da/dt*, is plotted versus *K* as illustrated in Fig. 2. These tests can be configured such that *K* increases with crack length (constant applied load), decreases with increasing crack length (constant crack mouth opening displacement), or is approximately constant as the crack length changes (special tapered samples). Each type of test has its advantages and disadvantages. However, in service, most SCC failures occur under constant-load conditions such that the stress intensity increases as the crack propagates. As a result, it is usually assumed in SCC discussions that the stress intensity is increasing with increasing crack length.

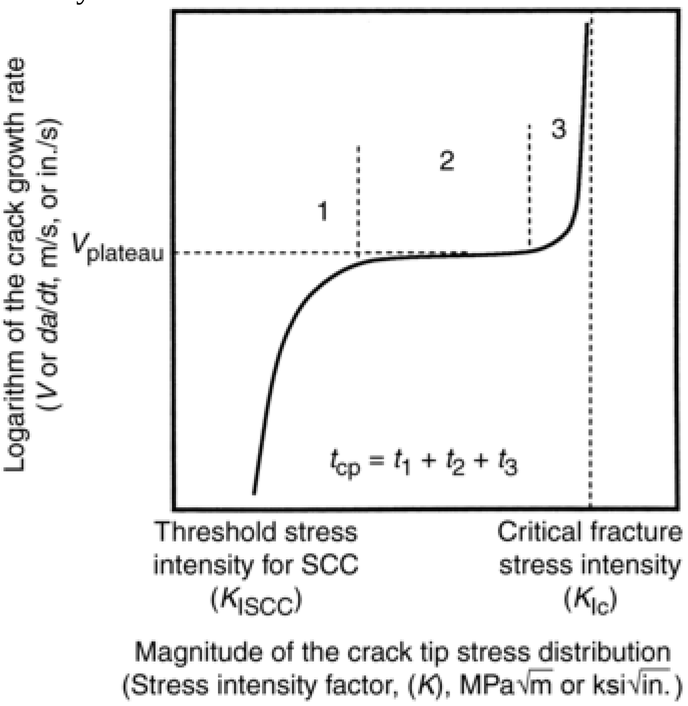

Fig. 2 Schematic of typical crack propagation rate as a function of crack tip stress-intensity behavior illustrating the regions of stages 1, 2, and 3 crack propagation, as well as identifying the plateau velocity and the threshold stress intensity

Typically, three regions of crack propagation rate versus stress-intensity level are found during crack propagation experiments. These regions are identified according to increasing stress-intensity factor as stage 1, 2, or 3 crack propagation (Fig. 2). No crack propagation is observed below some threshold stress-intensity level, K_{ISCC}. This threshold stress level is determined not only by the alloy but also by the environment and metallurgical condition of the alloy, and presumably, this level corresponds to the minimum required stress level for synergistic interaction with the environment. At low stress-intensity levels (stage 1), the crack propagation rate increases rapidly with the stress-intensity factor. At intermediate stress-intensity levels (stage 2), the crack propagation rate approaches some constant velocity that is virtually independent of the mechanical driving force. This plateau velocity, $V_{plateau}$, is characteristic of the alloy-environment combination and is the result of rate-limiting environmental processes such as mass transport of environmental species up the crack to the crack tip. In stage 3, the rate of crack propagation exceeds the plateau velocity as the stress-intensity level approaches the critical stress-intensity level for mechanical fracture in an inert environment, K_{Ic} (Ref 10).

Slow Strain Rate Testing. Stress-corrosion tests also can be conducted by slowly increasing the load or strain on either precracked or smooth samples. Usually, a tensile machine pulls a smooth sample that is exposed to the corrosive environment at a low cross head speed, 10^{-5} to 10^{-9} m/s. The strain to failure in the corrosive environment and the strain to failure in an inert environment can then be plotted against the strain rate, as shown in Fig. 3(a), or the ratio of these measurements can be plotted as shown in Fig. 3(b) for ductility. The ratio of other tensile property measurements, such as reduction in area and ultimate tensile strength, could also be plotted. These tests are known as *constant extension rates tests* (CERT), *slow strain rate tests,* or *straining electrode tests.* These tests are excellent for comparing the relative susceptibility of alloys to cracking in an

environment or for studying the influence of metallurgical variables on the susceptibility of an alloy. However, the application of this data to the prediction of actual in-service crack propagation rates is difficult and unreliable.

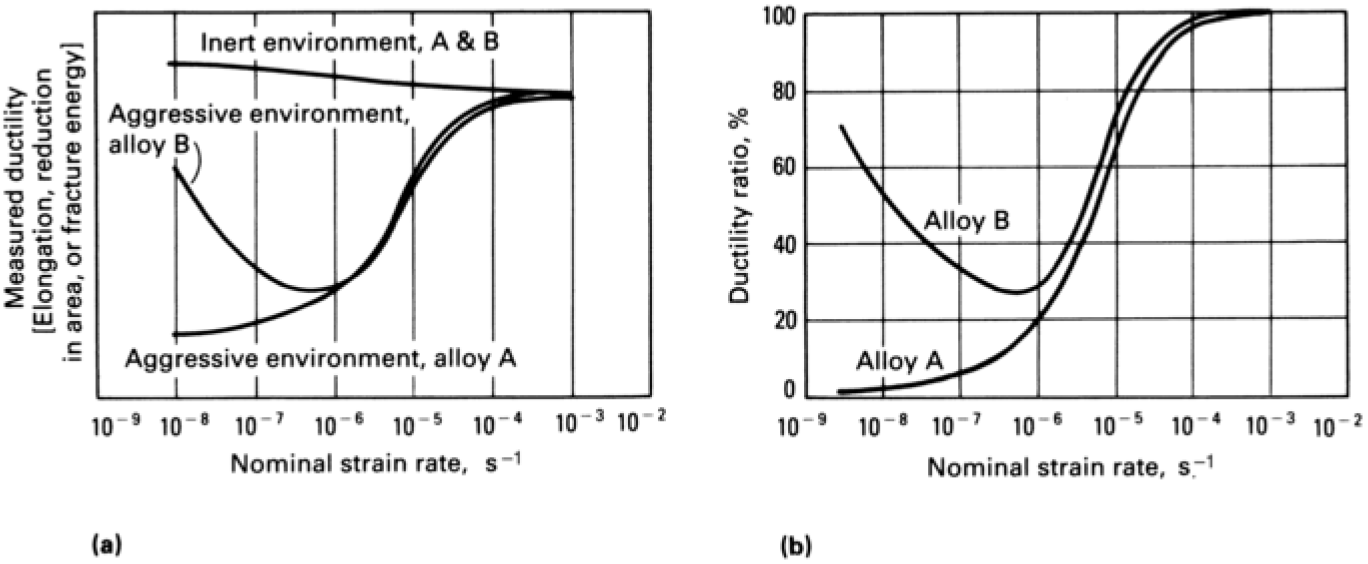

Fig. 3 Strain to failure plots resulting from slow strain rate testing. (a) Ductility of two alloys is measured by elongation, reduction in area, or fracture energy in the aggressive environment and an inert reference environment. (b) Schematic of typical ductility ratio of the effects of the aggressive over the inert reference environment versus strain rate behavior of two different types of alloys

References cited in this section

8. C.M. Chen, M.H. Froning, and E.D. Verink, in *Stress Corrosion—New Approaches,* STP 610, ASTM, 1976, p 289

9. C.J. Beevers, Ed., *The Measurement of Crack Length and Shape During Fracture and Fatigue,* Chameleon Press, 1980

10. E.N. Pugh, U. Bertocci, and R.E. Ricker, National Bureau of Standards, unpublished research, 1987

R.H. Jones, Stress-Corrosion Cracking, *Corrosion: Fundamentals, Testing, and Protection*, Vol 13A, *ASM Handbook*, ASM International, 2003, p 346–366

Stress-Corrosion Cracking

R.H. Jones, Battelle Pacific Northwest National Laboratory

The Phenomenon of SCC

Stress-corrosion cracking is a delayed failure process. That is, cracks initiate and propagate at a slow rate from 10^{-9} to 10^{-6} m/s (4×10^{-7} to 4×10^{-4} in./s), until the stresses in the remaining ligament of metal exceed the fracture strength. The sequence of events involved in the SCC process usually is divided into three stages:

- Crack initiation and stage 1 propagation
- Stage 2 or steady-state crack propagation
- Stage 3 crack propagation or final failure

Distinction among these stages is difficult because the transition occurs in a continuous manner and the division is therefore arbitrary. To enhance the understanding of this process, these steps are discussed in the context of typical experimental techniques and results. Stress-corrosion cracking experiments can be classified into three different categories:

- Tests on statically loaded smooth samples
- Tests on statically loaded precracked samples
- Tests using slowly straining samples

More detailed information on these tests can be found in the article "Evaluating Stress-Corrosion Cracking" in this Volume.
Tests on statically loaded smooth samples usually are conducted at various fixed stress levels, and the time to failure of the sample in the environment is measured. Figure 1 illustrates the typical results obtained from this type of test. In Fig. 1, the logarithm of the measured time to failure, t_f, is plotted against the applied stress, $\sigma_{applied}$, and the time to failure can be seen to increase rapidly with decreasing stress; a threshold stress, σ_{th}, is determined where the time to failure approaches infinity. The total time to failure at a given stress consists of the time required for the formation of a crack (the incubation or initiation time, t_{in}, and the time of crack propagation, t_{cp}. These experiments can be used to determine the maximum stress that can be applied to avoid SCC failure, to determine an inspection interval to confirm the absence of SCC crack propagation, or to evaluate the influence of metallurgical and environmental changes on SCC. However, the actual time for the formation or initiation of cracks is strongly dependent on a wide variety of parameters, such as surface finish and prior history. If a cracklike flaw or a crevice is present in the material, then the time to initiate a crack may be reduced dramatically (Ref 8).

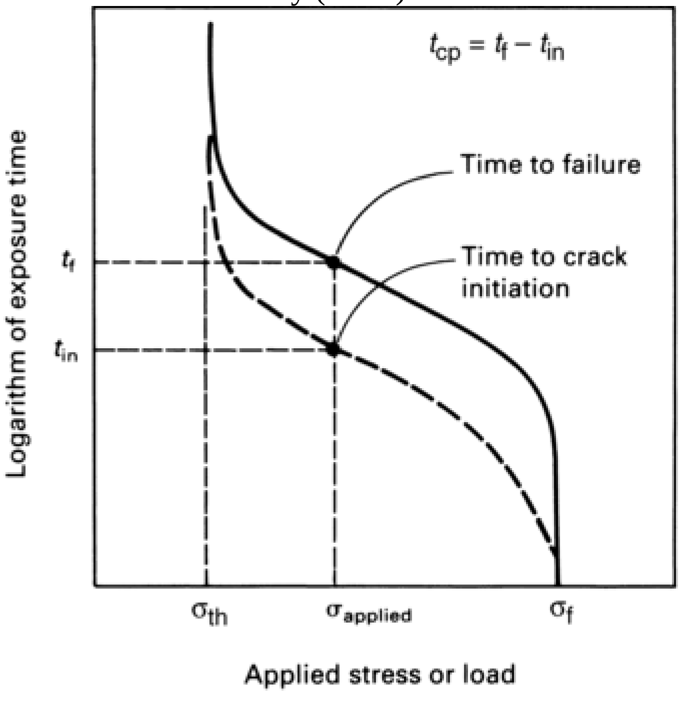

Fig. 1 Schematic of a typical time to failure as a function of initially applied stress for smooth sample stress-corrosion cracking tests

Tests on statically loaded precracked samples usually are conducted with either a constant applied load or with a fixed crack opening displacement, and the actual rate or velocity of crack propagation, *da/dt*, is measured (Ref 9). The magnitude of the stress distribution at the crack tip (the mechanical driving force for crack propagation) is quantified by the stress intensity factor, *K*, for the specific crack and loading geometry. As a result, the crack propagation rate, *da/dt*, is plotted versus *K* as illustrated in Fig. 2. These tests can be configured such that *K* increases with crack length (constant applied load), decreases with increasing crack length (constant crack mouth opening displacement), or is approximately constant as the crack length changes (special tapered samples). Each type of test has its advantages and disadvantages. However, in service, most SCC failures occur

under constant-load conditions such that the stress intensity increases as the crack propagates. As a result, it is usually assumed in SCC discussions that the stress intensity is increasing with increasing crack length.

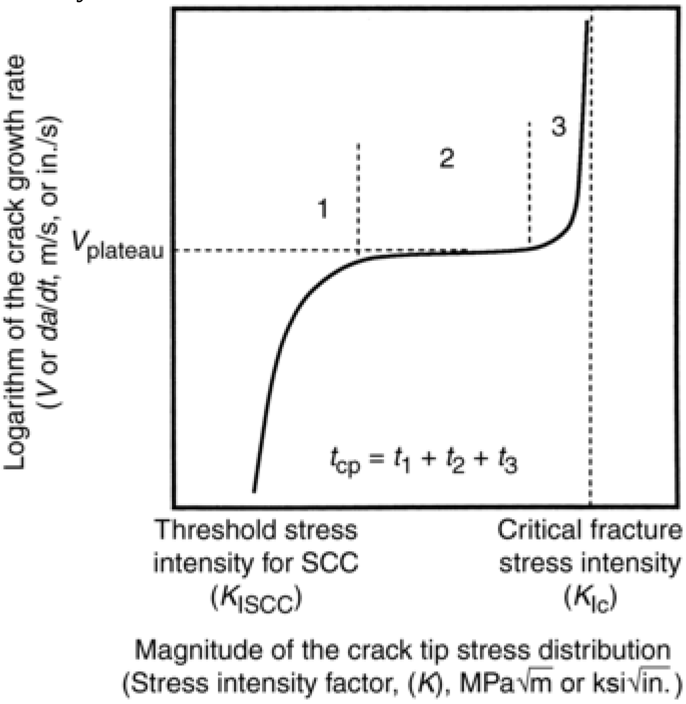

Fig. 2 Schematic of typical crack propagation rate as a function of crack tip stress-intensity behavior illustrating the regions of stages 1, 2, and 3 crack propagation, as well as identifying the plateau velocity and the threshold stress intensity

Typically, three regions of crack propagation rate versus stress-intensity level are found during crack propagation experiments. These regions are identified according to increasing stress-intensity factor as stage 1, 2, or 3 crack propagation (Fig. 2). No crack propagation is observed below some threshold stress-intensity level, K_{ISCC}. This threshold stress level is determined not only by the alloy but also by the environment and metallurgical condition of the alloy, and presumably, this level corresponds to the minimum required stress level for synergistic interaction with the environment. At low stress-intensity levels (stage 1), the crack propagation rate increases rapidly with the stress-intensity factor. At intermediate stress-intensity levels (stage 2), the crack propagation rate approaches some constant velocity that is virtually independent of the mechanical driving force. This plateau velocity, $V_{plateau}$, is characteristic of the alloy-environment combination and is the result of rate-limiting environmental processes such as mass transport of environmental species up the crack to the crack tip. In stage 3, the rate of crack propagation exceeds the plateau velocity as the stress-intensity level approaches the critical stress-intensity level for mechanical fracture in an inert environment, K_{Ic} (Ref 10).

Slow Strain Rate Testing. Stress-corrosion tests also can be conducted by slowly increasing the load or strain on either precracked or smooth samples. Usually, a tensile machine pulls a smooth sample that is exposed to the corrosive environment at a low cross head speed, 10^{-5} to 10^{-9} m/s. The strain to failure in the corrosive environment and the strain to failure in an inert environment can then be plotted against the strain rate, as shown in Fig. 3(a), or the ratio of these measurements can be plotted as shown in Fig. 3(b) for ductility. The ratio of other tensile property measurements, such as reduction in area and ultimate tensile strength, could also be plotted. These tests are known as *constant extension rates tests* (CERT), *slow strain rate tests,* or *straining electrode tests.* These tests are excellent for comparing the relative susceptibility of alloys to cracking in an environment or for studying the influence of metallurgical variables on the susceptibility of an alloy. However, the application of this data to the prediction of actual in-service crack propagation rates is difficult and unreliable.

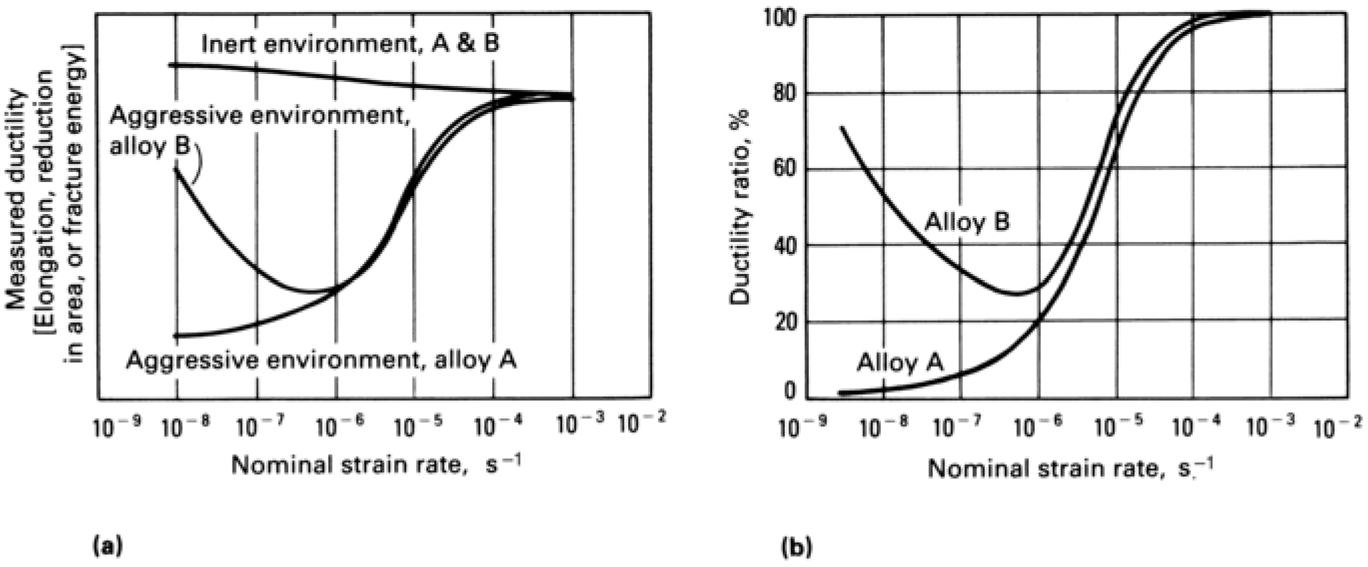

Fig. 3 Strain to failure plots resulting from slow strain rate testing. (a) Ductility of two alloys is measured by elongation, reduction in area, or fracture energy in the aggressive environment and an inert reference environment. (b) Schematic of typical ductility ratio of the effects of the aggressive over the inert reference environment versus strain rate behavior of two different types of alloys

References cited in this section

8. C.M. Chen, M.H. Froning, and E.D. Verink, in *Stress Corrosion—New Approaches,* STP 610, ASTM, 1976, p 289
9. C.J. Beevers, Ed., *The Measurement of Crack Length and Shape During Fracture and Fatigue,* Chameleon Press, 1980
10. E.N. Pugh, U. Bertocci, and R.E. Ricker, National Bureau of Standards, unpublished research, 1987

R.H. Jones, Stress-Corrosion Cracking, *Corrosion: Fundamentals, Testing, and Protection,* Vol 13A, *ASM Handbook,* ASM International, 2003, p 346–366

Stress-Corrosion Cracking

R.H. Jones, Battelle Pacific Northwest National Laboratory

Controlling Parameters

The mechanisms that have been proposed for SCC require that certain processes or events occur in sequence for sustained crack propagation to be possible. These requirements explain the plateau region in which the rate of crack propagation is independent of the applied mechanical stress. That is, a sequence of chemical reactions and processes is required, and the rate-limiting step in this sequence of events determines the limiting rate or plateau velocity of crack propagation (until mechanical overload fracture starts contributing to the fracture process in stage 3). Figure 4 illustrates a crack tip in which crack propagation results from reactions in metal ahead of the propagating crack. Close examination of Fig. 4 reveals that potential rate-determining steps include:

- Mass transport along the crack to the crack tip
- Reactions in the solution near the crack
- Surface adsorption at or near the crack tip
- Surface diffusion

- Surface reactions
- Absorption into the bulk
- Bulk diffusion to the plastic zone ahead of the advancing crack
- Chemical reactions in the bulk
- The rate of interatomic bond rupture

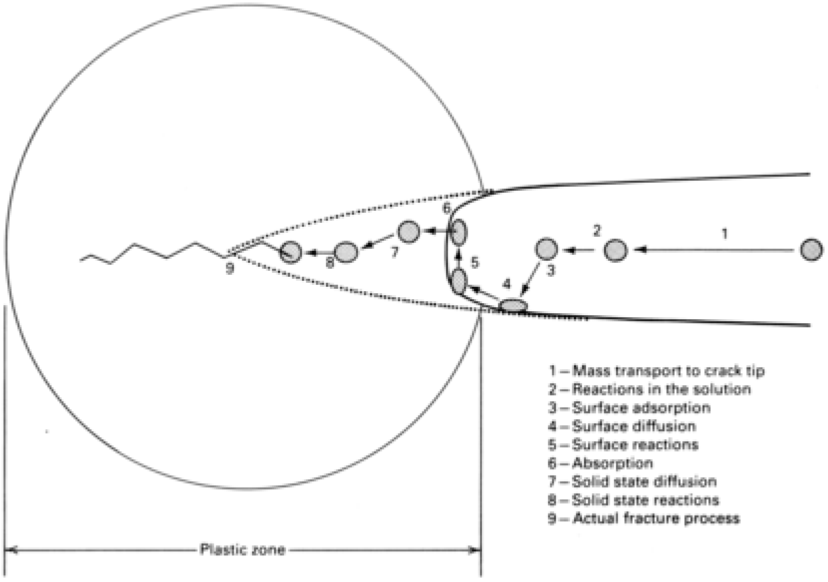

Fig. 4 Schematic of crack tip processes that may be the rate-determining step in environmentally assisted crack propagation

Changes in the environment that modify the rate-determining step will have a dramatic influence on the rate of crack propagation, while alterations to factors not involved in the rate-determining step or steps will have little influence, if any. However, significantly retarding the rate of any one of the required steps in the sequence could make that step the rate-determining step. In aqueous solutions, the rate of adsorption and surface reactions is usually very fast compared with the rate of mass transport along the crack to the crack tip. As a result, bulk transport into this region or reactions in this region frequently are believed to be responsible for determining the steady-state crack propagation rate or plateau velocity. In gaseous environments, surface reactions, surface diffusion, and adsorption may be rate limiting, as well as the rate of bulk transport to the crack tip (Ref 11, 12).
Several different environmental parameters are known to influence the rate of crack growth in aqueous solutions. These parameters include, but are not limited to:

- Temperature
- Pressure
- Solute species
- Solute concentration and activity
- pH
- Electrochemical potential
- Solution viscosity
- Stirring or mixing

Altering any of these parameters may alter the rate of the rate-controlling steps, either accelerating or reducing the rate of crack propagation. Also, it may be possible to arrest or stimulate crack propagation by altering the rate of an environmental reaction. It is well known and generally accepted that the environment at occluded sites, such as a crack tip, can differ significantly from the bulk solution. If an alteration to the bulk environment allows the formation of a critical SCC environment at crack nuclei, then crack propagation will result. If the bulk environment cannot maintain this local crack tip environment, then crack propagation will stop. As a result, slight changes to the environment may have a dramatic influence on crack propagation, while dramatic changes may have only a slight influence.

In addition to these environmental parameters, stress-corrosion crack propagation rates are influenced by:

- The magnitude of the applied stress or the stress-intensity factor
- The stress state, which includes plane stress and plane strain
- The loading mode at the crack tip (tension or torsion, for example)
- Alloy composition, which includes nominal composition, exact composition (all constituents), and impurity or tramp element composition
- Metallurgical condition, which includes strength level, second phases present in the matrix and at the grain boundaries, composition of phases, grain size, grain-boundary segregation, and residual stresses
- Crack geometry, which includes length, width, and aspect ratio; and crack opening and crack tip closure

References cited in this section

11. D.P. Williams and H.G. Nelson, *Metall. Trans.,* Vol 1 (No. 1), 1970, p 63

12. R.E. Ricker and D.J. Duquette, The Role of Environment on Time Dependent Crack Growth, *Micro and Macro Mechanics of Crack Growth,* K. Sadananda, B.B. Rath, and D.J. Michel, Ed., American Institute of Mining, Metallurgical, and Petroleum Engineers, 1982, p 29

R.H. Jones, Stress-Corrosion Cracking, *Corrosion: Fundamentals, Testing, and Protection,* Vol 13A, *ASM Handbook,* ASM International, 2003, p 346–366

Stress-Corrosion Cracking

R.H. Jones, Battelle Pacific Northwest National Laboratory

Important Fracture Features

Stress-corrosion cracks can initiate and propagate with little outside evidence of corrosion and no warning as catastrophic failure approaches. The cracks initiate frequently at surface flaws that are either preexisting or formed during service by corrosion, wear, or other processes. The cracks then grow with little macroscopic evidence of mechanical deformation in metals and alloys that are normally quite ductile. Crack propagation can be either intergranular or transgranular; sometimes, both types are observed on the same fracture surface. Crack openings and the deformation associated with crack propagation may be so small that the cracks virtually are invisible except in special nondestructive examinations. As the stress intensity increases, the plastic deformation associated with crack propagation increases, and the crack opening increases. When the final fracture region is approached, plastic deformation can be appreciable because corrosion-resistant alloys are frequently quite ductile. The features of stress-corrosion fracture surfaces are covered in greater detail in the article “Modes of Fracture” and the “Atlas of Fractographs” in *Fractography,* Volume 12 of *ASM Handbook,* formerly 9th Edition *Metals Handbook.*

R.H. Jones, Stress-Corrosion Cracking, *Corrosion: Fundamentals, Testing, and Protection,* Vol 13A, *ASM Handbook,* ASM International, 2003, p 346–366

Stress-Corrosion Cracking

R.H. Jones, Battelle Pacific Northwest National Laboratory

Phenomenology of Crack Initiation Processes

Crack Initiation at Surface Discontinuities. Stress-corrosion cracking frequently initiates at preexisting or corrosion-induced surface features. These features may include grooves, laps, or burrs resulting from fabrication processes. Examples of such features are shown in Fig. 5; these features were produced during grinding in the preparation of a joint for welding. The feature shown in Fig. 5(a) is a lap, which subsequently recrystallized during welding and could now act as a crevice at which deleterious cations concentrate. The highly sensitized recrystallized material could also more readily become the site of crack initiation by intergranular corrosion. A cold-worked layer and surface burrs, shown in Fig. 5(b), can also assist crack initiation.

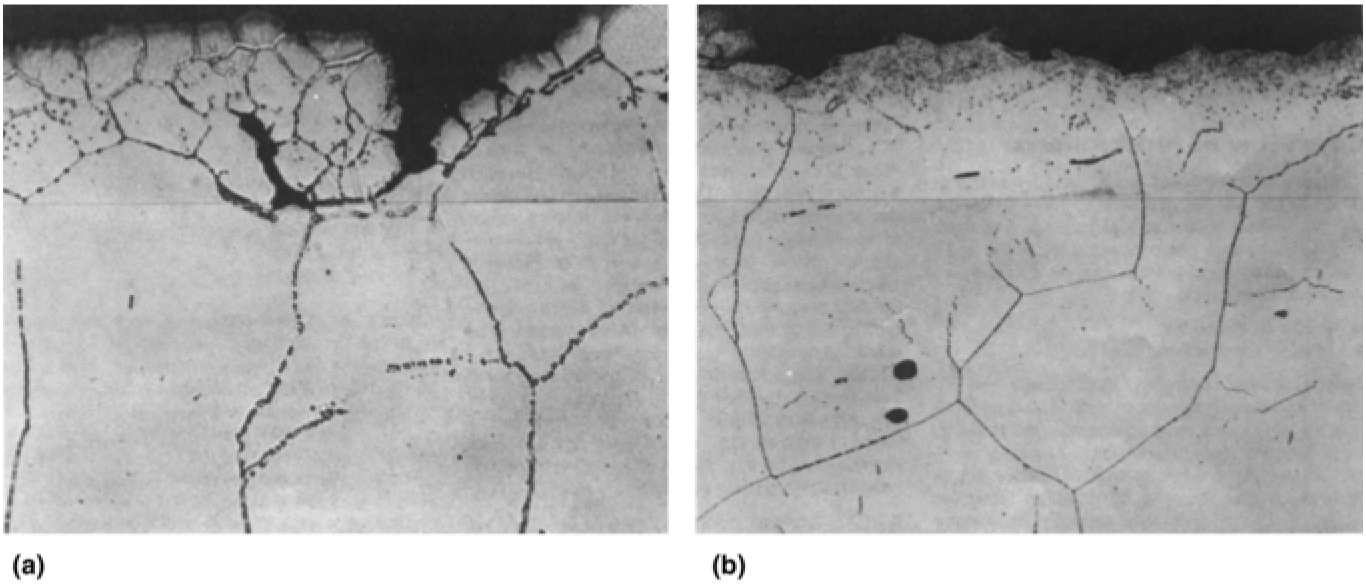

Fig. 5 Optical micrographs showing defects on the inner surface of type 304 stainless steel pipe near weld root (a) and near through crack (b). Both 670×

Crack Initiation at Corrosion Pits. Stress- corrosion cracks can also initiate at pits that form during exposure to the service environment (Fig. 6) or by prior cleaning operations, such as pickling of type 304 stainless steel before fabrication. Pits can form at inclusions that intersect the free surface or by a breakdown in the protective film. In electrochemical terms, pits form when the potential exceeds the pitting potential. It has been shown that the SCC potential and pitting potential were identical for steel in nitrite solutions (Ref 13).

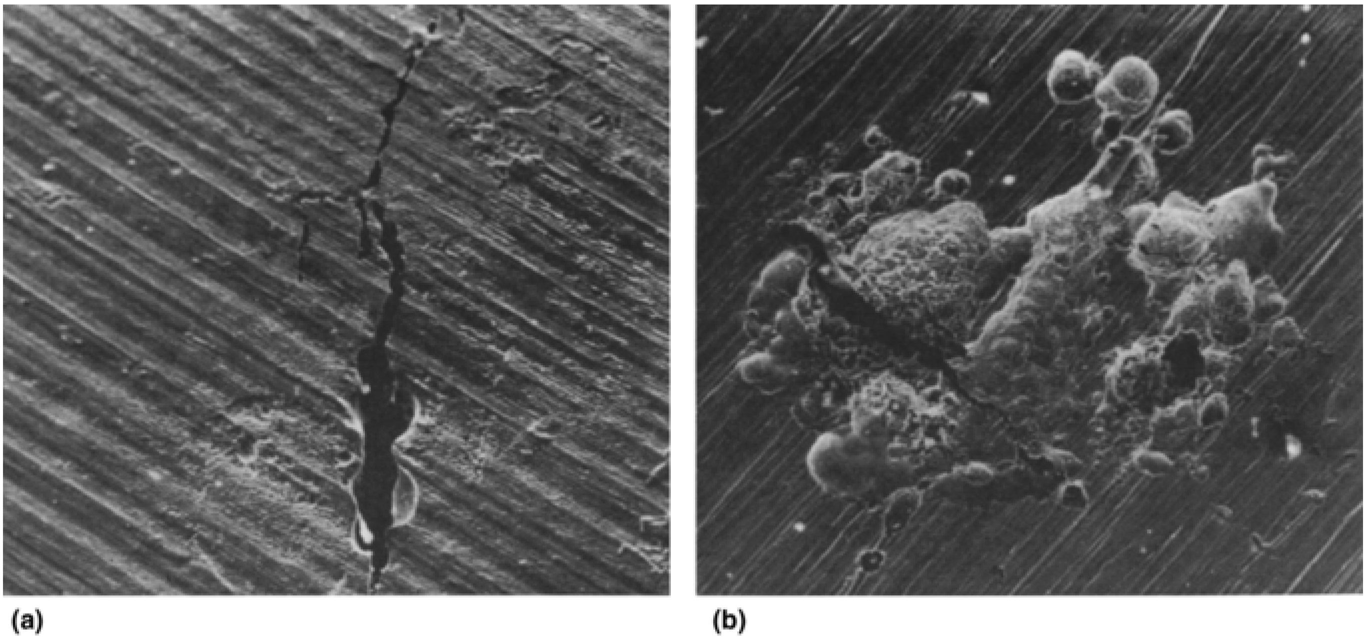

Fig. 6 Stress-corrosion crack initiating from a corrosion pit in a quenched-and-tempered high-strength turbine disk steel (3.39Ni-1.56Cr-0.63Mo-0.11V) test coupon exposed to oxygenated, demineralized water for 800 h under a bending stress of 90% of the yield stress. (a) 185×. (b) 248×. Courtesy of S.J. Lennon, ESCOM, and F.P.A. Robinson, University of the Witwatersrand

The transition between pitting and cracking is dependent on the same parameters that control SCC—that is, the electrochemistry at the base of the pit, pit geometry, chemistry of the material, and stress or strain rate at the base of the pit. A detailed description of the relationship between these parameters and crack initiation has not been developed because of the difficulty in measuring crack initiation. Methods for measuring short surface cracks are under development but are limited to detecting cracks that are beyond the initiation stage. The pit geometry is important in determining the stress and strain rate at the base of the pit. Generally, the aspect ratio between the penetration and the lateral corrosion of a pit must be greater than approximately 10 before a pit acts as a crack initiation site. A penetration to lateral corrosion ratio of 1 corresponds to uniform corrosion, and a ratio of about 1000 is generally observed for a growing stress- corrosion crack. As in the case of a growing crack, the pit walls must exhibit some passive film-forming capability in order for the corrosion ratio to exceed 1. A change in the corrosive environment and potential within a pit may also be necessary for the pit to act as a crack initiator. Pits can act as occluded cells similar to cracks and crevices, although in general their volume is not as restricted. There are a number of examples in which stress-corrosion cracks initiated at the base of a pit by intergranular corrosion. In these circumstances, the grain-boundary chemistry and the pit chemistry were such that intergranular corrosion was favored. Crack propagation was also by intergranular SCC in these cases.

Although the local stresses and strain rates at the base of the pit play a role in SCC initiation, there are examples of preexisting pits that did not initiate stress-corrosion cracks. This observation has led to the conclusion that the electrochemistry of the pit is more important than the local stress or strain rate (Ref 13). A preexisting pit may not develop the same local electrochemistry as one grown during service because the development of a concentration cell depends on the presence of an actively corroding tip that establishes the anion and cation current flows. Similarly, an inability to reinitiate crack growth in samples in which active growth was occurring before the samples were removed from solution, rinsed, dried, and reinserted into solution also suggests that the local chemistry is very important.

Crack Initiation by Intergranular Corrosion or Slip Dissolution. Stress-corrosion crack initiation can also occur in the absence of pitting by intergranular corrosion or slip-dissolution processes. Intergranular corrosion-initiated SCC requires that the local grain-boundary chemistry differ from the bulk chemistry. This condition occurs in sensitized austenitic stainless steels or with the segregation of impurities such as phosphorus, sulfur, or silicon in a variety of materials. Slip-dissolution-initiated SCC results from local corrosion at emerging slip planes and occurs primarily in low stacking fault materials. The processes of crack initiation and propagation by the slip-dissolution process are in fact very similar.

Reference cited in this section

13. R.M. Parkins, *Mater. Sci. Technol.,* Vol 1, 1985, p 480

R.H. Jones, Stress-Corrosion Cracking, *Corrosion: Fundamentals, Testing, and Protection*, Vol 13A, *ASM Handbook*, ASM International, 2003, p 346–366

Stress-Corrosion Cracking

R.H. Jones, Battelle Pacific Northwest National Laboratory

Crack Initiation Mechanisms

Although the features causing SCC initiation, such as pits, fabrication defects, and intergranular corrosion, are observed and identified easily, there are few well-developed models of SCC initiation. This lack of models for crack initiation mechanisms is the result of several complicating factors. For example, the initiation of a crack is difficult to measure experimentally, even though it is not difficult to detect the location from which a growing crack has emanated. Furthermore, crack initiation has not been defined precisely, and it is difficult to determine at what point a pit is actually a crack and when intergranular corrosion becomes intergranular SCC. Also, the fracture mechanics concept of design assumes preexisting flaws in materials, although these may not be surface flaws that can become stress-corrosion cracks. It has been demonstrated that the corrosion fatigue threshold of 12% Cr steels and 2.0% NiCrMoV steels could be related to the minimum depth of surface pits, as shown in Fig. 7. Using a linear-elastic fracture mechanics approach and relating a pit to a half-elliptical surface crack, one researcher has shown that the critical pit dimension could be expressed by the following relationship (Ref 14):

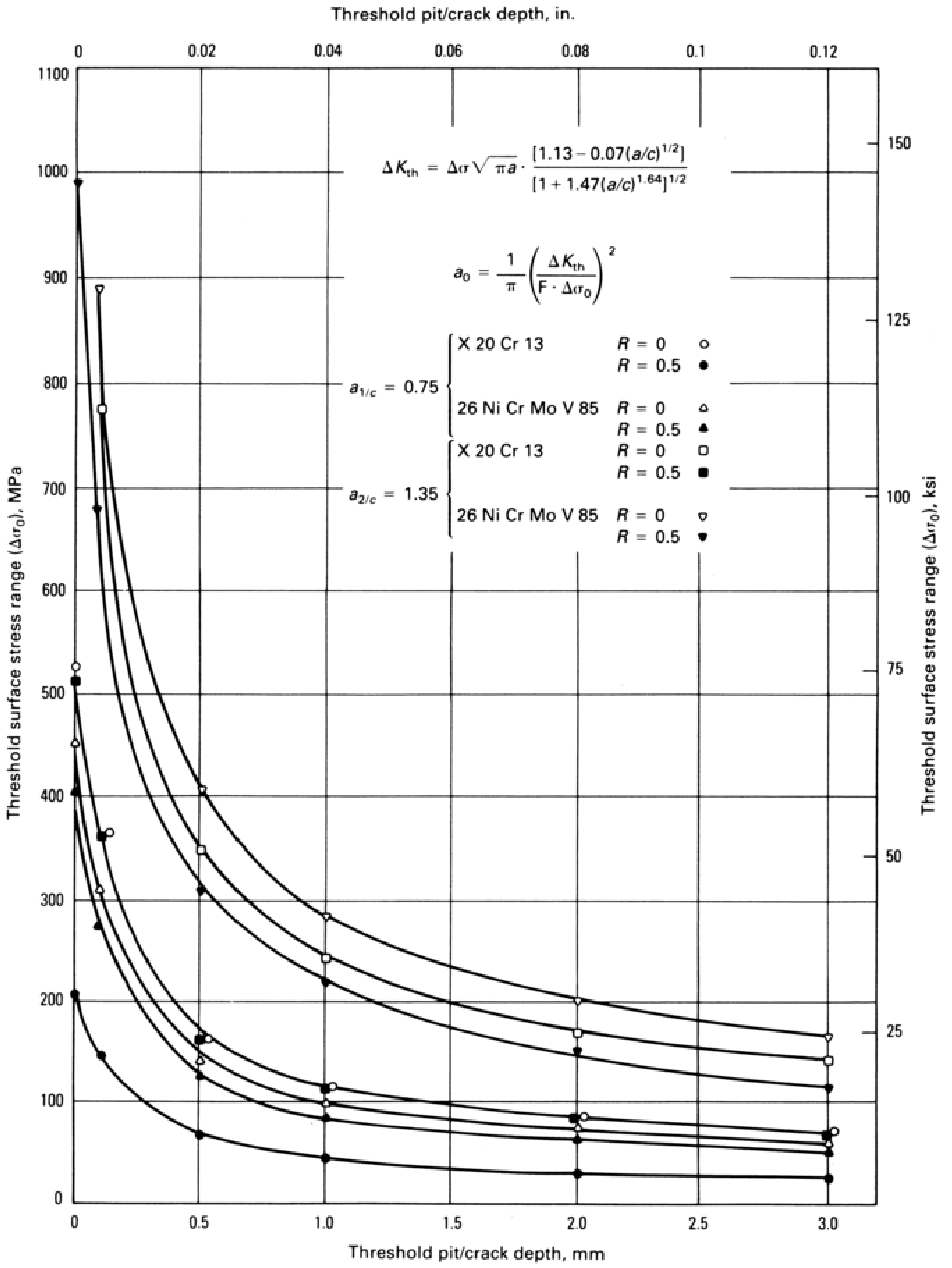

Fig. 7 Relationship between stress amplitude and minimum depth of surface defects for 12% Cr steel and a 2.0% NiCrMoV steel. Source: Ref 14

$$a_0 = \frac{1}{\pi}\left(\frac{\Delta K_{th}}{F\Delta\sigma_0}\right)^2 \qquad \text{(Eq 1)}$$

where ΔK_{th} is the corrosion fatigue threshold, F is a constant, and $\Delta\sigma_0$ is the alternating surface stress. A pit could be represented by a half-elliptical surface crack because it had intergranular corrosion at the base that caused the pit to have cracklike characteristics.

A model for stress-corrosion crack growth was developed from pits in brass tested in a non- tarnishing ammoniacal solution (Ref 15). The researchers evaluated the corrosion and stress aspects of a pit to develop a model for crack initiation. They assumed that the corrosion conditions in the base of the pit were essentially the same as those on a flat surface and that initiation required that a critical crack tip opening displacement be exceeded. Using linear-elastic fracture mechanics, the researchers developed the following relationship for the time to initiate a crack:

$$t_{inc} = \frac{(K_{ISCC})^2}{\pi B\left(\sigma^2 - \sigma_0^2\right)}\exp\left(\frac{-V_m}{V_0}\right) \qquad \text{(Eq 2)}$$

where K_{ISCC} is the stress-corrosion threshold for crack growth for brass in ammoniacal solution, σ is the applied stress, σ_0 is the stress needed to close the crack, B is a constant, $-V_m$ is the electrochemical potential of the sample, and V_0 is the reversible potential. However, the assumption that the pit corrosion conditions are equal to the flat surface conditions limits the applicability of this model, because generally it is accepted that the electrochemistry in a pit differs considerably from that of a flat surface. Also, this model does not describe explicitly the transition from a pit to a crack but treats a pit as a small crack in which the crack tip opening and crack depth are affected by corrosion.

The transition between intergranular corrosion and intergranular SCC was evaluated for nickel with segregated phosphorus and sulfur (Ref 16, 17). Because phosphorus and sulfur inhibit the formation of a passive film on nickel, it was expected that intergranular SCC would be similar in these two materials. It was observed, however, that only shallow intergranular corrosion to a depth of about 0.1 mm (0.004 in.) resulted in nickel in which sulfur was segregated to the grain boundary when tested at a strain rate of 10^{-6} s^{-1} in 1 *N* sulfuric acid (H_2SO_4). On the other hand, rapid intergranular SCC resulted in nickel in which phosphorus was segregated to the grain boundaries that was tested under similar conditions. Using crack tip chemistry modeling, it was shown that intergranular corrosion did not convert to a stress-corrosion crack in Ni+S because the sulfur remained on the crack walls, causing the electrolyte in the solution to become saturated and the crack tip corrosion rate to drop to zero. Starting from a flat surface, the corrosion current at the tip of the intergranular corrosion penetration was about 30 mA/cm^2 (195 mA/in.^{2}) and decreased to 0 at a depth of about 0.08 mm (0.003 in.), as shown in Fig. 8. A similar corrosion depth was measured for samples held at 900 mV for extended periods or for straining electrode samples, while for Ni+P a crack growth rate of 10^{-4} mm/s was measured. These results indicate the importance of electrochemistry in the base of a pit or an intergranular penetration and show that the occurrence of intergranular corrosion does not a priori indicate that intergranular SCC will follow.

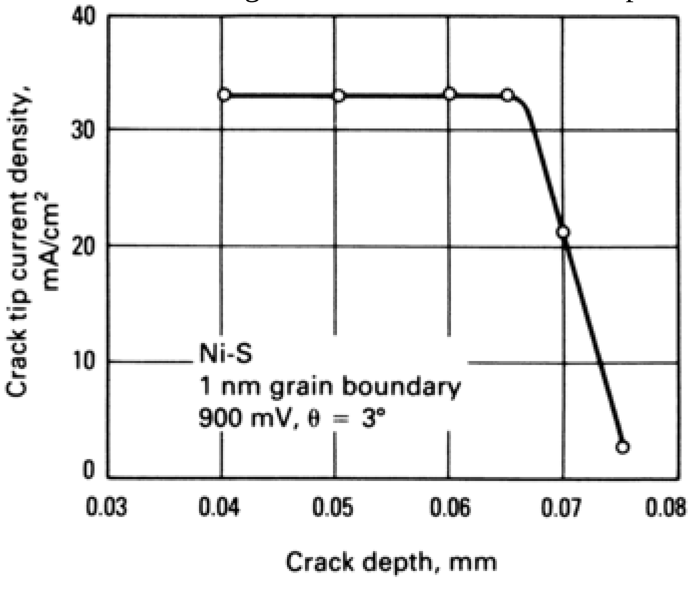

Fig. 8 Effect of crack depth on crack tip corrosion rates for nickel with actively corroding crack walls. θ, angle between the crack walls

References cited in this section

14. L. Hagn, Lifetime Prediction for Parts in Corrosion Environments, *Corrosion in Power Generating Equipment,* Plenum Press, 1983

15. O. Buck and R. Ranjan, Evaluation of a Crack-Tip-Opening Displacement Model Under Stress-Corrosion Conditions, *Modeling Environmental Effects on Crack Growth Processes,* R.H. Jones and W.W. Gerberich, Ed., The Metallurgical Society, 1986, p 209

16. M.J. Danielson, C. Oster, and R.H. Jones, *Corros. Sci.,* Vol 32 (No 1), 1991, p 1–21

17. R.H. Jones, M.J. Danielson, and D.R. Baer, *J. Mater. Energy Syst.,* Vol 8, 1986, p 185

R.H. Jones, Stress-Corrosion Cracking, *Corrosion: Fundamentals, Testing, and Protection,* Vol 13A, *ASM Handbook,* ASM International, 2003, p 346–366

Stress-Corrosion Cracking

R.H. Jones, Battelle Pacific Northwest National Laboratory

Phenomenology of Crack Propagation Processes

Crack initiation and propagation are related but different processes; however, by definition, if a crack initiates, it will propagate. As indicated in the section “Crack Initiation Mechanisms” in this article, cracks may initiate at preexisting surface flaws if the necessary electrochemical, mechanical, and metallurgical conditions are met, or corrosion processes may create a surface flaw by pitting or localized corrosion. The conditions that create a pit or localized corrosion at chemical inhomogeneities such as grain boundaries, inclusions, second phases, and interphase boundaries are not necessarily the same as those needed for sustained crack growth. For example, the electrochemical conditions near the surface of a material are similar to the bulk electrolyte conditions; electrolyte conditions in a propagating crack generally differ from the bulk electrolyte. If the conditions at the tip of the growing pit or localized corrosion penetration cannot achieve the proper pH, potential, or chemistry, crack propagation may not proceed. Also, if the pit aspect ratio is not greater than a critical value, then the local stresses and strains resulting from a sustained sharp crack are not attained and crack growth cannot occur. Lastly, for stress-corrosion crack growth resulting from cathodic hydrogen, a short crack may have to initiate by an anodic dissolution process, while propagation depends on hydrogen activity.

Although there are conditions under which local corrosion or pitting may not result in crack propagation, more frequently they do lead to cracking. Three conditions cited often as requirements for sustained SCC are a susceptible material, a corrosive environment, and an adequate stress. The list of susceptible material conditions and corrosive environments that are known to cause SCC has been expanding steadily. For example, pure metals are known to crack when impurities are segregated to grain boundaries, nonsensitized stainless steels crack in high-purity water, and ferritic steels crack in environments other than nitrate and caustic solutions. Similarly, the details of the microstructure and microchemistry of a susceptible material, specific ions and chemistry, pH, potential, the corrosion rates of the local crack tip associated with a corrosive environment, and the crack tip stresses, strains, and strain rates associated with cracking are better known today than they were previously. Knowledge and understanding of the factors and mechanisms of stress corrosion are continuing to expand; however, a number of factors are well established. The phenomenological description of stress corrosion based on these known factors is presented in this section.

Environmental Factors

Environmental effects on SCC are summarized frequently simply by listing alloy-environment combinations in which SCC has been observed, such as that in Table 1. In recent years, the number of such combinations has increased. Added to this list is the observation of the transgranular SCC of copper, the intergranular SCC of pure metals such as iron and nickel, and the SCC of materials in high-purity water in the absence of specific anions. Stress-corrosion cracking of pure metals was thought to be impossible in early lists of material-environment combinations, but it is now realized that specific environment/metal reactions occur that allow crack advance. In the case of intergranular SCC of iron and nickel, this reaction occurs between the environment and impurities segregated to the grain boundaries (a condition that exists in many pure metals and engineering alloys).

This increase in known susceptible materials can be attributed to the use of new SCC tests, refined crack propagation monitoring equipment, improved electrochemical control equipment, and, perhaps most importantly, the increased research activity in this field over the last 20 to 30 years.

Expectations for material performance have increased also with time as materials are used in more aggressive environments under more demanding loading conditions. Lists such as that given in Table 1 can be useful in materials selection for a design involving corrosive environments because it can lead the materials engineer to seek more specific information on the materials and environments in question. However, such lists can also be misleading because service conditions may differ markedly from those in which the susceptibility listed in Table 1 was determined. Because SCC is dependent on bulk alloy chemistry, microstructure, microchemistry, loading parameters, and specific environmental factors such as oxidizing potential and pH, lists of the type given in Table 1 should be used only for a general overview of SCC.

A complete description of SCC must treat both the thermodynamic requirements and kinetic aspects of cracking. A knowledge of the thermodynamic conditions will help determine whether cracking is feasible; kinetic information describes the rate at which cracks propagate. There are thermodynamic requirements for both anodically assisted SCC (where crack propagation is dependent either directly or indirectly on the oxidation of metal atoms from the crack tip and their dissolution in the electrolyte) and for hydrogen-assisted crack growth resulting from the reduction of hydrogen ions at the crack tip.

Thermodynamics of SCC. The thermodynamic conditions for anodically assisted SCC are that dissolution or oxidation of the metal and its dissolution in the electrolyte must be thermodynamically possible and that a protective film, such as an oxide or salt, must be thermodynamically stable. The first condition becomes a requirement because, without oxidation, crack advance by dissolution would not result. That a process is controlled by anodic dissolution does not a priori indicate that the total crack extension is the sum of the total number of coulombs of charge exchanged at the crack tip. There are crack advance processes in which the crack advance is controlled by anodic dissolution but in which the total crack length is greater than can be accounted for by the total charge transfer. These processes are covered in the section “Crack Propagation Mechanisms” in this article. However, it is important to note that if the brittle crack advance process is initiated and controlled by anodic dissolution, the crack growth rate will be zero if the anodic current density is zero and will increase with increasing current density. This also holds true for crack advance resulting from brittle crack jump.

The thermodynamic requirement of simultaneous film formation and oxidation for stress- corrosion crack growth can be understood from the diagram shown in Fig. 9, in which the ratio of the corrosion currents from the walls relative to the crack tip is the critical parameter. This ratio must be substantially less than 1 for a crack to propagate; otherwise, the crack will blunt, or the crack tip solution will saturate. Crack initiation can also be controlled by this ratio because a pit with a high wall corrosion rate will broaden as fast or faster than it will penetrate, resulting in general corrosion rather than crack growth. It is believed generally that the activity of the crack walls relative to the crack tip is a consequence of greater dynamic strain at the tip than along the walls.

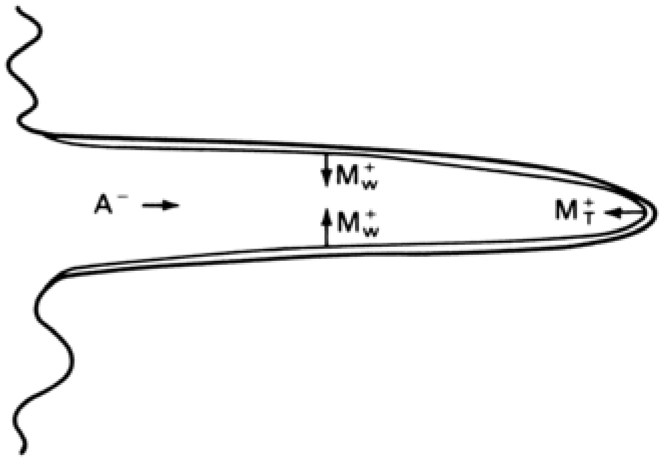

Fig. 9 Schematic of stress-corrosion crack showing important transport and corrosion reactions. A^- represents negatively charged anions migrating to the crack tip, M_w^+ represents metal ions entering the crack solution from the crack walls, and M_T^+ indicates metal ions entering the crack solution from the crack tip.

A thermodynamic requirement of simultaneous film formation and oxidation of the underlying material led to the identification of critical potentials for the presence or absence of SCC. An example of these critical potentials is shown in Fig. 10 for a passive film-forming material such as stainless steel. Zones 1 and 2 are those in which transgranular stress-corrosion crack growth is most likely to occur; intergranular stress-corrosion crack growth can occur over a wider range of potentials than these two zones can. Transgranular SCC occurs in zone 1 because the material is in transition from active corrosion to passive film formation such that the simultaneous conditions for film formation on the crack walls and corrosion at the crack tip are met. A similar condition exists in zone 2, with the added factor that these potentials are at or above the pitting potential so that cracks can initiate by pitting.

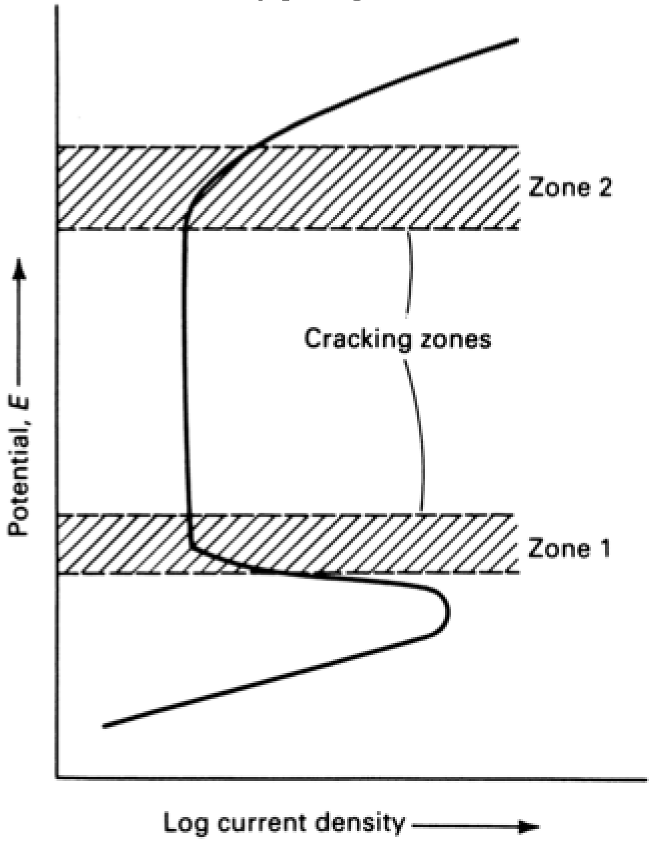

Fig. 10 Potentiokinetic polarization curve and electrode potential values at which stress-corrosion cracking appears

Intergranular SCC occurs over a wider range of potentials than those shown for zones 1 and 2 because chemical inhomogeneities at the grain boundary produce a different electrochemical response relative to the bulk material. Therefore, passive crack walls and active crack tips can result over the potential range from zone 1 to zone 2.

Examples of the critical potentials for SCC are shown in Fig. 11 for several materials. Identification of critical potentials for SCC has led to the use of electrochemical methods for assessing stress-corrosion susceptibility. Zones 1 and 2 are identified by determining the electrochemical potential versus current curves, as shown in Fig. 10 and 11. The shapes of these curves determined at high and low sweep rates are also used to indicate potentials at which the simultaneous conditions of film formation and metal oxidation occur.

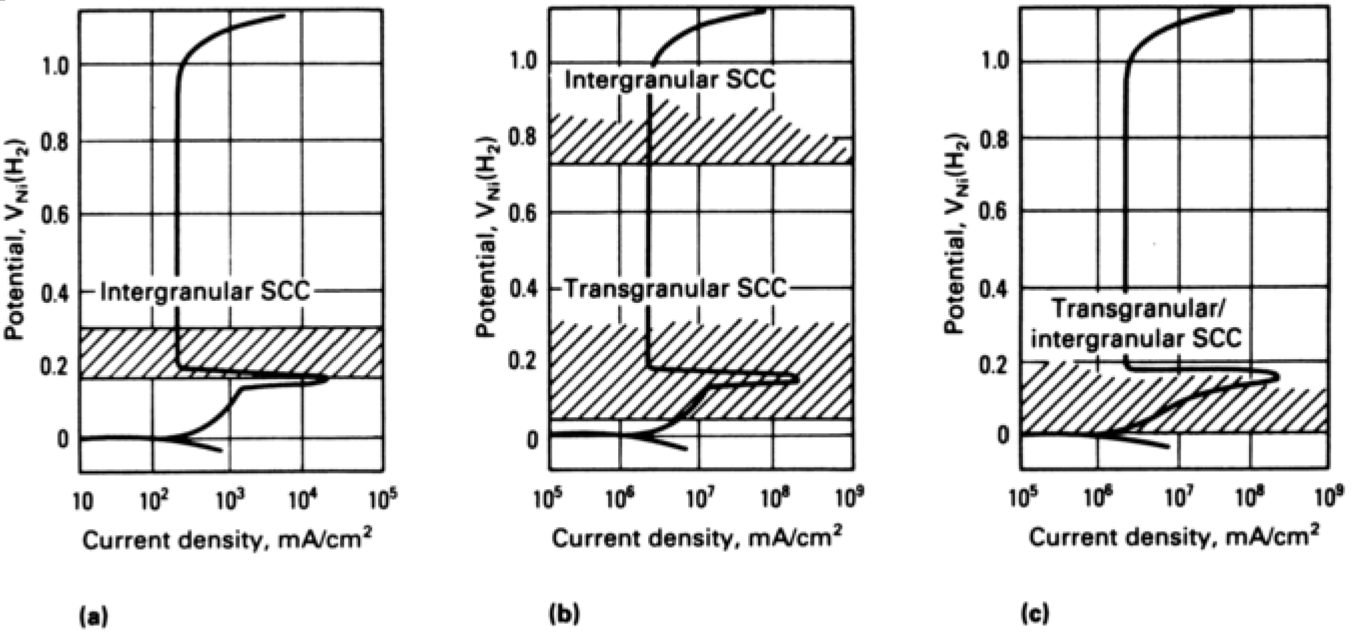

Fig. 11 Potentiokinetic polarization curve and electrode potential values at which intergranular and transgranular stress-corrosion cracking appear in a 10% NaOH solution at 288 °C (550 °F). (a) Alloy 600. (b) Alloy 800. (c) AISI type 304 stainless steel

Application of Potential-pH Diagrams. Critical potentials for SCC can also be related to potential-pH stability diagrams (Pourbaix diagrams) because these diagrams describe the conditions at which film formation and metal oxidation will occur. An example for carbon steel is given in Fig. 12, in which SCC is associated with potentials and pHs at which phosphate, carbonate, or magnetite films are thermodynamically stable while the species Fe^{2+} and $HFeO_2^-$ are metastable. A second example of the potential-pH regimes in which SCC occurs is given in Fig. 13 for a 70Cu-30Zn brass in a variety of solutions.

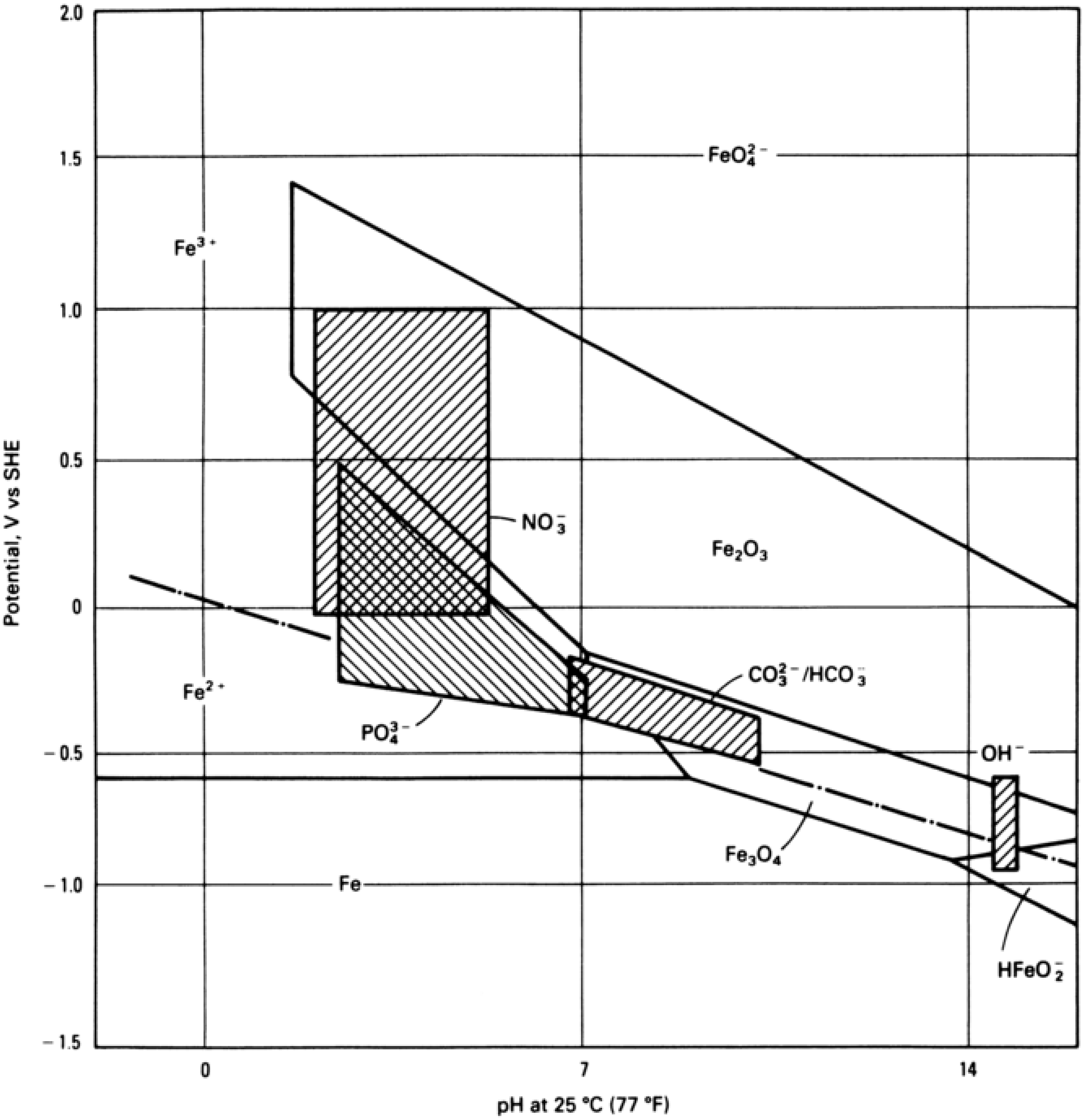

Fig. 12 Relationship between pH-potential conditions for severe cracking susceptibility of carbon steel in various environments and the stability regions for solid and dissolved species on the Pourbaix diagram. Note that severe susceptibility is encountered where a protective film (phosphate, carbonate, magnetite, etc.) is thermodynamically stable, but if ruptured, a soluble species (Fe^{2+}, $HFeO_2^-$) is metastable.

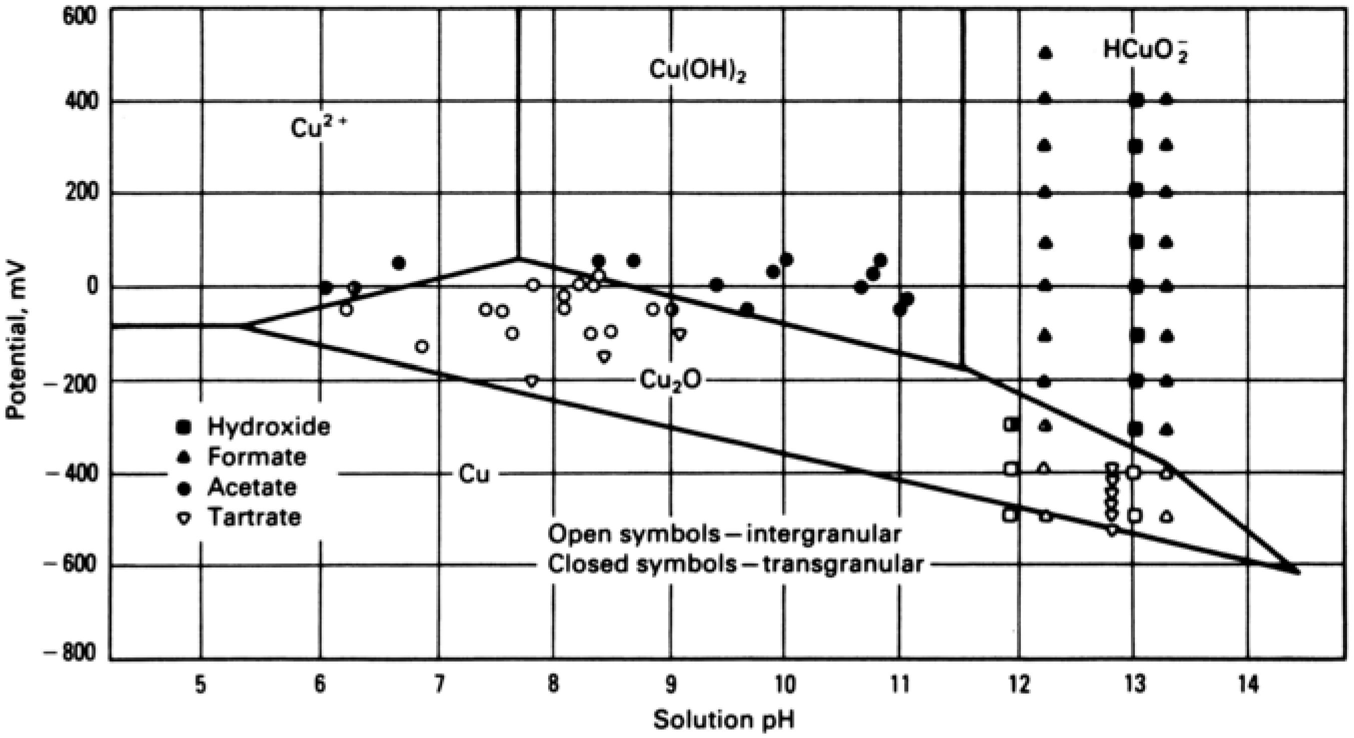

Fig. 13 Potential-pH diagram showing the domains of failure mode for 70Cu-30Ni brass in various solutions, together with the calculated positions of various boundaries relating to the domains of stability of different chemical species

The effect of many environmental parameters, such as pH, oxygen concentration, and temperature, on the thermodynamic conditions for SCC can be related to their effect on the potential-pH diagrams (as shown in Fig. 12 and 13) or on the material potential relative to the various stability regions. Using the potential-pH diagram for iron in water at 25 °C (77 °F) shown in Fig. 14, the effects of changing the pH and oxygen concentration can be illustrated. A decrease in the pH from 9 to 6 at a potential of -0.2 V versus standard hydrogen electrode (SHE) shifts iron from a region of stability to one of active corrosion. Based on the thermodynamic criteria for simultaneous stability and active corrosion, the critical pH would be expected to be 7, with decreasing susceptibility at higher pHs because of increased film stability and at lower pHs because of decreased film stability and the increase of general corrosion. Changes in the oxygen concentration generally alter the electrode potential, with increasing oxygen concentration resulting in more oxidizing conditions. The effects of temperature on the potential-pH diagram must be determined for each temperature of interest as the regions of stability shift with temperature.

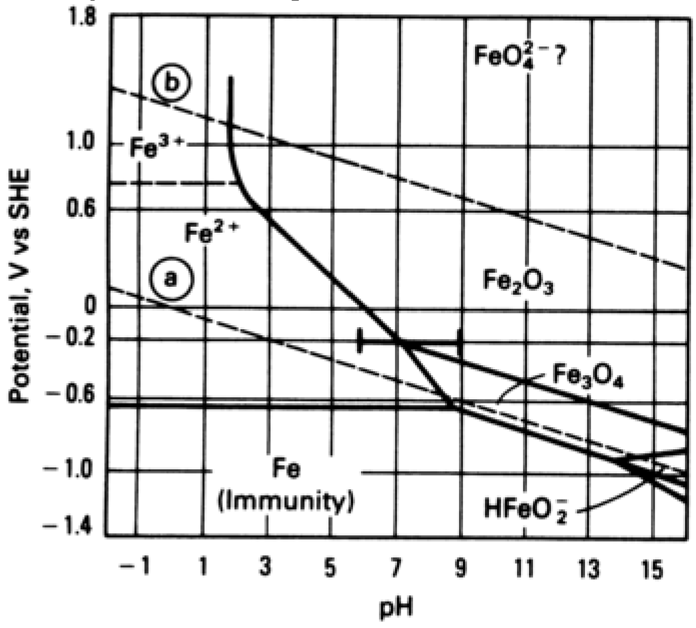

Fig. 14 Potential-pH diagram (Pourbaix) for iron in water at 25 °C (77 °F). A decrease in pH from 9 to 6 at potential of -0.2 V, which shifts iron from a region of stability to one of active corrosion, is indicated by the solid bar.

For materials in which SCC occurs by a hydrogen-induced subcritical crack growth mechanism, the thermodynamic requirement for crack growth is governed by the hydrogen reduction line shown by dashed line *a* in Fig. 14. Hydrogen reduction on iron in water at 25 °C (77 °F) occurs at potentials below this line, but not above it. Therefore, the range of potentials at which hydrogen is available to cause crack growth increases and becomes more oxidizing with decreasing pH.

Application of potential-pH diagrams for identifying specific conditions at which SCC will occur is limited by a number of factors, such as the availability of these diagrams for complex solutions and for the temperatures of interest and the substantial deviation of the chemistry of a crevice or crack from the bulk solution chemistry. Also, the electrode potential at the crack tip can differ from that of the free surface of the material. These differences arise from the need for diffusion of metal ions away from the actively corroding crack tip, migration of anions into the crack, reactions along the crack walls, convection of the electrolyte in the crack, reactions along the crack walls, and, in some cases, by gas bubble formation that causes potential drops. Efforts to measure the local crack tip chemistry and potentials are restricted by crack sizes, which can be substantially smaller than 1 μm. Therefore, mathematical modeling of transport within cracks and the resulting crack tip chemistry, reactions, and potentials have been pursued actively in recent years. The results of measurements in simulated crevices and modeling have shown clearly that the crack tip chemistry can differ from the bulk conditions, but the specifics of these differences are not well known and depend on the material and environment being considered.

For example, based on evaluations by one researcher, the pH within cracks and crevices of structural steels in marine environments ranged from 4 to 11, of stainless steel from 0 to 3, of aluminum from 3 to 4, and of titanium from 1 to 2 (Ref 18). Shifts of up to 300 mV in the crack tip potential in the anodic direction were observed for cathodically polarized steel, while other researchers found only a small shift in the crack tip potential relative to the external potential under steady-state conditions (Ref 16) or a 300 mV shift in the cathodic direction when the crevice walls were active, reducing to a small shift when the walls passivated (Ref 19). Therefore, the critical potentials at which cracking may occur can differ from those given by the bulk equilibrium conditions used to determine the potential-pH diagrams. Although it is possible to determine the equilibrium conditions based on the crack tip conditions, the current knowledge of crack tip conditions is fragmentary at best. Other factors that limit the usefulness of the equilibrium potential-pH diagrams are the lack of available diagrams for specific materials and environments and the variable temperatures, chemistries, and potentials common in many industrial applications.

Kinetics of SCC. A knowledge of the thermodynamic conditions at which SCC can occur is insufficient without a corresponding understanding of the kinetics of crack growth because the life of a component may be adequate if the crack growth rate is sufficiently slow, even though SCC is thermodynamically possible. As in the thermodynamic conditions for SCC, environmental parameters such as potential, pH, oxygen concentration, temperature, and crack tip chemistry have a strong effect on the crack growth kinetics. The crack tip reactions and the rate-determining steps controlling the crack growth rate are specific to alloy-environment combinations; although a discussion of each system is beyond the scope of this section, some general observations are made. Also, the crack growth rate depends on the crack advance process even though it is controlled by electrochemical reactions.

Detailed descriptions of various crack growth mechanisms are given in the section "Crack Propagation Mechanisms" in this article by categorizing these mechanisms as either anodic dissolution or mechanical fracture models. For the case of a crack growing by anodic dissolution alone, the total crack advance is a function of the total charge transfer at the crack tip, while the crack velocity is a function of the crack tip current density. For a crack growing with mechanical fracture, the total crack advance exceeds the total charge transfer at the crack tip, but the crack velocity may still be controlled by the crack tip current density. A limiting velocity, *da/dt*, can be described for a crack advancing under pure anodic dissolution by the following Faradaic relationship:

$$\frac{da}{dt} = \frac{i_a M}{zF\rho} \qquad \text{(Eq 3)}$$

where i_a is the anodic current density of a bare surface, M is the atomic weight, z is the valence, F is Faraday's constant, and ρ is the material density. It has been shown (Ref 20) that this relationship (Eq 3) between the bare surface current density and the crack propagation rate is applicable to a wide variety of materials, as presented in Fig. 15. Equation 2 assumes that the crack tip is maintained in a bare condition, while the crack walls are relatively inactive. A bare crack tip and passive walls can result from the difference between the electrochemical conditions at the tip and other regions in the crack, a difference in the local chemistry of the material at the crack tip that causes the tip to be more active than the crack walls (such as at a sensitized or segregated grain boundary), or a crack tip strain rate that is sufficiently high to prevent the formation of a protective film.

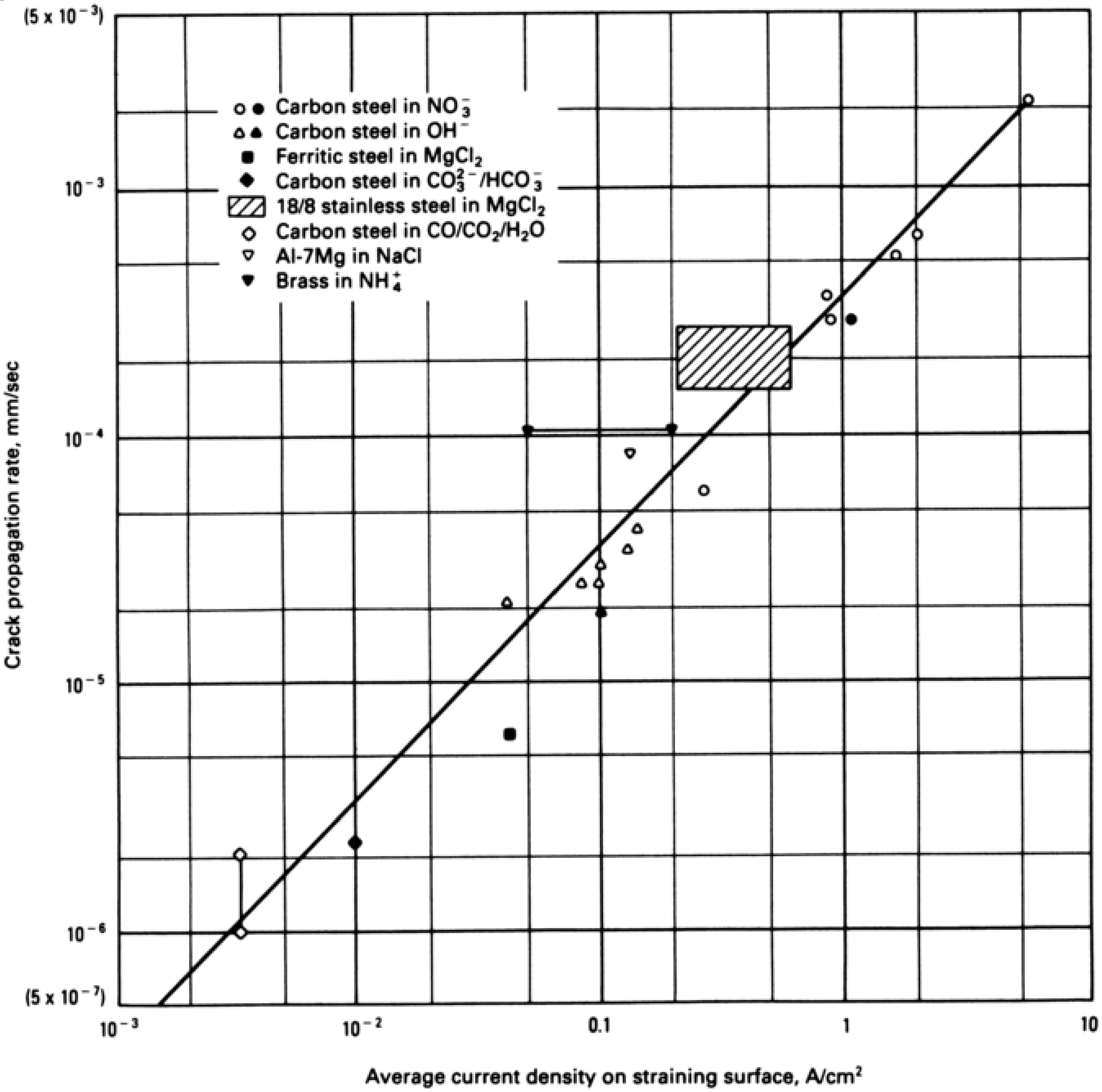

Fig. 15 Relationship between the average crack propagation rate and the oxidation (that is, dissolution and oxide growth) kinetics on a straining surface for several ductile alloy/aqueous environment systems

A number of factors can reduce the crack velocity below that given by Eq 3 and in Fig. 15. The most widely examined crack growth retardation process is that resulting from the crack tip being covered by a film for some fraction of time. The process of crack growth in the presence of a film at the crack tip has been described by several mechanisms, such as slip dissolution and passive film rupture, covered in the section "Crack Propagation Mechanisms" in this article. In general, the crack growth rate depends on the rate at which the film

is ruptured and reformed. The amount of corrosion that occurs between these two events has been used to describe the crack growth rate. This time period is determined by the crack tip strain rate, film fracture strain, repassivation rate of the surface, maximum corrosion rate while the tip is bare, and the corrosion rate decay with repassivation. Other factors that can reduce the crack growth rate below that given by Eq 3 are limits in the diffusion rate of species into and out of the crack tip, crack deflection away from the principal stress, and changes in the local material chemistry. Transport of species into and out of cracks is considered a major limitation to attaining the crack growth rate predicted by Eq 3. Factors such as the crack geometry or width, reactions or corrosion rate along the walls of the crack, diffusion rate of anions and cations, and metal salt solubility limits all contribute to transport-limited crack velocities.

A lack of clear knowledge about the specific conditions at the tip of a crack has limited the understanding of the role of specific species on crack growth rates. At this time, it is possible only to describe the effect of bulk electrolyte conditions on crack growth rate; the local conditions may vary significantly. However, knowledge of the local crack tip conditions is most important for understanding the mechanisms of cracking, although a knowledge of the external crack conditions is adequate for monitoring and controlling SCC. Using austenitic stainless steel as an example, the effects of electrochemical potential, oxygen content, and temperature are shown schematically in Fig. 16, 17, and 18. Similar relationships exist for other anion concentrations, such as halides and sulfur species, but the data base is not as well developed as the cases shown. It is important to note that these are not independent effects, because the effects of oxygen concentration and temperature are probably related to the potential. The details of this relationship are complex and are beyond the scope of this section.

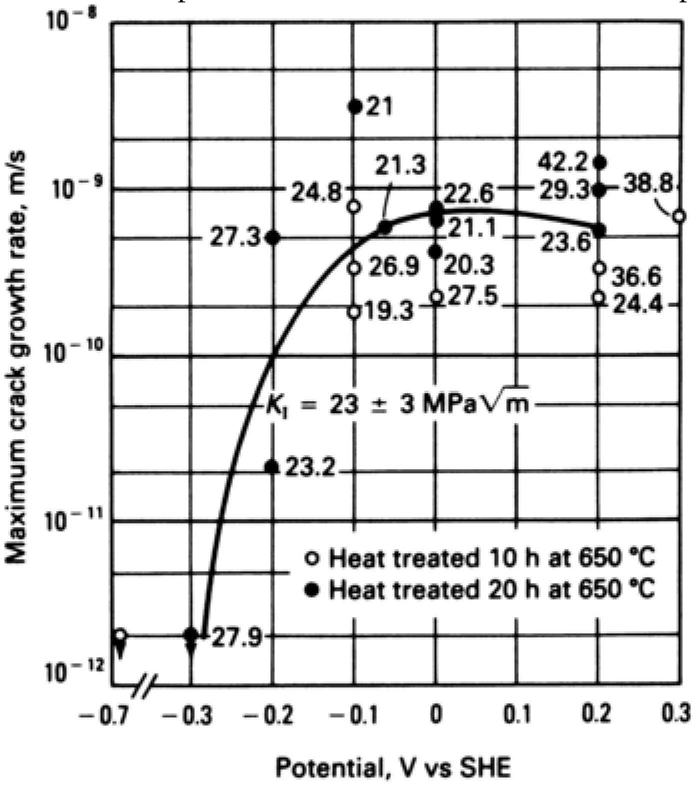

Fig. 16 Effect of potential on the maximum crack growth rate in sensitized type 304 stainless steel in 0.01 m Na_2SO_4 at 250 °C (480 °F). Numbers denote K_I values.

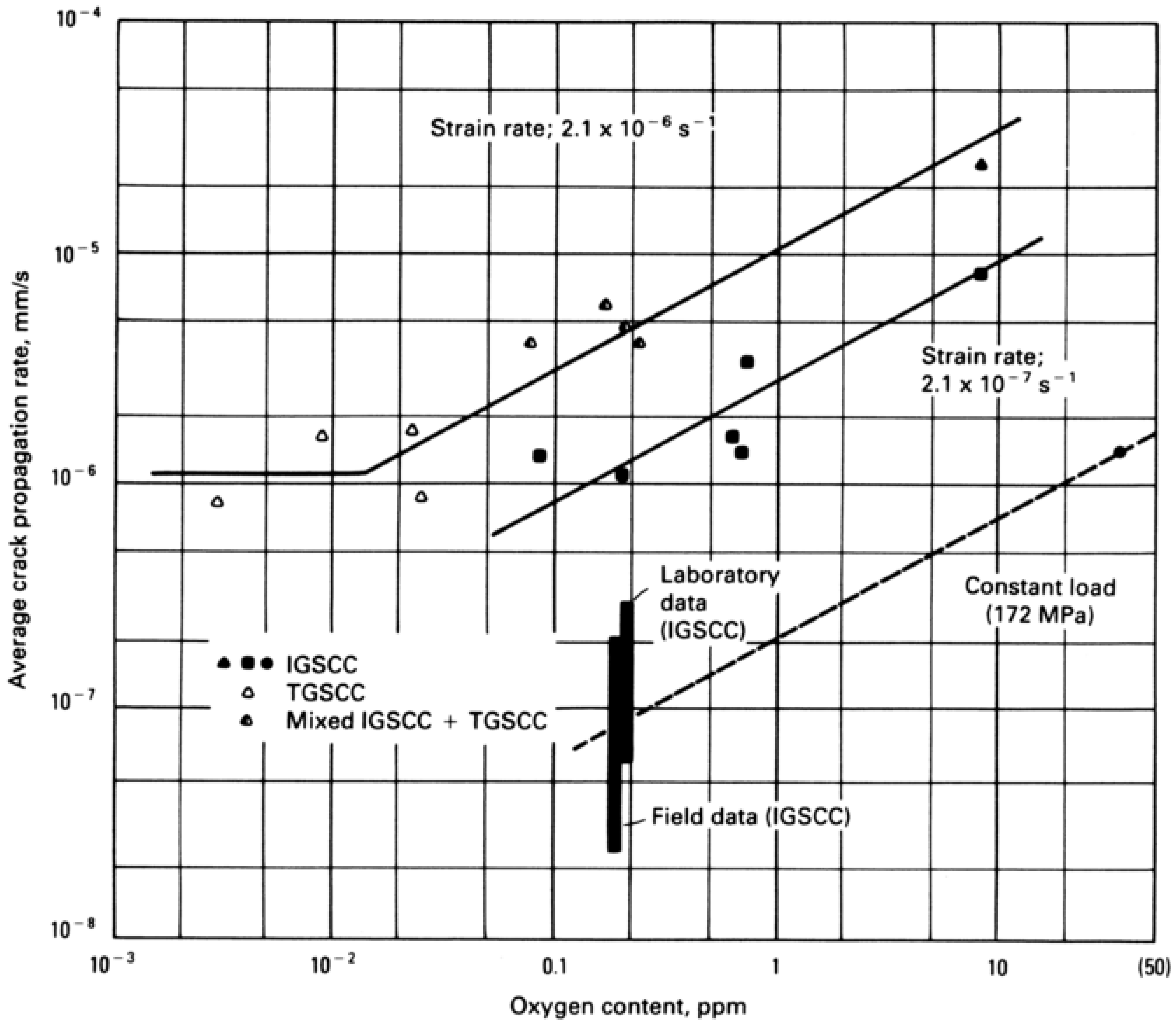

Fig. 17 Variation in the average crack propagation rate in sensitized type 304 stainless steel in water at 288 °C (550 °F) with oxygen content. Data are from both constant extension rate (CERT) tests, constant load, and field observations on boiling water reactor piping. IGSCC, intergranular SCC; TGSCC, transgranular SCC.

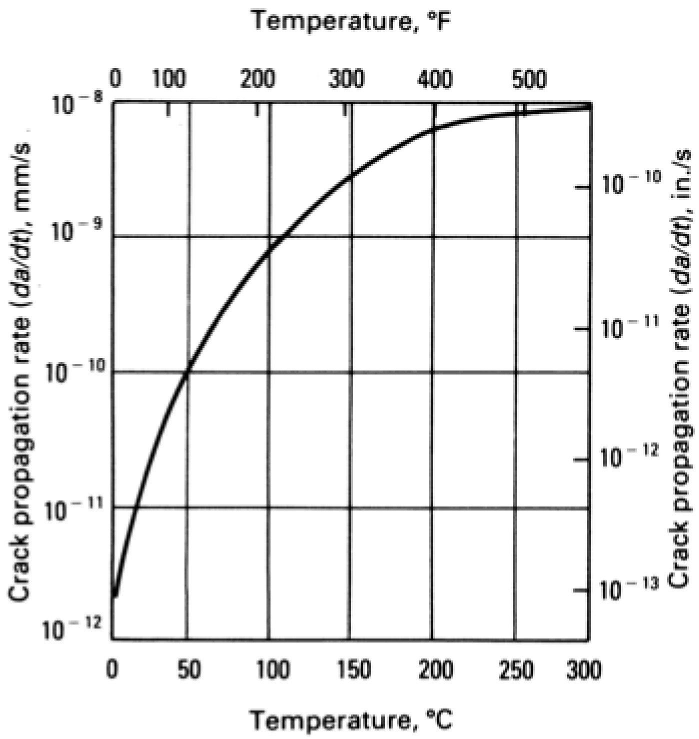

Fig. 18 Schematic of crack growth rate versus temperature for intergranular stress-corrosion cracking of type 304 stainless steel

A mechanical fracture process in SCC can produce crack velocities exceeding those given by Eq 3 by some magnification factor, which can be as large as 100. The mechanism of brittle fracture induced by SCC, which is covered in the section "Crack Propagation Mechanisms" in this article, is thought to involve the formation of a corrosion product at the crack tip in which a cleavage crack can initiate and propagate some depth into the ductile substrate. As mentioned earlier, this process would produce crack lengths that exceed those accounted for by the total charge transfer/metal oxidation process, but it would be dependent on the crack tip corrosion rate because the formation rate of the corrosion product would depend on the corrosion rate.

Early observations and proposals of this process have been made (Ref 21, 22, 23, 24, 25). A current list of materials in which SCC is thought to occur through a film-induced cleavage process as suggested in Ref 25 is given in Table 2, which shows a wide range of materials and environments. An attempt has been made to identify the corrosion product or layer that initiates the cleavage cracking process, but this identification must be considered speculative. The electrochemical conditions controlling the brittle SCC process have not been catalogued carefully; however, for many systems, the main issue is whether cracking can be described completely by anodic dissolution or whether a mechanical fracture process is involved. The greatest uncertainty involves the possibility of a transition between anodic and mechanical SCC processes that is affected by electrochemistry, material chemistry, or mechanics.

The electrochemical factors described in the previous paragraphs generally were drawn from examples of intergranular SCC, but many of the effects would be similar for brittle transgranular SCC. For example, the brittle transgranular crack growth rate follows closely the dependence of the anodic current density on potential. Whether there are critical potentials at which transgranular SCC may switch from a brittle mechanical fracture mode to a purely anodic dissolution mode is unknown. However, for many systems, the critical potentials describing SCC are valid control parameters even though the process associated with these critical potentials may be uncertain. For an anodic dissolution-controlled process, the critical potentials were associated with the need for an active tip and passive crack walls. These conditions are still necessary for a brittle SCC process because it is dependent on the anodic reaction to produce the corrosion reaction product. This product may be a film or a dealloyed layer, but the rate of formation and, therefore, the brittle crack growth rate are dependent on the crack tip current density.

Material Chemistry and Microstructure

The relationship between material chemistry and microstructure and SCC is equally as complex as the relationship between the environment and SCC. Bulk alloy composition can affect passive film stability and phase distribution (for example, chromium in stainless steel), minor alloying elements can cause local changes in passive film-forming elements (for example, carbon in stainless steel causing sensitization), impurity elements can segregate to grain boundaries and cause local differences in the corrosion rate (for example, phosphorus in nickel or nickel-base alloys), and inclusions can cause local crack tip chemistry changes as the crack intersects them (for example, manganese sulfide in steel). In addition, alloys can undergo dealloying, which is thought to be a primary method by which brittle SCC initiates. The following summary is divided into intergranular and transgranular effects because some of the primary factors can be best described in this way; however, it is important to recognize that many of the material chemistry factors can affect both intergranular and transgranular cracking.

Intergranular Stress-Corrosion Cracking. Material chemistry and microstructure effects on intergranular SCC can generally be divided into two categories: grain-boundary precipitation and grain-boundary segregation. Grain-boundary precipitation effects include carbide precipitation in austenitic stainless steels and nickel-base alloys, which causes a depletion of chromium adjacent to the grain boundary and intermetallic precipitation in aluminum alloys, which are anodically active. Grain-boundary segregation of impurities such as phosphorus, sulfur, carbon, and silicon can produce a grain boundary that is up to 50% impurity within a 1 to 2 nm thick region. These impurities can alter the corrosion and mechanical properties of the grain boundary and can therefore cause cracking by anodic dissolution and perhaps mechanical fracture.

Grain-Boundary Precipitation in Stainless Steels. Chromium carbide precipitation in stainless steels occurs in the temperature range 500 to 850 °C (930 to 1560 °F), with the rate of precipitation controlled by chromium diffusion. For intermediate times, such as occurs with heat treating and welding, chromium depletion occurs adjacent to the grain boundary during chromium carbide growth. This depletion can be described by the minimum chromium concentration adjacent to the carbide and the width of the depleted zone. Minimum chromium concentrations of 8 to 10 at.% have been measured by analytical electron microscopy, while the width of the depleted zone has been measured to range from 10 nm to hundreds of nanometers. After times long enough for carbide growth to reach completion, the chromium profile is eliminated, and the chromium concentration returns to the bulk value.

The intergranular SCC of austenitic stainless steel depends primarily on the nature of the chromium-depleted zone, which is explained generally by the depletion of a passive film-forming element along a continuous path through the material. The stress-corrosion susceptibility and crack growth rate of austenitic stainless steel can be described by the degree of sensitization (DOS) as measured by corrosion tests such as the Strauss or electrochemical potentiokinetic reactivation (EPR) tests. Quantitative comparisons between susceptibility as measured by the presence or absence of intergranular SCC in an SCC test or the crack growth rate and the DOS or chromium depletion parameters have been successful in cases in which sufficient data have been available, but these correlations are limited to specific alloys, environments, and stress conditions. Semiquantitative comparisons in which intergranular SCC is predicted for DOS values greater than some critical value are less costly to obtain and have been used more extensively.

An example of the time/temperature/DOS curves at several carbon concentrations is shown in Fig. 19. The curves represent the conditions necessary for the development of a constant degree of sensitization, with the strong effect of bulk carbon concentration on the time needed to develop a sensitized microstructure. Therefore, the most common method for reducing the possibility of developing a sensitized microstructure is to reduce the carbon concentration or to control the thermal history of the material. Given that the material is sensitized, control of the environment and stress conditions can be used to reduce the crack propagation rate.

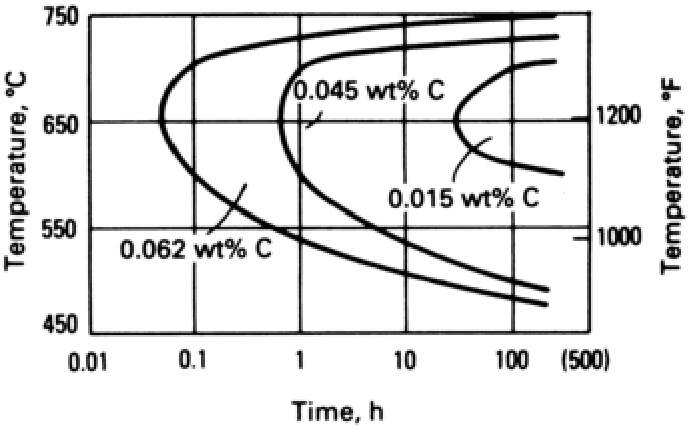

Fig. 19 Time/temperature/sensitization curves determined by EPR tests on type 304 stainless steel alloys of variable carbon contents

Clearly, chromium and carbon are the two most important elements involved in the development of sensitization; however, other elements can play a role. Molybdenum has an effect similar to that of chromium—incorporation into the carbides and depletion adjacent to the grain boundaries—although it is generally present in smaller concentrations (for example, in type 316 stainless steel) than chromium is. Nickel increases the activity of carbon in austenitic stainless steel; therefore, increases in nickel concentration can enhance sensitization for a given carbon concentration and thermal history. Manganese, silicon, and nitrogen have also been shown to affect sensitization, but the available data on these elements are comparatively sparse. Silicon has been shown to segregate to grain boundaries when present in sufficient quantities or by the nonequilibrium processes that occur when the material is irradiated with neutrons. The presence of silicon in the grain boundaries has been found to be deleterious in oxidizing environments.

Grain-Boundary Precipitation in Nickel Alloys. The cause of intergranular SCC in nickel- base alloys is more complex than it is in austenitic stainless steel. Chromium-carbide precipitation and chromium depletion occur in nickel-base alloys, such as alloy 600, as they do in austenitic stainless steels, but a clear connection between the presence of this microstructure and intergranular SCC has not been made. Carbon solubility is considerably lower and chromium diffusion is faster in nickel-base alloys than in austenitic stainless steels; therefore, the nose in the carbide precipitation or sensitization curves shown in Fig. 19 is shifted to shorter times and higher temperatures. Significant heat- to-heat variations in the chromium depletion of alloy 600 have been observed for a given heat treatment. This variation is attributed to the sensitivity of alloy 600 to carbon concentration and to the variability in mill-anneal heat treatment conditions. Chromium depletion is thought to accelerate cracking in oxygenated water but has not been identified as a controlling factor in deaerated water or caustic environments at 300 °C (570 °F). The rapid carbide precipitation kinetics in nickel-base alloys allows the development of a healed microstructure in which carbide growth is complete and the chromium profile is eliminated with relatively short heat treatment times.

Some significant differences between the intergranular SCC of nickel-base alloys and that of austenitic stainless steels include the positive effect of a semicontinuous distribution of carbides at the grain boundary in single-phase material and the galvanic couple between the γ' and γ phases in precipitation-hardened alloys. The beneficial effect of a semicontinuous distribution of carbides is thought to be related to dislocation generation from the carbides that results in a crack blunting or stress relaxation at the tip of a crack. The detrimental effect of the γ' phase is thought to result from a galvanic couple that polarizes the γ phase anodically relative to the γ' phase.

Grain-Boundary Precipitation in Aluminum Alloys. Aluminum alloys are also noted for the occurrence of intergranular SCC in aqueous environments, including sodium chloride (NaCl) solutions. The details of the intergranular SCC process in aluminum alloys are very complex and vary with alloy composition, but some features can be summarized. Grain-boundary precipitation has been identified as a contributing factor in the intergranular SCC in aluminum alloys; galvanic effects between the precipitates and matrix are considered to be important. In some cases, the precipitates are anodic, and in others, they are cathodic to the matrix. Peak- aged materials that give maximum hardnesses and microstructures in which slip bands are produced upon straining are considered to be vulnerable to SCC. Overaged structures are considered to be less susceptible. The mechanism of crack growth is thought to be a combination of local anodic dissolution and hydrogen

embrittlement. Whether crack extension is by anodic dissolution or by hydrogen embrittlement remains an open question; however, in aqueous solutions, the primary source of hydrogen is anodic dissolution.

Grain-Boundary Segregation in Aluminum Alloys. Grain-boundary enrichment of magnesium without precipitation of a magnesium-rich phase has been identified as a factor in the intergranular SCC of aluminum alloys (Ref 26, 27). This enrichment is associated with increased corrosion activity at the grain boundary and the possible formation of magnesium hydride (MgH) or enhanced hydrogen entry along the grain boundaries. Crack advance is thought to occur by discontinuous crack jumps (possibly nucleated by hydrides) and crack arrest after about 150 to 350 nm of advance, followed by repetition of this process.

Grain-Boundary Segregation in Ferrous and Nickel Alloys. Grain-boundary enrichment of impurities can contribute to the intergranular SCC of iron-base alloys, austenitic stainless steels, and nickel-base alloys. The extent of their effect depends on the electrochemical potential, the presence of other stress-corrosion processes such as chromium depletion, and their concentration in the grain boundary. The enrichment of impurities to grain boundaries by equilibrium segregation can be described by the enrichment ratio, as shown in Fig. 20 for a variety of impurity- alloy combinations (Ref 28). The enrichment ratio defines the upper bound to the grain-boundary concentration that will be achieved under equilibrium conditions, which can be very long times at low temperatures. It can be seen from Fig. 20 that enrichment ratios as high as 10^5 are possible for some impurities and that ratios greater than 10^2 are not uncommon. For the bulk impurity concentrations present in most engineering alloys, grain-boundary impurity concentrations of 10 to 20 at.% are possible. Therefore, an intergranular stress-corrosion crack can propagate along a grain boundary that has a composition vastly different from that of the bulk alloy.

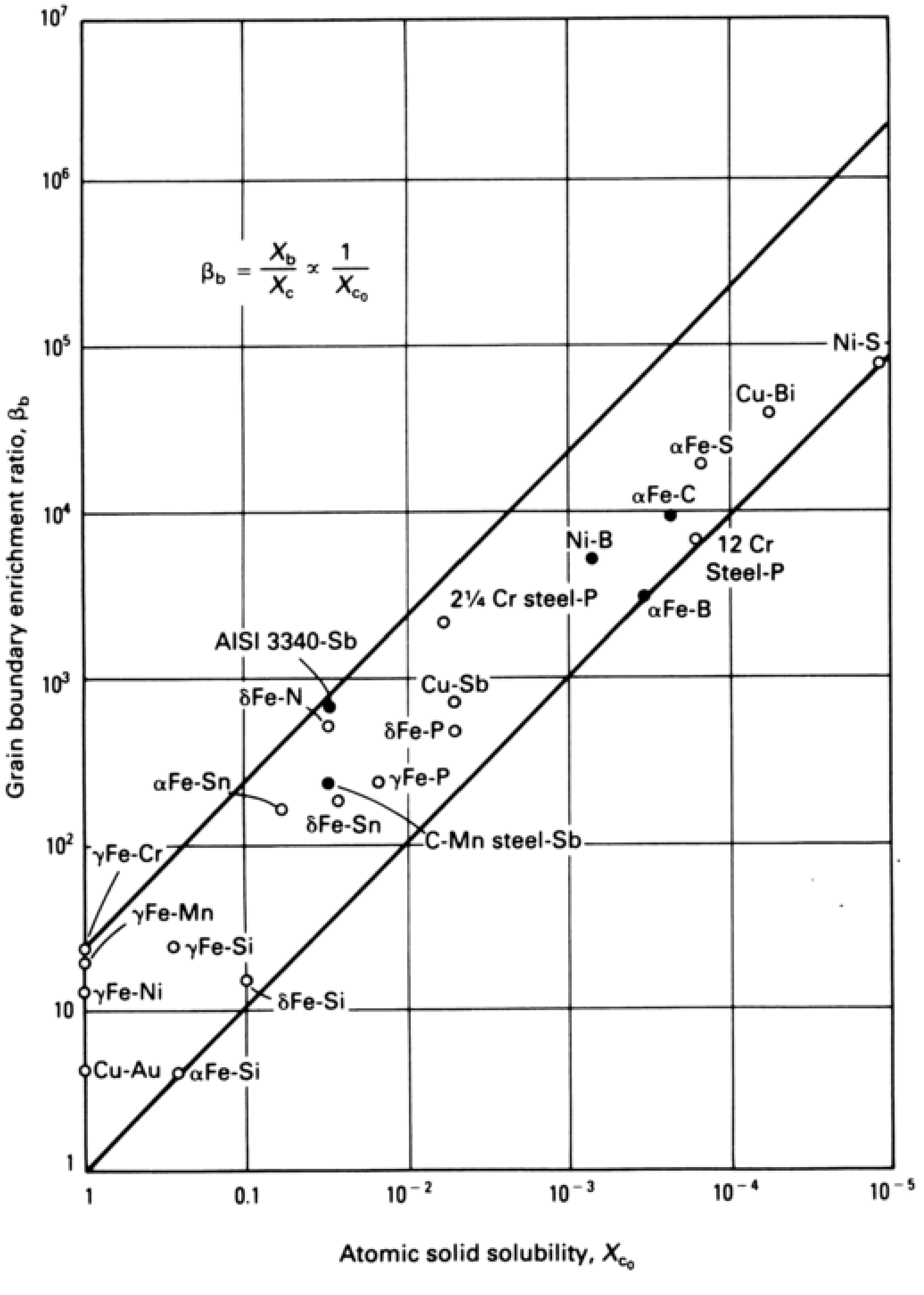

Fig. 20 Correlation between measured grain-boundary enrichment ratios, β, and the inverse of solid solubility, X_{c_0}. The symbols X_b and X_c represent the actual concentration of the species b and c in the bulk.

Ferritic steels exhibit intergranular SCC in hot nitrate, caustic, carbonate, and a variety of other environments. The presence of intergranular SCC is dependent on the electrochemical potential because intergranular SCC is predominant at potentials in the active-passive transition. Early studies of this effect identified carbon segregation as the primary element of concern where the carbon atoms were said to provide suitable imperfection sites for adsorption of nitrate in an adsorption-induced crack growth mechanism (Ref 29). More recently, phosphorus segregation has been associated with the intergranular SCC of iron alloys in nitrate and caustic solutions (Ref 30, 31); grain-boundary concentrations as low as 2 to 3 at.% have been sufficient to alter the passivity of iron in hot nitrate solutions. A complexity of SCC in ferritic steels is the susceptibility of such steels to intergranular SCC and to hydrogen-induced subcritical crack growth. The temperatures and electrochemical potentials at which intergranular SCC and cathodic hydrogen-induced subcritical crack growth

occur generally are not the same. Stress corrosion tends to dominate at temperatures above about 50 °C (120 °F) and at potentials in the active-passive transition; hydrogen effects are predominant at temperatures below 50 °C (120 °F), at more cathodic potentials, and at lower pH values. Examples of the effect of sulfur and phosphorus on the tendency toward intergranular fracture are given in Fig. 21 and 22, from which it can be seen that sulfur was more effective than phosphorus in causing intergranular fracture of iron at cathodic potentials (Ref 32, 33). For the conditions of this test, a sulfur concentration of about 13 at.% was sufficient to change the fracture mode from transgranular to intergranular.

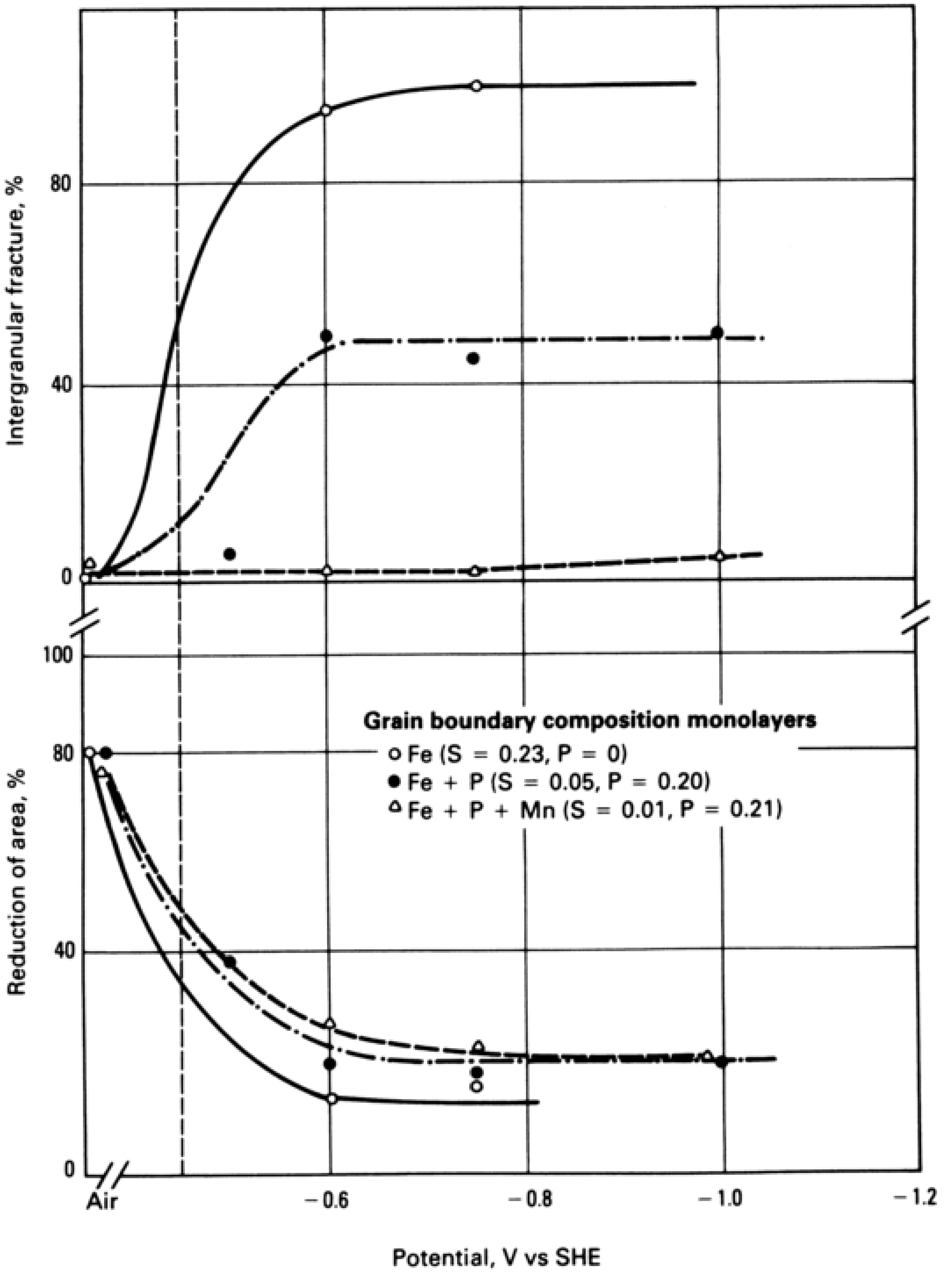

Fig. 21 Percent intergranular fracture, reduction of area, and strain to failure of iron, iron + phosphorus, and iron + phosphorus + manganese alloys tested at various cathodic potentials

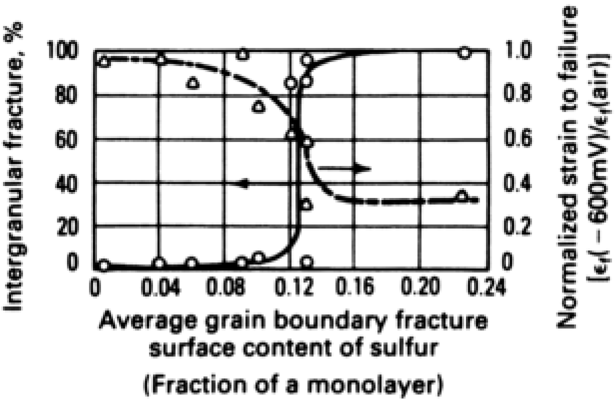

Fig. 22 Percent intergranular fracture and the normalized strain to failure plotted as a function of sulfur content at the grain boundary for straining electrode tests at a cathodic potential of -600 mV (SCE)

Grain-boundary impurity segregation of various impurities, including phosphorus, silicon, sulfur, and nitrogen, has been reported in austenitic stainless steels (Ref 34); however, no direct effect on intergranular SCC has been identified in high-temperature water. Phosphorus segregation has been shown to cause intergranular corrosion in highly oxidizing solutions, and impurity segregation of phosphorus and perhaps silicon has been suggested as a primary factor in irradiation-assisted SCC, which occurs in the oxidizing in-core environment of light water reactors (Ref 35). Phosphorus segregation apparently can contribute to the intergranular SCC of austenitic stainless steels in high-temperature water if the carbon concentration of the alloy is lower than 0.002%. At this low concentration, there is virtually no sensitization; therefore, the phosphorus segregation effect is observed.

Phosphorus is also the primary grain-boundary segregant in alloy 600 and has been shown to segregate by an equilibrium process (Ref 36). The grain-boundary composition versus temperature curves for alloy 600 and type 304 stainless steel are shown in Fig. 23, along with a calculated curve for equilibrium segregation in nickel (Ref 37). It can be seen that grain-boundary phosphorus concentrations to 15 at.% are possible. Grain-boundary segregation of sulfur, boron, nitrogen, and titanium also has been observed in alloy 600; however, a clear connection between the impurity segregation and intergranular SCC in nickel-base alloys has not been observed to date.

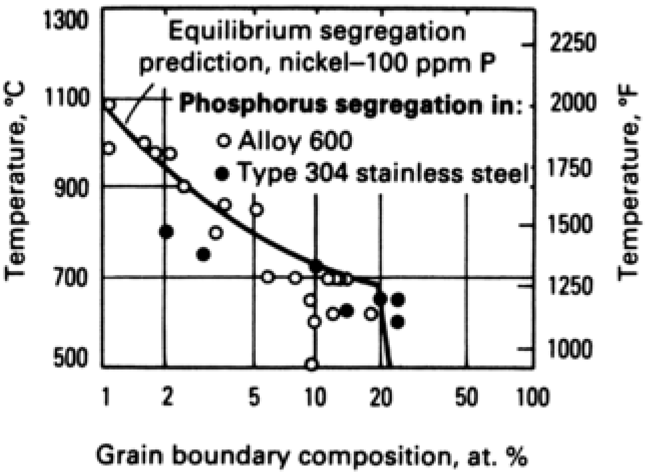

Fig. 23 Grain-boundary segregation measurements in Alloy 600 and type 304 stainless steel. Shown are auger electron spectroscopy measurements of phosphorus segregation in the two alloys as compared with model prediction for phosphorus segregation in nickel.

In contrast to the high-temperature water results for alloy 600, a clear effect of phosphorus segregation on the intergranular SCC of nickel was observed at oxidizing potentials in acidic solutions at 25 °C (77 °F) (Ref 18), as shown in Fig. 24. Intergranular SCC was observed at anodic potentials ranging from the active-passive transition to transpassive potentials in nickel with phosphorus-enriched grain boundaries but not sulfur-enriched grain boundaries. The role of phosphorus was identified with degradation of the passive film formed on nickel in acidic solutions. This example is a clear case of active- path corrosion; however, the cracking was clearly

stress dependent, as evidenced by a threshold stress intensity below which intergranular SCC did not occur and an alignment of cracks with the applied tensile stress. Because there were no grain-boundary carbides or chromium depletion in the nickel, these results illustrate the potential effect of impurities when other grain-boundary processes are absent. Therefore, it appears, as in the case of type 304 stainless steel cited earlier, that impurity segregation may induce intergranular SCC in the absence of carbides and chromium depletion.

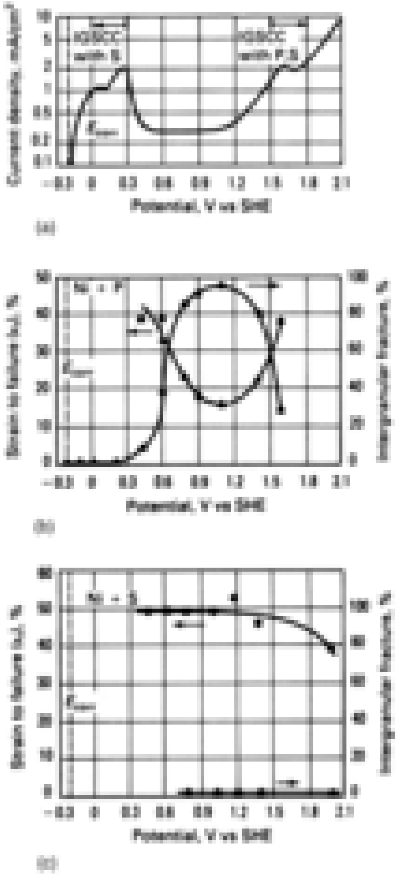

Fig. 24 Stress-corrosion cracking behavior of nickel with phosphorus and sulfur segregation. (a) Polarization curve for nickel in 1 *N* H_2SO_4 at 25 °C (77 °F). (b) Strain to failure and percent intergranular fracture for 26% phosphorus segregation at grain boundaries. (c) Strain to failure and percent intergranular fracture for 40% sulfur segregation at grain boundaries

Like ferritic materials, nickel-base alloys and austenitic stainless steels are susceptible to hydrogen-induced intergranular subcritical crack growth. Impurity segregation is thought to play a key role in this hydrogen-induced fracture, as the results for nickel shown in Fig. 25 illustrate. These results show the combined effect of sulfur segregation and cathodic hydrogen on the amount of intergranular fracture in nickel. For the conditions of these tests, a given amount of intergranular fracture resulted for different combinations of grain-boundary sulfur and hydrogen reduction rate. A decrease in the amount of sulfur could be compensated for by an increased hydrogen activity to give the same amount of intergranular fracture.

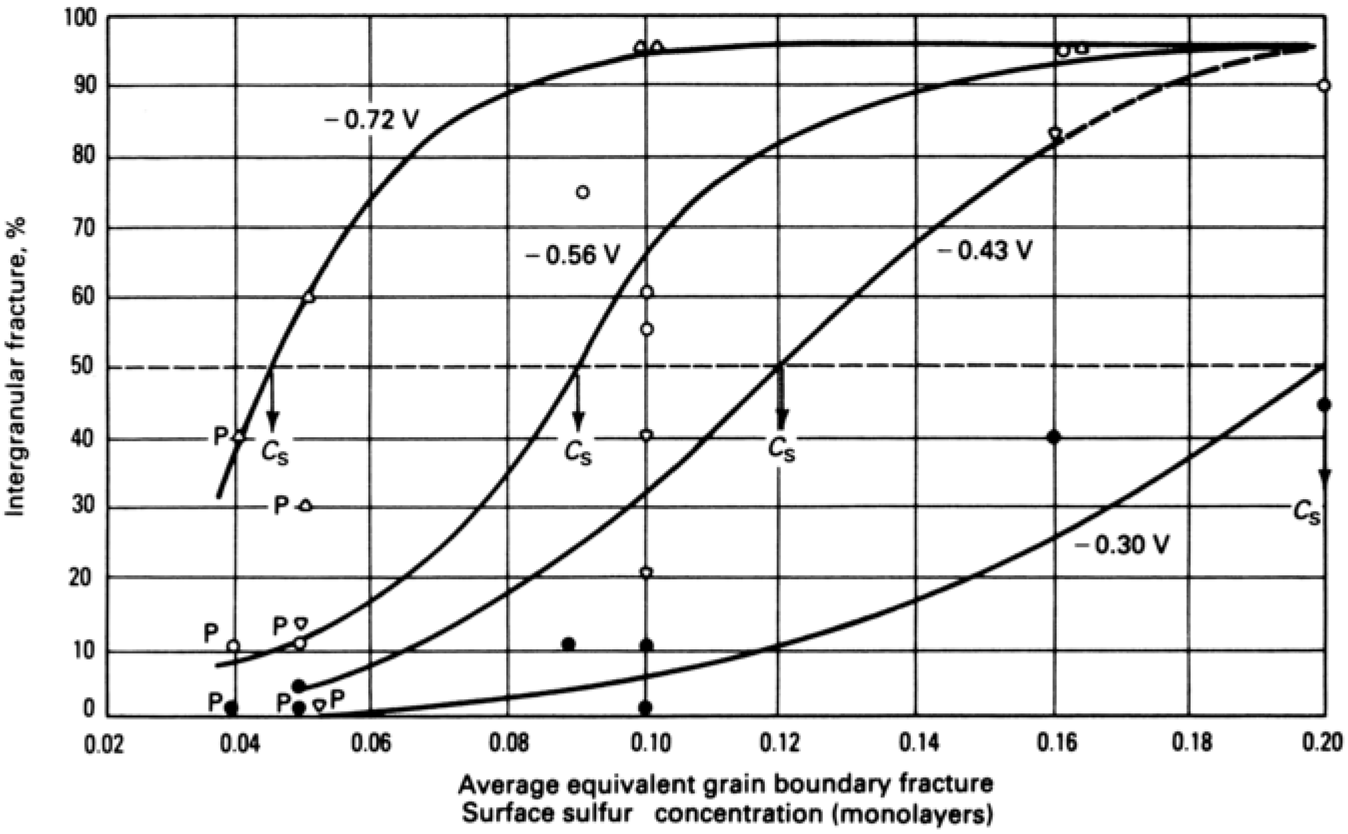

Fig. 25 Percent intergranular fracture and reduction of area versus grain-boundary composition of nickel for several cathodic test potentials. C_S is the critical sulfur concentration corresponding to 50% intergranular fracture. Points labeled P are equivalent sulfur concentrations for alloys with sulfur + phosphorus at the grain boundaries. Source: Ref 38

Transgranular Stress-Corrosion Cracking. Numerous metallurgical factors affect transgranular SCC, for example, crystal structure, anisotropy, grain size and shape, dislocation density and geometry, yield strength, composition, stacking fault energy, ordering, and phase composition. Some of these factors also affect intergranular SCC, as covered in the section "Intergranular Stress-Corrosion Cracking" in this article. Also, some of their effects on transgranular SCC are related to the corrosion behavior of the alloy, which can be understood from potential-pH diagrams or polarization curves. Because these effects are covered elsewhere, they are not discussed here. Similarly, yield strength effects are considered in the section "Mechanical Factors" in this article. Metallurgical factors in hydrogen-induced subcritical crack growth, such as crystal structure, hydride stability, and yield strength, are considered in the article "Hydrogen Damage" in this Volume. The effects of alloy composition on corrosion rate, hydrogen exchange current densities, and hydrogen absorption rates also influence the hydrogen-induced subcritical crack growth of materials in corrosive environments, but these are covered in the articles dealing with specific metals and alloys.

Alloying effects on slip planarity are a key metallurgical factor in transgranular SCC. Planar slip occurs in alloys with low stacking fault energy, alloys containing ordered phases, or alloys exhibiting short- or long-range ordering. The consequences of planar slip on transgranular SCC have been explained by the slip-dissolution model discussed in Ref 39. In this model, the passive film is ruptured by the emergence of a slip step. In high-chloride environments, evidence was presented that preferential corrosion occurred along the high dislocation density plane created by planar slip (Ref 40). A number of crack growth processes were suggested based on the planar slip localized corrosion process—for example, control of crack advance solely by anodic dissolution of the slip plane, brittle fracture of the corrosion product or tarnish film formed along the localized corrosion path, and the tunneling process by which corrosion along the slip plane branches out into tunnels accompanied by mechanical fracture of the remaining ligaments. The planar slip concept of transgranular SCC appears consistent with a number of observations, such as alloying and strain rate effects. Details of these mechanisms are presented in the section "Crack Propagation Mechanisms" in this article.

A significant difficulty associated with the slip-dissolution mechanism is the nature of the transgranular SCC fracture surfaces, which are generally not on the slip planes and have cleavage-like features. For example, for

admiralty brass tested in aqueous ammonia (NH_3) and Al- 5.5Zn-2.5Mg tested in aqueous NaCl, the primary fracture facets were (110) planes, while for stable austenitic stainless steel tested in aqueous magnesium chloride ($MgCl_2$) at 155 °C (310 °F), the primary facets were on (100) planes. There is also evidence that crack advance in brass occurs in a discontinuous manner (Ref 24). Several mechanisms for the development of a cleavage crack in ductile face-centered cubic (fcc) alloys have been presented, but a definite correlation has not emerged.

One concept that has received considerable attention is that proposed in Ref 25, in which a rapid crack advance that begins in a brittle film at the crack tip induces cleavage fracture of the ductile material ahead of the crack tip. The brittle films that are regarded as the initiating layers are given in Table 2. These include a dealloyed layer, oxide, nitride, carbide, or hydride. A dealloyed layer acting as a cleavage crack initiator is suggested for brass, copper-gold, and iron- chromium-nickel alloys. If this concept is supported by future research, the relative reactivity of the alloying elements will prove to be a key metallurgical factor in the transgranular SCC of materials. It has also been demonstrated that the dealloying rate of copper-aluminum and copper- zinc as a function of aluminum and zinc, respectively, corresponds to the crack growth rate in ammoniacal solution (Ref 25).

Mechanical Factors

There is more commonality in the mechanical aspects of stress corrosion between intergranular SCC and transgranular SCC and between various materials than there is in environmental and metallurgical aspects. As indicated earlier, many of the environmental or metallurgical factors are specific to a given material/environment combination such that a metallurgical factor may be significant in one environment, but not in another. Threshold stress intensities and stresses, the presence of a stress-independent crack growth regime, and a dependence of crack growth rate on strain rate are features common to a variety of environmentally induced crack growth processes and a variety of materials. Anodic and cathodic controlled processes show many of these common features.

The stress-intensity dependence of environmentally induced subcritical crack growth is shown schematically in Fig. 26, along with a relationship for the linear-elastic mode I stress intensity. The applied stress intensity is a function of the uniform stress and the crack length; therefore, for a constant-stress test, the stress intensity increases with increasing crack extension. For low-strength materials that form a significant plastic zone ahead of the crack, nonlinear fracture mechanics relationships must be used to calculate K. The subcritical crack growth behavior of many material/environment combinations is characterized by a threshold and by stages 1, 2, and 3 (see the article "Fracture Toughness and Fracture Mechanics" in *Mechanical Testing and Evaluation,* Volume 8 of *ASM Handbook,* for a detailed discussion of modes of crack formation).

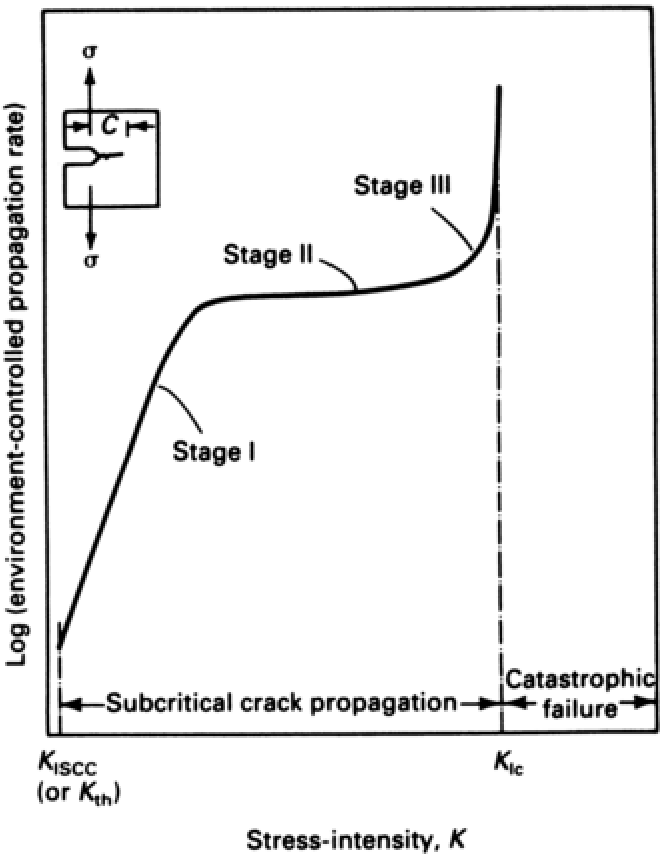

Fig. 26 Typical, subcritical crack propagation rate versus stress intensity relationship. Stress intensity, *K*, is defined as $K = A\sigma\sqrt{\pi C/B}$, where σ is the total tensile stress, *C* is the crack length, and A and B are geometrical constants.

In Fig. 26, the threshold is defined by the minimum detectable or reliably measured crack growth rate, while in some materials, stage 1 has a large *K* dependence such that a lower threshold does not result at lower crack velocities. There are a number of physical processes that can be associated with a threshold stress intensity, including a fracture strain for a passive film rupture mechanism, the critical resolved shear stress for the slip-dissolution mechanism, a fracture stress for a brittle film-induced cleavage mechanism, or a critical crack tip opening for transport of species in the crack. The threshold stress intensity generally is associated with the development of a plastic zone at the crack tip; however, calculations of crack tip strains are not very accurate, and experimental correlations between plastic zone development of K_{ISCC} have not been made.

Stage 1 subcritical crack growth is marked by a rapid increase in crack velocity with a small increase in *K*. Dependencies of crack velocity on stress intensity to the fourth power have been reported for a number of material/environment combinations. Changes in crack velocity of two orders of magnitude with small changes in *K* are not uncommon for the stage 1 regime. Few explanations for the *K* dependence of stage 1 have been put forth. One explanation is that in stage 1, the crack tip plastic strain rate is increasing rapidly with *K*, and another explanation is that the transport of species into and out of the crack increases rapidly with increasing crack volume in stage 1.

In metals tested in aqueous solutions, in transport of cations or anions in the crack electrolyte, or in passive film forming materials, the passive film rupture and repassivation rates are thought to be rate-limiting processes. Environmental parameters such as crack tip potential, corrosion rates, and pH also affect the stage 2 crack velocity so that in many systems the limiting velocity is a function of crack tip corrosion rate, strain rate, and transport rate. A steady-state crack transport calculation for intergranular SCC in nickel + phosphorus gave crack growth values within a factor of five of the measured stage 2 values (Ref 16). For transgranular SCC, there is increasing evidence that the crack velocity is a function of the corrosion rate, but that crack advance results from brittle crack jumps that exceed the depth of the corrosion reaction. In this case, the crack velocity may scale with the corrosion rate, but the crack length exceeds that determined from charge transfer.

Most stress-corrosion data have been obtained by using specimens loaded in a tensile mode in which the stress is perpendicular to the plane of the advancing crack; this condition is defined as mode 1 loading. In practice, a

component may have a complex loading mode such that torsion and shear components are present. The effect of mixed loading modes on SCC is therefore an important consideration in component design; however, very few SCC data exist for other than mode 1 loading. Some examples of SCC in modes 1 and 3 for aluminum in 3.5% NaCl and type 304 stainless steel in boiling $MgCl_2$ are shown in Fig. 27, in which it can be seen that mode 1 loading gives the lowest threshold stress or stress intensity. Also shown in Fig. 27(a) is a schematic of the test specimen used to perform mixed-mode SCC tests. In both cases, the researchers concluded that the lower thresholds and higher crack velocities in mode 1 tests of these materials indicate a hydrogen embrittlement component to SCC because hydrogen effects are more prominent under tensile loading conditions (Ref 41, 42). However, anodic stress- corrosion processes are also aided by the crack opening that results from mode 1 loading.

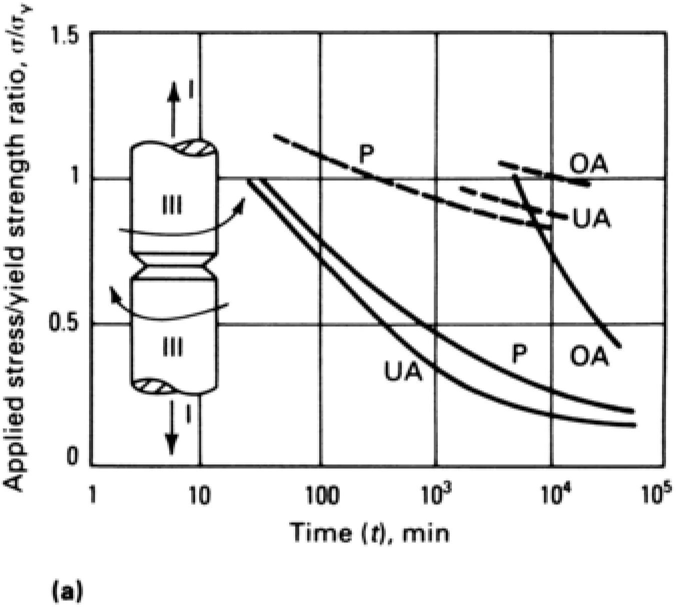

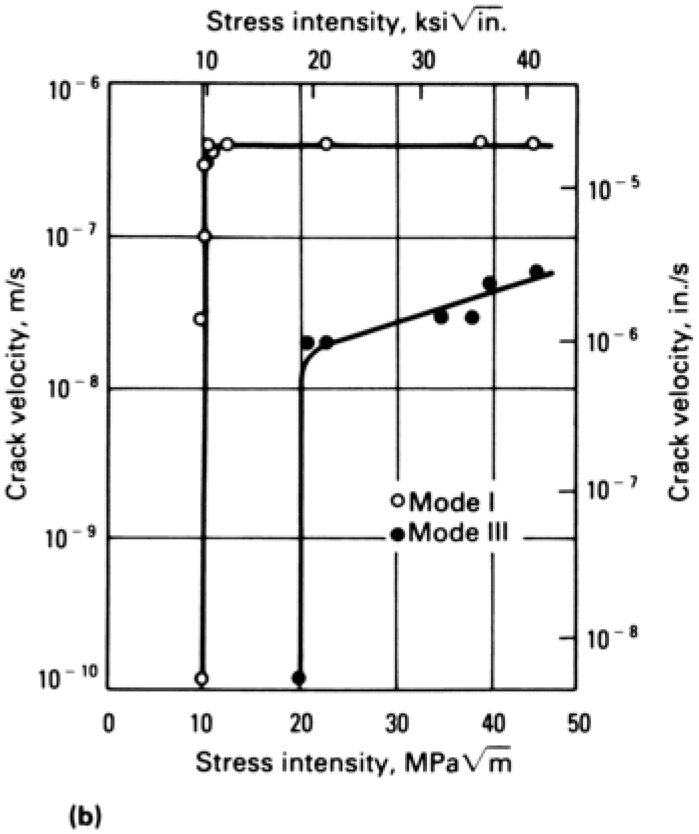

Fig. 27 Examples of SCC in mode 1 and mode 3. (a) Susceptibility of 7075 aluminum alloy to corrosion cracking in 3.5% NaCl solution tension. Mode 1 and torsion (solid lines). Mode 3 tests (dashed lines). P,

peak and aging; OA, overaged; UA, underaged. (b) Crack velocity versus stress intensity curves for stress-corrosion cracking of type 304 stainless steel in modes 1 and 3 in boiling $MgCl_2$

Stress-corrosion data are frequently given as applied stress versus time to failure, as shown in Fig. 28. These data are obtained with notched or unnotched specimens statically loaded in tension or bending. The threshold stress is sensitive to the environment, alloy composition, and structure and is not strictly a materials property. The threshold stress is related to the yield strength of the material, with thresholds generally being greater than one-half the yield strength, and in many cases, the threshold is a significant fraction (about 0.8) of the yield strength of the material. Therefore, most SCC tests performed with this technique are performed at values of about 80% or greater of the yield strength.

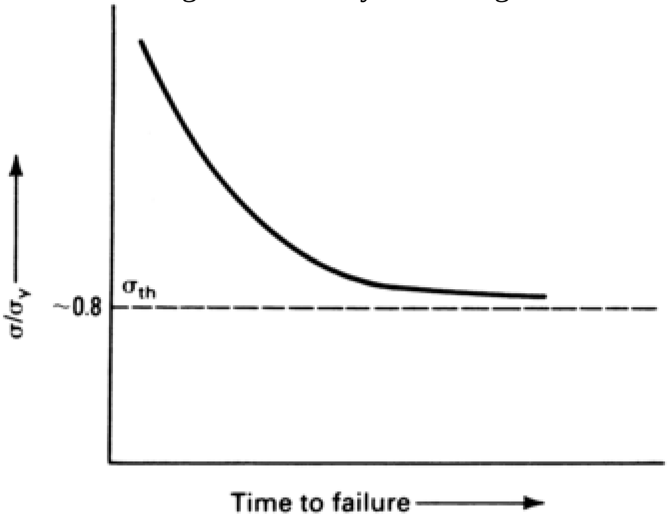

Fig. 28 Schematic diagram of time to failure versus applied stress, σ, normalized to the yield strength σ_y for stress corrosion

The data obtained with this method incorporate the stage 1, 2, and 3 regimes shown in Fig. 26 in addition to a crack initiation stage. Crack growth begins with the development of a pit or intergranular corrosion groove that raises the stress intensity to the K_{ISCC}. Because the stress is constant, the stress intensity increases with increasing crack length as given by the expression in Fig. 26 so that the crack progresses through stage 1 to stage 2 and ultimately to fracture in stage 3. Therefore, the failure time in a constant- stress test is dependent on the initiation rate, the value of the K_{ISCC}, the crack growth rate in stage 2, and the fracture toughness K_{Ic}. These test data are useful because they relate to the sequence that may occur in practice, but it is difficult to relate them to physical processes and rate-controlling steps. Crack growth rates are frequently estimated from constant-load tests based on the crack depth divided by the total test time. Crack velocities obtained in this manner are minimum values because the time for initiation is included so that instantaneous velocities will always be greater.

The threshold stress is perhaps the least complicated value obtained from constant-load tests. For film-forming materials, the threshold can be related to the film formation and rupture rate. Below the threshold stress, the film formation rate is sufficiently high to maintain the surface in a filmed condition; at higher stresses, the film rupture rate exceeds the reformation rate such that a pit or an intergranular corrosion groove can grow. For transgranular SCC initiated by a brittle corrosion film, the threshold stress could be related to the fracture stress of the film; however, this type of relationship has not been established for the brittle film-induced cleavage process.

Constant extension rate or slow strain rate tests have essentially replaced the use of the constant-stress test for stress-corrosion testing. This change has occurred because of the variability in times of failure with a constant-stress test and the long test times needed to define the stress threshold. Also, the concept that the crack growth rate is a function of the strain rate, as shown in Fig. 29 for intergranular type 304 stainless steel, has led to the use of a constant extension rate test. The CERT specimens will fail within a given period of time, thus eliminating specimens that do not fail because they are loaded to a stress below the threshold. The crack growth rates given in Fig. 29 are minimum values obtained from unnotched specimens, and the strain rate is the average applied rate. Clearly, once a crack develops, the crack tip strain rate will differ from the average

applied value. An example of the crack velocity as a function of the crack tip strain rate is given in Fig. 30 for intergranular SCC of a carbon-manganese steel tested in a carbonate solution. A threshold strain rate is evident in these results that is the same as a threshold stress intensity. A second threshold strain rate exists at high strain rates because mechanical fracture occurs before a crack can initiate and propagate to a measurable length. The two strain rate thresholds are illustrated in Fig. 31.

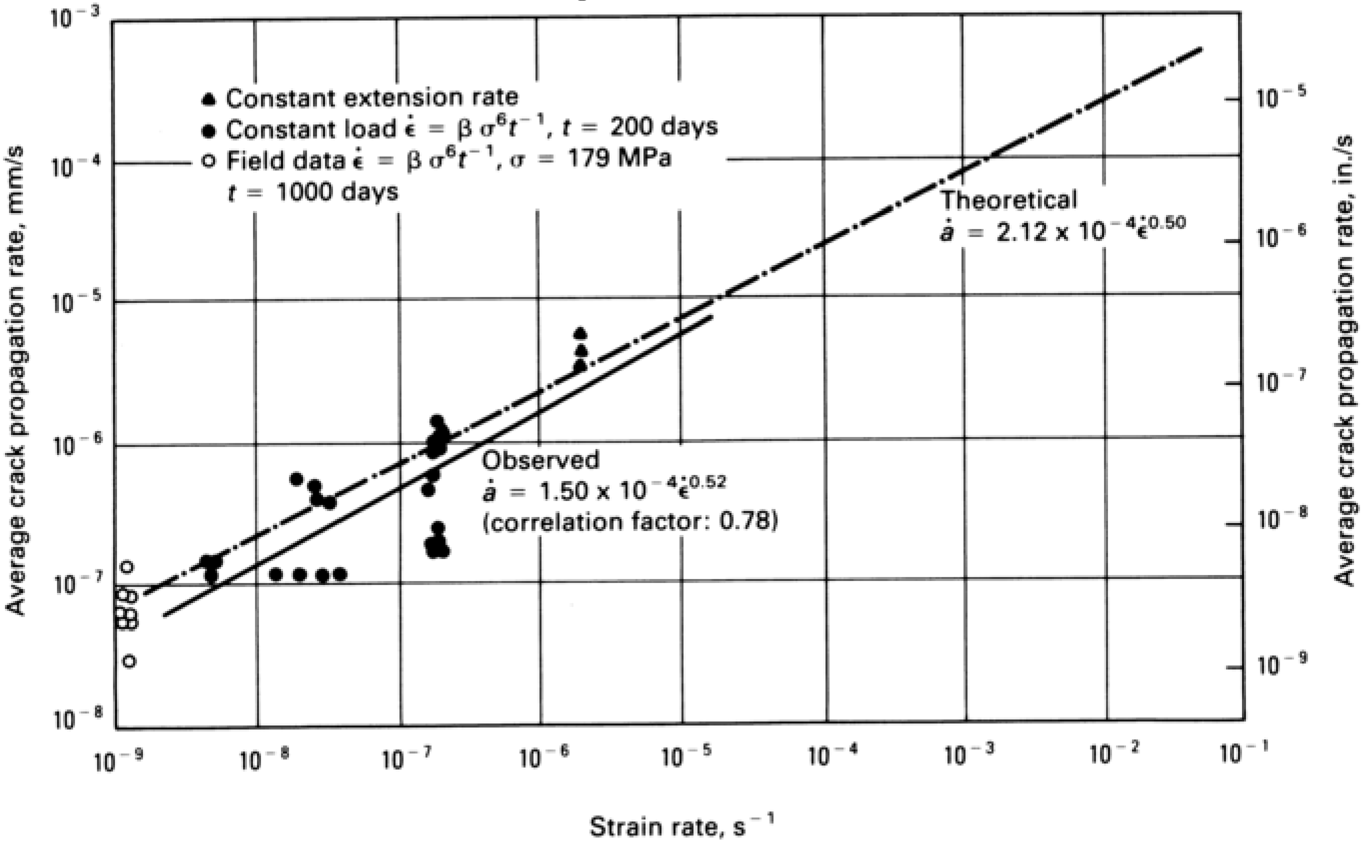

Fig. 29 Comparison between observed and theoretical crack propagation rate/strain rate ($\dot{a}/\dot{\epsilon}$) relationships for furnace-sensitized type 304 stainless steel in water/0.2 ppm oxygen at 288 °C (550 °F)

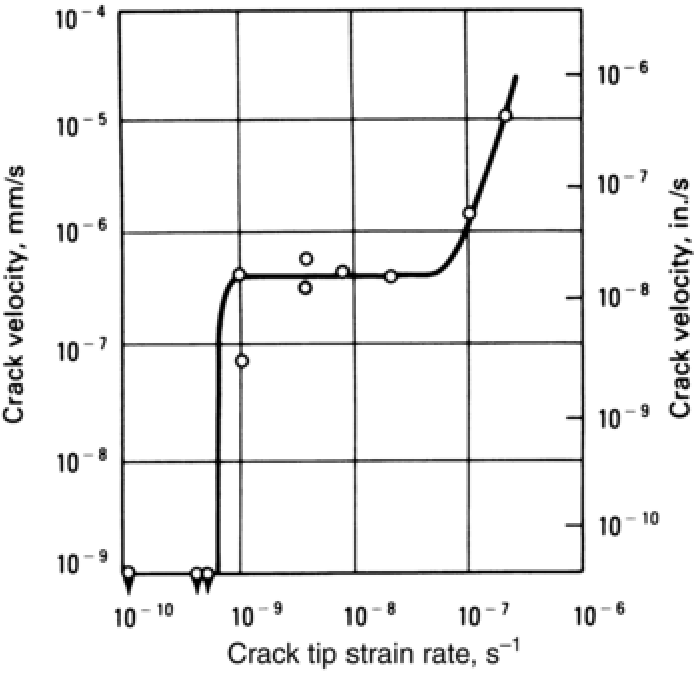

Fig. 30 Intergranular crack velocities for various applied crack tip strain rates in a carbon-manganese steel immersed in 1 *N* Na_2CO_3 + 1 *N* $NaHCO_3$ at -650 mV (SCE) and 75 °C (165 °F)

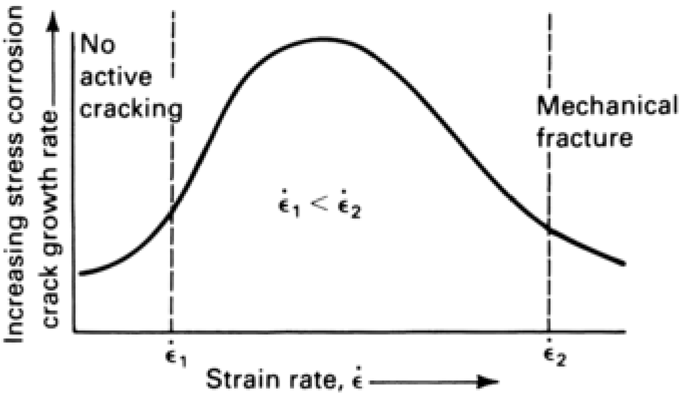

Fig. 31 Stress-corrosion crack growth as a function of the two strain rate thresholds, $\dot{\epsilon}_1$ and $\dot{\epsilon}_2$

It is important to distinguish between static and dynamic effects. For example, a sample could be plastically strained 10% and the load dropped to below the threshold stress before being immersed in a corrosive environment and SCC will not occur. However, a sample can be slowly strained 10% in a corrosive environment with the development of numerous cracks and perhaps even complete failure. Therefore, it is the dynamic strain and creation of fresh surface or dynamic fracture of a brittle film that is crucial to SCC. Corrosion current measurements corroborate these observations; the current density of a prestrained sample is usually very similar to an unstrained sample, while the current density measured during dynamic strain is considerably greater than that in the unstrained sample.

References cited in this section

16. M.J. Danielson, C. Oster, and R.H. Jones, *Corros. Sci.,* Vol 32 (No 1), 1991, p 1–21

18. A. Turnbull, Progress in the Understanding of the Electrochemistry in Cracks, *Embrittlement by the Local Crack Environment,* R.P. Gangloff, Ed., The Metallurgical Society, 1984, p 3

19. R.N. Parkins, Prevention of Environment Sensitive Fracture by Inhibition, *Embrittlement by the Local Crack Environment,* R.P. Gangloff, Ed., The Metallurgical Society, 1984, p 385

20. R.N. Parkins, *Br. Corros. J.,* Vol 14, 1979, p 5

21. C. Edeleneau and A.J. Forty, *Philos. Mag.,* Vol 46, 1960, p 521

22. J.A. Beavers and E.N. Pugh, *Metall. Trans. A,* Vol 11A, 1980, p 809

23. M.T. Hahn and E.N. Pugh, *Corrosion,* Vol 36, 1980, p 380

24. E.N. Pugh, On the Propagation of Transgranular Stress Corrosion Cracks, *Atomistics of Fracture,* R.M. Latanision and J.R. Pickens, Ed., Plenum Press, 1983, p 997

25. R.C. Newman and K. Sieradzki, “Film-Induced Cleavage During Stress-Corrosion Cracking of Ductile Metals and Alloys,” NATO Advanced Research Workshop on Chemistry and Physics of Fracture, June 1986

26. N.J.H. Holroyd and G.M. Scamans, *Scr. Metall.,* Vol 19, 1985, p 915

27. E.C. Pow, W.W. Gerberich, and L.E. Toth, *Scr. Metall.,* Vol 15, 1981, p 55

28. E.D. Hondros and M.P. Seah, *Int. Met. Rev.,* Dec 1977, p 262

29. L. Long and H. Uhlig, *J. Electrochem. Soc.,* Vol 112, 1965

30. J. Kuppa, H. Erhart, and H. Grabke, *Corros. Sci.,* Vol 21, 1981, p 227

31. N. Bandyopadhyay, R.C. Newman, and K. Sieradzdki, in *Proceedings of the Ninth International Congress on Metallic Corrosion* (Toronto, Canada), NACE, 1984

32. R.H. Jones, S.M. Bruemmer, M.T. Thomas, and D.R. Baer, Comparison of Segregated Phosphorus and Sulfur Effects on the Fracture Mode and Ductility of Iron Tested at Cathodic Potentials, *Scr. Metall.,* Vol 16, 1982, p 615

33. S.M. Bruemmer, R.H. Jones, M.T. Thomas, and D.R. Baer, Fracture Mode Transition of Iron in Hydrogen as a Function of Grain Boundary Sulfur, *Scr. Metall.,* Vol 14, 1980, p 137

34. A. Joshi and D.J. Stein, *Corrosion,* Vol 28 (No. 9), 1972, p 321

35. R.H. Jones, Some Radiation Damage-Stress Corrosion Synergisms in Austenitic Stainless Steels, *Proceedings of the Second International Symposium on Environmental Degradation of Materials in Nuclear Power Systems-Water Reactors,* American Nuclear Society, Sept 1985, p 173

36. M. Guttman, P. Dumoulin, Nguyen Tan Tai, and P. Fontaine, *Corrosion,* Vol 37, 1981, p 416

37. S.M. Bruemmer, L.A. Charlot, and C.H. Henager, Jr., "Microstructural Effects on Microdeformation and Primary-Side Stress Corrosion Cracking of Alloy 600 Tubing," EPRI Final Report, Project 2163-4, Electric Power Research Institute, Aug 1986

38. R.H. Jones, S.M. Bruemmer, M.T. Thomas, and D.R. Baer, Influence of Sulfur, Phosphorus, and Antimony Segregation on the Intergranular Hydrogen Embrittlement of Nickel, *Metall. Trans. A,* Vol 14A, 1983, p 223

39. R.W. Staehle et al., *Corrosion,* Vol 26 (No. 11), 1970, p 451

40. H.W. Pickering and P.R. Swann, *Corrosion,* Vol 19 (No. 3), 1963, p 373

41. A.W. Thompson and I.M. Bernstein, *Advances in Corrosion Sciences and Technology,* Vol 7, M.G. Fontana and R.W. Staehle, Ed., Plenum Press, 1980, p 53

42. R.M. Riecke, A. Athens, and I.O. Smith, *Mater. Sci. Technol.,* Vol 2, 1986, p 1066

R.H. Jones, Stress-Corrosion Cracking, *Corrosion: Fundamentals, Testing, and Protection*, Vol 13A, *ASM Handbook,* ASM International, 2003, p 346–366

Stress-Corrosion Cracking

R.H. Jones, Battelle Pacific Northwest National Laboratory

Crack Propagation Mechanisms

As indicated in the previous discussion, it is unlikely that a single mechanism of SCC exists; instead, there are probably two or three different operative mechanisms. Many models have been proposed, but only the more

prominent are discussed. The proposed mechanisms for crack propagation fall into two basic classifications: those based on dissolution as the principal cause of crack propagation and those that involve mechanical fracture in the crack propagation process.

Dissolution Models

According to models of this type, the crack advances by preferential dissolution at the crack tip. A number of models have been proposed to account for this process. For example, preferential dissolution at the crack tip has been attributed to the formation of active paths in the material, stresses at the crack tip, and chemical-mechanical interactions (Ref 43, 44, 45, 46, 47, 48). However, research has essentially eliminated all but one model from serious consideration, and the debate has recently centered on the details of this model.

Film Rupture. The film rupture model, also referred to as the *slip-dissolution model,* assumes that the stress acts to open the crack and rupture the protective surface film. Two investigators, working independently, first postulated that localized plastic deformation at the crack tip ruptures the passivating film, exposing bare metal at the crack tip (Ref 49, 50). The freshly exposed bare metal then dissolves rapidly, resulting in crack extension. Some investigators (Ref 51, 52, 53) assume that once propagation starts, the crack tip remains bare because the rate of film rupture at the crack tip is greater than the rate of repassivation (Fig. 32a). Others (Ref 54, 55, 56, 57) assume that the crack tip repassivates completely and is ruptured periodically by the emergence of slip steps (Fig. 32b).

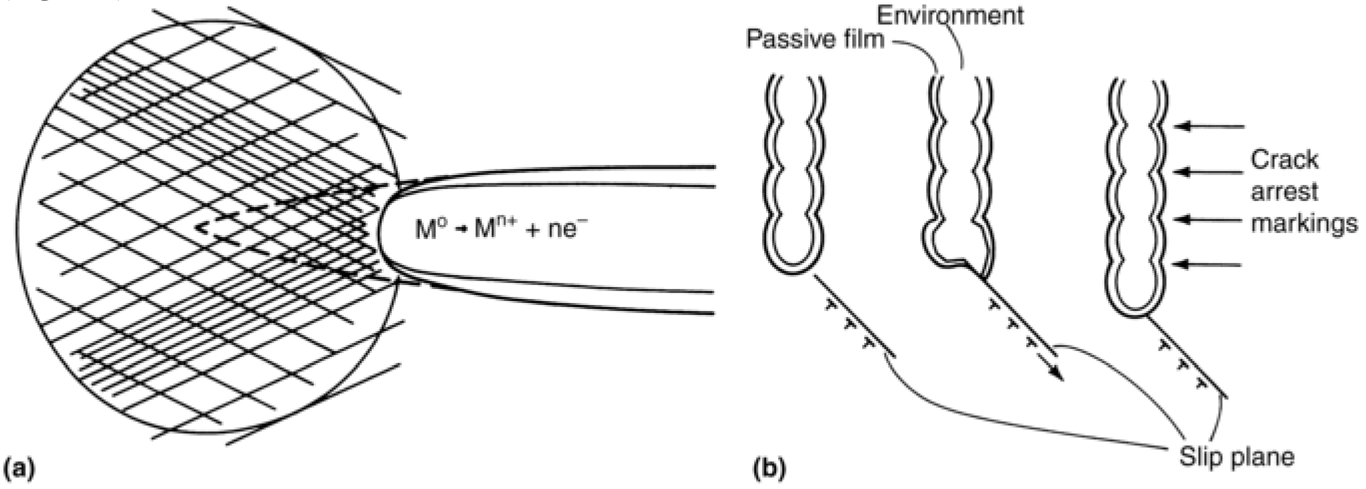

Fig. 32 Schematic representations of crack propagation by the film rupture model. (a) Ref 50. (b) Ref 56 and 57

Considerable evidence has been found to support these mechanistic models, and intergranular corrosion may be considered the low stress limiting case of this mechanism (Ref 43, 44, 45, 46, 47, 48, 49, 50, 51, 52, 53, 54, 55, 56, 57). However, the observation of discontinuous cracking and crack arrest markings (discussed previously) is an indication that crack propagation can be, and frequently is, discontinuous. Also, transgranular SCC fracture surfaces are flat, crystallographically oriented, and match precisely on opposite sides of the fracture surface (indicating very little dissolution during crack advance). As a result, film rupture and dissolution are accepted as viable mechanisms of intergranular SCC in some systems, but generally are not accepted as mechanisms of transgranular SCC (Ref 58).

Mechanical Fracture Models

Mechanical fracture models originally assumed that stress concentration at the base of corrosion slots or pits increased to the point of ductile deformation and fracture (Ref 48). These early proposals assumed that the crack essentially propagated by dissolution and that the remaining ligaments then failed by mechanical fracture (ductile or brittle). A refinement of this approach has been proposed (Ref 40, 59); it is generally known as the *corrosion tunnel model.*

The Corrosion Tunnel Model. In this model, it is assumed that a fine array of small corrosion tunnels form at emerging slip steps. These tunnels grow in diameter and length until the stress in the remaining ligaments

causes ductile deformation and fracture. The crack thus propagates by alternating tunnel growth and ductile fracture (Fig. 33). Cracks propagating by this mechanism should result in grooved fracture surfaces with evidence of microvoid coalescence on the peaks, as illustrated in Fig. 33(a). This theory is not consistent with the common fractographic features discussed previously. As a result, it was suggested (Ref 60) that the application of a tensile stress results in a change in the morphology of the corrosion damage from tunnels to thin flat slots, as shown in Fig. 33(b). The formation of slots was observed below the dealloyed sponge layer on the {110} type planes in austenitic stainless steels, and it was found that the formation of these slots required the presence of a tensile stress. The width of the corrosion slots was found to approach atomic dimensions, and as a result, close correspondence of matching fracture surfaces would be expected. It was concluded that transgranular SCC can be explained in terms of the formation and mechanical separation of corrosion slots (Ref 60).

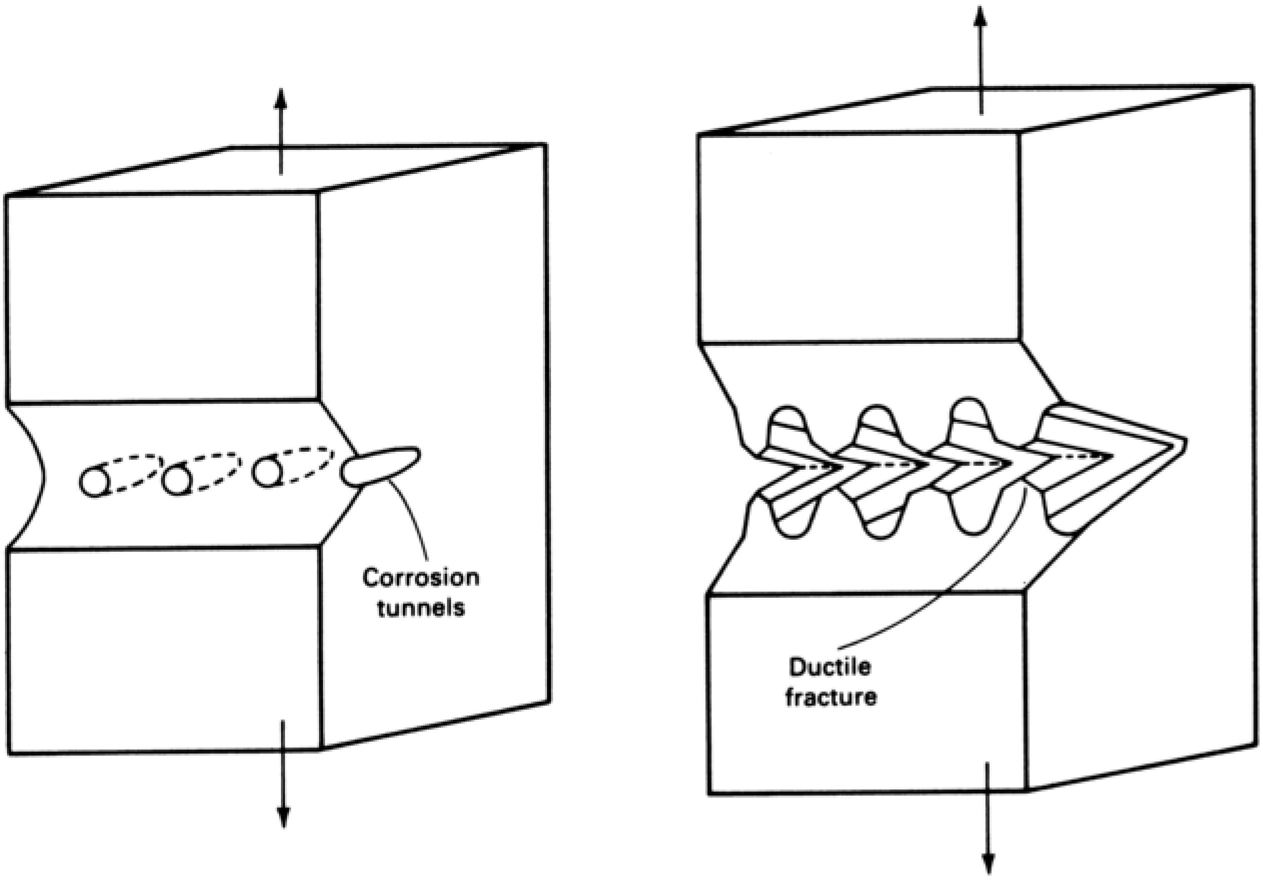
Corrosion
tunnels
Ductile
fracture

(a)

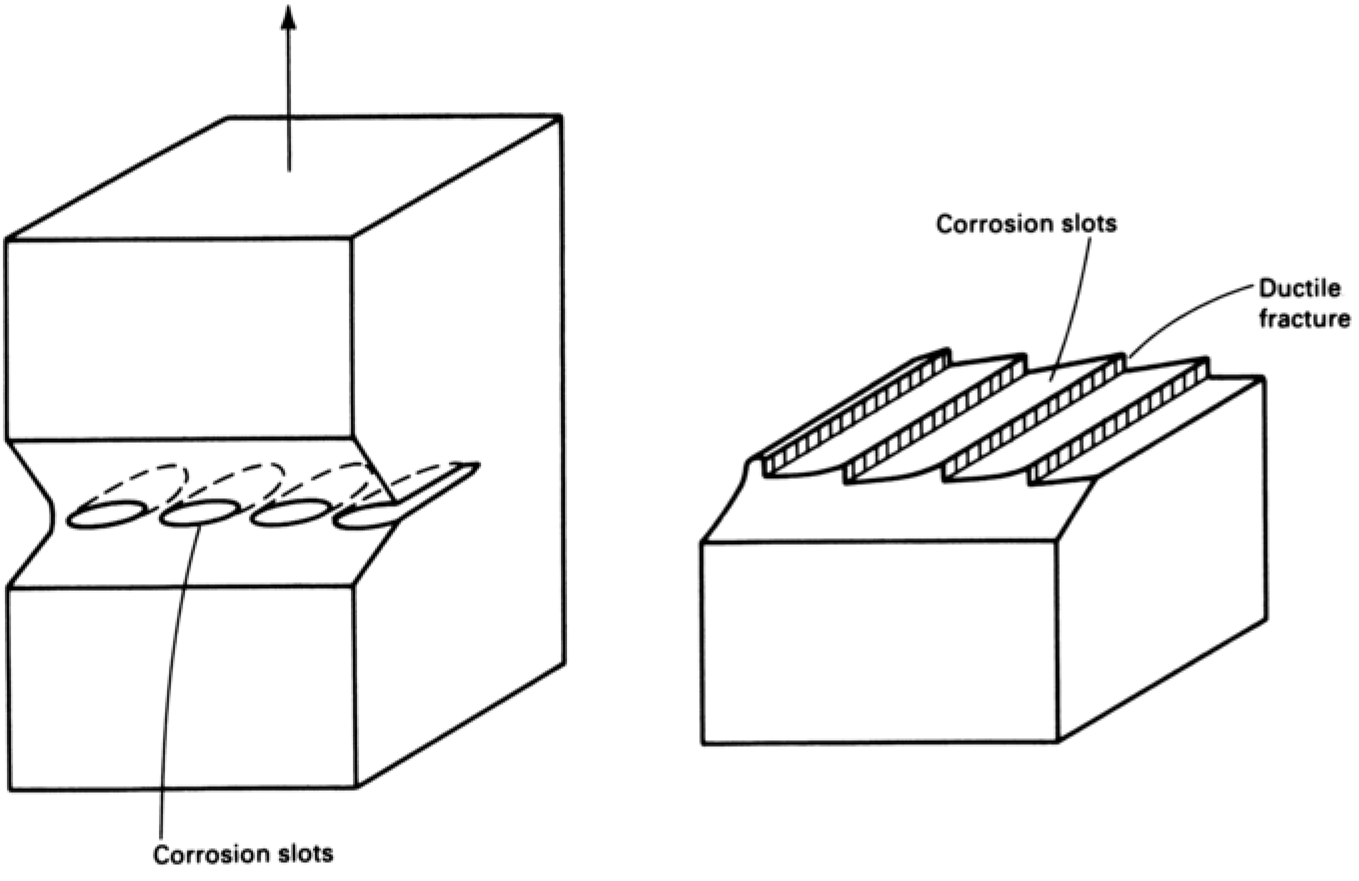
Corrosion slots
Ductile
fracture
Corrosion slots

(b)

Fig. 33 Corrosion tunnel models. (a) Schematic of tunnel model showing the initiation of a crack by the formation of corrosion tunnels at slip steps and ductile deformation and fracture of the remaining ligaments. (b) Schematic diagram of the tunnel mechanism of SCC and flat slot formation as proposed in Ref 60

Adsorption-Enhanced Plasticity. Studies of liquid-metal embrittlement (LME), hydrogen embrittlement, and SCC have led to the conclusion that similar fracture processes occur in each case (Ref 61, 62, 63). Because chemisorption is common to all three, this process was concluded to be responsible for the environmentally induced crack propagation (Ref 61). Based on fractographic studies, it was concluded that cleavage fracture is not an atomically brittle process but occurs instead by alternate slip at the crack tip in conjunction with formation of very small voids ahead of the crack. It was also proposed that chemisorption of environmental species facilitated the nucleation of dislocations at the crack tip, promoting the shear processes responsible for brittle cleavagelike fracture (Ref 61, 62, 63). The origin of crack arrest markings by this mechanism is, however, uncertain. Nevertheless, this mechanism promises to explain many similarities among SCC, LME, and hydrogen embrittlement.

The Tarnish Rupture Model. This model was first proposed (Ref 64) to explain transgranular SCC but was later modified by other researchers (Ref 65, 66, 67) to explain intergranular SCC. In the original model (Ref 64), a brittle surface film forms on the metal that fractures under the applied stress. Fracture of the film exposes bare metal, which rapidly reacts with the environment to re-form the surface film. The crack propagates by alternating film growth and fracture, as shown in Fig. 34(a). This hypothesis was later modified to explain intergranular SCC based on the assumption that the oxide film penetrates along the grain boundary ahead of the crack tip, as shown in Fig. 34(b). Again, crack propagation consists of alternating periods of film growth and brittle film fracture. Film growth requires transport of species across the film and, as a result, the thickness of the film is limited in the absence of stress (Ref 67). This model predicts crack arrest markings on intergranular fracture surfaces and discontinuous acoustic emission during crack propagation that are not always observed during intergranular SCC. Also, it assumed penetration of the film into the grain boundary ahead of the crack tip, which may not be the case for all systems (Ref 68). At present, experimental results are insufficient to confirm or refute this model (Ref 66, 67).

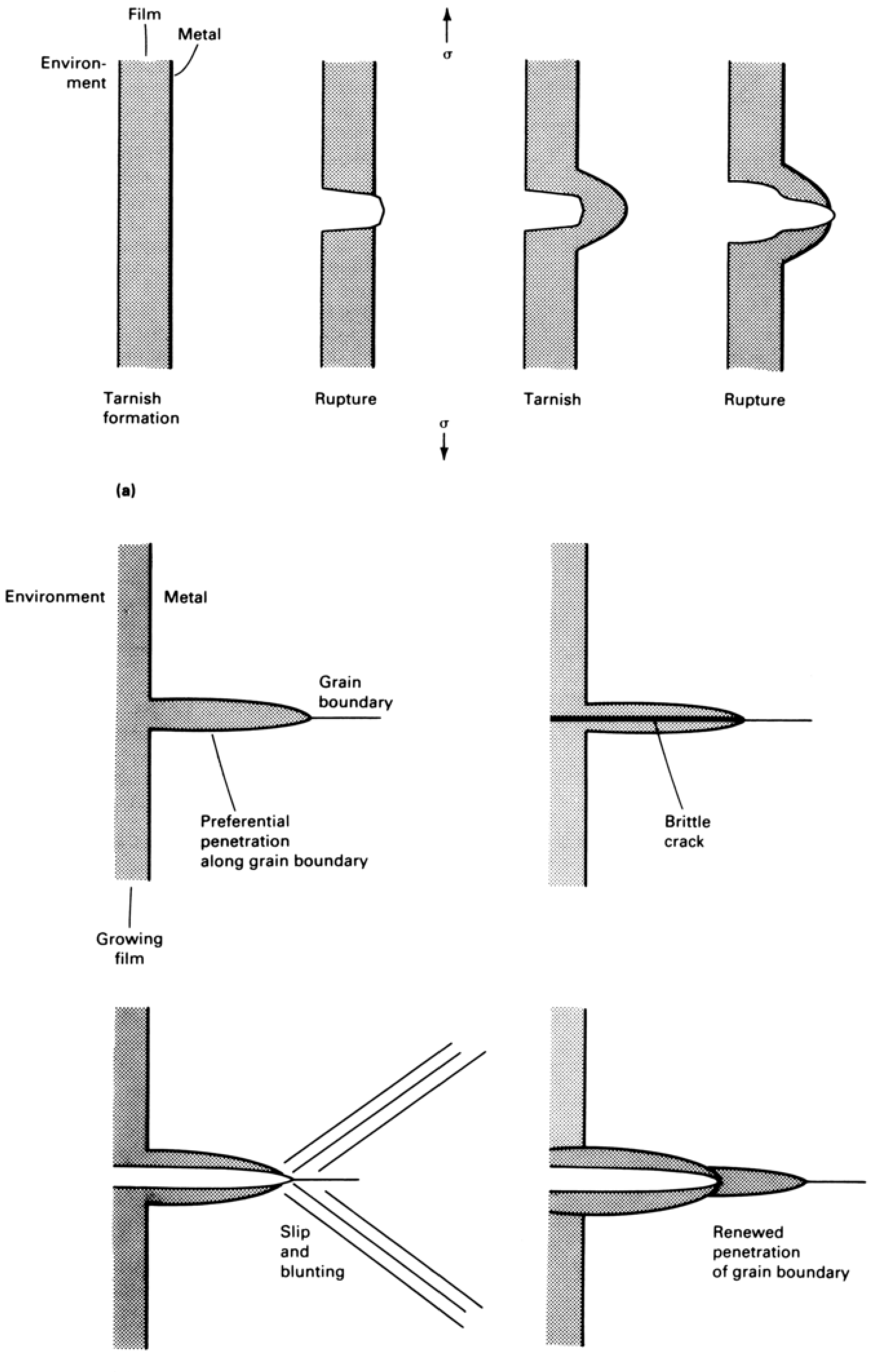
Film
Metal
Environ-
ment
σ
Tarnish
formation
Rupture
Tarnish
Rupture
σ
(a)
Environment
Metal
Grain
boundary
Preferential
penetration
along grain boundary
Growing
film
Brittle
crack
Slip
and
blunting
Renewed
penetration
of grain boundary

Fig. 34 Tarnish rupture models. (a) Schematic of the tarnish rupture model for SCC as proposed in Ref 64. (b) Modified tarnish rupture model of SCC for systems with intergranular oxide film penetration (Ref 66, 67)

The Film-Induced Cleavage Model. In 1959, the hypothesis was presented that dealloying and/or vacancy injection could induce brittle fracture (Ref 69). However, the exact nature of the interactions and how they could induce the observed crack propagation was not thoroughly evaluated. More recently, a model was developed based on the hypothesis that a surface film could induce cleavage fracture (Ref 70). This model assumes that:

- A thin surface film or layer forms on the surface
- A brittle crack initiates in this layer
- The brittle crack crosses the film/matrix interface with little loss in velocity
- Once in the ductile matrix, the brittle crack will continue to propagate
- This crack will eventually blunt and arrest, after which this process repeats itself

This model has the unique ability to explain the crack arrest markings, the cleavagelike facets on the fracture surface, and the discontinuous nature of crack propagation.

The hypothesis that a brittle crack will continue to propagate after it has entered the normally ductile matrix is a critical point. This allows a thin surface layer to induce brittle crack propagation over distances much greater than the film thickness. A critical examination of this hypothesis concluded that a brittle crack can propagate in a ductile matrix if the crack is sharp and is propagating at high velocities before entering the ductile matrix (Ref 71). A computer model was developed for this process, and it was concluded that a surface layer can initiate brittle fracture even if the layer is ductile (depending on lattice mismatch, etc.) (Ref 72). More research into surface films and brittle fracture is required before this model can be thoroughly evaluated.

Adsorption-Induced Brittle Fracture. This model, which was initially presented in Ref 46, is based on the hypothesis that adsorption of environmental species lowers the interatomic bond strength and the stress required for cleavage fracture. This model is frequently referred to as the stress-sorption model, and similar mechanisms have been proposed for hydrogen embrittlement and LME (Ref 73). This model predicts that cracks should propagate in a continuous manner at a rate determined by the arrival of the embrittling species at the crack tip. This model does not explain how the crack maintains an atomically sharp tip in a normally ductile material, because it does not include a provision for limiting deformation in the plastic zone. Also, the discontinuous nature of crack propagation is not explained by this model.

Hydrogen Embrittlement. Stress-corrosion cracking in some material/environment combinations can be a form of hydrogen-induced subcritical crack growth. Because the anodic reaction must have a corresponding cathodic reaction and because the reduction of hydrogen is frequently the cathodic reaction, hydrogen-induced subcritical crack growth can be the dominant stress-corrosion crack growth process in some materials. Many features of hydrogen-induced subcritical crack growth from cathodic hydrogen are very similar to those produced by gaseous or internal hydrogen. The mechanisms of hydrogen damage are discussed in the following section. However, a few features of hydrogen embrittlement from cathodic hydrogen that are different from other forms of hydrogen embrittlement are summarized.

Once hydrogen has been absorbed by a material, its effect, whether from a gaseous or cathodic source, is the same. This has been shown for a number of materials and a variety of properties. There are three primary differences between gaseous and cathodic hydrogen absorption processes. First, cathodic hydrogen adsorbs on the surface as atomic hydrogen (as reduced), while gaseous hydrogen adsorbs in the molecular form and must dissociate to form atomic hydrogen. Desorption of loosely bound molecular hydrogen is relatively easy, while the dissociation step can, in some cases, be the rate- determining step. Therefore, the desorption and absorption rates of gaseous and cathodic hydrogen may be substantially different for equal hydrogen activities. Second, the hydrogen activities produced by cathodic hydrogen can be quite large (thousands of psi) and are dependent on the anodic reaction rate, while gaseous hydrogen pressures are generally much lower. Lastly, the surface of the material at a crack tip may be substantially different under electrochemical corrosion conditions from that in the presence of gaseous hydrogen containing substantial quantities of other gases, such a O_2 and CO_2.

Hydrogen-induced crack growth as the dominant stress-corrosion mechanism has been suggested for ferritic steels, nickel-base alloys, titanium alloys, and aluminum alloys, although ferritic steels show the most evidence

of this mechanism. The effects of factors such as yield strength, impurity segregation, and temperature on the crack growth behavior of ferritic materials in aqueous environments all follow the trends of gaseous hydrogen embrittlement. For example, the crack growth rate of a 3% Ni steel as a function of temperature in water is shown in Fig. 35(a), while the crack growth rate of 4340 steel in gaseous hydrogen is shown in Fig. 35(b). The maximum crack growth rate occurs at about 20 °C (70 °F), with similar decreases at both higher and lower temperatures. However, anodic stress- corrosion processes become active at temperatures above 100 °C (212 °F) for the steel tested in water. Similar trends have been shown for impurity segregation effects on hydrogen-induced crack growth of materials where cathodic and gaseous hydrogen produce essentially similar results. Some of these results have been presented in the section “Material Chemistry and Microstructure” in this article.

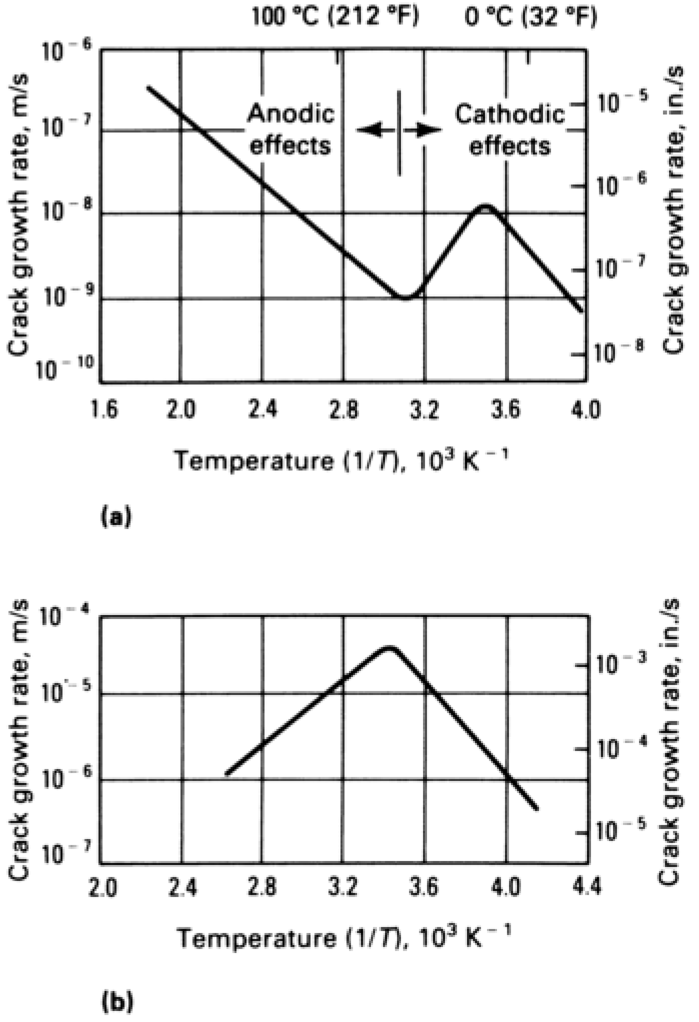

Fig. 35 Schematic of crack growth rate versus temperature for (a) 3% Ni steel in water (Ref 74) and (b) 4340 steel in gaseous hydrogen (Ref 75)

Specific mechanisms of cathodic hydrogen induced subcritical crack growth have not been developed because it has generally been sufficient merely to identify hydrogen as the cause for cracking. However, a mechanism was presented in which grain-boundary impurities act as hydrogen recombinant poisons and enhance the uptake of cathodic hydrogen (Ref 76). A schematic of this process is shown in Fig. 36, in which the tin and antimony that segregated to the grain boundaries of nickel enhance the hydrogen uptake kinetics. This mechanism does not propose a new mechanism by which hydrogen can cause cracking but merely proposes a mechanism by which impurity segregation can enhance hydrogen uptake. There may be circumstances in which such a mechanism could tip the balance between an anodically driven process and a cathodically driven process or could accelerate cracking to a value that is measurable or of practical significance. However, a review of the combined effects of impurity segregation and hydrogen embrittlement concluded that grain- boundary impurities behave the same with cathodic and gaseous hydrogen in that they enhance crack growth by a combined grain-boundary embrittlement processes but not by enhanced hydrogen uptake (Ref 77). It should be

noted, however, that a material with impurities such as sulfur, phosphorus, antimony, and tin segregated to their grain boundaries are more susceptible to all forms of hydrogen—cathodic, gaseous, or internal.

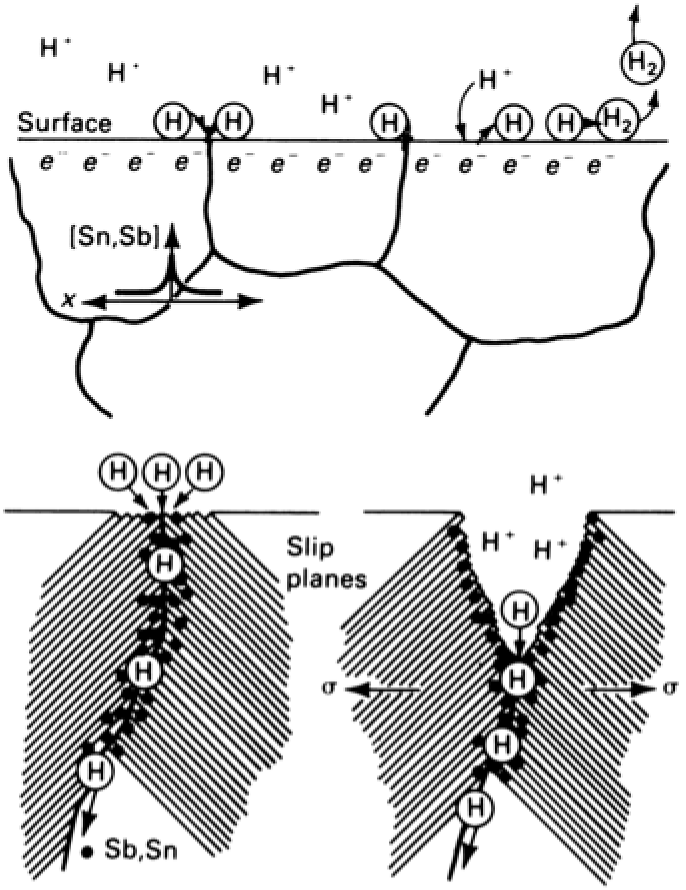

Fig. 36 Schematic showing effect of some impurities on mechanism by which intergranular embrittlement of nickel is presumed to occur at cathodic potentials

References cited in this section

40. H.W. Pickering and P.R. Swann, *Corrosion,* Vol 19 (No. 3), 1963, p 373

43. E.H. Dix, *Trans. AIME,* Vol 137 (No 11), 1940

44. R.B. Mears, R.H. Brown, and E.H. Dix, *Symposium on Stress-Corrosion Cracking of Metals,* ASTM and the American Institute of Mining, Metallurgical, and Petroleum Engineers, 1944, p 323

45. E.H. Dix, Jr., *Trans. ASM,* Vol 42, 1950, p 1057

46. H.H. Uhlig, *Physical Metallurgy of Stress Corrosion Fracture,* T.N. Rhodin, Ed., Interscience, 1959, p 1

47. L. Yang, G.T. Horne, and G.M. Pound, *Physical Metallurgy of Stress Corrosion Fracture,* T.N. Rhodin, Ed., Interscience, 1950, p 29

48. J.J. Harwood, *Stress Corrosion Cracking and Embrittlement,* W.D. Robertson, Ed., John Wiley & Sons, 1956, p 1

49. F.A. Champion, in *Symposium on Internal Stresses in Metals and Alloys,* Institute of Metals, 1948, p 468

50. H.L. Logan, *J. Res. Natl. Bur. Stand.,* Vol 48, 1952, p 99

51. E.W. Hart, *Surfaces and Interfaces II,* Syracuse University Press, 1968, p 210

52. H.J. Engle, in *The Theory of Stress Corrosion Cracking in Alloys,* North Atlantic Treaty Organization, 1971

53. J.C. Scully, *Corros. Sci.,* Vol 15, 1975, p 207

54. D.A. Vermilyea, *J. Electrochem. Soc.,* Vol 119, 1972, p 405

55. D.A. Vermilyea, *Stress Corrosion Cracking and Hydrogen Embrittlement of Iron Based Alloys,* NACE, 1977, p 208

56. R.W. Staehle, in *The Theory of Stress Corrosion Cracking in Alloys,* North Atlantic Treaty Organization, 1971, p 233

57. R.W. Staehle, *Stress Corrosion Cracking and Hydrogen Embrittlement of Iron Based Alloys,* NACE, 1977, p 180

58. E.N. Pugh, *Corrosion,* Vol 41 (No. 9), 1985, p 517

59. P.R. Swann and J.D. Embury, *High Strength Materials,* John Wiley & Sons, 1965, p 327

60. J.M. Silcock and P.R. Swann, *Environment- Sensitive Fracture of Engineering Materials,* Z.A. Foroulis, Ed., The Metallurgical Society, 1979, p 133

61. S.P. Lynch, *Hydrogen Effects in Metals,* A.W. Thompson and I.M. Bernstein, Ed., The Metallurgical Society, 1981, p 863

62. S.P. Lynch, *Met. Sci.,* Vol 15 (No. 10), 1981, p 463

63. S.P. Lynch, *J. Mater. Sci.,* Vol 20, 1985, p 3329

64. A.J. Forty and P. Humble, *Philos. Mag.,* Vol 8, 1963, p 247

65. A.J. McEvily and P.A. Bond, *J. Electrochem. Soc.,* Vol 112, 1965, p 141

66. E.N. Pugh, in *Stress Corrosion Cracking and Hydrogen Embrittlement of Iron Based Alloys,* National Association of Corrosion Engineers, 1977, p 37

67. J.A. Beavers, I.C. Rosenberg, and E.N. Pugh, in *Proceedings of the 1972 Tri-Service Conference on Corrosion,* MCIC-73- 19, Metals and Ceramics Information Center, 1972, p 57

68. T.R. Pinchback, S.P. Clough, and L.A. Heldt, *Metall, Trans. A,* Vol 7A, 1976, p 1241; *Metall. Trans. A,* Vol 6A, 1975, p 1479

69. A.J. Forty, *Physical Metallurgy of Stress Corrosion Fracture,* T.N. Rhodin, Ed., Interscience, 1959, p 99

70. K. Sieradzki and R.C. Newman, *Philos. Mag. A,* Vol 51 (No. 1), 1985, p 95

71. I.-H. Lin and R.M. Thomson, *J. Mater. Res.,* Vol 1 (No. 1), 1986

72. G.J. Dienes, K. Sieradzki, A. Paskin, and B. Massoumzadeh, *Surf. Sci.,* Vol 144, 1984, p 273

73. N.S. Stolloff, *Environment-Sensitive Fracture of Engineering Materials,* Z.A. Foroulis, Ed., The Metallurgical Society, 1979, p 486

74. M.O. Speidel and R.M. Magdowski, Stress Corrosion Cracking of Steam Turbine Steels—An Overview, *Proceedings of the Second International Symposium on Environmental Degradation of Materials in Nuclear Power Systems-Water Reactors,* American Nuclear Society, 1986, p 267

75. D.P. Williams and H.G. Nelson, *Metall. Trans.,* Vol 1, 1970, p 63

76. R.M. Latanision and H. Opperhauser, *Metall. Trans.,* Vol 5, Scientific and Technical Book Service, 1974, p 483

77. R.H. Jones, A Review of Combined Impurity Segregation-Hydrogen Embrittlement Processes, *Advances in the Mechanics and Physics of Surfaces,* R.M. Latanision and T.E. Fischer, Ed., Scientific and Technical Book Service, 1986

R.H. Jones, Stress-Corrosion Cracking, *Corrosion: Fundamentals, Testing, and Protection*, Vol 13A, *ASM Handbook*, ASM International, 2003, p 346–366

Stress-Corrosion Cracking

R.H. Jones, Battelle Pacific Northwest National Laboratory

Summary

Stress-corrosion cracking is a phenomenon in which time-dependent crack growth occurs when the necessary electrochemical, mechanical, and metallurgical conditions exist. Corrosion fatigue is a related process in which the load is cyclic in corrosion fatigue rather than static as in stress corrosion. When hydrogen is generated as a product of the corrosion reaction, crack growth can occur by a hydrogen embrittlement process in much the same way as if hydrogen were in the gaseous form. A common feature of each of these processes is the subcritical crack growth in which cracks grow from existing flaws or initiation sites and grow to a size at which catastrophic failure occurs. Catastrophic failure occurs because the combination of crack length and applied stress increases the stress intensity to the fracture toughness of the material. A second common feature of stress corrosion, corrosion fatigue, and hydrogen-induced crack growth is that these mechanisms do not require the entire component to become embrittled; the effect is localized to the crack tip region.

This article is intended to familiarize the reader with the phenomenological and mechanistic aspects of stress corrosion in order to enhance the use of other discussions in this Handbook on stress-corrosion evaluation and occurrence in specific industries and environments. The phenomenological description of crack initiation and propagation describes well-established experimental evidence and observations of stress corrosion, while the discussions on mechanisms describe the physical process involved in crack initiation and propagation. The physical processes involved in crack growth have received more evaluation and are better understood than the processes responsible for crack initiation. There is some phenomenological understanding of stress-corrosion crack initiation, but the detailed mechanistic information is not well known.

Stress-corrosion cracking occurs when certain critical conditions are achieved. These conditions include electrochemical, mechanical, and metallurgical factors that must exist simultaneously. A change in any one of these three factors is adequate for eliminating SCC; therefore, a clear knowledge of these critical factors is important in system design. The important electrochemical parameters include oxidizing potential, pH, impurity concentration, and temperature. The important mechanical parameters include stress, stress intensity, and strain rate. The important metallurgical factors include localized micro-chemistry (such as the depletion of passive

film forming elements or the enrichment of active corroding elements), bulk composition, deformation character, and yield strength.

There are a number of plausible mechanisms or physical processes that account for SCC. No single mechanism is adequate to describe stress corrosion in the variety of materials in which it has been observed. Stress-corrosion crack propagation mechanisms can be subdivided into dissolution and mechanical fracture models, with the mechanical fracture models further divided into ductile and brittle crack extension processes. Dissolution models include film-rupture and active-path processes, while ductile mechanical models include corrosion tunneling and adsorption-enhanced plasticity models. Brittle mechanical models include the tarnish rupture and film- induced cleavage models.

Stress-Corrosion Cracking

R.H. Jones, Battelle Pacific Northwest National Laboratory

Acknowledgment

This article is adapted from the article "Stress- Corrosion Cracking," by R.H. Jones and R.E. Ricker, in the previous edition, *Corrosion,* Volume 13 of the *ASM Handbook,* ASM International, 1987.

R.H. Jones, Stress-Corrosion Cracking, *Corrosion: Fundamentals, Testing, and Protection,* Vol 13A, *ASM Handbook*, ASM International, 2003, p 346–366

Stress-Corrosion Cracking

R.H. Jones, Battelle Pacific Northwest National Laboratory

References

1. T.A. Michalske and S.W. Freiman, *Nature,* Vol 295, 11 Feb 1982, p 511
2. J.F. Fellers and B.F. Kee, *J. Appl. Polymer Sci.,* Vol 18, 1974, p 2355
3. E.H. Andrews, *Developments in Polymer Science,* Applied Science, 1979
4. H.T. Sumison and D.P. Williams, in *Fatigue of Composite Materials,* STP 569, ASTM, 1975, p 226
5. C. Zeben, in *Analysis of the Test Methods for High Modulus Fibers and Composites,* STP 521, ASTM, 1973, p 65
6. K. Sieradski and R.C. Newman, *Philos. Mag. A,* Vol 5 (No. 1), 1985, p 95
7. T. Cassaigne, E.N. Pugh, and J. Kruger, National Bureau of Standards and Johns Hopkins University, unpublished research, 1987

8. C.M. Chen, M.H. Froning, and E.D. Verink, in *Stress Corrosion—New Approaches,* STP 610, ASTM, 1976, p 289

9. C.J. Beevers, Ed., *The Measurement of Crack Length and Shape During Fracture and Fatigue,* Chameleon Press, 1980

10. E.N. Pugh, U. Bertocci, and R.E. Ricker, National Bureau of Standards, unpublished research, 1987

11. D.P. Williams and H.G. Nelson, *Metall. Trans.,* Vol 1 (No. 1), 1970, p 63

12. R.E. Ricker and D.J. Duquette, The Role of Environment on Time Dependent Crack Growth, *Micro and Macro Mechanics of Crack Growth,* K. Sadananda, B.B. Rath, and D.J. Michel, Ed., American Institute of Mining, Metallurgical, and Petroleum Engineers, 1982, p 29

13. R.M. Parkins, *Mater. Sci. Technol.,* Vol 1, 1985, p 480

14. L. Hagn, Lifetime Prediction for Parts in Corrosion Environments, *Corrosion in Power Generating Equipment,* Plenum Press, 1983

15. O. Buck and R. Ranjan, Evaluation of a Crack-Tip-Opening Displacement Model Under Stress-Corrosion Conditions, *Modeling Environmental Effects on Crack Growth Processes,* R.H. Jones and W.W. Gerberich, Ed., The Metallurgical Society, 1986, p 209

16. M.J. Danielson, C. Oster, and R.H. Jones, *Corros. Sci.,* Vol 32 (No 1), 1991, p 1–21

17. R.H. Jones, M.J. Danielson, and D.R. Baer, *J. Mater. Energy Syst.,* Vol 8, 1986, p 185

18. A. Turnbull, Progress in the Understanding of the Electrochemistry in Cracks, *Embrittlement by the Local Crack Environment,* R.P. Gangloff, Ed., The Metallurgical Society, 1984, p 3

19. R.N. Parkins, Prevention of Environment Sensitive Fracture by Inhibition, *Embrittlement by the Local Crack Environment,* R.P. Gangloff, Ed., The Metallurgical Society, 1984, p 385

20. R.N. Parkins, *Br. Corros. J.,* Vol 14, 1979, p 5

21. C. Edeleneau and A.J. Forty, *Philos. Mag.,* Vol 46, 1960, p 521

22. J.A. Beavers and E.N. Pugh, *Metall. Trans. A,* Vol 11A, 1980, p 809

23. M.T. Hahn and E.N. Pugh, *Corrosion,* Vol 36, 1980, p 380

24. E.N. Pugh, On the Propagation of Transgranular Stress Corrosion Cracks, *Atomistics of Fracture,* R.M. Latanision and J.R. Pickens, Ed., Plenum Press, 1983, p 997

25. R.C. Newman and K. Sieradzki, “Film-Induced Cleavage During Stress-Corrosion Cracking of Ductile Metals and Alloys,” NATO Advanced Research Workshop on Chemistry and Physics of Fracture, June 1986

26. N.J.H. Holroyd and G.M. Scamans, *Scr. Metall.,* Vol 19, 1985, p 915

27. E.C. Pow, W.W. Gerberich, and L.E. Toth, *Scr. Metall.,* Vol 15, 1981, p 55

28. E.D. Hondros and M.P. Seah, *Int. Met. Rev.,* Dec 1977, p 262

29. L. Long and H. Uhlig, *J. Electrochem. Soc.,* Vol 112, 1965

30. J. Kuppa, H. Erhart, and H. Grabke, *Corros. Sci.,* Vol 21, 1981, p 227

31. N. Bandyopadhyay, R.C. Newman, and K. Sieradzdki, in *Proceedings of the Ninth International Congress on Metallic Corrosion* (Toronto, Canada), NACE, 1984

32. R.H. Jones, S.M. Bruemmer, M.T. Thomas, and D.R. Baer, Comparison of Segregated Phosphorus and Sulfur Effects on the Fracture Mode and Ductility of Iron Tested at Cathodic Potentials, *Scr. Metall.,* Vol 16, 1982, p 615

33. S.M. Bruemmer, R.H. Jones, M.T. Thomas, and D.R. Baer, Fracture Mode Transition of Iron in Hydrogen as a Function of Grain Boundary Sulfur, *Scr. Metall.,* Vol 14, 1980, p 137

34. A. Joshi and D.J. Stein, *Corrosion,* Vol 28 (No. 9), 1972, p 321

35. R.H. Jones, Some Radiation Damage-Stress Corrosion Synergisms in Austenitic Stainless Steels, *Proceedings of the Second International Symposium on Environmental Degradation of Materials in Nuclear Power Systems-Water Reactors,* American Nuclear Society, Sept 1985, p 173

36. M. Guttman, P. Dumoulin, Nguyen Tan Tai, and P. Fontaine, *Corrosion,* Vol 37, 1981, p 416

37. S.M. Bruemmer, L.A. Charlot, and C.H. Henager, Jr., "Microstructural Effects on Microdeformation and Primary-Side Stress Corrosion Cracking of Alloy 600 Tubing," EPRI Final Report, Project 2163-4, Electric Power Research Institute, Aug 1986

38. R.H. Jones, S.M. Bruemmer, M.T. Thomas, and D.R. Baer, Influence of Sulfur, Phosphorus, and Antimony Segregation on the Intergranular Hydrogen Embrittlement of Nickel, *Metall. Trans. A,* Vol 14A, 1983, p 223

39. R.W. Staehle et al., *Corrosion,* Vol 26 (No. 11), 1970, p 451

40. H.W. Pickering and P.R. Swann, *Corrosion,* Vol 19 (No. 3), 1963, p 373

41. A.W. Thompson and I.M. Bernstein, *Advances in Corrosion Sciences and Technology,* Vol 7, M.G. Fontana and R.W. Staehle, Ed., Plenum Press, 1980, p 53

42. R.M. Riecke, A. Athens, and I.O. Smith, *Mater. Sci. Technol.,* Vol 2, 1986, p 1066

43. E.H. Dix, *Trans. AIME,* Vol 137 (No 11), 1940

44. R.B. Mears, R.H. Brown, and E.H. Dix, *Symposium on Stress-Corrosion Cracking of Metals,* ASTM and the American Institute of Mining, Metallurgical, and Petroleum Engineers, 1944, p 323

45. E.H. Dix, Jr., *Trans. ASM,* Vol 42, 1950, p 1057

46. H.H. Uhlig, *Physical Metallurgy of Stress Corrosion Fracture,* T.N. Rhodin, Ed., Interscience, 1959, p 1

47. L. Yang, G.T. Horne, and G.M. Pound, *Physical Metallurgy of Stress Corrosion Fracture,* T.N. Rhodin, Ed., Interscience, 1950, p 29

48. J.J. Harwood, *Stress Corrosion Cracking and Embrittlement,* W.D. Robertson, Ed., John Wiley & Sons, 1956, p 1

49. F.A. Champion, in *Symposium on Internal Stresses in Metals and Alloys,* Institute of Metals, 1948, p 468

50. H.L. Logan, *J. Res. Natl. Bur. Stand.,* Vol 48, 1952, p 99

51. E.W. Hart, *Surfaces and Interfaces II,* Syracuse University Press, 1968, p 210

52. H.J. Engle, in *The Theory of Stress Corrosion Cracking in Alloys,* North Atlantic Treaty Organization, 1971

53. J.C. Scully, *Corros. Sci.,* Vol 15, 1975, p 207

54. D.A. Vermilyea, *J. Electrochem. Soc.,* Vol 119, 1972, p 405

55. D.A. Vermilyea, *Stress Corrosion Cracking and Hydrogen Embrittlement of Iron Based Alloys,* NACE, 1977, p 208

56. R.W. Staehle, in *The Theory of Stress Corrosion Cracking in Alloys,* North Atlantic Treaty Organization, 1971, p 233

57. R.W. Staehle, *Stress Corrosion Cracking and Hydrogen Embrittlement of Iron Based Alloys,* NACE, 1977, p 180

58. E.N. Pugh, *Corrosion,* Vol 41 (No. 9), 1985, p 517

59. P.R. Swann and J.D. Embury, *High Strength Materials,* John Wiley & Sons, 1965, p 327

60. J.M. Silcock and P.R. Swann, *Environment- Sensitive Fracture of Engineering Materials,* Z.A. Foroulis, Ed., The Metallurgical Society, 1979, p 133

61. S.P. Lynch, *Hydrogen Effects in Metals,* A.W. Thompson and I.M. Bernstein, Ed., The Metallurgical Society, 1981, p 863

62. S.P. Lynch, *Met. Sci.,* Vol 15 (No. 10), 1981, p 463

63. S.P. Lynch, *J. Mater. Sci.,* Vol 20, 1985, p 3329

64. A.J. Forty and P. Humble, *Philos. Mag.,* Vol 8, 1963, p 247

65. A.J. McEvily and P.A. Bond, *J. Electrochem. Soc.,* Vol 112, 1965, p 141

66. E.N. Pugh, in *Stress Corrosion Cracking and Hydrogen Embrittlement of Iron Based Alloys,* National Association of Corrosion Engineers, 1977, p 37

67. J.A. Beavers, I.C. Rosenberg, and E.N. Pugh, in *Proceedings of the 1972 Tri-Service Conference on Corrosion,* MCIC-73- 19, Metals and Ceramics Information Center, 1972, p 57

68. T.R. Pinchback, S.P. Clough, and L.A. Heldt, *Metall, Trans. A,* Vol 7A, 1976, p 1241; *Metall. Trans. A,* Vol 6A, 1975, p 1479

69. A.J. Forty, *Physical Metallurgy of Stress Corrosion Fracture,* T.N. Rhodin, Ed., Interscience, 1959, p 99

70. K. Sieradzki and R.C. Newman, *Philos. Mag. A,* Vol 51 (No. 1), 1985, p 95

71. I.-H. Lin and R.M. Thomson, *J. Mater. Res.,* Vol 1 (No. 1), 1986

72. G.J. Dienes, K. Sieradzki, A. Paskin, and B. Massoumzadeh, *Surf. Sci.,* Vol 144, 1984, p 273

73. N.S. Stolloff, *Environment-Sensitive Fracture of Engineering Materials,* Z.A. Foroulis, Ed., The Metallurgical Society, 1979, p 486

74. M.O. Speidel and R.M. Magdowski, Stress Corrosion Cracking of Steam Turbine Steels—An Overview, *Proceedings of the Second International Symposium on Environmental Degradation of Materials in Nuclear Power Systems-Water Reactors,* American Nuclear Society, 1986, p 267

75. D.P. Williams and H.G. Nelson, *Metall. Trans.,* Vol 1, 1970, p 63

76. R.M. Latanision and H. Opperhauser, *Metall. Trans.,* Vol 5, Scientific and Technical Book Service, 1974, p 483

77. R.H. Jones, A Review of Combined Impurity Segregation-Hydrogen Embrittlement Processes, *Advances in the Mechanics and Physics of Surfaces,* R.M. Latanision and T.E. Fischer, Ed., Scientific and Technical Book Service, 1986

R.H. Jones, Stress-Corrosion Cracking, *Corrosion: Fundamentals, Testing, and Protection*, Vol 13A, *ASM Handbook*, ASM International, 2003, p 346–366

Stress-Corrosion Cracking

R.H. Jones, Battelle Pacific Northwest National Laboratory

Selected References

General Reference

- R.P. Gangloff and M.B. Ives, Ed., "Environment-Induced Cracking of Metals," NACE- 10, NACE, 1988
- R.H. Jones, Ed., *Chemistry and Electrochemistry of Corrosion and Stress Corrosion Cracking: A Symposium Honoring the Contributions of R.W. Staehle,* TMS, 2001
- R.H. Jones, Ed., *Environmental Effects on Engineered Materials,* Marcel-Dekker, Inc., 2001
- R.H. Jones, Ed., *New Techniques for Characterizing Corrosion and Stress Corrosion,* TMS, Warrendale, PA, 1995
- R.H. Jones, Ed., *Stress-Corrosion Cracking Materials Performance and Evaluation,* ASM International, 1992
- R.D. Kane, Ed., "Environmentally Assisted Cracking: Predictive Methods for Risk Assessment and Evaluation of Materials, Equipment and Structures," STP 1401, ASTM, 2000

Analysis of SCC

- S.M. Bruemmer and L.E. Thomas, Insights into Environmental Degradation Mechanisms from High Resolution Characterization of Crack Tips, *Proceedings of Chemistry and Electrochemistry of Corrosion and Stress Corrosion Cracking,* R.H. Jones, Ed., TMS, Warrendale, PA, 2001, p 123
- R.H. Jones, H. Li, and J.P. Hirth, "Effects of Mixed Mode I/III Loading on Environmental- Induced Cracking," *Corrosion,* Vol 57 (No. 1), 2001, p 52

- T. Magnin, D. Tanguy, and D. Delafosse, Physical and Numerical Modeling of the Stress Corrosion Cracking Behavior of Austenitic Stainless Steel, Al-Mg and Nickel- Base Alloys in PWR and Chloride Solutions, *Proceedings of Chemistry and Electrochemistry of Corrosion and Stress Corrosion Cracking,* R.H. Jones, Ed., TMS, Warrendale, PA, 2001, p 45
- R.W. Staehle, Bases for Predicting the Earliest Failures Due to Stress Corrosion Cracking, *Proceedings of Chemistry and Electrochemistry of Corrosion and Stress Corrosion Cracking,* R.H. Jones, Ed., TMS, Warrendale, PA, 2001, p K-1

Specific Alloys and SCC

- N.J.H. Holroyd, Environment-Induced Cracking of High-Strength Aluminum Alloys, *Environment-Induced Cracking of Metals,* R.P. Gangloff and M.B. Ives, Ed., NACE, 1988, p 311
- R.H. Jones, D.R. Baer, M.J. Danielson, and J.S. Vetrano, Role of Mg in the Stress Corrosion Cracking of an Al-Mg Alloy, *Metals and Mater. Trans A,* Vol 32A, 2001, p 1699
- N. Sridhar, D.S. Dunn, and A. Anderko, “Prediction of Conditions Leading to Stress Corrosion Cracking of Gas Transmission Lines,” *Environmentally Assisted Cracking: Predictive Methods for Risk Assessment and Evaluation of Materials, Equipment and Structures,* STP 1401, R.D. Kane, Ed., ASTM, 2000

B. Craig, Hydrogen Damage, *Corrosion: Fundamentals, Testing, and Protection*, Vol 13A, *ASM Handbook*, ASM International, 2003, p 367–380

Hydrogen Damage

Bruce Craig, MetCorr

Introduction

HYDROGEN DAMAGE is a form of environmentally assisted failure that results most often from the combined action of hydrogen and residual or applied tensile stress. Hydrogen damage to specific alloys or groups of alloys manifests itself in many ways, such as cracking, blistering, hydride formation, and loss in tensile ductility. For many years, these failures have been collectively termed hydrogen embrittlement; this term persists even though it is improperly used to describe a multitude of failure modes involving hydrogen, several of which do not demonstrate the classical features of embrittlement (that is, reduced load-carrying capability or fracture below the yield strength). This section classifies the various forms of hydrogen damage, summarizes the various theories that seek to explain hydrogen damage, and reviews hydrogen degradation in specific ferrous and nonferrous alloys. Information on the effect of hydrogen on fracture characteristics is available in the article "Modes of Fracture" in *Fractography,* Volume 12 of *ASM Handbook,* formerly *Metals Handbook,* 9th ed.

B. Craig, Hydrogen Damage, *Corrosion: Fundamentals, Testing, and Protection*, Vol 13A, *ASM Handbook*, ASM International, 2003, p 367–380

Hydrogen Damage

Bruce Craig, MetCorr

Classification of Hydrogen Processes

The specific types of hydrogen damage have been categorized in order to enhance the understanding of the factors that affect this behavior in alloys and to provide a basis for development and analysis of theories regarding different hydrogen damage mechanisms (Ref 1). Table 1 presents one of these classifications schemes, describing the materials that are susceptible to the various forms of damage, the source of hydrogen, typical conditions for the occurrence of failure, and the initiation site. The mechanism for each of these failure modes is also described briefly. The first three classes are grouped together and designated hydrogen embrittlement because these are the failure modes that typically exemplify classical hydrogen embrittlement.

Table 1 Classifications of processes of hydrogen degradation of metals

	Hydrogen embrittlement			Hydrogen attack	Blistering	Shatter cracks, flakes, fisheyes	Micro-perforation	Degradation in flow properties	Metal hydride formation
	Hydrogen environment embrittlement	**Hydrogen stress cracking**	**Loss in tensile ductility**						
Typical materials	Steels, nickel-base alloys, metastable stainless steel, titanium alloys	Carbon and low-alloy steels	Steels, nickel-base alloys, Be-Cu bronze, aluminum alloys	Carbon and low-alloy steels	Steels, copper, aluminum	Steels (forgings and castings)	Steels (compressors)	Iron, steels, nickel-base alloys	V, Nb, Ta, Ti, Zr, U
Usual source of hydrogen (not exclusive)	Gaseous H_2	Thermal processing, electrolysis, corrosion	Gaseous hydrogen, internal hydrogen from electrochemical charging	Gaseous	Hydrogen sulfide corrosion, electrolytic charging, gaseous	Water vapor reacting with molten steel	Gaseous hydrogen	Gaseous or internal hydrogen	Internal hydrogen from melt; corrosion, electrolytic charging, welding
Typical conditions	10^{-12} to 10^2 MPa (10^{-10} to 10^4 psi) gas pressure	0.1 to 10 ppm total hydrogen content	0.1 to 10 ppm total hydrogen content range of gas pressure exposure	Up to 10^2 MPa (15 ksi) at 200–595 °C (400–1100 °F)	Hydrogen activity equivalent to 0.2 to 1 × 10^2 MPa (3–15 ksi) at 0–150 °C (30–300 °F)	Precipitation of dissolved ingot cooling	2 to 8 × 10^6 MPa (30–125 ksi) at 20–100 °C (70–210 °F)	1–10 ppm hydrogen content (iron at 20 °C, or 70 °F) up to 10^2 MPa (15 ksi) gaseous hydrogen (various metals, T > 0.5 melting point)	0.1 to 10^2 MPa (15–15,000 psi) gas pressure hydrogen activity must exceed solubility limit near 20 °C (70 °F)
	Observed at -100 to 700 °C (-150 to 1290 °F); most severe near 20 °C (70 °F)	Observed at -100 to 100 °C (-150 to 210 °F); most severe near 20 °C (70 °F)	Observed at -100 to 700 °C (-150 to 1290 °F)	…	…	…	…	…	…
	Strain rate	Strain rate	Occurs in	…	…	…	…	…	…

	important; embrittlement more severe at low strain rate; generally more severe in notched or precracked specimens	important; embrittlement more severe at low strain rate; always more severe in notched or precracked specimens	absence of effect on yield stress; strain rate important						
Failure initiation	Surface or internal initiation; incubation period not observed	Internal crack initiation	Surface and/or internal effect	Surface (decarburization); internal carbide interfaces (methane bubble formation)	Internal defect	Internal defect	Unknown	…	Internal defect
Mechanisms	Surface or subsurface processes	Internal diffusion to stress concentration	Surface or subsurface processes	Carbon diffusion (decarburization); hydrogen diffusion; nucleation and growth (bubble formation)	Hydrogen diffusion; nucleation and growth of bubble; steam formation	Hydrogen diffusion to voids	Unknown	Adsorption to dislocations; solid-solution effects	Hydride precipitation

T, temperature. Source: Ref 1

Hydrogen environment embrittlement occurs during the plastic deformation of alloys in contact with hydrogen-bearing gases or a corrosion reaction and is therefore strain-rate dependent. The degradation of the mechanical properties of ferritic steels, nickel-base alloys, titanium alloys, and metastable austenitic stainless steels is greatest when the strain rate is low and the hydrogen pressure and purity are high.

Hydrogen stress cracking, also referred to as hydrogen-induced cracking or static fatigue, is characterized by the brittle fracture of a normally ductile alloy under sustained load in the presence of hydrogen. Most often, fracture occurs at sustained loads below the yield strength of the material. This cracking mechanism depends on the hydrogen fugacity, strength level of the material, heat treatment/microstructure, applied stress, and temperature. For many steels, a threshold stress exists below which hydrogen stress cracking does not occur. This threshold is a function of the strength level of the steel and the specific hydrogen-bearing environment. Therefore, threshold stress or stress intensity for hydrogen stress cracking is not considered a material property. Generally, the threshold stress decreases as the yield strength and tensile strength of an alloy increase. Hydrogen stress cracking is associated with absorption of hydrogen and a delayed time to failure (incubation time), during which hydrogen diffuses into regions of high triaxial stress. Hydrogen stress cracking may promote one mode of fracture in an alloy rather than another form normally observed in benign environments. Thus, all modes of cracking have been observed in most commercial alloy systems; however, hydrogen stress cracking usually produces sharp, singular cracks in contrast to the extensive branching observed for stress-corrosion cracking (SCC). The catastrophic cracking of steels in hydrogen sulfide (H_2S) environments, referred to as sulfide stress cracking, is a special case of hydrogen stress cracking.

Loss in tensile ductility was one of the earliest recognized forms of hydrogen damage. Significant decreases in elongation and reduction in area are observed for steels, stainless steels, nickel-base alloys, aluminum alloys, and titanium alloys exposed to hydrogen. This mode of failure is most often observed in lower-strength alloys, and the extent of loss in tensile ductility is a function of hydrogen content of the material. Loss in tensile ductility behavior is strain-rate sensitive and becomes more pronounced as the strain-rate decreases.

Hydrogen attack is a high-temperature form of hydrogen damage that occurs in carbon and low-alloy steels exposed to high-pressure hydrogen at high temperatures for extended time. Hydrogen enters the steel and reacts with carbon either in solution or as carbides to form methane gas; this may result in the formation of cracks and fissures or may simply decarburize the steel, resulting in a loss in strength of the alloy. This form of damage is temperature dependent, with a threshold temperature of approximately 200 °C (400 °F).

Blistering occurs predominantly in low- strength alloys when atomic hydrogen diffuses to internal defects, such as laminations or nonmetallic inclusions, and then precipitates as molecular hydrogen (H_2). The pressure of molecular hydrogen can attain such high values that localized plastic deformation of the alloy occurs, forming a blister that often ruptures. Blisters are frequently found in low-strength steels that have been exposed to aggressive corrosive environments (such as H_2S) or cleaned by pickling.

Shatter cracks, flakes, and fisheyes are features common to hydrogen damage in forgings, weldments, and castings. They are attributed to hydrogen pickup during melting operations when the melt has a higher solubility for hydrogen than the solid alloy. During cooling from the melt, hydrogen diffuses to and precipitates in voids and discontinuities, producing the features that result from the decreased solubility of hydrogen in the solid metal. In many aspects, these features are comparable to blistering, and this could be considered a special case of that class.

Microperforation by high-pressure hydrogen occurs at extremely high pressures of hydrogen near room temperature. Microperforation occurs predominately in steels. This form of hydrogen damage manifests itself as a network of small fissures that allows permeation of the alloy by gases and liquids.

Degradation in flow properties in hydrogen environments has been found at ambient temperatures for iron and steel and at elevated temperature for several alloy systems. The steady- state creep rate under constant load has been observed to increase in the presence of hydrogen for some nickel-base alloys.

Hydride formation produces embrittlement in magnesium, tantalum, niobium, vanadium, uranium, thorium, zirconium, titanium, and their alloys, as well as many other less common metals and alloys. The degradation of mechanical properties and the cracking of these metals and their alloys are attributable to the precipitation of metal hydride phases. Hydrogen pickup often results from welding, heat treating, charging from corrosion processes, or during melting of the alloy. Hydride formation is enhanced for some metal-hydrogen systems by the application of stress—the so-called stress-induced hydride formation. Alloy systems that form hydrides are generally ductile at high, >300 K (80 °F), and low, <100 K(-280 °F), temperatures at which they fracture by ductile rupture. This temperature dependence is comparable to that observed for the hydrogen embrittlement of

ferrous and nickel alloys. Some of these alloys are also susceptible to failure in hydrogen by mechanisms other than hydriding. Some evidence exists that nickel and aluminum alloys may also form a highly unstable hydride that could contribute to hydrogen damage of these alloys; however, this possibility has not been confirmed.

Reference cited in this section

1. J.P. Hirth and H.H. Johnson, Hydrogen Problems in Energy Related Technology, *Corrosion*, Vol 32, 1976, p 3

B. Craig, Hydrogen Damage, *Corrosion: Fundamentals, Testing, and Protection*, Vol 13A, *ASM Handbook*, ASM International, 2003, p 367–380

Hydrogen Damage

Bruce Craig, MetCorr

Theories for Hydrogen Damage

As may be appreciated from the numerous classes of hydrogen damage, there are many explanations or theories for these various forms of degradation. The preeminent theories for hydrogen damage are based on pressure, surface adsorption, decohesion, enhanced plastic flow, hydrogen attack, and hydride formation. Although many other theories have been presented, most are variations on these basic models.

The pressure theory of hydrogen damage, or more specifically, hydrogen embrittlement, is one of the oldest models for hydrogen damage (Ref 2). This theory attributes hydrogen embrittlement to the diffusion of atomic hydrogen into the metal and its eventual accumulation at voids or other internal surfaces in the alloy, where it combines to form molecular hydrogen. As the concentration of hydrogen increases at these microstructural discontinuities, a high internal pressure is created that enhances void growth or initiates cracking. This model, although apparently reasonable for blistering and possibly appropriate for some aspects of loss in tensile ductility, does not explain many of the factors observed for classes of failure such as hydrogen stress cracking. However, it is a well-recognized phenomenon that charging hydrogen into steel or nickel alloys at high fugacity, either with high- pressure hydrogen gas or under extreme electrochemical charging, can create a significant density of voids and irreversible damage to the alloy consistent with a pressure-dependent model.

The surface adsorption theory suggests that hydrogen adsorbs on the free surfaces created adjacent to the crack tip, decreasing the surface free energy and thus the work of fracture (Ref 3). Reduction in the work of fracture would thus enhance crack propagation at stress levels below those typically experienced for a particular alloy in a benign environment. There are many arguments against this model. The principal criticism is that it greatly underestimates the work of fracture and does not account for the discontinuous crack growth that has been observed for hydrogen cracking.

Decohesion describes the effect of hydrogen on the cohesive force between atoms of the alloy matrix (Ref 4, 5, 6). Sufficiently high hydrogen concentrations that accumulate ahead of a crack tip are assumed to lower the maximum cohesive force between metal atoms such that the local maximum tensile stress perpendicular to the plane of the crack then becomes equivalent to or greater than the lattice cohesive force, and fracture results.

Enhanced plastic flow and instability are associated with hydrogen dislocation interactions and are primarily based on fractographic observations (Ref 7). This approach proposes that atomic hydrogen enhances dislocation motion (generally, screw dislocations) and the creation of dislocations at surfaces and/or crack tips, leading to softening of the material on a localized scale. Although this behavior has been observed in certain steels, hardening by hydrogen has also been found. Careful high-resolution electron microscopy of what appears to be brittle cleavage or intergranular fracture surfaces has revealed evidence of crack tip plasticity in support of this mechanism. Recently, it was proposed (Ref 8) that hydrogen may enhance plastic instability in the form of shear localization. Moreover, the coupling of shear-band propagation with the formation of microvoids at

second- phase particles that are intersected by these shear bands can produce significant reduction in the fracture toughness of an alloy, especially under mixed-mode loading.

Hydride formation is the degradation of Group Vb metals (niobium, vanadium, and tantalum) and zirconium, titanium, and magnesium in hydrogen environments by the formation of a brittle metal hydride at the crack tip. When sufficient hydrogen is available in the alloy, a metal hydride precipitates. Cracking of the hydride occurs, followed by crack arrest in the more ductile matrix or continued crack growth between hydrides by ductile rupture. Because hydride formation is enhanced by the application of stress, the stress field ahead of the crack tip may induce precipitation of additional hydrides that cleave. Thus, in some alloys, brittle crack propagation occurs by repeated precipitation of hydrides ahead of the crack tip, cleavage of these hydrides, precipitation of new hydrides, and so on until fracture is complete (Ref 9).

Hydrogen attack is one of the better understood mechanisms of hydrogen damage but is specific to a single class of damage by hydrogen at high temperature (Ref 10). Hydrogen attack may take two forms of damage: surface decarburization or internal decarburization. However, the mechanism is the same for both forms. At elevated temperatures, hydrogen diffuses into the steel or reacts at the surface with carbon in solid solution or that which has dissociated from carbides to form a hydrocarbon—typically methane. This chemical reaction is easily described thermodynamically, which sets this form of damage apart for the more complex forms of hydrogen damage. As expected, damage is dependent on temperature and hydrogen partial pressure. Surface decarburization occurs at temperatures above 540 °C (1000 °F) and internal decarburization at temperatures from 200 °C (400 °F) upward.

Hydrogen Trapping. Although numerous models exist, none adequately explains the behavior exhibited by alloys in different hydrogen-bearing systems. Until a universal theory is developed, one must rely on the phenomenological behavior between the more prominent alloy systems to understand hydrogen damage. One of the principal factors that determines the hydrogen damage susceptibility of ferrous alloys is a phenomenon referred to as trapping (Ref 11). Diffusion studies of iron and steels have shown an initial retardation in diffusion rate or lag time for hydrogen diffusion through these alloys before a steady-state diffusivity compatible with that expected theoretically is achieved. This lag time is generally considered to be related to the filling of traps by hydrogen. In fact, the apparent diffusivity of hydrogen in steels shows a precipitous decrease with increasing concentration of particles (traps), as shown in Fig. 1.

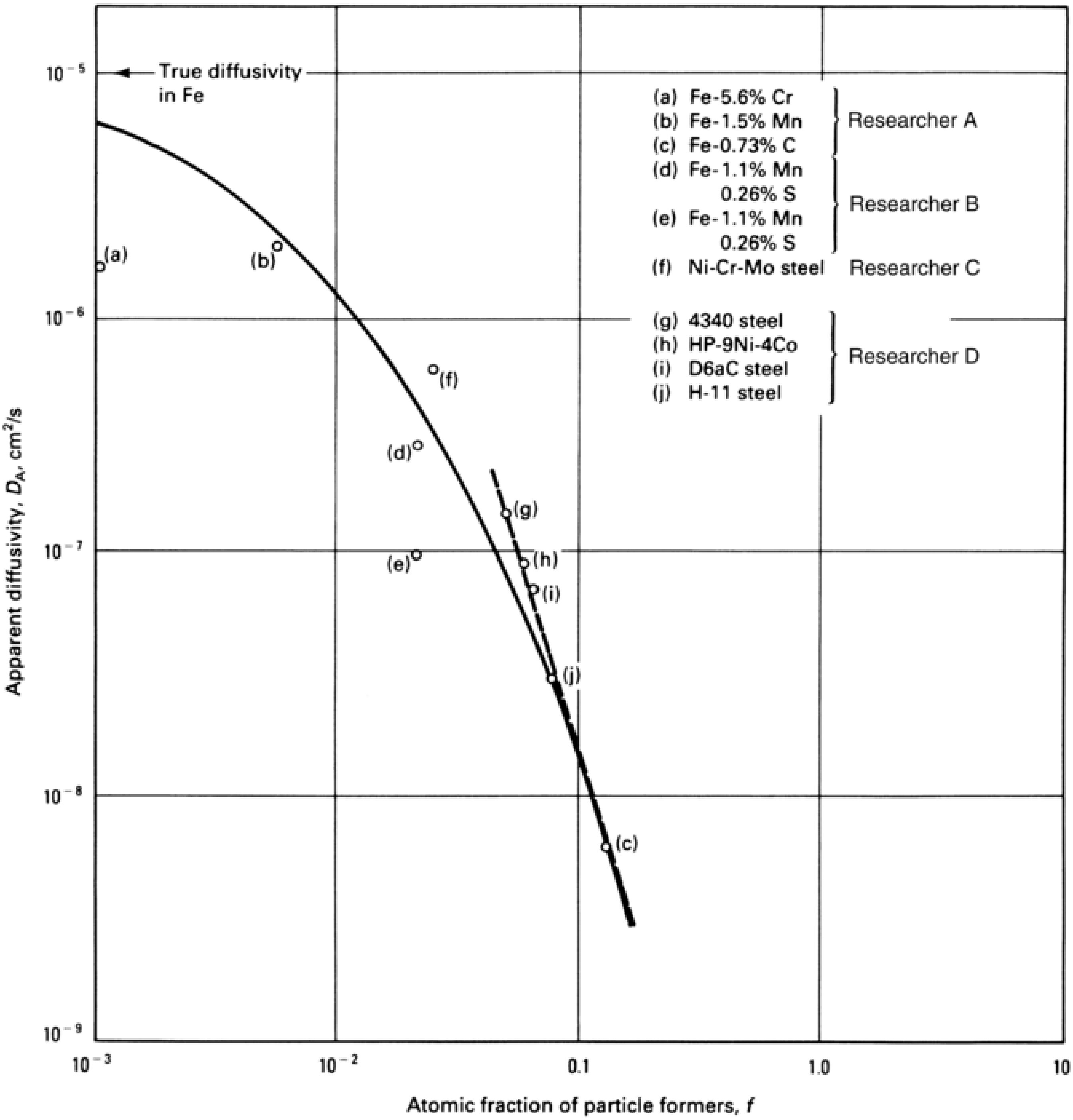

Fig. 1 Decrease in apparent hydrogen diffusivity with increased fraction of precipitate particles. Source: Ref 12

Hydrogen trapping may be considered the binding of hydrogen atoms to impurities, structural defects, or microstructural constituents in the alloy. Binding may be attributed to local electric fields and stress fields, temperature gradients, chemical potential gradients, or physical trapping. These hydrogen traps may be mobile (dislocations, stacking faults) or stationary (grain boundaries, carbide particles, individual solute atoms). They may also be reversible or irreversible traps. Short-duration trapping of hydrogen in which the occupancy time is limited is referred to as reversible. A long residency time for hydrogen characterized by a high binding energy is termed irreversible trapping. Table 2 presents a classification of hydrogen traps in steel. The concept and investigation of trapping have been developed primarily for steels; however, trapping may not be restricted to this system. Face- centered cubic (fcc) alloys show a similar trapping behavior, although at a somewhat reduced efficiency for trapping compared to steels.

Table 2 Classification of hydrogen traps in steels according to size

Trap class	Example of trap: Elements at the left of iron	Example of trap: Elements with a negative ε^{i}_{H} (a)	Interaction energy(b), eV	Character if known	Influence diameter, D_i
Point	…	Ni	(0.083)	Most probably reversible	A few inter-atomic spacings
	Mn	Mn	(0.09)		
	Cr	Cr	(0.10)		
	V	V	(0.16)		
	…	Ce	(0.16)		
	…	Nb	(0.16)	Reversible	
	Ti	Ti	0.27		
	…	(vacancy)	…	Getting more irreversible	
	Sc	O	(0.71)		
	Ca	Ta	(0.98)		
	K	Ia	(0.98)		
	…	Nd	(1.34)		
Linear	Dislocations		0.31	Reversible	3 nm for an edge dislocation
			0.25	Reversible	
			(average values)		
	Intersection of three grain boundaries	…	Depends on coherency	…	
Planar or bimensional	Particle-matrix interfaces				
	TiC (incoherent)		0.98	Irreversible, gets more reversible as the particle is more coherent	Diameter of the particle, or a little more as coherency increases
	$Fe^{3}C$		0.8–0.98		
	MnS		…		
	Grain boundaries		0.27	Reversible	Same as dislocation
			Average value 0.55–0.61 (high angle)	Reversible or irreversible	
	Twins		…	Reversible	A few interatomic spacings
	Internal surfaces (voids)		…	…	…
Volume	Voids		>0.22	…	Dimension of the defect
	Cracks		…	…	
	Particles		Depends on exothermicity of the dissolution of H by the particle	…	

(a) ε^{i}_{H} is the interaction coefficient. A negative ε^{i}_{H} means hydrogen is attracted.
(b) Values of interaction energies are either experimental or are calculated (when between parentheses) at room temperature. Source: Ref 13

References cited in this section

2. C. Zapffe and C. Sims, Hydrogen Embrittlement, Internal Stress and Defects in Steel, *Trans. AIME*, Vol 145, 1941, p 225

3. N.J. Petch and P. Stables, Delayed Fracture of Metals Under Static Load, *Nature,* Vol 169, 1952, p 842

4. A.R. Troiano, The Role of Hydrogen and Other Interstitials in the Mechanical Behavior of Metals, *Trans. ASM,* Vol 52, 1960, p 57

5. R.A. Oriani, A Mechanistic Theory of Hydrogen Embrittlement of Steels, *Bunsen-Gesellschaft Phys. Chemie,* Vol 76, 1972, p 848

6. J.F. Knott, Fracture Toughness and Hydrogen Assisted Crack Growth in Engineering Alloys, *Hydrogen Effects in Materials,* A.W. Thompson and N.R. Moody, Ed., TMS, 1996, p 387

7. C.D. Beachem, A New Model for Hydrogen Assisted Cracking (Hydrogen Embrittlement), *Metall. Trans.,* Vol 3, 1972, p 437

8. J.P. Hirth, The Role of Hydrogen in Enhancing Plastic Instability and Degrading Fracture Toughness of Steels, *Hydrogen Effects in Materials,* A.W. Thompson and N.R. Moody, Ed., TMS, 1996, p 507

9. S. Gahr, M.L. Grossbech, and H.K. Birnbaum, *Acta Metall.,* Vol 25, 1977, p 125

10. F.H. Vitovec, Modeling of Hydrogen Attack of Steel in Relation to Material and Environmental Variables, *Current Solutions to Hydrogen Problems in Steels,* C.G. Interrante and G.M. Pressouyre, Ed., American Society for Metals, 1982

11. G.M. Pressouyre and I.M. Bernstein, A Quantitative Analysis of Hydrogen Trapping, *Metall. Trans. A,* Vol 9, 1978, p 1571

12. W.W. Gerberich, Effect of Hydrogen on High Strength and Martensitic Steels, *Hydrogen in Metals,* I.M. Bernstein and A.W. Thompson, Ed., American Society for Metals, 1974, p 115

13. G.M. Pressouyre, A Classification of Hydrogen Traps in Steel, *Metall. Trans. A,* Vol 10, 1979, p 1571

B. Craig, Hydrogen Damage, *Corrosion: Fundamentals, Testing, and Protection*, Vol 13A, *ASM Handbook*, ASM International, 2003, p 367–380

Hydrogen Damage

Bruce Craig, MetCorr

Hydrogen Damage in Iron-Base Alloys

Pure Irons. Hydrogen damage may occur in relatively pure irons, such as Ferrovac E and other magnetically soft irons, producing either transgranular or intergranular fracture, depending on the heat treatment and the presence of impurities and solutes (carbon, oxygen, and nitrogen) at the grain boundaries. Hydrogen can also lower the yield strength and flow stress of high-purity iron at approximately room temperature or lead to hardening. Although the yield strength is reduced for impure iron, the flow stress may be increased under conditions of low hydrogen fugacity.

Ferrous Alloys. Many factors affect the behavior of ferrous alloys in hydrogen-bearing environments. Hydrogen concentration, temperature, heat treatment/microstructure, stress level (applied and yield stress), solution composition, and environment are the primary factors involved in determining susceptibility to hydrogen embrittlement. Figure 2 shows the effect of hydrogen concentration on the time to failure for a high-

strength steel. The longer the baking time, the lower the residual hydrogen in the steel matrix. In general, increasing the concentration of hydrogen in an alloy reduces time to failure and the stress level at which failure occurs.

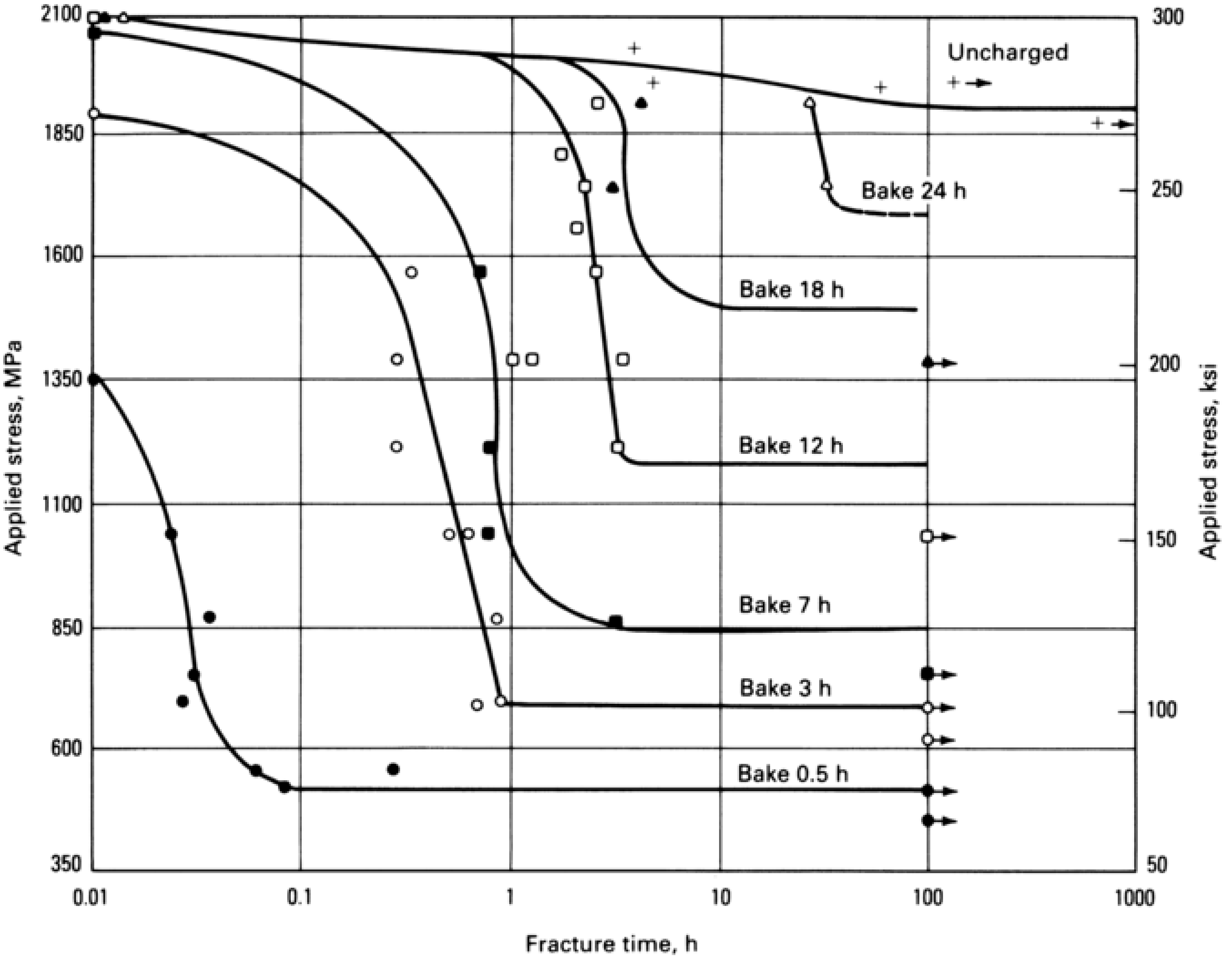

Fig. 2 Static fatigue curves for various hydrogen concentrations obtained by different baking times at 150 °C (300 °F). Sharp-notch high-strength steel specimens 1590 MPa (230 ksi); normal notch strength: 2070 MPa (300 ksi). Source: Ref 4

Hydrogen concentration in the alloy is a function of the fugacity or the approximate concentration of hydrogen at the surface exposed to the environment. Therefore, hydrogen embrittlement is controlled by the hydrogen gas pressure or pH of the environment as well as constituents within the environment that may accelerate or inhibit the entry of hydrogen into the alloy. Elements such as sulfur, phosphorus, antimony, tin, and arsenic and their compounds have been found to inhibit the hydrogen recombination reaction in aqueous solutions, thus increasing the charging of atomic hydrogen into the alloy. In contrast, small amounts of oxygen in gaseous hydrogen environments have demonstrated an inhibitive effect on crack growth of high- strength steels subject to hydrogen cracking.

Figure 3 shows the dependence of both the threshold stress intensity and the crack growth rate of high-strength American Iron and Steel Institute (AISI) 4130 (Unified Numbering System, or UNS, G41300) steel on hydrogen pressure. Increasing the hydrogen pressure reduces the threshold stress intensity for crack initiation and increases the crack growth rate for a specific stress-intensity value.

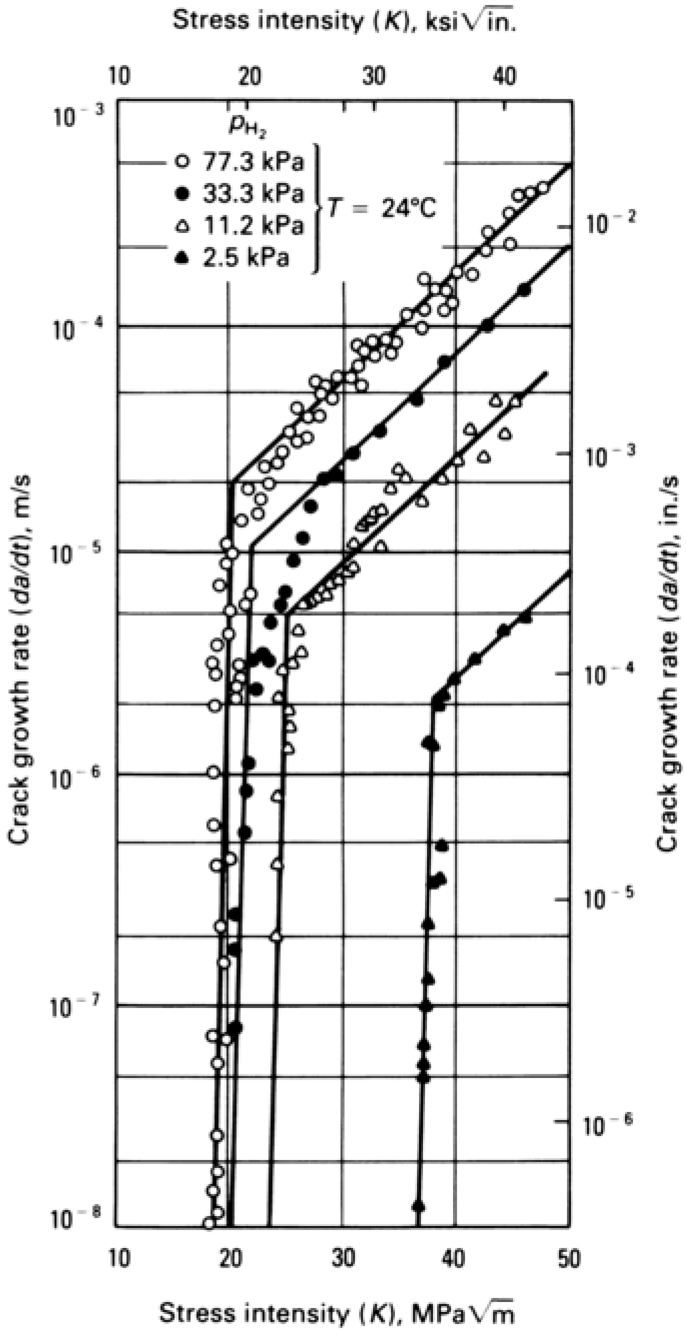

Fig. 3 The stress-intensity *K* dependence of crack growth rate da/dt at various hydrogen pressures at 24 °C (75 °F) for AISI 4340 steel. Source: Ref 14

Temperature also plays an important role in the hydrogen embrittlement of ferrous alloys. Embrittlement is most severe near room temperature (Ref 15) and becomes less severe or nonexistent at higher or lower temperatures (Fig. 4). At lower temperatures, the diffusivity of hydrogen is too sluggish to fill sufficient traps, but at high temperatures, hydrogen mobility is enhanced, and trapping is diminished. As can be seen in Fig. 4, embrittlement is also strongly strain-rate dependent. At high strain rates, fracture may proceed without the assistance of hydrogen, because the mobility of hydrogen is not sufficient to maintain a hydrogen atmosphere around moving dislocations.

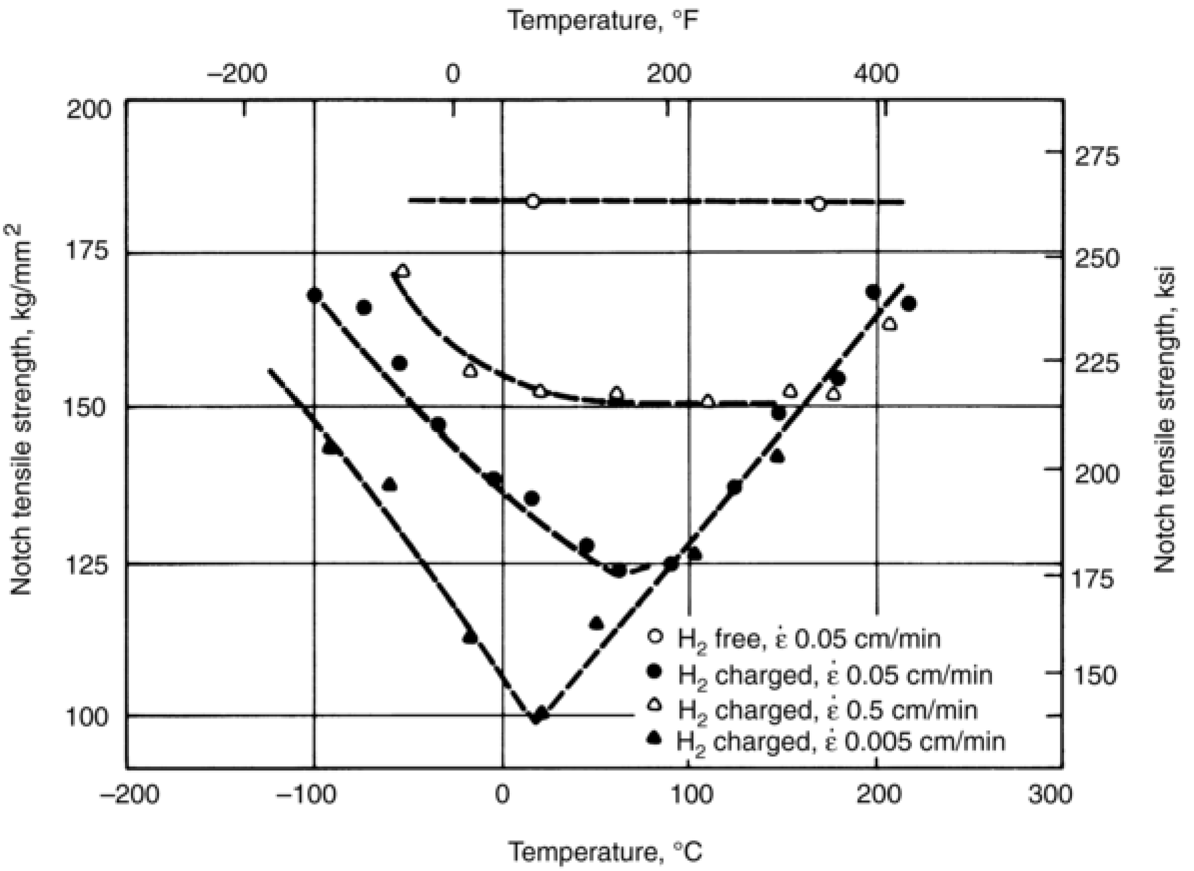

Fig. 4 Notch tensile strength of high-strength steel plotted against testing temperature for three strain rates (crosshead speeds, $\dot{\epsilon}$). Source: Ref 15

Figure 5 shows threshold stress intensity as a function of yield strength for a large number of steels in a variety of hydrogen-containing environments. It can be seen that the threshold stress intensity for crack growth generally decreases with increasing yield strength, regardless of environment, and that very high-strength steels are not usable in hydrogen environments. Threshold stress intensities and crack growth rates are a function of the specific hydrogen environments, with H_2S being one of the most severe environments (Fig. 6). At lower yield strengths, the mechanism for hydrogen-assisted failure apparently changes, and blistering becomes the more common feature of failure. The threshold stress intensities for high-strength steels subjected to hydrogen environments are significantly less than those thresholds measured under benign conditions. These lower thresholds lead to subcritical crack growth when compared to critical values expected from fracture mechanics. Therefore, it is common to designate these thresholds as K_{ISCC} or K_{IH}.

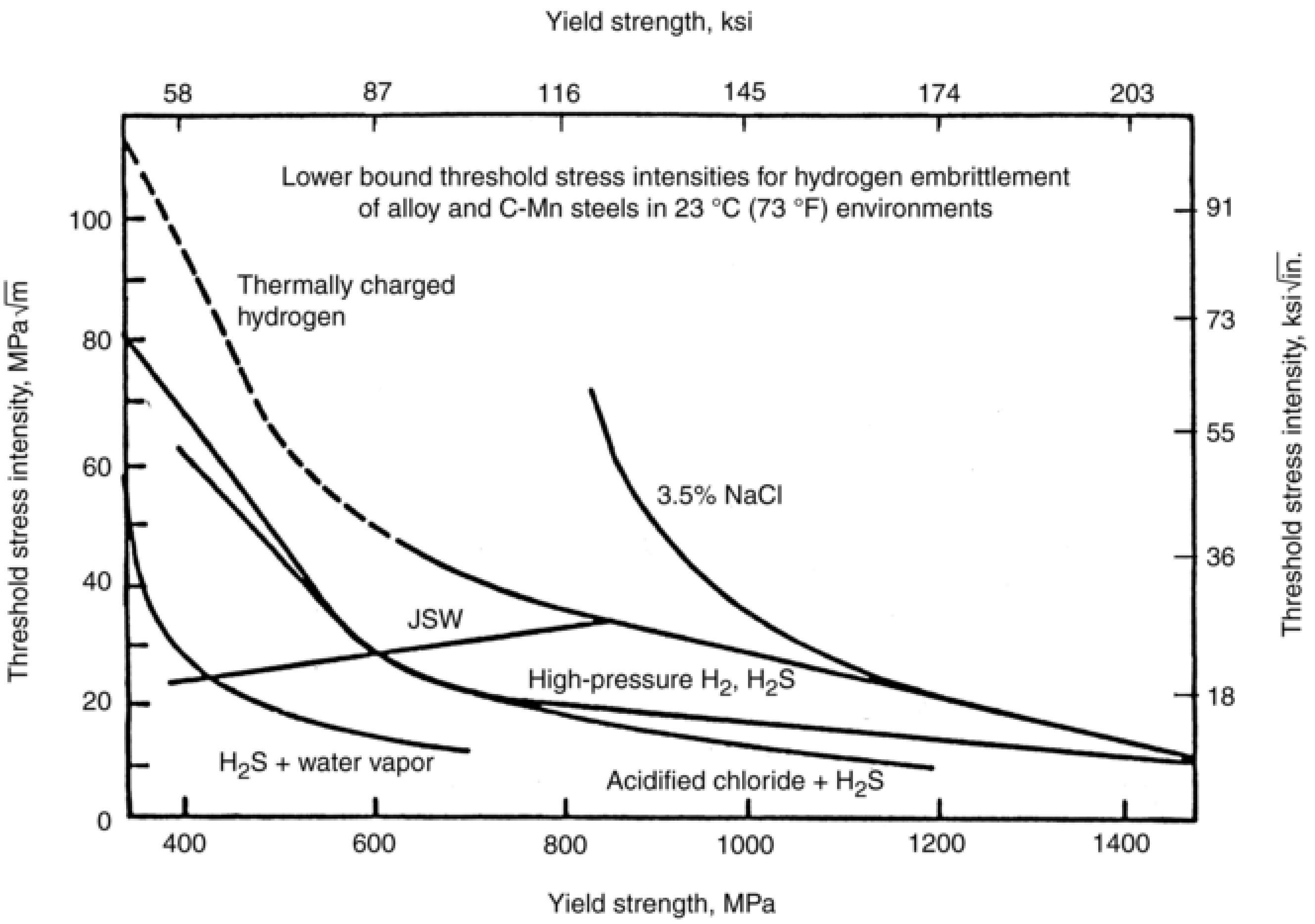

Fig. 5 **Lower bounds on threshold stress intensity versus yield strength for ferrite-pearlite, bainitic, and martensitic steels stressed in five hydrogen-producing environments. JSW, Japan Steel Works. Source: Ref 16**

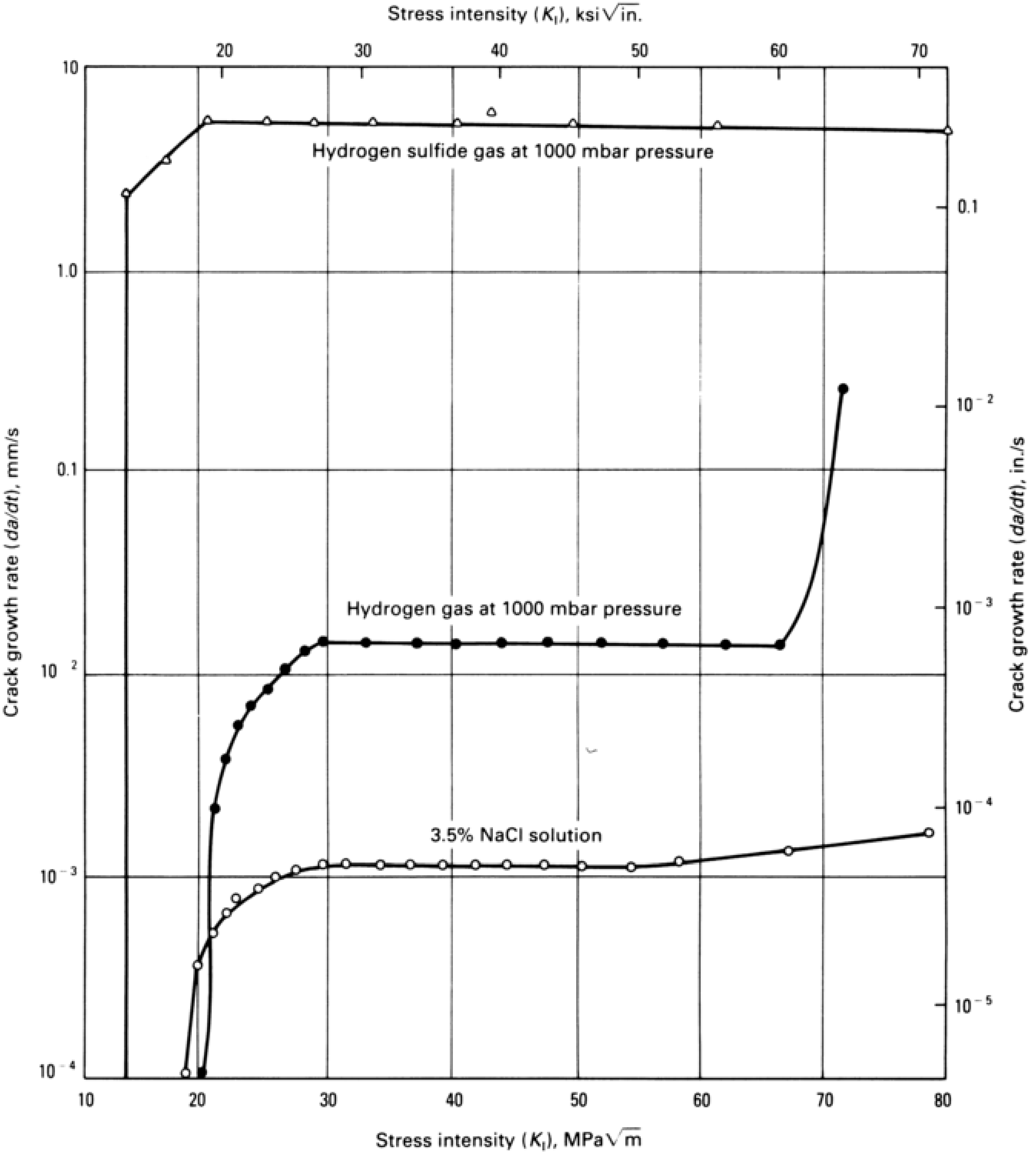

Fig. 6 Crack velocity as a function of stress intensity for a chromium-molybdenum-vanadium steel at 291 K (18 °C, or 64 °F). Source: Ref 17

In low-strength steels, 700 MPa (100 ksi) yield strength or less, hydrogen damage occurs predominately by loss in tensile ductility or blistering. For loss in tensile ductility, hydrogen promotes the formation and/or growth of voids by enhancing the decohesion of the matrix at carbide particle and inclusion interfaces.

At higher hydrogen fugacities and often in the absence of stress, blistering or a form of cracking also associated with inclusions—referred to as stepwise cracking, blister cracking, or hydrogen- induced cracking (HIC)—can occur. Stepwise cracking has been observed frequently in low- strength steels subjected to H_2S-containing environments in the absence of stress (Fig. 7). This type of cracking is not dependent on steel strength but is strictly a function of steel chemistry, processing, and the severity of the hydrogen environment (Ref 18). In H_2S environments, a cracking morphology has been observed in low-strength steels that combines the features of

hydrogen stress cracking and HIC and has been designated stress-oriented hydrogen-induced cracking (SOHIC) (Ref 19). It is unfortunate that too often when investigators observe a new morphology of cracking, they establish a new name for the cracking regardless whether this is justified mechanistically. The result is that the literature is cluttered with many names for the same phenomenon.

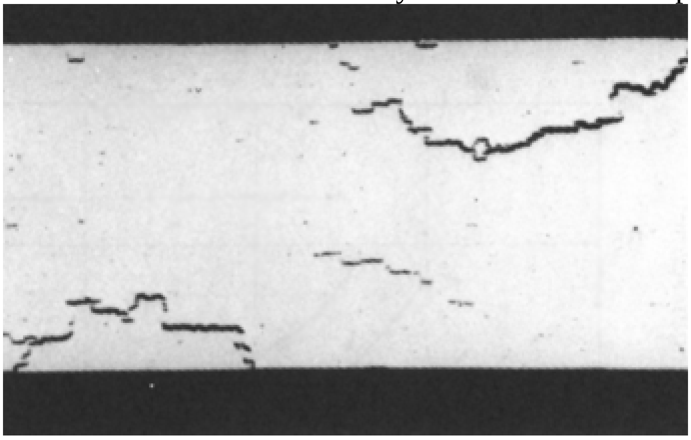

Fig. 7 Stepwise cracking of a low-strength pipeline steel exposed to H_2S. 6×

Fracture of low-strength steels in hydrogen environments may be characterized by ductile dimple rupture, tearing, cleavage, quasi-cleavage, and, less frequently under certain conditions, intergranular cracking. The article "Modes of Fracture" in *Fractography,* Volume 12 of *ASM Handbook,* formerly *Metals Handbook,* 9th ed., contains fractographs illustrating the effects of hydrogen on the fracture appearance of steels.

High-strength steels, those with yield strengths above 700 MPa (100 ksi), are prone to fracture either in an intergranular fashion or by quasi-cleavage, depending on the stress intensity. These steels commonly display an incubation time before fracture initiates under sustained loading, usually in association with regions of high triaxial stress. Because triaxial stresses are created at notch roots or under plane strain, fracture initiates internally in the steel. Intergranular fracture is promoted by the presence of impurity elements at prior-austenite or -ferrite grain boundaries. Elements such as phosphorus, sulfur, tin, antimony, and arsenic have been found to enhance the intergranular fracture of high- strength steels in hydrogen, and as expected, temper-embrittled steels are even more susceptible to hydrogen stress cracking than steels that are not embrittled.

Metallurgical structure can have a profound effect on the resistance of steels to hydrogen embrittlement. When compared at equivalent strength levels, a quenched-and-tempered fine- grain microstructure is more resistant to cracking than a normalized or bainitic steel. However, this is also dependent to a large extent on the strength level at which this comparison is made. In general, the most resistant microstructure is a highly tempered martensitic structure with equiaxed ferrite grains and spheroidized carbides evenly distributed throughout the matrix. Because microstructure is dependent on heat treatment and composition, these factors are not easily separated and must be considered together. There is also a grain size effect that produces enhanced resistance to hydrogen with decreasing prior- austenite grain size (Fig. 8). However, if the grain size is significantly larger than the plastic zone size, the reverse may be true.

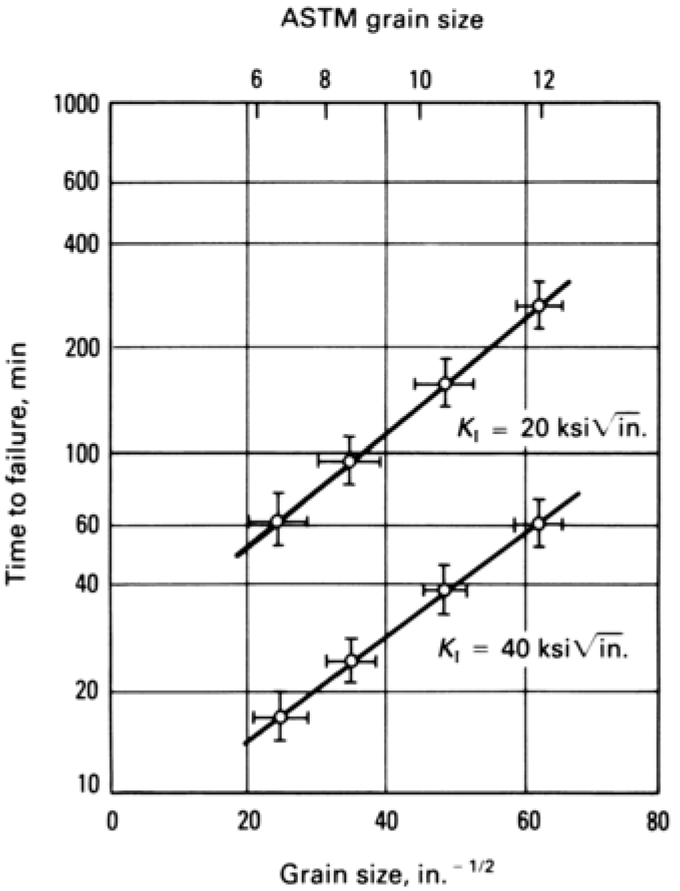

Fig. 8 Illustration of how a refinement in grain size improves resistance to hydrogen failure as measured by the time to failure of two strengths of AISI 4340 steels. Source: Ref 20

The role of alloying elements is quite complex and not easily distinguished from the effects of heat treatment, microstructure, and strength level. Depending on the microstructure and strength level, a specific alloying element may or may not contribute to the hydrogen embrittlement resistance of an alloy or may even increase susceptibility to cracking. The concentration of the alloying element is also a factor in the behavior of alloys in hydrogen. Molybdenum, for example, is beneficial in reducing susceptibility to sulfide stress cracking, a form of hydrogen stress cracking, in AISI 4130 steels up to approximately 0.75 wt%. However, beyond this concentration, a separate Mo_2C phase precipitates in the alloy after tempering at above 500 °C (930 °F), significantly reducing resistance to sulfide stress cracking.

In general, elements such as carbon, phosphorus, sulfur, manganese, and chromium impart greater susceptibility to hydrogen embrittlement in low-alloy steels. However, large increases in such elements as chromium, nickel, and molybdenum in order to produce stainless steels alter the crystal structure, microstructure, and subsequently the heat treatment requirements and therefore the hydrogen embrittlement behavior of this group of ferrous alloys.

Stainless Steels The response of stainless steels to hydrogen-bearing environments is basically related to their strength level. Ferritic stainless steels have excellent resistance to hydrogen embrittlement because of their low strength and enhanced ductility. However, if the ferritic stainless steels are cold worked, they may become susceptible to cracking in hydrogen environments. Similarly, austenitic stainless steels are highly resistant to hydrogen cracking in the annealed or lightly cold-worked condition but can become quite susceptible when heavily cold worked. This increased susceptibility to hydrogen cracking due to increasing yield strength from cold working is similar to the dependence of carbon and low-alloy steel on strength. Decreased resistance to hydrogen for highly cold- worked austenitic stainless steels is largely attributed to the deformation-induced formation of martensite. For those austenitic stainless steels having a very stable austenite phase and high yield strength, such as 21Cr-6Ni-9Mn (UNS S21900), susceptibility is considered to be solely a function of yield strength, similar to the body- centered cubic (bcc) low-alloy steel behavior.

Other factors that may affect the susceptibility of austenitic stainless steels to hydrogen damage are the possible formation of metastable hydride phase that would produce a hydride-based fracture path and the interaction of

hydrogen with stacking faults to reduce stacking fault energy in the austenite, leading to planar slip and brittle fracture. The degree of participation of any of these factors has not been established.

Just as a similarity exists between austenitic stainless steels and low-alloy steels at the high- strength end of the spectrum, the lower-strength austenitics behave in the same manner as the low-alloy steels in hydrogen by a reduction in ductility. Figure 9 shows the loss in reduction in area for several austenitic stainless steels in high-pressure hydrogen. It is apparent that a wide variation in hydrogen damage exists between these various austenitic alloys. Type 304L (UNS S30403) is the most susceptible to loss in tensile ductility, and the stable austenitic alloys, such as 15Cr-25Ni (UNS S66286), are almost unaffected. As observed in carbon and low-alloy steels, there is a temperature effect (~0 °C, or 32 °F) involved with the ductility loss in austenitic stainless steels, although it is somewhat lower than the room-temperature dependence observed for low-alloy steels.

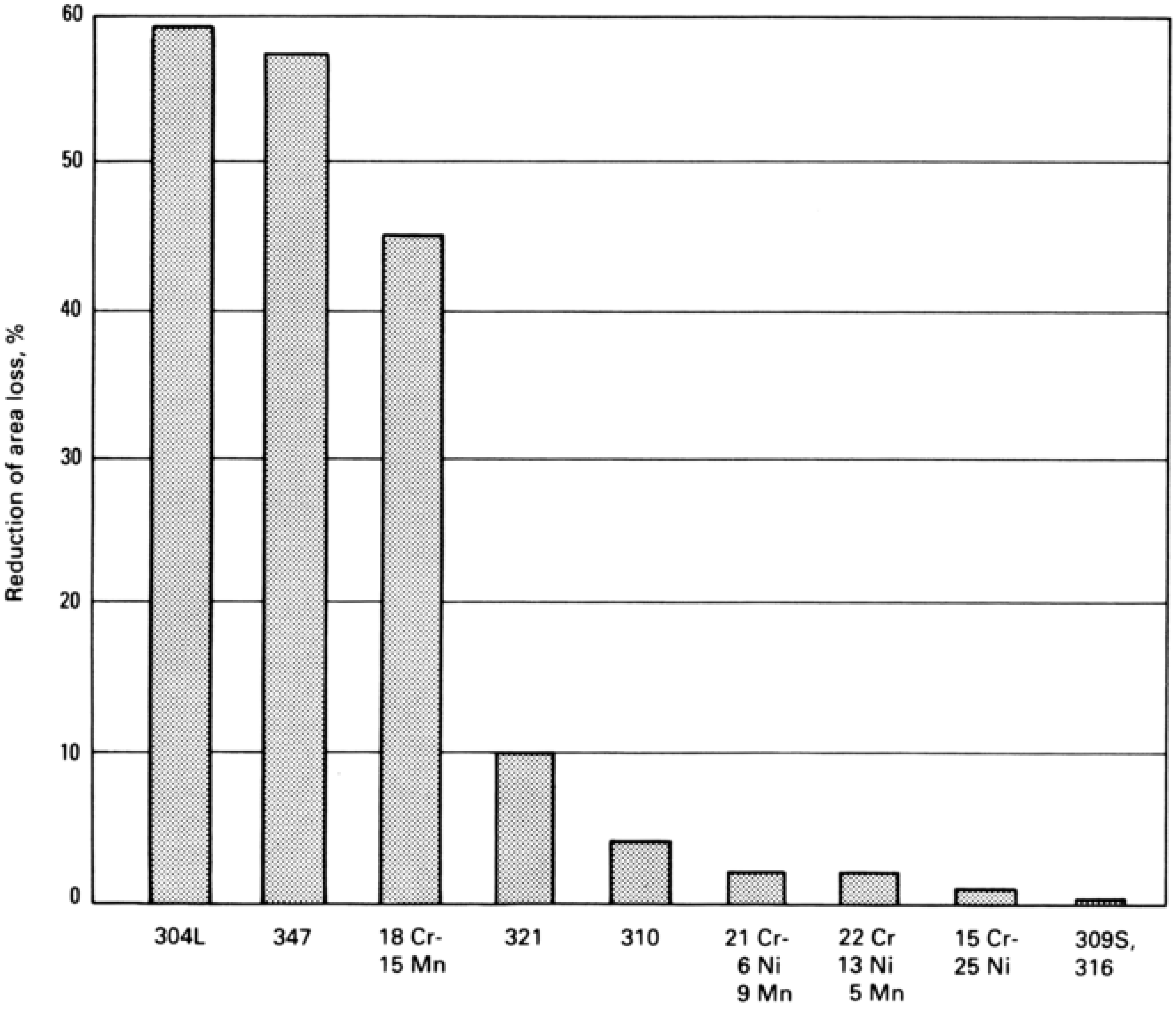

Fig. 9 Ductility loss for several austenitic stainless steels in high-pressure hydrogen. Source: Ref 21

Duplex stainless steels represent an interesting type of behavior in hydrogen as a result of their two-phase structure of ferrite and austenite. Because the solubilities and diffusivities of hydrogen are quite different between the austenite and ferrite phases, the response of the overall duplex alloy is significantly different than either a ferritic or austenitic stainless steel. Reference 22 compiles much of the data in the literature regarding the measured hydrogen diffusion coefficient in duplex stainless steels, as shown in Fig. 10. As could be expected, there is a large degree of scatter in these data as a result of factors such as the relative ferrite-to-austenite ratio, the grain- boundary areas, the volume fraction of precipitates, and so on.

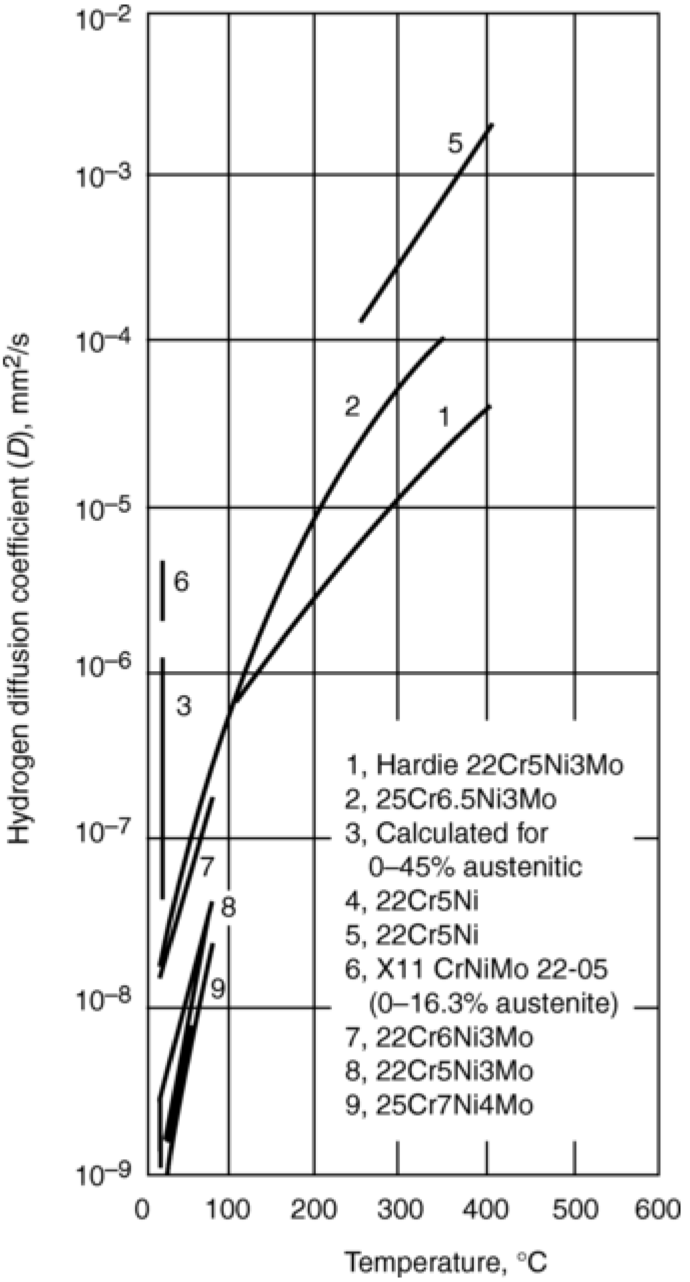

Fig. 10 Published values of hydrogen diffusion coefficients in duplex stainless steels. Data sources are identified in Ref 22. Curves 4 and 5 are from the same source. Curves 8 and 9 are from the same source: Ref 22

A theoretical analysis for hydrogen transport in these two-phase alloys (Ref 23) showed that the effective diffusivity of hydrogen in duplex stainless steels was reduced by a factor of approximately 400 compared to a fully ferritic steel, and that trapping at the ferrite-austenite interface was the most significant factor in explaining this reduced diffusivity of hydrogen in duplex stainless steels relative to ferritic steels. The behavior of hydrogen in duplex stainless steels is very complex, because a change in the ferrite- to-austenite ratio not only alters the relative interface area but also changes the volume fraction of each phase, thereby increasing the solubility and diffusivity of hydrogen in the alloy as a whole.

It is apparent that there are many similarities in behavior between stainless steels and carbon and low-alloy steels in hydrogen. Similarly, the martensitic and precipitation-hardening stainless steels exhibit the same dependence on strength level and microstructure as observed in low-alloy steels. Martensitic and precipitation-hardening stainless steels are extremely susceptible to hydrogen embrittlement with increasing yield strength. Figure 11 compares several grades of precipitation-hardening stainless steel with type 410 martensitic stainless steel tested in an aqueous environment saturated with H_2S. The numbers adjacent to each data point represent the tempering or aging treatment. Generally, the same trend of decreasing time to failure with increasing yield strength is observed as for low- alloy steels. The poor performance of the type 410 martensitic stainless steel

compared to precipitation-hardening stainless steels is typical of the behavior of most martensitic stainless steels, which also compare poorly with low-alloy steels at the same strength level. Even the newer family of martensitic stainless steels, recently introduced as Super 13 Cr, have relatively poor resistance to cracking in hydrogen-bearing environments. Figure 12 shows the regions of hydrogen-assisted cracking (HAC) and those that are not (no HAC) for a steel containing approximately 15% Cr, 4% Ni, and 1.5% Mo. Note that the hydrogen-generating power of the solution, given by the combination of pH and H_2S concentration, defines the boundary of cracking (Ref 25).

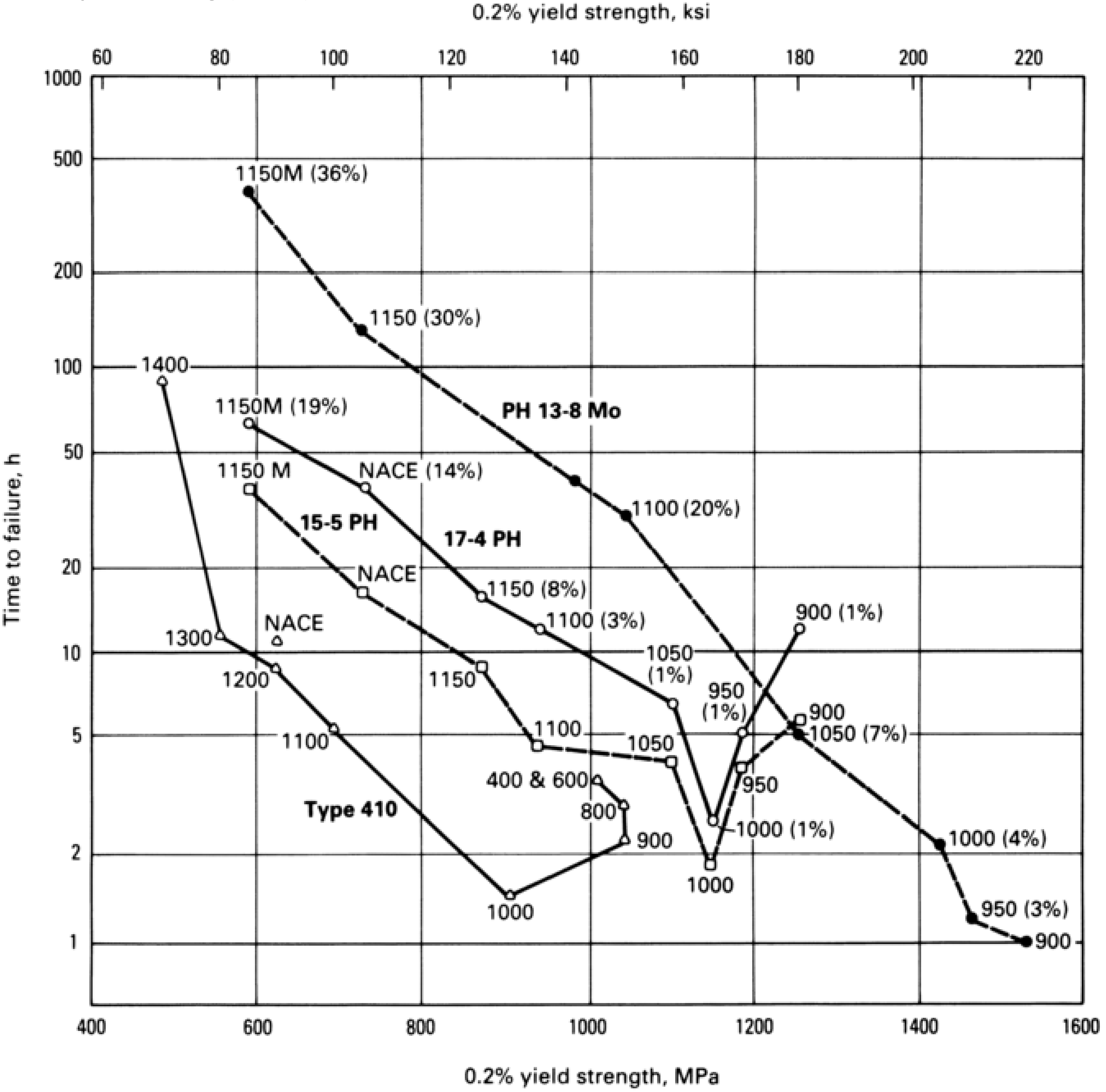

Fig. 11 Time to failure of various alloys as a function of yield strength when tested under 345 MPa (50 ksi) of applied stress in saturated H_2S. Numbers adjacent to data points represent tempering or aging treatment; parenthetical values indicate approximate amounts of austenite. Source: Ref 24

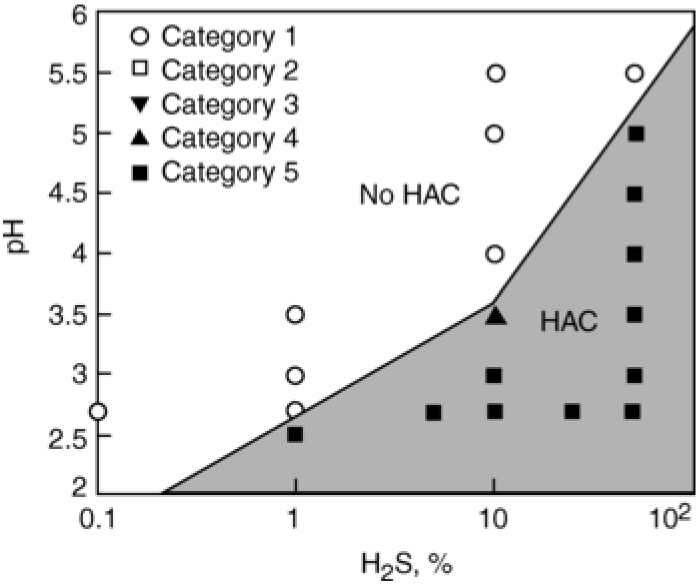

Fig. 12 The H_2S-pH tolerance of low-carbon martensitic stainless steel tested by the slow strain-rate technique. HAC, hydrogen-assisted cracking. Source: Ref 25

Ultrahigh-strength, >1400 MPa (200 ksi), martensitic stainless steels, low-alloy steels, and maraging steels are extremely susceptible to cracking in hydrogen environments, including aqueous solutions containing NaCl. Although chlorides are the primary cause of SCC in many alloy systems, it is generally accepted that the mechanism of cracking in ultrahigh-strength steels is related to hydrogen embrittlement.

Figure 13 compares the crack growth rate of AISI 4340 in several environments against grade 250 maraging steel. The maraging steel has much better resistance to crack propagation in 3.5% NaCl than 4340 and displays a high threshold stress intensity for crack propagation. For maraging steels, there is evidence that peak-aged condition or slight overaging may improve resistance to hydrogen embrittlement, but underaging is detrimental to resistance.

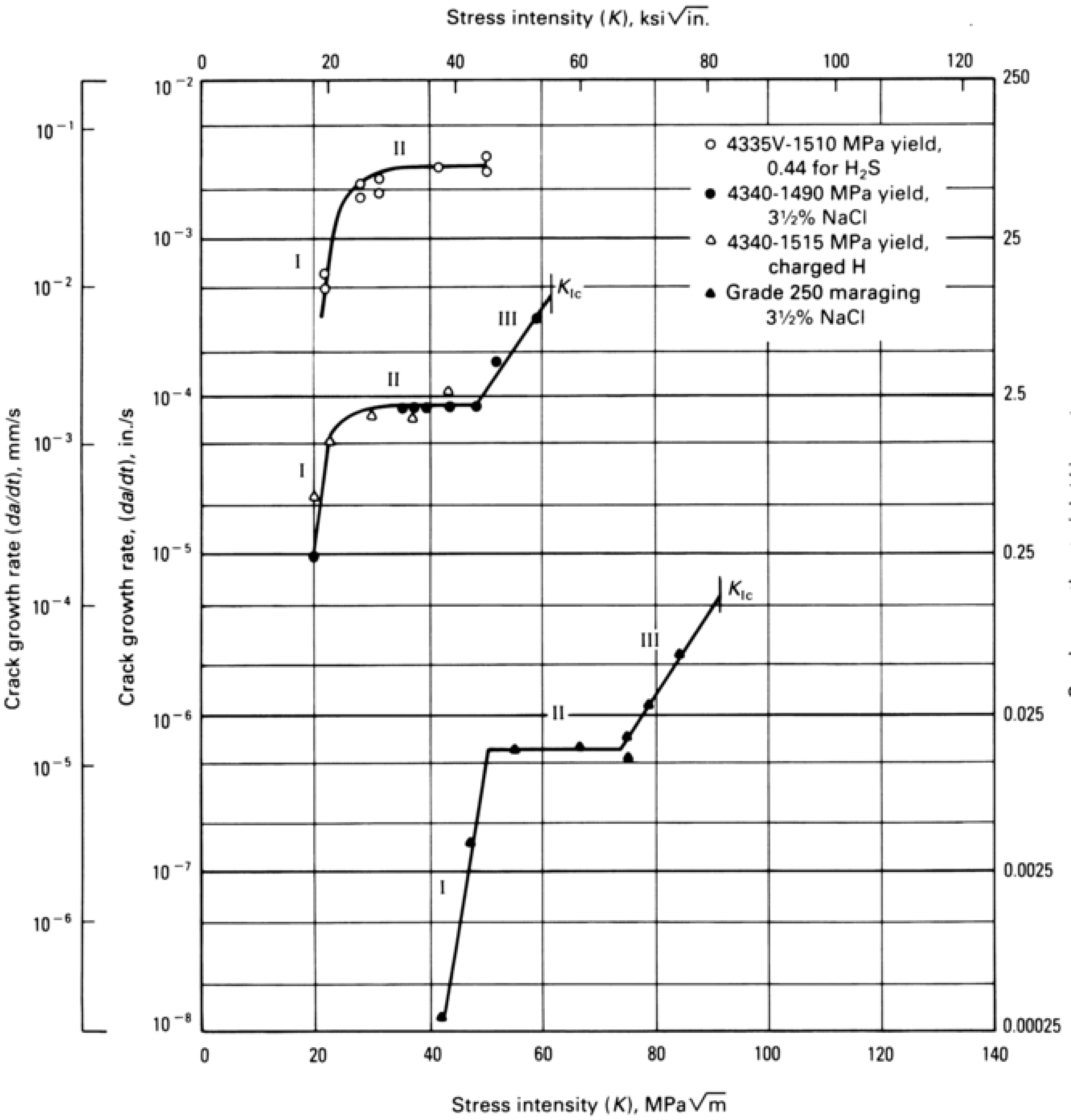

Fig. 13 Effect of material, environment, and stress-intensity level on crack growth. Source: Ref 12

Hydrogen attack is strictly a high-temperature form of hydrogen damage that primarily affects ferritic steels. Hydrogen attack is dependent on time, temperature, and hydrogen pressure. After a certain incubation time, a diminution of properties occurs with the onset of decarburization and cracking (Fig. 14). Resistance of steels to hydrogen attack is related to the stability of the carbides, and as such, the addition of carbide- stabilizing elements such as vanadium, titanium, niobium, and molybdenum enhance the resistance to this form of hydrogen damage.

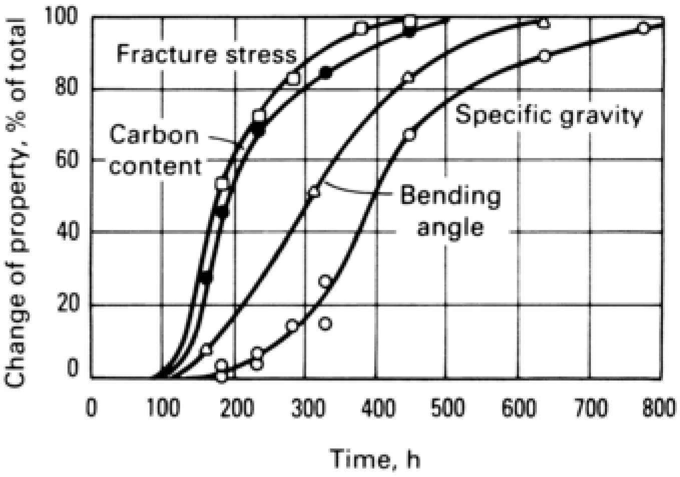

Fig. 14 Relative change of properties of a Society of Automotive Engineers (SAE) 1020 steel as a function of time of exposure to hydrogen at 427 °C (800 °F) and 6.2 MPa (900 psi) partial pressure. Source: Ref 10

Chromium-molybdenum steels have been found to be the most resistant to hydrogen attack for the cost involved; therefore, a great deal of industrial experience has been gained with these alloys. Much of this experience has been compiled and plotted to provide a guideline for steel selection as a function of temperature and hydrogen partial pressure and is presented as a series of curves often referred to as a Nelson diagram (Ref 26). As more experience is gathered on the use of these steels in hydrogen, this series of curves is periodically updated by the American Petroleum Institute.

References cited in this section

4. A.R. Troiano, The Role of Hydrogen and Other Interstitials in the Mechanical Behavior of Metals, *Trans. ASM,* Vol 52, 1960, p 57

10. F.H. Vitovec, Modeling of Hydrogen Attack of Steel in Relation to Material and Environmental Variables, *Current Solutions to Hydrogen Problems in Steels,* C.G. Interrante and G.M. Pressouyre, Ed., American Society for Metals, 1982

12. W.W. Gerberich, Effect of Hydrogen on High Strength and Martensitic Steels, *Hydrogen in Metals,* I.M. Bernstein and A.W. Thompson, Ed., American Society for Metals, 1974, p 115

14. H.G. Nelson and D.P. Williams, Quantitative Observations of Hydrogen Induced Slow Crack Growth in a Low Alloy Steel, *Stress Corrosion Cracking and Hydrogen Embrittlement of Iron Base Alloys,* National Association of Corrosion Engineers, 1977, p 390

15. B.A. Graville, R.G. Baker, and F. Watkinson, *Br. Weld. J.,* Vol 14, 1967, p 337

16. R.P. Gangloff, A Review and Analysis of the Threshold for Hydrogen Environment Embrittlement of Steel, *Corrosion Prevention and Control, Proc. 33rd Sagamore Army Materials Research Conf.* (MA), U.S. Army Materials Technology Laboratory, 1986

17. P. McIntyre, The Relationship Between Stress Corrosion Cracking and Sub Critical Flaw Growth in Hydrogen and Hydrogen Sulphide Gases, *Stress Corrosion Cracking and Hydrogen Embrittlement of Iron Base Alloys,* National Association of Corrosion Engineers, 1977, p 788

18. A. Ikeda, "Progress on the Metallurgical Investigation of HIC Phenomena and Development of HIC Resistant Steel," Second International Conf. on Interaction of Steels with Hydrogen in Petroleum Industry Pressure Vessel and Pipeline Service, 19 Oct 1994 (Vienna)

19. “Guidelines on Materials Requirements for Carbon Steels and Low Alloy Steels for H_2S Containing Environments in Oil and Gas Production,” European Federation of Corrosion Publication 16, Institute of Materials, London, 1995

20. R.P.M. Procter and H.W. Paxton, *Trans. ASM,* Vol 62, 1969, p 989

21. A.W. Thompson, “Hydrogen Embrittlement of Stainless Steels and Carbon Steels,” paper presented at the midyear meeting (Toronto, Canada), American Petroleum Institute, 1978

22. T. Boellinghaus, H. Hoffmeister, and C. Middel, “Scatterbands for Hydrogen Diffusion in Steels Having a Ferritic or Martensitic Microstructure and Steels Having an Austenitic Microstructure at Room Temperature,” *Weld. World,* Vol 37 (No.1), 1996, p 16–23

23. A. Turnbull and R.B. Hutchings, “Analysis of Hydrogen Atom Transport in a Two- Phase Alloy, *Mater. Sci. Eng.,* A177, 1994, p 161–171

24. R.R. Gaugh, “Sulfide Stress Cracking of Precipitation Hardening Stainless Steels,” Paper 109, presented at Corrosion/77, National Association of Corrosion Engineers, 1977

25. T. Boellinghaus, H. Hoffmeister, and S. Dietrich, “Slow Strain Rate Testing of Low Carbon Martensitic Stainless Steels,” EuroCorr '97, Sept 1997 (Tondheim, Norway), Institute of Materials, London

26. “Steels for Hydrogen Service at Elevated Temperatures and Pressures in Petroleum Refineries and Petrochemical Plants,” Publication 941, 2nd ed., American Petroleum Institute, June 1977

B. Craig, Hydrogen Damage, *Corrosion: Fundamentals, Testing, and Protection,* Vol 13A, *ASM Handbook*, ASM International, 2003, p 367–380

Hydrogen Damage

Bruce Craig, MetCorr

Nickel Alloys

Nickel and its alloys are susceptible to hydrogen damage in both aqueous and gaseous hydrogen environments. The same factors that affect hydrogen embrittlement susceptibility in ferrous alloys are also prevalent in nickel alloys, although to a lesser degree. In general, fcc metals, because of their greater ease of slip and reduced solute diffusivities as compared to bcc materials, are less susceptible to hydrogen damage. As with ferrous alloys, hydrogen in nickel and its alloys may introduce intergranular, transgranular, or quasi-cleavage cracking, and although the macroscopic features appear to be brittle, on a microscopic scale there is a high degree of local plasticity, suggesting that hydrogen enhances flow at the crack tip. Figure 15 shows the reduction in ductility associated with hydrogen charging a 72Ni-28Fe alloy as a function of strain rate. Almost identical behavior was observed for unalloyed nickel.

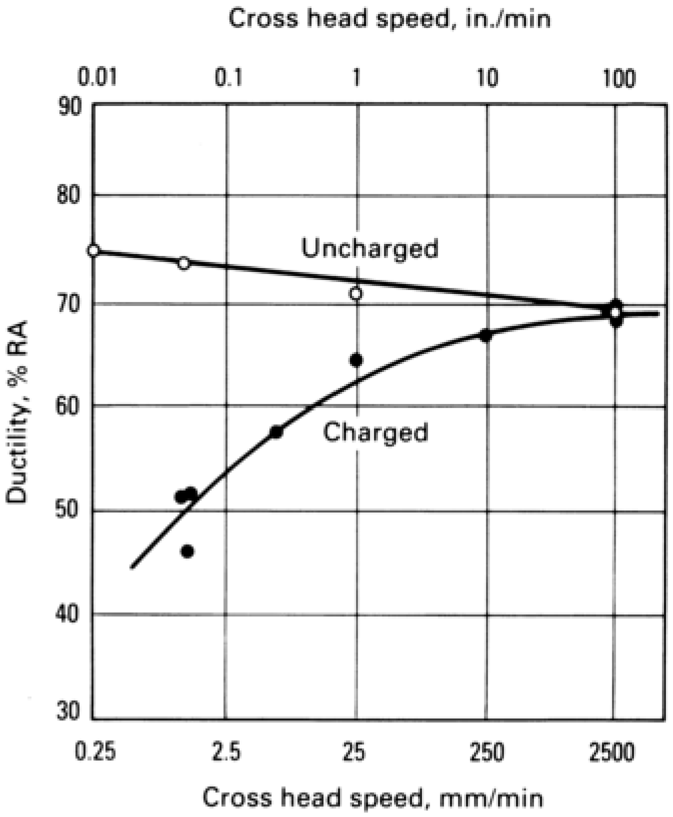

Fig. 15 Ductility at fracture as a function of strain rate in a hydrogen-charged and uncharged 72Ni-28Fe alloy. RA, reduction in area. Source: Ref 4

Alloys based on the ternary Fe-Ni-Cr system (Incoloy) and Inconel alloys show reductions in ductility when charged with hydrogen, depending on the specific thermomechanical treatments performed on the alloy. Generally, these alloys are more resistant to hydrogen stress cracking in the cold-worked and unaged condition as compared to the cold-worked and aged condition. Age-hardenable alloys show the least resistance to hydrogen when aged to their peak or near- peak strength. Stabilization treatments followed by aging reduce the resistance of these alloys as compared to direct aging. Increased cold work also produces a loss in tensile ductility. Hydrogen stress cracking of these alloys may also occur, rather than a loss in tensile ductility, when they possess high yield strengths or are under high hydrogen fugacity. The nickel-copper alloys (Monels) have also been found to be susceptible to hydrogen embrittlement, with increasing strength obtained by cold working or aging.

Figure 16 is a good comparison of the effect of hydrogen on the threshold cracking behavior of several stainless steels and nickel alloys (Ref 27). It is interesting to note that there is not an obvious distinction between single-phase alloy resistance and that of multiphase alloys. For example, the single-phase alloy 625 performs much the same as the precipitation-hardening alloy 718. Likewise, the single-phase alloy 310 is not significantly different from the age-hardening alloy A286. The significant reductions in the threshold stress-intensity factor (K_{th}) for types 301 and 304 are attributable to the strain-induced transformation to martensite in these alloys.

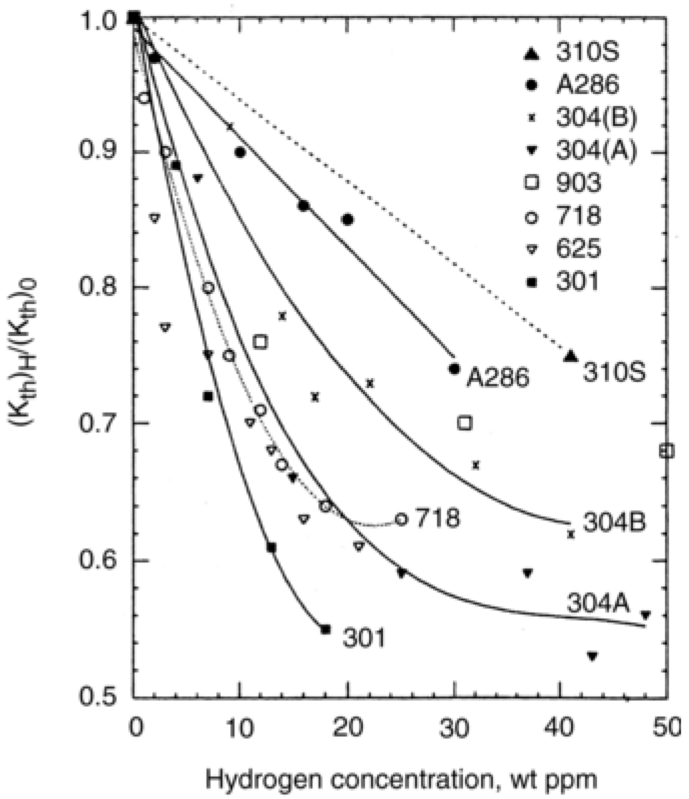

Fig. 16 Effect of hydrogen on the threshold stress intensity for crack propagation, normalized against the hydrogen-free values. Ref 27

Several nickel-base alloys are resistant to hydrogen stress cracking when cold worked to yield strengths in excess of 1240 MPa (180 ksi). However, when these alloys (Hastelloy alloy C- 276, Hastelloy alloy C-4, and Inconel alloy 625) are aged at low temperature, their resistance to hydrogen cracking is considerably diminished. This behavior is attributed to the segregation of phosphorus and sulfur to grain boundaries, which provide low-energy fracture paths (much the same as occurs in high-strength steels), or to an ordering reaction of the form $Ni_2(Cr, Mo)$. Figure 17 presents data that relate the reduction in area loss to ordering for the ordering alloy Ni_2Cr charged with hydrogen.

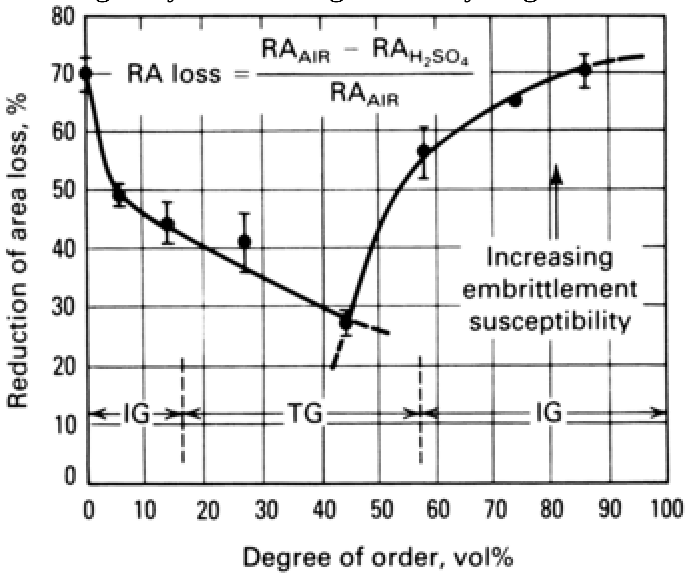

Fig. 17 Effect of the degree of order on the embrittlement susceptibility of Ni_2Cr. Regions of intergranular (IG) and ductile transgranular fracture (TG) are shown. RA, reduction of area. Source: Ref 28

References cited in this section

4. A.R. Troiano, The Role of Hydrogen and Other Interstitials in the Mechanical Behavior of Metals, *Trans. ASM*, Vol 52, 1960, p 57

27. P.D. Hicks and C.J. Altstetter, "Hydrogen- Enhanced Cracking of Superalloys," *Metall. Trans. A*, Vol 32, 1992, p 237–248

28. B.J. Berkowitz, M. Kurkela, and R.M. Latanision, Effect of Ordering on the Hydrogen Permeation and Embrittlement of Ni_2Cr, *Hydrogen Effects in Metals*, I.M. Bernstein and A.W. Thompson, Ed., American Society for Metals, 1981, p 411

B. Craig, Hydrogen Damage, *Corrosion: Fundamentals, Testing, and Protection*, Vol 13A, *ASM Handbook*, ASM International, 2003, p 367–380

Hydrogen Damage

Bruce Craig, MetCorr

Aluminum Alloys

Only recently has it been determined that hydrogen embrittles aluminum. For many years, all environmental cracking of aluminum and its alloys was represented as SCC; however, testing in specific hydrogen environments has revealed the susceptibility of aluminum to hydrogen damage. Hydrogen damage in aluminum alloys may take the form of intergranular or transgranular cracking or blistering. Blistering is most often associated with the melting or heat treatment of aluminum, where reaction with water vapor produces hydrogen. Blistering due to hydrogen is frequently associated with grain-boundary precipitates or the formation of small voids. Blister formation in aluminum is different from that in ferrous alloys in that it is more common to form a multitude of near-surface voids that coalesce to produce a large blister.

In a manner similar to the mechanism in iron- base alloys, hydrogen diffuses into the aluminum lattice and collects at internal defects. This occurs most frequently during annealing or solution treating in air furnaces prior to age hardening.

Dry hydrogen gas is not detrimental to aluminum alloys; however, with the addition of water vapor, subcritical crack growth increases dramatically (Fig. 18). The threshold stress intensity for cracking of aluminum also decreases significantly in the presence of humid hydrogen gas at ambient temperature (Fig. 19).

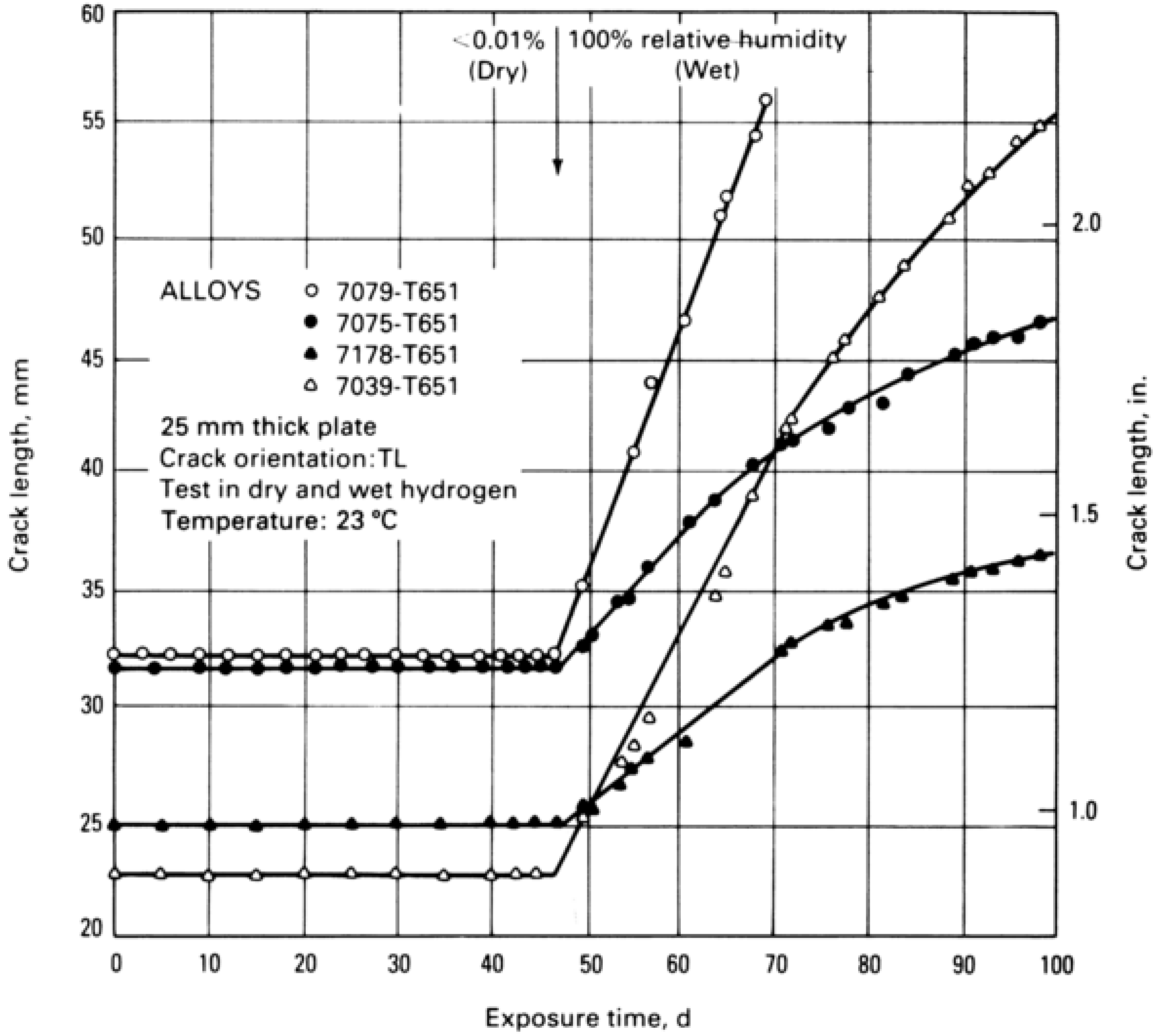

Fig. 18 Effect of humidity on subcritical crack growth of high-strength aluminum alloys in hydrogen gas. Source: Ref 29

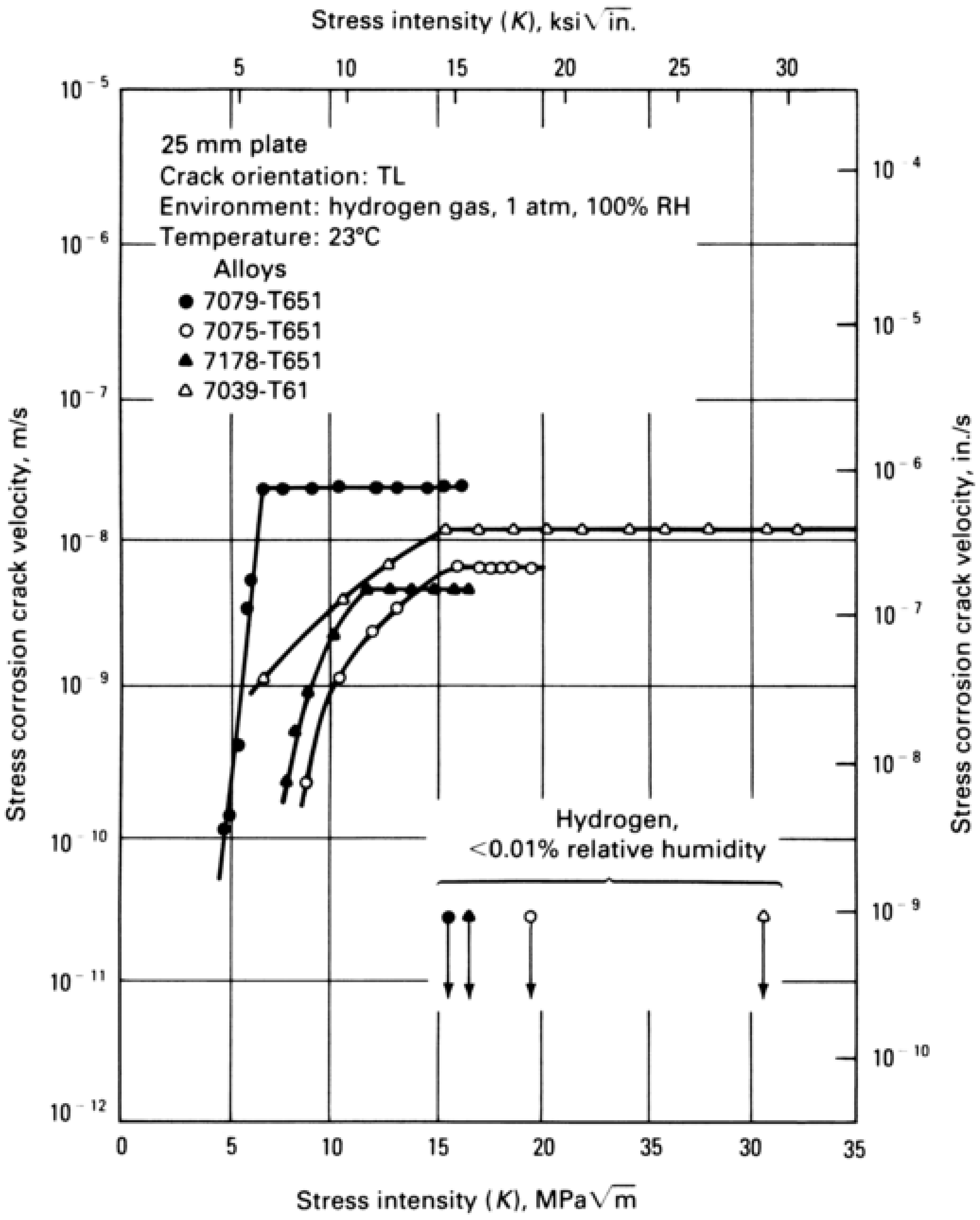

Fig. 19 Crack velocity of four high-strength aluminum alloys plotted as a function of crack-tip stress intensity in moist and dry hydrogen gas. Source: Ref 29

Crack growth in aluminum in hydrogen is also a function of hydrogen permeability, as in the iron-and nickel-base alloys. Hydrogen permeation and the crack growth rate are a function of potential, increasing with more negative potentials, as expected for hydrogen embrittlement behavior. Similarly, the ductility of aluminum alloys in hydrogen is temperature dependent, displaying a minimum in reduction in area below 0 °C (32 °F); this is similar to other fcc alloys (Ref 29).

Most of the work on hydrogen embrittlement of aluminum alloys has been on the 7000 series (Al-Zn-Mg); therefore, the full extent of hydrogen damage in aluminum alloys has not been determined or the mechanisms established. Some evidence for a metastable aluminum hydride has been found that would explain the brittle intergranular fracture of aluminum-zinc-magnesium alloys in water vapor. However, the instability of the hydride is such that is has been difficult to evaluate. Another explanation for intergranular fracture of these alloys is preferential decohesion of grain boundaries containing segregated magnesium. Overaging of these alloys increases their resistance to hydrogen embrittlement in much the same way as for highly tempered martensitic steels.

Reference cited in this section

29. M.O. Speidel, Hydrogen Embrittlement of Aluminum Alloys, *Hydrogen in Metals,* I.M. Bernstein and A.W. Thompson, Ed., American Society for Metals, 1974

B. Craig, Hydrogen Damage, *Corrosion: Fundamentals, Testing, and Protection*, Vol 13A, *ASM Handbook*, ASM International, 2003, p 367–380

Hydrogen Damage

Bruce Craig, MetCorr

Copper Alloys

A common form of hydrogen damage in copper has been known for years as steam embrittlement and is observed only when copper contains oxygen. Hydrogen entering the metal reacts with oxygen either in solid solution or at oxide inclusions to form water. At temperatures above the critical temperature for water, steam forms, and the pressure generated is sufficient to produce microcavity formation and cracking. The equation for reaction with cuprous oxide particles is $Cu_2O + 2H = 2Cu + H_2O(g)$. The circumstances under which this form of hydrogen damage occurs are typically related to the annealing of copper in a hydrogen atmosphere. At lower temperatures, steam is not generated and therefore does not create the problem. Although the use of oxygen-free copper essentially eliminates susceptibility to steam embrittlement, the heavy cold working of oxygen-free copper can result in grain-boundary void formation when hydrogen is introduced.

Compared to the ferrous and nickel alloys, relatively little work has been performed specific to the hydrogen embrittlement of copper-base alloys. There is some indication that age-hardenable alloys such as beryllium-copper are susceptible to embrittlement under severe charging conditions, producing a loss in tensile ductility. A systematic study of these alloys remains to be performed.

B. Craig, Hydrogen Damage, *Corrosion: Fundamentals, Testing, and Protection*, Vol 13A, *ASM Handbook*, ASM International, 2003, p 367–380

Hydrogen Damage

Bruce Craig, MetCorr

Titanium Alloys

Titanium and its alloys suffer hydrogen damage primarily by hydride-phase formation. Pure α-titanium is relatively unaffected by small concentrations (<200 ppm) of hydrogen; however, above this content, the impact toughness is impaired. The purity of the α-titanium is important to its behavior in hydrogen. Commercially pure titanium is much more sensitive to hydrogen than pure titanium is. The amount of hydrogen necessary to induce ductile-to-brittle transition behavior in commercially pure titanium is one- half the amount needed in pure titanium.

Loss in impact toughness also occurs in α/β- titanium and β-titanium alloys and is sometimes referred to as impact embrittlement. This hydrogen damage at high strain rates is the result of hydrides that precipitate after the high-temperature exposure of titanium to hydrogen.

Another mode of failure for titanium alloys in hydrogen predominates under slow strain-rate loading. Figure 20 shows the strain-rate behavior for an α/β alloy. As the strain rate increases, the effect of hydrogen is lost. As in steels, the reduction in area and the elongation of titanium alloys are diminished in hydrogen.

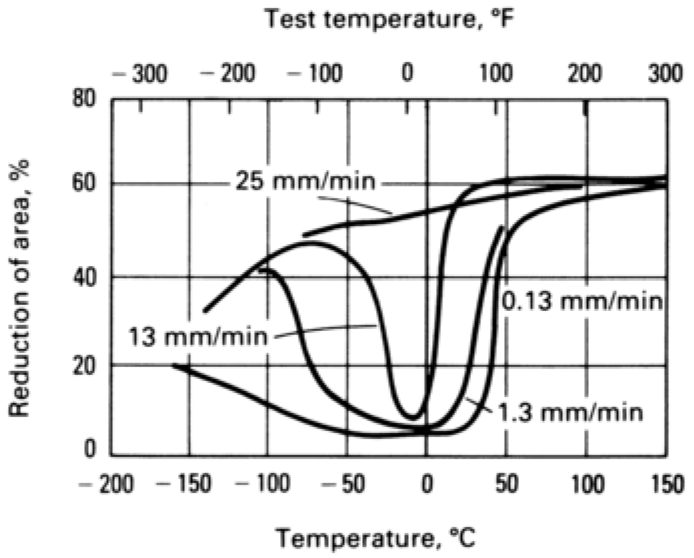

Fig. 20 Effects of hydrogen content (375 ppm), strain rate, and temperature on the tensile ductility of typical α/β-titanium alloy unnotched tensile specimens. Source: Ref 30

Both types of failure for titanium alloys in hydrogen are attributed to hydride-phase precipitation. The low strain-rate embrittlement is related to hydride formation caused by strain- enhanced precipitation, but embrittlement under impact is caused by hydride-phase formation after fabrication or heat treatment. Unlike many hydride-forming systems, titanium forms a stable hydride, but the kinetics of precipitation are slow compared to the Group Vb metals. Therefore, embrittlement is more prone to occur at low strain rates at which precipitation can proceed at a rate that is sufficient to provide a brittle crack path.

Because hydrogen solubility increases with temperature for these alloys, hydride embrittlement typically decreases as the temperature increases. Additionally, at higher temperatures, the hydride may become more ductile, reducing brittle crack initiation. As expected, the threshold stress intensity for crack propagation is also a function of the hydrogen content decreasing with increasing hydrogen.

The role of microstructure in the hydrogen damage of titanium is quite complex and is not fully understood. However, it has been determined that under slow strain rates, the α/β alloys fail by intergranular separation along boundaries but that completely α-alloys fracture by transgranular cleavage. Embrittlement is not as severe in α/β alloys with a continuous equiaxed α matrix as for those alloys with a continuous acicular β-matrix (Ref 31). However, this behavior is a function of hydrogen pressure and may be reversed at lower pressures (Ref 32).

References cited in this section

30. D.N. Williams, The Hydrogen Embrittlement of Titanium Alloys, *J. Inst. Met.,* Vol 91, 1963

31. H.G. Nelson, D.P. Williams, and J.E. Stein, Environmental Hydrogen Embrittlement of an α-β Titanium Alloy: Effect of Microstructure, *Hydrogen Damage,* C.D. Beachem, Ed., American Society for Metals, 1977

32. H.G. Nelson, in *Hydrogen in Metals,* I.M. Bernstein and A.W. Thompson, Ed., American Society for Metals, 1974, p 445

B. Craig, Hydrogen Damage, *Corrosion: Fundamentals, Testing, and Protection*, Vol 13A, *ASM Handbook*, ASM International, 2003, p 367–380

Hydrogen Damage

Bruce Craig, MetCorr

Zirconium Alloys

Zirconium and its alloys suffer hydrogen damage by hydride precipitation, especially in the presence of notches or at low temperatures in smooth specimens. Failure occurs by cracking of the brittle, precipitated hydride phase during straining. These fractured hydrides may then accelerate fracture by ductile microvoid formation and coalescence, primarily enhancing the latter. Similar to titanium, zirconium alloys precipitate stable hydrides. Depending on the hydrogen content of the alloy, one of two stable or one metastable hydride(s) may precipitate. The two stable zirconium hydrides are δ-hydride (fcc) and ε- hydride (face-centered tetragonal, or fct). The metastable gamma-hydride also has a fct structure (Ref 33).

As in other alloy systems, the tensile ductility generally diminishes with increasing hydrogen content (Fig. 21). Similarly, the hydrogen embrittlement of these alloys is dependent on stress state, becoming more pronounced as the stress state moves from uniaxial to biaxial to triaxial tension. For example, the local stress state ahead of a sharp notch can produce a region of biaxial or triaxial stress, thus increasing the susceptibility to hydrogen embrittlement.

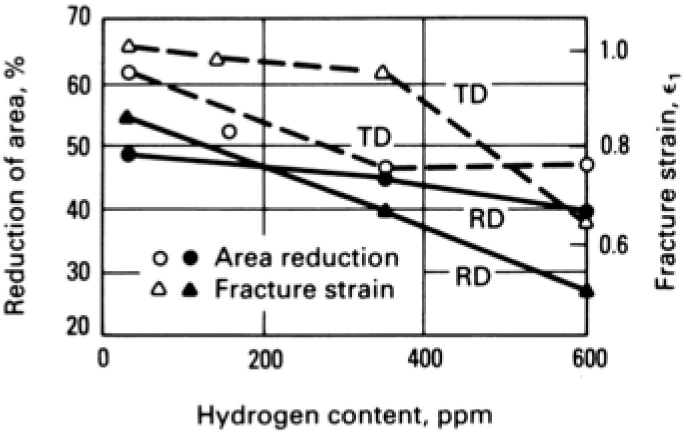

Fig. 21 Influence of hydrogen on the reduction of area at fracture and the true strain at fracture for Zircaloy-2. TD transverse direction; RD, rolling direction. Source: Ref 34

The embrittlement by zirconium hydride formation is a strong function of temperature, because increasing the temperature reduces the volume fraction of hydride due to the increased solid solubility of hydrogen with temperature. Ductile-to-brittle transition behavior has been observed in hydrided zirconium alloys, and the transition temperature has been found to be a function of hydrogen content, increasing with hydrogen concentration (Fig. 22).

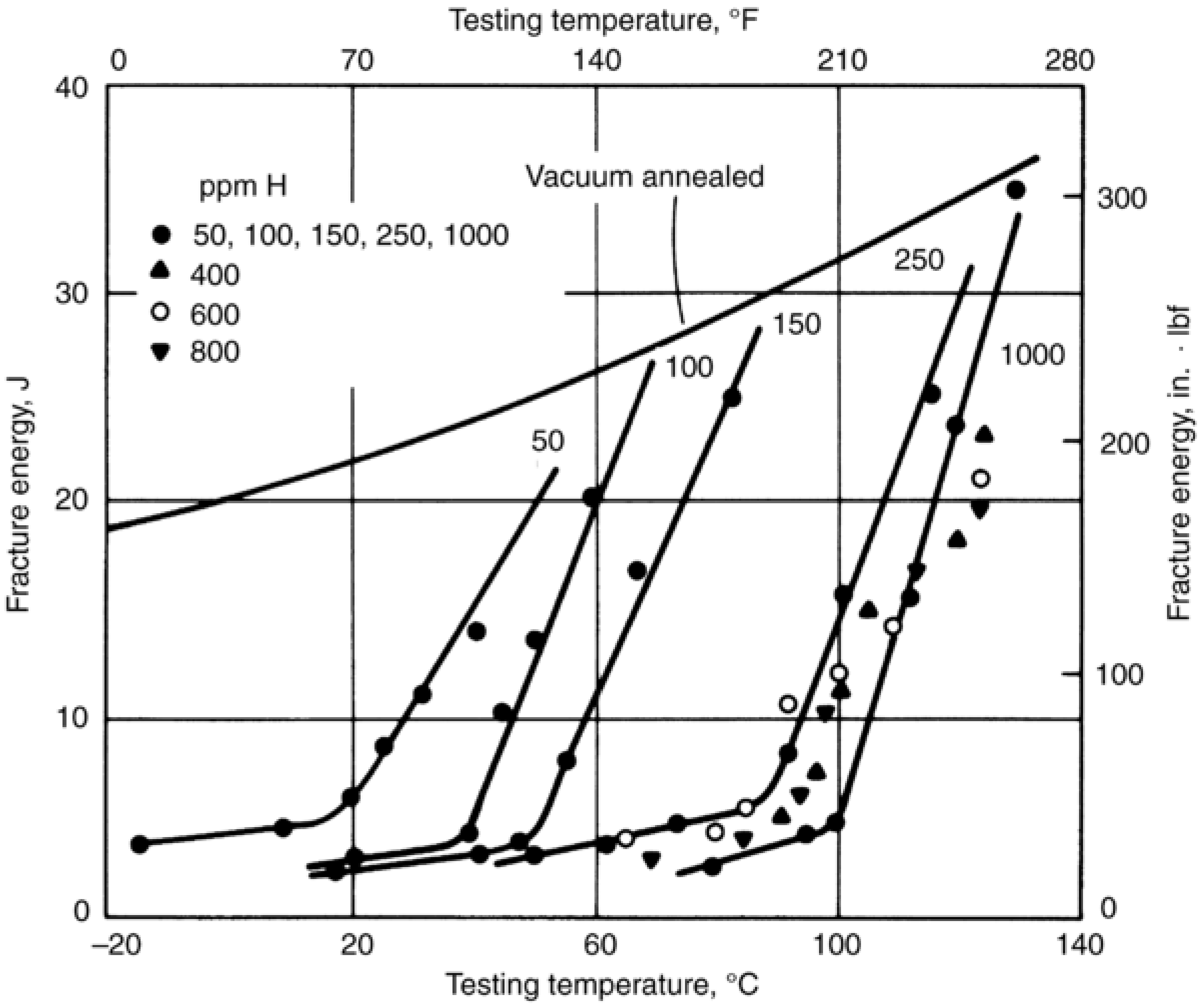

Fig. 22 Ductile-to-brittle transitions in hydrided zirconium. Source: Ref 35

Hydride distribution and morphology are other important factors in the extent of hydrogen damage in zirconium alloys. Because the brittle hydride phase provides an easy crack path for fracture, the distribution and morphology of this phase in relation to the sense of the applied tensile stress determine the degree of embrittlement. The shape and distribution of the hydrides are dependent on heat treatment prior to precipitation and cooling rate during precipitation. Rapid cooling produces a more uniform dispersion of hydrides, while slow cooling enhances the grain- boundary precipitation of the hydride platelets. Toughness is not as dramatically affected in the former case as in the latter.

References cited in this section

33. D. Northwood and U. Kosasih, Hydrides and Delayed Hydrogen Cracking in Zirconium and Its Alloys, *Int. Met. Rev.,* Vol 28, 1983, p 92

34. F. Yunchang and D.A. Koss, The Influence of Multiaxial States of Stress on the Hydrogen Embrittlement of Zirconium Alloy Sheet, *Metall. Trans. A,* Vol 16, 1985, p 675

35. D. Hardie, *J. Nucl. Mater.,* Vol 42, 1972, p 317

B. Craig, Hydrogen Damage, *Corrosion: Fundamentals, Testing, and Protection*, Vol 13A, *ASM Handbook*, ASM International, 2003, p 367–380

Hydrogen Damage

Bruce Craig, MetCorr

Vanadium, Niobium, Tantalum, and Their Alloys

These metals and alloys are all embrittled by hydrogen—primarily by hydride-phase formation; however, unlike titanium and zirconium alloys, these systems do not form a stable hydride. The introduction of hydrogen into unalloyed vanadium, niobium, and tantalum increases the yield strength of these metals and creates ductile-to-brittle transition behavior (Fig. 23).

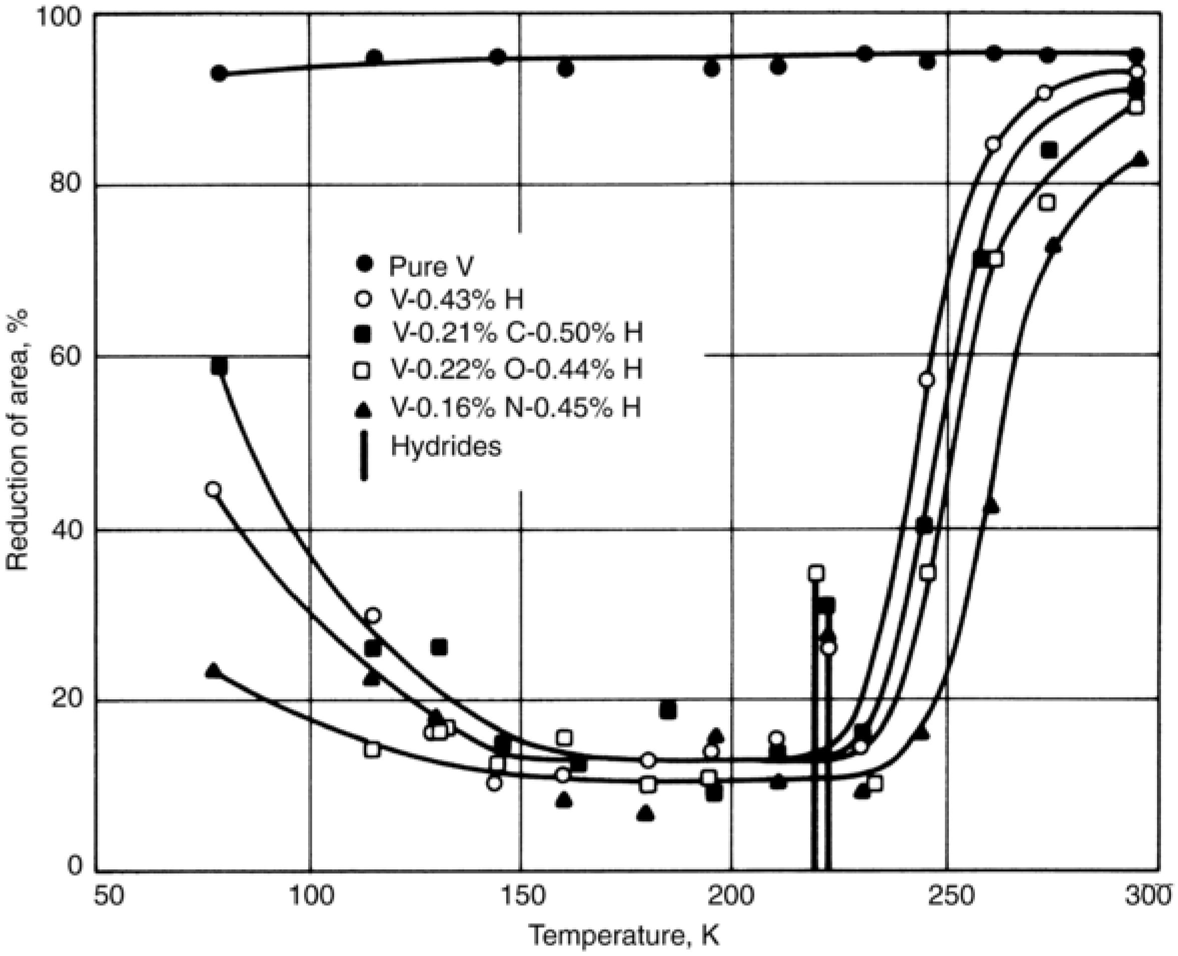

Fig. 23 Effect of hydrogen and combined carbon, nitrogen, or oxygen and hydrogen on the temperature dependence of ductility in vanadium. Source: Ref 36

Many of these alloy systems display ductile- to-brittle transition behavior in the presence of hydrogen in much the same manner as that described for zirconium and titanium. However, these alloys have been found to exhibit grain- boundary cracking when low levels of hydrogen are present in solid solution below the terminal solid-solubility limit. In fact, all of the hydride- forming systems exhibit hydrogen damage from solute hydrogen at low concentrations of hydrogen at which hydrides are not expected to precipitate. Although fracture transition is correlated with hydride formation in vanadium, other systems, such a niobium, zirconium, titanium, and tantalum, display more classical hydrogen embrittlement without a corresponding hydride- phase precipitation (Ref 33, 36).

Once the hydrogen content exceeds terminal solid solubility, damage may proceed by hydride precipitate formation. Below this solubility limit, the relative resistance to cracking or loss in tensile ductility is largely a function of the hydrogen concentration and alloying elements (Fig. 24). However, the terminal solid solubility for a particular metal-hydrogen system that forms hydrides is an extremely strong function of stress, so that reference to stress-free equilibrium phase diagrams for predicting hydride-phase behavior may be inaccurate (Ref 38).

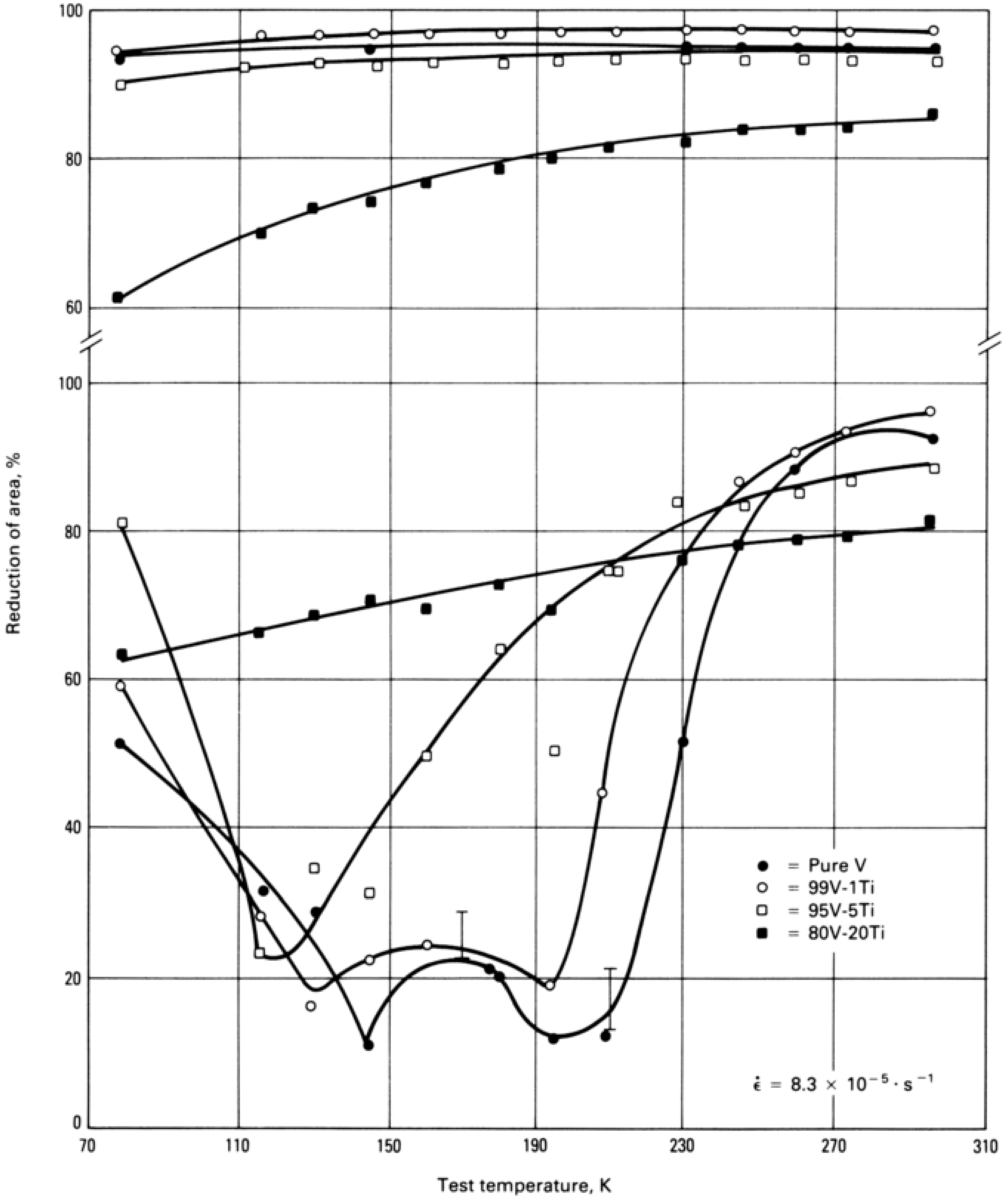

Fig. 24 Temperature dependence of reduction of area for selected hydrogen-charged (bottom) and uncharged (top) vanadium-titanium alloys. Source: Ref 37

There are many other metals and alloys that form hydrides (for example, thorium, uranium, and beryllium), but far less is known about these systems. Therefore, a great deal of investigation into the metal-hydrogen interactions in many alloy systems remains to be done, especially considering the trend in new materials for advanced technologies.

References cited in this section

33. D. Northwood and U. Kosasih, Hydrides and Delayed Hydrogen Cracking in Zirconium and Its Alloys, *Int. Met. Rev.,* Vol 28, 1983, p 92

36. W.A. Spitzig, C.V. Owen, and T.E. Scott, The Effects of Interstitials and Hydrogen Interstitial Interactions on Low Temperature Hardening and Embrittlement in V, Nb, and Ta, *Metall. Trans. A,* Vol 17, 1986, p 1179

37. C.V. Owen, T.J. Rowland, and O. Buck, Effects of Hydrogen on Some Mechanical Properties of Vanadium-Titanium Alloys, *Metall. Trans. A,* Vol 16, 1985, p 59

38. H.K. Birnbaum, Hydrogen Related Second Phase Embrittlement of Solids, *Hydrogen Embrittlement and Stress Corrosion Cracking,* American Society for Metals, 1984, p 153–177

B. Craig, Hydrogen Damage, *Corrosion: Fundamentals, Testing, and Protection*, Vol 13A, *ASM Handbook*, ASM International, 2003, p 367–380

Hydrogen Damage

Bruce Craig, MetCorr

Intermetallic Compounds

Since the late 1980s, there has been a significant effort to understand the behavior of intermetallic compounds when exposed to hydrogen- bearing environments. An excellent review of the subject is presented in Ref 39. Table 3, taken from that review, indicates that essentially all of the intermetallic compounds are embrittled by hydrogen.

Table 3 Intermetallic compounds embrittled by moisture or hydrogen at ambient temperature

Alloy	Agent	Crystal structure[a]
Ni_3(Al,Ti) single crystal	Moisture	$L1_2$
Ni_3Al + B	Moisture	$L1_2$
Ni_3Al + Be	Moisture	$L1_2$
Ni_3(Al,Mn)	Moisture	$L1_2$
Ni_3Si	Moisture	$L1_2$
Ni_3(Si,Ti)	Moisture	$L1_2$
Ni_3(Si,Ti) + B	Hydrogen	$L1_2$
$(Co,Fe)_3V$	Moisture	$L1_2$
Ni_3Fe	Hydrogen	$L1_2$
FeAl	Moisture	B2
Fe_3Al	Moisture	DO_3

(a) $L1_2$, ordered face-centered cubic; B2 and DO_3, body-centered cubic forms. Source: Ref 39

This hydrogen embrittlement occurs either by contact with hydrogen-containing environments or from direct hydrogen charging. Even exposure to moisture can induce hydrogen damage in some of these compounds. Moreover, many of these alloys are compromised by hydrogen regardless of whether they are in the ordered or disordered condition. Just as with conventional metallic alloys, intermetallic compounds that fail from hydrogen damage can demonstrate intergranular and transgranular cracking, cleavage, and formation of brittle hydrides. Likewise, factors such as composition, microstructure, temperature, and strain rate are important to these alloys and their behavior in hydrogen, as they are in metallic alloys.

Reference cited in this section

39. N.S. Stoloff, Environmental Embrittlement of Nickel-Based and Iron-Based Intermetallics, *Environmental Effects on Engineered Materials,* R.H. Jones, Ed., Marcel Dekker, 2001, p 275

B. Craig, Hydrogen Damage, *Corrosion: Fundamentals, Testing, and Protection*, Vol 13A, *ASM Handbook*, ASM International, 2003, p 367–380

Hydrogen Damage

Bruce Craig, MetCorr

References

1. J.P. Hirth and H.H. Johnson, Hydrogen Problems in Energy Related Technology, *Corrosion,* Vol 32, 1976, p 3
2. C. Zapffe and C. Sims, Hydrogen Embrittlement, Internal Stress and Defects in Steel, *Trans. AIME,* Vol 145, 1941, p 225
3. N.J. Petch and P. Stables, Delayed Fracture of Metals Under Static Load, *Nature,* Vol 169, 1952, p 842
4. A.R. Troiano, The Role of Hydrogen and Other Interstitials in the Mechanical Behavior of Metals, *Trans. ASM,* Vol 52, 1960, p 57
5. R.A. Oriani, A Mechanistic Theory of Hydrogen Embrittlement of Steels, *Bunsen-Gesellschaft Phys. Chemie,* Vol 76, 1972, p 848
6. J.F. Knott, Fracture Toughness and Hydrogen Assisted Crack Growth in Engineering Alloys, *Hydrogen Effects in Materials,* A.W. Thompson and N.R. Moody, Ed., TMS, 1996, p 387
7. C.D. Beachem, A New Model for Hydrogen Assisted Cracking (Hydrogen Embrittlement), *Metall. Trans.,* Vol 3, 1972, p 437
8. J.P. Hirth, The Role of Hydrogen in Enhancing Plastic Instability and Degrading Fracture Toughness of Steels, *Hydrogen Effects in Materials,* A.W. Thompson and N.R. Moody, Ed., TMS, 1996, p 507
9. S. Gahr, M.L. Grossbech, and H.K. Birnbaum, *Acta Metall.,* Vol 25, 1977, p 125
10. F.H. Vitovec, Modeling of Hydrogen Attack of Steel in Relation to Material and Environmental Variables, *Current Solutions to Hydrogen Problems in Steels,* C.G. Interrante and G.M. Pressouyre, Ed., American Society for Metals, 1982

11. G.M. Pressouyre and I.M. Bernstein, A Quantitative Analysis of Hydrogen Trapping, *Metall. Trans. A,* Vol 9, 1978, p 1571

12. W.W. Gerberich, Effect of Hydrogen on High Strength and Martensitic Steels, *Hydrogen in Metals,* I.M. Bernstein and A.W. Thompson, Ed., American Society for Metals, 1974, p 115

13. G.M. Pressouyre, A Classification of Hydrogen Traps in Steel, *Metall. Trans. A,* Vol 10, 1979, p 1571

14. H.G. Nelson and D.P. Williams, Quantitative Observations of Hydrogen Induced Slow Crack Growth in a Low Alloy Steel, *Stress Corrosion Cracking and Hydrogen Embrittlement of Iron Base Alloys,* National Association of Corrosion Engineers, 1977, p 390

15. B.A. Graville, R.G. Baker, and F. Watkinson, *Br. Weld. J.,* Vol 14, 1967, p 337

16. R.P. Gangloff, A Review and Analysis of the Threshold for Hydrogen Environment Embrittlement of Steel, *Corrosion Prevention and Control, Proc. 33rd Sagamore Army Materials Research Conf.* (MA), U.S. Army Materials Technology Laboratory, 1986

17. P. McIntyre, The Relationship Between Stress Corrosion Cracking and Sub Critical Flaw Growth in Hydrogen and Hydrogen Sulphide Gases, *Stress Corrosion Cracking and Hydrogen Embrittlement of Iron Base Alloys,* National Association of Corrosion Engineers, 1977, p 788

18. A. Ikeda, "Progress on the Metallurgical Investigation of HIC Phenomena and Development of HIC Resistant Steel," Second International Conf. on Interaction of Steels with Hydrogen in Petroleum Industry Pressure Vessel and Pipeline Service, 19 Oct 1994 (Vienna)

19. "Guidelines on Materials Requirements for Carbon Steels and Low Alloy Steels for H_2S Containing Environments in Oil and Gas Production," European Federation of Corrosion Publication 16, Institute of Materials, London, 1995

20. R.P.M. Procter and H.W. Paxton, *Trans. ASM,* Vol 62, 1969, p 989

21. A.W. Thompson, "Hydrogen Embrittlement of Stainless Steels and Carbon Steels," paper presented at the midyear meeting (Toronto, Canada), American Petroleum Institute, 1978

22. T. Boellinghaus, H. Hoffmeister, and C. Middel, "Scatterbands for Hydrogen Diffusion in Steels Having a Ferritic or Martensitic Microstructure and Steels Having an Austenitic Microstructure at Room Temperature," *Weld. World,* Vol 37 (No.1), 1996, p 16–23

23. A. Turnbull and R.B. Hutchings, "Analysis of Hydrogen Atom Transport in a Two- Phase Alloy, *Mater. Sci. Eng.,* A177, 1994, p 161–171

24. R.R. Gaugh, "Sulfide Stress Cracking of Precipitation Hardening Stainless Steels," Paper 109, presented at Corrosion/77, National Association of Corrosion Engineers, 1977

25. T. Boellinghaus, H. Hoffmeister, and S. Dietrich, "Slow Strain Rate Testing of Low Carbon Martensitic Stainless Steels," EuroCorr '97, Sept 1997 (Tondheim, Norway), Institute of Materials, London

26. "Steels for Hydrogen Service at Elevated Temperatures and Pressures in Petroleum Refineries and Petrochemical Plants," Publication 941, 2nd ed., American Petroleum Institute, June 1977

27. P.D. Hicks and C.J. Altstetter, "Hydrogen- Enhanced Cracking of Superalloys," *Metall. Trans. A,* Vol 32, 1992, p 237–248

28. B.J. Berkowitz, M. Kurkela, and R.M. Latanision, Effect of Ordering on the Hydrogen Permeation and Embrittlement of Ni_2Cr, *Hydrogen Effects in Metals,* I.M. Bernstein and A.W. Thompson, Ed., American Society for Metals, 1981, p 411

29. M.O. Speidel, Hydrogen Embrittlement of Aluminum Alloys, *Hydrogen in Metals,* I.M. Bernstein and A.W. Thompson, Ed., American Society for Metals, 1974

30. D.N. Williams, The Hydrogen Embrittlement of Titanium Alloys, *J. Inst. Met.,* Vol 91, 1963

31. H.G. Nelson, D.P. Williams, and J.E. Stein, Environmental Hydrogen Embrittlement of an α-β Titanium Alloy: Effect of Microstructure, *Hydrogen Damage,* C.D. Beachem, Ed., American Society for Metals, 1977

32. H.G. Nelson, in *Hydrogen in Metals,* I.M. Bernstein and A.W. Thompson, Ed., American Society for Metals, 1974, p 445

33. D. Northwood and U. Kosasih, Hydrides and Delayed Hydrogen Cracking in Zirconium and Its Alloys, *Int. Met. Rev.,* Vol 28, 1983, p 92

34. F. Yunchang and D.A. Koss, The Influence of Multiaxial States of Stress on the Hydrogen Embrittlement of Zirconium Alloy Sheet, *Metall. Trans. A,* Vol 16, 1985, p 675

35. D. Hardie, *J. Nucl. Mater.,* Vol 42, 1972, p 317

36. W.A. Spitzig, C.V. Owen, and T.E. Scott, The Effects of Interstitials and Hydrogen Interstitial Interactions on Low Temperature Hardening and Embrittlement in V, Nb, and Ta, *Metall. Trans. A,* Vol 17, 1986, p 1179

37. C.V. Owen, T.J. Rowland, and O. Buck, Effects of Hydrogen on Some Mechanical Properties of Vanadium-Titanium Alloys, *Metall. Trans. A,* Vol 16, 1985, p 59

38. H.K. Birnbaum, Hydrogen Related Second Phase Embrittlement of Solids, *Hydrogen Embrittlement and Stress Corrosion Cracking,* American Society for Metals, 1984, p 153–177

39. N.S. Stoloff, Environmental Embrittlement of Nickel-Based and Iron-Based Intermetallics, *Environmental Effects on Engineered Materials,* R.H. Jones, Ed., Marcel Dekker, 2001, p 275

B. Craig, Hydrogen Damage, *Corrosion: Fundamentals, Testing, and Protection,* Vol 13A, *ASM Handbook,* ASM International, 2003, p 367–380

Hydrogen Damage

Bruce Craig, MetCorr

Selected References

- P. Azou, Ed., *Third International Congress on Hydrogen and Materials,* Pergamon Press, 1982
- C.D. Beachem, Ed., *Hydrogen Damage,* American Society for Metals, 1977
- I.M. Bernstein and A.W. Thompson, Ed., *Hydrogen in Metals,* American Society for Metals, 1972

- I.M. Bernstein and A.W. Thompson, Ed., *Hydrogen Effects in Metals,* American Institute of Mining, Metallurgical, and Petroleum Engineers, 1981
- T. Magnin, Ed., *Corrosion-Deformation Interactions CDI '96,* Institute of Materials, United Kingdom, 1997
- T. Magnin and J.M. Gras, Ed., *Corrosion-Deformation Interactions,* Les Editions de Physiques, Les Ulis, France, 1993
- N.R. Moody and A.W. Thompson, Ed., *Hydrogen Effects on Material Behavior,* TMS, 1990
- N.R. Moody, A.W. Thompson, R.E. Ricker, and G.S. Was, Ed., *Hydrogen Effects on Material Behavior and Corrosion Deformation Interactions,* TMS, to be published 2003
- Special Issue on Hydrogen Effects on Material Behavior, *Eng. Fract. Mechan.,* Vol 68, 2001
- R.W. Staehle et al., Ed., *Stress Corrosion Cracking and Hydrogen Embrittlement of Iron Base Alloys,* National Association of Corrosion Engineers, 1977
- A.W. Thompson and N.R. Moody, Ed., *Hydrogen Effects in Materials,* TMS/AIME, 1996

D.G. Kolman, Liquid Metal Induced Embrittlement, *Corrosion: Fundamentals, Testing, and Protection,* Vol 13A*, ASM Handbook*, ASM International, 2003, p 381–392

Liquid Metal Induced Embrittlement

Revised by David G. Kolman, Los Alamos National Laboratory

Introduction

LIQUID METAL INDUCED EMBRITTLEMENT (LMIE), also known as liquid metal embrittlement, is the reduction of the fracture resistance of a solid material during exposure to a liquid metal. References in the literature to liquid metal embrittlement were first made over 100 years ago (Ref 1). Commonly, LMIE is described as the catastrophic brittle failure of a normally ductile metal when coated with a thin film of a liquid metal and subsequently stressed in tension. The fracture mode typically changes from a ductile to a brittle intergranular or brittle transgranular (cleavage) mode; however, there is no change in the yield and flow behavior of the solid metal. As shown in Fig. 1, embrittlement manifests itself as a reduction in fracture stress, strain, or both. Fracture can occur well below the yield stress of the solid. The stress required to propagate a sharp crack or a flaw is significantly lower than that necessary to initiate a crack in the liquid metal environment. In most cases, the initiation or the propagation of cracks appears to occur instantaneously, with the fracture propagating through the entire test specimen. The velocity of crack or fracture propagation can be as large as 10 to 100 cm/s (4 to 40 in./s) (Ref 2, 3, 4, 5).

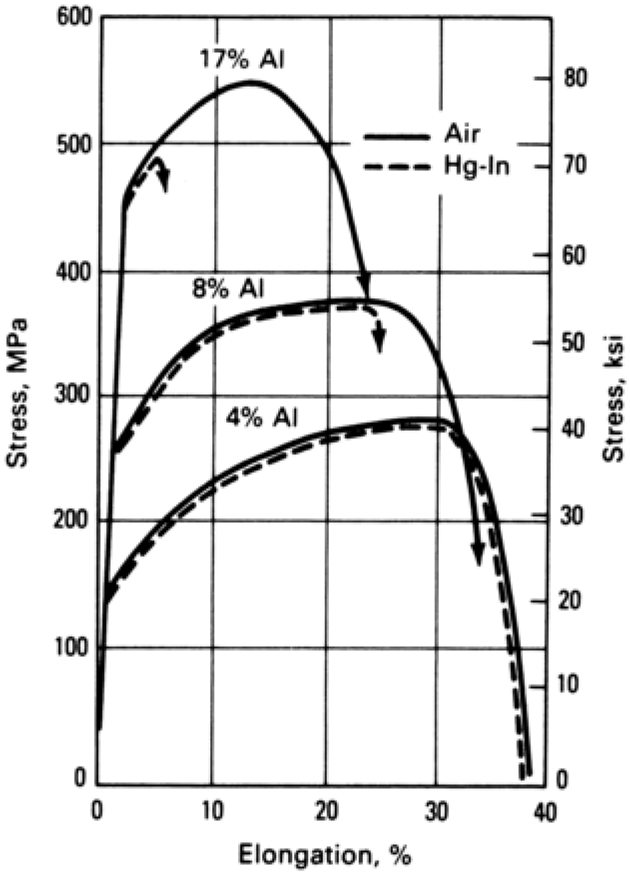

Fig. 1 Effects of environment on the yield stress and strain-hardening rate on various iron-aluminum alloys tested in air and mercury-indium solutions

Examination of LMIE fracture surfaces shows complete coverage by the liquid metal. Liquid metal is in intimate contact with the solid and is usually difficult to remove. The fracture mode becomes apparent when special techniques are used to remove the liquid (Ref 6). It should be emphasized that gross amounts of liquid are not necessary; even micrograms of liquid lead can cause LMIE in 75 mm (3 in.) thick steel tubes (Fig. 2). In fact, one monolayer is sufficient to cause LMIE (Ref 7). The fracture is usually brittle intergranular, with little indication of crack branching or striation to indicate slow crack propagation.

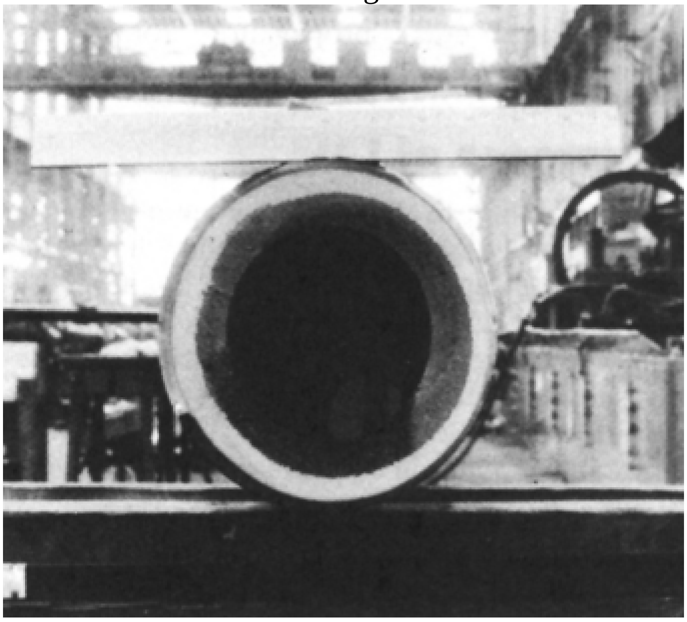

Fig. 2 Liquid lead induced brittle fracture of a 75 mm (3 in.) section of a 4340 steel pressure vessel tube

The presence of liquid at the moving crack tip appears necessary for fast fracture. However, in high-strength brittle metals, a crack initiated in the presence of liquid may propagate in a brittle manner in the absence of liquid. In low-strength metals, a transition may occur from brittle-to- ductile failure under similar circumstances. Although far less frequent than brittle fracture, embrittlement can also occur by a ductile dimpled rupture mode in certain steels, copper alloys, and aluminum alloys. The embrittlement then manifests itself as the degradation of the fracture properties of the solid metal. Fracture is not limited to polycrystalline metals and the presence of grain boundaries. Embrittlement of amorphous alloys (Ref 8, 9) and single crystals (Ref 10, 11) has been observed. Single crystals of zinc and cadmium exhibited brittle cleavage fracture as a result of LMIE (Fig. 3). These are but a few of the manifestations of LMIE.

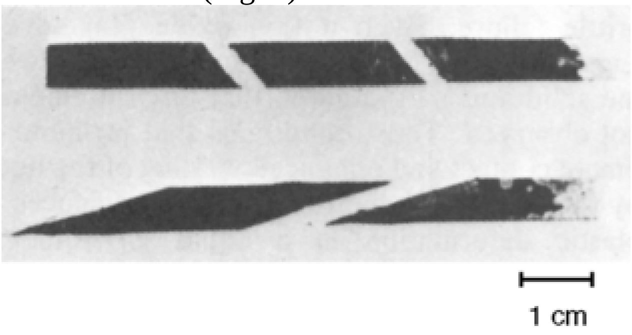

Fig. 3 Cleavage fracture of cadmium monocrystals at 25 °C (75 °F) following a coating with Hg-60In (at.%) solution

Embrittlement is not a corrosion, dissolution, or diffusion-controlled intergranular penetration process but is considered to be a special case of brittle fracture that occurs in the absence of an inert environment and at low temperatures. Time- and temperature-dependent processes are not considered to be responsible for the occurrence of LMIE. Also, in most cases of LMIE, little or no penetration of liquid metal into the solid metal is observed. The embrittlement of the solid metal coated with liquid metal or immersed in the liquid does not depend on the time of exposure to the liquid metal before testing (Fig. 4) or on whether the liquid is pure or presaturated with the solid. Usually, one of the prerequisites is that the solid has little or no solubility in the liquid and forms no intermetallic compound to constitute an embrittlement couple (Ref 12). However, exceptions to this empirical rule have been noted (Ref 72).

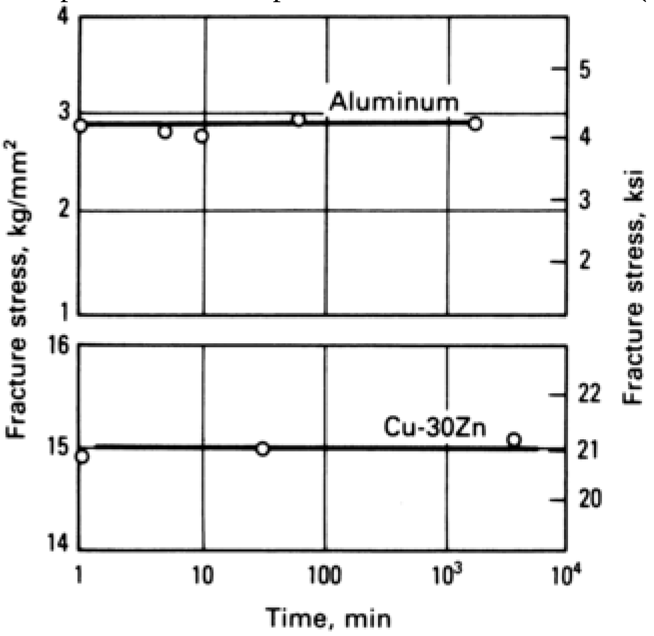

Fig. 4 Fracture stress of polycrystalline aluminum and Cu-30Zn brass as a function of exposure to liquid mercury before testing in this environment

An increase in test temperature usually decreases embrittlement, which leads to a brittle- to-ductile transition. Severe embrittlement occurs near the freezing temperature of the liquid. In fact, in iron lead, iron indium (Fig.

5), and many other metallic couples, embrittlement occurs below the melting temperature of the liquid. This phenomenon is called solid metal induced embrittlement (SMIE) of metals and is described in the following article in this Section. Gaseous metal embrittlement, not discussed here, has been noted as well.

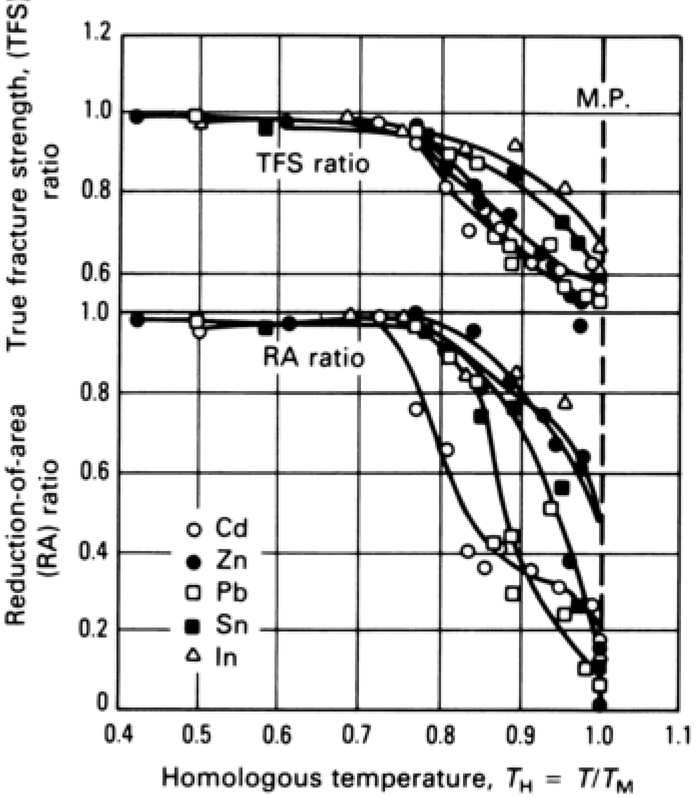

Fig. 5 Embrittlement of 4140 steel by various metals below their melting point. Comparison of normalized true fracture strength (TFS) ratio and the reduction-of-area (RA) ratio as a function of homologous temperature, T_H, where T and T_M are the test and the melting temperature of the embrittling metal, respectively. M.P., melting point. Source: Ref 13

The occurrence of LMIE is not a laboratory curiosity. Such failures have been observed in metals and alloys in the following industrial applications and processes:

- Small amounts of alloying elements, such as lead and tellurium, added to steel to improve machinability may lead to embrittlement (Fig. 6). Internally leaded steels have cracked at lead inclusions. For example, leaded steel gears have cracked during induction-hardening heat treatments, and warm punching of leaded steel shafts has resulted in unexpected fracture during the forming operation.
- Cadmium-plated titanium and steels are embrittled during high-temperature service by molten cadmium.
- Indium, used as a high-vacuum seal in steel chambers, has caused cracking during bakeout operations.
- Zircaloy tubes used in nuclear reactors have been cracked by both solid and liquid cadmium.
- Although infrequent, LMIE also occurs in petrochemical plants and in the steel industry during heat treatment, hot rolling, brazing, soldering, and welding (Ref 14, 15, 16, 17) operations.
- Embrittlement of steel occurs by electroplated or dipped cadmium, zinc, or tin—all of which provide corrosion resistance.
- In liquid metal cooled reactors, liquid lithium can cause LMIE in metals.

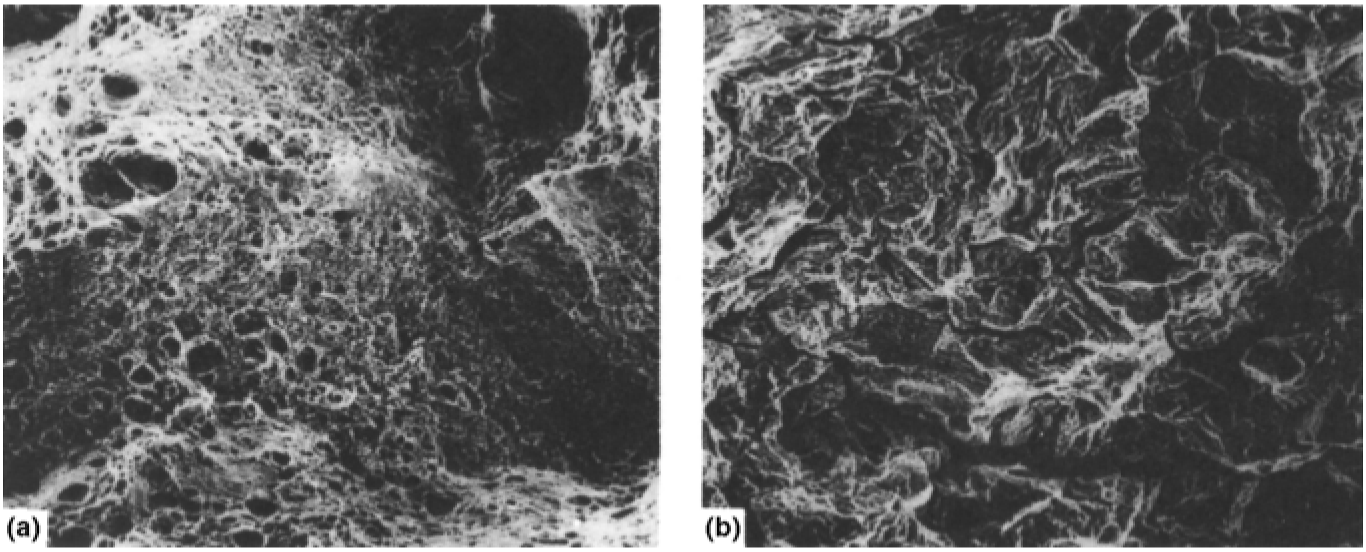

Fig. 6 Influence of lead on the fracture morphology of a 4340 steel. (a) Ductile failure after testing in argon at 370 °C (700 °F). (b) The same steel tested in liquid lead at 370 °C (700 °F) showing brittle intergranular fracture

As would be expected of embrittlement, the fracture is typically associated with a significant loss of macroscopic ductility. The fracture mode is often largely intergranular, although transgranular brittle fracture (cleavage) can occur. Intergranular (IG) fractures may also reveal dimples associated with the ductile mechanism of microvoid coalescence along the grain boundaries. This is referred to as dimpled intergranular (or intercrystalline) fracture.

Fracture surfaces from LMIE are easily distinguishable from those due to stress-corrosion cracking (SCC), and more details on the failure analysis of LMIE fractures are described in the article "Liquid Metal and Solid Metal Induced Embrittlement" in *ASM Handbook,* Volume 11 (2002), *Failure Analysis and Prevention.* The embrittlement is severe, and the propagation of fracture is typically very fast in the case of LMIE as compared to that in SCC. Thus, the predominant occurrence of brittle fracture surfaces, fast or catastrophic fracture, significant loss in ductility and strength/fracture toughness, and the presence of liquid at the tip of the propagating crack are some of the characteristics that may be used to distinguish LMIE from other environmentally induced failures. Detailed information on the mechanisms of LMIE and the susceptibility of specific metals and alloys to liquid metal induced failures can be found in Ref 8 and 18, 19, 20, 21, 22, 23, 24, 25, 26.

References cited in this section

1. W.H. Johnson, *Proc. R. Soc. (London) A,* Vol 23, 1874, p 168

2. D.A. Wheeler, R.G. Hoagland, and J.P. Hirth, Effect of Solid Metal Strength Level on the Liquid-Metal Embrittlement of Aluminum by Mercury, *Scr. Metall.,* Vol 22, 1988, p 533–538

3. B.A. Benson and R.G. Hoagland, Crack- Growth Behavior of a High-Strength Aluminum Alloy During LME by Gallium, *Scr. Metall.,* Vol 23, 1989, p 1943–1948

4. D.A. Wheeler, R.G. Hoagland, and J.P. Hirth, Evidence for Crack Tip Oxidation Effects During the Liquid-Metal Embrittlement of AA-7075 Aluminum-Alloy by Mercury, *Corrosion,* Vol 45, 1989, p 207–212

5. J.A. Kapp, in *Embrittlement by Liquid and Solid Metals,* M.H. Kamdar, Ed., TMS/ AIME, 1984, p 117–131

6. D.G. Kolman and R. Chavarria, “Liquid- Metal Embrittlement of 7075 Aluminum and 4340 Steel Compact Tension Specimens by Gallium,” *J. Test. Eval.,* Vol 30 (No. 5), 2002, p 452–456

7. P.H. Au-Yeung, J.T. Lukowski, L.A. Heldt, and C.L. White, An Auger Spectrometric Study of the Crack Tip Surface-Chemistry for Liquid-Metal Embrittlement: Beta-Brass Embrittled by Gallium, *Scr. Metall. Mater.,* Vol 24, 1990, p 95–100

8. N.S. Stoloff, in *Environment-Induced Cracking of Materials,* R.P. Gangloff and M.P. Ives Ed., NACE, 1990, p 31–41

9. S. Ashok, N.S. Stoloff, M.E. Glicksman, and T. Slavin, Liquid-Metal and Hydrogen Embrittlement of Amorphous Alloys, *Scr. Metall.,* Vol 15, 1981, p 331–337

10. S.P. Lynch, Hydrogen Embrittlement and Liquid-Metal Embrittlement in Nickel Single-Crystals, *Scr. Metall.,* Vol 13, 1979, p 1051–1056

11. C.F. Old and P. Trevena, *Met. Sci.,* Vol 13, 1979, p 487, 591–596

12. M.J. Kelley and N.S. Stoloff, Analysis of Liquid-Metal Embrittlement from a Bond- Energy Viewpoint, *Metall. Trans.,* Vol 6, 1975, p 159–166

13. J.C. Lynn, W.R. Warke, and P. Gordon, Solid Metal Induced Embrittlement of Steel, *Mater. Sci. Eng.,* Vol 18, 1975, p 51–62

14. W. Shih, J. King, and C. Raczkowski, Liquid-Copper/Zinc Embrittlement in Alloy 718, *Weld. J.,* Vol 77, 1998, p S219–S222

15. W.F. Savage, *Welding,* Vol 57, 1978, p s9–s16

16. R.M. Bruscato, Liquid-Metal Embrittlement of Austenitic Stainless-Steel When Welded to Galvanized Steel, *Weld. J.,* Vol 71, 1992, p S455–S459

17. W.F. Savage, E.F. Nippes, and M.C. Mushala, Liquid-Metal Embrittlement of Heat- Affected Zone by Copper Contamination, *Weld. J.,* Vol 57, 1978, p S237–S245

18. M.H. Kamdar, *Prog. Mater. Sci.,* Vol 15, 1973, p 289

19. M.H. Kamdar, in *Treatise on Materials Science and Technology,* Vol 25, C.L. Briant and S.K. Banerjee, Ed., Academic Press, 1983, p 361–459

20. W. Rostoker, J.M. McCaughey, and H. Markus, *Embrittlement by Liquid Metals,* Reinhold Publishing, 1960

21. B. Joseph, M. Picat, and F. Barbier, *Eur. Phys. J.-Appl. Phys.,* Vol 5, 1999, p 19–31

22. M.G. Nicholas, in *Embrittlement by Liquid and Solid Metals,* M.H. Kamdar, Ed., TMS/ AIME, 1984 p 27–50

23. M.G. Nicholas and C.F. Old, Liquid-Metal Embrittlement, *J. Mater. Sci.,* Vol 14, 1979, p 1–18

24. S.P. Lynch, Metal-Induced Embrittlement of Materials, *Mater. Charact.,* Vol 28, 1992, p 279–289

25. C.F. Old, Liquid-Metal Embrittlement of Nuclear-Materials, *J. Nucl. Mater.,* Vol 92, 1980, p 2–25

26. F.A. Shunk, Specificity as an Aspect of Liquid-Metal Embrittlement, W.R. Warke, Ed., *Scr. Metall.*, Vol 8, 1974, p 519–526

72. D.G. Kolman and R. Charvarria, “The Liquid Metal Embrittlement of 316L SS by Ga,” Los Alamos National Laboratory Report LA-UR-02-7774; Submitted to *Corrosion,* Dec. 2002

D.G. Kolman, Liquid Metal Induced Embrittlement, *Corrosion: Fundamentals, Testing, and Protection*, Vol 13A*, ASM Handbook,* ASM International, 2003, p 381–392

Liquid Metal Induced Embrittlement

Revised by David G. Kolman, Los Alamos National Laboratory

Mechanisms of Embrittlement

Several mechanisms have been proposed to explain LMIE, including stress-assisted dissolution of the solid at the crack tip, reduction in the surface energy of the solid by the liquid metal, and adsorption-enhanced plasticity. It has been suggested that embrittlement is associated with liquid metal adsorption-induced localized reduction in the strength of the atomic bonds at the crack tip or at the surface of the solid metal at sites of stress concentrations.

With this possibility in mind, consider the crack shown in Fig. 7. Crack propagation occurs by the breaking of $A\text{-}A_0$ bonds at the crack tip and, subsequently, the breaking of similar bonds at the propagating crack tip by the chemisorbed liquid metal atom B. (A vapor phase from a solid in a solid-solid metal embrittlement couple or an elemental gas, such as hydrogen, may also provide the embrittling atom B.) Next, assume that liquid metal atom B at the crack tip reduces the cohesive strength of $A\text{-}A_0$ bonds. The chemisorption process presumably occurs spontaneously or only after the $A\text{-}A_0$ bonds have been strained to some critical value. In any event, electronic rearrangement occurs because of adsorption, which weakens the bonds at the crack tip. The crack propagates when the applied stress is increased, so that it exceeds the reduced breaking strength of $A\text{-}A_0$ bonds. The liquid metal atom becomes stably chemisorbed on the freshly created surfaces. The surface diffusion of the liquid metal atoms over the chemisorbed liquid metal atoms feeds the advancing crack tip, thus propagating the crack at reduced stress and causing complete failure of the specimen.

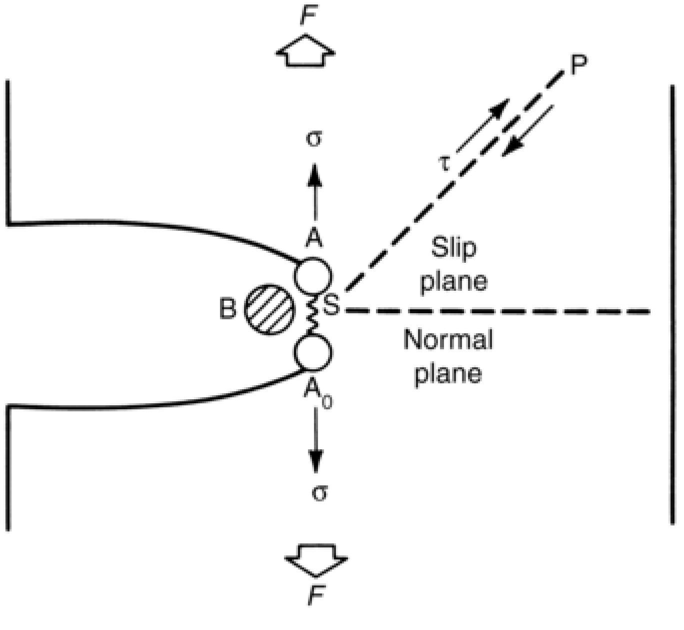

Fig. 7 Schematic illustrating displacement of atoms at the crack tip. The bond $A\text{-}A_0$ constitutes the crack tip, and B is the liquid metal atom.

In the previously mentioned mechanism, it is assumed that tensile decohesion is predominantly responsible for the occurrence of embrittlement, although both tensile as well as shear decohesion can occur. Embrittlement can also occur by the adsorption-induced reductions in the shear strength of the atomic bonds at the crack tip. The reduced shear strength facilitates nucleation of dislocations or slip at low stresses at or near the crack tip. Localized plasticity can result in void nucleation at precipitates, inclusions, or at other discontinuities (such as subboundaries in a single grain). The voids may grow and thus result in a rupture (i.e., an IG fracture) with the appearance of dimples on the fracture surfaces. The localized increased plasticity results in an overall reduction in the strain at failure as compared to that in the absence of liquid metal, thus causing embrittlement. For embrittlement due to reduced shear cohesion, lower strain at failure or subcritical crack growth by linkage of voids is the measure of LMIE.

A schematic representation of the previously mentioned process is given in Fig. 8, and supporting fractographic evidence is given for high- strength steel (Fig. 9a) and beryllium-copper alloys (Fig. 9b) broken in liquid metal environments. Conversely, Fig. 9(c–e) and Fig. 10 provide strong support for the reduced tensile cohesion mechanism.

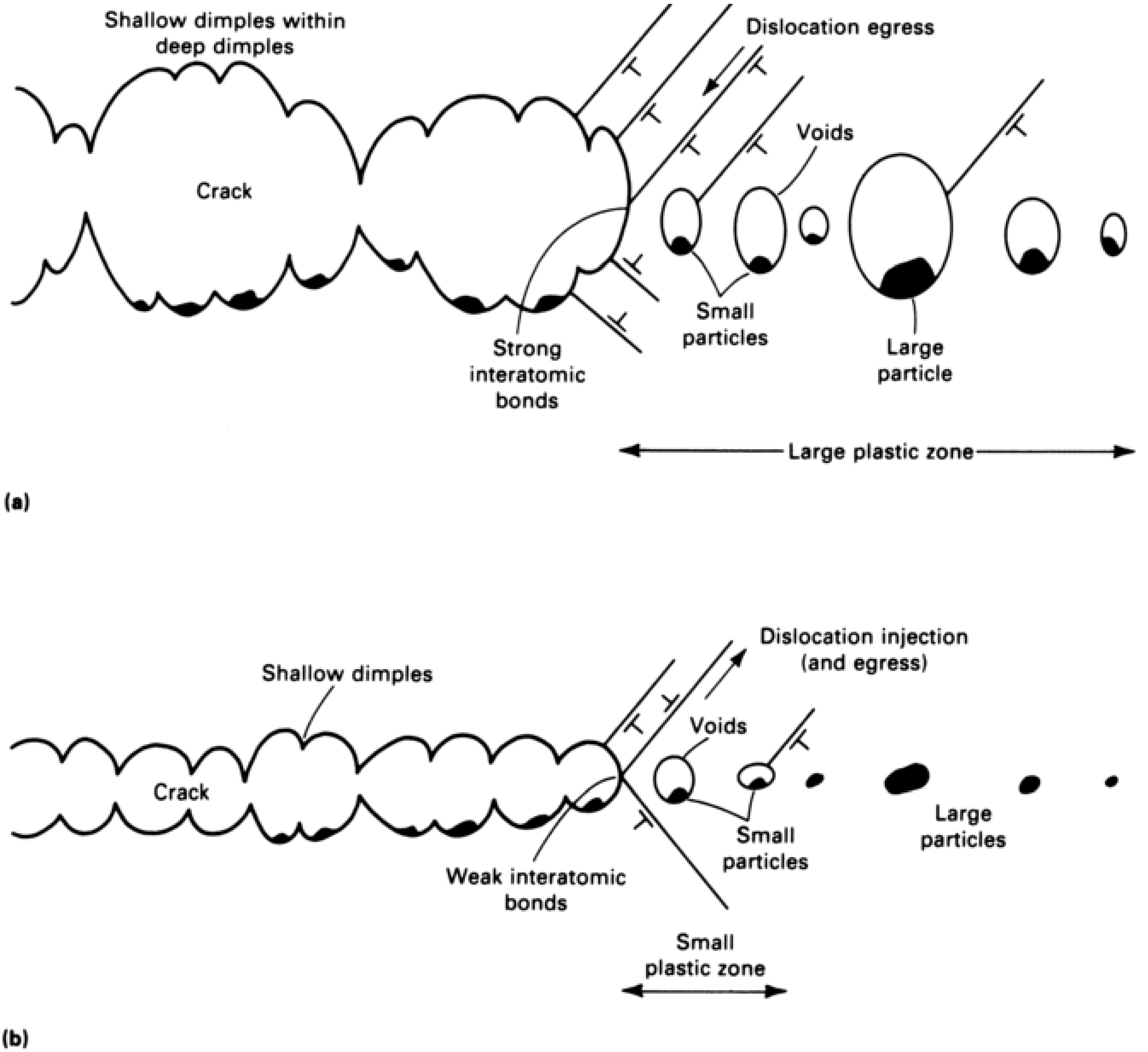

Fig. 8 Schematic illustrating the mechanisms of crack growth by microvoid coalescence. (a) Inert environment. (b) Embrittling liquid metal environment

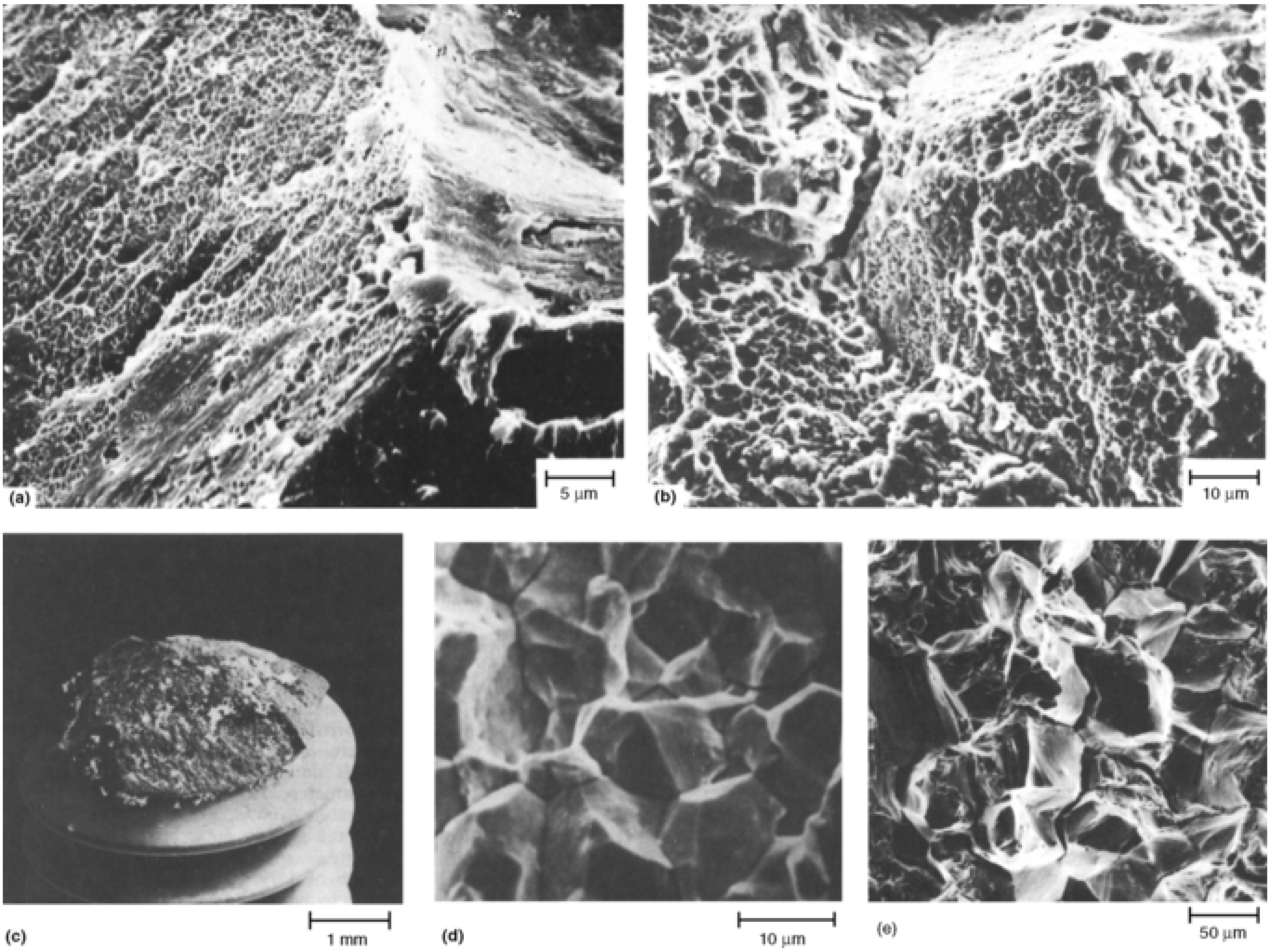

Fig. 9 Ductile and brittle fracture morphologies resulting from LMIE. (a) Fracture surface produced by subcritical cracking in D-6ac steel (tempered at 650 °C, or 1200 °F) in liquid mercury showing predominantly dimpled intercrystalline fracture along prior-austenite grain boundaries. (b) Fracture surface produced by rapid subcritical crack growth (~1 mm/s, or 0.4 in./s) in a Cu-1.9Be alloy in liquid mercury at 20 °C (70 °F) showing predominantly dimpled intercrystalline fracture. (c) Macrograph of a cadmium-plated fastener made from 1040 steel. Aerodynamic heating during descent of the solid fuel rocket engine resulted in brittle intergranular fracture. (d) Scanning electron micrograph of the failed machine screw shown in (c). (e) Fracture surface of a Monel specimen that failed in liquid mercury. The fracture is predominantly intergranular with some transgranular contribution.

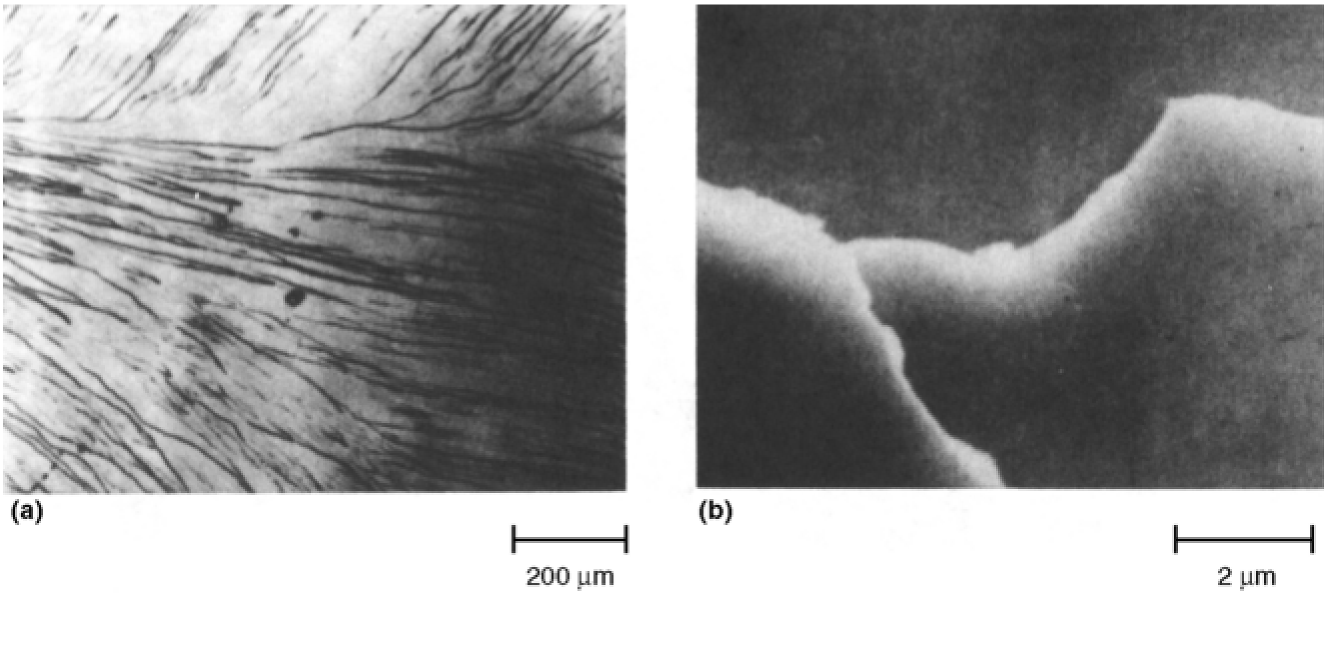

Fig. 10 Optical micrograph (a) and scanning electron micrograph (b) showing a cleavage fracture surface produced by cracking a zinc single crystal in liquid mercury

Most often, LMIE induces a brittle IG or cleavage fracture mode at reduced tensile stresses and thus supports the tensile decohesion mode. However, the dimpled IG fracture by LMIE should be considered an embrittling process in a failure analysis in which the reduction in the mechanical parameters at fracture is the measure of embrittlement. Although LMIE can occur by either a brittle or a ductile microscopic mechanism; both degrade the fracture properties of the solid metal. In addition, macroscopic fracture features may be a combination of macroscale ductile fracture (by microvoid coalescence) truncated by LMIE fracture from a transgranular brittle mechanism (cleavage) or IG mechanisms.

D.G. Kolman, Liquid Metal Induced Embrittlement, *Corrosion: Fundamentals, Testing, and Protection,* Vol 13A*, ASM Handbook,* ASM International, 2003, p 381–392

Liquid Metal Induced Embrittlement

Revised by David G. Kolman, Los Alamos National Laboratory

Role of Liquid in Crack Propagation

In the mechanism of embrittlement described previously, it was implied that once a crack is nucleated, subsequent crack propagation occurs mechanically with liquid absent at the crack tip or occurs by the continuous presence of the liquid metal atoms at the propagating crack tip caused by the surface diffusion of liquid metal atoms over chemisorbed liquid metal atoms. The role of liquid in embrittlement should be investigated by measuring the crack growth rate as a function of temperature and stress intensity. The velocity of crack propagation, or crack growth rate, in SCC has been extensively investigated. However, such investigations in liquid metal are limited (Ref 2, 3, 4, 5, 6, 27, 28, 29). Figure 11 shows that the velocity of crack growth in brass in liquid mercury was at least 2 orders of magnitude higher than that in an inert environment. The crack propagation activation energy for brass in liquid mercury is only 3 to 5 kcal/mol (Fig. 12). This corresponds to diffusion of liquid mercury over mercury adsorbed on brass. The very high velocities of crack propagation and very low activation energies are considered to be distinguishing features from similar investigations in SCC environments in the same metals. Such characteristics can be used to differentiate liquid metal induced crack propagation from stress- corrosion or hydrogen damage.

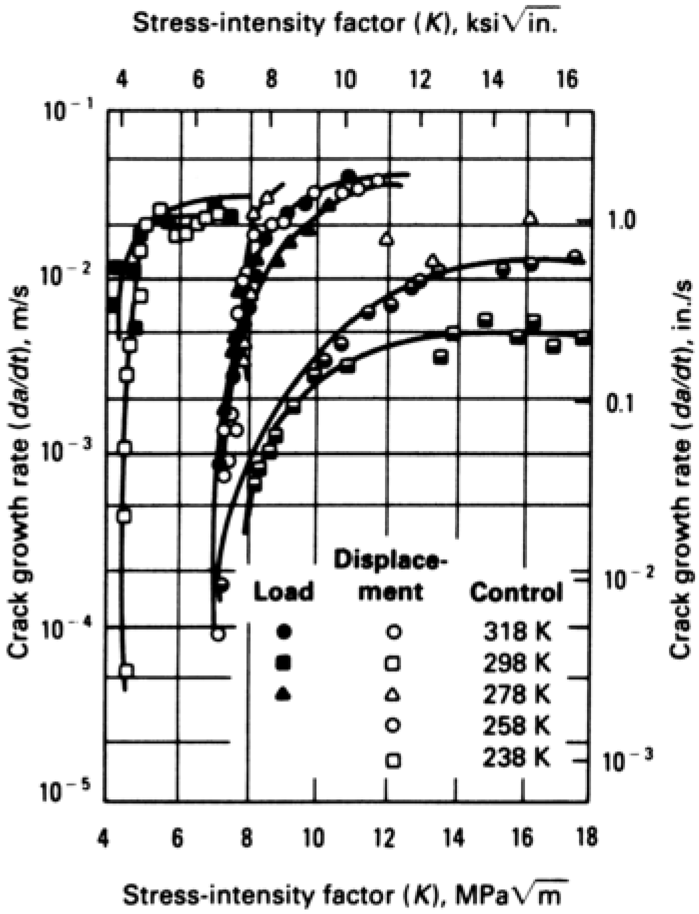

Fig. 11 Crack growth rate versus stress-intensity factor for brass in liquid mercury at various temperatures under load and displacement control conditions

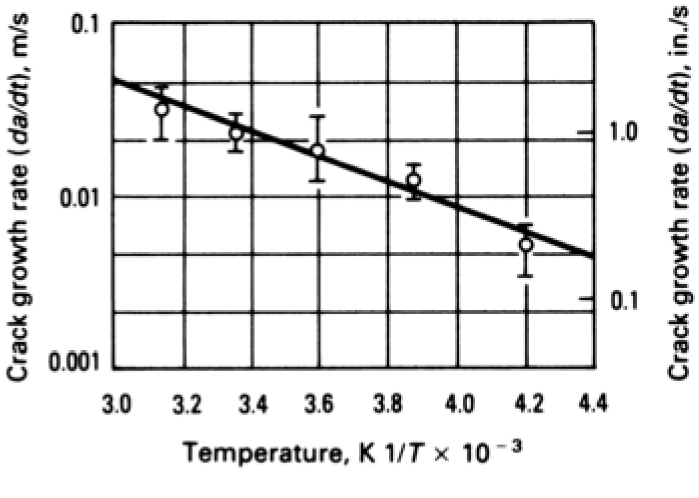

Fig. 12 Crack growth rate versus reciprocal of temperature for brass in liquid mercury. The activation energy, *Q*, is 4 kcal/mol.

References cited in this section

2. D.A. Wheeler, R.G. Hoagland, and J.P. Hirth, Effect of Solid Metal Strength Level on the Liquid-Metal Embrittlement of Aluminum by Mercury, *Scr. Metall.,* Vol 22, 1988, p 533–538

3. B.A. Benson and R.G. Hoagland, Crack- Growth Behavior of a High-Strength Aluminum Alloy During LME by Gallium, *Scr. Metall.,* Vol 23, 1989, p 1943–1948

4. D.A. Wheeler, R.G. Hoagland, and J.P. Hirth, Evidence for Crack Tip Oxidation Effects During the Liquid-Metal Embrittlement of AA-7075 Aluminum-Alloy by Mercury, *Corrosion,* Vol 45, 1989, p 207–212

5. J.A. Kapp, in *Embrittlement by Liquid and Solid Metals,* M.H. Kamdar, Ed., TMS/ AIME, 1984, p 117–131

6. D.G. Kolman and R. Chavarria, "Liquid- Metal Embrittlement of 7075 Aluminum and 4340 Steel Compact Tension Specimens by Gallium," *J. Test. Eval.,* Vol 30 (No. 5), 2002, p 452–456

27. P.J.L. Fernandes and D.R.H. Jones, The Effects of Loading Variables on Fatigue-Crack Growth in Liquid-Metal Environments, *Int. J. Fatigue,* Vol 17, 1995, p 501–505

28. J.J. Lewandowski, Y.S. Kim, and N.J.H. Holroyd, Lead-Induced Solid Metal Embrittlement of an Excess Silicon Al-Mg-Si Alloy at Temperatures of -4 °C to 80 °C, *Metall. Trans. A,* Vol 23, 1992, p 1679–1689

29. J.A. Kargol and D.L. Albright, Fracture Mechanics Method for Determining Crack- Propagation Resistance of Embrittled Aluminum Bicrystals, *J. Test. Eval.,* Vol 3, 1975, p 173–178

D.G. Kolman, Liquid Metal Induced Embrittlement, *Corrosion: Fundamentals, Testing, and Protection*, Vol 13A*, ASM Handbook,* ASM International, 2003, p 381–392

Liquid Metal Induced Embrittlement

Revised by David G. Kolman, Los Alamos National Laboratory

Occurrence of LMIE

Susceptibility to LMIE is unique to specific solid metal/liquid metal systems. For example, liquid gallium embrittles aluminum but not magnesium, and liquid mercury embrittles zinc but not cadmium. The equilibrium phase diagrams of most embrittlement couples show that they form binary systems with little or no solid solubility. Also, they form immiscible liquids in the liquid state, and they usually do not form intermetallic compounds. This is an empirical observation, valid for many embrittlement couples, although exceptions have been reported.

The most critical and mandatory condition for LMIE is that the liquid should be in intimate contact with the surface of the solid to initiate embrittlement and should subsequently be present at the tip of the propagating crack to cause brittle failure. Even a thin oxide film several angstroms thick may prevent interaction between the solid and the liquid so that embrittlement is not observed. Thus, conditions that promote intimate contact and enhanced wetting of the liquid by the solid, such as freshly created surfaces by plastic deformation in a liquid environment, breaking of oxide films, or other such factors, lead to LMIE of the solid. Indeed, investigators have used chemical (Ref 4, 30) and mechanical (Ref 2, 6, 31) depassivation techniques in order to achieve reliable wetting of specimens for testing.

The severity of embrittlement is not necessarily related to just the previously mentioned criteria and conditions, but it is related to the chemical nature of the embrittling species. For example, zinc can be embrittled more by liquid gallium than by mercury. In addition, the severity of embrittlement is related to the properties of the solid and depends on such factors as strength, alloying elements, grain size, and strain rate. The severity or occurrence or nonoccurrence of embrittlement depends on the type of test and whether the solid contains stress concentrators, such as preexisting cracks or flaws, or is smooth and free of stress raisers. By increasing the possibilities of maintaining high stress concentrations, the susceptibility of the solid to LMIE is also increased.

For example, smooth specimens of low-alloy low-strength steel are not embrittled by liquid lead, but the same steel containing a fatigue precrack is severely embrittled by liquid lead. Therefore, uniaxial tension tests provide a nonconservative assessment of LMIE susceptibility, and the use of fracture mechanics specimens and test techniques (Ref 2, 3, 4, 5, 6, 27, 28, 29, 32) is preferable. Note that fracture mechanics testing of specimens in liquid metal environments is much more challenging than uniaxial tension testing, due to difficulties with crack tip wetting, crack growth measurement, and data interpretation.

Certain other prerequisites must be fulfilled before fracture can initiate in a solid. For a ductile metal without a precrack, these are tensile stress, plastic deformation, and the presence of a stable obstacle to slip serving as a stress concentrator. This obstacle can be preexisting (for example, a grain boundary) or can be created during deformation (for example, a twin or kink band).

In addition, there should be an adequate supply of liquid metal to adsorb at the obstacle and subsequently at the propagating crack tip. Plastic deformation or yielding may mean localized deformation in few grains rather than general yielding of the solid metal. If a specimen contains a preexisting crack, then adsorption of the liquid at the crack tip and some tensile stress are necessary to propagate a crack. If the solid is notch brittle, LMIE can occur at reduced stress. In order for LMIE to occur, there must be an embrittler at the crack tip. However, once a crack is initiated, it may propagate further in a ductile or brittle manner in the absence of the liquid, depending on the constraints at the crack tip. Brittle fracture may occur after some ductile fracture in an inert environment. The changing constraint conditions may enable brittle crack propagation after the embrittler is exhausted, but only if, under the crack tip conditions, the material is intrinsically brittle. Thus, it may not be necessary for the liquid to be present during the entire process of crack propagation. The occurrence of LMIE in an embrittlement couple requires good wetting of the surface of the solid by the liquid, the presence of sufficient stress concentration to initiate or propagate a crack in liquid, and possible concurrence with the empirical observations mentioned previously.

References cited in this section

2. D.A. Wheeler, R.G. Hoagland, and J.P. Hirth, Effect of Solid Metal Strength Level on the Liquid-Metal Embrittlement of Aluminum by Mercury, *Scr. Metall.,* Vol 22, 1988, p 533–538

3. B.A. Benson and R.G. Hoagland, Crack- Growth Behavior of a High-Strength Aluminum Alloy During LME by Gallium, *Scr. Metall.,* Vol 23, 1989, p 1943–1948

4. D.A. Wheeler, R.G. Hoagland, and J.P. Hirth, Evidence for Crack Tip Oxidation Effects During the Liquid-Metal Embrittlement of AA-7075 Aluminum-Alloy by Mercury, *Corrosion,* Vol 45, 1989, p 207–212

5. J.A. Kapp, in *Embrittlement by Liquid and Solid Metals,* M.H. Kamdar, Ed., TMS/ AIME, 1984, p 117–131

6. D.G. Kolman and R. Chavarria, "Liquid- Metal Embrittlement of 7075 Aluminum and 4340 Steel Compact Tension Specimens by Gallium," *J. Test. Eval.,* Vol 30 (No. 5), 2002, p 452–456

27. P.J.L. Fernandes and D.R.H. Jones, The Effects of Loading Variables on Fatigue-Crack Growth in Liquid-Metal Environments, *Int. J. Fatigue,* Vol 17, 1995, p 501–505

28. J.J. Lewandowski, Y.S. Kim, and N.J.H. Holroyd, Lead-Induced Solid Metal Embrittlement of an Excess Silicon Al-Mg-Si Alloy at Temperatures of -4 °C to 80 °C, *Metall. Trans. A,* Vol 23, 1992, p 1679–1689

29. J.A. Kargol and D.L. Albright, Fracture Mechanics Method for Determining Crack- Propagation Resistance of Embrittled Aluminum Bicrystals, *J. Test. Eval.,* Vol 3, 1975, p 173–178

30. M.H. Kamdar, in *Embrittlement by Liquid and Solid Metals,* M.H. Kamdar, Ed., TMS, 1984 p 149–159

31. S.P. Lynch, Liquid-Metal Embrittlement in an Al 6-Percent Zn 3-Percent Mg Alloy, *Acta Metall.*, Vol 29, 1981, p 325–340

32. B. Cox and Y.M. Wong, Liquid Metal Embrittlement of Zr-2.5% Nb Alloy, *J. Nucl. Mater.*, Vol 245, 1997, p 34–43

D.G. Kolman, Liquid Metal Induced Embrittlement, *Corrosion: Fundamentals, Testing, and Protection*, Vol 13A, *ASM Handbook*, ASM International, 2003, p 381–392

Liquid Metal Induced Embrittlement

Revised by David G. Kolman, Los Alamos National Laboratory

Effects of Metallurgical, Mechanical, and Physical Factors

It has been shown that the prerequisites for liquid metal induced brittle fracture are the same as those for brittle fracture in an inert environment at low temperatures, that is, the need for plastic flow. Sufficient stress intensity and adsorption of liquid metal are necessary to initiate and/or propagate a crack. From the investigations reported for many embrittlement couples, including classic zinc-mercury couples, it has been concluded that adsorption-induced embrittlement can be regarded as a special case of brittle fracture that normally occurs in brittle materials at low temperatures in an inert environment. (Ductile fracture can also result by the adsorption-induced reductions in the shear strength of the atomic bonds at the crack tip.) Thus, the effects of yield stress, grain size, strain rate, temperature, and so on in a liquid metal environment follow trends similar to those noted for metals tested in an inert environment. The effects of a variety of metallurgical factors on LMIE can be found in (Ref 8).

Effects of Grain Size. The grain size dependence of fracture stress has been investigated for zinc mercury, cadmium gallium, brass and copper alloys in mercury, and low-carbon steel in lithium. In these and other instances, the fracture stress varied linearly with the reciprocal of the square root of grain size and followed the well- known Cottrell-Petch relationship of grain size dependence on fracture stress (Ref 8).

For the zinc-mercury couple shown in Fig. 13, fracture is nucleation controlled in region I, whereas in region II it is propagation controlled. Nucleation-controlled embrittlement implies the occurrence of unstable crack propagation; that is, once a crack is initiated, it propagates to failure in the presence or absence of the liquid metal at the crack tip. In propagation-controlled failure, stable crack propagation occurs such that microcracks are formed at some low stress in a liquid metal environment, but the microcracks propagate to failure only when a higher stress is reached. Thus, in propagation-controlled failure, unpropagated microcracks may be found beside the main fracture, and complete fracture of the specimen occurs only in the presence of liquid metal. The reverse is observed when fracture is initiation-controlled.

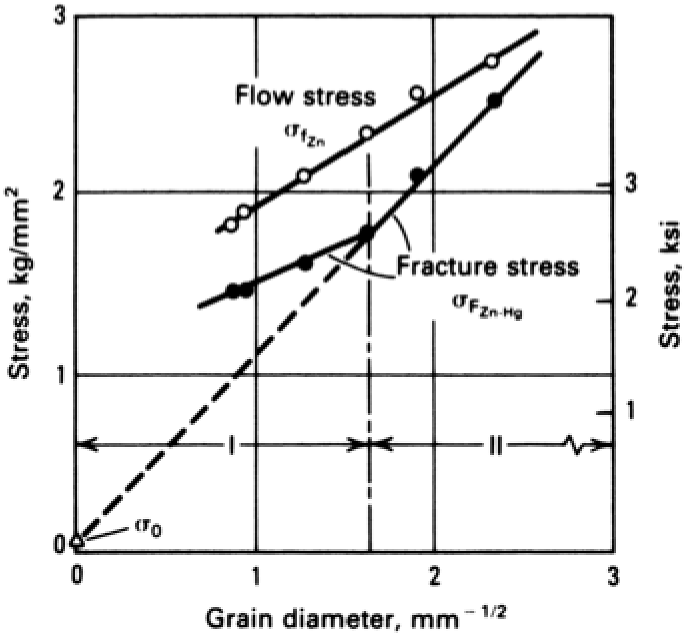

Fig. 13 Effect of grain size on LMIE. Variation of the flow stress of amalgamated zinc polycrystalline specimens, σ_{fZn}, and fracture stress of amalgamated zinc specimens, $\sigma_{FZn\text{-}Hg}$, as a function of grain size at 298 K

Effects of Temperature and Strain Rate. Liquid metal induced embrittlement occurs at the melting point of liquid metal. There are quite a few instances in which embrittlement occurs below the melting point of liquid by SMIE. In some instances, an embrittlement maximum is seen at intermediate temperatures (Ref 5, 11, 30, 33, 34, 35, 36, 37, 38, 39). In other cases, the susceptibility to embrittlement may remain essentially unchanged with temperature. At a sufficiently high test temperature, a brittle-to-ductile transition occurs when embrittlement ceases and ductility is restored to the solid. Such transitions do not occur at a sharply defined temperature and are not predictable on a theoretical basis or in terms of diffusion, dissolution, or other such embrittlement processes. It is generally accepted that a significant increase in temperature counteracts the inherent propensity for fracture in the embrittling liquid metal environment.

In smooth steel specimens tested in liquid lead, brittle-to-ductile transition occurs at approximately 510 °C (950 °F), 335 °C (600 °F) above the melting point of lead. In fracture-mechanics specimens of similar steel containing sharp notches tested in liquid lead, the transition occurs at approximately 650 °C (1200 °F), which is 140 °C (250 °F) higher than that for smooth specimens. Transition temperature in this case depends on the presence or absence of a stress raiser in the specimen and on the type of test method used. It should also be noted that this effect is probably related not just to stress concentration but also to constraint effects on the apparent flow stress of the material at the crack tip. This also promotes brittle behavior. Such brittle-to-ductile transitions also have been reported for zinc-mercury, aluminum-mercury, brass-mercury, titanium-cadmium, steel-lead, and steel-lead-antimony solution embrittlement couples.

Transition temperature also varies with strain rate and grain size in a manner similar to metals tested in an inert environment; that is, an increase in strain rate and a decrease in grain size increase the transition temperature. The effects of grain size on transition temperature have been reported for aluminum in Hg-3Sn solutions and brass-mercury embrittlement couples. The effects of strain rate on transition temperature have been reported for cadmium-gallium, zinc-mercury, aluminum-mercury, zinc-indium, brass- mercury, and titanium-cadmium embrittlement couples. Changes in the strain rate by orders of magnitude are usually required to change the transition temperature by 50 to 100 °C (90 to 180 °F). For example, in the titanium-cadmium couple, a change of approximately 60 °C (110 °F) occurs with a change of one to two orders of magnitude in the strain rate and corresponds to a comparable increase in yield stress with the strain rate. The effects of strain rate appear to be related to the increase in the yield stress. This corresponds to an increase in the embrittlement susceptibility and a decrease in the brittle-to- ductile transition temperature.

Effects of Stress. Static fatigue or delayed- failure tests are conducted to study the effects of time-dependent processes, such as diffusion penetration of the grain boundary, as the cause of embrittlement. Also, such tests are performed because they simulate service conditions of constant stress in an embrittling environment as a

function of time and assist in the failure analysis. Time-to-failure depends on the notch sensitivity of the alloy, and embrittlement may be independent of time-to-failure in notch-insensitive alloys. Conversely, the time-to-failure may be very sensitive to the stress level in other alloys. In notch-sensitive zinc tested in mercury, for example, complete failure can occur instantly at a stress slightly higher than a threshold stress.

These kinds of results indicate that time-dependent diffusion penetration or dissolution processes are not always dominant factors in LMIE. In isolated instances, grain-boundary penetration by the liquid has been the cause of embrittlement. For example, under no applied load (unstressed but with internal residual stress still possible), aluminum or commercial aluminum alloys disintegrate into individual grains when contacted with liquid gallium. Liquid antimony embrittles steel, and embrittlement increases with temperature; thus, diffusional processes cause antimony to embrittle steel. Liquid copper and liquid lithium embrittle steel in a similar manner (Fig. 14). However, in these cases, both diffusional and classic LMIE have been observed. Such behavior can be differentiated by the temperature dependence, by the susceptibility to embrittlement, or by embrittlement occurring in solid metal environments.

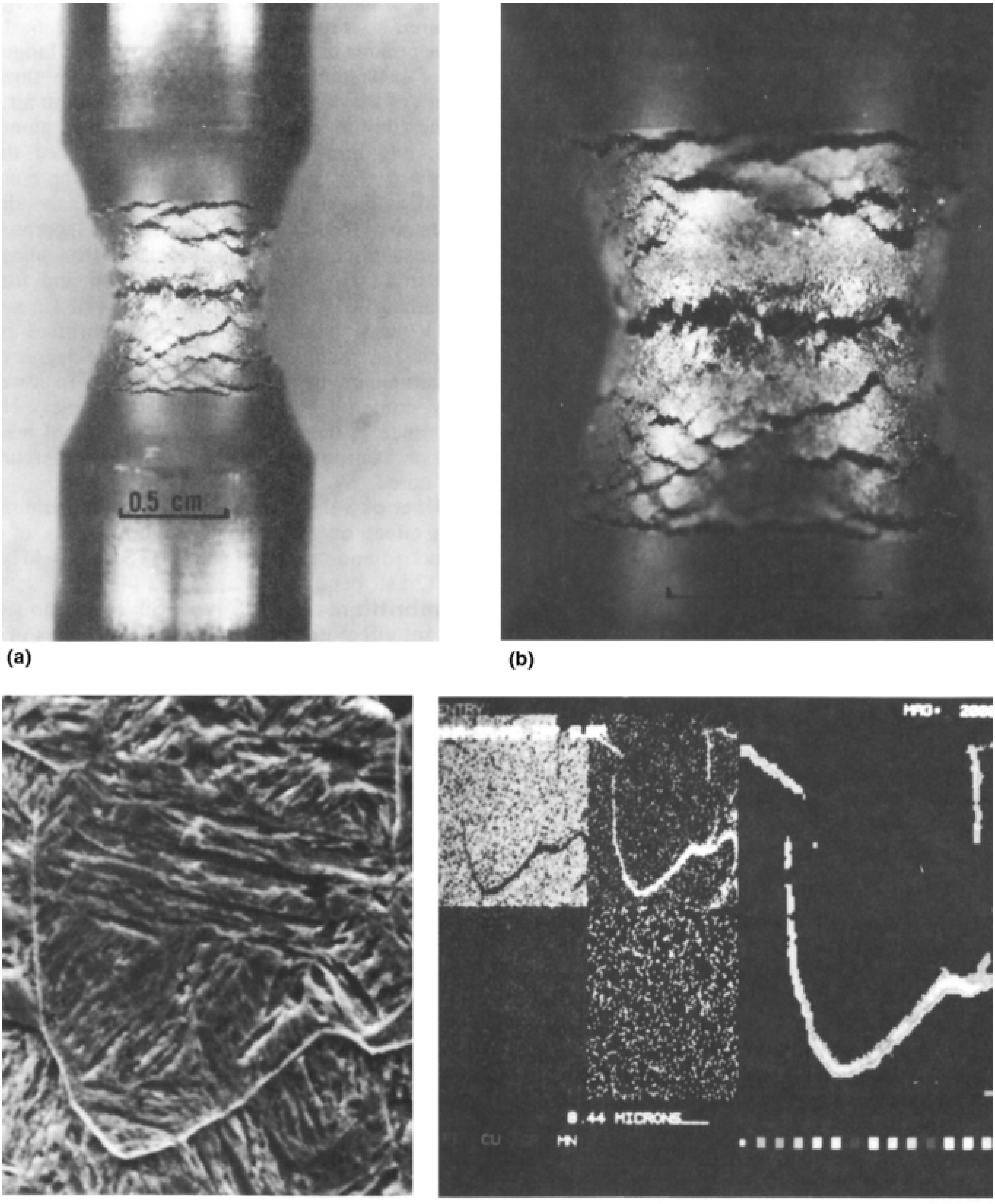

Fig. 14 Copper-induced LMIE of 4340 steel. (a) and (b) Copper-plated specimen that was pulled at 1100 °C (2010 °F) in a Gleeble hot tensile machine showing liquid copper embrittlement of steel. (c) Scanning electron micrograph of the pulled specimen. 1600×. (d) Computer-processed x-ray map showing the presence of copper in prior-austenite grain boundaries

Inert Carriers and LMIE. In some cases, investigation of the embrittlement behavior of a potential solid-liquid metal couple is not possible. The reason is that the solid metal at temperatures just above the melting temperature of the liquid metal is either too ductile to initiate and propagate a brittle crack or the solid is

excessively soluble in the liquid metal. It is possible, however, that a solid metal can be embrittled by a liquid metal of high melting point by dissolving it in an inert-carrier liquid metal of a lower melting point. Thus, the embrittling species is effectively in a liquid state at some temperature far below its melting point. In addition, it provides a means of investigating the variation in the degree of embrittlement induced in a solid metal as a function of the concentration and as a function of the chemical nature of the several active liquid metal species dissolved separately in a common inert-carrier liquid metal.

For example, mercury does not embrittle cadmium, but indium may embrittle cadmium (melting point: 325 °C, or 617 °F). However, cadmium is quite ductile at 156 °C (313 °F), the melting temperature of indium. Mercury dissolves up to 70% indium at room temperature. The indium in the mercury-indium solution at room temperature embrittles cadmium (Fig. 15). In fact, cadmium single crystals, which are ductile even at liquid helium temperature, can be embrittled by indium and cleaved in indium- mercury solutions (Fig. 3). Another example of embrittlement by inert carriers is that of Zircaloy nuclear fuel claddings used in liquid metal cooled nuclear reactors. In liquid cesium, Zircaloy claddings fail in a ductile manner; in cesium saturated with cadmium, Zircaloy is subject to brittle fracture (Ref 40).

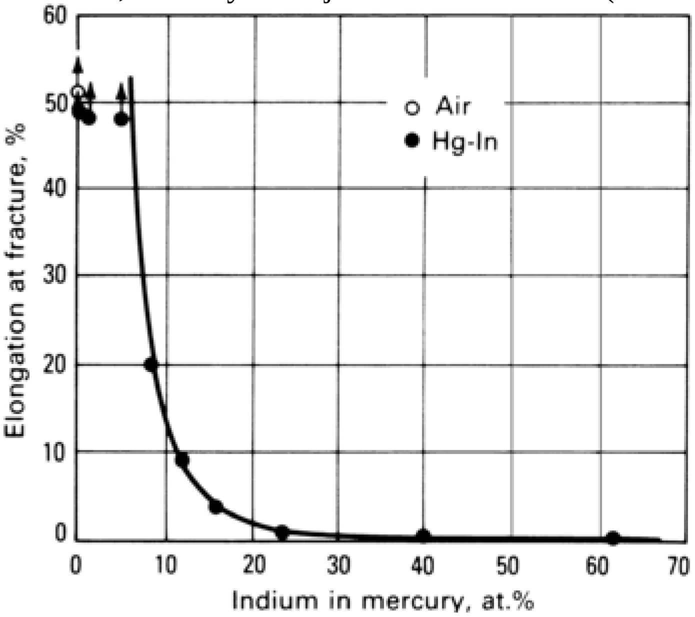

Fig. 15 Variation in ductility of polycrystalline cadmium as a function of indium content of mercury-indium surface coatings. Specimens were tested at 25 °C (75 °F) in air and in mercury-indium solution.

The concept of inert-carrier LMIE is useful in failure analysis where LMIE has occurred in a liquid solution—for example, solder rather than a pure liquid metal. The susceptibility of various species in the solder in causing LMIE can be investigated by incorporating each species in an inert liquid. This may suggest a means of preventing embrittlement by replacing the most potent embrittling agent with a nonembrittling species.

References cited in this section

5. J.A. Kapp, in *Embrittlement by Liquid and Solid Metals,* M.H. Kamdar, Ed., TMS/ AIME, 1984, p 117–131

8. N.S. Stoloff, in *Environment-Induced Cracking of Materials,* R.P. Gangloff and M.P. Ives Ed., NACE, 1990, p 31–41

11. C.F. Old and P. Trevena, *Met. Sci.,* Vol 13, 1979, p 487, 591–596

30. M.H. Kamdar, in *Embrittlement by Liquid and Solid Metals,* M.H. Kamdar, Ed., TMS, 1984 p 149–159

33. D.D. Perovic, G.C. Weatherly, and W.A. Miller, Influence of Temperature and Strain- Rate on Liquid-Metal Embrittlement of an Aluminum Alloy Containing Bismuth Inclusions, *Acta Metall.,* Vol 36, 1988, p 2249–2257

34. P. Skeldon, J.P. Hilditch, J.R. Hurley, and D.R. Tice, The Liquid-Metal Embrittlement of 9 Cr Steel in Sodium Environments and the Role of Nonmetallic Impurities, *Corros. Sci.,* Vol 36, 1994, p 593–610

35. H.G. Suzuki, Strain Rate Dependence of Cu Embrittlement in Steels, *ISIJ Int.,* Vol 37, 1997, p 250–254

36. P.L.J. Fernandes and D.R.H. Jones, The Effects of Microstructure on Crack Initiation in Liquid-Metal Environments, *Eng. Fail. Anal.,* Vol 4, 1997, p 195–204

37. D.D. Perovic, G.C. Weatherly, and W.A. Miller, On the Strain Rate Dependence of Ductility Troughs Observed Under Liquid- Metal Embrittlement and Creep Conditions, *Scr. Metall.,* Vol 21, 1987, p 345–347

38. N.N. Breyer and K.L. Johnson, Liquid- Metal Embrittlement of 4145 Steel by Lead- Tin and Lead-Antimony Alloys, *J. Test. Eval.,* Vol 2, 1974, p 471–477

39. V.Y. Abramov, S.N. Bozin, O.I. Eliseeva, G.M. Kalinin, V.I. Kalyandruk, and E.M. Lyutyi, Influence of a Lead Melt on Plastic- Deformation of High-Alloyed Heat-Resistant Steels, *Mater. Sci.,* Vol 30, 1994, p 465–469

40. W.T. Grubb, Cadmium Metal Embrittlement of Zircaloy-2, *Nature,* Vol 265, 1977, p 36–37

D.G. Kolman, Liquid Metal Induced Embrittlement, *Corrosion: Fundamentals, Testing, and Protection*, Vol 13A*, ASM Handbook*, ASM International, 2003, p 381–392

Liquid Metal Induced Embrittlement

Revised by David G. Kolman, Los Alamos National Laboratory

Fatigue in Liquid Metal Environments

Most studies of LMIE have been concerned with the effects of tensile loading on fracture. Investigations of fatigue behavior (Ref 2, 4, 5, 6, 8, 25, 27, 41, 42, 72) are important, because this test condition is more severe than other test conditions, including the tensile testing of metals. Thus, a solid tested in fatigue may become embrittled, but the same solid tested in tension may not exhibit embrittlement. This may be because at the high stress level corresponding to yield stress, which is a prerequisite for the occurrence of embrittlement in tough metals, the solid may be sufficiently ductile to prevent initiation of a crack in the liquid. Another explanation is that fatigue generates and maintains a sharper crack tip that gives rise to a greater stress intensity. Another explanation is that cyclic stress is more efficient at crack tip wetting than tensile stress (Ref 6).

For example, smooth specimens of high-purity chromium-molybdenum low-alloy steel with yield stress of approximately 690 MPa (100 ksi) are not embrittled by liquid lead, but the same steel specimens containing a fatigue precrack are severely embrittled by liquid lead. The fatigue life in liquid lead is reduced to 25% of that in an inert argon environment. Crack propagation in a liquid metal environment under fatigue and tensile loading can be significantly different. The stress intensity at failure of 7.7 MPa$\sqrt{m}$ (7 ksi $\sqrt{in.}$) for a 4340 steel specimen containing a fatigue precrack tested in cyclic fatigue in liquid lead was 5 times lower than that for the same specimen tested in tension in static fatigue and was 20 times lower than that in an inert argon environment. Furthermore, the 7.7 MPa$\sqrt{m}$ (7 ksi$\sqrt{in.}$) stress intensity was the same whether the specimen had a machined notch (0.13 mm, or 0.005 in., root radius) or a fatigue precrack at the root of the notch; that is, embrittlement was independent of root radius. These results indicate that embrittlement is very severe, and even blunt cracks can propagate to failure. Similar results have also been reported for the same steel tested in liquid mercury.

These results clearly indicate that fatigue testing of a notched or a fatigue precracked specimen provides the most severe test condition and therefore causes maximum susceptibility to embrittlement in a given liquid metal environment. To determine whether a solid is susceptible to LMIE in a particular liquid, it is advisable to test the solid metal with a stress raiser or a notch in a tension-tension fatigue test.

References cited in this section

2. D.A. Wheeler, R.G. Hoagland, and J.P. Hirth, Effect of Solid Metal Strength Level on the Liquid-Metal Embrittlement of Aluminum by Mercury, *Scr. Metall.,* Vol 22, 1988, p 533–538

4. D.A. Wheeler, R.G. Hoagland, and J.P. Hirth, Evidence for Crack Tip Oxidation Effects During the Liquid-Metal Embrittlement of AA-7075 Aluminum-Alloy by Mercury, *Corrosion,* Vol 45, 1989, p 207–212

5. J.A. Kapp, in *Embrittlement by Liquid and Solid Metals,* M.H. Kamdar, Ed., TMS/ AIME, 1984, p 117–131

6. D.G. Kolman and R. Chavarria, "Liquid- Metal Embrittlement of 7075 Aluminum and 4340 Steel Compact Tension Specimens by Gallium," *J. Test. Eval.,* Vol 30 (No. 5), 2002, p 452–456

8. N.S. Stoloff, in *Environment-Induced Cracking of Materials,* R.P. Gangloff and M.P. Ives Ed., NACE, 1990, p 31–41

25. C.F. Old, Liquid-Metal Embrittlement of Nuclear-Materials, *J. Nucl. Mater.,* Vol 92, 1980, p 2–25

27. P.J.L. Fernandes and D.R.H. Jones, The Effects of Loading Variables on Fatigue-Crack Growth in Liquid-Metal Environments, *Int. J. Fatigue,* Vol 17, 1995, p 501–505

41. T.M. Regan and N.S. Stoloff, Mercury Embrittlement of Cu-Al Alloys Under Cyclic Loading, *Metall. Trans. A,* Vol 8, 1977, p 885–890

42. M.G. Adamson, W.H. Reineking, and S. Vaidyanathan, Evidence for Liquid Cesium- Induced and Tellurium-Induced Fatigue Embrittlement of Cold-Worked AISI Type 316 Stainless Steel, *Trans. Am. Nucl. Soc.,* Vol 50, 1985, p 252–254

72. D.G. Kolman and R. Charvarria, "The Liquid Metal Embrittlement of 316L SS by Ga," Los Alamos National Laboratory Report LA-UR-02-7774; Submitted to *Corrosion,* Dec. 2002

D.G. Kolman, Liquid Metal Induced Embrittlement, *Corrosion: Fundamentals, Testing, and Protection*, Vol 13A*, ASM Handbook*, ASM International, 2003, p 381–392

Liquid Metal Induced Embrittlement

Revised by David G. Kolman, Los Alamos National Laboratory

Decrease or Elimination of LMIE Susceptibility

The decohesion mechanism of embrittlement is related to electron interactions, where by electron redistribution between the solid and the liquid metal atoms reduces cohesion and thus induces embrittlement. Such

interactions at the electron level are the inherent properties of the interacting atoms and are therefore difficult or impossible to change in order to reduce the susceptibility to LMIE.

One possibility is to introduce impurity atoms in the grain boundary that have more affinity for sharing electrons with the liquid metal atoms than for sharing electrons with the solid metal atoms. For example, phosphorus additions to Monel segregate to the grain boundaries and reduce the embrittlement of Monel by liquid mercury. Additions of lanthanides to internally leaded steels reduce lead embrittlement of steel. Another alternative is to electroplate or clad the solid surface with a metal as a barrier between the embrittling solid-liquid metal couple, making sure that the barrier metal is not embrittled by the liquid metal.

Another possibility is that a ceramic or a covalent material coating on the solid surface can inhibit embrittlement. Apparently, only materials with metallic bonding are susceptible to LMIE. The severity of embrittlement could be reduced by decreasing the yield stress of the solid below the stress required to initiate a crack or by cladding with a high-purity metal of the alloy that is embrittled but that has a very low yield stress. Thus, Zircaloy, which is clad with a high-purity zirconium, becomes immune to embrittlement by cadmium. The obvious possibility is to replace embrittling liquid metals or solutions by nonembrittling metals or solutions.

D.G. Kolman, Liquid Metal Induced Embrittlement, *Corrosion: Fundamentals, Testing, and Protection*, Vol 13A, *ASM Handbook*, ASM International, 2003, p 381–392

Liquid Metal Induced Embrittlement

Revised by David G. Kolman, Los Alamos National Laboratory

Embrittlement of Nonferrous Metals and Alloys

Zinc. Mercury, indium, gallium, and Pb-20Sn solder embrittle zinc. Mercury decreases the fracture stress of pure zinc by 50% and dilute zinc alloys (0.2 at.% Cu or Ag) by 5 times that in an inert environment. The fracture propagation energy for a crack in zinc single crystals in mercury is 60%, and in gallium it is 40% of that in air. Zinc is embrittled more severely by gallium than by indium or mercury.

Aluminum. Mercury embrittles both pure and alloyed aluminum. (Ref 2, 4, 5, 43). The tensile stress is decreased by some 20%. The fatigue life of 7075 aluminum alloy is reduced in mercury, and brittle-to-ductile transition occurs at 200 °C (390 °F). Additions of gallium and cadmium to mercury increase the embrittlement of aluminum. Delayed failure by LMIE occurs in mercury. Dewetting of aluminum by mercury has been found to inhibit embrittlement. The possible cause of dewetting is the dissolution of aluminum by mercury, the oxidation of fine aluminum particles by air, and the formation of aluminum oxide at the aluminum-mercury interface.

The aluminum-gallium system has been well studied (Ref 2, 6, 11, 44, 45, 46, 47, 48, 49, 50). As little as 1 MPa$\sqrt{m}$ (1 ksi$\sqrt{\text{in.}}$) can yield failure (Ref 3, 6). In some cases, gallium in contact with aluminum disintegrates aluminum alloys into individual grains in the absence of applied stress. Therefore, grain-boundary penetration of gallium is sometimes used to separate grains and to study topographical features and orientations of grains in aluminum.

Aluminum alloys are embrittled by tin-zinc and lead-tin alloys. The embrittlement susceptibility is related to heat treatment and the strength level of the alloy. There is some uncertainty about whether zinc embrittles aluminum. However, indium severely embrittles aluminum. Alkali metals, sodium, and lithium are known to embrittle aluminum. Aluminum alloys containing either lead, cadmium, or bismuth (Ref 33) inclusions embrittle aluminum when impact tested near the melting point of these inclusions. The severity of embrittlement increases from lead to cadmium to bismuth.

Copper. Mercury embrittles copper (Ref 41), and the severity of embrittlement increases when copper is alloyed with aluminum and zinc. Antimony, cadmium, lead, tin (Ref 51), and thallium are also reported to embrittle copper. Mercury embrittlement of brass is a classic example of LMIE. Embrittlement occurs in both tension and fatigue and varies with grain size and strain rate. Mercury embrittlement of brass and copper alloys

has been extensively investigated. Lead and tin inclusions in brass cause severe embrittlement when tested near the melting point of these inclusions. Lithium reduces the rupture stress and elongation at failure of solid copper. Sodium is reported to embrittle copper; however, cesium does not. The embrittling effects of bismuth for copper and their alloys are well documented. Gallium embrittles copper at temperatures ranging from 25 to 240 °C (75 to 465 °F) (Ref 7, 27, 36, 52). Gallium also embrittles single crystals of copper. Indium embrittles copper at 156 to 250 °C (313 to 480 °F).

Other Nonferrous Materials. Tantalum and titanium alloys are embrittled by mercury and by Hg-3Zn solution. Refractory metals and alloys, specifically W-25Re, molybdenum, and Ta-10W, are susceptible to LMIE when in contact with molten Pu-1Ga. Cadmium and lead are not embrittled by mercury. However, indium dissolved in mercury embrittles both polycrystalline and single-crystal cadmium (Fig. 3). The embrittlement of titanium and its alloys by both liquid and solid cadmium is well recognized by the aircraft industry. Cadmium-plated fasteners of both titanium and steel are known to fail prematurely below the melting point of cadmium. Cadmium- plated steel bolts have good stress-corrosion resistance, but cadmium is known to crack steel. Therefore, such bolts are not recommended for use. Zinc is reported to embrittle magnesium and titanium alloys. Silver, gold, and their alloys are embrittled by both mercury and gallium. Nickel and nickel alloys are embrittled by mercury (Ref 10, 53, 54), cadmium (Ref 55), bismuth (Ref 39), lithium (Ref 54), and sodium (Ref 54). Nickel is severely embrittled by cadmium dissolved in cesium. The fracture mode is brittle IG with bright grain-boundary fracture.

Embrittlement of Zircaloy by mercury (Ref 32, 56), calcium, strontium, zinc, cesium cadmium (Ref 57, 58), cadmium (Ref 40, 58), and iodine has been reported. Failure of Zircaloy tubes used as cladding material for nuclear fuel rods has been suspected to result from nuclear- interaction reaction products, such as iodine and cadmium carried by liquid cesium, which is used as a coolant in the reactor. Systematic investigation in the laboratory has shown that cadmium, both in the solid and the liquid state or as a carrier species dissolved in liquid cesium, causes severe LMIE and SMIE of zirconium and Zircaloy-2.

References cited in this section

2. D.A. Wheeler, R.G. Hoagland, and J.P. Hirth, Effect of Solid Metal Strength Level on the Liquid-Metal Embrittlement of Aluminum by Mercury, *Scr. Metall.,* Vol 22, 1988, p 533–538

3. B.A. Benson and R.G. Hoagland, Crack- Growth Behavior of a High-Strength Aluminum Alloy During LME by Gallium, *Scr. Metall.,* Vol 23, 1989, p 1943–1948

4. D.A. Wheeler, R.G. Hoagland, and J.P. Hirth, Evidence for Crack Tip Oxidation Effects During the Liquid-Metal Embrittlement of AA-7075 Aluminum-Alloy by Mercury, *Corrosion,* Vol 45, 1989, p 207–212

5. J.A. Kapp, in *Embrittlement by Liquid and Solid Metals,* M.H. Kamdar, Ed., TMS/ AIME, 1984, p 117–131

6. D.G. Kolman and R. Chavarria, "Liquid- Metal Embrittlement of 7075 Aluminum and 4340 Steel Compact Tension Specimens by Gallium," *J. Test. Eval.,* Vol 30 (No. 5), 2002, p 452–456

7. P.H. Au-Yeung, J.T. Lukowski, L.A. Heldt, and C.L. White, An Auger Spectrometric Study of the Crack Tip Surface-Chemistry for Liquid-Metal Embrittlement: Beta-Brass Embrittled by Gallium, *Scr. Metall. Mater.,* Vol 24, 1990, p 95–100

10. S.P. Lynch, Hydrogen Embrittlement and Liquid-Metal Embrittlement in Nickel Single-Crystals, *Scr. Metall.,* Vol 13, 1979, p 1051–1056

11. C.F. Old and P. Trevena, *Met. Sci.,* Vol 13, 1979, p 487, 591–596

27. P.J.L. Fernandes and D.R.H. Jones, The Effects of Loading Variables on Fatigue-Crack Growth in Liquid-Metal Environments, *Int. J. Fatigue,* Vol 17, 1995, p 501–505

32. B. Cox and Y.M. Wong, Liquid Metal Embrittlement of Zr-2.5% Nb Alloy, *J. Nucl. Mater.,* Vol 245, 1997, p 34–43

33. D.D. Perovic, G.C. Weatherly, and W.A. Miller, Influence of Temperature and Strain- Rate on Liquid-Metal Embrittlement of an Aluminum Alloy Containing Bismuth Inclusions, *Acta Metall.,* Vol 36, 1988, p 2249–2257

36. P.L.J. Fernandes and D.R.H. Jones, The Effects of Microstructure on Crack Initiation in Liquid-Metal Environments, *Eng. Fail. Anal.,* Vol 4, 1997, p 195–204

39. V.Y. Abramov, S.N. Bozin, O.I. Eliseeva, G.M. Kalinin, V.I. Kalyandruk, and E.M. Lyutyi, Influence of a Lead Melt on Plastic- Deformation of High-Alloyed Heat-Resistant Steels, *Mater. Sci.,* Vol 30, 1994, p 465–469

40. W.T. Grubb, Cadmium Metal Embrittlement of Zircaloy-2, *Nature,* Vol 265, 1977, p 36–37

41. T.M. Regan and N.S. Stoloff, Mercury Embrittlement of Cu-Al Alloys Under Cyclic Loading, *Metall. Trans. A,* Vol 8, 1977, p 885–890

43. X.M. Liu, Y.J. Su, L.J. Qiao, and W.Y. Chu, Transmission Electron Microscopic Observations of Embrittlement of an Aluminum Alloy by Liquid Metal, *Corrosion,* Vol 55, 1999, p 851–857

44. Y. Kodama, P.K. Choi, H. Koizumi, and S. Hyodo, Acoustic-Emission Associated with the Fracture of Al and Al-Alloy Embrittled by Liquid Gallium, *Mater. Sci. Eng. A,* Vol 176, 1994, p 231–235

45. C. Roques-Carmes, M. Aucouturier, and P. Lacombe, *Met. Sci.,* Vol 7, 1973, p 128–132

46. R.C. Hugo and R.G. Hoagland, Gallium Penetration of Aluminum: In-Situ TEM Observations at the Penetration Front, *Scr. Mater.,* Vol 41, 1999, p 1341–1346

47. R.C. Hugo and R.G. Hoagland, The Kinetics of Gallium Penetration into Aluminum Grain Boundaries: In Situ TEM Observations and Atomistic Models, *Acta Mater.,* Vol 48, 2000, p 1949–1957

48. W. Ludwig and D. Bellet, Penetration of Liquid Gallium into the Grain Boundaries of Aluminium: A Synchrotron Radiation Microtomographic Investigation, *Mater. Sci. Eng. A,* Vol 281, 2000, p 198–203

49. J.A. Kargol and D.L. Albright, Effect of Relative Crystal Orientation on Liquid- Metal Induced Grain-Boundary Fracture of Aluminum Bicrystals, *Metall. Trans. A,* Vol 8, 1977, p 27–34

50. W.Y. Chu, X.M. Liu, J.L. Luo, and L.J. Qiao, Mechanism of Embrittlement of Al Alloy by Liquid Metal Ga, *Can. Metall. Q.,* Vol 38, 1999, p 127–132

51. R.C. Muthiah, J.A. Pfaendtner, S. Ishikawa, and C.J. McMahon, Tin-Induced Dynamic Embrittlement of Cu-7%Sn Bicrystals with a Sigma 5 Boundary, *Acta Mater.,* Vol 47, 1999, p 2797–2808

52. J.T. Lukowski, D.B. Kasul, L.A. Heldt, and C.L. White, Discontinuous Crack Propagation in Ga-Induced Liquid-Metal Embrittlement of Beta-Brass, *Scr. Metall. Mater.,* Vol 24, 1990, p 1959–1964

53. V.I. Igoshev, L.G. Rogova, L.I. Trusov, and T.P. Khvostantseva, Embrittlement of Nanocrystalline Nickel by Liquid-Metals, *J. Mater. Sci.,* Vol 29, 1994, p 1569–1574

54. S.P. Lynch, A Fractographic Study of Hydrogen-Assisted Cracking and Liquid-Metal Embrittlement in Nickel, *J. Mater. Sci.,* Vol 21, 1986, p 692–704

55. D.W. Cameron, Failures in Large Gas Turbines Due to Liquid-Metal Embrittlement, *Mater. Charact.*, Vol 33, 1994, p 37–43

56. B. Cox, *Corrosion,* Vol 28, 1972, p 207–[fj 217

57. B. Cox, B.A. Surette, and J.C. Wood, in *Environmental Degradation of Engineering Materials in Aggressive Environments,* M.R. Louthan, R.P. McNitt, and R.D Sisson Ed., Laboratory for the Study of Environmental Degradation of Engineering Materials, 1981, p 293–302

58. S.W. Sharkawy, A.A. Abouzahra, and F.H. Hammad, Liquid-Metal Embrittlement of Zircaloy-2 Tubes by Cesium/Cadmium, *J. Nucl. Mater.,* Vol 126, 1984, p 184–189

D.G. Kolman, Liquid Metal Induced Embrittlement, *Corrosion: Fundamentals, Testing, and Protection,* Vol 13A, *ASM Handbook,* ASM International, 2003, p 381–392

Liquid Metal Induced Embrittlement

Revised by David G. Kolman, Los Alamos National Laboratory

Embrittlement of Ferrous Metals and Alloys

Embrittlement by Aluminum. Tensile and stress-rupture tests have been conducted on steels in molten aluminum at 690 °C (1275 °F). For short-term tensile tests, a reduced breaking stress and reduction of area were found as compared to the values in air. In the stress-rupture tests, the time to failure was dependent on the applied stress.

Embrittlement by Antimony. American Iron and Steel Institute (AISI) 4340 steel tested in fatigue in liquid Pb-35Sb at 540 °C (1000 °F) and in antimony at 675 °C (1250 °F) was very severely embrittled (Ref 30). The embrittlement in lead antimony occurred 165 to 220 °C (300 to 400 °F) higher than that observed for high-purity lead. Small additions of antimony (~5 wt%) to lead had no effect on embrittlement when tested in fatigue, although 0.002 to 0.2% Sb additions have caused a significant increase in the embrittlement of smooth AISI 4140 steel specimens tested in tension. Embrittlement by antimony increases with temperature and is thought to occur by the grain-boundary diffusion of antimony in steel.

Embrittlement by Bismuth. On testing in liquid bismuth at 300 °C (570 °F), no embrittlement was noted in bend tests on a quenched-and-tempered steel. No intercrystalline attack was noted on the low-carbon steel after stress-rupture time- to-failure testing.

Embrittlement by Cadmium. In several studies of the embrittlement of AISI 4340 steel, embrittlement occurred at 260 to 322 °C (500 to 612 °F) but not at 204 °C (399 °F) for high- strength steel. Cracks were observed in samples loaded to 90% of their yield stress at 204 °C (399 °F). The threshold stress required for cracking decreases with an increase in temperature. Cracking at 204 °C (399 °F) was strongly dependent on the strength level of the steel, and embrittlement was not observed for strength levels less than 1240 MPa (180 ksi). Delayed failure occurs in cadmium-plated high-strength steels (AISI 4340, 4140, 4130, and an 18% Ni maraging steel). Failures were observed at 232 °C (450 °F), which is approximately 90 °C (160 °F) below the melting point of cadmium. Static failure limits of 10 and 60% of the room-temperature notch strength have been reported for electroplated and vacuum-deposited cadmium, respectively, at 300 °C (570 °F). A discontinuous crack propagation mode was observed, consisting of a series of crack propagation steps separated by periods of no apparent growth. This slow crack growth region was characterized by cracks along the prior-austenite grain boundaries. Once the cracks reached a critical size, a catastrophic failure occurred that was characterized by a transgranular ductile fracture. An AISI 4130 steel exposed to cadmium has also been reported to fail at 316 °C (601 °F) (Ref 55).

Embrittlement of high-strength steels occurs when they are stress-rupture tested in liquid and solid cadmium. Cadmium produces a progressive decrease in the reduction of area at fracture of AISI 4140 steel over the temperature range of 170 to 321 °C (338 to 610 °F). Cadmium was identified as a more potent solid metal embrittling agent than lead, tin, zinc, or indium.

It has been reported that 304 stainless steel is immune to LMIE in cadmium and cadmium aluminum over a wide range of temperature and strain rate (Ref 59).

Embrittlement by Copper. The embrittlement of low-carbon steel by copper plate occurred at 900 °C (1650 °F) during a slow-bend test. The embrittling effects of the copper plate exceeded those encountered with brazing alloys. Similar observations have been made for plain carbon steels, silicon steels, and chromium steels at 1000 to 1200 °C (1800 to 2190 °F). Iron-36 Ni (Ref 35), 304 stainless steel (Ref 15, 17), and 316 stainless steel (Ref 17) also have been shown to be embrittled by copper.

The surface cracking produced during the hot working of some steels at 1100 to 1300 °C (2010 to 2370 °F) also has several characteristics of LMIE. It is promoted by surface enrichment of copper and other elements during oxidation and subsequent penetration along the prior-austenite grain boundaries. Elements such as nickel, molybdenum, tin, and arsenic that affect the melting point of copper or its solubility in austenite also influence embrittlement. A ductility trough has also been noted, with no cracking produced at temperatures above 1200 °C (2190 °F). Steel plated with copper and pulse heated to the melting point of copper in milliseconds was embrittled by both liquid and solid copper. Hot tensile testing in a Gleeble testing machine at high strain rates produced severe cracking in AISI 4340 steel by both the liquid and solid copper.

Embrittlement by Gallium. The alloy Fe-3Si is severely embrittled by gallium, as are the solid solutions of iron, AISI 4340 steel (Ref 6), and 316L stainless steel (Ref 72).

Embrittlement by Indium. Indium embrittles pure iron and carbon steels. Embrittlement depends on both the strength level and the microstructure. Pure iron was embrittled only at temperatures above 310 °C (590 °F), appreciably above the melting point of indium. However, other steels, such as AISI 4140 (ultimate tensile strength of 1379 MPa, or 200 ksi), were embrittled by both solid and liquid indium. Surface cracks were detected at temperatures below the melting temperature of indium. This was interpreted as a local manifestation of the underlying embrittlement mechanism, and it was assumed that the cracks must reach a critical size before the gross mechanical properties are affected.

Embrittlement by Lead. The influence of lead on the embrittlement of steel has been extensively investigated (Ref 30, 38, 39, 60, 61, 62) and has been found to be sensitive to both composition and metallurgical effects. The studies fall into two major classifications:

- Liquid metal induced embrittlement due to contact with an external source of liquid lead
- Internal LMIE in which the lead is present internally as inclusions or a minor second phase, as in leaded steels

Both external and internal lead-induced embrittlement exhibit similar characteristics, but for the purpose of simplicity, each is treated individually.

Liquid Metal Induced Embrittlement Due to External Lead. When exposed to pure lead, AISI 4145 and 4140 steels exhibit classic LMIE, as shown by substantial decreases in both the reduction of area and the elongation at fracture. The fracture stress and the reduction of area decreased at temperatures considerably below the melting point of lead and varied continuously through the melting point, suggesting that the same embrittlement mechanism is operative for both solid and liquid metal environments.

Additions of zinc, antimony, tin, bismuth, and copper increase the embrittling potency of lead. Additions of up to 9% Sn, 2% Sb, or 0.5% Zn to lead increased the embrittlement of AISI 4145 steel. In some cases, the embrittlement and failure occurred before the ultimate tensile strength (UTS) was reached. The extent of embrittlement increases with increasing impurity content. No correlation was observed between the degree of embrittlement and wettability. The lead-tin alloys readily wetted steels, but the more embrittling lead-antimony alloys did not.

Liquid Metal Induced Embrittlement Due to Internal Lead. Leaded steels are economically attractive, because lead increases the machining speed and the lifetime of the cutting tools. The first systematic investigation of embrittlement of leaded steels was reported in 1968 by Mostovoy and Breyer. Embrittlement characteristics similar to those promoted by external lead were observed. The degradation in the ductility began at approximately 120 °C (215 °F) below the melting point of lead, with the embrittlement trough present from 230

to 454 °C (446 to 849 °F). This was followed by a reversion to ductile behavior at approximately 480 °C (895 °F).
The severity of the embrittlement and the brittle-to-ductile transition temperature, T_R, have been shown to be dependent on the strength level of the steel, with the degree of embrittlement and T_R increasing with strength level. In these studies, IG fracture was produced, which was propagation controlled at low temperatures and nucleation controlled at high temperatures. The degree of embrittlement was critically dependent on the lead composition, and the influence of trace impurities completely masked any variations due to different carbon and alloy compositions of the steel. Lead embrittlement of a steel compressor disk was induced by bulk lead contents of 0.14 and 6.22 wt%. The lead is associated with the nonmetallic inclusions, and on yielding, microcracks form at the weak inclusion-matrix interface, releasing a source of embrittling agent to the crack tip that aids subsequent propagation. An electron microprobe analysis of the nonmetallic inclusions identified the presence of zinc, antimony, tin, bismuth, and arsenic. With the exception of arsenic, all these trace impurities have been shown to have a significant effect on the external LMIE of steel.
The two most promising methods of suppressing LMIE are the control of sulfide composition and morphology and the cold working of the steel. The addition of rare earth elements to the steel melt modifies the sulfide morphology and composition and can eliminate LMIE.
Embrittlement by Lithium. Exposure of AISI 4340 steel to lithium at 200 °C (390 °F) resulted in static fatigue, with the time to failure depending on the applied stress. A decreasing fracture stress and elongation to fracture were noted with increasing UTS of variously treated steels, and catastrophic failure occurred for those steels with tensile strengths exceeding 1034 MPa (150 ksi). The tensile ductility of low-carbon steel at 200 °C (390 °F) was drastically reduced in lithium, with IG failure after 2 to 3% elongation, but there was no effect on the yield stress or the initial work-hardening behavior. The fracture stress was shown to be a linear function of $d^{-1/2}$, where d is the average grain diameter, in accordance with the Petch relationship.
Embrittlement by Mercury. A variety of studies have examined the steel-mercury system (Ref 5, 9, 63, 64). It has been shown that mercury embrittlement is crack nucleation controlled and can be induced in low-carbon steel samples by the introduction of local stress raisers. The fracture toughness of a notched 1Cr-0.2 Mo steel was significantly decreased on testing in mercury. The effective surface energy required to propagate the crack was 12 to 16 times greater in air than in mercury. The fatigue life of AISI 4340 steel in mercury is reduced by 3 orders of magnitude as compared to that in air.
The addition of solutes (cobalt, silicon, aluminum, and nickel) to iron, which reduced the propensity for cross slip by decreasing the number of active slip systems and changed the slip mechanism from wavy to planar glide, increased the susceptibility to embrittlement. Iron alloys containing 2% Si, 4% Al, or 8% Ni and iron containing 20% V or iron containing 49% Co and 2% V have been shown to be embrittled by mercury in unnotched tensile tests. The degree of embrittlement behavior was extended to lower alloy contents by using notched samples. No difference in the embrittlement potency of mercury or a saturated solution of indium in mercury was noted.
Effect of Selenium. Selenium had no embrittling effect on the mechanical properties of a quenched-and-tempered steel (UTS ~1460 MPa, or 212 ksi) bend tested at 250 °C (480 °F).
Embrittlement by Silver. Silver had no significant effect on the mechanical properties of a range of plain carbon steels, silicon steels, and chromium steels tested by bending at 1000 to 1200 °C (1830 to 2190 °F). However, a silver- base filler metal containing 45% Ag, 25% Cd, and 15% Sn has been reported to embrittle A- 286 heat-resistant steel in static load tests above and below 580 °C (1076 °F), the melting point of the alloy.
Effect of Sodium. Unnotched tensile properties of low-carbon steel remained the same when tested in air and in sodium at 150 and 250 °C (300 and 480 °F). Similarly, Armco iron (Armco Inc.), low-carbon steel, and type 316 steel were not embrittled by sodium at 150 to 1600 °C (300 to 2910 °F). Sodium containing nonmetallic impurities was shown to be more aggressive than sodium alone for bainitic, martensitic, tempered martensitic, and ferritic/pearlitic steels (Ref 34, 65).
Embrittlement by Solders and Bearing Metals. A wide range of steels are susceptible to embrittlement and intercrystalline penetration by molten solders and bearing metals at temperatures under 450 °C (840 °F). Tensile tests have revealed embrittlement as a reduction in ductility. The embrittlement increased with grain size and strength level of the steel, except for temper-embrittled steels.
The tensile strength and ductility of carbon steel containing 0.13% C were decreased on exposure to the molten solders and bearing alloys. The embrittlement was concomitant with a change to a brittle IG fracture mode and penetration along prior-austenite grain boundaries. Ductile failure was observed with samples tested in air or in

the liquid metal at temperatures exceeding 450 °C (840 °F). No intercrystalline penetration of solder was noted in carbon steels containing 0.77 and 0.14% C at 950 °C (1740 °F).

It has been reported that solder embrittles steel more than Woods metal (a bismuth-base fusible alloy containing lead and tin), particularly if it contains 4% Zn. The bearing metals produced embrittlement similar to the solder-containing 4% Zn alloy.

Embrittlement by Tellurium. Tellurium-associated embrittlement has been reported for carbon and alloy steels. Hot shortness occurs in AISI 12L14 + Te steel, with the most pronounced loss in ductility between 810 and 1150 °C (1490 and 2100 °F), embrittlement being most severe at 980 °C (1795 °F). The embrittlement has been shown to occur by the formation of a lead-telluride film at the grain boundary, which melts at 923 °C (1693 °F). The mechanical test data and the examination of fracture surfaces by Auger electron spectroscopy and scanning electron microscopy indicated LMIE of steel by the lead-telluride compound. The embrittlement of austenitic stainless steel by tellurium and tellurium-cesium mixtures has been well documented (Ref 42, 66, 67, 68, 69, 70, 71).

Effect of Thallium. Thallium had no embrittling effects on the mechanical properties of a quenched-and-tempered steel (UTS ~1460 MPa, or 212 ksi) tested in bending at 325 °C (615 °F).

Embrittlement by Tin. The embrittling effect of tin has been observed in a range of austenitic and nickel-chromium steels, the degree of embrittlement increasing with strength level. Embrittlement depends on the presence of a tensile stress and is associated with intercrystalline penetration.

The embrittlement by solid tin occurs at approximately 120 °C (215 °F) below its melting point. The fracture surfaces exhibited an initial brittle zone perpendicular to the tensile axis that followed the prior-austenite grain boundaries. Layers of intermetallic compound present at the steel-tin interface did not impede the embrittlement process. Embrittlement has been observed in delayed-failure tests down to 218 °C (424 °F) (14 °C, or 25 °F, below the melting point of tin); however, in tensile tests, embrittlement by solid tin was effective at temperatures as low as 132 °C (270 °F), which is 100 °C (180 °F) below melting point.

An AISI 3340 steel doped with 500 ppm of phosphorus, arsenic, and tin has been tested in the presence of tin while in the segregated (temper embrittled) and the unsegregated states. Temper-embrittled steels were found to be more susceptible to embrittlement than steel heat treated to a nontempered state.

A lower fatigue limit and lifetime at stresses below the fatigue limit for low-carbon steel and for 18-8 stainless steel have been noted when tested in tin at 300 °C (570 °F). The exposure time to the tin before testing had no influence on the fatigue life of the steel.

Embrittlement of Austenitic Steels by Zinc. Two main types of interaction of zinc and austenitic stainless steel have been observed. Type I relates to the effects on unstressed material in which liquid metal penetration/erosion is the major controlling factor, and type II relates to stressed materials in which classic LMIE is observed.

Type I Embrittlement. Zinc slowly erodes unstressed 18-8 austenitic stainless steel at 419 to 570 °C (786 to 1058 °F) and penetrates the steel, with the formation of an intermetallic β nickel- zinc compound at 570 to 750 °C (1060 to 1380 °F). At higher temperatures, penetration along the grain boundaries occurs, with a subsequent diffusion of nickel into the zinc-rich zone. This results in a nickel-exposed zone adjacent to the grain boundaries, reducing the stability of the γ phase and causing it to transform to an α-ferrite; the associated volume change of the $\gamma \rightarrow \alpha$ transformation produces an internal stress that facilitates fracture along the grain boundaries. Similar behavior has been observed in an unstressed 316C stainless steel held 30 min at 750 °C (1380 °F), in which penetration occurred to a depth of 1 mm (0.04 in.), and in an unstressed type 321 steel held 2 h at 515 °C (960 °F), in which a penetration of 0.127 mm (0.005 in.) was observed.

Type II embrittlement occurs in stainless steel above 750 °C (1380 °F) and is characterized by an extremely fast rate of crack propagation that is several orders of magnitude greater than that of type I, with cracks propagating perpendicular to the applied stress. In laboratory tests, an incubation period was observed before the propagation of type II cracks, suggesting that they may be nucleated by type I cracks formed during the initial contact with zinc.

At 800 °C (1470 °F), a stressed type 316C stainless steel failed catastrophically when coated with zinc. Cracking was produced at a stress of 57 MPa (8 ksi) at 830 °C (1525 °F) and 127 MPa (18 ksi) at 720 °C (1330 °F), but failure was not observed at a stress of 16 MPa (2 ksi) at 1050 °C (1920 °F).

Liquid metal induced embrittlement may be produced by the welding of austenitic steels in the presence of zinc or zinc-base paints (Ref 16). Intercrystalline cracking has been observed in the heat-affected zone in areas heated from 800 to 1150 °C (1470 to 2100 °F), and electron microprobe analysis has been used to identify the

grain-boundary enrichment of nickel and zinc, together with the formation of a low-melting nickel-zinc compound. The embrittlement of sheet samples of austenitic steel coated with zinc dust dye and zinc chromate primer occurs at stresses of the order of 20 MPa (3 ksi).

Embrittlement of Ferritic Steels by Zinc. Embrittlement of ferritic steels and Armco iron by molten zinc has been reported in the temperature range of 400 to 620 °C (750 to 1150 °F). Long exposures and intercrystalline attack were needed to cause a reduction in the elongation to fracture; an iron-zinc intermetallic layer was formed that inhibited embrittlement until the layer was ruptured. High-alloy ferritic steels exhibit embrittlement by zinc at temperatures above 750 °C (1380 °F).

Delayed failure occurs in steel in contact with solid zinc at 400 °C (750 °F), which is 19 °C (34 °F) below the melting point of zinc. The slow crack growth region is characterized by intergranular mode of cracking.

Exposing AISI 4140 steel to solid zinc results in a decrease in the reduction of area and in fracture stress at 265 °C (510 °F), with no significant changes in the other mechanical properties. The tensile fracture initially propagates intergranularly, with the final failure occurring by shear. Liquid zinc embrittles 4140 steel at 431 °C (808 °F), and it has been shown that zinc is present at the crack tip.

Figure 16 shows a compilation of liquid metal embrittling and nonembrittling couples based on the theoretical calculations of the solubility parameter and the reduction in the fracture surface energy. The embrittlement curve is separated by brittle and ductile fracture. A concise summary of embrittlement couples is provided in Table 1. Both pure and alloyed solids are listed. References 8, 20, 22, 23, 24, and 26 are review articles that discuss embrittlement couples, some of which are not covered in Table 1.

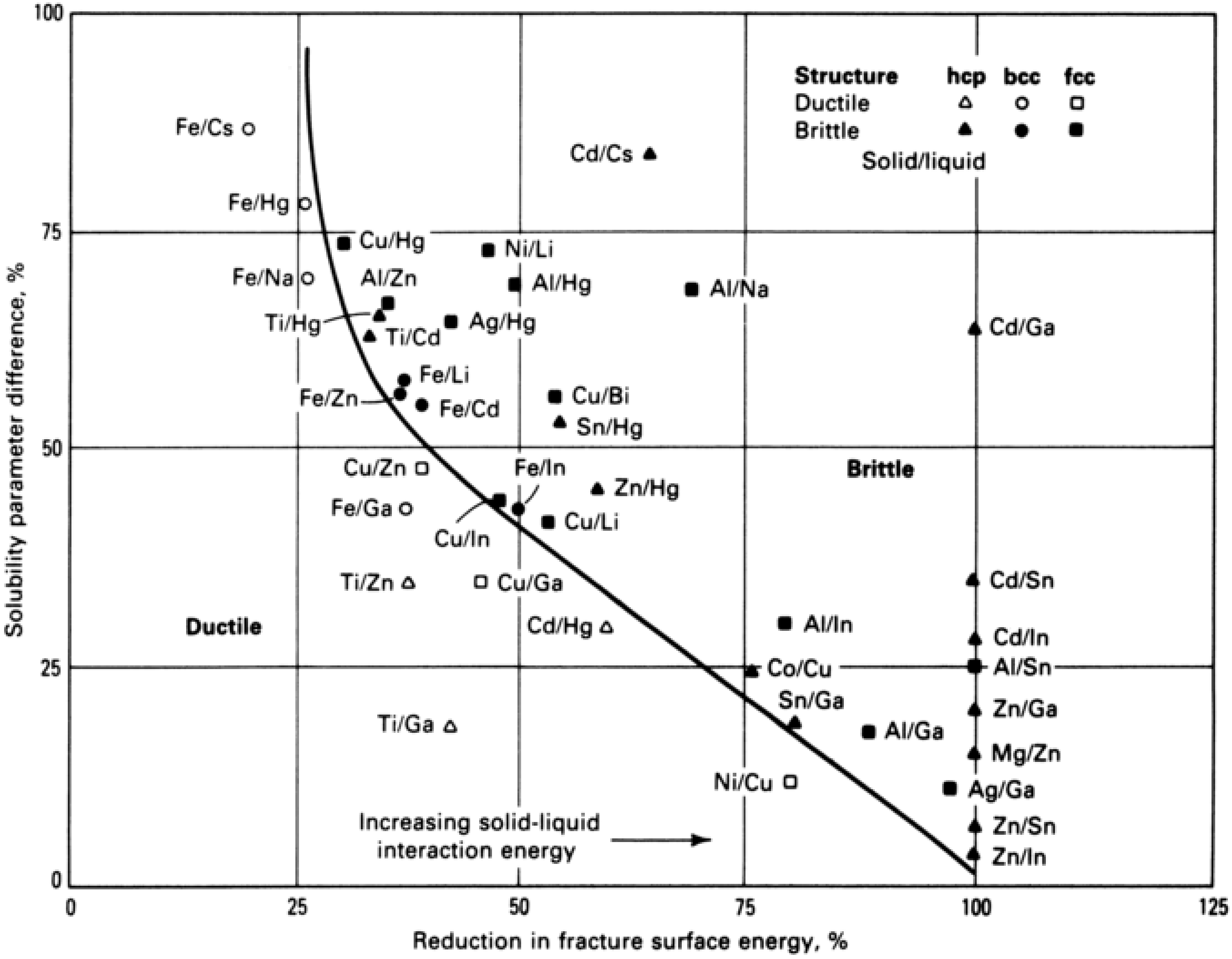

Fig. 16 Calculated reduction in the fracture surface energy relating to solubility parameter for many solid-liquid embrittlement couples. Note that the curve separates embrittlement couples from nonembrittled solid-liquid metal couples. hcp, hexagonal close-packed; bcc, body-centered cubic; fcc, face-centered cubic

Table 1 Summary of embrittlement couples

Solid		Liquid																				
		Hg		**Cs**	**Ga**		**Na**	**In**		**Li**	**Sn**		**Bi**		**Tl**	**Cd**	**Pb**		**Zn**	**Te**	**Sb**	**Cu**
		P	**A**	**P**	**P**	**A**	**P**	**P**	**A**	**P**	**P**	**A**	**P**	**A**	**P**	**P**	**P**	**A**	**P**	**P**	**P**	**P**
Sn	P	X	…	…	X	…	…	…	…	…	…	…	…	…	…	…	…	…	…	…	…	…
Bi	P	X	…	…	…	…	…	…	…	…	…	…	…	…	…	…	…	…	…	…	…	…
Cd	P	…	…	X	X	X	…	…	…	…	X	…	…	…	…	…	…	…	…	…	…	…
Zn	P	X	X	…	X	X	…	X	X	…	X	…	…	…	…	…	X	…	…	…	…	…
	LA	…	X	…	…	…	…	…	…	…	…	…	…	…	…	…	…	…	…	…	…	…
Mg	CA	…	…	…	…	…	X	…	…	…	…	…	…	…	…	…	…	…	X	…	…	…
Al	P	X	X	…	X	…	…	X	…	…	…	X	X	…	…	X	X	…	…	…	…	…
	CA	X	X	…	X	…	X	X	…	…	X	…	X	X	…	…	X	…	X	…	…	…
Ge	P	…	…	…	X	…	…	X	…	…	X	…	X	…	X	X	X	…	…	…	X	…
Ag	P	X	X	…	X	X	…	…	…	X	…	…	…	…	…	…	…	…	…	…	…	…
	LA	…	…	…	…	…	…	…	…	X	…	…	…	…	…	…	…	…	…	…	…	…
Cu	CP	X	X	…	…	…	X	…	…	X	…	…	X	X	…	…	X	…	…	…	…	…
	LA	X	…	…	X	…	…	…	…	…	…	…	…	…	…	…	…	…	…	…	…	…
	CA	X	X	…	X	…	…	X	X	X	X	(?)	X	…	…	…	X	…	…	…	…	…
Ni	P	X	…	…	…	…	…	…	…	X	…	…	…	…	…	…	X	…	…	…	…	…
	LA	…	…	…	…	…	…	…	…	X	…	…	…	…	…	…	…	…	…	…	…	…
	CA	…	…	…	…	…	…	…	…	…	X	…	…	…	…	…	X	…	…	…	…	…
Fe	P	…	…	…	…	…	…	…	…	…	…	…	…	…	…	…	…	…	…	…	…	X
	LA	X	X	…	X	…	…	X	X	X	…	…	…	…	…	…	…	…	…	…	…	…
	CA	…	…	…	X	…	…	X	…	X	X	…	…	…	…	X	X	X	X	X	X	X
Pd	P	…	…	…	…	…	…	…	…	X	…	…	…	…	…	…	…	…	…	…	…	…
	LA	…	…	…	…	…	…	…	…	X	…	…	…	…	…	…	…	…	…	…	…	…
Ti	CA	…	X	…	…	…	…	…	…	…	…	…	…	…	…	X	…	…	…	…	…	…

P, element (nominally pure): A, alloy; C, commercial; L, laboratory

References cited in this section

5. J.A. Kapp, in *Embrittlement by Liquid and Solid Metals,* M.H. Kamdar, Ed., TMS/ AIME, 1984, p 117–131

6. D.G. Kolman and R. Chavarria, "Liquid- Metal Embrittlement of 7075 Aluminum and 4340 Steel Compact Tension Specimens by Gallium," *J. Test. Eval.,* Vol 30 (No. 5), 2002, p 452–456

8. N.S. Stoloff, in *Environment-Induced Cracking of Materials,* R.P. Gangloff and M.P. Ives Ed., NACE, 1990, p 31–41

9. S. Ashok, N.S. Stoloff, M.E. Glicksman, and T. Slavin, Liquid-Metal and Hydrogen Embrittlement of Amorphous Alloys, *Scr. Metall.,* Vol 15, 1981, p 331–337

15. W.F. Savage, *Welding,* Vol 57, 1978, p s9–s16

16. R.M. Bruscato, Liquid-Metal Embrittlement of Austenitic Stainless-Steel When Welded to Galvanized Steel, *Weld. J.,* Vol 71, 1992, p S455–S459

17. W.F. Savage, E.F. Nippes, and M.C. Mushala, Liquid-Metal Embrittlement of Heat- Affected Zone by Copper Contamination, *Weld. J.,* Vol 57, 1978, p S237–S245

20. W. Rostoker, J.M. McCaughey, and H. Markus, *Embrittlement by Liquid Metals,* Reinhold Publishing, 1960

22. M.G. Nicholas, in *Embrittlement by Liquid and Solid Metals,* M.H. Kamdar, Ed., TMS/ AIME, 1984 p 27–50

23. M.G. Nicholas and C.F. Old, Liquid-Metal Embrittlement, *J. Mater. Sci.,* Vol 14, 1979, p 1–18

24. S.P. Lynch, Metal-Induced Embrittlement of Materials, *Mater. Charact.,* Vol 28, 1992, p 279–289

26. F.A. Shunk, Specificity as an Aspect of Liquid-Metal Embrittlement, W.R. Warke, Ed., *Scr. Metall.,* Vol 8, 1974, p 519–526

30. M.H. Kamdar, in *Embrittlement by Liquid and Solid Metals,* M.H. Kamdar, Ed., TMS, 1984 p 149–159

34. P. Skeldon, J.P. Hilditch, J.R. Hurley, and D.R. Tice, The Liquid-Metal Embrittlement of 9 Cr Steel in Sodium Environments and the Role of Nonmetallic Impurities, *Corros. Sci.,* Vol 36, 1994, p 593–610

35. H.G. Suzuki, Strain Rate Dependence of Cu Embrittlement in Steels, *ISIJ Int.,* Vol 37, 1997, p 250–254

38. N.N. Breyer and K.L. Johnson, Liquid- Metal Embrittlement of 4145 Steel by Lead- Tin and Lead-Antimony Alloys, *J. Test. Eval.,* Vol 2, 1974, p 471–477

39. V.Y. Abramov, S.N. Bozin, O.I. Eliseeva, G.M. Kalinin, V.I. Kalyandruk, and E.M. Lyutyi, Influence of a Lead Melt on Plastic- Deformation of High-Alloyed Heat-Resistant Steels, *Mater. Sci.,* Vol 30, 1994, p 465–469

42. M.G. Adamson, W.H. Reineking, and S. Vaidyanathan, Evidence for Liquid Cesium- Induced and Tellurium-Induced Fatigue Embrittlement of Cold-Worked AISI Type 316 Stainless Steel, *Trans. Am. Nucl. Soc.,* Vol 50, 1985, p 252–254

55. D.W. Cameron, Failures in Large Gas Turbines Due to Liquid-Metal Embrittlement, *Mater. Charact.,* Vol 33, 1994, p 37–43

59. J.K. Thomas, N.C. Iyer, H.B. Peacock, and J.A. Begley, Evaluation of Liquid-Metal Embrittlement of Stainless Steel 304 by Cadmium and Cadmium-Aluminum Solutions, *J. Nucl. Mater.,* Vol 210, 1994, p 216–225

60. A. Legris, G. Nicaise, J.B. Vogt, J. Foct, D. Gorse, and D. Vancon, Embrittlement of a Martensitic Steel by Liquid Lead, *Scr. Mater.,* Vol 43, 2000, p 997–1001

61. T. Sample and H. Kolbe, Liquid Metal Embrittlement (LME) Susceptibility of the 8–9% Cr Martensitic Steels and Their Simulated Welded Structures in Liquid Pb-17Li, *J. Nucl. Mater.,* Vol 283B, 2000, p 1336–1340

62. T. Sample, P. Fenici, and H. Kolbe, Liquid Metal Embrittlement Susceptibility of Welded MANET II (DIN 1.4914) in Liquid Pb-17Li, *J. Nucl. Mater.,* Vol 233–237, 1996, p 244–247

63. S.P. Lynch, Metal-Induced Embrittlement of Ductile Materials and Dislocation Emission from Crack Tips, *Scr. Metall.,* Vol 18, 1984, p 509–513

64. S.P. Lynch, A Fractographic Study of Gaseous-Hydrogen Embrittlement and Liquid- Metal Embrittlement in a Tempered-Martensitic Steel, *Acta Metall.,* Vol 32, 1984, p 79–90

65. J.P. Hilditch, J.R. Hurley, P. Skeldon, and D.R. Tice, The Liquid-Metal Embrittlement of Iron and Ferritic Steels in Sodium, *Corros. Sci.,* Vol 37, 1995, p 445–454

66. M.G. Adamson, E.A. Aitken, and S. Vaidyanathan, Synergistic Tellurium-Cesium Embrittlement of Type-316 Stainless Steel, *Nature,* Vol 295, 1982, p 49–51

67. M.G. Adamson and E.A. Aitken, On the Cs, Te Fission Product-Induced Attack and Embrittlement of Stainless Steel Cladding in Oxide Fuel Pins, *J. Nucl. Mater.,* Vol 132, 1985, p 160–166

68. J.A. Hemsworth, M.G. Nicholas, and R.M. Crispin, Tellurium Embrittlement of Type- 316 Steel, *J. Mater. Sci.,* Vol 25, 1990, p 5248–5256

69. M.G. Adamson, S. Vaidyanathan, T. Lauritzen, and W.H. Reineking, Evidence for Liquid-Metal Embrittlement of 20-Percent Cold-Worked Type 316 by Cesium-Tellurium Fission Products, *Trans. Am. Nucl. Soc.,* Vol 39, 1981, p 385–387

70. M.H. Adamson and W.H. Reineking, in *Embrittlement by Liquid and Solid Metals,* M.H. Kamdar, Ed., TMS-AIME, 1984, p 523–547

71. M.G. Adamson, W.H. Reineking, and S. Vaidyanathan, Liquid Cs, Te-Induced Fatigue Embrittlement of Cold-Worked 316 Stainless Steel, *Metall. Trans. A,* Vol 17, 1986, p 2090–2093

72. D.G. Kolman and R. Charvarria, "The Liquid Metal Embrittlement of 316L SS by Ga," Los Alamos National Laboratory Report LA-UR-02-7774; Submitted to *Corrosion,* Dec. 2002

D.G. Kolman, Liquid Metal Induced Embrittlement, *Corrosion: Fundamentals, Testing, and Protection*, Vol 13A, *ASM Handbook*, ASM International, 2003, p 381–392

Liquid Metal Induced Embrittlement

Revised by David G. Kolman, Los Alamos National Laboratory

Acknowledgment

This article was revised from M.H. Kamdar, Liquid Metal Embrittlement, in *Corrosion,* Vol 13, *Metals Handbook,* 9th ed., ASM International, 1987, p 171–184.

D.G. Kolman, Liquid Metal Induced Embrittlement, *Corrosion: Fundamentals, Testing, and Protection*, Vol 13A, *ASM Handbook*, ASM International, 2003, p 381–392

Liquid Metal Induced Embrittlement

Revised by David G. Kolman, Los Alamos National Laboratory

References

1. W.H. Johnson, *Proc. R. Soc. (London) A,* Vol 23, 1874, p 168

2. D.A. Wheeler, R.G. Hoagland, and J.P. Hirth, Effect of Solid Metal Strength Level on the Liquid-Metal Embrittlement of Aluminum by Mercury, *Scr. Metall.,* Vol 22, 1988, p 533–538

3. B.A. Benson and R.G. Hoagland, Crack- Growth Behavior of a High-Strength Aluminum Alloy During LME by Gallium, *Scr. Metall.,* Vol 23, 1989, p 1943–1948

4. D.A. Wheeler, R.G. Hoagland, and J.P. Hirth, Evidence for Crack Tip Oxidation Effects During the Liquid-Metal Embrittlement of AA-7075 Aluminum-Alloy by Mercury, *Corrosion,* Vol 45, 1989, p 207–212

5. J.A. Kapp, in *Embrittlement by Liquid and Solid Metals,* M.H. Kamdar, Ed., TMS/ AIME, 1984, p 117–131

6. D.G. Kolman and R. Chavarria, "Liquid- Metal Embrittlement of 7075 Aluminum and 4340 Steel Compact Tension Specimens by Gallium," *J. Test. Eval.,* Vol 30 (No. 5), 2002, p 452–456

7. P.H. Au-Yeung, J.T. Lukowski, L.A. Heldt, and C.L. White, An Auger Spectrometric Study of the Crack Tip Surface-Chemistry for Liquid-Metal Embrittlement: Beta-Brass Embrittled by Gallium, *Scr. Metall. Mater.,* Vol 24, 1990, p 95–100

8. N.S. Stoloff, in *Environment-Induced Cracking of Materials,* R.P. Gangloff and M.P. Ives Ed., NACE, 1990, p 31–41

9. S. Ashok, N.S. Stoloff, M.E. Glicksman, and T. Slavin, Liquid-Metal and Hydrogen Embrittlement of Amorphous Alloys, *Scr. Metall.,* Vol 15, 1981, p 331–337

10. S.P. Lynch, Hydrogen Embrittlement and Liquid-Metal Embrittlement in Nickel Single-Crystals, *Scr. Metall.,* Vol 13, 1979, p 1051–1056

11. C.F. Old and P. Trevena, *Met. Sci.,* Vol 13, 1979, p 487, 591–596

12. M.J. Kelley and N.S. Stoloff, Analysis of Liquid-Metal Embrittlement from a Bond- Energy Viewpoint, *Metall. Trans.,* Vol 6, 1975, p 159–166

13. J.C. Lynn, W.R. Warke, and P. Gordon, Solid Metal Induced Embrittlement of Steel, *Mater. Sci. Eng.,* Vol 18, 1975, p 51–62

14. W. Shih, J. King, and C. Raczkowski, Liquid-Copper/Zinc Embrittlement in Alloy 718, *Weld. J.,* Vol 77, 1998, p S219–S222

15. W.F. Savage, *Welding,* Vol 57, 1978, p s9–s16

16. R.M. Bruscato, Liquid-Metal Embrittlement of Austenitic Stainless-Steel When Welded to Galvanized Steel, *Weld. J.,* Vol 71, 1992, p S455–S459

17. W.F. Savage, E.F. Nippes, and M.C. Mushala, Liquid-Metal Embrittlement of Heat- Affected Zone by Copper Contamination, *Weld. J.,* Vol 57, 1978, p S237–S245

18. M.H. Kamdar, *Prog. Mater. Sci.,* Vol 15, 1973, p 289

19. M.H. Kamdar, in *Treatise on Materials Science and Technology,* Vol 25, C.L. Briant and S.K. Banerjee, Ed., Academic Press, 1983, p 361–459

20. W. Rostoker, J.M. McCaughey, and H. Markus, *Embrittlement by Liquid Metals,* Reinhold Publishing, 1960

21. B. Joseph, M. Picat, and F. Barbier, *Eur. Phys. J.-Appl. Phys.,* Vol 5, 1999, p 19–31

22. M.G. Nicholas, in *Embrittlement by Liquid and Solid Metals,* M.H. Kamdar, Ed., TMS/ AIME, 1984 p 27–50

23. M.G. Nicholas and C.F. Old, Liquid-Metal Embrittlement, *J. Mater. Sci.,* Vol 14, 1979, p 1–18

24. S.P. Lynch, Metal-Induced Embrittlement of Materials, *Mater. Charact.,* Vol 28, 1992, p 279–289

25. C.F. Old, Liquid-Metal Embrittlement of Nuclear-Materials, *J. Nucl. Mater.,* Vol 92, 1980, p 2–25

26. F.A. Shunk, Specificity as an Aspect of Liquid-Metal Embrittlement, W.R. Warke, Ed., *Scr. Metall.,* Vol 8, 1974, p 519–526

27. P.J.L. Fernandes and D.R.H. Jones, The Effects of Loading Variables on Fatigue-Crack Growth in Liquid-Metal Environments, *Int. J. Fatigue,* Vol 17, 1995, p 501–505

28. J.J. Lewandowski, Y.S. Kim, and N.J.H. Holroyd, Lead-Induced Solid Metal Embrittlement of an Excess Silicon Al-Mg-Si Alloy at Temperatures of -4 °C to 80 °C, *Metall. Trans. A,* Vol 23, 1992, p 1679–1689

29. J.A. Kargol and D.L. Albright, Fracture Mechanics Method for Determining Crack- Propagation Resistance of Embrittled Aluminum Bicrystals, *J. Test. Eval.,* Vol 3, 1975, p 173–178

30. M.H. Kamdar, in *Embrittlement by Liquid and Solid Metals,* M.H. Kamdar, Ed., TMS, 1984 p 149–159

31. S.P. Lynch, Liquid-Metal Embrittlement in an Al 6-Percent Zn 3-Percent Mg Alloy, *Acta Metall.,* Vol 29, 1981, p 325–340

32. B. Cox and Y.M. Wong, Liquid Metal Embrittlement of Zr-2.5% Nb Alloy, *J. Nucl. Mater.,* Vol 245, 1997, p 34–43

33. D.D. Perovic, G.C. Weatherly, and W.A. Miller, Influence of Temperature and Strain- Rate on Liquid-Metal Embrittlement of an Aluminum Alloy Containing Bismuth Inclusions, *Acta Metall.,* Vol 36, 1988, p 2249–2257

34. P. Skeldon, J.P. Hilditch, J.R. Hurley, and D.R. Tice, The Liquid-Metal Embrittlement of 9 Cr Steel in Sodium Environments and the Role of Nonmetallic Impurities, *Corros. Sci.,* Vol 36, 1994, p 593–610

35. H.G. Suzuki, Strain Rate Dependence of Cu Embrittlement in Steels, *ISIJ Int.,* Vol 37, 1997, p 250–254

36. P.L.J. Fernandes and D.R.H. Jones, The Effects of Microstructure on Crack Initiation in Liquid-Metal Environments, *Eng. Fail. Anal.,* Vol 4, 1997, p 195–204

37. D.D. Perovic, G.C. Weatherly, and W.A. Miller, On the Strain Rate Dependence of Ductility Troughs Observed Under Liquid- Metal Embrittlement and Creep Conditions, *Scr. Metall.,* Vol 21, 1987, p 345–347

38. N.N. Breyer and K.L. Johnson, Liquid- Metal Embrittlement of 4145 Steel by Lead- Tin and Lead-Antimony Alloys, *J. Test. Eval.,* Vol 2, 1974, p 471–477

39. V.Y. Abramov, S.N. Bozin, O.I. Eliseeva, G.M. Kalinin, V.I. Kalyandruk, and E.M. Lyutyi, Influence of a Lead Melt on Plastic- Deformation of High-Alloyed Heat-Resistant Steels, *Mater. Sci.,* Vol 30, 1994, p 465–469

40. W.T. Grubb, Cadmium Metal Embrittlement of Zircaloy-2, *Nature,* Vol 265, 1977, p 36–37

41. T.M. Regan and N.S. Stoloff, Mercury Embrittlement of Cu-Al Alloys Under Cyclic Loading, *Metall. Trans. A,* Vol 8, 1977, p 885–890

42. M.G. Adamson, W.H. Reineking, and S. Vaidyanathan, Evidence for Liquid Cesium- Induced and Tellurium-Induced Fatigue Embrittlement of Cold-Worked AISI Type 316 Stainless Steel, *Trans. Am. Nucl. Soc.,* Vol 50, 1985, p 252–254

43. X.M. Liu, Y.J. Su, L.J. Qiao, and W.Y. Chu, Transmission Electron Microscopic Observations of Embrittlement of an Aluminum Alloy by Liquid Metal, *Corrosion,* Vol 55, 1999, p 851–857

44. Y. Kodama, P.K. Choi, H. Koizumi, and S. Hyodo, Acoustic-Emission Associated with the Fracture of Al and Al-Alloy Embrittled by Liquid Gallium, *Mater. Sci. Eng. A,* Vol 176, 1994, p 231–235

45. C. Roques-Carmes, M. Aucouturier, and P. Lacombe, *Met. Sci.,* Vol 7, 1973, p 128–132

46. R.C. Hugo and R.G. Hoagland, Gallium Penetration of Aluminum: In-Situ TEM Observations at the Penetration Front, *Scr. Mater.,* Vol 41, 1999, p 1341–1346

47. R.C. Hugo and R.G. Hoagland, The Kinetics of Gallium Penetration into Aluminum Grain Boundaries: In Situ TEM Observations and Atomistic Models, *Acta Mater.,* Vol 48, 2000, p 1949–1957

48. W. Ludwig and D. Bellet, Penetration of Liquid Gallium into the Grain Boundaries of Aluminium: A Synchrotron Radiation Microtomographic Investigation, *Mater. Sci. Eng. A,* Vol 281, 2000, p 198–203

49. J.A. Kargol and D.L. Albright, Effect of Relative Crystal Orientation on Liquid- Metal Induced Grain-Boundary Fracture of Aluminum Bicrystals, *Metall. Trans. A,* Vol 8, 1977, p 27–34

50. W.Y. Chu, X.M. Liu, J.L. Luo, and L.J. Qiao, Mechanism of Embrittlement of Al Alloy by Liquid Metal Ga, *Can. Metall. Q.,* Vol 38, 1999, p 127–132

51. R.C. Muthiah, J.A. Pfaendtner, S. Ishikawa, and C.J. McMahon, Tin-Induced Dynamic Embrittlement of Cu-7%Sn Bicrystals with a Sigma 5 Boundary, *Acta Mater.,* Vol 47, 1999, p 2797–2808

52. J.T. Lukowski, D.B. Kasul, L.A. Heldt, and C.L. White, Discontinuous Crack Propagation in Ga-Induced Liquid-Metal Embrittlement of Beta-Brass, *Scr. Metall. Mater.,* Vol 24, 1990, p 1959–1964

53. V.I. Igoshev, L.G. Rogova, L.I. Trusov, and T.P. Khvostantseva, Embrittlement of Nanocrystalline Nickel by Liquid-Metals, *J. Mater. Sci.,* Vol 29, 1994, p 1569–1574

54. S.P. Lynch, A Fractographic Study of Hydrogen-Assisted Cracking and Liquid-Metal Embrittlement in Nickel, *J. Mater. Sci.,* Vol 21, 1986, p 692–704

55. D.W. Cameron, Failures in Large Gas Turbines Due to Liquid-Metal Embrittlement, *Mater. Charact.,* Vol 33, 1994, p 37–43

56. B. Cox, *Corrosion,* Vol 28, 1972, p 207–[fj 217

57. B. Cox, B.A. Surette, and J.C. Wood, in *Environmental Degradation of Engineering Materials in Aggressive Environments,* M.R. Louthan, R.P. McNitt, and R.D Sisson Ed., Laboratory for the Study of Environmental Degradation of Engineering Materials, 1981, p 293–302

58. S.W. Sharkawy, A.A. Abouzahra, and F.H. Hammad, Liquid-Metal Embrittlement of Zircaloy-2 Tubes by Cesium/Cadmium, *J. Nucl. Mater.,* Vol 126, 1984, p 184–189

59. J.K. Thomas, N.C. Iyer, H.B. Peacock, and J.A. Begley, Evaluation of Liquid-Metal Embrittlement of Stainless Steel 304 by Cadmium and Cadmium-Aluminum Solutions, *J. Nucl. Mater.,* Vol 210, 1994, p 216–225

60. A. Legris, G. Nicaise, J.B. Vogt, J. Foct, D. Gorse, and D. Vancon, Embrittlement of a Martensitic Steel by Liquid Lead, *Scr. Mater.,* Vol 43, 2000, p 997–1001

61. T. Sample and H. Kolbe, Liquid Metal Embrittlement (LME) Susceptibility of the 8–9% Cr Martensitic Steels and Their Simulated Welded Structures in Liquid Pb-17Li, *J. Nucl. Mater.,* Vol 283B, 2000, p 1336–1340

62. T. Sample, P. Fenici, and H. Kolbe, Liquid Metal Embrittlement Susceptibility of Welded MANET II (DIN 1.4914) in Liquid Pb-17Li, *J. Nucl. Mater.,* Vol 233–237, 1996, p 244–247

63. S.P. Lynch, Metal-Induced Embrittlement of Ductile Materials and Dislocation Emission from Crack Tips, *Scr. Metall.,* Vol 18, 1984, p 509–513

64. S.P. Lynch, A Fractographic Study of Gaseous-Hydrogen Embrittlement and Liquid- Metal Embrittlement in a Tempered-Martensitic Steel, *Acta Metall.,* Vol 32, 1984, p 79–90

65. J.P. Hilditch, J.R. Hurley, P. Skeldon, and D.R. Tice, The Liquid-Metal Embrittlement of Iron and Ferritic Steels in Sodium, *Corros. Sci.,* Vol 37, 1995, p 445–454

66. M.G. Adamson, E.A. Aitken, and S. Vaidyanathan, Synergistic Tellurium-Cesium Embrittlement of Type-316 Stainless Steel, *Nature,* Vol 295, 1982, p 49–51

67. M.G. Adamson and E.A. Aitken, On the Cs, Te Fission Product-Induced Attack and Embrittlement of Stainless Steel Cladding in Oxide Fuel Pins, *J. Nucl. Mater.,* Vol 132, 1985, p 160–166

68. J.A. Hemsworth, M.G. Nicholas, and R.M. Crispin, Tellurium Embrittlement of Type- 316 Steel, *J. Mater. Sci.,* Vol 25, 1990, p 5248–5256

69. M.G. Adamson, S. Vaidyanathan, T. Lauritzen, and W.H. Reineking, Evidence for Liquid-Metal Embrittlement of 20-Percent Cold-Worked Type 316 by Cesium-Tellurium Fission Products, *Trans. Am. Nucl. Soc.,* Vol 39, 1981, p 385–387

70. M.H. Adamson and W.H. Reineking, in *Embrittlement by Liquid and Solid Metals,* M.H. Kamdar, Ed., TMS-AIME, 1984, p 523–547

71. M.G. Adamson, W.H. Reineking, and S. Vaidyanathan, Liquid Cs, Te-Induced Fatigue Embrittlement of Cold-Worked 316 Stainless Steel, *Metall. Trans. A,* Vol 17, 1986, p 2090–2093

72. D.G. Kolman and R. Charvarria, “The Liquid Metal Embrittlement of 316L SS by Ga,” Los Alamos National Laboratory Report LA-UR-02-7774; Submitted to *Corrosion,* Dec. 2002

D.G. Kolman, Solid Metal Induced Embrittlement, *Corrosion: Fundamentals, Testing, and Protection,* Vol 13A, *ASM Handbook*, ASM International, 2003, p 393–397

Solid Metal Induced Embrittlement

Revised by David G. Kolman, Los Alamos National Laboratory

Introduction

EMBRITTLEMENT that occurs below the melting point, T_m, of the embrittling species is known as solid metal induced embrittlement (SMIE) of metals. The severity of embrittlement increases with temperature (Ref 1), with a sharp and significant increase in severity at the T_m of the embrittling agent. Above T_m, embrittlement has all the characteristics of liquid metal induced embrittlement (LMIE), as described in the previous article in this Section.

Although SMIE of metals has not been mentioned or recognized as an embrittlement phenomenon in industrial processes, many instances of loss in ductility, strength, and brittle fracture of metals and alloys have been reported for electroplated metals and coatings or inclusions of low-melting metals below their T_m (Ref 2). Delayed failure of cadmium-plated high-strength steel has been observed below the T_m of cadmium (Ref 3, 4). Accordingly, cadmium-plated steel bolts, despite their excellent resistance to corrosion, are not recommended for use above 230 °C (450 °F). Notched tensile specimens of various steels are embrittled by solid cadmium. Solid cadmium, silver, and gold embrittle titanium. Leaded steels are embrittled by solid lead, with considerable loss in ductility below the T_m of lead; this phenomenon accounts for numerous elevated-temperature failures of leaded steels, such as radial cracking of gear teeth during induction-hardening heat treatment, fracture of steel shafts during straightening at elevated temperature, and heat treatment failure of jet engine compressor disks. Liquid and solid cadmium metal environments, as well as cadmium dissolved in inert nonembrittling coolant liquid, serve to embrittle the Zircaloy-2 nuclear fuel cladding tubes used in nuclear reactors (Ref 5). Inconel vacuum seals are cracked by solid indium. These reports of brittle failure clearly indicate the importance of SMIE in industrial processes.

Solid metal induced embrittlement was first recognized and investigated in the mid-1960s and early 1970s by studying the delayed failure of steels and titanium in a solid cadmium environment (Ref 6, 7, 8). Results of these studies are shown in Fig. 1 and 2. A systematic investigation of SMIE (Ref 9) of steel by a number of solid metal embrittling species found that solid metal as an external environment can cause embrittlement and for steels represents a generalized phenomenon of embrittlement (see Fig. 3 in the article, "Liquid Metal Induced Embrittlement").

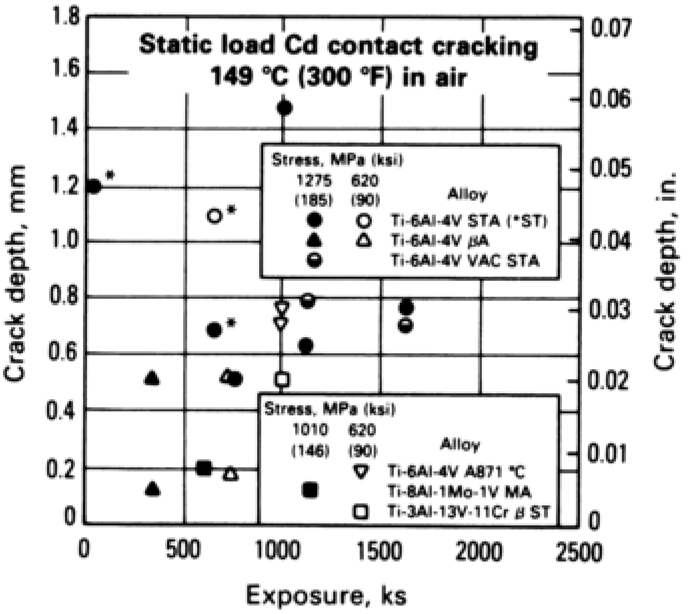

Fig. 1 Crack depth as a function of exposure time to solid cadmium environment for various titanium alloys at three stress levels. STA, solution treated and aged; ST, solution treated; VAC STA, vacuum solution treated and aged; βA, β-annealed; A, annealed; MA, mill annealed. Source: Ref 4

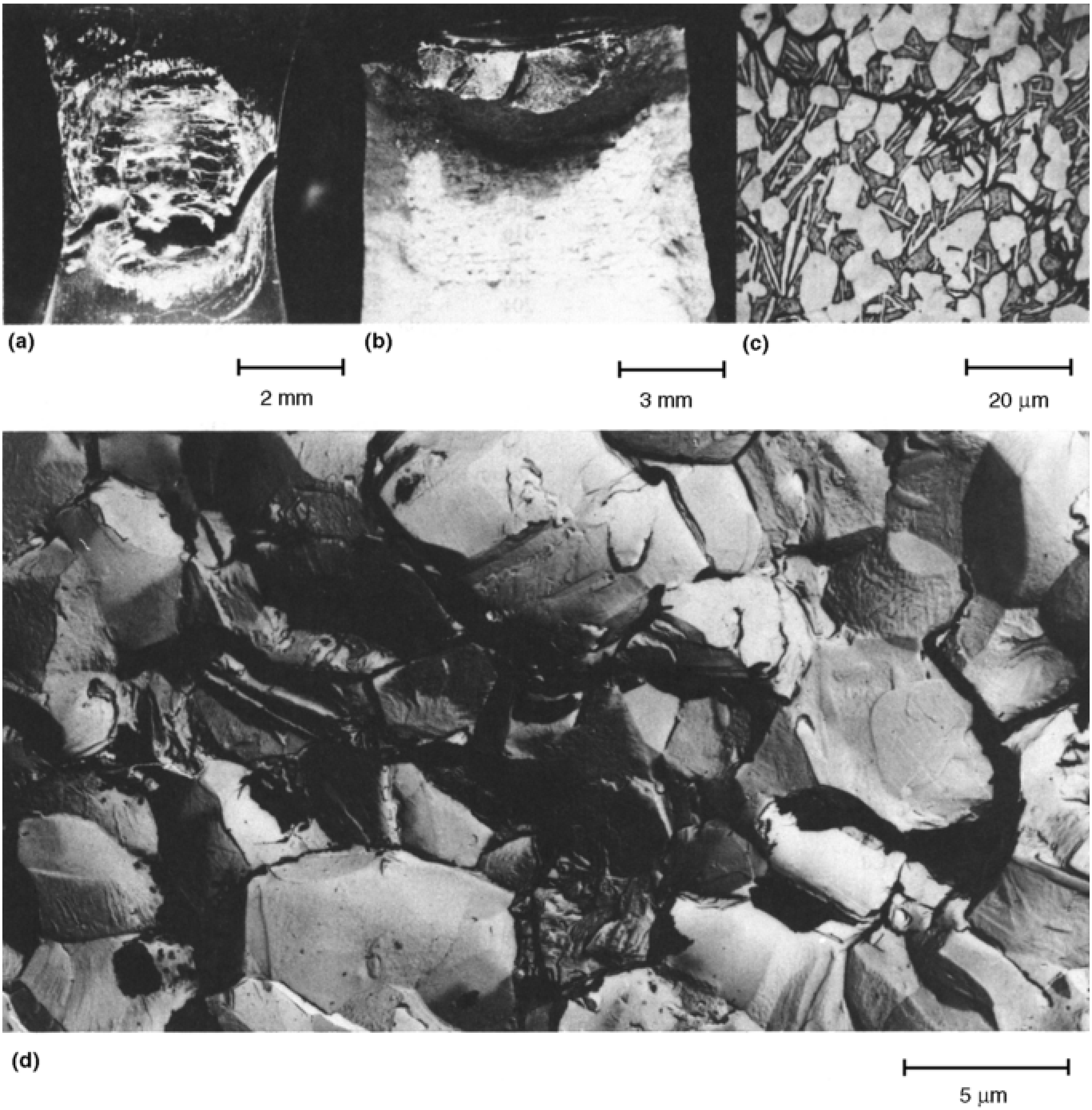

Fig. 2 Crack morphology for Ti-6Al-4V (solution treated and aged). (a) Typical specimen with multiple cracks in the indented area. (b) Fracture surface of (a) showing the depth of cadmium-induced cracking. (c) Cross section showing mixed intergranular cracking and α cleavage in cadmium-induced crack. Etched with Kroll's reagent. (d) Transmission electron microscopy fractograph (two-stage replica) of similar area showing intergranular cracking and cleavage. Courtesy of D.A. Meyn

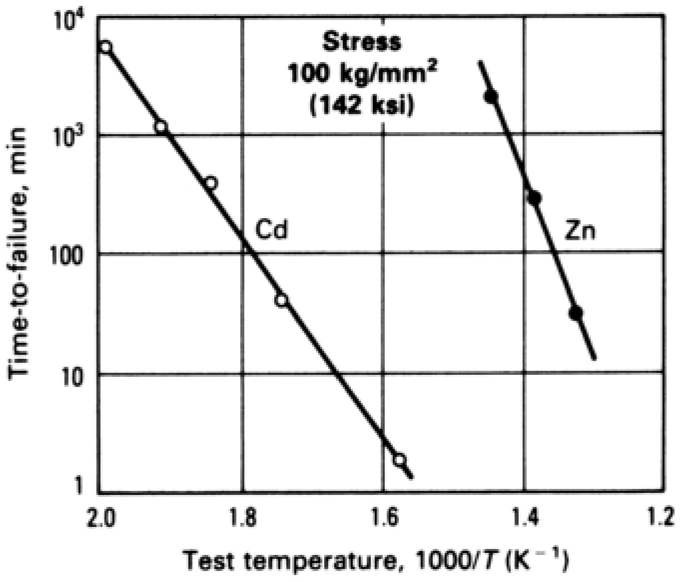

Fig. 3 Arrhenius plots of delayed failure in steel tested in cadmium and zinc. The activation energy, *Q*, is 39 kcal/mol for cadmium, 70 kcal/mol for zinc. Source: Ref 3

Solid metal induced embrittlement can also occur when the embrittling solid is an internal environment, that is, present in the solid as an inclusion (Ref 9). It has been clearly demonstrated that internally leaded steel is embrittled below the T_m of the lead inclusion of steel (Ref 9).

Brittle fracture in LMIE and SMIE is of significant scientific interest, because the embrittling species are in the vicinity of or at the tip of the crack and are not transported by dislocations or by slip due to plastic deformation into the solid, as is hydrogen in the hydrogen embrittlement of steels. Also, embrittling species are less likely to be influenced by the effects of grain- boundary impurities, such as antimony, phosphorus, and tin, which cause significant effects on the severity of hydrogen and temper embrittlement of metals. Investigations of SMIE and LMIE, therefore, can be interpreted less ambiguously than similar effects in other environments, such as hydrogen and temper embrittlement of metals. Thus, solid-liquid environmental effects provide a unique opportunity to study embrittlement mechanisms in a simple and direct manner under controlled conditions.

It is conceivable that a common mechanism may underlie solid, liquid, and gas phase induced embrittlement (Ref 10, 11, 12, 13, 14). The interactions at the solid-environment interface and the transport of the embrittling species to the crack tip may characterize a specific embrittlement phenomenon. A study of SMIE and LMIE may provide insights into the mechanisms of hydrogen and temper embrittlement. It is apparent that the phenomenon of SMIE is of both industrial and scientific importance. A review of the investigations of the occurrence and mechanisms of SMIE follows. See also the brief review paper by Lynch (Ref 1).

References cited in this section

1. S.P. Lynch, Metal-Induced Embrittlement of Materials, *Mater. Charact.,* Vol 28, 1992, p 279–289

2. S. Mostovoy and N.N. Breyer, *Trans. ASM,* Vol 61, 1968, p 219–232

3. Y. Asayama, in *Embrittlement by Liquid and Solid Metals,* M.H. Kamdar, Ed., American Institute of Mining, Metallurgical, and Petroleum Engineers, 1984

4. D.A. Meyn, *Corrosion,* Vol 29, 1973, p 192–196

5. W.T. Grubb, Cadmium Metal Embrittlement of Zircaloy-2, *Nature,* Vol 265, 1977, p 36–37

6. Y. Iwata, Y. Asayama, and A. Sakamoto, *J. Jpn. Inst. Met.,* Vol 31, 1967, p 73

7. D.N. Fager and W.F. Spurr, *Corrosion,* Vol 27, 1971, p 72

8. D.N. Fager and W. F. Spurr, *Corrosion,* Vol 26, 1970, p 409

9. J.C. Lynn, W.R. Warke, and P. Gordon, Solid Metal-Induced Embrittlement of Steel, *Mater. Sci. Eng.,* Vol 18, 1975, p 51–62

10. S.P. Lynch, Hydrogen Embrittlement and Liquid-Metal Embrittlement in Nickel Single Crystals, *Scr. Metall.,* Vol 13, 1979, p 1051–1056

11. S.P. Lynch, A Fractographic Study of Hydrogen-Assisted Cracking and Liquid-Metal Embrittlement in Nickel, *J. Mater. Sci.,* Vol 21, 1986, p 692–704

12. S.P. Lynch, A Fractographic Study of Gaseous-Hydrogen Embrittlement and Liquid- Metal Embrittlement in a Tempered-Martensitic Steel, *Acta Metall.,* Vol 32, 1984, p 79–90

13. S.P. Lynch and P. Trevena, Stress-Corrosion Cracking and Liquid-Metal Embrittlement in Pure Magnesium, *Corrosion,* Vol 44, 1988, p 113–124

14. S.P. Lynch, Mechanisms of Stress-Corrosion Cracking and Liquid-Metal Embrittlement in Al-Zn-Mg Bicrystals, *J. Mater. Sci.,* Vol 20, 1985, p 3329–3338

D.G. Kolman, Solid Metal Induced Embrittlement, *Corrosion: Fundamentals, Testing, and Protection,* Vol 13A, *ASM Handbook,* ASM International, 2003, p 393–397

Solid Metal Induced Embrittlement

Revised by David G. Kolman, Los Alamos National Laboratory

Characteristics of SMIE

To date, SMIE has been observed only in those couples in which LMIE occurs, suggesting that LMIE is a prerequisite for the occurrence of SMIE. Solid metal induced embrittlement may occur in the absence of LMIE if a brittle crack cannot be initiated at the T_m of the embrittling agent. A recent compilation of SMIE couples is given in Tables 1 and 2, which show that all solid metal embrittling agents are also known to cause LMIE.

Table 1 Occurrence of SMIE in steels

Base metal	Embrittler (melting point)	Onset of embrittlement		Test type[(a)]	Specimen type[(b)]
		°C	**°F**		
1041	Pb (327 °C, or 621 °F)	288	550	ST	S
1041 leaded	Pb	204	399	ST	S
1095	In (156 °C, or 313 °F)	100	212	ST	S
3340	Sn (232 °C, or 450 °F)	204	399	ST	N
	Pb	316	601	ST	N
4130	Cd (321 °C, or 610 °F)	300	572	DF	N
4140	Cd	300	572	DF	N
	Pb	204	399	ST	S
	Pb-Bi (NA)[(c)]	Below solidus		ST	S
	Pb-Zn (NA)	Below solidus		ST	S
	Zn (419 °C, or 786 °F)	254	489	DF	N

	Sn	218	424	DF	N
	Cd	188	370	DF	N
	Pb	160	320	DF	N
	In	Room temperature		DF	N
	Pb-Sn-Bi (NA)	Below solidus		ST	S
	In	80	176	DF	S
	Sn	204	399	ST	S
	Sn-Bi (NA)	Below solidus		ST	S
	Sn-Sb (NA)	Below solidus		ST	S
	In	110	230	DF	S
	In	93	199	DF	S
	In-Sn (118 °C, or 244 °F)	93	199	DF	S
4145	Sn	204	399	ST	S
	In	121	250	ST	S
	Pb-4Sn (NA)	204	399	ST	S
	Pb-Sn (NA)	204	399	ST	S
	Pb-Sb (NA)	204	399	ST	S
	Pb	288	550	ST	S
4145 leaded	Pb	204	399	ST	S
4340	Cd	260	500	DF	N
	Cd	300	572	DF	N
	Cd	38	100	DF	S
	Zn	400	752	DF	N
4340M	Cd	38	100	DF	S
8620	Pb	288	550	ST	S
8620 leaded	Pb	204	399	ST	S
A-4	Pb	288	550	ST	S
A-4 leaded	Pb	204	399	ST	S
D6ac	Cd	149	300	DF	N

(a) ST, standard tensile test; DF, delayed-failure tensile test.
(b) S, smooth specimen; N, notched specimen.
(c) NA, data not available. Courtesy of Dr. A. Druschitz

Table 2 Occurrence of SMIE in nonferrous alloys.

All test specimens were smooth type.

Base metal	Embrittler (melting point)	Onset of embrittlement		Test type[a]
		°C	**°F**	
Ti-6Al-4V	Cd (321 °C, or 610 °F)	38	100	DF
	Cd	149	300	BE
Ti-8Al-1Mo-1V	Cd	38	100	DF
	Cd	149	300	BE
Ti-3Al-14V-11Cr	Cd	149	300	BE
Ti-6Al-6V-2Sn	Cd	149	300	BE
	Ag (961 °C, or 1762 °F)	204–232	399–450	BE
	Au (1053 °C, or 1927 °F)	204–232	399–450	BE
Cu-Bi[b]	Hg (-39 °C, or -38 °F)	-84	-119	ST
Cu-Bi[c]	Hg	-87	-125	ST
Cu-3Sn[c]	Hg	-48	-54	ST
Cu-1Zn[c]	Hg	-46	-51	ST
Tin bronze	Pb (327 °C, or 621 °F)	200	392	IM
Zinc	Hg	-51	-60	ST

Inconel	In (156 °C, or 313 °F)	Room temperature		RE
Zircaloy-2	Cd	300	572	ST

(a) DF, delayed-failure tensile test; BE, bend test; ST, standard tensile test; IM, impact tensile test; RE, residual stress test.
(b) Heat treated to uniformly distribute solutes.
(c) Heat treated to segregate solutes to grain boundaries. Courtesy of Dr. A. Druschitz

Solid metal induced embrittlement (SMIE) and liquid metal induced embrittlement (LMIE) are strikingly similar phenomena. The prerequisites for SMIE are the same as those for LMIE: intimate contact between the solid and the embrittling agent, the presence of tensile stress, crack nucleation at the solid/embrittling agent interface from a barrier (such as a grain boundary), and the presence of embrittling species at the propagating crack tip. Also, metallurgical factors that increase brittleness in metals, such as grain size, strain rate, increases in yield strength, solute strengthening, and the presence of notches or stress raisers, all appear to increase embrittlement. The susceptibility to SMIE is stress and temperature sensitive and does not occur below a specific threshold value. Embrittlement by delayed failure is also observed for both LMIE and SMIE (Table 3).

Table 3 Delayed failure in SMIE and LMIE systems

Base metal	Liquid	Solid
Type A behavior: delayed failure observed		
4140 steel	Li	Cd
4340 steel	Cd	In
4140 steel	In	Cd
4140 steel	…	Pb
4140 steel	…	Sn
4140 steel	…	In
4140 steel	…	Zn
2024 Al	Hg	…
2424 Al	Hg-3Zn	…
7075 Al	Hg-3Zn	…
5083 Al	Hg-3Zn	…
Al-4Cu	Hg-3Zn	…
Cu-2Be	Hg	…
Cu-2Be	Hg	…
Type B behavior: delayed failure not observed		
Zn	Hg	…
Cd	Hg	…
Cd	Hg + In	…
Ag	Hg + In	…
Al	Hg	…

Courtesy of Dr. A. Druschitz

Some differences between LMIE and SMIE exist. Multiple cracks are formed in SMIE; in LMIE, a single crack usually propagates to failure. The fracture in SMIE is propagation controlled. However, crack propagation rates are at least 2 to 3 orders of magnitude slower than in LMIE. Brittle intergranular fracture changes to ductile shear because of the inability of the embrittling agent to keep up with the propagating crack tip. Incubation periods have been reported, indicating that the crack nucleation process may not be the same as in LMIE (Ref 15, 16, 17). Nucleation and propagation are two separate stages of fracture in SMIE.

These differences may arise because of the rate of reaction or interactions at the metal/embrittling agent interface and because the transport properties of solid and liquid metal embrittling agents are of significantly different magnitudes. It has been suggested that reductions in the cohesive strength of atomic bonds at the tip are responsible for both SMIE and LMIE (Ref 2, 15, 16, 18, 19). However, transport of the embrittling agent is the rate-controlling factor in SMIE. Another possibility is that stress-assisted penetration of the embrittling agent in the grain boundaries initiates cracking, but surface self- diffusion of the embrittling species similar to that proposed for LMIE controls crack propagation.

References cited in this section

2. S. Mostovoy and N.N. Breyer, *Trans. ASM,* Vol 61, 1968, p 219–232

15. P. Gordon, Metal-Induced Embrittlement of Metals: Evaluation of Embrittler Transport Mechanisms, *Metall. Trans. A,* Vol 9, 1978, p 267–273

16. P. Gordon and H.H. An, The Mechanisms of Crack Initiation and Crack-Propagation in Metal-Induced Embrittlement of Metal, *Metall. Trans. A,* Vol 13, 1982, p 457–472

17. A. Druschitz and P. Gordon, in *Embrittlement by Liquid and Solid Metals,* M.H. Kamdar, Ed., American Institute of Mining, Metallurgical, and Petroleum Engineers, 1984

18. A.R.C. Westwood and M.H. Kamdar, *Philos. Mag.,* Vol 8, 1963, p 787–804

19. N.S. Stoloff and T.L. Johnston, *Acta Metall.,* Vol 11, 1963, p 251–256

D.G. Kolman, Solid Metal Induced Embrittlement, *Corrosion: Fundamentals, Testing, and Protection,* Vol 13A, *ASM Handbook,* ASM International, 2003, p 393–397

Solid Metal Induced Embrittlement

Revised by David G. Kolman, Los Alamos National Laboratory

Investigations of SMIE

The first investigations of delayed failure were reported in cadmium-, zinc-, and indium-plated tensile specimens of 4340, 4130, 4140, and 18% Ni maraging steel in the temperature range of 200 to 300 °C (390 to 570 °F), as shown in Fig. 4 and 5. The results indicated that 4340 was the most susceptible and that 18% Ni maraging steel was the least susceptible alloy to cadmium embrittlement. The activation energy for steel-cadmium embrittlement was 39 kcal/mol (Fig. 3), which corresponded to diffusion of cadmium in the grain boundary. A thin, plated layer of nickel or copper has been reported to act as a barrier to the embrittling agent and to prevent SMIE of steel (Ref 3). Solid indium is reported to embrittle steels (Ref 16, 17), and an incubation period exists for crack nucleation.

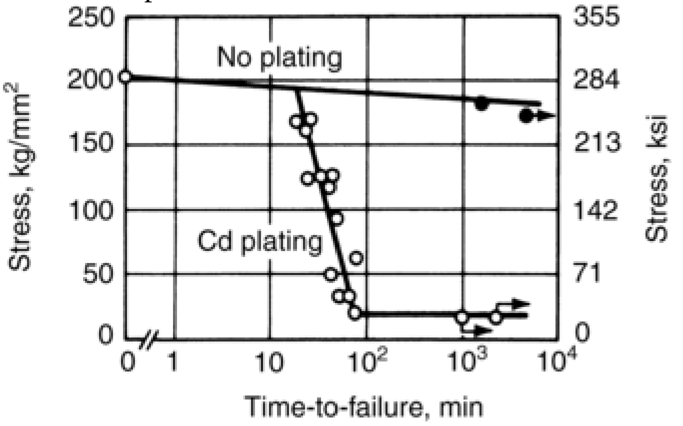

Fig. 4 Embrittlement behavior of cadmium-plated 4340 steel. Specimens were tested in delayed failure at 300 °C (570 °F) and unplated steel in air at 300 °C (570 °F). Source: Ref 3

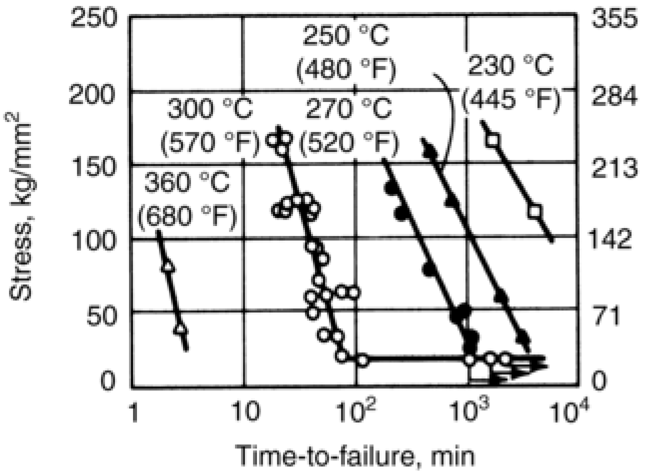

Fig. 5 Embrittlement behavior of cadmium-plated 4340 steel. Specimens were tested in delayed failure at temperatures ranging from 360 to 230 °C (680 to 445 °F). Source: Ref 3

Embrittlement of different steels in lead was investigated as both an external and internal (leaded steel) environment; SMIE was conclusively demonstrated to be a reproducible effect (Ref 2, 9). It was also demonstrated that SMIE is an extension of LMIE (Ref 2, 16). Internally leaded high-strength steels are susceptible to severe embrittlement in the range of the T_m of lead, and this embrittlement is a manifestation of LMIE. However, it was found that the onset of embrittlement occurs some 95 °C (200 °F) below the T_m of lead (330 °C, or 625 °F) and is continuous up to the T_m with no discontinuity or anomalies in the variation of the embrittlement with temperature (Ref 2). At the T_m of lead, a sharp increase occurs in the severity of embrittlement, and ductile-to-brittle transition occurs in the temperature range of 370 to 450 °C (700 to 840 °F). The same behavior was noted for pure lead as an external environment soldered onto 4140 steel, and such embrittlement has also been observed for surface coatings of zinc, lead, cadmium, tin, and indium on steel (Ref 2). Embrittlement manifests itself as a reduction in tensile ductility over a range of temperatures extending from approximately three-quarters of the absolute T_m of the embrittling agent up to the T_m (Ref 9). It has been shown that the embrittlement is caused by the growth of stable subcritical intergranular cracks and that crack propagation is the controlling factor in embrittlement (Ref 2, 16). This indicated that transport of embrittling agents to the crack tip was either by vapor phase or by surface or volume diffusion. In this study, the vapor pressure of the embrittling species at T_m varied widely and ranged from 20 to 6×10^{-36} Pa (1.5×10^{-1} to 4.5×10^{-38} torr) (Table 4). However, the crack propagation times for all embrittling agents were similar. The estimated values of the diffusion coefficients ranged in the vicinity of 10^{-4} to 10^{-6} cm²/s (6.5×10^{-4} to 6.5×10^{-6} in.²/s). These values are comparable to surface or self-diffusion of embrittling agent over embrittling agent and suggest that diffusion, not vapor transport, is the rate-controlling process.

Table 4 Embrittler vapor pressures and calculated vapor-transport times at the embrittler-melting temperatures

Embrittler	Vapor pressure		Time, s
	Pa	**torr**	
Zn	20	1.5×10^{-1}	5×10^{-3}
Cd	10	7.5×10^{-2}	1×10^{-2}
Hg[(a)]	0.3	2.25×10^{-3}	3×10^{-1}
Sb	4×10^{-4}	3.0×10^{-6}	3×10^{2}
K	1×10^{-4}	7.5×10^{-7}	1×10^{3}
Na	2×10^{-5}	1.5×10^{-7}	5×10^{3}
Ti	4×10^{-6}	3.0×10^{-8}	3×10^{4}
Pb	5×10^{-7}	3.75×10^{-9}	2×10^{5}
Bi	2×10^{-8}	1.5×10^{-10}	5×10^{6}
Li	2×10^{-8}	1.5×10^{-10}	5×10^{6}
In	3×10^{-19}	2.25×10^{-21}	3×10^{17}

Sn	8×10^{-21}	6.0×10^{-23}	1×10^{19}
Ga	6×10^{-36}	4.5×10^{-38}	2×10^{35}

(a) At room temperature. Courtesy of P. Gordon

There have been few studies of the SMIE of nonferrous alloys. A small amount of lead impurity has been shown to be detrimental to the failure resistance of an aluminum-magnesium- silicon alloy (Ref 20). Aluminum 7075 is embrittled by solid indium (Ref 21). A titanium alloy was shown to be susceptible to SMIE by cadmium, silver, and gold (Ref 22).

References cited in this section

2. S. Mostovoy and N.N. Breyer, *Trans. ASM,* Vol 61, 1968, p 219–232

3. Y. Asayama, in *Embrittlement by Liquid and Solid Metals,* M.H. Kamdar, Ed., American Institute of Mining, Metallurgical, and Petroleum Engineers, 1984

9. J.C. Lynn, W.R. Warke, and P. Gordon, Solid Metal-Induced Embrittlement of Steel, *Mater. Sci. Eng.,* Vol 18, 1975, p 51–62

16. P. Gordon and H.H. An, The Mechanisms of Crack Initiation and Crack-Propagation in Metal-Induced Embrittlement of Metal, *Metall. Trans. A,* Vol 13, 1982, p 457–472

17. A. Druschitz and P. Gordon, in *Embrittlement by Liquid and Solid Metals,* M.H. Kamdar, Ed., American Institute of Mining, Metallurgical, and Petroleum Engineers, 1984

20. J.J. Lewandowski, Y.S. Kim, and N.J.H. Holroyd, Lead-Induced Solid Metal Embrittlement of an Excess Silicon Al-Mg-Si Alloy at Temperatures of -4 °C to 80 °C, *Metall. Trans. A,* Vol 23, 1992, p 1679–1689

21. S.P. Lynch, Solid-Metal-Induced Embrittlement of Aluminum-Alloys and Other Materials, *Mater. Sci. Eng. A,* Vol 108, 1989, p 203–212

22. R.E. Stoltz and R.H. Stulen, Solid Metal Embrittlement of Ti-6Al-6V-2Sn by Cadmium, Silver, and Gold, *Corrosion,* Vol 35, 1979, p 165–169

D.G. Kolman, Solid Metal Induced Embrittlement, *Corrosion: Fundamentals, Testing, and Protection,* Vol 13A*, ASM Handbook*, ASM International, 2003, p 393–397

Solid Metal Induced Embrittlement

Revised by David G. Kolman, Los Alamos National Laboratory

Delayed Failure and Mechanism of SMIE

If a metal in contact with the embrittling species is loaded to a stress that is lower than that for fracture and is tested at various temperatures, then either the environment-induced fracture initiates and propagates instantaneously, as in a zinc-mercury LMIE couple, or delayed failure or static fatigue is observed. Examples of these two types of fracture processes are given in Table 3. Investigations of delayed failure provide an opportunity to separate crack nucleation from crack propagation and, specifically, to evaluate the transport-related role of the embrittling species. Solid metal induced embrittlement is a propagation-controlled fracture

process, and the time, temperature, and stress dependence of embrittlement presents an opportunity to study the kinetics of the cracking process.

The most critically investigated embrittlement system is 4140 steel embrittled by solid and liquid indium. Measurement of the decrease in electrical potential has been used to monitor crack initiation and propagation and to investigate the effects of temperature and stress level on delayed failure in 4140 steel by liquid and solid indium (Ref 15). The effects of temperature and stress level on the initiation time (incubation period for crack initiation) for both SMIE and LMIE are given in Fig. 6. The activation energy of the crack initiation process is approximately 37 kcal/mol and is essentially independent of the applied stress level. The activation energy represents the energy for stress-aided self-diffusion of both liquid and solid indium in the grain boundaries of the steel. Thus, crack initiation in both SMIE and LMIE occurs first by the adsorption of the embrittling agent at the site of crack initiation.

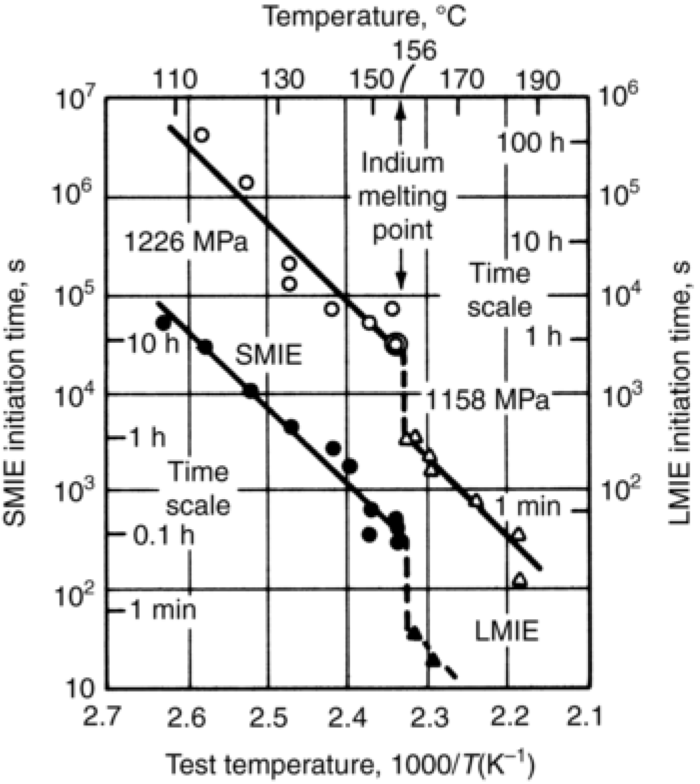

Fig. 6 Initiation time versus temperature in SMIE and LMIE of 4140 steel exposed to indium at two stress levels. Source: Ref 16

However, because of the presence of an incubation period, the rate-controlling process is stress-aided diffusion penetration of the base- metal grain boundaries. Such penetration reduces the stress necessary to initiate a crack, causing embrittlement of the base metal. On this basis, it is difficult to explain embrittlement of single crystals, which do not contain grain boundaries. Thus, rather than stress-aided diffusion penetration along grain boundaries, the embrittling species may reduce cohesion of atoms at the grain boundaries in accord with the reduction-in-cohesion mechanism. This mechanism would also explain SMIE of single crystals. Crack propagation time as a function of temperature and stress level for both SMIE and LMIE of steel by indium is plotted in Fig. 7. The activation energy for crack propagation for this couple was 5.6 kcal/mol, which represents the energy for self-diffusion of indium over indium. Thus, propagation is controlled by the diffusion of indium over several multilayers of indium adsorbed on the crack surface or by the so-called waterfall mechanism of embrittlement. This mechanism is a variation of that proposed and discussed in detail as the reduction-in-cohesion mechanism for LMIE.

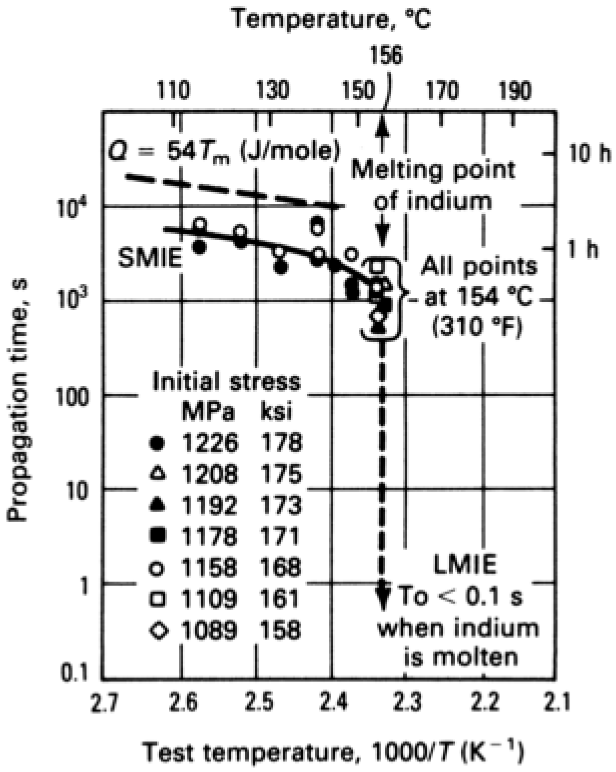

Fig. 7 Propagation time versus temperature for 4140 steel exposed to indium at various temperatures and stress levels. Note the occurrence of SMIE and LMIE and little dependence on stress level of test. Source: Ref 16

Adsorption of the embrittling agent at the solid surface is followed by the rate-controlling step of stress-aided diffusion of the embrittling agent in the grain boundary of the base metal. The embrittling agent reduces cohesion of the grain-boundary base-metal atoms, thus initiating a crack at a lower stress than that observed for the alloy in the absence of the embrittling species, resulting in embrittlement. Crack propagation occurs by multilayer self-diffusion of the embrittling species. These processes are valid for both LMIE and SMIE in the steel-indium embrittlement couple. It is clear that SMIE is similar to LMIE except that SMIE is a slower, embrittling agent transport-limited process. In this regard, the study of SMIE is important in eliminating the possibility in LMIE that a crack, once nucleated, may propagate in a brittle manner in the absence of the embrittling species at the tip of the crack. Solid metal induced embrittlement has only recently been recognized, and further research is needed concerning the effects of metallurgical, mechanical, and chemical parameters on embrittlement. However, it is clear that SMIE must be recognized as yet another phenomenon of environmentally induced embrittlement.

References cited in this section

15. P. Gordon, Metal-Induced Embrittlement of Metals: Evaluation of Embrittler Transport Mechanisms, *Metall. Trans. A,* Vol 9, 1978, p 267–273

16. P. Gordon and H.H. An, The Mechanisms of Crack Initiation and Crack-Propagation in Metal-Induced Embrittlement of Metal, *Metall. Trans. A,* Vol 13, 1982, p 457–472

D.G. Kolman, Solid Metal Induced Embrittlement, *Corrosion: Fundamentals, Testing, and Protection,* Vol 13A*, ASM Handbook,* ASM International, 2003, p 393–397

Solid Metal Induced Embrittlement

Revised by David G. Kolman, Los Alamos National Laboratory

Acknowledgment

This article was revised from M.H. Kamdar, Solid Metal Induced Embrittlement, in *Corrosion,* Vol 13, *Metals Handbook,* 9th ed., ASM International, 1987, p 184–189.

D.G. Kolman, Solid Metal Induced Embrittlement, *Corrosion: Fundamentals, Testing, and Protection,* Vol 13A*, ASM Handbook,* ASM International, 2003, p 393–397

Solid Metal Induced Embrittlement

Revised by David G. Kolman, Los Alamos National Laboratory

References

1. S.P. Lynch, Metal-Induced Embrittlement of Materials, *Mater. Charact.,* Vol 28, 1992, p 279–289
2. S. Mostovoy and N.N. Breyer, *Trans. ASM,* Vol 61, 1968, p 219–232
3. Y. Asayama, in *Embrittlement by Liquid and Solid Metals,* M.H. Kamdar, Ed., American Institute of Mining, Metallurgical, and Petroleum Engineers, 1984
4. D.A. Meyn, *Corrosion,* Vol 29, 1973, p 192–196
5. W.T. Grubb, Cadmium Metal Embrittlement of Zircaloy-2, *Nature,* Vol 265, 1977, p 36–37
6. Y. Iwata, Y. Asayama, and A. Sakamoto, *J. Jpn. Inst. Met.,* Vol 31, 1967, p 73
7. D.N. Fager and W.F. Spurr, *Corrosion,* Vol 27, 1971, p 72
8. D.N. Fager and W. F. Spurr, *Corrosion,* Vol 26, 1970, p 409
9. J.C. Lynn, W.R. Warke, and P. Gordon, Solid Metal-Induced Embrittlement of Steel, *Mater. Sci. Eng.,* Vol 18, 1975, p 51–62
10. S.P. Lynch, Hydrogen Embrittlement and Liquid-Metal Embrittlement in Nickel Single Crystals, *Scr. Metall.,* Vol 13, 1979, p 1051–1056
11. S.P. Lynch, A Fractographic Study of Hydrogen-Assisted Cracking and Liquid-Metal Embrittlement in Nickel, *J. Mater. Sci.,* Vol 21, 1986, p 692–704
12. S.P. Lynch, A Fractographic Study of Gaseous-Hydrogen Embrittlement and Liquid- Metal Embrittlement in a Tempered-Martensitic Steel, *Acta Metall.,* Vol 32, 1984, p 79–90

13. S.P. Lynch and P. Trevena, Stress-Corrosion Cracking and Liquid-Metal Embrittlement in Pure Magnesium, *Corrosion,* Vol 44, 1988, p 113–124

14. S.P. Lynch, Mechanisms of Stress-Corrosion Cracking and Liquid-Metal Embrittlement in Al-Zn-Mg Bicrystals, *J. Mater. Sci.,* Vol 20, 1985, p 3329–3338

15. P. Gordon, Metal-Induced Embrittlement of Metals: Evaluation of Embrittler Transport Mechanisms, *Metall. Trans. A,* Vol 9, 1978, p 267–273

16. P. Gordon and H.H. An, The Mechanisms of Crack Initiation and Crack-Propagation in Metal-Induced Embrittlement of Metal, *Metall. Trans. A,* Vol 13, 1982, p 457–472

17. A. Druschitz and P. Gordon, in *Embrittlement by Liquid and Solid Metals,* M.H. Kamdar, Ed., American Institute of Mining, Metallurgical, and Petroleum Engineers, 1984

18. A.R.C. Westwood and M.H. Kamdar, *Philos. Mag.,* Vol 8, 1963, p 787–804

19. N.S. Stoloff and T.L. Johnston, *Acta Metall.,* Vol 11, 1963, p 251–256

20. J.J. Lewandowski, Y.S. Kim, and N.J.H. Holroyd, Lead-Induced Solid Metal Embrittlement of an Excess Silicon Al-Mg-Si Alloy at Temperatures of -4 °C to 80 °C, *Metall. Trans. A,* Vol 23, 1992, p 1679–1689

21. S.P. Lynch, Solid-Metal-Induced Embrittlement of Aluminum-Alloys and Other Materials, *Mater. Sci. Eng. A,* Vol 108, 1989, p 203–212

22. R.E. Stoltz and R.H. Stulen, Solid Metal Embrittlement of Ti-6Al-6V-2Sn by Cadmium, Silver, and Gold, *Corrosion,* Vol 35, 1979, p 165–169

S.C. Dexter, Microbiologically Influenced Corrosion, *Corrosion: Fundamentals, Testing, and Protection*, Vol 13A, *ASM Handbook*, ASM International, 2003, p 398–416

Microbiologically Influenced Corrosion

Stephen C. Dexter, University of Delaware

Introduction

A GREAT VARIETY of microscopic organisms (microorganisms) are present in virtually all natural aqueous environments, such as bays, estuaries, harbors, coastal and open ocean seawaters, as well as rivers, streams, lakes, and ponds. The same could be said for all manner of aqueous industrial fluids and waste waters. These organisms include many species of bacteria, algae, and fungi. In all of these environments, the tendency is for microorganisms present in the water to attach to and grow on the immersed surfaces of structural materials, resulting in the formation of a biological film, or biofilm. Larger, macroscopic organisms, such as the well-known barnacles and mussels, are also present in many environments. The presence of such macroorganisms can result in a heavy encrustation of hard-shelled fouling organisms on structures in coastal seawater. There is a voluminous amount of literature on the formation of biofilms and their adverse effects (Ref 1, 2, 3, 4, 5). The emphasis of this article on microbiologically influenced corrosion (MIC) is on the effects of the microscopic organisms and the by-products they produce on the electrochemical corrosion of metals.

The biofilms that form on the surface of structural metals and alloys immersed in aqueous environments have the capability to influence the corrosion of those metals and alloys. This influence derives from the ability of the organisms to change the environmental variables such as pH, oxidizing power, velocity of flow, and concentration of chemical species at the metal surface. Thus, the value of a given parameter at the metal-water interface within the biofilm may be quite different from that in the bulk electrolyte away from the interface. The result can be the initiation of corrosion under conditions in which there would be none in the absence of the film, a change in the mode of corrosion (that is, from uniform to localized), or an increase or decrease in the corrosion rate, as shown in Fig. 1 (Ref 6). It is important to note, however, that the presence of a biofilm does not necessarily mean that there will always be a significant effect on corrosion.

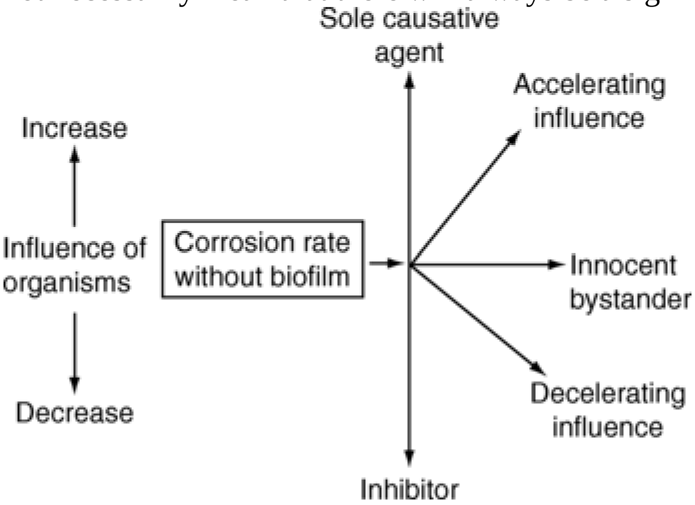

Fig. 1 Schematic showing that the influence microorganisms can have on corrosion ranges from sole causative agent to inhibitor. The most usual influence, however, is to change the mode of corrosion from general to localized and increase the rate of penetration. Source: Ref 6

Most of the documented cases in which biological organisms are the sole cause of, or an accelerating factor in, corrosion involve localized forms of attack. One reason for this is that organisms usually do not form in a continuous film on the metal surface. Additional information on biofilms can be found in the section “Community Structure and Formation of Biofilms” in this article. The large fouling organisms in marine environments settle as individuals, and it is often a period of months or even years before a complete cover is built up. A scatter of individual barnacles on a stainless steel surface creates oxygen concentration cells. The portion of the metal surface covered by the barnacle shell is shielded from dissolved oxygen in the water and thus becomes the anode through mechanisms described in the Section “Fundamentals of Corrosion” in this Volume. The result is crevice corrosion under the base of the barnacles, as shown in Fig. 2. A similar effect can take place on aluminum and, to a lesser extent, on structural steel. There is some evidence that the attack begins only after the animal dies (Ref 7).

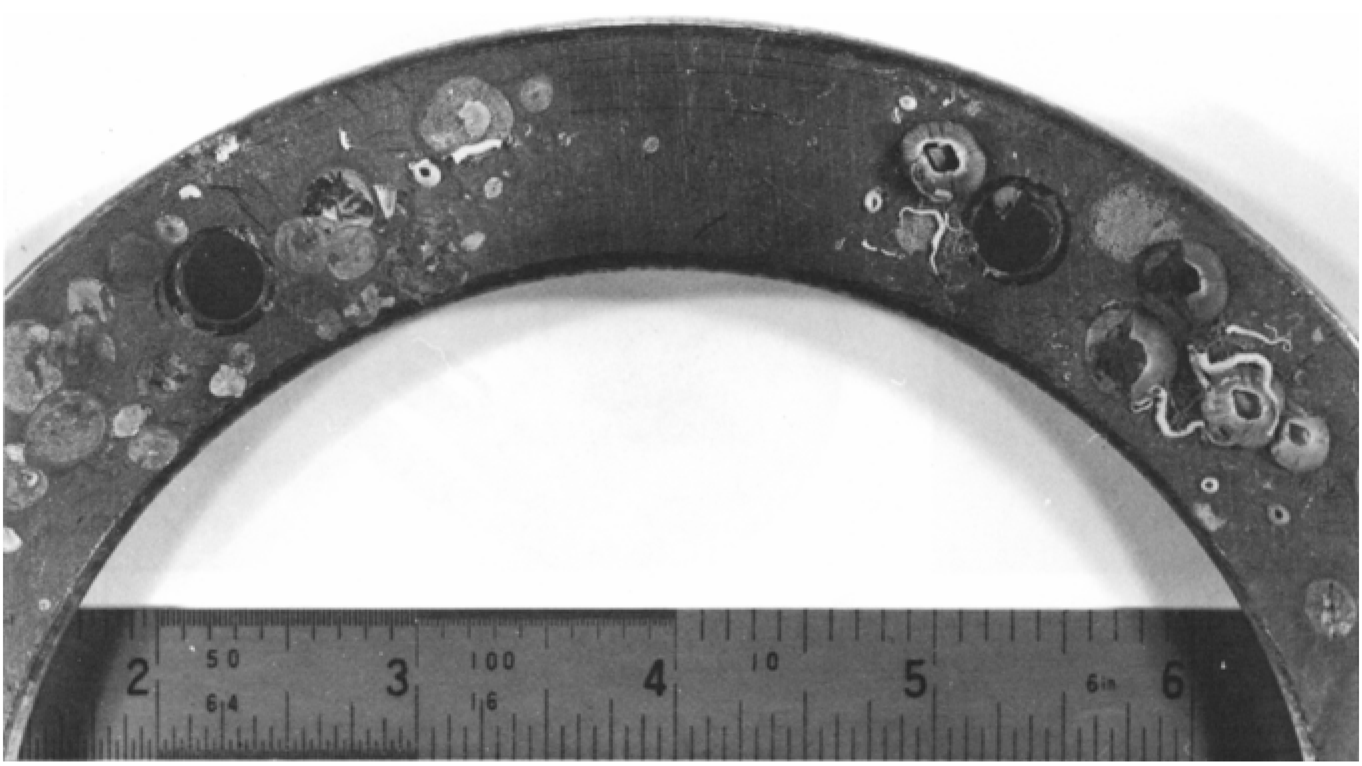

Fig. 2 Corrosion under a scatter of individual barnacles on a stainless steel surface

Microscopic organisms also tend to settle nonuniformly on metal surfaces. In some cases, they form discrete colonies; in other cases, they form biofilms with nominally complete coverage of the immersed surface. In the latter case, however, the distribution of organisms within the biofilm is usually extremely heterogeneous, leading to sharp chemical gradients both along the metal surface and perpendicular to it.

The purpose of this article is to consider in general the characteristics of organisms that allow them to interact with corrosion processes, the mechanisms by which organisms can influence the occurrence or rate of corrosion, and the types of corrosion most often influenced by microbes. In addition, the industries most often reported as being affected by microbiological corrosion are listed, along with the organisms usually implicated in the attack. The types of attack that have most commonly been documented are illustrated by generalized case histories for different classes of alloys. Cases that are still in the research stage or cases in which evidence for a primary role of the biofilm is not convincing are not covered. Sources of further information on MIC are listed in the Selected References and References at the end of this article.

References cited in this section

1. J.D. Costlow and R.C. Tipper, Ed., *Marine Biodeterioration: An Interdisciplinary Study,* Proceedings of the Symposium, Naval Institute Press, 1984

2. K.C. Marshall, *Interfaces in Microbial Ecology,* Harvard University Press, 1976

3. D.C. Savage and M. Fletcher, Ed., *Bacterial Adhesion,* Plenum Press, 1985

4. L.V. Evans, Ed., *Biofilms: Recent Advances in Their Study and Control,* Harwood Academic Publishers, 2000

5. B. Little, P. Wagner, and F. Mansfeld, Microbiologically Influenced Corrosion of Metals and Alloys, *Int. Mater. Rev.,* Vol 36 (No. 6), 1991, p 253–272

6. S.C. Dexter, Microbiological Effects, *Corrosion Tests and Standards,* 2nd ed., R. Baboian, Ed., *ASTM Manual 20,* ASTM, in press

7. M. Eashwar, G. Subramanian, P. Chandrasekaran, and K. Balakrishnan, Mechanism for Barnacle-Induced Crevice Corrosion in Stainless-Steel, *Corrosion,* Vol 48 (No. 7), 1992, p 608–612

S.C. Dexter, Microbiologically Influenced Corrosion, *Corrosion: Fundamentals, Testing, and Protection*, Vol 13A, *ASM Handbook*, ASM International, 2003, p 398–416

Microbiologically Influenced Corrosion

Stephen C. Dexter, University of Delaware

General Characteristics of Microbes

The organisms that are known to have an important impact on corrosion are mostly microorganisms such as bacteria, algae, and fungi (yeasts and molds). In this section, the general characteristics of the microorganisms that facilitate their influence on the electrochemistry of corrosion are discussed (Ref 8, 9, 10, 11).

Physical Characteristics. Microorganisms range in length from 0.1 to over 5 μm (some filamentous forms can be several hundred micrometers long) and up to approximately 3 μm in width. Many of them are motile; that is, they can "swim" to a favorable, or away from an unfavorable, environment. Because of their small size, they can reproduce themselves in a short time. Under favorable conditions, some bacteria can double in number every 20 min or less. Thus, a single bacterium can produce a mass of over one million microorganisms in less than 7 h.

In addition to rapid reproduction, the bacteria as a group can survive wide ranges of temperature (-10 to >100 °C, or 15 to >212 °F), pH (~0 to 10.5), dissolved oxygen concentration (0 to saturation), pressure (vacuum to >31 MPa, or 4500 psi), and salinity (tolerances vary from the parts per billion range to approximately 30% salt). Despite these wide ranges of tolerance for the microorganisms as a whole, most individual species have much narrower ranges. Most bacteria that have been implicated in corrosion grow best at temperatures of 15 to 45 °C (60 to 115 °F) and a pH of 6 to 8. Oxygen requirements vary widely with species. Microbes may be obligate aerobes (require oxygen for growth), microaerophilic (require minute levels of oxygen for growth), facultative anaerobes (grow with or without oxygen), or obligate anaerobes (grow only in the complete absence of oxygen).

Some microbes can produce spores that are resistant to a variety of environmental extremes, such as drying, freezing, and boiling. Spores have been known to survive for hundreds of years under arctic conditions and then to germinate and grow when conditions become favorable. Many microbes can adapt quickly to a wide variety of compounds as food sources. This gives them high survivability under changing environmental conditions.

Metabolic Characteristics. Many of the microorganisms implicated in corrosion are able to have an influence on the electrochemical reactions involved by virtue of chemical compounds consumed and the products produced during the course of their metabolism. A large percentage of them can form extracellular polymeric materials termed simply *polymer,* or *slime.* The slime is involved in attaching the organisms to the surface, trapping and concentrating nutrients for the microbes to use as food, and often, in shielding the organisms from the toxic effect of biocides. The slime film can influence corrosion by trapping or complexing heavy-metal ions near the surface. It can also act as a diffusion barrier for chemical species migrating to or from a metal surface, thus changing the chemical concentrations and pH at and near the solid-liquid interface where the corrosion takes place.

Some species of microbes can produce organic acids, such as formic and succinic, or mineral acids, such as H_2SO_4. These chemicals are corrosive to many metals. One series of bacteria is involved in metabolizing nitrogen compounds. As a group, they can reduce nitrates (NO^{-3}) (often used as corrosion inhibitors) to nitrogen (N_2) gas. Others can convert nitrates to nitrite, or vice versa, or they can break it down to form ammonia (NH_3). Still other series of bacteria are involved in the transformation of sulfur compounds (Fig. 3). They can oxidize sulfur or sulfides to sulfates (SO_4^{2-}) (or H_2SO_4), or they can reduce sulfates to sulfides, often producing corrosive H_2S as an end product.

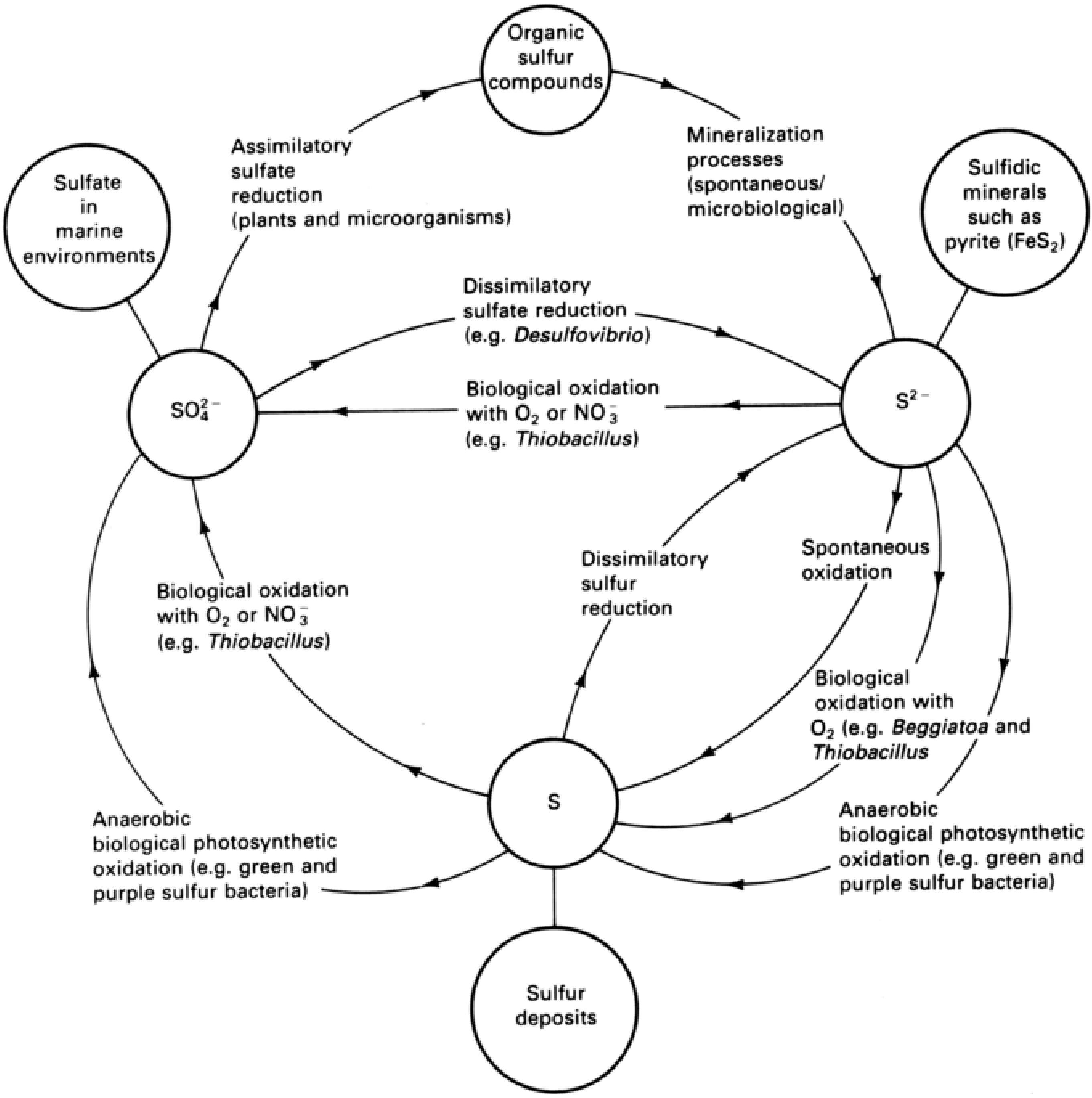

Fig. 3 The sulfur cycle showing the role of bacteria in oxidizing elemental sulfur to sulfate (SO_4^{2-}) and in reducing sulfate to sulfide (S^{2-}). Source: Ref 12

Organisms that have a fermentative type of metabolism produce carbon dioxide (CO_2) and hydrogen (H_2). Other microbes can use CO_2 and H_2 as sources of carbon and energy, respectively. Numerous species of bacteria and algae either produce or use oxygen. It is rare that a corrosion process does not depend on the concentration of at least one of these three dissolved gasses. Finally, some bacteria are capable of being directly involved in the oxidation or reduction of metal ions, particularly iron and manganese. Such bacteria can shift the chemical equilibrium between Fe, Fe^{2+}, and Fe^{3+}, which often influences the corrosion rate.

References cited in this section

8. D.H. Pope, D. Duquette, P.C. Wayner, and A.H. Johannes, "Microbiologically Influenced Corrosion: A State-of-the-Art-Review," Publication 13, Materials Technology Institute of the Chemical Process Industries, Inc., 1984

9. D.H. Pope, "A Study of Microbiologically Influenced Corrosion in Nuclear Power Plants and a Practical Guide for Countermeasures," EPRI NP-4582, Final Report, Electric Power Research Institute, 1986

10. J.D.A. Miller, Ed., *Microbial Aspects of Metallurgy,* Elsevier, 1970

11. H.A. Videla, *Manual of Biocorrosion,* CRC Press, Inc., 1996, p 13–45, 121–133, 160–173, 179–185, 228–237, 232

12. *Microbial Corrosion,* Proceedings of the Conference, National Physical Laboratory, The Metals Society, 1983

S.C. Dexter, Microbiologically Influenced Corrosion, *Corrosion: Fundamentals, Testing, and Protection,* Vol 13A*, ASM Handbook,* ASM International, 2003, p 398–416

Microbiologically Influenced Corrosion

Stephen C. Dexter, University of Delaware

Organisms Involved in MIC Corrosion

A select number of organisms are repeatedly reported as causing corrosion in environments in which there would be none without them, or accelerating corrosion, or changing a relatively slow rate of general corrosion into one with rapid localized penetration of the metal. These organisms are listed in Table 1.

Table 1   Microorganisms most commonly implicated in biological corrosion

Genus or species	pH range	Temperature range		Oxygen requirement	Metals affected	Action
		°C	**°F**			
Bacteria						
***Desulfovibrio* (best known: *D. desulfuricans*)**	4–8	10–40	50–105	Anaerobic	Iron and steel, stainless steels, aluminum, zinc, copper alloys	Use hydrogen in reducing SO_4^{2-} to S^{2-} and H_2S; promote formation of sulfide films
***Desulfotomaculum* (best known: *D. nigrificans,* also known as *Clostridium*)**	6–8	10–40 (some at 45–75)	50–105 (some at 115–165)	Anaerobic	Iron and steel, stainless steels	Reduce SO_4^{2-} to S^{2-} and H_2S (spore formers)
Desulfomonas	…	10–40	50–105	Anaerobic	Iron and steel	Reduce SO_4^{2-} to S^{2-} and H_2S
Acidithiobacillus thiooxidans	0.5–8	10–40	50–105	Aerobic	Iron and steel, copper alloys, concrete	Oxidizes sulfur and sulfides to form H_2SO_4; damages protective coatings

Acidithiobacillus ferrooxidans	1–7	10–40	50–105	Aerobic	Iron and steel	Oxidizes ferrous (Fe^{2+}) to ferric (Fe^{3+})
Gallionella	7–10	20–40	70–105	Aerobic	Iron and steel, stainless steels	Oxidizes ferrous to ferric ions and manganous to manganic ions; promotes tubercule formation
Siderocapsa* Type species: *S. treubii	Unknown	Unknown	Unknown	Low oxygen	Iron and carbon steel	Oxidizes iron
Leptothrix	6.5–9	10–35	50–95	Aerobic	Iron and steel	Oxidizes ferrous to ferric ions and manganous to manganic ions
Sphaerotilus	7–10	20–40	70–105	Aerobic	Iron and steel, stainless steels	Oxidizes ferrous to ferric ions and manganous to manganic ions; promotes tubercule formation
S. natans	…	…	…	…	Aluminum alloys	…
Pseudomonas	4–9	20–40	70–105	Aerobic	Iron and steel, stainless steels	Some strains can reduce Fe^{3+} to Fe^{2+}
P. aeruginosa	4–8	20–40	70–105	Aerobic	Aluminum alloys	…
Fungi						
Cladosporium resinae	3–7	10–45 (best at 30–35)	50–115 (best at 85–95)	…	Aluminum alloys	Produces organic acids in metabolizing certain fuel constituents

S.C. Dexter, Microbiologically Influenced Corrosion, *Corrosion: Fundamentals, Testing, and Protection*, Vol 13A, *ASM Handbook*, ASM International, 2003, p 398–416

Microbiologically Influenced Corrosion

Stephen C. Dexter, University of Delaware

Formation of Biofilms

Community Structure and Formation of Microbial Biofilms. The ability of an organism to survive on a surface and to influence corrosion is often related to associations between that organism and those of other species. The bacteria implicated in corrosion may begin their lives on a metal surface as a scatter of individual cells, as shown in Fig. 4(a). As the biofilm matures, however, the organisms are usually found as individuals or in

colonies embedded in the matrix of a semicontinuous and highly heterogeneous biofilm (Fig. 4 b,c). It is in this latter configuration that there is the most potential for survival and growth of the organisms capable of influencing corrosion.

(a)

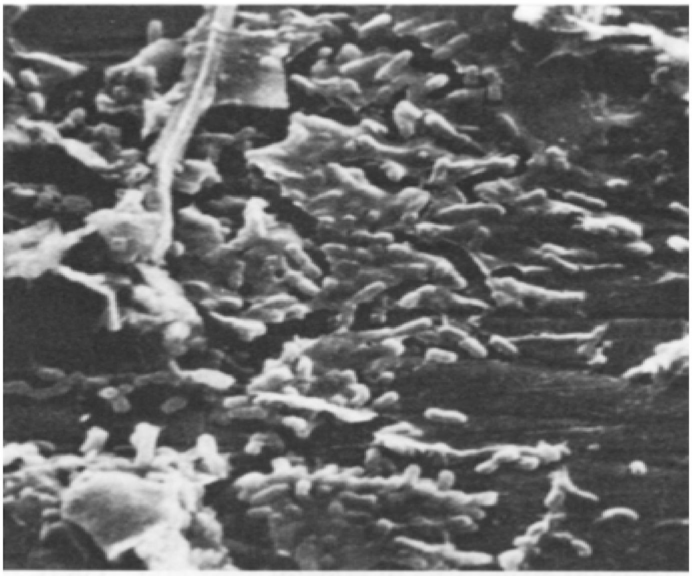

(b)

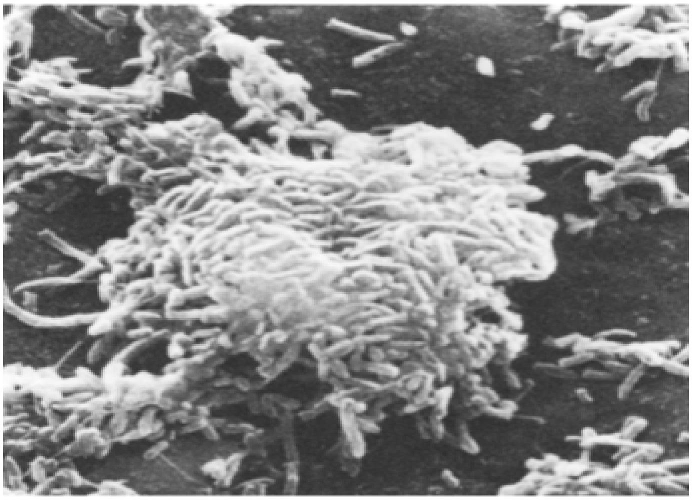

(c)

Fig. 4 Various forms of bacterial film that can influence corrosion. (a) Scatter of individual cells. 6050×. (b) Semicontinuous film of bacteria in slime. 3150×. (c) Bacterial cells in a colony. 2700×

Immersion of any solid surface in a natural aqueous environment, such as seawater or fresh water from lakes, rivers, streams, and ponds, initiates a continuous and dynamic process, beginning with adsorption of nonliving, dissolved organic material and continuing through the formation of bacterial and algal slime films. The process of colonization begins immediately on immersion with the adsorption of a nonliving organic conditioning film. This conditioning film is nearly complete within the first 2 h of immersion, at which time the initially colonizing bacteria begin to attach in substantial numbers. The bacterial, or primary, slime film develops over a period of 24 to 72 h in most natural waters, depending on the temperature, although further changes in the film can often be observed over more than a 2 month period.

The physical structure of the biofilm is heterogeneous, starting with a thin base layer of organisms embedded in extracellular polymeric substances. Depending on the velocity of fluid flow, that base layer may be anywhere from 10 to 100 μm in thickness, and it may cover from less than 20% to more than 90% of the metal surface. On top of the base film is a columnar, or cauliflower-like, structure extending out into the bulk fluid. Between and around the columnar entities is a network of microchannels through which water may flow (Ref 13, 14, 15), as shown in Fig. 5. Microscopic observations (Ref 15) indicate that such a biofilm may contain diverse microbial populations, including coccoidal, rod- shaped, chain-forming, and filamentous microorganisms (Fig. 6, 7, 8).

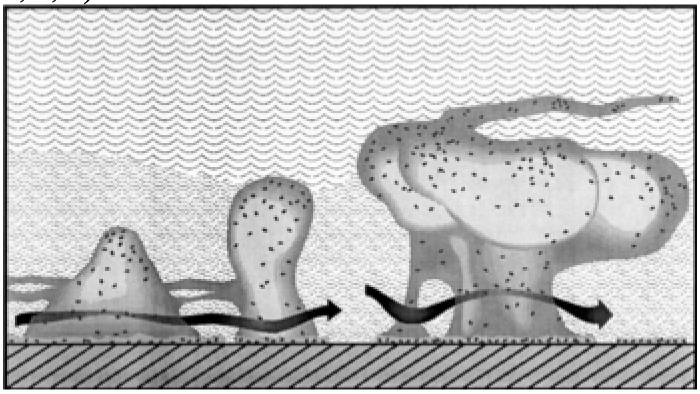

Fig. 5 Conceptual model of biofilm structure as determined by confocal scanning laser microscopy. The metal is shown crosshatched. Note the nearly continuous base film upon which sits a series of cauliflower-like cell clusters separated by voids through which bulk water can flow (arrows). Source: Ref 15

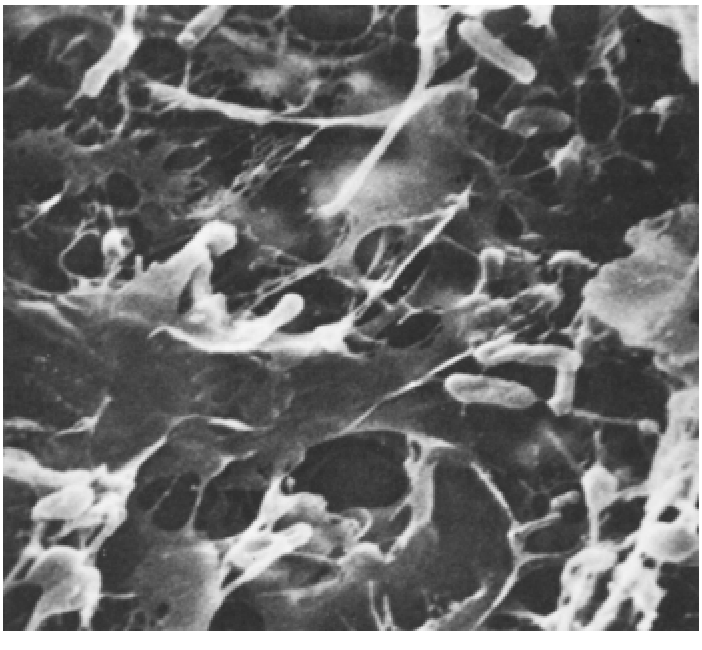

Fig. 6 Microbial film consisting of rod-shaped bacteria and slime. Courtesy of S.C. Dexter, University of Delaware

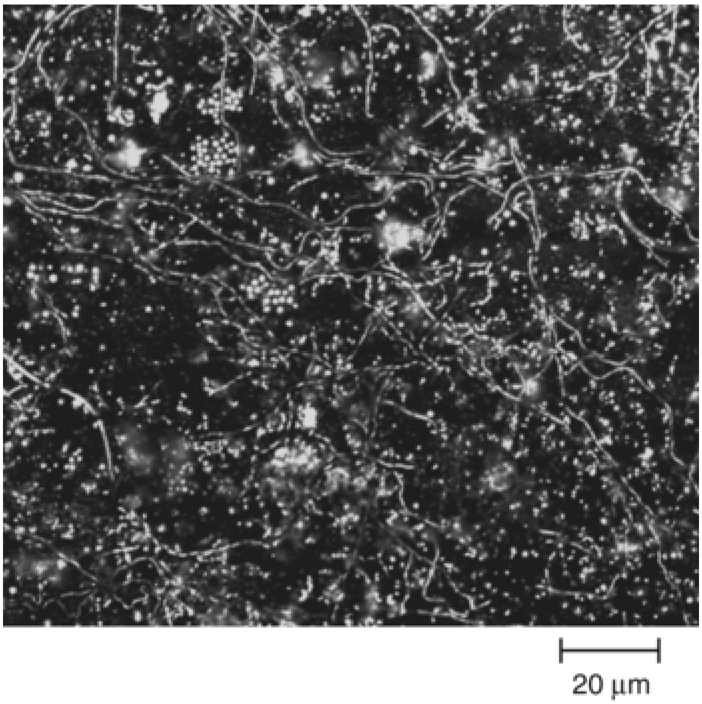

Fig. 7 Coccoidal microbial colonies and filamentous microorganisms observed on a Unified Numbering System (UNS) S20910 (Nitronic 50) alloy surface immersed in natural seawater for 28 days. Source: Ref 16

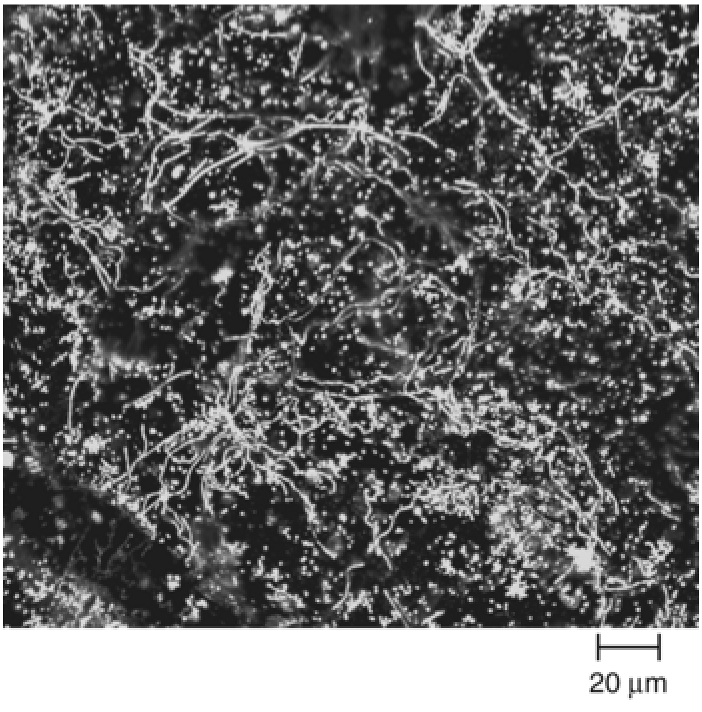

Fig. 8 Filamentous and coccoidal microorganisms observed on a UNS S20910 (Nitronic 50) alloy surface immersed in natural seawater for 42 days. Source: Ref 16

Mature biofilms in most aqueous environments including seawater are composed of microorganisms, the by-products of their metabolism, trapped detrital materials, and corrosion products. In the outer portions of the biofilm, aerobic heterotrophic bacteria consume oxygen and produce metabolites useful to other organisms residing nearby and beneath them in the biofilm. This produces favorable microenvironments for anaerobic microorganisms to grow in a synergistic community on an immersed metal surface (Ref 17, 18, 19, 20). For example, the sulfate- reducing bacteria (SRB) are implicated in the corrosion of iron-base alloys in a variety of environments (Ref 10, 12, 17, 21). The traditional view is that most SRB are obligate anaerobes, yet they are

known to accelerate corrosion in aerated environments. This becomes possible when the aerobic organisms in the outer portions of the columnar structure create an anaerobic microenvironment with the organic acids and nutrients necessary for growth of the SRB close to the metal surface (Fig. 9). Thus, the organisms influencing corrosion can often flourish at the corrosion site by associating with other organisms in a microbial colony or consortium, even when the bulk environment is not conducive to their growth. This traditional view is currently being challenged by recent research showing many SRB are microaerophillic and able to function under low oxygen conditions at any depth of the biofilm.

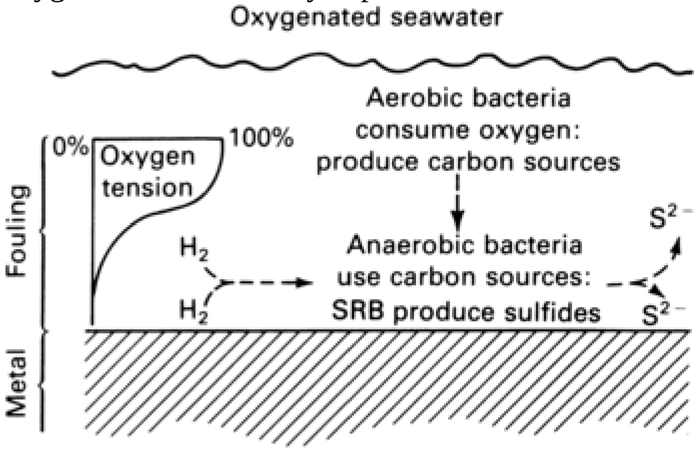

Fig. 9 Variations through the thickness of a bacterial film. Aerobic organisms near the outer surface of the film consume oxygen and create a suitable habitat for the sulfate-reducing bacteria (SRB) at the metal surface. Source: Ref 17

It should be noted that the dynamics of fluid flow past the metal surface can alter the form of the biofilm or even prevent its formation. This can result in acceleration or deceleration of corrosion, depending on the role of the biofilm. See the section “Corrosion Inhibition by Bacteria” in this article for additional information on inhibitive effects.

Formation of Macrofouling Films. In addition to the microbial biofilms discussed previously, natural seawater typical of coastal oceanic and estuarine environments worldwide supports the settlement and growth of a great variety of macroscopic plants and animals. In such marine environments, the fouling film, which starts with the formation of a microbial biofilm, often becomes dominated by the growth of the macroscopic organisms within weeks to months of immersion. The exact process of colonization is complex, depending on location, temperature, climate, and the nature of the surface being colonized. Additional information on the formation of macrofouling films is available (Ref 1, 2, 3, 4, 5).

A heavy encrustation of biofouling organisms on structural steel immersed in seawater often decreases the corrosion rate of the steel, as long as the cover of organisms remains complete and relatively uniform. The heavy fouling layer acts as a barrier film in limiting the amount of dissolved oxygen reaching the metal surface. A layer of hard-shelled organisms, such as barnacles or mussels, on steel in the splash zone (just above the high-tide level) also shields the metal from the damaging effect of wave action. It should be emphasized that these beneficial effects on general corrosion occur under a complete fouling layer. If coverage is incomplete, as shown in Fig. 10, the fouling film is then more likely to cause the initiation of localized corrosion by creating oxygen concentration cells. The beneficial effects may also be lost if the fouling film leads to a high activity of SRB at the metal surface. A heavy encrustation of these macroorganisms also can have a number of undesirable physical effects on marine structures. The fouling layer increases both weight and hydrodynamic drag on the structure. Interference with the functioning of moving parts also may occur.

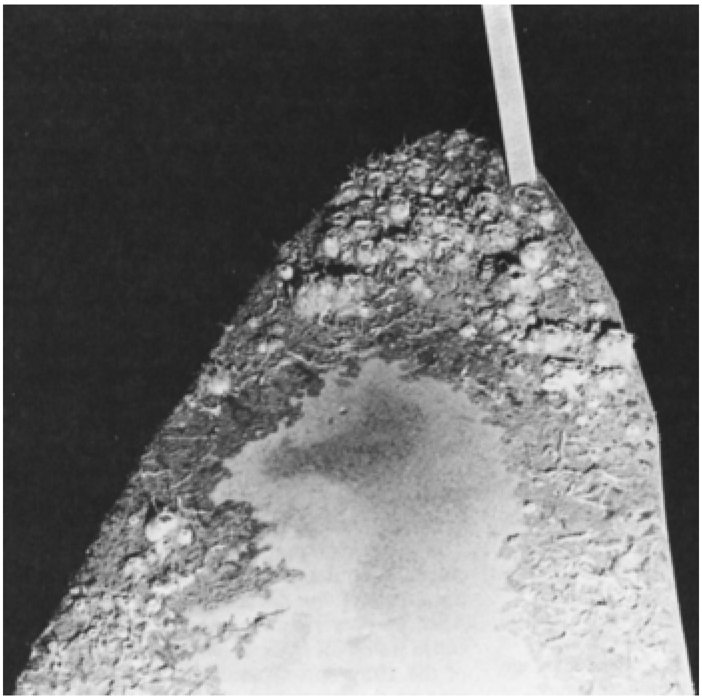

Fig. 10 Barnacles attached to the periphery of a high-strength steel rudder, which had originally been coated with an antifouling paint. During use, the paint around the edges had been removed by mechanical action, thus allowing the attachment of barnacles. Partial coverage of such macroorganisms can lead to localized corrosion. Complete coverage can sometimes provide a barrier film and limit corrosion. Courtesy of B. Little, Naval Ocean Research and Development Activity, Department of the Navy

As documented in the following sections, the influence of biofilms on the rate at which corrosion propagates can range from acceleration to inhibition. In a few well-documented situations, the organisms are the sole cause of corrosion, while in other cases, they may be innocent bystanders, having little to no effect. The challenge from the corrosion engineering perspective is to determine when the influence of the organisms is important enough that effective corrosion control cannot be achieved without specifically addressing the microbial effect.

References cited in this section

1. J.D. Costlow and R.C. Tipper, Ed., *Marine Biodeterioration: An Interdisciplinary Study,* Proceedings of the Symposium, Naval Institute Press, 1984

2. K.C. Marshall, *Interfaces in Microbial Ecology,* Harvard University Press, 1976

3. D.C. Savage and M. Fletcher, Ed., *Bacterial Adhesion,* Plenum Press, 1985

4. L.V. Evans, Ed., *Biofilms: Recent Advances in Their Study and Control,* Harwood Academic Publishers, 2000

5. B. Little, P. Wagner, and F. Mansfeld, Microbiologically Influenced Corrosion of Metals and Alloys, *Int. Mater. Rev.,* Vol 36 (No. 6), 1991, p 253–272

10. J.D.A. Miller, Ed., *Microbial Aspects of Metallurgy,* Elsevier, 1970

12. *Microbial Corrosion,* Proceedings of the Conference, National Physical Laboratory, The Metals Society, 1983

13. Z. Lewandowski, P. Stoodley, and S. Altobelli, *Water Sci. Technol.,* Vol 3, 1995, p 153–162

14. D. de Beer and P. Stoodley, Relation between the Structure of an Aerobic Biofilm and Transport Phenomena, *Water Sci. Technol.,* Vol 32 (No. 8), 1995, p 11–18

15. D. de Beer, P. Stoodley, and Z. Lewandowski, Liquid Flow and Mass Transport in Heterogeneous Biofilms, *Water Res.,* Vol 30 (No. 11), 1996, p 2761–2765

16. K. Xu, "Effect of Biofilm Heterogeneity on Corrosion Behavior of Passive Alloys in Seawater," Ph.D. dissertation, University of Delaware, 2000

17. W.A. Hamilton and S. Maxwell, Biological and Corrosion Activity of SRB in Natural Biofilms, *Proceedings of Biologically Induced Corrosion,* NACE International, 1986, p 131–136

18. J.W. Costerton and G.G. Geesey, The Microbial Ecology of Surface Colonization and of Consequent Corrosion, *Biological Induced Corrosion,* NACE-8, S.C. Dexter, Ed., NACE International, 1986, p 223–232

19. R.J. Parkes, *Soc. Gen. Microbiol. Symp.,* Vol 41, 1987, p 147–177

20. C.C. Gaylarde and H.A. Videla, *Int. Biodeterior.,* Vol 23, 1987, p 91–104

21. S.C. Dexter, Ed., Biologically Induced Corrosion, *Proceedings of the Conference,* National Association of Corrosion Engineers, 1986

S.C. Dexter, Microbiologically Influenced Corrosion, *Corrosion: Fundamentals, Testing, and Protection*, Vol 13A, *ASM Handbook*, ASM International, 2003, p 398–416

Microbiologically Influenced Corrosion

Stephen C. Dexter, University of Delaware

General Mechanisms by Which Biological Organisms Influence Corrosion

The presence of a biological film on a corroding metal surface does not introduce some new type of corrosion, but it may influence the occurrence and/or the rate of all currently known types of corrosion. The net effect of both micro- and macrobiofouling film formation on corrosion is variable. The most usual effect of both types of fouling is to make corrosion of the metal substratum more localized than it would be in water with the same bulk chemistry but without microorganisms. This effect is a consequence of the heterogeneity of the biofilm, which in turn leads to an increase in the variability of the chemical environment from place to place along the metal surface.

Microbial biofilms change the chemistry at the metal-liquid interface in a number of ways that have an important bearing on corrosion. As the biofilm grows, the bacteria in the film produce a number of by-products. Among these are organic acids, hydrogen sulfide, and protein-rich polymeric materials commonly known as *slime.* The first effect of the composite film of bacteria and associated polymer is to create a diffusion barrier between the metal-liquid interface and the bulk seawater. The barrier itself is over 90% water, so it does not truly isolate the interface. Instead, it supports strong concentration gradients, both parallel and perpendicular to the metal surface (Ref 22). Thus, the water chemistry at the interface may be different from that in the bulk water, although the two are closely coupled through diffusive processes. These biological influences can be divided into four general categories:

- Production of organic and inorganic acids as metabolic by-products

- Production of sulfides under oxygen-free (anaerobic) conditions
- Introduction of new redox reactions
- Production of oxygen or chemical concentration cells

Acid Production. The sulfur-oxidizing bacteria can produce up to approximately 10% H_2SO_4. This mineral acid, with its accompanying low pH, is highly corrosive to many metals, ceramics, and concrete. Other species of bacteria produce organic acids (e.g., acetic, citric, succinic, lactic) that are corrosive to metal surfaces (Ref 5). The acids produced by these organisms can also contribute to corrosion by aiding the breakdown of coatings systems. Alternatively, other organisms that have no direct influence on corrosion may be involved in the breakdown of coatings. The breakdown products are then sometimes usable as food by the acid-producing bacteria, ultimately leading to accelerated corrosion of the underlying metal. Organic acids produced by fungi were identified as the cause of pitting failures in painted carbon steel holds on a bulk carrier and aluminum fuel storage tanks (Ref 5). Acid production is discussed further in the section "Concrete" in this article.

Bacterial action on decaying organic matter in the slime film can also result in the production of ammonia and sulfides. Ammonia causes stress-corrosion cracking of copper alloys (Ref 23), and sulfides have been implicated in accelerated localized and/or uniform corrosion of both copper alloys and steels (Ref 5).

Anaerobic Sulfide Production. The most thoroughly documented case in which microbes are known to cause corrosion is that of iron and steel under anaerobic conditions in the presence of SRB. Based on electrochemistry, deaerated soils of near-neutral pH are not expected to be corrosive to iron and steel. However, if the soil contains SRB and a source of sulfates, rapid corrosion has been found to occur.

The classical mechanism originally proposed for this corrosion involved the removal of atomic hydrogen from the metal surface by the bacteria using the enzyme hydrogenase (Ref 24). The removed hydrogen was then supposedly used by the bacteria in the reduction of sulfates to sulfides. The following set of equations was proposed to explain this mechanism:

$Fe \rightarrow 4Fe^{2+} + 8e^-$ Anodic reaction	(Eq 1)
$8H_2O \rightarrow 8H^+ + 8OH^-$ Dissociation of water	(Eq 2)
$8H^+ + 8e^- \rightarrow 8H$ Cathodic reaction	(Eq 3)
$SO_4^{2-} + 8H \xrightarrow{SRB} S^{2-} + 4H_2O$ Cathodic depolarization	(Eq 4)
$Fe^{2+} + S^{2-} \rightarrow FeS$ Corrosion product	(Eq 5)
$3Fe^{2+} + 6OH^- \rightarrow 3Fe(OH)_2$ Corrosion product	(Eq 6)

Without SRB, the mechanism would stop after Eq 3, when the surface became covered by a monolayer of hydrogen. According to the theory, this hydrogen is stripped off by the bacteria, a process known as *cathodic depolarization;* this process allows corrosion to continue. It is now recognized that this original mechanism, although it undoubtedly plays an important role, does not represent the entire process (Fig. 11). It has been shown that the iron sulfide (FeS) film produced is protective if continuous, but that it causes galvanic corrosion of the bare iron underneath if defective. The bacteria thus transform a benign environment into an aggressive one in which steel corrodes quite rapidly. Other corrosive substances, such as H_2S, can also be produced. The SRB also have been identified as contributors to the corrosion of stainless, copper, and aluminum alloys (Ref 5, 12, 21).

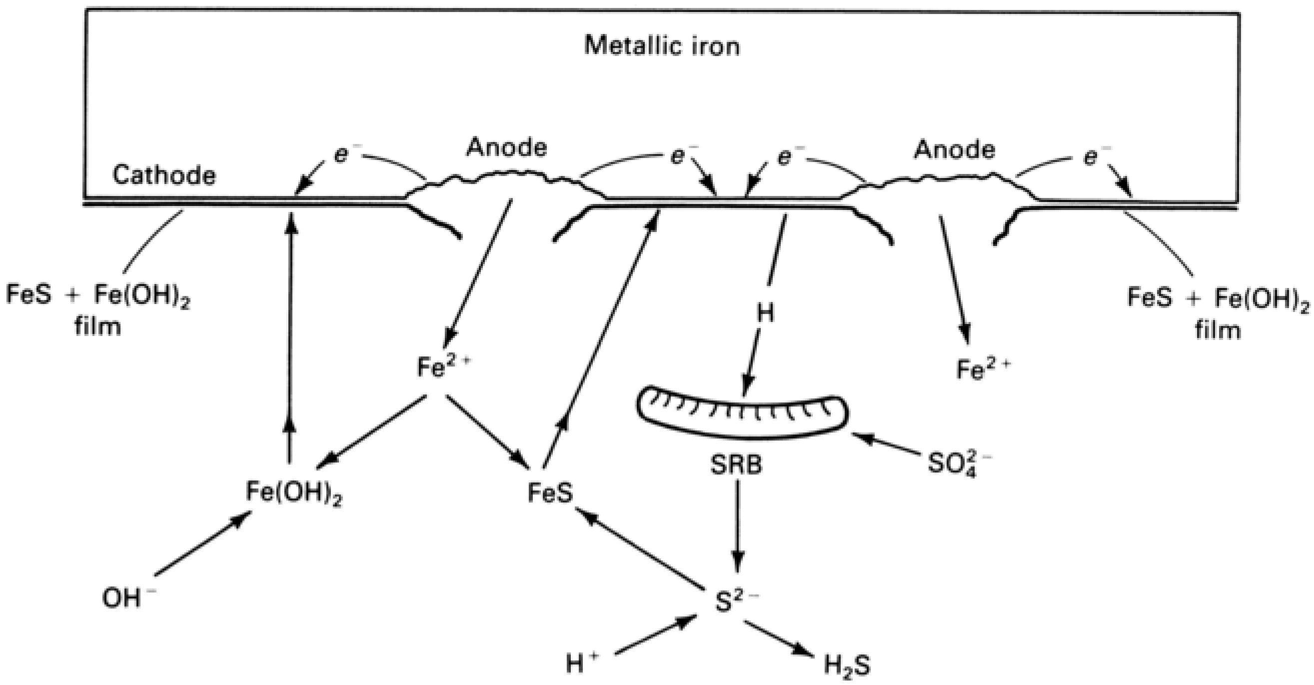

Fig. 11 Schematic of the anaerobic corrosion of iron and steel showing the action of sulfate-reducing bacteria (SRB) in removing hydrogen from the surface to form FeS and H_2S

Introduction of New Redox Reactions. Biofilms are able to accumulate ions, such as the heavy metals manganese and iron, in concentrations far above those in the surrounding bulk water. For example, the concentration of dissolved Mn^{2+} is in the nanomolar range in Lower Delaware Bay seawater (Ref 25). Within a biofilm grown on a passive alloy in that same seawater, the concentration is in the micromolar range (Ref 21), and the total manganese is in the millimolar range (Ref 25). The presence of these compounds makes new redox reactions available to the corrosion process, particularly to the cathodic reaction.

To use manganese again as an example, the following reactions have been proposed for the acceleration of corrosion reactions by manganese redox cycling within biofilms. Linhardt (Ref 26) originally proposed the two-electron transfer reduction of MnO_2 directly to Mn^{2+}. The one-electron transfer reduction of MnO_2 to solid MnOOH is discussed in Ref 27:

$$MnOOH + 3H^+ + e^- \rightarrow Mn^{2+} + 2H_2O \quad \text{(Eq 7)}$$

Or by disproportionation:

$$2MnOOH + 2H^+ \rightarrow MnO_2 + Mn^{2+} + 2H_2O \quad \text{(Eq 8)}$$

It was concluded that disproportionation of the solid MnOOH by Eq 8 was unlikely, because the free energy of formation was positive under the test conditions, and that reduction by Eq 7 would allow for reoxidation in the presence of manganese-oxidizing bacteria to keep the redox cycle going.

Alternately, the reduction of MnO_2 via a soluble Mn^{3+} intermediate is (Ref 25):

$$4H^+ + MnO_2 + 1e^- \rightarrow Mn^{3+} + 2H_2O \quad \text{(Eq 9)}$$

$$2H_2O + 2Mn^{3+} \rightarrow MnO_2 + Mn^{2+} + 4H^+ \quad \text{(Eq 10)}$$

$$2H_2O + Mn^{2+} + O_2 \rightarrow Mn^{3+} + 4OH^- + 1e^- \quad \text{(Eq 11)}$$

Equation 9 describes the one-electron reduction of MnO_2 to a soluble Mn^{3+} species, which is metastable and disproportionates quickly to Mn^{4+} and Mn^{2+} in seawater (Eq 10) unless complexed by strong organic ligands (Ref 25). These reactions explain the production of MnO_2 and Mn^{2+} in the absence of dissolved oxygen. If oxygen is present, it can reoxidize Mn^{2+} back to Mn^{3+} (Eq 11), where Eq 10 can occur again. If oxygen is not present, Mn^{3+} disproportionation alone can still account for the results, because MnO_2 can never be fully depleted. This manganese redox cycle can include both inorganic and biological processes.

Oxygen and Chemical Concentration Cells. Any biofilm that does not provide for complete, uniform coverage of the entire immersed surface of a metal or alloy has the potential to form concentration cells. Two chemical

species, oxygen and hydrogen, that are often implicated (or even rate controlling) in corrosion are also important in the metabolism of the bacteria. A given bacterial slime film can be a source or a sink for either oxygen or hydrogen. Moreover, these films are rarely continuous. Usually, they provide only spotty coverage of the metal surface. Thus, they are capable of inducing oxygen (or other chemical) concentration cells. In aerated environments, areas of the metal surface between the columnar structures of the biofilm may be in contact with oxygenated electrolyte. These areas with relatively high oxygen concentrations within the biofilm are cathodic relative to areas with less oxygen. Beneath a microbial colony, oxygen is depleted as it is used by the organisms in their metabolism. Oxygen from the bulk electrolyte is unable to replenish those areas because of a combination of effects. First, oxygen migration through the film is slowed by the diffusion barrier effect, and second, oxygen that does penetrate the film is immediately used by the microbial metabolism. Formation of such a corrosion cell, as shown in Fig. 12, causes a pit to form at the anodic area under the bacterial colony.

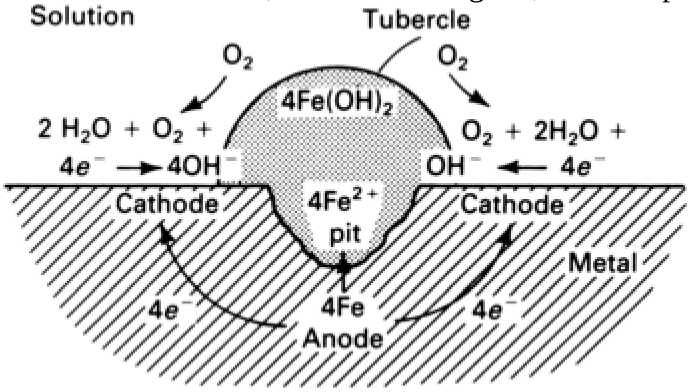

Fig. 12 Schematic of pit initiation and tubercle formation due to an oxygen concentration cell under a biological deposit. Source: Ref 21

As the pit grows, iron dissolves according to the anodic reaction:

$Fe \rightarrow Fe^{2+} + 2e^-$ (Eq 12)

The cathodic reaction is reduction of dissolved oxygen outside the pit to form OH^- according to:

$O_2 + 2H_2O + 4e^- \rightarrow 4OH^-$ (Eq 13)

The insoluble ferrous hydroxide corrosion product forms by the reaction:

$3Fe^{2+} + 6OH^- \rightarrow 3Fe(OH)_2$ (Eq 14)

Corrosion products mingle with polymer from the bacterial film to form a corrosion tubercule, which itself may cause a problem with obstruction of fluid flow in piping systems. In addition, if the previously mentioned process takes place in the presence of bacteria capable of oxidizing ferrous ions to ferric ions, the corrosion rate is accelerated, because the ferrous ions are removed from solution as soon as they are produced. This depolarizes the anode and accelerates corrosion of iron under the deposit. The ferric ions form ferric hydroxide ($Fe(OH)_3$), which contributes to the rapid growth of the tubercule. This process has been responsible for corrosion and plugging of iron water pipes.

If chlorides are present in the system, the pH of the electrolyte trapped inside the tubercule may become very acid by the autocatalytic process of metal hydrolysis similar to that described in the articles “Evaluating Pitting Corrosion ” and “Evaluating Crevice Corrosion” in this Volume. Chloride ions from the environment combine with ferric ions produced by corrosion in the presence of the bacteria to form a highly corrosive, acidic ferric chloride solution inside the tubercule. This has been responsible for severe pitting of stainless steel piping systems, as described in the section “MIC of Passive Alloys” in this article.

Another example of a chemical concentration cell is that between manganese- and sulfide-rich areas. Whenever microbial sulfate reduction and manganese deposition occur simultaneously within biofilms, then a differential potential cell is likely to form at the metal surface. The microbially mediated manganese redox cycle drives the metal open-circuit potential in the noble direction, whereas bacterial sulfide production drives it in the active direction. Thus, when a manganese-oxidizing microcolony and an SRB microcolony form at different sites on the same metal surface, a differential potential cell may be created. The area under sulfide species becomes anodic, while the area under manganese species becomes cathodic. Localized corrosion is likely to initiate at the metal surface as a result of the differential potential cell.

The cathodic site would be expected to form where manganese had accumulated and manganese-oxidizing microorganisms were active. The dominant cathodic reaction at this site would involve the reduction of Mn(III) or Mn(IV) complexes to Mn(II), according to a reaction of the type:

$$\text{Mn(III) complex} + e^- \rightarrow \text{Mn(II) complex} \qquad \text{(Eq 15)}$$

Conversely, the anode should form where SRB reside at the metal surface, leading to a neutral pH reaction such as:

$$HS^- + Fe \rightarrow FeS + H^+ + 2e^- \qquad \text{(Eq 16)}$$

The potential difference between these sulfide and Mn(III) or MnO_2 areas of the surface is larger than 500 mV (Ref 16). In comparison, differential aeration cells are quite weak. Even for an oxygen concentration differential of 10^4 between the aerated and deaerated areas, the potential difference is only approximately 60 mV.

In all of the previous examples, the biofilm is able to change the chemistry of the electrolyte substantially at the water-metal interface. Thus, the initiation of corrosion as well as the corrosion rate may depend more on the details of the electrolyte chemistry at the interface, including its heterogeneity, than it does on the ambient bulk water chemistry.

References cited in this section

5. B. Little, P. Wagner, and F. Mansfeld, Microbiologically Influenced Corrosion of Metals and Alloys, *Int. Mater. Rev.,* Vol 36 (No. 6), 1991, p 253–272

12. *Microbial Corrosion,* Proceedings of the Conference, National Physical Laboratory, The Metals Society, 1983

16. K. Xu, "Effect of Biofilm Heterogeneity on Corrosion Behavior of Passive Alloys in Seawater," Ph.D. dissertation, University of Delaware, 2000

21. S.C. Dexter, Ed., Biologically Induced Corrosion, *Proceedings of the Conference,* National Association of Corrosion Engineers, 1986

22. K. Xu, S.C. Dexter, and G.W. Luther III, Voltammetric Microelectrodes for Biocorrosion Studies, *Corrosion,* Vol 54 (No. 10), 1998, p 814

23. D.H. Pope, D.J. Duquette, A.H. Johannes, and P.C. Wayner, *Mater. Perform.,* Vol 23 (No. 4), 1984, p 14–18

24. C.A.H. Von Wolzogen Kuhr and L.S. Van der Vlugt, *Water, Den Haag,* Vol 18, 1934, p 147–165

25. D.T. Ruppel, S.C. Dexter, and G.W. Luther, *Corrosion,* Vol 57, 2001, p 863–873

26. P. Linhardt, Failure of Chromium-Nickel Steel in a Hydroelectric Power Plant by Manganese-Oxidizing Bacteria, *Microbially Influenced Corrosion of Materials,* E. Heitz et al., Ed., Springer-Verlag, 1996

27. B.H. Olesen, R. Avci, and Z. Lewandowski, Manganese Dioxide as a Potential Cathodic Reactant in Corrosion of Stainless Steels, *Corros. Sci.,* Vol 42, 2000, p 211–227

S.C. Dexter, Microbiologically Influenced Corrosion, *Corrosion: Fundamentals, Testing, and Protection,* Vol 13A, *ASM Handbook*, ASM International, 2003, p 398–416

Microbiologically Influenced Corrosion

Stephen C. Dexter, University of Delaware

Industries Affected

The various industries that have been affected by microbiological corrosion problems are listed in Table 2. References to problems in the chemical-processing, nuclear power, oil field (both onshore and offshore), and underground pipeline industries are most common in the published literature. This does not necessarily mean that these industries are more prone to problems of this type than other industries. It does mean that these industries have been quick to recognize the biological causes of some of their corrosion problems, to take steps to solve these problems, and to make the results public. More recently, biological corrosion represents a growing challenge to the fire protection industry.

Table 2 Industries affected by microbiologically influenced corrosion

Industry or structure	Problem areas
Chemical processing	Stainless steel tanks, pipelines, and flanged joints, particularly in welded areas after hydrotesting with natural river or well waters
Power generation: nuclear, hydro, fossil fuel, and geothermal	Carbon and stainless steel piping and tanks; copper-nickel, stainless, brass, and aluminum-bronze cooling water pipes and tubes, especially during construction, hydrotest, and outage periods
Onshore and offshore oil and gas	Mothballed and waterflood systems; oil- and gas-handling systems, particularly in those environments soured by sulfate-reducing-bacteria (SRB)-produced sulfides
Underground pipeline	Water-saturated clay-type soils of near-neutral pH with decaying organic matter and a source of SRB
Water treatment	Heat exchangers and piping
Sewage handling and treatment	Concrete and reinforced-concrete structures
Highway maintenance	Culvert piping
Buildings and stoneworks	Ancient and modern limestones, marbles, sandstones, granites, and mortars
Pulp and paper	Raw, process, and cooling water systems; paper machine headboxes and suction rolls
Hydraulic systems	Increased corrosivity of hydraulic oils with entrained water; fouling and corrosion of filters
Fire protection systems	Pinhole leaks in piping systems; plugging of piping and sprinkler heads
Aviation	Aluminum integral wing tanks and fuel storage tanks
Metalworking	Increased wear from breakdown of machining oils and emulsions

The frequency of literature reports of microbiological corrosion problems in these industries also does not mean that corrosion is accelerated everywhere microorganisms are present. Many bacteria existing in natural and man-made environments do not cause or accelerate corrosion. Bacteria may exist at the corrosion site only because the electrochemistry of corrosion creates a favorable environment for their growth.

S.C. Dexter, Microbiologically Influenced Corrosion, *Corrosion: Fundamentals, Testing, and Protection,* Vol 13A, *ASM Handbook*, ASM International, 2003, p 398–416

Microbiologically Influenced Corrosion

Stephen C. Dexter, University of Delaware

Microbiologically Influenced Corrosion of Various Materials

This section describes microbiologically influenced corrosion (MIC) of irons and steels, passive alloys (austenitic stainless steels), aluminum alloys, copper alloys, and composites.

Biological Corrosion of Irons and Steels

A large number of case histories involving the microbial acceleration of the localized corrosion of iron and steel have been presented in the literature. These are far too numerous to list in this article. An excellent introduction to the literature can be gained by referring to Ref 8, 9, 10, 11, 12, 21, 28, 29, 30, 31).

Anaerobic Corrosion. The corrosive action of the SRB from the genera *Desulfovibrio, Desulfotomaculum,* and *Desulfomonas* in anaerobic environments is well known. The morphology of attack is almost always localized and often looks very similar to the pitting shown for cast iron in Fig. 13.

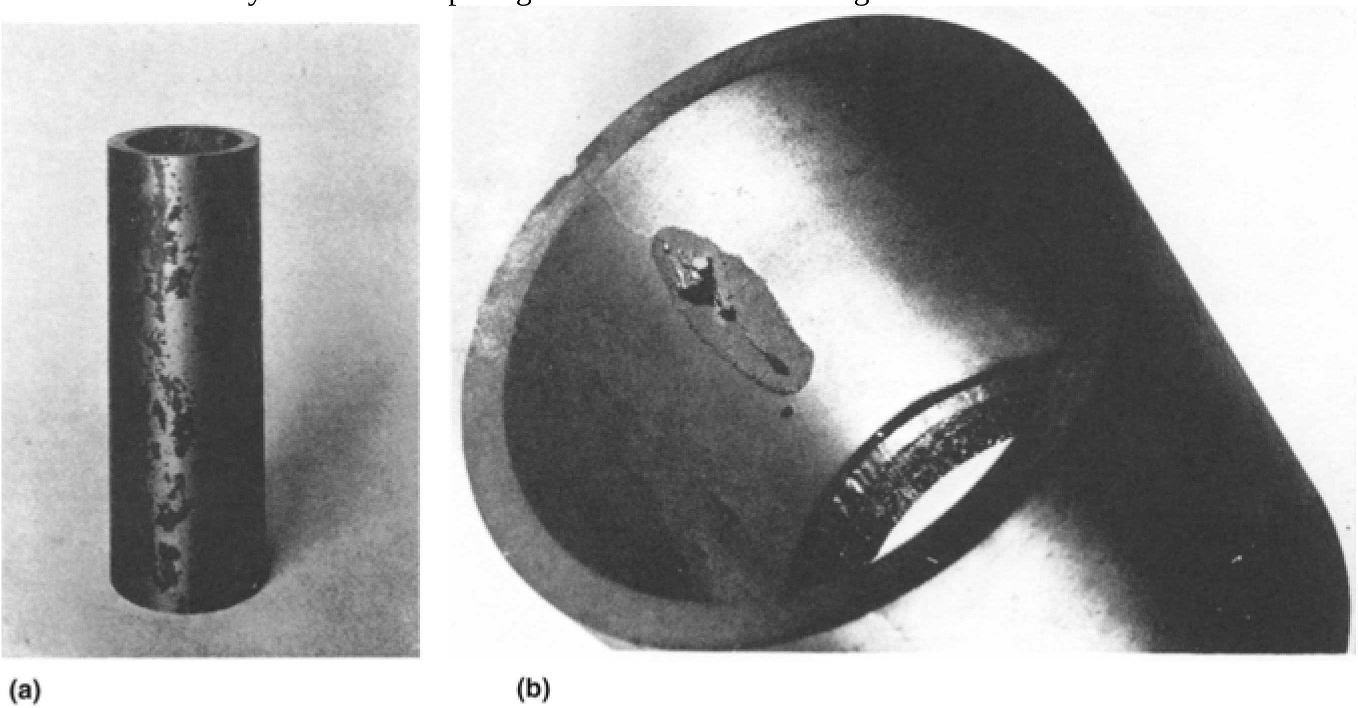

Fig. 13 Anaerobic biological corrosion of cast iron. (a) Cast iron pipe section exhibiting external pitting caused by bacteria. (b) Cast iron pipe showing penetration by bacteria-induced pitting corrosion. Source: Ref 10

In the early decades of this century, it was generally believed that the SRB could influence the corrosion of steel only in totally anaerobic environments such as deaerated soils and marine sediments. Recently, it has been recognized that anaerobic corrosion by SRB can take place in nominally aerated environments. In these latter cases, anaerobic microenvironments can exist under biodeposits of aerobic organisms, in crevices built into the structure, and at flaws in various types of coating systems. The most corrosive environments are often those in which alternate aerobic-anaerobic conditions exist because of the action of variable flow hydrodynamics or periodic mechanical action.

The anaerobic corrosion of iron and steel has been identified in such diverse environments as waterlogged soils of near-neutral pH; bottom muds of rivers, lakes, marshes, and estuaries (especially when these contain decaying organic material as a source of sulfates for the SRB); under marine fouling deposits and in various other offshore industrial environments (Ref 32); under nodules or tubercules in natural freshwaters and recirculating cooling waters; and under disbonded areas of pipeline coatings.
Unexpectedly rapid localized corrosion of steel bulkheads in marine harbor environments and of the ship hull plating of several tankers has been documented (Ref 33). In each case, the localized attack was found beneath macrofouling layers. The biofilm at and around the corrosion sites was populated with a rich consortium of aerobic and anaerobic microorganisms, and the SRB population was elevated by several orders of magnitude above that in the biofilm remote from the corrosion sites. These observations, coupled with the occurrence of corrosion rates too high to be explained by the usual metallurgical and electrochemical mechanisms, are the classic signs of biocorrosion.
A considerable amount of work has been done to assess the relative aggressiveness of various soils and sediments. The work in soils prior to 1970 is reviewed in Ref 34. Factors such as the presence or absence of SRB, soil resistivity, and water content were considered. It was discovered that SRB activity correlated well with soil redox potential, E_h, on the normal hydrogen scale (NHE), a variable that is much easier to measure than numbers of SRB. Aggressive soils tended to have mean resistivities of less than 2000 ohm · cm and a mean redox potential more negative than 400 mV on the NHE corrected to pH 7. Soils that were borderline based on these two tests tended to be aggressive if their water content was over 20%. With regard to redox potential alone, soil corrosivity varied, as shown in Table 3 (Ref 34).

Table 3 Dependence of soil corrosivity on redox potential

Soil E_h (NHE), mV	Corrosivity
<100	Severe
100–200	Moderate
200–400	Slight
>400	Noncorrosive

E_h, redox potential; NHE, normal hydrogen scale
Other attempts to assess the risk of corrosion by SRB have been sporadic. One investigation attempted to assess the severity of the SRB hazard on the inside of submarine pipelines carrying North Sea crude oil by measuring both the numbers of SRB present in the oil and the activity (or vigor of growth) of the organisms (Ref 35). The risk was assessed as extreme if both the numbers of organisms and their activity were rated high, and the risk was considered to be minimal if both were rated low.
Efforts to solve the anaerobic iron and steel corrosion problem, as outlined in Ref 34, include:

- Replacing the iron or steel with noncorrodible materials, such as fiberglass, polyvinyl chloride, polyethylene, and concrete
- Creating a nonaggressive environment around the steel by backfilling with gravel or clay-free sand to encourage good drainage (that is, oxygenating to suppress SRB), making the environment alkaline, or using biocides (in closed industrial systems)
- Using cathodic protection. Potentials of -0.95 V versus $Cu/CuSO_4$ (or even more negative) are often required. At these potentials, the risk of hydrogen cracking or blistering should be assessed.
- Use of various barrier coatings, sometimes including corrosion inhibitors and/or biocides

Aerobic Corrosion. Corrosion of iron and steel under oxygenated conditions generally involves the formation of acidic metabolites. The aerobic sulfur-oxidizing bacteria *Thiobacillus* can create an environment of up to approximately 10% H_2SO_4, thus encouraging rapid corrosion. Other organisms produce organic acids with similar results. This corrosion can be localized or general, depending on the distribution of organisms and metabolic products. If all the bacterial activity is concentrated at a break or delamination in a coating material, the corrosion is likely to be highly localized. If, on the other hand, the metabolic products are spread over the surface, the corrosion may be general, as has been reported for carbon steel tendon wires used to prestress a concrete vessel in a nuclear power plant (Ref 9). In this case, the wires were coated with a hygroscopic grease

prior to installation. A study to determine the cause of corrosion concluded that the wires, shown in Fig. 14, were corroded by formic and acetic acids excreted by bacteria in breaking down the grease.

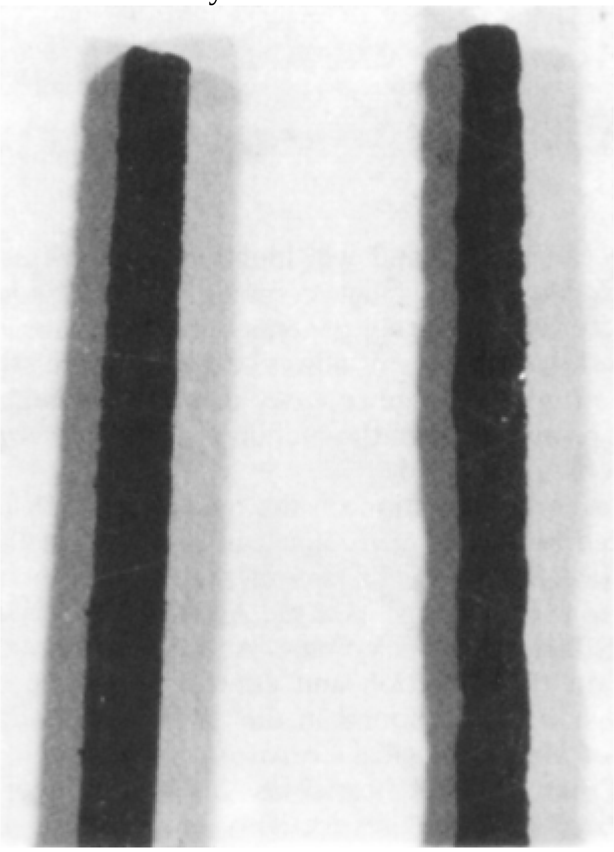

Fig. 14 Carbon steel wires from a prestressing tendon of a nuclear power plant showing the damage resulting from the formation of organic acids in the tendon due to the breakdown of grease by the bacteria present in the tendon. Source: Ref 9

Other cases of aerobic corrosion of iron and steel begin with the creation of oxygen concentration cells by deposits of slime-forming bacteria. Such corrosion is often accelerated by the iron-oxidizing bacteria in the formation of tubercules.

MIC of Passive Alloys

There are three general sets of conditions under which localized biological corrosion of austenitic stainless steel occurs (Fig. 15). These are illustrated by two generalized case histories. Typical examples of microbiologically induced localized corrosion of stainless steel are shown in Fig. 16.

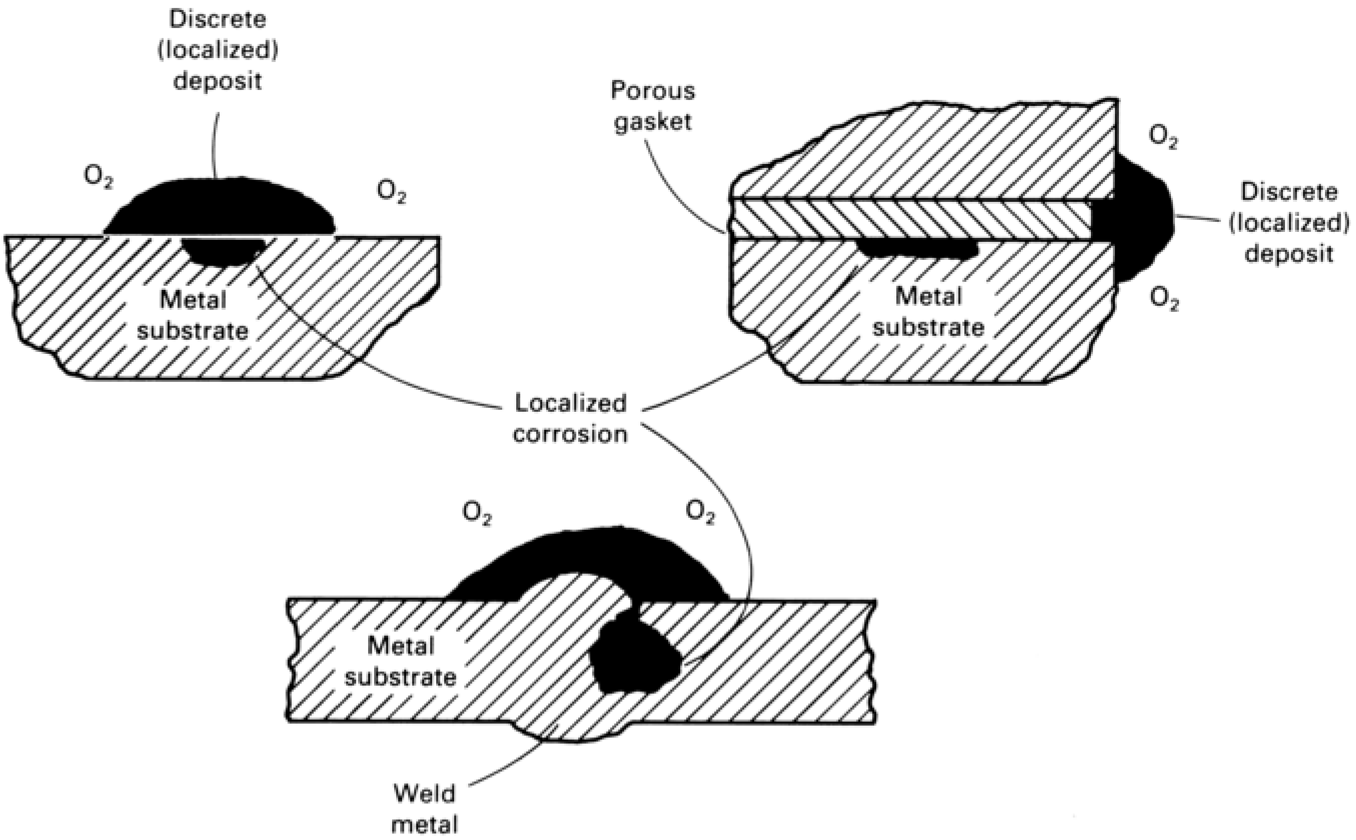

Fig. 15 The three most common forms of microbial corrosion. Source: Ref 40

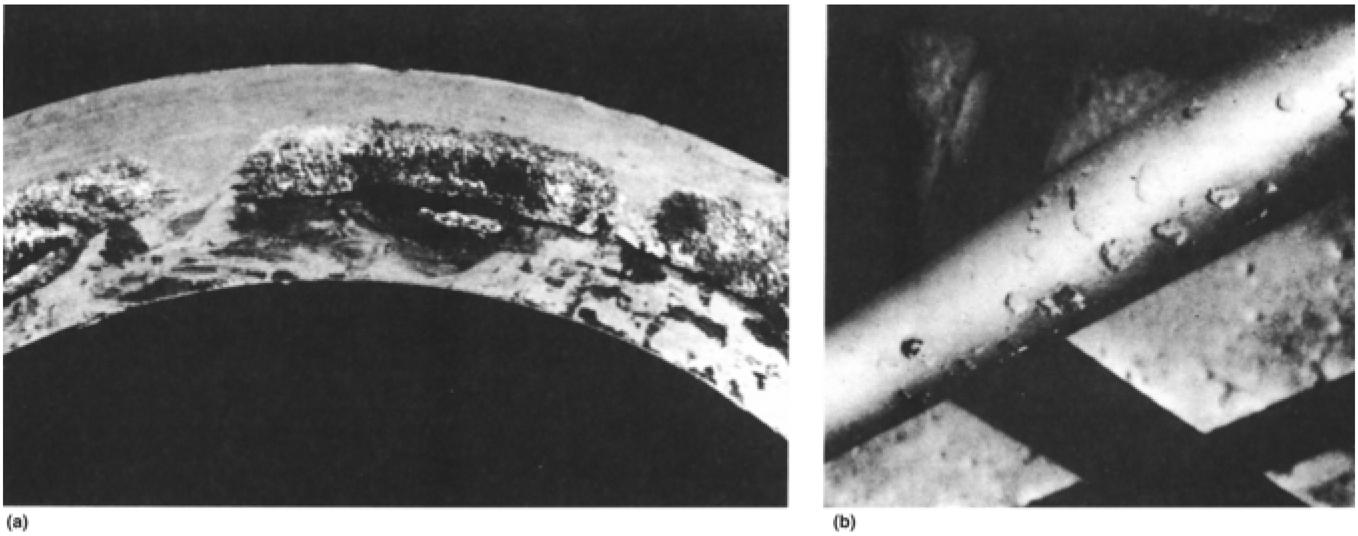

Fig. 16 Localized biological corrosion of austenitic stainless steel. (a) Crevice corrosion of type 304 stainless steel flange from a cooling water system. Staining shows evidence of adjacent biomounds. The corrosion attack reached a depth of 6 mm ($\frac{1}{4}$ in.). Courtesy of W.K. Link and R.E. Tatnall, E.I. Du Pont de Nemours & Co., Inc. (b) Pits on the underside of type 304 stainless steel piping used in a waste treatment tank (after sandblasting to remove biomounds). Courtesy of G. Kobrin and R.E. Tatnall, E.I. Du Pont de Nemours & Co., Inc.

Hydrotest or Outage Conditions. As originally reported in Ref 36, a new production facility required type 304L and 316L austenitic stainless steels for resistance to nitric and organic acids. All of the piping and flat-bottomed storage tanks were field erected and hydrostatically tested. The hydrotest water was plant well water containing 20 ppm chlorides and was sodium softened.

The pipelines were not drained after testing. The tanks were drained but were then refilled for ballast because of a hurricane threat. Two to four months after hydrotesting, water was found dripping from butt welds in the

nominally 3 mm ($\frac{1}{8}$ in.) wall piping. Internal inspection revealed numerous pits in and adjacent to welds under reddish-brown deposits in both piping and tanks. On cleaning off the deposit, the researchers found a large stained area with a pit opening. Metallographic sectioning showed a large subsurface cavity with only a small opening to the surface. Pitted welds in a type 316L tank showed some evidence of preferential attack of the delta- ferrite stringers, as shown in Fig. 17. It is not yet known exactly why such attack often concentrates at the weld line. Work by many investigators to characterize this phenomenon has been reviewed (see Borenstein, p 168–171 in “Selected References”). It is not always clear whether biological colonization precedes or follows the initiation of localized corrosion. What is clear is that once corrosion and biodeposits are both established, the attack proceeds more rapidly than would be expected due to electrochemical effects alone.

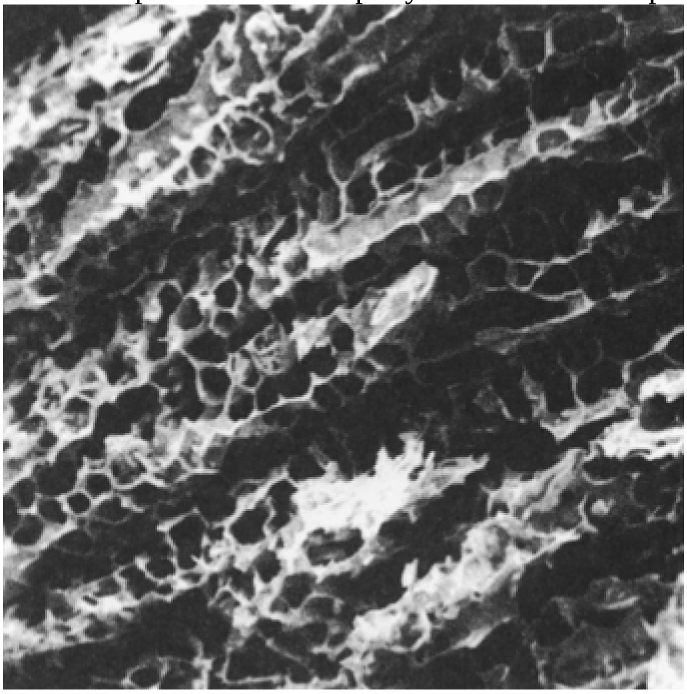

Fig. 17 Scanning electron micrograph showing matrix remaining after preferential corrosion of the δ-ferrite phase in a type 316 stainless steel. 300×. Courtesy of J.G. Stoecker, Monsanto Company

Well water and deposits both showed high counts of the iron bacteria *Gallionella* and the iron-manganese bacteria *Siderocapsa.* Deposits also contained thousands of parts per million of iron, manganese, and chlorides. Sulfate-reducing and sulfur-oxidizing bacteria were not present in either water or deposits. The proposed mechanism for the attack involves:

- Original colonization by the iron and manganese bacteria at the weld seams to create an oxygen concentration cell. Several investigators have confirmed that microorganisms are attracted to any site on a metallic surface having enhanced electrochemical activity, whether or not stable corrosion has initiated (Ref 37, 38).
- Dissolution of ferrous and manganous ions under the deposits
- Attraction of chloride ions as the most abundant anion to maintain charge neutrality
- Oxidation of the ferrous and manganous ions to ferric and manganic by the bacteria to form a highly corrosive acidic chloride solution in the developing pit

Many failures of this type have been reported in the chemical-processing industries in new equipment after hydrotesting but prior to commissioning in service. Similar failures have been reported in older equipment in both the chemical-processing and nuclear power industries when untreated well or river water was allowed to remain stagnant in the equipment during outage periods. Occasionally, the pitting is accompanied by what appear to be chloride stress-corrosion cracks under the deposits (Ref 9, 29). Examples of transgranular cracks in a type 304 stainless steel tank are shown in Fig. 18.

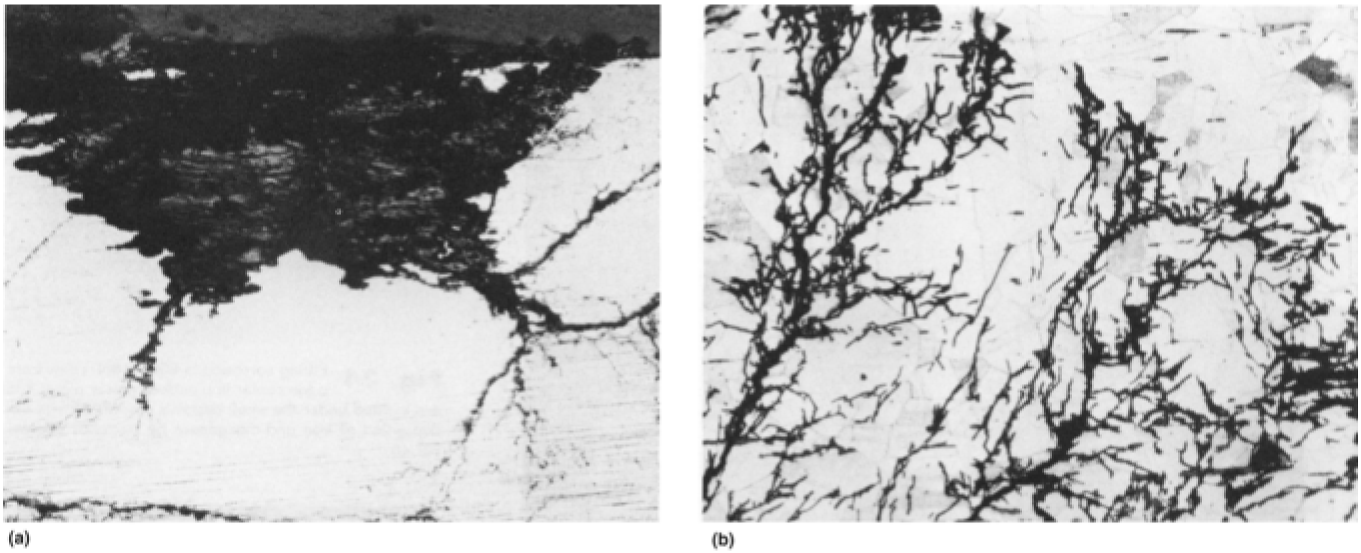

Fig. 18 Cracks emanating from pits in a type 304 stainless steel tank that was placed in hot demineralized water service with an operating temperature that fluctuated from 75 to 90 °C (165 to 195 °F). (a) Micrograph of a section through a typical biological deposit and pit in the wall of the tank. 25×. 10% oxalic acid etch. (b) Higher-magnification view of cracks. These branched transgranular cracks are typical of chloride stress-corrosion cracking of austenitic stainless steel. 250×. 10% oxalic acid etch. Source: Ref 39

Crevice or Gasket Conditions. A different set of conditions has led to the localized corrosion of asbestos-gasketed flanged joints in a type 304 stainless steel piping system (Ref 40). Inspection of the system after approximately 3 years of service in river water revealed severe crevice corrosion in and near the flanged and gasketed joints. The corrosion sites were covered by voluminous tan-to-brown, slimy biodeposits, as shown in Fig. 19(a). Under the deposits were broad, open pits with bright, active surfaces (Fig. 19b). The surfaces under the gasket material and adjacent to the corroded areas were covered with black deposits, which emitted H_2S gas when treated with HCl.

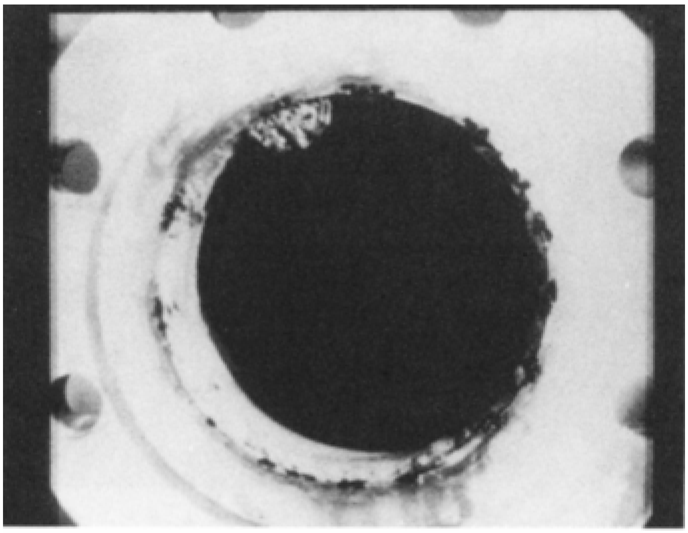

(a)

(b)

Fig. 19 Localized corrosion of asbestos-gasketed flanged joints in a type 304 stainless steel piping system. (a) Single remaining biodeposit adjacent to resulting corrosion on the flange. Numerous other similar deposits were dislodged in opening the joint. (b) Closeup of gouging-type corrosion under deposits shown in (a) after cleaning to remove black corrosion products. Source: Ref 40

The biological deposits were high in iron, silt- and slime-forming bacteria, and iron bacteria but not chloride, manganese, and sulfur compounds. Sulfate-reducing bacteria were found only in the black deposits. These bacteria had survived continuous chlorination (0.5 to 1.0 ppm residual), caustic adjustment of pH to 6.5 to 7.5, and continuous additions of a polyacrylate dispersant and a nonoxidizing biocide (quarternary amine plus tris tributyl tin oxide) (Ref 40).

The suspected mechanism involves:

- Colonization by slime-forming bacteria at low-velocity sites near gasketed joints
- Trapping of suspended solids rich in iron by the growing biodeposit, thus creating an environment conducive to growth of the filamentous iron bacteria
- Rapid depletion of oxygen in the crevice area by a combination of biological and electrochemical mechanisms (Ref 41), creating an environment for the SRB
- Breakdown of passivity by a combination of oxygen depletion and SRB activity, causing localized corrosion

Standard approved methods for controlling the biological corrosion of stainless alloys are currently being developed. Some general guidelines for avoiding problems in hydrotesting, however, are given in Ref 36. These guidelines are summarized as follows. First, demineralized water or high-purity steam condensate is used for the test water. The equipment should be drained and dried as soon as possible after testing. Second, if a natural freshwater must be used, it should be filtered and chlorinated, and the equipment should be blown or mopped dry within 3 to 5 days after testing.

Effects in the Marine Environment. The idea that natural seawater, with its full complement of organisms, is more corrosive than artificial seawater often has appeared in the corrosion literature. Many papers have been published since the late 1980s in documentation of this phenomenon. The material is organized into three categories giving the effects on:

- Open-circuit (OCP) and pitting potentials
- Initiation of localized corrosion
- Corrosion propagation

Effect of Biofilms on OCP and Pitting Potentials. During the past 15 years, many investigators from all over the world have documented the tendancy for biofilms to cause a noble shift in the OCP of passive alloys (Ref 42, 43, 44, 45, 46, 47, 48). The alloys tested include but are not limited to Unified Numbering System (UNS) S30400, S30403, S31600, S31603, S31703, S31803, N08904, N08367, S44660, S20910, S44735, N10276, and R50250. To a first approximation, the amount of ennoblement was independent of alloy composition as long as the alloy had an *n*-type semiconducting passive film. It has been shown that the noble shift in OCP for passive alloys with *p*- type passive films, such as alloy N06455 (C4), took place more slowly with a smaller total shift than alloys such as N08367 (6XN) with an *n*- type passive film (Ref 49).

Ennoblement of the OCP occurred in fresh, brackish, and seawaters as long as corrosion initiation did not interfere. The rate of ennoblement was slower in fresh water than in seawater, but the amount of ennoblement was inversely related to the salinity of the electrolyte (Ref 50). The most noble potentials reached were also highest and most consistent in freshwater. Thus, it was concluded that ennoblement of the OCP decreased the salinity level below which a given alloy should be resistant to localized corrosion initiation (Ref 50). Theoretically, this information could be used to decide the upper salinity limits for application of any given alloy. In practice, however, this is impractical for two reasons. First, there are seasonal and tidal salinity fluctuations in any natural estuarine environment. Second, complex industrial equipment, such as heat exchangers, that are often fabricated from passive alloys may themselves create salinity gradients due to variations in temperature and flow rate.

Research showed that the critical potential for pit initiation (E_{cpp}) on an open surface and the breakdown potential for initiation of localized corrosion (E_b) at occluded sites or the air-water interface are also affected by formation of biofilms (Ref 51). For alloy S30400, the average E_{cpp} of samples with biofilms (425 ± 24 mV saturated calomel electrode, or SCE) was 95 mV higher than that of the bare samples (330 ± 35 mV). This result is not surprising, because bacteria produce nitrates and sulfates. Further, many bacteria accumulate large amounts of inorganic phosphate in the form of granules of polyphosphate. When these bacteria die, those phosphates are released into the biofilm. Na_2SO_4 and $NaNO_3$ (concentrations as low as 0.0125 *M*) are known to be pitting inhibitors for stainless steels. For alloy S31600, the E_{cpp} values of the biofilmed samples (500 mV) were not much different than the bare metal samples (480 ± 17 mV). The reason for this is unknown, but it is possible that the inhibitor concentration produced in the biofilm was not high enough to affect the higher E_{cpp} for S31600.

The breakdown potential data for alloy S30400 showed that E_b increased from 60 mV for the bare sample to 260 ± 20 mV for those with biofilms. For alloy S31600, E_b increased a smaller amount, from 300 mV for the

bare sample to 390 ± 14 mV for those with biofilms. These values agreed favorably with the observation that corrosion at the air-water interface was observed for S30400 and S31600 after the corrosion potential reached potentials of 250 and 350 mV SCE, respectively. These data strongly suggest that critical pitting and breakdown potentials should be measured on samples with natural biofilms when the application involves exposure to waters from which they form.

Initiation of Pitting and Crevice Corrosion. Tests on crevice-corrosion samples of passive alloys S30400 and S31600 revealed that crevice initiation times were reduced when natural marine biofilms were allowed to form on the exposed external cathode surface (Ref 46, 52, 53, 54). Even though there was a lot of variability in the data, it was concluded from the tests that ennoblement of the OCP in the presence of natural biofilms usually caused the alloy to reach its breakdown potential for crevice initiation faster than when the test was repeated under control conditions without the biofilm.

Propagation of Crevice Corrosion. Many investigators have used potentiodynamic polarization curves to show that cathodic kinetics are increased during biofilm formation on passive alloy surfaces (Ref 46, 55, 56, 57). Tests have shown that this increase in kinetics results in higher propagation rates for crevice corrosion (Ref 52, 53, 54). Crevice propagation rates after initiation were enhanced significantly and consistently. Crevice propagation current densities were increased by 1 to 3 orders of magnitude versus the control for alloys S30400, S31603, S31725, and N08904. The effect was also reflected in greater weight loss as well as higher maximum and average depths of attack on test alloys with biofilms on the exterior cathode surface versus the control.

Effect of Biofilms on Galvanic Corrosion. The increase in cathodic kinetics due to the action of biofilms on passive alloy surfaces also can increase the propagation rate of galvanic corrosion. Researchers tested galvanic corrosion of copper, steel 3003, aluminum, and zinc anodes coupled to cathode panels of passive alloy N08367 (Ref 58). In one series of tests, natural marine microbial biofilms were allowed to form on the cathode surface. On the control tests, the action of the biofilm was prevented. Corrosion of the copper, steel, and aluminum anodes was significantly higher when connected to cathodes on which the biofilm was allowed to grow naturally. The largest effect was noted for the copper anodes. As shown in Fig. 20, the galvanic current for copper corrosion, as measured with a zero resistance ammeter, was 2 to 3 decades higher for copper couples with biofilms on the cathode than for the corresponding control couples. Weight loss values for the copper anodes were also significantly higher when coupled to cathodes with biofilms than on control coupons.

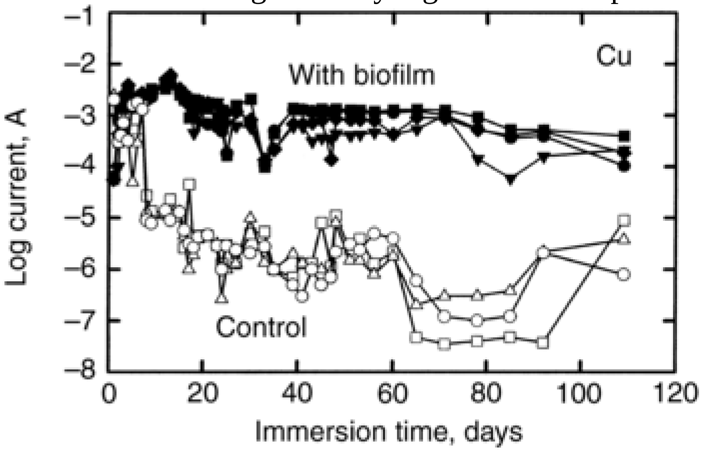

Fig. 20 Corrosion currents for galvanic couples of UNS C1100 copper anodes versus UNS N08367 stainless steel cathodes with and without (control) the influence of natural marine microbial biofilms. Source: Ref 58

Similar results were found for the steel and aluminum anodes. Average corrosion currents and weight losses were 5 to 8 times higher for the steel and aluminum anodes when biofilms were allowed to grow on the cathode surface than for the control without the biofilm. The galvanic currents measured for aluminum are shown in Fig. 21, and the aluminum anodes themselves are shown in Fig. 22.

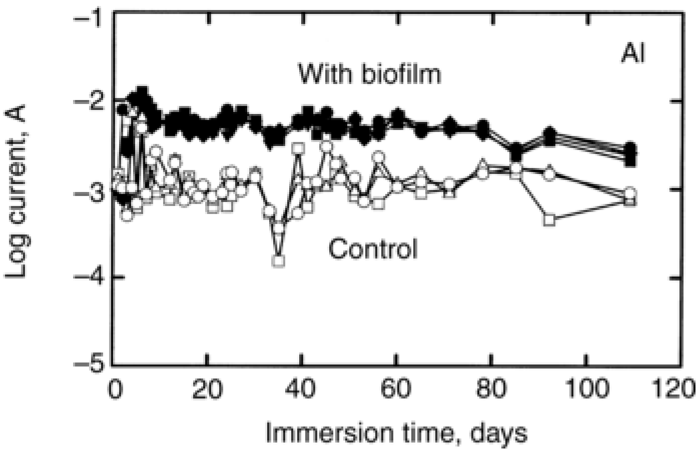

Fig. 21 Corrosion currents for galvanic couples of UNS A93003 aluminum alloy anodes versus UNS N08367 stainless steel cathodes with and without (control) the influence of natural marine microbial biofilms. Source: Ref 58

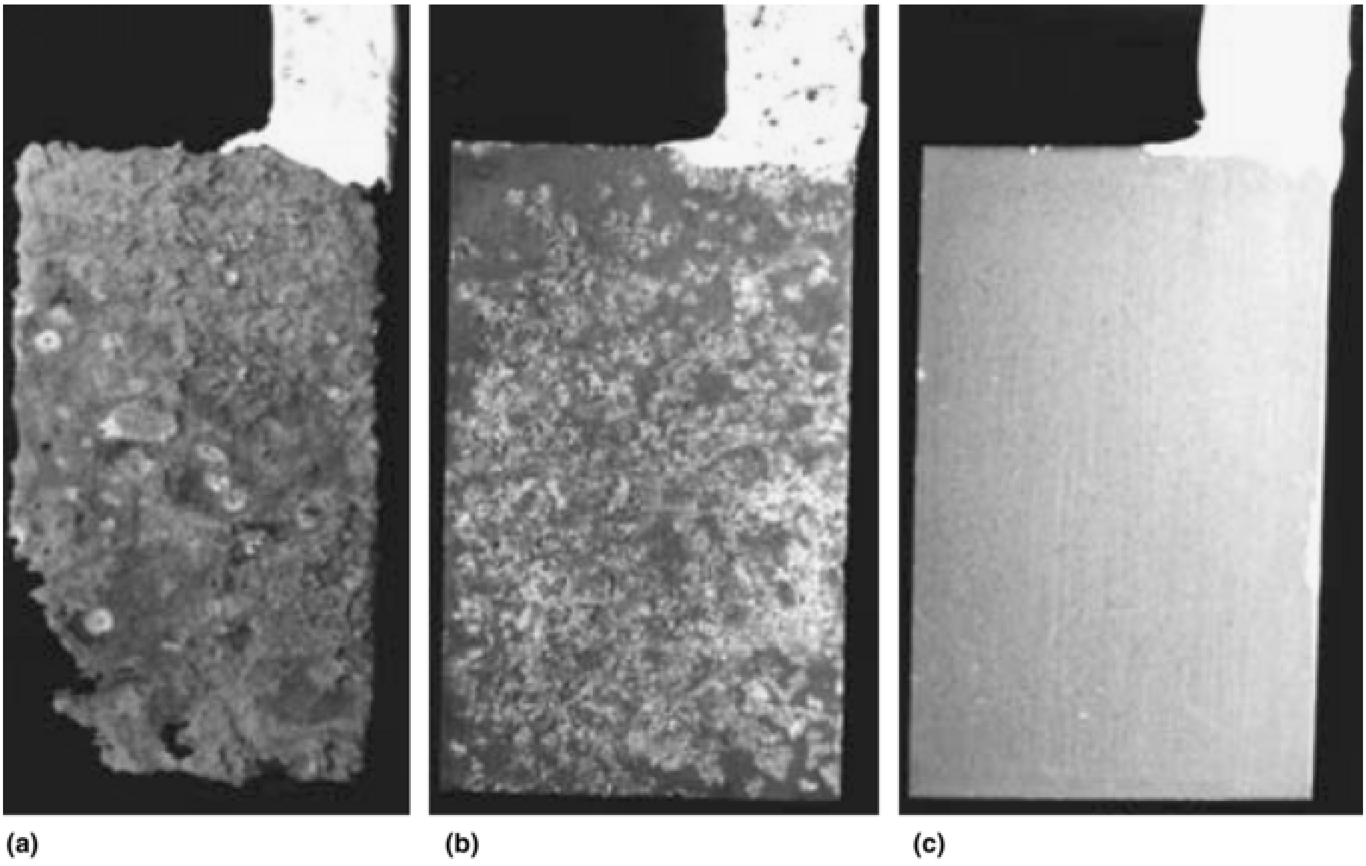

Fig. 22 UNS A93003 aluminum coupons after galvanic corrosion test and removal of corrosion products. (a) Coupled to stainless steel cathode with natural microbial biofilm. (b) Coupled to control stainless steel cathode without biofilm. (c) As originally prepared prior to immersion. Source: Ref 58

In contrast, the corrosion currents and weight loss values for all zinc couples, both with and without biofilms on the cathode, fell within the same scatter band. The reason why biofilms had no effect on galvanic corrosion of zinc anodes was not determined. It was speculated, however, that the zinc anodes generated a high enough pH at the cathode surface to interfere with the action of microorganisms within the biofilm.

MIC of Aluminum

Pitting corrosion of integral wing aluminum fuel tanks in aircraft that use kerosene-based fuels has been a problem since the 1950s (Ref 59). The fuel becomes contaminated with water by vapor condensation during

variable-temperature flight conditions. Attack occurs under microbial deposits in the water phase and at the fuel-water interface. The organisms grow either in continuous mats or sludges, as shown in Fig. 23, or in volcano-like tubercules with gas bubbling from the center, as shown schematically in Fig. 24.

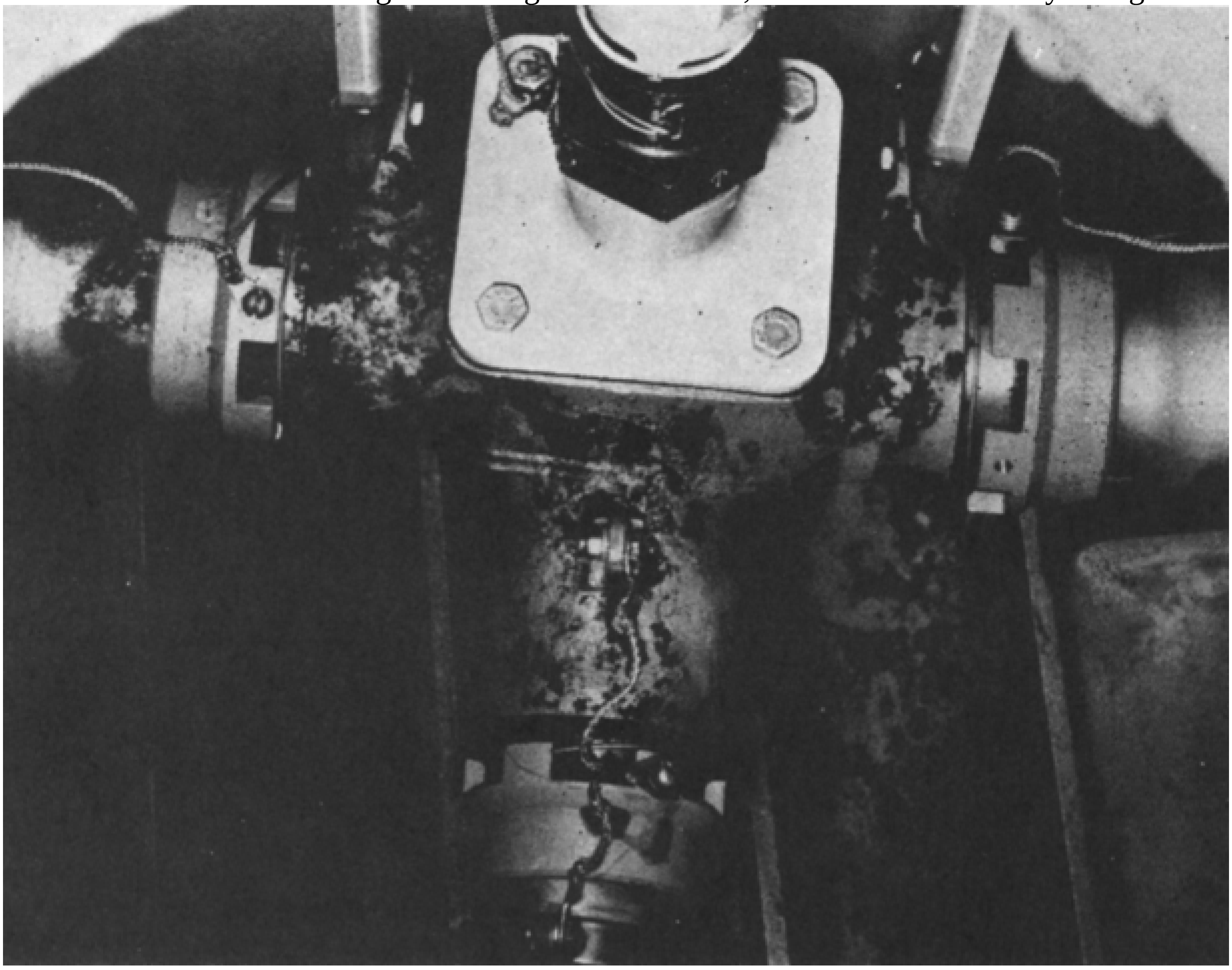

Fig. 23 Microbial growth in the integral fuel tanks of jet aircraft. Source: Ref 10

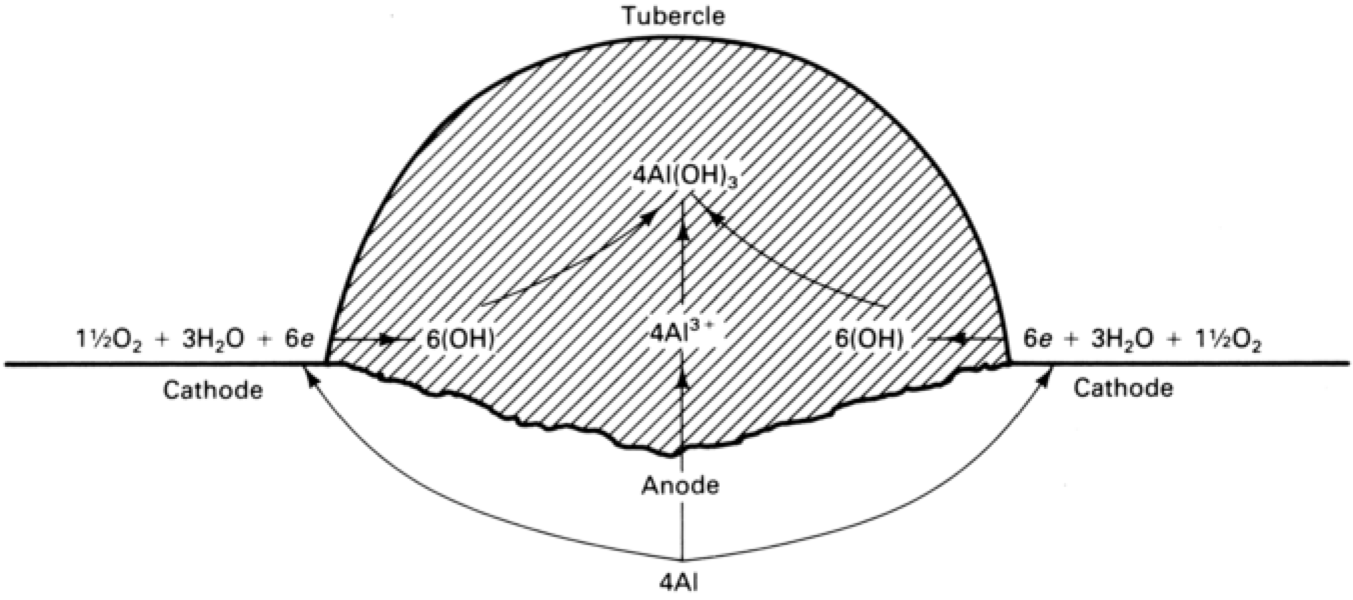

Fig. 24 Schematic of tubercle formed by bacteria on an aluminum alloy surface. Source: The Electrochemical Society

The organisms commonly held responsible are *Pseudomonas*, *Cladosporium*, and *Desulfovibrio.* These are often suspected of working together in causing the attack. *Cladosporium resinae* is usually the principal

organism involved; it produces a variety of organic acids (pH 3 to 4 or lower) and metabolizes certain fuel constituents. These organisms may also act in concert with the slime-forming *Pseudomonads* to produce oxygen concentration cells under the deposit. Active SRB have sometimes been identified at the base of such deposits. Control of this type of attack has usually focused on a combination of reducing the water content in fuel tanks; coating, inspecting, and cleaning fuel tank interiors; and using biocides and fuel additives. More information can be found in Ref 8 and 59.

MIC of Copper and Nickel Alloys

The well known toxicity of cuprous ions toward living organisms does not mean that the copper-base alloys are immune to biological effects in corrosion. It does mean, however, that only those organisms having a high tolerance for copper are likely to have a substantial effect. Thiobacillus thiooxidans, for example, can withstand copper concentrations as high as 2%. Localized corrosion of copper alloys by SRB in estuarine environments has been documented in published reports (Ref 60, 61). Cases of MIC of Cu-10Ni, Admiralty brass (Cu-30Zn-15Sn), and aluminum brass (Cu-20Zn-2Al) at electric generating facilities using fresh or brackish cooling waters also have been documented (Ref 62, 63, 64). Most of the reported cases of microbial corrosion of copper alloys are caused by the production of such corrosive substances as CO_2, H_2S, NH_3, and organic or inorganic acids (Ref 5, 23). Bacterial extracellular polymers play a role in the corrosion of copper alloys in freshwater distribution systems (Ref 65, 66).

Laboratory and field studies have been designed to evaluate corrosion in welds and heat- affected zones in Cu-Ni seawater piping systems exposed to estuarine and sea waters (Ref 61). It was demonstrated that welds provide unique environments for the colonization of SRB with the subsequent production of sulfides that affect the weld seam surface, the adjacent flow zone, and the downstream surface of the heat-affected zone. Exposure of sulfide-derived surfaces to fresh, aerated seawater resulted in rapid spalling on the downstream side of weld seams. The bared surfaces became anodic to the sulfide- coated weld root, accelerating corrosion.

Copper-nickel tubes from the fan coolers in a nuclear power plant were found to have pitting corrosion under bacterial deposits (Fig. 25). Slime-forming bacteria acting in concert with iron- and manganese-oxiding bacteria were responsible for the deposits.

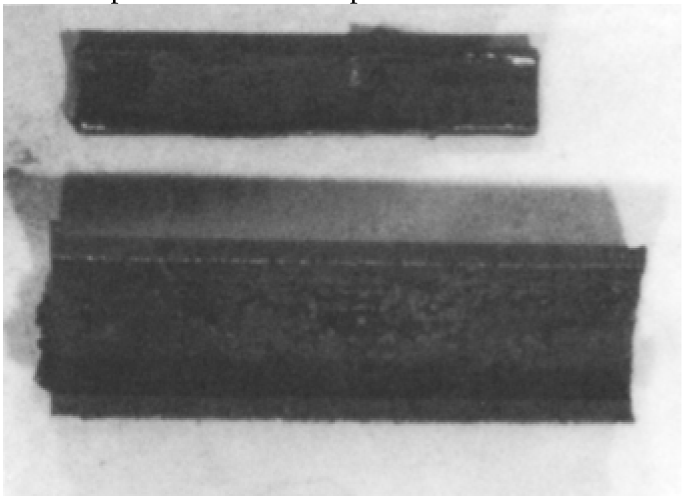

Fig. 25 Pitting corrosion in 90Cu-10Ni tubes from a fan cooler in a nuclear power plant. Pits are located under the small deposits associated with the deposition of iron and manganese by bacteria. Source: Ref 9

Monel 400 (66.5% Ni, 31.5% Cu, and 1.25% Fe) tubing was severely pitted after exposure to marine and estuarine waters containing SRB (Ref 67). Localized corrosion was attributed to a combination of differential aeration cells, a large cathode-to-anode area ratio, concentration of chlorides, development of acidity within the pits, and the specific reactions of the base metals with sulfides produced by the SRB. Chlorine and sulfur reacted selectively with the iron and nickel in the alloy, leaving a copper-rich, spongy pit interior (selective dealloying). Monel 400 (UNS N04400) was found to be highly susceptible to MIC attack in Arabian Gulf seawater by SRB (Ref 68). The SRB attack was in the form of circular cavities where an intergranular mode of corrosion took place and was accompanied by selective leaching of nickel and iron.

In another case, Monel heat-exchanger tubes were found to have severe pitting corrosion (Fig. 26) under discrete deposits rich in iron, copper, manganese, and silicon, with some nickel (Ref 9). Associated with the deposit were slime-forming bacteria, along with iron- and manganese- oxidizing bacteria. Several million SRB were found within each pit under the deposit. It was thought that the deposit-forming organisms created an environment conducive to growth of SRB, which then accelerated corrosion by the production of H_2S.

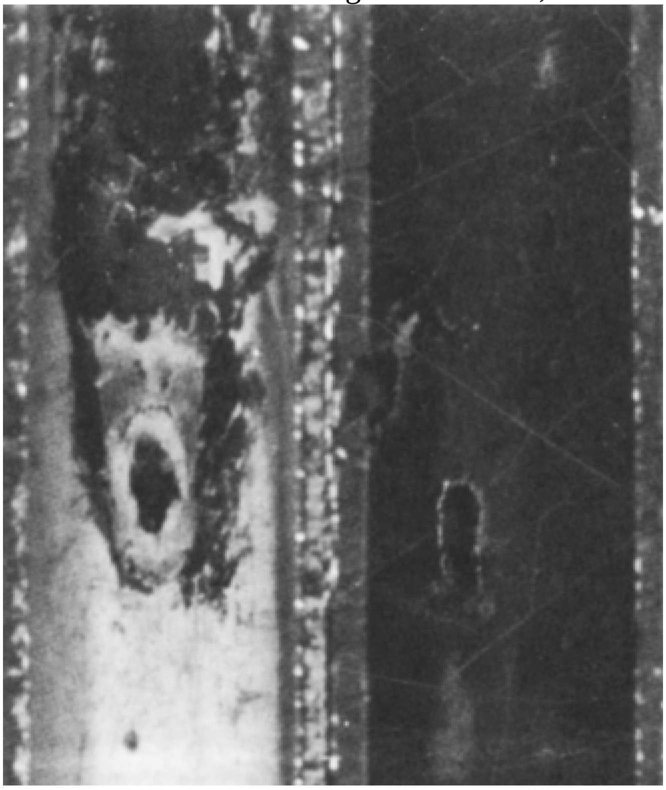

Fig. 26 Pitting corrosion in Monel tubes from a heat exchanger. Each pit was originally covered by a discrete deposit containing large numbers of SRB. Source: Ref 9

It is quite common to have bacterial slime films on the interior of copper alloy heat-exchanger and condenser tubing. Usually, these films are a problem only with heat transfer as long as the organisms are living. When they die, however, organic decomposition produces sulfides, which are notoriously corrosive to copper alloys. Occasionally, NH_3-induced stress-corrosion cracking has been directly attributed to microbial NH_3 production.

Biodeterioration of Nonmetallics, Composites, and Coatings

In addition to influencing the corrosion of metals and alloys, microorganisms have long been known for their ability to participate in the biodeterioration of wood, concrete, stone, polymers, asphalt, and various minerals (Ref 11). More recently, cases have been documented for the biodeterioration by bacteria and/or fungi of architectural building materials, stoneworks, fiber-reinforced composites, polymeric coatings, and concrete (Ref 69).

Building Materials and Stoneworks. As summarized in Ref 70, microbiological activity plays an important role in the overall process of deterioration for a variety of building materials. Weathering by rain, wind, freeze-thaw, and the ultraviolet component of sunlight begin to break down the surface and provide microorganisms with organic and inorganic nutrients. Biodeterioration then proceeds by the processes of staining, patina formation, pitting, etching, disaggregation, and exfoliation. Prevention measures under outdoor conditions include the application of biocides and other formulations based on a combination of silicones and biocides. Control of environmental variables, such as humidity, temperature, and light, also is used under some indoor conditions to minimize degradation.

The same types of processes are active in the biodeterioration of cultural heritage stoneworks at many locations worldwide (Ref 71). The attack is generally the result of interactions between microorganisms (bacteria, algae, fungi), macroorganisms (lichens and mosses), and physico-chemical mechanisms, including atmospheric pollution.

Composite Materials. It was reported that the glass fibers used in fiber-reinforced polyester (FRP) lost all rigidity when exposed to SRB for 90 days, although the glass itself and the epoxy and vinyl resin materials were not attacked (Ref 72, 73). Some attack on graphite fibers by soil bacteria (Ref 74) has been reported. A 10% loss in strength of a carbon-fiber-reinforced epoxy resin composite has been reported on exposure to SRB. It has also been shown that fungi can cause degradation of carbon-reinforced epoxies and other FRP due to *hyphae* penetration of the resin material (Ref 75).

Coatings. Many types of polymeric coatings can be subject to biodegradation. The attack is usually caused by acids or enzymes produced by bacteria or fungi. This often results in selective attack on one or more specific components of a coating system, with consequent increase in porosity and water or other ion transport through the coating and the formation of blisters, breaches, and disbonded areas. Many of these effects have recently been reviewed (Ref 72). It has been noted that the microbes responsible for damage to coatings may or may not be involved in corrosion initiation under the damaged coating (Ref 76). The electrochemical impedance and electrochemical noise techniques have been used for studying microbial deterioration of coatings (Ref 77, 78, 79). Blisters and delaminations in the coatings were usually associated with microorganisms in both natural marine and laboratory exposures. It was not clear, however, whether those organisms played any role in corrosion initiation under the coating. As already noted earlier in this article, both marine and freshwater microbes can be attracted to iron corrosion products or even sites of heightened electrochemical activity without necessarily being implicated in corrosion initiation. The mere observation that microbial attachment and corrosion occur at a common location on a metal surface is not enough evidence to assign cause and effect (Ref 80, 81).

Concrete can be damaged by the acids, sulfates, ammonium, and other materials produced by microorganisms. Perhaps the most prevalent concrete application in which significant biodeterioration problems have been encountered is municipal wastewater collection and treatment systems. Researchers have studied such systems in which the bacterially mediated sulfur cycle (Fig. 3) plays the major role (Ref 82, 83). In the anaerobic environment of the sewage itself, SRB convert sulfates to sulfides, causing hydrogen sulfide (H_2S) to be released into the aerobic environment near the top of the sewer pipe. The H_2S is in turn oxidized to sulfuric acid by the sulfur-oxidizing bacteria *Thiobacillus.* Bacterial acid production caused the pH in the vicinity of the sewer pipe crown to reach values as low as 2.0, resulting in acid attack on the concrete (Ref 82).

Steel reinforcing bar in concrete corrodes readily in such environments, once exposed by sufficient deterioration of the concrete. Even in the absence of acid attack on the concrete, it has been shown (Ref 84) that H_2S production by SRB can cause corrosion of the rebar in reinforced-concrete structures. If the H_2S is able to permeate the concrete, the normally passive iron oxide film on the rebar in the high-pH pore- water environment of the concrete is converted to a non-protective iron sulfide film.

References cited in this section

5. B. Little, P. Wagner, and F. Mansfeld, Microbiologically Influenced Corrosion of Metals and Alloys, *Int. Mater. Rev.,* Vol 36 (No. 6), 1991, p 253–272

8. D.H. Pope, D. Duquette, P.C. Wayner, and A.H. Johannes, "Microbiologically Influenced Corrosion: A State-of-the-Art-Review," Publication 13, Materials Technology Institute of the Chemical Process Industries, Inc., 1984

9. D.H. Pope, "A Study of Microbiologically Influenced Corrosion in Nuclear Power Plants and a Practical Guide for Countermeasures," EPRI NP-4582, Final Report, Electric Power Research Institute, 1986

10. J.D.A. Miller, Ed., *Microbial Aspects of Metallurgy,* Elsevier, 1970

11. H.A. Videla, *Manual of Biocorrosion,* CRC Press, Inc., 1996, p 13–45, 121–133, 160–173, 179–185, 228–237, 232

12. *Microbial Corrosion,* Proceedings of the Conference, National Physical Laboratory, The Metals Society, 1983

21. S.C. Dexter, Ed., Biologically Induced Corrosion, *Proceedings of the Conference,* National Association of Corrosion Engineers, 1986

23. D.H. Pope, D.J. Duquette, A.H. Johannes, and P.C. Wayner, *Mater. Perform.,* Vol 23 (No. 4), 1984, p 14–18

28. H.A. Videla and R.C. Salvarezza, *Introduction to Microbiological Corrosion,* Biblioteca Mosaico, 1984 (in Spanish)

29. D.H. Pope and J.G. Stoecker, Microbiologically Influenced Corrosion, *Process Industries Corrosion—Theory and Practice,* B.J. Moniz and W.I. Pollock, Ed., National Association of Corrosion Engineers, 1986, p 227–242

30. G. Kobrin, Ed., A Practical Manual on Microbiologically Influenced Corrosion, NACE International, 1994

31. J. Stoecker, Ed., *A Practical Manual on Microbiologically Influenced Corrosion,* Vol 2, NACE International, 2001

32. P.F. Sanders and W.A. Hamilton, Biological and Corrosion Activities of Sulfate-Reducing Bacteria in Industrial Process Plant, *Biologically Induced Corrosion,* S.C. Dexter, Ed., National Association of Corrosion Engineers, 1986, p 47–68

33. I.B. Beech, S.A. Campbell, and F.C. Walsh, Marine Microbial Corrosion, *A Practical Manual on Microbiologically Influenced Corrosion,* Vol 2, J. Stoecker, Ed., NACE International, 2001, p 11.3–11.14

34. J.D.A. Miller and A.K. Tiller, Microbial Corrosion of Buried and Immersed Metal, *Microbial Aspects of Metallurgy,* J.D.A. Miller, Ed., American Elsevier, 1970, p 61–106

35. R.A. King, J.D.A. Miller, and J.F.D. Stott, Subsea Pipelines: Internal and External Biological Corrosion, *Biologically Induced Corrosion,* S.C. Dexter, Ed., National Association of Corrosion Engineers, 1986, p 268–274

36. G. Kobrin, Reflections on Microbiologically Induced Corrosion of Stainless Steels, *Biologically Induced Corrosion,* S.C. Dexter, Ed., National Association of Corrosion Engineers, 1986, p 33

37. B.J. Little, P.A. Wagner, K.R. Hart, and R. Ray, "Spatial Relationships Between Bacterial and Localized Corrosion," Paper 278, Corrosion/96, NACE International, 1996

38. M. Eashwar and S.C. Dexter, "Relation of Bacterial Settlement Patterns to Anodic Activity on Stainless Steel Weldments," Paper 174, Corrosion/99, NACE International, 1999

39. J.G. Stoecker and D.H. Pope, Study of Biological Corrosion in High Temperature Demineralized Water, *Mater. Perform.,* June 1986, p 51–56

40. R.E. Tatnall, Case Histories: Bacteria Induced Corrosion, *Mater. Perform.,* Vol 20 (No. 8), 1981, p 41

41. S.C. Dexter, K.E. Lucas, and G.Y. Gao, Role of Marine Bacteria in Crevice Corrosion Initiation, *Biologically Induced Corrosion,* S.C. Dexter, Ed., National Association of Corrosion Engineers, 1986, p 144–153

42. P. Chandrasekaran and S.C. Dexter, "Thermodynamic and Kinetic Factors Influenced by Biofilm Chemistry Prior to Passivity Breakdown," Paper 482, Corrosion/ 94, NACE International, 1994

43. P. Chandrasekaran and S.C. Dexter, Factors Contributing to Ennoblement of Passive Metals Due to Biofilms in Seawater, *Proc. 12th International Corrosion Congress,* Vol 5B, NACE International, 1993, p 3696–3707

44. S.C. Dexter and G.Y. Gao, Effect of Seawater Biofilms on Corrosion Potential and Oxygen Reduction of Stainless Steel, *Corrosion,* Vol 44 (No. 10), 1988, p 717–723

45. S.C. Dexter, Effect of Biofilms on Marine Corrosion, *Bioextraction and Biodeterioration of Metals,* C. Gaylarde and H. Videla, Ed., Cambridge University Press, 1995, p 129–167

46. R. Johnson and E. Bardal, Cathodic Properties of Different Stainless Steels in Natural Seawater, *Corrosion,* Vol 41 (No. 5), 1985, p 296

47. V. Scotto, R. Dicintio, and G. Marcenaro, The Influence of Marine Aerobic Microbial Film on Stainless-Steel Corrosion Behavior, *Corros. Sci.,* Vol 25 (No. 3), 1985, p 185–194

48. S. Motoda, Y. Suzuki, T. Shinohara, and S. Tsujikawa, The Effect of Marine Fouling on the Ennoblement of Electrode Potential for Stainless Steels, *Corros. Sci.,* Vol 31, 1990, p 515–520

49. S.C. Dexter and S. Maruthamuthu, "Response of Passive Alloys with N- and P- Type Passive Films to Manganese in Biofilms," Paper 01256, Corrosion/2001, NACE International, 2001

50. S.C. Dexter and H.-J. Zhang, Effect of Biofilms on Corrosion Potential of Stainless Alloys in Estuarine Waters, *Proc. 11th Intl. Corrosion Congress,* April 1990 (Florence, Italy), Assoc. Italiana Di Metall., Milano, Italy, p 4.333

51. H.-J. Zhang and S.C. Dexter, Effect of Biofilms on Critical Pitting Potentials for Stainless Steels S30400 and S31600 in Seawater, *Proc. 1995 International Conference on Microbiologically Influenced Corrosion,* May 1995 (New Orleans, LA), P. Angel et al., Ed., NACE International, p 70/1–70/8

52. H.-J. Zhang and S.C. Dexter, "Effect of Marine Biofilms on Crevice Corrosion of Stainless Alloys," Paper 400, Corrosion/ 92, NACE International, 1992

53. H.-J. Zhang and S.C. Dexter, Effect of Biofilms on Crevice Corrosion of Stainless Alloys in Coastal Seawater, *Proc. 12th International Corrosion Congress,* Vol 5B, NACE International, 1993, p 3761–3772

54. H.-J. Zhang and S.C. Dexter, "Effect of Marine Biofilms on Initiation Time of Crevice Corrosion for Stainless Steels," Paper 285, Corrosion/95, NACE International, 1995

55. V. Scotto, Electrochemical Studies on Biocorrosion of Stainless Steel in Seawater, *EPRI Workshop on Microbial Induced Corrosion,* G. Licina, Ed., Electric Power Research Institute, p B.1–B.36

56. A. Mollica, G. Ventura, E. Traverso, and V. Scotto, "Cathodic Behavior of Nickel and Titanium in Natural Seawater," Seventh Intl. Biodeterioration Symp., International Biodeterioration Society (Cambridge, U.K.), 1987

57. S.C. Dexter, Effect of Biofilms on Crevice Corrosion, *Proc. COR/96 Topical Research Symposium on Crevice Corrosion,* NACE, 1996, p 367–383

58. S.C. Dexter and J.P. LaFontaine, Effect of Natural Marine Biofilms on Galvanic Corrosion, *Corrosion,* Vol 54 (No. 11), 1998, p 851–861

59. J.J. Elpjick, Microbial Corrosion in Aircraft Fuel Systems, *Microbial Aspects of Metallurgy,* J.D.A. Miller, Ed. American Elsevier, 1970, p 157–172

60. B. Little, P. Wagner, R. Ray, and M. McNeil, *J. Mar. Technol. Soc.,* Vol 24 (No. 3), 1990, p 10–17

61. B.J. Little, P. Wagner, and J. Jacobus, The Impact of Sulfate-Reducing Bacteria on Welded Copper-Nickel Seawater Piping Systems, *Mater. Perform.,* Vol 27 (No. 8), 1988, p 57–61

62. R.J. Soracco, D.H. Pope, J.M. Eggars, and T.N. Effinger, Microbiologically Influenced Corrosion Investigations in Electric Power Generating Stations, *Corrosion 1988,* Paper 83, NACE International, 1988

63. D.H. Pope, *Microbial Corrosion in Fossil- Fired Power Plants: A Study of Microbiologically Influenced Corrosion and a Practical Guide for Its Treatment and Prevention,* Electric Power Research Institute, Palo Alto, CA, 1987

64. D.H. Pope, A Study of Microbiologically Influenced Corrosion in Nuclear Power Plants and a Practical Guide for Countermeasures, EPRI Final Report NP-4582, Project 1166-6, Electric Power Research Institute, Palo Alto, CA, May 1986

65. G.G. Geesey, M.W. Mittleman, T. Iwaoka, and P.R. Griffiths, Role of Bacterial Exopolymers in the Deterioration of Metallic Copper Surfaces, *Mater. Perform.,* Vol 25 (No. 2), 1986, p 37–40

66. G.G. Geesey and P.J. Bremer, Evaluation of Copper Corrosion under Bacterial Biofilms, *Corrosion 91,* Paper 111, NACE International, 1991

67. B. Little, P. Wagner, R. Ray, and J.M. Jones, Microbiologically Influenced Corrosion of Copper Alloys in Saline Waters Containing Sulfate Reducing Bacteria, *Corrosion 91,* Paper 101, NACE International, 1991

68. V.K. Guoda, I.M. Banat, W.T. Riad, and S. Mansour, Microbiologically Induced Corrosion of UNS N04400 in Seawater, *Corrosion,* Vol 49 (No. 1), 1993, p 63–73

69. T.D. Perry, M. Breuker, and R. Mitchell, Biodeterioration of Concrete and Stone, *Proceedings of the Corrosion 2002 Research Topical Symposium: Microbiologically Influenced Corrosion,* NACE International, 2002, p 113–121

70. C. Saiz-Jimenez, The Biodeterioration of Building Materials, *A Practical Manual on Microbiologically Influenced Corrosion,* Vol 2, J.G. Stoecker, Ed., NACE International, 2001, p 4.1

71. C. Saiz-Jimenez and X. Arino, Microbial Corrosion of Cultural Heritage Stoneworks, *A Practical Manual on Microbiologically Influenced Corrosion,* Vol 2, J.G. Stoecker, Ed., NACE International, 2001, p 11.25

72. B. Little, R. Ray, and P. Wagner, Biodegradation of Nonmetallic Materials, *A Practical Manual on Microbiologically Influenced Corrosion,* Vol 2, J.G. Stoecker, Ed., NACE International, 2001, p 3.1

73. P.A. Wagner, R.I. Ray, B.J. Little, and W.C. Tucker, *Mater. Perform.,* Vol 33 (No. 4), 1994, p 46

74. J.P. Pendrys, *J. Electrochem. Soc.,* Vol 136, 1989, p 113C

75. J.D. Gu, T.E. Ford, K.E.G. Thorp, and R. Mitchell, Microbial Deterioration of Fiber Reinforced Composite Materials, *Proc. Intl. Conf. on Microbially Influenced Corrosion,* P. Angel et al., Ed., NACE International, 1995, p 25/1

76. J.M. Jones, M. Walch, and F. Mansfeld, “Microbial and Electrochemical Studies of Coated Steel Exposed to Mixed Microbial Communities,” Paper 108, Corrosion/91, NACE International, 1991

77. F. Mansfeld, H. Hiao, L.T. Han, C.C. Lee, C. Chen, J. Jones-Meehan, and B. Little, “Evaluation of Coating Degradation for Polymer Coated Steel Exposed to Seawater,” Paper 659, Corrosion/96, NACE International, 1996

78. B.J. Little, R.I. Ray, P.A. Wagner, J. Jones- Meehan, C.C. Lee, and F. Mansfeld, Spatial Relationships between Marine Bacteria and Localized Corrosion on Polymer Coated Steel, *Biofouling,* Vol 13 (No. 4), 1999, p 301–321

79. J.M. Jones, M. Walch, and F.B. Mansfeld, Microbial and Electrochemical Studies of Coated Steel Exposed to Mixed Microbial Communities, *Corrosion 91,* Paper 108, NACE International, 1991

80. S.C. Dexter, Role of Microfouling Organisms in Marine Corrosion, *Biofouling,* Vol 7, 1993, p 97–127

81. B. Little, R. Ray, P. Wagner, J. Jones-Meehan, C. Lee, and F. Mansfeld, Spatial Relationships Between Marine Bacteria and Localized Corrosion on Polymer Coated Steel, *Biofouling,* Vol 13 (No. 4), 1999, p 301

82. F. Mansfeld, H. Shih, A. Postyn, J. Devinny, R. Islander, and C.L. Chin, “Corrosion Monitoring and Control in Concrete Sewer Pipes,” Paper 113, Corrosion/90, NACE International, 1990

83. C.F. Kulpa and C.J. Baker, Involvement of Sulfur-Oxidizing Bacteria in Concrete Deterioration, *Microbially Influenced Corrosion and Biodeterioration,* N.J. Dowling, M.W. Mittleman, and J.C. Danko, Ed., Univ. of Tennessee, 1991, p 4–7

84. A.N. Moosavi, J.L. Dawson, and R.A. King, The Effect of Sulphate-Reducing Bacteria on the Corrosion of Reinforced Concrete, *Biologically Induced Corrosion,* S.C. Dexter, Ed., NACE International, 1986, p 291

S.C. Dexter, Microbiologically Influenced Corrosion, *Corrosion: Fundamentals, Testing, and Protection*, Vol 13A, *ASM Handbook*, ASM International, 2003, p 398–416

Microbiologically Influenced Corrosion

Stephen C. Dexter, University of Delaware

Testing for Microbiologically Influenced Corrosion

Electrochemical corrosion and biological film formation have often been treated as separate events. However, the presence of microorganisms on a metal surface, even in the early stages of biofilm formation, can change the chemistry at the interface where corrosion reactions take place. Thus, the biological effect can be substantial, and it can take place simultaneously with the electrochemical reactions. Testing for microbiologically influenced corrosion (MIC) is used to determine if the microbes are the cause of specific types of corrosion failures or if the microbes in a given environment result in an unacceptably high corrosion rate for a given alloy.

Just as there is no unique microbiological environment, there also is no uniquely definitive test for MIC. The question has often been asked: How can I determine whether the corrosion in my system is MIC or not? The question itself can be misleading. The presence of microorganisms in the environment at a corrosion site does

not introduce some new form of corrosion. Rather, the organisms are capable of enhancing all known types of corrosion. The real question is: Are the organisms present in my system having a strong enough influence on corrosion that no corrosion control program can be successful without specifically controlling the organisms? In order to prove that the organisms present were the sole cause of corrosion, one would have to show first that the organisms can reproduce the attack when introduced into a sterile system, and second, that the effect does not happen when the organisms are absent from an otherwise identical environment. There are only a few well-documented situations in which this is the case. In most cases, the organisms present exert an accelerating influence on corrosion, hence the name Microbiologically Influenced Corrosion.

No specific standards have been written for MIC testing (Ref 6). Four types of evidence— metallurgical, microbiological, chemical, and electrochemical—are generally used to determine if the influence of the organisms is important enough that it must be addressed for a corrosion control program to be successful.

Metallurgical Evidence. The metallurgical history of the alloy in use is important, as is the morphology of the corrosive attack. Some types of MIC are recognizable, in part, by the pattern of corrosion on the surface, as detailed elsewhere (Ref 85, 86). The distribution and morphology of the corrosive attack should be recorded photographically.

Microbiological Evidence. Even though no direct correlation can be made between numbers of organisms or their distribution along the surface of the metal and the probability of MIC, this information is important. Moreover, the data must be gathered while the corrosion site is still wet. If, as is often the case, the corroded component is removed from the system, discarded, and allowed to dry before it is examined, much of the important information is lost. It is important to photographically record the initial appearance of the corrosion site in color as soon as possible, so that the organisms are still alive. Sampling of biological materials and corrosion products must be done using proper procedures, which are well described elsewhere (Ref 86, 87).

Chemical Evidence. As much chemical information as possible should be gathered about the electrolytic environment and the microorganisms themselves. Particular attention should be given to recording the chemistry of the liquid phase and its variability, both spatially and with time in relation to the observed corrosive attack. Any localized inputs of chemicals or pollutants not normally present in the environment should be noted.

Detailed chemical information should also be gathered for the corrosion products and any biological mounds that may be present at or near the corrosion site. This information should include the color, texture, odor, and distribution of the materials as well as their organic and inorganic chemistries. Detailed procedures for doing this have also been published (Ref 86).

Electrochemical Evidence. Virtually all electrochemical tests described elsewhere in this Volume have proven useful within certain limitations for MIC testing. The procedures for performing such tests and interpreting the data in cases where MIC is suspected have been given in several prior publications (Ref 86, 87, 88, 89). Further information on MIC testing may be found in Ref 11, 86, and 90.

References cited in this section

6. S.C. Dexter, Microbiological Effects, *Corrosion Tests and Standards,* 2nd ed., R. Baboian, Ed., *ASTM Manual 20,* ASTM, in press

11. H.A. Videla, *Manual of Biocorrosion,* CRC Press, Inc., 1996, p 13–45, 121–133, 160–173, 179–185, 228–237, 232

85. S.W. Borenstein and P.B. Lindsay, MIC Failure Analyses, *A Practical Manual on Microbiologically Influenced Corrosion,* G. Kobrin, Ed., NACE International, 1994, p 189

86. B.J. Little, P.A. Wagner, and F. Mansfeld, Microbiologically Influenced Corrosion, *Corrosion Testing Made Easy,* Vol 5, B.C. Syrett, Series Ed., NACE International, 1997, p 23

87. B. Little and P. Wagner, Indicators for Sulfate-Reducing Bacteria in Microbiologically Influenced Corrosion, *Biofouling and Biocorrosion in Industrial Water Systems,* G.G. Geesey, Z. Lewandowski, and H.-C. Flemming, Ed., Lewis Publishers, CRC Press Inc., Boca Raton, FL, 1994, p 213–230

88. S.C. Dexter, D.J. Duquette, O.W. Siebert, and H.A. Videla, Use and Limitations of Electrochemical Techniques for Investigating Microbiological Corrosion, *Corrosion,* Vol 47 (No. 4), 1991, p 308

89. F. Mansfeld and B. Little, A Technical Review of Electrochemical Techniques Applied to Microbiologically Influenced Corrosion, *Corros. Sci.,* Vol 32 (No. 3), 1991, p 247

90. J.R. Kearns and B.J. Little, Ed., *Microbiologically Influenced Corrosion Testing,* Special Technical Publication 1232, ASTM, 1994

S.C. Dexter, Microbiologically Influenced Corrosion, *Corrosion: Fundamentals, Testing, and Protection*, Vol 13A, *ASM Handbook*, ASM International, 2003, p 398–416

Microbiologically Influenced Corrosion

Stephen C. Dexter, University of Delaware

Prevention of MIC

Much has been written over the past decade about prevention and control of biological corrosion. The purpose of this section is not a comprehensive review of the subject but rather to describe the general approaches taken and to point the reader to the literature for additional information.

The most effective general approach to biocorrosion control starts with the notion that it is easier to prevent biocorrosion problems than it is to fix them. The most important step in prevention is to start with a clean system and to keep it clean (Ref 11). The first encounter of a system with a biocorrosive electrolyte is often in the process of hydrostatic testing immediately after fabrication. Hydrotesting of fabricated stainless steel structures has often been done with untreated fresh well waters. Such waters may contain microorganisms, such as *gallionella,* which have been noted for causing corrosion. The use of biocides (see subsequent information) in the hydrotest water or complete drainage and drying of the structure after hydrotesting is necessary to avoid problems. Additional information about biocorrosion of weldments and during hydrotesting can be found in the section “MIC of Passive Alloys” in this article.

Subsequent to placing any structure in service under possible biocorrosion-conducive conditions, a successful biocorrosion prevention program should feature keeping the metallic surfaces of the system clean as the major priority. The reason this has been stressed by so many authors is that it is much easier to control microorganisms that are dispersed in the liquid phase than it is after they have settled on the surface in the form of a biofilm.

The general approaches to maintaining a system free of biocorrosion problems vary with the materials of construction, environment, economics, and duty cycle of the equipment. The most common approaches involve the use of coatings, cathodic protection, and biocides.

Cathodic protection is usually used together with coatings in order to decrease the cost of the applied current. (See the article “Cathodic Protection” in this Volume.) Coatings themselves can be subject to biodeterioration, as discussed previously. Cathodic protection can be of benefit for the prevention of some forms of biocorrosion. The cathodic current may be applied by means of sacrificial anodes or other direct-current power supply (e.g., solar cells) or by an external alternating-current power supply and rectifier system. In either case, the applied current opposes the naturally occurring corrosion current regardless of whether that current is influenced by biological processes. Only a few interactions between cathodic protection and biofilms have been documented in the literature.

The application of a cathodic current changes the pH at the metal surface, making it more basic due to the production of hydroxyl ions from the reduction of oxygen. An increase in pH above 9 to 10 is considered detrimental to many marine microorganisms (Ref 91). In the biocorrosion literature, cathodic currents are

known to both inhibit the growth of general aerobic microorganisms and stimulate the growth of SRB in anaerobic regions of metal surfaces (Ref 92, 93).

The increase in pH at the metal surface due to cathodic protection also decreases the solubility of calcium and magnesium salts in seawater, resulting in the precipitation of calcareous deposits. There is some evidence (Ref 94) that preexisting biofilms tend to make calcareous deposition more uniform. Theoretically, this could make the calcareous deposit more protective, and the biofilm could enhance cathodic protection. This possible benefit of a biofilm to cathodic protection must be balanced against the tendency of cathodic currents to stimulate the growth of SRB, which would be detrimental. Marine biofilms also have been shown to increase or decrease the effectiveness of cathodic protection, depending on the applied current density (Ref 95).

Two further examples serve to illustrate the detrimental effects biofilm formation can have on cathodic protection. First, it is generally recognized that biofilms increase the cathodic kinetics of stainless steel cathodes (Ref 46, 55, 56, 57, 58). In the North Sea offshore industry, where sacrificial iron anodes are used to cathodically protect stainless steel from localized corrosion, the enhanced cathodic kinetics due to biofilm growth on the stainless steel result in a higher-than-expected consumption of the anodes. Second, in the presence of SRB biofilms on stainless steel in seawater, cathodic protection is sometimes unable to prevent localized corrosion initiation even at very active cathodic potentials (Ref 96). Thus, in spite of some possible beneficial effects, the bulk of the evidence indicates that biofilm formation is detrimental to the process and economics of cathodic protection.

Biocides in Closed Systems. For many years, various chemicals with biocidal action have been widely used to control biofilm formation in closed systems, such as heat exchangers, cooling towers, and storage tanks. Such chemicals work by killing or disrupting the reproductive cycle of the target organisms. Biocides in very low concentrations are often sufficient to kill organisms suspended in the liquid phase (i.e., in the planktonic state). Once the organisms attach to a solid surface and form a biofilm, however, much higher concentrations of the biocide are needed to control them. There are two reasons for this effect. First, the extracellular polymeric substance materials secreted by the organisms in the biofilm are able to bind the biocidal entities and shield the organisms from their action. Second, microorganisms in the biofilm may become resistant to the biocide used (Ref 97). Thus, the biocides and corrosion inhibitors that are so often used together to control biocorrosion work best in a system that is kept clean.

The three main ways that biocides work are as enzyme poisons or protein denaturants, oxidizing agents, and surface-active agents (Ref 98). The enzyme poisons tend to act against specific groups of microbes. For example, bisthiocyanates are effective against all organisms having iron-containing cytochromes. These are suitable for incorporation into some coatings. Other compounds within this group are the isothiazolones, which react with the thiol groups in proteins, and the aldehydes, such as formaldehyde, which act on both proteins and lipopolysaccharides in the bacterial cell wall.

The oxidizing biocides are probably the most widely used in practice. These include chlorine, hypochlorite, chlorine dioxide, bromine, and ozone. Chlorine has been widely used in the water treatment industry for many decades. Recently, however, it has been coming under regulatory pressure, and its use is being limited. Moreover, this class of biocides has the ability to raise the OCP of passive alloys sufficiently to initiate localized corrosion in some cases, if used to excess. Ozone is coming into increasing use as a biocide in cooling water systems (Ref 99). It has the advantage over chlorination in that lower dosages are required to prevent biofilm formation or to remove existing biofilms (Ref 100).

The surface-active agents, such as the quaternary ammonium compounds (quats), work by targeting the surface structure of individual microbial cells, causing them to be damaged with eventual lysis. The hydrophobic and hydrophilic portions of the biocide molecules allow them to penetrate the lipid-containing cell wall of the microbes. An excellent table showing the advantages and disadvantages of the biocides most commonly used in the water treatment industry can be found in Ref 11 and 101. For additional information on the range of biocides available, the recommended selection criteria, and procedures for application, the reader is referred to Ref 10 and 102 to 104.

Monitoring for MIC. Any well-conceived and effective biocorrosion mitigation program needs to include monitoring as a periodic or continual means of assessing whether program goals are being achieved. This is especially true in industrial water-handling systems with known susceptibility to biocorrosion, such as cooling water and injection water systems, heat exchangers, wastewater treatment facilities, storage tanks, piping systems, and all manner of power plants, including those based on fossil fuels, hydroelectric, and nuclear.

Monitoring systems originally configured for use in programs to control scaling and inorganic corrosion do not necessarily provide the information needed to maintain control of biofouling and biocorrosion. Initial attempts to extend abiotic corrosion monitoring into the biocorrosion arena were geared toward assessing the number of microbes per unit volume of water sampled from the system. This data were combined with electrochemical corrosion measurements, using electrical resistance or polarization resistance probes sometimes together with weight loss measurements from sample coupons. The problem with this approach is that numbers of planktonic organisms in the water do not correlate well with the organisms present in biofilms on the metal surface where the corrosion actually takes place. The combined data indicate that something is happening to corrosion in the system but do not usually give sufficient information for control of either biofouling or biocorrosion.

An effective monitoring scheme for controlling both biofouling and biocorrosion should include the generation of as many of the following types of data as possible:

- Sessile bacterial counts of the organisms in the biofilm on the metal surface done by either conventional biological techniques (Ref 86) or optical microscopy
- Direct observation of the community structure of the biofilm. This can be done on metal coupons made from the same alloy used for the system. Several types of probe systems are commercially available for holding and inserting such coupons into the system (Ref 105, 106, 107, 108). Imaging of the organisms in the biofilm can be done by scanning electron microscopy, environmental scanning electron microscopy, epifluorescence optical microscopy, or confocal laser scanning microscopy.
- Identification of the microorganisms found in both the process water and on the metal surface. Methods for doing this are reviewed in some detail in Ref 86.
- Surface analysis to obtain chemical information on corrosion products and biofilms
- Evaluation of the morphology of the corrosive attack on the metal surface after removal of biological and corrosion product deposits. Conventional macrophotography as well as low-power stereomicroscopy, optical microscopy, metallography, and scanning electron microscopy may all be helpful in this regard.
- Electrochemical corrosion measurements from electrical resistance or polarization-resistance-type probes, as described elsewhere in this Volume
- Water quality and redox potential measurements
- Other types of information specific to each operational system, including duty cycle and downtime information, concentrations and timing for addition of biocides and other chemical inputs, local sources and nature of pollutants, and so on

Recent developments in biocorrosion monitoring have been reviewed (Ref 11, 109), including a detailed description of two case histories: one in a chemical industry cooling water system and the other for an oilfield water injection system in which the previously mentioned approach has been used successfully. In addition to the types of data discussed previously, several new on-line fouling and corrosion sensor systems have been developed (Ref 110, 111, 112, 113, 114). These systems use the interactions between biofouling and the electrochemistry of corrosion to generate data of interest in biocorrosion monitoring and control.

References cited in this section

10. J.D.A. Miller, Ed., *Microbial Aspects of Metallurgy,* Elsevier, 1970

11. H.A. Videla, *Manual of Biocorrosion,* CRC Press, Inc., 1996, p 13–45, 121–133, 160–173, 179–185, 228–237, 232

46. R. Johnson and E. Bardal, Cathodic Properties of Different Stainless Steels in Natural Seawater, *Corrosion,* Vol 41 (No. 5), 1985, p 296

55. V. Scotto, Electrochemical Studies on Biocorrosion of Stainless Steel in Seawater, *EPRI Workshop on Microbial Induced Corrosion,* G. Licina, Ed., Electric Power Research Institute, p B.1–B.36

56. A. Mollica, G. Ventura, E. Traverso, and V. Scotto, "Cathodic Behavior of Nickel and Titanium in Natural Seawater," Seventh Intl. Biodeterioration Symp., International Biodeterioration Society (Cambridge, U.K.), 1987

57. S.C. Dexter, Effect of Biofilms on Crevice Corrosion, *Proc. COR/96 Topical Research Symposium on Crevice Corrosion,* NACE, 1996, p 367–383

58. S.C. Dexter and J.P. LaFontaine, Effect of Natural Marine Biofilms on Galvanic Corrosion, *Corrosion,* Vol 54 (No. 11), 1998, p 851–861

86. B.J. Little, P.A. Wagner, and F. Mansfeld, Microbiologically Influenced Corrosion, *Corrosion Testing Made Easy,* Vol 5, B.C. Syrett, Series Ed., NACE International, 1997, p 23

91. F.M.M. Morel and B. Palenik, Aquatic Chemistry of Trace Metals in Biofilms, *Structure and Function of Biofilms,* W.G. Characklis and P.A. Wilderer, Ed., John Wiley, 1989, p 289

92. R.G.J. Edyvean, The Effects of Microbiologically Generated Hydrogen Sulfide in Marine Corrosion, *MTS J.,* Vol 24, 1990, p 5–9

93. J. Guezennec, Influence of Cathodic Protection of Mild Steel on the Growth of Sulphate-Reducing Bacteria at 35 °C in Marine Sediments, *Biofouling,* Vol 3, 1991, p 339

94. S.C. Dexter and S.-H. Lin, Effect of Marine Biofilms on Cathodic Protection, *Int. Biodeterior. Biodegrad.,* Vol 29, 1992, p 231

95. S.C. Dexter and S.-H. Lin, Calculation of Seawater pH at Polarized Metal Surfaces in the Presence of Surface Films, *Corrosion,* Vol 48, 1992, p 50

96. M.F.L. deMelle, S.G. Gomez de Saravia, and H.A. Videla, An Overview on Biofilms and Calcareous Deposits Interrelationships on Cathodically Protected Steel Surfaces, *Proc. 1995 Intl. Conf. on MIC,* P. Angel et al., Ed., NACE International, 1995, p 50-1

97. J.W. Costerton, The Formation of Biocide- Resistant Biofilms in Industrial, Natural and Medical Systems, *Dev. Ind. Microbiol.,* Vol 25, 1984, p 363–372

98. C.C. Gaylarde, Design, Selection and Use of Biocides, *Bioextraction and Biodeterioration of Metals,* C. Gaylarde and H. Videla, Ed., Cambridge University Press, 1995, p 327

99. R.G. Rice and J.F. Wilkes, "Fundamental Aspects of Ozone Chemistry in Recirculating Cooling Water Systems," Paper 205, Corrosion/91, NACE International, 1991

100. H.A. Videla, M.R. Viera, P.S. Guiamet, M.F.L. deMelle, and J.C. Staibano Alais, Biocidal Activity of Dissolved Ozone on Sessile and Planktonic Bacteria: Effects of Corrosion Behavior of Cooling Water Systems Structural Materials, *Proc. 1995 Intl. Conf. on MIC,* P. Angel et al., Ed., NACE International, 1995, p 62-1

101. H.C. Flemming, Biofouling in Water Treatment, *Biofouling and Biocorrosion in Industrial Water Systems,* H.C. Flemming and G.G. Geesey, Ed., Springer-Verlag, 1991, p 47

102. R.W. Lutey, Treatment for the Mitigation of MIC, *A Practical Manual on Microbiologically Influenced Corrosion,* Vol 2, J.G. Stoecker, Ed., NACE International, 2001, p 9.1

104. M.R.W. Brown and P. Gilbert, Sensitivity of Biofilms to Antimicrobial Agents, *J. Appl. Bacteriol. Symp. Suppl.,* Vol 74, 1993, p 87S–97S

105. H.A. Videla, F. Bianchi, M.M.S. Freitas, C.G. Canales, and J.F. Wilkes, Monitoring Biocorrosion and Biofilms in Industrial Waters: A Practical Approach, *Microbiologically Influenced Corrosion Testing,* Special Technical Publication 1232, J.R. Kearns and B.J. Little, Ed., ASTM, 1994, p 128

106. I. Ruseski, J. Robbins, and J.W. Costerton, Biocide Testing Against Corrosion-Causing Oil-Field Bacteria Helps Control Plugging, *Oil Gas J.,* Vol 80, 1982, p 253

107. P.F. Sanders and W.A. Hamilton, Biological and Corrosion Activities of Sulphate- Reducing Bacteria in Industrial Process Plant, *Biologically Induced Corrosion,* S.C. Dexter, Ed., NACE International, 1986, p 47

108. H.A. Videla, M.F.L. deMelle, R.A. Silva, F. Bianchi, and C. Gonzales Canales, "A Practical Approach to the Study of the Interaction Between Biofouling and Passive Layers on Mild Steel and Stainless Steel in Cooling Water," Paper 124, Corrosion/ 90, NACE International, 1990

109. T.P. Zintel, G.J. Licina, and T.R. Jack, "Techniques for MIC Monitoring," *A Practical Manual on Microbiologically Influenced Corrosion,* Vol 2, J.G. Stoecker, Ed., NACE International, 2001, p 10.1

110. P.S.N. Stokes, M.A. Winters, P.O. Zuniga, and D.J. Schlottenmier, Developments in on-line Fouling and Corrosion Surveillance, *Microbiologically Influenced Corrosion Testing,* Special Technical Publication 1232, J.R. Kearns and B.J. Little, Eds., ASTM, 1994

111. G.J. Licina, G. Nekoksa, and R.L. Howard, "An Electrochemical Method for On-Line Monitoring of Biofilm Activity in Cooling Tower," Paper 177, Corrosion/92, NACE International, 1992

112. G.J. Licina, G. Nekoksa, and R.L. Howard, "An Electrochemical Method for On-Line Monitoring of Biofilm Activity in Cooling Water Using the Bio-George™ Probe"

113. G.J. Licina and G. Nekoksa, "The Influence of Water Chemistry and Biocode Additions on the Response of an On-Line Biofilm Monitor," Paper 527, Corrosion/ 95, NACE International, 1995

114. A. Mollica and G. Ventura, Use of a Biofilm Electrochemical Monitoring Device for an Automatic Application of Anitfouling Procedures in Seawater, *Proc. 12th Intl. Corrosion Cong.,* NACE International, 1993, p 3807

S.C. Dexter, Microbiologically Influenced Corrosion, *Corrosion: Fundamentals, Testing, and Protection*, Vol 13A*, ASM Handbook,* ASM International, 2003, p 398–416

Microbiologically Influenced Corrosion

Stephen C. Dexter, University of Delaware

Corrosion Inhibition by Bacteria

As was shown in Fig. 1, the influence of microorganisms may not always be to cause or accelerate corrosion. There is also the possibility that they may be able to inhibit corrosion. Any such inhibitory effect occurs in the same type of complex and heterogeneous environment in which biocorrosion takes place. Thus, the same general biofilm formation processes that have been described earlier in this article as being important to biocorrosion also are in operation during corrosion inhibition. This is an important point to consider if one is

contemplating including a biological component to a corrosion control program. The objective of corrosion control strategies is usually to create a uniformly noncorrosive condition at the metal surface that can be maintained in that state with a minimum of effort and expense. Thus, the same highly variable and heterogeneous processes that lead to corrosion under a living biofilm work counter to the objective of corrosion control. Biofilms are not inherently uniform and stable. This may partially explain why some organisms found in biofilms can inhibit general corrosion, while other organisms in the same biofilm can cause localized corrosion. Moreover, the same organisms reported to cause MIC under one set of conditions can be protective under another. It has been noted that some strains of *Pseudomonas* increase the corrosion rate of iron and nickel (Ref 115), while under other conditions, they can have a protective effect (Ref 116).

Nevertheless, inhibition of corrosion by the action of microorganisms is an exciting new topic that is now being developed. The topic has recently been reviewed (Ref 11). At least in theory, microbial inhibition of corrosion could work in several ways, including:

- Forming or stabilizing protective films on the metal surface. This could include bacterial mediation of sulfide species at iron surfaces (Ref 11) and the stabilization of protective films on copper (Ref 117) and copper-nickel alloys (Ref 118).
- Decreasing the corrosiveness of the electrolyte. Just as microorganisms can create aggressive conditions by the formation of corrosive metabolites, they also can create benign conditions, for example, by decreasing the dissolved oxygen concentration (Ref 119) or changing the pH, as long as a uniform effect can be achieved.
- Altering or neutralizing corrosive substances. Organic compounds related to biofilm formation have been reported to decrease hydrogen embrittlement and cracking by hindering the dissolution, dissociation, and adsorption of hydrogen (Ref 120).

The concept of using regenerative biofilms for corrosion control in aluminum, brass, and steel systems is actively under investigation by several investigators (Ref 121, 122, 123, 124, 125, 126). It must be emphasized, however, that the process of corrosion control by bacteria is highly complex. As of the date of this publication, it cannot be predicted and controlled (Ref 127). Thus, considerable further research is required before this process can be used successfully as a reliable industrial corrosion control technique.

References cited in this section

11. H.A. Videla, *Manual of Biocorrosion,* CRC Press, Inc., 1996, p 13–45, 121–133, 160–173, 179–185, 228–237, 232

115. A. Pedersen, S. Kjelleberg, and M. Hermansson, *J. Microbiol. Meth.,* Vol 8, 1988, p 191

116. A. Pedersen and M. Hermansson, *Biofouling,* Vol 3, 1991, p 1

117. P. Angell, A. Sonnerson, P.A. Wagner, B.J. Little, and D.C. White, The Role of *Oceanospirillium* Exopolymer in Marine Copper Corrosion, *Proc. 1995 Intl. Conf. on MIC,* P. Angel et al., Ed., NACE International, 1995, p 74-1

118. H.A. Videla, Biocorrosion of Non-Ferrous Metal Surfaces, *Biofouling and Biocorrosion in Industrial Water Systems,* G.G. Geesey, Z. Lewandowski, and H.C. Flemming, Ed., Lewis Publishers, 1994, p 231

119. A. Jayaraman, E.T. Cheng, J.C. Earthman, and T.K. Wood, *Appl. Microbiol. Biotechnol.,* Vol 48, 1997, p 11–17

120. C.J. Thomas, R.G.J. Edyvean, and R. Brook, Biologically Enhanced Corrosion Fatigue, *Biofouling,* Vol 1, 1988, p 65

121. F. Mansfeld, C.H. Hsu, D. Ornek, T.K. Wood, and B.C. Syrett, Corrosion Control Using Regenerative Biofilms (CCURB) on Aluminum 2024 and Brass in Different Media, *Proc. Symp. on New Trends in Electrochemical Impedance Spectroscopy (EIS) and Electrochemical Noise Analysis (ENA), The Electrochem. Soc. Proc.,* Vol 2000–24, 2001, p 99–118

122. D. Ornek, A. Jayaraman, T.K. Wood, Z. Sun, C.H. Hsu, and F. Mansfeld, *Corros. Sci.,* Vol 43, 2001, p 2121–2133

123. A. Nagiub and F. Mansfeld, *Corros. Sci.,* Vol 43, 2001, p 2001–2009

124. F. Mansfeld, Z. Sun, and H.S. Hsu, *Electrochim. Acta,* Vol 46, 2001, p 3651–3664

125. K. Trandem, P.J. Arps, and J.C. Earthman, "Closed-Loop Sidestream Systems for Investigating Corrosion Control Using Regenerative Biofilms (CCURB) in Service Water," Paper 648, Corrosion/2000, NACE International, 2001

126. B.C. Syrett, P.J. Arps, J.C. Earthman, F. Mansfeld, and T. Wood, Biofilms That Prevent Corrosion, *Proceedings of the Corrosion 2002 Research Topical Symposium: Microbiologically Influenced Corrosion,* NACE Press, NACE International, 2002, p 145–162

127. B. Little and R. Ray, A Perspective on Corrosion Inhibition by Biofilms, *Corrosion,* Vol 58, 2002, p 424–428

S.C. Dexter, Microbiologically Influenced Corrosion, *Corrosion: Fundamentals, Testing, and Protection*, Vol 13A, *ASM Handbook*, ASM International, 2003, p 398–416

Microbiologically Influenced Corrosion

Stephen C. Dexter, University of Delaware

Further Reading

A list of recommended readings can be found immediately following the numbered references, in the section "Selected References."

S.C. Dexter, Microbiologically Influenced Corrosion, *Corrosion: Fundamentals, Testing, and Protection*, Vol 13A, *ASM Handbook*, ASM International, 2003, p 398–416

Microbiologically Influenced Corrosion

Stephen C. Dexter, University of Delaware

References

1. J.D. Costlow and R.C. Tipper, Ed., *Marine Biodeterioration: An Interdisciplinary Study,* Proceedings of the Symposium, Naval Institute Press, 1984

2. K.C. Marshall, *Interfaces in Microbial Ecology,* Harvard University Press, 1976

3. D.C. Savage and M. Fletcher, Ed., *Bacterial Adhesion,* Plenum Press, 1985

4. L.V. Evans, Ed., *Biofilms: Recent Advances in Their Study and Control,* Harwood Academic Publishers, 2000

5. B. Little, P. Wagner, and F. Mansfeld, Microbiologically Influenced Corrosion of Metals and Alloys, *Int. Mater. Rev.,* Vol 36 (No. 6), 1991, p 253–272

6. S.C. Dexter, Microbiological Effects, *Corrosion Tests and Standards,* 2nd ed., R. Baboian, Ed., *ASTM Manual 20,* ASTM, in press

7. M. Eashwar, G. Subramanian, P. Chandrasekaran, and K. Balakrishnan, Mechanism for Barnacle-Induced Crevice Corrosion in Stainless-Steel, *Corrosion,* Vol 48 (No. 7), 1992, p 608–612

8. D.H. Pope, D. Duquette, P.C. Wayner, and A.H. Johannes, “Microbiologically Influenced Corrosion: A State-of-the-Art-Review,” Publication 13, Materials Technology Institute of the Chemical Process Industries, Inc., 1984

9. D.H. Pope, “A Study of Microbiologically Influenced Corrosion in Nuclear Power Plants and a Practical Guide for Countermeasures,” EPRI NP-4582, Final Report, Electric Power Research Institute, 1986

10. J.D.A. Miller, Ed., *Microbial Aspects of Metallurgy,* Elsevier, 1970

11. H.A. Videla, *Manual of Biocorrosion,* CRC Press, Inc., 1996, p 13–45, 121–133, 160–173, 179–185, 228–237, 232

12. *Microbial Corrosion,* Proceedings of the Conference, National Physical Laboratory, The Metals Society, 1983

13. Z. Lewandowski, P. Stoodley, and S. Altobelli, *Water Sci. Technol.,* Vol 3, 1995, p 153–162

14. D. de Beer and P. Stoodley, Relation between the Structure of an Aerobic Biofilm and Transport Phenomena, *Water Sci. Technol.,* Vol 32 (No. 8), 1995, p 11–18

15. D. de Beer, P. Stoodley, and Z. Lewandowski, Liquid Flow and Mass Transport in Heterogeneous Biofilms, *Water Res.,* Vol 30 (No. 11), 1996, p 2761–2765

16. K. Xu, “Effect of Biofilm Heterogeneity on Corrosion Behavior of Passive Alloys in Seawater,” Ph.D. dissertation, University of Delaware, 2000

17. W.A. Hamilton and S. Maxwell, Biological and Corrosion Activity of SRB in Natural Biofilms, *Proceedings of Biologically Induced Corrosion,* NACE International, 1986, p 131–136

18. J.W. Costerton and G.G. Geesey, The Microbial Ecology of Surface Colonization and of Consequent Corrosion, *Biological Induced Corrosion,* NACE-8, S.C. Dexter, Ed., NACE International, 1986, p 223–232

19. R.J. Parkes, *Soc. Gen. Microbiol. Symp.,* Vol 41, 1987, p 147–177

20. C.C. Gaylarde and H.A. Videla, *Int. Biodeterior.,* Vol 23, 1987, p 91–104

21. S.C. Dexter, Ed., Biologically Induced Corrosion, *Proceedings of the Conference,* National Association of Corrosion Engineers, 1986

22. K. Xu, S.C. Dexter, and G.W. Luther III, Voltammetric Microelectrodes for Biocorrosion Studies, *Corrosion,* Vol 54 (No. 10), 1998, p 814

23. D.H. Pope, D.J. Duquette, A.H. Johannes, and P.C. Wayner, *Mater. Perform.,* Vol 23 (No. 4), 1984, p 14–18

24. C.A.H. Von Wolzogen Kuhr and L.S. Van der Vlugt, *Water, Den Haag,* Vol 18, 1934, p 147–165

25. D.T. Ruppel, S.C. Dexter, and G.W. Luther, *Corrosion,* Vol 57, 2001, p 863–873

26. P. Linhardt, Failure of Chromium-Nickel Steel in a Hydroelectric Power Plant by Manganese-Oxidizing Bacteria, *Microbially Influenced Corrosion of Materials,* E. Heitz et al., Ed., Springer-Verlag, 1996

27. B.H. Olesen, R. Avci, and Z. Lewandowski, Manganese Dioxide as a Potential Cathodic Reactant in Corrosion of Stainless Steels, *Corros. Sci.,* Vol 42, 2000, p 211–227

28. H.A. Videla and R.C. Salvarezza, *Introduction to Microbiological Corrosion,* Biblioteca Mosaico, 1984 (in Spanish)

29. D.H. Pope and J.G. Stoecker, Microbiologically Influenced Corrosion, *Process Industries Corrosion—Theory and Practice,* B.J. Moniz and W.I. Pollock, Ed., National Association of Corrosion Engineers, 1986, p 227–242

30. G. Kobrin, Ed., A Practical Manual on Microbiologically Influenced Corrosion, NACE International, 1994

31. J. Stoecker, Ed., *A Practical Manual on Microbiologically Influenced Corrosion,* Vol 2, NACE International, 2001

32. P.F. Sanders and W.A. Hamilton, Biological and Corrosion Activities of Sulfate-Reducing Bacteria in Industrial Process Plant, *Biologically Induced Corrosion,* S.C. Dexter, Ed., National Association of Corrosion Engineers, 1986, p 47–68

33. I.B. Beech, S.A. Campbell, and F.C. Walsh, Marine Microbial Corrosion, *A Practical Manual on Microbiologically Influenced Corrosion,* Vol 2, J. Stoecker, Ed., NACE International, 2001, p 11.3–11.14

34. J.D.A. Miller and A.K. Tiller, Microbial Corrosion of Buried and Immersed Metal, *Microbial Aspects of Metallurgy,* J.D.A. Miller, Ed., American Elsevier, 1970, p 61–106

35. R.A. King, J.D.A. Miller, and J.F.D. Stott, Subsea Pipelines: Internal and External Biological Corrosion, *Biologically Induced Corrosion,* S.C. Dexter, Ed., National Association of Corrosion Engineers, 1986, p 268–274

36. G. Kobrin, Reflections on Microbiologically Induced Corrosion of Stainless Steels, *Biologically Induced Corrosion,* S.C. Dexter, Ed., National Association of Corrosion Engineers, 1986, p 33

37. B.J. Little, P.A. Wagner, K.R. Hart, and R. Ray, "Spatial Relationships Between Bacterial and Localized Corrosion," Paper 278, Corrosion/96, NACE International, 1996

38. M. Eashwar and S.C. Dexter, "Relation of Bacterial Settlement Patterns to Anodic Activity on Stainless Steel Weldments," Paper 174, Corrosion/99, NACE International, 1999

39. J.G. Stoecker and D.H. Pope, Study of Biological Corrosion in High Temperature Demineralized Water, *Mater. Perform.,* June 1986, p 51–56

40. R.E. Tatnall, Case Histories: Bacteria Induced Corrosion, *Mater. Perform.,* Vol 20 (No. 8), 1981, p 41

41. S.C. Dexter, K.E. Lucas, and G.Y. Gao, Role of Marine Bacteria in Crevice Corrosion Initiation, *Biologically Induced Corrosion,* S.C. Dexter, Ed., National Association of Corrosion Engineers, 1986, p 144–153

42. P. Chandrasekaran and S.C. Dexter, "Thermodynamic and Kinetic Factors Influenced by Biofilm Chemistry Prior to Passivity Breakdown," Paper 482, Corrosion/ 94, NACE International, 1994

43. P. Chandrasekaran and S.C. Dexter, Factors Contributing to Ennoblement of Passive Metals Due to Biofilms in Seawater, *Proc. 12th International Corrosion Congress,* Vol 5B, NACE International, 1993, p 3696–3707

44. S.C. Dexter and G.Y. Gao, Effect of Seawater Biofilms on Corrosion Potential and Oxygen Reduction of Stainless Steel, *Corrosion,* Vol 44 (No. 10), 1988, p 717–723

45. S.C. Dexter, Effect of Biofilms on Marine Corrosion, *Bioextraction and Biodeterioration of Metals,* C. Gaylarde and H. Videla, Ed., Cambridge University Press, 1995, p 129–167

46. R. Johnson and E. Bardal, Cathodic Properties of Different Stainless Steels in Natural Seawater, *Corrosion,* Vol 41 (No. 5), 1985, p 296

47. V. Scotto, R. Dicintio, and G. Marcenaro, The Influence of Marine Aerobic Microbial Film on Stainless-Steel Corrosion Behavior, *Corros. Sci.,* Vol 25 (No. 3), 1985, p 185–194

48. S. Motoda, Y. Suzuki, T. Shinohara, and S. Tsujikawa, The Effect of Marine Fouling on the Ennoblement of Electrode Potential for Stainless Steels, *Corros. Sci.,* Vol 31, 1990, p 515–520

49. S.C. Dexter and S. Maruthamuthu, "Response of Passive Alloys with N- and P- Type Passive Films to Manganese in Biofilms," Paper 01256, Corrosion/2001, NACE International, 2001

50. S.C. Dexter and H.-J. Zhang, Effect of Biofilms on Corrosion Potential of Stainless Alloys in Estuarine Waters, *Proc. 11th Intl. Corrosion Congress,* April 1990 (Florence, Italy), Assoc. Italiana Di Metall., Milano, Italy, p 4.333

51. H.-J. Zhang and S.C. Dexter, Effect of Biofilms on Critical Pitting Potentials for Stainless Steels S30400 and S31600 in Seawater, *Proc. 1995 International Conference on Microbiologically Influenced Corrosion,* May 1995 (New Orleans, LA), P. Angel et al., Ed., NACE International, p 70/1–70/8

52. H.-J. Zhang and S.C. Dexter, "Effect of Marine Biofilms on Crevice Corrosion of Stainless Alloys," Paper 400, Corrosion/ 92, NACE International, 1992

53. H.-J. Zhang and S.C. Dexter, Effect of Biofilms on Crevice Corrosion of Stainless Alloys in Coastal Seawater, *Proc. 12th International Corrosion Congress,* Vol 5B, NACE International, 1993, p 3761–3772

54. H.-J. Zhang and S.C. Dexter, "Effect of Marine Biofilms on Initiation Time of Crevice Corrosion for Stainless Steels," Paper 285, Corrosion/95, NACE International, 1995

55. V. Scotto, Electrochemical Studies on Biocorrosion of Stainless Steel in Seawater, *EPRI Workshop on Microbial Induced Corrosion,* G. Licina, Ed., Electric Power Research Institute, p B.1–B.36

56. A. Mollica, G. Ventura, E. Traverso, and V. Scotto, "Cathodic Behavior of Nickel and Titanium in Natural Seawater," Seventh Intl. Biodeterioration Symp., International Biodeterioration Society (Cambridge, U.K.), 1987

57. S.C. Dexter, Effect of Biofilms on Crevice Corrosion, *Proc. COR/96 Topical Research Symposium on Crevice Corrosion,* NACE, 1996, p 367–383

58. S.C. Dexter and J.P. LaFontaine, Effect of Natural Marine Biofilms on Galvanic Corrosion, *Corrosion,* Vol 54 (No. 11), 1998, p 851–861

59. J.J. Elpjick, Microbial Corrosion in Aircraft Fuel Systems, *Microbial Aspects of Metallurgy,* J.D.A. Miller, Ed. American Elsevier, 1970, p 157–172

60. B. Little, P. Wagner, R. Ray, and M. McNeil, *J. Mar. Technol. Soc.,* Vol 24 (No. 3), 1990, p 10–17

61. B.J. Little, P. Wagner, and J. Jacobus, The Impact of Sulfate-Reducing Bacteria on Welded Copper-Nickel Seawater Piping Systems, *Mater. Perform.,* Vol 27 (No. 8), 1988, p 57–61

62. R.J. Soracco, D.H. Pope, J.M. Eggars, and T.N. Effinger, Microbiologically Influenced Corrosion Investigations in Electric Power Generating Stations, *Corrosion 1988,* Paper 83, NACE International, 1988

63. D.H. Pope, *Microbial Corrosion in Fossil- Fired Power Plants: A Study of Microbiologically Influenced Corrosion and a Practical Guide for Its Treatment and Prevention,* Electric Power Research Institute, Palo Alto, CA, 1987

64. D.H. Pope, A Study of Microbiologically Influenced Corrosion in Nuclear Power Plants and a Practical Guide for Countermeasures, EPRI Final Report NP-4582, Project 1166-6, Electric Power Research Institute, Palo Alto, CA, May 1986

65. G.G. Geesey, M.W. Mittleman, T. Iwaoka, and P.R. Griffiths, Role of Bacterial Exopolymers in the Deterioration of Metallic Copper Surfaces, *Mater. Perform.,* Vol 25 (No. 2), 1986, p 37–40

66. G.G. Geesey and P.J. Bremer, Evaluation of Copper Corrosion under Bacterial Biofilms, *Corrosion 91,* Paper 111, NACE International, 1991

67. B. Little, P. Wagner, R. Ray, and J.M. Jones, Microbiologically Influenced Corrosion of Copper Alloys in Saline Waters Containing Sulfate Reducing Bacteria, *Corrosion 91,* Paper 101, NACE International, 1991

68. V.K. Guoda, I.M. Banat, W.T. Riad, and S. Mansour, Microbiologically Induced Corrosion of UNS N04400 in Seawater, *Corrosion,* Vol 49 (No. 1), 1993, p 63–73

69. T.D. Perry, M. Breuker, and R. Mitchell, Biodeterioration of Concrete and Stone, *Proceedings of the Corrosion 2002 Research Topical Symposium: Microbiologically Influenced Corrosion,* NACE International, 2002, p 113–121

70. C. Saiz-Jimenez, The Biodeterioration of Building Materials, *A Practical Manual on Microbiologically Influenced Corrosion,* Vol 2, J.G. Stoecker, Ed., NACE International, 2001, p 4.1

71. C. Saiz-Jimenez and X. Arino, Microbial Corrosion of Cultural Heritage Stoneworks, *A Practical Manual on Microbiologically Influenced Corrosion,* Vol 2, J.G. Stoecker, Ed., NACE International, 2001, p 11.25

72. B. Little, R. Ray, and P. Wagner, Biodegradation of Nonmetallic Materials, *A Practical Manual on Microbiologically Influenced Corrosion,* Vol 2, J.G. Stoecker, Ed., NACE International, 2001, p 3.1

73. P.A. Wagner, R.I. Ray, B.J. Little, and W.C. Tucker, *Mater. Perform.,* Vol 33 (No. 4), 1994, p 46

74. J.P. Pendrys, *J. Electrochem. Soc.,* Vol 136, 1989, p 113C

75. J.D. Gu, T.E. Ford, K.E.G. Thorp, and R. Mitchell, Microbial Deterioration of Fiber Reinforced Composite Materials, *Proc. Intl. Conf. on Microbially Influenced Corrosion,* P. Angel et al., Ed., NACE International, 1995, p 25/1

76. J.M. Jones, M. Walch, and F. Mansfeld, "Microbial and Electrochemical Studies of Coated Steel Exposed to Mixed Microbial Communities," Paper 108, Corrosion/91, NACE International, 1991

77. F. Mansfeld, H. Hiao, L.T. Han, C.C. Lee, C. Chen, J. Jones-Meehan, and B. Little, "Evaluation of Coating Degradation for Polymer Coated Steel Exposed to Seawater," Paper 659, Corrosion/96, NACE International, 1996

78. B.J. Little, R.I. Ray, P.A. Wagner, J. Jones- Meehan, C.C. Lee, and F. Mansfeld, Spatial Relationships between Marine Bacteria and Localized Corrosion on Polymer Coated Steel, *Biofouling,* Vol 13 (No. 4), 1999, p 301–321

79. J.M. Jones, M. Walch, and F.B. Mansfeld, Microbial and Electrochemical Studies of Coated Steel Exposed to Mixed Microbial Communities, *Corrosion 91,* Paper 108, NACE International, 1991

80. S.C. Dexter, Role of Microfouling Organisms in Marine Corrosion, *Biofouling,* Vol 7, 1993, p 97–127

81. B. Little, R. Ray, P. Wagner, J. Jones-Meehan, C. Lee, and F. Mansfeld, Spatial Relationships Between Marine Bacteria and Localized Corrosion on Polymer Coated Steel, *Biofouling,* Vol 13 (No. 4), 1999, p 301

82. F. Mansfeld, H. Shih, A. Postyn, J. Devinny, R. Islander, and C.L. Chin, "Corrosion Monitoring and Control in Concrete Sewer Pipes," Paper 113, Corrosion/90, NACE International, 1990

83. C.F. Kulpa and C.J. Baker, Involvement of Sulfur-Oxidizing Bacteria in Concrete Deterioration, *Microbially Influenced Corrosion and Biodeterioration,* N.J. Dowling, M.W. Mittleman, and J.C. Danko, Ed., Univ. of Tennessee, 1991, p 4–7

84. A.N. Moosavi, J.L. Dawson, and R.A. King, The Effect of Sulphate-Reducing Bacteria on the Corrosion of Reinforced Concrete, *Biologically Induced Corrosion,* S.C. Dexter, Ed., NACE International, 1986, p 291

85. S.W. Borenstein and P.B. Lindsay, MIC Failure Analyses, *A Practical Manual on Microbiologically Influenced Corrosion,* G. Kobrin, Ed., NACE International, 1994, p 189

86. B.J. Little, P.A. Wagner, and F. Mansfeld, Microbiologically Influenced Corrosion, *Corrosion Testing Made Easy,* Vol 5, B.C. Syrett, Series Ed., NACE International, 1997, p 23

87. B. Little and P. Wagner, Indicators for Sulfate-Reducing Bacteria in Microbiologically Influenced Corrosion, *Biofouling and Biocorrosion in Industrial Water Systems,* G.G. Geesey, Z. Lewandowski, and H.-C. Flemming, Ed., Lewis Publishers, CRC Press Inc., Boca Raton, FL, 1994, p 213–230

88. S.C. Dexter, D.J. Duquette, O.W. Siebert, and H.A. Videla, Use and Limitations of Electrochemical Techniques for Investigating Microbiological Corrosion, *Corrosion,* Vol 47 (No. 4), 1991, p 308

89. F. Mansfeld and B. Little, A Technical Review of Electrochemical Techniques Applied to Microbiologically Influenced Corrosion, *Corros. Sci.,* Vol 32 (No. 3), 1991, p 247

90. J.R. Kearns and B.J. Little, Ed., *Microbiologically Influenced Corrosion Testing,* Special Technical Publication 1232, ASTM, 1994

91. F.M.M. Morel and B. Palenik, Aquatic Chemistry of Trace Metals in Biofilms, *Structure and Function of Biofilms,* W.G. Characklis and P.A. Wilderer, Ed., John Wiley, 1989, p 289

92. R.G.J. Edyvean, The Effects of Microbiologically Generated Hydrogen Sulfide in Marine Corrosion, *MTS J.,* Vol 24, 1990, p 5–9

93. J. Guezennec, Influence of Cathodic Protection of Mild Steel on the Growth of Sulphate-Reducing Bacteria at 35 °C in Marine Sediments, *Biofouling,* Vol 3, 1991, p 339

94. S.C. Dexter and S.-H. Lin, Effect of Marine Biofilms on Cathodic Protection, *Int. Biodeterior. Biodegrad.,* Vol 29, 1992, p 231

95. S.C. Dexter and S.-H. Lin, Calculation of Seawater pH at Polarized Metal Surfaces in the Presence of Surface Films, *Corrosion,* Vol 48, 1992, p 50

96. M.F.L. deMelle, S.G. Gomez de Saravia, and H.A. Videla, An Overview on Biofilms and Calcareous Deposits Interrelationships on Cathodically Protected Steel Surfaces, *Proc. 1995 Intl. Conf. on MIC,* P. Angel et al., Ed., NACE International, 1995, p 50-1

97. J.W. Costerton, The Formation of Biocide- Resistant Biofilms in Industrial, Natural and Medical Systems, *Dev. Ind. Microbiol.,* Vol 25, 1984, p 363–372

98. C.C. Gaylarde, Design, Selection and Use of Biocides, *Bioextraction and Biodeterioration of Metals,* C. Gaylarde and H. Videla, Ed., Cambridge University Press, 1995, p 327

99. R.G. Rice and J.F. Wilkes, “Fundamental Aspects of Ozone Chemistry in Recirculating Cooling Water Systems,” Paper 205, Corrosion/91, NACE International, 1991

100. H.A. Videla, M.R. Viera, P.S. Guiamet, M.F.L. deMelle, and J.C. Staibano Alais, Biocidal Activity of Dissolved Ozone on Sessile and Planktonic Bacteria: Effects of Corrosion Behavior of Cooling Water Systems Structural Materials, *Proc. 1995 Intl. Conf. on MIC,* P. Angel et al., Ed., NACE International, 1995, p 62-1

101. H.C. Flemming, Biofouling in Water Treatment, *Biofouling and Biocorrosion in Industrial Water Systems,* H.C. Flemming and G.G. Geesey, Ed., Springer-Verlag, 1991, p 47

102. R.W. Lutey, Treatment for the Mitigation of MIC, *A Practical Manual on Microbiologically Influenced Corrosion,* Vol 2, J.G. Stoecker, Ed., NACE International, 2001, p 9.1

103. G.C. White, *The Handbook of Chlorination and Alternative Disinfectants,* Van Nostrand Reinhold, New York, NY, 1992, 1308 p

104. M.R.W. Brown and P. Gilbert, Sensitivity of Biofilms to Antimicrobial Agents, *J. Appl. Bacteriol. Symp. Suppl.,* Vol 74, 1993, p 87S–97S

105. H.A. Videla, F. Bianchi, M.M.S. Freitas, C.G. Canales, and J.F. Wilkes, Monitoring Biocorrosion and Biofilms in Industrial Waters: A Practical Approach, *Microbiologically Influenced Corrosion Testing,* Special Technical Publication 1232, J.R. Kearns and B.J. Little, Ed., ASTM, 1994, p 128

106. I. Ruseski, J. Robbins, and J.W. Costerton, Biocide Testing Against Corrosion-Causing Oil-Field Bacteria Helps Control Plugging, *Oil Gas J.,* Vol 80, 1982, p 253

107. P.F. Sanders and W.A. Hamilton, Biological and Corrosion Activities of Sulphate- Reducing Bacteria in Industrial Process Plant, *Biologically Induced Corrosion,* S.C. Dexter, Ed., NACE International, 1986, p 47

108. H.A. Videla, M.F.L. deMelle, R.A. Silva, F. Bianchi, and C. Gonzales Canales, “A Practical Approach to the Study of the Interaction Between Biofouling and Passive Layers on Mild Steel and Stainless Steel in Cooling Water,” Paper 124, Corrosion/ 90, NACE International, 1990

109. T.P. Zintel, G.J. Licina, and T.R. Jack, “Techniques for MIC Monitoring,” *A Practical Manual on Microbiologically Influenced Corrosion,* Vol 2, J.G. Stoecker, Ed., NACE International, 2001, p 10.1

110. P.S.N. Stokes, M.A. Winters, P.O. Zuniga, and D.J. Schlottenmier, Developments in on-line Fouling and Corrosion Surveillance, *Microbiologically Influenced Corrosion Testing,* Special Technical Publication 1232, J.R. Kearns and B.J. Little, Eds., ASTM, 1994

111. G.J. Licina, G. Nekoksa, and R.L. Howard, “An Electrochemical Method for On-Line Monitoring of Biofilm Activity in Cooling Tower,” Paper 177, Corrosion/92, NACE International, 1992

112. G.J. Licina, G. Nekoksa, and R.L. Howard, “An Electrochemical Method for On-Line Monitoring of Biofilm Activity in Cooling Water Using the Bio-George™ Probe”

113. G.J. Licina and G. Nekoksa, “The Influence of Water Chemistry and Biocode Additions on the Response of an On-Line Biofilm Monitor,” Paper 527, Corrosion/ 95, NACE International, 1995

114. A. Mollica and G. Ventura, Use of a Biofilm Electrochemical Monitoring Device for an Automatic Application of Anitfouling Procedures in Seawater, *Proc. 12th Intl. Corrosion Cong.,* NACE International, 1993, p 3807

115. A. Pedersen, S. Kjelleberg, and M. Hermansson, *J. Microbiol. Meth.,* Vol 8, 1988, p 191

116. A. Pedersen and M. Hermansson, *Biofouling,* Vol 3, 1991, p 1

117. P. Angell, A. Sonnerson, P.A. Wagner, B.J. Little, and D.C. White, The Role of *Oceanospirillium* Exopolymer in Marine Copper Corrosion, *Proc. 1995 Intl. Conf. on MIC,* P. Angel et al., Ed., NACE International, 1995, p 74-1

118. H.A. Videla, Biocorrosion of Non-Ferrous Metal Surfaces, *Biofouling and Biocorrosion in Industrial Water Systems,* G.G. Geesey, Z. Lewandowski, and H.C. Flemming, Ed., Lewis Publishers, 1994, p 231

119. A. Jayaraman, E.T. Cheng, J.C. Earthman, and T.K. Wood, *Appl. Microbiol. Biotechnol.,* Vol 48, 1997, p 11–17

120. C.J. Thomas, R.G.J. Edyvean, and R. Brook, Biologically Enhanced Corrosion Fatigue, *Biofouling,* Vol 1, 1988, p 65

121. F. Mansfeld, C.H. Hsu, D. Ornek, T.K. Wood, and B.C. Syrett, Corrosion Control Using Regenerative Biofilms (CCURB) on Aluminum 2024 and Brass in Different Media, *Proc. Symp. on New Trends in Electrochemical Impedance Spectroscopy (EIS) and Electrochemical Noise Analysis (ENA), The Electrochem. Soc. Proc.,* Vol 2000–24, 2001, p 99–118

122. D. Ornek, A. Jayaraman, T.K. Wood, Z. Sun, C.H. Hsu, and F. Mansfeld, *Corros. Sci.,* Vol 43, 2001, p 2121–2133

123. A. Nagiub and F. Mansfeld, *Corros. Sci.,* Vol 43, 2001, p 2001–2009

124. F. Mansfeld, Z. Sun, and H.S. Hsu, *Electrochim. Acta,* Vol 46, 2001, p 3651–3664

125. K. Trandem, P.J. Arps, and J.C. Earthman, "Closed-Loop Sidestream Systems for Investigating Corrosion Control Using Regenerative Biofilms (CCURB) in Service Water," Paper 648, Corrosion/2000, NACE International, 2001

126. B.C. Syrett, P.J. Arps, J.C. Earthman, F. Mansfeld, and T. Wood, Biofilms That Prevent Corrosion, *Proceedings of the Corrosion 2002 Research Topical Symposium: Microbiologically Influenced Corrosion,* NACE Press, NACE International, 2002, p 145–162

127. B. Little and R. Ray, A Perspective on Corrosion Inhibition by Biofilms, *Corrosion,* Vol 58, 2002, p 424–428

S.C. Dexter, Microbiologically Influenced Corrosion, *Corrosion: Fundamentals, Testing, and Protection,* Vol 13A, *ASM Handbook,* ASM International, 2003, p 398–416

Microbiologically Influenced Corrosion

Stephen C. Dexter, University of Delaware

Selected References

- S.W. Borenstein, *Microbiologically Influenced Corrosion Handbook,* Industrial Press, Inc., 1994
- C. Gaylarde and H. Videla, Ed., *Bioextraction and Biodeterioration of Metals,* Cambridge University Press, Cambridge, U.K., 1995
- G.G. Geesey, Z. Lewandowski, and H.-C. Flemming, Ed., *Biofouling and Biocorrosion in Industrial Water Systems,* Lewis Publishers, CRC Press, Inc., Boca Raton, FL, 1994
- J.R. Kearns and B.J. Little, Ed., *Microbiologically Influenced Corrosion Testing,* Special Technical Publication 1232, ASTM, 1994
- G. Kobrin, Ed., *A Practical Manual on Microbiologically Influenced Corrosion,* NACE International, 1994
- B.J. Little and P.A. Wagner, Application of Electrochemical Techniques to the Study of MIC, *Modern Aspects of Electrochemistry,* No. 34, J.O. Bockris et al., Ed., Kluwer Academic/Plenum Publishers, 2001
- B.J. Little, P.A. Wagner, and F. Mansfeld, Microbiologically Influenced Corrosion, *Corrosion Testing Made Easy,* Vol 5, B.C. Syrett, Series Ed., NACE International, 1997

- D.H. Pope, D. Duquette, P.C. Wayner, and A.H. Johannes, “Microbiologically Influenced Corrosion: A State-of-the-Art Review,” MTI Publication 13, Materials Technology Institute of the Chemical Process Industries, Inc., June 1984
- J. Stoecker, Ed., *A Practical Manual on Microbiologically Influenced Corrosion,* Vol 2, NACE International, 2001
- H.A. Videla, *Manual of Biocorrosion,* CRC Press, Inc., 1996

B.S. Covino, Jr., Introduction to Corrosion Testing and Evaluation, *Corrosion: Fundamentals, Testing, and Protection*, Vol 13A, *ASM Handbook*, ASM International, 2003, p 419

Introduction to Corrosion Testing and Evaluation

Bernard S. Covino, Jr., Albany Research Center, U.S. Department of Energy

Introduction

"CORROSION TESTING AND EVALUATION" contains information on the how, why, and where of corrosion testing. There are step- by-step instructions for techniques, examples of actual test data, hints to help in interpretation, references, and selected references for further information. Because corrosion testing and evaluation is such an integral part of the job of all corrosion engineers, scientists, and technicians, this Section presents a uniform view of state-of- the-art corrosion testing and evaluation procedures that are currently being used by corrosionists.

There are many good reasons for having a uniform source of corrosion testing and evaluation procedures. Uniformity of testing and evaluation ensures that the worldwide corrosion community will speak the same language to its customers. Uniformity can be viewed as a form of quality control of the product that corrosionists present to their clients. On the other hand, active members of the corrosion community will always push the envelope to develop new corrosion testing techniques and ways of interpreting corrosion data. The challenge is to create and achieve acceptance and agreement for the new techniques that will become basic tools for future corrosionists.

The "Corrosion Testing and Evaluation" Section consists of five subsections: "Planning Corrosion Tests and Evaluating Results," "Laboratory Corrosion Testing," "Simulated Service Corrosion Testing," "In-Service Techniques for Damage Detection and Monitoring," and "Evaluating Forms of Corrosion." The articles in this Section have been extensively updated, plus there is more than 30% totally new material.

B.S. Covino, Jr., Introduction to Corrosion Testing and Evaluation, *Corrosion: Fundamentals, Testing, and Protection*, Vol 13A, *ASM Handbook*, ASM International, 2003, p 419

Introduction to Corrosion Testing and Evaluation

Bernard S. Covino, Jr., Albany Research Center, U.S. Department of Energy

Planning Corrosion Tests and Evaluating Results

This subsection contains vital information for the corrosionist. Properly designed and planned experiments can reduce the number of experiments and produce data that are subjected to statistical analysis. Statistically significant data can then be used to develop mechanistic- and knowledge-based models that are used, for example, as critical elements in life cycle management of equipment and structures.

B.S. Covino, Jr., Introduction to Corrosion Testing and Evaluation, *Corrosion: Fundamentals, Testing, and Protection*, Vol 13A, *ASM Handbook*, ASM International, 2003, p 419

Introduction to Corrosion Testing and Evaluation

Bernard S. Covino, Jr., Albany Research Center, U.S. Department of Energy

Laboratory Corrosion Testing

Laboratory procedures are used to screen metals and alloys for further testing and to develop data helpful to understanding corrosion processes. Immersion testing is the most frequently conducted procedure for evaluating corrosion resistance. However, when more information than corrosion rate is needed or accelerated testing is required, electrochemical techniques are often considered. Many electrochemical techniques are available, and their use has been made easier by the incorporation of computer software and hardware. Accelerated testing of materials is often conducted in salt spray, fog, and light exposure cabinets. Techniques for conducting microbiologically influenced corrosion tests are presented with an increased emphasis in this subsection.

B.S. Covino, Jr., Introduction to Corrosion Testing and Evaluation, *Corrosion: Fundamentals, Testing, and Protection*, Vol 13A, *ASM Handbook*, ASM International, 2003, p 419

Introduction to Corrosion Testing and Evaluation

Bernard S. Covino, Jr., Albany Research Center, U.S. Department of Energy

Simulated Service Corrosion Testing

Simulated service testing produces corrosion data with reliability second only to in-service exposures. This subsection considers corrosion testing techniques for three common environments: atmosphere, water, and soil. Changes in atmospheric corrosion testing are being driven by the need for more mechanistic and predictive information and by the development of corrosivity maps. Some of this predictive capability requires the determination of a mass balance for the corrosion reaction and the determination of the effect of atmospheric constituents on corrosion through the measurement of runoff water chemistry. Testing in waters is a mature science, and most applicable techniques are covered by NACE and ASTM standards. As in aqueous environments, immersion testing by using buried coupons is the most widely used practice for underground or soil corrosion tests.

B.S. Covino, Jr., Introduction to Corrosion Testing and Evaluation, *Corrosion: Fundamentals, Testing, and Protection*, Vol 13A, *ASM Handbook*, ASM International, 2003, p 419

Introduction to Corrosion Testing and Evaluation

Bernard S. Covino, Jr., Albany Research Center, U.S. Department of Energy

Simulated Service Corrosion Testing

Simulated service testing produces corrosion data with reliability second only to in-service exposures. This subsection considers corrosion testing techniques for three common environments: atmosphere, water, and soil. Changes in atmospheric corrosion testing are being driven by the need for more mechanistic and predictive information and by the development of corrosivity maps. Some of this predictive capability requires the determination of a mass balance for the corrosion reaction and the determination of the effect of atmospheric constituents on corrosion through the measurement of runoff water chemistry. Testing in waters is a mature science, and most applicable techniques are covered by NACE and ASTM standards. As in aqueous environments, immersion testing by using buried coupons is the most widely used practice for underground or soil corrosion tests.

B.S. Covino, Jr., Introduction to Corrosion Testing and Evaluation, *Corrosion: Fundamentals, Testing, and Protection*, Vol 13A, *ASM Handbook*, ASM International, 2003, p 419

Introduction to Corrosion Testing and Evaluation

Bernard S. Covino, Jr., Albany Research Center, U.S. Department of Energy

---

In-Service Techniques for Damage Detection and Monitoring

This subsection addresses corrosion and corrosivity sensing techniques that can be used in situ in addition to ex situ techniques for detecting corrosion. Direct testing of coupons is used frequently to monitor in-service corrosion because of the simplicity and accuracy of the technique. Electrochemical techniques such as linear polarization resistance and electrochemical noise have moved from the laboratory to the processing plant and beyond to help with the detection of general and localized corrosion. Electrical and inductive resistance probes are frequently used to measure general corrosion rates. Ex situ techniques, such as ultrasonic thickness measurements, work from the outside of the vessel. Emerging techniques, such as microwave and guided wave ultrasonic methods can be configured to detect corrosion under coatings or to measure the moisture content of the interior of structures. Infrared imaging is typically used to detect the presence of corrosion under a coating.

B.S. Covino, Jr., Introduction to Corrosion Testing and Evaluation, *Corrosion: Fundamentals, Testing, and Protection*, Vol 13A, *ASM Handbook*, ASM International, 2003, p 419

Introduction to Corrosion Testing and Evaluation

Bernard S. Covino, Jr., Albany Research Center, U.S. Department of Energy

---

Evaluating Forms of Corrosion

The articles in this subsection address the wide variety of corrosion phenomena experienced in the laboratory, in simulated service testing, and in in-service testing: uniform, pitting, crevice, galvanic, intergranular, exfoliation, cavitation, impingement, gaseous, and microbiologically influenced corrosion. Stress-corrosion cracking, hydrogen embrittlement, and erosion corrosion also are covered. This subsection describes specific tests and their interpretation for all of the aforementioned forms of corrosion. Substantial information is included on specialized test techniques not addressed in the subsections “Laboratory Corrosion Testing” or “Simulated Service Corrosion Testing,” for forms of corrosion such as stress-corrosion cracking, corrosion fatigue, and hydrogen embrittlement.

P.R. Roberge, Designing, Planning, and Preparing Corrosion Tests, *Corrosion: Fundamentals, Testing, and Protection*, Vol 13A, *ASM Handbook*, ASM International, 2003, p 420–424

Designing, Planning, and Preparing Corrosion Tests

P.R. Roberge, Royal Military College of Canada

Introduction

THE CORROSION BEHAVIOR of a given material depends on the environment and the conditions of exposure as well as the condition of the test material. The most reliable predictor of performance is service experience, followed closely by field testing, because both are based on the actual environment and its complex variations. Part of the testing philosophy involves whether the test is intended to reproduce a certain environment accurately or whether it is more advisable to use a corrosive environment that represents a worst-case situation. In either case, the corrosion investigator must do everything possible to make the test reproducible by documenting and exercising explicit control over environmental factors such as concentration of reactants and contaminants, solution pH, temperature, aeration, velocity, impingement, and bacteriological effects.

Corrosion behavior is often the result of complicated interactions between the conditions of a metallic surface and the adjacent environment to which it is exposed. Therefore, there is no universal corrosion test for all purposes. Many investigators have traditionally avoided the use of statistical techniques because the added reliability did not seem to offset the effort and time required to become familiar with the methodology or to perform the calculations. Most often, the results must be interpreted in terms of relative rankings. Such interpretations can be subjective and depend much on the judgment of the investigator. Therefore, it is advisable, when planning a corrosion-testing program, to select the testing conditions carefully in order to produce ranking parameters with minimal influence from testing conditions while rich in engineering significance.

P.R. Roberge, Designing, Planning, and Preparing Corrosion Tests, *Corrosion: Fundamentals, Testing, and Protection*, Vol 13A, *ASM Handbook*, ASM International, 2003, p 420–424

Designing, Planning, and Preparing Corrosion Tests

P.R. Roberge, Royal Military College of Canada

Test Objectives and Conditions

Properly conducted corrosion tests can mean the savings of important assets. They are the means of avoiding the use of a metal under unsuitable conditions or of using a more expensive material than is required. Corrosion tests also help in the development of new alloys that perform more inexpensively, more efficiently, longer, or more safely than the alloys currently in use. Corrosion testing programs can be simple and completed in a few minutes or hours, or they can be complex, requiring the combined work of a number of investigators over a period of years. Preliminary time and effort spent considering metallurgical factors, environmental variations, statistical treatment, and the interpretation of accelerated test results are often the most useful part of the test procedures. Typical corrosion test objectives include:

- Determining the best material to fill a need (material selection)
- Predicting the probable service life of a product or structure

- Evaluating the new commercial alloys and processes
- Assisting with development of materials with improved resistance to corrosion
- Conducting lot-release and acceptance tests to determine whether material meets specifications (quality control)
- Evaluating environmental variations and controls (inhibitors)
- Determining the most economical means of reducing corrosion (evaulate prevention methods)
- Studying corrosion mechanisms

Metal Composition and Metallurgical Condition. If commercial alloys are to be tested, the preferred procedure is to obtain mill-fabricated material representative of current production. If possible, a fabrication history should be obtained listing the major fabricating steps, together with an accurate analysis of the metal composition. Metallographic examination may also be necessary to ensure that the material is in a proper metallurgical condition. When nonstandard alloys or metallurgical treatments are to be evaluated, it may be economically impractical to have them fabricated with large production equipment. In such cases, laboratory casts or heats can be made in small quantities. Although this is a valid procedure for initial tests, a promising alloy candidate should be evaluated several times by using specimens from quantities of material large enough to be representative of typical production runs before it is produced commercially. Several production lots must be evaluated because promising results from a single lot of material are often not reproduced on subsequent fabrication runs.

Another preliminary decision is the form of metal to be tested. Metals are available in two basic forms: cast and wrought (worked). These two forms should not be interchanged in testing. The various methods of casting (such as die, permanent mold, and sand mold) and the various methods of working wrought products (drawing, extruding, forging, rolling) will affect grain structure and homogeneity, which consequently can affect corrosion resistance. The metal procured for the test should be, as nearly as possible, the type that will be used in the intended application.

Preparation of Test Specimens. The sampling of test materials and the preparation of test specimens are important variables in corrosion testing, because corrosion behavior can be significantly influenced by variations in metallurgical structure and the condition of the metal surface. These factors are especially pertinent when various forms of localized corrosion are under evaluation in complex alloys. The uniformity of the randomly chosen metal sample population should be verified as part of the plan for preparation of the test specimens. Problems resulting from lack of uniformity are less likely to be encountered with pure metals and homogeneous alloys.

The primary consideration should be the use of test specimens that are truly representative of the specified material, that is, alloy, metallurgical condition, and product form, rather than specimens that are the most expedient for the investigation. For example, it might seem advantageous to obtain flat, uniform disk specimens by machining slices from an extruded rod rather than by shearing or stamping test coupons from rolled sheet (and avoiding residual stresses in the sheared edges). However, the corrosion behavior of the end-grain surfaces of the machined disks could be different from that of the rolled surface of the sheet product.

Surface preparation by various machining or polishing methods and various chemical treatments can be a source of considerable variation in test results and must be controlled. In some cases, it may be desired to evaluate the metal in the mill-finished condition, although this approach will generally result in the greatest variability. As a general rule, corrosion-testing standards contain specific recommendations regarding appropriate surface treatments, depending on the metal alloy system. Judicious use of proper or standardized surface treatments will reduce variability in corrosion test results.

Assessment of Corrosion Damage. Appropriate methods of measuring degradation of metallic materials depend on the form of corrosion being observed. For example, the age-old method of measuring corrosion by determining weight loss and calculating average corrosion rates, which is adequate for metals that corrode uniformly, is not a realistic measure of localized forms of corrosion, such as pitting and intergranular attack. A serious consideration in the corrosion testing of metals is the use of suitable controls, both for the metal and for the test environment. With some materials, certain characteristics used for assessing corrosion damage will change with time, even in the absence of corrosion. In such cases, a set of control specimens must be provided for each period of corrosion testing. This set is then evaluated at the same time as the corroded specimens. Some alloys, for example, gradually change in strength over long periods of time at room temperature, and the strength of most metals is affected by time at elevated temperatures.

Another required control is a method of determining whether the corrosive medium maintains the intended degree of corrosivity. When an alloy is tested repeatedly by the same method, as in quality-control tests, the investigator may be sufficiently experienced to know whether the visual appearance and resultant data are of the order expected. This is often not the case with new alloys or products because their corrosion performance is unpredictable. The usual procedure is to expose a well-established previously tested alloy as a control to determine whether the results are consistent with past experience. If they are, the new alloy is considered to have received a valid exposure. However, if the effects of corrosion on the well-known alloy are not typical, the investigator is alerted to the possibility of an error in test environment and the necessity for a rerun of the test after corrective measures have been made.

Reliability of Corrosion Test Results. Corrosion rate results should be used with caution. Corrosion engineers frequently take the results of relatively short-term one-period exposure tests, divide the weight loss (or pit depth) of the metal by the time of exposure, and from this determine a constant rate of corrosion for the particular metal-environment combination. Such early one-point average rates are valid only when materials corrode linearly with time; however, this is the exception rather than the rule for metals in natural environments. The effect of film formation on the surface varies the corrosion rate with time in a large majority of cases. The creation of a film of corrosion product often shields the metal substrate from the corrosive environment, with a resulting decrease in corrosion rate. In this case, the projection of corrosion rates before a film has formed will be unduly pessimistic.

At best, the precision of corrosion test results leaves something to be desired because of the relative complexity of corrosion systems. This is particularly true when evaluating forms of localized corrosion, which can be related often to heterogeneous microstructures in the test material. As progress is being made in the standardization of corrosion test methods, more attention is being directed toward providing potential users of the methods with information to help them assess in general terms its usefulness in proposed applications. The American Society for Testing and Materials (ASTM) recently made it mandatory that statements on the precision (reproducibility) and bias (systematic error) be included in every standard for a test method. If this information is not currently available to the corrosion investigator, it should added as a requirement to the test plan.

P.R. Roberge, Designing, Planning, and Preparing Corrosion Tests, *Corrosion: Fundamentals, Testing, and Protection*, Vol 13A, *ASM Handbook*, ASM International, 2003, p 420–424

Designing, Planning, and Preparing Corrosion Tests

P.R. Roberge, Royal Military College of Canada

Design of Experiments

A strategy for planning research known as design of experiments was first introduced in the early 1920s when a scientist at a small agricultural research station in England, Sir Ronald Fisher, showed how one could conduct valid experiments in the presence of many naturally fluctuating conditions such as temperature, soil condition, and rainfall. The design principles that he developed for agricultural experiments have been successfully adapted to industrial and military applications since the 1940s.

Experimental design is an iterative process of analyzing test results in a systematic way to create, verify, and perfect models that can in turn serve to plan more efficient and less costly test programs. Applied to a corrosion problem, such a process can combine modern scientific principles with an appreciation of the mechanisms of degradation of the material being studied. Experimental design is an accepted methodology that can help to make the transition between simple but practical empirical models to the most sophisticated multiparameter mechanistic models.

The role of experimental design in acquiring the knowledge of a process (Fig. 1) emphasizes the iterative aspect of the process leading to the creation of realistic models. As expressed in this figure, the selection of an experimental strategy should precede and influence data acquisition. It is indeed difficult, if not impossible, to

retrofit experiments to satisfy the statistical considerations necessary for the construction of valid models. Any time spent in preparing a test program is a good investment. The most important consideration, at the initial planning stages, should be to integrate the available information in order to limit future setbacks. Table 1 expands on each of the elements in Fig. 1 by indicating many of the questions that should be asked at the three stages of a statistical design loop for acquiring knowledge of a process. See Ref 1 for a detailed description of the experimental design process.

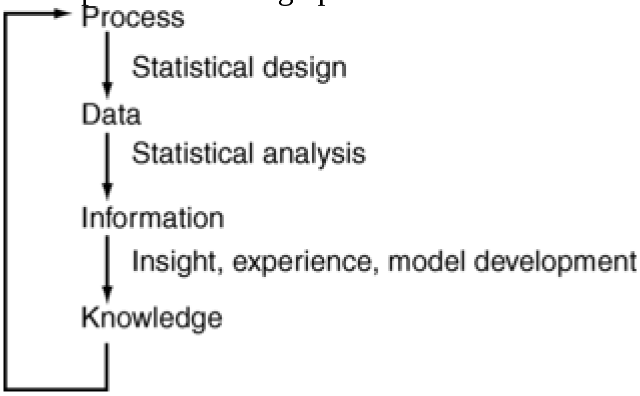

Fig. 1 Statistical design loop for acquiring knowledge of a process

Table 1 Elements of the iterative process for experimental design

Process step/Category	Question
Statistical design	
Process definition	What are the relevant material and environmental factors?
	What is the domain or operating envelope to be investigated?
	What is the expected outcome?
Preliminary questions	What are the experimental constraints?
	What systematic errors are expected?
	Should the trials be randomized?
	Is there an estimate for the experimental errors?
	Should all factors be investigated at once?
	Should there be a central point measurement?
Optimizing design	How many factors must be considered?
	Are interactions between factors expected?
	Should the design be complete or fractional?
	What is the most logical order of experiments?
Data—analysis of results	
Critical analysis	Are some results suspect (outliers)?
	Were the factor levels well set?
	Calculate the effects of the factors using statistical parameters.
	Check for ambiguities.
Follow-up	Should the experimental domain be modified?[a]
	Is a complementary test design required?[a]
	Is the chosen mathematical model appropriate?[a]
Information-model development	
Model development	Will complementary designs be encompassed?
	Are complementary trials required?
	Are new factors addressed?
	Can the operating envelope be expanded?
	Is a new model more suitable?
	Is the mathematical model optimized?

(a) If all three answers are “no,” the experiment can be stopped. If one is “yes,” the experimentation should continue.
It is believed that the systematic design of experiments can (Ref 2):

- Save time and money: fewer experiments are required per firm conclusion.
- Simplify data handling: data are digested in a readily reusable form.
- Establish better correlations: variables and their effects are isolated.
- Provide greater accuracy: the estimation of errors is cornerstone to statistical design.

While some of the factors leading to corrosion damage can be reproduced relatively easily by creating a situation favorable to their occurrence, other factors depend entirely on the development of local defects that often become visible only after long and highly variable periods of exposure. When an experiment or test is planned, many factors have to be considered. Some of the standard considerations for the design of a test program include (Ref 3):

- How should the results be interpreted?
- How can the information be integrated with earlier or other tests?
- How many specimens are available?
- What is the production schedule (batch, sequential)?
- How many factors control the behavior of the specimen?
- How many factors are to be included in the tests?
- Which of these factors interact and which have negligible interaction?
- What type of data is to be measured?
- Is the sample homogeneous?
- How representative is the sample?
- Are the tests destructive?
- How expensive are the tests and/or specimens?
- How much control is there over testing?
- How difficult would it be to compensate for human errors in the planning?

Out of all these questions and interrogations, a test protocol should be developed to transform the corrosion test design into a set of reliable and reproducible measurements that achieve the goals and objectives of the test. The test protocol can simply be a guide or “road map” to the collection of raw or uninterpreted measurements defining the methods and standards used. When measurements must meet legal, regulatory, or customer requirements, the test protocol may be codified into a quality assurance plan. The test protocol typically specifies criteria for precision, accuracy, completeness, representativeness, and comparability of the corrosion and related measurements. The test protocol can address sampling and analytical procedures, calibration procedures and standards, data reduction and processing methods, data validation, data reporting, and even data audits (Ref 4).
Experiment Design Strategies. Properly designed and executed experiments will generate more precise data while using substantially fewer experimental runs than alternative approaches. They will lead to results that can be interpreted using relatively simple statistical techniques, in contrast to the information gathered in observational studies, which can be exceedingly difficult to interpret. Corrosion scientists and engineers usually work with either controlled or uncontrolled experiments. Properly designed controlled experiments are much more amenable to statistical analysis of variance than are properly designed uncontrolled experiments (Ref 5).
Controlled Factorial Experiments. In controlled experiments, levels of independent variables are controlled, and the dependent variables showing the progress of a corrosion attack are measured with proper means. The framework of factors and subfactors presented in Table 1 of the article “Statistical Interpretation of Corrosion Test Results” in this Volume is an exhaustive list of the independent variables to control in a planned corrosion experiment. The results of an expert opinion poll highlighting the most important factors involved in various forms of corrosion failures presented in Table 2 of the same article could help shorten the list of actual variables of significance in given situations.
Each controlled variable with more than one controlled level is considered a factor in such experiments. The main advantage of a factorial design experiment is that interaction as well as direct effects can be studied with

less replication than several one-way analyses of variances. An example of an interaction effect is a change of slope of a corrosion-rate/relative-humidity curve with a change in temperature. Researchers use two-level factorial experiments to determine which variables or factors cause direct synergistic effects on the measured parameter. Each new factor introduced, however, doubles the number of test conditions. Thus, the need to include a large number of factors in a complete experimental design often results in an impractical number of test conditions. To circumvent this problem, statisticians can design fractional experiments that produce nearly all the information needed by confounding some possible effects such as higher-order interactions (Ref 5).
This efficiency is often lost when interactions exist. In the field of corrosion research, it is difficult to find combinations of three or more significant variables that will not produce at least one interaction. Sometimes interaction effects are more important than the separate variable effects. A particular example of such interactions in a corrosion situation is the occurrence of stress-corrosion cracking (SCC), which clearly involves three factors:

- Susceptibility of the material to SCC
- The presence of a corrosive environment conducive to SCC
- The presence of sustained stresses

Stress-corrosion cracking will not occur if any one of the three conditions is absent. Because interactions can be important, the factorial design determines what interactions occur and the magnitude of their effect. The two-level factorial design is excellent to use when several variables could affect the test outcome. This design determines what variables, combination of variables, or both, could have a significant effect on the results. In practice, all variables or factors that could possibly affect the test outcome should be included. If n is the number of variables, 2^n is the number of cases or conditions in the two- level factorial design. Replication of some of the conditions is necessary to establish an error variance (Ref 4). One disadvantage of two-level factorial designs is that the size of the study increases by a factor of two for each additional factor. For example, with eight factors, 2^8 or 256 runs would theoretically be necessary. Fortunately, because three-factor and higher-order interactions are rarely important, such intensive efforts are seldom required.
For most purposes, it is only necessary to evaluate the main effects of each variable and the two-factor interactions, which can be done with only a fraction of the runs in a full-factorial design. Such designs are called resolution V designs. If there are some two-factor interactions that are known to be impossible, one can further reduce the number of runs by using resolution IV designs.
Design resolution is defined in terms of which effects are unconfounded with which other effects. One ordinarily seeks fractional factorial experiments that have main effects (s = 1) and low-order interactions (say those involving s = 2 or 3 factors) unconfounded with other main effects and low-order interactions-equivalently, in which they are confounded only with high- order interactions.
The resolution of a design is usually denoted by uppercase Roman numerals (e.g. III, IV, V). A design in which main effects are not confounded with other main effects but are confounded with two-factor and higher-order interactions is a resolution-III design. Such a design is of resolution III because effects containing s = 1 factor are unconfounded with effects containing less than R - s = 3 - 1 = 2 factors. The only effects containing less than s = 2 factors are other main effects.
In a resolution-IV design, main effects are unconfounded with effects involving less than R - s = 4 - 1 = 3 factors, i.e., main effects and two-factor interactions. Two-factor interactions (s = 2) are unconfounded with effects involving less than R - s = 2 factors, i.e., main effects (s = 1). There are some two-factor interactions confounded with other two-factor interactions in R IV designs.
A design of resolution V has main effects and two-factor interactions (s = 1, 2) unconfounded with one another. Some main effects are confounded with four-factor and higher-order interactions. Some two-factor interactions are confounded with three-factor and higher-order interactions.
A good compromise for complex situations is to employ what is called a screening design technique to identify the most dominant factors, often with the intent to conduct a more extensive and systematic investigation (Ref 6). An important application of screening experiments is also to perform ruggedness tests that, once completed, will permit the control or limitation of environmental factors or test conditions that can easily influence a test program (Ref 7). There are, of course, many subtleties in designing experiments that may intimidate a person with limited familiarity of statistics. Fortunately, however, there are a number of software systems that will guide a user in a friendly manner through the process of designing experiments.

Uncontrolled Experiments. In the real world, materials are seldom exposed to controlled environments. In uncontrolled experiments such as atmospheric exposures, uncontrolled independent variables such as temperature and relative humidity are measured along with the dependent corrosion results. A properly designed uncontrolled experiment is one that considers all the possible effects of uncontrolled variables. The knowledge of physical and chemical processes is most valuable in this respect. If an important variable is missed, all the other data become less meaningful (Ref 5).

For proper subsequent analysis, uncontrolled experiments require the collection of considerable data. As an example, if one were to collect ten sets of data involving nine uncontrolled variables and the measured corrosion results, a total of 100 data points would have been collected for further analysis. If all the variables were included in that analysis, a perfect mathematical fit could be obtained; however, this fit would be both physically and statistically meaningless. The experimental design does not consider the possibility of nonlinear effects, interaction effects, or error effects. One approach to ensure that enough data sets are collected is to count all the physically and chemically (not mathematically) possible direct and interaction effects of the measured variables and multiply by 4 or 5 to account for possible nonlinearity and error (Ref 5).

Blocking. The more widely used statistical techniques typically assume that “independent” variables are not associated with each other and that their levels are fixed and have no measurement error. These assumptions are seldom true in practice. Often the independent variables studied as possible corrosion contributors are subject to measurement error and may have effects on each other as well as on corrosion performance. Too few or poor measurements of independent variables can result in an inability to show statistical association when an actual cause-effect relationship exits. The more data collected on the independent variables, the greater the probability that good relationships between these variables and corrosion performance can be established (Ref 4). It is well recognized that the planning activities that precede the actual test runs are critical to the successful resolution of the experimenter's problem. In planning an experiment, it is necessary to limit any bias that may be introduced by the experimental units or experimental conditions. Strategies such as randomization and blocking can be used to minimize the effect of nuisance or noise elements.

In some production processes, units are produced in natural “chunks” or blocks. Blocking can be used to prevent experimental results from being influenced by variations from batch to batch, machine to machine, day to day, or shift to shift. For example, when the process being investigated can only produce a fraction of the samples required for all runs in a planned experiment, it may be necessary to break up the experiment into blocks. However, it is not desired to run positive settings of all factors in one block, and all negative settings in the other. Otherwise, any incidental differences between blocks would systematically affect all estimates of the main effects of the factors of interest. Rather, it is advisable to distribute the runs over the blocks so that any differences between blocks (i.e., the blocking factor) do not bias the results for the factor effects of interest. This is accomplished by treating the blocking factor as another factor in the design. Consequently, another interaction effect is lost to the blocking factor, and the resultant design is of lower resolution. However, these designs often have the advantage of being statistically more powerful because they allow estimating and controlling the variability in the production process that is due to differences between blocks.

References cited in this section

1. J.L. Goupy, *Methods for Experimental Design,* Elsevier, Amsterdam, The Netherlands, 1993

2. P.R. Roberge, Better Corrosion Testing through Experimental Design, *Mater. Perform.,* Vol 34, 1995, p 7–9

3. D.K. Lloyd and M. Lipow, *Reliability: Management, Methods and Mathematics,* The American Society for Quality Control, 1984

4. J.W. Spence, S.D. Cramer, and F.H. Haynie, Planning and Design of Tests, *Corrosion Tests and Standards,* MNL 20, R. Baboian, Ed., American Society for Testing of Materials, 1995, p 33–39

5. F.H. Haynie, Statistical Treatment of Data, Data Interpretation, and Reliability. *Corrosion Tests and Standards,* MNL 20, R. Baboian, Ed., American Society for Testing of Materials, 1995, p 62–67

6. G.E.P. Box and N.R. Draper, *Empirical Model-Building and Response Surfaces,* John Wiley & Sons, 1987

7. R.L. Mason, R.F. Gunst, and J.L. Hess, *Statistical Design and Analysis of Experiments,* John Wiley & Sons, 1989

P.R. Roberge, Designing, Planning, and Preparing Corrosion Tests, *Corrosion: Fundamentals, Testing, and Protection*, Vol 13A, *ASM Handbook*, ASM International, 2003, p 420–424

Designing, Planning, and Preparing Corrosion Tests

P.R. Roberge, Royal Military College of Canada

Examples of Experimental Designs Applied to Corrosion Testing

Example 1: Selection of a Cast Superalloy. In this study, a series of cast nickel-base γ/γ' superalloys were systematically varied at selected levels of cobalt, chromium, molybdenum, tantalum, and aluminum and the alloys weight change performance was monitored (Ref 8). A full-factorial central experimental design was used, making up five sets of star points to completely map the response of these alloys. For five elemental variables, 43 alloy compositions were required. The results analyzed by regression analysis led to a complete second-degree equation describing the total variability of the alloy performance.

Example 2: Improved Cosmetic Corrosion Test. Within the efforts of the American Iron and Steel Institute's (AISI) Task Force on Automotive Corrosion, a design of experiments program was initiated. The aim of this program was to study the effects of a number of carefully selected test parameters on the performance of automotive steel sheet products subjected to a cyclic corrosion test and to “on-vehicle” tests (Ref 9). A review of the literature guided the initial selection of the seven test variables considered of major importance to corrosion performance of automotive steel. Triplicate 100 by 150 mm (4 by 6 in.) panels were exposed to eight test runs designed according to a Plackett-Burman partial factorial design. The results of these tests were to be used as a guide to develop an improved test procedure.

Example 3: Container Material for Nuclear Waste Disposal. In this project, a two-level factorial design was adopted to map the effects of five environmental factors (Cl^-, SO^{2-}_4, NO^-_3, F^-, and temperature) on a candidate material for containers in the Yucca Mountain repository site (Ref 10). The trial order was randomized before testing and a five-factor interaction was used to block the experiments, in terms of two different potentiostats used in the study, in order to verify the instrumental variability. A complete response surface of alloy 825 resistance to localized corrosion, estimated by cyclic polarization, was produced as a function of environmental variables.

Example 4: Managing Water Chemistry. Experimental design was also used to study mild steel corrosion in water containing various scaling agents and the addition of an organophosphorus inhibitor (Ref 11). The corrosion rates were measured in laboratory experiments with linear polarization. Mathematical models were generated relating the corrosion behavior to solution flow rate and the concentrations of Ca^{2+}, Cl^-, HCO^-_3, and the organic inhibitor. Two models were developed in this study: the first described the corrosion rates of mild steel and the second the scaling tendencies of the water. These models were then validated with pilot cooling tower experiments.

Example 5: Corrosivity in Complex Environments. Experimental design techniques were also used to develop models for understanding the effects of complex environments on materials considered for the operation of different processes such as wood pyrolysis (Ref 12), gas desulfurization (Ref 13), and continuous digesters (Ref 14). In these studies, it was demonstrated that designed experiments are essential to reduce the complexity of the environments (solution variables, constraints, etc.) to a manageable level. When properly done, the results of such studies can be used to predict the corrosion performance of alloys as a function of solution composition.

For the interested reader, Ref 14 gives many details on the actual statistical procedures used for a few typical designs in complex corrosion examples.

References cited in this section

8. C.A. Barrett, The Effects of Cr, Co, Al, Mo and Ta on the Cyclic Oxidation Behavior of a Prototype Cast Ni-Base Superalloy Based on a 25 Composite Statistically Designed Experiment, *Conf. High Temperature Corrosion Energy Systems,* The Metallurgical Society/AIME, 1984, p 667–680

9. L.A. Roudabush, H.E. Towsend, and D.C. McCune, Update on the Development of an Improved Cosmetic Corrosion Test by the Automotive and Steel Industries, *Proc. Sixth Automotive and Prevention Conf.,* P-268, SAE International, 1993, p 53–63

10. G.A. Gragnolino and N. Sridhar, Localized Corrosion of a Candidate Container Material for High-Level Nuclear Waste Disposal, *Corrosion,* Vol 47, 1991, p 464–472

11. R.V. Davis, Investigation of Factors Influencing Mild Steel Corrosion Using Experimental Design, *CORROSION/93,* Paper No. 280, NACE International, 1993

12. H. Aubin and C. Roy, Study on the Corrosiveness of Wood Pyrolysis Oils, *Fuel Sci. Technol. Int.,* Vol 8, 1990; p 77–86

13. G.H. Koch, N.G. Thompson, J.M. Spangler, and B.C. Syrett, Effect of Solution Species in Wet SO_2 Scrubber Environments on the Corrosion of Alloys, *CORROSION/86,* Paper No. 363, NACE International, 1986

14. G.H. Koch, J.M. Spangler, and N.G. Thompson, Corrosion Studies in Complex Environments, *The Use of Synthetic Environments for Corrosion Testing,* STP 970, P.E. Francis and T.S. Lee, Ed., American Society for Testing of Materials, 1988, p 3–17

P.R. Roberge, Designing, Planning, and Preparing Corrosion Tests, *Corrosion: Fundamentals, Testing, and Protection*, Vol 13A*, ASM Handbook*, ASM International, 2003, p 420–424

Designing, Planning, and Preparing Corrosion Tests

P.R. Roberge, Royal Military College of Canada

Acknowledgment

This article is based in part on “Planning and Preparation of Corrosion Tests” and “Interpretation and Use of Corrosion test Results” by D.O. Sprowls in *Corrosion,* Vol 13, *Metals Handbook,* ASM International, 1987.

P.R. Roberge, Designing, Planning, and Preparing Corrosion Tests, *Corrosion: Fundamentals, Testing, and Protection*, Vol 13A, *ASM Handbook*, ASM International, 2003, p 420–424

Designing, Planning, and Preparing Corrosion Tests

P.R. Roberge, Royal Military College of Canada

References

1. J.L. Goupy, *Methods for Experimental Design,* Elsevier, Amsterdam, The Netherlands, 1993
2. P.R. Roberge, Better Corrosion Testing through Experimental Design, *Mater. Perform.,* Vol 34, 1995, p 7–9
3. D.K. Lloyd and M. Lipow, *Reliability: Management, Methods and Mathematics,* The American Society for Quality Control, 1984
4. J.W. Spence, S.D. Cramer, and F.H. Haynie, Planning and Design of Tests, *Corrosion Tests and Standards,* MNL 20, R. Baboian, Ed., American Society for Testing of Materials, 1995, p 33–39
5. F.H. Haynie, Statistical Treatment of Data, Data Interpretation, and Reliability. *Corrosion Tests and Standards,* MNL 20, R. Baboian, Ed., American Society for Testing of Materials, 1995, p 62–67
6. G.E.P. Box and N.R. Draper, *Empirical Model-Building and Response Surfaces,* John Wiley & Sons, 1987
7. R.L. Mason, R.F. Gunst, and J.L. Hess, *Statistical Design and Analysis of Experiments,* John Wiley & Sons, 1989
8. C.A. Barrett, The Effects of Cr, Co, Al, Mo and Ta on the Cyclic Oxidation Behavior of a Prototype Cast Ni-Base Superalloy Based on a 25 Composite Statistically Designed Experiment, *Conf. High Temperature Corrosion Energy Systems,* The Metallurgical Society/AIME, 1984, p 667–680
9. L.A. Roudabush, H.E. Towsend, and D.C. McCune, Update on the Development of an Improved Cosmetic Corrosion Test by the Automotive and Steel Industries, *Proc. Sixth Automotive and Prevention Conf.,* P-268, SAE International, 1993, p 53–63
10. G.A. Gragnolino and N. Sridhar, Localized Corrosion of a Candidate Container Material for High-Level Nuclear Waste Disposal, *Corrosion,* Vol 47, 1991, p 464–472
11. R.V. Davis, Investigation of Factors Influencing Mild Steel Corrosion Using Experimental Design, *CORROSION/93,* Paper No. 280, NACE International, 1993
12. H. Aubin and C. Roy, Study on the Corrosiveness of Wood Pyrolysis Oils, *Fuel Sci. Technol. Int.,* Vol 8, 1990; p 77–86
13. G.H. Koch, N.G. Thompson, J.M. Spangler, and B.C. Syrett, Effect of Solution Species in Wet SO_2 Scrubber Environments on the Corrosion of Alloys, *CORROSION/86,* Paper No. 363, NACE International, 1986

14. G.H. Koch, J.M. Spangler, and N.G. Thompson, Corrosion Studies in Complex Environments, *The Use of Synthetic Environments for Corrosion Testing,* STP 970, P.E. Francis and T.S. Lee, Ed., American Society for Testing of Materials, 1988, p 3–17

P.R. Roberge, Statistical Interpretation of Corrosion Test Results, *Corrosion: Fundamentals, Testing, and Protection*, Vol 13A, *ASM Handbook*, ASM International, 2003, p 425–429

Statistical Interpretation of Corrosion Test Results

P.R. Roberge, Royal Military College of Canada

Introduction

IMPORTANT ASPECTS of any corrosion investigation are the credibility of the test results and user acceptance of the test methodology. When commercially competitive materials are evaluated or when corrosion tests are used for materials acceptance, the testing techniques come under close scrutiny and quick criticism in the marketplace. Public safety and producer liability are potent considerations in decisions involving materials selection and the determination of safe environments. A significant degree of confidence is justified only after an accumulation of sufficient experience in correlating test data with actual performance behavior under known conditions.

P.R. Roberge, Statistical Interpretation of Corrosion Test Results, *Corrosion: Fundamentals, Testing, and Protection*, Vol 13A, *ASM Handbook*, ASM International, 2003, p 425–429

Statistical Interpretation of Corrosion Test Results

P.R. Roberge, Royal Military College of Canada

Complexity of Test Conditions

Corrosion test results often show more scatter than many other types of tests because of a variety of factors, an important one being the effect on corrosion rates due to minor impurities in the materials themselves or in the testing environments (Ref 1). This intrinsic complexity has made the transformation of corrosion testing results into usable real-life functions for service applications a difficult task, because testing often results in the generation of unreliable data (Ref 2). The accuracy of data against testing time and number of factors, presented in Fig. 1, illustrates the relative difficulties associated with reproducing industrially realistic corrosion problems.

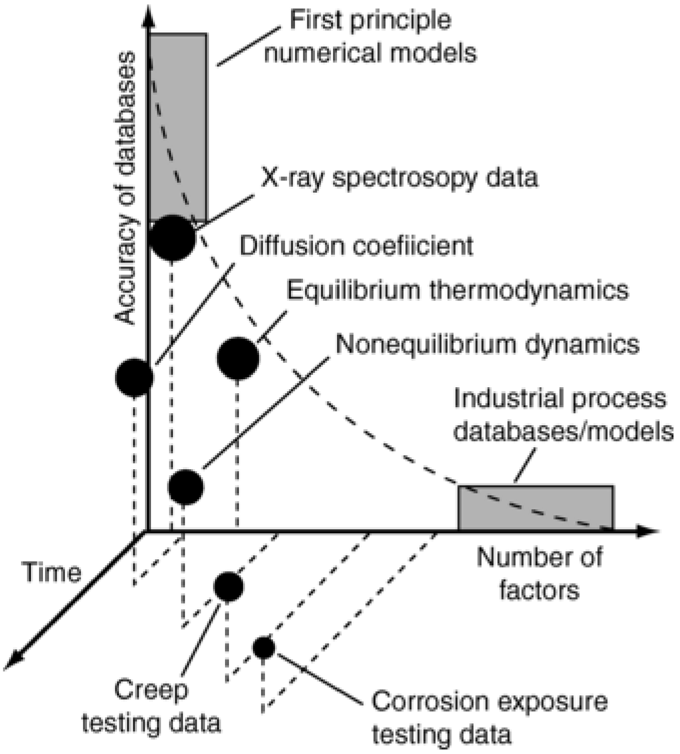

Fig. 1 Time and environment dependency of databases and models. Source: Ref 2

In the development of laboratory corrosion tests for alloy evaluation, for example, it is necessary to determine the dominant corrosion factors. Preferred practice is to design a test to represent a severe condition for the corrosion system involved, thus reducing the time for effects to be observed. One of the dominant factors is then chosen to be the rank-ordering factor. Study of alloy response as a function of this factor provides a means for comparing the corrosion resistance of different alloys. Following is a partial list of factors that have been used for evaluating the susceptibility of alloys to stress-corrosion cracking (Ref 3):

- Time to failure under constant load conditions
- Time to failure under constant strain conditions
- Threshold stress for failure
- Threshold stress for failure/yield strength
- Threshold strain for failure
- Threshold stress intensity
- Strain for 50% probability of failure
- Crack growth rate
- Time to failure (slow strain rate test)
- Loss of ductility (slow strain rate test)
- Fracture appearance (slow strain rate test)
- Work to failure (slow strain rate test)
- Critical strain rate

References cited in this section

1. "Standard Guide for Applying Statistics to Analysis of Corrosion Data," G 16 *Annual Book of ASTM Standards,* Vol 03.02, American Society for Testing of Materials, 1999

2. A. Tomiura, Lessons for a Case Study of Property Databases in Materials Development, *Computerization/Networking of Materials Databases,* STP 1311, S. Nishijima, S. Iwata, and C.H. Newton, Ed., American Society for Testing and Materials, 1996, p 3–20

3. R.S. Treseder, An Engineering View of Laboratory Corrosion Tests, *Laboratory Corrosion Tests and Standards,* STP 866, G.S. Haynes and R. Baboian, Ed., American Society for Testing of Materials, 1985, p 5–13

P.R. Roberge, Statistical Interpretation of Corrosion Test Results, *Corrosion: Fundamentals, Testing, and Protection*, Vol 13A, *ASM Handbook*, ASM International, 2003, p 425–429

Statistical Interpretation of Corrosion Test Results

P.R. Roberge, Royal Military College of Canada

Mechanistic Aspects

Developments in accelerated testing should be based on modern scientific principles and incorporate an appreciation of the mechanisms of service degradation of the metal being studied. In the course of carrying out a failure analysis, the analyst must consider a broad spectrum of possibilities or reasons for the failure occurrence. A large number of factors, frequently uncorrelated, have to be considered to determine the cause of the original failure. If the failure can be duplicated under controlled simulated service conditions, much can be learned about the initial reasons for its occurrence (Ref 4). Many considerations impact the validity and accuracy of information gathered from laboratory testing programs, however. In principle, accelerated life tests and performance degradation tests serve various purposes, ranging from quality control to measuring the reliability of manufactured products (Ref 5).

Acceleration Considerations. The continuous salt spray practice (Ref 6), for example, which was designed originally to test coatings on metals, has been used widely to evaluate the resistance of metals to corrosion in marine service or on exposed shore locations (Ref 7, 8). Extensive experience has shown that, although salt spray tests yield results somewhat similar to those in marine exposure, they do not reproduce all the factors causing corrosion in marine service. Reviews on this subject indicated that the salt spray test cannot realistically be used, for example, for parts with complicated shapes, because salt spray particles fall in vertical patterns, creating a strong orientation dependency (Ref 9, 10). Another major inadequacy of the test is the variable sensitivity of different metallic materials to the ions present in various service environments.

Many other cabinet tests have been developed to determine the corrosion performance of materials intended for use in natural atmospheres; see the article "Cabinet Testing" in this Volume. A series of ASTM International standards have been developed, for example, to relate different variations of creating and controlling fog and humidity in cabinets for corrosion testing of a broad spectrum of products. These products range from decorative electrodeposited coatings to the evaluation of the corrosivity of solder fluxes for copper tubing systems. The basic humidity test is most commonly used to evaluate the corrosivity of materials or the effects of residual contaminants. Cyclic humidity tests are conducted to simulate exposure to high humidity and heat typical of tropical environments.

More complex tests are based on controlled amounts of corrosive gases added to humidity to replicate more severe environments. Some of these tests are designed to reveal and amplify certain characteristics of a material by using very high concentrations of corrosive gases. Some amplify the presence of pores in gold or palladium coatings (Ref 11, 12). The moist SO_2 test is intended to produce corrosion in a form resembling that in industrial environments (Ref 13). A very sophisticated variation of these tests is the flowing of mixed gas test. Pollutants such as chlorine, hydrogen sulfide, and nitrogen dioxide are measured to a parts-per-billion precision in a chamber at controlled temperature and humidity (Ref 14). This test is particularly adapted to the needs of the electronics industry.

Framework of Factors. An increasingly accepted methodology consists of correlating the results obtained with these tests with actual service performance to verify that the corrosion mechanisms have indeed followed the same paths. Modern surface analysis techniques have been found to be quite useful to ascertain that the corrosion products have the same morphologies and crystallographic structures typically found on equipment

used in service. An interesting point of view is that all engineering materials are reactive chemicals and that the strength of materials depends on the extent to which environments influence the reactivity and subsequent degradation of these engineering materials (Ref 15). This concept was the subject of a major review with respect to stress-corrosion cracking (SCC), but the rationale behind the effort is universal and can be extended to all corrosion processes. The general framework consisted of the six factors presented in Table 1 (Ref 16). These factors represent independent variables affecting the intensity of SCC, with a number of subfactors, as shown in Table 1.

Table 1 Factors and subfactors controlling the occurrence of a stress-corrosion cracking failure

Factor	Subfactors and contributing elements
Material	Chemical composition of alloy Crystal structure Grain-boundary composition Surface condition
Environment	
Chemical definition	Type, chemistry, concentration, phase, conductivity of corrodent
Circumstance	Velocity of fluid, thin layer in equilibrium with relative humidity, cyclic wetting and drying, heat transfer, boiling, wear and fretting, deposits
Temperature	At metal surface exposed to environment Temperature fluctuation
Stress	
Stress definition	Mean stress, maximum stress, minimum stress, constant load, constant strain, strain rate, plane stress, plane strain, modes of deformation (I, II, III), biaxial, cyclic frequency, wave shape
Sources of stress	Intentional, residual, produced by reacted products, thermal cycling
Geometry	Discontinuities as stress intensifiers Creation of galvanic potentials Heterogeneous chemicals in crevices Gravitational settling of solids Restricted geometry, with heat transfer leading to concentration effects Orientation vs. environment
Time	Change in grain-boundary chemistry Change in structure Change in surface deposits, chemistry, or heat-transfer resistance Development of surface defects, pitting, or erosion Development of occluded geometry Relaxation of stress

Types of Corrosion Damage. A generally accepted classification scheme of corrosion damage is based on the appearance of a corrosion attack. The term *form* of corrosion generally is attributed to Ref 17. The eight basic forms of corrosion were considered, slightly expanded, and divided into three groups, based on their ease of identification (Ref 18):

Group 1: readily identifiable by ordinary visual examination	**Uniform corrosion** **Pitting** **Crevice corrosion** **Galvanic corrosion**
Group 2: may require supplementary means of examination	Erosion Cavitation Fretting Intergranular
Group 3: verification is usually required by microscopy	Exfoliation Dealloying Stress-corrosion cracking Corrosion fatigue

Many tests have been designed specifically to reveal the susceptibility of materials to one or more of these corrosion forms. However, the mechanisms behind a corrosion attack are controlled by factors similar to those listed in Table 1. Because there are actually no known studies specifically linking these two different frameworks, it was decided to carry out a survey following principles of knowledge engineering. Fifteen recognized corrosion experts completed an opinion poll concerning the main subfactors and the common forms of corrosion. Responses were then analyzed to determine the importance of factors in Table 1 to commonly accepted forms of corrosion failure (Table 2). A more detailed analysis of the responses obtained for pitting corrosion is shown as box-and-whisker plots in Fig. 2. (In a box-and-whisker plot, the whiskers represent the complete range of values. The median, also called the second quartile, is the vertical line within the box. The median of the lower part of the data is calculated. This is the first quartile, and it locates the left side of the box. Likewise, the median of the remaining upper part of the data is calculated. This is the third quartile, and it locates the right side of the box.) In Table 3, the responses are ranked in decreasing order of the median and sharpness of the responses (inverse of the breadth of the whiskers).

Table 2 Results of an expert opinion poll indicating the most important factors causing different types of corrosion failures

Factor	Important factors												
	Uniform	**Pitting**	**Crevice**	**Galvanic**	**Erosion**	**Cavitation**	**Fretting**	**Intergranular**	**Dealloying**	**SCC**	**Fatigue**	**Scaling**	**Internal attack**
Material													
Composition	X	X		X		X	X	X	X	X	X	X	X
Crystal structure								X					
Grain-boundary composition								X		X			
Surface condition		X								X			
Environmental													
Nominal	X	X		X	X			X	X	X	X	X	
Circumstantial		X	X							X			
Stress													
Applied										X	X		
Residual										X			
Product buildup										X			
Cyclic											X		
Geometry													
Galvanic potentials				X									
Restricted geometries			X										
Setting of solids		X											
Temperature													
Changing temperature												X	
Temperature of surface		X										X	X
Time													
Changes over time	X											X	X

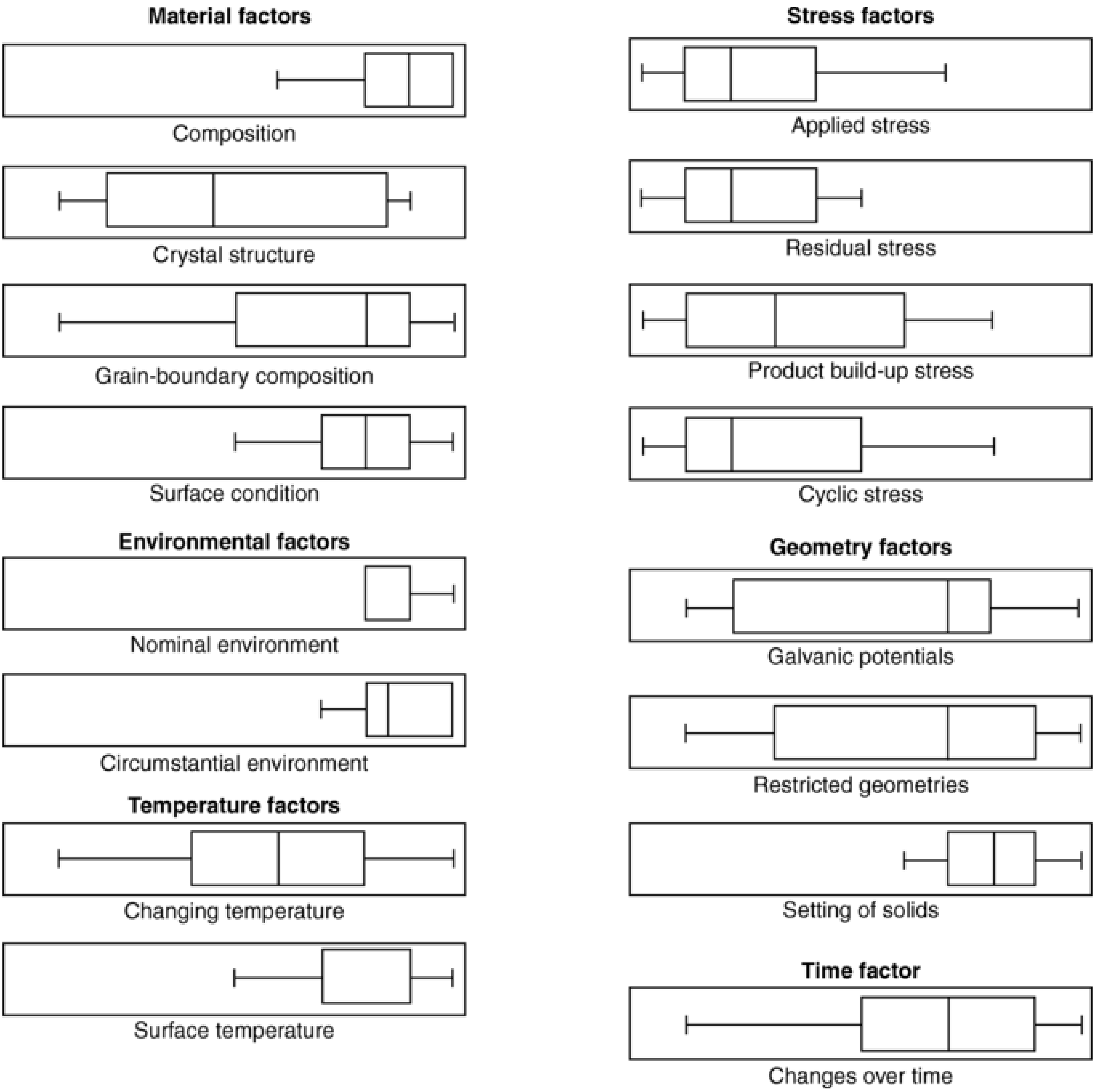

Fig. 2 Box-and-whisker plots of the survey results obtained for the factors and subfactors underlying the appearance of pitting corrosion

Table 3 Ranking of the subfactors causing pitting corrosion in decreasing order of importance and distribution sharpness

Factor	Subfactor
In order of decreasing importance	
Material	Composition
Temperature	Surface
Environment	Nominal Circumstantial
Material	Grain boundary Surface

Geometry	Setting Galvanic Restricted
Time	…
Temperature	Changing
Material	Microstructure
Stress	Product Applied Residual Cyclic
In order of decreasing sharpness	
Environment[(a)]	Nominal Circumstantial
Material	Composition
Geometry[(a)]	Settling
Temperature	Surface
Material	Surface
Stress	Residual Applied
Material	Microstructure
Stress	Product Cyclic
Material	Grain boundary
Geometry	Galvanic
Temperature	Changing
Geometry	Restricted
Time	…

(a) Presence of one suspect outlier

Such a simple survey reveals the lack of consensus that exists currently on the importance of many of the subfactors causing corrosion damage. Some of the ambiguities are probably due to the high level of context sensitivity that is a fundamental character of failure analysis. Pitting corrosion, which was selected here as an example, may assume different shapes. Pitting corrosion can produce pits with their mouth open (uncovered) or covered with a semipermeable membrane of corrosion products. Pits can be either hemispherical or cup-shaped. In some cases, they are flat walled, revealing the crystal structure of the metal, or they may have a completely irregular shape (Ref 19). In some instances, pits can be very damaging even at the micrometer level, while in other cases an inspector would only get nervous upon the appearance of pits at the macroscopic level.

References cited in this section

4. P.R. Roberge, What Is Accelerated in Accelerated Testing: A Framework for Definition, *Cyclic Cabinet Corrosion Testing,* STP 1238, G.S. Haynes and K. Tellefsen, Ed., American Society for Testing and Materials, 1995, p 18–30

5. W. Nelson, *Accelerated Testing, Statistical Models, Test Plans, and Data Analysis,* John Wiley and Sons, 1990

6. “Standard Practice for Operating Salt Spray (Fog) Apparatus,” B 117, *Annual Book of ASTM Standards,* American Society for Testing of Materials, 1997

7. J.A. Capp, A Rational Test for Metallic Protective Coatings, *Proc. ASTM,* Vol 14, 1914, p 474–481

8. A.N. Finn, Method of Making the Salt- Spray Corrosion Test, *Proc. ASTM,* Vol 18, 1918, p 237–238

9. F.L. LaQue, *Marine Corrosion: Causes and Prevention,* John Wiley & Sons, 1975

10. F.L. LaQue, A Critical Look at Salt Spray Tests, *Mater. Meth.,* Vol 35, 1952, p 77–81

11. “Standard Test Method for Porosity in Gold Coatings on Metal Substrates by Nitric Acid Vapor,” B 735, *Annual Book of ASTM Standards,* American Society for Testing of Materials, 2000

12. “Standard Test Method for Porosity in Gold or Palladium Coatings by Sulfurous Acid/ Sulfur-Dioxide Vapor,” B 799, *Annual Book of ASTM Standards,* American Society for Testing of Materials, 2000

13. “Standard Practice for Conducting Moist SO_2 Tests,” G 87, *Annual Book of ASTM Standards,* American Society for Testing of Materials, 1998

14. “Standard Practice for Conducting Mixed Flowing Gas (MFG) Environmental Tests,” B 827, *Annual Book of ASTM Standards,* American Society for Testing of Materials, 1997

15. R.W. Staehle, *Environmental Definition,* R.W. Revie, V.S. Sastri, E. Ghali, D.L. Piron, and P.R. Roberge, Ed., Pergamon Press, 1991, p 3–43

16. R.W. Staehle, Understanding “Situation-Dependent Strength”: A Fundamental Objective in Assessing the History of Stress-Corrosion Cracking, *Environment-Induced Cracking of Metals,* NACE International, 1989, p 561–612

17. M.G. Fontana, *Corrosion Engineering,* McGraw-Hill, 1986

18. C.P. Dillon, *Forms of Corrosion: Recognition and Prevention,* NACE International, 1982

19. Z. Szklarska-Smialowska, *Pitting Corrosion,* NACE International, 1986

P.R. Roberge, Statistical Interpretation of Corrosion Test Results, *Corrosion: Fundamentals, Testing, and Protection*, Vol 13A, *ASM Handbook*, ASM International, 2003, p 425–429

Statistical Interpretation of Corrosion Test Results

P.R. Roberge, Royal Military College of Canada

Probabilistic Aspects

The concept of probability distribution was first applied in a corrosion context in the 1930s (Ref 20, 21). A landmark paper (Ref 21) described a simple arrangement of metallic coupons subdivided in a multitude of small squares by masking with paraffin (Fig. 3). From this arrangement, the influence of 16 basic variables on the probability and relative velocity of corrosion attack was estimated. The probabilistic behavior of corrosion

processes has since been described to fall under one of several basic probability distributions, as indicated in Table 4 (Ref 22). The following descriptions highlight the main characteristics of some of these distributions.

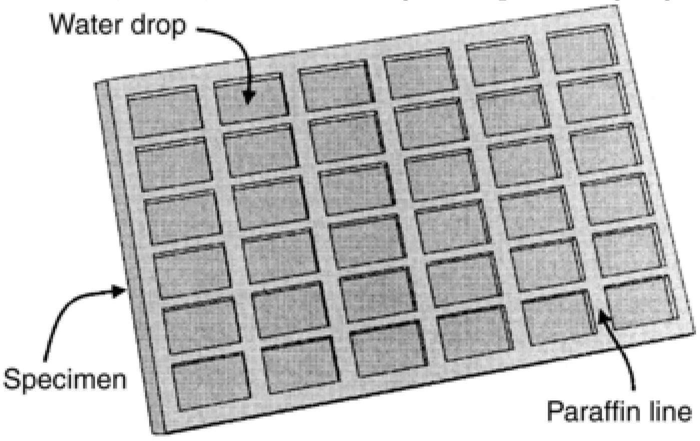

Fig. 3 Schematic representation of the test specimen used in the experiment to demonstrate the probabilistic nature of corrosion phenomena

Table 4 Main probability distributions observed in corrosion testing

Probability distribution	Corrosion phenomenon
Normal	Pitting potential
Log normal	Stress-corrosion cracking (SCC) failure time
Poisson	Two-dimensional distribution of pits
Exponential	Pit induction time SCC and hydrogen embrittlement failure time
Extreme value	Maximum pit depth SCC failure time Fatigue crack depth

Source: Ref 22

Normal Distribution. The normal probability distribution function has the familiar symmetrical bell shape and is the basis for the most common statistical techniques of experimental design and data analysis. A sample of test results of mass loss, mass gain, thickness loss, corrosion potential, corrosion rate, and pitting area may have a normal distribution. The following equations describe the normal probability distribution function, $f(x)$, and the cumulative normal probability function, $F(x)$:

$$f(x) = \frac{1}{\sigma\sqrt{2\pi}} \exp\left[-\frac{(x-\mu)^2}{2\sigma^2}\right] \quad \text{(Eq 1)}$$

$$F(x) = \int f(x)\,dx = \frac{1}{\sigma\sqrt{2\pi}} \int \exp\left[-\frac{(x-\mu)^2}{2\sigma^2}\right] dx \quad \text{(Eq 2)}$$

where μ is the mean, σ is the standard deviation, and x is the measured variable.

Log-Normal Distribution. In some cases, assuming a log-normal distribution can produce a more fitting analysis of the results. A log-normal distribution is simply data that have a normal distribution after they are converted to logarithms. The data can then be analyzed using normal statistical techniques. Some types of corrosion data that have been shown to be distributed in log-normal functions are weight loss, thickness loss,

time to initial stress-corrosion cracks, time to SCC failures, and polarization currents in the Tafel slope range. Some indicators that a process is best described by log-normal distribution are (Ref 23):

- Data values that physically cannot be negative
- Normal standard deviations that are proportional to arithmetic means
- Arithmetic means that are consistently greater than median values
- Dependent parameters whose logarithms are proportional to the values of independent parameters

The following equations describe the log-normal probability distribution function, *f*(*x*), and the cumulative log-normal probability function, *F*(*x*):

$$f(x) = \frac{1}{\sigma' x\sqrt{2\pi}} \exp\left[-\frac{(\ln x - \mu')^2}{2\sigma'^2}\right] \quad \text{(Eq 3)}$$

$$F(x) = \int f(x)\,dx = \frac{1}{\sigma'\sqrt{2\pi}} \int \frac{1}{x} \exp\left[-\frac{(\ln x - \mu')^2}{2\sigma'^2}\right] dx \quad \text{(Eq 4)}$$

where μ′ is the mean, σ′ is the standard deviation of data in logarithm form, and *x* is the measured variable.

Exponential distribution is widely used in reliability analysis. It is the simplest probability distribution because it is characterized by one parameter, a constant hazard rate (λ), which, in terms of frequency of occurrence, translates into a rapid decay from high initial values. Metastable pitting on stainless steels or on other noble alloys has often been characterized by such distribution. The electrochemical noise amplitude of singular events generated by corrosion processes has been shown to decay following an exponential distribution (Ref 24). The following equations describe the exponential probability distribution function, *f*(*x*), and the cumulative exponential probability function, *F*(*x*):

$$f(x) = \lambda \exp(-\lambda x) \quad \text{(Eq 5)}$$

$$F(x) = \int f(x)\,dx = 1 - \exp(-\lambda x) \quad \text{(Eq 6)}$$

where λ is the constant hazard rate, and *x* is the measured variable.

Poisson Distribution. Typically, a Poisson random variable is a count of the number of events that occur in a certain time interval or spatial area. The Poisson distribution is usually considered when the random or stochastic phenomena being observed occur on relatively rare occasions. Stable pit generation on stainless steel has been found to follow such a probability distribution (Ref 22). The following equations describe the Poisson probability distribution function, *f*(*x*), and the cumulative Poisson probability function, *F*(*x*):

$$f(x) = \frac{\lambda^x \exp(-\lambda)}{x!} \quad \text{(Eq 7)}$$

$$F(x) = \int f(x)\,dx = \sum_{i=0}^{x} \frac{\lambda^i \exp(-\lambda)}{i!} \quad \text{(Eq 8)}$$

where λ is the shape parameter defined by the number of events in a time-given interval, and *x* is the measured variable.

Extreme-Value Distribution. The depths of deepest pits on specimens, the times to first leaks in pipe lengths, the times to first SCC failures, and the number of cycles to first corrosion fatigue failures are, by definition, extreme values. The depth of the deepest pit on a specimen is the upper tail of the distribution of depths of all pits on that specimen (Ref 23). Engineers concerned with soil corrosion and underground steel piping are aware that the maximum pit depth found on a buried structure is somehow related to the percentage of the structure inspected. Finding the deepest actual pit requires a detailed inspection of the whole structure. As the area of the structure inspected decreases, so does the probability of finding the deepest actual pit. A number of statistical transformations have been proposed to quantify the distributions in pitting variables. Gumbel is given the credit

for the original development of extreme-value statistics (EVS) for the characterization of pit-depth distribution (Ref 25).

The EVS procedure is to measure maximum pit depths on several replicate specimens that have pitted, then arrange the pit-depth values in order of increasing rank. The Gumbel or extreme-value cumulative probability function is shown in Eq 9, where λ and α are the location and scale parameters, respectively. This probability function can be used to characterize the data set and estimate the extreme pit depth that possibly can affect the system from which the data was initially produced:

$$F(x) = \exp\left(-\exp\left[-\frac{x-\lambda}{\alpha}\right]\right) \quad \text{(Eq 9)}$$

In reality, there are three types of extreme- value probability functions (Ref 26):

- *Type 1:* exp(-exp[-x]), or the Gumbel distribution
- *Type 2:* exp(-x^{-k}), or the Cauchy distribution
- *Type 3:* exp(-[ω - x]^k), or the Weibull distribution

where x is a random variable, and k and ω are constants.

A goodness-of-fit test is required to verify which of these three distributions best fits a specific data set. The chi square test, or Kolmogorov-Simirnov test, has been used often for this purpose. A simpler graphical procedure is also possible using a generalized extreme-value distribution with a shape factor dependent on the type of distribution. There are two expressions for the generalized extreme-value cumulative probability function, that is, when $kx \leq (\alpha + \lambda k)$ and $k \neq 0$:

$$F(x) = \exp\left(-1 - k\frac{x-\lambda}{\alpha}\right)^{1/k} \quad \text{(Eq 10)}$$

and when $x \geq \lambda$ and $k = 0$:

$$F(x) = \exp\left(-\exp -\frac{x-\lambda}{\alpha}\right) \quad \text{(Eq 11)}$$

Some examples of corrosion situations have been reported where extreme-value distribution proved to be an adequate representation of the problems being addressed (Ref 27):

- For underground piping in a cathodic protection feasibility study
- For the evaluation of a gas distribution system and power plant condenser tubing
- During the assessment of stainless steel tube leaks
- The assessment of copper-nickel tube pitting performance

In another study, data from water injection pipeline systems and from the published literature were used to simulate the sample functions of pit growth on metal surfaces (Ref 28). The conclusions of that study were:

- Maximum pit depths were adequately characterized by extreme-value distribution.
- Corrosion rates for water injection systems could be modeled by a Gaussian distribution.
- An exponential pipeline leak growth model was appropriate for all operation regimes.

References cited in this section

20. U.R. Evans, R.B. Mears, and P.E. Queneau, Corrosion Probability and Corrosion Velocity, *Eng.,* Vol 136, 1933, p 689

21. R.B. Mears and U.R. Evans, The “Probability” of Corrosion, *Trans. Faraday Soc.,* Vol 31, 1935, p 527–542

22. T. Shibata, Corrosion Probability and Statistical Evaluation of Corrosion Data, *Uhlig's Corrosion Handbook,* R.W. Revie, Ed., Wiley-Interscience, 2000, p 367–392

23. F.H. Haynie, Statistical Treatment of Data, Data Interpretation, and Reliability, *Corrosion Tests and Standards,* MNL 20, R. Baboian, Ed., American Society for Testing of Materials, 1995, p 62–67

24. P.R. Roberge, The Analysis of Spontaneous Electrochemical Noise by the Stochastic Process Detector Method, *Corrosion,* Vol 50, 1994, p 502

25. E.J. Gumbel, "Statistical Theory of Extreme Values and Some Practical Applications," Mathematics series 33, National Bureau of Standards, 1954

26. T. Shibata, Statistical and Stochastic Approaches to Localized Corrosion, *Corrosion,* Vol 52, 1996, p 813–830

27. J.J. Meany and J.P. Ault, Extreme Value Analysis of Pitting Corrosion, *Life Prediction of Corrodible Structures,* Vol 1, R.N. Parkins, Ed., NACE International, 1994, p 306–319

28. A.K. Sheikh, J.K. Boah, and D.A. Hansen, Statistical Modeling of Pitting Corrosion and Pipeline Reliability, *Corrosion,* Vol 46, 1990, p 190–197

P.R. Roberge, Statistical Interpretation of Corrosion Test Results, *Corrosion: Fundamentals, Testing, and Protection*, Vol 13A, *ASM Handbook,* ASM International, 2003, p 425–429

Statistical Interpretation of Corrosion Test Results

P.R. Roberge, Royal Military College of Canada

Statistical Analysis

Most physical and chemical measurements, performed under nominally identical conditions, yield differing data. The results of corrosion tests are no exception. Sometimes, the difference between values is less than measurement precision and cannot be detected. At other times, the difference approaches the magnitude of the values. This variability can diminish greatly the confidence in using corrosion test data to predict lifetime or long-term corrosion behavior. The consequences are that structures must be overdesigned, or unexpected failures can occur if variability is not addressed adequately during corrosion testing. The most effective way to address variability is to use the appropriate number of replicate samples for each test performed (Ref 29). Some of the statistical concepts to produce effective test programs are:

- Population, sample, and replication
- Best estimate of variance and standard deviation
- Confidence limits for the mean
- Simple linear regression
- Multiple regression analysis and analysis of variance
- Covariance of independent variables
- A long list of secondary topics that are the fabric of statistical analysis

Most of the modern spreadsheet programs can now do complex regression analysis and often even provide information on the analytical processes themselves.
In this Volume, the article "Statistics for the Corrosionist" provides information on some of these concepts.

Reference cited in this section

29. S. Tait, Increase Your Confidence in Corrosion Test Data, *Mater. Perform.,* Vol 40, 2001, p 58–61

P.R. Roberge, Statistical Interpretation of Corrosion Test Results, *Corrosion: Fundamentals, Testing, and Protection*, Vol 13A, *ASM Handbook*, ASM International, 2003, p 425–429

Statistical Interpretation of Corrosion Test Results

P.R. Roberge, Royal Military College of Canada

Acknowledgment

This article is based, in part, on "Interpretation and Use of Corrosion Test Results" by D.O. Sprowls in *Corrosion, Metals Handbook* 9th ed., Vol 13, ASM International, 1987.

P.R. Roberge, Statistical Interpretation of Corrosion Test Results, *Corrosion: Fundamentals, Testing, and Protection*, Vol 13A, *ASM Handbook*, ASM International, 2003, p 425–429

Statistical Interpretation of Corrosion Test Results

P.R. Roberge, Royal Military College of Canada

References

1. "Standard Guide for Applying Statistics to Analysis of Corrosion Data," G 16 *Annual Book of ASTM Standards,* Vol 03.02, American Society for Testing of Materials, 1999
2. A. Tomiura, Lessons for a Case Study of Property Databases in Materials Development, *Computerization/Networking of Materials Databases,* STP 1311, S. Nishijima, S. Iwata, and C.H. Newton, Ed., American Society for Testing and Materials, 1996, p 3–20
3. R.S. Treseder, An Engineering View of Laboratory Corrosion Tests, *Laboratory Corrosion Tests and Standards,* STP 866, G.S. Haynes and R. Baboian, Ed., American Society for Testing of Materials, 1985, p 5–13
4. P.R. Roberge, What Is Accelerated in Accelerated Testing: A Framework for Definition, *Cyclic Cabinet Corrosion Testing,* STP 1238, G.S. Haynes and K. Tellefsen, Ed., American Society for Testing and Materials, 1995, p 18–30
5. W. Nelson, *Accelerated Testing, Statistical Models, Test Plans, and Data Analysis,* John Wiley and Sons, 1990
6. "Standard Practice for Operating Salt Spray (Fog) Apparatus," B 117, *Annual Book of ASTM Standards,* American Society for Testing of Materials, 1997
7. J.A. Capp, A Rational Test for Metallic Protective Coatings, *Proc. ASTM,* Vol 14, 1914, p 474–481
8. A.N. Finn, Method of Making the Salt- Spray Corrosion Test, *Proc. ASTM,* Vol 18, 1918, p 237–238

9. F.L. LaQue, *Marine Corrosion: Causes and Prevention,* John Wiley & Sons, 1975

10. F.L. LaQue, A Critical Look at Salt Spray Tests, *Mater. Meth.,* Vol 35, 1952, p 77–81

11. "Standard Test Method for Porosity in Gold Coatings on Metal Substrates by Nitric Acid Vapor," B 735, *Annual Book of ASTM Standards,* American Society for Testing of Materials, 2000

12. "Standard Test Method for Porosity in Gold or Palladium Coatings by Sulfurous Acid/ Sulfur-Dioxide Vapor," B 799, *Annual Book of ASTM Standards,* American Society for Testing of Materials, 2000

13. "Standard Practice for Conducting Moist SO_2 Tests," G 87, *Annual Book of ASTM Standards,* American Society for Testing of Materials, 1998

14. "Standard Practice for Conducting Mixed Flowing Gas (MFG) Environmental Tests," B 827, *Annual Book of ASTM Standards,* American Society for Testing of Materials, 1997

15. R.W. Staehle, *Environmental Definition,* R.W. Revie, V.S. Sastri, E. Ghali, D.L. Piron, and P.R. Roberge, Ed., Pergamon Press, 1991, p 3–43

16. R.W. Staehle, Understanding "Situation-Dependent Strength": A Fundamental Objective in Assessing the History of Stress-Corrosion Cracking, *Environment-Induced Cracking of Metals,* NACE International, 1989, p 561–612

17. M.G. Fontana, *Corrosion Engineering,* McGraw-Hill, 1986

18. C.P. Dillon, *Forms of Corrosion: Recognition and Prevention,* NACE International, 1982

19. Z. Szklarska-Smialowska, *Pitting Corrosion,* NACE International, 1986

20. U.R. Evans, R.B. Mears, and P.E. Queneau, Corrosion Probability and Corrosion Velocity, *Eng.,* Vol 136, 1933, p 689

21. R.B. Mears and U.R. Evans, The "Probability" of Corrosion, *Trans. Faraday Soc.,* Vol 31, 1935, p 527–542

22. T. Shibata, Corrosion Probability and Statistical Evaluation of Corrosion Data, *Uhlig's Corrosion Handbook,* R.W. Revie, Ed., Wiley-Interscience, 2000, p 367–392

23. F.H. Haynie, Statistical Treatment of Data, Data Interpretation, and Reliability, *Corrosion Tests and Standards,* MNL 20, R. Baboian, Ed., American Society for Testing of Materials, 1995, p 62–67

24. P.R. Roberge, The Analysis of Spontaneous Electrochemical Noise by the Stochastic Process Detector Method, *Corrosion,* Vol 50, 1994, p 502

25. E.J. Gumbel, "Statistical Theory of Extreme Values and Some Practical Applications," Mathematics series 33, National Bureau of Standards, 1954

26. T. Shibata, Statistical and Stochastic Approaches to Localized Corrosion, *Corrosion,* Vol 52, 1996, p 813–830

27. J.J. Meany and J.P. Ault, Extreme Value Analysis of Pitting Corrosion, *Life Prediction of Corrodible Structures,* Vol 1, R.N. Parkins, Ed., NACE International, 1994, p 306–319

28. A.K. Sheikh, J.K. Boah, and D.A. Hansen, Statistical Modeling of Pitting Corrosion and Pipeline Reliability, *Corrosion,* Vol 46, 1990, p 190–197

29. S. Tait, Increase Your Confidence in Corrosion Test Data, *Mater. Perform.,* Vol 40, 2001, p 58–61

P.R. Roberge, Modeling Corrosion Processes, *Corrosion: Fundamentals, Testing, and Protection*, Vol 13A, *ASM Handbook*, ASM International, 2003, p 430–445

Modeling Corrosion Processes

P.R. Roberge, Royal Military College of Canada

Introduction

RECORDING CORROSION INFORMATION presents multiple difficulties, ranging from the basic lack of details in failure analyses to the inherent complexity of the variables involved. The complexities associated with corrosion damage information are compounded by a general lack of standard schemes to represent materials in their operational environments. Data gathered in controlled laboratory environments can usually be obtained with more precision, and for such data, standards have been developed to streamline the exchange of information between organizations. For scientists and engineers developing materials, models have become an essential benchmarking element for the selection and life prediction associated with the introduction of new materials or processes. For systems managers, the corrosion performance or underperformance of materials has a very different meaning. In the context of life-cycle management, corrosion is only one element of the whole, and the main difficulty with corrosion information is its presentation at the system management level.

One of the principal goals of scientific discovery is the development of a theory, a coherent body of knowledge that can be used to provide explanations and predictions for a specific domain of knowledge. Theory development is a complex process involving three principal activities: theory formation, theory revision, and paradigm shift. A theory is first proposed from a collection of known observations. It then goes through a series of revisions aimed at reducing the shortcomings of the initial model. The initial theory can thus evolve into one that can provide sophisticated predictions, but such a theory can also become much more complex and difficult to use. In such cases, the problems can be partly eliminated by a paradigm shift, that is, a revolutionary change that involves a conceptual reorganization of the theory (Ref 1).

The Venn diagrams of Fig. 1 illustrate the three stages of a theory revision (Ref 2). In the first stage of theory revision (Fig. 1a), an anomaly is noted, a new observation that is not explained by the current model. In a subsequent stage (Fig. 1b), the old theory is reduced to its most basic or fundamental expression before it finally serves as the basis of a new theory formulation (Fig. 1c). Corrosion models have similarly evolved over the relatively short history of corrosion science and engineering. Modern understanding of corrosion phenomena and control of corrosion damages was greatly accelerated when the thermodynamic and kinetic behaviors of metallic materials were made explicit in what became known, respectively, as potential-pH diagrams and mixed-potential diagrams. These two fundamental models, which were both established in the 1940s, have become the basis of many models developed in an evolutionary fashion since then.

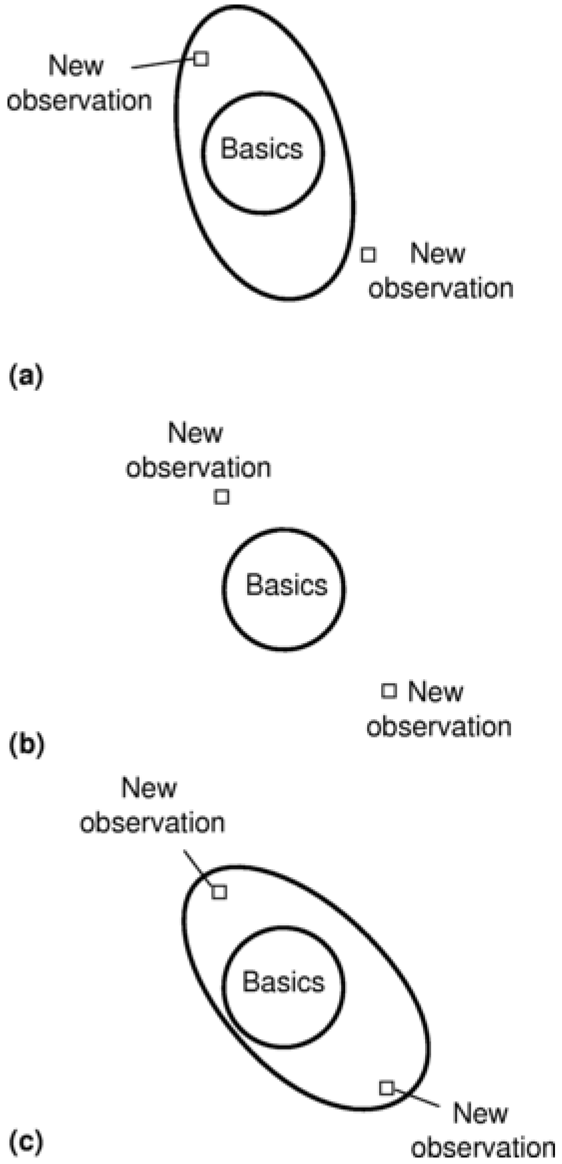

Fig. 1 Venn diagram theory revision using abduction for hypothesis formation. (a) First stage of theory with observed anomaly. (b) Theory reduced to fundamentals. (c) Theory reformulated to account for all known observations

References cited in this section

1. T. Kuhn, *The Structure of Scientific Revolutions,* University of Chicago Press, 1970

2. P. O'Rorke, S. Morris, and D. Schulenburg, Theory Formation by Abduction: A Case Study Based on the Chemical Revolution, *Computational Models of Scientific Discovery and Theory Formation,* J. Shrager and P. Langley, Ed., Morgan Kaufmann Publishing, 1990

P.R. Roberge, Modeling Corrosion Processes, *Corrosion: Fundamentals, Testing, and Protection*, Vol 13A, *ASM Handbook*, ASM International, 2003, p 430–445

Modeling Corrosion Processes

P.R. Roberge, Royal Military College of Canada

Mechanistic Models

Mechanistic models of corrosion processes have been developed to incorporate a range of chemical and electrochemical reactions with the complex interactions of diffusion and migration details. Some specific situations lend themselves to the development of useful mechanistic models to account for the main features governing corrosion processes. These models are most naturally expressed in terms of differential equations or in other nonexplicit forms of mathematics. However, modern developments in computing facilities and in mathematical theories of nonlinear and chaotic behaviors have made it possible to cope with relatively complex problems. A mechanistic model has the following advantages (Ref 3):

- It contributes to our understanding of the phenomenon under study.
- It usually provides a better basis for extrapolation.
- It tends to be parsimonious, that is, frugal in the use of parameters, and it provides better estimates of the system response.

The multidisciplinary nature of corrosion science is reflected in the multitude of approaches that have been proposed to explain and model fundamental corrosion processes. The following list illustrates some scientific disciplines, with examples of modeling efforts one can find in the literature:

- *Surface science:* atomistic model of passive films
- *Physical chemistry:* adsorption behavior of corrosion inhibitors
- *Quantum mechanics:* design tools for organic inhibitors
- *Solid-state physics:* scaling properties associated with hot corrosion
- *Water chemistry:* control model of inhibitors and antiscaling agents
- *Boundary-element mathematics:* cathodic protection

When the mechanisms underlying corrosion processes are not understood sufficiently well or are too complicated to allow an exact model to be built from theory, empirical models have proven to be quite useful. The degree of complexity of an empirical model can seldom be assessed in the initial phase of model development. A pragmatic model development approach is to start with a limited set of variables and increase its complexity as required by growing evidence and the need for increased confidence in the results.

Basic Principles of Mechanistic Models

Rates of general corrosion in aqueous environments depend on a multitude of factors, such as the chemistry of the aqueous solution, concentrations of components, temperature, presence of nonaqueous phases, hydrodynamic conditions, and metallurgical factors. Therefore, it is desirable to rationalize and predict the effects of these factors using mechanistic models.

Pourbaix Model. The first comprehensive model that summarized many of the basic variables underlying a corrosion situation became known as potential-pH (*E*-pH) diagrams, also called predominance or Pourbaix diagrams, which have been adopted universally since their introduction in late 1940s. These diagrams have repeatedly been proven an elegant way to represent the thermodynamic stability of chemical species in given aqueous environments. The *E*- pH diagrams are typically plotted for various equilibria on normal Cartesian coordinates, with potential, *E*, as the ordinate (*y*-axis) and pH as the abscissa (*x*-axis) (Ref 4).

Pourbaix diagrams have proven to be a convenient way to summarize a situation in terms of its thermodynamics and to provide a useful means of predicting electrochemical and chemical processes that could potentially occur in certain conditions of pressure, temperature, and chemical makeup. The following example illustrates potential corrosion damage to steel in water flowing through the radiators and pipes of an hydronic system (Ref 5). Given a pH range of 6.5 to 8 for mains water and the *E*-pH diagram in Fig. 2, it is apparent that minimal corrosion damage is to be expected if the corrosion potential remains below -0.65 V (standard hydrogen electrode) (Ref 6). While *E*-pH diagrams were initially designed for relatively simple situations involving pure metals and pure water at a single temperature, the availability of computing power and basic thermodynamic information has permitted the development of these diagrams for increasingly complex situations, such as interaction associated with multielement systems (Ref 7).

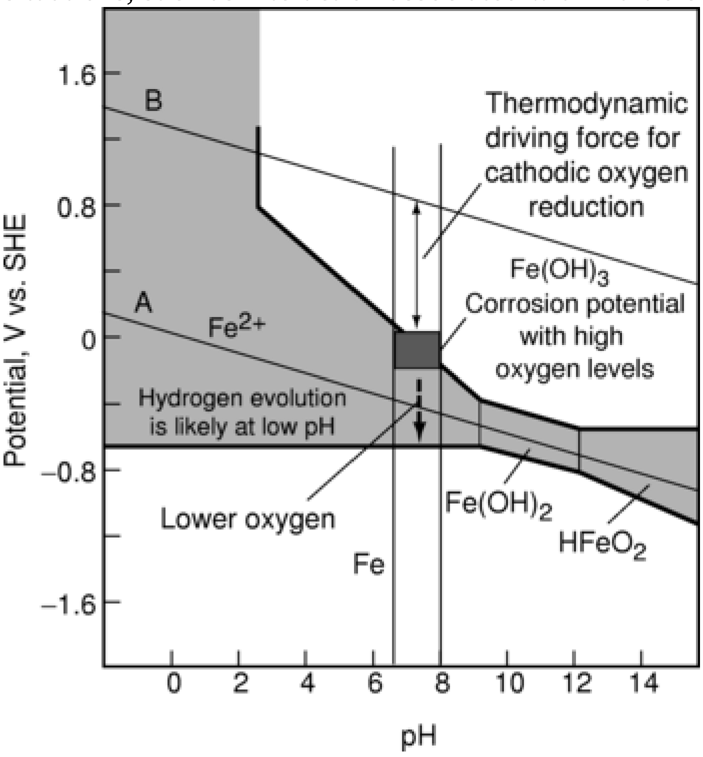

Fig. 2 Potential-pH diagram of iron in water at 25 °C (77 °F) highlighting the corrosion processes in the hydronic pH range. SHE, standard hydrogen electrode

Polarization Curves. The use of polarization curves for the study of corrosion reactions can be traced back to the 1930s (Ref 8). However, the representation of the mixed potential behavior is often associated with Professor Evans, who has popularized this representation of corrosion polarization measurements (Ref 9). These diagrams have become a reflection of our understanding of the corrosion basics in the most complex chemistries, as is illustrated in the following example.

Anodic protection of a kraft liquor tank was first successfully realized at the end of 1984, and the success of this system resulted in many commercial installations. Unfortunately, unexpectedly high corrosion rates were reported at localized areas in several of the tanks, even though the remainder of the surfaces corroded at rates less than 0.13 mm/yr (0.005 in./yr) (Ref 10). Most of the problems experienced have been attributed to incomplete understanding of the electrochemistry of carbon steel in these liquors and the coexistence of active and passive areas, which had not been addressed properly in earlier control strategies. An elegant yet simple model of passivation in caustic sulfide was developed to explain the role of sulfide in the process (Ref 11). According to the research, after the initial nucleation of Fe_3O_4, sulfide is incorporated as substitutional ions into the Fe_3O_4 spinel lattice, forming a nonprotective compound, $(Fe_3O_4)_{-x}S_x$, where x was predicted to be approximately 0.19 at the peak of the active-passive transition. Because passivation cannot occur until the sulfide in the film is completely removed by oxidation, high current densities are required to force this reaction. However, once devoid of sulfide, the film can remain stable if the potential is kept more positive than the Flade potential corresponding to the reduction reaction of oxidized sulfur species, such as $S_2O_3^{2-}$ and S_2^{2-} (Ref 10).

Figure 3 depicts one anodic and four cathodic idealized polarization curves, including the possible intersection points (Ref 6). The number and location of the intersection points creates four types of behavior, namely,

monostable (active), bistable, astable, and monostable (passive). A potentiodynamic curve of each of these types of behavior is shown, respectively, in Fig. 4(a–d). Astable behavior occurs infrequently, because it requires a single anodic-cathodic intersection on the negative resistance portion of the anodic curve. This is an unstable operating condition, resulting in continuous oscillations between active and passive potentials. Various alloys in elevated-temperature sulfuric acid are known to exhibit such behavior (Ref 10).

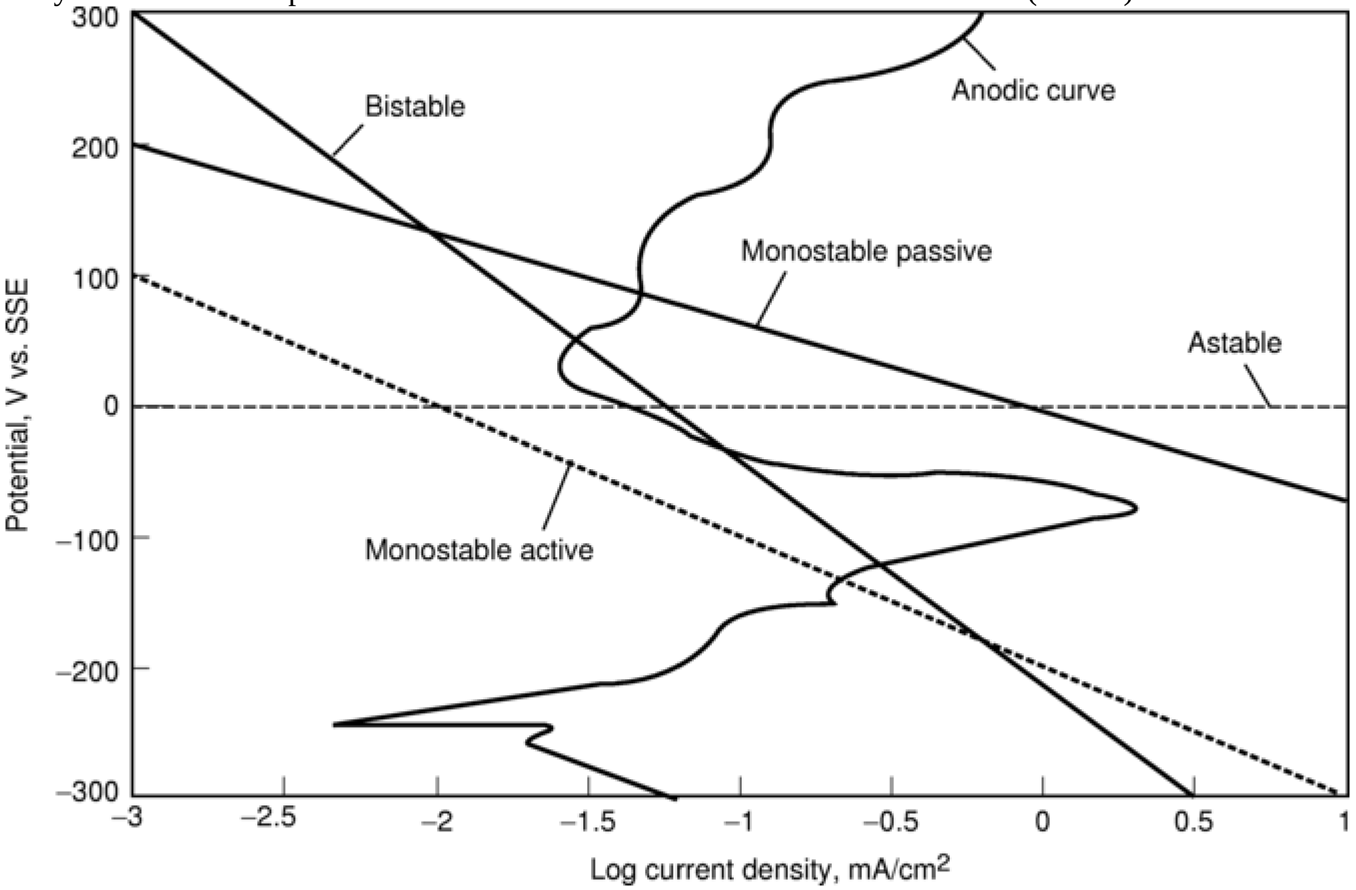

Fig. 3 Polarization curves with possible combinations of anodic-cathodic intersections in the mixed-potential representation of carbon steel exposed to kraft liquors. SSE, saturated mercury sulfate electrode

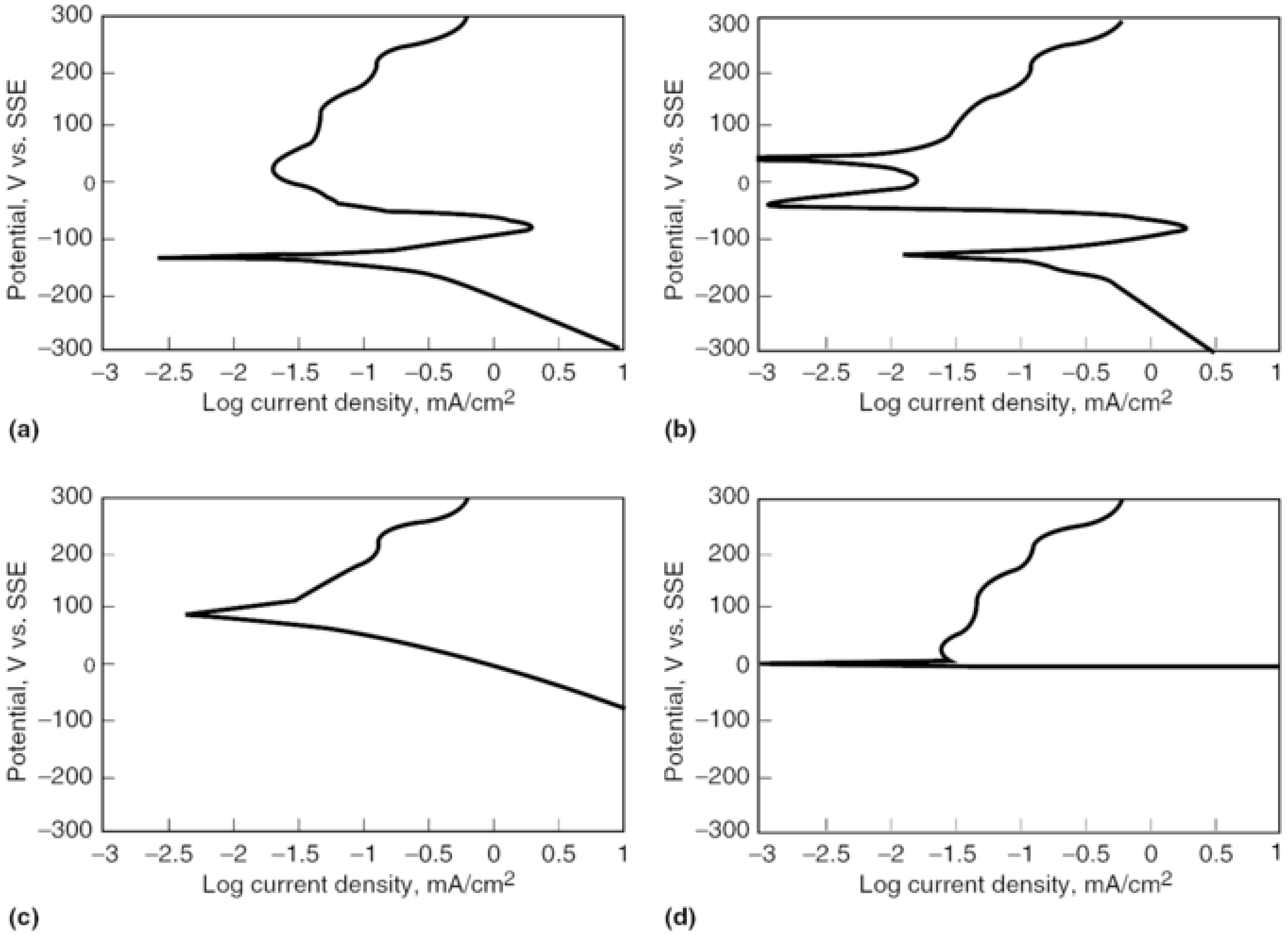

Fig. 4 Theoretical polarization curves illustrating the behavior of mild steel exposed to kraft liquors. (a) Monostable (active) behavior. (b) Bistable behavior. (c) Monostable (passive) behavior. (d) Astable behavior. SSE, saturated mercury sulfate electrode

Modeling the Efficiency of Corrosion Inhibitors

A mechanistic model has been developed for simulating the rates of general corrosion of selected metals in aqueous solutions. The model predictions have been verified for a number of systems that include corrosion inhibitors (Ref 12), carbon steel and stainless steel CO_2/H_2S corrosion (Ref 13), and systems containing concentrated brines (Ref 14). In all cases, good agreement with experimental data has been obtained. An assessment of the requirements to produce such an extensive model has indicated that the model should (Ref 12):

- Use a comprehensive thermodynamic model to compute the speciation and activities of species in the aqueous solution
- Use models for calculating transport properties, which are necessary to predict mass- transfer effects
- Represent the partial cathodic and anodic processes on the metal surface
- Reproduce the active-passive transition and the effect of active ions on passivity
- Reproduce experimental corrosion rates using parameters calibrated on the basis of a limited amount of data
- Be implemented in an easy-to-use program

The model presently contains a thermophysical module that provides comprehensive speciation calculations and an electrochemical module to predict the partial reduction and oxidation processes on the surface of the metal.

Thermophysical Module. This part of the model combines information about standard- state properties of all species of interest with a formulation for the excess Gibbs energy, which accounts for solution nonideality. The thermodynamic model is used to predict the concentrations and activities of both ionic and neutral species in multicomponent systems that may contain an aqueous phase, any number of solid phases, and, if necessary, a vapor and a nonaqueous liquid phase. The activities of individual species are further used in the electrochemical model. After completing speciation calculations, the thermophysical module computes several properties of the solution, including pH, density, electrical conductivity, viscosity, and diffusivity. The calculations included in this module have been described in detail elsewhere (Ref 15).

Electrochemical Module. The parameters of the electrochemical model have been determined by using a large number of experimental polarization and corrosion rate data. In particular, the parameters for the proton reduction, water reduction, oxygen reduction, and iron oxidation processes were determined from relevant data on the corrosion of iron and mild steel in various mineral acids, bases, and saline solutions. The parameters that represent the effect of several inhibiting ions have been calibrated using polarization data or experimental corrosion rate data that relate the corrosion inhibition to the solution concentration (Ref 12). Because the model contains empirical parameters obtained from experimental data, the quality of model predictions depends on the data on which the parameters are based. This is a common feature of all semiempirical models. The partial electrochemical processes are then combined into a total predicted polarization curve by applying the mixed-potential theory, which states that, in a freely corroding situation, the total cathodic current, i_c, is equal to the total anodic current, i_a:

$$\sum i_{c,i} = \sum i_{a,j} \quad \text{(Eq 1)}$$

where $i_{c,i}$ and $i_{a,j}$ denote the i-th cathodic and j- th anodic process. Once the corrosion potential is obtained by solving Eq 1, the corrosion current density is also computed. The model is implemented in two steps:

1. It calculates the speciation and thermodynamic properties. At the end of the speciation calculations, it also computes the transport properties that are necessary for modeling mass-transfer effects.
2. Then, the program uses the previously obtained speciation and transport properties to calculate the partial anodic and cathodic processes that are possible in the system. Finally, the partial electrochemical processes are combined, and the corrosion rate and potential are calculated using the mixed-potential theory.

The electrochemical module is capable of reproducing the active-passive transition and the effect of solution species on passivity. In order to simulate the effect of active ions on the passive current density, the electrochemical module relies on an approach developed for studying the chemical dissolution kinetics of oxides in aqueous media. Surface reactions between the passive oxide layer and the ions present in solution are considered in the development of a mathematical relationship between the activities of these aggressive or inhibitive ions and the passive-anodic current density.

Applications of the Model. To verify the performance of the model, corrosion rates have been calculated for carbon steel exposed to aerated water in the presence of several inhibitors. Figure 5 shows the dependence of the calculated corrosion rate on the concentration of three inhibitors; that is, monobasic phosphate (Fig. 5a), silicate (Fig. 5b), and chromate ions (Fig. 5c). In all cases, a fairly sharp transition to passive behavior is observed as the concentration of the inhibitor exceeds a certain threshold value. This threshold value is very low for chromates and substantially higher for phosphates and silicates. It is noteworthy that the model represents the experimental corrosion rates with very good accuracy. The presence of inhibitive ions counteracts the effect of halide ions and limits the current density. In this way, the model simultaneously takes into account the ions that promote the dissolution of the passive film and those that inhibit its dissolution.

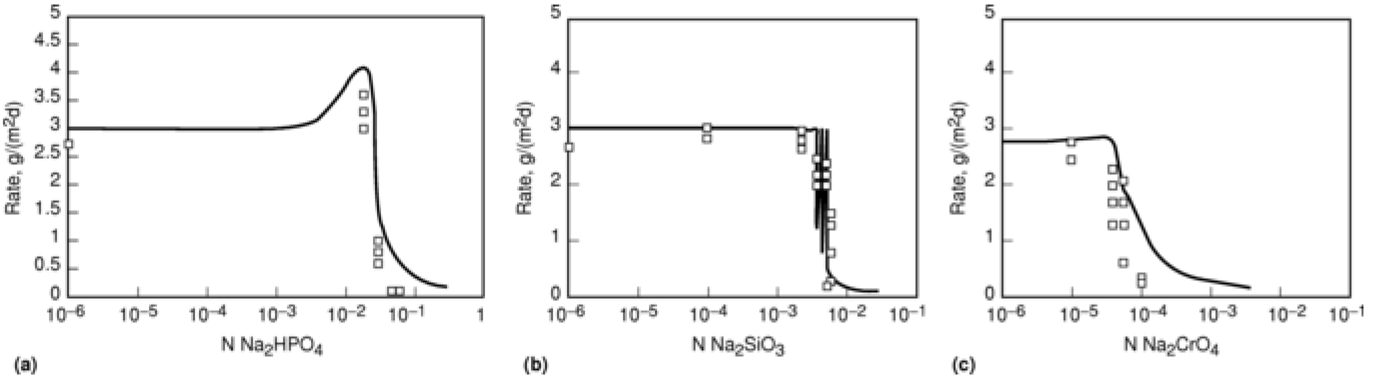

Fig. 5 Effect of various inhibitors on the corrosion rate of carbon steel in aerated water at 25 °C (77 °F). (a) HPO_4^{2-} ions. (b) SiO_3^{2-} ions. (c) CrO_4^{2-} ions. Line generated from electrochemical model and test data (squares) are given.

Figure 6, which shows the calculated current density versus potential relationships for three concentrations of silicate ions, illustrates how the model reproduces the competitive behavior between the local cathodic and anodic processes that are taken into account in the analysis. The dominant cathodic process, the reduction of oxygen, in this example, proceeds under mass- transfer control, as shown by the vertical portion of the oxygen reduction line. The iron oxidation process shows an active-passive transition, which is strongly influenced by the presence of inhibitors. Without silicate ions (Fig. 6a), the oxygen reduction line intersects the iron oxidation line in the range of active dissolution of iron. Correspondingly, the corrosion potential is low, and the corrosion rate is substantial.

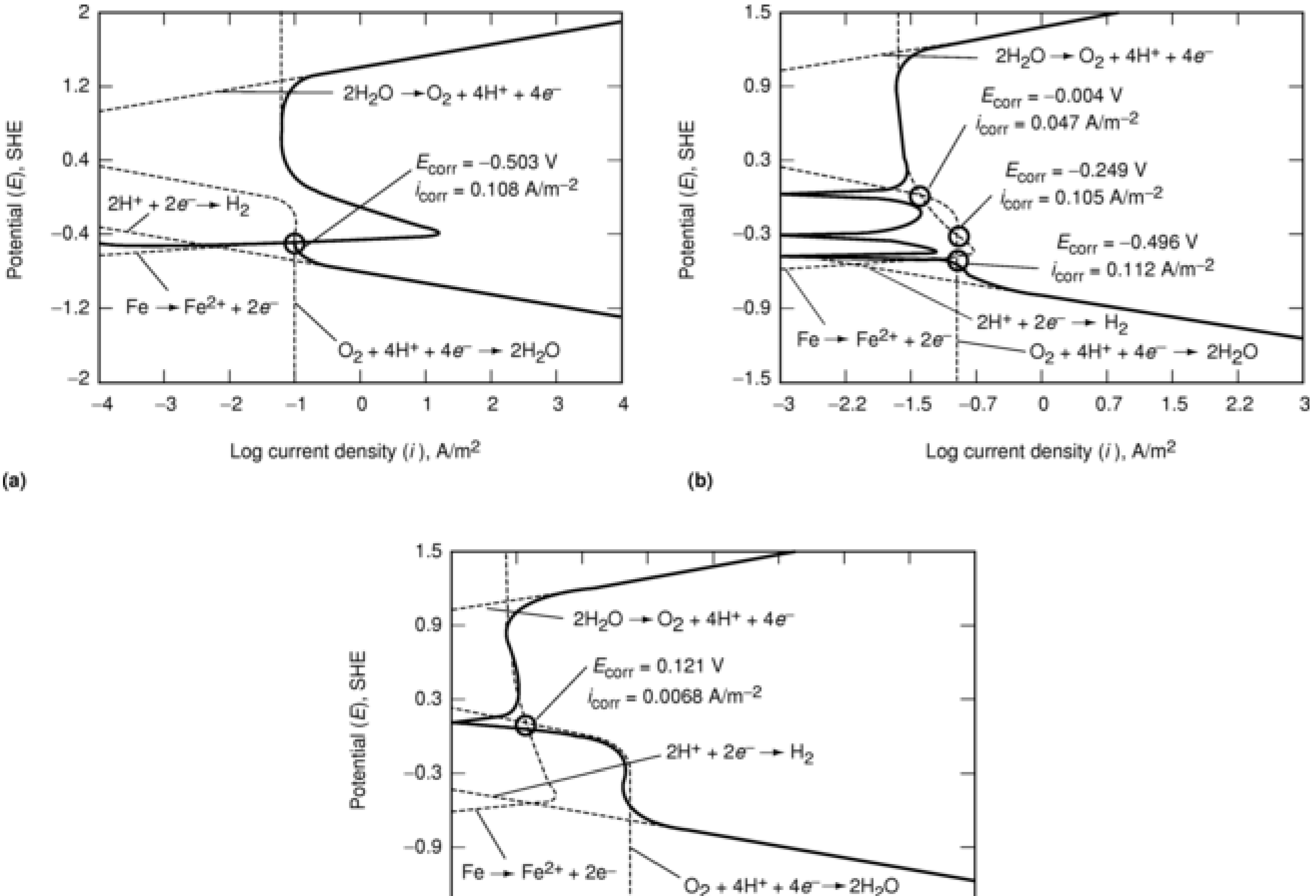

Fig. 6 Predicted current density/potential relationships, including partial anodic and cathodic processes, for carbon steel in aerated water with (a) no Na_2SiO_3, (b) 0.0014 *m* Na_2SiO_3, and (c) 0.008 *m* Na_2SiO_3. SHE, standard hydrogen electrode; E_{corr}, corrosion potential; i_{corr}, corrosion current

With a substantial concentration of silicate ions (Fig. 6c), both the passive current density and the critical current density are substantially reduced. Subsequently, the oxygen reduction line intersects the iron oxidation line within the passive range. The corrosion potential is substantially increased, and the corrosion rate is reduced. For intermediate concentrations of silicate ions (Fig. 6b), the shape of the predicted iron oxidation line is such that three mixed potentials are possible. This results in multiple steady states, and the system may oscillate between corrosion in the active and passive states. The electrochemical model was found to be particularly suitable for studying the synergistic effects of mixtures of inhibitors, such as mixtures of molybdate and nitrite inhibitors.

The ion association model has been in use by major water treatment companies since the early 1970s. Saturation indexes used routinely by water treatment chemists provide a measure of the thermodynamic driving force for a scalant to form; however, these indexes do not incorporate the capacity of the water for continued scaling. The water concentrations of various substances in dissolved, colloidal, or suspended forms are typically low but can vary considerably. Water can have a high saturation level with no visible scale formation. The driving force might be present, but there is insufficient mass for gross precipitation. Simple indexes include:

- Langelier saturation index (LSI)
- Ryznar stability index
- Stiff-Davis saturation index
- Oddo-Tomson index for calcium carbonate

Indexes have also been developed for other common scales, such as calcium sulfate and calcium phosphate. All these indexes provide an indicator of scale potential but lack accuracy, principally because they ignore the reduced availability of ions such as calcium, which is affected by association with sulfate, and other ions (Ref 16). This binding, or reduced availability of the reactants, decreases the effective ion activity product for a saturation level calculation. The most efficient method for modeling the speciation of a water is to proceed through numerous computer iterations for (Ref 17):

- The verification of electroneutrality via a cation-anion balance, and balancing with an appropriate ion (e.g., sodium or potassium for cation-deficient waters; sulfate, chloride, or nitrate for anion-deficient waters)
- Estimation of ionic strength, calculating and correcting activity coefficients and dissociation constants for temperature and correcting alkalinity for noncarbonate alkalinity
- Iterative calculation of the distribution of species in the water from dissociation constants. A partial listing of these ion pairs is given in Table 1.
- Verification of mass balance and adjusting ion concentrations to agree with analytical values
- Repetition of the process until corrections are insignificant
- Calculation of saturation levels based on the free concentrations of ions estimated, using the ion association model (ion pairing)

Table 1 Example ion pairs used to estimate free ion concentrations

Aluminum = $(Al^{3+}) + (Al(OH)^{2+}) + (Al(OH)_2^+) + (Al(OH)_4^-) + (AlF^{2+}) + (AlF_2^+) + (AlF_3) + (AlF_4^-) + (AlSO_4^+) + (Al(SO_4)_2^-)$
Barium = $(Ba^{2+}) + (BaSO_4) + (BaHCO_3^+) + (BaCO_3) + (Ba(OH)^+)$
Calcium = $(Ca^{2+}) + (CaSO_4) + (CaHCO_3^+) + (CaCO_3) + (Ca(OH)^+) + (CaHPO_4) + (CaPO_4^-) + (CaH_2PO_4^+)$
Iron = $(Fe^{2+}) + (Fe^{3+}) + (Fe(OH)^+) + (Fe(OH)^{2+}) + (Fe(OH)_3^-)$ + (FeHPO4+) + $(FeHPO_4) + (FeCl^{2+}) + (FeCl_2^+) + (FeCl_3) + (FeSO_4) + (FeSO_4^+) + (FeH_2PO_4^+) + (Fe(OH)_2^+) + (Fe(OH)_3) + (Fe(OH)_4^-) + (Fe(OH)_2) + (FeH_2PO_4^{2+})$

Magnesium = (Mg^{2+}) + $(MgSO_4)$ + $(MgHCO_3^+)$ + $(MgCO_3)$ + $(Mg(OH)^+)$ + $(MgHPO_4)$ + $(MgPO_4^-)$ + $(MgH_2PO_4^+)$ + (MgF^+)
Potassium = (K^+) + (KSO_4^-) + $(KHPO_4^-)$ + (KCl)
Sodium = (Na^+) + $(NaSO_4^-)$ + (Na_2SO_4) + $(NaHCO_3)$ + $(NaCO_3^-)$ + (Na_2CO_3) + $(NaCl)$ + $(NaHPO_4^-)$
Strontium = (Sr^{2+}) + $(SrSO_4)$ + $(SrHCO_3^+)$ + $(SrCO_3)$ + $(Sr(OH)^+)$

The use of ion pairing to estimate the concentrations of free species overcomes several of the major shortcomings of traditional indexes. Ion pairing takes into account the association that can occur between ions at concentrations far from infinite dilution, effectively reducing their availability in solution. Calcium, for example, may be paired with sulfate, bicarbonate, carbonate, phosphate, and other species. Bound ions are not readily available for scale formation. When indexes are used to establish operating limits, such as maximum concentration ratio or maximum pH, the differences between the use of indexes calculated using ion pairing can have some serious economic significance. For example, experience on a system with high total dissolved solids (TDS) water may be translated to a system operating with a lower TDS water. The high indexes that were found acceptable in the high TDS water may be unrealistic when translated to a water where ion pairing is less significant in reducing the apparent driving force for scale formation. Table 2 summarizes the impact of TDS on LSI when calculated using total analytical values for calcium and alkalinity and when calculated using the free calcium and carbonate concentrations calculated using an ion association model. Indexes based on ion association models provide a common denominator for comparing results between systems. For example, the calcite saturation level calculated using free calcium and carbonate concentrations has been used successfully as the basis for developing models that describe the minimum effective scale inhibitor dosage that maintains clean heat-transfer surfaces (Ref 18). The following example illustrates how silica, a very common compound, can greatly influence the fragile equilibria involved in cooling water and how this can be revealed with the use of a commercial software system (Ref 17).

Table 2 Impact of ion pairing on the Langelier scaling index (LSI)

Water type	Ion pairing	LSI		TDS impact on LSI
		Low TDS	**High TDS**	
High chloride	No pairing	2.25	1.89	-0.36
	With pairing	1.98	1.58	-0.40
High sulfate	No pairing	2.24	1.81	-0.43
	With pairing	1.93	1.07	-0.86

TDS, total dissolved solids

Guidelines for the upper silica operating limits have been well defined in water treatment practice and have evolved with treatment programs. In the days of acid chromate cooling system treatment, an upper limit of 150 ppm silica as SiO_2 was common. The limit increased to 180 ppm with the advent of alkaline treatments and pH control limits up to 9.0. Silica control levels approaching or exceeding 200 ppm as SiO_2 have been reported for the current high-pH, high-alkalinity, all-organic treatment programs, where pH is allowed to equilibrate at 9.0 or higher (Ref 19).

The evolution of silica control limits can be readily understood by reviewing the silica solubility profile. As depicted in Fig. 7, amorphous silica solubility increases with increasing pH. Silica solubility also increases with increasing temperature. In the pH range of 6.0 to 8.0 and temperature range of 20 to 30 °C (68 to 86 °F), cooling water is saturated with amorphous silica when the concentration reaches 100 ppm as SiO_2 (20 °C, or 68 °F) or 135 ppm (30 °C, or 86 °F). These concentrations correspond to a saturation level of 1.0. The traditional silica limit for this pH range has been 150 ppm as SiO_2. As outlined in Table 3, at pH 7.6, a limit of 150 ppm corresponds roughly to a saturation level of 1.4 at 20 °C (68 °F) and 1.1 at 30 °C (86 °F).

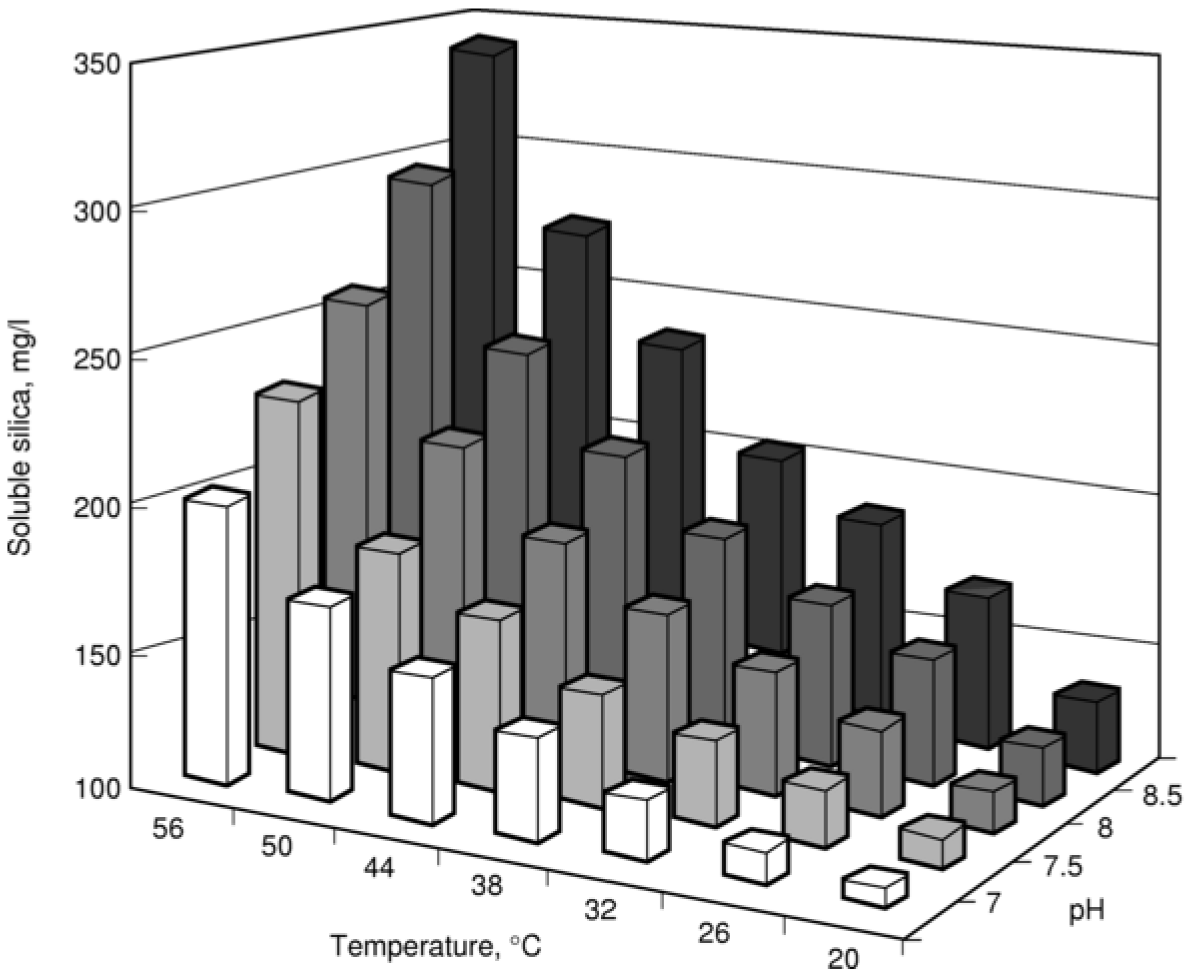

Fig. 7 Solubility of amorphous silica as a function of temperature and pH

Table 3 Silica limits for three treatment schemes

pH level	Temperature		Silica level, ppm	Saturation level limit
	°C	**°F**		
Low (6.0)	20	68	130	1.2
	30	86	150	1.1
Moderate (7.6)	20	68	150	1.4
	30	86	150	1.1
High (8.9)	20	68	>180	1.5
	30	86	>180	1.3

At the upper end of the cooling water pH range (9.0), silica solubility increases to 115 ppm (20 °C, or 68 °F) and 140 ppm (30 °C, or 86 °F). A control limit of 180 ppm corresponds to saturation levels of 1.5 and 1.3, respectively. In systems where concentration ratio is limited by silica solubility, it is recommended that the concentration ratio limit be reestablished seasonally based on amorphous silica saturation level or whenever significant temperature changes occur (Ref 19).

Boundary-Element Modeling

Early predictions of corrosion rates and estimates of adequate cathodic protection (CP) have traditionally been based on case studies and sample exposure tests. Applying these techniques to real structures usually involves extrapolations, use of large safety factors, and ongoing corrections and maintenance of the system. In the late 1960s, the finite-element method was applied to the problem by discretization of the electrolytically conductive environment with a mesh (Ref 20). The mathematical solution is found at the intersection points, or nodes, of the mesh. The solution is numerical, because an approximate form of Laplace's equation governs variations of the solution between adjacent nodes. However, creating a finite-element mesh can be an extremely tedious and

time-consuming process. Even when the mesh-generation process is automated, it is difficult to perform a simulation when there are large geometry scale differences in the model, which is exactly the case found in most corrosion control problems where anodes are small compared with the size of the structure and the problem areas are most likely in corners and areas of complex geometry.

In the late 1970s, boundary-element (BE) methods became available. As the name implies, this numerical method requires mesh elements to be created but now only on the boundary (or surfaces) of the object to be modeled (Fig. 8). The main advantages of boundary elements for impressed current cathodic protection (ICCP) analysis are (Ref 20):

- Meshes are now only on the surface; hence, only two-dimensional elements are required. Mesh generators can be used with confidence, and models can be constructed extremely quickly and inexpensively once the geometry is defined.
- Models can be created with fine detail of key or complex areas while course modeling the remaining structure or large volume of electrolyte.
- Boundary-element methods are very effective and accurate for modeling large or infinite domains, as is the case for CP analysis.

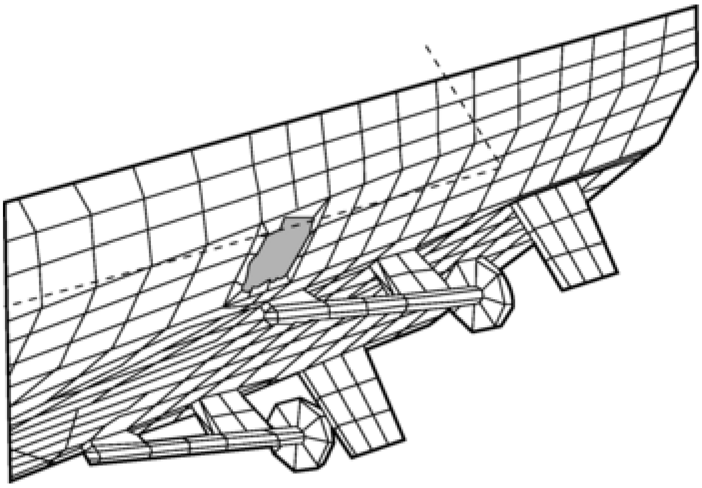

Fig. 8 Boundary-element model of the wetted surface of the propeller section of a ship showing the dark anode area in contrast with the protected cathodic surface

The design goal of an ICCP system is to produce an evenly distributed protection potential on the structure as well as to reduce the power consumption of the anodes to a minimum. The available design variables are the number of anodes, their location, and the location of the reference cells. The constraints on the design are the values of the potential on the structure. In order to provide adequate protection, the potential must be less than a specified value, for example, -800 mV. In order to prevent overprotection, the potential must be greater than a specified value, for example, -900 mV. By combining an automatic optimization procedure with the BE model of the ICCP system, an optimal solution can be obtained. The equation governing electrochemical corrosion for the wetted surface of a ship hull is (Ref 21):

$$k\nabla^2\Phi = 0 \quad \text{(Eq 2)}$$

where Φ is the potential, k is the conductivity of the electrolyte, and ∇^2 is the symbol for a Laplacian operator, a second-order, multidimensional, partial differential equation.

Equation 2 is valid if the electrolyte is homogeneous, there are no electrical sources or sinks, and the system is electroneutral. A shipboard ICCP system can be modeled in such a way to meet these conditions. Seawater is often represented as a uniform mixture of multiple components. Current source points and exposed metal can be represented by boundary conditions, eliminating the need to include sources and sinks in the model. Electroneutrality maintains charge equilibrium for the ship, surrounding water, and ICCP system. The solution space for the problem defined by Eq 2 used in the BE approach is the surface, Γ, which bounds the domain, Ω, as defined by:

$$\Gamma = \Gamma_A + \Gamma_C + \Gamma_I \quad \text{(Eq 3)}$$

where Γ_A is the anodic surface, Γ_C is the cathodic surface, and Γ_I is the insulated surface.
The surface, Γ, must be continuous, but all sections of one surface type do not have to be contiguous. An ICCP system consists of the surfaces to be protected, the anodes, the reference cells, and the power supply. Anodes are defined by maintaining the potential at a constant value, Φ_A:

$$\Phi(x, y) = \Phi_A \qquad \text{(Eq 4)}$$

defining the current density as a constant, q_A, on a surface:

$$\frac{\partial \Phi(x, y)}{\partial n(x, y)} = q_A \qquad \text{(Eq 5)}$$

where $\Phi(x, y)$ is the electrical potential at the point (x, y), and $n(x, y)$ is the normal to the surface at the point (x, y). Reference cells are defined as specific points on the hull where the mathematical solution is obtained.
It has been demonstrated that BE modeling can accurately predict experimental results. A major issue for accurate predictions is the availability of detailed polarization data. However, the lack of availability of accurate polarization data for a particular design condition does not eliminate all advantages associated with BE modeling. Reasonable polarization data can be used to obtain potential maps that identify good and bad regions of protection. Boundary-element methods also can be used to evaluate the effect of a single parameter on system performance. In this way, basic understanding of electrochemical corrosion and parameter interactions can be obtained. Several parametric studies have been completed to date (Ref 21):

- Damage levels in the propeller area
- Seawater conductivity
- Finite paint resistance
- Influence of stray current source on system performance

It is possible to design experiments that would account for the majority, if not all, of the factors that influence polarization response for the materials involved in ICCP. However, this approach quickly leads to impracticably large experimental programs. There are two processes for ICCP system design that rely on BEs but eliminate the need for a high degree of accuracy in polarization response. One proposed method defines the polarization response as an unknown to be solved in the BE process (Ref 21). Sensors provide potential information at specific locations. An inverse problem is defined in which the potential map of the ship hull is defined from the measured data and assumptions of behavior in the regions between sensor points. The solution, obtained through a series of BE evaluations, is the polarization data. Discrete areas of damage can be located based on differences in calculated potentials and measured values at the sensor locations. Once the polarization response is determined for a given ship geometry and service condition, anode strengths and power requirements can be readily obtained.
Combined Boundary Element and Physical Scale. The second proposed approach is a hybrid design combining BE and physical scale (PS) modeling techniques (Ref 21). In the first stage, BE modeling is used to develop best estimates of the layout of an ICCP system. Anode locations, anode numbers, reference cell locations, and reference cell numbers are factors that can be varied using computational analyses. The polarization response used in this phase does not have to duplicate service conditions but only has to be a reasonable approximation. The second stage of the ICCP design uses PS modeling. In PS modeling, the structural dimensions and the conductivity of the electrolyte are scaled by the same factor (Ref 22). In this process, the scaled model and the full-sized structure maintain identical current density values at points, identical potential differences at points, identical polarization potentials at the anode and cathode, and an identical potential drop across the electrolyte. The use of a best-estimate design eliminates multiple cycles of PS modeling. This approach enables the designer to exploit the advantages of both BE and PS modeling approaches.

Alloy Selection System for Elevated Temperatures

The task of providing reliable information on corrosion of metals and alloys in high-temperature gases is difficult, due to the diversity of corrosive environments and the lack of standardization for corrosion data. The Alloy Selection System for Elevated Temperatures (ASSET) information system is being developed to address many of these difficulties. The present system contains information on approximately 80 commercial alloys,

4900 corrosion data measurements, and over six million exposure hours. Data compilation in this interactive model has been organized to allow prediction of sound metal thickness losses by several corrosion mechanisms at high temperatures as functions of gas composition, temperature, time, and alloy type (Ref 23, 24). The equations, which correlate the corrosion measurements with exposure conditions and the data, are stored in databases. The corrosion mechanisms for which corrosion predictions can be made are:

- Sulfidation
- Sulfidation/oxidation
- Isothermal oxidation
- Carburization

The program stores the corrosion measurements, exposure conditions, and corrosion mechanisms and predicts alloy corrosion by accessing the stored data for that alloy and determining the parameters of the rate equation. A different equation is used for each corrosion mechanism. The software uses the alloy composition and the corrosive environment information to calculate the stable corrosion products and the equilibrium gas composition for a given combination of alloy and exposure conditions. The computations use the ChemSage program from FACT, a Gibbs free energy minimization program (Ref 25). Some of the potential solution or mixed corrosion product phases considered are MO, M_3O_4, M_2O_3, MS, M_2S_4, M_3C, $M_{23}C_6$, and M_7C_3, where M represents a combination of iron, nickel, and chromium in the compound.

The thermodynamic solution behaviors of the solid austenitic and ferritic alloys are also considered. Thermochemical characteristics such as the partial pressures $p_{O_2}$and $p_{S_2}$and the carbon activity of the environment, which help determine corrosion product stabilities, are also provided by the calculation. The software assists identification of the likely corrosion mechanism by knowing the stable corrosion products at the corrosion product/corrosive gas interface, the alloy in question, and the partial pressures, $p_{O_2}$and p_{S_2}. Different alloys in the same exposure conditions may exhibit different stable corrosion products and different corrosion mechanisms. In the absence of experimental data for the specific conditions of interest, predictions made by using this approach may be the best available for the corrosion mechanisms that are incorporated into the system, in comparison with those made using the traditional methods of literature review and data analysis. Examples of the accuracy using the ASSET system are shown in Fig. 9. They show how large amounts of corrosion data can be well correlated. The correlations are quite good for three decades of variation in corrosion penetration for several alloys and corrosion mechanisms, considering the uncertainty associated with these types of data.

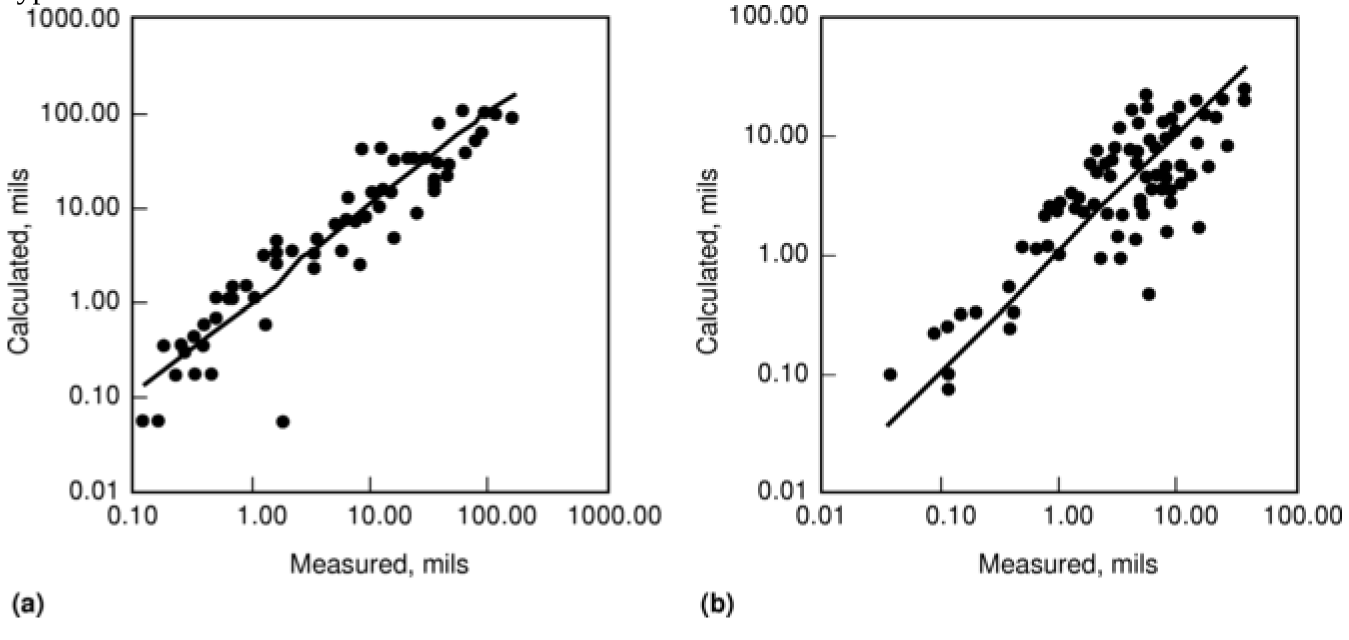

Fig. 9 Verification of the corrosion prediction capabilities of ASSET over three decades of experimental corrosion rate measurements at various temperatures and in different environments with (a) carbon steel oxidation and (b) American Iron and Steel Institute (AISI) 310 sulfidation/oxidation. (Note: 1 mil equals 0.0254 mm.)

Predicting the Life of Nuclear Waste Containers

In the United States and Canada, the regulations pertaining to the geologic disposal of high- level nuclear waste require that the radionucleides remain substantially contained within the waste package for 300 to 1000 years after permanent closure of the repository. The current concept of a waste package involves the insertion of spent fuel bundles inside a container that is then placed in a deep borehole, either vertically or horizontally, with a small air gap between the container and the borehole. For vitrified wastes, a pour canister inside the outer container acts as an additional barrier, making the successful performance of the container material crucial to fulfilling the containment requirements over long periods of time.

Providing that no failures occur as a result of mechanical effects, the main factor limiting survival of these containers is expected to be corrosion in the groundwater to which they would be exposed. Two general classes of container materials have been studied internationally: corrosion-allowance and corrosion-resistant materials. Corrosion-allowance materials possess a measurable general corrosion rate but are not susceptible to localized corrosion. By contrast, corrosion-resistant materials are expected to have very low general corrosion rates because of the presence of a protective surface oxide film. However, they may be susceptible to localized corrosion damage. A model developed to predict the failure of grade 2 titanium has considered two major corrosion modes (Ref 26):

- Failure by crevice corrosion
- Failure by hydrogen-induced cracking (HIC)

In this predictive model, a small number of containers are assumed to be defective and to fail within 50 years of emplacement. Each modeling parameter is assigned a range of values, resulting in a distribution of corrosion rates and failure times. The crevice corrosion rate is assumed to be solely dependent on properties of the material and the temperature of the vault. Crevice corrosion is also assumed to initiate rapidly on all containers and subsequently propagate without repassivation. Failure by HIC is assumed to be inevitable once a container temperature falls below 30 °C (86 °F). However, the concentration of atomic hydrogen to render a container susceptible to HIC would occur only very slowly and might even be negligible if that container had never been subject to crevice corrosion.

Figure 10 illustrates the thin-shell packed-particulate design chosen as a reference container for this study. The mathematical procedure to combine various probability functions and arrive at a failure probability of a hot container due to crevice corrosion at a certain temperature is illustrated in Fig. 11. The failure rate due to HIC in this model is arbitrarily assumed to have a triangular distribution in order to simplify the calculations and knowing that HIC is only a predicted marginal failure mode in the considered burial conditions. On the basis of these assumptions and the subsequent calculations, it was predicted that 96.7% of all containers would fail by crevice corrosion and the remaining by HIC. However, only 0.137% of the total number of containers was predicted to fail before 1000 years (0.1% by crevice corrosion and 0.037% by HIC), with the earliest failure after 300 years (Ref 26). For a view of nickel alloys in similar applications, see the article “Effects of Metallurgical Variables on the Corrosion of High-Nickel Alloys” in this Volume.

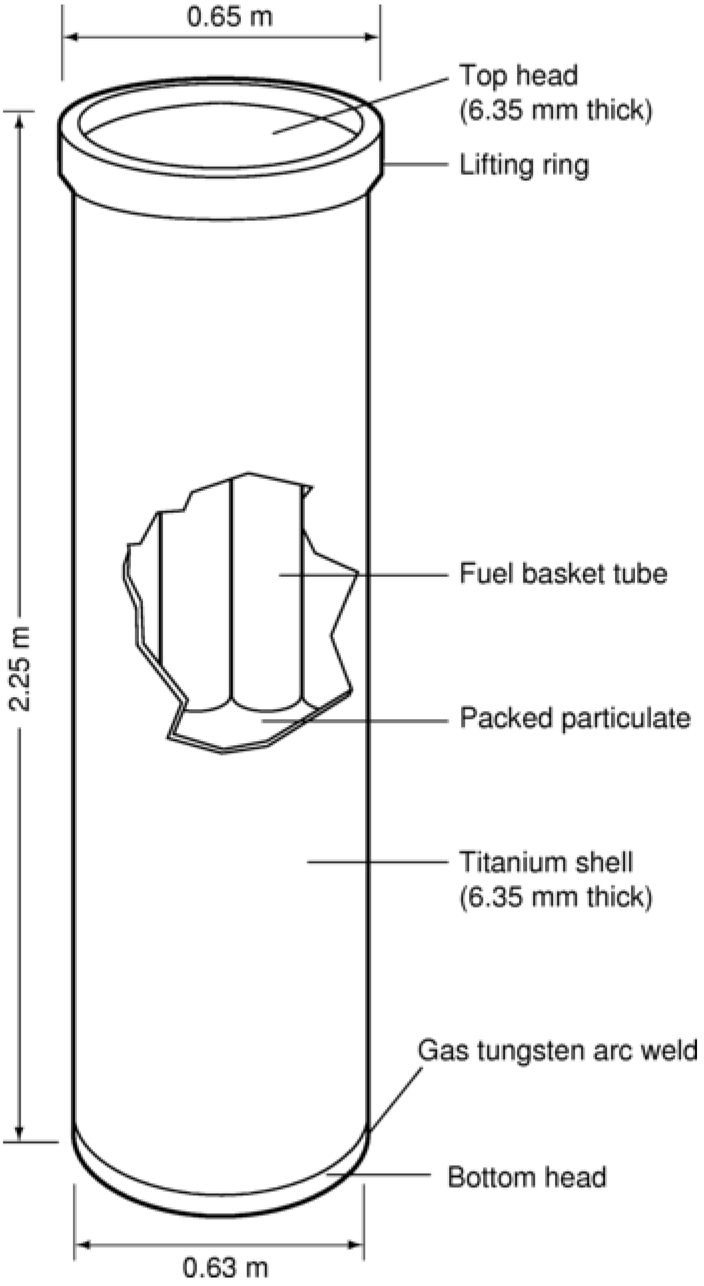

Fig. 10 Packed-particulate supported-shell container for waste nuclear fuel bundles

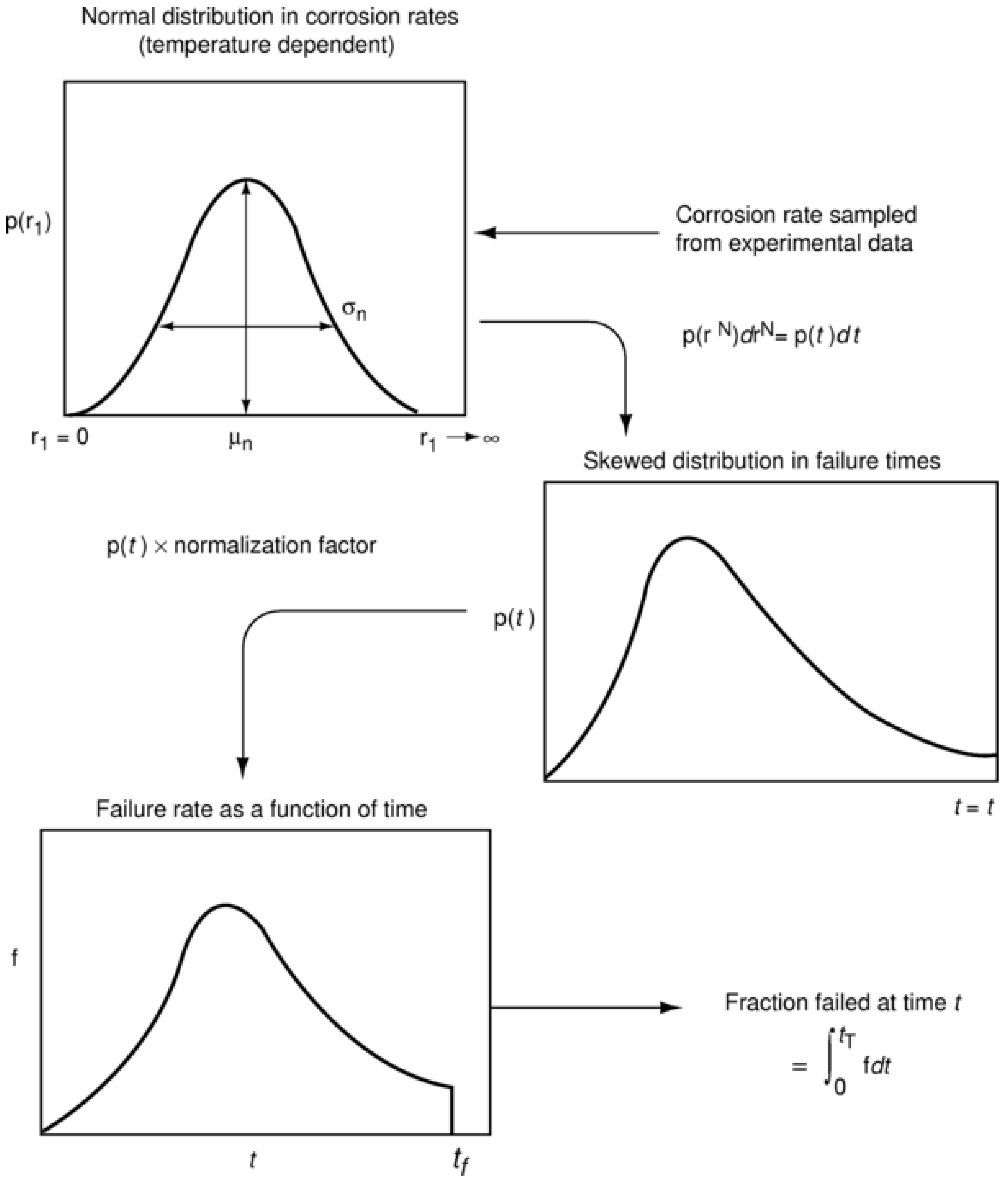

Fig. 11 Procedure used to determine the failure rate of hot containers as a function of time

Pitting Corrosion Fatigue (PCF) Models

The phases of life of a structure have been classified as follows (Ref 27):

- *Phase 1:* nucleation or formation of damage by a specific physical or corrosion damage process. Corrosion and other processes may act alone to create the damage.
- *Phase 2:* microstructurally dominated crack linkup and propagation
- *Phase 3:* crack propagation in the regime where various fracture mechanics methods may be applied, both for analysis and material characterization
- *Phase 4:* final instability of the system

Figure 12 illustrates these degradation processes, with the portion of life on the abscissa and the corresponding growth in discontinuity size plotted schematically on the ordinate. In a first model to estimate the number of fatigue cycles for a pit to reach the critical pit depth to nucleate a mode I crack, it was proposed that pit growth rate theory applied to data obtained with fatigue crack growth experiments in a corrosive environment would be sufficient. Using this model, the pit-to-crack transition length and cycles to failure for various stresses could be determined. However, there are many unknowns for the analysis of real components to estimate accurately the fatigue life under PCF conditions (Ref 27). Once critical-sized pits are formed, it is necessary to estimate the time or cycles for the pits to reach a critical condition or critical depth to nucleate fatigue cracks from those pits. Pit-to- crack transition length under various stresses using the stress-intensity threshold value from fatigue crack growth experiments can be estimated in a two-step process (Ref 27):

1. Pit-to-crack transition analysis
2. Estimation of fatigue cycles to failure

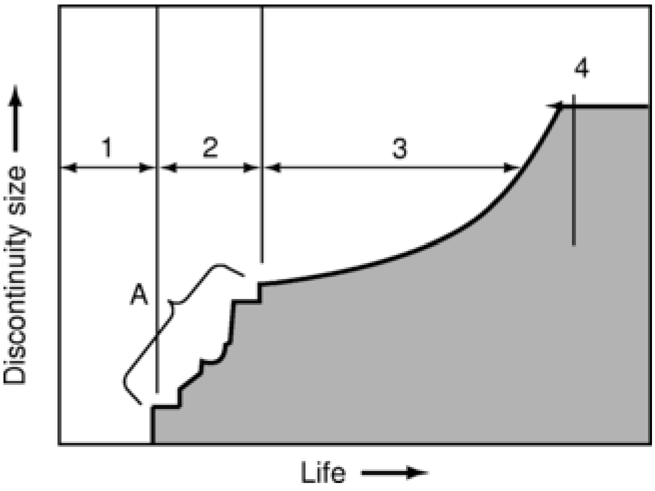

Fig. 12 Four phases involved in the degradation process of in-service components, where "A" corresponds to the first detectable crack, and the crack length progression steps correspond to (1) nucleation, (2) phase steps due to local anisotropy, (3) stress-dominated crack growth, and (4) crack to fracture. Source: Ref 27

The pit-to-crack transition analysis is first performed to determine the critical size of a pit in terms of pit depth that would transition to a crack (not necessarily a mode I crack) for different stresses. The stress values that could be used in the calculation are the estimated maximum applied stress that the component would be subjected to and the ultimate stress for the material in question. The PCF model can be used to determine the critical pit depth (Ref 27):

$$K_{sf} = 1.1\sigma\sqrt{\pi(a/Q)} \qquad \text{(Eq 6)}$$

where, K_{sf} is the stress-intensity factor for a surface discontinuity (MPa/m$^{0.5}$), σ is the applied stress (MPa), a is the size of the pit in terms of pit depth (μm or m), and Q is the dimensionless shape parameter.

In this calculation, it can be assumed that K_{sf} is equal to "short" crack stress-intensity threshold (ΔK_{scth}) for the material. It is recommended that the value of ΔK_{scth} be used, because the pit- to-crack transition first would result in a non- mode I crack, that is, in the short crack region. It is important to note that there is no standard value for the ΔK_{scth} in the short crack region for a particular material, because there is no standard test method to measure the fatigue crack growth rates in this regime. Therefore, this value can either be determined from conducting short fatigue crack growth experiments or determined from literature for a specific material. The shape parameter, Q, for a surface crack can be assumed, depending on the pit morphology. For different stress levels, ranging from the estimated applied stress for the component to the ultimate stress of the material, the critical pit depth, a, that would enable the transition of the pit to a short crack can be determined. The resultant value of a can be compared with the measured depth of the pit from the failure analysis of a similar component, if there is any. Moreover, the calculated value of a can be correlated to the experimentally generated pit growth rate curve to estimate the phase 1 life. A model has been proposed to estimate allowable stresses based on the

allowable stress-intensity threshold (Ref 28). This model is expressed in Eq 7, where the allowable stress, $\Delta\sigma_{all}$, at which the particular component can be operated is determined from the allowable stress-intensity threshold, ΔK_{all}, which itself is determined from corrosion fatigue experiments. The maximum pit depth, h_{max}, in Eq 7 is measured from corrosion pit growth rate experiments for a given machine-material-environment system:

$$\Delta\sigma_{all} = \frac{\Delta K_{all}}{F\sqrt{\pi h_{max}}} \qquad \text{(Eq 7)}$$

where, ΔK_{all} can be determined from a fatique crack growth rate, da/dN, versus stress-intensity factor, ΔK, plot for a material; h_{max} is the maximum pit depth; and F is a geometric factor. The total cycles to failure under corrosion fatigue conditions can subsequently be estimated using the well-known Paris equation:

$$da/dN = C\Delta K^n \qquad \text{(Eq 8)}$$

where, da/dN is the rate of crack growth per cycle (m/cycle), C and n are empirical parameters, and ΔK is the stress-intensity range (MPa $\cdot$ $m^{0.5}$)

The accuracy of the estimation can be improved if fatigue crack growth rate data under realistic corrosive environments are used in calculating the total cycles to failure. As well, the data on the effect of prior corrosion on the fatigue crack propagation also can help in getting more accurate estimation. The reader is referred to Ref 27 for a detailed example of the applicability of the PCF model in estimating the fatigue life of a real component.

References cited in this section

3. G.E.P. Box and N.R. Draper, *Empirical Model-Building and Response Surfaces,* John Wiley and Sons, 1987

4. M. Pourbaix, *Atlas of Electrochemical Equilibria in Aqueous Solutions,* NACE International, 1974

5. D.R.H. Jones, *Materials Failure Analysis: Case Studies and Design Implications,* Pergamon Press, 1993

6. P.R. Roberge, *Handbook of Corrosion Engineering,* McGraw Hill, 1999

7. W.T. Thompson, M.H. Kaye, C.W. Bale, and A.D. Pelton, Pourbaix Diagrams for Multielement Systems, *Uhlig's Corrosion Handbook,* R.W. Revie, Ed., Wiley Interscience, 2000, p 125–136

8. C. Wagner and W. Traud, Uber die deutung von korrosionvorgangen durch uberlagerung von elektrochemischen teilvorgangen und uber die potentialbildung an mischellektroden, *Z. Elektrochemie,* Vol 44, 1938, p 391-402

9. U.R. Evans, *An Introduction to Metallic Corrosion,* Edward Arnold, London, U.K., 1948

10. J.I. Munro, Anodic Protection of White and Green Liquor Tankage With and Without the Use of Protective Organic Linings, *Proceedings of the Seventh International Symposium on Corrosion in the Pulp and Paper Industry,* (Atlanta, GA), Technical Association of the Pulp and Paper Industry (TAPPI), 1992, p 117–130

11. D. Tromans, Anodic Polarization Behavior of Mild Steel in Hot Alkaline Sulfide Solutions, *J. Electrochem. Soc.,* Vol 127, 1980, p 1253–1256

12. A. Anderko, P. McKenzie, and R.D. Young, Computation of Rates of General Corrosion Using Electrochemical and Thermodynamic Models, *Corrosion,* Vol 57, 2001, p 202–213

13. A. Anderko and R.D. Young, "A Model for Calculating Rates of General Corrosion of Carbon Steel and 13% Cr Stainless Steel in CO_2/H_2S Environments," Paper 086, Corrosion 2001, NACE International, 2001

14. A. Anderko and R.D. Young, A Model for Corrosion of Carbon Steel in Lithium Bromide Absorption Refrigeration Systems, *Corrosion,* Vol 56, 2000, p 543–555

15. M. Rafal, J.W. Berthold, N.C. Scrivner, and S.L. Grise, Models for Electrolyte Solutions, *Models for Thermodynamic and Phase Equilibria Calculations,* S.I. Sandler, Ed., Marcel Dekker, 1995, p 601–670

16. A.H. Truesdell and B.F. Jones, A Computer Program for Calculating Chemical Equilibria of Natural Waters, *J. Res., US Geol. Surv.,* Vol 2, 1974, p 233–248

17. R.J. Ferguson, A.J. Freedman, G. Fowler, A.J. Kulik, J. Robson, and D.J. Weintritt, The Practical Application of Ion Association Model Saturation Level Indices to Commercial Water Treatmant Problem Solving, *Mineral Scale Formation and Inhibition,* Z. Amjad Ed., Plenum Press, 1995, p 323–340

18. R.J. Ferguson, O. Codina, W. Rule, and R. Baebel, "Real-Time Control of Scale Inhibitor Feed Rate," IWC-88-57, 49th Annual Meeting, (Pittsburg, PA). International Water Conference, 1988

19. R.J. Ferguson, "Computerized Ion Association Model Profiles Complete Range of Cooling System Parameters," IWC-91-47, 52nd Annual Meeting, (Pittsburg, PA), International Water Conference, 1991

20. R.A. Adey and J. Baynham, "Design and Optimization of Cathodic Protection Systems Using Computer Simulation," Paper 723, Corrosion 2000, NACE International, 2000

21. V.G. DeGiorgi and K.E. Lucas, Computational Design of ICCP Systems: Lessons Learned and Future Directions, *Designing Cathodic Protection Systems for Marine Structures and Vehicles,* STP 1370, H.P. Hack, Ed., ASTM, 1999, p 87–100

22. R.W. Ditchfield, J.N. McGrath, and D.J. Tighe-Ford, Theoretical Validation of the Physical Scale Modeling of the Electrical Potential Characteristics of Marine Impressed Current Cathodic Protection, *J. Appl. Electrochem.,* Vol 25, 1995, p 54–60

23. R.C. John, A.D. Pelton, A.L. Young, W.T. Thompson, I.G. Wright, and T.M. Besmann, Managing Corrosion Engineering Information for Metals in Hot Corrosive Gases, *Materials Design Approaches and Experiences,* J.C., Zhao, M. Fahrmann, and T.M. Pollock, Ed., 4–8 Nov 2001 (Indianapolis, IN), TMS, 2001, p 359–382

24. R.C. John, "Compilation and Use of Corrosion Data for Alloys in Various High- Temperature Gases," Paper 99073, Corrosion 99, NACE International, 1999

25. C.W. Bale, A.D. Pelton, and W.T. Thompson, Facility for the Analysis of Chemical Thermodynamics (F*A*C*T), Ecole Polytechnique/McGill University, Montreal, Canada, 1996

26. D.W. Shoesmith, B.M. Ikeda, and D.M. LeNeveu, Modeling the Failure of Nuclear Waste Containers, *Corrosion,* Vol 53, 1997, p 820–829

27. D.W. Hoeppner, V. Chandrasekaran, and A.M.H. Taylor, "Review of Pitting Corrosion Fatigue Models," ICAF '99, 12–16 July 1999 (Bellevue, WA), International Committee of Aeronautical Fatigue (ICAF), 1999

28. S. Kawai and K. Kasai, Considerations of Allowable Stress of Corrosion Fatigue (Focused on the Influence of Pitting), *Fatigue Fract. Eng. Mater. Struct.,* Vol 8, 1985, p 115–127

P.R. Roberge, Modeling Corrosion Processes, *Corrosion: Fundamentals, Testing, and Protection*, Vol 13A, *ASM Handbook*, ASM International, 2003, p 430–445

Modeling Corrosion Processes

P.R. Roberge, Royal Military College of Canada

Risk-Based Models

Some of the issues involved in deciding on a cost-effective solution for combating corrosion are generic to sound system management. Others are specifically related to the impact of corrosion damage on system integrity and operating costs. Risk assessments can be designed to answer many questions. Some have risk hierarchies with a limited number of variables to produce a quick screening of high-risk system components. Others consider the impact of a multitude of variables in their overall assessment. The danger in using too few variables is that the analysis becomes more qualitative than quantitative, approaching more of the fundamental indexing method. Similarly, when considering a large number of variables, the potential exists for diluting the impact of rare-occurrence events among the myriad of other potential problems. Therefore, the development and fine-tuning of the risk algorithm to ensure that potentially dangerous conditions are properly identified is the most critical step in any risk analysis program (Ref 29).

Basic Principles of Risk Management

Traditional risk management has been based on regulatory code compliance issues, and the decision to perform maintenance has been left up to a limited number of people, drawing off of their own experience and the limited amount of information they can access. Risk-based models use a systematic and structured approach based on the consequences of failure. As such, they represent a shift away from time-based tasks and emphasize the functional importance of system components and their failure/maintenance history. The following examples illustrate how these considerations are put into practice and integrated into efficient management systems.
Corrosion-Based Design (CBD) Applied to a Steam Generator. More industrial equipment is being designed or forced to perform for durations for which the environmental effects have never been seriously considered. An objective of the CBD method is to provide a framework within which materials and design disciplines can communicate effectively. The basic principles for conducting CBD are (Ref 30):

- All engineering materials are simply reactive chemicals that, in some environments, dissolve as rapidly as table salt in hot water. The surprise is never that materials fail; the surprise should be that these reactive materials work.
- Materials fail in the environments that are specifically adjacent to the surface and not in the bulk environment. These local environments are greatly influenced by prior history of exposure, flow, buildup of deposits, and local cells.
- What appears to be imponderable complexity in corrosion can be handled and bounded by explicit consideration of specific possible environments and modes of corrosion that can occur.

The CBD approach to predicting performance is a series of knowledge-elicitation steps that require detailed consideration on a multitude of topics. The two most important of these steps are shown in Fig. 13 and 14, which describe, respectively, the environment and the material definitions. Each of the numbers in brackets in Fig. 13 identifies an explicit action that needs to be considered in the step of environmental definition. The endpoint of the process is an input to a location-for-analysis (LA) matrix, whose locations in a steam generator are indicated in Fig. 15. A brief explanation of the individual elements in Fig. 13 follows:

1. Nominal chemistry refers to the bulk chemistry. For components exposed to ordinary air atmospheres, the major elements mean humid air. The minor elements refer to industrial contaminants, such as SO_2 and NO_2.

2. Prior chemistry history refers to exposures to environmental species that might still reside on the surfaces or inside crevices.
3. System sources refer to those environments that do not come directly from a component but from outside.
4. Physical features include occluded geometries, flow, and long-range electrochemical cells.
5. Transformations refer, for example, to microbial actions that can change relatively innocuous chemicals, such as sulfates, into very corrosive sulfide species that accelerate hydrogen entry and increase corrosion rates.
6. Concentration refers to accumulations much greater than that in the bulk environment due to various actions of wetting and drawing, evaporation, potential gradients, and crevice actions that prevent dilution.
7. Inhibition refers to actions taken to minimize corrosive actions. This usually involves additions of oxygen scavengers or species that interfere directly with anodic or cathodic reactions.

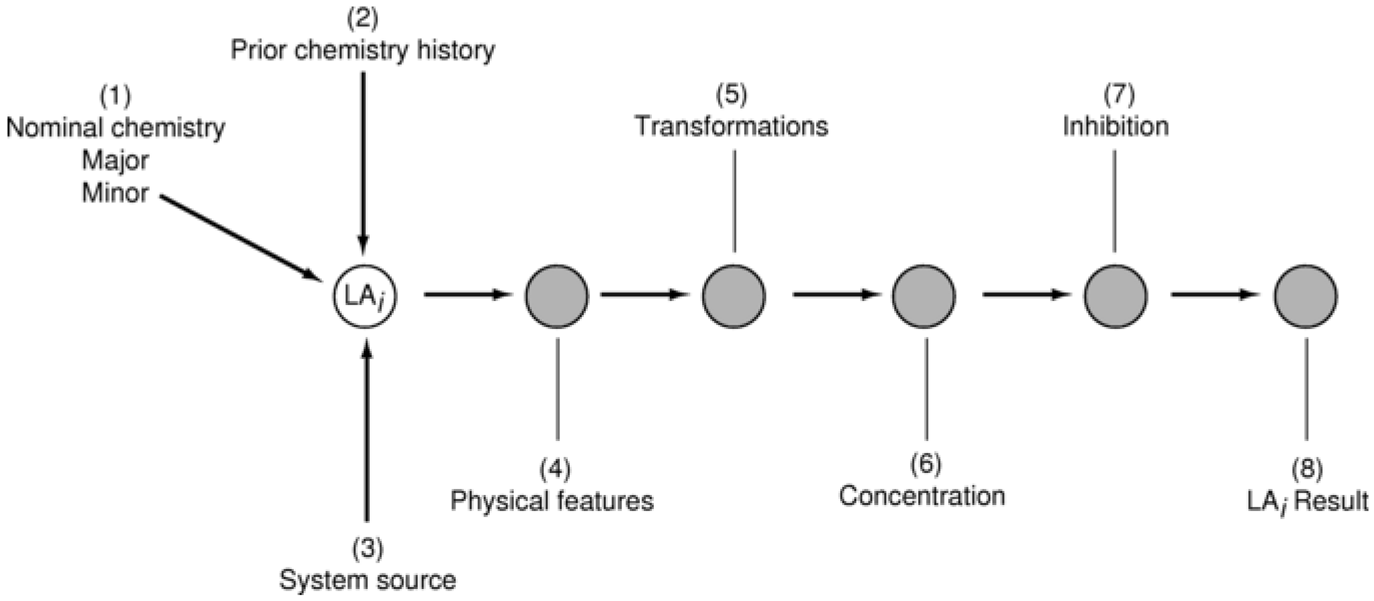

Fig. 13 Analysis sequence for determining environment at a location-for-analysis (LA) matrix. Details are given in text.

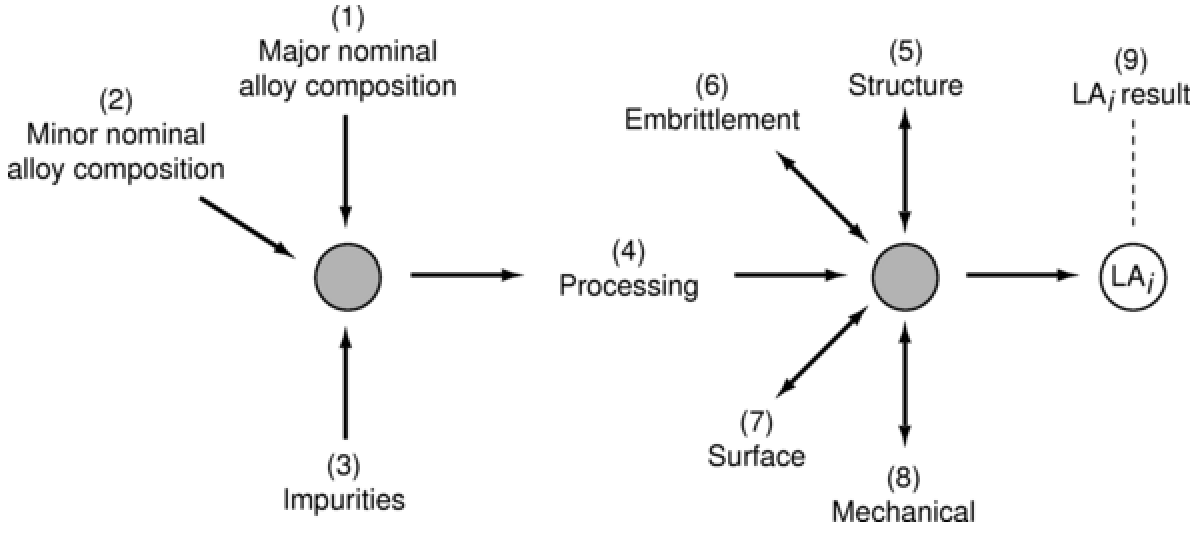

Fig. 14 Analysis sequence for determining materials at a location-for-analysis (LA) matrix. Details are given in text.

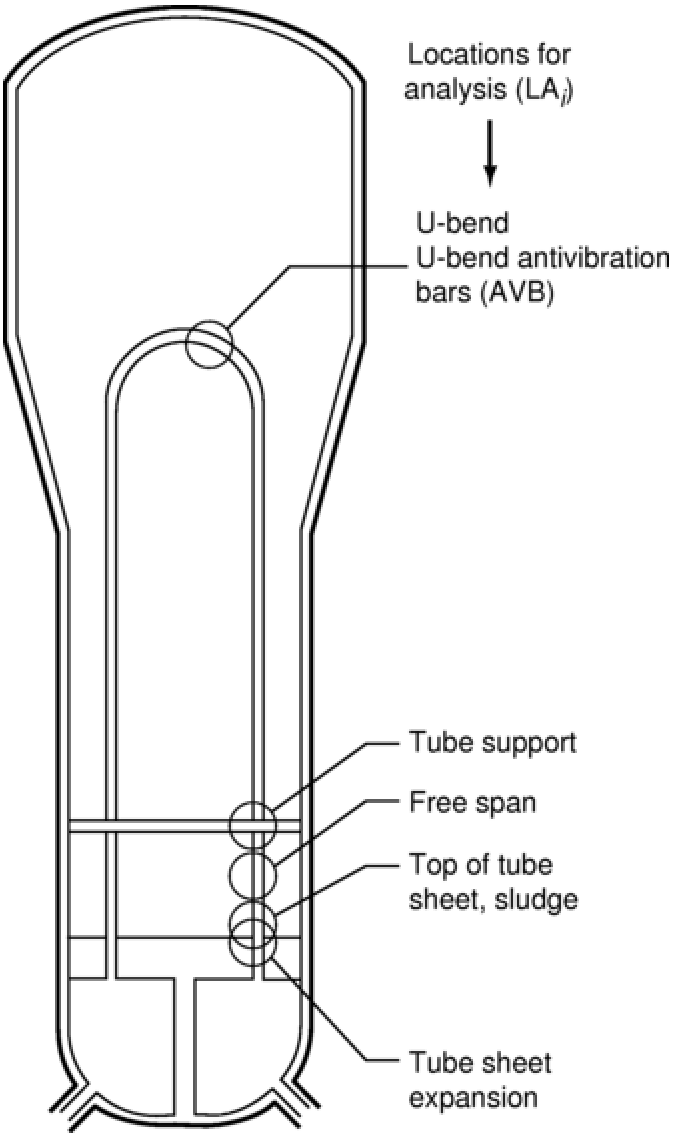

Fig. 15 Schematic view of steam generator indicating the locations for analysis considered in the template presented in Table 4

Defining materials characterizes those aspects that affect the modes of corrosion. A brief explanation of the individual elements in Fig. 14 follows:

1. Major nominal alloy composition includes those species added in relatively large concentrations, such as the iron, chromium, nickel, and molybdenum in type 316 stainless steel.
2. Minor nominal alloy composition includes species such as sulfur, nitrogen, phosphorus, silicon, and manganese usually found in steels, or the oxygen and nitrogen usually found in titanium.
3. Impurities include species such as arsenic, selenium, and similar elements that contribute to temper brittleness, or to excess oxygen and nitrogen picked up during welding of titanium.
4. Processing includes fabrication to shape, with associated times and temperatures of hot deformation and heat treatments, cold deformation to size, welding, machining, and grinding.
5. Structure includes single and multiple phases, anisotropy, second phases, and grain size.
6. Embrittlement includes grain-boundary composition and the formation of phases that embrittle, such as sigma phases in iron-chromium-base alloys.
7. Surface includes surface machining, surface stresses that result from thermal gradients, grinding, shot peening, and impurities absorbed at the surface.
8. Mechanical includes the mechanical properties of tensile strength, ductility, and toughness.

The LA template of the locations that correspond to the most likely failure sites along tubes in a steam generator of a pressurized-water nuclear power plant, indicated in Fig. 15, is illustrated in Table 4 for the main failure modes and submodes considered in such an analysis.

Table 4 Matrix for organizing mode-location cells

Locations for analysis (LA_i)	ID	OD	Modes (MD_j) and submodes (SD_j) to be considered												
			Submodes of SCC						**Submodes of IGC**						
			LPSCC (*j* = 1)	**HPSCC (*j* = 2)**	**AcSCC (*j* = 3)**	**MRSCC (*j* = 4)**	**AkSCC (*j* = 5)**	**PbSCC (*j* = 6)**	**HPIGC (*j* = 7)**	**AcIGC (*j* = 8)**	**AkIGC (*j* = 9)**	**Wastage (*j* = 10)**	**Pitting (*j* = 11)**	**Fatigue (*j* = 12)**	**Wear (*j* = 13)**
Tubular expansion (*i* = 1)	x	…	…	…	…	…	…	…	…	…	…	…	…	…	…
Tubular expansion (*i* = 2)	…	x	…	…	…	…	…	…	…	…	…	…	…	…	…
Top of tube sheet (*i* = 3)	x	…	…	…	…	…	…	…	…	…	…	…	…	…	…
Top of tube sheet (*i* = 4)	…	x	…	…	…	…	…	…	…	…	…	…	…	…	…
Sludge (*i* = 5)	…	x	…	…	…	…	…	…	…	…	…	…	…	…	…
Free span (*i* = 6)	x	…	…	…	…	…	…	…	…	…	…	…	…	…	…
Free span (*i* = 7)	…	x	…	…	…	…	…	…	…	…	…	…	…	…	…
Tube support (hot leg) (*i* = 8)	…	x	…	…	…	…	…	…	…	…	…	…	…	…	…
Tube support (cold leg) (*i* = 9)	…	x	…	…	…	…	…	…	…	…	…	…	…	…	…
U-bend (*i* = 10)	x	…	…	…	…	…	…	…	…	…	…	…	…	…	…
U-bend AVB (*i* = 11)	…	x	…	…	…	…	…	…	…	…	…	…	…	…	…

ID, inside diameter; OD, outside diameter; SCC, stress-corrosion cracking; IGC, intergranular corrosion; LP, low potential; HP, high potential; Ac, acidic; MR, midrange pH; AK, alkaline; Pb, lead; AVB, antivibration bars

A Fault Tree for the Risk Assessment of Gas Pipeline. A fault tree is a diagrammatic representation of the relationship between component-level failures and a system-level undesired event. A fault tree depicts how component-level failures propagate through the system to cause a system-level failure. The component-level failures are called the terminal events, primary events, or basic events of the fault tree. The system-level undesired event is called the top event of the fault tree. Figure 16 presents the most commonly used logic symbols and gates for the construction of fault trees (Ref 31). Fault tree analysis (FTA) is a very efficient method for reviewing and analytically examining a process or piece of equipment in its details to emphasize the lower-level fault occurrences that directly or indirectly contribute to a major fault or undesired event. By performing a FTA from lower-level failure mechanisms, a global overview of the system is achieved. Once completed, the fault tree allows the risk engineer to fully evaluate the safety or reliability of a system by altering the various lower-level attributes of the tree. Through this type of modeling, a number of variables may be visualized in a cost-effective manner.

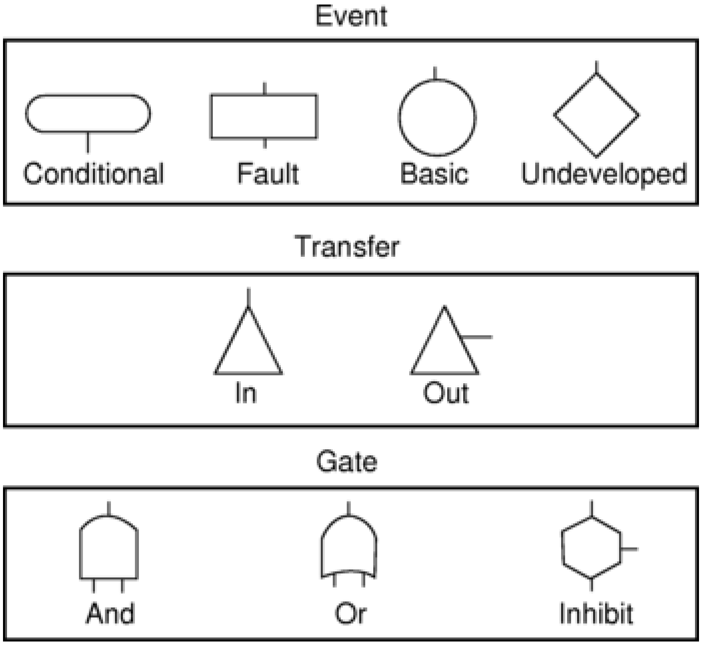

Fig. 16 Fault tree symbols for gates, transfers, and events

Figure 17 illustrates how Nova Corporation adopted FTA for the risk assessment of uniform corrosion on its 18,000 km (11,000 mile) gas pipeline network (Ref 32). The Nova rupture- risk FTA was normally performed for the review and analytical examination of systems or equipment to emphasize the lower-level fault occurrences, and the results of the FTA calculations were regularly validated with inspection results. These results also served to schedule maintenance operations, conduct surveys, and plan research and development efforts. Each element of each branch in Fig. 17 contains numeric probability information related to technical and historical data for each segment of the complete pipeline network. In some cases, it is simpler to assume some probability values for an entire system. The probabilities of operating at maximum permitted pressure and the presence of electrolyte were both set at value unity in Fig. 17, therefore forcing the focus on worst-case scenarios. Other, more verifiable variables can be fully developed, as is shown in Fig. 18 for two basic events describing the probable impact of a cathodic protection deficiency on the pipeline network.

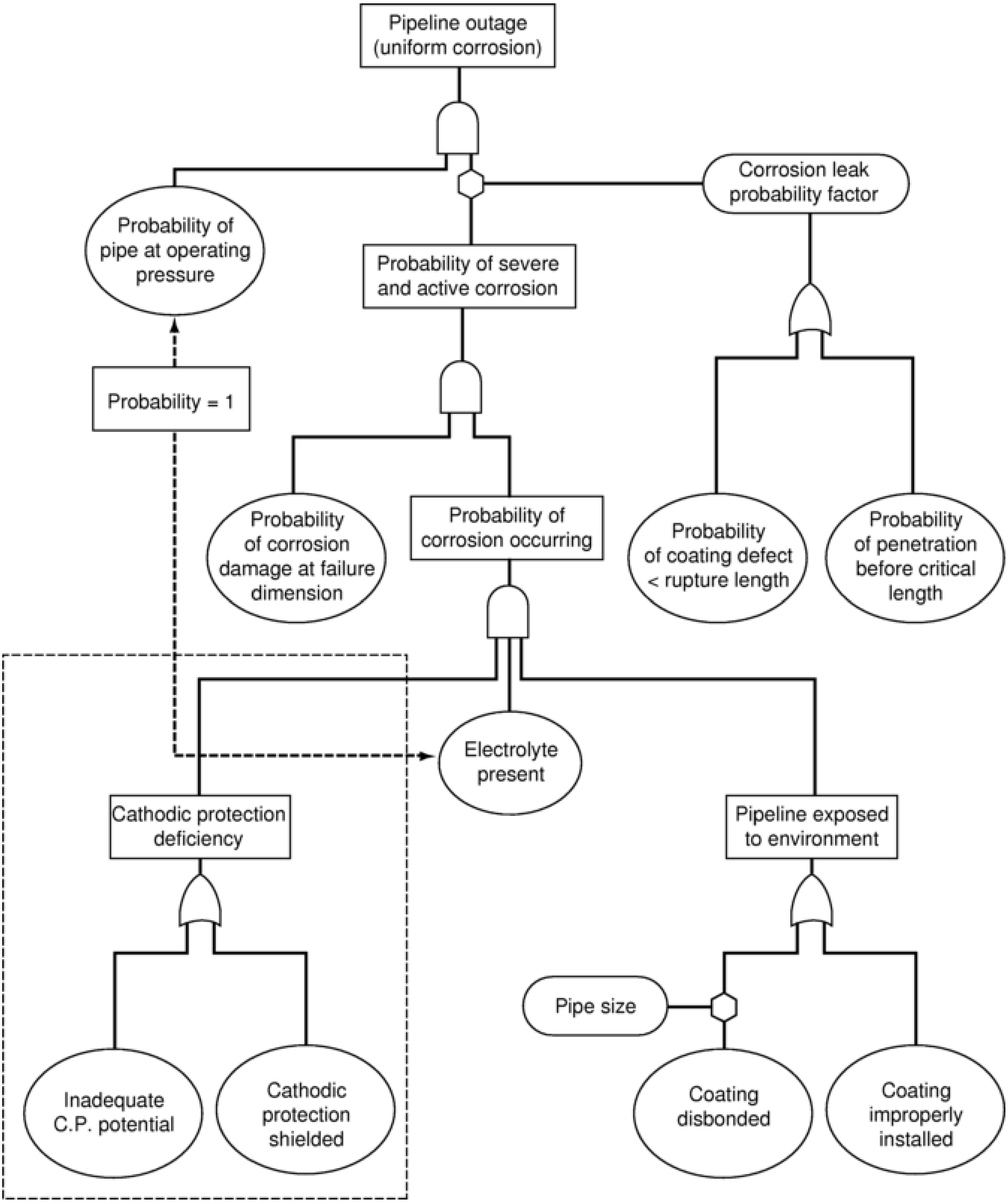

Fig. 17 Fault tree for natural gas pipeline outage due to general corrosion. C.P., cathodic protection

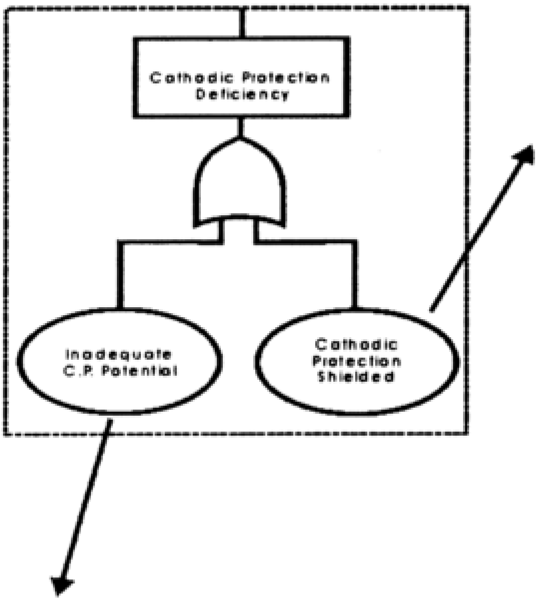


```
function PCPSH
private PCPSH_Value

 PCPSH_Value = 0.05
 if COAT1 = "FBE"
   PCPSH_Value = iif( DIST = 1, 0.05, PCPSH_Value )
   PCPSH_Value = iif( DIST = 2, 0.05, PCPSH_Value )
   PCPSH_Value = iif( DIST = 3, 0.05, PCPSH_Value )
   PCPSH_Value = iif( DIST = 4, 0.05, PCPSH_Value )
 endif

 if COAT1 = "EP "
   PCPSH_Value = iif( DIST = 1, 0.05, PCPSH_Value )
   PCPSH_Value = iif( DIST = 2, 0.05, PCPSH_Value )
   PCPSH_Value = iif( DIST = 3, 0.05, PCPSH_Value )
   PCPSH_Value = iif( DIST = 4, 0.05, PCPSH_Value )
 endif

 if COAT1 = "AE " .or. COAT1 = "CTE"
   PCPSH_Value = iif( DIST = 1, 0.46, PCPSH_Value )
   PCPSH_Value = iif( DIST = 2, 0.56, PCPSH_Value )
   PCPSH_Value = iif( DIST = 3, 0.30, PCPSH_Value )
   PCPSH_Value = iif( DIST = 4, 0.55, PCPSH_Value )
 endif

 if COAT1 = "PT " .or. COAT1 = "PT2" .or. ;
    COAT1 = "SRT" .or. COAT1 = "HHT"
   PCPSH_Value = iif( DIST = 1, 0.30, PCPSH_Value )
   PCPSH_Value = iif( DIST = 2, 0.88, PCPSH_Value )
   PCPSH_Value = iif( DIST = 3, 0.51, PCPSH_Value )
   PCPSH_Value = iif( DIST = 4, 0.79, PCPSH_Value )
 endif
```

```
function PCPINAD
private PCPINAD_Value

 PCPINAD_Value = 0.0
 PCPINAD_Value = iif( DIST = 1, 0.000152, PCPINAD_Value )
 PCPINAD_Value = iif( DIST = 2, 0.007100, PCPINAD_Value )
 PCPINAD_Value = iif( DIST = 3, 0.000134, PCPINAD_Value )
 PCPINAD_Value = iif( DIST = 4, 0.000388, PCPINAD_Value )
```

Fig. 18 Detailed code for the basic events leading to a cathodic protection (C.P.) deficiency

Maintenance Steering Group (MSG) System Applied to Aircraft. The aircraft industry and its controlling agencies have developed, over the past few decades, a comprehensive system to represent potential failures of aircraft components, the maintenance steering group (MSG). The first generation of formal air carrier maintenance programs was based on the belief that each part on an aircraft required periodic overhaul. As experience was gained, it became apparent that some components did not require as much attention as others, and new methods of maintenance control were developed. Condition monitoring was thus introduced in the decision logic of the initial MSG document (MSG-1) and was applied to Boeing 747 aircraft.

After several alterations to the system, industry and regulatory authorities began working together in 1991 to provide additional enhancements to MSG-3. As a result of these efforts, revision 2 was submitted to the Federal Aviation Administration (FAA) in September 1993 and was accepted a few weeks later (Ref 33). One particularly interesting addition in this revision is a procedure for incorporating corrosion damage in the MSG logic. The environmental deterioration analysis (EDA) involves the evaluation of the structure against probable exposure to adverse environments. The evaluation of deterioration is based on a series of steps supported by reference materials containing baseline data expressing the susceptibility of structural materials to various types of environmental damage, and it produces inputs for the structure maintenance program.

The MSG-3 (revision 2) structures analysis begins by developing a complete breakdown of the aircraft systems to the component level. All structural items are then either classified as structure-significant items (SSIs) or other structure. An item is classified as a SSI depending on consideration of consequences of failure and likelihood of failures as well as material, protection, and probable exposure to corrosive environments. All SSIs are then listed and categorized as damage-tolerant or safe-life items, to which life limits are assigned (Ref 34). Accidental damage, environmental deterioration, corrosion prevention and control, and fatigue damage evaluation are then performed for these SSIs, following the logic diagram illustrated in Fig. 19. Once the MSG-3 structure analysis is completed, each element of the structural analysis diagram (Fig. 19) can be expanded right to the individual components and associated inspection and maintenance tasks. The logic of the EDA,

illustrated in Fig. 20, requires the input of a multitude of parameters, such as component part number, location, material composition, and protective coating, that can be actuated in practical templates.

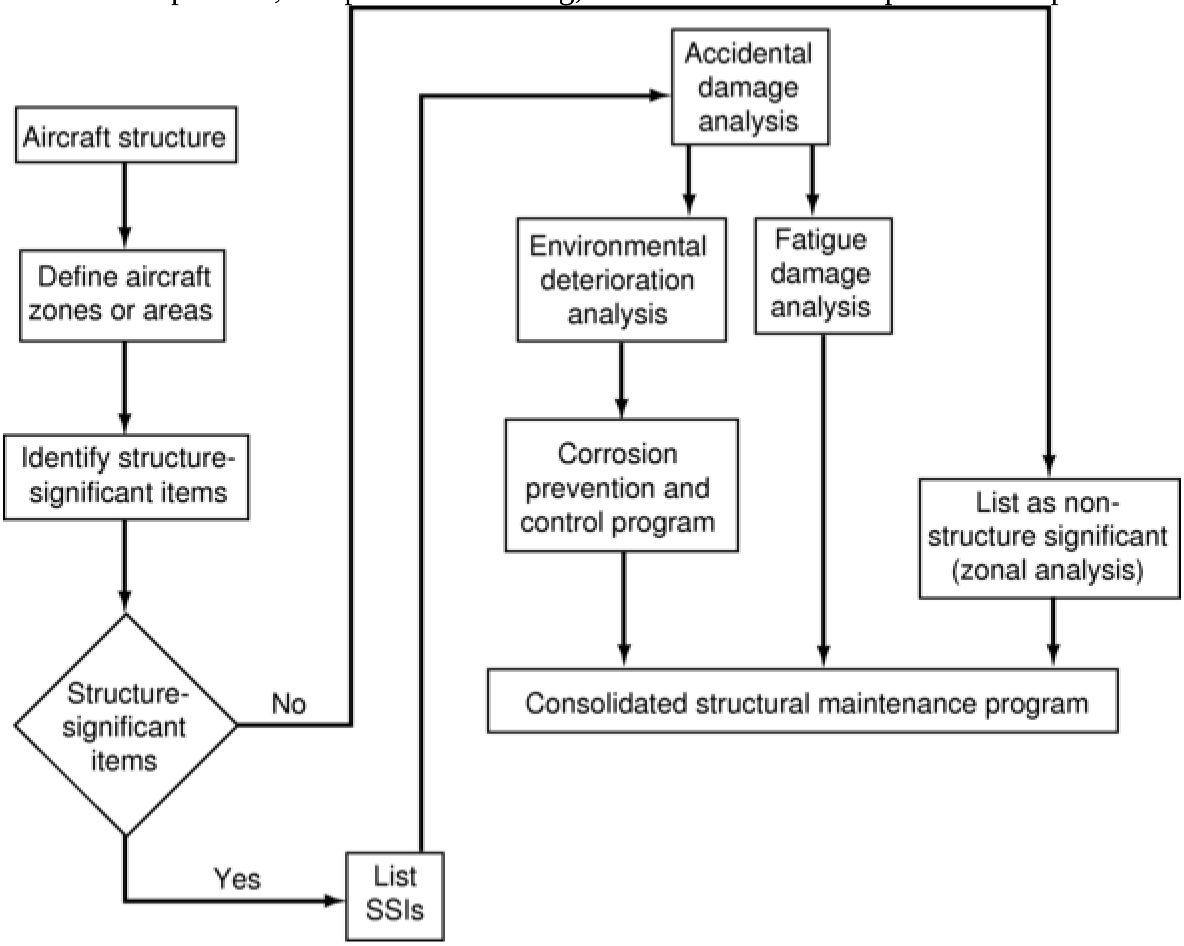

Fig. 19 Overall maintenance steering group (MSG-3), revision 2, structural analysis logic diagram for aircraft. SSIs, structure-significant items

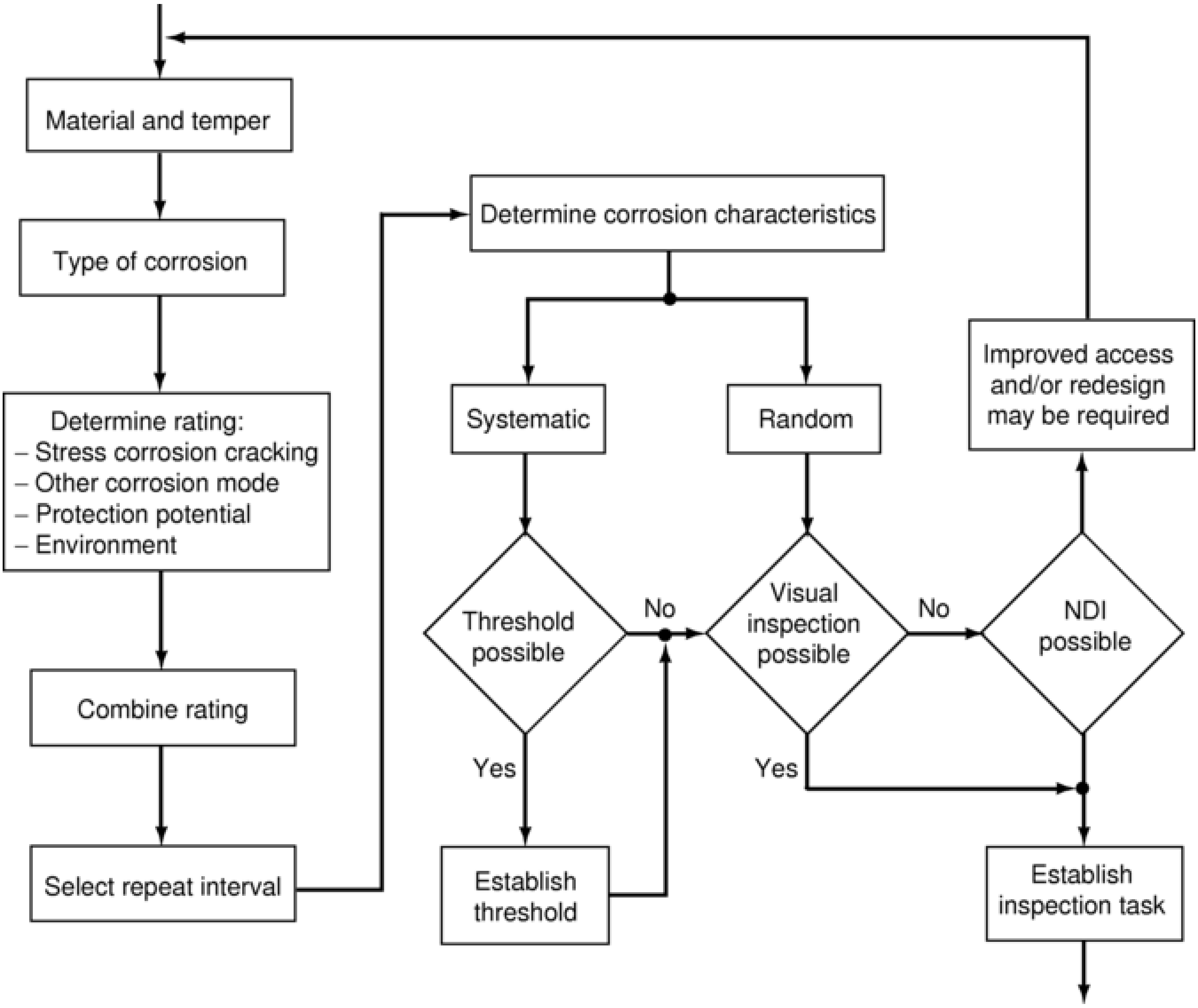

Fig. 20 Environmental deterioration analysis logic diagram. NDI, nondestructive inspection

Corrosion Index for Pipeline Risk Evaluation. The third example of comprehensive models is the pipeline risk assessment methodology, described in detail in (Ref 35). The methodology is based on subjective risk assessment, a method particularly well adapted to situations where knowledge is incomplete and judgments are based on opinions, experience, and other nonquantifiable resources. The technique used for quantifying risk factors is a hybrid of several methods, allowing the user to confide in scores obtained by combining statistical failure data with operator experience. The subjective scoring system allows the assessment of the pipeline risk picture in two general parts:

- A detailed itemization and relative weighting of all reasonably foreseeable events that may lead to the failure of a pipeline are carried out. The itemization is further broken down into the four indexes illustrated in Fig. 21, corresponding to typical categories of pipeline accident failures. By considering each item in each index, an expert evaluator arrives at a numerical value for that index. The four index values are then summed to obtain the total index value.
- A detailed analysis is made of potential consequences of each failure, considering product characteristics, pipeline operating conditions, and line location.

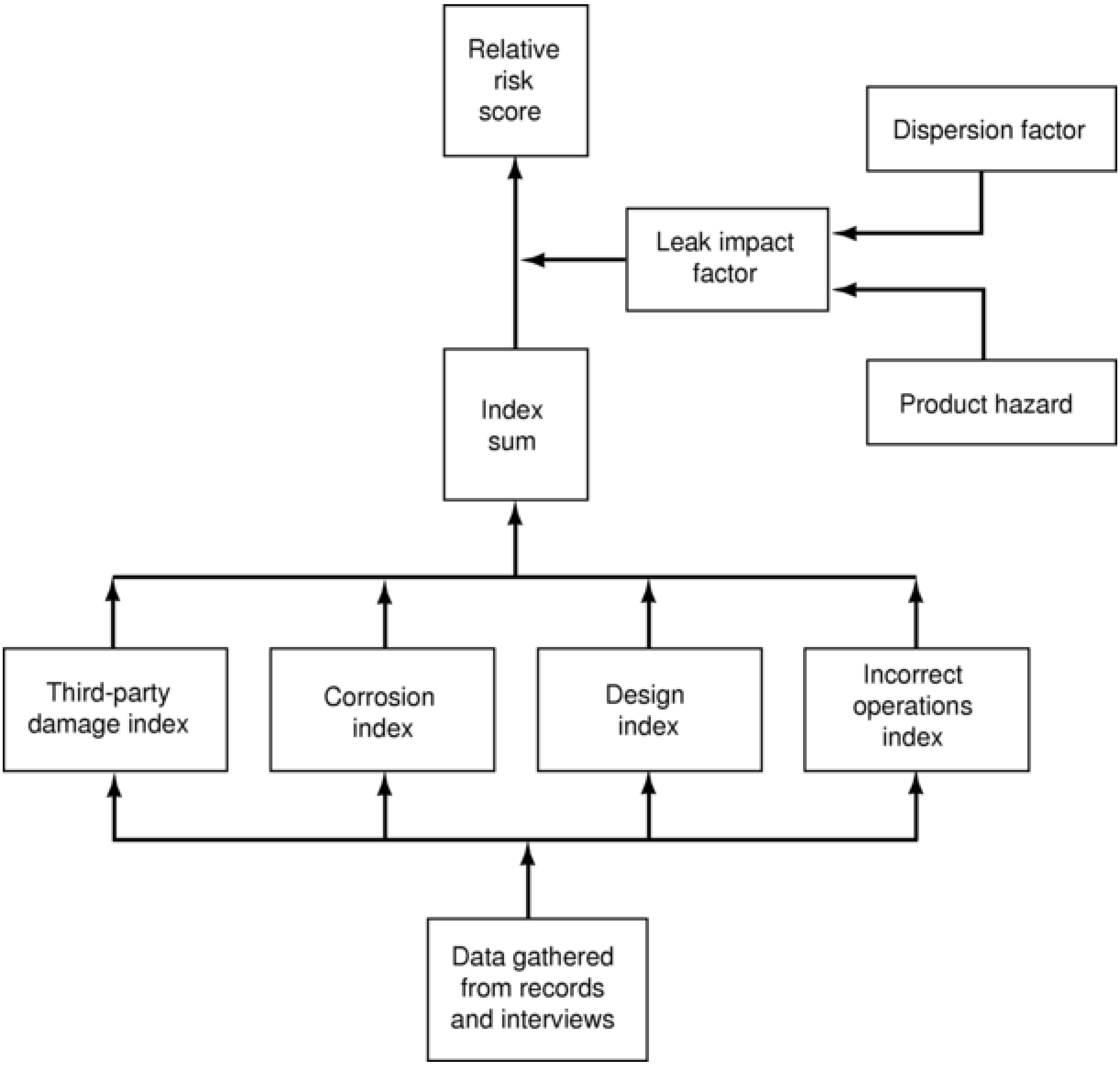

Fig. 21 Pipeline risk assessment model

The risk of a pipeline failure caused by corrosion, directly or indirectly, is probably the most common hazard associated with steel pipelines. The corrosion index was organized into three categories to reflect three types of environment to which pipelines are typically exposed, that is, atmospheric corrosion, soil corrosion, and internal corrosion. Table 5 contains the elements contributing to each type of environment and the suggested weighting factors. Building the risk assessment tool requires the following four steps:

1. *Sectioning:* dividing a system into smaller sections. The size of each section should reflect practical considerations of operation, maintenance, and cost of data gathering versus the benefit of increased accuracy.
2. *Customizing:* deciding on a list of risk contributors and risk reducers and their relative importance
3. *Data gathering:* building the database by completing an expert evaluation for each section of the system
4. *Maintenance:* identifying when and how risk factors can change and updating these factors accordingly

Table 5 Pipeline corrosion risk subjective assessment

Corrosion problem	Risk weight, points
Atmospheric corrosion	
Facilities	0–5
Atmospheric type	0–10
Coating/inspection	0–5

Total	0–20
Internal corrosion	
Product corrosivity	0–10
Internal protection	0–10
Total	0–20
Soil corrosion	
Cathodic protection	0–8
Coating condition	0–10
Soil corrosivity	0–4
Age of system	0–3
Other metals	0–4
AC-induced currents	0–4
SCC and HIC	0–5
Test leads	0–6
Close internal surveys	0–8
Inspection tool	0–8
Total	0–60
Total	0–100

AC, alternating current; SCC, stress-corrosion cracking; HIC, hydrogen- induced cracking

References cited in this section

29. S.F. Biagiotti, Jr. and M.P. Gloven, "Pipeline Risk Assessment and Effective Resource Allocation," Paper 481, Corrosion 2000, NACE International, 2000

30. R.W. Staehle, Lifetime Prediction of Materials in Environments, *Uhlig's Corrosion Handbook,* R.W. Revie, Ed., Wiley Interscience, 2000, p 27–84

31. *Fault Tree Analysis Application Guide,* Reliability Analysis Center, 1990

32. P.R. Roberge, Eliciting Corrosion Knowledge Through the Fault-Tree Eyeglass, *Modelling Aqueous Corrosion: From Individual Pits to Corrosion Management,* K.R. Trethewey and P.R. Roberge, Ed., Kluwer Academic Publishers, 1994, p 399–416

33. D. Nakata, MSG-3 Aircraft Systems/Powerplant Analysis Method, *Aircraft Maintenance and Reliability Seminar/Workshop,* Vol 1, Transportation Systems Consulting Corp., 1997

34. *BBAD Maintenance Program: Policy and Procedures Handbook,* Bombardier Inc., 1994

35. W.K. Muhlbauer, *Pipeline Risk Management Manual,* Gulf Publishing Co., 1996

P.R. Roberge, Modeling Corrosion Processes, *Corrosion: Fundamentals, Testing, and Protection*, Vol 13A, *ASM Handbook*, ASM International, 2003, p 430–445

Modeling Corrosion Processes

P.R. Roberge, Royal Military College of Canada

Knowledge Models

The adequate transfer and reuse of information involves the development of information- processing strategies that can become quite complex. Humans are accustomed to working with imprecise information. They naturally accept vague use of language, making continuous interpretations of the information they receive based on context. Ambiguity can cause problems. However, if the scope for ambiguity is provided, a question and answer clarifies the matter. For a machine to carry out the same tasks, unambiguous language must be defined. This, of course, is the first event in the creation of a traditional programming language, such as FORTRAN, PASCAL or C. The structuring of knowledge inevitably requires the definition of terms, statements of relationships between them, and elimination of ambiguity. Despite this, modern mathematics has devised techniques that do allow for imprecise or error-containing information, and, by means of fuzzy logic, some computers can now cope with such situations (Ref 36). Some of the artificial intelligence tools that have been developed in support of corrosion control and protection are reviewed in the following sections.

Basic Principles of Knowledge Models

From a practical point of view, all models of expertise have their place and possess special features designed to represent specific types of knowledge. Knowledge engineering research has produced a wide range of models of expertise, which have been classified into five major classes (Ref 37):

- *Heuristic models:* offer a symbolic, or representational, description of expertise that is seen as a combination of facts and heuristics. A rule-based or heuristic system would be an excellent choice, for example, when the hierarchy between facts and decisions is well established.
- *Deep models:* suggest that experts use a variety of deep knowledge structures represented differently from heuristic rules. Deep models of expertise are said to better represent the expert functions at each level of the expertise model hierarchy.
- *Implicit models:* offer a representational description with a particular emphasis on the implicitness or explicitness of knowledge. Implicit models have become increasingly popular, with the development of artificial neural networks.
- *Competence models:* are representation independent and principally distinguish between domain and task knowledge. The focus of competence models is usually on the strategy of a problem-solving process. These models provide an extension of a functional rule-based system from which the heuristic knowledge was extracted to generate an explicit knowledge-level description of a specialist's expertise (Ref 37).
- *Distributed models:* can be compared to negotiation schemes. The tools implementing this approach are still on the research bench, because many aspects of fuzzy systems development for fuzzification and defuzzification remain both attractive and mysterious to apply (Ref 36).

Expert Systems. During the 1970s, research in expert systems (ES) was mostly a laboratory curiosity. The research focus then was really centered on developing ways of representing and reasoning about knowledge in a computer and much less on designing actual systems (Ref 38). In 1985, approximately 50 systems were deployed and reported, but the success of some of these captured the attention of many organizations and individuals. The corrosion community reacted with interest to the advent of these new information-processing technologies by establishing programs to foster and encourage the introduction of ES in the workplace. While some of these programs were relatively modest, others were quite ambitious and important both in scope and in funding. The advantages and limitations of using ES technology were analyzed in great detail in one of the first reported efforts on combating corrosion with ES (Ref 39). The stress-corrosion cracking (SCC) ES (SCCES) had been created to calculate the risk of various factors involved in SCC, such as crack initiation, when the user supplied evidence. The main goal of this effort was to support the decision process of “general” materials engineers. The system would initially play the role of a consultant, but it was anticipated that SCCES had the potential to become:

- An intelligent checklist
- A trainer
- An expert sharpener
- A communication medium

- A demonstration vehicle

The transfer of corrosion expertise into ES has been realized in a multitude of projects. The NACE International Conference Proceedings, for example, regularly contain papers that illustrate the continuous interest in the application of knowledge engineering to corrosion. Unfortunately, many systems reported in the literature have never been commercialized. This has resulted in a lack of impartial and practical information concerning the performance and accuracy of these systems. It is indeed very difficult to believe everything that is said in a paper or, even more so, when the information is some form of publicity. To remedy this situation, the European Federation of Corrosion (EFC) and the Materials Technology Institute (MTI) have performed two surveys, between 1988 and l990, requesting recognized developers of ES in corrosion-related areas to provide very specific information concerning the availability, scope, and performance of their systems (Ref 40). A review of the information presented in these reports was summarized (Ref 41), and other developments in expert systems for corrosion prevention and control were reported subsequently (Ref 42).
Neural Networks. A modeling neural network essentially acts as a mapping operator or a transfer function, taking inputs normally fed to a process and computing its predicted output values (Ref 36). Because the input-output mapping can be either static or dynamic, the technology can be applied to a broad range of applications, being particularly efficient with real-time operations. However, neural networks are also well adapted to perform other implicit expert functions, such as pattern recognition and classification.
An artificial neural network (ANN) is a network of many very simple processors or neurons (Fig. 22), each possibility having a small amount of local memory. The interaction of the neurons in the network is roughly based on the principles of neural science. Unidirectional channels that carry numeric data based on the weights of connections connect these neurons, which operate only on their local data and on the inputs they receive via the connections. Most neural networks have some sort of training rule. The training algorithm adjusts the weights on the basis of presented patterns. In other words, neural networks “learn” from examples. Artificial neural networks excel particularly at problems where pattern recognition is important and precise computational answers are not required. When ANNs inputs and/or outputs contain evolved parameters, their computational precision and extrapolation ability significantly increases and can even outperform more traditional modeling techniques. Some applications of ANN to corrosion problems are briefly described below.

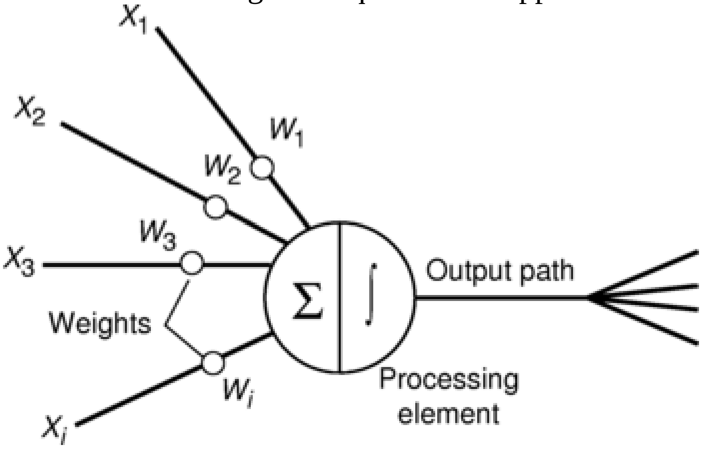

Fig. 22 Schematic of a single processor or neuron in an artificial neural network

Predicting the SCC Risk of Stainless Steels. The risk of encountering a SCC situation was functionalized in terms of the main environment variables (Ref 43). Case histories reflecting the influence of temperature, chloride concentration, and oxygen concentration have been analyzed by means of a back-propagation network. Three neural networks were developed. One was created to reveal the temperature and chloride concentration dependency (Fig. 23) and another to expose the combined effect of oxygen and chloride content in the environment. The third ANN was trained to explore the combined effect of all three parameters. During this project, ANNs were found to outperform traditional mathematical regression techniques, where the functions have to be specified before performing the analysis.

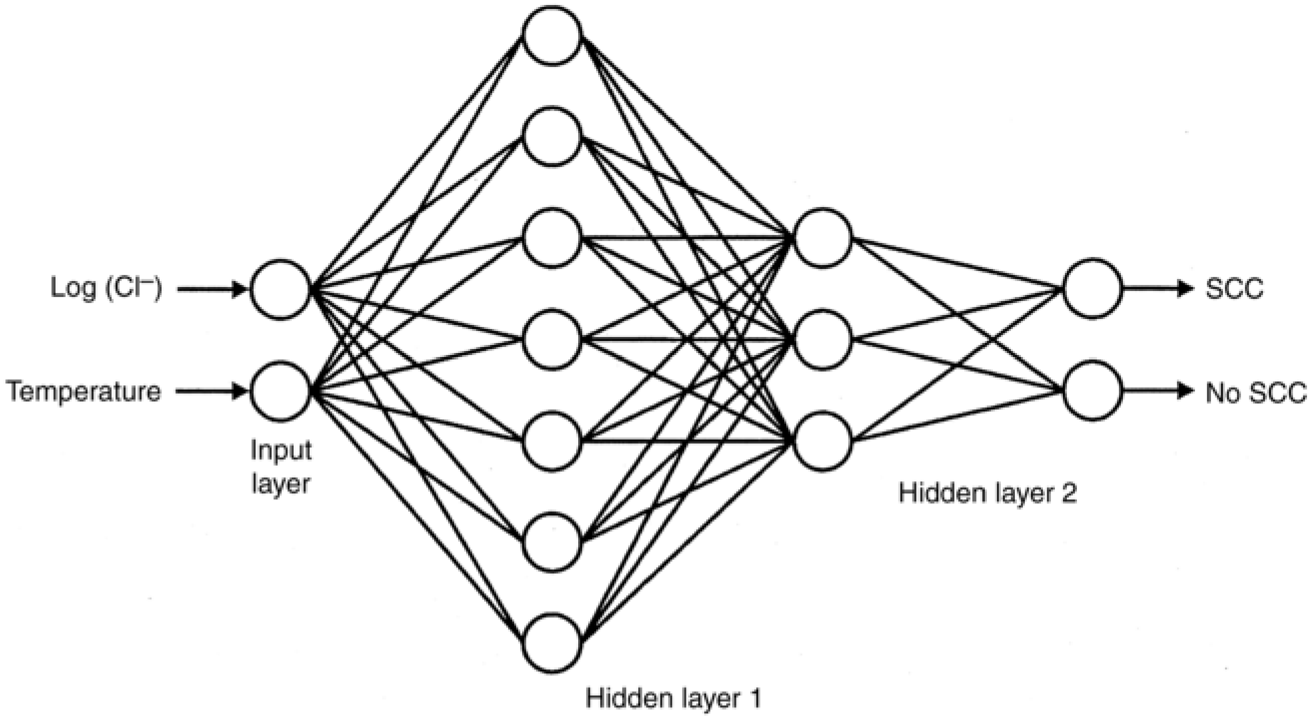

Fig. 23 Four-layer neural network architecture (one input, one output, and two middle computing hidden layers) for the prediction of stress-corrosion cracking (SCC) risk of austenitic stainless steels in industrial processes

Corrosion Prediction from Polarization Scans. An ANN was put to the task of recognizing certain relationships in potentiodynamic polarization scans in order to predict the occurrence of general or localized corrosion, such as pitting and crevice (Ref 44). The initial data inputs were derived by carefully examining a number of polarization scans for a number of systems and recording those features that were used for the predictions. Table 6 lists the initial inputs used and how the features were digitized for computer input. The variables shown were chosen because they were thought to be the most significant in relation to the predictions (Table 6). The final ANN proved to be able to make appropriate predictions using scans outside the initial training set. The resulting ANN was embedded in an ES to facilitate the input of data and the interpretation of the numerical output of the ANN.

Table 6 Data inputs and outputs for predicting corrosion out of polarization scans with an artificial neural network

Parameter	Value of feature
Input	
Repassivation potential	E_{prot} - E_{corr}
Pitting potential	E_{pit} - E_{corr}
Hysteresis	+1 = Positive
	0 = None
	-1 = Negative
Current density at scan reversal	μA/cm^2
Anodic nose	+1 = Yes
	0 = No
Passive current density	μA/cm^2
Potential at anodic-cathodic transition	$E_{a\ to\ c}$ - E_{corr}
Output	
Crevice corrosion predicted	+1 = Yes
	0 = No
Pitting predicted	+1 = Yes

	0 = No
Should general corrosion be considered	+1 = Yes
	0 = No

E_{prot}, repassivation (or protection) potential; E_{corr}, corrosion potential; E_{pit}, pitting potential; $E_{A\ to\ C}$, anodic to cathodic potential

Predicting the Degradation of Nonmetallic Lining Materials. An ANN was trained to recognize the pattern between results from a sequential immersion test for nonmetallic materials and the behavior of the same material in field applications (Ref 45). Eighty-nine cases were used for the supervised training of the network. Another 17 cases were held back for testing of the trained network. An effort was made to ensure that both sets had experimental data taken from the same test but using different samples. Appropriate choice of features enabled the ANN to mimic the expert with reasonable accuracy. The successful development of this ANN was another indication that ANNs could seriously aid in projecting laboratory results into field predictions.

Validation and Extrapolation of Electrochemical Impedance Data. The ANN developed in this project had three independent input vectors: frequency, pH, and the applied potential (Ref 46). The ANN was designed to learn from the invisible or hidden information at high and low frequencies and to predict in a lower frequency range than that used for training. Eight sets of impedance data acquired on nickel electrodes in phosphate solutions were used for this project. Five sets were used for training the ANN and three for its testing. The ANN proved to be a powerful technique for generating diagnostics at these conditions.

Modeling CO_2 Corrosion. A CO_2 corrosion worst-case model based on an ANN approach was developed and the model validated against a large experimental database (Ref 47). An experimental database was used to train and test the ANN. It consisted initially of six elemental descriptors (temperature, partial CO_2 pressure, ferrous and bicarbonate ion concentrations, pH, and flow velocity) and one output, that is, the corrosion rate. The system demonstrated superior interpolation performance compared to two well-known semiempirical models. The ANN model also demonstrated extrapolation capabilities comparable to a purely mechanistic electrochemical CO_2 corrosion model.

Pitting of Aluminum in Natural Waters. The development and testing of an ANN model for the prediction of pitting of aluminum alloy A91100 was demonstrated in the context of nuclear waste storage (Ref 48). The U.S. Department of Energy Savannah River site for the extended storage of aluminum-clad spent nuclear fuel, where most of this waste is stored in large water basins, is fully equipped with corrosion control programs. Vigilant monitoring and regulation of water chemistry has reduced the occurrence of pitting to essentially zero. Trained ANN models, based on the configuration described in Fig. 24, were used to predict pit depths for periods up to 1 year. Because the supply waters contained species not included in the training data of these models, correlation between predicted and actual pit depth deteriorated for longer time periods.

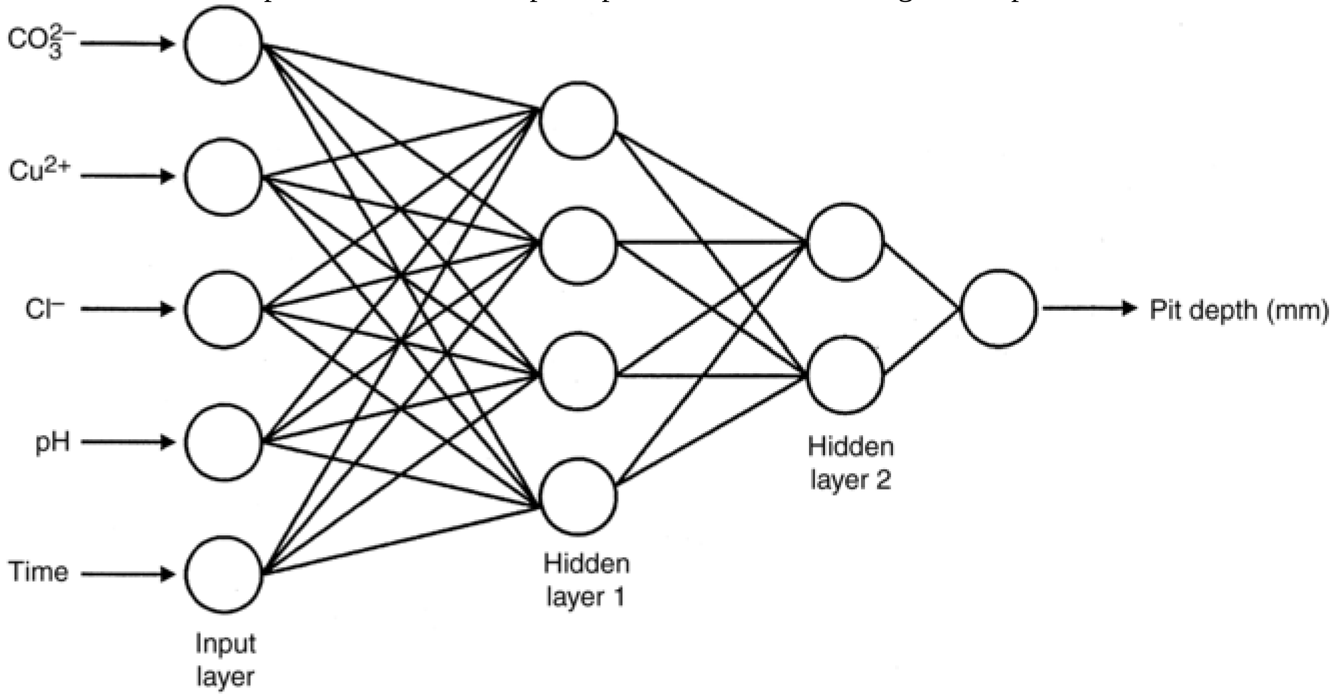

Fig. 24 Four-layer neural network architecture (one input, one output, and two middle computing hidden layers) for the prediction of pitting of aluminum as a function of water chemistry variables

References cited in this section

36. K.R. Trethewey and P.R. Roberge, Design and Structure of Knowledge-Based Systems for Improved Materials Performance, *Corros. Rev.,* Vol 15, 1997, p 71–94

37. P.E. Slatter, Models of Expertise in Knowledge Engineering, *Knowledge Engineering,* Vol 1, McGraw Hill, 1990

38. J. Durkin, *Expert Systems: Design and Development,* MacMillan Publishing Co., 1994

39. A. Basden, On the Applications of Expert Systems, *Int. J. Man Mach. Stud.,* Vol 19, 1983, p 461–472

40. *Report of Task Group 1 of the Working Party on Expert Systems in Materials Engineering,* Materials Technology Institute, 1990, p 1–124

41. P.R. Roberge, Bridging the Gap Between the World of Knowledge and the World That Knows, *Mater. Perform.,* Vol 33, 1994, p 52–56

42. P.R. Roberge, Expert Systems for Corrosion Prevention and Control, *Corros. Rev.,* Vol 15, 1997, p 1–14

43. H.M.G. Smets and W.F.L. Bogaerts, SCC Analysis of Austenitic Stainless Steels in Chloride-Bearing Water by Neutral Network Techniques, *Corrosion,* Vol 48, 1992, p 618–623

44. E.M. Rosen and D.C. Silverman, Corrosion Prediction from Polarization Scans Using Artificial Neural Network Integrated with an Expert System, *Corrosion,* Vol 48, 1992, p 734–745

45. D.C. Silverman, Artificial Neural Network Predictions of Degradation of Nonmetallic Lining Materials from Laboratory Tests, *Corrosion,* Vol 50, 1994, p 411–418

46. M. Urquidi-MacDonald and P.C. Egan, Validation and Extrapolation of Electrochemical Impedance Spectroscopy Data, *Corros. Rev.,* Vol 15, 1997, p 169–194

47. S. Nesic and M. Vrhovac, A Neural Network Model for CO_2 Corrosion of Carbon Steel, *J. Corros. Sci. Eng.,* Vol 1, 1998, p 1–11

48. J. Leifer and J.I. Mickalonis, Prediction of Aluminum Pitting in Natural Waters via Artificial Neural Network Analysis, *Corrosion,* Vol 56, 2000, p 563–571

P.R. Roberge, Modeling Corrosion Processes, *Corrosion: Fundamentals, Testing, and Protection*, Vol 13A, *ASM Handbook*, ASM International, 2003, p 430–445

Modeling Corrosion Processes

P.R. Roberge, Royal Military College of Canada

References

1. T. Kuhn, *The Structure of Scientific Revolutions,* University of Chicago Press, 1970

2. P. O'Rorke, S. Morris, and D. Schulenburg, Theory Formation by Abduction: A Case Study Based on the Chemical Revolution, *Computational Models of Scientific Discovery and Theory Formation,* J. Shrager and P. Langley, Ed., Morgan Kaufmann Publishing, 1990

3. G.E.P. Box and N.R. Draper, *Empirical Model-Building and Response Surfaces,* John Wiley and Sons, 1987

4. M. Pourbaix, *Atlas of Electrochemical Equilibria in Aqueous Solutions,* NACE International, 1974

5. D.R.H. Jones, *Materials Failure Analysis: Case Studies and Design Implications,* Pergamon Press, 1993

6. P.R. Roberge, *Handbook of Corrosion Engineering,* McGraw Hill, 1999

7. W.T. Thompson, M.H. Kaye, C.W. Bale, and A.D. Pelton, Pourbaix Diagrams for Multielement Systems, *Uhlig's Corrosion Handbook,* R.W. Revie, Ed., Wiley Interscience, 2000, p 125–136

8. C. Wagner and W. Traud, Uber die deutung von korrosionvorgangen durch uberlagerung von elektrochemischen teilvorgangen und uber die potentialbildung an mischellektroden, *Z. Elektrochemie,* Vol 44, 1938, p 391-402

9. U.R. Evans, *An Introduction to Metallic Corrosion,* Edward Arnold, London, U.K., 1948

10. J.I. Munro, Anodic Protection of White and Green Liquor Tankage With and Without the Use of Protective Organic Linings, *Proceedings of the Seventh International Symposium on Corrosion in the Pulp and Paper Industry,* (Atlanta, GA), Technical Association of the Pulp and Paper Industry (TAPPI), 1992, p 117–130

11. D. Tromans, Anodic Polarization Behavior of Mild Steel in Hot Alkaline Sulfide Solutions, *J. Electrochem. Soc.,* Vol 127, 1980, p 1253–1256

12. A. Anderko, P. McKenzie, and R.D. Young, Computation of Rates of General Corrosion Using Electrochemical and Thermodynamic Models, *Corrosion,* Vol 57, 2001, p 202–213

13. A. Anderko and R.D. Young, “A Model for Calculating Rates of General Corrosion of Carbon Steel and 13% Cr Stainless Steel in CO_2/H_2S Environments,” Paper 086, Corrosion 2001, NACE International, 2001

14. A. Anderko and R.D. Young, A Model for Corrosion of Carbon Steel in Lithium Bromide Absorption Refrigeration Systems, *Corrosion,* Vol 56, 2000, p 543–555

15. M. Rafal, J.W. Berthold, N.C. Scrivner, and S.L. Grise, Models for Electrolyte Solutions, *Models for Thermodynamic and Phase Equilibria Calculations,* S.I. Sandler, Ed., Marcel Dekker, 1995, p 601–670

16. A.H. Truesdell and B.F. Jones, A Computer Program for Calculating Chemical Equilibria of Natural Waters, *J. Res., US Geol. Surv.,* Vol 2, 1974, p 233–248

17. R.J. Ferguson, A.J. Freedman, G. Fowler, A.J. Kulik, J. Robson, and D.J. Weintritt, The Practical Application of Ion Association Model Saturation Level Indices to Commercial Water Treatmant Problem Solving, *Mineral Scale Formation and Inhibition,* Z. Amjad Ed., Plenum Press, 1995, p 323–340

18. R.J. Ferguson, O. Codina, W. Rule, and R. Baebel, “Real-Time Control of Scale Inhibitor Feed Rate,” IWC-88-57, 49th Annual Meeting, (Pittsburg, PA). International Water Conference, 1988

19. R.J. Ferguson, “Computerized Ion Association Model Profiles Complete Range of Cooling System Parameters,” IWC-91-47, 52nd Annual Meeting, (Pittsburg, PA), International Water Conference, 1991

20. R.A. Adey and J. Baynham, “Design and Optimization of Cathodic Protection Systems Using Computer Simulation,” Paper 723, Corrosion 2000, NACE International, 2000

21. V.G. DeGiorgi and K.E. Lucas, Computational Design of ICCP Systems: Lessons Learned and Future Directions, *Designing Cathodic Protection Systems for Marine Structures and Vehicles,* STP 1370, H.P. Hack, Ed., ASTM, 1999, p 87–100

22. R.W. Ditchfield, J.N. McGrath, and D.J. Tighe-Ford, Theoretical Validation of the Physical Scale Modeling of the Electrical Potential Characteristics of Marine Impressed Current Cathodic Protection, *J. Appl. Electrochem.,* Vol 25, 1995, p 54–60

23. R.C. John, A.D. Pelton, A.L. Young, W.T. Thompson, I.G. Wright, and T.M. Besmann, Managing Corrosion Engineering Information for Metals in Hot Corrosive Gases, *Materials Design Approaches and Experiences,* J.C., Zhao, M. Fahrmann, and T.M. Pollock, Ed., 4–8 Nov 2001 (Indianapolis, IN), TMS, 2001, p 359–382

24. R.C. John, “Compilation and Use of Corrosion Data for Alloys in Various High- Temperature Gases,” Paper 99073, Corrosion 99, NACE International, 1999

25. C.W. Bale, A.D. Pelton, and W.T. Thompson, Facility for the Analysis of Chemical Thermodynamics (F*A*C*T), Ecole Polytechnique/McGill University, Montreal, Canada, 1996

26. D.W. Shoesmith, B.M. Ikeda, and D.M. LeNeveu, Modeling the Failure of Nuclear Waste Containers, *Corrosion,* Vol 53, 1997, p 820–829

27. D.W. Hoeppner, V. Chandrasekaran, and A.M.H. Taylor, “Review of Pitting Corrosion Fatigue Models,” ICAF '99, 12–16 July 1999 (Bellevue, WA), International Committee of Aeronautical Fatigue (ICAF), 1999

28. S. Kawai and K. Kasai, Considerations of Allowable Stress of Corrosion Fatigue (Focused on the Influence of Pitting), *Fatigue Fract. Eng. Mater. Struct.,* Vol 8, 1985, p 115–127

29. S.F. Biagiotti, Jr. and M.P. Gloven, “Pipeline Risk Assessment and Effective Resource Allocation,” Paper 481, Corrosion 2000, NACE International, 2000

30. R.W. Staehle, Lifetime Prediction of Materials in Environments, *Uhlig's Corrosion Handbook,* R.W. Revie, Ed., Wiley Interscience, 2000, p 27–84

31. *Fault Tree Analysis Application Guide,* Reliability Analysis Center, 1990

32. P.R. Roberge, Eliciting Corrosion Knowledge Through the Fault-Tree Eyeglass, *Modelling Aqueous Corrosion: From Individual Pits to Corrosion Management,* K.R. Trethewey and P.R. Roberge, Ed., Kluwer Academic Publishers, 1994, p 399–416

33. D. Nakata, MSG-3 Aircraft Systems/Powerplant Analysis Method, *Aircraft Maintenance and Reliability Seminar/Workshop,* Vol 1, Transportation Systems Consulting Corp., 1997

34. *BBAD Maintenance Program: Policy and Procedures Handbook,* Bombardier Inc., 1994

35. W.K. Muhlbauer, *Pipeline Risk Management Manual,* Gulf Publishing Co., 1996

36. K.R. Trethewey and P.R. Roberge, Design and Structure of Knowledge-Based Systems for Improved Materials Performance, *Corros. Rev.,* Vol 15, 1997, p 71–94

37. P.E. Slatter, Models of Expertise in Knowledge Engineering, *Knowledge Engineering,* Vol 1, McGraw Hill, 1990

38. J. Durkin, *Expert Systems: Design and Development,* MacMillan Publishing Co., 1994

39. A. Basden, On the Applications of Expert Systems, *Int. J. Man Mach. Stud.,* Vol 19, 1983, p 461–472

40. *Report of Task Group 1 of the Working Party on Expert Systems in Materials Engineering,* Materials Technology Institute, 1990, p 1–124

41. P.R. Roberge, Bridging the Gap Between the World of Knowledge and the World That Knows, *Mater. Perform.,* Vol 33, 1994, p 52–56

42. P.R. Roberge, Expert Systems for Corrosion Prevention and Control, *Corros. Rev.,* Vol 15, 1997, p 1–14

43. H.M.G. Smets and W.F.L. Bogaerts, SCC Analysis of Austenitic Stainless Steels in Chloride-Bearing Water by Neutral Network Techniques, *Corrosion,* Vol 48, 1992, p 618–623

44. E.M. Rosen and D.C. Silverman, Corrosion Prediction from Polarization Scans Using Artificial Neural Network Integrated with an Expert System, *Corrosion,* Vol 48, 1992, p 734–745

45. D.C. Silverman, Artificial Neural Network Predictions of Degradation of Nonmetallic Lining Materials from Laboratory Tests, *Corrosion,* Vol 50, 1994, p 411–418

46. M. Urquidi-MacDonald and P.C. Egan, Validation and Extrapolation of Electrochemical Impedance Spectroscopy Data, *Corros. Rev.,* Vol 15, 1997, p 169–194

47. S. Nesic and M. Vrhovac, A Neural Network Model for CO_2 Corrosion of Carbon Steel, *J. Corros. Sci. Eng.,* Vol 1, 1998, p 1–11

48. J. Leifer and J.I. Mickalonis, Prediction of Aluminum Pitting in Natural Waters via Artificial Neural Network Analysis, *Corrosion,* Vol 56, 2000, p 563–571

F. Mansfeld, Electrochemical Methods of Corrosion Testing, *Corrosion: Fundamentals, Testing, and Protection*, Vol 13A, *ASM Handbook*, ASM International, 2003, p 446–462

Electrochemical Methods of Corrosion Testing

Florian Mansfeld, University of Southern California

Introduction

DURING CORROSION, at least two electrochemical reactions, an oxidation and a reduction reaction, occur at a metal-electrolyte interface. Because corrosion is due to an electrochemical mechanism, it is clear that electrochemical techniques can be used to study corrosion reactions and mechanisms. This article reviews the fundamentals of electrochemical corrosion test methods, preparations for electrochemical polarization experiments, and the various electrochemical techniques available for laboratory studies of corrosion phenomena.

F. Mansfeld, Electrochemical Methods of Corrosion Testing, *Corrosion: Fundamentals, Testing, and Protection*, Vol 13A, *ASM Handbook*, ASM International, 2003, p 446–462

Electrochemical Methods of Corrosion Testing

Florian Mansfeld, University of Southern California

Fundamentals

The basis of all electrochemical techniques lies in the principle of mixed-potential theory, which was clearly established in a classic paper published in 1938 (Ref 1). It was demonstrated that uniform corrosion occurs when anodic and cathodic reactions take place in constant change of location and time of the individual processes. In this concept, it is not necessary to postulate the presence of local anodes and cathodes for corrosion to occur. Nevertheless, in later years it has often been stated that corrosion occurs when local anodes and cathodes have been established, despite the obvious fact that, in this case, uniform corrosion is not possible. The corrosion potential, E_{corr}, or open-circuit potential (OCP), is a mixed potential; that is, it is the unique potential at which the rates of the anodic and cathodic reaction are exactly equal. The rate of the anodic or the cathodic reaction at E_{corr} equals the corrosion rate. Because the rates of these two reactions are independent of each other, it is possible to inhibit corrosion by reducing the rate of only one of the two reactions by using, for example, anodic or cathodic corrosion inhibitors. Cathodic protection in which the material to be protected is polarized cathodically in order to reduce the rate of the anodic metal dissolution reaction is another example. The concept of mixed-potential theory and its application in corrosion science and technology has been discussed in many textbooks (Ref 2, 3).

The use of mixed-potential theory for the monitoring of corrosion rates was also demonstrated by showing that the slope of a potential versus current density plot at E_{corr} can be used to determine the corrosion rate (Ref 1). Today, this technique is referred to as the polarization- resistance technique or, less precisely, as the linear polarization technique (Ref 4). From this research, it also becomes clear that corrosion current densities, i_{corr}, can be obtained from the analysis of anodic and cathodic polarization curves, which is often referred to as Tafel extrapolation (Ref 2, 3). This concept has been developed further (Ref 4, 5). In addition, mechanistic information can be obtained by analysis of the Tafel slopes that have characteristic values, depending on the nature of the rate-determining step in the corrosion mechanism (Ref 2, 4).

A large number of electrochemical techniques are available for laboratory studies of various corrosion phenomena as well as for corrosion monitoring (Ref 6, 7, 8, 9, 10). The National Association of Corrosion Engineers (NACE) series, *Corrosion Testing Made Easy,* contains several volumes that deal with the use of electrochemical methods (Ref 11, 12, 13). The advice given previously (Ref 14)—“Don't be afraid of electrochemical techniques, but use them with care”— applies for laboratory studies. Often, electrochemical techniques are considered to be overly complicated. However, recent developments by the manufacturers of hardware and software have made the use of these techniques quite simple. Most equipment contains software that enables the user to carry out an electrochemical test in a straightforward manner. Of course, interpretation of the results of such tests remains up to the user. Often, only the experimental results are presented; sometimes, the results of very simple measurements, such as E_{corr}, have been overinterpreted. It has to be remembered that electrochemical tests indicate that corrosion has happened but do not contain information concerning the cause of corrosion. Therefore, statements that certain electrochemical techniques such as the electrochemical noise (ECN) technique “offers unique capabilities that should allow quantification of microbial effects on corrosion,” and “ECN offers promise in identifying microbiologically influenced corrosion” (Ref 15) should be viewed with caution.

Electrochemical techniques available for laboratory studies of corrosion phenomena are summarized in Table 1. These techniques range from those in which no external signal is applied, such as E_{corr} and electrochemical noise analysis (ENA), to those in which only a small potential or current perturbation is applied, such as polarization resistance, R_p, and electrochemical impedance spectroscopy (EIS); to those in which the applied potential or current is varied over a wide range, such as anodic and cathodic polarization curves and pitting scans.

Table 1 Electrochemical corrosion testing techniques

Category	Test method
No applied signal	Open circuit or corrosion potential
	Dissimilar metal corrosion (galvanic corrosion)
	Electrochemical noise analysis
Small-signal polarization	Polarization resistance (linear polarization)
	Electrochemical impedance spectroscopy
Large-signal polarization	Potentiostatic and galvanostatic polarization
	Potentiodynamic and galvanodynamic polarization
Scanning electrode techniques	Potential scans
	Current scans
	Electrochemical impedance spectroscopy scans
Miscellaneous tests	Hydrogen permeation
	Anodized aluminum corrosion test
	Electrolytic corrosion test
	Paint adhesion on a scribed surface
	Impedance test for anodized aluminumodized
	Critical pitting temperature

The galvanic current flowing between two dissimilar metals can be monitored using a zero- resistance ammeter (ZRA). Diffusion of atomic hydrogen into metals, such as steel, that can cause failure can be evaluated with the electrochemical permeation method. Scanning electrode techniques can be used to determine the location of anodes and cathodes on electrodes. It has to be recognized that very simple techniques, such as those in which no external signal is applied, usually provide much less quantitative information concerning corrosion mechanisms than those in which a carefully controlled signal is applied to the system under investigation and the response of the system is analyzed. An example for this kind of approach is EIS, in which the frequency of the applied signal is used as an additional variable. ASTM Committee G-1 has published standard practices for most of the techniques listed in Table 1, describing the experimental approach and giving examples for the use of these methods.

References cited in this section

1. C. Wagner and W. Traud, *Z. Elektrochemie,* Vol 44, 1938, p 391
2. H. Kaesche, *The Corrosion of Metals,* NACE, 1985
3. D.A. Jones, *Principles and Prevention of Corrosion,* MacMillan Publishing Co., 1992
4. F. Mansfeld, The Polarization Resistance Technique for Measuring Corrosion Currents, *Advancements in Corrosion Science and Technology,* Vol 6, M.G. Fontana and R.W. Staehle, Ed., Plenum Press, 1976, p 163
5. M. Stern and A.L. Geary, *J. Electrochem. Soc.,* Vol 104, 1957, p 56
6. R. Baboian, Ed., *Electrochemical Techniques for Corrosion,* NACE, 1977
7. *Electrochemical Corrosion Testing,* STP 727, U. Bertocci and F. Mansfeld, Ed., ASTM, 1979
8. R. Baboian, Ed., *Electrochemical Techniques for Corrosion Engineers,* NACE, 1986
9. R. Baboian, Ed., *Corrosion Tests and Standards—Application and Interpretation,* ASTM, 1995
10. R.W. Revie, Ed., *Uhlig's Corrosion Handbook,* 2nd ed., Electrochemical Society Series, Wiley-Interscience, 2000
11. B.J. Little, P.A. Wagner, and F. Mansfeld, *Corrosion Testing Made Easy—Microbiologically Influenced Corrosion,* B.C. Syrett, Ed., NACE, 1997
12. N.G. Thompson and J.H. Payer, *Corrosion Testing Made Easy—dc Electrochemical Methods,* B.C. Syrett, Ed., NACE, 1998
13. R. Cottis and S. Turgoose, *Corrosion Testing Made Easy—Electrochemical Impedance and Noise,* B.C. Syrett, Ed., NACE, 1999
14. F. Mansfeld, *Corrosion,* Vol 44, 1988, p 856
15. G.G. Geesey, I. Beech, P.J. Bremer, B.J. Webster, and D.B. Wells, Biocorrosion, *Biofilms II: Process Analysis and Applications,* J.D. Bryers, Ed., Wiley, 2000, p 281

F. Mansfeld, Electrochemical Methods of Corrosion Testing, *Corrosion: Fundamentals, Testing, and Protection*, Vol 13A, *ASM Handbook*, ASM International, 2003, p 446–462

Electrochemical Methods of Corrosion Testing

Florian Mansfeld, University of Southern California

Preparing an Electrochemical Polarization Experiment

For the performance of most electrochemical tests discussed here, a potentiostat and an electrochemical cell are required. Open-circuit-potential measurements may be performed using only a high-input impedance voltmeter, while galvanic current and ECN measurements may be carried out using a ZRA instead of a potentiostat, as

discussed subsequently. The features and requirements of the instrumentation needed for an electrochemical test are discussed in brief. A more detailed description can be found in Ref 12.
The basic instrumentation needed for the electrochemical tests includes:

- Test or working electrode (WE)
- One or more counter electrodes (CE)
- Reference electrode (RE)
- Test cell
- Potentiostat
- Voltmeters for monitoring of potential and current (optional)
- Recording devices (strip chart or *x*-*y* recorders)
- Computer with software program and plotter (replacing the voltmeter and recording devices) (optional)
- Gas tank with nitrogen, argon, or another gas to deaerate the solution (optional)
- Thermostat with a constant temperature bath or heating mantle (optional)

In a potentiostatic experiment, the applied potential, E_{appl}, is maintained between the RE and WE. The WE is at virtual ground. Therefore, the sign of the potential displayed on the potentiostat is sometimes that of the RE to ground and opposite the potential of the WE. This fact, unfortunately, often leads to confusion concerning the sign of the measured potential. The instruction manual of the potentiostat to be used should be consulted regarding this point. The current flows between CE and WE and is usually displayed with the correct sign (positive for an anodic current). A simple test can be carried out using a zinc WE, which has a very negative E_{corr} versus any common RE, and for which a negative (cathodic) current is recorded when a potential $E < E_{corr}$ is applied.
The minimum requirements for a potentiostatic test are a test cell with WE, RE, CE, a potentiostat, and a recording device (Ref 11, 12). Potential and current can be monitored using voltmeters, although this is also possible with the built-in instruments in the potentiostat. In most current applications of polarization techniques, the experiment is carried out using software that is either supplied by the instrument manufacturer or is available from other commercial sources. This method is a very convenient practice that allows storage of many experimental data that can later be analyzed with appropriate analysis software.
Test or Working Electrode. The WE can be of various shapes, such as a cylinder or a flat disk. Often, the availability of a material as rod or sheet determines the shape of the electrode. When a cylinder is used, it has to be considered that edge effects can play a role due to different current distribution along the WE surface. The metallurgical properties may also be different for the sides and the bottom of the cylinder. Fewer problems occur with a flat disk, especially when care is taken that crevice corrosion does not occur. Not much attention is usually paid to the size of the electrode, with 1 cm^2 (0.2 $in.^2$) being a common test area. However, a much larger size is useful when very small currents have to be measured, while much smaller electrodes are useful when very large currents flow in the system. The error due to the ohmic drop between WE and RE is less when small electrodes are used.
The WE is connected to an electrode holder to which the lead to the potentiostat is attached. Details of the construction of electrode holders appear in Ref 11 and 12 and are not repeated here. It is important that only glass, synthetic fluorine-containing resin, or other nonmetallic materials are immersed as part of the electrode holder. Figure 1 shows electrode holders with a cylinder electrode (Fig. 1a) or a sheet electrode (Fig. 1b).

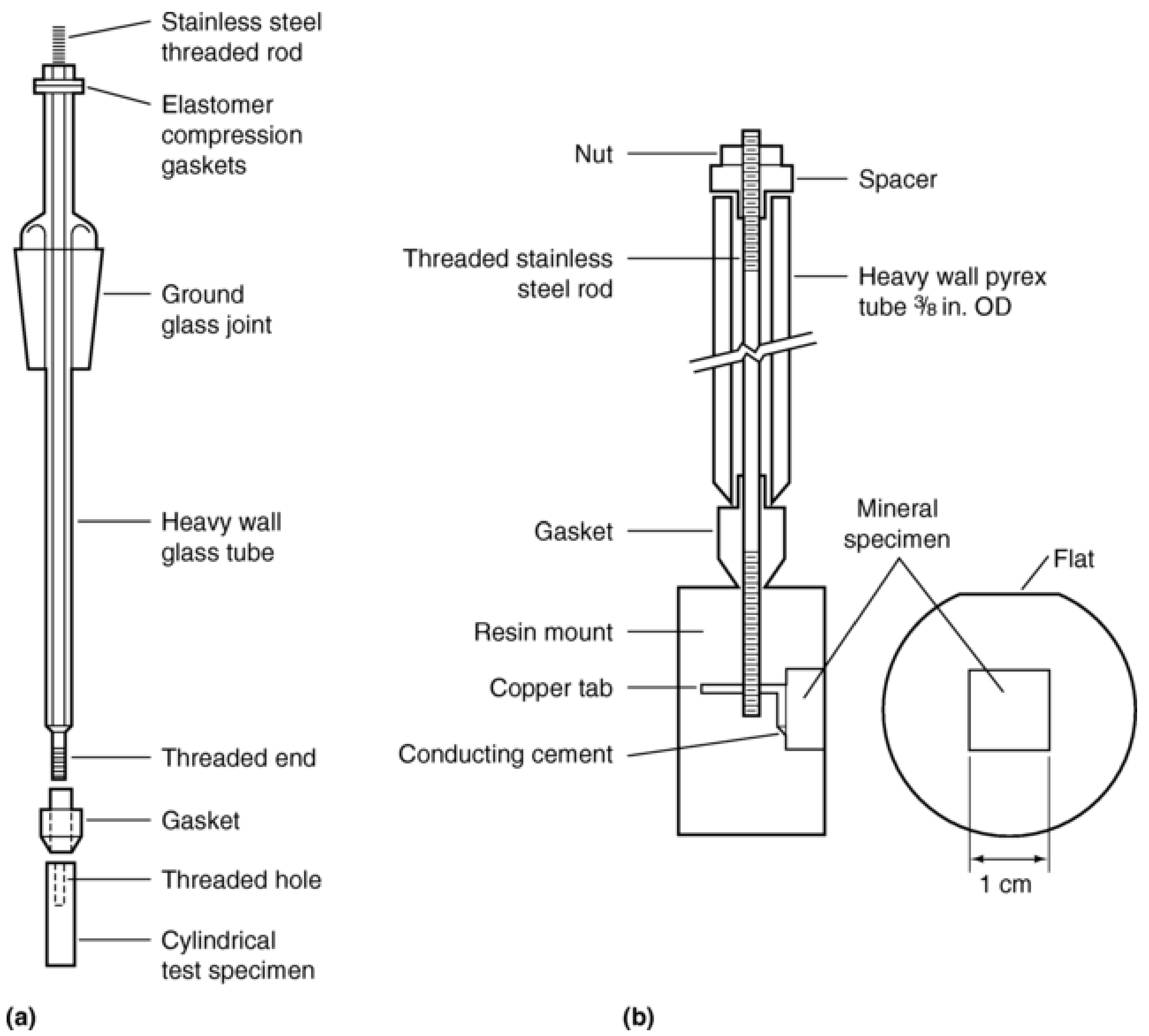

Fig. 1 Test electrodes and electrode holders. (a) Cylindrical electrodes. (b) Flat disk or sheet electrodes. OD, outside diameter

In neutral, aerated solutions, the cathodic reaction (reduction of oxygen) is usually under mass transport control. In this case, the electrochemical experiment should be carried out under controlled hydrodynamic conditions that can be achieved through the use of a rotating disk electrode (Fig. 2a) or a rotating cylinder electrode (RCE) (Fig. 2b). The RCE is preferred for corrosion studies because it provides very good current distribution. Polarization curves may be obtained at a constant rotation speed or as a function of rotation speed in studies where information concerning the details of the diffusion- controlled reduction reaction is required.

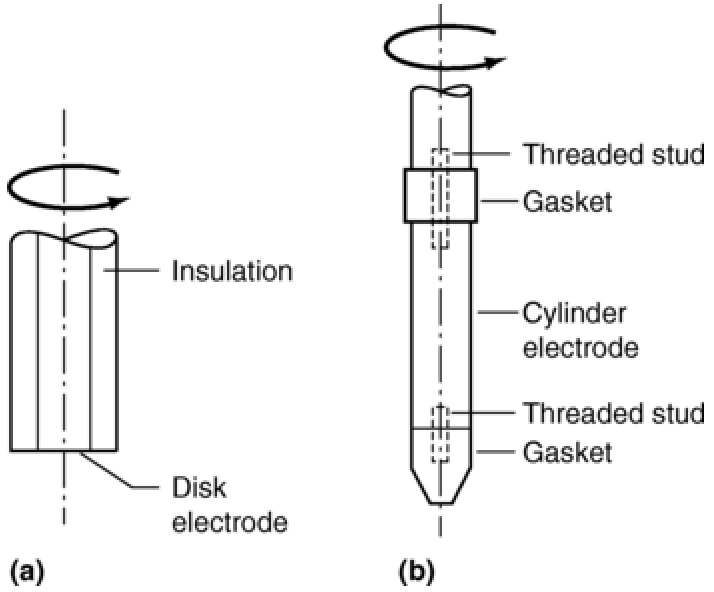

Fig. 2 Test electrodes. (a) Rotating disk electrodes. (b) Rotating cylinder electrodes

Counter Electrode. The choice of the CE is dictated by the requirement that the CE should be of good conductivity and should not dissolve as a result of current flow. Platinum is used in most experiments. Because it is desirable to use CEs that are much larger than the WE in order to reduce the current density at the CE and avoid contamination by reaction products of the electrolyte, less expensive materials, such as graphite, stainless steel, or titanium alloys, are often used as CEs. For the same reason, the CE should be placed in a separate compartment with a glass frit to the main cell. However, this precautionary measure is often neglected.

Reference Electrode. The saturated calomel electrode (SCE) is the most common RE used in studies of corrosion reactions, due to its stability and commercial availability. Care must be taken to avoid contamination of the test electrolyte by leakage of chloride ions from a SCE when tests are carried out in chloride ion-free test solutions. A mercury/mercurous sulfate electrode may be used when chloride ion contamination is not acceptable. Other REs are the Ag/AgCl and the Cu/ $CuSO_4$ electrodes. A luggin capillary is used to minimize the ohmic drop between WE and RE (Ref 11, 12).

A number of REs should be kept in the laboratory, with one RE being set aside as a calibration standard or the master RE, which is not used in actual potential tests. All other REs should be checked against this master RE before use by measuring the potential difference between the two electrodes, using a high-input impedance voltmeter. The potential difference should be less than 2 to 3 mV. Electrodes still showing a large potential difference after this procedure should be reconditioned or discarded.

Test Cell. The design of the test cell can be quite complicated for studies in deaerated solutions with constant temperature control, or very simple in tests with oxygenated solutions at room temperature. Three-compartment cells are often used in the first case, while an open beaker often gives satisfactory results in the second case. For larger sheet electrodes, such as those used in the evaluation of polymer coatings or anodic films (Ref 16), the simple cell with the flat sample exposed horizontally, as shown in Fig. 3, has been used by many authors. The Avesta cell has the advantage that its cell design allows crevice corrosion, which might be a problem with most other cell designs, to be avoided during the test. Important points to consider in assembly of a test cell are the correct placement of the luggin capillary for minimization of the ohmic drop and the CEs for satisfactory current distribution. Deaeration of the test solution is carried out by bubbling nitrogen gas or argon through the test cell for a sufficient time.

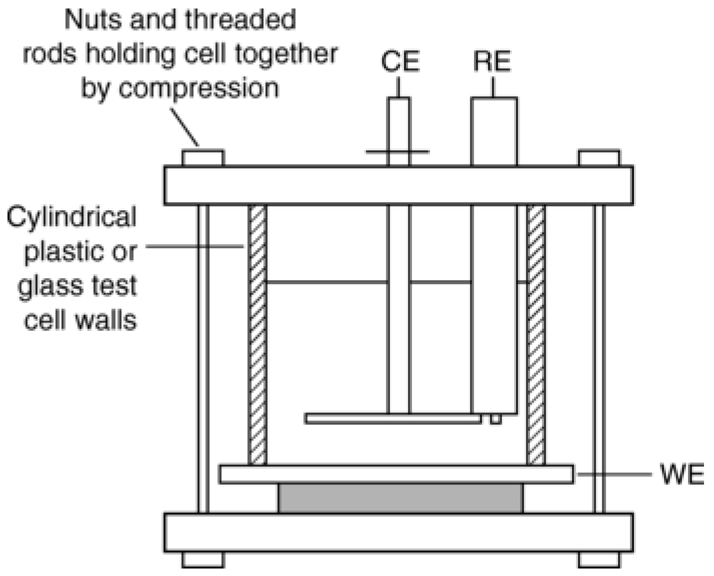

Fig. 3 Test cell for flat sheet electrodes. CE, counter electrode; RE, reference electrode; WE, working electrode

Potentiostat. A number of different potentiostats are available from different manufacturers. These instruments can be very sophisticated, allowing the recording of a number of electrochemical tests under computer control, or quite simple, with only the basic features in a low-cost model. Some newer instruments, using appropriate software, allow simultaneous recording of several experiments.

The main requirements of a potentiostat have been discussed elsewhere in detail (Ref 11, 12). The available range of E_{appl} should be at least ±2 V, and the current capability should be ±1 A. A larger range of E_{appl} may be required for some tests, such as the pitting of titanium alloys. The maximum cell voltage should be approximately 60 V. Outputs should be provided for monitoring of potential and current. For the latter purpose, the current should be provided as a voltage versus ground, which is important for recording of the current on a strip chart or *x-y* recorder. The positive feedback or the current interrupter technique can be used for elimination of the ohmic drop, which can be significant in studies in low-conductivity media such as very dilute solutions and nonaqueous media (Ref 17, 18). The possibility of conducting the experiment under computer control is highly desirable, especially for more complicated tests such as the potentiodynamic tests described subsequently.

Voltmeters. The values of potential and current usually are displayed on the front panel of the potentiostat. Often, only one of these parameters can be read at a given time. Therefore, it is sometimes convenient to observe both values on separate voltmeters, especially when meters with a digital display are used. If current-time (*I-t*) or potential-current (*E-I*) curves are recorded, the use of digital voltmeters is useful to ensure that these curves are recorded correctly.

If it is desired to determine the potential of an electrode directly with a voltmeter rather than from the potential output of the potentiostat, a high-input impedance voltmeter has to be used to prevent current flow and polarization of WE and RE due to the potential measurement. The potential can be recorded on a strip chart recorder using the output of such a voltmeter. In this case, the input impedance of the recorder is not important. However, direct connection of a recorder to the RE and WE should be avoided, because the input impedance of most recorders is quite low.

Recording Devices. For tests in which the current, *I*, is monitored at a fixed value of E_{appl} as a function of time, *t*, a strip chart recorder is needed for the recording of the *I-t* curve. In this case, the current output, which is provided in the potentiostat as a voltage versus ground, is connected to the recorder, with the appropriate settings of the current range on the potentiostat and the voltage range on the recorder.

For tests in which a number of potential steps are applied, increasing in the anodic or cathodic direction, a strip chart or an *x-y* recorder can be used for the recording of the *I-t* curve. In the latter case, the current output is connected to the *y*-axis, and the *x*-axis is set to a time scale that is appropriate for the time used for each potential step.

If a computerized system is used, recording devices are not needed. One of the advantages of the use of proper software is the fact that the electrochemical data are displayed on the screen as they are collected, which allows the researcher to stop an experiment that obviously is not running properly.

Computer with Software Program and Plotter. It is convenient and time saving to use a software program to record polarization data. Most commercial software programs contain a number of typical electrochemical tests, such as potentiostatic, potentiodynamic, galvanostatic polarization, and other tests, such as the measurement of the galvanic current, the electrochemical impedance, or ECN. The user can input the particular parameters that are desired for use in the test. Usually, default values are included in the program, which allows the running of a test with only a few inputs provided by the user.

For a potentiostatic test of type 1 (explained later in this article), the inputs are the applied potential, E_{appl}, and the time for which the potential is applied. Additional inputs depend on the particular software program to be used. The ***I-t*** curve is displayed on the computer screen with a current scale that has been selected by the program. After the test is completed, the ***I-t*** curve can be plotted after reformatting of the two axes into more convenient scales. In a galvanostatic test, a constant current, *I*, is applied for a certain time, and the ***E-t*** curve is monitored.

The potentiostatic test of type 2 (detailed later) requires additional inputs, such as the starting potential and the final potential as well as step height and length. Sometimes, for cleaning or other purposes, the test electrode is held at a preconditioning potential for a certain period before the test is started.

Figure 4 shows a typical arrangement for the application of electrochemical techniques in laboratory studies. The potentiostat connected to the test cell is controlled by a computer with suitable software; the experimental data can be printed out on the printer and/or displayed later, using software designed for analysis of the results of a given electrochemical test (Ref 11, 12).

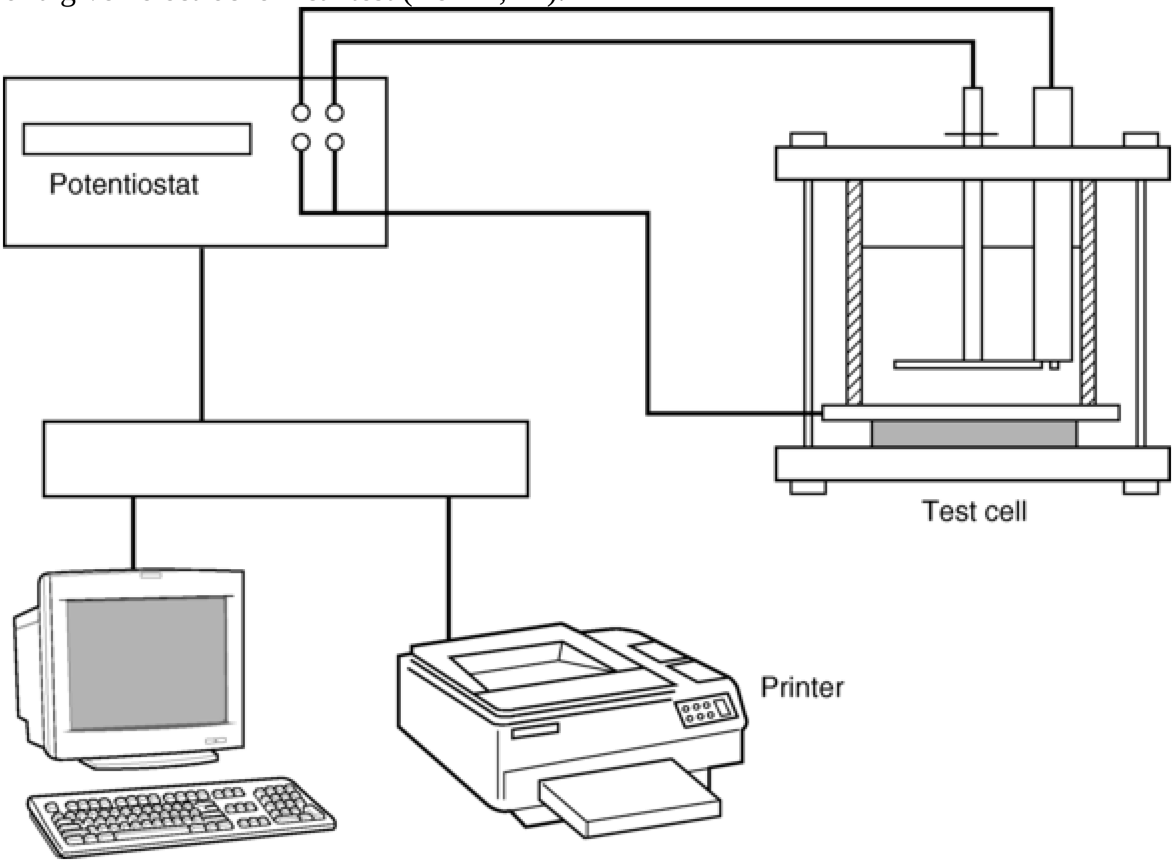

Fig. 4 Experimental arrangement for application of electrochemical techniques in laboratory tests

Thermostat. For studies that require carefully controlled temperatures, the test cell is placed in a constant-temperature bath, or a heating/cooling jacket is placed around the test cell.

References cited in this section

11. B.J. Little, P.A. Wagner, and F. Mansfeld, *Corrosion Testing Made Easy—Microbiologically Influenced Corrosion,* B.C. Syrett, Ed., NACE, 1997

12. N.G. Thompson and J.H. Payer, *Corrosion Testing Made Easy—dc Electrochemical Methods,* B.C. Syrett, Ed., NACE, 1998

16. F. Mansfeld and M.W. Kendig, *Corrosion,* Vol 41, 1985, p 490

17. F. Mansfeld, *Corrosion,* Vol 32, 1976, p 143

18. F. Mansfeld, M.W. Kendig, and S. Tsai, *Corros. Sci.,* Vol 22, 1982, p 455

F. Mansfeld, Electrochemical Methods of Corrosion Testing, *Corrosion: Fundamentals, Testing, and Protection*, Vol 13A, *ASM Handbook*, ASM International, 2003, p 446–462

Electrochemical Methods of Corrosion Testing

Florian Mansfeld, University of Southern California

No-Applied-Signal Tests

In measurements of OCP or E_{corr}, the galvanic current flowing between two dissimilar metals and ECN, no external electrochemical signal is applied. In one approach to the measurement of ECN data, the galvanic current flowing between two electrodes of the same material maintained at zero potential and the potential of this couple versus a stable RE are recorded simultaneously.

Open-Circuit or Corrosion Potential. Measurement of E_{corr} is the easiest electrochemical test to perform, but it provides the least amount of mechanistic information. Measurement of E_{corr} requires a stable reference electrode, such as a SCE, a high-impedance voltmeter, and, in most cases, a suitable recording device. Corrosion potential can be determined also by observing the digital display on the potentiostat, monitored by recording the potential output value from the potentiostat on a strip chart recorder as a function of exposure time or, if a suitable software program is used, by plotting the potential- time curve stored on a disk on a printer after the test is finished.

Open-circuit potential often increases with time for passive samples as passivity improves, and OCP often decreases when localized corrosion begins.

The time dependence of E_{corr} has been monitored by many groups investigating the effects of biofilm formation on localized corrosion of stainless steels in natural seawater (Ref 19). Most published data show a rapid ennoblement of E_{corr} (i.e., a shift to more positive values) during the first days of exposure.

The corrosion potential was monitored for Al 2024, mild steel, and cartridge brass during exposure to abiotic artificial seawater (AS) and to AS containing *Shewanella algae* or *Shewanella ana* (Ref 20). For Al 2024 (Fig. 5a) and brass (Fig. 5b), E_{corr} decreased in the presence of bacteria, while for mild steel (Fig. 5c), an increase of E_{corr} was observed. After exposure for 7 days to AS containing *S. ana*, kanamycin was added to kill the bacteria, and E_{corr} changed to the values observed in the abiotic AS for Al 2024 and brass but not for mild steel (Fig. 5). Electrochemical impedance spectroscopy was used to determine the corrosion mechanism of these systems in more detail (Ref 20).

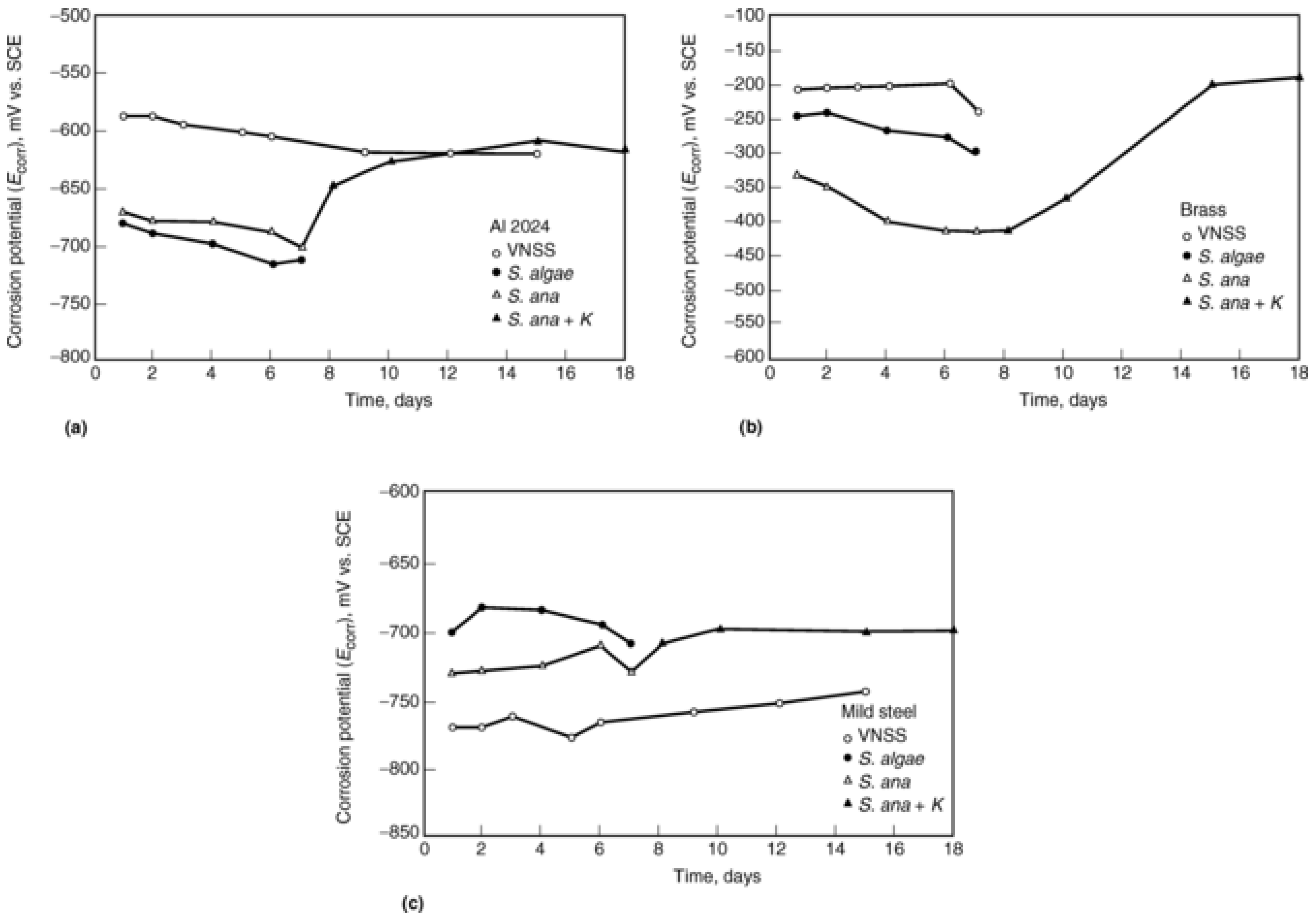

Fig. 5 Time dependence of corrosion potential (E_{corr}) for (a) Al 2024, (b) brass, and (c) mild steel exposed to artificial seawater with or without bacteria. VNSS, Väätänen nine salts solution. *K*, kanamycin. Source: Ref 20

The main problem with the use of E_{corr} measurements is overinterpretation. Based on information obtained with E_{corr} alone, it is not possible to determine whether corrosion rates have increased or decreased. Some authors have interpreted shifts of E_{corr} in the negative direction as a reduction of the rate of cathodic reaction or an increase of the rate of the anodic reactions. These are the two simplest possibilities that can be expected to lead to the observed result. However, without additional data, such as measurement of the polarization resistance (R_p), no valid mechanistic conclusions can be drawn.

Dissimilar Metal Corrosion (Galvanic Corrosion). Short-circuit currents between dissimilar metals or metals exposed to electrolytes of different composition need to be measured by means of a ZRA, because the introduction of a milliammeter with an internal resistance, R_i, in a low-resistance circuit may alter the total current by producing a potential difference, IR_i, between the two electrodes. The ZRA based on operational amplifiers, which was introduced in 1970 by Lauer and Mansfeld (Ref 21) for corrosion studies (Fig. 6), applies 0 mV potential difference between the two electrodes in the galvanic couple. The potential of the couple should be measured versus a RE in order to obtain additional information concerning the corrosion mechanism. A potentiostat can be used as a ZRA by setting the applied potential to 0 mV. The galvanic current is monitored as the current output of the potentiostat.

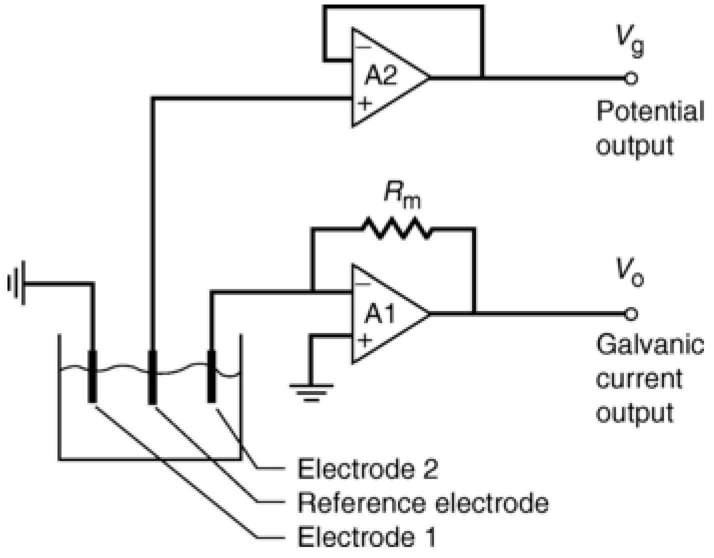

Fig. 6 Instrumental arrangement for continuous measurement of the galvanic current and potential. A1 and A2 represent operational amplifiers. R_m, measuring resistor; V_g, galvanic voltage; V_o, output voltage. Source: Ref 22

In using a ZRA based on operational amplifiers, one electrode is connected to the grounded input (Fig. 6). The galvanic current, I_g, needed to maintain 0 mV between the two electrodes is monitored as the output voltage $V_o = I_g R_m$, where R_m is the measuring resistor. The measuring resistor can be varied to maintain V_o in a convenient range, that is, 0 to 1 V. The potential V_g of the galvanic couple is measured with the voltage follower (A2 in Fig. 6), which determines the potential of the RE versus ground. Both V_o and V_g can be recorded on strip chart recorders or other devices. The advantage of the design in Fig. 6 is its low cost, which allows construction of several devices and monitoring of multiple test cells at the same time. Operational amplifiers can also be used to construct inexpensive and versatile potentiostats, as discussed elsewhere (Ref 22).

The galvanic current is a measure of the increase of the corrosion current of the anode due to the coupling to the cathode and does not allow calculation of the corrosion rate of either electrode (Ref 23). Simultaneous measurements of the galvanic current and the potential of the coupled electrodes using a RE allow determination of the changes of the kinetics of the corrosion reactions with exposure time. It has to be recognized that the magnitude of the measured galvanic current depends on the area ratio of anode and cathode, A^c to A^a. If this ratio is not 1, then the measured galvanic current, I_g, has to be normalized to determine the galvanic current densities, $i_g^a = I_g/A^a$ and $i_g^c = I_g/A^c$, which have different numerical values (Ref 24).

Detailed studies have been conducted on the galvanic corrosion of aluminum alloys coupled to a number of materials (Ref 25, 26). Figure 7 shows the time dependence of the galvanic current, I_g, (Fig. 7a) and the potential, E_g, (Fig. 7b) of different galvanic couples versus a SCE (Ref 25). Galvanic current flowing between Al 2024 and a dissimilar metal decreased in the sequence copper > 304 stainless steel > Ti-6Al-4V, indicating that copper acted as an efficient cathode, while the titanium did not cause significant galvanic corrosion of Al 2024. For couples involving cadmium or zinc, Al 2024 was protected cathodically (Fig. 7a). Except for the couple involving zinc, E_g remained close to E_{corr} of Al 2024 (Fig. 7b). Similar results were obtained for Al 7075 (Fig. 7). A ZRA has been used to evaluate the effect of dichromate additions on the galvanic corrosion of a brass-steel couple in aerated 20% NaCl (Ref 27).

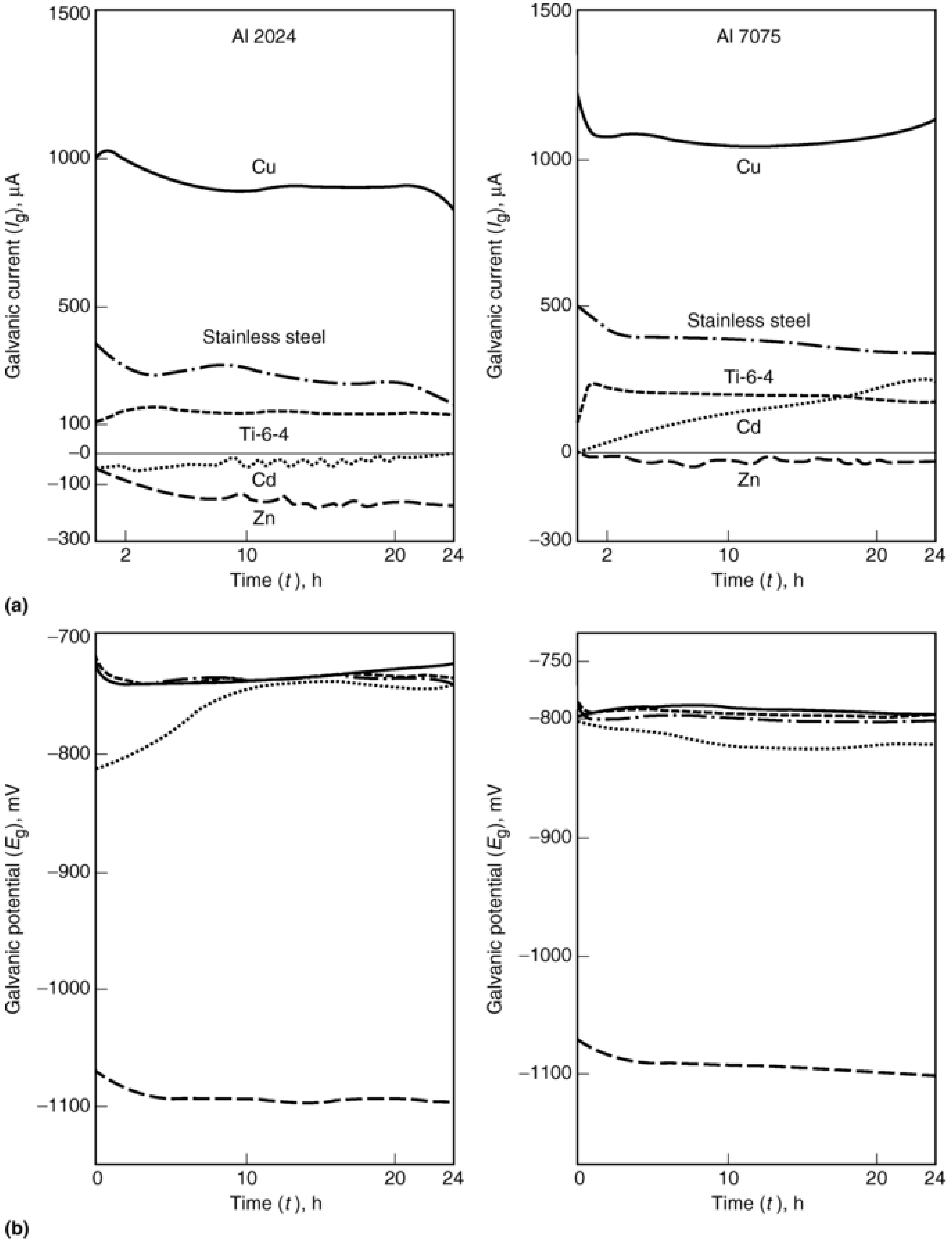

Fig. 7 Time dependence of (a) galvanic current (I_g) and (b) galvanic potential (E_g) for Al 2024 and Al 7075 coupled to different dissimilar materials in aerated 3.5% NaCl. Source: Ref 25

Electrochemical Noise Analysis (ENA). Electrochemical noise data can be obtained as fluctuations of E_{corr}; as fluctuations of the potential, E, at an applied current, I; or as fluctuations of I at an applied E. Recently, it has

become common practice—at least in laboratory studies—to measure potential and current fluctuations simultaneously, as shown in Fig. 8 (Ref 28, 29, 30, 31). In this approach, two electrodes of the same material are coupled through a ZRA. Current fluctuations are measured using the ZRA, while the potential fluctuations are measured with a high-impedance voltmeter between the two coupled electrodes and an RE, which could be a stable RE, such as an SCE, or a third electrode of the same material as the two test electrodes (Ref 28, 29). The latter approach is commonly used in corrosion monitoring. A review of different methods for collection of ECN data can be found in Ref 32.

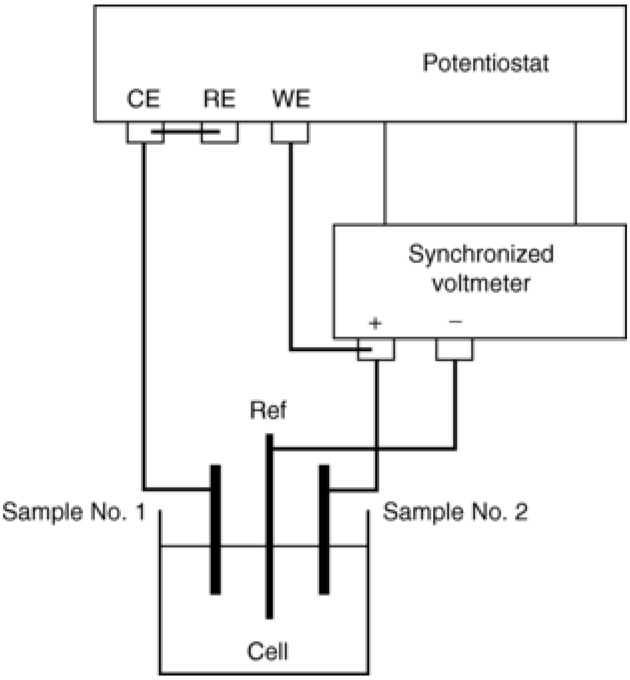

Fig. 8 Experimental arrangement for simultaneous collection of potential and current fluctuations. Source: Ref 30

Simultaneous collection of potential and current ECN data allows ENA in the time and the frequency domains. Various methods of data analysis have been discussed in detail (Ref 30, 31, 33, 34, 35). The parameters commonly determined in these analyses are listed in Table 2. Figure 9 shows experimental potential, *V*, (Fig. 9a) and current, *I*, (Fig. 9b) fluctuations for mild steel exposed to aerated 0.5 *N* NaCl as well as the power spectral density (PSD) plots for these data (Fig. 9c, d) (Ref 36). The drift in the raw experimental data that causes erroneous PSD slopes was removed using a linear method (Ref 36). From the PSD plots for potential and current fluctuations, the spectral noise or noise impedance plot (R_{sn}) (Fig. 9e) can be determined as the ratio of the fast Fourier transform of potential and current fluctuations, or the square root of the ratio of the potential and current PSD plots. Good agreement was observed between the impedance spectra and the spectral noise plots (Ref 36). Analysis of ECN data in the time domain results in values of the mean potential, E_{coup}, and the mean current, I_{coup}, of the coupled electrodes. In addition, the standard deviations σV and σI of the potential and current fluctuations, respectively, and the noise resistance $R_n = \sigma V/\sigma I$ are obtained. The localization index LI = $\sigma I/I_{rms}$, where I_{rms} is the root mean square value of the current fluctuations, can also be determined (Ref 32, 37). The suggestion that LI can be used to determine the prevailing corrosion mechanism should be viewed with great caution (Ref 35, 37).

Table 2 Statistical analysis of ECN data

Parameter	Formula
Mean	$\bar{x} = \frac{1}{N}\sum_{i=1}^{N} x_i$
Standard deviation	$\sigma = \sqrt{\frac{1}{N}\sum_{i=1}^{N}(x_i - \bar{x})^2}$
Root mean square	$rms = \sqrt{\frac{1}{N}\sum_{i=1}^{N} x_i^2}$

Localization index	$LI = \frac{\sigma I}{I_{rms}}$
Noise resistance	$R_n = \frac{\sigma V}{\sigma I}$
Skewness	[illegible]
Kurtosis	[illegible]

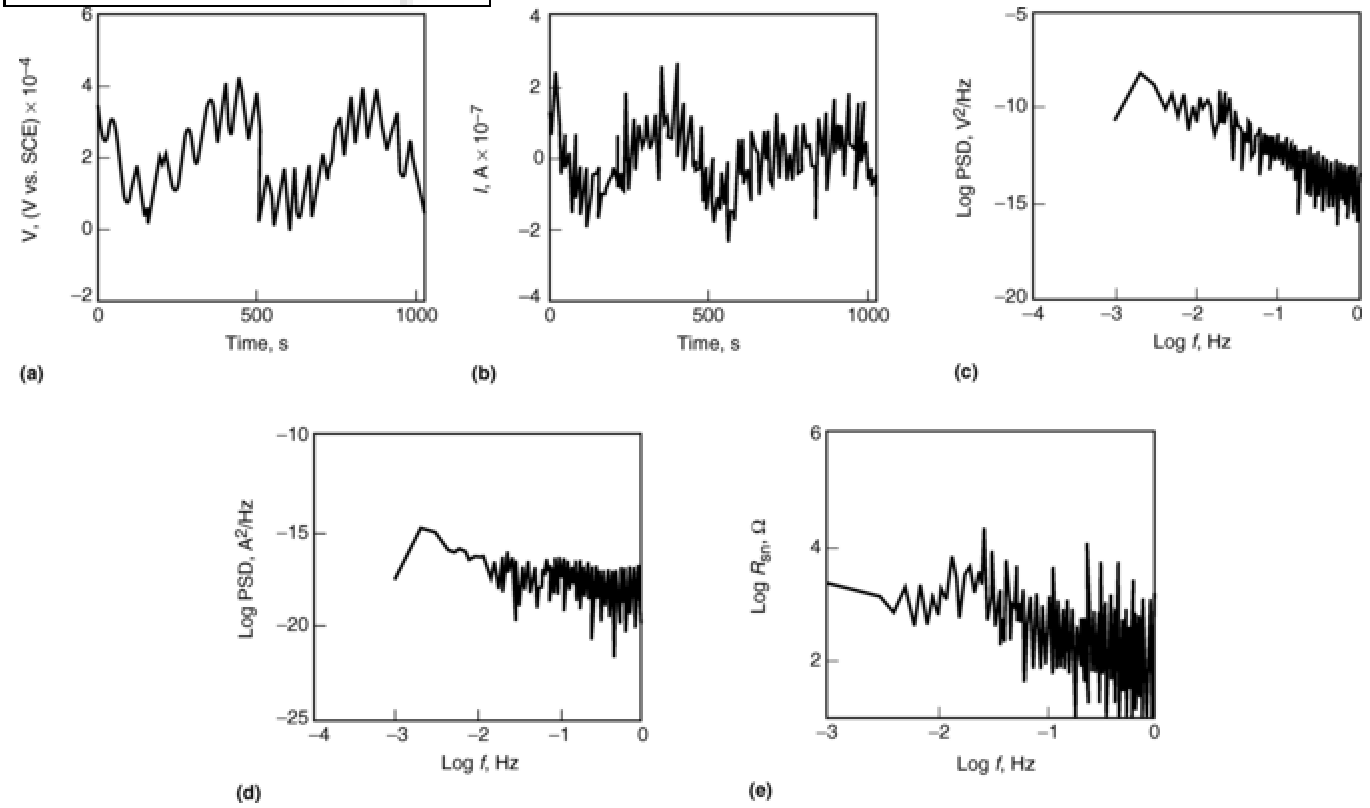

Fig. 9 Electrochemical noise data after trend removal for mild steel exposed to 0.5 *N* NaCl. (a) Voltage time history. Voltage is measured against SCE. (b) Current time history. (c) Power spectral density (PSD) plot from voltage data. (d) Power Spectral density plot from current data. (e) Spectral noise impedance, R_{sn}, derived from PSD. Source Ref 36

It has been assumed often that R_n is equal to R_p; however, it has been shown for passive systems, such as stainless steel or titanium alloys exposed to neutral media, that R_n was several orders of magnitude lower than R_p (Ref 35, 38). Similar results were reported for polymer- coated steel. In fact, for epoxy-polyamide- coated steel, no relationship between R_n and any properties of the coated steel sample could be found (Ref 29, 30, 31). Moreover, R_n was found to depend on bandwidth Δf of the noise measurement (Ref 30). In general, R_n is close to R_p only in those cases where the impedance is independent of frequency within Δf (Ref 30). Skewness and kurtosis of the ECN data can be used for a more detailed analysis of the ECN data. High kurtosis values are considered to be indicative of localized corrosion. Drift of ECN data can affect the slopes of PSD plots (Ref 39). It has been shown how to correct derived parameters such as σV, σI, and R_n for the effects of drift (Ref 36). A description of the background and application of the ECN technique, including detailed descriptions of the measurement procedure and different approaches to the analysis of ECN data, is available in Ref 13.

References cited in this section

13. R. Cottis and S. Turgoose, *Corrosion Testing Made Easy—Electrochemical Impedance and Noise,* B.C. Syrett, Ed., NACE, 1999

19. F. Mansfeld and B. Little, *Corros. Sci.,* Vol 32, 1991, p 247

20. A. Naguib and F. Mansfeld, *Electrochim. Acta,* Vol 37, 2002, p 2319

21. G. Lauer and F. Mansfeld, *Corrosion,* Vol 26, 1970, p 504

22. F. Mansfeld and R.V. Inman, *Corrosion,* Vol 35, 1979, p 21

23. F. Mansfeld, *Corrosion,* Vol 29, 1973, p 403

24. F. Mansfeld, *Corrosion,* Vol 27, 1971, p 436

25. F. Mansfeld, D.H. Hengstenberg, and J.V. Kenkel, *Corrosion,* Vol 30, 1974, p 343

26. F. Mansfeld and J.V. Kenkel, *Corros. Sci.,* Vol 15, 1975, p 183, 239

27. D.A. Jones, *Corrosion,* Vol 40, 1984, p 181

28. F. Mansfeld, L.T. Han, and C.C. Lee, *J. Electrochem. Soc.,* Vol 143, 1996, p L286

29. F. Mansfeld, L.T. Han, C.C. Lee, C. Chen, G. Zhang, and H. Xiao, *Corros. Sci.,* Vol 39, 1997, p 255

30. F. Mansfeld, L.T. Han, C.C. Lee, and G. Zhang, *Electrochim. Acta,* Vol 43, 1998, p 2933

31. F. Mansfeld, H. Xiao, L.T. Han, and C.C. Lee, *Prog. Org. Coatings,* Vol 30, 1997, p 89

32. D.A. Eden, "Electrochemical Noise—The First Two Octaves," Paper 386, Corrosion/ 98, NACE, 1998

33. U. Bertocci, C. Gabrielli, F. Huet, and M. Keddam, *J. Electrochem. Soc.,* Vol 144, 1997, p 31

34. U. Bertocci, C. Gabrielli, F. Huet, M. Keddam, and P. Rousseau, *J. Electrochem. Soc.,* Vol 144, 1997, p 37

35. F. Mansfeld, Z. Sun, E. Speckert, and C.H. Hsu, "Electrochemical Noise Analysis (ENA) for Active and Passive Systems," Paper 00418, Corrosion/2000, NACE, 2000

36. F. Mansfeld, Z. Sun, C.H. Hsu, and A. Nagiub, *Corros. Sci.,* Vol 43, 2001, p 341

37. F. Mansfeld and Z. Sun, *Corrosion,* Vol 55, 1999, p 915

38. C.C. Lee and F. Mansfeld, *Corros. Sci.,* Vol 40, 1998, p 959

39. C. Gabrielli, F. Huet, and M. Keddam, *Electrochim. Acta,* Vol 31, 1986, p 1025

F. Mansfeld, Electrochemical Methods of Corrosion Testing, *Corrosion: Fundamentals, Testing, and Protection*, Vol 13A, *ASM Handbook*, ASM International, 2003, p 446–462

Electrochemical Methods of Corrosion Testing

Florian Mansfeld, University of Southern California

Small-Signal Polarization Tests

In measurements of the polarization resistance and electrochemical impedance spectra, only a small electrochemical signal is applied in order to ensure that the system under investigation remains linear. This requirement also ensures that these measurements are nondestructive and therefore can be repeated many times on the same system.

Polarization-Resistance Method. Thorough reviews of background and application of the polarization-resistance technique for measuring corrosion currents are found in Ref 4 and 40. The polarization resistance (R_p) defined as:

$$R_p = (dE/di)_{E_{corr}} \quad \text{(Eq 1)}$$

is determined as the slope of a polarization curve at E_{corr}, where $i = 0$. Usually, potentiodynamic polarization curves collected in close vicinity of E_{corr} are used for this purpose. ASTM G 59, "Standard Practice for Conducting Potentiodynamic Polarization-Resistance Measurements," deals with experimental procedures for determining R_p according to Eq 1. This method describes an experimental procedure for polarization-resistance measurements that allows an investigator to calibrate equipment and test methods. Figure 10 shows standard polarization curves for type 430 stainless steel in 1.0 *N* H_2SO_4, deaerated with hydrogen, at 30 °C (85 °F). Experimental polarization curves must fall within curves 2 and 3; otherwise, experimental problems have occurred.

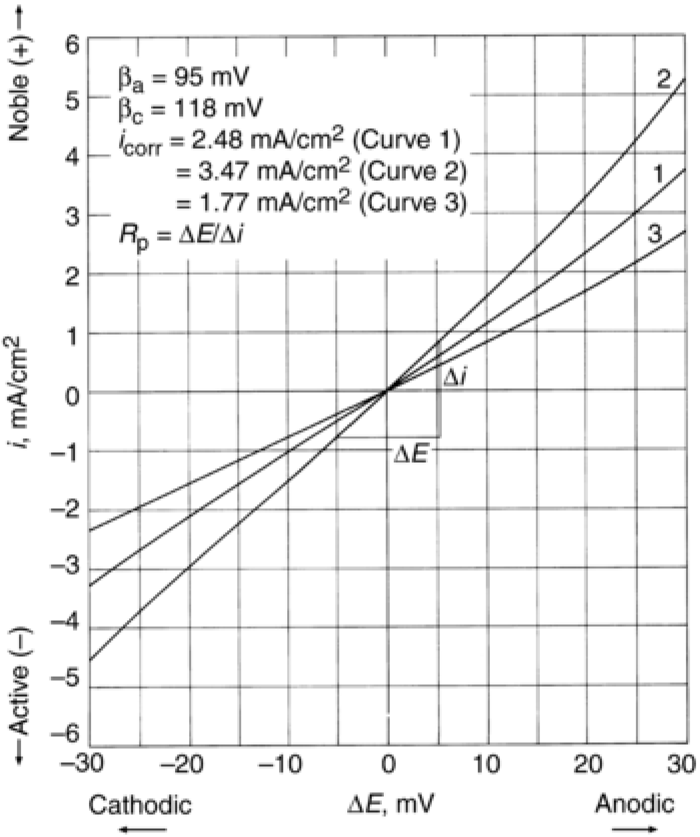

Fig. 10 Standard potentiodynamic polarization curves in the vicinity of E_{corr} for type 430 stainless steel in 1 *N* H_2SO_4, 30 °C (85 °F). Source: ASTM G 59

Applications of the R_p technique as a nondestructive method for monitoring corrosion rates have been discussed in detail in review articles (Ref 4, 40). The main advantage of the R_p technique over periodic weight-loss measurements is the possibility of continuously monitoring instantaneous corrosion rates of a metal exposed to a corrosive environment.

Polarization resistance can be converted to i_{corr} using the Stern-Geary equation:

$$i_{corr} = B/R_p \quad \text{(Eq 2)}$$

where B is a parameter calculated using the Tafel slopes:

$$B = \beta_a\beta_c/2.3(\beta_a + \beta_c) \quad \text{(Eq 3)}$$

where β_a and β_c are the anodic and cathodic Tafel slopes, respectively.

In order to obtain quantitative values of i_{corr} from experimental R_p data, B has to be known for the same experimental conditions. For qualitative estimates, a constant value of B between 13 and 26 mV often is used. Corrosion rates can be obtained from i_{corr} using Faraday's law.

In determining R_p values from polarization curves, scan rate and ohmic drop effects have to be considered. Experimental polarization curves can change with increasing scan rate. In general, R_p is underestimated (and corrosion rates overestimated) when scan rates are too high. Polarization resistance is overestimated (and corrosion rates underestimated) when the uncompensated resistance (R_s) is not considered, because the experimental value of R_p ($R_{p,exp}$) contains a contribution from R_s:

$$R_{p,exp} = R_p + R_s \quad \text{(Eq 4)}$$

The contribution from R_s can be eliminated during the measurement by using positive feedback or current interrupter techniques or by subtracting R_s from $R_{p,exp}$ as calculated from analysis of the polarization curve. Uncompensated resistance can be determined by applying a constant current pulse, I_{appl}, and observing the potential response on an oscilloscope (Fig. 11). The initial sharp rise of the potential $E = I_{appl}R_s$ due to ohmic drop is followed by a slower increase due to double-layer charging. Thus, $R_s = E/I_{appl}$.

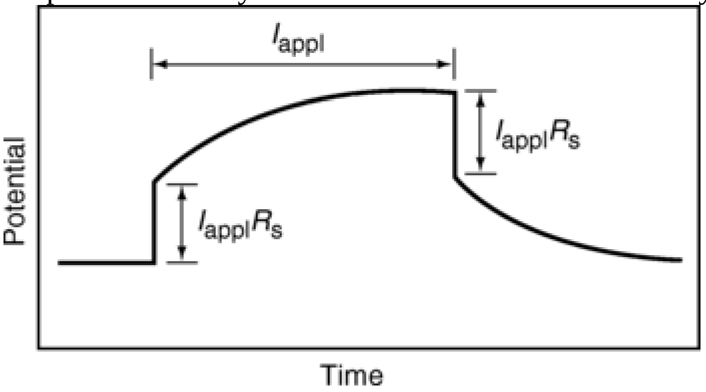

Fig. 11 Potential pulse method for determining the uncompensated resistance, R_s

The error $e = R_s/R_p$ due to the uncompensated resistance can have similar values for a system with high corrosion rates in a solution of high conductivity and for a system with low corrosion rates in a solution of low conductivity. Therefore, ohmic drop effects can be important in all systems. Experimentally, it has been observed that the largest errors due to the uncompensated resistance occur for systems with high corrosion rates and low conductivity, such as steel in acid/ alcohol mixtures.

The linear polarization technique is a variation of the polarization-resistance technique and forms the basis of commercial corrosion-rate monitors. In this approach, it is assumed that polarization curves are linear in the vicinity of E_{corr} (E_{corr} ± 10 mV). In this case, R'_p is defined as:

$$R'_p = \Delta E/i \quad \text{(Eq 5)}$$

where $\Delta E = E_{appl} - E_{corr}$, and i is the current density measured at the applied potential, E. Because ΔE is constant, i_{corr} is proportional to the measured current density, i:

$$i_{corr} = k \cdot i \quad \text{(Eq 6)}$$

where k is treated as a system constant.

In commercial instruments, positive and negative values of ΔE are applied, and the average value of i is used to determine the corrosion rate. The assumption that the polarization curve is linear with ΔE has been discussed, and the limitation of the technique has to be considered in each application (Ref 4, 40). Several commercial devices are available, and automatic ohmic drop compensation is available in some instruments.

Electrochemical impedance spectroscopy (EIS) data are recorded as a function of frequency of an applied alternating current (ac) signal at a fixed working point (E, i) of a polarization curve. In corrosion studies, this working point is often E_{corr} ($E = E_{corr}$, $i = 0$). Usually, a very large frequency range has to be investigated to obtain the complete impedance spectrum. In most corrosion studies, this frequency range extends from 100 kHz, the upper limit of commonly used frequency response analyzers (FRAs), to 1 mHz. Measurements at lower frequencies are very time consuming. Impedance data usually are determined with a three-electrode system, although it is also possible to use a two-electrode system in which both electrodes are of the same material. In this case, the EIS data are collected at E = 0 V. A potentiostat is used to apply the potential at

which the data are to be collected. The FRA is programmed to apply a series of sine waves of constant amplitude, small enough to remain in the linear potential region, and varying the frequency. Impedance data are determined by the FRA at each frequency and stored in its memory. Because a very large number of data points have to be collected, displayed, and analyzed, it is essential to use adequate software for these purposes. Such software is available from all major manufacturers of FRAs.

Information obtained with EIS differs from that determined with the other techniques previously described, because the corrosion system is analyzed at a fixed potential (or current). Properties of the system at this potential can then be determined through analysis of the frequency dependence of the impedance. One of the advantages of EIS is that only very small signals are applied, making it a nondestructive technique. In many cases, EIS data have shown that existing models for corrosion systems based on results of studies with direct-current (dc) techniques were too simplistic.

Experimental impedance spectra can be displayed using linear coordinates in complex plane plots in which the negative value of the imaginary impedance ($-Z''$) is plotted versus the real part (Z'). For a simple circuit consisting of a parallel combination of resistance, R_p, and capacitance, C_{dl}, with R_s in series (Fig. 12a), such a plot results in a semicircle (Fig. 12b). This approach neglects the fact that the impedance often changes over many orders of magnitude, and that the frequency dependence of the impedance cannot be recognized in complex plane plots. The preferred format for display of EIS data is therefore the Bode plot (Fig. 12c, d), in which log $|Z|$ and the phase angle (Φ) are plotted versus the logarithm of the frequency (f) of the applied signal, with $|Z|$ being the modulus of the impedance. In Fig. 12, the curves for $\alpha = 1$ refer to ideal capacitive behavior, while the curves for $\alpha = 0.9$ are typical for the often-observed deviations from ideal behavior. The constant phase element concept is often used in such cases. ASTM G 106, “Standard Practice for Verification of Algorithm and Equipment for Electrochemical Impedance Measurements,” describes an experimental procedure that may be used to check the instrumentation and technique for collection and presentation of EIS data. Reference impedance plots in both complex plane and Bode format are included for a dummy cell and for stainless steel type 430 in a solution containing 0.005 *M* sulfuric acid (H_2SO_4) and 0.495 *M* sodium sulfate (Na_2SO_4).

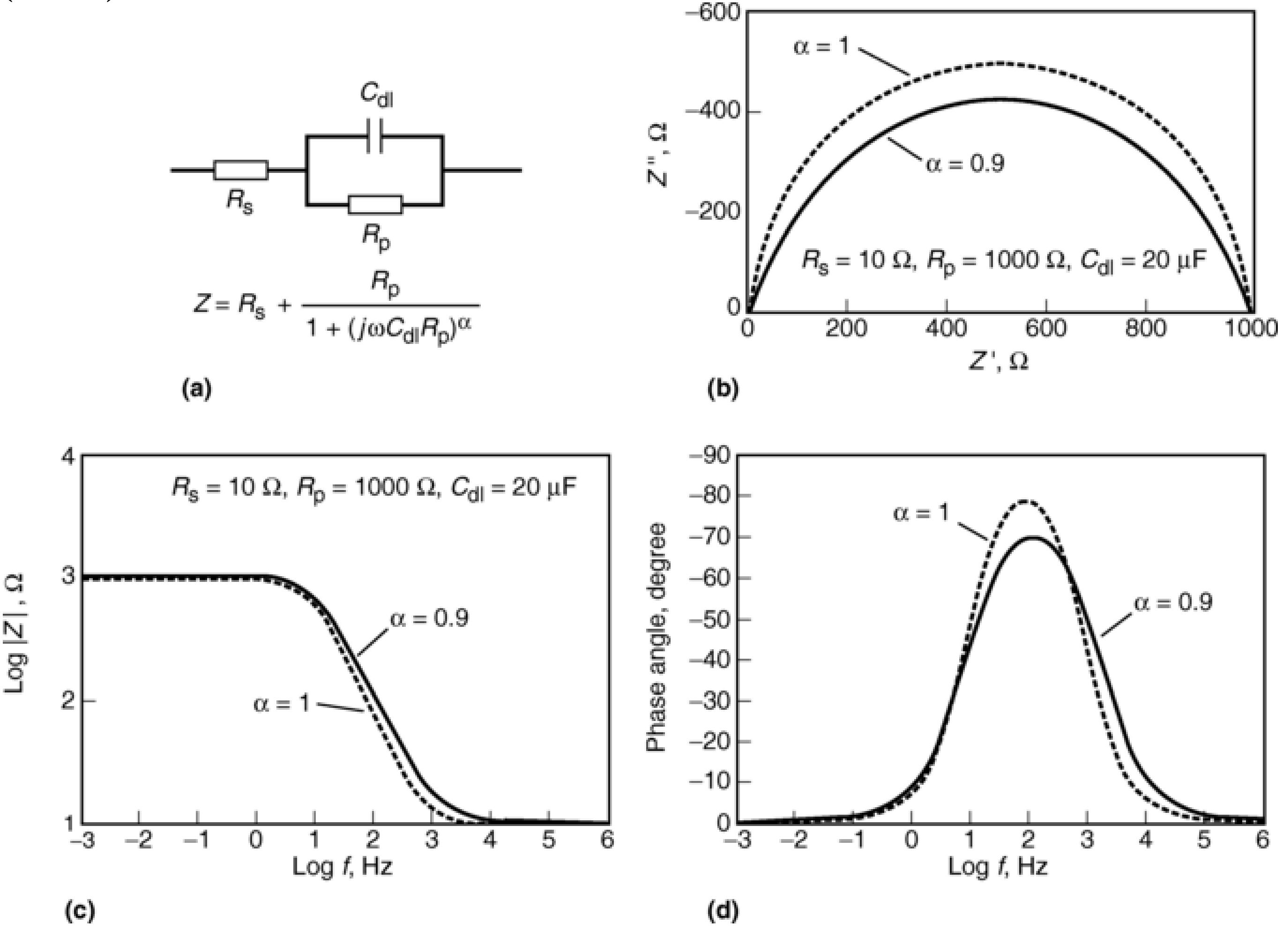

Fig. 12 Representations of a corroding electrode. (a) Equivalent circuit model. R_s, 10 Ω; R_p, 1000 Ω; C_{dl}, 20 μF. (b) The complex plane or Nyquist plot of the equivalent circuit for α = 1 and α = 0.9. Note the intercepts with the real axis occur at R_s and $R_s + R_p$. (c) Bode plot of the base 10 log of the magnitude of the impedance against the log of the frequency. The range of the impedance is between R_s and $R_s + R_p$. (d) Bode plot of the negative phase angle versus the log of the frequency

In order to perform a quantitative analysis of EIS data, it is necessary to use an appropriate equivalent circuit that describes accurately the physical properties of the system under investigation. Equivalent circuits for polymer-coated metals, anodized aluminum alloys, and localized corrosion of aluminum alloys have been described in the literature (Ref 41). The ANALEIS software contains modules that were designed for the analysis of EIS data for these systems (Ref 41).

The most successful application of EIS has probably been in the analysis of the properties of protective polymer coatings and their changes during exposure to corrosive environments (Ref 42, 43). Impedance spectra for polymer-coated metals exposed to corrosive media can be analyzed with the software module COATFIT, which is based on the equivalent circuit shown in Fig. 13(a). In this equivalent circuit, C_c is the capacitance of the coating, which depends on its dielectric constant, ε, and its thickness, d:

$$C_c = \varepsilon\varepsilon_o A/d \quad \text{(Eq 7)}$$

where ε_o is the dielectric constant of vacuum, and A is the exposed area. The variable R_{po} has been called the pore resistance, because it is considered to be due to the formation of ionically conducting paths in the polymer (Ref 44, 45). The variable R_p is the polarization resistance of the area at the polymer coating/metal interface at which corrosion occurs, and C_{dl} is the corresponding capacitance. An increase of C_c with time can be related to water uptake by the coating (Ref 43). The rate at which R_{po} decreases with increasing exposure time has been used to rank the efficiency of different pretreatments for steel in providing corrosion protection by a polybutadiene coating (Ref 44, 45). The changes of C_{dl} can be used to estimate the corroding delaminated area, A_{corr}, (Ref 46) and to calculate the specific polarization resistance $R^o_{po} = R_{po} A_{corr} (\mathrm{ohm cm}^2)$, from which an estimate of the corrosion rate of the delaminated area can be made. Figure 13(b) shows a comparison of experimental and fitted impedance spectra for polymer-coated Mg AZ31 that had been exposed to 0.5 N NaCl. Excellent agreement of the experimental and fitted data was observed. The use of EIS for lifetime prediction of organic coatings on steel is described in Ref 47. Damage functions based on the experimental values of A_{corr} have been determined and can be used for lifetime prediction of polymer-coated steel exposed to natural seawater for several years (Ref 48).

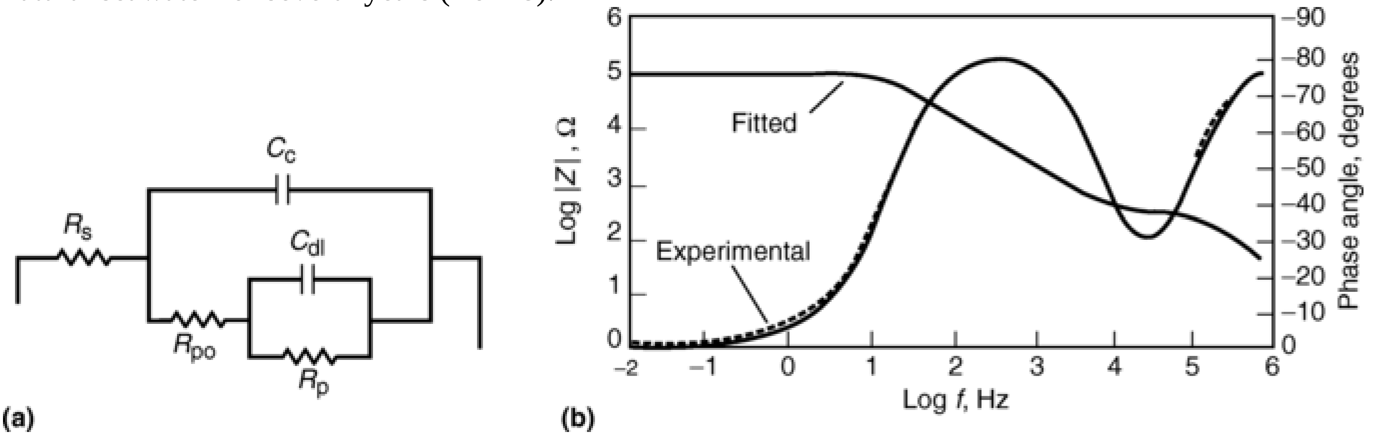

Fig. 13 (a) Equivalent circuit for polymer-coated metals exposed to a corrosive environment. (b) Comparison of an experimental and fitted impedance spectra for polymer-coated Mg AZ31 exposed to 0.5 N NaCl. (b) C_c, 5.129 pF; C_{dl}, 99.69 pF; R_{po}, 357.1 Ω; R_s, 3Ω; R_p, 102.1 kΩ. Source: Ref 41

Impedance spectra for anodized aluminum alloys can be analyzed with the module ANODAL (Ref 41). The analysis is based on the equivalent circuit in Fig. 14(a), where C_{po} is the capacitance of the outer porous layer, R_{po} is the resistance of the sealed pores, and C_b and R_b are the capacitance and resistance of the inner barrier layer, respectively (Ref 16, 49, 50, 51). Analysis of impedance spectra for a large number of anodized and sealed aluminum alloys has shown that the spectra fall into a narrow scatter band if the same anodizing and sealing procedures are followed. Electrochemical impedance spectroscopy has been recommended therefore as

a quality-control test for anodized and sealed aluminum alloys (Ref 16). It should be noted that for unsealed or dichromate sealed samples, R_{po} is very low. Therefore, C_{po} does not appear in the measured spectrum in these two cases (Ref 51).

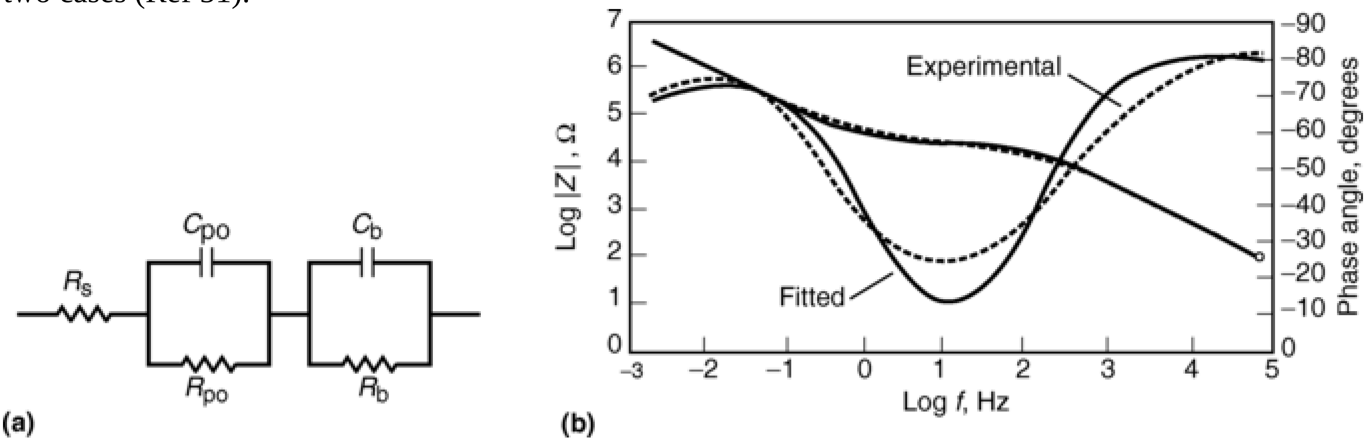

Fig. 14 (a) Equivalent circuit for anodized aluminum alloys. (b) Comparison of experimental and fitted spectra for Al 6061 (sulfuric acid anodized and hot water sealed) exposed to 0.5 *N* NaCl. C_{po}, 56.87 pF; C_b, 0.37 μF; R_{po}, 28.83 kΩ; R_b, 26.62 MΩ; R_s, 1Ω. Source: Ref 41

Figure 14(b) shows the result of a fit of experimental data for sulfuric-acid-anodized and hot-water-sealed Al 6061 that had been exposed to 0.5 *N* NaCl. Good agreement between the measured and fitted spectra was observed at the highest and lowest frequencies. However, significant deviations occurred in the frequency range between 1000 and 0.1 Hz. For a modified equivalent circuit in which R_{po} was replaced by a transmission line impedance $Z_{po} = K(j\omega)^n$ (Fig. 15a), excellent agreement between the experimental and fitted data was obtained (Fig. 15b). From the fitted values of C_b and C_{po}, the thickness of the barrier and the porous layer can be obtained. For the fit parameters in Fig. 15(b), a barrier layer thickness of 250 Å was calculated. The calculated thickness of 21 μm for the porous layer agreed very well with that obtained by observation in the scanning electron microscopy of the cross section of the anodized sample (Ref 41).

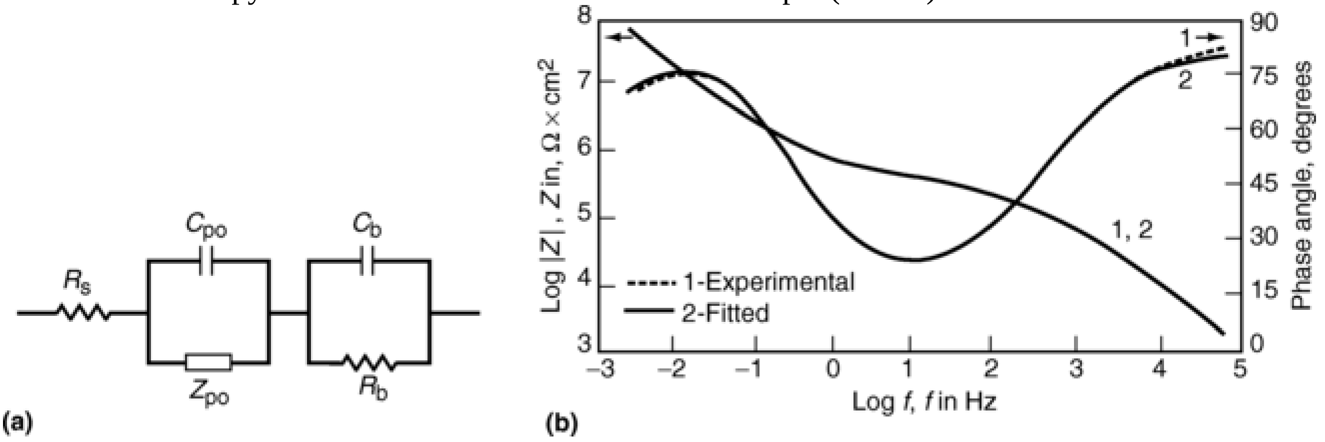

Fig. 15 (a) Modified equivalent circuit for anodized aluminum alloys. (b) Comparison of experimental and fitted spectra for Al 6061 (sulfuric acid anodized and hot water sealed) exposed to 0.5 *N* NaCl. Source: Ref 41

The experimental impedance spectra for aluminum alloys exposed to solutions containing chloride ions show characteristic changes when pits initiate and grow (Ref 52, 53, 54, 55). The spectra can be explained by the equivalent circuit in Fig. 16, where R_p and C_p are the polarization resistance and capacitance, respectively, of the passive surface; R_{pit} and C_{pit} are the corresponding values for the growing pits; $W = (K/F)(j\omega)^n$ is a transmission line impedance; and F is the area fraction at which pits have initiated. Figure 17 gives a comparison of experimental and fitted impedance spectra for Al 6061 after 24 h exposure to 0.5 *N* NaCl. As explained elsewhere (Ref 56), it is possible to obtain F from the time dependence of C_{pit}, which allows determination of the pitted area, A_{pit}, which can be used to normalize R_{pit} and obtain the specific pit polarization

resistance, R^{o}_{pit}. As a result of this procedure, it is possible to determine relative pit growth rates, the time dependence of which can be expressed as:

$$\log\left(1/R^{o}_{\mathrm{pit}}\right) = a + b\log\left(t - t_{o}\right) \quad \text{(Eq 8)}$$

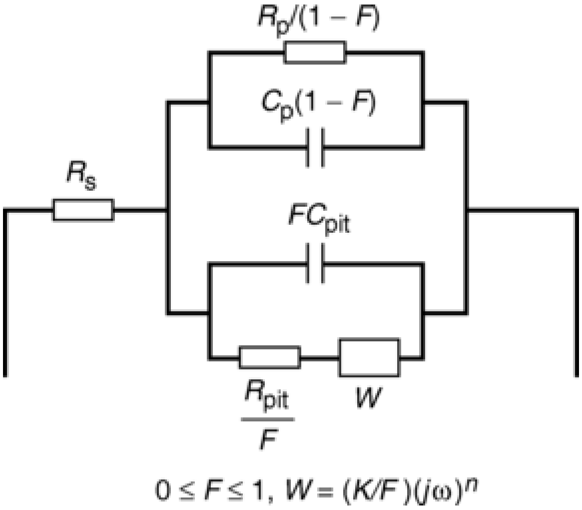

Fig. 16 Equivalent circuit for the impedance of aluminum alloys for which pits have been initiated. Source: Ref 41

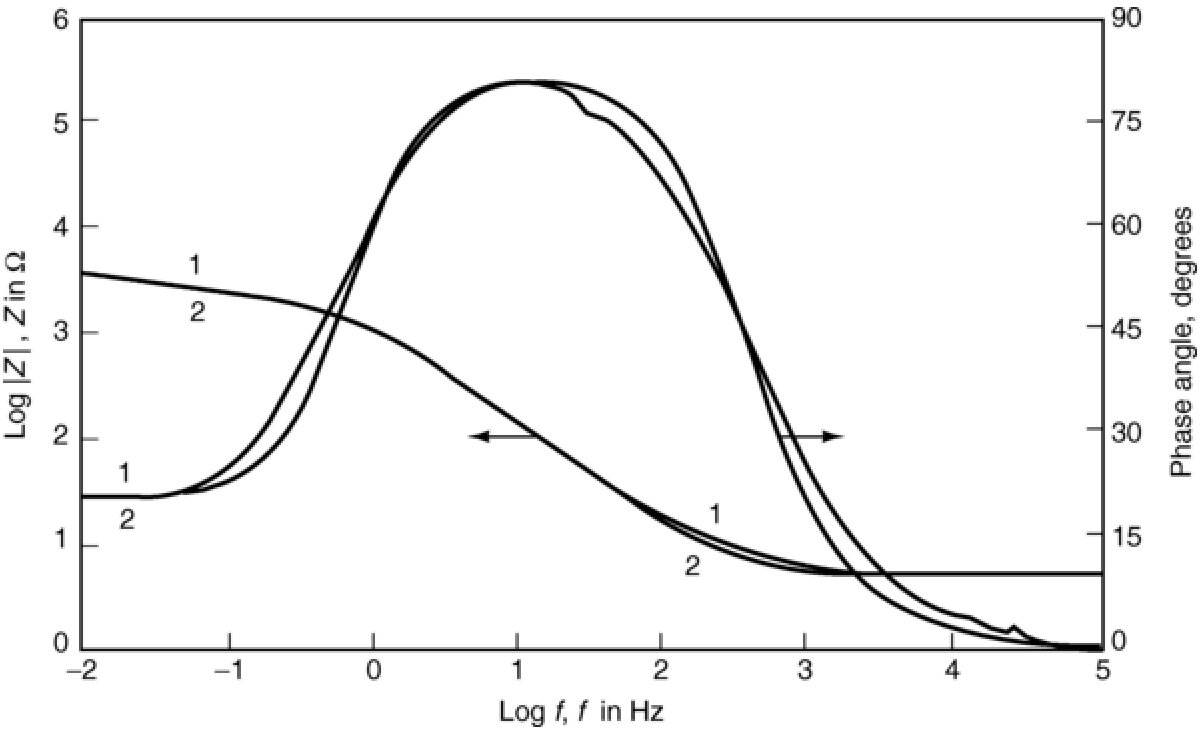

Fig. 17 Comparison of experimental (curve 1) and fitted (curve 2) impedance spectra for Al 6061 after 24 h exposure to 0.5 *N* NaCl. Source: Ref 41

The time dependence of log $\left(1/R^{o}_{\mathrm{pit}}\right)$ for Al 7075 that had been passivated in 1000 ppm $CeCl_3$ (Ref 55) in Fig. 18 agrees with the time law in Eq 8.

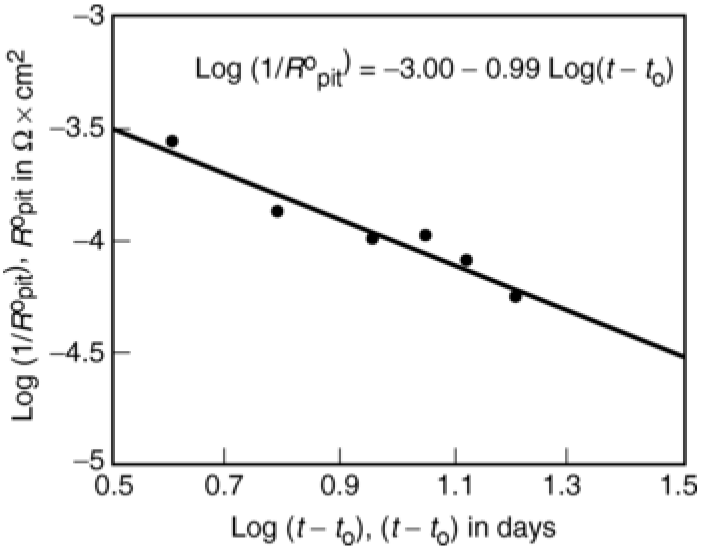

Fig. 18 Time dependence of R^{o}_{pit} for Al 7075 (passivated in $CeCl_3$) during exposure to 0.5 *N* NaCl. Source: Ref 41

Electrochemical impedance spectroscopy data have often been used only to determine R_p, which is defined as the limit of the real part of the impedance for $f = 0$ (Ref 41):

$$R_p = \lim_{f \to 0} Z'(f) - R_s \qquad \text{(Eq 9)}$$

In this case, all other important information contained in the impedance spectrum is ignored. Nevertheless, the nondestructive nature of EIS makes it an ideal tool for monitoring the corrosion behavior over extended time periods.

In Fig. 19(a), R_p values obtained for Al 2024 exposed to artificial seawater (AS) containing *S. algae* or *S. ana* are plotted as a function of exposure time, while the corresponding results for brass and mild steel are plotted in Fig. 19(b) and (c), respectively (Ref 20). For Al 2024 exposed to sterile AS, pitting was observed, and therefore, R^{o}_{pit} obtained by fitting of the experimental spectra to the equivalent circuit in Fig. 16 is shown in Fig. 19(a). Similar very high R^{o}_{p} values were obtained for Al 2024 in the presence of *S. algae* or *S. ana*, indicative of passive behavior. When kanamycin was added to the AS containing *S. ana* after 7 days, R_p did not change immediately (Fig. 19a). After 15 days, pitting was observed. These changes of R_p are different from those of E_{corr} in Fig. 5(a), where E_{corr} increased very shortly after addition of kanamycin. For brass, *S. algae* produced only a small increase of R^{o}_{p}, while a much larger effect was found for *S. ana* (Fig. 19b). As observed for Al 2024 (Fig. 19a), R^{o}_{p} did not change for several days after addition of kanamycin (Fig. 19b), while E_{corr} changed almost immediately (Fig. 5b). The changes of R^{o}_{p} due to the addition of the two different bacteria were quite similar for mild steel, and, as observed for Al 2024 and brass, R^{o}_{p} did not decrease to the levels observed in sterile AS for several days (Fig. 19c).

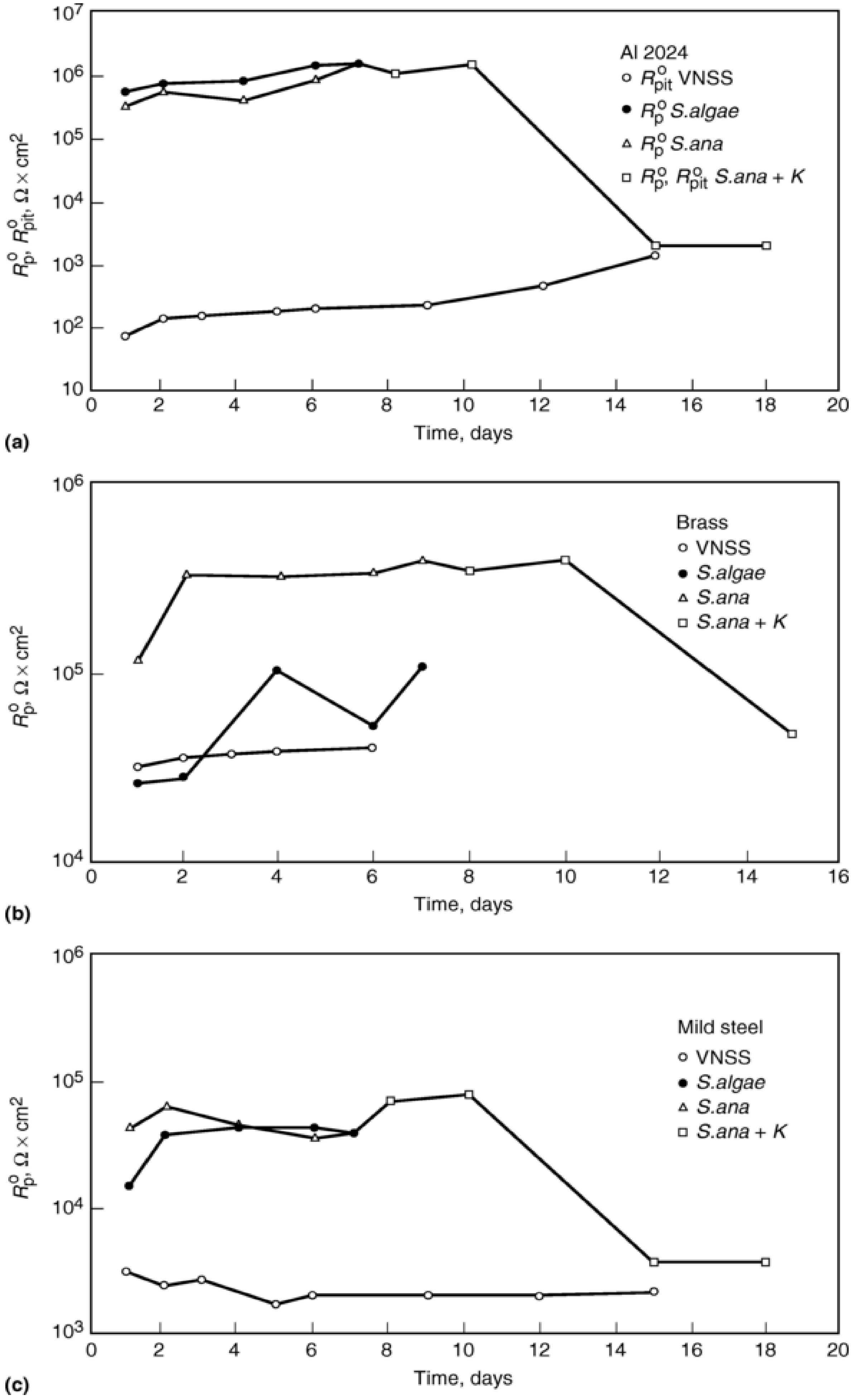

(a)
Al 2024
R_{pit}^{o} VNSS
R_{p}^{o} S.algae
R_{p}^{o} S.ana
R_{p}^{o}, R_{pit}^{o} S.ana + K
R_{p}^{o}, R_{pit}^{o}, $\Omega \times cm^2$
Time, days
(b)
Brass
VNSS
S.algae
S.ana
S.ana + K
R_{p}^{o}, $\Omega \times cm^2$
Time, days
(c)
Mild steel
VNSS
S.algae
S.ana
S.ana + K
R_{p}^{o}, $\Omega \times cm^2$
Time, days

Fig. 19 Time dependence of R_p for (a) Al 2024, (b) brass, and (c) mild steel during exposure to sterile artificial seawater and artificial seawater containing *S. algae* or *S. ana.* VNSS, Väätänen nine salts solution. *K,* kanamycin. Source: Ref 20

References cited in this section

4. F. Mansfeld, The Polarization Resistance Technique for Measuring Corrosion Currents, *Advancements in Corrosion Science and Technology,* Vol 6, M.G. Fontana and R.W. Staehle, Ed., Plenum Press, 1976, p 163

16. F. Mansfeld and M.W. Kendig, *Corrosion,* Vol 41, 1985, p 490

20. A. Naguib and F. Mansfeld, *Electrochim. Acta,* Vol 37, 2002, p 2319

40. J.R. Scully, *Corrosion,* Vol 56, 2000, p 199

41. F. Mansfeld, H. Shih, H. Greene, and C.H. Tsai, *Analysis of EIS Data for Common Corrosion Processes,* STP 1188, ASTM, 1993, p 37

42. F. Mansfeld, *J. Appl. Electrochem.,* Vol 25, 1995, p 187

43. F. Mansfeld and M. Kendig, *Electrochemical Impedance Tests for Protective Coatings,* STP 866, ASTM, 1985, p 122

44. F. Mansfeld, M. Kendig, and S.Tsai, *Corrosion,* Vol 38, 1982, p 478

45. M. Kendig, F. Mansfeld, and S. Tsai, *Corros. Sci.,* Vol 23, 1983, p 317

46. J. Titz, G.H. Wagner, H. Spaehn, M. Ebert, K. Juettner, and W.J. Lorenz, *Corrosion,* Vol 46, 1990, p 221

47. M. Kendig and F. Mansfeld, *Mat. Res. Soc. Symp. Proc.,* Vol 115, 1988, p 193

48. F. Mansfeld, C.C. Lee, L.T. Han, B.J. Little, P. Wagner, R. Ray, and J. Jones-Meehan, “The Impact of MIC on Protective Polymer Coatings,” Final Report, Contract N00014- 94-1-0026, The Office of Naval Research, Aug 1998

49. J. Hitzig, K. Juettner, W.J. Lorenz, and W. Paatsch, *Corros. Sci.,* Vol 24, 1984, p 945

50. J. Hitzig, K. Juettner, W.J. Lorenz, and W. Paatsch, *J. Electrochem. Soc.,* Vol 133, 1986, p 133

51. F. Mansfeld and M.W. Kendig, *J. Electrochem. Soc.,* Vol 135, 1988, p 828

52. F. Mansfeld, S. Lin, S. Kim, and H. Shih, *Corros. Sci.,* Vol 27, 1987, p 997

53. F. Mansfeld and H.Shih, *J. Electrochem. Soc.,* Vol 135, 1987, p 332

54. F. Mansfeld, S. Lin, S. Kim, and H. Shih, *Electrochim. Acta,* Vol 34, 1989, p 1123

55. F. Mansfeld, S. Lin, S. Kim, and H. Shih, *J. Electrochem. Soc.,* Vol 137, 1990, p 78

56. F. Mansfeld, H. Shih, H. Greene, and C.H. Tsai, *Detection and Monitoring of Localized Corrosion with EIS,* STP 1188, ASTM, 1993, p 297

F. Mansfeld, Electrochemical Methods of Corrosion Testing, *Corrosion: Fundamentals, Testing, and Protection*, Vol 13A, *ASM Handbook*, ASM International, 2003, p 446–462

Electrochemical Methods of Corrosion Testing

Florian Mansfeld, University of Southern California

Large-Signal Polarization Tests

In large-signal polarization tests, the applied potential is varied over a wide range, using either a series of applied potential steps or a change of potential at a constant rate. It is also possible to use a series of current steps or a constantly changing current; however, these techniques are less popular. Because polarization over a wide potential range might cause irreversible changes of the sample surface properties, it is not possible, in most cases, to repeat a large-signal polarization test on the same sample.
Potentiostatic Techniques. There are two types of potentiostatic techniques:

- *Type 1:* recording of the current as a function of time at a constant applied potential, E_{appl}
- *Type 2:* recording of the steady-state current as a function of E_{appl}

The data obtained in the type 1 test provide information about the time dependence of the rate of an electrochemical reaction at a given potential. The data collected with the type 2 test can be used to construct a polarization curve, which usually is plotted as E_{appl} versus the logarithm of the measured current density, *i*. Polarization curves also can be obtained by the potentiodynamic technique. Because the instrumentation and experimental procedures are quite similar for both techniques (Ref 11, 12), much of the discussion presented in this section is also valid for the following section. ASTM G 5, "Standard Reference Test Method for Making Potentiostatic and Potentiodynamic Anodic Polarization Measurements," is a classic document that has been used for many years in many countries. This test method describes experimental procedures for checking one's experimental technique and instrumentation. If followed, using ASTM-provided type 430 stainless steel in 1.0 *N* H_2SO_4, the method provides repeatable polarization curves that reproduce the curves shown in ASTM G 5. If discrepancies are found, the experiment has not been performed correctly, there might be problems with the test cell, and/ or the equipment might not function properly.
A complete polarization curve consists of a cathodic part and an anodic part. The cathodic portion of the polarization curve contains information concerning the kinetics of the reduction reaction(s) occurring for a particular system. Depending on the solution composition, a mass- transport-controlled region can be reached at more negative potentials, at which the reaction rate (the measured current density) depends only on the solution composition and the hydrodynamic conditions. The particular features of the anodic part of the polarization curve depend strongly on the metal-electrolyte system. Usually, a charge-transfer-controlled region occurs at potentials close to E_{corr}. So-called passive metals show an active-passive transition followed by a passive region and the region of oxygen evolution at the highest applied potentials. For those metals, which are susceptible to localized corrosion, a large increase of the current occurs in the passive region when the pitting potential, E_{pit}, has been exceeded. ASTM G 3, "Standard Practice for Conventions Applicable to Electrochemical Measurements in Corrosion Testing," provides conventions for reporting and displaying electrochemical data and contains theoretical and experimental polarization curves.
In general, only qualitative information, such as changes in the polarization characteristics in the passive region or changes of E_{pit} due to the presence of inhibitors or alloying, is extracted from a full polarization curve. However, it is possible to determine from such curves quantitative information that is related to the kinetics of the corrosion reactions and the corrosion rate.
The relationship between the applied potential, E_{appl}, and the measured current density, *i*, in the Tafel region is given by (Ref 2, 3):

$$E_{appl} = E_{corr} + \beta_a \log (i/i_{corr}) \quad \text{(Eq 10)}$$

for the anodic polarization curve and:

$E_{appl} = E_{corr} - \beta_c \log (i/i_{corr})$ (Eq 11)

for the cathodic polarization curve.

In Eq 10 and 11, the anodic Tafel slope, β_a, and the cathodic Tafel slope, β_c, are positive numbers. Plots of E_{appl} versus log *i* are called Tafel plots. The corrosion current density, i_{corr}, can be determined according to Eq 10 and 11 by extrapolation of the Tafel lines to $E_{appl} = E_{corr}$, where $i = i_{corr}$ (Fig. 20). This method of obtaining corrosion current density is called the Tafel extrapolation method. It is also possible to determine i_{corr} from either the anodic or the cathodic Tafel plot or from the intersection of both plots. It is advantageous to use computer software to record polarization curves and analyze the experimental data in terms of parameters such as β_a, β_c, and i_{corr}. From the numerical values of β_a and β_c, conclusions concerning the rate- determining step in the reaction mechanism can be made (Ref 2, 3, 4). From i_{corr}, the corrosion rate can be calculated using Faraday's law. ASTM G 102, "Standard Practice for Calculation of Corrosion Rates and Related Information from Electrochemical Measurements," provides guidance in converting the results of electrochemical measurements to rates of uniform corrosion.

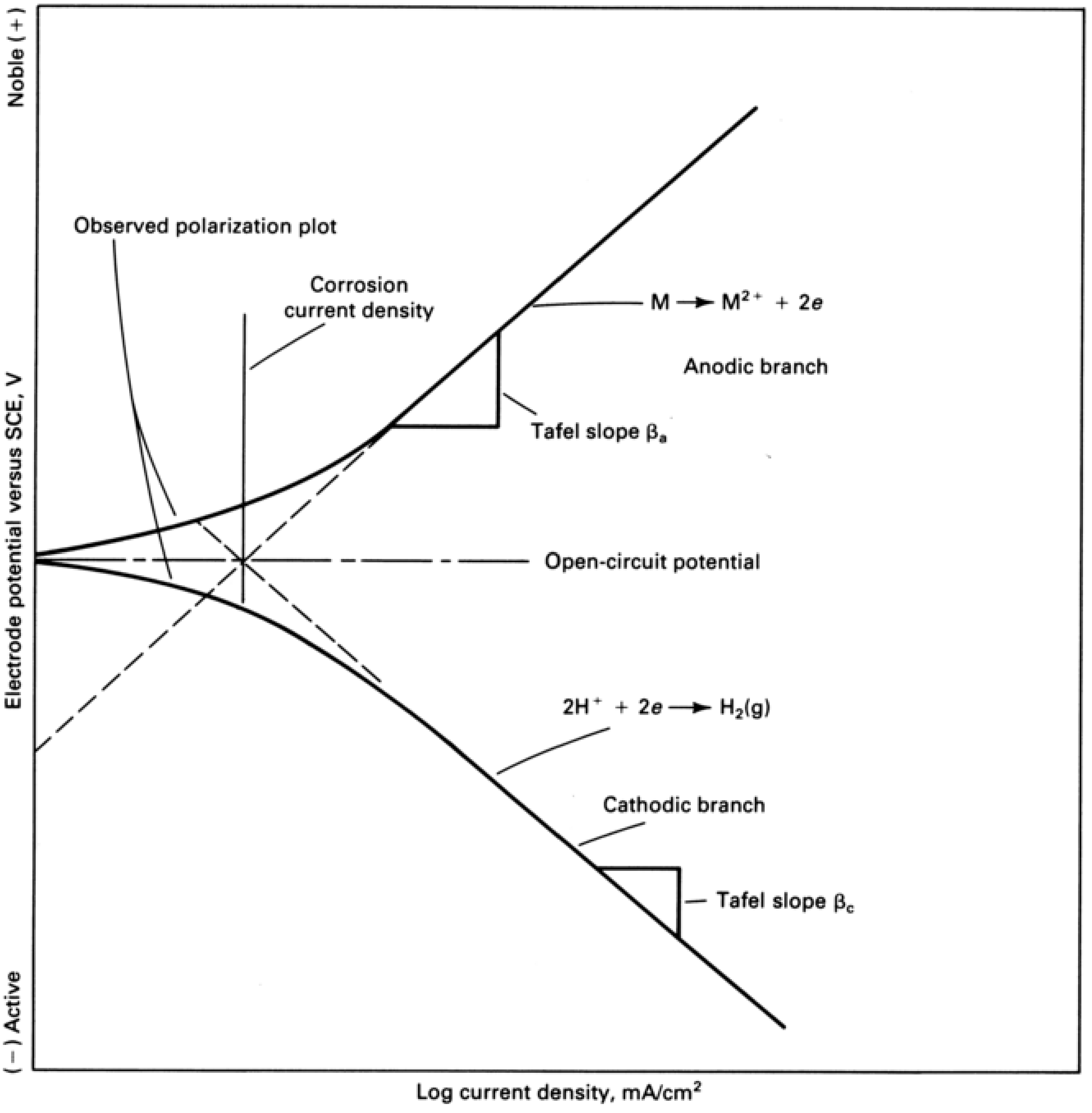

Fig. 20 Theoretical Tafel plots illustrating the Tafel extrapolation method. SCE, saturated calomel electrode; SHE, standard hydrogen electrode

An equivalent circuit for a three-electrode cell is shown in Fig. 21, where R_p is the polarization resistance of the test electrode; C is its capacitance; R_s is the resistance of the electrolyte between the surface of the test electrode and the tip of the Luggin capillary, which houses the reference electrode; and R_c is the resistance of the electrolyte between the test electrode and the counter electrode. The applied potential, E_{appl}, appears across $R_p + R_s$ and therefore always includes an ohmic drop, IR_s, where I is the current flowing as a result of polarization. This ohmic drop is an error in the measurement, because the potential E_{appl} set at the potentiostat differs from the true electrode potential E by IR_s. This fact has to be recognized in all polarization experiments. In many cases, where electrolytes with reasonable conductivity are used and IR_s is small compared to E_{appl}, this error can be neglected. In other cases, it can be eliminated by the positive feedback or current interrupter techniques (Ref 17, 18) that are available in most modern potentiostats.

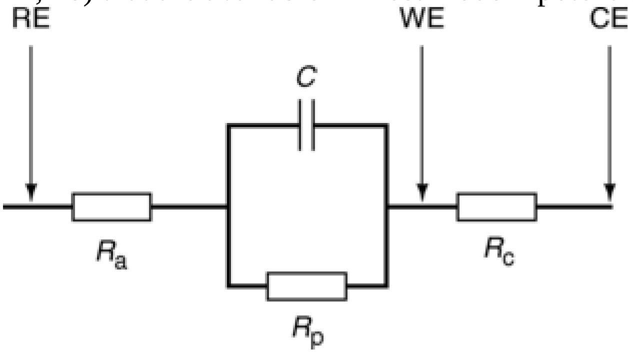

Fig. 21 Dummy cell for testing of potentiostat

Experimental Procedure for Potentiostatic Test Type 1. The experimental procedures for the two types of potentiostatic tests are described using the same types of electrodes and test cells. They differ insofar as type 2 involves the application of a series of potential steps. This requires changes of E_{appl} by hand, periodic adjustment of the sensitivity of the current-measuring device in the potentiostat, and sometimes, adjustment of the current scale of the recorder also. The procedure is greatly simplified if appropriate software is used and the experiment is carried out under computer control.

When the test cell has been assembled, the electrodes can be connected to the potentiostat. In most cases, E_{corr} is monitored before starting the potentiostatic test. When E_{corr} has reached a reasonable stable value, the potential can be applied and the corresponding current measured.

Often, a series of potential steps is applied to the same test electrode. This is the case in a test in which the pitting potential, E_{pit}, is determined as the potential at which the anodic current keeps increasing rather than decreasing after application of the potential step, as it would in the case for $E < E_{pit}$.

When the experiment is performed under computer control, the control parameters, such as the value of E_{appl} and the length of the potential step, have to be entered. Additional parameters related to the current measurement, such as the number of data points per second, might have to be entered. The experiment is performed then as programmed, and the current-time plot is displayed on the computer screen. After reformatting of the data, a printout of the ***I-t*** curve is obtained.

Experimental Procedure for Potentiostatic Test Type 2. The test is started by applying the first potential, which might be 10 to 50 mV more positive than E_{corr} if an anodic polarization curve is measured. After the current, which is recorded continuously throughout the test on a strip-chart recorder, has reached a steady-state value or after a predetermined time has elapsed, E_{appl} is increased to the next value, and the current is recorded. As increasing values of E_{appl} are used, it may become necessary to switch to less sensitive current scales. After the current at the final value of E_{appl} has been recorded, the polarization curve (E_{appl} versus log i) can be plotted using the final values of the current, I, at each potential and converting it into current density, i. Figure 22 shows the typical standard potentiostatic anodic polarization plot for type 430 stainless steel in 1.0 N H_2SO_4 at 30 °C (85 °F). Polarization curves performed according to ASTM G 5 with the standard ASTM sample have to fall within the scatter band shown in Fig. 22. Slightly different curves have been obtained with a new lot of samples introduced in recent years. Deviations from these standard plots point to deficiencies in the experimental technique, problems with the test cell, the equipment, and/or the operator.

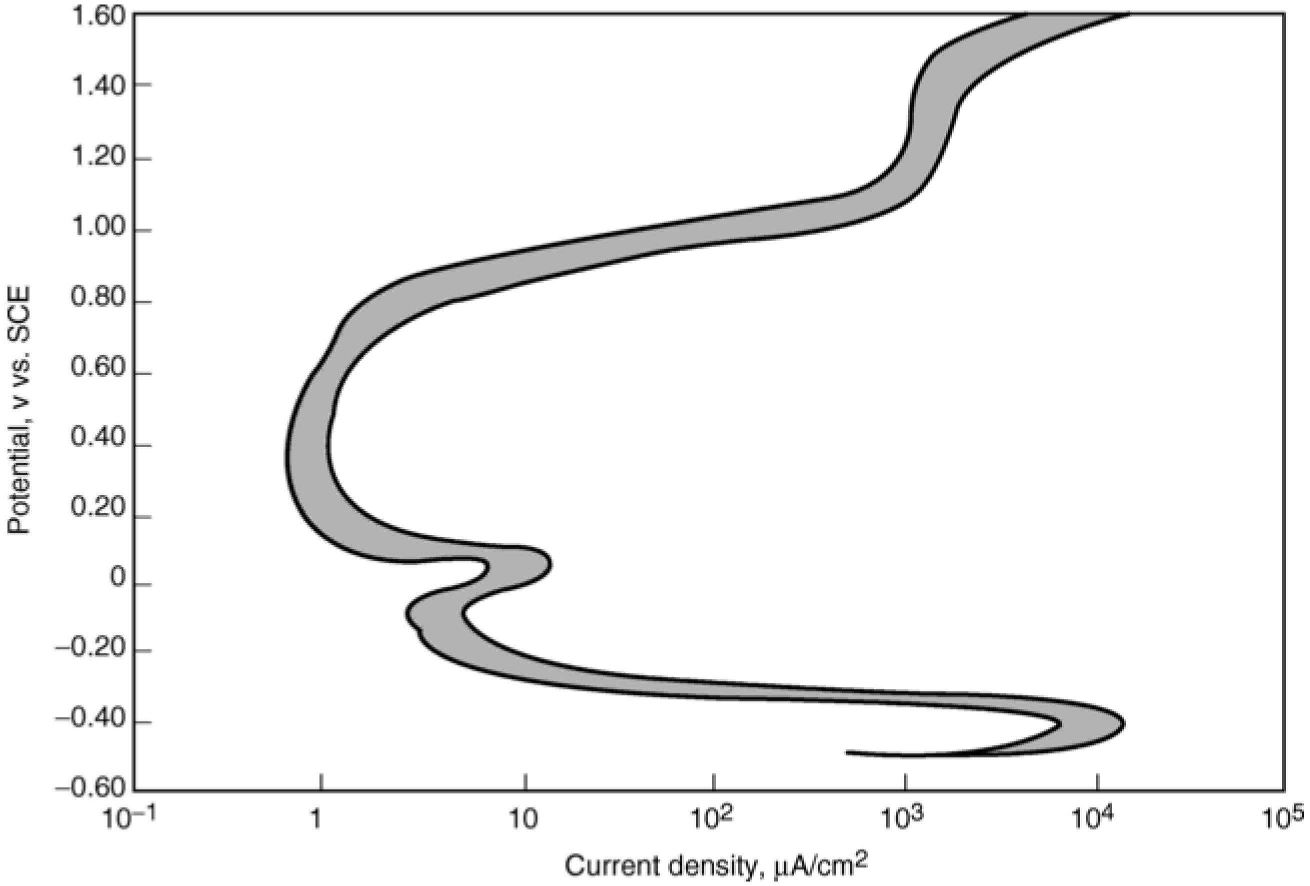

Fig. 22 Standard potentiostatic polarization curve for type 430 stainless steel in 1.0 *N* H_2SO_4, 30 °C (85 °F). Step rate, 50 mV for 5 min (each specimen). Source: ASTM G 5

Potentiodynamic Techniques. Potentiodynamic polarization curves can be obtained as a single sweep, that is, E_{appl} is increased at a constant scan rate, $s = dE_{appl}/dt$, between a starting potential, E_s, which often is E_{corr} or possibly below, and a final potential, E_f. Sometimes the scan is reversed when E_f or a preset maximum current density is reached, and stopped when the previous E_{corr} or a new value of E_{corr} is reached. Great care has to be taken in choosing an appropriate value of the scan rate (Ref 57). In general, less distortion of the true polarization curve occurs at the lowest scan rates. In ASTM G 5, a scan rate of 600 mV/h is recommended. Figure 23 shows the effects of varying scan rate on the shape of the anodic polarization curves for type 430 stainless steel in 1.0 *N* H_2SO_4 (Ref 14). Scan rates were increased from curve 1 to curve 4.

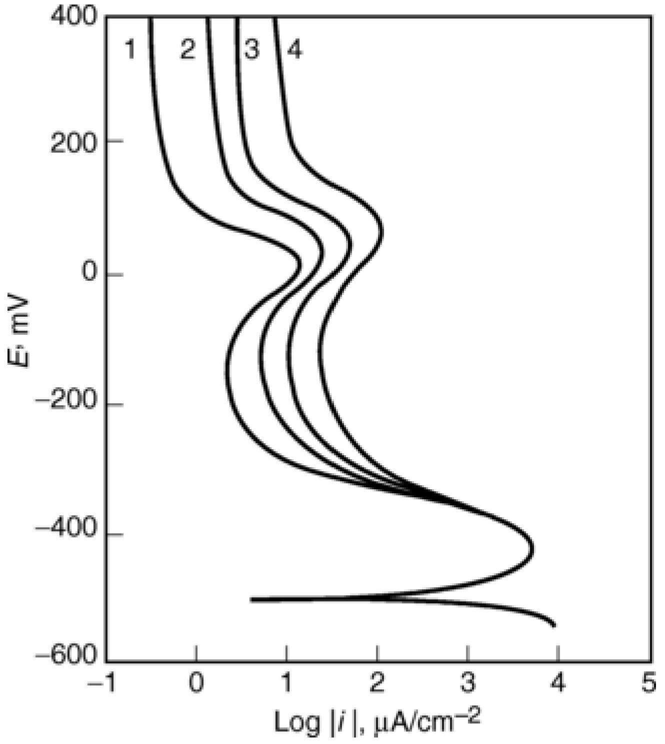

Fig. 23 Effect of scan rate on anodic polarization curve for type 430 stainless steel in 1.0 *N* H_2SO_4, 30 °C (85 °F). Scan rates, mV/s: 1) 0.03; 2) 0.17; 3) 0.34; 4) 1.00. Source: Ref 14

Single Sweeps. Anodic and cathodic polarization curves are usually determined at constant scan rate in a single sweep between two preset potentials, E_s and E_f. ASTM G 3 gives examples of polarization curves determined in this manner. Figure 24 shows the typical standard potentiodynamic anodic polarization plot for type 430 stainless steel in 1.0 *N* H_2SO_4 at 30 °C (85 °F). Anodic potentiodynamic polarization curves performed according to ASTM G 5 with the standard ASTM sample have to fall within the scatterband shown in Fig. 24. Slightly different curves have been obtained with a new lot of samples introduced in recent years. Deviations from these standard plots point to deficiencies in the experimental technique or problems with the test cell, the equipment, and/or the operator.

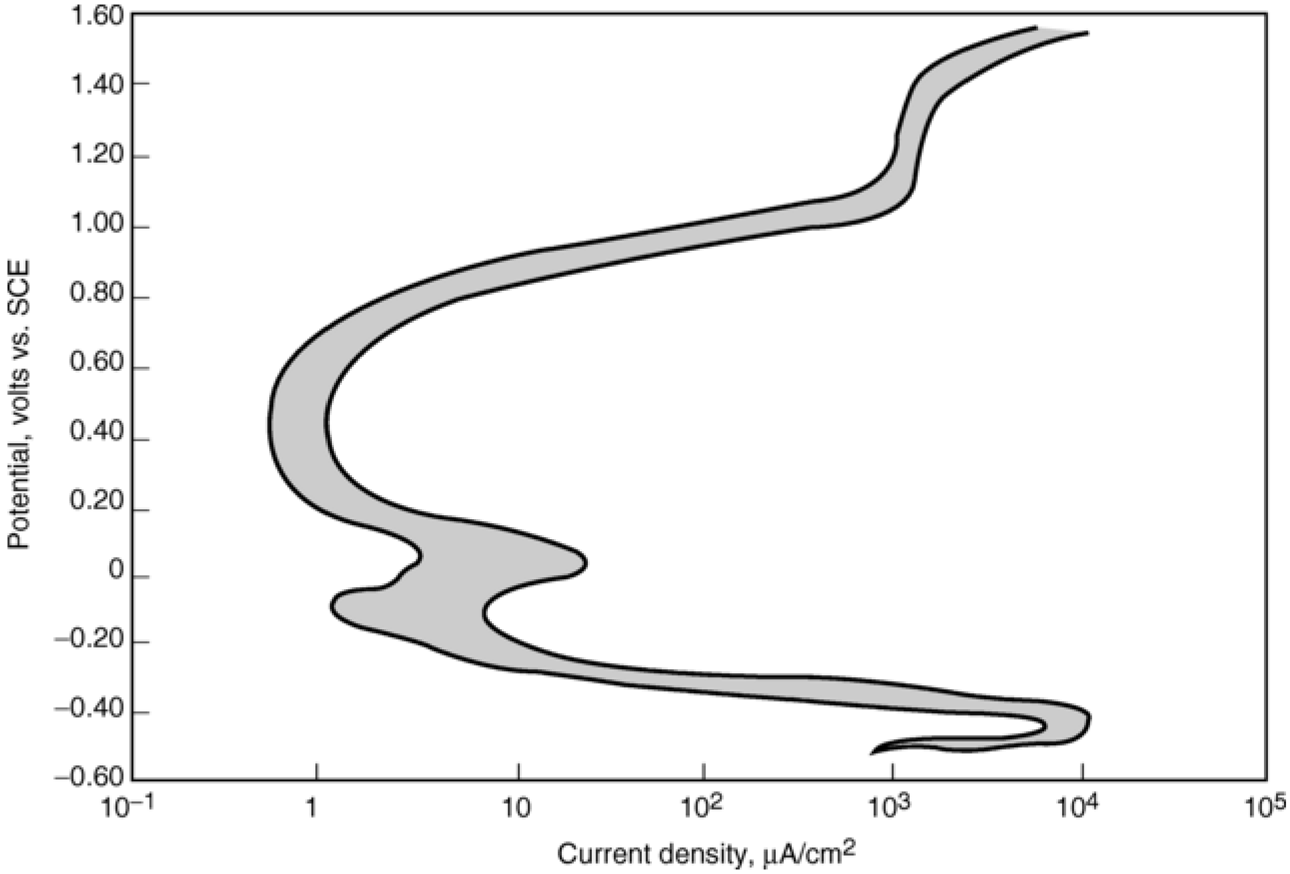

Fig. 24 Standard potentiodynamic polarization curve for type 430 stainless steel in 1.0 *N* H_2SO_4, 30 °C (85 °F). 0.6 V/h. Source: ASTM G 5

The results obtained by E_{corr} measurements and EIS suggest that the mechanism of microbiologically influenced corrosion inhibition (MICI) observed in the presence of *Shewanella algae* or *ana* is different for Al 2024 (Fig. 5a and 19a) and brass (Fig. 5b and 19b) on the one hand and mild steel (Fig. 5c and 19c) on the other. For Al 2024 and brass, the reduction of corrosion rates was accompanied by a shift of E_{corr} to more negative values, suggesting that MICI is due to a decrease of the rate of oxygen reduction in the presence of the biofilm. The increase of E_{corr} with a decrease of corrosion rates observed for mild steel can be explained only by a simultaneous decrease of the rates of the anodic and cathodic reactions. The former is assumed to be due to an increase of the Fe^{2+} concentration in the solution due to reduction of Fe^{3+} by *Shewanella,* leading to an increase of reversible potential, E_0, of the Fe/Fe^{2+} reaction, as discussed in Ref 58. This mechanism is shown schematically in Fig. 25, where it is assumed that the anodic reaction is under charge transfer control, while the cathodic reaction is under charge transfer control at low polarization and under mass- transport control at higher polarization. In the presence of the biofilm, the limiting current density, i_L, for oxygen reduction for Al 2024 and brass is decreased, but the rate of the anodic reaction remains unchanged. As a consequence, E_{corr} decreases from point 1 in Fig. 25 to point 2, and $i_L = i_{corr}$ decreases to i'_L. For mild steel, the rate of both reactions is decreased, and E_{corr} changes from point 1 to point 3, while i_L decreases to i'_L (Fig. 25).

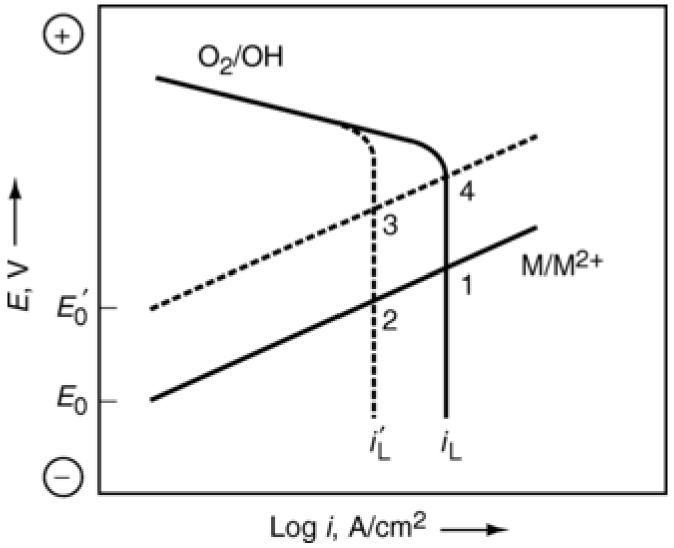

Fig. 25 Schematic polarization curves for a charge-transfer-controlled anodic reaction and a mass-transport-controlled cathodic reaction

The assumptions leading to the proposed mechanism have been confirmed by recording of potentiodynamic polarization curves after exposure to Väätänen nine salts solution (VNSS, pH 7.5) containing *Shewanella algae* for 7 days (Ref 20). For Al 2024 (Fig. 26) and brass (Fig. 27), a significant reduction of the rate of the cathodic reaction was observed, while for mild steel (Fig. 28), the rate of both reactions was reduced.

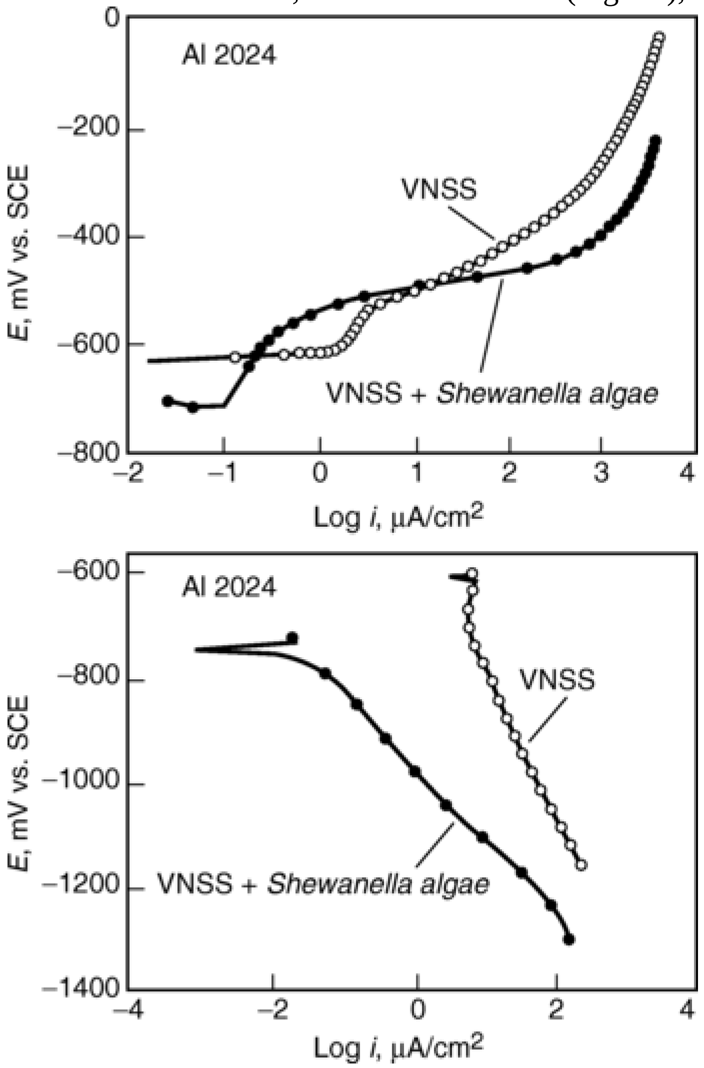

Fig. 26 Potentiodynamic polarization curves for Al 2024 exposed for 7 days to artificial seawater containing *S. algae.* VNSS, Väätänen nine salts solution. Source: Ref 20

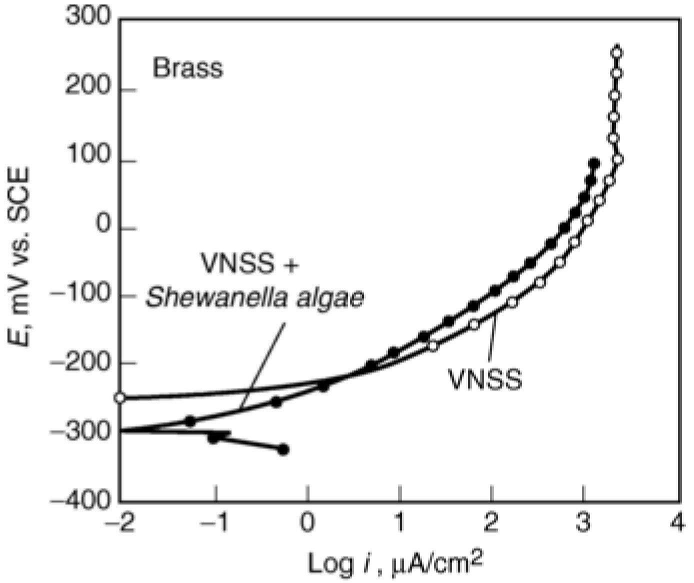

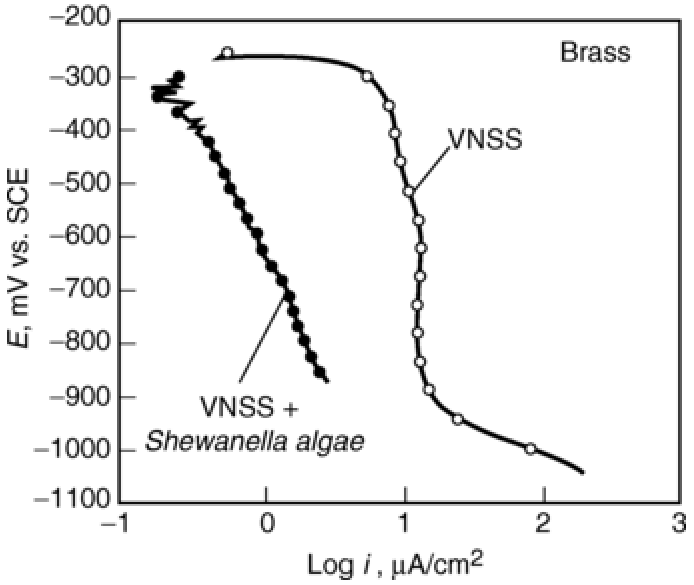

Fig. 27 Potentiodynamic polarization curves for brass exposed for 7 days to artificial seawater containing *S. algae.* VNSS, Väätänen nine salts solution. Source: Ref 20

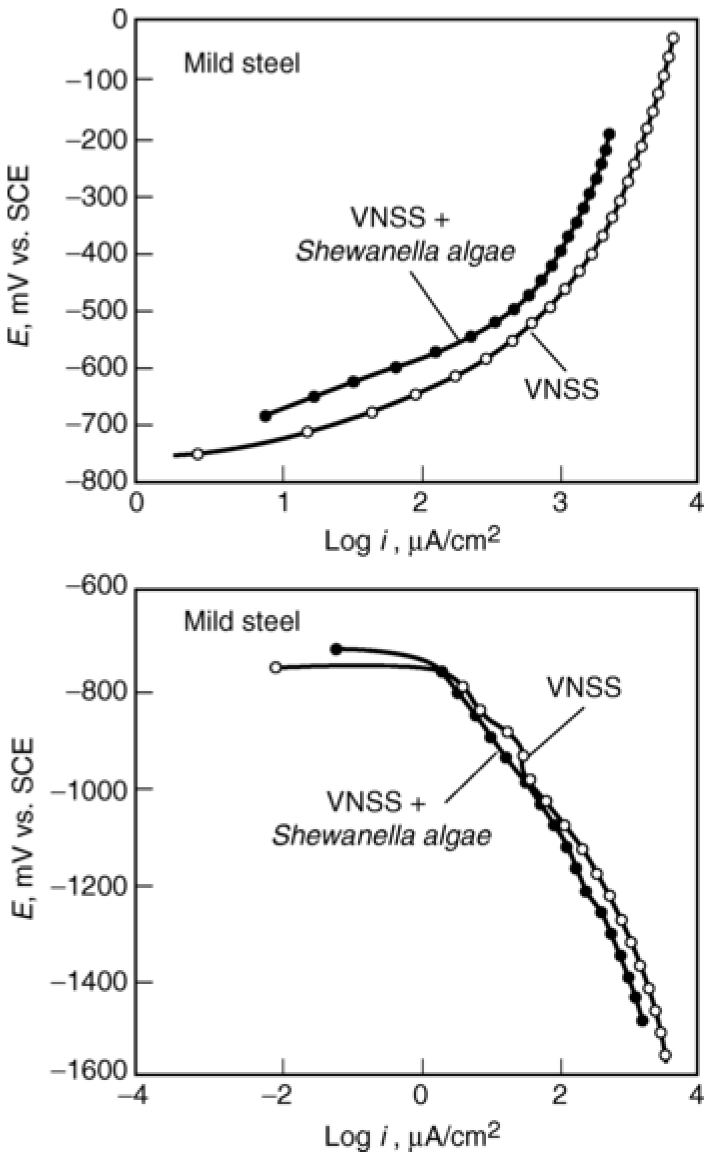

Fig. 28 Potentiodynamic polarization curves for mild steel exposed for 7 days to artificial seawater containing *S. algae.* Source: Ref 20

Pitting Scans. Pitting scans are carried out to determine E_{pit} and sometimes also the protection potential, E_{prot}. ASTM G 61, "Standard Test Method for Conducting Potentiodynamic Polarization Measurements for Localized Corrosion Susceptibility of Iron-, Nickel-, or Cobalt-Base Alloys," gives a procedure for conducting cyclic potentiodynamic polarization measurements to determine relative susceptibility to localized corrosion in the form of pitting or crevice corrosion. An indication of the susceptibility to localized corrosion is given by the potential, E_{pit}, at which the anodic current increases rapidly from the low values in the passive region. The more noble E_{pit} with respect to E_{corr}, the less susceptible is the alloy to initiation of localized corrosion (Ref 3, 11, 12). Figure 29 shows representative cyclic potentiodynamic polarization curves for type 304 stainless steel, which is susceptible to pitting and has a value of E_{pit} close to 0 mV versus SCE, and alloy C-276, which is immune to localized corrosion. The area under the curve for the forward and reverse scan for a susceptible alloy is a qualitative measure of corrosion damage due to pit growth. The difference between pitting and protection potentials is also used for this purpose.

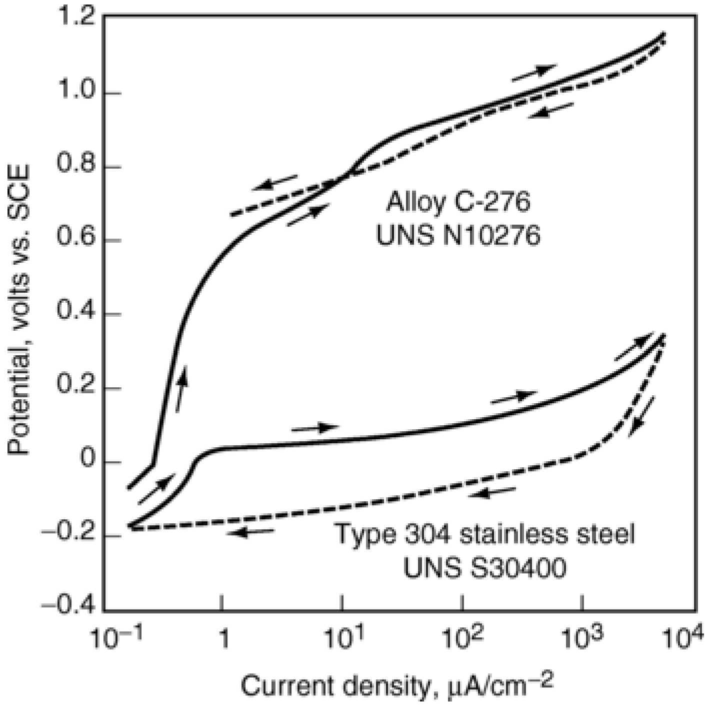

Fig. 29 Cyclic potentiodynamic polarization curves (pitting scans) for type 304 stainless steel and alloy C-276 in 3.54 wt% NaCl. Source: ASTM G 61

Evaluation of Alloy Sensitization. The electrochemical potentiokinetic reactivation (EPR) method, based on the original work found in Ref 59, has been developed for laboratory and field determination of the degree of sensitization of stainless steels (Ref 60, 61). The method is described in ASTM G 108, "Standard Test Method for Electrochemical Reactivation (EPR) for Detecting Sensitization of AISI Type 304 and 304L Stainless Steel." It also has been used successfully to evaluate sensitization of other stainless steels and nickel alloys. The EPR test is carried out using a reactivation potentiodynamic sweep from the passive region back to the active region, stopping at E_{corr}. The sweep is carried out in H_2SO_4 containing potassium thiocyanate (KSCN), which serves to activate the chromium- depleted grain boundaries. The current peak observed during the reactivation scan increases with the degree of sensitization. The charge Q passed is a measure of the degree of sensitization and can be used to determine a sensitization number, P_a, after normalization with the grain- boundary area. A modification of the EPR method is the double-loop electrokinetic repassivation test that involves a potentiodynamic scan from E_{corr} to the passive range, followed immediately by reverse polarization back to E_{corr} (Ref 62, 63). In this method, the degree of sensitization is determined by the ratio I_r/I_a of the maximum current generated in the reverse scan compared to that in the initial anodic scan. Figure 30 illustrates the principle of these two methods.

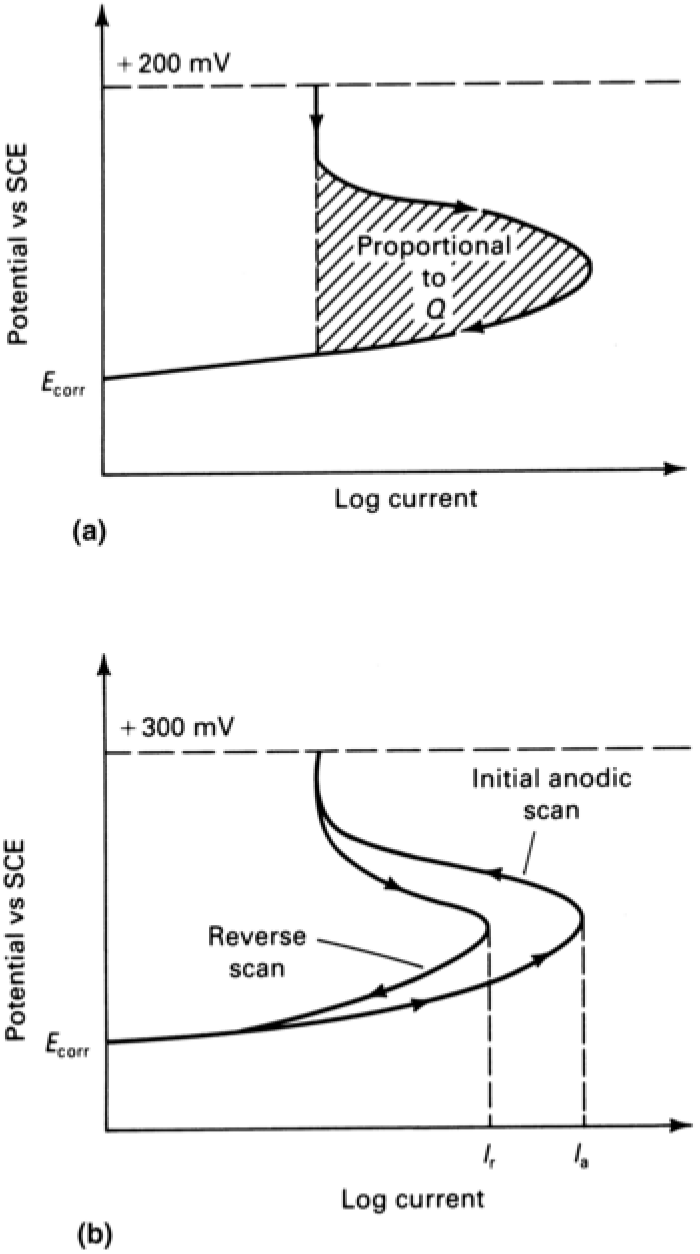

Fig. 30 Schematic potentiodynamic polarization curves for two methods for determination of the degree of sensitization. (a) Clarke et al method (Ref 61). (b) Akashi et al method (Ref 62)

Polarization curves obtained in the vicinity of E_{corr} can be analyzed by fitting of the experimental data to the equation that relates potential, E, and current density, i (Ref 2, 3):

$$i = i_{corr}\left[\exp\{2.3(E - E_{corr})/\beta_a\} - \exp\{2.3(E_{corr} - E)/\beta_c\}\right] \quad \text{(Eq 12)}$$

The polarization curves usually are obtained in the potentiodynamic mode. The results of the fit consist of experimental values of i_{corr}, β_a, and β_c. Several software programs have been described for carrying out this fit (Ref 64). Most potentiostat manufacturers supply software for this procedure. Because only a small polarization range $/E - E_{corr}/$ is applied (usually ±30 mV or less), this approach to obtain corrosion rates and Tafel slopes in the non-Tafel region is nondestructive and can be applied repeatedly without the danger of changing the properties of the surface under investigation. It is noted that the experimental approach is similar to that used in the determination of the polarization resistance, R_p. However, the kinetic data are obtained directly from the analysis of the measured polarization curve.

Galvanostatic and galvanodynamic techniques are used less commonly than the potentiostatic and potentiodynamic techniques described previously. In galvanostatic techniques, a constant current is applied, and

the potential is monitored as a function of time. It is also possible to record an entire polarization curve in the galvanostatic mode. A limitation of this approach for passive metals is that the passive region cannot be investigated. ASTM G 100, “Standard Test Method for Conducting Cyclic Galvanostaircase Polarization,” describes a method for determining E_{pit} for aluminum alloys, using a variation of the galvanostatic technique.

References cited in this section

2. H. Kaesche, *The Corrosion of Metals,* NACE, 1985

3. D.A. Jones, *Principles and Prevention of Corrosion,* MacMillan Publishing Co., 1992

4. F. Mansfeld, The Polarization Resistance Technique for Measuring Corrosion Currents, *Advancements in Corrosion Science and Technology,* Vol 6, M.G. Fontana and R.W. Staehle, Ed., Plenum Press, 1976, p 163

11. B.J. Little, P.A. Wagner, and F. Mansfeld, *Corrosion Testing Made Easy—Microbiologically Influenced Corrosion,* B.C. Syrett, Ed., NACE, 1997

12. N.G. Thompson and J.H. Payer, *Corrosion Testing Made Easy—dc Electrochemical Methods,* B.C. Syrett, Ed., NACE, 1998

14. F. Mansfeld, *Corrosion,* Vol 44, 1988, p 856

17. F. Mansfeld, *Corrosion,* Vol 32, 1976, p 143

18. F. Mansfeld, M.W. Kendig, and S. Tsai, *Corros. Sci.,* Vol 22, 1982, p 455

20. A. Naguib and F. Mansfeld, *Electrochim. Acta,* Vol 37, 2002, p 2319

57. F. Mansfeld and M. Kendig, *Corrosion,* Vol 37, 1981, p 545

58. M. Dubiel, C.H. Hsu, C.C. Chien, F. Mansfeld, and D.K. Newman, Microbial Iron Respiration Can Protect Steel from Corrosion, *Appl. Environ. Microbiol.,* submitted for publication

59. V. Cihal, A. Desestret, M. Froment, and G.H. Wagner, *Proc. Conf. European Federation of Corrosion* (Paris), European Federation of Corrosion, 1973, p 249

60. K. Osozawa, K. Bohnenkamp, and H.J. Engell, *Corros. Sci.,* Vol 6, 1966, p 421

61. W.L. Clarke, R.L. Cowan, and W.L. Walker, in *Intergranular Corrosion of Stainless Alloys,* STP 656, ASTM, 1978, p 99

62. M. Akashi, T. Kawamoto, and F. Umemura, *Corros. Eng. (Jpn.),* Vol 29, 1980, p 163

63. A.P. Majidi and M.A. Streicher, *Corrosion,* Vol 42, 1984, p 584

64. H. Shih and F. Mansfeld, STP 1154, ASTM, 1992, p 174

F. Mansfeld, Electrochemical Methods of Corrosion Testing, *Corrosion: Fundamentals, Testing, and Protection*, Vol 13A, *ASM Handbook*, ASM International, 2003, p 446–462

Electrochemical Methods of Corrosion Testing

Florian Mansfeld, University of Southern California

Scanning Electrode Techniques

The local distribution of anodic and cathodic sites can be evaluated using a number of electrochemical tests, such as the scanning reference electrode (SRET), the scanning vibrating electrode (SVET), local electrochemical impedance spectroscopy (LEIS), and the scanning Kelvin probe (SKP). While SRET and SVET allow measurements of the local corrosion currents, SKP provides a record of the surface potential distribution. The application of these techniques in electrochemistry and corrosion technology has recently been reviewed (Ref 65). A review of the early applications of scanning electrode techniques is found in Ref 8.

The SRET has been used mainly for investigation of local corrosion processes, such as pitting and crevice corrosion (Ref 8). The application of the SRET technique to localized corrosion phenomena is reviewed in Ref 66. More recently, SRET has also been used for the evaluation of delamination of organic coatings (Ref 67). The SRET technique is based on a microprobe that is capable of detecting local variations of the electrochemical properties of a metal surface with high lateral resolution. An optimized SRET has been used to evaluate the performance of several clear coatings, with good correlation between SRET signals and permeability as well as wet adhesion of these coatings (Ref 68).

The SVET offers a rapid method for monitoring the progress of corrosion of many metals and alloys exposed to corrosive solutions. The SVET technique has been shown to be a powerful tool for evaluating the efficiency of a variety of potential corrosion inhibitors as well as the determination of the current distribution in the vicinity of defects on polymer-coated metal surfaces (Ref 65, 69). It has also been used for determining the heterogeneous characteristics of consortia of bacteria and their possible influences on metallic substrates leading to microbiologically influenced corrosion (Ref 70).

The SKP. While SRET and SVET have to be used in immersion, the SKP is normally operated in (moist) air (Ref 71, 72). The SKP measures the Volta potential difference between a vibrating microreference electrode and the metallic surface under investigation. The corrosion potential can be derived from the Volta potential difference using a suitable calibration technique. One of the main advantages of the SKP technique is its nondestructive nature, while one disadvantage could be the fact that only potentials can be monitored. The SKP has been mainly applied to the study of polymer-coated metal surfaces, because it allows the detection of distinct potential differences between delaminated and intact areas (Ref 73). The SKP technique has been used to monitor the progress of filiform corrosion on a painted aluminum panel (Ref 65).

The SKP has been used to map the potential distribution under small drops of electrolyte in the classic Evans drop experiment (Ref 74, 75). Small drops of NaCl were placed on carbon steel, galvanized steel, stainless steel, and an aluminum alloy. In the absence of chromate, local anodes and cathodes were established in a short time. When dichromate was added to NaCl, very uniform potential distribution was found for stainless steel and Al 2024. The main driving force for the development of local anodes was considered to arise from oxygen reduction in very thin films of electrolyte surrounding the NaCl drop (Ref 74). The SKP technique has also been applied to the study of atmospheric corrosion processes (Ref 76).

References cited in this section

8. R. Baboian, Ed., *Electrochemical Techniques for Corrosion Engineers*, NACE, 1986

65. J.H.W. de Wit, D.H. van der Weijde, A.J. de Jong, F. Blekkenhorst, and S.D. Meijers, *Mat. Sci. Forum*, Vol 289–292, 1998, p 69

66. K.R. Trethewey, D.A. Sargeant, D.J. Marsh, and A.A. Tamimi, *Corros. Sci.*, Vol 35, 1993, p 127

67. F.J. Maile, T. Schauer, and C.D. Eisenbach, *Prog. Org. Coatings,* Vol 38, 2000, p 117

68. F.J. Maile, T. Schauer, and C.D. Eisenbach, *Farbe + Lack,* Vol 104 (No. 11), 1998, p 58

69. F. Zou, C. Barreau, R. Hellouin, D. Quantin, and D. Thierry, *Mat. Sci. Forum,* Vol 289–292, 1998, p 83

70. G. Chen, R.J. Palmer, and D.C. White, *Biodegrad.,* Vol 8, 1997, p 189

71. M. Stratmann, *Corros. Sci.,* Vol 27, 1987, p 869

72. M. Stratmann, *Corros. Sci.,* Vol 32, 1991, p 467

73. M. Stratmann, H. Streckel, and R. Feser, *Farbe + Lack,* Vol 97, 1991, p 9

74. C. Chen, C.B. Breslin, and F. Mansfeld, *Mater. Corros.,* Vol 49, 1998, p 1

75. U.R. Evans, *Met. Ind.,* Vol 29, 1926, p 481

76. M. Stratmann and H. Streckel, *Corros. Sci.,* Vol 30, 1990, p 681, 697, 715

F. Mansfeld, Electrochemical Methods of Corrosion Testing, *Corrosion: Fundamentals, Testing, and Protection*, Vol 13A, *ASM Handbook*, ASM International, 2003, p 446–462

Electrochemical Methods of Corrosion Testing

Florian Mansfeld, University of Southern California

Miscellaneous Techniques

A number of electrochemical techniques have been developed that allow evaluation of processes such as hydrogen embrittlement, especially of steels, or the susceptibility of metal and alloys to localized corrosion, such as pitting. Certain standard laboratory tests, such as the anodized aluminum corrosion test, the impedance test for anodized aluminum, the electrolytic corrosion test, as well as the paint adhesion on a scribed surface (PASS) test, are used mainly as quality-control tests.

Hydrogen Permeation Technique. The Devanathan-Stachurski method can be used to study parameters associated with the hydrogen embrittlement tendencies of metals and alloys (Ref 77). This method is described in ASTM G 148, "Standard Practice for Evaluation of Hydrogen Uptake, Permeation, and Transport in Metals by an Electrochemical Technique." The technique involves placing a thin metal foil between two electrochemical cells—a hydrogen charging cell and a hydrogen oxidation cell (Fig. 31). Hydrogen is generated on the side of the metal foil facing the charging cell by application of a sufficiently negative potential. For characterization of the hydrogen transport in the bulk of the material under investigation, galvanostatic charging is preferred. The hydrogen that diffuses through the foil is oxidized on the side of the foil that faces the oxidation cell. The potential of the foil is controlled at a sufficiently positive potential to ensure that the kinetics of the oxidation of hydrogen atoms are limited by the flux of hydrogen atoms. The total oxidation current is monitored as a function of time. It is the sum of the hydrogen oxidation current, which is the permeation current, and the background current due to dissolution of the metal foil. The latter needs to be kept small by choosing a proper electrolyte in the oxidation cell. For ferrous materials, an alkaline solution, such as 0.1 *M* NaOH, is used to ensure passive behavior.

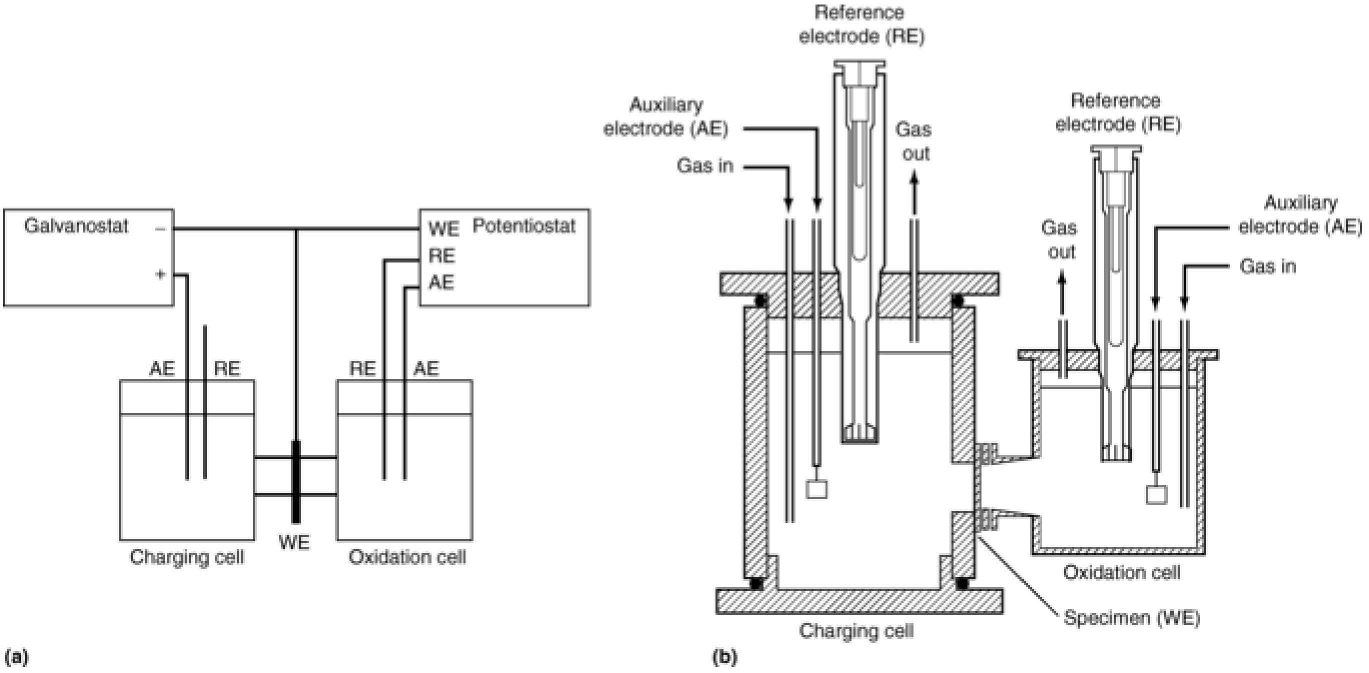

Fig. 31 Electrochemical hydrogen permeation cell assembly and measuring apparatus. (a) Schematic. (b) Polytetrafluoroethylene (PTFE) hydrogen permeation cell. Source: ASTM G 148

For a known foil thickness, L, the steady-state permeation current, J_{ss}, gives information concerning the subsurface concentration, C_H, at the charging surface:

$$J_{ss} = C_H D_l / L \quad \text{(Eq 13)}$$

where D_l is the lattice diffusion coefficient of hydrogen. ASTM G 148 gives a detailed description of the procedure for the analysis of the results of electrochemical hydrogen permeation results obtained from steady-state permeation current measurements or from permeation transient measurements.

The barnacle electrode assembly allows determination of the amount of mobile hydrogen atoms in a metallic structure that had been exposed previously to an aqueous or gaseous environment. In this case, only the hydrogen oxidation cell is used (Ref 78, 79).

Standard Laboratory Tests. Numerous ac and dc electrochemical methods have been used to study the performance and quality of protective coatings, including passive films on metallic substrates, and to evaluate the effectiveness of various surface pretreatments. Several of these methods are discussed subsequently.

The Anodized Aluminum Corrosion Test. The Ford anodized aluminum corrosion test (FACT) (Ref 80) involves cathodic polarization of the anodized aluminum surface by using a small, cylindrical, glass clamp-on cell and a special 5% NaCl solution containing cupric chloride ($CuCl_2$) acidified with acetic acid. A large voltage is applied across the cell by using a platinum auxiliary electrode. The alkaline conditions created by the cathodic polarization promote dissolution at small defects in the anodized aluminum surface. As the coating resistance is decreased, more current begins to flow, and the voltage decreases. The cell voltage (auxiliary electrode to test specimen voltage) is monitored for 3 min, and the parameter "cell voltage multiplied by time" is recorded. ASTM B 538, "Standard Method of FACT (Ford Anodized Aluminum Corrosion Test) Testing," describes the method in greater detail.

A similar test, known as the cathodic breakdown test, involves cathodic polarization to -1.6 versus SCE for a period of 3 min in acidified NaCl. The test was designed for anodized aluminum alloys, because the alkaline conditions created by the large applied currents promote the formation of corroding spots at defects in the anodized film.

The Electrolytic Corrosion Test. This test was designed for electrodeposits of, principally, nickel and chromium on less noble metals, such as zinc or steel (Ref 81). Special solutions are used, and the metal is polarized to +0.3 V versus SCE. The metal is taken through cycles of 1 min anodic polarization and 2 min unpolarized condition. An indicator solution is then used to detect the presence of pits that penetrate to the substrate. Each exposure cycle is assumed to simulate one year of exposure under atmospheric corrosion conditions. ASTM B 627, "Standard Method for Electrolytic Corrosion Testing (EC Test)," describes the method in greater detail.

The PASS test involves cathodic polarization of a small portion of a painted metal. The area exposed contains a scribed line that exposes a line of underlying bare metal. The sample is cathodically polarized for 15 min in 5% NaCl. At the end of this period, the amount of delaminated coating is determined using an adhesive-tape pulling procedure.

The Impedance Test for Anodized Aluminum. ASTM B 457, "Standard Method for Measurement of the Impedance of Anodic Coatings on Aluminum," is used to study the efficiency of the sealing process for anodized aluminum alloys (Ref 82, 83). In this sense, the test is similar to the FACT test, except that this method uses a 1 V_{rms}, 1 kHz signal source from an impedance bridge to determine the impedance of sealed, anodized aluminum. The impedance of the sealed, anodized aluminum alloy is determined in kΩ. The test area is defined with a portable cell, and a platinum or stainless steel auxiliary electrode is typically used. The sample is immersed in 3.5% NaCl. In contrast to the methods discussed previously, this quality-control test is essentially nondestructive and does not accelerate the corrosion process.

The Critical Pitting Temperature. The susceptibility of a material to pitting is usually evaluated based on the pitting potential, E_{pit}, that can be determined using a potentiostatic or potentiodynamic (pitting scan) technique. An alternative approach is based on the critical pitting temperature (CPT) that is described in ASTM G 150, "Standard Test Method for Electrochemical Critical Temperature Testing of Stainless Steels." The CPT is defined as the lowest temperature at which stable pit propagation occurs. The test method determines the potential-independent critical pitting temperature using a potentiostatic technique with a temperature scan. A specific sample holder is recommended that eliminates the occurrence of crevice corrosion. The test sample is exposed to a 1*M* NaCl solution that is initially maintained at 0 °C. The solution is then heated at a rate of 1 °C/min. The sample is polarized to a potential above the E_{pit} range during the entire temperature scan. The current is monitored during the temperature scan, and the CPT is defined as the temperature at which the current density exceeds 100 μA/ cm^2. The occurrence of pitting is confirmed visually after the test. The standard parameters recommended in ASTM G 150 are suitable for determining the CPT of austenitic stainless steels and other related alloys.

References cited in this section

77. M.A.V. Devanathan and Z. Stachurski, *Proc. R. Soc. (London) A,* Vol 270, 1962, p 90

78. D.A. Berman, J.J. DeLuccia, and F. Mansfeld, *Met. Prog.,* Vol 115, 1979, p 58

79. F. Mansfeld, S. Jeanjaquet, and D.K. Roe, *Mater. Perform.,* Vol 21 (No. 2), 1982, p 36

80. J. Stone, H.A. Tuttle, and H.N. Bogart, *Plating,* Vol 43, 1965, p 877

81. R.L. Saur and R.P. Basco, *Plating,* Vol 53, 1966, p 33, 320, 981

82. E.T. Englehart and G. Sowinski, Jr., *SAE J.,* Vol 72, 1974, p 51

83. E.T. Englehart and D.G. George, *Mater. Prot. (China),* Vol 3, 1964, p 25

F. Mansfeld, Electrochemical Methods of Corrosion Testing, *Corrosion: Fundamentals, Testing, and Protection*, Vol 13A, *ASM Handbook*, ASM International, 2003, p 446–462

Electrochemical Methods of Corrosion Testing

Florian Mansfeld, University of Southern California

References

1. C. Wagner and W. Traud, *Z. Elektrochemie,* Vol 44, 1938, p 391

2. H. Kaesche, *The Corrosion of Metals,* NACE, 1985

3. D.A. Jones, *Principles and Prevention of Corrosion,* MacMillan Publishing Co., 1992

4. F. Mansfeld, The Polarization Resistance Technique for Measuring Corrosion Currents, *Advancements in Corrosion Science and Technology,* Vol 6, M.G. Fontana and R.W. Staehle, Ed., Plenum Press, 1976, p 163

5. M. Stern and A.L. Geary, *J. Electrochem. Soc.,* Vol 104, 1957, p 56

6. R. Baboian, Ed., *Electrochemical Techniques for Corrosion,* NACE, 1977

7. *Electrochemical Corrosion Testing,* STP 727, U. Bertocci and F. Mansfeld, Ed., ASTM, 1979

8. R. Baboian, Ed., *Electrochemical Techniques for Corrosion Engineers,* NACE, 1986

9. R. Baboian, Ed., *Corrosion Tests and Standards—Application and Interpretation,* ASTM, 1995

10. R.W. Revie, Ed., *Uhlig's Corrosion Handbook,* 2nd ed., Electrochemical Society Series, Wiley-Interscience, 2000

11. B.J. Little, P.A. Wagner, and F. Mansfeld, *Corrosion Testing Made Easy—Microbiologically Influenced Corrosion,* B.C. Syrett, Ed., NACE, 1997

12. N.G. Thompson and J.H. Payer, *Corrosion Testing Made Easy—dc Electrochemical Methods,* B.C. Syrett, Ed., NACE, 1998

13. R. Cottis and S. Turgoose, *Corrosion Testing Made Easy—Electrochemical Impedance and Noise,* B.C. Syrett, Ed., NACE, 1999

14. F. Mansfeld, *Corrosion,* Vol 44, 1988, p 856

15. G.G. Geesey, I. Beech, P.J. Bremer, B.J. Webster, and D.B. Wells, Biocorrosion, *Biofilms II: Process Analysis and Applications,* J.D. Bryers, Ed., Wiley, 2000, p 281

16. F. Mansfeld and M.W. Kendig, *Corrosion,* Vol 41, 1985, p 490

17. F. Mansfeld, *Corrosion,* Vol 32, 1976, p 143

18. F. Mansfeld, M.W. Kendig, and S. Tsai, *Corros. Sci.,* Vol 22, 1982, p 455

19. F. Mansfeld and B. Little, *Corros. Sci.,* Vol 32, 1991, p 247

20. A. Naguib and F. Mansfeld, *Electrochim. Acta,* Vol 37, 2002, p 2319

21. G. Lauer and F. Mansfeld, *Corrosion,* Vol 26, 1970, p 504

22. F. Mansfeld and R.V. Inman, *Corrosion,* Vol 35, 1979, p 21

23. F. Mansfeld, *Corrosion,* Vol 29, 1973, p 403

24. F. Mansfeld, *Corrosion,* Vol 27, 1971, p 436

25. F. Mansfeld, D.H. Hengstenberg, and J.V. Kenkel, *Corrosion,* Vol 30, 1974, p 343

26. F. Mansfeld and J.V. Kenkel, *Corros. Sci.,* Vol 15, 1975, p 183, 239

27. D.A. Jones, *Corrosion,* Vol 40, 1984, p 181

28. F. Mansfeld, L.T. Han, and C.C. Lee, *J. Electrochem. Soc.,* Vol 143, 1996, p L286

29. F. Mansfeld, L.T. Han, C.C. Lee, C. Chen, G. Zhang, and H. Xiao, *Corros. Sci.,* Vol 39, 1997, p 255

30. F. Mansfeld, L.T. Han, C.C. Lee, and G. Zhang, *Electrochim. Acta,* Vol 43, 1998, p 2933

31. F. Mansfeld, H. Xiao, L.T. Han, and C.C. Lee, *Prog. Org. Coatings,* Vol 30, 1997, p 89

32. D.A. Eden, "Electrochemical Noise—The First Two Octaves," Paper 386, Corrosion/ 98, NACE, 1998

33. U. Bertocci, C. Gabrielli, F. Huet, and M. Keddam, *J. Electrochem. Soc.,* Vol 144, 1997, p 31

34. U. Bertocci, C. Gabrielli, F. Huet, M. Keddam, and P. Rousseau, *J. Electrochem. Soc.,* Vol 144, 1997, p 37

35. F. Mansfeld, Z. Sun, E. Speckert, and C.H. Hsu, "Electrochemical Noise Analysis (ENA) for Active and Passive Systems," Paper 00418, Corrosion/2000, NACE, 2000

36. F. Mansfeld, Z. Sun, C.H. Hsu, and A. Nagiub, *Corros. Sci.,* Vol 43, 2001, p 341

37. F. Mansfeld and Z. Sun, *Corrosion,* Vol 55, 1999, p 915

38. C.C. Lee and F. Mansfeld, *Corros. Sci.,* Vol 40, 1998, p 959

39. C. Gabrielli, F. Huet, and M. Keddam, *Electrochim. Acta,* Vol 31, 1986, p 1025

40. J.R. Scully, *Corrosion,* Vol 56, 2000, p 199

41. F. Mansfeld, H. Shih, H. Greene, and C.H. Tsai, *Analysis of EIS Data for Common Corrosion Processes,* STP 1188, ASTM, 1993, p 37

42. F. Mansfeld, *J. Appl. Electrochem.,* Vol 25, 1995, p 187

43. F. Mansfeld and M. Kendig, *Electrochemical Impedance Tests for Protective Coatings,* STP 866, ASTM, 1985, p 122

44. F. Mansfeld, M. Kendig, and S.Tsai, *Corrosion,* Vol 38, 1982, p 478

45. M. Kendig, F. Mansfeld, and S. Tsai, *Corros. Sci.,* Vol 23, 1983, p 317

46. J. Titz, G.H. Wagner, H. Spaehn, M. Ebert, K. Juettner, and W.J. Lorenz, *Corrosion,* Vol 46, 1990, p 221

47. M. Kendig and F. Mansfeld, *Mat. Res. Soc. Symp. Proc.,* Vol 115, 1988, p 193

48. F. Mansfeld, C.C. Lee, L.T. Han, B.J. Little, P. Wagner, R. Ray, and J. Jones-Meehan, "The Impact of MIC on Protective Polymer Coatings," Final Report, Contract N00014- 94-1-0026, The Office of Naval Research, Aug 1998

49. J. Hitzig, K. Juettner, W.J. Lorenz, and W. Paatsch, *Corros. Sci.,* Vol 24, 1984, p 945

50. J. Hitzig, K. Juettner, W.J. Lorenz, and W. Paatsch, *J. Electrochem. Soc.,* Vol 133, 1986, p 133

51. F. Mansfeld and M.W. Kendig, *J. Electrochem. Soc.,* Vol 135, 1988, p 828

52. F. Mansfeld, S. Lin, S. Kim, and H. Shih, *Corros. Sci.,* Vol 27, 1987, p 997

53. F. Mansfeld and H.Shih, *J. Electrochem. Soc.,* Vol 135, 1987, p 332

54. F. Mansfeld, S. Lin, S. Kim, and H. Shih, *Electrochim. Acta,* Vol 34, 1989, p 1123

55. F. Mansfeld, S. Lin, S. Kim, and H. Shih, *J. Electrochem. Soc.,* Vol 137, 1990, p 78

56. F. Mansfeld, H. Shih, H. Greene, and C.H. Tsai, *Detection and Monitoring of Localized Corrosion with EIS,* STP 1188, ASTM, 1993, p 297

57. F. Mansfeld and M. Kendig, *Corrosion,* Vol 37, 1981, p 545

58. M. Dubiel, C.H. Hsu, C.C. Chien, F. Mansfeld, and D.K. Newman, Microbial Iron Respiration Can Protect Steel from Corrosion, *Appl. Environ. Microbiol.,* submitted for publication

59. V. Cihal, A. Desestret, M. Froment, and G.H. Wagner, *Proc. Conf. European Federation of Corrosion* (Paris), European Federation of Corrosion, 1973, p 249

60. K. Osozawa, K. Bohnenkamp, and H.J. Engell, *Corros. Sci.,* Vol 6, 1966, p 421

61. W.L. Clarke, R.L. Cowan, and W.L. Walker, in *Intergranular Corrosion of Stainless Alloys,* STP 656, ASTM, 1978, p 99

62. M. Akashi, T. Kawamoto, and F. Umemura, *Corros. Eng. (Jpn.),* Vol 29, 1980, p 163

63. A.P. Majidi and M.A. Streicher, *Corrosion,* Vol 42, 1984, p 584

64. H. Shih and F. Mansfeld, STP 1154, ASTM, 1992, p 174

65. J.H.W. de Wit, D.H. van der Weijde, A.J. de Jong, F. Blekkenhorst, and S.D. Meijers, *Mat. Sci. Forum,* Vol 289–292, 1998, p 69

66. K.R. Trethewey, D.A. Sargeant, D.J. Marsh, and A.A. Tamimi, *Corros. Sci.,* Vol 35, 1993, p 127

67. F.J. Maile, T. Schauer, and C.D. Eisenbach, *Prog. Org. Coatings,* Vol 38, 2000, p 117

68. F.J. Maile, T. Schauer, and C.D. Eisenbach, *Farbe + Lack,* Vol 104 (No. 11), 1998, p 58

69. F. Zou, C. Barreau, R. Hellouin, D. Quantin, and D. Thierry, *Mat. Sci. Forum,* Vol 289–292, 1998, p 83

70. G. Chen, R.J. Palmer, and D.C. White, *Biodegrad.,* Vol 8, 1997, p 189

71. M. Stratmann, *Corros. Sci.,* Vol 27, 1987, p 869

72. M. Stratmann, *Corros. Sci.,* Vol 32, 1991, p 467

73. M. Stratmann, H. Streckel, and R. Feser, *Farbe + Lack,* Vol 97, 1991, p 9

74. C. Chen, C.B. Breslin, and F. Mansfeld, *Mater. Corros.,* Vol 49, 1998, p 1

75. U.R. Evans, *Met. Ind.,* Vol 29, 1926, p 481

76. M. Stratmann and H. Streckel, *Corros. Sci.,* Vol 30, 1990, p 681, 697, 715

77. M.A.V. Devanathan and Z. Stachurski, *Proc. R. Soc. (London) A,* Vol 270, 1962, p 90

78. D.A. Berman, J.J. DeLuccia, and F. Mansfeld, *Met. Prog.,* Vol 115, 1979, p 58

79. F. Mansfeld, S. Jeanjaquet, and D.K. Roe, *Mater. Perform.,* Vol 21 (No. 2), 1982, p 36

80. J. Stone, H.A. Tuttle, and H.N. Bogart, *Plating,* Vol 43, 1965, p 877

81. R.L. Saur and R.P. Basco, *Plating,* Vol 53, 1966, p 33, 320, 981

82. E.T. Englehart and G. Sowinski, Jr., *SAE J.,* Vol 72, 1974, p 51

83. E.T. Englehart and D.G. George, *Mater. Prot. (China),* Vol 3, 1964, p 25

T. Yau, Immersion Testing, *Corrosion: Fundamentals, Testing, and Protection,*, Vol 13A, *ASM Handbook*, ASM International, 2003, p 463–469

Immersion Testing

Te-Lin Yau, Te-Lin Yau Consultancy

Introduction

IMMERSION TESTING is the most frequently conducted test for evaluating the corrosion of metals in aqueous solutions. It appears simple: Totally immerse a test specimen in a corrosive solution for a period of time and then remove the specimen for examination. It is sometimes referred to as a "quick and dirty" test. However, a number of factors must be considered to achieve specific goals and to ensure adequate reproducibility of test results. The actual conditions of the test are usually determined by the nature of the problem at hand, the ingenuity of the investigator, and the budget of the test program. The following information is presented as a guide, so that some of the pitfalls of such testing may be avoided.

The methods and procedures described include basic factors that must be considered in sophisticated test procedures as well as in simple tests. Primary consensus standards for immersion corrosion testing of metals have been developed by ASTM International and NACE International. Applicable ASTM standards are given in Ref 1 to 9. The NACE method is given in Ref 10.

For proper planning of the test and interpretation of the test results, the specific influences of the following variables must be considered: solution composition, temperature, aeration, volume, velocity, and waterline effects; specimen surface preparation; method of immersion of specimens; duration of test; and method of cleaning specimens at the conclusion of the exposure.

In most cases, immersion tests are conducted to determine the corrosion rates of metals in a given environment. However, by employing specifically designed specimens and/or environments, immersion tests can also be conducted to evaluate the resistance of the metal to pitting, crevice corrosion, galvanic corrosion, hydrogen embrittlement, erosion, and stress-corrosion cracking. Sections of this Volume devoted to these topics have details on the specific testing methods.

References cited in this section

1. "Practice for Detecting Susceptibility to Intergranular Attack in Austenitic Stainless Steels," A 262, *Annual Book of ASTM Standards,* ASTM

9. "Standard Test Method for Visual Assessment of Exfoliation Corrosion Suscepti[chbility of 5*xxx* Series Aluminum Alloys,"[fj G 66, *Annual Book of ASTM Standards,* ASTM

10. "Laboratory Corrosion Testing of Metals," NACE TM-0169-2000, National Association of Corrosion Engineers

T. Yau, Immersion Testing, *Corrosion: Fundamentals, Testing, and Protection,*, Vol 13A*, ASM Handbook*, ASM International, 2003, p 463–469

Immersion Testing

Te-Lin Yau, Te-Lin Yau Consultancy

Total Immersion

Composition of Solution. Test solutions can be: (a) accurately prepared by combining chemicals according to the specifications of the Committee on Analytical Reagents of the American Chemical Society with distilled water, (b) naturally occurring solutions, or (c) samples of plant process solutions. The composition of the test solutions should be controlled to the fullest extent possible. They should be described as completely and accurately as possible in the test report. It helps to include information such as color, pH, and specific gravity before and after the test.

Evaporation losses can be controlled by a constant level device or by frequent addition of appropriate solution to maintain the original volume within ±1%. The use of a reflux condenser ordinarily, but not always, precludes the necessity of adding to the original kettle charge. Certain chemicals are too volatile to be quickly condensed.

The composition of the test solution sometimes changes as a result of catalytic decomposition or by reaction with the test specimens. For example, hydrogen peroxide may catalytically decompose, and hydrofluoric acid is quickly consumed by reacting with reactive metals such as titanium and zirconium. These changes should be determined if possible. Where required, the exhausted constituents should be added or a fresh solution provided during the course of the test. If problems are suspected, the composition of the test solutions should be checked by analysis at the end of the test to determine the extent of change in composition that took place from evaporation or reactions.

Corrosion products from the specimen may influence the corrosion rate of the metal or the corrosion rate of different metals exposed at the same time. For example, the accumulation of cupric ions in the testing of copper alloys in intermediate strength of sulfuric acid accelerates the corrosion of copper alloys, as compared to the rates that are found if the corrosion products are continually removed. Cupric ions may also exhibit a passivating effect on stainless steel specimens exposed at the same time. It is generally advisable to expose only the same type of alloys in the testing apparatus. Alloys in the same group may be quite different in chemical compositions. For example, there are copper-containing stainless steels, such as some of the precipitation-hardening and duplex stainless steels, and there are copper-free stainless steels.

Temperature of Solution. Temperature is a critical factor in corrosion. Accordingly, the temperature of the test solution and, if different, the temperature of the test specimen must be known. In many cases, corrosion increases rapidly with temperature. The corrosion of type 303 stainless steel by 65% nitric acid is shown in Table 1 (Ref 10). Corrosion increases from a low rate of less than 0.5 mm/yr (20 mils/yr) to over 100 mm/yr (4000 mils/yr) as a result of increasing the temperature 65 °C (120 °F). For some corrosion systems, the thermal effect is more complex. For example, the corrosion rate of Monel alloy in air- saturated sulfuric acid solutions increases sharply with rising temperature to a maximum at 80 °C (175 °F) and then decreases with a further increase in temperature. This is because of the decrease in dissolved oxygen in sulfuric acid, as indicated in Fig. 1 (Ref 11, 12).

Table 1 Effect of temperature on corrosion of type 303 stainless steel by 65% HNO_3

Temperature		Corrosion rate	
°C	**°F**	**mm/yr**	**mils/yr**
Up to 120	250	<0.5	<20
125	260	2.5	100
135	280	5.0	200
160	320	12.5	500
165	330	25	1000

185	370	125	5000

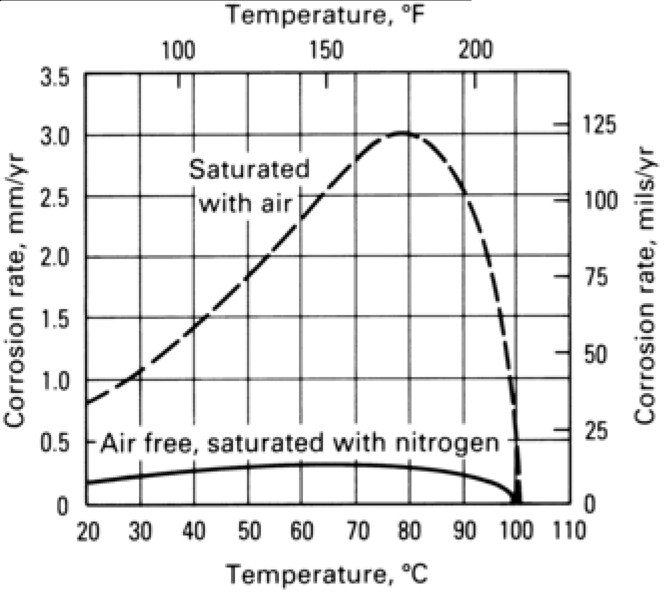

Fig. 1 Effect of temperature on the corrosion of Monel in 5 to 6% sulfuric acid. Solution velocity: 4.7 to 5 m/min (15.5 to 16.5 ft/min). Source: Ref 11, 12

Laboratory tests are often conducted in controlled-temperature water or oil baths. The temperature of the corroding solution should be controlled within ±1 °C (±1.8 °F) and must be stated in the report of test results.

If no specific temperature, such as a boiling point, is required or if a temperature range is to be investigated, the selected temperatures used in the test, as well as their respective durations, must be reported. Tests at ambient temperature should be conducted at the highest temperature anticipated. The variation in temperature should be reported also.

Accelerated corrosion tests often are conducted at temperatures above proposed operating temperatures in order to decrease the time of testing. Because the effect of temperature on corrosion rates may be great, there is a danger that economic, yet suitable materials may be eliminated. Also, as shown in the Monel example, if the temperature-corrosion-rate relation is nonlinear, an extrapolation of results based on increased temperature could lead to erroneous conclusions.

A common error involves the assumption that the environment temperature is the corroding temperature. This is particularly true in the case of materials for heating surfaces. The average temperature of the liquid in the tank may be 65 °C (150 °F), but the corroding or surface temperature of the steam heating coil is considerably higher. Therefore, tests conducted at 65 °C (150 °F) may provide erroneous results. Surface temperatures can often be estimated by considering heat-transfer coefficients.

Results of corrosion tests have shown that dissolution of borosilicate glass vessels in distilled water at temperatures above 60 °C (140 °F) lowers the corrosion rate of low-carbon steel significantly. Test apparatus has been designed that is capable of precise control and measurement of temperature (Ref 13).

Aeration of Solution. Aeration, or the presence of dissolved oxygen in a liquid environment, can influence corrosion rates profoundly. Accordingly, this factor should be considered carefully in a corrosion test program. In general, some metals and alloys are attacked more rapidly in the presence of oxygen, but others may show better corrosion resistance. Although this discussion is concerned primarily with the oxidizing effects of aeration, these effects could also be produced by other oxidizing agents. Figure 2 shows a generalized picture of several materials in different environments (Ref 14).

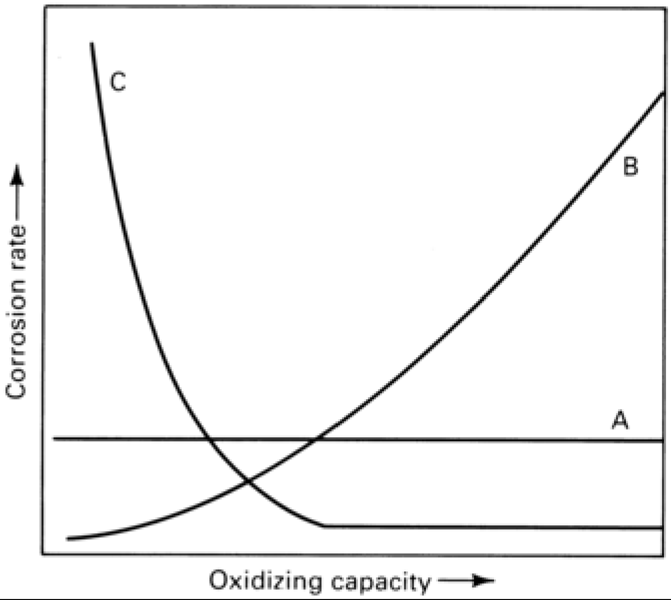

Curve A
1. Stainless steel in nitric acid
2. Aluminum in hydrogen peroxide
3. Hastelloy C in ferric chloride
Curve B
1. Monel in hydrochloric acid
2. Iron in water
3. Copper in sulfuric acid
Curve C
1. Stainless steel in sulfuric acid + copper sulfate
2. Stainless steel in sulfuric acid + nitric acid

Fig. 2 Effect of solution oxidizing capacity on corrosion rates of various metal-solution combinations. Source: Ref 14

Figure 1 shows the effect of aeration and deaeration on Monel. An interesting feature is the rapid decrease in corrosion as the temperature approaches the boiling point. The rates at the boiling points are essentially the same under the two conditions of test. The reason for this behavior is that the solubility of oxygen in boiling water or dilute aqueous solutions is practically nil. This feature is of interest from the practical standpoint, because a test at the boiling point is more convenient to conduct than one at an arbitrary temperature, such as 80 °C (175 °F), because the temperature is easily controlled and is reproducible. The operator might expect more severe results by running the test at the boiling point, but the actual results may be just the opposite.

Unless specified, the solution should not be aerated. Most tests related to process equipment should be conducted with the natural atmosphere inherent in the process, such as the vapors of the boiling liquid. If aeration is used, the specimens should not be located in the direct air stream from the sparger (perforated tube or pipe). Extraneous effects can be encountered if the air stream impinges on the specimens.

The simplest and most widely used aeration method consists of bubbling air through the solution. The solution is assumed then to be saturated with air. In most applications being simulated in the test, air is involved; therefore, air is used in the test. If air is not bubbled through the solution, the aeration effect depends on the air present in the solution at the start of the test and on its rate of removal or escape, if any. Air can also be absorbed from the atmosphere over the solution.

If oxygen saturation of the test solution is desired, this test can best be achieved by sparging with oxygen. Appropriate precautions should be taken when oxygen-rich gases are used, because many materials burn violently in pure oxygen. For other degrees of aeration, the solution should be sparged with synthetic mixtures of air or oxygen with an inert gas.

If complete exclusion of dissolved oxygen is necessary, specific techniques, such as prior heating of the solution and sparging with an inert gas (usually nitrogen), are required. A liquid atmospheric seal is often used on the test vessel to prevent air ingress.

Volume of Solution. The volume of the test solution should be large enough to avoid any appreciable change in its corrosivity during the test through exhaustion of corrosive constituents or by accumulation of corrosion products that may affect further corrosion. Typical minimum volume recommendations are solution-to-specimen area ratios of 200 L/m^2 of specimen surface when detecting susceptibility to intergranular attack of austenitic stainless steel (Ref 7) and 100 L/m^2 of specimen surface when evaluating the exfoliation corrosion susceptibility of 5*xxx* aluminum alloys (Ref 9).

When the objective of the test is to determine the effect of a metal alloy on the characteristics of the test solution (for example, to determine the effects of metals on dyes or the catalytic decomposition of hydrogen peroxide), it is desirable to reproduce the ratio of solution volume to exposed metal surface area that exists in practice. The actual time of contact of the metal with the solution must also be taken into account. Any necessary distortion of the test conditions must be considered when interpreting results.

Solution Velocity. The effect of velocity is not usually determined in normal laboratory tests, although specific tests have been designed for this purpose (Ref 11, 15, 16). However, for the sake of reproducibility, some velocity control is desirable. Tests at the boiling point should be conducted with the least heat input to avoid excessive turbulence and bubble impingement. In tests conducted below boiling point, thermal convection is generally the only source of liquid velocity. In test solutions with high viscosities, supplemental controlled stirring is needed to assure uniform conditions.

Method of Supporting Specimens. The supporting device and container should not be affected by or cause contamination of the test solution. The method of supporting specimens varies with the apparatus used for conducting the test, but supports should be designed to insulate the specimens from each other physically and electrically and to insulate the specimens from any metallic container or supporting device used within the apparatus.

The shape and form of the specimen support should ensure free contact of the specimen with the corroding solution, the liquid-vapor line, or the vapor phase (Fig. 3). If clad alloys are exposed, special procedures, such as coating of edges, are required to ensure that only the cladding is exposed, unless the purpose is to test the ability of the cladding to protect cut edges. Alternatively, a clad sample can be attached to an opening in a T-pipe so that only the clad surface is exposed to the test solution. Common supports include glass or ceramic rods, glass saddles, glass hooks, fluorocarbon plastic strings, and various insulated or coated metallic supports.

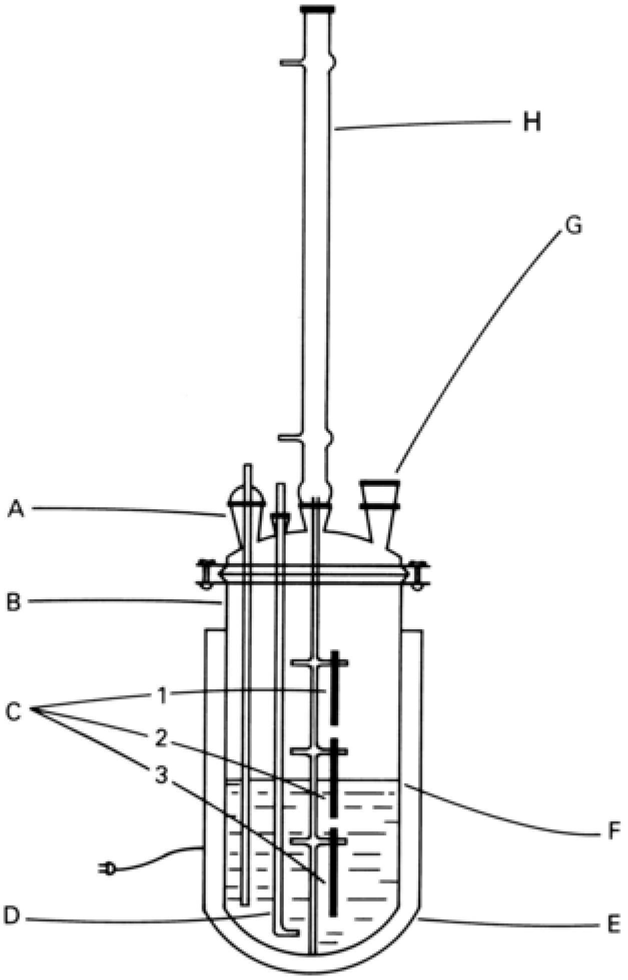

Fig. 3 Resin flask used to conduct simple immersion tests. A, thermowell; B, resin flask; C, specimens hung on supporting device (C-1, vapor phase; C-2, partial immersion; C-3, total immersion); D, air inlet; E, heating mantle; F, liquid interface; G, opening in flask for additional apparatus that may be required; H, reflux condenser. Source: Ref 7

In aqueous solutions under one atmosphere of air or oxygen pressure, it is desirable to position all specimens so that the oxygen supply is similar. This is especially important with corrosion systems in which the corrosion rate may be fairly high, such as for iron and steel in neutral salt solutions. In such tests, totally immersed specimens at a depth of less than 20 mm (0.8 in.) had markedly higher corrosion rates, but with deeper immersion, the rate was lower and variations in depth were unimportant (Ref 17). More detailed discussion of the factors that can affect corrosion behavior in immersion tests can be found in Ref 11.

References cited in this section

7. "Practice for Laboratory Immersion Corrosion Testing of Metals," G 31, *Annual Book of ASTM Standards,* ASTM

9. "Standard Test Method for Visual Assessment of Exfoliation Corrosion Suscepti[chbility of 5*xxx* Series Aluminum Alloys,"[fj G 66, *Annual Book of ASTM Standards,* ASTM

10. "Laboratory Corrosion Testing of Metals," NACE TM-0169-2000, National Association of Corrosion Engineers

11. F.A. Champion, *Corrosion Testing Procedures,* 2nd ed., John Wiley & Sons, 1965

12. O.B.J. Fraser, D.E. Ackerman, and J.W. Sands, *Ind. Eng. Chem.,* Vol 19, 1927, p 332

13. P.E. Francis and A.D. Mercer, Corrosion of a Mild Steel in Distilled Water and Chloride Solutions: Development of a Test Method, *Laboratory Corrosion Tests and Standards,* STP 866, G.S. Haynes and R. Baboian, Ed., ASTM, 1985, p 184–196

14. M.G. Fontana, "Corrosion Testing," Lesson 8 in home study and extension courses, American Society for Metals, 1969

15. W.H. Ailor, Ed., *Handbook on Corrosion Testing and Evaluation,* John Wiley & Sons, 1971

16. T.-L. Yau, Corrosion Test Loop, *Laboratory Corrosion Tests and Standards,* STP 866, G.S. Haynes and R. Baboian, Ed., ASTM, 1985, p 36–47

17. G.D. Bengough, U.R. Evand, T.P. Hoar, and F. Wormweff, *Chem. Ind.,* Nov 1938

T. Yau, Immersion Testing, *Corrosion: Fundamentals, Testing, and Protection*,, Vol 13A, *ASM Handbook*, ASM International, 2003, p 463–469

Immersion Testing

Te-Lin Yau, Te-Lin Yau Consultancy

Autoclave Tests

In order to improve conversion rate and yield, elevated temperature and pressure are employed in modern chemical technologies. Consequently, it is important to conduct corrosion tests at such elevated temperature and pressure. Autoclaves are often used for this type of test. They need to be manufactured in conformance with the American Society for Mechanical Engineers, or similar industry standards worldwide, and government regulations governing unfired pressure vessels. As shown in Fig. 4, the autoclave is fitted with devices for safety as well as measurement and control of pressure and temperature. The autoclave body should be made of a material that is compatible with the intended test environments. Structural materials include stainless steels, nickel-base alloys, titanium, zirconium, tantalum, and polytetrafluoroethylene-lined materials. Autoclaves are available in many sizes and types, ranging from hundreds of milliliters to several liters. They may be static, stirred, or refreshed. For refreshed autoclaves, there are additional devices, such as a high-pressure, constant-volume pump; a preheater; a back-pressure controller; and an overpressure protection system.

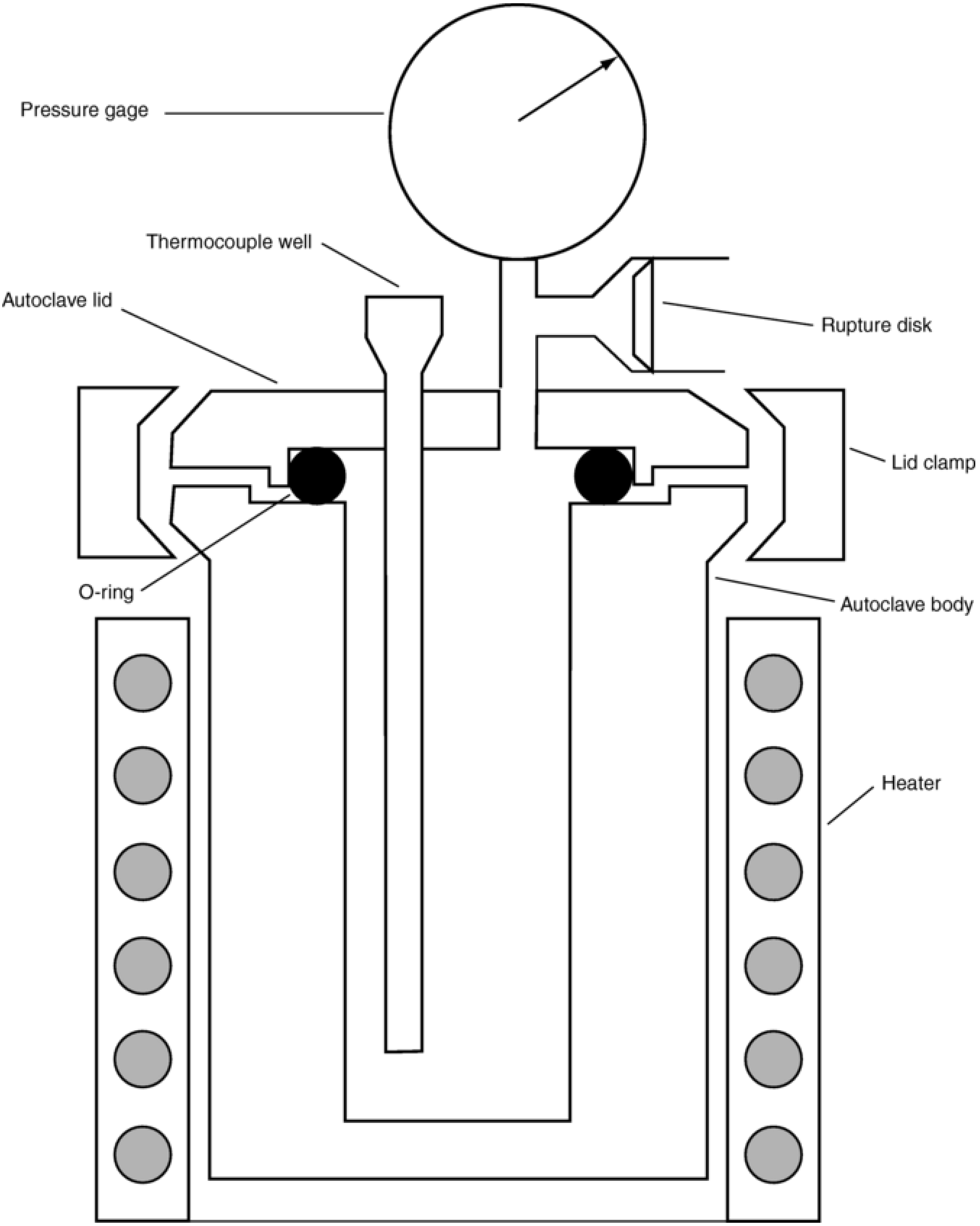

Fig. 4 An autoclave drawing showing common components

Temperature stability is a critical requirement in conducting autoclave tests. Temperature may fluctuate due to the heater, the control thermocouple, the heating rate, changes in external conditions, the degree of insulation, and the corrosion of specimens. The temperature measurement and recording systems should be calibrated to a specified accuracy at an established interval, such as every six months, to an accuracy of ±2.8 °C (±5 °F). Also, it is desirable to establish a vertical thermal profile for the autoclave, for example, every six months or whenever the heater or the control thermocouple is adjusted or replaced. Pressure affects the corrosion of

certain alloys under certain conditions. To accurately record the pressure, and for safety, the pressure gage should be calibrated.

Proper cleaning methods should be established for new autoclaves and for autoclaves after each test. Both chemical and mechanical methods should be considered, based on structural materials and test environments.

Because the autoclave body is often an alloy, the body itself is regarded as a test specimen. It may be difficult to follow the recommended minimum solution-volume-to-specimen area ratio, because this is dictated by the geometry of the autoclave. Still, the ratio should be as large as possible, and the test solution should be changed as frequently as practical.

A method for autoclave testing zirconium and hafnium in water or steam is given in Ref 18.

Reference cited in this section

18. “Standard Test Method for Corrosion Testing of Products of Zirconium, Hafnium, and Their Alloys in Water at 680 °F or in Steam at 750 °F,” G 2, *Annual Book of ASTM Standards*, ASTM

T. Yau, Immersion Testing, *Corrosion: Fundamentals, Testing, and Protection,*, Vol 13A, *ASM Handbook*, ASM International, 2003, p 463–469

Immersion Testing

Te-Lin Yau, Te-Lin Yau Consultancy

Partial Immersion to Vapor Phase

Laboratory tests under conditions of partial immersion and vapor phase are of practical importance, because such conditions are commonly found in service. Tests conducted in three locations in a resin flask, as shown in Fig. 3, can be used to determine the relative susceptibility of a material to localized corrosion at the liquid line and in the vapor phase. Partial-immersion conditions provide a very suitable accelerated test for such metals as aluminum alloys and others that develop concentrated attack at the liquid line (or splash zone in certain equipment). In certain alloy-environment systems, the vapor phase is more corrosive than the liquid phase.

T. Yau, Immersion Testing, *Corrosion: Fundamentals, Testing, and Protection,*, Vol 13A, *ASM Handbook*, ASM International, 2003, p 463–469

Immersion Testing

Te-Lin Yau, Te-Lin Yau Consultancy

Intermittent Immersion

The term *intermittent immersion* refers to alternate immersion and emersion in a liquid corrodent. The conditions are of practical importance, because they simulate the effects of the rise and fall of tidal waters and the movements of corrosive liquids in chemical plants. Also, they may provide a relatively rapid test for the effect of aqueous solutions, because a thin film of the solution, frequently renewed and almost saturated with oxygen, can be maintained on the test specimen during most of the period of exposure, even when the shape of the specimen is complex. Reference 11 contains a detailed discussion of the rather considerable research that has been done on various alternate immersion cycles and drying conditions for tests of metallic materials.

To simulate cyclic service conditions, the specimens should be dry before reimmersion, because this has an important effect on the protective character of films on the metal. For maximum corrosion, this drying should be done slowly, so that the film of the corrodent on the metal can be allowed the maximum time to act during immersion. In the interest of reproducibility, it is desirable to control the humidity and temperature of the atmosphere in order to ensure a constant rate of drying in successive cycles. When more thorough drying of the specimen is desired, forced-air circulation or radiant heating can be used to accelerate the drying. Artificial heating adds to the complexity of the test conditions, however, and may reduce the reproducibility of the test if it is not very carefully controlled.

Alternate Immersion in 3.5% NaCl. This test has gained widespread acceptance, particularly in the United States, and is described in ASTM G 44 (Ref 19). This practice uses a 1 h cycle that includes a 10 min period of immersion in an aqueous solution of 3.5% NaCl or a substitute ocean water (without heavy metals), followed by a 50 min emersion period. This 1 h cycle is continued 24 h/day for the test duration required for the particular test material. Aluminum and steel alloys are typically exposed from 10 to 90 days or longer, depending on the resistance of the alloy to corrosion by saltwater. Although this alternate-immersion test is considered to be an accelerated test representative of certain natural conditions (particularly marine environments), it is not intended to relate to specialized chemical environments.

Air circulation is an important consideration, because it affects the rate at which specimens dry and the loss of water by evaporation from the salt solution. The most important consideration consists of achieving moderate specimen drying conditions. Because various testing facilities use different immersion apparatuses and room sizes, individual experimentation is necessary to achieve adequate circulation. A mild circulation of air is recommended.

Specimen Drying. As with air circulation, no fixed procedure has been established and probably cannot be, unless a standardized immersion apparatus and test chamber are adopted. The objective, however, is to ensure that all specimens dry slowly during the 50 min emersion period. Because they all drain differently, specimens with different accrued corrosion films dry at different rates. New specimens with little accumulated corrosion products become dry in approximately 15 min, but other specimens with an accumulation of corrosion product and salt should be allowed approximately 40 min to dry.

Apparatus. The usual methods of immersion involve:

- Placing specimens on a movable rack that is periodically lowered into a stationary tank containing the solution (Fig. 5)
- Placing specimens on a hexagonal, semisubmerged Ferris wheel arrangement that rotates 60° every 10 min and thus passes the specimens through a stationary tank of solution
- Placing specimens in a stationary tray open to the atmosphere and having the solution moved by air pressure, nonmetallic pump, or gravity drain from a reservoir to the tray

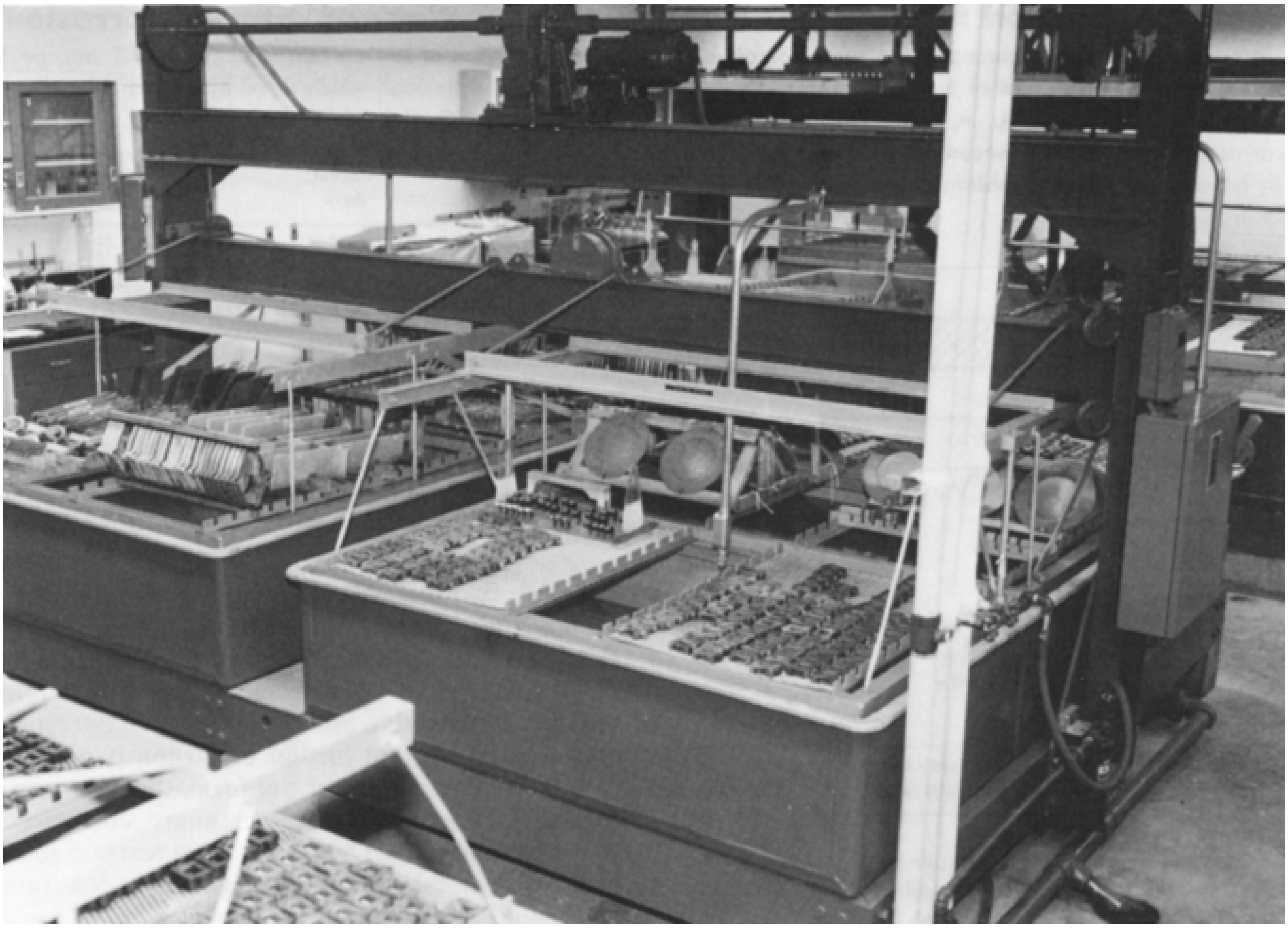

Fig. 5 Lift-type alternate-immersion apparatus. Courtesy of the Aluminum Company of America

Rate of Immersion. The rate of immersion and removal of the specimens from the solution should be as rapid as possible without jarring them. For purposes of standardization, an arbitrary limit is adopted, such that no more than 2 min elapse from the time the first portion of any specimen is covered or uncovered by solution.

Materials of construction that contact the salt solution are such that they are not affected by the corrodent to an extent that they can cause contamination of the solution and change its corrosiveness. Use of inert plastics or glass is recommended, where feasible. Metallic materials of construction should be selected from alloys that are recommended for marine use and are of the same general type as the metals being tested. Preferably, all metal parts should be protected with a suitable corrosion-resistant coating.

Specimen holders should be designed to electrically insulate the specimens from each other and from any other bare metal. When this is not possible, as with certain stressing bolts or jigs, the bare metal contacting the specimen should be isolated from the corrodent by a suitable coating. Protective coatings should be of a type that do not leach inhibiting or accelerating ions or protective oils over the noncoated portions of the specimen. Coatings containing chromates should be avoided. They should not obstruct airflow over the specimens, which retards the drying rate.

Solution Conditions. The salt solution is prepared by dissolving 3.5 ± 0.1 parts by weight of NaCl in 96.5 parts of water. The NaCl conforms to the specifications of the Committee on the Analytical Reagents of the American Chemical Society. Distilled or deionized water is used for compliance with the purity requirements of ASTM D 1193, type IV, reagent water (Ref 20).

When tests are to be made in substitute ocean water, it is prepared without heavy metals, in accordance with ASTM D 1141 (Ref 21). An advantage of the substitute ocean water in the case of stress-corrosion tests of certain high-strength aluminum alloys is that it causes less severe pitting than the 3.5% NaCl solution. It may be preferred in certain other cases, because the test results do (or are thought to) relate better to real marine environments.

Temperature. A freshly prepared solution should be allowed to come within 3 °C (5.4 °F) of the specified air temperature before being used. Thereafter, no control is required on the solution temperature. Instead, the air temperature is controlled, and the solution is allowed to reach temperature equilibrium.
Minimum Volume. The volume of the test solution should be large enough to avoid any appreciable change in its corrosiveness through exhaustion of corrosive constituents or through the accumulation of corrosion products or other constituents that might significantly affect further corrosion. A recommended arbitrary minimum ratio between the volume of the test solution and the surface area of the specimen(s) (including any uncoated accessories) is 320 L/m^2 (7.9 gal/ ft^2 or 206 mL/in^2).
Air Conditions. The air temperature is maintained at 27 ± 1 °C (80 ± 2 °F). The relative humidity is controlled at 45 ± 6%.

References cited in this section

11. F.A. Champion, *Corrosion Testing Procedures,* 2nd ed., John Wiley & Sons, 1965

19. "Standard Recommendation Practice for Alternate Immersion Stress Corrosion Testing in 3.5% Sodium Chloride Solution," G 44, *Annual Book of ASTM Standards,* ASTM

20. "Standard Specification for Reagent Water," D 1193, *Annual Book of ASTM Standards,* ASTM

21. "Standard Specification for Substitute Ocean Water," D 1141, *Annual Book of ASTM Standards,* ASTM

T. Yau, Immersion Testing, *Corrosion: Fundamentals, Testing, and Protection,*, Vol 13A, *ASM Handbook*, ASM International, 2003, p 463–469

Immersion Testing

Te-Lin Yau, Te-Lin Yau Consultancy

Specimen Preparation and Duration of Tests

The type, size, and shape of specimens vary with the purpose of the test, the nature of the test materials, and the apparatus used. Standard practices for preparing, cleaning, and evaluating corrosion test specimens are provided in ASTM G 1 (Ref 4). Corrosion is a surface phenomenon. Surface condition of specimens is critical in determining the outcome of tests. It is essential to know the quality of specimens (Ref 22). The knowledge of this effect is important in specifying surface finish for equipment. Surface condition of as-fabricated equipment is preferred in many tests. It can be rough with embedded impurities or smooth with post-fabrication cleaning.
Proper selection of appropriate lengths of exposure is important for any corrosion test, and misleading results may be obtained if the time factor is not considered. An excellent technique for investigating changes in corrosion rate with length of exposure is described in Ref 7, 10, and 14.
Planned interval tests involve the accumulated effects of corrosion at several times under a given set of conditions as well as the initial rate of corrosion of fresh metal, the more or less instantaneous corrosion rate of metal after long exposure, and the initial corrosion rate of fresh metal during the same period of time as the latter. The rates, or damage per unit time interval of one day, are shown in the diagram in Table 2 as A_1, A_2, and B, respectively. The exposure over several days is indicated as A_t and A_{t+1}. It would be desirable to have duplicate specimens for each interval. Further time extensions of the test should be made with similar added specimens and interval spacing if no changes occurred in the corrosion rate of the metal or the corrosiveness of the liquid during the first selection of test duration.

Table 2 Planned interval test

Identical specimens are placed in the same corrosive liquid; imposed conditions of test are constant for the entire time ($t + 1$); A_1, A_t, A_{t+1}, B, represent the corrosion damage experienced by each test specimen; A_2 is a calculated value obtained by subtracting A_t from A_{t+1}.

Corrosivity	Observed weight changes during corrosion testing	Criteria
Liquid corrosiveness	Unchanged	$A_1 = B$
	Decreased	$B < A_1$
	Increased	$A_1 < B$
Metal corrodibility	Unchanged	$A_2 = B$
	Decreased	$A_2 < B$
	Increased	$B < A_2$

Combinations of situations		
Liquid corrosiveness	**Metal corrodibility**	**Criteria**
Unchanged	Unchanged	$A_1 = A_2 = B$
Unchanged	Decreased	$A_2 < A_1 = B$
Unchanged	Increased	$A_1 = B < A_2$
Decreased	Unchanged	$A_2 = B < A_1$
Decreased	Decreased	$A_2 < B < A_1$
Decreased	Increased	$A_1 > B < A_2$
Increased	Unchanged	$A_1 < A_2 = B$
Increased	Decreased	$A_1 < B > A_2$
Increased	Increased	$A_1 < B < A_2$

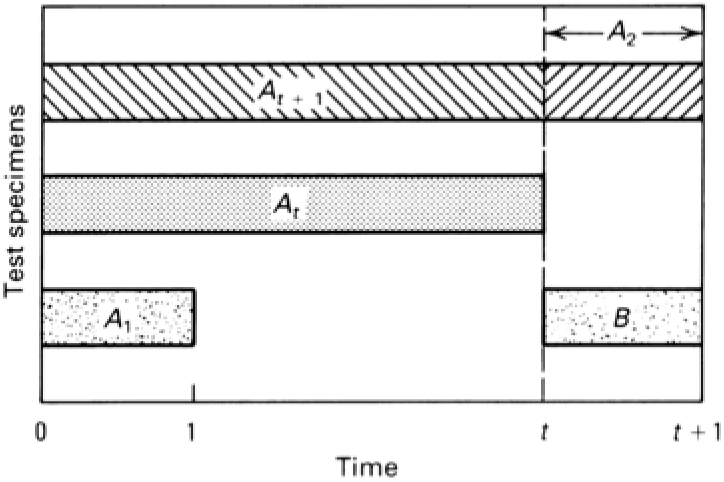

Comparison for corrosion damage A_1 on fresh metal in the time interval from 0 to 1 with corrosion damage B on fresh metal for the unit time interval from t to $t + 1$ shows the magnitude and direction of change in the corrosivity of the liquid that may have occurred during the total time of the test. Correspondingly, comparison of A_2 with B, where A_2 is the corrosion damage calculated by subtracting A_t from A_{t+1}, shows the magnitude and direction of change in corrodibility of the metal specimen during the test. These comparisons can be taken as criteria for the changes and are tabulated in Table 2. Also given in Table 2 are the criteria for all possible combinations of changes in the corrosivity of the liquid and corrodibility of the metal. The additional information obtained on occurrences in the course of the test justifies the additional effort involved. Table 3 lists the data obtained from a planned interval test of a carbon steel specimen in an aluminum chloride ($AlCl_3$)/antimony trichloride ($SbCl_3$) solution.

Table 3   Planned interval corrosion test

Duplicate strips of low-carbon steel (19 × 75 mm, or $\frac{3}{4}$× 3 in.) were immersed in 200 mL of 10% $AlCl_3$-90% $SbCl_3$ mixture through which dried hydrogen chloride gas was slowly bubbled at atmospheric pressure. Temperature: 90 °C (195 °F)

Value	Interval, days	Weight loss, mg	Penetration		Apparent corrosion rate	
			µm	**mils**	**mm/yr**	**mils/yr**
A_1	0–1	1080	42.9	1.69	15.7	620
A_t	0–3	1430	56.9	2.24	6.8	270
A_{t+1}	0–4	1460	58.2	2.29	5.3	210
B	3–4	70	2.8	0.11	1.02	40
A_2	Calculated 3–4	30	1.3	0.05	0.46	18

Analysis: $A_2 < B < A_1$, or 0.05 < 0.11 < 1.69. Conclusions: Liquid markedly decreased in corrosiveness during the test, and the formation of a partially protective scale on the steel was indicated; that is, metal became less corrodible.

The causes for the changes in corrosion rate as a function of time are not given by the planned interval test criteria. The corrosivity of the liquid may decrease as a result of corrosion during the course of a test because of the reduction in concentration of the corrosive agent, the depletion of a corrosive contaminant, the formation of inhibiting products, or other metal-catalyzed changes in the liquid. The corrosivity of the liquid may increase because of the formation of autocatalytic products, the destruction of corrosion-inhibiting substances, or other catalyzed changes in the liquid. Changes in the corrosiveness of the liquid may also arise from changes in composition that would occur under the test conditions, even in the absence of metal. To determine if the latter effect occurs, an identical test is run without test strips for the total time, *t*. Test strips are then added, and the test is continued for the unit time interval. Comparison with A_1 of corrosion damage from this test shows if the corrosive character of the liquid changes significantly in the absence of metal.

The corrodibility of the metal in a test may decrease as a function of time because of the formation of protective scale or the removal of a less resistant surface layer of metal. Metal corrodibility may increase because of the formation of corrosion-accelerating scale or the removal of a more resistant surface layer of metal. Indications of the causes of changes in corrosion rate can often be obtained from close observation of tests and corroded specimens as well as from special supplementary tests designed to reveal effects that may be involved.

Changes in liquid corrosiveness are not a factor in most plant tests that consist of once- through runs or where large ratios of solution volume to specimen area are involved. If the effect of corrosion on the mechanical properties of the metal or alloy is under consideration, a set of unexposed specimens is needed for comparison purposes.

Lengthy corrosion tests are generally not necessary to obtain accurate corrosion rates from materials that undergo severe corrosion. However, there are cases in which this assumption is not valid. For example, lead exposed to sulfuric acid initially corrodes at an extremely high rate while building a protective film; the rates then decrease considerably, so that further corrosion is negligible. The phenomenon of the formation of a protective film is observed with many corrosion-resistant materials. Therefore, short tests on such materials would indicate a high corrosion rate and would be completely misleading.

Short-term tests can also give misleading results on alloys that form passive films, such as stainless steels. With borderline conditions, a prolonged test may be needed to permit the breakdown of the passive film and the subsequent more rapid attack. Consequently, tests conducted for long periods are considerably more realistic than those conducted for short durations. This statement must be qualified by stating that corrosion should not proceed to the point at which the original specimen size or the exposed area is drastically reduced or the metal is perforated.

If anticipated corrosion rates are moderate or low, the following equation gives the suggested tests duration:

$$\text{Hours} = 50/(\text{corrosion rate in mm/yr})$$

$$\text{Hours} = 2000/(\text{corrosion rate in mils/yr})$$

For example, where the corrosion rate is 10 mils/yr (0.25 mm/yr), the test should run for at least 200 h. This method of estimating test duration is useful as an aid in deciding, after a test has been made, whether or not it is desirable to repeat the test for a longer period.

References cited in this section

4. “Practice for Preparing, Cleaning, and Evaluating Corrosion Test Specimens,” G 1, *Annual Book of ASTM Standards,* ASTM

7. “Practice for Laboratory Immersion Corrosion Testing of Metals,” G 31, *Annual Book of ASTM Standards,* ASTM

10. “Laboratory Corrosion Testing of Metals,” NACE TM-0169-2000, National Association of Corrosion Engineers

14. M.G. Fontana, “Corrosion Testing,” Lesson 8 in home study and extension courses, American Society for Metals, 1969

22. T.-L. Yau, J.A. Andrews, R. Henson, and D.R. Holmes, Practice for Conducting Corrosion Coupon Tests on Zirconium and Its Alloys, *Corrosion Tests and Evaluation: Silver Anniversary Volume,* STP 1000, R. Baboian and S.W. Dean, Ed., ASTM, 1990, p 303–311

T. Yau, Immersion Testing, *Corrosion: Fundamentals, Testing, and Protection,*, Vol 13A, *ASM Handbook*, ASM International, 2003, p 463–469

Immersion Testing

Te-Lin Yau, Te-Lin Yau Consultancy

Cleaning Corrosion Test Specimens

After corrosion testing, specimens should be properly cleaned to remove bulky deposits and corrosion products but not the metals. This must be done as soon as possible, so that the measured corrosion time interval is accurate. Corrosion may be continuing under the damp corrosion products until they are removed. Various mechanical, electrolytic, and chemical cleaning methods have been developed to clean different metals and alloys (Ref 4).

Reference cited in this section

4. “Practice for Preparing, Cleaning, and Evaluating Corrosion Test Specimens,” G 1, *Annual Book of ASTM Standards,* ASTM

T. Yau, Immersion Testing, *Corrosion: Fundamentals, Testing, and Protection,*, Vol 13A, *ASM Handbook*, ASM International, 2003, p 463–469

Immersion Testing

Te-Lin Yau, Te-Lin Yau Consultancy

Calculation of Corrosion Rate

The average corrosion rate may be obtained as follows:

$$\text{Corrosion rate} = (K \times W)/(A \times T \times D)$$

where K is a constant, T is the time of exposure in hours to the nearest 0.01 h, A is the area in cm^2 to the nearest 0.01 cm^2, W is the mass loss in grams to the nearest 1 mg, and D is the density in g/cm^3.
Several units are used to express corrosion rates. Using the previously mentioned units for *T*, *A*, *W*, and *D*, the corrosion rate can be calculated in a variety of units, with the following appropriate value of *K*:

Corrosion rate units desired	Constant, *K*
Mils per year (mils/yr)	3.45×10^6
Inches per year (in./yr)	3.45×10^3
Millimeters per year (mm/yr)	8.76×10^4
Micrometers per year (μm/yr)	8.76×10^7
Milligrams per square decimeter per day (mdd)	$2.40 \times 10^6 \times D$

Adapted from Ref 4
When expressing corrosion rates in years, the corrosionist must keep in mind the underlying assumption that the corrosion rate is uniform. When based on test data measured in hours, the extrapolation to years may not be valid. Also, by measuring the weight loss, an average loss of thickness is calculated. This may not be the most relevant characteristic.

Reference cited in this section

4. "Practice for Preparing, Cleaning, and Evaluating Corrosion Test Specimens," G 1, *Annual Book of ASTM Standards,* ASTM

T. Yau, Immersion Testing, *Corrosion: Fundamentals, Testing, and Protection,*, Vol 13A, *ASM Handbook*, ASM International, 2003, p 463–469

Immersion Testing

Te-Lin Yau, Te-Lin Yau Consultancy

Reporting the Data

The importance of reporting all data as completely as possible cannot be overemphasized. Expansion of the testing program in the future or correlating the results with tests of other investigators is possible only if all pertinent information is properly recorded, so the veracity of the data can be assured. The following checklist is a recommended guide for items that should be included in a standard report of immersion tests:

- Name of personnel and laboratory involved
- Date
- Identification of specimen material and number
- Form and metallurgical conditions of specimens (composition, quality grade)
- Cite standard methods employed (industry, government, or laboratory standards and guides)
- Treatment used to prepare specimens
- Visual-appearance remarks of each specimen before and after the corrosion testing
- Weights and dimensions of specimens before and after the corrosion testing
- Corrosive media and concentration (and any changes during test)
- Volume of test solution
- The color, pH, and specific gravity of the test solution before and after the corrosion testing
- Temperature (maximum, minimum, and average)

- Aeration (describe conditions or technique)
- Agitation (describe conditions or technique)
- Type of apparatus used for test. Include identification of measuring devices for auditing calibrations in accordance with established laboratory procedure.
- Duration of each test
- Number of specimens of each material tested, and whether specimens were tested separately or which specimens were tested in the same container
- Method used to clean specimens after exposure, and the extent of any error expected by this treatment. Use of a documented standard method is desirable.
- Evaluation of attack if other than general, such as crevice corrosion under support rod, pit depth and distribution, and results of microscopic examination or bend tests
- Corrosion rates for each specimen
- Minor occurrences or deviations from the proposed test program often can have significant effects and should be reported, if known.

T. Yau, Immersion Testing, *Corrosion: Fundamentals, Testing, and Protection,*, Vol 13A, *ASM Handbook*, ASM International, 2003, p 463–469

Immersion Testing

Te-Lin Yau, Te-Lin Yau Consultancy

Acknowledgment

Whereas this article was substantially revised, acknowledgment is made that it was adapted in part from the original article, "Immersion Testing," by D.O. Sprowls, *Corrosion,* Vol 13, ASM International, 1987, p 220.

T. Yau, Immersion Testing, *Corrosion: Fundamentals, Testing, and Protection,*, Vol 13A, *ASM Handbook*, ASM International, 2003, p 463–469

Immersion Testing

Te-Lin Yau, Te-Lin Yau Consultancy

References

1. "Practice for Detecting Susceptibility to Intergranular Attack in Austenitic Stainless Steels," A 262, *Annual Book of ASTM Standards,* ASTM

2. "Standard Guide for Descaling and Cleaning Titanium and Titanium Alloy Surfaces," B 600, *Annual Book of ASTM Standards,* ASTM

3. "Standard Guide for Descaling and Cleaning Zirconium and Zirconium Alloy Surfaces," B 614, *Annual Book of ASTM Standards,* ASTM

4. "Practice for Preparing, Cleaning, and Evaluating Corrosion Test Specimens," G 1, *Annual Book of ASTM Standards,* ASTM

5. "Guide for Conducting Corrosion Tests in Field Applications," G4, *Annual Book of ASTM Standards,* ASTM

6. "Guide for Applying Statistics to Analysis of Corrosion Data," G 16, *Annual Book of ASTM Standards,* ASTM

7. "Practice for Laboratory Immersion Corrosion Testing of Metals," G 31, *Annual Book of ASTM Standards,* ASTM

8. "Guide for Examination and Evaluation of Pitting Corrosion," G 46, *Annual Book of ASTM Standards,* ASTM

9. "Standard Test Method for Visual Assessment of Exfoliation Corrosion Suscepti[chbility of 5*xxx* Series Aluminum Alloys,"[fj G 66, *Annual Book of ASTM Standards,* ASTM

10. "Laboratory Corrosion Testing of Metals," NACE TM-0169-2000, National Association of Corrosion Engineers

11. F.A. Champion, *Corrosion Testing Procedures,* 2nd ed., John Wiley & Sons, 1965

12. O.B.J. Fraser, D.E. Ackerman, and J.W. Sands, *Ind. Eng. Chem.,* Vol 19, 1927, p 332

13. P.E. Francis and A.D. Mercer, Corrosion of a Mild Steel in Distilled Water and Chloride Solutions: Development of a Test Method, *Laboratory Corrosion Tests and Standards,* STP 866, G.S. Haynes and R. Baboian, Ed., ASTM, 1985, p 184–196

14. M.G. Fontana, "Corrosion Testing," Lesson 8 in home study and extension courses, American Society for Metals, 1969

15. W.H. Ailor, Ed., *Handbook on Corrosion Testing and Evaluation,* John Wiley & Sons, 1971

16. T.-L. Yau, Corrosion Test Loop, *Laboratory Corrosion Tests and Standards,* STP 866, G.S. Haynes and R. Baboian, Ed., ASTM, 1985, p 36–47

17. G.D. Bengough, U.R. Evand, T.P. Hoar, and F. Wormweff, *Chem. Ind.,* Nov 1938

18. "Standard Test Method for Corrosion Testing of Products of Zirconium, Hafnium, and Their Alloys in Water at 680 °F or in Steam at 750 °F," G 2, *Annual Book of ASTM Standards,* ASTM

19. "Standard Recommendation Practice for Alternate Immersion Stress Corrosion Testing in 3.5% Sodium Chloride Solution," G 44, *Annual Book of ASTM Standards,* ASTM

20. "Standard Specification for Reagent Water," D 1193, *Annual Book of ASTM Standards,* ASTM

21. "Standard Specification for Substitute Ocean Water," D 1141, *Annual Book of ASTM Standards,* ASTM

22. T.-L. Yau, J.A. Andrews, R. Henson, and D.R. Holmes, Practice for Conducting Corrosion Coupon Tests on Zirconium and Its Alloys, *Corrosion Tests and Evaluation: Silver Anniversary Volume,* STP 1000, R. Baboian and S.W. Dean, Ed., ASTM, 1990, p 303–311

T. Yau, Immersion Testing, *Corrosion: Fundamentals, Testing, and Protection,*, Vol 13A, *ASM Handbook*, ASM International, 2003, p 463–469

Immersion Testing

Te-Lin Yau, Te-Lin Yau Consultancy

Selected References

- R. Baboian, Ed., *Manual 20: Corrosion Tests and Standards: Application and Interpretation,* ASTM, 1995
- R. Baboian and S.W. Dean, Ed., *Corrosion Testing and Evaluation: Silver Anniversary Volume,* STP 1000, ASTM, 1990
- G. Cragnolino and N. Sridhar, Ed., *Application of Accelerated Corrosion Tests to Service Life Prediction of Materials,* STP 1194, ASTM, 1995
- E.D. Verink, *Corrosion Testing Made Easy: The Basics,* National Association of Corrosion Engineers, 1993

R. Singleton, Cabinet Testing, *Corrosion: Fundamentals, Testing, and Protection* ,Vol 13A, *ASM Handbook*, ASM International, 2003, p 470–477

Cabinet Testing

Raymund Singleton, The Singleton Corporation

Introduction

SALT SPRAY (FOG) TESTS have been used for over 100 years as accelerated tests for determining both the corrodibility of nonferrous and ferrous metals and the degree of protection afforded by both inorganic and organic coatings on metallic base (Ref 1).

The tests are utilized most often to compare the relative performance of metals and coatings to a known and retained standard for quality control purposes. The tests can be an indicator of the consistency of a production process and/or materials utilized. There has been extensive discussion of the salt fog test since its inception because of the reproducibility variances and the questionable correlation of results as related to actual "in-service" performance. This can be a result of the misapplication of the salt fog test with the expectation that the test atmosphere simulates a particular environment or service condition. Salt spray tests were not intended for this purpose, except in rare instances where corroborating data has been obtained to support such application. The test actually represents the application of a standardized amount of corrosive activity for comparing the relative performance of materials and/or coatings.

Many revisions and improvements to the salt spray test procedures, salt spray test chambers, and apparatus have been made over the years. A significant amount of the contributions result from efforts of ASTM International; The National Institute of Standards and Technology (NIST, formerly known as the U.S. National Bureau of Standards); other governmental agencies (including all branches of the U.S. Military); industry trade associations (such as The Society of Automotive Engineers; NACE International; SSPC: The Society for Protective Coatings, formerly The Steel Structures Painting Council); major automobile manufacturing companies and their suppliers, and various test equipment manufacturers. Some improvements have included the establishment of required test specifications, along with tolerance limits for test variables, which help

produce more reliably reproducible and meaningful test results. Even with the newly revised test procedures and modern designs of salt spray test equipment, there are still test procedures, support information, variables, and specifications of the tests that need to be examined for inclusion or evolved to improve the test standards.

Reference cited in this section

1. W.D., McMaster, “A History of the Salt Spray Tests,” Publication, General Motors Corporation, Sept 1965

R. Singleton, Cabinet Testing, *Corrosion: Fundamentals, Testing, and Protection* ,Vol 13A*, ASM Handbook*, ASM International, 2003, p 470–477

Cabinet Testing

Raymund Singleton, The Singleton Corporation

Applications and Use of Salt Spray (Fog) Testing

The salt spray type test has received its widest acceptance as a tool for evaluating the uniformity of thickness and degree of porosity of metallic and nonmetallic protective coatings. It has served this purpose with a great deal of success. The test is useful for evaluating different lots of the same product once a standard level of performance has been established. It is especially helpful as a screening test for revealing a particularly inferior coating. In recent years, certain cyclic acidified salt spray tests have been used to test the resistance of aluminum alloys to exfoliation corrosion. The salt spray test is, also, considered very useful as an accelerated laboratory corrosion test that attempts to simulate the effects of marine atmospheres on different metals, with or without protective coatings.

The most commonly used and accepted salt spray test methods in the United States and much of the rest of the world are the methods outlined in ASTM Standards B 117, B 368, and G 85 (Ref 2, 3, 4). U.S. Government agencies, professional associations, trade associations and groups, many industry groups, and automotive manufacturers and suppliers have established their own salt spray standards and procedures, but in the interest of utilizing existing successful technology, many of these standards largely conform to the details of the ASTM tests. Representative of these similar salt spray tests are GM 4298/Salt Fog and Mil Standard 810E, method 509.3. In addition, some international standards of similar type are DIN 50018 and ISO 9227, which includes salt fog, acetic-acid and copper accelerated salt spray (CASS) procedures.

It is important to note that it is possible to perform widely utilized humidity corrosion test standard procedures of similar type and operation to the “salt-fog” tests in the same type test apparatus when properly equipped. The humidity tests, however, use deionized water as the only corrosive agent and do not include a “salt- type,” corrosion-accelerator electrolyte in the test solution. Examples of domestic and international “humidity” corrosion tests are ASTM D 1735 (humidity-fog type)(Ref 5), ASTM D 2247 (100% condensing humidity) (Ref 6), GM 4465 (humidity-fog type), and ASTM G 60 (cyclic humidity) (Ref 7). See Table 1.

Table 1 Commonly used cabinet corrosion test methods

Test method	Designation	Electrolyte solution			Step number	Step title	Temperature		Relative humidity	Duration	Comments
		Content	Specific gravity	pH			°C	°F			
Static tests											
Salt fog	ASTM B 117	5% NaCl	1.0255–1.0400	6.5–7.2[(a)]	…	Salt fog	35	95	N/A	24 h/cycle[(b)]	…
Salt fog	DIN 50021-SS (Similar to ASTM B 117)	5% NaCl	1.0255–1.0400	6.5–7.2[(a)]	…	Salt fog	35	95	N/A	24 h/cycle[(b)]	…
Neutral salt fog	ISO 9227-NSS (Similar to ASTM B 117)	5% NaCl	1.029–1.036	6.5–7.2	…	Salt fog	35	95	N/A	24 h/cycle[(b)]	…
Salt fog	GM 4298P (Similar to ASTM B 117)	5% NaCl	1.0255–1.0400	6.5–7.2[(a)]	…	Salt fog	35	95	N/A	24 h/cycle[(b)]	…
Salt fog	Mil Std 810 E (Similar to ASTM B 117)	5% NaCl	1.0255–1.0400	6.5–7.2[(a)]	…	Salt fog	35	95	N/A	24 h/cycle[(b)]	…
Acetic-acid salt fog	ASTM G 85 A1	5% NaCl	1.0255–1.0400	3.1 to 3.3[(c)]	…	Salt fog	35	95	N/A	144–240 h	…
Acetic-acid salt fog	DIN 50021-ESS (Similar to ASTM G 85 A1)	5% NaCl	1.0255–1.0400	3.1 to 3.3[(c)]	…	Salt fog	35	95	N/A	TBD	…
Acetic-acid salt fog	DIN 50021-ESS (Similar to ASTM G 85 A1)	5% NaCl	1.0255–1.0400	3.1 to 3.3[(c)]	…	Salt fog	35	95	N/A	TBD	…
Acetic-acid salt fog	DIN 50021-ESS (Similar to ASTM G 85 A1)	5% NaCl	1.0255–1.0400	3.1 to 3.3[(c)]	…	Salt fog	35	95	N/A	TBD	…
Acetic-acid salt fog	ISO 9227-AASS (Similar to ASTM G 85 A1)	5% NaCl	1.029–1.036	3.1 to 3.3[(c)]	…	Salt fog	35	95	N/A	TBD	…

Test method	Designation	Electrolyte solution			Step number	Step title	Temperature		Relative humidity	Duration	Comments
		Content	Specific gravity	pH			°C	°F			
Copper-accelerated acetic acid salt fog (CASS Test)	ASTM B 368	5% NaCl 0.25 g CuCl/L solution	1.030–1.040	3.1–3.3[(a)(c)]	…	Salt fog	49	120	N/A	TBD	…
Copper-accelerated acetic acid salt fog	DIN 50021-CASS (Similar to ASTM B 368)	5% NaCl 0.25 g CuCl/L solution	1.030–1.040	3.1–3.3[(a)(c)]	…	Salt fog	50	122	N/A	TBD	…
Copper-accelerated acetic acid salt fog	ISO 9227-CASS (Similar to ASTM B 368)	5% NaCl 0.25 g CuCl/L solution	1.029–1.036	3.1–3.3[(a)(c)]	…	Salt fog	49	120	N/A	TBD	…
Humidity fog	ASTM D 1735	ASTM type IV water only	…	…	…	Humidity fog	38	100	N/A	24 h/cycle (com.)	Similar to ASTM B 117, except without the salt
Humidity fog	GM 4465P (Similar to ASTM D 1735)	ASTM type IV water only	…	…	…	Humidity fog	38	100	N/A	[(b)]	…
High humidity	ASTM D 2247	ASTM type IV water only	…	…	…	Soak	38	100	100%	Per customer	Use air distributor pipe or equivalent.
Corrodkote	ASTM B 380	Special slurry[(d)] (ASTM D 2247)	N/A	N/A	1	Slurry application	Ambient		>50%	1 h (to dry)	…
					2	Humidity fog	38	100	80–90%	20 h = 1 cycle	
Static or cyclic test											
Moist SO_2	ASTM G 87 (Kesternich)	Deionized water inside the cabinet for wet bottom is the only solution (ASTM D 2247)	…	…	1	SO_2 gas injection	Ambient		Ambient	0.2–2 L as required	…
					2	Soak[(e)]	40	104	N/A	Method A, 24 h; Method B, 8 h	
					3	Ambient[(f)] (method B only)	20–30	68–86	>75%	16 h	
Cyclic tests											
Moist SO_2	DIN 50018 (Kesternich)	Deionized water inside the	…	…	1	SO_2 gas injection	Ambient		Ambient	0.2 or 2 L as specified	…

Test method	Designation	Electrolyte solution			Step number	Step title	Temperature		Relative humidity	Duration	Comments
		Content	Specific gravity	pH			°C	°F			
	(Similar to ASTM G 87, method B)	cabinet for wet bottom is the only solution			2	Soak[e]	40	104	N/A	8 h	
					3	Ambient[f] (B only)	20–30	68–86	>75%	16 h	
Cyclic acidified acetic salt fog	ASTM G 85, A2	5% NaCl	1.0255–1.0400	2.8 to 3.0[g]	1	Salt fog	49	120	N/A (wet bottom)	¾ h	…
					2	Dry	49	120	7–40%	2 h	
					3	Soak	49	120	65–95%	3 ¼ h	
Acidified synthetic sea water (SWAAT test)	ASTM G 85, A3	Synthetic sea water with 10 mL glacial acetic acid/L	1.0255–1.0400	2.8 to 3.0	1	Salt fog	24–49 (TBD)	75–120 (TBD)	N/A (wet bottom)	½ h	…
					2	Soak	24–49 (TBD)	75–120 (TBD)	<98%	1 h	
Salt fog/SO_2	ASTM G 85, A4	5% NaCl or synthetic sea salt	1.0255–1.0400	2.5–3.2[a]	1	Salt fog	35	95	N/A	a. Constant b. ½ h[h]	…
					2	SO_2 addition	35	95	N/A	a. 1 h/6 h b. ½ h[h]	
					3	Soak	35	95	N/A	a. N/A b. 2 h[h]	
Dilute electrolyte fog/dry	ASTM G 85, A5	0.05% NaCl 0.35% $(NH_4)_2SO_4$	N/A	5.0–5.4[a]	1	Salt fog	Ambient		>75%	1 h	Humidifying tower is bypassed or drained with heat off
					2	Dry	35	95	N/A	1 h	
Scab corrosion creepback	GM 9511P	5% NaCl	N/A	N/A	1	Dry/immersion	60/ambient	140/ambient	N/A	1 h/15 min	Monday, 5 steps; Tuesday through Friday, first 3 steps only, 1 cycle = 24 h. Parts in humidity cabinet Saturday and Sunday
					2	Cold/ambient	-25/ambient	-13/ambient	N/A	30 min/75 min	
					3	Immersion/humidity	Ambient/60	Ambient/140	N/A/85%	15 min/ 22 h, 30 min	
					4	Ambient	N/A	N/A	75 min		
					5	Humidity	60	140	85%	21 h	
Cyclic corrosion test	CCT IV	5% NaCl	N/A	Not specified	1	Salt fog	50	122	N/A	10 min	Repeat steps 4 and 5 five times. No cycle <24 h, 10 min
					2	Dry	60	140	<30%	2 h 35 min	
					3	Humidity fog	60	140	95%	1 h 15 min	

Test method	Designation	Electrolyte solution			Step number	Step title	Temperature		Relative humidity	Duration	Comments
		Content	Specific gravity	pH			°C	°F			
					4	Dry	60	140	<30%	2 h 40 min	
					5	Humidity fog	60	140	95%	1 h 20 min	
Cyclic corrosion test	GM 9540P	0.9% NaCl, 0.1% $CaCl_2$, 0.25% $NaHCO_3$	N/A	6.0 to 9.0	1	Ambient	25	77	40–50%	8 h	Step 5 for 5 days/week, run only 4 times. Steps 1–4 for 7 days/week, run daily
					2	Spray	25	77	40–50%	During step 1, 4 sprays, 90 min apart	
					3	Humidity fog	49	120	100%	8 h	
					4	Dry	60	140	<30%	8 h	
					5	Ambient	25	77	40–50%	48 h	
Cyclic corrosion test	SAE J2334	0.5% NaCl, 0.1% $CaCl_2$, 0.075% $NaHCO_3$	N/A	N/A	1	Humidity fog	50	122	100%	6 h	Step 4 for 5 days/week, run only 4 times. Steps 1–3 for 7 days/week, run daily
					2	Spray (ambient)	25	77	40–50%	15 min	
					3	Dry	60	140	50%	17 h, 45 min	
					4	Dry	60	140	50%	48 h	
Cyclic corrosion test	Ford APGE	5% NaCl	N/A	6.0–8.0	1	Immersion	23	73	N/A	15 min	Step 4 for 5 days, run only 4 times. Steps 1–3 for 7 days, run daily
					2	Ambient	20–30	68–86	>75%	1 h, 15 min	
					3	Humidity fog	50	122	85–95%	22 h, 30 min	
					4	Humidity fog	50	122	85–95%	48 h (weekend)	
Cyclic UV-condensation/salt fog-dry exposure	ASTM D 5894 (Ref: ASTM D 4587, ASTM G 85, A5)	0.05% NaCl 0.35% $(NH_4)_2SO_4$	N/A	N/A	1	UV exposure(i)	60	140	N/A	4 h	Steps 1–2, 168 h, then steps 3–4, 168 h (total, 1 cycle)
					2	Condensation	50	122	N/A	4 h	
					3	Salt fog	Ambient		>75%	1 h	
					4	Dry	35	95	N/A	1 h	

N/A, not applicable.
TBD, to be determined.
(a) pH of collected condensate;
(b) Number of cycles by mutual agreement between buyer and seller;
(c) Solution adjusted to 3.1 to 3.3 pH with addition of glacial acetic acid;
(d) See specification for slurry make-up and application details;
(e) 90 min maximum ramp to soak;
(f) No heat, purge vapors, open cover;
(g) Solution adjusted to 2.8 to 3.0 pH with addition of glacial acetic acid;

(h) Examples only; test based on material specifications or by agreement between buyer and seller;
(i) Use UVA-340 bulbs.

There are two basic types of salt-spray/fog corrosion tests—“static” condition tests and “cyclic” condition tests. In tests classified as static type, the conditions and atmosphere are constant throughout the duration of the test exposure. Thus the test temperature, fog-density (as determined by condensate-collection rate), electrolyte solution pH, and specific gravity are all to remain constant within tolerance limits. Many organizations conducting static condition tests operate the equipment 24 hours a day, 7 days a week. After test specimens are placed into the test apparatus, they remain until they are subjected to the total duration time specified for each particular specimen. Each is then removed for study and analysis.

As with most endeavors, the field of corrosion testing is evolving. Current efforts are to design tests that correlate more closely, or simulate more realistically, actual environmental exposure and service conditions. With this in mind, most newer tests are cyclic. Cyclic tests subject specimens to a repeated sequence of timed, different-atmosphere steps until a predetermined time of exposure, or number of cycles, is achieved. A complete set of steps, before repetition of the sequence begins, makes up a cycle. These steps in each cycle usually incorporate (a) different temperatures (ambient, elevated, plus some lower than ambient); (b) varying levels of relative humidity (RH) from lower than 20 to 100% (that produce dry-off to saturated atmosphere conditions); and (c) various corrosive agents/pollutants/electrolytes (that can include any of a variety of different salts and gases to produce accelerated corrosion effects in the presence of moisture).

Some examples of the various exposure zone conditions used as steps in the cyclic tests are salt fog with and without compressed air humidification; humidity fog with and without compressed air humidification; controlled humidity, dry stage, ambient, specification-ambient with temperature and humidity control; and soak with maintained temperature, purge, solution spray, immersion, and dwell (no activity).

Representative of established standard cyclic salt spray (fog) type corrosion tests by industry and international groups are SAE J-2334, DIN 50018/SO2, GM 9540P, Ford APGE and CCT I, II, III, and IV from the Japanese automotive industry. (see Table 1 for a synopsis of test details for some of the tests). Using the SAE J-2334, GM 9540P, and CCT IV as examples, notice the similarity in Table 1 between these procedures and the common atmospheric conditions specified for some of their steps in the designated cycles.

References cited in this section

2. “Standard Practice for Operating Salt Spray (Fog) Apparatus,” B 117, *Annual Book of ASTM Standards,* ASTM International

3. “Standard Test Method for Copper-Accelerated Acetic Acid-Salt Spray (Fog) Testing (CASS Test),” B 368, *Annual Book of ASTM Standards,* ASTM International

4. ASTM G 85, “Standard Practice for Modified Salt Spray (Fog) Testing, Annex 1, Acetic-Acid Salt Spray Test, Continuous,” *Annual Book of ASTM Standards,* ASTM International

5. ASTM D 1735, “Standard Practice for Testing Water Resistance of Coatings Using Water Fog Apparatus,” *Annual Book of ASTM Standards,* ASTM International

6. “Standard Practice for Testing Water Resistance of Coatings in 100% Relative Humidity,” D 2247, *Annual Book of ASTM Standards,* ASTM International

7. “Standard Practice for Conducting Cyclic Humidity Tests,” G 60, *Annual Book of ASTM Standards,* ASTM International

R. Singleton, Cabinet Testing, *Corrosion: Fundamentals, Testing, and Protection* ,Vol 13A*, ASM Handbook*, ASM International, 2003, p 470–477

Cabinet Testing

Raymund Singleton, The Singleton Corporation

Static Atmosphere Condition Salt Spray (Fog) Tests

Salt Spray (Fog) Tests. ASTM B 117 is the most commonly used salt spray test for evaluating inorganic and organic coatings, especially where such tests are a part of material or product specifications. ASTM B 117 includes: DIN 50021-SS, GM 4298, and ISO 9227 (see Table 1).

There is quite a bit of commonality between the salt spray (fog) test and most of the other tests mentioned in this article as far as ingredients, specifications, apparatus, and procedures. As a result the salt spray (fog) test provides the best basis for the study of the other tests.

The ASTM B 117 test, when properly applied and performed, should yield a "standardized" amount and type of corrosive activity for comparison purposes. The test is not intended to correlate to any particular service environment or exposure condition unless long-term exposure data for a particular material or coating are available for comparison purposes. A criticism of the test as not being typically equivalent to "outdoor" exposure usually results when the procedure is misapplied or relied on to produce correlating results for which it was never intended.

The ASTM B 117 test consists of atomizing a specified sodium chloride aqueous solution to create a corrosive fog atmosphere in an enclosed chamber under controlled temperature. The use of ASTM D 1193, type IV reagent grade water is specified for makeup of the salt solution. Type IV reagent water must meet the following criteria: (a) pH in the range of 5 to 8 prior to use for testing purposes; (b) maximum electrical conductivity = 5.0 μs/cm at 298 K or 25 °C (77 °F); and (c) minimum electrical resistivity = 0.2 MΩ · cm at 298 K or 25 °C (77 °F). Limits for content of separate sodium and chloride in the type IV specification may be ignored because each would be insignificant once the sodium chloride salt was added. Other similar tests also use deionized (DI) water.

The aqueous test solution consists of 95% by weight of reagent water and 5% by weight of sodium chloride (NaCl), which contains not more than 0.1% by weight of sodium iodide, 0.3% by weight of total impurities, and 200 ppm total solids. In addition, the test solution needs to be substantially free (the operative term) of nickel and copper. This solution is representative for many "typical" fog type corrosion test procedures.

The salt used for many of these tests is a food grade sodium chloride with no anticaking agents. The use of food grade is specified because it produces scientifically valid results and is readily available.

Conditioned, humidified, and heated compressed air is used to atomize this solution to create the necessary corrosive fog atmosphere in the test chamber. When all specified test conditions are met, the resulting pH reading determined from the collected condensed-fog solution after atomization should be in the range of 6.5 to 7.2. The condensed-fog solution should be collected at a rate of 1 to 2 mL per collector (minimum of two collectors in the exposure zone) per hour of continuous operation. This verification of the density of the fog atmosphere helps establish the standardized test conditions. The temperature is maintained at 35 + 1.1 or -1.7 °C (95 + 2 or -3 °F) within the exposure zone of the closed salt spray chamber throughout the duration of the test. The duration of this test can range from 8 to 3000 h depending on the product or type of coating being tested.

The Acetic Acid-Salt Spray (Fog) Test. ASTM G 85, Annex A1, is also used for testing inorganic and organic coatings but is particularly applicable to the testing of decorative nickel- chromium or copper-nickel-chromium plating and cadmium plating on steel or zinc die castings. This test is usually used for the evaluation of the consistency of product quality (Ref 4).

As in the ASTM B 117 salt spray (fog) test, a 5% by weight of sodium chloride (NaCl) solution is used, but the solution is adjusted to a pH range of 3.1 to 3.3 by the addition of acetic acid. Note that the pH specification is for the solution obtained from the fog condensate collection devices after atomization. The temperature of the

salt spray chamber exposure zone is controlled to maintain 35 + 1.1 or -1.7 °C (95 + 2 or -3 °F) within the exposure zone of the closed chamber throughout the duration of the test.
This test can be as brief as 16 h, although it normally ranges from 144 to more than 240 h.
The copper-accelerated acetic acid-salt spray (fog) test or CASS test, ASTM B 368, (Ref 3), is primarily used for the relatively rapid testing of decorative copper-nickel-chromium or nickel-chromium plating on steel and zinc die castings. It is also useful in the testing of anodized, chromated, or phosphated aluminum. A 5% by weight of sodium chloride (NaCl) solution is used, with the addition of 1 g of copper II chloride ($CuCl_2{\cdot}2H_2O$) added to each 3.8 L of salt solution. The solution is then adjusted to a pH range of 3.1 to 3.3 by adding acetic acid. The exposure zone temperature of the CASS chamber is controlled to maintain 49 + 1.1 or -1.7 °C (120 + 2 or -3 °F) throughout the duration of the test, which ranges from 6 to 720 h.

References cited in this section

3. “Standard Test Method for Copper-Accelerated Acetic Acid-Salt Spray (Fog) Testing (CASS Test),” B 368, *Annual Book of ASTM Standards,* ASTM International

4. ASTM G 85, “Standard Practice for Modified Salt Spray (Fog) Testing, Annex 1, Acetic-Acid Salt Spray Test, Continuous,” *Annual Book of ASTM Standards,* ASTM International

---

R. Singleton, Cabinet Testing, *Corrosion: Fundamentals, Testing, and Protection* ,Vol 13A, *ASM Handbook*, ASM International, 2003, p 470–477

Cabinet Testing

Raymund Singleton, The Singleton Corporation

Cyclic and Other Atmosphere Condition Salt Spray (Fog) Tests

Many other cyclic salt spray (fog) test procedures have been developed in order to more closely approximate a specific application, service condition, or environment. Some of these are grouped as the ASTM G 85 “Modified Salt Spray (Fog) Testing” procedures. There are 5 Annexes of the G 85 standard: A1, the acetic acid salt spray (fog) test (a static condition test as mentioned in the previous section); A2, the cyclic acidified salt spray (fog) test; A3, the acidified synthetic seawater spray (fog) test; A4, the salt spray (fog)/sulfur dioxide (SO_2) test; and A5, the dilute electrolyte cyclic fog/dry test. Another test of significance is the ASTM moist sulfur dioxide (SO_2) test (ASTM G 87).
The cyclic acidified salt spray (fog) test (ASTM G 85, Annex 2) and the acidified synthetic sea water spray (fog) test (ASTM G 85, Annex 3) are each used, in part, for production control of exfoliation-resistant heat treatments for various aluminum alloys (Ref 8). The salt spray (fog)/SO_2 test (ASTM G 85, Annex 4) (Ref 9) is often used to test for the exfoliation corrosion resistance of various aluminum alloys and a wide range of nonferrous and ferrous materials and coatings, both inorganic and organic, when exposed to an SO_2-laden salt spray (fog) atmosphere. These conditions are encountered, for example, in shipboard and nearshore marine environments. As more of these, and other, cyclic-type tests are introduced and utilized, the development and implementation of capably sophisticated testing chambers and equipment will occur concurrently. Much newer equipment incorporates automatic functions to perform cyclic tests while largely unattended.
Some of the more widely used cyclic corrosion tests are for the automotive industry. However, their versatility and applicability have been demonstrated to the extent that their use is not limited to that industry. Some of these tests were developed to measure the cosmetic effects of corrosion of automotive painted, or coated, steel surfaces. Their success at evaluating the performance of these finishes by relative rank has led to wider use. Representative examples of these tests include (a) GM 9540 P, originating with General Motors yet used widely in addition by others including the U.S. Military; (b) SAE J2334, originating with the Society of Automotive

Engineers, and (c) CCT IV, originating with the Japanese automotive industry, yet containing many aspects in common with the two aforementioned cyclic test procedures. Note from Table 1 the similarities in exposure atmospheres and conditions between these tests.

Another popular cyclic corrosion test is the ASTM G 85 Annex 5 (Ref 10). It is used primarily to test paints for industrial maintenance coatings and architectural finishes.

The cyclic nature of the last group of tests simulates the effects of the changing nature of outdoor and in-service environmental conditions.

References cited in this section

8. S.J. Ketcham and I.S. Shaffer, Exfoliation Corrosion of Aluminum Alloys, *Localized Corrosion—Cause of Metal Failure,* STP 516, American Society for Testing and Materials (ASTM), 1972, p 3–16

9. "Standard Practice for Modified Salt Spray (Fog) Testing, Annex 4, SO_2 Salt Spray Test, Cyclic, G 85, *Annual Book of ASTM Standards,* ASTM International

10. "Standard Practice for Modified Salt Spray (Fog) Testing, Annex 5, Dilute Electrolyte Cyclic Fog Dry Test," G 85, *Annual Book of ASTM Standards,* ASTM International

---

R. Singleton, Cabinet Testing, *Corrosion: Fundamentals, Testing, and Protection* ,Vol 13A*, ASM Handbook*, ASM International, 2003, p 470–477

Cabinet Testing

Raymund Singleton, The Singleton Corporation

Combining Weathering (Light Exposure Apparatus) and Salt Spray (Fog) Type Corrosion Tests

An interesting practice that has proven useful in materials evaluation and research is the capability to study the degradation effects produced through the combination of accelerated weathering and corrosion testing procedures. This allows materials and coatings to be subjected to more complex accelerated effects. The following information indicates the significant differences in each type test used in the combined procedure.

Accelerated weathering testing generally attacks the coating material with various types of light exposures (from ultraviolet to infrared), along with heat, moisture, pollutant, and microbial attack to cause degradation and physical property changes to or within the coating or material. This type of procedure is often used to test nonmetallic polymer materials (Ref 11). Accelerated corrosion testing in this type testing, conversely, is usually used to examine the ability of a coating to protect a substrate by attacking the substrate material. Corrosion testing is often used to test metallic materials and coatings on metallic materials.

The combination of these two test types, where applicable, is very useful in the investigation of materials performance. A convenient, representative example of this type combined test standard is the ASTM D 5894, the UV condensation/salt spray (fog)-dry exposure test. The test comprises alternating one week of ASTM D 4587, UV-condensation exposure, and one week of ASTM G 85 Annex 5, salt-fog/dry exposure, to a predetermined total number of cycles. A complete cycle is made up of one week of each type test for a total of two weeks per cycle.

Reference cited in this section

11. W. Ketola, 3M Company, private communication, Minneapolis, MN

R. Singleton, Cabinet Testing, *Corrosion: Fundamentals, Testing, and Protection* ,Vol 13A*, ASM Handbook*, ASM International, 2003, p 470–477

Cabinet Testing

Raymund Singleton, The Singleton Corporation

Test Specimen Procedures for Salt Spray (Fog) Corrosion Tests

Corrosion test specimens for these tests include ferrous and non-ferrous metals in possible combinations with organic and inorganic coatings of various formulations, properties, and production and application methods. Test specimens are representative of items used in architectural, industrial, electrical and electronic, hardware, appliance, transportation, military, aerospace, marine, and other industrial applications. There are specific standardized procedures to be used for selecting, preparing, handling, cleaning, and storing test specimens prior to corrosion testing and after the tests have been completed. ASTM standards are a good starting point due to their wide use and acceptance. Industry specific standards for test specimen procedures often reference the ASTM standards as a basis.

A widely used document is ASTM G 1, "Standard Practice for Preparing, Cleaning and Evaluating Corrosion Test Specimens." This standard, as the title implies, provides good general information for those aspects of corrosion test specimen procedures for both pretest and posttest needs. Other standards, described in more detail subsequently, furnish examples of typically encountered aspects.

R. Singleton, Cabinet Testing, *Corrosion: Fundamentals, Testing, and Protection* ,Vol 13A*, ASM Handbook*, ASM International, 2003, p 470–477

Cabinet Testing

Raymund Singleton, The Singleton Corporation

Pretest Specimen Preparation for Salt Spray Corrosion Tests

ASTM D 609, Practice for Preparation of Cold-Rolled Steel Panels for Testing Paint, Varnish, Conversion Coatings and Related Coating Products (Ref 12), describes several cleaning procedures used prior to testing. These cleaning methods include vapor degreasing, solvent brushing, solvent wiping, and alkaline cleaning:

- *Procedure A, conversion coatings:* Preparation of test panels consists of one or more steps of cleaning, rinsing, or conditioning prior to the application of the coating. Additional water rinsing is required after the conversion coating is applied. Force air dry immediately after rinsing.
- *Procedure B, vapor degreasing:* Suspend panels in vapor-phase type degreaser using 1,1,1-trichloroethane. Prewipe with a clean, lintless cloth saturated with mineral spirits to remove solid particulate matter.
- *Procedure C, solvent brushing:* Power-brush scrub with mineral spirits. Dry at 52 to 93 °C (125 to 200 °F) before use or storage.
- *Procedure D, solvent wiping:* Remove all soluble and loosely adhering soil by rubbing the panel with a clean, lintless cloth wet with mineral spirits. Dry at 52 to 93 °C (125 to 200 °F) before use or storage.
- *Procedure E, alkaline cleaning:* Clean panels with alkaline solution by spray or immersion. One or more steps may be required. Force dry immediately after rinsing.

ASTM D 609 also provides information for materials and supplies. In addition, storing and handling methods are covered, such as the use of lint-free gloves when necessary, handling panels only by their edges, wrapping cleaned panels in paper treated with a corrosion inhibitor, and placement in a sealable plastic bag or envelope.

ASTM D 1654, Standard Test Method for Evaluation of Painted or Coated Specimens Subjected to Corrosive Environments furnishes information on both pretest and posttest procedures (Ref 13). This test method provides information necessary for test specimens. Pretreatment procedures include details on scribing, a deliberate simulation of coating failure, where applicable. Scribing is used to simulate the failure observed when coated products are subjected to abrasion or accidental damage and then exposed to corrosive influences.

The scribe tool consists of a “straight shank tungsten-carbide tip, lathe cutting tool (ANSI B94.50, Style E) or carbide tipped pencil type tool.” The apparatus for scribing also includes a straight-edge guide “of sufficient length and rigidity to guide the scribing tool in a straight line” (Ref 13). The scribe lines are often applied to test specimen panels by holding the tool at approximately 45 degrees from vertical and pulling along the straight edge guide to produce a uniform V-cut through the coating on the test piece. Scribe marks are applied to the surface of the test piece in vertical, diagonal, intersecting, or cross-hatch patterns. The uniformity in width and depth of the scribe mark is of great importance to the final test results.

Post-test operations for previously painted or coated specimens subjected to accelerated corrosion tests include their subsequent evaluation in respect to corrosion, blistering associated with corrosion, loss of adhesion at the scribe mark, or other coating failure. After testing it is necessary to clean the tested pieces and remove any loose coatings and corrosion products. A rigid spatula type scraping tool, a dull knife, or a similar instrument without sharp edges, is used for this purpose along with a compressed air source and air gun. The air gun should have necessary protective guards and be capable of delivering air at 10 ft^3/min at 80 psi. A scale or rule with 1 mm divisions is used to mark uniform increments along the scribed line. The extent of coating failure is then measured perpendicularly from the center of the scribe at each of the marks, either to one side or both sides of the scribe. The information from individual data points and averages are then entered into reports for further examination, processing, and analysis.

ASTM D 1654 covers preliminary treatment of scribed or unscribed test specimens. The standard provides information on the protection for cut edges with wax, tape, or other means. Posttest procedures prior to evaluation of test results detail cleaning methods such as rinsing, compressed air removal of corrosion products, and scraping and towel-drying or compressed-air drying. Directions for evaluation of the general surface condition, recording of data such as the percent of failed area, and the evaluation of unprotected edges are present also.

Post-Test Procedures for Test Specimen Evaluation. The ASTM D 1654 Standard directs the use of ASTM D 610 for evaluating the degree of rusting on painted steel surfaces and ASTM D 714 for evaluating the degree of blistering of paints. These two standards are representative of the type of evaluation and reporting necessary for some types of observed corrosion test results and provide examples of standardized rating methods for corrosion test results.

The ASTM D 610 Standard Test Method for Evaluating Degree of Rusting on Painted Steel Surfaces (Ref 14) includes a numerical evaluation scale to enable convenient rating of observed corrosion on tested pieces as follows:

Scale	Description
10	No rusting or <0.01% of surface rusted
9	Minute rusting <0.03% of surface rusted
8	Few isolated rust spots <0.1% of surface rusted
7	<0.3% of surface rusted
6	Extensive rust spots but <1% of surface
5	Rusting to the extent of 3% of surface rusted
4	Rusting to extent of 10% of surface rusted
3	Approximately $\frac{1}{6}$ of surface rusted
2	Approximately $\frac{1}{3}$ of surface rusted
1	Approximately $\frac{1}{2}$ of surface rusted
0	Approximately 100% of surface rusted

Pictorial reference images are also included to aid evaluation.

ASTM D 714, Standard Test Method for Evaluating Degree of Blistering of Paints (Ref 15) is similar to ASTM D 610 in that a numeric code is given for reporting type, size, and frequency of blistering as a result of testing. Reference photographic images are included to aid the evaluation. ASTM D 714 suggests the use of certain recommended descriptive terms, such as *medium*, *few,* and so forth in standardized reporting format. The photographic reference images illustrating blistering are to be used in conjunction with the following numeric reporting scale:

Size	Description
10	No blistering
8	Smallest size easily seen by unaided eye
6, 4, 2	Progressively larger sizes

Descriptive terms for frequency are dense, medium dense, medium, and few. Quantitative physical descriptions should include (by actual count):

- Size distribution by unit area
- Frequency of occurrence per unit area
- Pattern of distribution over surface

Descriptions of the shape of the blisters should include terms such as *small clusters* or *large patches.*

ASTM G 46, “Guide for Examination and Evaluation of Pitting Corrosion” (Ref 16) aids in evaluating this type of corrosion. Standards are included as references for reporting results.

After examinations, evaluations and interpretations of test results are performed, the information needs to be communicated. Industry- wide standardized report forms are generally used. There are, instead, many more specific, even proprietary, report forms designated by individual organizations, groups, and specific industries for particular materials and coatings. As a guide, some generalized information and categories recorded are listed subsequently.

Two areas of interest are the test environmental conditions produced in the exposure zone and test results observed on the tested specimens. Pertinent information to record for each follows:

Exposure data:

- Test identification/designation
- Type of salt and water used
- Exposure zone temperature
- Daily records of fog collection
- Volume of salt solution condensate collected (mL/h per 80 cm^2 collector)
- Salt concentration (% NaCl in H_2O) or specific gravity of collected condensed salt solution at 35 °C
- pH of collected solution

Test specimen data and observed results:

- Complete description of material/coating tested, including substrate used where appropriate
- Part identification/code/number/drawing reference
- Type of specimen
- Part dimensions
- Method of preparation/cleaning (before and after testing). Report cleaning standard identification number (example: ASTM D 609).
- Method of supporting or suspending test specimen in chamber
- Description of edge protection
- Exposure period (start and end times and dates of exposure)
- Interruptions in exposure: cause and length of time
- Results of all inspections

In addition to other formats, reporting of results can be enhanced with the inclusion of chart recorder output, photographs of the tested piece/ material illustrating corrosion effects, and digital scans (preferably color) of the surface of the tested piece/material illustrating corrosion effects.

References cited in this section

12. "Standard Practice for Preparation of Cold- Rolled Steel Panels for Testing Paint, Varnish, Conversion Coatings, and Related Coating Products," D 609, *Annual Book of ASTM Standards,* ASTM International

13. "Standard Test Method for Evaluation of Painted or Coated Specimens Subjected to Corrosive Environments," D 1654, *Annual Book of ASTM Standards,* ASTM International

14. "Standard Test Method for Evaluating Degree of Rusting on Painted Steel Surfaces," D 610, *Annual Book of ASTM Standards,* ASTM International

15. "Standard Test Method for Evaluating Degree of Blistering of Paints," D 714, *Annual Book of ASTM Standards,* ASTM International

16. "Standard Guide for Examination and Evaluation of Pitting Corrosion," G 46, *Annual Book of ASTM Standards,* ASTM International

---

R. Singleton, Cabinet Testing, *Corrosion: Fundamentals, Testing, and Protection* ,Vol 13A, *ASM Handbook*, ASM International, 2003, p 470–477

Cabinet Testing

Raymund Singleton, The Singleton Corporation

Salt Spray Test Chamber Apparatus

Salt spray cabinets are available from many manufacturers and range in size from extremely small bench-top cabinets to large walk-in and drive-in types. The ISO salt spray (fog) test specification (ISO 9227) indicates a minimum chamber size of 0.2 m^3 (8 ft^3) interior volume with a recommended minimum volume of 0.4 m^3 (16 ft^3). It has been found that small bench-top models are usually not practical since it can be difficult to obtain and control an adequate, uniform corrosive atmosphere. This is, in part, because of the small confined area used to produce the necessary homogeneous atmosphere. Larger walk-in or drive-in types (Fig. 1) are produced and are able to generate required test atmosphere specifications throughout the larger exposure zone.

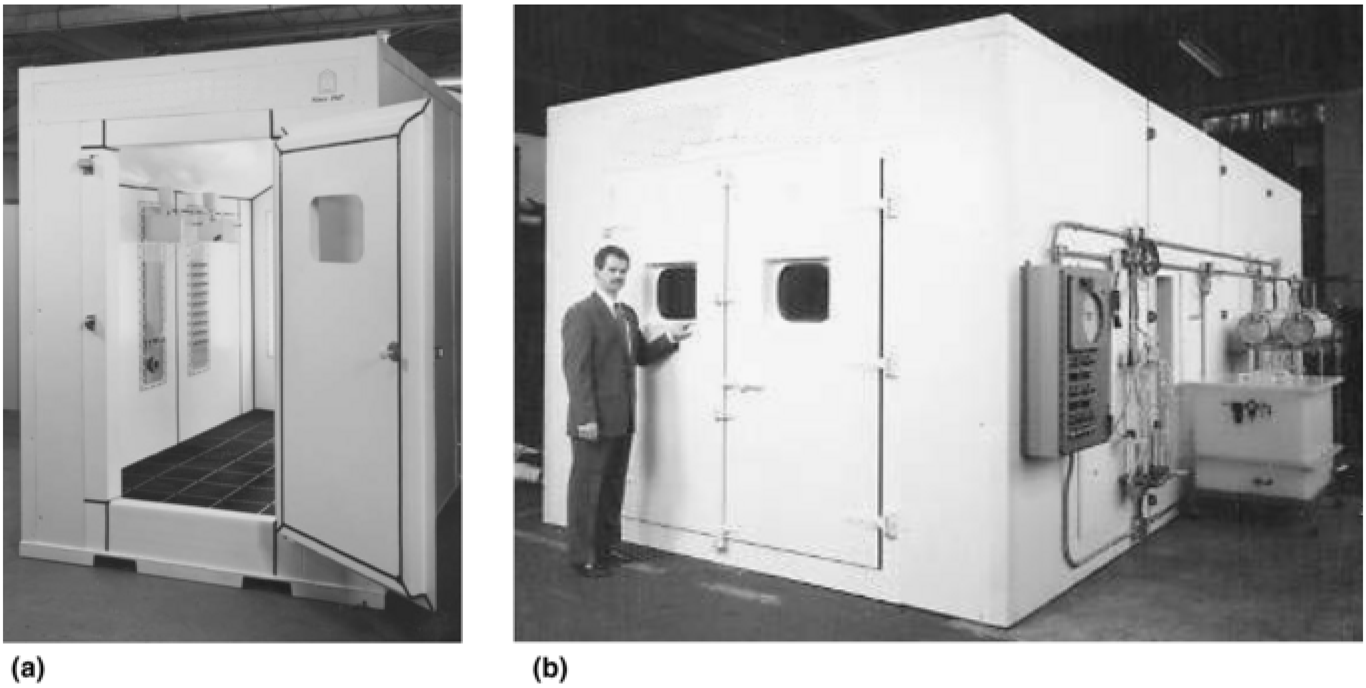

Fig. 1 Large test chambers. (a) Walk-in type. (b) Drive-in type

The most commonly used type of corrosion test chamber is the top-opening type (Fig. 2), which can range in size from 0.25 to 4.5 m^3 (9 to 160 ft^3) and larger. It should be large enough to hold the required number of parts adequately without overcrowding. Make sure also that adequate space is allowed for the size (length, width, and height) in required testing position, as well as the number of necessary test pieces.

Fig. 2 A commonly used open-top corrosion test chamber

Most corrosion test chambers are constructed of plastic (fabricated or molded), fiberglass (usually molded) (Fig. 3), or, more commonly, of steel with a plastic-lined interior (exposure zone) surface. It is important that all test chambers have no exposed metals or corrodible materials in the interior (exposure zone) testing area.

Fig. 3 A corrosion test chamber constructed of molded fiberglass

Major components of a corrosion test chamber consist of the components shown in Fig. 4 and described as follows:

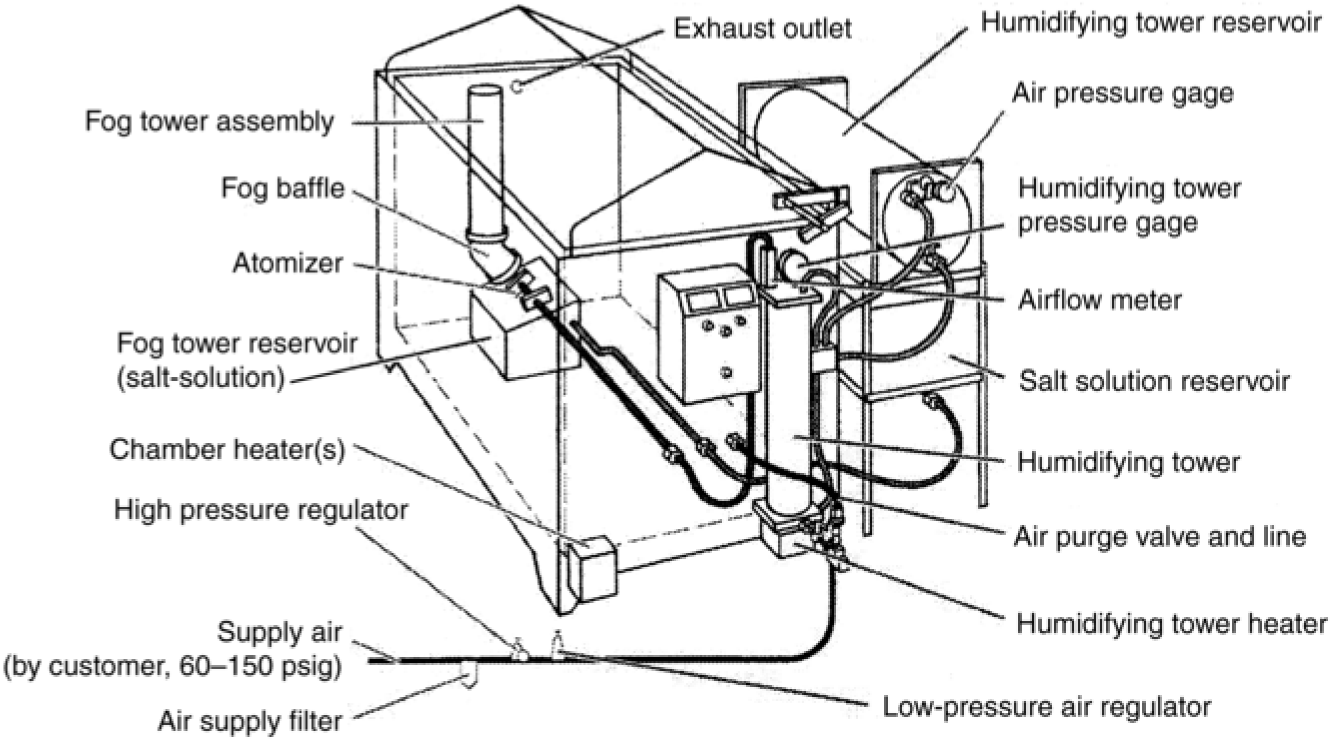

Fig. 4 A diagram of a standard salt-fog corrosion test chamber shows key components of the environment conditioning and control systems.

Compressed-air conditioning apparatus. Usually in the form of a tower, the conditioning apparatus is for heating and humidification (saturation) of the compressed-air supply. Since compressed-air is needed to atomize the salt (electrolyte) solution into the corrosive fog, it must be properly conditioned and controlled to promote uniformity and consistency of test results. To help accomplish this, the tower(s) must be equipped with suitable automatic controls to maintain (a) required temperature and (b) DI water-solution level. An uninterrupted supply of DI water is also necessary for the humidification process. The supply can take the form of (a) an automatic pressurized DI water supply system or (b) a refillable, DI water supply reservoir with

automatic level controls. The tower apparatus should properly condition the compressed air used to atomize the salt solution into a corrosive fog.

Exposure-zone heating apparatus. Along with suitable controls, the exposure-zone heating apparatus will properly maintain required chamber temperature(s). The controls should include temperature displays that indicate both (a) the humidifying (saturation) tower temperature and (b) the wet and dry bulb exposure zone temperatures (in order that RH may be determined for the tests).

A continuously available supply of salt (electrolyte) solution. Usually the salt-solution supply is from a reservoir system. It is necessary that an internal (exposure zone) reservoir be included in order that the salt solution can be preheated to meet the requirement that the solution be atomized at the test temperature. For this reason, the solution supply system requires automatic level controls.

Plastic atomizing nozzle(s). Usually such nozzles are mounted in a fog-generation tower(s) apparatus with adequate internal baffling to prevent direct impingement of the spray on the test pieces. The number of fog generation units (usually towers) required is dependent on the creation of enough fog density and uniformity, to produce 1 to 2 mL (for most test fog cycles) of fog condensate per hour of operation in each collection device (usually a plastic 100 mL graduated cylinder with an 80 cm^2 funnel mounted on top).

Specimen (test piece) supports are generally of inert material and can include fiberglass angle bars, plastic or wood bars, trays with angled slots or special mounting provisions, mesh tray panels of polypropylene, for example, and fishing line to tie or suspend test pieces (Fig. 5).

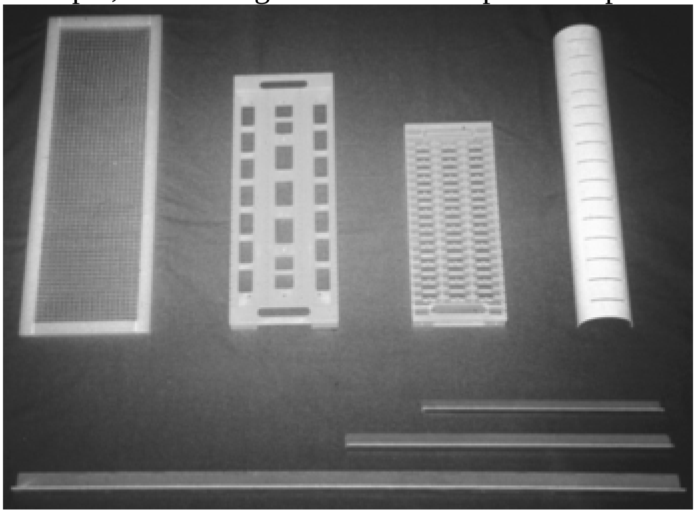

Fig. 5 Specimen supports used within test chambers. Trays, bar, and slotted fixtures are made of materials such as fiberglass and polypropylene that are inert in the test environment.

The dominant surface (principal surface of interest) of the test piece is generally mounted 15 to 30 degrees from the vertical. Sometimes the designation is either vertical or 6 degrees from vertical. Location, position, orientation, and fixturing of test specimens should be decided prior to the commencement of any testing. A good practice is to orient the dominant surface of the test piece(s) parallel with the principal direction of flow (the direction from the fog generation unit to the chamber exhaust) to reduce variability resulting from other orientations.

Another suggestion is to visually divide the exposure zone into at least four horizontal zones and locate the test pieces in each of the four zones for one quarter of the total test time. This procedure should maximize the repeatability of test results by assuring each test specimen receives uniform exposure.

Test specimens and collecting devices should be located no closer than 10 cm (4 in.) from the walls of the exposure zone. A separation of 20 cm (8 in.) should set apart the collecting device from the fog-generation (atomizing) tower(s). This allows the fog atmosphere to circulate evenly about all test specimen surfaces.

The top orifice of the collecting device should be located at the mean or average (vertical) height of the subject test pieces in the exposure zone. Leave adequate spacing (no less than 2.5 cm, or 1 in., is recommended) between adjacent average- or larger-sized, test specimens for proper flow of fog atmosphere to all surfaces. Do not position test pieces above others where dripping onto lower pieces would cause unpredictable or nonuniform patterns of corrosion and unrealistic results.

A bottom drain for the exposure zone should be provided in order to continuously dispose of the accumulating condensed fog. Some chamber drain systems are equipped with a trap that allows continuous draining while

maintaining approximately 2.5 cm (1 in.) of condensed solution in the bottom of the chamber. This is referred to as a “wet bottom” condition. The advantage is that the higher RH values necessary for proper fog collection are more easily achieved. The “wet bottom” condition is, however, not desirable for “dry off” cyclic test steps. For those situations, automatic, or manual valves are operated during those steps to allow the bottom to drain completely.

An exhaust system for the exposure zone vents the unit and eliminates the corrosive fog from entering the ambient atmosphere.

Temperature recording device(s) and/or data- logging software automatically reports test conditions on a continuous basis for record verification and auditing purposes.

In addition to including the previously mentioned features, most cyclic-capable corrosion test chambers incorporate computers and programmable logic controls (PLC) that allow the cyclic test sequences to be performed automatically without the need for an attendant.

Test chambers with computer (PLC or PC) control can include the ability to furnish controlled RH atmospheres. This ability is very useful for cyclic corrosion testing procedures that subject test specimens to a designated sequence of changed environmental conditions for more realistic test results. Computer controlled test chambers also may include the ability for automatic data logging and output for reporting purposes of test conditions. Data obtained can be used for real-time display in graph format or manipulated in spreadsheet-type software for use in reports.

Some corrosion test chambers equipped with computer control can be operated over a local area network (LAN) for remote monitoring and control of the tests. Operators of test chambers of this type can observe current test condition and data information, and they can change tests, adjust test set-point parameters remotely, and operate several test chambers from one PC.

R. Singleton, Cabinet Testing, *Corrosion: Fundamentals, Testing, and Protection* ,Vol 13A, *ASM Handbook*, ASM International, 2003, p 470–477

Cabinet Testing

Raymund Singleton, The Singleton Corporation

References

1. W.D., McMaster, “A History of the Salt Spray Tests,” Publication, General Motors Corporation, Sept 1965

2. “Standard Practice for Operating Salt Spray (Fog) Apparatus,” B 117, *Annual Book of ASTM Standards,* ASTM International

3. “Standard Test Method for Copper-Accelerated Acetic Acid-Salt Spray (Fog) Testing (CASS Test),” B 368, *Annual Book of ASTM Standards,* ASTM International

4. ASTM G 85, “Standard Practice for Modified Salt Spray (Fog) Testing, Annex 1, Acetic-Acid Salt Spray Test, Continuous,” *Annual Book of ASTM Standards*, ASTM International

5. ASTM D 1735, “Standard Practice for Testing Water Resistance of Coatings Using Water Fog Apparatus,” *Annual Book of ASTM Standards,* ASTM International

6. “Standard Practice for Testing Water Resistance of Coatings in 100% Relative Humidity,” D 2247, *Annual Book of ASTM Standards,* ASTM International

7. “Standard Practice for Conducting Cyclic Humidity Tests,” G 60, *Annual Book of ASTM Standards,* ASTM International

8. S.J. Ketcham and I.S. Shaffer, Exfoliation Corrosion of Aluminum Alloys, *Localized Corrosion—Cause of Metal Failure,* STP 516, American Society for Testing and Materials (ASTM), 1972, p 3–16

9. “Standard Practice for Modified Salt Spray (Fog) Testing, Annex 4, SO_2 Salt Spray Test, Cyclic, G 85, *Annual Book of ASTM Standards,* ASTM International

10. “Standard Practice for Modified Salt Spray (Fog) Testing, Annex 5, Dilute Electrolyte Cyclic Fog Dry Test,” G 85, *Annual Book of ASTM Standards,* ASTM International

11. W. Ketola, 3M Company, private communication, Minneapolis, MN

12. “Standard Practice for Preparation of Cold- Rolled Steel Panels for Testing Paint, Varnish, Conversion Coatings, and Related Coating Products,” D 609, *Annual Book of ASTM Standards,* ASTM International

13. “Standard Test Method for Evaluation of Painted or Coated Specimens Subjected to Corrosive Environments,” D 1654, *Annual Book of ASTM Standards,* ASTM International

14. “Standard Test Method for Evaluating Degree of Rusting on Painted Steel Surfaces,” D 610, *Annual Book of ASTM Standards,* ASTM International

15. “Standard Test Method for Evaluating Degree of Blistering of Paints,” D 714, *Annual Book of ASTM Standards,* ASTM International

16. “Standard Guide for Examination and Evaluation of Pitting Corrosion,” G 46, *Annual Book of ASTM Standards,* ASTM International

---

R. Singleton, Cabinet Testing, *Corrosion: Fundamentals, Testing, and Protection* ,Vol 13A, *ASM Handbook,* ASM International, 2003, p 470–477

Cabinet Testing

Raymund Singleton, The Singleton Corporation

Selected References

- S.J. Ketcham and I.S. Shaffer, Exfoliation Corrosion of Aluminum Alloys, *Localized Corrosion—Cause of Metal Failure,* STP 516, ASTM International, 1972, p 3–16
- W.D. McMaster, “A History of the Salt Spray Tests,” Publication GMR-497, General Motors Corporation, Sept 1965
- “Standard Method of Salt Spray (Fog) Testing,” B 117, *Annual Book of ASTM Standards,* ASTM International
- “Standard Practice for Modified Salt Spray (Fog) Testing,” G 85, *Annual Book of ASTM Standards,* ASTM International
- “Standard Practice for Operating Moist SO_2 Apparatus,” G 87, *Annual Book of ASTM Standards,* ASTM International
- “Standard Practice for Preparing, Cleaning, and Evaluating Corrosion Test Specimens,” G 1, *Annual Book of ASTM Standards,* ASTM International

- "Standard Specification For Reagent Water," D 1193, *Annual Book of ASTM Standards,* ASTM International
- "Standard Practice for Substitute Ocean Water," D 1141, *Annual Book of ASTM Standards,* ASTM International
- "Standard Test Method for Copper-Accelerated Acetic Acid-Salt Spray (Fog) Testing (CASS Test)," B 368, *Annual Book of ASTM Standards,* ASTM International

---

B.J. Little, F.B. Mansfeld, P.J. Arps and J.C. Earthman, Microbiologically Influenced Corrosion Testing *Corrosion: Fundamentals, Testing, and Protection*, Vol 13A, *ASM Handbook*, ASM International, 2003, p 478–486

Microbiologically Influenced Corrosion Testing

B.J. Little, Naval Research Laboratory; F.B. Mansfeld, University of Southern California; P.J. Arps and J.C. Earthman, University of California, Irvine

---

Introduction

CORROSION resulting from the presence and activities of microbes on metals and metal alloys is generally referred to as microbiologically influenced corrosion (MIC). Microbiologically mediated reactions can alter both rates and types of electrochemical reactions, but do not result in a unique manifestation of corrosion. Rather, MIC can produce a broad range of outcomes from severe localized corrosion to significant reductions in corrosion rate (Ref 1). Pitting, crevice corrosion, differential aeration cells, metal concentration cells, selective dealloying, enhanced erosion, and enhanced galvanic corrosion can result from MIC. Most MIC studies have focused on bacterial involvement; however, other single-celled organisms—such as fungi, yeast, and diatoms—can influence corrosion processes. Numerous test kits are available for culturing microorganisms known to influence corrosion. However, accurate diagnosis of MIC requires a combination of microbiological, surface analytical, and electrochemical techniques. Because microorganisms are ubiquitous and can be attracted to both anodic (Ref 2) and cathodic (Ref 3) sites, spatial relationships between microorganisms and corrosion products are not sufficient on their own to be interpreted as MIC. The following section describes biofilm formation and structure, microbial processes influencing corrosion, and electrochemical techniques used to study and monitor MIC.

References cited in this section

1. H.A. Videla, *Manual of Biocorrosion,* CRC Press, 1996

2. M.J. Franklin, D.C. White, B.J. Little, R.I. Ray, and R.K. Pope, *Biofouling,* Vol 15 (No. 1–3), 1999, p 13–23

3. B.J. Little and P.A. Wagner, The Interrelationship between Marine Biofouling, Cathodic Protection and Microbiologically Influenced Corrosion, *Mater. Sci. Forum,* Vol 192–194, pt. 1; *Electrochemical Methods in Corrosion Research V,* Fifth International Symposium, (Sesimbra, Portugal), 5–8 Sept 1994, Trans Tech Publications, 1995, p 433–446

B.J. Little, F.B. Mansfeld, P.J. Arps and J.C. Earthman, Microbiologically Influenced Corrosion Testing *Corrosion: Fundamentals, Testing, and Protection*, Vol 13A, *ASM Handbook*, ASM International, 2003, p 478–486

Microbiologically Influenced Corrosion Testing

B.J. Little, Naval Research Laboratory; F.B. Mansfeld, University of Southern California; P.J. Arps and J.C. Earthman, University of California, Irvine

Biofilm Formation

Cells attach to wet solid surfaces and produce a biofilm consisting of a matrix of polymeric substances and cells in microcolonies (Ref 4, 5, 6, 7, 8). Biofilm formation consists of a sequence of steps (Fig. 1) and begins with adsorption of macromolecules (proteins, polysaccharides, and humic acids) and smaller molecules (fatty acids, lipids) on solid surfaces. Adsorbed molecules or conditioning films alter physiochemical characteristics of the water/surface interface, including hydrophobicity and surface charge.

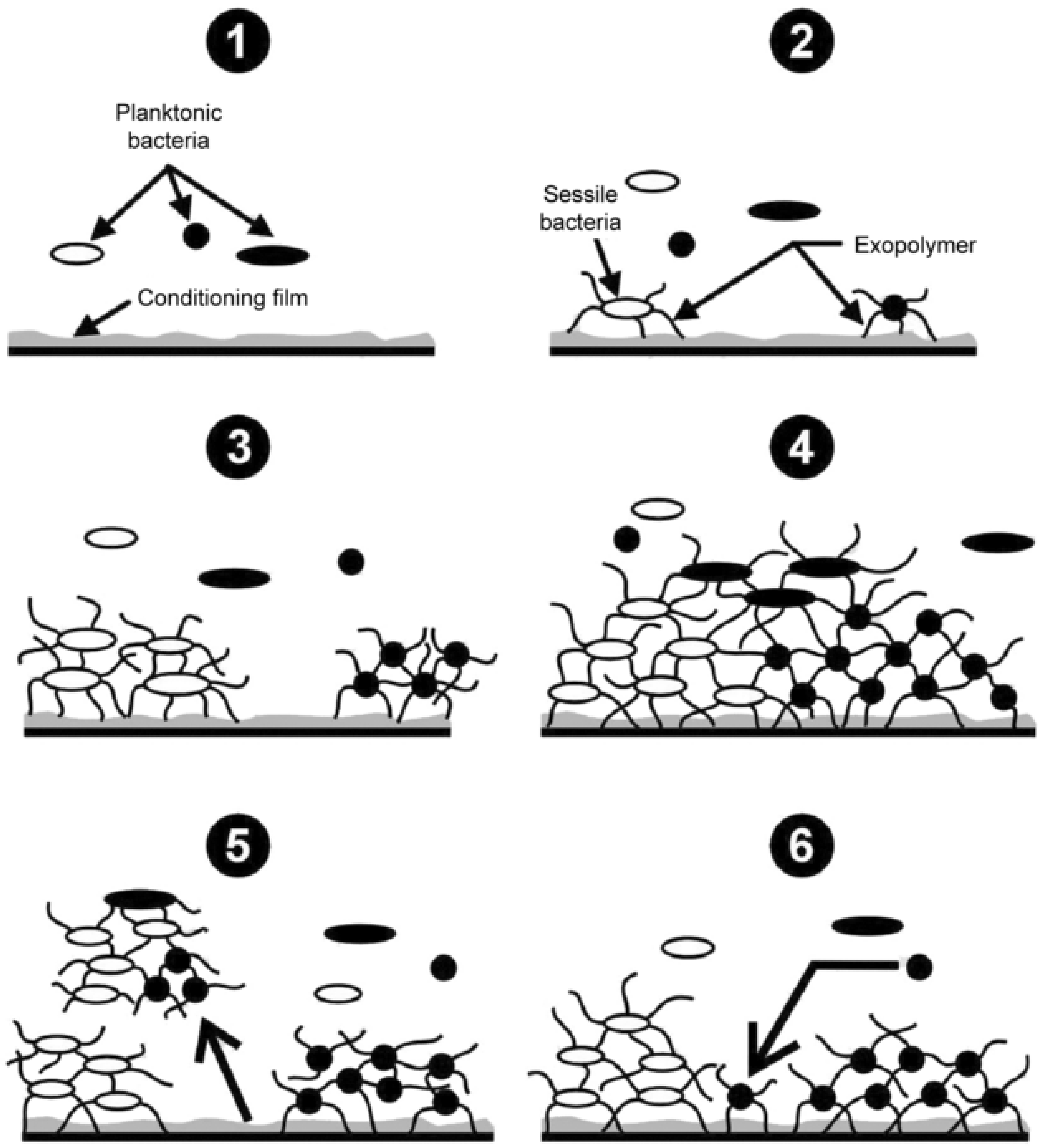

Fig. 1 Conceptual illustration of heterogeneous biofilm structure. (1) Initial attachment to substratum. (2) Synthesis of extracellular polymeric substances to establish more secure association with substratum. (3) Bacterial replication on the substratum and microcolony formation. (4) Formation of mature biofilm. (5) Sloughing and detachment of portions of biofilm. (6) Recolonization of areas of substratum exposed by sloughing events. Courtesy of the Center for Biofilm Engineering at Montana State University, Bozeman; Illustrator, P. Dirckx

Hydrodynamics play a major role in controlling the rate of microbial colonization during initial stages of biofilm formation. Transport of microorganisms to an interface and subsequent attachment are mediated by: diffusive transport due to Brownian motion, convective transport due to liquid flow, and active movement of motile bacteria near the interface. The influence of convective transport exceeds the other two mechanisms by several orders of magnitude. Once a microbial cell is in contact with a surface it may or may not adhere. The ratio of adhering cells to the total number of cells transported to an interface depends on substratum properties (including charge density), physiological state of the microbes, hydrodynamics, and nutritional signals from the environment. For many bacteria, attachment requires cell-surface appendages (fimbriae, pili) or adhesive substances (Ref 6, 7).

Immediately after attachment, microorganisms initiate production of adhesive substances, predominantly exopolysaccharides (Ref 7), collectively known as extracellular polymeric substances (EPS), that provide the biofilm matrix. Extracellular polymeric substances bridge microbial cells with the substratum and permit negatively charged bacteria to adhere to both negatively and positively charged surfaces.

Biofilm formation proceeds with division of cells and recruitment of planktonic cells to form a complicated architectural structure and ends with detachment of individual cells and aggregates (Fig. 1) (Ref 9, 10). The architectural structure is typically composed of pillar- and mushroom-shaped cell clusters separated by water channels that allow nutrients in and waste products out (see Fig. 2 in the article "Microbiologically Influenced Corrosion" in this Volume). Biofilm accumulation at surfaces is a self-perpetuating and continuous process. Initial colonization increases surface irregularity and promotes recruitment of additional free-swimming cells, promoting further surface irregularity. Each species in a biofilm has its own growth parameters, and there appear to be spatial distributions of growth (Ref 11). Development of specialized multicellular biofilm structures can involve cell-to-cell signaling (quorum sensing) among cells in close proximity (Ref 12, 13). Detachment includes two processes: sloughing and erosion. Sloughing is the process in which large pieces of biofilm are removed, exposing the underlying surface. Reasons for biofilm sloughing are not well understood. Biofilm erosion is the continuous removal of single cells or small groups of cells from the biofilm and is driven by shear stress at the biofilm/fluid interface. An increase in shear stress increases erosion rate and decreases biofilm accumulation rate. Empirical observations indicate that erosion rate is related to flow velocity, biofilm thickness, density, and tertiary structure (Ref 14).

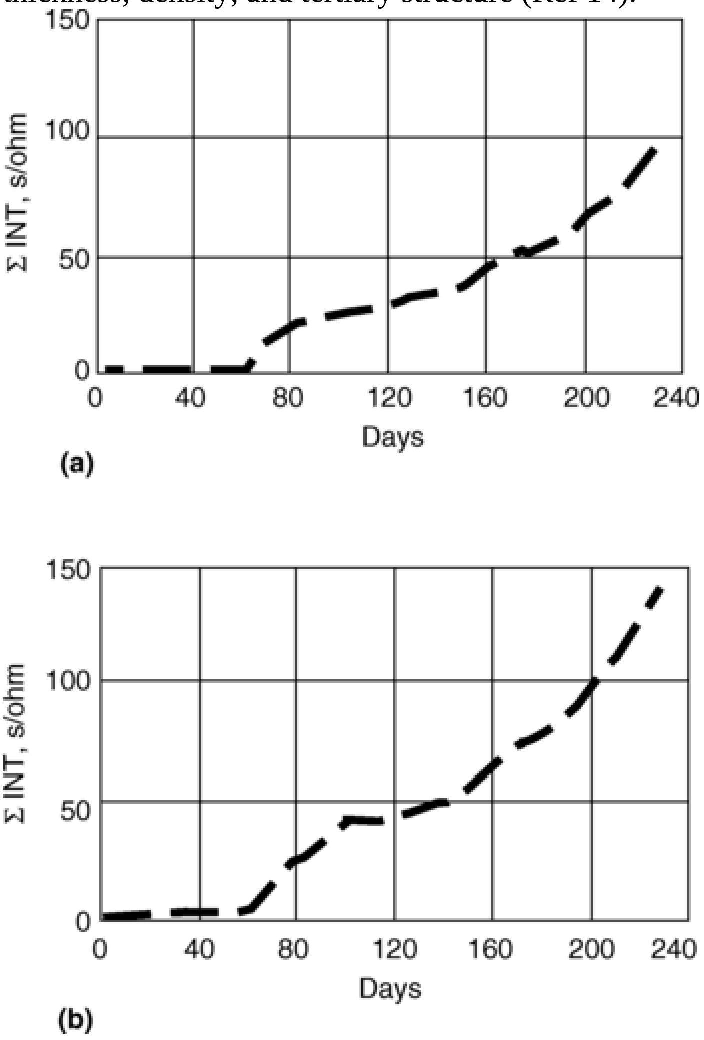

Fig. 2 Cumulative corrosion loss, ΣINT, for mild steel sensors embedded in concrete and exposed in a sewer bypass. (a) Control sample. (b) Flushed sample

Biofilms are capable of maintaining environments at biofilm/surface interfaces that are radically different from the bulk fluid in terms of pH, dissolved oxygen, and other organic and inorganic species. In some cases, these interfacial conditions could not be maintained in the bulk medium at room temperature near atmospheric

pressure. The consequence is that microorganisms within biofilms facilitate reactions that are not predicted by thermodynamic arguments based on the chemistry of the bulk medium.

References cited in this section

4. Y.H. An and R.J. Friedman, Ed., *Principles, Methods, and Applications, Handbook of Bacterial Adhesion,* Humana Press, 2000

5. J.D. Bryers, Ed., *Biofilms II: Process Analysis and Applications,* John Wiley & Sons, 2000

6. G.A. O'Toole and R. Kolter, Initiation of Biofilm Formation in *Pseudomonas fluorescens,* WCS365 Proceeds via Multiple, Convergent Signalling Pathways: A Genetic Analysis, *Mol. Microbiol.,* Vol 28, 1998, p 449–461

7. J.W. Costerton, Z. Lewandowski, D.E. Calwell, D.R. Korber, and H.M. Lappin-Scott, Microbial Biofilms, *Ann. Rev. Microbiol.,* Vol 49, 1995, p 711–745

8. R. Kolter and R. Losick, One for All and All for One, *Science,* Vol 280, 1998, p 226–227

9. J.R. Lawrence, D.R. Korber, B.D. Hoyle, J.W. Costerton, and D.E. Caldwell, Optical Sectioning of Microbial Biofilms, *J. Bacteriol.,* Vol 173, 1991, p 6558–6567

10. D. DeBeer, P. Stoodley, and Z. Lewandowski, Liquid Flow in Heterogeneous Biofilms, *Biotech. Bioeng.,* Vol 44, 1994, p 636–641

11. E.J. Wentland, P.S. Stewart, C.-T. Huang, and G.A. McFeters, Spatial Variations in Growth Rate within *Klebsiella pneumoniae* Colonies and Biofilm, *Biotechnol. Prog.,* Vol 12, 1996, p 316–321

12. D.G. Davies, M.R. Parsek, J.P. Pearson, B.H. Iglewski, J.W. Costerton, and E.P. Greenberg, The Involvement of Cell-to-Cell Signals in the Development of a Bacterial Biofilm, *Science,* Vol 280, 1998, p 295–298

13. G.M. Dunny and S.C. Winans, Ed., *Cell- Cell Signaling in Bacteria,* American Society of Microbiology, 1999

14. A. Ohashi, T. Koyama, K. Syutsubo, and H. Harada, A Novel Method for Evaluation of Biofilm Tensile Strength Resisting Erosion, *Water Sci. Technol.,* Vol 39 (No. 7), 1999, p 261–268

B.J. Little, F.B. Mansfeld, P.J. Arps and J.C. Earthman, Microbiologically Influenced Corrosion Testing *Corrosion: Fundamentals, Testing, and Protection*, Vol 13A, *ASM Handbook*, ASM International, 2003, p 478–486

Microbiologically Influenced Corrosion Testing

B.J. Little, Naval Research Laboratory; F.B. Mansfeld, University of Southern California; P.J. Arps and J.C. Earthman, University of California, Irvine

---

Mechanisms

The most serious MIC takes place in the presence of microbial consortia where many types of microorganisms are present within the structure of the biofilm. These include sulfate-reducing bacteria (SRB), metal-oxidizing and metal-reducing bacteria (MRB), acid-producing and slime-producing bacteria, hydrogen-consuming and hydrogen-producing bacteria, and metal-depositing bacteria, plus other forms of aerobic and anaerobic microbes (Fig. 3).

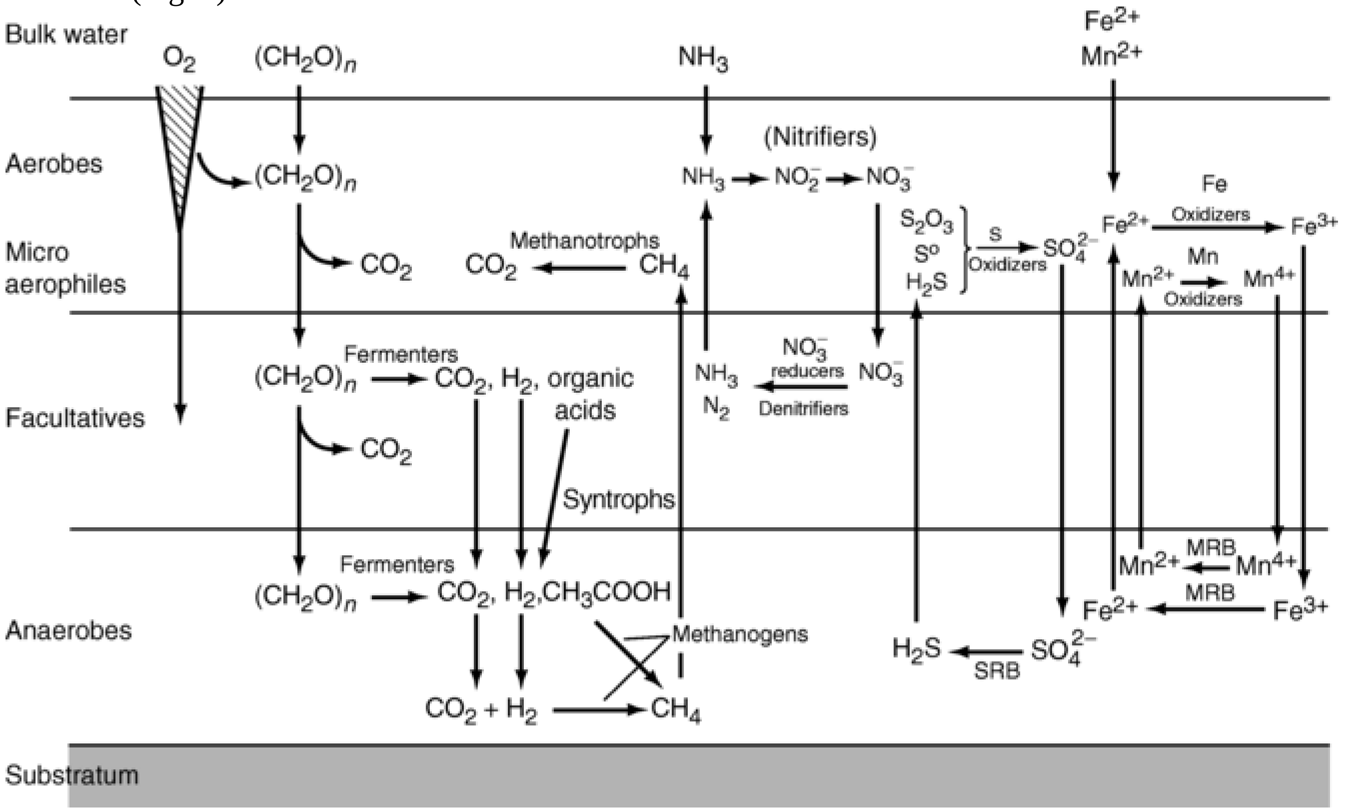

Fig. 3 Possible reactions that can occur in a biofilm

Sulfate-reducing bacteria are a phylogenetically diverse group of anaerobic bacteria found in natural and industrial environments. Sulfate- reducing bacteria use sulfate as the terminal electron acceptor during respiration and produce hydrogen sulfide. When the aerobic respiration rate within a biofilm is greater than the oxygen diffusion rate, the metal/biofilm interface can become anaerobic and provide a niche for SRB. The critical biofilm thickness required to produce anaerobic conditions depends on availability of oxygen and the respiration rates of organisms in the biofilm. The corrosion rate of iron and copper alloys in the presence of hydrogen sulfide is accelerated by the formation of iron sulfide minerals that stimulate the cathodic reaction.

Some microorganisms couple manganese and iron oxidation and reduction reactions to cell growth and metabolism of organic carbon. Manganese oxide deposited by microorganisms on stainless and mild steel alters the electrochemical properties pertaining to open-circuit potential or corrosion potential (E_{corr}) (Ref 15, 16). Iron-oxidizing bacteria produce tubercles of iron oxides and hydroxides creating oxygen-concentration cells that initiate a series of events that individually or collectively are very corrosive. Other microorganisms promote corrosion of iron and its alloys through dissimilatory metal reduction reactions that lead to the dissolution of protective iron oxide/hydroxide films on the metal surface. Passive layers are either lost or replaced by less stable films that allow further corrosion (Ref 17).

Bacteria and fungi produce a wide variety of organic acids (e.g., acetic, formic, lactic, succinic) as by-products of metabolism that are capable of initiating or accelerating corrosion (Ref 18, 19). Mineral acids, such as sulfuric, produced by some bacteria are very corrosive. The EPS may also control interfacial chemistry at a metal/ biofilm interface and thereby affect the rate of metal dissolution. Extracellular polymeric substances are also implicated in increased resistance of cells to biocides and other antimicrobial compounds (Ref 20, 21).

Inhibition of general corrosion by biofilms has been reported for mild steel, copper, aluminum, and stainless steels (Ref 22, 23, 24, 25, 26, 27). The mechanisms most frequently cited for the inhibition are:

- Formation of a diffusion barrier to corrosion products that stifles metal dissolution

- Consumption of oxygen by respiring aerobic microorganisms within the biofilm causing a diminution of that reactant at the metal surface
- Production of metabolic products that act as corrosion inhibitors (e.g., siderophores) or specific antibiotics that prevent proliferation of corrosion-causing organisms (e.g., SRB)
- Formation of passive layers that are unique to the presence of microorganisms

References cited in this section

15. B.H. Olesen, R. Avci, and Z. Lewandowski, Manganese Dioxide as a Potential Cathodic Reactant in Corrosion of Stainless Steels, *Corros. Sci.,* Vol 42, 2000, p 211–227

16. B.H. Olesen, P.H. Nielsen, and Z. Lewandowski, Effect of Biomineralized Manganese on the Corrosion Behavior of C1008 Mild Steel, *Corrosion,* Vol 56, 2000, p 80–89

17. B.J. Little, P.A. Wagner, K.R. Hart, R.I. Ray, D.M. Lavoie, K. Nealson, and C. Aguilar, "The Role of Metal Reducing Bacteria in Microbiologically Influenced Corrosion," Paper No. 215, Corrosion/97, NACE International, 1997

18. R.J. Soracco, D.H. Pope, J.M. Eggers, and T.N. Effinger, "Microbiologically Influenced Corrosion Investigations in Electric Power Generating Stations," Paper No. 83, Corrosion/88, National Association of Corrosion Engineers, 1988

19. B. Little, P. Wagner, and D. Duquette, Microbiologically Induced Increase in Corrosion Current Density of Stainless Steel under Cathodic Protection, *Corrosion,* Vol 44, 1988, p 270

20. G.G. Geesey and M.W. Mittelman, "The Role of High-Affinity, Metal-Binding Exopolymers of Adherent Bacteria in Microbial-Enhanced Corrosion," Paper No. 85, Corrosion/85, National Association of Corrosion Engineers, 1985

21. G.G. Geesey, M.W. Mittelman, T. Iwaoka, and P.R. Griffiths, Role of Bacterial Exopolymers in the Deterioration of Metallic Copper Surfaces, *Mater. Perform.,* Vol 25, 1986, p 37–40

22. B.W. Samuels, K. Sotoudeh, and R.T. Foley, *Corrosion,* Vol 37, 1981, p 92–97

23. G. Hernandez, V. Kucera, D. Thierry, A. Pedersen, and M. Hermansson, *Corrosion,* Vol 50, 1994, p 603–608

24. H.A. Videla, *Biofouling and Biocorrosion in Industrial Water Systems,* G.G. Geesey, Z. Lewandowski, and H.C. Flemmings, Ed., Lewis Publishers, 1994, p 231–241

25. A. Jayaraman, J.C. Earthman, and T.K. Wood, *Appl. Microbiol. Biotechnol.,* Vol 47, 1997, p 62–68

26. D. Ornek, T.K. Wood, B.C. Syrett, C.H. Hsu, and F. Mansfeld, "Corrosion Control Using Regenerative Biofilms (CCURB) on Al 2024 and 26000 Brass," Paper No. 1270, Corrosion/2001, NACE International, 2001

27. K. Trandem, Z.S. Farhangrazi, T.K. Wood, P.J. Arps, and J.C. Earthman, "Field Sidestream Investigations of Corrosion Control Using Regenerative Biofilms (CCURB)," Paper No. 1271, Corrosion/2001, NACE International, 2001

B.J. Little, F.B. Mansfeld, P.J. Arps and J.C. Earthman, Microbiologically Influenced Corrosion Testing *Corrosion: Fundamentals, Testing, and Protection*, Vol 13A, *ASM Handbook*, ASM International, 2003, p 478–486

Microbiologically Influenced Corrosion Testing

B.J. Little, Naval Research Laboratory; F.B. Mansfeld, University of Southern California; P.J. Arps and J.C. Earthman, University of California, Irvine

Electrochemical Techniques

Electrochemical techniques used to study MIC include those in which no external signal is applied (redox potential, E_{corr}, electrochemical noise, or ECN), those in which only a small potential or current perturbation is applied (polarization resistance, electrochemical impedance spectroscopy), and those in which the potential is scanned over a wide range (anodic and cathodic polarization curves, pitting scans). Galvanic current flowing between biotic and abiotic cells has also been measured using a dual-cell technique (also called "biological battery"). Current and potential mapping have been used to locate anodic and cathodic sites, and microsensors have been applied to determine concentration profiles in biofilms. Background for the most widely used electrochemical techniques and examples of applications to MIC are presented in the following sections.

Open-circuit or corrosion potential measurements require a stable reference electrode— usually assumed to be unaffected by biofilm formation—and a high-impedance voltmeter. E_{corr} values are difficult to interpret, especially when related to MIC (Ref 28). Despite this limitation, probably no other phenomenon has fascinated those studying MIC more than ennoblement, that is, the increase of E_{corr} due to formation of a biofilm on a metal surface.

Ennoblement has been observed mainly for stainless steels exposed to natural seawater (Fig. 4) (Ref 29, 30, 31, 32, 33, 34). Explanations for microbially influenced ennoblement include microbial production of hydrogen peroxide, corrosion inhibitors, extracellular substances, organometallic complexes, enzymes, and changes of cathodic properties of stainless steels as a result of microbial activity. Early explanations used thermodynamic arguments suggesting that the reversible potential (E^o) of the oxygen electrode increased in the presence of biofilms due to either an increase in partial pressure of oxygen or a decrease of surface pH. Since E^o increases only very slightly with an increase of oxygen pressure and since it is unlikely that acidification would increase passivity, those explanations were rejected.

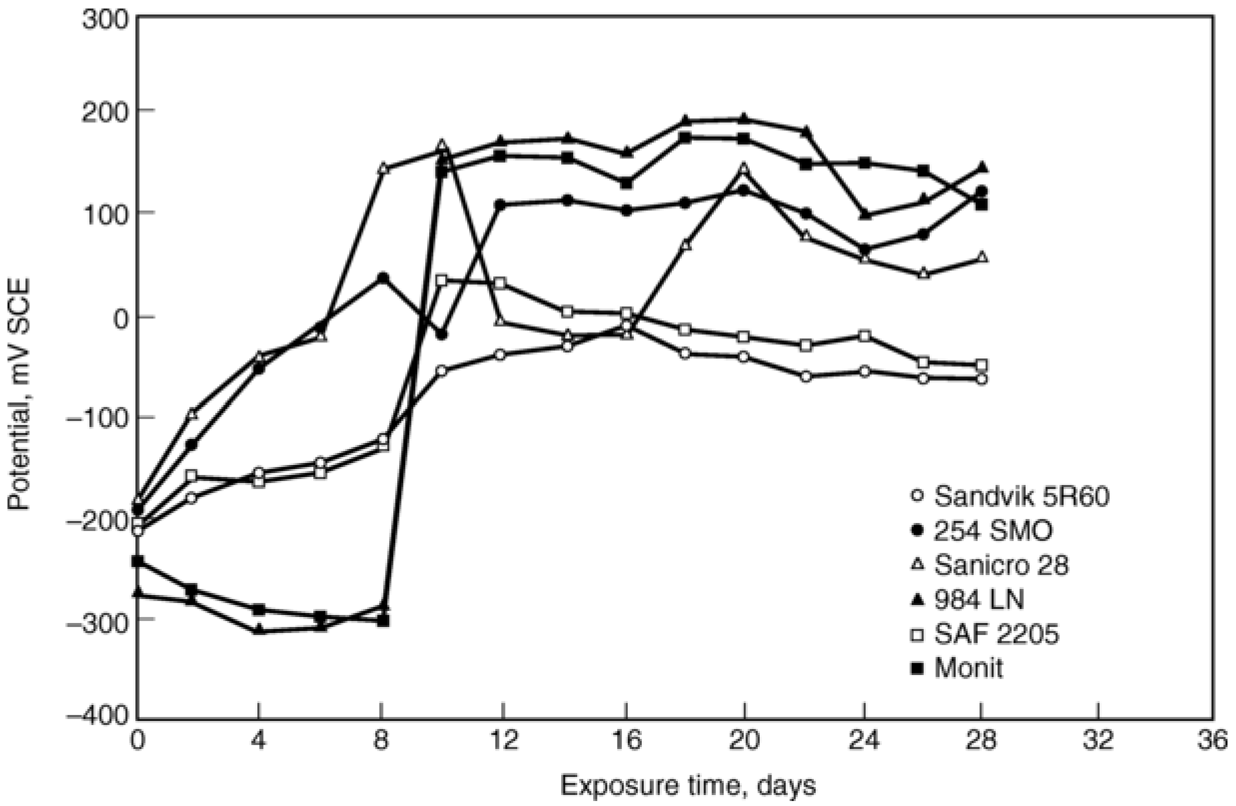

Fig. 4 Potential measured on freely exposed specimens in natural seawater at a velocity of 0.5 m/s. SCE, saturated calomel electrode

Results by Linhardt (Ref 35, 36), Olesen et al. (Ref 15, 16), and Dickinson et al. (Ref 37, 38) demonstrated ennoblement of stainless steels in river waters due to microbial deposition of MnO_2. Linhardt found large amounts of manganese minerals (mainly MnOOH and MnO_2) on severely pitted turbine runner blades in a hydroelectric plant and suggested that pitting was due to biomineralized manganese oxides. Von Rege et al. reported severe pitting around welds in type 316 stainless steel pipes used to pump cooling water from the Rhine River (Ref 39). He reported that the failure mechanism involved iron- and manganese-oxidizing bacteria causing ennoblement and pitting. Linhardt (Ref 36) concluded that ennoblement was due to the formation of MnO_2 according to:

$$Mn^{2+} + 2H_2O \rightarrow MnO_2 + 4H^+ + 2e^- \qquad \text{(Eq 1)}$$

Pitting occurred as a result of galvanic interaction between areas covered by manganese oxides acting as cathodes and bare stainless steel surfaces serving as anodes. Dickinson et al. (Ref 37, 38) observed an increase of E_{corr} from -150 mV to +350 mV versus saturated calomel electrode (SCE) for 316L stainless steel exposed to a fresh water creek over a 30 day period. The authors concluded that ennoblement was due to microbial deposition of manganese oxides.

The polarization resistance technique can be used to continuously monitor instantaneous corrosion rate of a metal or alloy exposed to a corrosive environment. Mansfeld (Ref 40) and more recently Scully (Ref 41) reviewed the background and use of polarization resistance (R_p) for measurement of corrosion currents. See the section “Polarization Resistance Method” in the article “Electrochemical Methods of Corrosion Testing” in this Volume for more details. R_p is defined as the slope of a potential (E) versus current density (i) curve at E_{corr}, where i = 0:

$$R_p = \left(\frac{dE}{di}\right)_{i=0} = 0 \qquad \text{(Eq 2)}$$

Corrosion current density (i_{corr}) is calculated from R_p by:

$$i_{corr} = B/R_p \qquad \text{(Eq 3)}$$

where

$$B = \beta_a\beta_c/2.303(\beta_a + \beta_c) \qquad \text{(Eq 4)}$$

The exact calculation of i_{corr} for a given time requires simultaneous measurements of R_p and anodic (β_a) and cathodic (β_c) Tafel slopes (Ref 42).

A simplification of the polarization resistance technique is the linear polarization technique in which it is assumed that the relationship between E and i is linear in a narrow range around E_{corr}. Usually only two points (E, i) are measured and B is assumed to have a constant value of about 20 mV. This approach is used in field tests and forms the basis of commercial corrosion rate monitors.

Keresztes et al. (Ref 43) studied the effect of *Desulfovibrio desulfuricans* on anaerobic corrosion of mild steel and brass using linear polarization and atomic force microscopy. The influence of biocides—*N*-hydroxy-methyl-glycine (GLY) and *N*-hydroxy-methylphenyl-alanine (PHE)—on corrosion rates was determined (Fig. 5). Corrosion rates for mild steel were lower in the presence of GLY. For brass, both biocides reduced corrosion rates compared to those observed for the sterile solution. The authors used these data in combination with results from polarization curves to obtain mechanistic information on the influence of biocides on MIC of mild steel and brass.

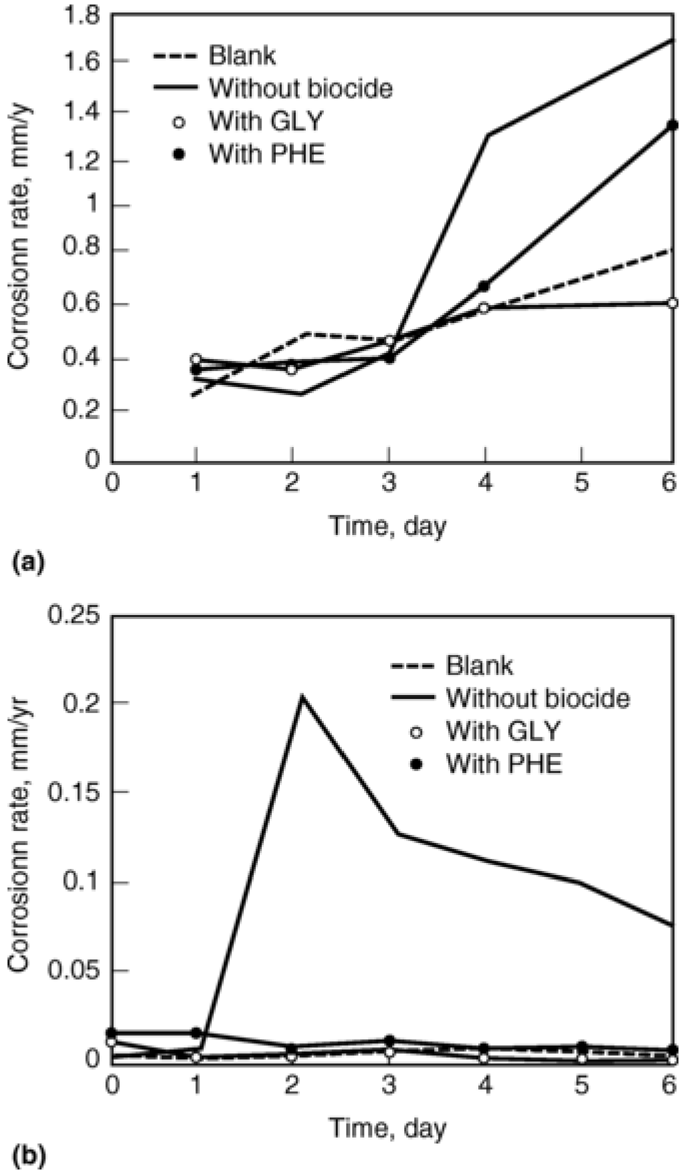

Fig. 5 Corrosion rate in the culture of *Desulfovibrio desulfuricans* for specimens with and without biocide treatment. (a) Mild steel. (b) Brass. GLY, *N*-hydroxy-methyl-glycine; PHE, *N*-hydroxy-methylphenyl-alanine

Mansfeld et al. (Ref 44) used linear polarization to determine R_p for mild steel sensors embedded in concrete exposed to a sewer environment. One concrete sample was periodically flushed with sewage to remove sulfuric acid (H_2SO_4) produced by sulfur-oxidizing bacteria. Another sample was used as a control. A data- logging system collected R_p at 10 min intervals simultaneously for the two corrosion sensors and two pH electrodes

placed at the concrete surface. Figure 2 shows the cumulative corrosion loss, ΣINT, obtained by integration of the $1/R_p$ versus time curves as:

$$\Sigma \text{INT} = \int \frac{1}{R_p} dt \qquad \text{(Eq 5)}$$

A qualitative measure of the corrosion rate can be obtained from the slope of the curves in Fig. 2. ΣINT is given in units of s/Ω. Because of uncompensated ohmic resistance and lack of precise values for Tafel slopes, data in Fig. 2 should be viewed as a qualitative measure of changes in corrosion rates. Corrosion losses remained low during the first two months followed by a large increase for both the flushed sample and the control sample. Increased corrosion rates of the embedded steel electrodes occurred when surface pH reached values of 1 or less due to accumulation of H_2SO_4. Total corrosion loss determined from integrated R_p data was less for the control sample than for the flushed sample.

Large signal polarization is applied to obtain potentiostatic or potentiodynamic polarization curves, as well as pitting scans. Polarization curves can be used to determine i_{corr} by Tafel extrapolation, while mass-transport-related phenomena can be evaluated based on the limiting current density (i_{lim}) Mechanistic information can be obtained from experimental values of β_a and β_c. In metal/electrolyte systems for which an active-passive transition occurs, the passive properties can be evaluated based on the critical potential (E_{crit}) and critical current density for passivation (i_{crit}), and the passive current density (i_{pass}). Pitting scans are used to determine pitting potential (E_{pit}) and protection potential (E_{prot}). A disadvantage of large-signal polarization is its destructive nature, that is, the irreversible changes of surface properties due to application of large anodic or cathodic potentials. Polarization curves are usually obtained for sterile solutions and solutions containing microorganisms (Ref 43) (Fig. 6).

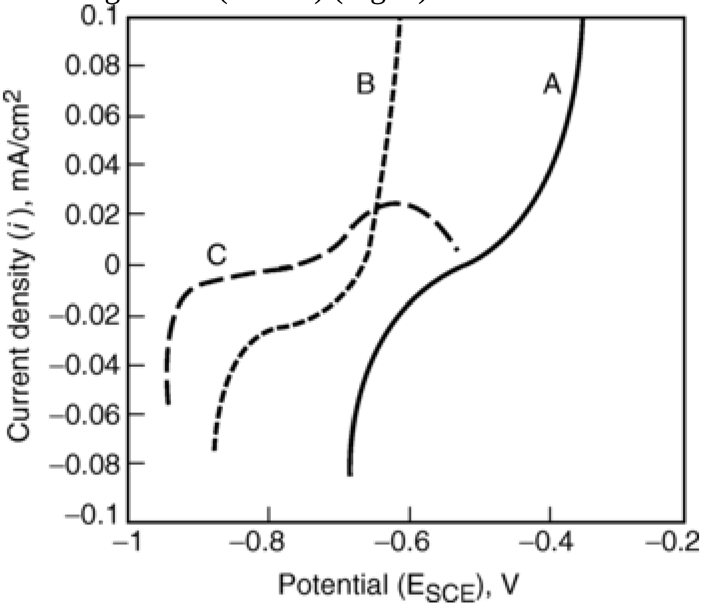

Fig. 6 Polarization curves measured on mild steel in the solution of biogenic and chemical sulfide. A, blank; B, biogenic sulfide; C, chemical sulfide

Electrochemical impedance spectroscopy (EIS) has been used in mechanistic studies of MIC (Ref 28). This development has been made possible in part by the availability of equipment that optimizes data collection in a wide range of frequencies and impedance values. In addition, software is available for fitting experimental data to appropriate equivalent circuits. The impact of microorganisms on corrosion protection of mild steel by polymer coatings was evaluated by Mansfeld and coworkers using EIS and electrochemical noise (ECN) to monitor coating degradation during exposure to natural seawater for periods up three years (Ref 45, 46). Figure 7 gives an example for impedance spectra over a seven-month period for a four coatings (thickness ≈ 200 μm). Impedance spectra show a gradual decrease of the impedance modulus $|Z|$ with time for all coatings except for an all-epoxy-polyamide system (Fig. 7d). Electrochemical impedance spectroscopy data for polymer coated steel are usually fit to the equivalent circuit shown in Fig. 8(a), where C_c is the coating capacitance, R_{po} is the pore resistance, C_{dl} is the capacitance of the delaminated area (A_d) and R_p is the corresponding polarization

resistance. Spectra for thick coatings should be fit to the open-boundary finite-length diffusion (OFLD) model (Fig. 8b) (Ref 46) in which C_c is replaced by a constant-phase element (CPE). The OFLD element is given by:

$$Z_{OFLD} = \frac{\tanh\left(B(j\omega)^{1/2}\right)}{Y_o (j\omega)^{1/2}} \quad \text{(Eq 6)}$$

where $B = l/(D)^{1/2}$ is the characteristic diffusion parameter, l is the diffusion length, D is the diffusion coefficient, ω is angular frequency ($\omega = 2\pi f$), and $Y_o = (\sigma(2)^{1/2})^{-1}$. For infinite values of l this model becomes the Randles circuit, in which the Warburg impedance (Z_w) is in series with R_p and is given by:

$$Z_w = \sigma(1 - j)\omega^{-1/2} \quad \text{(Eq 7)}$$

where σ is the Warburg coefficient.

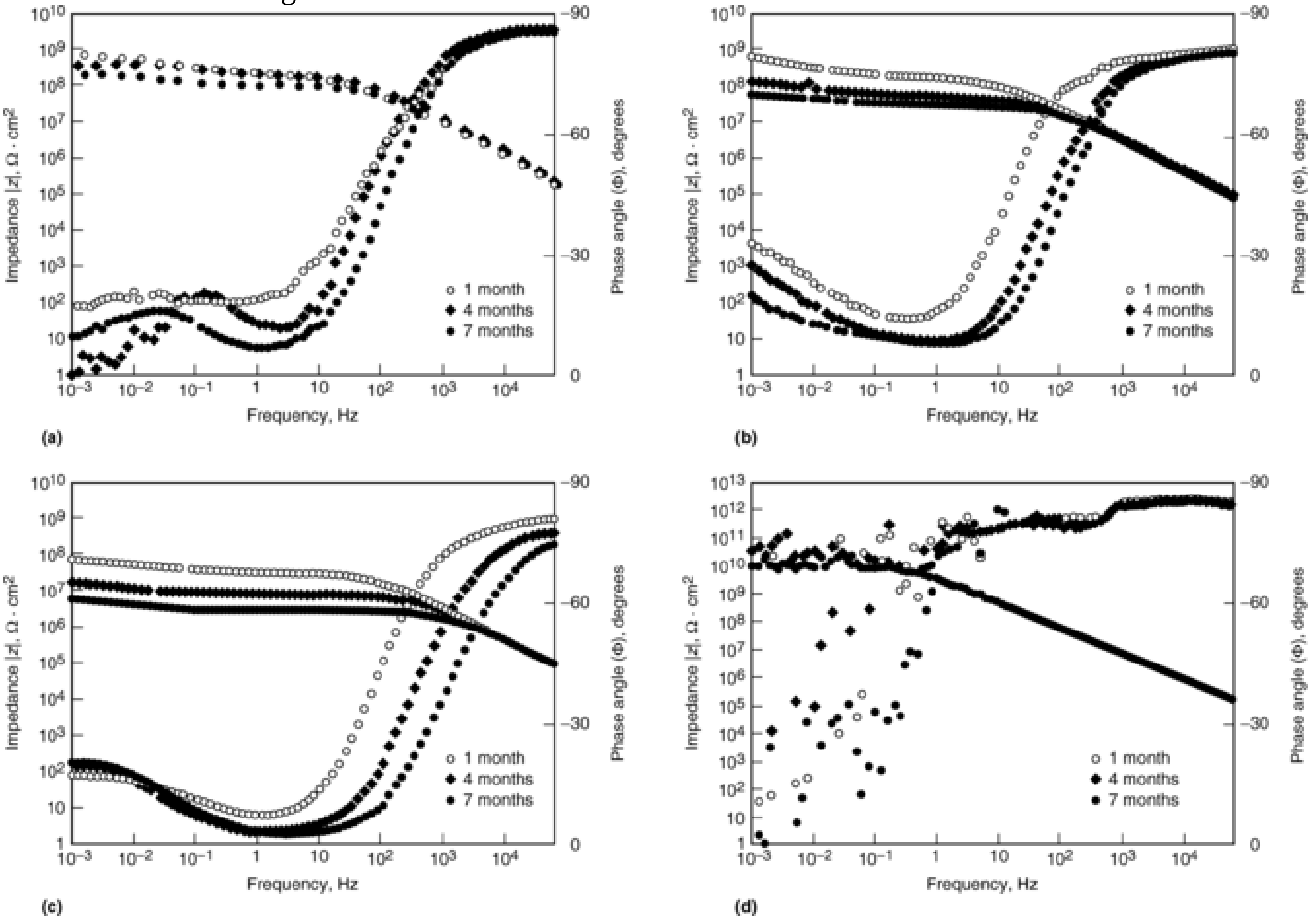

Fig. 7 Impedance spectra for coated steel exposed to natural seawater for 1, 4, and 7 months at Port Hueneme, CA. (a) Zinc primer, epoxy polyamide midcoat, urethane topcoat. (b) Zinc primer, epoxy polyamide, midcoat, latex topcoat. (c) Epoxy polyamide primer and midcoat, latex topcoat. (d) Epoxy polyamide primer, midcoat and topcoat

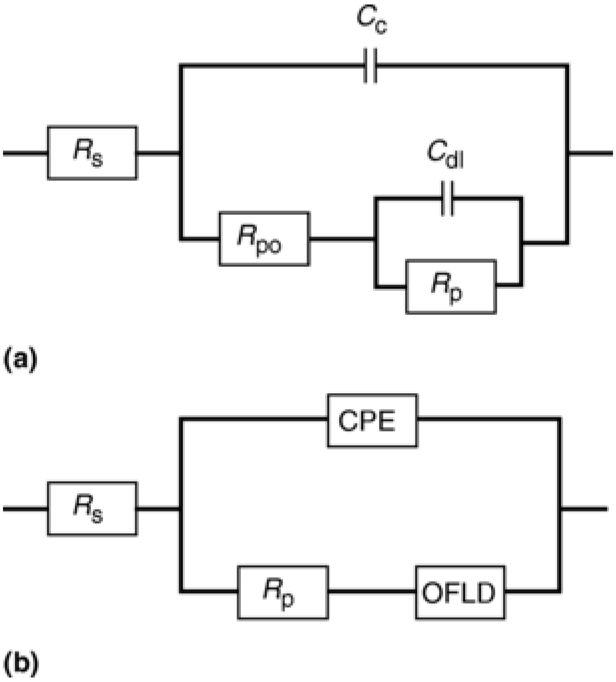

Fig. 8 Equivalent circuits for the analysis of impedance spectra for polymer-coated metals. (a) Coating model. (b) Open-boundary finite-length diffusion (OFLD) model for thick films, constant-phase element (CPE), equivalent resistance (R_s, R_p, R_{po}), equivalent capacitance (C_c, C_{dl})

Deterioration of protective coating properties can be followed by determination of A_d estimated from experimental values of R_{po}, C_{dl}, or R_p (Ref 47). In corrosion monitoring it is often not necessary to obtain a full analysis of all impedance spectra, and a simpler approach such as the break-point frequency (f_b) method can be used. A_d can be estimated from f_b, defined as:

$$f_b = \left(2\pi R_{po} C_c\right)^{-1} = A_d \left(2\pi R^o_{po} C_c\right)^{-1} = \Delta \left(2\pi R^o_{po} C^o_c\right)^{-1} \quad \text{(Eq 8)}$$

where R^o_{po} is the specific pore resistance (ohm · cm^2) and C^o_c is the specific coating capacitance (F/cm^2). The damage function, Δ, is equal to A_d/A_t where A_t is the total exposed area. Figure 9 gives a comparison of Δ values calculated based on Eq 8. The f_b data were converted into Δ values using the results of visual observation according to ASTM D 610 after about 110 days. Excellent agreement was observed between electrochemical and visual data for the remainder of the exposure period.

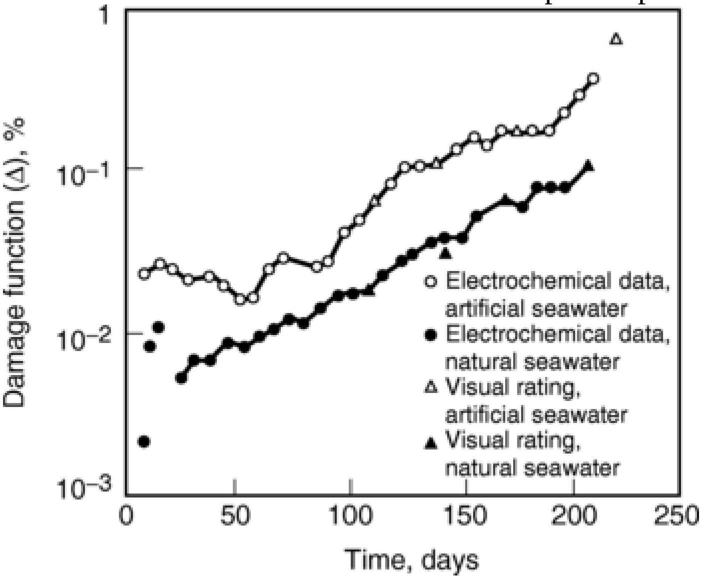

Fig. 9 Time dependence of damage function, Δ, based on electrochemical data and visual data for exposure to natural and artificial seawater

Electrochemical impedance spectroscopy has been used to evaluate genetically engineered bacteria as alternatives to biocides as inhibitors for MIC (Ref 26). Trandem et al. (Ref 27) used reciprocal polarization resistance ($1/R_p$) to compare corrosion rates of steel samples with and without engineered organisms (Fig. 10) tested in standard service water and service water inoculated with bacteria. Their data indicate that the engineered bacteria significantly reduced the corrosion rate of mild steel.

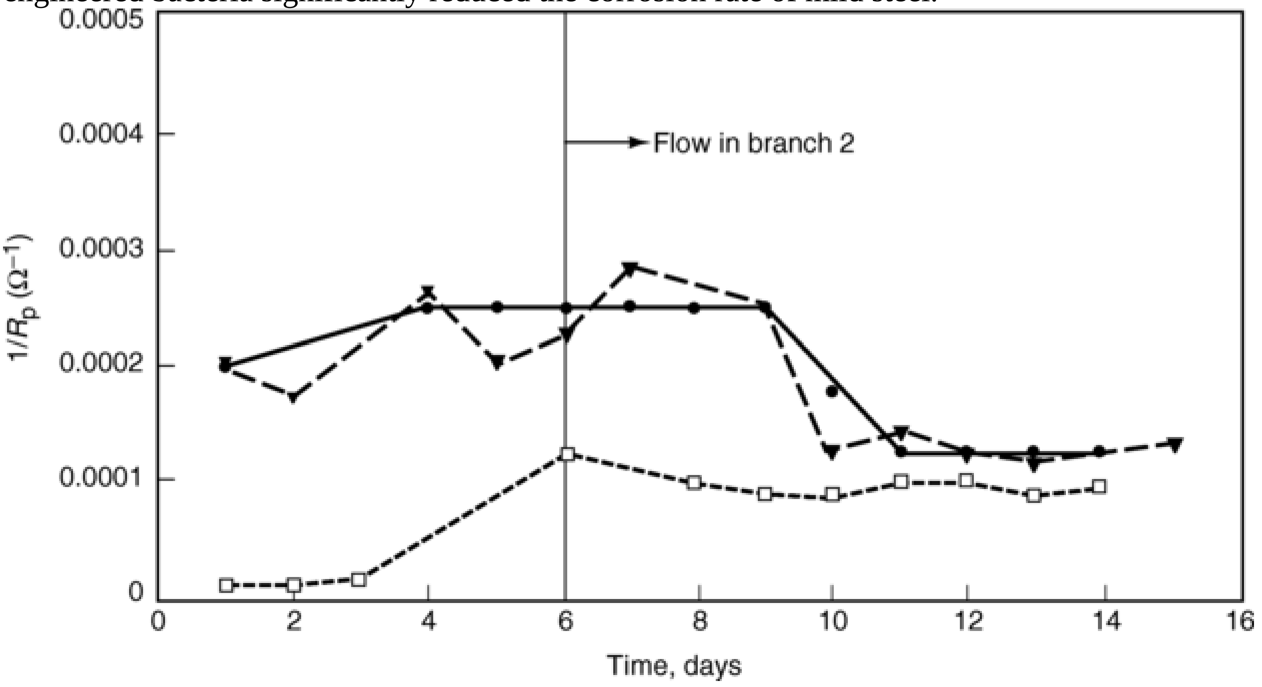

Fig. 10 Comparison of relative corrosion rates ($1/R_P$) for mild steel samples exposed to service water conditions (circle), to engineered bacteria with flow (inverted triangle), and to engineered bacteria without flow (square)

Electrochemical noise (ECN) can be studied as fluctuations of E_{corr}, as fluctuations of potential (E) at an applied current (I) or as the fluctuations of I at an applied E. In laboratory studies, it is possible to measure potential and current fluctuations simultaneously (Ref 49). In this approach, two electrodes of the same materials are coupled through a zero resistance ammeter (ZRA). Current fluctuations are measured using a ZRA, while the potential fluctuations are measured with a high-impedance voltmeter between the two coupled electrodes and a stable reference electrode. The reference electrode can be a SCE, or a third electrode of the same material as the two test electrodes. The latter approach is used commonly in corrosion monitoring. Eden reviewed methods for data collection (Ref 48).

Simultaneous collection of potential and current data allows analysis in time and frequency domains. Bertocci et al. (Ref 50, 51) and Mansfeld et al. (Ref 52) discussed methods of data analysis for this technique in detail. Experimental potential and current fluctuations for polymer-coated steel samples exposed to artificial seawater for 780 days are shown in Fig. 11(a) and (b), respectively, while the corresponding power spectral density (PSD) plots are shown in Fig. 11(c) and (d). The spectral noise plot— also called noise impedance plot—shown in Fig. 11(e) contains the impedance spectrum determined in an independent measurement. Figure 11(e) demonstrates excellent agreement between the two different types of electrochemical measurements.

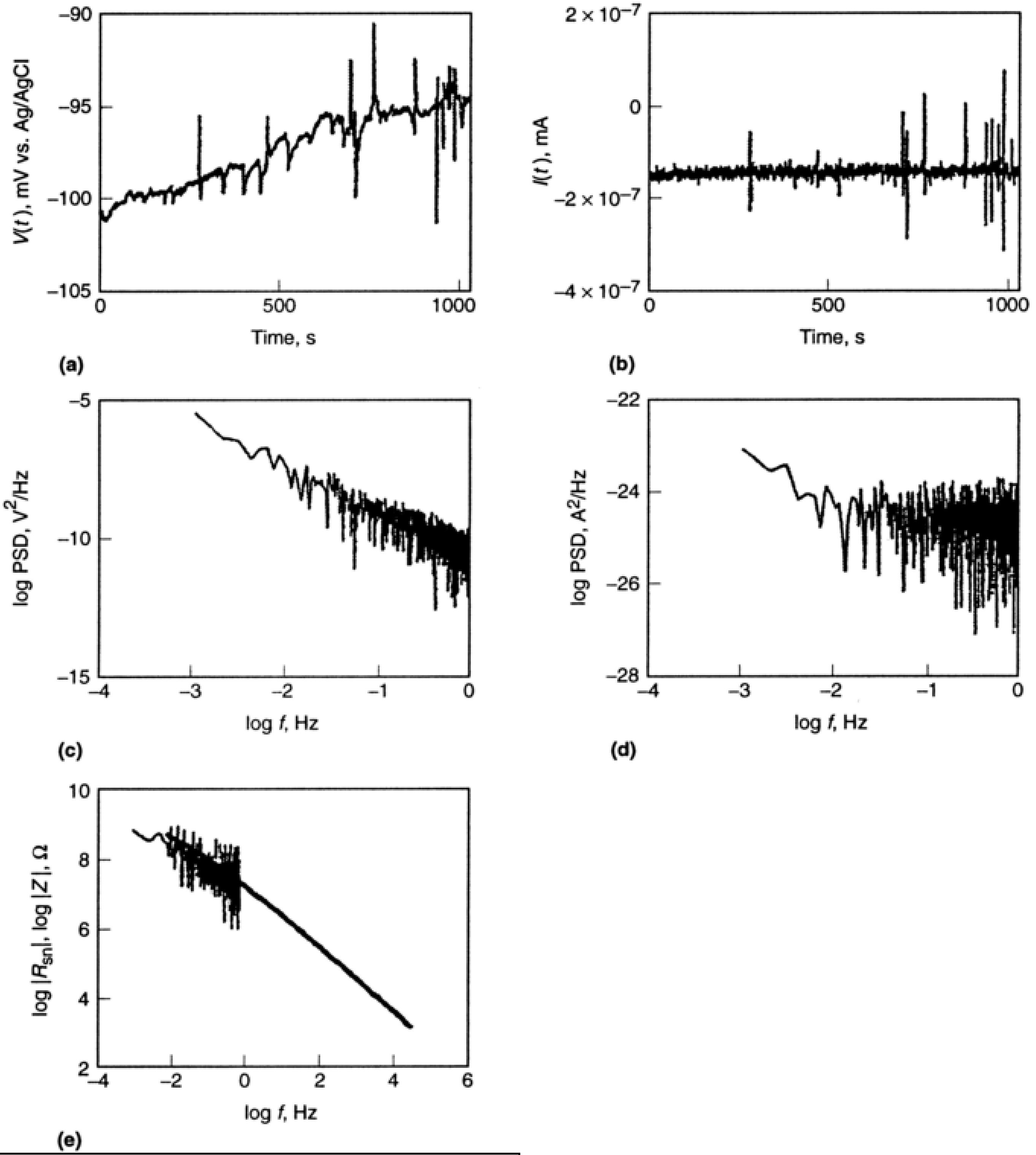

Mean potential (E_{coup}), V	**-0.0976**
Mean current (I_{coup}), A	-1.462×10^{-10}
SDev potential (σV), V	0.00199
SDev current (σ I), A	1.602×10^{-11}
Noise resistance (R_n), Ω	1.243×10^{8}
Spectral noise resistance (R^{o}_{sn}), Ω	4.023×10^{8}
Average of R_{sn} (R_{snave}), Ω	4.012×10^{7}

Fig. 11 Analysis of electrochemical noise data for an epoxy polyamide coating system exposed to artificial seawater for 780 days. (a) Voltage fluctuation with time *V*(*t*). (b) Current fluctuation with time, *I*(*t*). (c) Voltage power spectral density, PSD, versus log of frequency, *f*. (d) Current power spectral

density, PSD versus log of frequency, *f*. (e) Noise impedance plot, log of spectral noise, R_{sn}, and log of impedance, *Z*, versus log of frequency, *f*

Analysis of ECN data in the time domain results in values of the mean potential (E_{coup}) and the mean current (I_{coup}) of coupled electrodes. In addition, standard deviations of potential (σV) and current fluctuations (σI), and the noise resistance $R_n = \sigma V/\sigma I$ are obtained. The spectral noise resistance (R^o_{sn}) is defined as the direct-current (dc) limit of the spectral noise plot (Ref 53). The localization index (LI) = $\sigma I/I_{rms}$, where I_{rms} is the root-mean-square value of the current fluctuations, can also be determined (Ref 48). The suggestion that LI can be used to determine the prevailing corrosion mechanism should be viewed with caution (Ref 52).

It is often assumed that R_n is equal to R_p; however, it has been shown for passive systems such as stainless steel or titanium alloys exposed to neutral media that R_n was several orders of magnitude lower than R_p (Ref 52). Similar results were reported for polymer-coated steel. In fact, no relationship between R_n and any properties of the coated steel sample could be found for the epoxy-polyamide-coated steel sample in Fig. 11 (Ref 49).

The main application of ECN data has been in corrosion monitoring. Mansfeld et al. used ECN for remote on-line monitoring of carbon steel electrodes in a test loop of a surge water tank at a gas storage field (Fig. 12). R_n values were compared to corrosion rates obtained from weight loss of the electrodes used for the ECN measurements. R_n (Fig. 12c) and ΣINT (Fig. 12d) values were prepared for one of 19 three- electrode steel probes. ΣINT was converted to total weight loss (grams) as indicated in Fig. 12(d). The weight loss increased sharply in the first two weeks of exposure of fresh steel probes and then leveled off (Fig. 12d). Fairly good agreement between corrosion rates obtained by ENA (CR_{INT}) and weight loss (MCR) was observed as demonstrated in Fig. 12(e). The solid line in this figure was obtained by regression analysis. Results suggest that R_n can serve as useful measure of corrosion rate for systems exhibiting fairly high corrosion rates.

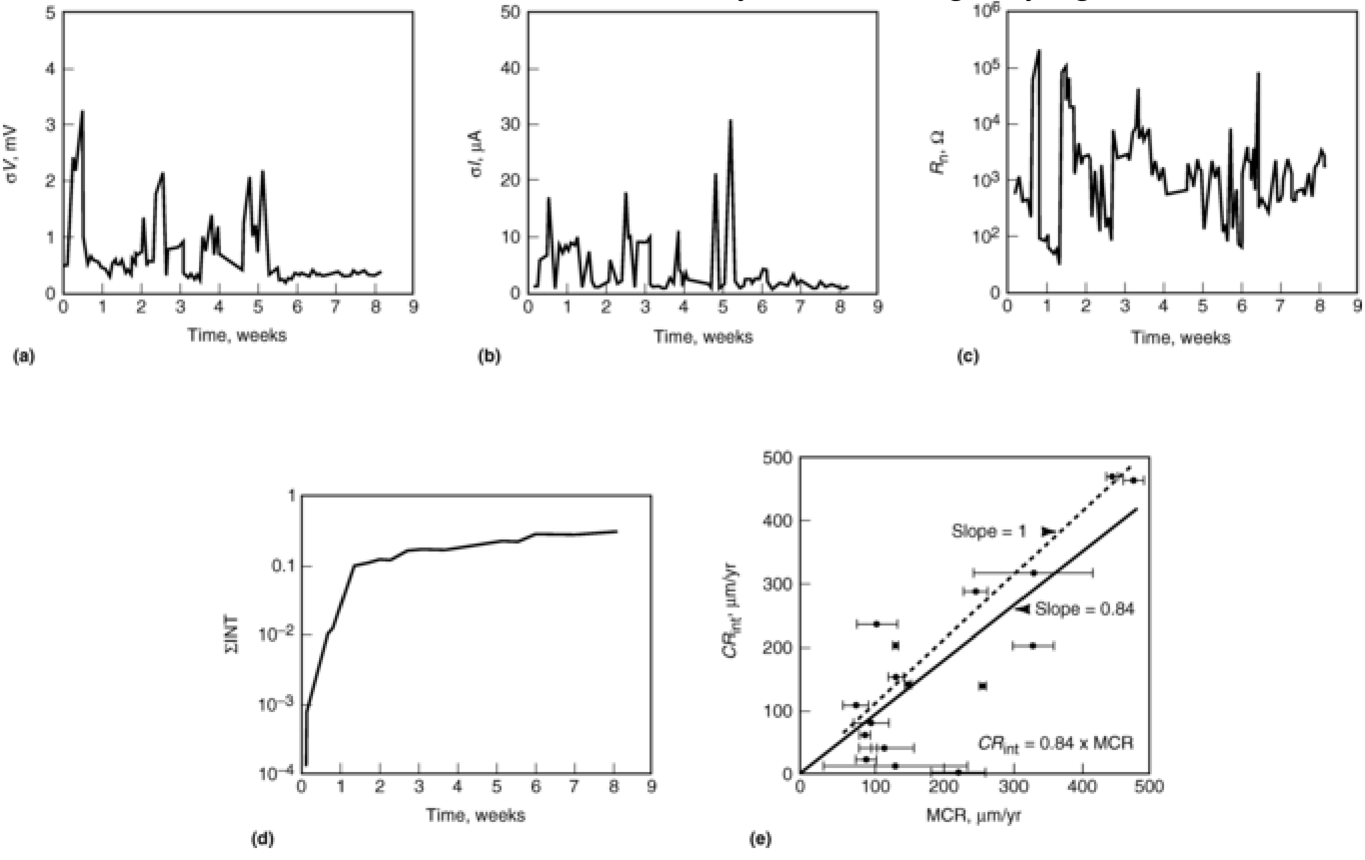

Fig. 12 Representative noise data as monitored for steel electrodes exposed in a test loop at a gas storage field. (a) Standard deviation of potential, σ*V*. (b) Standard deviation of current, σ*I*. (c) Noise resistance, R_n. (d) Cumulative corrosion loss, ΣINT. (e) CR_{INT} values for 19 noise probes compared with mean corrosion rates (MCR) determined from weight loss

Little et al. used EIS and ENA to examine spatial relationships between marine bacteria and localized corrosion on polymer-coated steel (Ref 54). Samples containing intentional defects in polymer coatings were exposed for 30 days in artificial and natural seawater with and without attached zinc coupons providing cathodic protection

to the exposed areas. R_n and R^o_{sn} increased with time for all cathodically protected samples. Electrochemical impedance spectroscopy suggested that increases were due to the formation of calcareous deposits in the defects. Surface analysis showed that very few bacteria were present in the defects of cathodically protected samples, while large amounts of bacteria were found in corrosion layers of the freely corroding samples.

Microsensors. Lee and de Beer (Ref 55) described ideal microsensors as having small tip diameters to prevent distortion of the local environment, small sensor surfaces for optimal spatial resolution, low noise levels, stable signal as well as high selectivity and strength to resist breakage. Lewandowski used microelectrodes to determine the oxygen concentration around a microcolony (Ref 56, 57) (Fig. 13). The microcolony was anoxic in the middle, but oxygen was detected at the bottom demonstrating transport via channels and voids.

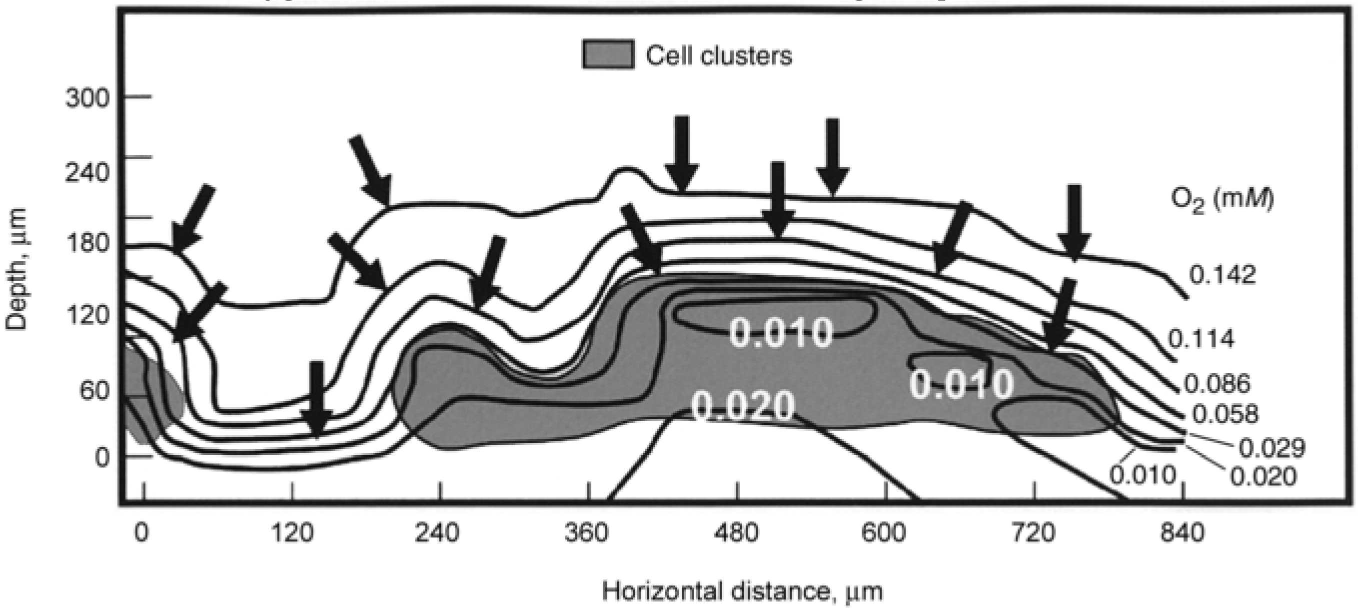

Fig. 13 Oxygen-concentration profiles around a colony of respiring aerobic organisms in an oxygenated environment. Continuous lines are isolines of equal oxygen concentration, while arrows indicate the direction of oxygen fluxes, always perpendicular to the active surface.

Dickinson et al. (Ref 58) used microelectrodes to measure dissolved oxygen and H_2O_2, and local E_{corr} values within biofilm on stainless steel surfaces exposed to river water. Ennoblement was not caused by elevated levels of dissolved oxidants. Measurements at various heights above the substratum and at numerous sites over the coupon surface showed H_2O_2 concentrations to be less than 2 μM. No significant variation in E_{corr} for the stainless steel microelectrode was detected at any site. Dissolved oxygen profiles in the same regions showed saturation levels at all sites.

Scanning vibrating electrode microscopy (SVEM) can provide a sensitive means of locating local anodic and cathodic currents using a vibrating microreference electrode and potential distributions associated with corrosion. Franklin et al. (Ref 2) used autoradiography of bacterial incorporated ^{14}C acetate to locate bacterial metabolic activity and SVEM to locate anodic and cathodic currents on colonized steel surface (Fig. 14). They demonstrated that pit propagation in carbon steel exposed to a phosphate-containing electrolyte required either stagnant conditions or microbial colonization of anodic regions. In sterile, continuously aerated medium, pits initiated and repassivated, while in the absence of aeration, pits initiated and propagated. Pit propagation was observed in continuously aerated medium inoculated with a heterotrophic bacterium. Sites of anodic activity coincided with sites of bacterial activity. Results suggest that bacteria may preferentially attach to the corrosion products formed over pits. Biofilms over anodic sites may create stagnant conditions within corrosion pits that result in pit propagation.

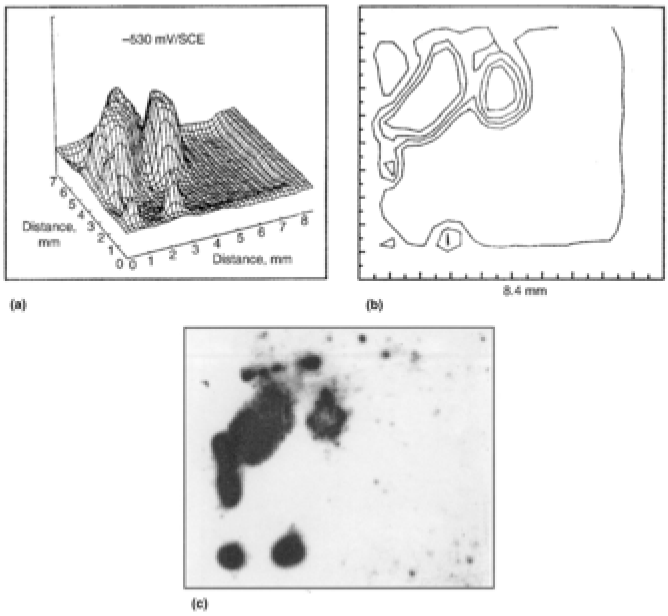

Fig. 14 Bacteria labeled by incubating with ^{14}C-acetate prior to exposure to corroding sample. Bacteria were associated primarily with anodic site. (a) Potential field map. (b) Contour map of potential fields. (c) Autoradiogram

References cited in this section

2. M.J. Franklin, D.C. White, B.J. Little, R.I. Ray, and R.K. Pope, *Biofouling,* Vol 15 (No. 1–3), 1999, p 13–23

15. B.H. Olesen, R. Avci, and Z. Lewandowski, Manganese Dioxide as a Potential Cathodic Reactant in Corrosion of Stainless Steels, *Corros. Sci.,* Vol 42, 2000, p 211–227

16. B.H. Olesen, P.H. Nielsen, and Z. Lewandowski, Effect of Biomineralized Manganese on the Corrosion Behavior of C1008 Mild Steel, *Corrosion,* Vol 56, 2000, p 80–89

26. D. Ornek, T.K. Wood, B.C. Syrett, C.H. Hsu, and F. Mansfeld, "Corrosion Control Using Regenerative Biofilms (CCURB) on Al 2024 and 26000 Brass," Paper No. 1270, Corrosion/2001, NACE International, 2001

27. K. Trandem, Z.S. Farhangrazi, T.K. Wood, P.J. Arps, and J.C. Earthman, "Field Sidestream Investigations of Corrosion Control Using Regenerative Biofilms (CCURB)," Paper No. 1271, Corrosion/2001, NACE International, 2001

28. B.J. Little and P.A. Wagner, Application of Electrochemical Techniques to the Study of MIC, Chapter 5, *Modern Aspects of Electrochemistry,* No. 34, J.O. Bockris et al., Ed., Kluwer Academic/Plenum Publishers, 2001

29. P. Chandrasekaran and S.C. Dexter, "Mechanism of Potential Ennoblement of Passive Metals by Seawater Biofilms," Paper No. 493, Corrosion/93, National Association of Corrosion Engineers, 1993

30. A. Mollica and A. Trevis, *Proc. Fourth Int. Congress on Marine Corrosion and Fouling,* Juan-Les-Pins. (Antibes, France), 1976, p 351–365

31. R. Johnsen and E. Bardal, *Corrosion,* Vol 41, 1985, p 296–302

32. V. Scotto, R. Di Cinto, and G. Marcenaro, *Corros. Sci.,* Vol 25, 1985, p 185–194

33. M. Eashwar, S. Maruthamutu, S. Sathyanarayanan, and K. Balakrishnan, *Proc. 12th Int. Corrosion Congress, 5b* (Houston, TX), National Association of Corrosion Engineers, 1993, p 3708–3716

34. M. Eashwar and S. Maruthamutu, *Biofouling,* Vol 8, 1995, p 203–213

35. P. Linhardt, *Werkst. Korros.,* Vol 45, 1994, p 79–83

36. P. Linhardt, Paper 398, *Proc. Corrosion 2000* (Houston, TX), NACE International, 2000, p 00398.1–00398.7

37. W.H. Dickinson, F. Caccavo, Jr., and Z. Lewandowski, *Corros. Sci.,* Vol 38, 1996, p 1407–1422

38. W.H. Dickinson and Z. Lewandowski, *Biofouling,* Vol 10, 1996, p 79–93

39. H. Von Rege, W. Sand, S. Bixter, H. Deckermann, and M. Renner, Paper 346, Corrosion 2000 (Houston, TX), NACE International, 2000, p 00346.1–00346.7

40. F. Mansfeld, The Polarization Resistance Technique for Measuring Corrosion Currents, *Advances in Corrosion Science and Technology,* Vol 6, M.G. Fontana and R.W. Staehle, Ed., Plenum Press, 1976, p 163–262

41. J.R. Scully, *Corrosion,* Vol 56, 2000, p 199–218

42. H. Shih and F. Mansfeld, *Computer Modeling in Corrosion,* STP 1154, R.S. Munn, Ed., American Society for Testing and Materials, 1992, p 174–185

43. Zs. Keresztes, J. Telegdi, J. Beczner, and E. Kalman, *Electrochim. Acta,* Vol 43, 1998, p 77–85

44. F. Mansfeld, H. Shih, A. Postyn, J. Devinny, R. Islander, and C.L. Chen, *Corrosion,* Vol 47, 1991, p 369–376

45. F. Mansfeld, C.C. Lee, L.T. Han, G. Zhang, B.J. Little, P. Wagner, R. Ray, and J. Jones- Meehan, "The Impact of Microbiologically Influenced Corrosion on Protective Polymer Coatings," Final Report, Contract No. N00014-94-1-0026, 1998

46. F. Mansfeld, L.T. Han, C.C. Lee, and G. Zhang, *Electrochim. Acta,* Vol 43, 1998, p 2933–2945

47. F. Mansfeld, *J. Appl. Electrochem.,* Vol 25, 1995, p 187–202

48. D.A. Eden, "Electrochemical Noise—The First Two Octaves," Paper No. 386, Corrosion/98, NACE International, 1998

49. F. Mansfeld, L.T. Han, C.C. Lee, C. Chen, G. Zhang, and H. Xiao, *Corros. Sci.,* Vol 39, 1997, p 255–279

50. U. Bertocci, C. Gabrielli, F. Huet, and M. Keddam, *J. Electrochem. Soc.,* Vol 144, 1997, p 31–37

51. U. Bertocci, C. Gabrielli, F. Huet, M. Keddam, and P. Rousseau, *J. Electrochem. Soc.,* Vol 144, 1997, p 37–43

52. F. Mansfeld, Z. Sun, E. Speckert, and C.H. Hsu, Paper No. 418, Corrosion/2000, NACE International, 2000

53. F. Mansfeld, C.C. Lee, C. Chen, and H. Xiao, *Corros. Sci.,* Vol 38, 1996, p 497–513

54. B.J. Little, R.I. Ray, P.A. Wagner, J. Jones- Meehan, C.C. Lee, and F. Mansfeld, *Biofouling,* Vol 13, 1999, p 301–321

55. W. Lee and D. de Beer, *Biofouling,* Vol 8, 1995, p 273–280

56. Z. Lewandowski, W.C. Lee, W.G. Characklis, and B. Little, Paper 93, Corrosion/88, National Association of Corrosion Engineers, 1988

57. Z. Lewandowski, Paper No. 400, Corrosion/ 2000, NACE International, 2000

58. W.H. Dickinson, Z. Lewandowski, and R.D. Geer, *Corrosion,* Vol 52, 1996, p 910–920

B.J. Little, F.B. Mansfeld, P.J. Arps and J.C. Earthman, Microbiologically Influenced Corrosion Testing *Corrosion: Fundamentals, Testing, and Protection*, Vol 13A, *ASM Handbook*, ASM International, 2003, p 478–486

Microbiologically Influenced Corrosion Testing

B.J. Little, Naval Research Laboratory; F.B. Mansfeld, University of Southern California; P.J. Arps and J.C. Earthman, University of California, Irvine

---

References

1. H.A. Videla, *Manual of Biocorrosion,* CRC Press, 1996

2. M.J. Franklin, D.C. White, B.J. Little, R.I. Ray, and R.K. Pope, *Biofouling,* Vol 15 (No. 1–3), 1999, p 13–23

3. B.J. Little and P.A. Wagner, The Interrelationship between Marine Biofouling, Cathodic Protection and Microbiologically Influenced Corrosion, *Mater. Sci. Forum,* Vol 192–194, pt. 1; *Electrochemical Methods in Corrosion Research V,* Fifth International Symposium, (Sesimbra, Portugal), 5–8 Sept 1994, Trans Tech Publications, 1995, p 433–446

4. Y.H. An and R.J. Friedman, Ed., *Principles, Methods, and Applications, Handbook of Bacterial Adhesion,* Humana Press, 2000

5. J.D. Bryers, Ed., *Biofilms II: Process Analysis and Applications,* John Wiley & Sons, 2000

6. G.A. O'Toole and R. Kolter, Initiation of Biofilm Formation in *Pseudomonas fluorescens,* WCS365 Proceeds via Multiple, Convergent Signalling Pathways: A Genetic Analysis, *Mol. Microbiol.,* Vol 28, 1998, p 449–461

7. J.W. Costerton, Z. Lewandowski, D.E. Calwell, D.R. Korber, and H.M. Lappin-Scott, Microbial Biofilms, *Ann. Rev. Microbiol.,* Vol 49, 1995, p 711–745

8. R. Kolter and R. Losick, One for All and All for One, *Science,* Vol 280, 1998, p 226–227

9. J.R. Lawrence, D.R. Korber, B.D. Hoyle, J.W. Costerton, and D.E. Caldwell, Optical Sectioning of Microbial Biofilms, *J. Bacteriol.,* Vol 173, 1991, p 6558–6567

10. D. DeBeer, P. Stoodley, and Z. Lewandowski, Liquid Flow in Heterogeneous Biofilms, *Biotech. Bioeng.,* Vol 44, 1994, p 636–641

11. E.J. Wentland, P.S. Stewart, C.-T. Huang, and G.A. McFeters, Spatial Variations in Growth Rate within *Klebsiella pneumoniae* Colonies and Biofilm, *Biotechnol. Prog.,* Vol 12, 1996, p 316–321

12. D.G. Davies, M.R. Parsek, J.P. Pearson, B.H. Iglewski, J.W. Costerton, and E.P. Greenberg, The Involvement of Cell-to-Cell Signals in the Development of a Bacterial Biofilm, *Science,* Vol 280, 1998, p 295–298

13. G.M. Dunny and S.C. Winans, Ed., *Cell- Cell Signaling in Bacteria,* American Society of Microbiology, 1999

14. A. Ohashi, T. Koyama, K. Syutsubo, and H. Harada, A Novel Method for Evaluation of Biofilm Tensile Strength Resisting Erosion, *Water Sci. Technol.,* Vol 39 (No. 7), 1999, p 261–268

15. B.H. Olesen, R. Avci, and Z. Lewandowski, Manganese Dioxide as a Potential Cathodic Reactant in Corrosion of Stainless Steels, *Corros. Sci.,* Vol 42, 2000, p 211–227

16. B.H. Olesen, P.H. Nielsen, and Z. Lewandowski, Effect of Biomineralized Manganese on the Corrosion Behavior of C1008 Mild Steel, *Corrosion,* Vol 56, 2000, p 80–89

17. B.J. Little, P.A. Wagner, K.R. Hart, R.I. Ray, D.M. Lavoie, K. Nealson, and C. Aguilar, "The Role of Metal Reducing Bacteria in Microbiologically Influenced Corrosion," Paper No. 215, Corrosion/97, NACE International, 1997

18. R.J. Soracco, D.H. Pope, J.M. Eggers, and T.N. Effinger, "Microbiologically Influenced Corrosion Investigations in Electric Power Generating Stations," Paper No. 83, Corrosion/88, National Association of Corrosion Engineers, 1988

19. B. Little, P. Wagner, and D. Duquette, Microbiologically Induced Increase in Corrosion Current Density of Stainless Steel under Cathodic Protection, *Corrosion,* Vol 44, 1988, p 270

20. G.G. Geesey and M.W. Mittelman, "The Role of High-Affinity, Metal-Binding Exopolymers of Adherent Bacteria in Microbial-Enhanced Corrosion," Paper No. 85, Corrosion/85, National Association of Corrosion Engineers, 1985

21. G.G. Geesey, M.W. Mittelman, T. Iwaoka, and P.R. Griffiths, Role of Bacterial Exopolymers in the Deterioration of Metallic Copper Surfaces, *Mater. Perform.,* Vol 25, 1986, p 37–40

22. B.W. Samuels, K. Sotoudeh, and R.T. Foley, *Corrosion,* Vol 37, 1981, p 92–97

23. G. Hernandez, V. Kucera, D. Thierry, A. Pedersen, and M. Hermansson, *Corrosion,* Vol 50, 1994, p 603–608

24. H.A. Videla, *Biofouling and Biocorrosion in Industrial Water Systems,* G.G. Geesey, Z. Lewandowski, and H.C. Flemmings, Ed., Lewis Publishers, 1994, p 231–241

25. A. Jayaraman, J.C. Earthman, and T.K. Wood, *Appl. Microbiol. Biotechnol.,* Vol 47, 1997, p 62–68

26. D. Ornek, T.K. Wood, B.C. Syrett, C.H. Hsu, and F. Mansfeld, "Corrosion Control Using Regenerative Biofilms (CCURB) on Al 2024 and 26000 Brass," Paper No. 1270, Corrosion/2001, NACE International, 2001

27. K. Trandem, Z.S. Farhangrazi, T.K. Wood, P.J. Arps, and J.C. Earthman, "Field Sidestream Investigations of Corrosion Control Using Regenerative Biofilms (CCURB)," Paper No. 1271, Corrosion/2001, NACE International, 2001

28. B.J. Little and P.A. Wagner, Application of Electrochemical Techniques to the Study of MIC, Chapter 5, *Modern Aspects of Electrochemistry,* No. 34, J.O. Bockris et al., Ed., Kluwer Academic/Plenum Publishers, 2001

29. P. Chandrasekaran and S.C. Dexter, "Mechanism of Potential Ennoblement of Passive Metals by Seawater Biofilms," Paper No. 493, Corrosion/93, National Association of Corrosion Engineers, 1993

30. A. Mollica and A. Trevis, *Proc. Fourth Int. Congress on Marine Corrosion and Fouling,* Juan-Les-Pins. (Antibes, France), 1976, p 351–365

31. R. Johnsen and E. Bardal, *Corrosion,* Vol 41, 1985, p 296–302

32. V. Scotto, R. Di Cinto, and G. Marcenaro, *Corros. Sci.,* Vol 25, 1985, p 185–194

33. M. Eashwar, S. Maruthamutu, S. Sathyanarayanan, and K. Balakrishnan, *Proc. 12th Int. Corrosion Congress, 5b* (Houston, TX), National Association of Corrosion Engineers, 1993, p 3708–3716

34. M. Eashwar and S. Maruthamutu, *Biofouling,* Vol 8, 1995, p 203–213

35. P. Linhardt, *Werkst. Korros.,* Vol 45, 1994, p 79–83

36. P. Linhardt, Paper 398, *Proc. Corrosion 2000* (Houston, TX), NACE International, 2000, p 00398.1–00398.7

37. W.H. Dickinson, F. Caccavo, Jr., and Z. Lewandowski, *Corros. Sci.,* Vol 38, 1996, p 1407–1422

38. W.H. Dickinson and Z. Lewandowski, *Biofouling,* Vol 10, 1996, p 79–93

39. H. Von Rege, W. Sand, S. Bixter, H. Deckermann, and M. Renner, Paper 346, Corrosion 2000 (Houston, TX), NACE International, 2000, p 00346.1–00346.7

40. F. Mansfeld, The Polarization Resistance Technique for Measuring Corrosion Currents, *Advances in Corrosion Science and Technology,* Vol 6, M.G. Fontana and R.W. Staehle, Ed., Plenum Press, 1976, p 163–262

41. J.R. Scully, *Corrosion,* Vol 56, 2000, p 199–218

42. H. Shih and F. Mansfeld, *Computer Modeling in Corrosion,* STP 1154, R.S. Munn, Ed., American Society for Testing and Materials, 1992, p 174–185

43. Zs. Keresztes, J. Telegdi, J. Beczner, and E. Kalman, *Electrochim. Acta,* Vol 43, 1998, p 77–85

44. F. Mansfeld, H. Shih, A. Postyn, J. Devinny, R. Islander, and C.L. Chen, *Corrosion,* Vol 47, 1991, p 369–376

45. F. Mansfeld, C.C. Lee, L.T. Han, G. Zhang, B.J. Little, P. Wagner, R. Ray, and J. Jones- Meehan, "The Impact of Microbiologically Influenced Corrosion on Protective Polymer Coatings," Final Report, Contract No. N00014-94-1-0026, 1998

46. F. Mansfeld, L.T. Han, C.C. Lee, and G. Zhang, *Electrochim. Acta,* Vol 43, 1998, p 2933–2945

47. F. Mansfeld, *J. Appl. Electrochem.,* Vol 25, 1995, p 187–202

48. D.A. Eden, "Electrochemical Noise—The First Two Octaves," Paper No. 386, Corrosion/98, NACE International, 1998

49. F. Mansfeld, L.T. Han, C.C. Lee, C. Chen, G. Zhang, and H. Xiao, *Corros. Sci.,* Vol 39, 1997, p 255–279

50. U. Bertocci, C. Gabrielli, F. Huet, and M. Keddam, *J. Electrochem. Soc.,* Vol 144, 1997, p 31–37

51. U. Bertocci, C. Gabrielli, F. Huet, M. Keddam, and P. Rousseau, *J. Electrochem. Soc.,* Vol 144, 1997, p 37–43

52. F. Mansfeld, Z. Sun, E. Speckert, and C.H. Hsu, Paper No. 418, Corrosion/2000, NACE International, 2000

53. F. Mansfeld, C.C. Lee, C. Chen, and H. Xiao, *Corros. Sci.,* Vol 38, 1996, p 497–513

54. B.J. Little, R.I. Ray, P.A. Wagner, J. Jones- Meehan, C.C. Lee, and F. Mansfeld, *Biofouling,* Vol 13, 1999, p 301–321

55. W. Lee and D. de Beer, *Biofouling,* Vol 8, 1995, p 273–280

56. Z. Lewandowski, W.C. Lee, W.G. Characklis, and B. Little, Paper 93, Corrosion/88, National Association of Corrosion Engineers, 1988

57. Z. Lewandowski, Paper No. 400, Corrosion/ 2000, NACE International, 2000

58. W.H. Dickinson, Z. Lewandowski, and R.D. Geer, *Corrosion,* Vol 52, 1996, p 910–920

S.D. Cramer and S.A. Matthes, Simulated Service Testing in the Atmosphere, *Corrosion: Fundamentals, Testing, and Protection*, Vol 13A, *ASM Handbook*, ASM International, 2003, p 487–494

Simulated Service Testing in the Atmosphere

Stephen D. Cramer and Steven A. Matthes, Albany Research Center, U.S. Department of Energy

---

Introduction

SIMULATED SERVICE TESTING is the most reliable predictor of corrosion behavior short of in-plant tests and actual service experience. Simulated service testing includes exposures of structural components and test specimens in outdoor environments that are representative of many general service situations. These so-called natural environments include exposures to the atmosphere, waters, and soil. They include the full spectrum of chemical, biological, meteorological, geological, and physical influences. Test materials are subjected to the cyclic effects of the weather, the complex chemistry of the atmosphere, the biochemical responses of water and soil, and the dynamic effects of the atmosphere and waters that cannot be realistically duplicated in the laboratory. This type of testing is important for objectives such as materials selection, predicting the probable service life of a product or structure, evaluating new commercial alloys and processes, and calibrating laboratory corrosion tests.

S.D. Cramer and S.A. Matthes, Simulated Service Testing in the Atmosphere, *Corrosion: Fundamentals, Testing, and Protection*, Vol 13A, *ASM Handbook*, ASM International, 2003, p 487–494

Simulated Service Testing in the Atmosphere

Stephen D. Cramer and Steven A. Matthes, Albany Research Center, U.S. Department of Energy

Atmospheric Corrosion

Corrosion or degradation of materials in the atmosphere occurs as the result of natural forces augmented by man-made (or anthropogenic) impacts. The degree of degradation varies for different materials and is influenced by a number of environmental factors. Many of these factors are natural in origin, such as meteorology (or climate), air chemistry, and seasonal and diurnal cycles, but some have man-made origins as well as natural origins. These include sulfur oxides, nitrogen oxides, hydrochloric acid, carbon dioxide, hydrocarbons, and particulate matter produced as fossil fuel and other organic material combustion products. They combine in a complex mix of chemical and physical processes that deliver reactive chemical species to exposed surfaces in wet and dry deposition processes that affect the corrosion or degradation of these surfaces (Ref 1).

While most atmospheric-corrosion studies focus on the growth of a protective corrosion product on metal surfaces, there is increasing interest in metal-environment interactions (weathering) related to wet and dry deposition that facilitate the loss of protective corrosion product and therefore affect the long-term performance or service life of metals (Ref 1, 2, 3, 4, 5, 6, 7, 8, 9, 10, 11, 12, 13, 14). These interactions lead to the formation of nonprotective, soluble minerals within the corrosion product layer that, in outdoor exposures, are typically removed in precipitation runoff (Ref 2, 3, 4, 5, 6, 7, 8, 9, 10, 11, 12, 13, 14, 15, 16, 17, 18, 19, 20). These interactions can accelerate atmospheric-corrosion processes and, by virtue of the removal of metal ions in precipitation runoff, can affect soil and water quality (Ref 14, 15, 16, 17, 18, 19, 20). Of particular interest in this regard is acid deposition or acid rain, which can accelerate corrosion damage of some widely used structural materials, including galvanized steel, zinc, copper, limestone, and marble (Ref 1, 2, 3, 4, 5, 6, 7, 8, 9, 10, 11, 12, 13, 14).

Over the years, considerable attention has been devoted to the weathering of building materials. Observations of materials corrosion performance in the atmosphere have ranged from those made on existing structures to carefully designed atmospheric exposure programs. These data represent an excellent base for understanding the behavior of materials in the atmosphere. However, much of the existing data suffer from two primary difficulties. First, many testing programs have been limited to characterizing a material for a specific application. This has resulted in variations in experimental designs, such that the results of one testing program cannot be compared unambiguously to the results of others. Second, and more seriously, test programs have generally been conducted without comprehensive environmental monitoring and characterization. This prevents the establishment of cause-and-effect relationships for atmospheric- corrosion phenomena and has precluded the establishment of a baseline understanding of the atmospheric environmental characteristics for which a considerable materials degradation database exists. The monitoring of relevant environmental parameters in association with controlled atmospheric exposures of materials is necessary to assess the impact of atmospheric variables on materials.

References cited in this section

1. Effects of Acidic Deposition on Materials, Report 19, *Terrestrial, Materials, Health and Visibility Effects,* Vol III, *Acidic Deposition: State of Science and Technology,* U.S. National Acid Precipitation Assessment Program, Washington, D.C., p. 19–1 to 19–280, 1991

2. W. He, I. Odenvall Wallinder, and C. Leygraf, A Comparison Between Corrosion Rates and Runoff Rates from New and Aged Copper and Zinc as Roofing Materials, *Water, Air Soil Pollut. Focus,* Vol 1, 2001, p 67–82

3. I. Odnevall Wallinder, P. Verbiest, W. He, and C. Leygraf, The Influence of Patina Age and Pollutant Levels on the Runoff Rate of Zinc from Roofing Materials, *Corros. Sci.,* Vol 40 (No. 11), 1998, p 1977–1982

4. I. Odnevall Wallinder, P. Verbiest, W. He, C. Leygraf, Effects of Exposure Direction and Inclination on the Runoff Rates of Zinc and Copper Roofs, *Corros. Sci.,* Vol 42, 2000 p 1471–1487

5. W. He, I. Odnevall Wallinder, and C. Leygraf, A Laboratory Study of Copper and Zinc Runoff during First Flush and Steady- State Conditions, *Corros. Sci.,* Vol 43, 2001, p 127–146

6. W. He, I. Odnevall Wallinder, and C. Leygraf, Runoff Rates of Zinc—A Four-Year Field and Laboratory Study, *Outdoor Atmospheric Corrosion,* STP 1421, H.E. Townsend, Ed., ASTM International, 2002, p 216–229

7. X. Zhang, W. He, I. Odnevall Wallinder, J. Pan, and C. Leygraf, Determination of Instantaneous Corrosion Rates and Runoff Rates of Copper from Naturally Patinated Copper during Continuous Rain Events, *Corros. Sci.,* Vol 44, 2002, p 2131–2151

8. I. Odnevall Wallinder and C. Leygraf, A Study of Copper Runoff in an Urban Atmosphere, *Corros. Sci.,* Vol 39 (No. 12), 1997, p 2039–2052

9. S.D. Cramer and L.G. McDonald, Atmospheric Factors Affecting the Corrosion of Zinc, Galvanized Steel, and Copper, *Corrosion Testing and Evaluation,* STP 1000, R. Baboian and S.W. Dean, Ed., American Society for Testing and Materials, 1990, p 208–224

10. J.W. Spence, F.H Haynie, F.W. Lipfert, S.D. Cramer, and L.G. McDonald, Atmospheric Corrosion Model for Galvanized Steel Structures, *Corrosion,* Vol 48 (No. 12), 1992, p 1009–1019

11. S.D. Cramer, L.G. McDonald, and J.W. Spence, Effects of Acidic Deposition on the Corrosion of Zinc and Copper, *Proceedings of the 12th International Corrosion Congress,* Vol 2, NACE International, 1993, p 722–733

12. S.D. Cramer, S.A. Matthes, G.R. Holcomb, B.S. Covino, Jr., and S.J. Bullard, “Precipitation Runoff and Atmospheric Corrosion,” Paper 00452, Corrosion/2000, NACE International, 2000

13. S.D. Cramer, S.A. Matthes, B.S. Covino, Jr., S.J. Bullard, and G.R. Holcomb, Environmental Factors Affecting the Atmospheric Corrosion of Copper, *Outdoor Atmospheric Corrosion,* STP 1421, H.E. Townsend, Ed., American Society for Testing and Materials, 2002, p 245–264

14. S.A. Matthes, S.D. Cramer, B.S. Covino, Jr., S.J. Bullard, and G.R. Holcomb, Precipitation Runoff from Lead, *Outdoor Atmospheric Corrosion,* STP 1421, H.E. Townsend, Ed., American Society for Testing and Materials, 2002, p 265–274

15. S.A. Matthes, S.D. Cramer, S.J. Bullard, B.S. Covino, Jr., and G.R. Holcomb, “Atmospheric Corrosion and Precipitation Runoff from Zinc and Zinc Alloy Surfaces,” Paper 03598, Corrosion/2003, 17–20 March 2003 (San Diego, CA), NACE International, 2003

16. H.T. Michels, B. Boulanger, and N.P. Nikolaidis, “Copper Roof Stormwater Runoff—Corrosion and the Environment,” Paper 02225, Corrosion/2002, NACE International, 2002

17. H.T. Michels, B. Boulanger, and N.P. Nikolaidis, Environmental Impact of Stormwater Runoff from a Copper Roof, *Mater. Perform.,* Vol 42 (No. 2) Feb 2003, p 70–74

18. M.C. Gromaire-Mertz, S. Garnaud, A. Gonzales, and G. Chebbo, Characterization of Urban Runoff Pollution in Paris, *Wat. Sci. Technol.,* Vol 39 (No. 2), 1999, p 1–8

19. T.S. Barron, "Architectural Uses of Copper—An Evaluation of Stormwater Pollution Loads and Best Management Practices," Palo Alto Regional Water Quality Control Plant, Palo Alto, CA, 2000

20. I. Odnevall Wallinder, C. Leygraf, C. Karlen, D. Heijerick, and C.R. Janssen, Atmospheric Corrosion of Zinc-Based Materials: Runoff Rates, Chemical Speciation and Ecotoxicity, *Corros. Sci.,* Vol 43, 2001, p 809–816

S.D. Cramer and S.A. Matthes, Simulated Service Testing in the Atmosphere, *Corrosion: Fundamentals, Testing, and Protection*, Vol 13A, *ASM Handbook*, ASM International, 2003, p 487–494

Simulated Service Testing in the Atmosphere

Stephen D. Cramer and Steven A. Matthes, Albany Research Center, U.S. Department of Energy

Types of Atmospheres

Before materials or materials data can be evaluated, the important atmospheric variables at the test site must be identified and then recorded during the exposure period. The variability of atmospheric-corrosion severity has been well documented (Ref 21, 22, 23). One way to address this is to characterize atmospheric exposures as occurring in rural, urban, industrial, or marine environments, or a combination of these. These designations reflect the level of chemical pollutants that are typical in the test environment. Table 1 lists typical rates for the deposition of SO_x and Cl^- on metal surfaces exposed to these environments (Ref 24).

Table 1 Typical activity ranges of SO_x and Cl^- measured in various atmospheres

These are average activity ranges measured over a 20–25 month period.

Type of atmosphere	mg SO_x/dm^2/d	mg Cl^-/m^2/d
Industrial	0.5–2	nil
Urban	0.5–4	nil
Rural (semi)	nil–2	nil
Marine	nil–0.5	25–150

Source: Ref 24

A rural atmosphere is normally classified as one that does not contain significant chemical pollutants but does contain organic and inorganic dusts. Its principal corrodents are moisture, oxygen, and carbon dioxide. Arid or tropical atmospheres are special cases of the rural environment because of their extremely low or high relative humidities (Ref 25). The rural atmosphere is generally the least corrosive of the atmospheric exposures encountered.

An urban atmosphere is similar to the rural environment in that it is thought to be away from sources of industrial pollution. Materials exposed to an urban atmosphere are subjected to the normal precipitation patterns and typical urban contaminants of SO_x and NO_x emitted by motor vehicles and the combustion of home fuels. However, pollution levels in urban atmospheres may, in fact, be similar to those in industrial atmospheres because of long-range transport of pollutants (Ref 1).

An industrial atmosphere is typically identified with heavy industrial manufacturing facilities. These atmospheres can contain significant concentrations of sulfur oxides, nitrogen oxides, chlorides, phosphates,

particulates, and other industrial emissions. These emissions can combine with precipitation or dew to form fairly corrosive solutions on metal surfaces.

A marine atmosphere is laden with fine particles of sea salt carried by the winds and deposited on materials. The marine atmosphere is usually one of the more corrosive atmospheric environments. It has been shown that the amount of salt (chlorides) in the marine environment decreases with increasing distance inland from the ocean and is greatly influenced by wind speed and direction (Ref 26).

Because long-range transport of pollutants can blur distinctions in atmospheric corrosivity (aggressivity) based on regional geography (rural, urban, industrial, marine), distinctions based on atmospheric chemistry may be more useful for predicting corrosion performance. The International Organization for Standardization (ISO) characterizes environments in ISO 9223 based on the level of pollutants in the environment (Ref 27, 28, 29). The pollutants measured are sulfur dioxide and chloride. Their concentration is determined by their deposition rate on standard surfaces. Deposition rates define four ranges of pollutant concentration, providing sixteen levels of corrosivity with which to characterize the performance of metals in the atmosphere. Field exposures of standard metals (carbon steel, zinc, copper, and aluminum) have been conducted to, in effect, calibrate the level of corrosion performance expected by exposure in each corrosivity category. Corrosion damage to the standard metals is ranked in five levels. A key factor determining corrosion performance in the corrosivity categories is the presence of moisture, characterized by the time of wetness (TOW).

Continuous air monitoring goes beyond discrete corrosivity categories to define atmospheric chemistry in terms of instantaneous or average measures of pollutant concentrations (sulfur and nitrogen oxides, hydrochloric acid, hydrocarbons, carbon dioxide, particulates) and environmental variables (temperature, wind speed and direction, relative humidity, precipitation rate and chemistry, solar radiation) (Ref 1, 9, 10, 11, 12, 13). While monitoring these variables can be expensive, it is often possible to co-locate atmospheric exposure test panels at or near local or regional monitoring sites that provide some or all of the needed information. This greatly enhances the usefulness of the resulting corrosion data for interpreting environmental effects and for modeling corrosion performance.

Indoor environments differ substantially from outdoor environments, with, in most cases, substantially lower levels of moisture, less dramatic variations in relative humidity and temperature, slower air movement, and complex air chemistry affected by a wide variety of sources and sinks for chemical species that can influence indoor corrosion (Ref 30). Indoor corrosion rates are typically lower than those outdoors and do not affect the structural integrity of most materials. They can, however, influence the performance of electronic devices and alter the surface of cultural artifacts.

References cited in this section

1. Effects of Acidic Deposition on Materials, Report 19, *Terrestrial, Materials, Health and Visibility Effects,* Vol III, *Acidic Deposition: State of Science and Technology,* U.S. National Acid Precipitation Assessment Program, Washington, D.C., p. 19–1 to 19–280, 1991

9. S.D. Cramer and L.G. McDonald, Atmospheric Factors Affecting the Corrosion of Zinc, Galvanized Steel, and Copper, *Corrosion Testing and Evaluation,* STP 1000, R. Baboian and S.W. Dean, Ed., American Society for Testing and Materials, 1990, p 208–224

10. J.W. Spence, F.H Haynie, F.W. Lipfert, S.D. Cramer, and L.G. McDonald, Atmospheric Corrosion Model for Galvanized Steel Structures, *Corrosion,* Vol 48 (No. 12), 1992, p 1009–1019

11. S.D. Cramer, L.G. McDonald, and J.W. Spence, Effects of Acidic Deposition on the Corrosion of Zinc and Copper, *Proceedings of the 12th International Corrosion Congress,* Vol 2, NACE International, 1993, p 722–733

12. S.D. Cramer, S.A. Matthes, G.R. Holcomb, B.S. Covino, Jr., and S.J. Bullard, “Precipitation Runoff and Atmospheric Corrosion,” Paper 00452, Corrosion/2000, NACE International, 2000

13. S.D. Cramer, S.A. Matthes, B.S. Covino, Jr., S.J. Bullard, and G.R. Holcomb, Environmental Factors Affecting the Atmospheric Corrosion of Copper, *Outdoor Atmospheric Corrosion,* STP 1421, H.E. Townsend, Ed., American Society for Testing and Materials, 2002, p 245–264

21. "Notice of Proposed Standard for Sulfur Oxide, Particulate Matter, Carbon Monoxide, Photochemical Oxidants, Hydrocarbons, and Nitrogen Oxides," 42 CFR, Part 410, Federal Register 36, Environmental Protection Agency, 1971, p 1502

22. F. Mansfield, "Regional Air Pollution Study Effects of Airborne Sulfur Pollutants on Materials," EPA 600/4-80-007, Environmental Protection Agency, Jan 1980

23. F.H. Haynie and J.B. Upham, Effects of Atmospheric Sulfur Dioxide on the Corrosion of Zinc, *Mater. Perform.,* Vol 9, 1970, p 35–40

24. H. Guttman and P.J. Sereda, Measurement of Atmospheric Factors Affecting the Corrosion of Metals, *Metal Corrosion in the Atmosphere,* STP 345, American Society for Testing and Materials, 1968, p 355–360

25. K.G. Compton, Atmospheric Corrosion, *NACE Basic Corrosion Course,* National Association of Corrosion Engineers, 1970, p 4-2

26. F.L. LaQue, Environment Factors in the Corrosion of Metals in Seawater and Sea Air, *Marine Corrosion,* John Wiley & Sons, 1975, p 103

27. D. Knotkova, V. Kucera, S.W. Dean, and P. Boschek, Classification of the Corrosivity of the Atmosphere—Standardized Classification System and Approach for Adjustment, *Outdoor Atmospheric Corrosion,* STP 1421, H.E. Townsend, Ed., American Society for Testing and Materials, 2002, p 109–124

28. J. Tidblad, V. Kucera, A.A. Mikhailov, and D. Knotkova, Improvement of the ISO Classification System Based on Dose-Response Functions Describing the Corrosivity of Outdoor Atmospheres, *Outdoor Atmospheric Corrosion,* STP 1421, H.E. Townsend, Ed., American Society for Testing and Materials, 2002, p 73–87

29. M. Morcillo, E. Almeida, B. Chico, and D. de la Fuente, Analysis of ISO Standard 9223, *Outdoor Atmospheric Corrosion,* STP 1421, H.E. Townsend, Ed., American Society for Testing and Materials, 2002, p 59–72

30. C. Leygraf and T.E. Graedel, *Atmospheric Corrosion,* Wiley-Interscience, 2000, p 109–115

S.D. Cramer and S.A. Matthes, Simulated Service Testing in the Atmosphere, *Corrosion: Fundamentals, Testing, and Protection,* Vol 13A, *ASM Handbook,* ASM International, 2003, p 487–494

Simulated Service Testing in the Atmosphere

Stephen D. Cramer and Steven A. Matthes, Albany Research Center, U.S. Department of Energy

---

Relative Corrosivity

Several programs have been conducted to assess the relative corrosivity of the environment at specific geographic locations over a finite period of time (Ref 24, 31, 32, 33). The use of calibration specimens to measure corrosivity can be traced to J.C. Hudson (Ref 32), who established the ranking of ten different environments based on the corrosion of wrought iron (Table 2). Table 3 summarizes additional site comparisons for the atmospheric-corrosion performance of steel and zinc (Ref 34).

Table 2 Relative corrosivity of atmospheres at different locations measured using wrought iron

Location	Type of atmosphere	Average weight loss of iron specimens in 1 year, mg/cm^2	Relative corrosivity
Khartoum, Sudan	Dry island (arid)	0.08	1
Singapore	Tropical/marine	0.69	9
State College, PA	Rural	1.90	25
Panama Canal Zone	Tropical/marine	2.28	31
Kure Beach, NC (250 m, or 800 ft, lot)	Marine	2.93	38
Kearny, NJ	Industrial	3.92	52
Pittsburgh, PA	Industrial	4.88	65
Frodingham, U.K.	Industrial	7.50	100
Daytona Beach, FL	Marine	10.34	138
Kure Beach, NC (25 m, or 80 ft, lot)	Marine	35.68	475

Source: Ref 32

Table 3 Measured atmospheric-corrosion rates for steel and zinc

Site	Location	Type of atmosphere	Relative corrosivity	
			Steel	**Zinc**
1	Normal Wells, Northwest Territory	Rural	0.02	0.2
2	Saskatoon, Saskatchewan	Rural	0.2	0.2
9	State College, PA[(a)]	Rural	1.0	1.0
17	Pittsburgh, PA (roof)	Industrial	1.8	1.5
18	London (Battersea), U.K.	Industrial	2.0	1.2
27	Bayonne, NJ	Industrial	3.4	3.1
28	Kure Beach, NC (250 m, or 800 ft, site)	Marine	3.6	1.9
31	London (Stratford), U.K.	Industrial	6.5	4.8
33	Point Reyes, CA	Marine	9.5	2.0
37	Kure Beach, NC (25 m, or 80 ft, site)	Marine	33.0	6.4

(a) The average weight losses on two 100 × 150 mm (4 × 6 in.) specimens after 1 year of bold exposure at the indicated site were used to calculate the relative corrosivity of the site. The losses in the rural atmosphere at State College, PA, were taken as unity, and the relative corrosiveness at each of the other sites is given in this table as a fraction or a multiple of unity. Source: Ref 34

References cited in this section

24. H. Guttman and P.J. Sereda, Measurement of Atmospheric Factors Affecting the Corrosion of Metals, *Metal Corrosion in the Atmosphere,* STP 345, American Society for Testing and Materials, 1968, p 355–360

31. F.L. LaQue, *Proc. ASTM,* Vol 51, 1951, p 495

32. J.C. Hudson, *J. Br. Iron Steel Inst.,* Vol 148, 1943, p 161

33. S.K. Coburn et al., Corrosiveness of Various Atmospheric Test Sites as Measured by Specimens of Steel and Zinc, *Metal Corrosion in the Atmosphere,* STP 435, American Society for Testing and Materials, 1968, p 326

34. *ASTM Mater. Res. Stand.,* Dec 1961, p 977

S.D. Cramer and S.A. Matthes, Simulated Service Testing in the Atmosphere, *Corrosion: Fundamentals, Testing, and Protection*, Vol 13A, *ASM Handbook*, ASM International, 2003, p 487–494

Simulated Service Testing in the Atmosphere

Stephen D. Cramer and Steven A. Matthes, Albany Research Center, U.S. Department of Energy

---

Environmental Factors

Methods have been developed for measuring many of the factors that affect atmospheric corrosion (Ref 1, 2, 3, 4, 5, 6, 7, 8, 9, 10, 11, 12, 13, 14, 24, 27, 28, 29, 30). Atmospheric chemistry, precipitation and particulate chemistry, meteorology, wet and dry deposition, precipitation runoff, and their variation with time can be determined continuously and by discrete measurements. Measurements can be site specific, regional, and global. Measurements can be instantaneous, short-time averages, daily, weekly, or annual. Identifying the important factors and interactions between factors that affect atmospheric corrosion is a challenging task. Often, annual average values of the important factors will suffice for environmental characterization. Environmental factors that should be considered for measurement include, but are not limited to, those listed in Table 4.

Table 4 Environmental parameters often considered as influences on the atmospheric degradation of materials

Category	Parameters
Wet deposition	pH
	Conductivity
	Cations: calcium (Ca^{2+}), magnesium (Mg^{2+}), sodium (Na^+), potassium (K^+), ammonium (NH_4^+), and hydrogen (H^+)
	Anions: sulfates (SO_4^{2-}), nitrates (NO_3^-), and chlorides (Cl^-)
Dry deposition	Sulfur dioxide (SO_2)
	Nitrogen dioxide (NO_2)
	Nitric acid (HNO_3)
	Ammonia (NH_3)
	Particulate matter, sulfates, nitrates
Meteorology	Ozone
	Wind speed
	Wind direction
	Relative humidity (dewpoint)
	Temperature
	Solar radiation
	Rainfall volume and intensity
Others	Test specimen surface temperature
	Time of wetness

Note: Time of wetness and the quantity of SO_2 and chloride are the most important variables in determining atmospheric corrosion. Such factors as hydrogen sulfide, nitrogen compounds, and other specific pollutants may be significant at specific sites if sources of these pollutants are located nearby.

References cited in this section

1. Effects of Acidic Deposition on Materials, Report 19, *Terrestrial, Materials, Health and Visibility Effects,* Vol III, *Acidic Deposition: State of Science and Technology,* U.S. National Acid Precipitation Assessment Program, Washington, D.C., p. 19–1 to 19–280, 1991

2. W. He, I. Odenvall Wallinder, and C. Leygraf, A Comparison Between Corrosion Rates and Runoff Rates from New and Aged Copper and Zinc as Roofing Materials, *Water, Air Soil Pollut. Focus,* Vol 1, 2001, p 67–82

3. I. Odnevall Wallinder, P. Verbiest, W. He, and C. Leygraf, The Influence of Patina Age and Pollutant Levels on the Runoff Rate of Zinc from Roofing Materials, *Corros. Sci.,* Vol 40 (No. 11), 1998, p 1977–1982

4. I. Odnevall Wallinder, P. Verbiest, W. He, C. Leygraf, Effects of Exposure Direction and Inclination on the Runoff Rates of Zinc and Copper Roofs, *Corros. Sci.,* Vol 42, 2000 p 1471–1487

5. W. He, I. Odnevall Wallinder, and C. Leygraf, A Laboratory Study of Copper and Zinc Runoff during First Flush and Steady- State Conditions, *Corros. Sci.,* Vol 43, 2001, p 127–146

6. W. He, I. Odnevall Wallinder, and C. Leygraf, Runoff Rates of Zinc—A Four-Year Field and Laboratory Study, *Outdoor Atmospheric Corrosion,* STP 1421, H.E. Townsend, Ed., ASTM International, 2002, p 216–229

7. X. Zhang, W. He, I. Odnevall Wallinder, J. Pan, and C. Leygraf, Determination of Instantaneous Corrosion Rates and Runoff Rates of Copper from Naturally Patinated Copper during Continuous Rain Events, *Corros. Sci.,* Vol 44, 2002, p 2131–2151

8. I. Odnevall Wallinder and C. Leygraf, A Study of Copper Runoff in an Urban Atmosphere, *Corros. Sci.,* Vol 39 (No. 12), 1997, p 2039–2052

9. S.D. Cramer and L.G. McDonald, Atmospheric Factors Affecting the Corrosion of Zinc, Galvanized Steel, and Copper, *Corrosion Testing and Evaluation,* STP 1000, R. Baboian and S.W. Dean, Ed., American Society for Testing and Materials, 1990, p 208–224

10. J.W. Spence, F.H Haynie, F.W. Lipfert, S.D. Cramer, and L.G. McDonald, Atmospheric Corrosion Model for Galvanized Steel Structures, *Corrosion,* Vol 48 (No. 12), 1992, p 1009–1019

11. S.D. Cramer, L.G. McDonald, and J.W. Spence, Effects of Acidic Deposition on the Corrosion of Zinc and Copper, *Proceedings of the 12th International Corrosion Congress,* Vol 2, NACE International, 1993, p 722–733

12. S.D. Cramer, S.A. Matthes, G.R. Holcomb, B.S. Covino, Jr., and S.J. Bullard, "Precipitation Runoff and Atmospheric Corrosion," Paper 00452, Corrosion/2000, NACE International, 2000

13. S.D. Cramer, S.A. Matthes, B.S. Covino, Jr., S.J. Bullard, and G.R. Holcomb, Environmental Factors Affecting the Atmospheric Corrosion of Copper, *Outdoor Atmospheric Corrosion,* STP 1421, H.E. Townsend, Ed., American Society for Testing and Materials, 2002, p 245–264

14. S.A. Matthes, S.D. Cramer, B.S. Covino, Jr., S.J. Bullard, and G.R. Holcomb, Precipitation Runoff from Lead, *Outdoor Atmospheric Corrosion,* STP 1421, H.E. Townsend, Ed., American Society for Testing and Materials, 2002, p 265–274

24. H. Guttman and P.J. Sereda, Measurement of Atmospheric Factors Affecting the Corrosion of Metals, *Metal Corrosion in the Atmosphere,* STP 345, American Society for Testing and Materials, 1968, p 355–360

27. D. Knotkova, V. Kucera, S.W. Dean, and P. Boschek, Classification of the Corrosivity of the Atmosphere—Standardized Classification System and Approach for Adjustment, *Outdoor Atmospheric Corrosion,* STP 1421, H.E. Townsend, Ed., American Society for Testing and Materials, 2002, p 109–124

28. J. Tidblad, V. Kucera, A.A. Mikhailov, and D. Knotkova, Improvement of the ISO Classification System Based on Dose-Response Functions Describing the Corrosivity of Outdoor Atmospheres, *Outdoor Atmospheric Corrosion,* STP 1421, H.E. Townsend, Ed., American Society for Testing and Materials, 2002, p 73–87

29. M. Morcillo, E. Almeida, B. Chico, and D. de la Fuente, Analysis of ISO Standard 9223, *Outdoor Atmospheric Corrosion,* STP 1421, H.E. Townsend, Ed., American Society for Testing and Materials, 2002, p 59–72

30. C. Leygraf and T.E. Graedel, *Atmospheric Corrosion,* Wiley-Interscience, 2000, p 109–115

S.D. Cramer and S.A. Matthes, Simulated Service Testing in the Atmosphere, *Corrosion: Fundamentals, Testing, and Protection*, Vol 13A, *ASM Handbook*, ASM International, 2003, p 487–494

Simulated Service Testing in the Atmosphere

Stephen D. Cramer and Steven A. Matthes, Albany Research Center, U.S. Department of Energy

---

Conducting Atmospheric-Corrosion Tests

The type of data or information required from the atmospheric-corrosion test dictates the specifics of the test program. For example, the test purpose could be to evaluate the general corrosion behavior of a material, the resistance to solar radiation, coating discoloration, pitting, galvanic effects, loss of strength, or the impact of environmental factors. The information to be obtained must be established in the planning stages of the work.

Materials To Be Exposed. Atmospheric-corrosion studies are generally carried out for periods of months and even years to measure environmental effects and to establish long-term performance. Therefore, it is important to select standard or reference materials (referred to as control specimens) that will be exposed alongside of the test materials, alloys, or coatings of interest. Control materials with a prior performance record in the exposure environment are extremely important for comparison purposes and for monitoring site corrosivity. The ISO recommends low-copper steel, commercial-purity aluminum, commercial-purity zinc, and commercial-purity copper as reference metals; they are representative of the engineering materials most widely used in indoor and outdoor exposures. They also have known performance records in various environments and documented corrosion behaviors when exposed to different atmospheric constituents and chemistries. With daily, seasonal, and long-term changes in air chemistry, precipitation chemistry, and meteorology, site corrosivity can change, and the use of reference materials provides a basis for quantifying these changes.

The number of replicate samples used depends on the exposure period and the number of scheduled sample removals. For visual observations, two samples for each environment are usually sufficient. More samples will

be needed for periodic removals. Samples that have been removed and cleaned should never be reexposed as part of the same test.

Atmospheric Specimens. ASTM International, NACE International, and ISO provide guidelines for sample design, preparation, exposure, postexposure cleaning, and evaluation (Table 5). These guidelines include standard sample designs for flat panels, stress corrosion, and other types of atmospheric-corrosion samples (Ref 35) (Table 6), such as the ISO wire helix sample (Fig. 1).

Table 5 Guidelines for atmospheric exposures

Procedure or guideline	Society or organization reference		
	ASTM International	**NACE International**	**ISO[(a)]**
Standard practice for conducting atmospheric tests on metals	G 50	…	ISO 8565:1992
Standard practice for recording data from atmospheric-corrosion tests of metallic-coated steel specimens	G 33	RP-02-81	…
		RP-0281-98	
Rating of electrodeposited panels subject to atmospheric exposure	B 537	…	…
Standard practices for preparing, cleaning, and evaluating corrosion test specimens	G 1	…	…
Standard definition of terms relating to corrosion and corrosion testing	G 15	…	ISO 8044:1999
Standard practice for applying statistics to analysis of corrosion data	G 16	…	…
Standard practice for examination and evaluation of pitting corrosion	G 46	…	ISO 111463:1995
Standard practice for making and using U-bend corrosion test specimens	G 30	…	ISO 7539-3:1989
Corrosion of metals and alloys—determination of bimetallic corrosion in outdoor exposure corrosion tests	…	…	ISO 7441:1984
Classification of corrosivity of atmospheres	…	…	ISO 9223:1992
Corrosion of metals and alloys—guidelines of values for the categorization of corrosive atmospheres	…	…	ISO 9224:1992
Corrosion of metals and alloys—aggressivity of atmospheres: methods of measurement of pollutant data(b)	G 91	…	ISO 9225:1992
Corrosion of metals and alloys—corrosivity of atmospheres: methods of determination of corrosion rate of standard specimens for the evaluation of corrosivity	…	…	ISO 9226:1992

(a) ISO, International Organization for Standardization. (b) The G 91 procedure is applicable only to SO_x-containing atmospheres.

Table 6 Recommendations for specimen design for atmospheric-corrosion testing

Type	Reference	Typical size[(a)]
Flat panel		
Flat panel	ASTM G 50 (Ref 36)	Ferrous: 100 × 150 mm (4 × 6 in.)
		Nonferrous: 100 × 200 mm (4 × 8 in.)

Stress corrosion		
U-bend	ASTM G 30 (Ref 37)	3 mm × 15 mm × 130 mm × 32 mm diam (0.12 in. × 0.6 in. × 5 in. × 1.25 in. diam)
Bent beam	ASTM G 39 (Ref 38)	3 point: 1 mm × 5 mm × 65 mm span (0.04 in. × 0.2 in. × 2.5 in. span); 2 point: 25 mm wide × 180 mm span (1 in. wide × 7 in. span)
C-ring	ASTM G 38 (Ref 39)	12 mm wide × 25 mm diam (0.5 in. wide × 1 in. diam)
Direct tension	ASTM G 49 (Ref 40)	Specimen size depends primarily on the dimensions of the product to be tested.
Welded	ASTM G 58 (Ref 41)	The thickness and size of the test specimen should represent the actual structural member.
Galvanic		
Disk	B-3 (Ref 42)	36 mm diam × 1.6 mm (1.4 in. diam × 0.06 in.), 33.5 mm diam × 1.6 mm (1.3 in. diam × 0.06 in.), 30 mm diam × 1.6 mm (1.2 in. diam × 0.06 in.), 25 mm diam × 1.6 mm (1 in. diam × 0.06 in.)
Plate	ISO/TC 156/WG3/N11 (Ref 43)	90 mm × 150 mm × 2 mm (3.5 in. × 6 in. × 0.08 in.), 70 mm × 25 mm × 2 mm (2.75 in. × 1 in. × 0.08 in.), 45 mm × 90 mm × 2 mm (1.8 in. × 3.5 in. × 0.08 in.), 25 mm × 70 mm × 2 mm (1 in. × 2.75 in. × 0.08 in.)
Open helix (metallic wire)	ISO/TC 156/WG4/N131 (Ref 44)	Wires with a diameter of 2–3 mm (0.08–0.12 in.) and 1000 mm (40 in.) long rolled into helix and attached to polyamide or metallic holder. See Fig. 1.

(a) The appropriate ASTM International or International Organization for Standardization (ISO) document should be consulted before selecting a specimen size. Source: Ref 35

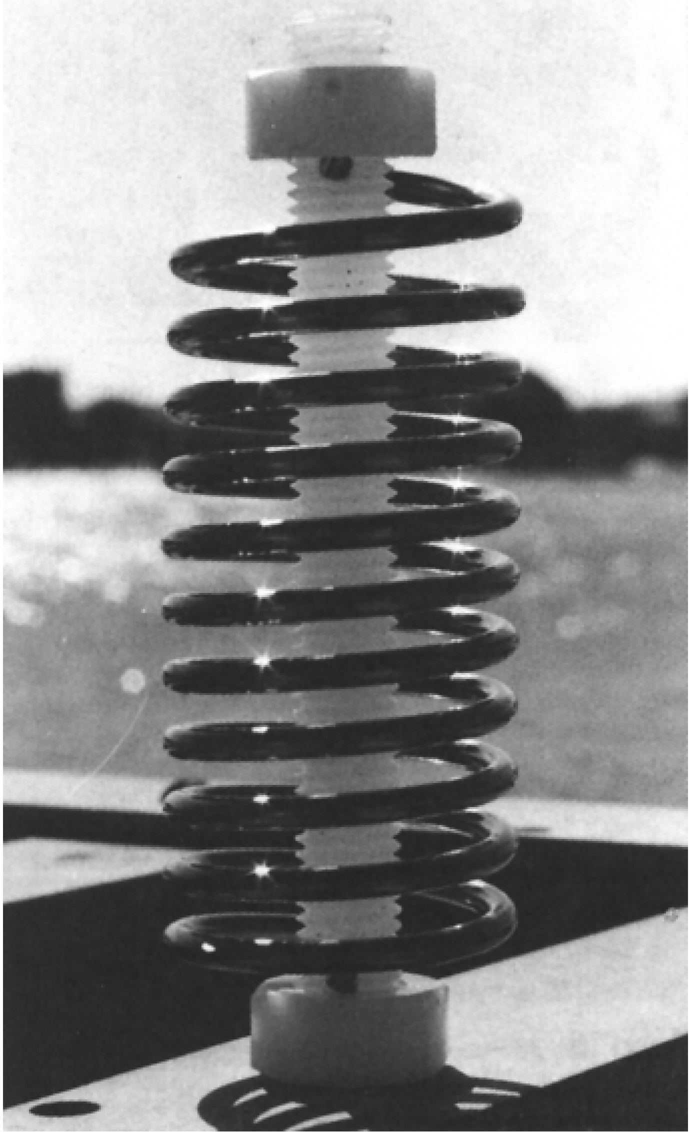

Fig. 1 International Organization for Standardization wire helix specimen

A suitable means of sample identification should be used. Stamped code numbers can be used for the more corrosion-resistant materials but will be lost on the more corrodible materials, such as steel. For these materials, drilled holes or side notches according to a number template can be used. A plastic tag affixed through a drilled hole with a nonmetallic tie has also been successfully used. In all cases, the method of identification of the sample should not bias the corrosion evaluation. It is also good practice to map the samples on the exposure rack; that is, draw, sketch, or list according to exposure the identity of each sample on the rack in case the codes or tags corrode away or are lost. Among the more important steps in atmospheric-corrosion testing is the documentation of results and observations for future reference and application. This reporting can take the form of internal company reports, technical papers, or presentations. In all cases, the objectives of the work, the exposure details, and the conclusions drawn from the analysis of the corrosion results should be documented. The chain of custody of this information and associated records is crucial to the completion of long-term exposure tests.

Exposure Guidelines. Atmospheric-corrosion samples are normally exposed on a test rack similar to that shown in Fig. 2. The rack is then attached to a frame or stand (ASTM G 50 or ISO DP8565). Sample sizes are normally 100 by 150 mm (4 by 6 in.) in these racks but can be any size necessary to properly evaluate the performance of the exposed material. For example, large panels (Fig. 3) and stress-corrosion cracking (SCC) U-bend samples (Fig. 4) are used in sizes and configurations necessary for the tests and environments of interest.

Fig. 2 Atmospheric-corrosion test rack

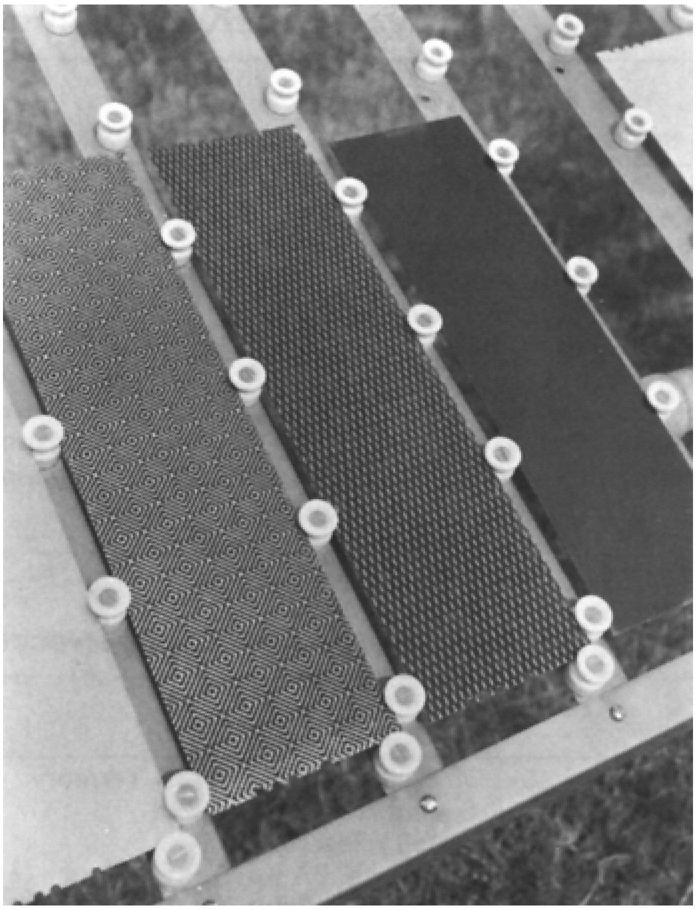

Fig. 3 Large atmospheric-corrosion test panels

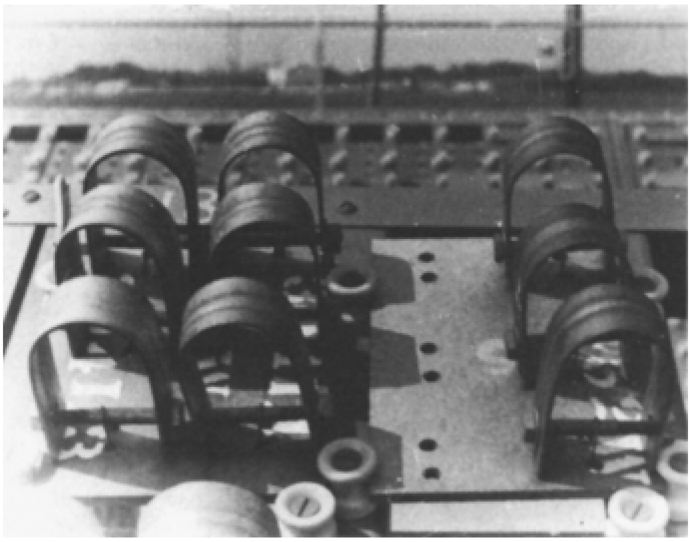

Fig. 4 U-bend specimens used for atmospheric-corrosion testing

For special situations, the exposure rack can be streamlined for small areas or for specialized exposures by using a corrosion spool rack similar to that shown in Fig. 5. In all cases, unless the objective of the exposure is to determine galvanic effects, the specimens should be electrically isolated from each other and from the exposure rack by nonconductive materials, such as porcelain or plastic insulators similar to those visible in Fig. 1, Fig. 2, Fig. 3, Fig. 4, Fig. 5.

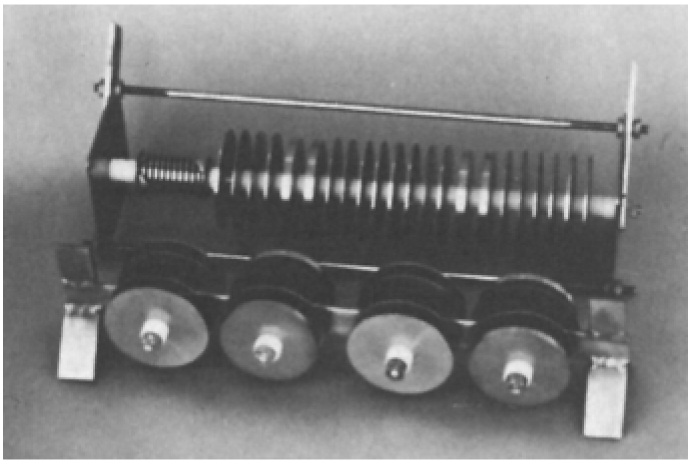

Fig. 5 Atmospheric-corrosion spool rack

The convention used for atmospheric-corrosion sample orientation is as follows: samples exposed in the northern hemisphere normally face south toward the sun; samples exposed in the southern hemisphere normally face north. It is also common practice to expose samples facing the most corrosive direction if the exposure site is close to a pollutant point source, such as sea coast, a fossil energy power plant, or the plume of pollutants downwind from an industrial site or even a city. ASTM G 50 recommends that samples be exposed on an angle 30° to the horizon (in Europe this angle is 45°). If maximum exposure to sunlight is desired, the specimens should be exposed at an angle to the horizon equal to the latitude of the site.

In order to fully characterize the effect of the environment on the corrosion process and to quantify the release of corrosion products into soils and groundwater, precipitation runoff may be studied (Ref 1, 2, 3, 4, 5, 6, 7, 8, 9, 10, 11, 12, 13, 14, 15, 16, 17, 18, 19, 20). Precipitation runoff is the precipitation containing dissolved corrosion products and environmental species that drain from a metal surface. Figure 6 shows a site where both atmospheric-corrosion and precipitation runoff measurements are made to provide a more complete characterization of the competing processes of corrosion film growth and corrosion film dissolution that accompany the corrosion process. Mass loss panels, typically one-sided with the downward side masked off to prevent corrosion, are exposed on an atmospheric-corrosion test rack such as that shown in Fig. 2. Precipitation is collected in a wet/dry collector. The collector is activated by a sensor that uncovers the bucket and collects precipitation during a rain event, then covers the bucket and seals it to prevent evaporation losses when the event stops. The sensor is heated so that the collection bucket remains open only as long as precipitation continues to wet the sensor. The collected precipitation provides a measure of precipitation rate, rain intensity, the wet deposition rate, and the chemistry of incident precipitation. The precipitation runoff panels are large, one-sided metal panels of the same materials as the mass loss panels and sit in a tray that collects and funnels all precipitation draining from the panel surface into runoff collection containers. The difference between the chemistry of the incident precipitation and the precipitation runoff is a measure of the rate that soluble corrosion product is removed from the panel surface. This difference in chemistry also gives a measure of the rate that environmental species such as sulfur and nitrogen oxides, chloride ion, ammonia, and particulate matter are dry deposited on the panel surface.

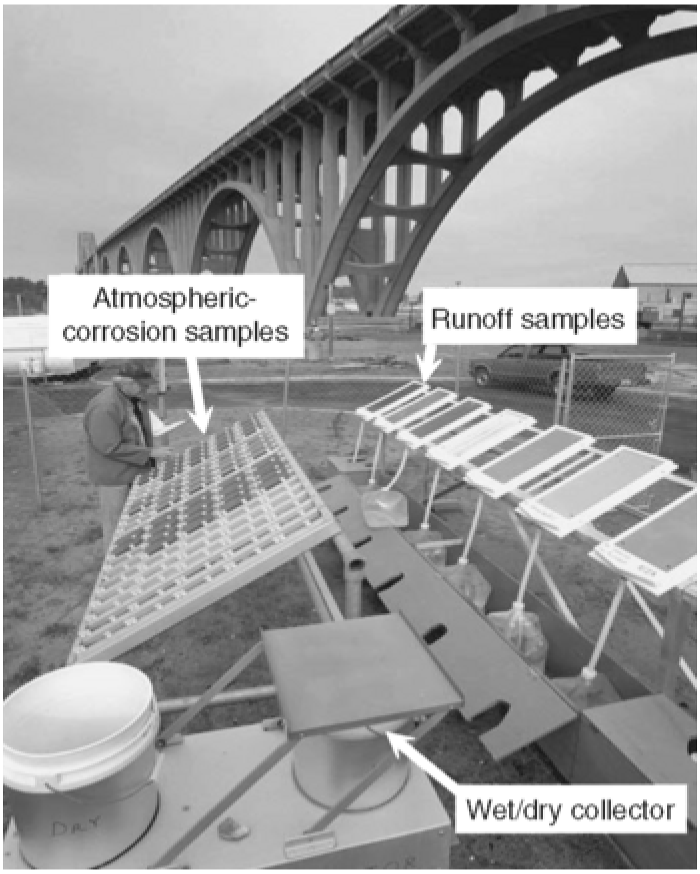

Fig. 6 Marine atmospheric-corrosion and precipitation runoff test site at Newport, OR

Evaluating Corrosion Panels and Precipitation Runoff. Exposed atmospheric-corrosion panels are evaluated in a variety of ways (Ref 45, 46, 47), beginning with a visual examination and progressing to other forms of analysis (Table 7). Coated samples are evaluated for undercutting of the coating, blistering, loss of surface finish, and protection of the substrate. Uncoated samples are evaluated for uniform corrosion, localized corrosion (pitting, crevice corrosion, SCC), or galvanic corrosion. Mass loss is quantified by chemical removal of corrosion product from the panel surface (something that was not done when atmospheric-corrosion studies were first attempted in the early 20th century) and determining the change in mass of the panel after exposure. The corrosion film is characterized by a variety of analytical techniques, such as wet chemistry, optical microscopy, scanning electron microscopy, x-ray fluorescence spectroscopy, x- ray diffraction, x-ray photoelectron spectroscopy, Auger electron spectroscopy, and other techniques. Precipitation and precipitation runoff chemistry is quantified by well-known wet chemical analytical techniques.

Table 7 Evaluation techniques for atmospheric-corrosion specimens

Technique	Value
Photographic documentation	Photographs of the specimens before and after cleaning give a permanent record of the performance of the material in the particular atmosphere.
Corrosion product analysis and surface deposits	Atmospheric-corrosion specimens usually have the corrosion product and airborne deposits on the surface at the time of removal. This adds a wealth of information to the observed behavior of the material.
Mass loss	For uniform corrosion, this is simple and can be converted to corrosion rate as $g/m^2/d$, mils per year, etc.
Pitting and localized corrosion	Yields information on the susceptibility of a material to localized attack. Pitting corrosion is often reported as average or maximum depth of attack and is usually measured with a dial depth gage or vernier microscope. Where possible, pitting data should be treated statistically with recognized methods covered in various standards. Weight loss data should not be used indiscriminately to calculate corrosion rates

	where the primary form of corrosion is localized.
Rust or rust stain	Data reveal the propensity of a material to rust and the degree of rust staining. Also, through cleaning procedures, it can be determined if the original appearance was retained.
Tensile test and other physical tests	Can often yield information on the atmospheric effect on the strength of materials, cracking behavior, etc.
Appearance	Effect of environment on appearance, color retention, etc.

References cited in this section

1. Effects of Acidic Deposition on Materials, Report 19, *Terrestrial, Materials, Health and Visibility Effects,* Vol III, *Acidic Deposition: State of Science and Technology,* U.S. National Acid Precipitation Assessment Program, Washington, D.C., p. 19–1 to 19–280, 1991

2. W. He, I. Odenvall Wallinder, and C. Leygraf, A Comparison Between Corrosion Rates and Runoff Rates from New and Aged Copper and Zinc as Roofing Materials, *Water, Air Soil Pollut. Focus,* Vol 1, 2001, p 67–82

3. I. Odnevall Wallinder, P. Verbiest, W. He, and C. Leygraf, The Influence of Patina Age and Pollutant Levels on the Runoff Rate of Zinc from Roofing Materials, *Corros. Sci.,* Vol 40 (No. 11), 1998, p 1977–1982

4. I. Odnevall Wallinder, P. Verbiest, W. He, C. Leygraf, Effects of Exposure Direction and Inclination on the Runoff Rates of Zinc and Copper Roofs, *Corros. Sci.,* Vol 42, 2000 p 1471–1487

5. W. He, I. Odnevall Wallinder, and C. Leygraf, A Laboratory Study of Copper and Zinc Runoff during First Flush and Steady- State Conditions, *Corros. Sci.,* Vol 43, 2001, p 127–146

6. W. He, I. Odnevall Wallinder, and C. Leygraf, Runoff Rates of Zinc—A Four-Year Field and Laboratory Study, *Outdoor Atmospheric Corrosion,* STP 1421, H.E. Townsend, Ed., ASTM International, 2002, p 216–229

7. X. Zhang, W. He, I. Odnevall Wallinder, J. Pan, and C. Leygraf, Determination of Instantaneous Corrosion Rates and Runoff Rates of Copper from Naturally Patinated Copper during Continuous Rain Events, *Corros. Sci.,* Vol 44, 2002, p 2131–2151

8. I. Odnevall Wallinder and C. Leygraf, A Study of Copper Runoff in an Urban Atmosphere, *Corros. Sci.,* Vol 39 (No. 12), 1997, p 2039–2052

9. S.D. Cramer and L.G. McDonald, Atmospheric Factors Affecting the Corrosion of Zinc, Galvanized Steel, and Copper, *Corrosion Testing and Evaluation,* STP 1000, R. Baboian and S.W. Dean, Ed., American Society for Testing and Materials, 1990, p 208–224

10. J.W. Spence, F.H Haynie, F.W. Lipfert, S.D. Cramer, and L.G. McDonald, Atmospheric Corrosion Model for Galvanized Steel Structures, *Corrosion,* Vol 48 (No. 12), 1992, p 1009–1019

11. S.D. Cramer, L.G. McDonald, and J.W. Spence, Effects of Acidic Deposition on the Corrosion of Zinc and Copper, *Proceedings of the 12th International Corrosion Congress,* Vol 2, NACE International, 1993, p 722–733

12. S.D. Cramer, S.A. Matthes, G.R. Holcomb, B.S. Covino, Jr., and S.J. Bullard, “Precipitation Runoff and Atmospheric Corrosion,” Paper 00452, Corrosion/2000, NACE International, 2000

13. S.D. Cramer, S.A. Matthes, B.S. Covino, Jr., S.J. Bullard, and G.R. Holcomb, Environmental Factors Affecting the Atmospheric Corrosion of Copper, *Outdoor Atmospheric Corrosion,* STP 1421, H.E. Townsend, Ed., American Society for Testing and Materials, 2002, p 245–264

14. S.A. Matthes, S.D. Cramer, B.S. Covino, Jr., S.J. Bullard, and G.R. Holcomb, Precipitation Runoff from Lead, *Outdoor Atmospheric Corrosion,* STP 1421, H.E. Townsend, Ed., American Society for Testing and Materials, 2002, p 265–274

15. S.A. Matthes, S.D. Cramer, S.J. Bullard, B.S. Covino, Jr., and G.R. Holcomb, "Atmospheric Corrosion and Precipitation Runoff from Zinc and Zinc Alloy Surfaces," Paper 03598, Corrosion/2003, 17–20 March 2003 (San Diego, CA), NACE International, 2003

16. H.T. Michels, B. Boulanger, and N.P. Nikolaidis, "Copper Roof Stormwater Runoff—Corrosion and the Environment," Paper 02225, Corrosion/2002, NACE International, 2002

17. H.T. Michels, B. Boulanger, and N.P. Nikolaidis, Environmental Impact of Stormwater Runoff from a Copper Roof, *Mater. Perform.,* Vol 42 (No. 2) Feb 2003, p 70–74

18. M.C. Gromaire-Mertz, S. Garnaud, A. Gonzales, and G. Chebbo, Characterization of Urban Runoff Pollution in Paris, *Wat. Sci. Technol.,* Vol 39 (No. 2), 1999, p 1–8

19. T.S. Barron, "Architectural Uses of Copper—An Evaluation of Stormwater Pollution Loads and Best Management Practices," Palo Alto Regional Water Quality Control Plant, Palo Alto, CA, 2000

20. I. Odnevall Wallinder, C. Leygraf, C. Karlen, D. Heijerick, and C.R. Janssen, Atmospheric Corrosion of Zinc-Based Materials: Runoff Rates, Chemical Speciation and Ecotoxicity, *Corros. Sci.,* Vol 43, 2001, p 809–816

35. S.W. Dean, Jr., Planning, Instrumentation and Evaluation of Atmospheric Corrosion Tests and a Review of ASTM Testing, *Atmospheric Corrosion,* John Wiley & Sons, 1982, p 195–216

36. "Standard Recommended Practice for Conducting Atmospheric Corrosion Tests on Metals," G 50, *Annual Book of ASTM Standards,* American Society for Testing and Materials

37. "Standard Recommended Practice for Making and Using U-Bend Stress Corrosion Test Specimens," G 30, *Annual Book of ASTM Standards,* American Society for Testing and Materials

38. "Standard Practice for Preparation and Use of Bent Beam Stress Corrosion Test Specimens," G 39, *Annual Book of ASTM Standards,* American Society for Testing and Materials

39. "Standard Recommended Practice for Making and Using C-Ring Stress Corrosion Test Specimens," G 38, *Annual Book of ASTM Standards,* American Society for Testing and Materials

40. "Standard Recommended Practice for Preparation and Use of Direct Tension Stress Corrosion Test Specimens," G 49, *Annual Book of ASTM Standards,* American Society for Testing and Materials

41. "Standard Practice for Preparation of Stress Corrosion Test Specimens for Weldments," G 58, *Annual Book of ASTM Standards,* American Society for Testing and Materials

42. R. Baboian, Final Report on the ASTM Study: Atmospheric Galvanic Corrosion of Magnesium Coupled to Other Metals, *Atmospheric Factors Affecting the Corrosion of Engineering Metals,* STP 646, S.K. Coburn, Ed., American Society for Testing and Materials, 1978, p 17–29

43. “Metals and Alloys—Test Methods for Contact Corrosion in Atmospheric Conditions,” ISO/TC 156/WG 3/N11, Third Working Draft, Proposal of USSR to ISO Technical Committee 156 WG 3, Nov 1979

44. “Corrosion of Metals and Alloys—Corrosivity of Atmospheres—Methods of Determination of Corrosion Rates of Standard Specimens for the Evaluation of Corrosivity,” ISO/TC 156 WG4/N131, German Proposal to ISO Technical Committee 156 WG3, 1979

45. T.E. Graedel, K. Nassau, and J.P. Franey, Copper Patinas Formed in the Atmosphere, Part I: Introduction, *Corros. Sci.,* Vol 27 (No. 7), 1987, p 639–657

46. T.E. Graedel, Copper Patinas Formed in the Atmosphere, Part II: Qualitative Assessment of Mechanisms, *Corros. Sci.,* Vol 27 (No. 7), 1987, p 721–740

47. T.E. Graedel, Copper Patinas Formed in the Atmosphere, Part III: A Semi-Quantitative Assessment of Rates and Constraints in the Greater New York Metropolitan Area, *Corros. Sci.,* Vol 27 (No. 7), 1987, p 741–769

S.D. Cramer and S.A. Matthes, Simulated Service Testing in the Atmosphere, *Corrosion: Fundamentals, Testing, and Protection*, Vol 13A, *ASM Handbook*, ASM International, 2003, p 487–494

Simulated Service Testing in the Atmosphere

Stephen D. Cramer and Steven A. Matthes, Albany Research Center, U.S. Department of Energy

---

Analyzing Atmospheric-Corrosion Tests

One of the principal goals of atmospheric-corrosion measurements is to have sufficient data to estimate the service life of the part being evaluated. Uniform corrosion is one of the most widely studied corrosion processes in atmospheric corrosion. In a mass balance for a metal surface in a bold, skyward exposure at any time, t, the total or cumulative corrosion loss, $M_T(t)$, is equal to the total metal present in the corrosion film, $M_F(t)$, plus the cumulative amount of metal in soluble corrosion product washed from the surface in precipitation runoff, $M_P(t)$; that is:

$$M_T(t) = M_F(t) + M_P(t) \qquad \text{(Eq 1)}$$

The time derivative of this equation is:

$$dM_T(t)/dt = dM_F(t)/dt + dM_P(t)/dt \qquad \text{(Eq 2)}$$

where $dM_T(t)/dt$ is the instantaneous corrosion rate, $dM_F(t)/dt$ is the rate of metal accumulation contributing to protective corrosion film growth, and $dM_P(t)/dt$ is the rate of metal loss from the corrosion film in precipitation runoff.

For materials such as nickel, steel, and stainless steel, the corrosion products are insoluble or not very soluble in precipitation, and the precipitation runoff loss rate is typically 0. Materials such as zinc, galvanized steel, copper, and aluminum have corrosion products soluble in precipitation. For these materials, if the atmospheric exposure is relatively short and corrosion film growth is the dominant process, the precipitation runoff loss rate is also effectively 0. Under these conditions, if the corrosion rate is assumed to be inversely proportional to the corrosion film thickness raised to some power n, that is:

$$dM_T(t)/dt \propto 1/M_F(t)^n \qquad \text{(Eq 3)}$$

integration of Eq 2 (with $M_F(t) = M_T(t)$) gives the well-known power model (Ref 48) describing the time variation of corrosion in the absence of precipitation runoff losses:

$M_T(t) = a_o t^{1/(n+1)}$ (Eq 4)

where a_o is a proportionality constant. When $n = 0$, the corrosion kinetics are linear, and the corrosion film is essentially non-protective; when $n = 1$, the corrosion kinetics are parabolic, and the corrosion film is protective. Data for a number of alloy steels exposed in a wide range of environments give n values ranging from 0 to roughly 2, or a little higher (Ref 48). Of course, expressed differently, Eq 4 is the bilogarithmic law for atmospheric corrosion:

$\log M_T(t) = \log a_o + [1/(n + 1)] \log t$ (Eq 5)

In other words, in the absence of precipitation runoff losses, the total corrosion plotted versus exposure time on logarithmic coordinates is a straight line with a slope of $[1/(n + 1)]$. Values of the slope generally fall in the range from 1 for $n = 0$ to $\frac{1}{3}$ for $n = 2$.

Equation 2 can also be integrated for conditions when soluble corrosion product is washed from the metal surface, that is, the precipitation runoff loss rate is nonzero, $dM_P(t)/dt > 0$. Independent measurements for metals such as zinc and copper (Ref 2, 3, 4, 6, 12, 13) that have corrosion products soluble in precipitation show that the cumulative precipitation runoff loss, $M_P(t)$, is essentially linear with respect to time, regardless of daily and seasonal variations in meteorology and air chemistry (Fig. 7). In other words, the precipitation runoff loss rate, $dM_P(t)/dt$, can be treated as a constant for a given geographic location or exposure site. Substituting Eq 3 with $n = 1$ into Eq 2 and integrating gives:

$M_T(t) = (\alpha/\beta)[1 - \exp\{-\beta M_T(t)/\alpha\}] + \beta t$ (Eq 6)

where β is the precipitation runoff loss rate, and α is a constant related to properties of the corrosion film.

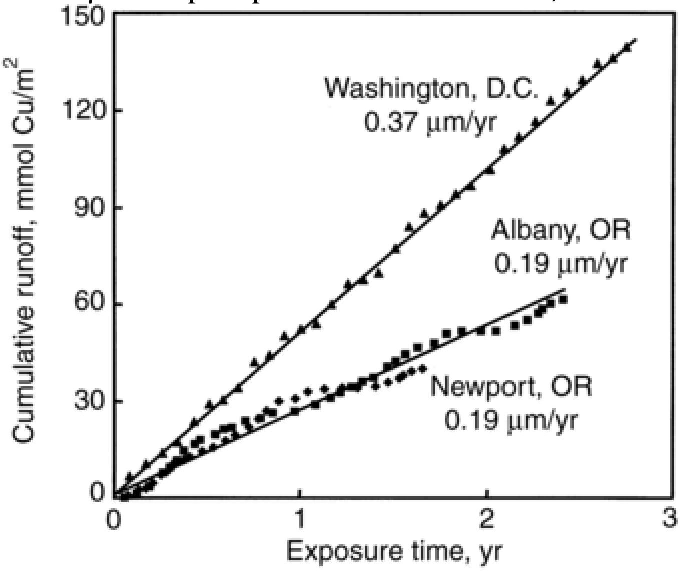

Fig. 7 Cumulative copper precipitation runoff losses at marine unpolluted and polluted sites as a function of exposure time

This empirical model describes the time variation of the total corrosion loss when the precipitation runoff loss rate is nonzero. It describes conditions where there is competition between corrosion film growth and corrosion film dissolution and removal in precipitation runoff. The precipitation runoff loss rate, β, describes the influence of environmental factors on corrosion film stability. The constant α describes the effect of intrinsic properties of minerals in the corrosion film on corrosion film stability. The ratio of the two terms, (α/β), describes the balance between the tendency for protective corrosion film growth and the environmental factors producing corrosion product losses in precipitation runoff. Equation 6 reduces to the parabolic form of Eq 4 in the limit where the precipitation runoff loss rate is 0.

With sufficient environmental data and limited geochemical modeling, contributions of environmental processes to the precipitation runoff rate can be estimated. This has been done for zinc (Ref 12) and copper (Ref 13) exposed in a polluted urban environment, a marine environment, and a rural environment. Figure 8 shows four contributions to copper corrosion in the polluted urban environment: (a) a strong acid contribution from wet deposition representing the effect of acid rain, (b) a weak acid contribution in wet deposition representing the effect of the carbon dioxide/bicarbonate/carbonate equilibia, (c) a dry deposition contribution representing

acid gases (sulfur dioxide, nitric acid, hydrochloric acid) and perhaps modified by the deposition of basic particulates, and (d) a precipitation of brochantite, $CuSO_4 \cdot 3Cu(OH)_2$, within the corrosion film as a result of weathering of the corrosion film. These contributions add together stoichiometrically to give the curve for the cumulative precipitation runoff loss, $M_P(t) = t\beta$.

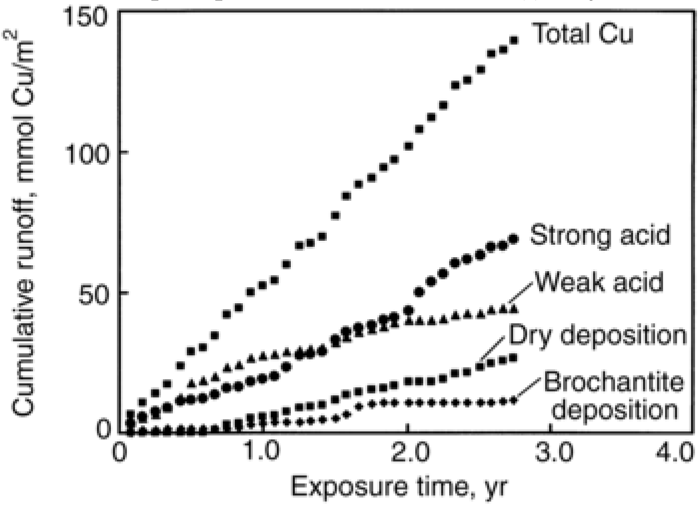

Fig. 8 Dry deposition, strong acid, weak acid, and brochantite deposition contributions to cumulative copper precipitation runoff loss as determined by geochemical modeling for the polluted Washington, D.C. site

Very long-term corrosion data that include both mass loss and corrosion film thickness and chemistry are not often available to test Eq 6. Data were available for a 100 year old copper roof in Stockholm, Sweden (Ref 5). Values of α and β were estimated, knowing that the ratio of the two values was equal to the steady-state thickness of the corrosion film. For an effective corrosion film thickness of 15.5 μm, the best estimates of the two values were (Ref 13) $\alpha = 13.9\ \mu m^2$/year and $\beta = 0.9\ \mu m$/year. The resulting curves for cumulative precipitation runoff loss, total corrosion mass loss, and the patina thickness are shown in Fig. 9 (Ref 13). This figure illustrates that corrosion film growth is the dominant process during the early exposure period. However, in long exposures, such as the 100 year old copper roof, a large fraction of the corrosion mass loss simply maintains the patina thickness so as to balance precipitation runoff losses. Of course, this is the result expected from Eq 2 for steady-state conditions where film growth has ceased, that is, $dM_F(t)/dt = 0$. In that case, the corrosion rate equals exactly the precipitation runoff loss rate.

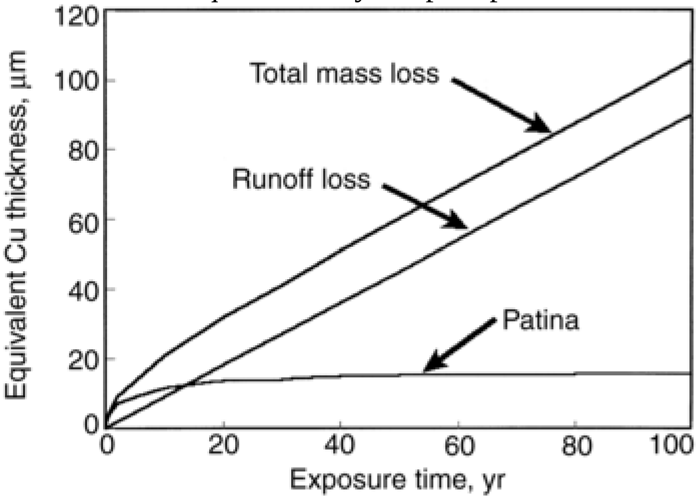

Fig. 9 Cumulative corrosion mass loss, corrosion film growth (patina), and precipitation runoff loss for a 100 year old copper roof exposed in Stockholm, Sweden

Finally, the parameters in Eq 6, α and β, can be used to define a dimensionless corrosion equation, that is:

$$M_T(t^*)^* = [1 - \exp\{-M_T(t^*)^*\}] + t^* \quad \text{(Eq 7)}$$

where $M_T(t^*)^* = M_T(t)\beta/\alpha$, dimensionless cumulative corrosion loss; $t^* = t\beta^2/\alpha$, dimensionless time; $M_{F,S} = \alpha/\beta$, the steady-state corrosion film or patina thickness; $t_c = \alpha/\beta^2$, a characteristic time (17.2 years for the example of the 100 year old copper roof).

The dimensionless corrosion equation gives the curve shown in Fig. 10 as a function of time (Ref 13). Early in the corrosion process, the corrosion kinetics are parabolic, and the slope of the curve is $\frac{1}{2}$. As the corrosion film matures and the corrosion process approaches steady state, the corrosion kinetics transition from parabolic kinetics to linear kinetics, and the slope changes from $\frac{1}{2}$to 1. In the framework of the dimensionless equation, short and long exposures are relative terms defined by the balance of environmental factors (β) and factors related to the mineralogy of the corrosion film (α).

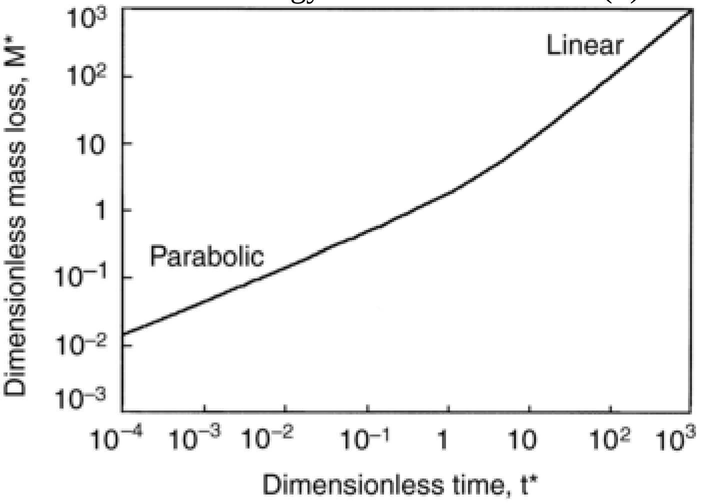

Fig. 10 Dimensionless empirical model for atmospheric corrosion with precipitation runoff losses showing effect of exposure time on cumulative mass loss and corrosion kinetics

References cited in this section

2. W. He, I. Odenvall Wallinder, and C. Leygraf, A Comparison Between Corrosion Rates and Runoff Rates from New and Aged Copper and Zinc as Roofing Materials, *Water, Air Soil Pollut. Focus,* Vol 1, 2001, p 67–82

3. I. Odnevall Wallinder, P. Verbiest, W. He, and C. Leygraf, The Influence of Patina Age and Pollutant Levels on the Runoff Rate of Zinc from Roofing Materials, *Corros. Sci.,* Vol 40 (No. 11), 1998, p 1977–1982

4. I. Odnevall Wallinder, P. Verbiest, W. He, C. Leygraf, Effects of Exposure Direction and Inclination on the Runoff Rates of Zinc and Copper Roofs, *Corros. Sci.,* Vol 42, 2000 p 1471–1487

5. W. He, I. Odnevall Wallinder, and C. Leygraf, A Laboratory Study of Copper and Zinc Runoff during First Flush and Steady- State Conditions, *Corros. Sci.,* Vol 43, 2001, p 127–146

6. W. He, I. Odnevall Wallinder, and C. Leygraf, Runoff Rates of Zinc—A Four-Year Field and Laboratory Study, *Outdoor Atmospheric Corrosion,* STP 1421, H.E. Townsend, Ed., ASTM International, 2002, p 216–229

12. S.D. Cramer, S.A. Matthes, G.R. Holcomb, B.S. Covino, Jr., and S.J. Bullard, “Precipitation Runoff and Atmospheric Corrosion,” Paper 00452, Corrosion/2000, NACE International, 2000

13. S.D. Cramer, S.A. Matthes, B.S. Covino, Jr., S.J. Bullard, and G.R. Holcomb, Environmental Factors Affecting the Atmospheric Corrosion of Copper, *Outdoor Atmospheric Corrosion,* STP 1421, H.E. Townsend, Ed., American Society for Testing and Materials, 2002, p 245–264

48. R.H. McCuen, P. Albrecht, and J. Cheng, A New Approach to Power-Model Regression of Corrosion Penetration Data, *Corrosion Forms and Control for Infrastructure,* STP 1137, V. Chaker, Ed., American Society for Testing and Materials, 1992, p 46–76

S.D. Cramer and S.A. Matthes, Simulated Service Testing in the Atmosphere, *Corrosion: Fundamentals, Testing, and Protection*, Vol 13A, *ASM Handbook*, ASM International, 2003, p 487–494

Simulated Service Testing in the Atmosphere

Stephen D. Cramer and Steven A. Matthes, Albany Research Center, U.S. Department of Energy

---

Acknowledgment

Portions of this article have been adapted from K.L. Money, Simulated Service Testing: Corrosion Testing in the Atmosphere, *Corrosion,* Vol 13, *Metals Handbook,* 9th ed., ASM International, 1987, p 205–206.

S.D. Cramer and S.A. Matthes, Simulated Service Testing in the Atmosphere, *Corrosion: Fundamentals, Testing, and Protection*, Vol 13A, *ASM Handbook*, ASM International, 2003, p 487–494

Simulated Service Testing in the Atmosphere

Stephen D. Cramer and Steven A. Matthes, Albany Research Center, U.S. Department of Energy

---

References

1. Effects of Acidic Deposition on Materials, Report 19, *Terrestrial, Materials, Health and Visibility Effects,* Vol III, *Acidic Deposition: State of Science and Technology,* U.S. National Acid Precipitation Assessment Program, Washington, D.C., p. 19–1 to 19–280, 1991

2. W. He, I. Odenvall Wallinder, and C. Leygraf, A Comparison Between Corrosion Rates and Runoff Rates from New and Aged Copper and Zinc as Roofing Materials, *Water, Air Soil Pollut. Focus,* Vol 1, 2001, p 67–82

3. I. Odnevall Wallinder, P. Verbiest, W. He, and C. Leygraf, The Influence of Patina Age and Pollutant Levels on the Runoff Rate of Zinc from Roofing Materials, *Corros. Sci.,* Vol 40 (No. 11), 1998, p 1977–1982

4. I. Odnevall Wallinder, P. Verbiest, W. He, C. Leygraf, Effects of Exposure Direction and Inclination on the Runoff Rates of Zinc and Copper Roofs, *Corros. Sci.,* Vol 42, 2000 p 1471–1487

5. W. He, I. Odnevall Wallinder, and C. Leygraf, A Laboratory Study of Copper and Zinc Runoff during First Flush and Steady- State Conditions, *Corros. Sci.,* Vol 43, 2001, p 127–146

6. W. He, I. Odnevall Wallinder, and C. Leygraf, Runoff Rates of Zinc—A Four-Year Field and Laboratory Study, *Outdoor Atmospheric Corrosion,* STP 1421, H.E. Townsend, Ed., ASTM International, 2002, p 216–229

7. X. Zhang, W. He, I. Odnevall Wallinder, J. Pan, and C. Leygraf, Determination of Instantaneous Corrosion Rates and Runoff Rates of Copper from Naturally Patinated Copper during Continuous Rain Events, *Corros. Sci.,* Vol 44, 2002, p 2131–2151

8. I. Odnevall Wallinder and C. Leygraf, A Study of Copper Runoff in an Urban Atmosphere, *Corros. Sci.,* Vol 39 (No. 12), 1997, p 2039–2052

9. S.D. Cramer and L.G. McDonald, Atmospheric Factors Affecting the Corrosion of Zinc, Galvanized Steel, and Copper, *Corrosion Testing and Evaluation,* STP 1000, R. Baboian and S.W. Dean, Ed., American Society for Testing and Materials, 1990, p 208–224

10. J.W. Spence, F.H Haynie, F.W. Lipfert, S.D. Cramer, and L.G. McDonald, Atmospheric Corrosion Model for Galvanized Steel Structures, *Corrosion,* Vol 48 (No. 12), 1992, p 1009–1019

11. S.D. Cramer, L.G. McDonald, and J.W. Spence, Effects of Acidic Deposition on the Corrosion of Zinc and Copper, *Proceedings of the 12th International Corrosion Congress,* Vol 2, NACE International, 1993, p 722–733

12. S.D. Cramer, S.A. Matthes, G.R. Holcomb, B.S. Covino, Jr., and S.J. Bullard, "Precipitation Runoff and Atmospheric Corrosion," Paper 00452, Corrosion/2000, NACE International, 2000

13. S.D. Cramer, S.A. Matthes, B.S. Covino, Jr., S.J. Bullard, and G.R. Holcomb, Environmental Factors Affecting the Atmospheric Corrosion of Copper, *Outdoor Atmospheric Corrosion,* STP 1421, H.E. Townsend, Ed., American Society for Testing and Materials, 2002, p 245–264

14. S.A. Matthes, S.D. Cramer, B.S. Covino, Jr., S.J. Bullard, and G.R. Holcomb, Precipitation Runoff from Lead, *Outdoor Atmospheric Corrosion,* STP 1421, H.E. Townsend, Ed., American Society for Testing and Materials, 2002, p 265–274

15. S.A. Matthes, S.D. Cramer, S.J. Bullard, B.S. Covino, Jr., and G.R. Holcomb, "Atmospheric Corrosion and Precipitation Runoff from Zinc and Zinc Alloy Surfaces," Paper 03598, Corrosion/2003, 17–20 March 2003 (San Diego, CA), NACE International, 2003

16. H.T. Michels, B. Boulanger, and N.P. Nikolaidis, "Copper Roof Stormwater Runoff—Corrosion and the Environment," Paper 02225, Corrosion/2002, NACE International, 2002

17. H.T. Michels, B. Boulanger, and N.P. Nikolaidis, Environmental Impact of Stormwater Runoff from a Copper Roof, *Mater. Perform.,* Vol 42 (No. 2) Feb 2003, p 70–74

18. M.C. Gromaire-Mertz, S. Garnaud, A. Gonzales, and G. Chebbo, Characterization of Urban Runoff Pollution in Paris, *Wat. Sci. Technol.,* Vol 39 (No. 2), 1999, p 1–8

19. T.S. Barron, "Architectural Uses of Copper—An Evaluation of Stormwater Pollution Loads and Best Management Practices," Palo Alto Regional Water Quality Control Plant, Palo Alto, CA, 2000

20. I. Odnevall Wallinder, C. Leygraf, C. Karlen, D. Heijerick, and C.R. Janssen, Atmospheric Corrosion of Zinc-Based Materials: Runoff Rates, Chemical Speciation and Ecotoxicity, *Corros. Sci.,* Vol 43, 2001, p 809–816

21. "Notice of Proposed Standard for Sulfur Oxide, Particulate Matter, Carbon Monoxide, Photochemical Oxidants, Hydrocarbons, and Nitrogen Oxides," 42 CFR, Part 410, Federal Register 36, Environmental Protection Agency, 1971, p 1502

22. F. Mansfield, “Regional Air Pollution Study Effects of Airborne Sulfur Pollutants on Materials,” EPA 600/4-80-007, Environmental Protection Agency, Jan 1980

23. F.H. Haynie and J.B. Upham, Effects of Atmospheric Sulfur Dioxide on the Corrosion of Zinc, *Mater. Perform.,* Vol 9, 1970, p 35–40

24. H. Guttman and P.J. Sereda, Measurement of Atmospheric Factors Affecting the Corrosion of Metals, *Metal Corrosion in the Atmosphere,* STP 345, American Society for Testing and Materials, 1968, p 355–360

25. K.G. Compton, Atmospheric Corrosion, *NACE Basic Corrosion Course,* National Association of Corrosion Engineers, 1970, p 4-2

26. F.L. LaQue, Environment Factors in the Corrosion of Metals in Seawater and Sea Air, *Marine Corrosion,* John Wiley & Sons, 1975, p 103

27. D. Knotkova, V. Kucera, S.W. Dean, and P. Boschek, Classification of the Corrosivity of the Atmosphere—Standardized Classification System and Approach for Adjustment, *Outdoor Atmospheric Corrosion,* STP 1421, H.E. Townsend, Ed., American Society for Testing and Materials, 2002, p 109–124

28. J. Tidblad, V. Kucera, A.A. Mikhailov, and D. Knotkova, Improvement of the ISO Classification System Based on Dose-Response Functions Describing the Corrosivity of Outdoor Atmospheres, *Outdoor Atmospheric Corrosion,* STP 1421, H.E. Townsend, Ed., American Society for Testing and Materials, 2002, p 73–87

29. M. Morcillo, E. Almeida, B. Chico, and D. de la Fuente, Analysis of ISO Standard 9223, *Outdoor Atmospheric Corrosion,* STP 1421, H.E. Townsend, Ed., American Society for Testing and Materials, 2002, p 59–72

30. C. Leygraf and T.E. Graedel, *Atmospheric Corrosion,* Wiley-Interscience, 2000, p 109–115

31. F.L. LaQue, *Proc. ASTM,* Vol 51, 1951, p 495

32. J.C. Hudson, *J. Br. Iron Steel Inst.,* Vol 148, 1943, p 161

33. S.K. Coburn et al., Corrosiveness of Various Atmospheric Test Sites as Measured by Specimens of Steel and Zinc, *Metal Corrosion in the Atmosphere,* STP 435, American Society for Testing and Materials, 1968, p 326

34. *ASTM Mater. Res. Stand.,* Dec 1961, p 977

35. S.W. Dean, Jr., Planning, Instrumentation and Evaluation of Atmospheric Corrosion Tests and a Review of ASTM Testing, *Atmospheric Corrosion,* John Wiley & Sons, 1982, p 195–216

36. “Standard Recommended Practice for Conducting Atmospheric Corrosion Tests on Metals,” G 50, *Annual Book of ASTM Standards,* American Society for Testing and Materials

37. “Standard Recommended Practice for Making and Using U-Bend Stress Corrosion Test Specimens,” G 30, *Annual Book of ASTM Standards,* American Society for Testing and Materials

38. “Standard Practice for Preparation and Use of Bent Beam Stress Corrosion Test Specimens,” G 39, *Annual Book of ASTM Standards,* American Society for Testing and Materials

39. “Standard Recommended Practice for Making and Using C-Ring Stress Corrosion Test Specimens,” G 38, *Annual Book of ASTM Standards,* American Society for Testing and Materials

40. “Standard Recommended Practice for Preparation and Use of Direct Tension Stress Corrosion Test Specimens,” G 49, *Annual Book of ASTM Standards,* American Society for Testing and Materials

41. “Standard Practice for Preparation of Stress Corrosion Test Specimens for Weldments,” G 58, *Annual Book of ASTM Standards,* American Society for Testing and Materials

42. R. Baboian, Final Report on the ASTM Study: Atmospheric Galvanic Corrosion of Magnesium Coupled to Other Metals, *Atmospheric Factors Affecting the Corrosion of Engineering Metals,* STP 646, S.K. Coburn, Ed., American Society for Testing and Materials, 1978, p 17–29

43. “Metals and Alloys—Test Methods for Contact Corrosion in Atmospheric Conditions,” ISO/TC 156/WG 3/N11, Third Working Draft, Proposal of USSR to ISO Technical Committee 156 WG 3, Nov 1979

44. “Corrosion of Metals and Alloys—Corrosivity of Atmospheres—Methods of Determination of Corrosion Rates of Standard Specimens for the Evaluation of Corrosivity,” ISO/TC 156 WG4/N131, German Proposal to ISO Technical Committee 156 WG3, 1979

45. T.E. Graedel, K. Nassau, and J.P. Franey, Copper Patinas Formed in the Atmosphere, Part I: Introduction, *Corros. Sci.,* Vol 27 (No. 7), 1987, p 639–657

46. T.E. Graedel, Copper Patinas Formed in the Atmosphere, Part II: Qualitative Assessment of Mechanisms, *Corros. Sci.,* Vol 27 (No. 7), 1987, p 721–740

47. T.E. Graedel, Copper Patinas Formed in the Atmosphere, Part III: A Semi-Quantitative Assessment of Rates and Constraints in the Greater New York Metropolitan Area, *Corros. Sci.,* Vol 27 (No. 7), 1987, p 741–769

48. R.H. McCuen, P. Albrecht, and J. Cheng, A New Approach to Power-Model Regression of Corrosion Penetration Data, *Corrosion Forms and Control for Infrastructure,* STP 1137, V. Chaker, Ed., American Society for Testing and Materials, 1992, p 46–76

S.D. Cramer and S.A. Matthes, Simulated Service Testing in the Atmosphere, *Corrosion: Fundamentals, Testing, and Protection*, Vol 13A, *ASM Handbook*, ASM International, 2003, p 487–494

Simulated Service Testing in the Atmosphere

Stephen D. Cramer and Steven A. Matthes, Albany Research Center, U.S. Department of Energy

---

Selected References

Special Technical Publications from ASTM International:

- R. Baboian and S.W. Dean, Jr., Ed., *Corrosion Testing and Evaluation*, STP 1000, 1990
- V. Chaker, Ed., *Corrosion Forms and Control for Infrastructure,* STP 1137, 1992
- S.K. Coburn, Ed., *Atmospheric Factors Affecting the Corrosion of Engineering Materials,* STP 646, 1978

- *Corrosion in Natural Environments,* STP 558, 1974
- S.W. Dean, Jr., G.H. Delgadillo, and J.B. Bushman, Ed., *Marine Corrosion in Tropical Environments,* STP 1399, 2000
- S.W. Dean, Jr. and T.S. Lee, Ed., *Degradation of Metals in the Atmosphere,* STP 965, 1988
- S.W. Dean, Jr. and E.C. Rhea, Ed., *Atmospheric Corrosion of Metals,* STP 767, 1982
- W.W. Kirk and H.H. Lawson, Ed., *Atmospheric Corrosion,* STP 1239, 1995
- *Metal Corrosion in the Atmosphere,* STP 435, 1968
- H.E. Townsend, Ed., *Outdoor Atmospheric Corrosion,* STP 1421, 2002

Publications from other sources:

- W.H. Ailor, Ed., *Atmospheric Corrosion,* Wiley-Interscience, 1982
- R. Baboian, Ed., *Materials Degradation Caused by Acid Rain,* ACS Symposium Series 318, American Chemical Society, 1986
- V. Kucera and E. Mattsson, Atmospheric Corrosion, *Corrosion Mechanisms,* F. Mansfeld, Ed., Marcel Dekker, 1987, p 211–284
- C. Leygraf and T.E. Graedel, *Atmospheric Corrosion,* Wiley-Interscience, 2000
- X.G. Zhang, *Corrosion and Electrochemistry of Zinc,* Plenum Press, 1996

Simulated Service Corrosion Testing in Water, *Corrosion: Fundamentals, Testing, and Protection*, Vol 13A, *ASM Handbook*, ASM International, 2003, p 495–496

Simulated Service Testing in Water

Introduction

SIMULATED SERVICE TESTING is the most reliable predictor of corrosion behavior short of actual service experience. This includes exposures of either structural components or test specimens in environments that are representative of many general service situations. Test materials are subjected to the cyclic effects of the weather, geographical influences, and bacteriological factors that cannot be realistically duplicated in the laboratory.

This type of testing is important for such objectives as materials selection, predicting the probable service life of a product or structure, evaluating new commercial alloys and processes, and calibrating laboratory corrosion tests. The type of information sought determines the selection of test specimens and the methods of assessing the corrosion effects.

As an environment in which corrosion occurs, water can be categorized as treated or natural. Regardless of the original intent for which a test has been developed, application can be extended to include any use. For example, ASTM G 78 (described in Table 1) is a guide for crevice corrosion testing of iron- and nickel-base alloys in seawater. The crevice assembly described could be installed on any alloy type in any environment if crevices are being studied. Only when quality control or acceptance stipulates a particular test method is there no room for departure. Some test methods involve the insertion of coupons or test panels into a conduit, with the environment at actual velocity and aeration. Other test methods involve the insertion of a test section into the flow line, especially if wall effects might be important. Still other tests require immersion of specimens in relatively open bodies of water.

Table 1 ASTM International and NACE methods for testing waters and materials in waters

Designation	Title	Description
ASTM standards		
D 1293	Standard Test Methods for pH of Water	These methods cover the determination of pH by electrometric measurement, using the glass electrode as the sensor. Two procedures are discussed. Method A covers the precise laboratory measurement of pH in water with the use of at least two of seven standard reference buffer solutions for equipment standardization. Method B concerns the routine or continuous measurement of pH in the laboratory and the measurement of pH under various continuous process conditions.
D 1498	Standard Practice for Oxidation-Reduction Potential of Water	This practice covers the apparatus and procedure for the electrometric measurement of oxidation-reduction potential in water.
D 2688	Standard Test Methods for Corrosivity of Water in the Absence of Heat Transfer (Weight Loss Methods)	These methods cover the determination of the corrosivity of water by evaluating pitting and by measuring the weight loss of metallic specimens. Additional information can be found in the articles “Pitting Corrosion” and “Evaluating Pitting Corrosion” in this Volume.
E 645	Standard Test Method for Efficacy of Microbiocides Used in Cooling Systems	This method covers the effect of bactericides and fungicides in controlling microbial growth in cooling water by using water collected from operational cooling water systems. Additional information can be found in the articles “Microbiologically Influenced Corrosion” and “Evaluating Microbiologically Influenced Corrosion” in this Volume.
G 52	Standard Practice for Exposing and Evaluating Metals and Alloys in Surface Seawater	This practice covers conditions for exposure of metals and alloys to surface seawater and presents the general procedures that should be followed in conducting seawater exposure tests so that meaningful comparisons can be made for different locations.
G 78	Standard Guide for Crevice Corrosion Testing of Iron-Base and Nickel-Base Stainless Alloys in Seawater and Other Chloride-Containing Aqueous Environments	This guide provides information for conducting crevice corrosion tests and identifies factors that may affect results and influence conclusions. These procedures can be used to identify the conditions that will most likely result in crevice corrosion and to provide a basis for assessing the relative resistance of various alloys to crevice corrosion under certain specified conditions. Additional information on crevice corrosion can be found in the articles “Crevice Corrosion” and “Evaluating Crevice Corrosion” in this Volume.
NACE standards		
TM 0174	Laboratory Methods for the Evaluation of Protective Coatings Used as Lining Materials in Immersion Service	This standard gives guidelines to assist manufacturers and users of protective coatings in selecting materials by providing standard test methods for evaluating protective coatings used as linings for immersion service. Two test methods are discussed for the evaluation of protective coatings on any substrate, such as steel, copper, or aluminum, so that both the factors of chemical resistance and permeability can be considered.
RP 0775	Preparation and Installation of Corrosion Coupons and Interpretation of Test Data in Oil	This standard emphasizes the use of uniform industry-proven methods to monitor corrosion in oil production systems. Procedures for preparing, analyzing, and installing

Production Practice	corrosion coupons are also outlined.

Tests used as criteria for acceptance and/or quality control may require a very specific water chemistry and values of such factors as hardness, pH, aeration, temperature, alkalinity, and specific dissolved ion concentrations. It is usually valuable to monitor some of these factors in testing any water because compositions and contaminants change with time as sources (well, river, estuary, storm drains) and climatic conditions (wind direction, temperature, acid rain) vary. A variation in the mixture of sources might change test results significantly. It is important to be aware of the factors that can affect test results when interpreting those results.

Unless galvanic action is being investigated (and it probably should be in most cases), specimens of differing alloy composition or thermomechanical treatment should be electrically isolated or insulated from each other and from the support framework. The factors that require consideration in water supplies are discussed in Ref 1, 2, 3, 4, 5. Many standardized and nonstandardized tests, methods, and practices are discussed in Ref 6, 7, 8, 9, 10. The ASTM International and NACE International standards that are directly or indirectly applicable to simulated service corrosion testing in water are listed and described in Table 1.

References cited in this section

1. F.N. Speller, in *Corrosion Handbook,* H. Uhlig, Ed., John Wiley & Sons, 1948, p 496
2. F.N. Speller, *Corrosion: Causes and Prevention,* McGraw-Hill, 1951, p 244
3. R.K. Swandby, *Corrosion Resistance of Metals and Alloys,* 2nd ed., F.L. LaQue and H.R. Copson, Ed., Reinhold, 1963, p 45
4. G. Butler and H.C.K. Ison, *Corrosion and Its Prevention in Waters,* Reinhold, 1966, p 18
5. *Prevention and Control of Water-Caused Problems in Building Potable Water Systems,* TPC 7, National Association of Corrosion Engineers, 1980
6. V.V. Kendall, in *Corrosion Handbook,* H. Uhlig, Ed., John Wiley & Sons, 1948, p 1058
7. F.L. LaQue, in *Corrosion Handbook,* H. Uhlig, Ed., John Wiley & Sons, 1948, p 1060
8. F.L. LaQue, in *Corrosion Resistance of Metals and Alloys,* 2nd ed., F.L. LaQue and H.R. Copson, Ed., Reinhold, 1963, p 107, 136
9. O.B.K. Fraser, in *Corrosion Handbook,* H. Uhlig, Ed., John Wiley & Sons, 1948, p 105
10. F.A. Champion, *Corrosion Testing Procedures,* 2nd ed., John Wiley & Sons, 1965

Simulated Service Corrosion Testing in Water, *Corrosion: Fundamentals, Testing, and Protection*, Vol 13A, *ASM Handbook*, ASM International, 2003, p 495–496

Simulated Service Testing in Water

Test Method Selection and Precautions

It is necessary to exercise sound judgment when selecting suitable testing procedures. For example, the results of static-immersion tests or alternate-immersion tests bear little relationship to pipelines flowing full within an operating plant. Test coupons inserted into an operating process line, or at least into a laboratory test loop using

process fluids at operating temperatures and velocities, will produce results that agree much better with actual plant experience. Because corrosion is often accelerated at metal/ liquid/vapor interfaces, these interfaces should be duplicated in the testing procedure if they are present in the plant or should be omitted from the testing if they are not an actual factor.

Simulated Service Corrosion Testing in Water, *Corrosion: Fundamentals, Testing, and Protection*, Vol 13A, *ASM Handbook*, ASM International, 2003, p 495–496

Simulated Service Testing in Water

Test Specimens

Specimen geometry, ratio of environment solution volume to exposed specimen area, or other shape and area factors should be as similar as possible to true plant conditions. Exposed, cut specimen edges, which are often attacked more rapidly than other parts, should be examined and discounted if edges are not exposed in plant equipment. Similarly, stamped specimen identification characters may suffer increased rates of attack or may be sites of stress-assisted or accelerated corrosion.

Virtually every specimen size has been used in immersion testing. Popular laboratory test specimen sizes range from 1 cm^2 (0.15 $in.^2$) of exposed surface to 25 × 100 mm (1 × 4 in.), both of which are used frequently, to 100 × 150 mm (4 × 6 in.). In-plant and seawater tests sometimes involve specimens measuring 150 × 250 mm (6 × 10 in.) or larger. When weldments or projections are of concern, either the weldment or the projection should be incorporated into the specimen. Entire components are seldom tested in the laboratory but may be installed in pilot plant or works scale operations (pumps, condensers, heat exchangers).

Simulated Service Corrosion Testing in Water, *Corrosion: Fundamentals, Testing, and Protection*, Vol 13A, *ASM Handbook*, ASM International, 2003, p 495–496

Simulated Service Testing in Water

Effect of Water Variables

To date, no compilation of relative rankings of alloy types in various aqueous environments is available. However, for iron-base alloys, the corrosion rate is relatively uniform in most waters, whether they are of high or low purity. The rate seems to vary more with aeration, that is, from less than 0.05 mm/yr (<2 mils/yr) in deaerated water to more than 1.25 mm/yr (>50 mils/ yr) in aerated water. In tap, brackish, or seawater, pitting tends to occur. In tap water and seawater, yellow brass tends to dezincify (especially when conditions are near stagnation), although corrosion rates are less than 0.05 mm/yr (<2 mils/yr) and more than 0.5 mm/yr (>20 mils/yr) for tap water and seawater, respectively. Detailed information on dezincification can be found in the article “Effects of Metallurgical Variables on Dealloying Corrosion” in this Volume.

There are no definite rules concerning the effect of flow rates, temperatures, and/or pH on the corrosion of alloys in water systems, although in waters free of passivators (including dissolved oxygen), increasing flow rates tend to erode any protective corrosion films that may have formed. Corrosion rates of most alloys over the pH range of 4 to 10 show little effect of pH. Outside this range, that is, 0 to 4 and 10 to 14, the environment cannot technically be considered water, except for some highly unusual acid rain cases. Increasing temperatures sometimes precipitate protective salts, such as calcium carbonate, which decrease corrosion rates in normal-to-hard waters.

Very pure or very soft waters are often excellent solvents for metallic ions, such as copper. If these waters are used to prepare laboratory solutions for test purposes, dissolved copper from copper water lines can deposit or

plate out on more active metal surfaces. In the case of aluminum alloys, this deposited copper can greatly accelerate corrosion immediately adjacent to the copper. The effect of dissolved copper ion on localized corrosion of aluminum is cited in ASTM Standards G 4, section 4.5 (Ref 11); G 52, section 6.2 (Ref 12); and G 71, section 4.2.1 (Ref 13). Similar effects of lesser intensity have been observed on most active metals.

Temperature differentials between points in a flow system can produce accelerated attack due to differences in ionic activity. Although this attack usually occurs at the point of higher temperature, protective scales occasionally precipitate on the high-temperature surface, with attack occurring at the cooler sites. In any system involving differential temperature, the investigator should be aware of this possible behavior.

Another temperature effect in open, aqueous systems is the decreasing solubility of gases, particularly oxygen, with increasing temperature. This effect reduces the cathodic action, or more exactly that portion due to oxygen reduction, and thus decreases the amount of anodic reaction that occurs.

Similarly, the solubility of air and oxygen in saline solutions decreases with increasing concentration of salt, but the solution conductivity increases with the dissolved salt concentration. The two effects combine in oxygen reduction cathodic systems to produce increasing corrosion rates up to about 3.5 wt% sodium chloride (NaCl) solutions and decreasing corrosion rates above that value. This particular effect is not observed in freshwater systems.

Natural waters, depending on the source, may contain variable concentrations of dissolved carbonates. These are principally calcium, magnesium, and/or sodium, with the solubility controlled by both the partial pressure of carbon dioxide and the solubility product of calcium carbonate as it varies with alkalinity and temperature. Deposition of a thin continuous film of carbonate can protect the underlying metal where a lack of the same would allow attack. On the other hand, a film that is too thick impedes heat transfer and can lead to reduced flow and ultimately to possible tube burn-out. Carbonate scaling, measurement through the Langelier Index, and controlling treatments are discussed in Ref 14.

References cited in this section

11. "Standard Guide for Conducting Corrosion Coupon Tests in Field Applications," G 4, *Annual Book of ASTM Standards,* American Society for Testing and Materials

12. "Standard Practice for Exposing and Evaluating Metals and Alloys in Surface Seawater," G 52, *Annual Book of ASTM Standards,* American Society for Testing and Materials

13. "Standard Guide for Conducting and Evaluating Galvanic Corrosion Tests in Electrolytes," G 71, *Annual Book of ASTM Standards,* American Society for Testing and Materials

14. H.H. Uhlig and R.W. Revie, *Corrosion and Corrosion Control,* 3rd ed., John Wiley & Sons, 1985, p 111–114, 415–420

Simulated Service Corrosion Testing in Water, *Corrosion: Fundamentals, Testing, and Protection*, Vol 13A, *ASM Handbook*, ASM International, 2003, p 495–496

Simulated Service Testing in Water

Acknowledgment

This article has been adapted from C.H. Baloun, Corrosion Testing in Water, *Corrosion,* Vol 13, *ASM Handbook* (formerly *Metals Handbook* 9th ed.,), ASM International, 1987, pages 207–208.

References

1. F.N. Speller, in *Corrosion Handbook,* H. Uhlig, Ed., John Wiley & Sons, 1948, p 496
2. F.N. Speller, *Corrosion: Causes and Prevention,* McGraw-Hill, 1951, p 244
3. R.K. Swandby, *Corrosion Resistance of Metals and Alloys,* 2nd ed., F.L. LaQue and H.R. Copson, Ed., Reinhold, 1963, p 45
4. G. Butler and H.C.K. Ison, *Corrosion and Its Prevention in Waters,* Reinhold, 1966, p 18
5. *Prevention and Control of Water-Caused Problems in Building Potable Water Systems,* TPC 7, National Association of Corrosion Engineers, 1980
6. V.V. Kendall, in *Corrosion Handbook,* H. Uhlig, Ed., John Wiley & Sons, 1948, p 1058
7. F.L. LaQue, in *Corrosion Handbook,* H. Uhlig, Ed., John Wiley & Sons, 1948, p 1060
8. F.L. LaQue, in *Corrosion Resistance of Metals and Alloys,* 2nd ed., F.L. LaQue and H.R. Copson, Ed., Reinhold, 1963, p 107, 136
9. O.B.K. Fraser, in *Corrosion Handbook,* H. Uhlig, Ed., John Wiley & Sons, 1948, p 105
10. F.A. Champion, *Corrosion Testing Procedures,* 2nd ed., John Wiley & Sons, 1965
11. "Standard Guide for Conducting Corrosion Coupon Tests in Field Applications," G 4, *Annual Book of ASTM Standards,* American Society for Testing and Materials
12. "Standard Practice for Exposing and Evaluating Metals and Alloys in Surface Seawater," G 52, *Annual Book of ASTM Standards,* American Society for Testing and Materials
13. "Standard Guide for Conducting and Evaluating Galvanic Corrosion Tests in Electrolytes," G 71, *Annual Book of ASTM Standards,* American Society for Testing and Materials
14. H.H. Uhlig and R.W. Revie, *Corrosion and Corrosion Control,* 3rd ed., John Wiley & Sons, 1985, p 111–114, 415–420

Simulated Service Corrosion Testing in Water, *Corrosion: Fundamentals, Testing, and Protection*, Vol 13A, *ASM Handbook*, ASM International, 2003, p 495–496

Simulated Service Testing in Water

Selected References

- J.F. Jenkins, Seawater Tests, *Corrosion Tests and Standards: Application and Interpretation,* R. Baboian, Ed., ASTM International, 1995, p 127–130
- W.T. Young and P. Fairer, Freshwater Tests, *Corrosion Tests and Standards: Application and Interpretation,* R. Baboian, Ed., ASTM International, 1995, p 131–136

M.K.A. Flitton, and E. Escalante, Simulated Service Testing in Soil, *Corrosion: Fundamentals, Testing, and Protection*, Vol 13A, *ASM Handbook*, ASM International, 2003, p 497–500

Simulated Service Testing in Soil

M.K. Adler Flitton, Idaho National Engineering and Environmental Laboratory; E. Escalante, Corrosion Group, National Institute of Science and Technology (retired)

Introduction

TEST METHODS for evaluating the durability of a metal in soil are described in this article. Specimen design, preparation, burial, and retrieval techniques are discussed. The type of information sought during soil-induced corrosion evaluation controls the design configuration and the nature of the corrosion measurements. Consideration of these factors during the planning stage will help the corrosion engineer obtain a maximum amount of information with a minimum number of problems.

The corrosion of metals in soils, which is also called underground corrosion, can be divided into two broad categories: corrosion in undisturbed soils and corrosion in disturbed soils. Corrosion in undisturbed soil is always low, regardless of soil conditions, and is limited only by the availability of the oxygen necessary for the cathodic reaction. Steel piles driven into soil fall under this category and therefore undergo limited corrosive attack. Corrosion of metals in disturbed soils is strongly affected by soil conditions. Soil electrical resistivity, mineral composition, dissolved salts, moisture content, total acidity or alkalinity (pH), redox potentials, microbiological activity, and concentration of oxygen play important roles in determining whether metal corrosion is a serious problem in soils (Table 1). Other, secondary factors are also important but are more difficult to define. Thus, simply testing metals and alloys in a variable pH solution or in aerated or deaerated solutions will not accurately simulate the conditions in soil (Ref 2).

Table 1 Numerical corrosivity scale

Point system for predicting soil corrosivity according to American Water Works Association C 105

Soil parameter	Value	Assigned points
Resistivity, Ω · cm	<700	10
	700–1000	8
	1000–1200	5
	1200–1500	2
	1500–2000	1
	>2000	0
pH	0–2	5
	2–4	3
	4–6.5	0
	6.5–7.5	0
	7.5–8.5	0
	>8.5	3
Redox potential, mV	>100	0

	50–100	3.5
	0–50	4
	<0	5
Sulfides	Positive	3.5
	Trace	2
	Negative	0
Moisture	Poor drainage, continuously wet	2
	Fair drainage, generally moist	1
	Good drainage, generally dry	0

When points in the American Water Works Association scale equal 10 or higher, protective measures have been recommended for cast iron alloys. Source: Ref 1

Any metal buried by backfilling is in a disturbed soil and is subject to corrosion attack, depending on the characteristics of the soil. Most metals in soil are exposed to disturbed-soil conditions. Because it is the more common of the two, only the disturbed-soil condition is discussed.

References cited in this section

1. "ANSI Standard for Polyethylene Encasement for Ductile-Iron Pipe Systems," C105/ A21.5-99, American Water Works Association, 1999
2. D.B. Craig and D.S. Anderson, Ed., *Handbook of Corrosion Data,* 2nd ed., ASM International, 1995, p 822–823

M.K.A. Flitton, and E. Escalante, Simulated Service Testing in Soil, *Corrosion: Fundamentals, Testing, and Protection*, Vol 13A*, ASM Handbook*, ASM International, 2003, p 497–500

Simulated Service Testing in Soil

M.K. Adler Flitton, Idaho National Engineering and Environmental Laboratory; E. Escalante, Corrosion Group, National Institute of Science and Technology (retired)

Soil Characteristics

Soil is a complex, dynamic environment that changes continuously and seasonally, both chemically and physically. Precipitation, plants, and animals all have their effects on the environment, but perhaps a greater effect results from human activities of building structures, roads, electric power lines, underground utilities, landfills, farming, snow removal with salts, and so on. Characterizing a soil for its corrosivity is difficult at best. However, certain empirically derived facts are known to affect the corrosivity of soils.

Soil electrical resistivity is recognized as an important parameter in underground corrosion (Ref 3). Ions from dissolved salts and minerals must migrate through the electrolyte in a soil to supply the metal surface with the electron donors or acceptors necessary for the corrosion reaction to proceed. Soil resistivity is a measure of the concentration of these ions and how easily they move through the soil environment (Ref 4). A high soil resistivity suggests a low corrosion rate, because the rate of ion diffusion is low. The nature of the ion species is also critical. Chlorides, for example, are known to enhance the breakdown of the protective oxide on some metals (Ref 5). Copper ions accelerate the attack on aluminum (Ref 6). Sulfates can provide oxidizers for microbiological corrosion (Ref 7). Other salts, such as carbonates, can affect the pH of the soil. Thus, the corrosivity of a soil can be strongly affected by the presence of certain chemical species, and a soil that is corrosive for one metal may not be corrosive for another metal. Table 2 shows the generally adopted corrosion severity ratings based on soil resistivity (Ref 8).

Table 2 Corrosivity ratings based on soil resistivity

Soil resistivity, Ω · cm	Corrosivity rating
>20,000	Essentially noncorrosive
10,000–20,000	Mildly corrosive
5,000–10,000	Moderately corrosive
3,000–5,000	Corrosive
1,000–3,000	Highly corrosive
<1,000	Extremely corrosive

pH. The acidity or the alkalinity of most soils is stable because of the buffering action of the soluble minerals available. However, soils across the United States, for example, can differ in pH from 5 to 10. This pH range has a small effect on general and pitting corrosion attack but has a large effect on the susceptibility of ferrous alloys to hydrogen embrittlement (Ref 9). Furthermore, some metals, such as zinc, copper, and aluminum, are amphoteric and can undergo corrosive attack at high and low pH values; by definition, these metals may be susceptible to attack in acid and alkaline soils (Ref 6). These effects on the corrosion process make it desirable to measure the pH of the soil at a test site (Ref 10).

Soil texture is dependent on the proportions of sand, silt, and clay mineral particles making up a soil. Clay, having the finest particle size and minimum pore volume between particles, tends to reduce the movement of air and water through the soil and can therefore develop conditions of poor aeration when wet. Sand has the largest particle size and promotes increased aeration and distribution of moisture. Soil texture is important as an influence on the diffusivity of soluble salts and gases. Internal drainage describes the water- retention properties of a soil and is related to soil texture. Internal drainage also is affected by the height of the water table and thus whether the soil is in a saturated or unsaturated condition. Soil texture and drainage also influence the movement of corrosion products within the soil environment and how corrosion products may change as they are transported away from the metal.

The ways in which soil resistivity, pH, and soil composition interact to determine soil corrosivity are not well understood despite extensive amounts of data that have been collected over the years (Ref 3, 11, 12). Soil temperature has been found to have a strong effect on soil resistivity and oxygen solubility. Because these are opposing effects competing to control the corrosion process, their cumulative effect on metal corrosion in soil is minimized (Ref 9). Clearly, many factors affect soil corrosivity, and their interrelationship is complex.

References cited in this section

3. M. Romanoff, "Underground Corrosion," NBS 579, NTIS PB 168,350, National Bureau of Standards, April 1957

4. "Standard Method for Field Measurement of Soil Resistivity Using the Wenner Four- Electrode Method," G 57, *Annual Book of ASTM Standards,* American Society for Testing and Materials, 1995

5. J.R. Galvele, Present State of Understanding of the Breakdown of Passivity and Repassivation, *Passivity of Metals,* The Electrochemical Society, Inc., 1978, p 258–327

6. H.H. Uhlig and R.W. Revie, *Corrosion and Corrosion Control,* 3rd ed., John Wiley & Sons, 1985, p 111–114, 415–420.

7. W.P. Iverson, An Overview of the Anaerobic Corrosion of Underground Metallic Structures: Evidence for a New Mechanism, *Underground Corrosion,* American Society for Testing and Materials, 1981, p 33–52

8. P.R. Roberge, *Handbook of Corrosion Engineering,* McGraw-Hill, 1999

9. E. Escalante, The Effect of Soil Resistivity and Soil Temperature on the Corrosion of Galvanically Coupled Metals in Soil, *Galvanic Corrosion,* STP 978, H. Hack, Ed., American Society for Testing and Materials, 1988

10. "Standard Test Method for Measuring pH of Soil for Use in Corrosion Testing," G 51, *Annual Book of ASTM Standards,* American Society for Testing and Materials, 1995.

11. W.J. Schwerdtfeger, Soil Resistivity as Related to Underground Corrosion and Cathodic Protection, *J. Res. Natl. Bur. Stand.,* Vol 69C (No. 1), Jan–March 1965

12. N.D. Tomashov, *Theory of Corrosion and Protection of Metals,* Macmillan, 1966, p 399–451.

M.K.A. Flitton, and E. Escalante, Simulated Service Testing in Soil, *Corrosion: Fundamentals, Testing, and Protection,* Vol 13A, *ASM Handbook,* ASM International, 2003, p 497–500

Simulated Service Testing in Soil

M.K. Adler Flitton, Idaho National Engineering and Environmental Laboratory; E. Escalante, Corrosion Group, National Institute of Science and Technology (retired)

Test Approach

Although soil characteristics give some indication of the corrosivity of a soil environment, the optimal test of metals is to bury specimens in the soil of interest. The concept is simple, but there are some important considerations. For example, the type of data sought and the data objectives will determine the design of specimens and the test procedure. Will the data be used as an analog for underground utilities or structures, or will they be used in models to determine long- term containment failure and contaminant transport into the soil environment? Interest in metal corrosion in soils extends to long-term stability of critical underground infrastructure, such as water, gas, oil, and waste pipelines and telephone and electric power distribution cables. Another even more pressing environmental issue concerns the long-term underground containment of legacy and newly generated hazardous chemical and nuclear wastes—wastes requiring isolation and containment for hundreds or even thousands of years.

In addition to buried specimens of metals, provision must be made for electrochemical corrosion measurements and for environmental measurements during the burial period. Periodic retrieval of specimens of an alloy requires that identical sets be buried, one set per retrieval. Each set must have statistically significant numbers of each alloy represented. It is necessary to mark the specimens for future identification and to mark the location of the specimens at the site. The importance of maintaining permanent, clear, detailed records cannot be overemphasized. These records become increasingly important for long-term burial periods where personnel and organizations may change. Loss of records can directly impact the uncertainties in the corrosion rate measurements.

M.K.A. Flitton, and E. Escalante, Simulated Service Testing in Soil, *Corrosion: Fundamentals, Testing, and Protection,* Vol 13A, *ASM Handbook,* ASM International, 2003, p 497–500

Simulated Service Testing in Soil

M.K. Adler Flitton, Idaho National Engineering and Environmental Laboratory; E. Escalante, Corrosion Group, National Institute of Science and Technology (retired)

Specimen Preparation

The type of data needed usually determines the design of the specimen. If corrosion of pipe is under consideration, then pipe material should be used. To minimize internal corrosion effects, the ends can be sealed with caps. Corrosion of a tank container suggests the use of sheet or plate material for testing. If welds are expected, then welded material should be included. If dissimilar metals will be in contact, then galvanically coupled materials are required. Stressed U-bend or C-ring specimens, for example, are necessary for stress-corrosion or hydrogen embrittlement studies. Control specimens should also be included. Control specimens could be uncoated metals when the effect of coatings is being evaluated. Similarly, unstressed specimens should be included when stressed specimens are being studied. Archived samples of the alloys being studied (not exposed in the test environment but kept in a protected environment such as a desiccant chamber) should be kept for comparative purposes.

Before cleaning and weighing, the specimen is marked for proper identification by stamping or notching the specimen. In the case of a brittle metal, chemical or laser etching of an identification mark is preferred. In addition to this identification on the specimen, a secondary identification method should be used. One method is to attach plastic tags to the specimen in case corrosion is sufficiently severe to destroy the identification markings. Because these tags are often lost during retrieval or transportation, they should not be the primary marking system. Another method for identification is placement of the specimen. Both the placement position and the location of the trench can be used to identify the specimen, as long as the installation records are maintained. Where retrievals are planned on a periodic basis, duplicate specimens must be provided, and each must have its own unique identification mark.

Electrical contact to a specimen is required when electrochemical measurements are made during the burial period. This contact can be achieved with a 14-gage (~1.9 mm, or 0.075 in., diameter) insulated metal conductor that extends above ground and is soldered or bolted to the specimen. Solder can be removed after retrieval and before reweighing by heating the joint and wiping away the solder, but this is possible only with high-melting-point metal specimens, such as ferrous alloys. To avoid galvanic attack of the specimen or the conductor during burial, the joint must be coated. Electrical conductors to both electrodes of a galvanic couple allow galvanic currents to be measured.

Another real-time measurement to consider for corrosion rate comparison is the use of electrical resistance probes made from the alloys being tested. Electrical resistance probes have one element exposed to the test environment while another element is sealed and protected from corrosion in an epoxy or plastic sheath. This allows a comparison of electrical resistance between the two elements. Sensitivity of the probe depends on the element configuration and thickness. Periodic measurements are made over the course of the test to determine corrosion rate.

M.K.A. Flitton, and E. Escalante, Simulated Service Testing in Soil, *Corrosion: Fundamentals, Testing, and Protection*, Vol 13A, *ASM Handbook*, ASM International, 2003, p 497–500

Simulated Service Testing in Soil

M.K. Adler Flitton, Idaho National Engineering and Environmental Laboratory; E. Escalante, Corrosion Group, National Institute of Science and Technology (retired)

Specimen Burial

A technique frequently used for shallow burial is to dig a trench up to 1.22 m (4 ft) deep that is long enough to allow placement of the specimens approximately 300 mm (12 in.) apart along its length (Fig. 1). For burial of specimens deeper than 1.22 m (4 ft), a large-diameter hole can be drilled. In deeper burials, caution should be used to ensure worker safety and cave-in protection (Fig. 2). If specimens are to be retrieved periodically, for example, after 1, 2, or 4 years exposure, then all specimens of a given retrieval increment should be grouped together; that is, all specimens to be recovered at the end of 1 year are grouped separately from those that are to be retrieved at the end of 2 years, and so on.

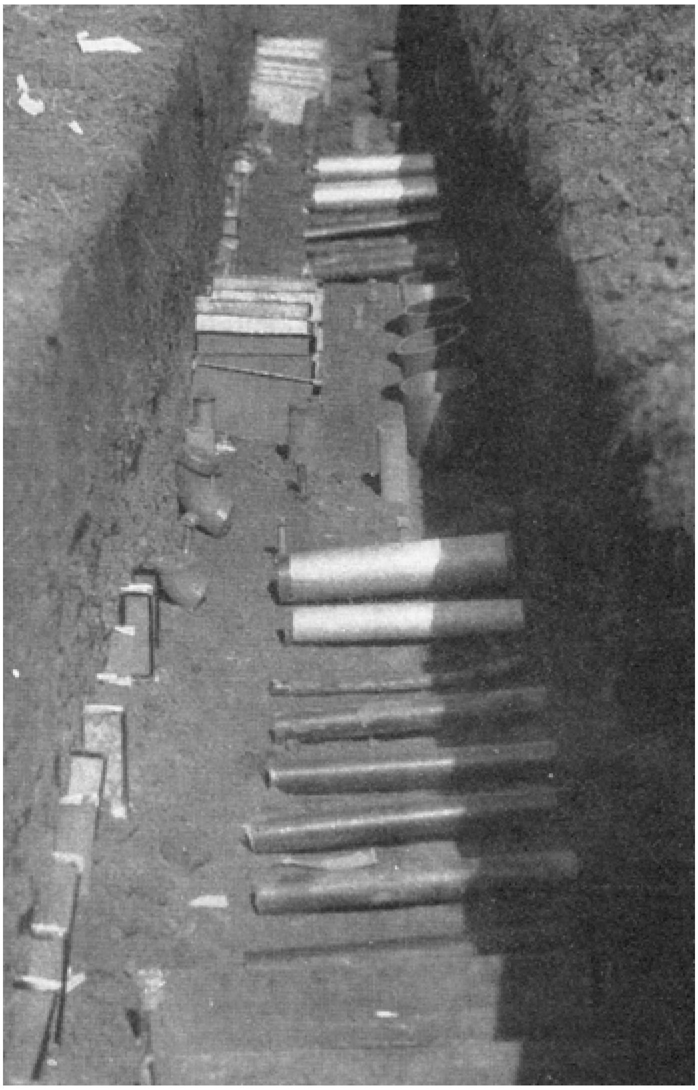

Fig. 1 Metal specimens in trench. Typical of underground corrosion studies, metal samples of sheet metal, pipes, and pipe fixtures are arranged in a shallow trench.

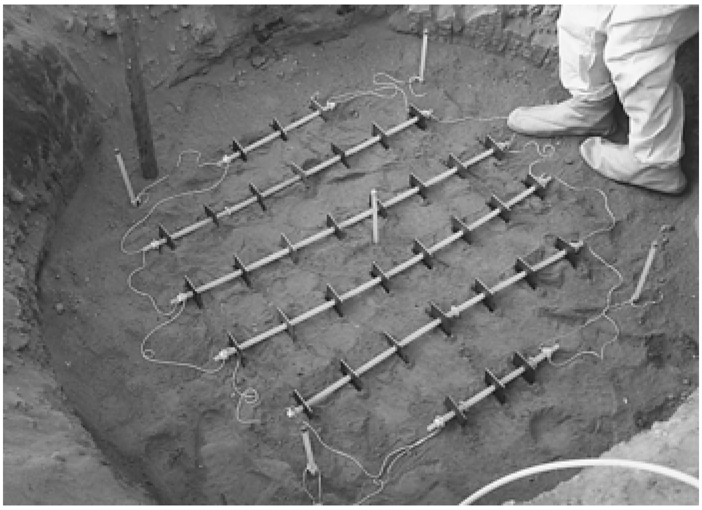

Fig. 2 Metal specimens in augured drill hole. Metal samples are arranged on inert rods arranged as an array in the hole. The rods are tethered to location rods with nylon cords. Other instrumentation, such as a pipe for moisture monitoring and a tube for soil gas sampling, are also pictured. Depths may vary, depending on the requirements of the underground corrosion to be investigated.

To facilitate retrieval of the specimens, it is useful to tie a small-diameter (3 mm, or 0.12 in.) nylon rope (or other nonconductive material) to each specimen in a retrieval group. Thus, when one specimen is found, digging can proceed by following the rope until all of the specimens are recovered. Wood posts can be used to mark the location of the ends of a group of specimens, and the rope can be tied to these posts. Where posts cannot be used, metal markers buried just below the surface of the ground are used to mark the location of the specimens. These markers can then be located with a metal detector. It is useful to have a clearly visible surface marker that identifies the site and an individual or company that can be contacted for further information about the test.

An accurate map of the area identifying the exact location of all specimens is mandatory. Global positioning system (GPS) coordinates can be used to identify the location of the specimens and markers on installation and again at the time of specimen retrieval. The GPS elevation data also can provide the depth of specimens in relationship to the elevation of the soil surface. This GPS data should be recorded on the specimen map of the test site. Although describing the details of burial and recovery may seem mundane, important data can be lost in long-term exposure tests because such information was not properly recorded and maintained.

Electrical conductors attached to the specimens, including those from installed probes, must be carefully and permanently marked for identification at the surface end of the conductor. These conductors can then be attached to contact points on the wood posts or secured through a stand-up pipe with a weather-protective instrument/terminal enclosure (Fig. 3).

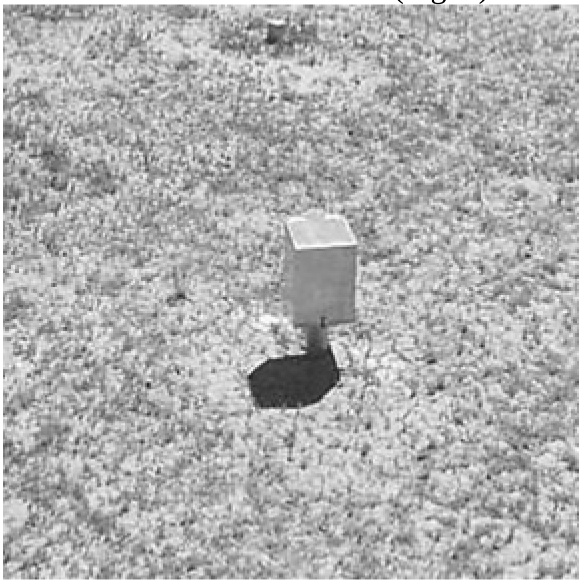

Fig. 3 Monitoring station. A protective enclosure houses instrumentation for environmental and corrosion monitoring.

M.K.A. Flitton, and E. Escalante, Simulated Service Testing in Soil, *Corrosion: Fundamentals, Testing, and Protection*, Vol 13A, *ASM Handbook*, ASM International, 2003, p 497–500

Simulated Service Testing in Soil

M.K. Adler Flitton, Idaho National Engineering and Environmental Laboratory; E. Escalante, Corrosion Group, National Institute of Science and Technology (retired)

Corrosion Measurements

Engineers are usually interested in obtaining data on the corrosion rate of a metal in soil, and this requires knowledge of mass loss and length of exposure. However, rate of pit growth may be the more important measurement if the material is to be used in construction of a fluid container or a pipeline. For some metals and

alloys, stress- corrosion cracking or hydrogen embrittlement may more likely be the mode of failure. Other aspects related to corrosion may also need to be examined, such as microbiological influences and transport of corrosion products away from the specimens and into the surrounding environment.

Uniform Corrosion. Gravimetric mass loss is the reference by which all mass loss measurements are judged when evaluating the uniform or general corrosive attack of a metal in soil. Gravimetric mass-loss determinations involve weighing the specimen before the exposure period and then reweighing it after retrieval. When properly carried out, the mass loss represents the average rate at which the metal is consumed by corrosion. This technique generally requires long exposures (years) so that the mass loss is measurable and significant. Specimens of 1000 g or less should be weighed to an accuracy of 0.5 mg. Sample size may be limited by the capacity of the balance available. An excellent source of information on preparing, cleaning, and evaluating specimens is ASTM G 1 (Ref 13).

If data are obtained through periodic retrievals, little can be learned about corrosion losses between retrieval times. One method of obtaining continuous corrosion rate data is to use electrical measurements that take advantage of the electrochemical nature of underground corrosion. Another method is to employ real-time electrical resistance corrosion probes.

In the polarization resistance technique, the potential of a metallic specimen is changed by 10 mV or less, and the amount of current applied to make this change is measured (Ref 14). Three electrodes are usually used: the working electrode (the metal of interest), the reference electrode (used to measure the potential of the working electrode), and the counterelectrode (used to apply current to the working electrode). Figure 4 illustrates the configuration of the three electrodes for a typical measurement in soil. The effects of the potential (*I*R) drop between the reference electrode and working electrode, an error that arises when measuring a potential in the presence of current (*I*) flowing through a resistive medium (R), must be considered (Ref 15). Details of this polarization technique are described in the article "Electrochemical Methods of Corrosion Testing" in this Volume.

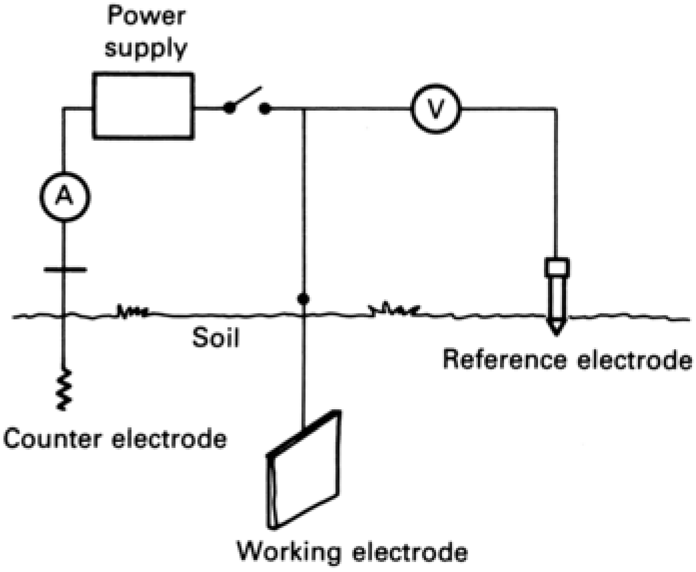

Fig. 4 Configuration of electrodes used in a polarization measurement of metals in soil

Pitting corrosion is typically measured after retrieval of the specimens, as described in ASTM G 46 (Ref 16). Large, shallow pits can be easily measured with pit micrometers. A narrow, deep pit is more difficult to measure, because a pit micrometer cannot be used. Scanning vertical interferometry is a method to precisely measure even small-diameter pits nondestructively. Another accurate but time-consuming method is to cross section the specimen and use an optical means to measure the pit. A micrometer stage on a low-power microscope is useful for this type of measurement.

Whichever method is used, the objective is to measure the deepest pits. By measuring the maximum pit depth of duplicate specimens over a period of time, a rate of maximum pit growth can be obtained. The distribution of the pits (percentage of surface pitted) may also be of interest. Time-to-perforation data can be obtained by designing a specimen that is pressurized with air. This pressure is then monitored over a period of time until failure is indicated by a pressure decrease (Ref 17). It is important to design the system so that the specimen being tested fails before the monitoring lines fail.

Stress-Corrosion Cracking and Hydrogen Embrittlement. Preparation of stressed specimens for underground performance studies is more time-consuming, because the specimen must be properly stressed before burial. Fixtures or bolts attached to the specimen must be nonmetallic, electrically insulated from the specimen, or coated to avoid galvanic effects. When hydrogen embrittlement specimens are cathodically charged by a sacrificial anode, it may be useful to monitor the current between the two electrodes and the electrical potential of the couple versus a reference electrode (Ref 18).

Time-to-failure data can be obtained by attaching a hollow tensile specimen to a stressing ring (Fig. 5) and monitoring the change in strain or diameter of the ring. Stress is applied to the tensile specimen by turning the stressing nuts so that the stressing ring is elastically deformed. The stressed tensile specimen is then embedded in the soil, with the stressing ring extending above ground (Fig. 5). This and other special designs can provide failure data before retrieval. Retrieval of the specimen soon after failure is important to prevent subsequent destruction of the failure surface by general corrosion attack. Examination of this surface can provide information on the mode of failure.

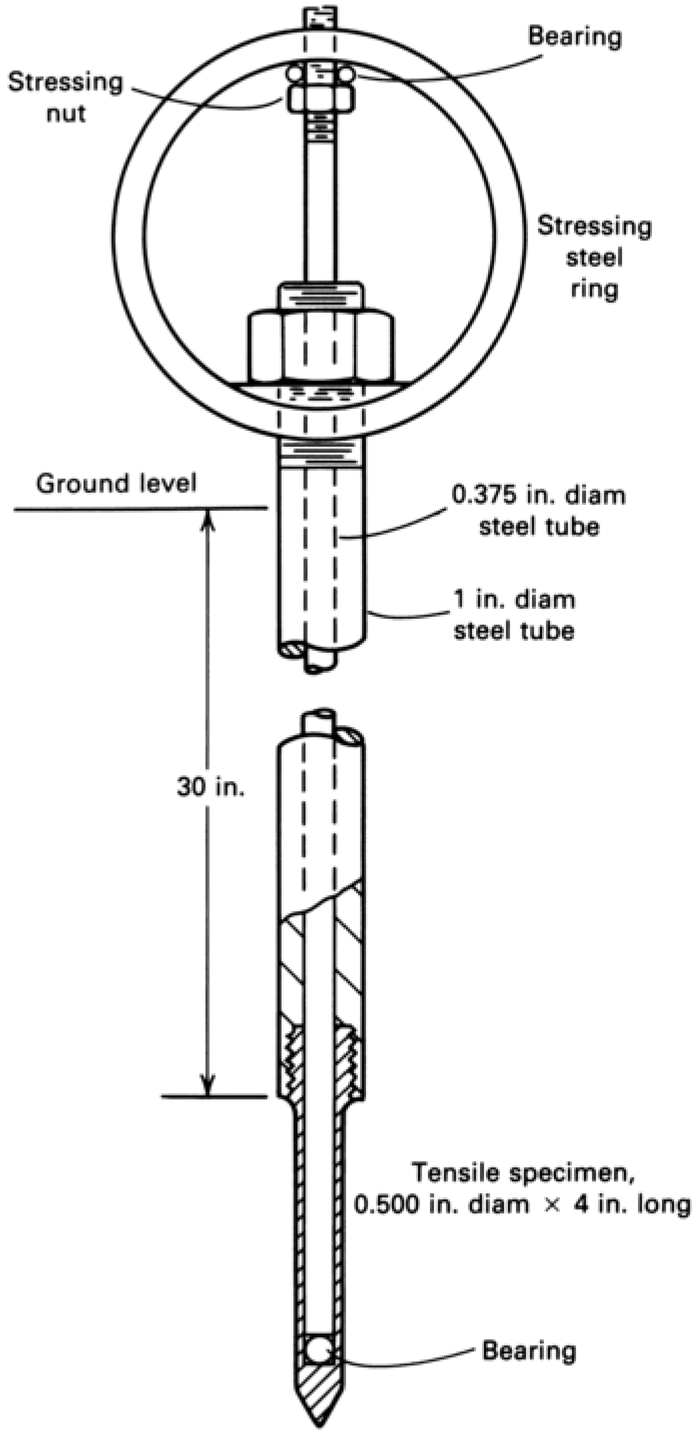

Fig. 5 Surface-monitored ring-stressed hollow specimen for stress-corrosion cracking and hydrogen embrittlement studies of metals in soil. The 10 cm (4 in.) long test specimen is placed approximately 75 cm (30 in.) beneath the surface of the soil. Source: Ref 19

References cited in this section

13. "Standard Practice for Preparing, Cleaning, and Evaluating Corrosion Test Specimens," G 1, *Annual Book of ASTM Standards,* American Society for Testing and Materials, 1990
14. D.A. Jones, Principles of Measurement and Prevention of Buried Metal Corrosion by Electrochemical Polarization, *Underground Corrosion,* STP 741, American Society for Testing and Materials, 1981, p 123–132
15. M.A. Hubbe, Polarisation Resistance Corrosivity Test with a Correction for Resistivity, *Br. Corros. J.*, Vol 15 (No. 4), 1980, p 193–197
16. "Standard Recommended Practice for Examination and Evaluation of Pitting Corrosion," G 46, *Annual Book of ASTM Standards,* American Society for Testing and Materials, 1994
17. J.B. Vrable, Unbonded Polyethylene Film for Protection of Underground Structures, *Mater. Prot. Perform.,* Vol 11 (No. 3), March 1972, p 26–28
18. E. Escalante and W.F. Gerhold, The Galvanic Coupling of Some Stressed Stainless Steels to Dissimilar Metals Underground, *Properties of Materials for Liquefied Natural Gas Tankage,* STP 579, American Society for Testing and Materials, 1976, p 88–93
19. J.B. Vrable, "Stress Corrosion Behavior of Line-Pipe Steels in Underground Environments," Project 59.001-001(2), United States Steel Corporation, July 1970

M.K.A. Flitton, and E. Escalante, Simulated Service Testing in Soil, *Corrosion: Fundamentals, Testing, and Protection*, Vol 13A*, ASM Handbook,* ASM International, 2003, p 497–500

Simulated Service Testing in Soil

M.K. Adler Flitton, Idaho National Engineering and Environmental Laboratory; E. Escalante, Corrosion Group, National Institute of Science and Technology (retired)

Specimen Retrieval

When the specimens are buried as described here, the retrieval process should proceed smoothly. The initial surface digging can be carried out with power equipment, but the final few centimeters of soil must be removed by careful hand shoveling to reduce the possibility of specimen damage, loss of corrosion products, or loss of identification labels. Corrosion product at or near the specimen surface needs to be collected once the specimen location is determined. The spatial distribution of corrosion product relative to the specimen will provide information on migration or transport of corrosion product in the surrounding soil. Microbial sampling of the specimens should be done immediately after retrieval for best results. A preliminary examination of specimens and a photographic record during the retrieval can be very useful. The preliminary examination helps identify changes that may occur in the time between excavation and final specimen examination in a laboratory.

M.K.A. Flitton, and E. Escalante, Simulated Service Testing in Soil, *Corrosion: Fundamentals, Testing, and Protection*, Vol 13A, *ASM Handbook*, ASM International, 2003, p 497–500

Simulated Service Testing in Soil

M.K. Adler Flitton, Idaho National Engineering and Environmental Laboratory; E. Escalante, Corrosion Group, National Institute of Science and Technology (retired)

Conclusions

Corrosion of metals in undisturbed soil is typically very low and is independent of soil characteristics. However, corrosion in disturbed soil is strongly influenced by the soil environment. Because determining soil corrosivity through soil characterization is difficult, and because data on specific alloys are needed, it is necessary to conduct underground corrosion studies. Information on the durability of metals in soil can be obtained by using physical and electrochemical measurements.

Gravimetric measurements and electrochemical polarization measurements provide information on deterioration due to uniform corrosion. Pit depth measurements and surface monitoring of pressurized vessels provide data that can be used to determine metal perforation rates. The susceptibility of metals to hydrogen embrittlement and stress-corrosion cracking can also be determined by physical measurements at the soil surface or by periodic retrieval of stressed specimens. Monitoring the potential and the galvanic current of cathodically charged stressed specimens can reveal the susceptibility of an alloy to hydrogen embrittlement.

Specimen design depends on the type of data sought. It is essential to mark burial specimens properly, to map burial sites, and to maintain permanent records. A reliable chain of custody of the records is particularly important in long-term exposure tests.

M.K.A. Flitton, and E. Escalante, Simulated Service Testing in Soil, *Corrosion: Fundamentals, Testing, and Protection*, Vol 13A, *ASM Handbook*, ASM International, 2003, p 497–500

Simulated Service Testing in Soil

M.K. Adler Flitton, Idaho National Engineering and Environmental Laboratory; E. Escalante, Corrosion Group, National Institute of Science and Technology (retired)

References

1. "ANSI Standard for Polyethylene Encasement for Ductile-Iron Pipe Systems," C105/ A21.5-99, American Water Works Association, 1999
2. D.B. Craig and D.S. Anderson, Ed., *Handbook of Corrosion Data,* 2nd ed., ASM International, 1995, p 822–823
3. M. Romanoff, "Underground Corrosion," NBS 579, NTIS PB 168,350, National Bureau of Standards, April 1957
4. "Standard Method for Field Measurement of Soil Resistivity Using the Wenner Four- Electrode Method," G 57, *Annual Book of ASTM Standards,* American Society for Testing and Materials, 1995
5. J.R. Galvele, Present State of Understanding of the Breakdown of Passivity and Repassivation, *Passivity of Metals,* The Electrochemical Society, Inc., 1978, p 258–327

6. H.H. Uhlig and R.W. Revie, *Corrosion and Corrosion Control,* 3rd ed., John Wiley & Sons, 1985, p 111–114, 415–420.

7. W.P. Iverson, An Overview of the Anaerobic Corrosion of Underground Metallic Structures: Evidence for a New Mechanism, *Underground Corrosion,* American Society for Testing and Materials, 1981, p 33–52

8. P.R. Roberge, *Handbook of Corrosion Engineering,* McGraw-Hill, 1999

9. E. Escalante, The Effect of Soil Resistivity and Soil Temperature on the Corrosion of Galvanically Coupled Metals in Soil, *Galvanic Corrosion,* STP 978, H. Hack, Ed., American Society for Testing and Materials, 1988

10. "Standard Test Method for Measuring pH of Soil for Use in Corrosion Testing," G 51, *Annual Book of ASTM Standards,* American Society for Testing and Materials, 1995.

11. W.J. Schwerdtfeger, Soil Resistivity as Related to Underground Corrosion and Cathodic Protection, *J. Res. Natl. Bur. Stand.,* Vol 69C (No. 1), Jan–March 1965

12. N.D. Tomashov, *Theory of Corrosion and Protection of Metals,* Macmillan, 1966, p 399–451.

13. "Standard Practice for Preparing, Cleaning, and Evaluating Corrosion Test Specimens," G 1, *Annual Book of ASTM Standards,* American Society for Testing and Materials, 1990

14. D.A. Jones, Principles of Measurement and Prevention of Buried Metal Corrosion by Electrochemical Polarization, *Underground Corrosion,* STP 741, American Society for Testing and Materials, 1981, p 123–132

15. M.A. Hubbe, Polarisation Resistance Corrosivity Test with a Correction for Resistivity, *Br. Corros. J.,* Vol 15 (No. 4), 1980, p 193–197

16. "Standard Recommended Practice for Examination and Evaluation of Pitting Corrosion," G 46, *Annual Book of ASTM Standards,* American Society for Testing and Materials, 1994

17. J.B. Vrable, Unbonded Polyethylene Film for Protection of Underground Structures, *Mater. Prot. Perform.,* Vol 11 (No. 3), March 1972, p 26–28

18. E. Escalante and W.F. Gerhold, The Galvanic Coupling of Some Stressed Stainless Steels to Dissimilar Metals Underground, *Properties of Materials for Liquefied Natural Gas Tankage,* STP 579, American Society for Testing and Materials, 1976, p 88–93

19. J.B. Vrable, "Stress Corrosion Behavior of Line-Pipe Steels in Underground Environments," Project 59.001-001(2), United States Steel Corporation, July 1970

M.K.A. Flitton, and E. Escalante, Simulated Service Testing in Soil, *Corrosion: Fundamentals, Testing, and Protection*, Vol 13A, *ASM Handbook*, ASM International, 2003, p 497–500

Simulated Service Testing in Soil

M.K. Adler Flitton, Idaho National Engineering and Environmental Laboratory; E. Escalante, Corrosion Group, National Institute of Science and Technology (retired)

Selected References

- M.K. Adler Flitton, R.E. Mizia, and C.W. Bishop, "Underground Corrosion of Activated Metals in an Arid Vadose Zone Environment," Paper 02531, NACE, April 2002
- N.C. Brady and R.R. Weil, *The Nature and Properties of Soils,* Prentice-Hall, 2002
- E. Escalante, Soils, *Corrosion Tests and Standards,* ASTM, 1995
- A. Klute, Ed., *Methods of Soil Analysis,* 2nd ed., American Society of Agronomy, Inc., 1986
- D.L. Sparks et al., *Methods of Soil Analysis, Part 3: Chemical Methods,* Soil Science Society of America, 1996

V.S. Agarwala, In-Service Techniques—Damage Detection and Monitoring, *Corrosion: Fundamentals, Testing, and Protection*, Vol 13A, *ASM Handbook*, ASM International, 2003, p 501–508

In-Service Techniques—Damage Detection and Monitoring

Vinod S. Agarwala, Naval Air Systems Command

Introduction

BECAUSE OF THE MAGNITUDE of the corrosion problem, its economic impact, and human safety factors, new methods for detecting and monitoring corrosion are being developed. Past efforts have resulted in new methods being used in the field or being tested for possible field use. The possibility of a "smart coating" that could detect corrosion, inhibit corrosion, and facilitate the repair of corroded areas is an industry goal. Wireless technology has resulted in the possible implantation of sensors that can be interrogated from remote locations and thus monitor areas that were previously inaccessible except by detailed examination and disassembly of the structure.

While the standard techniques of coupon evaluation for field studies of corrosive conditions are still valuable, they may be inconvenient, labor intensive, or too slow to monitor the corrosion process. Resistance and hydrogen probes monitor on-line corrosion in reactor cooling waters, oil pipelines, and refineries (Ref 1, 2). The location and monitoring of these probes are critical for obtaining meaningful data. NACE Standard, RP0189-95 discusses such methods for on- line monitoring of cooling waters (Ref 2). Figure 1 shows an on-line monitoring system. Parameters such as pH, temperature, conductivity, and corrosion currents are monitored. Other parameters, including heat-transfer rates across piping, water-flow rate, pressure-drop changes, and biofilm sensors, as well as electrochemical and optical sensors are reviewed in this article. This article covers some standard techniques, but also reviews some of the new methods that have been developed. At the time of publication, some of these newer methods were being field tested, while others were in development.

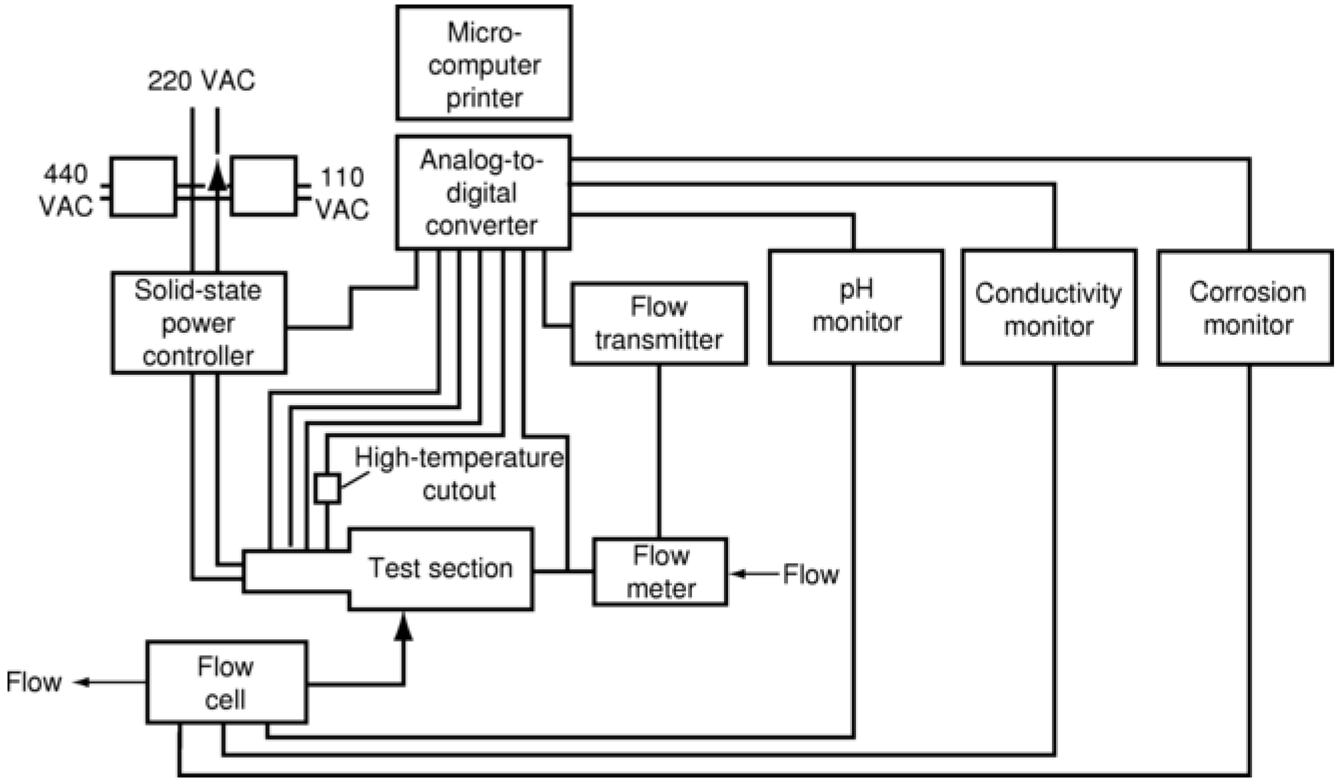

Fig. 1 Integrated on-line monitor

The most promising newer techniques are detailed in subsequent articles in this Handbook. In general, these techniques fall into such categories as electrochemical methods, electromagnetic or sound wave methods, and fiber-optic technology, along with visible, ultraviolet or infrared light, and some unique methods utilizing reflected and amplified light to look at surface topography, triboluminescent sensing, thermography, and the superconducting quantum interference device (SQUID). Reports describing these methods are included in NACE Symposia on corrosion monitoring (CORROSION/1994, Ref 3; CORROSION/1997, Ref 4; and CORROSION/2000, Ref 5). Agarwala and Ahmad (Ref 6) give detailed references to many of the corrosion-monitoring techniques mentioned in this article. For the management of corrosion data, Roberge and Tullmin show how to monitor corrosion in aging systems for maintenance and repair issues (Ref 7, 8).

References cited in this section

1. J.G. Knudsen, H.-Y. Jou, and K.W. Herman, Paper 358, presented at CORROSION/85, NACE International, 1985
2. "On-Line Monitoring of Cooling Waters," Standard RP0189-95, NACE International, 2001
3. Proceedings of Symposium, "Corrosion and Corrosivity Sensors," presented at CORROSION/1994, NACE International, 1994
4. Proceedings of Symposium, "Corrosion Sensing and Management of Aging Systems," presented at CORROSION 2000, NACE International, 2000
5. M. Tullmin, P.R. Roberge, and M.A. Little, "Sensors for Aircraft Corrosion—Review and Future," Paper 301, presented at CORROSION/97, 1997
6. V.S. Agarwala and S. Ahmad, Paper 00271, presented at CORROSION/2000, NACE International, 2000

7. M. Tullmin and P.R. Roberge, “Monitoring Corrosion in Aging Systems—New Possibilities and Old Fundamentals,” Paper 00282, presented at CORROSION 2000, NACE International, 2000

8. P.R. Roberge, Ed., *Handbook of Corrosion Engineering,* McGraw-Hill, 2000

V.S. Agarwala, In-Service Techniques—Damage Detection and Monitoring, *Corrosion: Fundamentals, Testing, and Protection*, Vol 13A, *ASM Handbook*, ASM International, 2003, p 501–508

In-Service Techniques—Damage Detection and Monitoring

Vinod S. Agarwala, Naval Air Systems Command

Electrochemical Methods

Polarization resistance measurement has been used to detect crevice corrosion under O-rings and at the ends of pipe. Crevice corrosion measured visually correlates well with polarization resistance (Ref 9). Embeddable microinstruments can measure resistance and other corrosive parameters and transmit data from remote locations (Ref 10). Figure 2 shows a 4 by 6 mm (0.16 by 0.24 in.) microinstrument, which includes potentiostat, zero-resistance ammeter (ZRA), analog-to-digital and the reverse (A/D- D/A) converters, and three on-chip electrodes. Results from the microinstruments to measure polarization resistance indicated good correlation to results from conventional instrumentation. Further development of microinstruments will include potentiometric measurements controlled by microprocessor. The microinstrument can be incorporated in on-line testing systems by attaching them to actual parts of interest.

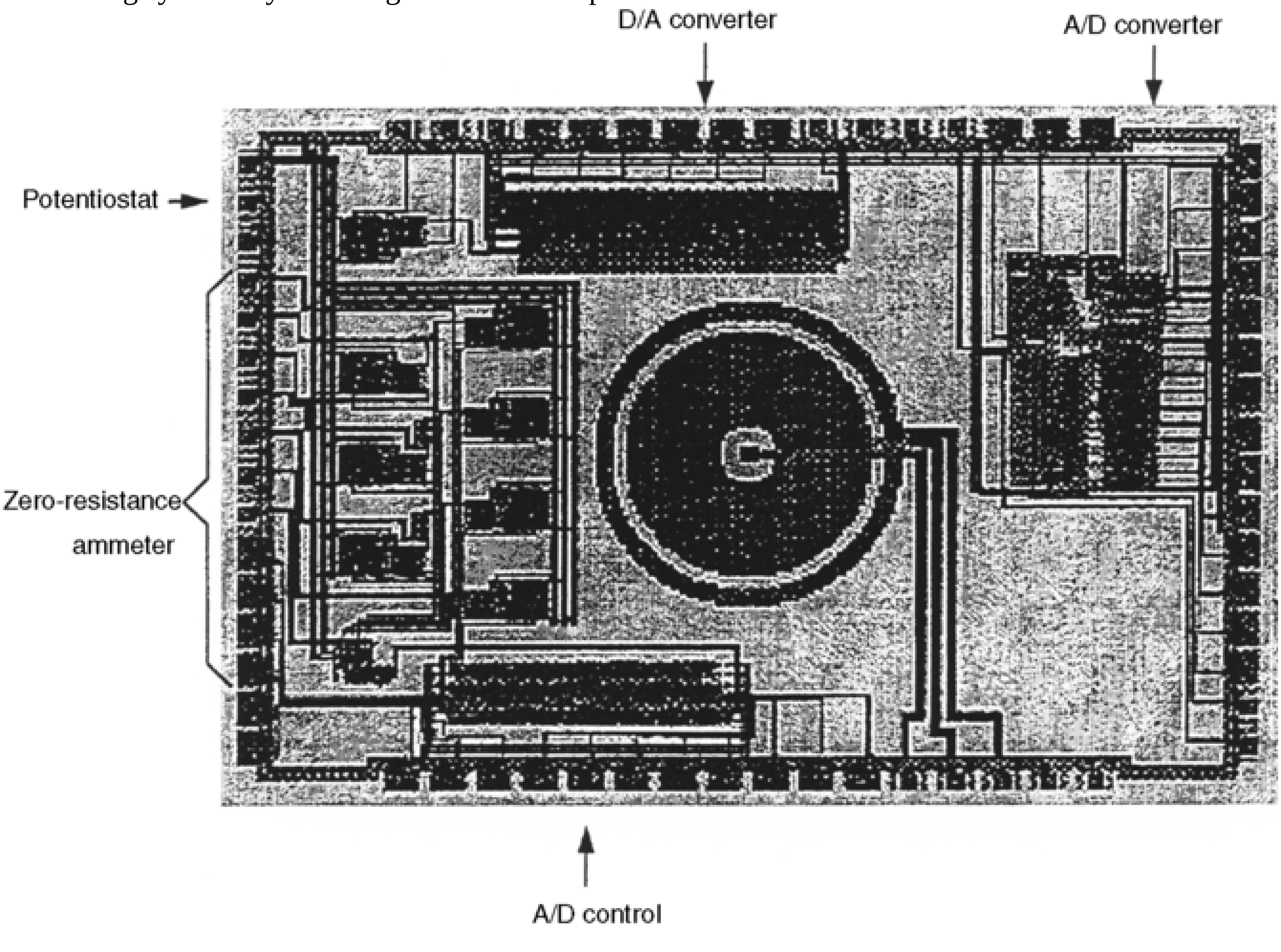

Fig. 2 Design of microcircuit containing integrated potentiostat/autoranging zero-resistance ammeter (ZRA), analog-to-digital and digital-to-analog (A/D-D/A) converters, and three on-chip electrodes. Size is about 4 × 6 mm (0.16 × 0.24 in.). Source: Ref 10

Corrosion potential and cathodic protection current monitoring was used to determine the extent of coating damage inside large ship tanks (Ref 11). This technique, combined with a camera on the probe for visual information, provided a convenient method to monitor corrosion damage to wastewater collection and ship ballast tanks. Access of the probe was through normal hatches in these ship tanks and off-the-shelf equipment was utilized. When the electromotive force (emf) or anodic current was monitored, limits could be established by correlating corrosion damage to that shown on the video camera. Software enhancements of the video recordings also produced images highlighting the corrosion damage itself. Figure 3 indicates the probe assembly inserted through the hatch with zinc anodes, reference electrodes, and associated data logger. Figure 4 indicates the acceptable levels for the potential to monitor corrosion; similar figures could have been developed in the work for monitoring the zinc electrode anodic current (Ref 11).

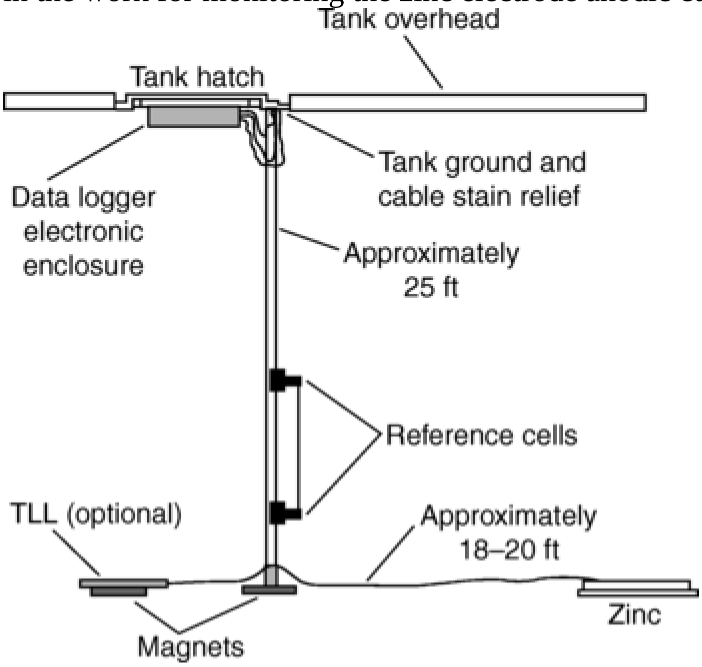

Fig. 3 Probe installation in ballast tank with zinc anodes, reference electrodes, and data logger. Source: Ref 11

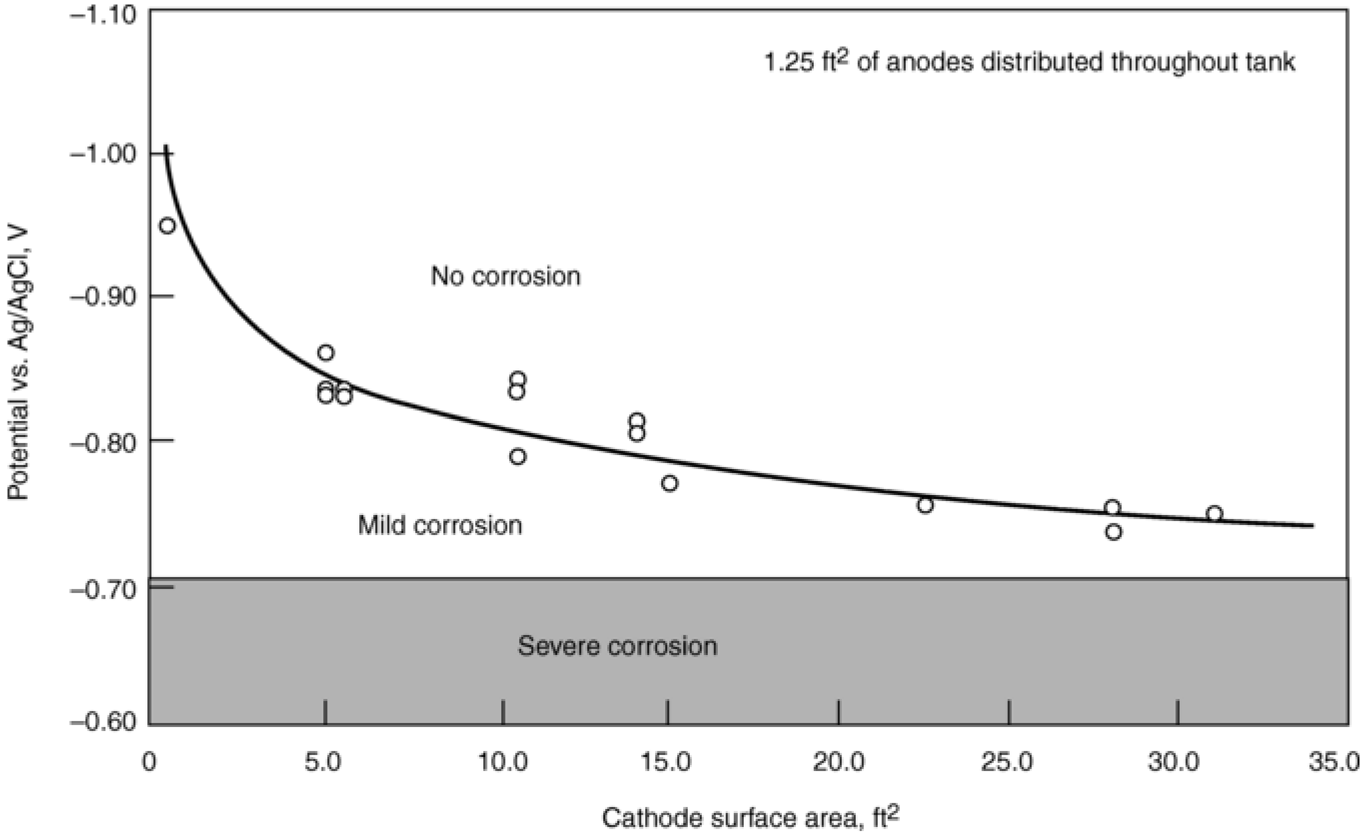

Fig. 4 Potential versus surface area of cathode with areas marked for no corrosion, mild corrosion, and serious corrosion

Electrochemical impedance measuring systems have been developed with implantable electrodes to monitor in situ corrosion of surfaces and interfaces (Ref 12). Figure 5 shows the information obtained from this implantable type of system at low frequency. Electrochemical noise (ECN) measurement has been used for corrosivity assessment. Interpretation of the results of ECN was difficult (Ref 13, 14). With advances in software, transform programs, and enhancement techniques, patterns of ECN are being correlated with the different types of corrosion.

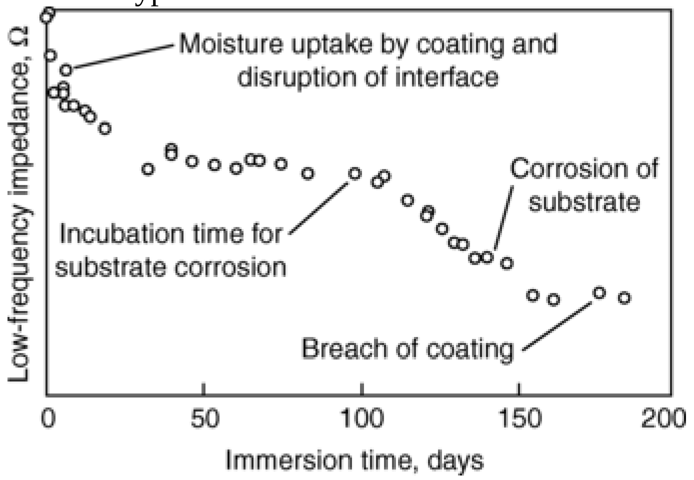

Fig. 5 Low-frequency impedance as a function of sample exposure time for immersed epoxy-coated aluminum. Three stages of coating degradation shown are moisture absorption, incubation, and substrate corrosion.

Voltammetric microelectrodes have been developed to measure corrosivity parameters such as metal ions, pH, sulfide ions, and oxygen (Ref 15, 16, 17, 18, 19). Figure 6 is an example of a microelectrode system that fits inside a standard rivet fastener. These measurements are indirect and very localized, but the possibility of

several outputs that can then be correlated to corrosion is possible and may become more reliable with the multiple signal outputs.

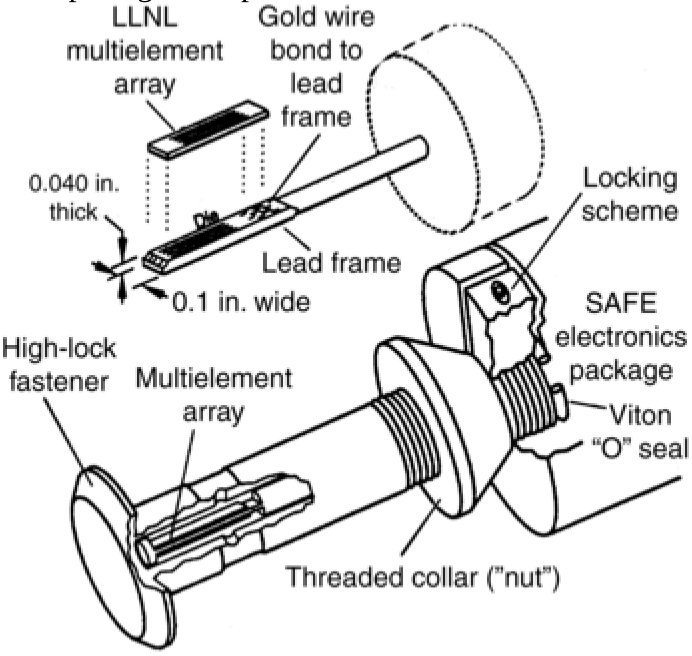

Fig. 6 Microelectrode array fitted into a rivet fastener

Coulometric measurements on a macroscale using copper cup, glass beads, and steel screens (Ref 19) or on a microscale with implantable bimetallic thin-film galvanic sensors (Ref 20, 21, 22, 23) have been developed and tested. The latter stand- alone, microthin film coulometer, called intelligent corrosivity sensor (ICS), is presently being validated to monitor hidden corrosion conditions inside aircraft using a wireless concept (Ref 20, 21, 22). The ICS measures galvanic current produced by the thin-film bimetallic elements, collects and stores data in its memory chip, and downloads data when queried through a radio frequency (RF) data-gathering transceiver (DGT) or transponder to a laptop computer. Figure 7 shows a composite picture of ICS components.

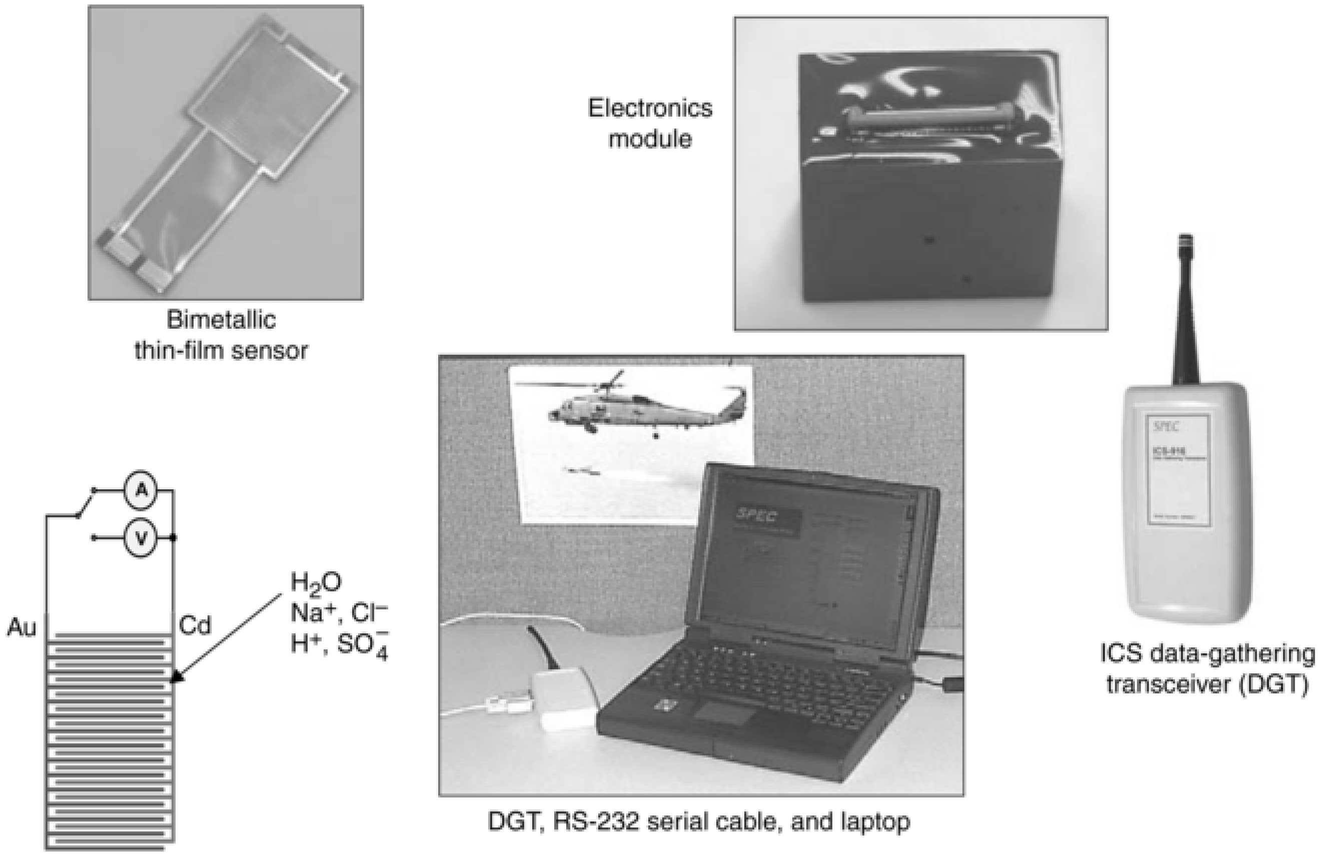

Fig. 7 The hardware components of intelligent corrosivity sensor (ICS). The schematic below thin-film sensor shows the sensing element with interdigitated metallic strips.

Figure 8(a) shows how sensors can be mounted in the most corrosion-prone interior of a P-3 aircraft. The technique measures corrosivity of the localized environment and is stand- alone for up to three years during military deployment. The data download is done through the DGT when desired or on the availability of the aircraft. The software is used to develop a real-time profile of current and then to transform it into coulombs to indicate corrosion rate as total possible corrosion damage with period of exposure, as shown in Fig. 8(b). This is finally used to develop a corrosion index for determining repair and maintenance calls.

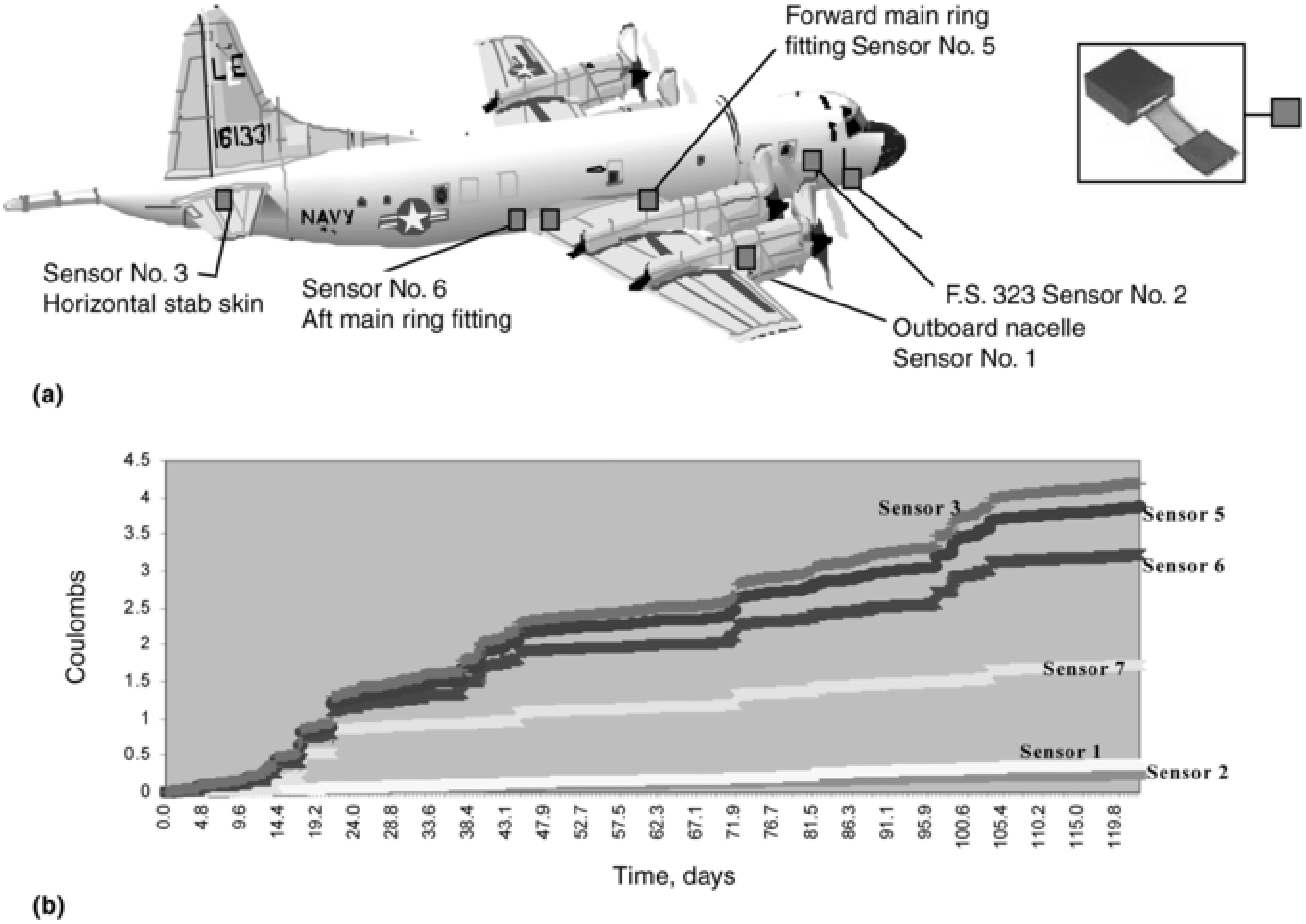

Fig. 8 Corrosion data recording on an aircraft. (a) Sensor locations. (b) Coulombs versus deployment time of data downloaded from each ICS (shown as square blocks mounted on P-3 aircraft) during service

References cited in this section

9. M. Inman, A.K. Rawat, E.J. Taylor, P.J. Moran, et al., "Detection of Crevice Corrosion Under an O-Ring by Polarization Resistance Measurements Using Electrodes Embedded in the O-Ring," Paper 296 and 312, presented at CORROSION/97, NACE International, 1997

10. R.G. Kelly, J. Yuan, S.H. Jones, W. Blanke, J.H. Aylor, W. Wang, A.P. Batson, A. Wintenberg, and G.G. Clemana, Embeddable Microinstruments for Corrosion Monitoring, Paper 294, *CORROSION/97*, NACE International, 1997

11. K.E. Lucas, P.F. Slebodnick, E.A. Hogan, E.D. Thomas, and A.I. Kaznoff, "Comprehensive Monitoring and Evaluation of Ballast Tank Coating Integrity for Life Prediction and Condition Based Maintenance," Paper 00299, presented at CORROSION 2000, NACE International, 2000

12. G. Davis, C.M. Dacres, and L.A. Krebs, "EIS Based In-Situ Sensors for the Early Detection of Coatings Degradation and Substrate Corrosion," Paper 00275, presented at CORROSION 2000, NACE International, 2000

13. P.R. Roberge, R.D. Klassen, and M. Tullmin, "Electrochemical Noise Analysis for Corrosivity Assessment," Paper 00282, presented at CORROSION 2000, NACE International, 2000

14. D.A. Eden, A.N. Rothwell, and J.L. Dawson, Paper 444, "Electrochemical Noise for Detection of Susceptibility to Stress Corrosion Cracking," CORROSION/91, NACE International, 1991

15. J.N. Schoess and C.A. Paul, Smart Fasteners Technology for Aging Aircraft, *Proc. SPIE Smart Structures and Materials Conference,* Vol 2444, Society of Photo-Optical Instrumentation Engineers, Feb 1995, p 192–197

16. J.N. Schoess and G. Seifert, Smart Aircraft Fastener Evaluation Systems: A Condition- Based Corrosion Detection System for Aging Aircraft, presented at *1995 Air Force Aging Aircraft Conference,* (Dayton, OH)

17. R.D. Granata, J.W. Fisher, and J.C. Wilson, "Update on Applications of Corrosion Coulometers" Paper 307, presented at CORROSION/97, NACE International, 1997

18. S.K. Chawla, T. Anguish, and J.H. Payer, Microsensors for Corrosion Control, *Mater. Perform.,* Vol 29 (No. 5), 1990

19. K. Xu, S.C. Dexter, and G.W. Luther, III, Paper 300, presented at CORROSION/97, NACE International, 1997

20. V.S. Agarwala, A Probe for Monitoring Corrosion in Marine Environments, *Atmospheric Corrosion in Marine Environments,* W.H. Ailor, Ed., J. Wiley & Sons, 1982, p 183–192

21. V.S. Agarwala, Sensors for Monitoring Corrosion in Aircraft Systems, Paper 431, *Proc. 13th ICC* (Melbourne, Australia), International Corrosion Congress (ICC), Dec 1996

22. B. Zollars, N. Salazar, J. Gilbert, and M. Sanders, "Remote Datalogger for Thin Film Sensors," Paper 313, presented at CORROSION/97, NACE International, 1997

23. A.V. Bray, H. Stretz, and S.C. Buckner, "Coating Effects in Microwave NDE in the Detection of Corrosion for Aircraft Applications," Paper 00268, presented at CORROSION 2000, NACE International, 2000

V.S. Agarwala, In-Service Techniques—Damage Detection and Monitoring, *Corrosion: Fundamentals, Testing, and Protection*, Vol 13A, *ASM Handbook*, ASM International, 2003, p 501–508

In-Service Techniques—Damage Detection and Monitoring

Vinod S. Agarwala, Naval Air Systems Command

Electromagnetic and Sonic Methods

Hidden corrosion damage detection has been the most difficult task where teardown inspection is cost prohibitive. In the past, nondestructive inspection (NDI) was at best 60% accurate. In the last decade, significant technical advancements have led to breakthroughs in the use of NDI techniques. The new microwave, ultrasonic, and acoustic techniques are finding much greater applications for monitoring hidden corrosion and cracks. For instance, a microwave corrosion detector (MCD) can scan and locate corrosion underneath paint using microwave sources and analyzing the reflected wave to determine the integrity of the coating/substrate interface (Ref 23). It is based on the principle that the energy of the reflected radar wave is different in corroded areas compared to a reference or noncorroded surface. The concept was derived from a police radar gun. Figure 9 shows the latest version of a MCD, which has been used for scanning surface corrosion under coatings.

Fig. 9 A handheld microwave corrosion detector (MCD) scanner

A typical eddy-current system measures the impedance of a very small area of a structure within its reach. In the presence of crack/corrosion damage, the eddy currents are interrupted, causing a change in the complex impedance of the test area in that location. Often this change or blip in the impedance spectra is skewed and becomes indeterminate when there are multilayers present. The new developments in this technology have made eddy current a better tool to find corrosion in multilayer aircraft structures (Ref 24) and in reinforced and prestressed concrete structures (Ref 25).

Acoustical monitoring of concrete bridges and pipelines with computer software analysis and remote sensing has been successfully used in identifying localized areas of deterioration (Ref 26). An array of acoustical sensors embedded/ installed on large structures such as bridges or buildings can be monitored from remote locations, detecting large cracks or other acoustical events and alerting personnel to inspect those sites.

Until recently, ultrasonics was the least used method because of the complex nature of the waves and noise signals generated during its application. The new developments in signal processing and the hardware and software designs of ultrasonic guided wave methods have made it possible to sense defects in inaccessible areas under coatings or in joints on aircraft structures (Ref 27, 28). Alloy wall thinning, microcracking, and debonding effects can be seen with this method as demonstrated on helicopter and fixed- wing aircraft surfaces. Figure 10 shows an example of lap splice inspection and detection of poor bonding in the splice joint. Recently, the use of piezoelectric films has miniaturized the transducers that produce ultrasonics; this makes the method more useful as a leave-in-place device for long-term monitoring of corrosion-assisted damage.

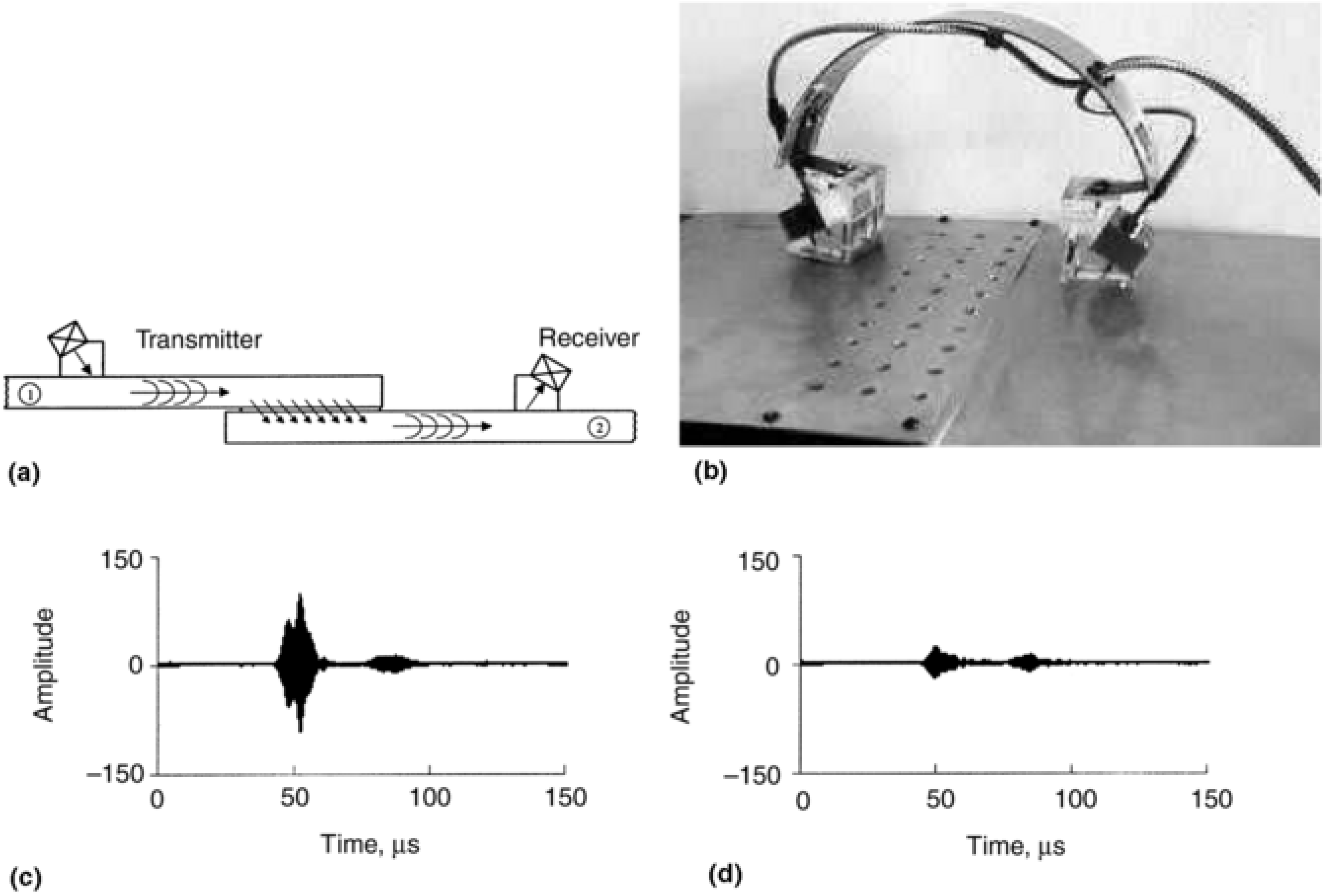

Fig. 10 Ultrasonic method for detecting poor bonding in a lap splice with ultrasonic guided waves. (a) Ultrasonic through-transmission approach for lap splice joint inspection. (b) Double-spring "hopping probe" used for the inspection of a lap splice joint. (c) Signal for a good bond. (d) Signal from a poorly bonded splice

References cited in this section

23. A.V. Bray, H. Stretz, and S.C. Buckner, "Coating Effects in Microwave NDE in the Detection of Corrosion for Aircraft Applications," Paper 00268, presented at CORROSION 2000, NACE International, 2000

24. J.M.S. Dubois, P.R. Roberge, and J.R.S. Giguere, "Eddy Current Sliding Probe Technology for the Detection of Corrosion on Multi-Layered Aircraft Structures," Paper 00296, presented at CORROSION 2000, NACE International, 2000

25. G. John, "Development of Inductive Imaging of Corrosion Damaged Reinforced and Prestressed Concrete Structures," Paper 293, presented at CORROSION 2000, NACE International, 2000

26. J.F. Elliot and M.W. Holley, "Continuous Acoustic Monitoring of Structures," Paper 00288, presented at CORROSION 2000, NACE International, 2000

27. J.L. Rose, L.E. Soley, T. Hay, and V.S. Agarwala, "Ultrasonic Guided Waves for Hidden Corrosion Detection in Naval Aircraft," Paper 00267, presented at CORROSION 2000, NACE International, 2000

28. J.L. Rose, D. Jiao, S.P. Pelt, J.N. Barshinger, and M.J. Quarry, "Hidden Corrosion Detection with Guided Waves," Paper 292, presented at CORROSION/97, NACE International, 1997

V.S. Agarwala, In-Service Techniques—Damage Detection and Monitoring, *Corrosion: Fundamentals, Testing, and Protection*, Vol 13A, *ASM Handbook*, ASM International, 2003, p 501–508

In-Service Techniques—Damage Detection and Monitoring

Vinod S. Agarwala, Naval Air Systems Command

Optical and Fiber-Optic Sensing

The change in optical properties of aluminum- clad fiber-optic probes as the aluminum corrodes has been tested at Boeing for monitoring hidden areas of aircraft for corrosion (Ref 29, 30). This method is adaptable to remote sensing and can be installed in new installations and on aging aircraft during maintenance in the corrosion-susceptible areas.

Uses of pigments that change color upon evolution of hydrogen have been tested as indicators of metal oxidation at a nearby site (Ref 31). These pigments could be incorporated into paint coatings to detect corrosion. A fiber-optic strain sensor has been used to detect changes in a metal surface due to corrosion, cracking, or joint failure (Ref 32, 33). Changes in pH can also be detected with fiber-optic probes (Ref 34). During corrosion of surfaces, the pH can increase or decrease in different areas.

References cited in this section

29. A.A. Panova, P. Pantano, and D.R. Walt, "In-Situ Fluorescence Imaging of Localized Corrosion with a pH-Sensitive Imaging Fiber," Paper 314, presented at CORROSION/ 97, NACE International, 1997

30. R. Ikegami, Boeing Defense & Space Group, Seattle, WA, private communications, 1993

31. Y. Bar-Cohen, R.V. Bugga, and A.I. Attia, "Corrosion Indicating Pigments and Probes", *NASA Tech Brief,* Vol 17 (No. 10), Item 15, 1993

32. N. Lagakos, H.N. Jones, S.G. Lambrakos, and P.P. Trzaskoma-Paulette, "A Fiber Optic Sensor for Detection of Degradation in Aircraft Lap Joints," Paper 00297, presented at CORROSION 2000, NACE International, 2000

33. I.M. Perez and V.S. Agarwala, "Corrosion Detection and Monitoring Method and Apparatus," U.S. Patent 5646400, 8 July 1997

34. A.A. Panova, P. Pantano, and D.R. Walt, In- Situ Fluorescence Imaging of Localized Corrosion with a pH-Sensitive Imaging Fiber, *Anal. Chem.,* Vol 69, 1997, p 1635–1641

V.S. Agarwala, In-Service Techniques—Damage Detection and Monitoring, *Corrosion: Fundamentals, Testing, and Protection*, Vol 13A, *ASM Handbook*, ASM International, 2003, p 501–508

In-Service Techniques—Damage Detection and Monitoring

Vinod S. Agarwala, Naval Air Systems Command

Fluorescence Methods

Fluorescence utilizes an excitation light source of a given wavelength and then measures the corresponding emission of fluorescence light at a lower wavelength. The light source can be ultraviolet, visible, or infrared light. The development of fiber-optic fluorescence in the red and infrared regions is a new approach to corrosion detection as only few natural materials fluoresce in the infrared (Ref 35). The fluorescence can detect pH changes as well as changes in concentration of specific analytes (metal ions, oxygen, carbon dioxide, etc.). Thus, fluorescent techniques have been developed that are sensitive to small-concentration species and are very selective. The methods of detection can also be varied from direct measurement of fluorescence emission to determine the ratio of emission at two wavelengths and even fluorescence lifetime measurements following the decay of emitted light after a pulse of excitation light. For corrosion detection, fluorescence can be used to monitor redox changes, pH changes, or the buildup of corrosion products (adsorption-type indicators) on selected surfaces.

The application of fluorescence methods to scan large areas for corrosion has been investigated by Agarwala and Johnson (Ref 36, 37, 38). The concept is based on the specificity of incorporated indicator material in a paint/coating that changes its fluorescent property when it either oxidizes or interacts with corrosion products. On many surfaces, corrosion is not easily seen because of surface coatings, limited access locations, or difficulty in inspecting large areas thoroughly. The incorporation of fluorophore into a coating would change its fluorescent properties during localized corrosion and could greatly enhance corrosion detection, providing economic and safety benefits. Large surfaces such as those on an aircraft could be scanned with an ultraviolet (UV) source, and the fluorescence could be monitored visually or with a recorder to note areas where corrosion may have occurred. These areas could then be checked in detail with other techniques if necessary. Figure 11 illustrates this method of scanning.

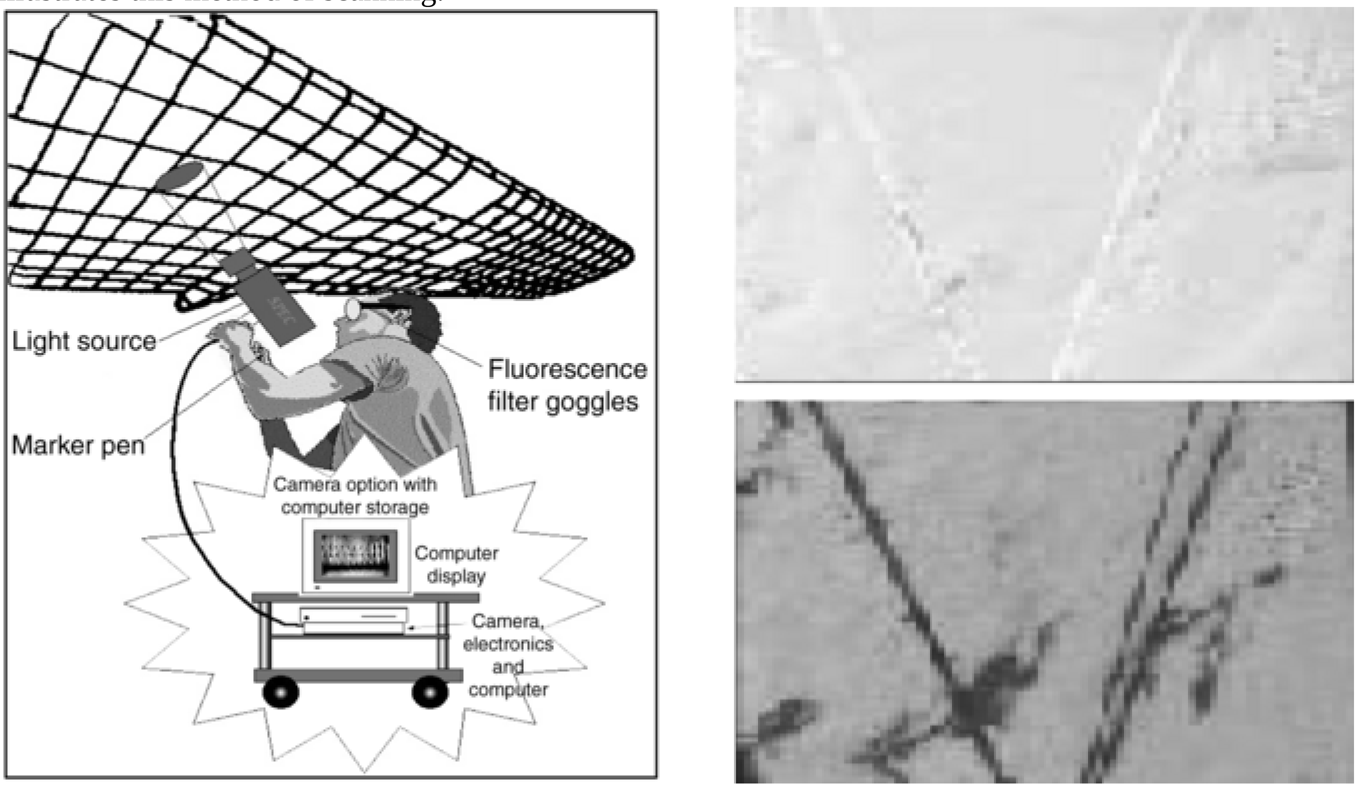

Fig. 11 Large-area scanning system for corrosion under coating using ultraviolet (UV) light source. Left: a camera option to visually inspect and record corrosion suspect areas on an aircraft wing. Right: a close-up picture of a panel showing corrosion under the coating. Fluorescence under UV is quite obvious as compared to the one in visible light.

Fluorophores such as fluorescein, oxine, and morin have been tested for this type of application. Fluorescein is highly fluorescent in high pH conditions and also in the oxidized state. Figure 12 shows the behavior of fluorescein when formulated in an epoxy and applied on an aluminum panel. Figure 12(a) shows the difference in fluorescence as the degree of corrosion increases. This painted panel was exposed to salt-spray conditions of varying degree to cause corrosion. Figure 12(b) shows the fluorescent spectra with high emissions for fluorescein in a broad range of 525 to 555 nm wavelengths.

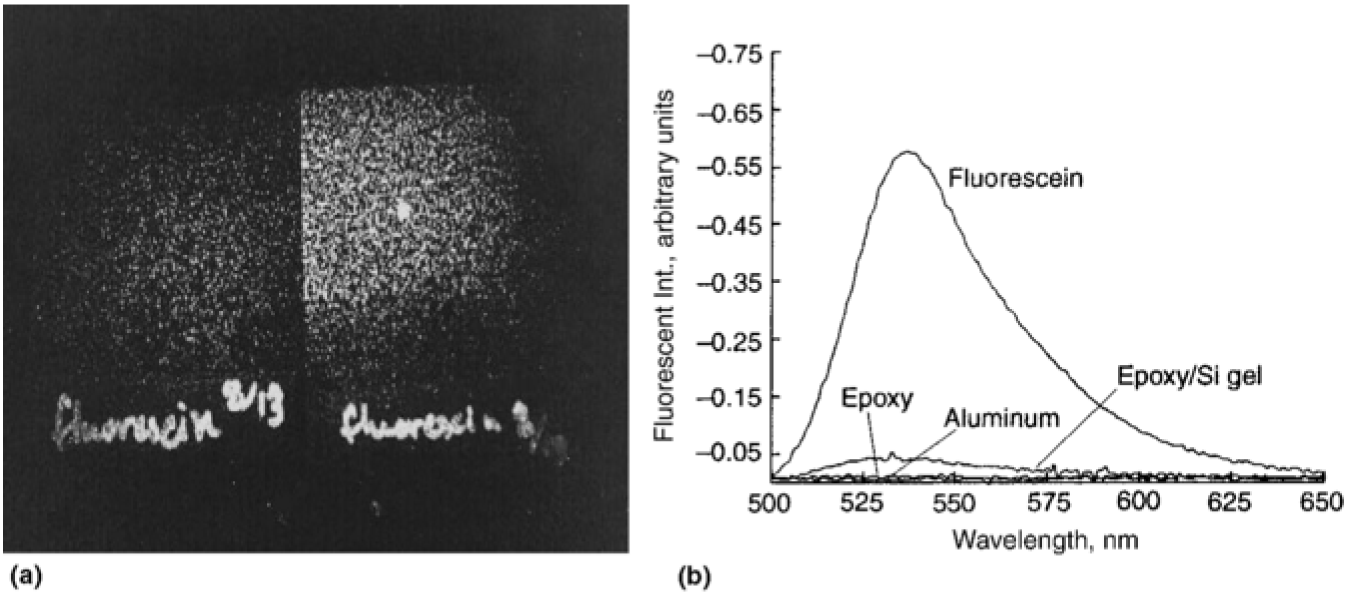

Fig. 12 The result of fluorescein test as indicator of corrosion. (a) Variance in fluorescence under ultraviolet light with varying degree of corrosion. (b) A broad range high emission for fluorescein

Oxine is an adsorption-type indicator, and when it adsorbs to aluminum oxide it fluoresces. The aluminum oxide must be in a granular state from localized corrosion and not the tight layer type that is present on all aluminum surfaces. Oxine has been shown to fluoresce more on a painted but nonchromated surface than on a chromate conversion coated 7075-T6 aluminum alloy. Morin is a complexing agent that binds to aluminum ions and becomes fluorescent. This fluorescence is an indication of the oxidation of aluminum on a surface.

There are also temperature-sensitive fluorophores that change color with temperature so that they can monitor small changes in surface temperature. They can monitor chemical reactions due to corrosion under the surface, or, with thermal imaging, they can sense temperature differences when the surface is subjected to a transient from a heat source.

References cited in this section

35. R.B. Thompson, Red and Near-Infrared Fluorometry, *Topics in Fluorescence Spectroscopy: Probe Design and Chemical Sensing,* Vol 4, J.R. Lakowicz, Ed., Plenum Press, 1994, p 151–181

36. R.E. Johnson and V.S. Agarwala, The Use of Fluorescence Compounds and Complexes of Metals as Early Warning Detectors of Corrosion, *Mater. Perform.*, Vol 33 (No. 4), 1994, p 25–29

37. R.E. Johnson, K.S. Rajan, and V.S. Agarwala, Fluorescence Based Sensors for Corrosion Detection, *The Role of Characterization in Understanding Environmental Degradation of Materials,* Vol 25, *Microstructural Science,* J.W. Simmons, J.A. Hawk, and D.E. Alman, Ed., ASM International, 1998, p 65–70

38. R.E. Johnson and V.S. Agarwala, et al., “Fluorescent Materials Utilized as Early Warning Sensors for Corrosion of Aluminum Alloys,” Paper 505, presented at CORROSION/99, NACE International, 1999

V.S. Agarwala, In-Service Techniques—Damage Detection and Monitoring, *Corrosion: Fundamentals, Testing, and Protection*, Vol 13A, *ASM Handbook*, ASM International, 2003, p 501–508

In-Service Techniques—Damage Detection and Monitoring

Vinod S. Agarwala, Naval Air Systems Command

Other Corrosion-Detection Methods

The Diffracto Sight, or D-Sight, is an optical method that uses a charge-coupled device (CCD) camera and a white light source. It measures reflected light from a low incident angle light on surfaces (Ref 39, 40). The reflected light is amplified by the collection method, and the resulting image magnifies surface topology so that pillowing (corrosion products) around rivets and other surface changes can easily be seen. Figure 13 indicates the difference seen by this method in a heavily corroded area and a noncorroded area.

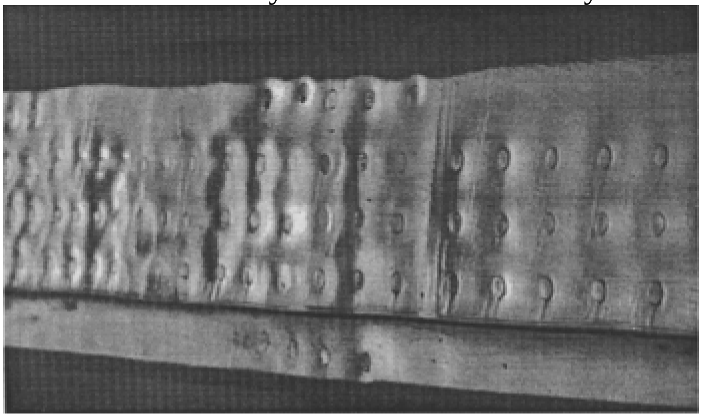

Fig. 13 The results of using Diffracto Sight (D-Sight) method in examining areas with heavy corrosion

Triboluminescent damage sensors detect the light emitted by materials upon fracturing (Ref 41). This is being looked at for detection of cracks and fretting/fatigue damage. Thermography senses thermal gradients from a surface after flashing it with a heat source (Ref 42). The thermal patterns will be different for areas with corrosion products, delaminations, and cracks compared to the noncorroded surface. Figure 14(a) shows a thermography setup for either reflection or transmission. Figure 14(b) is a thermograph of a lap joint showing hot spots and possible corrosion around two of the fastener areas.

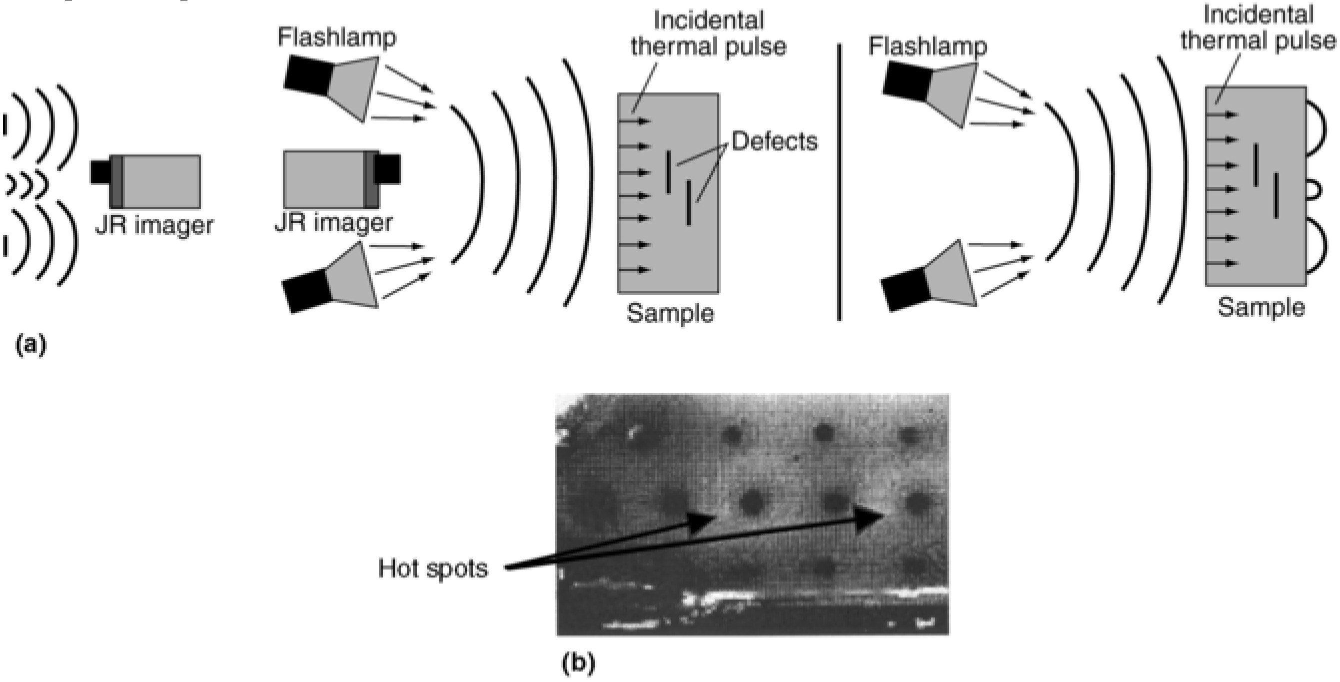

Fig. 14 Infrared thermography. (a) Standard setup of heat lamps, sample, and infrared detector for reflectance (left) or transmission mode (right). (b) A thermograph of a lap joint showing two hot spots at fasteners indicating possible corrosion products

The superconducting quantum interference device (SQUID) magnetometer can image changes in the magnetic fields of a surface caused by corrosion (Ref 43, 44). The setup for this method is shown in Fig. 15. In this novel approach, actual corrosion currents are detected. So far, this device can be used only in the laboratory and on conveniently sized surfaces. Even at this early stage, it could certainly identify problem areas that are more susceptible to corrosion (types of lap joints, fasteners, etc.) and should be monitored more carefully on larger surfaces.

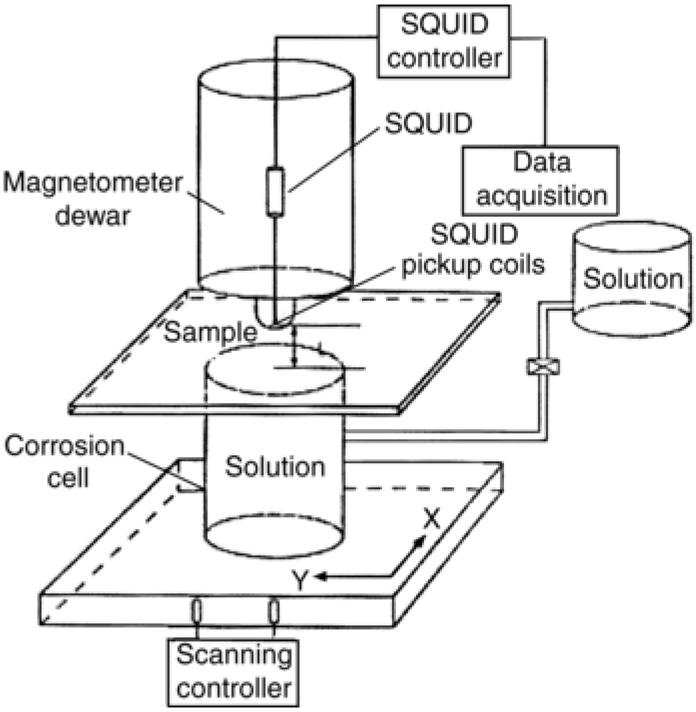

Fig. 15 Superconducting quantum interference device (SQUID) used for scanning samples

References cited in this section

39. D.J. Willie, "Applying D-Sight Technology to Aging Aircraft Corrosion NDI," Technical Paper Series 951140, Society of Automotive Engineers, 1994

40. "D-Sight Aircraft Inspection System," Diffracto Ltd., Windsor, Ontario, Canada

41. I. Sage, R. Badcock, L. Humberstone, N. Geddes, M. Kemp, and G. Bourhill, Triboluminescent Damage Sensors, *Smart Mater. Struct.,* Vol 8, 1999, p 504–510

42. I. Perez and P. Kulowitch, "Thermography for Characterization of Corrosion Damage," Paper 00290, presented at CORROSION 2000, NACE International, 2000

43. D. Li, Y.P. Ma, W.F. Flanagan, B.D. Lichter, and J.P. Wikswo, Jr., Detection of In-Situ Active Corrosion by a SQUID Magnetometer, *J. Min.,* Vol 47 (No. 9), 1995, p 36–39

44. J.P. Wikswo Jr., "Squid Magnetometers for Studying Corrosion and Corrosion Protection in Aircraft Aluminum," Paper 293, presented at CORROSION/97, NACE International, 1997

V.S. Agarwala, In-Service Techniques—Damage Detection and Monitoring, *Corrosion: Fundamentals, Testing, and Protection*, Vol 13A, *ASM Handbook*, ASM International, 2003, p 501–508

In-Service Techniques—Damage Detection and Monitoring

Vinod S. Agarwala, Naval Air Systems Command

Data Management and Expert System

Management of data collected by various methods is key to a successful corrosion prevention and control program. A good record of corrosion types, locations, and repair history is essential for determining trends and patterns of corrosion, according to Colavita et al. (Ref 45). Problems can be identified and prioritized. Of course, this would require creating a systematic approach to develop a good diagnostic solution for repair and maintenance. Handsy and coworkers (Ref 46, 47, 48) used this concept to develop a general-purpose statistical database management system for inspection, data collection, and analysis of military vehicles. Their Corrosion Expert System (CES) was designed to act as an intelligent assistant to a vehicle designer (Ref 48). Figure 16 shows the architecture used by CES. It is a hybrid rule-based production system and Bayesian network composed of seven parts:

- A hybrid production system composed of a long-term memory containing a knowledge base of rules formulated with the help of human experts through the knowledge acquisition facility; a working memory containing a global database of facts or evidence used by the rules; an agenda containing a prioritized list of rules created by the inference engine, whose patterns are satisfied by facts or objects in working; an inference engine that decides which rules are satisfied by the facts or objects, prioritizes the satisfied rules, and executes the rules with the highest priority; and a Bayesian network propagating uncertainty in the rules
- Computer-aided design/computer-aided engineering (CAD/CAE) system interface for converting geometry
- Geometry analyzer that uses a separate rule- based production system to determine some geometry-related facts such as the galvanic potential of the materials, area ratio, presence of crevices, poultice entrapment, and drainage
- Explanation facility for the expert system to explain its reasoning to the user
- Knowledge acquisition facility for automatically entering new knowledge into the system in the future
- An advisory system that utilizes information from the system explanation facility and the geometry analyzer in a separate rule-based production system to formulate proposed actions the user can take to avoid corrosion
- User interface for communication with the expert system, specifically, a Java-based graphical user interface (GUI)

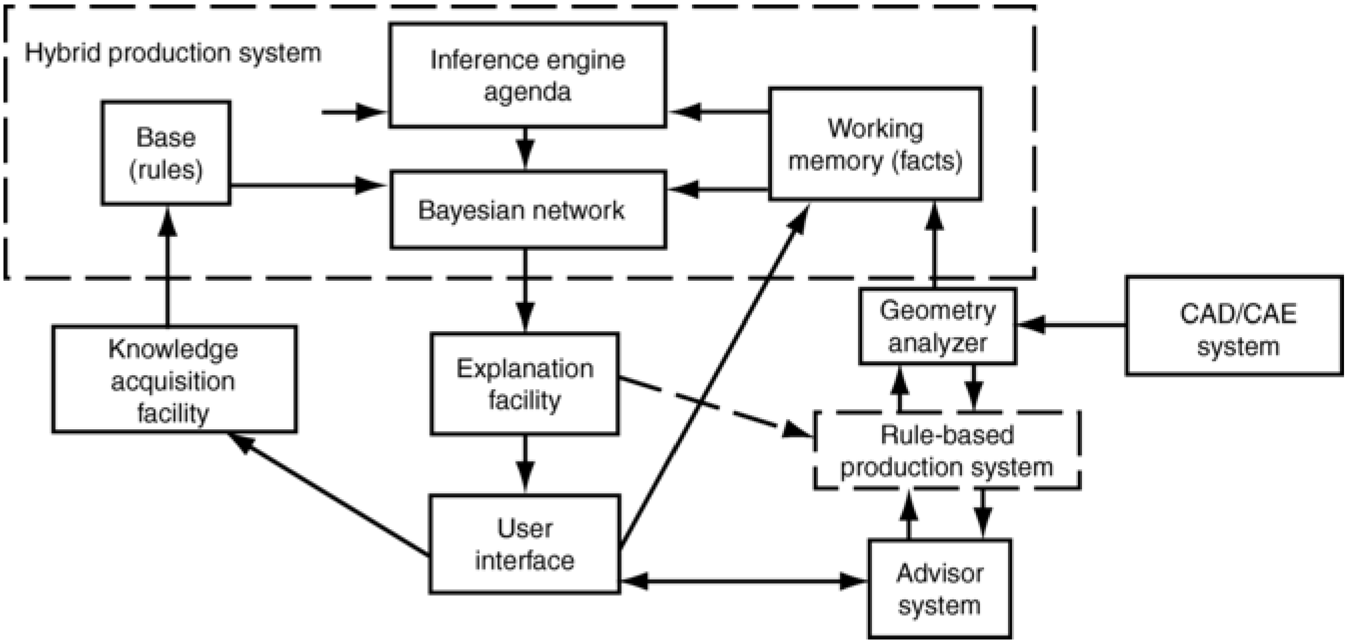

Fig. 16 Corrosion Expert System

References cited in this section

45. M. Colavita, "Italian Air Force Corrosion Data Management," Paper 00301, presented at CORROSION 2000, NACE International, 2000

46. C.T. Savell and I.C. Handsy, "CORRDBMS: How to Collect and Analyze Failure Data in an Uncontrolled Field Environment," Third Joint FAA/DOD/ NASA Conference on Aging Aircraft (Albuquerque, NM), Sept 1999

47. T. Hakkarainen, "Transferring Corrosion Knowledge to Computers: Models for Predicting Corrosion," Technical Paper 97396, NACE International, 1997

48. C.T. Savell, I.C. Handsy, and J.P. Ault, "Development of an Analytical Corrosion Expert System for Design," Proc. Fifth International Aircraft Corrosion Workshop (Solomons, MD), Naval Air Systems Command, Patuxent River, MD, Aug 2002

V.S. Agarwala, In-Service Techniques—Damage Detection and Monitoring, *Corrosion: Fundamentals, Testing, and Protection*, Vol 13A, *ASM Handbook*, ASM International, 2003, p 501–508

In-Service Techniques—Damage Detection and Monitoring

Vinod S. Agarwala, Naval Air Systems Command

Simulation and Modeling

Predictive modeling and simulation offer an economic and efficient way to investigate the appropriate procedures for incorporating the mechanisms of corrosion prevention into military hardware systems design and operation. This area addresses model development, model implementation, system simulation, visualization, and more. This includes, but is not limited to, performing failure modes and effects analysis, reliability modeling and analysis, fault-tree analysis for reliability and safety operations, man- machine models,

maintainability modeling and analysis, life-cycle predictions, behavioral projections, virtual-reality models, and safety-impact analysis for normal and abnormal environments. The Aircraft Structural Integrity Program (ASIP) of U.S. Air Force is perhaps the first effort based on this concept (Ref 49).

Reference cited in this section

49. C. Brooks, K. Honeycutt, S. Prost-Domasky, and D. Peeler, "Monitoring the Robustness of Corrosion & Fatigue Prediction," Technical Brief, 2001 Air Force Structural Integrity Program Conference, (Williamsburg, PA) 11–13 Dec 2001

V.S. Agarwala, In-Service Techniques—Damage Detection and Monitoring, *Corrosion: Fundamentals, Testing, and Protection*, Vol 13A, *ASM Handbook*, ASM International, 2003, p 501–508

In-Service Techniques—Damage Detection and Monitoring

Vinod S. Agarwala, Naval Air Systems Command

References

1. J.G. Knudsen, H.-Y. Jou, and K.W. Herman, Paper 358, presented at CORROSION/85, NACE International, 1985
2. "On-Line Monitoring of Cooling Waters," Standard RP0189-95, NACE International, 2001
3. Proceedings of Symposium, "Corrosion and Corrosivity Sensors," presented at CORROSION/1994, NACE International, 1994
4. Proceedings of Symposium, "Corrosion Sensing and Management of Aging Systems," presented at CORROSION 2000, NACE International, 2000
5. M. Tullmin, P.R. Roberge, and M.A. Little, "Sensors for Aircraft Corrosion—Review and Future," Paper 301, presented at CORROSION/97, 1997
6. V.S. Agarwala and S. Ahmad, Paper 00271, presented at CORROSION/2000, NACE International, 2000
7. M. Tullmin and P.R. Roberge, "Monitoring Corrosion in Aging Systems—New Possibilities and Old Fundamentals," Paper 00282, presented at CORROSION 2000, NACE International, 2000
8. P.R. Roberge, Ed., *Handbook of Corrosion Engineering,* McGraw-Hill, 2000
9. M. Inman, A.K. Rawat, E.J. Taylor, P.J. Moran, et al., "Detection of Crevice Corrosion Under an O-Ring by Polarization Resistance Measurements Using Electrodes Embedded in the O-Ring," Paper 296 and 312, presented at CORROSION/97, NACE International, 1997
10. R.G. Kelly, J. Yuan, S.H. Jones, W. Blanke, J.H. Aylor, W. Wang, A.P. Batson, A. Wintenberg, and G.G. Clemana, Embeddable Microinstruments for Corrosion Monitoring, Paper 294, *CORROSION/97*, NACE International, 1997

11. K.E. Lucas, P.F. Slebodnick, E.A. Hogan, E.D. Thomas, and A.I. Kaznoff, "Comprehensive Monitoring and Evaluation of Ballast Tank Coating Integrity for Life Prediction and Condition Based Maintenance," Paper 00299, presented at CORROSION 2000, NACE International, 2000

12. G. Davis, C.M. Dacres, and L.A. Krebs, "EIS Based In-Situ Sensors for the Early Detection of Coatings Degradation and Substrate Corrosion," Paper 00275, presented at CORROSION 2000, NACE International, 2000

13. P.R. Roberge, R.D. Klassen, and M. Tullmin, "Electrochemical Noise Analysis for Corrosivity Assessment," Paper 00282, presented at CORROSION 2000, NACE International, 2000

14. D.A. Eden, A.N. Rothwell, and J.L. Dawson, Paper 444, "Electrochemical Noise for Detection of Susceptibility to Stress Corrosion Cracking," CORROSION/91, NACE International, 1991

15. J.N. Schoess and C.A. Paul, Smart Fasteners Technology for Aging Aircraft, *Proc. SPIE Smart Structures and Materials Conference,* Vol 2444, Society of Photo-Optical Instrumentation Engineers, Feb 1995, p 192–197

16. J.N. Schoess and G. Seifert, Smart Aircraft Fastener Evaluation Systems: A Condition- Based Corrosion Detection System for Aging Aircraft, presented at *1995 Air Force Aging Aircraft Conference,* (Dayton, OH)

17. R.D. Granata, J.W. Fisher, and J.C. Wilson, "Update on Applications of Corrosion Coulometers" Paper 307, presented at CORROSION/97, NACE International, 1997

18. S.K. Chawla, T. Anguish, and J.H. Payer, Microsensors for Corrosion Control, *Mater. Perform.*, Vol 29 (No. 5), 1990

19. K. Xu, S.C. Dexter, and G.W. Luther, III, Paper 300, presented at CORROSION/97, NACE International, 1997

20. V.S. Agarwala, A Probe for Monitoring Corrosion in Marine Environments, *Atmospheric Corrosion in Marine Environments,* W.H. Ailor, Ed., J. Wiley & Sons, 1982, p 183–192

21. V.S. Agarwala, Sensors for Monitoring Corrosion in Aircraft Systems, Paper 431, *Proc. 13th ICC* (Melbourne, Australia), International Corrosion Congress (ICC), Dec 1996

22. B. Zollars, N. Salazar, J. Gilbert, and M. Sanders, "Remote Datalogger for Thin Film Sensors," Paper 313, presented at CORROSION/97, NACE International, 1997

23. A.V. Bray, H. Stretz, and S.C. Buckner, "Coating Effects in Microwave NDE in the Detection of Corrosion for Aircraft Applications," Paper 00268, presented at CORROSION 2000, NACE International, 2000

24. J.M.S. Dubois, P.R. Roberge, and J.R.S. Giguere, "Eddy Current Sliding Probe Technology for the Detection of Corrosion on Multi-Layered Aircraft Structures," Paper 00296, presented at CORROSION 2000, NACE International, 2000

25. G. John, "Development of Inductive Imaging of Corrosion Damaged Reinforced and Prestressed Concrete Structures," Paper 293, presented at CORROSION 2000, NACE International, 2000

26. J.F. Elliot and M.W. Holley, "Continuous Acoustic Monitoring of Structures," Paper 00288, presented at CORROSION 2000, NACE International, 2000

27. J.L. Rose, L.E. Soley, T. Hay, and V.S. Agarwala, "Ultrasonic Guided Waves for Hidden Corrosion Detection in Naval Aircraft," Paper 00267, presented at CORROSION 2000, NACE International, 2000

28. J.L. Rose, D. Jiao, S.P. Pelt, J.N. Barshinger, and M.J. Quarry, "Hidden Corrosion Detection with Guided Waves," Paper 292, presented at CORROSION/97, NACE International, 1997

29. A.A. Panova, P. Pantano, and D.R. Walt, "In-Situ Fluorescence Imaging of Localized Corrosion with a pH-Sensitive Imaging Fiber," Paper 314, presented at CORROSION/ 97, NACE International, 1997

30. R. Ikegami, Boeing Defense & Space Group, Seattle, WA, private communications, 1993

31. Y. Bar-Cohen, R.V. Bugga, and A.I. Attia, "Corrosion Indicating Pigments and Probes", *NASA Tech Brief,* Vol 17 (No. 10), Item 15, 1993

32. N. Lagakos, H.N. Jones, S.G. Lambrakos, and P.P. Trzaskoma-Paulette, "A Fiber Optic Sensor for Detection of Degradation in Aircraft Lap Joints," Paper 00297, presented at CORROSION 2000, NACE International, 2000

33. I.M. Perez and V.S. Agarwala, "Corrosion Detection and Monitoring Method and Apparatus," U.S. Patent 5646400, 8 July 1997

34. A.A. Panova, P. Pantano, and D.R. Walt, In- Situ Fluorescence Imaging of Localized Corrosion with a pH-Sensitive Imaging Fiber, *Anal. Chem.,* Vol 69, 1997, p 1635–1641

35. R.B. Thompson, Red and Near-Infrared Fluorometry, *Topics in Fluorescence Spectroscopy: Probe Design and Chemical Sensing,* Vol 4, J.R. Lakowicz, Ed., Plenum Press, 1994, p 151–181

36. R.E. Johnson and V.S. Agarwala, The Use of Fluorescence Compounds and Complexes of Metals as Early Warning Detectors of Corrosion, *Mater. Perform.,* Vol 33 (No. 4), 1994, p 25–29

37. R.E. Johnson, K.S. Rajan, and V.S. Agarwala, Fluorescence Based Sensors for Corrosion Detection, *The Role of Characterization in Understanding Environmental Degradation of Materials,* Vol 25, *Microstructural Science,* J.W. Simmons, J.A. Hawk, and D.E. Alman, Ed., ASM International, 1998, p 65–70

38. R.E. Johnson and V.S. Agarwala, et al., "Fluorescent Materials Utilized as Early Warning Sensors for Corrosion of Aluminum Alloys," Paper 505, presented at CORROSION/99, NACE International, 1999

39. D.J. Willie, "Applying D-Sight Technology to Aging Aircraft Corrosion NDI," Technical Paper Series 951140, Society of Automotive Engineers, 1994

40. "D-Sight Aircraft Inspection System," Diffracto Ltd., Windsor, Ontario, Canada

41. I. Sage, R. Badcock, L. Humberstone, N. Geddes, M. Kemp, and G. Bourhill, Triboluminescent Damage Sensors, *Smart Mater. Struct.,* Vol 8, 1999, p 504–510

42. I. Perez and P. Kulowitch, "Thermography for Characterization of Corrosion Damage," Paper 00290, presented at CORROSION 2000, NACE International, 2000

43. D. Li, Y.P. Ma, W.F. Flanagan, B.D. Lichter, and J.P. Wikswo, Jr., Detection of In-Situ Active Corrosion by a SQUID Magnetometer, *J. Min.,* Vol 47 (No. 9), 1995, p 36–39

44. J.P. Wikswo Jr., "Squid Magnetometers for Studying Corrosion and Corrosion Protection in Aircraft Aluminum," Paper 293, presented at CORROSION/97, NACE International, 1997

45. M. Colavita, “Italian Air Force Corrosion Data Management,” Paper 00301, presented at CORROSION 2000, NACE International, 2000

46. C.T. Savell and I.C. Handsy, “CORRDBMS: How to Collect and Analyze Failure Data in an Uncontrolled Field Environment,” Third Joint FAA/DOD/ NASA Conference on Aging Aircraft (Albuquerque, NM), Sept 1999

47. T. Hakkarainen, “Transferring Corrosion Knowledge to Computers: Models for Predicting Corrosion,” Technical Paper 97396, NACE International, 1997

48. C.T. Savell, I.C. Handsy, and J.P. Ault, “Development of an Analytical Corrosion Expert System for Design,” Proc. Fifth International Aircraft Corrosion Workshop (Solomons, MD), Naval Air Systems Command, Patuxent River, MD, Aug 2002

49. C. Brooks, K. Honeycutt, S. Prost-Domasky, and D. Peeler, “Monitoring the Robustness of Corrosion & Fatigue Prediction,” Technical Brief, 2001 Air Force Structural Integrity Program Conference, (Williamsburg, PA) 11–13 Dec 2001

V.S. Agarwala, In-Service Techniques—Damage Detection and Monitoring, *Corrosion: Fundamentals, Testing, and Protection*, Vol 13A, *ASM Handbook*, ASM International, 2003, p 501–508

In-Service Techniques—Damage Detection and Monitoring

Vinod S. Agarwala, Naval Air Systems Command

Selected References

- V.S. Agarwala and A. Fabiszewski, “Thin Film Microsensors for Integrity of Coatings, Composites and Hidden Structures,” Paper 342, presented at CORROSION/94, NACE International, 1994
- R.W. Bosch and W.F. Bogaerts, Instantaneous Corrosion Rate Measurement with Small Amplitude Potential Intermodulation Techniques, *Corrosion,* Vol 52 (No. 3), 1996, p 204–212
- J.C. Bovankovich, On-Line Corrosion Monitoring for Process Plant Control, *Mater. Perform.,* Vol 33, 1994, p 57–60
- J.F. Chen and W.F. Bogaerts, Electrochemical Emission Spectroscopy for Monitoring Uniform and Localized Corrosion, *Corrosion,* Vol 52, 1996, p. 753–759
- T.Y. Chen, M.R. Godfrey, and S.C. Avallone, “Corrosion and Corrosion Product Transport Monitoring in Boiler Condensate Systems,” Paper 336, presented at CORROSION/94, NACE International, 1994
- M. Forslund, J. Majoros, and C. Leygraf, A Sensor System for High Resolution In-Situ Atmospheric Corrosivity Monitoring in Field Environments, *J. Electrochem. Soc.,* Vol 144, 1997, p 2637–2642
- G. Glass, A.M. Hassanein, and N.R. Buenfeld, Monitoring the Passivation of Steel in Concrete Induced by Cathodic Protection, *Corros. Sci.,* Vol 39, 1997, p 1451–1458
- M.R. Godfrey and T.Y. Chen, Monitoring Corrosion in Boiler Systems with Colorimetric Tests for Ferrous and Total Iron, *Corrosion,* Vol 51, 1995, p 797–804
- R.D. Granata, J.W. Fisher, and J.C. Wilson, “Update on Applications of Corrosion Coulometers,” Paper 307, presented at CORROSION/97, NACE International, 1997
- J.A. Grandle and S.R. Taylor, Electrochemical Impedance Spectroscopy of Coated Aluminum Beverage Containers; Determination of an Optimal Parameter for Large Sample Evaluation, *Corrosion,* Vol 50, 1994, p 792–803
- K. Habib and F. Al-Sabti, Monitoring Pitting Corrosion by Holographic Interferometry, *Corrosion,* Vol 53, 1997, p 688–692

- H.S. Isaacs, Potential Transients, Transmission and Electrochemical Corrosion Detection, *NASA Tech. Rep.*, ID: 99 40011449 N (94N15922), Jan 1993
- R. Jasinski and K.D. Efird, Electrochemical Corrosion Probe for High Resistivity Hydrocarbon/Water Mixtures, *Corrosion*, Vol 44 (No. 9), 1988, p 658
- R.E. Johnson, and V.S. Agarwala, K.S. Rajan, A. Singh, and M.G. Durrett, "Fluorescent Materials Utilized as Early Warning Sensors for Corrosion of Aluminum Alloys," Paper 505, presented at CORROSION/99, NACE International, 1999
- N. Mehta and V.S. Agarwala, "Electrochemical Impedance Spectroscopy: A Tool for Evaluating Paint Film Persistency on Metal Surface," Paper 049, U.S. Navy and Industry Corrosion Technology Information Exchange (Louisville, KY), 1998
- A. Nishikata, Y. Ichihara, and T. Tsuru, An Application of Electrochemical Impedance Spectroscopy to Atmospheric Corrosion Study, *Corros. Sci.,* Vol 37, 1995, p 897–911
- A.A. Panova, P. Pantano, and D.R. Walt, In- Situ Fluorescence Imaging of Localized Corrosion with a pH-Sensitive Imaging Fiber, *Anal. Chem.,* Vol 69, 1997, p 1635–641
- J.H. Payer, K. Fink, and I. Song, "Metal- Metal Oxide pH Sensor: The Effect of Anions and Aeration on pH Measurements," Paper 308, presented at CORROSION/97, NACE International, 1997
- G. Rocchini, Corrosion Rate Monitoring of Metallic Materials Using the Linear Response, *Corros. Sci.*, Vol 36, 1994, p 1047–1061
- E.D. Schmauch, A Computerized Corrosion Monitoring System, *NASA Tech. Rep.*, ID 19930073667 N (93N71114), Jan 1986
- N. Sridhar, G.A. Cragnolino, J.C. Walton, and D. Dunn, *Application of Accelerated Corrosion Tests to Service Life Prediction of Materials,* G. Cragnolino and N. Sridhar, Ed., STP 1194, American Society for Testing and Materials, 1994
- M. Twomey, Inspection Techniques for Detecting Corrosion under Insulation, *Mater. Eval.,* Vol 55, 1997, p 129–132
- L. Veleva, S.A. Tomas, and E. Marin, On the Use of the Photoacoustic Technique for Corrosion Monitoring of Metals: Cu and Zn Oxides Formed in Tropical Environments, *Corros. Sci.,* Vol 39, Sept 1997, p 1641–655
- J.P. Wikswo, Jr., "Squid Magnetometers for Studying Corrosion and Corrosion Protection in Aircraft Aluminum," Paper 293, presented at CORROSION/97, NACE International 1997
- H. Xiao and F. Mansfeld, Evaluation of Coating Degradation with Electrochemical Impedance Spectroscopy and Electrochemical Noise Analysis, *J. Electrochem. Soc.*, Vol 141, 1994, p 2332–2337
- J. Zosel, W. Fichtner, H. Kaden, and B. Rau, Corrosion Monitoring with Electrochemical Sensors by Using Evolution-Inspired Optimization Techniques, *Werkst. Korros.*, Vol 47 (No. 6), 1996, p 299–306

G.D. Davis, C.M. Dacres, and L.A. Krebs, Electrochemical Techniques for In-Service Corrosion Monitoring, *Corrosion: Fundamentals, Testing, and Protection*, Vol 13A, *ASM Handbook*, ASM International, 2003, p 509–513

Electrochemical Techniques for In-Service Corrosion Monitoring

Guy D. Davis and Chester M. Dacres, DACCO SCI, INC.; Lorrie A. Krebs, Anderson Materials Evaluation, Inc.

Introduction

A VARIETY OF ELECTROCHEMICAL TECHNIQUES are used to detect and monitor material deterioration in service or in the field. Static or direct current (dc), potential or current measurements, are well established in a number of applications, including buried pipelines and storage tanks. Electrochemical impedance spectroscopy (EIS) and electrochemical noise (ECN) measurements are more common in the laboratory but are also finding applications in the field, especially for inspection of coatings.

G.D. Davis, C.M. Dacres, and L.A. Krebs, Electrochemical Techniques for In-Service Corrosion Monitoring, *Corrosion: Fundamentals, Testing, and Protection*, Vol 13A, *ASM Handbook*, ASM International, 2003, p 509–513

Electrochemical Techniques for In-Service Corrosion Monitoring

Guy D. Davis and Chester M. Dacres, DACCO SCI, INC.; Lorrie A. Krebs, Anderson Materials Evaluation, Inc.

Direct Current Electrochemical Techniques

The most commonly used electrochemical technique in corrosion detection of buried or immersed structures is to measure the corrosion potential or open-circuit potential of the corroding metal against a reference electrode and follow its variation with time. In general, if the corrosion potential of a buried pipeline falls to more active values, then corrosion is developing, but a shift in the positive or noble direction indicates a stifling of corrosion through passivation or the formation of insoluble protective corrosion products. For example, newly laid insulated steel pipelines may have an average potential in excess of -0.8 V with respect to a copper/copper sulfate reference electrode, whereas old corroded steel pipes may have an average potential in the order of -0.2 V (Ref 1). In this case, the old pipe with the less negative voltage, though corroded, is corroding at a slower rate.

The copper/copper sulfate half cell is commonly used as a reference electrode for underground metals—that is, those in contact with soil or concrete (Ref 2). Differences in potential values along the pipeline mean that galvanic currents are flowing through the soil between the anodic and cathodic points on the pipe. If all the pipe-to-soil potentials along the pipe were of equal value or if infinite circuit resistances existed, galvanic currents could not flow and the pipelines would not corrode. These ideal conditions do not exist. The rate of corrosion will depend on the magnitude of the galvanic currents flowing.

In addition to the corrosion information that the pipe-to-soil potential technique provides, potential surveys over various parts of the pipeline may determine such effects as current distribution, induced currents, and stray-current pickup. This information can be used to design a suitable corrosion protection system to prevent further pipeline degradation. In Fig. 1 (Ref 3), three reading locations are shown for a pipe-to-soil potential survey on

an insulated pipeline. If no corrosion were occurring, each potential reading would be essentially the same. However, because these measurements are affected by corrosion currents flowing to or from the pipe due to voltage drops in the soil in the immediate vicinity of the pipeline, pipeline corrosion is reflected in the voltage measurements.

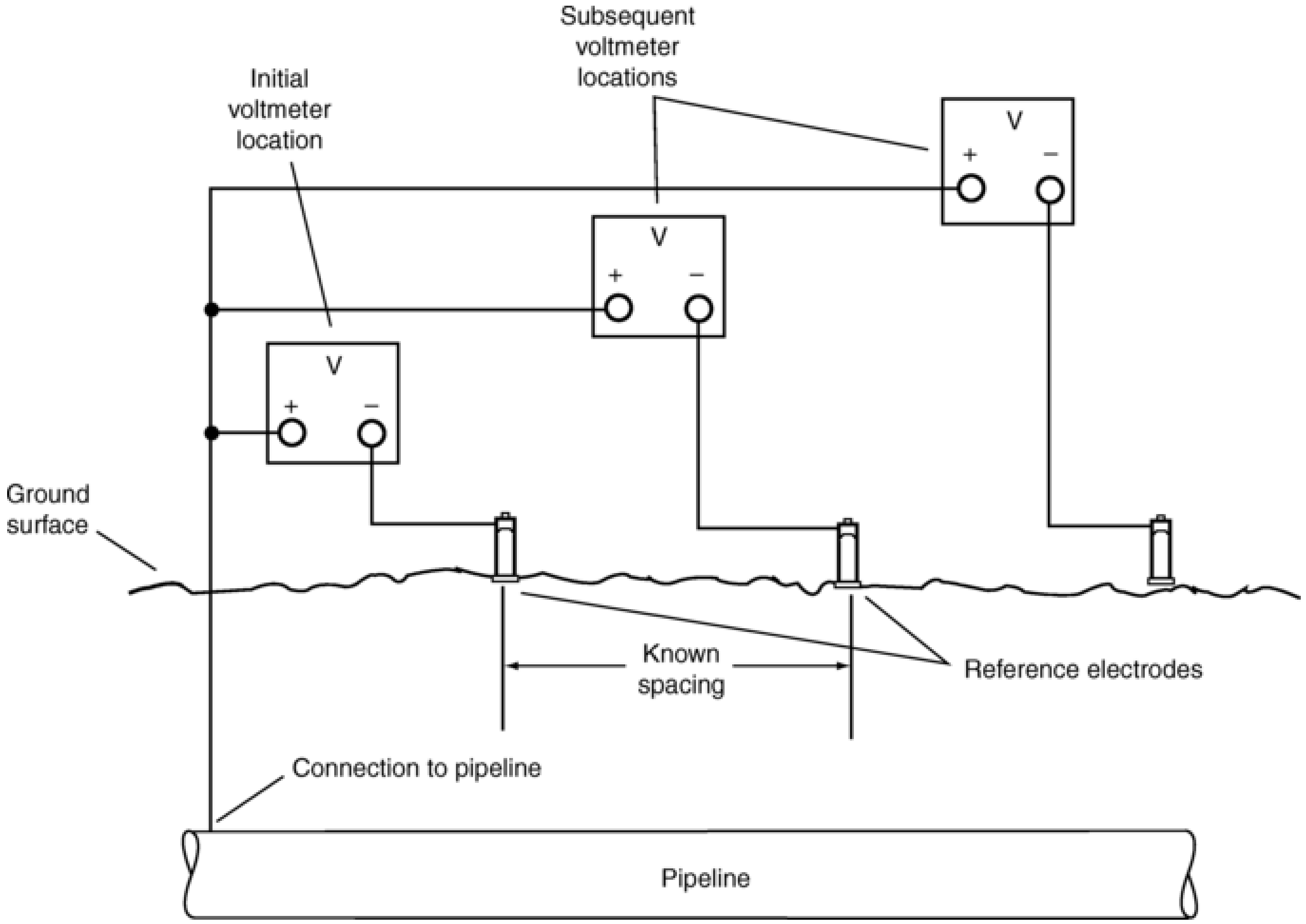

Fig. 1 Principle of pipe-to-soil potential survey

Figure 2 shows data from an actual field survey (Ref 3). Peaks in the plot (the most negative values) indicate locations to be suspected as corroding areas. Material variations that create peaks in the plots can be analyzed and corrosion rates developed with the aid of supporting electrochemical techniques such as EIS. These electrochemical techniques allow determination and correlation of the types of corrosion occurring.

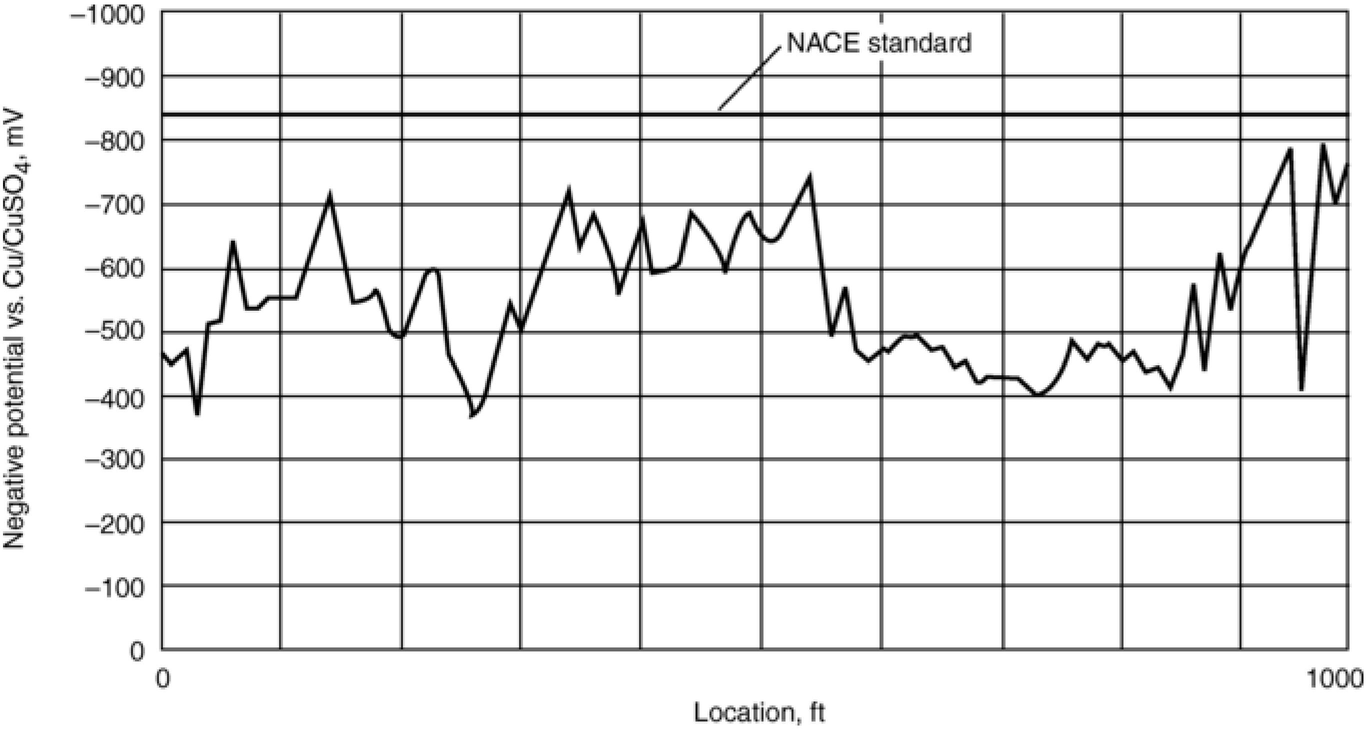

Fig. 2 Pipe-to-soil potential measurements.

If it is not possible to make direct electrical contact with the pipeline, then a closely matched pair of copper/copper sulfate electrodes can be used (Fig. 3) (Ref 1). This procedure can identify the location on the pipeline from which the corrosion current is coming—that is, top, side, or bottom.

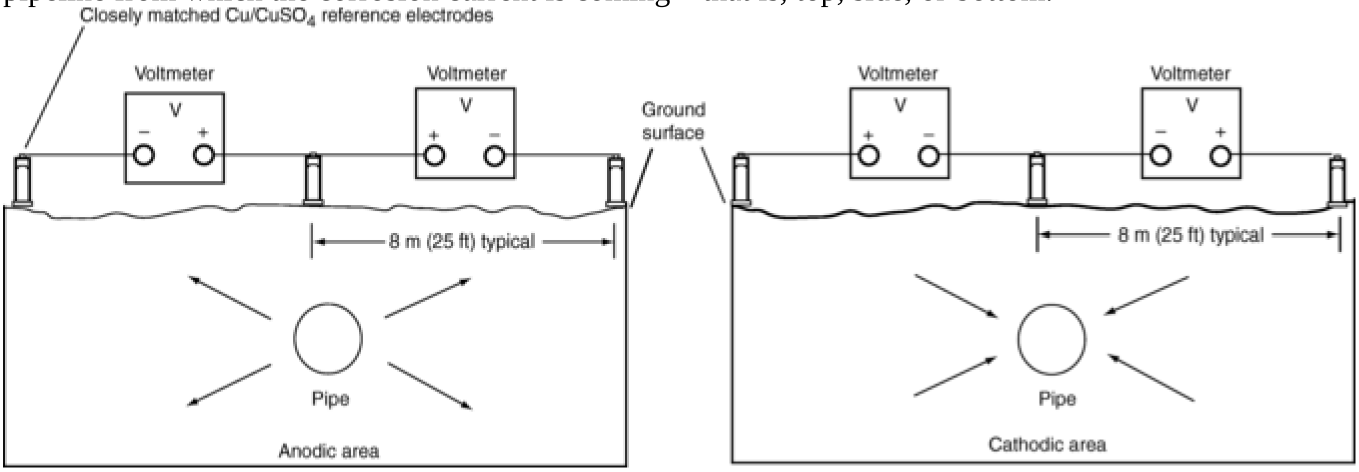

Fig. 3 Pipe-to-soil potential survey using two electrodes. The volt meter with electrodes is moved to take measurements on both sides of the pipe are as shown for anodic and cathodic areas.

For exposed insulated pipelines, prevention of moisture intrusion to the exterior wall will prevent corrosion. To detect moisture intrusion, a small conductivity probe can be pushed through the insulation to the outer surface of the pipe. By monitoring the local conductivity as a function of insulation depth, the amount and location of moisture can be determined. If sufficient moisture is present, potential measurements can be taken to assess the extent of corrosion, similar to those for buried pipelines. Additionally, small specific ion electrodes can detect the presence of different ions and thus help determine the degree of material degradation.

References cited in this section

1. J.A. Beavers, *Peabody's Control of Pipeline Corrosion*, 2nd ed., R.L. Bianchetti, Ed., National Association of Corrosion Engineers, 2001, p 4

2. J.A. Beavers, *Peabody's Control of Pipeline Corrosion*, 2nd ed., R.L. Bianchetti, Ed., National Association of Corrosion Engineers, 2001, p 302

3. C.M. Dacres and B.S. Wenner, personal communication, 1994

G.D. Davis, C.M. Dacres, and L.A. Krebs, Electrochemical Techniques for In-Service Corrosion Monitoring, *Corrosion: Fundamentals, Testing, and Protection*, Vol 13A, *ASM Handbook*, ASM International, 2003, p 509–513

Electrochemical Techniques for In-Service Corrosion Monitoring

Guy D. Davis and Chester M. Dacres, DACCO SCI, INC.; Lorrie A. Krebs, Anderson Materials Evaluation, Inc.

Electrochemical Impedance Spectroscopy

Electrochemical impedance spectroscopy, also known as ac impedance, involves applying a small alternating current voltage between the working electrode (specimen) and a counter electrode and measuring the current that is induced between the specimen and a reference electrode (Ref 4, 5, 6, 7, 8, 9, 10, 11). Both the magnitude and phase of the current relative to the voltage are measured, and a complex impedance is calculated. This measurement is repeated over a wide range of frequencies like 0.01 to 10,000 Hz. Corrosion and degradation of both bare and coated metals can be investigated. This technique is especially suited for coated metals because the coating acts as a capacitor and is amenable to ac but not to dc techniques.

It is common to model the impedance spectrum as an equivalent circuit. The equivalent circuit shown in Fig. 4 is very popular in describing a coating with defects. The left-most resistance and capacitance (RC) circuit represents the coating while the right-most RC circuit represents the interface. Initially, the coating resistance is very high so that the impedance spectrum is dominated by the coating capacitance. This is illustrated by the “good” spectrum of solid symbols in Fig. 5. In this Bode magnitude representation, the impedance has a slope of -1 and a high value, typically 10^8 to 10^{10} Ω, at low frequencies. The phase angle is close to -90° over most of the frequency range. As a coating degrades, moisture penetrates and allows conductance, so the coating resistance decreases. The impedance at low frequencies decreases by one or more orders of magnitude and becomes independent of frequency. In the phase angle plots, the phase is close to zero (purely resistive) at low frequencies and drops to near -90° (purely capacitive) at high frequencies. The “bad” spectrum of open symbols in Fig. 5 is an indication of a degrading coated metal. Once enough moisture reaches the interface, the metal can start to corrode. The interface circuit parameters will reflect this corrosion, and a second time constant can often be detected in the spectrum.

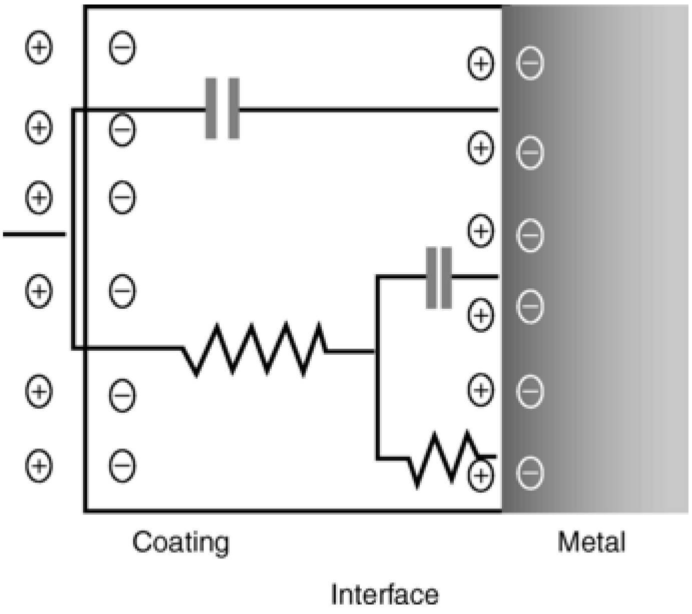

Fig. 4 Equivalent circuit for a defective coating

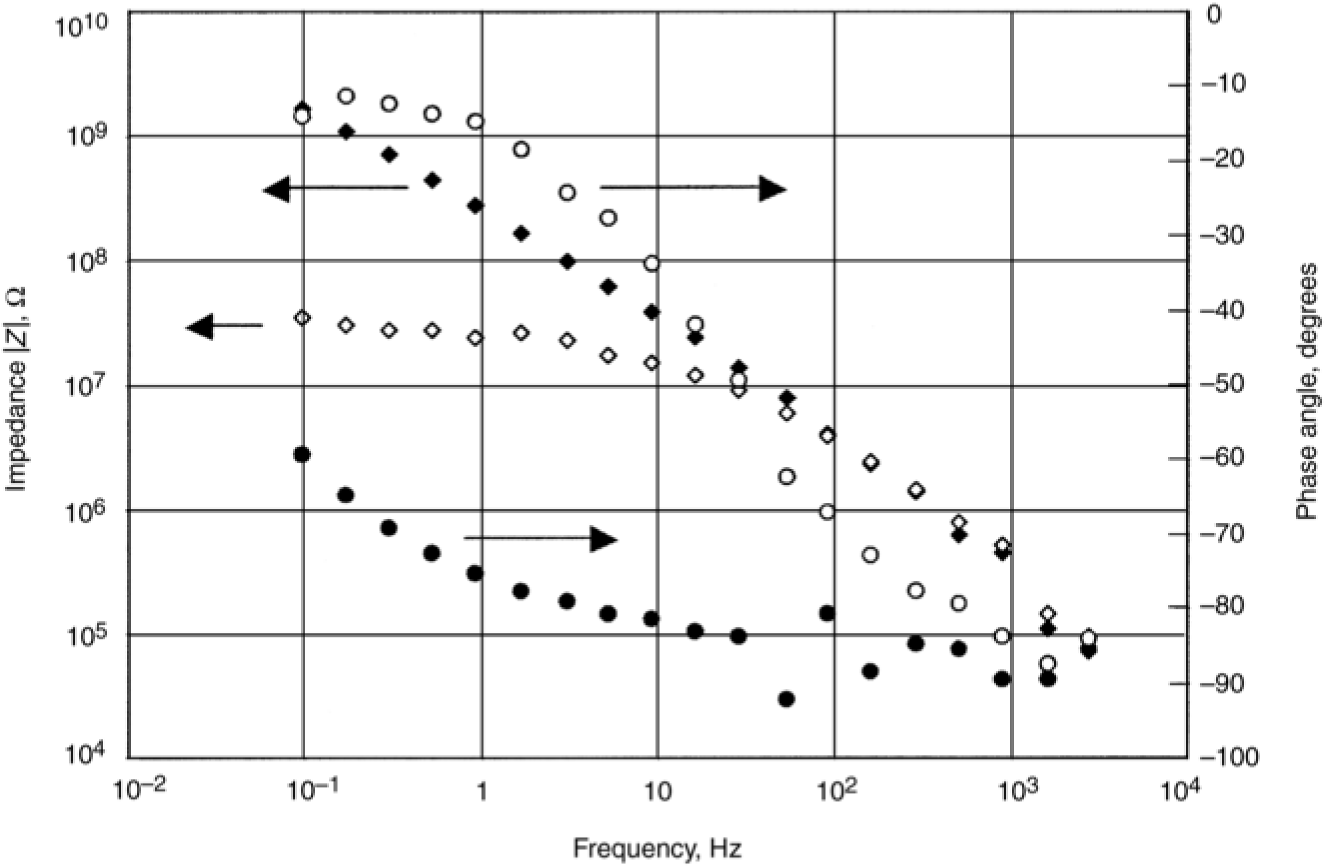

Fig. 5 Bode format for magnitude of impedance (diamonds) and phase angle (circles). A good coating is plotted with solid symbols, and a bad coating is indicated by the plots with open symbols.

The changes detected by EIS are well in advance of any visual signs of corrosion, such as, rust or blistering, so that EIS can be used to predict coating performance.

Good correlation has been reported between EIS measurements and long-term coating performance during immersion in different electrolytes (Ref 8, 12, 13, 14). This predictive capability is illustrated in Fig. 6. A variety of different coatings and substrates were prepared with a wide range of protective qualities and subjected to a cyclic laboratory corrosion test that automotive manufacturers have found predictive of service performance of materials. The time for the low-frequency impedance of the coating to decrease to 10^7 Ω

correlated very well to the amount of rust or corrosion on the panels at the end of the 100 cycle (5 month) test. Although there were no visible signs of corrosion on the panels at the time that the impedance had decreased to $10^7\ \Omega$, that time value was predictive of the effectiveness of the coating (Ref 15, 16). Similar measurements have shown that the 100-cycle test could be shortened by up to 40% without loss of information (Ref 15, 16, 17).

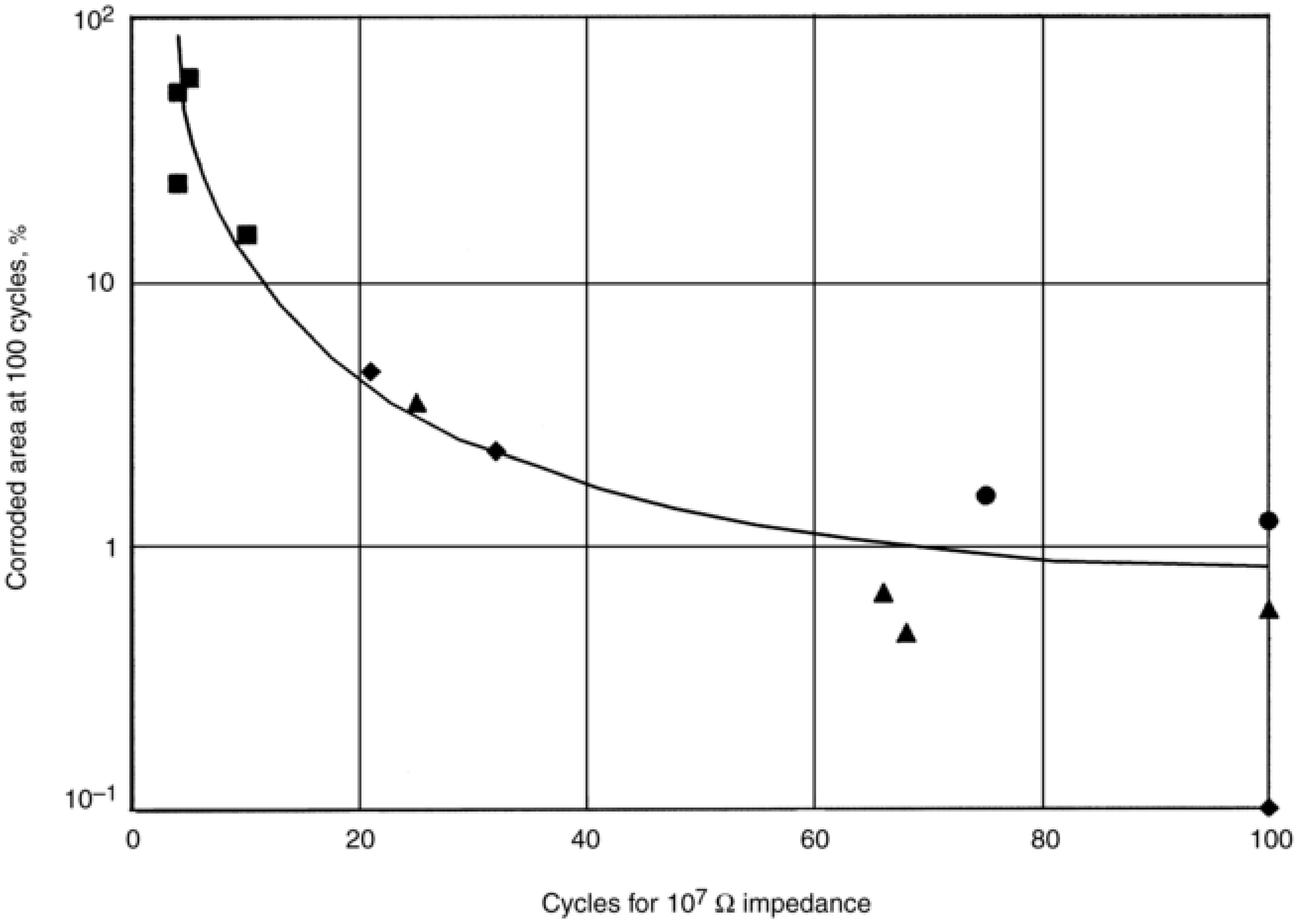

Fig. 6 Correlation of corroded area at end of cyclic laboratory corrosion test with the time for the low-frequency impedance to decrease to $10^7\ \Omega$. The different symbols represent different substrate materials.

Traditionally, EIS has been primarily a laboratory tool for several reasons. The electronics (potentiostats) needed to perform the measurements were bench-top size and inconvenient to take into the field. Furthermore, the specimens had to be immersed into an electrolyte along with the counter and reference electrodes. This process required small specimens. Recent developments have ameliorated these limitations. Portable electronics that can easily be taken into the field are available. Alternative means of inspecting large structures have also been introduced to expand the types of systems that can be examined by EIS. The first of these is a clamp-on electrochemical cell (essentially a bottomless beaker with an O-ring seal at the bottom) (Fig. 7, left) that can be attached to a flat, horizontal surface of a large structure (Ref 18, 19, 20). In a few cases, clamp-on cells containing sponges, gels, or similar materials impregnated with electrolyte have proven satisfactory and have eased the flat, horizontal surface requirement. The other approach is the use of in-situ corrosion sensors (Ref 15, 16, 21), either sensors of conductive paint that are applied directly to the surface of interest for long-term monitoring or handheld sensors that are pressed against the surface during measurement (Fig. 7, right). These sensors require no externally applied electrolyte and can be used on structures of any shape and size under ambient or accelerated laboratory conditions.

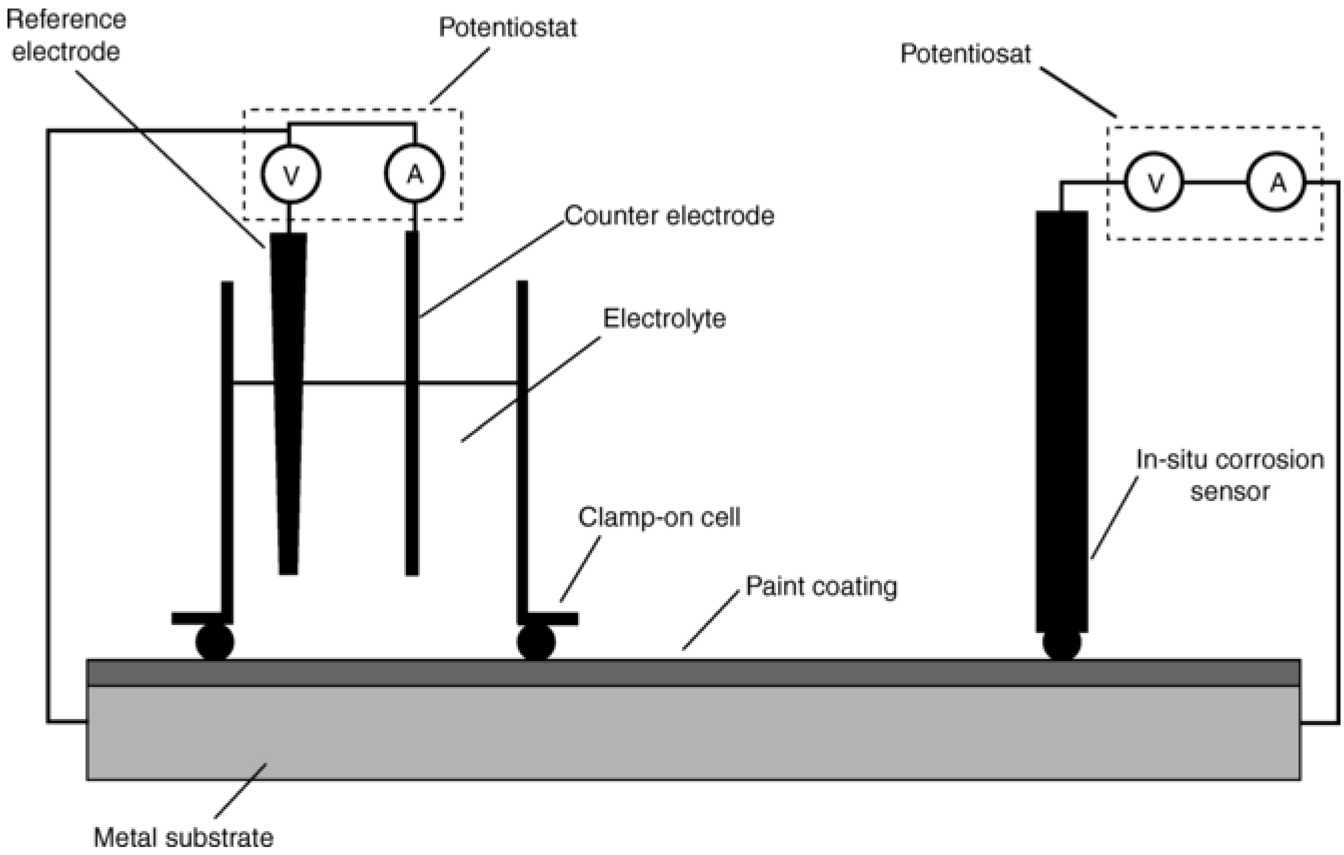

Fig. 7 Left: schematic representation of a clamp-on cell with O-ring seal that allows conventional EIS to be performed on areas of large structures. Right: schematic representation of in-situ corrosion sensor, which allows EIS to be performed under ambient conditions without electrolyte.

The ability to take measurements under arbitrary conditions enables EIS to become part of a condition-based maintenance (CBM) protocol or to directly and qualitatively compare coating degradation in different environments. This allows accelerated testing to be validated more readily than relying on visual comparison of specimens once extensive corrosion has occurred. This comparison is illustrated in Fig. 8. A series of coatings were subjected to salt fog (ASTM B 117), a cyclic laboratory accelerated test, and exposure on the beach at Kennedy Space Center (Ref 17). No correlation was seen between the beach exposure and salt fog; in fact, the correlation coefficient was -0.04, indicating a nearly random relationship. In contrast, the cyclic test exhibited a correlation coefficient of 0.97 with beach exposure. Although the relevance of salt fog testing to field exposures has long been questioned (Ref 22, 23, 24, 25, 26), the comparisons have generally involved visual observations, weight loss measurements, analyses of corrosion products, or other semiquantitative or late-stage measurements.

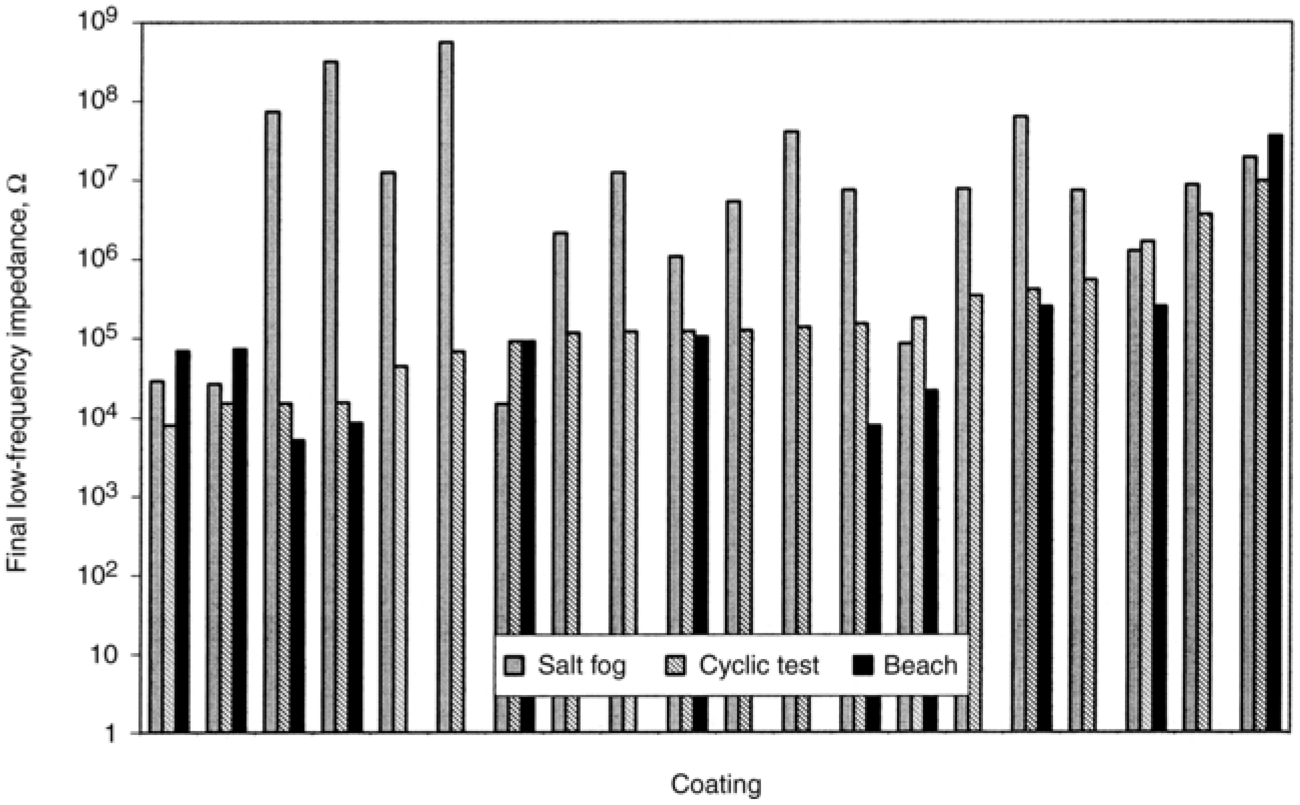

Fig. 8 The final low-frequency impedance for several coatings following exposure at Kennedy Space Center beach, salt fog testing, and cyclic test exposures. The coatings are ordered in increasing cyclic test values. Cyclic tests and the beach exposure correlate to each other, while the salt fog test results do not.

References cited in this section

4. A.J. Bard and L.R. Faulkner, *Electrochemical Methods: Fundamentals and Applications,* Wiley, 1980

5. F. Mansfeld, *Corrosion,* Vol 36, 1981,[fj p 301

6. G.W. Walter, *Corrosion Sci.,* Vol 26, 1986, p 681

7. F. Mansfeld, M.W. Kendig, and S. Tsai, *Corrosion,* Vol 38, 1982, p 570

8. J.R. Scully, *J. Electrochem. Soc.,* Vol 136, 1989, p 979

9. J.R. Scully, *Corrosion Testing and Evaluation: Silver Anniversary Issue,* STP 1000, R. Baboian and S.W. Dean, Ed., ASTM, 1990, p 351

10. U. Rammelt and G. Reinhard, *Prog. Org. Coat.,* Vol 21, 1992, p 205

11. J.N. Murray, *Prog. Org. Coat.,* Vol 31, 1997, p 375

12. W.S. Tait, *J. Coatings Technol.,* Vol 61, 1989, p 57

13. J.N. Murray and H.P. Hack, Paper 140 presented at *Corrosion/90,* National Association of Corrosion Engineers, 1990

14. J.A. Grandle and S.R. Taylor, *Corrosion,* Vol 50, 1994, p 792

15. G.D. Davis, C.M. Dacres, and L.A. Krebs, *Mater. Perform.,* Vol 39, 2000, p 46

16. G.D. Davis, C.M. Dacres, and L.A. Krebs, Paper 275 presented at Corrosion/2000, (Houston, TX) National Association of Corrosion Engineers

17. G.D. Davis, L.A. Krebs, and C.M. Dacres, *J. Coatings Technol.,* Vol 74 (No. 935), Dec 2002, p 69

18. A. Zdunek and X. Zhan, paper presented at the *Fourth World Congress on Coating Systems for Bridge and Steel Structures,* February 1995, (St. Louis, MO), Steel Structures Painting Council,

19. K. Homma et al., *Corrosion Forms and Control for Infrastructure,* STP 1137, V. Chaker, Ed., ASTM, 1992

20. P.C. Su, O.F. Devereux, and W. Madych, *Structural Integrity in Aging Aircraft,* AD- Vol 47, C.I. Chang and C.T. Sun, Ed., American Society of Mechanical Engineers, 1995

21. L.A. Krebs, G.D. Davis, and C.M. Dacres, Paper 1430 presented at Corrosion/2001, (Houston, TX), National Association of Corrosion Engineers, 2001

22. S.B. Lyon, G.E. Thompson, and J.B. Johnson, STP 1133, ASTM, p 20

23. M. Petschel, Jr., *Proc. Fifth Automotive Corrosion & Prevention Conf.,* 1991, p 179

24. B.S. Skerry, A. Alavi, and K.I. Lindgren, *J. Coatings Technol.,* Vol 60, 1988, p 97

25. H.E. Townsend, D.C. McClune, R.J. Neville, R.D. Granata, and W.A. Schumacher, *Proc. Fifth Automotive Corrosion and Prevention Conf.,* SAE. 1991, p 73

26. B.R. Appleman, *J. Prot. Coatings Linings,* October 1992, p 134

G.D. Davis, C.M. Dacres, and L.A. Krebs, Electrochemical Techniques for In-Service Corrosion Monitoring, *Corrosion: Fundamentals, Testing, and Protection*, Vol 13A, *ASM Handbook*, ASM International, 2003, p 509–513

Electrochemical Techniques for In-Service Corrosion Monitoring

Guy D. Davis and Chester M. Dacres, DACCO SCI, INC.; Lorrie A. Krebs, Anderson Materials Evaluation, Inc.

Electrochemical Noise

Tracking the perturbations in current and potential caused by random corrosion events is the focus of the electrochemical noise (ECN) method. Techniques include monitoring the changing potential of a corroding surface relative to a selected reference electrode, monitoring the current fluctuations between nominally identical electrodes in a corrosive environment, and comparing current and potential noise in order to determine electrochemical noise resistance or impedance. Refer to “Electrochemical Methods of Corrosion Testing” in this Volume for further details. For nearly two decades these methodologies have been practiced as a means of detecting and observing corrosion phenomena such as general corrosion, cavitation and erosion corrosion, crevice and pitting corrosion, coating degradation, microbiologically induced corrosion, stress-corrosion cracking, and inhibition (Ref 27, 28). The application of this technique for continuous in-plant corrosion monitoring has become more popular in recent years.

The earliest studies in electrochemical noise and its relationship to corrosion are attributed to Iverson (Ref 29), who examined potential transients associated with corroding metals and alloys. Many researchers have

subsequently studied the applicability of electrochemical noise measurement to the evaluation of corrosion rates and identification of corrosion mechanisms. Typically, current fluctuations are measured by connecting two identical electrodes through a zero-resistance ammeter (ZRA) (Ref 30). Variations in potential can be monitored by introducing a third electrode, either another nominally identical electrode or a standard reference electrode. Potential fluctuations may also be monitored by using two electrodes identical to, but electrically isolated from, the pair used for current measurement. These arrangements constitute the two-, three-, and four-electrode systems encountered in electrochemical noise measurement.

Statistical interpretation of current and potential fluctuation data may be employed to determine R_n, the noise resistance (Ref 27, 31). For example, the ratio of the standard deviations of the potential and current over a fixed time frame can be used to define R_n. R_n has been shown to be an indicator of the onset of localized corrosion, as well as to have an inverse relationship to corrosion rate.

Alternatively, a frequency domain analysis such as fast Fourier transform (FFT) or maximum entropy method (MEM) may be employed. The FFT analysis is better suited to long-term data where several transforms can be averaged, while MEM analysis is preferable for single data sets (Ref 27). The power spectral densities that result from frequency domain transforms may be used to calculate the spectral noise resistance (R_{sn}) as a function of frequency, or noise impedance. It has been shown experimentally that the frequency domain transform methods produce more quantitatively reliable results than statistical data analysis (Ref 31, 32). Statistical analysis methods may be useful when qualitative results are considered adequate (Ref 33).

Electrochemical noise techniques have been developed for on-line monitoring in a variety of industries, including power generation, nuclear waste containment, and water supply (potable and heating/cooling) (Ref 28, 34). The corrosion behavior of several metals and alloys has been characterized by the electrochemical noise technique in a variety of environments, and results have compared well with those characterized by more traditional techniques (Ref 28, 33, and 35). However, certain factors, including electrode asymmetry (material differences, bias voltages, coatings) and the influence of instrumental noise, may affect results and must be considered when employing electrochemical noise measurement as a monitoring tool (Ref 36, 37, 38).

References cited in this section

27. *Uhlig's Corrosion Handbook,* 2nd ed., R.W. Revie, Ed., New York, 2000, p 1227

28. *Electrochemical Noise Measurement for Corrosion Applications,* J.R. Kearns, J.R. Scully, P.R. Roberge, D.L. Reichert, and J.L. Dawson, Ed., ASTM, 1996, p 173

29. W.P. Iverson, *J. Electrochem. Soc.,* Vol 115, 1968, p 617

30. J.A. von Fraunhofer and C.H. Banks, *Potentiostat and Its Applications,* Butterworths, London, 1972.

31. U. Bertocci, C. Gabrielli, F. Huet, and M. Keddam, *J. Electrochem. Soc.* Vol 144, 1997, p 31

32. U. Bertocci, C. Gabrielli, F. Huet, M. Keddam, and P. Rousseau, *J. Electrochem. Soc.,* Vol 144, 1997, p 37

33. C. Monticelli, G. Trabanelli, and G. Meszaros, *J. Appl. Electrochem.,* Vol 28, 1998, p 963

34. D. Townley and S.J. Duranceau, Paper 01287 presented at Corrosion 2001, (Houston, TX), National Association of Corrosion Engineers, NACE 2001

35. P.R. Roberge and D.R. Lenard, *J. Appl. Electrochem.,* Vol 28, 1998, p 405

36. U. Bertocci and F. Huet, *J. Electrochem. Soc.,* Vol 144, 1997, p 2786

37. A. Bautista and F. Huet, *J. Electrochem. Soc.,* Vol 146, 1999, p 1730

38. A. Bautista, U. Bertocci, and F. Huet, *J. Electrochem. Soc.,* Vol 148, 2001, p B412

G.D. Davis, C.M. Dacres, and L.A. Krebs, Electrochemical Techniques for In-Service Corrosion Monitoring, *Corrosion: Fundamentals, Testing, and Protection*, Vol 13A, *ASM Handbook*, ASM International, 2003, p 509–513

Electrochemical Techniques for In-Service Corrosion Monitoring

Guy D. Davis and Chester M. Dacres, DACCO SCI, INC.; Lorrie A. Krebs, Anderson Materials Evaluation, Inc.

References

1. J.A. Beavers, *Peabody's Control of Pipeline Corrosion,* 2nd ed., R.L. Bianchetti, Ed., National Association of Corrosion Engineers, 2001, p 4
2. J.A. Beavers, *Peabody's Control of Pipeline Corrosion,* 2nd ed., R.L. Bianchetti, Ed., National Association of Corrosion Engineers, 2001, p 302
3. C.M. Dacres and B.S. Wenner, personal communication, 1994
4. A.J. Bard and L.R. Faulkner, *Electrochemical Methods: Fundamentals and Applications,* Wiley, 1980
5. F. Mansfeld, *Corrosion,* Vol 36, 1981,[fj p 301
6. G.W. Walter, *Corrosion Sci.,* Vol 26, 1986, p 681
7. F. Mansfeld, M.W. Kendig, and S. Tsai, *Corrosion,* Vol 38, 1982, p 570
8. J.R. Scully, *J. Electrochem. Soc.,* Vol 136, 1989, p 979
9. J.R. Scully, *Corrosion Testing and Evaluation: Silver Anniversary Issue,* STP 1000, R. Baboian and S.W. Dean, Ed., ASTM, 1990, p 351
10. U. Rammelt and G. Reinhard, *Prog. Org. Coat.,* Vol 21, 1992, p 205
11. J.N. Murray, *Prog. Org. Coat.,* Vol 31, 1997, p 375
12. W.S. Tait, *J. Coatings Technol.,* Vol 61, 1989, p 57
13. J.N. Murray and H.P. Hack, Paper 140 presented at *Corrosion/90,* National Association of Corrosion Engineers, 1990
14. J.A. Grandle and S.R. Taylor, *Corrosion,* Vol 50, 1994, p 792
15. G.D. Davis, C.M. Dacres, and L.A. Krebs, *Mater. Perform.,* Vol 39, 2000, p 46
16. G.D. Davis, C.M. Dacres, and L.A. Krebs, Paper 275 presented at Corrosion/2000, (Houston, TX) National Association of Corrosion Engineers
17. G.D. Davis, L.A. Krebs, and C.M. Dacres, *J. Coatings Technol.,* Vol 74 (No. 935), Dec 2002, p 69
18. A. Zdunek and X. Zhan, paper presented at the *Fourth World Congress on Coating Systems for Bridge and Steel Structures,* February 1995, (St. Louis, MO), Steel Structures Painting Council,

19. K. Homma et al., *Corrosion Forms and Control for Infrastructure,* STP 1137, V. Chaker, Ed., ASTM, 1992

20. P.C. Su, O.F. Devereux, and W. Madych, *Structural Integrity in Aging Aircraft,* AD- Vol 47, C.I. Chang and C.T. Sun, Ed., American Society of Mechanical Engineers, 1995

21. L.A. Krebs, G.D. Davis, and C.M. Dacres, Paper 1430 presented at Corrosion/2001, (Houston, TX), National Association of Corrosion Engineers, 2001

22. S.B. Lyon, G.E. Thompson, and J.B. Johnson, STP 1133, ASTM, p 20

23. M. Petschel, Jr., *Proc. Fifth Automotive Corrosion & Prevention Conf.,* 1991, p 179

24. B.S. Skerry, A. Alavi, and K.I. Lindgren, *J. Coatings Technol.,* Vol 60, 1988, p 97

25. H.E. Townsend, D.C. McClune, R.J. Neville, R.D. Granata, and W.A. Schumacher, *Proc. Fifth Automotive Corrosion and Prevention Conf.,* SAE. 1991, p 73

26. B.R. Appleman, *J. Prot. Coatings Linings,* October 1992, p 134

27. *Uhlig's Corrosion Handbook,* 2nd ed., R.W. Revie, Ed., New York, 2000, p 1227

28. *Electrochemical Noise Measurement for Corrosion Applications,* J.R. Kearns, J.R. Scully, P.R. Roberge, D.L. Reichert, and J.L. Dawson, Ed., ASTM, 1996, p 173

29. W.P. Iverson, *J. Electrochem. Soc.,* Vol 115, 1968, p 617

30. J.A. von Fraunhofer and C.H. Banks, *Potentiostat and Its Applications,* Butterworths, London, 1972.

31. U. Bertocci, C. Gabrielli, F. Huet, and M. Keddam, *J. Electrochem. Soc.* Vol 144, 1997, p 31

32. U. Bertocci, C. Gabrielli, F. Huet, M. Keddam, and P. Rousseau, *J. Electrochem. Soc.,* Vol 144, 1997, p 37

33. C. Monticelli, G. Trabanelli, and G. Meszaros, *J. Appl. Electrochem.,* Vol 28, 1998, p 963

34. D. Townley and S.J. Duranceau, Paper 01287 presented at Corrosion 2001, (Houston, TX), National Association of Corrosion Engineers, NACE 2001

35. P.R. Roberge and D.R. Lenard, *J. Appl. Electrochem.,* Vol 28, 1998, p 405

36. U. Bertocci and F. Huet, *J. Electrochem. Soc.,* Vol 144, 1997, p 2786

37. A. Bautista and F. Huet, *J. Electrochem. Soc.,* Vol 146, 1999, p 1730

38. A. Bautista, U. Bertocci, and F. Huet, *J. Electrochem. Soc.,* Vol 148, 2001, p B412

P.R. Roberge and R.D. Klassen, Corrosion Monitoring Techniques, *Corrosion: Fundamentals, Testing, and Protection*, Vol 13A, *ASM Handbook*, ASM International, 2003, p 514–518

Corrosion Monitoring Techniques

P.R. Roberge and R.D. Klassen, Royal Military College of Canada

Introduction

CORROSION MONITORING has become important in the operation of modern industrial plants and in the use and maintenance of expensive assets such as bridges and aircraft. Engineering and maintenance personnel need to be aware of both the cumulative damage caused by corrosion and the rate of the deterioration, because the costs associated with corrosion problems can be huge and the risks devastating. (See the article “Direct Costs of Corrosion in the United States” in this Volume). The term *on-line monitoring,* as used in this context, includes electrochemically based techniques for evaluating the progress or rate of corrosion. Nondestructive approaches for monitoring metal thickness are covered in the articles “Corrosion Monitoring Using Microwave and Guided Wave Nondestructive Evaluation” and “Corrosion Monitoring for Industrial Processes” in this Section.

P.R. Roberge and R.D. Klassen, Corrosion Monitoring Techniques, *Corrosion: Fundamentals, Testing, and Protection*, Vol 13A, *ASM Handbook*, ASM International, 2003, p 514–518

Corrosion Monitoring Techniques

P.R. Roberge and R.D. Klassen, Royal Military College of Canada

On-Line Corrosion Monitoring Techniques

Corrosion monitoring techniques can be divided into two categories, direct and indirect. Direct techniques measure parameters that are directly associated with the corrosion processes. These include coupons, electrical resistance (ER) and inductive resistance, linear polarization resistance (LPR), electrochemical impedance spectroscopy (EIS), zero-resistance ammetry (ZRA), electrochemical noise (ECN) and self- linear polarization resistance (SLPR). Indirect techniques measure parameters that are indirectly related to the rate of corrosion, such as monitoring the corrosion potential and the use of hydrogen probes. Further details on the corrosion potential, EIS, and ECN techniques are given in the article “Electrochemical Techniques for In-Service Corrosion Monitoring” in this Volume.
There are differences in the quality of information obtained between different corrosion monitoring techniques. Some techniques provide information on the average corrosion rate only (ER, LPR, and EIS), while other techniques can additionally provide information on the type of corrosive attack (ECN and SLPR). References 1, 2, 3, 4, 5 give reviews of on-line corrosion monitoring for process-plant control. A broad review of corrosion engineering is presented elsewhere (Ref 6).

References cited in this section

1. J.C. Bovankovich, “On-Line Corrosion Monitoring for Process Plant Control,” *Mater. Perform.,* Vol 33 (No. 11), 1994, p 57–60

2. *Corrosion Monitoring in Industrial Plants Using Nondestructive Testing and Electrochemical Methods,* STP 908, G.C. Moran and P. Labine, Ed., ASTM 1986

3. S.W. Dean, Overview of Corrosion Monitoring in Modern Industrial Plants, *Corrosion Monitoring in Industrial Plants Using Nondestructive Testing and Electrochemical Methods,* STP 908, G.C. Moran and P. Labine, Ed., ASTM, 1986a, p 197–220

4. S.W. Dean, Electrochemical Methods for Corrosion Testing in the Process Industries, *Electrochemical Corrosion Testing With Special Consideration of Practical Applications, Proc. of International Workshop,* E. Heintz, J.C. Rowlands, and F. Mansfeld, Ed., (Ferrara, Italy), DECHEMA, 1986b, p 1–15

5. C.P. Dillon, A.S. Krisher, and H. Wissenberg, Plant Corrosion Tests, *Handbook on Corrosion Testing and Evaluation,* W.H. Ailor, Ed., John Wiley & Sons, 1971, p 599–615

6. P.R. Roberge, *Handbook of Corrosion Engineering*, McGraw-Hill, 2000

P.R. Roberge and R.D. Klassen, Corrosion Monitoring Techniques, *Corrosion: Fundamentals, Testing, and Protection*, Vol 13A, *ASM Handbook*, ASM International, 2003, p 514–518

Corrosion Monitoring Techniques

P.R. Roberge and R.D. Klassen, Royal Military College of Canada

Direct Techniques

Corrosion Coupons. A simple and inexpensive method of corrosion monitoring involves the exposure and subsequent evaluation of actual metal specimens or "coupons." Small specimens are exposed to the environment of interest for a specific period of time and subsequently removed for weight-loss measurement and more detailed examination. ASTM G 4 (Ref 7) was designed to provide guidance for this type of testing, and Ref 8 gives additional details. Two disadvantages of this approach are that a long exposure period is required and only cumulative information is provided. Coupons are also commonly used to monitor the effectiveness of cathodic protection measures in buried pipelines. In this application the mass loss is not measured, but coupons are examined to determine the corrosion state of the exterior pipe wall.

Electrical and Inductive Resistance. Electrical resistance (ER) probes are specially designed corrosion coupons with electrical connections. The corrosion rate of the exposed element is calculated from a measurement of electrical resistance rather than mass loss. These measurements are made by installing a device fabricated from the material in question, such as a wire, in such a way that its electrical resistance can be measured. Resistance is a strong function of temperature and therefore must be accounted for with simultaneous temperature measurement. As corrosion processes reduce the metallic cross section of the exposed element, the electrical resistance increases with exposure time. The corrosion rate is obtained by taking the slope of a series of measurements made over a period of time. Generally, the sensitivity of ER probes is insufficient to qualify for real-time corrosion measurements because transients of short duration go undetected.

The inductive resistance probe is a recently introduced derivative of ER (Ref 6). The reduction in the thickness of a sensing element is measured by changes in the inductive resistance of a coil embedded in the sensor. Sensing elements with high magnetic permeability intensify the magnetic field around the coil; therefore, thickness changes affect the inductive resistance of the coil. The decrease in response time, or sensitivity, has been claimed to be several orders of magnitude higher than it is with comparable ER probes. Both techniques should be applied only to nonpitting environments.

Linear Polarization Resistance. The technique of LPR provides an estimate of the corrosion rate based on the Stern-Geary equation (Ref 9). The theory behind the technique is that the corrosion rate of a metal, in the

absence of diffusional resistances, is inversely proportional to the *polarization resistance*; that is, the slope of the potential/current response curve near the corrosion potential. The equation and Tafel plots are found in the article “Electrochemical Methods of Corrosion Testing” in this Volume. The proportionality factor, *B*, is a function of the anodic and cathodic Tafel slopes, which depend on temperature and the chemical species and concentration in the electrolyte. An external power supply gradually polarizes the specimen about 10 mV on both sides of the corrosion potential. The slope between the induced potential and the resulting current is interpreted as the polarization resistance. The time required for each resistance determination is a matter of minutes. Thus, this type of probe can provide corrosion rate feedback information with sufficient speed that it can be used in process control schemes.
The limitations to this approach include:

- A requirement that the electrolyte has a sufficiently high conductivity
- The vessel wall or pipe must be penetrated.
- The use of a stable reference electrode.

The latter limitation is usually not restrictive since three electrodes of the same material provides satisfactory service in most industrial applications. Even though the applied sensor perturbation is small, repeated application over a long period can lead to “artificial” surface damage. In addition, these systems cannot provide information on localized corrosion, such as pitting and stress-corrosion cracking (SCC).
An algorithm for evaluating the suitability of the ER versus LPR probes is shown in Fig. 1 (Ref 10). If the electrolyte is nonconductive, then ER is recommended over LPR. If the product of estimated corrosion rate and resistivity is less than 25 kΩ · cm · mil/year, then a two-electrode LPR probe is recommended. If the above product is greater than 250 kΩ · cm · mil/year, then a three-electrode LPR probe is recommended. (The kΩ · cm · mil/year units are those used in the original algorithm.) For intermediate values of the above product, an ER probe is recommended.

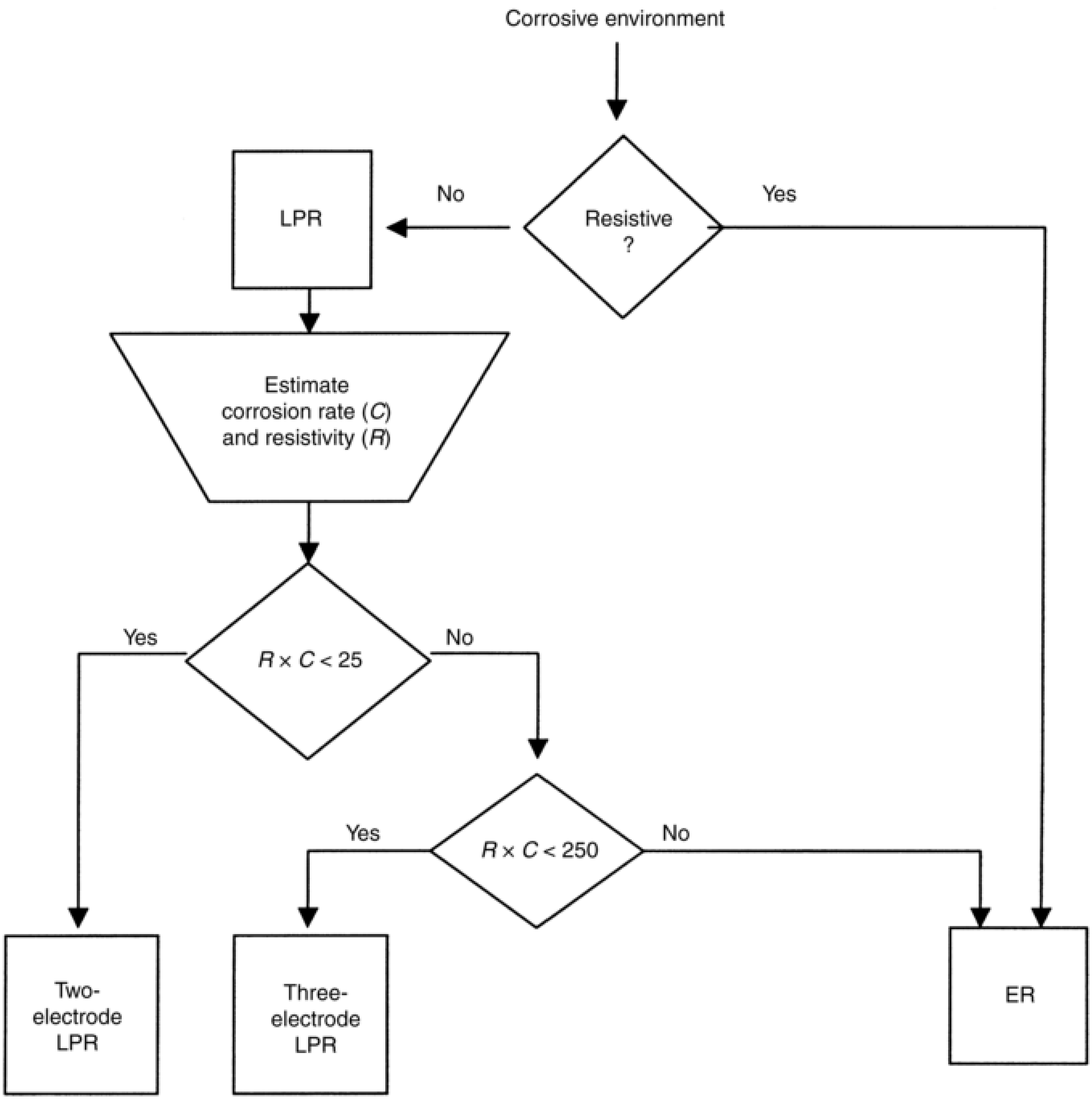

Fig. 1 Algorithm for suitability of electrical resistance (ER) and linear polarization resistance (LPR) corrosion monitoring techniques as a function of electrolyte conductivity and estimated corrosion rate. *R* is the electrolyte resistivity in kΩ · cm and *C* is the corrosion rate in mils per year. Source: Ref 10

Electrochemical Impedance Spectroscopy. In principle, the same type of probe used for linear polarization resistance measurements can be used for electrochemical impedance measurements. In order to characterize certain features of corrosion behavior in detail, measurements throughout the entire frequency range are required; that is, from 0.1 Hz to 100 kHz. This approach permits the separation of the electrolyte resistance, the corrosion reaction resistance, and mass-transfer resistances. Therefore this approach is viable for highly resistive electrolytes such as steam condensate. Although EIS is usually considered to measure uniform corrosion only, the pit depth has been found to correlate to a fitted model element, the constant phase angle (Ref 11).

Zero-Resistance Ammetry. In zero-resistance ammetry (ZRA), galvanic currents are usually measured between dissimilar materials with the current being proportional to the corrosion rate of the corroding element. The electronic circuitry for this task is simple and inexpensive (Ref 12). The dissimilarities between the sensor elements may be related to different compositions, heat treatments, stress levels, or surface conditions. As per

the Stern-Geary approximation, the measured or galvanic current is proportional to the corrosion current, the anodic and cathodic potential differences with E_{corr} and the Tafel slopes for the anodic and cathodic processes. Under conditions where the latter four factors are constant, the galvanic current is consistently proportional to the corrosion current.

Electrochemical Noise. In this technique, fluctuations in potential and current between freely corroding electrodes are measured. Because of the small scale of these fluctuations of interest (in many cases <1 μV and <1 nA), sensitive instrumentation is required. A measurement frequency of 1 or 2 Hz usually suffices. For simultaneous measurement of electrochemical potential and current noise, a three-electrode sensor is required. The current is measured between two of the sensor elements with a zero- resistance circuit, and the potential is measured between the third element and the other two elements, which are at the same nominal potential. For industrial corrosion monitoring purposes, each element is usually constructed from the same material.

While measurement of electrochemical noise (EN) is straightforward, data analysis can be complex. Such analysis is usually directed at distinguishing the different forms of corrosion, quantifying the noise signals, and processing the vast number of accumulated data points into a summarized format. Data processing approaches can involve both time-domain and frequency spectral analysis. A resistance parameter that is considered to be a polarization resistance and therefore a measure of the corrosion rate can be obtained from each approach (Ref 13); that is, noise resistance from the time domain and spectral noise resistance from the frequency domain.

Self-Linear Polarization Resistance. An alternate technique for extracting a polarization resistance from EN measurements in the time domain is self-linear polarization resistance (SLPR). Blocks of potential and current measurements are independently detrended and then plotted against each other. The slope of detrended potential versus detrended current is interpreted as a polarization resistance. It is understood that this treatment of EN data reveals perturbations from E_{corr} that are initiated by localized corrosion events. Comparison of mass loss and LPR measurements indicates that SLPR provides a better estimate of polarization resistance than noise resistance or spectral noise resistance Ref 14.

References cited in this section

6. P.R. Roberge, *Handbook of Corrosion Engineering,* McGraw-Hill, 2000

7. “Standard Method for Conducting Corrosion Coupon Tests in Plant Equipment,” G 4, *Annual Book of ASTM Standards,* ASTM

8. B.J. Boniz, “Field Coupon Corrosion Testing in Process Industries Corrosion-Theory and Practice”, NACE International, 1986

9. M. Stern and R.M. Roth, *J. Electrochem. Soc.,* Vol 104, 1958, p 440t

10. G.L. Cooper, Sensing Probes and Instruments for Electrochemical and Electrical Resistance Corrosion Monitoring, *Corrosion Monitoring in Industrial Plants Using Nondestructive Testing and Electrochemical Methods,* STP 908, G.C. Moran and P. Labine, Ed., ASTM, p 237–250

11. P.R. Roberge and V.S. Sastri, Laboratory and Field Evaluation of Organic Corrosion Inhibitors in Sour Media, *Corros. Sci.,* Vol 35 (No. 5–8), 1993, p 1503–1513

12. R. Baboian and P. Prew, Low-Cost Electronic Devices for Corrosion Measurements, *Mater. Perform.,* July 1993, p 56–59

13. R.A. Cottis, Interpretation of Electrochemical Noise Data, *Corrosion,* Vol 57 (No. 3), 2001, p 265–285

14. R.D. Klassen and P.R. Roberge, “Self Linear Polarization Resistance,” Paper 02330, presented at Corrosion 2002 (Denver), NACE International, 2002

P.R. Roberge and R.D. Klassen, Corrosion Monitoring Techniques, *Corrosion: Fundamentals, Testing, and Protection*, Vol 13A, *ASM Handbook*, ASM International, 2003, p 514–518

Corrosion Monitoring Techniques

P.R. Roberge and R.D. Klassen, Royal Military College of Canada

Indirect Techniques

Corrosion Potential. Measurement of corrosion potential is a relatively simple concept, and the underlying principle is widely used for monitoring the corrosion state of reinforcing steel in concrete and buried pipelines under cathodic protection. This approach can also be valuable in cases where an alloy could show both active and passive corrosion behavior in a given process stream. For example, stainless steels can provide excellent service as long as they remain passive. However, if an upset occurs that would introduce either chlorides or reducing agents into the process stream, stainless alloys may become active and exhibit excessive corrosion rates. Corrosion potential measurements can indicate the transition from passive to active corrosion.

The success of corrosion potential measurements depends on the long-term stability of a reference electrode. Such electrodes have been developed for continuous pH monitoring of process streams, and their application for measuring corrosion potentials is straightforward. However, temperature, pressure, electrolyte composition, pH, and other variables can limit the applications of these electrodes for corrosion-monitoring service. Also, while the technique may indicate changes in corrosion behavior over time, it does not provide any indication of corrosion rates.

Hydrogen Probes. The concept of the hydrogen probe is based on the fact that one of the cathodic reaction products in nonoxidizing acidic systems is hydrogen. The hydrogen atoms thus generated diffuse through the vessel wall and are liberated at the exterior surface. In one variation, a hydrogen probe contains a piece of palladium foil applied to the exterior surface and serving as both collector and catalyst for the subsequent oxidation of the hydrogen (Ref 15). This method is in practice limited to steel, which has a high hydrogen diffusivity and low solubility of hydrogen. This approach has another variation that consists of simply attaching a chamber to the exterior of the pipe and monitoring hydrogen liberation through increasing pressure of hydrogen gas (Ref 5).

Generic guidelines relating the measured hydrogen flux and actual damage (thickness loss, cracking, blistering) have not been established. This approach is also limited to systems in which the temperature outside of the pipe is moderate and the diffusion rate of hydrogen is high. Gas pipeline service is the most common application. In this case, corrosion can occur when hydrogen sulfide, water, and sometimes carbon dioxide (CO_2) are present.

References cited in this section

5. C.P. Dillon, A.S. Krisher, and H. Wissenberg, Plant Corrosion Tests, *Handbook on Corrosion Testing and Evaluation,* W.H. Ailor, Ed., John Wiley & Sons, 1971, p 599–615

15. R. Martin and E.C. French, "Corrosion Monitoring in Sour Systems Using Electrochemical Hydrogen Potential Probes," Paper 6657, presented at the Sour Gas Symposium of the Society of Petroleum Engineers (Dallas, TX), American Institute of Mining, Metallurgical and Petroleum Engineers, 1977

P.R. Roberge and R.D. Klassen, Corrosion Monitoring Techniques, *Corrosion: Fundamentals, Testing, and Protection*, Vol 13A, *ASM Handbook*, ASM International, 2003, p 514–518

Corrosion Monitoring Techniques

P.R. Roberge and R.D. Klassen, Royal Military College of Canada

System Considerations

In the selection of a corrosion monitoring method, a variety of factors should be considered. First, everyone concerned with the corrosion monitoring program should understand the purpose of the test. The costs and reliability of the methods under consideration should be understood. In many cases, it is desirable to include more than one method in order to provide more confidence in the information generated. Another question of importance is whether there is access to the process streams and equipment in question. If access is available, methods that involve probes or coupons become more feasible. Otherwise, nondestructive methods may be required.

An important factor in the selection of monitoring methods is the response time required to obtain the desired information from the method. Coupon methods and techniques that require plant shutdown tend to be relatively slow in generating information. On the other hand, equipment that measures instantaneous corrosion rates can provide fast results. A final consideration is one of safety. In an operating plant, equipment failure can lead to a leak, which can result in loss of product, a hazard potential, and possible shutdown of the plant. It is important for the monitoring apparatus to minimize the possibility of such an incident (Ref 16).

Probe Location

A principal part of any corrosion-monitoring program is deciding where to locate the corrosion monitoring devices. Because corrosion will probably not occur uniformly throughout a region of interest, it is desirable to find sites at which the highest corrosion rates will be experienced.

Example 1: Corrosion Monitoring of a Distillation Column. The problems involved in developing corrosion monitoring programs for a plant are illustrated in the example of a distillation column. The most logical points for corrosion monitoring in a distillation column are the feed point, the overhead product receiver, and the reboiler or bottoms product line. These points are the locations at which the highest and lowest temperatures are encountered, as well as the points at which the most and least volatile products are concentrated. However, these points are usually not the locations of the most severe corrosion. The species causing corrosion will often concentrate at an intermediate point in the column because of chemical reactions within the column. Therefore, if there is a possibility of concentrating a corrosive species within the distillation column, several monitoring points are required throughout the column for the corrosion monitoring program to be comprehensive. A monitoring program can be restricted to the most corrosive location within the column once this area has been identified. Another problem with distillation columns is that the liquid on trays tends to be frothy. This creates difficulties for electrochemical methods. One solution to this problem is to install bypass loops that remove liquid from the column, pass it over the corrosion-monitoring probes, and then reinject it at a lower point in the column. This practice avoids the problem of foam and froth and provides a more controlled flow rate over the corrosion monitoring equipment. Use of a bypass loop also allows removal of liquid samples at times of high corrosion rates for further analysis.

Example 2: Corrosion Monitoring of Piping with High-Velocity Gas Streams. High-velocity gas streams in pipes may cause problems with conventional monitoring systems. In this case, the presence of an aqueous phase is usually restricted to a thin layer on the surface of the pipe. A probe that protrudes into the pipe may miss the liquid layer that is present only close to the pipe wall. A flush-mounted surface probe can be used in such cases.

Example 3: Probe Location in Storage Tanks. Probe location is also critical in storage tanks containing nonaqueous liquids. The most corrosive location in these tanks may be at the liquid level if the liquid in the tank has a density exceeding that of water. In this case, the corrosion-monitoring probe should be mounted on a floating platform. In this way, the probe can detect the presence of a corrosive aqueous phase. However, when

the liquid stored in the tank is less dense than the water, the corrosion-monitoring device should probably be positioned at the bottom of the tank.
Leakage. Where vessel and piping walls must be penetrated in order to install probes, the potential for leaks exists. Leaks can cause hazards and can shut down operating plants. The corrosion monitoring system must be installed such that leaks from the probe can be handled with minimal interruption (Ref 17).

Installation Techniques

Coupons. A slip-in rack is designed to be inserted and removed from equipment that is in operation. A retractable coupon holder makes this type of rack especially useful (See Fig. 3 in the article "Corrosion Monitoring for Industrial Processes" in this Volume). The slip-in rack requires a gate valve and a suitable-sized nozzle to serve as a retraction chamber. A rod-shaped coupon holder is contained in the retraction chamber, which is flanged to the gate valve. The other end of the retraction chamber contains a packing gland through which the coupon holder passes. Coupons are mounted on the rod in the retracted position. The chamber is bolted to the gate valve, which is then opened to allow the coupons to be slid into the process stream. The sequence is reversed to remove the test coupons. Other appliances for installing coupons are the spool (birdcage) rack, the insert rack, and the slip-in rack (Ref 3, 4).

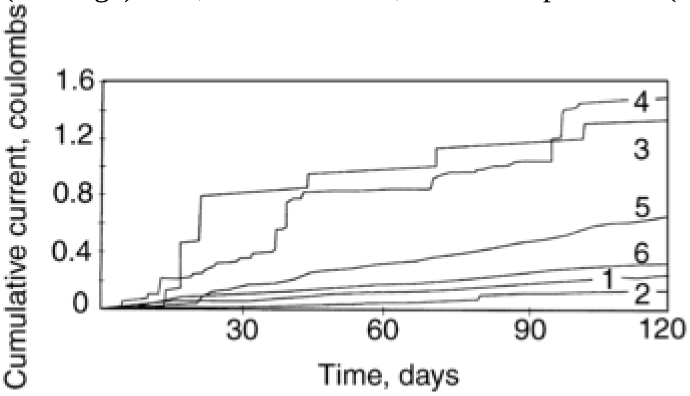

Fig. 2 Cumulative current, in coulombs, from the zero-resistance ammetry (ZRA) sensors at various location on the aircraft shown in Fig. 5. Source: Ref 17

Electrical Resistance Probe. A schematic of an electrical resistance probe is shown as Fig. 4 in the article "Corrosion Monitoring for Industrial Processes" in this Volume. The wire is fabricated from the material of concern in such a way that its electrical resistance or inductance can be measured. A temperature-compensating element of the same material is usually incorporated such that it is shielded from the corrosive environment but close to the same temperature environment as the exposed element.

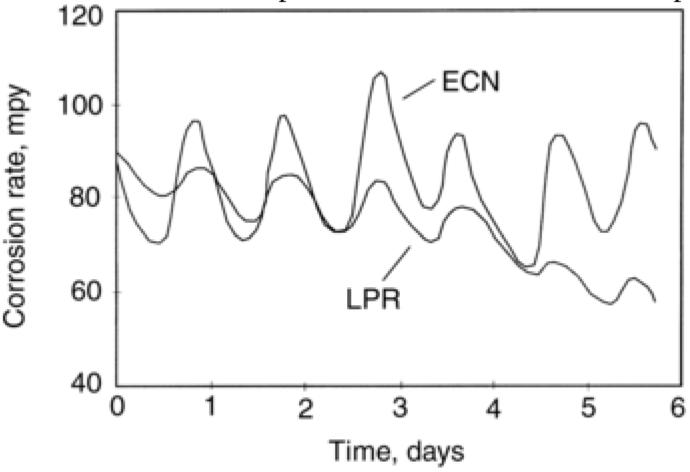

Fig. 3 Smoothed corrosion rates from electrochemical noise (ECN) and linear polarization resistance (LPR) measurements from the same probe within an oil/water separation plant. The oscillations correlated with daily operations of a vacuum truck. Source: Ref 18

Linear Polarization Resistance Probe. A schematic of a three-electrode linear polarization resistance probe is shown in Fig. 5(a) in the article "Corrosion Monitoring for Industrial Processes" in this Volume. The probe elements are constructed from the material of interest, similar to an ER probe. One method of exposing the probe elements in a process pipe is through a pipe tee, as shown in Fig. 5(c) in the article "Corrosion Monitoring for Industrial Processes" in this Volume.

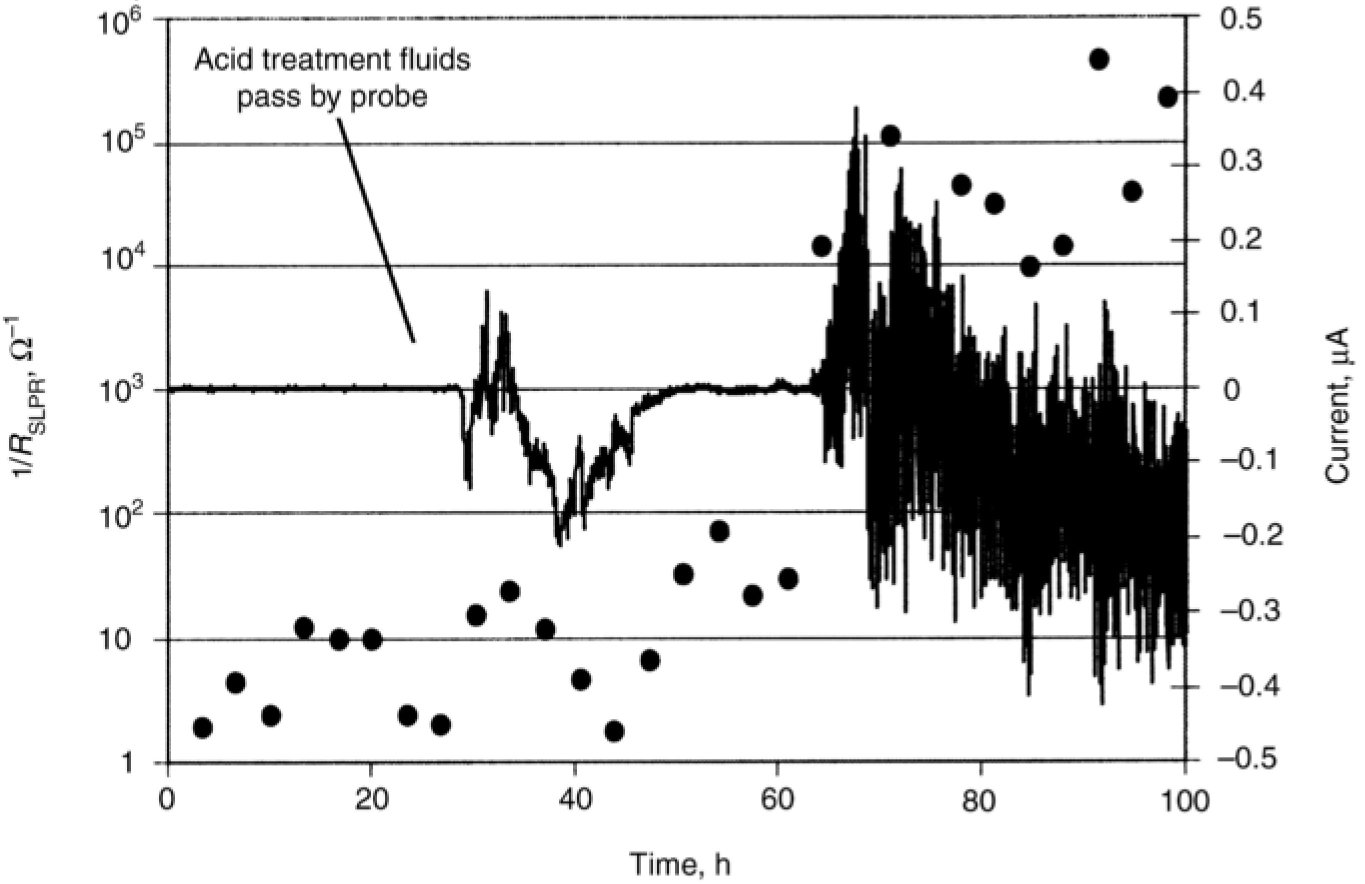

Fig. 4 Electrochemical noise data current (solid line) and $1/R_{SLPR}$ (dots) from a probe monitoring acid treatment fluids entering the Simonette battery. Source: Ref 21

Hydrogen Probe. A schematic of a hydrogen probe on the outside of a pipe is shown in Fig. 7 in the article "Corrosion Monitoring for Industrial Processes" in this Volume. The interface between the outside of the pipe wall and electrolyte is a foil of palladium. The foil is permeable to hydrogen gas escaping through the container wall and catalyzes its oxidation under an applied potential. The electrolyte is 90% sulfuric acid, and the counter electrodes for the oxidation reaction are stainless steel rods. The current that is required to oxidize the hydrogen is proportional to the corrosion rate of the interior of the vessel.

Wiring. A primary difficulty with corrosion- monitoring equipment is the need to install wires from the probes to the control room or to data storage systems. The cost of wiring usually exceeds the cost of probes and electronic instruments. In addition, wiring systems are often sources of problems due to breakage, moisture entry, and connection difficulties. Emerging wireless systems have great potential for enabling corrosion monitoring sensors to be more effectively deployed.

Corrosion Management

In-line corrosion monitoring requires skill in interpretation and reporting since important economic decisions are often based on the test results (Ref 17). Although there are a number of standards that provide guidelines for certain procedures, there is no standard that is comprehensive. To plan an appropriate test program, the investigator must know or have good advice on both the chemistry and the mechanics of the processes involved; that is, the investigator must understand the entire corrosion system. It is important to prepare detailed records of what was done as part of the experiment, and it is also important to document any unplanned changes that occur in the process stream or the equipment during the investigation. Without valid interpretation and

effective (timely) reporting, the price of the work can be significantly greater than the cost of time and materials. However, the consequences of corrosion failures go beyond these additional costs. Also involved are personal safety risks and liability, hazard potentials, decreased product quality, and pollution problems. Several technical and personnel requirements for the success of a corrosion monitoring program are given in Ref 16.

References cited in this section

3. S.W. Dean, Overview of Corrosion Monitoring in Modern Industrial Plants, *Corrosion Monitoring in Industrial Plants Using Nondestructive Testing and Electrochemical Methods,* STP 908, G.C. Moran and P. Labine, Ed., ASTM, 1986a, p 197–220

4. S.W. Dean, Electrochemical Methods for Corrosion Testing in the Process Industries, *Electrochemical Corrosion Testing With Special Consideration of Practical Applications, Proc. of International Workshop,* E. Heintz, J.C. Rowlands, and F. Mansfeld, Ed., (Ferrara, Italy), DECHEMA, 1986b, p 1–15

16. C.F. Britton and B.C. Tofield, Effective Corrosion Monitoring, *Mater. Perform.,* Vol 4, p 41–44

17. V.S. Agarwala, "Aircraft Corrosion in the Military: Maintenance and Repair Issues," Paper 597, presented at Corrosion 1998 (San Diego), NACE International, 1998

18. V.S. Agarwala, "In-Situ Corrosivity Monitoring of Military Hardware Environments," Paper 632 presented at Corrosion 1996 (Denver), NACE International, 1996

21. E.E. Barr, R. Goodfellow, and L.M. Rosenthal, "Noise Monitoring at Canada's Simonette Sour Oil Processing Facility," Paper 414, presented at Corrosion 2000 (Orlando), NACE International, 2000

P.R. Roberge and R.D. Klassen, Corrosion Monitoring Techniques, *Corrosion: Fundamentals, Testing, and Protection,* Vol 13A, *ASM Handbook,* ASM International, 2003, p 514–518

Corrosion Monitoring Techniques

P.R. Roberge and R.D. Klassen, Royal Military College of Canada

---

Examples of On-Line Corrosion Monitoring

In addition to the previous examples dealing with probe locations, the following examples illustrate various monitoring techniques.

Example 4: Smart Reinforced Concrete Structures. In the civil engineering and construction industry, corrosion measurements are usually limited to periodic inspections. While such measurements can be misleading, it is at times difficult to make a persuasive argument for continuous measurements, in view of the fact that rebar corrosion often only manifests after decades of service life. As a result of advances in corrosion monitoring technology and selected on-line monitoring studies that have demonstrated the highly time-dependent nature of rebar corrosion damage, continuous measurements may gradually find increasing application. Furthermore, the concept of smart reinforced concrete structures is gaining momentum through the utilization of a variety of diagnostic sensing systems. The integration of corrosion monitoring technology and information on the location of the damage appears to be a logical evolution (Ref 6).

The simplest electrochemical rebar corrosion monitoring technique is measurement of the corrosion potential. A measurement procedure and data interpretation procedure are described in ASTM C 876. The basis of this technique is that the corrosion potential of the rebar will shift in the negative direction if the surface changes

from the passive to the actively corroding state. A simplified interpretation of the potential readings is presented in Table 1.

Table 1 Significance of rebar corrosion potential values

Potential (volts vs. SCE), V	Significance
V > -0.20	Greater than 90% probability that no corrosion is occurring
-0.35 ≤ V ≤ -0.20	Uncertainty regarding corrosion activity
V < -0.35	Greater than 90% probability that corrosion is occurring

SCE, saturated calomel electrode. Source: ASTM C 876

Apart from its simplicity, a major advantage of this technique is that large areas of concrete can be mapped with the use of mechanized devices. This approach is typically followed on civil engineering structures such as bridge decks, for which potential "contour" maps are produced to highlight problem areas. The potential measurements are usually performed with the reference electrode at the concrete surface and an electrical connection to the rebar. However, the results obtained with this technique are only qualitative, without any information on actual corrosion rates. Highly negative rebar corrosion values are not always indicative of high corrosion rates, as the unavailability of oxygen may stifle the cathodic reaction. Also, interpreting the potential readings from epoxy-coated rebar is even more problematic.

Example 5: Atmospheric Corrosion in Aircraft. While corrosion inspection is mandated and nondestructive testing of aircraft are widely practiced, corrosion monitoring activity is only beginning to emerge, led by efforts in the military aircraft domain. In recent years, prototype corrosion monitoring systems have been installed on operational aircraft in the United States, Canada, Australia, the United Kingdom and South Africa. Several systems are in the laboratory and ground-level research and testing phases. The interest in aircraft corrosion monitoring activities is related to three potential application areas: reducing unnecessary inspections, optimizing certain preventative maintenance schedules and evaluating materials performance under actual operating conditions. The first application area arises from the fact that many corrosion-prone areas of an aircraft are difficult to access and costly to inspect. Typically, these areas are inspected on fixed schedules, regardless of whether corrosion has taken place or not on a particular aircraft. Unnecessary physical inspections could be delayed if there was a full understanding of when and where corrosion occurred (Ref 17).

A zero-resistance ammeter (ZRA)-based sensor for monitoring corrosive conditions for aircraft as well as other equipment was developed (Ref 18). It consisted of a novel thin film device (interdigitized bimetallic strips on a Kapton (E.I. DuPont de Nemours and Co.) polyimide film), which was galvanically coupled or short circuited through a ZRA and interfaced to a miniature data acquisition system. In most applications the active element was cadmium and the inert metal was gold. An underlying assumption is that atmospheric conditions that cause cadmium to corrode will also cause aluminum to corrode. In one trial, six sensors were installed in the interior of an aircraft as shown in Fig. 5 (Ref 19). These locations were (1) outboard vacelle, (2) fuselage near the nose, (3) within the horizontal stabilizer, (4) forward main ring fitting, (5) aft main ring fitting, and (6) heat exchanger. The cumulative current, expressed in coulombs over a three-month exposure period, is shown in Fig. 2 for each location. The results illustrate that locations on the same aircraft exposed to the same weather and outside environmental factors experience widely different degrees of atmospheric corrosivity. Sensors of this type can become a basis for condition-based maintenance of aircraft hardware in the future.

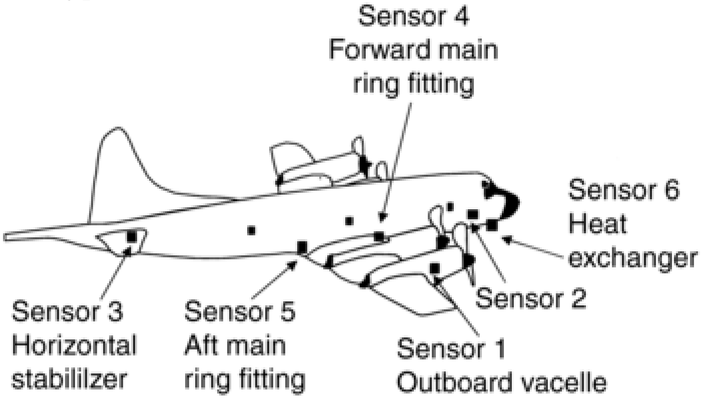

Fig. 5 Schematic of an aircraft showing locations where zero-resistance ammetry (ZRA) corrosivity sensors were placed. Source: Ref 17

Example 6: Electrochemical Noise Probes in Chemical Plants. Five probes with five elements each were installed at an oil/water separation facility (Ref 20). Each probe was designed to measure the corrosion rate by both LPR and ECN. Bridging between the elements by sludge and iron sulfide was a problem that was addressed by regular cleaning of the probe elements. Figure 3 shows variations in the corrosion rates, which were averaged over 5 min intervals and then smoothed. The oscillations were attributed to the effects of vacuum loading truck operations that occurred daily. These variations would not have been observable from corrosion coupon data, which give an integrated or cumulative view of corrosion damage.

Another example of field tests with ECN probes was described by Ref 21. One ECN probe was placed in a flow line between the well and processing plant. In order to reduce scaling problems, the well was treated with 3 m^3 (106 ft^2) of crude oil containing 15% hydrochloric acid combined with 13% xylene. Figure 4 shows the raw electrochemical current and $1/R_{SLPR}$ (analyzed by the SLPR method presented earlier, Ref 14) from the probe in the flow line just before and just after the line was “pigged.” The data indicates that fluctuations in the current and a large jump in corrosion rate ($1/R_{SLPR}$) did not occur until about 30 h after the oil/acid/xylene mixture had passed by.

References cited in this section

6. P.R. Roberge, *Handbook of Corrosion Engineering*, McGraw-Hill, 2000

14. R.D. Klassen and P.R. Roberge, “Self Linear Polarization Resistance,” Paper 02330, presented at Corrosion 2002 (Denver), NACE International, 2002

17. V.S. Agarwala, “Aircraft Corrosion in the Military: Maintenance and Repair Issues,” Paper 597, presented at Corrosion 1998 (San Diego), NACE International, 1998

18. V.S. Agarwala, “In-Situ Corrosivity Monitoring of Military Hardware Environments,” Paper 632 presented at Corrosion 1996 (Denver), NACE International, 1996

19. V.S. Agarwala and R. Wood, (2000). “Corrosion and Corrosivity Monitoring-An Update,” *Fourth International Aircraft Corrosion Workshop* (August 2000). [CD-ROM]. Navmar Applied Sciences Corporation (*mayer@navmar.com*)

20. G.E.C. Bell, L.M. Rosenthal, and K. Lawson, “Electrochemical Noise Corrosion Monitoring Field Trial at Cahn 3 Water Treatment Plant Lost Hills, California,” Paper 412, presented at Corrosion 2000 (Orlando), NACE International, 2000

21. E.E. Barr, R. Goodfellow, and L.M. Rosenthal, “Noise Monitoring at Canada's Simonette Sour Oil Processing Facility,” Paper 414, presented at Corrosion 2000 (Orlando), NACE International, 2000

P.R. Roberge and R.D. Klassen, Corrosion Monitoring Techniques, *Corrosion: Fundamentals, Testing, and Protection*, Vol 13A, *ASM Handbook*, ASM International, 2003, p 514–518

Corrosion Monitoring Techniques

P.R. Roberge and R.D. Klassen, Royal Military College of Canada

---

References

1. J.C. Bovankovich, "On-Line Corrosion Monitoring for Process Plant Control," *Mater. Perform.,* Vol 33 (No. 11), 1994, p 57–60

2. *Corrosion Monitoring in Industrial Plants Using Nondestructive Testing and Electrochemical Methods,* STP 908, G.C. Moran and P. Labine, Ed., ASTM 1986

3. S.W. Dean, Overview of Corrosion Monitoring in Modern Industrial Plants, *Corrosion Monitoring in Industrial Plants Using Nondestructive Testing and Electrochemical Methods,* STP 908, G.C. Moran and P. Labine, Ed., ASTM, 1986a, p 197–220

4. S.W. Dean, Electrochemical Methods for Corrosion Testing in the Process Industries, *Electrochemical Corrosion Testing With Special Consideration of Practical Applications, Proc. of International Workshop,* E. Heintz, J.C. Rowlands, and F. Mansfeld, Ed., (Ferrara, Italy), DECHEMA, 1986b, p 1–15

5. C.P. Dillon, A.S. Krisher, and H. Wissenberg, Plant Corrosion Tests, *Handbook on Corrosion Testing and Evaluation,* W.H. Ailor, Ed., John Wiley & Sons, 1971, p 599–615

6. P.R. Roberge, *Handbook of Corrosion Engineering,* McGraw-Hill, 2000

7. "Standard Method for Conducting Corrosion Coupon Tests in Plant Equipment," G 4, *Annual Book of ASTM Standards,* ASTM

8. B.J. Boniz, "Field Coupon Corrosion Testing in Process Industries Corrosion-Theory and Practice", NACE International, 1986

9. M. Stern and R.M. Roth, *J. Electrochem. Soc.,* Vol 104, 1958, p 440t

10. G.L. Cooper, Sensing Probes and Instruments for Electrochemical and Electrical Resistance Corrosion Monitoring, *Corrosion Monitoring in Industrial Plants Using Nondestructive Testing and Electrochemical Methods,* STP 908, G.C. Moran and P. Labine, Ed., ASTM, p 237–250

11. P.R. Roberge and V.S. Sastri, Laboratory and Field Evaluation of Organic Corrosion Inhibitors in Sour Media, *Corros. Sci.,* Vol 35 (No. 5–8), 1993, p 1503–1513

12. R. Baboian and P. Prew, Low-Cost Electronic Devices for Corrosion Measurements, *Mater. Perform.,* July 1993, p 56–59

13. R.A. Cottis, Interpretation of Electrochemical Noise Data, *Corrosion,* Vol 57 (No. 3), 2001, p 265–285

14. R.D. Klassen and P.R. Roberge, "Self Linear Polarization Resistance," Paper 02330, presented at Corrosion 2002 (Denver), NACE International, 2002

15. R. Martin and E.C. French, "Corrosion Monitoring in Sour Systems Using Electrochemical Hydrogen Potential Probes," Paper 6657, presented at the Sour Gas Symposium of the Society of Petroleum Engineers (Dallas, TX), American Institute of Mining, Metallurgical and Petroleum Engineers, 1977

16. C.F. Britton and B.C. Tofield, Effective Corrosion Monitoring, *Mater. Perform.,* Vol 4, p 41–44

17. V.S. Agarwala, "Aircraft Corrosion in the Military: Maintenance and Repair Issues," Paper 597, presented at Corrosion 1998 (San Diego), NACE International, 1998

18. V.S. Agarwala, "In-Situ Corrosivity Monitoring of Military Hardware Environments," Paper 632 presented at Corrosion 1996 (Denver), NACE International, 1996

19. V.S. Agarwala and R. Wood, (2000). "Corrosion and Corrosivity Monitoring-An Update," *Fourth International Aircraft Corrosion Workshop* (August 2000). [CD-ROM]. Navmar Applied Sciences Corporation (*mayer@navmar.com*)

20. G.E.C. Bell, L.M. Rosenthal, and K. Lawson, "Electrochemical Noise Corrosion Monitoring Field Trial at Cahn 3 Water Treatment Plant Lost Hills, California," Paper 412, presented at Corrosion 2000 (Orlando), NACE International, 2000

21. E.E. Barr, R. Goodfellow, and L.M. Rosenthal, "Noise Monitoring at Canada's Simonette Sour Oil Processing Facility," Paper 414, presented at Corrosion 2000 (Orlando), NACE International, 2000

P.R. Roberge and R.D. Klassen, Corrosion Monitoring Techniques, *Corrosion: Fundamentals, Testing, and Protection*, Vol 13A, *ASM Handbook*, ASM International, 2003, p 514–518

Corrosion Monitoring Techniques

P.R. Roberge and R.D. Klassen, Royal Military College of Canada

---

Selected References

- P.R. Roberge, *Handbook of Corrosion Engineering*, McGraw-Hill, 2000
- *Corrosion Monitoring in Industrial Plants Using Nondestructive Testing and Electrochemical Methods*, STP 908, G.C. Moran and P. Labine, Ed., ASTM, 1986, p 197–220

L. Yang and N. Sridhar, Monitoring of Localized Corrosion, *Corrosion: Fundamentals, Testing, and Protection*, Vol 13A, *ASM Handbook*, ASM International, 2003, p 519–524

Monitoring of Localized Corrosion

Lietai Yang and Narasi Sridhar, Southwest Research Institute

Introduction

LOCALIZED CORROSION, in the form of pitting and crevice corrosion, once initiated, can propagate rapidly and either result in component failure or trigger other modes of failures, such as stress-corrosion cracking. Because localized corrosion is isolated to certain areas and often has small lateral dimensions compared with its depth, detection methods that measure response over a large surface area, such as the widely used electrical resistance and linear polarization methods (Ref 1, 2, 3, 4, 5, 6), are not sufficiently sensitive. Development of suitable on-line monitoring tools for localized corrosion has been a challenge to researchers, plant engineers, and operators. The nature of localized corrosion must be understood to develop monitoring tools.

References cited in this section

1. V.S. Agarwala and S. Ahmad, "Corrosion Detection and Monitoring—A Review," Paper 271, Corrosion/2000, NACE International, 2000

2. L. Yang, X. Sun, and F. Steward, “An Electrical Resistance Probe for Monitoring Flow-Assisted Corrosion in Simulated Primary Coolant of Nuclear Reactors at 310 °C,” Paper 459, Corrosion/99, NACE International, 1999

3. G.K. Brown, J.R. Davies, and B.J. Hemblade, “Real-Time Metal Loss Internal Monitoring,” Paper 278, Corrosion/2000, NACE International, 2000

4. N. Sridhar, D.S. Dunn, C.S. Brossia, and O.C. Moghissi, “Corrosion Monitoring Techniques for Thermally Driven Wet and Dry Conditions,” Paper 283, Corrosion/ 2000, NACE International, 2000

5. F. Mansfeld, The Polarization Resistance Technique for Measuring Corrosion Currents, *Advances in Corrosion Engineering and Technology,* Vol 6, M.G. Fontana and R.W. Staehle, Ed., Plenum, 1976

6. F. Mansfeld, Polarization Resistance Measurements—Experimental Procedures and Evaluation of Testing Data, *Electrochemical Techniques for Corrosion Engineering,* R. Baboian, Ed., NACE International, 1987, p 18–26

L. Yang and N. Sridhar, Monitoring of Localized Corrosion, *Corrosion: Fundamentals, Testing, and Protection,* Vol 13A, *ASM Handbook,* ASM International, 2003, p 519–524

Monitoring of Localized Corrosion

Lietai Yang and Narasi Sridhar, Southwest Research Institute

Initiation of Localized Corrosion

A number of factors influence the initiation of localized corrosion:

- Presence of a critical concentration of an aggressive species (e.g., chloride) or inhibiting species (e.g., nitrate)
- Sufficiently high corrosion potential caused by the presence of oxidizing agents
- Sufficiently high temperature
- Stagnant regions
- Surface and microstructural heterogeneities (e.g., manganese sulfide inclusions)
- Microbial activity

While the early stages of localized corrosion processes are still not completely understood (Ref 7, 8, 9), the stable growth of localized corrosion has long been established to be a process where the dissolution sites (anodic sites) are separated spatially from the sites where oxidants in the environment are reduced (cathodic sites), with the electronic current flowing through the metal to couple these two processes. Therefore, many of the electrochemical techniques for studying localized corrosion processes rely on monitoring the current flow between these two sites (Ref 10). Some of these electrochemical methods have been adopted for on-line monitoring of localized corrosion. Nonelectrochemical methods also have been used for on-line monitoring of localized corrosion in recent years. The following section describes some of the methods that have been used or have the potential to be used for on-line, real-time monitoring of localized corrosion.

References cited in this section

7. P.M. Natishan, R.G. Kelly, G.S. Frankel, and R.C. Newman, Ed., *Critical Factors in Localized Corrosion II,* The Electrochemical Society, 1996

8. R.G. Kelly, G.S. Frankel, P.M. Natishan, and R.C. Newman, Ed., *Critical Factors in Localized Corrosion III,* The Electrochemical Society, 1999

9. G.S. Frankel and J.R. Scully, Ed., *Localized Corrosion,* Proceedings of the Corrosion/ 2001 Research Topical Symposium, NACE International, 2001

10. F.P. IJsseling, Electrochemical Methods in Crevice Corrosion Testing, *Br. Corros. J.,* Vol 15 (No. 2), 1980, p 51–69

L. Yang and N. Sridhar, Monitoring of Localized Corrosion, *Corrosion: Fundamentals, Testing, and Protection*, Vol 13A, *ASM Handbook*, ASM International, 2003, p 519–524

Monitoring of Localized Corrosion

Lietai Yang and Narasi Sridhar, Southwest Research Institute

Electrochemical Noise Method

The electrochemical noise (ECN) measurement technique (Ref 11) uses three electrodes comprising two normally identical working electrodes (electrodes 1 and 2) and a reference electrode (or, alternatively, a pseudoreference electrode manufactured from the same material as the working electrodes). Electrodes 1 and 2 are coupled through a zero resistance ammeter (ZRA), and the output from the current coupling is connected to an electrochemical current noise- monitoring device. Electrode 1 and the reference electrode are connected to an electrochemical potential-monitoring apparatus. This potential- monitoring device measures the electrochemical potential noise between the reference or pseudo- reference electrode and the coupled electrodes (electrodes 1 and 2). Both the electrochemical current noise and the electrochemical potential noise are connected to a signal processor, usually a personal computer.

Corrosion processes are stochastic in nature. The electrochemical reactions occurring at corroding surfaces generate low-frequency (<1 Hz) and low-amplitude random fluctuations (noise) of current (1 nA to 10 μA) and potential (0.1 μV to 10 mV) signals. The measurement and analysis of such noise signals provide useful information on the corrosion processes, including the type of corrosion and time of corrosion initiation (Ref 12, 13). The analyses of the electrochemical noise data usually are performed in the time and frequency domains. The pattern of the noise signals usually is used to evaluate the corrosion activity. Because automated pattern recognition requires sophisticated computer programming, statistical single parameters derived from the noise signals, such as mean potential, mean coupling current, standard deviations of the voltage and the current (or root mean square from an analog instrument), and noise resistance often are used as corrosion indicators for on-line applications (Ref 11, 14, 15, 16). In addition, pit index (Ref 15) and Kurtosis current (Ref 17) are used to evaluate the pitting activity.

The ECN method has many advantages in detecting localized corrosion. It is essentially non- perturbing. Measurements are carried out either at or close to the corrosion potential. It may have a mechanistic link to the stochastic nature of the localized corrosion-initiation processes and relies on the measurement of non-steady-state responses typical of early stages of localized corrosion. However, the measurement is not quantitative for localized corrosion rates and has not been reproducible in all cases. The pitting index, which is the ratio of the standard deviation of the current noise to the root mean square of the coupling current, has been shown not to correlate with the onset of pitting (Ref 18, 19). Furthermore, the noise signal between two identical electrodes is not highly sensitive to localized corrosion events in systems containing powerful redox agents (Ref 18).

References cited in this section

11. J.L. Dawson, Electrochemical Noise Measurement: The Definitive In-Situ Technique for Corrosion Applications?, *Electrochemical Noise Measurement for Corrosion Applications,* STP 1277, J.R. Kearns, J.R. Scully, P.R. Roberge, and D.L. Dawson, Ed., ASTM, 1996, p 3–35

12. J.C. Uruchurtu and J.L. Dawson, Noise Analysis of Pure Aluminum under Different Pitting Conditions, *Corrosion,* Vol 43 (No. 1), 1987, p 19–26

13. A.M.P. Simoes and M.G.S. Ferreira, Crevice Corrosion Studies on Stainless Steel Using Electrochemical Noise Measurements, *Br. Corros. J.,* Vol 22 (No.1), 1987, p 21–25

14. F. Mansfeld, L.T. Han, C.C. Lee, C. Chen, G. Zhang, and H. Xiao, Analysis of Electrochemical Impedance and Noise Data for Polymer-Coated Metals, *Corros. Sci.,* Vol 39 (No. 2), 1997, p 255–279

15. A.N. Rothwell, D.A. Eden, and G. Row, "Electrochemical Noise Techniques for Determining Corrosion Rates and Mechanisms," Paper 223, Corrosion/92, NACE International, 1992

16. J.B. Lumsden, M.W. Kendig, and S. Jeanjaquet, "Electrochemical Noise for Carbon Steel in Sodium Chloride Solutions—Effect of Chloride and Oxygen Activity," Paper 224, Corrosion/92, NACE International, 1992

17. E.E. Barr, A.H. Greenfield, and L. Pierard, "Application of Electrochemical Noise Monitoring to Inhibitor—Evaluation and Optimization in Field: Results from the Kaybob South Sour Gas Field," Paper 01288, Corrosion/2001, NACE International, 2001

18. R.G. Kelly, M.E. Inman, and J.L. Hudson, Analysis of Electrochemical Noise for Type 410 Stainless Steel in Chloride Solutions, *Electrochemical Noise Measurement for Corrosion Applications,* STP 1277, J.R. Kearns, J.R. Scully, P.R. Roberge, D.L. Reichert, and J.L. Dawson, Ed., ASTM, 1996, p 101–113

19. S.T. Pride, J.R. Scully, and J.L. Hudson, Analysis of Electrochemical Noise from Metastable Pitting in Aluminum, Aged Al- 2%Cu, and AA 2024-T3, *Electrochemical Noise Measurement for Corrosion Applications,* STP 1277, J.R. Kearns, J.R. Scully, P.R. Roberge, D.L. Reichert, and J.L. Dawson, Ed., ASTM, 1996, p 307

L. Yang and N. Sridhar, Monitoring of Localized Corrosion, *Corrosion: Fundamentals, Testing, and Protection*, Vol 13A, *ASM Handbook*, ASM International, 2003, p 519–524

Monitoring of Localized Corrosion

Lietai Yang and Narasi Sridhar, Southwest Research Institute

Galvanically Coupled Differential Flow Cell

The galvanically coupled differential flow cell (Ref 20, 21, 22, 23, 24) employs essentially a slow-moving (relative to solution) electrode and a fast-moving electrode, both being made of identical corrodible metals and coupled together through a ZRA, as shown in Fig. 1. In Fig. 1, a valve and two flow meters are used to regulate the flow rates through the two cells so that the slow-moving electrode is exposed to a slow-moving liquid, and the fast-moving electrode is exposed to a fast-moving liquid. The area ratio of the fast- moving electrode to the-slow moving electrode is in the range of 20:1 to 200:1. Because of the differences between the flow pattern on the surfaces and the geometries of the two electrodes, the slow-moving electrode acts as an anode and the fast-

moving electrode acts as a cathode in a localized corrosion environment. Thus, a current flows between the two electrodes. The localized corrosion rate (LCR) is calculated according to:

$$\text{LCR} = 11.7 \cdot I/A_{se} + \text{GCR} \quad \text{(Eq 1)}$$

where LCR is in μm/yr; 11.7 is a conversion factor for carbon steel; I is the ZRA reading in μA; A_{se} is the surface area of the slow-moving electrode, measured in cm^2; and GCR is the general corrosion rate in μm/yr. The general corrosion rate can be obtained from the slow-moving electrode by decoupling it from the fast-moving electrode and connecting it to a linear polarization resistance corrosion monitor. Usually, the contribution from the general corrosion rate is negligibly low.

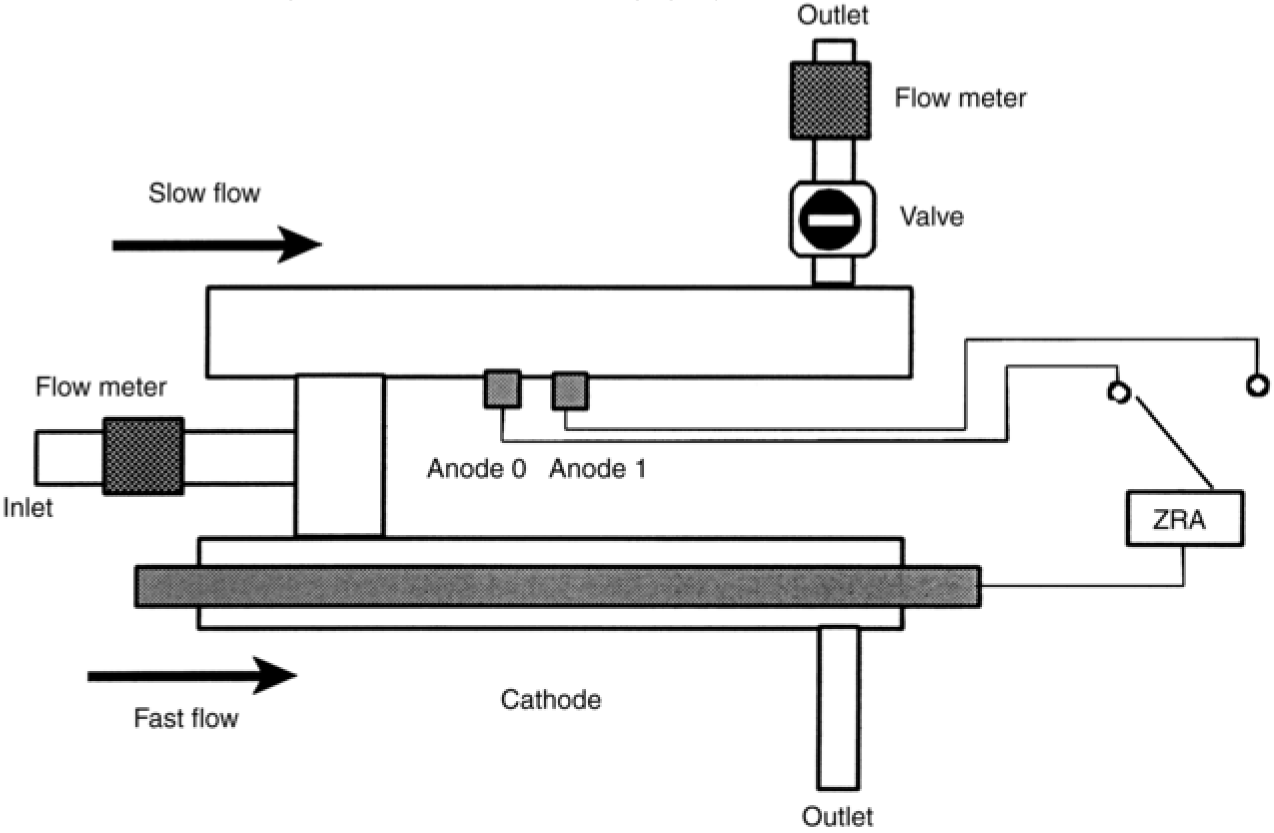

Fig. 1 Differential flow cell sensor for localized corrosion. Valve adjusts relative flow rates. Anode 0 and anode 1 are redundant, and zero resistance ammeter (ZRA) can be switched to either anode. Adapted from Ref 24, with permission from the National Association of Corrosion Engineers (NACE) International

This method has been tested for localized corrosion monitoring in cooling water systems (Ref 20, 21, 23, 24). The measurement conducted in a cooling water system of an integrated plastics plant (Ref 23) shows that the sensor responded to upset or nonideal operating conditions and the dosing of inhibitors. It was shown to be a useful tool in optimizing treatment performance and identifying upset conditions at the plant as well as providing field verification of the effectiveness of a new treatment program in reducing the localized corrosion rate of carbon steel. However, this method relies on the forced movement of the electrodes (or the solution), and the current between the slow-moving anode and the fast- moving cathode may not represent the true corrosion current flowing from a corroding site to a noncorroding site of a metal under localized corrosion conditions. Furthermore, localized corrosion, for example, pitting, usually focuses on an area that is significantly smaller than the large, slow-moving electrode (0.3 to 0.5 cm^2, or 0.05 to 0.08 $in.^2$) for the differential flow cell (Ref 20, 21, 22, 23, 24). It may not be reliable to predict a localized corrosion rate based on the current measured from a large surface area. The sensor has not been widely used either in laboratories or in the field.

References cited in this section

20. B. Yang, “A Novel Method for On-line Determination of Underdeposit Corrosion Rate in Cooling Water Systems,” Paper 335, Corrosion/94, NACE International, 1994

21. B. Yang, “Localized Corrosion Monitoring in Cooling Water Systems,” Paper 541, Corrosion/95, NACE International, 1995

22. B. Yang, “Real-Time Localized Corrosion Monitoring in Refinery Cooling Water Systems,” Paper 595, Corrosion/98, NACE International, 1998

23. B. Yang, “Minimizing Localized Corrosion via New Chemical Treatment and Performance-Based Treatment Optimization and Control,” Paper 307, Corrosion/99, NACE International, 1999

24. B. Yang, Real-Time Localized Corrosion Monitoring in Industrial Cooling Water Systems, *Corrosion*, Vol 56 (No. 7), 2000, p 743–756

L. Yang and N. Sridhar, Monitoring of Localized Corrosion, *Corrosion: Fundamentals, Testing, and Protection*, Vol 13A, *ASM Handbook*, ASM International, 2003, p 519–524

Monitoring of Localized Corrosion

Lietai Yang and Narasi Sridhar, Southwest Research Institute

Galvanically Coupled Crevice Cell

The galvanically coupled crevice cell has been used to study the crevice corrosion of stainless steel materials in seawater (Ref 25, 26, 27, 28). Figure 2 shows the schematic diagram of a coupled crevice cell system (Ref 27). In Fig. 2, there are three creviced stainless steel specimens and a large, noncreviced specimen that is similar to the creviced specimens in composition. Each of the three creviced specimens is coupled independently to the large, noncreviced specimen through a resistor. The crevice corrosion taking place in the crevices drives the electrode potential of the creviced specimen more negative (or anodic) than the large, noncreviced specimen (cathode). This process produces a coupled current from the large, non-creviced specimen to the creviced specimen. The coupled current is measured from its associated resistor and used to indicate the degree of crevice corrosion. The reference electrode in Fig. 2 is used to measure the potential of the coupled electrodes.

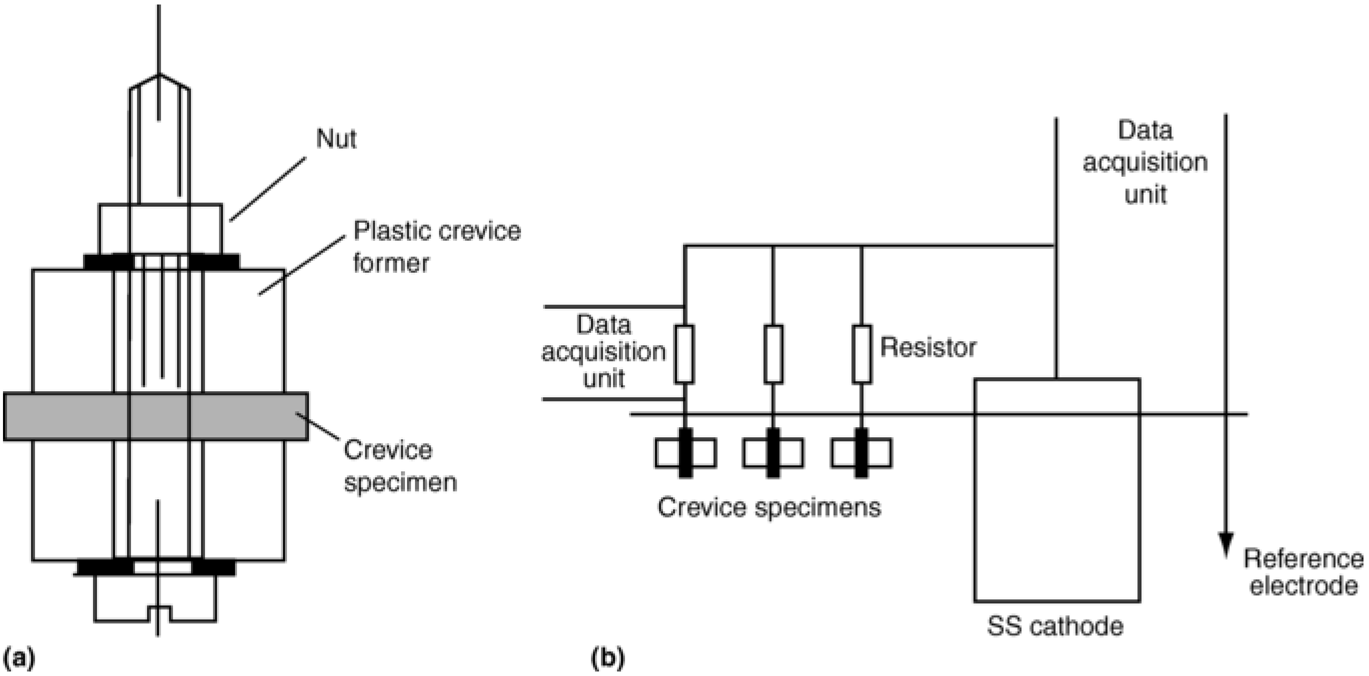

Fig. 2 Crevice cell system. (a) Cross section of crevice assembly. (b) Schematic diagram of crevice assemblies galvanically coupled to stainless steel (SS) cathode. Source: Ref 27, with permission from NACE International

Figure 3 shows typical results obtained with the crevice cell system (Ref 27). The measurement was conducted in a seawater test loop at 15 °C (59 °F), under which condition the specimen normally is not subject to crevice corrosion. The purpose of this measurement was to study the effect of temporary upset conditions on crevice corrosion of a welded stainless steel (UNS S31254) in seawater. Prior to the start of the measurement in Fig. 3, the crevice specimens were aged temporarily at high temperatures and high electrochemical potentials to initiate crevice corrosion. Figure 3 shows that the corrosion attack continued to propagate at 15 °C (59 °F) for 10 to 20 days before repassivation took place.

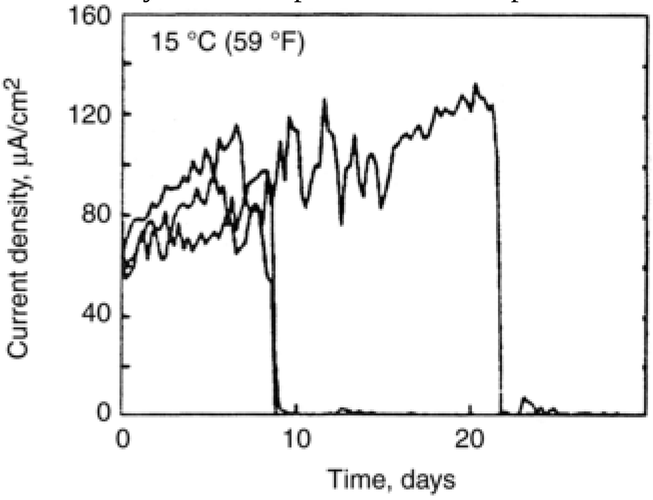

Fig. 3 Galvanic current densities of three creviced specimens of welded stainless steel (UNS S31254) and a cathode as a function of time in seawater at 15 °C (59 °F). This illustrates that repassivation occurs in approximately 10 to 20 days. Source: Ref 27, with permission from NACE International

This technique requires only straightforward voltage measurements and yet is capable of detecting the onset of localized corrosion under service conditions. Depending on the accuracy and resolution of the voltage-monitoring instrument, it may be able to detect localized corrosion in the early stages of degradation. The disadvantage of this method is that it cannot be used to determine the true rate of localized corrosion, due to the large surface area of the crevice (5.5 cm^2, or 0.85 $in.^2$). On-line application of this sensor remains to be demonstrated in the field.

References cited in this section

25. U. Steinsmo, The Effect of Temperature on Propagation of Crevice Corrosion of High Alloyed Stainless Steel in Natural Seawater, *Progress in the Understanding and Prevention of Corrosion,* Vol 2, Tenth Eur. Corros. Congr. Paper, J.M. Costa and A.D. Mercer, Ed., Institute of Materials, London, U.K., 1993, p 974–982

26. U. Steinsmo, T. Rogne, and J.M. Drugli, "Aspects of Testing and Selecting Stainless Steels for Seawater Applications," Paper 492, Corrosion/94, NACE International, 1994

27. U. Steinsmo, T. Rogne, and J. Drugli, Aspects of Testing and Selecting Stainless Steels for Seawater Applications, *Corrosion,* Vol 53 (No. 12), 1997, p 955–964

28. U. Steinsmo, Test Method for Localized Corrosion of Stainless Steel in Seawater, *Pitture Vernic. Eur.*, Vol 74 (No.14), 1998, p 15–18

L. Yang and N. Sridhar, Monitoring of Localized Corrosion, *Corrosion: Fundamentals, Testing, and Protection*, Vol 13A, *ASM Handbook*, ASM International, 2003, p 519–524

Monitoring of Localized Corrosion

Lietai Yang and Narasi Sridhar, Southwest Research Institute

Galvanically Coupled Crevice Cell

The galvanically coupled crevice cell has been used to study the crevice corrosion of stainless steel materials in seawater (Ref 25, 26, 27, 28). Figure 2 shows the schematic diagram of a coupled crevice cell system (Ref 27). In Fig. 2, there are three creviced stainless steel specimens and a large, noncreviced specimen that is similar to the creviced specimens in composition. Each of the three creviced specimens is coupled independently to the large, noncreviced specimen through a resistor. The crevice corrosion taking place in the crevices drives the electrode potential of the creviced specimen more negative (or anodic) than the large, noncreviced specimen (cathode). This process produces a coupled current from the large, non-creviced specimen to the creviced specimen. The coupled current is measured from its associated resistor and used to indicate the degree of crevice corrosion. The reference electrode in Fig. 2 is used to measure the potential of the coupled electrodes.

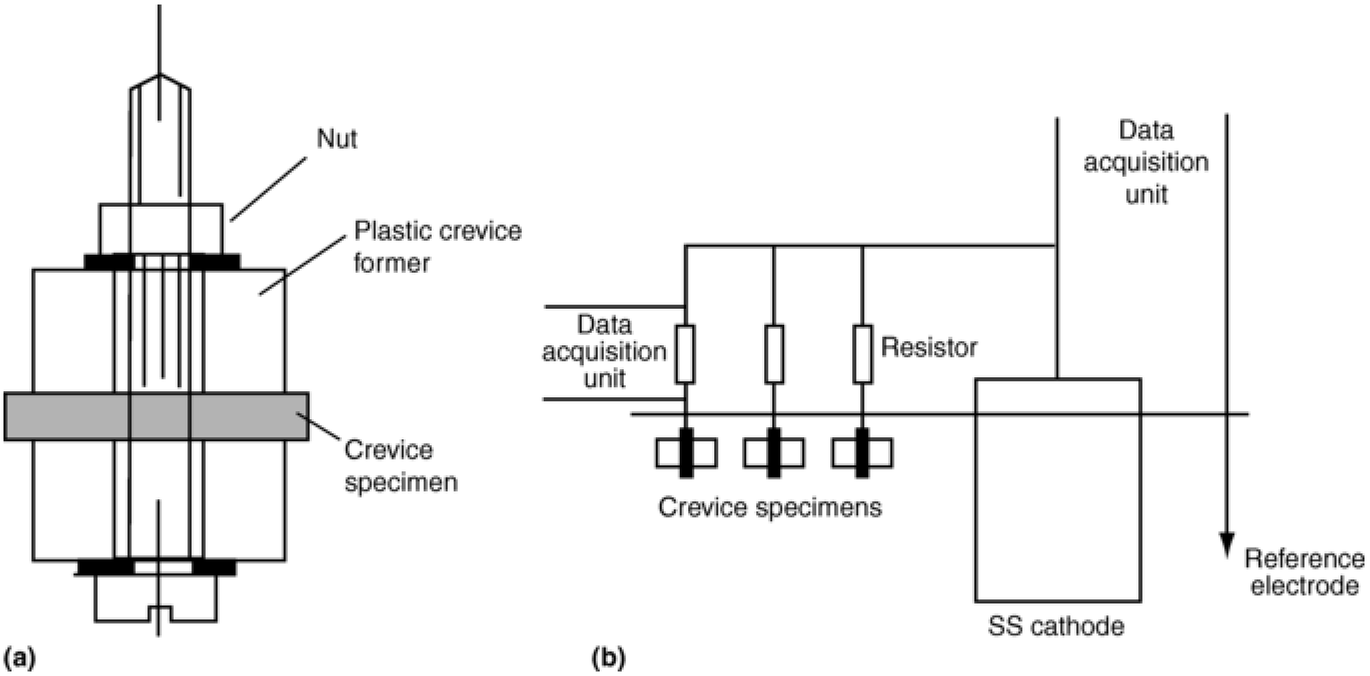

Fig. 2 Crevice cell system. (a) Cross section of crevice assembly. (b) Schematic diagram of crevice assemblies galvanically coupled to stainless steel (SS) cathode. Source: Ref 27, with permission from NACE International

Figure 3 shows typical results obtained with the crevice cell system (Ref 27). The measurement was conducted in a seawater test loop at 15 °C (59 °F), under which condition the specimen normally is not subject to crevice corrosion. The purpose of this measurement was to study the effect of temporary upset conditions on crevice corrosion of a welded stainless steel (UNS S31254) in seawater. Prior to the start of the measurement in Fig. 3, the crevice specimens were aged temporarily at high temperatures and high electrochemical potentials to initiate crevice corrosion. Figure 3 shows that the corrosion attack continued to propagate at 15 °C (59 °F) for 10 to 20 days before repassivation took place.

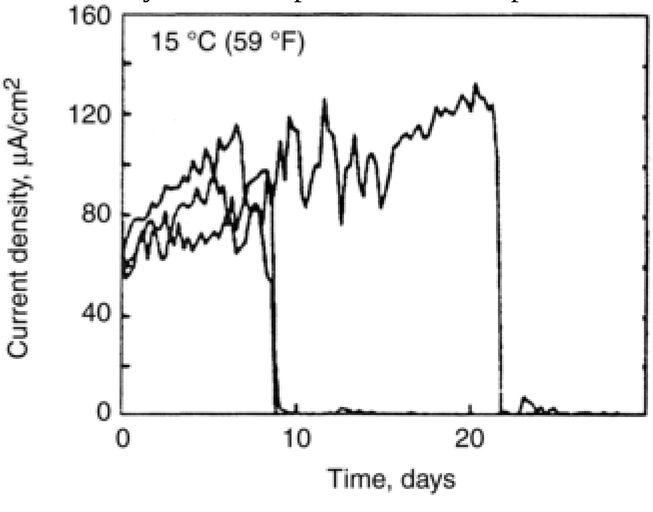

Fig. 3 Galvanic current densities of three creviced specimens of welded stainless steel (UNS S31254) and a cathode as a function of time in seawater at 15 °C (59 °F). This illustrates that repassivation occurs in approximately 10 to 20 days. Source: Ref 27, with permission from NACE International

This technique requires only straightforward voltage measurements and yet is capable of detecting the onset of localized corrosion under service conditions. Depending on the accuracy and resolution of the voltage-monitoring instrument, it may be able to detect localized corrosion in the early stages of degradation. The disadvantage of this method is that it cannot be used to determine the true rate of localized corrosion, due to the large surface area of the crevice (5.5 cm^2, or 0.85 $in.^2$). On-line application of this sensor remains to be demonstrated in the field.

References cited in this section

25. U. Steinsmo, The Effect of Temperature on Propagation of Crevice Corrosion of High Alloyed Stainless Steel in Natural Seawater, *Progress in the Understanding and Prevention of Corrosion*, Vol 2, Tenth Eur. Corros. Congr. Paper, J.M. Costa and A.D. Mercer, Ed., Institute of Materials, London, U.K., 1993, p 974–982

26. U. Steinsmo, T. Rogne, and J.M. Drugli, "Aspects of Testing and Selecting Stainless Steels for Seawater Applications," Paper 492, Corrosion/94, NACE International, 1994

27. U. Steinsmo, T. Rogne, and J. Drugli, Aspects of Testing and Selecting Stainless Steels for Seawater Applications, *Corrosion,* Vol 53 (No. 12), 1997, p 955–964

28. U. Steinsmo, Test Method for Localized Corrosion of Stainless Steel in Seawater, *Pitture Vernic. Eur.*, Vol 74 (No.14), 1998, p 15–18

L. Yang and N. Sridhar, Monitoring of Localized Corrosion, *Corrosion: Fundamentals, Testing, and Protection*, Vol 13A, *ASM Handbook*, ASM International, 2003, p 519–524

Monitoring of Localized Corrosion

Lietai Yang and Narasi Sridhar, Southwest Research Institute

Electrochemical Biofilm Activity Sensor

Microbially induced localized penetration of materials can occur due to a combination of microbially mediated electrochemical reactions, local generation of deleterious species, and geometrical restrictions produced by the biofilm. Through-wall penetration of piping and heat exchanger tubing at rates 10 to 1000 times more rapid than typical general corrosion rates can result (Ref 41). Figure 7 shows the schematic diagram of a sensor (Ref 41, 42, 43, 44, 45) developed to monitor localized corrosion due to microbiological activity.

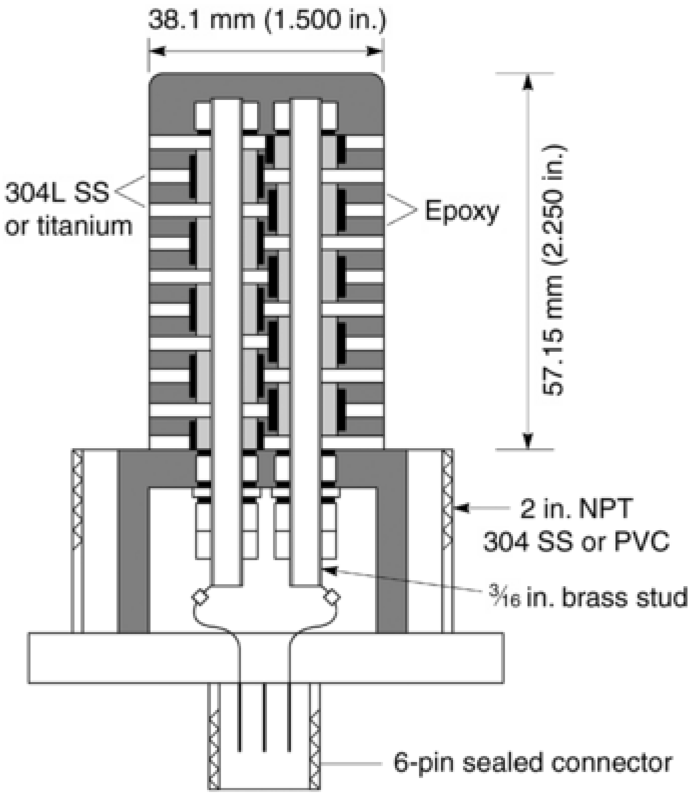

Fig. 7 Electrochemical biofilm activity monitoring probe. Probe is cylindrical, 38.1 mm (1.500 in.) in diameter, and 57.15 mm (2.250 in.) high. SS, stainless steel; NPT, American National Standard Taper Pipe Thread; PVC, polyvinyl chloride. Source: Ref 41, with permission from NACE International

The sensor consists of a stack of identical stainless steel discs (other passive metals, such as titanium, have also been used successfully) configured as a right-circular cylinder. The discs are divided into two groups, with each being connected to a brass stud to form an electrode. The electrodes are electrically isolated from each other and from the body of the probe, using an epoxy resin. One electrode (set of discs) is polarized relative to the other for a short period of time each day. The externally applied potential creates different local conditions on the stainless steel electrodes, conditions that cause different microbiological colonies to become established on the positive and negative electrodes. This polarization cycle produces slightly modified environments on the discs that are conducive to biofilm formation. Tracking the daily applied current and noting significant changes in that current provides one method to detect the onset of biofilm formation. The difference in the magnitude of the applied current from the baseline (i.e., the applied current when no biofilm is present) provides a measure of the localized corrosion due to biofilm activity. The generated current, the current that flows between the two electrodes when no external potential is applied, provides an additional, and often more sensitive, indicator of the effect of biofilm activity. In general, the onset of biofilm formation is signaled by an abrupt change in the generated current from the typical baseline value that is always very near zero. The magnitude of the deviation of the generated current from its baseline value provides a quantitative measure of the effect of biofilm activity on corrosion. It has been demonstrated in field measurements (Ref 41) that the biofilm activity sensor offers the system operator real-time information on the condition of microbiological fouling in the system so that injections of biocides or other mitigation activities can be based on measured effects of biofilm activity on a surface. However, its application in the field has been limited, and the reproducibility of the sensor remains to be seen.

References cited in this section

41. J.G. Licina, “Monitoring Biofilms on Metallic Surfaces in Real Time,” Paper 442, Corrosion/2001, NACE International, 2001

42. J.G. Licina and G. Nekoksa, “An Electrochemical Method for On-Line Monitoring of Biofilm Activity,” Paper 403, Corrosion/ 93, NACE International, 1993

43. J.G. Licina, "Experience with On-Line Monitoring of Biofilms in Power Plant Environments," Paper 257, Corrosion/94, NACE International, 1994

44. J.G. Licina and G. Nekoksa, "The Influence of Water Chemistry and Biocide Additions on the Response of an On-Line Biofilm Monitor," Paper 527, Corrosion/95, NACE International, 1995

45. J.G. Licina and L.P. Vehuis, "Biocide Optimization Using an On-Line Biofilm Detector," Paper 00-060, International Water Conference, Oct 2000 (Pittsburgh, PA), Engineers Society of Western Pennsylvania

---

L. Yang and N. Sridhar, Monitoring of Localized Corrosion, *Corrosion: Fundamentals, Testing, and Protection*, Vol 13A, *ASM Handbook*, ASM International, 2003, p 519–524

Monitoring of Localized Corrosion

Lietai Yang and Narasi Sridhar, Southwest Research Institute

Nonelectrochemical Methods

The electric field mapping technique (Ref 46) measures metal loss over a pipeline surface. An array of permanently installed pick-up wires is positioned around the outside of a pipe. A current is fed through a selected section of the pipe and an electric potential map is derived to correlate the change in wall thickness.
This method has the ability to monitor the localized corrosion of an actual component as it occurs. It gives the corrosion depth, pit size, and the actual location of the damage. It is also nonintrusive and non-perturbing to the corrosion metal-electrolyte interface or to the corrosion environment. The disadvantage of this method includes the requirement of special multichannel hardware and the associated software for data collection and data analysis. It also requires the installation of a large number of miniature electrodes on a small surface area of a pipe or equipment to obtain the high resolution for localized corrosion monitoring.
Magnetic Field Detection. Although not an ideal on-line detection tool, another nonelectrochemical technique that has been used to detect localized corrosion is the superconducting quantum interference device (SQUID) (Ref 47), which is a highly sensitive magnetic field detector that can detect fields less than approximately 2×10^{-8} of the terrestrial magnetic field. Originally, SQUID was developed using conventional superconducting materials and required cooling by liquid helium to 4 K. However, with the advent of ceramic superconductors, SQUIDs operating at liquid nitrogen temperature (77 K) are commercially available. The technique relies on sensitively detecting the magnetic fields generated by the currents at the anodic and cathodic areas during localized corrosion. The spatial separation of the anodic and cathodic areas aids in the detection of localized corrosion sites. The technique has been demonstrated for aluminum alloys used in aircraft systems (Ref 47). The advantages of this technique include its ability to detect corrosion without contacting the corroding metal; the potential for identifying corrosion on hidden surfaces, such as lap joints; and to develop some idea of the rate of corrosion. The disadvantages of the technique include its inability to be used on ferromagnetic metals or where ferromagnetic metals are in proximity, such as steel rivets on aluminum, and its inability to be used as a real-time monitor.

References cited in this section

46. R. Johnson, B.E. Bjornsen, D. Morton, D. Parr, and B. Ridd, "Weld Root Corrosion Monitoring with a New Electrical Field Signature Mapping Inspection Tool," Paper 00096, Corrosion/2000, 2000

47. D. Li, Y. Ma, W.F. Flanagan, B.D. Lichter, and J.P. Wikswo, Jr., Application of Superconducting Magnetometry in the Study of Aircraft Aluminum Alloy Corrosion, *Corrosion,* Vol 52 (No. 3) 1996, p 219–231

L. Yang and N. Sridhar, Monitoring of Localized Corrosion, *Corrosion: Fundamentals, Testing, and Protection*, Vol 13A, *ASM Handbook*, ASM International, 2003, p 519–524

Monitoring of Localized Corrosion

Lietai Yang and Narasi Sridhar, Southwest Research Institute

Conclusions

On-line monitoring of localized corrosion is still a challenge to researchers, plant engineers, and operators. The ECN method has been the most extensively studied method for localized corrosion monitoring. It may provide useful information on localized corrosion, including initiation and propagation. However, the results have not been reproducible in all cases. The differential flow cell and crevice cell methods may be used as qualitative but not quantitative sensors for localized corrosion, because the surface areas of the electrodes are significantly larger than the areas of localized attacks. The coupled multielectrode sensor offers promise as a localized corrosion sensor. However, it is a newly emerging technology, and its performance as a localized corrosion sensor remains to be judged by future work. Nonelectrochemical techniques that rely on electric or magnetic field detection are also being used in specific applications, such as underwater pipelines and aircraft lap joints.

L. Yang and N. Sridhar, Monitoring of Localized Corrosion, *Corrosion: Fundamentals, Testing, and Protection*, Vol 13A, *ASM Handbook*, ASM International, 2003, p 519–524

Monitoring of Localized Corrosion

Lietai Yang and Narasi Sridhar, Southwest Research Institute

References

1. V.S. Agarwala and S. Ahmad, “Corrosion Detection and Monitoring—A Review,” Paper 271, Corrosion/2000, NACE International, 2000

2. L. Yang, X. Sun, and F. Steward, “An Electrical Resistance Probe for Monitoring Flow-Assisted Corrosion in Simulated Primary Coolant of Nuclear Reactors at 310 °C,” Paper 459, Corrosion/99, NACE International, 1999

3. G.K. Brown, J.R. Davies, and B.J. Hemblade, “Real-Time Metal Loss Internal Monitoring,” Paper 278, Corrosion/2000, NACE International, 2000

4. N. Sridhar, D.S. Dunn, C.S. Brossia, and O.C. Moghissi, “Corrosion Monitoring Techniques for Thermally Driven Wet and Dry Conditions,” Paper 283, Corrosion/ 2000, NACE International, 2000

5. F. Mansfeld, The Polarization Resistance Technique for Measuring Corrosion Currents, *Advances in Corrosion Engineering and Technology,* Vol 6, M.G. Fontana and R.W. Staehle, Ed., Plenum, 1976

6. F. Mansfeld, Polarization Resistance Measurements—Experimental Procedures and Evaluation of Testing Data, *Electrochemical Techniques for Corrosion Engineering*, R. Baboian, Ed., NACE International, 1987, p 18–26

7. P.M. Natishan, R.G. Kelly, G.S. Frankel, and R.C. Newman, Ed., *Critical Factors in Localized Corrosion II,* The Electrochemical Society, 1996

8. R.G. Kelly, G.S. Frankel, P.M. Natishan, and R.C. Newman, Ed., *Critical Factors in Localized Corrosion III,* The Electrochemical Society, 1999

9. G.S. Frankel and J.R. Scully, Ed., *Localized Corrosion,* Proceedings of the Corrosion/ 2001 Research Topical Symposium, NACE International, 2001

10. F.P. IJsseling, Electrochemical Methods in Crevice Corrosion Testing, *Br. Corros. J.,* Vol 15 (No. 2), 1980, p 51–69

11. J.L. Dawson, Electrochemical Noise Measurement: The Definitive In-Situ Technique for Corrosion Applications?, *Electrochemical Noise Measurement for Corrosion Applications,* STP 1277, J.R. Kearns, J.R. Scully, P.R. Roberge, and D.L. Dawson, Ed., ASTM, 1996, p 3–35

12. J.C. Uruchurtu and J.L. Dawson, Noise Analysis of Pure Aluminum under Different Pitting Conditions, *Corrosion,* Vol 43 (No. 1), 1987, p 19–26

13. A.M.P. Simoes and M.G.S. Ferreira, Crevice Corrosion Studies on Stainless Steel Using Electrochemical Noise Measurements, *Br. Corros. J.,* Vol 22 (No.1), 1987, p 21–25

14. F. Mansfeld, L.T. Han, C.C. Lee, C. Chen, G. Zhang, and H. Xiao, Analysis of Electrochemical Impedance and Noise Data for Polymer-Coated Metals, *Corros. Sci.,* Vol 39 (No. 2), 1997, p 255–279

15. A.N. Rothwell, D.A. Eden, and G. Row, "Electrochemical Noise Techniques for Determining Corrosion Rates and Mechanisms," Paper 223, Corrosion/92, NACE International, 1992

16. J.B. Lumsden, M.W. Kendig, and S. Jeanjaquet, "Electrochemical Noise for Carbon Steel in Sodium Chloride Solutions—Effect of Chloride and Oxygen Activity," Paper 224, Corrosion/92, NACE International, 1992

17. E.E. Barr, A.H. Greenfield, and L. Pierard, "Application of Electrochemical Noise Monitoring to Inhibitor—Evaluation and Optimization in Field: Results from the Kaybob South Sour Gas Field," Paper 01288, Corrosion/2001, NACE International, 2001

18. R.G. Kelly, M.E. Inman, and J.L. Hudson, Analysis of Electrochemical Noise for Type 410 Stainless Steel in Chloride Solutions, *Electrochemical Noise Measurement for Corrosion Applications,* STP 1277, J.R. Kearns, J.R. Scully, P.R. Roberge, D.L. Reichert, and J.L. Dawson, Ed., ASTM, 1996, p 101–113

19. S.T. Pride, J.R. Scully, and J.L. Hudson, Analysis of Electrochemical Noise from Metastable Pitting in Aluminum, Aged Al- 2%Cu, and AA 2024-T3, *Electrochemical Noise Measurement for Corrosion Applications,* STP 1277, J.R. Kearns, J.R. Scully, P.R. Roberge, D.L. Reichert, and J.L. Dawson, Ed., ASTM, 1996, p 307

20. B. Yang, "A Novel Method for On-line Determination of Underdeposit Corrosion Rate in Cooling Water Systems," Paper 335, Corrosion/94, NACE International, 1994

21. B. Yang, "Localized Corrosion Monitoring in Cooling Water Systems," Paper 541, Corrosion/95, NACE International, 1995

22. B. Yang, "Real-Time Localized Corrosion Monitoring in Refinery Cooling Water Systems," Paper 595, Corrosion/98, NACE International, 1998

23. B. Yang, "Minimizing Localized Corrosion via New Chemical Treatment and Performance-Based Treatment Optimization and Control," Paper 307, Corrosion/99, NACE International, 1999

24. B. Yang, Real-Time Localized Corrosion Monitoring in Industrial Cooling Water Systems, *Corrosion,* Vol 56 (No. 7), 2000, p 743–756

25. U. Steinsmo, The Effect of Temperature on Propagation of Crevice Corrosion of High Alloyed Stainless Steel in Natural Seawater, *Progress in the Understanding and Prevention of Corrosion,* Vol 2, Tenth Eur. Corros. Congr. Paper, J.M. Costa and A.D. Mercer, Ed., Institute of Materials, London, U.K., 1993, p 974–982

26. U. Steinsmo, T. Rogne, and J.M. Drugli, "Aspects of Testing and Selecting Stainless Steels for Seawater Applications," Paper 492, Corrosion/94, NACE International, 1994

27. U. Steinsmo, T. Rogne, and J. Drugli, Aspects of Testing and Selecting Stainless Steels for Seawater Applications, *Corrosion,* Vol 53 (No. 12), 1997, p 955–964

28. U. Steinsmo, Test Method for Localized Corrosion of Stainless Steel in Seawater, *Pitture Vernic. Eur.,* Vol 74 (No.14), 1998, p 15–18

29. Z. Qingdong, A Novel Electrochemical Testing Method and Its Use in the Investigation of Underfilm Corrosion of Temporary Protective Oil Coating, *Corrosion,* Vol 56 (No. 7), 2000, p 722–726

30. Q. Zhong, Electrochemical Technique for Investigating Temporarily Protective Oil Coatings, *Prog. Org. Coatings,* Vol 30 (No. 4), 1997, p 213–218

31. Q. Zhong, Wire Beam Electrode: A New Tool for Investigating Electrochemical Inheterogeneity of Oil Coating, *Prog. Org. Coatings,* Vol 30 (No. 4), 1997, p 279–285

32. Y.J. Tan, A New Crevice Corrosion Testing Method and Its Use in the Investigation of Oil Stain, *Corrosion,* Vol 50 (No. 4), 1994, p 266–269

33. Y.J. Tan, Monitoring Localized Corrosion Processes and Estimating Localized Corrosion Rates Using a Wire-Beam Electrode, *Corrosion,* Vol 54 (No. 5), 1998, p 403–413

34. L. Yang, N. Sridhar, O. Pensado, and D. Dunn, An In-Situ Galvanically Coupled Multielectrode Array Sensor for Localized Corrosion, *Corrosion,* Vol 58 (No. 12), 2002, p 1004–1014

35. Y.J. Tan, Wire Beam Electrode: A New Tool for Studying Localized Corrosion and Other Inheterogeneity Electrochemical Processes, *Corros. Sci.,* Vol 41 (No. 2), 1999, p 229–247

36. Y.J. Tan, S. Bailey, B. Kinsella, and A. Lowe, Mapping Corrosion Kinetics Using the Wire Beam Electrode in Conjunction with Electrochemical Noise Resistance Measurements, *J. Electrochem. Soc.,* Vol 147 (No. 2), 2000, p 530–539

37. L. Yang, N. Sridhar, and O. Pensado, "Development of a Multielectrode Array Sensor for Monitoring Localized Corrosion," Abstract 182, Extended Abstract, Vol 1, presented at the 199th Meeting of the Electrochemical Society, 2001

38. L. Yang and D. Dunn, Evaluation of Corrosion Inhibitors in Cooling Water Systems Using a Coupled Multielectrode Array Sensor, Paper 004, Corrosion/2002, NACE International, 2002

39. L. Yang, N. Sridhar, and G. Cragnolino, “Comparison of Localized Corrosion of Fe- Ni-Cr-Mo Alloys in Concentrated Brine Solutions Using a Coupled Multielectrode Array Sensor,” Paper 545, Corrosion/2002, NACE International, 2002

40. Z. Szklarska-Smialowska, *Pitting Corrosion of Metals,* NACE International, 1986

41. J.G. Licina, “Monitoring Biofilms on Metallic Surfaces in Real Time,” Paper 442, Corrosion/2001, NACE International, 2001

42. J.G. Licina and G. Nekoksa, “An Electrochemical Method for On-Line Monitoring of Biofilm Activity,” Paper 403, Corrosion/ 93, NACE International, 1993

43. J.G. Licina, “Experience with On-Line Monitoring of Biofilms in Power Plant Environments,” Paper 257, Corrosion/94, NACE International, 1994

44. J.G. Licina and G. Nekoksa, “The Influence of Water Chemistry and Biocide Additions on the Response of an On-Line Biofilm Monitor,” Paper 527, Corrosion/95, NACE International, 1995

45. J.G. Licina and L.P. Vehuis, “Biocide Optimization Using an On-Line Biofilm Detector,” Paper 00-060, International Water Conference, Oct 2000 (Pittsburgh, PA), Engineers Society of Western Pennsylvania

46. R. Johnson, B.E. Bjornsen, D. Morton, D. Parr, and B. Ridd, “Weld Root Corrosion Monitoring with a New Electrical Field Signature Mapping Inspection Tool,” Paper 00096, Corrosion/2000, 2000

47. D. Li, Y. Ma, W.F. Flanagan, B.D. Lichter, and J.P. Wikswo, Jr., Application of Superconducting Magnetometry in the Study of Aircraft Aluminum Alloy Corrosion, *Corrosion,* Vol 52 (No. 3) 1996, p 219–231

L. Yang and N. Sridhar, Monitoring of Localized Corrosion, *Corrosion: Fundamentals, Testing, and Protection*, Vol 13A, *ASM Handbook*, ASM International, 2003, p 519–524

Monitoring of Localized Corrosion

Lietai Yang and Narasi Sridhar, Southwest Research Institute

Selected References

- R. Baboian Ed., *Electrochemical Techniques for Corrosion Engineering,* NACE International, 1987
- M.G. Fontana and R.W. Staehle, Ed., *Advances in Corrosion Engineering and Technology,* Vol 6, Plenum, 1976, Chap. 3
- J.R. Kearns, J.R. Scully, P.R. Roberge, and D.L. Dawson, Ed., *Electrochemical Noise Measurement for Corrosion Applications,* Special Technical Publication 1277, ASTM
- R.G. Kelly, G.S. Frankel, P.M. Natishan, and R.C. Newman, Ed., *Critical Factors in Localized Corrosion III,* Proceeding Vol 98–17, The Electrochemical Society, 1999
- Localized Corrosion, *Proceedings of the Corrosion/2001 Research Topical Symposium,* G.S. Frankel and J.R. Scully, Ed., NACE International, 2001
- P.M. Natishan, R.G. Kelly, G.S. Frankel, and R.C. Newman, Ed., *Critical Factors in Localized Corrosion II,* Proceeding Vol 95–15, The Electrochemical Society, 1996
- Z. Szklarska-Smialowska, *Pitting Corrosion of Metals,* NACE International, 1986

I. Perez, Infrared Imaging for Corrosion, Disbondments, and Cracks, *Corrosion: Fundamentals, Testing, and Protection*, Vol 13A, *ASM Handbook*, ASM International, 2003, p 525–528

Infrared Imaging for Corrosion, Disbondments, and Cracks

Ignacio Perez, Office of Naval Research

Introduction

ACTIVE INFRARED (IR) THERMOGRAPHY continues to gain acceptance as a nondestructive evaluation (NDE) tool for both in-service and manufacturing applications. For example, pulse thermography is the preferred method for in-service inspection of core cracks in E2-C propellers at Cherry Point Naval Depot and for inspection of metallic honeycomb structures during manufacturing at BF Goodrich Aerospace. This technique compares favorably to point-by-point nondestructive inspection (NDI) techniques such as eddy-current and ultrasonic methods. Positive aspects of IR pulse thermography include:

- Images of a relatively large area can be produced, which makes it a fast inspection technique (Ref 1).
- It is partially insensitive to curved surfaces (Ref 2).
- Images are easy to interpret, and it does not have liftoff effects.
- It has a wide range of material applicability: metals, composites, ceramics, and coatings.
- It is very easy to use as it does not require a couplant.
- Analytical and numerical models (Ref 3, 4, 5) together with computing speed and storage capacity have been steadily increasing.
- Cost of computers and IR cameras have been decreasing.

References cited in this section

1. H. Xiaoyan, L.D. Favro, and R.L. Thomas, Quantitative Defect Depth Measurements for NDE of Composites, *Proc. American Society for Composites,* R.F. Gibson and G.M. Newaz, Ed., Technomic Publishing Co., 1998, p 1077–1081

2. H. Xiaoyan, L.D. Favro, and R.L. Thomas, Thermal Wave NDI of Disbonds and Corrosion in Aircraft, *Second Joint NASA/FAA/ DOD Conf. Aging Aircraft,* NASA/CP- 1999-208982/Part 1, C.E. Harris, Ed., Langley Research Center, p 265–274

3. M.B. Saintey and D.P. Almond, Mathematical Modelling of Transient Thermography and Defect Sizing, *Review of Progress in QNDE,* Vol 15, D.O. Thompson and D.E. Chimenti, Ed., Plenum, 1996, p 503

4. L.D. Favro, X. Han, P.K. Kuo, and R.L. Thomas, Imaging the Early Time Behavior of Reflected Thermal Wave Pulses, in *Thermosense XVII,* Society of Photo-Optical Instrumentation Engineers, Vol 2473, 1995, p 162

5. X.P.V. Maldague, *Nondestructive Evaluation of Materials by IR Thermography,* Springer-Verlag, 1993, p 29

I. Perez, Infrared Imaging for Corrosion, Disbondments, and Cracks, *Corrosion: Fundamentals, Testing, and Protection*, Vol 13A, *ASM Handbook*, ASM International, 2003, p 525–528

Infrared Imaging for Corrosion, Disbondments, and Cracks

Ignacio Perez, Office of Naval Research

Infrared Thermography Equipment

There are three key components that are required to perform active thermography: an excitation source, a thermographic camera, and a computer with software that controls the instrumentation, acquires data, and displays the results. The challenge of active thermography is to match the thermal excitation source to the material and defect type being inspected. Some of the most common thermal excitation sources include:

- Arc lamps for detection of delaminations in composites and generalized corrosion in metals
- Hot air guns for detecting disbondments in weakly conducting materials
- Microwave sources for detection of trapped water in dielectric media
- More recently, ultrasonic welder guns for detection of cracks in materials

All of these thermal excitation techniques produce relative “hot spots” or large thermal contrasts on the specimen surface when there is a defect within the material. With the aid of the IR camera and associated equipment, the inspector makes a permanent record of these hot spots.
Figure 1 shows a laboratory setup of a pulse thermographic system with two arc lamps and an IR camera in between them. In a typical pulse thermographic experiment arrangement, the arc lamps are positioned as close as possible to the samples being inspected so as to deposit as much energy as possible over the sample's surface. The lamps are arranged to produce a uniform heating zone over the samples. The IR camera is situated to best capture images of the surface of the sample. Power to the lamps is provided by a capacitor bank that is charged to full capacity, typically 10 kJ. Just before discharging the capacitor through the arc lamps, the IR camera is triggered to start acquiring thermal images of the sample surface for background subtraction purposes. Usually ten frames suffice. After a few frames have been acquired with the sample at room temperature, the capacitor bank is discharged and the radiant energy produced by the lamps is deposited over the surface of the sample.

(a) (b)

Fig. 1 Typical infrared imaging equipment. (a) An infrared (IR) camera between two xenon arc lamps. (b) A highly portable commercially available system

The radiant pulse deposition time (τ_{dep}) should be made short enough so that only the surface of the sample increases in temperature initially, while the bulk of the sample remains at room temperature. Typically, the minimum τ_{dep} is approximately 5 ms. In general, the thermal excitation source should be capable of depositing the energy on the surface of the sample in a time comparable to or shorter than the lateral diffusion time (τ_{lat}) of the material being imaged. If τ_{dep} were much longer than the τ_{lat}, the resulting contrast temperature would be significantly lower than otherwise. Table 1 provides typical values of the normal and lateral diffusion times for an aluminum panel with two thickness values and with flat bottom holes of different radii to simulate defects.

Table 1 Infrared imaging time constants for a 7075 T6 aluminum sheet

Sheet thickness, *t*		Depth to hold, *d*		Normal diffusion time[(a)] (τ_{nor}), ms	Hole radius, *R*		Lateral diffusion time[(a)] (τ_{lat}), ms
mm	**in.**	**mm**	**in.**		**mm**	**in.**	
1.588	0.0625	0.3969	0.0156	1.6	12.7	0.5	1463
		0.7938	0.03125	2.8	6.35	0.25	366
		1.191	0.04688	1.6	3.175	0.125	91
3.175	0.125	0.3969	0.0156	2.2	1.588	0.0625	23
		0.7938	0.03125	6.5	0.7938	0.03125	5.8
		1.588	0.0625	11.5	0.3969	0.0156	1.5

(a) Based on $\rho c/k = 1.8$ s/cm^2

The pulse thermographic process can be described as follows. As soon as the radiant energy is deposited on the surface of the sample, it starts to diffuse into the bulk sample. Regions in the sample with delaminations, debonding, or corrosion will offer greater resistance to the flow of energy than regions with no defects. As a result, hot spots—or regions with large thermal contrast—will develop on the surface of the sample. These hot spots will be recorded by the IR camera system, which has been acquiring data throughout the experiment. It is the analysis of these hot spots that will allow the inspector to detect damage.

Figure 1(b) shows a portable version of the pulse thermographic system described previously. In this case, the IR camera and the arc lamp are integrated together in the same casing and situated on top of the tripod. The data-acquisition system and the capacitor bank are located on the adjacent dolly. The capacitor bank used in this system is significantly smaller than the one used in the laboratory to make the entire unit more portable. Typically, 2 to 3 kJ of energy storage is available in the portable unit compared to 10 kJ in the laboratory system. To compensate for the lower amount of energy and a potential drop in sensitivity, the inspection area is made proportionally smaller in order to maintain a similar energy density over the surface of the sample.

I. Perez, Infrared Imaging for Corrosion, Disbondments, and Cracks, *Corrosion: Fundamentals, Testing, and Protection*, Vol 13A, *ASM Handbook*, ASM International, 2003, p 525–528

Infrared Imaging for Corrosion, Disbondments, and Cracks

Ignacio Perez, Office of Naval Research

Thermographic Process

Simple models have been developed (Ref 6, 7, 8) describing the pulse thermographic process. They all are characterized by three distinctive phases:

- The energy-deposition phase characterized by the duration of the heat pulse
- The contrast-formation phase characterized by the diffusion of the surface thermal energy into the bulk of the material
- The contrast dissipation phase characterized by the lateral dissipation of energy

Each phase is characterized by a specific time constant τ_{dep}, τ_{nor}, and τ_{lat}, as shown in Fig. 2. In the limit of short pulse duration ($\tau_{dep} \ll \tau_{nor}$), the following simple relation characterizes the thermal contrast in terms of the parameters shown in Fig. 2:

$$\Delta T_{\max} = \frac{Q}{\rho c}\left(\frac{1}{d} - \frac{1}{t}\right)\cdot\left(\frac{\tau_{lat}}{\tau_{nor}}\right)^{\{1/[1-(\tau_{lat}/\tau_{nor})]\}}$$

where ΔT_{max} is the peak thermal contrast developed on a sample with a defect; $Q = J \cdot \tau_{dep}$, where Q is the amount of energy deposited on the surface of the sample per unit area, J is energy flux per unit area and time, and τ_{dep} is deposition time; ρc is the product of the density and specific heat of the material; d is the distance from the defect to the surface of the material; t is the thickness of the sample; R is the radius of defect; $\tau_{nor} = \rho c/k(d(t - d)/t)^2$ is the normal diffusion time; $\tau_{lat} = \rho c/k(R^2/2)$ is the lateral diffusion time; and k is thermal conductivity. For nonisotropic materials, k in the normal and lateral directions will have different values.

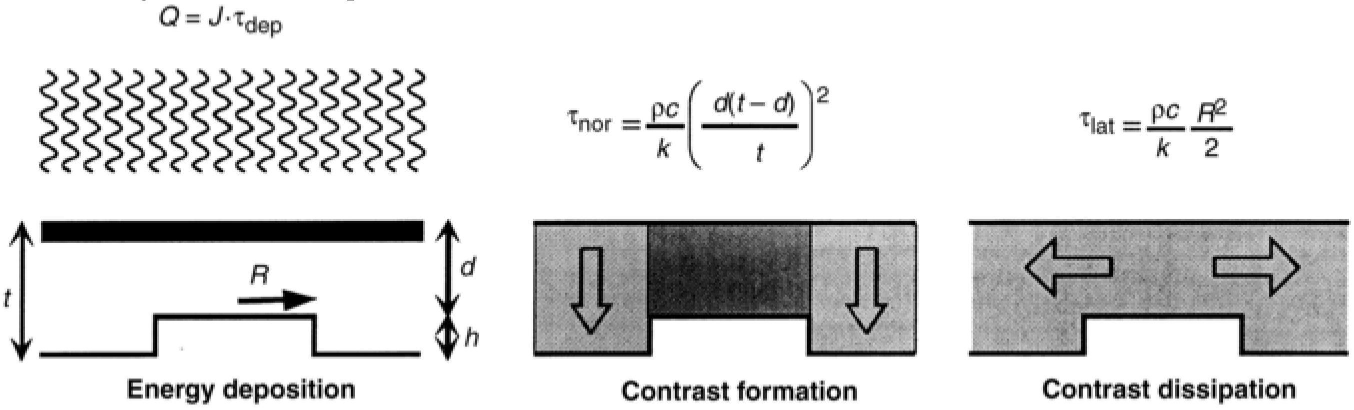

Fig. 2 The three phases characteristic of the pulse thermographic process and their respective characteristic time constant (a) deposition τ_{dep}; (b) contrast formation, τ_{nor}; (c) contrast dissipating, τ_{lat}. The key parameters characterizing the specimen and defect are: thickness, *t*; depth to defect, *d*; height of defect, *h*; radius of defect, *R*. Formulas are explained in the text.

These phases are not separated in time; rather, they all start at the same time. As soon as energy starts to be deposited over the surface of a panel, the energy will also start to diffuse into the panel. If there is a discontinuity in the panel, energy will begin to accumulate over the discontinuity and a thermal contrast will start forming. As soon as a contrast starts forming, it will also start dissipating laterally. All processes take place simultaneously. Depending on their relative duration, the contrast will be larger or smaller. The condition necessary to maximize the contrast temperature when a fixed amount of energy, Q, is deposited on the surface of a panel is obtained when:

$$\tau_{dep} \leq \tau_{nor} < \tau_{lat}$$

In other words, to maximize the amount of contrast formed one needs to deposit the energy in a time shorter than or comparable to the contrast formation time, which is largely controlled by the normal diffusion time constant. After this time, the lateral diffusion effects take hold and the contrast will not reach its maximum potential. For an isotropic material, the relation $\tau_{nor} < \tau_{lat}$ is equivalent to having the size of the defect (R) larger than the thickness of the plate; that is, $2R > t$. In this limit, the quantity

$$\left(\frac{\tau_{lat}}{\tau_{nor}}\right)^{\{1/[1-(\tau_{lat}/\tau_{nor})]\}}$$

approaches 1, and the thermal contrast approaches a very simple relation $\Delta T = Q/\rho c(1/d - 1/t)$. This relationship has been observed and reported in many scientific papers.

References cited in this section

6. I. Perez, R. Santos, P. Kulowitch, and M. Ryan, Calorimetric Modeling of Thermographic Data, in *Thermosense XX,* Society of Photo-Optical Instrumentation Engineers, Vol 3361, 1998, p 75

7. I. Perez, W.R. Davis, P. Kulowitch, and M.F. Dersch, Thermographic Modeling of Water Entrapment, *Thermosense XXI,* D.H. LeMieux and J.R. Snell, Jr., Society of Photo- Optical Instrumentation Engineers, April 1999, p 32–39

8. I. Perez and S. Shepard, Modeling of Pulsed Thermography in Anisotropic Media, *Review of Progress in QNDE,* Vol 18B, D.O. Thompson and D.E. Chimenti, Ed., Plenum Press, 1998, p 2063–2072

I. Perez, Infrared Imaging for Corrosion, Disbondments, and Cracks, *Corrosion: Fundamentals, Testing, and Protection,* Vol 13A, *ASM Handbook,* ASM International, 2003, p 525–528

Infrared Imaging for Corrosion, Disbondments, and Cracks

Ignacio Perez, Office of Naval Research

Imaging Results

The detection sensitivity of the pulse thermographic process, like ΔT_{max}, depends on the amount of energy deposited on the surface of the panel, the deposition time (Q, τ_{dep}), the size and depth of the flaw and thickness of the panel (R, d, t) (Ref 9). In general terms, the sensitivity increases linearly with the amount of energy, Q, and decreases inversely to the distance of the defect from the surface, d. Other factors that will significantly affect the sensitivity of the technique are edge effects, fasteners with different thermal conductivity than the base metal, and variations of an adhesive layer thickness in multilayered structures. Presently, the resolution achieved with the state-of-the-art system is about 3% thickness loss in laboratory environments inspecting flat panels and about 15 to 20% thickness loss under realistic field conditions inspecting structural components.

Pulse thermographic methods work best when inspecting materials with defects that are parallel to the surface such as disbondments, delaminations, and generalized corrosion because they disrupt the flow of energy very effectively. When the defect is perpendicular to the surface of the sample, such as with many types of cracks, pulse thermography does not work since disruption to the energy flow is minimal. Other thermographic methods are being developed for these types of defects such as line-scanning thermography and, more recently, sonic thermography.

Reference cited in this section

9. I. Perez and X. Han, Pulsed Thermography Modeling, *Review of Progress in QNDE,* Vol 21, D.O. Thompson and D.E. Chimenti, Ed., Plenum Press, 2002

I. Perez, Infrared Imaging for Corrosion, Disbondments, and Cracks, *Corrosion: Fundamentals, Testing, and Protection,* Vol 13A, *ASM Handbook,* ASM International, 2003, p 525–528

Infrared Imaging for Corrosion, Disbondments, and Cracks

Ignacio Perez, Office of Naval Research

Sonic Thermography for Crack Detection

Original work on sonic thermography started in the late 1970s with studies on the interaction between high-power ultrasonic sources and materials (Ref 10). It was found accidentally that when a cracked specimen was insonified with a high-power ultrasonic gun, cracks would be excited in such a way that they were easily detected with a thermal camera. Recent work in sonic thermography or thermosonics (Ref 11, 12) has demonstrated that this technique can also be applied to detect other forms of damage in materials, such as delamination in composites or corrosion in aluminum.

In the thermosonic method, a burst of high- power ultrasonic energy is applied to a sample. The energy quickly floods all corners of the sample. If a crack is present anywhere on the sample, energy will dissipate very effectively from it, creating a region of elevated temperature that can be imaged effectively with an IR camera (Fig. 3).

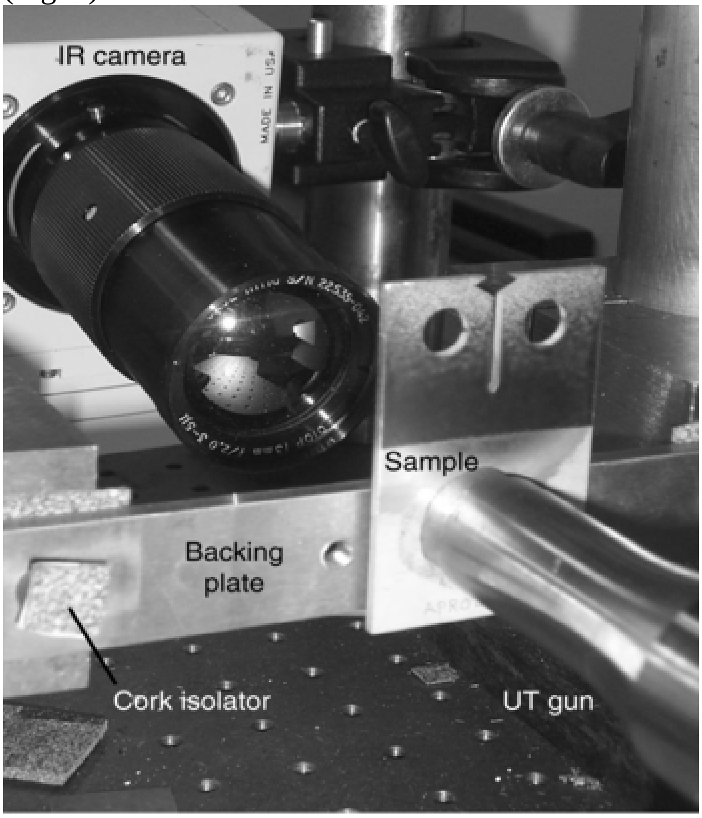

(a)

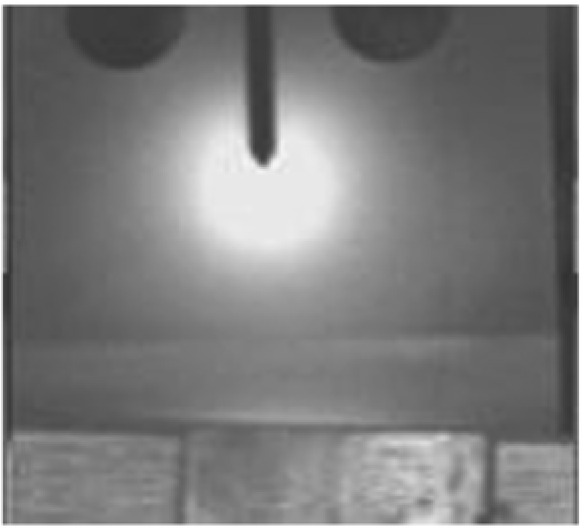

(b)

Fig. 3 Sonic thermography arrangement. (a) Ultrasonic (UT) gun energizes sample. Cork insulators mechanically isolate samples from the backing plate. Infrared (IR) camera captures images. (b) Thermograph from IR camera detects a crack at the root of the slot.

This mode of coupling energy to a sample is much more effective than the one used in the pulse thermographic method. In the pulse thermographic method, energy must be deposited uniformly over the entire surface of the sample being inspected, but it is only the energy that falls over the defective area that contributes to the thermographic signal. The remainder of the incident energy contributes to the background temperature, thereby reducing the maximum possible thermal contrast, since the thermal contrast is obtained by subtracting the background temperature from the temperature of the hot spot. In the thermosonic method, energy is coupled to the sample being inspected with an ultrasonic (UT) gun in contact with the sample at one point of its surface. The energy then quickly spreads to all corners of the sample, with the amplitude of vibration building up in the sample while the UT gun is on. If there is a crack present in the sample, vibrational energy will start dissipating through it. The dissipation mechanism is not completely understood, but it is believed to be related to rubbing or clapping of the facing surfaces of the crack. The net effect of this dissipation is that the area surrounding the crack will heat up, thereby allowing for its detection. This is a very effective use of the interrogation energy, since most of it is consumed in generating the thermosonic signal.

An analogy to detecting a crack by using the thermosonic process is finding a hole on a bicycle tire by using an air pressure gun. The analogy can be explained as follows. To find a hole in a tire, one applies air pressure through one point on the surface of the tire. The air quickly fills the entire volume of the tire and the pressure keeps building up in the tire while the pump remains on. If there is a small hole in the tire, air will leak through it, generating a small sound, thereby allowing for its detection. If there are several holes in the tire, each one will leak air, allowing for their detection. The higher the pressure in the tire, the stronger the sound produced by the hole. Continuing with the analogy, we know that a minimum amount of air pressure is required to detect a hole in a tire. Very small holes are effectively closed due to the elastic properties of rubber, and a minimum amount of air pressure is required to force air through the hole. Likewise in thermosonic experiments, a minimum amount of energy is required to excite cracks. This should be expected since closed cracks, such as hairline fatigue cracks that are almost invisible to the naked eye, would require a minimum amount of vibration amplitude to overcome the frictional forces produced by the mating surfaces. Evidence of this phenomena has been observed in laboratory experiments.

Figure 3 shows the experimental setup used by the author. A 1000 W power supply (not shown in the figure) was used, and the excitation frequency was 20 kHz. It would be desirable to have a system where the frequency of the UT gun could be adjusted depending on the particular characteristics of the sample and defect being inspected. Unfortunately, a recent search found all high-power commercial units had a fixed excitation frequency. This is because these units are engineered to achieve maximum amplitude displacements at the tip of the gun by stacking up a series of precisely cut piezoelectric crystals operating at the same resonant frequency. A steel horn (Fig. 3) is used in the UT gun to enhance the amplitude of vibration.

During a standard experiment, the controller is set to maximum power with pulse duration adjusted according to the experimental requirements, but limited to no more than 0.5 s because of hardware constraints. In fact, the longer the excitation, the stronger the thermosonic signal will be (Ref 13).

The UT gun was mounted on a platform to impede it from sliding over the surface of the sample and damaging the surface, while providing good load control via a pneumatic regulator. The load applied to the gun against the sample determines the amount of energy that couples into the sample and thereby determines the amplitude of the thermosonic signal. It was found in experiments that the thermosonic signal increased linearly with the applied load. Conservation of energy dictates that at some higher load value the thermosonic signal will saturate, but the available load capacity of 45 lb was far from saturation. As high loads tend to scourge the surface of the sample, a scientist at Wayne State University placed a thin coupling agent (a thin foil of copper) between the UT gun and the sample to minimize surface damage while maintaining good mechanical coupling. The appropriate choice of the coupling agent will determine if this technique is truly nondestructive and how much energy couples into the part being inspected. The infrared camera used in all the experiments discussed in this paper was a Radiance HS camera with a frame rate adjusted to capture thermal images at a rate of 120 frames/s.

Mechanical isolation of the sample is required in order to obtain an optimal thermosonic signal. If the sample being inspected rested directly over a backing plate of similar acoustic impedance or if the mechanical isolation between the sample and the backing plate was not significant, then the thermosonic signal would be minimal or not existing at all. This lack of thermosonic signal is understandable because the ultrasonic energy would leak out of the sample through the backing plate. Using the bicycle tire analogy, trying to detect a small fatigue crack in a sample in direct contact with a backing plate would correspond to trying to detect a small pinhole on

the tire when there was a large open gap in the tire. Air pressure would not be able to build in the tire due to the presence of the open gap in the tire. Similarly, good thermosonic signals are obtained when a piece of cork is placed between the sample and the backing plate to produce good mechanical isolation (Fig. 3) (Ref 13).

In practice, complete isolation, while desirable, is difficult to achieve. This does not mean that thermosonics is limited to the inspection of well-isolated components. As long as the energy leakage to the surrounding area is small compared to the energy required to excite a crack, thermosonics will be useful as an NDE technique.

There is still considerable experimental work and development to be done before thermosonics becomes a user-friendly NDE technique. The thermographic imaging techniques presented in this article and other techniques currently being developed are expanding the use of thermography into areas not previously considered.

References cited in this section

10. R.B. Mignogna, R.E. Green Jr., J.C. Duke Jr., E.G. Henneke II, and K.L. Reifsnider, *Ultrasonics,* Vol 19, 1981, p 159–163
11. L.D. Favro, X. Han, Z. Ouyang, G. Sun, H. Sui, and R.L. Thomas, *Rev. Sci. Instrum.,* Vol 71, 2000, p 2418
12. J. Rantala, D. Wu, and G. Busse, Amplitude Modulated Lock-in Vibrothermography for NDE of Polymers and Composites, *Research in Nondestructive Evaluation,* Vol 7, No. 4, 1995, p 215–228
13. I. Perez and W.R. Davis, Optimizing the Thermosonic Signal, *Review of Progress in QNDE,* Vol 23, D.O. Thompson and D.E. Chimenti, Ed., Plenum Press, 2003

I. Perez, Infrared Imaging for Corrosion, Disbondments, and Cracks, *Corrosion: Fundamentals, Testing, and Protection*, Vol 13A, *ASM Handbook*, ASM International, 2003, p 525–528

Infrared Imaging for Corrosion, Disbondments, and Cracks

Ignacio Perez, Office of Naval Research

Acknowledgment

The author would like to thank Dr. Robert Green from The Johns Hopkins University and Dr. Skip Favro and Dr. Xiaoyan Han from Wayne State University for insightful observations and valuable critiques of this article. Thanks to Mr. Richard Wood, Naval Air warfare center at Cherry Point for assistance with figures.

I. Perez, Infrared Imaging for Corrosion, Disbondments, and Cracks, *Corrosion: Fundamentals, Testing, and Protection*, Vol 13A, *ASM Handbook*, ASM International, 2003, p 525–528

Infrared Imaging for Corrosion, Disbondments, and Cracks

Ignacio Perez, Office of Naval Research

References

1. H. Xiaoyan, L.D. Favro, and R.L. Thomas, Quantitative Defect Depth Measurements for NDE of Composites, *Proc. American Society for Composites,* R.F. Gibson and G.M. Newaz, Ed., Technomic Publishing Co., 1998, p 1077–1081

2. H. Xiaoyan, L.D. Favro, and R.L. Thomas, Thermal Wave NDI of Disbonds and Corrosion in Aircraft, *Second Joint NASA/FAA/ DOD Conf. Aging Aircraft,* NASA/CP- 1999-208982/Part 1, C.E. Harris, Ed., Langley Research Center, p 265–274

3. M.B. Saintey and D.P. Almond, Mathematical Modelling of Transient Thermography and Defect Sizing, *Review of Progress in QNDE,* Vol 15, D.O. Thompson and D.E. Chimenti, Ed., Plenum, 1996, p 503

4. L.D. Favro, X. Han, P.K. Kuo, and R.L. Thomas, Imaging the Early Time Behavior of Reflected Thermal Wave Pulses, in *Thermosense XVII,* Society of Photo-Optical Instrumentation Engineers, Vol 2473, 1995, p 162

5. X.P.V. Maldague, *Nondestructive Evaluation of Materials by IR Thermography,* Springer-Verlag, 1993, p 29

6. I. Perez, R. Santos, P. Kulowitch, and M. Ryan, Calorimetric Modeling of Thermographic Data, in *Thermosense XX,* Society of Photo-Optical Instrumentation Engineers, Vol 3361, 1998, p 75

7. I. Perez, W.R. Davis, P. Kulowitch, and M.F. Dersch, Thermographic Modeling of Water Entrapment, *Thermosense XXI,* D.H. LeMieux and J.R. Snell, Jr., Society of Photo- Optical Instrumentation Engineers, April 1999, p 32–39

8. I. Perez and S. Shepard, Modeling of Pulsed Thermography in Anisotropic Media, *Review of Progress in QNDE,* Vol 18B, D.O. Thompson and D.E. Chimenti, Ed., Plenum Press, 1998, p 2063–2072

9. I. Perez and X. Han, Pulsed Thermography Modeling, *Review of Progress in QNDE,* Vol 21, D.O. Thompson and D.E. Chimenti, Ed., Plenum Press, 2002

10. R.B. Mignogna, R.E. Green Jr., J.C. Duke Jr., E.G. Henneke II, and K.L. Reifsnider, *Ultrasonics,* Vol 19, 1981, p 159–163

11. L.D. Favro, X. Han, Z. Ouyang, G. Sun, H. Sui, and R.L. Thomas, *Rev. Sci. Instrum.,* Vol 71, 2000, p 2418

12. J. Rantala, D. Wu, and G. Busse, Amplitude Modulated Lock-in Vibrothermography for NDE of Polymers and Composites, *Research in Nondestructive Evaluation,* Vol 7, No. 4, 1995, p 215–228

13. I. Perez and W.R. Davis, Optimizing the Thermosonic Signal, *Review of Progress in QNDE,* Vol 23, D.O. Thompson and D.E. Chimenti, Ed., Plenum Press, 2003

A.V. Bray, Corrosion Monitoring Using Microwave and Guided Wave Nondestructive Evaluation, *Corrosion: Fundamentals, Testing, and Protection*, Vol 13A, *ASM Handbook*, ASM International, 2003, p 529–532

Corrosion Monitoring Using Microwave and Guided Wave Nondestructive Evaluation

Alan V. Bray, Systems and Materials Research Consultancy (SMRC)

Introduction

TWO INTERESTING TECHNIQUES for finding hidden corrosion are emerging as viable in-service nondestructive evaluation (NDE) tools: microwave NDE and guided wave (GW) ultrasonic NDE methods. The in-service inspection scenario is complicated by the fact that corrosion is often hidden, and expensive disassembly can be required to complete an inspection. Microwave and GW NDE techniques have promise as methods that minimize disassembly in many common corrosion detection problems. Both methods are capable of detecting corrosion damage, cracks, and other defect types in inaccessible areas.

The most common corrosion-detection application of microwave NDE is inspecting under a coating or appliqué for corrosion. This corrosion detection is based on the physics of the way in which microwaves interact with the materials of the coating and the sublayers of corrosion. Paint, appliqués, and corrosion byproducts are all dielectric materials, and each influences a microwave signal differently. In addition, the damage caused by corrosion can change the distance from the coated surface to the base metal, and this change in height is also detectable. Aircraft coatings are critical targets because corrosion under a coating can ultimately result in loss of airframe integrity. Non-corrosion-related applications include inspection of composites and detection of moisture in nonconducting structures.

The NDE by GW differs from other ultrasonic methods in two distinct ways: GW evaluation is typically conducted at lower frequencies—often under 1 MHz, and GW signals travel long distances. Thus an area can be inspected from a significant distance. Some GW methods are aimed at detecting corrosion wastage from as far away as 20 m (65 ft) from a GW sensor array. Applications include inspection of insulated pipe runs while only removing a small portion of the insulation, and inspection of structures such as beams from a fixed set of GW sensors.

Like many NDE techniques, microwave and guided wave ultrasonic methods can be valuable tools for detecting hidden corrosion when used properly and interpreted with care. Much of the current research in applying these NDE methods to modern inspection problems centers on developing systems that are insensitive to errors and false alarms, and this often means systems that are specific to a given inspection scenario. As an example, a guided wave inspection system for insulated piping would be quite different than one used for detecting the presence of wing icing. Similarly, microwave NDE systems for detecting corrosion under coatings are configured differently than for moisture detection within a nonconducting structure like a honeycomb panel or a sandwich panel. Many of the basic system tools remain unchanged, but sensor configurations, frequency ranges, and analysis techniques can differ dramatically from one application to the next.

A.V. Bray, Corrosion Monitoring Using Microwave and Guided Wave Nondestructive Evaluation, *Corrosion: Fundamentals, Testing, and Protection*, Vol 13A*, ASM Handbook*, ASM International, 2003, p 529–532

Corrosion Monitoring Using Microwave and Guided Wave Nondestructive Evaluation

Alan V. Bray, Systems and Materials Research Consultancy (SMRC)

Microwave NDE Devices

Microwave transmitters provide the incident energy for an inspection. The most commonly used transmitters for corrosion detection are actually transceivers; diodes in the transmitter receive the reflected signal. The incident and reflected signals are separated in the device, and the reflected signals are then analyzed for evidence of corrosion. The presence of corrosion attenuates the received signal, as do changes in the distance from the metal substrate caused by wastage. A key to microwave NDE device design is keeping the sensor at a fixed distance from the inspection surface in order to avoid misinterpreting changes in standoff distance from actual corrosion features. The mechanical design, coupled with electronic processing of the reflected signal, are crucial in minimizing false alarms.

Open-ended waveguides are used often as microwave corrosion NDE sensors, although open- ended coaxial sensors (Ref 3) and strip-line antennae (Ref 4) have also successfully detected defects under coatings. Open ended rectangular waveguide sensors typically operate in the X- band (8 to 12.5 GHz) or K-band (12.5 to 40 GHz) frequency range. Corrosion detection sensitivity is dependent on frequency and standoff distance. Emerging microwave NDE tools for inspecting under coatings include small programmable logic devices that aid in distinguishing good and bad operating conditions (e.g., conditions that would lead to false alarms or missed detections).

Microwave devices sense the dielectric change that results when corrosion products are present under the coating. The amount/degree of corrosion has an influence that can also be sensed by the device. A heavily corroded area will attenuate the signal output more than a lightly corroded area will. Device displays can include a range of corrosion severity based on the extent of change in the returned signal. Defining the amount or degree of corrosion at the threshold of detection is difficult since it is defined by the corrosion itself. Some groups have used standard exposure methods such as ASTM G 34 specimens to define the lower detection limits in terms of hours of exposure under a defined regimen of corrosion (Ref 5).

Inspections with a microwave NDE device can be done with standard scanning systems, but handheld scanning is also possible. Any microwave scanning mechanism must be designed with altitude (standoff) distance and cant angle sensitivity in mind. Robust systems include logic to eliminate drastic changes that could be changes in altitude. As an example, the radius of curvature of the inspection surface can cause inaccuracies if the altitude control system has a wide enough footprint so that the distance to the sensor changes significantly with radius of curvature of the part.

Principles of Operation. Microwave NDE techniques depend on the interaction of incident microwave energy with a material or structure. This interaction involves the effect of the material on the electric and magnetic fields generated by the microwave device. Changes in the conductivity, permittivity, and permeability of the inspected material relative to its surroundings are sensed in these field changes, as well as changes in substrate morphology.

Figure 1 illustrates that the damage caused by corrosion of the substrate and the corrosion product itself both result in a change in the received signal. The bottom sketch portrays change caused by a change in the distance to the substrate, the top attenuation of the signal caused by the presence of corrosion products. Clearly, most detections are some combination of the two extremes. Corrosion products are typically dielectric materials, such as metal oxides—for example, iron and aluminum oxides. The dielectric nature of a material is described mathematically by its permittivity and loss factor, the real and imaginary components of the dielectric characteristic. Microwave NDE techniques for detecting corrosion under paints and appliqués exploit the contrast in the dielectric characteristics of corrosion versus that of the coating as well as the changes in substrate characteristics that indicate corrosion damage such as pitting and wastage.

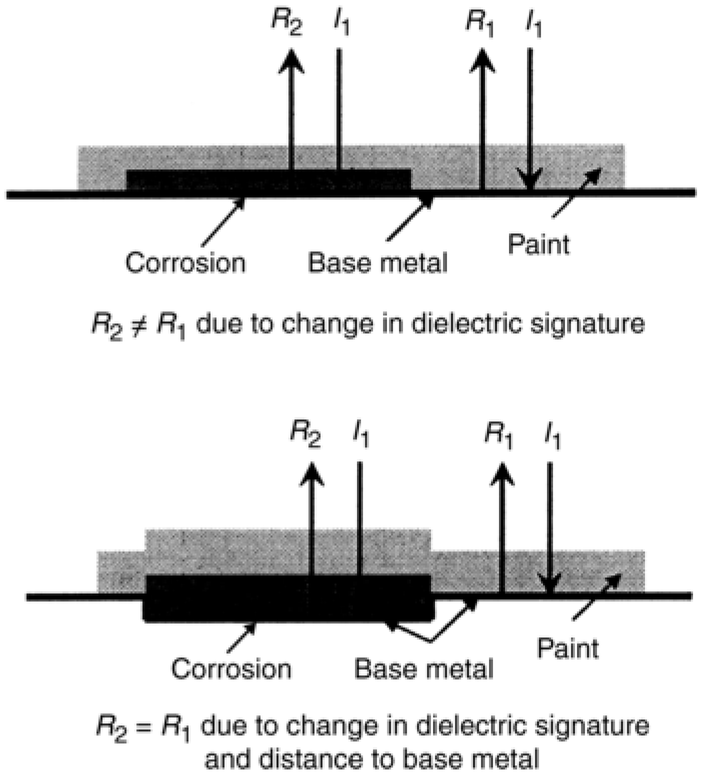

Fig. 1 The same incident signal (I_1) yields differing reflected signals (R_1 and R_2). R_1 is the return from an undamaged area, the base-line measurement. On the top, the change from R_1 to R_2 is due to the dielectric nature of the corrosion product. On the bottom the change is due to a combination of the dielectric change and a change in the transmission length.

In the microwave sensor, a three-port circulator or similar element is used to separate the incident and reflected signals. The drive signal for the microwave source is typically a continuous wave transmitter. These are low-power devices, typically under 0.5 mW; however, shielding the operator from stray microwave radiation is considered a good safety practice. Corrosion can be detected as an attenuation of the received signal relative to that for a noncorroded state.

Detecting Hidden Corrosion. Since microwaves are reflected by metals, they are not useful in inspecting under metal structures such as lap joints. Their primary use as a corrosion NDE tool is in inspecting under paints and appliqués applied to metallic substrates. Microwave NDE methods can be used to inspect deep into the material matrix of nonconducting structures such as fiberglass composites (e.g., Ref 6) for delaminations, voids, and the presence of moisture.

When scanning over a painted surface, corrosion products under the paint cause a change in the electromagnetic energy reflected back to the microwave device. It is this change that is then used to indicate the presence of corrosion (Ref 7). Microwaves are very sensitive to the presence of moisture, and this feature can be both a hindrance and a boon in NDE. Surfaces that are wet cannot be inspected without drying, yet the ability to find trapped moisture can be a valuable asset in some applications. Another scanning issue is inspection in corners and tight spots. The mechanical design used to maintain standoff control is rarely small enough to get into these tight spaces, yet these areas are a high priority in NDE because of their potential for corrosion. Special heads can be fitted to the wave guide of the device to maintain standoff control in corners, but it is difficult to include all the possible corner configurations in a single NDE device kit. In operations where the inspection geometry is constant from one unit to the next, such as inspection of a single aircraft type, a special set of heads can be developed to cover the various corners and tight spots.

In-service inspections can be done with a handheld device, and the power consumption is low enough for battery operation. Scanning speeds on a uniform surface such as an aircraft skin are surprisingly fast and are only limited by the electronic processing time. Scanning is typically done in a quick search mode that looks for any indication of degradation, and then the indicated area is inspected more carefully to ensure that it is not a false alarm and to get a rough determination of the severity and size of the corroded area.

Typical Applications. Microwave corrosion NDE applications that concentrate on inspection of the metallic substrate under coatings include shipboard painted or laminated structures (Ref 8), painted and appliquéd

aircraft skins (Ref 5), coated bridge structures (Ref 9), or any other metal component under a coating that would otherwise be difficult to inspect without removing the coating. Microwave sensors used for corrosion NDE are most often single-point devices. Focused microwave sensors have been successfully used in other applications such as inspection of fiber-reinforced plastic (FRP) jacketed concrete structures (Ref 10). Arrays of microwave sensors for inspecting large areas such as aircraft skins have potential applications, but sensor control (standoff and cant angle) can become problematic.

A spot microwave NDE sensor is a relatively simple device, and inspection rates are fast compared with those for most other NDE techniques. The reason for this is that there is very little integration time required to make a corrosion/no- corrosion decision. Scan speeds of 0.3 to 0.6 m/ s (1 to 2 ft/sec) have been reported, which is roughly the hand speed of moving a paint brush. A microwave NDE device with a 12 mm (0.5 in.) aperture can easily cover over 20 to 40 m^2 (200 to 400 ft^2) in an hour in the hands of a trained operator. Operator displays can be as simple as looking at a string of light-emitting diodes, hearing an audible alarm, or watching a meter. Even with modern digital logic built in, it is still important that an operator be able to discern the difference between changes in sensor altitude caused by rivets or seams, and changes due to corrosion. The low cost of microwave NDE sensors is attractive, but as with any NDE procedure, training is essential to ensure reliable corrosion detection.

References cited in this section

3. R. Zoughi, C. Huber, J. Easter, and K. Hayes, Microwave Detection of Surface Cracks in Metals Under Dielectric Coatings Using Open-Ended Coaxial Sensors: Preliminary Results, *ASNT, Topics on Nondestructive Evaluation Series,* Vol 2 (Jan 1998), p 53–60

4. J.A. Navarro and K. Chang, Inverted Stripline Antennas Integrated with Passive and Active Solid-State Devices, *Trans. Microwave Theory Techniques,* Vol 43 (No. 9), Sep 1995, p 2069–2065

5. A.V. Bray, H. Stretz, and S.C. Buckner, Coating Effects in Microwave NDE in the Detection of Corrosion in Aircraft, Paper 228-6200, presented in *Proc. National Association of Corrosion Engineers Symposium 2000* (Orlando, FL), NACE International, March 2000

6. J. M. Liu, Microwave Scattering for the Characterization of a Disc-Shape Void in Dielectric Materials and Composites, *Proc. of the 24th Annual Symposium on Quantitative Nondestructive Evaluation,* July 1997, p 699–703

7. N. Qaddoumi, L. Handjojo, T. Bigelow, J. Easter, A. Bray, and R. Zoughi, Microwave Corrosion Detection Using Open Ended Rectangular Waveguide Sensors, *Mater. Eval.,* Vol 58 (No. 2), February 2000, p 178–184

8. A.V. Bray, K.E. Jenne, N. Qaddoumi, J.K. Easter, T. Bigelow, and R. Zoughi, Microwave NDE Methods for Detecting Corrosion Under Paint, *Proc. of the American Society of Naval Engineers Condition Based Maintenance Symposium,* (Arlington, VA), June 1998. Available http:// www.navalengineers.org/Publications/ Pubs.html

9. R. Zoughi, Principles of and Applications of Microwave and Millimeter Wave NDE Methodologies: An Overview, *Nondestructive Evaluation of Materials and Composites,* Dec 1996, p 46–54

10. Y.J. Kim, F. Flavius, L. Jofre, and M.Q. Feng, *Proc. of the 46th Annual Society for the Advancement of Material and Process Engineering Symposium,* (Long Beach, CA), May 2001. Available http:// www.sampe.org/publicat.html#symposium

A.V. Bray, Corrosion Monitoring Using Microwave and Guided Wave Nondestructive Evaluation, *Corrosion: Fundamentals, Testing, and Protection*, Vol 13A*, ASM Handbook*, ASM International, 2003, p 529–532

Corrosion Monitoring Using Microwave and Guided Wave Nondestructive Evaluation

Alan V. Bray, Systems and Materials Research Consultancy (SMRC)

Guided Wave Ultrasonic Devices

Guided wave ultrasonic NDE methods have a loose microwave analog—the wave guide. Guided waves are generated by first flooding a structure with acoustic energy. This energy is reflected from the boundaries of the structure with small changes in frequency, and these signals constructively combine to form wave packets that travel within structure much like a wave guide. Some wave packets, or modes, can travel long distances without significant attenuation once they are formed (Ref 11), and these are the richest modes for detecting corrosion wastage. Figure 2 illustrates the manner in which GW modes are formed in a structure. There are many variations on the basic elements of GW systems of NDE; these include a wide range of frequency selection, drive pulse shapes, sensor arrays, and electronic display systems.

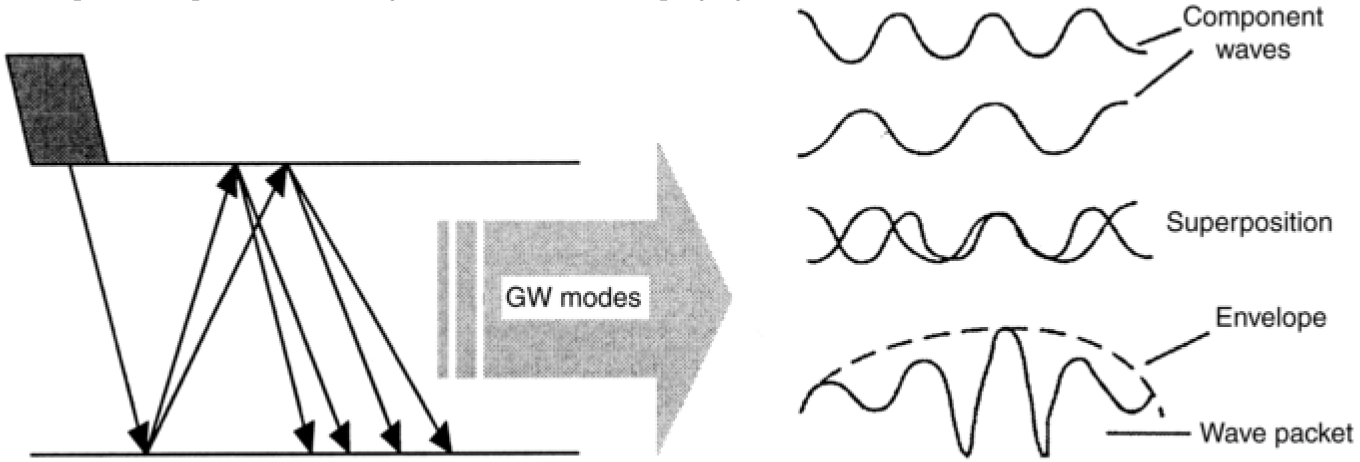

Fig. 2 The formation of a guided wave within a structure is shown on the left. Superposition of the component waves create the wave packet within the carrier envelope.

Guided waves are useful in inspection scenarios where an item is covered or encased. Examples include insulated piping, sandwiched structures such as lap joints, encapsulated pressure vessel walls, and applications such as wing icing where a guided wave is generated in the wing skin (Ref 12) and the presence of ice shows up as a change in the return signal. Guided wave NDE systematic “noise” sources include mode- coupling phenomena, array pattern dropouts or blind spots, and operator training and interpretation.

Principles of Operation. Most GW ultrasonic sensors are piezoelectric transducers in either crystalline or piezo-composite format. Guided wave transducers are driven by high- voltage (on the order of 1000 V in some applications) tone burst electronics. Detection of corrosion damage is done in pulse-echo or through-transmission modes, the latter requiring a separate receiving sensor or array. Common displays include amplitude versus time of arrival for a given frequency range. Each mode travels at a different speed, but in most inspections the frequency range is narrow enough that the time scale can be recalibrated in distance from the transducer.

Guided wave ultrasonic NDE sensors can be classified into two major designs—those that are in contact with the inspection surface and those that use standoff sensors such as electromagnetic acoustic transducers (EMATs) or laser generated/ received sound (Ref 13). Contact sensors can be used in such applications as insulated piping systems, but a section of the insulation must be removed from the transmitter and receiver sites. Electromagnetic acoustic transducers and laser devices can insert and receive sound through porous coatings up to the limiting distance for the device.

In many guided wave applications, arrays of GW sensors are driven in phase or with programmed delays for activating sensors in the array. The advantages of an array include larger cross-sectional coverage, increased distances of inspection, and the ability to tune the signal using array delay times to increase the probability of detecting corroded or cracked areas.

Detecting Hidden Corrosion. Pipe or pressure vessel wall thinning due to corrosion is a classic GW target. As the GW packets strike a thinned area, mode changes are induced that can be detected as changes in frequency content and time delay. Time delay changes result since each mode travels at a unique velocity. Mode diagrams of phase velocity versus $f \times d$, the product of frequency (f) and the dimension (d) of the "waveguide." In a pipe inspection, d is the pipe wall thickness. These mode diagrams in the frequency region of interest are an important tool in understanding inspection results. Tone burst systems are typically built on a personnel computer platform, and many of the analysis functions are programmed into the system.

The smallest defects that are detectable with NDE systems by GW method depend on the application. In pipe inspection scenarios, the lower defect limit is usually characterized as 5 to 7% of the cross-sectional area of the pipe wall (Ref 14). Since the distance of the defect from the transducer is known, it is a simple matter to pinpoint the defect location with a tape measure. This makes it an excellent tool for quickly scanning large lengths of pipe, tubing, and hidden aircraft structures to identify and locate in-service corrosion problems that can then be examined in detail with more conventional ultrasonic methods.

Typical Applications. Guided wave ultrasonic applications encompass a wide range of customized scenarios for corrosion and crack NDE. Monitoring existing structures with an array of guided wave leave-in-place (LIP) sensors is a relatively new technique (Ref 15). Small GW sensors are placed in the vicinity of a critical high stress region, and initial measurements record the state of the part at that point in time. As the part is used in service the "array" that was formed by the LIP sensors can be interrogated and compared to the initial state. This is a particularly pertinent technique for parts that have a history of failure under stress. Leave-in-place sensors for monitoring existing structures operate in the 200 KHz region. The sensors are relatively inexpensive, and they can be left in place for years.

As frequencies drop to accommodate larger structures, the GW sensor size naturally increases. In applications requiring a lower frequency approach, the sensor array is commonly moved from site to site and operated in pulse- echo mode. Trend analysis of inspection results is possible, but care must be taken to record the original array positions if time/frequency scans are to be compared over time. The pipe inspection application is an example of a low frequency GW NDE application employing this approach (Ref 16).

References cited in this section

11. D.N. Alleyne and P. Cawley, Long Range Propagation of Lamb Waves in Chemical Plant Pipework, *Mater. Eval.,* Vol 55 (No. 4), April 1997, p 504–508

12. D.D. Hongerholt, G. Willms, and J.L. Rose, "Summary of Results from an Ultrasonic In- Flight Wing Ice Detection System," presented at *American Society for Nondestructive Testing (ASNT) Quantitative Nondestructive Evaluation,* Brunswick, ME, July 2001

13. Z. Guo, J.D. Achenbach, and S. Krishnaswamy, EMAT Generation and Laser Detection of Single Lamb Wave Modes, *Proc. of the 24th Annual Symposium on Quantitative Nondestructive Evaluation,* July 1997, p 201–208

14. P.J. Mudge, "Field Application of the Teletest Long-Range Ultrasonic Testing Technique," *Insight,* Vol 43 (No 2), Feb 2001

15. J.L. Rose, and T. Hay, "New Technological Challenges in Ultrasonic Guided Wave NDE," presented at Tri-Service Corrosion Conference (San Antonio) 14–18 Jan 2002

16. A.V. Bray, L.H. Carbaugh, R.K. Austin, J.L Rose, M. Avioli, and M. Quarry, Detecting Corrosion Under Insulation In Shipboard Piping II, *Proc. of the U.S. Navy and Industry Corrosion Technology Information Exchange* (Louisville, KY), July 1999

A.V. Bray, Corrosion Monitoring Using Microwave and Guided Wave Nondestructive Evaluation, *Corrosion: Fundamentals, Testing, and Protection*, Vol 13A*, ASM Handbook*, ASM International, 2003, p 529–532

Corrosion Monitoring Using Microwave and Guided Wave Nondestructive Evaluation

Alan V. Bray, Systems and Materials Research Consultancy (SMRC)

References

1. R. Zoughi and S. Ganchev, *Microwave Nondestructive Evaluation, A State of the Art Review, NTIAC 95-01,* Nondestructive Testing Information Analysis Center. Available http://www.ntiac.com/pubs/micro.html

2. J.L. Rose, *Ultrasonic Waves in Solid Media,* Cambridge University Press, 1999

3. R. Zoughi, C. Huber, J. Easter, and K. Hayes, Microwave Detection of Surface Cracks in Metals Under Dielectric Coatings Using Open-Ended Coaxial Sensors: Preliminary Results, *ASNT, Topics on Nondestructive Evaluation Series,* Vol 2 (Jan 1998), p 53–60

4. J.A. Navarro and K. Chang, Inverted Stripline Antennas Integrated with Passive and Active Solid-State Devices, *Trans. Microwave Theory Techniques,* Vol 43 (No. 9), Sep 1995, p 2069–2065

5. A.V. Bray, H. Stretz, and S.C. Buckner, Coating Effects in Microwave NDE in the Detection of Corrosion in Aircraft, Paper 228-6200, presented in *Proc. National Association of Corrosion Engineers Symposium 2000* (Orlando, FL), NACE International, March 2000

6. J. M. Liu, Microwave Scattering for the Characterization of a Disc-Shape Void in Dielectric Materials and Composites, *Proc. of the 24th Annual Symposium on Quantitative Nondestructive Evaluation,* July 1997, p 699–703

7. N. Qaddoumi, L. Handjojo, T. Bigelow, J. Easter, A. Bray, and R. Zoughi, Microwave Corrosion Detection Using Open Ended Rectangular Waveguide Sensors, *Mater. Eval.,* Vol 58 (No. 2), February 2000, p 178–184

8. A.V. Bray, K.E. Jenne, N. Qaddoumi, J.K. Easter, T. Bigelow, and R. Zoughi, Microwave NDE Methods for Detecting Corrosion Under Paint, *Proc. of the American Society of Naval Engineers Condition Based Maintenance Symposium,* (Arlington, VA), June 1998. Available http:// www.navalengineers.org/Publications/ Pubs.html

9. R. Zoughi, Principles of and Applications of Microwave and Millimeter Wave NDE Methodologies: An Overview, *Nondestructive Evaluation of Materials and Composites,* Dec 1996, p 46–54

10. Y.J. Kim, F. Flavius, L. Jofre, and M.Q. Feng, *Proc. of the 46th Annual Society for the Advancement of Material and Process Engineering Symposium,* (Long Beach, CA), May 2001. Available http:// www.sampe.org/publicat.html#symposium

11. D.N. Alleyne and P. Cawley, Long Range Propagation of Lamb Waves in Chemical Plant Pipework, *Mater. Eval.,* Vol 55 (No. 4), April 1997, p 504–508

12. D.D. Hongerholt, G. Willms, and J.L. Rose, "Summary of Results from an Ultrasonic In- Flight Wing Ice Detection System," presented at *American Society for Nondestructive Testing (ASNT) Quantitative Nondestructive Evaluation,* Brunswick, ME, July 2001

13. Z. Guo, J.D. Achenbach, and S. Krishnaswamy, EMAT Generation and Laser Detection of Single Lamb Wave Modes, *Proc. of the 24th Annual Symposium on Quantitative Nondestructive Evaluation,* July 1997, p 201–208

14. P.J. Mudge, "Field Application of the Teletest Long-Range Ultrasonic Testing Technique," *Insight,* Vol 43 (No 2), Feb 2001

15. J.L. Rose, and T. Hay, "New Technological Challenges in Ultrasonic Guided Wave NDE," presented at Tri-Service Corrosion Conference (San Antonio) 14–18 Jan 2002

16. A.V. Bray, L.H. Carbaugh, R.K. Austin, J.L Rose, M. Avioli, and M. Quarry, Detecting Corrosion Under Insulation In Shipboard Piping II, *Proc. of the U.S. Navy and Industry Corrosion Technology Information Exchange* (Louisville, KY), July 1999

A.V. Bray, Corrosion Monitoring Using Microwave and Guided Wave Nondestructive Evaluation, *Corrosion: Fundamentals, Testing, and Protection,* Vol 13A*, ASM Handbook,* ASM International, 2003, p 529–532

Corrosion Monitoring Using Microwave and Guided Wave Nondestructive Evaluation

Alan V. Bray, Systems and Materials Research Consultancy (SMRC)

Selected References

- J.L. Rose, *Ultrasonic Waves in Solid Media,* Cambridge University Press, 1999
- R. Zoughi and S. Ganchev, *Microwave Nondestructive Evaluation, A State of the Art Review, NTIAC 95-01,* Nondestructive Testing Information Analysis Center. Available *http:/ /www.ntiac.com/*

S.W. Dean, Corrosion Monitoring for Industrial Processes, *Corrosion: Fundamentals, Testing, and Protection,* Vol 13A*, ASM Handbook,* ASM International, 2003, p 533–541

Corrosion Monitoring for Industrial Processes

Sheldon W. Dean, Dean Corrosion Technology, Inc.

Introduction

IN-SERVICE MONITORING of industrial manufacturing operations is the type of service- corrosion testing that presents the greatest challenge and for which there is a great need. In such operations, the expense of corrosion problems can be huge and the risks devastating. These expenses are summarized in the article "Direct Costs of Corrosion in the United States" in this Volume. The detailed report to the United States Congress is available (Ref 1). Corrosion monitoring has become an important aspect of the design and operation of modern industrial plants because it is one of several techniques that can be used to keep track of the degradation processes that may be occurring in an industrial operation. The most widely used application of in-service monitoring is to identify the occurrence of corrosive conditions that may be caused by unknown circumstances, such as a new catalyst that promotes corrosive chemicals formation, or a feed stock that may contain corrosive

impurities from time to time. In such circumstances, in-line monitoring can be an important tool to maintaining safe operation. Because of the high cost of installing in-line monitoring systems, and the need for regular maintenance, these systems are seldom used in well-behaved operations. In these cases, periodic inspections suffice to meet both the regulatory and management needs for a safe operation. However, in situations such as oil and gas production, where substantial variations in process fluids may occur in a relatively short time, the value of on-line monitoring is higher and can be essential to long- term safety and reliability.

This article, therefore, focuses on methods of monitoring corrosion in industrial plants. The term *monitoring,* as used in this context, includes any technique for evaluating the progress or rate of corrosion.

Reference cited in this section

1. G.H. Koch, M.P.H. Brongers, N.G. Thompson, Y.P. Virmani, and J.H. Payer, "Corrosion Cost and Preventive Strategies in the United States," FHWA-RD-01-156, Federal Highway Administration, U.S. Department of Transportation, Washington D.C., March 2002

S.W. Dean, Corrosion Monitoring for Industrial Processes, *Corrosion: Fundamentals, Testing, and Protection*, Vol 13A, *ASM Handbook*, ASM International, 2003, p 533–541

Corrosion Monitoring for Industrial Processes

Sheldon W. Dean, Dean Corrosion Technology, Inc.

Selecting a Corrosion-Monitoring Method

A large variety of techniques are available for corrosion monitoring in plant corrosion tests, and much has been written on the subject (Ref 2, 3, 4, 5, 6, 7, 8, 9, 10, 11, 12). The most widely used and simplest method of corrosion monitoring involves the exposure and evaluation of the actual test coupons (specimens). ASTM G 4 was developed to provide guidance for this type of testing (Ref 13). Additional detailed information on procedures from practical experience is given in Ref 10. Extensive overviews of some electrochemical methods of corrosion monitoring in industrial plants are given in Ref 7 and 8. ASTM G 96 (Ref 14) provides detailed information on the use of electrical and electrochemical monitoring methods. However, in view of the growing number of methods available, the selection of corrosion-monitoring methods may be somewhat arbitrary.

In the selection of a corrosion-monitoring method, a variety of factors should be considered. First, the purpose of the test should be understood by everyone concerned with the corrosion-monitoring program. The cost and applicability of the methods under consideration should be known, and it is important to consider the reliability of the method selected. In many cases, it is desirable to include more than one method in order to provide more confidence in the information generated.

Another key question is what type of access to the process streams and equipment is available. If access is available, methods that involve probes or coupons become more feasible. Otherwise, nondestructive methods may be required. An important factor in the selection of monitoring methods is the response time required to obtain the desired information from the method. Coupon methods and techniques that require plant shutdown for installation and retrieval of specimens tend to be relatively slow in generating information. On the other hand, equipment that measures instantaneous corrosion rates can provide rapid results, but often with a reduction in accuracy. A most important consideration is safety. In an operating plant, equipment failure can lead to a leak, which can result in loss of product, a hazard potential, and possible shutdown of the plant. It is important for the monitoring apparatus to be designed to minimize the possibility of such an incident and to have a plan in place to safely deal with any leak that might develop.

References cited in this section

2. C.P. Dillon, A.S. Krisher, and H. Wissenberg, Plant Corrosion Tests, *Handbook on Corrosion Testing and Evaluation,* W.H. Ailor, Ed., John Wiley & Sons, 1971, p 599–615

3. A.S. Couper, Methods in Oil-Refining Industries, *Handbook on Corrosion Testing and Evaluation,* W.H. Ailor, Ed., John Wiley & Sons, 1971, p 617–624

4. "Laboratory Corrosion Testing of Metals for the Process Industries," NACE TM-01-69, National Association of Corrosion Engineers, 1976

5. J.N. Wanklyn, *Corrosion Monitoring in the Oil and Petrochemical and Process Industries,* J. Wanklyn, Ed., Oyez Scientific and Technical Service Ltd., 1982

6. *Corrosion Monitoring in Industrial Plants Using Nondestructive Testing and Electrochemical Methods,* STP 908, G.C. Moran and P. Labine, Ed., American Society for Testing and Materials, 1986

7. S.W. Dean, Overview of Corrosion Monitoring in Modern Industrial Plants, *Corrosion Monitoring in Industrial Plants Using Nondestructive Testing and Electrochemical Methods,* STP 908, G.C. Moran and P. Labine, Ed., American Society for Testing and Materials, 1986, p 197–220

8. S.W. Dean, Electrochemical Methods for Corrosion Testing in the Process Industries, *Electrochemical Corrosion Testing with Special Consideration of Practical Applications,* E. Heintz, J.C. Rowlands, and F. Mansfeld, Ed., Proceedings of International Workshop, (Ferrara, Italy), DECHEMA, 1986, p 1–15

9. *Process Industries Corrosion—Theory and Practice,* National Association of Corrosion Engineers, 1986

10. B.J. Moniz, Field Coupon Corrosion Testing, *Process Industries Corrosion—Theory and Practice,* National Association of Corrosion Engineers, 1986

11. S.J. Pikul, T.S. Lee, and D.B. Anderson, "Field Corrosion Tests for Materials Evaluation in Chemical Process Industries," Paper 119, presented at Corrosion/86, National Association of Corrosion Engineers, 1986

12. A. Perkins, Industrial Applications, *Corrosion Tests and Standards,* Manual 20, ASTM International, 1995, p 143–148

13. "Standard Method for Conducting Corrosion Coupon Tests in Plant Equipment," G 4, *Annual Book of ASTM Standards,* Vol 03.02, ASTM International

14. "Standard Guide for On-Line Monitoring of Corrosion in Plant Equipment (Electrical and Electrochemical Methods)," G 96, *Annual Book of ASTM Standards,* Vol 03.02, ASTM International

---

S.W. Dean, Corrosion Monitoring for Industrial Processes, *Corrosion: Fundamentals, Testing, and Protection*, Vol 13A, *ASM Handbook*, ASM International, 2003, p 533–541

Corrosion Monitoring for Industrial Processes

Sheldon W. Dean, Dean Corrosion Technology, Inc.

Direct Testing of Coupons

Although they are not intended to replace laboratory tests, plant coupon tests usually are designed to monitor the damage rate occurring on existing equipment, to evaluate alternative materials of construction, and sometimes to determine the effects of process conditions that cannot be reproduced in the laboratory.

Advantages of Coupon Testing (Ref 10). Plant coupon testing provides several specific advantages over laboratory coupon testing. A large number of materials can be exposed simultaneously and can be ranked in actual process streams with actual process conditions. Testing can be used to monitor the corrosivity of process streams. The coupons can be designed for specific forms of corrosion, but the exposure time is usually determined by the plant operation.

Large Number of Coupons. Because many coupons can be exposed simultaneously, they can be tested in duplicate or triplicate (to measure scatter), and they can be fabricated to simulate such conditions as welding, residual stresses, or crevices. These variations can provide the engineer with increased confidence in selecting materials for new equipment, maintenance, or repair.

Actual process streams reveal the synergistic effects of combinations of chemicals or contaminants. In addition, the possibility is remote that the corrosion of specific coupons contaminates the process and affects the corrosion resistance of other coupons. However, one potential source of error that must be checked is contamination of the process stream by the corrosion of the existing equipment.

For example, in a hypothetical case, the equipment is fabricated from a nickel-base alloy, and the process is a reducing acid. Contamination of the process by nickel ions may result in an apparent improvement in the corrosion resistance of titanium test coupons. If the existing equipment is then replaced with titanium, based on these misleading test results, it may corrode rapidly without the beneficial effect of the nickel ions.

Monitoring of Inhibitor Programs. Coupons often are used to monitor inhibitor programs in, for example, water treatment or refinery overhead streams. With retractable coupon holders, the coupons can be extracted from the process without having to shut down in order to determine the corrosion rate.

Long Exposure Times. Some forms of localized corrosion, such as crevice corrosion, pitting, and stress-corrosion cracking (SCC), require time to initiate. To increase confidence in the test results, coupons can be exposed for as long as necessary to ensure that the initiation time has been exceeded.

Coupon design can be selected to test for specific forms of corrosion. Coupons can be designed to detect such phenomena as crevice corrosion, pitting, and dealloying corrosion. For example, some pulp mill bleach plant washer drums are protected electrochemically to mitigate crevice corrosion. Specifically designed crevice-corrosion test coupons are used to monitor the effectiveness of the electrochemical protection program. These coupons are removed periodically from the equipment and examined for evidence of crevice corrosion.

Disadvantages of Coupon Testing (Ref 10). Coupon testing has four main limitations:

- Coupon testing cannot be used to detect rapid changes in the corrosivity of a process.
- Localized corrosion cannot be guaranteed to initiate before the coupons are removed— even with extended test durations.
- Corrosion rate calculated from coupons may not reflect the corrosion of the plant equipment because of factors such as multiphase flow, where the aqueous phase is much more corrosive than the organic or vapor phase, or turbulence from mixers, elbows, valves, pumps, and other items that accelerate the corrosion in a specific location in the equipment removed from where the coupons were exposed.
- Coupons may be misleading in situations where the corrosion rate varies significantly over time because of unrealized process factors.

Contamination of the process fluid is an issue that must be addressed in the food, medical, and electronic equipment manufacturing industries, if coupons are introduced.

Rapid Changes in Corrosivity. The corrosion rate calculated from a coupon is an average over a specific period of time. Therefore, field coupon testing cannot detect process upsets as they occur. For real-time monitoring, electrochemical methods, such as the polarization-resistance technique, may be more appropriate (see the section “Polarization-Resistance Measurement” in this article).

Corrosion Rates of Coupons Compared with That of Equipment. The corrosion rate of plant equipment seldom equals that calculated on a matching test coupon because it is almost impossible to duplicate the equipment exposure with a coupon exposure. However, coupons are very helpful in many situations because they provide a clear view of the corrosion damage with information on the development of deposits, films, and localized

attack. In addition, coupon testing is probably the least complicated type of in-service testing and, consequently, requires the least operator skill.
Corrosion Forms Not Detected. The principal limitation of coupon testing is the simulation of erosion-corrosion and heat-transfer effects. Careful placement of the coupons in the process equipment can slightly offset these weaknesses.
Erosion-corrosion is related to process turbulence, and process turbulence is often a function of equipment design. Because coupons tend to shield one another from the effects of process turbulence, field coupon testing is not reliable as a method of simulating erosion-corrosion.
For heat-transfer effects, specially designed coupons are required that simulate effects such as those found in heating elements or condenser tubes. Coupons range in design from thermowell-shaped devices to sample tubes in a test heat exchanger. Thermowell-shaped devices are heated or cooled on the inside and project into the process stream (Ref 13). Heat-transfer tests can also be conducted in the laboratory. In this environment, the coupon forms part of the wall of the test vessel and can therefore be heated or cooled from one side. Because of the cost involved, heat-transfer coupon tests are usually carried out on only one (or perhaps two) alloys that have been selected from a larger group.
Coupon Options (Ref 10). The design of the coupon is an important part of any plant corrosion-testing program. Proper selection of the coupon shape, surface finish, metallurgical condition, and geometry allows evaluation of specific forms of corrosion.
Uniform Corrosion Coupons. The most common coupon shape for the evaluation of uniform corrosion is rectangular. Circular shapes are also used. Rectangular coupons are the most common because most alloys are available in plate or sheet form. Other shapes are used when there are restrictions on available product forms or when a specific material condition is required. Coupon identification must be legible and permanent. The simplest, and preferred, method of identification is stencil stamping.
Coupon finish represents a significant contribution to the overall cost. The least expensive finish that is consistent with the test requirements should be selected. For example, an inexpensive surface finish is acceptable where carbon steel coupons are used routinely to monitor additions of inhibitor in water treatment programs. This may be achieved by punching or shearing, followed by glass bead blasting. On the other hand, when it is necessary to rank alloys in a process environment, the coupons must be finished with ground or machined parallel edges and sanded faces.
A wide variety of coupon finishes are available, including:

- Mill finish
- Glass bead blasted
- Sandblasted
- Steel shotblasted
- Abrasive cloth or paper sanded
- Machined
- Electrolytically polished

Ideally, the surface finish of the coupon should match the finish of the equipment. This match is very difficult to achieve for several reasons. For example, there is the difference in surface finish between different mill product forms and even between different heats of the same metal or alloy. In addition, there can be wide variation among mill scale and surface deposits from processing operations. The principal requirement of testing is to assess the corrosion resistance of the test alloy in the condition that would be used in actual equipment.
Abrasive cloth or paper sanding is the most common practice of surface preparation. Sanding removes such surface deposits as mill scale and such defects as scratches or pits. A 120-grit finish, which is standard, can be produced easily without specialized equipment. Metallurgical changes that are heat induced, such as the sensitization of stainless steels or nickel-base alloys, can be prevented by keeping the coupon cool through wet sanding with progressively finer abrasives.
Clean polishing belts should be used to avoid contamination of the coupon surface. For example, a belt that has been used to polish a brass coupon should not be used to polish an aluminum coupon.
The corrosion resistance of some alloys can be enhanced by a special surface condition, for example, the oxide films that are formed on titanium or zirconium. For these alloys, conditioning of the coupons would take place

after mechanical surface preparation. However, some films that form during mill processing or chemical exposure actually reduce corrosion resistance. Certain forms of iron sulfide on carbon steel are examples of these types of films. The coupons must be specially treated in such cases.

Coupons that are cut by punching or shearing have cold-worked edges. The effects of cold work extend back from the cut edge a distance equal to the material thickness. These affected areas can be removed by grinding or machining. Cold-worked edges may affect the corrosion rate in some cases, and the residual stresses it induces may cause SCC in some materials. Extensive edge preparation can be a major contributor to the cost of the coupon.

Galvanic-Corrosion Coupons. Pairs of test coupons are coupled electrically to study the effects of galvanic corrosion. The relative areas exposed usually vary from 1:1 to 10:1 or greater. The area ratios should be reversed for complete assessment, that is, 10:1 and 1:10. This reversal may not be necessary when a specific effect is being studied, for example, simulation of the galvanic corrosion of dissimilar-metal fasteners in column trays.

A major concern with electrically coupled coupons is maintaining electrical continuity for the entire exposure period. Corrosion product films can wedge mechanically joined coupons apart, thereby eliminating the electrical contact and any galvanic corrosion effect. ASTM G 71 (Ref 15) provides valuable information on galvanic corrosion testing in both field and laboratory environments.

With metals that can become embrittled by hydrogen absorption—for example, titanium, zirconium, tantalum, and hardenable steels—the cathodic (protected) member of the galvanic couple may be subject to the greater damage. However, the typical mass-loss measurements would not reveal such damage.

Crevice-Corrosion Coupons. Equipment crevices, such as weld backing rings, tube-tubesheet joints, or flanged connections, are common sites for localized corrosion in the process environment. Many metals perform differently in crevices as opposed to unshielded areas. Behavior is dependent on several factors. These factors include how strongly oxygen reduction (cathode depolarization) controls the cathode reaction or how the crevice alters the bulk process chemistry by lowering the pH or concentrating aggressive species.

The most imaginative form of coupon-corrosion testing is the simulation of crevice corrosion (Ref 16). The various techniques that can be used for crevice-corrosion testing include rubber bands, spot-welded lap joints, and wire wrapped around threaded bolts. Each crevice test creates a particular crevice geometry between specific materials and has a particular anode/cathode area ratio. Thus, no crevice-corrosion test is universally applicable (see the article “Evaluating Crevice Corrosion” in this Volume).

The two most widely used crevice geometries in field coupon testing employ insulating spacers to separate and electrically insulate the coupons. Spacers are usually either flat washers or multiple-crevice washers. Either type of spacer can be made of materials ranging from hard ceramics to soft thermoplastic resins (Ref 17).

ASTM G 78 (Ref 17) and G 48 (Ref 18) provide valuable information on crevice corrosion specimen design and should be consulted before attempting a crevice-corrosion test.

Stress-Corrosion Coupons. Typical sources of sustained tensile stress that cause SCC of equipment in service are the residual stresses resulting from forming and welding operations and the assembly stresses associated with interference-fitted parts, especially in the case of tapered, threaded connections. Therefore, the most suitable coupons for plant tests are the self-stressed bending and residual-stress specimens described in the article “Evaluating Stress-Corrosion Cracking” in this Volume. Convenient coupons are the cup impression, U-bend (Ref 19), C-ring (Ref 20), tuning fork, and welded panel (Ref 21). The method of stressing for all of these coupons results in decreasing load as cracks form and begin to propagate. Therefore, complete fracture is seldom observed, and careful examination is required to detect cracking.

Welded Coupons. Because welding is a principal method of fabricating equipment, the use of welded coupons is often desirable. Aside from the effects of residual stresses, the primary concern is the behavior of the weld bead and the heat-affected zone (HAZ). In some alloys, the HAZ becomes sensitized to severe intergranular (sometimes called knife-line) attack, and in certain other alloys, the HAZ is anodic to the parent metal. When possible, it is more realistic to remove welded coupons from production-sized weldments than to weld the small coupons. Because the thermal conditions in both the weld metal and the HAZ are a function of the number of weld passes, the metal thickness, the weld position, and the welding technique, it is not usually considered good practice to use welded coupons to assess the possibility of sensitization from welding. It is generally better to carry out a sensitizing heat treatment on an unwelded coupon before it is tested and then look for evidence of intergranular corrosion or cracking.

Sensitized Metal. Sensitization is a metallurgical change that occurs when certain austenitic stainless steels, ferritic stainless steels, nickel- base alloys, and other alloys are heated under specific conditions. This results in the precipitation of carbides or other intermetallic phases at grain boundaries, which reduces corrosion resistance. Any heat-inducing process (for example, stress relief of weldments) may cause sensitization, which is time and temperature dependent. There is a specific temperature range over which each particular alloy sensitizes rapidly. Sensitization leads to intergranular corrosion in specific environments.

Welding is the most common cause of sensitization. However, welded coupons may not exhibit sensitization because they may be given insufficient weld passes (compared with actual process equipment). As a result, they spend insufficient time in the sensitizing temperature range, and susceptibility to intergranular corrosion may not be detected.

An appropriate sensitizing heat treatment guarantees that any corrosion susceptibility induced by welding or heat treatment is detected. The optimal temperature and time ranges for sensitization vary for different alloys. For example, 30 min at 650 °C (1200 °F) is usually sufficient to sensitize American Iron and Steel Institute (AISI) type 316 stainless steel.

Some of the corrosion-resistant aluminum- magnesium (5000-series) alloys containing 3 to 6% Mg are also subject to sensitization when heated at temperatures in the range of 65 to 175 °C (150 to 350 °F). Reference 22 describes a test method for susceptibility to this phenomenon. The effective time and temperature conditions depend on the alloy content and metallurgical condition (Ref 23).

The advantage of using sensitized coupons is that, if corrosion occurs, they indicate a potential problem. The user is thus obliged to consider how the equipment will be welded and heat treated and to determine whether high-temperature excursions will occur during operation.

Test Rack Design. It may be possible to expose corrosion coupons in stagnant or slowly flowing conditions by simply hanging them on an insulated wire or plastic cord, but this procedure is generally inadequate. Instead, specimen holders and test racks are usually used to support and insulate the coupons. These racks must hold coupons firmly in place to prevent mechanical damage and metal loss from causes other than corrosion. They must also electrically isolate the coupons from contact with each other and from the vessel itself to prevent unintentional electrochemical interactions. The basic types of racks are discussed briefly as follows. They are described in detail in Ref 2, 5, 10, and 12.

Spool (Birdcage) Rack. A typical spool rack is useful in open vessels, such as reactors and tanks, for which access to the spool is readily achieved (Fig. 1). It has the advantage that a relatively large number of coupons can be accommodated.

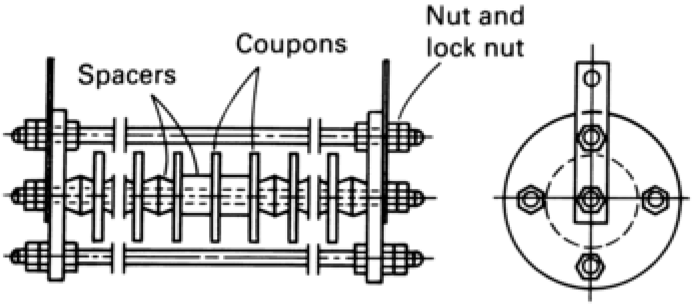

Fig. 1 Illustration of typical spool-type coupon rack. Source: Ref 13

The insert rack is convenient for use in pipes or other units that have flanged connections that allow easy access to the system. For larger-diameter pipes or nozzles, a dutchman-type rack can be used. Such a rack consists of a suitable spool-type piece with the coupons mounted crosswise on a bar (Fig. 2). In both cases, the equipment must be shut down during installation and removal of the racks, or a by-pass line added to the system that allows the process fluid to be routed around the specimens while they are being inserted or removed. It is very important to have good-quality shut-off valves and drain and flush provisions if a bypass is to be used.

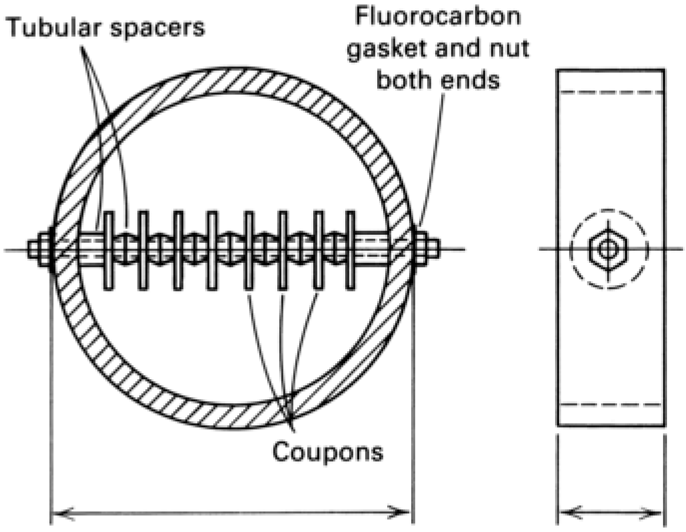

Fig. 2 Illustration of typical dutchman coupon rack. Source: Ref 13

A slip-in rack is designed to be inserted into and removed from equipment that is in operation. A retractable coupon holder makes this type of rack especially useful (Fig. 3). The slip-in rack requires a full-port gate valve and a suitable- sized nozzle to serve as a retraction chamber. A rod-shaped coupon holder is contained in the retraction chamber, which is flanged to the gate valve. The other end of the retraction chamber contains a packing gland through which the coupon holder passes. Coupons are mounted on the rod in the extended position and are then drawn into the retraction chamber. The chamber is bolted to the gate valve, which is then opened to allow the coupons to be slid into the process stream. The sequence is reversed to remove the test coupons. It is essential that the rod or handle be equipped with a restraining chain or other device to prevent the blowout of the specimen holder when retracting the specimens when the system is under pressure. Drain and flush ports are desirable additions to deal with the process fluid that is present in the retraction chamber before the specimens are removed. These ports are also useful to eliminate intrusion of air into the process fluid during insertion of the coupons.

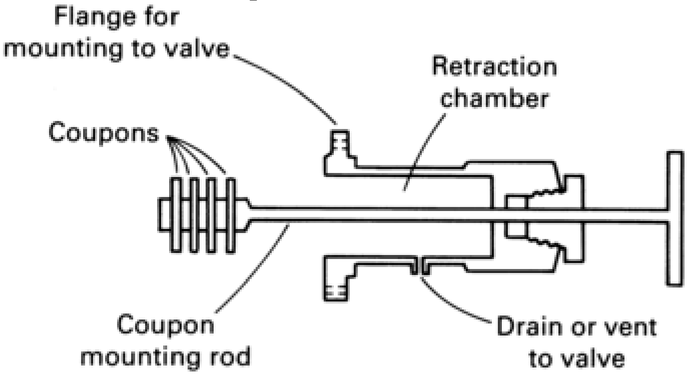

Fig. 3 Illustration of retractable coupon holder. Source: Ref 10

Coupon Cleaning and Evaluation. The test coupons should be cleaned as soon as possible after removal from the test. The procedures for cleaning and weighing, which depend on the test material and the extent of corrosion, are described in Ref 4, 10, and 24. These methods are overviewed in the article “Statistical Interpretation of Corrosion Test Results” in this Volume.

Examination of the coupons after cleaning and weighing reveals the forms of corrosion that may be expected in equipment made of the coupon material. Because the coupons used for calculating corrosion rates are usually small, they should be examined very carefully for signs of localized corrosion effects that could invalidate the mass- loss data. Coupons are examined with the unaided eye and then at increasing magnifications, up to 30 to 50×, with a binocular microscope. The scanning electron microscope is an extremely useful tool for detecting superficial localized effects.

In some cases, coupons must be bent and/or sectioned and metallographically examined to reveal certain types of corrosion damage. There are special localized corrosion effects that could not only jeopardize determination

of realistic corrosion rates but also signal other serious types of behavior. These effects include edge attack, crevice corrosion, stress corrosion near stenciled identification numbers, pitting, selective corrosion (such as dealloying), knife-line attack, blistering, intergranular corrosion, embrittlement, and erosion-corrosion. In addition to the various corrosion effects, there may be inadvertent mechanical or galvanic corrosion damage. Techniques for evaluating specific forms of corrosion are described in various articles in this Section.

References cited in this section

2. C.P. Dillon, A.S. Krisher, and H. Wissenberg, Plant Corrosion Tests, *Handbook on Corrosion Testing and Evaluation,* W.H. Ailor, Ed., John Wiley & Sons, 1971, p 599–615

4. "Laboratory Corrosion Testing of Metals for the Process Industries," NACE TM-01-69, National Association of Corrosion Engineers, 1976

5. J.N. Wanklyn, *Corrosion Monitoring in the Oil and Petrochemical and Process Industries,* J. Wanklyn, Ed., Oyez Scientific and Technical Service Ltd., 1982

10. B.J. Moniz, Field Coupon Corrosion Testing, *Process Industries Corrosion—Theory and Practice,* National Association of Corrosion Engineers, 1986

12. A. Perkins, Industrial Applications, *Corrosion Tests and Standards,* Manual 20, ASTM International, 1995, p 143–148

13. "Standard Method for Conducting Corrosion Coupon Tests in Plant Equipment," G 4, *Annual Book of ASTM Standards,* Vol 03.02, ASTM International

15. "Standard Guide for Conducting and Evaluating Galvanic Corrosion Tests in Electrolytes," G 71, *Annual Book of ASTM Standards,* Vol 03.02, ASTM International

16. W.D. France, Jr., Crevice Corrosion of Metals, *Localized Corrosion—Cause of Metal Failure,* STP 519, M. Henthorne, Ed., American Society for Testing and Materials, 1972, p 164–200

17. "Standard Guide for Crevice Corrosion Testing of Iron-Base and Nickel-Base Stainless Alloys in Seawater and Other Chloride- Containing Aqueous Environments," G 78, *Annual Book of ASTM Standards,* Vol 03.02, ASTM International

18. "Standard Test Methods for Pitting and Crevice Corrosion Resistance of Stainless Steels and Related Alloys by Use of Ferric Chloride Solution," G 48, *Annual Book of ASTM Standards,* Vol 03.02, ASTM International

19. "Standard Practice for Making and Using U- Bend Stress-Corrosion Test Specimens," G 30, *Annual Book of ASTM Standards,* Vol 03.02, ASTM International

20. "Standard Practice for Making and Using C- Ring Stress-Corrosion Test Specimens," G 38, *Annual Book of ASTM Standards,* Vol 0302, ASTM International

21. "Standard Practice for Preparation of Stress- Corrosion Test Specimens for Weldments," G 58, *Annual Book of ASTM Standards,* Vol 03.02, ASTM International

22. "Standard Practice for Determining the Susceptibility to Intergranular Corrosion of 5*xxx* Series Aluminum Alloys by Weight Loss After Exposure to Nitric Acid (NAWLT Test)," G 67, *Annual Book of ASTM Standards,* American Society for Testing and Materials

23. E.H. Dix, Jr., W.A. Anderson, and M.B. Shumaker, Influence of Service Temperature on the Resistance of Wrought Aluminum-Magnesium Alloys to Corrosion, *Corrosion,* Vol 15 (No. 2), 1959, p 55t–62t

24. "Standard Practice for Preparing, Cleaning, and Evaluating Corrosion Test Specimens," G 1, *Annual Book of ASTM Standards,* Vol 03.02, ASTM International

---

S.W. Dean, Corrosion Monitoring for Industrial Processes, *Corrosion: Fundamentals, Testing, and Protection*, Vol 13A, *ASM Handbook*, ASM International, 2003, p 533–541

Corrosion Monitoring for Industrial Processes

Sheldon W. Dean, Dean Corrosion Technology, Inc.

Electrical-Resistance Probes

Electrical-resistance probes (Fig. 4) are specially designed corrosion coupons; see ASTM G 96, method A (Ref 14). Their corrosion rate is calculated from measurement of electrical resistance rather than mass loss. These measurements are made by installing a wire or other device fabricated from the material in question in such a way that its electrical resistance can be conveniently measured. Corrosion reduces the cross section of the exposed element; therefore, its electrical resistance increases with exposure time, if corrosion is taking place. A temperature- compensating element should be incorporated in such a probe because the resistance of the probe is also influenced by the temperature.

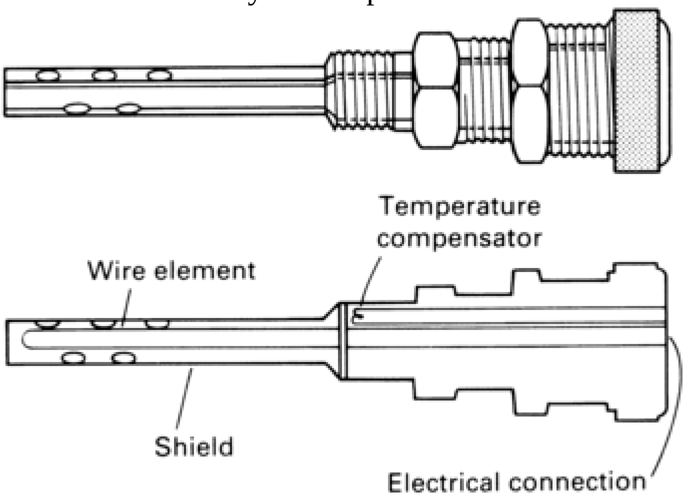

Fig. 4 Electrical-resistance probe. Source: Ref 7

When installing the probe, if galvanic corrosion is a concern, the probe should be tested for electrical isolation with adjacent metallic materials.

Electrical-resistance probes measure the remaining average metal thickness. To obtain the corrosion rate, a series of measurements are made over a period of time, and the results are plotted as a function of exposure time. The corrosion rate can be determined from the slope of the resulting plot.

There are several advantages to this approach. Because probes are relatively small, they can be installed easily. To determine the metal remaining, the probe can be wired directly to a control room location or to a portable resistance bridge at the probe location. For systems that are wired directly to control rooms, a computer system can be used to obtain the data and to reduce the results to corrosion rate values. Commercial electrical-resistance equipment is available. Use of electrical-resistance probes does not depend on the environment; there are two reasons for this. First, only the remaining metal is measured, and second, the conductivity of the corrosive environment is usually inconsequential. This is not true in, for example, molten salts or liquid metals;

the high conductivity of the environment in such systems precludes the use of electrical-resistance probes. Thus, no problems exist in measuring corrosion that occurs in liquid or vapor streams. Electrical-resistance probes are used in various applications, such as monitoring the corrosivity of cooling water systems (Ref 14).

However, there are some disadvantages to this approach. Vessel and piping walls must be penetrated in order to install the probes; such penetration results in the potential for leaks. It is expensive to direct wire the probe to a control room location, and such work must be carried out with care to avoid spurious signals and errors. On the other hand, it is time consuming and sometimes impossible to take measurements at the probe site with a portable bridge. The temperature-compensation device reacts slowly, and it can be a source of error if the temperature varies when the measurement is taken. Corrosion- rate measurements obtained in short periods of time can be inaccurate, because the method measures only the remaining metal, not the rate of attack; thus, the errors involved in estimating small differences between large numbers make this method inaccurate. This method provides no practical information on localized attack.

It is also very important to select the correct type of probe for the application. Cylindrical probes or wires may not detect corrosion of a pipe wall from a thin film of liquid on the pipe wall resulting from annular two-phase flow. A flush-mounted probe must be used in this case. Another major problem is finding leak-tight insulators that have sufficient corrosion resistance to the process fluids encountered. In some cases, it has been necessary to weld a nozzle with a flange over the external connection so that the area could be closed tightly if a leak developed during operation.

References cited in this section

7. S.W. Dean, Overview of Corrosion Monitoring in Modern Industrial Plants, *Corrosion Monitoring in Industrial Plants Using Nondestructive Testing and Electrochemical Methods*, STP 908, G.C. Moran and P. Labine, Ed., American Society for Testing and Materials, 1986, p 197–220

14. "Standard Guide for On-Line Monitoring of Corrosion in Plant Equipment (Electrical and Electrochemical Methods)," G 96, *Annual Book of ASTM Standards,* Vol 03.02, ASTM International

---

S.W. Dean, Corrosion Monitoring for Industrial Processes, *Corrosion: Fundamentals, Testing, and Protection*, Vol 13A, *ASM Handbook*, ASM International, 2003, p 533–541

Corrosion Monitoring for Industrial Processes

Sheldon W. Dean, Dean Corrosion Technology, Inc.

Ultrasonic Thickness Measurements

Ultrasonic thickness measurements can be used to monitor corrosion rates in situ. Ultrasonic thickness measurements involve placement of a transducer against the exterior of the vessel in question. The transducer produces an ultrasonic signal. This signal passes through the vessel wall, bounces off the interior surface, and returns to the transducer. The thickness is calculated by using the time that elapses between emission of the signal and its subsequent reception, along with the velocity of sound in the material. To obtain a corrosion rate, a series of measurements must be made over a time interval, and the metal loss per unit time must be determined.

One advantage of this method is that it is not necessary to penetrate the vessel to make the measurements. In addition, the results are obtained in terms of thickness. Small, handheld probes and reading devices are available for making these measurements and are relatively easy to use.

There are also several disadvantages. Ideally, a bare metal surface free of paint, thermal insulation, and corrosion products must be exposed. A coupling agent, such as grease, petroleum jelly, or oil, must be used so that the signal can pass from the probe into the metal and return. Problems may arise when vessel walls are at

high or low temperatures. Serious problems may exist in equipment that has a metallurgically bonded internal lining, because it is not obvious from which surface the returning signal originates.

Despite these drawbacks, the ultrasonic thickness approach is widely practiced where it is necessary to evaluate vessel life and suitability for further service. It must be kept in mind, however, that depending on the type of transducer used, the ultrasonic thickness method can overestimate metal thickness when the remaining thickness is under approximately 1.3 mm (0.05 in.).

S.W. Dean, Corrosion Monitoring for Industrial Processes, *Corrosion: Fundamentals, Testing, and Protection*, Vol 13A, *ASM Handbook*, ASM International, 2003, p 533–541

Corrosion Monitoring for Industrial Processes

Sheldon W. Dean, Dean Corrosion Technology, Inc.

Ultrasonic Thickness Measurements

Ultrasonic thickness measurements can be used to monitor corrosion rates in situ. Ultrasonic thickness measurements involve placement of a transducer against the exterior of the vessel in question. The transducer produces an ultrasonic signal. This signal passes through the vessel wall, bounces off the interior surface, and returns to the transducer. The thickness is calculated by using the time that elapses between emission of the signal and its subsequent reception, along with the velocity of sound in the material. To obtain a corrosion rate, a series of measurements must be made over a time interval, and the metal loss per unit time must be determined.

One advantage of this method is that it is not necessary to penetrate the vessel to make the measurements. In addition, the results are obtained in terms of thickness. Small, handheld probes and reading devices are available for making these measurements and are relatively easy to use.

There are also several disadvantages. Ideally, a bare metal surface free of paint, thermal insulation, and corrosion products must be exposed. A coupling agent, such as grease, petroleum jelly, or oil, must be used so that the signal can pass from the probe into the metal and return. Problems may arise when vessel walls are at high or low temperatures. Serious problems may exist in equipment that has a metallurgically bonded internal lining, because it is not obvious from which surface the returning signal originates.

Despite these drawbacks, the ultrasonic thickness approach is widely practiced where it is necessary to evaluate vessel life and suitability for further service. It must be kept in mind, however, that depending on the type of transducer used, the ultrasonic thickness method can overestimate metal thickness when the remaining thickness is under approximately 1.3 mm (0.05 in.).

S.W. Dean, Corrosion Monitoring for Industrial Processes, *Corrosion: Fundamentals, Testing, and Protection*, Vol 13A, *ASM Handbook*, ASM International, 2003, p 533–541

Corrosion Monitoring for Industrial Processes

Sheldon W. Dean, Dean Corrosion Technology, Inc.

Measurement of Corrosion Potentials

The use of corrosion-potential measurements for in-service corrosion monitoring is not as widespread as the use of polarization resistance. However, this approach can be valuable in some cases, particularly where an alloy could show both active and passive corrosion behavior in a given process stream. For example, stainless steels

can provide excellent service, as long as they remain passive. However, if an upset occurs that would introduce either chlorides or reducing agents into the process stream, stainless alloys may become active and may exhibit excessive corrosion rates. Corrosion-potential measurements would indicate the development of active corrosion, and they may be coupled with polarization-resistance measurements as additional confirmation of high corrosion rates (Ref 8).

The success of corrosion-potential measurements depends on the long-term stable performance of a standard reference electrode. Such electrodes have been developed for continuous pH monitoring of process streams, and their application for measuring corrosion potentials is straightforward. However, the conditions of temperature, pressure, electrolyte composition, pH, and other possible variables can limit the applications of these electrodes for corrosion-monitoring service.

Reference cited in this section

8. S.W. Dean, Electrochemical Methods for Corrosion Testing in the Process Industries, *Electrochemical Corrosion Testing with Special Consideration of Practical Applications,* E. Heintz, J.C. Rowlands, and F. Mansfeld, Ed., Proceedings of International Workshop, (Ferrara, Italy), DECHEMA, 1986, p 1–15

S.W. Dean, Corrosion Monitoring for Industrial Processes, *Corrosion: Fundamentals, Testing, and Protection*, Vol 13A, *ASM Handbook*, ASM International, 2003, p 533–541

Corrosion Monitoring for Industrial Processes

Sheldon W. Dean, Dean Corrosion Technology, Inc.

Measurement of Corrosion Potentials

The use of corrosion-potential measurements for in-service corrosion monitoring is not as widespread as the use of polarization resistance. However, this approach can be valuable in some cases, particularly where an alloy could show both active and passive corrosion behavior in a given process stream. For example, stainless steels can provide excellent service, as long as they remain passive. However, if an upset occurs that would introduce either chlorides or reducing agents into the process stream, stainless alloys may become active and may exhibit excessive corrosion rates. Corrosion-potential measurements would indicate the development of active corrosion, and they may be coupled with polarization-resistance measurements as additional confirmation of high corrosion rates (Ref 8).

The success of corrosion-potential measurements depends on the long-term stable performance of a standard reference electrode. Such electrodes have been developed for continuous pH monitoring of process streams, and their application for measuring corrosion potentials is straightforward. However, the conditions of temperature, pressure, electrolyte composition, pH, and other possible variables can limit the applications of these electrodes for corrosion-monitoring service.

Reference cited in this section

8. S.W. Dean, Electrochemical Methods for Corrosion Testing in the Process Industries, *Electrochemical Corrosion Testing with Special Consideration of Practical Applications,* E. Heintz, J.C. Rowlands, and F. Mansfeld, Ed., Proceedings of International Workshop, (Ferrara, Italy), DECHEMA, 1986, p 1–15

S.W. Dean, Corrosion Monitoring for Industrial Processes, *Corrosion: Fundamentals, Testing, and Protection*, Vol 13A, *ASM Handbook*, ASM International, 2003, p 533–541

Corrosion Monitoring for Industrial Processes

Sheldon W. Dean, Dean Corrosion Technology, Inc.

Alternating Current Impedance Measurements

Alternating current (ac) impedance-polarizing techniques are being increasingly used in electrochemical evaluation. In principle, the same probe elements used for polarization-resistance measurements can be used for ac impedance studies. As shown in Fig. 6, the ac impedance approach permits the separation and independent analysis of the resistive and capacitive elements of the electrochemical corrosion reaction (Ref 26). The method is particularly useful for high- resistivity electrolytes, such as steam condensate. In these cases, polarization-resistance measurements provide readings that are erroneously low, because the bulk resistance of the electrochemical cell adds to the measured resistance. This problem is minimized with the ac approach. ASTM G 96 (Ref 14) provides a very comprehensive discussion of this problem and gives practical guidance on dealing with it.

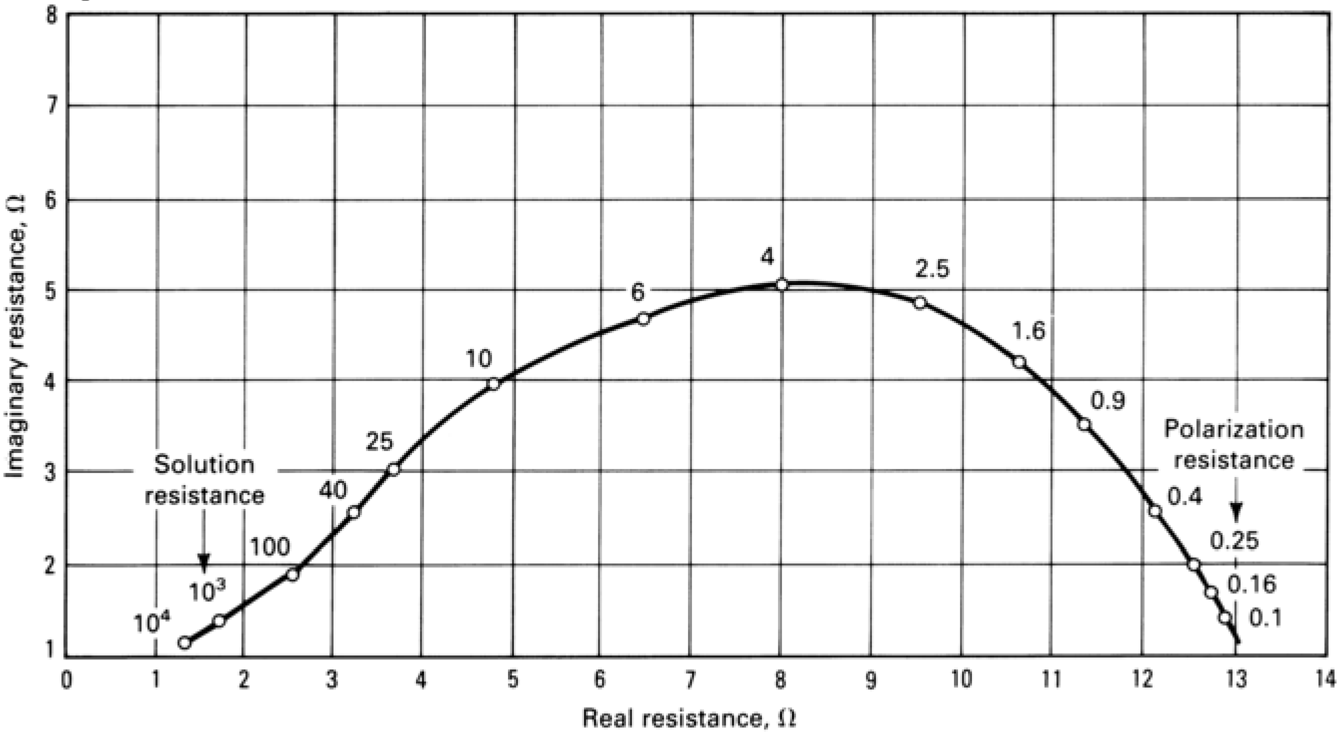

Fig. 6 Typical plot of ac impedance data in terms of real and imaginary resistance. The numbers on the curve indicate the frequency in hertz. Source: Ref 7

A sophisticated ac frequency generator and analyzer system is necessary to obtain results such as those shown in Fig. 6. Some investigators have suggested using only two frequencies to characterize ac impedance behavior (Ref 27). Although this minimizes the number of measurements, it does not reveal the details of the behavior. It is necessary to be familiar with the approach in order to interpret the results of ac impedance studies. The specimen designs used in commercial polarization-resistance probes have not been optimized for ac analysis. For this reason, a full frequency-response curve is desirable in order to verify that the behavior can be analyzed by conventional techniques, although it may take several hours to obtain a complete frequency-response curve. Thus, more development is necessary before the ac impedance technique achieves widespread acceptance for in-service corrosion monitoring. Another drawback is that the Stearn-Geary constant (Ref 25) or Tafel slopes must be known in order to convert ac impedance data into corrosion-rate information.

References cited in this section

7. S.W. Dean, Overview of Corrosion Monitoring in Modern Industrial Plants, *Corrosion Monitoring in Industrial Plants Using Nondestructive Testing and Electrochemical Methods,* STP 908, G.C. Moran and P. Labine, Ed., American Society for Testing and Materials, 1986, p 197–220

14. "Standard Guide for On-Line Monitoring of Corrosion in Plant Equipment (Electrical and Electrochemical Methods)," G 96, *Annual Book of ASTM Standards,* Vol 03.02, ASTM International

25. M. Stern and R.M. Roth, *J. Electrochem. Soc.,* Vol 104, 1958, p 440t

26. S.W. Dean, in *Electrochemical Techniques for Corrosion,* R. Baboian, Ed., National Association of Corrosion Engineers, 1977, p 52–60

27. S. Haruyama and T. Tsuru, in *Electrochemical Corrosion Testing,* STP 727, F. Mansfeld and U. Bertocci, Ed., American Society for Testing and Materials, 1981, p 167–186

S.W. Dean, Corrosion Monitoring for Industrial Processes, *Corrosion: Fundamentals, Testing, and Protection*, Vol 13A, *ASM Handbook*, ASM International, 2003, p 533–541

Corrosion Monitoring for Industrial Processes

Sheldon W. Dean, Dean Corrosion Technology, Inc.

Electrochemical Noise

Electrochemical noise refers to the natural fluctuations of either current or potential of a corroding specimen (Ref 28). If a specimen is electrically isolated and allowed to corrode, there are fluctuations of the corrosion potential as the corrosion proceeds. Likewise, if a corroding specimen is held at constant potential, fluctuations occur in the current required to maintain that potential. In one type of setup, three identical specimens are exposed to the environment. The potential between one of the specimens and the other two is monitored, while the current between the other two is also monitored by a zero- resistance ammeter. These signals are subsequently analyzed to obtain a standard deviation of the current noise and a standard deviation of the potential noise. The ratio of the potential standard deviation to the current standard deviation is believed to be equal to the polarization resistance, and this can then be converted to a corrosion rate through the Stearn-Geary relationship (Ref 25).

This approach has appealed to some investigators, because it does not involve any external polarization of the specimens and does not require the use of reference electrodes. Localized corrosion produces unique noise signals, and this has attracted attention because it gives this approach a chance of detecting these forms of corrosion while they are initiating. Pitting, for example, has been characterized by the ratio of the current standard deviation to the average corrosion current. Other analyses of the noise characteristics have been proposed but not universally accepted.

References cited in this section

25. M. Stern and R.M. Roth, *J. Electrochem. Soc.,* Vol 104, 1958, p 440t

28. J.R. Scully, Eletrochemical Tests, *Corrosion Tests and Standards,* Manual 20, ASTM International, 1995, p 75–90

S.W. Dean, Corrosion Monitoring for Industrial Processes, *Corrosion: Fundamentals, Testing, and Protection*, Vol 13A, *ASM Handbook*, ASM International, 2003, p 533–541

Corrosion Monitoring for Industrial Processes

Sheldon W. Dean, Dean Corrosion Technology, Inc.

Hydrogen Probe

The concept of the hydrogen probe is based on the fact that one of the cathodic reaction products in nonoxidizing acidic systems is hydrogen. The hydrogen atoms thus generated diffuse through the thickness of the vessel and are liberated at the exterior surface. A hydrogen probe—in one variation, the probe is a piece of palladium foil—is applied to the exterior surface. The probe serves as collector and catalyst for the subsequent oxidation of the hydrogen (Ref 26). The cell is attached to the palladium foil. The current employed in the oxidation reaction is supplied by a stainless steel working electrode (Fig. 7). The electrolyte is 90% sulfuric acid. The current that is required to oxidize the hydrogen is measured; it is directly proportional to the corrosion rate of the interior of the vessel.

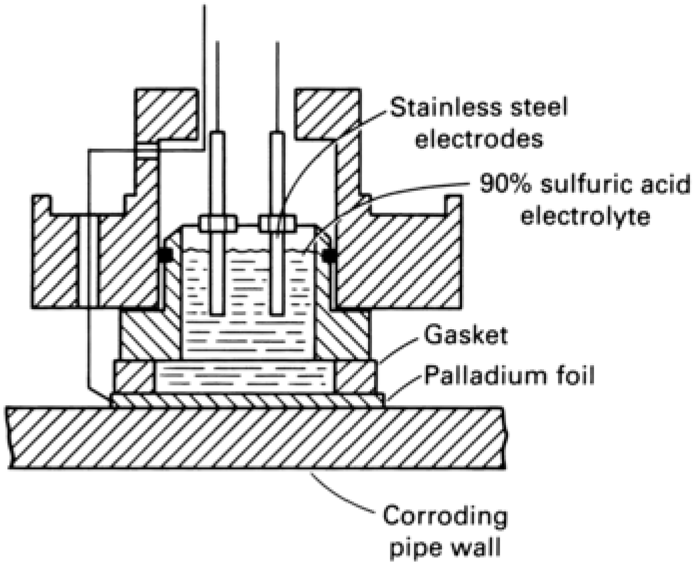

Fig. 7 Design of palladium foil hydrogen patch probe. Source: Ref 27

Hydrogen-probe analysis measures the corrosion rate, unlike ultrasonic thickness measurements and other techniques that measure remaining wall thickness. However, hydrogen-probe analysis is limited to systems in which the temperature is close to ambient and the diffusion rate of hydrogen is high. Gas pipeline service is the most common application. In this case, corrosion can occur when hydrogen sulfide, water, and sometimes carbon dioxide (CO_2) are present. This approach has another variation that consists of simply attaching a chamber to the exterior of the pipe and monitoring hydrogen liberation through increasing pressure (Ref 2).

One advantage of exterior hydrogen monitoring is that it does not require penetration of the pipe wall in order to obtain the corrosion rate. It is assumed in this method that all of the hydrogen liberated in the corrosion reaction diffuses through the steel vessel wall instead of being liberated as hydrogen gas at the surface, and this is true when hydrogen recombination poisons, such as hydrogen sulfide (H_2S), are present. Commercial devices are available for corrosion monitoring by this technique, although it is questionable whether such devices could be positioned and allowed to operate unattended for extended periods of time. In addition, these units have all of the problems associated with any electrochemical measuring device, namely the need for complex electronic equipment and wiring and the need for operators and installers with a sensitivity to the requirements of such equipment. Also, this method is, in practice, limited to steel, which has a high hydrogen diffusivity and low solubility of hydrogen.

Exterior hydrogen monitoring does not supply a quantitative measurement of hydrogen damage. However, it does provide a means of measuring the relative severity of corrosion damage and of evaluating the effects of process changes on the severity of corrosion.

References cited in this section

2. C.P. Dillon, A.S. Krisher, and H. Wissenberg, Plant Corrosion Tests, *Handbook on Corrosion Testing and Evaluation,* W.H. Ailor, Ed., John Wiley & Sons, 1971, p 599–615

26. S.W. Dean, in *Electrochemical Techniques for Corrosion,* R. Baboian, Ed., National Association of Corrosion Engineers, 1977, p 52–60

27. S. Haruyama and T. Tsuru, in *Electrochemical Corrosion Testing,* STP 727, F. Mansfeld and U. Bertocci, Ed., American Society for Testing and Materials, 1981, p 167–186

S.W. Dean, Corrosion Monitoring for Industrial Processes, *Corrosion: Fundamentals, Testing, and Protection*, Vol 13A, *ASM Handbook*, ASM International, 2003, p 533–541

Corrosion Monitoring for Industrial Processes

Sheldon W. Dean, Dean Corrosion Technology, Inc.

Analysis of Process Streams

Another useful in-service corrosion-monitoring technique is analysis of the process streams for the presence of corrosion products. This straight-forward approach usually does not require the installation of specialized equipment. For example, process streams from the bottom of the distillation column can be routinely sampled, and atomic absorption analysis techniques can be used to determine such heavy metals as iron, nickel, and chromium at very low levels. The concentration of such impurities is then directly proportional to the corrosion rate multiplied by the area of metal corroding, if the only source of metal ions is corrosion, and if the corrosion products are not precipitating. One problem is that the corroding area may not be known with certainty; therefore, the results are relative. However, they do help to determine whether conditions have improved.

S.W. Dean, Corrosion Monitoring for Industrial Processes, *Corrosion: Fundamentals, Testing, and Protection*, Vol 13A, *ASM Handbook*, ASM International, 2003, p 533–541

Corrosion Monitoring for Industrial Processes

Sheldon W. Dean, Dean Corrosion Technology, Inc.

Sentry Holes

In this monitoring technique, small sentry holes are drilled into the outside of a vessel or pipe at areas that are considered to be particularly susceptible to corrosion. The holes are drilled to the pressure-design thickness. Thus, when corrosion has almost consumed the corrosion allowance, the appearance of a small leak indicates that action must be taken to prevent a major failure. Sentry holes may be threaded or may have nipples attached

to facilitate plugging. Nondestructive testing is frequently performed in the area near the leak to determine the extent of the damage before repair or shutdown.
These holes are required in reinforcing pads applied to support nozzles in pressure vessels. In these cases, leakage from the hole signals corrosion or cracking of the nozzle weld and is an important safety feature of the design.

S.W. Dean, Corrosion Monitoring for Industrial Processes, *Corrosion: Fundamentals, Testing, and Protection*, Vol 13A, *ASM Handbook*, ASM International, 2003, p 533–541

Corrosion Monitoring for Industrial Processes

Sheldon W. Dean, Dean Corrosion Technology, Inc.

Side-Stream (Bypass) Loops

It is sometimes advantageous to operate a side-stream loop to determine the effect of chemical process changes without making these changes in the entire process system. This provides the advantage of an in-service corrosion test with product streams, yet permits evaluation of the effects of additives, inhibitors, and other changes in the environment without affecting the main process stream.
In the simplest case, a side stream from a major piece of equipment is run through a small tank or a widened section of the line in order to permit changes in the product stream and insertion of corrosion-monitoring devices. In such a case, the effluent from the side stream is usually discarded. In a more complicated installation, the entire cycle of the operation may be duplicated on a small scale using a portion of the mainstream. Obviously, a more sophisticated side-stream apparatus can approach the complexity and the expense of a pilot plant.

S.W. Dean, Corrosion Monitoring for Industrial Processes, *Corrosion: Fundamentals, Testing, and Protection*, Vol 13A, *ASM Handbook*, ASM International, 2003, p 533–541

Corrosion Monitoring for Industrial Processes

Sheldon W. Dean, Dean Corrosion Technology, Inc.

Strategies in Corrosion Monitoring

Monitoring Locations. A principal part of any corrosion-monitoring program is deciding where to locate the corrosion-monitoring devices. Because corrosion will probably not occur uniformly throughout the plant, it is desirable in any corrosion-monitoring program to find sites at which the highest corrosion rates will be experienced.
The problems involved in developing corrosion-monitoring programs for a plant are illustrated in the example of a distillation column. The most logical points for corrosion monitoring in a distillation column are the feed point, the overhead product receiver, and the reboiler or bottoms product line. These points are the locations at which the highest and lowest temperatures are encountered, as well as the points at which the most and least volatile products are concentrated. However, these points are usually not the locations of the most severe corrosion.
The species causing the corrosion often concentrates at an intermediate point in the column because of chemical changes within the column. Therefore, if there is a possibility of concentrating a corrosive species within the distillation column, several monitoring points would be required throughout the column for the corrosion-

monitoring program to be comprehensive (Fig. 8). A monitoring program can be restricted to the most corrosive location within the column, once this area has been identified (Ref 29).

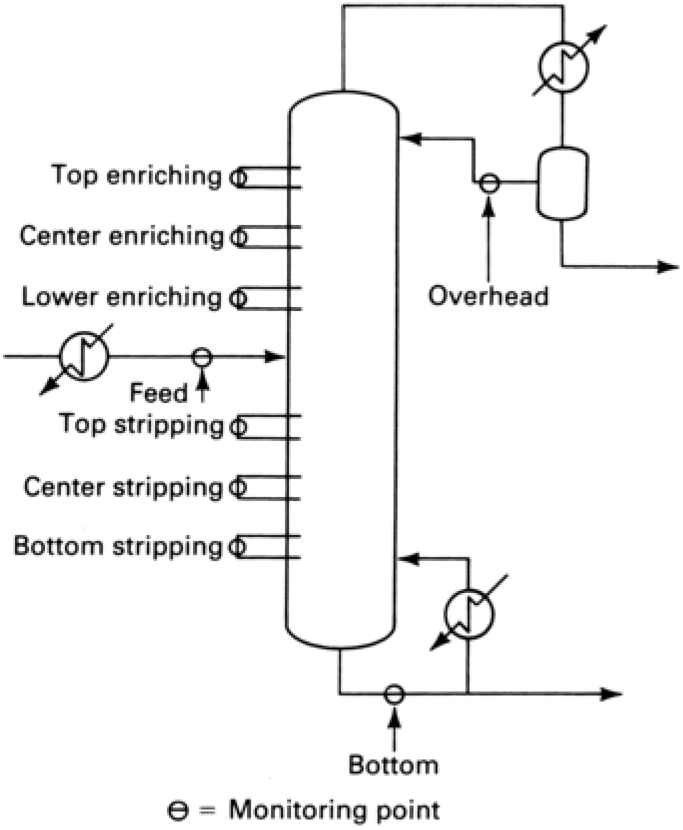

Fig. 8 Distillation column showing preferred locations of monitoring probes or other devices. Source: Ref 7

Another problem with distillation columns is that the liquid on trays tends to be frothy. This creates difficulties for electrochemical methods. One solution to this problem is to install bypass loops that remove liquid from the column, pass it over the corrosion-monitoring probes, and reinject it at a lower point in the column (Ref 2). This practice avoids the problem of foam and froth and provides a more controlled flow rate over the corrosion-monitoring equipment. Use of a bypass loop also allows removal of liquid samples at times of high corrosion rates (Fig. 9).

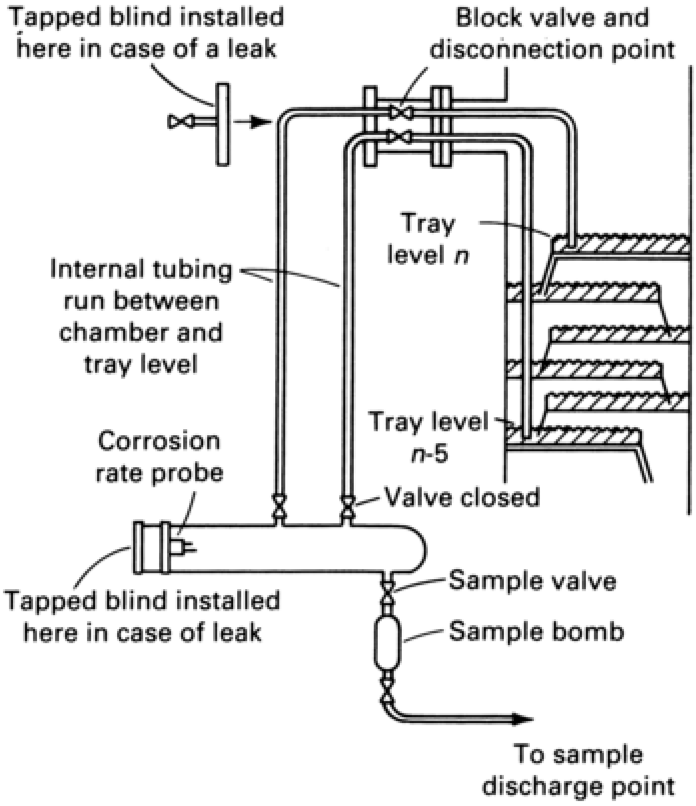

Fig. 9 Use of a side-stream (bypass) loop to monitor corrosion in a distillation column. Source: Ref 7

The process stream can be sampled in locations other than distillation columns. A sample tap can be helpful in conjunction with polarization-resistance devices. The alarm on polarization-resistance monitoring equipment can be used to signal the need to remove samples. This is particularly desirable in the case of pilot plant operation, in which wide variations in processing conditions are encountered. It is also helpful in plants that produce different products in the same equipment.

High-velocity gas streams in pipes may cause problems with conventional monitoring systems. In this case, the presence of an aqueous phase is usually restricted to a thin layer on the surface of the pipe. This condition is known as annular flow. A probe that protrudes into the pipe may miss the liquid layer that is present only close to the pipe wall. A flush-mounted surface probe can be used in such cases. This probe permits the measurement of polarization resistance in order to estimate the corrosion rate of the pipe wall (Ref 30).

Probe location is also critical in storage tanks containing nonaqueous liquids. The most corrosive location in these tanks may be at the liquid level, if the liquid in the tank has a density exceeding that of water. In this case, the corrosion- monitoring probe should be mounted on a floating platform. In this way, the probe can detect the presence of a corrosive aqueous phase. However, when the liquid stored in the tank is less dense than the water, the corrosion-monitoring device should probably be positioned at the bottom of the tank.

Ultrasonic Thickness Data Analysis. Ultrasonic thickness measurements are often obtained during turnaround periods when the plant is not operating. A well-designed program provides a series of thickness measurements at specified locations throughout the plant. Assuming that the original thickness of a vessel was constant, a diagram similar to that shown in Fig. 10 can be drawn. Figure 10 shows the inverse relationship between the average corrosion rate and the remaining thickness. It is then possible to estimate the remaining life of the vessel from the maximum corrosion rate and the remaining corrosion allowance. In cases in which corrosion rate varies randomly, the highest corrosion rate and the smallest remaining thickness can be estimated by using statistical analysis. This approach provides a rational method of estimating remaining life when faced with a quantity of thickness readings from an ultrasonic thickness survey.

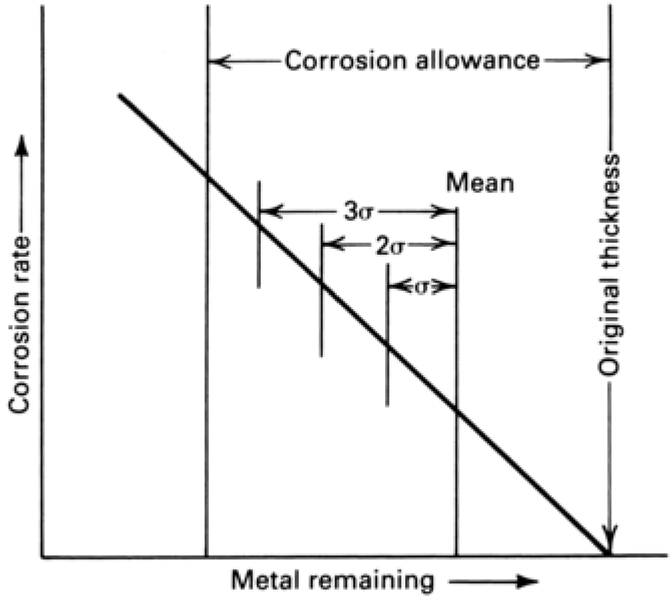

Fig. 10 Typical plot of metal thickness remaining versus calculated corrosion rate obtained from ultrasonic thickness data. Statistical analysis can be used to estimate the remaining corrosion allowance in terms of standard deviation σ. Source: Ref 7

Redundancy is also important in designing corrosion-monitoring programs. The use of at least two different types of corrosion-monitoring devices at any location is often desirable. For example, the use of an electrical-resistance probe with a polarization-resistance probe allows measurement of both instantaneous corrosion rates and an average corrosion rate. The data thus obtained can be correlated, and this is very helpful in identifying spurious or inaccurate readings.

In another approach, the polarization-resistance probe is weighed before and after the test in order to correlate mass loss with the average corrosion rate that the probe suffered. There is reason to expect that the electrochemical value is in error if the average corrosion rate and the mass loss of the probe do not agree. Also, to obtain time-average corrosion-rate values, independent coupons can be installed together with polarization-resistance probes.

A variety of corrosion-monitoring approaches must be used when designing pilot or demonstration plants. Coupon tests can be very helpful in selecting optimal materials for processes based on pilot-plant experience. Polarization-resistance monitoring is very useful for determining whether certain processing conditions cause corrosive situations to develop. Because the corrosion mechanisms are often not well understood, and because the result of erroneous information can be serious overdesign or exposure to unexpected hazards, redundancy in the design of such monitoring systems is important in pilot plants.

Other Issues. A primary difficulty with corrosion-monitoring equipment is the need to install wires from the probes to the control room or to the instruments and data-storage systems. Hardwire systems are usually more expensive than the probes and electronic instruments. In addition, wiring systems are often sources of problems due to breakage, moisture entry, and connection difficulties. One option is the use of devices to transform the data to coded citizens' band (CB) radio signals. These small, battery- operated units can be installed at probe locations, and they provide the desired information to the base station on command. The base station would be located in the control room. Acceptance of this approach may increase as such systems become more available and more reliable.

The problem of leaks is another important issue in corrosion-monitoring systems. Leaks can cause hazards and can shut down operating plants. The corrosion-monitoring system must be installed such that leaks from the probe can be handled with minimal interruption. A device that penetrates the wall of the vessel may leak; therefore, it is essential to have contingency plans for dealing with leaks before the devices are installed.

A related problem concerns packing glands on pressure vessels that have removable devices. The pressure within a system exerts a force on any removable device. Therefore, it is important to prevent the device from being blown out, which might injure personnel attempting to remove the device or would expose such personnel to the fluid within the vessel. For this reason, restraining rods, chains, and flush and drain ports must be used.

References cited in this section

2. C.P. Dillon, A.S. Krisher, and H. Wissenberg, Plant Corrosion Tests, *Handbook on Corrosion Testing and Evaluation,* W.H. Ailor, Ed., John Wiley & Sons, 1971, p 599–615

7. S.W. Dean, Overview of Corrosion Monitoring in Modern Industrial Plants, *Corrosion Monitoring in Industrial Plants Using Nondestructive Testing and Electrochemical Methods,* STP 908, G.C. Moran and P. Labine, Ed., American Society for Testing and Materials, 1986, p 197–220

29. R. Martin and E.C. French, "Corrosion Monitoring in Sour Systems Using Electrochemical Hydrogen Potential Probes," Paper 6657, presented at the Sour Gas Symposium of the Society of Petroleum Engineers (Dallas, TX), American Institute of Mining, Metallurgical and Petroleum Engineers, 1977

30. C.G. Arnold and D.R. Hixson, *Mater. Perform.,* Vol 21 (No. 4), April 1982, p 21–24

S.W. Dean, Corrosion Monitoring for Industrial Processes, *Corrosion: Fundamentals, Testing, and Protection*, Vol 13A, *ASM Handbook*, ASM International, 2003, p 533–541

Corrosion Monitoring for Industrial Processes

Sheldon W. Dean, Dean Corrosion Technology, Inc.

Interpretation and Reporting

In-service monitoring, more than any other type of corrosion testing, requires the utmost skill in interpretation and reporting. Important economic decisions are often based on the test results. Although there are a number of standards that provide guidelines for certain procedures, there is no standard that is comprehensive. To plan an appropriate test program, the investigator must know or have good advice on both the chemistry and the mechanics of the processes involved; that is, the investigator must understand the entire corrosion system. There must be a strong emphasis on the strategy of the program and a searching analysis of the test results. It is important to prepare detailed records of what was done as part of the experiment, and it is also important to document any unplanned changes that occur in the process stream or the equipment during the investigation. Without a valid interpretation and effective (timely) reporting, the price of the work can be significantly greater than the cost of time and materials. However, the consequences of corrosion failures go beyond additional costs. Also involved are personal safety risks (and liability), hazard potentials, process reliability, and product quality and pollution problems.

S.W. Dean, Corrosion Monitoring for Industrial Processes, *Corrosion: Fundamentals, Testing, and Protection*, Vol 13A, *ASM Handbook*, ASM International, 2003, p 533–541

Corrosion Monitoring for Industrial Processes

Sheldon W. Dean, Dean Corrosion Technology, Inc.

Acknowledgments

S.W. Dean reviewed and made substantial revisions to the original article, "In-Service Monitoring," by S.W. Dean and D.O. Sprowls, *Metals Handbook,* 9th edition, Vol 13, 1987, p 197. Portions of the original article were adapted with permission from S.W. Dean, Overview of Corrosion Monitoring in Modern Industrial Plants, *Corrosion Monitoring in Industrial Plants Using Non-Destructive Testing and Electrochemical Methods,* STP 908, G.C. Moran and P. Labine, Ed., American Society for Testing and Materials, 1986, p 197–220.

S.W. Dean, Corrosion Monitoring for Industrial Processes, *Corrosion: Fundamentals, Testing, and Protection*, Vol 13A, *ASM Handbook*, ASM International, 2003, p 533–541

Corrosion Monitoring for Industrial Processes

Sheldon W. Dean, Dean Corrosion Technology, Inc.

References

1. G.H. Koch, M.P.H. Brongers, N.G. Thompson, Y.P. Virmani, and J.H. Payer, "Corrosion Cost and Preventive Strategies in the United States," FHWA-RD-01-156, Federal Highway Administration, U.S. Department of Transportation, Washington D.C., March 2002

2. C.P. Dillon, A.S. Krisher, and H. Wissenberg, Plant Corrosion Tests, *Handbook on Corrosion Testing and Evaluation,* W.H. Ailor, Ed., John Wiley & Sons, 1971, p 599–615

3. A.S. Couper, Methods in Oil-Refining Industries, *Handbook on Corrosion Testing and Evaluation,* W.H. Ailor, Ed., John Wiley & Sons, 1971, p 617–624

4. "Laboratory Corrosion Testing of Metals for the Process Industries," NACE TM-01-69, National Association of Corrosion Engineers, 1976

5. J.N. Wanklyn, *Corrosion Monitoring in the Oil and Petrochemical and Process Industries,* J. Wanklyn, Ed., Oyez Scientific and Technical Service Ltd., 1982

6. *Corrosion Monitoring in Industrial Plants Using Nondestructive Testing and Electrochemical Methods,* STP 908, G.C. Moran and P. Labine, Ed., American Society for Testing and Materials, 1986

7. S.W. Dean, Overview of Corrosion Monitoring in Modern Industrial Plants, *Corrosion Monitoring in Industrial Plants Using Nondestructive Testing and Electrochemical Methods,* STP 908, G.C. Moran and P. Labine, Ed., American Society for Testing and Materials, 1986, p 197–220

8. S.W. Dean, Electrochemical Methods for Corrosion Testing in the Process Industries, *Electrochemical Corrosion Testing with Special Consideration of Practical Applications,* E. Heintz, J.C. Rowlands, and F. Mansfeld, Ed., Proceedings of International Workshop, (Ferrara, Italy), DECHEMA, 1986, p 1–15

9. *Process Industries Corrosion—Theory and Practice,* National Association of Corrosion Engineers, 1986

10. B.J. Moniz, Field Coupon Corrosion Testing, *Process Industries Corrosion—Theory and Practice,* National Association of Corrosion Engineers, 1986

11. S.J. Pikul, T.S. Lee, and D.B. Anderson, "Field Corrosion Tests for Materials Evaluation in Chemical Process Industries," Paper 119, presented at Corrosion/86, National Association of Corrosion Engineers, 1986

12. A. Perkins, Industrial Applications, *Corrosion Tests and Standards,* Manual 20, ASTM International, 1995, p 143–148

13. "Standard Method for Conducting Corrosion Coupon Tests in Plant Equipment," G 4, *Annual Book of ASTM Standards,* Vol 03.02, ASTM International

14. "Standard Guide for On-Line Monitoring of Corrosion in Plant Equipment (Electrical and Electrochemical Methods)," G 96, *Annual Book of ASTM Standards,* Vol 03.02, ASTM International

15. "Standard Guide for Conducting and Evaluating Galvanic Corrosion Tests in Electrolytes," G 71, *Annual Book of ASTM Standards,* Vol 03.02, ASTM International

16. W.D. France, Jr., Crevice Corrosion of Metals, *Localized Corrosion—Cause of Metal Failure,* STP 519, M. Henthorne, Ed., American Society for Testing and Materials, 1972, p 164–200

17. "Standard Guide for Crevice Corrosion Testing of Iron-Base and Nickel-Base Stainless Alloys in Seawater and Other Chloride- Containing Aqueous Environments," G 78, *Annual Book of ASTM Standards,* Vol 03.02, ASTM International

18. "Standard Test Methods for Pitting and Crevice Corrosion Resistance of Stainless Steels and Related Alloys by Use of Ferric Chloride Solution," G 48, *Annual Book of ASTM Standards,* Vol 03.02, ASTM International

19. "Standard Practice for Making and Using U- Bend Stress-Corrosion Test Specimens," G 30, *Annual Book of ASTM Standards,* Vol 03.02, ASTM International

20. "Standard Practice for Making and Using C- Ring Stress-Corrosion Test Specimens," G 38, *Annual Book of ASTM Standards,* Vol 0302, ASTM International

21. "Standard Practice for Preparation of Stress- Corrosion Test Specimens for Weldments," G 58, *Annual Book of ASTM Standards,* Vol 03.02, ASTM International

22. "Standard Practice for Determining the Susceptibility to Intergranular Corrosion of 5*xxx* Series Aluminum Alloys by Weight Loss After Exposure to Nitric Acid (NAWLT Test)," G 67, *Annual Book of ASTM Standards,* American Society for Testing and Materials

23. E.H. Dix, Jr., W.A. Anderson, and M.B. Shumaker, Influence of Service Temperature on the Resistance of Wrought Aluminum-Magnesium Alloys to Corrosion, *Corrosion,* Vol 15 (No. 2), 1959, p 55t–62t

24. "Standard Practice for Preparing, Cleaning, and Evaluating Corrosion Test Specimens," G 1, *Annual Book of ASTM Standards,* Vol 03.02, ASTM International

25. M. Stern and R.M. Roth, *J. Electrochem. Soc.,* Vol 104, 1958, p 440t

26. S.W. Dean, in *Electrochemical Techniques for Corrosion,* R. Baboian, Ed., National Association of Corrosion Engineers, 1977, p 52–60

27. S. Haruyama and T. Tsuru, in *Electrochemical Corrosion Testing,* STP 727, F. Mansfeld and U. Bertocci, Ed., American Society for Testing and Materials, 1981, p 167–186

28. J.R. Scully, Eletrochemical Tests, *Corrosion Tests and Standards,* Manual 20, ASTM International, 1995, p 75–90

29. R. Martin and E.C. French, “Corrosion Monitoring in Sour Systems Using Electrochemical Hydrogen Potential Probes,” Paper 6657, presented at the Sour Gas Symposium of the Society of Petroleum Engineers (Dallas, TX), American Institute of Mining, Metallurgical and Petroleum Engineers, 1977

30. C.G. Arnold and D.R. Hixson, *Mater. Perform.,* Vol 21 (No. 4), April 1982, p 21–24

31. E.C. French, *Oil Gas J.,* Vol 17, 1975, p 82–88

B. Phull, Evaluating Uniform Corrosion, *Corrosion: Fundamentals, Testing, and Protection,* Vol 13A, *ASM Handbook,* ASM International, 2003, p 542–544

Evaluating Uniform Corrosion

Revised by Bopinder Phull, Consultant

Introduction

UNIFORM CORROSION refers to attack on an exposed metal surface that results in homogeneous thickness loss. In other words, the metal loss is spread evenly over the surface rather than being localized as, for example, pitting or stress- corrosion cracking. Uniform corrosion is also known as general corrosion. Practical examples of uniform or general corrosion include dissolution of iron or zinc in dilute sulfuric acid, aluminum in sodium hydroxide solution, bare or galvanized steel in atmospheric environments, and so on. In terms of electrochemistry, the metal undergoing uniform corrosion can be regarded as a single electrode, which supports anodic and cathodic reactions concurrently. Furthermore, the anodic and cathodic sites can be considered as local with respect to each other, approximately equal in area, and fluctuating randomly in a stochastic manner over the metal surface. Corrosion occurs by local cell action, that is, metal dissolution of the anodic sites due to oxidation (electron loss), driven by charge-transfer reduction reaction(s) at the adjacent cathodic sites (electron consumption). Uniform corrosion can be mitigated by materials selection, coatings, inhibitors, cathodic protection, and in specific cases anodic protection. Another practical means of addressing uniform corrosion in many practical applications is to build in a corrosion allowance at the design stage. The most appropriate corrosion control method will depend on specific metal-environment considerations, application criticality, and economics.

Testing for uniform corrosion and its evaluation are relatively simple. Appropriate test specimens (also often referred to as corrosion coupons) are exposed to the environment of interest, and the metal loss is determined after a prescribed period by, for example, mass loss or measurement of thickness change. Convenience, practicality, safety considerations, and economics will typically dictate whether testing is performed in the laboratory and/or in actual service conditions. Laboratory testing usually consists of small specimens immersed in relatively small volumes of simulated or actual service environments. The advantage of this type of testing is that the tests can be controlled closely; thus, unintentional disturbances that could occur during in-plant tests can be avoided. These tests are usually designed to simulate expected service conditions. It should be recognized that the objective of testing is to determine the type and extent of corrosion incurred. There is no advance assurance that the test specimens will undergo uniform corrosion.

Service tests (field, in-plant, or on-line tests) involve placing test samples in actual service conditions for evaluation. The test specimens need to be mounted securely and are usually electrically isolated from each other and plant equipment to preclude galvanic interactions— unless the objective of the test is to investigate such effects. The advantage of service testing is that the test specimens are exposed to the actual service environment. However, in-plant testing is also fraught with limitations. For instance, it may be difficult to subject the test specimens to the same flow, pressure, or heat-transfer conditions as the actual plant equipment, such as in piping, pumps, valves, and condensers. Although techniques are available commercially for on-line

insertion and retrieval of test specimens, that is, without plant shutdown, they are not used routinely in all industries because of cost.

B. Phull, Evaluating Uniform Corrosion, *Corrosion: Fundamentals, Testing, and Protection*, Vol 13A, *ASM Handbook,* ASM International, 2003, p 542–544

Evaluating Uniform Corrosion

Revised by Bopinder Phull, Consultant

Mass-Loss Tests

For engineering applications, uniform corrosion rates are reported as loss of metal thickness per unit time. Corrosion rates are often calculated from mass-loss data. Mass loss is the difference between the original mass of the specimen and the mass after a prescribed or known exposure period. Before determining the mass loss after exposure, it is important to clean the specimens properly to remove corrosion product adhering to the surface. After cleaning, it is essential to examine the test specimens visually. Calculation of corrosion rates from mass-loss data will yield meaningful results for use in design only if the specimens have suffered uniform attack. Conversely, computation of corrosion rates from mass loss for specimens that have predominately incurred localized corrosion will give erroneous information to the designer or end-user.

It may be possible to measure the thickness changes in the test specimens or equipment directly, for example, by using calipers, micrometers, or ultrasonic gages. Ultrasonic thickness measurements are particularly suited to scheduled inspection of actual plant equipment such as piping, vessels, tanks, pump casings, and valve bodies. Uniform corrosion rates are usually expressed as thickness loss per unit time, for example, micrometers/year (μm/y), millimeters per year (mm/y), and mils per year (mpy; where 1 mil = 25.4 μm).

Specimen Preparation. The first step in testing is the selection and preparation of suitable test specimens. Clear and complete documentation of the test material is very important. This should include the chemical composition as well as the metallurgical condition of the specimens. The specimens are usually saw-cut from larger stock and the surfaces and edges ground and deburred. It is important to minimize introduction of stresses or metallurgical transformations (e.g., due to overheating) during specimen preparation. Laser cutting, while rapid and convenient, may introduce microstructural changes that make the heat-affected areas, for example, specimen edges or mounting holes, more or less prone to corrosion, depending on the material and test environment. Each sample should be clearly identified before testing. This is commonly done with identification codes that are stenciled (stamped or engraved) on the specimens. Stamped codes introduce stresses where cracking can occur in susceptible materials. Similarly, codes made by laser stenciling or electrical discharge machining (EDM) may increase corrosion propensity of associated areas. It is important to prepare a map sheet so that test specimens can still be identified even if the identification codes are obliterated by corrosion during the test.

The size and shape of the test specimens are often specified in such a manner as to make them easy to handle and allow for ease of surface preparation, cleaning, and weighing. Specimens 1.6 to 6.4 mm ($\frac{1}{16}$ to $\frac{1}{4}$in.) thick and a few inches square are not uncommon. While it may be desirable to protect specimen edges for some materials, this is not always practical in corrosion tests. Before exposure to the corrosive medium, the test specimen surface needs to be prepared and cleaned. The surface can be ground, grit or glass-bead blasted, or pickled. Ideally, the surface finish of the test specimen should be the same as that of the metal or alloy in service. Unfortunately, this is not always possible because of the variations in surface condition produced during fabrication. However, surface preparation of the test specimens ensures a standard surface condition during testing. Usually, sufficient material is removed to reach the bulk composition/ structure of the metal or alloy; that is, surface- depleted or -enriched layers nonrepresentative of bulk material are removed, unless influence of these variables is part of the investigation. After surface preparation, the specimens are degreased with a solvent such as acetone, dried, weighed, and either immediately exposed to the test medium or stored in a desiccator until test commencement. For most laboratory tests, specimens should ideally be weighed to a

precision of ±0.1 mg. Ideally, specimens with a large surface-area-to-volume ratio are preferred for accurate mass-loss determination, especially when the expected corrosion rate is low. Practical guidelines for preparing, cleaning, and evaluating corrosion test specimens are provided in ASTM G 1 (Ref 1).
Test Methods. The method and apparatus used to expose the test specimens to the test environment are very important and should meet the following guidelines:

- The corrosive medium should have easy access to the test specimens.
- The specimens should be well supported.
- The specimens should be electrically insulated from all other metals in the system.
- The specimens should be completely immersed, unless other effects are being studied.
- The specimens should be readily accessible.

Practical guidelines for laboratory immersion corrosion testing of metals are provided in ASTM G 31 (Ref 2) and NACE International TM0169-2000 (Ref 3).
It is important to plan the experimental technique so that the test specimens are removed and the mass loss determined after appropriate exposure duration. The corrosion rate may initially increase or decrease and eventually become constant with time. Exposure of many replicate specimens is usually necessary with the mass- loss test method to determine corrosion rate variations as a function of time. The following very rough rule of thumb suggested for test duration (in hours) is cited in Refs 2 and 3:

$$\text{Test duration(hours)} = 2000/(\text{expected corrosion rate in mpy}) \quad \text{(Eq 1)}$$

In addition to the sequential removal of specimens with time, a planned interval testing schedule can be used to obtain more information on the initial corrosion rates and on accumulated effects (see ASTM G 31, Ref 2). Planned interval testing involves exposing identical specimens to the test solution at various intervals during the test. By evaluating the results, initial corrosion rates and changes in solution corrosivity can be determined. Planned interval testing is an excellent example of good experimental planning. References 2 and 3 also include recommendations for minimum solution volume to use in the test per unit surface area of exposed specimen (e.g., 20 mL/cm^2, or 125 mL/in^2). This is to avoid depletion of corrodents and hence significant changes in solution corrosivity during the test.
Test Variables. Important variables that must be addressed during experimental planning include gases, temperature, solution volume and flow, and exposure time. The presence of dissolved gases, for example, O_2, CO_2, H_2S, SO_2, and so on, in the test solution can have a dramatic effect on the rate of corrosion. Dissolved gases are usually supplied by bubbling them through the solution. Running the test under pressure or partial vacuum will alter the dissolved gas concentration. If degassing is required, purified nitrogen or argon can be bubbled through the solution to displace dissolved gases.
The influence of temperature can be complicated in that it affects gas solubility, pH, corrosion product formation, and other parameters. Therefore, the temperature of the test should be monitored and controlled as necessary during the corrosion test.
The flow velocity of the solution also plays an important role in determining the corrosion rates. Corrosion rates may increase or decrease as the fluid velocity near the sample is increased. In any case, flow characteristics that represent the condition in service should be established during testing. This is often not a simple task, because the hydrodynamic conditions in service and their effect on the corrosion rate can be complex. Rotating disks and cylinders and jet-impingement apparati have been used to study corrosion rates under controlled hydrodynamic conditions (Ref 4, 5, 6, 7).
The type of exposure is also important in test design; total, partial, or intermittent exposure can change the mode and rate of corrosion. For immersion testing, all test specimens should be immersed at approximately the same depth in the test environment. Partially immersed samples can be used to study waterline corrosion. Samples can also be tested in the vapor phase.
Posttest Sample Cleaning, Data Acquisition, and Reporting. After the test specimens are removed from the exposure environment, they are cleaned to remove any corrosion products. The corrosion products must be removed with minimal additional corrosion of the test specimens. Sometimes, the corrosion products are not removed, and the mass gain is used to calculate corrosion rate. In principle, this approach has some appeal, because the specimen can be returned to the test after weighing (i.e., without removing corrosion products).

However, it assumes that all of the corrosion products formed from the inception of the test remain on the surface and that their stoichiometry is well known. Mass-gain testing has been used in high- temperature oxidation, gaseous, and atmospheric environments. However, the more common method is to remove the corrosion products by a combination of careful chemical and mechanical cleaning before determining mass loss. Detailed procedures and solutions for cleaning specimens after exposure are given in ASTM G 1 (Ref 1), including how to make corrections for mass loss incurred during cleaning.

It is essential to examine the test specimens visually to verify or characterize the type of corrosion attack suffered. This can generally be done with the unaided eye and does not usually require the aid of a microscope. If corrosion is uniform, the corrosion rate can be calculated from the mass-loss data as follows:

$$\text{Corrosion rate} = (K \times W)/(A \times t \times \rho) \qquad \text{(Eq 2)}$$

where K is a constant, W is mass loss, A is exposed specimen area, t is exposure time, and ρ is material density. Table 1 shows the various corrosion rate units and corresponding values of the constant K in Eq 2 when W is in grams, A is in cm^2, t is in hours, and ρ is in g/cm^3 (Ref 1, 2). ASTM G 1 also contains material density data for common metals and alloys. It must be reiterated that corrosion rates that reflect material-thinning rates should not be calculated from mass-loss data when corrosion attack is primarily localized, because they will lead to erroneous interpretation and conclusions. For example, calculation of corrosion rate from mass-loss data alone may indicate a negligible uniform corrosion rate for a given material, whereas, in reality, the subject test specimen may have been completely perforated by a few small-diameter pits. In other words, the low uniform corrosion rate would provide a false sense of confidence in the corrosion performance that would be contradicted by unexpected failure in service (e.g., heat-exchanger tubing). In the case of uniform and nonuniform corrosion, units such as $g/m^2 \cdot h$ or mdd (see Table 1) can be used for making relative comparisons of corrosion performance, for example, evaluation of solution corrosivity or determining efficacy of corrosion mitigation methods. However, the data should not be converted to thinning rates (e.g., mpy or mm/y) unless the corrosion is confirmed to be uniform.

Table 1 Values for constant *K* in the corrosion rate equation (Eq 2)

Corrosion rate units desired	Constant *K* in corrosion rate equation
Mils per year (mpy)	3.45×10^6
Inches per year (ipy)	3.45×10^3
Micrometers per year (µm/y)	8.76×10^7
Millimeters per year (mm/y)	8.76×10^4
Grams per square meter per hour ($g/m^2 \cdot h$)	$1 \times 10^4 \times \rho$
Milligrams per square decimeter per day (mdd)	$2.40 \times 10^6 \times \rho$

ρ is material density in g/cm^3.

Source: Ref 1

ASTM G 4 (Ref 8) provides guidelines on conducting corrosion coupon tests in field applications, particularly the use of test racks in plant applications.

References cited in this section

1. "Standard Practice for Preparing, Cleaning, and Evaluating Corrosion Test Specimens," G 1, *Wear and Erosion; Metal Corrosion,* Vol 03.02, *Annual Book of ASTM Standards,* American Society for Standards and Testing, 2002

2. "Standard Practice for Laboratory Immersion Corrosion Testing of Metals," G 31, *Wear and Erosion; Metal Corrosion,* Vol 03.02, *Annual Book of ASTM Standards,* American Society for Standards and Testing, 2002

3. "Standard Test Method: Laboratory Corrosion Testing of Metals," TM0169-2000, NACE International, 2000

4. J.S. Newman, *Electrochemical Systems,* Prentice-Hall, 1973

5. D.C. Silverman, Rotating Cylinder Electrode for Velocity Sensitivity Testing, *Corrosion,* Vol 40, 1984, p 220

6. A.J. Bard and L.R. Faulkner, in *Electrochemical Methods: Fundamentals and Applications,* J. Wiley & Sons, 1980, p 283–304

7. K.D. Efird, E.J. Wright, J.A. Boros, and T.G. Hailey, Correlation of Steel Corrosion in Pipe Flow with Jet Impingement and Rotating Cylinder Tests, *Corrosion,* Vol 49, 1993, p 992

8. "Standard Guide for Conducting Coupon Tests in Field Applications," G 4, *Wear and Erosion; Metal Corrosion,* Vol 03.02, *Annual Book of ASTM Standards,* American Society for Standards and Testing, 2002

B. Phull, Evaluating Uniform Corrosion, *Corrosion: Fundamentals, Testing, and Protection*, Vol 13A, *ASM Handbook*, ASM International, 2003, p 542–544

Evaluating Uniform Corrosion

Revised by Bopinder Phull, Consultant

Other Test and Evaluation Methods

If visual appearance indicates uniform corrosion on the test specimens, then periodic analysis for dissolved or insoluble corrosion products may be used to calculate corrosion rate (Ref 9). This is generally most meaningful for closed systems; that is, the test solution is not refreshed. This approach assumes that all of the corroded metal enters the test solution does not remain on the surfaces of the test specimens as corrosion product. For an alloy, it is assumed that its constituent elements enter the solution stoichiometrically. For material-environment combinations where hydrogen is evolved as a by-product, the hydrogen can be collected during the test, using a gas burette. Again, if corrosion is uniform, it may be possible to calculate the corrosion rate from the volume of hydrogen evolved, provided the correlation between metal loss and amount of gas liberated is known (Ref 9, 10).

If corrosion attack is uniform, useful estimates of corrosion rates can be obtained from electrochemical techniques such as linear polarization resistance (LPR). This technique is described in ASTM G 59 (Ref 11). Basically, a small voltage is applied between two small, identical electrodes made from the material of interest. The electrodes are usually incorporated in a probe, which is immersed in the environment. The current associated with the small voltage perturbation is measured. Polarization resistance is the ratio of applied voltage to the resultant current density and is inversely related to the corrosion rate via a Stern and Geary constant. This technique requires immersion of the probe in an aqueous (preferably conductive) medium. The LPR technique lends itself readily to monitoring uniform corrosion in laboratory tests or in-plant applications (Ref 12). Instrumentation ranges from portable, single-channel, hand-held units to multichannel systems installed in control rooms.

Another technique for monitoring uniform corrosion is the electrical resistance (ER) method. The change in the electrical resistance of a sensing element (e.g., wire, strip, or foil) made from the material of interest and exposed to the environment is monitored with a Kelvin- Wheatstone bridge as a function of time. The sensing element is usually incorporated into a suitable probe. The sensing element thins due to corrosion, with a corresponding increase in its electrical resistance. The corrosion rate is directly related to the slope of the curve from plotting resistance change versus time. A major attribute of the ER technique is that, unlike the LPR technique, it does not require an aqueous or conductive medium. Monitoring equipment for laboratory and on-line corrosion tests using the electrical resistance technique is available commercially (Ref 12).

References cited in this section

9. G. Wranglén, *An Introduction to Corrosion and Protection of Metals,* Chapman & Hall, 1985, p 229

10. R.L. Martin and E.C. French, Corrosion Monitoring in Sour Systems Using Electrochemical Hydrogen Patch Probes, *J. Pet. Technol.,* Nov 1978, p 1566–1570

11. "Standard Test Method for Conducting Potentiodynamic Polarization Resistance Measurements," G 59, *Wear and Erosion; Metal Corrosion,* Vol 03.02, *Annual Book of ASTM Standards,* American Society for Standards and Testing, 2002

12. "Standard Guide for On-Line Monitoring of Corrosion in Plant Equipment (Electrical and Electrochemical Methods)," G 96, *Wear and Erosion; Metal Corrosion,* Vol 03.02, *Annual Book of ASTM Standards,* American Society for Standards and Testing, 2002

B. Phull, Evaluating Uniform Corrosion, *Corrosion: Fundamentals, Testing, and Protection*, Vol 13A, *ASM Handbook*, ASM International, 2003, p 542–544

Evaluating Uniform Corrosion

Revised by Bopinder Phull, Consultant

Acknowledgment

This article has been adapted in part from C.A. Natalie, Evaluation of Uniform Corrosion, *Corrosion,* Vol 13, *ASM Handbook* (formerly *Metals Handbook,* 9th ed.), ASM International, 1987, p 229–230.

B. Phull, Evaluating Uniform Corrosion, *Corrosion: Fundamentals, Testing, and Protection*, Vol 13A, *ASM Handbook*, ASM International, 2003, p 542–544

Evaluating Uniform Corrosion

Revised by Bopinder Phull, Consultant

References

1. "Standard Practice for Preparing, Cleaning, and Evaluating Corrosion Test Specimens," G 1, *Wear and Erosion; Metal Corrosion,* Vol 03.02, *Annual Book of ASTM Standards,* American Society for Standards and Testing, 2002

2. "Standard Practice for Laboratory Immersion Corrosion Testing of Metals," G 31, *Wear and Erosion; Metal Corrosion,* Vol 03.02, *Annual Book of ASTM Standards,* American Society for Standards and Testing, 2002

3. "Standard Test Method: Laboratory Corrosion Testing of Metals," TM0169-2000, NACE International, 2000

4. J.S. Newman, *Electrochemical Systems,* Prentice-Hall, 1973

5. D.C. Silverman, Rotating Cylinder Electrode for Velocity Sensitivity Testing, *Corrosion,* Vol 40, 1984, p 220

6. A.J. Bard and L.R. Faulkner, in *Electrochemical Methods: Fundamentals and Applications,* J. Wiley & Sons, 1980, p 283–304

7. K.D. Efird, E.J. Wright, J.A. Boros, and T.G. Hailey, Correlation of Steel Corrosion in Pipe Flow with Jet Impingement and Rotating Cylinder Tests, *Corrosion,* Vol 49, 1993, p 992

8. "Standard Guide for Conducting Coupon Tests in Field Applications," G 4, *Wear and Erosion; Metal Corrosion,* Vol 03.02, *Annual Book of ASTM Standards,* American Society for Standards and Testing, 2002

9. G. Wranglén, *An Introduction to Corrosion and Protection of Metals,* Chapman & Hall, 1985, p 229

10. R.L. Martin and E.C. French, Corrosion Monitoring in Sour Systems Using Electrochemical Hydrogen Patch Probes, *J. Pet. Technol.,* Nov 1978, p 1566–1570

11. "Standard Test Method for Conducting Potentiodynamic Polarization Resistance Measurements," G 59, *Wear and Erosion; Metal Corrosion,* Vol 03.02, *Annual Book of ASTM Standards,* American Society for Standards and Testing, 2002

12. "Standard Guide for On-Line Monitoring of Corrosion in Plant Equipment (Electrical and Electrochemical Methods)," G 96, *Wear and Erosion; Metal Corrosion,* Vol 03.02, *Annual Book of ASTM Standards,* American Society for Standards and Testing, 2002

B. Phull, Evaluating Uniform Corrosion, *Corrosion: Fundamentals, Testing, and Protection*, Vol 13A, *ASM Handbook*, ASM International, 2003, p 542–544

Evaluating Uniform Corrosion

Revised by Bopinder Phull, Consultant

Selected References

- A.H. Ailor, Ed., *Handbook of Corrosion Testing and Evaluation,* J. Wiley & Sons, Inc., 1971
- R. Baboian, Ed., *Manual 20 Corrosion Tests and Standards: Application and Interpretation,* ASTM, West Conshohocken, PA, 1995
- M. Fontana, *Corrosion Engineering,* 3rd ed., McGraw-Hill, 1986
- P.A. Schweitzer, *Corrosion and Corrosion Protection Handbook,* Marcel Dekker, 1983
- R. Winston Revie, Ed., *Uhligh's Corrosion Handbook,* 2nd ed., J. Wiley & Sons, Inc., 2000

B. Phull, Evaluating Pitting Corrosion, *Corrosion: Fundamentals, Testing, and Protection*, Vol 13A, *ASM Handbook*, ASM International, 2003, p 545–548

Evaluating Pitting Corrosion

Revised by Bopinder Phull, Consultant

Introduction

PITTING is a form of localized corrosion that is often a concern in applications involving passivating metals and alloys in aggressive environments. Pitting can also occur in nonpassivating alloys with protective coatings or in certain heterogeneous corrosive media. It is a very damaging form of corrosion that is not readily evaluated by the methods used for characterizing metal loss caused by uniform corrosion. It should be recognized that accelerated laboratory test methods allow ranking of relative susceptibility or resistance to pitting corrosion but typically do not provide reliable predictions of time to failure in actual service environments.

B. Phull, Evaluating Pitting Corrosion, *Corrosion: Fundamentals, Testing, and Protection*, Vol 13A, *ASM Handbook*, ASM International, 2003, p 545–548

Evaluating Pitting Corrosion

Revised by Bopinder Phull, Consultant

Test Methods

ASTM G 48 gives procedures for determining the pitting (and crevice) corrosion resistance of stainless steels and related alloys when exposed to an oxidizing chloride environment, namely, 6% ferric chloride ($FeCl_3$) at 22 ± 2 or 50 ± 2 °C (70 ± 3.5 or 120 ± 3.5 °F) (Ref 1). Method A is a 72 h total-immersion test of small coupons that is designed to determine the relative pitting resistance of stainless steels and nickel-base chromium-bearing alloys. Method B is a crevice test under the same exposure conditions, and it can be used to determine both the pitting and crevice corrosion resistance of these alloys. These tests can be used for determining the effects of alloying additions, heat treatments, and surface finishes on pitting and crevice corrosion resistance. Methods A and B are designed to cause breakdown of type 304 stainless steel at room temperature. Methods C and D are used to determine the critical temperature to cause initiation of pitting and crevice corrosion, respectively, in 6% $FeCl_3$ + 1% HCl solution. In each of these methods, the use of $FeCl_3$ solution is justified on the basis that a similar electrolyte chemistry develops within the pits in susceptible ferrous alloys exposed to chloride-containing service environments. As a result, these tests can give misleading results for alloys intended for chloride-free service environments.

ASTM F 746 describes a procedure to determine the resistance to pitting or crevice corrosion of passive metals and alloys from which surgical implants will be produced (Ref 2). This is an electrochemical potentiostatic screening test that is used to rank surgical implant alloys in order of their resistance to localized corrosion in a 0.9% NaCl solution at 37 ± 1 °C (98.6 ± 1.8 °F) (average human body temperature). Using a potentiostat, an anodic potential is applied to a small test specimen in an effort to initiate localized corrosion; the current is then monitored as a function of time at a constant potential. With this method, alloys are ranked in terms of the critical potential for pitting; the more electropositive (more noble) this critical potential is, the more resistant the alloy is to passive film breakdown and to localized corrosion. The method was intentionally designed to cause breakdown of at least one alloy (type 316L stainless steel) that is currently considered acceptable for

surgical implant use. Those alloys that suffer pitting or crevice corrosion during more severe portions of the test do not necessarily suffer localized corrosion when placed within the human body as a surgical implant.

ASTM G 61 is an electrochemical test method for conducting cyclic potentiodynamic polarization measurements to determine susceptibility to localized corrosion (Ref 3) of iron-, nickel-, and cobalt-base alloys in chloride environments. A small test specimen is polarized using a potentiostat, a counter electrode, and a reference electrode. Commencing at the free (or open circuit) corrosion potential, a polarization curve is generated by scanning the potential of the test specimen in the anodic direction. (The potential versus log current density plot is usually recorded automatically.) The scan is reversed at some preset criterion (potential or current density). Breakdown potential for pitting, repassivation (protection) potential, and hysteresis behavior (difference between forward and reverse anodic scans) data are acquired from the polarization curve and used to compare the pitting (or crevice) corrosion resistance of test materials. Several different methods for determining the protection potential have been compared (Ref 4).

The general interpretation of the results is that pits initiate and grow at potentials more noble than the breakdown (pitting) potential of the passive film. In service environments, this can happen when the corrosion potential shifts sufficiently in the electropositive direction, for example, due to the influence of oxidizing species such as O_2, Fe^{3+}, OCl^-, and so on. At potentials more active or electronegative than the repassivation (protection) potential, pit initiation and growth are stifled. It should be noted that breakdown potential, repassivation potential, and hysteresis behavior are not material properties; they are empirical values, which are influenced by experimental technique and procedure. Nevertheless, they are useful in ranking alloy performance when nominally the same test procedure is followed. Criticisms of such tests for predicting long-term corrosion behavior are discussed in Ref 5, 6, 7.

ASTM G 100 gives a procedure for conducting cyclic galvanostaircase polarization (GSCP) to determine relative susceptibility to pitting (and crevice) corrosion of alloys (Ref 8). In this method, the current is increased and decreased and the potential is monitored. For some materials, specifically aluminum alloy 3003-H14 (UNS A93003), this method gives a more reproducible protection potential value compared to potentiodynamic methods such as ASTM G 61.

Although polarization test techniques such as ASTM G 61 or G 100 are used primarily in the laboratory, they can also be used successfully in the field. However, the risk of ground (earth) loops, which can affect measurement capabilities and hence results, is greater for in-plant (field) applications because of the possibility of the large electrical and magnetic fields often associated with industrial equipment. A common ground-loop problem can be circumvented by using a potentiostat that has a floating working (test) electrode terminal instead of a grounded one. Because of the large applied potentials used in these tests, the test specimens are usually irreversibly affected, at least in electrochemical terms. Thus, they are not considered as on-line techniques for routine monitoring of localized corrosion. There are on-line techniques (Ref 9), such as electrochemical linear polarization resistance (LPR) and electrical resistance (ER), but they are more suited to monitoring uniform rather than localized corrosion.

Electrochemical noise (EN) is a relatively new technique that is finding increasing use alongside the more traditional electrochemical methods, both in research and the field. Electrochemical potential noise (EPN) involves monitoring small shifts (typically μV to mV range) in the corrosion potential of a test electrode with respect to a suitable reference electrode. Initiation of pits is usually characterized by distinct shifts in potential; repassivation is indicated by potential recovery. Quantitative information on corrosion rate is given by electrochemical current noise (ECN) measurements in which the micro-galvanic current between two nominally identical test specimens made from the material of interest is monitored. References 10, 11, 12 provide additional information on EN techniques.

References cited in this section

1. "Standard Test Methods for Pitting and Crevice Corrosion Resistance of Stainless Steels and Related Alloys by the Use of Ferric Chloride Solution," G 48, *Wear and Erosion; Metal Corrosion,* Vol 03.02, *Annual Book of ASTM Standards,* American Society for Testing and Materials, 2002

2. "Standard Test Method for Pitting or Crevice Corrosion of Metallic Surgical Implant Materials," F 746, *Medical Devices, Emergency Medical Services,* Vol 13.01, *Annual Book of ASTM Standards,* American Society for Testing and Materials, 2002

3. "Standard Practice for Conducting Cyclic Potentiodynamic Polarization Measurements for Localized Corrosion," G 61, *Wear and Erosion; Metal Corrosion,* Vol 03.02, *Annual Book of ASTM Standards,* American Society for Testing and Materials, 2002

4. M. Hubbell, C. Price, and R. Heidersbach, Crevice and Pitting Corrosion Tests for Stainless Steels: A Comparison of Short- Term Tests With Longer Exposures, *Laboratory Corrosion Tests and Standards,* STP 866, G.S. Haynes and R. Baboian, Ed., American Society for Testing and Materials, 1985, p 324–336

5. B.E. Wilde, Critical Appraisal of Some Popular Laboratory Tests for Predicting the Localized Corrosion Resistance of Stainless Alloys in Sea Water, *Corrosion,* Vol 28 (No. 8), Aug 1972, p 283

6. F.L. LaQue and H.H Uhlig, An Essay on Pitting, Crevice Corrosion and Related Potentials, *Mater. Perform.,* Vol 22 (No. 8), Aug 1983, p 34

7. D. C. Silverman, Practical Corrosion Prediction Using Electrochemical Techniques, *Uhlig's Corrosion Handbook,* R.W. Revie, Ed., John Wiley & Sons, 2000, p 1179–1225

8. "Standard Test Method for Conducting Cyclic Galvanostaircase Polarization," G 100, *Wear and Erosion; Metal Corrosion,* Vol 03.02, *Annual Book of ASTM Standards,* American Society for Testing and Materials, 2002

9. "Standard Guide for On-Line Monitoring of Corrosion in Plant Equipment (Electrical and Electrochemical Methods)," G 96, *Wear and Erosion; Metal Corrosion,* Vol 03.02, *Annual Book of ASTM Standards,* American Society for Testing and Materials, 2002

10. D.A. Eden, Electrochemical Noise, *Uhlig's Corrosion Handbook,* R.W. Revie, Ed., John Wiley & Sons, 2000, p 1127–1238

11. J.R. Kearns and J.R. Scully, Ed., *Electrochemical Noise Measurement for Corrosion Applications,* STP 1277, American Society for Testing and Materials, 1996

12. R.G. Kelly, in *Corrosion Tests and Standards: Application and Interpretation,* R. Baboian, Ed., American Society for Testing and Materials, 1995, p 172

B. Phull, Evaluating Pitting Corrosion, *Corrosion: Fundamentals, Testing, and Protection*, Vol 13A, *ASM Handbook*, ASM International, 2003, p 545–548

Evaluating Pitting Corrosion

Revised by Bopinder Phull, Consultant

Examination of Pits

ASTM G 46 provides guidance for the identification and examination of pits and evaluating the extent of pitting corrosion (Ref 13). It is important to be able to determine the extent of pitting, either in service applications or in laboratory tests for ranking alloy performance. The following is a summary of the procedures described in detail in Ref 13. Additional guidelines can be found in Ref 14.

Identification and Examination of Pits

Visual examination of the corroded surface can be performed with the unaided eye or a low- power microscope. The corroded surface is usually photographed, and the size, shape, and density of the pits determined (Fig. 1, 2).

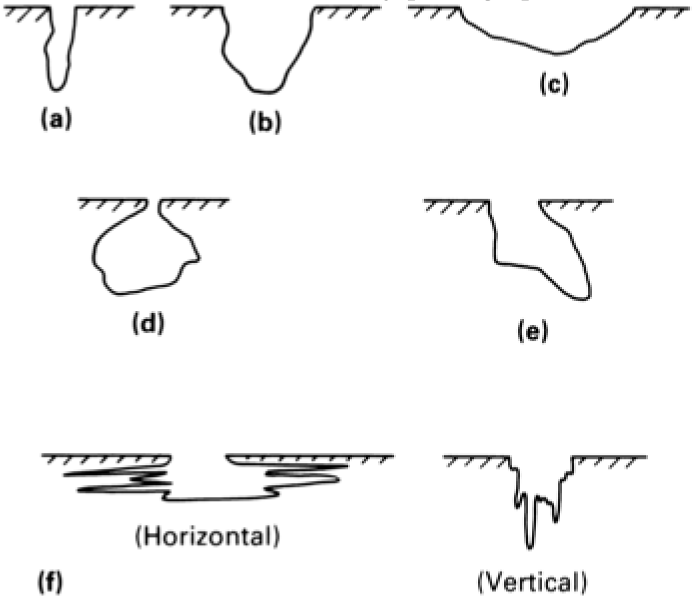

Fig. 1 Variations in the cross-sectional shape of pits. (a) Narrow and deep. (b) Elliptical. (c) Wide and shallow. (d) Subsurface. (e) Undercutting. (f) Shapes determined by microstructural orientation. Source: Ref 13

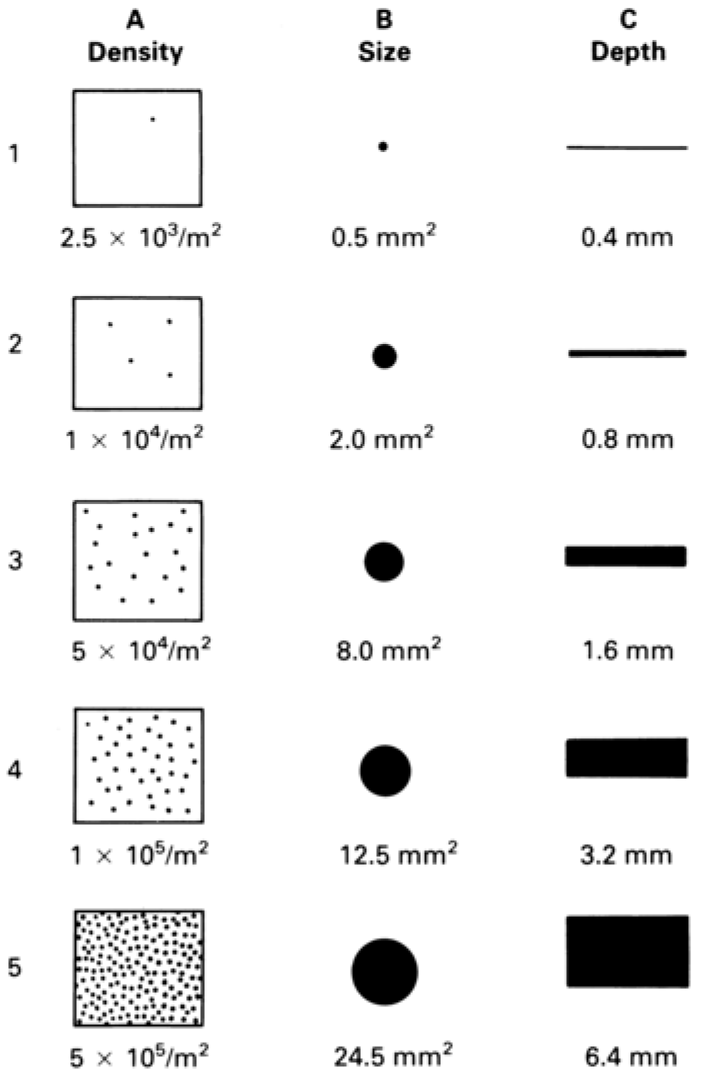

Fig. 2 Standard rating chart for pits. Source: Ref 13

Metallographic examination can be used to determine whether there is a correlation between pits and microstructure and whether the cavities are true pits or the result of another mechanism, such as intergranular corrosion or dealloying.

Nondestructive Inspection. Reference 13 outlines procedures for the nondestructive evaluation of pitted specimens. These include radiographic, electromagnetic, ultrasonic, and dye- penetrant inspection. These methods can be used to locate pits and to provide some information on their size, but they generally cannot detect small pits or differentiate between pits and other types of surface defects.

Extent of Pitting

Mass loss is generally not a good indication of the extent of pitting unless uniform corrosion is slight and pitting is fairly severe. If there is significant uniform corrosion, the contribution of pitting to total mass loss is small. Mass loss should not be ignored in every case, however. For example, measurement of mass loss, along with visual comparison of pitted surfaces, may be sufficient to rank the relative resistance of alloys in laboratory tests.

Pit depth measurement is generally a better indicator of the extent of localized attack than mass loss. Pit depth measurement can be accomplished by several methods, including metallographic examination, machining, use of a micrometer or depth gage, and microscopic measurements. In the microscopic method, a metallurgical microscope is focused on the lip of the pit and then on the bottom of the pit. The difference between the initial and final readings on the fine-focusing knob or stage vernier is the pit depth.

References cited in this section

13. "Standard Recommended Practice for Examination and Evaluation of Pitting Corrosion," G 46, *Wear and Erosion; Metal Corrosion,* Vol 03.02, *Annual Book of ASTM Standards,* American Society for Testing and Materials, 2002

14. F.A. Champion, *Corrosion Testing Procedures,* 2nd ed., John Wiley & Sons, 1965, p 197

B. Phull, Evaluating Pitting Corrosion, *Corrosion: Fundamentals, Testing, and Protection,* Vol 13A, *ASM Handbook*, ASM International, 2003, p 545–548

Evaluating Pitting Corrosion

Revised by Bopinder Phull, Consultant

Evaluation of Pitting

Pitting can be described in several ways. Reference 13 includes procedures for the use of standard charts, metal penetration, statistical analysis, and loss in mechanical properties to quantify the severity of pitting damage. More than one of these methods can be used. In fact, it is often found that no single method is sufficient by itself.

Standard charts such as shown in Fig. 2 can be used to rate pits in terms of density, size, and depth. Columns A and B in Fig. 2 are used to rate the density (that is, the number of pits per unit area on the specimen surface) and the average size of the pits, respectively. Column C rates the average depth of attack. An example of a rating using Fig. 2 might be A-3, B-2, C-3; this rating indicates a density of 5×10^4 pits/m^2, an average pit size of 2.0 mm^2, and an average pit depth of 1.6 mm.

Such charts facilitate communication among those who are familiar with the standard ratings and offer a simple means of storing data for comparison with other test results. However, it can be tedious and time-consuming to

measure all of the pits, and the time spent doing so is usually not justified, because maximum values (especially pit depths) are often more significant than average values.

Metal Penetration. In this method, the deepest pits are measured and metal penetration is expressed in terms of the maximum pit depth, an average of, for example, the ten deepest pits, or both. Metal penetration is especially significant when the metal is intended for service as an enclosure for gas or liquid and when a hole could result in loss of fluid.

Metal penetration can also be expressed in terms of a pitting factor, which is the ratio of the deepest metal penetration to the average metal penetration (determined from mass loss):

$$\text{Pitting factor} = \frac{\text{Deepest metal penetration}}{\text{Average metal penetration}} \qquad \text{(Eq 1)}$$

A pitting factor of 1 represents uniform corrosion. The larger the number, the greater the pit depth penetration. The pitting factor cannot be used when pitting or general corrosion is slight, because values of 0 or infinity are obtained in such situations, respectively.

The application of statistics to the analysis of corrosion data is covered in detail in ASTM G 16 (Ref 15). The subject is discussed briefly in Ref 13 to show how statistics can be used in the evaluation of pitting data.

The probability that pitting will initiate on a metal surface depends on a number of factors, including the pitting tendency of the metal, the corrosivity of the solution, the specimen area, and the duration of exposure. A pitting probability test can be used to determine the susceptibility of metals to pitting. However, this test will not provide information about the rate of propagation, and the results are applicable only to the conditions of exposure. Pitting probability *P* is expressed as a percentage and requires exposure of a number of specimens to a particular set of conditions (Ref 16, 17):

$$P = \frac{N_p}{N} \times 100 \qquad \text{(Eq 2)}$$

where N_p is the number of specimens that pit, and *N* is the total number of specimens.

The relationship between pit depth and area or time of exposure may vary with such factors as the environment and the metal exposed. Equations 3 and 4 are examples of the relationships that have been found to apply under certain exposure conditions. Equation 3 is the relationship between maximum pit depth *D* and the area *A* of a pipeline exposed to soil (Ref 18, 19, 20):

$$D = \mathrm{b}A^{\mathrm{a}} \qquad \text{(Eq 3)}$$

where a and b are constants (each > 0) derived from the slope and the *y*-intercept of a straight line obtained when the logarithm of the maximum or mean pit depth for successively increasing exposed areas on the pipeline are plotted against the logarithm of the corresponding pipeline areas. The dependence on exposed area is attributed to the increased chance for the deepest pit to be found when the size of the sample of pits is increased by an increase in the area of corroded surface.

There is a common but highly mistaken tendency to divide measured pit depth by exposure time to compute a pitting rate, for example, mils per year, millimeters per year, and so on. Unless independently corroborated by good data, this approach can be misleading and potentially hazardous in predicting time to failure by pitting corrosion. The maximum pit depth *D* of aluminum exposed to various waters was found to vary as the cube root of time *t*, as shown in Eq 4 (Ref 16, 21):

$$D = \mathrm{K}t^{1/3} \qquad \text{(Eq 4)}$$

where K is a constant that is dependent on the composition of the water and the alloy. Equation 4 has been found to apply to several aluminum alloys exposed to different waters.

Extreme value probability statistics (Ref 22, 23) have been successfully applied to estimate the maximum pit depth on a large area of material based on examination of only a small portion of that area (Ref 14, 16, 21). The procedure consists of measuring maximum pit depths on several replicate specimens and then arranging the pit depth values in order of increasing rank. A plotting position for each order of ranking is obtained by substitution in the relation $M/(n + 1)$, where *M* is the order of ranking of the specimen in question, and *n* is the total number of specimens or values. For example, the plotting position for the second value out of 10 would be 2/(10 + 1) = 0.1818. These values are plotted on the ordinate of extreme value probability paper versus corresponding maximum pit depths. A straight line indicates that extreme value statistics are applicable.

Extrapolation of the straight line can be used to determine the probability that a specific pit depth will occur or the number of observations that must be made to find a particular pit depth.

Loss in Mechanical Properties. If pitting is the predominant form of corrosion and if the density of pitting is relatively high, the change in a mechanical property relative to unexposed control specimens can be used to characterize degree of pitting. The typical properties considered for this purpose are tensile strength, elongation, fatigue strength, impact resistance, and burst pressure (Ref 24, 25).

The precautions that must be taken in the application of these mechanical test procedures are covered in most standard methods. However, it must be stressed that the exposed and unexposed specimens should replicate each other as closely as possible. Therefore, consideration should be given to such factors as specimen size, edge effects, direction of rolling, and surface finish.

Representative specimens of the metal are exposed to the same conditions except for the corrosive environment. The mechanical properties of the exposed and unexposed specimens are measured after the exposure, and the difference between the two results is attributed to corrosion damage.

Some of these methods are better suited to the evaluation of other forms of localized corrosion, such as intergranular or stress corrosion. Therefore, their limitations must be considered. The often erratic nature of pitting and the location of pits on the specimen can affect results. In some cases, the change in mechanical properties due to pitting may be too small to provide meaningful results. Perhaps one of the most difficult problems is to separate the effects due to pitting from those caused by other forms of corrosion.

References cited in this section

13. "Standard Recommended Practice for Examination and Evaluation of Pitting Corrosion," G 46, *Wear and Erosion; Metal Corrosion,* Vol 03.02, *Annual Book of ASTM Standards,* American Society for Testing and Materials, 2002

14. F.A. Champion, *Corrosion Testing Procedures,* 2nd ed., John Wiley & Sons, 1965, p 197

15. "Standard Recommended Practice for Applying Statistics to Analysis of Corrosion Data," G 16, *Annual Book of ASTM Standards,* American Society for Testing and Materials, 2002

16. B.R. Pathak, Testing in Fresh Waters, *Handbook on Corrosion Testing and Evaluation,* W.H. Ailor, Ed., John Wiley & Sons, 1971, p 553

17. P.M. Aziz and H.P. Godard, Influence of Specimen Area on the Pitting Probability of Aluminum, *J. Electrochem. Soc.,* Vol 102, Oct 1955, p 577

18. G.N. Scott, Adjustment of Soil Corrosion Pit Depth Measurements for Size of Sample, *Proceedings of the American Petroleum Institute,* Vol 14, Section IV, American Petroleum Institute, 1934, p 204

19. M. Romanoff, *Underground Corrosion,* National Bureau of Standards Circular 579, U.S. Government Printing Office, 1957, p 71

20. I.A. Denison, Soil Exposure Tests, *The Corrosion Handbook,* H.H. Uhlig, Ed., John Wiley & Sons, 1948, p 1048

21. H.P. Godard, The Corrosion Behavior of Aluminum in Natural Waters, *Can J. Chem. Eng.,* Vol 38, Oct 1960, p 1671

22. E.J. Gumbel, *Statistical Theory of Extreme Values and Some Practical Applications,* Applied Mathematics Series 33, U.S. Department of Commerce, 1954

23. P.M. Aziz, Application of the Statistical Theory of Extreme Values to the Analysis of Maximum Pit Depth Data for Aluminum, *Corrosion,* Vol 12, Oct 1956, p 495

24. T.J. Summerson, M.J. Pryor, D.S. Keir, and R.J. Hogan, Pit Depth Measurements as a Means of Evaluating the Corrosion Resistance of Aluminum in Sea Water, *Metals,* STP 196, American Society for Testing and Materials, 1957, p 157

25. R. Baboian, “Corrosion Resistant High- Strength Clad Metal System for Hydraulic Brake Line Tubing,” SAE Preprint 740290, Society for Automotive Engineers, 1972

B. Phull, Evaluating Pitting Corrosion, *Corrosion: Fundamentals, Testing, and Protection*, Vol 13A, *ASM Handbook*, ASM International, 2003, p 545–548

Evaluating Pitting Corrosion

Revised by Bopinder Phull, Consultant

Acknowledgment

This article has been adapted from D.O. Sprowls, Evaluation of Pitting Corrosion, *Corrosion,* Vol 13, *ASM Handbook* (formerly *Metals Handbook,* 9th ed.), ASM International, 1987, p 231–233.

B. Phull, Evaluating Pitting Corrosion, *Corrosion: Fundamentals, Testing, and Protection*, Vol 13A, *ASM Handbook*, ASM International, 2003, p 545–548

Evaluating Pitting Corrosion

Revised by Bopinder Phull, Consultant

Acknowledgment

This article has been adapted from D.O. Sprowls, Evaluation of Pitting Corrosion, *Corrosion,* Vol 13, *ASM Handbook* (formerly *Metals Handbook,* 9th ed.), ASM International, 1987, p 231–233.

B. Phull, Evaluating Pitting Corrosion, *Corrosion: Fundamentals, Testing, and Protection*, Vol 13A, *ASM Handbook*, ASM International, 2003, p 545–548

Evaluating Pitting Corrosion

Revised by Bopinder Phull, Consultant

Selected References

- A.H. Ailor, Ed., *Handbook of Corrosion Testing and Evaluation,* John Wiley & Sons, 1971
- R. Baboian, Ed., *Manual 20 Corrosion Tests and Standards: Application and Interpretation,* ASTM International, 1995
- M. Fontana, *Corrosion Engineering,* 3rd ed., McGraw-Hill, 1986

- H. P. Godard, W. B. Jepson, M. R. Bothwell, and R. L. Kane, *The Corrosion of Light Metals,* John Wiley & Sons, 1967
- Z. Szklarska-Smialowska, *Pitting Corrosion of Metals,* NACE International, 1986

R.M. Kain, Evaluating Crevice Corrosion, *Corrosion: Fundamentals, Testing, and Protection*, Vol 13A, *ASM Handbook*, ASM International, 2003, p 549–561

Evaluating Crevice Corrosion

R.M. Kain, Consultant

Introduction

CREVICE CORROSION is a form of localized corrosion that affects many alloys that normally exhibit passive behavior. Stainless steels, particularly those with little or no molybdenum, are especially prone to crevice corrosion. In neutral and acidic chloride-containing environments, some higher-alloyed stainless-type materials and related nickel-base alloys may also be susceptible to crevice attack. Although other materials, such as aluminum alloys, copper alloys, and titanium alloys, may also be susceptible to crevice-related corrosion, testing and test development have primarily focused on assessing the behavior of the stainless-type alloys. Much of this attention has been directed toward identification and development of more resistant alloys for marine applications and in certain process industries, such as pulp and paper. Over the years, diverse crevice corrosion testing methodologies have evolved and continue to find significant utility in simple immersion studies, electrochemical testing, and the development of mathematical modeling. This article discusses a number of the more frequently used crevice corrosion testing and evaluation procedures. It is recognized, however, that other techniques may exist and that their merits should be examined, especially in the context of the intended application.

R.M. Kain, Evaluating Crevice Corrosion, *Corrosion: Fundamentals, Testing, and Protection*, Vol 13A, *ASM Handbook,* ASM International, 2003, p 549–561

Evaluating Crevice Corrosion

R.M. Kain, Consultant

Aspects of Crevice Corrosion Testing

Because crevices are real space dimensions between mating materials, use of the term *artificial* crevice test is discouraged in favor of descriptors that identify the crevice former as naturally occurring (for example, a barnacle) or man-made (for example, a washer). Man-made crevice formers can be either a metal or nonmetal and recreate the geometry of some fabricated crevices. Man-made crevice formers may or may not reproduce all conditions found in service, particularly those that are naturally occurring.

Crevice corrosion tests are based on two accepted phases of crevice corrosion: initiation and propagation. Initiation refers to the breakdown of passivity and propagation or penetration as the actual occurrence of crevice corrosion. Under some conditions, breakdown may be followed by repassivation without any outward evidence of attack. For a given alloy-environment combination, the occurrence of crevice corrosion is highly dependent on the crevice geometry. Tighter crevices are more conducive to promoting initiation, but this factor may affect

the propagation behavior of materials in different ways (Ref 1). Environmental factors may affect the rate of crevice corrosion propagation. Although natural and synthetic seawater, for example, will both initiate crevice corrosion on type 316 (Unified Numbering System, or UNS, S31600) and many other stainless alloys, propagation in the two environments is often quite different (Ref 2). The overall size of the specimen in relation to the crevice (cathode-to-anode) surface area can also affect propagation behavior. Regardless of the purpose of crevice corrosion testing, the investigator should be aware that these and many other factors can affect test results.

Depending on availability, natural or actual process environments may be used in laboratory immersion tests. This provides a convenient opportunity to study, for example, the effects of temperature, crevice geometry, and other factors such as surface finish. Crevice corrosion tests can be conducted at marine corrosion test sites and at laboratories associated with chemical-processing facilities.

References cited in this section

1. T.S. Lee et al., Mathematical Modelling of Crevice Corrosion of Stainless Steels, *Corrosion and Corrosion Protection Proceedings,* Vol 81-8, The Electrochemical Society, 1981, p 213–224
2. R.M. Kain and T.S. Lee, Recent Developments in Test Methods for Investigating Crevice Corrosion, *Laboratory Corrosion Tests and Standards,* STP 866, American Society for Testing and Materials, 1985, p 299–323

R.M. Kain, Evaluating Crevice Corrosion, *Corrosion: Fundamentals, Testing, and Protection*, Vol 13A, *ASM Handbook*, ASM International, 2003, p 549–561

Evaluating Crevice Corrosion

R.M. Kain, Consultant

Guidelines for Crevice Corrosion Testing

Laboratory crevice corrosion screening tests play a valuable role in the ultimate use of stainless steels in corrosive environments. Laboratory immersion tests and electrochemical studies are important tools for investigating the effects of alloy content, surface preparation, and environmental variables. However, test results should be used judiciously so as not to limit materials that may otherwise not meet contrived conditions selected to accelerate test results. ASTM G 78 provides guidance for conducting crevice corrosion tests on stainless steels and related nickel-base alloys in seawater and other chloride-containing environments (Ref 3). While its origins grew out of attempts to standardize the use of multiple- crevice assemblies, described later in this article, this guide does not promote any particular crevice former but advises the reader to be aware that crevice corrosion test results can be affected by a number of interrelated factors. In particular, crevice geometry and specimen preparation are very important aspects of testing. This standard provides guidance in the conduct of tests for flat and cylindrical specimens as well as those having irregular surfaces, such as weldments. It also reviews evaluation and reporting considerations. Importantly, Ref 3 points out that the occurrence or absence of crevice corrosion in a given test is no assurance that it will not occur under other test conditions. This is especially true if the design fails to consider those factors that may affect initiation and/or propagation behavior.

Reference cited in this section

3. “Standard Guide for Crevice Corrosion Testing of Iron-Base and Nickel-Base Stainless Alloys in Seawater and Other Chloride Containing Aqueous Environments,” G 78, *Annual Book of ASTM Standards,* American Society for Testing and Materials

R.M. Kain, Evaluating Crevice Corrosion, *Corrosion: Fundamentals, Testing, and Protection*, Vol 13A, *ASM Handbook*, ASM International, 2003, p 549–561

Evaluating Crevice Corrosion

R.M. Kain, Consultant

Guidelines for Crevice Corrosion Testing

Laboratory crevice corrosion screening tests play a valuable role in the ultimate use of stainless steels in corrosive environments. Laboratory immersion tests and electrochemical studies are important tools for investigating the effects of alloy content, surface preparation, and environmental variables. However, test results should be used judiciously so as not to limit materials that may otherwise not meet contrived conditions selected to accelerate test results. ASTM G 78 provides guidance for conducting crevice corrosion tests on stainless steels and related nickel-base alloys in seawater and other chloride-containing environments (Ref 3). While its origins grew out of attempts to standardize the use of multiple- crevice assemblies, described later in this article, this guide does not promote any particular crevice former but advises the reader to be aware that crevice corrosion test results can be affected by a number of interrelated factors. In particular, crevice geometry and specimen preparation are very important aspects of testing. This standard provides guidance in the conduct of tests for flat and cylindrical specimens as well as those having irregular surfaces, such as weldments. It also reviews evaluation and reporting considerations. Importantly, Ref 3 points out that the occurrence or absence of crevice corrosion in a given test is no assurance that it will not occur under other test conditions. This is especially true if the design fails to consider those factors that may affect initiation and/or propagation behavior.

Reference cited in this section

3. “Standard Guide for Crevice Corrosion Testing of Iron-Base and Nickel-Base Stainless Alloys in Seawater and Other Chloride Containing Aqueous Environments,” G 78, *Annual Book of ASTM Standards,* American Society for Testing and Materials

R.M. Kain, Evaluating Crevice Corrosion, *Corrosion: Fundamentals, Testing, and Protection*, Vol 13A, *ASM Handbook,* ASM International, 2003, p 549–561

Evaluating Crevice Corrosion

R.M. Kain, Consultant

Specific Crevice Corrosion Tests

In-Plant and Field Testing. A considerable amount of crevice corrosion data has been obtained from in-plant and field test rack exposures of candidate alloys in various process streams and other industrial environments.

ASTM G 4 (Ref 4) provides guidance on specimen preparation, test rack assembly, and exposure considerations. Simple tetrafluoroethylene (TFE) fluorocarbon sleeves and washers, intended primarily as electrical insulating spacers between candidate alloy specimens, have proved to be effective crevice formers. Likewise, metal-to- metal configurations have also been used. Test results for square, rectangular, and circular spool disk specimens have identified the occurrence of crevice corrosion and the extent of penetration incurred during the exposure period. Although these and other tests lack definition with regard to actual times to initiation and rates of propagation, they are nonetheless quite effective in screening materials for further consideration. Some test racks are spring loaded, while others are not. It is generally recognized that rapid and severe attack on some specimens in a test assembly may influence crevice tightness on others in the same assembly.

One area in which test rack exposures have been extensively used is the pulp and paper industry. For example, Ref 5 discusses results from bleach plant exposure in which crevice corrosion susceptibility was identified for 24 of the 26 alloys tested. However, the crevices found in bleach plant equipment may be less severe than those on the test specimens. This is supported by the observation that some materials that exhibited less than 0.4 to 0.46 mm (15 to 18 mils) of crevice penetration in a 3 month test actually performed satisfactorily in service for up to 20 years.

Ferric Chloride Crevice Corrosion Tests. Ferric chloride tests involve exposure to a highly oxidizing acid chloride environment. The pH of the standard 6% $FeCl_3$ solution, according to ASTM G 48 (Ref 6), is approximately 1.2. This is less than the pH of the critical crevice solution, which can cause a breakdown of passivity for UNS S30400 and S31600 stainless steels. Critical crevice solution compositions for these alloys with respect to pH and chloride concentration have been identified as pH 2.0 at 1.5 *M* Cl^- and pH 1.7 at 3.5 *M* Cl^-, respectively (Ref 7, 8). Use of $FeCl_3$ eliminates the time factor for development of the aggressive crevice solution from the neutral pH of, for example, a chloride- containing natural water. The crevice prevents oxygen from maintaining the passive film. The combination of low pH and high Cl^- lowers the breakdown or critical potential for pitting in the crevice, while ferric ions (Fe^{3+}) maintain the potential of the alloy in the critical region that supports the cathodic reaction outside the crevice.

More resistant alloys do not exhibit a breakdown potential in the domain associated with Fe^{3+} reduction at ambient temperature. In some cases, the Fe^{3+} serves as a chemical potentiostat and holds the corrosion potential well within the passive region in the absence of oxygen. Increasing the $FeCl_3$ solution temperature to 50 °C (120 °F), for example, promotes breakdown and allows for ranking of more resistant alloys. Figure 1 shows schematically the polarization characteristics for stainless steels exposed to $FeCl_3$.

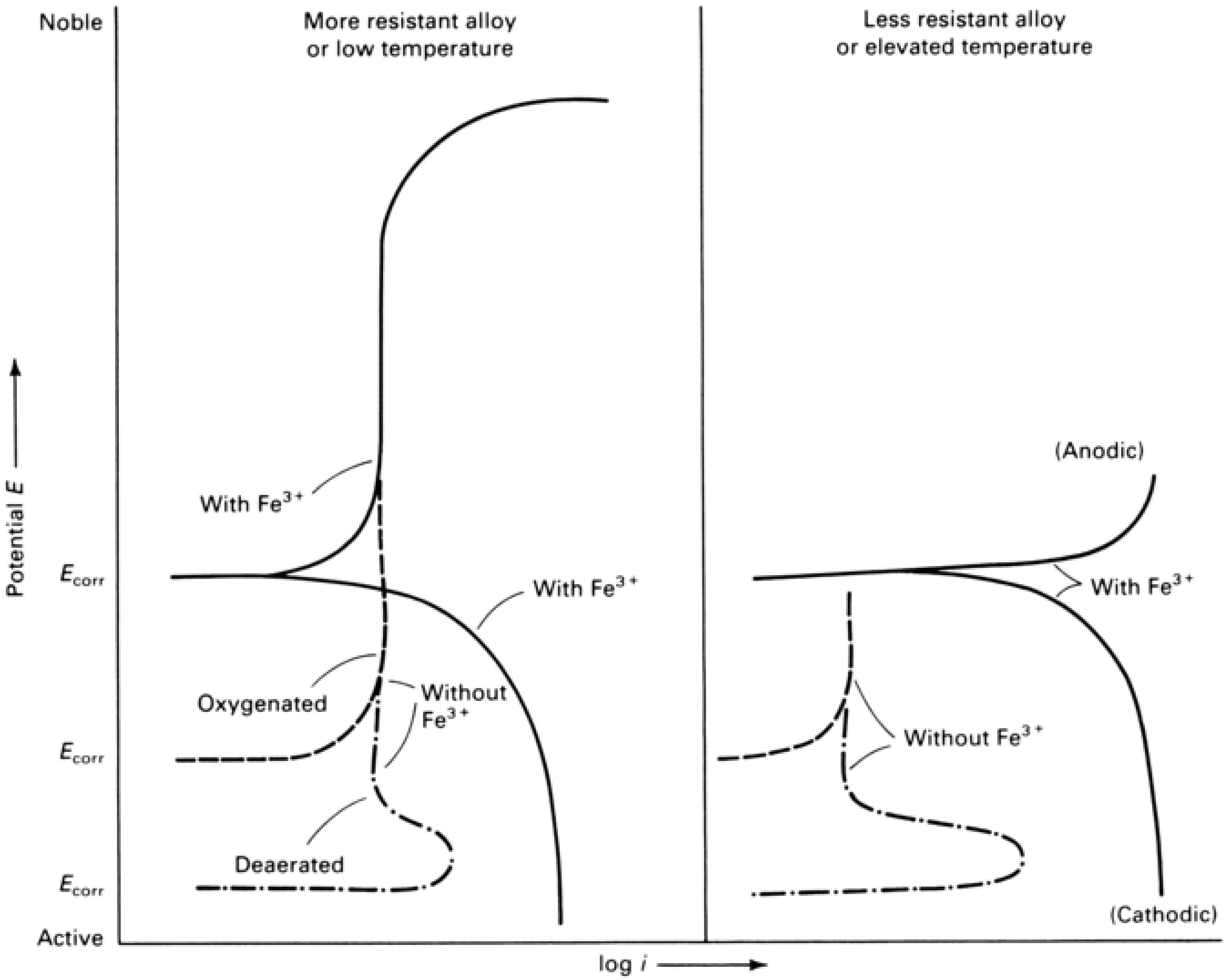

Fig. 1 Schematic showing the polarization characteristics of stainless-type materials in an acid chloride solution with and without Fe^{3+}. E_{corr}, corrosion potential; *i*, current density

ASTM and Materials Technology Institute (MTI) Test Methods. Both ASTM G 48 (method B) and MTI-2 (Ref 9) used a simple 6% ferric chloride solution prepared with $FeCl_3 \cdot 6H_2O$ and distilled water solutions. Both are intended for short-term testing within ambient and elevated- temperature ranges. In the G 48 (method B) procedure, crevices are formed by the placement of a polytetrafluoroethylene (PTFE) cylindrical block on each side of the test specimen and securing them in place with rubber bands. Tests at 22 ± 2 °C (72 ± 3.5 °F) are conducted for 72 h. Crevices in the MTI-2 method are created by the application of two modified multiple-crevice assemblies (serrated PTFE washers), each having 12 plateaus or contact sites. An assembly torque of 0.28 N · m (2.5 in. · lbf) was prescribed for tests of 24 h duration. The MTI-2 method calls for a series of tests so as to define a critical crevice temperature (CCT) within 2.5 °C (4.5 °F) increments. A CCT was one that produced at least a 0.025 mm (0.001 in.) deep attack at one or more of the available crevice sites.

There are currently two ASTM methods available for CCT testing: one intended primarily for nickel-base and chromium-containing alloys, G 48 (method D), and one for stainless steels, G 48 (method F). Corresponding standardized pitting tests appear under designations G 48 (methods A, C, and E). Both G 48 (methods D and F) use the serrated washer device mentioned previously. Method D specifies the original MTI-2 torque of 0.28 N · m (2.5 in. · lbf), while method E specifies a higher torque of 1.58 N · m (14 in. · lbf). Currently, the recommended test durations are 12 and 24 h, respectively. Both methods D and F use an acidified (1% HCl) solution of ferric chloride (6% $FeCl_2$), intended to provide stable pH conditions during elevated-temperature testing.

During modification of the original MTI-2 method, ASTM subcommittee G-01.05 adopted two alloy-chemistry-based equations useful in identifying a starting test temperature for the respective methods. Both G 48 (methods D and F) are intended to identify a CCT within the 0 to 85 °C (32 to 185 °F) range by the use of

fresh specimens for each exposure. If crevice corrosion is observed at the initial test temperature, methods D and F advise lowering the temperature for the next test by 5 °C (9 °F) and repeating the test. If no attack is found after the initial tests, the temperature is raised by 10 °C (18 °F) and a new specimen exposed. The process is repeated, as needed, until the CCT is identified. The criterion for crevice corrosion in these methods is a measured attack depth of ≥0.025 mm (0.001 in.).

Precision and bias statements exist for ASTM G 48 (methods D and F). For the purpose of alloy ranking, specimens tested by all three methods (B, D, and F) can be evaluated by mass loss, number of sites attacked, and the range of penetrations incurred. The user is cautioned that surface preparation can influence test results. Testing in ferric chloride solution with fresh specimens for each temperature increment resulted in lower CCT values than when the same specimen was reused without resurfacing (Ref 10). ASTM G 48 has been used for alloy development purposes as well as for quality control. Generally, acceptable criteria are established by agreement between alloy producer and the purchaser.

The value of CCT ranking for service life prediction remains limited. Some correlation has been reported for CCT and specific seawater test data (Ref 11, 12), but it does not take into account the effect of crevice geometry and the interrelationship with the natural environment. Although increasing temperature (for example, from 25 to 50 °C, or 77 to 120 °F) of the $FeCl_3$ solution is certainly detrimental, the same is not necessarily true with respect to crevice corrosion in seawater where bulk oxygen concentration decreases with increasing temperature (due to inverse solubility), and biological activity may increase initially but decreases drastically above a threshold temperature (Ref 13).

Sodium Chloride Crevice Corrosion Test. Materials Technology Institute method MTI-4 (Ref 9) involves testing in chloride solutions at eight concentrations, ranging from 0.1 to 3.0% NaCl, to establish a minimum (critical) Cl^- concentration that results in crevice corrosion at room temperature (20 to 24 °C, or 68 to 75 °F). Specimen requirements, crevice assembly procedure, and evaluation technique for the MTI-4 method are identical to those used in the MTI-2 method. The recommended test period for the MTI-4 method, however, is 1000 h, and suggested controls are UNS S30400 and S31600 stainless steel.

Both methods are acceptable screening tools and are well suited for alloy development purposes. However, extension of either method beyond its intended scope may be misleading. In the case of MTI-4, for example, deviations in crevice geometry from that of the serrated washer could significantly alter resistance to a given bulk Cl^- concentration. Tighter and/or larger crevices could promote initiation at lower Cl^- levels (Ref 14). Use of the serrated washer identified earlier, for example, has produced crevice initiation at Cl^- levels as low as 100 to 300 mg/L in a matter of a few days when assembled at an initial torque of 8.5 N · m (75 in. · lbf) (Ref 15). Metal-to-metal crevice sites can sometimes promote more rapid initiation and at lower Cl^- levels in comparison to nonmetal-to- metal crevices of comparable geometry (Ref 16).

References cited in this section

4. "Standard Guide for Conducting Corrosion Tests in Field Application," G 4, *Wear and Erosion; Metal Corrosion,* Vol 03.02, *Annual Book of ASTM Standards,* American Society for Testing and Materials

5. A.H. Tuthill, Resistance of Highly Alloyed Materials and Titanium to Localized Corrosion in Bleach Plant Environments, *Mater. Perform.,* Vol 24 (No. 9), 1985, p 43–49

6. "Standard Method for Pitting and Crevice Corrosion Resistance of Stainless Steels and Related Alloys by the Use of Ferric Chloride Solution," G 48, *Annual Book of ASTM Standards,* American Society for Testing and Materials

7. J.W. Oldfield and W.H. Sutton, Crevice Corrosion of Stainless Steels, Part II: Experimental Studies, *Br. Corros. J.,* Vol 13 (No. 3), 1978, p 104

8. R.M. Kain et al., Use of Electrochemical Techniques for the Study of Crevice Corrosion in Natural Seawater, Section 6: Localized Corrosion, *Electrochemical Techniques for Corrosion Engineering,* NACE Publication, 1986, p 261–279

9. R.S. Treseder and E.A. Kachik, MTI Corrosion Tests for Iron and Nickel-Base Corrosion Alloys, *Laboratory Corrosion Tests and Standards*, STP 866, American Society for Testing and Materials, 1985, p 373–399

10. E.L. Hibner, Modification of Critical Crevice Temperature Test Procedures for Nickel Alloys in a Ferric Chloride Environment, *Mater. Perform.,* Vol 26 (No. 3), 1987, p 37–40

11. A.P. Bond and H.J. Dundas, Resistance of Stainless Steels to Crevice Corrosion in Seawater, *Mater. Perform.,* Vol 23 (No. 7), 1984, p 39–43

12. A. Garner, Crevice Corrosion of Stainless Steel in Seawater: Correlation of Field Data with Laboratory Ferric Chloride Tests, *Corrosion,* Vol 37 (No. 3), 1981, p 178–184

13. T.S. Lee et al., The Effect of Environmental Variables on Crevice Corrosion of Stainless Steels in Seawater, *Mater. Perform.,* Vol 23 (No. 7), 1984, p 9–15

14. R.M. Kain, Crevice Corrosion Behavior of Stainless Steel in Seawater and Related Environments, *Corrosion,* Vol 40 (No. 6), 1984, p 313–321

15. R.M. Kain et al., The Resistance of Type 304 and Type 316 Stainless Steel to Crevice Corrosion Natural Waters, *J. Mater. Energy Syst.,* Vol 5 (No. 4), 1984, p 205–211

16. J.W. Oldfield and W.H. Sutton, New Technique for Predicting the Performance of Stainless Steels in Seawater and Other Chloride Containing Environments, *Br. Corros. J.,* Vol 15 (No. 1), 1980, p 31–34

R.M. Kain, Evaluating Crevice Corrosion, *Corrosion: Fundamentals, Testing, and Protection*, Vol 13A, *ASM Handbook,* ASM International, 2003, p 549–561

Evaluating Crevice Corrosion

R.M. Kain, Consultant

Multiple-Crevice Assembly Testing

The multiple-crevice assembly (MCA) technique was originally introduced in the mid- 1970s as a rapid and economical screening tool for establishing resistance to crevice corrosion in natural seawater (Ref 17). Testing was specifically intended to be severe enough to produce some indication of alloy susceptibility or resistance instead of relying on other factors, such as fouling and seasonal variation in temperature. It was also desirable that the MCA demonstrate recognized differences in alloy capabilities, such as those between UNS S30400 and S31600 stainless steels, as well as the exceptional degree of performance expected of highly corrosion-resistant alloys. Unlike some other popular crevice corrosion tests, the MCA test relied solely on naturally occurring processes and required neither outside electrochemical nor chemical stimulation.

It was argued that because crevice corrosion appeared to be random in its occurrence, the creation of a number of identical crevice sites on a given set of specimens would provide a basis for statistical analysis. Therefore, the MCA design and the use of the probability-of-attack concept gained appeal (Ref 18). Early concerns with geometrical factors primarily addressed the size of the specimen in terms of boldly exposed area (cathode) to shielded or crevice area (anode) (Ref 17). Subsequent research, especially through mathematical modeling (Ref 1, 14, 16), showed that the occurrence of crevice corrosion was dependent on a number of interrelated factors, while the probability concept suggested only a material (i.e., alloy) property. Because crevice geometry factors, such as crevice tightness, could be overriding considerations (Ref 19, 20), proponents and users of the MCA

generally abandoned the probability concept in describing the occurrence of crevice corrosion. However, as evidenced by the number of investigations reported in the literature (for example, see Ref 21, 22, 23, 24), the MCA technique remained popular, because it enabled the investigator to report results in terms of initiation and propagation. For example, resistance to initiation could be expressed as the number of crevice sites or the percentage of sites exhibiting attack in a given test period. Because attack, when it occurs, is located at specific sites (Fig. 2), penetration measurements could be made at each site and reported as a maximum depth. This can be accomplished by using an appropriate dial depth gage or focusing microscope. Results have been reported as a range of these maximum values or their average value. Table 1, for example, gives data describing the effect of molybdenum content on both initiation and propagation resistance for a series of controlled-chemistry heats of a nickel- base alloy containing 30% Cr. Multiple-crevice test results have been reported in bar graph form as mean values plus and minus one standard deviation of the percentage of sites initiated and maximum depth of attack (Ref 25).

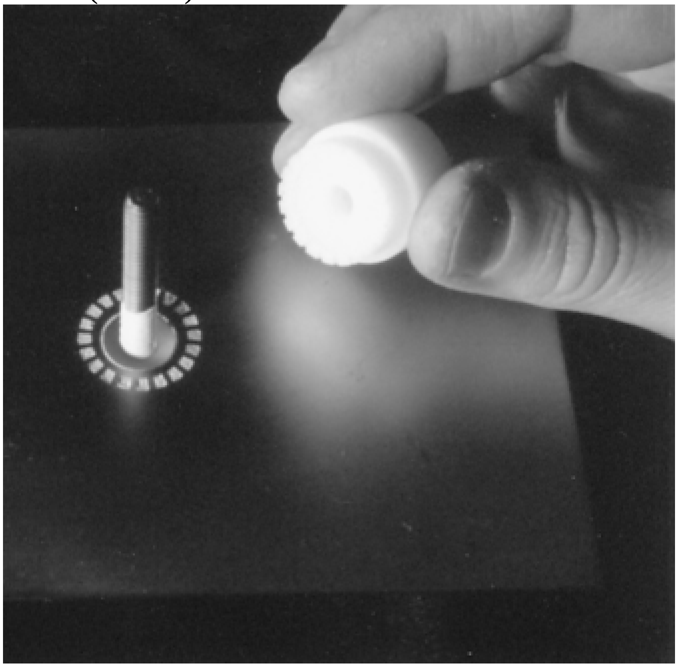

Fig. 2 Example of crevice attack associated with 20 plateau multiple-crevice assembly. Courtesy of the LaQue Center for Corrosion Technology, Inc.

Table 1 Multiple-crevice assembly test results showing the beneficial effects of molybdenum in nickel-base alloys containing 30% Cr

Results of 30 day test in filtered, natural seawater at 30 °C (85 °F)

Alloy	Alloy molybdenum content, %	Initiation resistance			Penetration resistance			
		Time observed, h		**Average number of sites visibly corroded**	**Maximum depth**		**Average depth**	
		Earliest	**Average**		**mm**	**mils**	**mm**	**mils**
A	0	52	76	10–11	1.75	69	0.8	31.5
B	0.5	52	76	11	1.65	65	0.48	19
C	0.9	100	115	9–10	1.2	47	0.4	16
D	2.6	100	115	8–9	0.8	31.5	0.2	8
E	4.9	ND	ND	1	0.05	2	0.05	2

ND, not detected during 30 day test. Source: Ref 21

Reference 26, which was prepared under a grant from the National Institute of Standards and Technology (NIST), provides a critical review on the significance and use of MCAs for testing in natural seawater. The report traces the development and changes in design and application of the acetal resin device shown in Fig. 2. Included in Ref 26 are results of an ASTM International subcommittee G-01.09 round-robin test aimed at standardization of the MCA test procedure. Triplicate specimens of four different alloys, with wet-ground (120-grit SiC) surfaces and MCAs tightened to an initial torque of 8.5 N · m (75 in. · lbf), were exposed for 30 days

in natural seawater. Of the eight participants with access to natural seawater, seven were located on the U.S. east coast at latitudes ranging from Key West, FL, to New England. The eighth test location was the California coast. All except two test sites provided some degree of seawater filtration; three were unable to provide temperature control. As expected, some differences in seawater chemistry (for example, chloride and dissolved oxygen) and ambient temperatures were reported.

Although the purpose of these tests was to determine the reproducibility of results for different classes of materials, the test alloys were also ranked for corrosion susceptibility. None of the participants reported any incidence of crevice corrosion for nickel alloy C-276 (UNS N10276), which contains ~15% Mo. On the other hand, at least one specimen of alloy G (UNS N06007), which contains ~6% Mo, initiated attack at all eight test locations. Overall, the actual number of crevice sites attacked and the range and maximum depth of penetration for UNS N06007 were both found to be quite minimal. For UNS S30400 and S31600 stainless steels, however, crevice corrosion occurred on all specimens except for one UNS S31600. In general, identification of alloy susceptibility was quite reproducible. However, in terms of the actual number of sites that initiated crevice corrosion, much variability was observed, particularly with respect to test location and participant.

Because of the variability in the round-robin test results, a second set of tests with five participants was conducted at one location. The test was restricted to UNS S30400 and S31600 stainless steels. Actual assembly and conduct of the test were performed by individuals with different degrees of experience in MCA testing. All of the tests were conducted at the same time in natural seawater at 25 ± 2 °C (77 ± 3.5 °F). The results of these tests are shown in Fig. 3. Overall, the degree of variability is consistent with that observed from data provided from the original round-robin testing at different test locations. In addition, penetrations measured for the two stainless steels in the latter round-robin test were comparable to those in the original.

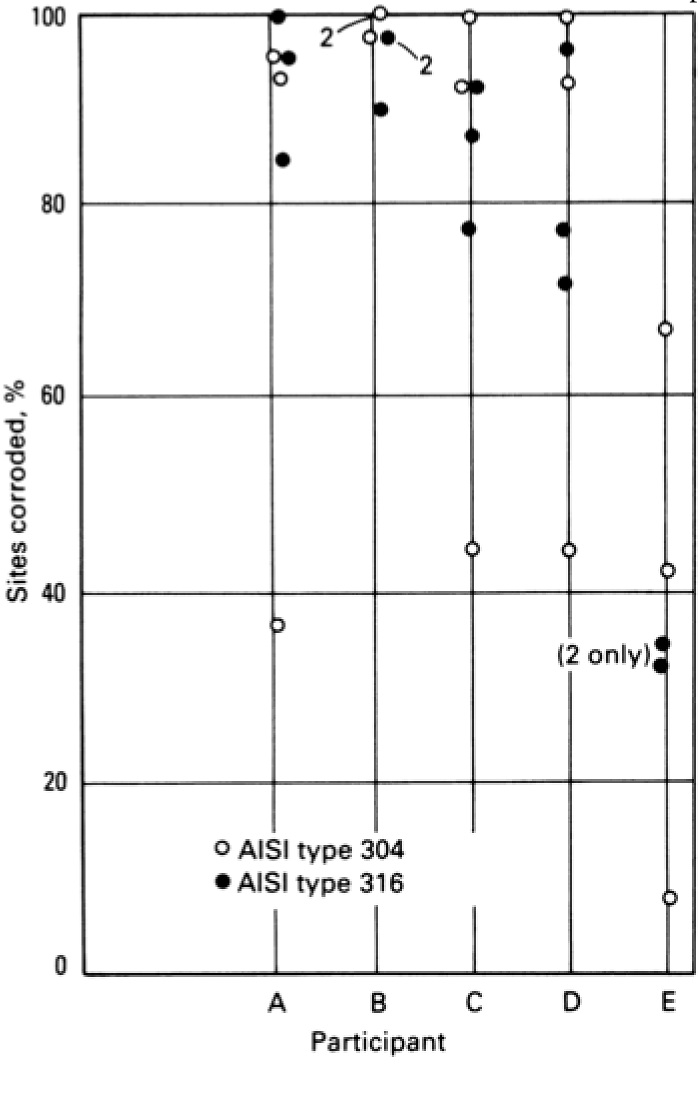

Fig. 3 Multiple-crevice assembly round-robin results from 30 day test conducted simultaneously at one ASTM International selected seawater site. AISI, American Iron and Steel Institute

In another series of 30 day comparative tests (Ref 27), 13 participants used MCAs in round- robin testing of UNS S30400 in 3.5% NaCl at 30 °C (85 °F). Crevice assembly design and initial torque were the same as in the ASTM International committee G-01.09 round-robin test. Again, considerable variability was evident from one participant to another. Crevice sites that exhibited initiation out of 120 available crevice sites ranged from 20 to 86%. Although some exceptions were noted, a number of individual participants reported good reproducibility among replicate specimens. Compared to attack in natural seawater, penetrations in 3.5% NaCl tests did not exceed 0.23 mm (9 mils). Average penetrations for triplicate specimens varied by only a few hundredths of a millimeter.

The degree of variability described previously is likely to be encountered in any type of crevice corrosion test. When conducted in a conscientious manner, MCA tests can generate meaningful results for ranking of alloys and identifying the effects of other exposure variables. The MCA test cannot and should not be used to predict alloy performance under other conditions.

Another test series involved exposure of several grades of stainless steel in different to pulp- bleaching environments. Testing was performed in accordance with a procedure developed by NACE International T-5H-6 task group ("Test Methods for Measuring Crevice Corrosion Rates"). Multiple exposures involved the use of a Rulon (Saint-Gobain Performance Plastics) crevice device similar to that shown in Fig. 2 but with somewhat larger plateaus. Participants used specimens of a given size, and the assemblies were torqued to prescribed levels. Because only a few crevice sites initiated, and reproducibility was poor, it was concluded that the method was not useful in warm (up to 82 °C, or 180 °F), low- pH (1 to 5), low-chloride (50 to 2000 ppm) environments. However, these conditions actually fit well with the premise that a range of tight crevice gaps exists for each type of assembly. Mathematical modeling has shown an interrelationship between bulk chloride level and crevice gap (Ref 14). For the relatively small depth of a MCA site and the low-level chlorides present in the bleach plant, only the tightest of sites should be expected to initiate crevice corrosion.

References cited in this section

1. T.S. Lee et al., Mathematical Modelling of Crevice Corrosion of Stainless Steels, *Corrosion and Corrosion Protection Proceedings,* Vol 81-8, The Electrochemical Society, 1981, p 213–224

14. R.M. Kain, Crevice Corrosion Behavior of Stainless Steel in Seawater and Related Environments, *Corrosion,* Vol 40 (No. 6), 1984, p 313–321

16. J.W. Oldfield and W.H. Sutton, New Technique for Predicting the Performance of Stainless Steels in Seawater and Other Chloride Containing Environments, *Br. Corros. J.,* Vol 15 (No. 1), 1980, p 31–34

17. D.B. Anderson, Statistical Aspects of Crevice Corrosion in Seawater, *Galvanic and Pitting Corrosion—Field and Laboratory Studies,* STP 576, American Society for Testing and Materials, 1976, p 261

18. A.P. Bond et al., Corrosion Resistance of Stainless Steels in Seawater, *Advanced Materials in Seawater Applications,* Climax Molybdenum Company, Piacenza, Italy, Feb 1980, p 1

19. J.W. Oldfield, "Crevice Corrosion of Stainless Steels: The Importance of Crevice Geometry and Alloys Composition," presented at 19th Journees de Aciers Speciaux, (Saint Etienne, France), May 1980, Met. Corros.- Ind., April 1981, No. 668, p 134–147

20. T. Sydberger, *Werkst. Korros.,* Vol 32 (No. 3), 1981, p 119

21. R.M. Kain, "Effect of Alloy Content on the Localized Corrosion Resistance of Several Nickel Base Alloys in Seawater," Paper 229, presented at Corrosion/86, National Association of Corrosion Engineers, 1986

22. R.M. Kain, "Crevice Corrosion and Metal Ion Concentration Cell Corrosion Resistance of Candidate Materials for OTEC Heat Exchangers," ANL/OTEC-BCM-022, Argonne National Laboratory and the U.S. Department of Energy, May 1981

23. G.O. Davis and M.A. Streicher, "Initiation of Chloride Crevice Corrosion on Stainless Alloys," Paper 205, presented at Corrosion/ 85, National Association of Corrosion Engineers, 1985

24. H.P. Hack, Crevice Corrosion Behavior of 45 Molybdenum Containing Stainless Steels in Seawater, *Mater. Perform.*, Vol 22 (No. 6), 1983, p 24–30

25. T.S. Lee and R.M. Kain, "Factors Influencing the Crevice Corrosion Behavior of Stainless Steels in Seawater," Paper 69, presented at Corrosion/83, National Association of Corrosion Engineers, 1983

26. R.M. Kain, Crevice Corrosion Testing in Natural Seawater: Significance and Use of Multiple Crevice Assemblies, *J. Test. Eval.*, Sept 1990, p 309–319

27. U. Hideki et al., "Crevice Corrosion of Stainless Steels in Chloride Solutions," Paper 117, presented at Corrosion/89, National Association of Corrosion Engineers, 1989

R.M. Kain, Evaluating Crevice Corrosion, *Corrosion: Fundamentals, Testing, and Protection*, Vol 13A, *ASM Handbook*, ASM International, 2003, p 549–561

Evaluating Crevice Corrosion

R.M. Kain, Consultant

Continuous Crevice Formers

Perspex Crevice Assemblies. While MCAs were being used extensively in the 1980s to investigate crevice corrosion in marine and paper mill environments, another type of device was developed as a research tool. The Perspex crevice assembly (PCA) was initially devised and used to provide immersion test verification data for the development of mathematical models of crevice corrosion (Ref 7). Perspex is a British trade name (Imperial Chemical Industries, UK) for a hard plastic, polymethyl methacrylate (PMMA). This material and related plastics, such as Plexiglas (ATOFINA Chemicals, Inc.), can be machined as a continuous-type crevice former with depth dimensions that are intentionally varied. The design shown in Fig. 4 was prepared with bored holes that enabled access of the test medium to the inside diameter (ID), creating an effective crevice depth equivalent to one-half the PCA annular dimension. The most common- size PCAs reported in the literature are those measuring 40 mm outside diameter (OD) by 20 mm ID (1.6 by 0.8 in.) and a smaller version measuring 30 mm OD by 20 mm ID (1.2 by 0.8 in.) (Ref 3, 28). Because of the translucent nature of the acrylic plastic, the earliest stages of crevice corrosion development can be detected in situ. This led to greater accuracy in reporting times to initiation and the extent of measured propagation.

Fig. 4 Perspex crevice assembly with ports to allow aqueous environment access to inside diameter. Courtesy of the LaQue Center for Corrosion Technology, Inc.

Perspex crevice assemblies have been used extensively in comparing alloy performance and in tests to investigate variations in Cl^- and SO_4^{2-} levels in simulated natural waters, crevice geometry, test temperature, alloy surface conditions, and cathode-to-anode area ratio (Ref 28, 29, 30, 31, 32).
Perspex crevice assemblies have been used in the smooth, polished, ground, and machine- grooved condition to vary the severity of the geometry formed at a particular assembly torque, usually 2.8 N · m (25 in. · lbf). In some tests, crevice conditions were made even more severe by introducing a deformable insert (plastic tape) between the hard plastic and the test metal surface. Effects of the previously mentioned variations on alloy performance in natural seawater are reported in Ref 31 and 32. Results for several alloys that have diverse chemistries are shown in Table 2.

Table 2 Identification of metallurgical/ geometrical test conditions that promoted crevice corrosion of various alloys in 60 day natural seawater Perspex crevice assembly test

Test material		Alloy resistance (R) or susceptibility (S) for indicated test conditions[(a)]							
UNS No.	**CRN[(b)]**	**A**	**B**	**C**	**D**	**E**	**F**	**G**	**H**
S31603	24	S	S	S	S	S	S	S	S
S32550	37	R	R	R	R	R	R	S	S
S31254	43	R	R	R	R	R	R	S	R
Alloy VI	43	R	S	R	R	R	R	S	S
N08926	45	R	R	R	R	R	R	R	S
N08367	45	R	R	R	R	R	R	R	R
Alloy VIII	46	R	R	R	R	R	R	S	S
N08031	51	R	S	R	R	R	R	R	R
S32654	56	R	R	R	R	R	R	R	R
N10276	69	R	R	R	R	R	R	S	R
N06059	73	R	R	R	R	R	R	R	R

UNS, Unified Numbering System.

(a) A, specimen surface, as-produced mill; Perspex crevice assembly (PCA) washer finish, 0.05 μm alumina polish. B, specimen surface, as-produced mill; PCA washer finish, A and tape insert. C, specimen surface, as-

produced mill; PCA washer finish, 600-grit SiC. D, specimen surface, as-produced mill; PCA washer finish, 120-grit SiC. E, specimen surface, as-produced mill; PCA washer finish, 60-grit SiC. F, specimen surface, as-produced mill; PCA washer finish, lathe turned (R_a, 15 μm). G, specimen surface, ground (120-grit SiC); PCA washer finish, 0.05 μm alumina polish. H, specimen surface, ground and pickled (10 min in 15% HNO_3 + 6% HF at 40 °C, or 105 °F); PCA washer finish, 0.05 μm alumina polish.

(b) CRN, corrosion resistance number (%Cr + 3.3 × %Mo + 16 × %N), equal to pitting resistance equivalent number, PREN. Source: Ref 32

For the most part, PCAs have been assembled with simple nut, bolt, and washer assemblies of a corrosion-resistant material such as UNS N10276 or titanium Gr-2 (UNS R50400). As described, for example, in Ref 19, precision washers have also been used to ensure a constant pressure.

At least one investigation (Ref 33) has employed continuous washers of the 30 mm OD by 20 mm ID (1.2 by 0.8 in.) design but fashioned from other polymers, including PTFE, Rulon, and fiber-impregnated PTFE. In these tests, the crevice formers were made without access holes and thus had a nominal crevice depth of 5.0 mm (0.2 in.) as contrasted with the 2.5 mm (0.1 in.) depth inherent with the original PCA. Unlike the translucent, polished acrylic plastic, PCAs made from the previously mentioned materials do not permit detection of the early stages of crevice corrosion initiation.

Gaskets. Over the years, gaskets have been a perennial source of crevice corrosion at flanged surfaces and other mounting sites where a nonmetallic was used for sealing or for electrical isolation purposes. In early seawater tests, for example, crevice corrosion often developed beneath Bakelite (Georgia Pacific Corp.) insulators used to mount specimens on test racks.

As reported in Ref 34, PTFE and cloth fiber- filled rubber gaskets were used in an extensive U.S. Navy program to evaluate candidate valve materials for seawater service. Materials considered for valve body applications were tested with grooved surfaces and the fiber-filled rubber gaskets. Other material considered for valve trim hardware was tested in the surface-ground condition with PTFE gaskets. In both tests, the respective metal surface roughness was quantified. Both types of gasket were ~50 mm OD by 13 mm ID (2 by 0.5 in.) and held in place on both sides of the 100 mm by 150 mm (4 by 6 in.) testpieces, as shown in Fig. 5. Tables 3 and 4 summarize the results of a 6 month test conducted in filtered seawater at 25 ± 5 °C (77 ± 9 °F).

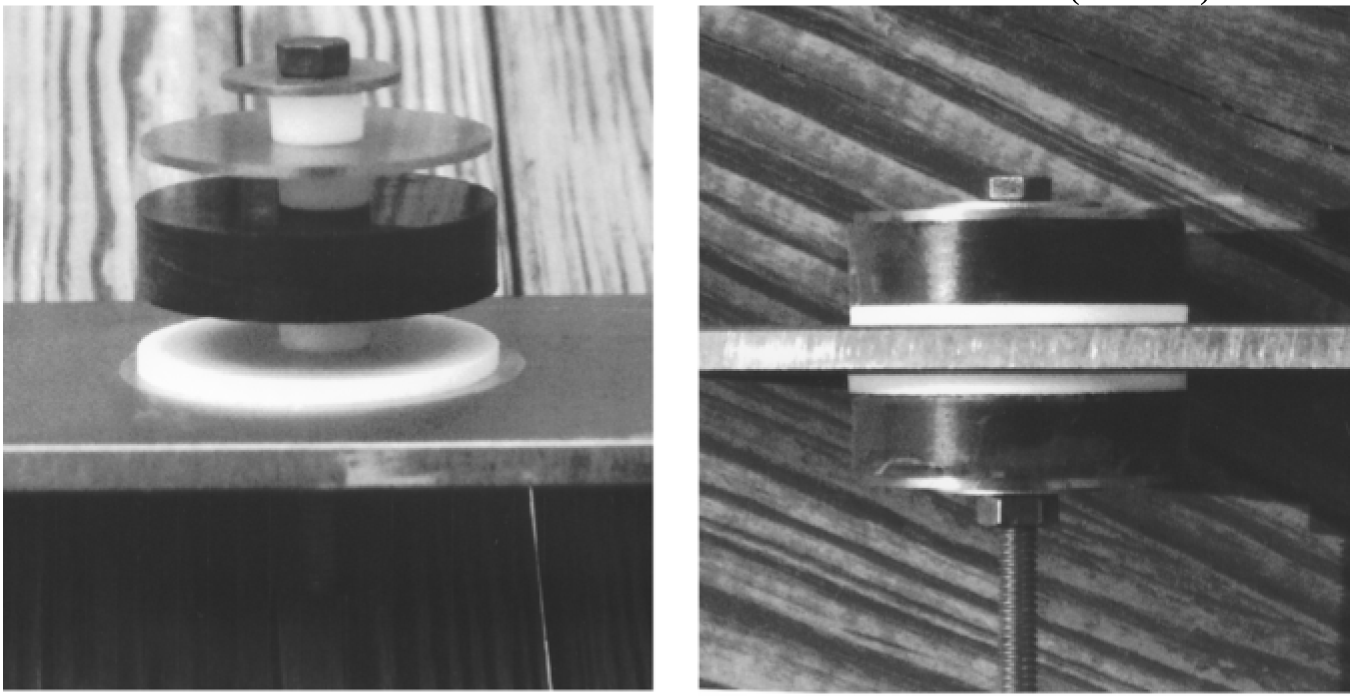

(a) (b)

Fig. 5 Exploded (a) and completed (b) views of gasket crevice assembly of the type used in Ref 34 and elsewhere. Gasket held in place with polyvinyl chloride and titanium retainer. Courtesy of the LaQue Center for Corrosion Technology, Inc.

Table 3 Summary of results for wrought stainless steel and nickel-base alloys in 6 month natural seawater tests with polytetrafluoroethylene (PTFE) gaskets

UNS No. or other designation	Number of sites attacked (4 max)	Maximum depth of attack	
		mm	**in.**
S31603	4	2.27	0.089
N08367	3	1.17	0.046
S31254	4	1.73	0.068
S32654	0	0.0	0.000
S39275	4	1.04	0.041
S32760	4	0.98	0.039
S21000	2	0.59	0.023
N06625	3	0.18	0.007
N10276	2	0.13	0.005
N06022	0	0.00	0.000
N06686	0	0.00	0.000
N06059	0	0.00	0.000
C-2000	0	0.00	0.000
N07716	4	0.43	0.017
N07718	3	1.18	0.046
N09925	4	3.18	0.125

Note: PTFE gasket site machined to 0.5 to 1.5 μm finish. UNS, Unified Numbering System. Source: Ref 34

Table 4 Summary of results for various cast alloys in 6 month natural seawater test with cloth-impregnated rubber gaskets

UNS No. or other designation	Number of sites attacked (4 max)	Maximum depth of attack	
		mm	**in.**
C92200	2	0.34	0.013
C95800	4	0.60	0.024
N24135	4	0.71	0.028
C96400	4	0.25	0.010
J92800	4	3.75	0.148
N08007[(a)]	4	3.97	0.156
J94651	4	3.39	0.133
J93254[(a)]	4	3.31	0.130
N26625	2	1.66	0.065
N30002	3	2.83	0.111
N26022	1	0.98	0.039
Alloy 59 cast	0	0.00	0.000

Note: Except for cast alloy 59, all other materials were thin-section investment castings and tested in as-cast condition. UNS, Unified Numbering System.

(a) UNS N08007 and J93254 were tested with smooth surfaces (Table 3), while all others were tested with a coarse phonographic finish. Source: Ref 34

The effect of gasket material on the crevice corrosion resistance of cast (UNS J92800) and wrought (UNS S31600) stainless steel was investigated in seawater and a less aggressive Cl^-- and SO_4^{2-} -containing water (Ref 35). Identification of 11 gasket materials (plus PCA controls) and seawater test results for J92800 flanges are provided in Table 5. In seawater, the propensity for attack favored crevices formed with nitrile and PTFE-type gaskets. The nominal cathode-to- crevice area ratio in the tests was smaller than in many of the other crevice corrosion tests cited here.

Table 5 Effect of selected gasket material on the crevice corrosion initiation and propagation behavior of cast alloy UNS J92800 (CF3M) flanges in seawater

Gasket material	Number of flanges attacked	Maximum depth of attack

		mm	in.
Amaride fiber + nitrile	2/2	2.10	0.083
Glass-filled PTFE	1/2	1.40	0.055
PTFE	2/2	1.05	0.041
Carbon fiber + nitrile	2/2	0.77	0.030
Graphite/stainless steel	1/2	0.69	0.027
EPDM	1/2	0.05	0.002
Nitrile	1/2	0.03	0.001
PCA-type control	2/2	0.01	0.000
Red rubber	1/2	0.01	0.000
Fluoroelastomer	0/2	0.00	0.000
Butyl rubber	0/2	0.00	0.000
Neoprene	0/2	0.00	0.000

UNS, Unified Numbering System; PTFE, polytetrafluoroethylene; EPDM, ethylene-propylene-diene monomer (rubber); PCA, Perspex crevice assembly. Note: Flanges surface ground (R_a, 0.4 μm). Testing comprised 21 days exposure to flowing (0.7 m/s, or 2.3 ft/s) seawater, followed by 7 days wet lay-up, resulting in stagnant conditions. Source: Ref 35

Irregular Surfaces. The use of rigid crevice formers with deformable inserts, for example, PCAs and gasket assemblies, can generally produce tight crevices on metals with irregular surfaces associated with coarse grinding, machining, and heavy acid pickling. However, these types of devices are generally not applicable to testing autogenous welds, raised weld beads, or unfinished weld overlays. Some success has been achieved by using O-rings or rods (Ref 36) made of deformable polymers. In each case, some type of holder or retainer is needed to position and secure the crevice former over the desired section of weldment. This may be achieved by bolting through a hole drilled in the test specimen or by using a clamping device.

Another, more adaptable method involves the use of an epoxy-type coating. Reference 37 describes the application of an epoxy coating to assess the crevice corrosion behavior of weld metal and adjacent heat-affected zones on cruciform-shaped specimens in seawater. Reference 37 discusses the repeatability aspects of the testing performed on UNS S31603, S20910, and N08367. Elsewhere, a paint marking pen was successfully used to create crevice conditions and assess the performance of seal-welded tube- to-tube sheet assemblies fabricated with unidentified stainless steel components (Ref 38). Figure 6 shows before-and-after views of a tested section. The use of dried plastic from a felt tip pen to produce crevice sites is discussed in Ref 39. Some of the attributes described for this technique include a constant critical geometry, no need for fixturing, a crevice area that can be varied, and simple specimens having concave, convex, or uneven surfaces.

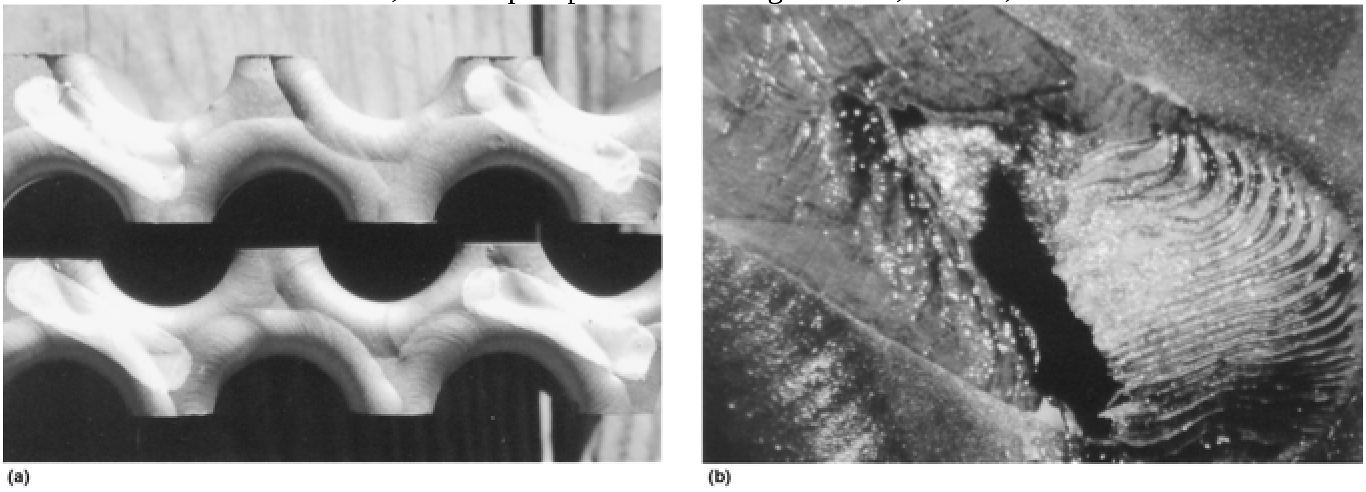

Fig. 6 Example of the use of paint marker (a) to create crevice site on irregular weld surface and (b) resulting attack after exposure to seawater. Courtesy of the LaQue Center for Corrosion Technology, Inc.

There appears to be some similarity in the undulated pattern of attack found beneath coatings (see Fig. 6b) and that associated with heat tint on as-welded stainless steel exposed to seawater and other chloride-containing solutions.

References cited in this section

3. "Standard Guide for Crevice Corrosion Testing of Iron-Base and Nickel-Base Stainless Alloys in Seawater and Other Chloride Containing Aqueous Environments," G 78, *Annual Book of ASTM Standards,* American Society for Testing and Materials

7. J.W. Oldfield and W.H. Sutton, Crevice Corrosion of Stainless Steels, Part II: Experimental Studies, *Br. Corros. J.,* Vol 13 (No. 3), 1978, p 104

19. J.W. Oldfield, "Crevice Corrosion of Stainless Steels: The Importance of Crevice Geometry and Alloys Composition," presented at 19th Journees de Aciers Speciaux, (Saint Etienne, France), May 1980, Met. Corros.- Ind., April 1981, No. 668, p 134–147

28. J.W. Oldfield et al., Avoiding Crevice Corrosion of Stainless Steels, *Proc. Stainless Steel '84 Symposium,* (Gotenberg, Sweden), Chalmers University of Technology and Jernkontoret (Sweden) and The Metals Society (UK), 1984

29. R.M. Kain and J.W. Oldfield, "Prediction of Crevice Corrosion Resistance of Stainless Steels in Aqueous Environments—A Corrosion Engineering Guide," presented at 12th International Corrosion Congress, Localized Corrosion Session, (Houston, TX), NACE International, 1993

30. J.W. Oldfield and R.M. Kain, Assessment of the Corrosion Resistance of Austenitic Stainless Steels in Industrial Waters, *Proc. International Corrosion Congress,* (Florence, Italy), Associazione Italiana Di Metallurgia, 1990

31. R.M. Kain, "Effects of Surface Finish on the Crevice Corrosion Resistance of Stainless Steels in Seawater and Related Environments," Paper 508, presented at Corrosion/ 91, National Association of Corrosion Engineers, 1991

32. R.M. Kain, Seawater Testing to Assess the Crevice Corrosion Resistance of Stainless Steels and Related Alloys, *Proc. 12th International Corrosion Congress, Localized Corrosion Session,* Vol 3, (Houston, TX), 1993, NACE International, p 1889–1900

33. P.A. Klein et al., "The Effect of Electrolytic Chlorination on the Crevice Corrosion Behavior of 70/30 Copper-Nickel and Nickel- Copper Alloy 400," Paper 509, presented at Corrosion/91, National Association of Corrosion Engineers, 1991

34. D.M. Aylor et al., "Crevice Corrosion Performance of Candidate Naval Ship Seawater Valve Materials in Quiescent and Flowing Natural Seawater," Paper 329, presented at Corrosion/99, NACE International, 1999

35. R.M. Kain, Gasket Materials and Other Factors Influencing the Crevice Corrosion Resistance of Stainless Steel Flanges, *Mater. Perform.,* Vol 37 (No. 8), 1998, p 62–66

36. R.A. Buchanan and C.D. Lundin, New Method for Crevice Corrosion Testing of Welds with Reinforcements, *Corrosion,* Vol 58 (No. 5), 2002, p 448

37. R.M. Kain, Use of Coatings to Assess the Crevice Corrosion Resistance of Stainless Steels in Warm Seawater, *Marine Corrosion in Tropical Environments,* STP 1399, American Society for Testing and Materials, 2000

38. LaQue Center for Corrosion Technology, Inc., Unpublished test report, 2000

39. T. Degerbeck and T. Gille, Crevice Corrosion—A New Crevice Former, *Corros. Sci.,* Vol 19, 1979, p 1113–1114

R.M. Kain, Evaluating Crevice Corrosion, *Corrosion: Fundamentals, Testing, and Protection*, Vol 13A*, ASM Handbook,* ASM International, 2003, p 549–561

Evaluating Crevice Corrosion

R.M. Kain, Consultant

Evaluating Cylindrical Materials and Products

It is often desirable to evaluate the crevice corrosion resistance of product forms other than flat sheet and plate. Crevice corrosion testing of rod and barstock as well as alloy tubing and pipe can be accomplished by the use of devices that can produce a crevice on the OD of the test material. Such devices exist as off-the-shelf fittings or other products that can be cut and adapted to meet test needs. Among those available are wood collars, O-rings, ferrule and sleeve-type compression fittings, polyvinyl chloride (PVC) compression fittings with internal rubber glands, various flexible hose products, snap-type hose clamps, packing materials, and epoxy coatings.

The selection of an appropriate crevice former should take into account the purpose of the tests, for example, direct one-on-one alloy evaluations, assessing environmental variables, or evaluating product performance under conditions likely to be found in service. The selection depends heavily on the size (OD) of the product being tested and the available size of the crevice- forming material. The fact that rod and barstock can be machined to specific dimensions gives the investigator some control over the test design. In contrast, the testing of tubular products may be dictated by the available mill-produced OD and whether the products are formed to English or metric dimensions. The combination of product form and selected crevice device can accurately reproduce or closely approximate the crevice geometries found in some service applications.

O-Rings. The simplest method of crevice corrosion testing of cylindrical specimens, including tubulars, is by the application of O-rings (PTFE, rubber, Viton [DuPont Dow Elastomers] or other polymer). The crevice can be made more or less severe by varying the size of the O-ring with respect to the OD of the alloy product. It should be recognized that excessive stretching of an O-ring may alter its width and, accordingly, the depth of the crevice formed. O-rings of different thicknesses allow the crevice depth to be varied. One advantage of O-rings is that they do not require tightening and thus eliminate a source of variation found in some other types of devices. However, O-rings should not be overstretched.

Another advantage of O-rings is that results from simple immersion tests can be correlated with electrochemical tests, such as ASTM F 764 (Ref 40), that use a rod-shaped electrode with an O-ring crevice former. A disadvantage is that the crevice depth is limited. The shallow depth of an O-ring is less likely to promote attack of more highly alloyed stainless steels and nickel-base alloys that otherwise may be more susceptible with deeper crevices, for example, with gasket or washer-type crevice formers. As a rule, deep- tight crevices are considered to be more severe than shallow-loose crevices.

Wood Collars. Collars fashioned from water- resistant redwood (but not copper-chromium- arsenate-treated lumber) have been used to assess the relative resistance of stainless alloy shaft stock to crevice corrosion in seawater (Ref 41). In this case, the redwood was drilled to provide holes of the same diameter as the OD of the barstock tested. The lumber was then split to provide two half-bracelets and further cut into the shape of collars analogous to a penal stock. The collars were positioned over a length of barstock material and tightly secured with corrosion-resistant fasteners. The crevice depth can be intentionally changed by varying the lumber thickness. The cathode-to-anode (crevice) area ratio can be varied by varying the bar length or by adding multiple collars.

Packing Material. Packing glands are sites where crevice corrosion could occur, for example, on boat and pump shafts. Reference 42 details a method for comparing the effect of different types of packing materials on the crevice corrosion resistance of stainless steel shafting under static and dynamic conditions. In brief, the packing material was cut into lengths approximately one-half the circumference of the test material. The lengths of packing were freely shaped to form a collar or gland around the test-piece and held tightly in place within a retainer fashioned from a PVC fitting. Some internal machining of the fitting may be required to ensure a tight fit of the packing around the testpiece.

Sleeve Assemblies. The use of sleeves (Fig. 7) produced from polymer and rubber tubing or from hose and applied to the OD of cylindrical specimens allows crevices of varying tightness and depth to be formed. Under simple immersion conditions, these nonmetallic sleeves can be used alone, without the need for additional clamping. For direct alloy comparisons, the OD of all test specimens should be the same, so that crevice tightness is not a variable.

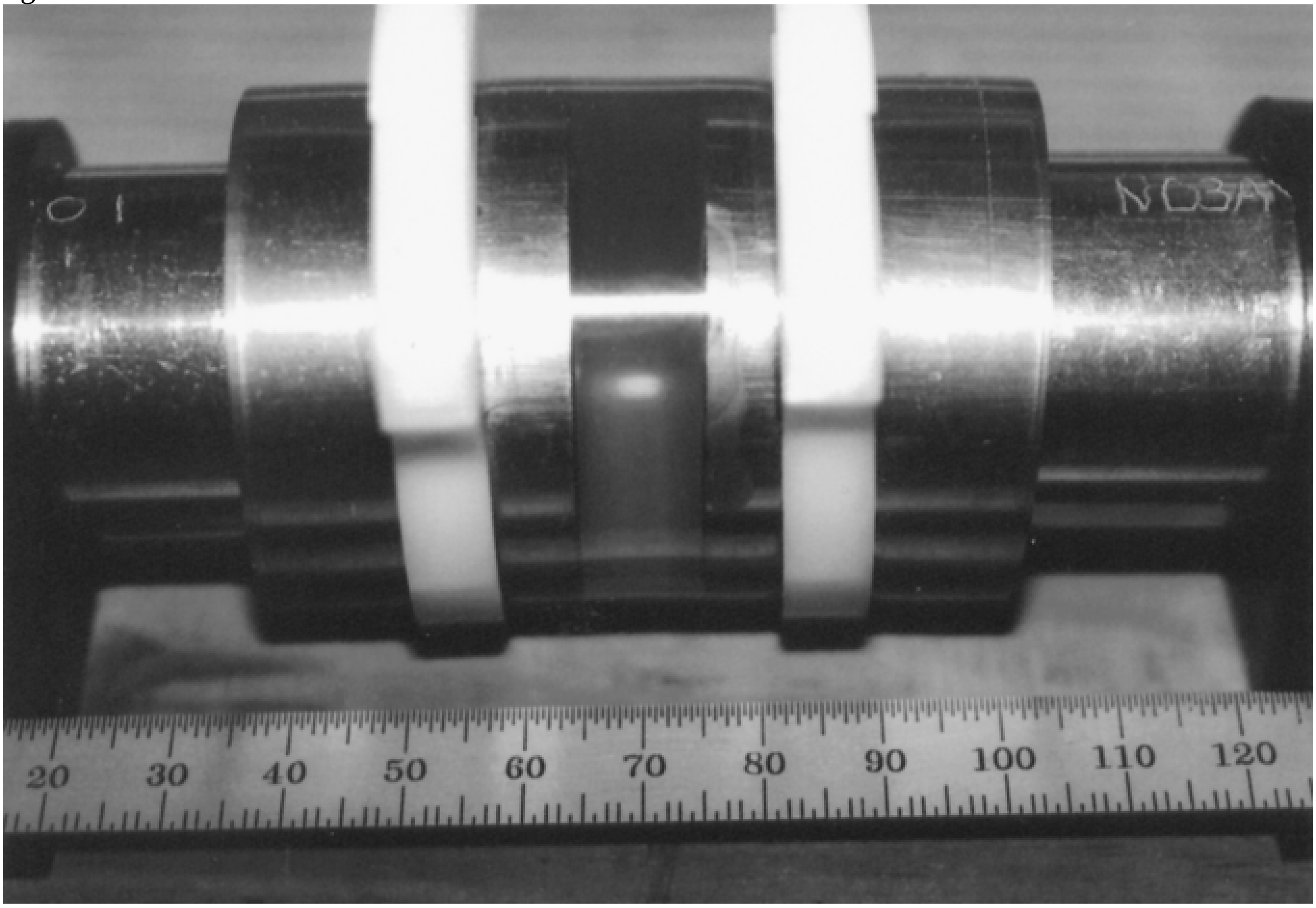

Fig. 7 Translucent vinyl sleeve assembly applied to pipe or tube outside diameter for crevice corrosion testing under static or dynamic flow conditions. Courtesy of the LaQue Center for Corrosion Technology, Inc.

The vinyl sleeve test method offers several advantages. These include ease of preparation, ability to produce tight crevices, and the translucent nature, which facilitates detection of crevice corrosion initiation at the earliest stages.

A number of investigations (Ref 43, 44, 45, 46, 47, 48) have used vinyl sleeves (Tygon tubing, Saint-Gobain Performance Plastics) and/or rubber hose to test alloy tube and pipe sections under dynamic conditions. In those tests, seawater (treated and untreated) flowed through a series of alloy tubes or pipes connected by the vinyl sleeves. In dynamic tests, it is essential that the sleeves be clamped to the specimens to prevent separation due to line pressure. The spacing between specimens should be minimal to prevent any bulging of the sleeve that could vary crevice geometry. In tests of this design, the wetted interior pipe surface (ID) serves as the cathode and the shielded portion of the pipe OD as the crevice (anode).

Ideally, all tubular specimens should be of the same size and schedule. However, this is not always possible. Reference 45 describes one seawater crevice corrosion test program that examined the performance of a series

of high-alloy stainless steel produced to English and metric dimensions. In these tests, the IDs of the vinyl sleeves either matched or were smaller than the ODs of the tubular test specimens. Testing proceeded with the understanding that the severity of the crevices was different. In Table 6, those specimens tested with the tightest fit were identified as severe (S) and those with matching ID/ ODs as moderately severe (MS). The differences in seawater velocity associated with each specimen ID dimension are also noted in Table 6.

Table 6 Crevice corrosion resistance exhibited by 10 different stainless-type tubing alloys in 60 day flowing seawater/vinyl sleeve tests

UNS No.	Seawater velocity		Crevice severity[a]	Initiation resistance	
	m/s	**ft/s**		**Earliest detection, days**	**Number of sites attacked[b] (6 max)**
S31603	2.4	7.9	MS	4	6
S31703	2.4	7.9	MS	4	6
S31254	4.0	13.1	MS	7	6
S32750	2.4	7.9	MS	14	3
N08925	3.3	10.8	S	14	3
N08367	2.0	6.6	MS	14	3
S32550	2.4	7.9	MS	43	4
N08926	1.6	5.2	S	53	2
S32760	2.4	7.9	MS	OK at 60	0
S39724	2.4	7.9	MS	OK at 60	0

UNS, Unified Numbering System.
(a) MS, moderately severe; S, severe.
(b) Maximum depth (0.57 mm, or 0.022 in.) found on UNS S31703 tube; all others ≤0.22 mm (0.0087 in.). Source: Ref 45

Large-Diameter Pipe. Testing the crevice corrosion resistance of large-diameter pipe (e.g., 250 mm, or 10 in.) creates challenges for the investigator. In a previously unreported case (Ref 49), large-diameter pipes prepared by different metallurgical processes were tested in seawater in lengths measuring approximately 750 mm (30 in.). Equally spaced holes were drilled along the length of the pipe at 0°, 90°, 180°, and 270°. To accommodate the inner and outer curvature of the pipes, sections of 25.4 mm diameter by 6.4 mm (1 by 0.25 in.) wall vinyl tubing were split and punched into 25.4 mm (1 in.) OD diameter disks with a 6.4 mm (0.25 in.) center hole. To create the desired crevice on the OD and ID of the test pipe, these disks were then mated with the ID and OD of the pipe at the location of the drilled holes and bolted in place with micarta retainers. The resulting conditions produced crevice corrosion of alloy UNS N06625 within 60 days and revealed no significant effect of the metallurgical processes that were investigated.

Compression Fittings. A disadvantage of vinyl sleeves is their cost relative to that of other crevice formers, particularly when testing larger, for example, >25.4 mm (1 in.), alloy tubulars. One option is to use inexpensive PVC compression fittings with internal rubber glands. The width of the gland increases with the pipe size of the fitting. Some variability in crevice geometry may result during assembly and tightening of the compression nuts on either end. Selection of this type of crevice-forming device, while economical, sacrifices the ability for early in situ detection of crevice attack available with the translucent vinyl sleeve device. However, if the attack is significant, corrosion products may become evident at the compression nut/tube interface. References 50 and 51 cite results of two seawater test programs aimed at examining benefits of surface treatment to enhance the crevice corrosion resistance of stainless steel and nickel-base alloy UNS N06625. In another test program (Ref 52), the effects of alternating flow and stagnant seawater conditions on the behavior of 90/10 copper-nickel (UNS C71500) and alloy- 400 (UNS N04400) were investigated with this type of crevice former. Elsewhere, the behavior of stainless alloy tubing fitted with PVC compression fittings was investigated in aerated, deaerated, and sulfide-containing seawater (Ref 52).

Other types of readily available but more costly compression fittings containing internal ferrules and sleeves have also been used. One test program (Ref 53) used UNS S31600 stainless steel compression fittings to test the resistance of two versions of a 6Mo-containing stainless steel in a tube-to-tubesheet simulation. Nylon compression fittings of this type have also been used to compare alloy resistance to natural and chlorinated

seawater (Ref 43). Results were compared with those from concurrent tests with vinyl sleeves and those made from Buna-N (E.I. Dupont) tubing.

The ferrule-and-sleeve devices actually create at least three different crevice geometries within an assembly: a shallow-tight one beneath the ferrule, a deeper-tight crevice at the sleeve, and a considerably deeper but less tight crevice between the tube wall and fitting annulus. Depending on alloy sensitivity, attack may occur at all locations or only at one or both of the tighter crevice sites.

Due to their opaqueness and need for tightening, the ferrule-and-sleeve-type devices share the same limitations as the PVC/rubber gland devices. On the other hand, some versions are available in both English and metric unit dimensions and are therefore suitable for testing tubular and other cylindrical products.

Metal-to-Metal Assemblies. Reference 52 describes metal-to-metal crevice corrosion testing of stainless steel tubulars fitted with compression fittings. A test simulating a tube-to-tube support sheet (Fig. 8) configuration with 0.13 mm (0.005 in.) clearance was reported in Ref 45. While both tubes and plate comprising UNS S30400 stainless steel were attacked within 60 days, no attack of AL-6XN (UNS N08367) tubes or mating tube support plates of UNS S31603 or alloy 2507 (UNS S37250) occurred.

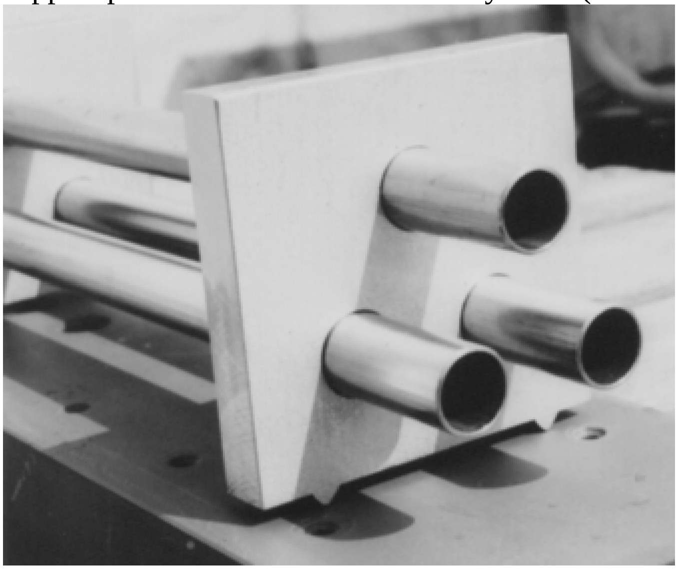

Fig. 8 Example of mixed-metal crevice assembly intended to mimic actual tube and tube support plate conditions (described in Ref 45). Courtesy of the LaQue Center for Corrosion Technology, Inc.

Coatings, such as a marine-grade epoxy, have been used to create crevice conditions on both cylindrical and flat specimens (Ref 37, 54, 55). This is a relatively inexpensive approach for testing of tubulars of all sizes under simple immersion conditions. The coating can be applied to as-produced and prepared tubular surfaces (Ref 54). Anode-to-cathode area ratio effects can be investigated by varying the percentage of tube surface area coated (Fig. 9). In general, the interface between the coating (edge) and the bare metal serves as the crevice mouth and from which corrosion product inevitably appears if the material is susceptible. Once initiated, the attack may continue further inward beneath the coating, progressively disbonding it.

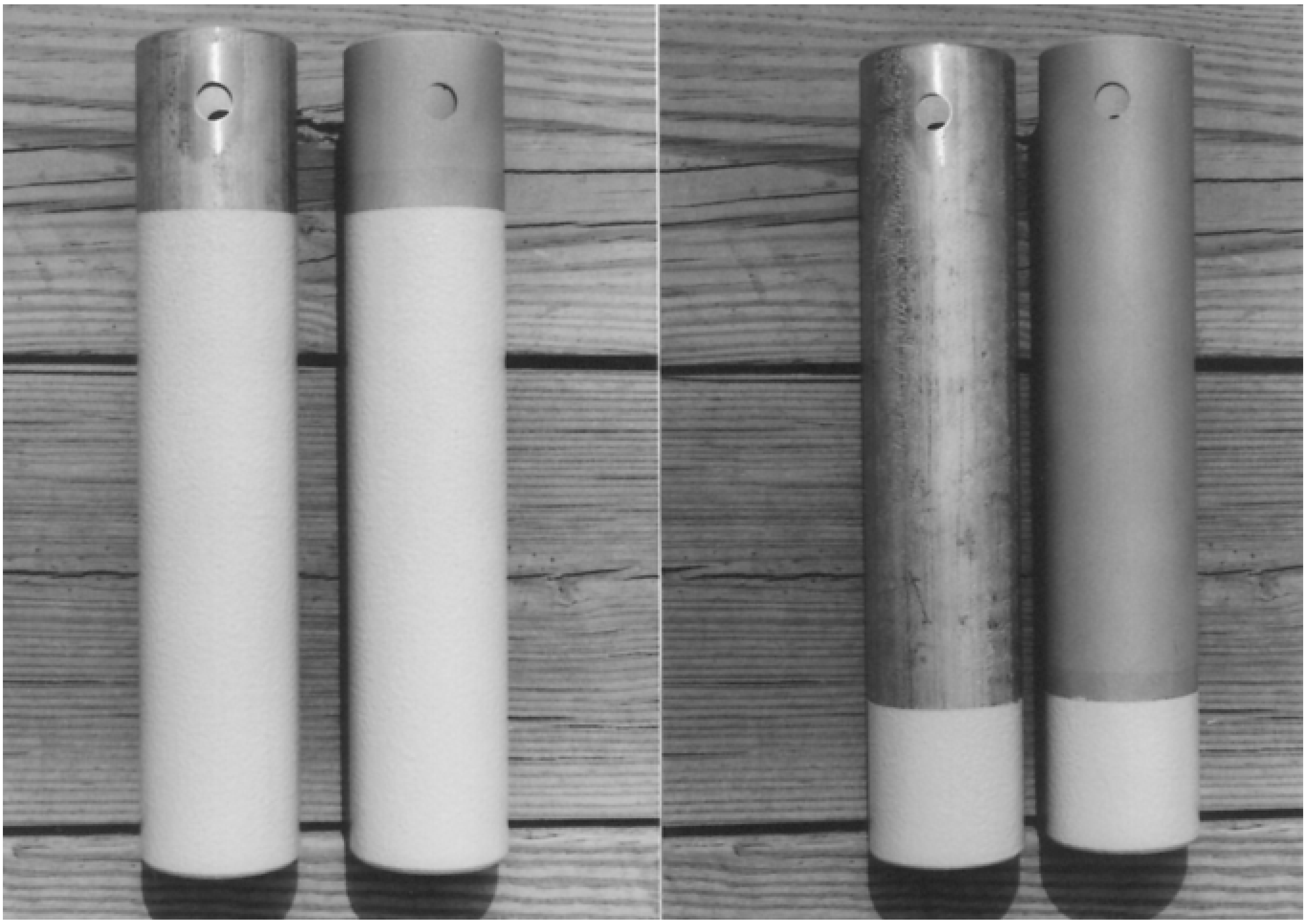

Fig. 9 Use of epoxy coating to create crevice conditions on alloy pipe specimen. Coated surface varied to investigate area ratio effect. Courtesy of the LaQue Center for Corrosion Technology, Inc.

Assessing Corrosion Damage on Cylindrical Specimens. As with flat-panel-type specimens, cylindrical and tubular specimens can be evaluated by their resistance to initiation and propagation. Initial resistance can be reported according to the observed times to visible attack as well as the number or percent of crevice sites attacked. Depending on the size of the specimens, it may be possible to determine mass loss. In addition, affected crevice area and the depth of attack (penetration) can be determined. Affected area can be measured (or estimated) by placing a transparent grid over the crevice site and counting the number of area units (e.g., millimeters squared). Measuring the depth of attack for a cylindrical specimen can be more challenging than for a flat specimen. One method entails placing the cylindrical specimen in a lathe and rotating the specimen manually. A dial depth gage mounted on the traversing tool post is then used to measure depth of attack along the circumference and axis of the specimen. For example, depth of attack can be measured along a line at various degrees of rotation, for example, every 15°, 30°, or 45°.

References cited in this section

37. R.M. Kain, Use of Coatings to Assess the Crevice Corrosion Resistance of Stainless Steels in Warm Seawater, *Marine Corrosion in Tropical Environments,* STP 1399, American Society for Testing and Materials, 2000

40. "Standard Test Method for Pitting or Crevice Corrosion of Metallic Surgical Implant Materials," F 746, *Annual Book of ASTM Standards,* Vol 13.01, American Society for Testing and Materials

41. LaQue Center for Corrosion Technology, Inc., Unpublished test report, 1978

42. R.M. Kain and I. Dunoff, “Influence of Packing Material on the Corrosion Resistance of Stainless Steel Boat Shafting and Related Materials,” Paper 639, presented at Corrosion/2000, NACE International, 2000

43. R.M. Kain et al., “Crevice Corrosion of Nickel-Chromium-Molybdenum Alloys in Natural and Chlorinated Seawater,” Paper 112, presented at Corrosion/89, National Association of Corrosion Engineers, 1989

44. R.M. Kain and P.A. Klein, “Crevice Corrosion Propagation Studies for Alloy N06625: Remote Crevice Assembly Testing in Flowing Natural and Chlorinated Seawater,” Paper 158, presented at Corrosion/90, National Association of Corrosion Engineering, 1990

45. R.M. Kain and A. Zeuthen, Crevice Corrosion Testing of Austenitic, Superaustenitic, Superferritic and Superduplex Stainless Type Alloys in Seawater, *Corrosion Testing in Natural Waters,* STP 1300, American Society for Testing and Materials, 1996

46. M.E. Inman et al., “Detection of Crevice Corrosion in Natural Seawater Using Polarization Resistance Measurements,” Paper 297, presented at Corrosion/97, NACE International, 1997

47. D.C. Agarwal, “Solving Critical Problems in Marine Environments by an Advanced Ni-Cr-Mo Alloy 59 UNS N06059,” Paper 635, presented at Corrosion/2000, NACE International, 2000

48. R.M. Kain, “Testing for Crevice Corrosion Susceptibility,” presented at research symposium at Corrosion/96, NACE International, 1996

49. LaQue Center for Corrosion Technology, Inc., Unpublished test report, 1993

50. R.M. Kain and M.B. Ives, “Surface Treatments Benefiting the Crevice Corrosion Resistance of Nickel Alloy N06625 in Natural and Chlorinated Seawater,” Paper 330, presented at Corrosion/99, NACE International, 1999

51. R.M. Kain et al., “Localized and General Corrosion Resistance of Candidate Metallic Materials for RO-Membrane Cartridges,” Paper 268, presented at Corrosion/95, NACE International, 1995

52. R.M. Kain, A. Zeuthen, and J. Maurer, “Localized Corrosion Resistance of Stainless Type Materials in Aerated, Deaerated, and Stagnant Sulfide Bearing Seawater,” Paper 423, presented at Corrosion/97, NACE International, 1997

53. P.A. Klein et al., “A Localized Corrosion Assessment of 6% Molybdenum Stainless Steel Condenser Tubing at the Calvert Cliffs Nuclear Power Plant,” Paper 490, presented at Corrosion/94, National Association of Corrosion Engineers, 1994

54. R.M. Kain, “Crevice Corrosion Behavior of Coated Stainless Steel in Natural Seawater,” Paper 827, presented at Corrosion/2000, NACE International, 2000

55. R.M. Kain, “Seawater Crevice Corrosion Resistance of Stainless Steels Coated with Silane and Antifouling Paint Systems,” Paper 187, presented at Corrosion/2002, NACE International, 2002

R.M. Kain, Evaluating Crevice Corrosion, *Corrosion: Fundamentals, Testing, and Protection*, Vol 13A, *ASM Handbook*, ASM International, 2003, p 549–561

Evaluating Crevice Corrosion

R.M. Kain, Consultant

Component Testing

In some cases, it may be possible to test manufactured components or assemblies and assess their resistance to crevice corrosion. These may comprise nonmetal-to-metal or metal-to-metal joints. In the latter case, like-metal or dissimilar- metal couples may be involved. Testing of flanges with gaskets or O-rings and fasteners are common examples. In an unpublished test (Ref 56), a number of highly torqued like-metal and dissimilar-metal nut, bolt, and washer assemblies were tested by alternate immersion in seawater for 25 weeks. Fasteners comprising all UNS N06625 components exhibited some evidence of crevice attack at mated nut-to-washer, bolthead-to-washer, washer-to-washer, nut-to- bolthead and nut-to-bolt-thread surfaces. When NiCu alloy UNS N04400 washers were substituted for UNS N06625, no attack on the latter occurred, due to galvanic protection (sacrificial corrosion) provided by the NiCu alloy. In another case using UNS N06625 washers in an otherwise all-titanium assembly, attack of the nickel-base alloy was limited to the mated washer surfaces. No attack was found at the titanium-to-UNS N06625 crevice sites created at bolt-head and nut locations. In a metal-to-metal configuration, hydrolysis reactions involving corrosion products from both surfaces in a crevice can contribute to changes in the crevice electrolyte chemistry, leading to breakdown of passivity (Ref 7). Only the UNS N06625 surface in the preceding example would be a contributor of pH-lowering chromium ions.

Reference 57 describes seawater testing of alloy 686 (UNS N08686) bolting securely fastened to large plates of UNS N06625. Specimens were exposed with and without cathodic protection from zinc anodes.

References cited in this section

7. J.W. Oldfield and W.H. Sutton, Crevice Corrosion of Stainless Steels, Part II: Experimental Studies, *Br. Corros. J.,* Vol 13 (No. 3), 1978, p 104

56. LaQue Center for Corrosion Technology, Inc., Unpublished test report, 1998

57. E.L. Hibner and L.E. Shoemaker, "High Strength Corrosion Resistance Alloy 686 for Seawater Fastener Service," Paper 195, presented at Corrosion/2002, NACE International, 2002

R.M. Kain, Evaluating Crevice Corrosion, *Corrosion: Fundamentals, Testing, and Protection*, Vol 13A, *ASM Handbook*, ASM International, 2003, p 549–561

Evaluating Crevice Corrosion

R.M. Kain, Consultant

Electrochemical Tests

ASTM Standard Methods. ASTM G 61 is recommended primarily for investigating localized corrosion on iron-, nickel-, or cobalt-base alloys (Ref 58). Crevices are formed on a 16 mm (0.63 in.) diameter disk test electrode by a TFE- fluorocarbon gasket/mounting assembly. Other gasket materials can also be used. The test electrode

is the anodic member of a polarization cell containing a deaerated 3.5% NaCl solution. After a 1 h period of free corrosion, the test specimen electrode potential is scanned in the noble direction at a rate of 0.6 V/h. Current density and potential are continuously plotted. On reaching an anodic current density of 5 mA/cm^2, the scan direction is reversed and the scan continued back to its original potential. Susceptibility to crevice corrosion is identified by the occurrence of positive hysteresis during the reverse scan. Relative alloy resistance can be established by comparing the forward and reverse scan potential-current domains with UNS N10276 and S30400 stainless steel standards. ASTM G 61 provides standard polarization plots for comparison and equipment performance verification. Some degree of variability is expected. Several factors may affect results, most notably the actual time between specimen preparation and exposure as well as the degree of tightness used in assembling the test electrode holder.

Nonstandard variations of ASTM G 61, such as the use of different electrode assemblies and/ or polarization scan rates, may significantly affect the measured response (Ref 59). Some correlations have been made between cyclic polarization tests performed according to ASTM G 61 and immersion crevice tests in seawater (Ref 60). For the most part, cyclic polarization tests are able to differentiate between highly alloyed, resistant materials (for example, the high-molybdenum nickel-base alloys UNS N06625 and N10276) and lower-alloy materials (for example, 300-series stainless steel). Correlation for alloys with intermediate compositions may be more difficult, because they exhibit resistance to a broader range of environments (that is, Cl^- concentration and crevice geometry) than the 300- series stainless steels but less than that for nickel-base chromium plus high-molybdenum alloys.

Previously mentioned ASTM F 746 describes procedures for evaluating the pitting and crevice corrosion resistance of metallic surgical implant materials (Ref 40). Testing is again limited to making relative rankings of performance. The procedure calls for the use of a cylindrical electrode with crevices formed by a mounting compression gasket and an intentional crevice-forming collar. Corrosion is induced by a polarization step to +0.8 V versus a saturated calomel reference electrode (SCE). Provisions are established for current monitoring and subsequent potential-time increments. The test is designed to produce corrosion for a control electrode of UNS S31600 stainless steel. Alloys can be compared relative to breakdown, propagation, and repassivation tendencies.

Other Potentiostatic and Potentiodynamic Polarization Tests. A potentiostatic test procedure (Ref 61) identifies alloy crevice corrosion resistance according to an established critical crevice temperature (CCT). Tests have been conducted in neutral NaCl solution and synthetic seawater under constant applied potentials, for example, +600 mV versus SCE. In this automated test, the equipment is programmed to increase the solution temperature in 5 °C (9 °F) increments until a specific critical current level is reached in a given period, for example, 15 to 20 min.

Test results obtained with the previously mentioned method using MCAs are summarized in Table 7 (Ref 62). Also given in Table 7 is a CCT ranking determined in 72 h $FeCl_3$ tests performed according to ASTM G 48 (rubber band test) and another ranking based on the total number of crevice corrosion sites initiated in 30 day natural seawater MCA tests. The three procedures gave the same ranking merit for only 3 of the 12 test materials, numbers 1, 2, and 6. In several cases, two procedures provided the same ranking for a given alloy. In the Santron test, the noble potential is intended to mimic the redox potential of $FeCl_3$. In natural seawater, such potentials would never be achieved without chemical stimulation. In the absence of crevice corrosion, nickel-base chromium-molybdenum alloys as well as some stainless steels have achieved potentials in the +300 to +400 mV range versus SCE in ambient temperature seawater (Ref 55, 63, 64).

Table 7 Initiation of crevice corrosion in immersion tests in seawater, $FeCl_3$, and synthetic seawater

All specimens were ground with 120-grit SiC.

Alloy	Filtered seawater[a]		$FeCl_3$[b]			Synthetic seawater[c]		
			Failure temperature		**Rank**	**Failure temperature**		**Rank**
	Number of sites	**Rank**	**°C**	**°F**		**°C**	**°F**	
29-4C	0	1	55	131	1	90.0	195	1
Monit	0	2	47	117	2	67.5	155	2
SC-1	1	3	45	113	4	60.0	140	5

Ferralium 255	2	4	37	99	5	60.0	140	4
Haynes No. 20 Mod	6	5	28	82	8	47.5	120	7
AL6X	11	6	37	99	6	57.5	135	6
254SMO	18	7	46	115	3	62.5	145	3
904L	36	8	22	72	10	42.5	110	9
JS700	47	9	31	88	7	45.0	115	8
JS777	60	10	14	57	12	30.0	85	12
AISI type 329	73	11	25	77	9	40.0	105	11
Nitronic 50	112	12	15	59	11	40.0	105	10

(a) 30 day test at 30 °C (85 °F).

(b) 72 h test in 10% $FeCl_3 \cdot 6H_2O$.

(c) Santron test; 20 min measuring time. Source: Ref 62

Potentiodynamic polarization tests for crevice-free electrodes in a series of increasingly aggressive simulated crevice solutions have been used to rank alloys according to a criterion associated with anodic peak current density (Ref 7). Such information has been used in mathematical modeling to identify the localized environment or critical crevice solution (CCS) that can cause breakdown of passivity and the conditions leading up to it (Ref 28, 30). In addition, as shown in Fig. 10, a plot of log current versus pH has been used to characterize propagation resistance for several cast alloys (Ref 65). Alloy propagation behavior can be ranked according to the slope of the log *i*/pH plot. For the previously mentioned tests, the electrode and its wire lead connection are potted with a thermosetting resin. After curing, the electrode surface is ground, then wiped with a coat of resin to fill gaps, and reground or polished prior to testing.

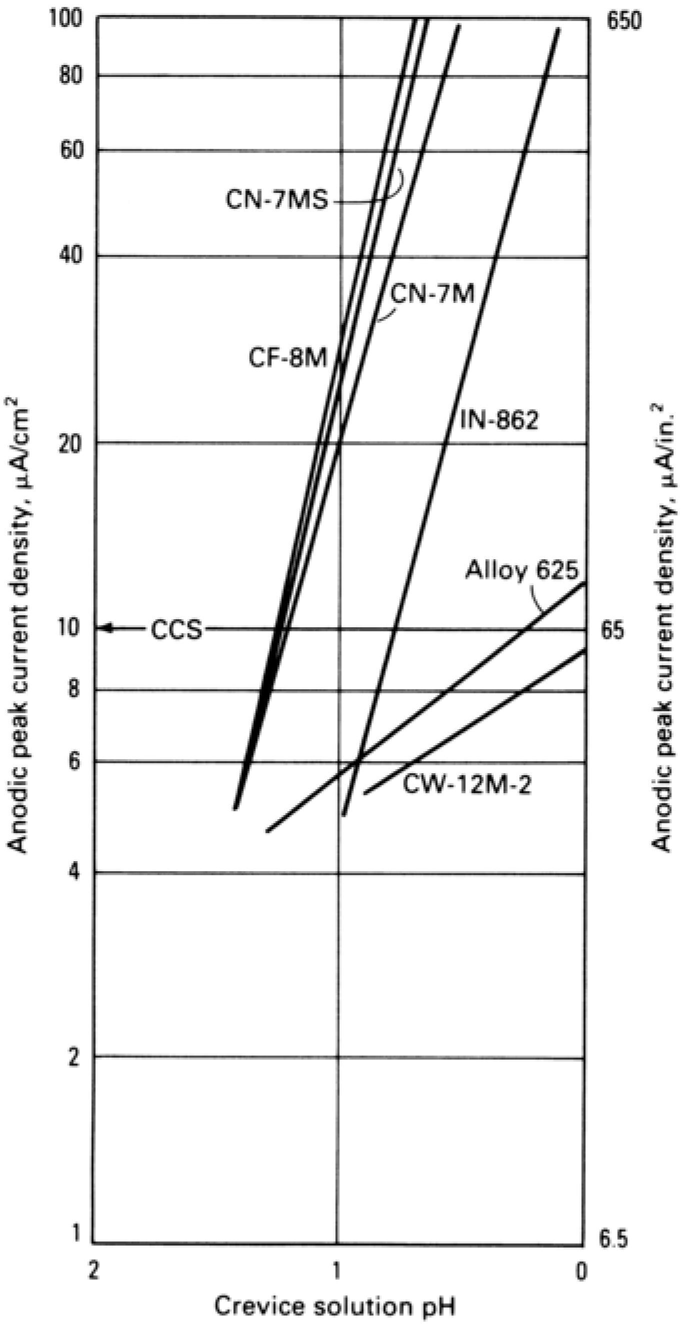

Fig. 10 Plot of anodic peak current density versus simulated crevice solution pH used to determine the composition (pH) of the critical crevice solution (CCS) according to the 10 μA/cm^2 (64.5 μA/in.^{2}) criterion. Source: Ref 8

While not intended for the previously mentioned purpose, ASTM G 150 (Ref 66) may also have some utility in CCS identification. ASTM G 150 was developed to produce a crevice-free electrode for the study of critical pitting temperature. While a crevice gap is present between the test electrode and its holder, this space is continuously flushed with purified water to prevent the buildup of aggressive H^+ and Cl^- ions that would otherwise contribute to breakdown of passivity and lead to crevice attack.

Remote Crevice Assemblies. An electrochemical procedure requiring no stimulation other than that provided by the bulk environment/alloy reaction has been described in the literature. Techniques have been identified as either remote crevice or remote cathode tests (Ref 44, 65, 67, 68). Remote crevice assembly tests involve the physical separation but electrical connection of a small anode or crevice member and a larger cathodic member. Both are exposed in the bulk environment. Current between the two members can be monitored through a zero-resistance ammeter. The technique is quite capable of accurately identifying the time to initiation and subsequent propagation.

Unlike other techniques, this procedure is able to separate the initiation and propagation phases of crevice corrosion. This capability is summarized by the plot of corrosion current normalized for initiation time in Fig. 11. Results show good reproducibility in both the trend of increasing current once initiation has occurred as well as the magnitude of current. The total charge (coulombs) is a measure of propagation, which is directly proportional to mass loss due to crevice corrosion.

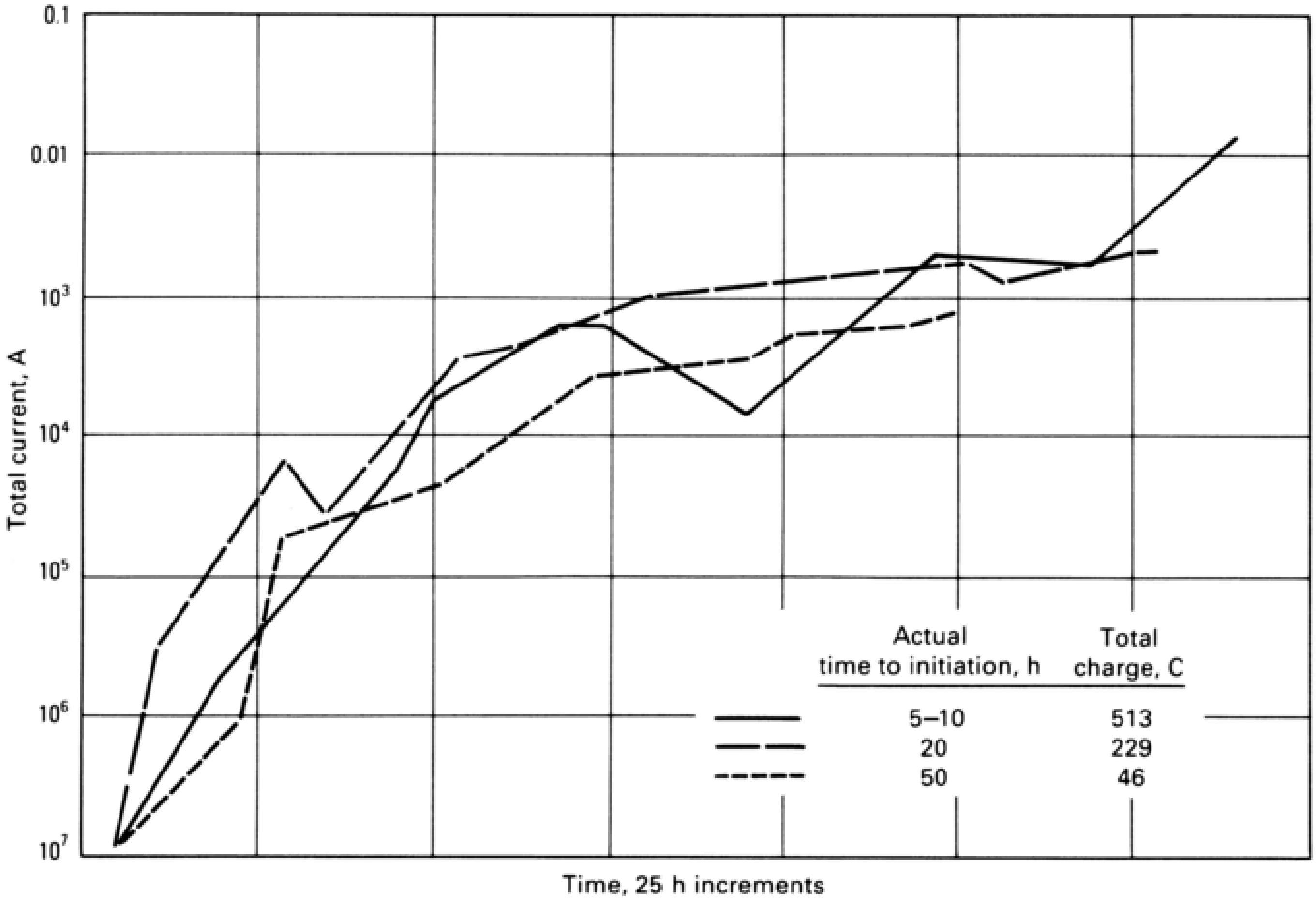

Fig. 11 Comparison of crevice corrosion propagation currents for UNS S31603 stainless steel remote crevice assemblies after normalizing initiation times. Source: Ref 2

Other Electrochemical Techniques. Other specialized tests have been developed, with varying degrees of success. One test involves the use of compartmentalized cells with anode and cathode members exposed to actual or simulated environments (Ref 69). Such tests have been used to evaluate the effects of changes in solution chemistry and surface area ratios. In addition, a vibrating electrode technique has been used to map variations in current density above a creviced stainless steel specimen of known crevice geometry (Ref 70). Such tests are more expensive and perhaps more conducive to mechanistic studies rather than for routinely characterizing alloy resistance to crevice corrosion. A number of electrochemical techniques that may be considered for crevice corrosion testing are reviewed in Ref 71 and 72.

References cited in this section

2. R.M. Kain and T.S. Lee, Recent Developments in Test Methods for Investigating Crevice Corrosion, *Laboratory Corrosion Tests and Standards,* STP 866, American Society for Testing and Materials, 1985, p 299–323

7. J.W. Oldfield and W.H. Sutton, Crevice Corrosion of Stainless Steels, Part II: Experimental Studies, *Br. Corros. J.,* Vol 13 (No. 3), 1978, p 104

8. R.M. Kain et al., Use of Electrochemical Techniques for the Study of Crevice Corrosion in Natural Seawater, Section 6: Localized Corrosion, *Electrochemical Techniques for Corrosion Engineering,* NACE Publication, 1986, p 261–279

28. J.W. Oldfield et al., Avoiding Crevice Corrosion of Stainless Steels, *Proc. Stainless Steel '84 Symposium,* (Gotenberg, Sweden), Chalmers University of Technology and Jernkontoret (Sweden) and The Metals Society (UK), 1984

30. J.W. Oldfield and R.M. Kain, Assessment of the Corrosion Resistance of Austenitic Stainless Steels in Industrial Waters, *Proc. International Corrosion Congress,* (Florence, Italy), Associazione Italiana Di Metallurgia, 1990

40. "Standard Test Method for Pitting or Crevice Corrosion of Metallic Surgical Implant Materials," F 746, *Annual Book of ASTM Standards,* Vol 13.01, American Society for Testing and Materials

44. R.M. Kain and P.A. Klein, "Crevice Corrosion Propagation Studies for Alloy N06625: Remote Crevice Assembly Testing in Flowing Natural and Chlorinated Seawater," Paper 158, presented at Corrosion/90, National Association of Corrosion Engineering, 1990

55. R.M. Kain, "Seawater Crevice Corrosion Resistance of Stainless Steels Coated with Silane and Antifouling Paint Systems," Paper 187, presented at Corrosion/2002, NACE International, 2002

58. "Standard Practice for Conducting Cyclic Potentiodynamic Polarization Measurements for Localized Corrosion," G 61, *Annual Book of ASTM Standards,* Vol 03.02, American Society for Testing and Materials

59. R.M. Kain, "Localized Corrosion Behavior in Natural Seawater: A Comparison of Electrochemical and Crevice Testing of Stainless Steel," Paper 70, presented at Corrosion/80, National Association of Corrosion Engineers, 1980

60. B.E. Wilde, A Critical Appraisal of Some Popular Laboratory Electrochemical Tests for Predicting the Localized Corrosion Resistance of Stainless Alloys in Sea Water, *Corrosion,* Vol 28 (No. 8), 1972, p 283

61. S. Bernhardsson, Paper 85, presented at Corrosion/80, National Association of Corrosion Engineers, 1980

62. N.S. Nagaswami and M.A. Streicher, "Accelerated Laboratory Tests for Crevice Corrosion of Stainless Alloys," Paper 7, presented at Corrosion/83, National Association of Corrosion Engineers, 1983

63. J.M. Kroughman and F.P. Ijsseling, Crevice Corrosion of Stainless Steels and Nickel Alloys in Seawater, *Proc. Fifth International Congress on Marine Corrosion and Fouling,* G. Londres, Ed., (Barcelona, Spain), 1980, p 214

64. A. Mollica et al., Cathodic Performance of Stainless Steels in Natural Seawater as a Function of Microorganism Settlement and Temperature, *Corrosion,* Vol 48 (No. 1), 1998, p 48–56

65. T.S. Lee et al., Use of Electrochemical Techniques for the Study of Crevice Corrosion in Natural Seawater, *Electrochemical Techniques for Corrosion Engineering,* National Association of Corrosion Engineering, 1986

66. "Standard Test Method for Electrochemical Critical Pitting Temperature Testing of Stainless Steels," G 150, *Wear and Erosion, Metal Corrosion,* Vol 03.02, *Annual Book of ASTM Standards,* American Society for Testing and Materials

67. T.S. Lee, A Method of Quantifying the Initiation and Propagation Stages of Crevice Corrosion, *Electrochemical Corrosion Testing,* STP 727, American Society for Testing and Materials, 1981, p 43–68

68. R.M. Kain, Electrochemical Measurement of the Crevice Corrosion Propagation Resistance of Stainless Steels: Effect of Environmental Variables, *Mater. Perform.,* Vol 23 (No. 2), 1984, p 24

69. R.M. Kain and T.S. Lee, "The Effect of Crevice Solution pH on Corrosion Behavior of Stainless Steels," Paper 27, presented at Corrosion/84, National Association of Corrosion Engineers, 1984

70. H.S. Issacs, "Application of the Vibration Probe to Localized Current Measurements," Paper 55, presented at Corrosion/85, National Association of Corrosion Engineers, 1985

71. J. Postlewaite, *Can. Metall. Q.,* Vol 22 (No. 1), 1983, p 133

72. F.P. Ijsseling, Electrochemical Methods in Crevice Corrosion Testing, *Br. Corros. J.,* Vol 15 (No. 2), 1980, p 51

R.M. Kain, Evaluating Crevice Corrosion, *Corrosion: Fundamentals, Testing, and Protection*, Vol 13A, *ASM Handbook,* ASM International, 2003, p 549–561

Evaluating Crevice Corrosion

R.M. Kain, Consultant

Mathematical Modeling

Mathematical models have been developed to serve as research and predictive tools describing the many interrelated factors known to influence crevice corrosion behavior in chloride-containing environments (Ref 7, 73, 74). Model development is heavily dependent on input from laboratory confirmation tests using some of the evaluation methods described in this article. The PCA test, for example, was used extensively in support of the Sutton-Oldfield model (Ref 7, 16) and its subsequent refinements (Ref 73). In addition, results from potentiodynamic polarization tests were used to model passive current and CCS chemistries (Ref 16).

Figure 12 shows a sample model output describing the influence of crevice geometry on initiation behavior of UNS S31803 stainless steel (Ref 73). Figure 13 shows a sample model prediction of expected resistance for UNS S31600 in various chloride- and sulfate-containing waters (Ref 73).

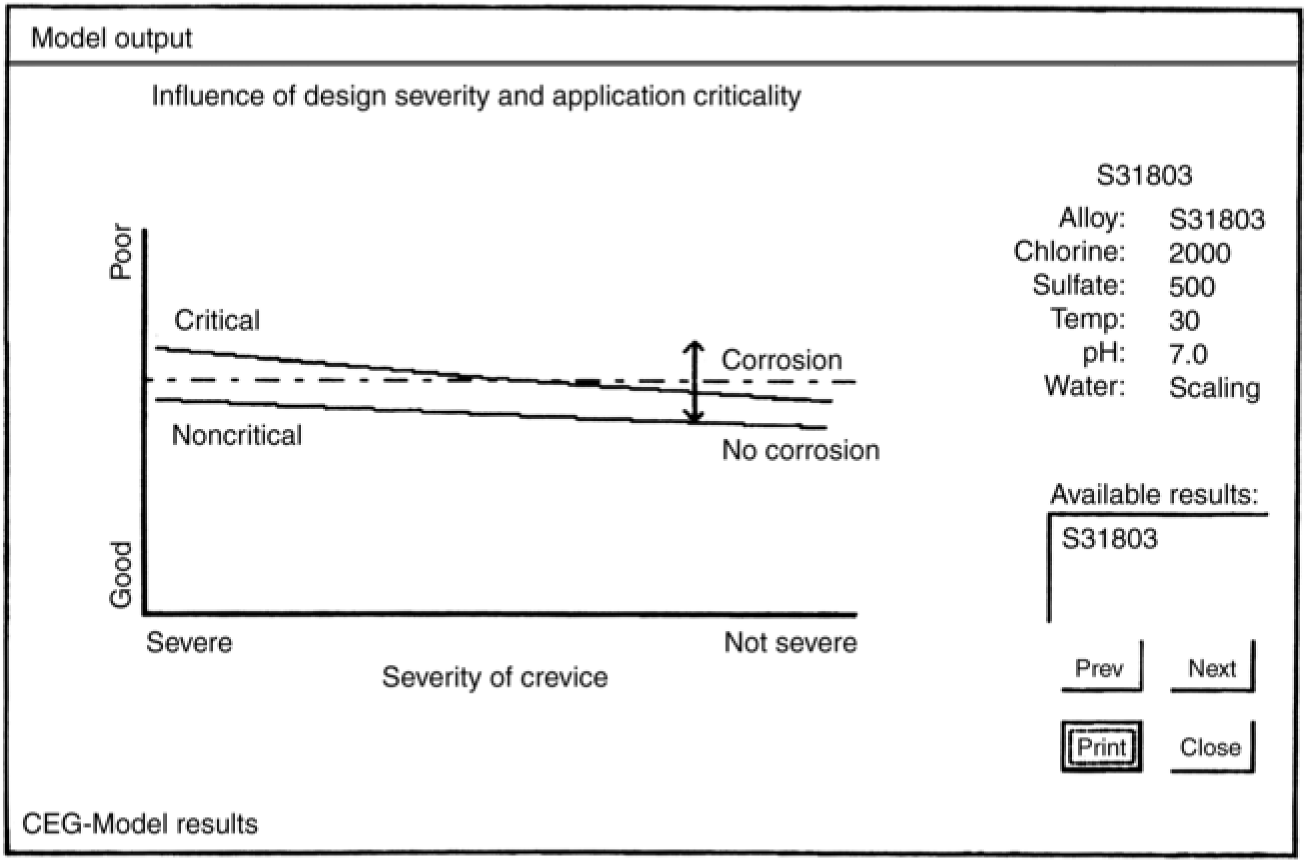

Fig. 12 Example of *Crevice Corrosion Engineering Guide* (Ref 73) model output describing effect of crevice geometry on stainless steel resistance

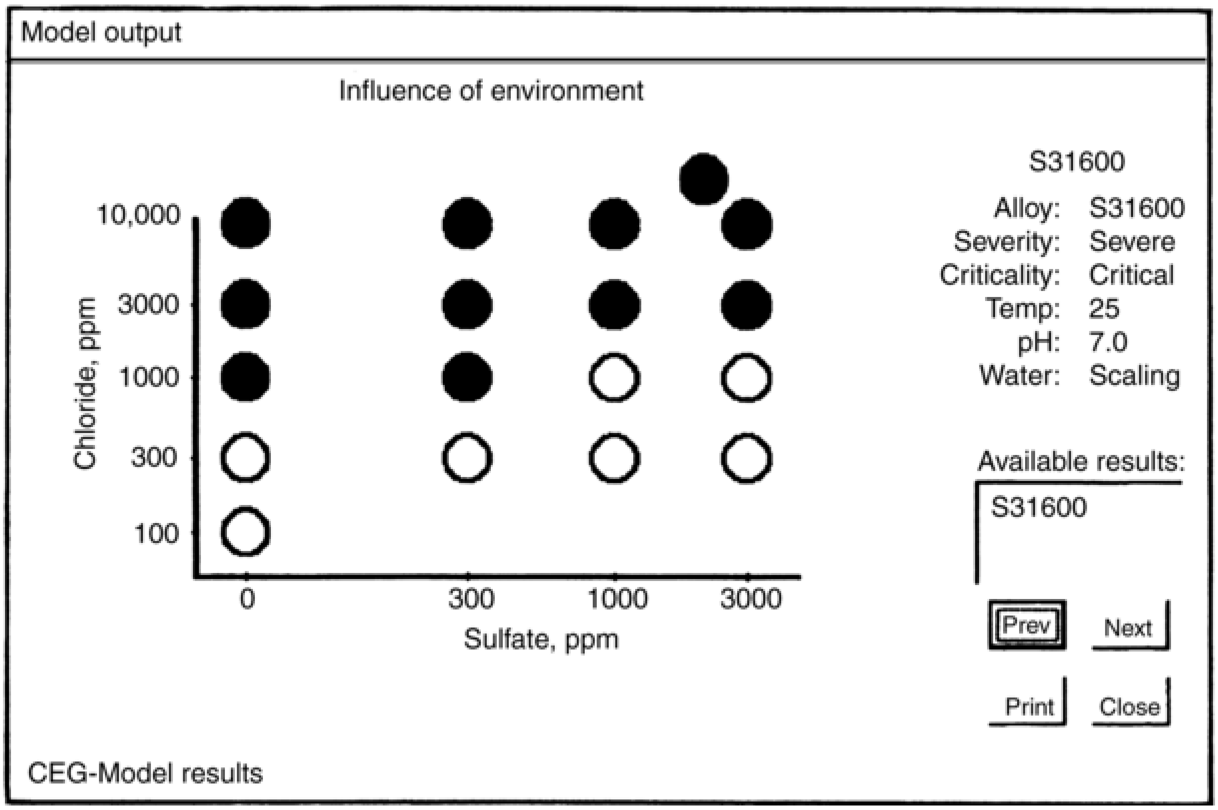

Fig. 13 Model prediction showing effect of chloride and sulfate ion on a range of stainless steels

Reference 74 describes a model that addresses both crevice corrosion initiation and propagation as well as passivation. A number of citations provided in Ref 74 and 75 offer additional reading on this subject.

References cited in this section

7. J.W. Oldfield and W.H. Sutton, Crevice Corrosion of Stainless Steels, Part II: Experimental Studies, *Br. Corros. J.,* Vol 13 (No. 3), 1978, p 104

16. J.W. Oldfield and W.H. Sutton, New Technique for Predicting the Performance of Stainless Steels in Seawater and Other Chloride Containing Environments, *Br. Corros. J.,* Vol 15 (No. 1), 1980, p 31–34

73. J.W. Oldfield and R.M. Kain, Prediction of Crevice Corrosion Resistance of Stainless Steels in Aqueous Environments—A Corrosion Engineering Guide, *Proc. 12th International Corrosion Congress,* National Association of Corrosion Engineers, 1993, p 1876

74. P.O. Gartland, Modelling Crevice Corrosion of Fe-Cr-Ni-Mo Alloys in Chloride Solutions, *Proc. 12th International Corrosion Congress,* Vol 3B, National Association of Corrosion Engineers, 1993, p 1901–1914

75. B. Shaw, P. Moran, and P.O. Gartland, Crevice Corrosion of a Nickel-Based Super Alloy in Natural and Chlorinated Seawater, *Proc. 12th International Corrosion Congress,* Vol 3B, National Association of Corrosion Engineers, 1993, p 1915–1928

R.M. Kain, Evaluating Crevice Corrosion, *Corrosion: Fundamentals, Testing, and Protection*, Vol 13A, *ASM Handbook,* ASM International, 2003, p 549–561

Evaluating Crevice Corrosion

R.M. Kain, Consultant

References

1. T.S. Lee et al., Mathematical Modelling of Crevice Corrosion of Stainless Steels, *Corrosion and Corrosion Protection Proceedings,* Vol 81-8, The Electrochemical Society, 1981, p 213–224

2. R.M. Kain and T.S. Lee, Recent Developments in Test Methods for Investigating Crevice Corrosion, *Laboratory Corrosion Tests and Standards,* STP 866, American Society for Testing and Materials, 1985, p 299–323

3. "Standard Guide for Crevice Corrosion Testing of Iron-Base and Nickel-Base Stainless Alloys in Seawater and Other Chloride Containing Aqueous Environments," G 78, *Annual Book of ASTM Standards,* American Society for Testing and Materials

4. "Standard Guide for Conducting Corrosion Tests in Field Application," G 4, *Wear and Erosion; Metal Corrosion,* Vol 03.02, *Annual Book of ASTM Standards,* American Society for Testing and Materials

5. A.H. Tuthill, Resistance of Highly Alloyed Materials and Titanium to Localized Corrosion in Bleach Plant Environments, *Mater. Perform.,* Vol 24 (No. 9), 1985, p 43–49

6. "Standard Method for Pitting and Crevice Corrosion Resistance of Stainless Steels and Related Alloys by the Use of Ferric Chloride Solution," G 48, *Annual Book of ASTM Standards,* American Society for Testing and Materials

7. J.W. Oldfield and W.H. Sutton, Crevice Corrosion of Stainless Steels, Part II: Experimental Studies, *Br. Corros. J.,* Vol 13 (No. 3), 1978, p 104

8. R.M. Kain et al., Use of Electrochemical Techniques for the Study of Crevice Corrosion in Natural Seawater, Section 6: Localized Corrosion, *Electrochemical Techniques for Corrosion Engineering,* NACE Publication, 1986, p 261–279

9. R.S. Treseder and E.A. Kachik, MTI Corrosion Tests for Iron and Nickel-Base Corrosion Alloys, *Laboratory Corrosion Tests and Standards,* STP 866, American Society for Testing and Materials, 1985, p 373–399

10. E.L. Hibner, Modification of Critical Crevice Temperature Test Procedures for Nickel Alloys in a Ferric Chloride Environment, *Mater. Perform.,* Vol 26 (No. 3), 1987, p 37–40

11. A.P. Bond and H.J. Dundas, Resistance of Stainless Steels to Crevice Corrosion in Seawater, *Mater. Perform.,* Vol 23 (No. 7), 1984, p 39–43

12. A. Garner, Crevice Corrosion of Stainless Steel in Seawater: Correlation of Field Data with Laboratory Ferric Chloride Tests, *Corrosion,* Vol 37 (No. 3), 1981, p 178–184

13. T.S. Lee et al., The Effect of Environmental Variables on Crevice Corrosion of Stainless Steels in Seawater, *Mater. Perform.,* Vol 23 (No. 7), 1984, p 9–15

14. R.M. Kain, Crevice Corrosion Behavior of Stainless Steel in Seawater and Related Environments, *Corrosion,* Vol 40 (No. 6), 1984, p 313–321

15. R.M. Kain et al., The Resistance of Type 304 and Type 316 Stainless Steel to Crevice Corrosion Natural Waters, *J. Mater. Energy Syst.,* Vol 5 (No. 4), 1984, p 205–211

16. J.W. Oldfield and W.H. Sutton, New Technique for Predicting the Performance of Stainless Steels in Seawater and Other Chloride Containing Environments, *Br. Corros. J.,* Vol 15 (No. 1), 1980, p 31–34

17. D.B. Anderson, Statistical Aspects of Crevice Corrosion in Seawater, *Galvanic and Pitting Corrosion—Field and Laboratory Studies,* STP 576, American Society for Testing and Materials, 1976, p 261

18. A.P. Bond et al., Corrosion Resistance of Stainless Steels in Seawater, *Advanced Materials in Seawater Applications,* Climax Molybdenum Company, Piacenza, Italy, Feb 1980, p 1

19. J.W. Oldfield, "Crevice Corrosion of Stainless Steels: The Importance of Crevice Geometry and Alloys Composition," presented at 19th Journees de Aciers Speciaux, (Saint Etienne, France), May 1980, Met. Corros.- Ind., April 1981, No. 668, p 134–147

20. T. Sydberger, *Werkst. Korros.,* Vol 32 (No. 3), 1981, p 119

21. R.M. Kain, "Effect of Alloy Content on the Localized Corrosion Resistance of Several Nickel Base Alloys in Seawater," Paper 229, presented at Corrosion/86, National Association of Corrosion Engineers, 1986

22. R.M. Kain, "Crevice Corrosion and Metal Ion Concentration Cell Corrosion Resistance of Candidate Materials for OTEC Heat Exchangers," ANL/OTEC-BCM-022, Argonne National Laboratory and the U.S. Department of Energy, May 1981

23. G.O. Davis and M.A. Streicher, "Initiation of Chloride Crevice Corrosion on Stainless Alloys," Paper 205, presented at Corrosion/ 85, National Association of Corrosion Engineers, 1985

24. H.P. Hack, Crevice Corrosion Behavior of 45 Molybdenum Containing Stainless Steels in Seawater, *Mater. Perform.,* Vol 22 (No. 6), 1983, p 24–30

25. T.S. Lee and R.M. Kain, "Factors Influencing the Crevice Corrosion Behavior of Stainless Steels in Seawater," Paper 69, presented at Corrosion/83, National Association of Corrosion Engineers, 1983

26. R.M. Kain, Crevice Corrosion Testing in Natural Seawater: Significance and Use of Multiple Crevice Assemblies, *J. Test. Eval.,* Sept 1990, p 309–319

27. U. Hideki et al., "Crevice Corrosion of Stainless Steels in Chloride Solutions," Paper 117, presented at Corrosion/89, National Association of Corrosion Engineers, 1989

28. J.W. Oldfield et al., Avoiding Crevice Corrosion of Stainless Steels, *Proc. Stainless Steel '84 Symposium,* (Gotenberg, Sweden), Chalmers University of Technology and Jernkontoret (Sweden) and The Metals Society (UK), 1984

29. R.M. Kain and J.W. Oldfield, "Prediction of Crevice Corrosion Resistance of Stainless Steels in Aqueous Environments—A Corrosion Engineering Guide," presented at 12th International Corrosion Congress, Localized Corrosion Session, (Houston, TX), NACE International, 1993

30. J.W. Oldfield and R.M. Kain, Assessment of the Corrosion Resistance of Austenitic Stainless Steels in Industrial Waters, *Proc. International Corrosion Congress,* (Florence, Italy), Associazione Italiana Di Metallurgia, 1990

31. R.M. Kain, "Effects of Surface Finish on the Crevice Corrosion Resistance of Stainless Steels in Seawater and Related Environments," Paper 508, presented at Corrosion/ 91, National Association of Corrosion Engineers, 1991

32. R.M. Kain, Seawater Testing to Assess the Crevice Corrosion Resistance of Stainless Steels and Related Alloys, *Proc. 12th International Corrosion Congress, Localized Corrosion Session,* Vol 3, (Houston, TX), 1993, NACE International, p 1889–1900

33. P.A. Klein et al., "The Effect of Electrolytic Chlorination on the Crevice Corrosion Behavior of 70/30 Copper-Nickel and Nickel- Copper Alloy 400," Paper 509, presented at Corrosion/91, National Association of Corrosion Engineers, 1991

34. D.M. Aylor et al., "Crevice Corrosion Performance of Candidate Naval Ship Seawater Valve Materials in Quiescent and Flowing Natural Seawater," Paper 329, presented at Corrosion/99, NACE International, 1999

35. R.M. Kain, Gasket Materials and Other Factors Influencing the Crevice Corrosion Resistance of Stainless Steel Flanges, *Mater. Perform.,* Vol 37 (No. 8), 1998, p 62–66

36. R.A. Buchanan and C.D. Lundin, New Method for Crevice Corrosion Testing of Welds with Reinforcements, *Corrosion,* Vol 58 (No. 5), 2002, p 448

37. R.M. Kain, Use of Coatings to Assess the Crevice Corrosion Resistance of Stainless Steels in Warm Seawater, *Marine Corrosion in Tropical Environments,* STP 1399, American Society for Testing and Materials, 2000

38. LaQue Center for Corrosion Technology, Inc., Unpublished test report, 2000

39. T. Degerbeck and T. Gille, Crevice Corrosion—A New Crevice Former, *Corros. Sci.,* Vol 19, 1979, p 1113–1114

40. “Standard Test Method for Pitting or Crevice Corrosion of Metallic Surgical Implant Materials,” F 746, *Annual Book of ASTM Standards,* Vol 13.01, American Society for Testing and Materials

41. LaQue Center for Corrosion Technology, Inc., Unpublished test report, 1978

42. R.M. Kain and I. Dunoff, “Influence of Packing Material on the Corrosion Resistance of Stainless Steel Boat Shafting and Related Materials,” Paper 639, presented at Corrosion/2000, NACE International, 2000

43. R.M. Kain et al., “Crevice Corrosion of Nickel-Chromium-Molybdenum Alloys in Natural and Chlorinated Seawater,” Paper 112, presented at Corrosion/89, National Association of Corrosion Engineers, 1989

44. R.M. Kain and P.A. Klein, “Crevice Corrosion Propagation Studies for Alloy N06625: Remote Crevice Assembly Testing in Flowing Natural and Chlorinated Seawater,” Paper 158, presented at Corrosion/90, National Association of Corrosion Engineering, 1990

45. R.M. Kain and A. Zeuthen, Crevice Corrosion Testing of Austenitic, Superaustenitic, Superferritic and Superduplex Stainless Type Alloys in Seawater, *Corrosion Testing in Natural Waters,* STP 1300, American Society for Testing and Materials, 1996

46. M.E. Inman et al., “Detection of Crevice Corrosion in Natural Seawater Using Polarization Resistance Measurements,” Paper 297, presented at Corrosion/97, NACE International, 1997

47. D.C. Agarwal, “Solving Critical Problems in Marine Environments by an Advanced Ni-Cr-Mo Alloy 59 UNS N06059,” Paper 635, presented at Corrosion/2000, NACE International, 2000

48. R.M. Kain, “Testing for Crevice Corrosion Susceptibility,” presented at research symposium at Corrosion/96, NACE International, 1996

49. LaQue Center for Corrosion Technology, Inc., Unpublished test report, 1993

50. R.M. Kain and M.B. Ives, “Surface Treatments Benefiting the Crevice Corrosion Resistance of Nickel Alloy N06625 in Natural and Chlorinated Seawater,” Paper 330, presented at Corrosion/99, NACE International, 1999

51. R.M. Kain et al., “Localized and General Corrosion Resistance of Candidate Metallic Materials for RO-Membrane Cartridges,” Paper 268, presented at Corrosion/95, NACE International, 1995

52. R.M. Kain, A. Zeuthen, and J. Maurer, “Localized Corrosion Resistance of Stainless Type Materials in Aerated, Deaerated, and Stagnant Sulfide Bearing Seawater,” Paper 423, presented at Corrosion/97, NACE International, 1997

53. P.A. Klein et al., “A Localized Corrosion Assessment of 6% Molybdenum Stainless Steel Condenser Tubing at the Calvert Cliffs Nuclear Power Plant,” Paper 490, presented at Corrosion/94, National Association of Corrosion Engineers, 1994

54. R.M. Kain, “Crevice Corrosion Behavior of Coated Stainless Steel in Natural Seawater,” Paper 827, presented at Corrosion/2000, NACE International, 2000

55. R.M. Kain, “Seawater Crevice Corrosion Resistance of Stainless Steels Coated with Silane and Antifouling Paint Systems,” Paper 187, presented at Corrosion/2002, NACE International, 2002

56. LaQue Center for Corrosion Technology, Inc., Unpublished test report, 1998

57. E.L. Hibner and L.E. Shoemaker, "High Strength Corrosion Resistance Alloy 686 for Seawater Fastener Service," Paper 195, presented at Corrosion/2002, NACE International, 2002

58. "Standard Practice for Conducting Cyclic Potentiodynamic Polarization Measurements for Localized Corrosion," G 61, *Annual Book of ASTM Standards,* Vol 03.02, American Society for Testing and Materials

59. R.M. Kain, "Localized Corrosion Behavior in Natural Seawater: A Comparison of Electrochemical and Crevice Testing of Stainless Steel," Paper 70, presented at Corrosion/80, National Association of Corrosion Engineers, 1980

60. B.E. Wilde, A Critical Appraisal of Some Popular Laboratory Electrochemical Tests for Predicting the Localized Corrosion Resistance of Stainless Alloys in Sea Water, *Corrosion,* Vol 28 (No. 8), 1972, p 283

61. S. Bernhardsson, Paper 85, presented at Corrosion/80, National Association of Corrosion Engineers, 1980

62. N.S. Nagaswami and M.A. Streicher, "Accelerated Laboratory Tests for Crevice Corrosion of Stainless Alloys," Paper 7, presented at Corrosion/83, National Association of Corrosion Engineers, 1983

63. J.M. Kroughman and F.P. Ijsseling, Crevice Corrosion of Stainless Steels and Nickel Alloys in Seawater, *Proc. Fifth International Congress on Marine Corrosion and Fouling,* G. Londres, Ed., (Barcelona, Spain), 1980, p 214

64. A. Mollica et al., Cathodic Performance of Stainless Steels in Natural Seawater as a Function of Microorganism Settlement and Temperature, *Corrosion,* Vol 48 (No. 1), 1998, p 48–56

65. T.S. Lee et al., Use of Electrochemical Techniques for the Study of Crevice Corrosion in Natural Seawater, *Electrochemical Techniques for Corrosion Engineering,* National Association of Corrosion Engineering, 1986

66. "Standard Test Method for Electrochemical Critical Pitting Temperature Testing of Stainless Steels," G 150, *Wear and Erosion, Metal Corrosion,* Vol 03.02, *Annual Book of ASTM Standards,* American Society for Testing and Materials

67. T.S. Lee, A Method of Quantifying the Initiation and Propagation Stages of Crevice Corrosion, *Electrochemical Corrosion Testing,* STP 727, American Society for Testing and Materials, 1981, p 43–68

68. R.M. Kain, Electrochemical Measurement of the Crevice Corrosion Propagation Resistance of Stainless Steels: Effect of Environmental Variables, *Mater. Perform.,* Vol 23 (No. 2), 1984, p 24

69. R.M. Kain and T.S. Lee, "The Effect of Crevice Solution pH on Corrosion Behavior of Stainless Steels," Paper 27, presented at Corrosion/84, National Association of Corrosion Engineers, 1984

70. H.S. Issacs, "Application of the Vibration Probe to Localized Current Measurements," Paper 55, presented at Corrosion/85, National Association of Corrosion Engineers, 1985

71. J. Postlewaite, *Can. Metall. Q.,* Vol 22 (No. 1), 1983, p 133

72. F.P. Ijsseling, Electrochemical Methods in Crevice Corrosion Testing, *Br. Corros. J.,* Vol 15 (No. 2), 1980, p 51

73. J.W. Oldfield and R.M. Kain, Prediction of Crevice Corrosion Resistance of Stainless Steels in Aqueous Environments—A Corrosion Engineering Guide, *Proc. 12th International Corrosion Congress,* National Association of Corrosion Engineers, 1993, p 1876

74. P.O. Gartland, Modelling Crevice Corrosion of Fe-Cr-Ni-Mo Alloys in Chloride Solutions, *Proc. 12th International Corrosion Congress,* Vol 3B, National Association of Corrosion Engineers, 1993, p 1901–1914

75. B. Shaw, P. Moran, and P.O. Gartland, Crevice Corrosion of a Nickel-Based Super Alloy in Natural and Chlorinated Seawater, *Proc. 12th International Corrosion Congress,* Vol 3B, National Association of Corrosion Engineers, 1993, p 1915–1928

R.M. Kain, Evaluating Crevice Corrosion, *Corrosion: Fundamentals, Testing, and Protection*, Vol 13A, *ASM Handbook*, ASM International, 2003, p 549–561

Evaluating Crevice Corrosion

R.M. Kain, Consultant

Selected References

- F.L. LaQue, Marine Corrosion—Causes and Prevention, *Crevice Corrosion,* J. Wiley & Sons, 1975, p 164
- A.J. Sedriks, Corrosion of Stainless Steel, *Crevice Corrosion,* 2nd ed., Wiley Interscience, 1996

H.P. Hack, Evaluation Galvanic Corrosion, *Corrosion: Fundamentals, Testing, and Protection*, Vol 13A, *ASM Handbook*, ASM International, 2003, p 562–567

Evaluating Galvanic Corrosion

Harvey P. Hack, Northrop Grumman Corporation

Introduction

GALVANIC CORROSION, although listed as one of the forms of corrosion, should instead be considered a type of corrosion mechanism, because galvanic effects can accelerate any of the other forms of corrosion. Any of the tests used for the more conventional forms of corrosion, therefore, such as uniform attack, pitting, or stress corrosion, can be used with modifications to determine galvanic-corrosion effects. The modifications can be as simple as connecting a second metal to the system or as complex as necessary to evaluate the appropriate parameters. A change in the method of data interpretation is often all that is needed to convert conventional test methods into galvanic-corrosion tests.
This article discusses component, model, electrochemical, and specimen tests.

H.P. Hack, Evaluation Galvanic Corrosion, *Corrosion: Fundamentals, Testing, and Protection*, Vol 13A, *ASM Handbook*, ASM International, 2003, p 562–567

Evaluating Galvanic Corrosion

Harvey P. Hack, Northrop Grumman Corporation

Component Testing

Component testing is an especially useful technique for galvanic corrosion prediction. The materials in a system are often selected primarily for reasons other than galvanic compatibility. In complex components, such as valves or pumps, many different materials can be used in a geometric configuration that is extremely difficult to model. In more complicated cases, even the most basic prediction, such as which materials will suffer increased corrosion due to galvanic effects, may not be possible from simple laboratory tests. Therefore, component testing becomes the best method for predicting galvanic corrosion behavior in complex systems.

Conducting component tests for galvanic corrosion is similar to conducting component tests for any other type of corrosion. The same care must be taken to ensure that the materials, the operation of the component, and the environment are similar to those in service. However, one important difference with regard to galvanic corrosion is the relationship between the component being tested and the other elements of the system. It would, for example, be a waste of effort to expose a complicated piece of machinery in order to look for galvanic corrosion when the whole device is cathodically protected as a result of being attached to a protected structure. Alternatively, incorrect results would be obtained for the exposure of an isolated bronze mixed-material valve when the ultimate use is in a piping system made of a more noble metal that could accelerate the corrosion of the entire valve galvanically. When outside interactions of this type are possible, the interacting materials must be made part of the corrosion system by exposing the appropriate surface area of those materials electrically connected to, and in the same electrolyte as, the component being tested.

The principal advantages of component testing are the ease of interpretation of results and the lack of scaling or modeling uncertainties. The disadvantages include the high cost and the need for extremely sensitive measures of corrosion damage to obtain results within reasonable time periods.

H.P. Hack, Evaluation Galvanic Corrosion, *Corrosion: Fundamentals, Testing, and Protection*, Vol 13A, *ASM Handbook*, ASM International, 2003, p 562–567

Evaluating Galvanic Corrosion

Harvey P. Hack, Northrop Grumman Corporation

Modeling

Even when the galvanic behavior of panels of the materials of interest is known, the geometrical arrangement of these materials may make galvanic-corrosion prediction difficult because of the effects of solution (electrolyte) resistance on the corrosion rates. An example of this is a heat-exchanger tube in a tubesheet. Assuming the tube to be anodic to the tubesheet, areas of the tube near the tubesheet will have low solution resistance to the cathode and will corrode rapidly, but areas away from the tubesheet will have a large solution resistance to the cathodic metal and will therefore corrode more slowly. In the reverse case, in which the tubesheet is anodic to the tube, the areas of the cathodic tube near the tubesheet will drive the galvanic corrosion of the tubesheet much more than distant areas will.

Computer Modeling. Geometrical effects can be modeled in computers by using such techniques as finite elements, boundary elements, and finite differences. The best computer models solve a version of the Laplace

equation for the electrolyte surrounding the corroding materials and use the polarization behavior of the material in question as boundary conditions at the metal/ electrolyte interface. The analysis is similar to the heat flow analysis, with potential analogous to temperature, current analogous to heat flux, and the polarization boundary condition analogous to a special nonlinear type of temperature- dependent convective flux.

The only data this type of model requires are the geometry, electrolyte conductivity, and polarization characteristics of the materials involved. The program generates potentials and current densities as a function of location, either of which can be related back to corrosion rate. The nonlinear boundary conditions make this type of computer modeling difficult to perform unless sufficient computing power is available. Computer modeling provides an excellent predictive tool for geometrical effects; however, it is still seen as less satisfying than physical scale- model exposures.

Physical scale modeling must model the solution resistance effects and the relative effects of polarization resistance and solution resistance to obtain accurate geometrical predictive capability. When solution resistance is important, the best type of scale modeling is the scaled conductivity exposure. In this type of exposure, the model is reduced in size by some factor from the original. To maintain proper potential and current distribution scaling, the electrolyte conductivity must also be reduced by the same factor. Any resistive coatings such as paints must also have their conductivity scaled similarly. In the case of paints, this can be accomplished by applying a thinner layer, reduced by the same scaling factor used for size, than the thickness used in practice.

For example, a one-tenth-scale model of a heat exchanger designed to operate in seawater with a conductivity of 4 S/cm should be placed in seawater diluted to a conductivity of 0.4 S/cm. In this case, the observed potential and current distributions will be the same between the model and the full-scale heat exchanger. For physical scale modeling, measurements that can be taken include potential distribution by the use of a movable reference electrode, corrosion depth as a function of location, and, if the model design permits, current to different parts of the structure and mass loss of certain model components.

Although less expensive than full-scale component testing, physical scale modeling has many of the disadvantages of component testing. In addition, a great inaccuracy in conductivity scaling stems from the fact that the polarization resistance of the materials in the system of interest is often a function of solution conductivity. Thus, changing solution conductivity may influence polarization resistance sufficiently to make the results of the model inaccurate. There is no experimental way to avoid this shortcoming.

H.P. Hack, Evaluation Galvanic Corrosion, *Corrosion: Fundamentals, Testing, and Protection*, Vol 13A, *ASM Handbook*, ASM International, 2003, p 562–567

Evaluating Galvanic Corrosion

Harvey P. Hack, Northrop Grumman Corporation

Laboratory Testing

Laboratory tests fall into two categories: electrochemical tests in which the data are analyzed and reported in a way that assists galvanic-corrosion predictions and specimen exposures that may or may not be electrochemically monitored.

Electrochemical Tests

The use of electrochemical techniques to predict galvanic corrosion is summarized in Ref 1. The details that relate to testing techniques are discussed in the following paragraphs.

Galvanic Series. When the only information needed is which of the materials in the system are possible candidates for galvanically accelerated corrosion and which will be unaffected or protected, the information from a galvanic series in the appropriate medium is useful. Such a series is a list of freely corroding potentials of the materials of interest in the environment of interest arranged in order of potential (Fig. 1). The galvanic series is easy to use and is often all that is required to answer a simple galvanic-corrosion question. The

material with the most negative, or anodic, corrosion potential has a tendency to suffer accelerated corrosion when electrically connected to a material with a more positive, or noble, potential. The disadvantages include:

- No information is available on the rate of corrosion.
- Active-passive metals may display two widely differing potentials.
- Small changes in electrolyte can change the potentials significantly.
- Potentials may be time dependent.

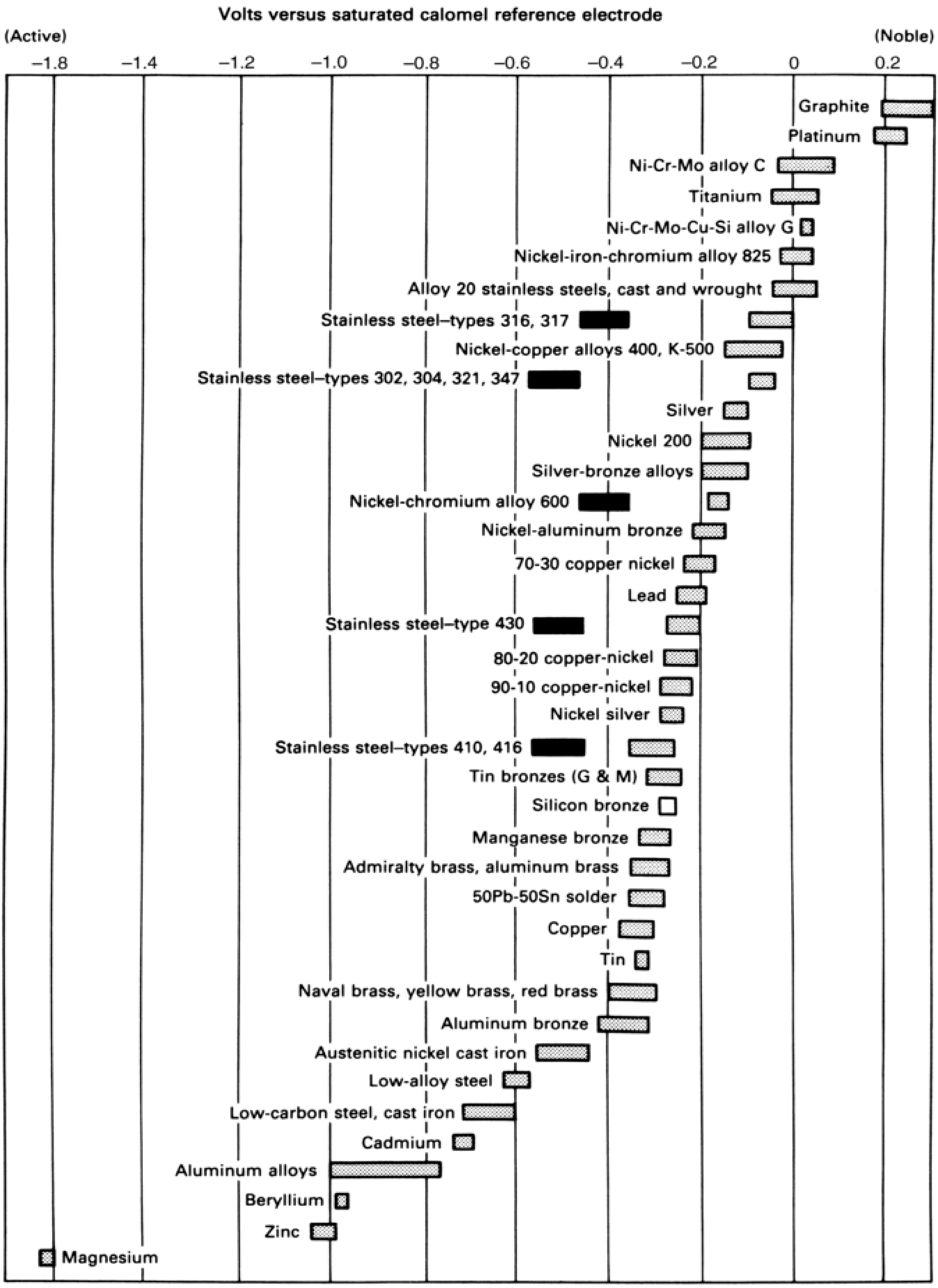

Fig. 1 Galvanic series for seawater. Dark boxes indicate active behavior of active-passive alloys.

Creating a galvanic series is a matter of measuring the corrosion potential of various materials of interest in the electrolyte of interest against a reference electrode half-cell, such as saturated calomel. This procedure is described in Ref 2. The details of such factors as meter resistance, reference cell selection, and measurement duration are also addressed in Ref 2. There is little difference from a normal reading of corrosion potential except for the measurement duration and the creation of a list ordered by potential.

To prepare a galvanic series that will be valid for the materials and environment of interest in service, all of the factors that affect the potential of those materials in that environment must be accounted for. These factors include material composition, heat treatment, surface preparation (mill scale, coatings surface finish, etc.), environmental composition (trace contaminants, dissolved gases, etc.), temperature, and flow rate. One important effect is exposure time, particularly on materials that form corrosion product layers. All of the precautions and warnings regarding the generation and use of a galvanic series are given in Ref 2.

Polarization Curves. More useful information on the rate of galvanic corrosion can be obtained by investigating the polarization behavior of the materials involved. This can be done by generating stepped potential or potentiodynamic polarization curves or by obtaining potentiostatic information on polarization behavior. The objective is to obtain a good indication of the amount of current required to hold each material at a given potential. Because all materials in the galvanic system must be at the same potential in systems with low solution resistivity, such as seawater, and because the sum of all currents flowing between the materials must equal 0 by Kirchoff's Law, the coupled potential of all materials and the galvanic currents flowing can be uniquely determined for the system. Faraday's Law can then be used to relate the corrosion rate to the galvanic current if the resulting potential of the anodic materials is well away from their corrosion potential, or the corrosion rate can be found as a function of potential by independent measurement.

Potentiodynamic polarization curves are generated by connecting the specimen of interest to a scanning potentiostat. This device applies whatever current is necessary between the specimen and a counterelectrode to maintain that specimen at a given potential versus a reference electrode half-cell placed near the specimen. The current required is plotted as a function of potential over a range that begins at the corrosion potential and proceeds in the direction (anodic or cathodic) required by that material. Such curves would be generated for each material of interest in the system. Additional information on the method for generating these curves is available in the article "Electrochemical Methods of Corrosion Testing" in this Volume and in Ref 3. The scan rate for potential must be chosen such that sufficient time is allowed for completion of electrical charging at the interface.

Potentiodynamic polarization is particularly effective for materials with time-independent polarization behavior. It is fast, relatively easy, and gives a reasonable, quantitative prediction of corrosion rates in many systems. However, potentiostatic techniques are preferred for time-dependent polarization. To establish polarization characteristics for time-dependent polarization, a series of specimens is used, each held to one of a series of constant potentials with a potentiostat while the current required is monitored as a function of time. After the current has stabilized or after a preselected time period has elapsed, the current at each potential is recorded. Testing of each specimen results in the generation of one potential/current data pair, which gives a point on the polarization curve for that material. The data are then interpolated to trace out the full curve. This technique is very accurate for time- dependent polarization but is expensive and time consuming. The individual specimens can be weighed before and after testing to determine corrosion rate as a function of potential, thus enabling the errors from using Faraday's Law to be easily corrected.

The process of predicting galvanic corrosion from polarization behavior can be illustrated by the example of a steel-copper system. Steel has the more negative corrosion potential and will therefore suffer increased corrosion on coupling to copper, but the amount of this corrosion must be predicted from polarization curves. If the polarization of each material is plotted as the absolute value of the log of current density versus potential and if the current density axis of each of these curves is multiplied by the wetted surface area of that material in the service application, then the result will be a plot of the total anodic current for steel and the total cathodic current for copper in this application as a function of potential (Fig. 2).

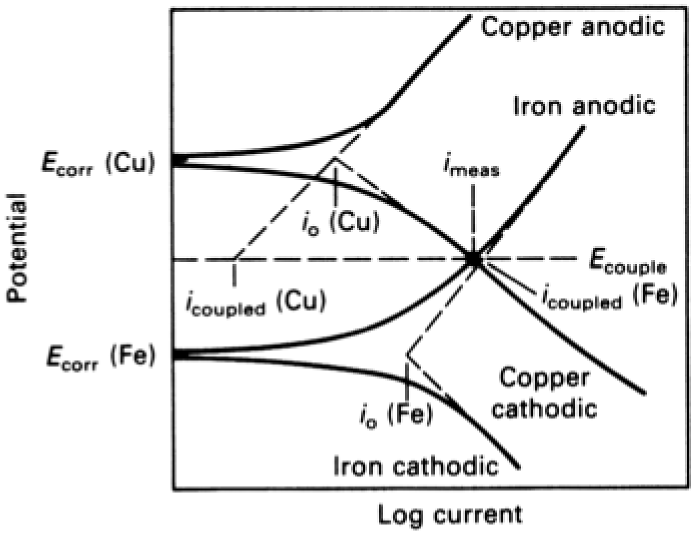

Fig. 2 Prediction of coupled potential and galvanic current from polarization diagrams. ***i*****, current;** $\boldsymbol{i_o}$**, exchange current;** $\boldsymbol{E_{corr}}$**, corrosion potential**

Furthermore, when the two metals are electrically connected, the anodic current to the steel must be supplied by the copper; that is, the algebraic sum of the anodic and cathodic currents must equal 0. If the polarization curves for the two materials, normalized for surface area as described previously, are plotted together, this current condition is satisfied where the two curves intersect. This point of intersection allows for the prediction of the coupled potential of the materials and the galvanic current flowing between them from the intersection point. This procedure works if there is no significant electrolyte resistance between the two metals; otherwise, this resistance must be taken into account as described in Ref 4.

Specimen Exposures

Specimens for galvanic-corrosion testing include panels, wires, pieces of actual components, and other configurations of the materials of interest that are exposed in a process stream, a simulated service environment, or the actual environment. Specimens of the materials of interest are usually exposed in the same ratios of wetted or exposed areas as in the service application. The different materials are either placed in physical contact to provide electrical connection or are wired together such that the current between the materials can be monitored, usually as a function of time. Seldom can the effects of electrolyte resistance be included in this type of test, and the resistance is usually kept extremely low by appropriate relative placement of the materials.

Immersion. There are virtually no standardized tests for galvanic corrosion under immersion conditions, partly because the type of information needed, the extent of modeling of the service situation, and the type of system studied vary widely. This makes development of a standard test difficult. However, some general guidelines for galvanic-corrosion specimen testing in liquid electrolytes are given in Ref 5.

Immersion testing always involves an electrical connection between at least two dissimilar metals. This is usually accomplished with a wire, as in Fig. 3, although threaded mounting rods such as the assembly shown in Fig. 4 have also been used successfully for electrical connection. Soldered or brazed connections have the best electrical integrity.

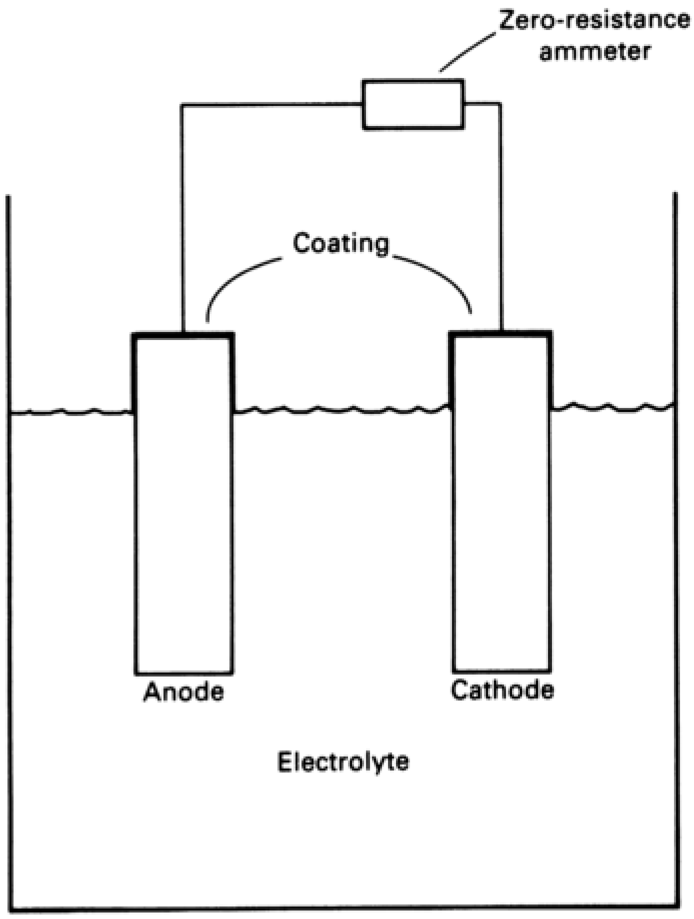

Fig. 3 Typical galvanic-corrosion immersion test setup using wire connections

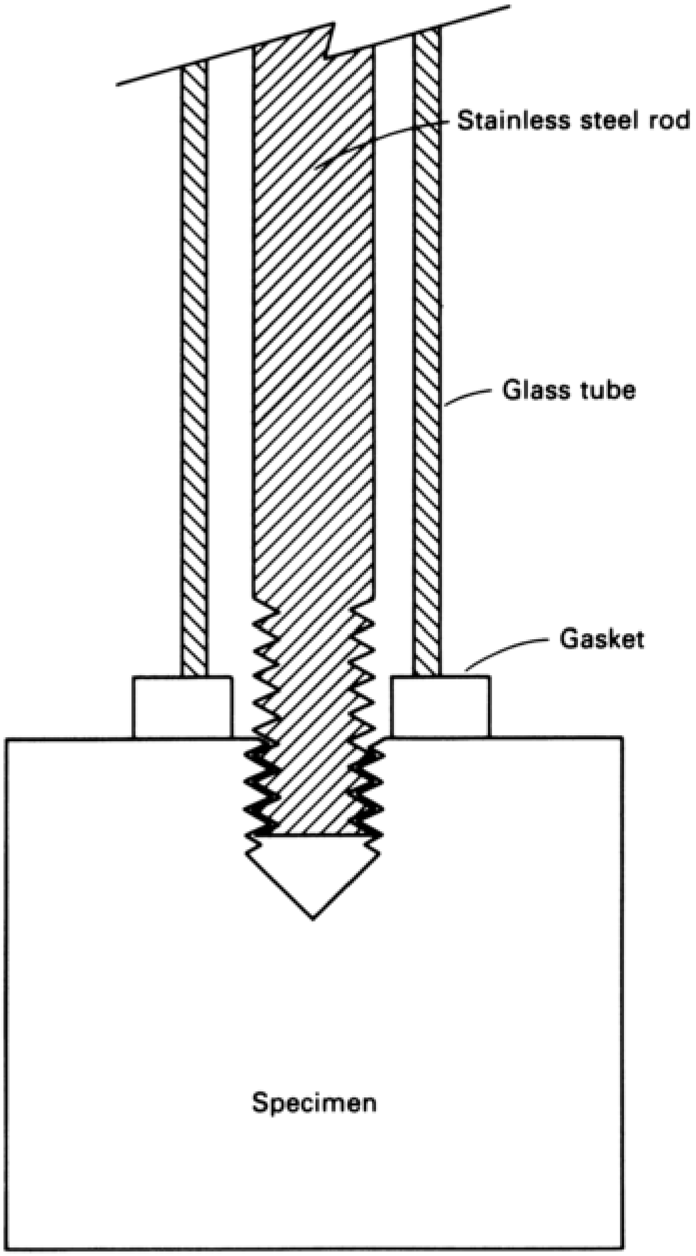

Fig. 4 Typical galvanic-corrosion test specimen using a threaded rod for mounting and electrical connection

The electrolyte must be excluded from the contact area by applying a sealant, such as silicone or epoxy; by keeping the joint area out of the electrolyte by partial immersion of the specimen, in which case a waterline area is created; or by use of a tube and gasket or O-ring seal, in the case of a threaded mounting rod. Mounting the specimen in a specially formulated epoxy has been found to be effective in minimizing crevice corrosion while maintaining a dry electrical connection. However, selection of the best epoxy formulation is difficult. Care must be taken that the sealant or gasket material is stable in the electrolyte being studied.

Almost any sealing procedure will create a potential area for crevice corrosion; thus, it is very difficult to study galvanic behavior independent of crevice-corrosion behavior. Control specimens may be run with similar crevices and no electrical connection, but because the reproducibility of crevice-corrosion behavior is not good, data scatter will be large. Under some circumstances, the galvanic effect of importance may be the acceleration of crevice-corrosion attack.

The relative wetted surface areas of the materials being tested will have an important effect on the magnitude of the galvanic attack. The larger the cathode-to-anode area ratio is, the larger the degree of attack will be; therefore, it would at first seem reasonable to accelerate the test by using a large ratio. This should not be done, because accelerating the attack may also change the mechanism of the attack, which would lead to erroneous conclusions. It is far more appropriate to use more accurate measurement techniques to determine the extent of

the attack over a short period than to accelerate the test to obtain measurable attack quickly. If soldered or brazed connections are used for electrical connection, subsequent evaluation by weight loss is difficult; therefore, if weight loss is to be used to measure attack, threaded and sealed connections are preferred.

Measurement of the electrical current flowing between the metals can give a very sensitive indication of the extent of the galvanic attack and will allow the attack to be monitored over time. Coupled potential is another parameter that is useful to follow during the course of the exposure. The effect of exposure time on the rate of attack should be properly considered. Initially high rates of galvanic attack may decay to acceptable levels in a short period of time, or initially low attack rates may increase to unacceptable levels over time.

Current can be measured by inserting a resistor of 1 to 10 Ω in the current circuit and measuring the potential drop across this resistor with a voltmeter having an internal resistance of at least 1000 Ω. The resistor should be sized such that the voltage across it does not exceed 5 mV; thus, the resistor will not significantly impede the current flow. Alternatively, a zero-resistance ammeter (ZRA) can be used instead of the resistor. This device is an operational amplifier connected to maintain 0 V across its input terminals (Fig. 5). A current-measuring resistor placed in the feedback circuit may be as large as the amplifier will allow, thus enabling currents in the nanoampere range to be easily measured. One simple way of creating a zero-resistance ammeter is by using a potentiostat with the counter- electrode and reference electrode leads shorted together and set to a working electrode potential of 0 V (Fig. 6).

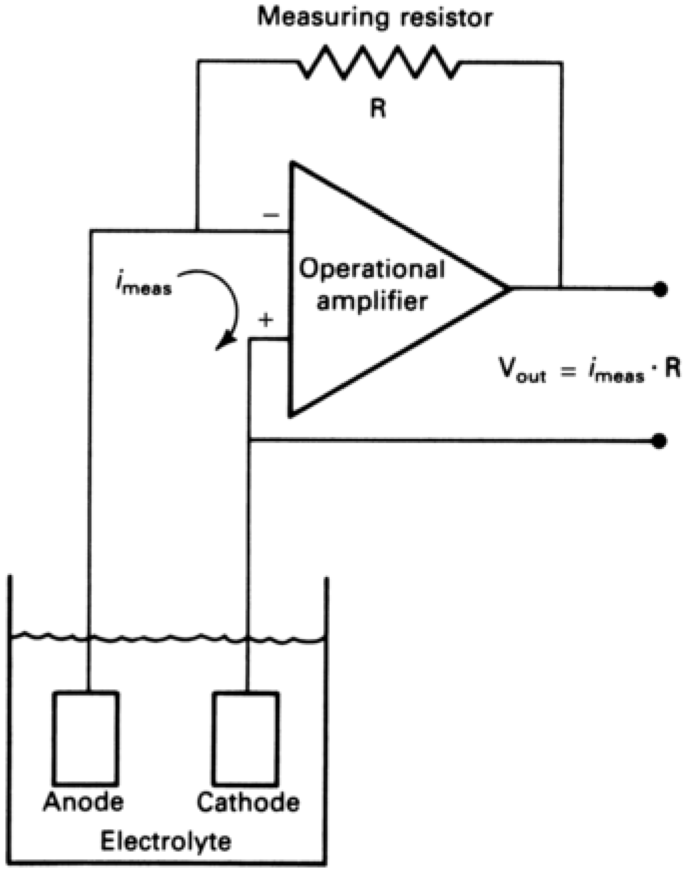

Fig. 5 Basic circuit for a zero-resistance ammeter

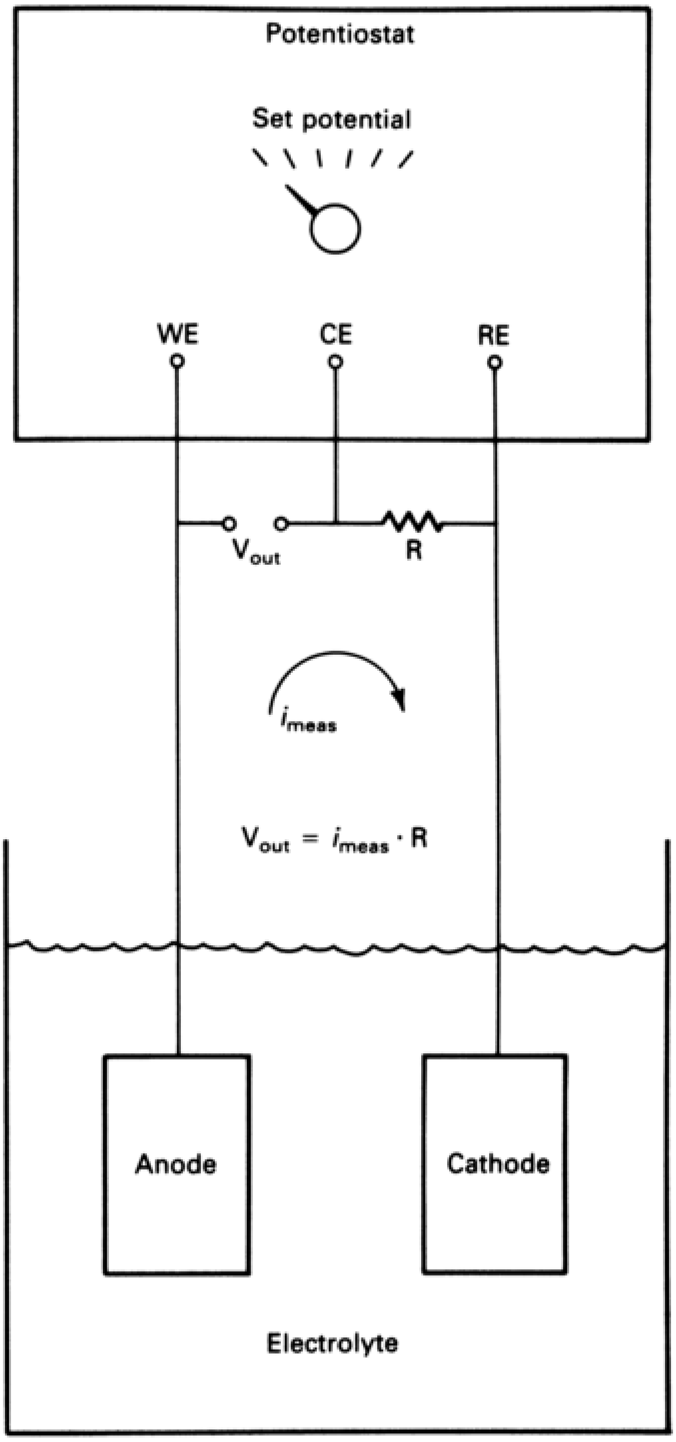

Fig. 6 Conversion of a potentiostat into a zero-resistance ammeter. WE, working electrode; CE, counter electrode; RE, reference electrode

For most electrochemical reactions it is possible to convert reaction current to corrosion rate using the expression:

$$CR = 0.1288 i_g EW/d$$

where CR is corrosion rate in mils per year, i_g is current density in microamperes per square centimeter, *EW* is equivalent weight of the corroding material, and *d* is density in grams per cubic centimeter. This conversion will frequently be inaccurate for calculating galvanic corrosion rate from galvanic current because corrosion may not be uniform, some current may go toward reactions at the anode other than metal loss, such as valence change of ions in solution, and additional corrosion at the anode is generated by cathodic reactions on the anode not measured by the galvanic current. Therefore, the preceding calculation will frequently underestimate the total corrosion of an anode in a galvanic corrosion cell. Estimation of galvanic corrosion rate from galvanic

current is worse for materials with high self-corrosion, such as metals in acids, and best when the anode and cathode open-circuit potentials are far apart so that after coupling, little cathodic activity occurs on the anode.

The importance of electrolyte flow in galvanic corrosion should not be overlooked in establishing the test procedure. A test apparatus should be used that reproduces the flow under service conditions. If this is not possible and flow must be scaled, the exact scaling method will depend on the assumed corrosion processes. Cathodic reactions, such as oxygen reduction, that are controlled by diffusion through a fluid boundary layer are likely to be properly scaled by reproducing the hydrodynamic boundary layer of the service application in the test. This should reproduce the diffusion boundary layer that controls the reaction.

Alternatively, the rates of reactions controlled by films such as anodic brightening of copper alloys, other passivation-type reactions, or control by calcareous-deposit formation in seawater, may depend more on the shear stress at the surface required to strip off the film. In this case, surface shear stress may be a better hydrodynamic parameter to reproduce in the test.

Many different types of flow apparatus have been used, such as concentric tubes, in-line tubes, rotating cylinders, rotating ring-disks, rectangular flow channels with specimens mounted in the walls, and circulating foils. Each of these has its own hydrodynamic peculiarities, but one common area of concern is the leading edge of the specimen. It is difficult, even for specimens recessed in the walls of a flow channel, to avoid a step or gap that can create unexpected hydrodynamic conditions at the specimen surfaces downstream. Also, mounting to allow electrical connection must be considered, and crevice effects are essentially impossible to eliminate.

Atmospheric Tests. General testing guidelines become more complex when considering atmospheric or cabinet exposures. Testing in these environments differs markedly from immersion tests in a number of ways, most of which involve the insufficiency of electrolyte. Many of the variables that influence the behavior of specimens in the atmosphere are discussed in Ref 6.

The thinness of the electrolyte film and the normally low conductivity of the electrolyte combine to limit galvanic effects for bare metals to within approximately 5 mm (0.2 in.) of the dissimilar-metal interface (Ref 7). This distance may be somewhat greater if nonconductive coatings are present. Area ratio effects thus become relatively unimportant. Sealing the electrical connections becomes relatively less important than in immersion testing if the connections are more than 5 mm (0.2 in.) from the area to be evaluated and if corrosion products will not interfere with the continuity of the connection. Periodic checks of electrical continuity in atmospheric galvanic-corrosion tests are recommended. Geometrical effects also become unimportant, except as they relate to the entrapment of moisture. However, specimen orientation effects must be considered. The behavior of the galvanic couples will depend on whether they are exposed on the top or the bottom of the panel, whether they are sheltered or not, or other considerations, such as the effect of specimen mass on condensation.

It is surprising that several standard tests have emerged for atmospheric galvanic corrosion, since there are no standardized tests for galvanic corrosion immersed in electrolytes even though more testing has been done in this area. One of these tests is an International Organization for Standardization (ISO) standard (Ref 8). This test uses a 100 × 400 mm (4 × 16 in.) panel of the anodic material to which a 50 × 100 mm (2 × 4 in.) strip of the cathodic material is bolted (Fig. 7). After exposure, the anodic material can be evaluated for material degradation by weight loss and other corrosion measurements as well as by degradation of such mechanical properties as ultimate tensile strength.

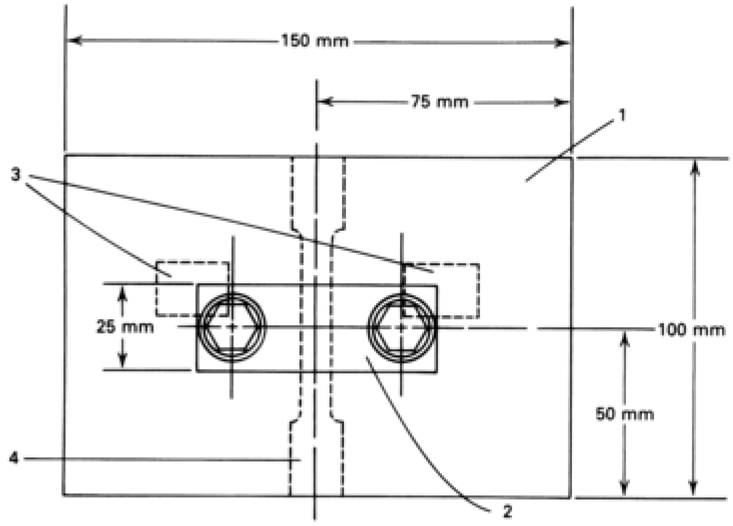

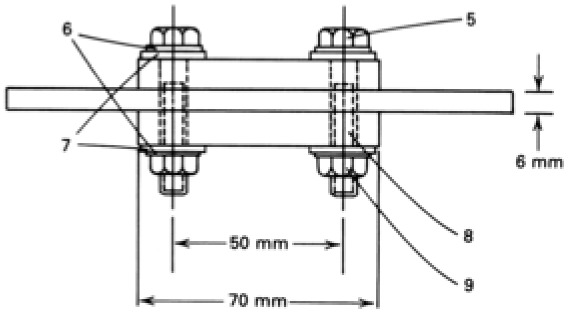

Fig. 7 Specimen configuration for the ISO test for atmospheric galvanic corrosion. 1, anodic plate, 1 piece; 2, cathodic plate, 2 pieces; 3, microsection, 2 pieces; 4, tensile test specimen; 5, bolt, 8 × 40 mm, 2 pieces; 6, washers, 1 mm thick, 16 mm diameter, 4 pieces; 7, insulating washers, 1 to 3 mm thick, 18 to 20 mm diameter, 4 pieces; 8, insulating sleeve, 2 pieces; 9, nut, 2 pieces.

This test is relatively easy to perform but requires the availability of plates of the materials of interest and a prior knowledge of which material is anodic. Like any atmospheric galvanic- corrosion test, crevice effects cannot be adequately separated from galvanic effects in some cases; therefore, a coating is sometimes applied between the anode and cathode plates. The disadvantage of this test is the time required to obtain results; for systems with moderate corrosion rates, exposures of 1 to 5 years are not unusual.

Another commonly used atmospheric galvanic-corrosion test is the wire-on-bolt test, sometimes referred to as the CLIMAT test (Ref 9, 10, 11). In this test, a wire of the anodic material is wrapped around a threaded rod of the cathodic material (Fig. 8). Because corrosion can be rapid in this test, exposure duration should usually be limited. This makes the test ideal for measuring atmospheric corrosivity as well as material corrosion properties. Not all materials of interest are available in the required wire and threaded rod forms, and analysis is usually restricted to weight-loss measurement and observation of pitting. When the required materials are available, this test is less expensive and easier to conduct than the ISO plate test.

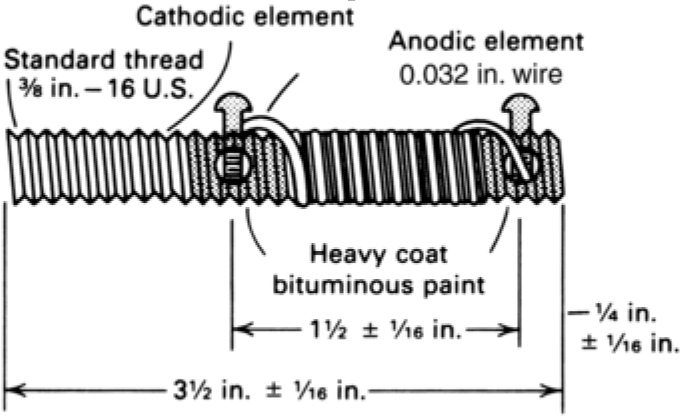

Fig. 8 Specimen configuration for the wire-on-bolt test for atmospheric galvanic corrosion

A third atmospheric galvanic-corrosion test has been used extensively by ASTM International but has not been standardized. This test (Ref 12) involves the use of 25 mm (1 in.) diameter washers of the materials of interest bolted together as shown in Fig. 9. The bolt that holds the washers together can also be used to secure the assembly in position. After exposure, the washers can be disassembled for weight loss determination. The materials needed for this test are not as large as those for the ISO plate test, but testing can take as long and cannot provide mechanical properties data.

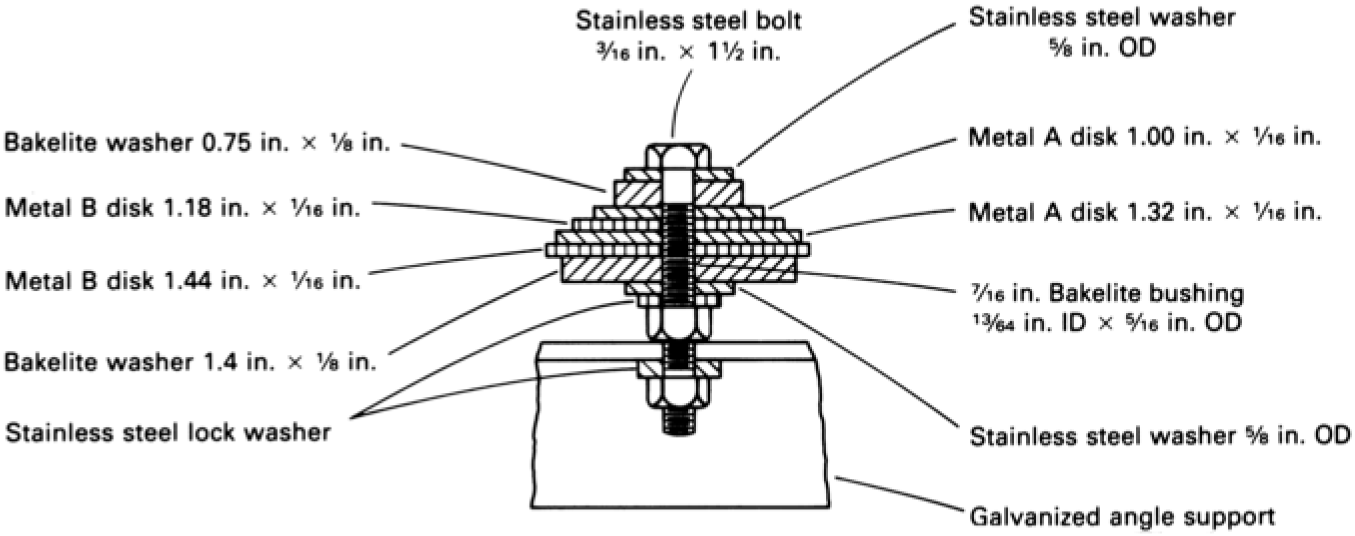

Fig. 9 Specimen configuration for the washer test for atmospheric galvanic corrosion

References cited in this section

1. R. Baboian, Electrochemical Techniques for Predicting Galvanic Corrosion, *Galvanic and Pitting Corrosion—Field and Laboratory Studies,* STP 576, ASTM International, 1976, p 5–19

2. "Standard Guide for Development and Use of a Galvanic Series for Predicting Galvanic Corrosion Performance," G 82, *Annual Book of ASTM Standards,* ASTM International

3. "Standard Reference Test Method for Making Potentiostatic and Potentiodynamic Anodic Polarization Measurements," G 5, *Annual Book of ASTM Standards,* ASTM International

4. H.P. Hack, P.J. Moran, and J.R. Scully, Influence of Electrolyte Resistance on Electrochemical Measurements and Procedures to Minimize or Compensate for Resistance Errors, *The Measurement and Correction of Electrolyte Resistance in Electrochemical Tests,* STP 1056, L.L. Scribner and S.R. Taylor, Ed., ASTM International, Jan 1990, p 5–26

5. "Standard Guide for Conducting and Evaluating Galvanic Corrosion Tests in Electrolytes," G 71, *Annual Book of ASTM Standards,* ASTM International

6. "Standard Practice for Conducting Atmospheric Corrosion Tests of Metals," G 50, *Annual Book of ASTM Standards,* ASTM International

7. V. Kucera and E. Mattson, *Atmospheric Corrosion of Bimetallic Structures in Atmospheric Corrosion,* W.H. Aylor, Ed., John Wiley & Sons, 1982, p 567

8. "Corrosion of Metals and Alloys—Determination of Bi-Metallic Corrosion in Outdoor Exposure Corrosion Tests," ISO 7441, International Organization for Standards

9. K.G. Compton, A. Mendizza, and W.W. Bradley, Atmospheric Galvanic Couple Corrosion, *Corrosion,* Vol II, 1955, p 383

10. H.P. Godard, Galvanic Corrosion Behavior of Aluminum in the Atmosphere, *Mater. Prot.,* Vol 2 (No. 6), 1963, p 38

11. D.P. Doyle and T.E. Wright, Rapid Methods for Determining Atmospheric Corrosivity and Corrosion Resistance, *Atmospheric Corrosion,* W.H. Aylor, Ed., John Wiley & Sons, 1982, p 227

12. R. Baboian, Final Report on the ASTM Study: Atmospheric Galvanic Corrosion of Magnesium Coupled to Other Metals, *Atmospheric Factors Affecting the Corrosion of Engineering Metals,* STP 646, S.K. Coburn, Ed., ASTM International, 1978, p 17–29

H.P. Hack, Evaluation Galvanic Corrosion, *Corrosion: Fundamentals, Testing, and Protection*, Vol 13A, *ASM Handbook*, ASM International, 2003, p 562–567

Evaluating Galvanic Corrosion

Harvey P. Hack, Northrop Grumman Corporation

References

1. R. Baboian, Electrochemical Techniques for Predicting Galvanic Corrosion, *Galvanic and Pitting Corrosion—Field and Laboratory Studies,* STP 576, ASTM International, 1976, p 5–19
2. "Standard Guide for Development and Use of a Galvanic Series for Predicting Galvanic Corrosion Performance," G 82, *Annual Book of ASTM Standards,* ASTM International
3. "Standard Reference Test Method for Making Potentiostatic and Potentiodynamic Anodic Polarization Measurements," G 5, *Annual Book of ASTM Standards,* ASTM International
4. H.P. Hack, P.J. Moran, and J.R. Scully, Influence of Electrolyte Resistance on Electrochemical Measurements and Procedures to Minimize or Compensate for Resistance Errors, *The Measurement and Correction of Electrolyte Resistance in Electrochemical Tests,* STP 1056, L.L. Scribner and S.R. Taylor, Ed., ASTM International, Jan 1990, p 5–26
5. "Standard Guide for Conducting and Evaluating Galvanic Corrosion Tests in Electrolytes," G 71, *Annual Book of ASTM Standards,* ASTM International
6. "Standard Practice for Conducting Atmospheric Corrosion Tests of Metals," G 50, *Annual Book of ASTM Standards,* ASTM International
7. V. Kucera and E. Mattson, *Atmospheric Corrosion of Bimetallic Structures in Atmospheric Corrosion,* W.H. Aylor, Ed., John Wiley & Sons, 1982, p 567
8. "Corrosion of Metals and Alloys—Determination of Bi-Metallic Corrosion in Outdoor Exposure Corrosion Tests," ISO 7441, International Organization for Standards
9. K.G. Compton, A. Mendizza, and W.W. Bradley, Atmospheric Galvanic Couple Corrosion, *Corrosion,* Vol II, 1955, p 383
10. H.P. Godard, Galvanic Corrosion Behavior of Aluminum in the Atmosphere, *Mater. Prot.,* Vol 2 (No. 6), 1963, p 38
11. D.P. Doyle and T.E. Wright, Rapid Methods for Determining Atmospheric Corrosivity and Corrosion Resistance, *Atmospheric Corrosion,* W.H. Aylor, Ed., John Wiley & Sons, 1982, p 227
12. R. Baboian, Final Report on the ASTM Study: Atmospheric Galvanic Corrosion of Magnesium Coupled to Other Metals, *Atmospheric Factors Affecting the Corrosion of Engineering Metals,* STP 646, S.K. Coburn, Ed., ASTM International, 1978, p 17–29

H.P. Hack, Evaluation Galvanic Corrosion, *Corrosion: Fundamentals, Testing, and Protection*, Vol 13A, *ASM Handbook*, ASM International, 2003, p 562–567

Evaluating Galvanic Corrosion

Harvey P. Hack, Northrop Grumman Corporation

Selected References

- R. Francis, *Galvanic Corrosion: A Practical Guide for Engineers,* NACE International, 2001
- *Galvanic Corrosion,* STP 978, H.P. Hack, Ed., ASTM International, 1988
- H.P. Hack, *Galvanic Corrosion Test Methods,* NACE International, 1993

B. Phull, Evaluating Intergranular Corrosion, *Corrosion: Fundamentals, Testing, and Protection*, Vol 13A, *ASM Handbook,* ASM International, 2003, p 568–571

Evaluating Intergranular Corrosion

Revised by Bopinder Phull, Consultant

Introduction

INTERGRANULAR CORROSION (IGC) is preferential attack of either grain boundaries or areas immediately adjacent to grain boundaries in a material exposed to a corrosive environment but with little corrosion of the grains themselves. *Intergranular corrosion* is also known as *intergranular attack* (IGA). *End-grain attack, grain dropping,* and *"sugaring"* are additional terms that are sometimes used to describe IGC. In certain materials, corrosion progressing laterally along planes parallel to rolled surfaces is known as exfoliation, and it generally occurs along grain boundaries—hence, intergranular corrosion. A layered appearance is a common manifestation of exfoliation (also referred to as *layer corrosion*), resulting from voluminous corrosion products prying open the material; for example, in aluminum alloys.

Most alloys are susceptible to IGA when exposed to specific environments. This is because grain boundaries are sites for precipitation and segregation, which make them chemically and physically different from the grains themselves. Intergranular attack is defined as the selective dissolution of grain boundaries or closely adjacent regions without appreciable attack of the grains themselves. This is caused by potential differences between the grain-boundary region and any precipitates, intermetallic phases, or impurities that form at the grain boundaries. The actual mechanism and degree of attack differs for each alloy system.

Precipitates that form as a result of the exposure of metals at elevated temperatures (for example, during production, fabrication, heat treatment, and welding) often nucleate and grow preferentially at grain boundaries. If these precipitates are rich in alloying elements that are essential for corrosion resistance, the regions adjacent to the grain boundary are consequently depleted of these elements. The metal is thus sensitized and is susceptible to IGA in one or more specific corrosive environments. For example, in austenitic stainless steels such as Type 304, intergranular attack is often associated specifically with precipitation of chromium-rich carbides ($Cr_{23}C_6$) at grain boundaries in the heat- affected zone. Precipitation of such carbides is often referred to as *sensitization.* When chromium-rich precipitates form, the surrounding areas are depleted in chromium. As a result, the depleted areas are more susceptible to corrosion in specific environments than regions away from the grain boundaries. Another example of grain boundary segregation is sigma-phase formation that results in a

Cr- and Mo-rich constituent at grain boundaries in Cr- and Mo-containing alloys. Sigma-phase is usually more difficult to resolve visually in the microstructure than Cr-carbides.

Impurities that segregate at grain boundaries may promote galvanic action in a corrosive environment by serving either as anodic or cathodic sites. For example, in 2000-series (2*xxx*) aluminum alloys, the copper-depleted (anodic) band on either side of the grain boundary is dissolved while the grain boundary is cathodic due to the $CuAl_2$ precipitates. Conversely, in the 5000-series (5*xxx*) aluminum alloys, intermetallic precipitates such as Mg_2Al_3 (anodic) are attacked when they form a continuous phase in the grain boundary. During exposures to chloride solutions, the galvanic couples formed between these precipitates and the alloy matrix can lead to severe intergranular attack. Actual susceptibility to intergranular attack and degree of corrosion depends on the corrosive environment and on the extent of intergranular precipitation, which is a function of alloy composition, fabrication, and heat treatment parameters.

B. Phull, Evaluating Intergranular Corrosion, *Corrosion: Fundamentals, Testing, and Protection*, Vol 13A, *ASM Handbook*, ASM International, 2003, p 568–571

Evaluating Intergranular Corrosion

Revised by Bopinder Phull, Consultant

The Purpose of Testing

There is a perception in much of the industry that testing for susceptibility to IGA is equivalent to evaluating the resistance of the alloy to general and localized corrosion. Although the tests used for evaluating susceptibility to IGA are severe, they are not intended to duplicate conditions for the wide range of chemical exposures present in an industrial plant, even though some of these tests do simulate service conditions.

Testing for susceptibility to IGA, however, is useful for determining whether a vendor has supplied the correct material and in the proper metallurgical condition. There are some problems associated with quality assurance programs for purchased materials. Such programs are sometimes based on faith in what is supplied by a vendor or production mill and what is certified in the documentation sent with the material. However, such confidence may be misplaced. For example, there have been a number of accounts in which alloys have been substituted, resulting in premature failure. In one case, this occurred when Hastelloy B (UNS N10001) valves were substituted for the Hastelloy C-276 (UNS N10276) valves that were ordered to handle a hypochlorite solution. Not surprisingly, the Hastelloy B valves failed in about 3 months because this alloy is usually specified for reducing environments (e.g., HCl), whereas alloy C-276 is typically more suited to oxidizing environments (e.g., hypochlorite).

In addition, there are many examples in which the material supplied does not conform to its certified analysis. The problem of getting reliable certified analyses increases when documentation goes from a mill to an alloy supplier. In one case, for example, Type 304L stainless steel (UNS S30403) valves were ordered, but the vendor, having few orders for this alloy, substituted Type 316L stainless steel (UNS S31603) valves and sent certifications that purposely omitted the molybdenum analysis. Normally, this would have been a good substitution for improved corrosion resistance at a bargain price, but these valves were destined for hot, concentrated HNO_3 service and failed prematurely.

Therefore, it is essential that, for critical service, the correct alloys must be specified and in optimum metallurgical condition to resist IGA and other forms of corrosion associated with precipitates at the grain boundaries.

B. Phull, Evaluating Intergranular Corrosion, *Corrosion: Fundamentals, Testing, and Protection*, Vol 13A, *ASM Handbook*, ASM International, 2003, p 568–571

Evaluating Intergranular Corrosion

Revised by Bopinder Phull, Consultant

Tests for Stainless Steels and Nickel-Base Alloys

The austenitic and ferritic stainless steels, as well as most nickel-base alloys, are generally supplied in a heat treated condition such that they are free of carbide precipitates that are detrimental to corrosion resistance. However, these alloys are susceptible to sensitization from welding, improper heat treatment, and service in the sensitizing temperature range. The theory and application of acceptance tests for detecting the susceptibility of stainless steels and nickel-base alloys to intergranular attack are extensively reviewed in Ref 1, 2, 3. Corrosion tests for evaluating the susceptibility of an alloy to IGA are typically classified as either simulated-service or accelerated tests. The original laboratory tests for detecting IGA were simulated-service exposures. These were first used in 1926 when IGA was detected in an austenitic stainless steel in a copper sulfate-sulfuric acid ($CuSO_4$-H_2SO_4) pickling tank (Ref 4). Another simulated-service test for alloys intended for service in nitric acid (HNO_3) plants is described in Ref 5. In this case, for accelerated results, iron-chromium alloys were tested in a boiling 65% HNO_3 solution.

Over the years, specific accelerated tests have been developed and standardized for evaluating the susceptibility of various alloys to IGA. For example, ASTM A 262 contains six practices for detecting susceptibility to IGC in austenitic stainless steels (Ref 6). Practice A is an electrolytic oxalic-acid-etch screening test that can be performed in minutes on prepared samples followed by microscopic examination of the etched microstructure for $Cr_{23}C_6$ sensitization. Practice B is a 120 hour test in a boiling solution of ferric sulfate [$Fe_2(SO_4)_3$] + sulfuric acid (H_2SO_4); the weight-loss corrosion rate indicates degree of IGA due to $Cr_{23}C_6$ precipitation. A 240 hour test in boiling 65% HNO_3 constitutes Practice C; the degree of IGC due to $Cr_{23}C_6$ and sigma-phase formation is indicated by weight-loss corrosion rates. Practice D, which was an immersion test in 10% HNO_3 + 3% HF solution at 70 °C has been removed from ASTM A 262 (Ref 6). Practice E is a 24 hour test in boiling 6% $CuSO_4$ + 10% H_2SO_4 solution to which metallic copper is added; evaluation of IGC due to $Cr_{23}C_6$ formation is based on postexposure visual examination of specimens for fissures after bending. In Practice F, a 120 hour boiling test in $CuSO_4$ + 50% H_2SO_4 solution (with metallic copper present), weight-loss corrosion rates indicate the degree of sensitization due to $Cr_{23}C_6$ precipitation for molybdenum-bearing stainless steels.

Similarly, tests for detecting susceptibility to IGC in ferritic stainless steels have been incorporated into ASTM A 763 (Ref 7) and for wrought Ni-rich, Cr-bearing alloys, into ASTM G 28 (Ref 8). Acceptance criteria for ferritic and austenitic stainless steels, high nickel-base alloys, and aluminum alloys are summarized in Table 1.

Table 1 Appropriate evaluation tests and acceptance criteria for wrought alloys

UNS No.	Alloy name	Sensitizing treatment	Applicable tests (ASTM standards)	Exposure time, h	Criteria for passing, appearance or maximum allowable corrosion rate, mm/month (mils/month)
S43000	Type 430	None	Ferric sulfate (A 763-X)	24	1.14 (45)
S44600	Type 446	None	Ferric sulfate (A 763-X)	72	0.25 (10)
S44625	26-1	None	Ferric sulfate (A 763-X)	120	0.05 (2) and no significant grain dropping
S44626	26-1S	None	Cupric sulfate (A 763-Y)	120	No significant grain dropping
S44700	29-4	None	Ferric sulfate (A	120	No significant grain dropping

			763-X)		
S44800	29-4-2	None	Ferric sulfate (A 763-X)	120	No significant grain dropping
S30400	Type 304	None	Oxalic acid (A 262-A)	…	[a]
			Ferric sulfate (A 262-B)	120	0.1 (4)
S30403	Type 304L	1 h at 675 °C (1250 °F)	Oxalic acid (A 262-A)	…	[a]
			Nitric acid (A 262-C)	240	0.05 (2)
S30908	Type 309S	None	Nitric acid (A 262-C)	240	0.025 (1)
S31600	Type 316	None	Oxalic acid (A 262-A)	…	[a]
			Ferric sulfate (A 262-B)	120	0.1 (4)
S31603	Type 316L	1 h at 675 °C (1250 °F)	Oxalic acid (A 262-A)	…	[a]
			Ferric sulfate (A 262-B)	120	0.1 (4)
S31700	Type 317	None	Oxalic acid (A 262-A)	…	[a]
			Ferric sulfate (A 262-B)	120	0.1 (4)
S31703	Type 317L	1 h at 675 °C (1250 °F)	Oxalic acid (A 262-A)	…	[a]
			Ferric sulfate (A 262-B)	120	0.1 (4)
S32100	Type 321	1 h at 675 °C (1250 °F)	Nitric acid (A-262-C)	240	0.05 (2)
S34700	Type 347	1 h at 675 °C (1250 °F)	Nitric acid (A 262-C)	240	0.05 (2)
N08020	20Cb-3	1 h at 675 °C (1250 °F)	Ferric sulfate (G 28-A)	120	0.05 (2)
N08904	904L	None	Ferric sulfate (G 28-A)	120	0.05 (2)
N08825	Incoloy 825	1 h at 675 °C (1250 °F)	Nitric acid (A 262-C)	240	0.075 (3)
N06007	Hastelloy G	None	Ferric sulfate (G 28-A)	120	0.043 (1.7) sheet, plate, and bar; 0.05 (2) pipe and tubing
N06985	Hastelloy G-3	None	Ferric sulfate (G 28-A)	120	0.043 (1.7) sheet, plate, and bar; 0.05 (2) pipe and tubing
N06625	Inconel 625	None	Ferric sulfate (G 28-A)	120	0.075 (3)
N06690	Inconel 690	1 h at 540 °C (1000 °F)	Nitric acid (A 262-C)	240	0.025 (1)
N10276	Hastelloy C-276	None	Ferric sulfate (G 28-A)	24	1 (40)
N06455	Hastelloy C-4	None	Ferric sulfate (G 28-A)	24	0.43 (17)
N06110	Allcorr	None	Ferric sulfate (G 28-B)	24	0.64 (25)

N10001	Hastelloy B	None	20% hydrochloric acid	24	0.075 (3) sheet, plate, and bar; 0.1 (4) pipe and tubing
N10665	Hastelloy B-2	None	20% hydrochloric acid	24	0.05 (2) sheet, plate, and bar; 0.086 (3.4) pipe and tubing
A95005–A95657	Aluminum Association 5*xxx* alloys	None	Concentrated nitric acid (G 67)	24	(b)

(a) See ASTM A 262, practice A.
(b) See ASTM G 67, section 4.1.

Because sensitized alloys may inadvertently be used, acceptance tests are implemented as a quality-control check to evaluate stainless steels and nickel-base alloys when:

- Different alloys, or alloys with "high" carbon content, are substituted for the low-carbon grades (for example, Type 316 substituted for Type 316L), and when welding or heat treatment are involved
- An improper heat treatment during fabrication results in the formation of intermetallic phases.
- The specified limits for carbon and/or nitrogen contents of an alloy are inadvertently exceeded.

Some standard tests include acceptance criteria, but others do not (Ref 4, 5). Suitable criteria are needed that can clearly separate material susceptible to IGA from that resistant to attack. Table 1 lists evaluation tests and acceptance criteria for various stainless steels and nickel-base alloys. Despite establishment of "standard" acceptance/rejection criteria, the buyer and seller can agree on a different criterion that meets their particular needs.

ASTM G 108 describes a laboratory procedure for conducting a nondestructive electrochemical reactivation (EPR) test on Types 304 and 304L stainless steel to quantify the degree of sensitization (Ref 9). The metallographically mounted and highly polished test specimen is potentiodynamically polarized from the normally passive condition, in 0.5 *M* H_2SO_4 + 0.01 *M* KSCN solution at 30 ± 1 °C, to active potentials—a process known as reactivation. The amount of charge passed is related to the degree of IGC associated with $Cr_{23}C_6$ precipitation, which occurs predominately at the grain boundaries. After the single loop EPR test, the microstructure is examined and:

1. The grain boundary area is calculated from the grain size and the total exposed area of the test specimen.
2. Relative proportions of grain boundary attack and non-grain-boundary pitting are determined.

A charge per unit grain-boundary area of <0.1 C/cm^2 (0.016 C/in.^{2}) generally indicates unsensitized microstructure, and >0.4 C/cm^2 (0.062 C/in.^{2}) indicates a heavily sensitized alloy. Although a double loop EPR method has been proposed (Ref 10, 11) to eliminate non-grain- boundary pitting and surface-finish effects, often observed in the single loop method, the double- loop technique is not presently included in ASTM G 108.

References cited in this section

1. M. Henthorne, *Localized Corrosion—Cause of Metal Failure,* STP 516, ASTM International, 1972, p 66–119

2. M.A. Streicher, *Intergranular Corrosion of Stainless Alloys,* STP 656, ASTM International, 1978, p 3–84

3. M.A. Streicher, Intergranular Corrosion, *Corrosion Tests and Standards: Application and Interpretation,* R. Baboian, Ed., ASTM International, 1995, p 197–217

4. W.H. Hatfield, *J. Iron Steel Inst.,* Vol 127, 1933, p 380–383

5. W.R. Huey, *Trans. Am. Soc. Steel Treat.,* Vol 18, 1930, p 1126–1143

6. "Practices for Detecting Susceptibility to Intergranular Corrosion in Austenitic Stainless Steels," A 262, *Steel—Plate, Sheet, Strip, Wire; Stainless Steel Bar*, *Annual Book of ASTM Standards 2002,* Vol 1.03, ASTM International, 2002

7. "Practices for Detecting Susceptibility to Intergranular Corrosion in Ferritic Stainless Steels", A 763, *Steel—Plate, Sheet, Strip, Wire; Stainless Steel Bar, Annual Book of ASTM Standards 2002,* Vol 1.03, ASTM International, 2002

8. "Standard Test Methods for Detecting Susceptibility to Intergranular Corrosion in Wrought, Nickel-Rich, Chromium-Bearing Alloys," G 28, *Wear and Erosion; Metal Corrosion, Annual Book of ASTM Standards 2002,* Vol 3.02, ASTM International, 2002

9. "Standard Test Method for Electrochemical Reactivation (EPR) for Detecting Sensitization of AISI Type 304 and 304L Stainless Steel," G 108, *Wear and Erosion; Metal Corrosion, Annual Book of ASTM Standards 2002,* Vol 3.02, ASTM International, 2002

10. A.P. Majidi and M.A. Striecher, *Corrosion,* Vol 40, 1984, p 584–592

11. M. Akashi, T. Kawamoto, and F. Umemura, *Corros. Eng.*, (Jpn.), Vol 29, 1980, p 163

B. Phull, Evaluating Intergranular Corrosion, *Corrosion: Fundamentals, Testing, and Protection*, Vol 13A, *ASM Handbook*, ASM International, 2003, p 568–571

Evaluating Intergranular Corrosion

Revised by Bopinder Phull, Consultant

Tests for Aluminum Alloys

The electrochemically active paths at the grain boundaries of aluminum alloy materials can be either the solid solution or closely spaced anodic second-phase intermetallic particles. The identities of the specific actively corroding paths vary with the alloy composition and metallurgical condition of the product, as discussed in Ref 12 and 13. The most serious forms of such structure-dependent corrosion are stress-corrosion cracking (SCC) and exfoliation. Stress-corrosion cracking requires the presence of a sustained (residual and/or service) tensile stress, and exfoliation occurs only in wrought products with a directional grain structure. Not all materials that are susceptible to IGA, however, are susceptible to SCC or exfoliation.

Strain-Hardened 5*xxx* (Al-Mg) Alloys. Alloys in this series that contain more than approximately 3% Mg are rendered susceptible to IGA (sensitization) by certain manufacturing conditions or by being subjected to elevated temperatures up to approximately 175 °C (350 °F). This is the result of the continuous grain-boundary precipitation of the highly anodic Mg_2Al_3 phase, which corrodes preferentially in most corrosive environments.

ASTM G 67 is a method that provides a quantitative measure of the susceptibility to IGA of these alloys (Ref 14). This method consists of immersing test specimens in concentrated HNO_3 at 30 °C (85 °F) for 24 h and determining the mass loss per unit area of exposed surfaces as the measure of intergranular susceptibility. When the second phase is precipitated in a relatively continuous network along grain boundaries, the preferential attack of the network causes whole grains to drop out of the specimens. Such dropping out causes relatively large mass losses of the order of 25 to 75 mg/cm^2 (3.9 - 12 mg/in.^{2}), whereas specimens of materials resistant to IGC lose only about 1 to 15 mg/cm^2 (0.2 - 2.3 mg/in.^{2}). Intermediate mass losses occur when the precipitate is randomly distributed. The parallel relationship between the susceptibility to intergranular attack, SCC, and exfoliation of these particular alloys makes ASTM G 67 a useful screening test for alloy and process

development studies. A problem arises, however, in selecting a pass-or-fail value in relation to the performance of intermediate materials in environments other than HNO_3.

Heat Treated High-Strength Alloys. Materials problems caused by SCC, exfoliation, or corrosion fatigue of the early 2*xxx* (aluminum- copper) alloys were related to IGC, and the blame came to be associated with improper heat treatment. In 1944, an accelerated test for detecting susceptibility to IGC was incorporated into a U.S. Government specification for the heat treatment of aluminum alloys. Military Specification MIL-H-6088F has superseded this specification. Tests are required for periodic monitoring of 2*xxx* and 7*xxx* series alloys in all rivets and fastener components as well as sheet, bar, rod, wire, and shapes under 6.4 mm (0.25 in.) thick. Specimen preparation, test procedure, and evaluation criteria are detailed in Ref 15.

Other Tests for Aluminum Alloys. The volume of hydrogen evolved on immersion of etched 2*xxx* series (aluminum-copper-magnesium) alloys in a solution containing 3% sodium chloride (NaCl) and 1% hydrochloric acid (HCl) for a stipulated time has been used as a quantitative measure of the severity of IGA. A problem with this approach is that the correlation between the amount (or the rate) of hydrogen evolved is influenced by a number of factors, including alloy composition, temper, and grain size (Ref 16, 17).

Applied current or potential in neutral chloride solutions (for example, 0.1 *N* NaCl) provides another direct method of assessing the degree of susceptibility to intergranular attack when accompanied by a microscopic examination of metallographic sections (Ref 16, 18, 19).

As stated earlier, exfoliation is a form of corrosion that can occur in layers parallel to rolled surfaces, especially on aluminum alloys, and attack is generally along grain boundaries. ASTM G 34 is an accelerated test method to determine exfoliation corrosion susceptibility of 2*xxx* and 7*xxx* aluminum alloys (Ref 20); this is sometimes known as the EXCO test. Specimens of wrought material are immersed in 4 *M* NaCl + 0.5 *M* KNO_3 + 0.1 *M* HNO_3 solution at 25 ± 3 °C. Immersion times are 96 and 48 h for 2*xxx* and 7*xxx* alloys, respectively. Performance ratings are established by reference to standard photographs. An analogous exfoliation test for wrought 5*xxx* aluminum alloys, containing ≥2% Mg, is covered by ASTM G 66 in which test specimens are immersed in 1 *M* NH_4Cl + 0.25 *M* NH_4NO_3 + 0.01 *M* $(NH_4)_2C_4H_4O_6$ + 0.09 *M* H_2O_2 for 24 h at 65 ± 1 °C, followed by visual comparison with standard photographs (Ref 21). This test is sometimes known as "ASSET," an abbreviation for assessment of exfoliation corrosion test.

References cited in this section

12. T.J. Summerson and D.O. Sprowls, Corrosion Behavior of Aluminum Alloys, *Aluminum Alloys: Their Physical and Mechanical Properties,* Vol III, E.A. Starke, Jr. and T.H. Sanders, Jr., Ed., Engineering Materials Advisory Services Ltd., 1986, p 1576–1662

13. B.W. Lifka and D.O. Sprowls, *Localized Corrosion—Cause of Metal Failure,* STP 516, ASTM International, 1972, p 120–144

14. "Standard Test Method for Detecting Susceptibility to Intergranular Corrosion of 5*xxx* Series Aluminum Alloys by Mass Loss After Exposure to Nitric Acid (NAMLT Test)", G 67, *Wear and Erosion; Metal Corrosion, Annual Book of ASTM Standards 2002,* Vol 3.02, ASTM International, 2002

15. "Heat Treatment of Aluminum Alloys," Military Specification MIL-H-6088F, United States Government Printing Office

16. F.A. Champion, *Corrosion Testing Procedures,* 2nd ed., John Wiley & Sons, 1965, p 365, 366

17. G.J. Schafer, *J. Appl. Chem.,* Vol 10, 1960, p 138

18. S. Ketcham and W. Beck, *Corrosion,* Vol 16, 1960, p 37

19. M.K. Budd and F.F. Booth, *Corrosion,* Vol 18, 1962, p 197

20. “Standard Test Method for Exfoliation Corrosion Susceptibility in 2*xxx* and 7*xxx* Series Aluminum Alloys (EXCO Test)”, G 34, *Wear and Erosion; Metal Corrosion, Annual Book of ASTM Standards 2002,* Vol 3.02, ASTM International, 2002

21. “Standard Test Method for Visual Assessment of Exfoliation Corrosion Susceptibility in 5*xxx* Series Aluminum Alloys (ASSET Test)”, G 66, *Wear and Erosion; Metal Corrosion, Annual Book of ASTM Standards 2002,* Vol 3.02, ASTM International, 2002

B. Phull, Evaluating Intergranular Corrosion, *Corrosion: Fundamentals, Testing, and Protection*, Vol 13A, *ASM Handbook,* ASM International, 2003, p 568–571

Evaluating Intergranular Corrosion

Revised by Bopinder Phull, Consultant

Tests for Other Alloys

Although IGC is present to some extent in metallic materials other than stainless steels and aluminum alloys, incidences of attack associated with this form of corrosion are few and are generally not of practical importance. Therefore, no attempts have been made to develop and standardize specific tests for detecting susceptibility to IGC in these alloys. However, certain media have been commonly used for evaluating the susceptibility to IGC of magnesium, copper, lead, and zinc alloys (Ref 16). These media are listed in Table 2. The presence or absence of attack in these tests is not necessarily a measure of the performance of the material in any other corrosive (test or service) environments.

Table 2 Media for testing susceptibility to intergranular corrosion

Alloy	Medium	Concentration %	Temperature °C (°F)
Magnesium alloys	Sodium chloride plus hydrochloric acid	…	Room
Copper alloys	Sodium chloride plus sulfuric or nitric acid	1 NaCl, 0.3 acid	40–50 (105–120)
Lead alloys	Acetic acid or hydrochloric acid	…	Room
Zinc alloys	Humid air	100% relative humidity	95 (205)

Source: Ref 16

Magnesium Alloys. There are rare instances of reported IGC of magnesium alloys, as in the case of chromic acid contaminated with chlorides or sulfates.

The copper alloys that appear to be the most susceptible to IGC are Muntz metal, admiralty brass, aluminum brasses, and silicon bronzes. Admiralty alloys have been observed to suffer IGC on exposure to saline cooling waters, although the incidence of attack is very low. The antimony-doped grades are reportedly superior to the arsenical grades in this respect. Similarly, arsenical and phosphorized grades of aluminum brass have been observed to suffer IGC in seawater-type exposures.

Zinc die casting alloys have reportedly suffered IGC in certain steam atmospheres. A laboratory test for simulating service failures, and particularly for alloy development work, has been in use for testing the susceptibility of zinc- base die-castings to IGC (Ref 22). The test consists of exposing samples to air at 95 °C (205 °F) and 100% relative humidity for 10 days under conditions permitting condensation of hot water on the metal. Susceptibility to IGC is assessed by the effect on mechanical properties, such as impact strength.

Experience has shown that castings with mechanical properties and dimensions that are not significantly altered by the 10 day exposure in this test will not suffer IGA in atmospheric service.
Intergranular corrosion at elevated temperatures can occur by formation of low melting phases (in certain alloy-environment combinations) that result in rapid attack commonly at grain boundaries. For example, the formation of nickel-sulfides in nickel-base alloys can cause catastrophic failures in high-temperature, sulfur-rich gaseous environments. This phenomenon is commonly referred to as sulfidation. Deep penetration can occur rapidly, including through the full thickness of the metal. The techniques for evaluating this type of IGC include (a) x-ray mapping during examination in a scanning electron microscope (equipped with an energy-dispersive x-ray detector) and (b) transmission electron microscopy.

References cited in this section

16. F.A. Champion, *Corrosion Testing Procedures,* 2nd ed., John Wiley & Sons, 1965, p 365, 366

22. H.H. Uhlig, *Corrosion Handbook,* John Wiley & Sons, 1948

Acknowledgment

This article has been adapted from Donald O. Sprowls, Evaluation of Intergranular Corrosion, *Corrosion,* Volume 13, *ASM Handbook* (formerly 9th ed. *Metals Handbook*), ASM International, 1987, pages 239 to 241.

B. Phull, Evaluating Intergranular Corrosion, *Corrosion: Fundamentals, Testing, and Protection*, Vol 13A, *ASM Handbook*, ASM International, 2003, p 568–571

Evaluating Intergranular Corrosion

Revised by Bopinder Phull, Consultant

References

1. M. Henthorne, *Localized Corrosion—Cause of Metal Failure,* STP 516, ASTM International, 1972, p 66–119

2. M.A. Streicher, *Intergranular Corrosion of Stainless Alloys,* STP 656, ASTM International, 1978, p 3–84

3. M.A. Streicher, Intergranular Corrosion, *Corrosion Tests and Standards: Application and Interpretation,* R. Baboian, Ed., ASTM International, 1995, p 197–217

4. W.H. Hatfield, *J. Iron Steel Inst.,* Vol 127, 1933, p 380–383

5. W.R. Huey, *Trans. Am. Soc. Steel Treat.,* Vol 18, 1930, p 1126–1143

6. “Practices for Detecting Susceptibility to Intergranular Corrosion in Austenitic Stainless Steels,” A 262, *Steel—Plate, Sheet, Strip, Wire; Stainless Steel Bar, Annual Book of ASTM Standards 2002,* Vol 1.03, ASTM International, 2002

7. “Practices for Detecting Susceptibility to Intergranular Corrosion in Ferritic Stainless Steels”, A 763, *Steel—Plate, Sheet, Strip, Wire; Stainless Steel Bar, Annual Book of ASTM Standards 2002,* Vol 1.03, ASTM International, 2002

8. “Standard Test Methods for Detecting Susceptibility to Intergranular Corrosion in Wrought, Nickel-Rich, Chromium-Bearing Alloys,” G 28, *Wear and Erosion; Metal Corrosion, Annual Book of ASTM Standards 2002,* Vol 3.02, ASTM International, 2002

9. “Standard Test Method for Electrochemical Reactivation (EPR) for Detecting Sensitization of AISI Type 304 and 304L Stainless Steel,” G 108, *Wear and Erosion; Metal Corrosion, Annual Book of ASTM Standards 2002,* Vol 3.02, ASTM International, 2002

10. A.P. Majidi and M.A. Striecher, *Corrosion,* Vol 40, 1984, p 584–592

11. M. Akashi, T. Kawamoto, and F. Umemura, *Corros. Eng.,* (Jpn.), Vol 29, 1980, p 163

12. T.J. Summerson and D.O. Sprowls, Corrosion Behavior of Aluminum Alloys, *Aluminum Alloys: Their Physical and Mechanical Properties,* Vol III, E.A. Starke, Jr. and T.H. Sanders, Jr., Ed., Engineering Materials Advisory Services Ltd., 1986, p 1576–1662

13. B.W. Lifka and D.O. Sprowls, *Localized Corrosion—Cause of Metal Failure,* STP 516, ASTM International, 1972, p 120–144

14. “Standard Test Method for Detecting Susceptibility to Intergranular Corrosion of 5*xxx* Series Aluminum Alloys by Mass Loss After Exposure to Nitric Acid (NAMLT Test)”, G 67, *Wear and Erosion; Metal Corrosion, Annual Book of ASTM Standards 2002,* Vol 3.02, ASTM International, 2002

15. “Heat Treatment of Aluminum Alloys,” Military Specification MIL-H-6088F, United States Government Printing Office

16. F.A. Champion, *Corrosion Testing Procedures,* 2nd ed., John Wiley & Sons, 1965, p 365, 366

17. G.J. Schafer, *J. Appl. Chem.,* Vol 10, 1960, p 138

18. S. Ketcham and W. Beck, *Corrosion,* Vol 16, 1960, p 37

19. M.K. Budd and F.F. Booth, *Corrosion,* Vol 18, 1962, p 197

20. “Standard Test Method for Exfoliation Corrosion Susceptibility in 2*xxx* and 7*xxx* Series Aluminum Alloys (EXCO Test)”, G 34, *Wear and Erosion; Metal Corrosion, Annual Book of ASTM Standards 2002,* Vol 3.02, ASTM International, 2002

21. “Standard Test Method for Visual Assessment of Exfoliation Corrosion Susceptibility in 5*xxx* Series Aluminum Alloys (ASSET Test)”, G 66, *Wear and Erosion; Metal Corrosion, Annual Book of ASTM Standards 2002,* Vol 3.02, ASTM International, 2002

22. H.H. Uhlig, *Corrosion Handbook,* John Wiley & Sons, 1948

B. Phull, Evaluating Intergranular Corrosion, *Corrosion: Fundamentals, Testing, and Protection*, Vol 13A, *ASM Handbook*, ASM International, 2003, p 568–571

Evaluating Intergranular Corrosion

Revised by Bopinder Phull, Consultant

Selected References

- A.H. Ailor, Ed., *Handbook of Corrosion Testing and Evaluation,* J. Wiley & Sons, Inc., 1971
- R. Baboian, Ed., *Manual 20 Corrosion Tests and Standards: Application and Interpretation,* ASTM International, 1995
- M. Fontana, *Corrosion Engineering,* 3rd ed., McGraw-Hill, 1986
- *High Temperature Corrosion,* NACE International, 1983
- G.Y. Lai, *High Temperature Corrosion of Engineering Alloys,* ASM International, 1990

B. Phull, Evaluating Exfoliation Corrosion, *Corrosion: Fundamentals, Testing, and Protection,* Vol 13A, *ASM Handbook,* ASM International, 2003, p 572–574

Evaluating Exfoliation Corrosion

Revised by Bopinder Phull, Consultant

Introduction

EXFOLIATION is a structure-dependent form of localized (usually) intergranular corrosion that is most idiosyncratic in certain alloys and tempers of aluminum. It is also called layer corrosion or lamellar corrosion and is a form of subsurface attack that follows narrow paths (often grain boundaries) in the rolling direction of wrought materials and parallel to the rolled surfaces. Exfoliation corrosion often initiates at laterally sheared edges exposed to the environment. The corrosion products tend to swell or pry open the material, revealing alternate layers or leafing of corroded and uncorroded structure. Highly cold-worked materials, which have elongated grain boundaries, and thin-gage product forms tend to be most affected. Swelling associated with exfoliation corrosion can stress adjacent parts and cause overload failures—a phenomenon akin to packout rusting (Ref 1).

The occurrence of exfoliation in susceptible materials is influenced to a marked degree by environmental conditions. Figure 1 illustrates the broad range of behavior of aluminum alloy 2124 plate in different types of environments (Ref 2). The plate was heat treated to be susceptible to exfoliation. Performance can vary significantly, depending on the environment. For example, forged truck wheels made of an aluminum-copper alloy (2024-T4) give corrosion- free service for many years in the warm climates of the southern and western United States, but they exfoliate severely in only 1 or 2 years in the northern states, where deicing salts are used on the highways during the winter months.

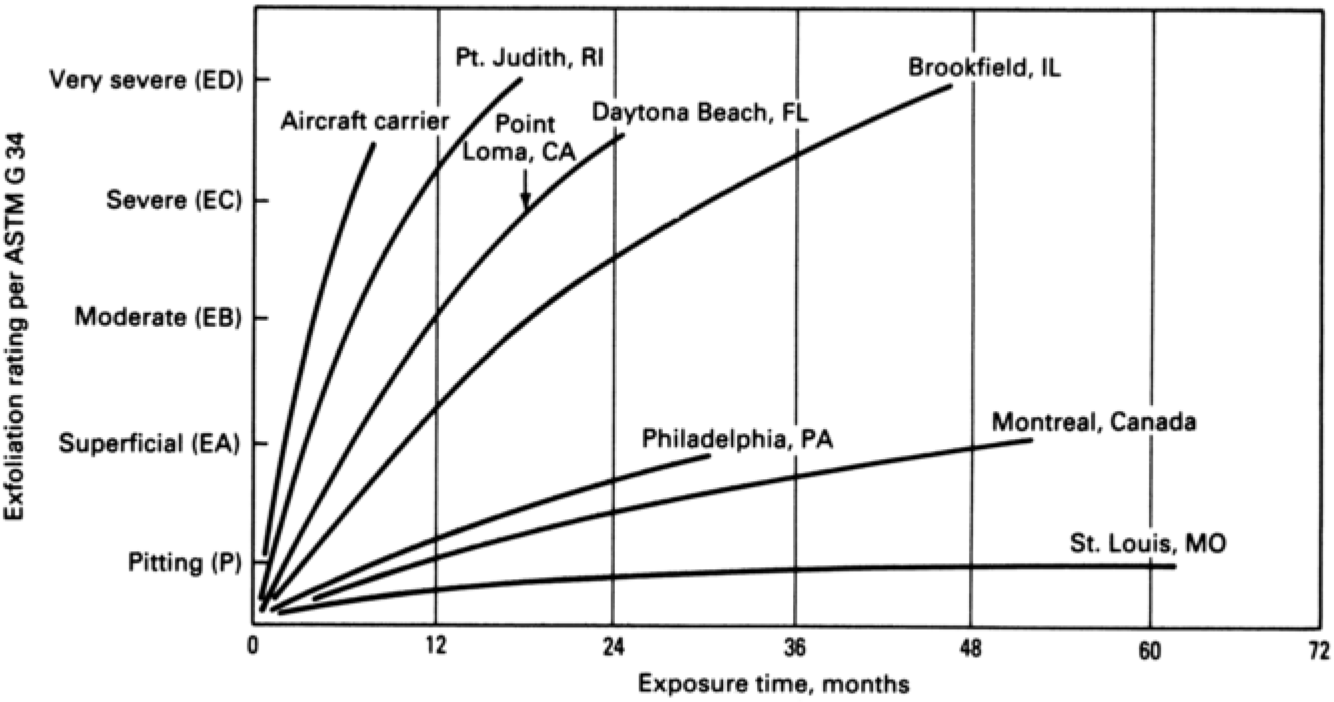

Fig. 1 Comparison of exfoliation of aluminum alloy 2124 (heat treated to be susceptible; EXCO ED rating) in various seacoast and industrial environments. Specimens were 13 mm ($\frac{1}{2}$ in.) plate. Source: Ref 2

Accelerated laboratory tests do not precisely predict long-term corrosion behavior; however, answers are needed quickly in the development of new materials. For this reason, accelerated tests are used to screen candidate alloys before conducting atmospheric exposures or other field tests. They are also sometimes used for quality- control tests. Several new laboratory tests for exfoliation corrosion have been standardized under the jurisdiction of American Society for Testing and Materials International (ASTM International) Committee G-1 on the Corrosion of Metals.

References cited in this section

1. J.B. Vrable, R.T. Jones, and E.H. Phelps, "The Application of High Strength Low Alloy Steels in the Chemical Industry," *Mater. Perform.,* Vol 18 (No. 1), Jan 1979, p 39–44
2. S.J. Ketcham and E.J. Jankowsky, Developing an Accelerated Test: Problems and Pitfalls. *Laboratory Corrosion Tests and Standards,* STP 866, G.S. Haynes and R. Baboian, Ed., American Society for Testing and Materials, 1985, p 14–23

B. Phull, Evaluating Exfoliation Corrosion, *Corrosion: Fundamentals, Testing, and Protection*, Vol 13A, *ASM Handbook*, ASM International, 2003, p 572–574

Evaluating Exfoliation Corrosion

Revised by Bopinder Phull, Consultant

Spray Tests

Three cyclic acidified salt spray tests have been widely used in the aluminum and aircraft industries. These are covered by the procedures described in Annexes A2, A3, and A4 of ASTM G 85 (Ref 3). This standard does not prescribe the particular practice, test specimen, or exposure period to be used for a specific product, nor does it define the interpretation to be given to the test results. These considerations are prescribed by specifications covering the material or product being tested or by agreement between the purchaser and the seller.

Annex A2 describes a cyclic salt spray test that uses a 5% sodium chloride (NaCl) solution, acidified to pH 3 with acetic acid, in a spray chamber at a temperature of 49 ± 1 °C (120 ± 2 °F). This test is applicable for exfoliation testing of 2*xxx* (dry-bottom operation) and 7*xxx* (wet-bottom operation; that is, with approximately 25 mm, or 1 in., of water present in the bottom of the test chamber) aluminum alloys with a test duration of 1 to 2 weeks. Results with 7075 and 7178 alloys in various metallurgical conditions have been shown to correlate well with results obtained in a seacoast atmosphere (4 year exposure at Point Judith, RI) (Ref 4).

Annex A3 describes another cyclic salt spray test that uses a 5% synthetic sea salt solution, acidified to pH 3 with acetic acid, in a spray chamber at a temperature of 49 °C (120 °F). The test is applicable to the production control of exfoliation-resistant tempers of the 2*xxx*, 5*xxx*, and 7*xxx* aluminum alloys (Ref 5, 6). Wet-bottom operating conditions are recommended with test durations of 1 to 2 weeks.

Annex A4 describes a salt/sulfur dioxide (SO_2) spray test that uses either 5% NaCl or 5% synthetic sea salt solution in a spray chamber at a temperature of 35 °C (95 °F). The spray may be either cyclic or constant. This, along with the type of salt solution and the test duration, is subject to agreement between the purchaser and the seller. The test is applicable for 2*xxx* and 7*xxx* aluminum alloys. Test duration is 2 to 4 weeks (Ref 2).

References cited in this section

2. S.J. Ketcham and E.J. Jankowsky, Developing an Accelerated Test: Problems and Pitfalls. *Laboratory Corrosion Tests and Standards,* STP 866, G.S. Haynes and R. Baboian, Ed., American Society for Testing and Materials, 1985, p 14–23

3. “Standard Practice for Modified Salt Spray (Fog) Testing,” G 85, *Wear and Erosion; Metal Corrosion,* Vol 03.02, *Annual Book of ASTM Standards 2002,* American Society for Testing and Materials, 2002

4. B.W. Lifka and D.O. Sprowls, Relationship of Accelerated Test Methods for Exfoliation Resistance in 7*xxx* Aluminum Alloys with Exposure to a Seacoast Atmosphere. *Corrosion in Natural Environments,* STP 558, American Society for Testing and Materials, 1974, p 306–333

5. H.B. Romans, An Accelerated Laboratory Test to Determine the Exfoliation Corrosion Resistance of Aluminum Alloys, *Mater. Res. Stand.,* Vol 9 (No. 11), 1969, p 31–34

6. S.J. Ketcham and P.W. Jeffrey, Exfoliation Corrosion Testing of 7178 and 7075 Aluminum Alloys, *Localized Corrosion— Cause of Metal Failure,* STP 516, American Society for Testing and Materials, 1972, p 273–302

B. Phull, Evaluating Exfoliation Corrosion, *Corrosion: Fundamentals, Testing, and Protection*, Vol 13A, *ASM Handbook*, ASM International, 2003, p 572–574

Evaluating Exfoliation Corrosion

Revised by Bopinder Phull, Consultant

Immersion Tests

Total-immersion tests were developed to provide simpler, more easily controlled test methods. Chloride solutions did not cause exfoliation during reasonable periods of immersion. However, formulations of chloride-nitrate solutions were found that produced severe exfoliation of susceptible alloys in only 1 or 2 days. Optimal test conditions differed for separate alloy families (Ref 7).

ASTM G 66 describes a procedure for the continuous-immersion exfoliation testing of 5*xxx* alloys containing 2.0% or more magnesium (Ref 8). Specimens are immersed for 24 h at 65 ± 1 °C (150 ± 2 °F) in a solution of 1 *M* ammonium chloride, 0.25 *M* ammonium nitrate, 0.01 *M* ammonium tartrate, and 0.09 *M* hydrogen peroxide. Susceptibility to exfoliation is determined by visual examination, using performance ratings established by reference to standard photographs. This method is stated to provide reliable prediction of the exfoliation corrosion behavior of 5*xxx* alloys in marine environments (Ref 9). The test is also useful for alloy development studies and quality control of mill products such as sheet and plate (Ref 10).

ASTM G 34 provides an accelerated exfoliation corrosion test for 2*xxx* and 7*xxx* aluminum alloys through the continuous immersion of test materials in an aqueous solution of 4 *M* NaCl, 0.5 *M* potassium nitrate, and 0.1 *M* nitric acid at 25 ± 3 °C (77 ± 5 °F) (Ref 11). Maximum recommended exposure periods for the 2*xxx* and 7*xxx* aluminum alloys are 96 and 48 h, respectively. Susceptibility to exfoliation is determined by visual examination, using performance ratings established by reference to standard photographs. This constant immersion exfoliation corrosion test method, also known as the EXCO test, is primarily used for research and development and quality control of such mill products as sheet and plate (Ref 10). However, it should not be construed as the optimal method for quality acceptance.

The ASTM G 34 method provides a useful prediction of the exfoliation behavior of 2*xxx* and 7*xxx* aluminum alloys in various types of outdoor service, especially in marine and industrial environments (Ref 4, 12). The test solution is very corrosive and represents the more severe types of environment service (Fig. 1). However, it remains to be determined whether correlations can be established between EXCO test ratings and practical service conditions for a given alloy. It has been reported that samples of 7*xxx* (Al-Zn- Mg-Cu) alloys rated EA (superficial exfoliation) or P (pitting) in a 48 h EXCO test did not develop more than superficial exfoliation (EA rating) during 6 to 9 year exposures to seacoast atmospheres, while EC- and ED-rated (severe and very severe exfoliation, respectively) materials developed severe exfoliation within 1 to 7 years at the seacoast (specimens rated EA to ED are shown in Fig. 2, Fig. 3, Fig. 4, Fig. 5) (Ref 12).

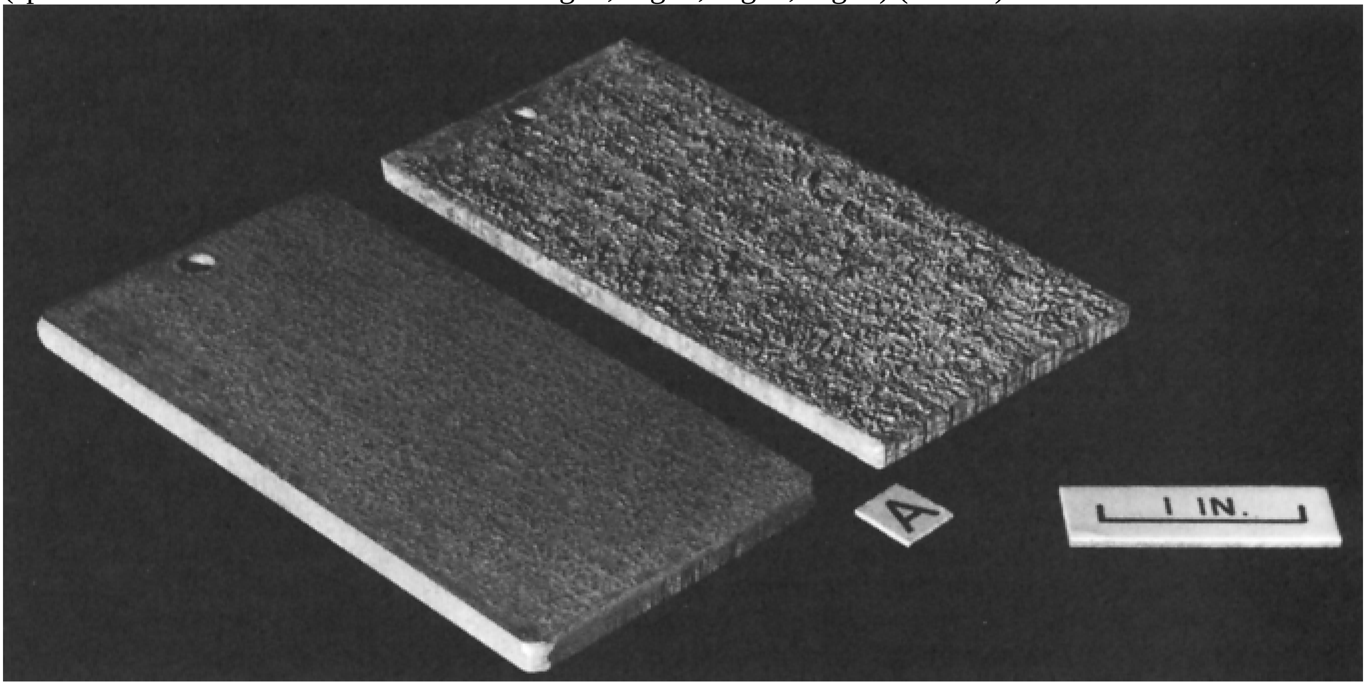

Fig. 2 Examples of exfoliation rating EA (superficial). Specimens exhibit tiny blisters, thin slivers, flakes, or powder, with only slight separation of metal. Source: Ref 11

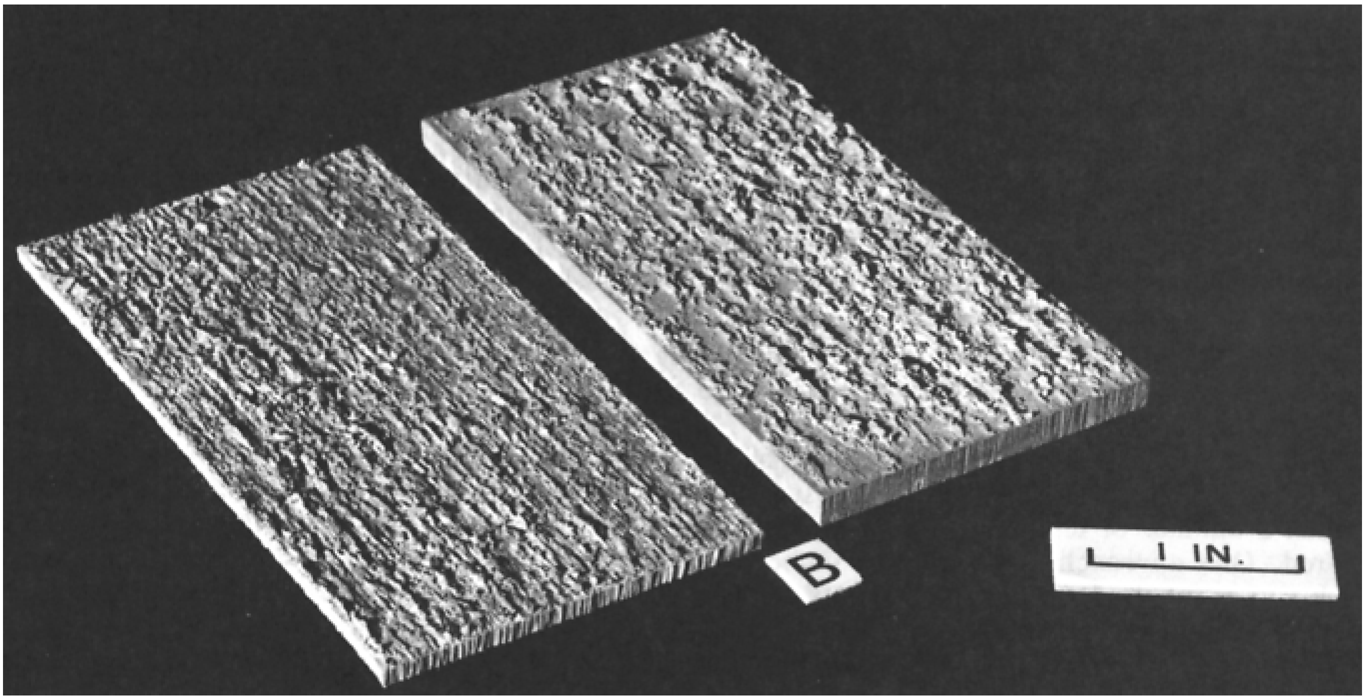

Fig. 3 Examples of exfoliation rating EB (moderate). Specimens show notable layering and penetration into the metal. Source: Ref 11

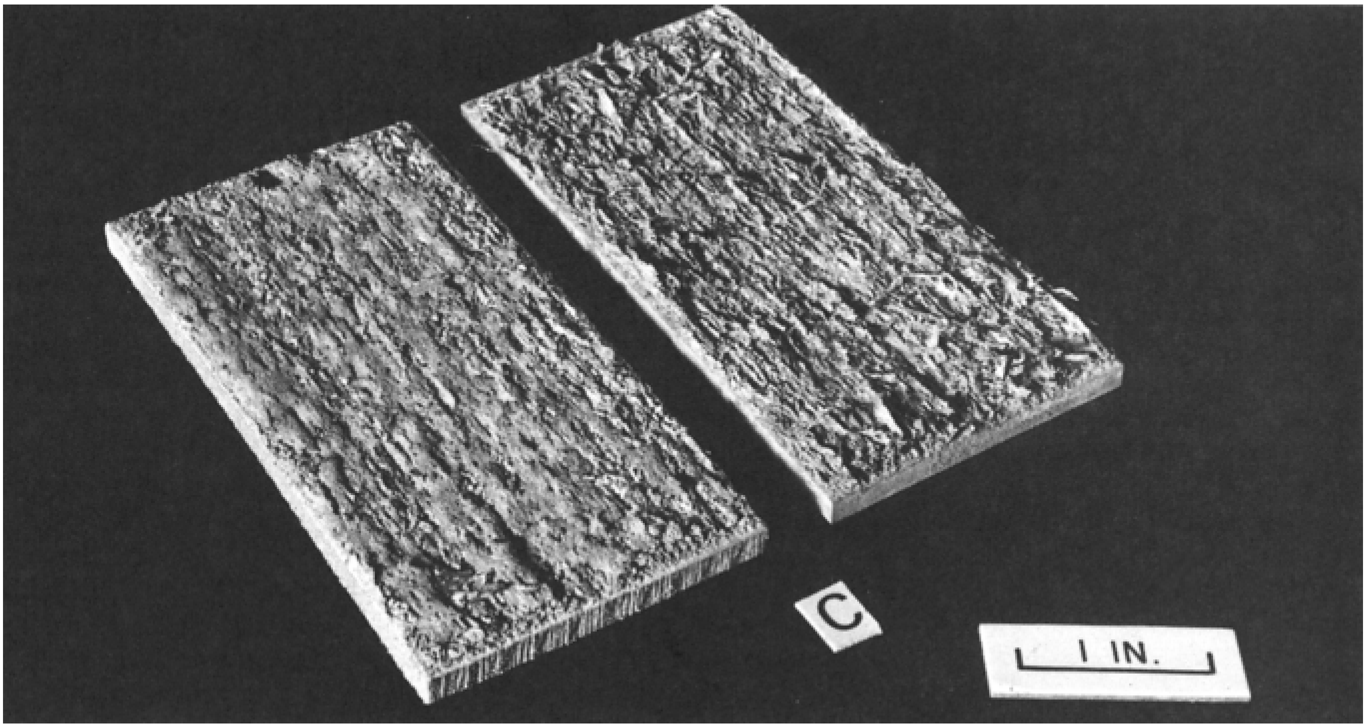

Fig. 4 Examples of exfoliation rating EC (severe). There is penetration to a considerable depth into the metal. Source: Ref 11

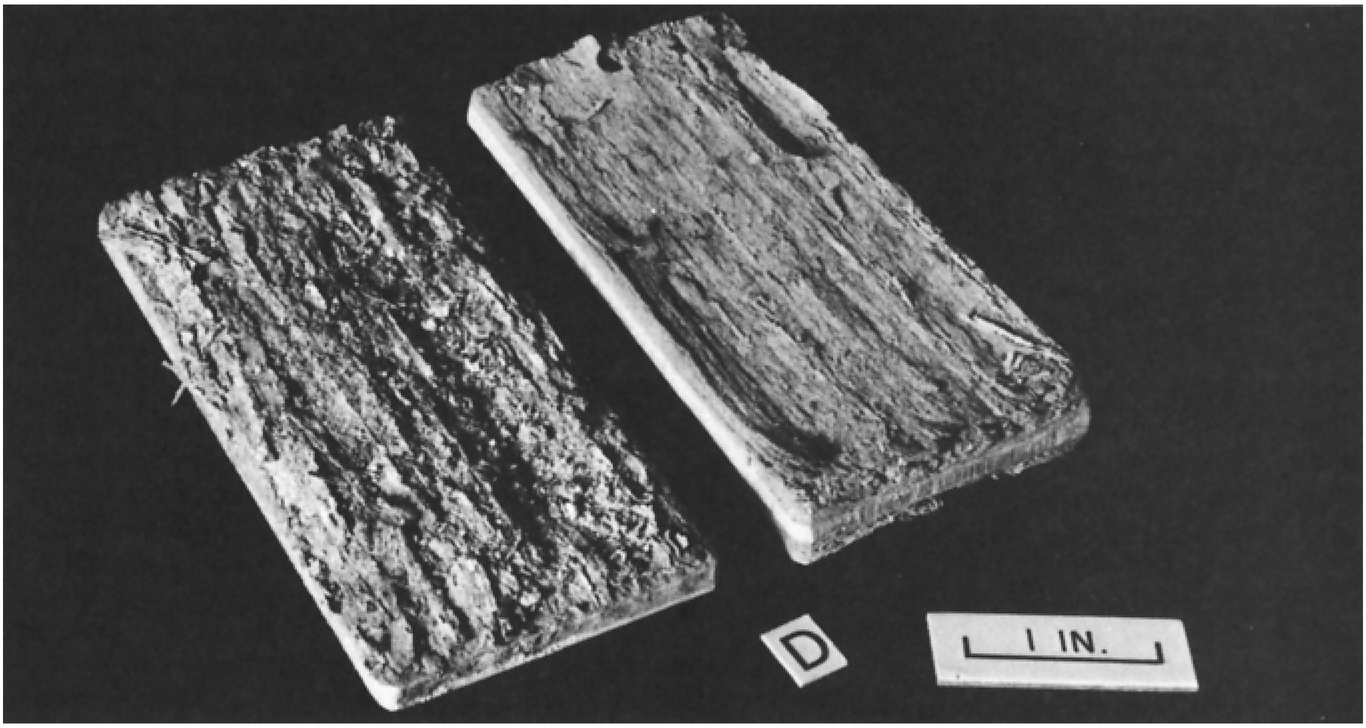

Fig. 5 Examples of exfoliation rating ED (very severe). Specimens appear similar to EC except for much greater penetration and loss of metal. Source: Ref 11

Performance differences between practical service and the EXCO test have been noted and indicate that the EXCO test may be too severe for some of the more recently developed 2*xxx* and 7*xxx* alloys. The testing program for evaluating new alloy materials should consist of multiple tests with one of the less aggressive ASTM G 85 salt spray methods supplemented by outdoor exposure tests. Caution must be exercised in setting limits for material procurement specifications based on accelerated tests (Ref 13).

References cited in this section

4. B.W. Lifka and D.O. Sprowls, Relationship of Accelerated Test Methods for Exfoliation Resistance in 7*xxx* Aluminum Alloys with Exposure to a Seacoast Atmosphere. *Corrosion in Natural Environments,* STP 558, American Society for Testing and Materials, 1974, p 306–333

7. D.O. Sprowls, J.D. Walsh, and M.B. Shumaker, Simplified Exfoliation Testing of Aluminum Alloys, *Localized Corrosion— Cause of Metal Failure,* STP 516, American Society for Testing and Materials, 1972, p 38–65

8. "Standard Test Method for Visual Assessment of Exfoliation Corrosion Susceptibility of 5*xxx*-Series Aluminum Alloys (ASSET Test)," G 66, *Wear and Erosion; Metal Corrosion,* Vol 03.02, *Annual Book of ASTM Standards 2002,* American Society for Testing and Materials, 2002

9. T.J. Summerson, Interim Report, Aluminum Association Task Group on Exfoliation and Stress-Corrosion Cracking of Aluminum Alloys for Boat Stock, *Proceedings of the Tri-Service Corrosion Military Equipment Conference,* Technical Report AFML-TR- 75-42, Vol II, Air Force Materials Laboratory, 1975, p 193–221

10. "Specification for Aluminum and Aluminum-Alloy Sheet and Plate," B 209, *Aluminum and Magnesium Alloys,* Vol 02.02, *Annual Book of ASTM Standards 2002,* American Society for Testing and Materials, 2002

11. “Standard Test Method for Exfoliation Corrosion Susceptibility in 2*xxx* and 7*xxx*-Series Aluminum Alloys (EXCO Test),” G 34, *Wear and Erosion; Metal Corrosion,* Vol 03.02, *Annual Book of ASTM Standards 2002,* American Society for Testing and Materials, 2002

12. D.O. Sprowls, T.J. Summerson, and F.E. Loftin, Exfoliation Corrosion Testing of 7075 and 7178 Aluminum Alloys—Interim Report on Atmospheric Exposure Tests (Report of ASTM G01.05.02 Interlaboratory Testing Program in Cooperation with the Aluminum Association), *Corrosion in Natural Environments,* STP 558, American Society for Testing and Materials, 1974, p 99–113

13. B.W. Lifka, “Corrosion Resistance of Aluminum Alloy Plate in Rural, Industrial, and Seacoast Atmospheres,” Paper 420, Corrosion/87, NACE International, 1987

B. Phull, Evaluating Exfoliation Corrosion, *Corrosion: Fundamentals, Testing, and Protection*, Vol 13A, *ASM Handbook*, ASM International, 2003, p 572–574

Evaluating Exfoliation Corrosion

Revised by Bopinder Phull, Consultant

Acknowledgment

This article has been adapted from D.O. Sprowls, Evaluation of Exfoliation Corrosion, *Corrosion,* Vol 13, *ASM Handbook* (formerly *Metals Handbook,* 9th ed.), ASM International, 1987, p 242–244

B. Phull, Evaluating Exfoliation Corrosion, *Corrosion: Fundamentals, Testing, and Protection*, Vol 13A, *ASM Handbook*, ASM International, 2003, p 572–574

Evaluating Exfoliation Corrosion

Revised by Bopinder Phull, Consultant

Acknowledgment

This article has been adapted from D.O. Sprowls, Evaluation of Exfoliation Corrosion, *Corrosion,* Vol 13, *ASM Handbook* (formerly *Metals Handbook,* 9th ed.), ASM International, 1987, p 242–244

B. Phull, Evaluating Exfoliation Corrosion, *Corrosion: Fundamentals, Testing, and Protection*, Vol 13A, *ASM Handbook*, ASM International, 2003, p 572–574

Evaluating Exfoliation Corrosion

Revised by Bopinder Phull, Consultant

References

1. J.B. Vrable, R.T. Jones, and E.H. Phelps, “The Application of High Strength Low Alloy Steels in the Chemical Industry,” *Mater. Perform.,* Vol 18 (No. 1), Jan 1979, p 39–44

2. S.J. Ketcham and E.J. Jankowsky, Developing an Accelerated Test: Problems and Pitfalls. *Laboratory Corrosion Tests and Standards,* STP 866, G.S. Haynes and R. Baboian, Ed., American Society for Testing and Materials, 1985, p 14–23

3. “Standard Practice for Modified Salt Spray (Fog) Testing,” G 85, *Wear and Erosion; Metal Corrosion,* Vol 03.02, *Annual Book of ASTM Standards 2002,* American Society for Testing and Materials, 2002

4. B.W. Lifka and D.O. Sprowls, Relationship of Accelerated Test Methods for Exfoliation Resistance in 7*xxx* Aluminum Alloys with Exposure to a Seacoast Atmosphere. *Corrosion in Natural Environments,* STP 558, American Society for Testing and Materials, 1974, p 306–333

5. H.B. Romans, An Accelerated Laboratory Test to Determine the Exfoliation Corrosion Resistance of Aluminum Alloys, *Mater. Res. Stand.,* Vol 9 (No. 11), 1969, p 31–34

6. S.J. Ketcham and P.W. Jeffrey, Exfoliation Corrosion Testing of 7178 and 7075 Aluminum Alloys, *Localized Corrosion— Cause of Metal Failure,* STP 516, American Society for Testing and Materials, 1972, p 273–302

7. D.O. Sprowls, J.D. Walsh, and M.B. Shumaker, Simplified Exfoliation Testing of Aluminum Alloys, *Localized Corrosion— Cause of Metal Failure,* STP 516, American Society for Testing and Materials, 1972, p 38–65

8. “Standard Test Method for Visual Assessment of Exfoliation Corrosion Susceptibility of 5*xxx*-Series Aluminum Alloys (ASSET Test),” G 66, *Wear and Erosion; Metal Corrosion,* Vol 03.02, *Annual Book of ASTM Standards 2002,* American Society for Testing and Materials, 2002

9. T.J. Summerson, Interim Report, Aluminum Association Task Group on Exfoliation and Stress-Corrosion Cracking of Aluminum Alloys for Boat Stock, *Proceedings of the Tri-Service Corrosion Military Equipment Conference,* Technical Report AFML-TR- 75-42, Vol II, Air Force Materials Laboratory, 1975, p 193–221

10. “Specification for Aluminum and Aluminum-Alloy Sheet and Plate,” B 209, *Aluminum and Magnesium Alloys,* Vol 02.02, *Annual Book of ASTM Standards 2002,* American Society for Testing and Materials, 2002

11. “Standard Test Method for Exfoliation Corrosion Susceptibility in 2*xxx* and 7*xxx*-Series Aluminum Alloys (EXCO Test),” G 34, *Wear and Erosion; Metal Corrosion,* Vol 03.02, *Annual Book of ASTM Standards 2002,* American Society for Testing and Materials, 2002

12. D.O. Sprowls, T.J. Summerson, and F.E. Loftin, Exfoliation Corrosion Testing of 7075 and 7178 Aluminum Alloys—Interim Report on Atmospheric Exposure Tests (Report of ASTM G01.05.02 Interlaboratory Testing Program in Cooperation with the Aluminum Association), *Corrosion in Natural Environments,* STP 558, American Society for Testing and Materials, 1974, p 99–113

13. B.W. Lifka, “Corrosion Resistance of Aluminum Alloy Plate in Rural, Industrial, and Seacoast Atmospheres,” Paper 420, Corrosion/87, NACE International, 1987

B. Phull, Evaluating Exfoliation Corrosion, *Corrosion: Fundamentals, Testing, and Protection*, Vol 13A, *ASM Handbook*, ASM International, 2003, p 572–574

Evaluating Exfoliation Corrosion

Revised by Bopinder Phull, Consultant

References

1. J.B. Vrable, R.T. Jones, and E.H. Phelps, "The Application of High Strength Low Alloy Steels in the Chemical Industry," *Mater. Perform.,* Vol 18 (No. 1), Jan 1979, p 39–44

2. S.J. Ketcham and E.J. Jankowsky, Developing an Accelerated Test: Problems and Pitfalls. *Laboratory Corrosion Tests and Standards,* STP 866, G.S. Haynes and R. Baboian, Ed., American Society for Testing and Materials, 1985, p 14–23

3. "Standard Practice for Modified Salt Spray (Fog) Testing," G 85, *Wear and Erosion; Metal Corrosion,* Vol 03.02, *Annual Book of ASTM Standards 2002,* American Society for Testing and Materials, 2002

4. B.W. Lifka and D.O. Sprowls, Relationship of Accelerated Test Methods for Exfoliation Resistance in 7*xxx* Aluminum Alloys with Exposure to a Seacoast Atmosphere. *Corrosion in Natural Environments,* STP 558, American Society for Testing and Materials, 1974, p 306–333

5. H.B. Romans, An Accelerated Laboratory Test to Determine the Exfoliation Corrosion Resistance of Aluminum Alloys, *Mater. Res. Stand.,* Vol 9 (No. 11), 1969, p 31–34

6. S.J. Ketcham and P.W. Jeffrey, Exfoliation Corrosion Testing of 7178 and 7075 Aluminum Alloys, *Localized Corrosion— Cause of Metal Failure,* STP 516, American Society for Testing and Materials, 1972, p 273–302

7. D.O. Sprowls, J.D. Walsh, and M.B. Shumaker, Simplified Exfoliation Testing of Aluminum Alloys, *Localized Corrosion— Cause of Metal Failure,* STP 516, American Society for Testing and Materials, 1972, p 38–65

8. "Standard Test Method for Visual Assessment of Exfoliation Corrosion Susceptibility of 5*xxx*-Series Aluminum Alloys (ASSET Test)," G 66, *Wear and Erosion; Metal Corrosion,* Vol 03.02, *Annual Book of ASTM Standards 2002,* American Society for Testing and Materials, 2002

9. T.J. Summerson, Interim Report, Aluminum Association Task Group on Exfoliation and Stress-Corrosion Cracking of Aluminum Alloys for Boat Stock, *Proceedings of the Tri-Service Corrosion Military Equipment Conference,* Technical Report AFML-TR- 75-42, Vol II, Air Force Materials Laboratory, 1975, p 193–221

10. "Specification for Aluminum and Aluminum-Alloy Sheet and Plate," B 209, *Aluminum and Magnesium Alloys,* Vol 02.02, *Annual Book of ASTM Standards 2002,* American Society for Testing and Materials, 2002

11. "Standard Test Method for Exfoliation Corrosion Susceptibility in 2*xxx* and 7*xxx*-Series Aluminum Alloys (EXCO Test)," G 34, *Wear and Erosion; Metal Corrosion,* Vol 03.02, *Annual Book of ASTM Standards 2002,* American Society for Testing and Materials, 2002

12. D.O. Sprowls, T.J. Summerson, and F.E. Loftin, Exfoliation Corrosion Testing of 7075 and 7178 Aluminum Alloys—Interim Report on Atmospheric Exposure Tests (Report of ASTM G01.05.02 Interlaboratory Testing Program in Cooperation with the Aluminum Association), *Corrosion in Natural Environments,* STP 558, American Society for Testing and Materials, 1974, p 99–113

13. B.W. Lifka, "Corrosion Resistance of Aluminum Alloy Plate in Rural, Industrial, and Seacoast Atmospheres," Paper 420, Corrosion/87, NACE International, 1987

B. Phull, Evaluating Stress-Corrosion Cracking, *Corrosion: Fundamentals, Testing, and Protection*, Vol 13A, *ASM Handbook,* ASM International, 2003, p 575–616

Evaluating Stress-Corrosion Cracking

Revised by Bopinder Phull, Consultant

Introduction

THERE ARE A NUMBER of corrosion-related causes of the premature fracture of structural components. The most common of these are compared in Fig. 1. Cracking due to corrosion fatigue occurs only under cyclic or fluctuating operating loads, while failure resulting from the other processes shown occurs under static or slowly rising loads. With certain alloy systems, hydrogen embrittlement may have a contributory role in each of these failure processes. Appropriate tests for the different failure modes are discussed in other articles in this Section.

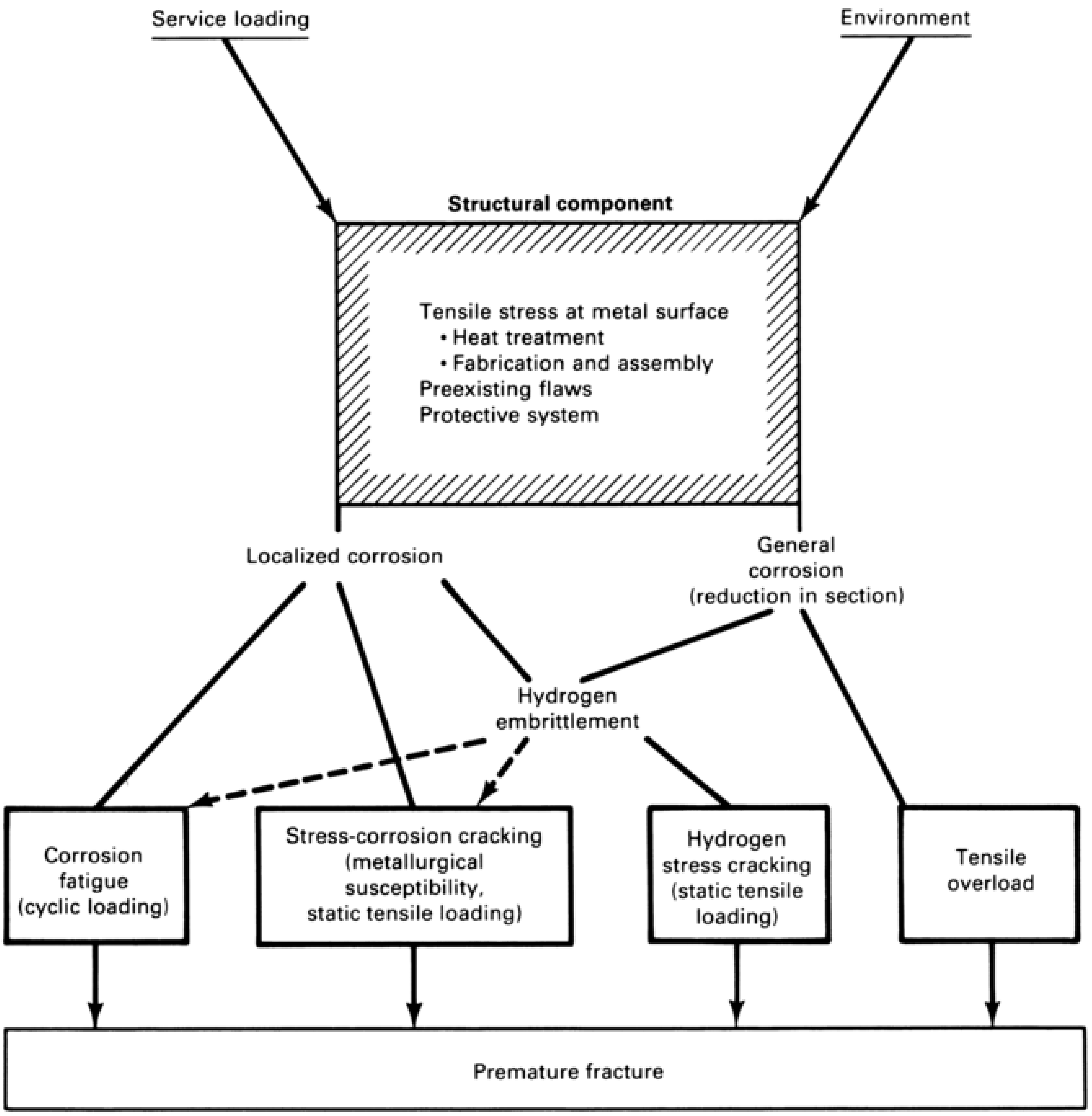

Fig. 1 Causes of premature fracture influenced by the corrosion of a structural component

The materials presented here are organized according to the following broad outline:

- General state-of-the-art
- Static loading of smooth specimens
- Static loading of precracked specimens
- Dynamic loading: slow-strain-rate testing
- Selection of test environments
- Appropriate tests for various alloy systems
- Interpretation of test results

B. Phull, Evaluating Stress-Corrosion Cracking, *Corrosion: Fundamentals, Testing, and Protection*, Vol 13A, *ASM Handbook*, ASM International, 2003, p 575–616

Evaluating Stress-Corrosion Cracking

Revised by Bopinder Phull, Consultant

Static Loading of Smooth Specimens

Tests for predicting the stress-corrosion performance of an alloy in a particular service application should be conducted with a stress system similar to that anticipated in service. Table 1 lists the numerous sources of sustained tension that are known to have initiated SCC in service and the applicable methods of stressing. Most of the SCC service problems involve tensile stresses of unknown magnitude that are usually very high. Tests that incorporate a high total strain are usually the most realistic in terms of duplicating service.

Table 1 Stressing methods applicable to various sources of sustained tension in service

Source of sustained tension in service	Constant strain	Constant load
Residual stress		
Quenching after heat treatment	X	…
Forming	X	…
Welding	X	…
Misalignment (fit-up stresses)	X	…
Interference fasteners	X	…
Interference bushings		
Rigid	X	…
Flexible	…	X
Flareless fittings	X	…
Clamps	X	…
Hydraulic pressure	X	X
Deadweight	…	X
Faying surface corrosion	X	X

Note: The greatest hazard arises when residual, assembly, and operating stresses are additive.

The results are strongly influenced by the mechanical aspects of the tests, such as method of loading and specimen size. These mechanical aspects can have variable effects on the initiation and propagation lifetimes and can influence estimates of a threshold stress. Therefore, an apparent threshold stress for SCC is not a material property, and threshold estimates must be qualified with regard to the test conditions and the significance level.

Constant-Strain versus Constant-Load Tests

Constant-strain (fixed-displacement) tests are widely used, primarily because a variety of simple and inexpensive stressing jigs can be devised. However, there is poor reproducibility of the exposure stress with some of these techniques. Therefore, sophisticated procedures have been developed to improve this facet of testing.

Constant-strain tests are sometimes called decreasing-load tests, because after the onset of SCC in small test specimens the gross section exposure stress decreases. This results from the opening of the crack (or cracks) under the high stress concentration at the crack tip (or tips) and causes some of the applied elastic strain to change to plastic strain, with an attendant reduction in the initial load (Ref 6, 7). Such trends in changing stress during crack growth are shown in Fig. 4.

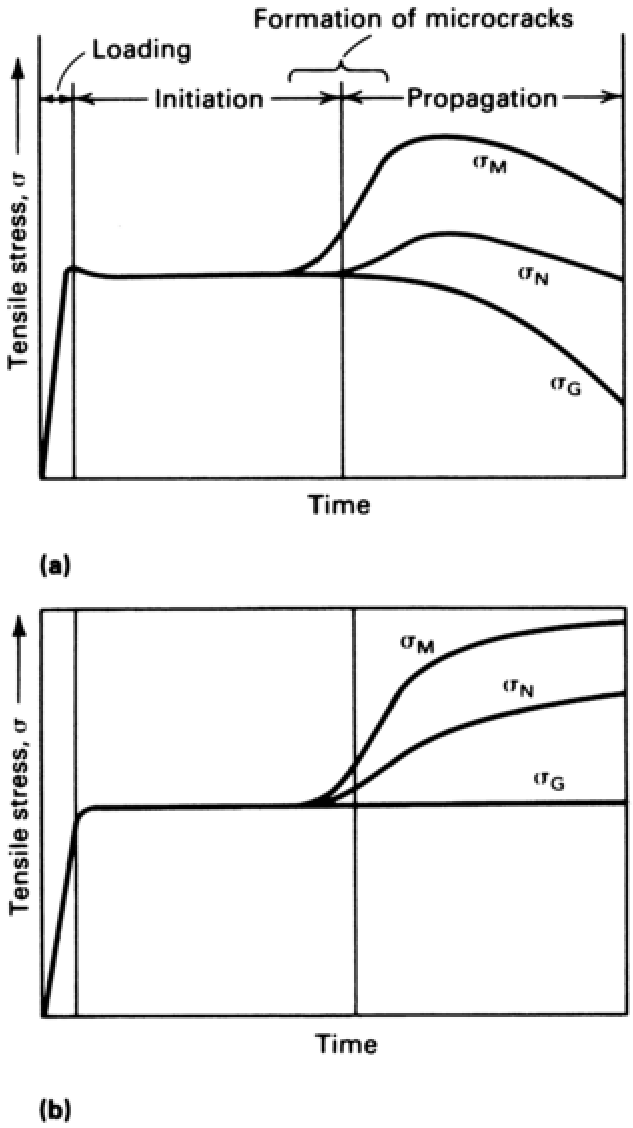

Fig. 4 Comparison of changing stress during initiation and growth of isolated SCC in constant-strain and constant-load tests of a uniaxially loaded tension specimen. (a) Constant-strain test. (b) Constant-load test. σ_M is the maximum stress at crack tip, σ_N is the average stress in the net section, and σ_G is the applied stress to the gross section. Source: Ref 7

Comparison of the stress trends for a constant- strain test (Fig. 4a) with those for a constant-load test (Fig. 4b) reveals that neither method of loading provides a constant-stress test after growth of microcracks has occurred. True constant-load (dead-load) tests result in increasing stress levels as cracking progresses and are more likely to lead to earlier failure with complete fracture and lower estimates of a threshold stress than constant-strain tests. Figures 4(a) and (b) illustrate basic trends that may be applied to all types of test specimens, including precracked specimens. Specific curves, however, will differ depending on other test conditions.

The stiffness of the combined stressing frame/ test specimen system can have a significant effect on materials evaluation if identical test procedures are not used (Ref 6). Many so-called constant-strain tests are not actually constant- strain tests, particularly if a spring is included in the stressing system, because a significant amount of elastic strain energy may be contained in the stressing system. Depending on the “softness” of the spring or the elasticity of the stressing jig, the stiffness (compliance) of the stressing system can be varied greatly between zero stiffness (dead load) and infinite stiffness (true constant total strain). Figure 5 shows the typical change in net section stress with the onset of SCC in an intermediate-stiffness stressing frame used in ASTM G 49 for loading direct-tension stress-corrosion test specimens (Ref 8).

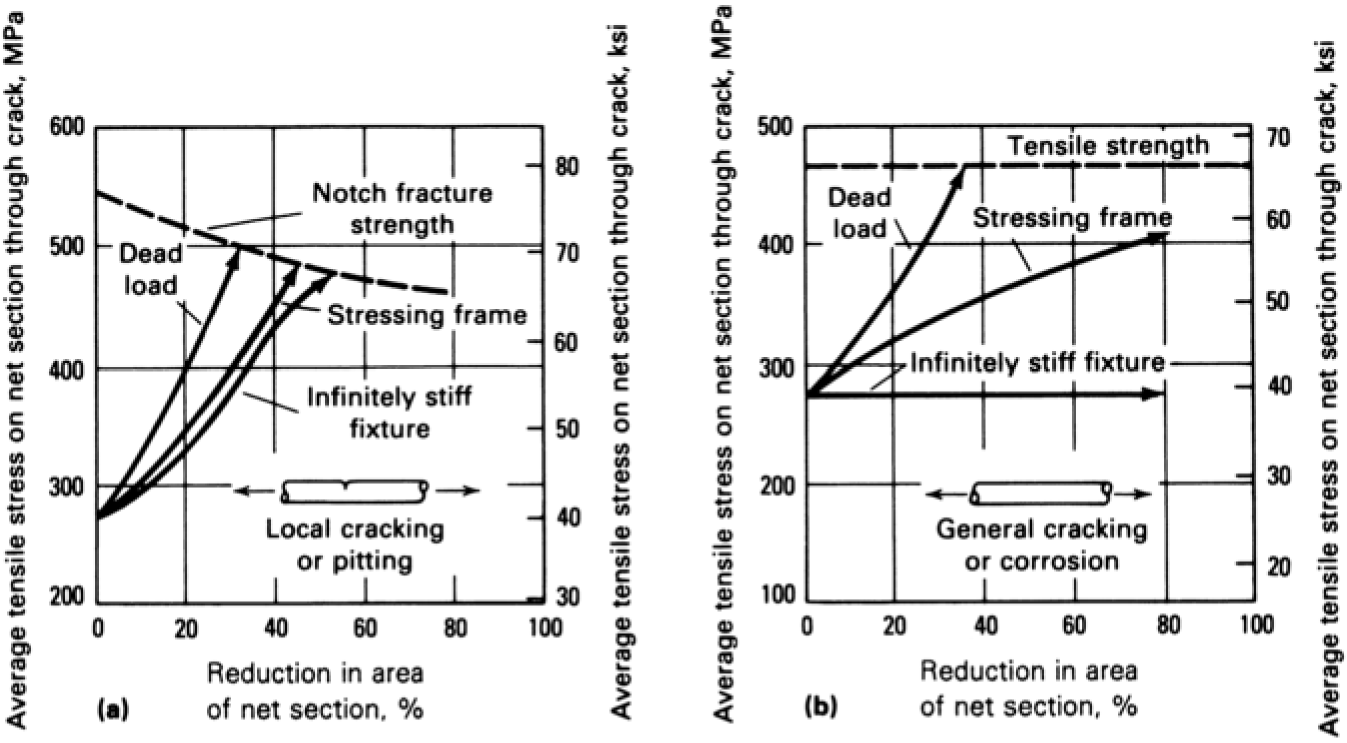

Fig. 5 Effect of loading method and extent of cracking or corrosion pattern on average net section stress in a uniaxially loaded tension specimen. Behavior is generally representative, but curves will vary with specific alloys and tempers. (a) Localized cracking. (b) General cracking. Source: Ref 8

The corrosion pattern on the test specimen, particularly the number and distribution of cracks, can impair the precision of results obtained by either constant-strain or constant-load tests. When isolated stress-corrosion cracks propagate in a specimen stressed by either method, the average tensile stress on the net section increases rapidly until the notch fracture strength is reached and the specimen breaks (Fig. 5a). Less penetration is required for fracture of specimens under dead load; this indicates that specimen life is shorter with lower-stiffness stressing frames. When microcracks initiate close to one another, their individual stress concentrations interact and are relaxed. Consequently, there may not be a sufficient stress concentration in the true constant-strain test to propagate further SCC, and the specimen will not break (Fig. 5b). Under a constant load, however, the growth of many cracks continues, and the specimen ultimately breaks.

With general cracking, crack propagation can be strongly influenced by frame stiffness. Therefore, SCC comparison of specimens tested at stress levels just above their thresholds is complicated by random variations in the cracking pattern, particularly when tested with a relatively stiff stressing system.

Although constant-load stressing appears to be advantageous for testing materials with relatively high resistance to SCC, difficulties arise when small-diameter specimens are utilized to avoid the use of massive loads or lever systems. In some test environments, highly stressed specimens may fail from general or pitting corrosion and an attendant increase in the effective stress. Such non-SCC failures complicate interpretation of test results, unless failure by SCC is confirmed by examination using a light microscope and/or a scanning electron microscope. Such extraneous failures are less likely to occur with specimens loaded under constant strain.

Therefore, small test specimens, which are generally preferred for laboratory screening tests and research studies, must be used with caution when estimates of serviceability are required. To determine serviceability, larger specimens should be used, and a stressing system should be selected that best duplicates the anticipated service conditions.

Bending versus Uniaxial Tension

Historically, the most extensively used stressing systems have incorporated constant-deformation specimens stressed by bending. This method is versatile because of the variety of simple techniques that can be used to test most metal products in all types of corrosive environments. The state of stress in a bend specimen, however, is

much more complex than in a tension specimen. Theoretically, tensile stress is uniform throughout the cross section in the tension specimen, except at corners in rectangular sections, but the tensile stress in bend specimens varies through the specimen thickness.

Tensile stress is at a maximum on the convex surface and decreases steeply to zero at the neutral axis. It then changes to a compressive stress, which reaches a maximum on the concave surface. Thus, only about 50% of the metal surface is under tension, and stress can vary from maximum to zero, depending on the stressing system. As SCC penetrates the metal, the stress gradient through the section thickness produces changes in stresses and strains that are different from those in a uniaxial tension specimen. This tendency yields significantly different SCC responses for the two types of stressing (Fig. 6).

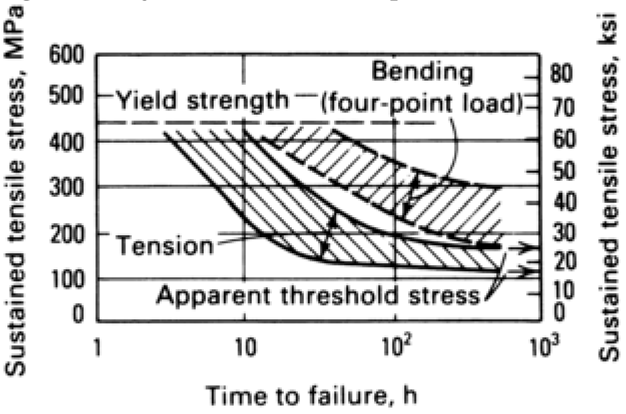

Fig. 6 Comparison of the SCC response with bending versus direct tension stressing under constant load for Al-5.3Zn-3.7Mg-0.3Mn-0.1Cr T6 temper alloy sheet. Tested to failure in 3% NaCl plus 0.1% H_2O_2. Source: Ref 9

Bending stress specimens experience other sources of variability in stress that are not present with direct tension stressing. Variations occur in the principal longitudinal stress across the width of the specimen as well as with the presence of biaxial stresses, both of which are influenced by the design of the specimen. Therefore, just as in the case of constant-load stressing, optimal control of stress and more severe testing conditions are provided by uniaxial tension stressing.

Statically loaded, smooth test specimens for SCC tests can be divided into three general categories: elastic-strain specimens, plastic-strain specimens, and residual-stress specimens. The commonly used specimen geometries for each of these categories are discussed in the sections that follow.

Elastic-Strain Specimens

To control the surface tensile stress applied by deformation loading, strain is usually restricted to the elastic range for the test material. The magnitude of the applied stress can then be calculated from the measured strain and modulus of elasticity. In constant-load stressing, the load typically is measured directly, and the stress is calculated by using the appropriate formula for the specimen configuration and the method of loading. Load cells or calibrated springs may be useful for applying and monitoring possible changes in load during the test. The commonly used types of specimens for tests under elastic- range stress are described in this section.

Bent-beam specimens can be used to test a variety of product forms. The bent-beam configuration is primarily used for sheet, plate, or flat extruded sections, which conveniently provide flat specimens of rectangular cross section, but it is also used for cast materials, rod, pipe, or machined specimens of circular cross section. This method is applicable to specimens of any metal that are stressed to levels less than the elastic limit of the material; therefore, the applied stress can be calculated or measured accurately (ASTM G 39, Ref 10; and ISO 7539-2, Ref 11).

Stress calculations by this method are not applicable to plastically stressed specimens. Bent- beam specimens are usually tested under constant-strain conditions, but constant-load conditions can also be used. In either case, local changes in the curvature of the specimen when cracking occurs result in changes in stress and strain during crack propagation. The “test stress” is taken as the highest surface tensile stress existing at the start of the test, that is, before the initiation of SCC.

Several configurations of bent-beam specimens and stressing systems are illustrated in Fig. 7 and are described in detail in ASTM G 39 (Ref 10) and in ISO 7539-2 (Ref 11). When specimens are tested at elevated temperatures, the possibility of stress relaxation should be investigated.

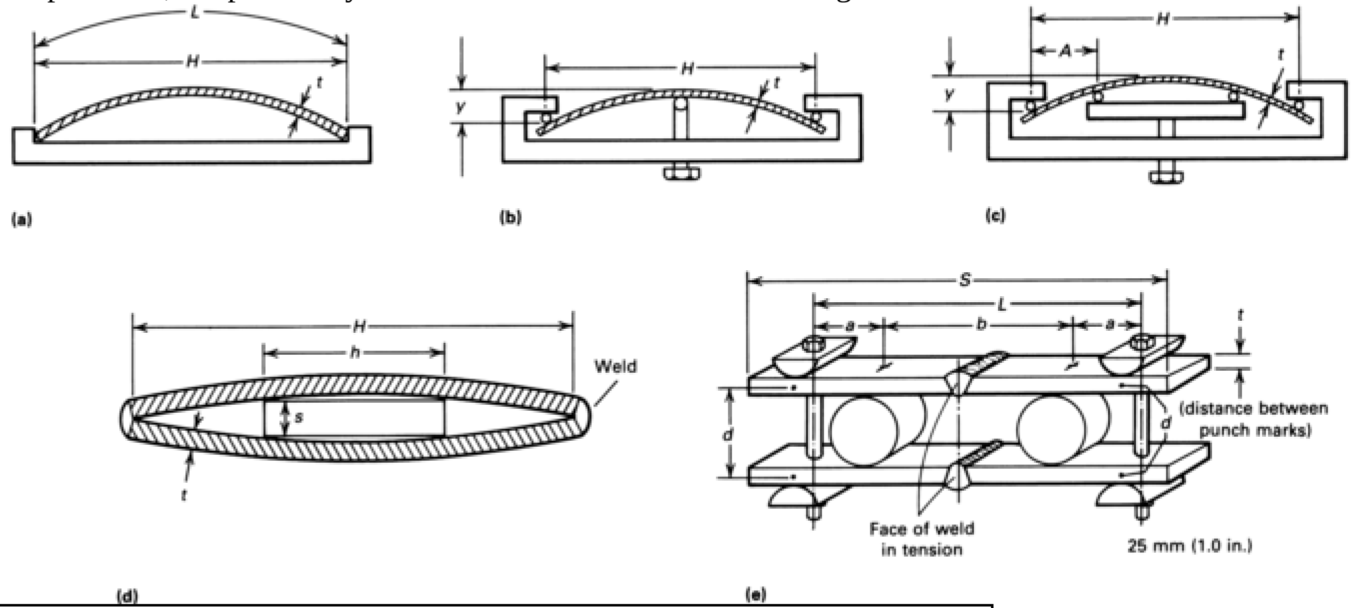

Bolt loaded double-beam specimen dimensions for various plate thicknesses									
t		***a***		***b***		***L***		***S***	
mm	in.	mm	in.	mm	in.	mm	in.	mm	in.
3.2	0.125	100	4.0	50	2.0	250	10.0	305	12.0
6.4	0.25	100	4.0	50	2.0	250	10.0	305	12.0
9.5	0.375	120	4.75	90	3.5	330	13.0	380	15.0
13	0.5	120	4.75	90	3.5	330	13.0	380	15.0
19	0.75	140	5.5	150	6.0	430	17.0	480	19.0
25	1.0	150	6.0	200	8.0	510	20.0	560	22.0
38	1.5	165	6.5	305	12.0	635	25.0	685	27.0

Fig. 7 Specimen and holder configurations for bent-beam stressing. (a) Two-point loaded specimen. (b) Three-point loaded specimen. (c) Four-point loaded specimen. (d) Welded double-beam specimen. (e) Bolt-loaded double-beam specimen. Formula for stressing specimen (e): $\Delta d = 2fa/3Et(3L - 4a)$, where Δd is deflection (in inches), f is nominal stress (in pounds per square inch), and E is modulus of elasticity (in pounds per square inch). Source: Ref 12

Two-point loaded specimens can be used for materials that do not deform plastically when bent to $(L - H)/H = 0.01$. The specimens should be approximately 25 × 250 mm (1 × 10 in.) flat strips cut to appropriate lengths to produce the desired stress after bending, as shown in Fig. 7(a). The maximum stress occurs at the midlength of the specimen and decreases to zero at specimen ends.

Three-point loaded specimens are flat strips that are typically 25 to 51 mm (1 to 2 in.) wide and 127 to 254 mm (5 to 10 in.) long. The thickness of a specimen is usually dictated by the mechanical properties of the material and the available product form. The specimen should be supported at the ends and bent by forcing a screw (equipped with a ball or knife-edge tip) against it at a point halfway between the end supports, as shown in Fig. 7(b). In a three-point loaded specimen, the maximum stress occurs at the midlength of the specimen and decreases linearly to zero at the outer supports.

Two- and four-point loaded specimens are often preferred over the three-point loaded specimen, because crevice corrosion often occurs at the central support of the three-point loaded specimen. Because this corrosion site is very close to the point of highest tensile stress, it may cathodically protect the specimen and prevent possible crack formation, or it may cause hydrogen embrittlement. Furthermore, the pressure of the central support at the point of highest load introduces biaxial stresses at the area of contact and can introduce tensile stresses where compressive stresses are normally present.

Four-point loaded specimens are flat strips that are typically 25 to 51 mm (1 to 2 in.) wide and 127 to 254 mm (5 to 10 in.) long. The thickness of a specimen is usually dictated by the mechanical properties of the material and the available product form. The specimen is supported at the ends and is bent by forcing two inner supports against it, as shown in Fig. 7(c). The two inner supports are located symmetrically around the midpoint of the specimen.

In a four-point loaded specimen, the maximum stress occurs between the contact points of the inner supports; the stress is uniform in this area. From the inner supports, the stress decreases linearly toward zero at the outer supports. The four-point loaded specimen is preferred over the three-point and two-point loaded specimens, because it provides a large area of uniform stress.

Welded double-beam specimens consist of two flat strips 25 to 51 mm (1 to 2 in.) wide and 127 to 254 mm (5 to 10 in.) long. The strips are bent against each other over a centrally located spacer until both ends touch. The strips are held in position by welding the ends together, as shown in Fig. 7(d).

In a welded double-beam specimen, the maximum stress occurs between the contact points of the spacer; the stress is uniform in this area. From contact with the spacer, the stress decreases linearly toward zero at the ends of the specimen, similar to a four-point loaded specimen.

A bolt-loaded double-beam specimen is shown in Fig. 7(e), along with suggested specimen dimensions for various thicknesses of plate and the formula for stressing such specimens (Ref 12). The beam deflections required to develop the intended tensile stress are calculated with the formula and are then applied by bolting the ends of the beams together. The deflections are measured with a dial gage to within ±0.0127 mm (±0.0005 in.). Thus, the error in stress application—if the beams are of homogeneous material and if the cross sections are uniform—is within 2%. The precision of the deflection measurement is within 0.5%, and the error in determining the modulus of elasticity, *E*, is within 1%.

Constant-moment beam specimens are designed such that a constant moment exists from one end to the other when the specimen is bent in the manner shown in Fig. 8 (Ref 13). This bending produces equal stress along the length of the specimen. The width-to-thickness ratio is less than 4 so that biaxial stresses are eliminated.

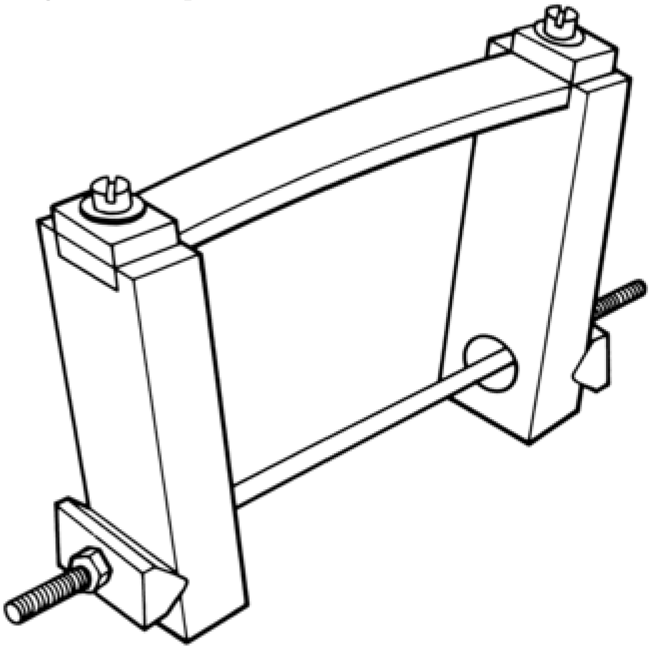

Fig. 8 Bent beam designed to produce pure bending. Source: Ref 13

This type of specimen offers the advantage of a relatively large area of material under a uniform stress. Such specimens can be used when the dimensions of the specimen are too small for other bent-beam specimens—for example, when specimens are taken in the short-transverse direction in plate (see Fig. 9c). The elastic stress σ in the convex surface is calculated by using:

$$\sigma = \frac{4Ety}{h^2} \quad \text{(Eq 1)}$$

where *h* is the distance between inner edges of the supports, *y* is the maximum deflection between inner edges of the supports, *t* is the thickness of the specimen, and *E* is the modulus of elasticity.

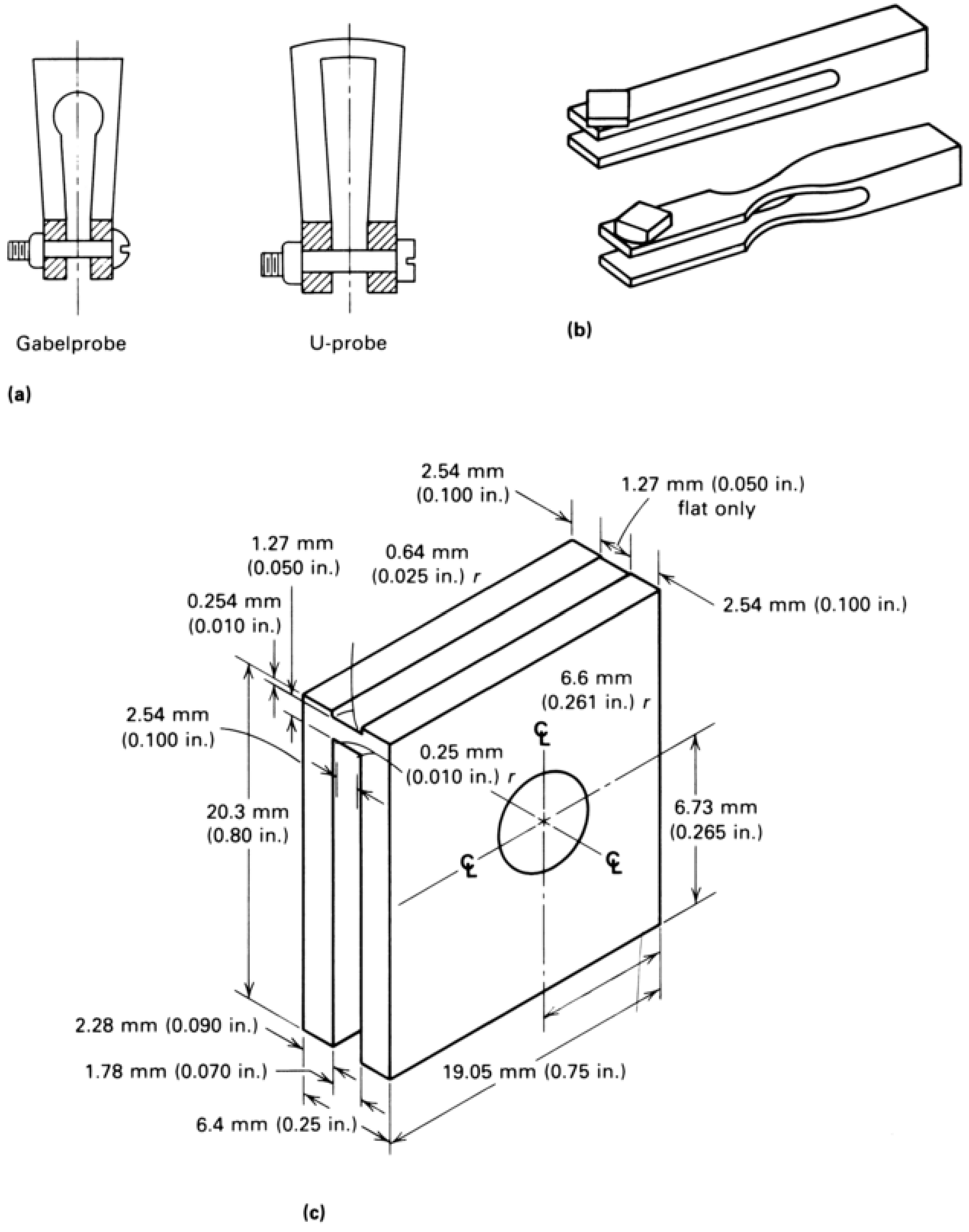

Fig. 9 Typical tuning-fork SCC test specimens. (a) Source: Ref 24. (b) Source: Ref 1. (c) Source: Ref 25

C-Ring Specimens. As discussed in ASTM G 38 (Ref 14), the C-ring is a versatile, economical specimen for quantitatively determining the susceptibility to SCC of all types of alloys in a wide variety of product forms. It is particularly well suited for testing tubing and for making short- transverse tests on various product forms, as shown in Fig. 10. The sizes of C-rings can be varied over a wide range, but rings with outside diameters less than about 16 mm ($\frac{5}{8}$ in.) are not recommended because of increased difficulties in machining and decreased precision in stressing. The C-ring specimen is also covered by ISO 7539-5 (Ref 15).

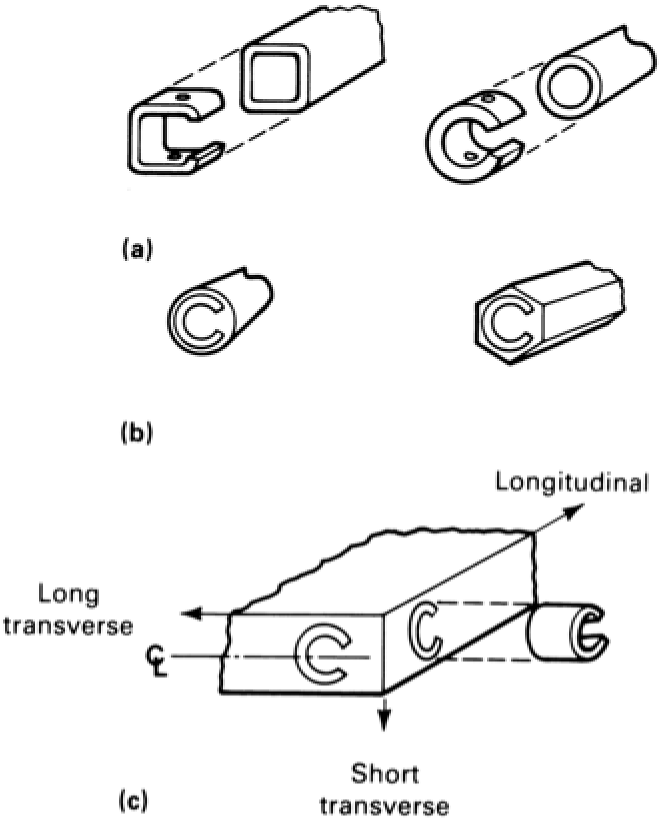

Fig. 10 Sampling procedure for testing various products with C-rings. (a) Tube. (b) Rod and bar. (c) Plate Source: Ref 14

The C-ring is typically a constant-strain specimen with tensile stress produced on the exterior of the ring by the tightening of a bolt centered on the diameter of the ring. However, an almost constant load can be developed by placing a calibrated spring on the loading bolt. C-rings can also be stressed in the reverse direction by spreading the ring and creating a tensile stress on the inside surface. These methods of stressing are shown in Fig. 11.

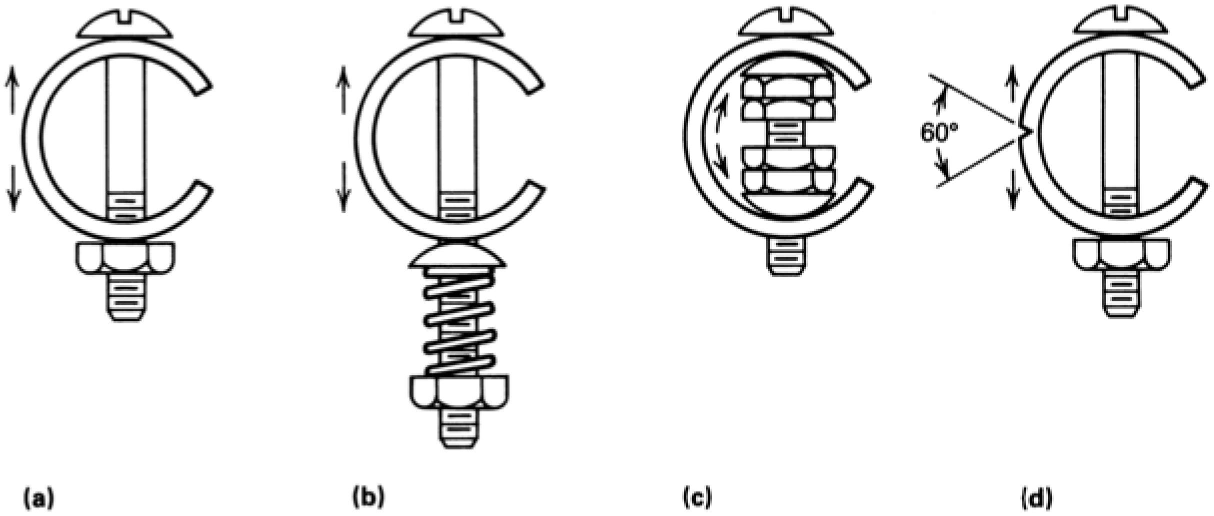

Fig. 11 Methods of stressing C-rings. (a) Constant strain. (b) Constant load. (c) Constant strain. (d) Notched C-ring; a similar notch could be used on the side of (a), (b), or (c). Source: Ref 14

Circumferential stress is of principal interest in the C-ring specimen. This stress is not uniform (Ref 16), as discussed previously in the section "Elastic-Strain Specimens" in this article. The stress varies around the circumference of the C-ring from zero at each bolt hole to a maximum at the middle of the arc opposite the stressing bolt. In a notched C-ring, a triaxial stress state is present adjacent to the root of the notch (Ref 17). For

all notches, the circumferential stress at the root of the notch is greater than the nominal stress and can generally be expected to be in the plastic range.

Generally, the C-ring can be stressed with high precision. The most accurate stressing procedure consists of attaching circumferential and transverse electrical strain gages to the surface stressed in tension, followed by tightening the bolt until the strain measurements indicate the desired circumferential stress.

The amount of compression required on the C-ring to produce elastic straining and the degree of elastic strain can be predicted theoretically. Therefore, C-rings can be stressed by calculating the deflection required to develop a desired elastic stress (ASTM G 38) (Ref 14). In notched specimens, a nominal stress is estimated using a ring outside diameter measured at the root of the notch and by taking into consideration the stress-concentration factor, K_t, for the specific notch.

O-ring specimens (Fig. 12) are used to develop a hoop stress in a particular part—for example, a cylindrical die forging in which a critical end-grain structure associated with the parting plane of the forging exists only at the surface of the forging. A relatively large surface area of metal is placed under a uniform tensile stress, and the O-ring stressing plug assembly simulates service conditions in structures containing interference-fit components. Stressed O- rings have also been used to evaluate protective treatments for the prevention of SCC (Ref 18).

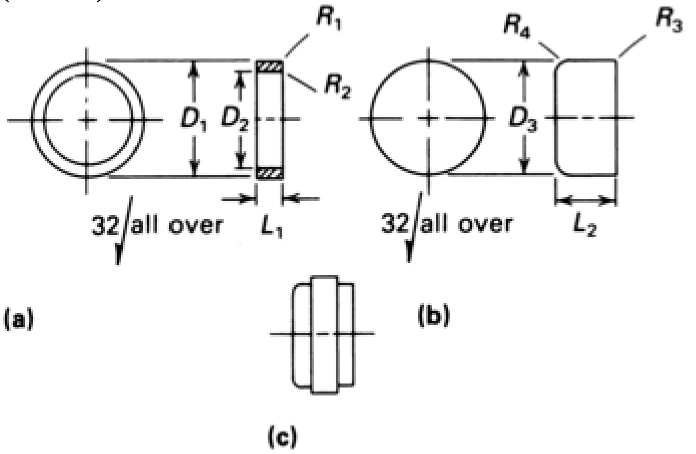

Fig. 12 O-ring SCC test specimen (a) and stressing plug (b). The O-ring is stressed by pressing it onto the plug, as shown in (c).

An O-ring is stressed by pressing it onto an oversized plug that is machined to a predetermined diameter to develop the desired stress at the outside surface of the ring. The nominal dimensions of this specimen can be varied to suit the part being tested, but certain characteristics should be observed to achieve adequate control of the stresses. The ring width should not be more than four times the wall thickness in order to ensure maximum uniformity of the hoop stress from the centerline to the edges of the ring. The tensile stress varies through the thickness of the ring and is highest at the inside surface. Interference required for stressing an O-ring can be calculated by using:

$$I = \frac{F(OD)^2}{E(ID)} \quad \text{(Eq 2)}$$

where I is the interference (on the diameter) between the O-ring and the plug, E is the modulus of elasticity, ID is the inside diameter, OD is the outside diameter, and F is the circumferential stress desired on the outside surface. Additional information regarding the design and stressing of O-ring specimens is given in Ref 19.

Tension Specimens. Specimens used to determine tensile properties in air are well suited and easily adapted to SCC, as discussed in ASTM G 49 (Ref 8) and ISO 7539-4 (Ref 20). When uniaxially loaded in tension, the stress pattern is simple and uniform, and the magnitude of the applied stress can be accurately determined. Specimens can be quantitatively stressed by using equipment for application of either a constant load, a constant strain, or an increasing load or strain.

This type of test is one of the most versatile methods of SCC testing because of the flexibility permitted in the type and size of the test specimen, the stressing procedures, and the range of stress level. It allows the simultaneous exposure of unstressed specimens (no applied load) with stressed specimens and subsequent tension testing to distinguish between the effects of true SCC and mechanical overload.

A wide range of test specimen sizes can be used, depending primarily on the dimensions of the product to be tested. Stress-corrosion test results can be significantly influenced by the cross section of the test specimen. Although large specimens may be more representative of most structures, they often cannot be prepared from the available product forms being evaluated. They also present more difficulties in stressing and handling in laboratory testing.

Smaller cross-sectional specimens are widely used. They have a greater sensitivity to SCC initiation, usually yield test results rapidly, and permit greater convenience in testing. However, the smaller specimens are more difficult to machine, and test results are more likely to be influenced by extraneous stress concentrations resulting from nonaxial loading, corrosion pits, and so on. Therefore, use of specimens less than about 10 mm (0.4 in.) in gage length and 3 mm (0.12 in.) in diameter is not recommended, except when testing wire specimens.

Tension specimens containing machined notches can be used to study SCC and hydrogen embrittlement. The presence of a notch induces a triaxial stress state at the root of the notch, in which the actual stress will be greater by a concentration factor that is dependent on the notch geometry. The advantages of such specimens include the localization of cracking to the notch region and acceleration of failure. However, unless directly related to practical service conditions, the results may not be relevant.

Tension specimens can be subjected to a wide range of stress levels associated with either elastic or plastic strain. Because the stress system is intended to be essentially uniaxial (except in the case of notched specimens), great care must be exercised in the construction of stressing frames to prevent or minimize bending or torsional stresses.

The simplest method of providing a constant load consists of a deadweight hung on one end of the specimen. This method is particularly useful for wire specimens. For specimens of larger cross section, however, lever systems such as those used in creep-testing machines are more practical. The primary advantage of any deadweight loading device is the constancy of the applied load.

A constant-load system can be modified by the use of a calibrated spring, such as that shown in Fig. 13. The proving ring, as used in the calibration of tension testing machines, has also been adapted to SCC testing to provide a simple, compact, easily operated device for applying axial load (Fig. 14). The load is applied by tightening a nut on one of the bolts and is determined by carefully measuring the change in ring diameter.

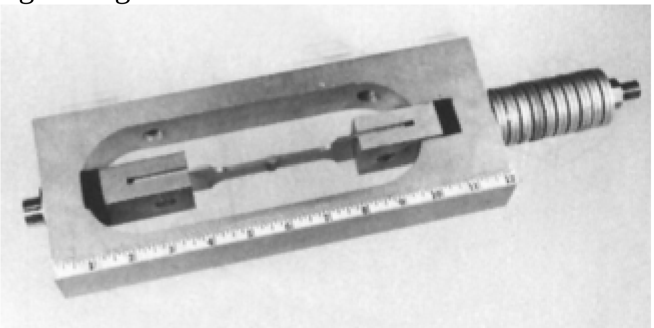

Fig. 13 Spring-loaded fixture used to stress 3.2 mm (0.125 in.) thick sheet tensile specimens in direct tension. Source: Ref 12

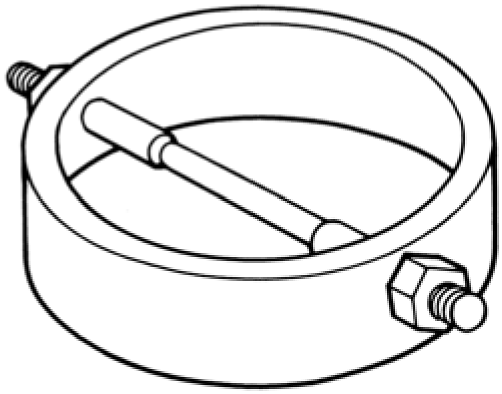

Fig. 14 Ring-stressed tension specimen for field testing. Source: Ref 1

Constant-strain SCC tests are performed in low-compliance tension-testing machines. The specimen is loaded to the required stress level, and the moving beam is then locked in position. Other laboratory stressing frames have been used, generally for testing specimens of smaller cross section. Figure 15(a) shows an exploded view of such a stressing frame, and Fig. 15(b) illustrates a special loading device developed to ensure axial loading with minimal torsion and bending of the specimen.

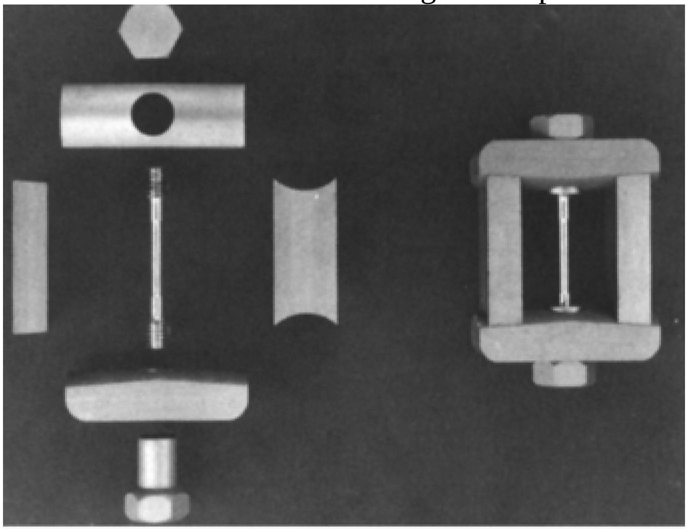

(a)

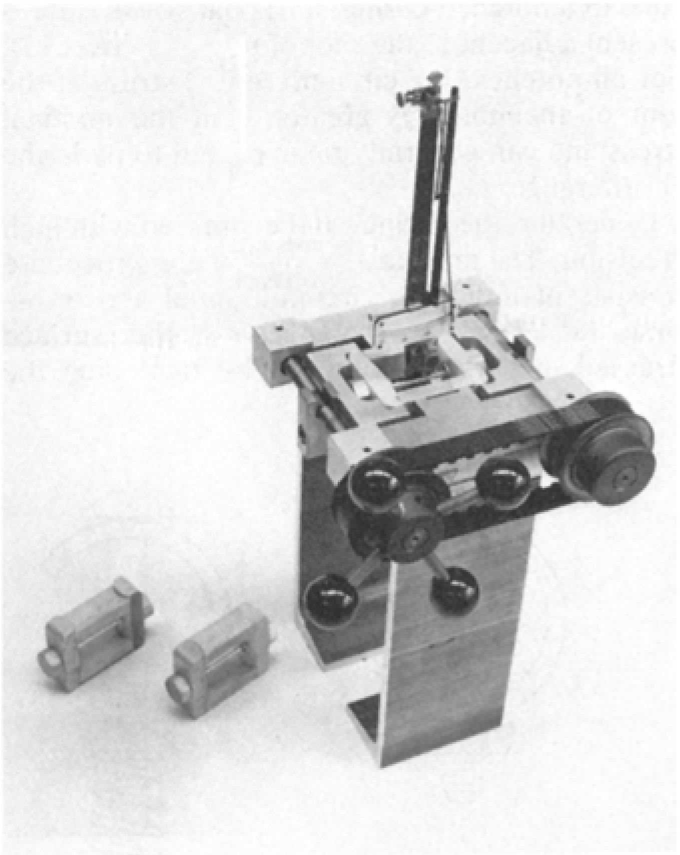

(b)

Fig. 15 Equipment for constant-strain SCC testing. (a) Constant-strain SCC testing frame. Exploded view (left) showing the 3.2 mm (0.125 in.) diam tension specimen and various parts of the stressing frame. Final stressed assembly (right). Source: Ref 21. (b) Synchronous loading device used to stress specimens. The specimen is loaded to a prescribed strain value determined from a clip-on gage. The applied stress is given by the product of the strain and the material elastic modulus. A stressed assembly and one assembled finger-tight ready for stressing are shown.

For stressing frames that do not contain any mechanism for the measurement of load, the stress level can be determined from measurement of the strain. However, only when the intended stress is below the elastic limit of the test material is the average linear stress (σ) proportional to the average linear strain (ε), $\sigma/\varepsilon = E$, where E is the modulus of elasticity.

When tests are conducted at elevated temperatures with constant-strain loaded specimens, consideration should be given to the possibility of stress relaxation. When stress relaxation or creep occurs in the test specimen, some of the elastic strain is converted to plastic strain and the nominal applied test stress is reduced. This effect is particularly important when the coefficients of thermal expansion are different for the specimen and stressing frame. Frequently, nonmetallic (plastic) insulators are used between the specimen and stressing frame to avoid galvanic action. If such plastic insulators are part of the stress-bearing system, creep (even at room temperature) can significantly alter the applied load on the specimen.

Even though eccentricity in loading can be minimized to levels acceptable for tension-testing machines, tensile stress around the circumference of round specimens and at the corners of sheet-type specimens varies to some extent. Several factors may introduce bending moments on specimens, such as longitudinal curvature and misalignment of threads on threaded-end round specimens. These factors have a greater effect on specimens with smaller cross sections. Tests should be made on specimens with strain gages affixed to the specimen surface around the circumference of 90° or 120° intervals to verify strain and stress uniformity and to determine if machining practices and stressing jigs are of adequate tolerance and quality.

When SCC occurs, it generally results in complete fracture of the specimen, which is easy to detect. However, when testing relatively ductile materials at stress levels close to the threshold of susceptibility, fracture may not occur during the period of exposure. The presence of SCC in such cases must be determined by mechanical tests or by metallographic examination, as discussed previously.

To study trends in SCC susceptibility, such as in alloy development research, it is often necessary to detect small differences in susceptibility. For this purpose, it is advantageous to use replicate sets of specimens stressed at several levels, including zero applied stress. The sets are then removed for metallographic examination or tension tests after appropriate periods of exposure.

Figure 16 illustrates the use of this procedure with samples of 7075 aluminum alloy that have been given different thermal treatments to decrease susceptibility to SCC. Analysis of these breaking stress data by extreme value statistics enables calculation of survival probabilities and the estimation of a threshold stress, without depending on failures during exposure. By using an elastic-plastic fracture mechanics model, an effective flaw size is calculated from the mean breaking stress, the strength, and the fracture toughness of the test material. The effective flaw size corresponds to the weakest link in the specimen at the time of the tension test, and it therefore represents the maximum penetration of the SCC. An advantage to using flaw depth to examine SCC performance is that the effects of specimen size and alloy strength and toughness can be normalized. In contrast, the specimen lifetime and breaking strength are biased by those mechanical (non-SCC) factors.

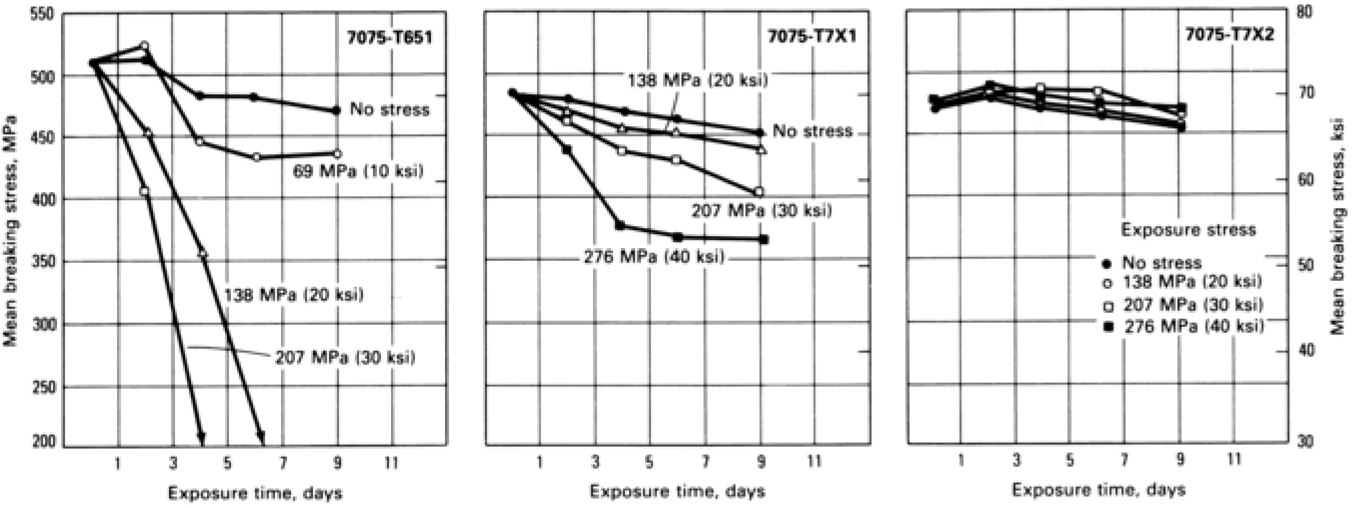

Fig. 16 Mean breaking stress versus exposure time for short-transverse 3.2 mm (0.125 in.) diam aluminum alloy 7075 tension specimens tested according to ASTM G 44 at various exposure stress levels. Each point represents an average of five specimens. Source: Ref 3

Mean trends in the 207 MPa (30 ksi) exposure data for the three temper variants of aluminum alloy 7075 examined in Fig. 16 are shown in Fig. 17. These results clearly illustrate that the thermal treatments used to reduce the SCC susceptibility of the 7075-T651 decreased the SCC penetration (Ref 22). The equivalent performance of the 7075-T7X1 3.2 and 5.7 mm (0.125 and 0.225 in.) diam specimens is evident. In contrast, Fig. 18 shows the specimen biases in SCC ratings obtained by traditional pass-fail methods (Ref 23).

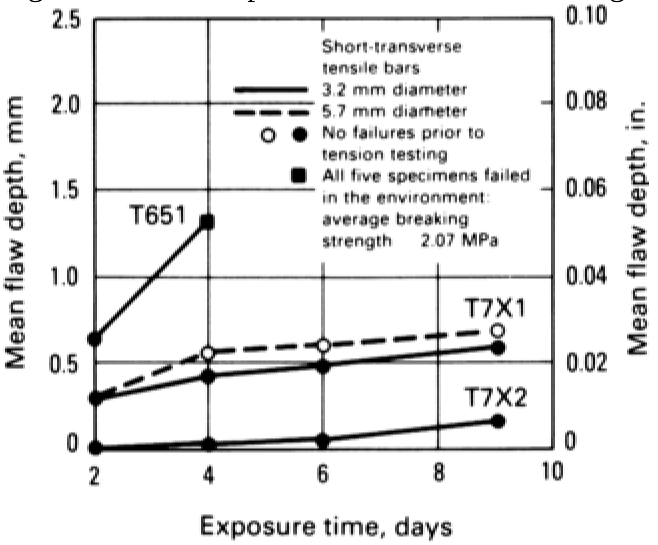

Fig. 17 Effect of temper on SCC performance of aluminum alloy 7075 subjected to alternate immersion in 3.5% NaCl solution at a stress of 207 MPa (30 ksi). Mean flow depth was calculated from the average breaking strength of five specimens subjected to identical conditions. Source: Ref 22

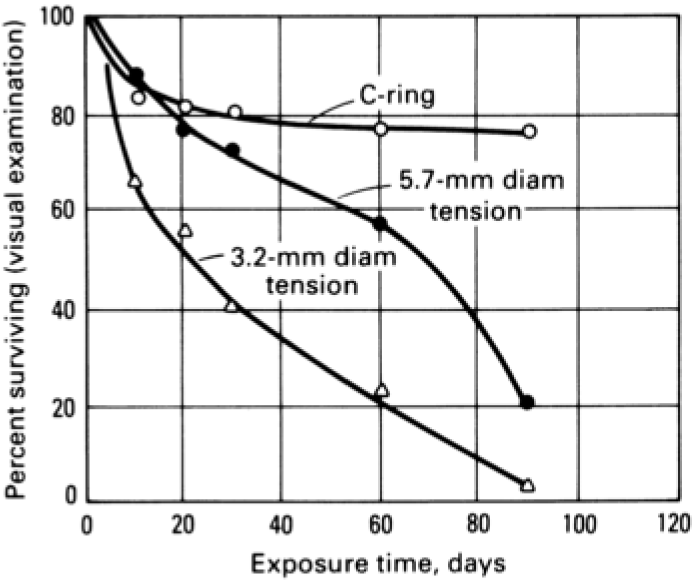

Fig. 18 Influence of specimen configuration on SCC test performance (alternate immersion in 3.5% sodium chloride per ASTM G 44). Aluminum alloy 7075-T7X51 specimens stressed 310 MPa (45 ksi); each point represents 60 to 90 specimens. Source: Ref 23

Tuning-fork specimens are special-purpose specimens with numerous modifications (Fig. 9). In Europe, the metal is strained into the plastic range, and stresses and strains are usually not measured (Ref 24, 26). In the United States, however, these specimens have been used with measured strains in the elastic and plastic ranges. Specimens of the type shown in Fig. 9(b) are convenient when a small self-contained specimen is required that will afford some insight into the applied stresses. Such a specimen is particularly well suited for testing thin plate material in the longitudinal or long-transverse direction while keeping the original mill-finished surface intact.

Tuning-fork specimens are stressed by closing the specimen tines and restraining them in the closed position with a bolt placed at the tine ends. The amount of closure is determined from Eq 3, which was derived from the data obtained with strain gages placed at the base of the tines on calibration specimens (Ref 1):

$$S = A\,\Delta x t \qquad \text{(Eq 3)}$$

where S is the maximum tension stress in the outer fiber of either tine, A is the calibration constant, Δx is the total amount of closure at the tine ends, and t is the thickness of the tines.

The stress on tuning forks with straight tines is greatest in a small area at the base of the tines. In tuning forks with tapered tines, the maximum stress extends uniformly along the tapered section. Tuning forks must be given the same consideration with regard to biaxial stresses as other flexurally loaded specimens.

The miniature tuning fork shown in Fig. 9(c) was devised to conduct short-transverse tests on sections that are too thin for tensile specimens or C-rings to be obtained (Ref 25). As with other tuning-fork specimens, the relationship between strain on the grooved surface and the deflection at the ends of the legs can be determined through the use of strain gages.

Plastic-Strain Specimens

Many accelerated SCC tests are performed with plastically deformed specimens, because these specimens are simple and economical to manufacture and use. These specimens are convenient for multiple replication tests of self- stressed (fixed-deflection) specimens in all environments. Because they usually contain large amounts of elastic and plastic strain, they provide one of the most severe tests available for smooth SCC test specimens.

Generally, the stress conditions are not known precisely. However, the anticipated high level of stress can be obtained consistently only if the precautions described for each type of specimen are observed. Another consideration is that the cold work required to form the test specimen can change the metallurgical condition and the SCC behavior of certain alloys.

Tests of this type are primarily used as screening tests to detect large differences between the SCC resistance of one alloy in several environments, one alloy in several metallurgical conditions in a given environment, and different alloys in the same environment. These tests are sometimes claimed to be too severe and therefore unsuitable for many applications, but the stress conditions are nevertheless representative of the high locked-in fabrication and assembly stresses frequently responsible for SCC in service.

U-bend specimens are rectangular strips bent approximately 180° around a predetermined radius and maintained in this plastically (and elastically) deformed condition during the test. Standardized test methods for this type of specimen are described in ASTM G 30 (Ref 27) and ISO 7539-3 (Ref 28). Bends slightly less than or greater than 180° are also used, but the term U- bend is generally applied to test specimens that are bent beyond their elastic limits. Figure 19 illustrates typical U-bend configurations showing several different methods of maintaining the applied stress.

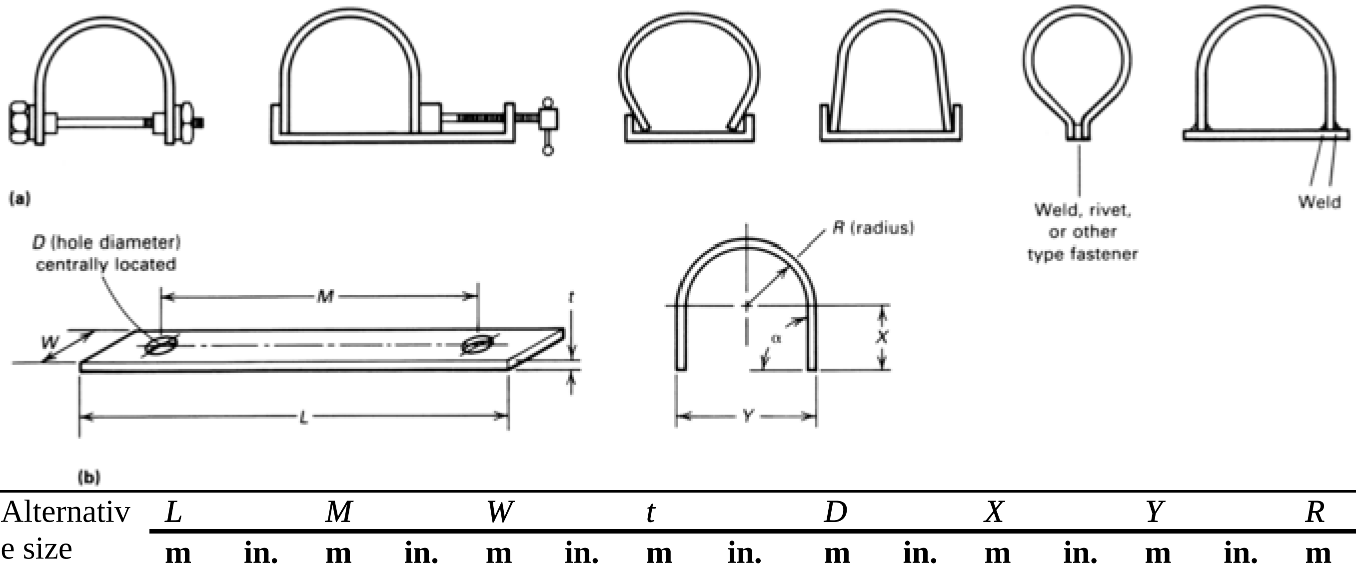

Alternative size	*L*		*M*		*W*		*t*		*D*		*X*		*Y*		*R*	
	mm	**in.**	**mm**	**in.**	**mm**	**in.**	**mm**	**in.**	**mm**	**in.**	**mm**	**in.**	**mm**	**in.**	**mm**	**in.**
A	80	3.2	50	2.0	20	0.8	2.5	0.098	10	0.4	32	1.26	14	0.55	5	0.2

B	100	4.0	90	3.5	9	0.35	3.0	0.12	7	0.28	25	0.98	38	1.50	16	0.6
C	120	4.7	90	3.5	20	0.8	1.5	0.06	8	0.31	35	1.4	35	1.4	16	0.6
D	130	5.1	100	4.0	15	0.6	3.0	0.12	6	0.24	45	1.77	32	1.26	13	0.51
E	150	5.9	140	5.5	15	0.6	0.8	0.03	3	0.12	61	2.40	20	0.8	9	0.35
F	310	12.2	250	9.8	25	0.98	13.0	0.51	13	0.51	105	4.13	90	3.5	32	1.26
G	510	20.1	460	18.1	25	0.98	6.5	0.26	13	0.51	136	5.35	165	6.5	76	3.0

Note: α = 1.57 rad

Fig. 19 Typical U-bend SCC specimens. (a) Various methods of stressing U-bends. (b) Typical U-bend specimen dimensions. Source: Ref 27

U-bend specimens can be used for all materials sufficiently ductile to be formed into a U- configuration without cracking. A U-bend specimen is most easily made from strips of sheet, but specimens can be machined from plate, bar, wire, castings, and weldments. Of primary interest in U-bend specimens is circumferential stress, which is not uniform, as discussed previously in the section on “Bent-Beam Specimens” in this article. Stress distribution in the U- bend specimen is discussed in detail in Ref 29.

A good approximation of applied strain ε can be obtained by:

$$\varepsilon = \frac{t}{2R} \text{ when } t < R \qquad \text{(Eq 4)}$$

where *t* is the specimen thickness, and *R* is the radius of curvature at the point of interest. Knowledge of the stress-strain curve is necessary to determine the stress. When a U-bend specimen is formed, the material in the outer fibers of the bend is strained into the plastic portion of the true-stress/true-strain curve, such as in section AB in Fig. 20(a). Several other stress-strain relationships that can exist in the outer fibers of a stressed U-bend test specimen are shown in Fig. 20(b) through (e). The actual relationship obtained depends on the method of stressing used.

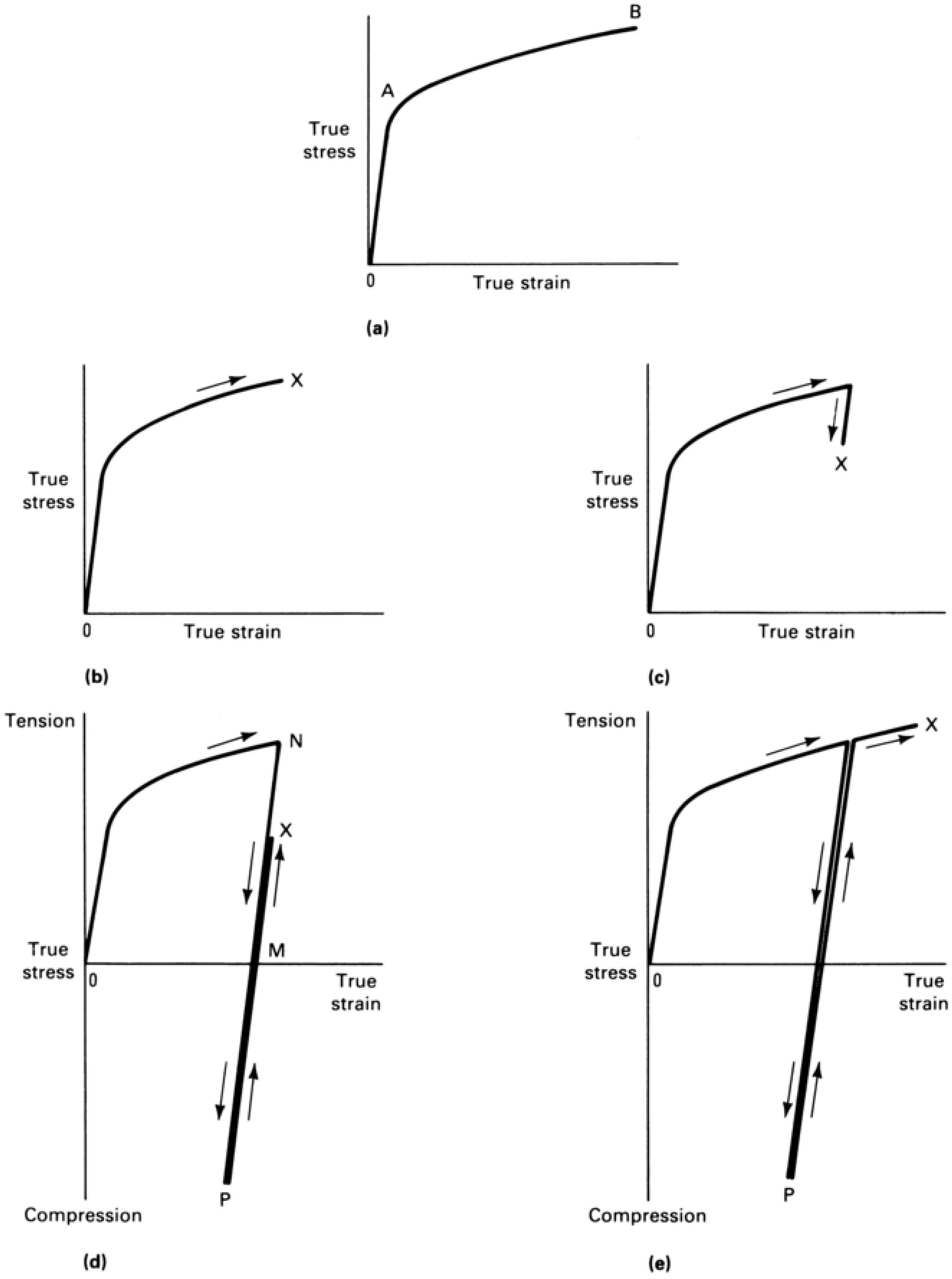

Fig. 20 True-stress/true-strain relationships for stressed U-bends. See text for discussion of (a) to (e). Source: Ref 27

Stressing is usually achieved by a one- or two- stage operation. Single-stage stressing is accomplished by bending the specimen into shape and maintaining it in that shape. The two types of stress conditions that can be obtained by single- stage stressing are defined by point X in Fig. 20(b) and (c). In Fig. 20(c), some elastic-strain relaxation has occurred by allowing the U-bend legs to spring back slightly at the end of the stressing sequence.
Two-stage stressing involves forming the approximate U-shape and then allowing the elastic strain to relax completely before the second stage of applying the test stress. The applied test strain can be a percentage (from 0 to 100%) of the tensile elastic strain that occurred during preforming (Fig. 20d) or can involve additional plastic strain (Fig. 20e). The convex specimen surface is stressed in tension in the region 0NM (Fig. 20d), and the concave surface is in compression. In the region MP, the situation is reversed; that is, compression is on the convex surface, and tension is on the concave surface.
The slope MN of the curve shown in Fig. 20(d) is steep. Therefore, it is often difficult to apply reproducibly a constant percentage of the total elastic prestrain, and the specimen surface may remain under compressive stress. Accordingly, the stress conditions in Fig. 20(b) and (e) are recommended because they result in a more severe test (that is, higher applied stress). Thus, the final applied strain prior to testing consists of plastic and elastic strain. To achieve the conditions illustrated in Fig. 20(b) and (e), springback of the U-bend legs after achieving the final plastic strain must be avoided. For materials with relatively low creep resistance, there will be some strain relaxation. It is important that the net residual stress be tensile. Compressively stressed surfaces are not normally prone to SCC. In fact, shot peening is a practical method for mitigating SCC by imparting a residual compressive stress on the metal surface before exposure to the service environment.

Residual-Stress Specimens

Most industrial SCC problems are associated with residual tensile stresses developed in the metal during such processes as heat treatment, fabrication, and welding. Therefore, residual- stress specimens simulating anticipated service conditions are useful for assessing the SCC performance of some materials in particular structures and in specific environments.
Plastic Deformation Specimens. Residual stresses resulting from such fabricating operations as forming, straightening, and swaging that involve localized plastic deformation at room temperature can exceed the elastic limit of the material. Examples of specimens of this type that have been used are shown in Fig. 21 and 22. Other specimen types used include panels with sheared edges, punched holes, or stamped identification numbers and specimens that show evidence of other practical fabricating operations.

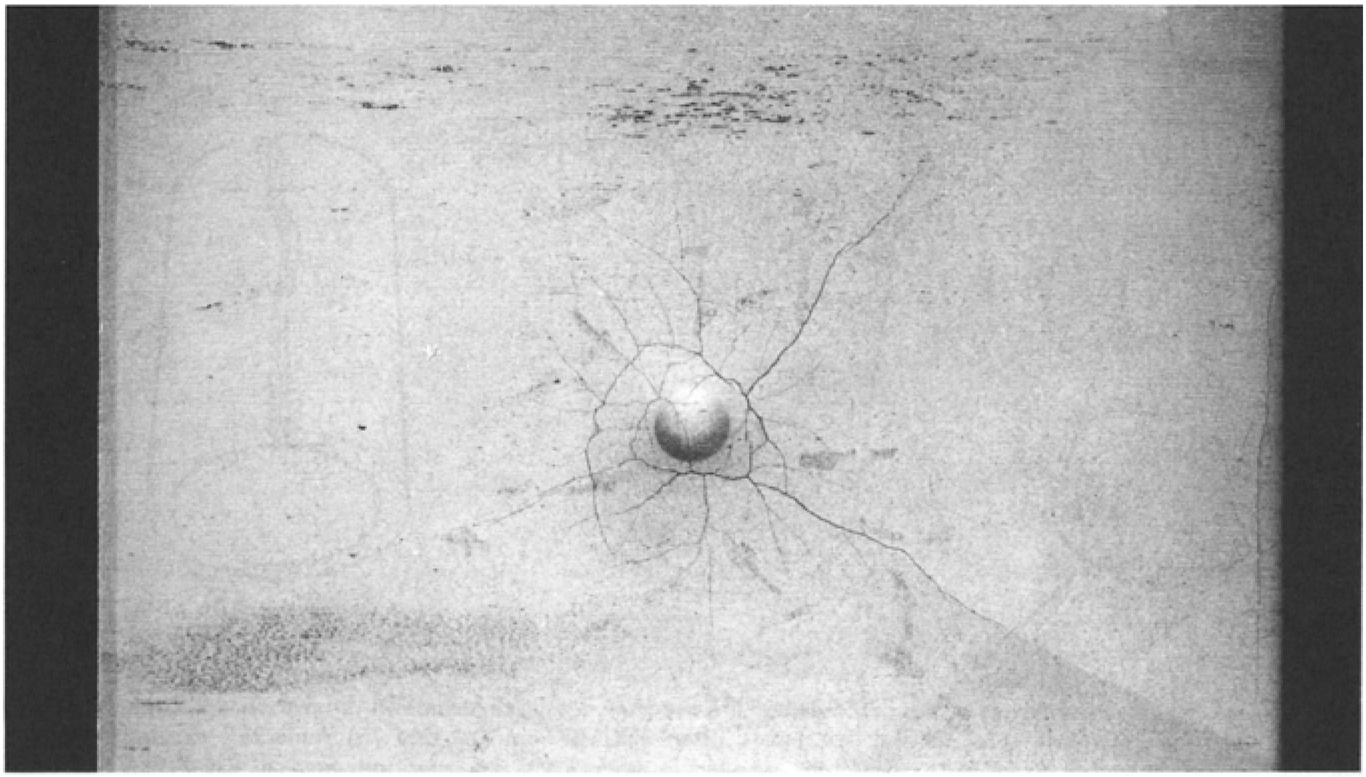

(a)

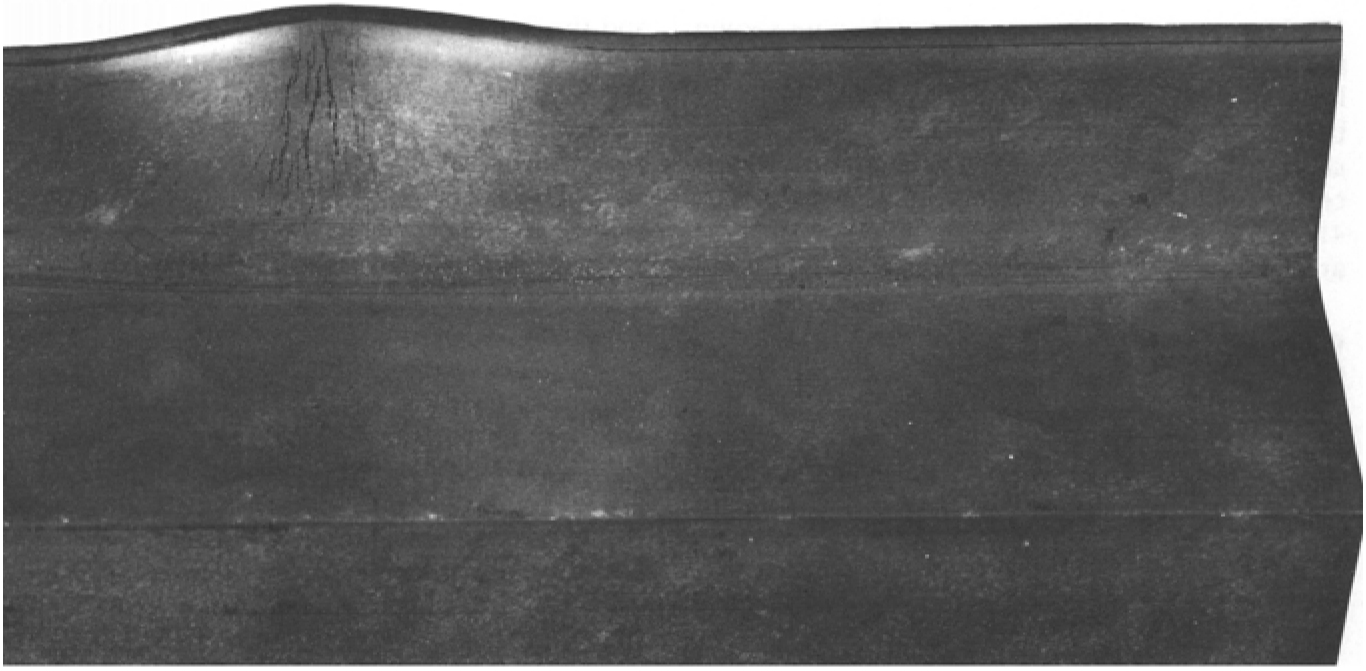

(b)

Fig. 21 SCC test specimens containing residual stresses from plastic deformation. (a) Cracked cup specimen (Ericksen impression). Source: Ref 1. (b) Joggled extrusion containing SCC in the plastically deformed region. Source: Ref 9

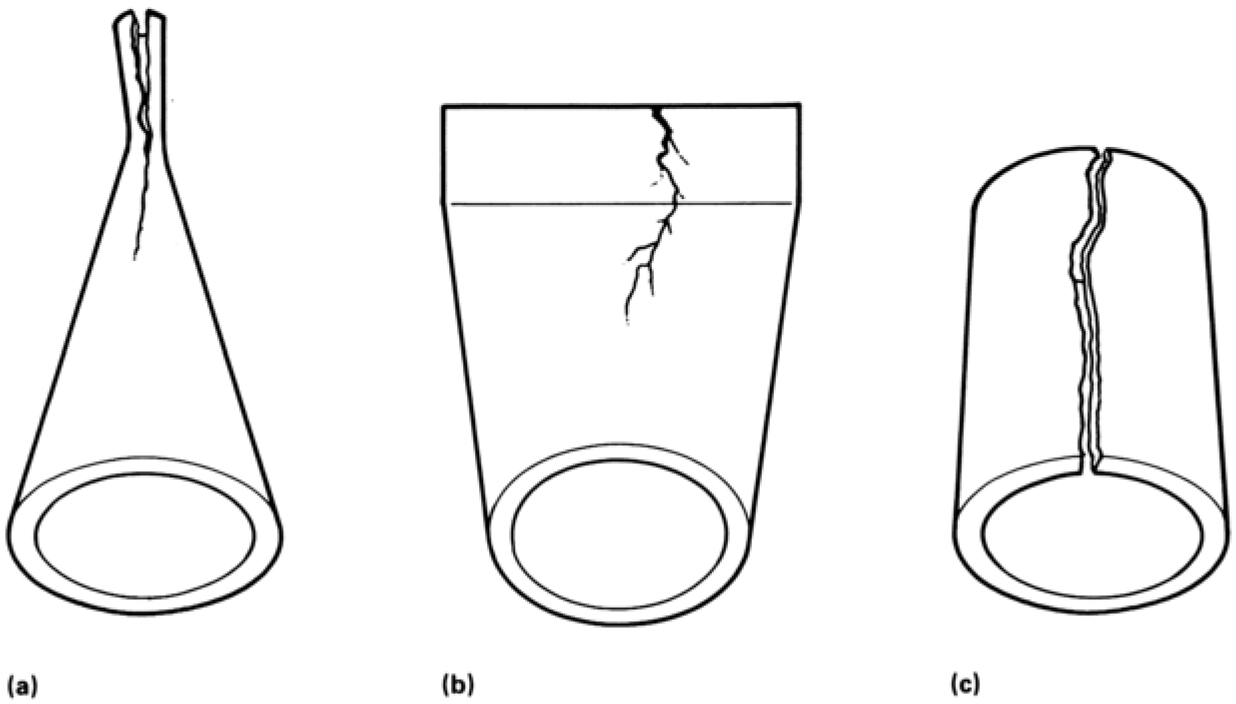

Fig. 22 SCC test specimens containing residual stresses from plastic deformation. Shown are 12.7 mm (0.5 in.) diam stainless steel tubular specimens after SCC testing. (a) and (b) Annealed tubing that was cold formed before testing. (c) Cold-worked tubing tested in the as-received condition. Source: Ref 1

Weld Specimens. Residual stresses developed in and adjacent to welds are frequently a source of SCC in service. Longitudinal stresses in the vicinity of a single weld are unlikely to be as large as stresses developed in plastically deformed weldments, because stress in the weld metal is limited by the yield strength of the hot metal that shrinks as it cools. High stresses can be built up, however, when two or more weldments are joined into a more complex structure.

Test specimens containing residual welding stresses are shown in Fig. 23. In fillet welds, residual tensile stress transverse to the weld can be critical, as indicated in Fig. 23(a) for a situation in which the tension stress acts in the short-transverse direction in an Al-Zn-Mg alloy plate.

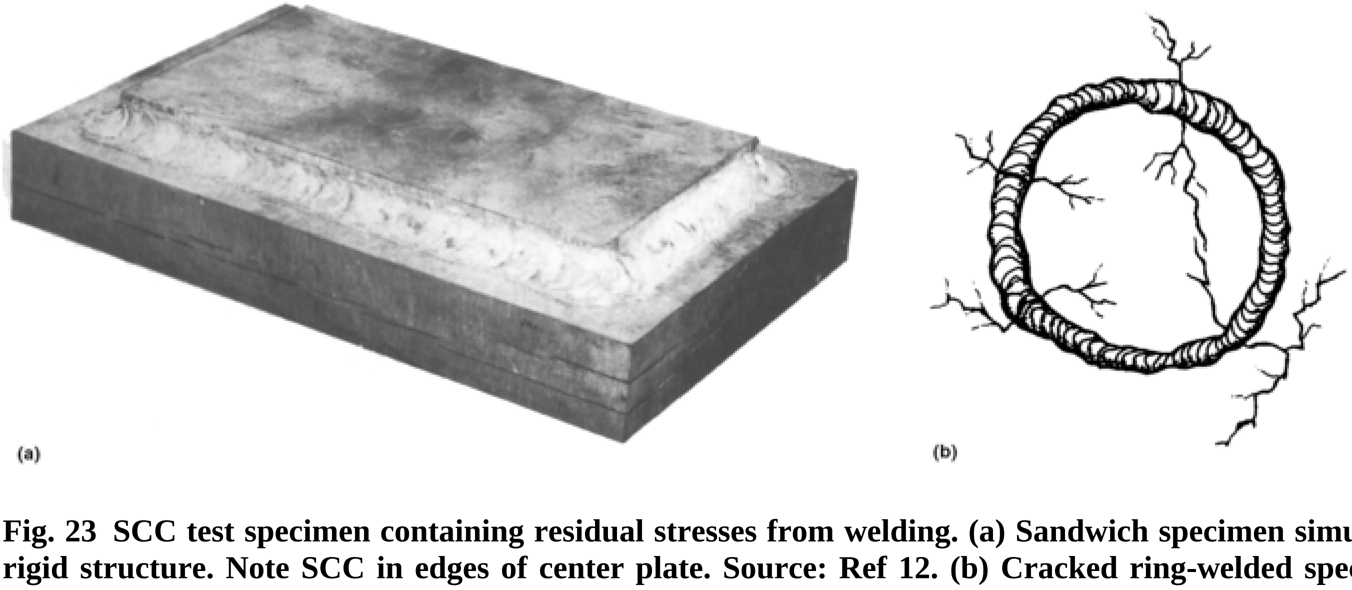

Fig. 23 SCC test specimen containing residual stresses from welding. (a) Sandwich specimen simulating rigid structure. Note SCC in edges of center plate. Source: Ref 12. (b) Cracked ring-welded specimen. Source: Ref 1

References cited in this section

1. A.W. Loginow, Stress Corrosion Testing of Alloys, *Mater. Prot.,* Vol 5 (No. 5), 1966, p 33–39

3. D.O. Sprowls et al., “A Study of Environmental Characterization of Conventional and Advanced Aluminum Alloys for Selection and Design: Phase II—The Breaking Load Test Method,” Contract NASI- 16424, NASA Contractor Report 172387, Aug 1984

6. R.N. Parkins, Stress Corrosion Test Methods—Physical Aspects, *The Theory of Stress Corrosion Cracking in Alloys,* J.C. Scully, Ed., NATO Scientific Affairs Division, 1971, p 449–468

7. G. Vogt, Comparative Survey of Type of Loading and Specimen Shape for Stress Corrosion Tests, *Werkst. Korros.,* Vol 29, 1978, p 721–725

8. “Practice for Preparation and Use of Direct Tension Stress-Corrosion Test Specimens,” G 49, *Metal Corrosion, Erosion, and Wear,* Vol 03.02, *Annual Book of ASTM Standards,* American Society for Testing and Materials

9. H.L. Craig, Jr., D.O. Sprowls, and D.E. Piper, Stress-Corrosion Cracking, *Handbook on Corrosion Testing and Evaluation,* W.H. Ailor, Ed., John Wiley & Sons, 1971, p 259

10. “Practice for Preparation and Use of Bent- Beam Stress-Corrosion Test Specimens,” G 39, *Metal Corrosion, Erosion, and Wear,* Vol 03.02, *Annual Book of ASTM Standards,* American Society for Testing and Materials

11. “Corrosion of Metals and Alloys—Stress Corrosion Testing—Part 2: Preparation and Use of Bent-Beam Specimens,” ISO 7539-2, International Organization for Standardization

12. M.B. Shumaker et al., Evaluation of Various Techniques for Stress Corrosion Testing Welded Aluminum Alloys, *Stress Corrosion Testing,* STP 425, American Society for Testing and Materials, 1967, p 317–341

13. R.A. Davis, Stress Corrosion Cracking Investigation of Two Low Alloy, High Strength Steels, *Corrosion,* Vol 19 (No. 2), 1963, p 45t–55t

14. “Practice for Making and Using C-Ring Stress-Corrosion Test Specimens,” G 38 *Metal Corrosion, Erosion, and Wear,* Vol 03.02, *Annual Book of ASTM Standards,* American Society for Testing and Materials

15. “Corrosion of Metals and Alloys—Stress Corrosion Testing—Part 5: Preparation and Use of C-Ring Specimens,” ISO 7539- 5, International Organization for Standardization

16. S.O. Fernandez and G.F. Tisinai, Stress Analysis of Un-notched C-rings Used for Stress Cracking Studies, *J. Eng. Ind.,* Feb 1968, p 147–152

17. F.S. Williams, W. Beck, and E.J. Jankowsky, A Notched Ring Specimen for Hydrogen Embrittlement Studies, *Proc. ASTM,* Vol 60, American Society for Testing and Materials, 1960, p 1192

18. D.O. Sprowls et al., “Investigation of the Stress Corrosion Cracking of High Strength Aluminum Alloys,” Final Technical Report for U.S. Government NASA Contract NAS-8-5340, Control No. 1-4-50-001167-01(lf), CPB-02-1215-64, 1967

19. Report of Task Group 1, of ASTM Subcommittee B-3/X, Stress Corrosion Testing Methods, *Stress Corrosion Testing,* STP 425, American Society for Testing and Materials, 1967, p 3–20; *Proc. ASTM,* Vol 65, 1965, p 182–197

20. “Corrosion of Metals and Alloys—Stress Corrosion Tests—Part 4: Preparation and Use of Uniaxially Loaded Tension Specimens,” ISO 7539-4, International Organization for Standardization

21. B.W. Lifka and D.O. Sprowls, Stress Corrosion Testing of 7079-T6 Aluminum Alloy in Various Environments, *Stress Corrosion Testing,* STP 425, American Society for Testing and Materials, 1967, p 342–362

22. R.J. Bucci et al., The Breaking Load Method: A New Approach for Assessing Resistance to Growth of Early Stage Stress Corrosion Cracks, *Corrosion Cracking,* V.S. Goel, Ed., *Proc. Int. Conf. and Exposition on Fatigue, Corrosion Cracking, Fracture Mechanics, and Failure Analysis,* American Society for Metals, 1986, p 267–277

23. D.O. Sprowls et al., Evaluation of a Proposed Standard Method of Testing for Susceptibility to SCC of High Strength 7XXX Series Aluminum Alloy Products, *Stress- Corrosion—New Approaches,* STP 610, H.L. Craig, Jr., Ed., American Society for Testing and Materials, 1976, p 3–31

24. "Testing of Light Metals, Stress Corrosion Test," German Standard DIN 50908, 1964

25. F.H. Haynie et al., "A Fundamental Investigation of the Nature of Stress Corrosion Cracking in Aluminum Alloys," Technical Report AFML 66-267, USAF Contract No. AF 33(615)-1710 Air Force Materials Laboratory, June 1966

26. P. Brenner, Realistic Stress Corrosion Testing, *Metallurgy,* Vol 23 (No. 9), 1969, p 879–886

27. "Practice for Making and Using U-Bend Stress-Corrosion Test Specimens," G 30 *Metal Corrosion, Erosion, and Wear,* Vol 03.02, *Annual Book of ASTM Standards,* American Society for Testing and Materials

28. "Corrosion of Metals and Alloys—Stress Corrosion Testing—Part 3: Preparation and Use of U-Bend Specimens," ISO 7539-3, International Organization for Standardization

29. H. Nathorst, Stress Corrosion Cracking in Stainless Steels, Part II—An Investigation of the Suitability of the U-Bend Specimen, *Weld. Res. Counc. Bull.,* Series No. 6, Oct 1950

B. Phull, Evaluating Stress-Corrosion Cracking, *Corrosion: Fundamentals, Testing, and Protection*, Vol 13A, *ASM Handbook*, ASM International, 2003, p 575–616

Evaluating Stress-Corrosion Cracking

Revised by Bopinder Phull, Consultant

Static Loading of Precracked (Fracture Mechanics) Specimens

The use of precracked (fracture mechanics) specimens is based on the concept that large structures with thick components are apt to contain cracklike defects. After a stress-corrosion crack begins to grow, or if the specimen is provided with a mechanical precrack, classical stress analysis is inadequate for determining the response of the material subjected to stress in the presence of a corrodent.

The mechanical driving force for cracks can be measured with linear elastic fracture mechanics theory in terms of the crack-tip stress-intensity factor, *K*, which is expressed in terms of the remotely applied loads, crack depth, and test specimen geometry. At or above a certain level of *K*, SCC in a susceptible material will initiate and grow in certain environments, but below that level no measurable propagation is observed (Ref 30).

The apparent threshold stress intensity for the propagation of SCC (assuming that crack nuclei form in a manner that cannot be described by fracture mechanics, such as localized corrosion) is designated K_{ISCC} (or

K_{th}). Therefore, in terms of linear elastic fracture mechanics theory, for a surface crack in a large plate remotely loaded in tension, the shallowest crack (of a shape that is long compared to its depth) that will propagate as a stress-corrosion crack is $a_{cr} = 0.2(K_{ISCC}/\ TYS)^2$, where *TYS* is tensile yield strength. Thus, a crack that is shallower than this critical value will not propagate under the given environmental conditions.
The value of a_{cr} incorporates the SCC resistance, K_{ISCC}, and the contribution of stress levels (of the order of the yield strength) to SCC that are due to residual or assembly stresses in thick component sections (Ref 4). Therefore, the application of fracture mechanics does not provide independent information about SCC; it simply provides a usable method for treating the stress factor in the presence of a crack.
When the rate of SCC propagation is determined and plotted as a function of K_t (the crack- opening mode), the test results for a highly susceptible alloy will exhibit the general trend shown in Fig. 3. Actual curves vary depending on the SCC resistance and fracture toughness of the alloy.
Although precracking may shorten or modify the initiation period, it does not circumvent it. Therefore, this method of testing also requires arbitrary and sometimes long exposure periods.

Test Specimen Selection

Almost all standard plane-strain fracture toughness test specimens can be adapted to SCC testing. These standard configurations should be used to ensure valid fracture analyses. Comprehensive discussions on SCC testing with precracked specimens can be found in Ref 31, 32, 33. Precracked specimens are shown in Fig. 24 where they are classified with respect to loading methods and the relationship with the stress-intensity factor as SCC propagates. Preparation of fracture toughness test specimens and test procedures are detailed in ASTM E 399 (Ref 34), E 1820 (Ref 35), and G 168 (Ref 36). Some exemplar test specimen dimensions and tolerances are given in Fig. 25(a)(a) to (c). Minor modifications to accommodate different loading arrangements and to facilitate mechanical precracking can be made to these configurations without invalidating the plane-strain constraints on the specimens. Figure 26 illustrates alternative chevron-notch and face-groove designs.

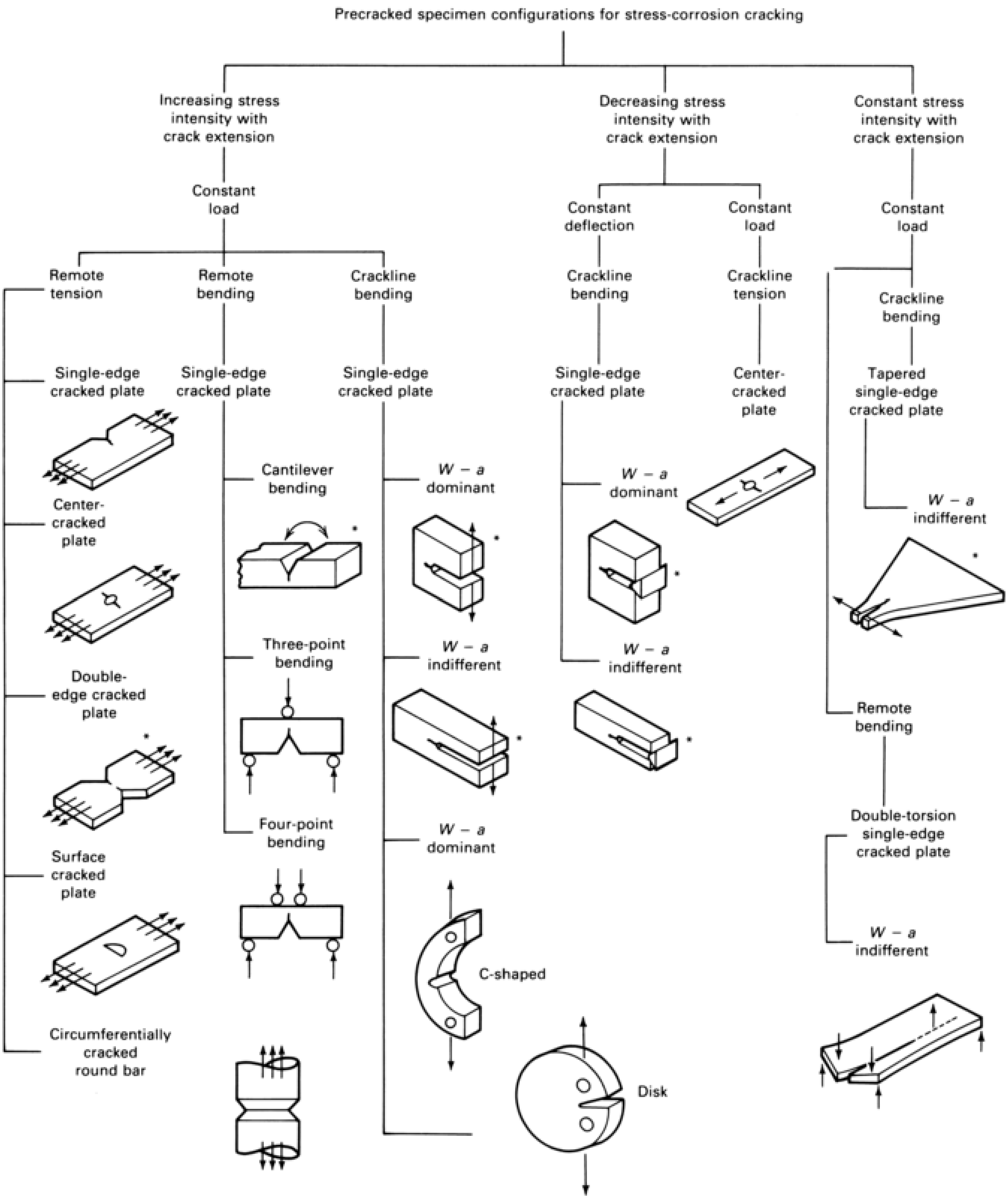

Fig. 24 Classification of precracked specimens for SCC testing. Asterisks denote commonly used configurations. Source: Ref 33

ASTM E 1681 (Ref 37) covers the determination of environment-assisted cracking threshold stress-intensity parameters, K_{IEAC} and K_{EAC} for metallic materials, using fatigue precracked beam or compact fracture specimens. Standard terminology relating to fracture testing is included in ASTM Standard E1823 (Ref 38).

Cantilever bend specimens (Fig. 25(a)a), sometimes referred to as single-edge-notched cantilever bend specimens, have been used in constant-load tests (K-increasing) for characterizing high-strength steels and titanium alloys (Ref 39). Equations 5, 6, 7 are recommended (Ref 40, 41):

$$K = \frac{6M}{BW^2}\left(\frac{2W}{\pi a}\tan\frac{\pi a}{2W}\right)^{1/2} \times \left[\frac{0.923+0.199\left(1-\sin\frac{\pi a}{2W}\right)^4}{\cos\frac{\pi a}{2W}}\right] \quad \text{(Eq 5)}$$

$$\frac{EBW(2V_0)}{M} = e^x \quad \text{(Eq 6)}$$

$$\frac{EBWV_{LL}}{M} = e^y \quad \text{(Eq 7)}$$

where e is the base of natural logarithm (2.718), $x = [0.1426 + 11.92(a/W) - 17.42(a/W)^2 + 15.84(a/W)^3 - 2.235(a/W)^4]$, $y = [6.188 + 12.98(a/W) - 41.19(a/W)^2 + 54.98(a/W)^3 - 22.28(a/W)^4]$. M is the applied bending moment, B is the specimen thickness (face grooves, when present, may be accounted for by replacing B with $\sqrt{BB_n}$, where B_n is the net thickness at the base of the face grooves; see Fig. 26b), W is the depth of the specimen, a is the depth of the notch plus crack, E is the modulus of elasticity, $2V_0$ is the total crack mouth opening displacement at the top face of the specimen, and V_{LL} is the total crack mouth opening displacement measured at the point of load application, which will vary depending on the load arm length.

Equation 5 is an expression for the stress intensity of a rectangular beam in pure bending and is valid over a wide range of *a/W* values. It applies to mode I loading only, however, and the usual tests include a mode II component from resulting shear stresses.

Equations 6 and 7 were determined by fitting experimental compliance data for cantilever bend specimens with a polynomial equation expressing the natural log of the normalized compliance as a function of *a/W*. These experimental values are in excellent agreement with those determined from Eq 5 for pure bending, even though the stress state at the crack tip will differ for cantilever bending. It has been suggested that analyses using pure bending expressions related to compliance measurement are suitable for testing with the cantilever bend configuration (Ref 40).

Crack growth measurements can be made with clip gage readings in conjunction with the crack- opening displacement calibrations given previously or by any other method that can be verified within ±0.127 mm (±0.005 in.). Examples of various methods are given in Ref 40 and 42.

Modified compact specimens (*K*-decreasing or *K*-increasing), as shown in Fig. 25(b)(b), are frequently referred to as 1T-WOL (wedge-opening loaded) or modified WOL specimens. Although most frequently used with constant-displacement (bolt) loading (Ref 39, 43), these specimens have also been used with constant load (Ref 3, 44, 45).

Equations 8, 9, 10, 11 can be used to calculate stress-intensity levels and normalized crack- opening displacements for fatigue precracking, for initiation of stress-corrosion testing, and for subsequent intervals during the test. These equations are based on boundary colocation values determined for this type of specimen configuration with face grooves and bolt loading (threaded bolt against a rigid loading tip) (Ref 40). The polynomial regression equation agrees with experimentally determined colocation values within 1% for 0.2 = *a/W* = 0.95:

$$K_{Io} = \frac{P\left(2+\frac{a_0}{W}\right)}{B\sqrt{W}\left(1-\frac{a_0}{W}\right)^{3/2}}\left[1.308+5.278\left(\frac{a_0}{W}\right) - 19.67\left(\frac{a_0}{W}\right)^2 + 24.57\left(\frac{a_0}{W}\right)^3 - 10.27\left(\frac{a_0}{W}\right)^4\right] \quad \text{(Eq 8)}$$

$$2V_0 = \frac{P}{EB}\times e^x \quad \text{(Eq 9)}$$

where $x = [1.830 + 4.307(a/W) + 5.871(a_0/ W)^2 - 17.53(a_0/W)^3 + 14.57(a_0/W)^4]$.

$$2V_{LL} = 2V_0 \times \frac{e^y}{e^x} \quad \text{(Eq 10)}$$

where $y = [1.623 + 3.352(a_0/W) + 8.205(a_0/ W)^2 - 19.59(a_0/W)^3 + 15.23(a_0/W)^4]$.

$$K_{Ii} = \frac{E\left(2V_{LL}\right)\left(2+\frac{a_i}{W}\right)}{\sqrt{W}\left(1-\frac{a_i}{W}\right)^{3/2}}\left\{\left[1.308+5.278\left(\frac{a_i}{W}\right) - 19.67\left(\frac{a_i}{W}\right)^2 + 24.57\left(\frac{a_i}{W}\right)^3 - 10.27\left(\frac{a_i}{W}\right)^4\right] \div e^z\right\} \quad \text{(Eq 11)}$$

where $z = [1.623 + 3.352(a_i/W) + 8.205(a_i/ W)^2 - 19.59(a_i/W)^3 + 15.23(a_i/W)^4]$. In Eq 8, Eq 9, Eq 10, Eq 11, K_{Io} is the desired starting stress intensity, a_0 is the starting crack length, P is the load calculated to develop K_{Io} with measured a_0, W is the net width of the specimen measured from the load line, K_{Ii} is the stress-intensity after time interval i, a_i is the crack length after time interval i, and $2V_{LL}$ is the total crack mouth opening displacement at the load line. All other quantities are as defined previously.

Double-beam specimens (*K*-decreasing or *K*-increasing), which are also referred to as double-cantilever beam specimens, are similar to modified compact specimens, but because of their greater width or length, they are well suited for studying SCC growth rates over a greater range of K_I values. The smaller height of these specimens (Fig. 25(c)c) allows more versatility in performing short-transverse tests from moderate thicknesses of material. Like compact specimens, double-beam specimens are generally used with constant-displacement (bolt) loading for convenience, but they can also be used with constant load.

Bolt-loaded specimens used with a test procedure similar to that described in Ref 46 have been extensively employed for short-transverse tests of aluminum alloy products (Ref 45, 47, 48). Equation 12, Equation 13, Equation 14, Equation 15 are recommended for general use with double-beam specimens:

$$K_{Io} = \frac{P\sqrt{12}}{B\sqrt{H}}\left[\frac{a_0}{H}+0.6728+0.0377\left(\frac{H}{a_0}\right)^2\right] \quad \text{(Eq 12)}$$

$$2V_0 = \frac{4K_{I_0}\sqrt{H}}{\sqrt{3}E}\left(\frac{a_0}{H}+0.6728\right)^2 \times \left[1+1.5\left(\frac{C_0}{a_0}\right)-1.15\left(\frac{C_0}{a_0}\right)^2\right] \quad \text{(Eq 13)}$$

$$2V_{LL} = \frac{2V_0}{1+1.5\left(\frac{C_0}{a_0}\right)-1.15\left(\frac{C_0}{a_0}\right)^2} \quad \text{(Eq 14)}$$

$$K_i = \frac{\sqrt{3}E(2V_{LL})}{4\sqrt{H}\left(\frac{a_i}{H}+0.6728\right)^2} \quad \text{(Eq 15)}$$

Equation 12 is an expression reported in Ref 49. The simplified Eq 15 provides more versatility with high accuracy for a wider range of specimen configurations and *K* values (crack growth) than equations previously published (Ref 46).

Two early K_I calibrations based on stress analysis (Ref 50) and compliance (Ref 51) are shown in Fig. 27 and are in excellent agreement. The shape of these curves can also be used as a design guide for preparing specimens. If the test must be completed in the shortest possible time, a_0 should be short to capitalize on the fact that the rate of decrease of K_I with crack extension is maximum for shallow cracks. However, if maximum accuracy is desired, a deeper crack (effective notch length *M*, Fig. 25(c)(c) should be chosen so that errors in crack length measurement do not cause significant errors in K_I.

In early work with aluminum alloys (Ref 46, 47) a relatively short effective notch length was used ($a_0/H \approx 0.9$), followed later by deeper notches ($a_0/H \approx 1.2$ to 2.2), all with a 2*H* value of 25.4 mm (1.0 in.) (Ref 3, 45, 47, 48). The recommended starting *a*/*H* value shown in Fig. 25(c)(c) is about 2 to 2.2, depending on the length of the precrack. Limited tests of a smaller beam height of 2*H* = 12.7 mm (0.5 in.) have shown little effect on the amount and rate of crack growth in aluminum alloy 7075 plate (Ref 52).

An alternative double-cantilever beam specimen has been developed for testing relatively thin sections (typically 6.4 mm, or $\frac{1}{4}$in., thick) of low-alloy steels (Ref 53). The specimen is stressed by forcing an appropriately dimensioned wedge into the slot. These specimens have been used to determine the effect of hardness of low-alloy steels on their resistance to SCC in environments containing hydrogen sulfide.

Constant K_I specimens are well suited for studying the mechanisms of SCC, because the stress intensity, K_I, is not dependent on crack depth and can be neglected in kinetic studies. Other attractive features are the relatively simple expressions for stress intensity and compliance and the apparent retention of plane-strain conditions in thin plate and sheet specimens. The cost of specimen preparation and instrumentation, however, prohibits its use for extensive SCC characterizations.

Reference 33 provides equations for the analysis of two types of constant K_I specimens: the tapered double-beam specimen and the double- torsion-loaded single-edge cracked specimen. A recent evaluation of the double-torsion method (Ref 54) used Al-Zn-Mg alloy sheet 3.2 mm (0.125 in.) thick. By using the double-torsion specimen, *V-K* curves were produced for aluminum alloy 7075-T651 sheet with conventional two-stage growth and plateau velocities that were only slightly higher than those for conventional double-cantilever beam tests of plate.

Other precracked specimen configurations, such as those shown in Fig. 24, can be used for special testing conditions. Information on the preparation and use of these specimens and the related fracture mechanics equations are given in Ref 33 and 55, 56, 57.

Preparation of Precracked Specimens

When using precracked SCC test specimens, the investigator must consider the dimensional (size) requirements of the specimen, its crack configuration and orientation, and machining and precracking of the specimen. These considerations are discussed in the sections that follow. Additional guidelines and recommendations on

specimen preparation in conjunction with fracture toughness testing are given in Ref 33, 34, 35, 36, 37 and 55, 56, 57.

Dimensional Requirements. A basic requirement of all precracked specimen configurations is that the dimensions be sufficient to maintain predominantly triaxial stress (plane- strain) conditions, in which plastic deformation is limited to a very small region in the vicinity of the crack tip. Experience with fracture toughness testing has shown that for a valid K_{Ic} measurement neither the crack depth a nor the thickness B should be less than $2.5(K_{Ic}/YS)^2$, where YS is the yield strength of the material (Ref 34, 39). Because of the uncertainty regarding a minimum thickness for which an invariant value of K_{ISCC} can be obtained, guidelines for designing fracture mechanics test specimens should be tentatively followed for SCC test specimens. The threshold stress-intensity value should be substituted for K_{Ic} in the aforementioned expression as a test of its validity.

If specimens are to be used for determination of K_{ISCC}, the initial specimen size should be based on an estimate of the K_{ISCC} of the material. Overestimation of the K_{ISCC} value is recommended; therefore, a larger specimen should be used than may eventually be necessary. When determining stress-corrosion crack growth behavior as a function of stress intensity, specimen size should be based on the highest stress intensity at which crack growth rates are to be measured (substitute K_{Io} in the $2.5(K_{Ic}/YS)^2$ expression).

Notch Configuration and Orientation. For SCC testing, the depth of the initial crack-starter notch—that is, the machined slot with a fatigue or mechanical pop-in crack at its apex—can be as short as $0.2W$. Guidelines for the depth of the notch depend on the limits of accurate K_I calibration with respect to the range of a/W or a/H and the considerations discussed previously for double-beam specimens.

Several designs of crack-starter notches are available for most plate specimens. The machined slot is used to simulate a crack, because it is impractical to produce plane cracks of sufficient size and accuracy in plate specimens. ASTM E 399 (Ref 34) recommends that the notch root radius should not be greater than 0.127 mm (0.005 in.), unless the chevron form is used, in which case it may be 0.25 mm (0.01 in.) or less (Fig. 26). This tolerance can be easily achieved with conventional milling and grinding equipment.

A significant factor in the SCC testing of thick sections of some metals, such as aluminum and titanium, is the direction of applied stress relative to the grain structure. A standardized plan for identifying the loading direction, the fracture plane, and the direction of crack propagation is shown in Fig. 28.

Machining. Specimens of the required orientation should be machined from products in the fully heat treated and stress-relieved condition to avoid complications due to residual stresses in the finished specimens. Safeguards against the presence of residual stresses are especially important for precracked specimens because these specimens are usually bulky and contain notches that are machined deep into the metal. For specimens of material that cannot easily be completely machined in the fully heat treated condition, the final thermal treatment can be given before the notching and finishing operations. However, fully machined specimens should be heat treated only when the heat treatment will not result in distortion, residual stress, quench cracking, or detrimental surface conditions.

Precracking. Fatigue precracking should be done in accordance with ASTM E 399, E 1820, G 168, and E 1681 (Ref 34, 35, 36, 37, respectively). The K level used for precracking each specimen should not exceed about two-thirds of the intended starting K-value for the environmental exposure. This prevents fatigue damage or residual compressive stress at the crack tip, which may alter the SCC behavior, particularly when testing at a K level near the threshold stress intensity for the specimen.

Aluminum alloy specimens can also be precracked by pop-in methods (wedge-opening loaded to the point of tensile overload), but steel and titanium alloys are usually too strong and tough to pop in without breaking off one of the specimen arms. Chevron notches are usually used to facilitate starting such mechanical precracks, and face grooves are sometimes necessary to produce straight precracks in tougher alloys (Fig. 26). These modifications may also be necessary to control fatigue precracking of some materials.

When a specimen is mechanically precracked by pop in, the load should be maintained and should not be reduced for testing at a lower initial K-value. Reducing the load (crack mouth opening displacement) required for pop in will result in residual compressive stress at the crack tip, which could interfere with SCC initiation. When testing specimens at a relatively low fraction of K_{Ic}, fatigue precracking is recommended.

Testing Procedure

For all methods using precracked specimens, the primary objective is usually to determine K_{ISCC} or K_{th}, threshold stress intensity for SCC for the alloy and environment combination. One procedure, similar to that

used with smooth specimens, depends on the initiation of SCC at various levels of applied K_{Io} values. Both constant- load (K-increasing) and constant-displacement (K-decreasing) tests can be used. The latter procedure, which is unique to precracked specimens, involves crack arrest. This technique requires a K-decreasing constant-displacement test. These methods are compared in Fig. 29, which illustrates the shift in the stress-intensity factor as SCC growth occurs.

K-Increasing versus K-Decreasing Tests. In constant-load specimens (K-increasing tests), stress parameters can be quantified with confidence. Because crack growth results in an increasing crack opening, there is less likelihood that corrosion products will block the crack or wedge it open. Crack-length measurements can be made readily with several continuous-monitoring methods.

A wide selection of constant-load specimen geometries are available to suit the test material, experimental facilities, and test objective. Therefore, crack growth can be studied under either bend or tension loading conditions. Specimens can be used to determine K_{ISCC} by the initiation of a stress-corrosion crack from a preexisting fatigue crack using a series of specimens or to measure crack growth rates.

The principal disadvantages of constant-load specimens are the expense and bulk associated with the need for an external loading system. Bend specimens can be tested in relatively simple cantilever beam equipment, but specimens subjected to tension loading require constant- load creep-rupture equipment or similar testing machines. In this case, expense can be minimized by testing chains of specimens connected by loading links that are designed to prevent unloading upon failure of individual specimens. Because of the size of these loading systems, it is difficult to test constant-load specimens under operating conditions, but they can be tested in environments obtained from operating systems.

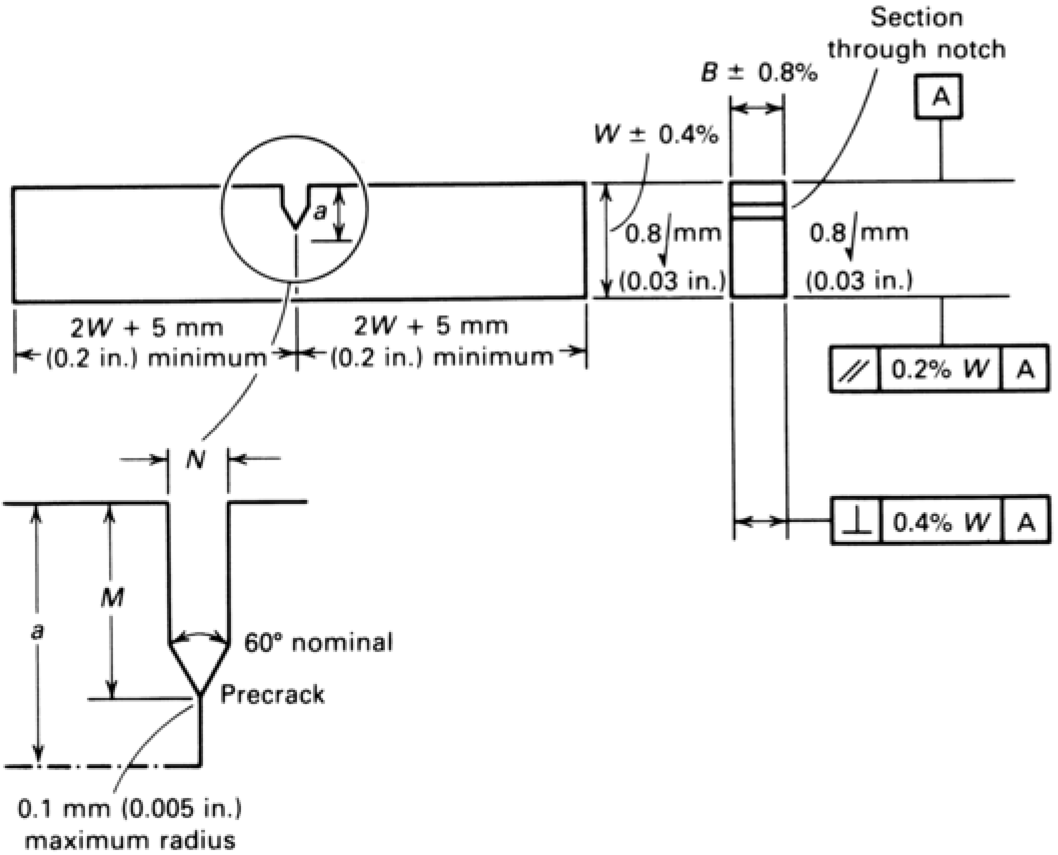

Fig. 25(a) Proportional dimensions and tolerances for cantilever bend test specimens. Width = *W*; thickness (*B*) = 0.5*W*; half loading span (*L*) = 2*W*; notch width (*N*) = 0.065*W* maximum if *W* >25 mm (>1.0 in.); *N* = 1.5 mm (0.06 in.) maximum if *W* = 25 mm (1.0 in.); effective notch length (*M*) = 0.25 to 0.45*W*; effective crack depth (*a*) = 0.45 to 0.55 *W*

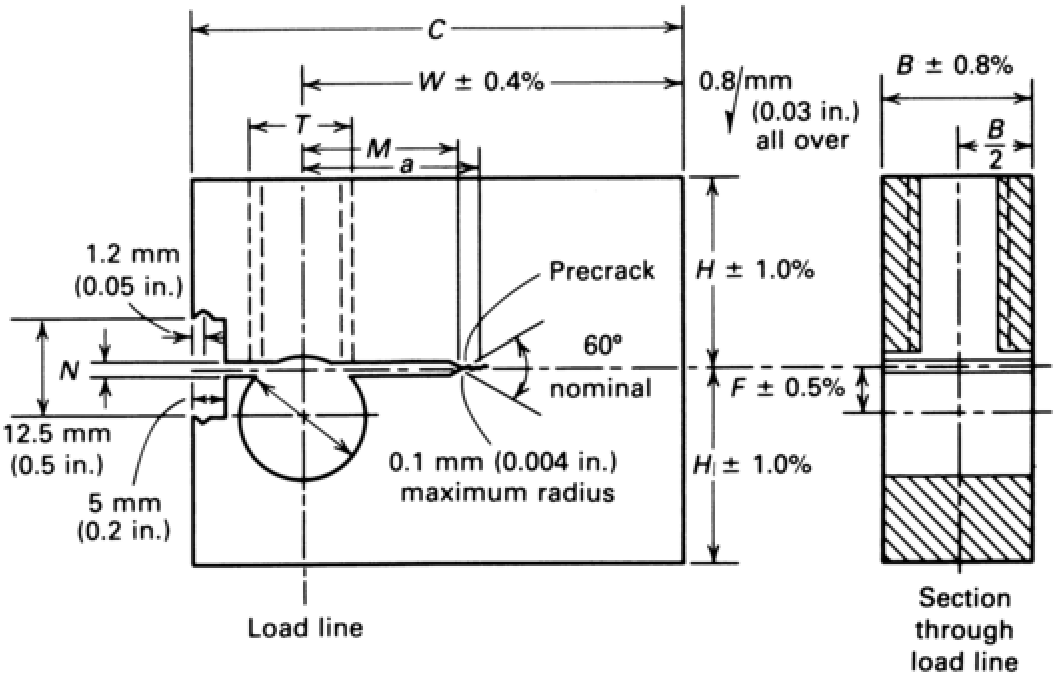

Fig. 25(b) Proportional dimensions and tolerances for modified compact specimens. Surfaces should be perpendicular and parallel as applicable to within 0.002*H* TIR. The bolt centerline should be perpendicular to the specimen centerline within 1°. Bolt of material similar to specimen where practical; fine threaded, square or Allen head. Thickness = *B*; net width (*W*) = 2.55*B*; total width (*C*) = 3.20*B*; half height (*H*) = 1.24*B*; hole diameter (*D*) = 0.718*B* + 0.003*B*; effective notch length (*M*) = 0.77*B*; notch width (*N*) = 0.06*B*; thread diameter (*T*) = 0.625*B*

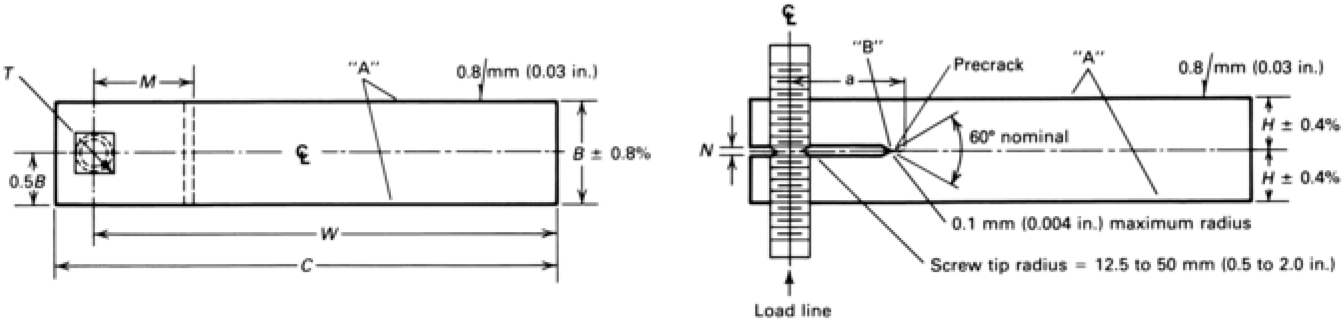

Fig. 25(c) Proportional dimensions and tolerances for double-beam specimens. "A" surfaces should be perpendicular and parallel as applicable to within 0.002*H* TIR. At each side, the point "B" should be equidistant from the top and bottom surfaces to within 0.001*H*. The bolt centerline (load line) should be perpendicular to the specimen centerline to within 1°. Bolt of material similar to specimen where practical; fine threaded, square or Allen head. Half height = *H*; thickness (*B*) = 2*H*; net width (*W*) = 10*H* minimum; total width (*C*) = *W* + *T*; thread diameter (*T*) = 0.75 *H* minimum; notch width (*N*) = 0.14*H* maximum; effective notch length (*M*) = 2*H*

Constant-displacement specimens (*K*-decreasing tests) are self-loaded; therefore, external stressing equipment is not required. Their compact dimensions also facilitate exposure to operating service environments. They can be used to determine K_{ISCC} by the initiation of stress-corrosion cracks from the fatigue precrack, in which case a series of specimens must be used to bracket the threshold value. This can also be achieved by the arrest of a propagating crack, because under constant-displacement testing conditions stress intensity decreases progressively as crack propagation occurs. In this case, a single specimen suffices in principle; in practice, the use of several replicate specimens is recommended to assess variability in test results.

Constant-displacement specimens are subject to several inherent disadvantages. Oxide formation or corrosion products can wedge the crack surfaces open, thus changing the applied displacement and load. Oxide formation or corrosion products can also block the crack mouth, thus preventing the entry of corrodent, and can impair the

accuracy of crack length measurements by electrical resistance methods. Applied loads can be measured only indirectly by displacement changes or by other sophisticated instrumentation. Crack arrest must be defined by an arbitrary crack growth rate below which it is impractical to measure cracks accurately (commonly about 10^{-10} m/s, or 1.5×10^{-5} in./h).

Loading Arrangements and Crack Measurement. To monitor crack propagation rate as a function of decreasing stress intensity when testing constant-displacement loaded specimens, two of the three testing variables must be measured—crack depth (a_i) or load (P_i) and crack- opening displacement at the load line (V_{LL}). Although crack initiation and growth can be detected from change in either load or crack length, load change is usually more sensitive to these conditions. Therefore, crack advance is easier to detect in specimens loaded in a testing machine, an elastic loading ring, or an instrumented bolt than in specimens loaded with a bolt or wedge. Figures 30(a)(a) and (b) illustrate typical loading arrangements for which load changes can be automatically monitored (Ref 3, 44, 58).

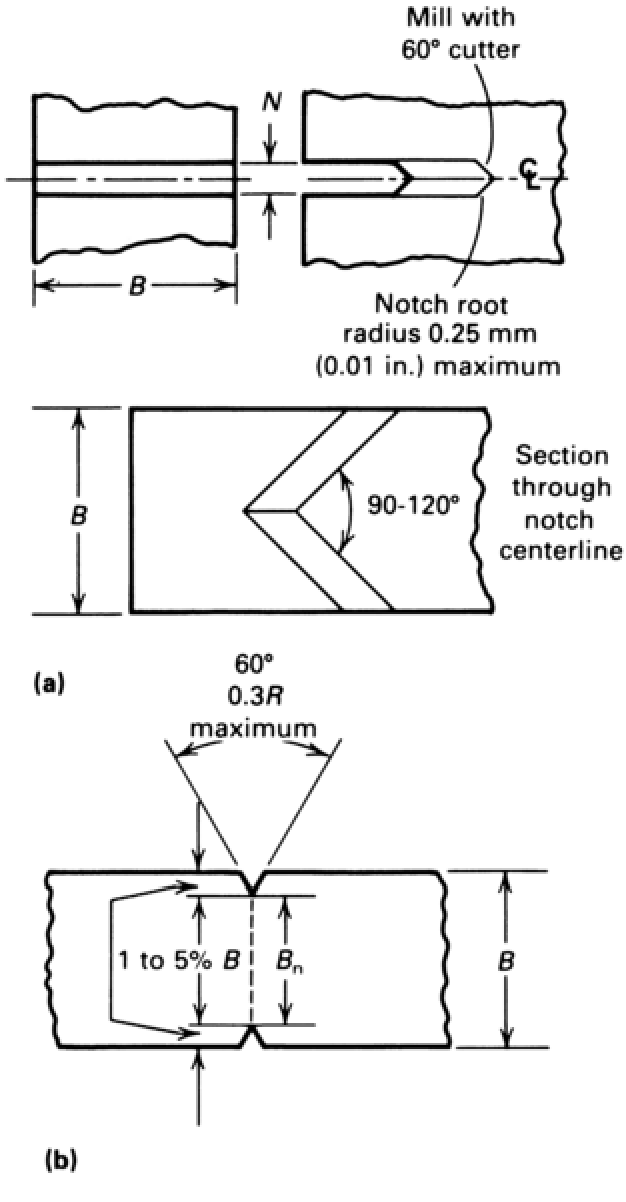

Fig. 26 Alternative chevron notch (a) and face grooves (b) for single-edge cracked specimens

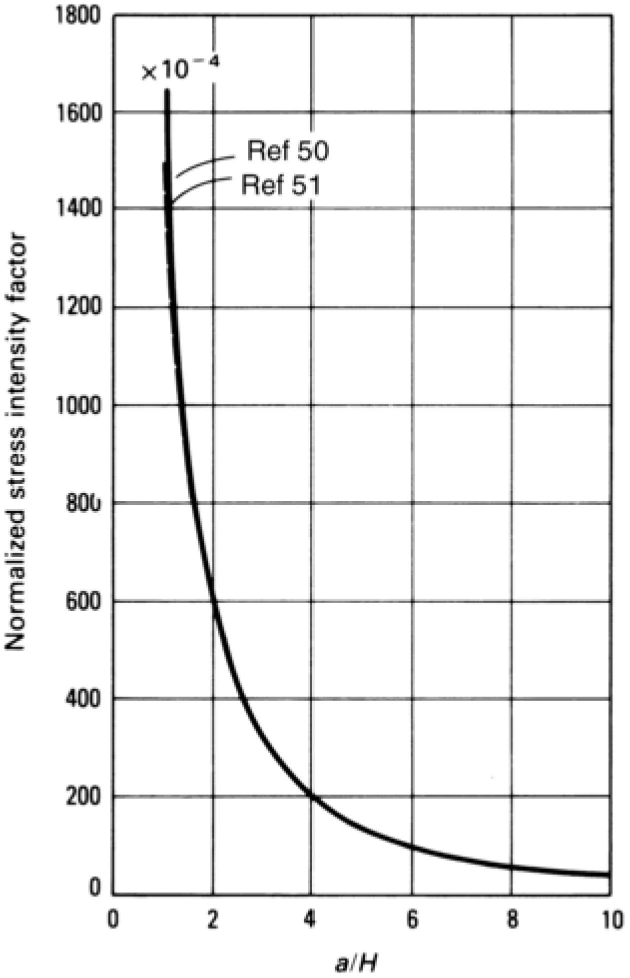

Fig. 27 Configuration and K_I calibration of a double-beam plate specimen. Normalized stress intensity K_I plotted against a/H ratio. (W - a) indifferent, crackline-loaded, single-edge cracked specimen. Source: Ref 33

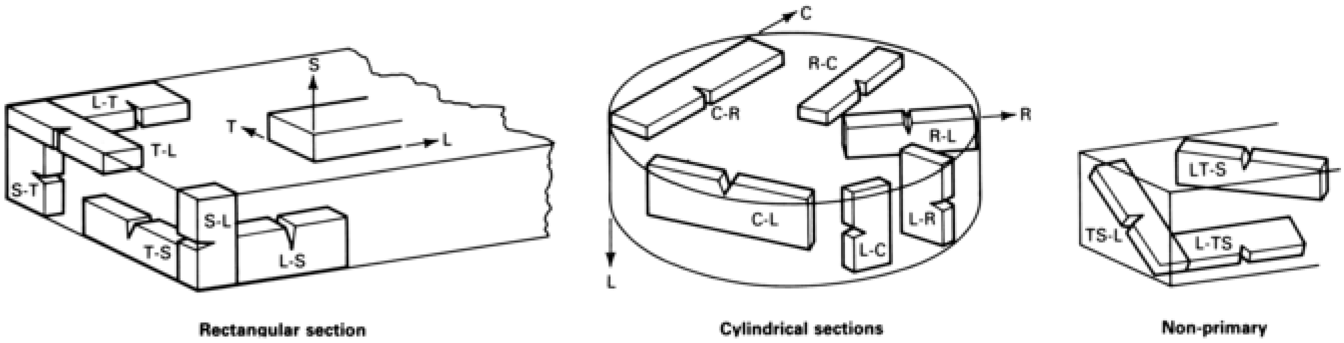

Fig. 28 Specimen orientation and fracture plane identification. L, length, longitudinal, principal direction of metal working (rolling, extrusion, axis of forging); T, width, long-transverse grain direction; S, thickness, short-transverse grain direction; C, chord of cylindrical cross section; R, radius of cylindrical cross section. First letter: normal to the fracture plane (loading direction); second letter: direction of crack propagation in fracture plane. Source: Ref 34

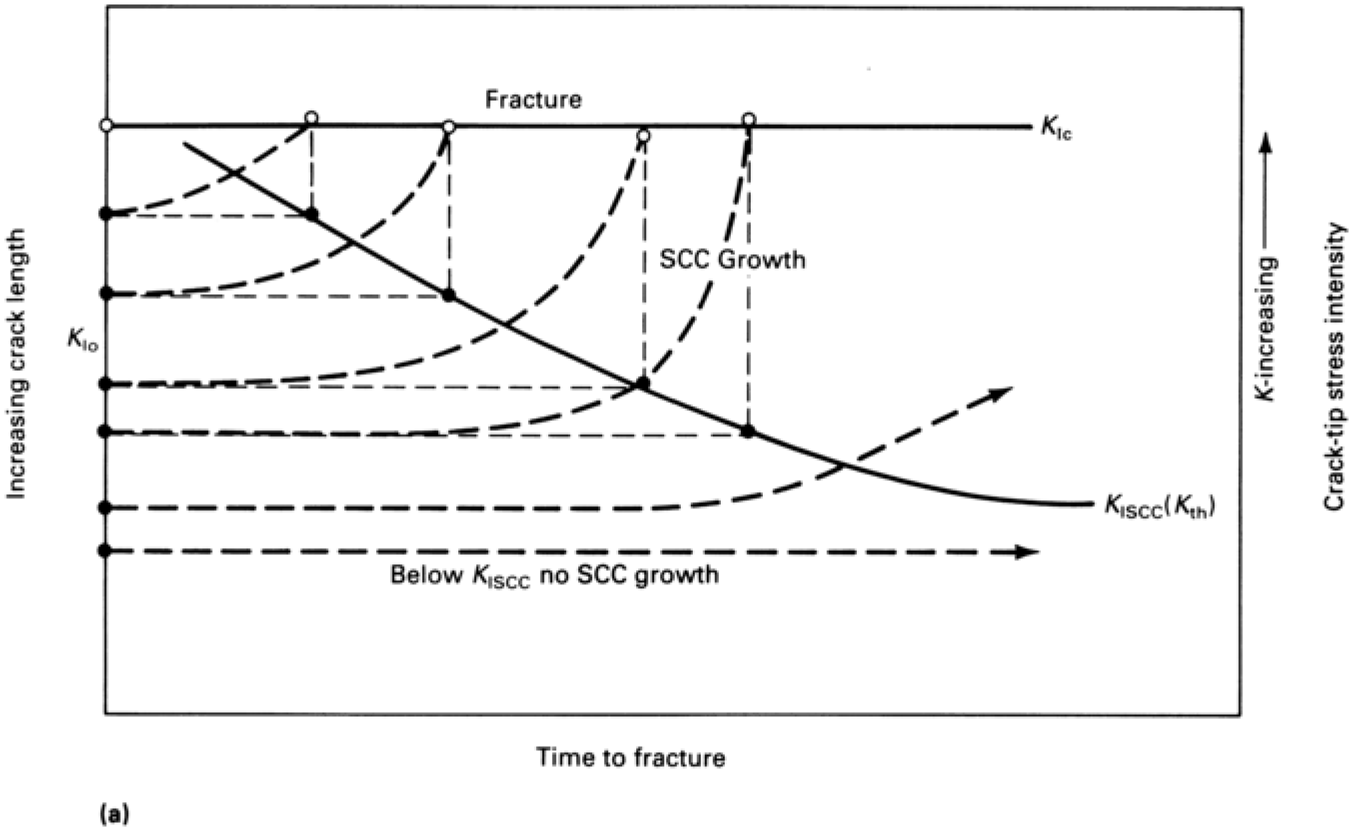

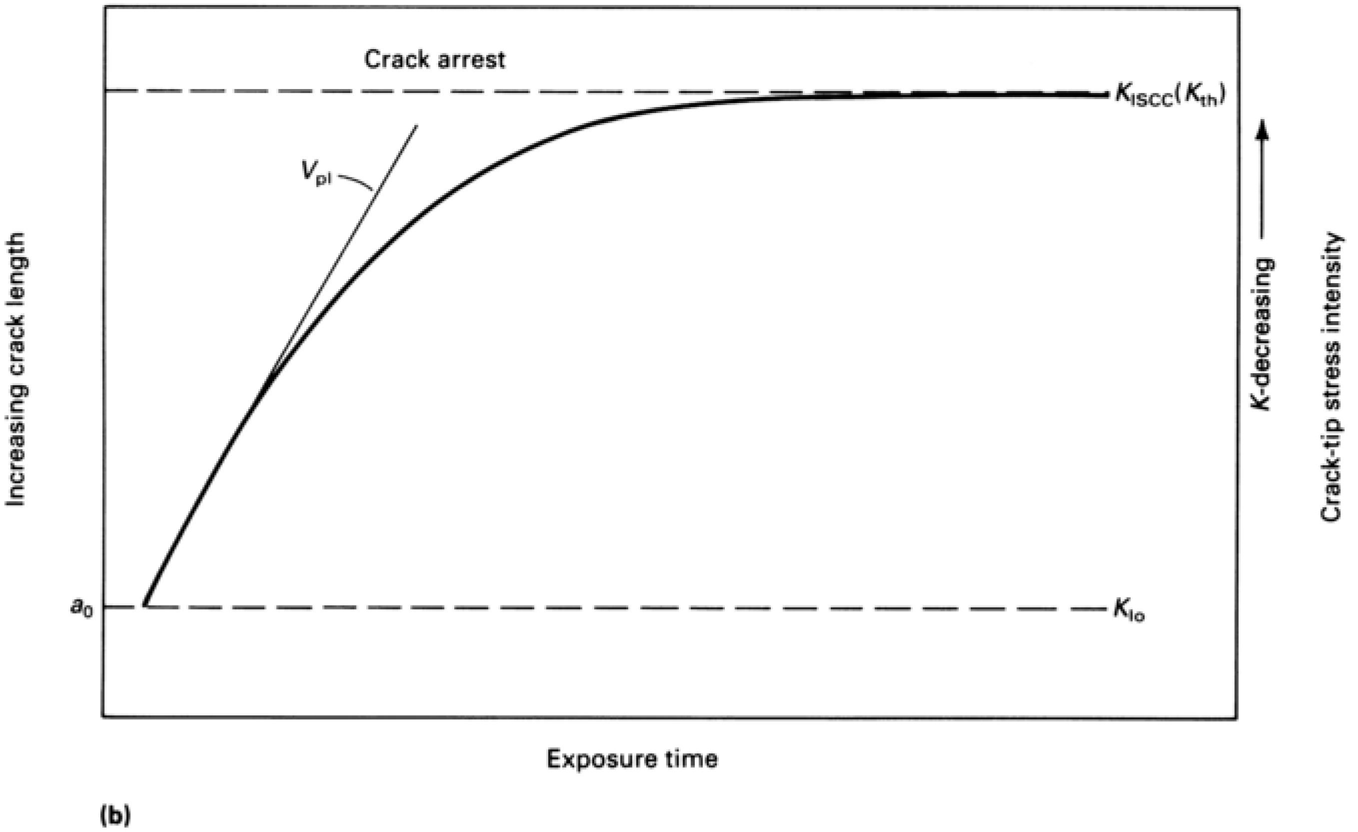

Fig. 29 Comparison of determination of K_{ISCC} by crack initiation versus crack arrest. (a) Constant-load test. (b) Constant crack-opening displacement test. a_0 = depth of precrack associated with the initial stress intensity K_{Io}; V_{pl} = plateau velocity

Figure 31 illustrates an ultrasonic method of measuring crack length at the interior (midwidth and quarter widths) of a bolt-loaded double- beam specimen. This method provides a more accurate measure of crack depth

than visual measurements made on the specimen surfaces. Various other techniques have been used, such as measurement of beam deflection for cantilever beam specimens (Ref 40) and changes in electrical resistance. Such arrangements, however, require calibration. It is feasible and desirable to obtain crack length measurements with a precision of at least ±0.127 mm (±0.005 in.).

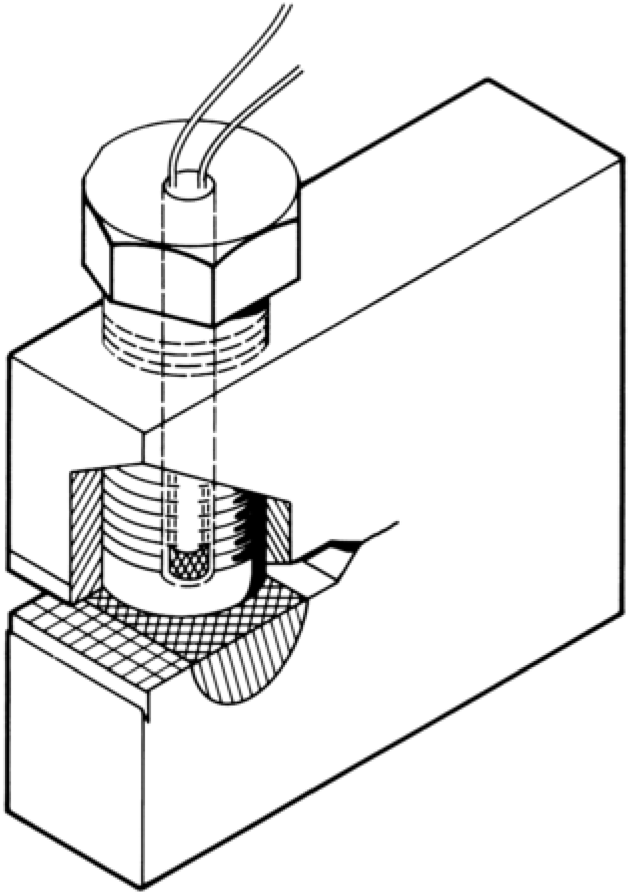

Fig. 30(a) Wedge-opening load specimen loaded with instrumented bolt. Source: Ref 58

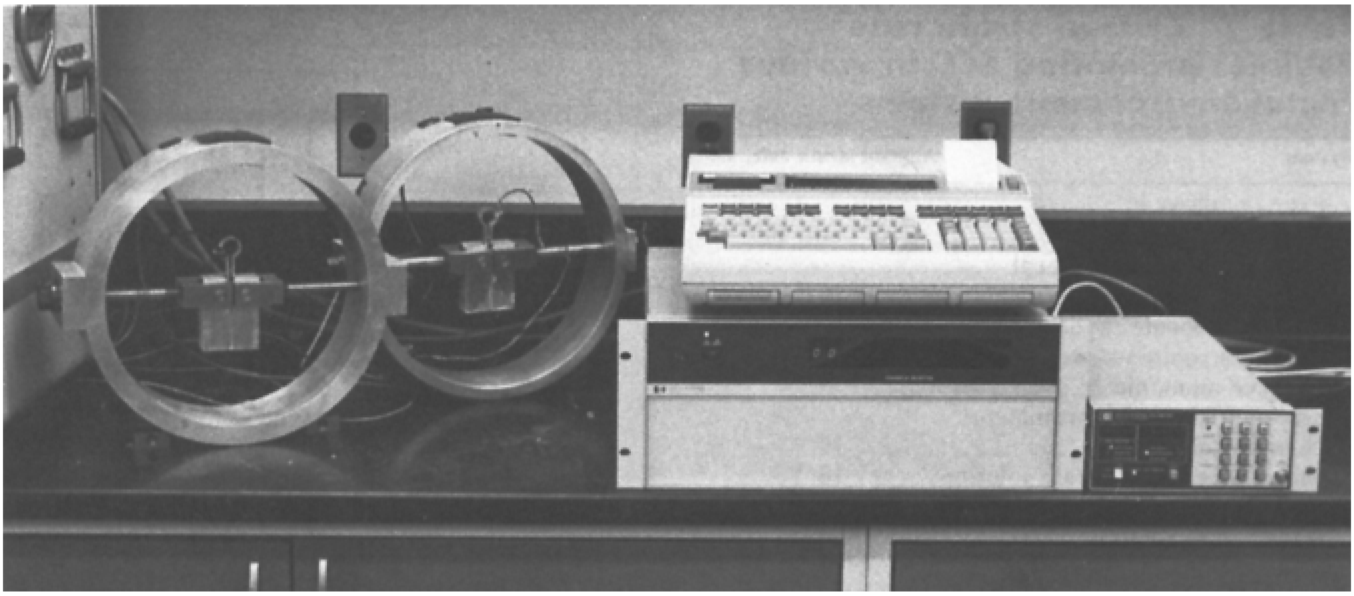

Fig. 30(b) Ring-loaded wedge-opening load specimen test setup. Box to the left of loading rings contains analog signal conditioning for load and displacement signals. The digital data-acquisition system consists of a scanner connected to the analog load and displacement signals, a digital voltmeter, and a portable computer used to read and store data and to control the other instruments. Source: Ref 3

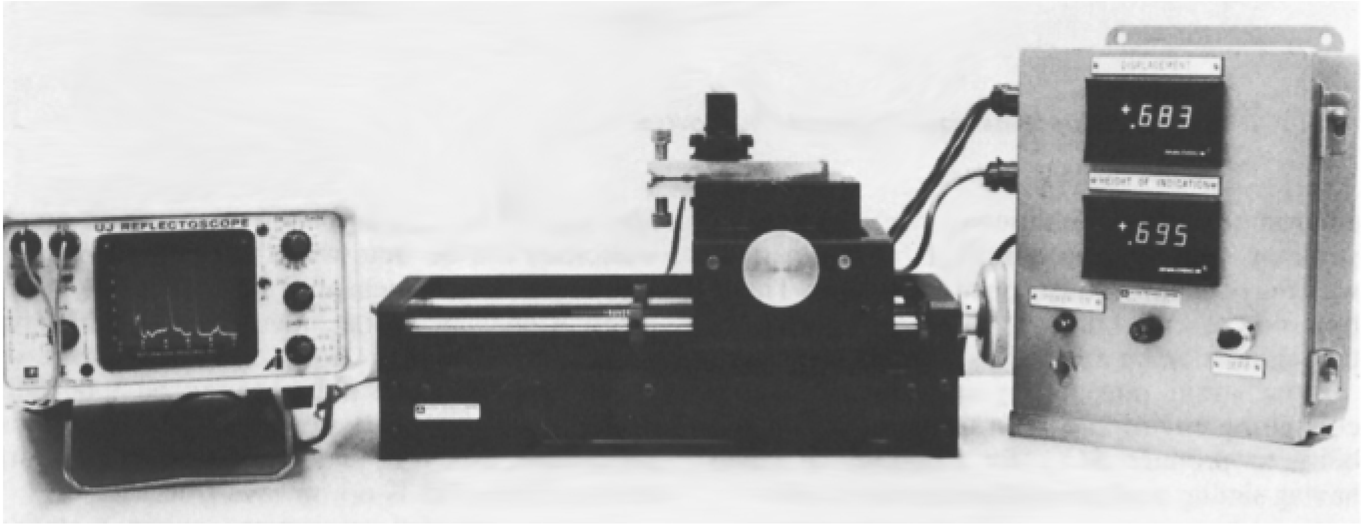

Fig. 31 Ultrasonic crack measurement system for double-beam specimens. Bolt-loaded specimen is mounted on translation stage at center. Ultrasonic transducer is located above specimen, and the oscilloscope at left indicates (left to right) the top of the specimen, the crack plane, and the bottom face reflection. Digital readouts of stage position and peak height for the crack front measurement used to make consistent positioning measurements are shown (right). This system has a crack growth resolution of approximately 0.127 mm (0.005 in.). Source: Ref 3

Exposure to Environment. When practical for laboratory accelerated testing, the test environment should be brought into contact with the specimen before it is stressed or immediately afterward; this enhances access of the corrodent to the crack tip to promote earlier initiation of SCC and to decrease variability in test results. Similarly, in certain cases, it may also be beneficial to introduce the corrodent even earlier, that is, during precracking. However, unless facilities are available to begin environmental exposure immediately after precracking, corrodent remaining at the crack tip may promote blunting due to corrosive attack. In addition, corrosion of the specimen surfaces in the small volume of the precrack or the advancing stress-corrosion crack will change the composition of the environment that is in contact with the crack tip and can significantly affect the test results. For example, hydrolysis reactions can drastically reduce the pH of the aqueous test environment (Ref 59) and can induce embrittlement of some steels by corrosion-product hydrogen.

Selection of an appropriate test duration presents problems that vary with the testing system; this includes the alloy and metallurgical condition, the test environment, and the loading method. Errors in interpretation of the test results can be caused by test durations that are either too short or too long. The optimal length of exposure can be best approached through recognition of meaningful crack propagation rates. What is considered meaningful depends on the available precision of measurement of crack lengths and an acceptably low rate for the criterion of a stress-intensity threshold (Fig. 3). A problem also exists with the correlation of SCC crack growth rates in the laboratory test and in an anticipated service environment. The question leads ultimately to the intended application and a determination of what is a tolerable amount of SCC growth for a given length of time.

Calculation of Crack Growth Rates. There are several procedures for calculating crack growth rate, da/dt, as a function of stress intensity from crack growth curves. The simplest is a graphical $\Delta a/\Delta t$ technique that may incorporate smoothing of the a versus t curve (Ref 46, 47, 48). Another widely used approach is smoothing of the crack growth curve by computer techniques for curve fitting the entire a versus t curve by a multiple-term polynomial function (Ref 40). ASTM E 647 (Ref 60) is also a useful resource, although it is specifically for measuring fatigue crack growth rates.

Other techniques include a secant method and an incremental polynomial method, in which derivatives of the smoothed crack growth curve are calculated at various points to determine instantaneous crack growth rates. Instantaneous growth rates are then plotted against the instantaneous stress intensities, K_{Ii}, at corresponding time intervals to obtain graphs similar to that shown in Fig. 3.

A limited study of the aforementioned four methods of treating crack growth data is presented for a high-strength aluminum alloy in Ref 3. All of the methods used to calculate crack growth rates produced the same general results, which were difficult to interpret because of large amounts of scatter resulting from the use of

small crack growth increments. Moreover, the significance of such graphs is dubious when the corrosivity of the environment and the length of exposure can invalidate the estimate of K by causing gross corrosion-product wedging effects and/or crack branching.

Reduction of crack length data becomes useless without prior subjective interpretation of crack length versus time curves. Allowances should be made for extraneous effects caused by erratic or apparent initiation of stress-corrosion crack growth, scatter in the measurement data due to excessive crack front curvature, multiple crack planes, crack-tip branching, and gross wedging caused by corrosion products.

A simple method of comparing materials by using crack growth curves is based on average growth rates taken from an exposure time of zero to an arbitrary time that is sufficient to achieve significant crack extension in the most SCC-susceptible materials being compared (Ref 52). This method not only rapidly identifies materials with relatively low resistance to SCC, but also provides numerical test results for highly resistant materials that may not develop a K_I versus da/dt curve with a definite plateau (see the section "Testing of Aluminum Alloys" in this article).

References cited in this section

3. D.O. Sprowls et al., "A Study of Environmental Characterization of Conventional and Advanced Aluminum Alloys for Selection and Design: Phase II—The Breaking Load Test Method," Contract NASI- 16424, NASA Contractor Report 172387, Aug 1984

4. B.F. Brown, "Stress Corrosion Cracking Control Measures," National Bureau of Standards Monograph 156, U.S. Department of Commerce, June 1977

30. R.P. Wei, S.R. Novak, and D.P. Williams, Some Important Considerations in the Development of Stress Corrosion Cracking Test Methods, *Mater. Res. Stand.,* Vol 12, 1972, p 25

31. "Characterization of Environmentally Assisted Cracking for Design—State of the Art," National Materials Advisory Board Report No. NMAB-386, National Academy of Sciences, 1982

32. B.F. Brown, The Application of Fracture Mechanics to Stress Corrosion Cracking, *Met. Rev.,* Vol 13, 1968, p 171–183

33. H.R. Smith and D.E. Piper, Stress Corrosion Testing with Precracked Specimens, *Stress Corrosion Cracking in High Strength Steels and in Titanium and Aluminum Alloys,* B.F. Brown, Ed., Naval Research Laboratory, 1972, p 17–78

34. "Standard Method Test for Plane-Strain Fracture Toughness of Metallic Materials," E 399, *Annual Book of ASTM Standards,* Vol 03.01, American Society for Testing and Materials

35. "Standard Test Method for Measurement of Fracture Toughness," E 1820, *Annual Book of ASTM Standards,* Vol 03.01, American Society for Testing and Materials

36. "Standard Practice for Making and Using Precracked Double Beam Stress Corrosion Specimens," G 168, *Annual Book of ASTM Standards,* Vol 03.02, American Society for Testing and Materials

37. "Standard Test Method for Determining Threshold Stress Intensity Factor for Environment-Assisted Cracking of Metallic Materials," E 1681, *Annual Book of ASTM Standards,* American Society for Testing and Materials

38. "Standard Terminology Relating to Fatigue and Fracture Testing," E 1823, *Annual Book of ASTM Standards,* American Society for Testing and Materials

39. J.A. Hauser, H.R.W. Judy, Jr., and T.W. Crooker, “Draft Standard Method of Test for Plane-Strain Stress-Corrosion-Cracking Resistance of Metallic Materials in Marine Environments,” NRL Memorandum Report 5295, Naval Research Laboratory, March 1984

40. W.B. Lisagor, Influence of Precracked Specimen Configuration and Starting Stress Intensity on the Stress Corrosion Cracking of 4340 Steel, *Environment-Sensitive Fracture: Evaluation and Comparison of Test Methods,* STP 821, S.W. Dean, E.N. Pugh, and G.M. Ugiansky, Ed., American Society for Testing and Materials, 1984, p 80–97

41. H. Tada, P. Paris, and G. Irwin, *The Stress Analysis of Cracks Handbook,* Del Research Corporation, 1973

42. J.A. Joyce, D.F. Hasson, and C.R. Crowe, Computer Data Acquisition Monitoring of the Stress Corrosion Cracking of Depleted Uranium Cantilever Beam Specimens, *J. Test. Eval.,* Vol 8 (No. 6), 1980, p 293–300

43. S.R. Novak and S.T. Rolfe, Modified WOL Specimen for K_{ISCC} Environmental Testing, *J. Met.,* Vol 4 (No. 3), 1969, p 701–728

44. J.G. Kaufman, J.W. Coursen, and D.O. Sprowls, An Automated Method for Evaluating Resistance to Stress-Corrosion Cracking with Ring-Loaded Precracked Specimens, *Stress Corrosion—New Approaches,* STP 610, H.L. Craig, Jr., Ed., American Society for Testing and Materials, 1976, p 94–107

45. C. Micheletti and M. Buratti, New Testing Methods for the Evaluation of the Stress- Corrosion Behavior of High-Strength Aluminum Alloys by the Use of Precracked Specimens, *Symposium Proc., Aluminum Alloys in the Aircraft Industry* (Turin, Italy), Oct 1976, Technicopy Ltd., 1978, p 149–159

46. M.V. Hyatt, Use of Precracked Specimens in Stress Corrosion Testing of High Strength Aluminum Alloys, *Corrosion,* Vol 26 (No. 11), 1970, p 487–503

47. D.O. Sprowls et al., “Evaluation of Stress Corrosion Cracking Susceptibility Using Fracture Mechanics Techniques,” Contract NAS 8-21487, Contractor Report NASA CR-124469, May 1973

48. R.C. Dorward and K.R. Hasse, “Flaw Growth of 7075, 7475, 7050, and 7049 Aluminum Plate in Stress Corrosion Environments,” Final Technical Report for U.S. Government Contract NAS 8-30890, Oct 1976; *Corrosion,* Vol 34 (No. 11), 1978, p 386–395

49. W.B. Fichter, The Stress Intensity Factor for the Double Cantilever Beam, *Int. J. Fract.,* Vol 22, 1983, p 133–143

50. J.E. Srawley and B. Gross, Stress Intensity Factors for Crackline-Loaded Edge-Crack Specimens, *Mater. Res. Stand.,* Vol 7 (No. 4), 1967, p 155–162

51. S. Mostovoy, R.B. Crosley, and E.J. Ripling, Use of Crackline Loaded Specimens for Measuring Plane Strain Fracture Toughness, *J. Mater.,* Vol 2 (No. 3), 1967, p 661–681

52. D.O. Sprowls and J.D. Walsh, Evaluating Stress-Corrosion Crack Propagation Rates in High Strength Aluminum Alloys with Bolt Loaded Precracked Double Cantilever Beam Specimens, *Stress Corrosion—New Approaches,* STP 610, H.L. Craig, Jr., Ed., American Society for Testing and Materials, 1976, p 143–156

53. R.B. Heady, Evaluation of Sulfide Corrosion Cracking Resistance in Low Alloy Steels, *Corrosion,* Vol 33 (No. 3), 1977, p 98–107

54. T.L. Bond, R.A. Yeske, and E.N. Pugh, Studies of Stress Corrosion Crack Growth in Al-Zn-Mg Alloys by the Double Torsion Method, *Environment-Sensitive Fracture: Evaluation and Comparison of Test Methods,* STP 821, S.W. Dean, E.N. Pugh, and G.M. Ugiansky, Ed., American Society for Testing and Materials, 1984, p 128–149

55. J.C. Lewis and G. Sines, Ed., *Fracture Mechanics: Fourteenth Symposium, Vol II, Testing and Application,* STP 791, American Society for Testing and Materials, 1983

56. S.W. Dean, E.N. Pugh, and G.M. Ugiansky, Ed., *Environment-Sensitive Fracture: Evaluation and Comparison of Test Methods,* STP 821, American Society for Testing and Materials, 1984

57. J.H. Underwood, S.W. Freiman, and F.I. Baratta, Ed., *Chevron-Notched Specimens: Testing and Stress Analysis,* STP 855, American Society for Testing and Materials, 1984

58. W.B. Gilbreath and M.J. Adamson, Aqueous Stress Corrosion Cracking of High Toughness D6AC Steel, *Stress-Corrosion—New Approaches,* STP 610, H.L. Craig, Jr., Ed., American Society for Testing and Materials, 1976, p 176–187

59. B.F. Brown, Concept of Occluded Corrosion Cells, *Corrosion,* Vol 26 (No. 8), 1970, p 249

60. “Standard Test Method for Measurement of Fatigue Crack Growth Rates,” E 647, *Annual Book of ASTM Standards,* American Society for Testing and Materials

B. Phull, Evaluating Stress-Corrosion Cracking, *Corrosion: Fundamentals, Testing, and Protection*, Vol 13A, *ASM Handbook*, ASM International, 2003, p 575–616

Evaluating Stress-Corrosion Cracking

Revised by Bopinder Phull, Consultant

Dynamic Loading: Slow-Strain-Rate Testing

An important method for accelerating the SCC process in laboratory testing involves relatively slow-strain-rate tension (SSRT) testing of a specimen during exposure to appropriate environmental conditions. In other words, the test specimen is stretched monotonically in axial tension at a slow rate until failure. This method is also known as constant extension-rate tensile (CERT) testing. The application of slow dynamic strain exceeding the elastic limit assists in the SCC initiation. This accelerated technique is consistent with the various proposed general mechanisms of SCC, most of which involve plastic microstrain and film rupture.

Slow-strain-rate tests can be used to test a wide variety of product forms, including parts joined by welding. Tests can be conducted in tension, in bending, or with plain, notched, or precracked specimens. The principal advantage of slow-strain-rate testing is the rapidity with which the SCC susceptibility of a particular alloy and environment can be assessed.

Slow-strain-rate testing is not terminated after an arbitrary period of time. Testing always ends in specimen fracture, and the mode of fracture is then compared with the criteria of SCC susceptibility for the test material. In addition to its timesaving benefits, generally less scatter occurs in the test results. Comprehensive discussions on the slow-strain-rate testing technique can be found in Ref 61, 62, 63, 64. Procedures for conducting SSRT tests are described in ASTM G 129 (Ref 65).

Critical Strain Rate. The most significant variable in slow-strain-rate testing is the magnitude of strain rate. If the strain rate is too high, ductile fracture will occur before the necessary corrosion reactions can take place. Therefore, relatively low strain rates must be used. However, at too low a strain rate, corrosion may be prevented because of repassivation or film repair so that the necessary reactions of bare metal cannot be sustained, and SCC may not occur. Although typical critical strain rates range from 10^{-5} to 10^{-7} s^{-1} depending on the alloy and environment system, the most severe strain rate must be determined in each case.

The repassivation reaction that is observed at very low strain rates and that prevents the formation of anodic SCC does not occur when cracking is the result of embrittlement by corrosion-product hydrogen. This mechanistic difference can be used to distinguish between anodic SCC (active path corrosion) and cathodic SCC (hydrogen embrittlement) as shown in Fig. 32.

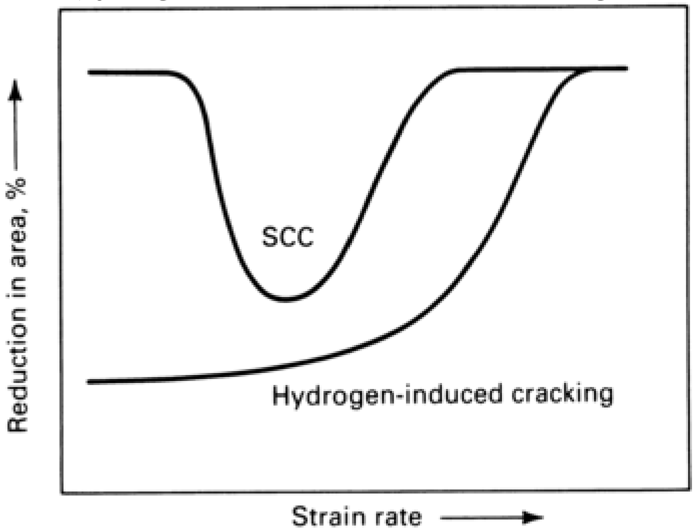

Fig. 32 Effect of strain rate on SCC and hydrogen-induced cracking. Source: Ref 66

The fastest strain rate that will promote SCC in a given system depends on crack velocity. Generally, the lower the SCC velocity, the slower the strain rate required. Applied strain rates known to have promoted SCC in metal/ environment systems are listed in Table 2.

Table 2 Critical strain rate regimes promoting SCC in various metal/ environment systems

System	Applied strain rate, s^{-1}
Aluminum alloys in chloride solutions	10^{-4} and 10^{-7}
Copper alloys in ammoniacal and nitrite solutions	10^{-6}
Steels in carbonate, hydroxide, or nitrate solutions and liquefied ammonia	10^{-6}
Magnesium alloys in chromate/chloride solutions	10^{-5}
Stainless steels in chloride solutions	10^{-6}
Stainless steels in high-temperature solutions	10^{-7}
Titanium alloys in chloride solutions	10^{-5}

The most relevant strain rates for various aluminum alloys are shown in Fig. 33. These trends illustrate that slow-strain-rate tests should be performed in a strain-rate regime that is appropriate for the given alloy and environment system.

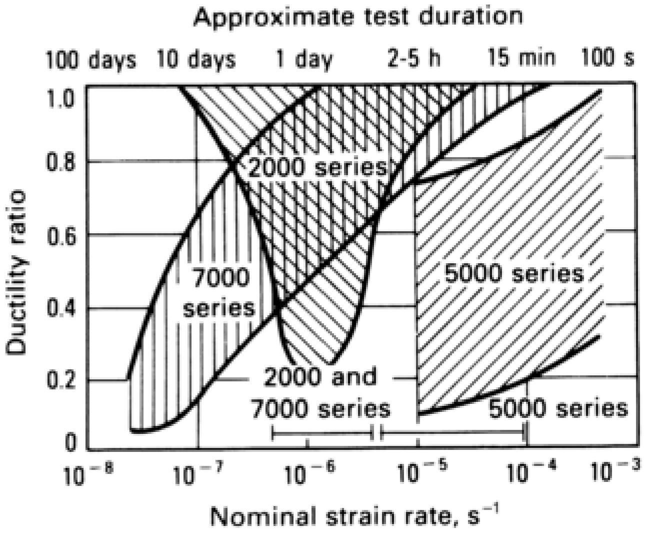

Fig. 33 Strain-rate regimes for studying SCC of various aluminum alloys. Corrodent: 3% sodium chloride plus 0.3% hydrogen peroxide. Source: Ref 64

Test Specimen Selection. Standard tension specimens (ASTM E 8) (Ref 67) are generally recommended for use with the specified conditions of gage lengths, radii, and so on, unless specialized studies are being conducted. For initially smooth specimens, the strain rate at the onset of the test is clearly defined: however, once cracks have initiated and grown, straining is likely to concentrate in the vicinity of the crack tip, and the effective strain rate is unknown. Rigorous solutions for determining the strain rate at crack tips or notches are not available, but effective strain rates are likely to be higher than for the same deflection rate applied to plain specimens.

Notched or precracked specimens can be used to restrict cracking to a given location—for example, when testing the heat-affected zone associated with a weld. Notched or precracked specimens can also be used to restrict load requirements where bending, as opposed to tensile loading, may offer an added benefit. The section thickness or diameter of such specimens is usually relatively small, so the testing duration is short.

Testing Equipment. Constant-strain-rate apparatus requirements include sufficient stiffness to resist significant deformation under the loads necessary to fracture the test specimens, a system to provide reproducible, constant strain rates over the range of 10^{-4} to 10^{-8} s^{-1}, and a cell to contain the test solution. Auxiliary equipment is used to control environmental conditions and to record test data. The testing equipment can also be instrumented to record load-elongation curves, which is convenient when testing at various strain rates. A typical constant-strain-rate unit is shown in Fig. 34. Various types of corrosion cells may be required to control the test conditions for specific studies.

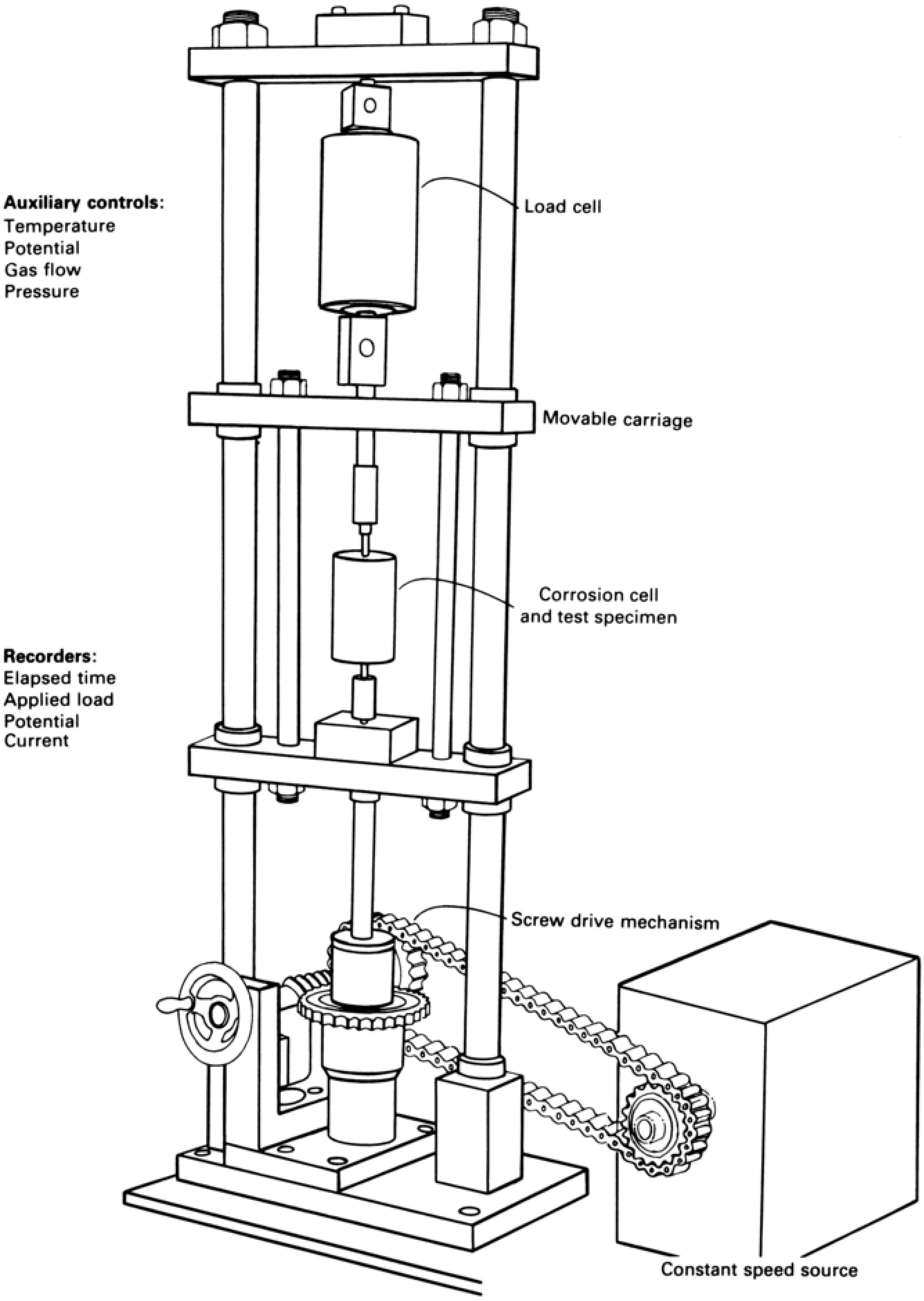

Fig. 34 Typical slow-strain-rate test apparatus. Source: Ref 63

In addition to uniaxial tensile units, cantilever constant-strain-rate apparatus has also been used in which an extension arm attached to a cantilever beam specimen is lowered at a constant rate. This technique has been successfully used to study SCC of low-carbon steel in carbonate- bicarbonate environments to determine crack velocity, critical strain rates, and inhibitor effectiveness (Ref 68). Additional information on slow-strain-rate testing equipment and procedures is available in Ref 56 and 61.

Assessment of Results. Historically, the principal methods of SCC assessment derived from SSRT testing were based on time to failure, maximum gross section stress developed during the tension test, percent elongation, fracture energy (area bounded by the load-elongation curve), and reduction in area. Figure 35 depicts stress-elongation curves that illustrate how stress-corrosion cracks influence the elongation to fracture as well as the maximum load.

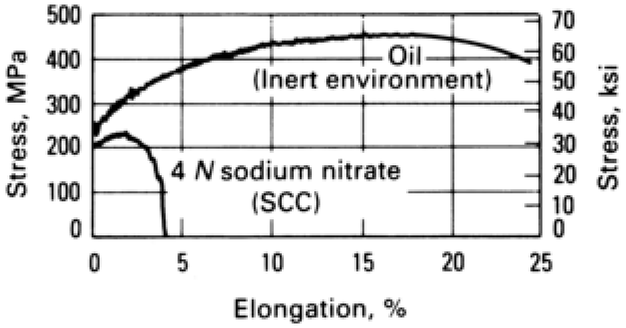

Fig. 35 Nominal stress versus elongation curves for carbon-manganese steel in slow-strain-rate test in boiling 4 *N* sodium nitrate and in oil at the same temperature. Source: Ref 62

To eliminate non-SCC effects, parallel tests are conducted in an inert environment, and a ratio of the result obtained in the corrodent divided by the result obtained in the inert environment is commonly used as an index of SCC susceptibility. For example, in Fig. 33, higher SCC resistance is denoted by higher ductility ratios.

Figure 36 shows a stress-corroded specimen containing many secondary stress-corrosion cracks and reduced ductility at fracture. Some alloys experience rapid deterioration of mechanical properties on contact with certain corrosive environments; any additional effect of applied straining can best be assessed by comparison with the behavior of unstrained specimens. Therefore, it is essential that the cause of environmental degradation be verified as SCC.

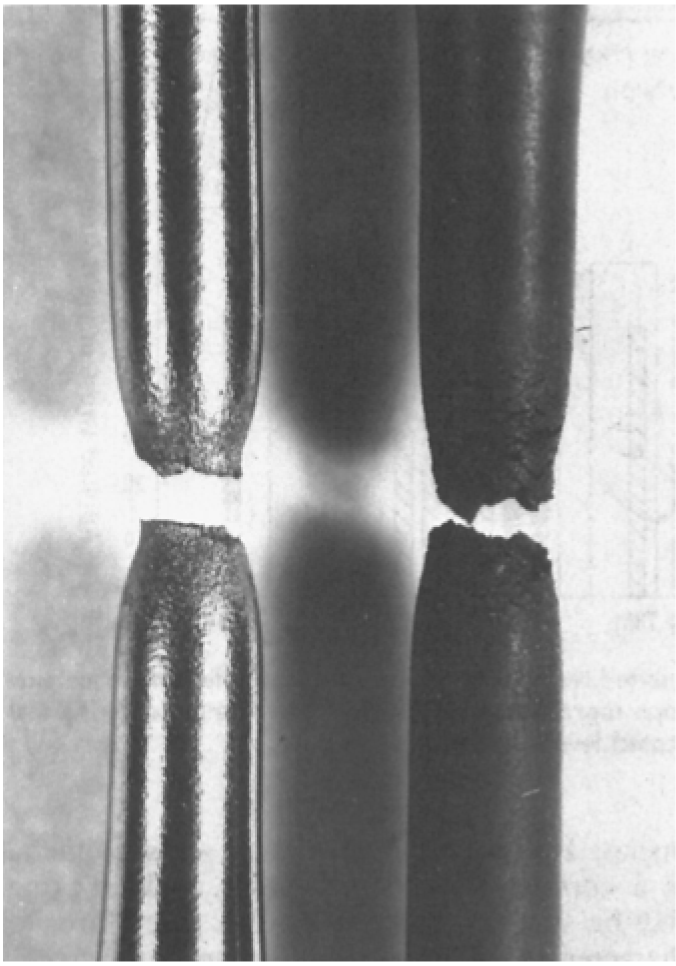

Fig. 36 Macrographs of two carbon steel specimens after slow-strain-rate tests conducted at a strain rate of 2.5 × 10^{-6} s^{-1} and 80 °C (180 °F). The ductility ratio in this example was 0.74 (original diameter: 2.54 mm, or 0.100 in.). Left: Ductile fracture in oil. Right: SCC in carbonate solution

Slow-strain-rate testing is very efficient in comparing environments in terms of their capability to produce SCC, for example, in steels having similar metallurgical characteristics. However, such comparisons are difficult and not very reliable when applied to groups of steels with different characteristics (Ref 66).

Slow-strain-rate testing as generally used does not provide data that can be used for design purposes. Recent work, however, has shown that average SCC velocities, threshold stresses, and threshold strain rates can be obtained with modified techniques combined with microscopy (Ref 62, 68, 69). For example, average SCC crack velocities can be determined from the depth of the largest crack measured on the fracture surfaces of specimens that have failed completely, or in longitudinal sections on the diameter of specimens that have not experienced total failure, divided by the time of testing. With this procedure, SCC is assumed to initiate at the start of the test, which is not always true.

With precracked specimens, other methods can be used to monitor crack growth and thus allow determination of crack velocities. The SCC behavior of a pipeline steel (Fig. 37) has been studied by using a precracked cantilever bend specimen in terms of threshold strain rate for crack growth and also in terms of crack growth rates analogous to the stage II plateau velocity shown in Fig. 3. Material properties, such as strength and toughness, that influence SCC performance when measured by tension testing are eliminated as factors; therefore, valid comparisons can be made of alloys with widely different structures and mechanical properties. Additional information on this method of assessment and the effects of strain rate can be found in Ref 70, 71, 72. Screening of alloys for sour oilfield service by the SSRT technique is covered by a NACE International test method (Ref 73). Reference 74 describes limitations of SSRT testing for evaluating SCC in the chemical-process industry.

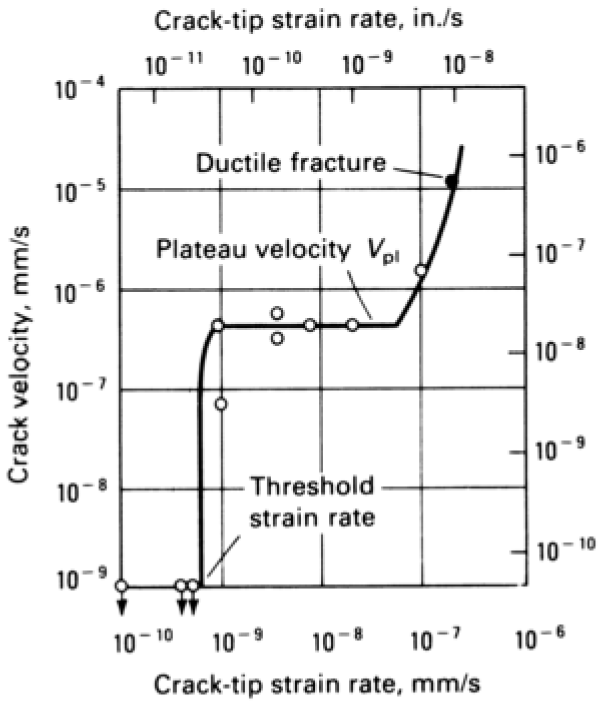

Fig. 37 Effects of beam deflection rate on stress-corrosion crack velocity in precracked cantilever bend specimens of a carbon-manganese steel. Tested in a carbonate-bicarbonate solution at 75 °C (165 °F) and at a potential of -650 mV versus SCE. Source: Ref 62

References cited in this section

56. S.W. Dean, E.N. Pugh, and G.M. Ugiansky, Ed., *Environment-Sensitive Fracture: Evaluation and Comparison of Test Methods,* STP 821, American Society for Testing and Materials, 1984

61. G.M. Ugiansky and J.H. Payer, Ed., *Stress Corrosion Cracking—The Slow Strain- Rate Technique,* STP 665, American Society for Testing and Materials, 1979

62. R.N. Parkins, Development of Strain-Rate Testing and Its Implications, *Stress-Corrosion Cracking—The Slow Strain-Rate Technique,* STP 665, G.M. Ugiansky and J.H. Payer, Ed., American Society for Testing and Materials, 1979, p 5–25

63. J.H. Payer, W.E. Berry, and W.K. Boyd, Constant Strain Rate Technique for Assessing Stress-Corrosion Susceptibility, *Stress-Corrosion—New Approaches,* STP 610, H.L. Craig, Jr., Ed., American Society for Testing and Materials, 1976, p 82–93

64. N.J.H. Holroyd and G.M. Scamans, Slow- Strain-Rate Stress Corrosion Testing of Aluminum Alloys, *Environment-Sensitive Fracture: Evaluation and Comparison of Test Methods,* STP 821, S.W. Dean, E.N. Pugh, and G.M. Ugiansky, Ed., American Society for Testing and Materials, 1984, p 202–241

65. "Practice for Slow Strain Rate Testing to Evaluate the Susceptibility of Metallic Materials to Environmentally Assisted Cracking," G 129, *Metal Corrosion, Erosion, and Wear,* Vol 03.02, *Annual Book of ASTM Standards,* American Society for Testing and Materials

66. C.D. Kim and B.E. Wilde, A Review of Constant Strain-Rate Stress Corrosion Cracking Test, *Stress Corrosion Cracking—The Slow Strain Rate Technique,* STP 665, G.M. Ugianski and J.H. Payer, Ed., American Society for Testing and Materials, 1979, p 97–112

67. "Standard Methods of Tension Testing of Metallic Materials," E 8, *Annual Book of ASTM Standards,* Vol 03.01, American Society for Testing and Materials

68. R.N. Parkins, “Fifth Symposium on Line Pipe Research,” Catalog No. L30174, U1- 40, American Gas Association

69. W.R. Wearmouth, G.P. Dean, and R.N. Parkins, Role of Stress in the Stress Corrosion Cracking of a Mg-Al Alloy, *Corrosion,* Vol 29 (No. 6), 1973, p 251–258

70. R.N. Parkins and Y. Suzuki, Environment Sensitive Cracking of a Nickel-Aluminum Bronze under Monotonic and Cyclic Loading Conditions, *Corros. Sci.,* Vol 23 (No. 6), 1983, p 577–599

71. R.N. Parkins, A Critical Evaluation of Current Environment-Sensitive Fracture Test Methods, *Environment-Sensitive Fracture: Evaluation and Comparison of Test Methods,* STP 821, S.W. Dean, E.N. Pugh, and G.M. Ugiansky, Ed., American Society for Testing and Materials, 1984, p 5–31

72. J. Yu, N.J.H. Holroyd, and R.N. Parkins, Application of Slow-Strain-Rate Tests to Defining the Stress for Stress Corrosion Crack Initiation in 70/30 Brass, *Environment-Sensitive Fracture: Evaluation and Comparison of Tests Methods,* STP 821, S.W. Dean, E.N. Pugh, and G.M. Ugiansky, Ed., American Society for Testing and Materials, 1984, p 288–309

73. “Slow Strain Rate Test Method for Screening Corrosion-Resistant Alloys (CRAs) for Stress Corrosion Cracking in Sour Oilfield Service,” NACE TM-01-98, NACE International, 1998

74. J.A. Beavers and G.H. Koch, *Limitations of the Slow Strain Rate Test for Stress Corrosion Cracking Testing,* MTI Publication No. 39, Materials Technology Institute of the Chemical Process Industries, 1994

B. Phull, Evaluating Stress-Corrosion Cracking, *Corrosion: Fundamentals, Testing, and Protection*, Vol 13A, *ASM Handbook,* ASM International, 2003, p 575–616

Evaluating Stress-Corrosion Cracking

Revised by Bopinder Phull, Consultant

Selection of Test Environments

The primary environmental factors in SCC testing are the nature and concentration of anions and cations in aqueous solutions, electrochemical potential, solution pH, the partial pressure and nature of species in gaseous mixtures, and temperature. Separately or in combination, environmental variables can have a profound effect on the thermodynamics and kinetics of the electrochemical processes that control environmentally assisted fracture. Therefore, the choice of environmental conditions provides an important basis for developing accelerated SCC test methods.

The environmental requirements for SCC vary with different alloys. Although a mechanical precrack or a critical strain rate provides a worst case for SCC from a mechanical standpoint, there does not appear to be a generally applicable worst case from an environmental standpoint. However, because the presence of moisture and saltwater is universal, the SCC characteristics of alloys in these environments—as well as in any special environment a given engineering structure may experience—are always of interest.

Figure 38 illustrates that electrochemical factors can override mechanical factors in determining SCC initiation sites. Three cantilever beam specimens of PH13-8Mo stainless steel were tested in saltwater. Specimen A was tested at a high K level. With the participation of the chloride ions, the protective oxide film ruptured at the bottom of the precrack and initiated SCC, which was halted before the beam fractured completely. Specimen B was loaded at a lower K level. After 1300 h, a stress-corrosion crack initiated, but not in the precrack. Crack

initiation occurred under the wall of the cell that surrounded the central portion of the specimen and contained the saltwater.

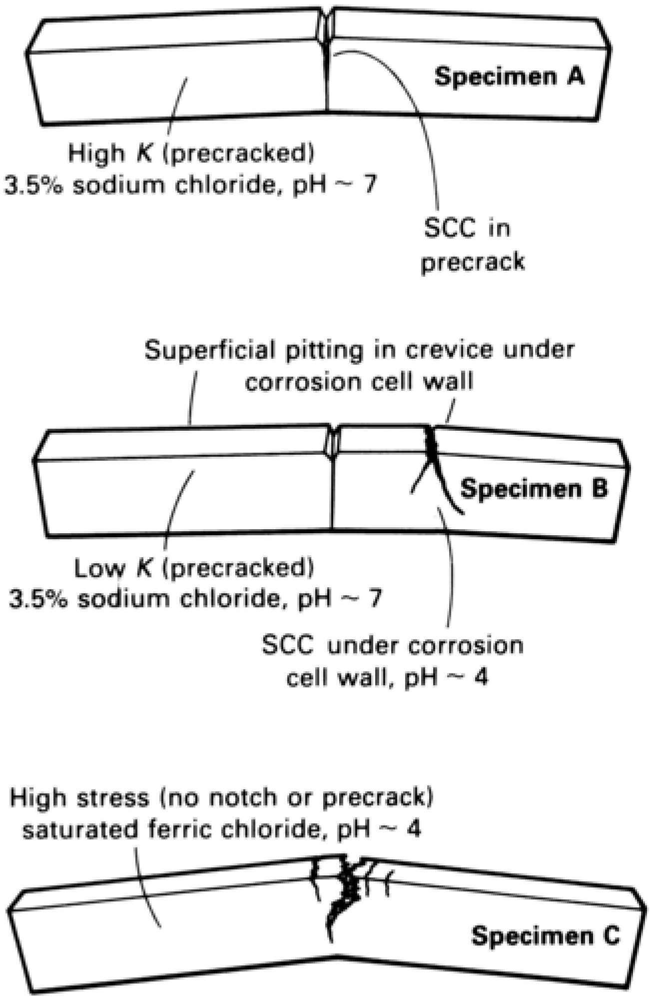

Fig. 38 Cantilever beam specimens of PH13-8Mo stainless steel after testing. Experiments demonstrate that electrochemical factors can override mechanical factors in determining initiation sites of SCC. See text for details. Source: Ref 75

Careful examination of this specimen and replicate specimens revealed small crevice-corrosion pits under the wall that initiated SCC in an almost smooth surface. Even if these small pits had been as sharp as a fatigue crack, the *K* level would have been much lower than at the machined and fatigued notch. In the stagnant situation under the cell wall, the stainless steel reacted with the saltwater to form hydrochloric acid and other corrosion products from the metal. Therefore, the low pH in a crevice, due to the hydrolysis of chromium corrosion product, overcame the mechanical disadvantage of the lack of a precrack. Specimen C was then tested to verify the effectiveness of electrochemical conditions in crack initiation. Saturated ferric chloride was selected to lower the pH to the range inside an active corrosion pit in the stainless steel; application of the solution to the unnotched beam resulted in the immediate initiation of many cracks in the smooth surface. Hydrochloric acid was found to be equally effective.

Stress-corrosion tests can be divided into two broad environmental classes: those conducted in actual service environments and those conducted under laboratory conditions.

Service Environments and Field Testing. The following examples illustrate the value, and in some cases the necessity, of exposure tests performed in actual service environments as an adjunct to laboratory evaluation. The standard 3.5% sodium chloride alternate immersion test data for aluminum alloys 2024 and 7075 proved useless in predicting the serviceability of these aluminum alloys for handling rocket propellant oxidizers such as nitrogen tetroxide and inhibited red fuming nitric acid (Ref 76). The alternate immersion test showed 2024-T351 and 7075- T651 to be susceptible to SCC at low short-transverse stresses, but 2024-T851 and 7075-T7351 were quite resistant even at high stresses. These data were supported by outdoor field tests in seacoast and industrial atmospheres.

However, in proof tests consisting of exposure to the actual service environment—inhibited red fuming nitric acid at 74 °C (165 °F)—SCC occurred in both tempers of 7075 alloy and did not occur in either temper of 2024 alloy (Fig. 39). There were no unexpected failures with the 2219-T87 and 6061-T651 materials, however.

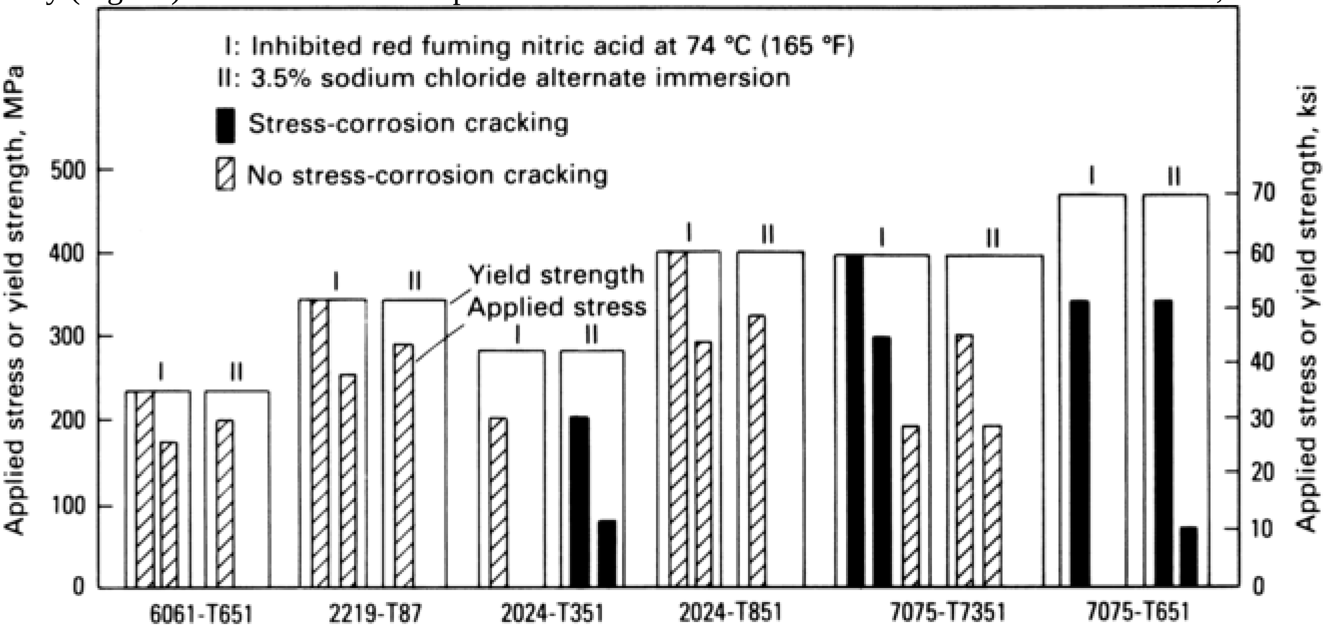

Fig. 39 SCC resistance of various aluminum alloys in inhibited red fuming nitric acid versus alternate immersion in 3.5% NaCl solution. Each bar graph represents an individual short-transverse C-ring test specimen machined from rolled plate and stressed at the indicated level. Source: Ref 76

Simulated-service tests should be conducted under conditions duplicating the service environment exactly, as illustrated by the following example with Ti-6Al-4V alloy pressure tanks for propellant-grade nitrogen tetroxide (<0.20 wt% moisture) (Ref 77). Preliminary laboratory SCC tests using specimens of Ti-6Al-4V demonstrated satisfactory compatibility with the nitrogen tetroxide and gave no indication of SCC.

In subsequent tests of actual pressurized tanks, however, SCC occurred rapidly, and the tanks failed. It was subsequently shown that the nitrogen tetroxide used in the tanks was of a higher- purity grade than that used in the laboratory tests. When test specimens were exposed to this grade of nitrogen tetroxide, they also failed. The small quantities of water and nitric oxide (impurities) present in the nitrogen tetroxide used in previous studies were sufficient to inhibit SCC of Ti-6Al- 4V in nitrogen tetroxide.

Field testing consists of placing a metal specimen in an environment in which conditions represent those anticipated in service. Typical examples include immersion in seawater, exposure to the atmosphere at marine or industrial sites, chemical plant streams, and so on. Field tests can be performed with test coupons or with actual or simulated structural components.

Laboratory Environments. Accelerated testing is conducted extensively in controlled laboratory environments for developmental studies in which it is not considered necessary that the test medium duplicate a particular service environment. Reliance should not be placed on such test results, however, unless they can be correlated with practical service experience or with the results of appropriate field tests.

Ideally, the results of a short exposure in a laboratory test will enable a reliable prediction of the SCC performance of an alloy over a long service period under particular environmental conditions. To fulfill this function, test conditions should be selected with regard to the anticipated service conditions. However, accelerated test media that yield reliable results for one alloy may not yield dependable results for another alloy, even though both alloys are of the same basic metal (Ref 9, 71). Therefore, caution must be exercised in the development and use of standardized test media. Recommended test media for various metals and alloys are discussed in later sections.

Mercury, other liquid-metal systems, and molten salts can also cause failure by cracking of metal under stress. In many cases of this type, oxidation-reduction reactions (corrosion) may not be involved; thus, the mechanisms of cracking under such conditions could be quite different from that of “classical” SCC.

Cracking caused by hydrogen embrittlement has been found to occur in titanium-base alloys and many high-strength ferrous alloys in various service environments. Hydrogen, under some conditions, enters the stressed

metal without the presence of a corrosion reaction, and cracking ensues. Hydrogen can also enter stressed metal as a corrosion reaction product, and cracking may be stimulated or may ensue. Therefore, to characterize adequately the environmental cracking of such alloys under sustained tensile stress, testing should be performed both with and without conditions that could involve hydrogen damage.

Length of Exposure. The question of appropriate test durations for the different material- environment combinations and the apparent need to establish them experimentally on a case- by-case basis has been a major stumbling block in the adoption of standard SCC test methods. The situation becomes acute when the results of an SCC test must be evaluated before all replicate specimens have cracked. In these cases, when a statistical probability evaluation must be performed, it should be recognized that time to failure is often normally distributed with respect to the logarithm of test time (see the section "Interpretation of Test Results" in this article). Exposure periods that are too short can result in a test that is trifling; when too long, they can introduce extraneous effects. An example is the excessive pitting of smooth test specimens that leads to failure by a different (and possibly unsuspected) mode of SCC, or by mechanical overload rather than by SCC (Ref 23). Problems in the case of precracked specimens can result from test periods being too short to develop a proper estimate of an apparent threshold stress intensity, especially in *K*-increasing tests; on the other hand, periods that are too long may result in corrosion-product wedging or crack tip blunting, both of which can invalidate calculations of the effective stress intensity and SCC growth rates in *K*-decreasing tests (Ref 32, Ref 47, Ref 48). Therefore, it is necessary to scrutinize test results carefully so that extraneous effects can be excluded from the analysis of the test results.

Electrochemical Tests. Recognition of the importance of electrical potential as one of the controlling parameters in SCC has resulted in increasing use of tests with potentiostatic control or impressed electrical current. No standards exist for such electrochemical tests, although several methods are routinely used. These tests involve specific conditions that are applicable only to given alloy and environment systems under consideration. These types of tests offer greater rapidity and precision than free corrosion tests.

Sophisticated approaches for studying systems involving active path corrosion use potentiodynamic methods. Anodic polarization curves can provide reasonably accurate predictions of the critical potential ranges and kinetic factors controlling SCC in a given system. One procedure (Ref 78) involves first scanning a range of potentials in the anodic direction at a relatively high scan rate (~1000 mV/min) to determine regions with high current density, in which intense anodic activity is likely. This is followed by a relatively low scan rate (~20 mV/min), which indicates regions where relative inactivity is likely.

Scans should be started at a potential at which the surface is film free. The rapid scan minimizes film formation so that the observed currents relate to relatively film-free conditions. The slow scan allows time for filming to occur. Comparison of the two curves reveals any ranges of potential within which high anodic activity in the film-free region reduces to insignificant activity when the time requirements for film formation are met, thus indicating the critical potential range in which SCC is likely.

Figure 40 illustrates this type of experiment for a low-carbon steel in a carbonate-bicarbonate solution with the predicted domains of behavior. Establishing a precise range of critical potentials for SCC requires subjective determination of boundary conditions relating to the current densities.

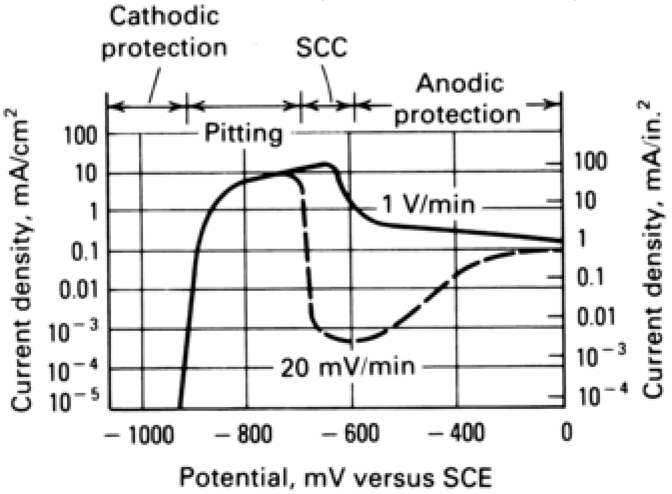

Fig. 40 Potentiodynamic polarization curves for carbon-manganese steel in 1 *N* sodium carbonate plus 1 *N* sodium bicarbonate at 90 °C (195 °F) showing the domains of behavior predicted from the curves. Source: Ref 78

A different approach with the use of anodic polarization curves has been used to characterize the SCC behavior of aluminum alloys (Ref 79). Corrosion of a susceptible microstructure in aqueous chloride solutions was exclusively intergranular only for a limited range of potentials between the first and second breakdown potentials, E_{BR}, determined from the anodic polarization curve, where E_{BR1} approximates the critical pitting potential of the active corrosion path at the grain boundaries and E_{BR2} approximates the critical pitting potential of the grain bodies. Figure 41 depicts an anodic polarization curve for aluminum alloy 7075-T651, illustrating the predicted domains of behavior.

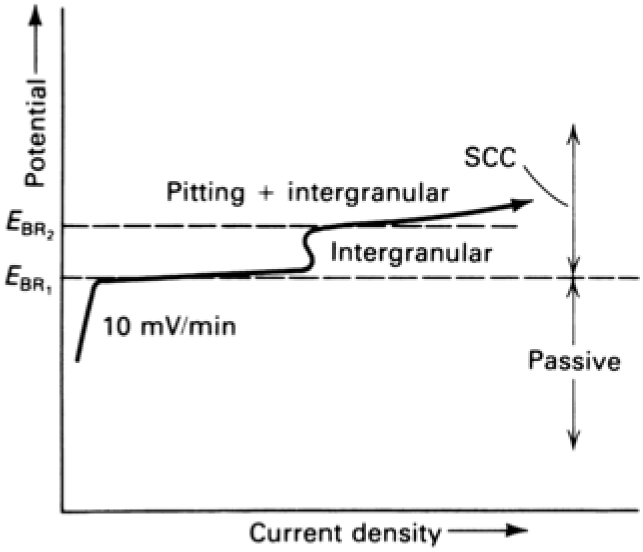

Fig. 41 Anodic polarization curves for aluminum alloy 7075-T651 in deaerated 3.5% sodium chloride solution showing the domains of behavior predicted from the curve. Source: Ref 80

The use of anodic polarization curves and related measurements is discussed in ASTM G 5 (Ref 81). Information obtained from the anodic polarization curve can be useful for screening environmental test media to reduce the number of actual SCC tests required. However, such electrochemical tests are concerned with testing a bulk environment in contact with an exposed surface, and it should not be assumed that such measurements represent the crack tip under conditions of crack growth. Therefore, even when an environment is identified as innocuous, a potent local environment may exist, such as in a pit when the pitting potential is exceeded or in a crevice or precrack.

Moreover, when laboratory SCC tests involve cracks or crevices, the potential at the crack tip may differ appreciably from that measured at the surface where the crack or crevice emerges. In laboratory tests, it must be considered whether or not environmental changes in composition or potential are involved and how they may relate to service conditions (Ref 71).

References cited in this section

9. H.L. Craig, Jr., D.O. Sprowls, and D.E. Piper, Stress-Corrosion Cracking, *Handbook on Corrosion Testing and Evaluation,* W.H. Ailor, Ed., John Wiley & Sons, 1971, p 259

23. D.O. Sprowls et al., Evaluation of a Proposed Standard Method of Testing for Susceptibility to SCC of High Strength 7XXX Series Aluminum Alloy Products, *Stress- Corrosion—New Approaches,* STP 610, H.L. Craig, Jr., Ed., American Society for Testing and Materials, 1976, p 3–31

32. B.F. Brown, The Application of Fracture Mechanics to Stress Corrosion Cracking, *Met. Rev.,* Vol 13, 1968, p 171–183

47. D.O. Sprowls et al., “Evaluation of Stress Corrosion Cracking Susceptibility Using Fracture Mechanics Techniques,” Contract NAS 8-21487, Contractor Report NASA CR-124469, May 1973

48. R.C. Dorward and K.R. Hasse, “Flaw Growth of 7075, 7475, 7050, and 7049 Aluminum Plate in Stress Corrosion Environments,” Final Technical Report for U.S. Government Contract NAS 8-30890, Oct 1976; *Corrosion,* Vol 34 (No. 11), 1978, p 386–395

71. R.N. Parkins, A Critical Evaluation of Current Environment-Sensitive Fracture Test Methods, *Environment-Sensitive Fracture: Evaluation and Comparison of Test Methods,* STP 821, S.W. Dean, E.N. Pugh, and G.M. Ugiansky, Ed., American Society for Testing and Materials, 1984, p 5–31

75. B.F. Brown. The Contributions of Physical Metallurgy and of Fracture Mechanics to Containing the Problem of Stress Corrosion Cracking, *Philos. Trans. R. Soc. (London) A,* Vol 282 (No. 1307), 1976, p 235–245

76. D.O. Sprowls and R.H. Brown, Stress Corrosion Mechanisms for Aluminum Alloys, *Fundamental Aspects of Stress-Corrosion Cracking,* R.W. Staehle, A.J. Forty, and D. van Rooyen, Ed., National Association of Corrosion Engineers, 1969, p 466–512

77. J.D. Jackson, W.K. Boyd, and R.W. Staehle, “Corrosion of Titanium,” DMIC Memorandum 218, Defense Metals Information Center, Battelle Memorial Institute, Sept 1966

78. R.N. Parkins, Predictive Approaches to Stress Corrosion Cracking Failure, *Corros. Sci.,* Vol 20, 1980, p 147–166

79. J.R. Galvele and S.M. DeMichelli, Mechanism of Intergranular Corrosion of Al-Cu Alloys, *Corros. Sci.,* Vol 10, 1970, p 795–807

80. S. Maitra and G.C. English, Mechanism of Localized Corrosion of 7075 Alloy Plate, *Metall. Trans. A,* Vol 12, March 1981, p 535–541

81. “Test Method for Jaw Crusher Gouging Abrasion Test,” G 5, *Metal Corrosion, Erosion, and Wear,* Vol 03.02, *Annual Book of ASTM Standards,* American Society for Testing and Materials

---

B. Phull, Evaluating Stress-Corrosion Cracking, *Corrosion: Fundamentals, Testing, and Protection*, Vol 13A, *ASM Handbook*, ASM International, 2003, p 575–616

Evaluating Stress-Corrosion Cracking

Revised by Bopinder Phull, Consultant

Testing of Aluminum Alloys

Stress-corrosion cracking of susceptible high- strength aluminum alloys can occur in moist air, seawater, and potable waters, and it varies with the alloy and temper and the magnitude of sustained tensile stress. Chloride solutions are generally favored for laboratory tests because sodium chloride is widely distributed in nature, and the test results are potentially relatable to stress- corrosion behavior in natural environments.

Testing with Smooth Specimens

Historically, stress-corrosion testing of aluminum alloys has been done with smooth (notch-free) specimens, and most published SCC ratings of aluminum alloys are based on such tests.

Alternate Immersion in 3.5% Sodium Chloride. Exposure to 3.5% sodium chloride or to substitute ocean water (ASTM D 1141) by alternate immersion (ASTM G 44) (Ref 82) is a widely used procedure for testing smooth specimens of aluminum alloys. Aeration of the specimens, achieved by the alternate immersion, enhances the corrosion potential (Ref 83) and produces more rapid SCC of most aluminum alloys than continuous immersion. The ASTM G 44 standard practice consists of a 1 h cycle that includes a 10 min soak in the aqueous solution followed by a 50 min period out of solution in air at 27 °C (80 °F) and 45% relatively humidity, during which time the specimens are air dried. This 1 h cycle is repeated continuously for the total number of days recommended for the particular alloy being tested. Typically, aluminum alloys are exposed from 20 to 90 days, depending on the resistance of the alloy to corrosion by saltwater. This test method is widely used for testing most types of aluminum alloys with all types of smooth specimens.

The alternate immersion test is primarily used for alloy development studies and for quality control of alloys with improved resistance to SCC (Ref 9, 84). This test method is specified in ASTM G 47 (Ref 85), which covers the method of sampling, type of specimen, specimen preparation, test environment, and method of exposure for determining the susceptibility to SCC of high-strength 2000-series alloys (1.8 to 7.0% Cu) and 7000-series alloys (0.4 to 2.8% Cu). Alternate immersion in 3.5% sodium chloride is also specified in ASTM G 64 for SCC testing of heat treatable aluminum alloys (Ref 86).

The parallel SCC behavior of a variety of aluminum alloys in the ASTM G 44 test and in a severe seacoast atmosphere is shown in Table 3. Additional comparisons may be found in Ref 23 and Ref 88. The relatively conservative estimate of the SCC behavior of an intermediate-resistance alloy in the ASTM G 44 test compared to that in various atmospheric environments is shown in Fig. 42, which also illustrates the wide range of behaviors in various atmospheric environments.

Table 3 Comparison of the SCC behavior of various aluminum alloys in the ASTM G 44 test and after 5 years in a seacoast atmosphere

3.2 mm ($\frac{1}{8}$ in.) diam short-transverse tension specimens obtained from 64 mm (2.5 in.) thick hot-rolled plate; nine replicate specimens per test stress

Alloy and temper	Applied stress			Number of failures		Time to first and median failure, days				
				ASTM G 44[(a)]	**Seacoast atmosphere[(b)]**	**ASTM G 44[(a)]**		**Seacoast atmosphere[(b)]**		
	MPa	**ksi**	**% of yield strength**			**First**	**Median**	**First**	**Median**	
	2024-T351	145	21	50	9	9	7	7	37	37
		87	12.6	30	9	9	7	7	37	37
2024-T851	295	42.8	75	8	8	37	65	37	266	
	197	28.6	50	0	2	…	…	643	…	
5456-H116	156	22.6	75	0	0	…	…	…	…	
6061-T651	254	36.8	90	0	0	…	…	…	…	
7050-T7651	227	32.9	50	0	0	…	…	…	…	
	136	19.7	30	0	0	…	…	…	…	
	91	13.2	20	0	0	…	…	…	…	
7050-T7451	217	31.5	50	0	0	…	…	…	…	
	130	18.9	30	0	0	…	…	…	…	

	87	12.6	20	0	0	…	…	…	…
7075-T651	221	32	50	…	9	…	…	7	7
	154	22.3	35	9	9	7	7	7	15
	88	12.8	20	9	9	7	67	7	37
7075-T7651	300	43.5	75	8	6	69	77	709	1491
	200	29	50	0	1	…	…	1069	…
	120	17.4	30	…	0	…	…	…	…
7075-T7351	335	48.6	90	6	2	67	80	1866	…
	273	39.6	75	0	0	…	…	…	…
	183	26.5	50	…	0	…	…	…	…

(a) Alternate immersion in 3.5% sodium chloride solution for 84 days: see Ref 82.
(b) Point Judith, RI.
Source: Ref 87

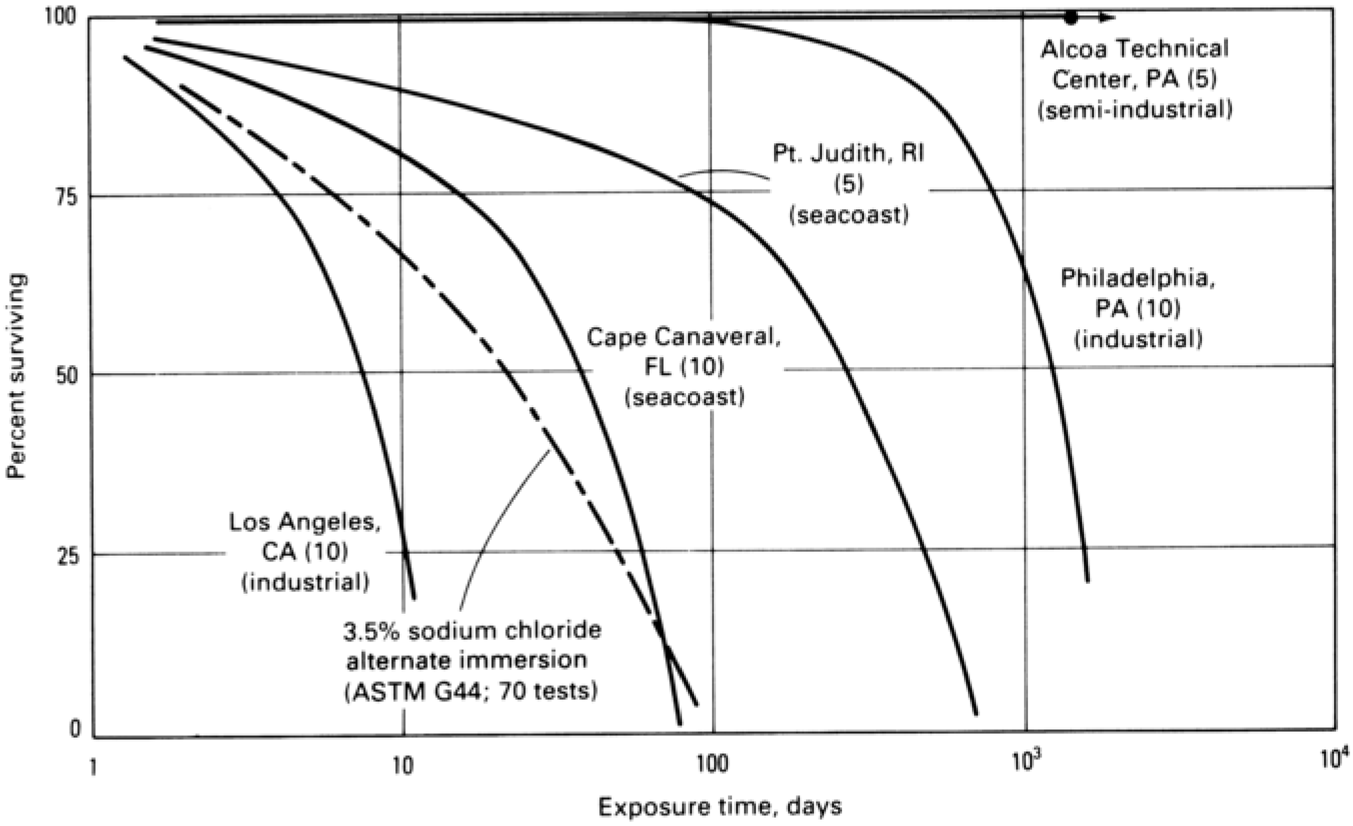

Fig. 42 Effect of variations in atmospheric environment on the probability and time to failure by SCC of a material with an intermediate susceptibility. Tests were made on short-transverse 3.2 mm (0.125 in.) diam tension specimens from 7075-T7651 type plate stressed 310 MPa (45 ksi). Parenthetical values indicate replication of tests. Source: Ref 3

Although ASTM G 44 is a good general-purpose test for aluminum alloys, it is not equally discriminating of all alloys at near-threshold stress levels. This tendency has been reported for 7000-series (Al-Zn-Mg-Cu) alloys containing less than about 1% Cu (Ref 9, 21, 88). Also, the test is not representative of special chemical environments, such as inhibited red fuming nitric acid (Fig. 39).

Continuous Immersion in Boiling 6% Sodium Chloride. A four-day exposure by continuous immersion in boiling 6% sodium chloride solution is widely used by U.S. aluminum producers for testing smooth specimens of 7000- series alloys containing no more than 0.26% Cu. Comparison of this test and a modified ASTM G 44 test to the industrial atmospheric exposure shown in Fig. 43 illustrates the advantage of the boiling salt test, ASTM G 103 (Ref 89).

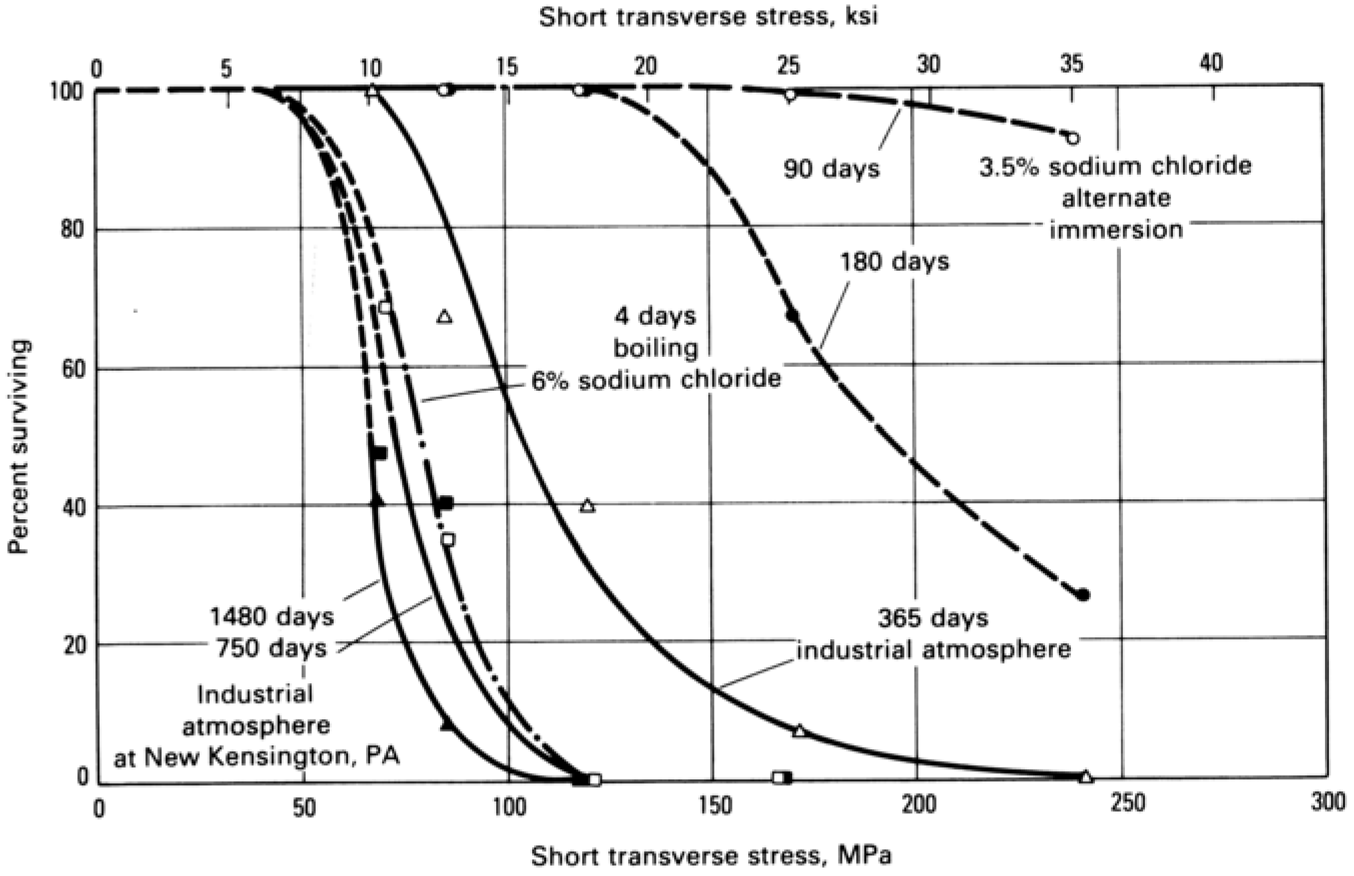

Fig. 43 Correlation of accelerated test media with service environment (industrial atmosphere). Combined data for five lots of rolled plate of aluminum alloy 7039-T64 (4.0Zn-2.8Mg-0.3Mn-0.2Cr). Tests in 3.5% sodium chloride were similar to ASTM G 44, except salt solution was made with commercial grade sodium chloride and New Kensington tap water. Source: Ref 9

This test is not effective for, and therefore not recommended for, the 2000-series (aluminum- copper) alloys, or the 5000-series (aluminum- magnesium) alloys. It is intended for statically loaded smooth nonwelded or welded specimens of 7000-series (Al-Zn-Mg-Cu) alloys containing <0.26% Cu. It appears to correlate better with outdoor atmospheric exposure than the ASTM G 44 procedure for the foregoing 7000-series aluminum alloys.

The impressed-current test for 5000-series alloys was developed for rapid evaluation of smooth coupon specimens of the 5000-series (aluminum-magnesium) alloys. The test solution is 3.5% sodium chloride, and the acceleration is provided by impressing on the test specimen a dc electrical current of 6.2×10^{-2} mA/mm^2 (40 mA/in.^{2}) of specimen surface. Good correlation with natural environment exposures is reported in Ref 90.

Other Testing Media. Although nitrates and sulfates, when dissolved in distilled water, tend to retard SCC, their presence in chloride environments can produce a synergistic stimulation of intergranular corrosion and SCC (Ref 80, 91, 92). Stress-corrosion cracking can also be accelerated for certain alloys by increasing acidity (lower pH), increasing temperature, adding oxidants, or electrochemically driving the SCC process by impressing an appropriate potential or electrical current density. These procedures, either singly or in combination, have been used to create various special-purpose tests:

- Continuous immersion test for 7000-series (Al-Zn-Mg) alloys (Ref 93): aqueous solution containing 3% sodium chloride, 0.5% hydrogen peroxide (30%), 100 mL/L 1 *N* sodium hydroxide, and 20 mL/L acetic acid (100%); pH 4.0

- Continuous immersion test for high-strength aircraft alloys (Ref 94): aqueous solution containing 2% sodium chloride plus 0.5% sodium chromate
- Impressed-current test for 7000-series (Al- Zn-Mg) alloys (Ref 95): aqueous solution containing 2% sodium chloride plus 0.5% sodium chromate; pH 8.1, current density 4.65×10^{-4} mA/mm^2 (0.3 mA/in.^{2}); 30 day maximum exposure time
- Alternate immersion test using an aqueous solution containing 2.86% sodium chloride plus 0.52% magnesium chloride (total chloride equal to that in ocean water): proposed in Ref 96 as a less corrosive substitute for 3.5% sodium chloride solution for ASTM G 44
- Continuous immersion test for 2000-series (aluminum-copper) and 7000 series (Al-Zn- Mg-Cu) alloys (Ref 97): aqueous 1% sodium chloride plus 2% potassium dichromate at 60 °C (140 °F); 168 h maximum exposure time
- Continuous immersion test for 2000-series (aluminum-copper) and 7000-series (Al-Zn- Mg-Cu) alloys (Ref 47, 48): aqueous solution containing 0.6 *M* sodium chloride, 0.02 *M* sodium dichromate, 0.07 *M* sodium acetate, plus acetic acid to pH 4; used principally for testing precracked specimens

Testing with Precracked Specimens

Testing aluminum alloys with precracked specimens, especially the bolt-loaded double- beam type, has been performed extensively, and the ranking of materials by this method is generally in good agreement with that established with smooth specimen tests. However, a number of problems in the interpretation of test results must be taken into account (Ref 45, 46, 47, 48, 98, 99, 100, 101).

The bolt-loaded *K*-decreasing type of test is attractive because no complicated apparatus is required to perform the tests, and the results appear to be relatable to the control of SCC problems in engineering structures. Distinction among test materials or test environments is based on the amount and the rate of penetration by SCC, with the results being expressed in terms of crack depth, a threshold stress-intensity factor (K_{ISCC} or K_{th}), or plateau velocity (V_{pl}) (Fig. 3).

For example, the relative susceptibilities of various alloys can be determined from crack depth versus time curves after testing for exposure periods as short as 150 to 200 h (Ref 46). This is shown for an extreme range of susceptibilities in Fig. 44. Plateau velocities in this example are indicated by graphical estimates of the average slopes of the initial portions of the crack growth curves, beginning at the time when growth started and extending until the curves definitely started to bend over toward an arrest. An arrest would indicate K_{th}, but real arrests (zero crack growth) may not occur; therefore, it is customary to define K_{th} as the crack tip stress intensity at which the crack growth rate has decreased to the limit of measuring capability. This is usually about 10^{-10} m/s (1 to 2×10^{-5} in./h), that is, where the growth is less than 0.2 mm (0.008 in.) within 30 days.

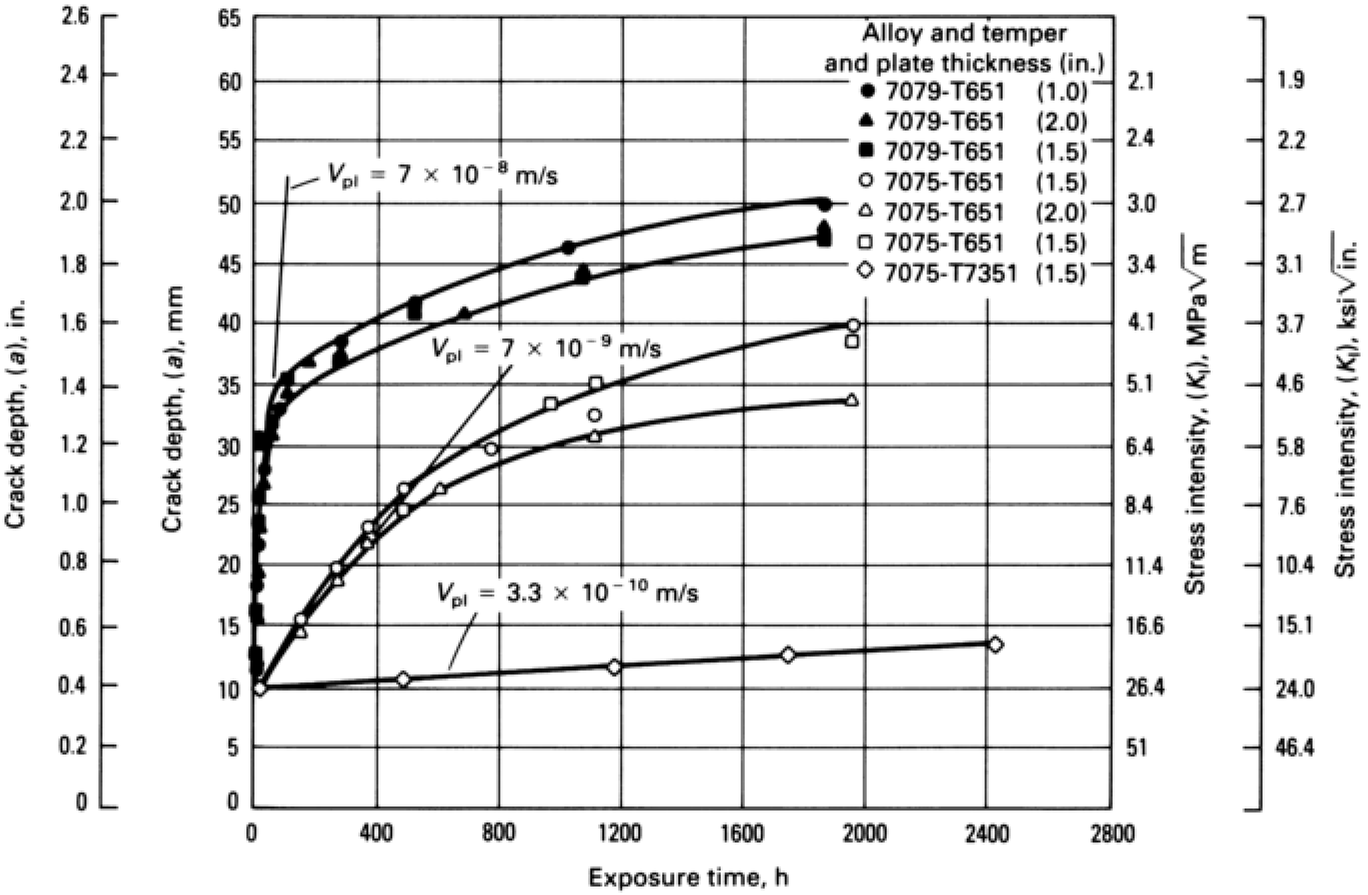

Fig. 44 Crack depth and stress intensity versus time curves for double-beam specimens of aluminum alloys 7075-T651, 7079-T651, and 7075-T7351 having nearly identical deflections and starting crack depths. Specimens with S-L orientation (see Fig. 28) measuring 25 × 25 × 127 mm (1 × 1 × 5 in.) bolt loaded to pop-in and wetted three times daily with 3.5% sodium chloride. Source: Ref 46

Plateau velocities can be readily determined for materials having a relatively low resistance to SCC, such as 7075-T651 and 7079-T651 alloy plates when stressed in the short-transverse direction. Such tests have been effectively used for the evaluation of corrosive environments and the study of SCC trends with the artificial aging of 7000-series (Al-Zn-Mg-Cu) alloys (Ref 98, 99). However, the use of plateau velocities for comparing materials with higher resistance to SCC becomes complicated when only small amounts of crack growth occur in normal exposure periods. In such cases, the initial penetration of SCC, even at near-critical stress intensities, may be delayed by an initiation (incubation) period and then may begin at small independent sites along an uneven mechanical crack front. The crack measurements are erratic, and the interpretation of the crack growth curves is subjective. Comparisons among relatively resistant materials are difficult.

Figure 45 shows a number of crack growth curves for several resistant materials. It is evident that the estimated plateau velocities are quite variable and do not correlate consistently with the total crack growth in a given exposure time. For these more SCC-resistant materials, average growth rates for the first 15 days of exposure appear to relate much better to the actual amount of crack growth and to smooth specimen ratings according to ASTM G 64 (Table 4).

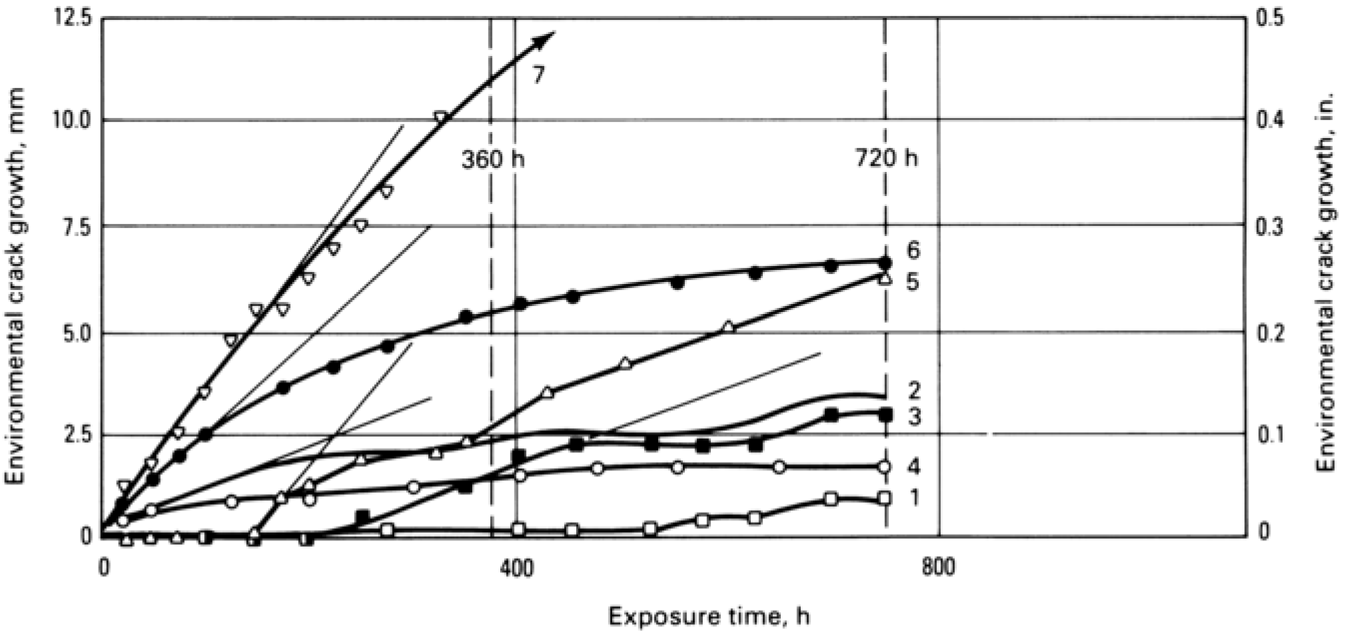

Fig. 45 Examples of SCC crack growth in various aluminum alloys with relatively high resistance to SCC. S-L (see Fig. 28) double-beam specimens bolt-loaded to pop-in and wetted with 3.5% sodium chloride three times daily; relative humidity 45%. The numbers 1 to 7 indicate different test materials listed in order of decreasing resistance to SCC (see Table 4); dashed lines indicate plateau velocities. The alloy 2 specimen failed by mechanical fracture rather than intergranular SCC. Source: Ref 47, 52

Table 4 Correlation of SCC plateau crack velocities with smooth specimen SCC ratings

Alloy	Smooth specimen rating[(a)]	Plateau crack velocity			
		First growth		**Average (0 to 15 days)**	
		m/s	**in. × 10^{-5}/h**	**m/s**	**in. × 10^{-5}/h**
1	A	6×10^{-10}	10	2×10^{-10}	3
2	A	7×10^{-9}	100[(b)]	1.8×10^{-9}	27[(b)]
3	B	2.1×10^{-9}	30	1.2×10^{-9}	19
4	B	4.2×10^{-9}	60	1.3×10^{-9}	20
5	B	7×10^{-9}	100	2.1×10^{-9}	30
6	C	6.3×10^{-9}	90	4.2×10^{-9}	60
7	D	1.1×10^{-8}	160	8.4×10^{-9}	120

Note: S-L (see Fig. 28) double-beam specimens bolt-loaded to pop-in and wetted three times daily with 3.5% sodium chloride.

(a) Short-transverse ratings per ASTM G 64 (Ref 86).

(b) Fractographic examination revealed mechanical fracture rather than the intergranular SCC verified in all other materials. Source: Ref 52

The performance of alloy 2 in Table 4 indicates another potential problem with tests performed at very high stress intensities; that is, with some very resistant materials, environmental crack growth will possibly be the result of mechanical fracture rather than of SCC. Therefore, it is necessary when testing SCC-resistant materials to verify that the crack growth is in fact SCC.

The determination of threshold stress intensities by the arrest method is frequently complicated by corrosion-product wedging, which changes the stress state at the tip of the crack and invalidates the calculation of effective stress intensities from the crack lengths. With low-resistance alloys, such as 7075-T651, an arrest may never occur, because the crack is continually driven ahead by the advancing wedge of insoluble corrosion products (Ref 47, 99). An indication of this was shown by the initiation of SCC in precracked specimens exposed with no applied load for just a few months in a seacoast atmosphere (Ref 47). Experimental evidence of a threshold stress intensity will depend on the amount of corrosion occurring in a given alloy/ environment system (Fig. 46).

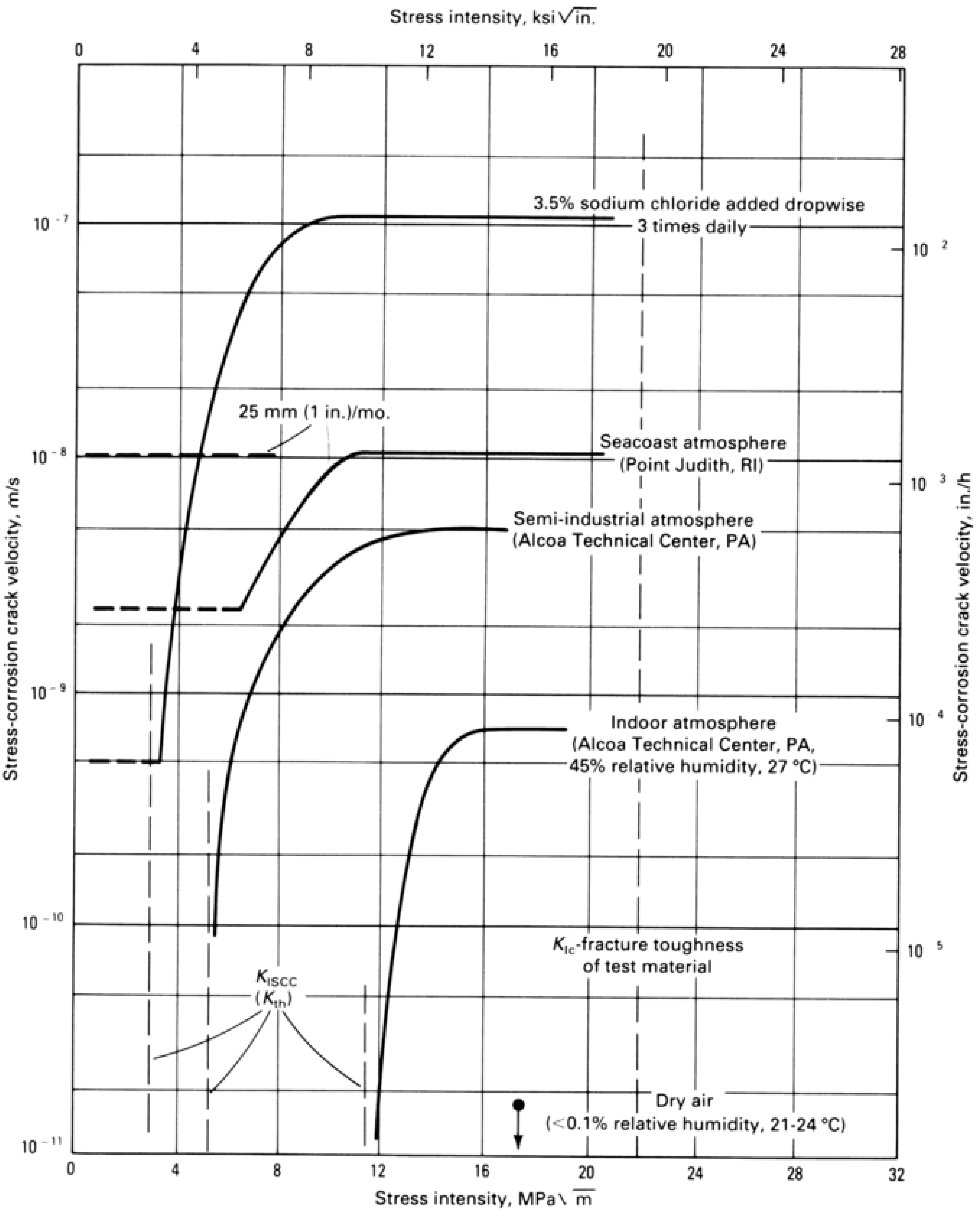

Fig. 46 Effect of corrosive environment on SCC velocity and threshold stress intensity for 7079-T651 plate (64 mm, or 2.5 in., thick) stressed in the short-transverse direction (S-L; see Fig. 28). Double-beam specimens bolt-loaded to pop-in. No SCC occurred during 3 years of exposure to dry air in a desiccator; however, the plateau velocity (horizontal part of each curve) and the apparent threshold stress intensity (K_{ISCC} or K_{th}) vary with the environment. Dashed portions of the curves represent the effect of corrosion-product wedging. Source: Ref 52

With intermediate-resistance materials, the growth curves may develop prominent steps indicative of temporary arrests. Figure 47 shows some of the various curves that may be obtained, depending on the resistance to corrosion and SCC of the test material, the corrosivity of the test medium, the magnitude of the applied stress intensity, and the length of exposure. The significant portion of the curve is that which goes from the beginning of the test to the first appreciable cessation of the crack growth. It is assumed that if it were not for the intervention of the corrosion-product wedging the curve would proceed to an arrest.

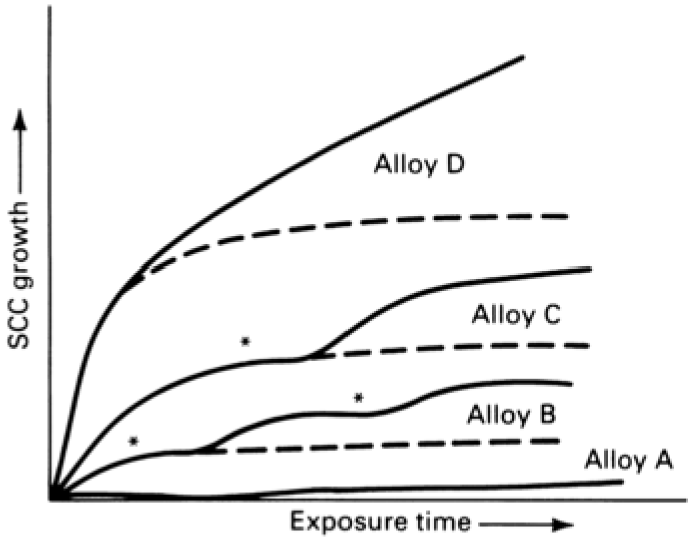

Fig. 47 The variable effects of corrosion-product wedging on SCC growth curves in a *K*-decreasing test. Solid lines: measured curve. Dashed lines: estimated true curve excluding the effect of corrosion-product wedging. Asterisks indicate temporary crack arrests.

The threshold stress intensities determined by this method can be useful for ranking materials, but usually cannot be considered valid. Therefore, they cannot be used in design calculations based on fracture mechanics. Displays of complete *V*–*K* curves provide convenient comparisons of various materials, as shown in Fig. 48. Problems with the control of the testing procedure and of correlations with service conditions have impeded the standardization of this test method (Ref 31, Ref 45).

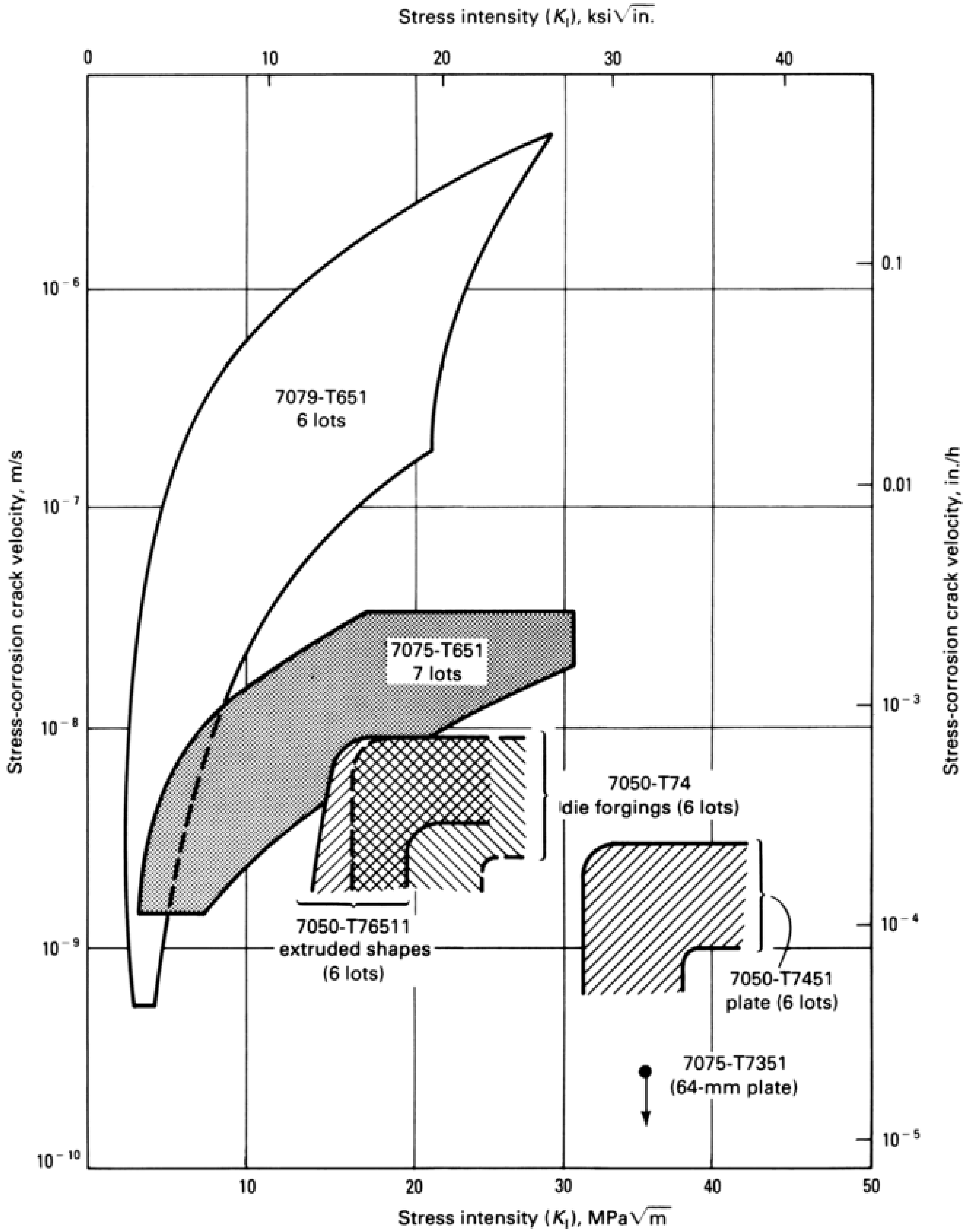

Fig. 48 SCC propagation rates for various aluminum alloy 7050 products. Double-beam specimens (S-L; see Fig. 28) bolt-loaded to pop-in and wetted three times daily with 3.5% NaCl. Plateau velocity averaged over 15 days. The right-hand end of the band for each product indicates the pop-in starting stress intensity (K_{Io}) for the tests of that material. Data for alloys 7075-T651 and 7079-T651 are from Ref 46. Source: Ref 102

Deadweight loading, or a simulated deadweight loading system used in conjunction with automatic data logging equipment (Fig. 30(b)b), has proved to be a rigorous method for evaluating threshold stress intensities by SCC initiation (Ref 44, 45). Because crack growth results in increasing stress intensity and an increasing crack opening, corrosion-product wedging is minimal, and each test usually has a definite end point (fracture). In these tests, fatigue precracked compact or modified compact specimens (Fig. 25(c)b) are loaded to various initial stress intensities K_{Io} and exposed until fracture or until completion of a designated time period (Fig. 29). The designated cutoff period should be long enough for extended initiation times and yet not long enough to allow corrosion-product wedging to exert a dominant influence.
The test results shown in Fig. 49 indicate that near-threshold values were reached within 1200 h, as judged by the flattening tendency of the curves. The slight downward slope of some of the curves after 1200 h may be the result of wedging by corrosion products, but this was not determined. The effect of such wedging would be to give lower estimates of the threshold stress intensity.

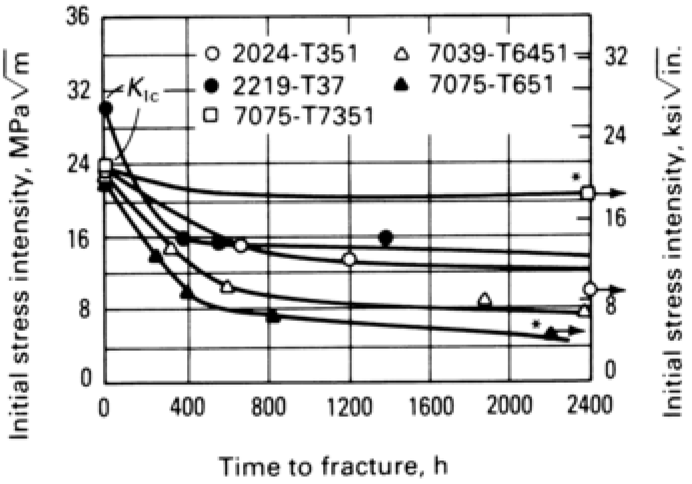

Fig. 49 Initial stress intensity versus time to fracture for S-L (see Fig. 28) compact specimens of various aluminum alloys exposed to an aqueous solution containing 0.06 *M* sodium chloride, 0.02 *M* sodium dichromate, 0.07 *M* sodium acetate, and acetic acid to pH 4. Asterisk indicates metallographic examination showed that SCC had started. Source: Ref 44

The testing of longitudinal (L-T, L-S in Fig. 28) and long-transverse (T-L, T-S in Fig. 28) specimens presents special problems with materials having typical directional grain structures. Stress-corrosion cracking growth is small and tends to be in the L-T plane, which is perpendicular to the plane of the precrack (Ref 103). Such out-of-plane crack growth invalidates calculations of the plane-strain threshold stress intensity K_{ISCC}. On the other hand, the testing of materials having an equiaxed grain structure also presents problems with stress-intensity calculations because of gross crack branching; this would be applicable to specimens of any orientation.
The most widely used corrodent for testing precracked specimens is 3.5% sodium chloride solution applied dropwise to the precrack two or (usually) three times daily (Ref 45, 46, 47, 48). This intermittent wetting technique accelerates SCC growth, but it also causes troublesome corrosion of the mechanical precrack. Less *aggressive* corrodents that have been used include substitute ocean water (ASTM D 1141) and an inhibited salt solution containing 0.06 *M* sodium cloride, 0.02 *M* sodium dichromate, 0.07 *M* sodium acetate, and acetic acid to pH 4 (Ref 48, 101). Some investigators have tested 7000-series alloys in distilled water (Ref 98) and in water vapor at 40 °C (104 °F) (Ref 104). Typical test durations that have been used range from 200 to 2500 h.
With low-resistance alloys, both of the first two corrodents listed in the preceding paragraph ranked alloys similarly and in agreement with exposure to a seacoast and an inland industrial atmosphere. Plateau velocities in the laboratory tests were about five to ten times faster than in the seacoast atmosphere and ten times faster than in the industrial atmosphere. In these *K*-decreasing laboratory tests, corrosion-product wedging effects dominated after exposure periods of about 200 to 800 h. The length of exposure time before the intervention of corrosion-product wedging varies with several factors, including the magnitude of K_{Io} and the inherent resistance to crevice corrosion of the test material in the corrosive environment (Ref 52).

Slow-Strain-Rate Testing

Slow-strain-rate testing is covered by ASTM G 129 (Ref 65). If there is no specific environment of interest, a 3.5% sodium chloride solution is often used. More corrosive test media can be used, including oxidant additions to the sodium chloride solution or more acidic solutions, such as aluminum chloride (Ref 64, 105).

In a round-robin testing program using several aluminum alloy types and several corrodents, a solution containing 3% sodium chloride plus 0.3% hydrogen peroxide was considered the most promising candidate for possible standardization (Fig. 33). Additional study is needed to determine the optimal composition of these constituents. Another promising candidate was a solution of 2% sodium chloride plus 0.5% sodium chromate having a pH of 3.

References cited in this section

3. D.O. Sprowls et al., "A Study of Environmental Characterization of Conventional and Advanced Aluminum Alloys for Selection and Design: Phase II—The Breaking Load Test Method," Contract NASI- 16424, NASA Contractor Report 172387, Aug 1984

9. H.L. Craig, Jr., D.O. Sprowls, and D.E. Piper, Stress-Corrosion Cracking, *Handbook on Corrosion Testing and Evaluation,* W.H. Ailor, Ed., John Wiley & Sons, 1971, p 259

21. B.W. Lifka and D.O. Sprowls, Stress Corrosion Testing of 7079-T6 Aluminum Alloy in Various Environments, *Stress Corrosion Testing,* STP 425, American Society for Testing and Materials, 1967, p 342–362

23. D.O. Sprowls et al., Evaluation of a Proposed Standard Method of Testing for Susceptibility to SCC of High Strength 7XXX Series Aluminum Alloy Products, *Stress- Corrosion—New Approaches,* STP 610, H.L. Craig, Jr., Ed., American Society for Testing and Materials, 1976, p 3–31

31. "Characterization of Environmentally Assisted Cracking for Design—State of the Art," National Materials Advisory Board Report No. NMAB-386, National Academy of Sciences, 1982

44. J.G. Kaufman, J.W. Coursen, and D.O. Sprowls, An Automated Method for Evaluating Resistance to Stress-Corrosion Cracking with Ring-Loaded Precracked Specimens, *Stress Corrosion—New Approaches,* STP 610, H.L. Craig, Jr., Ed., American Society for Testing and Materials, 1976, p 94–107

45. C. Micheletti and M. Buratti, New Testing Methods for the Evaluation of the Stress- Corrosion Behavior of High-Strength Aluminum Alloys by the Use of Precracked Specimens, *Symposium Proc., Aluminum Alloys in the Aircraft Industry* (Turin, Italy), Oct 1976, Technicopy Ltd., 1978, p 149–159

46. M.V. Hyatt, Use of Precracked Specimens in Stress Corrosion Testing of High Strength Aluminum Alloys, *Corrosion,* Vol 26 (No. 11), 1970, p 487–503

47. D.O. Sprowls et al., "Evaluation of Stress Corrosion Cracking Susceptibility Using Fracture Mechanics Techniques," Contract NAS 8-21487, Contractor Report NASA CR-124469, May 1973

48. R.C. Dorward and K.R. Hasse, "Flaw Growth of 7075, 7475, 7050, and 7049 Aluminum Plate in Stress Corrosion Environments," Final Technical Report for U.S. Government Contract NAS 8-30890, Oct 1976; *Corrosion,* Vol 34 (No. 11), 1978, p 386–395

52. D.O. Sprowls and J.D. Walsh, Evaluating Stress-Corrosion Crack Propagation Rates in High Strength Aluminum Alloys with Bolt Loaded Precracked Double Cantilever Beam Specimens, *Stress Corrosion—New Approaches,* STP 610, H.L. Craig, Jr., Ed., American Society for Testing and Materials, 1976, p 143–156

64. N.J.H. Holroyd and G.M. Scamans, Slow- Strain-Rate Stress Corrosion Testing of Aluminum Alloys, *Environment-Sensitive Fracture: Evaluation and Comparison of Test Methods,* STP 821, S.W. Dean, E.N. Pugh, and G.M. Ugiansky, Ed., American Society for Testing and Materials, 1984, p 202–241

65. "Practice for Slow Strain Rate Testing to Evaluate the Susceptibility of Metallic Materials to Environmentally Assisted Cracking," G 129, *Metal Corrosion, Erosion, and Wear,* Vol 03.02, *Annual Book of ASTM Standards,* American Society for Testing and Materials

80. S. Maitra and G.C. English, Mechanism of Localized Corrosion of 7075 Alloy Plate, *Metall. Trans. A,* Vol 12, March 1981, p 535–541

82. "Practice for Evaluating Stress Corrosion Cracking Resistance of Metals and Alloys by Alternate Immersion in 3.5% Sodium Chloride Solution," G 44, *Metal Corrosion, Erosion, and Wear,* Vol 03.02, *Annual Book of ASTM Standards,* American Society for Testing and Materials

83. H. Bohni and H.H. Uhlig, Environmental Factors Affecting the Critical Pitting Potential of Aluminum, *J. Electrochem. Soc.,* Vol 116, Part II, 1969, p 906–910

84. R.H. Brown, D.O. Sprowls, and M.B. Shumaker, The Resistance of Wrought High Strength Aluminum Alloys to Stress Corrosion Cracking, *Stress-Corrosion Cracking of Metals—A State of the Art,* STP 518, American Society for Testing and Materials, 1972, p 87–118

85. "Practice for Modified Salt Spray (Fog) Testing," G 47, *Metal Corrosion, Erosion, and Wear,* Vol 03.02, *Annual Book of ASTM Standards,* American Society for Testing and Materials

86. "Classification of Resistance to Stress- Corrosion Cracking of Heat-Treatable Aluminum Alloys," G 64, *Metal Corrosion, Erosion, and Wear,* Vol 03.02, *Annual Book of ASTM Standards,* American Society for Testing and Materials

87. B.W. Lifka, Corrosion Resistance of Aluminum Alloy Plate in Rural, Industrial, and Seacoast Atmospheres, unpublished

88. D.O. Sprowls and R.H. Brown, What Every Engineer Should Know about the Stress Corrosion of Aluminum, *Met. Prog.,* Vol 81 (No. 4), April 1962, p 79–85; Vol 81 (No. 5), May 1962, p 77–83

89. "Test Method for Performing a Stress-Corrosion Cracking Test of Low Copper Containing Al-Zn-Mg Alloys in Boiling 6% Sodium Chloride Solution," G 103, *Metal Corrosion, Erosion, and Wear,* Vol 03.02, *Annual Book of ASTM Standards,* American Society for Testing and Materials

90. F.F. Booth and H.P. Godard, An Anodic Stress-Corrosion Test for Aluminum-Magnesium Alloys, *First International Congress on Metallic Corrosion,* Butterworths, 1962, p 703–712

91. A.H. Le, B.F. Brown, and R.T. Foley, The Chemical Nature of Aluminum Corrosion, IV: Some Anion Effects on SCC of AA7075-T651, *Corrosion,* Vol 36 (No. 12). Dec 1980, p 673–679

92. D.O. Sprowls, J.D. Walsh, and M.B. Shumaker, Simplified Exfoliation Testing of Aluminum Alloys, *Localized Corrosion— Cause of Metal Failure,* STP 516, American Society for Testing and Materials, 1972, p 38–65

93. W. Pistulka and G. Lang, Accelerated Stress Corrosion Test Methods for Al-Zn- Mg Type Alloys, *Aluminum,* Vol 53 (No. 6), 1977, p 366–371

94. "Stress-Corrosion Cracking Testing of Aluminum Alloys for Aircraft Parts," German Aircraft Standard LN 65666, July 1974 (in German)

95. P.W. Jeffrey, T.E. Wright, and H.P. Godard, An Accelerated Laboratory Stress Corrosion Test for Al-Zn-Mg Alloys, *Proc. Fourth Int. Congress on Corrosion,* National Association of Corrosion Engineers, 1969, p 133–139

96. T.S. Humphries and J.E. Coston, "An Improved Stress Corrosion Test Medium for Aluminum Alloys," NASA Technical Memorandum NASA TM-82452, George C. Marshall Space Flight Center, Nov 1981

97. W.J. Helfrich, "Development of a Rapid Stress Corrosion Test for Aluminum Alloys," Final Summary Report, Contract No. NAS 8-20285, George C. Marshall Space Flight Center, May 1968

98. M.V. Hyatt and M.O. Speidel, High Strength Aluminum Alloys, *Stress Corrosion Cracking in High Strength Steels and in Titanium and in Aluminum Alloys,* B.F. Brown, Ed., Naval Research Laboratory, 1972, p 148–244

99. M.O. Speidel, Stress Corrosion Cracking of Aluminum Alloys, *Metall. Trans. A,* Vol 6, April 1975, p 631–651

100. L. Schra and J. Faber, "Influence of Environments on Constant Displacement Stress-Corrosion Crack Growth in High Strength Aluminum Alloys," NLR TR 81138 U, National Aerospace Laboratory NLR, 1981

101. J.R. Pickens, Techniques for Assessing the Corrosion Properties of Aluminum Powder Metallurgy Alloys, *Rapidly Solidified Powder Aluminum Alloys,* STP 890, M.E. Fine and E.A. Starke, Jr., Ed., American Society for Testing and Materials, 1986, p 381–409

102. R.E. Davies, G.E. Nordmark, and J.D. Walsh. "Design Mechanical Properties, Fracture Toughness, Fatigue Properties Exfoliation and Stress Corrosion Resistance of 7050 Sheet, Plate, Extrusions, Hand Forgings and Die Forgings," Final Report, Naval Air Systems, Contract N00019-72-C-0512, July 1975

103. R.C. Dorward and K.R. Hasse, Long- Transverse Stress-Corrosion Cracking Behavior of Aluminum Alloy AA7075, *Br. Corros. J.,* Vol 13 (No. 1), 1978, p 23–27

104. G.M. Scamans, Discontinuous Propagation of Stress Corrosion Cracks in Al-Zn- Mg Alloys, *Scr. Metall.,* Vol 13, 1979, p 245–250

105. S. Maitra, Determination of SCC Resistance of Al-Cu-Mg Alloys by Slow Strain Rate and Alternate Immersion Testing, *Corrosion,* Vol 37 (No. 2), 1981, p 98–103

B. Phull, Evaluating Stress-Corrosion Cracking, *Corrosion: Fundamentals, Testing, and Protection,* Vol 13A, *ASM Handbook,* ASM International, 2003, p 575–616

Evaluating Stress-Corrosion Cracking

Revised by Bopinder Phull, Consultant

Testing of Copper Alloys (Smooth Specimens)

Testing in Mattsson's Solution. According to ASTM G 37 (Ref 106), a stressed test specimen must be completely and continuously immersed in an aqueous solution containing 0.05 g-atom/L of Cu^{2+} and 1 g-mol/L

of ammonium ion (NH_4^+) with a pH of 7.2. The copper is added as hydrated copper sulfate, and the NH_4^+ is added as a mixture of ammonium hydroxide and ammonium sulfate. The ratio of the latter two compounds is adjusted to achieve the desired pH.

Mattsson's pH 7.2 solution is recommended only for brasses (copper-zinc base alloys). This test environment may give erroneous results for other copper alloys and is not recommended. This is particularly true for alloys containing aluminum or nickel.

This test environment is believed to provide an accelerated ranking of the relative or absolute degree of susceptibility to SCC for different brasses. The test environment correlates well with the corresponding service ranking in environments that cause SCC, which may be due to the combined presence of traces of moisture and ammonia vapor. The extent to which the accelerated ranking correlates with the ranking obtained after long-term exposure to environments containing corrodents other than ammonia is not known. Such environments may be severe marine atmospheres (chloride), severe industrial atmospheres (predominantly sulfur dioxide), or superheated ammonia-free steam.

It is currently not possible to specify a time to failure in Mattsson's pH 7.2 solution that corresponds to a distinction between acceptable and unacceptable SCC behavior in brass alloys. Such correlations must be determined on an individual basis. Generally, the longest recommended test duration is 1000 h since failures are not usually observed after this period.

Mattsson's pH 7.2 solution may also cause some stress-independent general and intergranular corrosion of brasses. Therefore, SCC failure may possibly be confused with mechanical failure induced by corrosion-reduced net cross section. This is most likely with small cross-sectional specimens, high applied stress levels, long exposure times, and SCC-resistant alloys. Careful metallographic examination is recommended for accurate determination of the cause of failure. Alternatively, unstressed control specimens can be exposed to corrosive environments in order to determine the extent to which stress-independent corrosion degrades mechanical properties.

Other Testing Media. The most widely used SCC agent for copper and copper alloys is ammonia (NH_3) (Ref 107). The NH_4^+ ion does not appear to cause cracking in a stable salt, such as ammonium sulfate. Cracking will occur in a salt that dissociates (such as ammonium carbonate) to form ammonia.

The $Cu(NH_3)_x^{2+}$ ion (*x* is usually 4 to 5) is thought to be necessary to induce SCC in copper metals (Ref 108). Amine groups also cause cracking or are easily converted to ammonia. Amines and sulfamic acid also cause cracking. Dry ammonia does not cause SCC of brass, as demonstrated by the successful use of brass valves and gages on tanks of anhydrous ammonia.

Stress-corrosion cracking of copper metals in ammonia will not occur in the absence of oxygen or an oxidizing agent. Carbon dioxide is also a requisite (Ref 109). Therefore, air rather than pure oxygen is necessary, and as a practical matter, moisture is essential. When other factors are favorable, a very small amount of NH_3 is sufficient to cause cracking. The controlling factor may therefore be moisture, because cracking may appear to be caused by the presence of a condensed moisture film.

Other than ammonia, the most effective agents for causing cracking are the fumes from nitric acid or moist nitrogen dioxide. Sulfur dioxide will also crack brass; however, both maximum and minimum concentration limits exist, and the reaction is slow (Ref 107). Alloy development studies have been conducted with a moist ammoniacal test atmosphere containing 80% air, 16% NH_3, and 4% water vapor at 35 °C (95 °F). However, none of these corrodents has received the attention that ammonia has garnered (Ref 108).

Historically, immersion of a copper alloy product in a mercurous nitrate solution has been used to test for residual stresses (Ref 110, 111). Because these residual stresses are possible sources of failure by SCC in other environments, some have regarded this test as a stress-corrosion test. However, it is only an indirect method of identifying SCC tendencies and does not correlate to the presence of SCC as well as test methods based on specific attack by ammonia (Ref 107). It does indicate, however, that mercury and other low-melting liquid metals can cause embrittlement and failure due to cracking.

References cited in this section

106. “Practice for Use of Mattsson's Solution of pH 7.2 to Evaluate the Stress-Corrosion Cracking Susceptibility of Copper-Zinc Alloys,” G 37, *Metal Corrosion, Erosion, and Wear,* Vol 03.02, *Annual Book of ASTM Standards,* American Society for Testing and Materials

107. D.H. Thompson, Stress Corrosion Cracking of Copper Metals, *Stress Corrosion Cracking of Metals—A State of the Art,* STP 518, American Society for Testing and Materials, 1972, p 39–57

108. E.N. Pugh, J.V. Craig, and A.J. Sedricks, The Stress-Corrosion Cracking of Copper, Silver, and Gold Alloys, *Proc. Conf. Fundamental Aspects of Stress-Corrosion Cracking,* National Association of Corrosion Engineers, 1969, p 118–158

109. G. Edmunds, E.A. Anderson, and R.K. Waring, Ammonia and Mercury Stress- Corrosion Cracking Tests for Brass, *Symposium on Stress-Corrosion Cracking of Metals,* American Society for Testing and Materials and the American Institute of Mining, Metallurgical, and Petroleum Engineers, 1944, p 7–18

110. "Standard Method of Mercurous Nitrate Test for Copper and Copper Alloys," B 154, *Annual Book of ASTM Standards,* American Society for Testing and Materials, 1984, p 352–354

111. "Tubing of Copper and Copper Alloys for Condensers and Heat Exchangers," German Standard DIN-1785 (available from ANSI), 1983

B. Phull, Evaluating Stress-Corrosion Cracking, *Corrosion: Fundamentals, Testing, and Protection*, Vol 13A, *ASM Handbook,* ASM International, 2003, p 575–616

Evaluating Stress-Corrosion Cracking

Revised by Bopinder Phull, Consultant

Testing of Carbon and Low-Alloy Steels

Generally, steels with lower strengths are susceptible to SCC only upon exposure to a small number of specific environments, such as the hot caustic solutions encountered in steam boilers, hot nitrate solutions, anhydrous ammonia, and hot carbonate-bicarbonate solutions (Ref 112, 113).

Boiler Water Embrittlement Detector Testing. Caustic cracking failures frequently originate in welded structures in the vicinity of faying surfaces, where small leaks cause soluble salts to accumulate in high local concentrations of caustic soda and silica. As a general rule, crevices or splash areas on hot metal surfaces where the concentration of dissolved soluble salts can occur are likely sites for SCC. This type of intergranular cracking failure has been produced with concentrations of sodium hydroxide as low as 5%, but a concentration of 15 to 30% is usually required at 200 to 250 °C (390 to 480 °F) to produce this phenomenon. The apparatus and procedures used to determine the embrittling or nonembrittling characteristics of the water in an operating boiler are detailed in ASTM D 807 (Ref 114).

Other Testing Media. Caustic cracking occurs in digester vessels used in the chemical-processing industries, and laboratory studies have been conducted using sodium hydroxide concentrations of about 30 to 35% (Ref 115). Tests in boiling nitrate solutions have frequently been used to study the effects of composition and metallurgical variables (Ref 113). In studies of low- carbon steel in boiling nitrate solutions having different cations, solutions containing the more acidic cations in greater concentrations were found to be the most potent. This tendency is illustrated by the apparent threshold stresses for failure of a 0.05% C steel in nitrate solutions with a range of concentrations, as shown in Table 5.

Table 5 Apparent threshold stress values for 0.05% C steel in nitrate solutions of varying concentrations

Nitrate solution	Apparent threshold stress values at a solution concentration of:							
	8 *N*		**4 *N***		**2.5 *N***		**1 *N***	
	MPa	**ksi**	**MPa**	**ksi**	**MPa**	**ksi**	**MPa**	**ksi**
Ammonium nitrate	14	2	21	3	48	7	83	12
Calcium nitrate	34	5	48	7	83	12	159	23
Lithium nitrate	34	5	55	8	131	19 at 2 *N*	159	23
Potassium nitrate	41	6	62	9	97	14	165	24
Sodium nitrate	55	8	131	19	152	22	179	26

Source: Ref 113

Cracking can be accelerated by the addition of small amounts of acid or oxidizing agents, such as potassium permanganate, manganese sulfate, sodium nitrite, and potassium dichromate, but hydroxides and other salts, particularly those forming insoluble iron products, such as sodium carbonate or sodium hydrogen phosphate, retard or prevent failure. Sodium nitrite is also a known inhibitor if the nitrite concentration is equal to that of the nitrate ion. A standard test environment has not been established, and conditions should be tailored to individual testing requirements.

The ranking of a given series of alloys may vary with exposure conditions (Ref 71). Consequently, selection of a particular alloy for use in an environment that varies from that used in laboratory ranking tests may result in unexpected service failure. This tendency is illustrated by the effects of alloying additions in ferritic steels on cracking in two different environments (Fig. 50). Figure 50(a) shows that each of the alloying additions is beneficial in the carbonate-bicarbonate solutions, with molybdenum having the greatest effect. However, the molybdenum addition has an adverse effect in the 35% sodium hydroxide solution, although the beneficial effects of nickel and chromium additions remain the same (Fig. 50b). Although nickel additions are beneficial in the above example, a similar addition of nickel to a carbon-manganese steel produced susceptibility to SCC in boiling magnesium chloride; this did not occur in the steel without the addition of nickel (Ref 117).

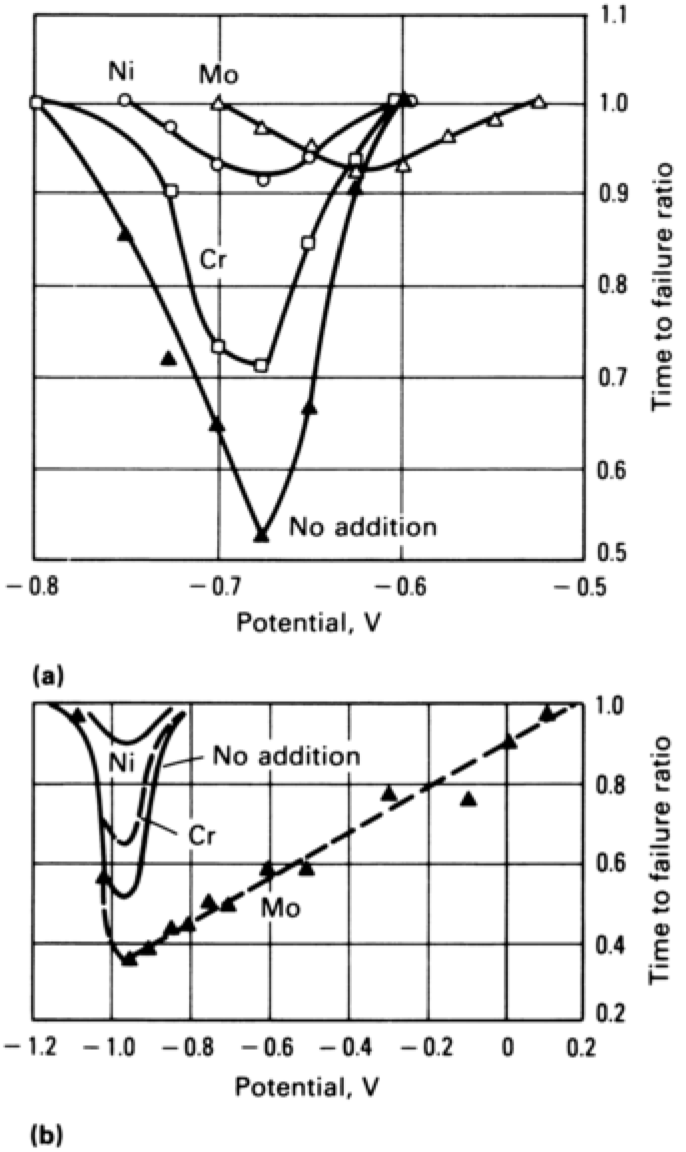

Fig. 50 Effect of various alloying elements on the SCC behavior of a low-alloy ferritic steel in two different corrosive environments. Behavior indicated by time-to-failure ratios in a slow-strain-rate test. (a) Immersed in 1 *N* sodium carbonate plus 1 *N* sodium bicarbonate at 75 °C (165 °F). (b) Immersed in boiling 35% sodium hydroxide. Source: Ref 116

The use of laboratory testing media that duplicate service conditions is equally important when accelerated tests are used for quality control through the acceptance or rejection of production lots of a particular alloy. Reference 118 discusses tests of prestressing steels intended for use as concrete reinforcing bars (rebars) in which an ammonium thiocyanate solution was used to discriminate between heats of steel.

Use of the carbonate-bicarbonate solutions for testing pipeline steels by the slow-strain-rate method revealed that the susceptibility to SCC was dependent on the electrochemical potential of the specimen surface in the test environment, as shown in Fig. 50(a). A critical range in which SCC occurred was established. The critical range varies with the test environment and alloy composition. Several tests at various carbonate-bicarbonate concentrations, temperatures, pH levels, and corrosion potentials indicated that test conditions using an impressed potential of -650 mV versus the saturated calomel electrode (SCE) and a temperature of 75 °C (165 °F) were optimal for SCC (Fig. 37).

References cited in this section

71. R.N. Parkins, A Critical Evaluation of Current Environment-Sensitive Fracture Test Methods, *Environment-Sensitive Fracture: Evaluation and Comparison of Test Methods,* STP 821, S.W. Dean, E.N. Pugh, and G.M. Ugiansky, Ed., American Society for Testing and Materials, 1984, p 5–31

112. H.L. Logan, *The Stress Corrosion of Metals,* John Wiley & Sons, 1966

113. R.N. Parkins, Stress Corrosion Cracking of Low Carbon Steels, *Proc. Conf. Fundamental Aspects of Stress Corrosion Cracking,* National Association of Corrosion Engineers, 1969, p 361–373

114. "Assessing the Tendency of Industrial Boiler Waters to Cause Embrittlement (USBM Embrittlement Detector Method)," D 807, *Annual Book of ASTM Standards,* American Society for Testing and Materials

115. M.J. Humphries and R.N. Parkins, Stress Corrosion Cracking of Mild Steels in Sodium Hydroxide Solutions Containing Various Additional Substances, *Corros. Sci.,* Vol 7, 1967, p 747–761

116. R.N. Parkins, P.W. Slattery, and B.S. Poulson, The Effects of Alloying Additions to Ferritic Steels Upon Stress-Corrosion Cracking Resistance, *Corrosion,* Vol 37 (No. 11), 1981, p 650–664

117. B.S. Poulson and R.N. Parkins, Effect of Nickel Additions upon the Stress Corrosion of Ferritic Steels in a Chloride Environment, *Corrosion,* Vol 29, Nov 1973, p 414–422

118. "Stress Corrosion Cracking Resistance Test for Prestressing Tendons," Technical Report 5, Proc. Federation Internationale de la Preconstrainte, Eighth Congress, Cement and Concrete Association, 1978

B. Phull, Evaluating Stress-Corrosion Cracking, *Corrosion: Fundamentals, Testing, and Protection*, Vol 13A, *ASM Handbook*, ASM International, 2003, p 575–616

Evaluating Stress-Corrosion Cracking

Revised by Bopinder Phull, Consultant

Testing of High-Strength Steels (Ref 4, Ref 119)

For steels with yield strengths greater than about 690 MPa (100 ksi)—such as low-alloy and alloy steels, hot-work die steels, maraging steels, and martensitic and precipitation-hardenable stainless steels—the environments that cause SCC are not specific. In many alloy systems, the phenomena of SCC and hydrogen embrittlement cracking are indistinguishable (Fig. 1). This is particularly the case in environments that contain sulfides or other promoters of hydrogen entry.

Environments of major concern are natural waters—for example, rainwater, seawater, and atmosphere moisture. Any of these environments may become contaminated, which significantly increases the likelihood of SCC. Contamination with hydrogen sulfide is particularly serious; consequently, the presence of hydrogen sulfide in high concentrations in saltwater associated with certain deep oil wells (termed sour wells) places an upper limit of approximately 620 MPa (90 ksi) on the yield strength that can be tolerated in stressed steel in such environments without cracking.

Sulfide Stress Cracking. Determination of sulfide stress cracking is covered in NACE TM- 01-77 (Ref 120). Stressed specimens are immersed in acidified 5% sodium chloride solution saturated with hydrogen sulfide at ambient pressure and temperature. The solution is acidified with the addition of 0.5% acetic acid, yielding an initial pH of approximately 3. Applied stress at convenient increments of the yield strength is used to obtain cracking data that are plotted as shown in Fig. 51. A 30-day test period is considered sufficient to reveal failure of susceptible material in most cases.

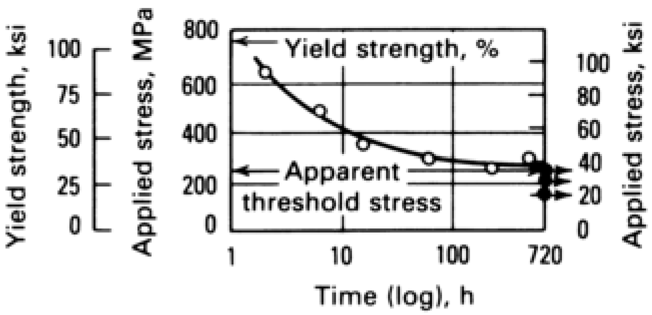

Fig. 51 Method of plotting results of sulfide stress cracking tests. Open symbols indicate failure; closed symbols indicate runouts. Source: Ref 120

The purpose of this test standard is to facilitate conformity in testing. Evaluation of data requires individual judgment on several points based on the specific requirements of the end use. Consequently, the test should not be used as a single criterion for evaluating an alloy for use in environments containing hydrogen sulfide or other hydrogen-charging elements. Attention should be paid to other factors that may affect SCC, such as pH, temperature, hydrogen sulfide concentration, corrosion potential, and stress level, when determining the suitability of a metal for use.

The NACE test method recommends the use of smooth, small-diameter tension specimens stressed with constant-load or sustained-load devices (Ref 120). However, different types of beam and fracture mechanics specimens may be included in the testing standard in the future.

Another test method, known as the Shell Bent Beam Test, has been used for 45 years in the petrochemical industry to rank various materials for use in sour environments (Ref 121). However, acceptance has not been sufficient to generate the interest for standardization.

Testing in sodium chloride solution constitutes a worst-case determination for high- strength steels; as such, it is generally considered unrealistically aggressive for the useful ranking of steels in service environments that do not contain hydrogen sulfide or other conditions favoring entry of hydrogen. Tests are usually performed in 3.5% sodium chloride solution, artificial seawater, natural seawater (rarely), or a marine atmosphere (Ref 4), unless specific environmental conditions are under study. ASTM G 44 (Ref 82) is used where applicable.

In saltwater and freshwater, a true threshold K_{ISCC} exists for high-strength steels that is useful for characterizing resistance to SCC. Ideally, K_{ISCC} defines the combination of applied stress and defect size below which SCC will not occur under static loading conditions in a given alloy and environment system. However, the reported value of K_{ISCC} for a given system often reflects the initial K_I level and the exposure time associated with the testing. Table 6 shows the risk of overestimating K_{ISCC} by terminating the exposure test too soon when using the SCC initiation method (Ref 30, Ref 31). A similar risk exists in tests conducted with the arrest method. Table 7 shows that K_{ISCC} values determined by the initiation and arrest methods may be the same when testing times are sufficiently long and when compatible criteria are used for establishing the threshold (Ref 31).

Table 6 Influence of cutoff time on apparent K_{ISCC} using the SCC initiation method

Exposure time, h	Apparent K_{ISCC}	
	MPa$\sqrt{m}$	**ksi**$\sqrt{in.}$
100	187	170
1000	127	110
10,000	28	25

Note: The initiation method was used on a constant-load cantilever bend specimen (K-increasing) of alloy steel with a yield strength of 1240 MPa (180 ksi). Test environment was synthetic seawater at room temperature. Source: Ref 31

Table 7 Comparison of K_{ISCC} values determined by initiation and arrest methods

Steel alloy	K_{ISCC}, MPa$\sqrt{m}$ (ksi$\sqrt{in.}$)	
	Initiation	**Arrest**
10Ni, normal purity	24 (22)	26 (24)
10Ni, high purity	59 (54)	57 (52)
18Ni, normal purity	22–33 (20–30)	28 (25)
18Ni, high purity	<33 (<30)	<33 (<30)

Note: Based on a crack growth rate of 2.5×10^{-4} mm/h (10^{-5} in./h). Modified compact specimens: constant load for initiation and wedge- loaded with a bolt for arrest. Test environment: saltwater at room temperature. Source: Ref 31

Figure 52 illustrates a method used to compare various high-strength steels (Ref 4, 122). Data were obtained in saltwater or seawater, and K_{ISCC} values are plotted versus yield strength. Envelopes are used to enclose all known valid data for the various steels. The crosshatched envelopes or individual data points represent the featured steels, which allows comparison with characteristics of the other steels. The straight lines in Fig. 52 illustrate how K_{ISCC} values relate to the maximum depth of long surface flaws that can be tolerated without stress-corrosion crack growth.

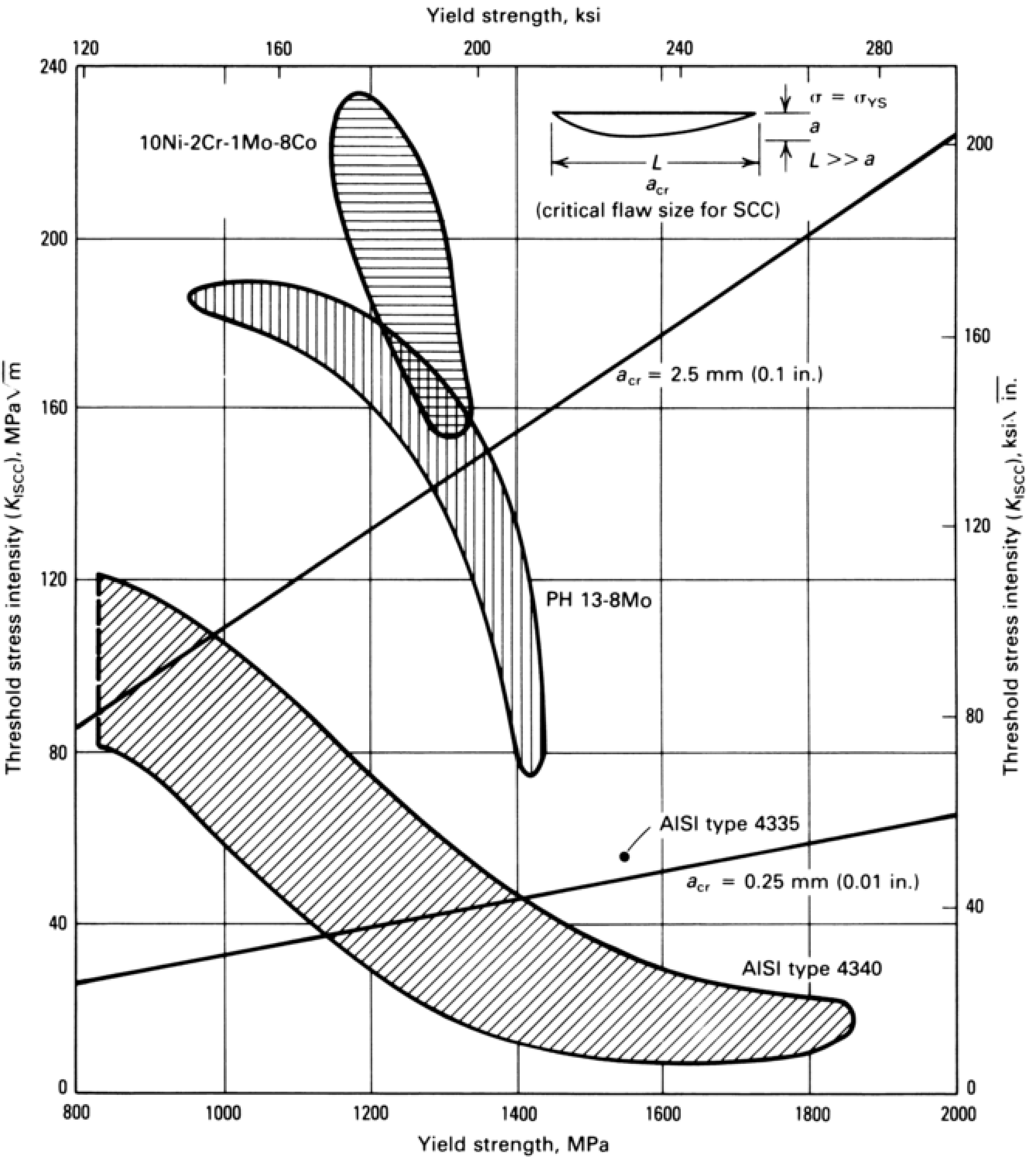

Fig. 52 Comparison of SCC behavior of several high-strength steels based on threshold stress-intensity (K_{ISCC}) values in saltwater. Source: Ref 122

Electrochemical Polarization. Although the mechanism of cracking in hydrogen sulfide environments is predominantly one of hydrogen embrittlement, the mechanism of environmentally induced failures in environments not containing sulfides or other promoters of hydrogen entry is not clearly agreed upon (Ref 119). Time to failure in a sodium chloride solution depends on the corrosion potential (Ref 4, 123), which determines whether failure results from active path corrosion or hydrogen embrittlement cracking. Electrochemical studies have shown that embrittlement of high-strength steels by corrosion-product hydrogen occurs when, for a given environment, the electrochemical potential of the metal is equal to or more electronegative than the reversible hydrogen potential, that is, for thermodynamic conditions that favor the deposition of hydrogen on the surface of the steel.

Figure 53 compares the various types of cracking behavior that can be expected from electrochemical polarization (Ref 124). All of the curves except curve G were obtained experimentally. Curve A represents the case in which only hydrogen embrittlement is obtained; curve B shows only active path corrosion. Both processes are shown in curves C and D.

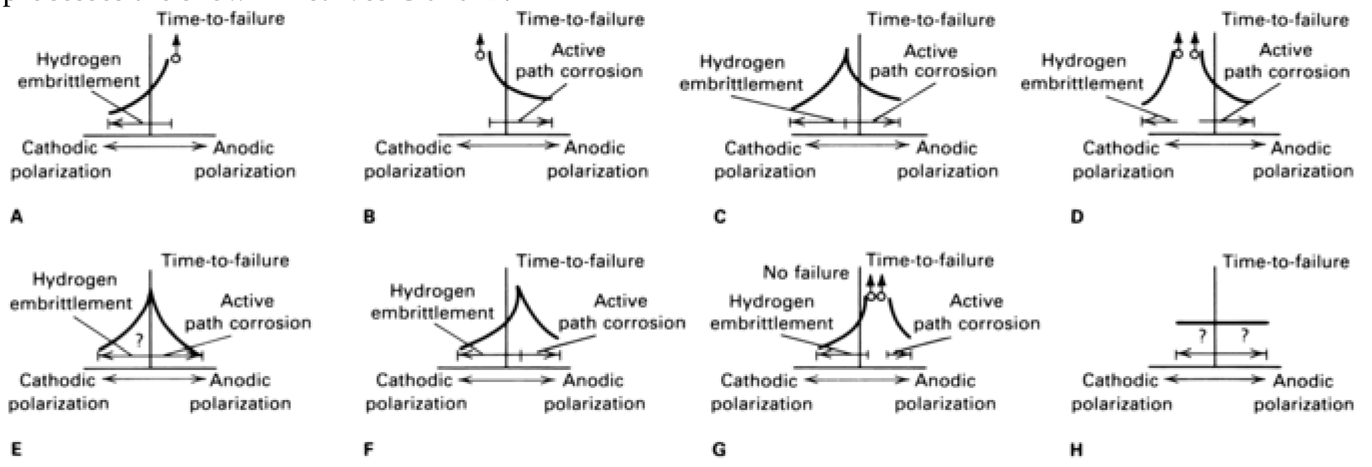

Fig. 53 Use of electrochemical polarization to distinguish between SCC and hydrogen embrittlement mechanisms in a high-strength steel immersed in sodium chloride solution. See text for explanation of curves A through H. Source: Ref 124

When both anodic and cathodic polarization shorten the cracking time, as in curve E, it is not possible to determine which mechanism prevails without applied current. Curves F and G can be expected in acid solutions when the corrosion potential is anodic to the reversible hydrogen potential.

In curve H, neither anodic nor cathodic polarization has any effect on cracking time. Therefore, it is possible that a hydrogen embrittlement mechanism is involved. However, the mechanism by which hydrogen enters the steels is not electrochemical. To perform realistic accelerated tests, the end use of the material and the environmental conditions involved should be considered so that the test procedure involves the appropriate cracking mechanism. It should be noted that hydrogen embrittlement cracking can also occur as a result of galvanic action between the test specimen and components of the stressing system. In all SCC testing, therefore, all electrical contact between the specimen and ancillary fixtures must be avoided, except when galvanic effects are desired.

References cited in this section

4. B.F. Brown, "Stress Corrosion Cracking Control Measures," National Bureau of Standards Monograph 156, U.S. Department of Commerce, June 1977

30. R.P. Wei, S.R. Novak, and D.P. Williams, Some Important Considerations in the Development of Stress Corrosion Cracking Test Methods, *Mater. Res. Stand.,* Vol 12, 1972, p 25

31. "Characterization of Environmentally Assisted Cracking for Design—State of the Art," National Materials Advisory Board Report No. NMAB-386, National Academy of Sciences, 1982

82. "Practice for Evaluating Stress Corrosion Cracking Resistance of Metals and Alloys by Alternate Immersion in 3.5% Sodium Chloride Solution," G 44, *Metal Corrosion, Erosion, and Wear,* Vol 03.02, *Annual Book of ASTM Standards,* American Society for Testing and Materials

119. E.H. Phelps, A Review of the Stress Corrosion Behavior of Steels with High Yield Strength, *Proc. Conf. Fundamental Aspects of Stress Corrosion Cracking,* National Association of Corrosion Engineers, 1969, p 398–410

120. "Test Method for Testing of Metals for Resistance to Sulfide Stress Cracking at Ambient Temperatures," TM-01-77, National Association of Corrosion Engineers, 1977, p 77–84

121. J.P. Fraser, G.G. Eldredge, and R.S. Treseder, Laboratory and Field Methods for Quantitative Study of Sulfide Corrosion Cracking, *Corrosion,* Vol 14, 1958, p 517t–523t

122. G. Sandoz, High Strength Steels, *Stress Corrosion Cracking in High Strength Steels and in Titanium and in Aluminum Alloys,* B.F. Brown, Ed., Naval Research Laboratory, Washington, D.C., 1972, p 79–145

123. H.J. Bhatt and E.H. Phelps, The Effect of Electrochemical Polarization on the Stress Corrosion Behavior of Steels with High Yield Strength, *Proc. Third Int. Congress on Metallic Corrosion,* 16–26 May 1966

124. H.J. Bhatt and E.H. Phelps, Effect of Solution pH on the Mechanism of Stress Corrosion Cracking of a Martensitic Stainless Steel, *Corrosion,* Vol 17, 1961, p 430t–434t

---

B. Phull, Evaluating Stress-Corrosion Cracking, *Corrosion: Fundamentals, Testing, and Protection*, Vol 13A, *ASM Handbook*, ASM International, 2003, p 575–616

Evaluating Stress-Corrosion Cracking

Revised by Bopinder Phull, Consultant

Testing of Non-Heat-Treatable Stainless Steels

The environments causing SCC that are encountered in the chemical industry are specific and are limited primarily to chloride and caustic solutions at elevated temperatures and sulfide environments at ambient temperatures. In seawater at or near room temperature, austenitic (Fe-Cr-Ni) and ferritic (Fe-Cr) steels do not generally experience SCC. However, occasionally, SCC of susceptible austenitic stainless steels can occur in ambient-temperature chloride-containing environments due to development of locally acidic conditions, for example, in pits and crevices. Fully ferritic stainless steels are highly resistant to SCC in chloride and caustic environments that cause austenitic stainless steels to crack. However, laboratory studies have shown small additions of nickel or copper to ferritic steels may render them susceptible to SCC in severe environments (Ref 4).

Testing in Boiling Magnesium Chloride Solution. ASTM G 36 (Ref 125) is applicable to wrought, cast, and welded austenitic stainless steels and related nickel-base alloys. This method determines the effects of composition, heat treatment, surface finish, microstructure, and stress on the susceptibility of these materials to chloride SCC. Although this test can be performed with various concentrations of magnesium chloride, ASTM G 36 specifies a test solution maintained at a constant boiling temperature of 155.0 ± 1.0 °C (311.0 ± 1.8 °F), that is, approximately 45% magnesium chloride. Also described is a test apparatus capable of maintaining solution concentration and temperature within the recommended limits for extended periods of time. Typical exposure times are up to 1000 h. However, historically, most of the SCC data on austenitic stainless steels were obtained by using a boiling 42% $MgCl_2$ solution (boiling point: 154 °C, or 309 °F). For this reason, testing is still done at the lower concentration.

Most chloride cracking testing has been carried out in accelerated test media such as boiling magnesium chloride (Ref 4, 126, 127). All austenitic stainless steels are susceptible to chloride cracking as shown in Fig. 54. It is noteworthy, however, that the higher-nickel types 310 and 314 were appreciably more resistant than the others (Fig. 55). Although this solution causes rapid cracking, it does not necessarily simulate the cracking observed in field applications.

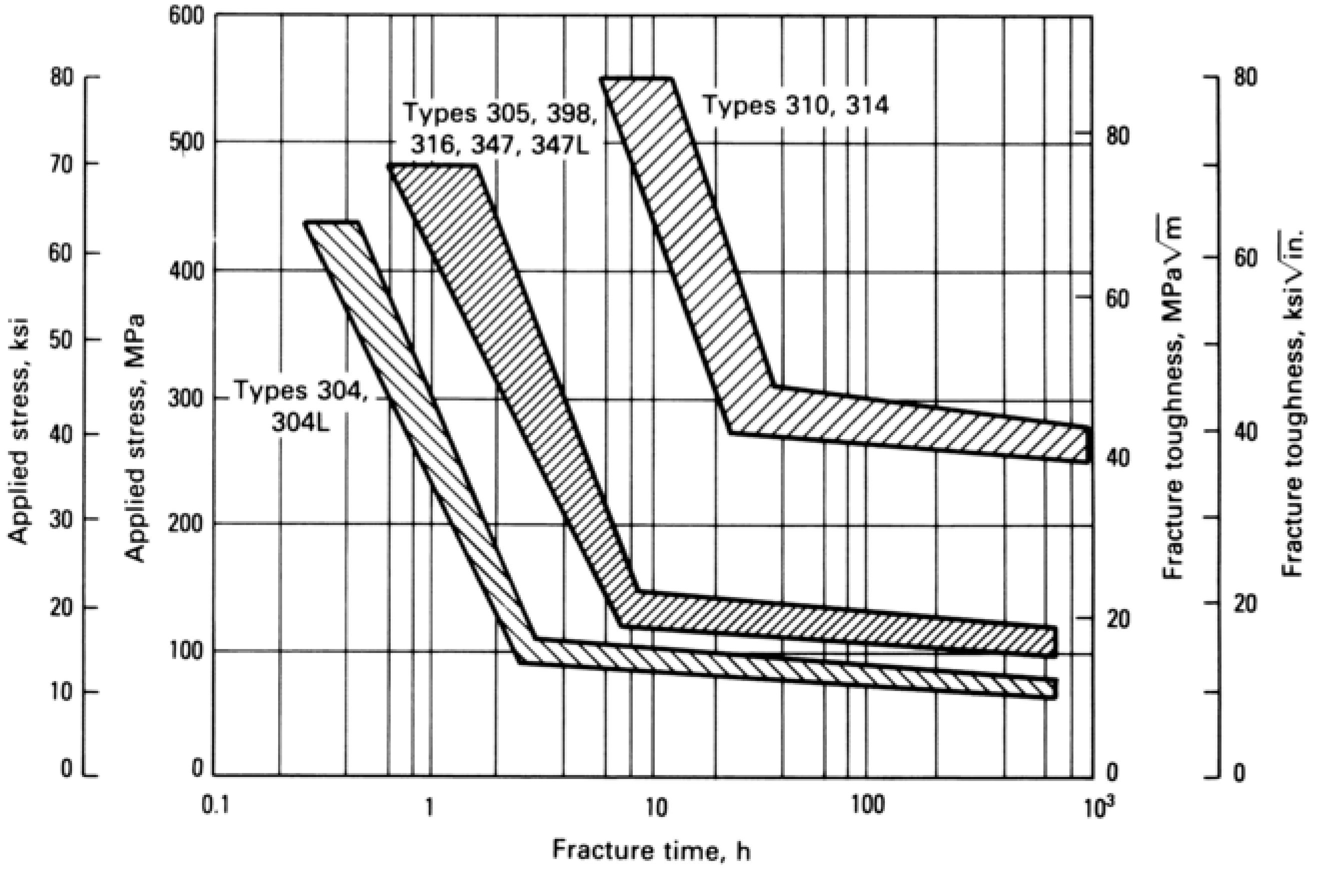

Fig. 54 Relative SCC behavior of austenitic stainless steels in boiling magnesium chloride. Source: Ref 128

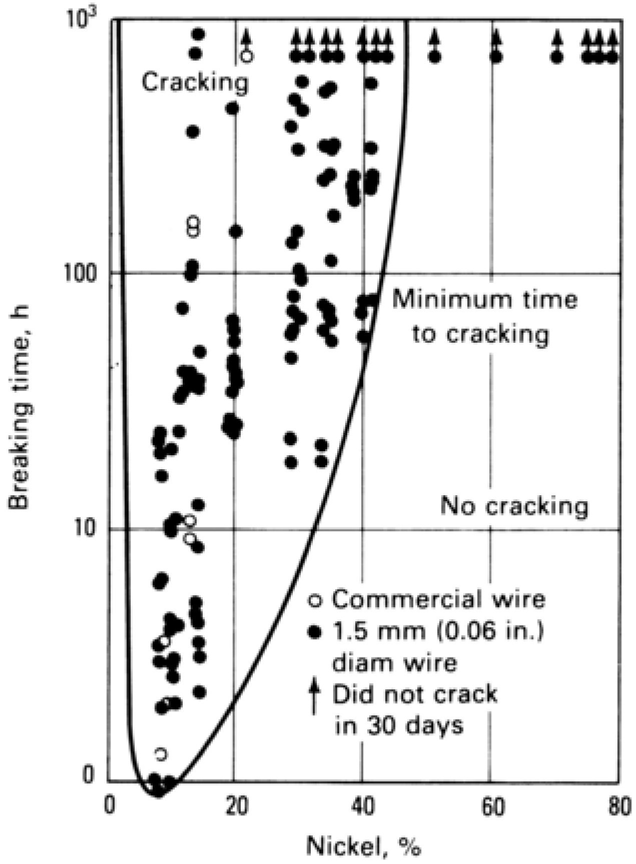

Fig. 55 Effect of nickel additions to a 17 to 24% Cr steel on resistance to SCC in boiling 42% magnesium chloride. 1.5 mm (0.06 in.) diam wire specimens deadweight loaded to 228 or 310 MPa (33 or 45 ksi). Source: Ref 129

Other ions in addition to chloride can cause cracking. Of all halogen ions, chlorides cause the most cases of SCC in austenitic stainless steels. Known cases of fluoride and bromide SCC are few, and iodide is not known to produce SCC. In addition, cations, such as Li^{+}, Ca^{2+}, Zn^{2+}, NH_4^{+}, Ni^{2+}, and Na^{+}, affect test results to varying degrees (Ref 130). Although chloride SCC occurs primarily at temperatures above about 90 °C (190 °F), acidified chloride solutions can produce SCC at lower temperatures (Ref 130, 131, 132). Therefore, in diagnosing service failures, it is necessary to establish which ions (and other environmental and stress conditions as well) have caused the failure. In this manner, an appropriate test procedure can be designed for the evaluation of alternative materials.

Reference 133 discusses laboratory reproduction of an environment that caused SCC at the top of a distillation tower in a crude oil refinery. The service environment consisted of a very dilute hydrochloric acid solution (36 ppm chloride) with a pH of 3 saturated with hydrogen sulfide gas at 80 °C (175 °F). In this test environment, austenitic stainless steels, such as type 304 or 316 failed, but the ferritic types 430 and type 434 did not.

ASTM G 123 (Ref 134) covers a procedure for evaluating SCC of stainless alloys, with different nickel content, in boiling 25% NaCl solution acidified to pH 1.5 with phosphoric acid. U-bend specimens are used, and the test method is designed to provide better correlation with chemical-process industry experience for stainless steels than the more severe boiling $MgCl_2$ test of ASTM G 36. Although the test can be run for as long as necessary, 6 weeks (~1000 hs) is expected to be sufficient to crack susceptible materials. Samples of susceptible materials, for example, type 304 or 316 stainless steel, are recommended as controls when evaluating more resistant materials.

Testing in Polythionic Acids. Petrochemical refinery equipment is subject to polythionic acid cracking, which may occur after shutdown. Polythionic acid forms by the decomposition of sulfides on metal walls in the presence of oxygen and water. ASTM G 35 (Ref 135) describes procedures for preparing and conducting exposures to polythionic acids ($H_2S_nO_6$ where n is usually 2 to 5) at room temperature to determine the relative susceptibility of sensitized stainless steels or related materials (high Ni-Cr-Fe alloys) to intergranular SCC.

This test method can be used to evaluate stainless steels or other materials in the as-received condition or after high-temperature service (480 to 815 °C, or 900 to 1500 °F) for prolonged periods of time. Wrought products, castings, and weldments of stainless steels or other related materials used in environments containing sulfur or sulfides can also be evaluated. Other materials that are capable of being sensitized can also be tested.

A variety of smooth SCC test specimens, surface finishes, and methods of applying stress can be used. Stressed specimens are immersed in the polythionic acid solution, which can be prepared by passing a slow current of hydrogen sulfide gas for 1 h through a fritted glass tube into a flask containing chilled (0 °C, or 32 °F) 6% sulfurous acid, after which the liquid is kept in a stoppered flask for 48 h at room temperature. Solutions can also be prepared by passing a slow current of sulfur dioxide gas through a fritted glass bubbler submerged in a container of distilled water at room temperature. This is continued until the solution becomes saturated. The hydrogen sulfide gas is then slowly bubbled into the sulfurous acid solution.

Prior to use, the polythionic acid solution should be filtered to remove elemental sulfur and then tested for acid content. This can be done by analytical tests or by using a control test specimen of sensitized type 302 or 304 stainless steel. The control should fail by cracking in less than 1 h.

The wick test can be used to evaluate the chloride cracking characteristics of thermal insulation for applications in the chemical-process industry. ASTM C 692 (Ref 136) covers the methodology and apparatus used to conduct this procedure. When a dilute aqueous solution is transmitted to a metal surface by capillary action through an absorbent fibrous material, the process is called wicking. Cracking occurs at much lower temperatures when alternate wetting and drying is used than when the specimens are kept wet continuously.

Other Testing Media. Hot concentrated caustic solutions are another type of environment encountered in chemical industries that causes SCC of stainless steels. However, the conditions leading to caustic cracking are more restrictive than those leading to chloride cracking, and caustic environments have not received the attention that chlorides have. There is little difference in the susceptibilities among types 304, 304L, 316, 316L, 347, and USS 18-18-2 austenitic steels. All of these alloys crack rapidly in solutions of 10 to 50% sodium hydroxide at 150 to 370 °C (300 to 700 °F) (Ref 4, 127, 137).

Certain strong acid solutions containing chlorides, such as 5 *N* sulfuric acid plus 0.5 *N* sodium chloride, 3 *N* perchloric acid plus 0.5 *N* sodium chloride, and 0.5 to 1.0 *N* hydrochloric acid, are capable of causing SCC in austenitic stainless steels at room temperature (Ref 4). Cracking in these environments is similar to the type of cracking that occurs in hot chloride environments.

Electrochemical Polarization. Stress-corrosion cracking in austenitic and ferritic stainless steels can be delayed or prevented by the application of cathodic current; however, if ferritic and martensitic steels are overprotected by relatively large cathodic current, they are apt to blister or crack due to the hydrogen discharged by the cathodic protection action. Anodic polarization significantly accelerates the initiation of SCC, but appears to have a smaller accelerating effect on crack propagation (Ref 138).

References cited in this section

4. B.F. Brown, "Stress Corrosion Cracking Control Measures," National Bureau of Standards Monograph 156, U.S. Department of Commerce, June 1977

125. "Practice for Evaluating Stress-Corrosion- Cracking Resistance of Metals and Alloys in a Boiling Magnesium Chloride Solution," G 36, *Annual Book of ASTM Standards,* American Society for Standards and Materials

126. R.M. Latanision and R.W. Staehle, Stress Corrosion Cracking of Iron-Nickel-Chromium Alloys, *Proc. Conf. Fundamental Aspects of Stress Corrosion Cracking,* National Association of Corrosion Engineers, 1969, p 214–307

127. S.W. Dean, Review of Recent Studies on the Mechanism of Stress Corrosion Cracking in Austenitic Stainless Steels, *Stress Corrosion—New Approaches,* STP 610, H.L. Craig, Jr., Ed., American Society for Testing and Materials, 1976, p 308–337

128. E. Denhard, Effect of Composition and Heat Treatment on the Stress Corrosion Cracking of Austenitic Stainless Steels, *Corrosion,* Vol 16 (No. 7), 1960, p 131–141

129. H.R. Copson, Effect of Composition on Stress Corrosion Cracking of Some Alloys Containing Nickel, *Physical Metallurgy of Stress Corrosion Fracture,* T.N. Rhodin, Ed., Interscience, 1959, p 247–272

130. A.W. Loginow, J.F. Bates, and W.L. Mathay, New Alloy Resists Chloride Stress Corrosion Cracking, *Mater. Prot. Perform.,* Vol 11 (No. 5), 1972, p 35–40

131. N.A. Nielsen, Observations and Thoughts on Stress Corrosion Mechanism, *J. Met.,* Vol 5, 1970, p 794–829

132. J.D. Harston and J.C. Scully, Stress Corrosion of Type 304 Steel in H_2SO_4/NaCl Environments at Room Temperature, *Corrosion,* Vol 25 (No. 12), 1969, p 493–501

133. S. Takemura, M. Onoyama, and T. Ooka, Stress Corrosion Cracking of Stainless Steels in Hydrogen Sulfide Solutions, *Corrosion,* Vol 16 (No. 7), 1960, p 338–348

134. "Test Method for Evaluating Stress-Corrosion Cracking of Stainless Alloys with Different Nickel Content in Boiling Acidified Sodium Chloride Solution," G 123, *Metal Corrosion, Erosion, and Wear,* Vol 03.02, *Annual Book of ASTM Standards,* American Society for Testing and Materials

135. "Practice for Determining the Susceptibility of Stainless Steels and Related Nickel- Chromium-Iron Alloys to Stress-Corrosion Cracking in Polythionic Acids," G 35, *Metal Corrosion, Erosion, and Wear,* Vol 03.02, *Annual Book of ASTM Standards,* American Society for Testing and Materials

136. “Standard Test Method for Evaluating the Influence of Thermal Insulations on External Stress Corrosion Cracking Tendency of Austenitic Stainless Steel,” C 692, *Annual Book of ASTM Standards,* American Society for Testing and Materials

137. J.L. Wilson, F.W. Pement, and R.G. Aspden, Effect of Alloy Structure, Hydroxide Concentration, and Temperature on the Caustic Stress-Corrosion Cracking of Austenitic Stainless Steel, *Corrosion,* Vol 30 (No. 4), 1974, p 139–149

138. H. Kohl, A Contribution to the Examination of Stress-Corrosion Cracking of Austenitic Stainless Steel in Magnesium Chloride Solution, *Corrosion,* Vol 23 (No. 12), 1967, p 39–49

B. Phull, Evaluating Stress-Corrosion Cracking, *Corrosion: Fundamentals, Testing, and Protection,* Vol 13A, *ASM Handbook*, ASM International, 2003, p 575–616

Evaluating Stress-Corrosion Cracking

Revised by Bopinder Phull, Consultant

Testing of Magnesium Alloys

There is no standard accelerated test environment recommended for assessing the susceptibility of magnesium-base alloys to SCC. Exposure of stressed specimens to the atmosphere has generally been used to determine the SCC susceptibility of specific products.

The chloride-containing solutions typically used in accelerated tests for aluminum alloys are unsatisfactory for SCC tests of magnesium alloys because of excessive general corrosion. In one investigation, a chromate-inhibited chloride solution (35 g/L sodium chloride plus 20 g/L potassium chromate; pH 8) was found to be suitable for testing magnesium alloys (Ref 139). Good correlation was observed between the SCC behavior of Mg-Al-Zn alloys exposed by total immersion in this solution and the behavior of the same alloys exposed to an industrial atmosphere. Cracking of highly stressed susceptible alloys occurs within a few hours, but exposures can be continued up to 1000 h without incurring excessive pitting. Laboratory tests also have been conducted using potassium hydrogen fluoride and a dilute solution of sodium chloride plus sodium bicarbonate as the test medium (Ref 140).

References cited in this section

139. G.F. Sager, R.H. Brown, and R.B. Mears, Tests for Determining Susceptibility to Stress Corrosion Cracking, *Symposium on Stress Corrosion Cracking of Metals,* American Society for Testing and Materials and the American Institute of Mechanical Engineers, 1945, p 255–272

140. H.B. Romans, Stress Corrosion Test Environments and Test Durations, *Stress Corrosion Testing,* STP 425, American Society for Testing and Materials, 1967, p 182–208

B. Phull, Evaluating Stress-Corrosion Cracking, *Corrosion: Fundamentals, Testing, and Protection*, Vol 13A, *ASM Handbook*, ASM International, 2003, p 575–616

Evaluating Stress-Corrosion Cracking

Revised by Bopinder Phull, Consultant

Testing of Magnesium Alloys

There is no standard accelerated test environment recommended for assessing the susceptibility of magnesium-base alloys to SCC. Exposure of stressed specimens to the atmosphere has generally been used to determine the SCC susceptibility of specific products.

The chloride-containing solutions typically used in accelerated tests for aluminum alloys are unsatisfactory for SCC tests of magnesium alloys because of excessive general corrosion. In one investigation, a chromate-inhibited chloride solution (35 g/L sodium chloride plus 20 g/L potassium chromate; pH 8) was found to be suitable for testing magnesium alloys (Ref 139). Good correlation was observed between the SCC behavior of Mg-Al-Zn alloys exposed by total immersion in this solution and the behavior of the same alloys exposed to an industrial atmosphere. Cracking of highly stressed susceptible alloys occurs within a few hours, but exposures can be continued up to 1000 h without incurring excessive pitting. Laboratory tests also have been conducted using potassium hydrogen fluoride and a dilute solution of sodium chloride plus sodium bicarbonate as the test medium (Ref 140).

References cited in this section

139. G.F. Sager, R.H. Brown, and R.B. Mears, Tests for Determining Susceptibility to Stress Corrosion Cracking, *Symposium on Stress Corrosion Cracking of Metals,* American Society for Testing and Materials and the American Institute of Mechanical Engineers, 1945, p 255–272

140. H.B. Romans, Stress Corrosion Test Environments and Test Durations, *Stress Corrosion Testing,* STP 425, American Society for Testing and Materials, 1967, p 182–208

B. Phull, Evaluating Stress-Corrosion Cracking, *Corrosion: Fundamentals, Testing, and Protection*, Vol 13A, *ASM Handbook*, ASM International, 2003, p 575–616

Evaluating Stress-Corrosion Cracking

Revised by Bopinder Phull, Consultant

Testing of Titanium Alloys

Although titanium alloys are not susceptible to SCC in either boiling 42% magnesium chloride or boiling 10% sodium hydroxide solutions, which are commonly used to study SCC in stainless steels, the susceptibility of titanium and its alloys to SCC has been demonstrated in several environments. This information is given in Table 9.

Table 9 Environments and temperatures conducive to SCC of titanium alloys

Environment	Temperature, °C (°F)
Hot dry chloride salts	260–480 °C (500–900 °F)
Seawater, distilled water, and aqueous solutions	Ambient
Nitric acid, red fuming	Ambient
Nitrogen tetroxide	Ambient to 75 °C (165 °F)
Methanol, ethanol	Ambient
Chlorine	Elevated
Hydrogen chloride	Elevated
Hydrochloric acid, 10%	Ambient to 40 °C (105 °F)
Trichloroethylene	Elevated
Trichlorofluoroethane	Elevated
Chlorinated diphenyl	Elevated

Testing in a Hot Salt Environment. The hot salt test consists of exposing a stressed salt- coated test specimen to an elevated temperature for various predetermined lengths of time. The exposure periods are determined by the alloy, stress level, temperature, and selected damage criterion (that is, embrittlement, cracking, or rupture, or a combination of these phenomena). Exposures are typically carried out in laboratory ovens or furnaces equipped with loading equipment for stressing specimens. Environmental conditions, the degree of control required, and the means for obtaining control are described in ASTM G 41 (Ref 144).

This test method can be used to test all metals if service conditions warrant. The test limits maximum operating temperatures and stress levels, or it categorizes different alloys according to their susceptibility if hot salt damage has been found to accelerate failure by creep, fatigue, or rupture. Although limited evidence relates this phenomenon to actual service failures, cracking under stress in a hot salt environment is a potential design-controlling factor.

The hot salt test should not be construed as being related to the SCC of materials in other environments. It should be used only in an environment that may be encountered in service.

Hot salt testing can be used for alloy screening to determine the relative susceptibility of metals to embrittlement and cracking and to determine the time-temperature-stress threshold levels for the onset of embrittlement and cracking. However, certain types of specimens are more suitable for each of these types of characterizations. Precracked specimens are unsuitable for testing of titanium alloys, because cracking reinitiates at salt/metal/air interfaces and results in many small cracks that extend independently. Therefore, smooth specimens are recommended.

Testing in Water and Aqueous Solutions. Water, seawater, and almost any neutral aqueous solution (except atmospheric water vapor) can cause SCC in many titanium alloys in the presence of preexisting cracklike flaws, although susceptibility in these environments cannot be detected by smooth specimens. Therefore, fracture mechanics type characterizations are necessary. For titanium alloys, the extremely rapid growth of stress-corrosion cracks in saltwater and the dependency on specimen geometry preclude the possibility of using crack growth rate data for design purposes.

Therefore, ranking of materials must be based on K_{ISCC} values, and a true threshold stress intensity for SCC apparently does exist (Ref 145). Titanium alloys do not exhibit stage I type crack growth kinetics (Fig. 3) in neutral aqueous solutions. Tests have been performed for sufficient periods of time to allow detection of crack growth rates of 10^{-9} m/s (1.4×10^{-4} in./h), but SCC has not been observed. The slowest crack velocity that has been detected is 10^{-8} m/s (1.4×10^{-3} in./h). Therefore, in neutral aqueous solutions, a threshold K_{ISCC} exists at which SCC will not propagate (Ref 4, 145). The above rates, however, are not as slow as those observed in high-susceptibility aluminum alloys (Fig. 46). Tests are commonly performed in water containing about 3.5% sodium chloride, artificial seawater, or natural seawater unless specific environments are being tested.

Electrochemical Polarization. The halide ions (chloride, bromide, and iodide) are SCC agents unique for titanium alloys in aqueous solutions at room temperature. The crack initiation load and velocity are controlled by the applied potential, as illustrated for the crack initiation load in Fig. 56. At potentials more negative than about -700 to -1400 mV, depending on the solution, specimens were cathodically protected. Sodium fluoride solution and solutions of the other anions that do not produce SCC (hydroxide, sulfide, sulfate, nitrite, nitrate, perchlorate, cyanide, and thiocyanate) yielded results at all potentials in the same scatterband as the air values.

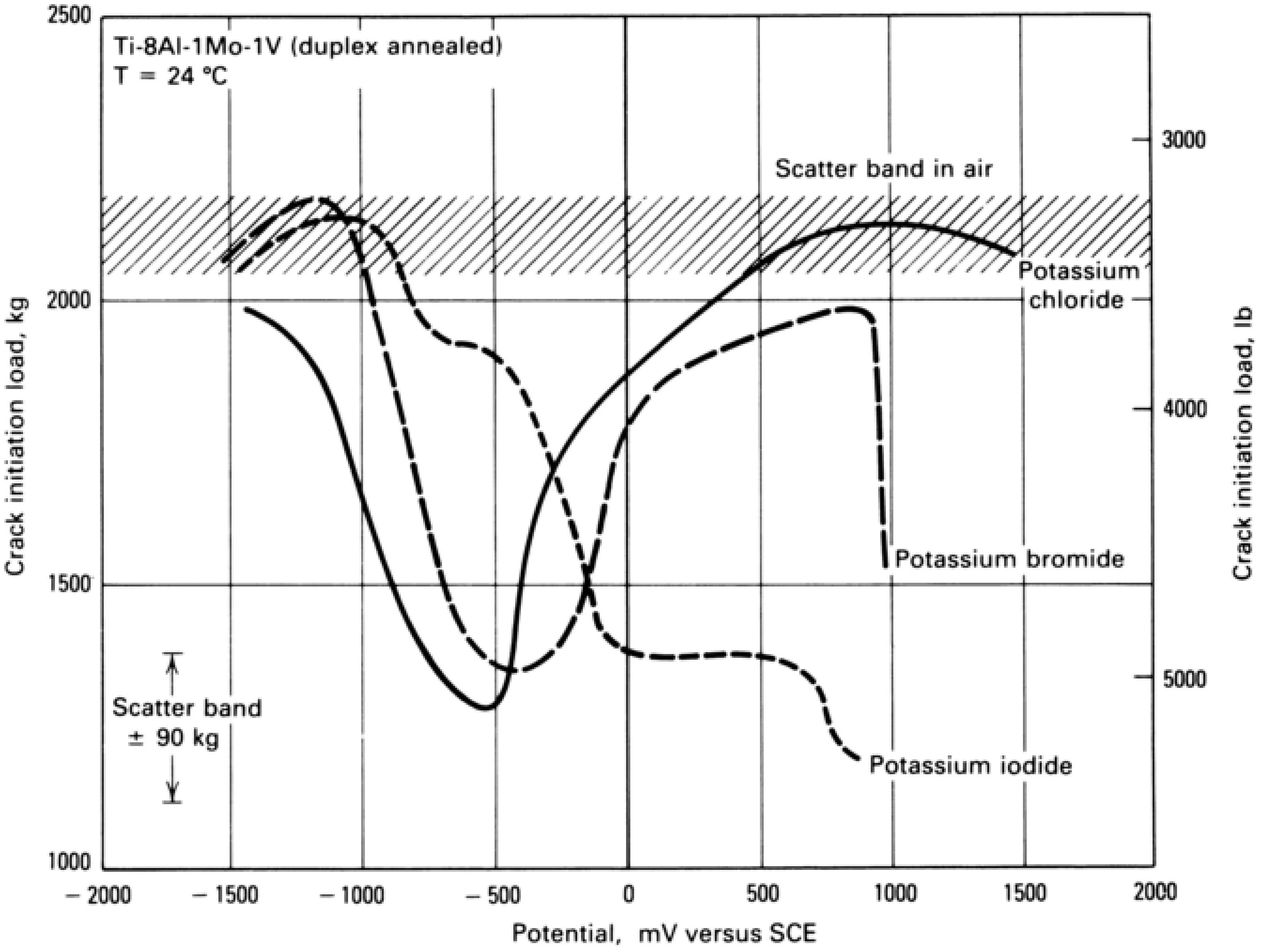

Fig. 56 Variation of crack initiation load with potential in 0.6 *M* halide solutions for Ti-8Al-1Mo-1V. Specimen: single-edge cracked sheet that was tension loaded by constant displacement. Source: Ref 145, 146

At potentials more positive than the above values, susceptibility of varying degrees occurred in the chloride, bromide, and iodide solutions. The width of the critical potential range and the potential for maximum susceptibility varies with the anion. A region of anodic protection occurred in the chloride and bromide solutions, but not in the iodide solution.

Crack propagation can be halted by switching the potential to either the anodic or cathodic protection zone. The corrosion potential of titanium alloys in 3.5% sodium chloride and seawater—about -80 mV versus SCE—is similar (slightly more negative) to the potential at which SCC susceptibility reaches a maximum (Ref 145).

Testing in Organic Fluids. A wide variety of organic fluids can cause SCC in some titanium alloys under specific test conditions (Table 9). Most of these fluids attack the passive surface film that is characteristic of titanium alloys. Consequently, precracked specimens do not have to be used to accelerate the SCC initiation. A standard environment does not exist; test conditions must be selected with appropriate consideration given to the type of environmental service required.

Sustained-Load Cracking in Inert Environments. High-strength titanium alloys for use in highly stressed components for military aircraft and other similar applications may be susceptible to sustained-load cracking in inert environments (including dry air). Sustained-load cracking is similar to SCC except that it is much slower and occurs in the total absence of a reactive environment. Sustained-load cracking is caused by, or is greatly aggravated by, hydrogen dissolved in the titanium during processing. Vacuum annealing can reduce the hydrogen level to less than 10 ppm, at which concentration the tendency toward sustained-load cracking is greatly reduced (Ref 4, 147).

Figure 57 illustrates an example of sustained- load cracking in mill-annealed plate of Ti-8Al- 1Mo-1V containing 48 ppm hydrogen. As shown in Fig. 57, the threshold stress-intensity factor for sustained-load cracking in dry air is designated K_{IH} because it is attributed to hydrogen in the metal. When the hydrogen

concentration was reduced to 2 ppm by vacuum annealing, the K_{IH} value was increased to equal the inherent plane-strain fracture toughness, K_{Ic}. However, the K_{ISCC} value was not affected (Ref 148). Therefore, in addition to the practical importance of sustained-load cracking, its potential contribution to cracking should be taken into account when evaluating environmental effects, particularly in mechanistic studies.

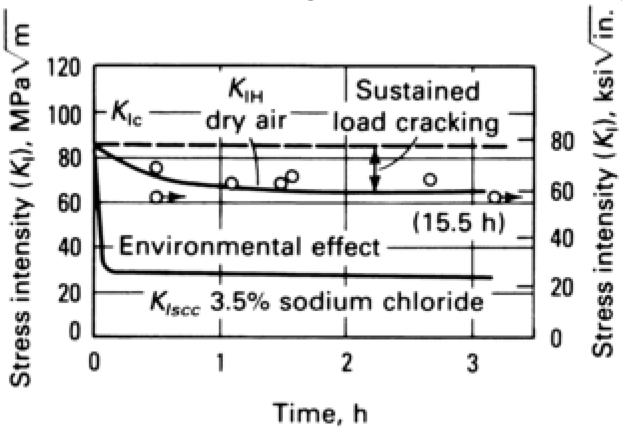

Fig. 57 Effect of sustained-load cracking compared to SCC in Ti-8Al-1Mo-1V mill-annealed sheet. Hydrogen concentration, 48 ppm; yield strength, 850 MPa (123 ksi); cantilever bend specimen (T-S); *B* = 6.35 mm (0.25 in.). See Fig. 28 for an explanation of specimen orientation and fracture plane identification. Source: Ref 148

References cited in this section

4. B.F. Brown, "Stress Corrosion Cracking Control Measures," National Bureau of Standards Monograph 156, U.S. Department of Commerce, June 1977

144. "Practice for Determining Cracking Susceptibility of Metals Exposed under Stress to a Hot Salt Environment," G 41, *Metal Corrosion, Erosion, and Wear,* Vol 03.02, *Annual Book of ASTM Standards,* American Society for Testing and Materials

145. M.J. Blackburn, W.H. Smyrl, and J.A. Sweeny, Titanium Alloys, *Stress Corrosion Cracking in High Strength Steels and in Titanium and in Aluminum Alloys,* B.F. Brown, Ed., Naval Research Laboratory, 1972, p 246–363

146. T.R. Beck, Electrochemical Aspects of Titanium Stress Corrosion, *Proc. Conf. Fundamental Aspects of Stress Corrosion Cracking,* National Association of Corrosion Engineers, 1969, p 605–619

147. D.A. Meyn, Effect of Hydrogen on Fracture and Inert Environment Sustained Load Cracking Resistance of Alpha-Beta Titanium Alloys, *Metall. Trans.,* Vol 5 (No. 11), 1974, p 2405–2414

148. G. Sandoz, Subcritical Crack Propagation in Ti-8Al-1Mo-1V Alloy in Organic Environments, Salt Water and Inert Environments, *Proc. Conf. Fundamental Aspects of Stress Corrosion Cracking,* National Association of Corrosion Engineers, 1969, p 684–690

B. Phull, Evaluating Stress-Corrosion Cracking, *Corrosion: Fundamentals, Testing, and Protection*, Vol 13A, *ASM Handbook*, ASM International, 2003, p 575–616

Evaluating Stress-Corrosion Cracking

Revised by Bopinder Phull, Consultant

Special Considerations for Testing of Weldments

ASTM G 58 (Ref 149) covers test specimens in which stresses are developed by the welding process only (that is, residual stress, Fig. 23), an externally applied load in addition to the stresses due to welding (Fig. 7e), and an externally applied load only, with residual welding stresses removed by annealing.

The National Materials Advisory Board Committee on Environmentally Assisted Cracking Test Methods for High-Strength Weldments published the following guidelines on SCC testing of weldments (Ref 31). Fracture mechanics of cracked bodies was found to be a valid and useful approach for designing against environmentally assisted cracking, although several limitations and difficulties must be taken into consideration. For static loading, K_{ISCC} and *da*/ *dt* versus K_I are useful parameters. They are specified to a material, temperature, and metal/ environment system and are functions of local chemical composition, microstructure, and so on.

Superimposed minor load fluctuations and infrequent changes in load can alter environmental cracking response. This effect, which cannot be predicted from K_{ISCC} and *da*/*dt* values, may be significant and detrimental. Reexamination of static loading as a design premise may be required. Existing test methodology or environmentally assisted cracking tendency is applicable to the evaluation of weldments. As in other structural components, residual stress must be treated in a quantitative and realistic manner.

The National Materials Advisory Board report supports current design emphasis based on the presumption of preexisting cracklike flaws in the structure and covers testing with precracked (fracture mechanics) specimens only. It contains a critical assessment of the problems associated with environmentally assisted cracking in high- strength alloys and of state-of-the-art design and test methodology.

References cited in this section

31. "Characterization of Environmentally Assisted Cracking for Design—State of the Art," National Materials Advisory Board Report No. NMAB-386, National Academy of Sciences, 1982

149. "Practice for Preparation of Stress-Corrosion Test Specimen for Weldments," G 58, *Metal Corrosion, Erosion, and Wear,* Vol 03.02, *Annual Book of ASTM Standards,* American Society for Testing and Materials

B. Phull, Evaluating Stress-Corrosion Cracking, *Corrosion: Fundamentals, Testing, and Protection*, Vol 13A, *ASM Handbook*, ASM International, 2003, p 575–616

Evaluating Stress-Corrosion Cracking

Revised by Bopinder Phull, Consultant

Surface Preparation of Smooth Specimens

The pronounced effect of surface conditions on the time required to initiate SCC in test specimens is well known (Ref 5). Unless the as-fabricated surface is being studied, the final surface preparation generally

preferred is a mechanical process followed by degreasing. However, chemical etches or electrochemical polishes can be used to remove heat treating films or thin layers of surface metal that may have become distorted during machining.
Care should be exercised to select an etchant that will not selectively attack constituents or phases in the metal and that will not deposit undesirable residues on the surface. Etching or pickling should not be used with alloys that are susceptible to hydrogen embrittlement.
Precautions should be taken when machining specimens to avoid overheating, plastic deformation, or the development of residual stress in the metal surface. Machining should be performed in stages so that the final cut leaves the principal surface with a clean finish of 0.7 μm (30 μin.) rms or smoother. The required machining sequences, types of tools, and feed rate depend on the alloy and metallurgical condition of the test piece. Lapping, mechanical polishing, and similar operations that produce flow of the metal should be avoided.

Reference cited in this section

5. R.N. Parkins et al., Report Prepared for the European Federation of Corrosion Working Party on Stress Corrosion Test Methods, *Br. Corros. J.,* Vol 7, July 1982, p 154–167

B. Phull, Evaluating Stress-Corrosion Cracking, *Corrosion: Fundamentals, Testing, and Protection*, Vol 13A, *ASM Handbook*, ASM International, 2003, p 575–616

Evaluating Stress-Corrosion Cracking

Revised by Bopinder Phull, Consultant

Interpretation of Test Results

This is the most fallible part of SCC testing and evaluation; it includes the analysis that leads to the conclusions and recommendations. Stress- corrosion test data are at best imprecise and test dependent, and they must be qualified with the testing conditions. It is important to verify the mode of environmental cracking (Fig. 1) and then to review the data to exclude all extraneous results, as discussed previously with the individual test methods. Following are some comments on the nature of the test dependency of the most commonly used criteria of SCC behavior.

Criteria of SCC Behavior

Specimen Life (Time to Failure). Stress-corrosion testing frequently involves determining the lives of specimens under specific test conditions. This includes the initiation (or incubation) of a stress-corrosion crack and its propagation to the point of fracture (Fig. 2). Such a determination is easily accomplished when only a single crack forms and the specimen fractures within the chosen test period. However, it often happens that SCC occurs but the specimen does not fracture. This is especially likely when testing relatively low-strength materials by constant strain loading (Fig. 5b) and when testing at applied-stress or stress-intensity levels only slightly above the threshold (Fig. 29a). Cracks may initiate at multiple sites in constant-strain loaded smooth specimens with relatively low applied stress, and a difficult problem arises in deciding when to consider a specimen failed if it does not fracture visibly.
It is often found that the majority of specimens in a set of replicates in a test fail rapidly; this leaves a few specimens that fail at much longer times or do not fail at all before the test is discontinued. Such behavior presents difficulties, both theoretical and practical, in deciding when to terminate a test, choosing a satisfactory representative value, and comparing such values.
The arithmetic mean specimen life is widely used for smooth specimens because it can be manipulated algebraically and can be used in many standard statistical tests of significance. It should be remembered,

however, that extremely large or extremely small values may cause the mean to be atypical of the true distribution. Moreover, in using the arithmetic mean, it is assumed that the population is normally or very nearly normally distributed. The median, on the other hand, has the advantage that it is influenced less by extreme values, requires no assumption about the population distribution, and can be obtained much faster than arithmetic mean values because only about half the number of replicates exposed need to be tested to failure. The median is used in a German specification (Ref 24) that also provides for the use of the geometric mean if the replication is small.

References 1 and 150 contain examples for highly susceptible steel and aluminum alloys, respectively; these examples demonstrate the normal distributions for the logarithms of the specimen lives. With such distributions, a geometric mean would be the best representative value of the specimen life. It has also been shown that a Weibull distribution can be appropriate for the nonnormally distributed test data for a relatively resistant aluminum alloy (Ref 151). Thus, it should not be assumed that any one distribution is applicable for all testing situations.

Comparisons of alloys with differing strength and fracture toughness based on time to failure can be completely misleading. For example, SCC growth curves are shown in Fig. 58 for alloys with different fracture toughnesses. Curves A, B, and C represent materials with decreasing toughness, with curve C showing fast fracture initiated by corrosion pits or fissures with no SCC.

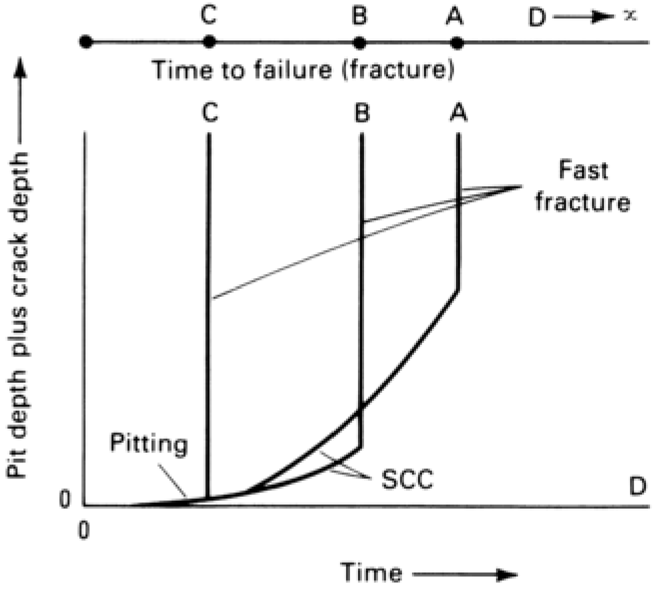

Fig. 58 Various processes in SCC as influenced by the fracture toughness of the metal. Kinetics for pitting (or, in material D, nonpitting), SCC (materials A and B only), and fast fracture. Line at top illustrates how time to failure data can be misleading. Source: Ref 152

The behavior of a material that does not develop localized pitting or intergranular attack is represented by a line coincident with the abscissa, designated D in Fig. 58. The time-to-failure ranking above the graph indicates D as best and A, B, and C as poorest. Actually, the SCC responses of C and D were not measured, and the true SCC ranking of A and B (indicated by depth of SCC at the time of fracture) exhibits a trend opposite to that inferred from the time-to- failure data above.

Further difficulties may arise, because the total time to fracture is also influenced by non- SCC factors, such as specimen type and size, method of loading, initial stress level, and initiation behavior of the alloy. Consequently, the SCC ranking of materials may vary among investigators using different testing techniques. Nevertheless, comparisons of specimen lives derived from smooth specimens can be useful in certain mechanistic studies and in tests for comparing environmental variations if the mechanical aspects of the investigation are held constant.

Threshold Stress (Stress-Time Curve). More information about the resistance to SCC of a material can be obtained when testing smooth specimens by using a range of applied stresses. Such data are usually presented graphically with the applied gross section stress plotted against specimen life (Fig. 54). The primary interest is generally in the long-life portion of the curve to obtain an estimate of the threshold stress.

A common method of estimating threshold stress involves the experimental determination of the lowest stress at which cracking occurs in at least one specimen and the highest stress at which cracking does not occur in several specimens (for example, three or more, depending on variability). An average of the lowest failure and highest no-failure stresses is usually taken as the threshold stress. Such determinations of critical stresses are carried out at specified test times that are known through experience or preliminary tests to be sufficient to produce SCC in the alloy- environment system of interest. Statistical methods are available for determining threshold stresses more precisely (for example, the Probit method or staircase method) and are commonly used for the determination of fatigue limits. However, the additional testing involved can be quite extensive.

Apparent threshold stresses determined in laboratory tests of coupon specimens are useful for ranking the SCC susceptibility of various materials, but, because such data are dependent on test conditions, they are not realistic for the purpose of engineering design (Ref 4). Also, when using such data as an aid in selecting the material for a specific structure, caution should be exercised in trying to relate the laboratory test conditions to the anticipated service conditions. Not only the environmental condition but also the geometry and size of the test specimens and the method of stressing should be compared (Fig. 6, 18). Further, threshold stresses obtained with statically loaded smooth specimens are likely to be nonconservative; it has been shown in tests on carbon-manganese steel that the threshold stress obtained by static loads is reduced by applied constant slow strain rates and that it can be reduced even further with cyclic loading (Ref 61). With appropriate frequency, load change, and temperature, average creep rates can be sustained over extended periods, but with static loading, the creep rate may fall below the level needed to promote SCC. In general, experimentally determined threshold stresses for materials with only limited susceptibility to SCC are more sensitive to variations in testing conditions than in the case of highly susceptible materials.

Percent Survival (Curve). This method of analyzing stress-corrosion test results is especially useful when some of the specimens in a group survive the duration of the test. Examples of various comparisons by this technique are shown in Fig. 18, 42, and 43. Although the curves can be drawn on regular coordinate graph paper, the percent survival values will often lie along a straight line when plotted on normal probability paper, as shown in Fig. 59. The linearity of this plot indicates that the statistical distribution of the test results is logarithmic-normal. The vertical positions of the lines indicate the cracking ability of the environment, which can be represented by median cracking times. The slopes of the lines correspond to the variance, which can be used to calculate confidence limits.

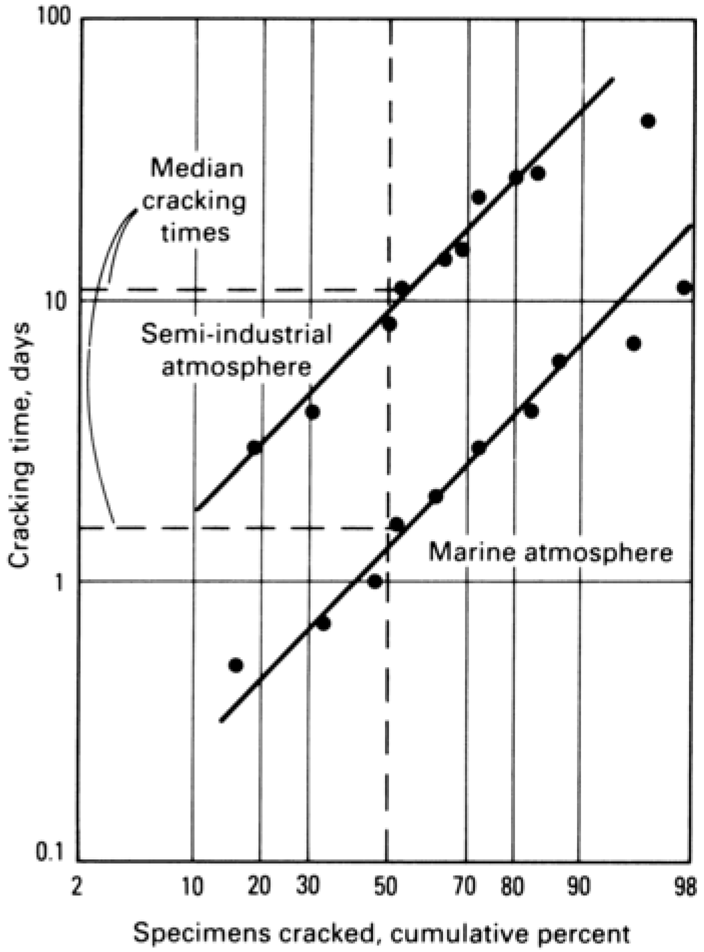

Fig. 59 Distribution of SCC test results for a stainless steel. Source: Ref 1, 153

Threshold Stress Intensity (K_{ISCC}, K_{th}). Linear elastic fracture mechanics is well established as a basis for materials characterization, including environmental cracking (Ref 31, 154, 155). In practice, it is most practical to define K_{ISCC} as the K_I level associated with some generally acceptable and definably low rate of crack growth that is commensurate with the design service life. When K_{ISCC} values are reported, the criterion for their assessment and the exposure time in the environment must accompany the threshold values. A rational approach to the development of useful data for design is to establish an operational definition of K_{ISCC} that is appropriate for the structure under consideration.

Such characterization requires that linear elastic fracture mechanics and plane-strain conditions be satisfied. However, for certain low- strength steels and aluminum alloys, existing data show that SCC can occur under conditions that deviate substantially from plane strain, and that SCC is by no means limited to or is most severe under plane-strain loading conditions (Ref 156, 157). In these cases, the application of linear elastic fracture mechanics is no longer valid, and the parameter K_{ISCC} is no longer meaningful. Similarly, when testing materials with a high resistance to SCC, loading to high percentages of K_{Ic} may cause a relaxation of stress due to creep. In this case also, the apparent K_{ISCC} values are meaningless. Constant-load tests, therefore, are preferred for lower-strength materials (Ref 158).

The symbol K_{th} has been used to identify threshold stress-intensity factors developed under test conditions that do not satisfy all the requirements for plane-strain stress. Design calculations using such values should not be employed unless it is clear that the laboratory tests exhibit the same stress state as that for the intended application. Nevertheless, properly determined K_{th} values can be useful for ranking materials.

In principle, experimentally determined K_{ISCC} values should be the same whether they are determined by the initiation or the arrest test method (Fig. 29). In both tests, there are dimensional requirements for ensuring that the test results are independent of geometrical effects (see the section “Preparation of Precracked Specimens” in this article). However, precautions must be exercised during testing to avoid the potential problems involved with the environmental exposure (incubation, corrosion-product wedging, crack branching, crack tip blunting, and so on). Comparisons of K_{ISCC} values determined for selected steels by both methods, along with examples

of overestimated values resulting from insufficient length of exposure, are shown in Tables 6 and 7. It is advisable, when practicable, to use a test that matches the type of loading encountered in the anticipated service.

From the parameter K_{ISCC}, a value of a_{cr} can be calculated using the relation $a_{cr} = 0.2\ (K_{ISCC}/\ \mathrm{TYS})^2$ (see the section "Static Loading of Precracked (Fracture Mechanics) Specimens" in this article). This is the shallowest crack (surface length is long compared to its depth) that will propagate as a stress-corrosion crack at a yield strength level of gross stress under the given environmental conditions. This can be a very useful parameter for comparing materials, especially when the measured a_{cr} values can be related to the capability of the flaw inspection system used for a given engineering structure (Fig. 52). Straight lines representing assumed values of a_{cr} in Fig. 52 illustrate how K_{ISCC} values for the various steel alloys relate to the maximum depth of long surface flaws that can be tolerated without growth of SCC.

Such a plot can be used as follows. If the inspection system to be used can detect all long surface flaws deeper than 0.25 mm (0.01 in.), then the materials engineer would select an alloy with a K_{ISCC} above the 0.25 mm (0.01 in.) line. Conversely, if the K_{ISCC} and tensile yield strength of a material are known, the equation can be used to estimate the maximum tolerable flaw size. Substitution of an anticipated design stress in terms of percentage of tensile yield strength in the formula for a_{cr} will generate a new series of a_{cr} lines of lower slope.

Alternatively, the following method, which is specific for a given loading method, can be used, inasmuch as the flaw depth and applied stress are uniquely related for a specific loading situation, a family of curves for constant K_{th} values can be developed within these parameters. Figure 60 shows such curves for long, shallow flaws; the curves were generated according to the following equations (Ref 160, 161, 162):

$$K_1 = M_B \sqrt{\frac{\pi a}{Q}} \quad \text{(Eq 16)}$$

$$M_B = \frac{Y}{6}\sqrt{\frac{t}{\pi a}} \quad \text{(Eq 17)}$$

$$Y = \sqrt{139\frac{a}{t} - 221\left(\frac{a}{t}\right)^2 + 783\left(\frac{a}{t}\right)^3} \quad \text{(Eq 18)}$$

where K_I is stress intensity, *s* is applied stress, *a* is flaw depth, *Q* is a shape parameter, and *t* is thickness. When K_{th} is substituted into Eq 16 and a flaw shape is assumed ($Q = 0.8$), this parameter is related to the flaw size and the applied stress. In this representation, SCC growth will not occur below the curve for the appropriate K_{th}. For example, for a steel with K_{th} of 60.5 MPa$\sqrt{m}$ (55 ksi$\sqrt{in.}$), a very deep flaw (6 mm, or 0.25 in.) would be required to cause crack propagation in hydrogen gas of a steel component stressed to 360 MPa (52 ksi) in bending. Such representations are useful for relating test data and K_{th} in design and in the development of crack inspection requirements, as well as for ranking alloys.

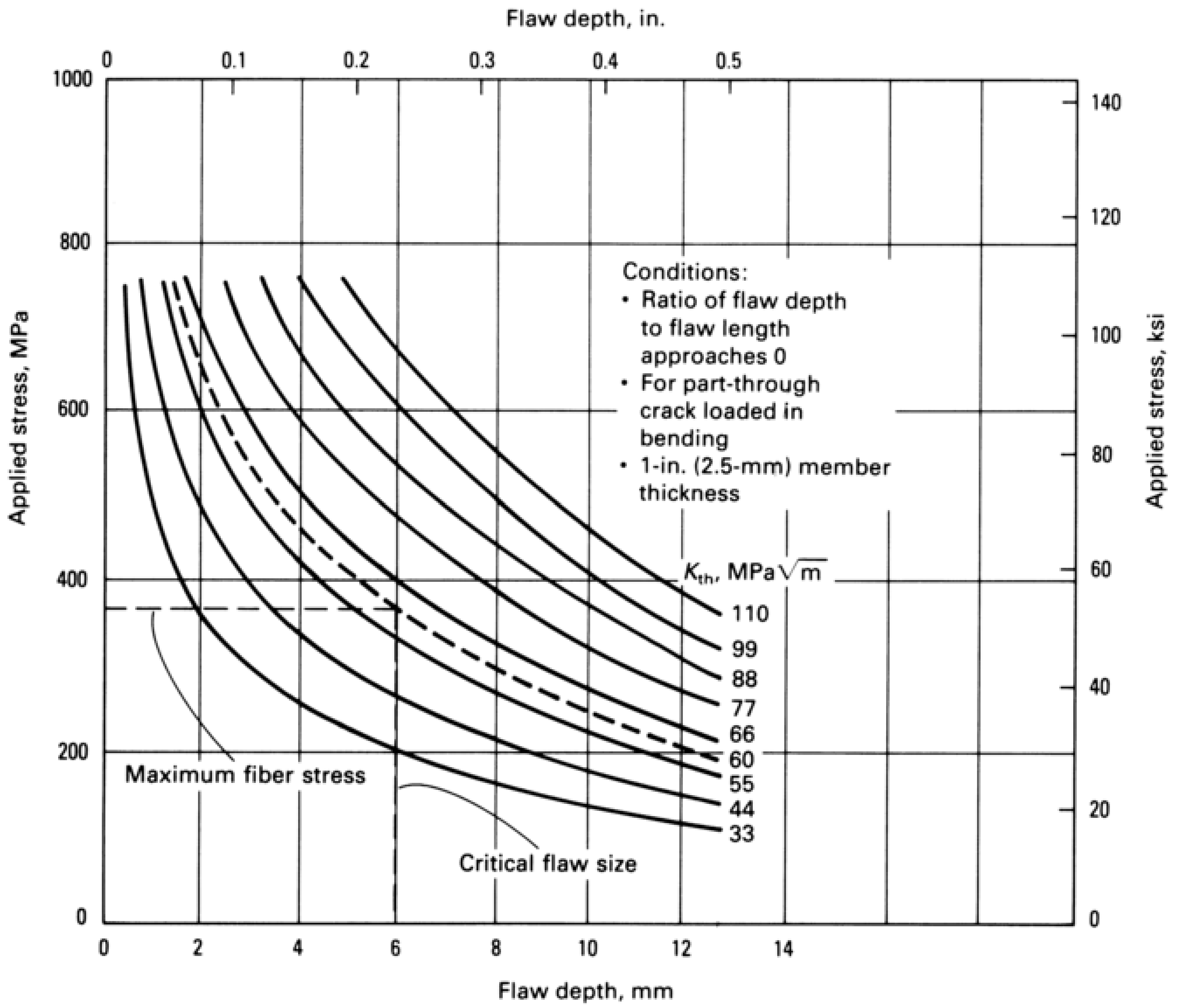

Fig. 60 Relationship of applied stress and flaw depth to crack propagation in hydrogen gas. Dashed lines show an example of the use of such a chart for a steel with K_{th} of 60.5 MPa$\sqrt{m}$ (55 ksi$\sqrt{in}$. at an operating stress of 359 MPa (52 ksi). Source: Ref 159

The requirements for K_{ISCC} tests, as well as for other fracture mechanics tests, include very explicit criteria regarding the minimum crack length for ensuring that the test results can be analyzed properly using existing linear fracture mechanics concepts. Therefore, a typical K_{ISCC} test uses a relatively large starting crack of the order of 25 mm (1 in.) long in a 25 mm (1 in.) thick specimen. In many types of service, however, initial defects of this size are rare. For example, damage-tolerant design criteria for military aircraft specify a flaw size of the order of 1.27 mm (0.05 in.) as the initial worst-case damage assumption upon introduction of a new part into service (Ref 155). Experimental work on high-strength steels exposed to hydrogen sulfide gas indicates that for a given combination of materials and applied stress there may indeed be a defect size below which the direct applicability of linear elastic fracture mechanics is questionable (Ref 163). Because of their susceptibility to SCC, however, high-strength steels should not be contemplated for service in the presence of hydrogen sulfide.

For example, Fig. 61 represents a concept of combining SCC thresholds based on smooth specimen and linear elastic fracture mechanics tests of aluminum alloy plate to give a conservative estimate of materials for design. As shown in Fig. 61, the threshold stress-intensity analysis breaks down in the small flaw region (ABE) when the smooth specimen threshold stress is exceeded. Therefore, the definition of a safe zone requires results from both types of tests; the exclusive use of either one of the test methods can yield nonconservative conclusions. It is anticipated that application and further development of elastic-plastic fracture mechanics theory will lead to

improved estimates of critical-stress/flaw-size combinations for the onset of SCC and tensile fracture, as proposed in Fig. 62.

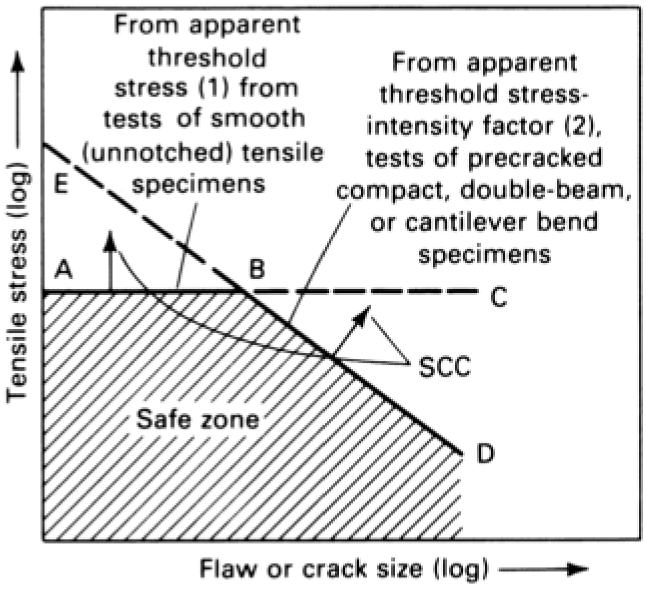

Fig. 61 Concept for combining SCC thresholds obtained on smooth and linear elastic fracture mechanics specimens to yield a conservative assessment of materials. (1) Minimum stress at which small tensile specimens fail by SCC when stressed in environment of interest. (2) Minimum stress intensity at which significant stress-corrosion crack growth occurs in environment of interest. Source: Ref 164

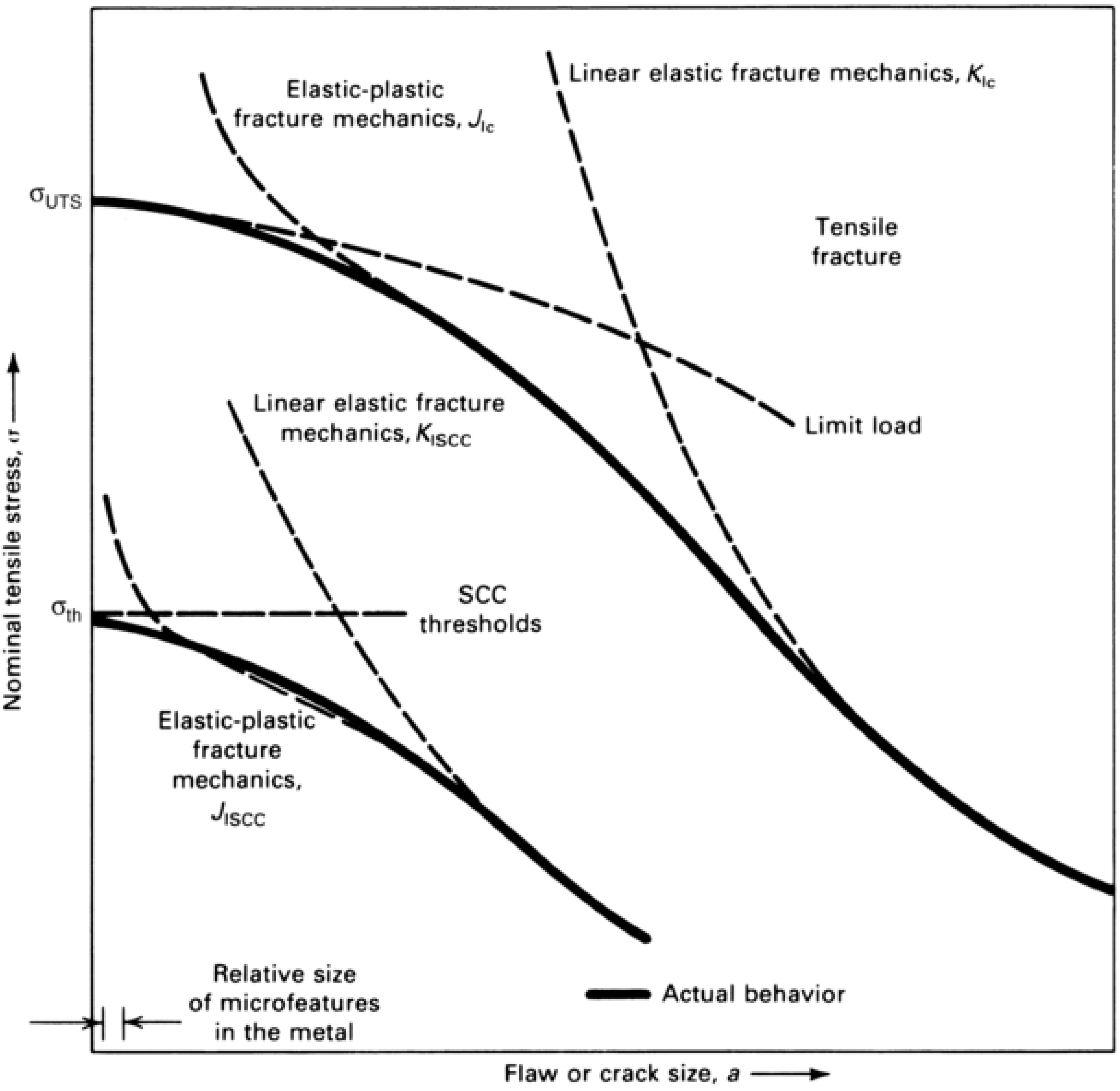

Fig. 62 Proposed linear-elastic and elastic-plastic models for describing critical combinations of stress and flaw size at SCC thresholds and at the onset of rapid tensile fracture. Source: Ref 3

SCC Velocity (V-K_I Curves). The issues of crack initiation and crack growth must be addressed for proper consideration of SCC response (Fig. 2). The use of mechanically precracked specimens provides a convenient approach for kinetic measurements where the crack growth rate can be determined as a function of the crack-tip stress-intensity factor (Fig. 3). Current emphasis, however, is on the identification of a steady-state response (plateau velocity) for the ranking of materials (Fig. 46). A disadvantage of this approach is that in some testing situations a plateau velocity is not observed (Fig. 63). However, for design purposes, the phenomena of incubation and the non-steady state response (stage 1, Fig. 3) must also be taken into account. However, these latter requirements are not well understood.

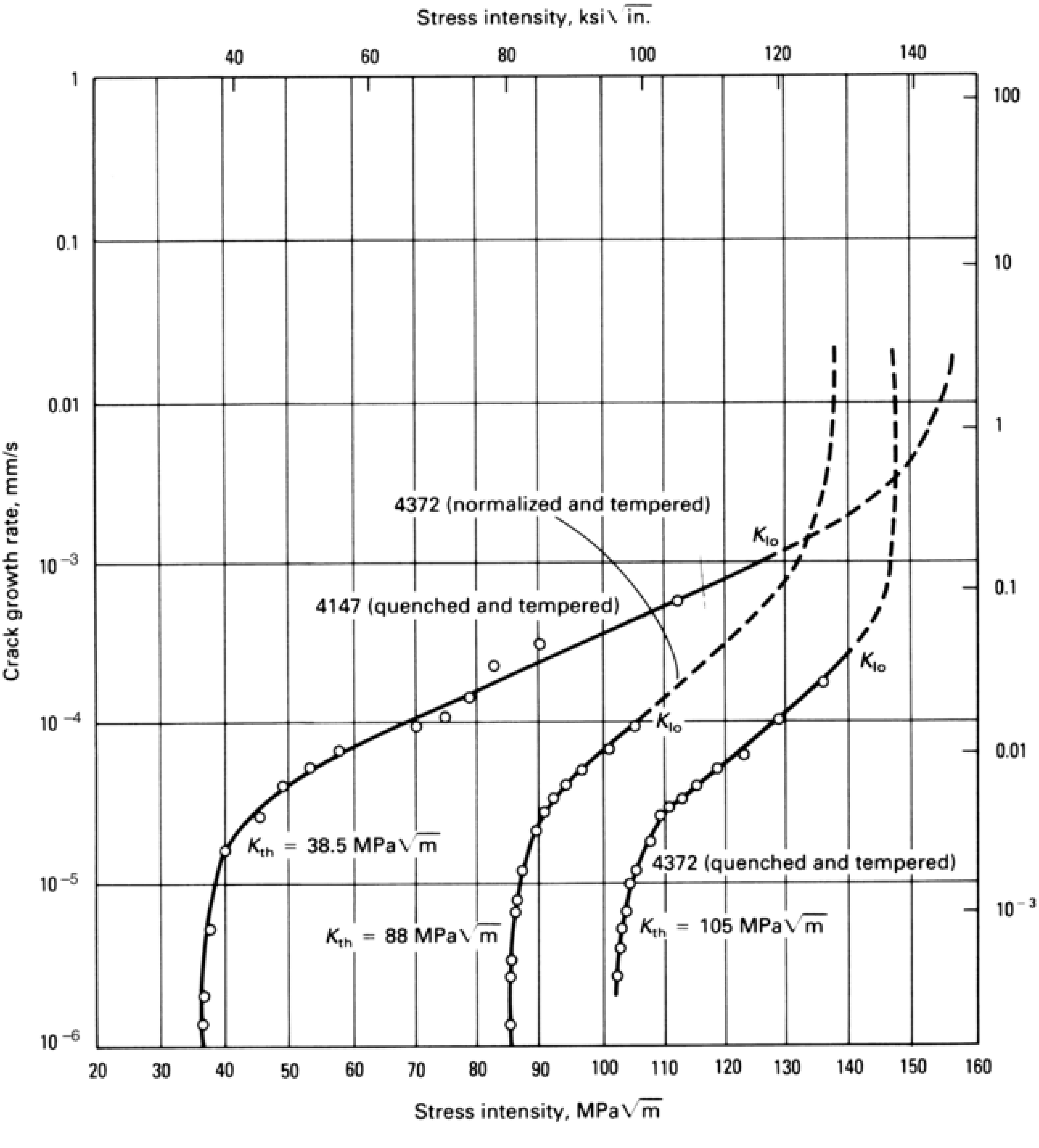

Fig. 63 Crack growth kinetics of three steels in hydrogen at 21 MPa (3000 psi). Source: Ref 159

An approximate approach to this problem of involving both the time of incubation (initiation) and the maximum crack growth rate of SCC at high stress intensities (plateau velocity) was proposed earlier in this article for use with testing of aluminum alloys with constant crack-opening displacement tests (Fig. 45 and Table 4). This involves a simple average rate taken from time zero to a judiciously chosen test duration. Useful ranking of materials can be displayed on V-K_I diagrams such as that shown in Fig. 48.

Another approach to the average velocity concept is available through an elastic-plastic fracture mechanics interpretation of breaking load test data obtained from stress corrosion tests of smooth tension specimens (Ref 22). The stress- corrosion crack growth rates estimated from the slopes of the curves in Fig. 17 from 0 to 4 or 6 days are shown in Table 10 to agree reasonably well with the plateau (*K*-independent) growth rates determined from conventional fracture mechanics tests using bolt-loaded double-beam specimens. It is also noteworthy that a distinction between the intermediate resistance T7X1 temper and the nearly immune T7X2 temper was made more readily using either the smooth specimen test or the average crack growth over 42 days with the double-beam specimen. Fractographic examination confirmed that this was a correct distinction.

Table 10 Stress-corrosion crack growth rates in aluminum alloy 7075 obtained by different test methods

Test method	Stress-corrosion crack growth rate					
	7075-T651		**7075-T7X1**		**7075-T7X2**	
	m/s	**in. × 10^{-5}/h**	**m/s**	**in. × 10^{-5}/h**	**m/s**	**in. × 10^{-5}/h**
Breaking load test using smooth tensile bar stressed 207 MPa (30 ksi); 4 or 6 days	>3.8 × 10^{-9}	>54(a)	7 × 10^{-10}	10(b)	1.3 × 10^{-10}	2(b)
Bolt-loaded double-beam, pop-in stress	3.1 × 10^{-9}	44	7.5 × 10^{-10}	11	(c)	(c)
Plateau velocity obtained from V-K_I curves						
Average growth 0–15 days	3.4 × 10^{-9}	48	4 × 10^{-10}	6	4 × 10^{-10}	6
Average growth 0–42 days	2.8 × 10^{-9}	40	4 × 10^{-10}	6	2 × 10^{-10}	3

(a) Over 4 days.
(b) Over 6 days.
(c) No plausible estimate could be made, because of the slight crack growth.
Source: Ref 3

The implication here, which needs further investigation, is that from a single test method it is possible to compare materials (1) on the basis of their probabilities of initiating and propagating SCC flaws to an arbitrary depth or (2) by their respective crack growth rates, both being meaningful engineering descriptors of SCC damage. An additional advantage to this approach is that the effects of specimen size and alloy strength and toughness can be normalized (Fig. 17).

Ductility Ratio (DR versus Strain-Rate Curves). Various ratio criteria, such as reduction of area, elongation, fracture stress, fracture energy, and time to failure, have been found to be useful in environmental studies with the slow- strain-rate test method. However, such criteria have limited use in comparing various materials because of their dependence on the strength and toughness of the alloy and the specificity of the critical strain rate and the environmental species (Fig. 33 and Table 2). Recent work has shown that average SCC growth rates, threshold stresses, and threshold strain rates can be obtained with modified techniques combined with microscopy. (Ref 62, 68, 69).

Other Criteria. Several other more specialized criteria can be found in the literature, such as:

- The Jones Stress Corrosion Index (Ref 90, 165)
- Critical Strain (Ref 121)
- Mean Critical Stress (Ref 166)

Precision of SCC Data

Variability in the measured values for SCC behavior arises from three primary sources: uncertainties associated with the measurement methods, variation in the test materials, and variation in the test environment. Suitable investigations must minimize the contributions from the first source and allow for quantitative assessment of the latter.

In the production of sophisticated high- strength and high-toughness alloys, close metallurgical control of the fabricating and thermal treatments is necessary to ensure that the required mechanical properties satisfy specifications. It is equally important from the standpoint of SCC that the metallurgical condition of the alloy be properly controlled. Just as there is a range of applicable mechanical properties for a given alloy and metallurgical condition (temper), a range in the SCC behavior can be expected from one heat (or lot) to another. Also, there can be an appreciable variation in the behavior of different-size mill products of the same material. An example of the variations in the SCC behavior of different lots and various mill products is shown in Fig. 48 for aluminum alloy 7050. When selecting a material for a particular structural component, SCC tests should be made on the specific products and sizes that will be required. Costly mistakes have been made in the past in the evaluation of prototype structures by testing parts fabricated from different products for economic expediency.

It is an unfortunate circumstance that the precision of SCC test results is generally lower for materials with an intermediate resistance to SCC than for materials with a very low or a very high resistance. This presents a special challenge in the comparison of competitive materials with improved resistance to SCC. Unfortunately, there is a scarcity of test data for determining what portion of the scatterbands shown in Fig. 48 is due to material variations and how much is due to the precision of the test measurements.

Variability can occur even in carefully controlled investigations. Reference 167 reports results of measurements of K_{ISCC} for a 4340 steel made in numerous laboratories by different test methods.

In another investigation, the precision in the measurement of plateau velocities was determined for a number of replicate bolt-loaded double-beam specimens of short-transverse orientation from a sample of 25 mm (1 in.) thick 7075-T651 aluminum alloy plate (Ref 168). Tension pop-in specimens were exposed by continuous immersion in aqueous solutions of 1 *M* sodium chloride and 1 *M* sodium perchlorate. For six tests in the chloride solution, the mean plateau velocity was 1.4×10^{-8} m/s (1×10^{-3} in./h) with a standard deviation of 0.2×10^{-8} m/s (0.1×10^{-3} in./h), and the range was 1 to 2×10^{-8} m/s (7×10^{-4} to 1.4×10^{-3} in./h) (±35%). For nine tests in the perchlorate solution, the mean plateau velocity was 8×10^{-9} m/s (6×10^{-4} in./h) with a standard deviation of 0.2×10^{-9} m/s (1.4×10^{-4} in./h), and the range was 5×10^{-9} to 1×10^{-8} m/s (4 to 8×10^{-4} in./h) (±31%).

Normalizing SCC Data

It is often necessary to normalize test results with respect to one of the mechanical properties of critical interest for a given engineering structure in order to place the SCC response in proper perspective. This is commonly done by expressing the exposure stress (or stress intensity) and the apparent threshold values in terms of percent yield strength (or percent critical stress intensity) rather than in absolute units. This process can sometimes result in a different ranking order of alloys, and controversy can arise over which ranking is more pertinent. The use of normalized data is usually most appropriate when the utmost resistance to SCC is required; that is, the material should be resistant even when stressed to nearly 100% of the normalizing property. For alloy development screening tests, consideration should be given to evaluating materials in both ways.

Predicting Service Life

Life predictions are difficult and should be made with caution because there are no workable mathematical models. The field is plagued with confusion created to a large extent by:

- The complex, multifaceted nature of the phenomenon, which involves metallurgy, mechanics, chemistry, and time
- The large number of variables known to affect SCC behavior
- Relatively poor correlation between laboratory test results and service experience
- Extensive data scatter
- Difficulty in assessing precisely the service conditions that the part must withstand

Designing to avoid SCC has traditionally taken the approach of preventing the initiation of SCC (safe-life concept). There is considerable service experience to justify this; one factor is that the materials that have given the most service problems are capable of developing relatively high SCC propagation rates (of the order of 25 mm, or 1 in., per month as shown in Fig. 46). Growth rates of this order, combined with relatively low thresholds of stress or stress intensity, make the fail-safe concept rather impractical. However, with the availability of advanced materials with higher thresholds for initiation of SCC and lower propagation rates, the damage- tolerant concept of design may become more practical for SCC and corrosion fatigue.

References cited in this section

1. A.W. Loginow, Stress Corrosion Testing of Alloys, *Mater. Prot.,* Vol 5 (No. 5), 1966, p 33–39

3. D.O. Sprowls et al., “A Study of Environmental Characterization of Conventional and Advanced Aluminum Alloys for Selection and Design: Phase II—The Breaking Load Test Method,” Contract NASI- 16424, NASA Contractor Report 172387, Aug 1984

4. B.F. Brown, “Stress Corrosion Cracking Control Measures,” National Bureau of Standards Monograph 156, U.S. Department of Commerce, June 1977

22. R.J. Bucci et al., The Breaking Load Method: A New Approach for Assessing Resistance to Growth of Early Stage Stress Corrosion Cracks, *Corrosion Cracking,* V.S. Goel, Ed., *Proc. Int. Conf. and Exposition on Fatigue, Corrosion Cracking, Fracture Mechanics, and Failure Analysis,* American Society for Metals, 1986, p 267–277

24. “Testing of Light Metals, Stress Corrosion Test,” German Standard DIN 50908, 1964

31. “Characterization of Environmentally Assisted Cracking for Design—State of the Art,” National Materials Advisory Board Report No. NMAB-386, National Academy of Sciences, 1982

61. G.M. Ugiansky and J.H. Payer, Ed., *Stress Corrosion Cracking—The Slow Strain- Rate Technique,* STP 665, American Society for Testing and Materials, 1979

62. R.N. Parkins, Development of Strain-Rate Testing and Its Implications, *Stress-Corrosion Cracking—The Slow Strain-Rate Technique,* STP 665, G.M. Ugiansky and J.H. Payer, Ed., American Society for Testing and Materials, 1979, p 5–25

68. R.N. Parkins, “Fifth Symposium on Line Pipe Research,” Catalog No. L30174, U1- 40, American Gas Association

69. W.R. Wearmouth, G.P. Dean, and R.N. Parkins, Role of Stress in the Stress Corrosion Cracking of a Mg-Al Alloy, *Corrosion,* Vol 29 (No. 6), 1973, p 251–258

90. F.F. Booth and H.P. Godard, An Anodic Stress-Corrosion Test for Aluminum-Magnesium Alloys, *First International Congress on Metallic Corrosion,* Butterworths, 1962, p 703–712

121. J.P. Fraser, G.G. Eldredge, and R.S. Treseder, Laboratory and Field Methods for Quantitative Study of Sulfide Corrosion Cracking, *Corrosion,* Vol 14, 1958, p 517t–523t

150. F.F. Booth and G.E. Tucker, Statistical Distribution of Endurance in Electrochemical Stress-Corrosion Tests, *Corrosion,* Vol 21 (No. 5), 1965, p 173–177

151. J.H. Harshbarger, A.I. Kemppinen, and B.W. Strum, Statistical Treatment of Nonnormally Distributed Stress-Corrosion Data, *Handbook on Corrosion Testing and Evaluation,* W.H. Ailor, Ed., John Wiley & Sons, 1971, p 87–100

152. B.F. Brown, Chapter 1, *Stress Corrosion Cracking in High Strength Steels and in Titanium and in Aluminum Alloys,* B.F. Brown, Ed., Naval Research Laboratory, 1972, p 13

153. B.F. Brown, “Stress Corrosion Cracking and Related Phenomena in High Strength Steels,” NRL Report 6041, Naval Research Laboratory, Nov 1963

154. “Military Specification for Airplane Damage Tolerance Requirements,” MIL-A- 83444 U.S. Air Force, 2 July 1974

155. *Damage Tolerant Handbook, A Compilation of Fracture and Crack-Growth Data for High-Strength Alloys,* Vol 1, MCIC- HB-O1R, Battelle Columbus Laboratories, Dec 1983

156. S.R. Novak, Effect of Prior Uniform Plastic Strain on the K_{ISCC} of High-Strength Steels in Sea Water, *J. Eng. Fract. Mech.,* Vol 5, 1973, p 727–763

157. W.G. Clark, Jr., Some Problems in the Application of Fracture Mechanics, *Fracture Mechanics—13th Conference,* STP 743, R. Roberts, Ed., American Society for Testing and Materials, 1981, p 269

158. M.O. Speidel, Fracture Mechanics and Stress Corrosion, *Blech Rohre Profile,* Vol 25 (No. 1), 1978, p 14–18 (in German)

159. A.W. Loginow and E.H. Phelps, Steels for Seamless Hydrogen Pressure Vessels, *Corrosion,* Vol 31 (No. 11), 1975, p 404–412

160. C.F. Tiffany, J.N. Masters, and F. Pall, Some Fracture Considerations in the Design of Spacecraft Pressure Vessels, *Proc. ASM Metals Congress,* American Society for Metals, 1966

161. G.M. Sinclair and S.T. Rolfe, "Analytical Procedure for Relating Subcritical Crack Growth to Inspection Requirements," Proc. ASME Metals Engineering Division Conference, American Society of Mechanical Engineers, 1969

162. F.W. Smith, "Stress-Intensity Factors for a Semi-Elliptical Surface Flaw," Structural Development Research Memorandum 17, The Boeing Company, 1966

163. W.G. Clark, Jr., Applicability of the K_{ISCC} Concept to Very Small Defects, *Cracks and Fracture (Ninth Conference),* STP 601, American Society for Testing and Materials, 1976, p 138–153

164. J.G. Kaufman, Stress Corrosion—Traditional Versus Fractured Mechanicians, *Corrosion,* Vol 35 (No. 4), April 1979, p i

165. E.L. Jones, Stress Corrosion of Aluminum Magnesium Alloys II—Method for Expressing Stress Corrosion Susceptibility on a Comparative Basis, *J. Appl. Chem.,* Jan 1954, p 7–10

166. J.T. Staley, Evaluating New Aluminum Alloy Forging Alloys, *Met. Eng. Q.,* Vol 14 (No. 4), 1974, p 50–55

167. R.P. Wei and S.R. Novak, Interlaboratory Evaluation of K_{ISCC} Measurement Procedures for Steels, *Environment-Sensitive Fracture: Evaluation and Comparison of Test Methods,* STP 821, S.W. Dean, E.N. Pugh, and G.M. Ugiansky, Ed., American Society for Testing and Materials, 1984, p 75–79

168. A.H. Le and R.T. Foley, Stress Corrosion Cracking of AA7075-T651 in Various Electrolytes—Statistical Treatment of Data Obtained Using DCB Precracked Specimens, *Corrosion,* Vol 39 (No. 10), 1983, p 379–383

B. Phull, Evaluating Stress-Corrosion Cracking, *Corrosion: Fundamentals, Testing, and Protection*, Vol 13A, *ASM Handbook*, ASM International, 2003, p 575–616

Evaluating Stress-Corrosion Cracking

Revised by Bopinder Phull, Consultant

Selection of Test Method

The SCC test method selected should not be so severe that it rejects a material that is adequate for a particular application. On the other hand, the test should not be so mild that it passes materials that will fail in service. For tests of new and unfamiliar materials or environments, it is expedient to perform more than one type of test. Although standardized tests, which can be specified for screening tests in alloy or process development or quality control, are an essential link between research and engineering, there is a need for much freer choice of test conditions for research studies of SCC mechanisms.

The appropriate SCC test method is the one that is best adapted to test the material product form to be evaluated and the one that will yield the type of test results that best address the test objective(s). The newer methods that use fracture mechanics type specimens and loading by means of a constant slow strain rate are more severe, when applicable, than the older techniques that use smooth (defect-free) specimens. However, the results of all tests require interpretation. The application of linear elastic fracture mechanics has opened the way to the correlation of the mechanical aspects of SCC test methods. It is anticipated that further development of the science of elastic-plastic fracture mechanics will enhance the application of test data to service needs.

B. Phull, Evaluating Stress-Corrosion Cracking, *Corrosion: Fundamentals, Testing, and Protection*, Vol 13A, *ASM Handbook*, ASM International, 2003, p 575–616

Evaluating Stress-Corrosion Cracking

Revised by Bopinder Phull, Consultant

Acknowledgment

This article has been adapted from D.O. Sprowls, Evaluation of Stress-Corrosion Cracking, *Corrosion,* Vol 13, *ASM Handbook* (formerly 9th ed. *Metals Handbook*), ASM International, 1987, p 245–282.

B. Phull, Evaluating Stress-Corrosion Cracking, *Corrosion: Fundamentals, Testing, and Protection*, Vol 13A, *ASM Handbook*, ASM International, 2003, p 575–616

Evaluating Stress-Corrosion Cracking

Revised by Bopinder Phull, Consultant

References

1. A.W. Loginow, Stress Corrosion Testing of Alloys, *Mater. Prot.,* Vol 5 (No. 5), 1966, p 33–39

2. E.H. Dix, Jr., Aluminum-Zinc-Magnesium Alloys, Their Development and Commercial Production, *Trans. ASM,* Vol 42, 1950, p 1057–1127

3. D.O. Sprowls et al., “A Study of Environmental Characterization of Conventional and Advanced Aluminum Alloys for Selection and Design: Phase II—The Breaking Load Test Method,” Contract NASI- 16424, NASA Contractor Report 172387, Aug 1984

4. B.F. Brown, “Stress Corrosion Cracking Control Measures,” National Bureau of Standards Monograph 156, U.S. Department of Commerce, June 1977

5. R.N. Parkins et al., Report Prepared for the European Federation of Corrosion Working Party on Stress Corrosion Test Methods, *Br. Corros. J.,* Vol 7, July 1982, p 154–167

6. R.N. Parkins, Stress Corrosion Test Methods—Physical Aspects, *The Theory of Stress Corrosion Cracking in Alloys,* J.C. Scully, Ed., NATO Scientific Affairs Division, 1971, p 449–468

7. G. Vogt, Comparative Survey of Type of Loading and Specimen Shape for Stress Corrosion Tests, *Werkst. Korros.,* Vol 29, 1978, p 721–725

8. “Practice for Preparation and Use of Direct Tension Stress-Corrosion Test Specimens,” G 49, *Metal Corrosion, Erosion, and Wear,* Vol 03.02, *Annual Book of ASTM Standards,* American Society for Testing and Materials

9. H.L. Craig, Jr., D.O. Sprowls, and D.E. Piper, Stress-Corrosion Cracking, *Handbook on Corrosion Testing and Evaluation,* W.H. Ailor, Ed., John Wiley & Sons, 1971, p 259

10. “Practice for Preparation and Use of Bent- Beam Stress-Corrosion Test Specimens,” G 39, *Metal Corrosion, Erosion, and Wear,* Vol 03.02, *Annual Book of ASTM Standards,* American Society for Testing and Materials

11. “Corrosion of Metals and Alloys—Stress Corrosion Testing—Part 2: Preparation and Use of Bent-Beam Specimens,” ISO 7539-2, International Organization for Standardization

12. M.B. Shumaker et al., Evaluation of Various Techniques for Stress Corrosion Testing Welded Aluminum Alloys, *Stress Corrosion Testing,* STP 425, American Society for Testing and Materials, 1967, p 317–341

13. R.A. Davis, Stress Corrosion Cracking Investigation of Two Low Alloy, High Strength Steels, *Corrosion,* Vol 19 (No. 2), 1963, p 45t–55t

14. “Practice for Making and Using C-Ring Stress-Corrosion Test Specimens,” G 38 *Metal Corrosion, Erosion, and Wear,* Vol 03.02, *Annual Book of ASTM Standards,* American Society for Testing and Materials

15. “Corrosion of Metals and Alloys—Stress Corrosion Testing—Part 5: Preparation and Use of C-Ring Specimens,” ISO 7539- 5, International Organization for Standardization

16. S.O. Fernandez and G.F. Tisinai, Stress Analysis of Un-notched C-rings Used for Stress Cracking Studies, *J. Eng. Ind.,* Feb 1968, p 147–152

17. F.S. Williams, W. Beck, and E.J. Jankowsky, A Notched Ring Specimen for Hydrogen Embrittlement Studies, *Proc. ASTM,* Vol 60, American Society for Testing and Materials, 1960, p 1192

18. D.O. Sprowls et al., "Investigation of the Stress Corrosion Cracking of High Strength Aluminum Alloys," Final Technical Report for U.S. Government NASA Contract NAS-8-5340, Control No. 1-4-50-001167-01(lf), CPB-02-1215-64, 1967

19. Report of Task Group 1, of ASTM Subcommittee B-3/X, Stress Corrosion Testing Methods, *Stress Corrosion Testing,* STP 425, American Society for Testing and Materials, 1967, p 3–20; *Proc. ASTM,* Vol 65, 1965, p 182–197

20. "Corrosion of Metals and Alloys—Stress Corrosion Tests—Part 4: Preparation and Use of Uniaxially Loaded Tension Specimens," ISO 7539-4, International Organization for Standardization

21. B.W. Lifka and D.O. Sprowls, Stress Corrosion Testing of 7079-T6 Aluminum Alloy in Various Environments, *Stress Corrosion Testing,* STP 425, American Society for Testing and Materials, 1967, p 342–362

22. R.J. Bucci et al., The Breaking Load Method: A New Approach for Assessing Resistance to Growth of Early Stage Stress Corrosion Cracks, *Corrosion Cracking,* V.S. Goel, Ed., *Proc. Int. Conf. and Exposition on Fatigue, Corrosion Cracking, Fracture Mechanics, and Failure Analysis,* American Society for Metals, 1986, p 267–277

23. D.O. Sprowls et al., Evaluation of a Proposed Standard Method of Testing for Susceptibility to SCC of High Strength 7XXX Series Aluminum Alloy Products, *Stress- Corrosion—New Approaches,* STP 610, H.L. Craig, Jr., Ed., American Society for Testing and Materials, 1976, p 3–31

24. "Testing of Light Metals, Stress Corrosion Test," German Standard DIN 50908, 1964

25. F.H. Haynie et al., "A Fundamental Investigation of the Nature of Stress Corrosion Cracking in Aluminum Alloys," Technical Report AFML 66-267, USAF Contract No. AF 33(615)-1710 Air Force Materials Laboratory, June 1966

26. P. Brenner, Realistic Stress Corrosion Testing, *Metallurgy,* Vol 23 (No. 9), 1969, p 879–886

27. "Practice for Making and Using U-Bend Stress-Corrosion Test Specimens," G 30 *Metal Corrosion, Erosion, and Wear,* Vol 03.02, *Annual Book of ASTM Standards,* American Society for Testing and Materials

28. "Corrosion of Metals and Alloys—Stress Corrosion Testing—Part 3: Preparation and Use of U-Bend Specimens," ISO 7539-3, International Organization for Standardization

29. H. Nathorst, Stress Corrosion Cracking in Stainless Steels, Part II—An Investigation of the Suitability of the U-Bend Specimen, *Weld. Res. Counc. Bull.,* Series No. 6, Oct 1950

30. R.P. Wei, S.R. Novak, and D.P. Williams, Some Important Considerations in the Development of Stress Corrosion Cracking Test Methods, *Mater. Res. Stand.,* Vol 12, 1972, p 25

31. "Characterization of Environmentally Assisted Cracking for Design—State of the Art," National Materials Advisory Board Report No. NMAB-386, National Academy of Sciences, 1982

32. B.F. Brown, The Application of Fracture Mechanics to Stress Corrosion Cracking, *Met. Rev.,* Vol 13, 1968, p 171–183

33. H.R. Smith and D.E. Piper, Stress Corrosion Testing with Precracked Specimens, *Stress Corrosion Cracking in High Strength Steels and in Titanium and Aluminum Alloys,* B.F. Brown, Ed., Naval Research Laboratory, 1972, p 17–78

34. “Standard Method Test for Plane-Strain Fracture Toughness of Metallic Materials,” E 399, *Annual Book of ASTM Standards,* Vol 03.01, American Society for Testing and Materials

35. “Standard Test Method for Measurement of Fracture Toughness,” E 1820, *Annual Book of ASTM Standards,* Vol 03.01, American Society for Testing and Materials

36. “Standard Practice for Making and Using Precracked Double Beam Stress Corrosion Specimens,” G 168, *Annual Book of ASTM Standards,* Vol 03.02, American Society for Testing and Materials

37. “Standard Test Method for Determining Threshold Stress Intensity Factor for Environment-Assisted Cracking of Metallic Materials,” E 1681, *Annual Book of ASTM Standards,* American Society for Testing and Materials

38. “Standard Terminology Relating to Fatigue and Fracture Testing,” E 1823, *Annual Book of ASTM Standards,* American Society for Testing and Materials

39. J.A. Hauser, H.R.W. Judy, Jr., and T.W. Crooker, “Draft Standard Method of Test for Plane-Strain Stress-Corrosion-Cracking Resistance of Metallic Materials in Marine Environments,” NRL Memorandum Report 5295, Naval Research Laboratory, March 1984

40. W.B. Lisagor, Influence of Precracked Specimen Configuration and Starting Stress Intensity on the Stress Corrosion Cracking of 4340 Steel, *Environment-Sensitive Fracture: Evaluation and Comparison of Test Methods,* STP 821, S.W. Dean, E.N. Pugh, and G.M. Ugiansky, Ed., American Society for Testing and Materials, 1984, p 80–97

41. H. Tada, P. Paris, and G. Irwin, *The Stress Analysis of Cracks Handbook,* Del Research Corporation, 1973

42. J.A. Joyce, D.F. Hasson, and C.R. Crowe, Computer Data Acquisition Monitoring of the Stress Corrosion Cracking of Depleted Uranium Cantilever Beam Specimens, *J. Test. Eval.,* Vol 8 (No. 6), 1980, p 293–300

43. S.R. Novak and S.T. Rolfe, Modified WOL Specimen for K_{ISCC} Environmental Testing, *J. Met.,* Vol 4 (No. 3), 1969, p 701–728

44. J.G. Kaufman, J.W. Coursen, and D.O. Sprowls, An Automated Method for Evaluating Resistance to Stress-Corrosion Cracking with Ring-Loaded Precracked Specimens, *Stress Corrosion—New Approaches,* STP 610, H.L. Craig, Jr., Ed., American Society for Testing and Materials, 1976, p 94–107

45. C. Micheletti and M. Buratti, New Testing Methods for the Evaluation of the Stress- Corrosion Behavior of High-Strength Aluminum Alloys by the Use of Precracked Specimens, *Symposium Proc., Aluminum Alloys in the Aircraft Industry* (Turin, Italy), Oct 1976, Technicopy Ltd., 1978, p 149–159

46. M.V. Hyatt, Use of Precracked Specimens in Stress Corrosion Testing of High Strength Aluminum Alloys, *Corrosion,* Vol 26 (No. 11), 1970, p 487–503

47. D.O. Sprowls et al., “Evaluation of Stress Corrosion Cracking Susceptibility Using Fracture Mechanics Techniques,” Contract NAS 8-21487, Contractor Report NASA CR-124469, May 1973

48. R.C. Dorward and K.R. Hasse, “Flaw Growth of 7075, 7475, 7050, and 7049 Aluminum Plate in Stress Corrosion Environments,” Final Technical Report for U.S. Government Contract NAS 8-30890, Oct 1976; *Corrosion,* Vol 34 (No. 11), 1978, p 386–395

49. W.B. Fichter, The Stress Intensity Factor for the Double Cantilever Beam, *Int. J. Fract.,* Vol 22, 1983, p 133–143

50. J.E. Srawley and B. Gross, Stress Intensity Factors for Crackline-Loaded Edge-Crack Specimens, *Mater. Res. Stand.,* Vol 7 (No. 4), 1967, p 155–162

51. S. Mostovoy, R.B. Crosley, and E.J. Ripling, Use of Crackline Loaded Specimens for Measuring Plane Strain Fracture Toughness, *J. Mater.,* Vol 2 (No. 3), 1967, p 661–681

52. D.O. Sprowls and J.D. Walsh, Evaluating Stress-Corrosion Crack Propagation Rates in High Strength Aluminum Alloys with Bolt Loaded Precracked Double Cantilever Beam Specimens, *Stress Corrosion—New Approaches,* STP 610, H.L. Craig, Jr., Ed., American Society for Testing and Materials, 1976, p 143–156

53. R.B. Heady, Evaluation of Sulfide Corrosion Cracking Resistance in Low Alloy Steels, *Corrosion,* Vol 33 (No. 3), 1977, p 98–107

54. T.L. Bond, R.A. Yeske, and E.N. Pugh, Studies of Stress Corrosion Crack Growth in Al-Zn-Mg Alloys by the Double Torsion Method, *Environment-Sensitive Fracture: Evaluation and Comparison of Test Methods,* STP 821, S.W. Dean, E.N. Pugh, and G.M. Ugiansky, Ed., American Society for Testing and Materials, 1984, p 128–149

55. J.C. Lewis and G. Sines, Ed., *Fracture Mechanics: Fourteenth Symposium, Vol II, Testing and Application,* STP 791, American Society for Testing and Materials, 1983

56. S.W. Dean, E.N. Pugh, and G.M. Ugiansky, Ed., *Environment-Sensitive Fracture: Evaluation and Comparison of Test Methods,* STP 821, American Society for Testing and Materials, 1984

57. J.H. Underwood, S.W. Freiman, and F.I. Baratta, Ed., *Chevron-Notched Specimens: Testing and Stress Analysis,* STP 855, American Society for Testing and Materials, 1984

58. W.B. Gilbreath and M.J. Adamson, Aqueous Stress Corrosion Cracking of High Toughness D6AC Steel, *Stress-Corrosion—New Approaches,* STP 610, H.L. Craig, Jr., Ed., American Society for Testing and Materials, 1976, p 176–187

59. B.F. Brown, Concept of Occluded Corrosion Cells, *Corrosion,* Vol 26 (No. 8), 1970, p 249

60. "Standard Test Method for Measurement of Fatigue Crack Growth Rates," E 647, *Annual Book of ASTM Standards,* American Society for Testing and Materials

61. G.M. Ugiansky and J.H. Payer, Ed., *Stress Corrosion Cracking—The Slow Strain- Rate Technique,* STP 665, American Society for Testing and Materials, 1979

62. R.N. Parkins, Development of Strain-Rate Testing and Its Implications, *Stress-Corrosion Cracking—The Slow Strain-Rate Technique,* STP 665, G.M. Ugiansky and J.H. Payer, Ed., American Society for Testing and Materials, 1979, p 5–25

63. J.H. Payer, W.E. Berry, and W.K. Boyd, Constant Strain Rate Technique for Assessing Stress-Corrosion Susceptibility, *Stress-Corrosion—New Approaches,* STP 610, H.L. Craig, Jr., Ed., American Society for Testing and Materials, 1976, p 82–93

64. N.J.H. Holroyd and G.M. Scamans, Slow- Strain-Rate Stress Corrosion Testing of Aluminum Alloys, *Environment-Sensitive Fracture: Evaluation and Comparison of Test Methods,* STP 821, S.W. Dean, E.N. Pugh, and G.M. Ugiansky, Ed., American Society for Testing and Materials, 1984, p 202–241

65. “Practice for Slow Strain Rate Testing to Evaluate the Susceptibility of Metallic Materials to Environmentally Assisted Cracking,” G 129, *Metal Corrosion, Erosion, and Wear,* Vol 03.02, *Annual Book of ASTM Standards,* American Society for Testing and Materials

66. C.D. Kim and B.E. Wilde, A Review of Constant Strain-Rate Stress Corrosion Cracking Test, *Stress Corrosion Cracking—The Slow Strain Rate Technique,* STP 665, G.M. Ugianski and J.H. Payer, Ed., American Society for Testing and Materials, 1979, p 97–112

67. “Standard Methods of Tension Testing of Metallic Materials,” E 8, *Annual Book of ASTM Standards,* Vol 03.01, American Society for Testing and Materials

68. R.N. Parkins, “Fifth Symposium on Line Pipe Research,” Catalog No. L30174, U1- 40, American Gas Association

69. W.R. Wearmouth, G.P. Dean, and R.N. Parkins, Role of Stress in the Stress Corrosion Cracking of a Mg-Al Alloy, *Corrosion,* Vol 29 (No. 6), 1973, p 251–258

70. R.N. Parkins and Y. Suzuki, Environment Sensitive Cracking of a Nickel-Aluminum Bronze under Monotonic and Cyclic Loading Conditions, *Corros. Sci.,* Vol 23 (No. 6), 1983, p 577–599

71. R.N. Parkins, A Critical Evaluation of Current Environment-Sensitive Fracture Test Methods, *Environment-Sensitive Fracture: Evaluation and Comparison of Test Methods,* STP 821, S.W. Dean, E.N. Pugh, and G.M. Ugiansky, Ed., American Society for Testing and Materials, 1984, p 5–31

72. J. Yu, N.J.H. Holroyd, and R.N. Parkins, Application of Slow-Strain-Rate Tests to Defining the Stress for Stress Corrosion Crack Initiation in 70/30 Brass, *Environment-Sensitive Fracture: Evaluation and Comparison of Tests Methods,* STP 821, S.W. Dean, E.N. Pugh, and G.M. Ugiansky, Ed., American Society for Testing and Materials, 1984, p 288–309

73. “Slow Strain Rate Test Method for Screening Corrosion-Resistant Alloys (CRAs) for Stress Corrosion Cracking in Sour Oilfield Service,” NACE TM-01-98, NACE International, 1998

74. J.A. Beavers and G.H. Koch, *Limitations of the Slow Strain Rate Test for Stress Corrosion Cracking Testing,* MTI Publication No. 39, Materials Technology Institute of the Chemical Process Industries, 1994

75. B.F. Brown. The Contributions of Physical Metallurgy and of Fracture Mechanics to Containing the Problem of Stress Corrosion Cracking, *Philos. Trans. R. Soc. (London) A,* Vol 282 (No. 1307), 1976, p 235–245

76. D.O. Sprowls and R.H. Brown, Stress Corrosion Mechanisms for Aluminum Alloys, *Fundamental Aspects of Stress-Corrosion Cracking,* R.W. Staehle, A.J. Forty, and D. van Rooyen, Ed., National Association of Corrosion Engineers, 1969, p 466–512

77. J.D. Jackson, W.K. Boyd, and R.W. Staehle, “Corrosion of Titanium,” DMIC Memorandum 218, Defense Metals Information Center, Battelle Memorial Institute, Sept 1966

78. R.N. Parkins, Predictive Approaches to Stress Corrosion Cracking Failure, *Corros. Sci.,* Vol 20, 1980, p 147–166

79. J.R. Galvele and S.M. DeMichelli, Mechanism of Intergranular Corrosion of Al-Cu Alloys, *Corros. Sci.,* Vol 10, 1970, p 795–807

80. S. Maitra and G.C. English, Mechanism of Localized Corrosion of 7075 Alloy Plate, *Metall. Trans. A,* Vol 12, March 1981, p 535–541

81. “Test Method for Jaw Crusher Gouging Abrasion Test,” G 5, *Metal Corrosion, Erosion, and Wear,* Vol 03.02, *Annual Book of ASTM Standards,* American Society for Testing and Materials

82. “Practice for Evaluating Stress Corrosion Cracking Resistance of Metals and Alloys by Alternate Immersion in 3.5% Sodium Chloride Solution,” G 44, *Metal Corrosion, Erosion, and Wear,* Vol 03.02, *Annual Book of ASTM Standards,* American Society for Testing and Materials

83. H. Bohni and H.H. Uhlig, Environmental Factors Affecting the Critical Pitting Potential of Aluminum, *J. Electrochem. Soc.,* Vol 116, Part II, 1969, p 906–910

84. R.H. Brown, D.O. Sprowls, and M.B. Shumaker, The Resistance of Wrought High Strength Aluminum Alloys to Stress Corrosion Cracking, *Stress-Corrosion Cracking of Metals—A State of the Art,* STP 518, American Society for Testing and Materials, 1972, p 87–118

85. “Practice for Modified Salt Spray (Fog) Testing,” G 47, *Metal Corrosion, Erosion, and Wear,* Vol 03.02, *Annual Book of ASTM Standards,* American Society for Testing and Materials

86. “Classification of Resistance to Stress- Corrosion Cracking of Heat-Treatable Aluminum Alloys,” G 64, *Metal Corrosion, Erosion, and Wear,* Vol 03.02, *Annual Book of ASTM Standards,* American Society for Testing and Materials

87. B.W. Lifka, Corrosion Resistance of Aluminum Alloy Plate in Rural, Industrial, and Seacoast Atmospheres, unpublished

88. D.O. Sprowls and R.H. Brown, What Every Engineer Should Know about the Stress Corrosion of Aluminum, *Met. Prog.,* Vol 81 (No. 4), April 1962, p 79–85; Vol 81 (No. 5), May 1962, p 77–83

89. “Test Method for Performing a Stress-Corrosion Cracking Test of Low Copper Containing Al-Zn-Mg Alloys in Boiling 6% Sodium Chloride Solution,” G 103, *Metal Corrosion, Erosion, and Wear,* Vol 03.02, *Annual Book of ASTM Standards,* American Society for Testing and Materials

90. F.F. Booth and H.P. Godard, An Anodic Stress-Corrosion Test for Aluminum-Magnesium Alloys, *First International Congress on Metallic Corrosion,* Butterworths, 1962, p 703–712

91. A.H. Le, B.F. Brown, and R.T. Foley, The Chemical Nature of Aluminum Corrosion, IV: Some Anion Effects on SCC of AA7075-T651, *Corrosion,* Vol 36 (No. 12). Dec 1980, p 673–679

92. D.O. Sprowls, J.D. Walsh, and M.B. Shumaker, Simplified Exfoliation Testing of Aluminum Alloys, *Localized Corrosion— Cause of Metal Failure,* STP 516, American Society for Testing and Materials, 1972, p 38–65

93. W. Pistulka and G. Lang, Accelerated Stress Corrosion Test Methods for Al-Zn- Mg Type Alloys, *Aluminum,* Vol 53 (No. 6), 1977, p 366–371

94. “Stress-Corrosion Cracking Testing of Aluminum Alloys for Aircraft Parts,” German Aircraft Standard LN 65666, July 1974 (in German)

95. P.W. Jeffrey, T.E. Wright, and H.P. Godard, An Accelerated Laboratory Stress Corrosion Test for Al-Zn-Mg Alloys, *Proc. Fourth Int. Congress on Corrosion,* National Association of Corrosion Engineers, 1969, p 133–139

96. T.S. Humphries and J.E. Coston, “An Improved Stress Corrosion Test Medium for Aluminum Alloys,” NASA Technical Memorandum NASA TM-82452, George C. Marshall Space Flight Center, Nov 1981

97. W.J. Helfrich, “Development of a Rapid Stress Corrosion Test for Aluminum Alloys,” Final Summary Report, Contract No. NAS 8-20285, George C. Marshall Space Flight Center, May 1968

98. M.V. Hyatt and M.O. Speidel, High Strength Aluminum Alloys, *Stress Corrosion Cracking in High Strength Steels and in Titanium and in Aluminum Alloys,* B.F. Brown, Ed., Naval Research Laboratory, 1972, p 148–244

99. M.O. Speidel, Stress Corrosion Cracking of Aluminum Alloys, *Metall. Trans. A,* Vol 6, April 1975, p 631–651

100. L. Schra and J. Faber, “Influence of Environments on Constant Displacement Stress-Corrosion Crack Growth in High Strength Aluminum Alloys,” NLR TR 81138 U, National Aerospace Laboratory NLR, 1981

101. J.R. Pickens, Techniques for Assessing the Corrosion Properties of Aluminum Powder Metallurgy Alloys, *Rapidly Solidified Powder Aluminum Alloys,* STP 890, M.E. Fine and E.A. Starke, Jr., Ed., American Society for Testing and Materials, 1986, p 381–409

102. R.E. Davies, G.E. Nordmark, and J.D. Walsh. “Design Mechanical Properties, Fracture Toughness, Fatigue Properties Exfoliation and Stress Corrosion Resistance of 7050 Sheet, Plate, Extrusions, Hand Forgings and Die Forgings,” Final Report, Naval Air Systems, Contract N00019-72-C-0512, July 1975

103. R.C. Dorward and K.R. Hasse, Long- Transverse Stress-Corrosion Cracking Behavior of Aluminum Alloy AA7075, *Br. Corros. J.,* Vol 13 (No. 1), 1978, p 23–27

104. G.M. Scamans, Discontinuous Propagation of Stress Corrosion Cracks in Al-Zn- Mg Alloys, *Scr. Metall.,* Vol 13, 1979, p 245–250

105. S. Maitra, Determination of SCC Resistance of Al-Cu-Mg Alloys by Slow Strain Rate and Alternate Immersion Testing, *Corrosion,* Vol 37 (No. 2), 1981, p 98–103

106. “Practice for Use of Mattsson's Solution of pH 7.2 to Evaluate the Stress-Corrosion Cracking Susceptibility of Copper-Zinc Alloys,” G 37, *Metal Corrosion, Erosion, and Wear,* Vol 03.02, *Annual Book of ASTM Standards,* American Society for Testing and Materials

107. D.H. Thompson, Stress Corrosion Cracking of Copper Metals, *Stress Corrosion Cracking of Metals—A State of the Art,* STP 518, American Society for Testing and Materials, 1972, p 39–57

108. E.N. Pugh, J.V. Craig, and A.J. Sedricks, The Stress-Corrosion Cracking of Copper, Silver, and Gold Alloys, *Proc. Conf. Fundamental Aspects of Stress-Corrosion Cracking,* National Association of Corrosion Engineers, 1969, p 118–158

109. G. Edmunds, E.A. Anderson, and R.K. Waring, Ammonia and Mercury Stress- Corrosion Cracking Tests for Brass, *Symposium on Stress-Corrosion Cracking of Metals,* American Society for Testing and Materials and the American Institute of Mining, Metallurgical, and Petroleum Engineers, 1944, p 7–18

110. “Standard Method of Mercurous Nitrate Test for Copper and Copper Alloys,” B 154, *Annual Book of ASTM Standards,* American Society for Testing and Materials, 1984, p 352–354

111. "Tubing of Copper and Copper Alloys for Condensers and Heat Exchangers," German Standard DIN-1785 (available from ANSI), 1983

112. H.L. Logan, *The Stress Corrosion of Metals,* John Wiley & Sons, 1966

113. R.N. Parkins, Stress Corrosion Cracking of Low Carbon Steels, *Proc. Conf. Fundamental Aspects of Stress Corrosion Cracking,* National Association of Corrosion Engineers, 1969, p 361–373

114. "Assessing the Tendency of Industrial Boiler Waters to Cause Embrittlement (USBM Embrittlement Detector Method)," D 807, *Annual Book of ASTM Standards,* American Society for Testing and Materials

115. M.J. Humphries and R.N. Parkins, Stress Corrosion Cracking of Mild Steels in Sodium Hydroxide Solutions Containing Various Additional Substances, *Corros. Sci.,* Vol 7, 1967, p 747–761

116. R.N. Parkins, P.W. Slattery, and B.S. Poulson, The Effects of Alloying Additions to Ferritic Steels Upon Stress-Corrosion Cracking Resistance, *Corrosion,* Vol 37 (No. 11), 1981, p 650–664

117. B.S. Poulson and R.N. Parkins, Effect of Nickel Additions upon the Stress Corrosion of Ferritic Steels in a Chloride Environment, *Corrosion,* Vol 29, Nov 1973, p 414–422

118. "Stress Corrosion Cracking Resistance Test for Prestressing Tendons," Technical Report 5, Proc. Federation Internationale de la Preconstrainte, Eighth Congress, Cement and Concrete Association, 1978

119. E.H. Phelps, A Review of the Stress Corrosion Behavior of Steels with High Yield Strength, *Proc. Conf. Fundamental Aspects of Stress Corrosion Cracking,* National Association of Corrosion Engineers, 1969, p 398–410

120. "Test Method for Testing of Metals for Resistance to Sulfide Stress Cracking at Ambient Temperatures," TM-01-77, National Association of Corrosion Engineers, 1977, p 77–84

121. J.P. Fraser, G.G. Eldredge, and R.S. Treseder, Laboratory and Field Methods for Quantitative Study of Sulfide Corrosion Cracking, *Corrosion,* Vol 14, 1958, p 517t–523t

122. G. Sandoz, High Strength Steels, *Stress Corrosion Cracking in High Strength Steels and in Titanium and in Aluminum Alloys,* B.F. Brown, Ed., Naval Research Laboratory, Washington, D.C., 1972, p 79–145

123. H.J. Bhatt and E.H. Phelps, The Effect of Electrochemical Polarization on the Stress Corrosion Behavior of Steels with High Yield Strength, *Proc. Third Int. Congress on Metallic Corrosion,* 16–26 May 1966

124. H.J. Bhatt and E.H. Phelps, Effect of Solution pH on the Mechanism of Stress Corrosion Cracking of a Martensitic Stainless Steel, *Corrosion,* Vol 17, 1961, p 430t–434t

125. "Practice for Evaluating Stress-Corrosion- Cracking Resistance of Metals and Alloys in a Boiling Magnesium Chloride Solution," G 36, *Annual Book of ASTM Standards,* American Society for Standards and Materials

126. R.M. Latanision and R.W. Staehle, Stress Corrosion Cracking of Iron-Nickel-Chromium Alloys, *Proc. Conf. Fundamental Aspects of Stress Corrosion Cracking,* National Association of Corrosion Engineers, 1969, p 214–307

127. S.W. Dean, Review of Recent Studies on the Mechanism of Stress Corrosion Cracking in Austenitic Stainless Steels, *Stress Corrosion—New Approaches,* STP 610, H.L. Craig, Jr., Ed., American Society for Testing and Materials, 1976, p 308–337

128. E. Denhard, Effect of Composition and Heat Treatment on the Stress Corrosion Cracking of Austenitic Stainless Steels, *Corrosion,* Vol 16 (No. 7), 1960, p 131–141

129. H.R. Copson, Effect of Composition on Stress Corrosion Cracking of Some Alloys Containing Nickel, *Physical Metallurgy of Stress Corrosion Fracture,* T.N. Rhodin, Ed., Interscience, 1959, p 247–272

130. A.W. Loginow, J.F. Bates, and W.L. Mathay, New Alloy Resists Chloride Stress Corrosion Cracking, *Mater. Prot. Perform.,* Vol 11 (No. 5), 1972, p 35–40

131. N.A. Nielsen, Observations and Thoughts on Stress Corrosion Mechanism, *J. Met.,* Vol 5, 1970, p 794–829

132. J.D. Harston and J.C. Scully, Stress Corrosion of Type 304 Steel in H_2SO_4/NaCl Environments at Room Temperature, *Corrosion,* Vol 25 (No. 12), 1969, p 493–501

133. S. Takemura, M. Onoyama, and T. Ooka, Stress Corrosion Cracking of Stainless Steels in Hydrogen Sulfide Solutions, *Corrosion,* Vol 16 (No. 7), 1960, p 338–348

134. "Test Method for Evaluating Stress-Corrosion Cracking of Stainless Alloys with Different Nickel Content in Boiling Acidified Sodium Chloride Solution," G 123, *Metal Corrosion, Erosion, and Wear,* Vol 03.02, *Annual Book of ASTM Standards,* American Society for Testing and Materials

135. "Practice for Determining the Susceptibility of Stainless Steels and Related Nickel- Chromium-Iron Alloys to Stress-Corrosion Cracking in Polythionic Acids," G 35, *Metal Corrosion, Erosion, and Wear,* Vol 03.02, *Annual Book of ASTM Standards,* American Society for Testing and Materials

136. "Standard Test Method for Evaluating the Influence of Thermal Insulations on External Stress Corrosion Cracking Tendency of Austenitic Stainless Steel," C 692, *Annual Book of ASTM Standards,* American Society for Testing and Materials

137. J.L. Wilson, F.W. Pement, and R.G. Aspden, Effect of Alloy Structure, Hydroxide Concentration, and Temperature on the Caustic Stress-Corrosion Cracking of Austenitic Stainless Steel, *Corrosion,* Vol 30 (No. 4), 1974, p 139–149

138. H. Kohl, A Contribution to the Examination of Stress-Corrosion Cracking of Austenitic Stainless Steel in Magnesium Chloride Solution, *Corrosion,* Vol 23 (No. 12), 1967, p 39–49

139. G.F. Sager, R.H. Brown, and R.B. Mears, Tests for Determining Susceptibility to Stress Corrosion Cracking, *Symposium on Stress Corrosion Cracking of Metals,* American Society for Testing and Materials and the American Institute of Mechanical Engineers, 1945, p 255–272

140. H.B. Romans, Stress Corrosion Test Environments and Test Durations, *Stress Corrosion Testing,* STP 425, American Society for Testing and Materials, 1967, p 182–208

141. W.K. Boyd and W.E. Berry, Stress Corrosion Cracking of Nickel and Nickel Alloys, *Stress Corrosion Cracking of Metals—A State of the Art,* STP 518, American Society for Testing and Materials, 1972, p 58–78

142. R.C. Newman, R. Roberge, and R. Bandy, Evaluation of SCC Test Methods for Inconel 600 in Low-Temperature Aqueous Solutions, *Environment-Sensitive Fracture: Evaluation and Comparison of Test Methods,* STP 821, S.W. Dean, E.N. Pugh, and G.M. Ugiansky, Ed., American Society for Testing and Materials, 1984, p 310–322

143. A.I. Asphahani, Slow Strain-Rate Technique and Its Applications to the Environmental Stress Cracking of Nickel-Base and Cobalt-Base Alloys, *Stress Corrosion Cracking—The Slow Strain Rate Technique,* STP 665, G.M. Ugiansky and J.H. Payer, Ed., American Society for Testing and Materials, 1979, p 279–293

144. "Practice for Determining Cracking Susceptibility of Metals Exposed under Stress to a Hot Salt Environment," G 41, *Metal Corrosion, Erosion, and Wear,* Vol 03.02, *Annual Book of ASTM Standards,* American Society for Testing and Materials

145. M.J. Blackburn, W.H. Smyrl, and J.A. Sweeny, Titanium Alloys, *Stress Corrosion Cracking in High Strength Steels and in Titanium and in Aluminum Alloys,* B.F. Brown, Ed., Naval Research Laboratory, 1972, p 246–363

146. T.R. Beck, Electrochemical Aspects of Titanium Stress Corrosion, *Proc. Conf. Fundamental Aspects of Stress Corrosion Cracking,* National Association of Corrosion Engineers, 1969, p 605–619

147. D.A. Meyn, Effect of Hydrogen on Fracture and Inert Environment Sustained Load Cracking Resistance of Alpha-Beta Titanium Alloys, *Metall. Trans.,* Vol 5 (No. 11), 1974, p 2405–2414

148. G. Sandoz, Subcritical Crack Propagation in Ti-8Al-1Mo-1V Alloy in Organic Environments, Salt Water and Inert Environments, *Proc. Conf. Fundamental Aspects of Stress Corrosion Cracking,* National Association of Corrosion Engineers, 1969, p 684–690

149. "Practice for Preparation of Stress-Corrosion Test Specimen for Weldments," G 58, *Metal Corrosion, Erosion, and Wear,* Vol 03.02, *Annual Book of ASTM Standards,* American Society for Testing and Materials

150. F.F. Booth and G.E. Tucker, Statistical Distribution of Endurance in Electrochemical Stress-Corrosion Tests, *Corrosion,* Vol 21 (No. 5), 1965, p 173–177

151. J.H. Harshbarger, A.I. Kemppinen, and B.W. Strum, Statistical Treatment of Nonnormally Distributed Stress-Corrosion Data, *Handbook on Corrosion Testing and Evaluation,* W.H. Ailor, Ed., John Wiley & Sons, 1971, p 87–100

152. B.F. Brown, Chapter 1, *Stress Corrosion Cracking in High Strength Steels and in Titanium and in Aluminum Alloys,* B.F. Brown, Ed., Naval Research Laboratory, 1972, p 13

153. B.F. Brown, "Stress Corrosion Cracking and Related Phenomena in High Strength Steels," NRL Report 6041, Naval Research Laboratory, Nov 1963

154. "Military Specification for Airplane Damage Tolerance Requirements," MIL-A- 83444 U.S. Air Force, 2 July 1974

155. *Damage Tolerant Handbook, A Compilation of Fracture and Crack-Growth Data for High-Strength Alloys,* Vol 1, MCIC- HB-O1R, Battelle Columbus Laboratories, Dec 1983

156. S.R. Novak, Effect of Prior Uniform Plastic Strain on the K_{ISCC} of High-Strength Steels in Sea Water, *J. Eng. Fract. Mech.,* Vol 5, 1973, p 727–763

157. W.G. Clark, Jr., Some Problems in the Application of Fracture Mechanics, *Fracture Mechanics—13th Conference,* STP 743, R. Roberts, Ed., American Society for Testing and Materials, 1981, p 269

158. M.O. Speidel, Fracture Mechanics and Stress Corrosion, *Blech Rohre Profile,* Vol 25 (No. 1), 1978, p 14–18 (in German)

159. A.W. Loginow and E.H. Phelps, Steels for Seamless Hydrogen Pressure Vessels, *Corrosion,* Vol 31 (No. 11), 1975, p 404–412

160. C.F. Tiffany, J.N. Masters, and F. Pall, Some Fracture Considerations in the Design of Spacecraft Pressure Vessels, *Proc. ASM Metals Congress,* American Society for Metals, 1966

161. G.M. Sinclair and S.T. Rolfe, "Analytical Procedure for Relating Subcritical Crack Growth to Inspection Requirements," Proc. ASME Metals Engineering Division Conference, American Society of Mechanical Engineers, 1969

162. F.W. Smith, "Stress-Intensity Factors for a Semi-Elliptical Surface Flaw," Structural Development Research Memorandum 17, The Boeing Company, 1966

163. W.G. Clark, Jr., Applicability of the K_{ISCC} Concept to Very Small Defects, *Cracks and Fracture (Ninth Conference),* STP 601, American Society for Testing and Materials, 1976, p 138–153

164. J.G. Kaufman, Stress Corrosion—Traditional Versus Fractured Mechanicians, *Corrosion,* Vol 35 (No. 4), April 1979, p i

165. E.L. Jones, Stress Corrosion of Aluminum Magnesium Alloys II—Method for Expressing Stress Corrosion Susceptibility on a Comparative Basis, *J. Appl. Chem.,* Jan 1954, p 7–10

166. J.T. Staley, Evaluating New Aluminum Alloy Forging Alloys, *Met. Eng. Q.,* Vol 14 (No. 4), 1974, p 50–55

167. R.P. Wei and S.R. Novak, Interlaboratory Evaluation of K_{ISCC} Measurement Procedures for Steels, *Environment-Sensitive Fracture: Evaluation and Comparison of Test Methods,* STP 821, S.W. Dean, E.N. Pugh, and G.M. Ugiansky, Ed., American Society for Testing and Materials, 1984, p 75–79

168. A.H. Le and R.T. Foley, Stress Corrosion Cracking of AA7075-T651 in Various Electrolytes—Statistical Treatment of Data Obtained Using DCB Precracked Specimens, *Corrosion,* Vol 39 (No. 10), 1983, p 379–383

B. Phull, Evaluating Hydrogen Embrittlement, *Corrosion: Fundamentals, Testing, and Protection*, Vol 13A, *ASM Handbook*, ASM International, 2003, p 617–624

Evaluating Hydrogen Embrittlement

Revised by Bopinder Phull, Consultant

Introduction

HYDROGEN EMBRITTLEMENT of metals is an old, frequently encountered, and often misunderstood phenomenon. It is most commonly thought to occur by subcritical crack growth, often producing time-delayed fractures in production parts, even with no externally applied stress. Many problems still exist, starting with a basic definition of hydrogen embrittlement, in addition to identifying its source, controlling its effects, and preventing its occurrence. This wide range of problems makes the evaluation of hydrogen embrittlement a multifaceted technical activity.

Research investigations on the phenomenon range from studies of crack nucleation and growth, including such parameters as incubation time, crack growth rates, and threshold stress intensities, to studies on the relative susceptibility of materials to hydrogen embrittlement. Practical implications of hydrogen embrittlement are discussed in the article "Hydrogen Damage and Embrittlement" in *ASM Handbook*, Volume 11 (2002), *Failure Analysis and Prevention.*

B. Phull, Evaluating Hydrogen Embrittlement, *Corrosion: Fundamentals, Testing, and Protection*, Vol 13A, *ASM Handbook*, ASM International, 2003, p 617–624

Evaluating Hydrogen Embrittlement

Revised by Bopinder Phull, Consultant

Toward a Definition (Ref 1)

Much confusion exists in the published literature over the definition of hydrogen embrittlement. Metal processing, chemical, and petrochemical industries have experienced various types of hydrogen problems for many years. The aerospace industry has experienced new and unexpected hydrogen embrittlement problems, principally in dealing with high-strength steels. There are many sources of hydrogen, several types of embrittlement, and various theories for explaining the observed effects.

Hydrogen embrittlement is often classified into three types:

- Internal reversible hydrogen embrittlement
- Hydrogen environment embrittlement
- Hydrogen reaction embrittlement

If specimens have been precharged with hydrogen from any source or in any manner and embrittlement is observed during mechanical testing, then embrittlement is caused by either internal reversible embrittlement or by hydrogen reaction embrittlement. If hydrides or other new phases containing hydrogen form during testing in gaseous hydrogen, then embrittlement is attributed to hydrogen reaction embrittlement. For all embrittlement determined during mechanical testing in gaseous hydrogen other than internal reversible and hydrogen reaction embrittlement, hydrogen environment embrittlement is assumed to be responsible.

Internal reversible hydrogen embrittlement has also been termed *slow strain rate embrittlement* and *delayed failure.* This is the classical type of hydrogen embrittlement that has been studied quite extensively. Widespread attention has been focused on the problem resulting from electroplating, particularly of cadmium, on high-strength steel components. Other sources of hydrogen are processing treatments such as melting and pickling. More recently, the embrittling effects of many stress-corrosion processes have been attributed to corrosion-produced hydrogen. Hydrogen that is absorbed from any source is diffusible within the metal lattice. To be fully reversible, embrittlement must occur without the hydrogen undergoing any type of chemical reaction after it has been adsorbed within the lattice.

Internal reversible hydrogen embrittlement can occur after a very small average concentration of hydrogen has been absorbed from the environment. However, local concentrations of hydrogen can be substantially greater than the average bulk value. For steels, embrittlement is usually most severe at room temperature during either delayed failure or slow strain rate tension testing. This time-dependent nature (incubation period) of internal reversible embrittlement suggests that diffusion of hydrogen within the lattice controls this type of embrittlement. Cracks initiate internally, usually below the root of a notch at the region where the triaxial stress (tensile hydrostatic stress) is maximum. Embrittlement in steel is reversible (ductility can be stored) by relieving the applied stress and aging at room temperature, provided microscopic cracks have not yet initiated. Internal reversible hydrogen embrittlement has also been observed in a wide variety of materials, including nickel-base alloys and austenitic stainless steels, provided they are severely charged with hydrogen.

Hydrogen environment embrittlement was recognized as a serious problem in the mid- 1960s when the National Aeronautics and Space Administration (NASA) and its contractors experienced failure of ground-based hydrogen storage tanks. These tanks were rated for hydrogen at pressures of 35 to 70 MPa (~5 to 10 ksi). Consequently, the failures were attributed to high-pressure hydrogen embrittlement. Because of these failures and the anticipated use of hydrogen in advanced rocket and gas turbine engines and auxiliary power units, NASA initiated both in-house and contractual research. The contractual effort had to define the relative susceptibility of structural alloys to hydrogen environment embrittlement. A substantial amount of research was concerned with the mechanism of the embrittlement process. Disagreement remains on whether hydrogen environment embrittlement is a form of internal reversible hydrogen embrittlement or is truly a distinct type of embrittlement.

Hydrogen Reaction Embrittlement. Although the sources of hydrogen may be any of those mentioned previously, this type of embrittlement is quite distinct from hydrogen environment embrittlement. Once hydrogen is adsorbed, it may react near the surface or diffuse substantial distances before it reacts. Hydrogen can react with itself, with the matrix, or with a foreign element in the matrix. The chemical reactions that comprise this type of embrittlement or attack are well known and are encountered frequently. The new phases formed by these reactions are usually quite stable, and embrittlement is not reversible during room temperature aging treatments.

Atomic hydrogen (H) can react with the matrix or with an alloying element to form a hydride (MH_x). Hydride phase formation can be either spontaneous or strain induced. Atomic hydrogen can combine to form molecular hydrogen (H_2). This problem is frequently encountered after steel processing and welding; it has been termed *flaking* or "*fisheyes.*" Atomic hydrogen can also react with a foreign element in the matrix to form a gas. A prime example is the reaction with carbon in low-alloy steels to form methane (CH_4) bubbles. Another example is the reaction of atomic hydrogen with oxygen in copper to form steam (H_2O), resulting in blistering and a porous metal component.

Although hydrogen reaction embrittlement is not a major topic in this article, its definition is included for the sake of completeness and in the hope of establishing a single definition for each of the various hydrogen embrittlement phenomena to avoid problems with semantics.

Further confusion results from the relation of stress-corrosion cracking (SCC) to hydrogen embrittlement, because the crack-growth mechanism is often found to be the same in both cases. On the surface, the active corrosion process produces the hydrogen that is the cause of the failure. In SCC, the pits or crevices (polarized anodically) are initiation sites, and therefore, although the growth mechanisms are the same, the method of prevention based on initiation can be different.

Reference cited in this section

1. L. Raymond, Ed., *Hydrogen Embrittlement Testing,* STP 543, ASTM International, 1974

B. Phull, Evaluating Hydrogen Embrittlement, *Corrosion: Fundamentals, Testing, and Protection*, Vol 13A, *ASM Handbook*, ASM International, 2003, p 617–624

Evaluating Hydrogen Embrittlement

Revised by Bopinder Phull, Consultant

Sources of Hydrogen

Hydrogen embrittlement generally occurs in service either in association with self-corrosion in acidic environments or when the part is being protected from corrosion; for example, during cathodic protection of high-strength steel. Atomic hydrogen is generated at the metal surface either due to reduction of hydrogen ions (in acidic environments) or due to dissociation of water in neutral-pH environments (e.g., when cathodic protection is applied). Failures that occur after a period of time are related to the diffusion of atomic hydrogen into the metal. The fracture path is usually intergranular in steels. Not all intergranular failures in steels however, are due to hydrogen embrittlement. In addition, not all hydrogen embrittlement failures in other metals and alloys are intergranular.

Time-delayed embrittlement failures are caused by the residual atomic hydrogen in the steel from the making or melting process and the atomic hydrogen introduced into the steel during processing and subsequent manufacture (for example, plating, machining with hydrocarbon- based oils, pickling, and welding). The atomic, diffusible, or nascent hydrogen (H) is the cause of the problem, not the total hydrogen that includes molecular hydrogen (H_2). Also necessary is applied stress or residual stress from welding or heat treating. Hydrogen embrittlement is generally found in high-strength steels, but hydrogen stress cracking (HSC) has been reported for other materials, such as refractory metals, superalloys, and even austenitic steels, when tested under high-pressure hydrogen gas.

B. Phull, Evaluating Hydrogen Embrittlement, *Corrosion: Fundamentals, Testing, and Protection*, Vol 13A, *ASM Handbook*, ASM International, 2003, p 617–624

Evaluating Hydrogen Embrittlement

Revised by Bopinder Phull, Consultant

Source of Stress

Cracking studies of high-strength steels in aqueous chloride solutions at potentials more electronegative than the open-circuit potential of about -0.6 V versus a saturated calomel electrode (SCE) are, in reality, hydrogen embrittlement tests, because the steel is at a cathodic potential; that is, hydrogen is produced at the surface of the steel. The worst case, or the most severe condition that produces cracking, is generated when atomic hydrogen is produced while the part (or test coupon) is under stress. This is the reason hardware is processed (plated) with no stress (except unavoidable manufacturing-induced residual stresses) and then stress relieved or baked before being placed in service. If residual stresses exist during plating, the part could break or at least have microcracks that subsequently lead to an early service failure.

Hydrogen relief or baking treatments can be effective in removing atomic hydrogen from steel. However, this does not ensure that hydrogen is removed from the part. The hydrogen can reside as molecular hydrogen at the interface between the steel part and a plating or coating. Sulfur, in the form of manganese-sulfide inclusions commonly found in steel, can act as a poison to dissociate the molecular hydrogen to atomic hydrogen. At the point of high stress, atomic hydrogen will then diffuse back into the steel part and eventually lead to time-delayed hydrogen embrittlement failure.

Because there are three sources of hydrogen— the manufacture of steel (melting), processing and manufacturing, and in-service (environment)—and because there are three sources of stress—applied, residual from heat treatment, and residual from welding or plastic deformation—nine possible combinations exist. Therefore, it is not always easy to identify the specific cause of a hydrogen embrittlement service failure. A comprehensive evaluation of hydrogen embrittlement service failures should include all nine possibilities. An evaluation of the possible controls that avoid in-service hydrogen embrittlement failures must focus on either eliminating the sources of hydrogen or operating at a sufficiently low stress (below the threshold) to prevent cracking.

Current hydrogen embrittlement prevention and control procedures are primarily directed at the plating process and use of in-service maintenance chemicals. These procedures are covered in ASTM F 519 (Ref 2). Over 30 military and federal specifications include hydrogen embrittlement relief treatments. Hardware, such as springs or structural fasteners, is tested directly by sustained or step-load stress tests to evaluate the effectiveness of the hydrogen embrittlement relief treatments.

Reference cited in this section

2. "Standard Method for Mechanical Hydrogen Embrittlement Testing of Plating Processes and Aircraft Maintenance Chemicals," F 519, *Annual Book of ASTM Standards,* ASTM International

---

B. Phull, Evaluating Hydrogen Embrittlement, *Corrosion: Fundamentals, Testing, and Protection,* Vol 13A, *ASM Handbook,* ASM International, 2003, p 617–624

Evaluating Hydrogen Embrittlement

Revised by Bopinder Phull, Consultant

Testing

Tests for hydrogen embrittlement are performed to determine the effect of hydrogen damage in combination with residual or applied stresses. In the past decade, conventional testing methods have been modified to incorporate fracture mechanics, and the various types of hydrogen damage have been further classified in terms of crack nucleation, crack growth rates, and threshold stress intensity measurements.

This section discusses the current methods of hydrogen embrittlement testing and focuses on accelerated small-specimen testing methods for failure analysis and production control of hydrogen embrittlement. Additional information on hydrogen damage in metals and on test methods for hydrogen embrittlement can be found in Ref 1, 2, 3, 4, 5, 6, 7, 8, 9.

Standardized Tests. The only current ASTM standards for hydrogen embrittlement testing are F 519 (Ref 2) and F 326 (Ref 3). These standards are based on (a) not putting hydrogen into the steel by keeping the hydrogen in the plating bath at acceptably low levels (ASTM F 326) and (b) using mechanical tests to ensure that the amount of residual hydrogen after baking is below acceptably low levels (ASTM F 519).

ASTM F 326. This standard method covers an electronic hydrogen-detection instrument procedure for the measurement of plating permeability to hydrogen, a variable that is related to hydrogen absorbed by steel during plating and to the hydrogen permeability of the plate during post-plate baking. A specific application of this method involves controlling cadmium-plating processes in which the plate porosity relative to hydrogen is critical, such as for high-strength steels.

This method uses a metal-shelled vacuum probe as an ion gage. A section of the probe shell is cadmium plated at the lowest current density encountered in the electroplating process. The probe ion current, proportional to hydrogen pressure, is recorded as a function of time during subsequent baking. The slope of this curve has an empirical relationship to failure data, such as those discussed in ASTM F 519.

ASTM F 519. This method covers the evaluation of the hydrogen-generating potential of fluids (aircraft maintenance chemicals) and the hydrogen embrittlement control of electroplating processes. Test specimens are installed to indirectly monitor the amount of hydrogen in the plating bath when actual hardware is being plated. The acceptable level of hydrogen is determined by a go/no-go situation established by the failure of a sustained-loaded, stressed specimen that has been baked at 191 °C ± 14 °C (375 °F ± 25 °F) for a minimum of 23 h. The procedures and requirements are specified for the following five types of AISI 4340 steel test specimens:

- Type 1a: notched round bars, stressed in tension, under constant load
- Type 1b: notched round bars loaded in tension with stressed O-rings
- Type 1c: notched round bars loaded in bending with loading bars
- Type 1d: notched C-rings loaded in bending with loading bolt
- Type 2a: unnotched ring specimens loaded in bending with displacement bars

For plated parts, no stress is applied until they have been baked; baking is specified to occur within 1 h after plating. For maintenance chemicals and cleaners, stress is applied before the test specimens are exposed to the environment. The latter condition is much more severe and discriminates against much lower levels of hydrogen but is more representative of the end use of a part.

The cantilever beam (CB) test is a constant- load test in which a V-notched specimen of a rectangular cross section is subjected to a bending load via a moment arm. A precrack at the root of the V-notch is initiated and extended by fatigue before testing. The area with the precrack is enclosed by an environmental chamber, which contains the environment during the test (Fig. 1a). The specimen is subjected to a constant load over a predetermined time period. The actual stress intensity, K_I, is a complex function of the bending moment, crack length, and specimen geometry:

$$K_1 = 4.12 \cdot M_0 \cdot \sqrt{\left(1/\alpha^3 - \alpha^3\right)/\left(B \cdot W^{3/2}\right)} \qquad \text{(Eq 1)}$$

where $\alpha = 1 - (a/W)$ and where M_0, B, and W are as defined in Fig. 1(b). The range of applicability for Eq 1 is $0.2 \leq (a/W) \leq 0.6$. ASTM E 1681 provides detailed descriptions of specimen preparation, testing, and interpretation of results (Ref 11). Other methods of loading or using nonrectangular test specimens are described in ASTM E 399 (Ref 12). As the crack grows, the stress intensity increases. Time to failure is plotted versus applied stress intensity. The lower limit of the resultant curve is a threshold stress intensity for hydrogen embrittlement, K_{IHE}, as shown in Fig. 2.

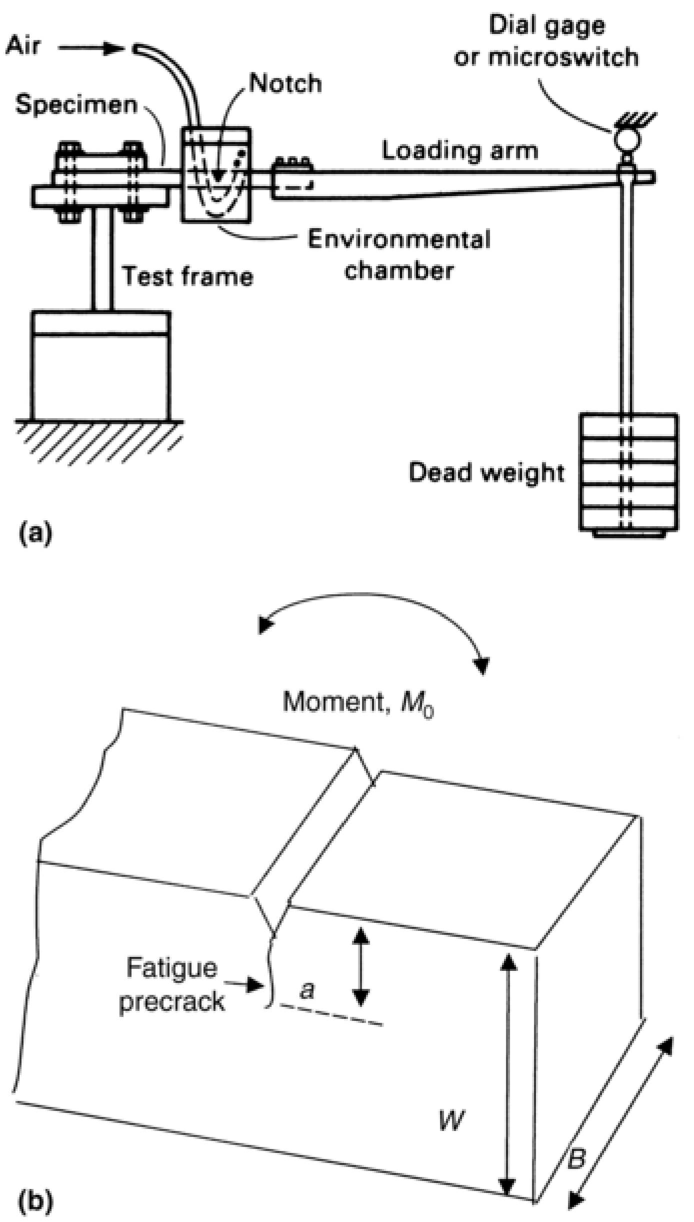

Fig. 1 Cantilever beam testing. (a) Fatigue-cracked cantilever beam test specimen and fixtures. Source: Ref 10. (b) Determination of stress intensity (K_I) for precracked cantilever beam specimens where 0.2 ≤ a/W ≤ 0.6. See text for discussion. Courtesy of U.S. Naval Research Laboratory

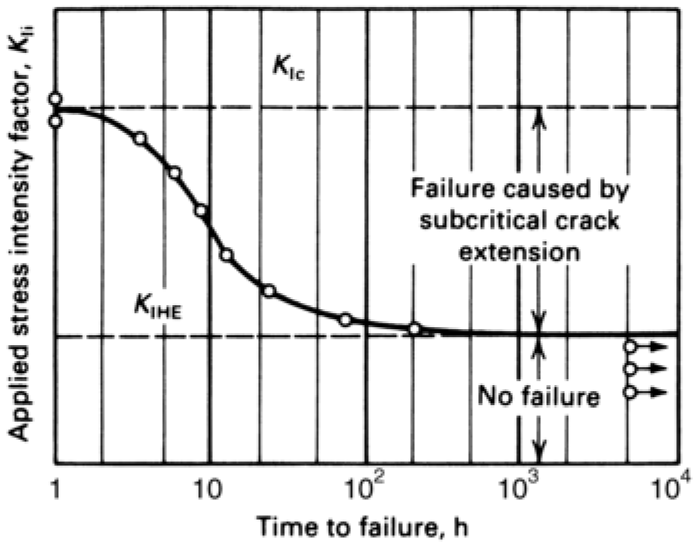

Fig. 2 Procedure to obtain K_{IHE} with precracked cantilever beam test specimen. Source: Ref 10

The K_{IHE} results of a cantilever beam test depend on how much time elapses before the test is terminated. Recommended test periods for establishing the true stress intensity threshold range from 200 h, which is typical for hydrogen embrittlement testing, to as long as 5000 h (Ref 13). Another limitation of this test method is that it can be expensive in terms of materials and machining. As many as 12 specimens placed under different loads in separate test machines are needed for each test in order to obtain valid K_{IHE} values.

The wedge-opening load (WOL) test applies a constant wedge- or crack-opening displacement. The actual stress intensity is a complex function of load, crack length, and specimen geometry. As the crack extends, stress intensity decreases until crack arrest occurs (Fig. 3). Crack growth can be monitored either by direct optical means (e.g., vernier microscope) or indirectly from strain gages attached to the back face. The initial load is assumed to be slightly above K_{IHE}. The specimen is maintained under these conditions for about 5000 h to establish the threshold. The crack grows to a point after which further growth is not measurable (K_{IHE}). However, it is difficult to determine precisely when the no- growth criterion is met. In some cases, it may be necessary to assume some minimum threshold crack growth rate such as 10^{-7} mm/s. Crack tip opening displacement should also be monitored. Corrosion reactions, accompanied by expansion in volume, may occur at the crack tip. This changes the opening displacement and increases the load, thus altering the desired testing conditions.

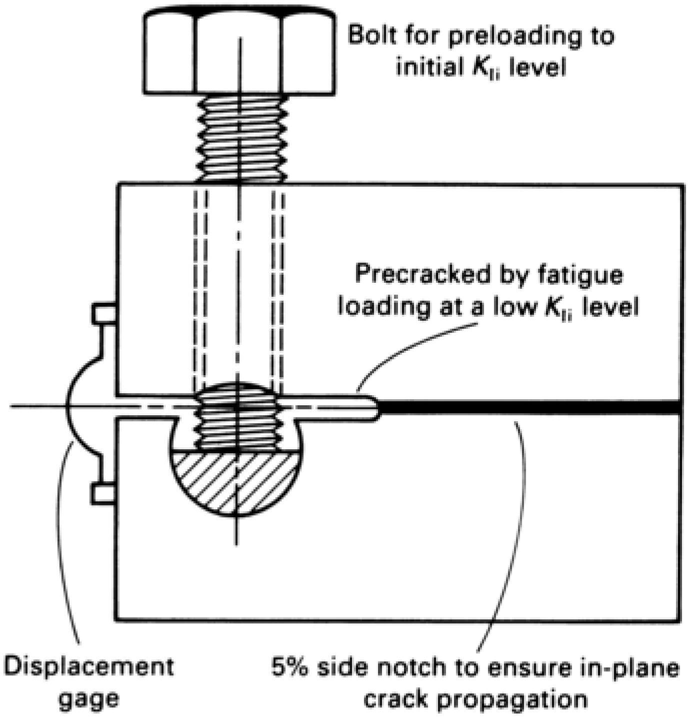

Fig. 3 Schematic showing basic principle of modified wedge-opening load test specimen

As subcritical crack extension occurs, stress intensity increases in the cantilever beam test and decreases in the WOL test (Fig. 4). Generally, the threshold stress intensity measured with the WOL test is lower than that measured with the cantilever beam test (Ref 14). A major advantage of the WOL test is that, in principle, only one specimen is required to measure K_{IHE}. In practice, if possible, it is prudent to test several replicate specimens concurrently.

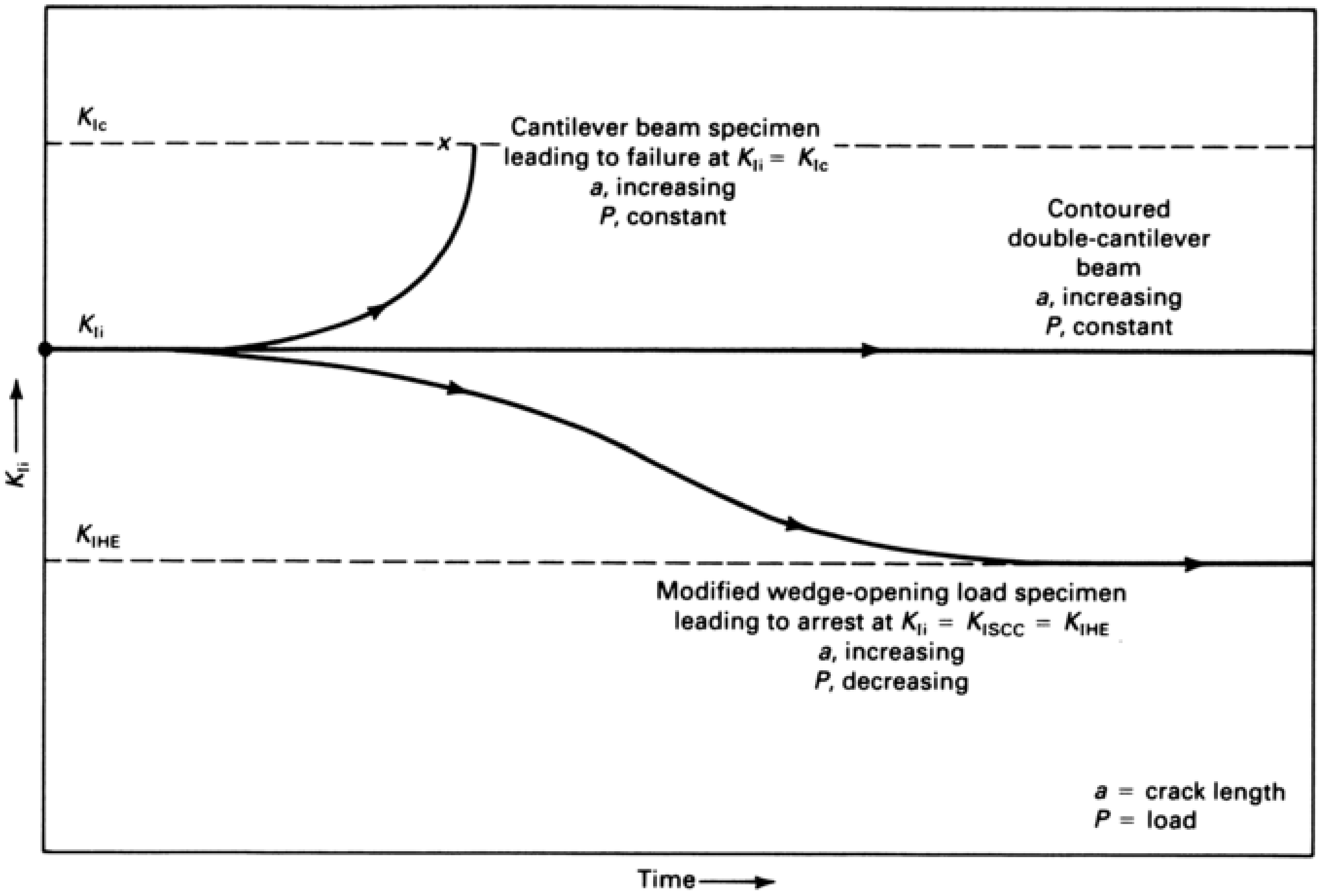

Fig. 4 Influence of time, crack extension, and load on stress-intensity behavior of modified wedge-opening load, cantilever beam, and contoured double-cantilever beam test specimens. Source: Ref 10

In long-term tests, it is essential to ensure that the concentration and the composition of the environmental solution do not change over time. For example, evaporation increases concentration and possible “salting” out at the waterline. Ultimately the solution level may drop below the crack line of the specimen. Such factors can render the test results invalid.

Figure 5 shows the results of WOL and cantilever beam tests on 25.4 mm (1 in.) thick iron- nickel-cobalt alloy steel specimens. The data imply that the wedge-opening load K_{IHE} crack- arrest result is the lower limit for the cantilever- beam K_{IHE} threshold.

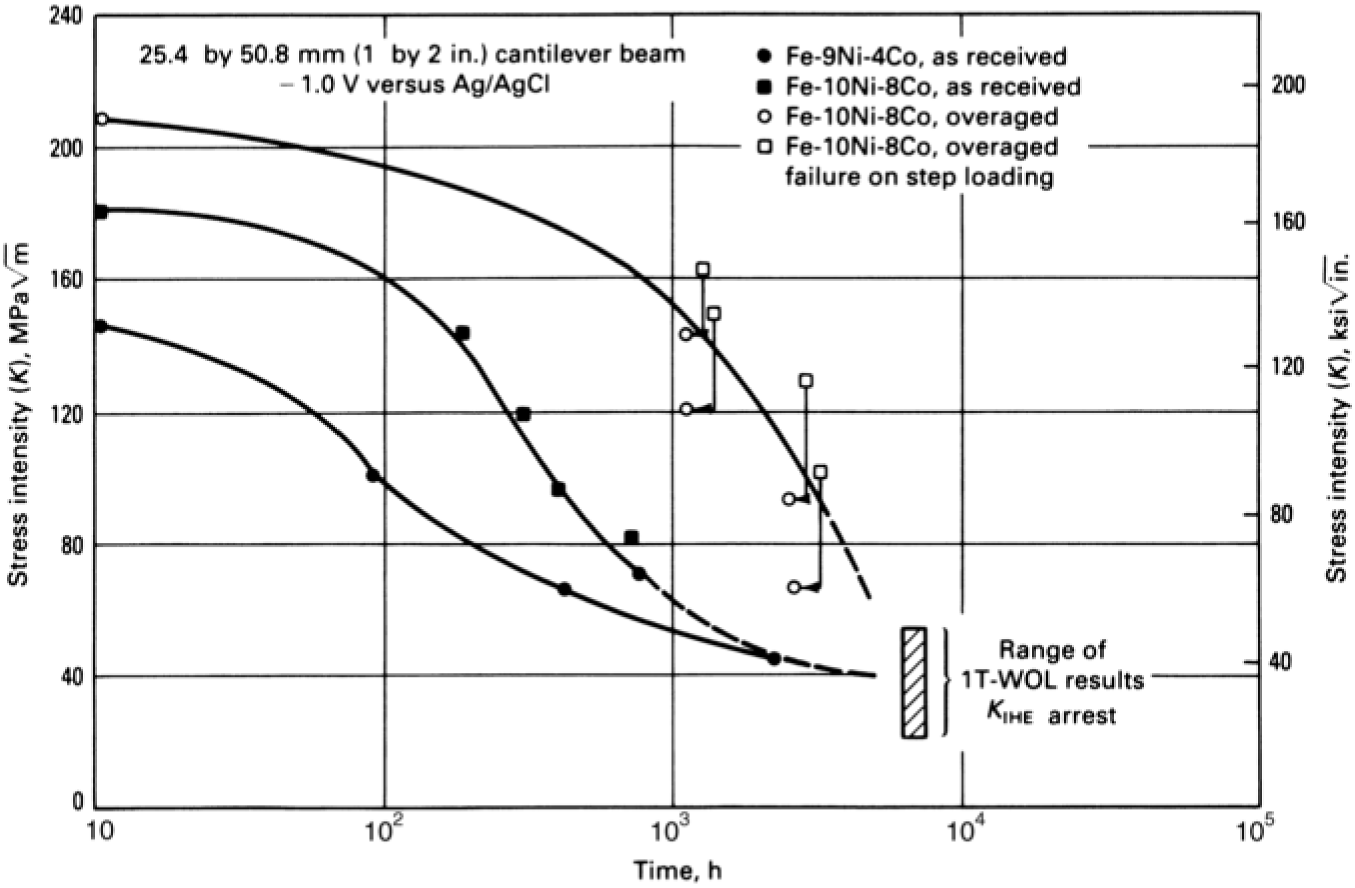

Fig. 5 Comparison of single-edge-notched cantilever beam and wedge-opening load test results for hydrogen embrittlement cracking of iron-nickel-cobalt steels. Source: Ref 15

The open circles in Fig. 5 represent "no fracture" at various exposure times for an overaged Fe-10Ni-8Co alloy in a cantilever beam test. The open squares indicate failure at increased stress intensities, following step loading at various exposure times at the lower stress intensity. The results suggest that increasing the load during the test produces more aggressive hydrogen-embrittlement conditions than a constant load.

This may be due to the possible formation of an oxide film on the surface. When the load is increased, the oxide film is broken, exposing fresh metal; more hydrogen is produced at the crack tip. For this reason, the test should use a rising load, because the constant-load cantilever beam test does not provide worst-case (fresh- metal-exposed) loading conditions.

The data also suggest that the cantilever beam test can generate an artificially high K_{IHE} threshold, depending on the time limit selected. If the test had been terminated at 200 h rather than at 5000 h, the reported K_{IHE} values from the cantilever beam test (Fig. 5) would have been four times higher than those measured after the longer time period. Similarly, the incubation period may not be exceeded, and no crack growth will occur if insufficient time is allowed in the wedge-opening load test.

Both testing methods require costly and time- consuming steps and result in a parameter, K_{IHE}, whose design significance is questionable. However, the parameter does provide a relative ranking of susceptibility to hydrogen embrittlement and, more generally, to SCC.

The contoured double-cantilever beam (DCB) test is used to measure crack growth rate at a constant stress intensity factor. This test simplifies the calculation of stress intensity by using a contoured specimen so that stress intensity is proportional to the applied load and is independent of the crack length. Thus, under a constant load, stress intensity remains constant with crack extension. For the test geometry shown in Fig. 6, the stress intensity factor equals 20 times the load ($K = 20P$).

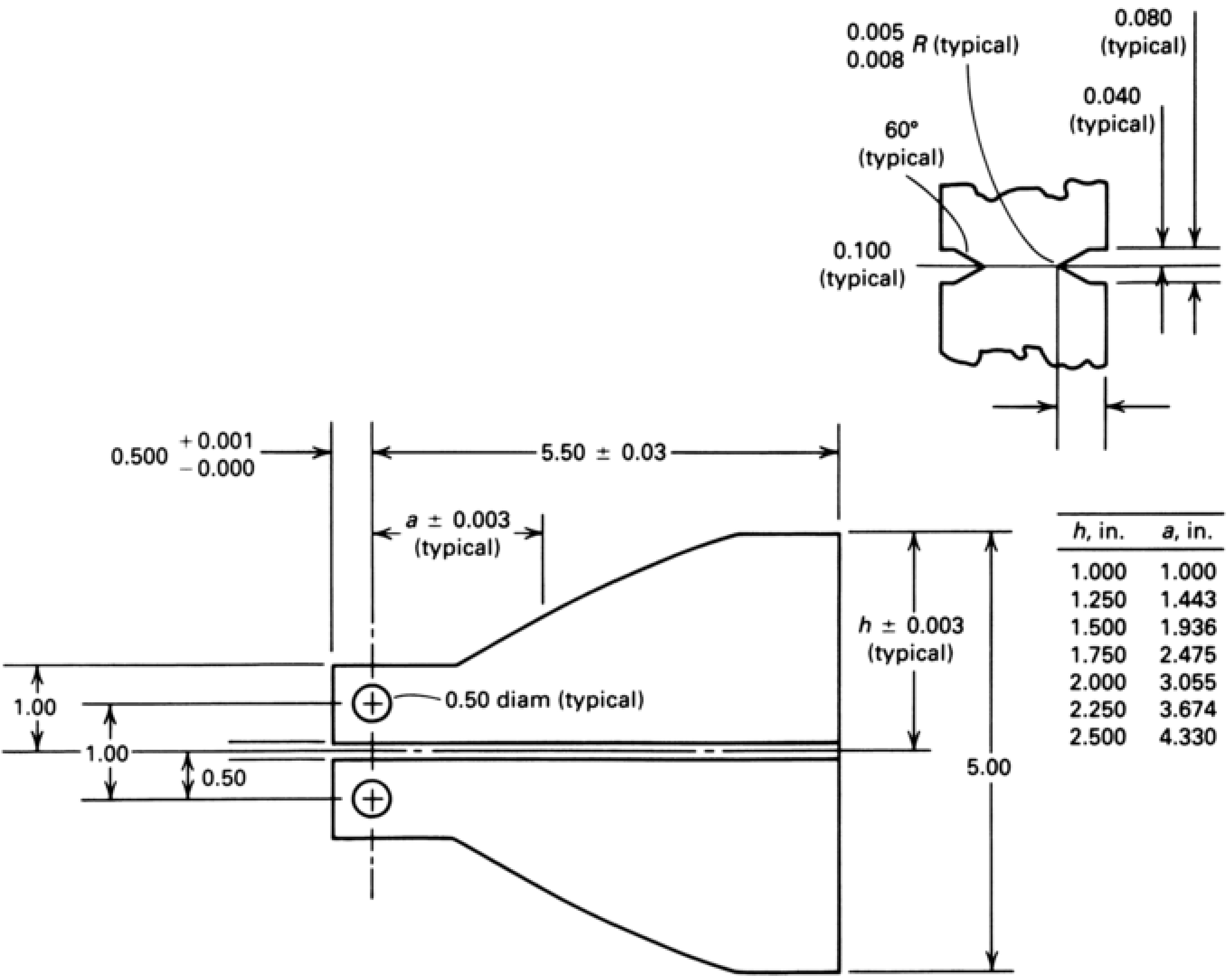

Fig. 6 Dimensions and configuration for double-cantilever beam test specimen. Specimen contoured to $3a^2/h^3 + 1/h = C$, where *C* is a constant. All values given in inches (1.0 in. = 25.4 mm)

Data on hydrogen embrittlement can be obtained with specimens of lower thickness (Ref 16) that do not otherwise meet the ASTM requirement of $K^2_{max} < 0.4\ B/(YS)^2$ (where *B* is the thickness and YS is the yield strength of the specimen), by using side grooves. Side grooves provide additional constraint on the material being tested. They also enable the maintenance of a plane-strain condition in a thin specimen by enhancing the triaxial state of the stress. This method has been extensively used to study the effect of heat treatment (hardness) and environment on the hydrogen stress cracking (HSC) of AISI 4340 steels (Fig. 7).

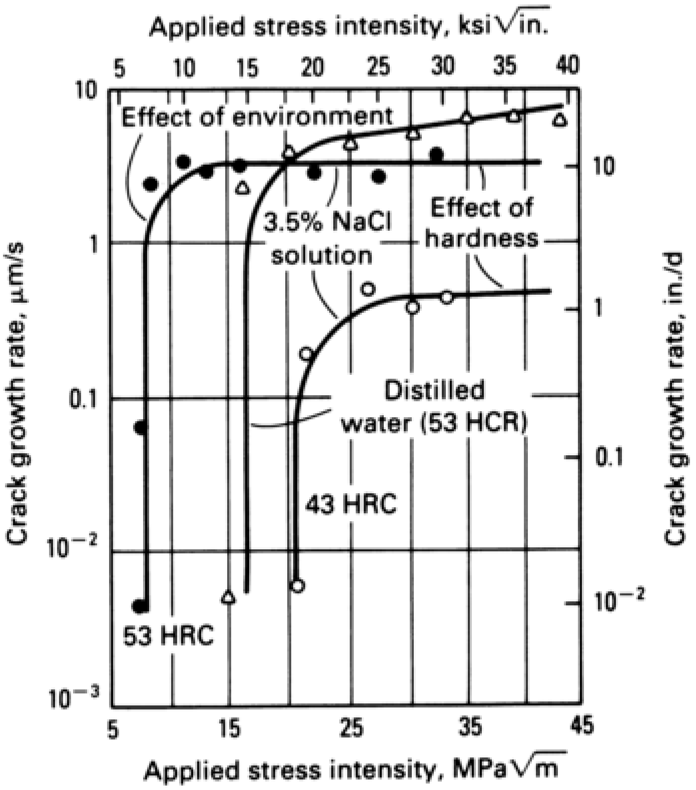

Fig. 7 Hydrogen embrittlement crack growth rate as a function of applied stress intensity for two different hardnesses and environments for an AISI 4340 steel, contoured double-cantilever beam test specimen

The contoured double-cantilever beam test has also been used to study the stress history effect that produces an incubation time before HSC. Figure 8 shows that incubation time is dependent on the type of steel. A decrease in the stress intensity factor from 44 to 22 MPa$\sqrt{m}$ (40 to 20 ksi$\sqrt{in.}$) may change the incubation time from less than 1 h for AISI 4340 steel to about 1 year for type D6-AC steel.

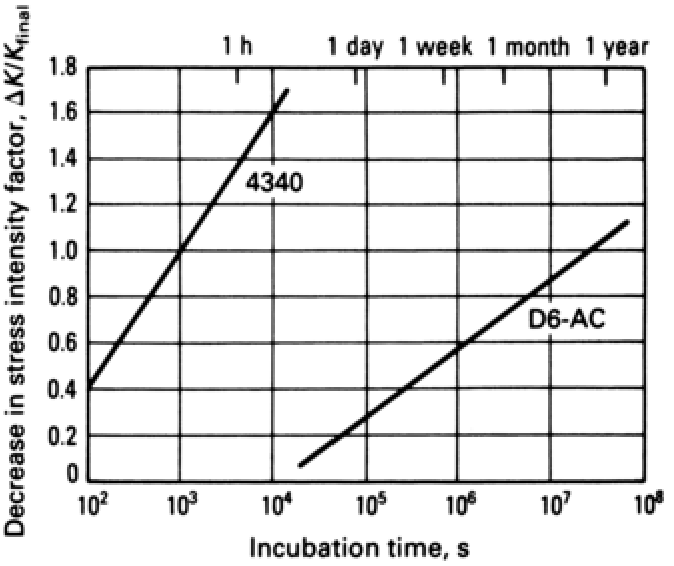

Fig. 8 Incubation time for crack growth in AISI type 4340 and type D6-AC steel contoured double-cantilever beam test specimens as a function of decrease in stress intensity. Source: Ref 17

Three-Point and Four-Point Bend Tests. The contoured double-cantilever beam test uses a constant load to maintain a constant stress intensity factor with crack extension. The same effect can be produced by using a three- or four- point bend test under displacement control. These tests use heavily side-grooved Charpy V-notch specimens (Fig. 9). Because crack-opening displacement is constant as the crack extends, the load

decreases. However, there is a slight initial increase in stress intensity to a maximum value that drops slightly as the ratio of crack depth to specimen width exceeds 0.5. Typically, stress intensity is constant within a small range. Figure 10 compares the change in stress intensity factor with crack extension for load control to that of displacement control for a three-point bend specimen.

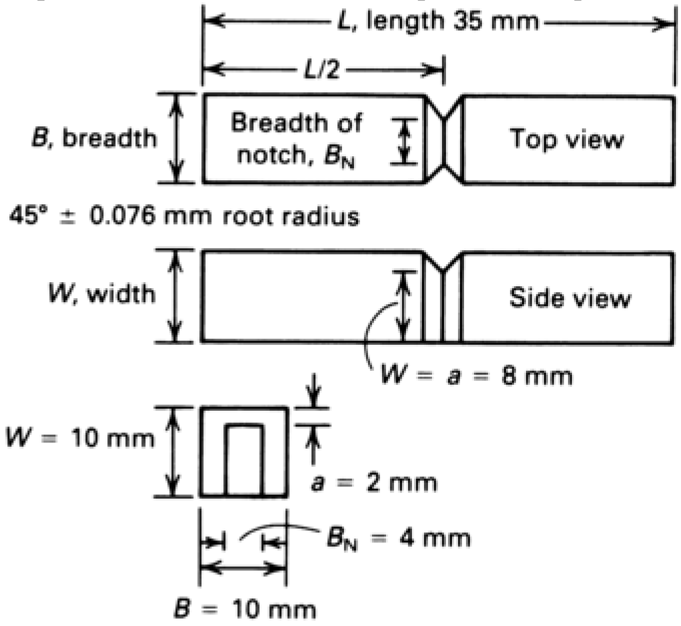

Fig. 9 Side-grooved Charpy V-notch test specimen used for three- and four-point bend tests

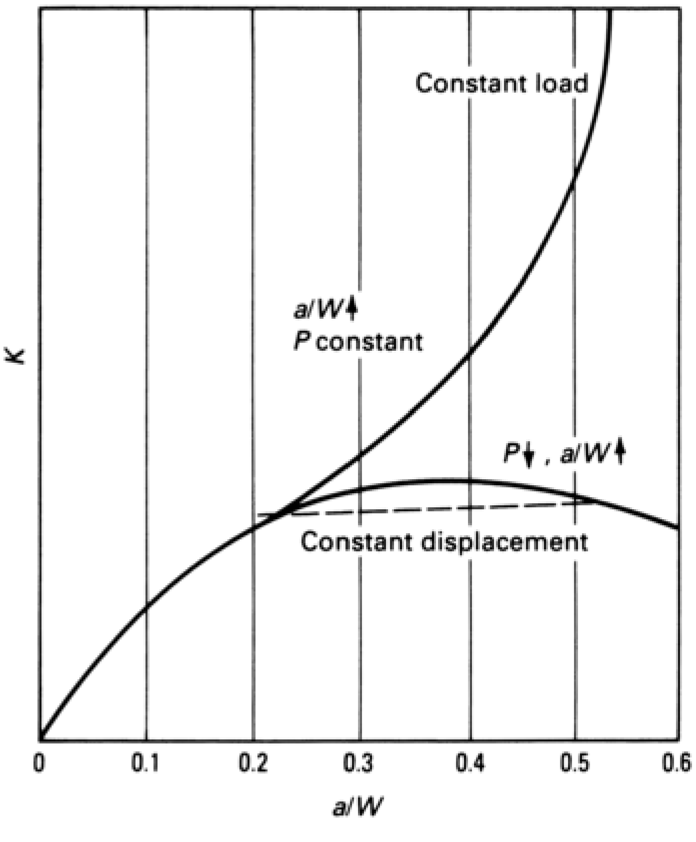

Fig. 10 Change in stress intensity factor with crack extension as a function of load control and displacement control for a three-point bend specimen

The rising step-load test provides a stress intensity that is different at each load but remains constant with crack extension as the load level is sustained. Crack initiation is signaled by a drop in load (Fig. 11). The rising step-load test was developed as an accelerated low-cost test for measuring the resistance of steels (particularly weldments) to hydrogen embrittlement (Ref 13, 17). The threshold obtained by this method could be slightly

higher if the test duration of each load is too short, but the test duration can be extended near the initiation loads in duplicate tests in order to obtain a more accurate measurement.

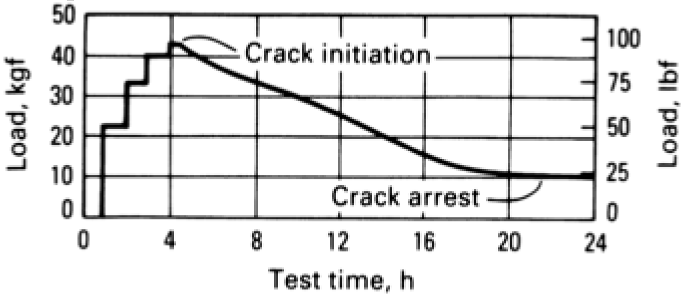

Fig. 11 Typical load-time record for four-point rising step-load test. Source: Ref 18

To index susceptibility to hydrogen-assisted cracking, the test should last no longer than 24 h, and the hydrogen source should reflect the most aggressive environment. In one experiment, a 3.5% sodium chloride solution was selected to simulate seawater, and a cathodic potential of -1.2 V versus SCE was used to generate hydrogen in order to reflect worst-case conditions of cathodic protection on a ship hull.

A Charpy specimen was chosen because such specimens are small and easy to machine and handle. In this test, however, the specimen was modified. Instead of using fatigue precrack, the notch-root radius was machined to less than 7.6 μm (3 mils). This was done to lower the cost and to give less ambiguous environmental conditions at the crack tip. Also, hydrogen cracks nucleate below the surface.

The specimen was deeply side grooved, a common practice used in crack growth rate tests to prevent the crack from branching. Side grooves are also used in crack-opening displacement or *J*-integral testing in order to cause load displacement curves to increase monotonically to fracture by inducing a highly triaxial stress field at the crack tip. Because a Charpy specimen is small, deep side grooves produce a triaxial stress field at the notch and thus promote crack initiation. The extent of the side grooving is such that the remaining ligament is only 40% of the original thickness. The modified Charpy specimen dimensions are shown in Fig. 9.

The specimen was loaded by means of beams and an instrumented bolt (Fig. 12). Four-point bending under constant displacement control and stress intensity results in crack growth. Once cracking initiates at the notch (a/W = 0.2, where a is crack length and W is width of the specimen), arrest does not occur until the crack is nearly through the specimen. The load is manually increased at 1 h intervals. An environmental chamber encompasses the specimen and includes a potentiostat to produce hydrogen while the specimen is under stress.

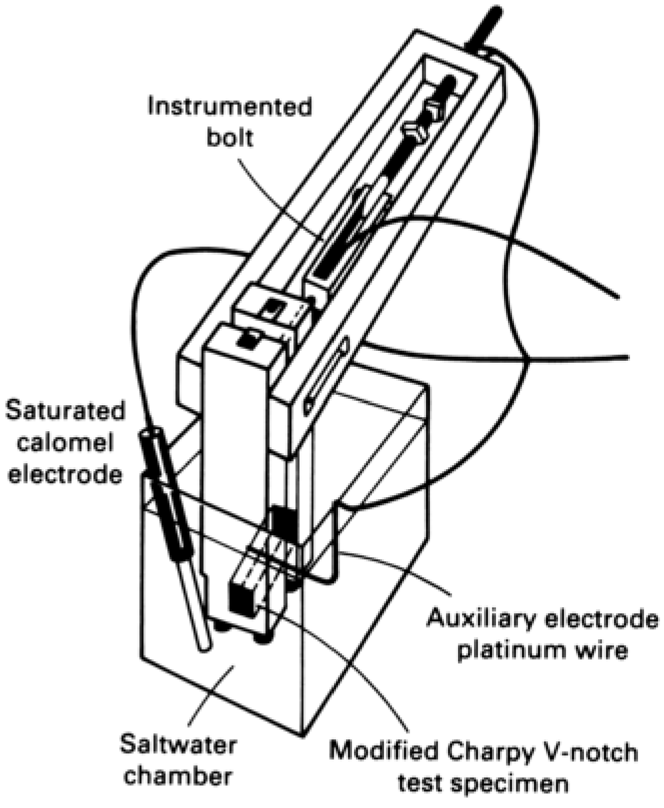

Fig. 12 Loading frame used for rising step-load test

The rising step-load test was used to evaluate high-strength HY ship steels and weldments in an environment simulating seawater under conditions of cathodic protection commonly employed to protect ship hulls (Ref 17). Samples from the heat-affected zone (HAZ) and other locations in the weld metal were tested. Interlayer gas tungsten arc heating was evaluated as a means of providing a refined, homogeneous, tempered microstructure with improved resistance to HSC. As a baseline, HY-130 and HY- 180 steels were compared.

Figure 13 plots rising step-load test results for HY-130 and HY-180 base metals, in addition to combinations of modified HY steel compositions and programmed-cooling-rate thermal cycles for the base metal and the weld wire. The vertical axis is a plot of a parameter derived from the specimen strength ratio in ASTM E 399— that is, 6 $P_{max}/B(W - a)^2$YS, where P_{max} is the maximum load that the specimen is able to sustain, *B* is the specimen thickness, *W* is the specimen width, *a* is the crack length, and YS is the yield strength in tension. For the data shown in Fig. 13, P_{max} was replaced by the crack initiation load. The horizontal axis is a ratio of K_{IHE}/YS, which was measured in a separate test program with cantilever beam and wedge-opening load specimens.

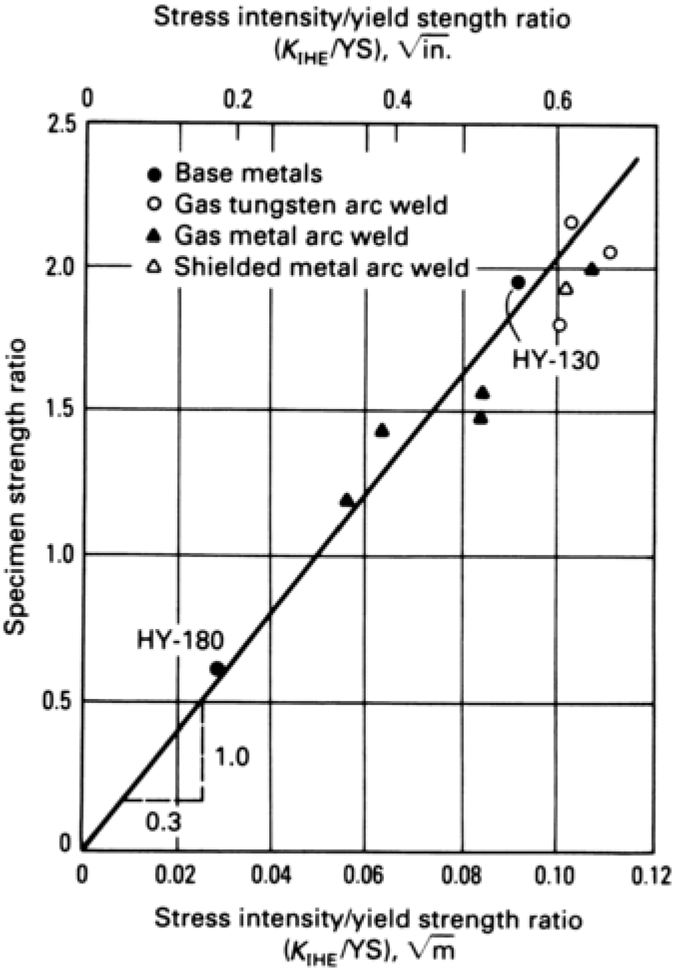

Fig. 13 Analytical correlation of strength ratio with threshold stress intensity data

The resistance to hydrogen embrittlement of the two base metals and six locations in HY-130 weldments was ranked by using this testing method. Test results showed that HY-180 is more susceptible to HSC than HY-130 and that the resistance to hydrogen embrittlement of specimens taken from the HAZ and the fusion line is consistently higher than that of weld metal specimens. The HSC resistance of the weld metal is affected by grain structure. Interlayer gas tungsten arc reheating homogenized the weld structure but did not temper the weld metal. Specimens from the gas tungsten arc reheated weldment consistently exhibited higher hardness and lower resistance to hydrogen embrittlement than similar specimens from the standard HY- 130 weld metal (Ref 14, 19).

The disk-pressure testing method measures the susceptibility to hydrogen embrittlement of metallic materials under a high-pressure gaseous environment (Ref 20). The test is used for the selection and quality control of materials, protective coatings, surface finishes, and other processing variables.

In this test, a thin disk of the metallic material to be tested is placed as a membrane in a test cell and subjected to helium pressure until it bursts. Because helium is inert, the fracture is caused by mechanical overload; no secondary physical or chemical action is involved. An identical disk is placed in the same test cell and subjected to hydrogen pressure until it bursts. Metallic materials that are susceptible to environmental hydrogen embrittlement fracture at a pressure lower than the helium-burst pressure. Materials that are not susceptible fracture under the same pressure for both hydrogen and helium.

The ratio, S_{H2}, between the helium-burst pressure, P_{He}, and the hydrogen-burst pressure, P_{H2}, indicates the susceptibility of the material to environmental hydrogen embrittlement: $S_{H2} = P_{He}/P_{H2}$. If S_{H2} is equal to or less than 1, the material is not susceptible to environmental hydrogen embrittlement. When S_{H2} is greater than 2, the material is considered to be highly susceptible. At values between 1 and 2, the material is moderately susceptible, with failure expected after long exposure to hydrogen. The material must be protected against such exposure.

A compilation of test results is shown in Fig. 14. The alloys having little or no sensitivity are 7075-T6 aluminum; Haynes 188 (cobalt base); beryllium copper (copper base); types 304, 316, and 310 austenitic stainless steel; type 430 ferritic steel; and age-hardened austenitic A 286 steel. Titanium-base alloy Ti-6Al-4V exhibits moderate sensitivity. Alloys with high sensitivity are Haynes 25 (cobalt base) and iron-base alloys, including medium- and high-strength steels. Conventional testing methods, such as the cantilever beam, wedge-opening load, and contoured double-cantilever beam tests, have also been adapted for testing in high-pressure gaseous hydrogen environments.

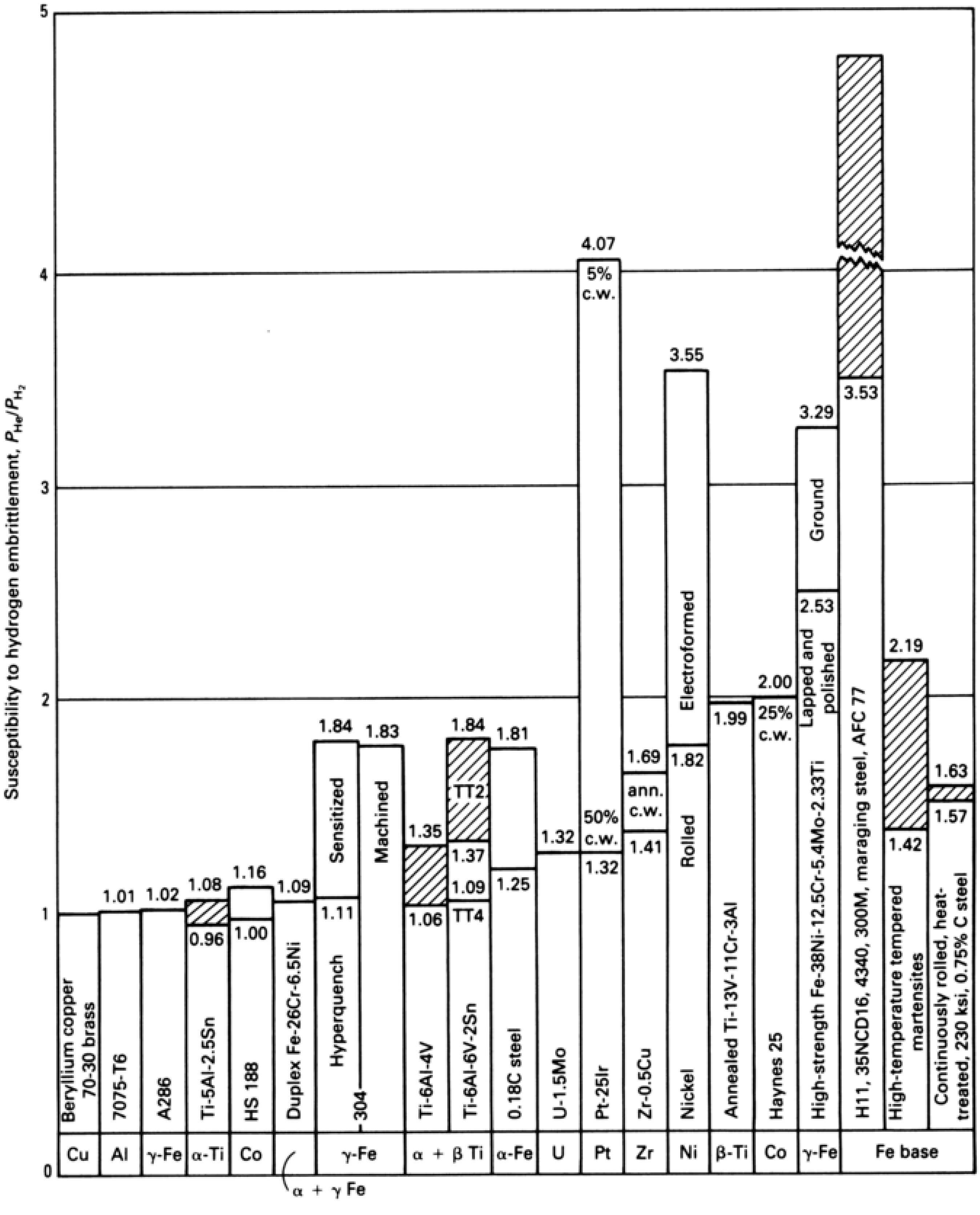

Fig. 14 Relative hydrogen susceptibility of various metals and alloys tested at a rate of 65 bars/min at room temperature. c.w., cold worked; ann., annealed. Source: Ref 20

Slow strain rate tensile tests can be used to evaluate many product forms, including plate, rod, wire, sheet, and tubing, as well as welded parts. Smooth, notched, or precracked specimens can be used. The principal advantage of this standardized test is that the susceptibility to HSC for a particular metal-environment combination can be rapidly assessed (Ref 21).

A variety of specimen shapes and sizes can be used. The most common is a smooth bar tensile coupon, as described in ASTM E 8 (Ref 22). The specimen is exposed to the environment and stressed monotonically at a slow but constant rate until complete fracture occurs. Typically, the output is a stress versus elongation. Tests are usually conducted over a range of strain rates; for example, 10^{-5} to 10^{-8} mm/mm/s. Interpretation of test results is based on one or more of the following parameters:

- Time to failure
- Ductility, for example, % elongation and/or reduction in cross-sectional area at the fracture
- Maximum stress (ultimate tensile strength, or UTS) achieved
- Fracture energy; that is, the area bounded by the stress-elongation curve

Potentiostatic Slow Strain Rate Tensile Testing. Studies have been conducted on the use of dissociated water under potentiostatic conditions that produce hydrogen on the surface of the tensile test specimen while under slow strain rate displacement control. Results suggest that hydrogen is the most significant parameter in hydrogen-sulfide SCC found in oil fields (Ref 23).

References cited in this section

1. L. Raymond, Ed., *Hydrogen Embrittlement Testing,* STP 543, ASTM International, 1974

2. "Standard Method for Mechanical Hydrogen Embrittlement Testing of Plating Processes and Aircraft Maintenance Chemicals," F 519, *Annual Book of ASTM Standards,* ASTM International

3. "Standard Method for Electronic Hydrogen Embrittlement Test for Cadmium-Electroplating Processes," F 326, *Annual Book of ASTM Standards,* ASTM International

4. I.M. Bernstein and A.W. Thompson, Ed., *Hydrogen in Metals,* American Society for Metals, 1973

5. C.D. Beachem, Ed., *Hydrogen Damage,* American Society for Metals, 1977

6. C.G. Interrante and G.M. Pressouyre, Ed., *Current Solutions to Hydrogen Problems in Steels,* American Society for Metals, 1983

7. R. Gibala and F. Hehemann, Ed., *Hydrogen Embrittlement and Stress Corrosion Cracking,* American Society for Metals, 1984

8. L. Raymond, Ed., *Hydrogen Embrittlement: Prevention and Control,* STP 962, ASTM International, 1987

9. A.R. Troiano, The Role of Hydrogen and Other Interstitials in the Mechanical Behavior of Metals, *Trans. ASM,* Vol 52, 1960, p 54–80

10. S.T. Rolfe and I.M. Barsom, *Fracture and Fatigue Control in Structures,* Prentice-Hall, 1977

11. "Standard Test Method for Determining Threshold Stress Intensity Factor for Environment-Assisted Cracking of Metallic Materials," E 1681, *Annual Book of ASTM Standards,* Vol 3.01, Metals—Mechanical Testing; Elevated and Low-Temperature Tests; Metallography, ASTM International 2002

12. ASTM E 399, "Standard Test Method for Plane-Strain Fracture Toughness of Metallic Materials," *Annual Book of ASTM Standards,* Vol 3.01, Metals—Mechanical Testing; Elevated and Low-Temperature Tests; Metallography, ASTM International, 2002

13. R.P. Wei, S.R. Novak, and D.R. Williams, Some Important Considerations in the Development of Stress Corrosion Cracking Test Methods, *Mater. Res. Stand.,* Vol 12 (No. 9), Sept 1972, p 25

14. C.A. Zanis, Subcritical Cracking in High Strength Steel Weldments—A Materials Approach, *SAMPE Q.*, Jan 1978, p 8–12

15. C.A. Zanis, P.W. Holsberg, and E.C. Dunn, Jr., Seawater Subcritical Cracking of HY- Steel Weldments, *Weld. J. Res. Suppl.*, Vol 59, Dec 1980

16. "Rapid Inexpensive Tests for Determining Fracture Toughness," NMAB-328, National Academy of Sciences, 1976

17. D.L. Dull and L. Raymond, Stress History Effect on Incubation Time for Stress Corrosion Crack Growth in AISI 4340 Steel, *Metall. Trans.*, Vol 3, Nov 1972, p 2943–2947

18. D.L. Dull and L. Raymond, Electrochemical Techniques, *Hydrogen Embrittlement and Testing*, STP 543, ASTM International, 1974, p 20–33

19. P.J. Fast, C.S. Susskind, and L. Raymond, "Charpy V-Notched Specimens for Indexing Stress Corrosion Cracking in HY Ship Steels and Weld Metals," Final report under contract F04701-78-C-0079, The Aerospace Corporation, Aug 1979

20. J.P. Fiddle, R. Bernardi, R. Broudeur, C. Roux, and M. Rapin, Disk Pressure Testing of Hydrogen Environment Embrittlement, *Hydrogen Embrittlement Testing*, STP 543, ASTM International, 1974, p 221–253

21. "Recommendations for Conducting Slow Strain Rate Corrosion Tests," Document ISO/TC 156/WG 2, International Organization for Standardization, British Standards Institute

22. "Standard Methods of Tension Testing of Metallic Materials," E 8, *Annual Book of ASTM Standards*, ASTM International

23. D.L. Dull and L. Raymond, Surface Cracking of Inconel 718 During Cathodic Charging, *Metall. Trans.*, Vol 4, June 1973, p 1635–1638

B. Phull, Evaluating Hydrogen Embrittlement, *Corrosion: Fundamentals, Testing, and Protection*, Vol 13A, *ASM Handbook*, ASM International, 2003, p 617–624

Evaluating Hydrogen Embrittlement

Revised by Bopinder Phull, Consultant

Interpretation of Test Results

The phenomenon of hydrogen embrittlement or SCC is very complex. The test results depend on environmental conditions (potential, pH, oxygenation level, temperature, environment), material and melting procedure (air, vacuum, electroslag remelting, vacuum arc remelting, and so on); test specimen geometry (notched tensile or bend specimens, cantilever beam specimens, wedge-opening loaded specimens), and specimen preparation (grinding, polishing, fatigue precracking, etc.). Because of the complex interactions between these factors, characterization of resistance (or conversely, susceptibility) to HE in absolute terms is almost impossible. The purpose of testing is to address a very specific set of conditions. Evaluation is, therefore, typically based on comparing data from controls (not subjected to HE) and specimens exposed to hydrogen—usually for various time periods.

The existing standard, ASTM F 519, is based on the assumption that air-melted AISI 4340 (Rockwell hardness 53 ± 1 HRC) is a worst- case condition. If no fracture occurs in this specimen after 200 h at 75% of the notched strength, then other 4340 steels processed by alternate melting processes (even steels with higher hardness levels because of vacuum melting) will not have residual levels of atomic hydrogen that would produce sustained-load failure in the environment of concern. Data to support this claim are shown in Fig. 15, which shows the extreme susceptibility of air melted 4340 steel as compared to electroslag remelted or vacuum arc remelted 4340 steel. This test is a “go/no-go” test intended to indicate relative susceptibility to HE of air-melted 4340 according to MIL S-5000E.

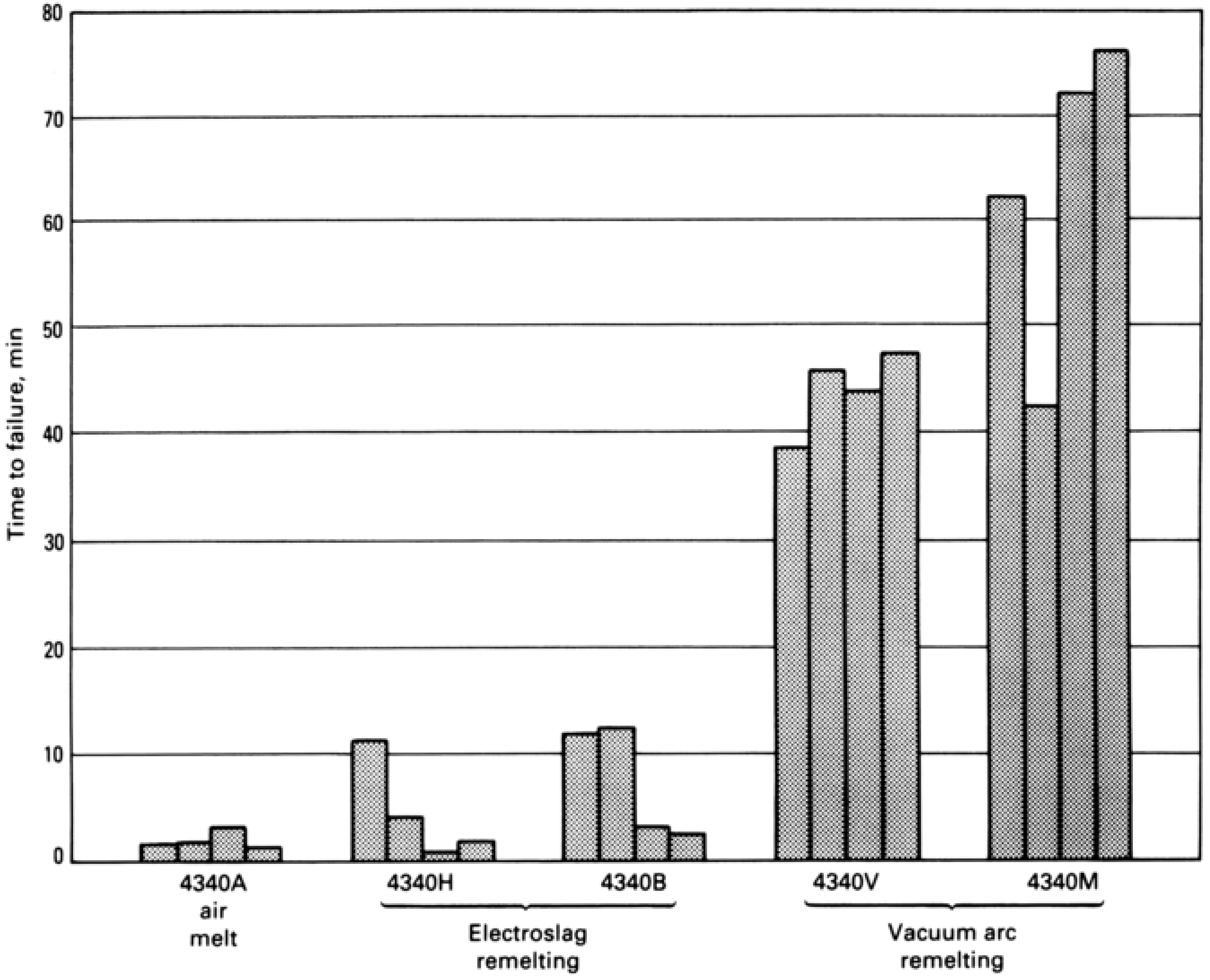

Fig. 15 Time to failure for AISI 4340 high-strength steels with an ultimate tensile strength range of 1790–2070 MPa (260–300 ksi) using ASTM F 519, Type 1c bend specimens. Source: Ref 24

This quality-control method suffers from the fact that manufacturing-induced stresses in the part might not be the same as in the representative test coupon. This is why stress-relief before plating is advised. If the coupon is stress free but the parts have a high residual stress, the coupons will pass the 200 h sustained-load test, but the parts, which might have cracked during plating, may inadvertently be put into service, or vice- versa.

To prevent misrepresentation, hardware or parts are often tested directly, such as in the case of fasteners or springs, and the use of representative test coupons is completely avoided. The problem with testing actual hardware is twofold. First, the test is destructive and can be costly, depending on the type of hardware being evaluated. Second, the method of applying the stress and the magnitude of the applied stress are not always easily obtained. It can be dangerous to reuse parts that have been proof tested by the application of a stress above the anticipated service stresses.

Reference cited in this section

24. L. Raymond and C. Beneker, “Evaluation of the Relative Hydrogen Embrittlement Susceptibility of ESR 4340 and Its Heat Treat Distortion Properties,” Final Report AM- MRC TR 82-49, Material Technology Laboratory, Sept 1982

B. Phull, Evaluating Hydrogen Embrittlement, *Corrosion: Fundamentals, Testing, and Protection*, Vol 13A, *ASM Handbook*, ASM International, 2003, p 617–624

Evaluating Hydrogen Embrittlement

Revised by Bopinder Phull, Consultant

Prevention and Control

The potential for hydrogen embrittlement must be evaluated before any prevention and control procedures are implemented (Ref 25). The sources of hydrogen must be examined with regard to three possibilities: the manufacture of the alloy, the manufacture and processing of the part, and the environmental service conditions. A source of hydrogen and a sufficient stress must exist in order for hydrogen embrittlement to occur. If either condition is eliminated, hydrogen embrittlement will not occur.

From a control viewpoint, the attempt is first made to eliminate the hydrogen and to ensure that no hydrogen is introduced during the manufacture and processing of the part. It is then anticipated that no problem will exist in service. This approach focuses on the hydrogen embrittlement process that has classically been referred to as internal hydrogen embrittlement, which is introduced, for example, during the manufacture and processing of the steel part. Once the part is in service, potential hydrogen embrittlement failure can result from hydrogen produced from a corrosion reaction, electrochemical (cathodic) protection, or from operation in high-pressure hydrogen. This is referred to as environmental hydrogen embrittlement.

Hydrogen embrittlement failures are prevented by controlling the amount of hydrogen introduced during the manufacture and processing of the hardware or part. Consideration must be given to the amount of hydrogen introduced during the melting of the alloy, the manufacture of the part, and the in-service environment, which should also include cleaners and paint strippers. The necessary controls are covered in ASTM F 519. The major difficulty appears to involve identifying the manufacturing-induced residual stresses that result from heat treatment and, especially, welding. Much more attention must be given to evaluating the potential for hydrogen embrittlement failures in the presence of residual stresses. The source of the residual stress must be identified in each piece of production hardware, or the assumption of high residual stresses in the manufactured part, especially in welded structures, must be included in the design analysis.

The usefulness of the threshold stress-intensity parameter, K_{IHE}, has yet to be established. Its main function appears to be its use in designing against the service-induced or application- induced possibilities of hydrogen embrittlement failure. This can be done only by controlling the applied stress and geometrical factors, such as root radius, in a given environment in order to maintain the effective applied stress intensity at a level below the threshold for subcritical crack growth. Although methodology for measuring K_{ISCC} is gradually being standardized, its significance in design is not yet completely understood.

Reference cited in this section

25. L. Raymond, Hydrogen Embrittlement Control, *ASTM Standard. News,* Vol 13 (No. 12), Dec 1985, p 46

B. Phull, Evaluating Hydrogen Embrittlement, *Corrosion: Fundamentals, Testing, and Protection*, Vol 13A, *ASM Handbook*, ASM International, 2003, p 617–624

Evaluating Hydrogen Embrittlement

Revised by Bopinder Phull, Consultant

Acknowledgment

This article has been adapted from L. Raymond, Evaluation of Hydrogen Embrittlement, *Corrosion,* Volume 13, *ASM Handbook* (formerly 9th edition *Metals Handbook*), ASM International, 1987, pages 283–290.

B. Phull, Evaluating Hydrogen Embrittlement, *Corrosion: Fundamentals, Testing, and Protection*, Vol 13A, *ASM Handbook*, ASM International, 2003, p 617–624

Evaluating Hydrogen Embrittlement

Revised by Bopinder Phull, Consultant

References

1. L. Raymond, Ed., *Hydrogen Embrittlement Testing,* STP 543, ASTM International, 1974
2. "Standard Method for Mechanical Hydrogen Embrittlement Testing of Plating Processes and Aircraft Maintenance Chemicals," F 519, *Annual Book of ASTM Standards,* ASTM International
3. "Standard Method for Electronic Hydrogen Embrittlement Test for Cadmium-Electroplating Processes," F 326, *Annual Book of ASTM Standards,* ASTM International
4. I.M. Bernstein and A.W. Thompson, Ed., *Hydrogen in Metals,* American Society for Metals, 1973
5. C.D. Beachem, Ed., *Hydrogen Damage,* American Society for Metals, 1977
6. C.G. Interrante and G.M. Pressouyre, Ed., *Current Solutions to Hydrogen Problems in Steels,* American Society for Metals, 1983
7. R. Gibala and F. Hehemann, Ed., *Hydrogen Embrittlement and Stress Corrosion Cracking,* American Society for Metals, 1984
8. L. Raymond, Ed., *Hydrogen Embrittlement: Prevention and Control,* STP 962, ASTM International, 1987
9. A.R. Troiano, The Role of Hydrogen and Other Interstitials in the Mechanical Behavior of Metals, *Trans. ASM,* Vol 52, 1960, p 54–80
10. S.T. Rolfe and I.M. Barsom, *Fracture and Fatigue Control in Structures,* Prentice-Hall, 1977

11. "Standard Test Method for Determining Threshold Stress Intensity Factor for Environment-Assisted Cracking of Metallic Materials," E 1681, *Annual Book of ASTM Standards,* Vol 3.01, Metals—Mechanical Testing; Elevated and Low-Temperature Tests; Metallography, ASTM International 2002

12. ASTM E 399, "Standard Test Method for Plane-Strain Fracture Toughness of Metallic Materials," *Annual Book of ASTM Standards,* Vol 3.01, Metals—Mechanical Testing; Elevated and Low-Temperature Tests; Metallography, ASTM International, 2002

13. R.P. Wei, S.R. Novak, and D.R. Williams, Some Important Considerations in the Development of Stress Corrosion Cracking Test Methods, *Mater. Res. Stand.,* Vol 12 (No. 9), Sept 1972, p 25

14. C.A. Zanis, Subcritical Cracking in High Strength Steel Weldments—A Materials Approach, *SAMPE Q.,* Jan 1978, p 8–12

15. C.A. Zanis, P.W. Holsberg, and E.C. Dunn, Jr., Seawater Subcritical Cracking of HY- Steel Weldments, *Weld. J. Res. Suppl.,* Vol 59, Dec 1980

16. "Rapid Inexpensive Tests for Determining Fracture Toughness," NMAB-328, National Academy of Sciences, 1976

17. D.L. Dull and L. Raymond, Stress History Effect on Incubation Time for Stress Corrosion Crack Growth in AISI 4340 Steel, *Metall. Trans.,* Vol 3, Nov 1972, p 2943–2947

18. D.L. Dull and L. Raymond, Electrochemical Techniques, *Hydrogen Embrittlement and Testing,* STP 543, ASTM International, 1974, p 20–33

19. P.J. Fast, C.S. Susskind, and L. Raymond, "Charpy V-Notched Specimens for Indexing Stress Corrosion Cracking in HY Ship Steels and Weld Metals," Final report under contract F04701-78-C-0079, The Aerospace Corporation, Aug 1979

20. J.P. Fiddle, R. Bernardi, R. Broudeur, C. Roux, and M. Rapin, Disk Pressure Testing of Hydrogen Environment Embrittlement, *Hydrogen Embrittlement Testing,* STP 543, ASTM International, 1974, p 221–253

21. "Recommendations for Conducting Slow Strain Rate Corrosion Tests," Document ISO/TC 156/WG 2, International Organization for Standardization, British Standards Institute

22. "Standard Methods of Tension Testing of Metallic Materials," E 8, *Annual Book of ASTM Standards,* ASTM International

23. D.L. Dull and L. Raymond, Surface Cracking of Inconel 718 During Cathodic Charging, *Metall. Trans.,* Vol 4, June 1973, p 1635–1638

24. L. Raymond and C. Beneker, "Evaluation of the Relative Hydrogen Embrittlement Susceptibility of ESR 4340 and Its Heat Treat Distortion Properties," Final Report AM- MRC TR 82-49, Material Technology Laboratory, Sept 1982

25. L. Raymond, Hydrogen Embrittlement Control, *ASTM Standard. News,* Vol 13 (No. 12), Dec 1985, p 46

B. Phull, Evaluating Hydrogen Embrittlement, *Corrosion: Fundamentals, Testing, and Protection*, Vol 13A, *ASM Handbook*, ASM International, 2003, p 617–624

Evaluating Hydrogen Embrittlement

Revised by Bopinder Phull, Consultant

Selected References

- *Corrosion of Metals and Hydrogen-Related Phenomena,* J. Flis, Ed., Materials Science Monograph Series, Vol 59, Elsevier-Science, 1991
- Hydrogen Embrittlement: Prevention and Control, L. Raymond, editor, ASTM STP 962, American Society for Testing and Materials, West Conshohocken, PA, 1988
- *Mechanical Hydrogen Embrittlement Methods for Evaluation and Control for Fasteners,* ASTM International, 2001

B. Phull, Evaluating Corrosion Fatigue, *Corrosion: Fundamentals, Testing, and Protection*, Vol 13A, *ASM Handbook*, ASM International, 2003, p 625–638

Evaluating Corrosion Fatigue

Revised by Bopinder Phull, Consultant

Introduction

FATIGUE is a common cause of the premature fracture of structural components. In corrosive environments, susceptible materials can fail even more quickly due to corrosion fatigue. Corrosion-fatigue cracking (CFC) is not limited to certain metallurgical conditions of the metal or to critical environmental species, as are other forms of environmentally assisted cracking. Classical CFC, stress-corrosion cracking (SCC), and hydrogen embrittlement cracking (HEC) failures are separated by a spectrum of behaviors dictated by a large number of factors, for example, metallurgical condition of the material, the method of stressing, and the electrochemistry of the metal-environment system.

B. Phull, Evaluating Corrosion Fatigue, *Corrosion: Fundamentals, Testing, and Protection*, Vol 13A, *ASM Handbook*, ASM International, 2003, p 625–638

Evaluating Corrosion Fatigue

Revised by Bopinder Phull, Consultant

Relationship between Corrosion- Fatigue Cracking, Stress-Corrosion Cracking, and Hydrogen Embrittlement Cracking

Figure 1 (Ref 1) illustrates a conceptual interrelationship of corrosion fatigue, stress corrosion, and hydrogen embrittlement. The most serious practical situations involving ductile-alloy/ environment systems are in the crosshatched regions. These regions indicate the combination of any two failure mechanisms. In the center, all three phenomena interact, which is probably representative of many practical situations involving ductile-alloy/aqueous environment systems. For example, in CFC and SCC, a surface pit constitutes a stress raiser, especially in the initiation process. Electrode potential and pH at an active crack tip may be significantly different from those on boldly exposed surfaces of a material. On the one hand, low-pH conditions can lead to local dissolution of metal and crack-tip blunting, which reduces stress-concentration effects. In contrast, low-pH conditions favor hydrogen generation and, consequently, increased risk of HEC. Reduction in local ductility associated with HEC is more likely to produce sharp crack tips, which, in turn, can exacerbate stress-concentration effects for any synergistic SCC or CFC. For materials that exhibit classical active- passive behavior, passivation is more conducive under static rather than dynamic conditions. For the latter, frequency of cyclic loading is often one of the critical factors that influences CFC in corrosive environments. Conversely, for corrosion control, cathodic protection generally mitigates CFC and SCC but increases the probability of HEC of susceptible materials. Thus, it is apparent from the foregoing that complex relationships can exist between CFC, SCC, and HEC. Although much research has been published in this area (Ref 1, 2, 3, 4, 5, 6, 7, 8, 9, 10, 11, 12, 13, 14, 15, 16, 17), many unanswered questions remain. It has been postulated that the danger of cracking in practical situations and the applicability of various testing techniques can be assessed from a mechanistic base as well as from the existing foundation of empirical experience (Ref 1). Some of the experimental evidence relating CFC to SCC is cited in later sections of this article that discuss specific aspects of corrosion-fatigue testing.

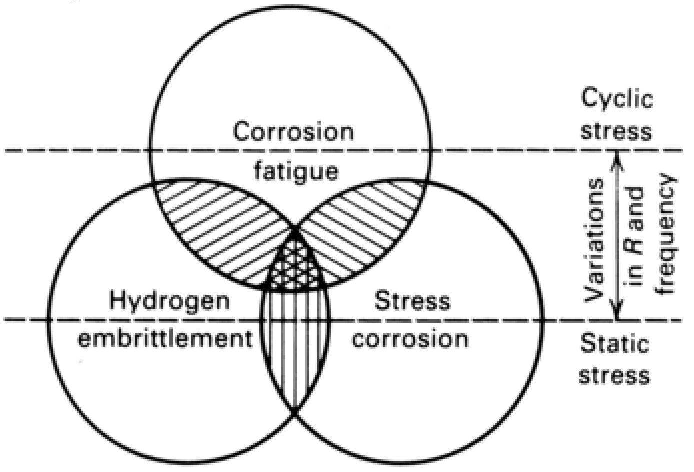

Fig. 1 Venn diagram illustrating the interrelationship among stress corrosion, corrosion fatigue, and hydrogen embrittlement. *R*, ratio of minimum stress to maximum stress. Source: Ref 1

References cited in this section

1. F.P. Ford, Current Understanding of the Mechanism of Stress Corrosion and Corrosion Fatigue, *Environment-Sensitive Fracture*, STP 821, S.W. Dean, E.N. Pugh, and G.M. Ugianski, Ed., American Society for Testing and Materials, 1984, p 32–51

2. O. Devereux, A.J. McEvily, and R.W. Staehle, Ed., *Corrosion Fatigue—Chemistry, Mechanics, and Microstructure,* Proceedings of NACE Conference, June 1971 (Storrs, CT), National Association of Corrosion Engineers, 1972

3. H.L. Craig, Jr., T.W. Crooker, and D.W. Hoeppner, Ed., *Corrosion-Fatigue Technology,* STP 642, American Society for Testing and Materials, 1978

4. R.W. Staehle and M.O. Speidel, Ed., *Stress Corrosion and Corrosion Fatigue Handbook,* ARPA Contract M00014-75-C-0703, Advanced Research Project Agency of the Department of Defense

5. P.R. Swann, F.P. Ford, and A.R.C. Westwood, Ed., *Mechanisms of Environment Sensitive Cracking of Materials,* Proceedings of Metals Society Conference, April 1977 (University of Surrey, U.K.), The Metals Society, 1979

6. R.N. Parkins and Ya. M. Kolotyrkin, Ed., *Corrosion Fatigue,* Proceedings of the First USSR-U.K. Seminar on Corrosion Fatigue of Metals, May 1980 (Lvov, USSR), The Metals Society, 1983

7. T.W. Crooker and B.N. Leis, Ed., *Corrosion Fatigue: Mechanics, Metallurgy, Electrochemistry and Engineering,* STP 801, American Society for Testing and Materials, 1983

8. S.W. Dean, E.N. Pugh, and G.M. Ugiansky, Ed., *Environment-Sensitive Fracture,* STP 821, American Society for Testing and Materials, 1984

9. R.N. Parkins, "A Critical Evaluation of Current Environment-Sensitive Fracture Test Methods," *Environment-Sensitive Fracture,* STP 821, S.W. Dean, E.N. Pugh, and G.M. Ugiansky, Ed., American Society for Testing and Materials, 1984, p 5–31

10. R.P. Gangloff, Ed., *Embrittlement by the Localized Crack Environment,* Proceedings of the TMS-AIME/MDS-ASM Symposium on Localized Crack Chemistry and Mechanics in Environment-Assisted Cracking, Oct 1983 (Philadelphia, PA), The Metallurgical Society, 1984

11. D.A. Jones, A Unified Mechanism of Stress Corrosion and Corrosion Fatigue Cracking, *Metall. Trans. A,* Vol 16, June 1985, p 1133–1141

12. R.P. Gangloff, Corrosion Fatigue Crack Propagation in Metals, *Environment-Induced Cracking of Metals,* R.P. Gangloff and M.B. Ives, Ed., NACE-10, NACE International, 1990, p 45

13. S.A. Shipilov, "Comparison Between Hydrogen-Enhanced Corrosion Fatigue Cracking Growth Rates and Critical Distances Ahead of a Growing Crack," Paper 00375, Corrosion/2000, NACE International, 2000

14. G.R. Engelhardt and D.D. MacDonald, "Modeling Corrosion Fatigue Crack Propagation," Paper 01115, Corrosion/2001, NACE International, 2001

15. D.D. MacDonald and G.R. Engelhardt, "Towards a Mechanism Based Theory for Crack Initiation," Paper 01116, Corrosion/2001, NACE International, 2001

16. T. Havn and H. Osvoll, "Corrosion Fatigue of Steel in Sea Water," Paper 02431, Corrosion/2001, NACE International, 2002

17. Y. Wang and R. Akid, Role of Nonmetallic Inclusions in Fatigue, Pitting, and Corrosion Fatigue, *Corrosion,* Vol 52 (No. 2), 1996, p 92–102

B. Phull, Evaluating Corrosion Fatigue, *Corrosion: Fundamentals, Testing, and Protection*, Vol 13A, *ASM Handbook*, ASM International, 2003, p 625–638

Evaluating Corrosion Fatigue

Revised by Bopinder Phull, Consultant

Prediction of Corrosion-Fatigue Life

While significant advances have been made, the methodology for the interpretation and use of standard test method data for environmental cracking is not fully developed. Moreover, to the extent that the two phenomena can interact synergistically under some conditions, existing approaches to standard test development may produce nonconservative data in some cases (Ref 18). A scientific basis for a reliable estimate of fatigue life for all conceivable load and environmental combinations remains elusive, despite the estimated billions of dollars spent combating fatigue (Ref 19).

A designer may rely on experience with similar components in service. However, such know- how is not available routinely. Therefore, fatigue data are often generated from accelerated laboratory tests. Fracture mechanics test specimens, for example, now provide very useful data for design engineers as well as for understanding fatigue behavior.

References cited in this section

18. T.W. Crooker, Environmental Cracking in Structural Alloys: A Look at Standards for Corrosion Fatigue and Stress-Corrosion Cracking, *ASTM Stand. News*, Vol 13 (No. 11), Nov 1985, p 54–58

19. J.T. Fong, Fatigue Research: Needs and Opportunities, *ASTM Stand. News*, Vol 13 (No. 11), Nov 1985, p 59–63

B. Phull, Evaluating Corrosion Fatigue, *Corrosion: Fundamentals, Testing, and Protection*, Vol 13A, *ASM Handbook*, ASM International, 2003, p 625–638

Evaluating Corrosion Fatigue

Revised by Bopinder Phull, Consultant

Types of Corrosion-Fatigue Tests

Laboratory corrosion-fatigue tests can be classified as either cycles-to-failure (complete fracture) or crack propagation (crack growth) tests. In cycles-to-failure testing, specimens or parts are subjected to a sufficient number of stress cycles to initiate and propagate cracks until complete fracture occurs. Such data are usually obtained by testing smooth or notched specimens. However, it is difficult to distinguish between CFC initiation and CFC propagation life with this type of testing.

In crack propagation testing, fracture mechanics methods are used to determine the crack growth rates of preexisting cracks under cyclic loading. Preexisting cracks or sharp defects in a material reduce or eliminate the crack initiation portion of the fatigue life of the component. Both types of testing are important. However, it appears that crack initiation is of more significance in the failure process of relatively thin sections, while crack growth appears to dominate thick- section component endurance (Ref 20).

The usual approach to corrosion-fatigue testing is to perform a state-of-the-art fatigue test in the presence of the environment of interest. This article emphasizes important factors that should be recognized and controlled in corrosion-fatigue tests and provides references to published standard methods and recommended practices.

Reference cited in this section

20. H.J. Westwood and W.K. Lee, Corrosion- Fatigue Cracking in Fossil-Fueled Boilers, *Corrosion Cracking,* Proceedings of the International Conference on Fatigue, Corrosion Cracking, Fracture Mechanics and Failure Analysis, Dec 1985 (Salt Lake City, UT), American Society for Metals, 1986, p 23–34

B. Phull, Evaluating Corrosion Fatigue, *Corrosion: Fundamentals, Testing, and Protection*, Vol 13A, *ASM Handbook*, ASM International, 2003, p 625–638

Evaluating Corrosion Fatigue

Revised by Bopinder Phull, Consultant

Standards and Recommended Practices for Fatigue Testing

Only a few standardized procedures for fatigue testing are available, because many of the testing machines are custom built. However, several types of fatigue-testing machines, testing methods, and test specimens are accepted as standard. In the United States, the ASTM International issues voluntary standards and recommended practices. Those related to fatigue testing are:

ASTM designation	Title	Ref
E 206	"Standard Definitions of Terms Relating to Fatigue Testing and the Statistical Analysis of Fatigue Data"	21
E 466	"Standard Practice for Conducting Force-Controlled Constant Amplitude Axial Fatigue Tests of Metallic Materials"	22
E 467	"Standard Practice for Verification of Constant Amplitude Dynamic Forces in an Axial Load Fatigue Testing System"	23
E 468	"Standard Practice for Presentation of Constant Amplitude Fatigue Test Results for Metallic Materials"	24
E 606	"Standard Practices for Strain-Controlled Fatigue Testing"	25
E 647	"Standard Test Method for Measurement of Fatigue Crack Growth Rates"	26
E 739	"Standard Practice for Statistical Analysis of Linear or Linearized Stress-Life (*S*-*N*) and Strain-Life (ε-*N*) Fatigue Data"	27
E 1823	"Standard Terminology Relating to Fatigue and Fracture Testing"	28
E 1942	"Standard Guide for Evaluating Data Acquisition Systems Used in Cyclic Fatigue and Fracture Mechanics Testing"	29
F 1801	"Standard Practice for Corrosion Fatigue Testing of Metallic Implant Materials"	30

References cited in this section

21. "Standard Practice for Conducting Force Controlled Constant Amplitude Axial Fatigue Tests of Metallic Materials," ASTM E 466, *Metals—Mechanical Testing; Elevated and Low-Temperature Tests; Metallography,* Vol 03.01 *2002 Annual Book of ASTM Standards,* American Society for Testing and Materials, 2002

22. "Standard Practice for Verification of Constant Amplitude Dynamic Forces in an Axial Load Fatigue Testing System," ASTM E 467, *Metals—Mechanical Testing; Elevated and Low-Temperature Tests; Metallography,* Vol 03.01, *2002 Annual Book of ASTM Standards,* American Society for Testing and Materials, 2002

23. "Standard Practice for Presentation of Constant Amplitude Fatigue Test Results for Metallic Materials," ASTM E 468, *Metals— Mechanical Testing; Elevated and Low- Temperature Tests; Metallography,* Vol 03.01, *2002 Annual Book of ASTM Standards,* American Society for Testing and Materials, 2002

24. "Standard Practices for Strain-Controlled Fatigue Testing," ASTM E 606, *Metals— Mechanical Testing; Elevated and Low- Temperature Tests; Metallography,* Vol 03.01, *2002 Annual Book of ASTM Standards,* American Society for Testing and Materials, 2002

25. "Standard Test Method for Measurement of Fatigue Crack Growth Rates," ASTM E 647, *Metals—Mechanical Testing; Elevated and Low-Temperature Tests; Metallography,* Vol 03.01, *2002 Annual Book of ASTM Standards,* American Society for Testing and Materials, 2002

26. "Standard Practice for Statistical Analysis of Linear or Linearized Stress-Life (*S-N*) and Strain-Life (ε-*N*) Fatigue Data," ASTM E 739, *Metals—Mechanical Testing; Elevated and Low-Temperature Tests; Metallography,* Vol 03.01, *2002 Annual Book of ASTM Standards,* American Society for Testing and Materials, 2002

27. "Standard Terminology Relating to Fatigue and Fracture Testing," ASTM E 1823, *Metals—Mechanical Testing; Elevated and Low-Temperature Tests; Metallography,* Vol 03.01, *2002 Annual Book of ASTM Standards,* American Society for Testing and Materials, 2002

28. "Standard Guide for Evaluating Data Acquisition Systems Used in Cyclic Fatigue and Fracture Mechanics Testing," ASTM E 1942, *Metals—Mechanical Testing; Elevated and Low-Temperature Tests; Metallography,* Vol 03.01, *2002 Annual Book of ASTM Standards,* American Society for Testing and Materials, 2002

29. "Standard Practice for Corrosion Fatigue Testing of Metallic Implant Materials," ASTM F 1801, *Metals—Medical Devices; Emergency and Medical Services,* Vol 13.01, *2002 Annual Book of ASTM Standards,* American Society for Testing and Materials, 2002

30. "Standard Test Method for Shear and Bending Fatigue Testing of Calcium Phosphate and Metallic Medical Coatings," ASTM F 1160, *Metals—Medical Devices; Emergency and Medical Services,* Vol 13.01, *2002 Annual Book of ASTM Standards,* American Society for Testing and Materials, 2002

B. Phull, Evaluating Corrosion Fatigue, *Corrosion: Fundamentals, Testing, and Protection,* Vol 13A, *ASM Handbook,* ASM International, 2003, p 625–638

Evaluating Corrosion Fatigue

Revised by Bopinder Phull, Consultant

Cycles-to-Failure Tests

In cycles-to-failure (crack initiation followed by propagation) tests, a specimen or part is subjected to cyclic loading until complete fracture results. A large portion of the total number of cycles in these tests is associated

with crack initiation. Although cycles-to-failure tests conducted on small specimens do not precisely establish the fatigue life of a large part, such tests do provide empirical data on the intrinsic fatigue crack initiation behavior of a metal or alloy. As a result, such data can be used to compare the effects of alloying additions, heat treatments, surface finishes, corrosion-control methods, and so on, and to develop empirical failure-prevention criteria for engineering design. Examples of the use of small-specimen fatigue test data can be found in the basis of the fatigue design codes for boilers and pressure vessels; complex welded, riveted, or bolted structures; and automotive and aerospace components.

Fatigue-Testing Regimes

The magnitude of the nominal applied stress on a cyclically loaded component is often measured by the amount of overstress, that is, the amount by which the nominal stress exceeds the fatigue limit or the long-life fatigue strength of the material used in the component. The number of load cycles that a component under low overstress can endure is high; therefore, high-cycle fatigue is often applied. Because high-cycle fatigue tests require uninterrupted operation for long periods of time, test machines that are simple and reliable are used. Either constant-load amplitude or constant deflection tests can be conducted.

As the magnitude of the nominal applied stress increases, the initiation of multiple cracks is more likely. Also, the spacing between fatigue striations, which indicate the progressive growth of the crack front, is increased, and the region of final fast fracture is increased in size.

Low-cycle fatigue is the regime characterized by high overstress. The commonly accepted dividing line between high-cycle and low-cycle fatigue is considered to be typically in the range of 10^4 to 10^5 cycles. In practice, this distinction is made by determining whether the dominant component of the strain imposed during cyclic loading is elastic (high cycle) or plastic (low cycle), which in turn depends on the properties of the metal as well as the magnitude of the nominal applied stress.

Different test techniques may be required for the control and monitoring of low-cycle fatigue tests. Typically, strain-controlled tests (constant strain amplitude) are used, and often, the test specimen is subjected to alternating tension and compression loading cycles.

In routine low- and high-cycle fatigue crack initiation testing, complete fracture of a small specimen is generally the failure criterion. Approximately 30 to 40% of the low-cycle fatigue life and approximately 80 to 90% of the high- cycle fatigue life, measured by cycles to failure, involve nucleation of the dominant fatigue crack that eventually causes failure.

Loading Parameters

Most laboratory fatigue testing is done either with axial loading or in bending. The stress is usually cycled between a maximum and a minimum tensile stress or between a maximum tensile stress and a maximum compressive stress. The latter is considered a negative tensile stress, is given an algebraic minus sign, and is therefore known as the minimum stress.

Applied stresses are described by three parameters. The mean stress, S_m, is the algebraic average of the maximum and minimum stresses in 1 cycle, $S_m = (S_{max} + S_{min})/2$. In the completely reversed cycle test, the mean stress is 0. The range of stress, S_r, is the algebraic difference between the maximum and minimum stresses in 1 cycle, $S_r = S_{max} - S_{min}$. The stress amplitude, S_a, is one-half the range of stress, $S_a = S_r/2 = (S_{max} - S_{min})/2$.

During a fatigue test, the stress cycle is usually maintained constant so that the applied stress conditions can be written $S_m \pm S_a$, where S_m is the static or mean stress, and S_a is the stress amplitude, which is equal to half the stress range. The nomenclature used to describe test parameters involved in cyclic stress testing is shown in Fig. 2.

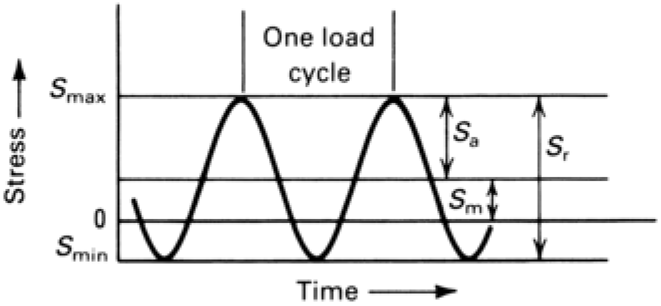

Fig. 2 Nomenclature used to describe test parameters involved in cyclic stress testing. S_a, stress amplitude; S_m, mean stress; S_r, stress range

The stress ratio is the algebraic ratio of two specified stress values in a stress cycle. Two commonly used stress ratios are the ratio *A* of the stress amplitude to the mean stress ($A = S_a/ S_m$) and the ratio *R* of the minimum stress to the maximum stress ($R = S_{min}/S_{max}$).

If the stresses are fully reversed, the stress ratio *R* becomes -1; if the stresses are partially reversed, *R* becomes a negative number less than 1. If the stress is cycled between a maximum stress and no load, *R* becomes 0. If the stress is cycled between two tensile stresses, *R* becomes a positive number less than 1. A stress ratio *R* of 1 indicates no variation in stress, making the test a sustained-load SCC test rather than a corrosion-fatigue test.

Presentation of Fatigue Data

High-cycle fatigue data are presented graphically as *S-N* curves, where *S* is stress and *N* is cycles to failure.

S-N Curves. The results of fatigue-cycles-to- failure tests are usually plotted as maximum stress, minimum stress, or stress amplitude versus number of cycles, *N*, to failure, using a logarithmic scale for the number of cycles. Stress is plotted on either a linear or a logarithmic scale. Three typical *S-N* curves are shown in Fig. 3.

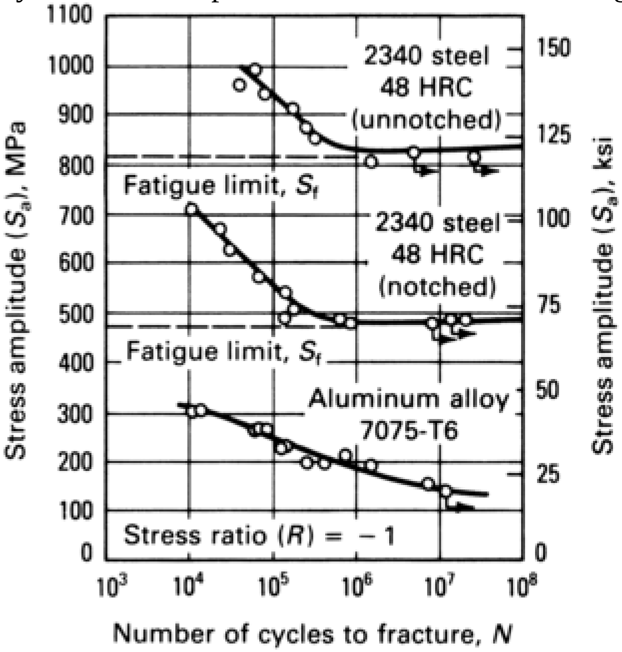

Fig. 3 Typical *S-N* curves for constant amplitude and sinusoidal loading

Fatigue Limit and Fatigue Strength. The horizontal portion of a *S-N* curve represents the maximum stress that the metal can withstand for an infinitely large number of cycles with 50% probability of failure. This maximum stress is known as the fatigue (endurance) limit, S_f. Most nonferrous metals do not exhibit a fatigue limit. Instead, their *S-N* curves continue to drop at a slow rate at high numbers of cycles, as shown by the curve for aluminum alloy 7075-T6 in Fig. 3.

For these types of metals, fatigue strength, rather than fatigue limit, is reported. Fatigue strength is the stress to which the metal can be subjected for a specified number of cycles. Because there is no standard number of cycles, each table of fatigue strengths must specify the number of cycles for which the strengths are reported. The fatigue strength of nonferrous metals at 10^8 or 5×10^8 cycles is sometimes erroneously called the fatigue limit.

Low-Cycle Fatigue. For the low-cycle fatigue region ($N < 10^4$ cycles), tests are conducted with controlled cycles of elastic plus plastic (total) strain range, rather than with controlled load or stress cycles. Under controlled-strain testing, fatigue-life behavior is represented by a log-log plot of the total strain range, $\Delta\varepsilon_t$, versus the number of cycles, *N*, to failure (Fig. 4).

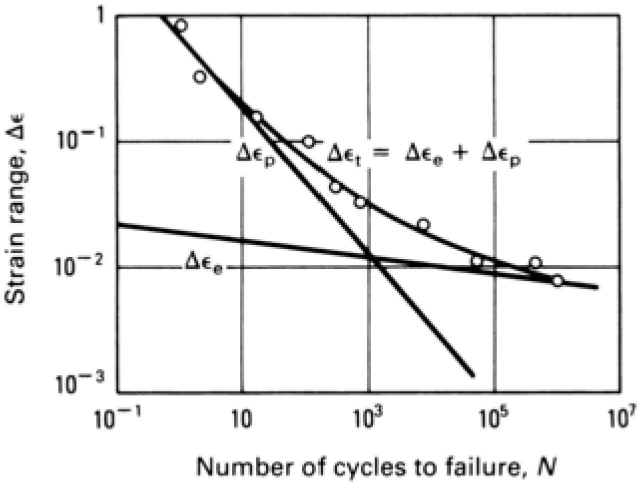

Fig. 4 Typical plot of strain range versus cycles to failure for low-cycle fatigue. $\Delta\varepsilon_t$, total strain range; $\Delta\varepsilon_e$, elastic strain range; $\Delta\varepsilon_p$, plastic strain range

The total strain range may be separated into elastic and plastic components. For many metals and alloys, the elastic strain range, $\Delta\varepsilon_e$, is equal to the stress range divided by the modulus of elasticity. The plastic strain range, $\Delta\varepsilon_p$, is the difference between the total strain range and the elastic strain range.

When curves are drawn for fatigue data, the equation and the method of the curve fit should be indicated. Any presentation of corrosion-fatigue data should include the following pertinent information, when applicable, regarding the material and the test:

- Material identification (product form)
- Mechanical properties, for example, yield strength (YS), ultimate tensile strength (UTS), percent elongation, hardness
- Orientation of the specimen
- Surface condition
- Notch description (stress-concentration factor)
- Type of fatigue test (mode of loading)
- Controlled test parameters
- Stress ratio
- Stress cycle frequency
- Stress wave shape
- Test temperature and environment

Fatigue Test Specimens

A typical fatigue test specimen has three areas: the test section and the two grip ends. The grip ends are designed to transfer load from the test machine grips to the test section and may be identical, particularly for axial fatigue tests. The transition from the grip ends to the test area is designed with large, smoothly blended radii to eliminate stress concentrations in the transition.

The design and type of specimen depend on the fatigue-testing machine and the objective of the fatigue study. The test section in the specimen is reduced in cross section to prevent failure in the grip ends and should be proportioned to use the middle to upper ranges of the load capacity of the fatigue machine. That is, it is best to avoid low load amplitudes where sensitivity and response of the system are decreased. Several types of fatigue test specimens are illustrated in Fig. 5.

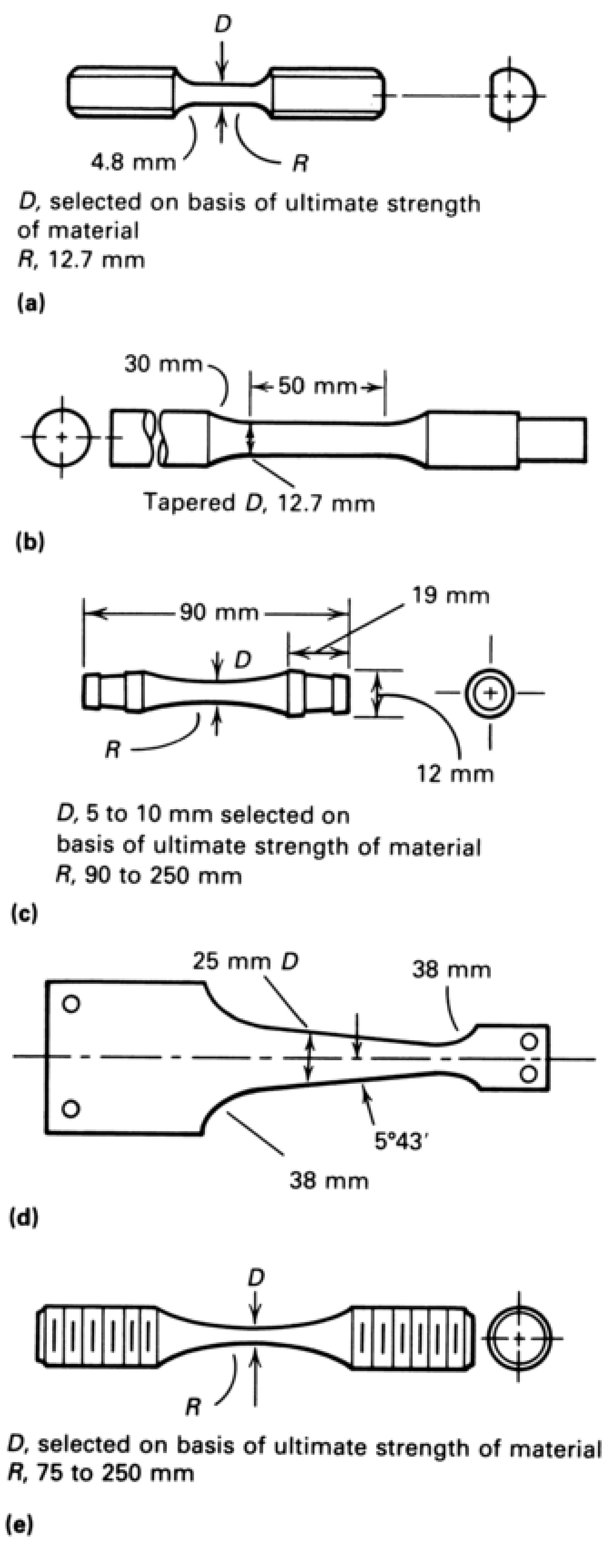

Fig. 5 Typical fatigue test specimens. (a) Torsional specimen. (b) Rotating cantilever beam specimen. (c) Rotating beam specimen. (d) Plate specimen for cantilever reverse bending. (e) Axial loading specimen. *R*, radius; *D*, diameter

Cylindrical Specimens. Three types of specimens with circular cross sections are commonly used:

- Specimens with a continuous radius between the grip ends with the minimum diameter at the center (Fig. 5c, e); referred to as hourglass specimens

- Specimens with tangentially blending fillets between the test section and the grip ends (Fig. 5a)
- Specimens for use in cantilever beam loading with tapered diameters proportioned to produce nominally constant stress along the test section (Fig. 5b), sometimes known as McAdam specimens

The design of the grip ends depends on the machine design and the gripping devices used. Round specimens for axial fatigue machines may be threaded, buttonhead, or constant-diameter types for clamping in V-wedge pressure grips.
For rotating-beam machines, short, tapered grip ends with internal threads are used, and the specimen is pulled into the grip by a draw bar. A long constant-diameter grip end shank is used on machines with lathe-type collet chucks as grips. Torsional fatigue specimens are generally cylindrical; however, there is usually a flat or keyway in the grip ends to transmit torque from the machine into the specimen (Fig. 5a).
Flat Sheet and Plate Specimens. Flat specimens for either axial or bending fatigue tests are generally reduced in width in the test section but may also have thickness reductions. The most commonly used types include:

- Specimens with tangentially blending fillets between the test section and the grip ends; used in both axial and bending fatigue tests
- Specimens with a continuous radius between the grip ends; also used in both axial and bending fatigue tests
- Specimens for use in cantilever reverse bending tests with tapered widths (Fig. 5d).

Flat specimens are generally clamped in flat wedge-type grips, or they can be held with a stiff bolted clamp/joint friction grip for reversed axial loading. Pin loading can be used when compression loads are not encountered. When pin loading is used, the holes drilled in the grip end must be designed to avoid shear or bearing failures at the holes, tensile failure between the holes at maximum load, and fatigue cracking at the holes in the grip end. In the axial fatigue testing of flat sheet specimens, the test length must be designed to prevent premature buckling of the specimen.

Effect of Test Specimen Size (Ref 31)

It is difficult to predict the fatigue performance of large machine members directly from the results of laboratory tests on small specimens. In most cases, a size effect exists; that is, the fatigue strength of large members is lower than that of small specimens. Even if the microstructure is the same, simply increasing specimen size increases the surface area and hence the probability of containing manufacturing flaws, which represent potential fatigue or corrosion- fatigue initiation sites. In reality, it is extremely difficult to prepare geometrically similar specimens of increasing diameter that have the same metallurgical structure and residual-stress distribution throughout the cross section. The problems in fatigue testing of large specimens are considerable, and few fatigue machines can accommodate specimens with a wide range of cross sections.
Changing the size of a fatigue specimen usually results in variations of two factors. First, increasing the diameter increases the volume and surface area of the specimen. The change in amount of surface is significant, because fatigue failures usually initiate at the surface. Second, for smooth or notched specimens loaded in bending or torsion, an increase in diameter usually decreases the stress gradient across the diameter and increases the volume of material that is highly stressed.
Experimental data on the size effect in fatigue typically show that the fatigue limit decreases with increasing specimen diameter. The data for steel shafts tested in reversed bending given in Table 1 show that the fatigue limit can be appreciably reduced in large section sizes.

Table 1 Effect of specimen size on the fatigue limit of normalized plain carbon steel in reversed bending

Specimen diameter		Fatigue limit	
mm	**in.**	**MPa**	**ksi**
7.6	0.30	248	36
38	1.50	200	29
152	6.00	144	21

Source: Ref 32

No size effect was found for smooth fatigue specimens of plain carbon steel with diameters ranging from 5 to 35 mm (0.2 to 1.4 in.) when tested in axial tension-compression loading (Ref 33). However, when a notch was introduced into the specimen, so that a stress gradient was produced, a definite size effect was observed. Therefore, it can be concluded that a size effect in fatigue is primarily due to the existence of a stress gradient.

The fact that large specimens with shallow stress gradients have lower fatigue limits supports the concept that a critical value of stress must be exceeded over a given finite depth of material for failure to occur. This appears to be a more realistic criterion of size effect than the ratio of the change in surface area to the change in specimen diameter. The importance of stress gradients in size effect explains why correlation between laboratory results and service failure is often poor. Actual failures in large parts are usually directly related to stress concentrations, either intentional or accidental, and it is usually impossible to duplicate the same stress concentration and stress gradient in a small laboratory specimen.

Effect of Stress Concentration

Fatigue strength is significantly reduced by the introduction of a stress raiser, such as a notch, hole, or corrosion pit. Because actual machine elements invariably contain such stress raisers as fillets, keyways, screw threads, press fits, and holes, fatigue cracks in structural parts usually initiate at such geometrical irregularities.

An optimal means of minimizing fatigue failure is the reduction of avoidable stress raisers through careful design and the prevention of accidental stress raisers by careful machining and fabrication. Stress concentration can also arise from surface roughness and metallurgical stress raisers, such as porosity, inclusions, local overheating in grinding, and decarburization. The effect of stress raisers on fatigue is generally studied by testing specimens containing a notch, usually a V-notch or a U-notch. The presence of a notch in a specimen under uniaxial load introduces three effects:

- There is an increase or concentration of stress at the root of the notch.
- A stress gradient is set up from the root of the notch toward the center of the specimen.
- A triaxial state of stress is produced at the notch root.

The ratio of the maximum stress in the region of the notch (or other stress concentration) to the corresponding nominal stress is the stress-concentration factor, K_t. In some situations, values of K_t can be calculated by using the theory of elasticity or can be measured by using photoelastic plastic models. Values for K_t are reported in Ref 34, 35, 36, 37.

The effect of notches on fatigue strength is determined by comparing the *S-N* curves of notched and unnotched specimens (Fig. 3). The data for notched specimens are usually plotted in terms of nominal stress based on the net cross section of the specimen. The severity of the notch in decreasing the fatigue limit is expressed by the fatigue notch factor, K_f. This factor is the ratio of the fatigue limit of unnotched specimens to the fatigue limit of notched specimens.

For materials that do not exhibit a fatigue limit, the fatigue notch factor is based on the fatigue strength at a specified number of cycles. Values of K_f have been found to vary with the severity of the notch, the type of notch, the material, the type of loading, and the stress level. Published values of K_f are subject to considerable variability and should be carefully examined for their limitations and restrictions. However, two general trends are usually observed for test conditions of completely reversed loading. First, K_f is usually less than K_t, and second, the ratio of K_f/K_t decreases as K_t increases.

The notch sensitivity of a material in fatigue is expressed by a notch sensitivity factor, q:

$$q = \frac{K_f - 1}{K_t - 1} \quad \text{(Eq 1)}$$

A material that experiences no reduction in fatigue behavior due to a notch ($K_f = 1$) has a factor of $q = 0$, but a material in which the notch has its full theoretical effect ($K_f = K_t$) has a factor of $q = 1$. However, q is not a true material constant, because it varies with the severity and type of notch, the size of the specimen, and the type of loading. As shown in Fig. 6, notch sensitivity increases with tensile strength. Therefore, it is sometimes possible to degrade fatigue performance by increasing the hardness or tensile strength of a material.

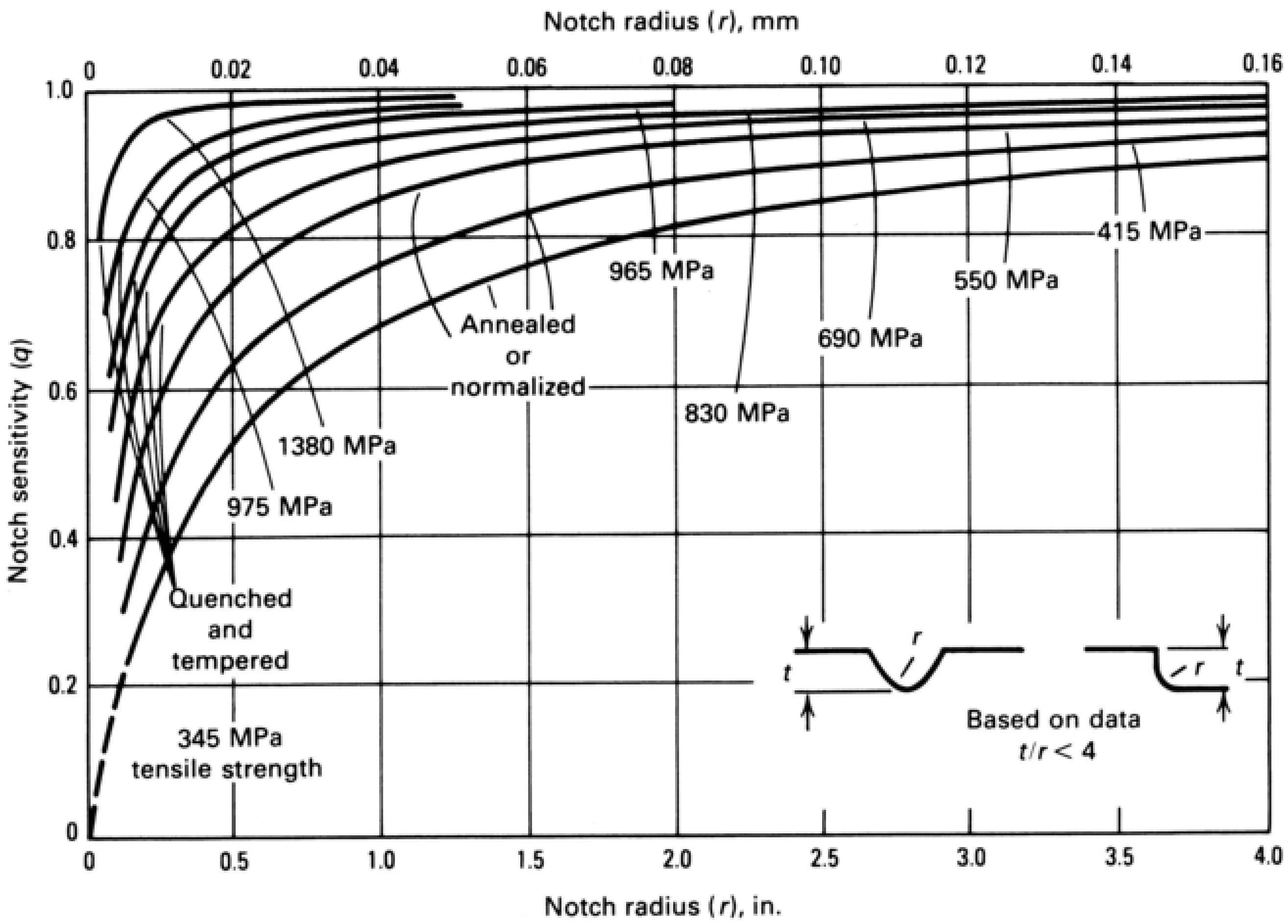

Fig. 6 Variation of notch sensitivity index with notch radius for steels tested in bending or axial fatigue loading. *t*, thickness. Source: Ref 38

Surface Effects and Fatigue

Fatigue properties are generally very sensitive to surface conditions. Except in special cases involving internal defects or case hardening, all fatigue cracks initiate at the surface. Factors that affect the surface of a corrosion-fatigue specimen can be divided into four categories:

- Surface roughness or stress raisers at the surface
- Changes in the properties of the surface metal
- Changes in the residual stress condition of the surface
- Corrosion

Surface Roughness. In general, fatigue life increases as the magnitude of surface roughness decreases. Fatigue life is the number of cycles of a specified character that a given specimen sustains before failure of a specified nature occurs, for example, crack initiation to a given depth, reaching a certain crack growth rate, or complete fracture. Decreasing surface roughness minimizes local stress raisers. Therefore, special attention must be given to the surface preparation of smooth, unnotched fatigue test specimens. Typically, a metallographic finish, free of machining grooves and grinding scratches, is required. Figure 7 illustrates the effect various surface conditions have on the fatigue properties of steel.

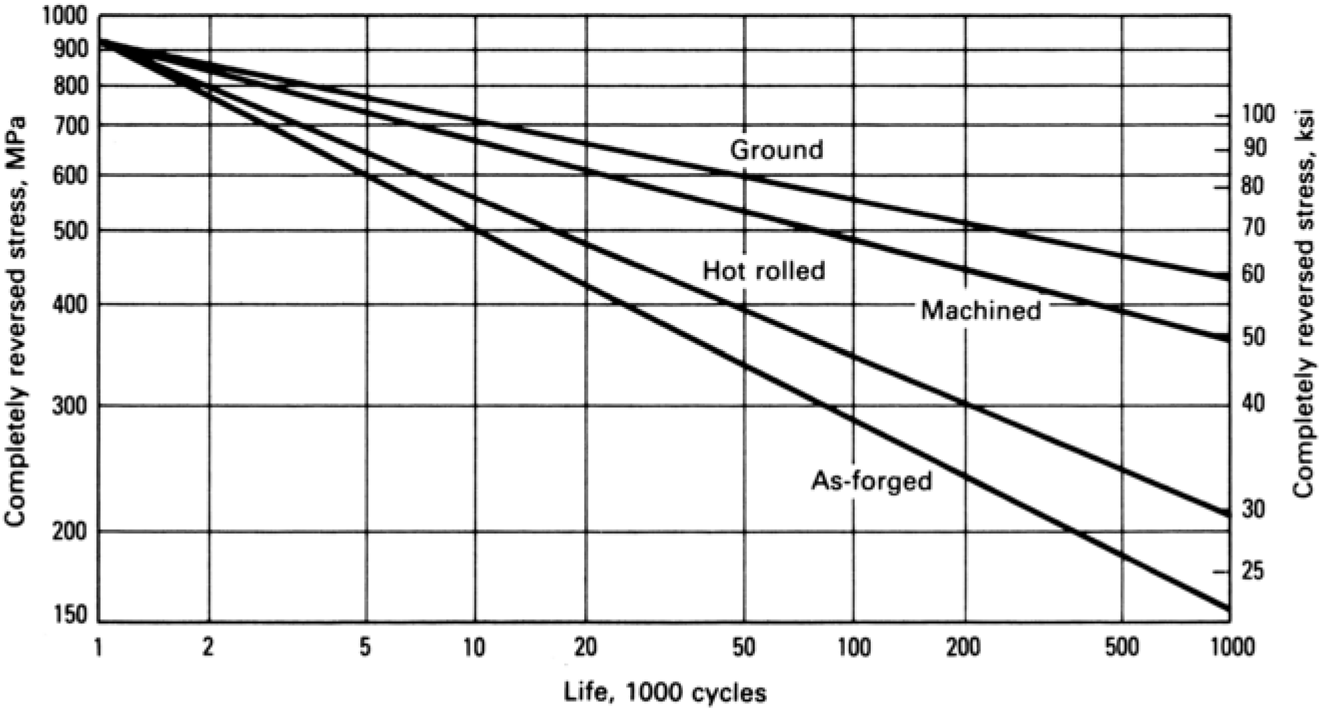

Fig. 7 Effect of surface conditions on the fatigue properties of steel (302 to 321 HB)

Changes in Surface Properties. Because fatigue failure is dependent on surface condition, any phenomenon that changes the fatigue strength of the surface material will greatly alter fatigue properties. For example, decarburization of the surface of heat treated steel is particularly detrimental to fatigue performance. Similarly, the fatigue strength of aluminum alloy sheet is reduced when a soft aluminum coating (cladding) is applied to the stronger age-hardenable aluminum alloy sheet.

Marked improvements in fatigue properties can result from the formation of harder and stronger surfaces on steel parts by carburizing and nitriding (Ref 39). However, because favorable compressive residual stresses are produced in the surface by these processes, the improved fatigue properties are not exclusively due to the formation of higher-strength material on the surface. The effectiveness of carburizing and nitriding in improving fatigue performance is greater when a high stress gradient exists (as in bending or torsion) than in an axial fatigue test.

The greatest improvement in fatigue performance occurs in notched fatigue specimens that are nitrided. The amount of strengthening depends on the diameter of the part and the depth of surface hardening. Improvements in fatigue properties similar to those caused by carburizing and nitriding may also be produced by flame hardening and induction hardening. In surface- hardened parts, failure initiates at the interface between the hard case and the softer core, rather than at the surface.

Electroplating of the surface generally decreases the fatigue limit of steel, because the coating, especially chromium plating, inherently contains cracks. The plating conditions used to produce an electroplated surface can have a significant effect on fatigue properties, because large changes in the residual stress, adhesion, porosity, and hardness of the plate can result. Anodized coatings on aluminum alloys may also decrease fatigue strength.

Surface Residual Stresses. Processing, such as grinding, polishing, and machining, that work hardens or increases residual stress on the surface can influence fatigue strength. However, there is no generalization that predicts the extent of improved fatigue strength from the results of work hardening and residual stress. Compressive residual surface stresses generally increase fatigue strength; tensile residual surface stresses do not. There may be a gradual decrease in residual stress if the cyclic stresses cause some plastic deformation. Compressive residual surface stress provides greater improvement in the fatigue strength of harder materials (such as alloy spring steel). In softer materials (such as low- carbon steel), work hardening effectively improves fatigue strength.

In a notched high-strength steel, the beneficial effect of prestretching and the detrimental effect of precompression are much greater than in a plain carbon steel because of the type of residual stress present at the

notch. In addition, compressive residual stress introduced during quenching from a tempering temperature will increase the fatigue strength, particularly in notched specimens.

In general, residual stresses are introduced by the poor fit of structural parts, a change in the specific volume of a metal accompanying phase changes, a change in shape following plastic deformation, or thermal stresses resulting from rapid temperature changes, such as occur in quenching. The influence of residual stress on fatigue strength is similar to that of an externally applied static stress. A static compressive surface stress increases the fatigue strength, and static tensile surface stress reduces it.

Specimen Preparation. Because both fatigue crack initiation and corrosion are typically surface dependent, proper machining and surface preparation of test specimens is critical. Unless care is taken, scatter caused by variable surface conditions will mask the scatter that is typical for the material being studied.

One of the primary aims of fatigue or corrosion-fatigue testing is the comparative performance of materials. Therefore, uniform specimen-preparation procedures must be established. Machining operations must not alter the surface structure of the metal. Heat generation, heavy cutting, and severe grinding are prohibited. For as-machined surfaces, the final machining direction should be oriented in the direction of the stress. Transition fillets must be blended into the test area without steps or undercutting. Surface polishing using metallographic techniques is preferred for smooth specimens, in which machining marks are removed by a sequence of grinding steps.

The final polishing is not a buffing operation but a cutting operation that uses lapping compounds or aluminum oxide powder in a liquid medium to remove grinding scratches. For flat sheet or plate specimens, edges should be slightly rounded and ground to eliminate nicks, dents, cuts, and sharp edges, which cause early crack initiation.

References cited in this section

31. G.E. Dieter, *Mechanical Metallurgy,* McGraw-Hill, 1976, p 426–427

32. O.J. Horger, Fatigue Characteristics of Large Sections, *Fatigue,* American Society for Metals, 1953

33. C.E. Phillips and R.B. Heywood, *Proc. Inst. Mech. Eng. (London),* Vol 165, 1951, p 113–124

34. R.E. Peterson, *Stress Concentration Design Factors,* John Wiley & Sons, 1974

35. H. Neuber, "Theory of Notch Stresses: Principles for Exact Calculation of Strength with References to Structural Form and Material," Springer, 1958, AEC-Tr-4547; available through NTIS, U.S. Dept. of Commerce

36. R.J. Roark, *Formulas for Stress and Strain,* 4th ed., McGraw-Hill, 1965

37. T. Topper, R. Wetzel, and J. Morrow, Neuber's Rule Applied to Fatigue of Notched Specimens, *J. Mater.,* Vol 4 (No. 1), 1969

38. G. Sines and J.R. Weisman, Ed., *Metal Fatigue,* McGraw-Hill, 1959

39. J.B. Bidwell et al., *Fatigue Durability of Carburized Steel,* American Society for Metals, 1957

B. Phull, Evaluating Corrosion Fatigue, *Corrosion: Fundamentals, Testing, and Protection*, Vol 13A, *ASM Handbook*, ASM International, 2003, p 625–638

Evaluating Corrosion Fatigue

Revised by Bopinder Phull, Consultant

Environmental Effects and Fatigue

In corrosion fatigue, the magnitude of the cyclic stress and the number of times it is applied are not the only critical loading parameters. Time-dependent environmental effects are also of primary importance. When failure occurs by corrosion fatigue, stress cycle frequency, stress wave shape, stress amplitude, and stress ratio all affect the cracking processes, depending on the resistance to SCC of the material.

Environmental Effects on Fatigue Strength. For any given material, the fatigue strength, or fatigue life at a given value of maximum stress, generally decreases in the presence of an environment that is aggressive to the material. This effect varies widely, depending primarily on the characteristics of the material-environment combination. The environment affects the probability of fatigue crack initiation, crack growth rate, or both. For many materials, the stress range required to cause fatigue failure diminishes progressively with increasing time and with the number of cycles of applied stress.

A corrosive environment reduces the crack initiation time by any form of localized attack to form a stress concentration. Corrosion attack is favored at new unfilmed metal surfaces formed at established slip bands, inclusions, second- phase particles, and so on. A clear example of the importance of stress concentration due to corrosion is illustrated in Fig. 8, which shows fatigue endurance results for plain and notched specimens of a 13% Cr ferritic steel in distilled water and saltwater. These environments are seen to cause a massive reduction in the endurance limit of the smooth specimens but only a relatively modest effect on the notched specimens. The importance of surface finish and the adverse effect of corrosion, even when only allowed to occur before a fatigue test, is of course well known and included in standard texts on fatigue test design (Ref 41).

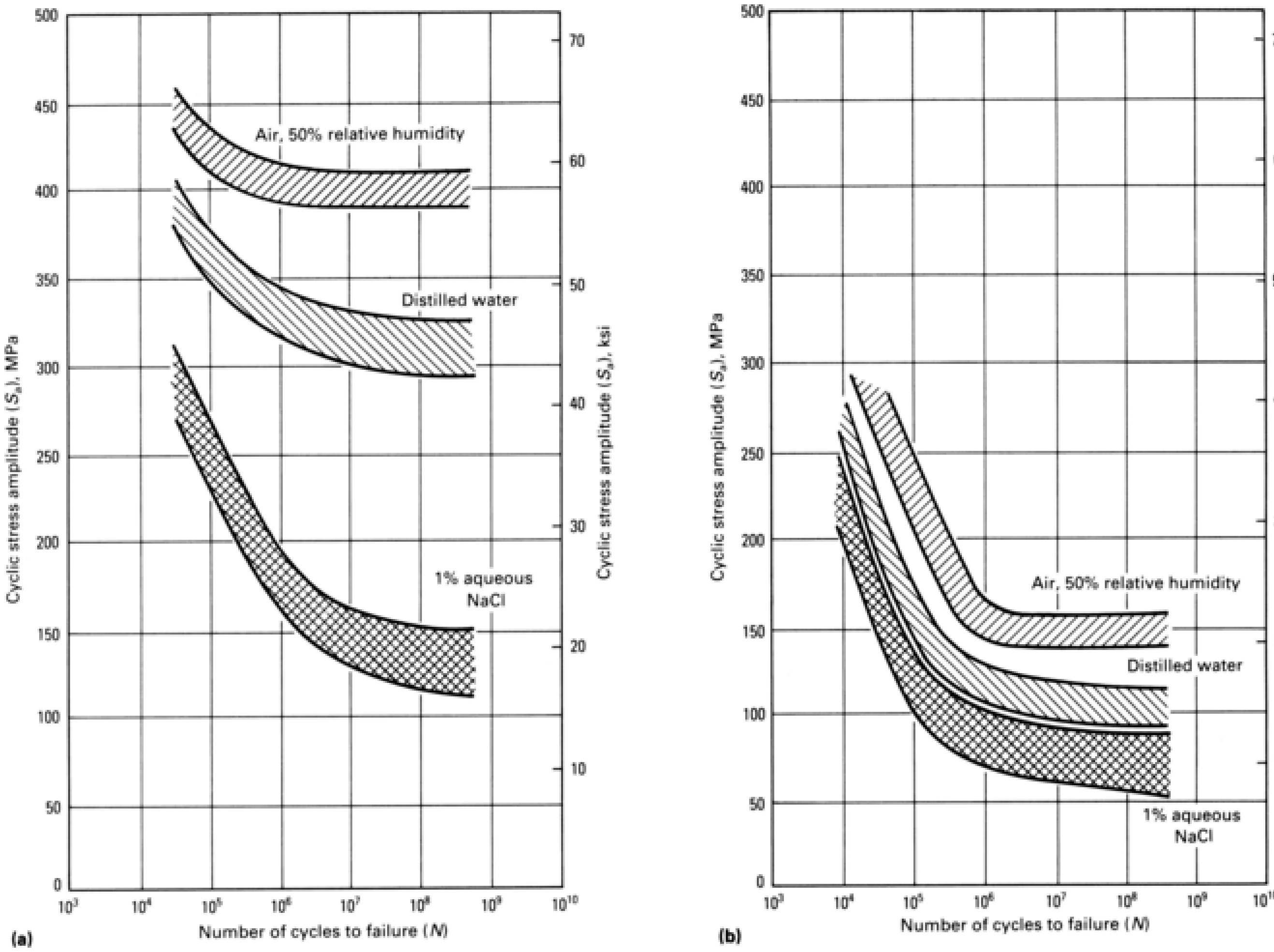

Fig. 8 Corrosion-fatigue endurance data for specimens of 13% Cr steel. Rotating bending tested (mean load zero) at a frequency of 50 Hz and temperature of 23 °C (73 °F). (a) Smooth specimens. (b) Notched specimens. Source: Ref 40

Effect of Frequency and Stress Wave Form. In nonaggressive environments, stress cycle frequency generally has little effect on fatigue behavior. On the other hand, in aggressive environments, fatigue strength is strongly dependent on frequency. Corrosion-fatigue strength will generally decrease as the cycle frequency is decreased. This effect is generally most prevalent at frequencies less than 10 Hz.

The frequency dependence of corrosion fatigue is thought to result from the fact that the interaction of a material with its environment is essentially a rate-controlled process. Low frequencies, especially at low strain amplitudes or when there is substantial elapsed time between changes in stress levels, allow longer times for interaction between material and environment. At high frequencies, particularly when high strain amplitude is also involved, the effects of corrosion may be masked, because contact time with the environment is short. In other words, mechanical failure due to high frequency and stress levels can occur well before significant corrosion effects can initiate and have a significant influence on the fatigue process.

The effect of stress frequency on low-cycle corrosion fatigue is also very dependent on susceptibility to SCC. For example, at low intermediate frequencies, material sensitive to SCC can fracture by the propagation of fatigue cracks; but at even lower frequencies, damage due to SCC during the period of maximum strain can become greater. In fact, the fatigue strength at extremely low frequencies can be markedly decreased. For example, in one case, for materials that were insensitive to SCC, failure occurred due to the propagation of CFC over the entire range of stress frequencies tested (0.02 to 17.3 cycles/min, or cpm) (Ref 42).

Historically, CFC is not considered to be a problem at very high frequencies. However, an ultrasonic corrosion-fatigue-testing system now exists for examining the corrosion-fatigue strength of engineering materials in the very high cycle regime (10^9 to 10^{10} cycles) typical of many design lifetimes. Central to this resonant fatigue-testing system is a high-efficiency, large-displacement piezoelectric transducer that operates at a frequency of 20 kHz. This transducer enables the accumulation of large numbers of cycles within a reasonable amount of time. The apparatus, environmental controls, and testing method are described in Ref 43.

Experimental 20 kHz and low-frequency corrosion-fatigue results obtained with this method for a number of engineering materials, including a 12% Cr stainless steel, show similar reductions in fatigue limit despite differences in frequency. The results hold for a variety of aqueous environments with and without electrochemical controls imposed during testing. The data illustrate the capabilities of the ultrasonic corrosion-fatigue technique and are analyzed to assess its advantages and limitations.

In some cases, corrosion-fatigue strength is strongly affected by the form of the stress wave as well as by the stress frequency. The period of zero stress, the period during which the stress changes, and the period of application of maximum stress in a single cycle each have an effect on the specimen life. Corrosion-fatigue damage is greatest during the period in which the stress is changing, while the protective effect of the stress-free time decreases the damage.

Effect of Stress Amplitude. In general, a low amplitude of cyclic stress favors relatively long fatigue life, permitting greater opportunity for involvement of the environment in the fatigue process. However, environmental interaction in certain alloy-environment systems may be insignificant unless the strain rate is in a critical range for SCC.

Stress amplitude must be considered together with mean stress and frequency. Low stress levels may allow more time for environmental interaction, but if the frequency is high, the crack tip may not be exposed to the environment for a time sufficient for the corrosion processes to do significant damage.

References cited in this section

40. M.O. Speidel, Corrosion Fatigue in Fe-Ni- Cr Alloys, *Proceedings of the International Conference on Stress Corrosion and Hydrogen Embrittlement of Iron-Base Alloys,* June 1973 (Unieux-Firminy, France), National Association of Corrosion Engineers, 1977, p 1071–1094

41. “Metallic Materials and Elements for Aerospace Vehicle Structures,” MIL-HDBK-5B, Vol 1, U.S. Department of Defense, Sept 1971, p 2–29

42. K. Endo and K. Komai, Effects of Stress Wave Form and Cycle Frequency on Low Cycle Corrosion Fatigue, *Corrosion Fatigue: Chemistry, Mechanics, and Microstructure,* O. Devereux, A.J. McEvily, and R.W. Staehle, Ed., Conference held at the University of Connecticut, June 1971, National Association of Corrosion Engineers, 1972, p 437–450

43. L.D. Roth and L.E. Willertz, Application of Ultrasonic Fatigue Testing Techniques to the Evaluation of the Corrosion-Fatigue Strength of Materials, *Environment-Sensitive Fracture,* STP 821, S.W. Dean, E.N. Pugh, and G.M. Ugianski, Ed., American Society for Testing and Materials, 1984, p 497–512

B. Phull, Evaluating Corrosion Fatigue, *Corrosion: Fundamentals, Testing, and Protection,* Vol 13A, *ASM Handbook,* ASM International, 2003, p 625–638

Evaluating Corrosion Fatigue

Revised by Bopinder Phull, Consultant

Crack Propagation Tests

In large structural components, the existence of a crack does not necessarily imply imminent failure of the part. Significant structural life may remain in the cyclic growth of the crack to a size at which a critical failure occurs. The objective of corrosion-fatigue crack propagation testing is to determine the rates at which subcritical cracks grow under cyclic loading before reaching a size that is critical for fracture under specified environmental conditions.

Fracture Mechanics Approach to Corrosion Fatigue

Fracture mechanics provides the basis for many modern fatigue crack growth studies. Fracture mechanics is based on the concept of similitude, in which cracks of different geometries grow at equal rates when subjected to equal near- tip driving forces, usually ΔK. ΔK is the stress- intensity range (K_{max} - K_{min}), where K is the magnitude of the mathematically ideal crack-tip stress field in a homogeneous, linear-elastic body; K is a function of applied load and crack geometry. The growth or extension of a fatigue crack under cyclic loading is principally controlled by maximum load and stress ratio (minimum/maximum stress). However, as in crack initiation, there are a number of additional factors that may exert a strong influence, especially with the presence of an aggressive environment. Most CFC growth-rate investigations attempt to follow the general provisions of standard test method ASTM E 647 (Ref 25).

In this constant-load-amplitude method, crack length is measured visually or by an equivalent method as a function of elapsed cycles, and these data are subjected to numerical analysis to establish the rate of crack growth. Crack growth rates are then expressed as a function of crack tip stress-intensity range, ΔK, which is calculated from expressions based on linear-elastic stress analysis.

Background information on the rationale for employing linear-elastic fracture mechanics for this purpose is given in Ref 44. Expressing the crack growth rate da/dN (where a is crack length and N is number of cycles) as a function of ΔK provides results that are independent of specimen geometry, and this enables the exchange and comparison of data obtained from a variety of specimen configurations and loading conditions. Moreover, this feature enables da/dN versus ΔK data to be used in the design and evaluation of engineering structures. It is important in the generation of CFC growth data, however, that there be judicious selection, monitoring, and control of mechanical, chemical, and electrochemical test variables in order to ensure that the data are truly applicable to the intended use.

Results of fatigue crack growth rate tests for many metallic structural materials have shown that complete da/dN versus ΔK curves have three distinct regions of behavior (Fig. 9). In an inert (or benign) environment, the rate of crack growth depends strongly on K at K levels approaching K_{Ic} (plane-strain fracture toughness) at the high end (region III) and at levels approaching an apparent threshold, ΔK_{th}, at the lower end (region I), with an intermediate region II that depends on some power of K or ΔK of the order of 2 to 10 (Ref 44). This is described by the power-law relationship:

$$\frac{da}{dN} = C(\Delta K)^n \quad \text{(Eq 2)}$$

where C and n are constants for a given material and stress ratio. In an aggressive environment, the CFC growth curve can be quite different from the pure fatigue curve, depending on the sensitivity of the material to the given environment and the occurrence of various static stress- fracture mechanisms. The environmental effects are quite strong above some threshold for SCC (K_{ISCC}) and may be negligible below this level (K_{ISCC} is the stress-intensity threshold for plane- strain environment-assisted cracking). In addition, certain loading factors, such as frequency, stress ratio, and stress waveform, can have marked effects on the crack growth curves in aggressive environments. Therefore, a variety of curves can be expected from the broad range of material-environment-loading systems that produce various CFC behaviors.

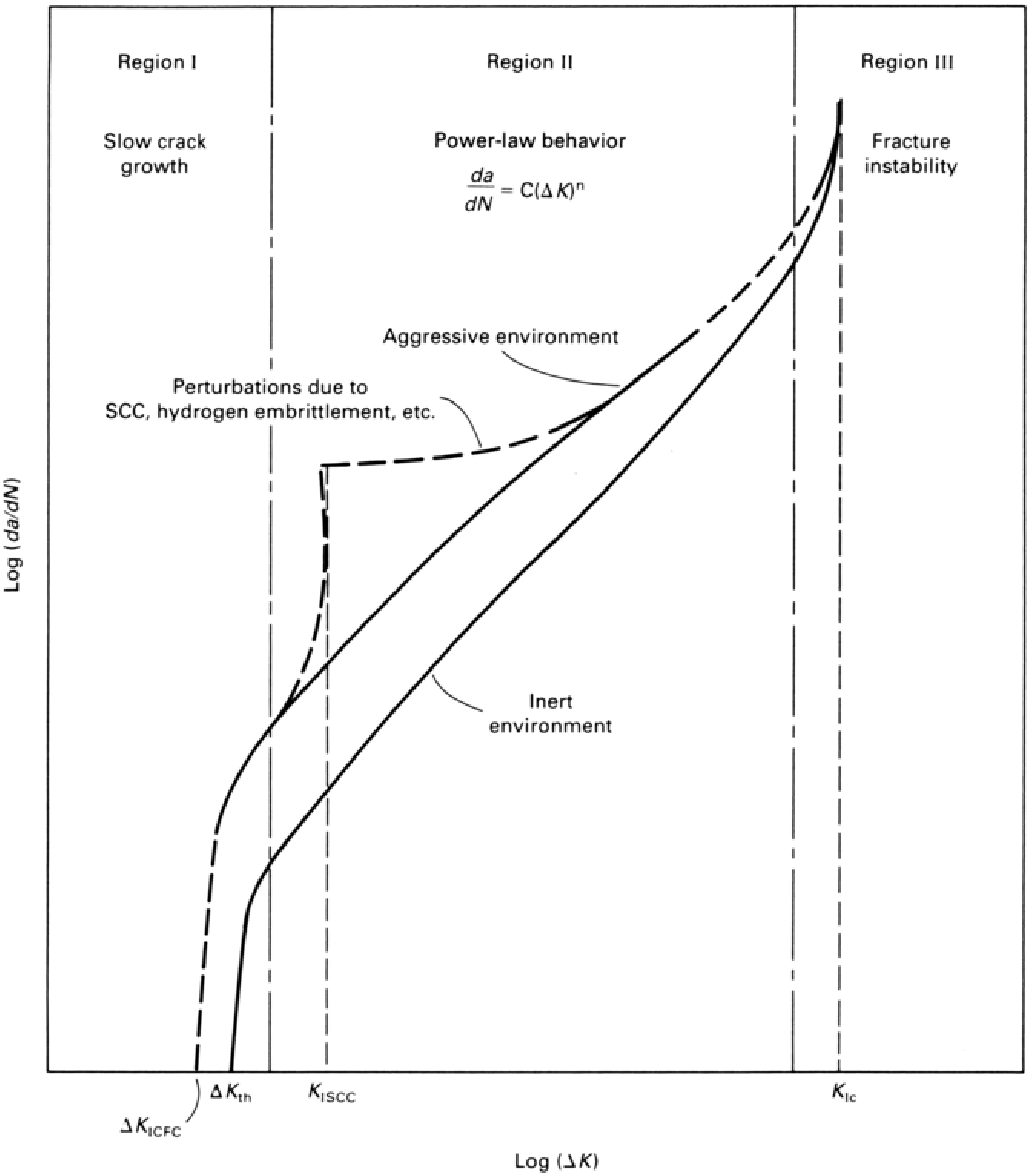

Fig. 9 Corrosion-fatigue crack propagation rate (*da*/*dN*) as a function of the cyclic crack tip stress-intensity range (Δ*K*). See the text for an explanation of the variables. Source: Ref 45

Figure 10 shows an example of a high- strength aluminum alloy with a high resistance to SCC. This alloy had a CFC growth rate ranging up to 1 order of magnitude higher in 3.5% sodium chloride (NaCl) solution compared to that in dry air. These data also illustrate that CFC behavior is similar when tested in the same environment with either a *K*-increasing (remote load) or a *K*-decreasing (wedge force) loading method.

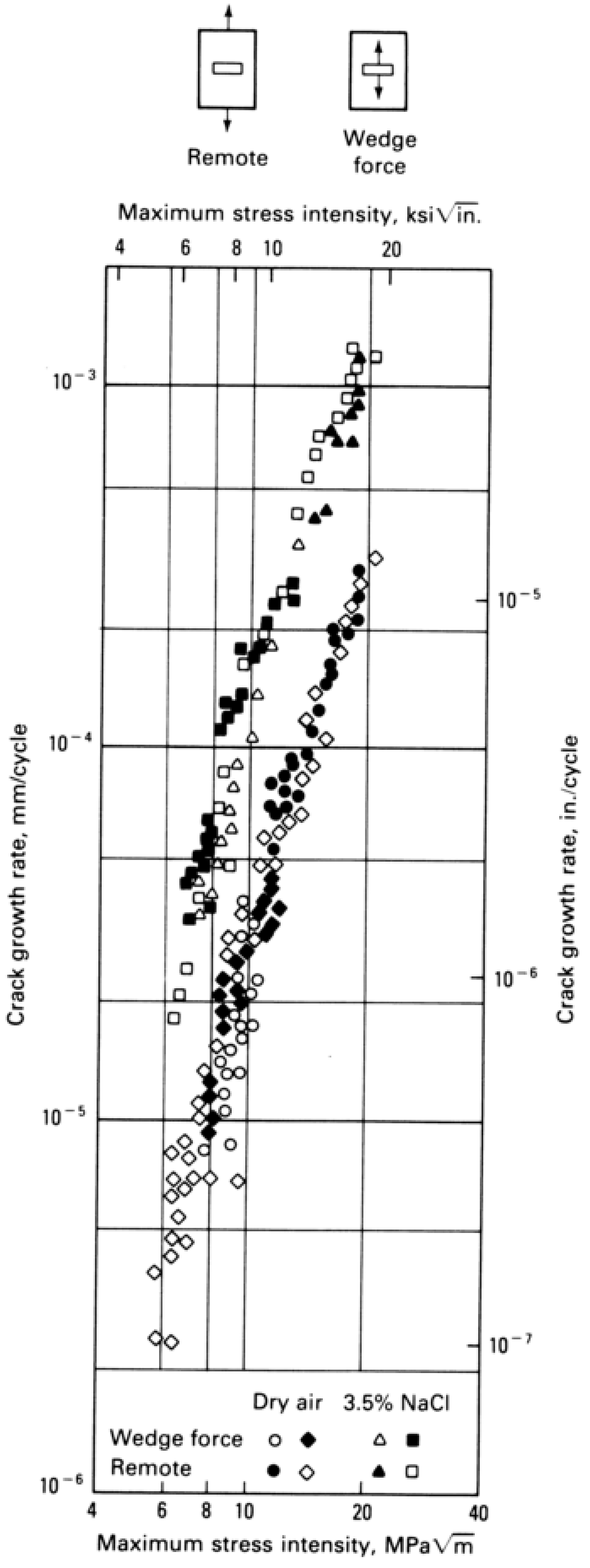

Fig. 10 Crack tip stress-intensity control of fatigue crack propagation in 7075-T6 aluminum alloy sheet—long-transverse loading. Remote and wedge force methods of loading specimens in aqueous 3.5% sodium chloride environment and benign dry air environment. Source: Ref 46

Corrosion-fatigue growth rate versus stress- intensity data have been extensively produced (Ref 2, 3, 4, 5, 6, 7, 8, 47, 48) and can be used for mitigating corrosion fatigue from several perspectives. Laboratory crack growth rate data are scalable quantitatively for predicting component performance. The da/dN versus ΔK curve for a given material and environment is integrated; it is then used in conjunction with the stress-intensity solution for a component to predict corrosion-fatigue life (Ref 44). A specific example reported in Ref 49 is illustrated in Fig. 11. The predicted 85 year life of a welded pipe is based on week-long laboratory measurements of da/dN versus ΔK for steel in an oil environment.

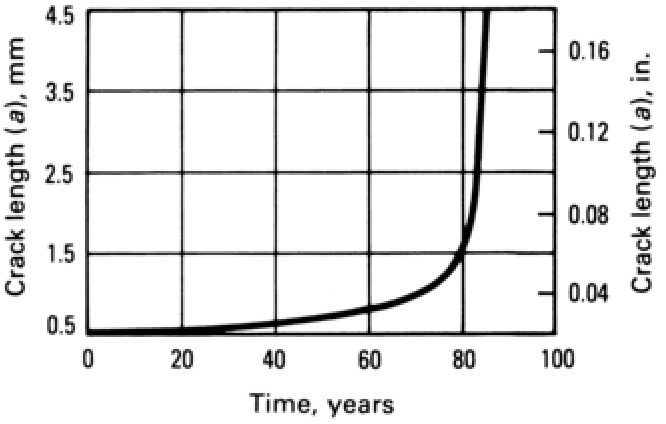

Fig. 11 Predicted fatigue crack extension from a weld toe crack in an American Petroleum Institute (API) 5LX52 carbon steel pipeline carrying hydrogen-sulfide-contaminated oil. Temperature: 23 °C (73 °F). Source: Ref 49

Alloy development for optimized corrosion- fatigue resistance, defined in terms of da/dN versus ΔK for different metallurgical conditions, is directly related to component life goals based on fracture mechanics. Similarly, the effects of mechanical and chemical variables on corrosion fatigue and component performance are defined through measured changes in crack growth rate at different applied stress-intensity levels.

Crack growth rate data are important to fundamental studies of corrosion-fatigue mechanisms. The fracture mechanics approach isolates crack propagation from initiation in terms of a precise near-tip mechanical driving force, ΔK. Crack growth rates are related directly to the kinetics of mass transport and the chemical reactions that constitute embrittlement. As shown in Fig. 12, prediction of the effect of loading frequency on crack growth rate in saltwater (normalized to vacuum) identifies important rate- limiting crack tip electrochemical reactions. Modeling and measurements in Fig. 12 provide a sound basis for extrapolating short-term laboratory data in order to predict long-term component cracking.

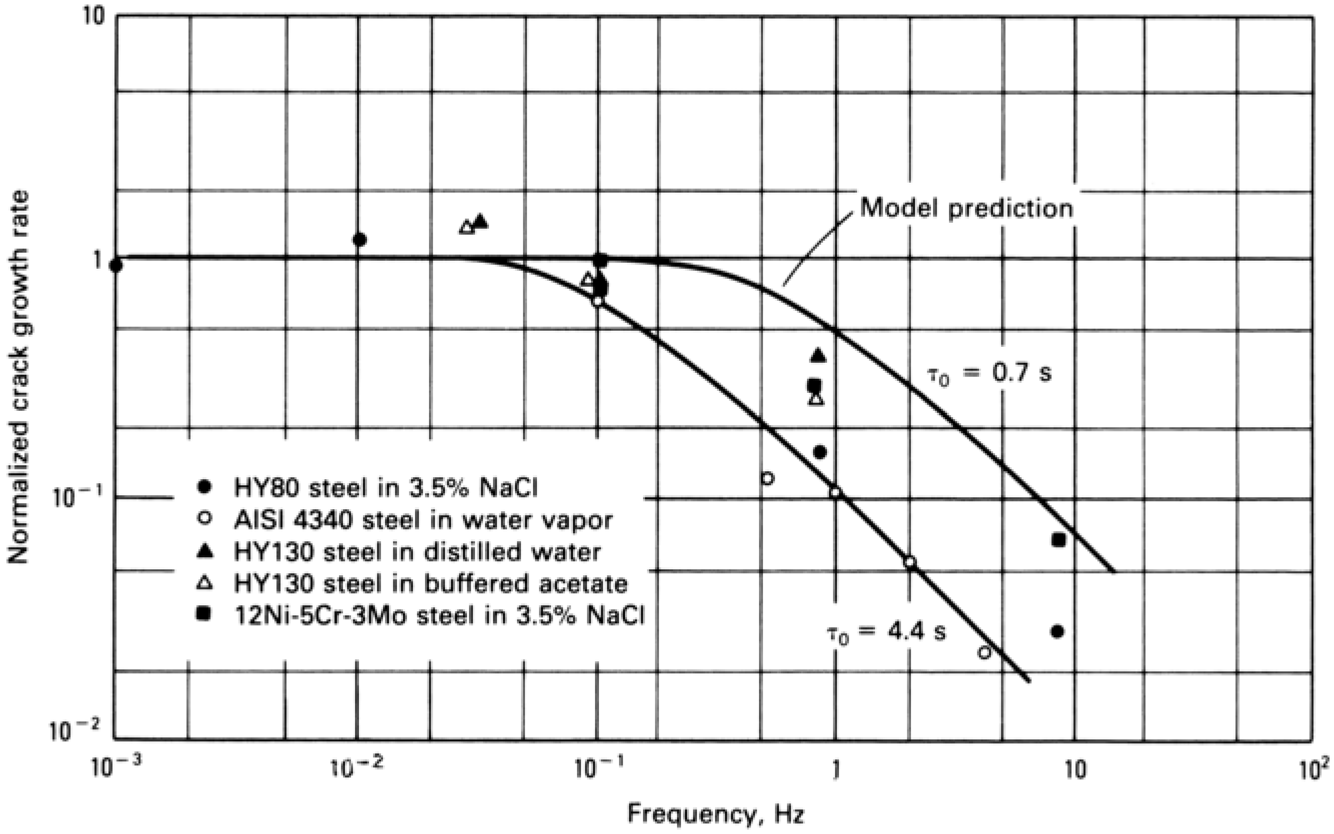

Fig. 12 Modeled effect of loading frequency on corrosion-fatigue crack growth in alloy steels in an aqueous chloride solution. The determination of the normalized crack growth rate and the time constants, τ_0, from the model can be found in Ref 50.

However, the fracture mechanics approach to corrosion fatigue is not valid in all cases. Discussion in this article is limited to crack growth in conjunction with net section elastic loading and small-scale plasticity confined to the crack tip. Studies of crack growth under large-scale cyclic plasticity have not been extended to consider environmental effects (Ref 51, 52). Also, while stress intensity provides a mechanical description of similitude, it may not completely describe crack growth because of interacting chemical and mechanical driving forces.

Results of investigations indicate that simple *K*-based approaches can be compromised for (a) small corrosion-fatigue cracks below 5 mm (0.2 in.), (b) cases in which varying crack shape and load transients alter crack chemistry and embrittlement, and (c) situations in which surface roughness or corrosion products impede crack displacement (Ref 51, 52, 53, 54, 55). Reference 51, 52, 53, 54, 55 should be consulted if an application includes plasticity, small crack, load transient, or crack closure effects.

Variables Influencing Corrosion Fatigue

Although corrosion-fatigue phenomena are diverse and specific to the environment, several variables are known to influence crack growth rate. The following factors must be considered in any study of corrosion fatigue:

- Stress-intensity range
- Load frequency
- Stress ratio
- Electrode potential in aqueous environment
- Environment composition
- Alloy composition, microstructure, and yield strength

Moreover, the effects of such variables as temperature, load history and waveform, stress state, and environment composition may be unique to specific materials and environments.

Stress-Intensity Range. Corrosion-fatigue crack growth rates generally increase with increasing stress intensity; however, the precise dependence varies markedly. It is incorrect to assume that the three regimes (near threshold, power law, and fast fracture; see Fig. 9) of fatigue cracking observed for benign environments simply shift to higher crack speeds at all ΔK levels. Although such behavior may actually occur, as illustrated in Fig. 10 for the aluminum/dry air system, the data provided in Fig. 13 and Fig. 14 are more typical of complex stress-intensity dependencies for aggressive environments.

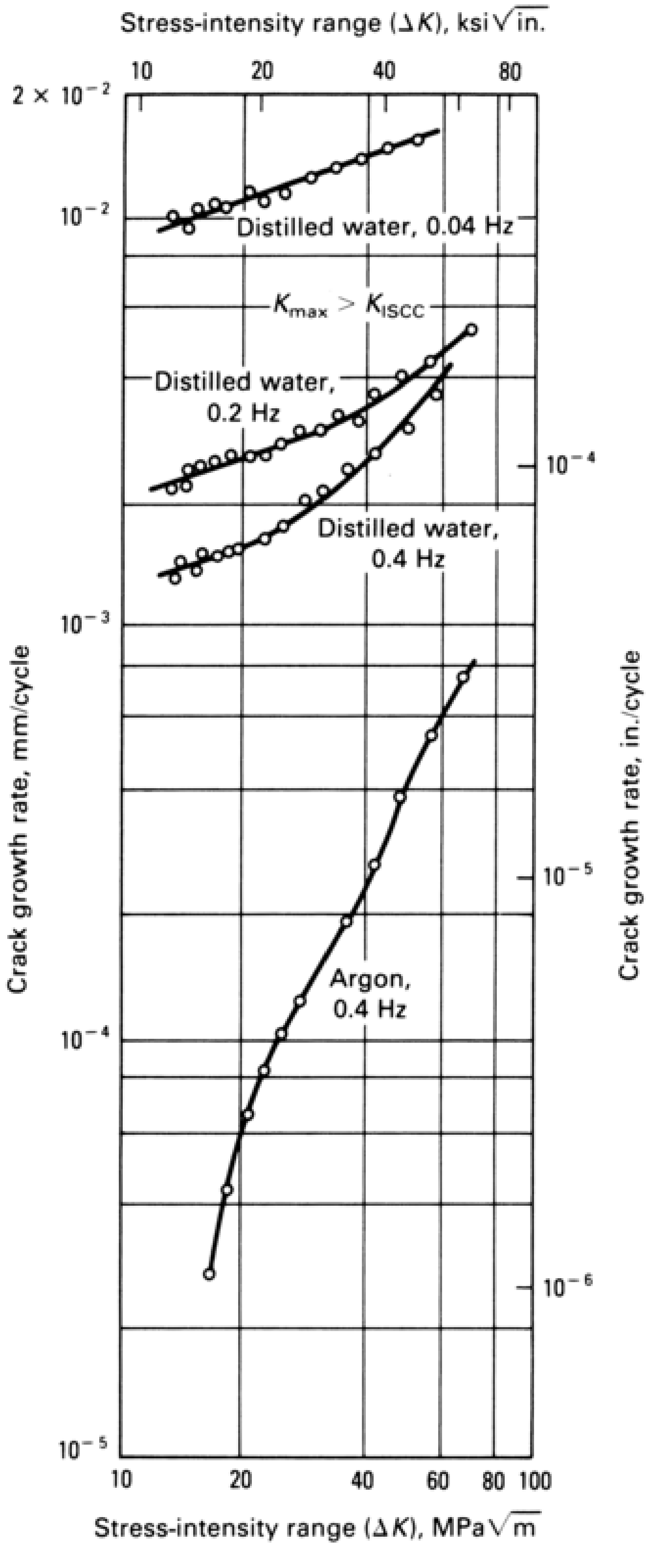

Fig. 13 Effect of stress-intensity range and loading frequency on corrosion-fatigue crack growth in ultrahigh-strength 4340 steel exposed to distilled water at 23 °C (73 °F). K_{max}, maximum stress-intensity factor; K_{ISCC}, threshold stress intensity for stress-corrosion cracking. Source: Ref 56

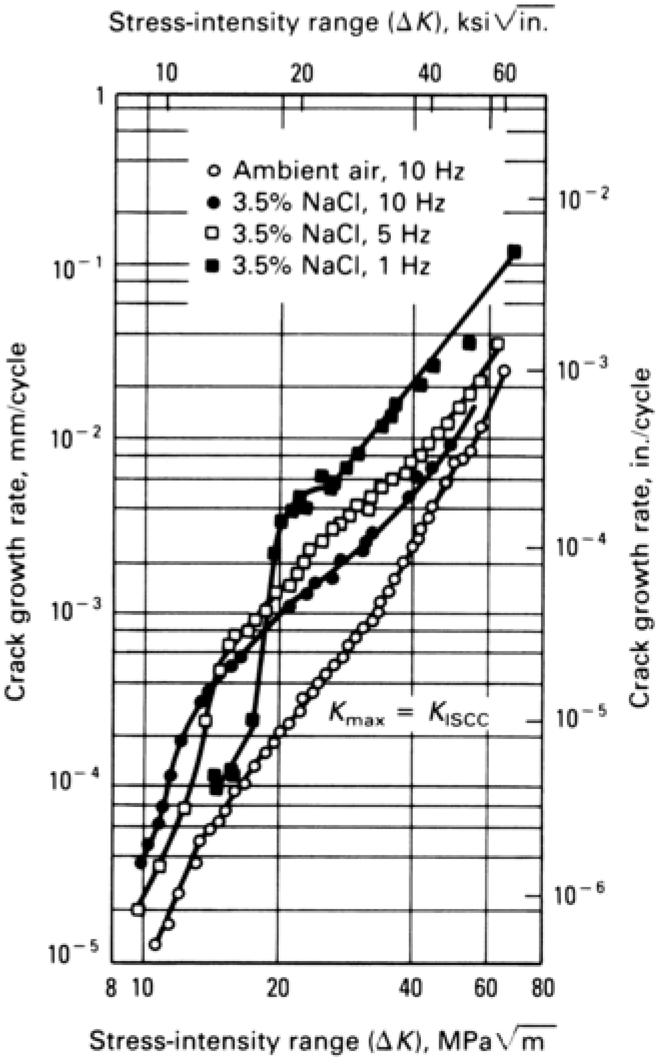

Fig. 14 Effects of stress intensity and frequency on corrosion fatigue in Ti-6Al-4V in aqueous sodium chloride at 23 °C (73 °F). Stress ratio: *R* = 0.1. K_{max}, maximum stress-intensity factor; K_{ISCC}, threshold stress intensity for stress-corrosion cracking. Source: Ref 57

Materials that are extremely environment sensitive, such as ultrahigh-strength steel in distilled water (Fig. 13), are characterized by high crack growth rates that are influenced less by ΔK. Time-dependent corrosion-fatigue crack growth occurs predominantly above the threshold stress intensity for static load cracking and is modeled through linear superposition of SCC and inert environment fatigue rates (Ref 28, 34). Time- dependent crack growth is the part of the crack extension that is attributable to the constant or rising-load portion of the cyclic load cycle, when SCC and hydrogen embrittlement mechanisms may be operative. Factors such as stress wave form and stress hold-time are particularly significant under these circumstances.

Cycle-dependent corrosion-fatigue crack propagation often occurs below the threshold for time-dependent SCC (Ref 57). Typical ΔK dependencies for this mode of cracking are complex, as illustrated in Fig. 14 for Ti-6Al-4V exposed to aqueous sodium chloride. The mechanistic implications of the various stress- intensity dependencies are detailed in Ref 28, 57, and 58. The influences of such variables as frequency, stress ratio, and metallurgical factors depend on the proportions of time- and cycle-dependent corrosion fatigue.

Frequency. The frequency of cyclic loading is the most important variable that influences CFC for most material, environment, and stress- intensity conditions. The rate of environmental cracking above that produced in vacuum generally increases with decreasing frequency. Frequencies exist above which CFC is diminished. The dominance of frequency is directly related to the time dependence of mass transport and chemical reaction steps required for environmental cracking. Basically, insufficient time is available for chemical embrittlement at rapid loading rates, that is, high frequencies, when damage is only mechanical and is equivalent to crack growth in vacuum. It is impossible to predict the frequency range at which corrosion fatigue is severe because of the numerous chemical processes. It is also difficult to extrapolate short- term (high-frequency) laboratory crack growth rate data in order to predict long-term component performance.

The literature provides qualitative guidance in terms of frequency effects on CFC. Crack growth in environmentally sensitive materials stressed above the stress-corrosion threshold proceeds at rapidly increased rates with decreasing frequency, as illustrated in Fig. 13. The frequency effect is predicted through the integration of static load data throughout each load cycle (Ref 50). For such systems, the chemical contribution to fatigue cracking is suppressed above 0.5 to 5 Hz, with higher critical frequencies associated with more aggressive environments and sensitive microstructures.

Frequency effects on cycle-dependent cracking are complex and unpredictable. The data given in Fig. 12 and 14 provide typical examples. For steels in saltwater (Fig. 12), CFC is suppressed at approximately 10 Hz. Crack speed increases with decreasing frequency and reaches a plateau between 0.5 and 0.1 Hz. In contrast, CFC in Ti-6Al-4V occurs at loading frequencies at least as high as 10 Hz (Fig. 14).

Stress Ratio. The rates of corrosion-fatigue crack propagation generally are increased by higher stress ratios. The deleterious effect of increased stress ratio is illustrated in Fig. 15 for carbon steel stressed cyclically in pressurized nuclear reactor water at 288 °C (550 °F). The extent of the corrosion-fatigue effect relative to dry air increased from approximately a factor of 4 at low *R* (0.11 to 0.24) to as much as 20- to 30-fold at high *R* (0.61 to 0.71) (Ref 59). Corrosion fatigue in this system probably proceeds by repeated passive film formation and rupture. Increased stress ratio at constant ΔK results in increased crack tip strain and strain rate, enhanced film rupture, and therefore increased corrosion-fatigue crack propagation (Ref 60).

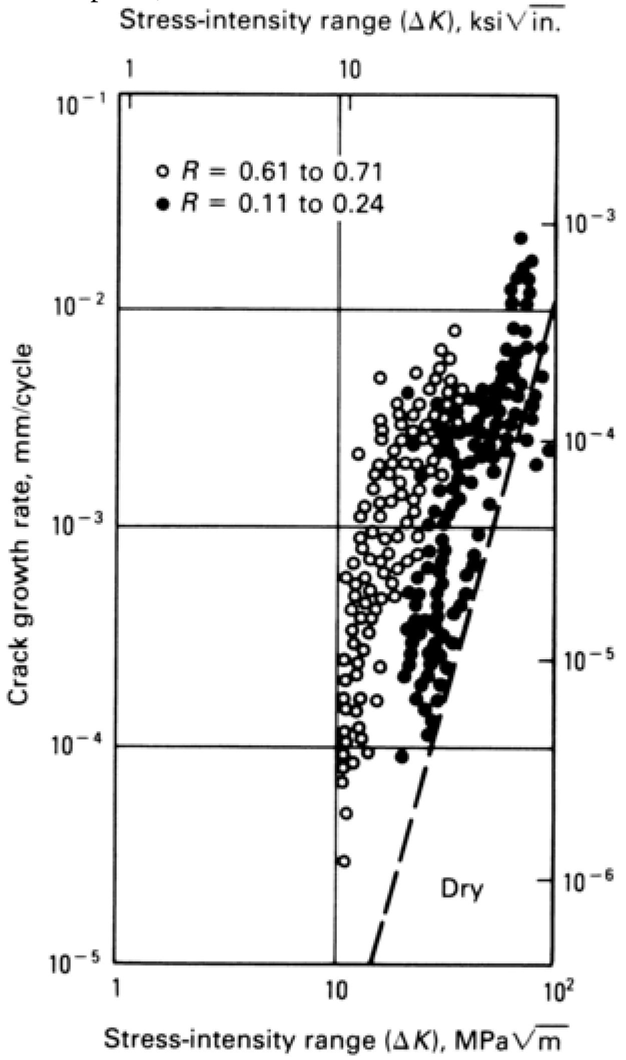

Fig. 15 Effect of stress ratio (*R*) on corrosion-fatigue crack propagation in ASTM A533 B and A508 carbon steels exposed to pressurized high-purity water at 288 °C (550 °F). Frequency: 0.017 Hz. Average behavior in air is represented by the dashed line labeled "Dry." Source: Ref 59

Electrode Potential. Like loading frequency, electrode potential strongly influences rates of corrosion-fatigue crack propagation for alloys in aqueous environments. Controlled changes in the potential of a specimen can result in either the complete elimination or the dramatic increase of fatigue cracking. The precise influence

depends on the mechanism of the environmental effect and on the anodic or cathodic magnitude of the applied potential.

For ferrous alloys that crack by hydrogen embrittlement when stressed in aqueous solutions, CFC is increased by high cathodic polarization from the free corrosion potential. Specific data are given in Fig. 16 for three steels stressed at constant ΔK in aqueous chloride environments (Ref 51, 61, 62). For each steel, the crack growth rate in saltwater is approximately three times faster than that reported for air at the free corrosion potential and is enhanced by a factor of 5 at a very high cathodic potential. For the low- strength BS4360:50D grade (similar to Unified Numbering System, or UNS, K02601), intermediate potentials appear to be mildly beneficial. Corrosion fatigue parallels electrode-potential- induced changes in the amount of cathodically evolved hydrogen in the crack tip. Precise modeling of this reaction sequence is complex and only partially completed (Ref 63).

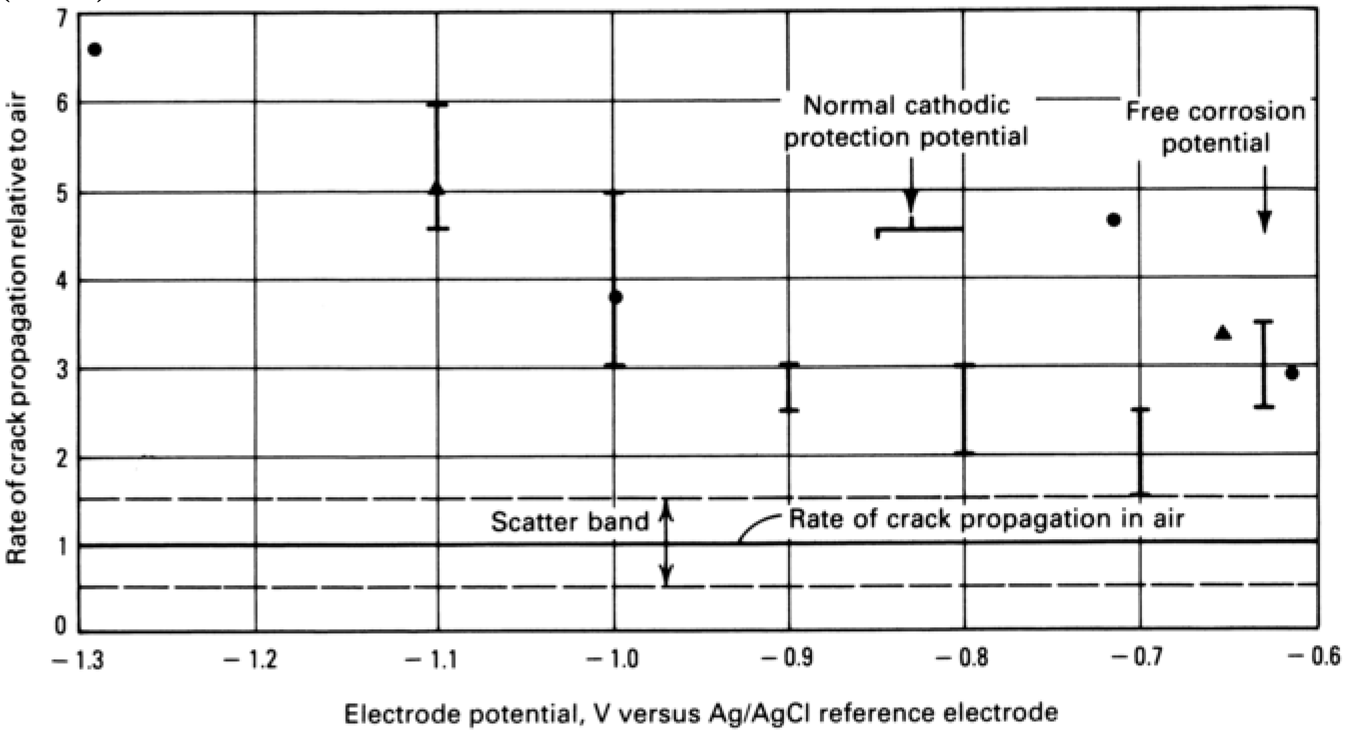

Fig. 16 Effect of applied electrode potential on corrosion-fatigue crack propagation in several steels exposed to seawater or 3% sodium chloride at constant ΔK between 20 and 40 MPa$\sqrt{m}$ (18 and 36 ksi$\sqrt{in.}$). Temperature: 23 °C (73 °F); frequency: 0.1 Hz; stress ratio: R = 0.1[ep[ol6p]

Material tested	Symbol	Yield strength MPa	Yield strength ksi	Environment	Ref
BS4360:50D	I	450	65	Seawater	60
HY80	•	600	85	3% NaCl	61
AISI 4130	▲	750	110	3% NaCl	62

Electrode potential control can suppress corrosion fatigue for alloys that crack through anodic dissolution/film rupture or anion adsorption mechanisms (Ref 64). For example, corrosion fatigue of austenitic stainless steel in chloride solutions at elevated temperatures is probably suppressed by polarization active to the critical potential for SCC.

Another example is illustrated in Fig. 17. Aluminum alloy 7079-T651 is degraded by corrosion fatigue in several aqueous halide solutions at the free corrosion potential. Compared to dry argon, cracking in potassium iodide is enhanced by more than an order of magnitude (Fig. 17a). The CFC growth rate was further increased by anodic polarization at potentials more electropositive than -0.6 V versus standard hydrogen electrode (SHE) but was suppressed by cathodic polarization (Fig. 17b).

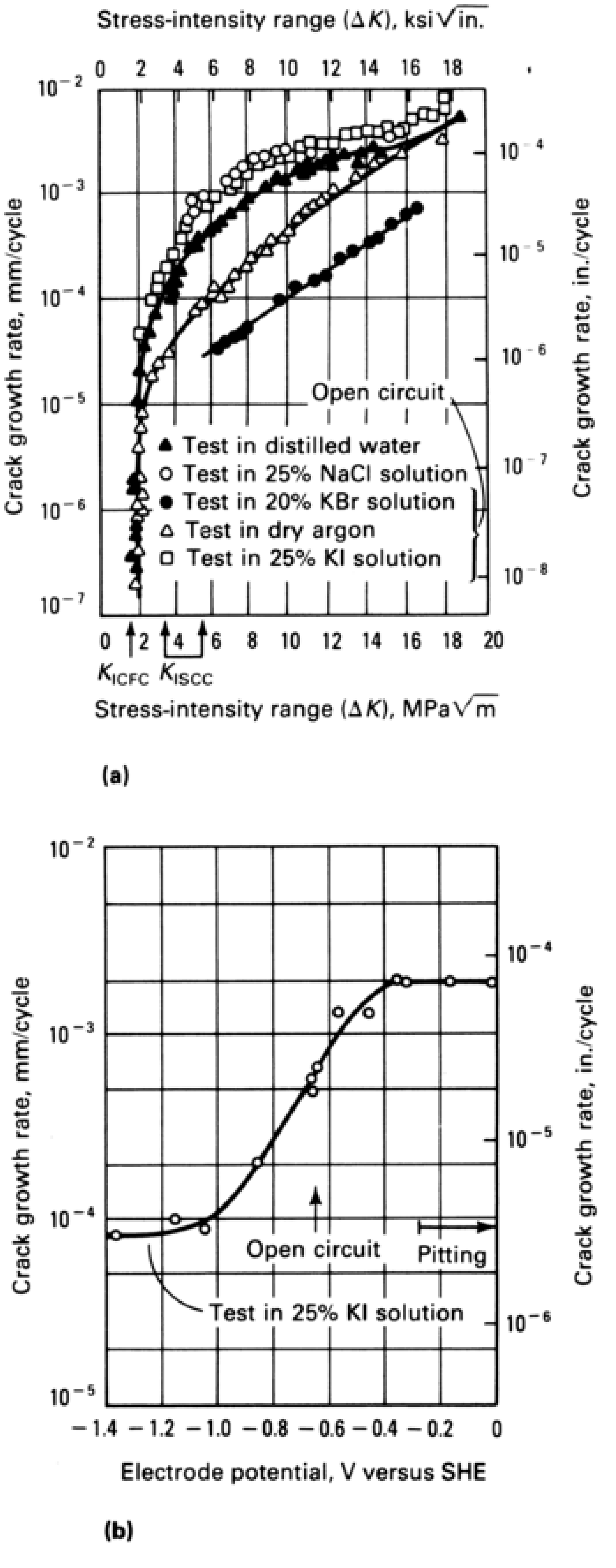

Fig. 17 Corrosion-fatigue behavior of aluminum alloy 7079-T651 plate (S-L orientation). Temperature: 23 °C (73 °F); frequency: 4 cycles/s; stress ratio: R = 0. (a) Effect of stress- intensity range on crack growth rate Threshold stress intensity for corrosion-fatigue cracking (K_{ICFC}) and a range of threshold intensity for stress-corrosion cracking (K_{ISCC}) are indicated at the bottom. (b) Effect of electrode

potential at ΔK of 6.7 MPa $\sqrt{m}$(6 ksi $\sqrt{in.}$) in 25% potassium iodide solution. SHE, standard hydrogen electrode. Source: Ref 65

Electrode potential should be monitored and, if appropriate, maintained constant during corrosion-fatigue testing. Apparent effects of variables, such as the dissolved oxygen content of the solution, flow rate, ion concentration, and alloy composition on corrosion fatigue, can often be traced to changing electrode potential.

Crack Closure Effects. Premature crack surface contact during unloading, or crack closure, can greatly reduce rates of fatigue crack propagation. The true (or effective) crack tip driving force is reduced below the applied Δ*K* because of the reduced crack tip displacement range. Closure phenomena are produced by a variety of mechanisms and are particularly relevant to fatigue crack propagation in the near-threshold regime, after large load excursions, and for embrittling corrosive mechanisms, as reviewed in Ref 53, 66, and 67.

Two mechanisms of crack closure are relevant to corrosion fatigue. Rough, intergranular crack surfaces, typical of environmental embrittlement, promote crack closure because uniaxially loaded cracks open in a complex three-dimensional mode, allowing for surface interactions and load transfer. Roughness-induced closure is most relevant to corrosion fatigue at low Δ*K* and at stress ratio levels where absolute crack opening displacements (0.5 to 3 μm) are less than fractured grain heights (5 to 50 μm).

Alternatively, crack closing is impeded by dense corrosion products within the pulsating fatigue crack. For mildly oxidizing environments, such as moist air, this closure mechanism is relevant at low stress-intensity levels and contributes to the formation of a threshold, as described in Ref 67.

For corrosive bulk environments, cracking at high Δ*K* values may be retarded below growth rates observed for air or vacuum due to corrosion product formation within the crack. The engineering significance of beneficial crack closure influences depends on the stability of the corrosion product during complex tension-compression loading and fluid conditions. An example of crack closure is presented in Fig. 18 for ASTM A 471 steel exposed to either moist air or steam at 100 °C (212 °F). Crack growth is reduced for the latter environment because of crack surface oxidation and enhanced closure. It should be noted that oxide-induced closure influences cracking even at a relatively high stress ratio of 0.35. The data presented in Fig. 18 were obtained at a high loading frequency of 100 Hz, and chemically enhanced crack growth was essentially precluded.

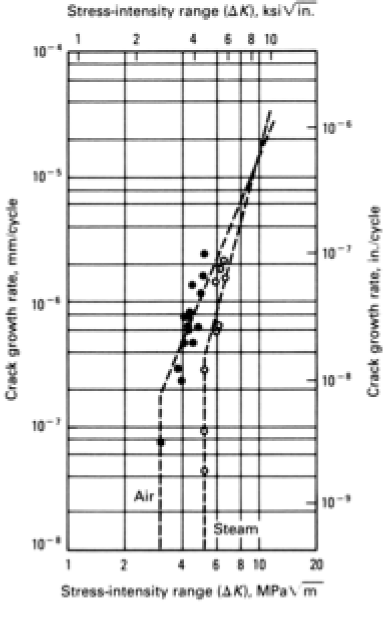

Fig. 18 Corrosion-fatigue crack propagation in ASTM A 471 steel exposed to moist air and steam. Temperature: 100 °C (212 °F); frequency: 100 Hz; stress ratio: *R* = 0.35. Source: Ref 68

Crack growth at lower frequencies could be deleteriously influenced by metal embrittlement and beneficially influenced by increased oxide formation and closure. The complexity of predicting environmentally enhanced cracking is clear, as emphasized by data given in Fig. 19 for a 2.25Cr-1Mo steel (ASTM A 542, class 3) stressed in dry hydrogen at 23 °C (73 °F). At high Δ*K* levels and low loading frequencies, cracking was accelerated in hydrogen as compared to moist air. This was due to classical hydrogen embrittlement. For low stress intensities, cracking was also increased by hydrogen exposure; however, the effect was not due to hydrogen embrittlement because of the rapid loading frequencies. Oxides form on crack surfaces through a

fretting mechanism during cycling in air, and crack growth rates are reduced by oxide-induced closure. However, oxide formation is precluded for cycling in pure hydrogen, crack closure is absent, and growth rates are increased relative to those in moist air. Equally rapid rates of fatigue cracking have been reported for low ΔK cycling in hydrogen and in helium. Equal rates of cracking are observed for hydrogen, helium, and moist air at high R (stress ratio) levels where closure was absent (Ref 66, 67).

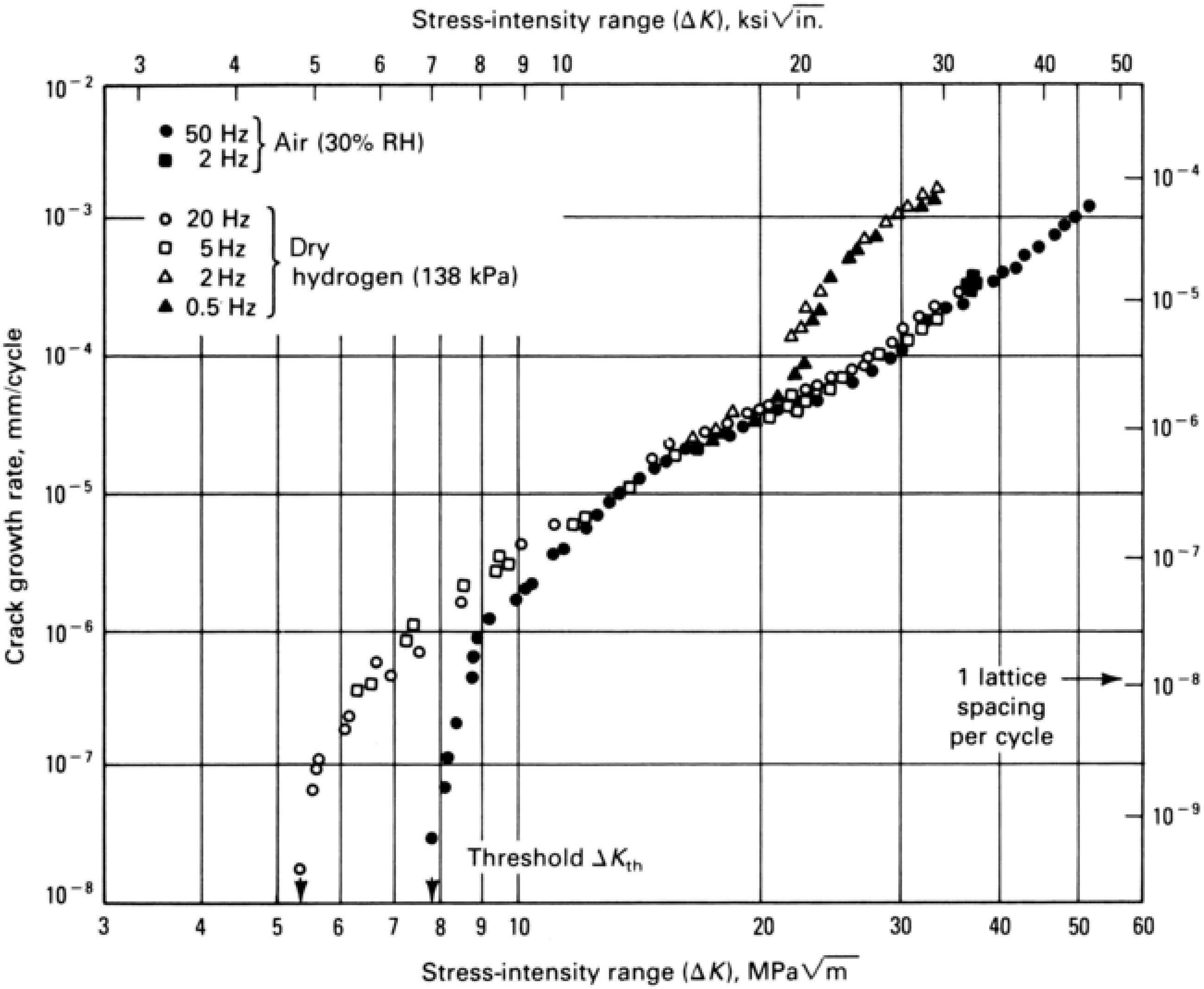

Fig. 19 Corrosion fatigue in 2.25Cr-lMo pressure vessel steel in dry hydrogen at 23 °C (73 °F) due to hydrogen embrittlement at high ΔK and to reduced oxide-induced closure at low ΔK. Stress ratio: R = 0.05. RH, relative humidity. Source: Ref 66

CFC Growth Characterization

Experimental characterizations of corrosion- fatigue crack propagation are complicated by the numerous variables that influence the failure process. Both the mechanics of loading and the composition of the environment must be controlled. Standard methods of measurement and fracture mechanics analysis of fatigue crack propagation in benign environments can be found in ASTM E 647 (Ref 25).

Four problem areas are relevant to corrosion- fatigue testing. First, the environment must be contained about the cracked specimen without affecting loading, crack monitoring, or specimen-environment composition. Parameters such as environmental purity, composition, temperature, and electrode potential must be monitored and controlled.

Second, the deleterious effect of low cyclic frequency dictates that crack growth rates be measured at low frequencies (often <0.2 Hz). This leads to long test times—often several days to weeks. Load-controlled equipment, crack- monitoring sensors and signal conditioners, and test environment composition must be stable throughout long-term tests.

Third, crack length must be measured for calculations of stress intensity and crack growth rate. Optical methods are often precluded by the environment and test chamber. Indirect methods, which are based on specimen compliance (Ref 69) or electrical potential difference (Ref 70), have been successfully applied to the monitoring of crack growth in a wide variety of hostile environments. Experimental and analytical requirements, however, are complex for indirect crack monitoring.

Nonvisual techniques will often have greater accuracy and less variability in crack length measurement than optical observations. In addition, the nonvisual techniques are generally more consistent and reliable, especially where long periods of unattended testing are anticipated. Beyond that, nonvisual techniques are absolutely essential where the test temperature or the environment prohibits direct visual observation. Nonvisual methods are more precise than visual techniques and allow for automation of the test beyond the mere acquisition of the crack growth rate data (Ref 71, 72).

Finally, specimen geometry and size requirements for ΔK-based crack propagation data, which are scalable to components through similitude, have not been established completely for subcritical crack growth. In-plane yielding must be limited to the crack tip by ensuring that net section stress is below yield and that the maximum plastic zone size, defined as approximately 0.2 $(K_{max}/\sigma_{YS})^2$ (where σ_{YS} is yield strength), is much less (for example, 10- to 50- fold) than the uncracked ligament. Specimen thickness, as it influences the degree of plane-strain constraint, and crack size, as it influences the chemical driving force, may affect corrosion- fatigue crack speeds. Such effects are currently unpredictable, and specimen thickness and crack geometry must be treated as variables.

CFC Growth in Specific Environments

Corrosion-fatigue crack growth studies in aqueous solutions and gaseous environments at ambient temperature present fewer problems experimentally than many of the other environments considered in this article. Nevertheless, simulation of practical conditions in relation to a specific engineering application requires careful consideration if the data are to be relevant. Similarly, in an academic investigation, comparison of the results of different pieces of work is possible only if the mechanical, metallurgical, and chemical variables are properly characterized and controlled. It is often the case, however, that the most frequent problem in determining the validity of corrosion-fatigue data lies with the control and monitoring of the bulk environment chemistry and the monitoring and recording of the electrochemical potential in aqueous solutions.

Corrosion-fatigue crack growth data are required for practical engineering applications in many diverse and specialized environments. An excellent overview of the following eight specific types of environments is given in *Mechanical Testing and Evaluation,* Volume 8 of *ASM Handbook,* and will not be repeated in this article:

- Vacuum and gaseous environments at ambient temperatures
- Vacuum and oxidizing gases at elevated temperatures
- Aqueous solutions at ambient temperatures
- Acidified chloride environments at ambient and elevated temperatures
- High-temperature pure water under aerated conditions
- High-temperature pure water under deaerated conditions
- Liquid metal environments
- Steam or boiling water with contaminants

References cited in this section

2. O. Devereux, A.J. McEvily, and R.W. Staehle, Ed., *Corrosion Fatigue—Chemistry, Mechanics, and Microstructure,* Proceedings of NACE Conference, June 1971 (Storrs, CT), National Association of Corrosion Engineers, 1972

3. H.L. Craig, Jr., T.W. Crooker, and D.W. Hoeppner, Ed., *Corrosion-Fatigue Technology,* STP 642, American Society for Testing and Materials, 1978

4. R.W. Staehle and M.O. Speidel, Ed., *Stress Corrosion and Corrosion Fatigue Handbook,* ARPA Contract M00014-75-C-0703, Advanced Research Project Agency of the Department of Defense

5. P.R. Swann, F.P. Ford, and A.R.C. Westwood, Ed., *Mechanisms of Environment Sensitive Cracking of Materials,* Proceedings of Metals Society Conference, April 1977 (University of Surrey, U.K.), The Metals Society, 1979

6. R.N. Parkins and Ya. M. Kolotyrkin, Ed., *Corrosion Fatigue,* Proceedings of the First USSR-U.K. Seminar on Corrosion Fatigue of Metals, May 1980 (Lvov, USSR), The Metals Society, 1983

7. T.W. Crooker and B.N. Leis, Ed., *Corrosion Fatigue: Mechanics, Metallurgy, Electrochemistry and Engineering,* STP 801, American Society for Testing and Materials, 1983

8. S.W. Dean, E.N. Pugh, and G.M. Ugiansky, Ed., *Environment-Sensitive Fracture,* STP 821, American Society for Testing and Materials, 1984

25. "Standard Test Method for Measurement of Fatigue Crack Growth Rates," ASTM E 647, *Metals—Mechanical Testing; Elevated and Low-Temperature Tests; Metallography,* Vol 03.01, *2002 Annual Book of ASTM Standards,* American Society for Testing and Materials, 2002

28. "Standard Guide for Evaluating Data Acquisition Systems Used in Cyclic Fatigue and Fracture Mechanics Testing," ASTM E 1942, *Metals—Mechanical Testing; Elevated and Low-Temperature Tests; Metallography,* Vol 03.01, *2002 Annual Book of ASTM Standards,* American Society for Testing and Materials, 2002

34. R.E. Peterson, *Stress Concentration Design Factors,* John Wiley & Sons, 1974

44. A.J. McEvily and R.P. Wei, Fracture Mechanics and Corrosion Fatigue, *Corrosion Fatigue: Chemistry, Mechanics and Microstructure,* O. Devereux, A.J. McEvily, and R.W. Staehle, Ed., National Association of Corrosion Engineers, 1973, p 381–395

45. P.M. Scott, Chemistry Effects in Corrosion Fatigue, *Corrosion Fatigue: Mechanics, Metallurgy, Electrochemistry and Engineering,* STP 801, T.W. Crooker and B.N. Leis, Ed., American Society for Testing and Materials, 1983, p 319–350

46. J.A. Feeney, J.C. McMillan, and R.P. Wei, Environmental Fatigue Crack Propagation of Aluminum Alloys at Low Stress Intensity Levels, *Metall. Trans.,* Vol 1, 1970, p 1741–1757

47. *Corrosion Cracking,* Proceedings of International Conference on Fatigue, Corrosion Cracking, Fracture Mechanics and Failure Analysis, Dec 1985 (Salt Lake City, UT), American Society for Metals, 1986

48. Z.A. Foroulis, Ed., *Environment-Sensitive Fracture of Engineering Materials,* The Metals Society and the American Institute of Mining, Metallurgical, and Petroleum Engineers, 1978

49. O. Vosikovsky and R.J. Cooke, An Analysis of Crack Extension by Corrosion Fatigue in a Crude Oil Pipeline, *Int. J. Pressure Vessels Piping,* Vol 6, 1978, p 113–129

50. R.P. Wei and G. Shim, Fracture Mechanics and Corrosion Fatigue, *Corrosion Fatigue: Mechanics, Metallurgy, Electrochemistry and Engineering,* STP 801, T.W. Crooker and B.N. Leis, Ed., American Society for Testing and Materials, 1984, p 5–25

51. M.H. El Haddad, T.H. Topper, and B. Mukherjee, Review of New Developments in Crack Propagation Studies, *J. Test Eval.,* Vol 9, 1981, p 65–81

52. N.E. Dowling, Crack Growth During Low Cycle Fatigue of Smooth Axial Specimens, *Cyclic Stress-Strain and Plastic Deformation Aspects of Fatigue Crack Growth,* STP 637, American Society for Testing and Materials, 1977, p 97–121

53. R.P. Gangloff and R.O. Ritchie, Environmental Effects Novel to the Propagation of Short Fatigue Cracks, *Fundamentals of Deformation and Fracture,* K.J. Miller, Ed., Cambridge University Press, 1987

54. S.J. Hudak, Jr. and R.P. Wei, Consideration of Nonsteady State Crack Growth in Material Evaluation and Design, *Int. J. Pressure Vessels Piping,* Vol 9, 1981, p 63–74

55. R.P. Gangloff, Crack Size Effects on the Chemical Driving Force for Aqueous Corrosion Fatigue, *Metall. Trans. A,* 1987

56. C.S. Kortovich, Corrosion Fatigue of 4340 and D6AC Steels Below K_{ISCC}, *Proceedings of the 1974 Triservice Conference on Corrosion of Military Equipment,* AFML-TR- 75-42, Air Force Materials Laboratory, Wright-Patterson Air Force Base, 1975

57. D.B. Dawson and R.M. Pelloux, Corrosion Fatigue Crack Growth of Titanium Alloys in Aqueous Environments, *Metall. Trans. A,* Vol 5, 1974, p 723–731

58. J.M. Barsom, Corrosion Fatigue Crack Propagation Below K_{ISCC}, *Eng. Fract. Mech.,* Vol 3, 1971, p 15–25

59. B. Tompkins and P.M. Scott, Environment Sensitive Fracture: Design Considerations, *Met. Technol.,* Vol 9, 1982, p 240–248

60. P.M. Scott, Effects of Environment on Crack Propagation, *Developments in Fracture Mechanics—II,* G.G. Shell, Ed., Applied Science, 1979, p 221–257

61. J.P. Gallagher, "Corrosion Fatigue Crack Growth Rate Behavior Above and Below K_{ISCC}," Report NRL-7064, Naval Research Laboratory, 1970

62. R.P. Gangloff, Exxon Research and Engineering Company, unpublished research, 1984

63. A. Turnbull, Progress in the Understanding of the Electrochemistry in Cracks, *Embrittlement by the Localized Crack Environment,* R.P. Gangloff, Ed., The Metals Society and the American Institute of Mining, Metallurgical, and Petroleum Engineers, 1984, p 3–31

64. R.N. Parkins, Prevention of Environment Sensitive Cracking by Inhibition, *Embrittlement by the Localized Crack Environment,* R.P. Gangloff, Ed., The Metals Society and the American Institute of Mining, Metallurgical, and Petroleum Engineers, 1984, p 385–404

65. M.O. Speidel, M.J. Blackburn, T.R. Beck, and J.A. Feeney, Corrosion Fatigue and Stress Corrosion Crack Growth in High Strength Aluminum Alloys, Magnesium Alloys and Titanium Alloys Exposed to Aqueous Solutions, *Corrosion Fatigue: Chemistry, Mechanics and Microstructure,* O. Devereux, A.J. McEvily, and R.W. Staehle, Ed., National Association of Corrosion Engineers, 1973, p 324–345

66. R.O. Ritchie, Application of Fracture Mechanics to Fatigue, Corrosion Fatigue and Hydrogen Embrittlement, *Analytical and Experimental Fracture Mechanics,* G.C. Sih, Ed., Sithoff and Noorohoff, 1981, p 81–108

67. S. Suresh and R.O. Ritchie, The Propagation of Short Fatigue Cracks, *Int. Met. Rev.,* 1987

68. L.K.L. Tu and B.B. Seth, Threshold Corrosion Fatigue Crack Growth in Steels, *J. Test. Eval.,* Vol 6, 1978, p 66–74

69. S.J. Hudak, Jr. and R.J. Bucci, Ed., *Fatigue Crack Growth Measurement and Data Analysis,* STP 738, American Society for Testing and Materials, 1981

70. R.P. Gangloff, Electrical Potential Monitoring of the Formation and Growth of Small Fatigue Cracks in Embrittling Environments, *Advances in Crack Length Measurement,* C.J. Beevers, Ed., Engineering Materials Advisory Services, 1982, p 175–230

71. J.K. Donald, Fatigue Crack Propagation and the Role of Automated Testing, *ASTM Stand. News,* Vol 13 (No. 11), Nov 1985, p 50–53

72. C.J. Beevers, Ed., *Advances in Crack Length Assessment,* Engineering Materials Advisory Service, 1982

B. Phull, Evaluating Corrosion Fatigue, *Corrosion: Fundamentals, Testing, and Protection*, Vol 13A, *ASM Handbook*, ASM International, 2003, p 625–638

Evaluating Corrosion Fatigue

Revised by Bopinder Phull, Consultant

Crack Propagation Tests

In large structural components, the existence of a crack does not necessarily imply imminent failure of the part. Significant structural life may remain in the cyclic growth of the crack to a size at which a critical failure occurs. The objective of corrosion-fatigue crack propagation testing is to determine the rates at which subcritical cracks grow under cyclic loading before reaching a size that is critical for fracture under specified environmental conditions.

Fracture Mechanics Approach to Corrosion Fatigue

Fracture mechanics provides the basis for many modern fatigue crack growth studies. Fracture mechanics is based on the concept of similitude, in which cracks of different geometries grow at equal rates when subjected to equal near- tip driving forces, usually ΔK. ΔK is the stress- intensity range (K_{max} - K_{min}), where K is the magnitude of the mathematically ideal crack-tip stress field in a homogeneous, linear-elastic body; K is a function of applied load and crack geometry. The growth or extension of a fatigue crack under cyclic loading is principally controlled by maximum load and stress ratio (minimum/maximum stress). However, as in crack initiation, there are a number of additional factors that may exert a strong influence, especially with the presence of an aggressive environment. Most CFC growth-rate investigations attempt to follow the general provisions of standard test method ASTM E 647 (Ref 25).

In this constant-load-amplitude method, crack length is measured visually or by an equivalent method as a function of elapsed cycles, and these data are subjected to numerical analysis to establish the rate of crack growth. Crack growth rates are then expressed as a function of crack tip stress-intensity range, ΔK, which is calculated from expressions based on linear-elastic stress analysis.

Background information on the rationale for employing linear-elastic fracture mechanics for this purpose is given in Ref 44. Expressing the crack growth rate da/dN (where a is crack length and N is number of cycles) as a function of ΔK provides results that are independent of specimen geometry, and this enables the exchange and comparison of data obtained from a variety of specimen configurations and loading conditions. Moreover, this feature enables da/dN versus ΔK data to be used in the design and evaluation of engineering structures. It is important in the generation of CFC growth data, however, that there be judicious selection, monitoring, and

control of mechanical, chemical, and electrochemical test variables in order to ensure that the data are truly applicable to the intended use.

Results of fatigue crack growth rate tests for many metallic structural materials have shown that complete da/dN versus ΔK curves have three distinct regions of behavior (Fig. 9). In an inert (or benign) environment, the rate of crack growth depends strongly on K at K levels approaching K_{Ic} (plane-strain fracture toughness) at the high end (region III) and at levels approaching an apparent threshold, ΔK_{th}, at the lower end (region I), with an intermediate region II that depends on some power of K or ΔK of the order of 2 to 10 (Ref 44). This is described by the power-law relationship:

$$\frac{da}{dN} = C(\Delta K)^n \quad \text{(Eq 2)}$$

where C and n are constants for a given material and stress ratio. In an aggressive environment, the CFC growth curve can be quite different from the pure fatigue curve, depending on the sensitivity of the material to the given environment and the occurrence of various static stress- fracture mechanisms. The environmental effects are quite strong above some threshold for SCC (K_{ISCC}) and may be negligible below this level (K_{ISCC} is the stress-intensity threshold for plane- strain environment-assisted cracking). In addition, certain loading factors, such as frequency, stress ratio, and stress waveform, can have marked effects on the crack growth curves in aggressive environments. Therefore, a variety of curves can be expected from the broad range of material-environment-loading systems that produce various CFC behaviors.

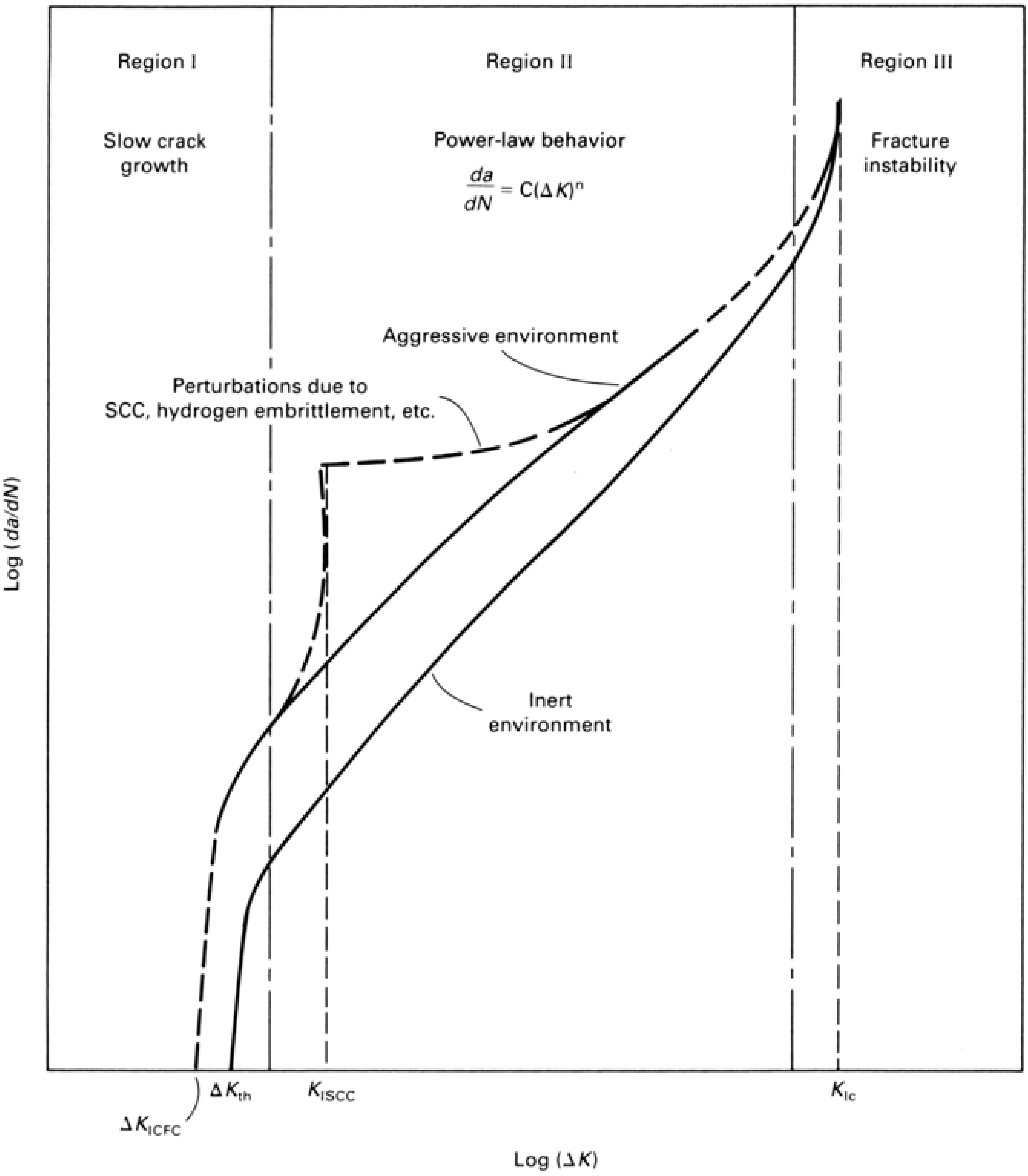

Fig. 9 Corrosion-fatigue crack propagation rate (*da*/*dN*) as a function of the cyclic crack tip stress-intensity range (Δ*K*). See the text for an explanation of the variables. Source: Ref 45

Figure 10 shows an example of a high- strength aluminum alloy with a high resistance to SCC. This alloy had a CFC growth rate ranging up to 1 order of magnitude higher in 3.5% sodium chloride (NaCl) solution compared to that in dry air. These data also illustrate that CFC behavior is similar when tested in the same environment with either a *K*-increasing (remote load) or a *K*-decreasing (wedge force) loading method.

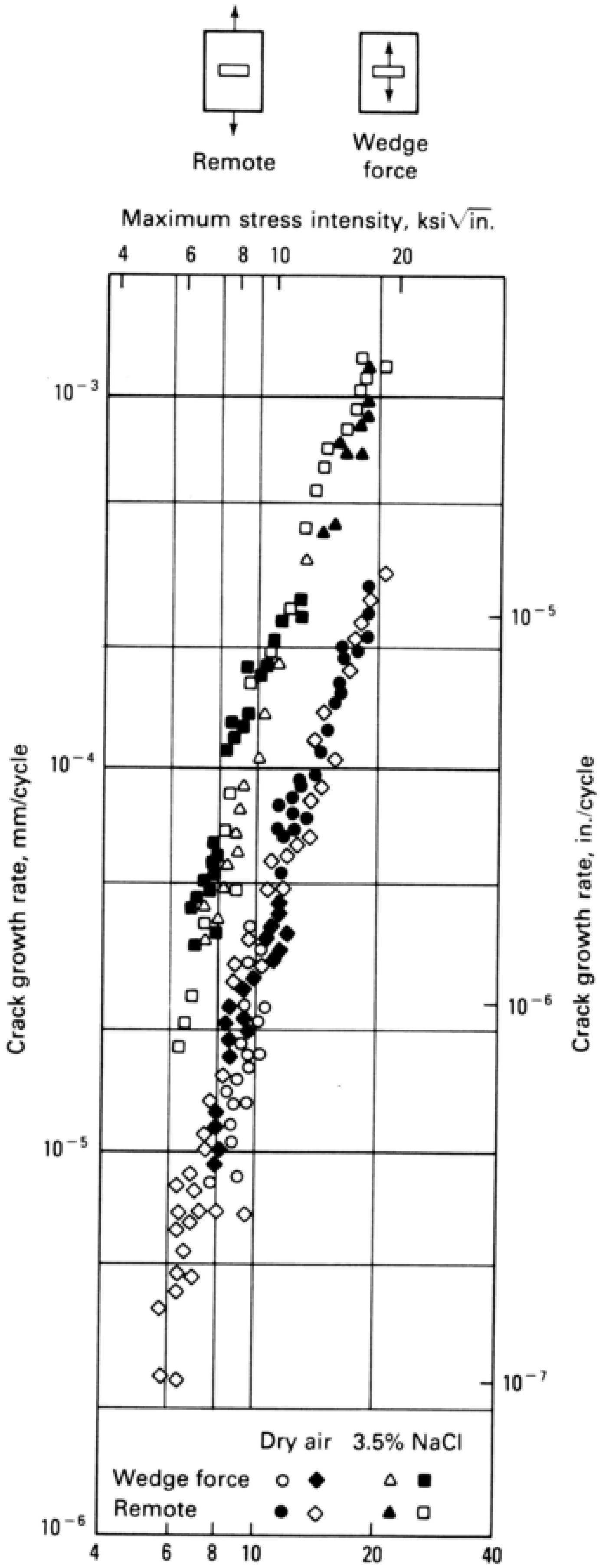

Fig. 10 Crack tip stress-intensity control of fatigue crack propagation in 7075-T6 aluminum alloy sheet—long-transverse loading. Remote and wedge force methods of loading specimens in aqueous 3.5% sodium chloride environment and benign dry air environment. Source: Ref 46

Corrosion-fatigue growth rate versus stress- intensity data have been extensively produced (Ref 2, 3, 4, 5, 6, 7, 8, 47, 48) and can be used for mitigating corrosion fatigue from several perspectives. Laboratory crack growth rate data are scalable quantitatively for predicting component performance. The *da*/*dN* versus Δ*K* curve for a given material and environment is integrated; it is then used in conjunction with the stress-intensity solution for a component to predict corrosion-fatigue life (Ref 44). A specific example reported in Ref 49 is illustrated in Fig. 11. The predicted 85 year life of a welded pipe is based on week-long laboratory measurements of *da*/*dN* versus Δ*K* for steel in an oil environment.

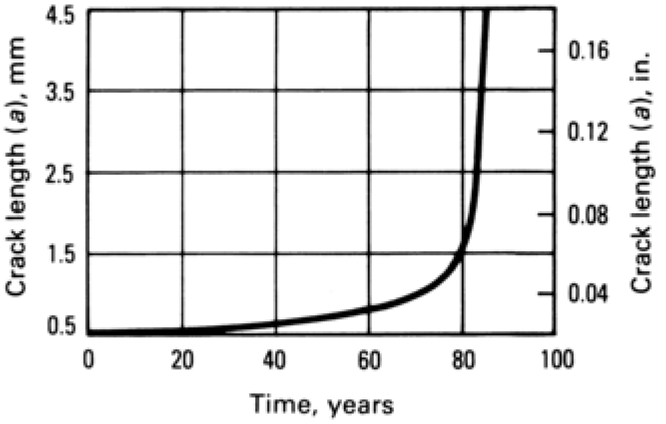

Fig. 11 Predicted fatigue crack extension from a weld toe crack in an American Petroleum Institute (API) 5LX52 carbon steel pipeline carrying hydrogen-sulfide-contaminated oil. Temperature: 23 °C (73 °F). Source: Ref 49

Alloy development for optimized corrosion- fatigue resistance, defined in terms of *da*/*dN* versus Δ*K* for different metallurgical conditions, is directly related to component life goals based on fracture mechanics. Similarly, the effects of mechanical and chemical variables on corrosion fatigue and component performance are defined through measured changes in crack growth rate at different applied stress-intensity levels.

Crack growth rate data are important to fundamental studies of corrosion-fatigue mechanisms. The fracture mechanics approach isolates crack propagation from initiation in terms of a precise near-tip mechanical driving force, Δ*K*. Crack growth rates are related directly to the kinetics of mass transport and the chemical reactions that constitute embrittlement. As shown in Fig. 12, prediction of the effect of loading frequency on crack growth rate in saltwater (normalized to vacuum) identifies important rate- limiting crack tip electrochemical reactions. Modeling and measurements in Fig. 12 provide a sound basis for extrapolating short-term laboratory data in order to predict long-term component cracking.

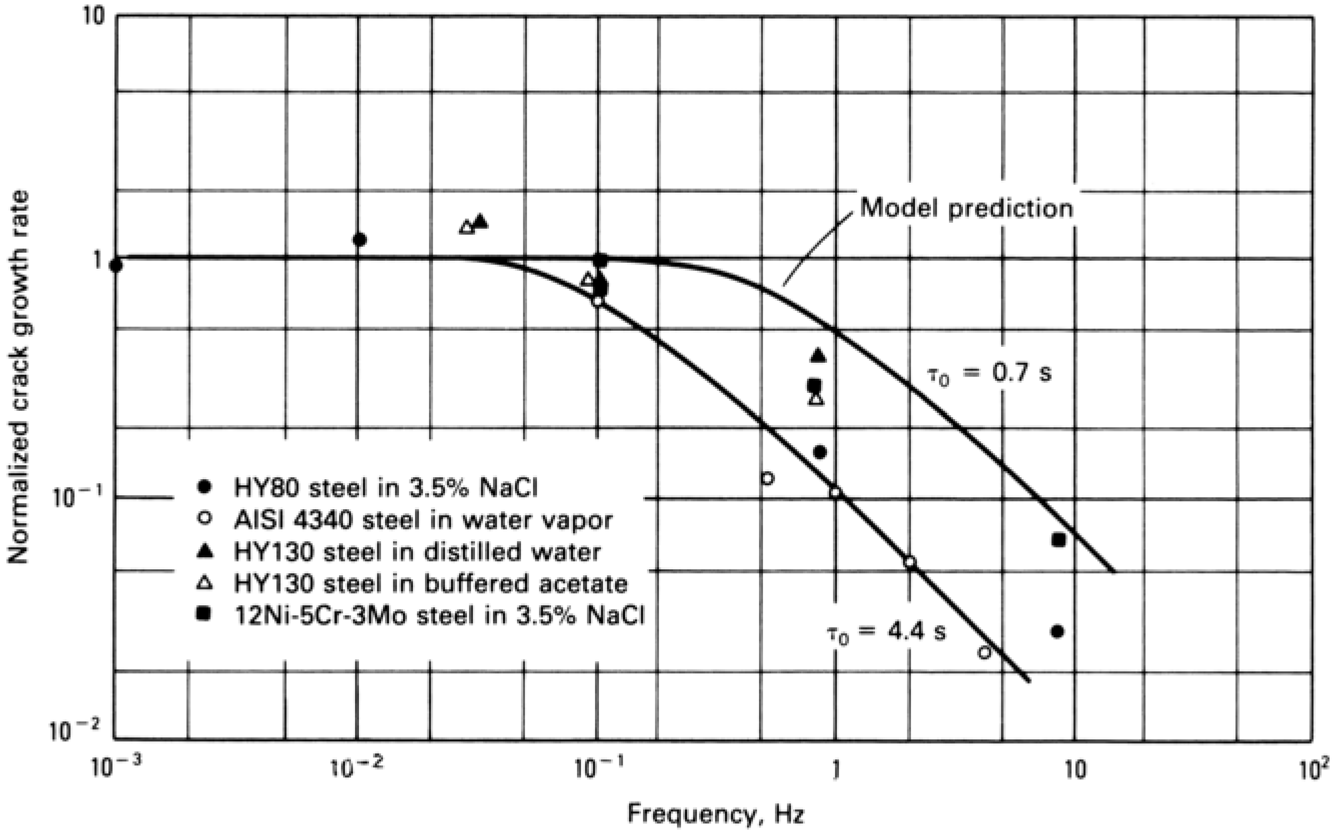

Fig. 12 Modeled effect of loading frequency on corrosion-fatigue crack growth in alloy steels in an aqueous chloride solution. The determination of the normalized crack growth rate and the time constants, τ_0, from the model can be found in Ref 50.

However, the fracture mechanics approach to corrosion fatigue is not valid in all cases. Discussion in this article is limited to crack growth in conjunction with net section elastic loading and small-scale plasticity confined to the crack tip. Studies of crack growth under large-scale cyclic plasticity have not been extended to consider environmental effects (Ref 51, 52). Also, while stress intensity provides a mechanical description of similitude, it may not completely describe crack growth because of interacting chemical and mechanical driving forces.

Results of investigations indicate that simple *K*-based approaches can be compromised for (a) small corrosion-fatigue cracks below 5 mm (0.2 in.), (b) cases in which varying crack shape and load transients alter crack chemistry and embrittlement, and (c) situations in which surface roughness or corrosion products impede crack displacement (Ref 51, 52, 53, 54, 55). Reference 51, 52, 53, 54, 55 should be consulted if an application includes plasticity, small crack, load transient, or crack closure effects.

Variables Influencing Corrosion Fatigue

Although corrosion-fatigue phenomena are diverse and specific to the environment, several variables are known to influence crack growth rate. The following factors must be considered in any study of corrosion fatigue:

- Stress-intensity range
- Load frequency
- Stress ratio
- Electrode potential in aqueous environment
- Environment composition
- Alloy composition, microstructure, and yield strength

Moreover, the effects of such variables as temperature, load history and waveform, stress state, and environment composition may be unique to specific materials and environments.

Stress-Intensity Range. Corrosion-fatigue crack growth rates generally increase with increasing stress intensity; however, the precise dependence varies markedly. It is incorrect to assume that the three regimes (near threshold, power law, and fast fracture; see Fig. 9) of fatigue cracking observed for benign environments simply shift to higher crack speeds at all ΔK levels. Although such behavior may actually occur, as illustrated in Fig. 10 for the aluminum/dry air system, the data provided in Fig. 13 and Fig. 14 are more typical of complex stress-intensity dependencies for aggressive environments.

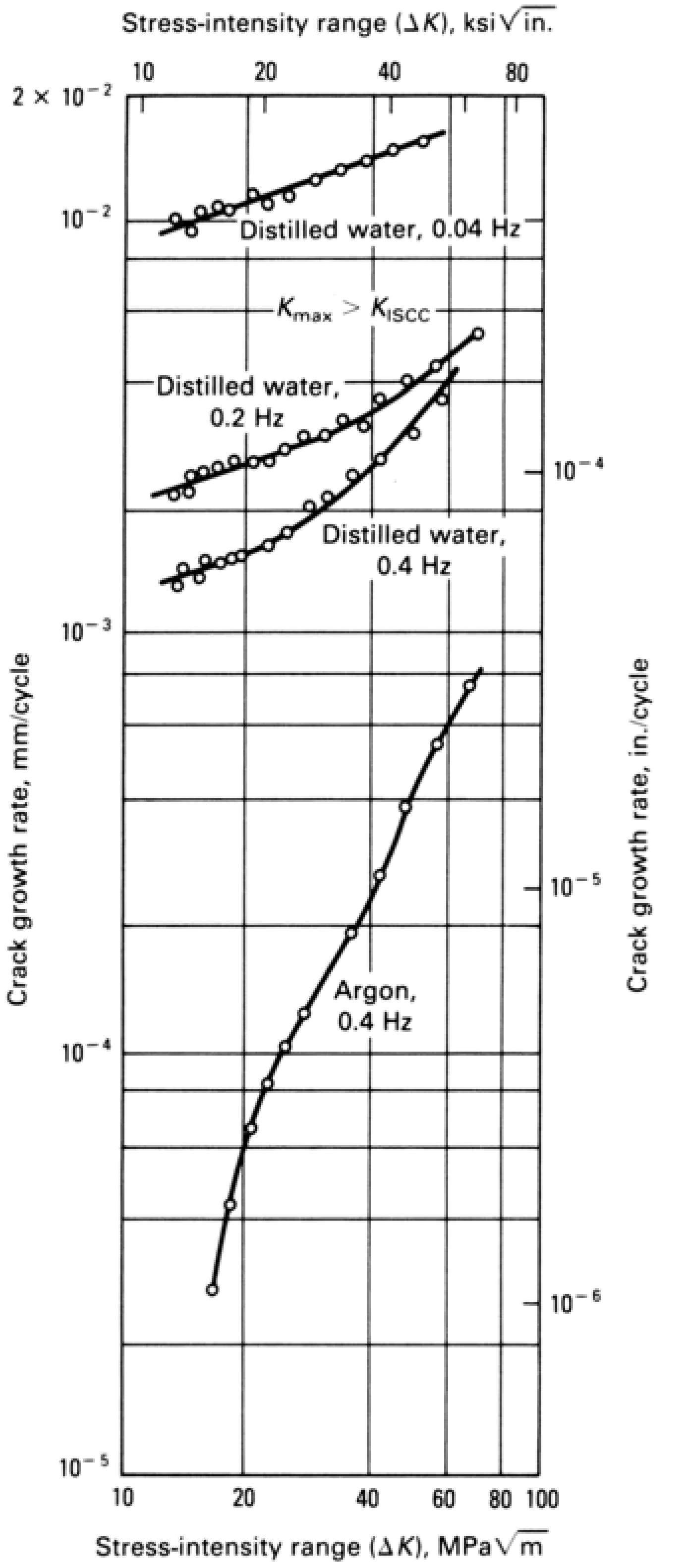

Fig. 13 Effect of stress-intensity range and loading frequency on corrosion-fatigue crack growth in ultrahigh-strength 4340 steel exposed to distilled water at 23 °C (73 °F). K_{max}, maximum stress-intensity factor; K_{ISCC}, threshold stress intensity for stress-corrosion cracking. Source: Ref 56

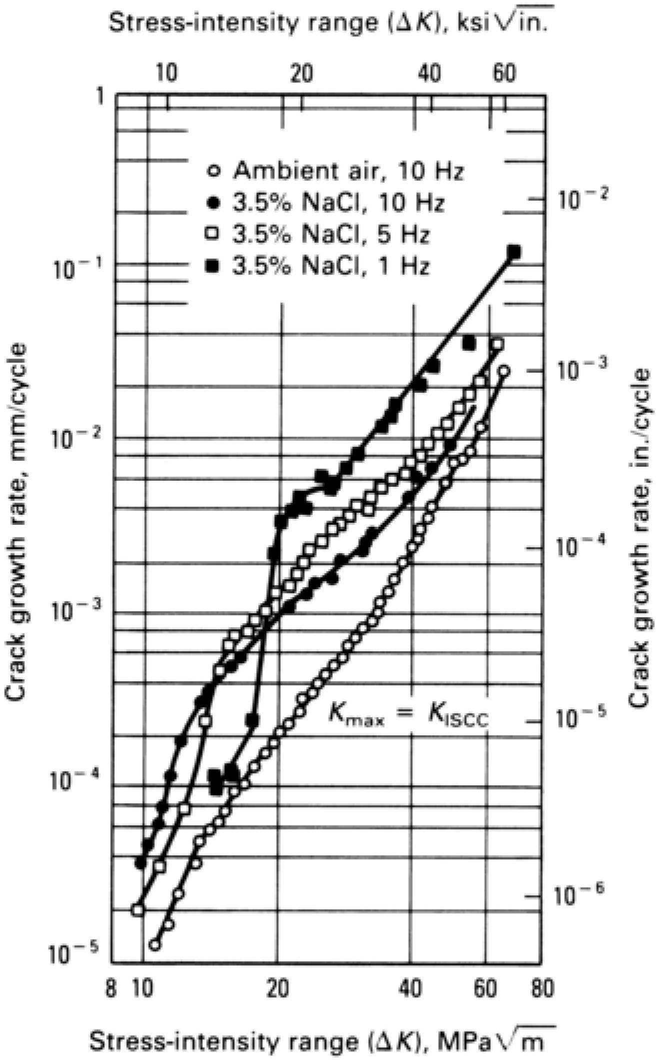

Fig. 14 Effects of stress intensity and frequency on corrosion fatigue in Ti-6Al-4V in aqueous sodium chloride at 23 °C (73 °F). Stress ratio: R = 0.1. K_{max}, maximum stress-intensity factor; K_{ISCC}, threshold stress intensity for stress-corrosion cracking. Source: Ref 57

Materials that are extremely environment sensitive, such as ultrahigh-strength steel in distilled water (Fig. 13), are characterized by high crack growth rates that are influenced less by ΔK. Time-dependent corrosion-fatigue crack growth occurs predominantly above the threshold stress intensity for static load cracking and is modeled through linear superposition of SCC and inert environment fatigue rates (Ref 28, 34). Time- dependent crack growth is the part of the crack extension that is attributable to the constant or rising-load portion of the cyclic load cycle, when SCC and hydrogen embrittlement mechanisms may be operative. Factors such as stress wave form and stress hold-time are particularly significant under these circumstances.

Cycle-dependent corrosion-fatigue crack propagation often occurs below the threshold for time-dependent SCC (Ref 57). Typical ΔK dependencies for this mode of cracking are complex, as illustrated in Fig. 14 for Ti-6Al-4V exposed to aqueous sodium chloride. The mechanistic implications of the various stress- intensity dependencies are detailed in Ref 28, 57, and 58. The influences of such variables as frequency, stress ratio, and metallurgical factors depend on the proportions of time- and cycle-dependent corrosion fatigue.

Frequency. The frequency of cyclic loading is the most important variable that influences CFC for most material, environment, and stress- intensity conditions. The rate of environmental cracking above that produced in vacuum generally increases with decreasing frequency. Frequencies exist above which CFC is diminished. The dominance of frequency is directly related to the time dependence of mass transport and chemical reaction steps required for environmental cracking. Basically, insufficient time is available for chemical embrittlement at rapid loading rates, that is, high frequencies, when damage is only mechanical and is equivalent to crack growth in vacuum. It is impossible to predict the frequency range at which corrosion fatigue is severe because of the numerous chemical processes. It is also difficult to extrapolate short- term (high-frequency) laboratory crack growth rate data in order to predict long-term component performance.

The literature provides qualitative guidance in terms of frequency effects on CFC. Crack growth in environmentally sensitive materials stressed above the stress-corrosion threshold proceeds at rapidly increased rates with decreasing frequency, as illustrated in Fig. 13. The frequency effect is predicted through the integration of static load data throughout each load cycle (Ref 50). For such systems, the chemical contribution to fatigue cracking is suppressed above 0.5 to 5 Hz, with higher critical frequencies associated with more aggressive environments and sensitive microstructures.

Frequency effects on cycle-dependent cracking are complex and unpredictable. The data given in Fig. 12 and 14 provide typical examples. For steels in saltwater (Fig. 12), CFC is suppressed at approximately 10 Hz. Crack speed increases with decreasing frequency and reaches a plateau between 0.5 and 0.1 Hz. In contrast, CFC in Ti-6Al-4V occurs at loading frequencies at least as high as 10 Hz (Fig. 14).

Stress Ratio. The rates of corrosion-fatigue crack propagation generally are increased by higher stress ratios. The deleterious effect of increased stress ratio is illustrated in Fig. 15 for carbon steel stressed cyclically in pressurized nuclear reactor water at 288 °C (550 °F). The extent of the corrosion-fatigue effect relative to dry air increased from approximately a factor of 4 at low *R* (0.11 to 0.24) to as much as 20- to 30-fold at high *R* (0.61 to 0.71) (Ref 59). Corrosion fatigue in this system probably proceeds by repeated passive film formation and rupture. Increased stress ratio at constant ΔK results in increased crack tip strain and strain rate, enhanced film rupture, and therefore increased corrosion-fatigue crack propagation (Ref 60).

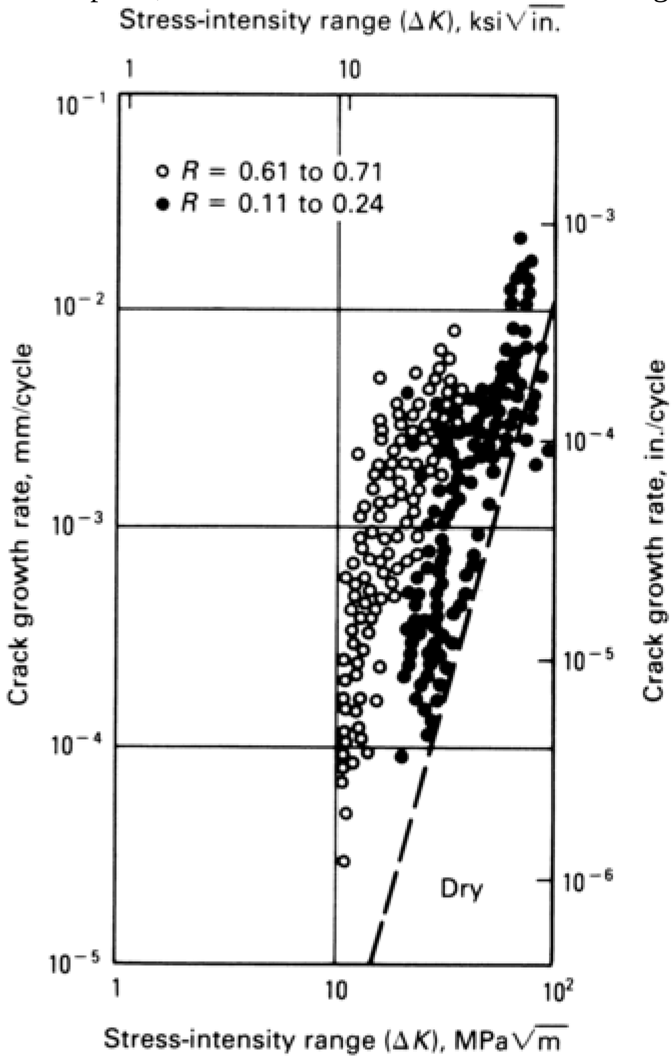

Fig. 15 Effect of stress ratio (*R*) on corrosion-fatigue crack propagation in ASTM A533 B and A508 carbon steels exposed to pressurized high-purity water at 288 °C (550 °F). Frequency: 0.017 Hz. Average behavior in air is represented by the dashed line labeled "Dry." Source: Ref 59

Electrode Potential. Like loading frequency, electrode potential strongly influences rates of corrosion-fatigue crack propagation for alloys in aqueous environments. Controlled changes in the potential of a specimen can result in either the complete elimination or the dramatic increase of fatigue cracking. The precise influence

depends on the mechanism of the environmental effect and on the anodic or cathodic magnitude of the applied potential.

For ferrous alloys that crack by hydrogen embrittlement when stressed in aqueous solutions, CFC is increased by high cathodic polarization from the free corrosion potential. Specific data are given in Fig. 16 for three steels stressed at constant ΔK in aqueous chloride environments (Ref 51, 61, 62). For each steel, the crack growth rate in saltwater is approximately three times faster than that reported for air at the free corrosion potential and is enhanced by a factor of 5 at a very high cathodic potential. For the low- strength BS4360:50D grade (similar to Unified Numbering System, or UNS, K02601), intermediate potentials appear to be mildly beneficial. Corrosion fatigue parallels electrode-potential- induced changes in the amount of cathodically evolved hydrogen in the crack tip. Precise modeling of this reaction sequence is complex and only partially completed (Ref 63).

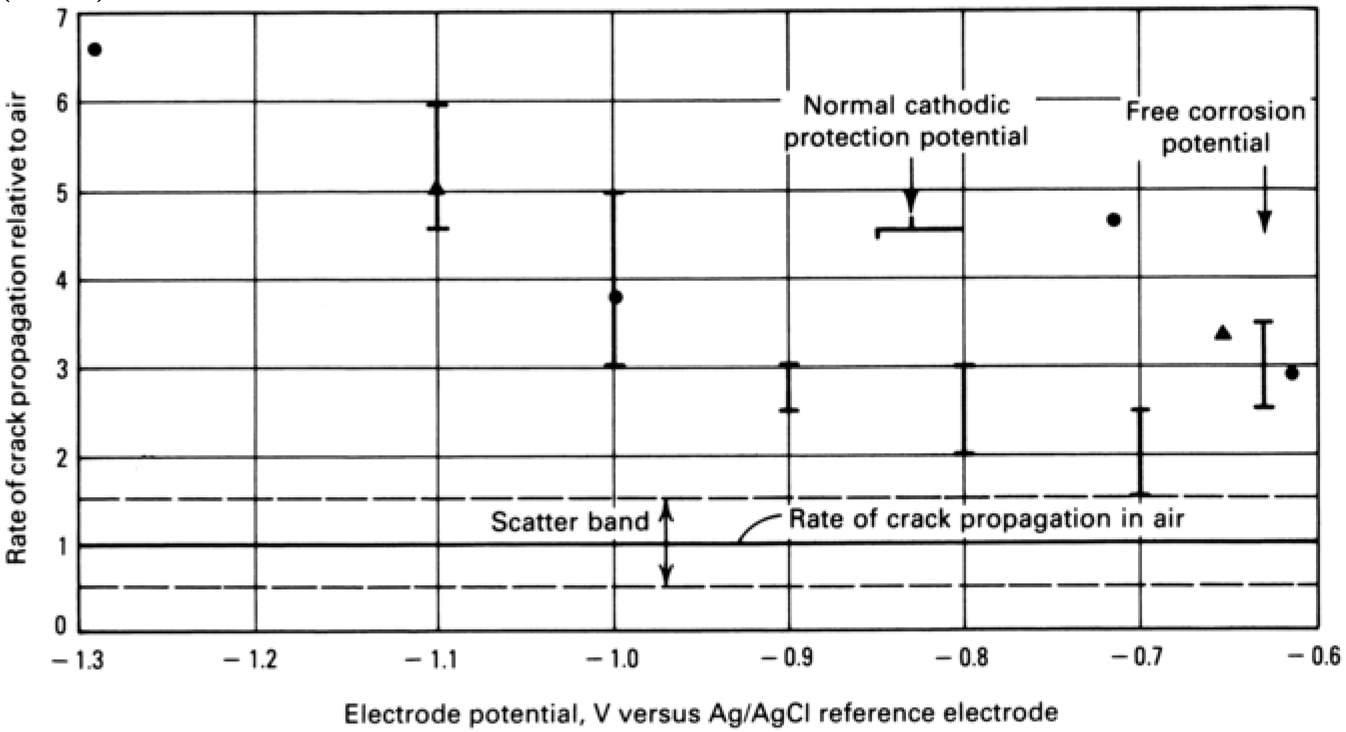

Fig. 16 Effect of applied electrode potential on corrosion-fatigue crack propagation in several steels exposed to seawater or 3% sodium chloride at constant ΔK between 20 and 40 MPa$\sqrt{m}$ (18 and 36 ksi$\sqrt{in.}$). Temperature: 23 °C (73 °F); frequency: 0.1 Hz; stress ratio: R = 0.1[ep[ol6p]

Material tested	Symbol	Yield strength MPa	Yield strength ksi	Environment	Ref
BS4360:50D	I	450	65	Seawater	60
HY80	•	600	85	3% NaCl	61
AISI 4130	▲	750	110	3% NaCl	62

Electrode potential control can suppress corrosion fatigue for alloys that crack through anodic dissolution/film rupture or anion adsorption mechanisms (Ref 64). For example, corrosion fatigue of austenitic stainless steel in chloride solutions at elevated temperatures is probably suppressed by polarization active to the critical potential for SCC.

Another example is illustrated in Fig. 17. Aluminum alloy 7079-T651 is degraded by corrosion fatigue in several aqueous halide solutions at the free corrosion potential. Compared to dry argon, cracking in potassium iodide is enhanced by more than an order of magnitude (Fig. 17a). The CFC growth rate was further increased by anodic polarization at potentials more electropositive than -0.6 V versus standard hydrogen electrode (SHE) but was suppressed by cathodic polarization (Fig. 17b).

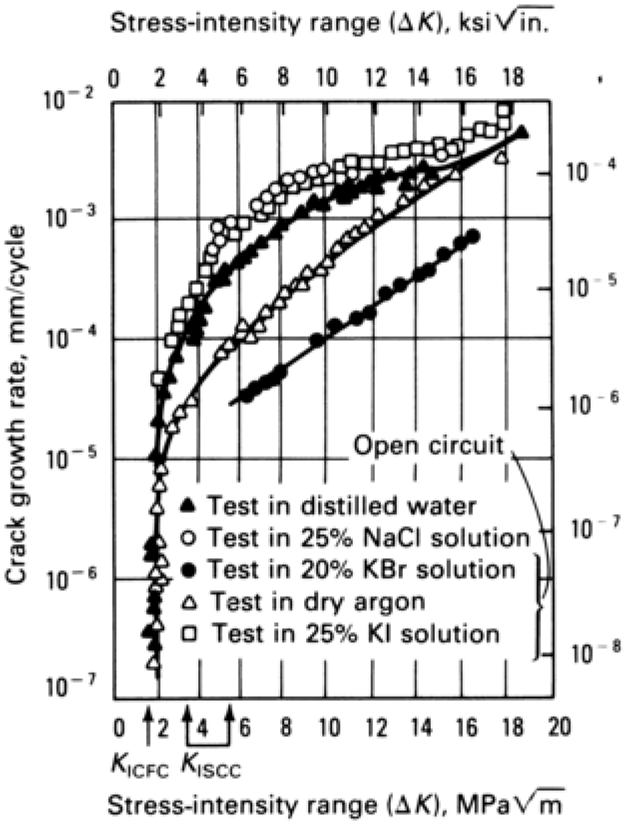

(a)

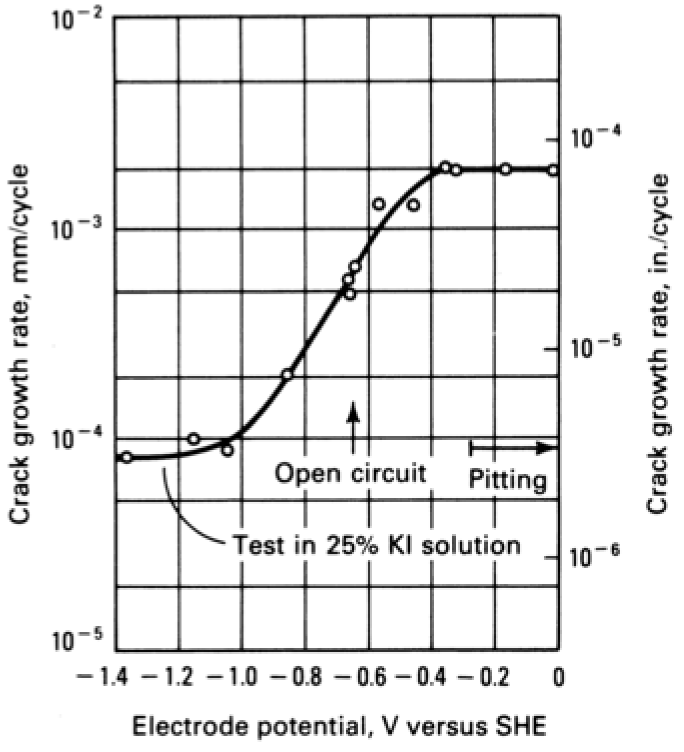

(b)

Fig. 17 Corrosion-fatigue behavior of aluminum alloy 7079-T651 plate (S-L orientation). Temperature: 23 °C (73 °F); frequency: 4 cycles/s; stress ratio: *R* = 0. (a) Effect of stress- intensity range on crack growth rate Threshold stress intensity for corrosion-fatigue cracking (K_{ICFC}) and a range of threshold intensity for stress-corrosion cracking (K_{ISCC}) are indicated at the bottom. (b) Effect of electrode

potential at ΔK of 6.7 MPa $\sqrt{m}$(6 ksi $\sqrt{in.}$) in 25% potassium iodide solution. SHE, standard hydrogen electrode. Source: Ref 65

Electrode potential should be monitored and, if appropriate, maintained constant during corrosion-fatigue testing. Apparent effects of variables, such as the dissolved oxygen content of the solution, flow rate, ion concentration, and alloy composition on corrosion fatigue, can often be traced to changing electrode potential.

Crack Closure Effects. Premature crack surface contact during unloading, or crack closure, can greatly reduce rates of fatigue crack propagation. The true (or effective) crack tip driving force is reduced below the applied Δ*K* because of the reduced crack tip displacement range. Closure phenomena are produced by a variety of mechanisms and are particularly relevant to fatigue crack propagation in the near-threshold regime, after large load excursions, and for embrittling corrosive mechanisms, as reviewed in Ref 53, 66, and 67.

Two mechanisms of crack closure are relevant to corrosion fatigue. Rough, intergranular crack surfaces, typical of environmental embrittlement, promote crack closure because uniaxially loaded cracks open in a complex three-dimensional mode, allowing for surface interactions and load transfer. Roughness-induced closure is most relevant to corrosion fatigue at low Δ*K* and at stress ratio levels where absolute crack opening displacements (0.5 to 3 μm) are less than fractured grain heights (5 to 50 μm).

Alternatively, crack closing is impeded by dense corrosion products within the pulsating fatigue crack. For mildly oxidizing environments, such as moist air, this closure mechanism is relevant at low stress-intensity levels and contributes to the formation of a threshold, as described in Ref 67.

For corrosive bulk environments, cracking at high Δ*K* values may be retarded below growth rates observed for air or vacuum due to corrosion product formation within the crack. The engineering significance of beneficial crack closure influences depends on the stability of the corrosion product during complex tension-compression loading and fluid conditions. An example of crack closure is presented in Fig. 18 for ASTM A 471 steel exposed to either moist air or steam at 100 °C (212 °F). Crack growth is reduced for the latter environment because of crack surface oxidation and enhanced closure. It should be noted that oxide-induced closure influences cracking even at a relatively high stress ratio of 0.35. The data presented in Fig. 18 were obtained at a high loading frequency of 100 Hz, and chemically enhanced crack growth was essentially precluded.

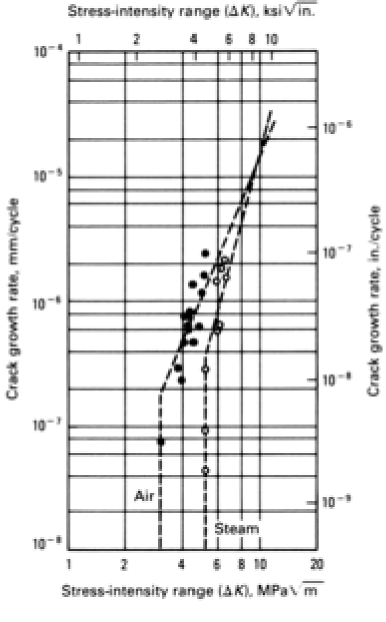

Fig. 18 Corrosion-fatigue crack propagation in ASTM A 471 steel exposed to moist air and steam. Temperature: 100 °C (212 °F); frequency: 100 Hz; stress ratio: *R* = 0.35. Source: Ref 68

Crack growth at lower frequencies could be deleteriously influenced by metal embrittlement and beneficially influenced by increased oxide formation and closure. The complexity of predicting environmentally enhanced cracking is clear, as emphasized by data given in Fig. 19 for a 2.25Cr-1Mo steel (ASTM A 542, class 3) stressed in dry hydrogen at 23 °C (73 °F). At high Δ*K* levels and low loading frequencies, cracking was accelerated in hydrogen as compared to moist air. This was due to classical hydrogen embrittlement. For low stress intensities, cracking was also increased by hydrogen exposure; however, the effect was not due to hydrogen embrittlement because of the rapid loading frequencies. Oxides form on crack surfaces through a

fretting mechanism during cycling in air, and crack growth rates are reduced by oxide-induced closure. However, oxide formation is precluded for cycling in pure hydrogen, crack closure is absent, and growth rates are increased relative to those in moist air. Equally rapid rates of fatigue cracking have been reported for low Δ*K* cycling in hydrogen and in helium. Equal rates of cracking are observed for hydrogen, helium, and moist air at high *R* (stress ratio) levels where closure was absent (Ref 66, 67).

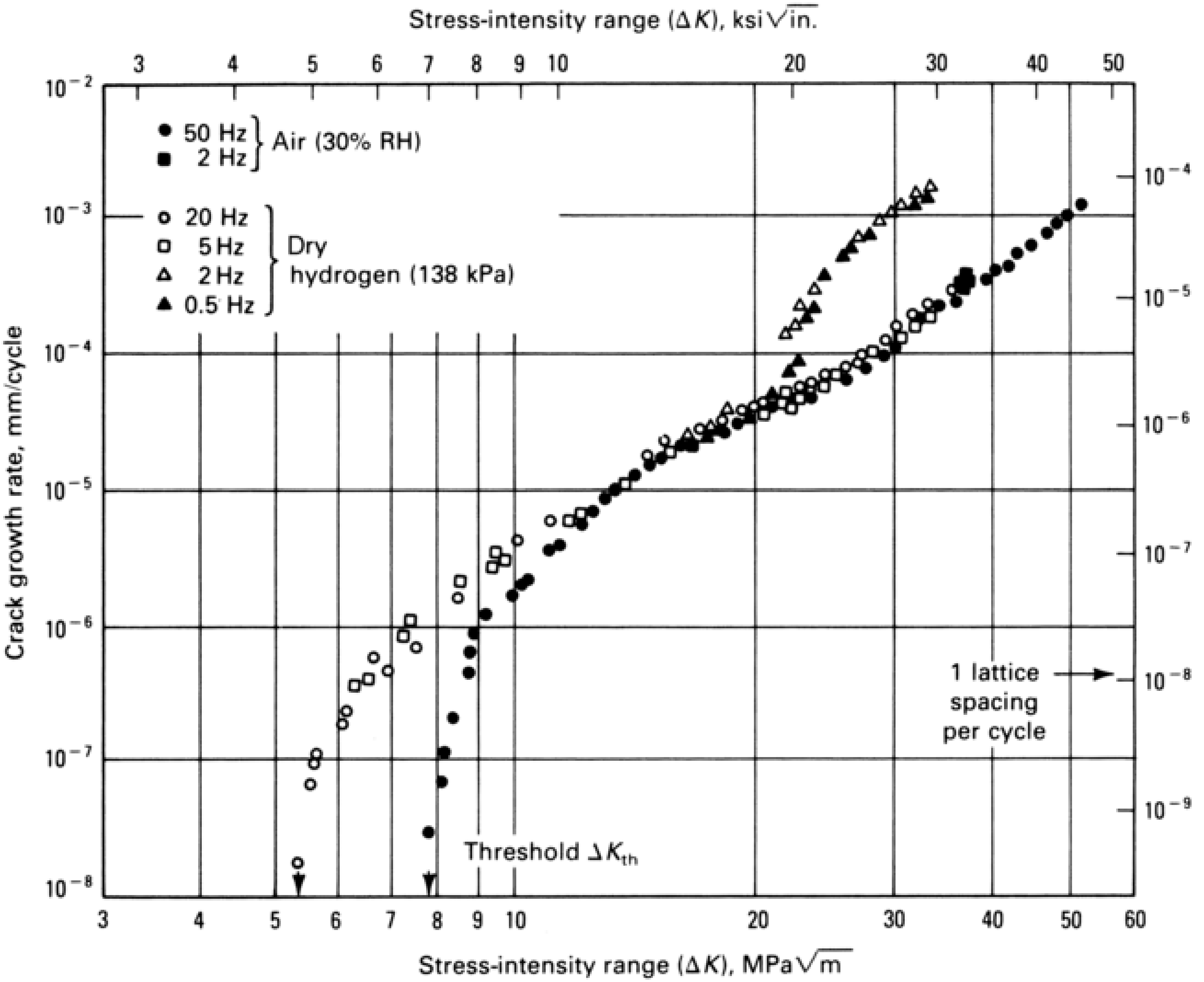

Fig. 19 Corrosion fatigue in 2.25Cr-lMo pressure vessel steel in dry hydrogen at 23 °C (73 °F) due to hydrogen embrittlement at high Δ*K* and to reduced oxide-induced closure at low Δ*K*. Stress ratio: *R* = 0.05. RH, relative humidity. Source: Ref 66

CFC Growth Characterization

Experimental characterizations of corrosion- fatigue crack propagation are complicated by the numerous variables that influence the failure process. Both the mechanics of loading and the composition of the environment must be controlled. Standard methods of measurement and fracture mechanics analysis of fatigue crack propagation in benign environments can be found in ASTM E 647 (Ref 25).

Four problem areas are relevant to corrosion- fatigue testing. First, the environment must be contained about the cracked specimen without affecting loading, crack monitoring, or specimen-environment composition. Parameters such as environmental purity, composition, temperature, and electrode potential must be monitored and controlled.

Second, the deleterious effect of low cyclic frequency dictates that crack growth rates be measured at low frequencies (often <0.2 Hz). This leads to long test times—often several days to weeks. Load-controlled equipment, crack- monitoring sensors and signal conditioners, and test environment composition must be stable throughout long-term tests.

Third, crack length must be measured for calculations of stress intensity and crack growth rate. Optical methods are often precluded by the environment and test chamber. Indirect methods, which are based on specimen compliance (Ref 69) or electrical potential difference (Ref 70), have been successfully applied to the monitoring of crack growth in a wide variety of hostile environments. Experimental and analytical requirements, however, are complex for indirect crack monitoring.

Nonvisual techniques will often have greater accuracy and less variability in crack length measurement than optical observations. In addition, the nonvisual techniques are generally more consistent and reliable, especially where long periods of unattended testing are anticipated. Beyond that, nonvisual techniques are absolutely essential where the test temperature or the environment prohibits direct visual observation. Nonvisual methods are more precise than visual techniques and allow for automation of the test beyond the mere acquisition of the crack growth rate data (Ref 71, 72).

Finally, specimen geometry and size requirements for ΔK-based crack propagation data, which are scalable to components through similitude, have not been established completely for subcritical crack growth. In-plane yielding must be limited to the crack tip by ensuring that net section stress is below yield and that the maximum plastic zone size, defined as approximately 0.2 $(K_{max}/\sigma_{YS})^2$ (where σ_{YS} is yield strength), is much less (for example, 10- to 50- fold) than the uncracked ligament. Specimen thickness, as it influences the degree of plane-strain constraint, and crack size, as it influences the chemical driving force, may affect corrosion- fatigue crack speeds. Such effects are currently unpredictable, and specimen thickness and crack geometry must be treated as variables.

CFC Growth in Specific Environments

Corrosion-fatigue crack growth studies in aqueous solutions and gaseous environments at ambient temperature present fewer problems experimentally than many of the other environments considered in this article. Nevertheless, simulation of practical conditions in relation to a specific engineering application requires careful consideration if the data are to be relevant. Similarly, in an academic investigation, comparison of the results of different pieces of work is possible only if the mechanical, metallurgical, and chemical variables are properly characterized and controlled. It is often the case, however, that the most frequent problem in determining the validity of corrosion-fatigue data lies with the control and monitoring of the bulk environment chemistry and the monitoring and recording of the electrochemical potential in aqueous solutions.

Corrosion-fatigue crack growth data are required for practical engineering applications in many diverse and specialized environments. An excellent overview of the following eight specific types of environments is given in *Mechanical Testing and Evaluation,* Volume 8 of *ASM Handbook,* and will not be repeated in this article:

- Vacuum and gaseous environments at ambient temperatures
- Vacuum and oxidizing gases at elevated temperatures
- Aqueous solutions at ambient temperatures
- Acidified chloride environments at ambient and elevated temperatures
- High-temperature pure water under aerated conditions
- High-temperature pure water under deaerated conditions
- Liquid metal environments
- Steam or boiling water with contaminants

References cited in this section

2. O. Devereux, A.J. McEvily, and R.W. Staehle, Ed., *Corrosion Fatigue—Chemistry, Mechanics, and Microstructure,* Proceedings of NACE Conference, June 1971 (Storrs, CT), National Association of Corrosion Engineers, 1972

3. H.L. Craig, Jr., T.W. Crooker, and D.W. Hoeppner, Ed., *Corrosion-Fatigue Technology,* STP 642, American Society for Testing and Materials, 1978

4. R.W. Staehle and M.O. Speidel, Ed., *Stress Corrosion and Corrosion Fatigue Handbook,* ARPA Contract M00014-75-C-0703, Advanced Research Project Agency of the Department of Defense

5. P.R. Swann, F.P. Ford, and A.R.C. Westwood, Ed., *Mechanisms of Environment Sensitive Cracking of Materials,* Proceedings of Metals Society Conference, April 1977 (University of Surrey, U.K.), The Metals Society, 1979

6. R.N. Parkins and Ya. M. Kolotyrkin, Ed., *Corrosion Fatigue,* Proceedings of the First USSR-U.K. Seminar on Corrosion Fatigue of Metals, May 1980 (Lvov, USSR), The Metals Society, 1983

7. T.W. Crooker and B.N. Leis, Ed., *Corrosion Fatigue: Mechanics, Metallurgy, Electrochemistry and Engineering,* STP 801, American Society for Testing and Materials, 1983

8. S.W. Dean, E.N. Pugh, and G.M. Ugiansky, Ed., *Environment-Sensitive Fracture,* STP 821, American Society for Testing and Materials, 1984

25. "Standard Test Method for Measurement of Fatigue Crack Growth Rates," ASTM E 647, *Metals—Mechanical Testing; Elevated and Low-Temperature Tests; Metallography,* Vol 03.01, *2002 Annual Book of ASTM Standards,* American Society for Testing and Materials, 2002

28. "Standard Guide for Evaluating Data Acquisition Systems Used in Cyclic Fatigue and Fracture Mechanics Testing," ASTM E 1942, *Metals—Mechanical Testing; Elevated and Low-Temperature Tests; Metallography,* Vol 03.01, *2002 Annual Book of ASTM Standards,* American Society for Testing and Materials, 2002

34. R.E. Peterson, *Stress Concentration Design Factors,* John Wiley & Sons, 1974

44. A.J. McEvily and R.P. Wei, Fracture Mechanics and Corrosion Fatigue, *Corrosion Fatigue: Chemistry, Mechanics and Microstructure,* O. Devereux, A.J. McEvily, and R.W. Staehle, Ed., National Association of Corrosion Engineers, 1973, p 381–395

45. P.M. Scott, Chemistry Effects in Corrosion Fatigue, *Corrosion Fatigue: Mechanics, Metallurgy, Electrochemistry and Engineering,* STP 801, T.W. Crooker and B.N. Leis, Ed., American Society for Testing and Materials, 1983, p 319–350

46. J.A. Feeney, J.C. McMillan, and R.P. Wei, Environmental Fatigue Crack Propagation of Aluminum Alloys at Low Stress Intensity Levels, *Metall. Trans.,* Vol 1, 1970, p 1741–1757

47. *Corrosion Cracking,* Proceedings of International Conference on Fatigue, Corrosion Cracking, Fracture Mechanics and Failure Analysis, Dec 1985 (Salt Lake City, UT), American Society for Metals, 1986

48. Z.A. Foroulis, Ed., *Environment-Sensitive Fracture of Engineering Materials,* The Metals Society and the American Institute of Mining, Metallurgical, and Petroleum Engineers, 1978

49. O. Vosikovsky and R.J. Cooke, An Analysis of Crack Extension by Corrosion Fatigue in a Crude Oil Pipeline, *Int. J. Pressure Vessels Piping,* Vol 6, 1978, p 113–129

50. R.P. Wei and G. Shim, Fracture Mechanics and Corrosion Fatigue, *Corrosion Fatigue: Mechanics, Metallurgy, Electrochemistry and Engineering,* STP 801, T.W. Crooker and B.N. Leis, Ed., American Society for Testing and Materials, 1984, p 5–25

51. M.H. El Haddad, T.H. Topper, and B. Mukherjee, Review of New Developments in Crack Propagation Studies, *J. Test Eval.,* Vol 9, 1981, p 65–81

52. N.E. Dowling, Crack Growth During Low Cycle Fatigue of Smooth Axial Specimens, *Cyclic Stress-Strain and Plastic Deformation Aspects of Fatigue Crack Growth,* STP 637, American Society for Testing and Materials, 1977, p 97–121

53. R.P. Gangloff and R.O. Ritchie, Environmental Effects Novel to the Propagation of Short Fatigue Cracks, *Fundamentals of Deformation and Fracture,* K.J. Miller, Ed., Cambridge University Press, 1987

54. S.J. Hudak, Jr. and R.P. Wei, Consideration of Nonsteady State Crack Growth in Material Evaluation and Design, *Int. J. Pressure Vessels Piping,* Vol 9, 1981, p 63–74

55. R.P. Gangloff, Crack Size Effects on the Chemical Driving Force for Aqueous Corrosion Fatigue, *Metall. Trans. A,* 1987

56. C.S. Kortovich, Corrosion Fatigue of 4340 and D6AC Steels Below K_{ISCC}, *Proceedings of the 1974 Triservice Conference on Corrosion of Military Equipment,* AFML-TR- 75-42, Air Force Materials Laboratory, Wright-Patterson Air Force Base, 1975

57. D.B. Dawson and R.M. Pelloux, Corrosion Fatigue Crack Growth of Titanium Alloys in Aqueous Environments, *Metall. Trans. A,* Vol 5, 1974, p 723–731

58. J.M. Barsom, Corrosion Fatigue Crack Propagation Below K_{ISCC}, *Eng. Fract. Mech.,* Vol 3, 1971, p 15–25

59. B. Tompkins and P.M. Scott, Environment Sensitive Fracture: Design Considerations, *Met. Technol.,* Vol 9, 1982, p 240–248

60. P.M. Scott, Effects of Environment on Crack Propagation, *Developments in Fracture Mechanics—II,* G.G. Shell, Ed., Applied Science, 1979, p 221–257

61. J.P. Gallagher, "Corrosion Fatigue Crack Growth Rate Behavior Above and Below K_{ISCC}," Report NRL-7064, Naval Research Laboratory, 1970

62. R.P. Gangloff, Exxon Research and Engineering Company, unpublished research, 1984

63. A. Turnbull, Progress in the Understanding of the Electrochemistry in Cracks, *Embrittlement by the Localized Crack Environment,* R.P. Gangloff, Ed., The Metals Society and the American Institute of Mining, Metallurgical, and Petroleum Engineers, 1984, p 3–31

64. R.N. Parkins, Prevention of Environment Sensitive Cracking by Inhibition, *Embrittlement by the Localized Crack Environment,* R.P. Gangloff, Ed., The Metals Society and the American Institute of Mining, Metallurgical, and Petroleum Engineers, 1984, p 385–404

65. M.O. Speidel, M.J. Blackburn, T.R. Beck, and J.A. Feeney, Corrosion Fatigue and Stress Corrosion Crack Growth in High Strength Aluminum Alloys, Magnesium Alloys and Titanium Alloys Exposed to Aqueous Solutions, *Corrosion Fatigue: Chemistry, Mechanics and Microstructure,* O. Devereux, A.J. McEvily, and R.W. Staehle, Ed., National Association of Corrosion Engineers, 1973, p 324–345

66. R.O. Ritchie, Application of Fracture Mechanics to Fatigue, Corrosion Fatigue and Hydrogen Embrittlement, *Analytical and Experimental Fracture Mechanics,* G.C. Sih, Ed., Sithoff and Noorohoff, 1981, p 81–108

67. S. Suresh and R.O. Ritchie, The Propagation of Short Fatigue Cracks, *Int. Met. Rev.,* 1987

68. L.K.L. Tu and B.B. Seth, Threshold Corrosion Fatigue Crack Growth in Steels, *J. Test. Eval.,* Vol 6, 1978, p 66–74

69. S.J. Hudak, Jr. and R.J. Bucci, Ed., *Fatigue Crack Growth Measurement and Data Analysis,* STP 738, American Society for Testing and Materials, 1981

70. R.P. Gangloff, Electrical Potential Monitoring of the Formation and Growth of Small Fatigue Cracks in Embrittling Environments, *Advances in Crack Length Measurement,* C.J. Beevers, Ed., Engineering Materials Advisory Services, 1982, p 175–230

71. J.K. Donald, Fatigue Crack Propagation and the Role of Automated Testing, *ASTM Stand. News,* Vol 13 (No. 11), Nov 1985, p 50–53

72. C.J. Beevers, Ed., *Advances in Crack Length Assessment,* Engineering Materials Advisory Service, 1982

B. Phull, Evaluating Corrosion Fatigue, *Corrosion: Fundamentals, Testing, and Protection*, Vol 13A, *ASM Handbook*, ASM International, 2003, p 625–638

Evaluating Corrosion Fatigue

Revised by Bopinder Phull, Consultant

References

1. F.P. Ford, Current Understanding of the Mechanism of Stress Corrosion and Corrosion Fatigue, *Environment-Sensitive Fracture,* STP 821, S.W. Dean, E.N. Pugh, and G.M. Ugianski, Ed., American Society for Testing and Materials, 1984, p 32–51

2. O. Devereux, A.J. McEvily, and R.W. Staehle, Ed., *Corrosion Fatigue—Chemistry, Mechanics, and Microstructure,* Proceedings of NACE Conference, June 1971 (Storrs, CT), National Association of Corrosion Engineers, 1972

3. H.L. Craig, Jr., T.W. Crooker, and D.W. Hoeppner, Ed., *Corrosion-Fatigue Technology,* STP 642, American Society for Testing and Materials, 1978

4. R.W. Staehle and M.O. Speidel, Ed., *Stress Corrosion and Corrosion Fatigue Handbook,* ARPA Contract M00014-75-C-0703, Advanced Research Project Agency of the Department of Defense

5. P.R. Swann, F.P. Ford, and A.R.C. Westwood, Ed., *Mechanisms of Environment Sensitive Cracking of Materials,* Proceedings of Metals Society Conference, April 1977 (University of Surrey, U.K.), The Metals Society, 1979

6. R.N. Parkins and Ya. M. Kolotyrkin, Ed., *Corrosion Fatigue,* Proceedings of the First USSR-U.K. Seminar on Corrosion Fatigue of Metals, May 1980 (Lvov, USSR), The Metals Society, 1983

7. T.W. Crooker and B.N. Leis, Ed., *Corrosion Fatigue: Mechanics, Metallurgy, Electrochemistry and Engineering,* STP 801, American Society for Testing and Materials, 1983

8. S.W. Dean, E.N. Pugh, and G.M. Ugiansky, Ed., *Environment-Sensitive Fracture,* STP 821, American Society for Testing and Materials, 1984

9. R.N. Parkins, "A Critical Evaluation of Current Environment-Sensitive Fracture Test Methods," *Environment-Sensitive Fracture*, STP 821, S.W. Dean, E.N. Pugh, and G.M. Ugiansky, Ed., American Society for Testing and Materials, 1984, p 5–31

10. R.P. Gangloff, Ed., *Embrittlement by the Localized Crack Environment,* Proceedings of the TMS-AIME/MDS-ASM Symposium on Localized Crack Chemistry and Mechanics in Environment-Assisted Cracking, Oct 1983 (Philadelphia, PA), The Metallurgical Society, 1984

11. D.A. Jones, A Unified Mechanism of Stress Corrosion and Corrosion Fatigue Cracking, *Metall. Trans. A,* Vol 16, June 1985, p 1133–1141

12. R.P. Gangloff, Corrosion Fatigue Crack Propagation in Metals, *Environment-Induced Cracking of Metals,* R.P. Gangloff and M.B. Ives, Ed., NACE-10, NACE International, 1990, p 45

13. S.A. Shipilov, "Comparison Between Hydrogen-Enhanced Corrosion Fatigue Cracking Growth Rates and Critical Distances Ahead of a Growing Crack," Paper 00375, Corrosion/2000, NACE International, 2000

14. G.R. Engelhardt and D.D. MacDonald, "Modeling Corrosion Fatigue Crack Propagation," Paper 01115, Corrosion/2001, NACE International, 2001

15. D.D. MacDonald and G.R. Engelhardt, "Towards a Mechanism Based Theory for Crack Initiation," Paper 01116, Corrosion/2001, NACE International, 2001

16. T. Havn and H. Osvoll, "Corrosion Fatigue of Steel in Sea Water," Paper 02431, Corrosion/2001, NACE International, 2002

17. Y. Wang and R. Akid, Role of Nonmetallic Inclusions in Fatigue, Pitting, and Corrosion Fatigue, *Corrosion,* Vol 52 (No. 2), 1996, p 92–102

18. T.W. Crooker, Environmental Cracking in Structural Alloys: A Look at Standards for Corrosion Fatigue and Stress-Corrosion Cracking, *ASTM Stand. News,* Vol 13 (No. 11), Nov 1985, p 54–58

19. J.T. Fong, Fatigue Research: Needs and Opportunities, *ASTM Stand. News,* Vol 13 (No. 11), Nov 1985, p 59–63

20. H.J. Westwood and W.K. Lee, Corrosion- Fatigue Cracking in Fossil-Fueled Boilers, *Corrosion Cracking,* Proceedings of the International Conference on Fatigue, Corrosion Cracking, Fracture Mechanics and Failure Analysis, Dec 1985 (Salt Lake City, UT), American Society for Metals, 1986, p 23–34

21. "Standard Practice for Conducting Force Controlled Constant Amplitude Axial Fatigue Tests of Metallic Materials," ASTM E 466, *Metals—Mechanical Testing; Elevated and Low-Temperature Tests; Metallography,* Vol 03.01 *2002 Annual Book of ASTM Standards,* American Society for Testing and Materials, 2002

22. "Standard Practice for Verification of Constant Amplitude Dynamic Forces in an Axial Load Fatigue Testing System," ASTM E 467, *Metals—Mechanical Testing; Elevated and Low-Temperature Tests; Metallography,* Vol 03.01, *2002 Annual Book of ASTM Standards,* American Society for Testing and Materials, 2002

23. "Standard Practice for Presentation of Constant Amplitude Fatigue Test Results for Metallic Materials," ASTM E 468, *Metals— Mechanical Testing; Elevated and Low- Temperature Tests; Metallography,* Vol 03.01, *2002 Annual Book of ASTM Standards,* American Society for Testing and Materials, 2002

24. “Standard Practices for Strain-Controlled Fatigue Testing,” ASTM E 606, *Metals— Mechanical Testing; Elevated and Low- Temperature Tests; Metallography,* Vol 03.01, *2002 Annual Book of ASTM Standards,* American Society for Testing and Materials, 2002

25. “Standard Test Method for Measurement of Fatigue Crack Growth Rates,” ASTM E 647, *Metals—Mechanical Testing; Elevated and Low-Temperature Tests; Metallography,* Vol 03.01, *2002 Annual Book of ASTM Standards,* American Society for Testing and Materials, 2002

26. “Standard Practice for Statistical Analysis of Linear or Linearized Stress-Life (*S-N*) and Strain-Life (ε-*N*) Fatigue Data,” ASTM E 739, *Metals—Mechanical Testing; Elevated and Low-Temperature Tests; Metallography,* Vol 03.01, *2002 Annual Book of ASTM Standards,* American Society for Testing and Materials, 2002

27. “Standard Terminology Relating to Fatigue and Fracture Testing,” ASTM E 1823, *Metals—Mechanical Testing; Elevated and Low-Temperature Tests; Metallography,* Vol 03.01, *2002 Annual Book of ASTM Standards,* American Society for Testing and Materials, 2002

28. “Standard Guide for Evaluating Data Acquisition Systems Used in Cyclic Fatigue and Fracture Mechanics Testing,” ASTM E 1942, *Metals—Mechanical Testing; Elevated and Low-Temperature Tests; Metallography,* Vol 03.01, *2002 Annual Book of ASTM Standards,* American Society for Testing and Materials, 2002

29. “Standard Practice for Corrosion Fatigue Testing of Metallic Implant Materials,” ASTM F 1801, *Metals—Medical Devices; Emergency and Medical Services,* Vol 13.01, *2002 Annual Book of ASTM Standards,* American Society for Testing and Materials, 2002

30. “Standard Test Method for Shear and Bending Fatigue Testing of Calcium Phosphate and Metallic Medical Coatings,” ASTM F 1160, *Metals—Medical Devices; Emergency and Medical Services,* Vol 13.01, *2002 Annual Book of ASTM Standards,* American Society for Testing and Materials, 2002

31. G.E. Dieter, *Mechanical Metallurgy,* McGraw-Hill, 1976, p 426–427

32. O.J. Horger, Fatigue Characteristics of Large Sections, *Fatigue,* American Society for Metals, 1953

33. C.E. Phillips and R.B. Heywood, *Proc. Inst. Mech. Eng. (London),* Vol 165, 1951, p 113–124

34. R.E. Peterson, *Stress Concentration Design Factors,* John Wiley & Sons, 1974

35. H. Neuber, “Theory of Notch Stresses: Principles for Exact Calculation of Strength with References to Structural Form and Material,” Springer, 1958, AEC-Tr-4547; available through NTIS, U.S. Dept. of Commerce

36. R.J. Roark, *Formulas for Stress and Strain,* 4th ed., McGraw-Hill, 1965

37. T. Topper, R. Wetzel, and J. Morrow, Neuber's Rule Applied to Fatigue of Notched Specimens, *J. Mater.,* Vol 4 (No. 1), 1969

38. G. Sines and J.R. Weisman, Ed., *Metal Fatigue,* McGraw-Hill, 1959

39. J.B. Bidwell et al., *Fatigue Durability of Carburized Steel,* American Society for Metals, 1957

40. M.O. Speidel, Corrosion Fatigue in Fe-Ni- Cr Alloys, *Proceedings of the International Conference on Stress Corrosion and Hydrogen Embrittlement of Iron-Base Alloys,* June 1973 (Unieux-Firminy, France), National Association of Corrosion Engineers, 1977, p 1071–1094

41. “Metallic Materials and Elements for Aerospace Vehicle Structures,” MIL-HDBK-5B, Vol 1, U.S. Department of Defense, Sept 1971, p 2–29

42. K. Endo and K. Komai, Effects of Stress Wave Form and Cycle Frequency on Low Cycle Corrosion Fatigue, *Corrosion Fatigue: Chemistry, Mechanics, and Microstructure,* O. Devereux, A.J. McEvily, and R.W. Staehle, Ed., Conference held at the University of Connecticut, June 1971, National Association of Corrosion Engineers, 1972, p 437–450

43. L.D. Roth and L.E. Willertz, Application of Ultrasonic Fatigue Testing Techniques to the Evaluation of the Corrosion-Fatigue Strength of Materials, *Environment-Sensitive Fracture,* STP 821, S.W. Dean, E.N. Pugh, and G.M. Ugianski, Ed., American Society for Testing and Materials, 1984, p 497–512

44. A.J. McEvily and R.P. Wei, Fracture Mechanics and Corrosion Fatigue, *Corrosion Fatigue: Chemistry, Mechanics and Microstructure,* O. Devereux, A.J. McEvily, and R.W. Staehle, Ed., National Association of Corrosion Engineers, 1973, p 381–395

45. P.M. Scott, Chemistry Effects in Corrosion Fatigue, *Corrosion Fatigue: Mechanics, Metallurgy, Electrochemistry and Engineering,* STP 801, T.W. Crooker and B.N. Leis, Ed., American Society for Testing and Materials, 1983, p 319–350

46. J.A. Feeney, J.C. McMillan, and R.P. Wei, Environmental Fatigue Crack Propagation of Aluminum Alloys at Low Stress Intensity Levels, *Metall. Trans.,* Vol 1, 1970, p 1741–1757

47. *Corrosion Cracking,* Proceedings of International Conference on Fatigue, Corrosion Cracking, Fracture Mechanics and Failure Analysis, Dec 1985 (Salt Lake City, UT), American Society for Metals, 1986

48. Z.A. Foroulis, Ed., *Environment-Sensitive Fracture of Engineering Materials,* The Metals Society and the American Institute of Mining, Metallurgical, and Petroleum Engineers, 1978

49. O. Vosikovsky and R.J. Cooke, An Analysis of Crack Extension by Corrosion Fatigue in a Crude Oil Pipeline, *Int. J. Pressure Vessels Piping,* Vol 6, 1978, p 113–129

50. R.P. Wei and G. Shim, Fracture Mechanics and Corrosion Fatigue, *Corrosion Fatigue: Mechanics, Metallurgy, Electrochemistry and Engineering,* STP 801, T.W. Crooker and B.N. Leis, Ed., American Society for Testing and Materials, 1984, p 5–25

51. M.H. El Haddad, T.H. Topper, and B. Mukherjee, Review of New Developments in Crack Propagation Studies, *J. Test Eval.,* Vol 9, 1981, p 65–81

52. N.E. Dowling, Crack Growth During Low Cycle Fatigue of Smooth Axial Specimens, *Cyclic Stress-Strain and Plastic Deformation Aspects of Fatigue Crack Growth,* STP 637, American Society for Testing and Materials, 1977, p 97–121

53. R.P. Gangloff and R.O. Ritchie, Environmental Effects Novel to the Propagation of Short Fatigue Cracks, *Fundamentals of Deformation and Fracture,* K.J. Miller, Ed., Cambridge University Press, 1987

54. S.J. Hudak, Jr. and R.P. Wei, Consideration of Nonsteady State Crack Growth in Material Evaluation and Design, *Int. J. Pressure Vessels Piping,* Vol 9, 1981, p 63–74

55. R.P. Gangloff, Crack Size Effects on the Chemical Driving Force for Aqueous Corrosion Fatigue, *Metall. Trans. A,* 1987

56. C.S. Kortovich, Corrosion Fatigue of 4340 and D6AC Steels Below K_{ISCC}, *Proceedings of the 1974 Triservice Conference on Corrosion of Military Equipment,* AFML-TR- 75-42, Air Force Materials Laboratory, Wright-Patterson Air Force Base, 1975

57. D.B. Dawson and R.M. Pelloux, Corrosion Fatigue Crack Growth of Titanium Alloys in Aqueous Environments, *Metall. Trans. A,* Vol 5, 1974, p 723–731

58. J.M. Barsom, Corrosion Fatigue Crack Propagation Below K_{ISCC}, *Eng. Fract. Mech.,* Vol 3, 1971, p 15–25

59. B. Tompkins and P.M. Scott, Environment Sensitive Fracture: Design Considerations, *Met. Technol.,* Vol 9, 1982, p 240–248

60. P.M. Scott, Effects of Environment on Crack Propagation, *Developments in Fracture Mechanics—II,* G.G. Shell, Ed., Applied Science, 1979, p 221–257

61. J.P. Gallagher, "Corrosion Fatigue Crack Growth Rate Behavior Above and Below K_{ISCC}," Report NRL-7064, Naval Research Laboratory, 1970

62. R.P. Gangloff, Exxon Research and Engineering Company, unpublished research, 1984

63. A. Turnbull, Progress in the Understanding of the Electrochemistry in Cracks, *Embrittlement by the Localized Crack Environment,* R.P. Gangloff, Ed., The Metals Society and the American Institute of Mining, Metallurgical, and Petroleum Engineers, 1984, p 3–31

64. R.N. Parkins, Prevention of Environment Sensitive Cracking by Inhibition, *Embrittlement by the Localized Crack Environment,* R.P. Gangloff, Ed., The Metals Society and the American Institute of Mining, Metallurgical, and Petroleum Engineers, 1984, p 385–404

65. M.O. Speidel, M.J. Blackburn, T.R. Beck, and J.A. Feeney, Corrosion Fatigue and Stress Corrosion Crack Growth in High Strength Aluminum Alloys, Magnesium Alloys and Titanium Alloys Exposed to Aqueous Solutions, *Corrosion Fatigue: Chemistry, Mechanics and Microstructure,* O. Devereux, A.J. McEvily, and R.W. Staehle, Ed., National Association of Corrosion Engineers, 1973, p 324–345

66. R.O. Ritchie, Application of Fracture Mechanics to Fatigue, Corrosion Fatigue and Hydrogen Embrittlement, *Analytical and Experimental Fracture Mechanics,* G.C. Sih, Ed., Sithoff and Noorohoff, 1981, p 81–108

67. S. Suresh and R.O. Ritchie, The Propagation of Short Fatigue Cracks, *Int. Met. Rev.,* 1987

68. L.K.L. Tu and B.B. Seth, Threshold Corrosion Fatigue Crack Growth in Steels, *J. Test. Eval.,* Vol 6, 1978, p 66–74

69. S.J. Hudak, Jr. and R.J. Bucci, Ed., *Fatigue Crack Growth Measurement and Data Analysis,* STP 738, American Society for Testing and Materials, 1981

70. R.P. Gangloff, Electrical Potential Monitoring of the Formation and Growth of Small Fatigue Cracks in Embrittling Environments, *Advances in Crack Length Measurement,* C.J. Beevers, Ed., Engineering Materials Advisory Services, 1982, p 175–230

71. J.K. Donald, Fatigue Crack Propagation and the Role of Automated Testing, *ASTM Stand. News,* Vol 13 (No. 11), Nov 1985, p 50–53

72. C.J. Beevers, Ed., *Advances in Crack Length Assessment,* Engineering Materials Advisory Service, 1982

B. Phull, Evaluating Corrosion Fatigue, *Corrosion: Fundamentals, Testing, and Protection*, Vol 13A, *ASM Handbook*, ASM International, 2003, p 625–638

Evaluating Corrosion Fatigue

Revised by Bopinder Phull, Consultant

Selected References

- C. Amzallag, Ed., *Automation in Fatigue and Fracture Testing and Analysis,* STP 1231, American Society for Testing and Materials, 2002
- *Fatigue and Fracture,* Vol 19, *ASM Handbook,* ASM International, 1996
- S. Kalluri and P.J. Bonacuse, Ed., *Multiaxial Fatigue and Deformation: Testing and Prediction,* STP 1387, American Society for Testing and Materials, 2000
- R.I. Stephens, A. Fatemi, R.R. Stephens, and H.O. Fuchs, *Metal Fatigue in Engineering,* 2nd ed., J. Wiley & Sons, 2001
- S. Suresh, *Fatigue of Metals,* 2nd ed., Cambridge University Press, 1998

D. Aylor, Evaluating Erosion Corrosion, Cavitation, and Impingement, *Corrosion: Fundamentals, Testing, and Protection*, Vol 13A, *ASM Handbook*, ASM International, 2003, p 639–643

Evaluating Erosion Corrosion, Cavitation, and Impingement

Revised by Denise Aylor, Naval Surface Warfare Center, Carderock Division, and Bopinder Phull, Consultant

Introduction

EROSION, CAVITATION, AND IMPINGEMENT are mechanically assisted forms of material degradation. Erosion, in the context of this article, is defined as the progressive loss of material from a solid surface due to mechanical interaction between that surface and a fluid; therefore, any equipment that is exposed to moving fluids may be susceptible to erosion. Cavitation is caused by the formation and collapse of vapor bubbles in a liquid near a metal surface. Impingement refers to damage caused by liquid jets, droplets, or solid particles impacting a solid surface.

Mechanical damage to metal surfaces removes protective films. These films can be air- formed passive oxides, as in the case of stainless steels, nickel-base alloys, and titanium alloys; or corrosion-product films, as in the case of copper- base alloys. Any process that removes the protective films and interferes with their quick reformation exposes the substrate to electrochemical corrosion. Hence the terms *erosion corrosion, cavitation corrosion,* and *impingement corrosion* connote material damage caused by the conjoint action of mechanical and electrochemical factors. More information on the mechanisms of these forms of attack is available in Ref 1 and 2.

Erosion, cavitation, impingement, and even corrosive wear are often “interrelated,” which is why it is not always possible to easily distinguish between them, especially in actual component failures in service environments. The presence of entrained solids can also contribute significantly to erosion (abrasive wear) of materials. Laboratory tests used to evaluate erosion, cavitation, and impingement damage on metals include the following (Ref 3, 4, 5, 6, 7, 8, 9):

- High-velocity flow tests, including venturi tubes, rotating disks, and ducts containing specimens in throat sections
- High-frequency vibratory tests using either magnetostriction devices or piezoelectric devices
- Impinging jet tests using either stationary or rotating specimens exposed to high-speed jet or droplet impact

These tests are generally designed to provide high-erosion intensities on small specimens in relatively short times. These methods may not closely simulate service conditions, but they are useful for ranking candidate materials.

References cited in this section

1. M.G. Fontana, *Corrosion Engineering,* 3rd ed., McGraw-Hill, 1986
2. Wear Failures, *Failure Analysis and Prevention,* Vol 11, *ASM Handbook,* ASM International, 2002, p 899–1043
3. J.Z. Lichtman, D.H. Kallas, and A. Rufolo, Evaluating Erosion (Cavitation) Damage, *Handbook of Corrosion Testing and Evaluation,* W.H. Ailor, Ed., John Wiley & Sons, 1971, p 453–472

4. "Standard Method of Vibratory Cavitation Erosion Test," G 32, *Annual Book of ASTM Standards,* ASTM International

5. "Standard Practice for Liquid Impingement Erosion Testing," G 73, *Annual Book of ASTM Standards,* ASTM International

6. "Standard Test Method for Determination of Slurry Abrasivity (Miller Number) and Slurry Abrasion Response of Materials (SAR Number)," G 75, *Annual Book of ASTM Standards,* ASTM International

7. "Standard Test Method for Conducting Erosion Tests by Solid Particle Impingement Using Gas Jets," G 76, *Annual Book of ASTM Standards,* ASTM International

8. "Standard Test Method for Erosion of Solid Materials by a Cavitating Liquid Jet," G 34, *Annual Book of ASTM Standards,* Vol 03.01, *Wear and Erosion, Metal Corrosion,* ASTM International, 2002

9. F.L. LaQue, *Marine Corrosion; Causes and Prevention,* J. Wiley & Sons, New York, 1975, p 53–71

D. Aylor, Evaluating Erosion Corrosion, Cavitation, and Impingement, *Corrosion: Fundamentals, Testing, and Protection,* Vol 13A, *ASM Handbook,* ASM International, 2003, p 639–643

Evaluating Erosion Corrosion, Cavitation, and Impingement

Revised by Denise Aylor, Naval Surface Warfare Center, Carderock Division, and Bopinder Phull, Consultant

---

Standard Test Methods

There are four ASTM International standards related to the evaluation of erosion, cavitation, and impingement. These are designations G 32 (Ref 4), G 73 (Ref 5), G 75 (Ref 6), and G 76 (Ref 7). All of these standards include definitions of terms related to cavitation, erosion, and impingement as well as information on specimen preparation, test conditions and procedures, and data interpretation.

ASTM G 32 is based on the generation and collapse of cavitation bubbles on a specimen surface vibrating at high frequency. It is used to evaluate the relative resistances of different materials to cavitation erosion.

Test Specimen. Reference 4 specifies a test specimen measuring 15.9 mm ± 0.05 mm (0.625 ± 0.002 in.) in diameter and not less than 4 mm (0.157 in.) and not more than 10 mm (0.393 in.) in thickness. More details on specimen requirements are provided in Ref 4.

The test apparatus (Fig. 1) produces axial oscillation of the test specimen, which is partially immersed in the test liquid. This is accomplished using either a magnetostrictive or piezoelectric transducer driven by an electronic oscillator or amplifier. The transducer vibrates at a frequency of 20 kHz. The apparatus must include some method of measuring the displacement amplitude of the transducer as well as a means of maintaining the specified test temperature.

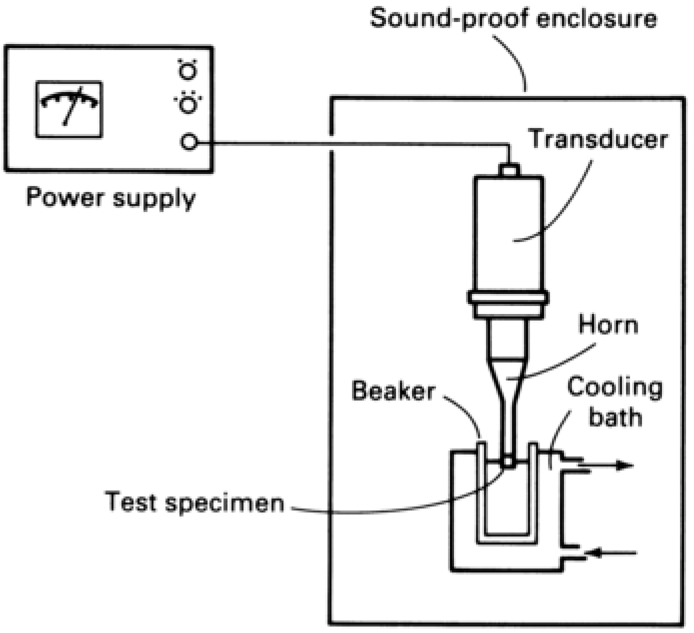

Fig. 1 Schematic of a typical vibratory erosion/cavitation test apparatus. Source: Ref 4

Test Conditions. The standard test liquid is distilled or other reagent water meeting the specifications of ASTM D 1193 ("Standard Specification for Reagent Water") maintained at a temperature of 25 ± 2 °C (77 ± 3.6 °F). Air is maintained over the test liquid at a pressure of not less than 6% from one standard atmosphere (101.3 kPa; 760 mm, or 29.92 in., of mercury). A peak-to-peak displacement amplitude of 0.05 mm (0.002 in.) ± 5% is specified for the oscillation of the test specimen. Alternatively, for weak, brittle, or nonmetallic materials that may be damaged too rapidly, a peak-to-peak displacement amplitude of 0.025 mm (0.001 in) is suggested.

Test conditions can be varied by using different test liquids, temperatures, and pressures. Any such variations must be noted when results are reported. Liquids other than reagent water that have been used include petroleum derivatives, glycerin, and liquid metals. Tests have shown that the erosion rate peaks strongly at a temperature about midway between the freezing point and the boiling point of the test liquid. Therefore, the erosion rate of a material in water at normal atmospheric pressure peaks at about 50 °C (122 °F) and falls off on either side of this value. The decrease in erosion rate is most dramatic as temperature rises above 50 °C (122 °F).

Test Procedure. The specimen must be cleaned and accurately weighed before testing, then immersed in the test liquid to a depth of 12 ± 4 mm (0.47 ± 0.16 in). The peak-to-peak displacement amplitude should be monitored constantly. The test should be interrupted periodically to determine the mass loss of the specimen, which should be carefully cleaned and dried before reweighing. The time between measurements should be such that a plot of cumulative mass loss versus exposure time can be established. The time between measurements, therefore, depends on the specimen material; softer materials (for example, aluminum alloys) can be examined every 15 min, while the interval between measurements for a harder material, such as Stellite alloy 6B, may range from 8 to 10 h. Testing should be continued at least until the erosion rate reaches a maximum and begins to diminish. When several materials are being compared, all should be tested until they reach comparable mean depths of erosion.

Data Acquisition and Reporting. The mean depth of erosion of the specimen should be calculated based on the full area of the test surface of the specimen. The report should include the following information:

- Alloy type, metallurgical condition, composition, and mechanical properties (including hardness)
- Specimen preparation, preferably including initial surface roughness measurement
- The number of specimens tested
- Tabulation of cumulative mass losses and cumulative exposure time for each specimen
- Plots of cumulative mean depth versus cumulative exposure time for each specimen

To facilitate comparisons between different materials, results are often expressed in terms of a single number based on the erosion resistance of the test specimen relative to that of a standard reference material. These types of ratings are discussed more fully in Ref 5.

The report should also include information on any deviations from the standard test procedure; for example, test liquid, temperature, or pressure as well as any unusual occurrences or observations. In addition, each test should include at least one of the standard reference materials to facilitate calculation of the normalized erosion resistance of the test materials. Annealed wrought Nickel 200 (UNS N02200), conforming to ASTM B 160, is a standard reference material. Reference materials of lesser and greater resistance, respectively, are: aluminum alloy 6061-T6 (UNS A96061) and annealed Type 316 stainless steel (UNS S31600; hardness 150–175 HV). These materials are also used to calibrate the testing apparatus.

ASTM G 134 (Ref 8) provides an alternative to ASTM G 32. A submerged cavitating jet, emanating from a nozzle, impinges on a test specimen causing cavities to collapse on it. This method allows comparison of the relative cavitation erosion resistance of solid materials as may be encountered in pumps, valves, ship propellers, diesel engines, and so forth. Although the test fluid is usually water, this test method can be used to compare the cavitation capacity in other liquids. The test apparatus, test specimens, reference materials, calculations, and data interpretation are detailed in Ref 8.

ASTM G 73 provides guidelines for liquid drop or jet impingement testing that, in addition to evaluating the resistance of metals, can be used to evaluate the degradation of optical properties of window materials and the destruction of coatings by the impinging liquid (Ref 5). The standard does not outline a single test method or apparatus but instead gives guidelines for setting up tests and specifies test and analysis procedures and the reporting of data.

Test Specimens. Metallic test specimens can be chosen to present a curved (airfoil or cylindrical) or flat surface to the impinging liquid. They can be machined from a solid bar or can be cut from sheet. If specimens are machined, care should be taken to avoid work hardening of the surface. Surface finish should range from 0.4 to 1.6 μm (16 to 63 μin.) rms (root mean square). If another surface finish is employed, it should be noted in the test report.

Test Apparatus. ASTM G 73 mainly addresses liquid-drop or jet-impingement test devices of the rotating disk type. In these tests, the specimen or specimens are attached to a rotating disk or arm, and their circular paths pass through one or more liquid jets or sprays, resulting in discrete impacts between the specimen and the droplets or the cylindrical surface of the jets. Peripheral velocities (and therefore impact velocities) ranging from about 50 m/s (165 ft/s) to as high as 1000 m/s (3280 ft/s) may be obtained, depending on the particular apparatus used. Figure 2 illustrates two examples of rotating disk test apparatuses.

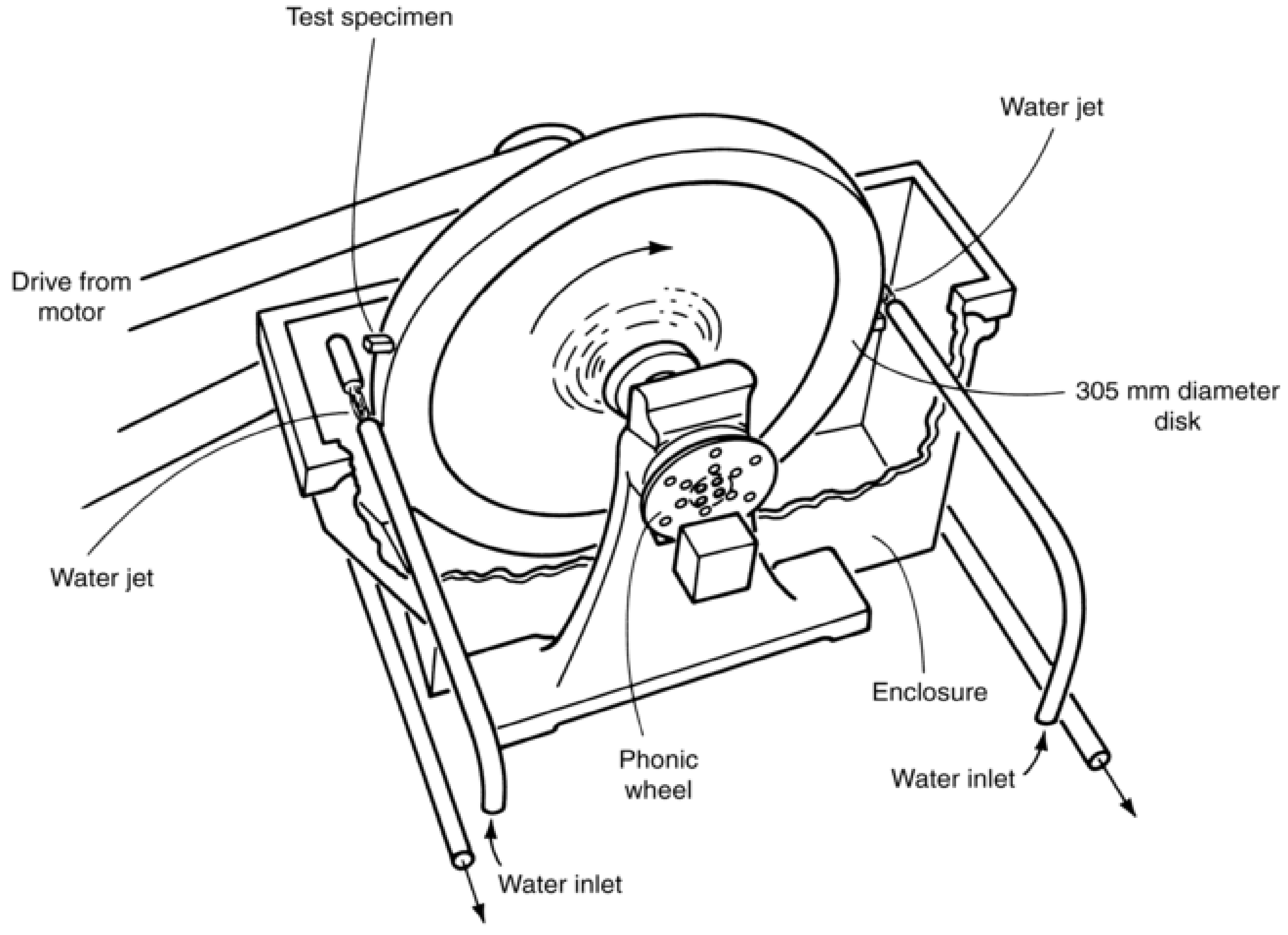
Test specimen
Water jet
Drive from motor
305 mm diameter disk
Water jet
Enclosure
Phonic wheel
Water inlet
Water inlet

(a)

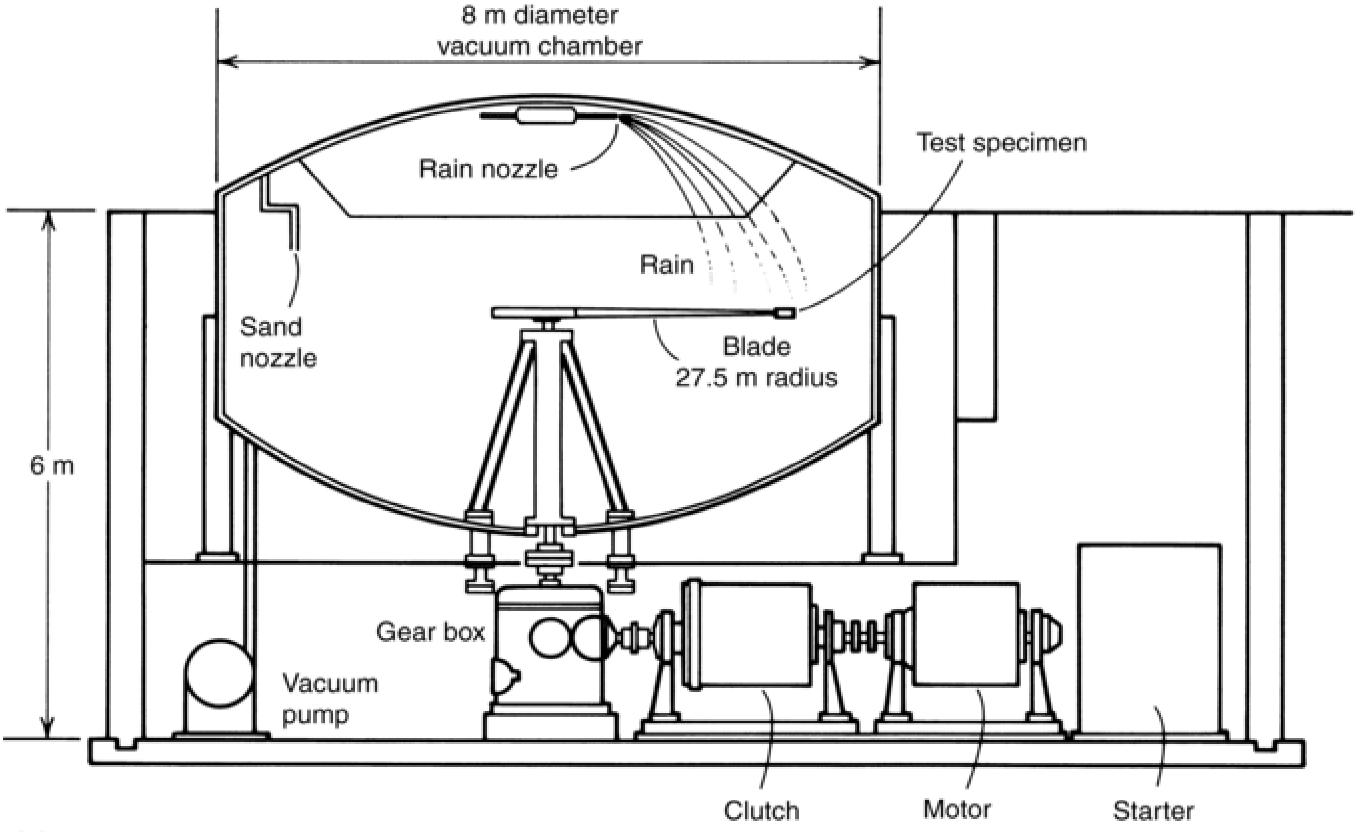
8 m diameter vacuum chamber
Test specimen
Rain nozzle
Rain
Sand nozzle
Blade 27.5 m radius
6 m
Gear box
Vacuum pump
Clutch
Motor
Starter

(b)

Fig. 2 Examples of rotating disk and rotating arm erosion/cavitation test apparatuses. (a) Small, relatively low-speed rotating disk and jet apparatus. (b) Large, high-speed rotating arm spray apparatus. Source: Ref 5

Droplet or jet diameters also vary from about 0.1 to 5 mm (0.004 to 0.2 in.). Droplets can be generated by spray nozzles, vibrating hollow needles, or rotating disks with water fed onto their surfaces. The typical droplet or jet diameter and the volume of liquid impacting the specimen per unit time should be determined within 10%. Jet diameter is usually assumed to be the same as the nozzle diameter. Other types of liquid-impact erosion test devices are also briefly described in Ref 5.

Test procedures for various materials vary to some extent. The standard gives procedures for structural materials and coatings, including metals, structural plastics, composites, and metals with ceramic or metallic coatings; elastomeric coatings; window materials; and transparent thin-film coatings on window materials. Details on these procedures are outlined in the standard.

Calculation of Erosion Resistance. Because it is currently not possible to define “absolute” erosion resistance, most investigators use comparative evaluations of different materials to quantify relative erosion resistance. ASTM G 73 details several approaches for calculating and presenting relative or normalized measures of erosion resistance for the various classes of materials considered. These include evaluation based on time to failure, total material loss, erosion rate-time patterns, incubation period, maximum erosion rate, and terminal erosion rate. Results for different materials can also be normalized by direct comparison to one of the designated reference materials: aluminum alloys 1100-0 or 6061-T6; annealed commercially pure 99.98% nickel (Nickel 270 used originally in the development of the standard may no longer be available; the alternative material is Ni 200, which has erosion resistance ~40% higher and incubation time ~60% greater than Ni 270); and Type 316 stainless steel, with a hardness between 155 and 170 HV. Indirect comparison to a standardized reference scale may also be done. Details on these procedures, as well as on the calculation of an apparatus severity factor, are given in ASTM G 73.

A jet-impingement test specifically designed for evaluating erosion-corrosion resistance of heat-exchanger tubing alloys is described in Ref 9. A submerged jet of liquid, emerging from a small orifice in a disc (made from a highly erosion-resistant material, e.g., titanium), is directed at a stationary test-specimen target. The degree of erosion corrosion is determined from overall mass loss and depth of attack at the impact area. The mean jet velocity is varied by using orifices of different sizes and selecting the appropriate liquid pressure. Multiple specimens can be tested at the same time at different impingement velocities. In addition to comparing performance of different alloys, the basic test setup can be used to evaluate efficacy of other corrosion control methods for mitigating erosion corrosion, for example, coatings, corrosion inhibitors, and cathodic protection.

ASTM G 75 (Ref 6) provides a test method to determine the relative abrasivity of a slurry or the resistance of different materials to the abrasivity of different slurries. Abrasion specifically refers to erosion caused by solid particles. The data are used to calculate a Miller number (slurry abrasivity) or a SAR number (material response to slurry abrasivity). These calculations provide useful information in selecting pumps and other equipment as well as in predicting the service life of pumps and related parts. The Miller number, which ranks abrasivity of slurries based on the wear of a standard reference block, increases as the wear damage on the reference block increases. The SAR number ranks the abrasion response of a material when tested in a slurry of interest and can be used to determine the most appropriate materials for use in particular slurries. Like the Miller number, the SAR number increases as the slurry damage on the test specimen increases.

Test Specimen. The test specimen used in assessing the slurry abrasivity (Miller number) is a standard wear reference block of a proprietary iron-chromium alloy (nominally 28% Cr, 2.5% C, 1% Mn, 0.8% V, 0.6% Si, 0.3% Mo, 0.25% Ni). The reference block is heat treated and machined to an approximate 25 × 13 × 5 to 7 mm (1 × 0.5 × 0.20 to 0.28 in.) size. The same specimen configuration is used for the SAR number test specimen, machined from the selected candidate material(s). Specimens should be wet ground flat using 320-grit silicon carbide paper prior to testing to remove any damage due to machining. After grinding, specimens should be scrubbed with detergent and water, rinsed, dried with a clean cloth, put under a heat lamp or blown dry for about 5 min, and then weighed.

Test Apparatus and Procedure. The test apparatus, which may be obtained commercially, positions the test specimen on a pivoted arm with a direct load applied. The specimen is driven in a horizontal, reciprocating motion along the bottom of a tray containing the slurry material. Each apparatus contains two to four operating arms, with a separate plastic tray for each arm. The specimen is lifted at one end of each stroke to allow fresh

slurry to flow underneath. Each tray holds about 300 mL (10.6 fluid oz) of slurry. The test is conducted in 2 h increments for a total test time of 6 h. Before each 2 h run, any slurry that has settled in the bottom of the trays is remixed using a suitable paddle. After each 2 h run, the specimens are removed from the test machine, scrubbed in water and detergent, rinsed, dried under a heat lamp or in an oven at about 175 °C (347 °F) for 15 min, and weighed. The specimens are then repositioned in the test machine at a 180° orientation to the first 2 h run. This method of alternating the specimen orientation before each 2 h run provides an averaging of the wear pattern on the specimen surface. A schematic of a typical Miller number test machine is included in Fig. 3.

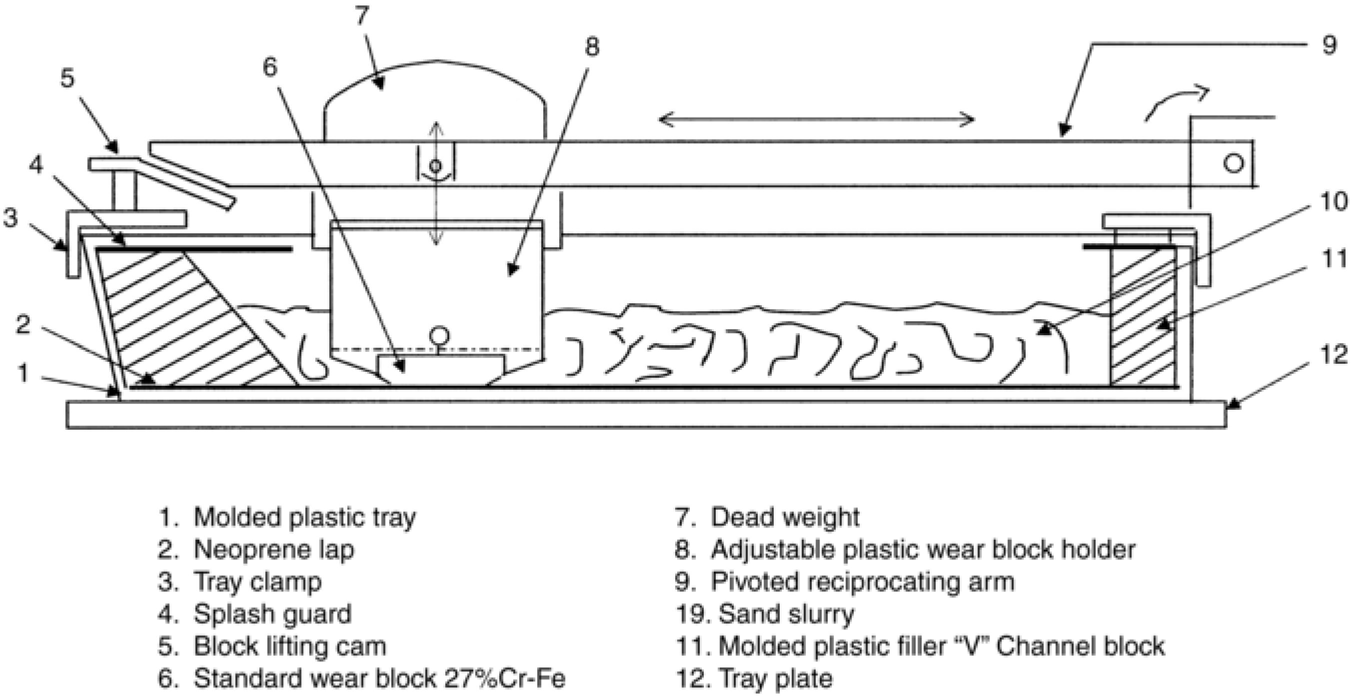

Fig. 3 Miller number machine layout. Source: Ref 6

Calculation of Miller Number and SAR Number. Mass measurements are recorded for the specimens initially and after a cumulative test time of 2, 4, and 6 h. The cumulative mass losses are averaged based on duplicate runs in a given slurry material. These test data are used to calculate both the Miller number and the SAR number. The Miller number is an index measuring slurry abrasivity and is related to the mass loss rate of duplicate reference-material wear blocks in a given slurry material. The SAR number is an index measuring material response to slurry abrasivity and is related to the mass loss rate of duplicate materials in a given slurry. Specifics of calculating these indexes are found in Ref 6; a computer program for calculating these indexes is also included in this standard.

ASTM Standard G 76 (Ref 7) describes a set of standard laboratory test conditions to determine material erosion from solid-particle impingement. This method can be used as a screening tool for evaluation of solid-particle erosion rates of different materials in simulated service environments. The test consists of repeatedly impacting gas-containing abrasive particles against the surface of a test specimen.

Test Specimen. A range of specimen sizes and configurations can be used for this test method as long as they are documented. A rectangular strip of size 10 × 30 × 2 mm (0.4 × 1.2 × 0.1 in.) is suggested as an appropriate specimen for this method.

Test Apparatus. The solid-particle erosion equipment available commercially must be capable of eroding material from a test specimen under controlled exposure conditions. A schematic of the equipment is shown in Fig. 4. The test apparatus must have the capability of controlling and adjusting the impact velocity of the particles, the particle flux, and the positioning of the specimen in relation to the impinging particle stream. Various systems, such as a vibrator-controlled hopper or a screw-feed system, can be utilized for injecting particles into the gas stream; however, the particle feed must be uniform and adjustable to allow the intended particle flow rate. The nozzle should be made of an erosion-resistant material like tungsten carbide or aluminum oxide, and the recommended size is 1.5 mm (0.06 in.) inner diameter by 50 mm (2.0 in.) long. The nozzle length-to-diameter ratio should be a minimum of 25 to 1 so that the particle velocity distribution in the gas stream is adequate.

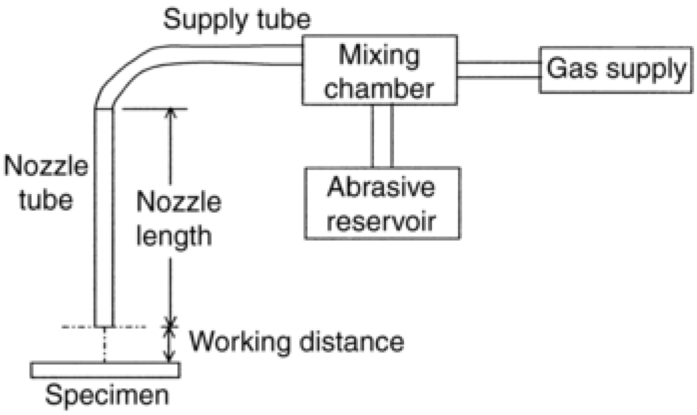

Fig. 4 Schematic drawing of solid particle erosion equipment. Source: Ref 7

The test apparatus must be calibrated to confirm satisfactory performance of the equipment. Calibration is recommended after every 50 tests or at the beginning of a new test program if the equipment has been inactive for a period of time. The calibration procedure utilizes Type 1020 steel specimens with 50 μm (0.002 in.) Al_2O_3 particles.
Test Conditions and Procedure. A summary of standard test conditions specified in ASTM G 76 is provided here:

- Nozzle tube dimensions: diameter 1.5 ± 0.075 mm (0.06 ± 0.003 in.); length, ≥50 mm (≥2 in.)
- Test gas: dry air, -50 °C (-60 °F) dew point or lower
- Abrasive particles: nominal 50 μm angular Al_2O_3; particles used only once
- Particle velocity: 30 ± 2 m/s (100 ± 7 ft/s)
- Gas flow rate ~8 L/min (0.3 ft^3/min) at 140 kPa (20 psig)
- Particle feed rate: 2.0 ± 0.5 g/min
- Test temperature: ambient (approximately 18–28 °C, or 65 to 80 °F)
- Test time: minimum 10 min to achieve steady state conditions; longer times permitted if final erosion crater no deeper than 1 mm (0.04 in.)
- Angle between nozzle axis and specimen surface: 90° ± 2°
- Distance from specimen surface to nozzle end: 10 ± 1 mm (0.4 ± 0.04 in.)

The test specimens are prepared for testing by grinding to a final surface roughness of 1 μm (40 μin.) rms or smaller. Specimens are then cleaned, weighed, and subjected to the particle impingement stream for a selected time interval. After each interval, specimens are removed from the test apparatus, recleaned, and reweighed. At least four test intervals are required for a total time of 10 min or more. For type 1020 steel, recommended cumulative test times are 2, 4, 8, and 16 min. Specimen mass loss is then plotted as a function of time, and the steady-state erosion rate of the material is determined from the slope of this plot.

References cited in this section

4. "Standard Method of Vibratory Cavitation Erosion Test," G 32, *Annual Book of ASTM Standards,* ASTM International

5. "Standard Practice for Liquid Impingement Erosion Testing," G 73, *Annual Book of ASTM Standards,* ASTM International

6. "Standard Test Method for Determination of Slurry Abrasivity (Miller Number) and Slurry Abrasion Response of Materials (SAR Number)," G 75, *Annual Book of ASTM Standards,* ASTM International

7. "Standard Test Method for Conducting Erosion Tests by Solid Particle Impingement Using Gas Jets," G 76, *Annual Book of ASTM Standards,* ASTM International

8. “Standard Test Method for Erosion of Solid Materials by a Cavitating Liquid Jet,” G 34, *Annual Book of ASTM Standards,* Vol 03.01, *Wear and Erosion, Metal Corrosion,* ASTM International, 2002

9. F.L. LaQue, *Marine Corrosion; Causes and Prevention,* J. Wiley & Sons, New York, 1975, p 53–71

D. Aylor, Evaluating Erosion Corrosion, Cavitation, and Impingement, *Corrosion: Fundamentals, Testing, and Protection,* Vol 13A, *ASM Handbook,* ASM International, 2003, p 639–643

Evaluating Erosion Corrosion, Cavitation, and Impingement

Revised by Denise Aylor, Naval Surface Warfare Center, Carderock Division, and Bopinder Phull, Consultant

---

Other Tests

Numerous other techniques are available for evaluating cavitation, erosion, and impingement in the laboratory. Most of these are variations on the methods already described, employing rotating disks, vibrating devices, or venturi tubes to achieve the required fluid velocities (Ref 10). Another device used to produce cavitation, erosion, and impingement is the liquid gun, which projects short, discrete slugs of liquid from a nozzle onto the specimen (Ref 11). Another method includes evaluation of materials or prototype components in simulated service conditions such as seawater valves in a test piping loop (Ref 12). Details of other nonstandard test procedures are available in Ref 13 to 16.

References cited in this section

10. C.M. Preece, Ed., *Erosion,* Vol 16, *Treatise on Materials Science and Engineering,* Academic Press, 1979

11. M.C. Rochester and J.H. Brunton, Influence of Physical Properties of the Liquid on the Erosion of Solids, *Erosion, Wear, and Interfaces With Corrosion,* STP 567, ASTM International, 1974, p 128–147

12. R.L. Ruedisueli and D.M. Aylor, “Erosion Resistance Testing for Candidate Seawater Valve Materials, Paper 468, NACE International, 2001

13. M. Matsumura, Y. Oka, S. Okumoto, and H. Furuya, Jet-in-Slit Test for Studying Erosion-Corrosion, *Laboratory Corrosion Tests and Standards,* STP 866, G.S. Haynes and R. Baboian, Ed., ASTM International, 1985, p 358–372

16. B.W. Madsen and R. Blickensderfer, “A New Flow-Through Slurry Erosion Wear Test,” *Slurry Erosion: Uses, Applications and Test Methods,* STP 946, ASTM International, 1987, p 169–183

D. Aylor, Evaluating Erosion Corrosion, Cavitation, and Impingement, *Corrosion: Fundamentals, Testing, and Protection*, Vol 13A, *ASM Handbook*, ASM International, 2003, p 639–643

Evaluating Erosion Corrosion, Cavitation, and Impingement

Revised by Denise Aylor, Naval Surface Warfare Center, Carderock Division, and Bopinder Phull, Consultant

Effects of Test Parameters (Ref 10)

Test conditions—including the temperature, pressure, flow velocity of the test liquid, frequency, amplitude, and distance between the specimen and the vibrating surface in a vibrating fluid—all influence the incubation and intensity of cavitation. The effects of varying these test parameters are described in the following paragraphs.

Variations in velocity and pressure should not be considered separately, because the intensity of erosion cavitation is a function of both parameters. Generally, erosion rates increase with velocity. A common technique used to evaluate the effect of velocity is to determine the number and size of pits produced in a soft material, such as aluminum, per unit time as velocity is varied (Ref 17). Although the number of pits observed increases over a wide range with velocity, the variation in pit size is relatively insignificant.

The influence of pressure has been investigated for both flow and vibratory cavitation (Ref 18, 19). In the former investigation, velocity was held constant and pressure was increased. Cavitation damage increased to a maximum and then decreased to zero at the pressure corresponding to cavitation inception (Ref 18). In vibratory testing, the erosion rate increased steadily with increasing pressure up to 4 atm, the maximum pressure obtainable in the device used (Ref 19). The authors noted, however, that at sufficient pressure, the cavitation rate would in fact drop to zero.

Temperature. As mentioned earlier in this article, erosion rate increases with temperature to a maximum and then decreases near the boiling point of the test liquid. The decrease in erosion rate near the boiling point is attributed to the increase in vapor pressure of the test liquid (Ref 10). The effect of temperature on the erosion rate of plain carbon steel in three aqueous environments is shown in Fig. 5.

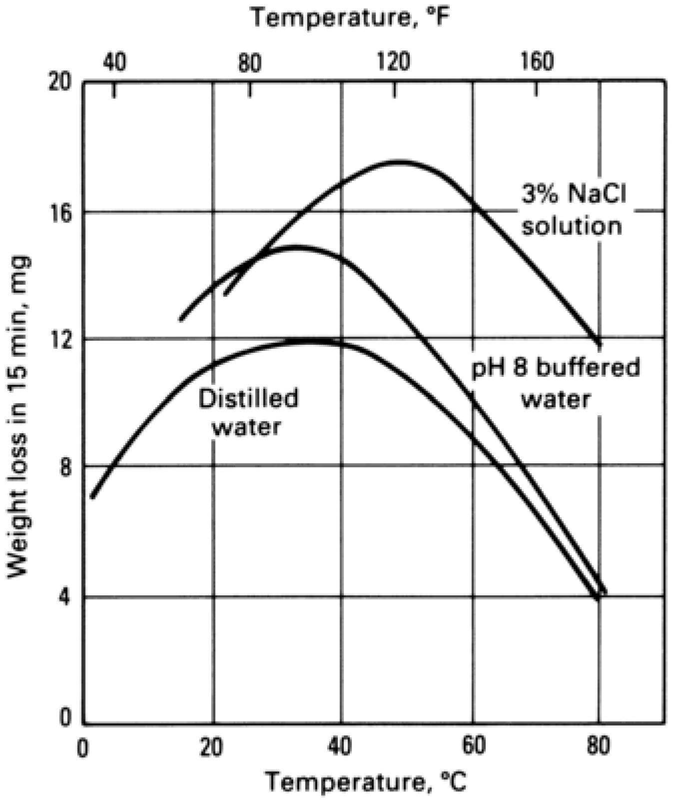

Fig. 5 Influence of temperature on the erosion rate of plain carbon steel in a vibratory cavitation device. Source: Ref 10

Amplitude and frequency in vibratory devices influence the degree of damage. In tests at constant frequency, erosion rate increased slightly with increasing amplitude (Ref 20). The incubation period for damage decreased with increasing amplitude.

Most vibratory devices operate at the resonant frequency of a piezoelectric crystal. Therefore, frequency cannot be easily varied over a significant range. In one investigation, three different devices with frequencies of 10, 20, and 30 kHz were used to determine the effect of frequency on erosion rate (Ref 20). The stress produced by the cavitation increased as frequency decreased, but the effect was not as significant as that caused by changes in amplitude.

Distance between Specimen and Vibrating Surface. The amount of erosion damage to a specimen rises to a maximum as the distance between the specimen and the vibrating surface decreases. At a frequency of 20 kHz, the position that results in maximum erosion rates is approximately 0.5 mm (0.02 in.) from the vibrating surface (Ref 10). The position of the maximum is independent of amplitude, but no data are available on the influence of frequency on this position.

The influence of fluid properties has been studied by several investigators. Unfortunately, most of them made little attempt to identify those properties of the fluid that affect erosion rates. One investigator, however, considered fluid viscosity, vapor pressure, surface tension, and specific gravity for water, gasoline, and the sodium- potassium eutectic (Ref 21). The temperature dependence of erosion rates was attributed to the effects of velocity and surface tension at low temperatures and to the increase in vapor pressure at high temperatures. By comparing the temperature dependence of properties of the different fluids, he was able to predict the variation in erosion damage in the three fluids. The resulting equation, however, cannot be used to predict erosion rates in other fluids.

References cited in this section

10. C.M. Preece, Ed., *Erosion,* Vol 16, *Treatise on Materials Science and Engineering,* Academic Press, 1979

17. R.T. Knapp, J.W. Daly, and F.G. Hammitt, *Cavitation,* McGraw-Hill, 1970

18. M.J. Robinson and F.G. Hammitt, *Trans. ASME D,* Vol 89, 1967, p 161

19. F.G. Hammitt and D.O. Rogers, *J. Mech. Eng. Sci.,* Vol 12, 1970, p 432

20. B. Vyas and C.M. Preece, *J. Appl. Phys.,* Vol 47, 1976, p 5133

21. W.C. Leith, *Proc. ASTM,* Vol 65, 1965, p 789

D. Aylor, Evaluating Erosion Corrosion, Cavitation, and Impingement, *Corrosion: Fundamentals, Testing, and Protection*, Vol 13A, *ASM Handbook*, ASM International, 2003, p 639–643

Evaluating Erosion Corrosion, Cavitation, and Impingement

Revised by Denise Aylor, Naval Surface Warfare Center, Carderock Division, and Bopinder Phull, Consultant

---

Data Correlations

Correlations among Test Methods (Ref 3). Investigations have indicated that there are considerable differences in the erosion intensities produced by different test techniques (that is, high-velocity flow, vibratory, and impingement) and test parameters (vibratory frequency and specimen size and shape). There is, however, general agreement on the ranking of test materials. When the erosion resistance of a material is expressed as a

normalized erosion resistance (NER), which is the ratio of the erosion rate of the test material to that of a standard material, results from different test methods and different laboratories can be directly compared and are reasonably consistent (Ref 22). Calculation of NER values and statistical analysis of erosion- rate data are discussed in detail in Ref 5, which also reports on the results of interlaboratory testing using a liquid impingement testing method at three specified velocities.

Correlations between Laboratory Results and Service (Ref 3). Methods to identify service-erosion intensities under conditions of controlled operation include: aluminum panels attached to hydraulic turbine vanes (Ref 23), a strain gage technique for measuring the relative intensities of laboratory and service devices (Ref 24), and the use of a radioactive paint to correlate the erosion intensity of an operating turbine with an erosion-rate index (Ref 25). This latter investigation led to the establishment of relative resistance scales, in which laboratory exposures of 1 to 2 h in a vibratory apparatus can be compared with 16 to 100 h exposures in a venturi apparatus and with months of operation in full-scale turbines. Another investigation (Ref 26) used a combination approach to determine erosion characteristics by (1) measuring (with the aid of a magnetic thickness gage) "wear" of an epoxy coating applied to a pump casing and impeller and (2) computing "wear" of the substrate metal by the thin-layer-activation technique (i.e., monitoring loss of radionuclides induced on the original surfaces).

References cited in this section

3. J.Z. Lichtman, D.H. Kallas, and A. Rufolo, Evaluating Erosion (Cavitation) Damage, *Handbook of Corrosion Testing and Evaluation,* W.H. Ailor, Ed., John Wiley & Sons, 1971, p 453–472

22. F.J. Heymann, "Toward Quantitative Prediction of Erosion Damage," Report E-1463, Westinghouse Electric Corporation, Development Engineering Department, June 1969

23. R.T. Knapp, "Accelerated Field Tests of Cavitation Intensities," Paper 56-A-57, American Society of Mechanical Engineers, 1956

24. R. Canavelis, The Investigation of Cavitation Damage by Means of Resistance Gages, *Cavitation Research Facilities and Techniques,* J.W. Holt and G.M. Wood, Ed., American Society of Mechanical Engineers, 1964

25. S.L. Kerr and K. Rosenberg, An Index of Cavitation Erosion by Means of Radioisotopes, *Trans. ASME,* Vol 80 (No. 6), Aug 1958, p 1308–1314

26. M.C. Rocco, P. Nair, and G.R. Addie, "Test Approach for Dense Slurry Erosion", *Slurry Erosion: Uses, Applications and Test Methods,* STP 946, ASTM International, 1987, p 185–210

D. Aylor, Evaluating Erosion Corrosion, Cavitation, and Impingement, *Corrosion: Fundamentals, Testing, and Protection*, Vol 13A, *ASM Handbook*, ASM International, 2003, p 639–643

Evaluating Erosion Corrosion, Cavitation, and Impingement

Revised by Denise Aylor, Naval Surface Warfare Center, Carderock Division, and Bopinder Phull, Consultant

---

Acknowledgment

This article has been adapted from Evaluation of Erosion and Cavitation, *Corrosion,* Volume 13, *ASM Handbook* (formerly 9th ed. *Metals Handbook*), ASM International, 1987, pages 311 to 313.

D. Aylor, Evaluating Erosion Corrosion, Cavitation, and Impingement, *Corrosion: Fundamentals, Testing, and Protection*, Vol 13A, *ASM Handbook*, ASM International, 2003, p 639–643

Evaluating Erosion Corrosion, Cavitation, and Impingement

Revised by Denise Aylor, Naval Surface Warfare Center, Carderock Division, and Bopinder Phull, Consultant

References

1. M.G. Fontana, *Corrosion Engineering,* 3rd ed., McGraw-Hill, 1986
2. Wear Failures, *Failure Analysis and Prevention,* Vol 11, *ASM Handbook,* ASM International, 2002, p 899–1043
3. J.Z. Lichtman, D.H. Kallas, and A. Rufolo, Evaluating Erosion (Cavitation) Damage, *Handbook of Corrosion Testing and Evaluation,* W.H. Ailor, Ed., John Wiley & Sons, 1971, p 453–472
4. "Standard Method of Vibratory Cavitation Erosion Test," G 32, *Annual Book of ASTM Standards,* ASTM International
5. "Standard Practice for Liquid Impingement Erosion Testing," G 73, *Annual Book of ASTM Standards,* ASTM International
6. "Standard Test Method for Determination of Slurry Abrasivity (Miller Number) and Slurry Abrasion Response of Materials (SAR Number)," G 75, *Annual Book of ASTM Standards,* ASTM International
7. "Standard Test Method for Conducting Erosion Tests by Solid Particle Impingement Using Gas Jets," G 76, *Annual Book of ASTM Standards,* ASTM International
8. "Standard Test Method for Erosion of Solid Materials by a Cavitating Liquid Jet," G 34, *Annual Book of ASTM Standards,* Vol 03.01, *Wear and Erosion, Metal Corrosion,* ASTM International, 2002
9. F.L. LaQue, *Marine Corrosion; Causes and Prevention,* J. Wiley & Sons, New York, 1975, p 53–71
10. C.M. Preece, Ed., *Erosion,* Vol 16, *Treatise on Materials Science and Engineering,* Academic Press, 1979
11. M.C. Rochester and J.H. Brunton, Influence of Physical Properties of the Liquid on the Erosion of Solids, *Erosion, Wear, and Interfaces With Corrosion,* STP 567, ASTM International, 1974, p 128–147
12. R.L. Ruedisueli and D.M. Aylor, "Erosion Resistance Testing for Candidate Seawater Valve Materials, Paper 468, NACE International, 2001
13. M. Matsumura, Y. Oka, S. Okumoto, and H. Furuya, Jet-in-Slit Test for Studying Erosion-Corrosion, *Laboratory Corrosion Tests and Standards,* STP 866, G.S. Haynes and R. Baboian, Ed., ASTM International, 1985, p 358–372
14. J.M. Hobbs, Report 69, National Engineering Laboratory, 1962
15. J.W. Holt and G.M. Wood, Ed., *Cavitation Research Facilities and Techniques,* American Society of Mechanical Engineers, 1964

16. B.W. Madsen and R. Blickensderfer, "A New Flow-Through Slurry Erosion Wear Test," *Slurry Erosion: Uses, Applications and Test Methods,* STP 946, ASTM International, 1987, p 169–183

17. R.T. Knapp, J.W. Daly, and F.G. Hammitt, *Cavitation,* McGraw-Hill, 1970

18. M.J. Robinson and F.G. Hammitt, *Trans. ASME D,* Vol 89, 1967, p 161

19. F.G. Hammitt and D.O. Rogers, *J. Mech. Eng. Sci.,* Vol 12, 1970, p 432

20. B. Vyas and C.M. Preece, *J. Appl. Phys.,* Vol 47, 1976, p 5133

21. W.C. Leith, *Proc. ASTM,* Vol 65, 1965, p 789

22. F.J. Heymann, "Toward Quantitative Prediction of Erosion Damage," Report E-1463, Westinghouse Electric Corporation, Development Engineering Department, June 1969

23. R.T. Knapp, "Accelerated Field Tests of Cavitation Intensities," Paper 56-A-57, American Society of Mechanical Engineers, 1956

24. R. Canavelis, The Investigation of Cavitation Damage by Means of Resistance Gages, *Cavitation Research Facilities and Techniques,* J.W. Holt and G.M. Wood, Ed., American Society of Mechanical Engineers, 1964

25. S.L. Kerr and K. Rosenberg, An Index of Cavitation Erosion by Means of Radioisotopes, *Trans. ASME,* Vol 80 (No. 6), Aug 1958, p 1308–1314

26. M.C. Rocco, P. Nair, and G.R. Addie, "Test Approach for Dense Slurry Erosion", *Slurry Erosion: Uses, Applications and Test Methods,* STP 946, ASTM International, 1987, p 185–210

D. Aylor, Evaluating Erosion Corrosion, Cavitation, and Impingement, *Corrosion: Fundamentals, Testing, and Protection*, Vol 13A, *ASM Handbook*, ASM International, 2003, p 639–643

Evaluating Erosion Corrosion, Cavitation, and Impingement

Revised by Denise Aylor, Naval Surface Warfare Center, Carderock Division, and Bopinder Phull, Consultant

---

Selected References

- Abrasive Erosion and Corrosion of Hydraulic Machinery, C.G. Duan and V.Y. Karelin, Ed., Imperial College Press, London, 2002
- W.H. Ailor, Ed., *Handbook of Corrosion Testing and Evaluation,* J. Wiley & Sons, Inc., 1971
- R. Baboian, Ed., *Manual 20 Corrosion Tests and Standards: Application and Interpretation,* ASTM International, 1995
- P. Blau, Ed., *Friction, Lubrication, and Wear Technology,* Vol 18, *ASM Handbook,* ASM International, 1992
- R.W. Revie, Ed., *Uhlig's Corrosion Handbook,* 2nd Ed., J. Wiley & Sons, 2000

J.F.D. Stott, Evaluating Microbiologically Influenced Corrosion, *Corrosion: Fundamentals, Testing, and Protection*, Vol 13A, *ASM Handbook*, ASM International, 2003, p 644–649

Evaluating Microbiologically Influenced Corrosion

James F.D. Stott, CAPCIS Ltd., Manchester, United Kingdom

Introduction

MICROBIOLOGICAL CORROSION, more accurately termed microbiologically influenced corrosion (MIC), is not fundamentally different from other types of aqueous electrochemical corrosion; it is simply that the chemical or physical conditions giving rise to the aggressive environment are produced by microorganisms as by- products of their energy-obtaining metabolism. This may involve the production of an aggressive chemical agent such as hydrogen sulfide (H_2S) or acidity. Microorganisms may also consume chemical species that are important in corrosion reactions (e.g., oxygen or nitrite inhibitors). Alternatively, their physical presence may form a slime or poultice, which leads to differential aeration cell attack or crevice corrosion. They may also break down the desirable physical properties of lubricating oils or protective coatings (Ref 1, 2, 3). Microorganisms can therefore be viewed as catalytic entities, effectuating chemical reactions that would otherwise be negligible because of their high activation energy.

Microorganisms, including the corrosion-inducing microorganisms, are present almost everywhere in soils, freshwater, seawater, and air. Therefore, the mere detection of microorganisms in an environment does not necessarily indicate a corrosion problem. What is important is the number of microorganisms of the relevant types.

The salient characteristics of microorganisms from the engineer's viewpoint are that they are small, ubiquitous, potentially very rapid growing, and subject to certain common restraints, such as temperature, pH, and nutrient availability. A problem exists only when conditions become favorable for a specific microbial population to explode, giving rise to thousands or even millions of cells per gram of environmental material. Even then, most microorganisms are harmless from the standpoint of the corrosion engineer; therefore, it is important that the microbiological assessment is type-specific.

The purpose of this article is to address the issue of how an engineer might go about assessing the risk of MIC in an industrial situation. It is not the author's intent to describe in detail the mechanisms of microbiologically mediated corrosion nor to address remedial measures. The role of microorganisms in the corrosion of metals was the subject of a number of classic review articles in the 1970s and 1980s (Ref 4, 5, 6, 7). For more detailed recent reviews of the subject, the reader is referred to the article “Microbiologically Influenced Corrosion” in this Volume and the articles cited under the Selected References at the end of this article. However, it is useful to begin with some limited background information about MIC.

References cited in this section

1. R.T. Ross, J.R. Sladen, and L.A. Wienart, in *Biodeterioration of Materials,* A.H. Walters and J.J. Elphick, Ed., Elsevier, 1975, p 127–136

2. E.C. Hill, in *Biodeterioration of Materials,* A.H. Walters and J.J. Elphick, Ed., Elsevier, 1975, p 157–172

3. E.C. Hill, Biodeterioration of Petroleum Products, *Microbial Aspects of the Deterioration of Materials,* D.W. Lovelock and R.J. Gilbert, Ed., Academic Press, 1975, p 127–136

4. J.D.A. Miller and K.A. Tiller, *Microbial Aspects of Metallurgy,* Aylesbury, Medical and Technical Publishing Co., 1971, p 61–105

5. W.P. Iverson, *Microbial Iron Metabolism,* J.B. Niedlands, Ed., Academic Press, 1974

6. V. Kucera, *Microbial Corrosion—A Literature Survey,* Swedish Corrosion Institute, Stockholm, 1980

7. D.H. Pope, D. Duquette, P.C. Wayner, and H.J. Arland, Microbially Influenced Corrosion. A State-of-the-Art Review, Publication 13, Materials Technology Institute, Columbus, Ohio, 1984

J.F.D. Stott, Evaluating Microbiologically Influenced Corrosion, *Corrosion: Fundamentals, Testing, and Protection,* Vol 13A*, ASM Handbook,* ASM International, 2003, p 644–649

Evaluating Microbiologically Influenced Corrosion

James F.D. Stott, CAPCIS Ltd., Manchester, United Kingdom

Attack by Sulfate-Reducing Bacteria

The most important group of bacteria associated with corrosion is the sulfate-reducing bacteria (SRB). Most reviewers have approached the subject of MIC from the viewpoint of the microbiologist and have emphasized the complexity and diversity of metabolic processes. In practice, the great majority of MIC failures are related to the activities of SRB. Sulfate-reducing bacteria are anaerobic (oxygen-free) bacteria that obtain their required carbon from organic nutrients and their energy from the reduction of sulfate ions to sulfide.

Sulfate-reducing bacteria will only flourish and cause damage if they obtain sufficient sulfate. Sulfate is abundant in freshwaters, seawater, and soils. Sulfide appears as H_2S (dissolved or gaseous), HS^- ions, S^{2-} ions, metal sulfides, or a combination of these, according to conditions. Sulfides are highly corrosive to many materials. In the case of iron and mild steel, the characteristic black iron sulfide (FeS) corrosion products liberate H_2S on acid treatment, distinguishing them from black iron oxide (magnetite). The corrosion products are often loose and, when dislodged, exhibit pits lined with bright metal corresponding to areas of anodic dissolution.

Bacteria of this type can also use hydrogen by sulfate reduction:

$$4H_2 + SO_4^{2-} \rightarrow S^{2-} + 4H_2O$$

The most commonly encountered SRB type is known as *Desulfovibrio* (Fig. 1).

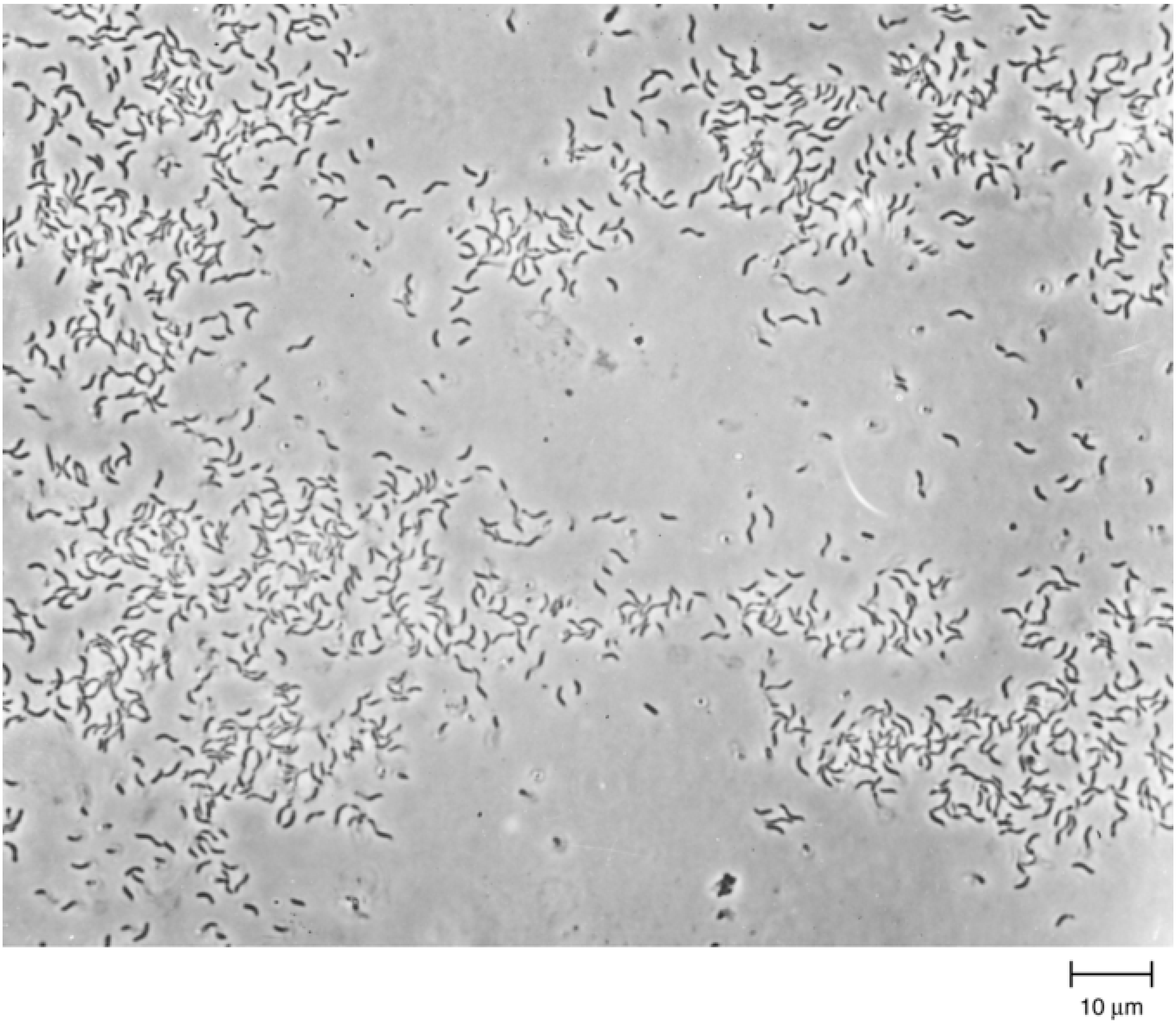

Fig. 1 Sulfate-reducing bacteria from the water bottom of an offshore oil storage tank

In natural conditions, SRB grow in association with other microorganisms and use a range of carboxylic acids and fatty acids, which are common by-products of other micro-organisms. Biological slimes are commonly found in the water phases of industrial process plants (Fig. 2). A wide range of common bacteria (e.g., *Pseudomonas* and *Flavobacterium*) can secrete large amounts of organic material under both aerobic and oxygen-free (anaerobic) conditions. Conditions at the base of even thin slimes (biofilms) can be ideal for the growth of SRB, with high organic nutrient status, no oxygen, low redox potential, and protection from biocidal agents. Figure 3 illustrates the steps in biofilm formation. The SRB can thereby produce active sulfide corrosion even in systems where the bulk liquid phase has a low nutrient status, a high oxygen concentration, and will not support growth of anaerobic bacteria.

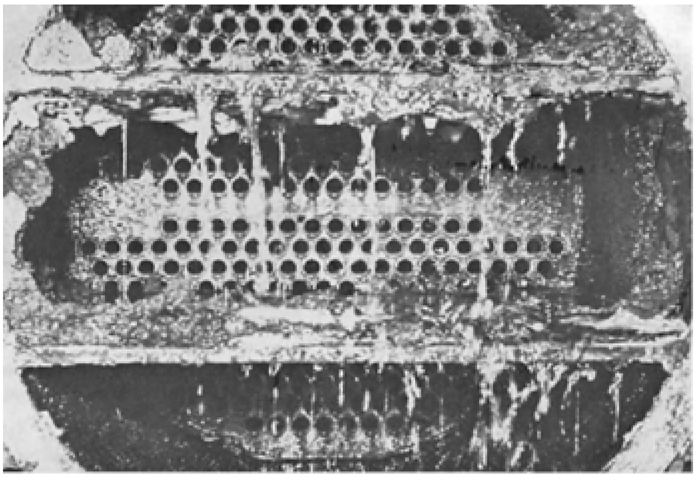

Fig. 2 Biofouling in a heat exchanger

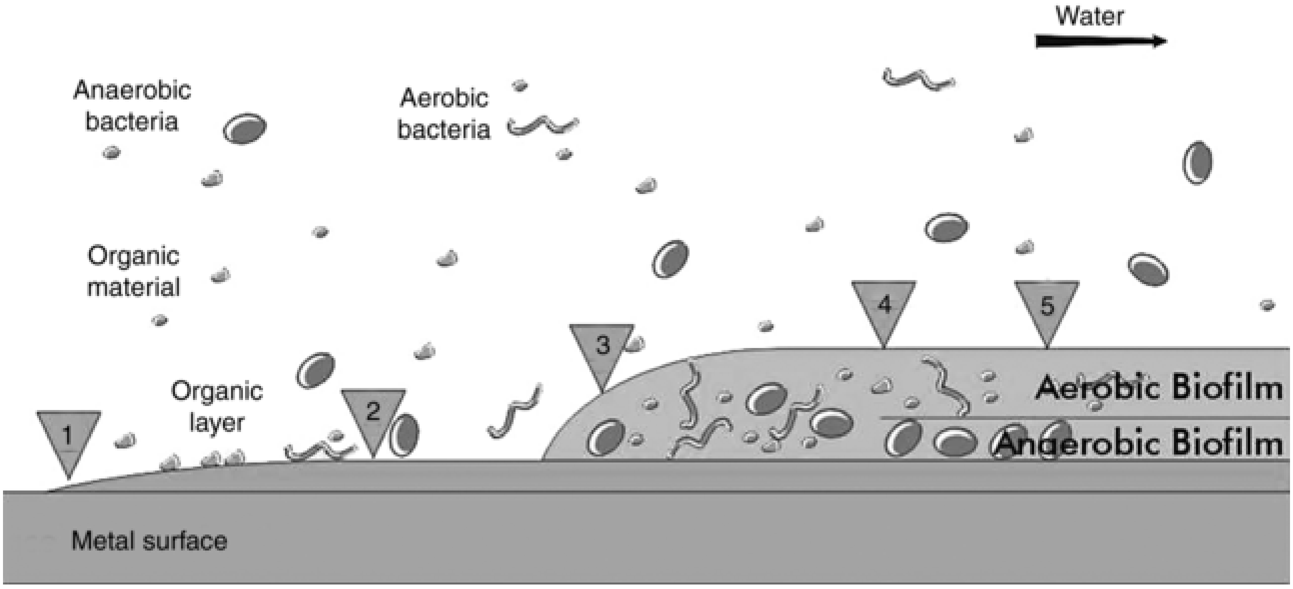

Fig. 3 Steps in biofilm formation

Most *Desulfovibrio* will only grow in the pH range 5 to 10 and the temperature range 5 to 45 °C (40 to 115 °F), up to a pressure limit of approximately 50 MPa (500 atm) (Ref 8). Some less common groups of SRB have the ability to grow at elevated temperatures up to at least 70 °C (160 °F). Reference 9 cites two cases of corrosion by thermophilic SRB activity: one case being in a tank of hot molasses at a sugar refinery, the second being a transformer tank buried in London clay, where the temperature was 60 to 80 °C (140 to 175 °F) for long periods.

Systems that are susceptible to the effects of MIC by SRB include oil fields (due to use of contaminated drilling mud and injection water), low-velocity lines and storage tanks, aircraft jet fuel tanks and lines, hydrotest waters, cooling waters, and wastewaters.

The petroleum-production industry has been particularly plagued by the activities of SRB, because it handles large volumes of deaerated water. These waters can become very sour with H_2S if infection with SRB occurs. The situation in the oil industry is the subject of a useful, practical review by NACE International (Ref 10). The phenomenon of unexpected increase in H_2S levels in produced fluids from petroleum reservoirs (reservoir souring) has been observed over a period of many years in different areas of the world (Ref 11, 12, 13, 14, 15, 16). Most workers in the field have directed attention to the activities of the SRB, and considerable money has been invested in biocide treatment programs for water injection, with the principal aim of killing or controlling this group of microorganisms (Ref 8).

The mechanism of SRB-mediated sulfide corrosion of ferrous metals has been well reviewed (Ref 17). It involves H_2S and FeS. Corrosion rates tend to be slow at first and then accelerate with time (Ref 18).

The muddy bottom of any relatively stagnant body of water with a high biological oxygen demand often supports massive growth of SRB, as may waterlogged soils. Any metallic installations buried or immersed in such environments can be expected to suffer badly from microbiological corrosion. The most serious economic problem is to pipelines, although sheet piles, hulls of ships, piers, and so on are frequently attacked. In some instances, cast iron pipes of 6.3 mm (0.25 in.) thickness have become perforated within 1 year under such conditions, while perforation in 3 years is common.

A large-scale study of many factors at 59 sites in the United Kingdom (Ref 19, 20) led to the suggestion that aggressive sites were characterized by soil resistivity of less than 20 Ω · m (2000 Ω · cm) or a mean redox potential more negative than +400 mV (on the hydrogen scale) at pH 7. Borderline cases were classified according to water content—those containing more than 20% water being deemed aggressive soils. Similarly, all soils with a mean soluble iron content of over 120 μg/g were found to be aggressive. A particularly corrosive situation is when H_2S diffuses upward into the aerated zone, where it becomes oxidized by air to sulfur (Ref 21).

There is a widespread belief that copper and its alloys are toxic to microorganisms and therefore are not susceptible to MIC. This notion is false. Copper alloys are much less toxic to bacteria than they are to macrofouling organisms, such as seaweed or shellfish, and suffer severe attack by sulfide if conditions allow the growth of SRB. A gun-metal impeller that was located in a polluted harbor (Fig. 4) failed in a matter of weeks after the pump was switched off, due to the growth of SRB in the stagnant pump. The component had previously given 2 years of trouble-free operation in aerated seawater.

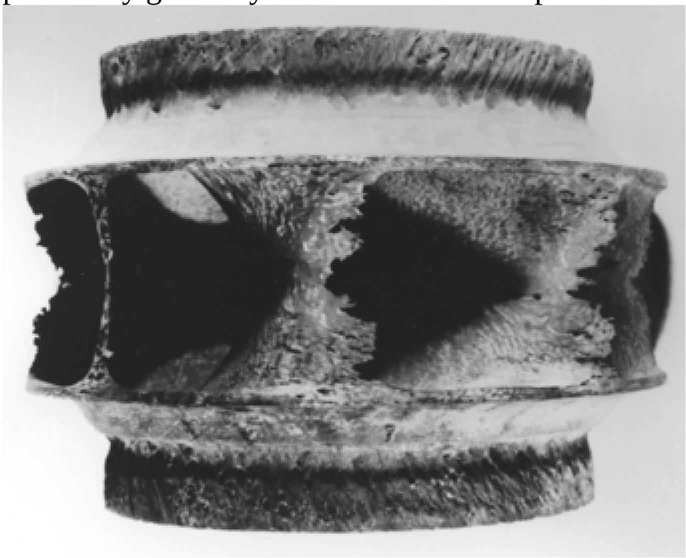

Fig. 4 Copper alloy impeller failure due to sulfate-reducing bacteria in stagnant seawater

Cases of mysterious underdeposit or underfouling pitting corrosion of copper-nickel heat-exchanger tubes have been observed. Many of these failures are demonstrably due to biogenic sulfide produced by SRB. When copper alloys are electrically linked into a cathodic protection system, they tend to lose their antifouling properties and become susceptible to attack by SRB colonies underneath the consequent fouling mat if insufficient protective current is reaching the substrate surface to polarize it into the immunity zone. Silver suffers very severe attack by SRB in a similar way to copper.

Numerous examples of corrosion of stainless steel and higher active/passive alloys involving sulfide production by SRB have been published (Ref 22, 23). This phenomenon is best termed microbiologically assisted, chloride-induced pitting attack. Active/passive alloys are susceptible to localized pitting by chloride ions. Reduced sulfur compounds produced by SRB appear to bind to the metal surface and catalyze the initiation of this process at much lower chloride concentration and at lower temperatures than would otherwise be the case.

Once a pit is established, the anodic reaction generates acidic conditions, accelerating the corrosion rate and causing flask-shaped cavities to form (Fig. 5). This is totally different from the shallow pitting attack of low-alloy materials exemplified in Fig. 6. The pits may be concealed beneath ferric hydroxide, and the process is often associated with copious amounts of brown-colored biological slime containing iron-oxidizing bacteria known as *Gallionella.* A typical example is shown in Fig. 7.

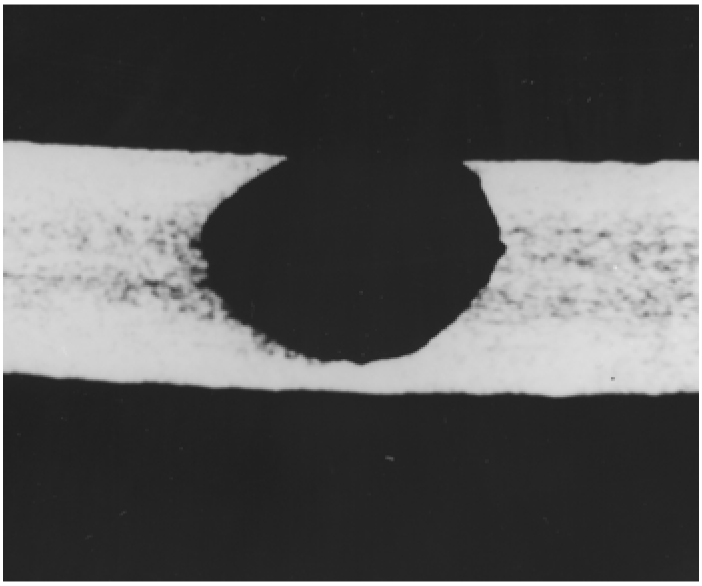

Fig. 5 Flask-shaped pit in an American Iron and Steel Institute (AISI) 304 (Unified Numbering System, or UNS, S30400) stainless steel pipe of 5 mm (0.2 in.) wall thickness

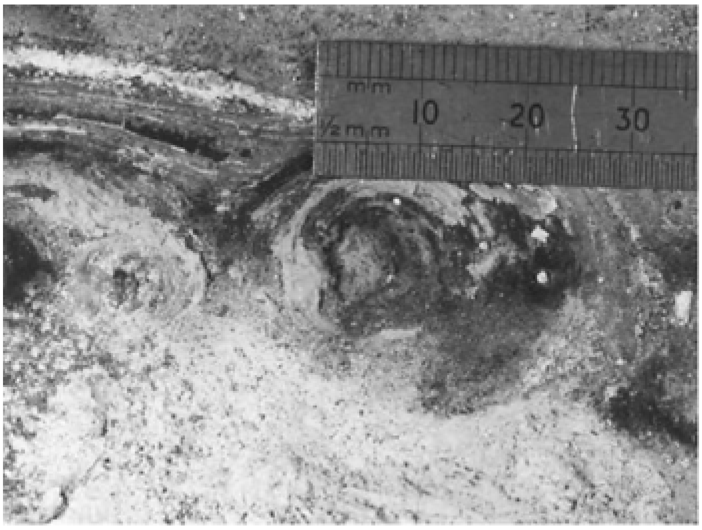

Fig. 6 Microbiologically influenced corrosion in a water pipe due to sulfate-reducing bacteria

Fig. 7 Slime formation by iron bacteria, *Gallionella,* in the pitted stainless steel pipe shown in Fig. 5

Bacterial metabolism is only involved in the pit initiation stage. Once the pit has formed and acidic chloride conditions develop within, the pit propagation process is the same as with any other case of chloride-induced pitting. Claims that MIC of stainless steels is characterized by a particular pit morphology, different from conventional chloride-induced pitting attack, should therefore be viewed with some skepticism.

References cited in this section

8. J.F.D. Stott and B.N. Herbert, *J. Appl. Bacteriol.,* Vol 60, 1986, p 57–66
9. J.R. Postgate, *The Sulphate-Reducing Bacteria,* Cambridge University Press, 1979
10. "The Role of Bacteria in the Corrosion of Oilfield Equipment," NACE TPC 3, National Association of Corrosion Engineers, 1976
11. R.L. Ginter, *Bull. Am. Assoc. Petrol. Geol.,* Vol 14, 1930, p 139
12. *Oil Gas J.,* Nov 1964, p 207
13. G.L. Gates and C.F. Parent, *Oil Gas J.,* Aug 1976, p 115
14. B.H. Moore, *World Oil,* March 1984, p 100
15. F.D.S. Al Sawaf, *Econ. Geol.,* Vol 72, 1977, p 608
16. S.L. Ege, C.J. Houghton, and P.T. Tucker, Second Annual Workshop on Secondary Recovery Technology, June 1985 (London)
17. J.A. Costello, "The Mechanism of the Corrosive Effect of SRB," Ph.D. dissertation, University of Cape Town, South Africa, 1975
18. R.A. King and J.D.A. Miller, *Nature,* Vol 233, 1972, p 491
19. G.H. Booth, A.W. Cooper, and P.M. Cooper, *Br. Corros. J.,* Vol 2, 1967, p 104
20. G.H. Booth, A.W. Cooper, and D.S. Wakerley, *Br. Corros. J.,* Vol 2, 1967, p 109
21. E. Schaschl, *Mater. Perform.,* Vol 19, 1989, p 9
22. G. Kobrin, *Mater. Perform.,* Vol 15, 1976, p 38–43
23. R.E. Tatnall, *Mater. Perform.,* Vol 19, 1989, p 88

J.F.D. Stott, Evaluating Microbiologically Influenced Corrosion, *Corrosion: Fundamentals, Testing, and Protection*, Vol 13A, *ASM Handbook*, ASM International, 2003, p 644–649

Evaluating Microbiologically Influenced Corrosion

James F.D. Stott, CAPCIS Ltd., Manchester, United Kingdom

Attack by Organisms Other Than SRB

As already discussed, biological slimes are commonly found in the water phases of industrial process plants. A wide range of bacteria can secrete large amounts of organic material under both aerobic and anaerobic conditions.

Some components of slimes also use nitrogen- containing compounds as an energy source. They are involved in the cycling of nitrogen in the environment. Ammonia and amines are produced by microbial decomposition of organic matter under both aerobic and anaerobic conditions (ammonification). These compounds are oxidized to nitrite and nitrate by aerobic bacteria such as *Nitrosomonas* or *Nitrobacter* species. *Nitrobacter* is very efficient at destroying the corrosion-inhibition properties of nitrite-based corrosion inhibitors by oxidation, unless a biocidal agent is included in the formulation (Ref 24). The detrimental effects on brass of the release of ammonia at the surfaces of heat-exchanger tubes have also been highlighted (Ref 25).

The bacteria of the genus *Thiobacillus,* of which there are several types, belong to an unusual group of microorganisms called chemolithotrophs. These organisms obtain energy not by oxidation of organic compounds but by oxidation of inorganic sulfur compounds (including sulfides) to sulfuric acid. The organisms build up their cell material by fixation of carbon dioxide. The following interlinked reactions are performed by mixed cultures of *Thiobacilli* acting on elemental sulfur or sulfides (Ref 26):

$$2H_2S + 2O_2 \rightarrow H_2S_2O_3 + H_2O$$

$$5S_2O_3^{2-} + 4O_2 + 4H_2O \rightarrow 5SO_4^{2-} + H_2SO_4 + 4S$$

$$4S + 3O_2 + 2H_2O \rightarrow 2H_2SO_4$$

Certain of the *Thiobacilli* will also leach metal sulfide ores according to the following reaction (Ref 27):

$$4FeS_2 + 15O_2 + 2H_2O \rightarrow 2Fe_2(SO_4)_3 + 2H_2SO_4$$

The important points to note are that these bacteria require oxygen (the opposite of the situation with SRB) and a source of reduced sulfur. The end product is sulfuric acid; one species (*Thiobacillus thioxidans*) is said to remain active at pH 0.7, corresponding to more than 5% sulfuric acid (Ref 28).

Although fairly commonly encountered in nature, *Thiobacillus* proliferation only causes problems in a relatively few specialized industrial situations. One such condition can arise in sewage systems, in which sulfide concentration may be high, owing to the action of putrefactive bacteria, unless aeration is efficient. Suitable conditions can also arise locally in made-up ground into which industrial waste material sometimes finds its way. For this reason, sulfuric acid corrosion of underground pipelines is sporadic and unpredictable.

Attack by sulfuric acid produced by sulfur- oxidizing bacteria such as *Thiobacillus* can be a severe problem in concrete sewers, mortar-lined ductile iron pipes, concrete manholes, and wastewater treatment plants and equipment (Fig. 8).

Fig. 8 Corrosion of a mortar-lined ductile iron wastewater pipe

Figure 9 illustrates schematically the typical corrosion/deterioration of septic sewage systems in hot climates such as the Middle East. The problem starts with growth of anaerobic SRB in the sewage, producing H_2S. This gas migrates to the air space at the top of the line, where it is oxidized into sulfuric acid in the water droplets at the crown of the pipe by *Thiobacillus.* The corrosion problem is due to the combination of the bacterial action that results in dissolution of the alkaline mortar by the acid, followed by corrosion of the ductile iron.

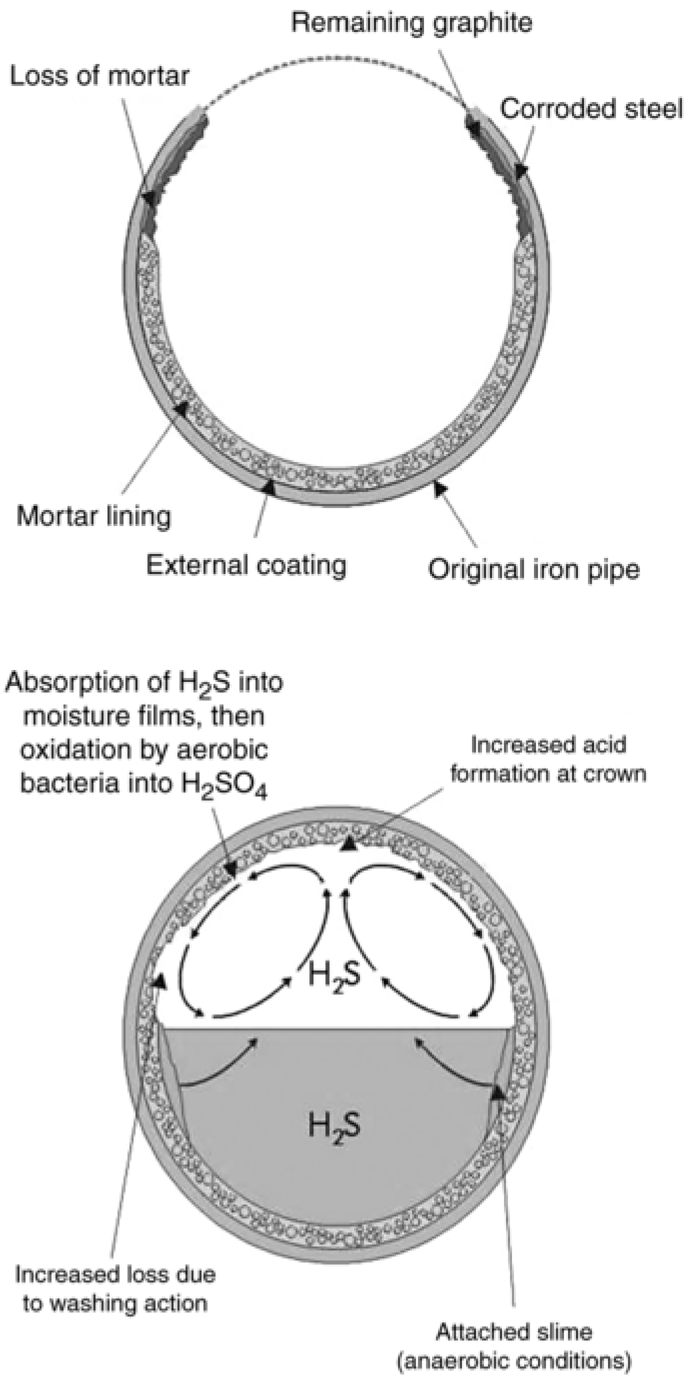

Fig. 9 Microbiologically influenced corrosion processes leading to collapse of a ductile iron sewer

A completely different type of organism from the various groups of bacteria are the fungi. The cells are much larger and grow in dense mats of material. Filamentous fungi are aerobic in nature and are involved in a wide range of biodeterioration problems.

Timber, paper, fuel oils, cloth, and so on can be attacked by fungi. Fungal activity generates organic acids, leading to a low pH in the water and under the microbial mat. In addition to direct acid corrosion, oxygen concentration cells are set up between zones of metal covered with oxygen-depleted fungal mats and those areas where no fungi are present. This electrochemical cell drives the metal dissolution reaction beneath the fungal mat.

By far, the most troublesome fungus in engineering systems is a type commonly called *Cladosporium resinae*, although now reclassified as *Hormoconis resinae* (Fig. 10). *Hormoconis resinae* has the ability to thrive in the presence of kerosene and other hydrocarbons, which it uses as a carbon source for oxidation. It also produces spores, which can survive extremes of temperature, only to germinate when more moderate conditions prevail. *Hormoconis resinae* is a continuing problem in fuel storage tanks and in aluminum integral fuel tanks of aircraft (Ref 29).

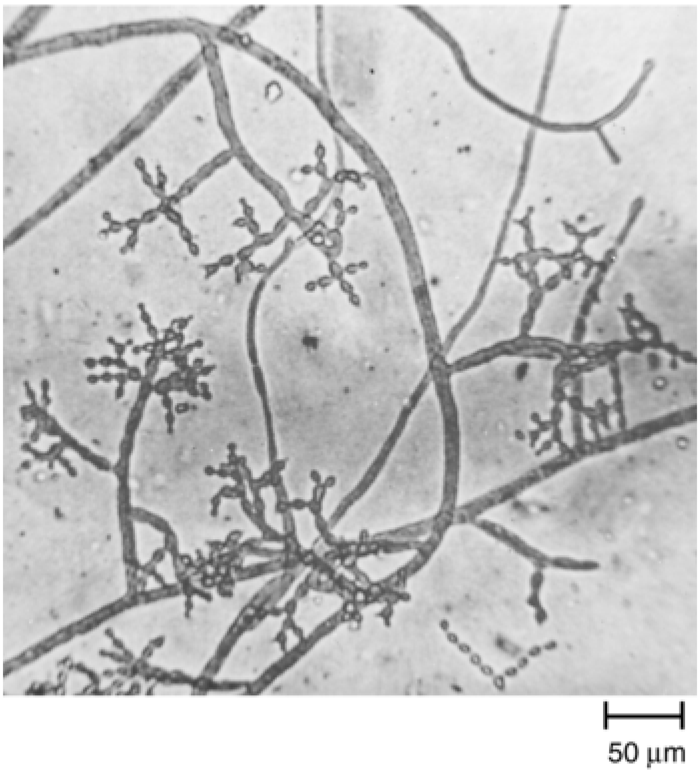

Fig. 10 ***Cladosporium resinae*** **from an aircraft fuel tank**

Brown, slimy mats of *Hormoconis resinae* may cover large areas of aluminum alloy (Fig. 11), causing pitting, exfoliation, and intergranular attack due to organic acids produced by the microbes and the differential aeration cells. This type of problem is largely confined to tropical, humid locations and is particularly severe in short-haul aircraft and those that experience a lot of idle time, where condensation builds up.

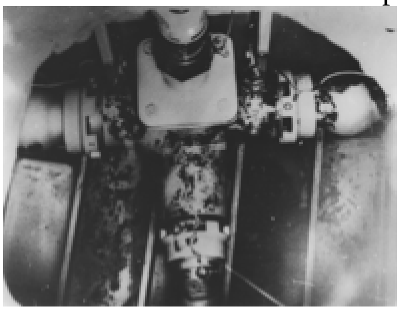

Fig. 11 Example of fungal growth in a jet aircraft fuel tank

The previously mentioned problem was unknown until the 1950s, when it became prevalent after the introduction of gas-turbine-engined aircraft, which use kerosene rather than gasoline as a fuel, and the adoption of integral or wet wing fuel tanks to replace the earlier rubberized fabric bay tanks (Ref 28). The problem of fungal growth in the fuel tanks of jet aircraft has generally diminished as the design of fuel tanks has improved to facilitate better drainage of condensed water and as biocides such as organoboranes have gained acceptance as fuel additives.

References cited in this section

24. L.A. Tarbuck and C.H.E. Wyborn, Proc. Condenser Biofouling Control Symp., March 1979 (Atlanta, GA), Electric Power Research Institute

25. T.P. Hoar, *Corrosion,* Vol 14, 1957, p 1036–1046

26. B.D. Purkiss, in *Biodeterioration of Materials,* A.H. Walters and J.J. Elphick, Ed., Elsevier, 1975, p 107–128

27. N.W. Le Roux, A.A. North, and J.C. Wilson, *Tenth International Mineral Processing Congress,* London Institute of Mining and Metallurgy, 1974, p 1051

28. E.S. Kempner, *J. Bacteriol.,* Vol 92, 1966, p 1842

29. J.J. Elphink, in *Biodeterioration of Materials,* A.H. Walters and J.J. Elphick, Ed., Elsevier, 1975, p 157–172

J.F.D. Stott, Evaluating Microbiologically Influenced Corrosion, *Corrosion: Fundamentals, Testing, and Protection*, Vol 13A, *ASM Handbook,* ASM International, 2003, p 644–649

Evaluating Microbiologically Influenced Corrosion

James F.D. Stott, CAPCIS Ltd., Manchester, United Kingdom

Testing for Microbiological Activity

Assessment of a microbiological population is generally carried out using culture techniques using specific growth media. Enumeration of SRB and total viable bacteria is most commonly by a serial extinction dilution technique using vials containing specially formulated SRB growth medium (Ref 30). The test comprises a serial dilution step followed by an incubation step. Ideally, the serial dilution part of the test should be carried out within a few hours of obtaining the subject samples (typically done on site); however, that is frequently not possible. The results become less reliable with increasing sample age. At the end of the incubation period, the SRB population density in the original sample is determined to the nearest order of magnitude by the number of vials in each dilution series that turn black due to bacterial sulfide production. An example is shown in Fig. 12.

Fig. 12 Test used to enumerate sulfate-reducing bacteria populations

Similar serial dilution tests, using a different type of growth medium, are used to enumerate total bacteria; the vials that show growth turn cloudy rather than black, often accompanied by a color change of an indicator dye to indicate organic acid production.

For the most accurate assessment, threefold or fivefold replicate serial dilution enumeration is carried out; this allows the mean probable number (MPN) of bacteria to be derived from standard MPN tables.

Test kits are commercially available, sometimes in a simplified form. There are also some rapid assay kits based on antibody reactions to SRB enzymes that do not require an incubation period to obtain a result. All simplified and rapid kits compromise accuracy and reliability to a greater or lesser degree. They should be regarded as no more than crude indicators, unless calibrated against standard serial dilution techniques for a specific environment.

Microorganisms that float or swim in water are called planktonic, whereas those that attach to the metal surface in biofilms are called sessile microorganisms. Most of the SRB and other bacteria present in water systems are sessile. Microbiologically influenced corrosion usually occurs as a result of the local environment created by the activity of bacteria attached to the metal surface. Planktonic bacterial counts are often misleadingly low, whereas much larger populations may be concealed in sediments, deposits, and biofilms on metal surfaces.

Increasingly, there is a trend to monitor SRB and microorganisms, using metal coupons similar to corrosion test coupons. Indeed, coupons may serve a dual purpose of corrosion monitoring and biofilm monitoring. Such coupons are sometimes termed bioprobes or biostuds and, for ease of recovery, are often placed in side-stream devices in flowing pipelines. One such sidestream device incorporating biostuds is known as the Robbins device.

If surface deposits or coupons are available, they should be sonicated or scraped into vials of culture medium, serially diluted on site, then incubated in the manner of water samples. In order of priority, samples from industrial systems should be taken from bottoms, metal surfaces, dead ends, and sumps. Sampling should be on a regular basis—weekly, monthly, or quarterly, depending on the extent of concern.

Low sessile population counts of below ~1000 SRB colony-forming units (cfu) per gram of deposit or per square centimeter of surface are not levels about which much concern needs to be expressed. However, regular testing should be undertaken to check trends. Populations will oscillate, but if they show a general upward drift, then action will be necessary sooner or later.

Planktonic SRB counts provide a less reliable indicator than sessiles. However, recurrent counts of greater than approximately 10 cfu/mL, any general upward trend, or any positive planktonic SRB counts in a nominally biocide-treated system are cause at least for further investigation of sessiles. Any planktonic SRB counts above approximately 1,000 cfu/mL is indicative of a heavy proliferation somewhere in the system, probably in deposits on surfaces, especially in stagnant or low-flow areas.

Total viable bacteria counts are usually much higher than SRB counts. Planktonic counts of up to 100,000/mL are common in many natural waters and industrial systems. Population densities higher than 100,000/mL probably indicate a significant buildup of slime somewhere. In biocide- treated systems, total viable bacteria counts should be several orders of magnitude lower than in the untreated water. The incubation period for total viable bacteria counts is only approximately 3 days, considerably shorter than SRB. Therefore, these counts can give a useful early warning of any problem with biocide-treatment efficiency.

Sulfate-reducing bacteria counts and total viable bacteria counts are relatively straightforward, routine analytical techniques. Tests for nitrite-utilizing bacteria or sulfur oxidizers are more complex, specialist techniques. However, problems associated with these organisms are usually clearly evident from the undesirable chemical changes they bring about.

As a supplement to microbiological testing, it is useful to carry out some chemical analyses. An important test is for sulfide in black corrosion deposits, such as those shown in Fig. 6 and 13. In the case of iron sulfide, a simple test is to warm a small sample of the solid with a few milliliters of hydrochloric acid in a glass test tube. If sulfide is present in the deposit, a slightly moistened strip of lead acetate paper in the mouth of the tube will turn brown, indicating H_2S evolution. If a lot of sulfide is present, the characteristic “bad egg” odor will also be apparent. This test needs to be undertaken within a short time of removing samples of deposit from the corrosion site, because wet or damp iron sulfide will eventually oxidize in air to brown rust. The color change of corrosion deposits from black to brown is, in itself, a good indication of sulfide corrosion product. Any such deposits that are taken back to the laboratory for more sophisticated chemical analysis should be preserved in anaerobic bags to prevent the oxidation of FeS that would otherwise occur.

Fig. 13 Iron sulfide on carbon steel tubulars from the stagnant annulus of a sulfate-reducing-bacteria-infected deep water well

Tests for sulfate, total organic carbon (TOC), pH, and oxygen concentration are also useful indicators of the potential for SRB growth. If sulfate concentration is low, then there is little hazard of SRB activity. The pH range most suited to SRB growth is 5 to 10. Outside these limits, bulk phase growth of SRB is very limited. Oxygen concentration will also affect SRB growth in bulk phases, but a high value does not mean that SRB are not present in pockets or under debris. A high oxygen concentration may allow other organisms to develop. The interpretation of those tests, together with other operating parameters, is discussed in the following section of this article.

Reference cited in this section

30. "Field Monitoring of Bacterial Growth in Oilfield Systems," NACE Standard Test Method, TM0-194-94, NACE International, 1994

J.F.D. Stott, Evaluating Microbiologically Influenced Corrosion, *Corrosion: Fundamentals, Testing, and Protection*, Vol 13A, *ASM Handbook*, ASM International, 2003, p 644–649

Evaluating Microbiologically Influenced Corrosion

James F.D. Stott, CAPCIS Ltd., Manchester, United Kingdom

Risk Assessment Based on Operating Conditions

Frequently, an engineer may be required to make an appraisal of the MIC risk with limited information on the corrosion history and little or no historic microbiological test data. The conclusions that may be drawn about the risk of MIC in such cases are largely based on consideration of operating parameters. This is often the situation with the assessment of the internal corrosion risks of hydrocarbon pipelines, water- handling systems, or process plants. The discussion that follows refers specifically to SRB-related problems, which are, by far, the most common MIC issue.

A group of researchers at Shell Petroleum Company have developed an approach to risk assessment of carbon steel pipelines, based on the details of water chemistry and operation parameters (Ref 31). Their MIC corrosion rate (CR) calculation is based on the following equation:

$$\text{CR(mm/year)} = C \times F^{\text{p}}$$

with

$$F = f_1 \times f_2 \times, \ldots, f_n$$

where C is a constant (C = 2 mm/year, or 0.08 in./year), the fs are factors for the various influencing parameters, and p is a power-law index (0.57).

While such an approach does provide a valuable empirical recognition of the relative contribution of the factors that encourage or inhibit MIC, the calculation of actual corrosion rates on such a basis should be viewed with great caution, given the present limited understanding of the imbricated effects of the various factors.

Presence of Water. All bacteria require free water in order to proliferate. In the case of oil pipelines, MIC needs only to be considered under separated flow conditions; if all water is entrained in the hydrocarbon, there is no risk of MIC (Ref 31).

In the author's experience, it is unwise to rely on dispersions to provide fully oil-wetted surfaces when the bottom solids and water content is in the order of 2% or greater, except under very turbulent hydrodynamic conditions. It is best to take an empirical and conservative view as to whether lines may be wet enough to sustain SRB growth at the present time and during their future operating life.

Salinity. According to results presented in Ref 9, if the salinity of water, expressed as weight percent NaCl, is more than approximately 7%, there is unlikely to be any SRB growth. That observation broadly agrees with the author's own experience, and a similar statement is reiterated in the more recent Shell Petroleum Company work (Ref 31). However, it should be noted that other workers have suggested that some SRB strains may be tolerant to much higher salt concentration.

Temperature. Most types of SRB grow optimally at temperatures between 10 and 45 °C (50 and 115 °F), which is the highest risk-temperature range. However, there are thermophilic strains of SRB that grow at higher temperatures, up to at least 70 °C (160 °F), and their activity cannot be discounted.

pH. Generally, there is unlikely to be SRB proliferation below pH 5 or above approximately pH 10, although the pH range for SRB that are protected in heavy deposits may be somewhat wider.

Anaerobic Conditions. Sulfate-reducing bacteria will only proliferate and produce sulfide in the absence of oxygen. Clearly, anaerobic situations are most at risk; however, there are many cases of SRB causing problems in slimes and deposits where the bulk water phase is essentially aerobic, for example, in cooling waters. This is especially the case for static or slow-flow conditions.

Nutrient Status of Water Phase. Sulfate-reducing bacteria growth is much less likely if the aqueous sulfate concentration or the organic carbon content is below approximately 10 mg/L or the ammoniacal nitrogen (not nitrate or nitrite) is below approximately 1 mg/L. An exception, in the author's experience, is the case of a plant under long-term lay-up with static, high-sulfate water (e.g., seawater), where a corrosive black water condition may develop over a period of months, even with very low organic carbon content. This is believed to be due to the reduction of sulfate by SRB using cathodic hydrogen formed by corrosion on steel surfaces.

Flow rate influences the nature of biofilm formation and the rate of nutrient delivery. As flow rate increases, biofilms become less bulky, and only the more adherent films remain on the metal surface. However, above a certain threshold, the initiation of biofilm formation is significantly limited. The transition zone is considered to be between 2 and 3 m/s (6.5 and 9.8 ft/s). At the other extreme, stagnation is often associated with the severest MIC incidents.

Cleaning Frequency. In order to initiate the MIC process, the free-floating, planktonic SRB cells need to attach themselves to a metal surface, that is, become sessile and proliferate to form a biofilm with its own entrained microenvironment. This process is disturbed by regular physical cleaning, such as brush pigging of pipelines. The incipient biofilm is disrupted and largely removed, and this is the most effective means of minimizing SRB growth and obviating MIC. Microbiologically influenced corrosion is uncommon in pipelines that are frequently pigged, even without biocide treatment. The more frequent the pig runs, the less time the biofilm has to recover.

Biocide Treatment. Any operation that disrupts the biofilm and thereby limits its proliferation will act to alleviate MIC. Biocide treatment is one such factor, provided the concentration, duration, and frequency of that biocide treatment is adequate. Just because some form of biocide treatment is in use, it should not be assumed that it must be effective. Biocides have very limited ability to penetrate existing deposits and are therefore much more effective when used in conjunction with frequent pigging or other cleaning processes.

The first stage of biocide selection is a laboratory evaluation of candidate biocides, using a time-kill test (Ref 30). In the case of once- through cooling water systems, the choice is between continuous low-dose treatment with oxidizing biocides (e.g., chlorine, bromine, chlorine dioxide peroxide, or ozone) or periodic shock dosing with much higher concentrations of organic biocide. Environmental constraints sometimes negate the latter possibility. Continuous low-level injection of organic biocide is of no value. Indeed, continuous low-level exposure may possibly be detrimental in the long term, because there is some possibility that it may encourage the development of more biocide-tolerant strains of bacteria.

For recirculating systems and hydrotest waters, organic biocides are often the treatment of choice. After the completion of laboratory tests for biocides in a given application (which should include economic considerations and chemical compatibility tests), a program of site monitoring is recommended.

The site monitoring should ensure that the chemical injection rate is giving the correct concentration of biocide and is changed accordingly when water throughput rate is altered and should monitor any major perturbations of the system that may affect biocide efficiency. Such perturbations include changes in contact time; flow rates; temperature; pH, use of a new chemical, for example, corrosion inhibitor, scale inhibitor, or oxygen scavenger; or shutdown periods.

References cited in this section

9. J.R. Postgate, *The Sulphate-Reducing Bacteria,* Cambridge University Press, 1979

30. "Field Monitoring of Bacterial Growth in Oilfield Systems," NACE Standard Test Method, TM0-194-94, NACE International, 1994

31. B.F.M. Pots, R.C. John, I.J. Rippon, J.J. Maarten, S. Thomas, S.D. Kapusta, M.M. Girgis, and T. Whitham, Paper 02235, NACE 2002, NACE International, 2002

J.F.D. Stott, Evaluating Microbiologically Influenced Corrosion, *Corrosion: Fundamentals, Testing, and Protection,* Vol 13A, *ASM Handbook,* ASM International, 2003, p 644–649

Evaluating Microbiologically Influenced Corrosion

James F.D. Stott, CAPCIS Ltd., Manchester, United Kingdom

References

1. R.T. Ross, J.R. Sladen, and L.A. Wienart, in *Biodeterioration of Materials,* A.H. Walters and J.J. Elphick, Ed., Elsevier, 1975, p 127–136

2. E.C. Hill, in *Biodeterioration of Materials,* A.H. Walters and J.J. Elphick, Ed., Elsevier, 1975, p 157–172

3. E.C. Hill, Biodeterioration of Petroleum Products, *Microbial Aspects of the Deterioration of Materials,* D.W. Lovelock and R.J. Gilbert, Ed., Academic Press, 1975, p 127–136

4. J.D.A. Miller and K.A. Tiller, *Microbial Aspects of Metallurgy,* Aylesbury, Medical and Technical Publishing Co., 1971, p 61–105

5. W.P. Iverson, *Microbial Iron Metabolism,* J.B. Niedlands, Ed., Academic Press, 1974

6. V. Kucera, *Microbial Corrosion—A Literature Survey,* Swedish Corrosion Institute, Stockholm, 1980

7. D.H. Pope, D. Duquette, P.C. Wayner, and H.J. Arland, Microbially Influenced Corrosion. A State-of-the-Art Review, Publication 13, Materials Technology Institute, Columbus, Ohio, 1984

8. J.F.D. Stott and B.N. Herbert, *J. Appl. Bacteriol.,* Vol 60, 1986, p 57–66

9. J.R. Postgate, *The Sulphate-Reducing Bacteria,* Cambridge University Press, 1979

10. "The Role of Bacteria in the Corrosion of Oilfield Equipment," NACE TPC 3, National Association of Corrosion Engineers, 1976

11. R.L. Ginter, *Bull. Am. Assoc. Petrol. Geol.,* Vol 14, 1930, p 139

12. *Oil Gas J.,* Nov 1964, p 207

13. G.L. Gates and C.F. Parent, *Oil Gas J.,* Aug 1976, p 115

14. B.H. Moore, *World Oil,* March 1984, p 100

15. F.D.S. Al Sawaf, *Econ. Geol.,* Vol 72, 1977, p 608

16. S.L. Ege, C.J. Houghton, and P.T. Tucker, Second Annual Workshop on Secondary Recovery Technology, June 1985 (London)

17. J.A. Costello, "The Mechanism of the Corrosive Effect of SRB," Ph.D. dissertation, University of Cape Town, South Africa, 1975

18. R.A. King and J.D.A. Miller, *Nature,* Vol 233, 1972, p 491

19. G.H. Booth, A.W. Cooper, and P.M. Cooper, *Br. Corros. J.,* Vol 2, 1967, p 104

20. G.H. Booth, A.W. Cooper, and D.S. Wakerley, *Br. Corros. J.,* Vol 2, 1967, p 109

21. E. Schaschl, *Mater. Perform.,* Vol 19, 1989, p 9

22. G. Kobrin, *Mater. Perform.,* Vol 15, 1976, p 38–43

23. R.E. Tatnall, *Mater. Perform.,* Vol 19, 1989, p 88

24. L.A. Tarbuck and C.H.E. Wyborn, Proc. Condenser Biofouling Control Symp., March 1979 (Atlanta, GA), Electric Power Research Institute

25. T.P. Hoar, *Corrosion,* Vol 14, 1957, p 1036–1046

26. B.D. Purkiss, in *Biodeterioration of Materials,* A.H. Walters and J.J. Elphick, Ed., Elsevier, 1975, p 107–128

27. N.W. Le Roux, A.A. North, and J.C. Wilson, *Tenth International Mineral Processing Congress,* London Institute of Mining and Metallurgy, 1974, p 1051

28. E.S. Kempner, *J. Bacteriol.,* Vol 92, 1966, p 1842

29. J.J. Elphink, in *Biodeterioration of Materials,* A.H. Walters and J.J. Elphick, Ed., Elsevier, 1975, p 157–172

30. "Field Monitoring of Bacterial Growth in Oilfield Systems," NACE Standard Test Method, TM0-194-94, NACE International, 1994

31. B.F.M. Pots, R.C. John, I.J. Rippon, J.J. Maarten, S. Thomas, S.D. Kapusta, M.M. Girgis, and T. Whitham, Paper 02235, NACE 2002, NACE International, 2002

J.F.D. Stott, Evaluating Microbiologically Influenced Corrosion, *Corrosion: Fundamentals, Testing, and Protection,* Vol 13A*, ASM Handbook,* ASM International, 2003, p 644–649

Evaluating Microbiologically Influenced Corrosion

James F.D. Stott, CAPCIS Ltd., Manchester, United Kingdom

Selected References

- S.W. Borenstein, *Microbiologically Influenced Corrosion Handbook,* Industrial Press, 1994
- "Microbiologically Influenced Corrosion and Biofouling in Oilfield Equipment," TCP 3, NACE, 1990
- C.A.C. Sequeira, Ed., "Microbial Corrosion," European Federation of Corrosion, Report 29, Institute of Materials, London, 2000
- J.G. Stoeckler II, Ed., *A Practical Manual on Microbiologically Influenced Corrosion,* Vol 2, NACE, 2001

D.A. Shifler, High-Temperature Gaseous Corrosion Testing, *Corrosion: Fundamentals, Testing, and Protection*, Vol 13A, *ASM Handbook*, ASM International, 2003, p 650–681

High-Temperature Gaseous Corrosion Testing

David A. Shifler, Naval Surface Warfare Center

Introduction

HIGH-TEMPERATURE CORROSION occurs in various environments and is affected by numerous factors, such as temperature, alloy or protective coating composition, time, and gas composition. High-temperature exposure of materials occurs in many applications, such as power plants (coal, oil, natural gas, and nuclear), pulp and paper mills, petrochemical and chemical industries, land-based gas turbine and diesel engines, gas turbine engines for aircraft, marine gas turbine engines for shipboard use, waste incineration, high-temperature fuel cells, and spacecraft components. Exposure in high-temperature environments can cause materials degradation and lead to problems that often bring about unscheduled outages, resulting in loss of reliability, decreased safety, and increased economic costs.

Predicting corrosion of metals and alloys or coated alloys is often difficult because of the range of composition of the corrosive gaseous or molten environments and the variety of materials that may be used. Moreover, corrosion prediction is further complicated, because materials often degrade in a high-temperature environment of a given application by more than a single corrosion mechanism.

There is a great need for materials testing, both for research and development of new materials (alloys, high-temperature coatings, refractories, etc.) and processes and to simulate industrial and application environments to understand the interactions that occur with current materials choices. There are, in general, few standards or guidelines for materials testing for high-temperature corrosion, which lead to errors in performance evaluation and a wide range of results on oxidation and corrosion-resistance measurements.

The goals of laboratory and field testing are to characterize materials performance in specific applications and to evaluate the effects of environmental changes on candidate materials. The test conditions should simulate, as much as possible, the environment of the specific application of interest. This includes duplicating the chemical composition of the atmosphere, liquid, or molten salt, the temperature and thermal cycle profiles, the stress states of the materials, fatigue conditions, and the design parameters.

The objective for performing a given high- temperature corrosion test should be identified during the initial phase of designing the testing procedure. Testing should be properly planned, relevant, and correlated with actual field use. Accelerated tests often provide useful information, but degradation processes in such tests may not reflect the actual corrosion mechanisms by which the materials naturally deteriorate. Testing may require laboratory, field, simulated service evaluations, or a combination of the tests. Details on general test planning are found in Ref 1.

Test parameters that should be considered include specimen size and preparation, isothermal or thermal cycling, test environment versus service environment, geometry, temperature, flow velocity, potential, and type of corrosion.

There also should be an idea of the type and degree of complexity of testing desired (Ref 1). In general, before testing components in most practical applications, one should be knowledgeable of the corrosion properties of

possible candidate materials and understand the possible materials interactions that a component may have with other material components in order to interpret and translate the test results into the requirements of the service application.

The high-temperature corrosion behavior of materials is often evaluated in the laboratory rather than in an actual service environment due to time and/or budget limitations. Laboratory evaluation is generally of relatively short duration and is often used to study environmental effects on the corrosion behavior of a metal, because the specific environmental conditions can be controlled. The major disadvantage of testing in the laboratory is that the actual service environment and conditions may not be evaluated. When service conditions are being simulated, certain assumptions are usually made. It is important when testing in the laboratory to correlate field data with laboratory data, so that the validity of the laboratory information can be assessed.

In-service testing provides the advantage of examining the corrosion behavior of a metal in the actual service environment. However, in-service testing is generally expensive, and variables are usually not well characterized or controllable. Small-specimen testing allows a large number of variables to be evaluated at minimal cost. Small specimens can be designed to determine specific types of corrosion. Although small-specimen testing allows examination in the actual service environment, the corrosion rate determined on small specimens may not be consistent with the corrosion rate of a large-scale piece of equipment, predominantly because it is difficult to duplicate all of the metallurgical conditions and the local environment of the large equipment on a small specimen. Similar to in- service testing, simulated service testing provides the advantage of exposure to the actual environment.

Reference cited in this section

1. J.W. Spence, S.D. Cramer, and F.H. Haynie, Planning and Design of Tests, *Corrosion Tests and Standards—Application and Interpretation,* R. Baboian, Ed., American Society of Testing and Materials, 1995, p 33

D.A. Shifler, High-Temperature Gaseous Corrosion Testing, *Corrosion: Fundamentals, Testing, and Protection*, Vol 13A, *ASM Handbook*, ASM International, 2003, p 650–681

High-Temperature Gaseous Corrosion Testing

David A. Shifler, Naval Surface Warfare Center

Factors Affecting High-Temperature Corrosion and Materials Properties

The rate by which a material may degrade in a high-temperature environment will depend on the reaction or range of operative reactions, the reaction thermodynamics, kinetics, and chemical and physical properties of the material exposed to this environment. A material can degrade at high temperatures on exposure to gaseous, liquid (molten ash, salts, or metal/alloys), or solid-state reaction processes, such as diffusion and interdiffusion, precipitation, and creep.

Thermodynamics

The thermodynamics of high-temperature corrosion reactions reveals what reactions are possible under certain conditions and is dependent on reactants and the possible products that may form. The overall driving force for any chemical reaction can be assessed by the change in the Gibbs free energy, ΔG, for that reaction. Strictly on the grounds of thermodynamics, a reaction will proceed from left to right, as written, if its ΔG is negative. For a metal (M) reacting with oxygen to form an oxide, the reaction is:

$$xM + yO_2 \rightarrow M_xO_y \quad \text{(Eq 1)}$$

For this reaction, the free energy may be written as:

$$\Delta G_{yO_2/MO} = \Delta G^o_{yO_2/MO} + RT \ln \frac{a_{M_xO_y}}{(a^x_M)(a^y_{O_2,MO})} \quad \text{(Eq 2)}$$

where ΔG^o is the standard free energy change when all reactant and product species are in their standard states, a_i is the chemical activity of species *i*, *R* is the gas constant (8.314 J/mol · K), and *T* is the absolute temperature (Ref 2). If the standard state for the reacting O_2 in Eq 1 is taken to be 1 atm, then the O_2 activity can be equated to its partial pressure, p_{O_2}, in Eq 2. Further, because the activity of stable pure solids is defined as unity at all temperatures and pressures, and $\Delta G = 0$ at equilibrium, the free energy of the simple oxidation reaction given in Eq 1 simplifies to:

$$\Delta G_{O_2/MO} = RT \ln p_{O_2/MO} \quad \text{(Eq 3)}$$

Thus, Eq 3 defines the free energy change, $\Delta G_{O_2/MO}$, for the formation of a pure oxide, M_xO_y, on the base metal, M, and the characteristic equilibrium pressure, $p_{O_2/MO}$for the dissociation of that oxide at some defined temperature. Because $\Delta G = \Delta H + T\Delta S$, where ΔH and ΔS are changes in enthalpy and entropy, respectively, a plot of ΔG versus *T* approximates a straight line, with changes in slope where new phases form, such as occurs during melting, boiling, or sublimation. The oxygen dissociation pressures leading to oxide formation or reduction for pure metals can be found graphically using an Ellingham diagram, such as the one shown in Fig. 1 (Ref 3). The procedure consists of passing a straight line through the point "O" (upper left-hand corner of the diagram) and a second point that intersects the temperature of interest for the metal/oxide system and extending the line to the oxygen nomographic scale, the intersection of which gives the dissociation p_{O_2}. Because oxidation can occur in the presence of water vapor and carbon dioxide, the diagram also displays nomographic scales with differing CO-to-CO_2 and H_2-to-H_2O ratios. Ellingham or Gibbs free energy-temperature diagrams for selected oxides are given in Ref 2. Similar Gibbs energy-temperature diagrams are available for other gaseous reactions such as sulfur, fluorine, chlorine, bromine, iodine, and nitrogen (Ref 4). A practical limitation of the Ellingham diagrams is that they are completely thermodynamic and therefore do not provide any information pertaining to the kinetics of a given metal corrosion reaction.

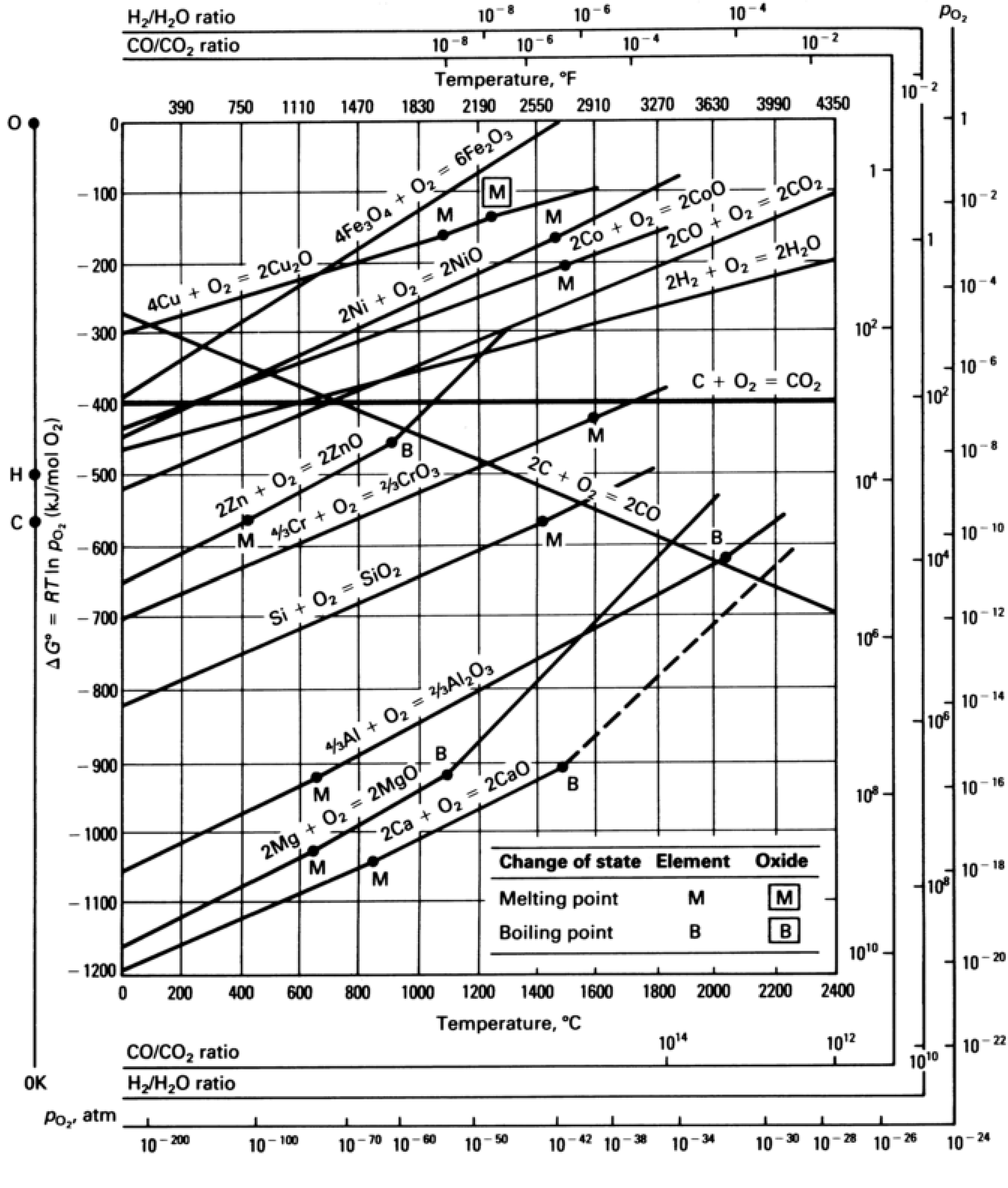

Fig. 1 Ellingham diagrams of selected oxides as a function of temperature. 1 atm = 101.3 kPa

The thermodynamics of a high-temperature reaction such as oxidation was described in the previous paragraph as a function of temperature, with pressure considered constant. If there are no volumetric changes in a given reaction, pressure will have no effect on corrosion thermodynamics. However, for some high-temperature applications, pressure is an important factor in determining which reactions transpire. For a metal at a constant temperature, the change in the free energy of a reaction (Ref 5) is due to a change in pressure from P_1 to P_2 and can be written as:

$$\left(\Delta G^\circ\right)_T = VdP = nRT\frac{dP}{P} = nRT\ln\frac{P_2}{P_1} \quad \text{(Eq 4)}$$

where *V* is volume and *n* is the number of molecules.

Isothermal stability diagrams are used for more complicated situations where a metal may be exposed to more than one oxidizing gas or when an alloy is exposed to a gaseous environment. In these situations, it is customary to fix the temperature at some practical value and plot variations of gas pressure or alloy composition against each other. This produces isothermal stability diagrams, or predominance area diagrams, that will illustrate the phases or species that are most stable in any set of circumstances.

One Metal and Two Gases (Ref 6). These diagrams, often called Kellogg diagrams, are constructed from the standard Gibbs free energies of formation, ΔG^o, of all elements and compounds likely to be present in the system. For example, in the Ni-O-S system, ΔG^o values of nickel monoxide (NiO[s]), nickel monosulfide (NiS[l]), nickel sulfate ($NiSO_4$[s]), sulfur dioxide (SO_2[g]), sulfur trioxide (SO_3[g]), and sulfur (S[l]) are needed.

In Fig. 2, the boundary between the Ni(s) and the NiO(s) regions represents the reaction Ni(s) + $\frac{1}{2}O_2$(g) ↔ NiO(s) at equilibrium; therefore, the diagram shows that at 1250 K (1790 °F) and O_2 pressure above approximately 10^{-11} atm, NiO will tend to form from the metallic nickel if p_{S_2} is low. Similarly, S_2 gas pressure greater than approximately 10^{-7} atm will form NiS from nickel at low p_{O_2}. A mixed gas of 10^{-5} atm each of S_2 and O_2 should form nearly the equilibrium ratio of NiO(s) and $NiSO_4$(s).

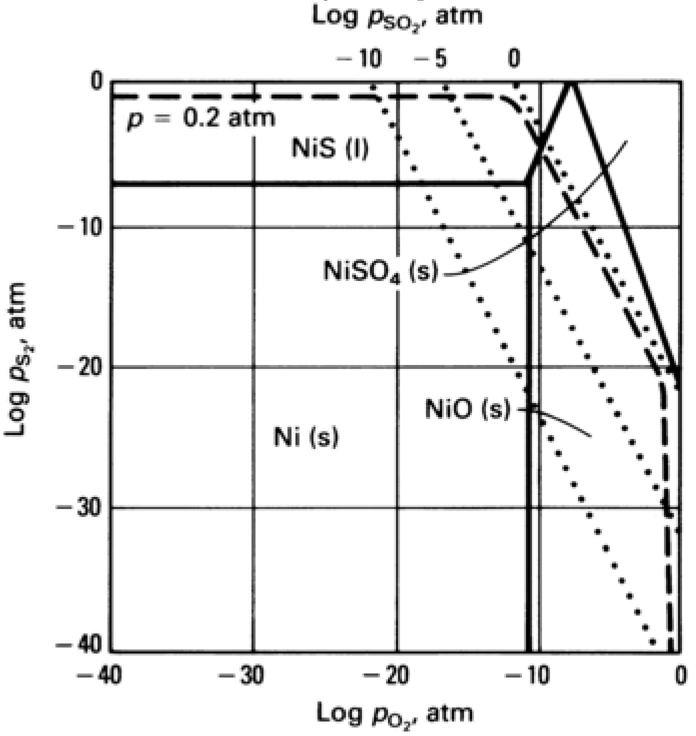

Fig. 2 The Ni-O-S system at 1250 K (1790 °F). Source: Ref 6

If the principal gases of interest were SO_2 and O_2 the same ΔG^o could be used to construct a diagram of log p_{O_2} versus log p_{SO_2}, or, as in Fig. 2, p_{SO_2} isobars can be added to the figure (dotted lines). Thus, a mixed gas of 10^{-5} atm each of SO_2 and O_2 will form only NiO at 1250 K (1790 °F), with neither the sulfide nor the sulfate being as stable.

When nickel metal is heated to 1250 K (1790 °F) in the open air with sulfur-containing gases, $p_{SO_2} + p_{S_2} + p_{O_2} \approx$ 0.2 atm. The situation is shown by the dashed line in Fig. 2 labeled "*p* = 0.2 atm."

An Alloy System and a Gas (Ref 6). Isothermal stability diagrams for oxidation of many important alloy systems have been worked out, such as the Fe-Cr-O system shown in Fig. 3. In this diagram, the mole fraction of chromium in the alloy is plotted against the log p_{O_2}, so that for any alloy composition, the most stable oxide or mixture of oxides is shown at any gas pressure.

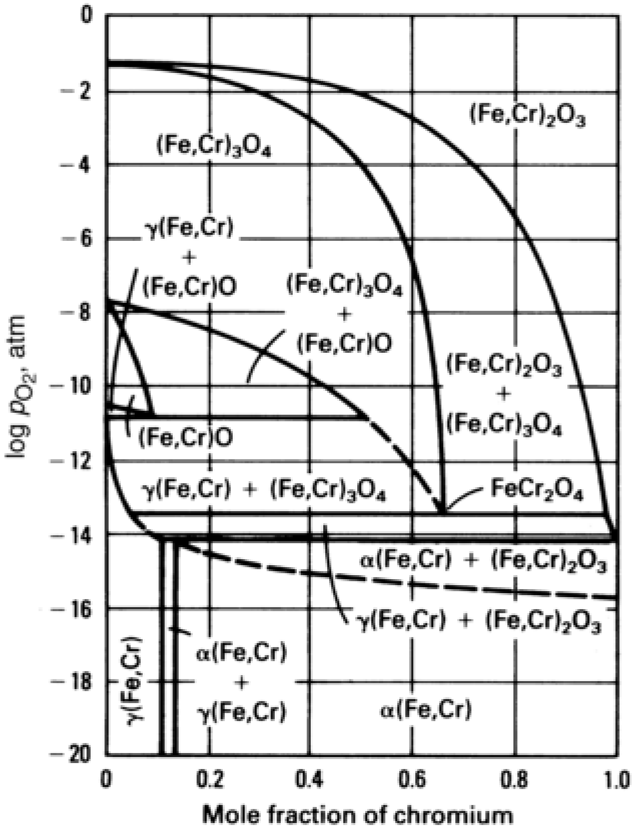

Fig. 3 Stability diagram of the Fe-Cr-O system at 1300 °C (2370 °F). Source: Ref 6

For any alloy system in a gaseous environment containing more than one reactive component, the pressures of all but one of the gases must be fixed at practical values to be able to construct an isothermal stability diagram in two dimensions. Figure 4 shows an example of such a situation: the iron-zinc system in equilibrium with sulfur and oxygen-containing gases, with SO_2 pressure set at 1 atm (101.3 kPa) and temperature held at 1164 K (1636 °F).

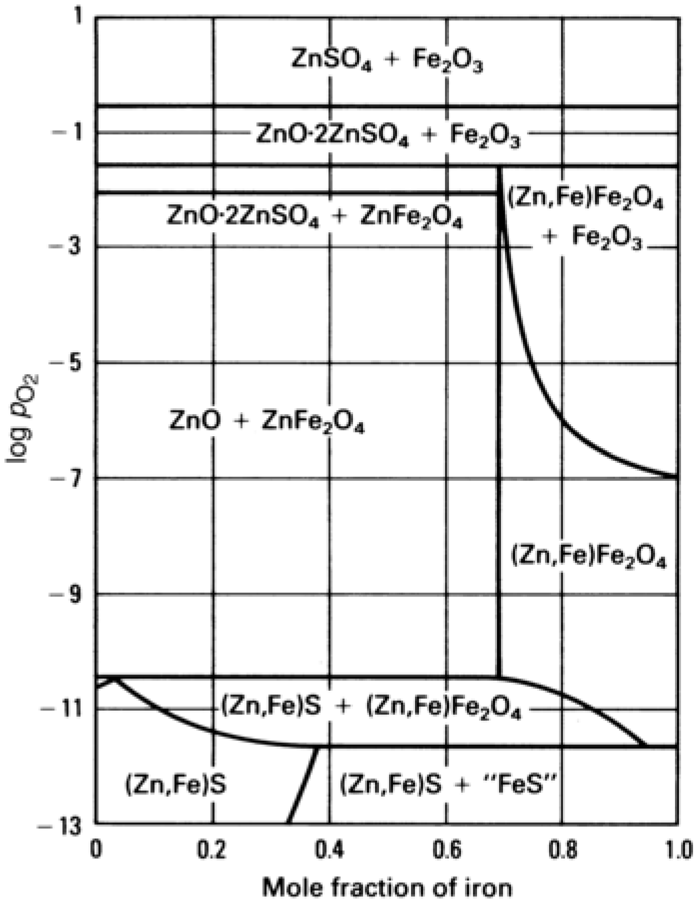

Fig. 4 The Fe-Zn-S-O system for p_{SO2} = 1 and temperature at 1164 K (1636 °F). Source: Ref 6

Use of Isothermal Stability Diagrams. Each area on the diagram is labeled with the stable phase that is in contact with the environment at the specified temperature and pressure conditions; other phases may also be stable beneath this outer phase. The boundary line between two phases shows the conditions for their equilibrium, that is, coexistence as stable products.
As with all thermodynamic diagrams, the use of these isothermal stability, or predominance area diagrams have specific rules that must be understood:

- Each area on the diagram is labeled with the predominant phase that is stable under the specified conditions of pressure or temperature. Other phases may also be stable in that area but in smaller concentrations.
- The boundary line between two predominance areas shows the conditions of equilibrium between the two phases.

The use of thermodynamically derived diagrams has limitations:

- The diagrams are based on thermodynamic data and do not predict reaction kinetics.
- The diagrams are for equilibrium conditions. Equilibrium may be reached quickly in high- temperature oxidation, but if the metal or alloy is then cooled, equilibrium may not be reestablished.
- Microenvironments, such as gases in voids or cracks, may create conditions that differ considerably from the diagram situations expected for the bulk reactant phases.
- The diagrams also do not show the effects that minor impurities or alloy additions may have on corrosion performance.

The Gibbs free energy change of a high-temperature reaction that is experienced in a high- temperature application or during a high-temperature test can be understood by considering the chemical potential ($\mu_i = [\partial G/\partial n_i]_{T,p,nj}$) of the species participating in the reaction. For multicomponent systems, the Gibbs free energy is

a function of temperature, pressure, and composition, such that $G = f(T, p, n_1, n_2, \ldots)$, where n_i is the number of moles of the ith component. Fundamentally, the free energy change can be written as (Ref 7):

$$dG = \sum_i n_i d\mu_i + \mu_i dn_i \quad \text{(Eq 5)}$$

$$dG = -SdT + Vdp + \sum_i \mu_i dn_i \quad \text{(Eq 6)}$$

For a process with fixed compositions and carried out under isothermal and isobaric conditions and at equilibrium, then $(dG)_{T,p,n} = 0$, leaving:

$$\Sigma n_i d\mu_i = -SdT + Vdp = 0$$
$$n_1 d\mu_1 + n_2 d\mu_2 = 0 \quad \text{(Eq 7)}$$

which is referred to as the Gibbs-Duhem equation (Ref 7, 8). The equation is extremely important in solution or molten electrolyte chemistry.

The accuracy of using thermodynamics to predict possible reactions of a metal or an alloy that may occur in a given environment are dependent on the similarity of the test environment with the available thermodynamic data used to construct a diagram. The performance of alloys in a given test environment is affected by the environment and/or the similarity of the alloy performance to that of a metal in a given environment.

Kinetics

While thermodynamics predicts what reactions may be possible, kinetics explains how fast these possible reactions will proceed. The reaction rate is affected by a number of complex interactions between the test material and the test environment during the test. Environmental contributions that affect reaction kinetics include (Ref 9):

- Temperature
- Time/thermal cycle conditions
- Corrosive species and their activity (concentration)
- Chemisorption and dissociation characteristics
- Stress states and cyclic strains

Materials characteristics that can affect high- temperature corrosion and other high-temperature materials processes include (Ref 9):

- Free energy of formation of scales (oxides, sulfides, chlorides, nitrides, etc.) of the alloying elements
- Scale integrity
- Alloy composition
- Alloy structure
- Alloy transformations, if any, that may occur in the operational service or test temperature
- Presence of materials combinations, such as high-temperature coatings on superalloys
- Material interdiffusion coefficients between the materials and its high-temperature reaction product or between two dissimilar materials (i.e., coatings on superalloys)
- Coefficient of thermal expansion differences in the scale and the materials substrate
- Scale adhesion
- Mechanical strength of the scale
- Solubility of gaseous products of the environment in the scale and the substrate
- Scale formation during different stages of the test
- Specimen size and shape

Materials frequently undergo changes in corrosion mechanisms that complicate reaction kinetics and the explanation of the reactions that may occur. High-temperature corrosion reactions are usually classified as following one of the reaction kinetics: linear, parabolic, logarithmic, or cubic (Ref 10). However, high-

temperature oxidation and corrosion processes may deviate from these rate-law kinetics, or the high-temperature reactions may be a combination of more than one rate.

Linear kinetics are typically associated with either a surface reaction step being rate controlling or nonprotective scaling. In the case of the latter, the corroding material may form a scale that is porous, crackprone, or nonadherent. The integrated rate equation describing linear kinetics is:

$x = k_L t$ (Eq 8)

where x is the scale thickness or mass gain per unit area, k_L is the linear rate constant, and t is time. The units of k_L depend on the test parameters used in measuring the kinetics: if the scale thickness is measured, k_L has units of centimeters per second, while if mass gain is measured, the rate constant has the units of $g/cm^2 \cdot s$. Figure 5 shows the linear relationship between mass gain versus oxidation time.

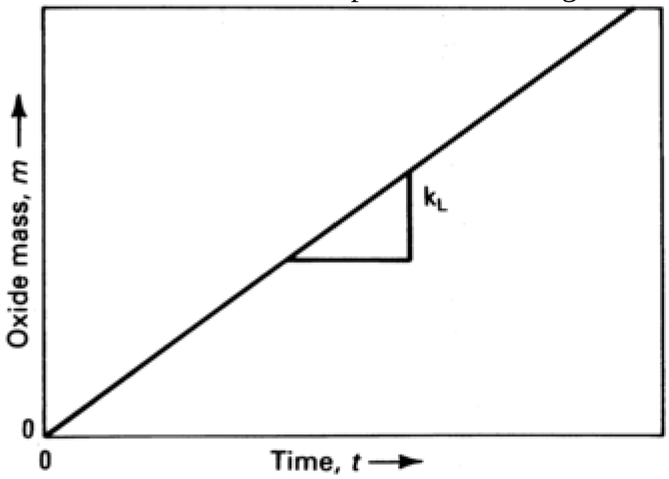

Fig. 5 Linear oxidation kinetics showing relationship between oxide mass and time

Parabolic kinetics describe high-temperature corrosion reactions where the rate-determining step is the diffusion of ions, either inward toward or outward from the substrate, with a chemical potential gradient as the driving force. Integrated, the parabolic rate equation is:

$x^2 = k_p t$ (Eq 9)

where k_p is the parabolic rate constant, and x is the thickness (centimeters per second) or mass gain per unit area ($g/cm^2 \cdot s$). Figure 6 shows the parabolic relationship between mass gain versus oxidation time. The high-temperature corrosion resistance of most chromia (Cr_2O_3) and alumina (Al_2O_3) scale-forming alloys follows parabolic rate kinetics.

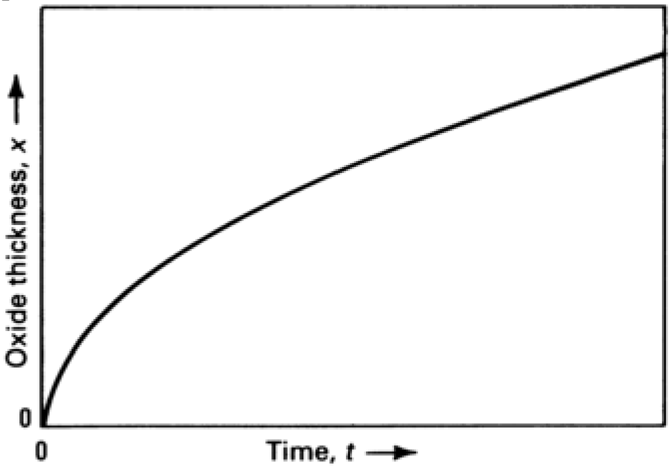

Fig. 6 Parabolic oxidation kinetics

Periodic cracking of a protective oxide results in the parabolic oxidation being interrupted by a sudden increase in rate, when the gas can react directly with the bare metal surface. As oxide begins to cover the metal surface again, parabolic oxidation is resumed. The time periods between successive parabolic steps are sometimes

fairly uniform, because a critical scale thickness is reached that causes cracks to be initiated. The overall oxidation of the metal becomes approximately a slow linear process.

Internal penetration and attack often can be described by parabolic kinetics (Ref 9). This characterizes the formation of precipitates (either intra- or intergranular) by the interaction of one or more species from the environment with the substrate. Internal penetration occurs when the reactive substrate component diffuses outwardly more slowly than the gaseous species diffuses inwardly. A simplified equation to describe internal attack in the absence of any external scale formation has been proposed (Ref 11):

$$X = \left[\frac{2N^S D^t}{\nu N_B^i}\right]^{1/2} \quad \text{(Eq 10)}$$

where *X* is the depth of internal penetration at time, *t*, N^s is the mole fraction of reactive gaseous species in the substrate at the surface, *D* is the diffusion coefficient of the oxidant in the substrate, ν is the atom ratio of oxidant to metal for the internally precipitating phase BO_ν, and N_B^i is the mole fraction of reactive component in the bulk substrate.

Logarithmic kinetics are often associated with the initial stages of oxidation, low-temperature service tests, or conditions where cavities and precipitates in a thick scale interfere with ion or vacancy diffusion mechanisms. Logarithmic scaling behavior on alloys is affected by precipitates that grow slowly within the scale or at the scale-substrate interface and restrict the growth of a scaling constituent (Ref 9). Growth stresses in the scale may cause development of cracks in the scale parallel to the substrate, thus leading to logarithmic or inverse logarithmic kinetics from the transport of electrons or ions. The rate equations describing logarithmic reaction kinetics are:

Logarithmic $x = k_{log} \log(t + t_o) + A$ (Eq 11)

Inverse logarithmic $1/x = B - k_{inv} \log t$ (Eq 12)

where A, B, k_{log}, and k_{inv} are constants at isothermal temperatures. Figure 7 shows the variation of direct logarithmic and inverse logarithmic kinetics.

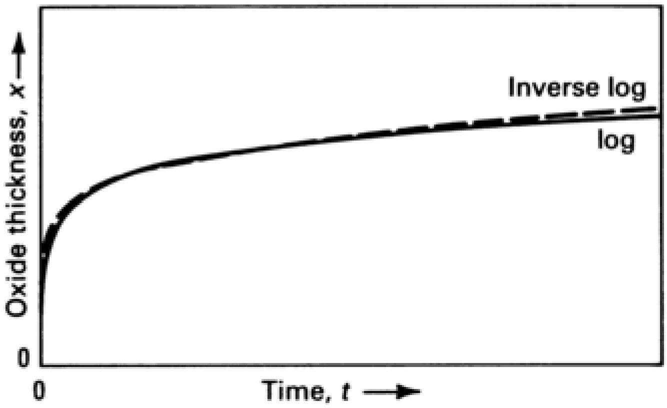

Fig. 7 Logarithmic and inverse logarithmic oxidation kinetics

Cubic Kinetics. In certain situations, scales form on some metals according to a cubic rate law:

$x^3 = k_c t$ (Eq 13)

where k_c is the cubic rate constant. Usually, such behavior is limited to short exposures (Ref 10). The cubic kinetics reported for the oxidation of zirconium or hafnium are explained as a combination of diffusion-limited scale formation and oxygen dissolution into the metal (Ref 12). In other cases, cubic kinetics have been explained as a superposition of a morphological complication and ionic diffusion through the scale (Ref 12). Figure 8 shows the comparison of the cubic rate kinetics with linear, parabolic, and logarithmic rate kinetics.

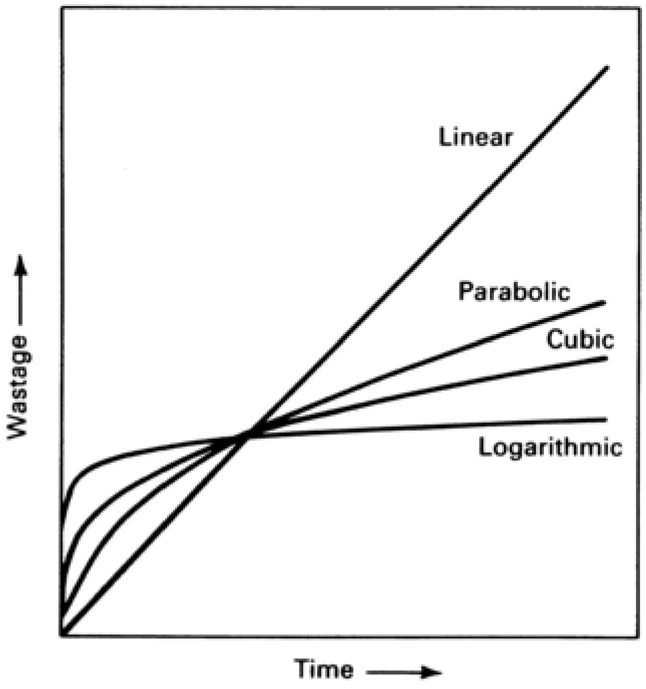

Fig. 8 Comparison of linear, logarithmic, parabolic, and cubic kinetics found in various thermal degradation processes. Source: Ref 13

Some high-temperature corrosion reactions cannot be described by the simple rate equations discussed previously. Occasionally, a metal oxidizes parabolically until the scale cracks or spalls off, and from that time on, until a new scale is formed, the oxidation is linear. Breakaway corrosion often occurs when numerous cracks continuously form through the scale to the substrate or when the principal component for forming the most stable scale is either effectively depleted at the alloy surface through repeated scale formation and spallation cycles or through selective internal compound formation.

Catastrophic corrosion occurs when a liquid phase is a product of a corrosion process. This may happen as a result of metal or alloy exposure to vapors of a low-melting compound or during the substrate corrosion, when one or more components of the material forms a low-melting compound with one or more corrosive species of a test or service gaseous environment. The liquid phase first forms at the scale/atmosphere interface and permeates through the scale to the substrate along defects such as grain boundaries and pores. Once at the substrate/scale interface, the molten phase spreads by capillary action and destroys scale adhesion (Ref 9). Table 1 lists oxides, sulfides, and chlorides that may lead to catastrophic corrosion.

Table 1 Low-melting compounds and eutectics that may lead to catastrophic corrosion

Potentially catastrophic corrosion species	**Melting point**	
	°C	**°F**
Oxides		
V_2O_5	674	1245
MoO_3	795	1463
Bi_2O_3	817	1503
PbO	885	1625
WO_3	1470	2678
Chlorides		
$MoCl_5$	194	381
WCl_5	240	464
$MnCl_2$	652	1206
$FeCl_2$	676	1249
$CoCl_2$	740	1364
$NiCl_2$	1030	1886

Metal-sulfide eutectics		
$Ni-Ni_3S_2$	645	1193
$Co-Co_4S_3$	877	1611
Fe-FeS	988	1810
$Cu-Cu_2S$	1067	1953

Source: Ref 9

Diffusion

Diffusion occurs due to the differences in chemical potential to the extent that a component always diffuses down its potential gradient. Note that by this definition, it is possible in multi- component systems for a given component to diffuse up its concentration gradient. When two isolated chambers kept at different temperatures are suddenly connected, the temperature in each chamber rises or falls to a common, equilibrated temperature that is driven by thermodynamics. Chemical, compositional, or defect differences in materials exposed to high-temperature gaseous environments will attempt to equilibrate via diffusion to form oxides, sulfides, and other metal-anion species or to level compositional differences.

Diffusion processes in solids play a key role in oxidation and other gaseous reactions with metals. Mass transfer may be the result of metal ion diffusion from the metal surface through the oxide, nitride, sulfide, or chloride (and other such metal compounds) layer to the absorbed anions at the oxide, nitride, sulfide, or chloride/gas interface or the result of diffusion of anions inward through the scale to the metal or alloy. Within the alloy, the diffusion of reacting metal atoms toward the surface and the back diffusion of unreactive atoms from the metal surface inward to the unaltered alloy can occur. The diffusion of interstitial atoms such as carbon, nitrogen, hydrogen, and oxygen can also be involved.

Atoms or ions can diffuse through solids by several mechanisms. The most common is vacancy diffusion, because a metal crystal always contains a high concentration of point defects, such as atomic vacancies, while ionic oxides contain Schottky and Frenkel defects that involve vacancies. An atom or ion sitting on a lattice site can diffuse by jumping to adjacent vacant sites. For metal atoms, this is relatively easy because of the short jump distances. The jump distances in ionic crystals are much longer, because cation and anion sites are surrounded by oppositely charged species.

Small, interstitial atoms diffuse readily from one interstitial position to another. In ionic oxides, the cations may diffuse interstitially, but the anions are usually not small enough to do so. In ionic crystals, an interstitial ion may crowd into a regular lattice site, displacing an ion, which is forced to move into an interstitial position or to the next lattice site.

Diffusion can be described by Fick's two laws, as noted in many texts (Ref 6, 14, 15). Fick's first law states that the rate of mass transfer is proportional to the concentration gradient:

$$J = D\left(\frac{\partial C}{\partial t}\right) \qquad \text{(Eq 14)}$$

The flux, J, is the mass diffusing per second through a unit cross-sectional area due to the concentration gradient, ($\partial C/\partial t$), and D is the diffusion coefficient, expressed in square centimeters per second. The diffusion coefficient is a function of diffusing atoms, the structure through which the diffusion takes place, and the temperature.

Under most conditions, the concentration gradient does not remain fixed with time and distance. For instance, the concentration of carbon diffusing into a metal (for example, a steel) changes with time and depth into the metal. Fick's second law describes this change under isothermal conditions as:

$$\frac{\partial C}{\partial t} = \frac{\partial}{\partial x}\left(D\frac{\partial C}{\partial x}\right) \qquad \text{(Eq 15)}$$

The diffusion coefficient is assumed to be independent of distance, x, to a first approximation, and the concentration, C, is dependent on the distance x. Equation 14 must be solved for the particular geometry and boundary conditions involved (flat, round, or spherical specimens, etc.). For carbon atoms diffusing inward from a flat surface, with constant composition-independent diffusivity, no subsurface phase change in the metal or movement of the metal surface, and a constant surface concentration, the solution to Eq 14 for the concentration of carbon at any distance x from the metal surface is:

$$\frac{C_M - C_X}{C_M - C_o} = \text{erf}\left(\frac{x}{2\sqrt{Dt}}\right) \quad \text{(Eq 16)}$$

where C_M is the carbon concentration at the metal/carburizing environment interface, C_X is the concentration at time t and distance x from the surface, and C_o is the initial constant concentration at any distance x when $t = 0$. The concentrations here are in moles of carbon per cubic centimeter of metal. The error function of the argument z, erf(z), is tabulated in many books on probability. As carburization proceeds, C_M and C_o remain constant; therefore, for any fixed value of C_X, the depth of penetration, x, of the carburization diffusion reaction is dependent on diffusion time:

$$x \propto \sqrt{t}$$

The diffusion coefficient D in rather stoichiometric compounds can usually be assumed to be proportional to the defect concentration. The diffusion coefficient can also vary with crystal orientation in noncubic crystals. For oxides that are epitaxial or have a preferred orientation, the diffusivity can be several times more or less than it would be for a random oxide. Temperature has a major effect on D by increasing it exponentially, according to the Arrhenius equation:

$$D = D_o e^{(-Q/RT)} \quad \text{(Eq 17)}$$

where D_o is a temperature-independent constant called the frequency factor that is a function of the diffusing species and the diffusion medium, and Q is the activation energy for the diffusion (Ref 6).

The activation energy is a measure of the temperature dependence of a diffusion process. A high value of Q means that diffusion proceeds much more rapidly at high temperatures but very slowly at low temperatures. Typical values of D_o and Q in oxides are listed in Table 2 of the article “Kinetics of Gaseous Corrosion Processes” in this Volume.

When two metals with a large difference in their diffusion coefficients interact, there is a net transport of material across a plane that initially separated them. This phenomenon is called the Kirkendall effect. Multicomponent interdiffusion is a complex process that requires use of multivariable diffusion couples in a phase field approach (Ref 16) or knowledge of diffusion pathways in multicomponent phase diagrams (Ref 17) to model the process and provide an understanding of the contributions to interdiffusion. These methods are based on the formalism of Fick's law, which includes diffusion interactions among the chemical species (Ref 18).

Protective coatings and superalloy substrates generally have widely diverse compositions due to the intended balancing between mechanical properties and corrosion resistance. Depending on the actual temperature, chemical gradients between the coating and superalloy substrate may cause interdiffusion phenomena to occur. Interdiffusion between the coating and the substrate (Ref 19) can modify the oxidation and corrosion resistance of the coating and the mechanical properties of the coating-substrate system. Interdiffusion slowly changes the chemical composition of both the coating and the alloy and subsequently may alter the microstructure of the coating and/or the substrate. In addition, selective oxidation reactions can induce alloy phase transformations (Ref 20, 21). In a hot corrosion environment, the formation of metal sulfides in the protective coating may eventually lead to diffusion via grain boundaries or other relatively easy diffusion pathways into the coating, which may alter the long-term performance of a coating/alloy system versus that observed in an oxidation environment.

In gaseous reactions with metals and alloys, metal ions are formed at the metal/scale interface, and the gaseous species, such as oxygen, is reduced at the scale/gas interface. All metal oxides, nitrides, and sulfides conduct both ions and electrons that are associated with diffusion processes. The electronic conductivities of oxides are usually several orders of magnitude greater than their corresponding ionic conductivities; thus, the diffusion of cations or gaseous ions (i.e., oxygen, sulfur, nitrogen, hydrogen, etc.) controls the reaction rate (Ref 12). Almost without exception, cations and gaseous ions do not diffuse at comparable rates in a given scale, because lattice defects for one of the component species typically predominate. Thus, growth of the scale for gaseous reactions with a metal or alloy should result in scale growth at either the metal-scale or the scale-gas interface if the reactions are controlled by diffusion (Ref 12).

In general, all oxides, sulfides, nitrides, and so on are nonstoichiometric compounds, because their actual, compositions deviate from their respective ideal molecular formulas. Some scales have an excess and others have a deficiency of metallic ions or a corresponding deficiency or excess of gaseous ions.

Nickel oxide (NiO) is an example of a metal- deficient oxide. For each nickel cation vacancy, there are two trivalent nickel cations in the normal lattice positions, as shown in Fig. 2 of the article “Kinetics of Gaseous Corrosion Processes” in this Volume. The trivalent ions are considered the combination of a divalent nickel cation and an associated positive-charged electron hole, or absence of an electron (Ref 12); hence, this is termed a *p*-type semiconductor. Ionic transport occurs by the diffusion of nickel vacancies from the nickel/gas interface to the Ni/ NiO interface. Electronic conduction occurs by the predominant diffusion of the electron holes. Accordingly, electrons migrate from the metal surface, by electron holes, to the adsorbed oxygen atoms, which then become oxygen anions. In this way, while Ni^{2+} cations and electrons move outward through the scale toward the gas, cation vacancies and electron holes move inward toward the metal. Consequently, as the scale thickens, cation vacancies may tend to accumulate to form voids at the nickel/NiO interface.

A metal-excess oxide carries the excess as either interstitial cations or as oxygen anion vacancies. Interstitial cations are small enough to fit into interstitial spaces in the oxide lattice and jump from one interstitial position to another during diffusion. Beryllium oxide (BeO) typifies a cation-excess, *n*-type semiconductor oxide, because the beryllium ion (Be^{2+}) is small enough to move interstitially through the BeO scale. Its structure is shown in Fig. 3 of the article “Kinetics of Gaseous Corrosion Processes” in this Volume.

Oxygen in the gas adsorbs on the BeO surface and picks up free electrons from the BeO to become adsorbed O^{2-} ions, which then react with excess Be^{2+} ions that are diffusing interstitially from the beryllium metal. The free electrons generated at the metal surface from beryllium ionization travel rapidly through vacant high-energy levels. As with *p*-type oxides, the cation-excess, *n*-type oxides grow at the oxide/gas interface as cations diffuse outwardly through the scale (Ref 6).

For *n*-type semiconducting oxides where the cations are too large or too highly charged to assume an interstitial position, anion vacancies are required to form the metal-excess structure. This group of anion-deficient, *n*-type semiconducting oxides is exemplified by zirconium dioxide (ZrO_2). In this case, although most of the cations are contributing four electrons to the ionic bonding, a small fraction of the zirconium cations only contributes two electrons to become zirconium ion, Zr^{2+}. Therefore, to maintain electrical neutrality, an equal number of anion vacancies must be present in the oxide. This arrangement is shown in Fig. 4 of the article “Kinetics of Gaseous Corrosion Processes” in this Volume. The oxide grows at the metal/oxide interface by inward diffusion of O^{2-} through the anion vacancies in the oxides (Ref 6, 22).

A number of compounds that can be nonstoichiometric with either a deficiency of cations or a deficiency of anions are amphoteric. An example is lead sulfide (PbS), which has a minimum in electrical conductivity at the stoichiometric composition. Thus, if the composition is $Pb_{1-x}S$, it is *p*-type, and if it is PbS_{1+x}, it is *n*- type. Similarly, intrinsic semiconductors, such as cupric oxide (CuO), have a few electron holes in their valence band and an equal number of free electrons in their nearly vacant conduction band. Electronic current is carried both by migration of electron holes in the low-energy bonding levels and by free electrons in the higher-energy conduction levels (Ref 6). Examples of *p*-type, *n*-type, and amphoteric superconducting sulfides, oxides, and nitrides are listed in Table 1 of the article “Kinetics of Gaseous Corrosion Processes” in this Volume.

All oxides contain some substitutional impurity cations from the alloy before oxidation or other gaseous high-temperature reaction. Although the solubility limit for foreign ions is low, they can have a great effect on diffusivity in the oxide and consequently, on the oxidation rate. By doping alloys with certain elemental additions, high-temperature gaseous reaction rates can be reduced.

In the very early stages of oxidation and especially at low temperatures, some oxides appear to grow with an amorphous structure. In general, these oxide glasses contain more oxygen than metal in their formulas, so that oxygen networks form around each of the metal ions. The random network ring structures that result allow large anions or molecular oxygen to move through them more readily than the smaller cations do. Amorphous oxides tend to crystallize as they age. Examples are silicon dioxide (SiO_2), Al_2O_3, tantalum pentoxide (Ta_2O_5), and niobium pentoxide (Nb_2O_5).

As a crystalline oxide grows on a metal surface, the oxide often aligns its crystal structure to be compatible with the structure of the metal substrate. This epitaxy finds the best fit, but not a perfect fit, between the oxide or scale and the substrate crystal structures.

Additional Aspects of Scale Growth

Stress develops in an epitaxial scale layer as it grows, due to the slight misfit between the scale and metal crystals. The stress is likely to produce dislocation arrays in the scale that could be paths of mass transport

through the film via diffusion. A mosaic structure, consisting of small crystallites with orientations very slightly tilted or twisted with respect to each other, may develop in the scale because of the growth stresses. The boundaries between the crystallites are dislocation arrays that serve as easy diffusion paths (Ref 6). Recrystallization of either the scale or the substrate may alter the stress conditions substantially.

Stresses in epitaxial layers increase as the films grow thicker, until, at some point, the bulk scale tends to become polycrystalline, and epitaxy is gradually lost. Epitaxy may last up to approximately 50 nm in many cases, but it is seldom strong over 100 nm. As the scale grows thicker, crystals that are favorably oriented for growth will grow at the expense of their neighboring grains until the scale surface consists of a few large grains with similar orientation. The variation in growth rate of different scale grains produces the roughening of the scaled surface that is commonly observed (Ref 6).

A pure metal that can oxidize to more than one valence will form a series of oxides, usually in separate layers. For example, iron has valences of +2 and +3 at high temperatures and forms wustite (FeO), magnetite (Fe_3O_4), and hematite (Fe_2O_3) scale layers. The scale layers will be arranged with the most metal-rich oxide species appearing next to the metal, and progressively less metal content is found in each succeeding layer toward the outside layer. In addition, a concentration gradient exists with each layer, with higher metal ion concentration closest to the metal/scale interface.

If the oxygen partial pressure in the gas is so low that it is below the dissociation pressures of the outer oxygen-rich oxides, then only the thermodynamically stable inner oxides will form. In general, the lowest-valence inner oxide will usually be *p*-type because of the ease with which electron holes and cation vacancies can form. The outermost oxide is often *n*-type because of its anion vacancies. A scale consisting of an inner layer with cations diffusing outward and an outer layer with anions diffusing inward will grow at the oxide/oxide interface (Ref 6).

Polycrystalline oxides develop stresses along their grain boundaries because of enhanced growth of oxide grains in preferred orientations. Short-circuit diffusion along grain boundaries may lead to oxide or high-temperature scale formation at the boundaries that imparts increased compressive stresses. Second-phase inclusions may oxidize at a different rate than the parent metal or alloy and lead to high stresses within the scale. Composition variations within a high- temperature coating or within gaseous-formed scales may also create stresses within the scale. Alloying constituents may react to a gaseous environment at different rates, leading to preferential growth of a scale from one or more elemental metal components. If diffusion is too slow to maintain constant composition within the scale, stress can develop in the alloy (Ref 6).

The activation energies for diffusion along line and surface defects in solids are much less than those for volume diffusion. Dislocations, grain boundaries, porosity networks, and external surfaces offer rapid diffusion paths at low temperatures, at which volume diffusion is extremely slow. In metals, diffusion along dislocations is more important than volume diffusion below approximately one-half of the absolute melting point. At high temperatures, volume diffusion predominates in both metals and oxides.

At very high temperatures, oxides and high- temperature scales may evaporate entirely or limit the protective nature of these protective scales. Platinum and refractory metals tend to have volatile oxides (Ref 6). As evaporation removes material from the scale layer, diffusion through the scale increases until the evaporation and diffusion rates are equal. The scale thickness remains constant, and the scale or oxide of the metal or alloy grows paralinearly. If more than one oxide or scale layer protects the substrate, the higher-valent outermost oxide/scale always has the higher vapor pressure and is thus more volatile.

Sample geometry may influence the stresses within a scale. The stress state (compressive or tensile) depends on whether the surface profile of the sample is convex or concave and whether the scale grows at the scale/gas interface or at the metal/scale interface. Figure 9 shows how the stress state may be altered in an oxide scale as it grows, assuming the original growth stresses were compressive. Other scales formed from gaseous reactions will behave similarly.

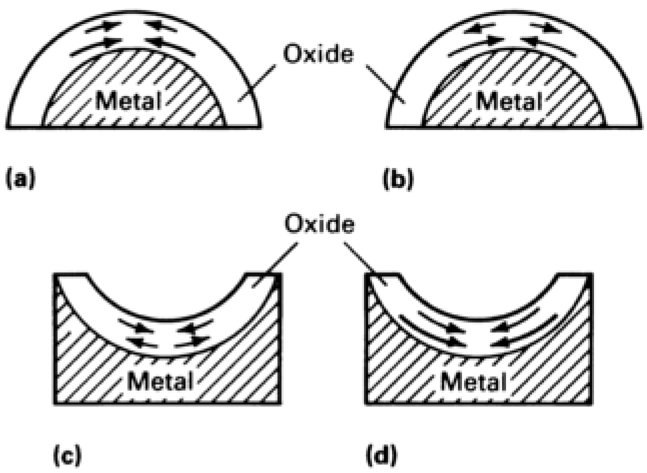

Fig. 9 Stress development on curved surfaces. (a) Oxide grows by cation diffusion on a convex surface. (b) Oxide grows by anion diffusion on a convex surface. (c) Oxide grows by cation diffusion on a concave surface. (d) Oxide grows by anion diffusion on a concave surface

In Fig. 9(a), for a convex surface on which oxide grows at the oxide/gas interface by cation diffusion outward through the scale, the metal surface will gradually recede, increasing the compressive stresses at the metal/oxide interface. If adhesion is to be maintained, the oxide has to follow the retreating interface, generating further compressive stresses in the scale. Stress relief can occur by either shear fracture, if the scale is extremely adherent, or by oxide buckling due to decohesion that could lead to local tensile failure. Figure 9(b) shows oxidation of a convex surface on which the oxide grows at the metal/ oxide interface by anion diffusion inward. The compressive stresses that develop at the metal/ oxide interface are due only to the volume change of the reaction oxide (volume generated is greater than the volume of metal consumed). Oxide that is pushed away from the growth area will gradually reduce its compressive stress until the outer surface may even be in tension. This may lead to the development of a laminated oxide structure, because new oxide forms under the older, buckled, decoherent oxide layer (Ref 6, 15).

For concave surfaces,Fig. 9(c) illustrates oxide growth at the oxide/gas interface by outward diffusion of cations. As the metal surface recedes, the compressive stresses due to oxide growth are reduced. If further adhesion is weak, further oxidation may lead to spallation of the oxide. If adhesion forces at the oxide/substrate interface are strong, further scale growth will cause development of tensile stresses in the oxide adjacent to the substrate. Figure 9(d) shows growth on a concave surface by anion diffusion inward for reaction at the metal-oxide interface. Very high compressive stresses develop during growth, until they exceed the cohesive strength of the oxide, and shear cracking results (Ref 6, 15).

A preferential reaction of a gaseous species (oxygen, sulfur, nitrogen, etc.) with one constituent in an alloy or refractory may alter the chemical composition of the material to the point where crystallographic phase transformation is experienced. A change in temperature may also cause transformations. Volume changes associated with these phase transformations can induce significant stresses in both the alloy and scale or high-temperature coating.

For oxides that grow by cation diffusion outward through cation vacancies (*p*-type oxides, such as NiO), the vacancies are created at the oxide/gas interface and diffuse inward through the scale as they exchange places with an equal number of outward-diffusing cations. The vacancies are annihilated within the oxide, at the metal/oxide interface, or within the metal, depending on the type of oxide system. In some oxides, the vacancies collect together within the oxide to form approximately spherical cavities. The preferred sites for cavity formation are along paths of rapid diffusion, such as grain boundaries and dislocation lines.

Vacancies that are annihilated at the metal/oxide interface may cause detachment of the scale, because voids that form reduce oxide-to-metal adhesion. If attachment is only partial, the oxidation rate slows down, because the cross-sectional area available for diffusion decreases (Ref 6).

References cited in this section

2. N. Birks and G.H. Meier, *Introduction to High Temperature of Metals,* Edward Arnold, London 1983

3. B. Mishra, Extractive Metallurgy, *Metals Handbook Desk Edition,* 2nd ed., ASM International, 1998, p 718

4. G.Y. Lai, Corrosion by Halogens, *High Temperature Corrosion of Engineering Metals,* ASM International, 1990, p 85–115

5. W.J. Moore, *Physical Chemistry,* 4th ed., Prentice-Hall, 1972, p 99–101

6. S.A. Bradford, Fundamentals of Corrosion in Gases, *Corrosion,* Vol 13, *Metals Handbook,* 9th ed., ASM International, 1987, p 61–76

7. G.W. Castellan, *Physical Chemistry,* 2nd ed., Addison-Wesley, 1971, p 257–258

8. L.L. Sheir and G.T. Burstein, *Corrosion: Corrosion Control,* Vol 2, 3rd ed., L.L. Sheir, J.A. Jarman, and G.T. Burstein, Ed., Butterworth-Heinemann, 1994, p 20:65–20:66

9. G.D. Smith, High Temperature, *Corrosion Tests and Standards—Application and Interpretation,* R. Baboian, Ed., American Society of Testing and Materials, 1995, p 149

10. L.R. Scharfstein and M. Henthrone, Testing at High Temperatures, *Handbook on Corrosion Testing and Evaluation,* W.H. Ailor, Ed., John Wiley & Sons, 1971, p 291–366

11. C. Wagner, Types of Reaction in the Oxidation of Alloys, *Z. Elektroch.,* Vol 63, 1959, p 772–782

12. M.G. Fontana, *Corrosion Engineering,* 3rd ed., McGraw-Hill, 1986, p 505–520

13. I.G. Wright, High Temperature Corrosion, *Corrosion,* Vol 13, *Metals Handbook,* 9th ed., ASM International, 1987, p 97–103

14. R.E. Reed-Hill and R. Abbaschian, *Physical Metallurgy Principles,* 3rd ed., PWS- Kent Publishing, 1992, p 360–420

15. A.S. Khanna, *Introduction to High-Temperature Oxidation and Corrosion,* ASM International, 2002, p 40–60, 172–201, 205–214

16. K. Wu, Y. Wang, and J.E. Morral, Predicting Interdiffusion Microstructure Using the Phase Field Approach, *Elevated Temperature Coatings: Science and Technology IV,* N.B. Dahotre, J.M. Hampikian, and J.E. Morral, Ed., The Minerals, Metals and Materials Society, 2001, p 133

17. E. Basuki, A. Crosky, and B. Gleeson, Interdiffusion Behaviour in Aluminide- Coated René 80H at 1150 °C, *Mater. Sci. Eng. A,* Vol 224, 1997, p 27–32

18. L. Onsager, Reciprocal Relations in Irreversible Processes, Part I, *Phys. Rev.,* Vol 37, 1931, p 405–426; Reciprocal Relations in Irreversible Processes, Part II, *Phys. Rev.,* Vol 38, 1931, p 2265–2279

19. A. Sanz, L. Llanes, J.P. Bernadou, M. Anglada, and M.B. Rapaccini, Influence of the Stress State on the Diffusion Phenomena Across the Interface Between a Protective Coating and a Single Crystal Superalloy, *Elevated Temperature Coatings: Science and Technology II,* N.B. Dahotre and J.M. Hampikian, Ed., The Minerals, Metals and Materials Society, 1996, p 373

20. D.J. Young and B. Gleeson, Alloy Phase Transformations Driven by High Temperature Corrosion Processes, *Corros. Sci.,* Vol 44, 2002, p 345–357

21. J.-G. Duh and J.-W. Lee, Diffusion-Related Kinetics in the Oxidation-Induced Phase Transformation of Fe-9Al-3Cr- 31Mn Alloys, *J. Electrochem. Soc.,* Vol 136, 1989, p 847–853

22. D.A. Jones, *Principles and Prevention of Corrosion,* 2nd ed., McGraw-Hill, 1996, p 412–415

D.A. Shifler, High-Temperature Gaseous Corrosion Testing, *Corrosion: Fundamentals, Testing, and Protection*, Vol 13A, *ASM Handbook*, ASM International, 2003, p 650–681

High-Temperature Gaseous Corrosion Testing

David A. Shifler, Naval Surface Warfare Center

Measurement of High-Temperature Degradation

Sample Preparation for Testing

For high-temperature testing, samples need to be prepared and processed in a similar manner as they would for actual service. The materials should be characterized by chemical composition, fabrication history, and by morphology or microstructure (Ref 23).

The size and shape of laboratory and field test samples can vary, but samples should be large enough to obtain meaningful quantitative information on exposure to the test environment. The samples should be large enough that the corrosion reaction being tested does not fully consume the material exposed. Geometry asperities, such as corners and edges, should be eliminated, if possible, because they tend to be less corrosion resistant than planar surfaces. The geometry, on the other hand, should reflect the part, component, or system as much as possible. Samples need to be identified, but any markings should not influence the test performance of the sample.

The samples should be prepared for testing in a specified manner so that the sample surfaces are clean, uniform, and defect-free to minimize conditions that may affect the testing results. Carburized, decarburized, or cold-worked layers should be removed (Ref 23). The samples should be handled carefully to avoid contamination. Before testing, each sample must be measured precisely to calculate the surface area and/or accurately weighed (for small samples, generally to a precision of 0.1 mg). Testing will alter the dimensions or the mass during exposure. After measuring the samples, they should be either inserted into the test setup or stored in a dessicator until needed.

Because deviations in test parameters may vary slightly over time and with sample placement within the test apparatus, replication is necessary. Samples in duplicate or triplicate will often be sufficient, but larger sample sizes are strongly advised when the test materials are highly variable. The consistency of the test results will be improved and the test result scatter decreased when the test parameters are tightly controlled and multiple samples are used (Ref 23).

If a test is often repeated, a pedigreed control sample should be used to calibrate the experimental laboratory or service test. This will verify whether test parameter abnormalities exist or if breakdown in operational controls has occurred during a test. Use of the control samples provides this measure of assurance. Control samples should be thoroughly characterized (chemical composition, fabrication history, microstructure, and physical and mechanical properties) (Ref 23).

Mass Change

Mass changes, either losses or gains, are determined by calculating the weight change per unit area, usually as a function of time, temperature, and pressure. Mass change is calculated as follows:

$$\text{Mass change} = \frac{W_f - W_o}{A} \quad \text{(Eq 18)}$$

where W_f is the final weight in grams, W_o is the initial weight in grams, and A is the original area in centimeters squared or meters squared. A plus or minus sign indicates a net gain or loss. It is important to record whether the test sample has been descaled or not and by what method. The scale may be difficult to remove if it is tightly adhered or part of an oxide substructure. There are standard methods used for descaling.

It is misleading if single data point or single analytical measurements are made over a long time duration, because corrosion rates and modes usually vary with time. The use of the mass change method to measure corrosion rate will also be inaccurate if spallation of the surface layer occurs during the test duration. Three additional limitations of the mass change method are that (a) it lacks the registering of subsurface attack, such as intergranular attack, which, at times, is quite deep; (b) deep localized corrosion (e.g., pitting) is averaged over the weight of the entire specimen, and thus, the extent of the attack is minimized; and (c) weight gains due to oxygen or sulfur absorption would interfere with weight loss measurements.

Structural Changes

Structural changes in a high-temperature test sample can result in depletion of a constituent in the material or thermal effects on the stability of the material. An example of alloy depletion is the dissolution of carbides near the substrate surface because of high-temperature exposure. A common thermal effect is the precipitation of topologically close-packed phases, such as mu, Laves, and sigma, over time within certain temperature ranges. Analytical methods, discussed later, can be used to confirm these structural changes.

Metallographic Analysis

Analysis can be most easily performed by optical metallography but may be done using scanning electron microscopy or transmission microscopy. Metal loss is defined as one-half the difference between the original thickness and the remaining thickness after exposure, as shown in Fig. 10 (Ref 24). Thickness extends to just beneath the scale/surface surface and excludes the thickness of internal attack:

$$\text{Metal loss} = \frac{t_o - t_m}{2} \quad \text{(Eq 19)}$$

where t_o is the original thickness or diameter, and t_m is the sample thickness or diameter after a term of exposure.

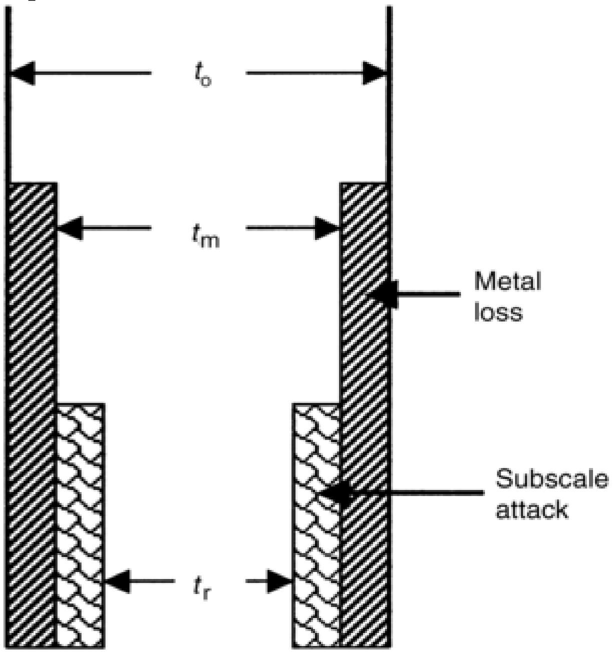

Fig. 10 Schematic showing thickness measurements t_o, original thickness; t_m, sample thickness after a term of exposure; and t_r is the remaining good metal thickness. Source: Ref 24

Depth of attack describes the formation of voids, internal precipitation, or penetration due to corrosion. This is termed depth of penetration or, in the case of oxidation, as internal oxidation. This attack may be due to loss of a material constituent to a high-temperature gaseous environment or internal reaction in the material. Voids are often associated with grain boundaries, because the boundaries are a major route for fast diffusion of the alloying element lost. Alloying elements of high vapor pressure or those that form volatile products with the gaseous environment are prone to cause voids.

It often is more convenient to test round samples, such as rods or pins. Corrosion attack of such test samples can be measured by metallographic examination at a specified magnification at designated intervals around the specimen circumference. The readings at each site around the circumference consist of the outer diameter of the remaining material and the inner reading marking the maximum corrosion penetration at a specific interval site. The measurements reported for round samples are described subsequently, with differences noted based on whether or not the samples are coated.

Uncoated alloy pin measurements affected by corrosion include average material loss on a radius and maximum material penetration.

Average Material Loss on a Radius. This is the combination of the average change of specimen diameter (original diameter minus the remaining diameter after full test exposure) and the average radius of corrosion loss due to all forms of oxidation and sulfidation ([outer diameter minus inner diameter]/2), as shown in Fig. 11. This measurement is usually averaged from a total of all measurements; however, because of the occasional variations in the original pin diameters, the average material loss on a radius is measured at specified intervals of each test specimen. Because these measurements are performed at discrete sites around the circumference, the average material loss on a radius is a statistical average:

$$\text{Average metal loss} = \frac{1}{N}\sum_{i}^{i=N}\left(\frac{D - D_1}{2}\right) \qquad \text{(Eq 20)}$$

where D is the original diameter, D_1 is the diameter of the structurally intact alloy, and N is the number of measurements on the test sample. Measurements are made to the nearest 0.02 mm (0.001 in.).

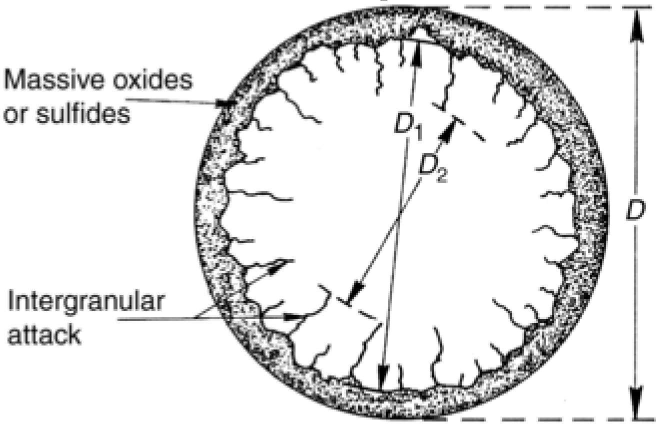

Fig. 11 Schematic of measuring high-temperature corrosion of uncoated metals and alloys on round specimens

Maximum Material Penetration. This measurement includes surface loss plus the depth of all oxides and sulfides that may be scattered or in local concentrations, such as grain boundaries. Only the greatest depth value is reported as the maximum penetration, that is:

$$\text{Maximum material penetration} = \frac{D - D_2}{2} \qquad \text{(Eq 21)}$$

where D is the original diameter, and D_2 is the diameter of the alloy pin unaffected by oxides and sulfides or any other form of corrosion (such as intergranular corrosion or void formation) caused by the high-temperature exposure. Measurements are made to the nearest 0.02 mm (0.001 in.). This type of measurement is most relevant to high-stress applications, such as turbine blades or critical incinerator components. Subsurface attack in local areas may also promote failures through fatigue or thermal cycling.

Coating Measurements Affected by Corrosion. High-temperature components are sometimes coated to provide improved protection. Depth of attack can be measured for these materials as well. Measurements of interest are average coating loss on a radius and maximum coating penetration on a radius.

Average Coating Loss on a Radius. This measurement reflects loss in coating thickness due to all forms of oxidation and sulfidation. An average of all measurements is made per test specimen, as depicted in Fig. 12:

$$\text{Average coating loss on a radius} = \frac{1}{N}\sum_{i}^{i=N}\left(C_o - (X_1 - Y_1)\right) \quad \text{(Eq 22)}$$

where C_0 is the original coating thickness, X_1 is the coating attack due to all forms of oxidation and corrosion, and Y_1 is the coating-substrate interface.

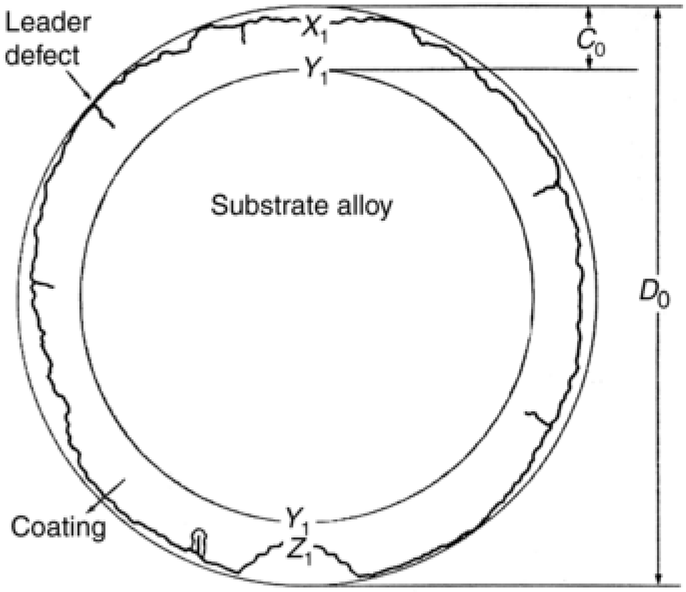

Fig. 12 Schematic of measuring high-temperature corrosion of coated materials on round specimens. C_0, original coating thickness; D_0, original coating plus substrate diameter; X_1, coating attack; Y_1, coating/substrate interface; Z_1, maximum coating attack

Maximum Coating Penetration on a Radius. This is a measurement of the deepest attack found anywhere along the test sample (Eq 23). This number yields a measurement of maximum depth-of-coating attack. Maximum penetration numbers are typically used to rank coating performance in these tests, under the assumption that once the coating has been completely penetrated, it no longer provides the intended protection to the substrate. Although average coating loss may be considerably less than the maximum penetration, the greatest degree of attack is determined to be the most critical measurement for coating assessments.

$$\text{Maximum coating penetration on a radius} = C_0 - (Y_1 - Z_1) \quad \text{(Eq 23)}$$

where C_0 is the original coating thickness, Z_1 is the maximum coating attack due to all forms of oxidation and corrosion, and Y_1 is the coating- substrate interface. Unlike the average coating loss, which is an average of a number of measurements, the maximum coating loss is a single measurement where the penetration was greatest.

Round specimens are preferred because they can be measured accurately by metallographic techniques across any diameter, which is an important consideration, because an uneven attack frequently occurs. Round specimens also minimize the influence of thermal stresses on the corrosion properties of materials. Sharp corners on test specimens may initiate spalling and premature oxide/coating failure that may not be characteristic of the material in actual service. Wedge, airfoil, or other unevenly shaped specimens are generally more difficult to analyze, except when using the weight-change method for measuring the degree of corrosion. However, weight change is not always an accurate quantification of the corrosion process.

Statistical Analysis of Corrosion Measurements. For better assurance of uncoated or coated corrosion measurements, multiple test specimens are recommended. Five multiple samples provide good statistical averaging (Ref 25). Because of the redundancy of the multiple test specimens, it is possible to perform a statistical analysis of the measurement data (Ref 26). This is accomplished by using the two-sample t-test, unequal variance, for examining the existence of real versus random differences between the corrosion data of any two given coatings or alloys. This statistical method tests the hypothesis (commonly referred to as the null hypothesis) that the means of the sets of data from two alloys or coating samples are equal against the alternative hypothesis that the mean on one alloy or coating set of data is greater than that of the second set. This statistical test is performed at a specified probability level (usually set at 90%) that the differences in the means are real and are not due to random variations. This statistical analysis does not project which alloy or coating is better or worse; it only examines the probability that the observed difference is real and not due to random variations. See also the articles "Statistical Interpretation of Corrosion Test Results" and "Statistics for the Corrosionist" in this Volume.

Analysis of Corrosion Products. It is usually desirable to analyze corrosion products and degradation phenomena for both composition and morphology. Such analysis may be performed by in situ methods or ex situ techniques that may require special handling and sample preparation. Compositional analysis can be done by wet chemistry, x-ray diffraction, high- and low-energy electron diffraction, x-ray fluorescence, electron probe microanalysis, inductively coupled atomic emission spectroscopy, atomic absorption spectroscopy, Fourier transform infrared spectroscopy, mass spectroscopy, and other methods. Structural morphology and analysis may be done using light microscopy image analysis, microhardness measurements, transmission electron microscopy, scanning electron microscopy, scanning Auger microscopy, field emission microscopy, plus other techniques. For details of these analytical methods, see *Materials Characterization,* Volume 10 of *ASM Handbook,* and Ref 10.

References cited in this section

10. L.R. Scharfstein and M. Henthrone, Testing at High Temperatures, *Handbook on Corrosion Testing and Evaluation,* W.H. Ailor, Ed., John Wiley & Sons, 1971, p 291–366

23. G.D. Smith, P. Ganesan, C.S. Tassen, and C. Conder, High Temperature Gases, *Corrosion Tests and Standards—Application and Interpretation,* R. Baboian, Ed., American Society of Testing and Materials, 1995, p 359

24. "Practice for Simple Oxidation Testing," G 54, ASTM International

25. I. Miller and J.E. Freund, *Probability and Statistics for Engineers,* 3rd ed., Prentice- Hall, 1985, p 188

26. J.R. Nicholls and P. Hancock, The Analysis of Oxidation and Hot Corrosion Data— A Statistical Approach, *High Temperature Corrosion,* NACE-6, R.A. Rapp, Ed., NACE International, 1983, p 198–210

D.A. Shifler, High-Temperature Gaseous Corrosion Testing, *Corrosion: Fundamentals, Testing, and Protection,* Vol 13A, *ASM Handbook,* ASM International, 2003, p 650–681

High-Temperature Gaseous Corrosion Testing

David A. Shifler, Naval Surface Warfare Center

High-Temperature Corrosion and Degradation Processes

Testing of high-temperature corrosion requires a degree of understanding of the major corrosion processes, based in large part on the material being exposed and the environment to which the material is exposed, along with the other basic factors discussed earlier. It must be realized that actual service environments and conditions may be far more complicated than simple laboratory tests may provide. High-temperature corrosion or degradation of materials may occur through a number of potential processes:

- Oxidation
- Carburization and metal dusting
- Nitridation
- Sulfidation
- Hot corrosion
- Chloridation and other halogenization reactions
- Hydrogen interactions
- Molten metals
- Molten salts
- Aging reactions, such as sensitization
- Creep
- Erosion-corrosion and wear
- Environmental cracking (stress-corrosion cracking and corrosion fatigue)

Oxidation. Most metals and alloys oxidize on exposure to temperatures above 300 °C (570 °F) in environments containing greater than 1 vol% O_2. Alloys are protected to varying degrees by the oxide layer. The thickness of the protective oxide often follows parabolic rate kinetics. Gas composition influences the rate of oxidation. The effects of oxygen concentration and temperature are specific to each alloy. Scale growth rates increase with a rise in temperature. Oxidation environments may be classified on the basis of the oxygen activity. Oxidizing environments contain an excess of free oxygen, while reducing environments contain no free oxygen at equilibrium in the gas mixture. Mixed-oxidant environments that are reducing tend to be more corrosive than oxidizing conditions.

Preferential grain-boundary oxidation, thermal cycling, the presence of moisture, and chloride- or sulfur-containing gases cause service lives much shorter than those predicted from isothermal oxidation. Small additions of rare earths, such as lanthanum, cerium, and yttrium, or the presence of dispersed oxides, such as yttria, ceria, zirconia, and lanthania, improve the scale adhesion and scale resilience of chromia-forming alloys to cyclic oxidation of Cr_2O_3-forming alloys, such as austenitic stainless steels and chromium-nickel alloys (Ref 27). These effects may include (a) more rapid formation of a continuous Cr_2O_3 scale, (b) reduction in the oxidation rate, (c) improved scale adherence, and (d) a change in the scale-forming reaction location from the scale-gas interface to the scale-alloy interface. Reactive elements are known to improve the oxidation resistance of many high-temperature alloys, particularly if the resistance is dependent on Cr_2O_3 formation.

Loss of oxide adhesion and integrity may be caused by mechanical damage via spallation or cracking of the oxide film from cyclic oxidation of chromia and alumina oxides formed on nickel-base alloys due to the mismatch of thermal expansion coefficients between the oxide and the base alloy (Ref 28).

Carburization of metals and alloys is a form of internal attack where the formation of carbide corrosion products occurs on exposure to temperatures above approximately 760 °C (1400 °F) in gases containing methane, carbon monoxide, hydrocarbons, carbon, or other carbonaceous compounds. Carburization alone usually does not result in corrosion or alloy wastage, but adsorption and diffusion of carbon into the base alloy can lead to significant changes in the alloy mechanical properties, leading to possible alloy embrittlement. Variables that affect the carburization rate are the temperature, exposure time, alloy composition, and the partial pressures of H_2, CH_4, and H_2S. The H_2S tends to slow alloy carburization rates.

Carburization is usually controlled by both carbon and oxygen activities. Carbon activity is a function of both the environment and of the metal or alloy. The carbon activity of a metal or alloy can be determined by thermodynamics. Generally, the lower the oxygen activity, the greater the tendency for carburization to occur. Carburization is a diffusion-controlled reaction where the maximum carbon gradient occurs at the reaction surface. Grain-boundary diffusion of carbon tends to be significantly faster than intragranular diffusion (Ref 23). It is often observed that there is a change of the carbide species from the surface to the interior.

Carbon dioxide produced in an oxidizing environment is less corrosive than carbon monoxide, CO, which is the prevalent carbonaceous gaseous species in a reducing environment. Reducing or oxidizing environments will usually be dependent on the stability of the oxide formed; the relative oxidizing or reducing atmosphere can be determined, to a first approximation, by use of the Ellingham diagrams discussed earlier.

Under simultaneous oxidizing and carburizing conditions where hydrocarbons are present in the gas stream and/or with the introduction of oily components, stainless steels and nickel-base alloys are susceptible to severe carburization called green rot (Ref 29). Green rot occurs when internal chromium carbides are formed during carburization; subsequent oxidizing of the carbides at the grain boundaries may result in embrittlement. Corrosion products in the pits consist of metal carbides, metal oxides, and graphite. The attack is localized, and carburization is confined to the pit.

Carburization may be tested in several gaseous environments, such as CH_4-H_2 (reducing) or CO_2-H_2-H_2O mixtures, or under pack carburization, where active charcoal is packed around the sample in a steel box and tested to the desired testing temperature. The carbon reacts with open pockets of air to generate carbon monoxide, which, in turn, disproportionates via the Boudouard reaction—C (s) + CO_2 (g) = 2CO (g), where "s" and "g" represent solid and gas, respectively—into an oxidizing mixture of carbon dioxide and carbon.

Carburization testing in the laboratory offers the convenience of access to the necessary equipment for precise control of conditions along with the ability to control measurement schedules. However, the laboratory test may not mimic all environmental and mechanical conditions, such as stress, design effects (corners, crevices, dead zones, etc.), thermal fluctuations in service abrasive damage, flow stream effects, and metal-to-metal contact reactions. Thus, the investigator may not be able to reproduce the complete atmosphere that is being simulated in the laboratory and thereby runs the risk of missing a key element in determining the rate of carburization degradation. Reference 30 reviews the phenomenon of carburization and procedures for testing and evaluating carburization.

Metal dusting can be described as a catastrophic form of carburization occurring under conditions where the carbon activity (a_C) in the gaseous atmosphere is much greater than that in the metal. The degradation takes place in strongly carburizing atmospheres (a_C » l). Although metal dusting has taken place at temperatures as high as 1095 °C (2000 °F) in strongly reducing gaseous environments, it generally occurs at temperatures from 480 to 815 °C (900 to 1500 °F). Deterioration and material wastage by metal dusting in carburizing gases at 425 to 815 °C (800 to 1500 °F) result in pitting and overall wastage of stainless steels with or without an oxidizing environment (Ref 31, 32, 33, 34, 35).

Slight modifications in the process conditions may significantly affect the occurrence and extent of metal dusting attack. The phenomenon can produce rapid metal wastage, producing pits and grooves as the affected metal disintegrates into a mixture of powdery carbon and metal particles. Metal dusting corrosion occurs in processes from numerous industries that include petrochemical processing (processes involving steam reforming of methane or natural gas, such as ammonia and methanol production), direct iron-ore reduction, coal degasification, and heat treating.

Nitridation of alloys in ammonia environments is well known in ammonia and heat treating industries (Ref 36). Nitridation characteristics are similar to carburization but are not as commercially common in occurrence. As with carburization environments, increasing oxygen activity decreases nitridation at a given temperature. It has been shown that the kinetics of nitridation in N_2 are much higher than that found in contact with NH_3 at high temperatures (980 to 1090 °C, or 1800 to 2000 °F) (Ref 37). Heat treating furnaces and accessories for heat treating powder metal products are typically exposed to N_2 or N_2-H_2 atmospheres at elevated temperatures (≈1090 °C, or 2000 °F). Alloys can be susceptible to nitridation attack in combustion environments even when such environments are oxidizing.

The internal precipitation of nitrides in heat- resisting alloys containing chromium or aluminum has been known to follow parabolic kinetics, indicating the diffusion of nitrogen is the rate-controlling step. Thermal cycling, which leads to cracking of the oxide scale and/or spallation, destroys the effectiveness of the barrier oxide, leading to internal nitridation.

Sulfidation is most often a reaction of a metal or alloy with gaseous species, although reaction with molten sulfur-containing species is possible. Sulfidation produces a metal-sulfur compound that forms on or beneath the surface of the material. The extent of corrosion depends on the partial pressure of sulfur relative to oxygen at a given temperature and the relative stability of the oxides and the sulfides at the same temperature.

Sulfidation may involve the formation of oxides plus sulfides in reducing gases, such as hydrogen/hydrogen sulfide mixtures, or in oxidizing gases, such as air-sulfur dioxide or air-sulfur dioxide water. In most

environments, Al_2O_3 or Cr_2O_3 form preferentially to the sulfides, but destructive sulfidation attack may occur at oxide crack sites (Ref 38). The reduced species, H_2S, is more corrosive than the oxidized species, SO_2 Gaseous reactions or molten phases, such as low-melting-point metal-sulfide eutectics, cause sulfidation. Sulfidation of nickel results in the formation of eutectic Ni_3S_2 that has a melting point of 635 °C (1175 °F) with a sulfur solubility of 0.005% (Ref 39). The eutectic formation causes the initiation and propagation of intergranular corrosion. The sulfidation rate of metals and alloys is usually many times higher than the corresponding oxidation rate. Metal sulfides generally are more complex and have lower melting temperatures than the corresponding oxides (Ref 40).

Adding chromium improves resistance to sulfide attack and increases the operating temperature limit of an alloy in a sulfidizing environment. Chromium sulfide formed below the surface of the protective oxide layer may lead to depletion of chromium and breakaway corrosion of the alloy. Once sulfur has entered into the alloy, sulfur tends to react preferentially with chromium or aluminum to form additional sulfides; this may cause redistribution of the scale-forming elements or interfere with the formation of protective oxide scales. Nickel-chromium alloys have been successfully used at service temperatures of 750 to 1200 °C (1400 to 2200 °F). Manganese, silicon, and aluminum additions improve the resistance of nickel alloys to sulfur attack (Ref 41).

Scaling rates of high-temperature stainless steels are higher in dry sulfur dioxide environments than in air, due to the formation of chromium sulfides below the protective chromia scale. The introduction of water vapor into air- sulfur dioxide environments accelerates sulfidation attack (Ref 13).

Sulfur can be transported through the Al_2O_3 and Cr_2O_3 protective scales under certain conditions, resulting in discrete sulfide precipitates observed at the scale/alloy interface. Sulfide concentrations above approximately 10 to 20 ppm have been shown to modify the adhesion strength and cyclic oxidation resistance of the protective oxide scales. Generally, cobalt-chromium binary alloys have resistance to sulfidation superior to nickel-chromium binary alloys because of the slower outward diffusion of cobalt ions through the scale during sulfidation and the relatively high melting point of the cobalt-Co_4S_3 eutectic (Ref 42).

Hot corrosion is a complex process involving both sulfidation and oxidation (Ref 43). Hot corrosion is a form of accelerated oxidation that affects alloys and coatings exposed to high-temperature gases contaminated with sulfur and alkali metal salts (Ref 44). These contaminants combine in the gas phase to form alkali metal sulfates; if the temperature of the alloy is below the dewpoint of the alkali sulfate vapors and above the sulfate melting points, molten sulfate deposits are formed (Ref 44). Molten sodium sulfate is the principal agent in causing hot corrosion (Ref 45, 46). Sulfide formation results from the interaction of the metallic substrate with a thin film of fused salt of sodium sulfate (Ref 47, 48, 49). Sulfur compounds come from two sources in a marine gas turbine engine: sulfur from the combustion fuel, which often ranges from 0.1 to 1 wt% (or more), depending on the grade of fuel, and sulfate salts contained in marine air that are ingested into the hot section of the turbine engine.

Chloride salts can act as a fluxing agent and dissolve protective oxide films or cause alloy oxides to fracture and spall. Air in a marine environment ingested into the combustion zone of any marine gas turbine engine will be laden with chlorides unless properly filtered. Sodium chloride (NaCl) has been viewed as an aggressive constituent in the hot corrosion of gas turbine components in the marine environment (Ref 50, 51).

Two general forms of sulfate hot corrosion exist. Type I, high-temperature hot corrosion (HTHC), occurs through multiple mechanisms. It is generally thought to transpire by basic fluxing and subsequent dissolution of the normally protective oxide scales by molten sulfate deposits that accumulate on the surfaces of high-temperature components, such as hot section turbine blades and vanes. The HTHC usually occurs at metal temperatures ranging from 850 to 950 °C (1560 to 1740 °F). Type I hot corrosion involves general broad attack caused by internal sulfidation above 800 °C (1470 °F); alloy depletion is generally associated with the corrosion front. This basic fluxing attack involves raising the Na_2O activity in the molten sulfate by formation of metal sulfides (Ref 52). Very small amounts of sulfur and sodium or potassium can produce sufficient Na_2SO_4 or K_2SO_4. In gas turbine environments, a sodium threshold level below 0.008 ppm by weight precluded type I hot corrosion (Ref 13).

Type II, low-temperature hot corrosion (LTHC), occurs in the temperature range of 650 to 750 °C (1200 to 1380 °F) where p_{SO_3} is relatively high or melts are deficient in the oxide ion concentration, leading to acidic fluxing of metal oxides, which results in pitting attack (Ref 53). Sulfides are found in the pitted area (Ref 54). The LTHC may involve a gaseous reaction of SO_3 or SO_2 with CoO and NiO, which results in pitting from the formation of low-melting mixtures of Na_2SO_4 and $NiSO_4$ or Na_2SO_4 and $CoSO_4$ in nickel-chromium, cobalt-

chromium, cobalt-chromium-aluminum, and nickel-chromium-aluminum alloys (Ref 13, 55). The interaction of these oxidation products with salt deposits forms a complex mixture of salts with a lower melting temperature (Ref 15). When the salt mixture melts, the corrosion rate increases rapidly. If other reactants are added, melting temperatures of the resultant salts can be further lowered. High chromium content (>25 to 30 wt% Cr) is required, generally, for good corrosion resistance to hot corrosion. Nickel-base alloys with both chromium and aluminum show further improvement in hot corrosion resistance.

Acid-base oxide reactions with molten sulfate through the measurement of oxide solubilities as a function of Na_2O activity in fused Na_2SO_4 were examined (Ref 56). Oxide solubility is dependent on Na_2O activity, which also serves to rank the acid-base character of individual oxides.

Other impurities, such as vanadium (≥0.4 ppm), phosphorus, lead, chlorides, and unburned carbon, can be involved in lowering salt melting temperatures, altering the sulfate activity, or changing the solution chemistry and acidity/basicity that leads to accelerating hot corrosion. Vanadic hot corrosion appears to be potentially more complex, because five compounds exist in the sodium, vanadium, oxygen system (Ref 57). The high-temperature reaction of sulfate and vanadium with ceramic oxides involved a Na_2O- V_2O_5 system that could be explained by Lewis acid-base chemistry (Ref 58). Basic zirconia (ZrO_2)-stabilizing oxides, such as Y_2O_3, do not react with Na_3VO_4 (or $3Na_2O$-V_2O_5) but do react with the V_2O_5 component of $NaVO_3$ (Na_2O- V_2O_5) and V_2O_5 itself to form YVO_4 (Ref 59). Acidic oxides, such as Ta_2O_5, react with the Na_2O component of Na_2VO_4 and $NaVO_3$ to form sodium tantalates and yield α-$TaVO_5$ with V_2O_5. The vanadate that is most corrosive in the initiation of vanadic attack will depend on the acidity/basicity of the coating or alloy oxide. No reaction occurs when the acid-base properties of a stabilizing oxide are equal (Ref 60). The thermochemistry of vanadate and sulfate melts and reaction with different stabilizing oxides with SO_3-$NaVO_3$ was studied (Ref 61).

High chromium content (>25 to 30% Cr) is required for good resistance to hot corrosion. Nickel alloys with both chromium and aluminum show improved hot corrosion resistance. However, inspection of phase stability diagrams for the systems M-Na-O-S, where M can be nickel, cobalt, iron, aluminum, or chromium, indicates that there are no combinations of melt basicity and oxygen activity where these metals, absent of a protective oxide film, are stable in contact with fused sodium sulfate (Ref 62). The relative hot corrosion resistance of a number of alloys has been evaluated in incinerator environments where hot corrosion can occur (Ref 38, 63, 64).

Yttria-stabilized zirconia (YSZ) is attacked at high temperatures and destabilized by phosphorus impurities in fuel (Ref 65). The acid P_2O_5 reacts with basic Y_2O_3 to form the salt YPO_4. Zirconia also synergistically reacts with sodium and P_2O_5 to form $NaZr_2(PO_4)_3$. The YSZ thermal barrier coatings (TBCs) have been exposed to $PbSO_4$-Na_2SO_4 molten salts without observable destabilization or reaction with this ceramic (Ref 66). However, lead, as PbO, appears to cause TBC failures by reacting with chromium in the NiCrAlY bond coat to form $PbCrO_4$.

Chloridation. Chlorides often accumulate rapidly on metallic surfaces of test samples. In one study, typical deposits contained 21 to 27% Cl when the flue gas contained 40 to 140 ppm HCl (Ref 67). Municipal wastes were characterized as having a 0.5% halide dry content, of which 60 wt% was derived from organic polymer sources (Ref 68). Chloride salts have melting temperatures as low as 175 °C (347 °F), which can act as fluxing agents that dissolve protective oxide films. High-temperature components exposed to air from a marine environment will be laden with chlorides. The following compounds may cause rapid corrosion of carbon steel, if present:

Compound	Melting point	
	°C	**°F**
Molten $SnCl_2$	246	474
$SnCl_2$ + NaCl	199	390
$ZnCl_2$	283	541
Eutectic $PbCl_2$/$FeCl_3$	175	347
Eutectic $ZnCl_2$/NaCl	262	504

Attack by halogens at elevated temperatures occurs through the volatility of the reaction products. Oxides that form in combustion gases will be porous and prone to fracture. Stainless steels are generally passive, but surface pitting may occur in chloride-containing environments. Nickel- base alloys can be expected to have superior corrosion resistance, as compared to stainless steel alloys (Ref 69). Clay containing aluminum silicate may inhibit chloride-related corrosion by raising the melting points of chloride salts through the formation of sodium aluminum silicates, which expel HCl and SO_3 (Ref 70). Problems with chlorides can be mitigated if

plastics and other sources of halogens are removed or minimized from the waste stream. Increasing the oxygen content and adding water vapor has also reduced the corrosion rate of various alloys by chlorides in a simulated waste incinerator environment (Ref 67). Hydrogen chloride can be formed from the combustion from chlorine-containing polymers and can dissociate into hydrogen and chlorine gases. Low pCl_2 will generate a reducing environment. However, HCl can react with oxygen (generally, catalyzed by surface oxides) to generate water and possibly very high Cl_2 pressures. The corrosion products of chloridation tend to be volatile and have low melting points. Other halogens may also affect metals and alloys in a manner similar to chlorides.

Laboratory halogenization testing environments are divided into two groups: those possessing no measurable oxygen and those containing measurable oxygen. In the oxygen-free environments, liquid phases and volatile reaction products may lead to erratic corrosion attack. Halogen-plus-oxygen environments often exhibit paralinear behavior as oxide scale and volatile halide reactions occur simultaneously.

Corrosion-resistance testing of materials is properly conducted in electrically heated furnaces using ceramic tubes with end caps containing pusher rods to manipulate the corrosion specimens under atmosphere. The end caps should be coated with a castable material to protect them from corrosion. Gas composition may be either purchased or synthesized from the components, using halogen-resistant electronic flow controllers or mixers. The specimens may be in the form of pins with dimensions similar to those mentioned for sulfidation testing. Gas flow streams of a total flow rate of 500 cm^3/min (30.5 $in.^3$/min) are considered adequate to ensure a consistent environment for all specimens. The effluent stream should be reacted with a caustic solution before venting to remove the reacted and unreacted halogens. At the completion of testing, the specimens should be examined metallographically for evidence of voiding or liquid-phase corrosion. Scale identification by x- ray diffraction or electron-dispersive spectrometry can be helpful in clarifying reaction mechanisms.

Hydrogen Interactions. In selected high- temperature reactions, steam may decompose on metal surfaces to form hydrogen and oxygen. The resulting chemisorbed hydrogen may diffuse into the metal to an appreciable level. Loss in tensile ductility of steels and nickel-base alloys has been observed in gaseous environments with a total hydrogen content of 0.1 to 10 ppm at -100 to 700 °C (-150 to 1300 °F). Hydrogen attack occurs when hydrogen diffuses into the metal (typically steel) and reacts with the carbides to form methane, $4H + Fe_3C \rightarrow CH_4 + 3Fe$; the methane causes subsequent internal microcracks that lead to brittle rupture. The larger methane gas molecules also tend to concentrate at the grain boundaries. When methane gas pressures exceed the cohesive strength of the grains, a network of discontinuous, intergranular microcracks is produced. The reaction rate depends on the amount of carbon in the alloy, the hydrogen concentration, diffusion, total gaseous pressure, and temperatures in the range of 200 to 600 °C (400 to 1110 °F). Hydrogen damage has been observed in utility boilers at temperatures as low as 316 °C (600 °F) (Ref 71). Hydrogen damage can occur in high-strength alloys, resulting in loss of tensile ductility. Nickel-base alloys are much less susceptible to hydrogen damage than ferrous-base alloys.

Nickel and nickel-base alloys are susceptible to attack in gaseous hydrogen environments. The same factors that affect hydrogen interactions in ferrous alloys are also operative for nickel-base alloys, although to a slightly lesser degree, because face-centered cubic metals have a greater number of slip planes and have lower solubilities for hydrogen than body-centered cubic metals (Ref 72). Hydrogen in nickel-base alloys may lead to intergranular, transgranular, or quasi- cleavage cracking. The Fe-Ni-Cr (Incoloy) and Inconel alloys show ductility reductions when exposed to hydrogen, particularly age-hardenable alloys (Ref 72).

Molten Metals. Corrosion may cause dissolution of an alloy surface directly, by intergranular attack, or by leaching. Liquid metal attack may also initiate alloying, compound reduction, or interstitial or impurity reactions. Carbon and low-alloy steels are susceptible to various molten metals or alloys, such as brass, aluminum, bronze, copper, zinc, lead-tin solders, indium, and lithium, at temperatures from 260 to 815 °C (500 to 1500 °F). Plain carbon steels are not satisfactory for long-term use with molten aluminum. Stainless steels are generally attacked by molten aluminum, zinc, antimony, bismuth, cadmium, and tin (Ref 73). Nickel, nickel-chromium, and nickel-copper alloys generally have poor resistance to molten metals, such as lead, mercury, and cadmium. In general, nickel-chromium alloys also are not suitable for use in molten aluminum (Ref 74). There are no metals or alloys known to be totally immune to attack by liquid aluminum (Ref 75). Liquid metal embrittlement (LME) is a special case of brittle fracture that occurs in the absence of an inert environment and at low temperatures (Ref 76). Decreased stresses can reduce the possibility of failure in certain embrittling molten alloys. Stainless steels suffer from LME by molten zinc. Small amounts of lead will embrittle nickel alloys, but molybdenum additions appear to improve lead LME resistance. The selection of fabricating processes must be chosen carefully for nickel- base superalloys. Liquid metal embrittlement can

occur when brazing precipitation-strengthened alloys, such as Unified Numbering System (UNS) N07041 (Ref 77). Many nickel superalloys crack when subjected to tensile stresses in the presence of molten (B-Ag) brazing filler alloys.

Molten salts are often involved in sulfidation, chloridation, hot corrosion, or high-temperature coatings, as discussed previously. The corrosiveness of the environment depends on the surface temperature and the condition of and/or the corrosive ingredients in the medium. Molten salts are employed in a number of applications, including metal heat treating; nuclear, fossil, and solar energy systems; reactive-metal extraction; high-temperature batteries; and fuel cells.

Molten salts tend to flux the inherent scale that forms on heat-resistant alloys. In the presence of molten ash products, the oxide, even in oxidizing environments, becomes unstable and dissolves. Oxygen and water vapor tend to accelerate molten salt corrosion. Molten salt corrosion can take the macroscopic form of uniform thinning, pitting, or internal or intergranular attack.

Alkali sulfates deposited on the fireside surfaces of boilers may react with SO_3 or SO_2 to form mixtures of alkali pyrosulfates (melting point: 400 to 480 °C, or 750 to 900 °F) or alkali- iron trisulfates (melting point: 550 °C, or 1020 °F) that cause fireside corrosion of reheater and superheater tubes (Ref 78). Molten sodium pyrosulfates ($Na_2S_2O_7$) (melting point: 400 °C, or 750 °F) or potassium pyrosulfates ($K_2S_2O_7$) (melting point: <300 °C, or 570 °F) react with carbon steels by dissolving the protective oxide film and then reacting with iron to cause accelerated wastage. A few parts per million of vanadium accelerate this reaction. The melting point of these deposits on waterwall tubes ranges from 300 to 410 °C (570 to 770 °F).

Testing is often done in quartz or platinum crucibles, either in air or in a controlled atmosphere. Molten salts can induce significant mass transport due to thermal gradients within the crucible. Molten salt corrosion generally involves dissolution of an alloying element in the higher- temperature regions and subsequent deposition of the element in the cooler parts of the system.

Aging Reactions. Long-term aging effects in service can cause metallurgical changes that alter the mechanical and corrosion properties of materials. Testing should reflect long-term aging effects on materials properties. Graphitization is a microstructural change that can occur in carbon and low-alloy steels. Pearlite (alternating ferrite and Fe_3C platelet structure) normally found in such steels will transform in time to graphite and ferrite at temperatures above 425 °C (800 °F), which causes loss of ductility and promotes embrittlement. Alloying additions of at least 0.7% Cr and 0.5% Mo markedly improve resistance of carbon steels to graphitization. Weld sites are particularly susceptible to graphitization. Treatments or operating conditions that heat ferritic and austenitic stainless steels to 500 to 900 °C (930 to 1650 °F) can cause segregation at the grain boundaries by the precipitation of complex chromium carbides (if carbon content is less than approximately 0.03 wt%), the formation of sigma phase, or the precipitation of other deleterious phases. Nickel-base superalloys are also susceptible to grain-boundary segregation. Nickel-base superalloys can be embrittled by less than 20 ppm sulfur segregation to alloy grain boundaries.

Grain-boundary segregation may result in localized corrosion if the grain boundaries are not as resistant as the alloy matrix, which may be a consequence of segregation causing depletion of corrosion-resistant elements. Pitting is another form of localized corrosion. Both dissolved oxygen and carbon dioxide can promote pitting of carbon steels. An alkaline pH can diminish corrosion, with the evolved gases likely to be neutral to acidic. Ash deposition, thermally induced stress, and particulate erosion may cause conditions that accelerate localized corrosion by cracking the protective oxide layer.

Iron, nickel, and cobalt superalloys owe their unique strength, up to a fairly high threshold temperature, to the presence of strengthening particles, such as inert oxide dispersoids, carbides, coherent ordered precipitates, and solid- solution-strengthening agents, in a face-centered cubic (with appropriate nickel additions) structure. Introduction of precipitates into the alloy through solid-solution reactions requires specific alloy chemistries and heat treatments to achieve the desired mechanical properties. However, at prolonged exposures to high temperatures (760 to 1000 °C, or 1400 to 1830 °F), the phase rule alone suggests that a large number of new phases could nucleate within multicomponent superalloys to form a number of microstructural instabilities (Ref 79). These instabilities can include transformation of a metastable phase to a more stable but incoherent phase, as in carbide transformation, stress-induced differential diffusion of solute atoms (coarsening of $M_{23}C_6$ at grain boundaries), or dissolution of strengthening precipitates in critical areas of the microstructure. Structural instabilities of austenitic high-temperature alloys at elevated temperatures can also include the formation of new topologically close-packed (tcp) phases, such as sigma, mu, and Laves phases, which are brittle and possess

cracklike morphologies that can adversely affect alloy tensile and stress-rupture ductility and impair resistance of the alloy to crack growth (Ref 79).

Intergranular corrosion occurs at or adjacent to grain boundaries, with little corresponding corrosion of the grains. Intergranular corrosion can be caused by impurities at the grain boundaries or enrichment or depletion of one of the alloying elements in the grain-boundary area. Austenitic stainless steels, such as type 304 (UNS S30400), become sensitized or susceptible to intergranular corrosion when heated in the range of 510 to 790 °C (950 to 1450 °F). In this temperature range, $Cr_{23}C_6$ precipitates, thus depleting chromium from an area along the grain boundaries below the level required to maintain stainless mechanical and corrosion-resistant properties. The depleted area is a region of relatively poor corrosion resistance. Controlling intergranular corrosion of austenitic stainless steels occurs through: (a) employing high-temperature solution heat treatment; (b) adding elements (stabilizers) such as titanium, niobium, or tantalum that are stronger carbide formers than chromium; and (c) lowering the carbon content below 0.03%.

Creep. Dislocations form in the oxide as it grows epitaxially on the metal because of the crystallographic lattice mismatch between oxide and metal. As the growth continues, these glissile slip dislocations move out into the oxide by the process of glide. Once out in the oxide, they become sessile growth dislocations. Creep may also develop in the alloy. Creep can affect the alloy, the protective films formed on the alloy, or the coating performance.

Although dislocations are present in the oxide, slip is not an important process in relieving growth stress (Ref 79). Plastic deformation of the oxide occurs only at high temperatures, at which creep mechanisms become operative. The three important creep mechanisms in oxides are grain-boundary sliding, Herring-Nabarro creep, and climb (Ref 80). Grain-boundary sliding allows relative motion along the inherently weak boundaries. Herring-Nabarro creep allows grain elongation by diffusion of ions away from grain- boundary areas in compression over to boundaries in tension (Ref 81). Within the grains, dislocation climb is controlled by diffusion of the slower-moving ions. The creep rate increases with the amount of porosity in the oxide.

The strength of a component within the creep range decreases rapidly when the material temperature increases. Creep entails a time-dependent deformation involving grain sliding and atom movement. When sufficient strain has developed at the grain boundaries, voids and microcracks develop. With continued operation at high temperatures, these voids and microcracks will grow and coalesce to form larger and larger cracks, until failure occurs. The creep rate will increase and the projected time to rupture will decrease when the stress and/or the metal temperature are increased. In gas turbines, the use of directionally solidified or single-crystal alloys with chemistries that promote high-temperature strength minimize degradation by creep.

Creep may be affected by gaseous reactions. Metal components in steam turbines and jet engines must withstand high stresses for long times at high temperatures. Specimens undergoing creep testing should be representative of a service component. A creep test is generally run under constant load and constant temperature for periods of 1000 to 10,000 h or more. Because the creep rate is a function of stress, a rise in stress will normally cause a corresponding increase in the creep rate. The temperature should be maintained within close tolerances, such as specified by the ASTM E 139, “Standard Test Methods for Conducting Creep, Creep Rupture and Stress-Rupture Tests of Metallic Materials.”

A stepped isothermal method has been developed to predict long-term creep performance in much less time than the traditional constant-load test. This test avoids stress variations by using single specimens and performs the tests within days. It forecasts long-term creep performance by increasing the temperature in steps; the creep curve is mapped out in sections, and change in creep rate between each temperature step determines the level of acceleration. This creep test method also provides a rapid method of studying creep behavior, residual strength, and the effects of other forms of degradation.

Erosion-corrosion and wear accelerate or increase the deterioration of a metal because of the relative movement between a corrosive fluid and the metal surface. Erosion may accelerate corrosion of high-temperature components discussed previously. Generally, mechanical wear, abrasion, or abrupt changes in flow direction are involved. Metal or alloy loss results when the protective, passive surface films are damaged or worn, and rapid attack comes about. Metals or alloys that are soft and readily damaged or mechanically worn, such as copper or lead, are susceptible to erosion. Impingement by solid particles may contribute to erosion-corrosion, which accelerates several forms of corrosion in the various gaseous or molten environments. Other factors controlling the rate of metal loss are related to the quantity, impact angle, speed, and density of the eroding medium.

The appearance of erosion-corrosion is characterized by grooves, gullies, waves, and rounded holes, which usually exhibit a directional pattern. Increases in velocity may cause no increase in attack until a critical velocity is reached. Erosion-corrosion can occur on metals and alloys that are completely resistant to a particular environment at low velocities. Greater velocity may either increase or decrease attack, depending on the nature of the corrosion or passivating mechanisms. Increasing the oxygen, carbon dioxide, or hydrogen sulfide concentration in contact with the metal surface may accelerate the attack of steel. Reduced attack may occur from increased velocity either by raising the diffusion or transfer of ions that diminish the stagnant surface film or by preventing deposition of salt or dirt that could cause crevice corrosion. Coal-fired generation systems are subject to erosion-corrosion conditions. Several laboratory techniques and methodologies have been established to study erosion-corrosion (erosion-oxidation and erosion-sulfidation) at high temperatures. How these laboratory methods simulate plant conditions and the limitations of each method are reviewed in Ref 82.

Wear is defined as damage to a solid surface that generally involves progressive loss of material and is due to relative motion between that surface and a contacting substance or substances. Tribocontacts cause damage to surfaces at high temperature, usually by many consecutive steps by several different mechanisms. Material loss from the surface can cause wear marks. Fundamental causes of material removal can be shear fracture, extrusion, fracture, chip formation, tearing, brittle fracture, fatigue fracture, chemical dissolution, and diffusion (Ref 83). The rate at which surfaces wear depends on the characteristics of each surface, the presence of abrasives, the speed and angle of contact, and other environmental conditions. There are several modes of wear (abrasive, polishing, solid-particle erosion, cavitation erosion, liquid impingement, slurry erosion, sliding and adhesive wear, fretting, corrosive and oxidative wear, and others) that are discussed in more detail in *Friction, Lubrication, and Wear Technology,* Volume 18 of *ASM Handbook.* Wear tests designed to closely simulate the condition of specific processes are discussed in Ref 84. There are no standardized tests for wear at high temperatures at this time.

Environmental cracking can occur with a wide variety of metals and alloys in specific environments. Environmental cracking is defined as the spontaneous brittle fracture of a susceptible material (usually quite ductile itself) under tensile stress in a specific environment over a period of time. Stress-corrosion cracking (SCC) and corrosion fatigue are two forms of environmental cracking that can lead to failure.

Stress-corrosion cracking results from the conjoint, synergistic interaction of residual or applied tensile stress and a specific corrodent for an otherwise ductile alloy. The tensile stress may be either applied (such as caused by internal pressure) or residual (such as induced during forming processes, assembly, or welding). Stress-corrosion cracking involves the concentration of stress and/or the concentration of the specific corrodent at the fracture site. Stress-corrosion cracking fractures may be oriented either longitudinally or circumferentially, but the fractures are always perpendicular to the stresses. Stress-corrosion cracking may be reduced either by removing applied or residual stresses or by avoiding concentrated corrodents.

Alloy composition, heat treatment, the exposure time, temperature, and solution media affect SCC. Fluctuating temperatures can accelerate SCC of austenitic stainless steels in the presence of chlorides, particularly at high-stress points from design, operation, or fabrication. Nickel alloys exhibit improved resistance to environmental cracking, as compared to carbon and stainless steels, although nickel alloys are not immune to SCC. Stress-corrosion cracking of certain nickel alloys has occurred in high-temperature halogen ion environments, high-temperature waters, and high-temperature alkaline systems and environments containing acids and H_2S. Stress-corrosion cracking of nickel-base alloys is dependent on the stress level, chloride concentration, alloy composition, and temperature. Susceptible temperature ranges vary from 175 to 330 °C (345 to 625 °F). Higher temperatures tend to lower the chloride threshold concentration and stress levels required for cracking. Ferritic stainless steels are usually not considered susceptible to SCC, but stressed martensitic stainless steel grades can crack in chloride environments.

Fatigue involves cyclic stresses applied to the component or system during service. Cyclic stresses below the yield stress of a material can reduce its expected life through the initiation and propagation of transgranular cracks. The number of cycles required to produce cracking depends on the level of strain and the environment. Vibration and thermal cycling can lead to initiation and propagation of fatigue degradation. Vibration fatigue cracks originate and propagate as a result of flow-induced vibration. Circumferential orientations are common to vibration fatigue cracks.

Corrosion fatigue failures are caused by the combined effects of a corrosive environment and cyclic stresses of sufficient magnitude. A corrosive environment accentuates this form of degradation by initiating stress raisers

for corrosion fatigue to start and/or lowering the stress necessary to continue the propagation of this cracking process. Corrosion usually lowers the minimum stress level and/or the number of cycles that will cause failure, compared to an inert environment. Corrosion fatigue cracks may develop at stress-concentration sites (stress raisers) such as pits, notches, or other surface irregularities. Corrosion fatigue is commonly associated with rigid restraints or attachments.

Thermal fatigue cracks develop from excessive strains induced by rapid cycling and sudden fluid temperature changes in contact with the tube metal across the tube wall thickness. This can be caused by rapid thermal fluctuations above proper process operational parameter limits. Water quenching by spraying also can induce thermal fatigue cracks by suddenly cooling component surfaces. This causes high tensile stresses between the component surface and the bulk metal or alloy; the cooled surface metal tends to contract, while this metal surface becomes restricted by the hotter metal below the surface.

Stress Rupture. Although not strictly a corrosion-related phenomenon, stress rupture is often involved when the component is subjected to high temperatures where changes in the microstructure or corrosion of the substrate reduce the effective thickness of the component to the point where failure occurs. Stress and temperature influence the useful life of materials in a given gaseous environment.

Most metals and alloys in an oxidizing environment are protected to varying degrees by an oxide layer. Alloy oxidation from air or steam forms an oxide scale along the metal surface that grows and thickens with time. The degree of protection of these formed surface scales and resistance of the alloy in a given environment will depend on factors such as chemical composition, thermodynamic stability, cation or anion transport through the scale, ionic defect structure, and morphological features of the scale.

References cited in this section

13. I.G. Wright, High Temperature Corrosion, *Corrosion,* Vol 13, *Metals Handbook,* 9th ed., ASM International, 1987, p 97–103

15. A.S. Khanna, *Introduction to High-Temperature Oxidation and Corrosion,* ASM International, 2002, p 40–60, 172–201, 205–214

23. G.D. Smith, P. Ganesan, C.S. Tassen, and C. Conder, High Temperature Gases, *Corrosion Tests and Standards—Application and Interpretation,* R. Baboian, Ed., American Society of Testing and Materials, 1995, p 359

27. D.P. Whittle and J. Stringer, *Philos. Trans. R. Soc.* (*London*) *A,* Vol 295, 1980, p 309

28. M. Shütze, Mechanical Properties of Oxide Scales, *Oxid. Met.,* Vol 44, 1995, p 29

29. R.A. Smith, Nickel and Its Alloys: Carburization and Attack by Carbon-Containing Gases, *Corrosion,* 2nd ed, L.L. Sheir, Ed., Newes-Butterworths, 1976, p 7:101

30. H.J. Grabke, *Carburization: A High Temperature Corrosion Phenomenon,* MTI 52, Materials Technology Institute of the Chemical Process Industries, Inc., 1998

31. W.B. Hoyt and R.H. Caughey, High Temperature Metal Deterioration in Atmospheres Containing Carbon-Monoxide and Hydrogen, *Corrosion,* Vol 15, 1959, p 627t

32. P.A. Lefrancois and W.B. Hoyt, Chemical Thermodynamics of High Temperature Reactions in Metal Dusting Corrosion, *Corrosion,* Vol 19, 1963, p 360t

33. H.J. Grabke, Metal Dusting of Low- and High-Alloy Steels, *Corrosion,* Vol 51 (No. 9), 1995, p 711

34. H.J. Grabke, E.M. Müller-Lorenz, B. Eltester, and M. Lucas, Formation of Chromium Rich Oxide Scales for Protection Against Metal Dusting, *Mater. High Temp.,* Vol 17 (No. 2), 2000, p 339

35. M. Maier, J.F. Norton, and P. Puschek, A Study of the Factors Contributing to the Metal Dusting of Fe-Cr-Ni Alloys in Highly Carburizing Atmospheres, *Mater. High Temp.,* Vol 17 (No. 2), 2000, p 347

36. K.M. Verma, H. Ghosh, and J.S. Rai, Behaviour of Materials of Construction During Cracking of Ammonia at 600 °C, *Br. Corros. J.,* Vol 13 (No. 4), 1978, p 173–176

37. G.Y. Lai, Nitridation of Several Combustor Alloys in a Simulated Gas Turbine Combustion Environment, *Advanced Materials and Coatings for Combustion Turbines,* V.P. Swaminathan and N.S. Cheruvu, Ed., ASM International, 1994, p 113–121

38. S. Mrowec, The Problem of Sulfur in High-Temperature Corrosion, *Oxid. Met.,* Vol 44, 1995, p 177

39. R.A. Smith, Nickel and Its Alloys: Sulphidation, *Corrosion,* 2nd ed., L.L. Sheir, Ed., Newes-Butterworths, 1976, p 7:90

40. F.H. Stott, G.C. Wood, and J. Stringer, Influence of Alloying Elements on the Development of Protective Scales, *Oxid. Met.,* Vol 44, 1995, p 113

41. *Materials of Construction for Shipboard Waste Incinerators,* National Research Council, National Academy of Sciences, Washington, D.C., 1977, p 91–92

42. K.N. Strafford and P.K. Datta, Design of Sulphidation Resistant Alloys, *Mater. Sci. Technol.,* Vol 5, Aug 1989, p 765

43. A.U. Seybolt, P.A. Bergman, and M. Kaufman, "Hot Corrosion Mechanism Study, Phase II," Final report under contract N600 (61533) 65595, MEL 2591, Assignment 87-122, prepared for Naval Ship Research and Development Center, Annapolis, MD, 30 June 1966 to 31 Oct 1967

44. S.R.J. Saunders, Corrosion in the Presence of Melts and Solids, *Guidelines for Methods of Testing and Research in High Temperature Corrosion: Working Party Report,* H.J. Grabke and D.B. Meadowcroft, Ed., European Federation of Corrosion, 14, The Institute of Materials, 1995, p 85–103

45. E.L. Simons, G.V. Browning and H.A. Liebhafsky, Sodium Sulfate in Gas Turbines, *Corrosion,* Vol 11 (No. 12), 1955, p 505t

46. R.K. Ahluwalia and K.H. Im, Aspects of Mass Transfer and Dissolution Kinetics of Hot Corrosion Induced by Sodium Sulphate, *J. Inst. Energy,* Vol 64 (No. 461), 1991, p 186

47. J.A. Goebel and F.S. Pettit, Na_2SO_4-Induced Accelerated Oxidation (Hot Corrosion) of Nickel, *Metall. Trans.,* Vol 1 (No. 7), 1970, p 1943

48. N.S. Bornstein and M.A. DeCrescente, The Relationship Between Compounds of Sodium and Sulfur and Sulfidation, *Trans. Metall. Soc. (AIME),* Vol 245 (No. 9), 1969, p 1947–1954

49. N.S. Bornstein and M.A. DeCrescente, The Role of Sodium in the Accelerated Oxidation Phenomenon Termed Sulfidation, *Metall. Trans.,* Vol 2 (No. 10), 1971, p 2875

50. J.F. Condé and B.A. Wareham, *Proceedings: Gas Turbine Materials in the Marine Environment Conference,* MCIC-75-27, 1974, p 73

51. D.A. Shores, D.W. McKee, and H.S. Spacil, *Proceedings: Properties of High Temperature Alloys with Emphasis on Environmental Effects,* PV 77-1, Z.A. Foroulis and F.S. Pettit, Ed., The Electrochemical Society, 1976, p 649

52. J.A. Goebel, F.S. Pettit, and G.W. Goward, Mechanisms for the Hot Corrosion of Nickel-Base Alloys, *Metall. Trans.*, Vol 4, 1973, p 261–278

53. K.L. Luthra and D.A. Shores, Mechanisms of Na_2SO_4 Induced Corrosion at 600–900 °C, *J. Electrochem. Soc.*, Vol 127, 1980, p 2202

54. K.T. Chiang, F.S. Pettit, and G.H. Meier, Low Temperature Corrosion, *High Temperature Corrosion*, NACE-6, R.A. Rapp, Ed., NACE International, 1983, p 519

55. H. Lewis and R.A. Smith, Corrosion of High Temperature Nickel-Base Alloys by Sulfate-Chloride Mixtures, *First International Congress on Metallic Corrosion*, 10–15 April 1961, Butterworths, 1962, p 202

56. R.A. Rapp, Chemistry and Electrochemistry of Hot Corrosion of Metals, *Mater. Sci. Eng.*, Vol 87, 1987, p 319–327

57. R.L. Jones, Low-Quality Fuel Problems with Advanced Engine Materials, *High Temp. Technol.*, Vol 6, 1988, p 187; NRL Memorandum Report 6252, 9 Aug 1988

58. R.L. Jones, C.E. Williams, and S.R. Jones, Reaction of Vanadium Compounds with Ceramic Oxides, *J. Electrochem. Soc.*, Vol 133, 1986, p 227–230

59. R.L. Jones and R.F. Reidy, Development of Hot Corrosion Resistant Scandia-Stabilized Zirconia Thermal Barrier Coatings, *Proceedings of Elevated Temperature Coatings: Science and Technology I*, N.B. Dahotre, J.M. Hampikian, and J.J. Stiglich, Ed., The Minerals, Metals and Materials Society, 1995, p 23

60. R.L. Jones, Oxide Acid-Base Reactions in Ceramic Corrosion, *High Temp. Sci.*, Vol 27, 1990, p 369–380

61. R.L. Jones, "Vanadate-Sulfate Melt Thermochemistry Relating to Hot Corrosion of Thermal Barrier Coatings," NRL/MR/ 6170-97-8103, Naval Research Laboratory, 30 Oct 1997

62. R.A. Rapp, Hot Corrosion of Materials: A Fluxing Mechanism?, *Corros. Sci.*, Vol 44, 2002, p 209–221

63. G. Wacker and W.L. Wheatfall, *Corrosion Problems Associated with Shipboard Waste Incineration Systems*, 1976 Tri-Service Corrosion Conference, DoD Tri-Service Committee on Corrosion, 26–28 Oct 1976 (Philadelphia, PA), p 185

64. P. Elliott, Materials Performance in High- Temperature Waste Combustion Systems, *Mater. Perform.*, Vol 32, 1993, p 82

65. S.C. Singhal and R.J. Bratton, Stability of a $ZrO_2(Y_2O_3)$ Thermal Barrier Coating in Turbine Fuel with Contaminants, *J. Eng. Power (Trans. ASME)*, Vol 102 (No. 10), 1980, p 770–775

66. D.W. McGee, K.L. Luthra, P. Siemers, and J.E. Palko, *Proceeding of the First Conference on Advanced Materials for Alternative Fuel Capable Directly Fired Heat Engines*, J.W. Fairbanks and J. Stringer, Ed., CONF-790749, National Technical Information Service, 1979, p 258

67. P. Ganesan, G.D. Smith, and L.E. Shoemaker, "The Effects of Excursions of Oxygen and Water Vapor Contents on Nickel- Containing Alloy Performance in a Waste Incineration Environment," Paper 248, Corrosion/91, NACE International, 1991

68. H.H. Krause, High Temperature Corrosion Problems in Waste Incineration Systems, *J. Mater. Energy Syst.,* Vol 7, 1986, p 322

69. G.D. Smith, P. Ganesan, and L.E. Shoemaker, "The Effect of Environmental Excursions within the Waste Incinerator on Nickel-Containing Alloy Performance," Paper 280, Corrosion/90, NACE International, 1990

70. C.T. Wall, J.T. Groves, and E.J. Roberts, How to Burn Salty Sludges, *Chem. Eng.,* Vol 7, 14 April 1975

71. F. Wilkes and D.A. Shifler, "Historical Perspectives of Intergranular Corrosion of Boiler Metal by Water," Paper 44, Corrosion/93, NACE International, 1993

72. B. Craig, Hydrogen Damage, *Corrosion,* Vol 13, *Metals Handbook,* 9th ed., ASM International, 1987, p 169

73. R.M. Davison, T. Debold, and M.J. Johnson, Corrosion of Stainless Steels, *Corrosion,* Vol 13, *Metals Handbook,* 9th ed., ASM International, 1987, p 559

74. R.A. Smith and S.R.J. Saunders, *Corrosion,* 3rd ed., L.L. Sheir, R.A. Jarman, and G.T. Burstein, Ed., Butterworth-Heinemann, 1994, p 7:136

75. M.G. Fontana and N.D. Greene, *Corrosion Engineering,* 2nd ed., McGraw-Hill, 1978, p 294

76. M.H. Kamdur, Liquid Metal Embrittlement, *Corrosion,* Vol 13, *Metals Handbook,* 9th ed., ASM International, 1987, p 171

77. E.F. Bradley, Ed., *Superalloys—A Technical Guide,* ASM International, 1988

78. W.T. Reid, *External Corrosion and Deposits—Boilers and Gas Turbines,* Elsevier, 1971

79. S.T. Wlodek, The Stability of Superalloys, *Proceedings on Long Term Stability of High Temperature Materials,* G.E. Fuchs, K.A. Dannemann, and T.C. Deragon, The Mineral, Metals and Materials Society, 1999, p 3

80. D.L. Douglass, Exfoliation and Mechanical Behavior of Scales, *Oxidation of Metals and Alloys,* ASM International, 1971, p 137–156

81. R.E. Reed-Hill and R. Abbaschian, Thermally Activated Plastic Deformation, *Physical Metallurgy Principles,* 3rd ed., PWS-Kent Publishing, 1992, p 836–899

82. J.R. Nicholls, Laboratory Studies of Erosion-Corrosion Processes Under Oxidizing and Oxidizing/Sulphidizing Conditions, *Mater. High Temp.,* Vol 14, 1997, p 289–306

83. S. Hogmark, S. Jacobson, and O. Vingsbo, Surface Damage, *Friction, Lubrication, and Wear Technology,* Vol 18, *ASM Handbook,* ASM International, 1992, p 176–292

84. F.H. Stott, Corrosion and Wear or Erosion, *Guidelines for Methods of Testing and Research in High Temperature Corrosion: Working Party Report,* H.J. Grabke and D.B. Meadowcroft, Ed., European Federation of Corrosion, 14, The Institute of Materials, 1995, p 85–103

D.A. Shifler, High-Temperature Gaseous Corrosion Testing, *Corrosion: Fundamentals, Testing, and Protection*, Vol 13A, *ASM Handbook*, ASM International, 2003, p 650–681

High-Temperature Gaseous Corrosion Testing

David A. Shifler, Naval Surface Warfare Center

High-Temperature Materials

High-temperature coatings provide a barrier from corrosive or highly oxidative environments that may degrade the substrate alloy. To provide optimal performance, coatings need to have good adherence to the substrate, ductility to resist thermal cycling, few or no defects that may provide easy pathways to deleterious gases, good compatibility with the substrate, and maintain corrosion resistance over the design life of the high-temperature component. There is a wide range of coatings and coating processes for protecting components in a variety of operating conditions (Ref 85).

Diffusion Coatings. Aluminide coatings on transition metals and alloys based on iron, nickel, and cobalt are β-FeAl, β-NiAl, and β- CoAl, respectively. Diffusion aluminide coatings are typically processed via pack cementation, slurry diffusion, or chemical vapor deposition (Ref 86). Subsequent heat treatments help develop the proper mechanical properties and trigger further diffusion within the coating. The principal protective oxide generated by the high- temperature oxidation of these aluminide intermetallics is Al_2O_3, which causes subsequent improved oxidation and corrosion resistance of aluminide coatings; however, less-protective oxides can form if other alloying elements are present in the substrate, either in solution or as precipitated phases (Ref 87).

Modified aluminide coatings designate an aluminide class that is altered by the addition of a secondary element such as chromium, platinum, a reactive element, or a combination of these elements (Ref 89). These coatings are generated either by incorporating the secondary element into the coating by pack codeposition or by deposition of the modifying element prior to an aluminization process by electroplating, electrophoresis sputtering, chemical vapor deposition, or pack cementation (Ref 86).

Overlay coatings are MCrAlY-type coatings (where M is iron, cobalt, nickel, or a combination of these elements) applied by either electron beam physical vapor deposition (EB-PVD) or by thermal or plasma spraying. Typically, these coatings initially contained cobalt or nickel, with 15 wt% Cr, 12 wt% Al, and 0.1 to 0.9 wt% Y. To improve its resistance to low-temperature type II hot corrosion, the cobalt was partially replaced with nickel, the aluminum content was reduced somewhat, and the chromium content was increased from 15 to 20 wt% to almost 32 wt%. Hafnium was used as a replacement for yttrium in some MCrAlX coatings, where X (yttrium or hafnium) promoted coating adhesion and oxidation resistance under thermal cycling conditions. The MCrAlY coatings have been air plasma sprayed (APS) as a cost-savings procedure, but it often produces a poor-quality coating. There are various procedures and methods by which plasma spraying may be done, many of which are proprietary or patent protected. Low-pressure plasma spraying (LPPS) and argon-shielded spraying produce better-quality coatings.

The principal oxide in the outer portion of a MCrAlY overlay coating is Al_2O_3. Yttrium is more prevalent in the outer scale and promotes oxidation resistance. Hafnium also promotes oxidation resistance and prevents sulfur from segregating to the coating-substrate interface, thus providing one mechanism of improving the overlay coating adhesion.

Nickel, cobalt, or both and chromium are found in the inner half of the coating nearer to the coating-substrate interface. Increases in chromium content improve both the hot corrosion resistance and the oxidation resistance of the overlay coating but tend to make the coating less ductile.

Thermal barrier coatings (TBCs) usually consist of a porous layer of zirconia, ZrO_2, that is stabilized in the metastable tetragonal phase by approximately 8 wt% yttria, Y_2O_3. The yttria- stabilized zirconia (YSZ) is applied using either plasma spraying or by EBPVD over a bond coat, which is usually MCrAlY (where M is cobalt and/or nickel) or a diffusion aluminide. The bond layer is typically 75 to 125 μm (0.003 to 0.005 in.), and the TBC is 125 to 375 μm (0.005 to 0.015 in.) thick. Application of the TBC system to hot section components in a gas turbine has been able to decrease metal surface temperature by approximately 150 °C.

(270 °F). The TBCs also smooth out hot spots, thus reducing thermal fatigue stresses. A thermally grown oxide (TGO) layer is formed between the bond coat and the TBC during fabrication and tends to grow thicker on high-temperature exposure of the TBC.

The EB-PVD-applied TBCs tend to produce a columnar structure with fine, ribbonlike voids, porosity within the columns aligned normal to the plane of the coating, and superior compliance to residual stresses. Plasma-sprayed TBCs have disklike voids aligned parallel to the coating plane and promoting superior insulating efficiency.

There are a number of degradation modes that can limit the life of a TBC (Ref 54) as a result of oxidation due to the possible porosity network in the TBC. By understanding the specific thermomechanical failure modes, TBCs can be designed for greater reliability and durability (Ref 88). The EB-PVD thermal barrier coatings tend to spall at the TGO/bond coat interface or in the alumina layer (Ref 89). It was observed that intermittent water vapor degraded the adherence of alumina to the bond coat under a TBC layer more severely than alumina formed on the same bond coat in the absence of a TBC (Ref 57).

Hot corrosion exposure to vanadium salts and sulfur trioxide promotes corrosion of stabilized zirconia by acid leaching of yttria. Yttria loss destabilizes the zirconia, and thermal cycling causes rapid coating failures. This is potentially serious when burning low-grade fuels (Ref 90). For engine use, ZrO_2 must be stabilized in its high-temperature tetragonal structure to avoid a destructive monoclinic-to-tetragonal phase transformation at 1100 °C (2010 °F). Scandia, Sc_2O_3, improves vanadate hot corrosion resistance of stabilized zirconia (Ref 59).

Refractories. The corrosion resistance of refractories is based on the thermodynamics of the potential corrosion reactions, the reaction rates and kinetics of these possible reactions, the composition and form of the refractory material, and the surface chemistry of the refractory with corrosive gaseous, liquid, or solid environments. The spontaneous direction of the possible corrosion chemical reactions can be calculated, which can indicate the reactions that are theoretically possible. The reaction kinetics will be dependent on the specific environment (gaseous, liquid, or solid), surface chemistry, the material microstructure and composition, refractory phase(s), and the temperature. All ceramics or refractories used in an oxygen-rich environment are oxides or develop a protective oxide on their surface (such as SiO_2 on SiC or Si_3N_4). Although oxide ceramics are inert and resist oxidation and reduction, they are not chemically inert. Ceramic corrosion between ceramic oxides and molten salt deposits generally can be explained as oxide/ acid-base reactions (Ref 57).

To determine if a particular slag is acidic or basic, the ratio of lime to silica in the slag is commonly used. As a general rule, the slag is basic if the CaO-to-SiO_2 ratio (or CaO + MgO to SiO_2 + Al_2O_3 ratio) is greater than 1. If the ratio is less than 1, the slag is considered acidic (Ref 91). Gases and liquids can penetrate deeply into highly porous refractories that can exacerbate spalling and accelerated corrosion. Oxidizing gases, such as NO_x, Cl_2, O_2, CO_2, H_2O, and SO_2, reducing gases (NH_3, H_2, C_xH_y, CO, and H_2S), and vapors of volatile elements and compounds may react with different refractories. Hydrodynamic mass transport by either convection or diffusion can markedly affect the corrosion rate of a refractory in an environment. Nonwetting refractories are relatively resistant to corrosion with liquids or gases. Molten aluminum, iron, silica, and other constituents derived from the incinerator waste streams can react with refractories to form new compounds or phases that can have different melting temperatures, dimensional stabilities, and corrosion resistances. The new phases or compounds can cause dimensional changes that can cause problems in the chamber. High-purity refractories are more corrosion resistant, because certain minor impurity components have microstructures, phases, and defect structures that can introduce significant corrosion. High-purity refractories improve corrosion resistance by avoiding low-melting eutectics. Alkali impurities should be minimized as much as possible. Solids, either as fine particulates or dust, can cause degradation of refractories through abrasion or deposition.

Test Standards. Since the 1990s, worldwide work has focused on formulating standard tests for physical and mechanical property determinations (Ref 92). Oxidation and corrosion standards have received attention more recently. Oxidation should be relatively straightforward, thus allowing current test methodologies to be used. Methodologies for hot corrosion resistance of superalloys can be adaptable to ceramics; guidelines for hot corrosion testing have been published by a technical working group of the Versailles Agreement on Advanced Materials and Standards (VAMAS) (Ref 93). The Japanese Industrial Standard JIS R 1609, “Testing Methods for Oxidation Resistance of Nonoxide High-Performance Ceramics,” published in 1990, was the first standard developed for ceramics.

ASTM International has several standards for measuring corrosion resistance:

ASTM designation	Title
C 621	"Standard Test Method for Isothermal Corrosion Resistance of Refractories to Molten Glass"
C 863	"Standard Test Method for Evaluation Oxidation Resistance of Silicon Carbide Refractories at Elevated Temperatures"
C 288	"Standard Test Method for Disintegration of Refractories in an Atmosphere of Carbon Monoxide"
C 454	"Standard Practice for Disintegration of Carbon Refractories by Alkali"

More information on ceramic corrosion testing can be found in Ref 94.

References cited in this section

54. K.T. Chiang, F.S. Pettit, and G.H. Meier, Low Temperature Corrosion, *High Temperature Corrosion,* NACE-6, R.A. Rapp, Ed., NACE International, 1983, p 519

57. R.L. Jones, Low-Quality Fuel Problems with Advanced Engine Materials, *High Temp. Technol.,* Vol 6, 1988, p 187; NRL Memorandum Report 6252, 9 Aug 1988

59. R.L. Jones and R.F. Reidy, Development of Hot Corrosion Resistant Scandia-Stabilized Zirconia Thermal Barrier Coatings, *Proceedings of Elevated Temperature Coatings: Science and Technology I,* N.B. Dahotre, J.M. Hampikian, and J.J. Stiglich, Ed., The Minerals, Metals and Materials Society, 1995, p 23

85. G.W. Goward, Protective Coatings—Purpose, Role, and Design, *Mater. Sci. Technol.,* Vol 2, 1986, p 194–200

86. R. Streiff, Aluminides: Yesterday's and Tomorrow's Coatings for Materials in Aggressive Environments, *Elevated Temperature Coatings: Science and Technology II,* N.B. Dahotre and J.M. Hampikian, Ed., The Minerals, Metals and Materials Society, 1996, p 407

87. G.W. Goward, Protective Coatings for High Temperature Alloys: State of Technology, *Proceedings of the Symposium on Properties of High Temperature Alloys,* Z.A. Foroulis and F.S. Pettit, Ed., PV 77- 1, The Electrochemical Society, 1976, p 806

88. P.K. Wright and A.G. Evans, Mechanism Governing the Performance of Thermal Barrier Coatings, *Curr. Opin. Solid State Mater. Sci.,* Vol 4, 1999, p 255–265

89. M.J. Stiger, N.M. Yanar, F.S. Pettit, and G.H. Meier, Mechanism of Failure of EB- PVD Thermal Barrier Coating Induced by High Temperature Oxidation, *Elevated Temperature Coatings: Science and Technology III,* J.M. Hampikian and N.B. Dahotre, Ed., TMS, 1999, p 51

90. S. Bose and J. DeMasi-Marcin, *Thermal Barrier Coating Experience in Gas Turbine Engines at Pratt & Whitney,* Thermal Barrier Coating Workshop, NASA CP 3312, National Aeronautics Space Administration, 1995, p 63

91. *Handbook of Refractory Practice,* 1st ed., Harbison-Walker/Indresco Inc, 1992, p PR-12

92. D.J. Baxter, *Oxidation/Corrosion of Advanced Ceramics: A Review of the Progress Towards Test Method Standardization, Working Party Report,* H.J. Grabke and D.B. Meadowcroft, Ed., European Federation of Corrosion, 14, The Institute of Materials, 1995, p 136–146

93. S. Schneider, Ed., *International Survey on the Classification of Advanced Ceramics,* VAMAS Report 5, ISSN 1016-2186, Versailles Agreement on Advanced Materials and Standards, 1991

94. R.A. McCauley, *Corrosion of Ceramics,* Marcel Dekker, 1995, p 109–128

D.A. Shifler, High-Temperature Gaseous Corrosion Testing, *Corrosion: Fundamentals, Testing, and Protection*, Vol 13A, *ASM Handbook*, ASM International, 2003, p 650–681

High-Temperature Gaseous Corrosion Testing

David A. Shifler, Naval Surface Warfare Center

Testing Methods Used for Materials at High Temperatures

As mentioned previously, high-temperature corrosion may occur in numerous environments and is affected by numerous factors, such as temperature, alloy or protective coating composition, time, and gas composition. There is a great need for materials testing, both for research and development of new materials (alloys, high-temperature coatings, refractories, etc.) and processes and to simulate industrial and application environments to understand the interactions that occur with current materials choices. The goals of laboratory and field testing are to characterize materials performance in specific applications and to evaluate the effects of environmental changes on candidate materials. The test conditions should simulate, as much as possible, the environment of the specific application of interest.

In the case of gas turbines, fuel and air quality and the specific engine environment in which it operates influence the corrosion of turbine components significantly. Aeroengines use relatively pure fuels with low sulfur contents, and the air quality is generally good, unless there are recurrent low-altitude flights or operations over marine environments. Industrial and shipboard turbine engines use lower-grade fuels with 0.3 to 1.0 wt% S content as well as other less-pure fuels. Unfiltered air intake for marine gas turbines may contain up to 2600 ppm Na_2SO_4, 19,000 ppm NaCl, and possibly, sand-derived deposits. Filtration may reduce the NaCl content in air to ≤0.01 ppm, but this is still sufficient to generate Na_2SO_4 (as well as Na_2SO_4 directly created from sulfur in the fuel), which can lead to sulfidation and hot corrosion. Fuel quality may vary during the service life of the engine. The use of less- refined, heavy fuels may contain up to 200 ppm vanadium that, when combined with Na_2SO_4, accelerates hot corrosion reactions. Engine temperatures may also vary with operational loads by 400 to 500 °C (720 to 900 °F) on going from idle to full power (Ref 95). The engine may ingest solid particles (sand, ash, dust, and sea salt) or generate pyrolytic carbon from uncombusted or poor oxidizing conditions that will contribute to metal wastage by erosion and impact turbine components. Carbon may also accentuate corrosion by reducing sodium sulfate to sulfides. Thermal cycling or transient conditions may further increase the corrosivity of salt deposits by cracking protective oxide layers. The complexity of the turbine operating environment and other high-temperature applications makes it impossible to develop simple tests to simulate all the pertinent parameters. Figure 13 shows the variation of the chemical species within the combustion flame as a function of the fuel-to-air ratio at a given turbine pressure and inlet temperature (Ref 96). Changing the fuel source, the amount of salt in the intake air, the inlet temperature, and/or the turbine pressure will change the speciation and the relative distribution of the chemical products.

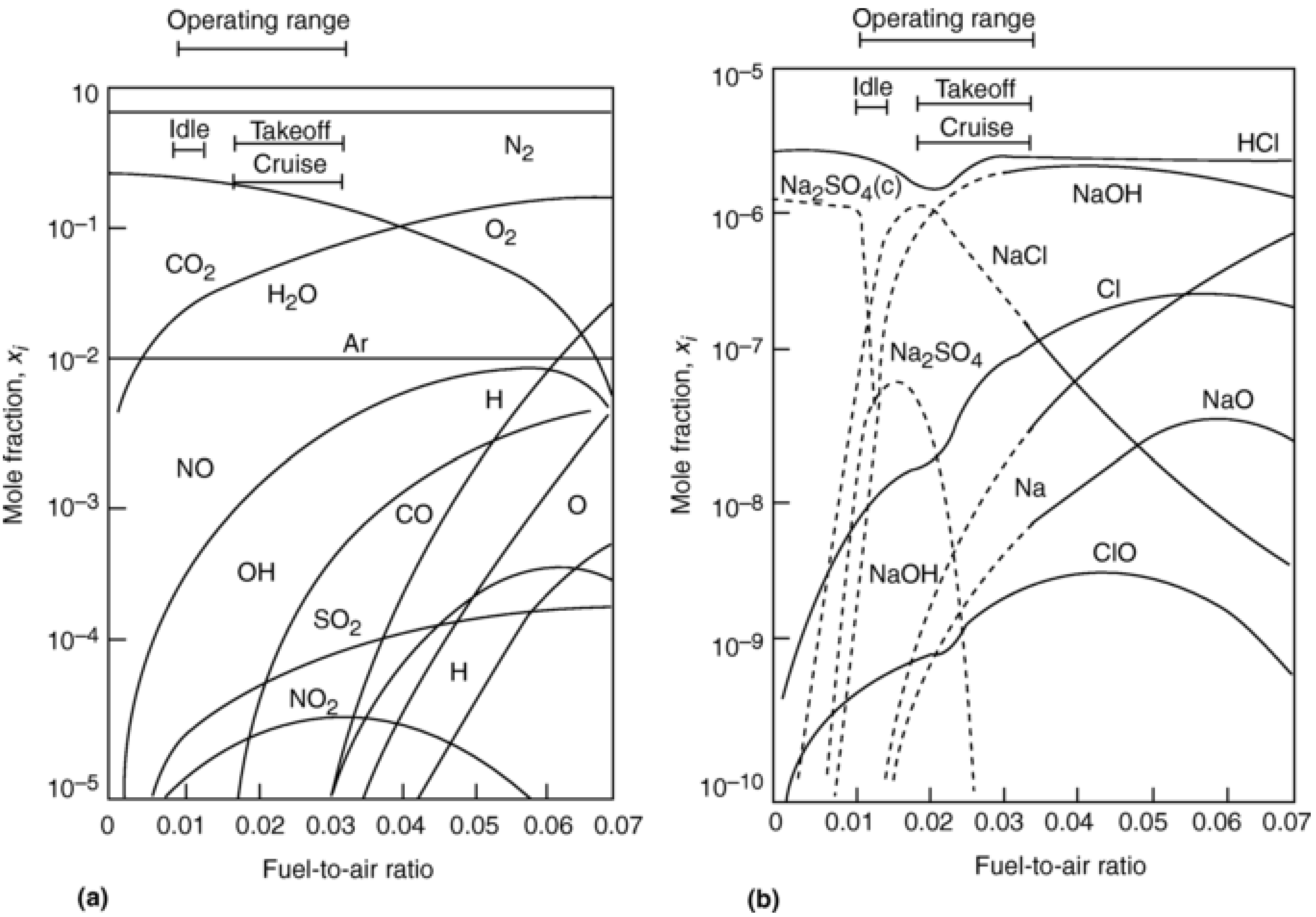

Fig. 13 Variation in equilibrium composition of the combustion flame as a function of the fuel-to-air ratio when pressure p = 22.1 atm (2.24 MPa) and the inlet temperature T_0 = 811 K (1000 °F) (for fuel jet A + 0.3% S; air, 5 ppm sea salt). (a) The major products formed. (b) Sodium- and chlorine-containing species. Source: Ref 96, 97, 98

Incinerators are also inherently complex high- temperature environments. The corrosiveness of the incinerator environment depends on the relative stream of wastes that are generated and the efficiency of removing potential wastes that have been proven to be severely corrosive, such as chlorine-containing plastics.

However, laboratory tests can be representative of in-service conditions by choosing the appropriate deposit or gas compositions, the temperature, and other operational aspects that can be controlled with a given test apparatus. Testing may include furnace testing, crucible tests, thermogravimetry or its derivatives, various burner rig tests, or autoclave testing with a host of analytical techniques to evaluate corrosion products or materials chemistries. Because some high-temperature reactions are electrochemical in nature, electrochemical tests (corrosion-potential monitoring, current measurements, and polarization to determine the acido-basicity of salts) can be employed in test programs (Ref 56, 99).

Furnace Tests

Both horizontal and vertical furnace geometries are widely used in high-temperature testing. High-temperature oxidation generally leads to external oxide scale together with the formation of internal oxidation products, particularly in mixed-oxidant or under salt deposit conditions. Furnace exposure methods may involve isothermal oxidation in air, oxygen, or reduced pO_2 conditions; cyclic oxidation exposures; gas-phase corrosion; hot salt corrosion (crucible, salt coat method, or burner rig testing); or diffusion studies at a temperature range of 250 to 1500 °C (480 to 2730 °F) or higher, depending on the focus of the parameter, material, and environment being tested. In conjunction with a thermobalance and other ancillary equipment (discussed later), furnace tests can generate kinetic data and analyze the corrosion products formed as a result of high- temperature gaseous reactions.

Furnace testing has been used to evaluate and measure the diffusion of chromium to the alloy- scale interface in several chromia-forming alloys during extended exposures at elevated temperatures. When the alloys were placed into a furnace and exposed to air at 1050 °C (1920 °F) for 720 h, the depth of chromium depletion could be measured due to the chromium interdiffusion to the surface. Other alloying elements can have a marked effect on chromium interdiffusion rate (Ref 100).

Another furnace test involves spraying an aqueous solution, saturated with salt, on specimens heated to a moderate temperature (approximately 200 °C, or 392 °F) to form a dry salt layer. Once samples are coated with this salt layer, testing can occur in a furnace at the prescribed temperature in a controlled atmosphere and a given length of time to monitor the corrosion on the sample (Ref 99). It is fairly simple to recoat coupons with Na_2SO_4 or other salts at various intervals in a furnace test.

Molten Salt Tests

The molten salt test is used to determine the susceptibility of materials (alloys, ceramics, and protective coatings) to corrosion attack from molten salts (Ref 55, 101). It consists of immersing selected samples in the molten salt for a given period of time and then examining the samples for evidence of attack. The half-cell potentials are measured in some molten salt immersion tests to study film integrity as a function of such parameters as oxide thickness, salt composition, and atmosphere. Test parameters in a crucible test are well defined and can be closely monitored.

For gas turbine applications, experiments are conducted in a resistance-wound electric furnace containing a high-purity platinum crucible with approximately 50 g (1.8 oz) of reagent-grade sodium sulfate (Na_2SO_4), as shown in Fig. 14. Potential measurements are made using platinum as a reference electrode that monitors the corrosion activity, because in molten salts, corrosion occurs via electrochemical processes (Ref 99). For sulfidation of alloys, a sustained rise in potential can be observed (Ref 99). A new batch of sodium sulfate is prepared prior to each exposure to eliminate any possible contamination from other sample immersions. All specimens are immersed in the molten Na_2SO_4 for up to 1000 h. A sample examination can be made after 500 h, and, if desired, the samples can be returned to the molten salt bath for an additional 500 h. The molten Na_2SO_4 salt temperature typically is maintained at 899 °C (1650 °F). The melting temperature of Na_2SO_4 is 884 °C (1623 °F). Still air or argon are used as atmospheres over the molten salts to achieve two levels of oxidizing conditions (Ref 101). Adding NaCl to the sodium sulfate can test the effects of slag. The crucible test is the simplest evaluation method to discern the relative resistances of materials in sulfidation and hot corrosion environments.

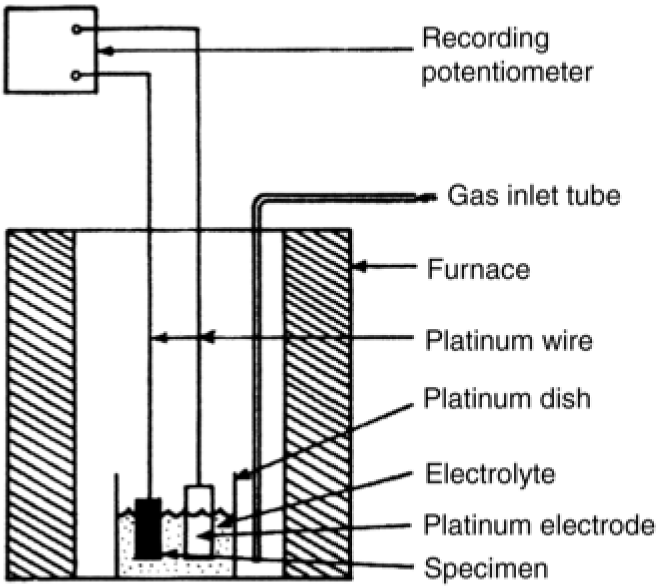

Fig. 14 Schematic of molten salt test apparatus with test specimen. Source: Ref 101

In molten salt tests, if the test sample is not completely immersed, there may be three distinct environments to which the test specimen is exposed. The first is immersion in the molten salt, the second is at the interface between the molten salt and its vapor, and the third specimen exposure is to the salt vapor. In the Dean test,

Na_2SO_4 is heated to above 1100 °C (2012 °F) to establish an appropriate vapor pressure, and the sample is maintained at a temperature below the dewpoint where condensation occurs, so that the SO_2/SO_3 in the furnace atmosphere should be controlled (Ref 102).
Table 2 shows how the crucible and other hot test methods compare to actual gas turbine service environments in terms of simulation, cost, and time (Ref 103). Stability of samples can be monitored by electrochemical-potential measurements.

Table 2 Accuracy of simulations of hot corrosion test methods, cost, and test times as compared to service experience of actual gas turbine engines

Type of test	Simulation with respect to:[(a)]					Cost[(b)]	Test time[(b)]
	Chemistry		**Aerodynamics**				
	Gas	**Solid or liquid species**	**System pressure**	**Gas velocity**	**Deposition rate (*dm*/*dt*) of condensable species**		
Engine	10	10	10	10	10	1	1
High pressure, high velocity	10	9	10	9	8	2	2
High velocity	5	8	4	9	7	3	7
Burner rigs	5	7	3	2	4	7	8
Thermogravimetric analysis	5	6	3	1	2	7	3
Crucible	2	5	1	1	1	10	10

(a) Simulation: 10 is best simulation of given factor; 1 is worst simulation of actual service.
(b) Relative cost, test time: 10 is lowest cost, shortest time; 1 is highest cost, longest time. Source: Ref 103

It has been found that certain molten mixtures of NaCl and Na_2SO_4 are more corrosive to superalloys than Na_2SO_4 alone (Ref 55). Sodium chloride (NaCl) also lowers the melting temperature of the NaCl-Na_2SO_4 mixtures relative to Na_2SO_4. The possibility exists that turbine components downstream of the power turbine will be exposed to both NaCl and Na_2SO_4. The NaCl is usually not deposited in the hot sections of the marine gas turbine engine, but sodium sulfate does form deposits in the hot sections. Vapors of NaCl react with SO_2 and SO_3 (formed from sulfur in the fuel) to produce Na_2SO_4. Thermodynamic equations for the formation of Na_2SO_4 are (Ref 104):

$$2NaCl + SO_2 + \frac{1}{2}O_2 + H_2O \leftrightarrow Na_2SO_4 + 2HCl(g) \quad \text{(Eq 24)}$$

$$2NaCl + SO_3 + H_2O \leftrightarrow Na_2SO_4 + 2HCl(g) \quad \text{(Eq 25)}$$

Sample preoxidation before molten salt testing can prolong the period of time before the oxide is penetrated and the onset of sulfidation begins (Ref 100). The half-cell potential measurements rise with the initiation of corrosion and generally correlate well with sulfidation attack. Other salts, such as V_2O_5, that are found in some fuels in service can be tested in a molten salt crucible test (Ref 105).
After exposure, samples are cleaned of salt by prolonged boiling in distilled or deionized water, oven dried, and weighed (samples are initially weighed before the molten salt test). The weight change is recorded. Optical microscopy or scanning electron microscopy is used, where warranted, to examine the specimen surface. X-ray energy-dispersive spectroscopy, x-ray diffraction, and/or emission spectroscopy are used to identify the corrosion products formed on the surface. Figure 15 show the relative resistance of two different nickel-base alloys after immersion for 150 h in a molten salt bath of 75 wt% Na_2SO_4-25 wt% NaCl at 899 °C (1650 °F). Figure 15(a) shows the broad corrosion front and the associated development of porosity and void formation that is typical of high-temperature type I hot corrosion. Figure 15(b) shows catastrophic corrosion of another nickel-base alloy.

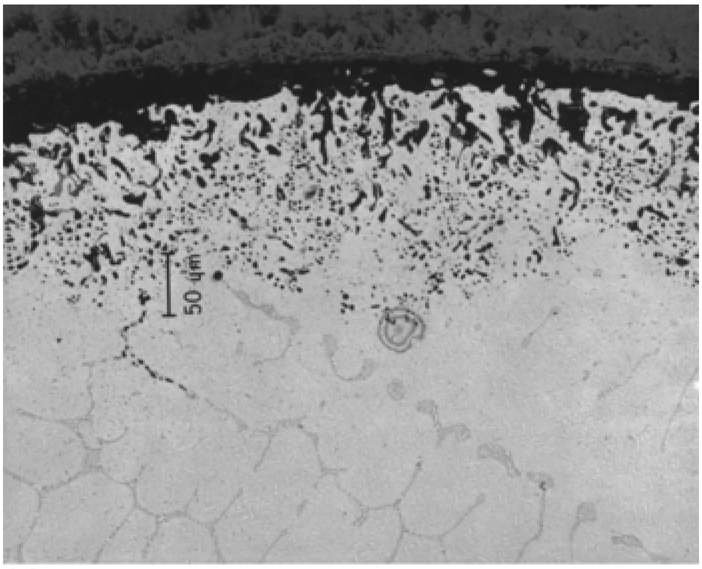

(a)

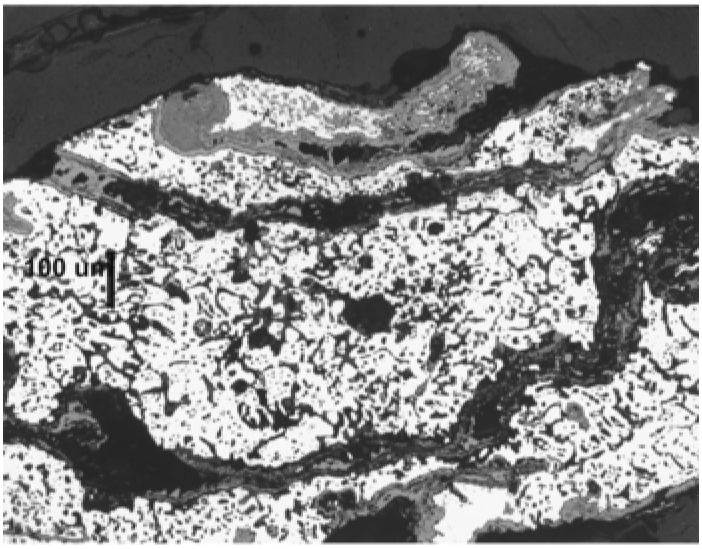

(b)

Fig. 15 Corrosion performance of two different nickel-base alloys after 150 h in molten Na_2SO_4-NaCl at 899 °C (1650 °F). Alloy (a) shows typical type I hot corrosion attack, while alloy (b) shows catastrophic corrosion attack.

Crucible tests are also conducive to studying the corrosion resistance of alloys in molten chlorides (NaCl-KCl) and eutectics of several mixed salts, such as NaCl-KCl-Na_2SO_4-K_2SO_4. The actual composition and the ratio of components in salt mixtures can vary the degree of acidity or basicity. This will determine, in large part, the stability of oxides when exposed to a corrosive environment such as a waste incinerator. The stability of Cr_2O_3, NiO, Co_3O_4, Fe_3O_4, and SiO_2 has been studied in different molten salt bath combinations with varying basicity that represent possible waste incinerator environmental interactions, as described in Ref 106.

Sodium sulfate can be described by acid-base chemistry in a similar manner as for pH in aqueous solutions. Specifically, the dissociation of sodium sulfate can be written as $Na_2SO_4 = Na_2O + SO_3$, for which the $\log_{10}$ of the condensed Na_2O activity is a quantitative measure of melt basicity, and the $\log_{10}$ of the gaseous SO_3 activity defines the melt acidity (Ref 62). In the same way as aqueous corrosion, corrosion in fused sodium sulfate is an electrochemical process. The soluble oxidant, SO_3 or $S_2O_7^{2-}$, is reduced in the cathodic step for acidic melts. The sites where cathodic reduction occurs result in a local increase in basicity, to the extent that a sulfide corrosion product may result. In salt films containing significant concentrations of multivalent transition-metal cations, the oxidation reaction can occur at the substrate/salt interface, and the cathodic reaction can occur at the salt/ gas interface through the interactions of the cations, in deference to SO_3, with a counterdiffusion of these metal ions carrying the current through the salt film (Ref 106). Electrochemical reactions affect the acid-

base chemistry of salt films. Electrochemical reactions in molten Na_2SO_4 have been monitored by a doped zirconia-oxygen sensor and Ag/Ag^+ mullite-sodium sensor during potentiodynamic polarization and cyclic voltammetry experiments (Ref 107).

Acid-base oxide reactions with molten sulfate through the measurement of oxide solubilities as a function of Na_2O activity in fused Na_2SO_4 were examined (Ref 56). Oxide solubility is dependent on Na_2O activity, which also serves to rank the acid-base character of individual oxides. The solubilities of NiO, Co_3O_4, Fe_2O_3, CeO_2, Cr_2O_3, Al_2O_3, and SiO_2 have been determined as a function of melt basicity for fused Na_2SO_4 at fixed temperatures (Ref 108, 109, 110, 111, 112, 113, 114, 115). The presence of more than one oxide contained in a salt film will cause greater dissolution than if only one oxide was present. The more basic oxide would exhibit acidic dissolution that releases oxide ions as corrosion products. The more acidic oxides would react with the oxide ions to promote basic dissolution (Ref 62).

The melt acidity can be determined by measuring the potential between a reference electrode and a working electrode contacting a melt of the same composition (Ref 107). Researchers proposed that a negative solubility gradient was a general criterion for hot corrosion to continue (Ref 116).

There are two major drawbacks to crucible test results when related to gas turbine engines (Ref 96). First, with the exception of the Dean test, the procedures involve a one-time application of Na_2SO_4, whereas in service, there is continuous or near-continuous deposition of Na_2SO_4 in turbine engines. Secondly, during service, material surfaces are exposed to temperatures, pressures, velocities, or gas compositions that vary significantly and rapidly with time, which cannot be easily reproduced in a furnace or crucible (Ref 96, 99, 117, 118).

Thermogravimetric Analysis

Thermogravimetric analysis (TGA), also known as thermogravimetry (TG), can complement the laboratory testing of materials in gaseous, high-temperature corrosive environments by determining the kinetics and mechanisms of high-temperature corrosion by measuring the oxide growth and associated change of sample mass over time at temperature (Ref 119). In this technique, changes in the mass of a sample are studied while the sample is subjected to a controlled-temperature program. The temperature program is most often a linear increase in temperature, but isothermal studies can also be carried out, when the changes in sample mass with time are followed. Thermogravimetry is inherently quantitative and therefore an extremely powerful thermal technique, but it gives no direct chemical information. Test temperatures may range up to 1700 °C (3092 °F).

The ability to analyze the volatile products during a weight loss is of great value. Additional information can be obtained by integrating mass spectroscopy or Fourier transform infrared spectroscopy (FTIR) with the TGA instrumentation. The main high-temperature processes amenable to TGA study (either by measuring weight losses or weight gains as a function of time) are listed in Table 3.

Table 3 Processes measurable by thermogravimetric analysis

Process	Weight gain	Weight loss
Adsorption or absorption	X	…
Desorption	…	X
Dehydration/desolvation	…	X
Sublimation	…	X
Vaporization	…	X
Decomposition	…	X
Solid-solid reactions	…	X
Solid-gas reactions	X	X

The essential components of the TGA instrument are an electrobalance, furnace, temperature programmer, sample holder, an enclosure for establishing the required atmosphere, and a means of recording and displaying the data (Ref 120). Balance sensitivity is usually approximately 1 μg, with a total capacity of a few hundred milligrams. In oxidation or high-temperature corrosion tests, depending on the capacity of the balance (500 mg to 100 g), the sample size, and other experimental factors, the actual sensitivity may be a few micrograms to 100 to 200 μm. A typical operating range for the furnace is ambient to 1000 °C (1832 °F), with heating rates up to 100 °C/min (212 °F/min), but materials may be exposed and measured by TGA to 1700 °C (3100 °F). The control of the furnace atmosphere requires careful attention, particularly the ability to establish an inert

(oxygen-free) atmosphere, and it is useful to be able to quickly change the nature of the atmosphere. Compatibility between the materials of construction, the sample, its decomposition products, and the gaseous atmosphere must be considered. Sample holder materials commonly available include aluminum, platinum, silica, and alumina. Indication of the sample temperature is by a thermocouple close to the sample. Careful calibration for temperature is important, especially for kinetic studies. Various means are available for temperature calibration, which is not a trivial matter, although reproducibility is often more important than absolute accuracy. Weight calibration is readily achieved using standard weights.

Many factors influence the shape of the TG curve, both sample- and instrument-related, some of which are interactive. The two primary factors are heating rate and sample size, an increase in either of which tends to increase the temperature at which sample decomposition occurs and to decrease the resolution between successive mass losses. The particle size of the sample material, the way in which it is packed, the crucible shape, and the gas flow rate can also affect the progress of the reaction. Careful attention to consistency in experimental details normally results in good repeatability. On the other hand, studying the effect of deliberate alterations in such factors as the heating rate can give valuable insights into the nature of the observed reactions.

Table 4 lists a set of recommended atmospheres and temperatures for testing materials by TGA under conditions closely related to certain environments or processes (Ref 119). Continuous TG permits the automatic recording of mass change for a single sample over a period that is generally 1 to 100 h. Discontinuous thermogravimetry (DTG) is more widely used when there is an attempt to simulate industrial service. This is particularly true for complex gaseous atmospheres, under salt deposits, or for long term (100 to >10,000 h in oxidation or corrosion studies) (Ref 122). Discontinuous methods do present mass gain data per specimen and impose a thermal shock when the specimens are removed from measurement, but they provide a simple experiment to be exposed to complex environments and to evaluate a wide variety of alloys in a single test.

Table 4 Recommended testing atmospheres and temperatures for testing materials by thermogravimetric analysis

Environment	Gas composition	Temperature	
		°C	**°F**
Air	Air, 2.5% H_2O	450–1200	850–2200
Flue gas	Air, 2.5% H_2O, 0.1–1% SO_2	400–1000	750–1850
Waste incineration	Air, 2.5% H_2O, 0.1–1% SO_2, 0.05–0.1% HCl	400–850	750–1550
Sulfidizing environment	0.1–1% H_2S, balance H_2	300–600	570–1100
Carburizing environment	1% CH_4, balance H_2, dew-point -45 °C (-50 °F)	800–1100	1450–2000
Nitriding environment	90% N_2, 10% H_2, dewpoint -45 °C (-50 °F)	800–1300	1450–2350
Metal dusting environment	25% CO, 73% H_2, 2% H_2O	350–750	660–1380
Coal gasification (wet)	0.1–1% H_2S, 5% CO, 2.5% H_2O, balance H_2	400–700	750–1300
Coal gasification (dry)	0.1–1% H_2S, 70% CO, 2.5% H_2O, 25% H_2	400–700	750–1300
Waste gasification (pyrolysis)	90% H_2O, 5% H_2, 5% CO, 0.1% HCl, 0.05% H_2S	400–700	750–1300

Source: Ref 121

The ability of TGA to generate fundamental quantitative data from almost any class of materials has led to its widespread use in every field of science and technology. Key application areas are:

- *Thermal stability:* Related materials can be compared at elevated temperatures under the required atmosphere. The TG curve can help to elucidate decomposition mechanisms.
- *Kinetic studies:* A variety of methods exist for analyzing the kinetic features of all types of weight loss or gain, either with a view to predictive studies or to understanding the controlling chemistry.
- *Materials characterization:* The TG and DTG curves can be used to “fingerprint” materials for identification or quality control.
- *Corrosion studies:* Thermogravimetry provides an excellent means of studying oxidation or reaction with other reactive gases or vapors.
- *Simulation of industrial processes:* The thermobalance furnace may be thought of as a mini-reactor, with the ability to mimic the conditions in some types of industrial reactor.

- *Compositional analysis:* By careful choice of temperature programming and gaseous environment, many complex materials or mixtures may be analyzed by selectively decomposing or removing their components. This approach is regularly used to analyze, for example, filler content in polymers, carbon black in oils, ash and carbon in coals, and the moisture content of many substances.

Differential thermal analysis (DTA) measures the temperature difference between a reactive sample and a nonreactive reference and is determined as a function of time, providing useful information about the temperatures, thermodynamics, and kinetics of reactions. The DTA is a dynamic method detecting the heat of reaction (exothermic or endothermic) of a physical or chemical change of the measured system. A sample to be analyzed and an inert substance are heated up in a furnace simultaneously under the same conditions. Within the sample and the inert substance there are mounted thermocouples that are connected against each other, so that the temperature difference between sample and inert substance is measured.

Differential scanning calorimetry (DSC) measures temperature and heat flows associated with thermal transitions in a material. It is thus the most generally applicable of all thermal analysis methods, because every physical or chemical change involves a change in heat flow. Differential scanning calorimetry involves recording the energy necessary to establish a zero temperature difference between a substance and a reference material against either time or temperature as each specimen is subjected to an identical temperature regime in an environment heated or cooled at a controlled rate. The resulting DSC curve represents the amount of heat applied per unit time as the ordinate value against either time or temperature as the abscissa; this is related to the kinetics of the process (Ref 123).

Temperature calibration is carried out by running standard materials, usually, very pure metals with accurately known melting points. Energy calibrations may be carried out by using either known heats of fusion for metals, commonly indium, or known heat capacities. Synthetic sapphire (corundum or aluminum oxide) is readily available as a heat capacity standard, and the values for this have been accurately determined over a wide temperature range. Typical purge gases are air and nitrogen, although helium is useful for efficient heat transfer and removal of volatiles. Argon is preferred as an inert purge when examining samples that can react with nitrogen. Experiments can also be carried out under vacuum or under high pressure, using instruments of the appropriate design.

In the absence of any discrete physical or chemical transformations, the baseline signal in DSC is related to the heat capacity of the sample. Differential scanning calorimetry allows this parameter to be determined with good accuracy over a wide temperature range. The conventional approach is to compare the signal obtained for the sample above that given by an empty pan, with the signal obtained for a standard material, usually sapphire, under the same conditions. Careful experimental technique is required to obtain accurate results, but heat capacities can be routinely measured to an accuracy of better than ±1%.

Other techniques are available for heat capacity measurement by DSC. Accurate data can be obtained in narrow temperature intervals by using a nonequilibrium pulse technique, which is particularly useful when measurements need to be made in a region constrained by adjacent complicating phase transitions. Less time-consuming experiments than those described previously can generate data more rapidly but at the expense of accuracy and precision, which may be adequate for a given purpose. Modulated- temperature differential scanning calorimetry (MTDSC), a recent enhancement of DSC, routinely generates heat capacity data from a standard experiment and can, in fact, measure this in a nominally isothermal condition. However, the classical method is still recommended for the best-quality results.

Use of DSC provides a cost-effective method for obtaining kinetic and thermodynamic data for condensed phase phenomena. Observable processes include simple phase transitions, characterization of polymorphism, and the kinetics and thermochemistry for a variety of complex reactions. Thermodynamic data for pure substances include melting and boiling points, heat capacity, heat of fusion, heat of solution, and heat of vaporization.

The DSC-DTA curve may show an exothermic or endothermic peak. The enthalpy changes associated with the events occurring are given by the area under the peaks. In general, the heat capacity will also change over the region, and problems may arise in the correct assignment of the baseline. In many cases, the change is small, and techniques have been developed for reproducible measurements in specific systems.

Some possible processes giving enthalpy peaks are listed in Table 5.

Table 5 Type of peaks related to different processes detected by differential thermal analysis and differential scanning calorimetry

Process	Exothermic	Endothermic
Solid-solid transition	X	X
Crystallization	X	…
Melting	…	X
Vaporization	…	X
Sublimation	…	X
Adsorption	X	…
Desorption	…	X
Desolvation (drying)	…	X
Decomposition	X	X
Solid-solid reaction	X	X
Solid-liquid reaction	X	X
Solid-gas reaction	X	X
Curing	X	…
Polymerization	X	…
Catalytic reactions	X	…

Burner Rig Testing

Experiences in the 1960s and 1970s led to the discoveries of severe high-temperature corrosion in shipboard gas turbine engines that usually did not occur in aircraft turbine engines. Early observations noted severe corrosion attack on the first-stage blade and vane components of a shipboard marine gas turbine engine was sufficiently rapid to cause engine failure in several hundred hours (Ref 124). The ingestion of sea salt and the combustion of fuels containing some measure of sulfur by gas turbine engines operating in marine environments can lead to corrosion of hot section components, particularly turbine vanes (nozzles) and blades (buckets). This attack was documented in the early open literature as hot corrosion, as discussed earlier (Ref 124, 125, 126). Accelerated high-temperature corrosion was later observed in shipboard waste incinerators (Ref 41, 63).

The laboratory technique that was found to most nearly approximate the operating conditions of a gas turbine engine was the burner rig (Ref 117). Burner rig tests provide a compromise between simple laboratory and field tests (Ref 96). Burner rigs are versatile: they may be used with very-low-sulfur fuel to simulate oxidation conditions at high temperatures; they may be used with 1 to 6 wt% S, vanadium, and/or high- carbon-residue fuels to simulate sulfidation and hot corrosion conditions; and they may be used with injection of NaCl to simulate hot corrosion conditions in a marine environment. Laboratory evaluations are employed as a sorting test for materials (alloys and coatings) resistant to hot corrosion, sulfidation, and other high-temperature gaseous corrosion reactions. The basic definition of a burner rig is a device that burns fuel to produce the high-temperature corrosive environment. There are several variations of burner rigs, each compromising certain aspects of a gas turbine environment while minimizing costs for testing (Ref 117). There are basically three types of burner rigs: low-velocity atmospheric pressure rigs, high-velocity atmospheric pressure rigs, and high-velocity, high-pressure rigs. Table 6 compares the test parameters of low-velocity atmospheric pressure, high-velocity atmospheric pressure, and high-velocity, high-pressure burner rigs in use (Ref 117).

Table 6 Typical operating parameters for burner rigs (low-velocity atmospheric pressure; high-velocity atmospheric pressure; high velocity, high pressure) simulating gas turbine environments

Users	Type	Sea salt concentration, ppm	Fuel	Fuel sulphur content, wt%	Metal temperature		Air/fuel ratio	Pressure, atm	Gas velocity, m/s	Thermal cycle	Test time, h	Specimens		
					°C	°F						Type	Number/test	Exposure
Low-velocity atmospheric pressure														
DTNSRDC, INCO and General Electric Co.	Ducted	10	Marine diesel or JP-5 doped with tertiary butyl disulfide	0.4–2	700 and 900	1290 and 1650	30/1	1	5	1/24 h	300–1000	Fin	42	Rotating carousel
Johnson Matthey & Co. Ltd. (U.K.)	Ducted	24	Natural gas (SO_4 added -1.56 l h^{-1})	…	…	…	30/1	1	…	1/1 h	500	Rod	…	Rotating carousel
National Physical Laboratory (U.K.)	Ducted	20 continuous, 9000 intermittent	BS 2869	1.0	Varies	Varies	28/1	1	0.1	1/22 h	300–1000	6.35 mm (0.25 in.) pin	24	Rotating carousel
Naval Air Propulsion Center	Ducted	10	JP-5	…	900–925	1650–1700	30/1	1	8	Yes—variable	600	Fin	20	Rotating carousel
Pratt & Whitney Aircraft Group, United Technologies Corp.	Ducted	20	Jet A (SO, gas added with primary air)	1.3	700 and 900	1290 and 1650	30/1	1	100 at nozzle, much lower at specimen	1/20 h	100–300	Aerofoil	7	Rotating carousel
Rolls Royce Leavesdon (U.K.)	Ducted	Measured as salt flux	Aviation-grade kerosene	0.3	900–1100	1650–2010	…	1	…	None	100–500	Pin blade	…	Rotating carousel
Societé Nationale d'Etude et de Construction de Moteurs d'Aviation (SNECMA) (France)	…	1.9 (Na)	…	…	850	1560	…	1	10	…	…	…	…	…

Users	Type	Sea salt concentration, ppm	Fuel	Fuel sulphur content, wt%	Metal temperature		Air/fuel ratio	Pressure, atm	Gas velocity, m/s	Thermal cycle	Test time, h	Specimens		
					°C	°F						Type	Number/test	Exposure
High-velocity atmospheric pressure														
Admirality Research Establishment (U.K.)	Ducted	0.1	NATO-F 16 naval distillate	1.0	650–900	1200–1650	50/1	0.76	165	1/25 h	2.5–1200	6.35 mm (0.25 in.) rod	33	Rotating carousel
Avco/Lycoming Division	Ducted	6	JP-4R	0.2	785–955	1445–1750	28/1 to 33/1	1	215	Yes—complex	Varies	Paddle	12	Rotating carousel
Brown Bovari and CIE (Germany)	…	15 (Na)	…	0.3–0.4	…	…	…	1	90	…	300	…	…	…
Cranfield Institute of Technology (U.K.)	Ducted	0.06	Diesel fuel	0.3–1.0	750–850	1380–1560	65/1	1	120–130	12/100 h	100	6.35 mm (0.25 in.) rod	33	Rotating carousel
DTNSROC	Ducted	…	JP4, JP5, or marine diesel	1.0	700 and 900	1290 and 1650	50/1	1	65–265	1/24 h	500	6.35 mm (0.25 in.) pin	18	Rotating carousel
Howmet Turbine Components Corp.	Unducted	5 or 50	JP-5R (doped with tertiary butyl disulfide)	0.3	785–955	1445–1750	36/1 to 44/1	1	215	Yes—complex	Varies	Paddle	12	Rotating carousel
NASA, Lewis Research Center	Unducted	0.5 Na as NaCl	Jet A (generally without additives)	0.03–0.07	700–1260	1290–2300	20/1 to 50/1	1	100 and 330	3 min forced air cooling/1 h	1–500	Cylinder or wedge	1–8	Single stationary, rotating, or carousel
National Aerospace Lab (The Netherlands)	Unducted	0–20	JP4 and jet A1	<0.05	<1100	<2010	40/1	1	230	1040—30 °C (85 °F) hold 6 s	150	Turbine blade	2–26	Cascade
Rolls Royce, Derby (U.K.)	Unducted	0.5–4	Standard aviation kerosene D Eng RD 2494	0.2	870–1100	1600–2010	45/1	1	200	None	120–600	Rod	12	Rotating carousel
Solar Turbine	Ducted	3 and 35	JP-5 and	0.04–	900–	1650–	…	1	280	1/1 h	150	Paddle	…	Rotating

Users	Type	Sea salt concentration, ppm	Fuel	Fuel sulphur content, wt%	Metal temperature		Air/fuel ratio	Pressure, atm	Gas velocity, m/s	Thermal cycle	Test time, h	Specimens		
					°C	°F						Type	Number/test	Exposure
International			diesel	0.25	980	1800								carousel
Sulzer (Switzerland)	…	15 (Na)	…	0.3–0.4	…	…	…	1	90	…	300	…	…	…
High velocity, high pressure														
Admiralty Research Establishment (U.K.)	Ducted	0.1–0.5	NATO-F 76 naval distillate	1.0	650–1000	1200–1830	60/1	1–10 (25 max)	230	1/5 h	100	6.35 mm (0.25 in.) rod	20	Rotating or stationary blade
Central Electricity Research Laboratories (U.K.)	Ducted	1.3 (Na)	Low-sodium gas oil	0.3–0.8	850–900	1560–1650	…	Up to 21	20–135	…	300+	…	…	…
NASA, Lewis Research Center	Ducted	0.5 Na or NaCl	Jet A (generally without additives)	0.03–0.07	700–1260	1290–2300	20/1 to 50/1	4 and 50	100	3 min forced air cooling/1 h	1–500	Cylinder or wedge	1–8	Single stationary, rotating, or carousel
Rolls Royce, Bristol (U.K.)	Ducted	None	Avtur	…	Up to 1260	Up to 2300	40/1	17	305	Yes	Varies	Aerofoil	9	Rotating carousel
Westinghouse	Ducted	…	GT-2 diesel	0.35	1100	2010	…	3	155	13/250 h	250	Rectangular bars	…	…

Note: 1 atm = 101.3 kPa. Source: Ref 117

The flow and heat-transfer characteristics around a cylindrical specimen are well documented and can be readily reproduced from one laboratory to another (Ref 96). Therefore, cylindrical test pins are normally used for burner rig testing. Specimens are usually rotated to keep all specimens at the same temperature and to ensure uniform exposure of contaminants from the combustion stream. In general, the specimens are removed from the test chamber periodically and cooled to achieve thermal cycling. Test cycles may range from every 10 min to once every 24 h, depending on the laboratory and the service application that is being simulated during the burner rig test. There is no accepted specification for burner rig testing. A recommended test practice was issued by the working group on hot salt corrosion testing of the Versailles Agreement on Advanced Materials and Standards (VAMAS) (Ref 127).

Likely, the most important factor as to how well a burner rig simulates gas turbine conditions is the contaminant flux rate deposited on the test specimens (Ref 102, 128, 129). The corrosion rate dependence on salt deposition rate is nonlinear and depends on the composition of the salt and the substrate alloy or coating (Ref 130).

There appears to be no unique salt level at which burner rigs are conducted in different laboratories, and there are wide variations of salt concentration used. In simulation tests, 1 ppm salt is considered realistic, but 10 ppm is often used. The corrosion rate typically increases with an increase in salt levels from 0 to 10 ppm. However, according to one report, varying the salt concentration from 10 to 50 ppm in air has little effect on low-temperature type II hot corrosion (Ref 131).

Due to the complexity of the turbine service environment and the impossibility for any burner rig test to fully simulate the service conditions, the results from burner rig testing should be used to rank the relative corrosion performance of alloys and of high-temperature coatings and should not be used to predict the actual corrosion rates or service life of these materials in an operating turbine.

Low-velocity atmospheric pressure burner rigs (LVBR) operate at low velocity (0.1 to 10 m/s, or 0.33 to 33 ff/s) (Ref 101). In ducted rigs, specimens are directly exposed to the hot gases from the combustion flame in an unrestricted manner. Under such conditions, it is impossible to maintain the critical partial pressure of SO_3/ SO_2 for hot corrosion to proceed (Ref 96).

Ducted LVBR rigs are used to gain better control of the test environment. The dimensions of a ducted combustion environment influence the aerodynamic flow and the heat-transfer characteristics around the test specimens (Ref 131). The combination of duct configuration, specimen design, and flow characteristics can alter the boundary layer at the specimen surface sufficiently to give variations in deposition rates (Ref 96). The Lynn ducted burner rig is shown in Fig. 16.

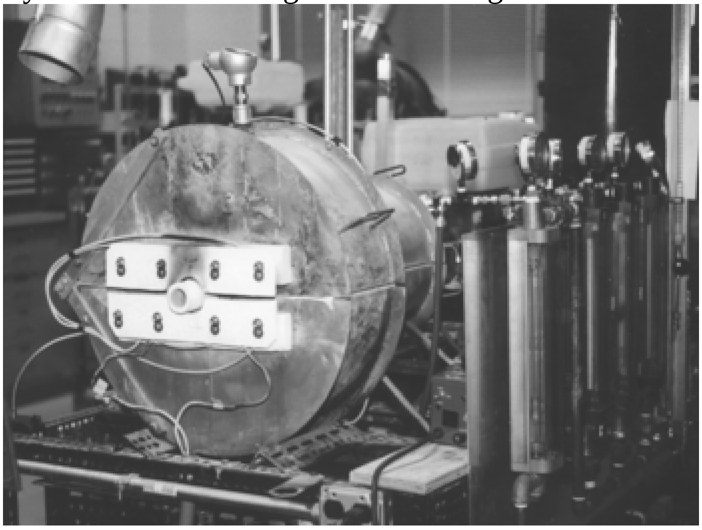

Fig. 16 Lynn ducted low-velocity atmospheric pressure burner rig used for hot corrosion testing

As shown in the LVBR schematic diagram (Fig. 17), the air, fuel, and sea salt are injected into the burner rig. The spray is injected into the forward combustion zone to duplicate high-temperature reactions occurring in gas turbines. The LVBR has been used for testing with 0.5, 5.0, 10, 100, and 200 ppm sea salt. The lower salt tests are run for 500 and 1000 h, the 100 ppm salt level for 100 to 500 h (Ref 132), and the 200 ppm salt tests for 100 h. The higher sea salt tests, especially at 200 ppm, are heavily oriented toward sulfidation effects; oxidation

does not appear to play a dominant role. On the other hand, the 0.5 ppm sea salt test yields more of an oxidation-oriented reaction, as evidenced in past efforts to more oxides and smaller (and fewer) sulfides.

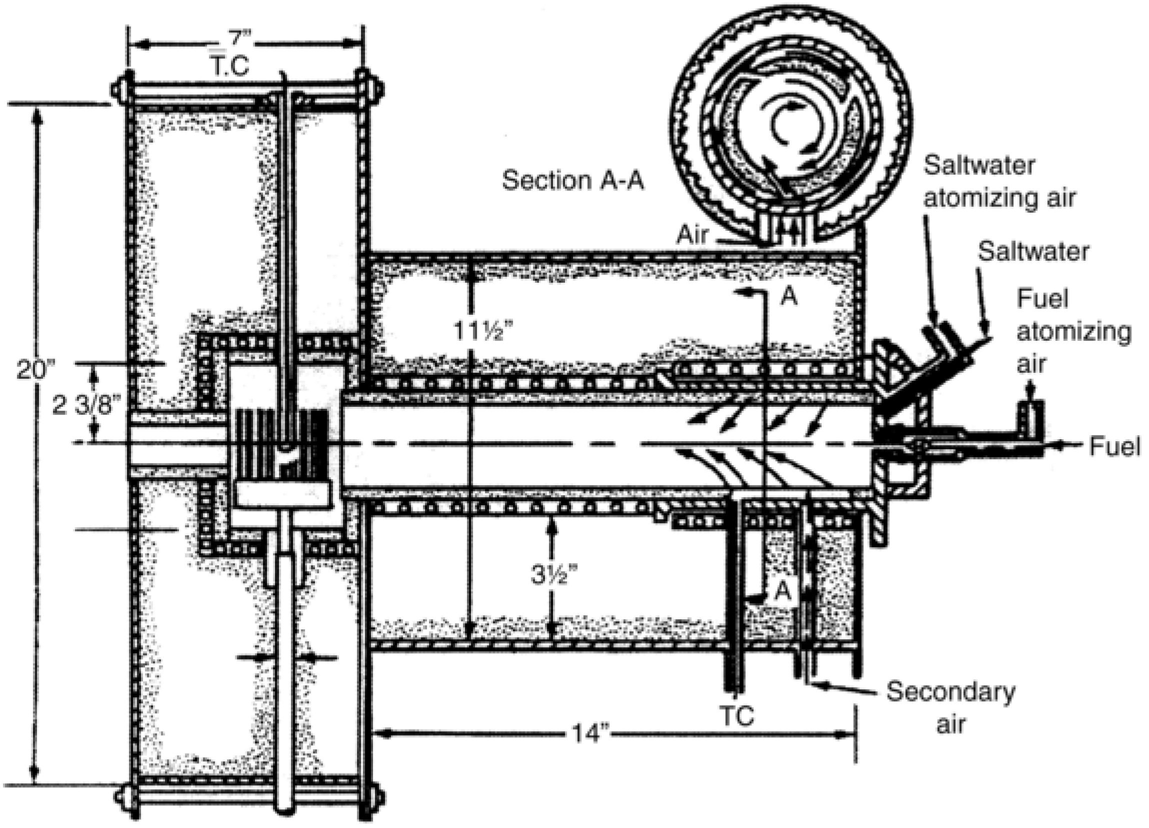

Fig. 17 Schematic of a low-velocity atmospheric pressure burner rig. TC, thermocouple

The important factors that influence hot corrosion in gas turbines are composition of the gas, condensate composition and deposition rate, and temperature. In order to simulate gas turbine conditions in a LVBR, it is desirable to duplicate all the variables. However, it is not possible to duplicate exactly, due to the pressure differentials between the gas turbine (5 to 15 atm, or 500 to 1500 kPa) and the 1 atm (101 kPa) LVBR (Ref 131). Table 7 shows a comparison of the partial pressures of gaseous species in the gas turbine and the LVBR. The corrosion rate depends on the salt deposition rate, which is nonlinear, and the corrosion depends on the composition of the salt and the substrate alloy or coating (Ref 130). It is desirable to represent an accelerated test of the turbine conditions with LVBR testing. This is accomplished by using impurity concentrations of the gas composition and the salt condensate that are similar between the rig and the turbine and by having a salt deposition rate that is higher in the rig, usually by a factor of 10, than occurs under turbine operating conditions.

Table 7 Typical operating conditions for gas turbines and low-velocity atmospheric pressure burner rigs (LVBR)

	Gas turbine conditions	LVBR conditions
Fuel	$CH_{1.7}$	$CH_{1.7}$
Air-to-fuel ratio (by weight)	60	30
Pressure, atm (MPa)	12 (1.2)	1(0.1)
pO_2**, atm (MPa)**	1.89 (0.192)	0.10 (0.01)
pN_2**, atm (MPa)**	9.34 (0.946)	0.76 (0.077)
pCO_2**, atm (MPa)**	0.42 (0.043)	0.068 (0.0069)
pH_2O**, atm (MPa)**	0.35 (0.035)	0.058 (0.0059)

Source: Ref 130

The SO_2/SO_3 equilibrium is a function of the partial pressure of oxygen. Because of the pressure differential between the gas turbine and the LVBR, the SO_2/SO_3 partial-pressure ratio in a LVBR cannot be equivalent to that in the turbine, and it is not possible to simulate the partial pressures of both SO_2 and SO_3. To simulate the

turbine conditions as nearly as possible in an LVBR environment, the choices are to use (SO_3 + SO_2) summation of partial pressures or the partial pressure of only SO_3 or SO_2 (Ref 130). The sulfur levels must be much higher than in the turbine because of the pressure difference. For an equivalent air/fuel ratio, the sulfur level in the 1 atm (101 kPa) LVBR test should be p times higher than in the turbine if the use of (SO_3 + SO_2) partial pressures are simulated, where p is the pressure in the turbine (Ref 130).

In actual operation, metered fuel is atomized and injected into the combustion chamber. Sea salt or other soluble contaminants are atomized and injected into the forward combustion area, as shown in Fig. 17. The gases, sea salt, or other solutions added to the fuel stream are thoroughly mixed by the swirl action of air entering through tangential slots in the combustion tube. This design precludes stagnation or stratification of the combustion gases. Downstream, the test specimens are exposed to the products of combustion and sea salt (or other contaminants, such as artificial urea).

Diesel and high-distillate fuels (NATO F76, JP4, and JP5) (Ref 129), as well as other commercial-grade liquid fuels, have been used for burner rig testing. Di-tertiary butyl disulfide may be added to NATO F76 diesel fuel to increase the sulfur concentration to 1% by weight, the maximum prescribed sulfur level for this military-specified fuel. Other contaminants (vanadium, carbon residue, or other species) can be added to study the individual or synergistic effects on the resistance of alloys (Ref 133) or protective coatings (Ref 134, 135) to high-temperature corrosion reactions. As discussed earlier, sulfur and sulfur-containing species have been shown to be a major reactant in hot corrosion. Fuel flow may be in the range of 4 to 6 cm^3/min, or approximately 1.5 to 2.3 gal, during a 24 h period. The fuel is atomized into a fine dispersion by low-pressure air and introduced into the forward combustion end of the furnace. The combination of a fine spray of fuel, excess air, and sufficiently high temperatures achieves instantaneous combustion.

Temperature is attained by the combustion of the fuel and is supplemented by heat from heating elements that surround the test chamber. The heaters reduce temperature gradients and provide stable, controllable temperatures between 815 and 1150 °C (1500 and 2100 °F). One control thermocouple is used, which is positioned in the center of the rotating specimen carousel approximately 25 mm (1 in.) above the refractory surface and is connected to a controller. The thermocouple allows the rig to normally run at its set temperature ±2 °C (±4 °F). Test temperatures for type I hot corrosion are run between 800 and 950 °C (1472 and 1742 °F), while type II hot corrosion tests are run between 600 and 800 °C (1112 and 1472 °F). Because of small variations of construction and operating parameters between LVBR test apparatuses and variations in carousel configurations, each rig should be calibrated prior to testing.

Air/fuel ratios are often set at 30 to 1 but may range from 15 to 1 (approximately stochiometric conditions) to approximately 60 to 1. Within very specific limits, temperature changes can be made without changing combustion conditions. Flame impingement on the specimens is always avoided. On the other hand, fuel-rich conditions or flame impingement can be obtainable as a special test condition.

The LVBR uncoated or coated test specimens (Fig. 18) are electrically and thermally isolated from one another by insertion into a moldable ceramic that is placed into a metallic carousel. The carousel rotates at a speed (such as 30 rpm) sufficient to assure equal thermal exposure of all test specimens.

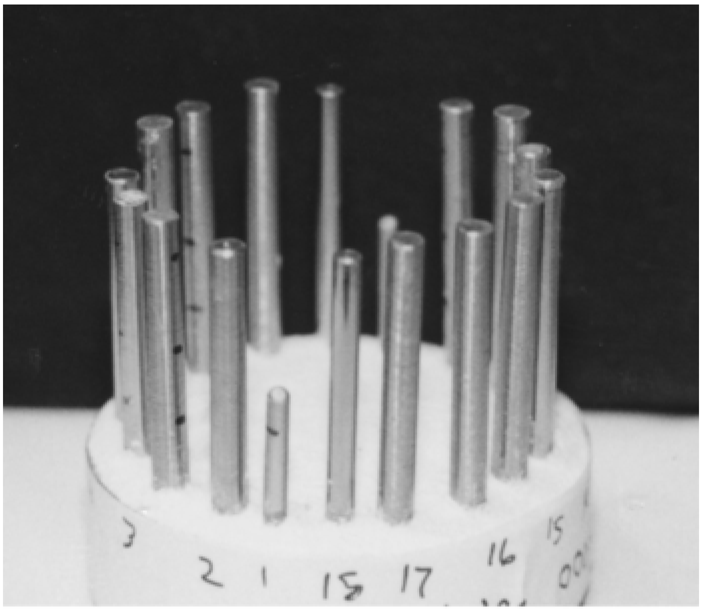

(a)

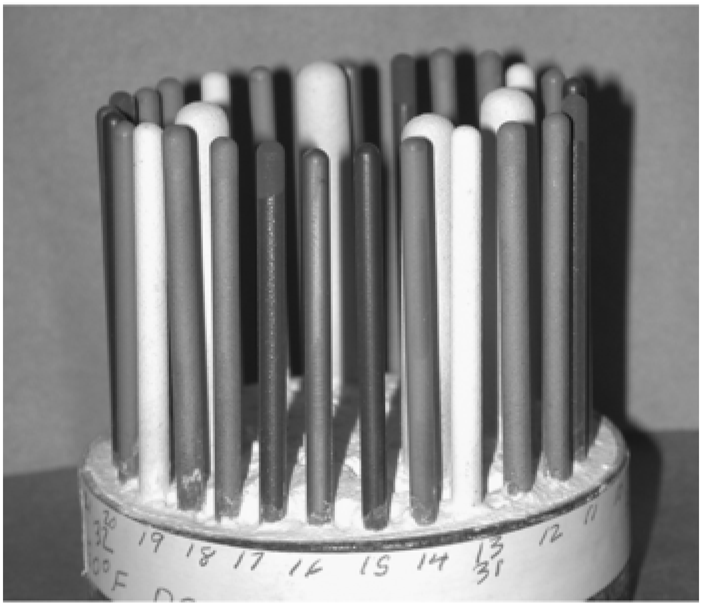

(b)

Fig. 18 Untested low-velocity atmospheric pressure burner rig test specimens. (a) Uncoated nickel-base alloys. (b) Coated superalloys

The LVBR tests are used to simulate gas turbine conditions and, more recently, the high- temperature, hot corrosion environment that occurs in waste incinerators. For laboratory testing of the waste environment, urine, if available, or artificial urine is used to duplicate the corrosive conditions on shipboard incinerators. Sea salt should be added to either urine solution to further simulate this corrosive marine environment. Therefore, all contaminants (fuel sulfur content, sea salt, urine, and others) should be determined during the design of the accelerated test to best simulate the environment under consideration.

Figure 19 shows the effects of type I hot corrosion on materials after 1000 h LVBR exposures at 899 °C (1650 °F). Type I high-temperature hot corrosion (HTHC) occurs through basic fluxing and subsequent dissolution of the normally protective oxide scales by the molten sulfate deposits at metal temperatures ranging from 850 to 950 °C (1562 to 1742 °F); alloy or coating depletion is generally associated with the corrosion front caused by type I hot corrosion.

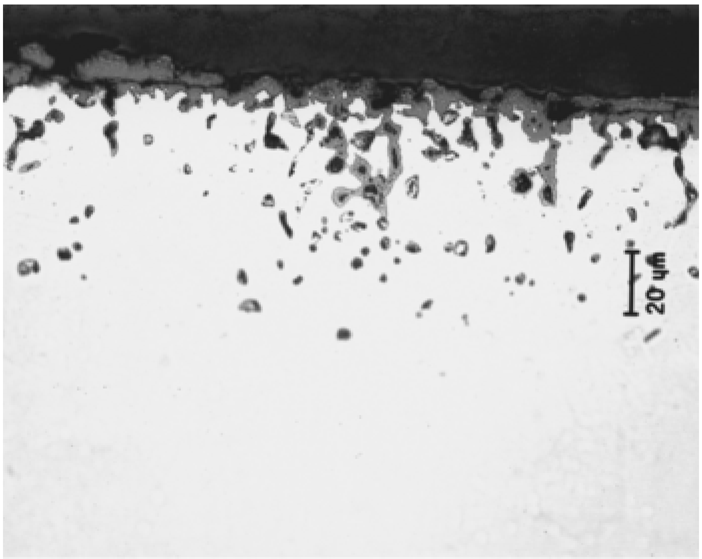

(a)

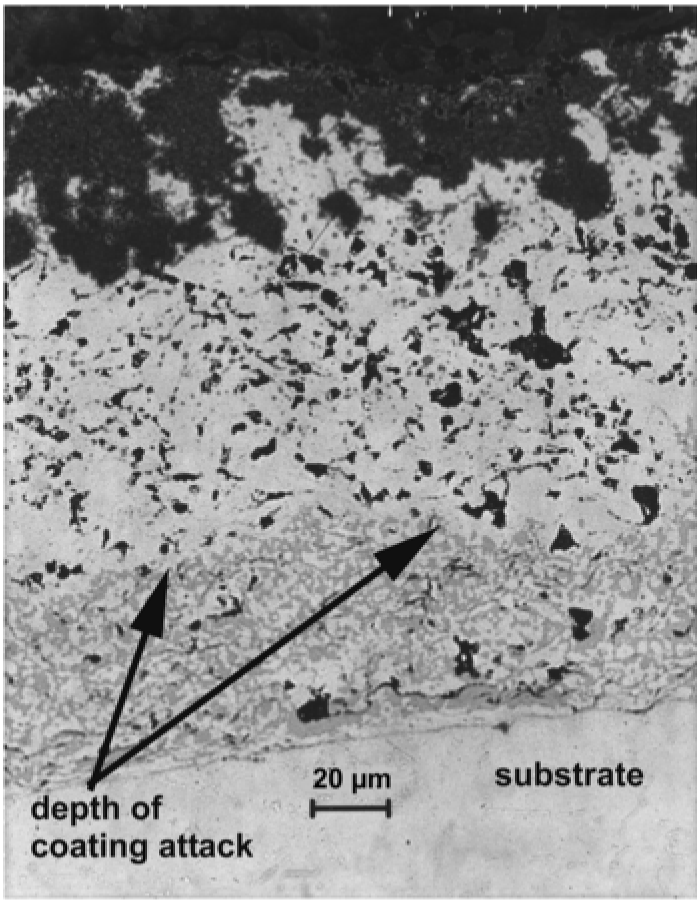

(b)

Fig. 19 Low-velocity atmospheric pressure burner rig test results at 900 °C (1650 °F). The nickel-base alloy (a) and the CoCrAlY-type coating (b) were both attacked by type I hot corrosion. Depletion of an alloy constituent or coating phase was found along a broad front, with an associated generation of small voids when the constituent/phase is depleted. Depth of penetration in the coating is 115 to 125 µm (4.5 to 5 mils).

As mentioned previously, the use of cheaper, lower-grade fuels may have some undesired consequences. The use of a LVBR test can determine whether certain fuel contaminants have an adverse effect on the performance and service life of hot section turbine coatings. Figure 20 shows the effects on a diffusion nickel aluminide coating after a 1000 h LVBR test conducted at 704 °C (1300 °F). The fuel parameter being tested in this case

was the fuel carbon residue (on 10% bottoms). Increased carbon residue content in the fuel, in this case, led to enhanced type II low- temperature hot corrosion (LTHC) (Ref 135). Type II corrosion occurs in the temperature range of 650 to 750 °C (1202 to 1382 °F), where p_{SO_3} is relatively high or melts are deficient in the oxide ion concentration, leading to acidic fluxing that results in pitting attack where the sulfides are found in the pitted area. The carbon may cause erosion, or its presence in the deposit may promote reduction of sodium sulfate to sodium sulfide. At a threshold fuel carbon-residue content between 0.19 and 0.33 wt%, type II hot corrosion vastly increases the average coating loss on a radius (from 23 to 30 μm, or 0.9 to 1.2 mils, to approximately 70 μm, or 2.75 mils), as shown in Fig. 21 (Ref 135) by enhancing the effective sulfate activity.

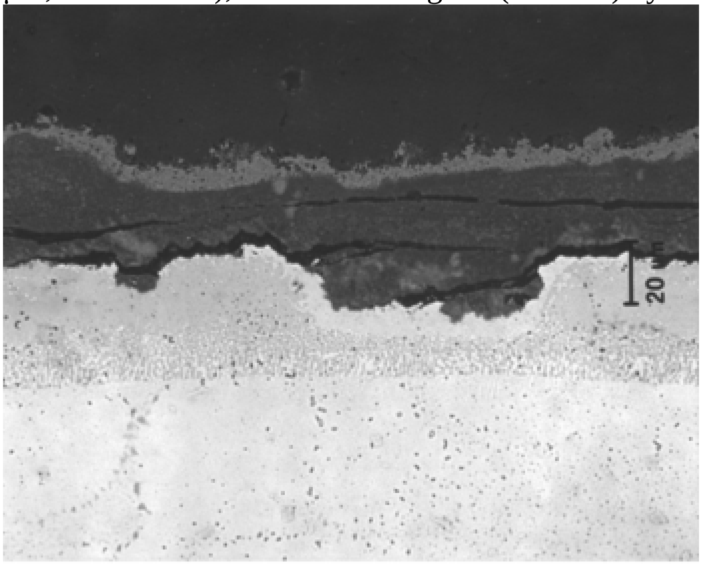

(a)

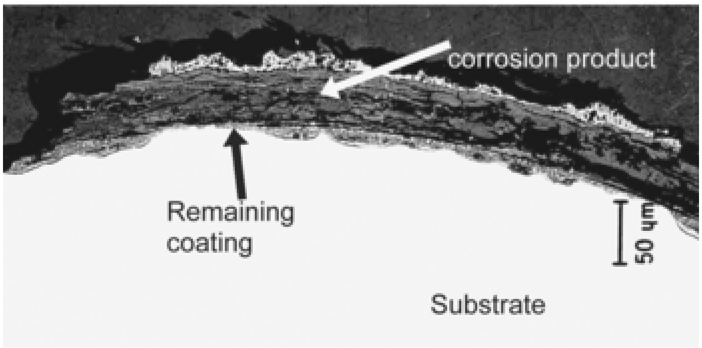

(b)

Fig. 20 Low-velocity atmospheric pressure burner rig pins after 1000 h exposure to combustion gases from fuel containing (a) 0.099 wt% C residue and (b) 0.33 wt% C residue. Increased carbon residue has a vast effect on aluminide coating performance.

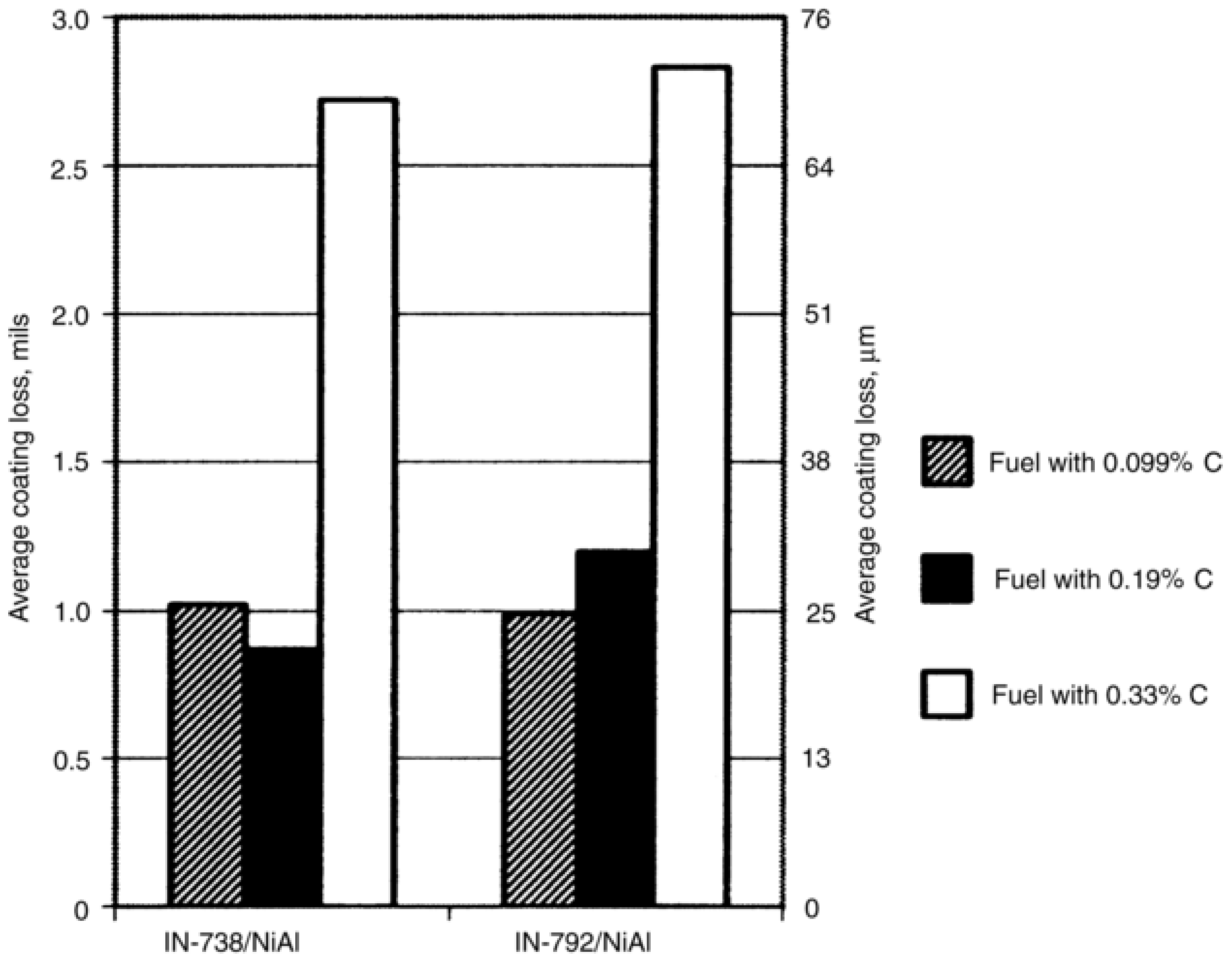

Fig. 21 Effects of fuel carbon residue (10% bottoms) on type II hot corrosion of nickel aluminide high-temperature coatings. Source: Ref 135

High-velocity atmospheric pressure burner rigs (HVBR) shown as a schematic in Fig. 22, operate at a velocity of approximately 0.5 Mach (331 m/s or 1086 ft/s). Other HVBR listed earlier in Table 8 operate from 65 to 330 m/s (213 to 1080 ft/s). Test rigs delivering pressures slightly above atmospheric pressure (up to 1.45 bar or 145 kPa) operate between 0.2 to 0.75 Mach (132 to 496 m/s or 433 to 1630 ft/s) (Ref 160). Like LVBR apparatus, HVBR test setups may be unducted or ducted. A HVBR can evaluate materials of various geometries and chemical compositions from 371 to 1371 °C (700 to 2500 °F) under oxidation or corrosive environments. The test temperature at the center of the specimen carousel is maintained to ±15 °C (±27 °F) (Ref 136).

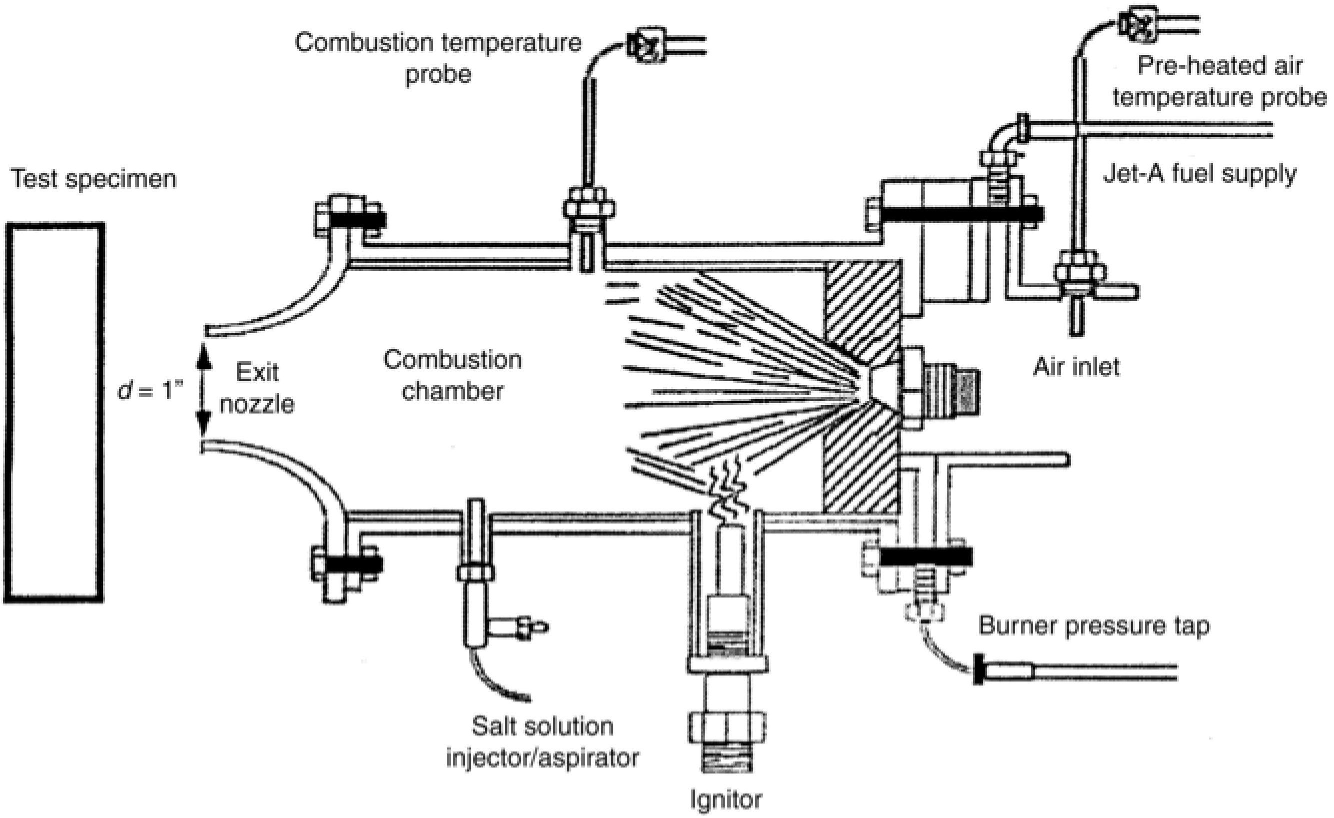

Fig. 22 Schematic of an unducted high-velocity atmospheric pressure burner rig

Table 8 Burner rig deposition rates for high-velocity and low-velocity types

Rig type	Temperature		Velocity		Na in combustion gas, ppm		Cl in combustion gas, ppm		SO_2/SO_3 in gas, vpm	Deposition rate, μg/cm^2 · h	Sodium mass flux, mg/cm^2 · h		Chloride mass flux, mg/cm^2 · h	
	°C	**°F**	**m/s**	**ft/s**	**Background**	**Average**	**Background**	**Average**			**Background**	**Average**	**Background**	**Average**
High-velocity (HV) burner rigs[(a)]														
HV_{MS}	700	1292	220	720	0.019	0.20	0.038	0.40	123	31	0.13	1.38	0.23	2.41
HV_{M}	750	1382	240	790	0.017	0.017	0.035	0.035	134	…	0.12	0.12	0.21	0.21
HV_{MS}	…	…	…	…	0.017	0.18	0.035	0.36	…	28	0.12	1.27	0.21	2.18
HV_{MS}	…	…	…	…	0.017	0.17	0.033	0.35	…	13	0.12	1.21	0.20	2.07
HV_{MH}	…	…	…	…	0.17	0.17	0.33	0.33	…	…	1.15	1.15	1.97	1.97
HV_{MS}	899	1650	270	890	0.015	0.16	0.031	0.33	153	5	0.10	1.09	0.19	1.96
Low-velocity (LV) burner rigs[(b)]														
LV_{M}	750	1382	0.1	0.3	20	112	36	200	325	188	0.30	1.67	0.55	3.0
LV_{M}	850	1562	0.1	0.3	20	112	36	200	325	165	0.30	1.67	0.55	3.0
LV_{A}	850	1562	0.1	0.3	13	13	20	20	47	50	0.19	0.19	0.30	0.30
LV_{A}	950	1742	0.1	0.3	13	13	20	20	47	7	0.19	0.19	0.30	0.30

(a) M, marine; MH, high-load marine; MS, marine + salt-shedding simulation of salt from compressor.

(b) A, low-sulfur fuel, jet engine simulation; M, 1% S fuel, marine. Source: Ref 136

Hot corrosion burner rig tests help to evaluate the potential durability of turbine engine materials, which are expected to breathe sea salt air from aircraft carriers and coastal bases of operation. This test is accomplished by injecting a controlled amount of sodium chloride solution into the burner flame.

Materials are subject to thermal cycling that duplicates the flight cycles experienced by aircraft making many takeoffs and landings daily. The test rigs can heat advanced materials and coatings to the extreme temperatures and hostile environments in which they are expected to operate by only burning several gallons of jet fuel per hour rather than full-scale engine tests.

Corrosion rates in HVBR and LVBR correlate with the contaminant flux rate and the amount of salt present on the test sample surfaces (Ref 117). Deposition efficiency changes with temperature from 10 to 12% at 750 °C (1382 °F) to 8 to 9% at 850 °C (1562 °F) and approximately 4% at 900 to 950 °C (1652 to 1742 °F) (Ref 137). Under high-velocity conditions at temperatures of 750 °C (1382 °F) and below, injection of salt particulates has been shown to result in increased corrosion of corrosion-resistant alloys, while no effect was noted for less resistant alloys. Such behavior is consistent with mechanical damage to the protective scale formed on corrosion-resistant alloys by particulate impact (Ref 138, 139). At 850 °C (1562 °F), the salt was semi- molten and therefore would more likely deposit on the surface rather than fracture the oxide.

To generate similar corrosion rates, salt deposition rates in LVBR tests were required to be much higher than the contaminant flux in HVBR tests. Table 8 compares the burner rig deposition rates, sodium, and chlorine mass fluxes (Ref 136).

If the contaminant fluxes are similar, material losses will be higher in the HVBR tests than observed in the LVBR in the type II hot corrosion existing at 750 °C (1382 °F). In the temperature regime where the type I hot corrosion predominates, the HVBR metal losses are higher than LVBR results exposed to low-salt fluxes, but the LVBR results are equal to or higher than the HVBR results, as shown in Table 9 (Ref 136).

Table 9 Maximum metal loss as a function of rig and of sodium flux

Alloy	Temperature		Average sodium flux, mg/cm^2 · h	Maximum metal loss, μm/1000 h	
	°C	**°F**		**LVBR**	**HVBR**
IN-738LC	750	1382	0.1–0.2	…	130
	750	1382	1–2	6	200
	850	1562	0.1–0.2	60	620
	850	1562	1–2	84; 142	100
IN-939	750	1382	1–2	1	10
	850	1562	0.1–0.2	28	250
	850	1562	1–2	79; 177	200
IN-100	750	1382	1–2	2,625	1,000
	850	1562	0.1–0.2	7,030; 8,510	3,000
	850	1562	1–2	18,245	3,380

LVBR, low-velocity atmospheric pressure burner rig; HVBR, high-velocity atmospheric pressure burner rig. Source: Ref 136

Due to the impact of salt particulates, discussed previously, the incubation time for hot corrosion to initiate is generally shorter in the HVBR test environment than noticed in LVBR tests. Although the metal losses from HVBR tests are lower than those measured after LVBR exposures, the test time was 2 to 15 times shorter in the HVBR tests compared to the LVBR test runs. The propagation rates for the two alloys illustrated in Table 10 were similar in both burner rigs.

Table 10 Comparison of incubation times and propagation rates exposed to low-velocity atmospheric pressure burner rig and high-velocity atmospheric pressure burner rig at 850 °C (1560 °F), with sodium mass flux of 1 to 2 mg/cm^2 · h

Alloy	Low-velocity burner rig				High-velocity burner rig			
	Metal loss, µm		**Propagation rate, µm/1000 h**	**Incubation time, h**	**Metal loss, µm**		**Propagation rate, µm/1000 h**	**Incubation time, h**
	1100 h	**1500 h**			**100 h**	**500 h**		
IN-738LC	93	213	322	790	24	161	345	30
IN-939	87	266	448	905	20	156	340	41

Source: Ref 136

The HVBR tests are also conducive to other gaseous reaction studies. Nitridation of several nickel-base alloys used as transition liners in the combustor section of a gas turbine engine was tested in a dynamic oxidation high-velocity (100 m/s, or 330 ft/s) burner rig operating for 100 h at 980 °C (1796 °F) (Ref 37). In this test, a fuel oil mixture was burned with an air-to-fuel ratio of approximately 50 to 1. The specimens were removed from the test chamber every 30 min and rapidly fan cooled for 2 min before returning the specimens to the test chamber. Due to the high- velocity combustion gas stream with frequent thermal cycling, all test specimens experienced oxide spallation and relatively uniform metal loss. The internal attack, measured by metallography, included both internal oxidation and nitridation, as shown in Fig. 23. Bulk carbon and nitrogen for the test specimens were analyzed. Iron, aluminum, and titanium alloying additions were found to be detrimental to resisting nitridation attack.

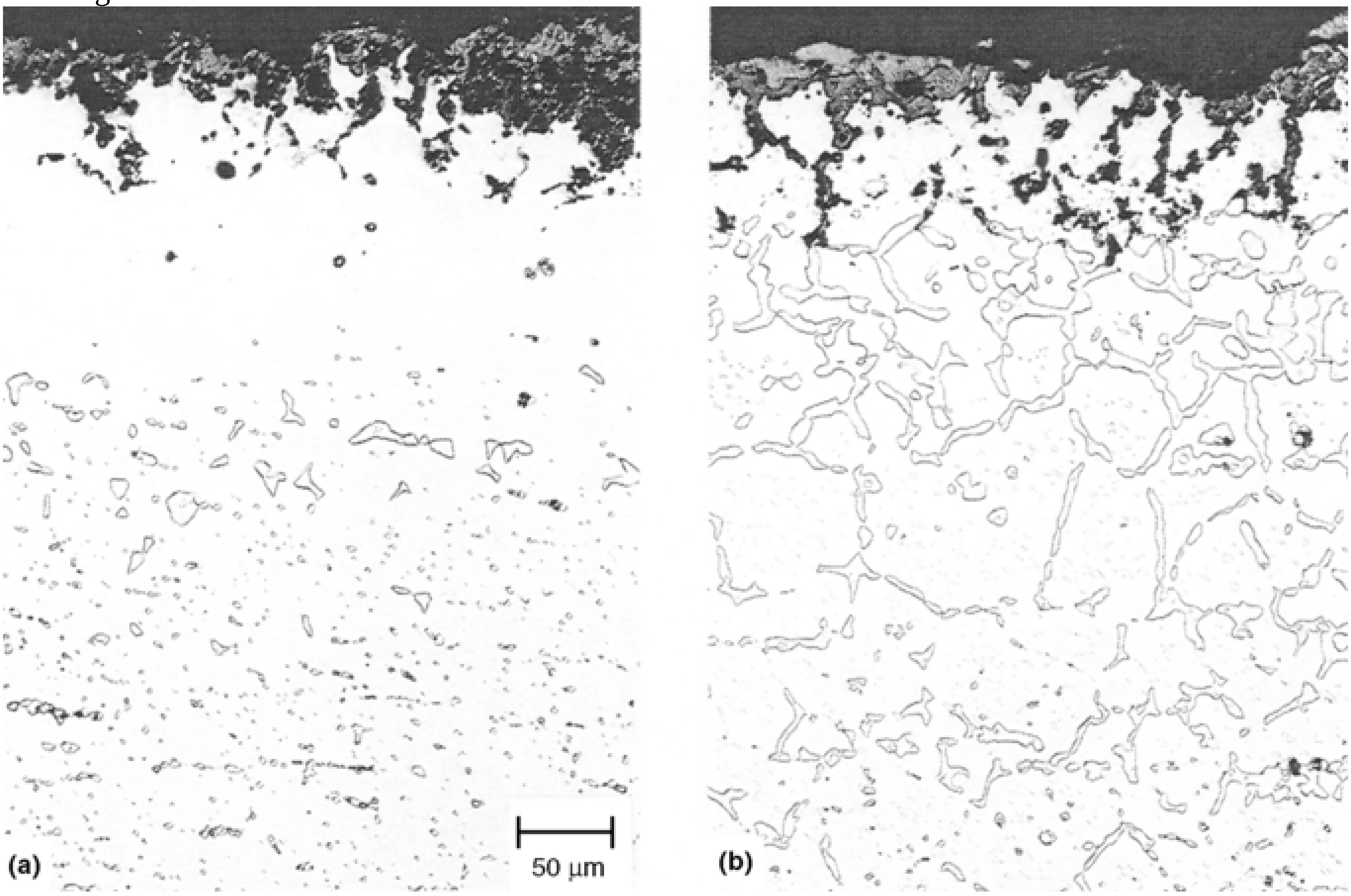

Fig. 23 Optical micrographs showing internal oxidation and nitridation after the dynamic oxidation burner rig testing at 980 °C (1800 °F) for 1000 h with 30 min cycling. (a) 230 alloy. Note blocky nitrides below carbide-depleted zone; fine carbide precipitates were due to aging during the test. (b) Alloy X

High-velocity, high-pressure burner rigs (HPBR), such as the one shown in Fig. 24, are more complex than the previous two rigs, but this test apparatus most accurately simulates the high-pressure, high-temperature

conditions in a gas turbine engine. Pressure and temperature can be adjusted to duplicate the conditions of a given engine. A HPBR requires compressors and other ancillary equipment to maintain the desired conditions in the combustor and the specimen chamber. The combustor and the specimen chamber must be designed to withstand the imposed pressures at the test temperatures.

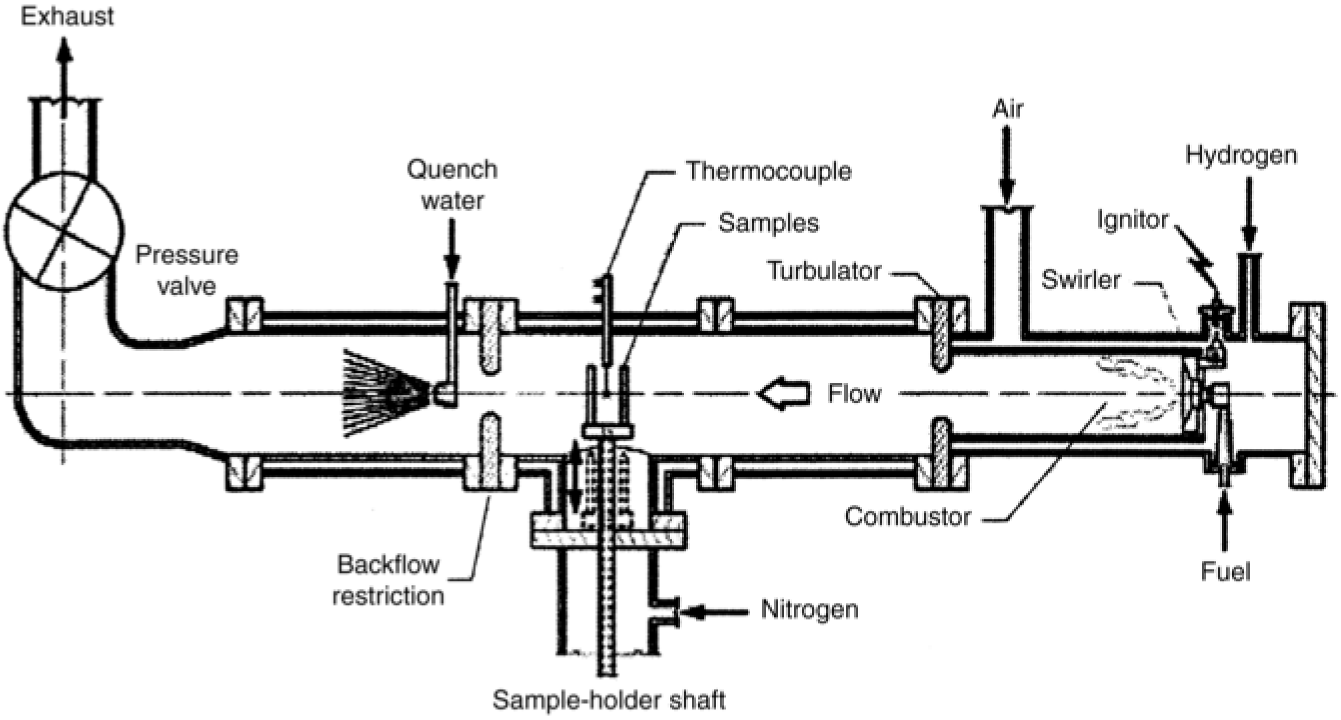

Fig. 24 Schematic of high-velocity, high-pressure burner rig

The HPBR is a combustion test rig used for high-temperature environmental durability studies of materials for advanced aircraft. The facility burns jet fuel and air in controlled ratios to produce combustion gas chemistries and temperatures that are realistic to those in gas turbine engines. In addition, the test section is also capable of simulating the pressures and gas velocities representative of today's aircraft. Test samples are easily accessible for ongoing inspection and documentation of weight change, thickness, cracking, and other metrics. The test pressures range from 3 to 50 atm (304 to 5066 kPa) and with gas flow velocities of 20 to 305 m/s (65 to 1000 ft/sec) (Ref 117). Conditions of one rig reportedly operated at pressures up to 30 bars (3000 kPa) with gas velocities of 0.25 to 0.9 Mach (166 to 596 m/s or 544 to 1960 ft/s) and temperatures between 700 to 1100 °C (1292 to 2012 °F) (Ref 161).

Testing at High Temperature, High Pressure

Test temperature and total system pressure (and the partial pressures of various soluble gaseous species) are two major factors affecting materials corrosion. There are several commercial and industrial processes that occur at both high temperatures (HT) and high pressures (HP). Table 11 lists a number of common commercial HT/HP environments (Ref 140). For simple HT/ HP exposure tests involving aqueous or nonaqueous phases, the total pressure of the constituents in the test chamber varies with temperature.

Table 11 Typical commercial high-temperature/high-pressure service conditions

Application	Environment	Temperature		Pressure	
		°C	**°F**	**MPa**	**bar**
Nuclear power	High-purity water/steam/H_2	280–500	536–932	≤17	≤170
Fluidized bed combustion	Air, gas, coal	600–750	1112–1382	1	10
Oil and gas production	Brine, H_2S, CO_2, S	20–250	68–482	≤130	≤1300
Aerospace propulsion	Hydrogen	-200–900	-328–1652	0.2–67	1–670
	Oxygen	-200–480	-328–896	≤8	≤80
Petroleum refining	H_2, H_2S, hydrocarbons	350–650	662–1202	≤10	≤100
Compressed natural gas storage	Methane with trace H_2S	0–100	32–212	≤8	≤80
Thermodynamic power generation	NH_3, H_2O	100–650	212–1202	≤1.5–15	≤15–150
Geothermal power	Brine, steam, H_2S	≤370	≤698	≤17	≤170
Steam boiler	Water, steam	≤300	≤572	≤9	≤90

Source: Ref 140

The simplest type of HT/HP corrosion test involves a sealed, static, pressurized autoclave vessel, as shown in Fig. 25. The test vessel contains a solution and vapor space above the solution. The ratio of liquid to gaseous phases is determined by the amount of each constituent, the vapor pressures of the constituents, and the temperature. Corrosion samples may be placed in the liquid phase, the gaseous phase(s), or at the phase interfaces, depending on the type of information required (Ref 140).

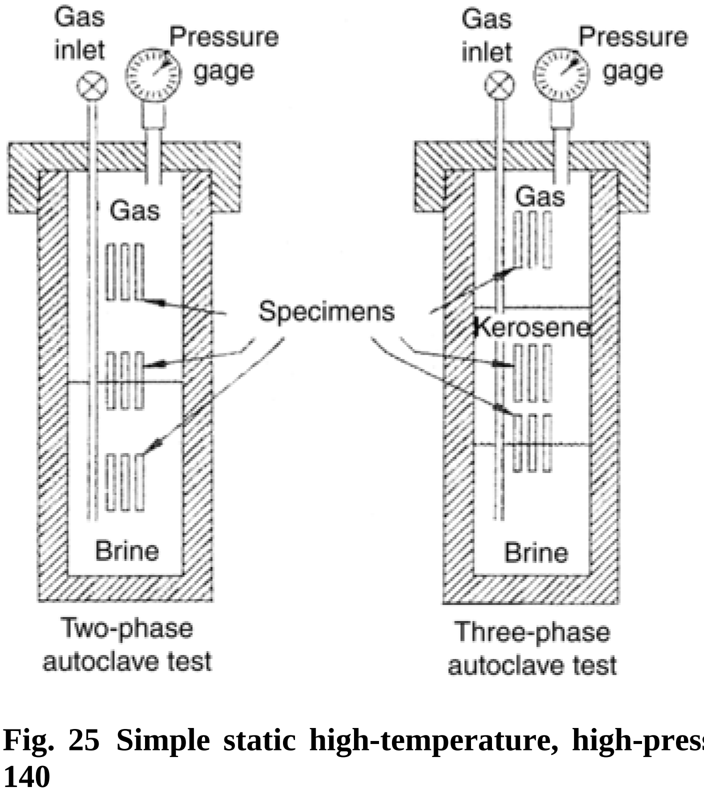

Fig. 25 Simple static high-temperature, high-pressure autoclave test vessel configuration. Source: Ref 140

In cases where susceptibility to hydrogen embrittlement cracking (HEC), Stress-corrosion cracking (SCC), liquid metal embrittlement (LME), or other environmentally assisted cracking (EAC) mechanisms may be suspected, it is common to evaluate the actual mechanical behavior of the alloys under consideration in the corrosive environment of interest. Slow strain rate testing (SSRT) or constant extension rate testing (CERT) may be used in a HT/HP environment. The important aspect of such techniques is the requirement for these

tests to be conducted in a range of strain rate or cross-head extension rate in which the material under evaluation is going to experience cracking, if it is susceptible (Ref 140).

In general, it is necessary to conduct such tests slowly enough so that the environment has adequate time to affect the material and produce cracking. These strain rates are typically in the range of 10^{-4} to 10^{-7}/s for SCC in many common metal-environment systems. For HEC, the critical strain rate is somewhat higher (i.e., 10^{-2} to 10^{-4}/s) in most susceptible iron, nickel, and titanium alloys. The SSRT is particularly adapted to HT/HP in simulated environments (Ref 140). Because the test is accelerated mechanically by the application of the dynamic straining, it is possible to use simulated test environments rather than the overly aggressive chemical environments commonly used in conventional standardized tests.

Figure 26 shows a vessel that can be used to conduct SSRT under HT/HP conditions. In aqueous environments, the heating is accomplished from the outside of the vessel to uniformly heat the entire test solution surrounding the specimen. For high-temperature gaseous environments, it may be possible to heat the specimen within the pressurized test vessel.

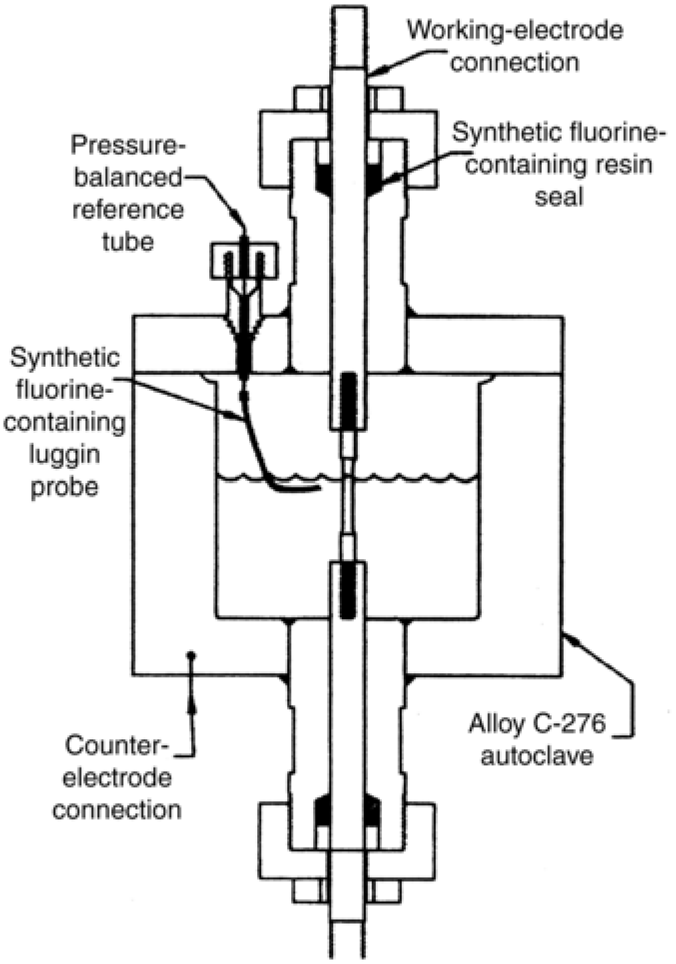

Fig. 26 High-temperature, high-pressure test vessel for slow strain rate testing. Source: Ref 140

In some cases, it may be possible to use the similarly designed HT/HP test vessel to conduct fracture or fatigue loading or both (Ref 140). For such tests, accommodations must be made to be able to handle the generally larger specimen configuration of fracture mechanics specimens. Additionally, there is the need to closely monitor crack opening displacement or crack growth or both directly, using various methods that include (a) pressure and environmentally compatible clip gages, (b) mechanical fixtures that exit the pressure vessel, or (c) potential drop across the specimen. In the case of potential-drop techniques, as the specimen cross section is reduced due to crack growth, the electrical resistance measured across the cracked region increases and can be monitored as a measure of crack growth. Alternately, in some cases, direct measurements of crack opening displacement can be conducted, using special mechanical feedthroughs in the test vessel. This technique, while cumbersome, is preferred where the test environment is particularly corrosive and may attack clip gages and interfere with electrical penetrations for the use with potential-drop techniques.

ASTM G 111, "Guide for Corrosion Tests in High-Temperature or High-Pressure Environment, or Both," establishes basic considerations that are necessary for conducting corrosion tests on metallic materials under conditions of high pressure or a combination of high temperature and pressure, and that will promote consistency in laboratory results.

Thermal Cycling

Many applications of high-temperature materials require repeated heating and cooling cycles that demand that materials be resistant to the mechanical stresses and subsequent damage during cycling. As noted in earlier sections, stresses are generated in the oxide or other gaseous-derived scale formed on metals and alloys in isothermal exposures. Alloys operating in high-temperature applications can exist if protective oxide films are formed or protective coatings are applied. For alloys with oxides, operation conditions usually apply large compressive stresses in the oxide scales due to the thermal expansion coefficients between substrates and oxides differing by 30 to 50%. A third source of stress in the oxide scale can be from scale growth itself, because of geometric effects or intrinsic oxide growth from counterdiffusion of oxide-forming species (Ref 28, 141). Table 12 gives the expansion coefficients of some metal-oxide systems. Figure 27 illustrates the strains that are generated by differential thermal expansion.

Table 12 Linear expansion coefficients of metals and oxides

System	Oxide coefficient ($\times 10^{-6}\ \alpha_o$)	Temperature range		Metal coefficient ($\times 10^{-6}\ \alpha_m$)	Temperature range		Ratio (α_m/α_o)
		°C	**°F**		**°C**	**°F**	
Fe/FeO	12.1	100–1000	212–1832	15.3	0–900	32–1652	1.25
Fe/Fe_2O_3	14.9	20–900	68–1652	15.3	0–900	32–1652	1.03
Ni/NiO	17.1	20–1000	68–1832	17.6	0–1000	32–1832	1.03
Co/CoO	15.0	20–1000	68–1832	14.0	25–350	77–662	0.93
Cr/Cr_2O_3	7.3	100–1000	212–1832	9.5	0–1000	32–1832	1.30
Cu/Cu_2O	4.3	20–750	68–1382	18.6	0–800	32–1473	4.32
Cu/CuO	9.3	20–600	68–1112	18.6	0–800	32–1473	2.0

Source: Ref 15

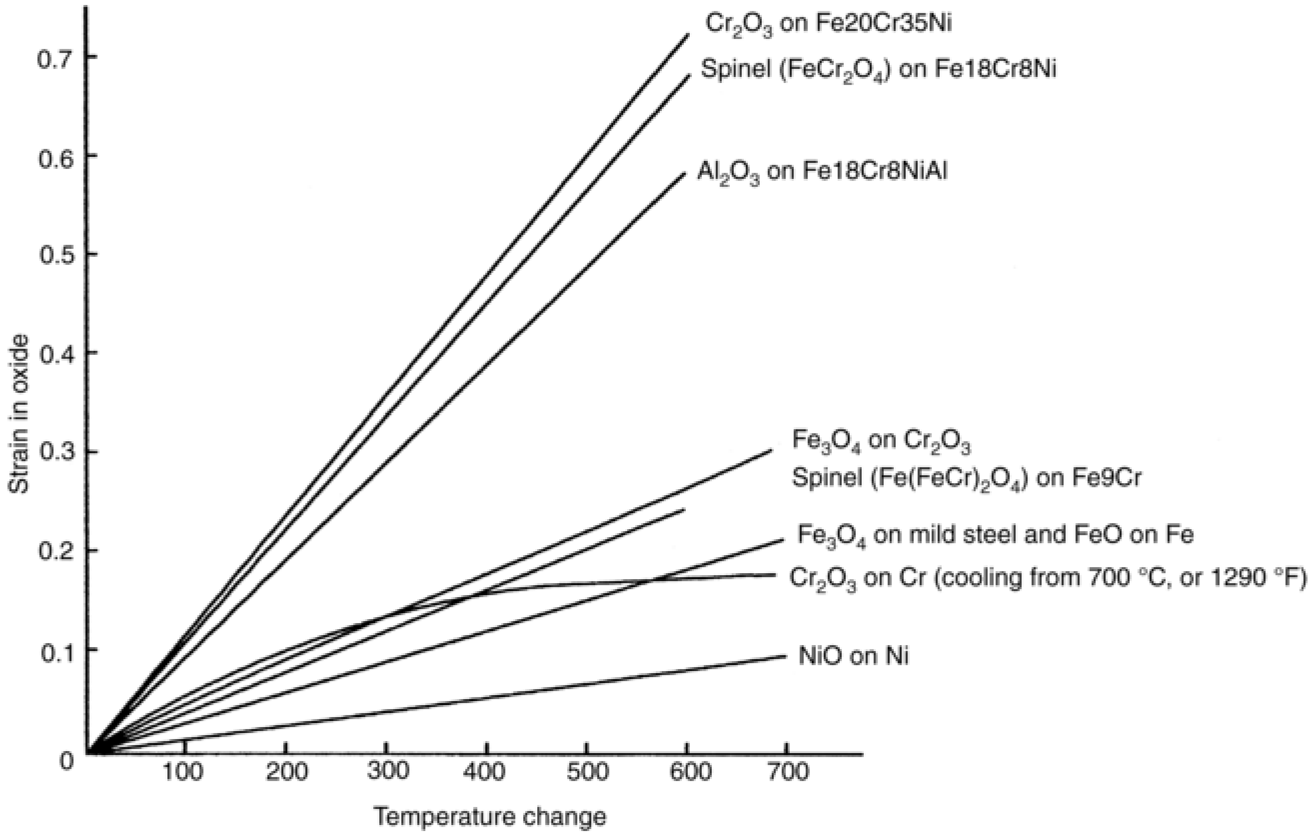

Fig. 27 Strains generated at the interface between various oxides and substrates by differential thermal expansion. Source: Ref 15

However, when metals and alloys are exposed in an oxidizing environment subjected to thermal changes, additional stresses impact on the high- temperature scale, which may alter its service life. If the sum of all these stresses reaches a critical value, the scales crack, detach, or spall, depending on the stress state (Ref 141) and the fracture toughness of the interface. The greater the disparity of coefficients of thermal expansion between the alloy and the oxide, the less adherent the oxide becomes during cooling, although other factors, such as fracture toughness of the interface, also can contribute to loss of adherence.

It is desirable that product scales, such as metal oxides or high-temperature coatings covering alloys that are subjected to stresses during thermal cycles, are resistant and adherent during these thermal cycles. It has been shown that degradation of an aluminized MAR-M-200 subjected to small, 2.8 °C (5 °F) rms wave, temperature variations at 1150 °C (2102 °F) suffered severe weight loss in 150 h (Ref 142). There have been several reviews on the effects of thermal cycling on high-temperature materials (Ref 143, 144, 145, 146, 147). Discussion of the mechanisms and testing methods for evaluating thermal cycling effects occurred during a recent workshop (Ref 143).

Thermal cycling of the test samples is preferred to simulate operations that exist in many high-temperature applications. The imposition of thermal cycling during oxidation or other gaseous reaction leads to enhanced metal-gas reaction rates due to scale failure from either decohesion or cracking and subsequent exposure of the newly bared alloy to the gaseous environment. Stresses related to thermal cycling increase the spallation of surface oxides, thereby increasing the propensity toward high-temperature corrosion. Thermal cycling can also lead to the growth and volume changes of the thermally grown oxide, leading to spallation of thermal barrier coatings (Ref 148). The effect of cycle frequency is highly dependent on the scale adherence to the substrate, the type of defect controlling spallation, the total test time, and probably, the test temperature. Water vapor and humidity may also alter the performance of alloy protective scale during prolonged cooling cycles away from the furnace; cold spalling may occur. Cycle frequency also affects how the cycling test is performed (Ref 149, 150, 151). A rapid temperature cycling (over 100 cycles/day) was developed to evaluate coated parts from 600 to 1000 °C (1112 to 1832 °F) in air, depending on the alloy substrate. This procedure was able to predict performance of these coated parts (Ref 152).

Computer programs have been developed to predict cyclic oxidation behavior of superalloys (weight change, amounts of retained and spalled oxide, total oxygen and metal consumed, and terminal rates of weight loss and metal consumption), based on models of oxidation-growth laws and input on spalling geometry, oxide phase, growth rate, spall constant, and cycle-duration parameters. This has provided success in some alloy systems, but such programs may not predict behavior in all systems (Ref 153, 154).

Table 13 lists the performance of several nickel-base and cobalt-base alloys in different corrosive environments (Ref 155). Exposure to dynamic oxidation generally causes accelerated corrosion or metal loss, as compared to static, isothermal oxidation tests. Depending on the composition of the alloy, the corrosion resistance may be superior in some environments but suffer severely in other high-temperature corrosive atmospheres.

Table 13 Corrosion of selected alloys in various high-temperature environments

Test	Temperature		Results for indicated UNS alloy								
	°C	**°F**	**S31008**	**N06601**	**N06625**	**N06690**	**N07214**	**N08120**	**R30556**	**N06230**	**R30188**
Static oxidation in air[(a)], average metal affected, mils	980	1800	1.1	1.3	0.7	…	0.2	3.7	1.1	0.7	0.6
	1090	2000	…	2.6	…	…	…	7.7	…	…	…
	1204	2200	10.3	7.5[(b)]	>47.6	…	0.7	…	>150	7.9	>21.7
Dynamic oxidation in air[(c)], average metal affected, mils	980	1800	16.5	20.0	7.6	…	1.2	…	6.2	3.5	4.2
Reducing sulfidation[(d)], maximum depth of attack, mils	871	1600	14	>21.7 perforated	…	…	…	…	35.6	…	23.6
Reducing sulfidation[(e)], maximum depth of attack, mils	593	1100	…	…	…	…	…	…	121	…	151
Hot corrosion[(f)], maximum metal affected, mils	675	1250	12	…	5	…	…	…	2.5	…	…
Hot corrosion[(g)], average corrosion rate, mils (maximum penetration, mils)	760	1400	13.0 (35)	…	…	2.8 (nil)	…	…	…	…	46.6 (9)
Chloridation[(h)], average metal affected, mils	900	1650	…	9.0	10.5	…	6.0	…	6.0	…	…
	1000	1830	…	…	…	…	…	…	11.8	…	…
Carburization[(i)], mg/cm^2 (depth in mils)	980	1800	7.7 (84.2)	…	…	…	…	0 (0)	1.0 (18.0)	0.4	0.5

Note: UNS, Unified Numbering System.

(a) Static oxidation in air; lab test for 1008 h, with specimens cycled to room temperature once every 168 h.

(b) Large internal voids not included for N06601 reading.

(c) Dynamic oxidation in air; lab test for 1000 h, with specimens cycled to room temperature once every 30 min.

(d) Ar, 5% H_2, 5% CO, 1% CO_2, 0.15% H_2S; $p_{O2} = 3 \times 10^{-19}$ atm; duration 500 h, except for 310 stainless steel, which was for 215 h.

(e) H_2, 46% CO, 0.8% CO_2, 1.7% H_2S at designated temperatures.

(f) Recuperator of aluminum remelting furnace flue gases. Mode of corrosion: combined attack by alkali sulfates, chlorides, with oxidation for 1150 h.

(g) Burner rig test with combustion products of No. 2 fuel oil (1.0% S); thermal shock frequency $\frac{11}{500}$h; corrodent urine.

(h) Ar + 20% O_2, 0.25% Cl_2 for 400 h at 1000 °C (1830 °F).

(i) Carburization resistance for 500 h in packed graphite. Source: Ref 155

Service Testing

Simulating the environment of an industrial process or application is a compromise in most situations. Most atmospheres consist of mixed oxidants of varying partial pressures (activities), temperature gradient profiles, and, in some cases, velocity and erosion parameters as well. Key application variables should be identified and care should be taken to see that these variables are suitably simulated in the service test. Characterization of gas composition is as essential as the control of temperature and gas flow rate. Atmosphere synthesis may require a stream of apparatuses consisting of such units as an inlet saturator, exhaust condensers, gas preheater beds, catalyst beds, heat shields, bubblers, mass flow meters, and analytical instrumentation. Corrosive gases, such as sulfur trioxide, will require corrosion-resistant materials of construction (Ref 9).

One standard wire-heater test is described by ASTM B 76, "Accelerated Life of Nickel-Chromium and Nickel-Chromium-Iron Alloys for Electrical Heating." The useful life of a material is determined by electrically heating a section of wire in air to a given temperature, where it is held for 2 min, followed by 2 min of cooling. This cycle is repeated until a 10% increase in electrical resistance is noted and reported as the useful life of the material. This testing can take approximately 1 week.

ASTM G 79, "Standard Practice for Evaluation of Metals Exposed to Carburization Environments," covers procedures for the identification and measurement of the extent of carburization in a metal sample and for the interpretation and evaluation of the effects of carburization. It applies mainly to iron- and nickel- base alloys for high-temperature applications. Four methods are described: method A, total mass gain; method B, metallographic evaluation; method C, carbon diffusion profile; and method D, change in mechanical properties.

Carburization testing in the field usually requires dedicating all or a portion of a particular piece of equipment for evaluating alloy performance or for evaluating the effect of process variables on the materials of construction (Ref 23). Such testing is performed to confirm laboratory data because of a lack of access to laboratory equipment or professional material expertise, or because of difficulty in duplicating certain carburization conditions in the laboratory. Atmospheres of low oxygen potential have proven difficult to duplicate in the laboratory. Direct simulation of ethylene furnaces is difficult in the laboratory because of the simultaneous interaction of long-term creep and high-temperature corrosion by carbonaceous atmospheres on the inner diameter and by oxidizing combustion gases on the outer diameter of the furnace tubes (Ref 23). A new carburization standard test method has been developed to generate carburization data for different materials under the same test parameters and procedures (Ref 156). This test method is conducted at 982 °C (1800 °F) for 96 h in H_2 containing 2% CH_4.

An excellent example of field testing in conjunction with laboratory testing to solve a heat- exchanger corrosion problem in an industrial chlorinated solvent incinerator is described in Ref 157. A corrosion rack containing three stainless steels, two high-nickel austenitic alloys, and three nickel-base alloys was placed within the gas hot stream of a heat exchanger containing HCl and chlorine. The in-situ test results were correlated with laboratory tests of the same alloys for this application.

Waste incinerator effluent streams contain halogen compounds arising principally from the burning of plastics and organic matter. A 10 year study of candidate alloy boiler tubes in several field test sites is described in Ref 158. Again, these field tests were confirmed by simulated laboratory test. Metallography and scanning electron microscopy were used to define the corrosion modes of this mixed-oxidant environment. Ultrasonic thickness-measuring equipment was used to follow the tube corrosion/ erosion rates at the field site. Tubes were periodically removed from service for laboratory evaluation. Test tracks have proven to be a valuable source of performance information on candidate materials in waste incinerator environments (Ref 3, 159).

References cited in this section

3. B. Mishra, Extractive Metallurgy, *Metals Handbook Desk Edition,* 2nd ed., ASM International, 1998, p 718

9. G.D. Smith, High Temperature, *Corrosion Tests and Standards—Application and Interpretation,* R. Baboian, Ed., American Society of Testing and Materials, 1995, p 149

15. A.S. Khanna, *Introduction to High-Temperature Oxidation and Corrosion,* ASM International, 2002, p 40–60, 172–201, 205–214

23. G.D. Smith, P. Ganesan, C.S. Tassen, and C. Conder, High Temperature Gases, *Corrosion Tests and Standards—Application and Interpretation,* R. Baboian, Ed., American Society of Testing and Materials, 1995, p 359

28. M. Shütze, Mechanical Properties of Oxide Scales, *Oxid. Met.,* Vol 44, 1995, p 29

37. G.Y. Lai, Nitridation of Several Combustor Alloys in a Simulated Gas Turbine Combustion Environment, *Advanced Materials and Coatings for Combustion Turbines,* V.P. Swaminathan and N.S. Cheruvu, Ed., ASM International, 1994, p 113–121

41. *Materials of Construction for Shipboard Waste Incinerators,* National Research Council, National Academy of Sciences, Washington, D.C., 1977, p 91–92

55. H. Lewis and R.A. Smith, Corrosion of High Temperature Nickel-Base Alloys by Sulfate-Chloride Mixtures, *First International Congress on Metallic Corrosion,* 10–15 April 1961, Butterworths, 1962, p 202

56. R.A. Rapp, Chemistry and Electrochemistry of Hot Corrosion of Metals, *Mater. Sci. Eng.,* Vol 87, 1987, p 319–327

62. R.A. Rapp, Hot Corrosion of Materials: A Fluxing Mechanism?, *Corros. Sci.,* Vol 44, 2002, p 209–221

63. G. Wacker and W.L. Wheatfall, *Corrosion Problems Associated with Shipboard Waste Incineration Systems,* 1976 Tri-Service Corrosion Conference, DoD Tri-Service Committee on Corrosion, 26–28 Oct 1976 (Philadelphia, PA), p 185

95. S.R.J. Saunders, Correlation Between Laboratory Corrosion Rig Testing and Service Experience, *Mater. Sci. Technol.,* Vol 2, 1986, p 282–289

96. A.K Gupta, J.P. Immarigeon, and P.C. Patnaik, A Review of Factors Controlling the Gas Turbine Hot Section Environment and Their Influence on Hot Salt Corrosion Test Methods, *High Temp. Technol.,* Vol 7 (No. 4), 1989, p 173–186

97. F.J. Kohl, C.A. Stearns, and G.C. Fryburg, The Role of NaCl in Flame Chemistry, in the Deposition Process, and Its Reaction with Protective Oxides, *Fourth U.S./U.K. Navy Conference on Gas Turbine Materials in a Marine Environment,* Vol 2, U.S. Naval Sea Command, Annapolis MD, 1979, p 565

98. F.J. Kohl, C.A. Stearns, and G.C. Fryburg, "Sodium Sulphate: Vaporization Thermodynamics and Reactions in Corrosive Flames," NASA-TM-X-71641, NASA Scientific and Technical Information Branch, Washington D.C., 1975

99. P. Steinmetz, C. Duret, and R. Morbioli, Laboratory Tests for Hot Corrosion Studies, *Mater. Sci. and Technol.,* Vol 2, 1986, p 262–271

100. M.A. Harper and L.R. Walker, "Chromium Depletion in High Temperature Alloys During Elevated Temperature Exposure," Paper 01154, Corrosion/2001, NACE International, 2001

101. W.L. Wheatfall, H. Doering, and G.J. Danek, Jr., Behavior of Superalloy Oxide Films in Molten Salts, *Hot Corrosion Problems Associated with Gas Turbine,* STP 421, ASTM, 1967, p 206

102. A.V. Dean, "Investigation into the Resistance of Various Nickel and Cobalt Base Alloys to Sea Salt Corrosion at Elevated Temperatures," National Gas Turbine Establishment Report, Royal Aircraft Establishment, Pyestock, Hants Jan 1964

103. H. Doering, Test Methods in Hot Corrosion, *1972 Conference Gas Turbine Materials,* Naval Ship Engineering Center, Naval Air Systems Command, Washington, D.C., 1972, p 143–151

104. M.A. DeCrescente and N.S. Bornstein, Formation and Reactivity Thermodynamics of Sodium Sulfate with Gas Turbine Alloys, *Corrosion,* Vol 24 (No. 5), May 1969, p 127

105. N.S. Bornstein, M.A. DeCrescente, and H.A. Roth, Accelerated Corrosion in Gas Turbine Engines, *1972 Conference Gas Turbine Materials,* Naval Ship Engineering Center, Naval Air Systems Command, Washington, D.C., 1972, p 3–16

106. T. Ishitsuka and K. Nose, Stability of Protective Oxide Films in Waste Incinerator Environment: Solubility Measurement of Oxides in Molten Chlorides, *Corros. Sci.,* Vol 44, 2002, p 247–263

107. C.O. Park and R.A. Rapp, Electrochemical Reactions in Molten Na_2SO_4 at 900 °C, *J. Electrochem. Soc.,* Vol 133, 1986, p 1636–1641

108. D.K. Gupta and R.A. Rapp, “The Solubilities of NiO, Co_3O_4, and Ternary Oxides in Fused Na_2SO_4 at 1200 °K, *J. Electrochem. Soc.,* Vol 127, 1980, p 2194

109. D.K. Gupta and R.A. Rapp, The Solubilities of NiO, Co_3O_4, and Ternary Oxides in Fused Na_2SO_4 at 1200 °K—Erratum, *J. Electrochem. Soc.,* Vol 127, 1980, p 2656

110. Y.S. Zhang and R.A. Rapp, Solubilities of α-Fe_2O_3 in Fused Na_2SO_4 at 1200 K, *J. Electrochem. Soc.,* Vol 132, 1985, p 734

111. Y.S. Zhang and R.A. Rapp, Solubilities of α-Fe_2O_3 and Fe_3O_4 in Fused Na_2SO_4 at 1200 K, *J. Electrochem. Soc.,* Vol 132, 1985, p 2498

112. Y.S. Zhang and R.A. Rapp, Solubilities of CeO_2, HfO_2, and Y_2O_3 in Fused Na_2SO_4- 30 mol% $NaVO_3$ and CeO_2 in Pure Na_2SO_4 at 900 °C, *Corrosion,* Vol 43 (No. 6), 1987, p 348

113. Y.S. Zhang, Solubilities of Cr_2O_3 in Fused Na_2SO_4 at 1200 K, *J. Electrochem. Soc.,* Vol 133, 1986, p 655

114. P.D. Jose, D.K. Gupta, and R.A. Rapp, Solubilities of α-Al_2O_3 in Fused Na_2SO_4 at 1200 K, *J. Electrochem. Soc.,* Vol 132, 1985, p 735

115. D.Z. Shi and R.A. Rapp, The Solubility of SiO_2 in Fused Na_2SO_4 at 900 °C, *J. Electrochem. Soc.,* Vol 133, 1986, p 849

116. R.A. Rapp and K.S. Goto, in *Proceedings of the Second International Symposium on Molten Salts,* J. Braunstein and J.R. Selman, Ed., PV-81-10, The Electrochemical Society, 1981, p 159

117. G.C. Booth and R.L. Clarke, Evaluation of Corrosion Resistance of Coated Superalloys in Rig Tests, *Mater. Sci. and Technol.,* Vol 2, March 1986, p 272

118. S.R.J. Saunders and J.R. Nicholls, Hot Corrosion Test Procedures and Coating Evaluation, *Thin Solid Films,* Vol 119, 1984, p 247

119. H.J. Grabke, Thermogravimetry, *Guidelines for Methods of Testing and Research in High Temperature Corrosion: Working Party Report,* H.J. Grabke and D.B. Meadowcroft, Ed., European Federation of Corrosion, 14, The Institute of Materials, 1995

120. C.J. Keattch and D. Dollimore, *An Introduction to Thermogravimetry,* 2nd ed., Heyden & Son, Ltd., 1975

121. H.J. Grabke, Definition and Preparation of Gas Atmospheres, *Guidelines for Methods of Testing and Research in High Temperature Corrosion: Working Party Report,* H.J. Grabke and D.B. Meadowcroft, Ed., European Federation of Corrosion, 14, The Institute of Materials, 1995, p 62–84

122. J.R. Nicholls, Discontinuous Measurement of High Temperature Corrosion, *Guidelines for Methods of Testing and Research in High Temperature Corrosion: Working Party Report,* H.J. Grabke and D.B. Meadowcroft, Ed., European Federation of Corrosion, 14, The Institute of Materials, 1995, p 11–36

123. J.L. McNaughton and C.T. Mortimer, Differential Scanning Calorimetry, *IRS; Physical Chemistry Series 2,* Vol 10, Butterworths, 1975

124. G.J. Danek, Jr., State-of-the-Art Survey on Hot Corrosion in Marine Gas Turbine Engines, *Nav. Eng. J.,* Vol 77, Dec 1965, p 859

125. "Hot Corrosion Problems Associated with Gas Turbines," from Symposium at 69th Annual Meeting ASTM, 26 June to 1 July 1966 (Atlantic City, NJ), Special Publication 421, ASTM, Sept 1967

126. N.S. Bornstein and M.A. DeCrescente, "Sulfidation in Gas Marine Engines," Paper 165, Corrosion/75, NACE International, 1975

127. J.R. Nicholls and S.R.J. Saunders, *Guidelines for Hot Salt Corrosion Burner Rig Tests,* Versailles Agreement on Advanced Materials and Standards (VAMAS), National Physical Laboratory, England, 1988

128. P. Hancock, The Use of Laboratory and Rig Tests to Simulate Gas Turbine Corrosion Problems, *Corros. Sci.,* Vol 22, 1982, p 51–65

129. S.R.J. Saunders, M.K. Hossain, and J.M. Ferguson, *Proceedings of the Conference on High Temperature Alloys in Gas Turbines,* (Liège, Belgium), Centre de Recherches Métallurgiques, Oct 1982, p 177

130. K.L. Luthra, Simulation of Gas Turbine Environments in Small Burner Rigs, *High Temp. Technol.,* Vol 7, 1989, p 187–192

131. D.J. Wortman, R.E. Fryxell, K.L. Luthra, and P. Bergman, Mechanisms of Low Temperature Hot Corrosion: Burner Rig Studies, *Proceedings of the Fourth U.S./U.K. Navy Conference on Gas Turbine Materials in a Marine Environment,* Vol 1, U.S. Naval SEA Command, 1979, p 379

132. W.L. Wheatfall and R.C. Schwab, "Hot- Corrosion Behavior of Several Newly Developed Nickel-Base Superalloys—A Preliminary Study," Naval Ship Research and Development Center Report 3199, Feb 1970

133. G.Y. Lai, J.J. Barnes, and J.E. Barnes, "A Burner Rig Investigation of the Hot Corrosion Behavior of Several Wrought Superalloys and Intermetallics," 91-GT-21, International Gas Turbine and Aeroengine Congress, American Society of Mechanical Engineers, 1991

134. D.A. Shifler, "Effects of Fuel Dye on the Hot Corrosion Resistance of Marine Gas Turbine Materials," Paper 167, Corrosion/ 2001, NACE International, 2001

135. D.A. Shifler, The Influence of Fuel Carbon Residue on Hot Corrosion, *Proceedings 2002 Tri-Service Corrosion Conference,* 14–18 Jan 2002 (San Antonio, TX), Department of Defense Tri-Service Corrosion Committee

136. J.R. Nicholls and S.R.J. Saunders, Comparison of Hot-Salt Corrosion Behaviour of Superalloys in High and Low Velocity Burner Rigs, *High Temp. Technol.,* Vol 7, 1989, p 193–201

137. “Military Specification Fuel, Naval Distillate,” MIL-F-16884J, 31 May 1995

138. P. Hancock and J.R. Nicholls, *Proceedings of the Fourth Conference on Gas Turbine Materials in a Marine Environment,* Naval Sea Systems Command, Washington, D.C., June 1979, p 403–422

139. D.J. Stephenson, J.R. Nicholls, and P. Hancock, The Erosion of Gas Turbine Blade Materials by Solid Sea Salt, *Corros. Sci.,* Vol 25, 1985, p 1181–1192

140. R.D. Kane, High Temperature and High Pressure, *Corrosion Tests and Standards— Application and Interpretation,* R. Baboian, Ed., American Society of Testing and Materials, 1995, p 106

141. M. Schütze, Mechanical Interactions in Oxide Scales, *Proceedings on High Temperature Corrosion and Materials Chemistry,* P.Y. Hou, M.J. McNallan, R. Oltra, E.J. Opila, and D.A. Shores, Ed., PV 98- 9, The Electrochemical Society, 1998, p 3

142. R.R. Dils and P.S. Follansbee, Dynamic Oxidation and Corrosion in Power Generating Units, *Corrosion,* Vol 33 (No. 11), 1977, p 385

143. P. Hancock and R.C. Hurst, in *Advances in Corrosion Science and Technology,* Vol 4, Plenum Press, 1974, p 1–84

144. D.J. Baxter and K. Natesan, *Rev. High- Temp. Mater.,* Vol 5 (No. 3/4) 1983, p 149–250

145. J. Stringer, Stress Generation and Relief in Growing Oxide Films, *Corros. Sci.,* Vol 10, 1970, p 513–543

146. R. Mevrel, Cyclic Oxidation of High Temperature Alloys, *Mater. Sci. Technol.,* Vol 3, 1987, p 531

147. M. Schütze and E.J. Quadakkers, Ed., *Cyclic Oxidation of High Temperature Materials: Mechanisms, Testing Methods, Characterization, and Life Time Estimation,* proceedings of a European Federation of Corrosion workshop, (Frankfurt/Main), EPC 27, IOM Communications Ltd., 1999

148. R. Anton, S.K. Jha, D. Clemens, W. Mallener, L. Singheiser, and W.J. Quadakkers, Thermal Cycling Testing of Thermal Barrier Coatings, *Cyclic Oxidation of High Temperature Materials,* proceedings of a European Federation of Corrosion Workshop, EPC 27, M. Schütze and W.J. Quadakkers, Ed., IOM Communications Ltd., 1999, p 339–356

149. B.A. Pint, P.F. Tortorelli, and I.G. Wright, Effect of Cycle Frequency on High Temperature Oxidation Behaviour of Alumina- and Chromia-Forming Alloys, *Cyclic Oxidation of High Temperature Materials,* proceedings of a European Federation of Corrosion workshop, EPC 27, M. Schütze and W.J. Quadakkers, Ed., IOM Communications Ltd., 1999, p 111–132

150. B.A. Pint, P.F. Tortorelli, and I.G. Wright, Effect of Cycle Frequency on High Temperature Oxidation Behaviour of Alumina- Forming Alloys, *Oxid. Met.,* Vol 58, 2002, p 73–102

151. G.M. Kim, N.M. Yanar, E.N. Hewitt, F.S. Pettit, and G.H. Meier, The Effect of the Type of Thermal Exposure on the Durability of Thermal Barrier Coatings, *Scr. Mater.,* Vol 46, 2002, p 489

152. A.L. Cabrera and J.F. Kirner, A Rapid- Temperature-Cycling Apparatus for Oxidation Testing, *Oxid. Met.,* Vol 35, 1991, p 471–479

153. J.L. Smialek, J.A. Nesbitt, C.A. Barrett, and C.E. Lowell, Cyclic Oxidation Testing and Modelling: A NASA Lewis Perspective, *Cyclic Oxidation of High Temperature Materials,* proceedings of a European Federation of Corrosion workshop, EPC 27, M. Schütze and W.J. Quadakkers, Ed., IOM Communications Ltd., 1999, p 148–168

154. J.L. Smialek and J.V. Auping, COSP for Windows—Strategies for Rapid Analyses of Cyclic-Oxidation Behavior, *Oxid. Met.,* Vol 57, 2002, p 559–581

155. "High Temperature Product Literature" and "Hastelloy Corrosion-Resistant Alloy Product Literature," Haynes International, 1991–1996

156. G. Lai, B. Li, B. Gleeson, and H.L. Craig, "Proposed Standard Carburization Test Method," Paper 03473, Corrosion/2003, NACE International, 2003

157. B.A. Baker, Heat Exchanger Corrosion in a Chlorinated Solvent Incinerator, *Handbook of Case Histories in Failure Analysis,* ASM International, 1992, p 118–123

158. J.A. Harris, W.G. Lipscomb, and G.D. Smith, "Field Experience of High Nickel Containing Alloys in Waste Incinerators," Paper 402, Corrosion/87, NACE International, 1987

159. G.D. Smith and C.S. Tassen, Performance of Alloys 825 and 625 in Waste Incinerator Environments, *Mater. Perform.,* Vol 28 (No. 12), 1989, p 41–43

160. R.J.H. Wanhill, A.J.A. Mom, H.J.C. Hersbach, G.A. Kool, and J.A.M. Boogers, NLR Experience with High Velocity Burner Rig Testing 1979–1989, *High Temp. Technol.,* Vol 7, 1989, p 201–211

161. G.C. Booth, J.C. Galsworthy, and A.F. Taylor, Low and High Pressure Rig Testing of Materials and Coatings, *Proceedings of the 4th Conference on Gas Turbine Materials in a Marine Environment,* Naval Sea Systems Command, Vol 1, June 1979, p 259–272

D.A. Shifler, High-Temperature Gaseous Corrosion Testing, *Corrosion: Fundamentals, Testing, and Protection,* Vol 13A*, ASM Handbook,* ASM International, 2003, p 650–681

High-Temperature Gaseous Corrosion Testing

David A. Shifler, Naval Surface Warfare Center

References

1. J.W. Spence, S.D. Cramer, and F.H. Haynie, Planning and Design of Tests, *Corrosion Tests and Standards—Application and Interpretation,* R. Baboian, Ed., American Society of Testing and Materials, 1995, p 33

2. N. Birks and G.H. Meier, *Introduction to High Temperature of Metals,* Edward Arnold, London 1983

3. B. Mishra, Extractive Metallurgy, *Metals Handbook Desk Edition,* 2nd ed., ASM International, 1998, p 718

4. G.Y. Lai, Corrosion by Halogens, *High Temperature Corrosion of Engineering Metals,* ASM International, 1990, p 85–115

5. W.J. Moore, *Physical Chemistry,* 4th ed., Prentice-Hall, 1972, p 99–101

6. S.A. Bradford, Fundamentals of Corrosion in Gases, *Corrosion,* Vol 13, *Metals Handbook,* 9th ed., ASM International, 1987, p 61–76

7. G.W. Castellan, *Physical Chemistry,* 2nd ed., Addison-Wesley, 1971, p 257–258

8. L.L. Sheir and G.T. Burstein, *Corrosion: Corrosion Control,* Vol 2, 3rd ed., L.L. Sheir, J.A. Jarman, and G.T. Burstein, Ed., Butterworth-Heinemann, 1994, p 20:65–20:66

9. G.D. Smith, High Temperature, *Corrosion Tests and Standards—Application and Interpretation,* R. Baboian, Ed., American Society of Testing and Materials, 1995, p 149

10. L.R. Scharfstein and M. Henthrone, Testing at High Temperatures, *Handbook on Corrosion Testing and Evaluation,* W.H. Ailor, Ed., John Wiley & Sons, 1971, p 291–366

11. C. Wagner, Types of Reaction in the Oxidation of Alloys, *Z. Elektroch.,* Vol 63, 1959, p 772–782

12. M.G. Fontana, *Corrosion Engineering,* 3rd ed., McGraw-Hill, 1986, p 505–520

13. I.G. Wright, High Temperature Corrosion, *Corrosion,* Vol 13, *Metals Handbook,* 9th ed., ASM International, 1987, p 97–103

14. R.E. Reed-Hill and R. Abbaschian, *Physical Metallurgy Principles,* 3rd ed., PWS- Kent Publishing, 1992, p 360–420

15. A.S. Khanna, *Introduction to High-Temperature Oxidation and Corrosion,* ASM International, 2002, p 40–60, 172–201, 205–214

16. K. Wu, Y. Wang, and J.E. Morral, Predicting Interdiffusion Microstructure Using the Phase Field Approach, *Elevated Temperature Coatings: Science and Technology IV,* N.B. Dahotre, J.M. Hampikian, and J.E. Morral, Ed., The Minerals, Metals and Materials Society, 2001, p 133

17. E. Basuki, A. Crosky, and B. Gleeson, Interdiffusion Behaviour in Aluminide- Coated René 80H at 1150 °C, *Mater. Sci. Eng. A,* Vol 224, 1997, p 27–32

18. L. Onsager, Reciprocal Relations in Irreversible Processes, Part I, *Phys. Rev.,* Vol 37, 1931, p 405–426; Reciprocal Relations in Irreversible Processes, Part II, *Phys. Rev.,* Vol 38, 1931, p 2265–2279

19. A. Sanz, L. Llanes, J.P. Bernadou, M. Anglada, and M.B. Rapaccini, Influence of the Stress State on the Diffusion Phenomena Across the Interface Between a Protective Coating and a Single Crystal Superalloy, *Elevated Temperature Coatings: Science and Technology II,* N.B. Dahotre and J.M. Hampikian, Ed., The Minerals, Metals and Materials Society, 1996, p 373

20. D.J. Young and B. Gleeson, Alloy Phase Transformations Driven by High Temperature Corrosion Processes, *Corros. Sci.,* Vol 44, 2002, p 345–357

21. J.-G. Duh and J.-W. Lee, Diffusion-Related Kinetics in the Oxidation-Induced Phase Transformation of Fe-9Al-3Cr- 31Mn Alloys, *J. Electrochem. Soc.,* Vol 136, 1989, p 847–853

22. D.A. Jones, *Principles and Prevention of Corrosion,* 2nd ed., McGraw-Hill, 1996, p 412–415

23. G.D. Smith, P. Ganesan, C.S. Tassen, and C. Conder, High Temperature Gases, *Corrosion Tests and Standards—Application and Interpretation,* R. Baboian, Ed., American Society of Testing and Materials, 1995, p 359

24. "Practice for Simple Oxidation Testing," G 54, ASTM International

25. I. Miller and J.E. Freund, *Probability and Statistics for Engineers,* 3rd ed., Prentice- Hall, 1985, p 188

26. J.R. Nicholls and P. Hancock, The Analysis of Oxidation and Hot Corrosion Data— A Statistical Approach, *High Temperature Corrosion,* NACE-6, R.A. Rapp, Ed., NACE International, 1983, p 198–210

27. D.P. Whittle and J. Stringer, *Philos. Trans. R. Soc.* (*London*) *A,* Vol 295, 1980, p 309

28. M. Shütze, Mechanical Properties of Oxide Scales, *Oxid. Met.,* Vol 44, 1995, p 29

29. R.A. Smith, Nickel and Its Alloys: Carburization and Attack by Carbon-Containing Gases, *Corrosion,* 2nd ed, L.L. Sheir, Ed., Newes-Butterworths, 1976, p 7:101

30. H.J. Grabke, *Carburization: A High Temperature Corrosion Phenomenon,* MTI 52, Materials Technology Institute of the Chemical Process Industries, Inc., 1998

31. W.B. Hoyt and R.H. Caughey, High Temperature Metal Deterioration in Atmospheres Containing Carbon-Monoxide and Hydrogen, *Corrosion,* Vol 15, 1959, p 627t

32. P.A. Lefrancois and W.B. Hoyt, Chemical Thermodynamics of High Temperature Reactions in Metal Dusting Corrosion, *Corrosion,* Vol 19, 1963, p 360t

33. H.J. Grabke, Metal Dusting of Low- and High-Alloy Steels, *Corrosion,* Vol 51 (No. 9), 1995, p 711

34. H.J. Grabke, E.M. Müller-Lorenz, B. Eltester, and M. Lucas, Formation of Chromium Rich Oxide Scales for Protection Against Metal Dusting, *Mater. High Temp.,* Vol 17 (No. 2), 2000, p 339

35. M. Maier, J.F. Norton, and P. Puschek, A Study of the Factors Contributing to the Metal Dusting of Fe-Cr-Ni Alloys in Highly Carburizing Atmospheres, *Mater. High Temp.,* Vol 17 (No. 2), 2000, p 347

36. K.M. Verma, H. Ghosh, and J.S. Rai, Behaviour of Materials of Construction During Cracking of Ammonia at 600 °C, *Br. Corros. J.,* Vol 13 (No. 4), 1978, p 173–176

37. G.Y. Lai, Nitridation of Several Combustor Alloys in a Simulated Gas Turbine Combustion Environment, *Advanced Materials and Coatings for Combustion Turbines,* V.P. Swaminathan and N.S. Cheruvu, Ed., ASM International, 1994, p 113–121

38. S. Mrowec, The Problem of Sulfur in High-Temperature Corrosion, *Oxid. Met.,* Vol 44, 1995, p 177

39. R.A. Smith, Nickel and Its Alloys: Sulphidation, *Corrosion,* 2nd ed., L.L. Sheir, Ed., Newes-Butterworths, 1976, p 7:90

40. F.H. Stott, G.C. Wood, and J. Stringer, Influence of Alloying Elements on the Development of Protective Scales, *Oxid. Met.,* Vol 44, 1995, p 113

41. *Materials of Construction for Shipboard Waste Incinerators,* National Research Council, National Academy of Sciences, Washington, D.C., 1977, p 91–92

42. K.N. Strafford and P.K. Datta, Design of Sulphidation Resistant Alloys, *Mater. Sci. Technol.,* Vol 5, Aug 1989, p 765

43. A.U. Seybolt, P.A. Bergman, and M. Kaufman, “Hot Corrosion Mechanism Study, Phase II,” Final report under contract N600 (61533) 65595, MEL 2591, Assignment 87-122, prepared for Naval Ship Research and Development Center, Annapolis, MD, 30 June 1966 to 31 Oct 1967

44. S.R.J. Saunders, Corrosion in the Presence of Melts and Solids, *Guidelines for Methods of Testing and Research in High Temperature Corrosion: Working Party Report,* H.J. Grabke and D.B. Meadowcroft, Ed., European Federation of Corrosion, 14, The Institute of Materials, 1995, p 85–103

45. E.L. Simons, G.V. Browning and H.A. Liebhafsky, Sodium Sulfate in Gas Turbines, *Corrosion,* Vol 11 (No. 12), 1955, p 505t

46. R.K. Ahluwalia and K.H. Im, Aspects of Mass Transfer and Dissolution Kinetics of Hot Corrosion Induced by Sodium Sulphate, *J. Inst. Energy,* Vol 64 (No. 461), 1991, p 186

47. J.A. Goebel and F.S. Pettit, Na_2SO_4-Induced Accelerated Oxidation (Hot Corrosion) of Nickel, *Metall. Trans.,* Vol 1 (No. 7), 1970, p 1943

48. N.S. Bornstein and M.A. DeCrescente, The Relationship Between Compounds of Sodium and Sulfur and Sulfidation, *Trans. Metall. Soc. (AIME),* Vol 245 (No. 9), 1969, p 1947–1954

49. N.S. Bornstein and M.A. DeCrescente, The Role of Sodium in the Accelerated Oxidation Phenomenon Termed Sulfidation, *Metall. Trans.,* Vol 2 (No. 10), 1971, p 2875

50. J.F. Condé and B.A. Wareham, *Proceedings: Gas Turbine Materials in the Marine Environment Conference,* MCIC-75-27, 1974, p 73

51. D.A. Shores, D.W. McKee, and H.S. Spacil, *Proceedings: Properties of High Temperature Alloys with Emphasis on Environmental Effects,* PV 77-1, Z.A. Foroulis and F.S. Pettit, Ed., The Electrochemical Society, 1976, p 649

52. J.A. Goebel, F.S. Pettit, and G.W. Goward, Mechanisms for the Hot Corrosion of Nickel-Base Alloys, *Metall. Trans.,* Vol 4, 1973, p 261–278

53. K.L. Luthra and D.A. Shores, Mechanisms of Na_2SO_4 Induced Corrosion at 600–900 °C, *J. Electrochem. Soc.,* Vol 127, 1980, p 2202

54. K.T. Chiang, F.S. Pettit, and G.H. Meier, Low Temperature Corrosion, *High Temperature Corrosion,* NACE-6, R.A. Rapp, Ed., NACE International, 1983, p 519

55. H. Lewis and R.A. Smith, Corrosion of High Temperature Nickel-Base Alloys by Sulfate-Chloride Mixtures, *First International Congress on Metallic Corrosion,* 10–15 April 1961, Butterworths, 1962, p 202

56. R.A. Rapp, Chemistry and Electrochemistry of Hot Corrosion of Metals, *Mater. Sci. Eng.,* Vol 87, 1987, p 319–327

57. R.L. Jones, Low-Quality Fuel Problems with Advanced Engine Materials, *High Temp. Technol.,* Vol 6, 1988, p 187; NRL Memorandum Report 6252, 9 Aug 1988

58. R.L. Jones, C.E. Williams, and S.R. Jones, Reaction of Vanadium Compounds with Ceramic Oxides, *J. Electrochem. Soc.,* Vol 133, 1986, p 227–230

59. R.L. Jones and R.F. Reidy, Development of Hot Corrosion Resistant Scandia-Stabilized Zirconia Thermal Barrier Coatings, *Proceedings of Elevated Temperature Coatings: Science and Technology I,* N.B. Dahotre, J.M. Hampikian, and J.J. Stiglich, Ed., The Minerals, Metals and Materials Society, 1995, p 23

60. R.L. Jones, Oxide Acid-Base Reactions in Ceramic Corrosion, *High Temp. Sci.,* Vol 27, 1990, p 369–380

61. R.L. Jones, “Vanadate-Sulfate Melt Thermochemistry Relating to Hot Corrosion of Thermal Barrier Coatings,” NRL/MR/ 6170-97-8103, Naval Research Laboratory, 30 Oct 1997

62. R.A. Rapp, Hot Corrosion of Materials: A Fluxing Mechanism?, *Corros. Sci.,* Vol 44, 2002, p 209–221

63. G. Wacker and W.L. Wheatfall, *Corrosion Problems Associated with Shipboard Waste Incineration Systems,* 1976 Tri-Service Corrosion Conference, DoD Tri-Service Committee on Corrosion, 26–28 Oct 1976 (Philadelphia, PA), p 185

64. P. Elliott, Materials Performance in High- Temperature Waste Combustion Systems, *Mater. Perform.,* Vol 32, 1993, p 82

65. S.C. Singhal and R.J. Bratton, Stability of a $ZrO_2(Y_2O_3)$ Thermal Barrier Coating in Turbine Fuel with Contaminants, *J. Eng. Power (Trans. ASME),* Vol 102 (No. 10), 1980, p 770–775

66. D.W. McGee, K.L. Luthra, P. Siemers, and J.E. Palko, *Proceeding of the First Conference on Advanced Materials for Alternative Fuel Capable Directly Fired Heat Engines,* J.W. Fairbanks and J. Stringer, Ed., CONF-790749, National Technical Information Service, 1979, p 258

67. P. Ganesan, G.D. Smith, and L.E. Shoemaker, “The Effects of Excursions of Oxygen and Water Vapor Contents on Nickel- Containing Alloy Performance in a Waste Incineration Environment,” Paper 248, Corrosion/91, NACE International, 1991

68. H.H. Krause, High Temperature Corrosion Problems in Waste Incineration Systems, *J. Mater. Energy Syst.,* Vol 7, 1986, p 322

69. G.D. Smith, P. Ganesan, and L.E. Shoemaker, “The Effect of Environmental Excursions within the Waste Incinerator on Nickel-Containing Alloy Performance,” Paper 280, Corrosion/90, NACE International, 1990

70. C.T. Wall, J.T. Groves, and E.J. Roberts, How to Burn Salty Sludges, *Chem. Eng.,* Vol 7, 14 April 1975

71. F. Wilkes and D.A. Shifler, “Historical Perspectives of Intergranular Corrosion of Boiler Metal by Water,” Paper 44, Corrosion/93, NACE International, 1993

72. B. Craig, Hydrogen Damage, *Corrosion,* Vol 13, *Metals Handbook,* 9th ed., ASM International, 1987, p 169

73. R.M. Davison, T. Debold, and M.J. Johnson, Corrosion of Stainless Steels, *Corrosion,* Vol 13, *Metals Handbook,* 9th ed., ASM International, 1987, p 559

74. R.A. Smith and S.R.J. Saunders, *Corrosion,* 3rd ed., L.L. Sheir, R.A. Jarman, and G.T. Burstein, Ed., Butterworth-Heinemann, 1994, p 7:136

75. M.G. Fontana and N.D. Greene, *Corrosion Engineering,* 2nd ed., McGraw-Hill, 1978, p 294

76. M.H. Kamdur, Liquid Metal Embrittlement, *Corrosion,* Vol 13, *Metals Handbook,* 9th ed., ASM International, 1987, p 171

77. E.F. Bradley, Ed., *Superalloys—A Technical Guide,* ASM International, 1988

78. W.T. Reid, *External Corrosion and Deposits—Boilers and Gas Turbines,* Elsevier, 1971

79. S.T. Wlodek, The Stability of Superalloys, *Proceedings on Long Term Stability of High Temperature Materials,* G.E. Fuchs, K.A. Dannemann, and T.C. Deragon, The Mineral, Metals and Materials Society, 1999, p 3

80. D.L. Douglass, Exfoliation and Mechanical Behavior of Scales, *Oxidation of Metals and Alloys,* ASM International, 1971, p 137–156

81. R.E. Reed-Hill and R. Abbaschian, Thermally Activated Plastic Deformation, *Physical Metallurgy Principles,* 3rd ed., PWS-Kent Publishing, 1992, p 836–899

82. J.R. Nicholls, Laboratory Studies of Erosion-Corrosion Processes Under Oxidizing and Oxidizing/Sulphidizing Conditions, *Mater. High Temp.,* Vol 14, 1997, p 289–306

83. S. Hogmark, S. Jacobson, and O. Vingsbo, Surface Damage, *Friction, Lubrication, and Wear Technology,* Vol 18, *ASM Handbook,* ASM International, 1992, p 176–292

84. F.H. Stott, Corrosion and Wear or Erosion, *Guidelines for Methods of Testing and Research in High Temperature Corrosion: Working Party Report,* H.J. Grabke and D.B. Meadowcroft, Ed., European Federation of Corrosion, 14, The Institute of Materials, 1995, p 85–103

85. G.W. Goward, Protective Coatings—Purpose, Role, and Design, *Mater. Sci. Technol.,* Vol 2, 1986, p 194–200

86. R. Streiff, Aluminides: Yesterday's and Tomorrow's Coatings for Materials in Aggressive Environments, *Elevated Temperature Coatings: Science and Technology II,* N.B. Dahotre and J.M. Hampikian, Ed., The Minerals, Metals and Materials Society, 1996, p 407

87. G.W. Goward, Protective Coatings for High Temperature Alloys: State of Technology, *Proceedings of the Symposium on Properties of High Temperature Alloys,* Z.A. Foroulis and F.S. Pettit, Ed., PV 77- 1, The Electrochemical Society, 1976, p 806

88. P.K. Wright and A.G. Evans, Mechanism Governing the Performance of Thermal Barrier Coatings, *Curr. Opin. Solid State Mater. Sci.,* Vol 4, 1999, p 255–265

89. M.J. Stiger, N.M. Yanar, F.S. Pettit, and G.H. Meier, Mechanism of Failure of EB- PVD Thermal Barrier Coating Induced by High Temperature Oxidation, *Elevated Temperature Coatings: Science and Technology III,* J.M. Hampikian and N.B. Dahotre, Ed., TMS, 1999, p 51

90. S. Bose and J. DeMasi-Marcin, *Thermal Barrier Coating Experience in Gas Turbine Engines at Pratt & Whitney,* Thermal Barrier Coating Workshop, NASA CP 3312, National Aeronautics Space Administration, 1995, p 63

91. *Handbook of Refractory Practice,* 1st ed., Harbison-Walker/Indresco Inc, 1992, p PR-12

92. D.J. Baxter, *Oxidation/Corrosion of Advanced Ceramics: A Review of the Progress Towards Test Method Standardization, Working Party Report,* H.J. Grabke and D.B. Meadowcroft, Ed., European Federation of Corrosion, 14, The Institute of Materials, 1995, p 136–146

93. S. Schneider, Ed., *International Survey on the Classification of Advanced Ceramics,* VAMAS Report 5, ISSN 1016-2186, Versailles Agreement on Advanced Materials and Standards, 1991

94. R.A. McCauley, *Corrosion of Ceramics,* Marcel Dekker, 1995, p 109–128

95. S.R.J. Saunders, Correlation Between Laboratory Corrosion Rig Testing and Service Experience, *Mater. Sci. Technol.,* Vol 2, 1986, p 282–289

96. A.K Gupta, J.P. Immarigeon, and P.C. Patnaik, A Review of Factors Controlling the Gas Turbine Hot Section Environment and Their Influence on Hot Salt Corrosion Test Methods, *High Temp. Technol.,* Vol 7 (No. 4), 1989, p 173–186

97. F.J. Kohl, C.A. Stearns, and G.C. Fryburg, The Role of NaCl in Flame Chemistry, in the Deposition Process, and Its Reaction with Protective Oxides, *Fourth U.S./U.K. Navy Conference on Gas Turbine Materials in a Marine Environment,* Vol 2, U.S. Naval Sea Command, Annapolis MD, 1979, p 565

98. F.J. Kohl, C.A. Stearns, and G.C. Fryburg, "Sodium Sulphate: Vaporization Thermodynamics and Reactions in Corrosive Flames," NASA-TM-X-71641, NASA Scientific and Technical Information Branch, Washington D.C., 1975

99. P. Steinmetz, C. Duret, and R. Morbioli, Laboratory Tests for Hot Corrosion Studies, *Mater. Sci. and Technol.,* Vol 2, 1986, p 262–271

100. M.A. Harper and L.R. Walker, "Chromium Depletion in High Temperature Alloys During Elevated Temperature Exposure," Paper 01154, Corrosion/2001, NACE International, 2001

101. W.L. Wheatfall, H. Doering, and G.J. Danek, Jr., Behavior of Superalloy Oxide Films in Molten Salts, *Hot Corrosion Problems Associated with Gas Turbine,* STP 421, ASTM, 1967, p 206

102. A.V. Dean, "Investigation into the Resistance of Various Nickel and Cobalt Base Alloys to Sea Salt Corrosion at Elevated Temperatures," National Gas Turbine Establishment Report, Royal Aircraft Establishment, Pyestock, Hants Jan 1964

103. H. Doering, Test Methods in Hot Corrosion, *1972 Conference Gas Turbine Materials,* Naval Ship Engineering Center, Naval Air Systems Command, Washington, D.C., 1972, p 143–151

104. M.A. DeCrescente and N.S. Bornstein, Formation and Reactivity Thermodynamics of Sodium Sulfate with Gas Turbine Alloys, *Corrosion,* Vol 24 (No. 5), May 1969, p 127

105. N.S. Bornstein, M.A. DeCrescente, and H.A. Roth, Accelerated Corrosion in Gas Turbine Engines, *1972 Conference Gas Turbine Materials,* Naval Ship Engineering Center, Naval Air Systems Command, Washington, D.C., 1972, p 3–16

106. T. Ishitsuka and K. Nose, Stability of Protective Oxide Films in Waste Incinerator Environment: Solubility Measurement of Oxides in Molten Chlorides, *Corros. Sci.,* Vol 44, 2002, p 247–263

107. C.O. Park and R.A. Rapp, Electrochemical Reactions in Molten Na_2SO_4 at 900 °C, *J. Electrochem. Soc.,* Vol 133, 1986, p 1636–1641

108. D.K. Gupta and R.A. Rapp, “The Solubilities of NiO, Co_3O_4, and Ternary Oxides in Fused Na_2SO_4 at 1200 °K, *J. Electrochem. Soc.,* Vol 127, 1980, p 2194

109. D.K. Gupta and R.A. Rapp, The Solubilities of NiO, Co_3O_4, and Ternary Oxides in Fused Na_2SO_4 at 1200 °K—Erratum, *J. Electrochem. Soc.,* Vol 127, 1980, p 2656

110. Y.S. Zhang and R.A. Rapp, Solubilities of α-Fe_2O_3 in Fused Na_2SO_4 at 1200 K, *J. Electrochem. Soc.,* Vol 132, 1985, p 734

111. Y.S. Zhang and R.A. Rapp, Solubilities of α-Fe_2O_3 and Fe_3O_4 in Fused Na_2SO_4 at 1200 K, *J. Electrochem. Soc.,* Vol 132, 1985, p 2498

112. Y.S. Zhang and R.A. Rapp, Solubilities of CeO_2, HfO_2, and Y_2O_3 in Fused Na_2SO_4- 30 mol% $NaVO_3$ and CeO_2 in Pure Na_2SO_4 at 900 °C, *Corrosion,* Vol 43 (No. 6), 1987, p 348

113. Y.S. Zhang, Solubilities of Cr_2O_3 in Fused Na_2SO_4 at 1200 K, *J. Electrochem. Soc.,* Vol 133, 1986, p 655

114. P.D. Jose, D.K. Gupta, and R.A. Rapp, Solubilities of α-Al_2O_3 in Fused Na_2SO_4 at 1200 K, *J. Electrochem. Soc.,* Vol 132, 1985, p 735

115. D.Z. Shi and R.A. Rapp, The Solubility of SiO_2 in Fused Na_2SO_4 at 900 °C, *J. Electrochem. Soc.,* Vol 133, 1986, p 849

116. R.A. Rapp and K.S. Goto, in *Proceedings of the Second International Symposium on Molten Salts,* J. Braunstein and J.R. Selman, Ed., PV-81-10, The Electrochemical Society, 1981, p 159

117. G.C. Booth and R.L. Clarke, Evaluation of Corrosion Resistance of Coated Superalloys in Rig Tests, *Mater. Sci. and Technol.,* Vol 2, March 1986, p 272

118. S.R.J. Saunders and J.R. Nicholls, Hot Corrosion Test Procedures and Coating Evaluation, *Thin Solid Films,* Vol 119, 1984, p 247

119. H.J. Grabke, Thermogravimetry, *Guidelines for Methods of Testing and Research in High Temperature Corrosion: Working Party Report,* H.J. Grabke and D.B. Meadowcroft, Ed., European Federation of Corrosion, 14, The Institute of Materials, 1995

120. C.J. Keattch and D. Dollimore, *An Introduction to Thermogravimetry,* 2nd ed., Heyden & Son, Ltd., 1975

121. H.J. Grabke, Definition and Preparation of Gas Atmospheres, *Guidelines for Methods of Testing and Research in High Temperature Corrosion: Working Party Report,* H.J. Grabke and D.B. Meadowcroft, Ed., European Federation of Corrosion, 14, The Institute of Materials, 1995, p 62–84

122. J.R. Nicholls, Discontinuous Measurement of High Temperature Corrosion, *Guidelines for Methods of Testing and Research in High Temperature Corrosion: Working Party Report,* H.J. Grabke and D.B. Meadowcroft, Ed., European Federation of Corrosion, 14, The Institute of Materials, 1995, p 11–36

123. J.L. McNaughton and C.T. Mortimer, Differential Scanning Calorimetry, *IRS; Physical Chemistry Series 2,* Vol 10, Butterworths, 1975

124. G.J. Danek, Jr., State-of-the-Art Survey on Hot Corrosion in Marine Gas Turbine Engines, *Nav. Eng. J.,* Vol 77, Dec 1965, p 859

125. “Hot Corrosion Problems Associated with Gas Turbines,” from Symposium at 69th Annual Meeting ASTM, 26 June to 1 July 1966 (Atlantic City, NJ), Special Publication 421, ASTM, Sept 1967

126. N.S. Bornstein and M.A. DeCrescente, “Sulfidation in Gas Marine Engines,” Paper 165, Corrosion/75, NACE International, 1975

127. J.R. Nicholls and S.R.J. Saunders, *Guidelines for Hot Salt Corrosion Burner Rig Tests,* Versailles Agreement on Advanced Materials and Standards (VAMAS), National Physical Laboratory, England, 1988

128. P. Hancock, The Use of Laboratory and Rig Tests to Simulate Gas Turbine Corrosion Problems, *Corros. Sci.,* Vol 22, 1982, p 51–65

129. S.R.J. Saunders, M.K. Hossain, and J.M. Ferguson, *Proceedings of the Conference on High Temperature Alloys in Gas Turbines,* (Liège, Belgium), Centre de Recherches Métallurgiques, Oct 1982, p 177

130. K.L. Luthra, Simulation of Gas Turbine Environments in Small Burner Rigs, *High Temp. Technol.,* Vol 7, 1989, p 187–192

131. D.J. Wortman, R.E. Fryxell, K.L. Luthra, and P. Bergman, Mechanisms of Low Temperature Hot Corrosion: Burner Rig Studies, *Proceedings of the Fourth U.S./U.K. Navy Conference on Gas Turbine Materials in a Marine Environment,* Vol 1, U.S. Naval SEA Command, 1979, p 379

132. W.L. Wheatfall and R.C. Schwab, “Hot- Corrosion Behavior of Several Newly Developed Nickel-Base Superalloys—A Preliminary Study,” Naval Ship Research and Development Center Report 3199, Feb 1970

133. G.Y. Lai, J.J. Barnes, and J.E. Barnes, “A Burner Rig Investigation of the Hot Corrosion Behavior of Several Wrought Superalloys and Intermetallics,” 91-GT-21, International Gas Turbine and Aeroengine Congress, American Society of Mechanical Engineers, 1991

134. D.A. Shifler, “Effects of Fuel Dye on the Hot Corrosion Resistance of Marine Gas Turbine Materials,” Paper 167, Corrosion/ 2001, NACE International, 2001

135. D.A. Shifler, The Influence of Fuel Carbon Residue on Hot Corrosion, *Proceedings 2002 Tri-Service Corrosion Conference,* 14–18 Jan 2002 (San Antonio, TX), Department of Defense Tri-Service Corrosion Committee

136. J.R. Nicholls and S.R.J. Saunders, Comparison of Hot-Salt Corrosion Behaviour of Superalloys in High and Low Velocity Burner Rigs, *High Temp. Technol.,* Vol 7, 1989, p 193–201

137. “Military Specification Fuel, Naval Distillate,” MIL-F-16884J, 31 May 1995

138. P. Hancock and J.R. Nicholls, *Proceedings of the Fourth Conference on Gas Turbine Materials in a Marine Environment,* Naval Sea Systems Command, Washington, D.C., June 1979, p 403–422

139. D.J. Stephenson, J.R. Nicholls, and P. Hancock, The Erosion of Gas Turbine Blade Materials by Solid Sea Salt, *Corros. Sci.,* Vol 25, 1985, p 1181–1192

140. R.D. Kane, High Temperature and High Pressure, *Corrosion Tests and Standards— Application and Interpretation,* R. Baboian, Ed., American Society of Testing and Materials, 1995, p 106

141. M. Schütze, Mechanical Interactions in Oxide Scales, *Proceedings on High Temperature Corrosion and Materials Chemistry*, P.Y. Hou, M.J. McNallan, R. Oltra, E.J. Opila, and D.A. Shores, Ed., PV 98- 9, The Electrochemical Society, 1998, p 3

142. R.R. Dils and P.S. Follansbee, Dynamic Oxidation and Corrosion in Power Generating Units, *Corrosion,* Vol 33 (No. 11), 1977, p 385

143. P. Hancock and R.C. Hurst, in *Advances in Corrosion Science and Technology,* Vol 4, Plenum Press, 1974, p 1–84

144. D.J. Baxter and K. Natesan, *Rev. High- Temp. Mater.,* Vol 5 (No. 3/4) 1983, p 149–250

145. J. Stringer, Stress Generation and Relief in Growing Oxide Films, *Corros. Sci.,* Vol 10, 1970, p 513–543

146. R. Mevrel, Cyclic Oxidation of High Temperature Alloys, *Mater. Sci. Technol.,* Vol 3, 1987, p 531

147. M. Schütze and E.J. Quadakkers, Ed., *Cyclic Oxidation of High Temperature Materials: Mechanisms, Testing Methods, Characterization, and Life Time Estimation,* proceedings of a European Federation of Corrosion workshop, (Frankfurt/Main), EPC 27, IOM Communications Ltd., 1999

148. R. Anton, S.K. Jha, D. Clemens, W. Mallener, L. Singheiser, and W.J. Quadakkers, Thermal Cycling Testing of Thermal Barrier Coatings, *Cyclic Oxidation of High Temperature Materials,* proceedings of a European Federation of Corrosion Workshop, EPC 27, M. Schütze and W.J. Quadakkers, Ed., IOM Communications Ltd., 1999, p 339–356

149. B.A. Pint, P.F. Tortorelli, and I.G. Wright, Effect of Cycle Frequency on High Temperature Oxidation Behaviour of Alumina- and Chromia-Forming Alloys, *Cyclic Oxidation of High Temperature Materials,* proceedings of a European Federation of Corrosion workshop, EPC 27, M. Schütze and W.J. Quadakkers, Ed., IOM Communications Ltd., 1999, p 111–132

150. B.A. Pint, P.F. Tortorelli, and I.G. Wright, Effect of Cycle Frequency on High Temperature Oxidation Behaviour of Alumina- Forming Alloys, *Oxid. Met.,* Vol 58, 2002, p 73–102

151. G.M. Kim, N.M. Yanar, E.N. Hewitt, F.S. Pettit, and G.H. Meier, The Effect of the Type of Thermal Exposure on the Durability of Thermal Barrier Coatings, *Scr. Mater.,* Vol 46, 2002, p 489

152. A.L. Cabrera and J.F. Kirner, A Rapid- Temperature-Cycling Apparatus for Oxidation Testing, *Oxid. Met.,* Vol 35, 1991, p 471–479

153. J.L. Smialek, J.A. Nesbitt, C.A. Barrett, and C.E. Lowell, Cyclic Oxidation Testing and Modelling: A NASA Lewis Perspective, *Cyclic Oxidation of High Temperature Materials,* proceedings of a European Federation of Corrosion workshop, EPC 27, M. Schütze and W.J. Quadakkers, Ed., IOM Communications Ltd., 1999, p 148–168

154. J.L. Smialek and J.V. Auping, COSP for Windows—Strategies for Rapid Analyses of Cyclic-Oxidation Behavior, *Oxid. Met.,* Vol 57, 2002, p 559–581

155. "High Temperature Product Literature" and "Hastelloy Corrosion-Resistant Alloy Product Literature," Haynes International, 1991–1996

156. G. Lai, B. Li, B. Gleeson, and H.L. Craig, "Proposed Standard Carburization Test Method," Paper 03473, Corrosion/2003, NACE International, 2003

157. B.A. Baker, Heat Exchanger Corrosion in a Chlorinated Solvent Incinerator, *Handbook of Case Histories in Failure Analysis,* ASM International, 1992, p 118–123

158. J.A. Harris, W.G. Lipscomb, and G.D. Smith, "Field Experience of High Nickel Containing Alloys in Waste Incinerators," Paper 402, Corrosion/87, NACE International, 1987

159. G.D. Smith and C.S. Tassen, Performance of Alloys 825 and 625 in Waste Incinerator Environments, *Mater. Perform.,* Vol 28 (No. 12), 1989, p 41–43

160. R.J.H. Wanhill, A.J.A. Mom, H.J.C. Hersbach, G.A. Kool, and J.A.M. Boogers, NLR Experience with High Velocity Burner Rig Testing 1979–1989, *High Temp. Technol.,* Vol 7, 1989, p 201–211

161. G.C. Booth, J.C. Galsworthy, and A.F. Taylor, Low and High Pressure Rig Testing of Materials and Coatings, *Proceedings of the 4th Conference on Gas Turbine Materials in a Marine Environment,* Naval Sea Systems Command, Vol 1, June 1979, p 259–272

D.A. Shifler, High-Temperature Gaseous Corrosion Testing, *Corrosion: Fundamentals, Testing, and Protection,* Vol 13A*, ASM Handbook,* ASM International, 2003, p 650–681

High-Temperature Gaseous Corrosion Testing

David A. Shifler, Naval Surface Warfare Center

Selected References

- R.A. Ainworth and G.A. Webster, *High Temperature Component Life Assessment,* Kluwer Academic Publishers, 1994
- C.M. Branco, R. Richie, and V. Sklenicka, Ed., *Mechanical Behaviour of Materials at High Temperature,* NATO Science Partnership Sub-Series 3, *High Technology,* Vol 15, Kluwer Academic Publishers, 1996
- *Characterization of High Temperature Materials: Microstructural Characterization,* Vol 1, Maney Publishers, 1989
- *Coatings for High-Temperature Structural Materials: Trends and Opportunities,* Committee on Coatings for High-Temperature Structural Materials, National Research Council, National Academies Press, 1996
- N.B. Dahotre and J.M. Hampikian, Ed., *Elevated Temperature Coatings: Science and Technology II,* The Minerals, Metals and Materials Society, 1996
- N.B. Dahotre, J.M. Hampikian, J.E. Morral, Ed., *Elevated Temperature Coatings: Science and Technology IV,* The Minerals, Metals and Materials Society, 2001
- N.B. Dahotre, J.M. Hampikian, and J.J. Stiglich, Ed., *Elevated Temperature Coatings: Science and Technology I,* The Minerals, Metals and Materials Society, 1995
- M.J. Donachie and S.J. Donachie, *Superalloys: A Technical Guide,* 2nd ed., ASM International, 2002
- G.R. Edwards, D.L. Olson, R. Visawantha, T. Stringer, and P. Bollinger, *Proceedings of the Workshop on Materials and Practice to Improve Resistance to Fuel Derived Environmental Damage in Land and Sea Based Turbines,* 22–23 Oct 2002, Electric Power Research Institute, 2003
- P. Elliot, Practical Guide to High-Temperature Alloys, *Mater. Perform.* Vol 28, 1989, p 57
- R.J. Fordham, Ed., *High Temperature Corrosion of Technical Ceramics,* Kluwer Academic Publishers, 1990

- G.E. Fuchs, K.A. Dannemann, and T.C. Deragon, Ed., *Long Term Stability of High Temperature Materials,* The Minerals, Metals and Materials Society, 1999
- B. Gleeson, High-Temperature Corrosion of Metallic Alloys and Coatings, *Corrosion and Environmental Degradation of Materials,* M. Schütze, Ed., Vol 19, *Materials Science and Technology,* R.W. Cahn, P. Haasen, and E.J. Kramer, Ed., Wiley-VCH, 2000, p 173–228
- S. Grainger and J. Blunt, Ed., *Engineering Coatings: Design and Application,* 2nd ed., Woodhead Publishing Ltd., 1999
- J.M. Hampikian and N.B. Dahotre, Ed., *Elevated Temperature Coatings: Science and Technology III,* The Minerals, Metals and Materials Society, 1999
- P.Y. Hou, T. Maruyama, M.J. McNallan, T. Narita, E.J. Opila, and D.A. Shores, *High Temperature Corrosion and Materials Chemistry: Per Kofstad Memorial Symposium,* PV 99-38, The Electrochemical Society, 2000
- P.Y. Hou, M.J. McNallan, R. Oltra, E.J. Opila, and D.A. Shores, *High Temperature Corrosion and Materials Chemistry,* PV 98-9, The Electrochemical Society, 1998
- W.B. Johnson and R.A. Rapp, Ed., *Proceedings of the Symposium on High Temperature Materials Chemistry V,* PV 90-18, The Electrochemical Society, 1990, p 1–98
- A.S. Khanna, *Introduction to High Temperature Oxidation and Corrosion,* ASM International, 2002
- G.Y. Lai, *High Temperature Corrosion of Engineering Alloys,* ASM International, 1990
- A.V. Levy, *Solid Particle Erosion and Erosion-Corrosion of Materials,* ASM International, 1995
- K.G. Nickel, Ed., *Corrosion of Advanced Ceramics: Measurement and Modeling,* Kluwer Academic Publishers, 1994
- E.J. Opila, P.Y. Hou, T. Maruyama, B. Pieraggi, M.J. McNallan, E. Wuchina, and D.A. Shifler, *High Temperature Corrosion and Materials Chemistry IV,* PV 2003-12, The Electrochemical Society, 2003
- E.J. Opila, M.J. McNallan, D.A. Shores, and D.A. Shifler, *High Temperature Corrosion and Materials Chemistry III,* PV 2001-12, The Electrochemical Society, 2001
- L. Remy and J. Petit, Ed., *Temperature-Fatigue Interaction,* Elsevier International Series on Structural Integrity, Vol 29, Elsevier Science, 2002
- M. Schütze, W.J. Quaddakers, and J.R. Nicholls, *Lifetime Modelling of High Temperature Corrosion Processes: Proceedings of a European Federation of Corrosion Workshop,* EFC 34, Maney Publishers, 2001
- S.C. Singhal, Ed., *High Temperature Protective Coatings,* The Metallurgical Society of AIME, 1982
- K.H. Stern, Ed., *Metallurgical and Ceramic Protective Coatings,* Kluwer Academic Publishers, 1996
- G. Sumner and V.B. Livesey, *Techniques for High Temperature Fatigue Testing,* Elsevier Applied Science, 1985
- Y. Tamarin, *Protective Coatings for Turbine Blades,* ASM International, 2002
- P.F. Tortorelli, I.G. Wright, and P.Y. Hou, Ed., *John Stringer Symposium on High Temperature Corrosion,* ASM International, 2003
- M.H. Van de Voorde and G.W. Meethan, *Materials for High Temperature Engineering Applications (Engineering Materials),* Springer Verlag, 2000
- R. Viswanathan, *Damage Mechanism and Life Assessment of High-Temperature Components,* ASM International, 1989

P. Natishan, Introduction to Methods of Corrosion Protection, *Corrosion: Fundamentals, Testing, and Protection*, Vol 13A, *ASM Handbook*, ASM International, 2003, p 685–686

Introduction to Methods of Corrosion Protection

Paul Natishan, Naval Research Laboratory

Introduction

CORROSION is an oxidation reaction where the corroding metal is the anode in an electrochemical cell. In addition to the anode, there are three other components that are necessary for corrosion to occur: an aggressive environment, a cathode where the reduction reaction occurs, and an electron-conducting path between the anode and the cathode. The basic concept for most methods of corrosion protection is to remove one or more of these cell components so that the pure metal or metal alloy of interest will not corrode. Another widely used corrosion protection approach is to change the nature of the anode so that it becomes the cathode (cathodic protection). These methods of corrosion protection are briefly reviewed as follows.

P. Natishan, Introduction to Methods of Corrosion Protection, *Corrosion: Fundamentals, Testing, and Protection*, Vol 13A, *ASM Handbook*, ASM International, 2003, p 685–686

Introduction to Methods of Corrosion Protection

Paul Natishan, Naval Research Laboratory

Factors Affecting Corrosion Behavior

A primary factor in determining corrosion behavior of metals is their chemical composition. Alloying, which is adding other element(s) to a metal, is one of the major means used to improve the corrosion resistance of the base material. Alloys with varying degrees of corrosion resistance have been developed in response to an ever-increasing number of severe service environments. An example of improved corrosion resistance by modifying the chemical composition is the alloying of steels. Carbon and low-alloy steels are less costly but also less corrosion-resistant. At the higher end of the alloying scale are the more costly and significantly more corrosion-resistant stainless steels. The corrosion resistance of stainless steels is due to the protective nature of the surface oxide film that forms a barrier between the environment and the alloy. The physical and chemical properties of the oxide film and the service environment determine the corrosion resistance of the alloy. In addition to alloying, there are metallurgical factors, often referred to as microstructure, such as crystal form, grain size and shape, grain heterogeneity, second phases, impurity inclusions, and residual stress that can influence corrosion. In addition, mechanical treatments can have effects on the corrosion properties, both positive and negative. Thus, alloying, metallurgical treatments, and mechanical treatments can greatly affect the corrosion resistance of the resulting alloy.

P. Natishan, Introduction to Methods of Corrosion Protection, *Corrosion: Fundamentals, Testing, and Protection*, Vol 13A, *ASM Handbook*, ASM International, 2003, p 685–686

Introduction to Methods of Corrosion Protection

Paul Natishan, Naval Research Laboratory

Galvanic Couples

Galvanic corrosion occurs when two or more dissimilar metals or alloys immersed in the same electrolyte are in electrical contact. The metal in the galvanic couple with the lower corrosion (electrochemical) potential has its potential pulled in the positive direction by the metal that has the higher corrosion potential. This generally causes the metal or alloy with the lower potential to experience accelerated corrosion. On the other hand, the metal with the higher corrosion potential undergoes a negative shift in potential, causing it to support additional cathodic reaction and thus to corrode less. The principles of galvanic corrosion can be and often are used as means of corrosion protection. In this case, a sacrificial metal (a sacrificial anode) is attached to a structure having a higher corrosion potential to intentionally lower the potential of the higher- potential metal or alloy and thus decrease the corrosion rate. This type of protection is called sacrificial cathodic protection (SACP). The lowering of potential can also be accomplished by applying a direct electrical current from an external source. This is impressed-current cathodic protection (ICCP). An undesired consequence of excessive cathodic protection (CP) or the use of cathodic protection with an inappropriate metal is that the potential can be pulled down to values where the hydrogen evolution reaction occurs. This, in turn, can lead to one of the forms of corrosion called hydrogen-induced cracking.

The lower-potential metal in a galvanic couple does not always have its corrosion rate accelerated. For metals that form a passive film, coupling with another metal of higher potential can cause the potential of the film-forming metal to shift from a value where it corrodes to one where a passive film is formed. When this is done intentionally, the procedure is referred to as anodic protection. Corrosion protection is achieved by moving the potential of the component to be protected in the positive direction. The passive film that forms acts as a barrier between the environment and the more active metal. However, the higher-potential metal in a galvanic couple is not always rendered less corrodible. A passive metal can sometimes be pulled out of its passive region and into a more corrosive region. A break in the passive film can lead to aggressive localized corrosion.

P. Natishan, Introduction to Methods of Corrosion Protection, *Corrosion: Fundamentals, Testing, and Protection*, Vol 13A, *ASM Handbook*, ASM International, 2003, p 685–686

Introduction to Methods of Corrosion Protection

Paul Natishan, Naval Research Laboratory

Coatings

Coatings generally protect the metal by imposing a physical barrier between the metal substrate and the environment. Three common types of coatings are organic, inorganic, and metallic.

Organic coatings afford protection by providing a physical barrier between the metal and the environment. These coatings can also contain corrosion inhibitors. Organic coatings include paints, resins, lacquers, and varnishes. The properties of the coating depend on the formulation of the coating. To achieve the desired protection, the proper application of an organic coating on an appropriately prepared substrate is required. Organic coatings protect more metal on a weight basis than any other means of corrosion protection.

Inorganic coatings are also used to provide a barrier between the environment and the metal. Inorganic coatings include enamels, glass linings, and conversion coatings. Porcelain enamel coatings are inert in water and resistant to most weather. They are common on appliances and plumbing fixtures. Glass-lined metals are used in process industries where there is concern over corrosion or contamination of the product. Conversion coatings are produced by intentionally corroding the metal surface in a controlled manner. This is done to produce an adherent corrosion product that protects the metal from further corrosion. Anodization of aluminum, one of the more commonly used conversion coating techniques, produces a protective aluminum oxide film on the aluminum metal. Another example of a chemical conversion coating is phosphatizing for the protection of automobile bodies.

Metallic coatings create a barrier between the metal substrate and the environment. In addition, metallic coatings can sometimes provide cathodic protection when the coating is compromised. Metallic coatings and other inorganic coatings are produced using a variety of techniques, including hot dipping, electroplating, cladding, thermal spraying, chemical vapor deposition, or surface modification using directed energy (laser or ion) beams.

P. Natishan, Introduction to Methods of Corrosion Protection, *Corrosion: Fundamentals, Testing, and Protection*, Vol 13A, *ASM Handbook*, ASM International, 2003, p 685–686

Introduction to Methods of Corrosion Protection

Paul Natishan, Naval Research Laboratory

Inhibitors

Corrosion inhibitors are substances that slow or prevent corrosion when added to an environment in which a metal usually corrodes. The effectiveness of corrosion inhibitors is dependent on the metal to be protected as well as on the operating environment. In addition, many inhibitors, most notably, chromates, are toxic, and environmental regulations limit the use of these agents. Some inhibitor types include anodic, cathodic, organic, precipitation, and vapor-phase inhibitors.

An understanding of the means of corrosion and corrosion protection methods can aid in the selection of materials and design of systems to protect the materials in their service environment. The following articles discuss traditional and emerging techniques used to improve corrosion resistance.

P. Natishan, Introduction to Corrosion Resistance of Bulk Materials, *Corrosion: Fundamentals, Testing, and Protection*, Vol 13A, *ASM Handbook*, ASM International, 2003, p 687–688

Introduction to Corrosion Resistance of Bulk Materials

Paul Natishan, Naval Research Laboratory

Introduction

THE CORROSION RESISTANCE of metallic materials can be influenced greatly by alloying, metallurgical treatments, and mechanical treatments. The following articles consider methods of preventing corrosion based on these factors, as applicable, for a number of technologically important alloy systems.

P. Natishan, Introduction to Corrosion Resistance of Bulk Materials, *Corrosion: Fundamentals, Testing, and Protection*, Vol 13A, *ASM Handbook*, ASM International, 2003, p 687–688

Introduction to Corrosion Resistance of Bulk Materials

Paul Natishan, Naval Research Laboratory

Alloying

Chemical composition is a primary factor in determining corrosion behavior of metals. Alloying has been the major means used to change the properties of metals (including corrosion). Alloys with varying degrees of corrosion resistance have been developed in response to ever- changing service environments. A good example of how corrosion resistance has been changed successfully by modifying the chemical composition is the alloying of iron to produce steels. Steels at the lower end of the alloying scale are less costly but also less corrosion resistant. These alloys are iron-base and contain a small amount (usually in the 0.5 to 3.0 wt% range) of nickel, molybdenum, chromium, or copper. They also generally have small amounts of phosphorus, nitrogen, and sulfur. At the higher end of the alloying scale are the more costly and significantly more corrosion-resistant stainless steels. Stainless steels contain a minimum amount (approximately 10.5 wt%) of chromium and, depending on the alloy, other elements such as nickel, molybdenum, and nitrogen. Figure 1 shows the effects of selected alloying elements on a 19Cr-9Ni stainless steel casting alloy. The corrosion resistance of stainless steels is based on the protective nature of the surface oxide film. The physical and chemical properties of the oxide film and the service environment determine the corrosion resistance of the alloy. Additional details on the stainless steels are presented in the following articles.

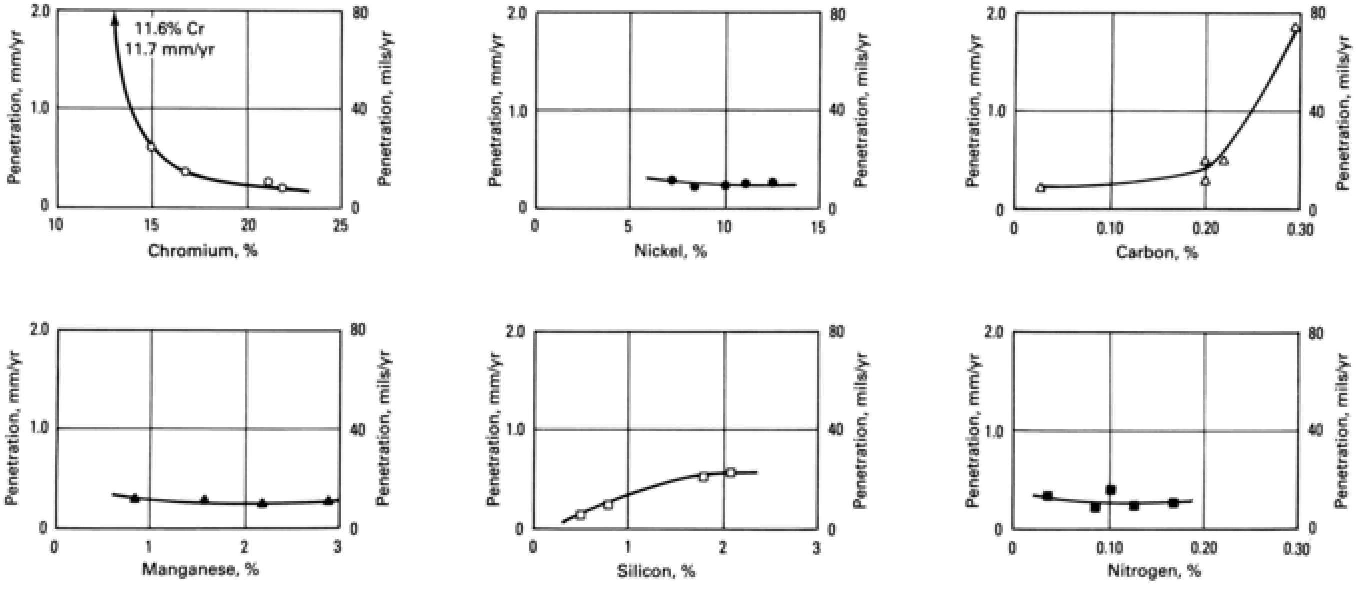

Fig. 1 The effect of alloying is shown as the influence that various elements have on the corrosion rate of a base 19Cr-9Ni casting alloy in boiling 65% nitric acid. The specimens were solution annealed and quenched. Composition of the base alloy was 19Cr, 9Ni, 0.09C, 0.8Mn, 1.0Si, 0.04P (max), 0.035S (max), and 0.06N (Ref 1).

Alloying does not always lead to better corrosion resistance. This can occur if the element being alloyed for corrosion resistance has a low solubility in the metal/alloy to which it is being added. The low solubility can result in the formation of a second phase, which can degrade, rather than enhance, the corrosion properties. This is the case for most aluminum alloys. Alloying elements that are typically used to increase the corrosion resistance have low solubility in aluminum when alloyed using conventional techniques.

Reference cited in this section

1. M. Blair, Cast Stainless Steels, *Properties and Selection: Irons, Steels, and High Performance Alloys,* Vol 1, *ASM Handbook,* ASM International, 1990, p 913

P. Natishan, Introduction to Corrosion Resistance of Bulk Materials, *Corrosion: Fundamentals, Testing, and Protection,* Vol 13A, *ASM Handbook,* ASM International, 2003, p 687–688

Introduction to Corrosion Resistance of Bulk Materials

Paul Natishan, Naval Research Laboratory

Metallurgical Factors

In addition to alloying, there are metallurgical factors, such as crystallography, grain size and shape, grain heterogeneity, second phases, impurity inclusions, and residual stress, that can influence corrosion. Most metals/alloys of technological importance are polycrystalline aggregates, with each individual crystal referred to as a *grain.* Grain orientation can affect corrosion resistance, as evidenced by metallographic etching rates and pitting behavior. Grain shape and size likewise may vary greatly, depending on the alloy and processing history. Alloys, particularly in the as-cast condition, generally exhibit chemical inhomogeneity, such that there is segregation of alloying elements and impurities to the grain-boundary regions. These heterogeneities, which can also develop during subsequent processing such as welding or heat treatment, can produce different electrochemical characteristics at the grain boundary relative to the grain interior and can lead to intergranular corrosion. This problem can be of great practical importance, especially to wrought stainless steels and nickel alloys. Second phases, such as ferrite grains in an otherwise austenitic stainless steel and beta grains in an otherwise alpha brass, can be of considerable importance in some alloy systems and to some forms of corrosion. Figure 2 illustrates the relationship between microstructure and corrosion behavior.

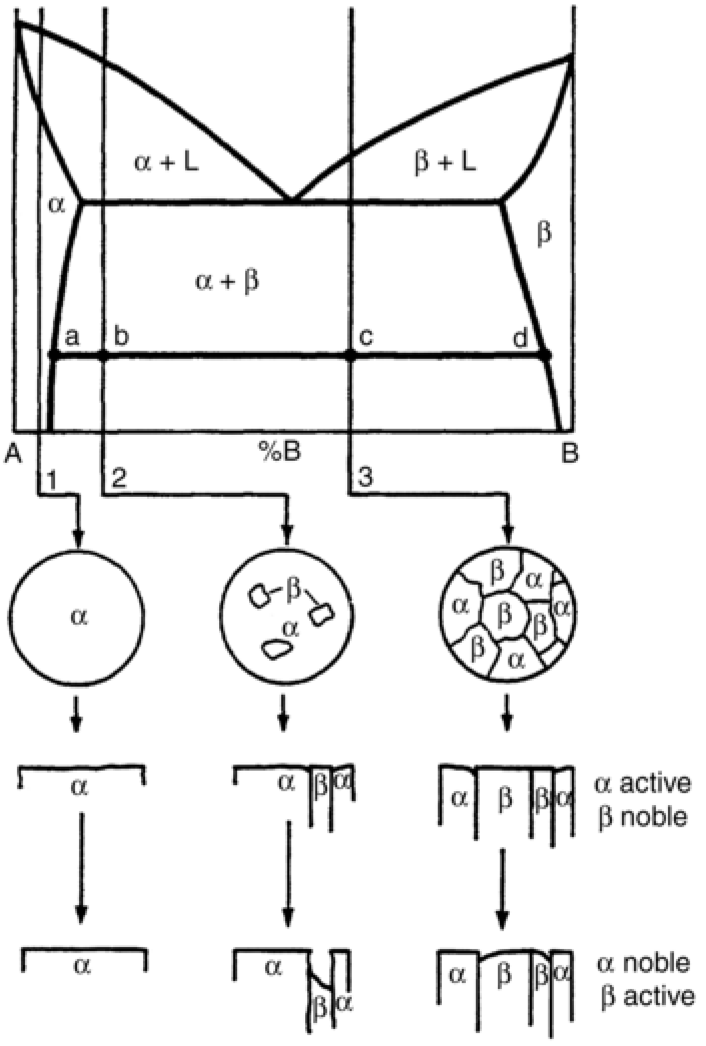

Fig. 2 The relationship between microstructure and corrosion behavior. From the phase diagram (top), alloys with differing compositions—and thus differing relative amounts of alpha and beta phase particles—are selected. A profile of the material in a corrosive medium is shown when alpha is active and beta is noble. The bottom line illustrates when alpha is more noble than beta (adapted from Ref 2).

Reference cited in this section

2. J. Davis, Ed., *Corrosion: Understanding the Basics,* ASM International, 2000, p 31

P. Natishan, Introduction to Corrosion Resistance of Bulk Materials, *Corrosion: Fundamentals, Testing, and Protection*, Vol 13A, *ASM Handbook*, ASM International, 2003, p 687–688

Introduction to Corrosion Resistance of Bulk Materials

Paul Natishan, Naval Research Laboratory

Mechanical Treatments

Mechanical treatments can have both positive and negative effects on the corrosion properties. Residual stresses from cold working or other sources can lead to increased corrosion rates and are also important in causing

stress-corrosion cracking. On the other hand, processes such as shot peening can be used to improve the corrosion behavior in some systems.

P. Natishan, Introduction to Corrosion Resistance of Bulk Materials, *Corrosion: Fundamentals, Testing, and Protection*, Vol 13A, *ASM Handbook*, ASM International, 2003, p 687–688

Introduction to Corrosion Resistance of Bulk Materials

Paul Natishan, Naval Research Laboratory

References

1. M. Blair, Cast Stainless Steels, *Properties and Selection: Irons, Steels, and High Performance Alloys*, Vol 1, *ASM Handbook*, ASM International, 1990, p 913
2. J. Davis, Ed., *Corrosion: Understanding the Basics*, ASM International, 2000, p 31

J. Snodgrass, Corrosion Resistance of Aluminum Alloys, *Corrosion: Fundamentals, Testing, and Protection*, Vol 13A, *ASM Handbook*, ASM International, 2003, p 689–691

Corrosion Resistance of Aluminum Alloys

Jack Snodgrass and Jim Moran, Alcoa, Inc.

Introduction

THIS ARTICLE addresses the general effects of composition, mechanical treatment, surface treatment, and processing on the corrosion resistance of aluminum and aluminum alloys. Most of the techniques used to alter the properties of aluminum are intended to improve mechanical and physical properties, but these techniques may actually cause degradation of corrosion resistance.

Most aluminum alloys can be produced with good corrosion resistance in natural atmospheres, such as freshwater, seawater, many soils and chemicals, and most foods. Thin-walled aluminum food containers, however, are coated to resist perforation (Ref 1). Corrosion resistance of a material must be defined in terms of the use of the material. For example, a pinhole perforation in a thin-walled food or beverage container is a corrosion failure, whereas pits of the same dimensions in an aluminum plate would not be considered corrosion failure. On the other hand, an aluminum roofing sheet may experience some shallow pitting and staining to the extent that its appearance changes. This can be considered either an aesthetic corrosion failure or acceptable corrosion resistance, because the roof has no perforations.

Thermodynamically, aluminum is a very active metal. Pure aluminum and all aluminum alloys depend on a naturally occurring aluminum oxide film to provide corrosion protection. This oxide film is adherent, transparent, stable in the pH range of approximately 4 to 9, self-healing, and an electrical insulator. While being protected from uniform corrosion, the most common form of corrosion found on aluminum alloys is localized pitting. This form of corrosion occurs when a corrosive species such as chloride ions compromises the integrity of the oxide film at local sites.

Reference cited in this section

1. J.E. Hatch, Ed., *Aluminum: Properties and Physical Metallurgy,* American Society for Metals, 1984, p 242, 301, 306–309

J. Snodgrass, Corrosion Resistance of Aluminum Alloys, *Corrosion: Fundamentals, Testing, and Protection*, Vol 13A, *ASM Handbook*, ASM International, 2003, p 689–691

Corrosion Resistance of Aluminum Alloys

Jack Snodgrass and Jim Moran, Alcoa, Inc.

Alloying to Improve Corrosion Resistance

There are five major alloying elements—copper, manganese, silicon, magnesium, and zinc— that significantly influence the properties of aluminum alloys. Other alloying components that are less significant from a corrosion-resistance standpoint are iron, chromium, titanium, zirconium, lithium, and nickel. These are frequently included to improve mechanical and other physical properties. The effects of each of the five major alloying elements are discussed briefly. Some aluminum alloys are binary, while others are multiconstituent, containing three or four major alloying additions. The alloys are grouped by series, based on the alloy designations for wrought aluminum of The Aluminum Association International (Ref 2). The following sections describe the corrosion behavior of each general alloy class. While this discussion is specifically focused on wrought product forms, castings of similar compositions generally behave similarly.

1*xxx* Series. The alloys in this series are at least 99% pure aluminum. These materials are really not alloys but rather are pure aluminum with various levels of impurities. The major impurities are iron and silicon. These materials are relatively corrosion resistant. In compositions with higher iron content, there is a tendency toward pitting corrosion, especially in aqueous chloride solutions.

2*xxx* Series. The alloys in this series contain primarily copper, up to 7%. Several also contain magnesium and/or manganese. The alloys in this series are strengthened by thermal processing. These alloys attain high strengths and are used in sheet, plate, and extruded forms, primarily in aerospace applications. Copper in aluminum alloys generally decreases the resistance to general corrosion and pitting. With proper heat treatment, quenching, and aging, these alloys can achieve moderately good resistance to stress- corrosion cracking and other forms of intergranular corrosion. The resistance to general and pitting corrosion is strongly influenced by the copper content in these alloys, regardless of thermal processing control. Several of the alloys in this series contain lithium (<2.5%), and a few also contain silver (<1%). The corrosion resistance of these low-density alloys is similar to other alloys in this series. A special group of alloys in this series contains nickel (<2.5%), which imparts high-temperature corrosion resistance for applications such as internal combustion engine pistons.

3*xxx* Series. The alloys in this series contain primarily manganese, up to 1.5%. Several also contain magnesium, up to 1.5%. The alloys in this series are strengthened by work hardening and are produced in extruded, sheet, and plate forms. Manganese has minimal impact on the corrosion resistance of aluminum alloys. These alloys have only moderate strengths and good corrosion resistance. Alloys in this series find use in beverage and food containers, building products, heat-exchanger tubing, and other general uses requiring good corrosion resistance.

4*xxx* Series. The alloys in this series contain primarily silicon, up to 14%. Because of their low melting points, these alloys are used primarily for braze and weld filler applications. These alloys are usually produced as sheet or wire and are found in the as-cast condition following a thermal joining process. The silicon in these alloys generally does not promote corrosion of the alloy itself. However, when used in a thermal joining process, there have been cases where the silicon has diffused into the grain boundaries of the materials being joined, causing decreased corrosion resistance.

5*xxx* Series. The alloys in this series contain primarily magnesium, up to 6%. Several of the alloys also contain manganese. Alloys in this series are strengthened by work hardening and are produced primarily as sheet and

plate. Several of the alloys that are produced as drawn wire are used in the production of window screens and as weld filler. The magnesium additions generally improve the corrosion resistance of these alloys, especially in saltwater. The 5*xxx* series of alloys can be divided into two groups: low magnesium (under 3%) and high magnesium (3 to 6%). The low-magnesium alloys have very good corrosion resistance in a broad range of environments. The high-magnesium alloys have greater strength than the low-magnesium alloys, and they have outstanding corrosion resistance in saltwater environments. The only drawback to the high-magnesium alloys is that they can be susceptible to intergranular forms of corrosion, including exfoliation and stress-corrosion cracking. This corrosion susceptibility can be avoided by using particular tempers and by limiting the maximum service temperatures to 65 °C (150 °F). The high- magnesium alloys are used extensively in marine vessels and structures.

6*xxx* Series. The alloys in this series contain primarily magnesium (<2%) and silicon (<2%), which form a strengthening constituent, magnesium silicide. Several of the alloys in this series also contain copper (<1.2%) and/or manganese (<1.2%). The alloys in this series are strengthened by thermal processing to have moderate strength; they generally have good corrosion resistance. Those that contain copper have somewhat poorer corrosion resistance than those without copper. The range of alloys in this series is very broad. Some of the alloys are produced only as sheet products for applications such as automotive body panels; others are produced only as extrusions for use as structural shapes. Still others are produced as extrusions and sheet. At least one of the alloys is produced as extrusions, sheet, and plate.

7*xxx* Series. The alloys in this series all contain zinc, up to 9%. In addition, nearly all of these alloys contain magnesium (<4%), and many of them contain copper (<3%). The alloys in this series are strengthened by thermal processing, resulting in several that are among the strongest commercially available aluminum alloys. Most of the alloys in this series are produced in both sheet and plate products; several of the alloys are also produced as extrusions. Because of their significant copper content, most of these alloys have only moderate resistance to general corrosion and pitting. When overaged tempers are used, these alloys have good-to-excellent exfoliation and stress-corrosion-cracking resistance. A few of the alloys in this series have very little copper and are used for special corrosion-related applications, such as sacrificial cladding on alclad sheet products.

8*xxx* Series. The alloys in this series do not fit into any of the previous series. Most of these alloys contain significant quantities of iron (<10%). A number of these alloys are produced as foils for consumer and commercial food wraps. In these applications, the alloys have very good corrosion resistance. Also, several of these alloys contain copper (<2%), magnesium (<2%), and lithium (<3%), with little or no iron. The lithium is added to reduce the density of the alloys for weight-critical aerospace applications. These low-density alloys are produced as sheet and plate that are thermally processed to develop strength. These alloys have corrosion resistance similar to many of the 7*xxx* alloys.

Reference cited in this section

2. *Aluminum Standards and Data,* The Aluminum Association, 1997, p 1–3

J. Snodgrass, Corrosion Resistance of Aluminum Alloys, *Corrosion: Fundamentals, Testing, and Protection*, Vol 13A, *ASM Handbook*, ASM International, 2003, p 689–691

Corrosion Resistance of Aluminum Alloys

Jack Snodgrass and Jim Moran, Alcoa, Inc.

Mechanical Treatments to Improve Corrosion Resistance

The major impact of mechanical treatment on corrosion of aluminum alloys is the application or removal of stresses that could lead to stress- corrosion cracking. Operations such as forming, bending, and machining can

create residual stress in aluminum alloys. Assembly will inpart stresses on components. When tolerances are tight for interference fits or loose due to misalignment, stresses are introduced. Stresses created by forming and machining can be relieved by shot peening the stressed area. This replaces the surface tensile stress with compressive stress that will not cause stress-corrosion cracking. Care should be taken when shot peening to avoid embedding metallic particles into the relatively soft aluminum surface. Fit-up stresses can be minimized by careful selection of tolerances during design and by applying adequate quality- control procedures during manufacture of parts.

J. Snodgrass, Corrosion Resistance of Aluminum Alloys, *Corrosion: Fundamentals, Testing, and Protection*, Vol 13A, *ASM Handbook*, ASM International, 2003, p 689–691

Corrosion Resistance of Aluminum Alloys

Jack Snodgrass and Jim Moran, Alcoa, Inc.

Surface Treatment to Improve Corrosion Resistance

Surface treatments that aid in preventing corrosion are of several different types. There are organic coatings or paints that provide a barrier between a corrosive environment and the aluminum surface. (See the article “Organic Coatings and Linings” in this Volume.) There are inorganic coatings, including claddings, and enhanced oxides, such as anodized films, Boehmite films, and conversion coatings. Each of these is discussed in more detail in the following paragraphs.

Organic coating systems are frequently applied to aluminum for strictly decorative purposes. For example, they are applied to aluminum siding and exposed automobile body panels to obtain desired color and to prevent natural weathering that is aesthetically unacceptable but structurally insignificant. Organic coatings may also be applied to aluminum for corrosion protection in special situations. In both cases, adequate surface preparation and careful coating selection are important to achieve the desired coating life.

Most organic coatings provide corrosion protection by forming a physical barrier between the aluminum surface and the environment. Some contain inhibitors, such as chromate primers. Aluminum insulation jacketing and refrigerator liners are coated on the back with a vapor barrier to prevent poultice and crevice corrosion when condensation collects between foamed insulation and the aluminum. Clear organic coatings are used where the look of a natural aluminum surface is desired and where weathering must be prevented. Temporary organic coatings are sometimes used to protect aluminum surfaces from corrosion during storage and transit. Heavy organic coatings, such as mastics and coal tars, are sometimes used to protect aluminum surfaces that are embedded in soils and concrete.

The performance of organic coating systems can be maximized by following the specific recommendations of suppliers regarding surface preparation; pretreatment; selection of compatible conversion coat, primer, and topcoat; application; and curing. If continuing maximum corrosion protection is required, the organic coating systems must be maintained.

Alclad aluminum is a duplex product in which a thin surface layer of one aluminum alloy (usually 5 to 10% of the total thickness) is metallurgically bonded to the main core alloy selected for strength. In order to ensure effective sacrificial cathodic protection of the core alloy, the clad alloy is usually selected to be at least 100 mV anodic to the core (Ref 3).

The surface layer is normally 1*xxx* for 2*xxx* cores, or 7072 for 3*xxx,* 5*xxx,* 6*xxx,* and 7*xxx* cores. The alclad aluminum alloys provide resistance to perforation by pitting corrosion. Pits do not penetrate into the core alloy, so loss of mechanical properties on long-term exposure to corrosive atmospheres is minimized. As an example, a kitchen kettle fabricated from sheet with a 5% layer of 7072 alloy on a 3003 core alloy resisted perforation in an aggressive water for 5 to 10 times the life of an unclad 3003 alloy kettle in the same water. Another example is the alclad 3004 roofing and siding on the hangar for Howard Hughes' *Spruce Goose* in a Long Beach, CA harbor that, after 33 years, had pitted only to the depth of the clad layer, 76 μm (3 mils). Further, the cladding

of thin-wall (1.5 mm, or 0.060 in.) irrigation pipe and culvert sheet greatly extends the time to perforation in aggressive waters.

Anodized Films. A commercial surface treatment unique to aluminum is anodizing. (See the article “Aluminum Anodizing” in this Volume.) The object to be treated is immersed as the anode in an acid electrolyte, and a direct current is applied. Oxidation of the surface occurs to produce a greatly thickened, hard, porous film of aluminum oxide. This film is then normally immersed in boiling water to seal the porosity and render the film impermeable (Ref 1).

Before sealing, the film can be colored by impregnation with dyes or pigments. Special electrolytes are sometimes used to produce colored anodic films directly in the anodizing bath. The degree of protection conferred to the surface depends on the thickness of the film, which may be 8 μm (0.3 mils) in the case of shiny automobile trim moldings, to 25 μm (1.0 mil) or more on the aluminum facade of a monumental building. These represent a thickening of the natural oxide film by a factor of approximately 1000 and 3000 times, respectively.

Architectural aluminum, such as handrails, doors, windows, and facades, is often anodized. The surface retains less atmospheric dirt and is much easier to clean. The anodic film has the same chemical characteristics as the natural oxide film and is corroded by strong alkalis and strong acids. In industrial atmospheres, the film tends to pit, with the time to initiation depending on the film thickness. To preserve the initial appearance of anodized aluminum facades, thick anodic films are coated with clear organic coating. The main virtues of an anodic film are its decorative appeal and the ease of cleaning. Anodizing is rarely the solution to a field corrosion problem.

Boehmite Films. The natural surface oxide film can be thickened by exposure to moving water, hot soft water, or steam. If this is done before exposure to a pitting-type environment, pitting is sometimes prevented. In one experiment, a specimen of 1200 alloy sheet that had previously been exposed for 1 year in a nonpitting freshwater with an estimated film thickness of 80 nm failed to pit in 16 days when immersed in a very aggressive water that produced a 965 μm (38 mil) pit on a fresh sheet specimen in the same period (Ref 1).

Conversion Coatings. A number of proprietary chemical immersion treatments, such as Alodine (Henkel Surface Technologies), Bonderite (Henkel Surface Technologies), Iridite (MacDermid Inc.), and others, are used to produce a complex surface conversion coating approximately 20 nm thick on aluminum sheet and extrusions before painting in a factory operation, compared to 5 nm for an untreated surface. The proprietary solutions are acidic and contain chromates, phosphates, and other chemicals. Such films greatly improve paint adhesion (Ref 1). (See the article “Chromate and Chromate-Free Conversion Coatings” in this Volume.)

The films, which contain chromates, have corrosion-preventive properties in their own right and are used on some aircraft and automotive components. However, they are relatively soft and can be used for corrosion prevention without overcoating only where there is no abrasion expected in service.

References cited in this section

1. J.E. Hatch, Ed., *Aluminum: Properties and Physical Metallurgy,* American Society for Metals, 1984, p 242, 301, 306–309

3. J.R. Davis, Ed., *Corrosion of Aluminum and Aluminum Alloys,* ASM International, 1999, p 202

J. Snodgrass, Corrosion Resistance of Aluminum Alloys, *Corrosion: Fundamentals, Testing, and Protection*, Vol 13A, *ASM Handbook*, ASM International, 2003, p 689–691

Corrosion Resistance of Aluminum Alloys

Jack Snodgrass and Jim Moran, Alcoa, Inc.

Processing to Improve Corrosion Resistance

Processing steps that lead to improved corrosion resistance fall into two groups: those that increase the uniformity of the distribution of alloying elements, constituents, and impurities, and those that decrease residual stresses. Nearly all of these are thermal processing steps that occur either during production of sheet, plate, and extrusions or following fabrication of the sheet, plate, and extrusions into semifinished or finished parts. The steps that can have relatively significant impact on corrosion resistance are enumerated in the following paragraphs.

Homogenization. Following casting, extrusion billets and rolling ingots are homogenized to make the composition more uniform and to improve workability. The uniformity of composition generally leads to improved corrosion resistance. This step includes holding the cast shape at an elevated temperature for a period of time that is usually measured in hours.

Rolling and Extrusion Temperatures. The temperature at which rolling and extrusion are performed can have an impact on intergranular corrosion resistance of the resulting product. The temperature at which products exit the deformation process can have an especially significant impact on the grain morphology and the composition at the grain boundaries. These temperatures are especially important for the 3*xxx*- and 5*xxx*-series alloys, because they are work hardened and often receive no further thermal treatments.

Quenching. The rate of cooling (quench rate) of aluminum products following either elevated- temperature fabrication or heat treatment can have a significant impact on the corrosion resistance of heat treated alloys. Rapid quenching generally freezes the metal with a more uniform composition than if the quench is slow, which allows composition gradients at grain boundaries. This is especially true for 2*xxx*- and 7*xxx*- series alloys that can be susceptible to intergranular forms of corrosion (exfoliation and stress-corrosion cracking) if not quenched properly. The 6*xxx*-series alloys can also have intergranular corrosion problems if not quenched properly, although the corrosion problems are not as severe as those found with the 2*xxx*- and 7*xxx*-series alloys.

Aging. The artificial aging process that is used to strengthen the heat treatable 2*xxx*-, 6*xxx*-, and 7*xxx*-series alloys can have a significant impact on corrosion resistance, even though it is conducted at relatively low temperatures. In many cases, the peak aged condition that provides maximum strength also provides reduced corrosion resistance, especially in the 7*xxx*-series alloys. By overaging, there is a small decrease in strength but a significant improvement in exfoliation and stress-corrosion-cracking resistance. Careful aging can also improve the corrosion resistance of several of the 6*xxx*-series alloys that find use as automotive body sheet. The aging of the automotive body sheet alloys is frequently accomplished by the paint bake cycle that is applied during the coating process. In addition to impacting grain-boundary chemistry, aging may serve to relieve stresses created in the material during rolling or extrusion.

Annealing is a moderate temperature treatment that relieves residual stress, lowers strength, and increases ductility and formability. Annealing improves corrosion resistance, but the accompaning loss of strength may be too great to be practical. In applications where strength is not of primary importance, aluminum alloys in the annealed condition provide the best corrosion resistance available.

J. Snodgrass, Corrosion Resistance of Aluminum Alloys, *Corrosion: Fundamentals, Testing, and Protection*, Vol 13A, *ASM Handbook*, ASM International, 2003, p 689–691

Corrosion Resistance of Aluminum Alloys

Jack Snodgrass and Jim Moran, Alcoa, Inc.

Selection of Fabrication Operations

Fabrication operations that create residual stress, change grain shape, and alter boundary composition can negatively impact corrosion resistance. Operations of particular concern include bending, stretching, shearing, punching, and welding. All of these operations increase residual tensile stresses. To reduce the impact of these operations on stress-corrosion-cracking resistance, the material can be stress relieved following the operation by the controlled application of heat or by shot peening. Alternately, the fabrication operation can be performed on

a material with a lower-strength temper, followed by an appropriate thermal strengthening treatment to the desired temper. In some alloys, especially those that are work hardened, several of these operations can cause changes in grain structure, such as grain growth and grain-boundary composition changes. Attention to these details can improve corrosion resistance.

J. Snodgrass, Corrosion Resistance of Aluminum Alloys, *Corrosion: Fundamentals, Testing, and Protection*, Vol 13A, *ASM Handbook*, ASM International, 2003, p 689–691

Corrosion Resistance of Aluminum Alloys

Jack Snodgrass and Jim Moran, Alcoa, Inc.

References

1. J.E. Hatch, Ed., *Aluminum: Properties and Physical Metallurgy,* American Society for Metals, 1984, p 242, 301, 306–309
2. *Aluminum Standards and Data,* The Aluminum Association, 1997, p 1–3
3. J.R. Davis, Ed., *Corrosion of Aluminum and Aluminum Alloys,* ASM International, 1999, p 202

B.A. Shaw, Corrosion Resistance of Magnesium Alloys, *Corrosion: Fundamentals, Testing, and Protection*, Vol 13A, *ASM Handbook*, ASM International, 2003, p 692–696

Corrosion Resistance of Magnesium Alloys

Revised by Barbara A. Shaw, Pennsylvania State University

Introduction

MAGNESIUM AND MAGNESIUM ALLOYS are often thought of as rapidly corroding metals because of their active positions in both the electromotive force (EMF) series (Table 1) and the galvanic series for seawater (see Fig. 1 in the article “Evaluating Galvanic Corrosion” in this Volume). However, depending on the environment and certain design considerations, the corrosion of magnesium can be well within acceptable design limits. Knowledge of environmental factors that influence degradation, types of corrosion to which magnesium alloys are most susceptible, protection schemes, and design considerations can significantly minimize corrosion and increase use of this family of lightweight structural metals.

Table 1 Standard reduction potentials

Electrode	Reaction	Potential, V
Li, Li^+	$Li^+ + e^- \rightarrow Li$	-3.02
K, K^+	$K^+ + e^- \rightarrow K$	-2.92
Na, Na^+	$Na^+ + e^- \rightarrow Na$	-2.71
Mg, Mg^{2+}	$Mg^{2+} + e^- \rightarrow Mg$	-2.37

Al, Al^{3+}	$Al^{3+} + e^- \rightarrow Al$	-1.71
Zn, Zn^{2+}	$Zn^{2+} + e^- \rightarrow Zn$	-0.76
Fe, Fe^{2+}	$Fe^{2+} + e^- \rightarrow Fe$	-0.44
Cd, Cd^{2+}	$Cd^{2+} + e^- \rightarrow Cd$	-0.40
Ni, Ni^{2+}	$Ni^{2+} + e^- \rightarrow Ni$	-0.24
Sn, Sn^{2+}	$Sn^{2+} + e^- \rightarrow Sn$	-0.14
Cu, Cu^{2+}	$Cu^{2+} + e^- \rightarrow Cu$	0.34
Ag, Ag^+	$Ag^+ + e^- \rightarrow Ag$	0.80

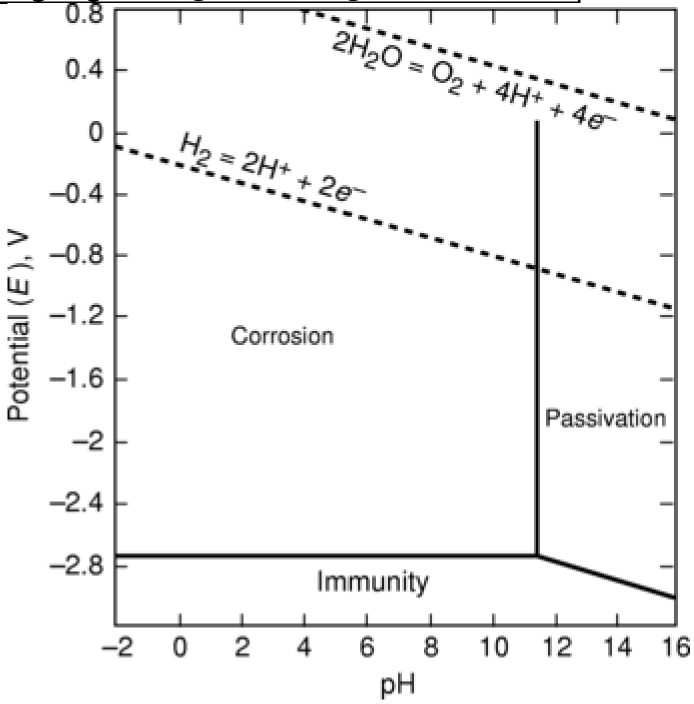

Fig. 1 Potential-pH (Pourbaix) diagram for the system of magnesium and water at 25 °C (77 °F), showing the theoretical domains of corrosion, immunity, and passivation. Source: Ref 1

When unalloyed magnesium is exposed to the air at room temperature, a gray oxide forms on its surface. Moisture converts this oxide to magnesium hydroxide, which is stable in the basic range of pH values, but is not in the neutral or acid ranges as shown in the Pourbaix diagram (Fig. 1). The immunity region of the diagram is well below the region of water stability; as a result, in neutral and low pH environments magnesium dissolution is accompanied by hydrogen evolution. In basic environments, passivation is possible as a result of the formation of a $Mg(OH)_2$ layer on the metal surface. Since the films that form on unalloyed magnesium are slightly soluble in water, they do not provide long-term protection (Ref 2). When chloride, bromide, sulfate, and chlorate are present, the surface films break down. Likewise, as the CO_2 in air acidifies water, the films are not stable. Corrosion potentials for magnesium electrodes in a variety of aqueous solutions are presented in Table 2, while corrosion rate data in water and several other media are presented in Fig. 2 and Table 3.

Table 2 Rest potential of magnesium electrodes under various aqueous solutions

Electrolyte	E_R (vs NHE)
***N* NaCl**	-1.72
***N* Na_2SO_4**	-1.75
***N* Na_2CrO_4**	-0.96
***N* HCl**	-1.68
***N* HNO_3**	-1.49
***N* NaOH**	-1.47
***N* NH_3**	-1.43
$Ca(OH)_2$ saturated	-0.95

$Ba(OH)_2$ saturated	-0.88

N, normal. Source: Ref 3

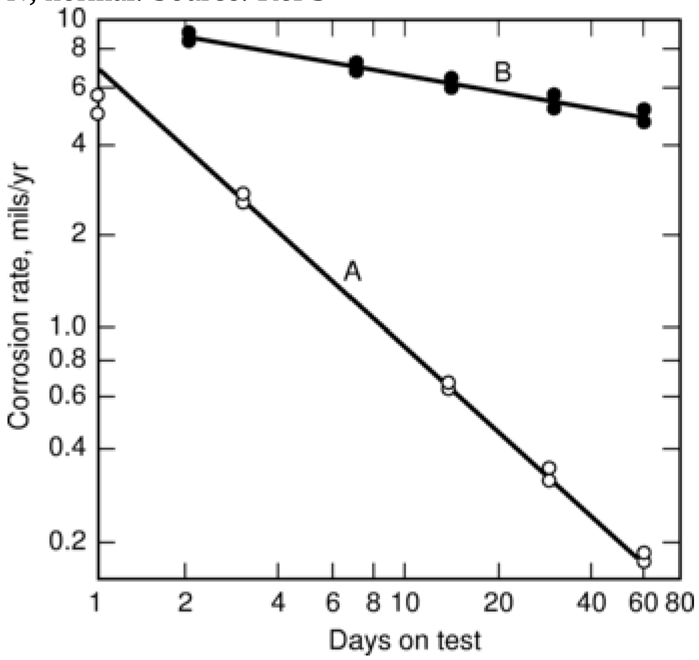

Fig. 2 Corrosion rates as a function of time for commercially pure magnesium. Curve A, distilled water vented to air through a caustic trap; curve B, distilled water vented to atmospheric CO_2. Source: Ref 2

Table 3 Corrosion rate of commercially pure magnesium in various media

Medium	Corrosion rate	
	mm/yr	**mils/yr**
Humid air	1.0×10^{-5}	0.0004
Humid air with condensation	1.5×10^{-2}	0.6
Distilled water	1.5×10^{-2}	0.6
Distilled water exposed to acid gases	0.03–0.3	1.2–12
Hot deionized water (100 °C) (14 days stagnant immersion)	16	640
Hot deionized water inhibited with 0.25 NaF	5.5×10^{-2}	2.2
Seawater	0.25	10
3*M* $MgCl_2$ solution	300	12×10^{3}
3*M* NaCl (99.99% high-purity Mg with <10 ppm Fe)	0.3	12

Grades 9980, 9990, 9991, 9995, 9998 except for NaCl solution.
Source: Compiled from Chapters 21–32 in Ref 4

Unalloyed magnesium is not extensively used for structural purposes. Consequently, the corrosion resistance of magnesium alloys is of primary concern. Two major magnesium alloy systems are available to the designer.

The first includes alloys containing 2 to 10% Al, combined with minor additions of zinc and manganese. These alloys are widely available at moderate cost, and their room-temperature mechanical properties are maintained to 95 to 120 °C (200 to 250 °F). Beyond this, elevated temperatures adversely affect mechanical properties and the corrosion properties deteriorate rapidly with increasing temperature.

The second group consists of magnesium alloyed with various elements (rare earths, zinc, thorium, and silver) except aluminum, all containing a small but effective zirconium content that imparts a fine grain structure and thus improved mechanical properties. These alloys generally possess much better elevated-temperature properties, but the more costly elemental additions combined with the specialized manufacturing technology required result in significantly higher costs. Table 4 lists some of the compositions commonly available in both systems. Note the aluminum group alloy designations begin with “A.”

Table 4 Typical magnesium alloy systems and nominal compositions

Alloy No.		Element(a), %							Product form(b)
ASTM	**UNS**	**Al**	**Zn**	**Mn**	**Ag**	**Zr**	**Th**	**Re**	
AM60	M10600	6	…	0.2	…	…	…	…	C
AZ31	M11310	3	1	0.2	…	…	…	…	W
AZ61	M11610	6	1	0.2	…	…	…	…	W
AZ63	M11630	6	3	0.2	…	…	…	…	C
AZ80	M11800	8	0.5	0.2	…	…	…	…	C, W
AZ91	M11910	9	1	0.2	…	…	…	…	C
EZ33	M12331	…	2.5	…	…	0.5	…	2.5	C
ZM21	…	…	2	1	…	…	…	…	W
HK31	M13310	…	0.1	…	…	0.5	3	…	C, W
HZ32	M13320	…	2	…	…	0.5	3	…	C
QE22	M18220	…	…	…	2.5	0.5	…	2	C
QH21	M18210	…	…	…	2.5	0.5	1	1	C
ZE41	M16410	…	4.5	…	…	0.5	…	1.5	C
ZE63	M16630	…	5.5	…	…	0.5	…	2.5	C
ZK40	M16400	…	4.0	…	…	0.5	…	…	C, W
ZK60	M16600	…	6.0	…	…	0.5	…	…	C, W

(a) For details, see alloying specifications.
(b) C, castings; W, wrought products

References cited in this section

1. M. Pourbaix, *Atlas of Electrochemical Equilibria in Aqueous Solutions,* National Association of Corrosion Engineers, 1974, p 139

2. H.P. Godard, W.P. Jepson, M.R. Bothwell, and R.L. Lane, Ed., *The Corrosion of Light Metals,* John Wiley & Sons, 1967, p 283

3. R.B. Mears and C.D. Brown, *Corrosion,* Vol 1, 1945, p 113

4. H.P. Godard, W.P. Jepson, M.R. Bothwell, and R.L. Lane, Ed., *The Corrosion of Light Metals,* John Wiley & Sons, 1967, Chap. 21

B.A. Shaw, Corrosion Resistance of Magnesium Alloys, *Corrosion: Fundamentals, Testing, and Protection,* Vol 13A, *ASM Handbook,* ASM International, 2003, p 692–696

Corrosion Resistance of Magnesium Alloys

Revised by Barbara A. Shaw, Pennsylvania State University

Metallurgical Factors

Chemical Composition. As the galvanic series in seawater reveals, magnesium is anodic to all other structural metals and, as a result, galvanic interactions between magnesium and other metals are a serious concern. The influence of cathodic iron impurities on the corrosion of commercially pure magnesium is presented in Fig. 3. Above the tolerance level of 170 ppm for iron in magnesium, the corrosion rate increases dramatically. Figure 4 shows the effects of iron and 13 other elements on the saltwater corrosion performance of magnesium in binary alloys with increasing levels of the individual elements. Six of the elements included in Fig. 4 (aluminum,

manganese, sodium, silicon, tin, and lead), as well as thorium, zirconium, beryllium, cerium, praseodymium, and yttrium, have little if any deleterious effect on the basic saltwater corrosion performance of pure magnesium when present at levels exceeding their solid solubility or up to a maximum of 5% (Ref 6). Four elements in Fig. 4 (cadmium, zinc, calcium, and silver) have mild-to-moderate accelerating effects on corrosion rates, whereas four others (iron, nickel, copper, and cobalt) have extremely deleterious effects because of their low solid-solubility limits and their ability to serve as active cathodic sites for the reduction of water at the sacrifice of elemental magnesium. Although cobalt is seldom encountered at detrimental levels and cannot be introduced even through the long immersion of cobalt steels in magnesium melts, iron, nickel, and copper are common contaminants that can be readily introduced through poor molten-metal-handling practices. These elements must be held to levels under their individual solubility limits, or their activity must be moderated through the use of alloying elements such as manganese or zinc, to obtain good corrosion resistance. These limits are stated in Table 5 for die-cast products.

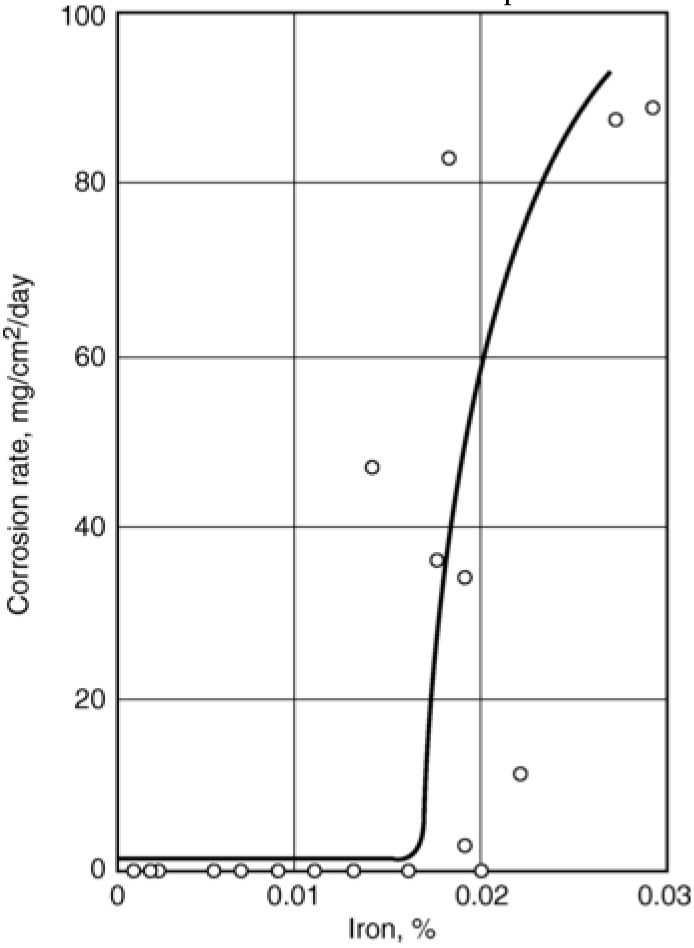

Fig. 3 Effect of iron content on the corrosion rate of commercially pure magnesium subjected to alternate immersion in 3% NaCl. Source: Ref 4

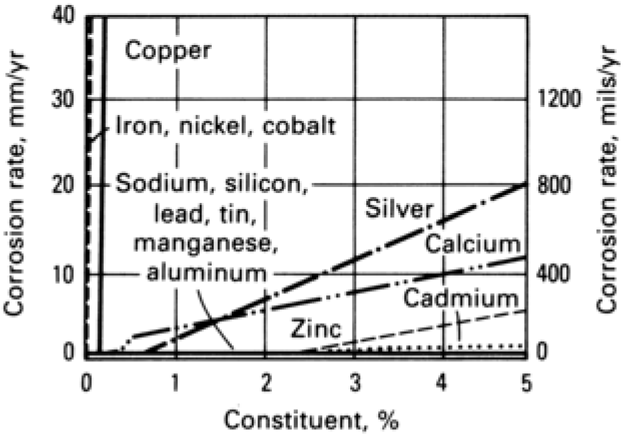

Fig. 4 Effect of alloying and contaminant metals on the corrosion rate of magnesium as determined by alternate immersion in 3% NaCl solution. Source: Ref 5

Table 5 Contaminant tolerances and manganese limits for magnesium die castings

Alloy	Critical contaminant limit (max), %			Mn limit, %
	Cu	**Ni**	**Fe**	
AM50A	0.010	0.002	0.004[(a)]	0.26–0.6[(a)]
AM60A	0.35	0.03	…	0.13–0.6
AM60B	0.10	0.002	0.005[(a)]	0.24–0.6[(a)]
AS41A	0.06	0.03	…	0.20–0.50
AS41B	0.02	0.002	0.0035	0.35–0.7
AZ91A	0.10	0.03	0.30[(b)]	0.13–0.50
AZ91B	0.35	0.03	0.3[(b)]	0.13–0.50
AZ91D	0.30	0.002	0.005[(a)]	0.15–0.50[(b)]

Per ASTM B 94.

(a) In alloys AS41B, AM50A, AM60B, and AZ91D, if either the minimum manganese limit or the maximum iron limit is not met, then the iron/manganese ratio shall not exceed 0.010, 0.015, 0.021, and 0.032, respectively.

(b) Not specified, but included in the limits for "other metals"

Figure 5 illustrates the effect of increasing iron, nickel, and copper contamination on the standard ASTM B 117 salt-spray performance of die-cast AZ91 test specimens as compared to the range of performance observed for cold-rolled steel and die-cast aluminum alloy 380 samples. Such results have led to the definition of the critical contaminant limits for two magnesium-aluminum alloys in both low- and high-pressure cast form and the introduction of improved high- purity versions of the alloys. Table 6 lists some of the critical contaminant limits defined to date. The iron tolerance for the magnesium-aluminum alloys depends on the manganese present, a fact suggested many years ago but only recently proved. For AZ91 with a manganese content of 0.15%, this means that the iron tolerance would be 0.0048% (0.032 × 0.15%) (Ref 11).

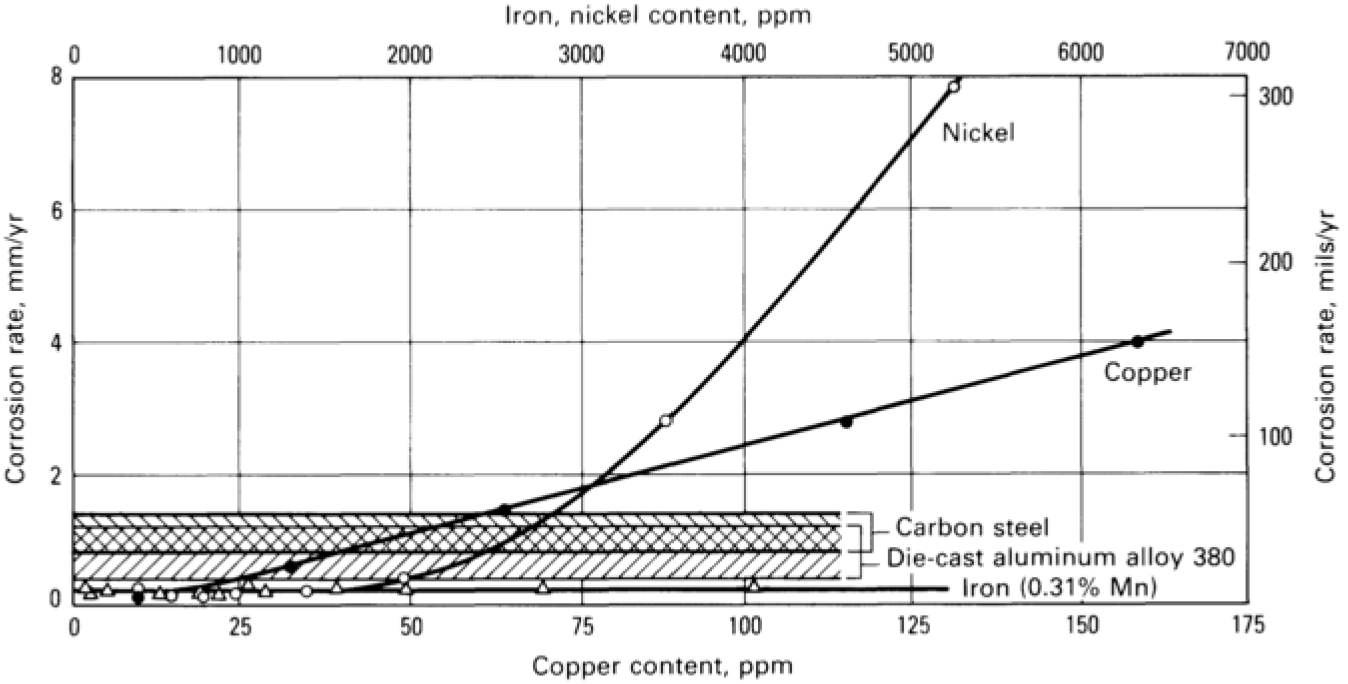

Fig. 5 Effect of nickel and copper contamination on the salt-spray corrosion performance of die-cast AZ91 alloy. Source: Ref 7

Table 6 Known contaminant tolerance limits in high- and low-pressure cast forms

Alloy/form	Grain size, μm	Critical contaminant limit, %			Ref
		Fe	**Ni**	**Cu**	
Unalloyed magnesium	…	0.015	0.0005	0.1	5
AZ91/high pressure	5–10	0.032 Mn[(a)]	0.0050	0.040	8
AZ91/low pressure	100–200	0.032 Mn[(a)]	0.0010	0.040	8
AM60/high pressure	5–10	0.021 Mn[(b)]	0.0030	0.010	7
AM60/low pressure	100–200	0.021 Mn[(b)]	0.0010	0.010	9
AZ63/low pressure	…	0.003[(c)]	0.0040	>0.45	5
K1A/low pressure	…	>0.003	0.003	…	10

(a) Iron tolerance equals manganese content of alloy times 0.032.

(b) Iron tolerance equals manganese content of alloy times 0.021.

(c) Magnesium content of AZ63 reported as 0.2%

It should also be noted that the nickel tolerance depends strongly on the cast form, which influences grain size, with the low-pressure cast alloys showing just a 10 ppm tolerance for nickel in the as-cast (F) temper. Therefore, alloys intended for low-pressure cast applications should be of the lowest possible nickel level (Ref 8). The low tolerance limits for the contaminants in AM60 alloy when compared to AZ91 alloy can be related to the absence of zinc. Zinc is thought to improve the tolerance of magnesium-aluminum alloys for all three contaminants, but it is limited to 1 to 3% Zn because of its detrimental effects on microshrinkage porosity and its accelerating effect on corrosion above 3%.

For magnesium-rare earth, -thorium, and -zinc alloys containing zirconium, the normal saltwater corrosion resistance is only moderately reduced when compared to high-purity magnesium and magnesium-aluminum alloys—0.5 to 0.76 mm/yr (20 to 30 mils/yr) as opposed to less than 0.25 mm/yr (10 mils/yr) in 5% salt spray—but contaminants again must be controlled. The zirconium alloying element is effective in this case because it serves as a strong grain refiner for magnesium alloys, and it precipitates the iron contaminant from the alloys before casting. However, if alloys containing more than 0.5 to 0.7% Ag or more than 2.7 to 3% Zn are used, a sacrifice in corrosion resistance should be expected (Fig. 4). Nevertheless, when properly finished these alloys provide excellent service in harsh environments.

Heat Treating, Grain Size, and Cold-Work Effects. Heating influences the salt-spray corrosion rate of die-cast commercial magnesium-aluminum alloys as shown in Fig. 6, which shows that alloys with higher residual-element (iron, nickel, and copper) concentrations were more negatively impacted by temperature. Using controlled-purity AZ91 alloy cast in both high- and low-pressure forms, the contaminant-tolerance limits have been defined as summarized in Table 7 for the as-cast (F), the solution treated (T4, held 16 h at 410 °C, or 775 °F, and quenched), and the solution treated and aged (T6, held 16 h at 410 °C, or 775 °F, quenched, and aged 4 h at 215 °C, or 420 °F).

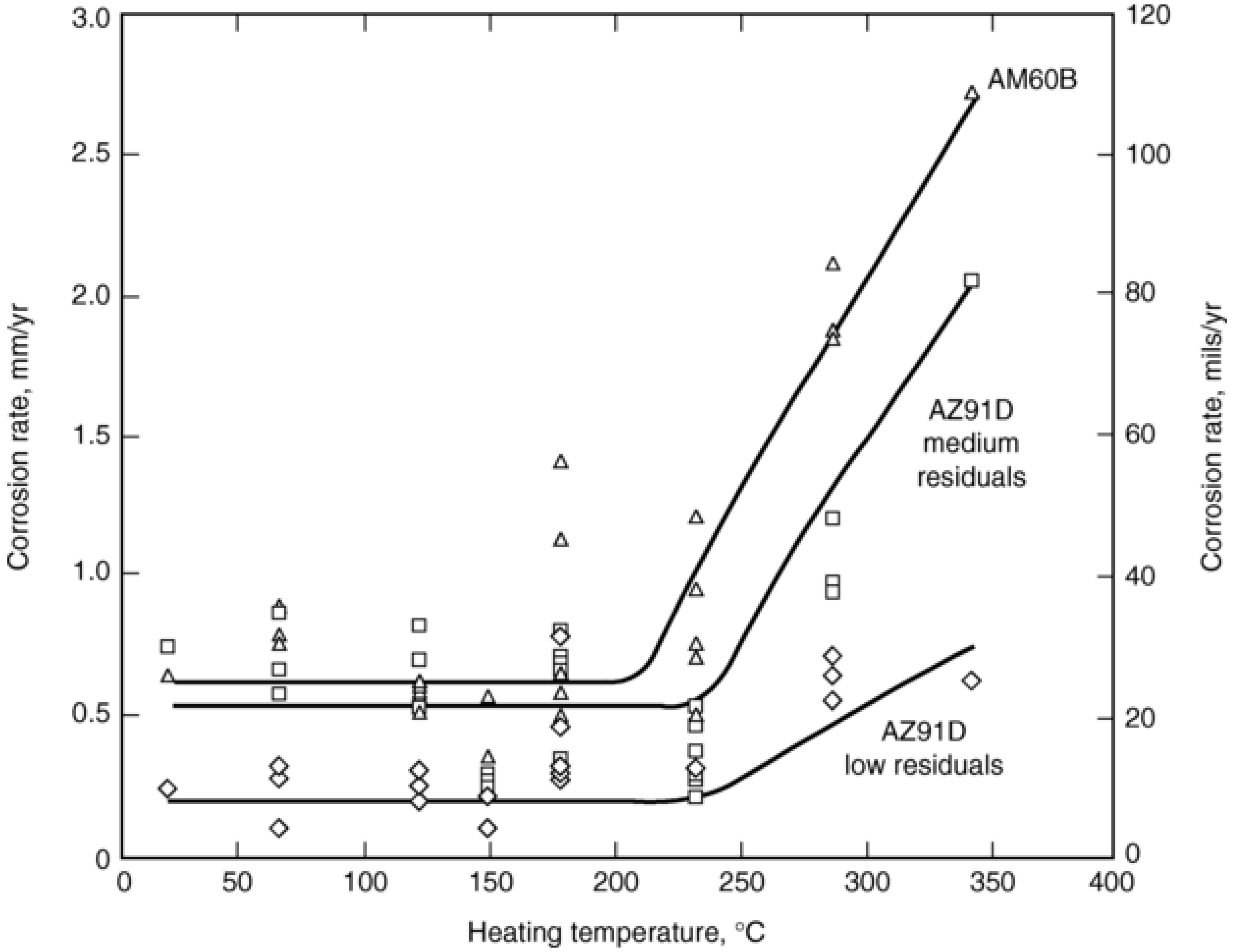

Fig. 6 Effect of heating temperature on corrosion rate of die-cast AZ91D and AM60B in salt-spray test for 10 days using ASTM B 117 method. Data are for test specimens that were heated from 0.5 to 36 h. Source: Ref 12

Table 7 Contaminant tolerance limits versus temper and cast form for AZ91 alloy

High-pressure die cast, 5–10 μm average grain size; low- pressure cast, 100–200 μm average grain size

Contaminant, %	Critical contaminant limit(a)			
	High pressure	**Low pressure**		
	F	**F**	**T4**	**T6**
Iron	0.032 Mn	0.032 Mn	0.035 Mn	0.046 Mn
Nickel	0.0050	0.0010	0.001	0.001
Copper	0.040	0.040	<0.010	0.040

(a) Tolerance limits expressed in wt% except for iron, which is expressed as the fraction of the manganese content (for example, the iron tolerance of 0.2% Mn alloy = 0.0064% Fe in F temper)

Table 8 compares the average 5% salt-spray corrosion performance of sand-cast samples produced in a standard AZ91C and a high-purity AZ91E composition. The alloys were cast with and without standard grain-refining practices used to evaluate physical and compositional effects. The cast samples were then tested in the F, T4, T6, and T5 (aged 4 h at 215 °C, or 420 °F) tempers. In the case of the high-iron-containing AZ91C, none of the variations tested significantly affected the poor corrosion performance resulting from an iron level two to three times the alloy tolerance. In the case of the high-purity alloy, however, the T5 and T6 tempers consistently gave salt-spray corrosion rates less than 0.25 mm/yr (10 mils/yr), whereas the as-cast and solution-treated samples exhibited an inverse response to grain size and/or the grain-refining agents. Welds on Mg-Al-Zn alloys should be aged or should be solution treated and aged to obtain good corrosion resistance in harsh environments and to reduce the risk of failure due to stress-corrosion cracking (SCC).

Table 8 Typical corrosion rates versus temper and grain size for two magnesium alloys

ASTM B 117 salt-spray test

Alloy	Grain size, μm	Mn, %	Fe[(a)]	Temper corrosion rate							
				F		**T4**		**T6**		**T5**	
				mm/yr	**mils/yr**	**mm/yr**	**mils/yr**	**mm/yr**	**mils/yr**	**mm/yr**	**mils/yr**
AZ91C (untreated)	187	0.18	0.087	18	700	15	600	15	600	…	…
AZ91C (degassed and grain refined)	66	0.16	0.099	17	690	18	700	15	600	…	…
AZ91E (untreated)	146	0.23	0.008	0.64	25	4	160	0.15	6	0.12	5
AZ91E (degassed and grain refined)	78	0.26	0.008	2.2	90	1.7	70	0.12	5	0.12	5
AZ91E (untreated)	160	0.33	0.004	0.35	14	3	120	0.22	9	0.12	5
AZ91E (degassed and grain refined)	73	0.35	0.004	0.72	29	0.82	33	0.1	4	0.1	4

(a) Iron is expressed as a fraction of analyzed manganese content.

Source: Ref 8, 9, 10

Cold working of magnesium alloys, such as stretching or bending, has no appreciable effect on corrosion rate. Shot- or grit-blasted surfaces often exhibit poor corrosion performance—not from induced cold work but from embedded contaminants. Acid pickling to a depth of 0.01 to 0.05 mm (0.0004 to 0.002 in.) can be used to remove reactive contaminants, but unless the process is carefully controlled, reprecipitation of the contaminant is possible, particularly with steel shot residues. Therefore, fluoride anodizing is often used when complete removal of the contaminant is essential (Ref 9).

References cited in this section

4. H.P. Godard, W.P. Jepson, M.R. Bothwell, and R.L. Lane, Ed., *The Corrosion of Light Metals,* John Wiley & Sons, 1967, Chap. 21

5. J.D. Hanawalt, C.E. Nelson, and J.A. Peloubet, Corrosion Studies of Magnesium and Its Alloys, *Trans. AIME,* Vol 147, 1942, p 273–299

6. M.R. Bothwell, in *The Corrosion of Light Metals,* John Wiley & Sons, 1967, p 269

7. J.E. Hillis and K.N. Reichek, Paper 870288, Society of Automotive Engineers, 1986

8. K.N. Reichek, K.J. Clark, and J.E. Hillis, Paper 850417, Society of Automotive Engineers, 1985

9. Dow Chemical Co., unpublished research

10. E.F. Emley, *Principles of Magnesium Technology,* Pergamon Press, 1966, p 692–695

11. I. Lunder, T.K. Aune, and K. Nisancioglu, Paper 382, presented at Corrosion/85 Conference, National Association of Corrosion Engineers, 1985

12. C. Suman, Paper 900794, Society of Automotive Engineers, 1990

B.A. Shaw, Corrosion Resistance of Magnesium Alloys, *Corrosion: Fundamentals, Testing, and Protection*, Vol 13A, *ASM Handbook*, ASM International, 2003, p 692–696

Corrosion Resistance of Magnesium Alloys

Revised by Barbara A. Shaw, Pennsylvania State University

Causes of Corrosion Failures in Magnesium Alloys

Causes of corrosion failures typically include heavy-metal contamination, blast residues, flux inclusions, and galvanic attack.

Heavy-metal contamination often results in general pitting attack that is unassociated with fasteners or dissimilar-metal attachments. The rate of attack on unpainted surfaces will be essentially unaltered by surface condition, that is, freshly sanded, machined, or acid pickled. Figure 7 illustrates the effect of heavy-metal contamination on the ASTM salt-spray corrosion performance of low-pressure cast AZ91.

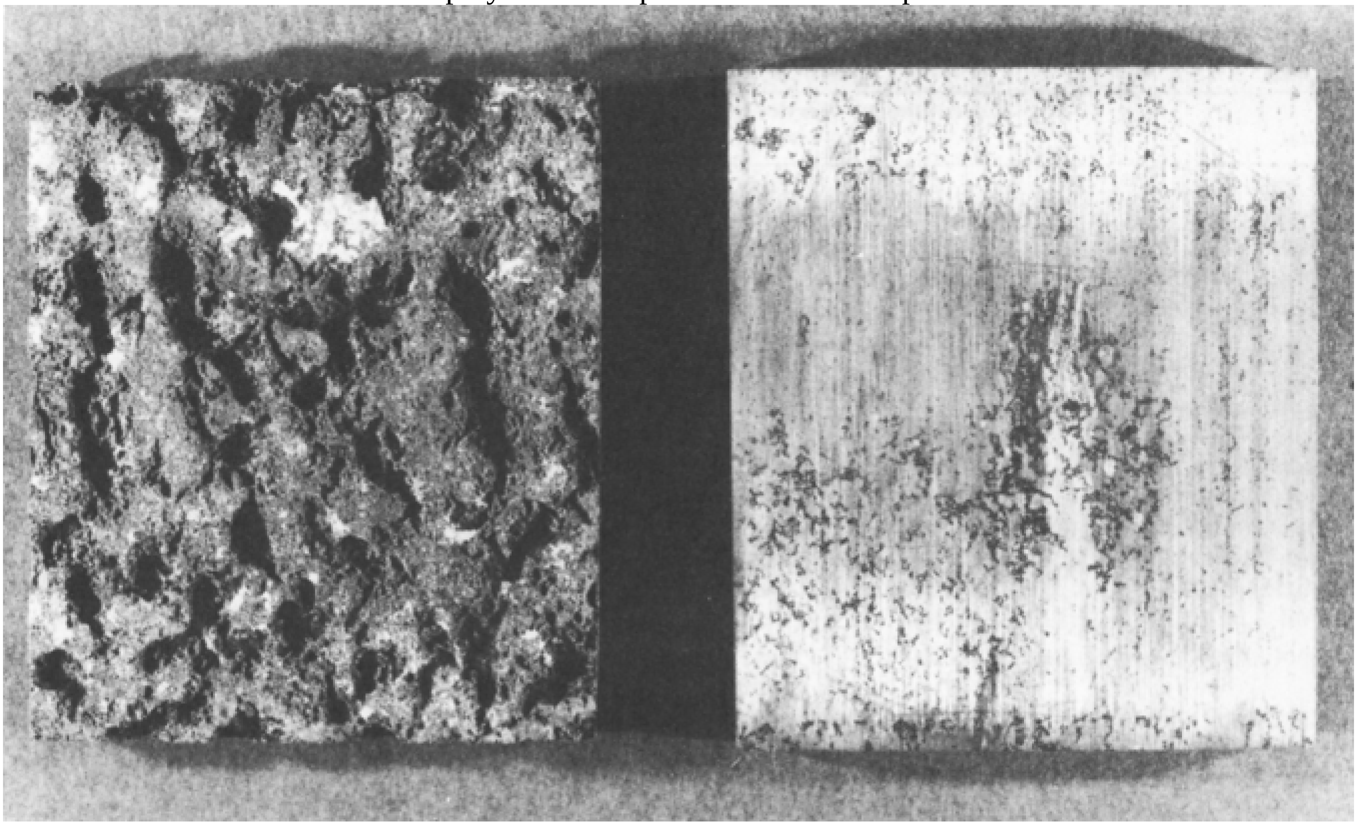

Fig. 7 Effect of heavy-metal contamination on the salt-spray performance of sand-cast AZ91 samples in the T6 temper, as determined by ASTM B 117 method. The samples, containing less than 10 ppm Ni and less than 100 ppm Cu, were simultaneously exposed for 240 h. The sample at left contained 160 ppm Fe and had a corrosion rate of 15 mm/yr (591 mils/yr). The sample at right contained 19 ppm Fe, and the corrosion rate was 0.15 mm/yr (5.9 mils/yr).

Blast residues can cause general pitting attack in saline environments. Attack is normally limited to unmachined surfaces of sand castings. Sanded or acid-etched (2% H_2SO_4 for 15 to 30 s) samples will show vastly improved performance in saltwater immersion or salt-spray tests because of removal of the contaminant. Scanning electron microscopy and energy-dispersive x-ray analysis samples cleaned in chromic acid (H_2CrO_4) can be used to confirm and identify the presence of the contaminant, which is usually iron (from steel shot blasting) or silica (from sand blasting).

Flux inclusions result in localized attack that is clustered or distributed randomly on machined surfaces of castings. Freshly machined surfaces exposed to 70 to 90% relative humidity will develop active corrosion sites

overnight. Scanning electron microscopy/energy-dispersive x-ray analysis of a freshly machined surface (free of fingerprints or other sources of contamination) will reveal pockets of magnesium and potassium chloride, as well as possible traces of calcium, barium, and sulfur. In zirconium-bearing alloys, elemental zirconium and zirconium-iron compounds may also be associated with the deposits. Chromic-acid pickling followed by chemical treatment and surface sealing can alleviate the problem of inclusions in finished castings. With the use of sulfur hexafluoride (SF_6) rapidly replacing fluxes for the protection of melts during casting, this problem should be eliminated in the future.

Galvanic attack is usually observed as heavy localized attack on the magnesium, normally within 3.2 to 4.8 mm ($\frac{1}{8}$ to $\frac{3}{16}$in.) of fasteners or an interface with other parts of dissimilar metal. Proper design and assembly methods, especially in the area of joints, can minimize galvanic attack.

Acknowledgment

This article was adapted from the article by Allan Froats, Terje Kr. Aune, David Hawke, William Unsworth, and James Hillis, “Corrosion of Magnesium and Magnesium Alloys,” which appeared in Volume 13, Corrosion, *Metals Handbook,* 9th ed., 1987; as well as the article by David L. Hawke, James E. Hillis, Mihiriban Pekguleryuz, and Isao Nakatsugawa, “Corrosion Behavior,” in *ASM Specialty Handbook: Magnesium and Magnesium Alloys,* ASM International, 1999.

B.A. Shaw, Corrosion Resistance of Magnesium Alloys, *Corrosion: Fundamentals, Testing, and Protection*, Vol 13A, *ASM Handbook*, ASM International, 2003, p 692–696

Corrosion Resistance of Magnesium Alloys

Revised by Barbara A. Shaw, Pennsylvania State University

References

1. M. Pourbaix, *Atlas of Electrochemical Equilibria in Aqueous Solutions,* National Association of Corrosion Engineers, 1974, p 139
2. H.P. Godard, W.P. Jepson, M.R. Bothwell, and R.L. Lane, Ed., *The Corrosion of Light Metals,* John Wiley & Sons, 1967, p 283
3. R.B. Mears and C.D. Brown, *Corrosion,* Vol 1, 1945, p 113
4. H.P. Godard, W.P. Jepson, M.R. Bothwell, and R.L. Lane, Ed., *The Corrosion of Light Metals,* John Wiley & Sons, 1967, Chap. 21
5. J.D. Hanawalt, C.E. Nelson, and J.A. Peloubet, Corrosion Studies of Magnesium and Its Alloys, *Trans. AIME,* Vol 147, 1942, p 273–299

6. M.R. Bothwell, in *The Corrosion of Light Metals,* John Wiley & Sons, 1967, p 269

7. J.E. Hillis and K.N. Reichek, Paper 870288, Society of Automotive Engineers, 1986

8. K.N. Reichek, K.J. Clark, and J.E. Hillis, Paper 850417, Society of Automotive Engineers, 1985

9. Dow Chemical Co., unpublished research

10. E.F. Emley, *Principles of Magnesium Technology,* Pergamon Press, 1966, p 692–695

11. I. Lunder, T.K. Aune, and K. Nisancioglu, Paper 382, presented at Corrosion/85 Conference, National Association of Corrosion Engineers, 1985

12. C. Suman, Paper 900794, Society of Automotive Engineers, 1990

A.J. Sedriks, Corrosion Resistance of Stainless Steels and Nickel Alloys, *Corrosion: Fundamentals, Testing, and Protection*, Vol 13A, *ASM Handbook*, ASM International, 2003, p 697–702

Corrosion Resistance of Stainless Steels and Nickel Alloys

A. John Sedriks, Office of Naval Research

Introduction

STAINLESS STEELS AND NICKEL-BASE ALLOYS are recognized for their resistance to general corrosion and other categories of corrosion. The effects of specific alloying elements, listed in Tables 1 and 2, metallurgical structure, and mechanical conditioning on corrosion resistance are examined in this article.

Table 1 Compositions of selected stainless steels and related higher alloys

UNS No.	AISI type or common name	Composition, %									
		C	**Mn**	**P**	**S**	**Si**	**Cr**	**Ni**	**Mo**	**Others**[(a)]	**PREN**[(b)]
Austenitic											
S30215	302B	0.15	2.0	0.05	0.03	2.00–3.00	17.00–19.00	8.00–10.00	…	…	18.00
S30400	304	0.08	2.0	0.05	0.03	1.00	18.00–20.00	8.00–10.50	…	…	19.00
S30403	304L	0.03	2.0	0.05	0.03	1.00	18.00–20.00	8.00–12.00	…	…	19.00
S30600	18-15	0.018	2.00	0.02	0.02	3.70–4.30	17.0–18.5	14.0–15.5	0.20	0.35 Cu	18.08
S30601	18-17-LC	0.015	1.0	0.030	0.013	5.00–5.60	17.0–18.0	17.0–18.0	…	…	17.9
S31000	310	0.25	2.0	0.045	0.03	1.50	24.00–26.00	19.00–22.00	…	…	25.00
S31008	310S	0.08	2.0	0.05	0.03	1.50	24.00–	19.00–	…	…	25.00

							26.00	22.00			
Ferritic											
S40900	409	0.08	1.00	0.045	0.045	1.00	10.50–11.75	0.50	…	Ti: 6 × C - 0.75	11.13
S43000	430	0.12	1.00	0.04	0.03	1.00	16.00–18.00	…	…	…	17.00
S44627	XM-27 E-Brite	0.010	0.40	0.020	0.020	0.40	25.0–27.0	0.50	0.75–1.50	0.05–0.20 Nb, 0.20 Cu, 0.015 N	29.82
Martensitic											
S41000	410	0.15	1.00	0.04	0.03	1.00	11.50–13.50	…	…	…	12.50
Superaustenitic											
S31254	254SMO	0.02	1.00	0.03	0.01	0.80	19.50–20.50	17.50–18.50	6.0–6.5	0.5–1.0 Cu, 0.18–0.22 N	43.83
N08367	Al-6XN	0.03	2.00	0.04	0.03	1.00	20.0–22.0	23.50–25.50	6.0–7.0	0.18–0.25 N	45.89
N08925	925hMo	0.02	1.00	0.045 max	0.03	0.50	19.0–21.0	24.0–26.0	6.00–7.00	0.80–1.50 Cu, bal Fe, 0.10–0.20 N	43.85
S32654	654SMO	0.02	2.00–4.00	0.03	0.005	0.50	24.0–25.0	21.0–23.0	7.00–8.00	0.30–0.60 Cu, 0.45–0.55 N	57.25
Superferritic											
S44635	Monit	0.025	1.00	0.04	0.03	0.75	24.5–26.0	3.50–4.50	3.50–4.50	0.035 N, Nb + Ti: 0.20 + 4(C + N) - 0.80	38.72
S44660	Sea-Cure	0.025	1.00	0.04	0.03	1.00	25.0–27.0	1.50–3.50	2.50–3.50	0.035 N, Nb + Ti: 0.20 + 4(C + N) - 0.08	36.17
S44735	AL-29-4C	0.03	1.00	0.04	0.03	1.00	28.0–30.0	1	3.60–4.20	0.045 N, Nb + Ti: 6(C + N)	42.22
Superduplex											
S39274	DP-3W	0.03	1.0	0.03	0.02	0.80	24.0–26.0	6.0–8.0	2.50–3.50	0.20–0.80 Cu, 1.50–2.50 W, 0.24–0.32 N	42.68
S32520	Uranus 52N+	0.03	1.5	0.035	0.02	0.8	24.0–26.0	5.5–8.0	3.0–5.0	0.5–3.00 Cu, 0.20–0.35 N	42.6
S32550	Ferralium 255	0.04	1.5	0.04	0.03	1.00	24.0–27.0	4.50–6.50	2.00–4.00	1.5–2.5 Cu, 0.1–0.25 N	38.28
S32750	SAF 2507	0.03	1.2	0.035	0.02	0.80	24.0–	6.0–	3.0–	0.24–0.32	42.68

							26.0	8.0	5.0	N	
S32760[c]	Zeron 100	0.03	1.0	0.03	0.01	1.00	24.0–26.0	6.0–8.0	3.0–4.0	0.5–1.0 Cu, 0.2–0.3 N, 0.5–1.0 W	41.79
Cast austenitic											
J95150	CN-7M	0.07	1.50	…	…	1.50	19.0–22.0	27.5–30.5	2.0–3.0	3.0–4.0 Cu	28.75
J94224	HK	0.20–0.60	2.00	0.04	0.04	2.00	24.0–28.0	18.0–22.0	…	…	26.0
High silicon											
S32615	SX	0.07	2.00	0.045	0.030	4.8–6.0	16.0–21.0	17.5–22.5	0.3–1.5	1.5–2.5 Cu	21.47

Composition is for identification only. Single values are maximum values, unless otherwise stated. UNS, Unified Numbering System; AISI, American Iron and Steel Institute.

(a) The balance of all alloys is iron.

(b) PREN, pitting-resistance equivalent number. PREN = %Cr + 3.3(%Mo) + 16(%N) + 1.65(%W) using mid-value of specified ranges or 50% of maximum specified value.

(c) Specified minimum PREN, 40

Table 2 Compositions of selected copper-nickel and nickel-base alloys

UNS No.	Common name	Composition, %														
		Ni	Cr	Cu	Fe	Co	Mo	W	Nb	Ti	Al	C	Mn	Si	B	Other
C70600	706	10.0–11.0	…	bal	1.0–2.0	Included with Cu	…	…	…	…	…	0.05	0.50–1.0	…	…	0.01 Pb, 0.05 S, Cu + named elements > 99.5
C71500	715	29.0–33.0	…	bal	0.40–1.0	Included with Cu	…	…	…	…	…	…	1.0	…	…	0.05 Pb, 1.0 Zn, Cu + named elements > 99.5. If welded, see spec for additional limits.
N02200	200	99.2 min	…	0.25 max	0.4 max	…	…	…	…	0.1 max	…	0.1	…	0.15	…	…
N02201	201	99.0 min	…	0.25 max	0.4 max	…	…	…	…	0.1 max	…	0.02	…	0.15	…	…
N04400	400	63.0–70.0	…	bal	2.50	…	…	…	…	…	…	0.3	2.00	0.50	…	0.024 S
N04405	R-405	63.0–70.0	…	bal	2.50	…	…	…	…	…	…	0.30	2.0	0.50	…	0.025–0.060 S
N05500	K-500	63.0–70.0	…	bal	2.00	…	…	…	…	0.35–0.85	2.30–3.15	0.25	1.50	0.50	…	0.01 S
N06022	C-22	bal	20.0–22.5	…	2.0–6.0	2.5	12.5–14.5	2.5–3.5	…	…	…	0.015	0.5	…	…	0.02 P, 0.02 S, 0.35 V
N06025	602CA	bal	24.0–26.0	0.1	8.0–11.0	…	0.15	…	…	0.1–0.2	1.8–2.4	0.15–0.25	0.15	0.5	…	0.020 P, 0.010 S, 0.05–0.12 Y, 0.01–0.10 Zr
N06030	G-30	43	28.0–31.5	2	15	…	4.0–6.0	1.5–4.0	0.8	…	…	0.03	…	1	…	…
N06045	45TM	45.0 min	26.0–29.0	0.3	21.0–25.0	…	…	…	…	…	…	0.05–0.12	1.00	2.5–3.0	…	0.05–0.12 N, 0.020 P, 0.010 S, total rare earth (RE) 0.05–0.15; approx 50% of RE is cerium

UNS No.	Common name	Composition, %													
		Ni	Cr	Cu	Fe	Co	Mo	W	Nb	Ti	Al	C	Mn	Si	B	Other
N06059	59	bal	22.0–24.0	…	1.5	0.3	15.0–16.5	…	…	…	0.1–0.4	0.010	0.5	0.10	…	0.015 P, 0.010 S
N06200	2000	bal	22.0–24.0	1.3–1.9	3.0	2.0	15.0–17.0	…	…	…	0.50	0.010	0.50	0.08	…	0.025 P, 0.010 S
N06600	600	bal	14.00–17.00	0.5 max	8	…	…	…	…	0.3 max	…	0.08	…	0.5	…	…
N06601	601	58.0–63.0	21.0–25.0	1	bal	…	…	…	…	…	1.0–1.7	0.1	1	0.5	…	…
N06617	617	44.5 min	20.0–24.0	0.5	3	10.0–15.0	8.0–10.0	…	…	0.6	0.8–1.5	0.05–0.15	1	1	0.006	…
N06625	625	58.0 min	20.0–23.0	…	5	1	8.0–10.0	…	3.15–4.15	0.4	0.4	0.1	0.5	0.5	…	…
N06686	686	bal	19.0–23.0	…	5.0	…	15.0–17.0	3.0–4.4	…	0.02–0.25	…	0.010	0.75	0.08	…	0.04 P, 0.02 S
N06690	690	58.0 min	27.0–31.0	0.5	7.0–11.0	…	…	…	…	…	…	0.05	0.05	0.5	…	…
N06985	G-3	bal	21.0–23.5	1.5–2.5	18.0–21.0	5.0	6.0–8.0	1.5 max	…	…	…	0.015	1.0	1.0	…	0.04 P, 0.03 S, Nb + Ta ≤ 0.50
N07214	214	bal	15.0–17.0	…	2.0–4.0	2.0	0.5	0.5 max	…	0.5	4.0–5.0	0.05	0.5	0.2	0.006	0.05 Zr, 0.002–0.040 Y, 0.015 P, 0.015 S
N07725	725	55.0–59.0	19.0–22.5	…	bal	…	7.00–9.50	…	2.75–4.00	1.00–1.70	0.35	0.03	0.35	0.20	…	0.015 P, 0.010 S
N07750	X-750	bal	14.0–17.0	…	5.0–9.0	…	…	…	0.9	2.5	…	…	…	…	…	…
N07754	MA 754	78	19.0–23.0	…	1	…	…	…	…	0.5	0.3	0.05	…	…	…	0.6 yttrium oxide
N08020	20Cb-3	32.0–38.0	19.0–21.0	3.0–4.0	bal	…	2.0–3.0	…	1	…	…	0.07	2	1	…	…
N08024	20Mo-4	35.0–40.0	22.5–25.0	0.5–1.5	bal	…	3.5–5.0	…	0.15–0.35	…	…	0.03	1	0.5	…	…
N08028	28	30.0–34.0	26.0–28.0	0.6–1.4	bal	…	3.0–4.0	…	…	…	…	0.03	2.50	1.00	…	0.030 P max, 0.030 S
N08031	3127hMo	30.0–32.0	26.0–28.0	1.0–1.4	bal	…	6.00–7.00	…	…	…	…	0.015	2.0	0.05	…	0.03 P max, 0.005 S max,

UNS No.	Common name	Composition, %														
		Ni	Cr	Cu	Fe	Co	Mo	W	Nb	Ti	Al	C	Mn	Si	B	Other
																0.15–0.25 N
N08330	RA-330	34.0–37.0	17.0–20.0	1.00	bal	…	…	…	…	…	…	0.08	2.00	0.75–1.50	…	0.03 P max, 0.03 S max, 0.025 Sn, 0.005 Pb
N08800	800	30.0–35.0	19.0–23.0	…	39.5 min	…	…	…	…	0.15–0.60	0.15–0.60	0.1	1.5	1	…	…
N08825	825	38.0–46.0	19.5–23.5	1.5–3.0	bal	…	2.5–3.5	…	…	0.6–1.2	0.2	0.05	1	0.5	…	0.04 P, 0.03 S
N08904	904L	23.0–28.0	19.0–23.0	1.00–2.00	bal	…	4.00–5.00	…	…	…	…	0.020	2.00	1.00	…	0.045 P max, 0.035 S
N10276	C-276	bal	14.5–16.5	…	5.5	…	15.0–17.0	3.0–4.5	…	…	…	0.01	…	0.08	…	…
N10665	B-2	bal	1.0 max	…	2.0 max	…	26.0–30.0	…	…	…	…	0.01	…	0.1	…	…

Composition is for identification only. Single values are maximum values, unless otherwise stated. UNS, Unified Numbering System

A.J. Sedriks, Corrosion Resistance of Stainless Steels and Nickel Alloys, *Corrosion: Fundamentals, Testing, and Protection*, Vol 13A, *ASM Handbook*, ASM International, 2003, p 697–702

Corrosion Resistance of Stainless Steels and Nickel Alloys

A. John Sedriks, Office of Naval Research

Stainless Steels

Stainless steels are corrosion-resistant iron- base alloys containing a maximum of 1.2% carbon and a minimum of 10.5% chromium by weight. This is the minimum amount of chromium that prevents the formation of rust in humid, unpolluted atmospheres, hence the designation “stainless.” The corrosion resistance of stainless steels is provided by a very thin and protective surface film, known as the passive film, which, when damaged, is self-healing in the presence of a wide variety of environments.

The Fe-Cr-Ni and Fe-Cr-Ni-Mn-N grades of stainless steels are austenitic and are popularly known by the former American Iron and Steel Institute (AISI) type numbers in the 300 and 200 series, respectively. The Fe-Cr grades are martensitic at lower chromium levels, ferritic at higher chromium levels, and are known by numbers in the 400 series. The most popular austenitic, ferritic, and martensitic grades have been type 304 (containing 19% Cr, 10% Ni, and also known by the Unified Numbering System (UNS) number, S30400), type 430 (17% Cr, S43000), and type 410 (12% Cr, S41000), respectively. Another popular grade has been type 409 (11% Cr, S40900) because of its use in automobile exhaust systems. Duplex grades (containing approximately 50% austenite and 50% ferrite) and precipitation-hardening grades (mostly martensitic) are also available for higher strength applications.

Stainless steels are used for consumer products; for machinery; in architecture; for military applications (particularly for nonmagnetic hulls of submarines and mine countermeasure vessels); and for equipment in the petroleum, chemical, aerospace, power, and process industries. Environmental initiatives, such as flue gas desulfurization in the power industry and the adoption of closed-loop (zero discharge) processes in the pulp and paper industry, have increased the demand for stainless steels.

The manufacturers of stainless steels have tended to specialize as either flat-product producers or long-product producers. Flat products include plate, sheet, strip, and foil, whereas long products include bar, rod, wire, and forging billets. Products such as forgings, welded pipe and tube, seamless pipe and tube, fittings, and weld fillers are made from either long or flat products by mills dedicated to their production. Castings and powder metallurgy products are typically custom melted by specialty producers. Some 180 different alloys can be recognized as belonging to the stainless steel group and currently are produced, with alloy content adjusted to give improved resistance to pitting and crevice corrosion, intergranular corrosion caused by sensitization, stress-corrosion cracking (SCC) and hydrogen embrittlement, general corrosion, and attack by high-temperature gases (Fig. 1).

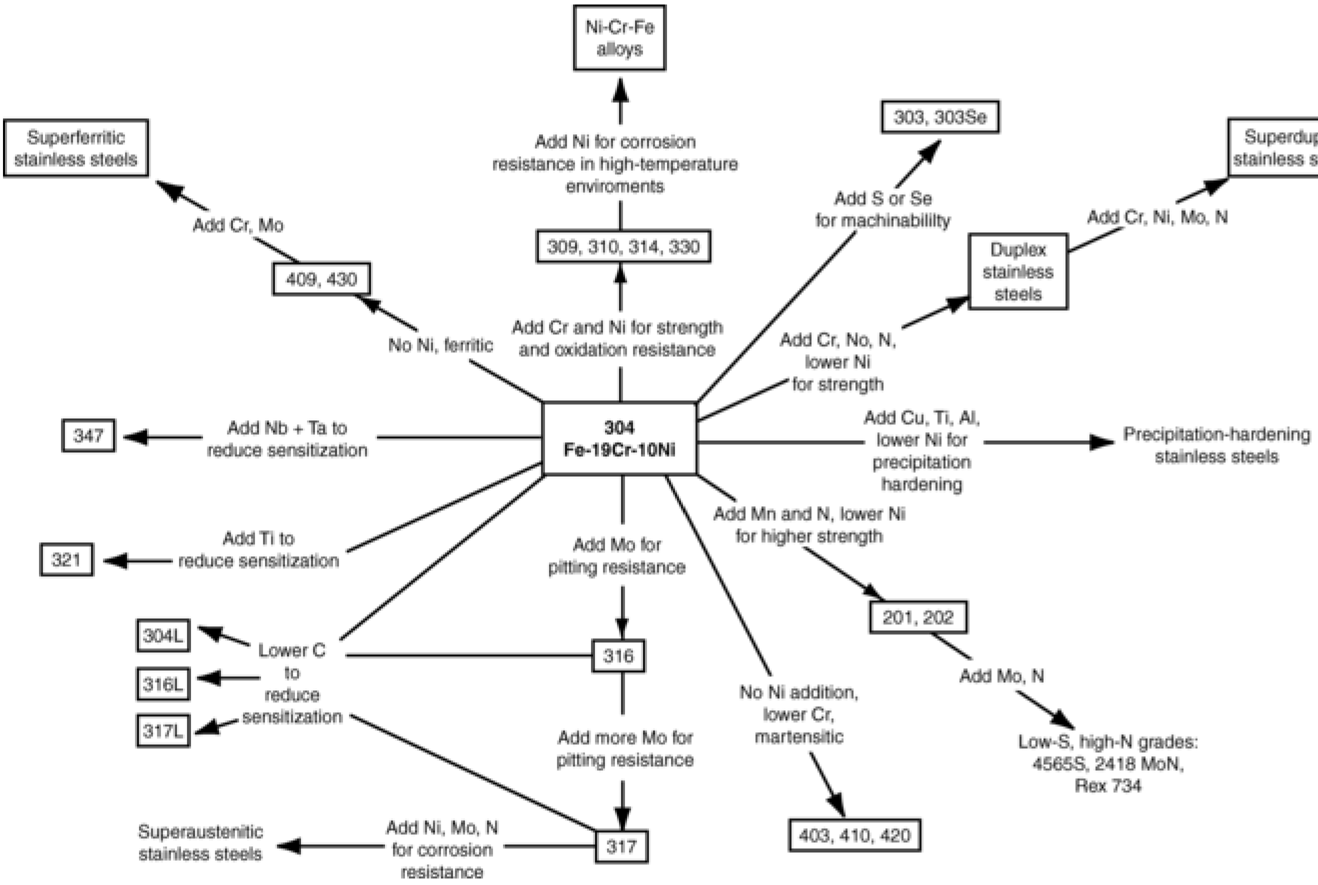

Fig. 1 Compositional and property linkages for stainless steels

Pitting and Crevice Corrosion. Resistance to pitting and crevice corrosion usually is improved by alloying the austenitic and duplex grades further with chromium, molybdenum, and nitrogen, and the ferritic grades with chromium and molybdenum. The beneficial effects of these alloying elements are complex and interactive. Attempts have been made by suppliers of stainless steels and nickel-base alloys to develop a compositionally derived pitting- and crevice-corrosion-resistance index known as the pitting-resistance equivalent number (PREN). The PREN is given by the alloying-element parameter %Cr + 3.3%Mo + 16%N + 1.65%W. In general, the larger the numerical value of PREN is, the higher the pitting and crevice-corrosion resistance will be, although a high numerical value of PREN should not be viewed as an absolute guarantee of freedom from localized attack. The major drawback in using a parameter based only on alloy content is that it ignores the often-found detrimental effects of microstructural constituents such as manganese sulfide inclusions, sigma and chi phases, chromium depleted zones, and alloying element segregation due to coring produced by weld solidification. However, PREN provides some guidance for alloy selection for service in oxidizing chloride or acidic environments. Among the proprietary stainless steels with a large numerical value of PREN are the superaustenitics, such as 254SMO (S31254), AL6XN (N08367), 925hMo (N08925), and 654SMO (S32654); the superferritics, such as 29-4C (S44735), Sea-Cure (S44660), and Monit (S44635); and the superduplexes, such as DP-3W (S39274), Ferralium 255 (S32550), SAF 2507 (S32750), Zeron 100 (S32760), and Uranus 52N+ (S32520).

Intergranular corrosion results from chromium depletion in the alloy matrix near grain- boundary chromium carbides (and sometimes nitrides). These can be precipitated during welding or some other high-temperature exposure. This depletion occurs at certain time-temperature combinations that are sufficient to precipitate chromium carbide but insufficient to rediffuse chromium back into the austenite near the carbide. For example, heating type 304 stainless steel containing 0.039% carbon for 10 h at 700 °C (1290 °F) results in the formation of chromium carbides that reduce the chromium level from 19% to less than 13% in the region next to the grain-boundary carbide precipitate, resulting in a loss of corrosion resistance in this region. This depletion is known as *sensitization.* Similar chromium depletion occurs in high-nitrogen duplex stainless steels due to the formation of chromium nitrides. Remedial measures for sensitization include alloying-element control procedures such as lowering the carbon content to 0.03% maximum, as in 304L (S30403), or stabilizing with titanium or niobium plus tantalum alloying additions (Fig. 1), or metallurgical treatments such as postweld

annealing to re-diffuse chromium back into the depleted regions. It should be noted that duplex stainless steels do not exhibit sensitization at the austenite-ferrite grain boundaries because of faster chromium diffusion and carbide growth kinetics in the ferrite phase. Nickel-base alloys are generally resistant to sensitization, because they are usually made either with sufficiently low carbon content or are stabilized with niobium.

Stress-corrosion cracking may occur in the presence of a tensile stress and a specific corrodent. Corrodents known to cause SCC in stainless steels are chloride solutions at elevated temperatures, caustic solutions, acids, aqueous solutions containing sulfur compounds, and high-temperature (300 °C, or 570 °F) water containing traces of dissolved oxygen. For SCC caused by sensitization, the remedies are the same as for intergranular corrosion. In other cases, susceptibility to SCC can be minimized or eliminated by alloying additions, metallurgical treatments, mechanical treatments, and chemical/electrochemical treatments. For example, susceptibility to SCC can be minimized by increasing the nickel content of the alloy (for austenitics only), selecting a suitable ferritic or duplex stainless steel instead of an austenitic one, lowering the service temperature, stress-relief annealing, shot peening to introduce compressive surface stresses, adding chemical corrosion inhibitors to the service environment, and cathodic protection. The last procedure should not be used for martensitic or precipitation-hardening stainless steels, which crack by a hydrogen embrittlement mechanism. For martensitic or precipitation-hardening stainless steels, tempering heat treatments to produce lower strengths may improve cracking resistance.

General corrosion (i.e., nonlocalized corrosion) can be encountered in strong acids or alkalies. Corrosion resistance in sulfuric and organic acids is promoted by alloying with copper, molybdenum, and nickel. Among alloys used in the chemical industry for sulfuric acid service are the copper-containing stainless steels and higher alloys, such as alloy 904L (N08904), 20Cb-3 (N08020), alloy 825 (N08825), and the cast stainless steel CN-7M (J95150), whereas higher-silicon stainless steel, such as S32615, has been used for handling hot, concentrated sulfuric acid. Phosphoric acid is handled by high- molybdenum grades, such as alloy 28 (N08028), G-30 (N06030), and 3127hMo (N08031). Nitric acid at most concentrations and temperatures can be handled by less highly alloyed stainless steels, such as type 304L (S30403), although higher- chromium stainless steels, such as type 310S (S31008) and alloy 800 (N08800), as well as silicon-containing stainless steels, such as S30600 and S30601, have been used for very hot, concentrated nitric acid. The ferritic stainless steel E-Brite (S44627) as well as the low-carbon version of commercially pure nickel, Nickel 201 (N02201), have been used to handle elevated- temperature caustic environments.

High-Temperature Corrosion. The various types of attack by high-temperature gases usually are referred to as oxidation, sulfidation, carburization, nitriding, and halogen-gas corrosion. In oxidizing, sulfidizing, and carburizing gases, high chromium contents, such as in type 310 (25% Cr, S31000) or its cast variant HK (J94224), improve resistance to attack. In addition, alloying with aluminum and silicon can be beneficial to oxidation resistance, as in type 406 (3.5% Al) and in type 302B (S30215, 2.5% Si), respectively. Resistance to nitriding is improved by alloying with nickel, as in RA-330 (N08330). For stainless steels, the upper temperature limit for operation in dry chlorine is approximately 320 °C (600 °F), with the presence of water vapor accelerating corrosion.

A.J. Sedriks, Corrosion Resistance of Stainless Steels and Nickel Alloys, *Corrosion: Fundamentals, Testing, and Protection*, Vol 13A, *ASM Handbook*, ASM International, 2003, p 697–702

Corrosion Resistance of Stainless Steels and Nickel Alloys

A. John Sedriks, Office of Naval Research

Nickel-Base Alloys

Nickel-base alloys make up an important segment of the corrosion-resistant materials, taking over from stainless steels and other alloys as service temperature or environment corrosivity increases. Commercially pure nickel, Nickel 200 (N02200), or its low-carbon version, Nickel 201 (N02201), is used as a corrosion-resistant material in food processing and in high-temperature caustic and gaseous chlorine or chloride environments.

However, alloying of nickel with other elements (e.g., chromium, copper, or molybdenum) greatly broadens its use in corrosion- resistant applications (Fig. 2).

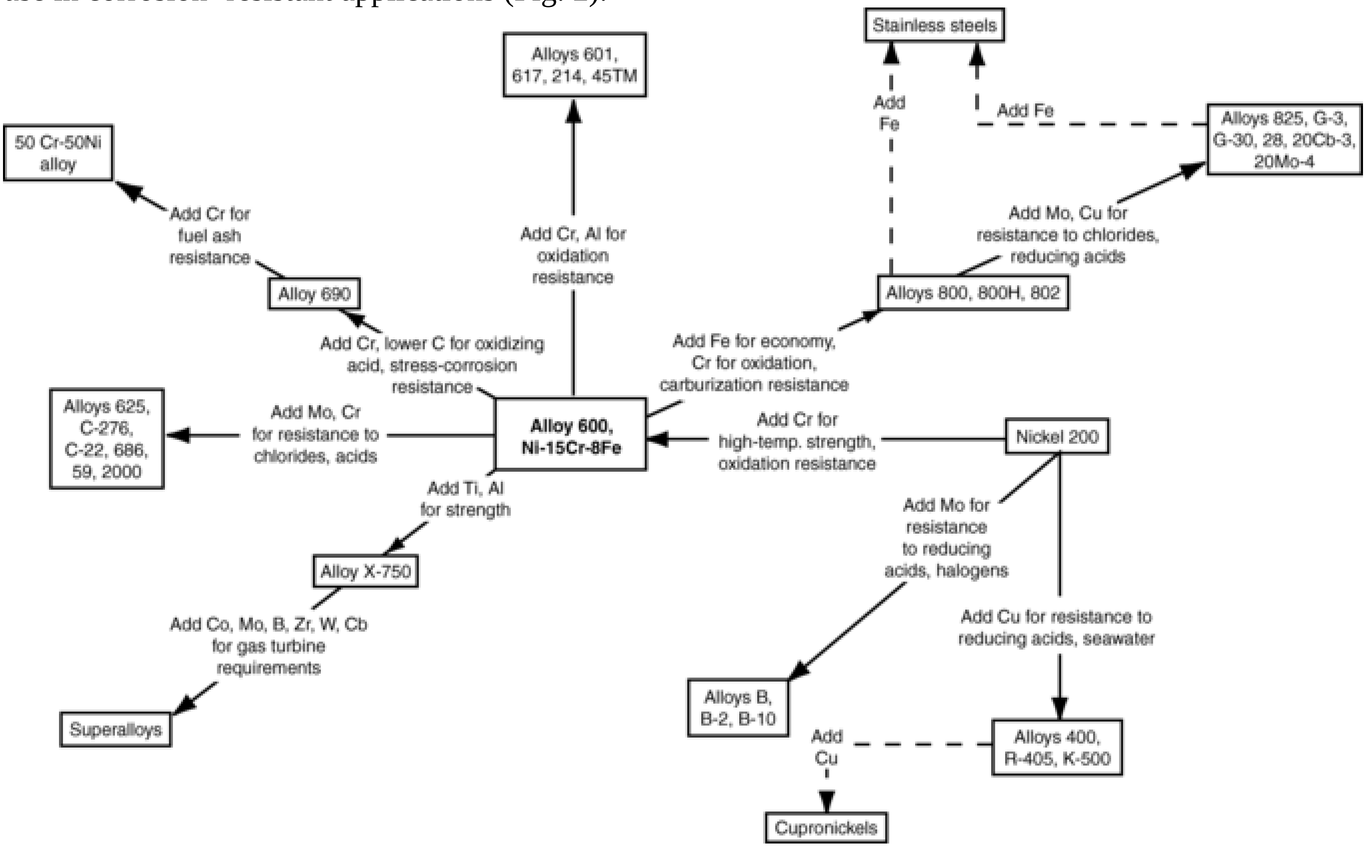

Fig. 2 Compositional and property linkages for nickel-base alloys

Nickel-Chromium Alloys. By far, the largest family of nickel alloys is that based on the nickel-chromium system, with alloy 600 (N06600) being the prototype (Fig. 2). Chromium imparts resistance to oxidizing environments and high-temperature strength. Increasing chromium to 30%, as in alloy 690 (N06690), also increases resistance to SCC in high-temperature (300 °C, or 570 °F) water and to corrosion in nitric acid solutions, steam, oxidizing gases, and shipboard waste-incinerator environments. Increasing chromium to 50%, as in IN- 657 (N07765), increases resistance to melting sulfates and vanadates found in fuel ash.

High-temperature oxidation resistance of nickel-chromium alloys is improved further by alloying with aluminum, as in alloys 601 (N06601) and 617 (N06617). Alloying additions of silicon and rare earth elements (e.g., cerium, yttrium, and lanthanum) also increase oxidation resistance. Among alloys that take advantage of the benefits of rare earth element additions on oxidation resistance are the silicon-containing alloys, such as 353MA (S35315) and 45TM (N06045), and the aluminum-containing alloys, such as 602CA (N06025) and 214 (N07214).

Of importance for use in aqueous reducing acids, oxidizing chloride solutions, and seawater in the presence of crevices and tight joints are the Ni-Cr-Mo alloys, such as 625 (N06625), C-276 (N10276), C-22 (N06022), 59 (N06059), 686 (N06686), and C-2000 (N06200). For these alloys to exhibit the maximum resistance to crevice corrosion in seawater environments, they should be free of deleterious precipitate phases and chromium-depleted surface layers. It is important, therefore, to remove by pickling, electropolishing, or mechanical processes, such as abrasion or grinding, any surface layers that have become depleted in chromium during high-temperature (above 980 °C, or 1800 °F) manufacturing steps.

Low-level titanium and aluminum alloying additions to nickel-chromium alloys and to Ni- Cr-Mo alloys result in strengthening by the precipitation of the γ' phase, without loss of corrosion resistance, as in alloys X-750 (N07750) and 725 (N07725), respectively.

Cobalt and other alloying additions provide to jet engine materials (superalloys) a combination of high-temperature strength and creep resistance, with oxidation and sulfidation resistance. Oxide dispersion strengthening, in addition to γ' strengthening, is used in the mechanically alloyed materials MA 754 (N07754) to provide high-temperature strength and oxidation resistance at the very high temperatures (approximately 1200 °C, or 2200 °F) encountered in molten glass processing and in reheating furnaces used in steel production.

Nickel-molybdenum alloys, such as B-2 (N10665), have excellent corrosion resistance in hydrochloric acid with low oxidizer content, whereas nickel-silicon alloys, such as D-207, have good corrosion resistance in hot, concentrated sulfuric acid.

Another technologically important group of materials are the lower-nickel (30 to 40%) Ni- Cr-Fe alloys that were originally developed to conserve nickel. The prototype, alloy 800 (N08800), is a general-purpose alloy with good high-temperature strength and good corrosion resistance in steam and in oxidizing or carburizing gases. Further alloying with molybdenum and copper, as in alloys 825 (N08825), G-3 (N06985), G-30 (N06030), 28 (N08028), 20Cb- 3 (N08020), and 20Mo-4 (N08024), improves resistance to localized corrosion in chlorides and resistance to general corrosion in reducing acids.

Nickel alloys exhibit high resistance to corrosive attack under nitriding conditions (e.g., in dissociated ammonia) and in chlorine or chloride gases. Corrosion in the latter at elevated temperatures proceeds by the formation and volatilization of chloride scales. High nickel contents in the alloys are beneficial, because nickel forms one of the least volatile chlorides. Conversely, in sulfidizing environments, high-nickel alloys without chromium can undergo corrosive attack due to the formation of a low-melting-point eutectic.

Nickel-copper alloys represent another technologically important group of materials. At higher nickel contents are alloys 400 (N04400), R-405 (N04405), and K-500 (N05500), which are used for certain corrosive chemicals, such as hydrofluoric acid, and for seawater. At higher copper contents are the cupronickels, such as 706 (C70600) and 715 (C71500), which are widely used for seawater applications because of their corrosion resistance and the ease with which marine fouling can be removed by mechanical processes.

A.J. Sedriks, Corrosion Resistance of Stainless Steels and Nickel Alloys, *Corrosion: Fundamentals, Testing, and Protection*, Vol 13A, *ASM Handbook*, ASM International, 2003, p 697–702

Corrosion Resistance of Stainless Steels and Nickel Alloys

A. John Sedriks, Office of Naval Research

Selected References

- “Corrosion Engineering Bulletin 1–6,” International Nickel Company, Inc., 1962–1980
- J.R. Davis, Ed., *ASM Specialty Handbook: Stainless Steels,* ASM International, 1994
- C.P. Dillon, *Corrosion Resistance of Stainless Steels,* Dekker, 1995
- M.G. Fontana and N.D. Greene, *Corrosion Engineering,* 2nd ed., McGraw-Hill, 1979
- W.Z. Friend, *Corrosion of Nickel and Nickel- Base Alloys,* Wiley, 1979
- F.L. LaQue and H.R. Copson, Ed., *Corrosion Resistance of Metals and Alloys,* 2nd ed., Reinhold, 1963
- D. Peckner and I.M. Bernstein, Ed., *Handbook of Stainless Steels,* McGraw-Hill, 1977
- A.J. Sedriks, *Corrosion of Stainless Steels,* 2nd ed., Wiley, 1996

S. Yu, Corrosion Resistance of Titanium Alloys, *Corrosion: Fundamentals, Testing, and Protection*, Vol 13A, *ASM Handbook*, ASM International, 2003, p 703–711

Corrosion Resistance of Titanium Alloys

Steven Yu, 3M Company

Introduction

TITANIUM AND ITS ALLOYS are valuable engineering materials due to their combination of light weight, high strength-density ratio, and stability in a wide range of environmental conditions (Ref 1, 2, 3, 4, 5, 6). Yet, historically high cost per weight has limited the use of titanium and titanium-base alloys to mission-critical engineering applications such as aerospace, military, or biomedical industries. Recent availability of commercial-grade titanium from the Russian Federation and the People's Republic of China has made the application of titanium-base alloys more accessible for the general consumer industry. Information on the engineering applications of titanium, its mechanical properties, and its alloy variants is readily available in literature (Ref 1, 2, 3, 4, 5, 6). The scope of this article is to provide the reader with a background in the complex relationship between titanium and its alloys with aqueous environments, which is dictated by the presence of a passivating oxide film.

References cited in this section

1. M.J. Donachie, Jr., *Titanium: A Technical Guide,* 2nd ed., ASM International, 2000
2. C.R. Brooks, *Heat Treatment, Structure and Properties of Nonferrous Alloys,* American Society for Metals, 1982
3. R. Boyer, G. Welsch, and E.W. Collings, Ed., *Materials Properties Handbook: Titanium Alloys,* ASM International, 1994
4. T.P. Hoar and D.C. Mears, Corrosion-Resistant Alloys in Chloride Solutions: Materials for Surgical Implants, *Proc. R. Soc. (London) A,* Vol 294 (No. 1438), 1966, p 486–510
5. A. McQuillan, *Titanium Science and Technology,* Plenum Press, 1973, p 915–922
6. R. Schutz, An Overview of Beta Titanium Alloy Environmental Behavior, *Beta Titanium Alloys in the 1990's,* D. Eylon, R. Boyer, and D. Koss, Ed., Minerals, Metals and Materials Society, 1993, p 75–91

S. Yu, Corrosion Resistance of Titanium Alloys, *Corrosion: Fundamentals, Testing, and Protection*, Vol 13A, *ASM Handbook*, ASM International, 2003, p 703–711

Corrosion Resistance of Titanium Alloys

Steven Yu, 3M Company

Corrosion Resistance of Titanium and Titanium-Base Alloys in Aqueous Environments

Pure titanium is highly corrosion resistant in aqueous environments that encompass any pH > 2, even those that contain aggressive anionic species (including Cl^-) (Ref 6, 7). Nevertheless, metallic titanium is thermodynamically reactive, as indicated by its relatively negative reversible potential on the electromotive force (emf) scale (E_0 = -1.63 V_{NHE}). (NHE is normal hydrogen electrode.) As a result of its reactivity, metallic titanium readily oxidizes during exposure to air as well as during exposure to aqueous and nonaqueous electrolytes (Ref 6, 8, 9, 10, 11, 12, 13, 14, 15). Such oxidation leads to the formation of titanium-base oxides, hydrated complexes, or aqueous cationic species as a result of active anodic dissolution. The oxide and hydrated-complex layers function as barriers between the surrounding environment and the underlying metallic titanium, which inhibit the subsequent oxidation of metallic titanium across the metal/barrier layer/solution interface. Therefore, further oxidation of titanium can only occur by anion and cation movement across the oxide through diffusion and migration by potential field-assisted movement through this barrier (Ref 15, 16, 17, 18).

Coherent titanium oxide films resist uniform corrosion in many environments, such as all natural waters, including distilled, fresh, and seawater (aerated and deaerated), as well as brine solutions, to temperatures in excess of 200 °C (390 °F) (Ref 6). Furthermore, titanium is generally corrosion resistant in the presence of oxidizing-acid media. Oxidizing acids, including chromic, nitric, perchloric, and hypochloric acids, readily oxidize titanium to form thermodynamically stable TiO_2 where oxide formation and further oxide thickening promotes additional passivity. In contrast, passivated titanium exhibits poor resistance to corrosion in reducing-acid environments, such as hydrochloric or sulfuric acids, where the passivating TiO_2 can be reduced to a soluble form of oxidized titanium. Therefore, alloying additions that can promote the stability of protective titanium oxide films in reducing-acid environments are beneficial in inhibiting corrosion of titanium-base alloys.

References cited in this section

6. R. Schutz, An Overview of Beta Titanium Alloy Environmental Behavior, *Beta Titanium Alloys in the 1990's,* D. Eylon, R. Boyer, and D. Koss, Ed., Minerals, Metals and Materials Society, 1993, p 75–91

7. M. Pourbaix, *Atlas of Electrochemical Equilibria in Aqueous Solutions,* 1st ed., NACE, 1974

8. R.W. Schutz and J.S. Grauman, “Compositional Effects on Titanium Alloy Repassivation Potential in Chloride Media,” Second International Conference on Localized Corrosion, (Orlando, FL) NACE, 1987

9. P.Y. Park et al., The Corrosion Behavior of Sputter-Deposited Mo-Ti Alloys in Concentrated Hydrochloric Acid, *Corros. Sci.,* Vol 38 (No. 10), 1996 p 1649–1667

10. V. Andreeva et al., Investigation of the Corrosion Resistance and the Electrochemical and Mechanical Properties of Titanium-Niobium Alloys, *Corrosion of Metals and Alloys,* N. Tomashov and E. Nirolybev, Ed., Israel Program for Scientific Translation, Jerusalem, 1966, p 34–47

11. P.J. Bania, *Beta-Titanium Alloys and Their Role in Titanium Industry,* D. Eylon, R. Boyer, and D. Koss, Ed., TMS, 1993, p 4

12. M. Levy and G. Sklover, Anodic Polarization of Titanium and Titanium Alloys in Hydrochloric Acid, *J. Electrochem. Soc.,* Vol 116 (No. 3), 1969, p 323–328

13. M. Itagaki, R. Oltra, and B. Vuillemin, Quantitative Analysis of Iron Dissolution During Repassivation of Freshly Generated Metallic Surfaces, *J. Electrochem. Soc.,* Vol 144 (No. 1), 1997, p 64–72

14. A. Mazhar, F. Heakal, and A. Gad-Allah, Anodic Behavior of Titanium in Aqueous Media, *Corros. Sci.,* Vol 44, 1988, p 705–710

15. D. Tomashov et al., The Passivation of Alloys on Titanium Bases, *Electrochim. Acta,* Vol 19, 1974, p 159–172

16. P.A. Mausli, S.G. Steinemann, and J.P. Simpson, “Properties of Surface Oxides on Titanium and Some Titanium Alloys,” Proceedings of the Sixth World Conference on Titanium (France), P. LaCombe, R. Tricot, and G. Bèranger, Ed., Sociètè Francaise de Métallurgie, 1988

17. N. Khalil and J.S.L. Leach, The Anodic Oxidation of Valve Metals, Part I: Determination of Ionic Transport Numbers by Alpha Spectrometry, *Electrochim. Acta,* Vol 31 (No. 10), 1986, p 1279–1285

18. J. Leach and B. Pearson, The Effect of Foreign Ions upon the Electrical Characteristics of Anodic ZrO_2 Films, *Electrochim. Acta,* Vol 29 (No. 9), 1984, p 1271–1282

S. Yu, Corrosion Resistance of Titanium Alloys, *Corrosion: Fundamentals, Testing, and Protection*, Vol 13A, *ASM Handbook*, ASM International, 2003, p 703–711

Corrosion Resistance of Titanium Alloys

Steven Yu, 3M Company

Passivating Titanium Oxides

Titanium is one of the thermodynamically reactive metals generally described as valve metals due to the ability of these metals to allow relatively fast cathodic reaction rates while limiting the reaction rate of the anodic reactions (Ref 19). Limited anodic reaction rates result from the formation of thermodynamically or kinetically stable oxide films. Such oxide films reduce reactivity and enhance corrosion resistance of titanium within a wide range of pH, as shown in Fig. 1. Moreover, titanium oxides, formed near the respective open-circuit potentials (OCPs) of titanium, have been generally agreed on to be amorphous (Ref 20, 21, 22). The amorphous nature of titanium oxide is attributed to a cation egress mechanism due to an applied potential field gradient, which results in the formation of the oxide primarily at the solution-oxide interface (Ref 22, 23). Therefore, there is limited epitaxial constraint to form a crystalline oxide. However, titanium oxides can undergo a phase transformation from amorphous to one of the following crystalline structures during anodic polarization or during heat treatments: (a) anatase (tetragonal), (b) rutile (tetragonal), or (c) brookite (orthorhombic) (Ref 22, 24). The lattice parameters of TiO_2 are presented in Table 1.

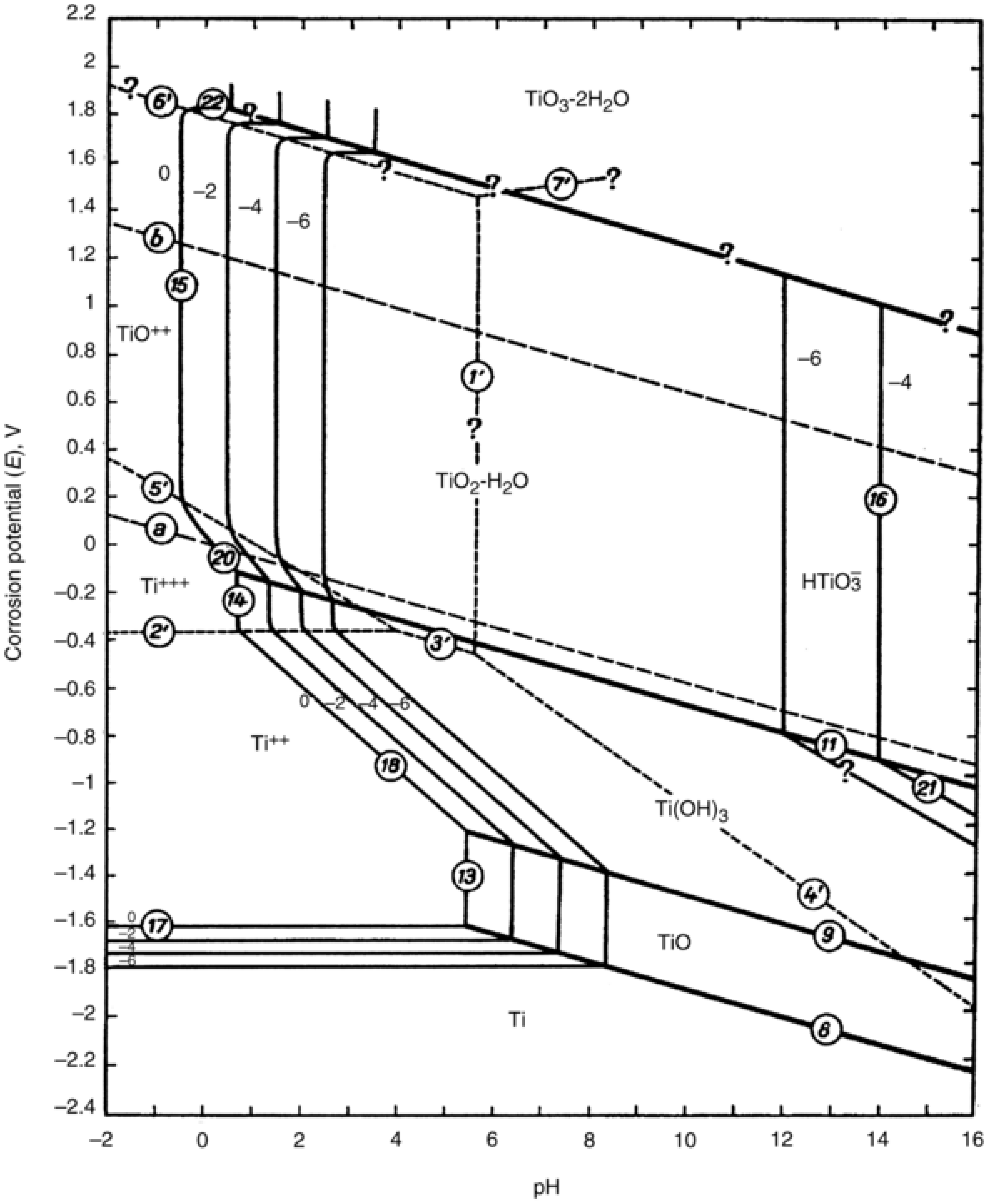

Fig. 1 Potential-pH equilibrium diagram for the titanium-water system at 25 °C (77 °F). The diagram was established by considering, as derivatives of the tri- and tetravalent titanium, the hydroxide $Ti(OH)_3$ and the hydrated oxide TiO_2-H_2O. Lines a and b establish the stability region of water. Consult Ref 7 for further explanation.

Table 1 Lattice parameters of crystalline titanium oxide

Crystal structure		Lattice constant a, nm	Lattice constant b, nm	Lattice constant c, nm
TiO_2-(anatase)	**tetragonal**	0.3733	…	0.937

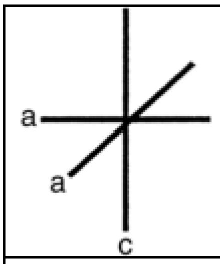			
TiO_2-(rutile) tetragonal	0.4584	…	0.2953
TiO_2-(brookite) orthorhombic 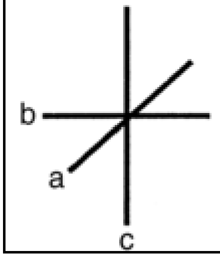	0.5436	0.9166	0.5135

The morphology of anodically formed oxides on valve metals, specifically titanium, has been described as a dual-layered oxide structure (Ref 14, 15, 25). The dual-layered oxide structure is composed of the following: (a) an inner compact and protective oxide at the metal-oxide interface, and (b) a porous outer oxide structure. The inner compact layer is primarily responsible for the passivation behavior of the oxide and is also responsible for the majority of the potential drop across the oxide film. The outer layer is a defected and porous oxide that has limited passivation characteristics (Ref 15). However, anodic polarization to more noble potentials within the passive potential range of titanium results in the thickening of the compact protective oxide by the following: (a) growth of the thin and protective oxide by metal cation egress, and/or (b) the conversion of the outer oxide into the more protective oxide (Ref 15).

Alloying additions, which can improve the efficiency of passivation, enhance the resistance of the passivating films to chemical dissolution, and/or inhibit the direct electrochemical dissolution of titanium through the oxide, should reduce passive current densities. This becomes crucial for cases of non-steady-state or rapid oxide formation, during which a majority of the anodic charge (~95%) is accounted for by the introduction of oxidized titanium into solution through the direct anodic dissolution of titanium (Ref 15, 26).

References cited in this section

7. M. Pourbaix, *Atlas of Electrochemical Equilibria in Aqueous Solutions,* 1st ed., NACE, 1974

14. A. Mazhar, F. Heakal, and A. Gad-Allah, Anodic Behavior of Titanium in Aqueous Media, *Corros. Sci.,* Vol 44, 1988, p 705–710

15. D. Tomashov et al., The Passivation of Alloys on Titanium Bases, *Electrochim. Acta,* Vol 19, 1974, p 159–172

19. M.J. Chappell and J.S.L. Leach, Passivity and Breakdown of Passivity of Valve Metals, *Passivity of Metals,* R.P. Frankenthal and J. Kruger, Ed., Electrochemical Society, 1978, p 1003–1034

20. E.J. Kelly and H.R. Bronstein, Kinetics and Mechanism of the Hydrogen Evolution Reaction of Titanium in Acidic Media, *J. Electrochem. Soc.,* Vol 131 (No. 10), 1984, p 2232–2238

21. N. Khalil, A. Bowen, and J.S.L. Leach, The Anodic Oxidation of Valve Metals, Part II: The Influence of the Anoidizing Conditions on the Transport Processes During the Anodic Oxidation of Zirconium, *Electrochim. Acta,* Vol 33 (No. 12), 1988, p 1721–1727

22. T. Shibata and Y. Zhu, The Effect of Film Formation Conditions of the Structure and Composition of Anodic Oxide Films on Titanium, *Corros. Sci.,* Vol 37 (No. 2), 1995, p 253–270

23. J.A. Davies et al., The Migration of Metal and Oxygen During Anodic Film Formation, *J. Electrochem. Soc.,* Vol 112 (No. 7), 1965, p 675–680

24. G.V. Samsonov, *The Oxide Handbook,* 2nd ed., IFI/Plenum, 1982

25. J. Pan, D. Thierry, and C. Leygraf, Electrochemical Impedance Spectroscopy Study of the Passive Oxide Film on Titanium for Implant Applications, *Electrochim. Acta,* Vol 41 (No. 7/8), 1996, p 1143–1153

26. D.G. Kolman and J.R. Scully, Electrochemistry and Passivty of a Ti-15Mo-3Nb-3Al Beta-Titanium Alloy in Ambient Temperature Aqueous Chloride Solutions, *J. Electrochem. Soc.,* Vol 140 (No. 10), 1993, p 2771

S. Yu, Corrosion Resistance of Titanium Alloys, *Corrosion: Fundamentals, Testing, and Protection*, Vol 13A, *ASM Handbook*, ASM International, 2003, p 703–711

Corrosion Resistance of Titanium Alloys

Steven Yu, 3M Company

Corrosion Vulnerability of Titanium and Titanium Oxides: The Effect of Selected Environments

The presence of a coherent air-formed or an anodically formed titanium oxide surface film inhibits corrosion and reduces active dissolution rates of metallic titanium. However, titanium oxide films are susceptible to failures that lead to accelerated mass loss rates. Oxide failure mechanisms can be classified in the following categories:

- Spatially localized oxide film breakdown by the ingress of aggressive anions, such as chlorides (Cl^-) and bromides (Br^-)
- Spatially local or homogenous chemical dissolution of the oxide in a strong reducing-acid environment
- Mechanical disruptions or depassivation, such as scratching, abrading, or fretting

Aggressive Anions. The presence of TiO_2 is a formidable barrier to uniform corrosion, but it can fail and lead to localized corrosion, including pitting, in the presence of aggressive anion species. Aggressive anion species, especially halide ions such as Cl^-, cause pitting (Ref 6, 22, 27, 28, 29). A possible mechanism of TiO_2 failure, which subsequently leads to pitting, is anion migration to the Ti/TiO_2 interface to form Ti/Ti-X/ TiO_2, where X is the aggressive anion species. According to one theory, the internal stresses associated with the Ti-X formation lead to rupture of the covering oxide film (Ref 19, 30). However, pitting of passivated titanium is limited to high anodic overpotentials, $E_{app} > 5$ V above OCP, even in aggressive halide-containing solutions, as indicated in Table 2. It is evident that titanium is highly resistant to pitting in solutions containing aggressive anion species, including Cl^- and Br^-, at temperatures of 25 °C to 100 °C (77 to 212 °F) and pH > 0.

Table 2 Pitting potential of commercially pure titanium

Environment	Temperature		Pitting potential	Source
	°C	**°F**		
1 *M* NaBr	30	86	+6 V_{SCE}	Ref 31
5% NaCl-HCl, pH = -0.05	25	77	+8.5 V_{SCE}	Ref 30
5% NaCl-HCl, pH = 3.5	**Boiling**		+6 V_{SCE}	Ref 6
1 *M* KCl	25	77	+14 V_{SCE}	Ref 33

Potential reference is saturated calomel electrode (SCE).

In addition to a resistance to pitting, titanium exhibits resistance to crevice corrosion that is a result of: (a) deaeration, (b) separation of anode and cathode, (c) metal-ion hydrolysis, (d) localized acidification, and (e) a breakdown mechanism. As a general rule, titanium is not susceptible to crevice corrosion at $T < 70$ °C (158 °F), regardless of the solution pH or chemistry, as shown in Fig. 2 (Ref 6, 34). At $T > 70$ °C (158 °F), initiation of crevice corrosion on titanium can be attributed to crystallization of titanium oxide, and increased passive dissolution, which lead to the five-stage process discussed previously (Ref 34). The anodically formed titanium oxide is amorphous at $T < 60$ °C (140 °F). The phase transformation of amorphous titanium oxide to a crystalline oxide can occur by anodic polarization (Ref 15, 22, 35). However, at $T > 60$ °C (140 °F), compressive stresses within the oxide can cause crystallization of the oxide. The resulting crystalline oxide film contains defects such as grain boundaries and intersections of screw dislocations with free surfaces, which can act as preferential sites for oxide failure or dissolution (Ref 9, 13, 36). The formation of grain boundaries, which can act as ionic diffusion pathways, allows for anion transport into the oxide (Ref 34). Moreover, increased passive dissolution at elevated temperatures can lead to metal-ion hydrolysis that generates acidity in an occluded geometry (Ref 22). Consequently, titanium with crystalline oxide films can be susceptible to crevice corrosion as well as pitting corrosion. Nevertheless, resistance to crevice corrosion at $T < 70$ °C (158 °F) does not preclude the possibility of a localized solution acidification mechanism leading to accelerated passive dissolution, because anodic dissolution rates of active and passive titanium are inversely proportional to related solution pH (Ref 12). The topic of local acidification is addressed subsequently. Note that alloying additions of molybdenum, zirconium, and palladium to titanium do raise the critical temperature of 70 °C (158 °F), as shown in Fig. 2.

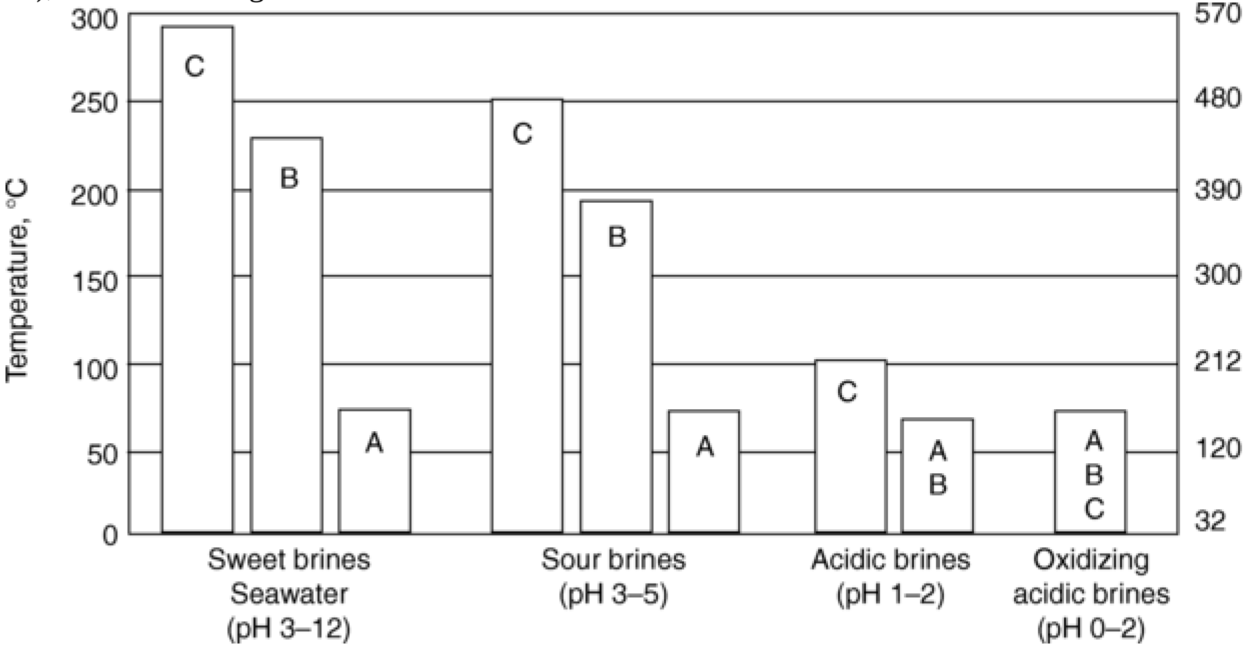

Fig. 2 Approximate temperature limits for crevice corrosion resistance of titanium alloys by group in various chloride brines. Group A: commercially pure titanium (grade 2) and beta titanium alloys. Group B: Beta-C (Ti-3%Al-8%V-6%Cr-4%Zr-4%Mo), Transage-207 (Ti-8%Mo-2.5%Al-9%Zr-2%Sn), and Ti-8-8-2-3 (Ti-8%Mo-8%V-2%Fe-3%Al). Group C: Beta-C/Pd (Ti-3%Al-8%V-6%Cr-4%Zr-4%Mo-0.05%Pd), Beta-21S (Ti-15%Mo-2.7%Nb-3%Al-0.2%Si), Ti-15-5 (Ti-15%Mo-5%Zr), and Beta III (Ti-

11.5%Mo-6%Zr-4.5%Sn). It is evident that the alloying additions of molybdenum, zirconium, and palladium were beneficial in raising the 70 °C (158 °F) threshold for crevice corrosion. Source: Ref 6

Reducing Acids. Titanium is generally corrosion resistant in the presence of oxidizing-acid media but exhibits performance limitations in the presence of reducing-acid media. Oxidizing acids, such as chromic, nitric, perchloric, and hypochloric acids, can oxidize titanium to form TiO_2, where further oxide thickening promotes passivity. In contrast, passivated titanium may undergo activation through the dissolution of TiO_2 in a reducing environment. As Ti^{4+} is reduced to a more soluble Ti^{3+}, passive film dissolution can occur, as previously discussed. The dissolution of titanium in the form of Ti^{3+} can occur in reducing acids such as hydrochloric acid. Interestingly, alloying additions can improve the corrosion resistance of titanium-base alloys in such an environment (Ref 6, 15). Some common acids, which are classified as reducing acids, are hydrochloric, sulfuric, phosphoric, and hydrofluoric acids.

The breakdown of anodic or air-formed titanium oxide has been correlated with the conversion of TiO_2 to hydrated TiOOH and the presence of Ti^{3+} (Ref 37, 38). It has been proposed (Ref 37) that the formation of Ti^{3+} in the form of TiOOH or its hydrated form of $TiOOH \cdot H_2O$, for example, $Ti(OH)_3$, through the reduction of Ti^{4+} in TiO_2 can occur at the oxide-solution interface. This can result in oxide film failure, because $TiOOH \cdot H_2O$ should readily dissolve in acidic solutions. The potential-pH equilibrium diagram for the Ti-H_2O system should be modified to include TiH_2 (Ref 39). In such a case, an equilibrium involving only the hydrated form of trivalent titanium may occur between the regions of TiO_2 and TiH_2 equilibrium (Ref 37). The formation of Ti^{3+} is critical, due to the higher solubility of Ti^{3+} at low pH in comparison to Ti^{4+}, as shown in Fig. 1. The solubility of Ti^{3+} accounts for active anodic dissolution of titanium in reducing acids.

Mechanical Attack. Mechanical disruption of TiO_2 by scratching, abrading, or fretting can also result in the exposure of the underlying thermodynamically reactive metallic titanium to an aqueous environment. However, repassivation can occur to reform an oxide layer to isolate the underlying reactive metal from the aqueous environment. When repassivation occurs, the high current densities associated with repassivation do not all go into the formation of passive oxides. Current densities have been recorded as high as 100 A/cm^2 (645 A/in.^{2}) for thin-film fracture tests of metallic titanium in deaerated 5 *M* HCl at 25 °C (77 °F) (Ref 40). However, it was recorded that the overall current efficiency for oxide formation on decay to steady state was less than 10% (Ref 40). Therefore, a majority of the repassivation charge went into metallic titanium dissolution, either as Ti^{3+} or TiO^{2+} (Ref 40, 41). Consequently, there can be a significant introduction of dissolved metallic ionic species into the local solution chemistry during repassivation. Within a tight geometry, such influx of titanium ions or other metal ions can lead to localized solution acidification by metal-ion hydrolysis. The low current efficiency associated with repassivation contrasts the near 100% charge efficiency associated with the slower passive film growth during anodic potentiostatic polarization of titanium in 0.5 *M* H_2SO_4 at temperatures ranging from 303 to 353 K (86 to 176 °F) (Ref 22). Therefore, reactivation current efficiency during repassivation and film growth during exposure to reducing acids may depend critically on the rate of oxidation and the disordered state of the oxide.

The release of titanium ions into the surrounding aqueous environment, as a result of metallic dissolution, is a critical issue with respect to corrosion in reducing acids. Introduction of titanium ions into the surrounding aqueous environment can lead to solution acidification by metallic-ion hydrolysis (Ref 42). It was shown that the dominant dissolved titanium species resulting from scratch-repassivation of titanium disks was Ti^{3+}, which was reported as being hydrolyzable (Ref 41, 42). In addition, it has been shown that the production of Ti^{3+} occurs over the duration of repassivation, due to the low overall current efficiency of TiO_2 formation immediately after rapid mechanical depassivation of microelectrodes that enabled high dissolution rates (Ref 40). Trivalent titanium ions (Ti^{3+}) can undergo metal-ion hydrolysis primarily by the following reaction:

$$Ti^{3+} + H_2O \rightarrow TiOH^{2+} + H^+ \quad \text{(Eq 1)}$$

The resulting hydrolysis of Ti^{3+} can produce a solution with a pH as low as 0, as shown when 1 *M* $TiCl_3$ is added to deaerated water (Ref 40). Indeed, the pH near a crack tip in Ti-8%Al- 1%Mo-1%V has been reported to be as low as 1.7 (Ref 43). Also, a pH < 1.3 was reported near a corroding pit on titanium that was exposed to neutral chloride solution (Ref 41). The decrease in localized solution pH due to hydrolysis can lead to enhanced titanium dissolution in reducing acid that, in turn, further acidifies the surrounding solution and causes even more dissolution of titanium, because the active and passive dissolution rates for titanium are well known to be functions of pH, as shown in Fig. 3 (Ref 26, 41, 44).

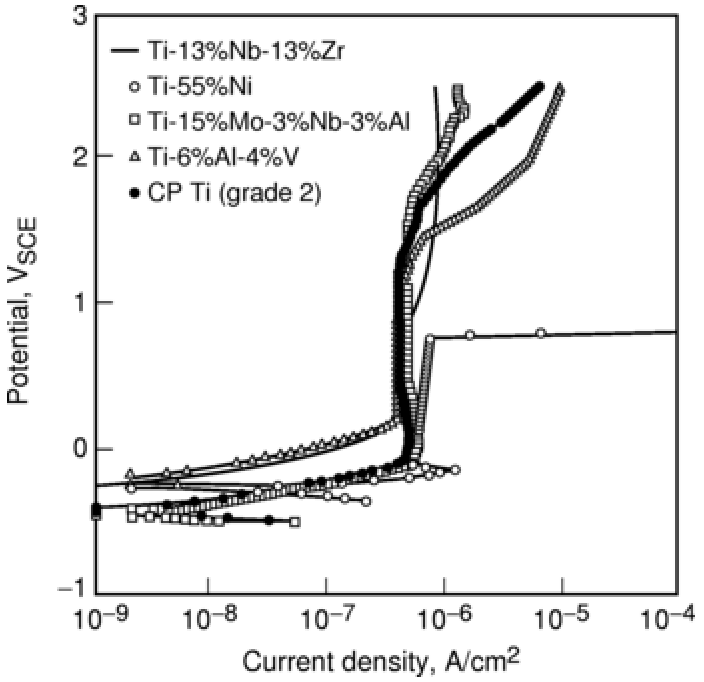

Fig. 3 Electrochemical polarization tests of titanium and titanium-base alloys, including Ti-6%Al-4%V (Ti-6-4), Ti-15%Mo-3%Nb-3%Al (Ti-15-3-3), Ti-13%Nb-13%Zr (Ti-13-13), Ti-55%Ni, and commercially pure (CP) titanium (grade 2), revealed that titanium and titanium-base alloys are spontaneously passive in a deaerated 0.1 *M* NaCl solution. The potentiodynamic scans were conducted at a scan rate of 0.1 mV/s. SCE, saturated calomel electrode

The resulting critical corrosion-related issues for titanium alloys include the possibility of: (a) occluded site deaeration, (b) partial or complete separation of anode and cathode sites, and (c) the metal dissolution/hydrolytic acidification/chloride ion (Cl^-) migration mechanism promoting a local buildup of acidity and high Cl^- concentrations adjacent to the alloy structures. In titanium applications that combine abrasive actions in a crevice, local acidification may be accelerated by the film rupture and repassivation mechanisms. The issues of local solution acidification and Cl^- accumulation do point toward crevice corrosion. However, crevice corrosion, which is defined by local depassivation and active dissolution in the absence of active abrasion, is not expected of titanium unless it is exposed to low- pH solutions at temperatures above 70 °C (158 °F), (Ref 1, 6, 34, 45, 46, 47, 48). It is yet unknown whether abrasion in crevice geometry could activate crevice corrosion at $T < 70$ °C (158 °F).

References cited in this section

1. M.J. Donachie, Jr., *Titanium: A Technical Guide,* 2nd ed., ASM International, 2000

6. R. Schutz, An Overview of Beta Titanium Alloy Environmental Behavior, *Beta Titanium Alloys in the 1990's,* D. Eylon, R. Boyer, and D. Koss, Ed., Minerals, Metals and Materials Society, 1993, p 75–91

9. P.Y. Park et al., The Corrosion Behavior of Sputter-Deposited Mo-Ti Alloys in Concentrated Hydrochloric Acid, *Corros. Sci.,* Vol 38 (No. 10), 1996 p 1649–1667

12. M. Levy and G. Sklover, Anodic Polarization of Titanium and Titanium Alloys in Hydrochloric Acid, *J. Electrochem. Soc.,* Vol 116 (No. 3), 1969, p 323–328

13. M. Itagaki, R. Oltra, and B. Vuillemin, Quantitative Analysis of Iron Dissolution During Repassivation of Freshly Generated Metallic Surfaces, *J. Electrochem. Soc.,* Vol 144 (No. 1), 1997, p 64–72

15. D. Tomashov et al., The Passivation of Alloys on Titanium Bases, *Electrochim. Acta,* Vol 19, 1974, p 159–172

19. M.J. Chappell and J.S.L. Leach, Passivity and Breakdown of Passivity of Valve Metals, *Passivity of Metals,* R.P. Frankenthal and J. Kruger, Ed., Electrochemical Society, 1978, p 1003–1034

22. T. Shibata and Y. Zhu, The Effect of Film Formation Conditions of the Structure and Composition of Anodic Oxide Films on Titanium, *Corros. Sci.,* Vol 37 (No. 2), 1995, p 253–270

26. D.G. Kolman and J.R. Scully, Electrochemistry and Passivty of a Ti-15Mo-3Nb-3Al Beta-Titanium Alloy in Ambient Temperature Aqueous Chloride Solutions, *J. Electrochem. Soc.,* Vol 140 (No. 10), 1993, p 2771

27. N. Casillas et al., Pitting Corrosion of Titanium, *J. Electrochem. Soc.,* Vol 141 (No. 3), 1994, p 636–642

28. P. McKay and D. Mitton, An Electrochemical Investigation of Localized Corrosion on Titanium in Chloride Environments, *Corrosion,* Vol 41 (No. 1), 1985, p 52–61

29. G. Burstein and R. Souto, Observations of Localized Instability of Passive Titanium in Chloride Solution, *Electrochim. Acta,* Vol 40 (No. 12), 1995, p 1881–1888

30. J. Yahalom and A. Poznansky, Surface Energy and the Stability of the Passive Layer, *Passivity of Metals,* R.P. Frankenthal and J. Kruger, Ed., Electrochemical Society, 1978, p 328–336

31. T. Shibata and Y. Zhu, The Effect of Film Formation Potential on the Stochastic Processes of Pit Generation on Anodized Titanium, *Corros. Sci.,* Vol 36(No. 1), 1994, p 153–163

33. I. Dugdale and J. Cotton, The Anodic Polarization of Titanium in Halide Solutions, *Corros. Sci.,* Vol 4, 1964, p 397–411

34. J.J. Noel et al., Passive Oxide Film on Titanium in Aqueous Chloride Solution Probed by Electrochemistry, XPS, and In- Situ Neutron Reflectometry, *Surface Oxide Films,* The Electrochemical Society, 1996

35. R.D. Armstrong and R.E. Firman, Impedance of Titanium in the Active-Passive Transition, *J. Electroanal. Chem. Interfacial Electrochem.,* Vol 34, 1972, p 391–397

36. J.R. Galvele, Present State of Understanding of the Breakdown of Passivity and Repassivation, *Passivity of Metals,* R.P. Frankenthal and J. Kruger, Ed., Electrochemical Society, 1978, p 285–323

37. C.K. Dyer and J.S.L. Leach, Reversible Reactions Within Anodic Oxide Films on Titanium Electrodes, *Electrochim. Acta,* Vol 23, 1978, p 1387–1394

38. D.J. Blackwood and L.M. Peter, Stability and Open Circuit Breakdown of the Passive Oxide Film on Titanium, *Electrochim. Acta,* Vol 33 (No. 8), 1988, p 1143–1149

39. T.R. Beck, Electrochemistry of Freshly- Generated Titanium Surfaces, Part I: Scraped Rotating Disk Experiment, *Electrochim. Acta,* Vol 18, 1973, p 807

40. D. Kolman and J. Scully, On the Repassivation Behavior of High Purity Titanium and Selected Alpha, Beta, Alpha + Beta Titanium Alloys in Aqueous Chloride Solutions, *J. Electrochem. Soc.,* Vol 143 (No. 6), 1996, p 1847–1859

41. T.R. Beck, *Localized Corrosion,* B.F. Brown, Ed., NACE, 1974, p 644

42. C. Baes and R. Mesmer, *The Hydrolysis of Cations,* John Wiley & Sons, 1976, p 147–168

43. B.F. Brown, C.T. Fujii, and E.F. Dahlberg, *J. Electrochem. Soc.,* Vol 116 (No. 218), 1969, p 218

44. M. Stern and H. Wissenberg, The Electrochemical Behavior and Passivity of Titanium, *J. Electrochem. Soc.,* Vol 106 (No. 9), 1959, p 755–759

45. P. Mckay, Crevice-Corrosion Kinetics on Titanium and a Ti-Ni-Mo Alloy in Chloride Solutions at Elevated Temperatures, *Corrosion Chemistry Within Pits, Crevices, and Cracks,* HMSO Books, 1987

46. R.W. Schutz, "Understanding and Preventing Crevice Corrosion," Corrosion 91, (Cincinnati, OH), NACE, 1991

47. L.A. Yao and F.X. Gan, Microelectrode Monitoring the Crevice Corrosion in Titanium, *Corrosion,* Vol 47 (No. 6), 1991, p 420–423

48. H. Shizhong and M. Xiaoxiong, Localized Corrosion in Titanium in Marine Environments, *Corrosion and Corrosion Control for Offshore and Marine Construction,* Pergamon Press, 1988

S. Yu, Corrosion Resistance of Titanium Alloys, *Corrosion: Fundamentals, Testing, and Protection*, Vol 13A, *ASM Handbook*, ASM International, 2003, p 703–711

Corrosion Resistance of Titanium Alloys

Steven Yu, 3M Company

Effects of Alloying on Active Anodic Corrosion of Titanium

Titanium alloys can be classified into three primary groups: (a) α titanium alloys with hexagonal close-packed (hcp) crystallographic structure; (b) β titanium alloys with body-centered cubic (bcc) crystallographic structures, including metastable β alloys; (c) and α+β titanium alloys, including near-α and near-β titanium alloys. Details regarding the alloy families are described in Ref 2 and 3. For titanium- base alloys containing β stabilizing elements, a molybdenum equivalency has been determined as:

$$\begin{aligned}\%\text{Mo(equivalent)} = \text{Mo} + 0.67(\%\text{V}) \\ + 0.28(\%\text{Nb}) + 2.9(\%\text{Fe}) \\ + 1.6(\%\text{Cr}) + 0.9(\%\text{Ni}) \\ - \text{Al(wt\%)}\end{aligned} \quad \text{(Eq 2)}$$

where approximately 10% Mo equivalency is sufficient to stabilize completely the beta phase on quenching to room temperature from above the beta-transus temperature.

Active Anodic Polarization Behavior of Titanium and Titanium-Base Alloys. Electrochemical polarization tests of titanium and titanium-base alloys, including Ti-6%Al-4%V (Ti-6-4), Ti-15%Mo-3%Nb-3%Al (Ti-15-3-3), Ti-13%Nb-13%Zr (Ti-13-13), Ti-55%Ni, and Ti-50%Cr, showed that titanium and the tested titanium-base alloys are spontaneously passive in a deaerated 0.1 *M* NaCl solution, as shown in Fig. 3. This is consistent with the stability of dominant TiO_2 at these OCP values and pH, as shown in Fig. 1. From OCP to +2.5 V_{SCE}, the tested alloys exhibited similar passive current densities of ~5×10^{-7} A/cm^2 (3.2×10^{-6} A/ in.^{2}).

The corrected critical current densities (i_{crit}) of the solution-treated alloys Ti-13-13, Ti-15-3-3, as well as commercially pure (CP) titanium (grade 2) were compared as functions of their respective molybdenum equivalency, as shown in Fig. 4. The corrected i_{crit} was defined as the following:

$$\text{Corrected } i_{crit} = i_{crit}(\text{measured}) + i_{cathodic} \quad \text{(Eq 3)}$$

where the $i_{cathodic}$ can be determined by Tafel extrapolation to the E_{app}, where the apparent i_{crit} is observed. The i_{crit} determined from the anodic polarization data, shown in Fig. 4, has been corrected to account for the cathodic current densities. Of the three alloys, solution-treated (ST) Ti-15-3-3, a metastable beta alloy, exhibited the lowest i_{crit} in 5 *M* HCl. Moreover, ST Ti-15-3-3 did not exhibit an active/passive transition in the 5 *M* HCl, as shown in Fig. 4. Instead, spontaneous passivity was observed at the OCP of Ti- 15-3-3. Researchers also reported that Ti-15-3-3 was spontaneously passive at its OCP in 5 *M* HCl at room temperature (Ref 40).

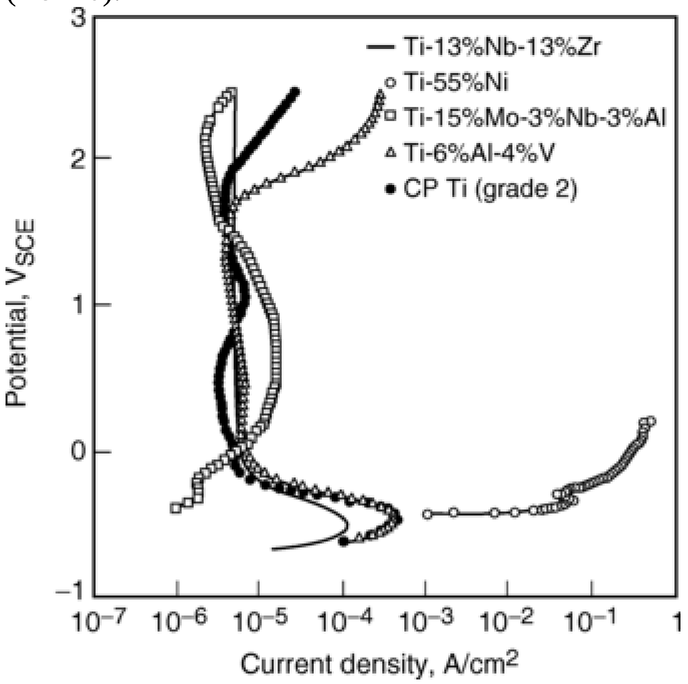

Fig. 4 Electrochemical polarization tests of titanium and titanium-base alloys, including Ti-6%Al-4%V (Ti-6-4), Ti-15%Mo-3%Nb-3%Al (Ti-15-3-3), Ti-13%Nb-13%Zr (Ti-13-13), Ti-55%Ni, and commercially pure (CP) titanium (grade 2), in a deaerated 5 *M* HCl solution. The potentiodynamic scans were conducted at a scan rate of 0.1 mV/s. SCE, saturated calomel electrode

Depassivation and Activation: Effects of Alloying Additions on Titanium at OCP. The dissolution of the respective native oxides and the subsequent surface activation of CP titanium as well as binary alloys, including Ti-45%Nb and Ti-50%Zr with native air-formed oxides (~2 to 3 nm in thickness) in 5 *M* HCl, were indicated by decreasing OCP. The decreasing OCP was followed by a sudden potential drop, as shown in Fig. 5 and 6. In 5 *M* HCl, the OCPs of CP titanium, Ti-45%Nb, and Ti-50%Zr were within the thermodynamically stable region of Ti^{3+} after the 12 h immersion, that is, after the potential drop, as revealed by the overlay of the OCPs onto the revised Pourbaix diagram of titanium at 37 °C (99 °F), as shown in Fig. 7. Similar decreases and step-function drops in OCPs of titanium were recorded in sulfuric and hydrochloric acids (Ref 38, 49, 50). It was confirmed that the OCP breakdown of the passive film on titanium was by chemical dissolution (Ref 38). The potential drops were not observed in deaerated 0.1 *M* NaCl (pH $\cong$6.8) for CP titanium and the titanium-base alloys (Fig. 5, 6). In this near-neutral pH solution, the air-formed oxides of all these materials were thermodynamically stable and resisted chemical dissolution, in contrast to what was experienced in deaerated 5 *M* HCl for the titanium-base materials (Fig. 5, 6). An overlay of the OCPs of CP titanium, Ti-45%Nb, and Ti-50%Zr on the Pourbaix diagram of titanium at 37 °C (99 °F) indicates that at pH = 6.8, CP titanium and the alloys were well within the thermodynamic stability regime of TiO_2 at 37 °C (99 °F), as shown in Fig. 7. The stability of the air- formed oxides in 0.1 *M* NaCl is confirmed by the spontaneous passivity of titanium, niobium, zirconium and the titanium-niobium- and titanium-zirconium-base alloys.

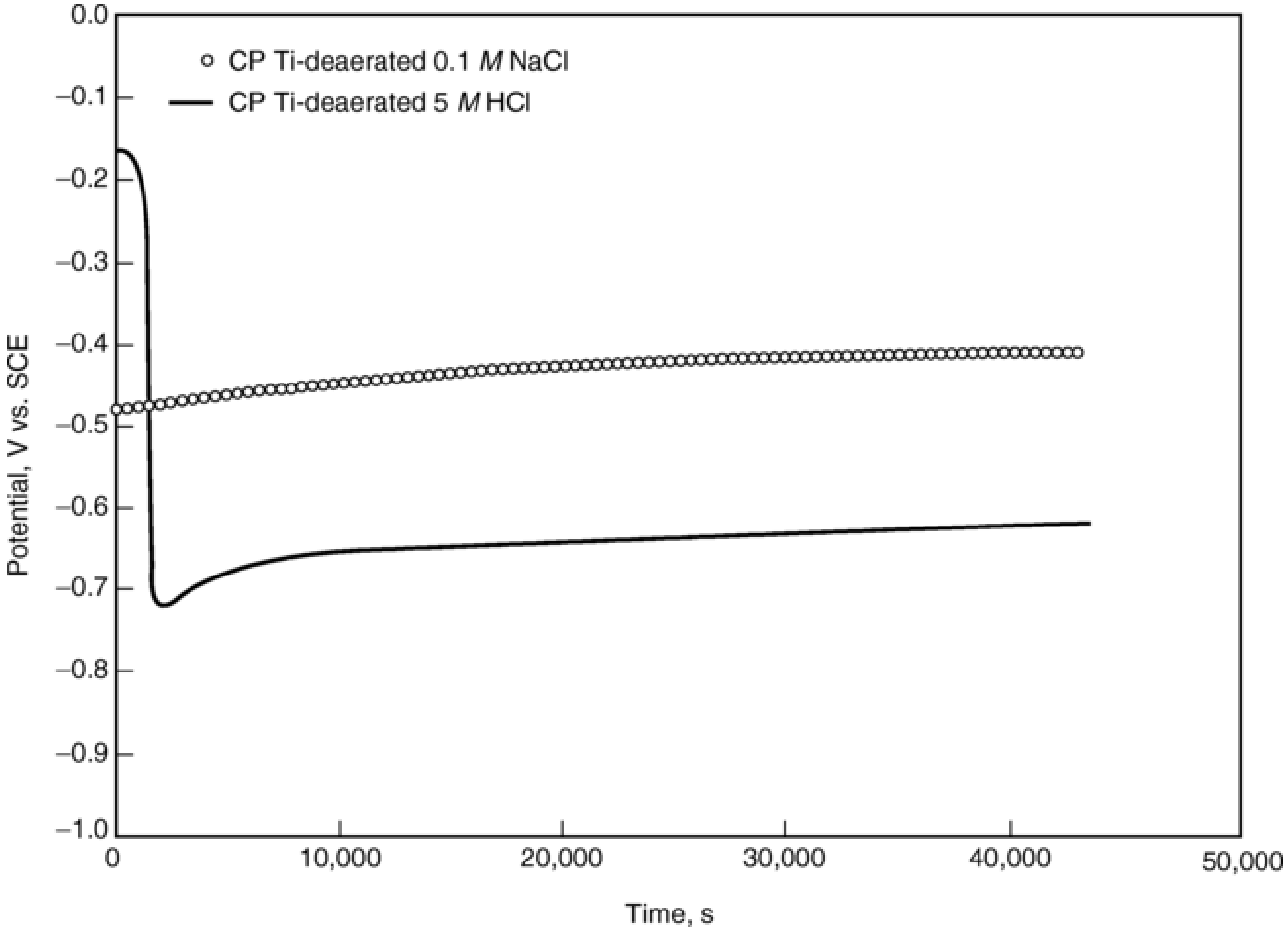

Fig. 5 **Open-circuit potentials of commercially pure (CP) titanium in deaerated 0.1 *M* NaCl solution and deaerated 5 *M* HCl solution at 37 °C (99 °F). In 0.1 *M* NaCl, CP titanium did not exhibit the drop in open-circuit potential that is characteristic of surface activation after oxide dissolution. SCE, saturated calomel electrode**

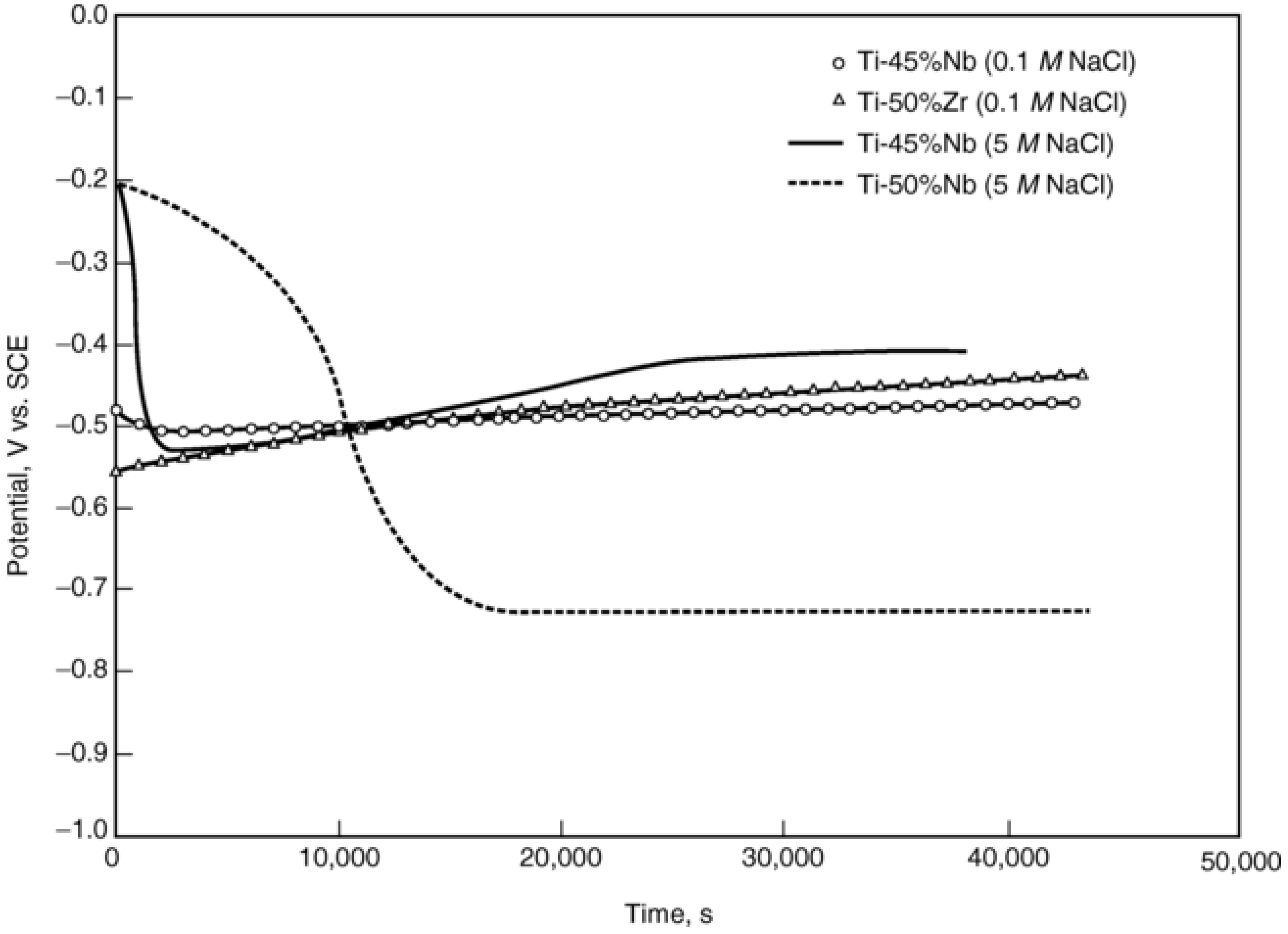

Fig. 6 Open-circuit potentials of Ti-45%Nb and Ti-50%Zr (bulk alloys), initially with air-formed oxides, in deaerated 0.1 *M* NaCl and 5 *M* HCl solutions at 37 °C (99 °F). Ti-45% Nb and Ti-50%Zr did not exhibit surface reactivation in 0.1 *M* NaCl solution (pH ~ 6.8). In contrast, both alloys exhibited surface reactivation in 5 *M* HCl due to chemical dissolution of the oxide. SCE, saturated calomel electrode

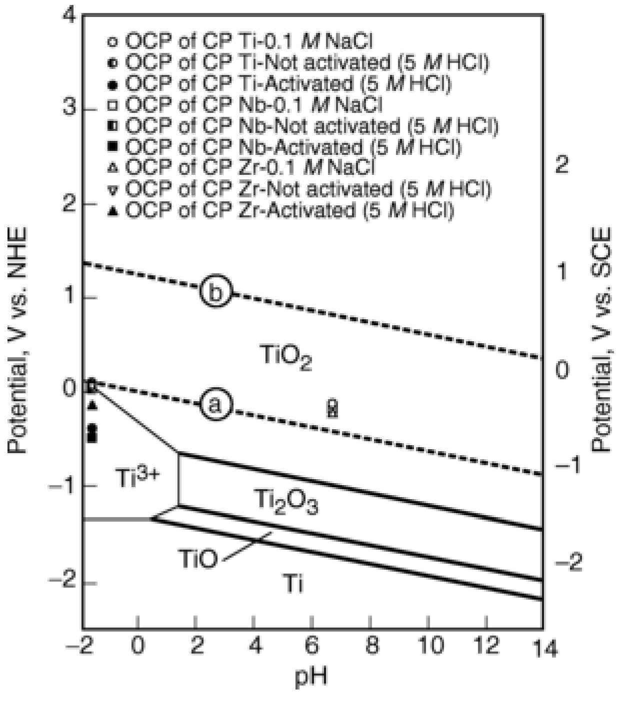

Fig. 7 Potential-pH equilibrium diagram for Ti-H_2O system of 37 °C (99 °F). The dissolved titanium species are at an activity of 10^{-6}. Lines a and b define the region of water stability. The experimentally recorded open-circuit potentials (OCP) of commercially pure (CP) titanium, Ti-45%Nb, and Ti-50%Zr

in deaerated 0.1 *M* NaCl and 5 *M* HCl solutions before and after surface activation at 37 °C (99 °F) are presented. SCE, saturated calomel electrode. NHE, normal hydrogen electrode

References cited in this section

2. C.R. Brooks, *Heat Treatment, Structure and Properties of Nonferrous Alloys,* American Society for Metals, 1982

3. R. Boyer, G. Welsch, and E.W. Collings, Ed., *Materials Properties Handbook: Titanium Alloys,* ASM International, 1994

38. D.J. Blackwood and L.M. Peter, Stability and Open Circuit Breakdown of the Passive Oxide Film on Titanium, *Electrochim. Acta,* Vol 33 (No. 8), 1988, p 1143–1149

40. D. Kolman and J. Scully, On the Repassivation Behavior of High Purity Titanium and Selected Alpha, Beta, Alpha + Beta Titanium Alloys in Aqueous Chloride Solutions, *J. Electrochem. Soc.*, Vol 143 (No. 6), 1996, p 1847–1859

49. E. Kelly, Anodic Dissolution and Passivation of Titanium in Acidic Media, *J. Electrochem. Soc.,* Vol 126 (No. 12), 1979, p 2064

50. N. Thomas and K. Nobe, The Electrochemical Behavior of Titanium, *J. Electrochem. Soc.,* Vol 116 (No. 12), 1969, p 1748–1751

S. Yu, Corrosion Resistance of Titanium Alloys, *Corrosion: Fundamentals, Testing, and Protection*, Vol 13A, *ASM Handbook*, ASM International, 2003, p 703–711

Corrosion Resistance of Titanium Alloys

Steven Yu, 3M Company

Effects of Alloying Additions on Titanium Passivity

The exact manner in which alloying additions improve passivating oxides is yet unclear. Therefore, possible mechanisms by which alloying additions can enhance the resistance to active anodic dissolution and inhibit the chemical dissolution of passive films are reviewed. The following theories are by no means the only theories with regards to passivity and effects of alloying additions on passivation.

Promoting Active/Passive Transition. The alloying addition of small concentrations of palladium to titanium induces spontaneous passivation of titanium-palladium alloys in reducing environments where titanium, by itself, exhibits active/passive transitions, as shown in Fig. 8. (Ref 16, 17, 33). In such cases, spontaneous passivation of titanium is due to enhanced cathodic kinetics associated with hydrogen evolution instead of expanded thermodynamic stability of oxide passivity. The presence of palladium and other noble-metal additions, such as iridium, platinum, and rhodium, at the solution-metal or solution/oxide/metal interface modify the kinetics of hydrogen evolution by: (a) increasing the exchange current density of hydrogen evolution, and/or (b) reducing the cathodic Tafel slope associated with hydrogen evolution. Increased cathodic exchange current densities and/or reduced cathodic Tafel slopes can result in passivity if the resulting OCP is above the active/passive transition potential of the binary alloy (i.e., TiO_2 is not converted to TiOOH). Moreover, changes in the cathodic Tafel slope of titanium- palladium alloys would indicate that the rate-determining step during hydrogen evolution is no longer a slow discharge reaction step, as described for

titanium (Ref 49). Instead, the rate- determining step during hydrogen evolution on titanium-palladium alloys is more consistent with the chemical hydrogen recombination step (Ref 49).

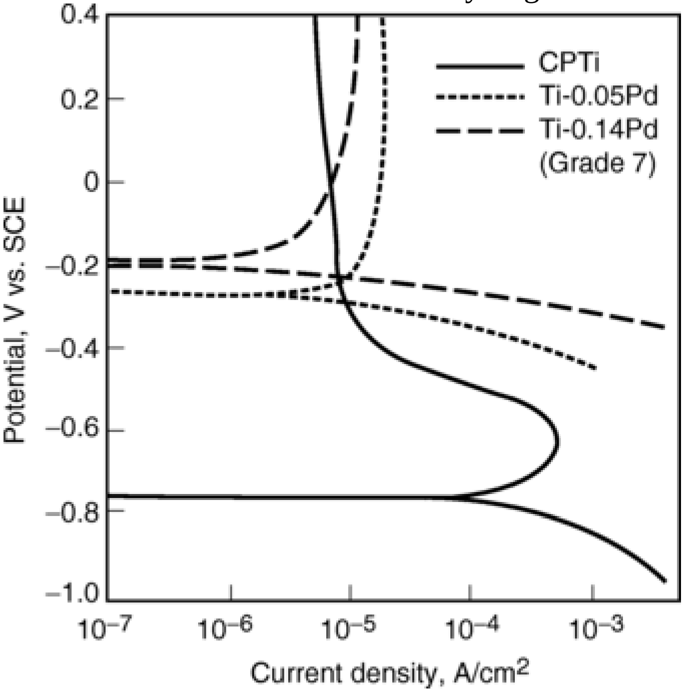

Fig. 8 Polarization measurement of titanium-palladium alloys in acidic sodium chloride solution (deaerated, sweep rate = 0.2 V/min, NaCl = 250 g/L, pH = 0.5, and boiling). SCE, saturated calomel electrode; CP, commercially pure. Source: Ref 51

References cited in this section

16. P.A. Mausli, S.G. Steinemann, and J.P. Simpson, "Properties of Surface Oxides on Titanium and Some Titanium Alloys," Proceedings of the Sixth World Conference on Titanium (France), P. LaCombe, R. Tricot, and G. Bèranger, Ed., Socièté Francaise de Métallurgie, 1988

17. N. Khalil and J.S.L. Leach, The Anodic Oxidation of Valve Metals, Part I: Determination of Ionic Transport Numbers by Alpha Spectrometry, *Electrochim. Acta,* Vol 31 (No. 10), 1986, p 1279–1285

33. I. Dugdale and J. Cotton, The Anodic Polarization of Titanium in Halide Solutions, *Corros. Sci.,* Vol 4, 1964, p 397–411

49. E. Kelly, Anodic Dissolution and Passivation of Titanium in Acidic Media, *J. Electrochem. Soc.,* Vol 126 (No. 12), 1979, p 2064

51. S. Kitayama et al., "Effect of Small Pd Addition on the Corrosion Resistance of Ti and Ti Alloys in Severe Gas and Oil Environments," Corrosion 92, NACE, 1992

S. Yu, Corrosion Resistance of Titanium Alloys, *Corrosion: Fundamentals, Testing, and Protection*, Vol 13A, *ASM Handbook*, ASM International, 2003, p 703–711

Corrosion Resistance of Titanium Alloys

Steven Yu, 3M Company

Formation of Amorphous or Vitreous Oxide

It has been asserted that alloying additions such as chromium and manganese that reduce passive current densities do so by reducing the density of crystal defects in oxide films and thereby reducing the ionic conductivity across the oxide (Ref 15). For example, the improved corrosion resistance associated with the addition of 12 wt% chromium to iron to form stainless steel can be attributed to the formation of an amorphous iron-chromium-base oxide (Ref 52). The formation of an amorphous oxide or possibly a vitreous oxide film, for example, short- range order and structure, can offer improved resistance to ion migration due to the absence of grain boundaries and dislocations that can act as low-energy conduits for ion migration (Ref 52). Moreover, the formation of either an amorphous or vitreous oxide enhances resistance to corrosion due to the flexibility of the atomic bonds between metallic cations with O^{2-} or OH^-. The benefits of bond flexibility are the following: (a) it allows for tolerance of the misfit strain associated with the presence of halide, specifically Cl^-, at the oxide-metal interface, and (b) almost all the surface atoms can bond with oxygen or OH^- without requiring an almost perfect epitaxial relationship between metal and oxide (Ref 52). Chromium and molybdenum also have been shown to improve the corrosion resistance of base metals such as iron and titanium by inhibiting anodic dissolution and enhancing passivation in reducing environments such as 6 and 12 *M* HCl, respectively (Ref 9, 53). Researchers associated the enhanced corrosion resistance and the improved passivity due to the formation of a passivating film consisting of double oxyhydroxides of molybdenum-titanium and chromium-titanium, which have a ratio of O^{2-} to OH^- of approximately 2. The double oxyhydroxides on molybdenum-titanium and chromium-titanium have been shown to be amorphous in structure, where molybdenum or chromium ions are bonded directly to titanium ions (Ref 9, 53). The amorphous and homogenous structure of the oxyhydroxides may account for the enhanced resistance to anodic dissolution in comparison to the respective molybdenum, chromium, and titanium oxides. The formation of oxyhydroxides will be helpful for construction of homogenous surface films without defects, which act as weak points for corrosion (Ref 53). Furthermore, it has been shown that zirconium, when alloyed with molybdenum and anodically polarized in 12 *M* HCl, will form complex double oxyhydroxides, where zirconium and molybdenum are covalently bonded as first nearest neighbors (Ref 54). Therefore, the alloying additions of niobium and zirconium may lead to the formation of amorphous oxyhydroxides when alloyed with titanium.

References cited in this section

9. P.Y. Park et al., The Corrosion Behavior of Sputter-Deposited Mo-Ti Alloys in Concentrated Hydrochloric Acid, *Corros. Sci.,* Vol 38 (No. 10), 1996 p 1649–1667

15. D. Tomashov et al., The Passivation of Alloys on Titanium Bases, *Electrochim. Acta,* Vol 19, 1974, p 159–172

52. A.G. Revesz and J. Kruger, The Role of Noncrystalline Films in Passivation and Breakdown of Passivation, *Passivity of Metals,* R.P. Frankenthal and J. Kruger, Ed., The Electrochemical Society, 1978, p 137–155

53. X. Li et al., Spontaneously Passivated Films on Sputter-Deposited Cr-Ti Alloys in 6 *M* HCl Solution, *Corros. Sci.,* Vol 39 (No. 5), 1997, p 935–948

54. P.Y. Park et al., The Corrosion Behavior of Sputter-Deposited Amorphous Mo-Zr Alloys in 12 *M* HCl, *Corros. Sci.*, Vol 37 (No. 2), 1995, p 307–320

S. Yu, Corrosion Resistance of Titanium Alloys, *Corrosion: Fundamentals, Testing, and Protection*, Vol 13A, *ASM Handbook*, ASM International, 2003, p 703–711

Corrosion Resistance of Titanium Alloys

Steven Yu, 3M Company

Reduction of the Potential Gradient across Surface Film

Anodic dissolution of metal is controlled by the applied electrode potential difference between metal and electrolyte. On a bare metal surface in contact with solution, the potential difference is located across a thin electrical double layer, the Helmholtz layer, which separates the bare metal surface from the hydrated ions and is approximately 0.5 nm in thickness (Ref 55). However, the presence of a compact oxide surface film results in a multilayered interface consisting of metal/compact surface film/double layer/solution, as shown in Fig. 9. Therefore, on an oxide-covered surface, metal dissolution reaction transpires as a series of consecutive reaction steps: (a) metal ions are transferred from the underlying surface of the metal to the metal- oxide interface, (b) ions migrate through the oxide film, and then, (c) metal ions are transferred across the Helmholtz double layer to the film- solution interface under the applied potential field. It is generally accepted that the last step, the transfer of ions across the Helmholtz double layer to the film-solution interface, which results in the hydration of the metal ions, is the rate- controlling step in metal dissolution across an oxide-covered interface (Ref 55). The potential difference (φ_c) across the Helmholtz double layer between a thin compact oxide and electrolyte is a function of the overall potential difference between the metal and solution (φ_m) as well as the geometry and physical characteristics of the multilayered film (Ref 55). The relationship between φ_c and φ_m has been defined as the following:

$$\phi_c = \phi_m \left(1 + \frac{L}{\delta_{dl}} \frac{\varepsilon_H}{\varepsilon_m}\right)^{-1} \quad \text{(Eq 4)}$$

where L is the semiconductor film thickness, ε_H is the dielectric constant of the Helmholtz layer, ε_m is the dielectric constant of the metal oxide, and δ_{dl} is the thickness of the Helmholtz layer. Therefore, if there is no oxide (surface) film, then $\varphi_c = \varphi_m$. However, the presence of a thin oxide film can reduce φ_c and therefore reduce the driving force necessary for metal-ion transfer across the Helmholtz layer and consequently reduce metallic dissolution. Two factors can be controlled with respect to the oxide: first, oxide thickness (L) and second, the oxide dielectric constant (ε_m). Thus, it is possible to reduce the potential drop across the Helmholtz layer and, accordingly, the potential field-driven anodic dissolution of the underlying metal by increasing the oxide thickness and/or decreasing the oxide dielectric constant. Consequently, any alloying additions that can increase the compact oxide thickness and/or reduce the dielectric constant of the oxide film can reduce anodic dissolution and enhance corrosion resistance.

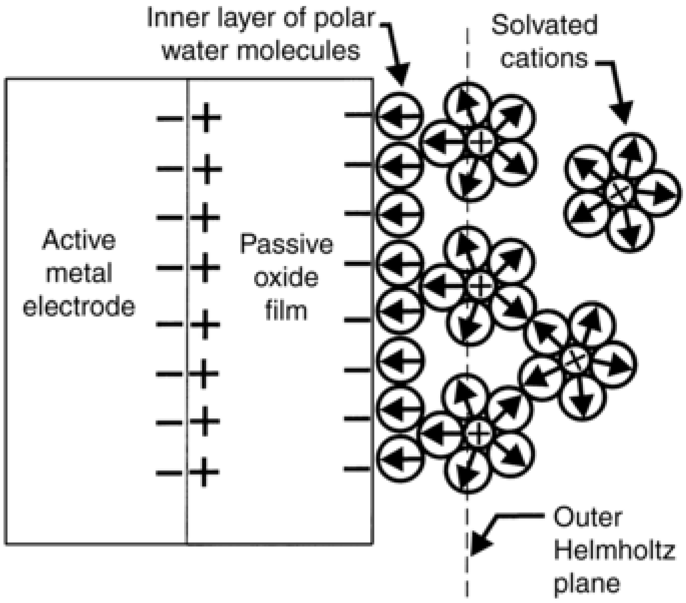

Fig. 9 Schematic of the active metal/passive oxide/Helmholtz double layer/solution interfaces that are present on a passivated metal surface

Reference cited in this section

55. N. Sato and G. Okamoto, Electrochemical Passivation of Metals, *Eletrochemical Materials Science,* J.O.M. Bockris, Ed., Plenum Press, 1981, p 193–245

S. Yu, Corrosion Resistance of Titanium Alloys, *Corrosion: Fundamentals, Testing, and Protection,* Vol 13A, *ASM Handbook,* ASM International, 2003, p 703–711

Corrosion Resistance of Titanium Alloys

Steven Yu, 3M Company

Enhancement of Atomic Bond Strength

The resistance of metals to dissolution and the propensity for passivation are functions of the atomic bond strengths (Ref 56). Metallic-to-metallic atom bonds and bonds between metallic atoms and oxygen or hydroxyl ions form an adsorbed hydroxyl layer (Ref 56). Relative metallic-to-metallic atom bond strength ($\varepsilon_{M\text{-}M}$) is shown in Eq 5. Similarly, the relative bond strengths between metallic atoms and oxygen can be approximated by the enthalpies (ΔH) of oxygen adsorption at a surface coverage (θ) of zero:

$$\varepsilon_{M\text{-}M} = \frac{\Delta H_{sub}}{\left(\frac{Z}{2}\right)} \quad \text{(Eq 5)}$$

where Z is the coordination number of atom M. The specific enthalpies of oxygen adsorption are provided in Table 3. In comparing the enthalpy of sublimation (ΔH_{sub}) and the enthalpy of oxygen adsorption, one can determine the relative abilities of elements to resist dissolution by creating strong metal-to-metal bonds and to enhance passivity by increasing the bond strengths between metal and oxygen. A high probability of passive oxide formation is indicated by: (a) a high negative energy change associated with oxygen adsorption, for example, metal bonding with oxygen; and (b) the ease by which initial metal-metal bonds can be broken, for

example, low enthalpy of sublimation. A net negative energy change as a result of a metal-metal bond breaking and a metal-oxygen bond forming would indicate the thermodynamic propensity for the formation of oxides. However, the presence of weak metal-metal bonds implies a high rate of metallic dissolution when bare metal is exposed to solution. In contrast, a metal with high metal-metal bond strengths is less likely to undergo dissolution (Ref 56, 57). Such metal will resist the formation of strong bonds with oxygen in favor of forming strong bonds between metallic atoms (Ref 56). Therefore, the mechanisms for stable passivity and stable resistance to dissolution are competitive. As such, two types of alloying elements exist: (a) passivity promoters that possess high enthalpies of oxygen adsorption and relatively low metal-metal bond strength, and (b) dissolution blockers that have high metal-metal bond strengths to inhibit metallic bond failures. However, by adding alloying elements with both characteristics, it would be possible to create an alloy that exhibits both resistance to anodic dissolution and stable passivity.

Table 3 Data for enthalpy of adsorption (oxygen), ΔH_{ads}, and atomic bond strength, $\varepsilon_{M\text{-}M}$, for a selection of metals

$\varepsilon_{M\text{-}M}$ was calculated from the heat of sublimation of the metals at 25 °C (77 °F).

Atomic number	Element	Structure[(a)]	Coordination number	Heat of sublimation ($\Delta H^{25\ °C}$, or $\Delta H^{77\ °F}$), kJ/mole	$\varepsilon_{M\text{-}M}$, kJ/mole	Heat of adsorption of oxygen (at $\theta \rightarrow 0$)[(b)], kJ/mole
13	Al	fcc	12	326.4	54.4	900
22	Ti	hcp	12	469.9	78.3	992
24	Cr	bcc	8	396.6	99.1	737
26	Fe	bcc	8	416.3	104.1	571
28	Ni	fcc	12	429.7	71.6	461
29	Cu	fcc	12	338.3	56.4	293
30	Zn	hcp	12	130.7	21.8	277
41	Nb	bcc	8	725.9	181.5	875
42	Mo	bcc	8	658.1	164.5	718
73	Ta	bcc	8	782.0	195.5	900
74	W	bcc	8	849.4	212.3	819
78	Pt	fcc	12	565.3	94.2	285
140	Zr	hcp	12	453.0	91.0	NA[(c)]

(a) fcc, face-centered cubic; hcp, hexagonal close-packed; bcc, body-centered cubic.
(b) θ, surface coverage.
(c) NA, not applicable.
Source: Ref 56

A classic example of both alloying types being used is chromium and molybdenum in stainless steels. Chromium, with its high enthalpy of oxygen adsorption, is added to iron to enhance oxide formation on stainless steel, as shown in Table 3. It is possible that chromium easily promotes the nucleation of chromium oxides on the surface of stainless steels at lower anodic overpotentials in comparison to the passive potentials of iron, thereby widening the potential range of passivity of iron-chromium-base alloys. In addition, molybdenum has a high metal-metal bond strength that indicates high resistance to reduce metallic dissolution, as shown in Table 3. Niobium exhibits a heat of adsorption of oxygen of 875 kJ/mole, which would classify niobium as a strong oxide former. Therefore, the alloying addition of niobium to titanium should result in improved passivation characteristics in comparison to pure titanium.

References cited in this section

56. P. Marcus, On Some Fundamental Factors in the Effect of Alloying Elements on Passivation of Alloys, *Corros. Sci.*, Vol 36 (No. 12), 1994, p 2155–2158

57. Y. Okazaki et al., Effect of Alloying Elements on Anodic Polarization Properties of Titanium Alloys in Acid Solutions, *Mater. Trans., JIM*, Vol 35 (No. 1), 1994, p 58–66

S. Yu, Corrosion Resistance of Titanium Alloys, *Corrosion: Fundamentals, Testing, and Protection*, Vol 13A, *ASM Handbook*, ASM International, 2003, p 703–711

Corrosion Resistance of Titanium Alloys

Steven Yu, 3M Company

Lowering of the pH of Zero Charge

The relationship between the resistance of an oxide to anion uptake and the pH of zero charge (pH_{pzc}) has been investigated on aluminum-base alloys (Ref 58). An important parameter governing the surface charge and, consequently, the adsorption characteristic of an oxide is the pH_{pzc} (Ref 58, 59). The pH_{pzc} of an oxide is the pH at which the surface has no net charge. Therefore, at a pH lower than the pH_{pzc}, the surface has a net positive charge, and aggressive anions are electrostatically attracted to the surface and can be adsorbed, which can possibly lead later to oxide failure. In contrast, at a pH higher than the pH_{pzc}, the surface has a net negative charge, and cations are attracted to the surface. Therefore, alloys containing elements that form oxides, which have relatively low pH_{pzc}, should exhibit superior resistance to aggressive anion uptake. The alloying additions of niobium and zirconium, which exhibit pH_{pzc} of 2.8 and 5.5, respectively, to aluminum, with a pH_{pzc} of 9.4, have been shown to enhance the resistance to anion uptake, for example, increase the pitting potential (Ref 58). Consequently, an alloy of niobium (pH_{pzc} ~ 2.8) to titanium (pH_{pzc} ~ 5), when oxidized, should exhibit superior resistance to chloride uptake and possible oxide failure in comparison to titanium. In contrast, it is possible that zirconium should have no measurable benefit to oxide failure resistance due to the similarity of the pH_{pzc} of titanium and zirconium. A limitation of the pH_{pzc} theory is its inability to predict a pH_{pzc} for mixed oxides.

References cited in this section

58. P. Natishan, E. McCafferty, and G.K. Hubler, Surface Charge Considerations in the Pitting of Ion-Implanted Aluminum, *J. Electrochem. Soc.*, Vol 135 (No. 2), 1988, p 321–327

59. P.M. Natishan, E. McCafferty, and W. O' Grady, A Study of Passive Film Using X-Ray Photoelectron and X-Ray Absorption Spectroscopy, *Applications of Surface Analysis Methods to Environmental/Materials Interactions*, R. Baer, G.D. Davis, and C.R. Clayton, Ed., Electrochemical Society, 1991, p 421

S. Yu, Corrosion Resistance of Titanium Alloys, *Corrosion: Fundamentals, Testing, and Protection*, Vol 13A, *ASM Handbook*, ASM International, 2003, p 703–711

Corrosion Resistance of Titanium Alloys

Steven Yu, 3M Company

Repassivation Behavior of Titanium and Titanium-Base Alloys

The electrochemical behavior of bare metal surfaces and their repassivation properties are important factors in environmentally assisted cracking (EAC), erosion-corrosion, and tribological applications. With the exception of gold, all metals oxidize reactive in aqueous environments, and almost all are protected from corrosion by the formation of a surface oxide film or an adsorbed film structure. This passivating behavior is clearly seen in valve metals, including titanium, niobium, zirconium, tantalum, and aluminum, that rely on kinetic barriers to

oxidation instead of thermodynamic stability of the metal for corrosion resistance. Therefore, passivating oxide films are crucial in the technological utility of valve metals. However, the failure of such oxides as a result of mechanical abrasion, anion interaction, or chemical dissolution is a dilemma that must be addressed.

The formation of a passivating film transpires in parallel with the active dissolution of the bare metal. During the formation of passivating film, the following steps can occur: (1) adsorbed film formation, (2) formation and growth of islands of oxides to cover the surface, (3) oxide film thickening, and (4) minimization of disorder in the oxide film. Opposing such reactions during passive film formation, the following reactions can occur: (a) active dissolution of metal across the passivating film; (b) dissolution in bare areas, which undercuts the islands of oxides; and (c) allocation of anodic charge to other competing oxidation reactions that do not contribute to oxide formation or consolidation of a compact oxide. Therefore, repassivation of the activated metal surface is achieved when the reaction rates for the formation of passivating film are greater than the rates of reactions opposing stabilization and thickening of the film. However, if the active dissolution mechanism dominates the net anodic reaction at such a site, then this site can become a stable location for localized corrosion. Therefore, an understanding of the mechanisms behind repassivation kinetics as well as the competing reactions are important for understanding the resistance of a metal to EAC, erosion-corrosion, localized corrosion, and tribology.

Repassivation Kinetics. During the repassivation of titanium, a minimum of four reactions can occur on the newly formed bare metal surface in deaerated reducing acid (Ref 39, 60):

$$Ti \rightarrow Ti^{3+} + 3e^{-} \quad \text{(Eq 6)}$$

$$Ti + 2H_2O \rightarrow TiO_2 + 4H^{+} + 4e^{-} \quad \text{(Eq 7)}$$

$$H^{+} + e^{-} \rightarrow H \quad \text{(Eq 8)}$$

$$Ti^{3+} + H_2O \rightarrow TiO^{2+} + 2H^{+} + e^{-} \quad \text{(Eq 9)}$$

The extent to which the anodic charge is consumed by Eq 6 can be addressed by inductively coupled plasma (ICP) solution analysis and gravimetric mass loss measurements. The thickening of titanium oxide, as described in Eq 7, can be measured by methods including electrochemical impedance spectroscopy (EIS). In contrast, nascent hydrogen formation cannot be measured by the experimental methods that are available to this researcher. However, the hydrogen-evolution reaction step is not possible at potentials greater than $E(V_{NHE})$ = 0.0 - 0.06 pH. Further oxidation of dissolved Ti^{3+} to Ti^{4+} in the form of TiO^{2+} can be measured by a scratched disk/gold ring oxidation test, as described in Ref 60.

The reaction step described by Eq 6 is reported to be the dominant mechanism that occurs during the repassivation of titanium in reducing acids, where greater than 90% of the applied anodic charge prior to steady-state passivation is consumed by the dissolution of metallic titanium into Ti^{3+} (Ref 40, 60). Moreover, the active anodic dissolution of titanium to Ti^{3+} occurs both on the bare metal surface and through the reforming oxide layer, due to the large potential gradient across the oxide. The following are possible reaction steps for metallic titanium dissolution to Ti^{3+} in deaerated solution, as described by Eq 6:

$$Ti \rightarrow Ti^{2+} + 2e^{-} \quad \text{(Eq 10)}$$

$$Ti^{2+} + H^{+} \rightarrow [Ti^{3+}H]_{ads} \quad \text{(Eq 11)}$$

$$[Ti^{3+}H]_{ads} \rightarrow Ti^{3+} + H^{+} + e^{-} \quad \text{(Eq 12)}$$

where the final product is aqueous Ti^{3+} at low potentials (Ref 7, 50). The alloying additions of species such as molybdenum, niobium, and zirconium to titanium could reduce active anodic dissolution rates of titanium-base alloys in comparison to pure titanium by enhancing the atomic bond strengths between titanium, molybdenum, niobium, and zirconium. Suffice it to say that molybdenum, niobium, and zirconium alloying additions can be beneficial in reducing the active anodic dissolution of titanium (Ref 56, 57). It is reasonable to assume that alloying additions of molybdenum, niobium, and zirconium to titanium increase the activation energy that is necessary to remove the valence electrons from titanium that are bonded to molybdenum, niobium, or zirconium in comparison to titanium bonded to titanium. This increase in activation energy required to oxidize titanium in titanium- molybdenum, titanium-niobium, and titanium- zirconium alloys is attributable to confirmed stronger *d*-*d*-level electron interaction between titanium-molybdenum, titanium-niobium, and titanium-zirconium near-neighbors in comparison to titanium-titanium. Therefore, the reaction rates for the

titanium-molybdenum, titanium-niobium, and titanium-zirconium alloys undergoing active anodic dissolution should be reduced in comparison to pure titanium.

Effects of Alloying Additions on Repassivation Kinetics of Titanium. Active anodic dissolution consumed approximately 90% of the total anodic charge for titanium, Ti-45%Nb, and Ti-50%Zr during galvanostatic polarization at 1 A/cm^2 (6.5 A/in.^{2}) (Ref 61). Similar high anodic-dissolution-charge consumption was recorded by researchers during repassivation tests of titanium, which indicates that the majority of the applied anodic charge density was consumed by active anodic dissolution of titanium, niobium, and zirconium from the bare surface (Ref 15, 40, 60). However, the anodic charge densities associated with active anodic dissolution diminished to approximately 10% of the total applied charge densities for Ti-45%Nb and Ti-50%Zr at lower anodic current densities approaching steady-state passivation densities, albeit at a high potential. In contrast, titanium still exhibited greater anodic dissolution charge densities at low current densities, which clearly indicates that the rapidly formed oxides on the titanium-niobium and titanium-zirconium binary alloys are more protective in comparison to TiO_2 formed on CP titanium.

Mechanisms by which Alloying Elements Inhibit Active Anodic Dissolution during Repassivation. It is reasonable to assume that similar dissolution inhibition mechanisms, as described in “Effects of Alloying on Active Anodic Corrosion of Titanium” are also applicable in inhibiting active anodic dissolution during repassivation. Researchers have explored the issue of enhanced resistance to metallic dissolution, from an atomic bonding approach (Ref 56, 57). They hypothesized that the formation of strong covalent bonds between the titanium and alloying species such as molybdenum, niobium, and zirconium atoms results in reduced rates of active metallic dissolution. Therefore, it reasonable to assume that the reaction rates for titanium-molybdenum, titanium-niobium, and titanium-zirconium alloys, which govern the active anodic dissolution, should be diminished, even at high- voltage driving force, in comparison to pure titanium.

Once a passive film has formed, the potential gradient across the metal/passive film/double layer/solution interface is defined by Eq 4, which is dependent on the oxide thickness, the Helmholtz double-layer thickness, as well as the dielectric constants of the oxide and the double layer. It can be assumed that the dielectric constant of the mixed oxides on titanium-base alloys will remain relatively constant (Ref 61). Moreover, assuming that the Helmholtz double-layer thickness as well as the dielectric constant of the double layer remain constant, the primary variable in determining the potential gradient across the oxide film is the oxide thickness (d_{ox}). An evaluation of the oxide-thickening ratios for titanium, Ti-45%Nb, and Ti-50%Zr revealed that both Ti-45%Nb and Ti-50%Zr exhibited higher oxide-thickening ratios, 3.1 and 2.2 nm/V, respectively, in comparison to titanium, which exhibited a $\Delta d_{ox}/\Delta E_{app}$ ratio of approximately 1.1 nm/V (Ref 61). Subsequently, there is a reduced potential gradient driving anodic dissolution of the underlying metal on Ti-45%Nb and Ti- 50%Zr in comparison to CP titanium. It is evident that such a primary condition for the high field model, for example, ~100% charge efficiency during oxide formation, is violated during galvanostatic polarization at high current densities, that is, $i > 0.0001$ A/cm^2 (0.00065 A/in.^{2}) (Ref 61). All of the tested samples exhibited significant active anodic dissolution, as measured by gravimetric mass loss measurements and ICP solution analysis. Therefore, the high field approximation for oxide growth cannot be used to describe the repassivation behavior of titanium and its alloys, including Ti-45%Nb and Ti- 50%Zr.

References cited in this section

7. M. Pourbaix, *Atlas of Electrochemical Equilibria in Aqueous Solutions,* 1st ed., NACE, 1974

15. D. Tomashov et al., The Passivation of Alloys on Titanium Bases, *Electrochim. Acta,* Vol 19, 1974, p 159–172

39. T.R. Beck, Electrochemistry of Freshly- Generated Titanium Surfaces, Part I: Scraped Rotating Disk Experiment, *Electrochim. Acta,* Vol 18, 1973, p 807

40. D. Kolman and J. Scully, On the Repassivation Behavior of High Purity Titanium and Selected Alpha, Beta, Alpha + Beta Titanium Alloys in Aqueous Chloride Solutions, *J. Electrochem. Soc.,* Vol 143 (No. 6), 1996, p 1847–1859

50. N. Thomas and K. Nobe, The Electrochemical Behavior of Titanium, *J. Electrochem. Soc.,* Vol 116 (No. 12), 1969, p 1748–1751

56. P. Marcus, On Some Fundamental Factors in the Effect of Alloying Elements on Passivation of Alloys, *Corros. Sci.,* Vol 36 (No. 12), 1994, p 2155–2158

57. Y. Okazaki et al., Effect of Alloying Elements on Anodic Polarization Properties of Titanium Alloys in Acid Solutions, *Mater. Trans., JIM,* Vol 35 (No. 1), 1994, p 58–66

60. T.R. Beck, Reactions and Kinetics of Newly Generated Titanium Surfaces and Relevance to Stress Corrosion Cracking, *Corrosion,* Vol 30 (No. 11), 1974, p 408–414

61. S.Y. Yu, "Mechanisms for Enhanced Active Dissolution Resistance and Passivity of Ti Alloyed with Nb and Zr," Department of Material Science and Engineering, University of Virginia, 1998

S. Yu, Corrosion Resistance of Titanium Alloys, *Corrosion: Fundamentals, Testing, and Protection*, Vol 13A, *ASM Handbook*, ASM International, 2003, p 703–711

Corrosion Resistance of Titanium Alloys

Steven Yu, 3M Company

References

1. M.J. Donachie, Jr., *Titanium: A Technical Guide,* 2nd ed., ASM International, 2000

2. C.R. Brooks, *Heat Treatment, Structure and Properties of Nonferrous Alloys,* American Society for Metals, 1982

3. R. Boyer, G. Welsch, and E.W. Collings, Ed., *Materials Properties Handbook: Titanium Alloys,* ASM International, 1994

4. T.P. Hoar and D.C. Mears, Corrosion-Resistant Alloys in Chloride Solutions: Materials for Surgical Implants, *Proc. R. Soc. (London) A,* Vol 294 (No. 1438), 1966, p 486–510

5. A. McQuillan, *Titanium Science and Technology,* Plenum Press, 1973, p 915–922

6. R. Schutz, An Overview of Beta Titanium Alloy Environmental Behavior, *Beta Titanium Alloys in the 1990's,* D. Eylon, R. Boyer, and D. Koss, Ed., Minerals, Metals and Materials Society, 1993, p 75–91

7. M. Pourbaix, *Atlas of Electrochemical Equilibria in Aqueous Solutions,* 1st ed., NACE, 1974

8. R.W. Schutz and J.S. Grauman, "Compositional Effects on Titanium Alloy Repassivation Potential in Chloride Media," Second International Conference on Localized Corrosion, (Orlando, FL) NACE, 1987

9. P.Y. Park et al., The Corrosion Behavior of Sputter-Deposited Mo-Ti Alloys in Concentrated Hydrochloric Acid, *Corros. Sci.,* Vol 38 (No. 10), 1996 p 1649–1667

10. V. Andreeva et al., Investigation of the Corrosion Resistance and the Electrochemical and Mechanical Properties of Titanium-Niobium Alloys, *Corrosion of Metals and Alloys,* N. Tomashov and E. Nirolybev, Ed., Israel Program for Scientific Translation, Jerusalem, 1966, p 34–47

11. P.J. Bania, *Beta-Titanium Alloys and Their Role in Titanium Industry,* D. Eylon, R. Boyer, and D. Koss, Ed., TMS, 1993, p 4

12. M. Levy and G. Sklover, Anodic Polarization of Titanium and Titanium Alloys in Hydrochloric Acid, *J. Electrochem. Soc.,* Vol 116 (No. 3), 1969, p 323–328

13. M. Itagaki, R. Oltra, and B. Vuillemin, Quantitative Analysis of Iron Dissolution During Repassivation of Freshly Generated Metallic Surfaces, *J. Electrochem. Soc.,* Vol 144 (No. 1), 1997, p 64–72

14. A. Mazhar, F. Heakal, and A. Gad-Allah, Anodic Behavior of Titanium in Aqueous Media, *Corros. Sci.,* Vol 44, 1988, p 705–710

15. D. Tomashov et al., The Passivation of Alloys on Titanium Bases, *Electrochim. Acta,* Vol 19, 1974, p 159–172

16. P.A. Mausli, S.G. Steinemann, and J.P. Simpson, “Properties of Surface Oxides on Titanium and Some Titanium Alloys,” Proceedings of the Sixth World Conference on Titanium (France), P. LaCombe, R. Tricot, and G. Bèranger, Ed., Sociètè Francaise de Métallurgie, 1988

17. N. Khalil and J.S.L. Leach, The Anodic Oxidation of Valve Metals, Part I: Determination of Ionic Transport Numbers by Alpha Spectrometry, *Electrochim. Acta,* Vol 31 (No. 10), 1986, p 1279–1285

18. J. Leach and B. Pearson, The Effect of Foreign Ions upon the Electrical Characteristics of Anodic ZrO_2 Films, *Electrochim. Acta,* Vol 29 (No. 9), 1984, p 1271–1282

19. M.J. Chappell and J.S.L. Leach, Passivity and Breakdown of Passivity of Valve Metals, *Passivity of Metals,* R.P. Frankenthal and J. Kruger, Ed., Electrochemical Society, 1978, p 1003–1034

20. E.J. Kelly and H.R. Bronstein, Kinetics and Mechanism of the Hydrogen Evolution Reaction of Titanium in Acidic Media, *J. Electrochem. Soc.,* Vol 131 (No. 10), 1984, p 2232–2238

21. N. Khalil, A. Bowen, and J.S.L. Leach, The Anodic Oxidation of Valve Metals, Part II: The Influence of the Anoidizing Conditions on the Transport Processes During the Anodic Oxidation of Zirconium, *Electrochim. Acta,* Vol 33 (No. 12), 1988, p 1721–1727

22. T. Shibata and Y. Zhu, The Effect of Film Formation Conditions of the Structure and Composition of Anodic Oxide Films on Titanium, *Corros. Sci.,* Vol 37 (No. 2), 1995, p 253–270

23. J.A. Davies et al., The Migration of Metal and Oxygen During Anodic Film Formation, *J. Electrochem. Soc.,* Vol 112 (No. 7), 1965, p 675–680

24. G.V. Samsonov, *The Oxide Handbook,* 2nd ed., IFI/Plenum, 1982

25. J. Pan, D. Thierry, and C. Leygraf, Electrochemical Impedance Spectroscopy Study of the Passive Oxide Film on Titanium for Implant Applications, *Electrochim. Acta,* Vol 41 (No. 7/8), 1996, p 1143–1153

26. D.G. Kolman and J.R. Scully, Electrochemistry and Passivty of a Ti-15Mo-3Nb-3Al Beta-Titanium Alloy in Ambient Temperature Aqueous Chloride Solutions, *J. Electrochem. Soc.,* Vol 140 (No. 10), 1993, p 2771

27. N. Casillas et al., Pitting Corrosion of Titanium, *J. Electrochem. Soc.,* Vol 141 (No. 3), 1994, p 636–642

28. P. McKay and D. Mitton, An Electrochemical Investigation of Localized Corrosion on Titanium in Chloride Environments, *Corrosion,* Vol 41 (No. 1), 1985, p 52–61

29. G. Burstein and R. Souto, Observations of Localized Instability of Passive Titanium in Chloride Solution, *Electrochim. Acta,* Vol 40 (No. 12), 1995, p 1881–1888

30. J. Yahalom and A. Poznansky, Surface Energy and the Stability of the Passive Layer, *Passivity of Metals,* R.P. Frankenthal and J. Kruger, Ed., Electrochemical Society, 1978, p 328–336

31. T. Shibata and Y. Zhu, The Effect of Film Formation Potential on the Stochastic Processes of Pit Generation on Anodized Titanium, *Corros. Sci.,* Vol 36(No. 1), 1994, p 153–163

32. T. Watanabe, H. Naito, and Y. Nakamura, Crevice Corrosion Behavior of Commercially Pure Titanium in NaCl-HCl Solutions, *J. Jpn. Inst. Met.,* Vol 50 (No. 9), 1986, p 822–827

33. I. Dugdale and J. Cotton, The Anodic Polarization of Titanium in Halide Solutions, *Corros. Sci.,* Vol 4, 1964, p 397–411

34. J.J. Noel et al., Passive Oxide Film on Titanium in Aqueous Chloride Solution Probed by Electrochemistry, XPS, and In- Situ Neutron Reflectometry, *Surface Oxide Films,* The Electrochemical Society, 1996

35. R.D. Armstrong and R.E. Firman, Impedance of Titanium in the Active-Passive Transition, *J. Electroanal. Chem. Interfacial Electrochem.,* Vol 34, 1972, p 391–397

36. J.R. Galvele, Present State of Understanding of the Breakdown of Passivity and Repassivation, *Passivity of Metals,* R.P. Frankenthal and J. Kruger, Ed., Electrochemical Society, 1978, p 285–323

37. C.K. Dyer and J.S.L. Leach, Reversible Reactions Within Anodic Oxide Films on Titanium Electrodes, *Electrochim. Acta,* Vol 23, 1978, p 1387–1394

38. D.J. Blackwood and L.M. Peter, Stability and Open Circuit Breakdown of the Passive Oxide Film on Titanium, *Electrochim. Acta,* Vol 33 (No. 8), 1988, p 1143–1149

39. T.R. Beck, Electrochemistry of Freshly- Generated Titanium Surfaces, Part I: Scraped Rotating Disk Experiment, *Electrochim. Acta,* Vol 18, 1973, p 807

40. D. Kolman and J. Scully, On the Repassivation Behavior of High Purity Titanium and Selected Alpha, Beta, Alpha + Beta Titanium Alloys in Aqueous Chloride Solutions, *J. Electrochem. Soc.,* Vol 143 (No. 6), 1996, p 1847–1859

41. T.R. Beck, *Localized Corrosion,* B.F. Brown, Ed., NACE, 1974, p 644

42. C. Baes and R. Mesmer, *The Hydrolysis of Cations,* John Wiley & Sons, 1976, p 147–168

43. B.F. Brown, C.T. Fujii, and E.F. Dahlberg, *J. Electrochem. Soc.,* Vol 116 (No. 218), 1969, p 218

44. M. Stern and H. Wissenberg, The Electrochemical Behavior and Passivity of Titanium, *J. Electrochem. Soc.,* Vol 106 (No. 9), 1959, p 755–759

45. P. Mckay, Crevice-Corrosion Kinetics on Titanium and a Ti-Ni-Mo Alloy in Chloride Solutions at Elevated Temperatures, *Corrosion Chemistry Within Pits, Crevices, and Cracks,* HMSO Books, 1987

46. R.W. Schutz, “Understanding and Preventing Crevice Corrosion,” Corrosion 91, (Cincinnati, OH), NACE, 1991

47. L.A. Yao and F.X. Gan, Microelectrode Monitoring the Crevice Corrosion in Titanium, *Corrosion,* Vol 47 (No. 6), 1991, p 420–423

48. H. Shizhong and M. Xiaoxiong, Localized Corrosion in Titanium in Marine Environments, *Corrosion and Corrosion Control for Offshore and Marine Construction,* Pergamon Press, 1988

49. E. Kelly, Anodic Dissolution and Passivation of Titanium in Acidic Media, *J. Electrochem. Soc.,* Vol 126 (No. 12), 1979, p 2064

50. N. Thomas and K. Nobe, The Electrochemical Behavior of Titanium, *J. Electrochem. Soc.,* Vol 116 (No. 12), 1969, p 1748–1751

51. S. Kitayama et al., “Effect of Small Pd Addition on the Corrosion Resistance of Ti and Ti Alloys in Severe Gas and Oil Environments,” Corrosion 92, NACE, 1992

52. A.G. Revesz and J. Kruger, The Role of Noncrystalline Films in Passivation and Breakdown of Passivation, *Passivity of Metals,* R

K. Ogle, and M. Wolpers, Phosphate Conversion Coatings, *Corrosion: Fundamentals, Testing, and Protection*, Vol 13A, *ASM Handbook*, ASM International, 2003, p 712–719

Phosphate Conversion Coatings

Kevin Ogle, Irsid, Arcelor R&D (Maizières-lès-Metz, France); Michael Wolpers, Henkel KGaA (Düsseldorf, Germany)

Introduction

PHOSPHATING is used in the metalworking industry to treat substrates like iron, steel, galvanized steel, aluminum, copper, and magnesium and its alloys. Most automobile bodies are zinc phosphated prior to painting to increase corrosion resistance and paint adhesion. The cold extrusion of steel would not be economically feasible without phosphating as a lubrifying film. Other applications include providing temporary corrosion resistance for unpainted metal and electrical resistance (Ref 1, 2, 3). This article gives an overview of the types, uses, and theory of phosphate coatings and their formation. It also discusses the composition of phosphating baths, phosphate layers, and their analysis, as well as the process hardware necessary to realize these treatments.

References cited in this section

1. W. Rausch, *Die Phosphatierung von Metallen* (*The Phosphating of Metals*), Eugen G. Leuze Verlag, 1988; ASM International and Finishing Publications Ltd., 1990

2. M. Bastian, P. Kuhm, and G. Meyer, *Metalloberfläche,* Vol 53 (No. 1), p 10–15; Vol 53 (No. 2), p 10–14; Vol 53 (No. 3), 1999, p 10–14

3. P.E. Tegehall, “The Chemistry of Zinc Phosphating of Steel,” Ph.D. thesis, Chalmers University of Technology, Göteborg, Sweden, 1990

K. Ogle, and M. Wolpers, Phosphate Conversion Coatings, *Corrosion: Fundamentals, Testing, and Protection*, Vol 13A, *ASM Handbook*, ASM International, 2003, p 712–719

Phosphate Conversion Coatings

Kevin Ogle, Irsid, Arcelor R&D (Maizières-lès-Metz, France); Michael Wolpers, Henkel KGaA (Düsseldorf, Germany)

Structure and Function of the Phosphate Film

Phosphate conversion coatings are composed of insoluble tertiary metal (Me) phosphates, $Me_3(PO_4)_2 \cdot xH_2O$. In this formula, Me represents divalent metallic cations of one or more metallic elements. The phosphate layer or coating is formed on a metal substrate by exposing the metal to a phosphating bath.

A summary of different types of phosphate layers is given in Table 1. A major distinction can be made between crystalline and amorphous phosphate layers. Figure 1 shows the morphological differences between crystalline and amorphous phosphate layers on zinc coated steel substrates. X-ray diffraction (XRD) spectra support the crystalline and amorphous character of the layer respectively. In Fig. 1(a) (on the left side), the phosphate crystals are clearly visible, giving a characteristic XRD pattern. By contrast, in Fig. 1(b) (on the right side), the amorphous layer is characterized by irregular structure in the scanning electron micrograph (SEM) and no pattern in the XRD spectra.

Table 1 Characteristics of different types of phosphate coatings and associated processes (general formulas)

Free acid is defined as the number of mL of 0.1 *M* NaOH required to reach the first endpoint during titration of 10 mL bath sample. Total acid is related to the second endpoint.

Characteristic	Amorphous phosphate layers		Crystalline phosphate layers		
	Alkali phosphating (iron phosphating)	**No-rinse-phosphating (dry-in-place phosphating)**	**Low-zinc phosphating Standard-zinc phosphating[(a)]**	**Heavy phosphating**	
				Zn cation	**Mn cation**
Coating weight, g/m²	0.1–1.0	0.1–4	1–7	5–30	<60
Conditioning	None	None	Titanium phosphate	None	None
Primary use	Temporary corrosion protection; paint base for low-corrosion environments	Forming	Temporary corrosion protection; paint base for high-corrosion environments	Unpainted applications	Unpainted applications; forming
Limitations	Low painted corrosion resistance; low unpainted corrosion resistance	Poor unpainted corrosion resistance; low painted corrosion resistance	Poor unpainted corrosion resistance	Expensive, long processing times	
Materials	Low-carbon steel	Stainless steel;	Stainless steel;	Stainless steel	Stainless steel

needed for tanks		glass fiber reinforced plastic	glass fiber reinforced plastic	or low-carbon steel	or low-carbon steel
Application method	Spray and immersion	Roll-on	Spray and immersion	Immersion(b)	Immersion(b)
Temperature, °C	40–55	Room temperature	32–60	50–80	80–98
Free acid	-2.0–2.0	30–50	0.6–3.0	4–8	9–12
pH	3–5	2–2.5	3–3.4	2.5–3	2–3
Total acid	5–10	~150+	18–35	40–50+	60–70
c(Zn^{2+}), g/L	…	5–15	0.5–2.0 [3–7]	20–40+	…
c(Fe^{2+}), g/L	~0.3	…	Approx 0–0.3	Approx 0–3	<8
c(Mn^{2+}), g/L	…	15–25	0–1.5	(c)	80
c(Ni^{2+}), g/L	…	1–5	0–1.5	(c)	15
c(Ca^{2+}), g/L(d)	…	…	<2.0	…	…
c(Mg^{2+}), g/L(d)	…	…	<1.0	…	…
c(Cu^{2+}), mg/L(d)	…	…	<10	…	…
c(Na^{+}), g/L	~2	…	<2.0	…	…
c(NO_3^{-}), g/L	~2	…	2–25	50–80	<120

(a) The standard zinc phosphating is comparable to the low-zinc process. Values in angular brackets belong to the standard-zinc phosphating. The main differences are the zinc and the phosphate concentrations. Standard zinc baths contain 3–7 g/L Zn^{2+} and 6–9 g/L PO_4^{3-}, and low-zinc baths contain 0.5–2 g/L Zn^{2+} and 12–16 g/L PO_4^{3-}. These ranges are not strict.
(b) In several cases the deposition of phosphate takes place under galvanostatic polarization.
(c) Small concentrations are possible.
(d) These ions are mainly used instead of manganese and/or nickel.

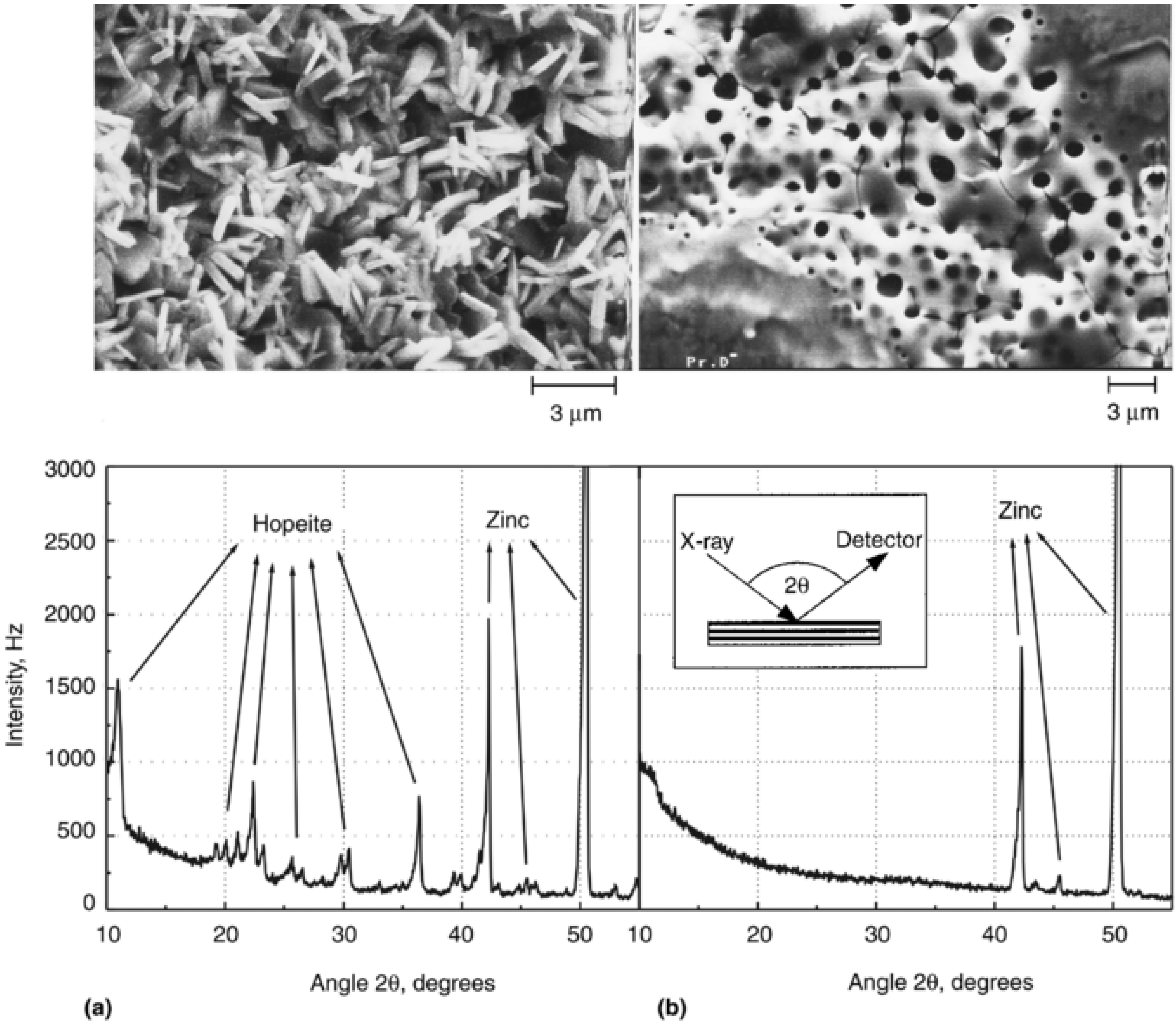

Fig. 1 Scanning electron micrographs and x-ray diffraction patterns comparing crystalline and amorphous phosphate layer. (a) Tri-cation phosphate layer of a spray process. (b) Tri-cation phosphate layer of a no-rinse process. Substrate is electrogalvanized steel.

The amorphous layers are commonly used for temporary corrosion protection, with coating weight ranging from 0.1 to 4.0 g/m^2 (0.00033 to 0.013 oz/ft^2). These layers are formed by alkali phosphating or by no-rinse phosphating. No- rinse phosphatation is mainly used in the coil- coating industry and means that the phosphating solution is applied directly to steel strips and dried without rinsing. Amorphous phosphate layers are formed using both iron- and zinc- based solutions.

Crystalline phosphate layers are most easily categorized by their intended application. For underpaint applications zinc-based phosphate layers formed by low-zinc or standard-zinc processes are used with coating weights ranging from 1 to 7 g/m^2 (0.0033 to 0.023 oz/ft^2). Values around 7 g/m^2 can be obtained on galvannealed and high-strength-steels. For cold forming and lubrification, coating weights of up to 60 g/m^2 (0.20 oz/ft^2) are common. These layers are sometimes referred to as "heavy phosphating" and are often, but not always, based on manganese- rather than zinc-phosphate layers.

Table 2 gives the formula for a number of different phosphate compounds that are theoretically possible in crystalline phosphate layers. The hopeite and phosphophyllite compounds are the most commonly observed. At the time of this writing, most commercial "state of the art" conversion coatings (pretreatment for painting) consist of Zn^{2+} in combination with one or more coatings of Mn^{2+}, Ni^{2+}, and Fe^{2+} (Ref 4).

Table 2 Phosphate compounds found in conversion coatings

Compound name[(a)]	Chemical formula	Structure
Vivanite	$Fe_3(PO_4)_2 \cdot 8H_2O$	Monoclinic
Iron-hureaulite[(b)]	$Fe_5H_2(PO_4)_4 \cdot 4H_2O$	Monoclinic
Strengite	$FePO_4 \cdot 2H_2O$	Orthorhombic
Hopeite	$Zn_3(PO_4)_2 \cdot 4H_2O$	Orthorhombic
Phosphophyllite[(b)]	$Zn_2Fe(PO_4)_2 \cdot 4H_2O$	Monoclinic
Scholzite	$Zn_2Ca(PO_4)_2 \cdot 4H_2O$	Orthorhombic
Phosphonicollite[(c)]	$Zn_2Ni(PO_4)_2 \cdot 4H_2O$	Orthorhombic
Phosphomangallite[(b)]	$Zn_2Mn(PO_4)_2 \cdot 4H_2O$	Orthorhombic
Manganese-hureaulite[(b)]	$Mn_5H_2(PO_4)_4 \cdot 4H_2O$	Monoclinic
Klinovariscite, variscite	$AlPO_4 \cdot 2H_2O$	Orthorhombic

(a) Hopeite and phosphophyllite are the most common.
(b) Phosphophyllite is (Fe, Mn)$Zn_2(PO_4)_2 \cdot 4H_2O$; hureaulite is (Mn, Fe_5)$H_2(PO_4)_4 \cdot 4H_2O$. The names used in this article were chosen to avoid confusion as to the actual composition.
(c) No mineralogical name known

The "crystalline" phosphate layer is not a simple film. The surface consists of an array of distinct phosphate crystals, which are often a mix of crystalline and x-ray amorphous phases. Figure 2 shows typical electron micrographs of crystalline phosphate films on steel, galvanized steel, and aluminum substrates. In between the phosphate crystals, bare metal may be exposed, but often it is not the metal of the original substrate. Ni^{2+}, Co^{2+}, or Cu^{2+} ions are frequently added to the phosphate bath, and these will deposit by a cementation reaction on the exposed metal surface (Ref 5). Further, the metallic surface between the crystals may be passivated by an amorphous phosphate film. In the case of phosphating followed by a passivating rinse, a chromate or other conversion coating may form between the crystals. The use of a chromate posttreatment may alter the outer surface of the phosphate crystals by producing a thin chromate-containing layer of enhanced chemical stability.

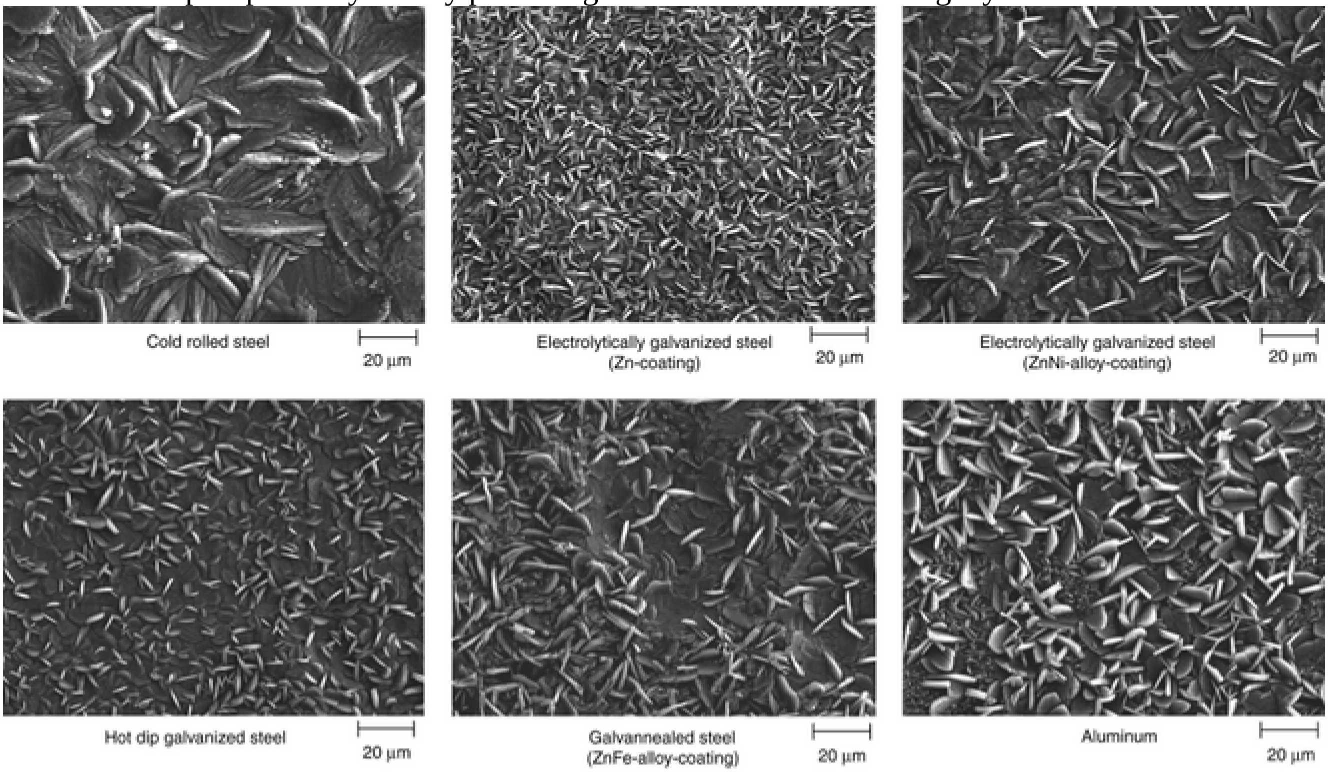

Fig. 2 SEM pictures of crystalline phosphate layers on steel, four different types of galvanized steel, and aluminum. All micrographs are shown at the same magnification.

Several functions may be attributed to the "crystalline" phosphate layer. The nonconducting nature of the phosphate crystal imparts a barrier property with excellent corrosion protection. The voids between the crystals provide anchorage for paint layers, increasing paint adherence. The exposed metal between the crystals is important for providing enough conducting surface to permit the cathodic deposition of paint primers as used in

the automotive industry. The fact that the paints are electrophoretic ensures that the deposition process begins at the bottom of the pore and builds up toward the exterior.

For the purpose of lubrication, the porosity of the surface leads to very good oil retention. Further, the oil may chemically bind to the phosphate layer by a saponification reaction. Lastly, on compression, the crystals can form a glass phase at the surface of the metal, imparting extremely low friction for deep drawing applications.

Figure 3 compares creepage behavior of three different painted steel products with and without phosphatation. Creepage is the distance between an artificial damage (scratch, cut, edge, stone chipping) and the border of the delaminated paint. The delaminated paint can be easily removed by scalpel.

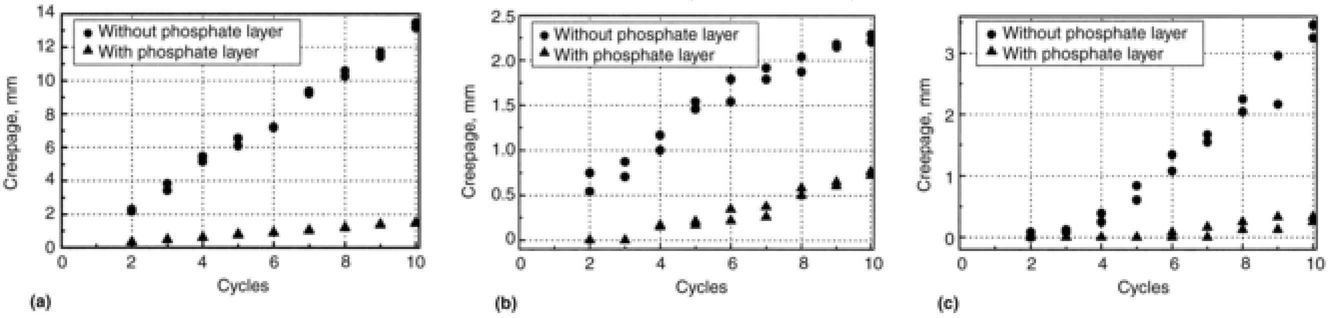

Fig. 3 Trend of paint delamination of steel products. (a) Cold rolled steel. (b) Hot dip galvanized steel. (c) Galvannealed steel (Fe-Zn alloy). Coating is approximately 25 µm electrophoretic paint with and without phosphate treatment. Artificial damage by Van Laar scratch, scalpel comparable to a ball-point pen, then exposed in a cyclic corrosion test. Test cycle was 1 day salt spray fog, plus 4 days condensed water exposure plus 2 days dry period. Creepage is defined as the distance between the artificial damage and the border of delamination. Note that the y-axes are different in scale. Source: Ref 6

Crystalline phosphate layers are often classified by the types of divalent cations present in the phosphating bath: mono-cation (essentially Zn^{2+}), bi-cation (Zn^{2+} and either Ni^{2+}, Ca^{2+}, Mg^{2+}, or Mn^{2+}) and tri-cation (Zn^{2+}, Ni^{2+}, Mn^{2+}). In these formulas, Ni^{2+} is sometimes replaced by Cu^{2+} for environmental reasons, as copper can be used at much lower concentrations. Tri-cation phosphating is considered the state of the art, giving the overall best performance in corrosion resistance and paint adhesion. A comparison of the corrosion behavior of some different types of phosphate layers is given in Fig. 4.

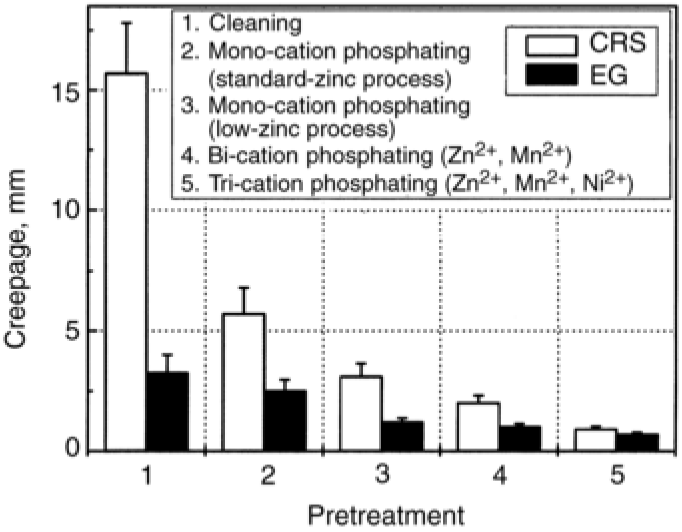

Fig. 4 Delamination of painted steel substrates treated with different zinc phosphatations after 1 year outdoor exposure. Substrate CRS, cold rolled steel; EG, electrogalvanized. Coating electrophoretic paint + filler + top-coat. Artificial damage by Clemen scratch, like a cut with a scalpel

Alkali phosphating, which mostly leads to amorphous coatings, is very different in terms of application and use (Ref 7) from crystalline phosphating. It is usually only applied as a pretreatment for iron and steel, but in principle it could also be applied for zinc, zinc- coated steel, and aluminum. It is used as a low-cost

pretreatment for paint or sometimes as an acidic cleaner. The general characteristics of alkali phosphatings are given in Table 1.

There are different types of alkali phosphate layers. On iron or steel, the phosphate layers are a mixture of iron phosphate ($Fe_3(PO_4)_2 \cdot 8H_2O$), iron oxides, and iron hydroxides. The treated surfaces may appear shiny and iridescent with temper colors. The phosphate coating weight lies between 0.1 and 0.4 g/m^2 (0.00033 to 0.0013 oz/ ft^2). Due to organic accelerators such as nitrobenzenesulfonic acid, it is possible to achieve phosphate-coating weights up to 1.0 g/m^2 (0.0033 oz/ft^2). In these cases the surfaces have a gray and dull appearance. The use of additional accelerators and chromium-free posttreatments leads to an optimization of corrosion resistance and paint adhesion. Figure 5 illustrates this development.

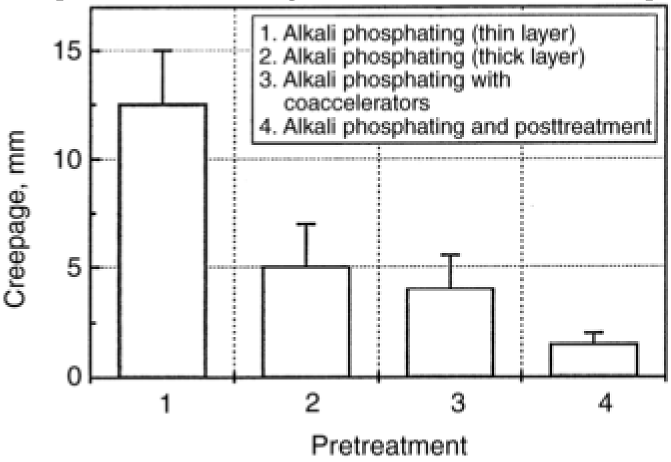

Fig. 5 Delamination of painted steel substrates treated with four different alkali phosphatations after 504 h exposure in salt spray fog. Coating, electrophoretic paint + filler + top-coat. Artificial damage, Van Laar scratch

References cited in this section

4. W.A. Roland and K.H. Gottwald, *Metalloberfläche,* Vol 42, 1988

5. E. Klusmann, U. König, and J.W. Schultze, *Mater. Corros.,* Vol 46, 1995, p 83

6. VDA Prüfblatt 621-415: Prüfung des Korrosionsschutzes von Kraftfahrzeuglackierungen bei zyklisch wechselnder Beanspruchung (Community of the German Car Producers, Test Instruction 621-415, Test of the Corrosion Protection of Paintings under Cyclic Changing Conditions)

7. T. Molz, *Metalloberfläche,* Vol 51, 1997, p 638–643

K. Ogle, and M. Wolpers, Phosphate Conversion Coatings, *Corrosion: Fundamentals, Testing, and Protection,* Vol 13A, *ASM Handbook,* ASM International, 2003, p 712–719

Phosphate Conversion Coatings

Kevin Ogle, Irsid, Arcelor R&D (Maizières-lès-Metz, France); Michael Wolpers, Henkel KGaA (Düsseldorf, Germany)

Phosphating Steps

There are four chemically important steps in the phosphating sequence: cleaning, activation or conditioning (mainly for zinc phosphating), phosphating, and posttreatment plus standard rinsing steps. When used as a pretreatment for paint, the phosphate layer may also undergo phase changes associated with dehydration

reactions during painting. Table 3 gives the integration of phosphating processes in different applications, and Fig. 6 illustrates the process sequence and application conditions for the car industry.

Table 3 Typical process sequences in different industries

Industry	Typical process sequence
Car, truck	Cleaning, water rinsing, activating, zinc phosphating, water rinsing, sealing, water rinsing, drying
Galvanizing line	Activating, zinc phosphating, water rinsing, drying
Coil coating line	Cleaning, water rinsing, alkali phosphating (or alternative activating, zinc phosphating), water rinsing, sealing, water rinsing, drying
Household, appliance	Cleaning, water rinsing, alkali phosphating (or alternative activating, zinc phosphating), water rinsing, sealing, water rinsing, drying
Wire-drawing	Pickling, water rinsing, plating, water rinsing, manganese phosphating (not always electrochemical), posttreatment with lime, borax or soaps, water rinsing, drying

Conditioning is an alternative term for activation.

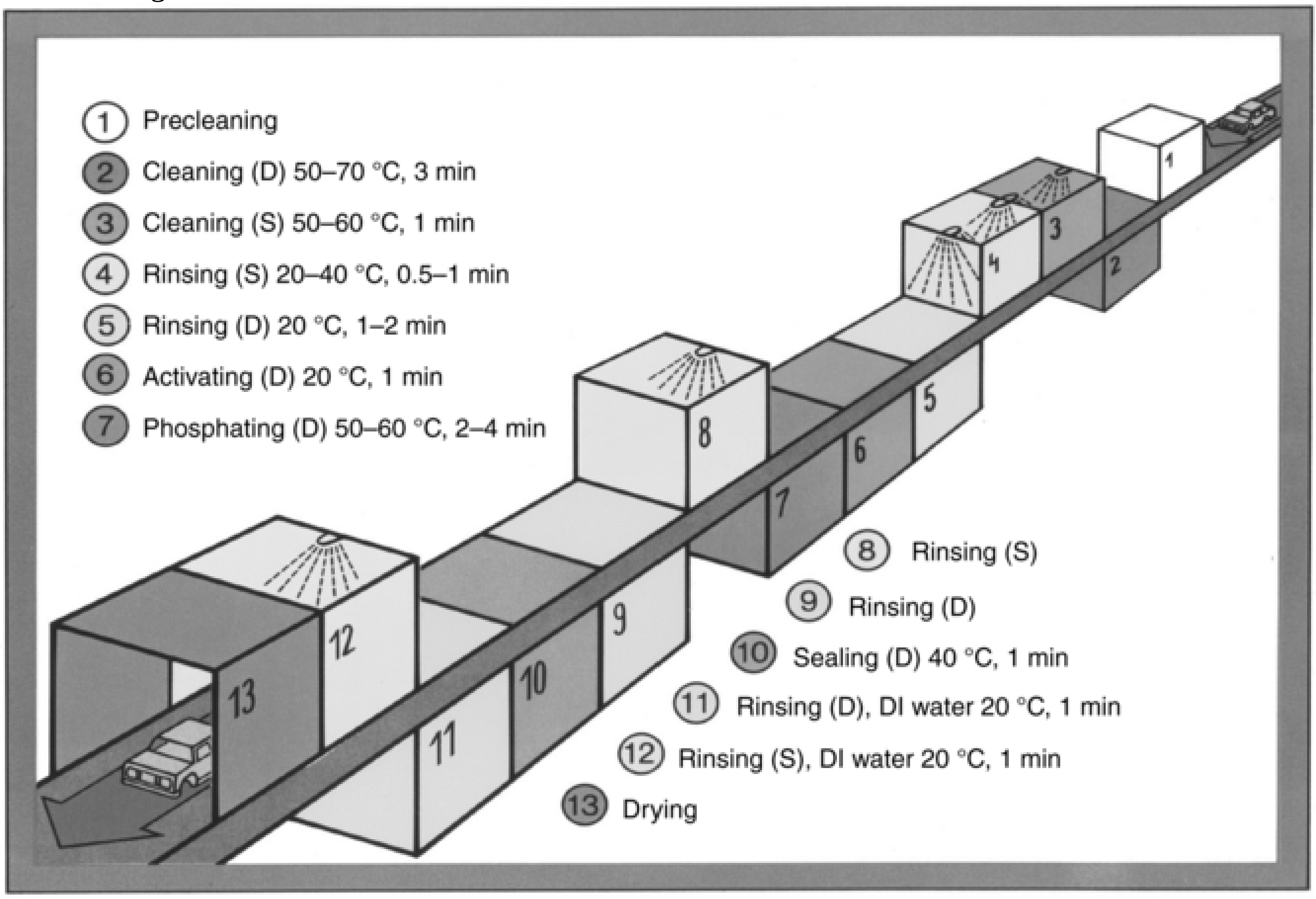

Fig. 6 Typical sequence of pretreatment process for car bodies. D, dipping; S, spraying; DI, deionized water

Cleaning

The degreasing process using aqueous solutions or organic solvents is an extremely important preconditioning step for phosphating (Ref 8, 9). Chlorinated hydrocarbons are very effective at removing oils and grease, but environmental laws strictly limit the use of such solvents. Treatment with alkaline solutions is also quite effective in removing oils and grease and also serves to increase the wettability of the metal surface and to remove oxide layers.

Alkaline degreasing agents consist of builders, complexants, and surfactants. Builders are inorganic salts and hydroxides. NaOH and KOH are responsible for the high pH values and make the primary contribution to the

ionic conductivity of the aqueous solutions. NaOH and KOH will also hydrolyze animal and plant oil and grease. Degreasing baths using these bases are usually in the pH 12 to 14 range. Iron and steel are normally passive in these high pH cleaning baths. Zinc and aluminum are normally degreased at lower pH because of their increased corrosion rate at high pH.

Commercial alkaline degreasing baths contain numerous additives. Silicates have good emulsifying action and dispersing properties. During cleaning of aluminum, zinc, and zinc-coated steel, a thin layer of silicate deposits on the surface and inhibits the attack of the metal by the alkaline solution. Phosphates, pyrophosphates, and polyphosphates soften the water and partly remove metal oxides and hydroxides. Borates and carbonates have good buffering properties, stabilize the pH, and inhibit the alkaline attack. Zinc and aluminum are normally degreased using cleaning systems based on borates and carbonates.

Surfactants are organic molecules composed of hydrophilic and hydrophobic groups. Due to this structure they cluster at the metal/solution interface. Depending on whether the hydrophilic group is cationic or anionic, the surfactant is called cation-active or anion-active. Nonionics are built up of polyethylene glycol or polypropylene glycol groups and aliphatic chain molecules, and aromatic groups. The surfactants dissolve and emulsify non-hydrolyzable components like mineral oils. Complexing agents like ethylenediamine tetraacetic acid (EDTA), nitrilotriacetic acid (NTA) or gluconates are added to cleaning baths to reduce undesirable precipitation. Table 4 gives an overview of degreasing solution additives.

Table 4 General formulas of alkaline cleaning products

Treated metals	pH(a)	Components	Temperature		Time, s(a)	Comments
			°C	**°F**		
Steel	7–14	Alkali, carbonates, phosphates, silicates, borates, complexing agents, surfactants	50–80	122–176	5–300	…
Zinc	7–11 [12–13]	Phosphates, carbonates, borates, silicates, complexing agents, surfactants	50–60	122–140	120–240 [3–15]	Pickling rate rises with alkalinity
Aluminum	7–10 [11–13]	Phosphates, carbonates, borates, complexing agents, surfactants	50–60	122–140	120–240 [3–15]	Pickling rate rises with alkalinity, mostly in combination with acid pickling
Prephosphated substrates	7–9	Phosphates, silicates, borates	50–60	122–140	120–240	Phosphate layer could be removed at higher pH, no tripolyphosphate
Magnesium	12–14	Alkali, carbonates	50–60	122–140	…	Mg is stable at higher pH. Alkaline cleaning is usually followed by acid pickling to remove hydroxide layers.

(a) Values in brackets belong to short processes, like coil coating lines

Activation (or Conditioning)

The activation step consists of exposure to a titanium colloid solution of near-neutral pH (Ref 10). The Ti colloids adsorb on the surface of the metal and serve as nucleation sites for the growth of the phosphate layer. Aqueous dispersions of sodium titanium phosphate are well suited for this preconditioning. A number of other chemicals, such as oxalic acid, amine soaps, or finely ground zinc phosphates have a similar effect. Activation increases the number of phosphate crystals per unit area while decreasing crystal size, coating weight, and the minimum reaction time. Many zinc phosphating systems are totally dependent on the preconditioning stage to deposit a beneficial zinc-phosphate layer. The preconditioner can be applied either as a portion of the final cleaning stage or, preferably, as a separate stage immediately before phosphating. Due to their colloidal character, the activation dispersions are not stable, and the colloids have a tendency to coagulate. This lowers

the frequency of nucleation and thus the rate of film growth. The coagulation process is very sensitive to pH, temperature, and water hardness, and these parameters must be precisely controlled (Ref 11, 12).
Phosphate layer nucleation and the effect of the activation step are not clearly understood. It is known from atomic force microscopy (AFM) studies that the colloids in the aqueous dispersion are disc-shaped and adsorb physically with the flat side against the metal surface (Ref 13). It is thought that an ion-exchange reaction occurs on the colloid surface between the sodium ions of the colloids and the zinc ions of the phosphating solution (Ref 14) and that this reaction initiates the growth of the phosphate layer.

Phosphating

The function of the constituents is described in the following discussion.
Basic Function of the Bath. The zinc phosphating bath consists mainly of phosphoric acid and divalent metal cations. The rate controlling step for the growth of the phosphate film is the reaction of H^+ ion and/or other oxidizing agents present as additives at the metal surface. The solution is inherently aggressive to the substrate metal, and the acidic attack of the metal surfaces leads to a local increase in pH and metal ion concentration (Ref 15, 16). When the solubility product of the tertiary metal phosphate is reached, then the corresponding phosphate compound will precipitate. In the case of zinc, the solubility product is $K_L\{Zn_3(PO_4)_2 \cdot 4H_2O\} = 5 \times 10^{-36}$. Additionally, the stability constants of $ZnH_2PO_4^+ (10^{3.3})$ and $ZnHPO_4 (10^{1.6})$ have to be taken into account (Ref 17, 18). The basic chemical reactions involved in the phosphating process are:

$$Me \rightarrow Me^{2+} + 2e^- \quad \text{Metal dissolution}$$

$$2H^+ + 2e^- \rightarrow H_2 \quad \text{Hydrogen evolution}$$

$$\left.\begin{array}{l} H_3PO_4 \leftrightarrow H_2PO_4^- + H^+ \\ H_2PO_4^- \leftrightarrow HPO_4^{2-} + H^+ \\ HPO_4^{2-} \leftrightarrow PO_4^{3-} + H^+ \end{array}\right\} \quad \text{Protolytic equilibria of phosphoric acid}$$

$$2PO_4^{3-} + 3Me^{2+} + 4H_2O \rightarrow Me_3(PO_4)_2 \cdot 4H_2O \downarrow$$

Metal phosphate layer precipitation

where Me^{2+} is one of several possible metal ions. The growth of the phosphate crystals continues until the coverage of the surface stops by self-inhibition as insoluble phosphate crystals block the metal dissolution and the consumption of H^+. The formation of $Me_3(PO_4)_2 \cdot 4H_2O$ is applicable to many crystalline phosphate coatings. Other phosphates may also precipitate, such as:

$$5Me^{2+} + 2HPO_4^{2-} + 2PO_4^{3-} + 4H_2O \rightarrow Me_5H_2(PO_4)_4 \cdot 4H_2O \downarrow$$

Metal Ions. In the phosphate layer, metal ions come from both the substrate metal and from the solution. For example, a zinc phosphate bath used to treat steel will contain hopeite ($Zn_3(PO_4)_2 \cdot 4H_2O$) and phosphophyllite ($Zn_2Fe(PO_4)_2 \cdot 4H_2O$), where the Fe^{2+} in the later species comes from the steel substrate. Other metal ions used in the phosphating bath are Mn^{2+}, Ni^{2+}, Co^{2+}, Cu^{2+}, Ca^{2+}, and Mg^{2+}. More noble metal ions like Ni^{2+}, Co^{2+}, or Cu^{2+} deposit by a cementation reaction on substrates like steel, zinc, and aluminum (Ref 5, 19, 20).
The development of zinc phosphating began with the so-called standard-zinc process. These baths contain approximately 3 to 7 g/L zinc and 6 to 9 g/L phosphate. It has been found, however, that a reduction of zinc (to ~1 g/L) and an increase of phosphate (to ~15 g/l) significantly improve the performance of the phosphate layers because of the greater formation of phosphophyllite or phosphonicollite. These processes are called low-zinc phosphatation. The concentration ranges are not so strict and could overlap in some cases.
Metal Surface. The reactivity of the metal surface being treated plays an important role in the phosphating process. Zinc and steel are readily attacked by phosphoric acid solution and are fairly easy to treat. Magnesium is highly reactive, which may cause problems. Aluminum requires the addition of fluoride ions to maintain sufficient reactivity. Passivating materials like stainless steel are difficult to phosphate. In general, the effect of alloying elements on the phosphating process can be predicted by their effect on the overall reactivity of the metal being treated. For the steel surface, most segregated oxides will block the phosphating reaction (for

instance, Cr_xO_y, Si_xO_y, Al_xO_y, …) (Ref 21, 22); occasionally this is a problem. Some oxides, in particular manganese oxides, actually increase the reactivity of the steel surface and are incorporated into the phosphate layer, yielding particularly good phosphating activity. Additionally, the roughness of the surface being treated plays an important role in the phosphating reactivity. For instance, skin passing is a rolling-mill process that increases surface roughness and substrate hardness. It breaks up oxide layers and increases the surface reactivity.

Accelerators. Modern phosphating baths use additives called accelerators to hasten the phosphating process. In the absence of accelerators, H^+ ion is the principal oxidant, and the formation of hydrogen bubbles at the surface disturbs the phosphating process. Therefore, it is necessary to suppress hydrogen evolution by another suitable reaction in order to accelerate the phosphatation step. Oxidants such as nitrate, nitrite, chlorate, bromate, peroxy compounds, ozone, organic nitro substances, hydroxylamine, and molybdate can play the role of a cathodic depolarizer. These substances are consumed reductively prior to the hydrogen evolution. Some of these reactions are:

$$NO_2^- + 2H^+ + e^- \rightarrow NO + H_2O$$
$$NO_3^- + 10H^+ + 8e^- \rightarrow NH_4^+ + 3H_2O$$
$$R - NO_2 + 6H^+ + 6e^- \rightarrow R - NH_2 + 2H_2O$$

where R is an organic group

$$ClO_3^- + 6H^+ + 6e^- \rightarrow Cl^- + 3H_2O$$
$$BrO_3^- + 6H^+ + 6e^- \rightarrow Br^- + 3H_2O$$
$$H_2O_2 + 2H^+ + 2e^- \rightarrow 2H_2O$$
$$O_3 + 2H^+ + 2e^- \rightarrow O_2 + 2H_2O$$

$$NH_2OH + 3H^+ + 2e^- \rightarrow NH_4^+ + H_2O \qquad \text{Disproportionation}$$
$$2NH_2OH \rightarrow N_2O + H_2O + 4H^+ + 4e^-$$

$$2MoO_4^{2-} + 10H^+ + 2e^- \rightarrow 2Mo(OH)_3 + 2H_2O$$

In the redox system (NO_2^-, NO_3^-), a variety of oxidation states between +5 and −3 are possible. Hydroxylamine has both oxidative and reductive properties (disproportionation reaction), whereas the others show only oxidative behavior. Molybdates are only used in the amorphous alkali phosphating process. Molybdenum could also vary in the oxidation state, which is again related to the color and iridescent appearance of the alkali phosphate coating.

These accelerators will readily oxidize iron so that it will precipitate as $FePO_4$ and be eliminated from the bath. The advantages and disadvantages of common accelerators are listed in Table 5. Many phosphating processes use combinations of two or more accelerators. Common combinations are nitrite/nitrate, nitrite/chlorate/ nitrate, peroxide/chlorate, and chlorate/nitrobenzene sulfonic acid. Some accelerators form by- products that build up in a bath and, over time, could be detrimental to performance.

Table 5 Comparison of accelerators used in the phosphating process

System	Nitrite/nitrate	Hydroxylamine	Peroxide	Nitroguanidine	Chlorate, nitrobenzene sulfonic acid
Concentration	0.05–0.1 g/L NO_2^-	0.5–1.5 g/L	30–50 mg/L	0.1–1.0 g/L	1–3 g/L ClO_3^- 0.4–1.0 g/L $C_6H_4(SO_3H)NO_2$
Control	Simple, often	Simple, sporadic	Complex, often	Sporadic, very complex	Sporadic, very complex
Replenishment	Separately	Internal	Separately	Separately	Separately

By-products	NO_3^-	NH_4^+, N_2O	…	Aminoguanidine, urea, others	Cl^-, azo colors, metanil acid
Relative coating weight	Middle	High	Low	High	Middle
Danger designation	Toxic, environmentally harmful, fire supporting	Noxious, environmentally harmful	Irritant	Explosive by an impulse	Fire supporting (ClO_3^-); noxious (ClO_3^-); irritant ($C_6H_4(SO_3H)NO_2$)
Relative cost	Low	Middle–high	Middle	Middle	High

Fluorides. When phosphating aluminum, high-strength steels containing silicon and/or aluminum or galvanized steel using zinc-aluminum alloys, such as hot-dip galvanized (0.14 to 0.30% Al-Zn), Galfan (5% Al- Zn), Galvalume (40% Al-Zn) or Galvannealed (Fe-Al-Zn), sufficient fluoride ions must be available to remove silicon oxide or aluminum oxide layers and complex the Al^{3+} or the Si^{4+} ion. Once in the bath, the aluminum will precipitate in the form of cryolithe, Na_3AlF_6, or elpasolithe, NaK_2AlF_6. Aluminum ions must be removed from the phosphating bath, because Al^{3+} disturbs the phosphating reaction. Fluorides can be added as HF, NaF, KF, HBF_4, or H_2SiF_6.

$$AlOOH + 3HF \rightarrow Al^{3+} + 3\,F^- + 2H_2O$$

$$Al^{3+} + 6F^- + 3Na^+ \rightarrow Na_3AlF_6\downarrow$$

Bath Pollution. There are several ions and substances that may disturb the phosphating reaction, and their build up in the bath must be avoided. Table 6 gives an overview of the problem ions. In the presence of such compounds, passivation, inhibition, complexation, cementation, or pitting corrosion (technical term: *white spotting*) (Ref 23) may occur instead of the phosphating reaction (Ref 24).

Table 6 Common pollutants for the phosphating reaction

Compound	Limiting concentration, mg/L	Consequence
Al^{3+}	3	Amorphous layer
V^{6+}	3	Passivation
Cr^{6+}	3	Passivation
Cr^{3+}	10	Passivation
Mo^{6+}	15	Passivation
Pb^{2+}	10	Cementation
As^{3+}, As^{5+}	3	Passivation
Ti^{4+}	5	Passivation
Zr^{4+}	5	Passivation
Sn^{2+}	5	Cementation
Cl^-	30–40	White spotting (pitting corrosion)
Cationic surfactants	20	Inhibition
Polyphosphate	20	Complexation, inhibition

Posttreatment. The pores between the phosphate crystals, although necessary to allow sufficient conduction for the electrodeposition of paint, may also represent failure points (Ref 2, 19, 25). A subsequent post treatment step may therefore prove necessary to protect these spaces. Sealing is done by substances that form insoluble oxides, hydroxides, phosphates, and so forth on the metal surface. Historically, the sealer of choice is chromate. The aqueous acidic solutions of chromium (VI) compounds and additives are applied in a kind of rinsing process on the phosphated metallic surface. Chromium (VI) is reduced to the basic chromium (III) and leads to a deposition of a gel-like film containing primarily chromium (III), with smaller amounts of chromium (VI), cations of the treated metal, and other components. The final phosphate conversion layer is completed after aging and drying.

There are two basic types of chromate sealing rinses. One type contains only chromic acid, and the other is a mixture of CrO_4^{2-} and Cr(III). Similar results can be obtained with solutions containing only Cr(III) (chromitation). Due to ecological hazard and noxious problems of Cr(VI), alternative treatments are needed.

Such posttreatments can contain other polyvalent metal cations and/or organic compounds such as monomers, oligomers, or polymers. Some popular examples are the fluoro-complexes of Zr^{4+} and Ti^{4+}, Cu^{2+} ions, MoO_4^{2-} (Ref 26), polyacrylates, silanes, and other organic compounds. Regardless which final rinse is used, the optimum pH is in the range of 3.8 to 5.0 to avoid dissolving the phosphate layer.

References cited in this section

2. M. Bastian, P. Kuhm, and G. Meyer, *Metalloberfläche,* Vol 53 (No. 1), p 10–15; Vol 53 (No. 2), p 10–14; Vol 53 (No. 3), 1999, p 10–14

5. E. Klusmann, U. König, and J.W. Schultze, *Mater. Corros.,* Vol 46, 1995, p 83

8. E. Lutter, *Die Entfettung,* Eugen G. Leuze Verlag, 1990

9. K. Wittel, *Metalloberfläche,* Vol 42, 1988, p 263–267

10. G. Jernstedt, *Trans. Electrochem. Soc.,* Vol 83, 1943, p 361

11. G. Lagaly, *Colloids in Ullmann's Encyclopedia of Industrial Chemistry,* Vol A7, VCH, 1986

12. M. Wolpers and J. Angeli, *Appl. Surf. Sci.,* Vol 179, 2001, p 281–291

13. I. Van Roy, H. Terryn, and G. Goeminne, *Colloids Surf. A,* Vol 136, 1998, p 89–96

14. P.E. Tegehall, *Colloids Surf.,* Vol 49, 1990, p 373

15. P.E. Tegehall and N.G. Vannerberg, *Corros. Sci.,* Vol 32 (No. 5/6), 1991, p 635–652

16. K. Ogle, C. Gabrielli, M. Keddam, and H. Pierrot, *J. Electrochem. Soc.,* Vol 141, 1994, p 2655

17. R.M. Smith and A.E. Martell, *Critical Stability Constants,* Vol 4, *Inorganic Complexes,* Plenum Press, 1976

18. J.O. Nrlagu, *Geochim. Cosmochim. Acta,* Vol 37, 1973, p 2357–2361

19. K.H. Stellnberger, M. Wolpers, T. Fili, C. Reinartz, T. Paul, and M. Stratmann, *Faraday Discuss.,* Vol 107, 1997, p 307

20. T. Sugama and T. Takahashi, *J. Mater. Sci.,* Vol 30, 1995, p 809–823

21. P.E. Augustsson, I. Olefjord, and Y. Olefjord, *Werkstoffe und Korrosion,* Vol 34, 1983, p 563

22. G. Angeli, “Oberflächenausscheidungen an kontinuierlich geglühtem Kaltband,” Ph.D. thesis, Technical University of Vienna, Austria, 2001

23. P.R. Levey, *40th MWSP Conf. Proc.,* ISS, 1998, p 171

24. S. Dietz, *JOT,* Vol 3, 2001, p 48–56

25. J.W. Schultze and N. Müller, *Metalloberflä che,* Vol 53, 1999, p 17–22

26. K. Aramski, *Corrosion,* Vol 55 (No. 11), 1999, p 1020

K. Ogle, and M. Wolpers, Phosphate Conversion Coatings, *Corrosion: Fundamentals, Testing, and Protection*, Vol 13A, *ASM Handbook*, ASM International, 2003, p 712–719

Phosphate Conversion Coatings

Kevin Ogle, Irsid, Arcelor R&D (Maizières-lès-Metz, France); Michael Wolpers, Henkel KGaA (Düsseldorf, Germany)

Physical and Chemical Properties

Gravimetric Analysis. Coating weight per unit area is the most characteristic measure of phosphate layers. Phosphated panels are weighed before and after stripping the phosphate layer. Oil, wax, grease, organic anticorrosive agents, and lacquer coatings must be removed prior to the analysis using organic solvents, and great care must be taken to ensure that the phosphate layer is not damaged in the process. Table 7 gives a list of phosphate-stripping solutions for a variety of phosphate layers and metals. In general, coating weight alone is a poor indicator of quality. It is more useful as a test of the consistency of the bath.

Table 7 Stripping solutions for phosphate layers

Metal	Stripping solution composition, wt%	Temperature		Time, min	Total metal removed, g · m^2
		°C	**°F**		
Iron, steel	12Na_4-EDTA, 4TEA, 9NaOH, 75H_2O	70	158	2–5	0.1
	5CrO_3, 95H_2O	70	158	15	0.05
Zinc	2.2$(NH_4)_2Cr_2O_7$, 27.4NH_3, 70.4H_2O	25	77	5	0.01
	5CrO_3, 95H_2O	25	77	5	0.05
Aluminum	65HNO_3, 35H_2O	25 (75)	77 (167)	15 (5)	0.1
Magnesium	0.5CrO_3, 99.5 H_2O	25	77	1–3	(a)

(a) Insufficient experience available

Chemical Analysis. The composition of the phosphate layer influences its performance and is therefore an important property. Elemental composition can be analyzed by wet analysis, x- ray fluorescence spectroscopy, and glow-discharge optical emission spectroscopy. Phase analysis is performed by x-ray diffraction and sometimes by Raman spectroscopy. Oxidation states and molecular information may be obtained from x-ray photoelectron or Auger electron spectroscopy (Ref 19). Wet chemical analysis of stripping solutions is typically used for determination of the composition of phosphate layers.

Structure and Morphology. A further consideration in the quality of crystalline phosphate layers is the structure of the coating (Ref 27). It is desirable that the phosphate crystals cover the surface homogeneously and have a fine crystalline, needle-, and shingle-like structure. Characterization includes light microscopy, scanning electron microscopy (SEM), field emission microscopy (FEM), and atomic force microscopy (AFM). The use of SEM is preferred over light microscopy because of the higher depth of focus, while FEM permits characterization of the phosphated surface with very low excitation voltage, yielding a higher surface sensitivity. A three-dimensional picture of the phosphated surface can be obtained by AFM or confocal laser microscopy.

Coverage. Complete coverage of the metal surface is also an important property of phosphate coatings, because paint adhesion is based on the mechanical locking of the paint into the voids between the crystals (Ref 25). Therefore, characterization of the so-called porosity of the layer and the determination of the degree of coverage and the volume of the pores is important. The simplest method is the visual or microscopic observation. Phosphated surfaces should appear dull and matte; the presence of shiny areas indicates the absence of the phosphate film.

More sophisticated chemical and electrochemical methods rely on the principle that a specific reaction may occur on the "free" metal surface. Turnbull's blue reaction (on steel substrates) and the cementation of copper (on zinc and zinc coated steel) are popular techniques to detect uncovered spots. The metallic surface between

the crystals may also be characterized by electrochemical methods since the phosphate layers are electronic insulators. Typical examples of experiments are the diffusion-limited currents for the reduction of oxygen (Ref 28), anodic charging curves corresponding to the oxidation of the metal surface (Ref 29), estimation of the polarization or charge transfer resistance (Ref 30), and measurement of the double-layer capacitance (Ref 27).

Thermal Analysis. The behavior of phosphate layers at higher temperatures is of technical importance. For example, at the drying temperatures of electrophoretic paints (150 to 200 °C or 302 to 392 °F), (Ref 31), the dehydration of hopeite occurs in two steps. Two crystal water molecules are lost in the temperature range of 80 to 120 °C (176 to 248 °F). The remaining two water molecules are lost around 250 °C (482 °F). The first dehydration step is reversible in the presence of moisture. After rehydration, the phosphate crystals are finer and orientations are different. Manganese and nickel increase the temperature of dehydration. In contrast to hopeite, the phosphophyllite phase becomes amorphous and the dehydration is irreversible.

Alkaline Resistance. An important chemical property of phosphate layers is their resistance to alkaline electrolytes (Ref 31, 32, 33, 34). Such an exposure may occur during cathodic deposition of paint (cathodic polarization of the substrate), during alkaline degreasing processes (for example prephosphated steel products) and under the paint coating during cathodic delamination (Ref 35, 36, 37). In these cases the stability of the phosphate layer can be increased by modifying the phosphating bath with Mn^{2+}, Ni^{2+}, Fe^{2+}, Mg^{2+}, Cu^{2+}, and Co^{2+}. The alkaline resistance of phosphophyllite is higher than that of hopeite.

References cited in this section

19. K.H. Stellnberger, M. Wolpers, T. Fili, C. Reinartz, T. Paul, and M. Stratmann, *Faraday Discuss.,* Vol 107, 1997, p 307

25. J.W. Schultze and N. Müller, *Metalloberflä che,* Vol 53, 1999, p 17–22

27. H. Bubert, H. Pulm, and H. Puderbach, *Mikrochim. Acta I,* 1987, p 355–364

28. A. Losch and J.W. Schultze, *J. Electroanal. Chem.* Vol 359, 1993, p 39

29. W. Machu, *Korrosion Metall.,* Vol 20, 1944, p 6–11; p 12–16

30. W. Machu, *Korrosion Metall.* Vol 17, 1941, p 157

31. W.J. Van Ooij and A. Sabata, *J. Coatings Technol.,* Vol 61, 1989, p 52–65

32. J.P. Servais, B. Schmitz, and V. Leroy, *Corrosion/88 Conf.* (St. Louis, MO), NACE, Vol 41

33. W.J. Van Ooij and A. Sabata, *Surf. Coat. Technol.,* Vol 39/40, 1989, p 667–674

34. S. Millow, *Metalloberfläche,* Vol 50, 1996, p 50–55; p 506–512

35. S. Maeda, *Prog. Org. Coatings,* Vol 11, 1983, p 1–18

36. H. Leidheiser, Jr., *J. Adhesion Sci. Technol.,* Vol 1, 1987, p 79–98

37. U. Stieglitz, W.D. Schulz, and W.D. Kaiser, *JOT,* Vol 4, 1995, p 44–49

K. Ogle, and M. Wolpers, Phosphate Conversion Coatings, *Corrosion: Fundamentals, Testing, and Protection*, Vol 13A, *ASM Handbook*, ASM International, 2003, p 712–719

Phosphate Conversion Coatings

Kevin Ogle, Irsid, Arcelor R&D (Maizières-lès-Metz, France); Michael Wolpers, Henkel KGaA (Düsseldorf, Germany)

Processing Equipment and Control

Phosphating solutions are usually applied by spraying or immersion, and the choice depends on the number, size, and shape of the parts to be treated. At coil coating or galvanizing lines, zinc-coated steel strips may be phosphated by a roll-on, dry-in-place, or no-rinse-process, during which the phosphating solution is applied to the strip and is dried without rinsing.

Spray Treatment. Spray phosphating is done in cabinets or tunnels. It involves pumping the bath through a series of risers that have spray nozzles aligned to coat all areas of the workpiece. Depending on the work being treated, different kinds of spray nozzles are used, such as flat-jet nozzles, full-cone nozzles, hollow-cone nozzles, and spoon nozzles. The spray treatment leads to rapid formation of the phosphate layer, because spraying guarantees a good exchange of the solution at the surface due to the strong solution impingement with the metal surface. Complex parts are difficult to treat. Movable robotic arms equipped with tank nozzles spraying in all directions are used to treat the internal areas of car bodies.

At coil coating or galvanizing lines, spraying is mainly used to phosphate zinc-coated steel strips. The solutions are applied in cabinets with spray beams on the top and bottom sides of the strip. Different spray zones are separated by squeeze rollers to avoid delay in the following stages.

Immersion Treatment. The advantages of the immersion treatment method are better treatment of surfaces of the workpiece (box sections), better drainage between stages with less drag- through of contaminants from one stage of the process to another, less maintenance and repair, lower bath-heating costs, and generally better coating performance than that for sprayed work. Also, large baths are less sensitive to changes such as depletion of chemicals or bath contamination; temperatures are more stable in the larger baths. Both facts are important for controlling and monitoring the bath. There are two major disadvantages. First, dipping is slower because mass transfer at the solution-metal interface is less intensive. Second, dipping requires the use of a larger volume of bath than spraying. This, in turn, implies more floor space, higher equipment costs, and a higher cost for recharging and waste disposal.

The process engineering of immersion treatment is comparable to spray treatment. The baths are aligned in series in cabinets or a tunnel with access at the entrance and exit. In the car industry, different engineering systems have been developed:

- Simple horizontal dipping
- Combination of dipping and spraying, with upper part sprayed and bottom part dipped
- To save floor space and shorten the treatment line, vertical dipping of car bodies. This process is called VERTAK (Dürr) and is a special technology for the phosphating process.
- To remove sludge on horizontal surfaces and to avoid air bubbles under roofs, the RO-DIP (Dürr) process involves the turning of car bodies several times.
- To improve the streaming behavior at the solution-metal interface, the installation of wing lamellas on the interior sides of the bath provides a constant and uniform stream to the part to be treated.

Materials. Tanks may be made from low-carbon steel for alkali cleaners, conditioners, and final rinses. If deionized water is used for these processes, stainless steel or plastic is indispensable. Phosphate systems may require stainless steel, depending on the presence of F^- or NO_3^-, acidity, operating temperature, and the desired lifetime of the tank. Nozzles must be stainless steel. Polypropylene, glass-fiber reinforced plastic, synthetic fluorine-containing resins, or plastic-lined steel can be substituted for stainless steel in some circumstances, but the use of plastics is limited to lower-temperature applications. These materials can also be used for pipes, pumps, and storage tanks.

Removal of Sludge and Scale. Sludge is formed by the undesirable precipitation of metal ions in the phosphating solution. One source of sludge is the oxidation of iron or manganese to form insoluble phosphates. In addition, precipitation for coating formation may produce phosphate that does not deposit on the workpiece. Scale is the phosphate coating that forms on processing equipment. A major cause of scale is excessive heating of the bath. Because most divalent metal phosphates are less soluble at higher temperatures, the localized heating that occurs with raising or maintaining the bath temperature can cause scale to form on heating elements. Sludge usually settles to the bottom; it can then be pumped to a filtration unit. In some cases, solution is pumped to a temporary storage tank and the sludge-rich solution from the bottom is removed. Scale is more difficult to remove. The most expedient method is to use an inhibited acid to dissolve it.

Solution Heating and Mixing. The optimum method of heating depends on the process equipment, but the following points should be kept in mind:

- Because phosphates precipitate at higher temperature, heating surfaces should be easy to clean.
- Spot heating should be avoided.
- The heat source should not be at the bottom of the tank, since settling sludge will insulate it.

Direct heating such as steam, electric, or gas heating should be avoided, because phosphates can precipitate on the surfaces of the heating system, blocking further heat transfer. Secondary heating—for example, external heat exchangers with hot water or oil—gives more satisfactory results. The temperature difference (ΔT) across heat exchanger plates (between the phosphating solution and the heating media) should be in the range of 5 °C (9 °F) to avoid scaling. The ΔT should never exceed 15 °C (27 °F).

For immersion phosphating, the last method would also be a useful source of solution mixing. The solution must be pumped in spray phosphating, but solution pumping is also necessary to obtain optimum results in some immersion systems. Barrel phosphating can provide considerable mixing around the part by rotation of the barrel; additional mixing is usually not required. Conveyor applications may or may not need additional mixing.

Replenishment. The solution should be replenished continuously to get a uniform coating. Automatic devices, such as dosing pumps which run continuously, are useful in controlling solution composition. Replenishment should be done in places in the phosphating system where rapid mixing occurs. It is not useful to dose the replenisher on the pressure side of the phosphating system, especially before the heating system. This can lead to additional sludge and scale and, therefore, to poor heating efficiency.

Chemical Analysis and Bath Control. The primary methods of bath control are acid-base titrations that measure the amount and type of acid present. Phosphoric acid has three dissociation steps. The so-called free acid is related to the first point of equivalence and is the amount (in milliliters) of 0.1 *N* sodium hydroxide (NaOH) needed to neutralize the strong acidity from 10 mL of the bath. The total acid correlates to the second dissociation step, a weak end point. It is the amount (in milliliters) of 0.1 *N* NaOH needed to neutralize all the acid in 10 mL of solution including the acidic metal-aquo complexes. The third dissociation equilibrium is not detectable by NaOH titration. Under several circumstances a back titration with 0.1 *N* sulfuric acid (H_2SO_4) is necessary to determine the free acid. In these cases the free acid becomes negative. Results are stated in points; for example, 2 mL = 2 points.

Metal concentrations can be checked by spectroscopic methods like atomic absorption spectroscopy, inductively coupled plasma atomic emission spectroscopy, flame emission spectroscopy, and so forth. Zinc concentration can be determined by a potentiometric titration with $K_4[Fe(CN)_6]$.

Accelerator concentrations are often determined by redox titration. The following methods are commonly used:

- Permanganate titration for NO_2^-
- Gas generation with urea and sulfamic acid for NO_2^-
- Acid-base titration of the free acid without and with acetone for NH_2OH
- Thiosulfate titration with potassium iodide for H_2O_2

Fluoride (F^-) is determined most efficiently by the use of an ion-sensitive electrode. This is of particular interest when processing aluminum, because one of the important uses of F^- is to keep the concentration of aluminum down by the formation of AlF_6^{3-} ions.

Ionic conductivity measurements can be related to the concentration of the solution constituents in the phosphating bath and, thus, can serve as a test for replenishment.
Conductivity measurements are simple to run on a phosphate bath; therefore, they are more widely used than titrometric-type controllers are. Unfortunately, because conductivity does not directly measure the relevant parameters, some systems require adjustment of replenishment levels as the phosphate bath ages and require recalibration when a new bath is built up.

K. Ogle, and M. Wolpers, Phosphate Conversion Coatings, *Corrosion: Fundamentals, Testing, and Protection*, Vol 13A, *ASM Handbook*, ASM International, 2003, p 712–719

Phosphate Conversion Coatings

Kevin Ogle, Irsid, Arcelor R&D (Maizières-lès-Metz, France); Michael Wolpers, Henkel KGaA (Düsseldorf, Germany)

References

1. W. Rausch, *Die Phosphatierung von Metallen* (*The Phosphating of Metals*), Eugen G. Leuze Verlag, 1988; ASM International and Finishing Publications Ltd., 1990
2. M. Bastian, P. Kuhm, and G. Meyer, *Metalloberfläche,* Vol 53 (No. 1), p 10–15; Vol 53 (No. 2), p 10–14; Vol 53 (No. 3), 1999, p 10–14
3. P.E. Tegehall, "The Chemistry of Zinc Phosphating of Steel," Ph.D. thesis, Chalmers University of Technology, Göteborg, Sweden, 1990
4. W.A. Roland and K.H. Gottwald, *Metalloberfläche,* Vol 42, 1988
5. E. Klusmann, U. König, and J.W. Schultze, *Mater. Corros.,* Vol 46, 1995, p 83
6. VDA Prüfblatt 621-415: Prüfung des Korrosionsschutzes von Kraftfahrzeuglackierungen bei zyklisch wechselnder Beanspruchung (Community of the German Car Producers, Test Instruction 621-415, Test of the Corrosion Protection of Paintings under Cyclic Changing Conditions)
7. T. Molz, *Metalloberfläche,* Vol 51, 1997, p 638–643
8. E. Lutter, *Die Entfettung,* Eugen G. Leuze Verlag, 1990
9. K. Wittel, *Metalloberfläche,* Vol 42, 1988, p 263–267
10. G. Jernstedt, *Trans. Electrochem. Soc.,* Vol 83, 1943, p 361
11. G. Lagaly, *Colloids in Ullmann's Encyclopedia of Industrial Chemistry,* Vol A7, VCH, 1986
12. M. Wolpers and J. Angeli, *Appl. Surf. Sci.,* Vol 179, 2001, p 281–291
13. I. Van Roy, H. Terryn, and G. Goeminne, *Colloids Surf. A,* Vol 136, 1998, p 89–96
14. P.E. Tegehall, *Colloids Surf.,* Vol 49, 1990, p 373
15. P.E. Tegehall and N.G. Vannerberg, *Corros. Sci.,* Vol 32 (No. 5/6), 1991, p 635–652

16. K. Ogle, C. Gabrielli, M. Keddam, and H. Pierrot, *J. Electrochem. Soc.,* Vol 141, 1994, p 2655

17. R.M. Smith and A.E. Martell, *Critical Stability Constants,* Vol 4, *Inorganic Complexes,* Plenum Press, 1976

18. J.O. Nrlagu, *Geochim. Cosmochim. Acta,* Vol 37, 1973, p 2357–2361

19. K.H. Stellnberger, M. Wolpers, T. Fili, C. Reinartz, T. Paul, and M. Stratmann, *Faraday Discuss.,* Vol 107, 1997, p 307

20. T. Sugama and T. Takahashi, *J. Mater. Sci.,* Vol 30, 1995, p 809–823

21. P.E. Augustsson, I. Olefjord, and Y. Olefjord, *Werkstoffe und Korrosion,* Vol 34, 1983, p 563

22. G. Angeli, "Oberflächenausscheidungen an kontinuierlich geglühtem Kaltband," Ph.D. thesis, Technical University of Vienna, Austria, 2001

23. P.R. Levey, *40th MWSP Conf. Proc.,* ISS, 1998, p 171

24. S. Dietz, *JOT,* Vol 3, 2001, p 48–56

25. J.W. Schultze and N. Müller, *Metalloberflä che,* Vol 53, 1999, p 17–22

26. K. Aramski, *Corrosion,* Vol 55 (No. 11), 1999, p 1020

27. H. Bubert, H. Pulm, and H. Puderbach, *Mikrochim. Acta I,* 1987, p 355–364

28. A. Losch and J.W. Schultze, *J. Electroanal. Chem.* Vol 359, 1993, p 39

29. W. Machu, *Korrosion Metall.,* Vol 20, 1944, p 6–11; p 12–16

30. W. Machu, *Korrosion Metall.* Vol 17, 1941, p 157

31. W.J. Van Ooij and A. Sabata, *J. Coatings Technol.,* Vol 61, 1989, p 52–65

32. J.P. Servais, B. Schmitz, and V. Leroy, *Corrosion/88 Conf.* (St. Louis, MO), NACE, Vol 41

33. W.J. Van Ooij and A. Sabata, *Surf. Coat. Technol.,* Vol 39/40, 1989, p 667–674

34. S. Millow, *Metalloberfläche,* Vol 50, 1996, p 50–55; p 506–512

35. S. Maeda, *Prog. Org. Coatings,* Vol 11, 1983, p 1–18

36. H. Leidheiser, Jr., *J. Adhesion Sci. Technol.,* Vol 1, 1987, p 79–98

37. U. Stieglitz, W.D. Schulz, and W.D. Kaiser, *JOT,* Vol 4, 1995, p 44–49

K. Ogle, and M. Wolpers, Phosphate Conversion Coatings, *Corrosion: Fundamentals, Testing, and Protection*, Vol 13A, *ASM Handbook*, ASM International, 2003, p 712–719

Phosphate Conversion Coatings

Kevin Ogle, Irsid, Arcelor R&D (Maizières-lès-Metz, France); Michael Wolpers, Henkel KGaA (Düsseldorf, Germany)

Selected References

- D.B. Freeman, *Phosphating and Metal Pre- Treatment*, Industrial Press Inc., New York, 1986
- K. Ogle and R.G. Buchheit, *Conversion Coatings,* 5.3, p 460–499 in M. Stratmann and G.S. Frankel, *Corrosion and Oxide Film,* Vol 4, in A.J. Bard and M. Stratmann, Ed., *Encyclopedia of Electrochemistry,* Wiley-VCH Verlag GmbH & Co., KGaA, Weinheim, 2003
- W. Rausch, *Die Phosphatierung von Metallen* (*The Phosphating of Metals*), Eugen G. Leuze Verlag, 1988; ASM International and Finishing Publications Ltd., 1990
- W. Rausch, *The Phosphating of Metals,* Finishing Publication Ltd. and ASM International, 1990

R.G. Buchheit and A.E. Hughes, Chromate and Chromate-Free Conversion Coatings, *Corrosion: Fundamentals, Testing, and Protection*, Vol 13A, *ASM Handbook*, ASM International, 2003, p 720–735

Chromate and Chromate-Free Conversion Coatings

R.G. Buchheit, The Ohio State University; A.E. Hughes, CSIRO

Introduction

CHROMATE CONVERSION COATINGS (CCCs) are thin (0.01 to 3 μm, or 0.0004 to 0.012 mil) amorphous inorganic films formed by contacting a metallic surface with an aqueous solution whose main film-forming agent is a soluble chromate species. Chromate conversion coatings form spontaneously without application of current or voltage and are applied most commonly to aluminum-, zinc-, magnesium-, iron-, cadmium-, and tin-base alloys. The coatings are primarily used to improve adhesion of subsequently applied organic coatings or to impart corrosion resistance during atmospheric exposure. Two important coating subtypes are chromium chromate and chromium phosphate coatings. Coatings consist of mixed metal oxides and hydroxides derived from chemical oxidation of the substrate and electrochemical and chemical reaction of species present in the coating solution. Coating thickness, color, and corrosion resistance depend on contact times, temperatures, solution chemistry, application method, and substrate composition. Certain types of CCCs contain labile hexavalent chromium (Cr(VI)), which can leach from the coating into an attacking liquid environment. Leached Cr(VI) can be transported through a contacting liquid phase to coating defects, where it may act to stifle further corrosion. In this sense, some CCCs are “self- healing.” The self-healing effect diminishes as CCCs dehydrate. As a result, the corrosion protection provided by stand-alone CCCs may decrease during exposure to ambient environments and elevated temperatures.

R.G. Buchheit and A.E. Hughes, Chromate and Chromate-Free Conversion Coatings, *Corrosion: Fundamentals, Testing, and Protection*, Vol 13A, *ASM Handbook*, ASM International, 2003, p 720–735

Chromate and Chromate-Free Conversion Coatings

R.G. Buchheit, The Ohio State University; A.E. Hughes, CSIRO

Historical Perspective

The use of inorganic chromate surface treatments can be traced to the early 20th century (Ref 1, 2). Alkaline carbonate-chromate solutions were devised for early aluminum-copper alloys in the 1920s (Ref 3, 4). Chromium phosphate coatings evolved prior to and during World War II (Ref 4). Formulations of this type are still in use today for zinc and zinc-aluminum metallic coatings on steel. Chromium chromate coatings with excellent corrosion resistance were developed in the 1950s (Ref 5, 6). These types of coatings were among the first to be recognized as self-healing (Ref 7). Accelerated chromium chromate formulations were introduced around 1970 (Ref 8) and are commonly used with aluminum alloys for stand-alone corrosion protection or as a base for paints.

The primary film-forming agent in CCC baths is Cr(VI). This compound is a potent human toxin and known cancer-causing agent (Ref 9, 10, 11, 12, 13, 14). There is a great demand to eliminate chromium from conversion coating processes to reduce health risks in the workplace and to reduce the potential for damage to the environment. Since the 1980s, there has been significant growth in research and development efforts aimed at identifying chromate-free coatings that match the ease of applicability and excellent performance of CCCs. While chromate replacement has occurred in certain applications (Ref 15), CCCs are still used in the most demanding applications.

References cited in this section

1. T. Biestek and J. Weber, *Electrolytic and Chemical Conversion Coatings,* Porticullis Press Limited-Redhill, Surrey, UK, 1976
2. S. Wernick, R. Pinner, and P.G. Sheasby, *The Surface Treatment and Finishing of Aluminum and its Alloys,* Vol 1, 5th ed., ASM International, 1987, p 220
3. O. Bauer and O. Vogel, German Patent Specification, 226776, 1923
4. O. Bauer and O. Vogel, German Patent Specification, 423758, 1923
5. W. Marchand, *Electroplat. Met. Finish.,* Vol 14, 1961, p 439
6. S. Spring and K. Woods, *Met. Finish.,* Vol 79, 1981, p 49
7. G.W. Ostrander, *Plating,* Vol 38, 1951, p 1033
8. J.N.J. Newhard, *Met. Finish.,* Vol 70, 1972, p 69
9. M. Krumploc and J. Rocek, *J. Am. Chem. Soc.,* Vol 101, 1979, p 3206
10. P. Lay and A. Levina, *J. Am. Chem. Soc.*, Vol 120, 1998, p 6704
11. P. O. O'Brien and A. Kortenkamp, *Transit. Met. Chem.,* Vol 20, 1995, p 636
12. D. Stearns and K. Wetterhahn, *Chem. Res. Toxicol.,* Vol 7, 1994, p 219

13. Y. Suzuki and K. Fukuda, *Arch. Toxicol.*, Vol 64, 1990, p 169

14. Y. Suzuki, *Ind. Health*, Vol 28, 1990, p 9

15. J.W. Bibber, *J. Electrochem. Soc.*, Vol 91, 1993, p 46

R.G. Buchheit and A.E. Hughes, Chromate and Chromate-Free Conversion Coatings, *Corrosion: Fundamentals, Testing, and Protection*, Vol 13A, *ASM Handbook*, ASM International, 2003, p 720–735

Chromate and Chromate-Free Conversion Coatings

R.G. Buchheit, The Ohio State University; A.E. Hughes, CSIRO

Chromate Conversion Coating Formation

The following factors affect the formation of CCCs.

Bath pH and Cr(VI) Concentration. Cr(VI) speciation in coating baths is an important variable in CCC formation. Cr(VI) in solution speciates via hydrolysis and dimerization to chromate, CrO_4^{2-}, dichromate, $Cr_2O_7^{2-}$, or bichromate $HCrO_4^{-}$(Ref 16). The predominant species present depends on Cr(VI) concentration and pH as shown in Fig. 1. Formation of chromium chromate coatings is normally carried out at pH values where dichromate is the predominant Cr(VI) species. Solution concentrations of 50 mM Cr(VI) and a pH of 1.2 to 3.0 are typical of modern commercial CCC bath formulations, because the most robust coatings form under these conditions. The total chromate concentration in the coating bath solution may vary by a factor of two or more without a significant impact on film formation rate (Ref 17).

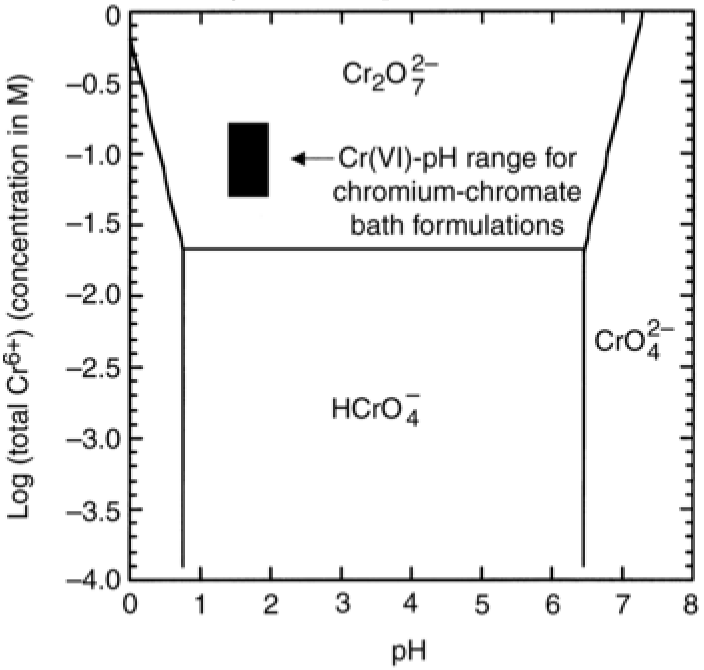

Fig. 1 Speciation of soluble Cr(VI) as a function of pH and concentration. The labels indicate the predominant soluble chromium species in a given pH-concentration domain. Many commercial CCC bath formulations have Cr(VI) concentrations that fall in the shaded box so that the primary film-forming species is dichromate. (Equilibrium constants from Ref 16)

Activators and Accelerators. CCC formation is greatly aided by "activating" species such as fluoride, sulfate, nitrate, formate, and acetate, among others (Ref 2). Fluoride is particularly effective in promoting film growth and is often added to both chromium chromate and chromium phosphate baths. Fluoride is typically added as NaF and mixed metal fluoride salts whose total concentration is in the 30 to 40 mM range. Fluoride attacks existing surface films, particularly on aluminum. It readily complexes Al^{3+} in solution and has the effect of lowering the aluminum content in CCCs (Ref 18). Consequently, CCCs are thicker and richer in chromium when F^- is added to the bath.

The use of "accelerators" in chromium chromate coating formulations began about 1970 (Ref 8). Accelerators used in commercial CCC formulations include: ferricyanides, acetates, formates, and chlorides, among others (Ref 17). Of these, potassium ferricyanide, $K_3Fe(CN)_6$, has been widely studied and described in the scientific and technical literature. Potassium ferricyanide is added to CCC formulations in 2 to 5 mM concentrations to increase coating weight. The active component in this compound is the ferricyanide anion, $Fe(CN)_6^{3-}$, which accelerates chromate reduction reaction kinetics, which are otherwise slow on oxide-covered surfaces (Ref 19). For example, on aluminum, $Fe(CN)_6^{3-}$ is readily reduced to ferrocyanide, $Fe(CN)_6^{4-}$. Ferrocyanide is oxidized by Cr(VI), which reduces to Cr(III) and contributes to film formation. Coupling substrate oxidation to chromate reduction by this mediation mechanism increases the film formation rate, which results in a more corrosion-resistant coating. Ferricyanide is also incorporated into the CCC, with iron-to-chromium ratios of 1 to 10 reported in at least two studies (Ref 19, 20). Ferricyanide has also been proposed to exist as mixed metal cyanide in CCCs (Ref 21, 22, 23). Direct effects of these compounds on coating corrosion resistance or paint adhesion have not been clearly established.

Experimental evidence from Raman spectroscopy suggests that ferricyanide adsorbs preferentially on copper-rich inclusions in Al-Cu-Mg alloys in a way that can interfere locally with CCC formation (Ref 24). This adsorbed layer forms rapidly and appears to suppress the Cr(VI) to Cr(III) reduction process that leads to film growth. This results in a thinner, chromium-deficient coating on the inclusion. How this affects subsequent corrosion protection has not been clearly established.

Chromium Chromate Coatings. Modern coating chemistries typically consist of 50 mM CrO_3, 30 to 40 mM mixture of fluoride and fluoro salts, and 2 to 5 mM potassium ferricyanide. Commercial formulations often include other minor ingredients and may have alternate activators and accelerators. The bath may be acidified with addition of nitric acid to bring the pH into the desired range.

In the case of aluminum alloys, and probably zinc and magnesium as well, chromium chromate conversion coating formation involves both chemical and electrochemical reactions. The classic formation reaction for a chromium chromate coating on aluminum is stated as (Ref 25):

$$Cr_2O_7^{2-} + 2Al + 2H^+ + H_2O \rightarrow 2CrOOH(s) + 2AlOOH(s) \quad \text{(Eq 1)}$$

This reaction scheme illustrates the coupling of aluminum oxidation to chromate reduction and the subsequent formation Cr(III) or mixed chromium/aluminum hydroxide, but chromium chromate coatings are usually more chromium-rich than the stoichiometry of Eq 1 suggests (Ref 26, 27). CCCs also contain Cr(VI), which is not indicated by Eq 1.

CCC formation does not occur entirely by electrochemical reaction. Rather, there appears to be two distinguishable phases to CCC growth: one that is characterized by intense net electrochemical activity and one that occurs with comparative electrochemical quiescence (Ref 28, 29). At times less than 30 s, coating growth occurs with significant detectable electrochemical activity (Ref 29). Coating weight (Ref 30) and thickness (Ref 18) are observed to increase rapidly. Cr(III) and Cr(VI) are detected in the coating (Ref 31), and coating morphology is characterized by a compact mass of nodules that cover the surface very quickly at the beginning of coating growth (Ref 32, 33, 34). Preferential nucleation and growth of the coating on local cathodic sites defined by local impurity element enrichment, and second-phase particle inclusions have also been reported (Ref 28, 34) (Fig. 2). Coatings formed in just several seconds confer useful levels of corrosion resistance, but are not as corrosion resistant as coatings formed by longer immersion times. At coating times greater than 30 s, detectable electrochemical activity diminishes. Coating weight continues to increase, but coating thickening slows (Ref 30) or stops (Ref 18). The Cr(III) and Cr(VI) concentrations in the coating both increase, but the Cr(VI) to Cr(III) ratio also increases indicating a greater rate of Cr(VI) uptake (Ref 27, 29). Terminal Cr(VI) concentrations expressed as a percentage of total chromium in the coating are typically about 30% (Ref 27).

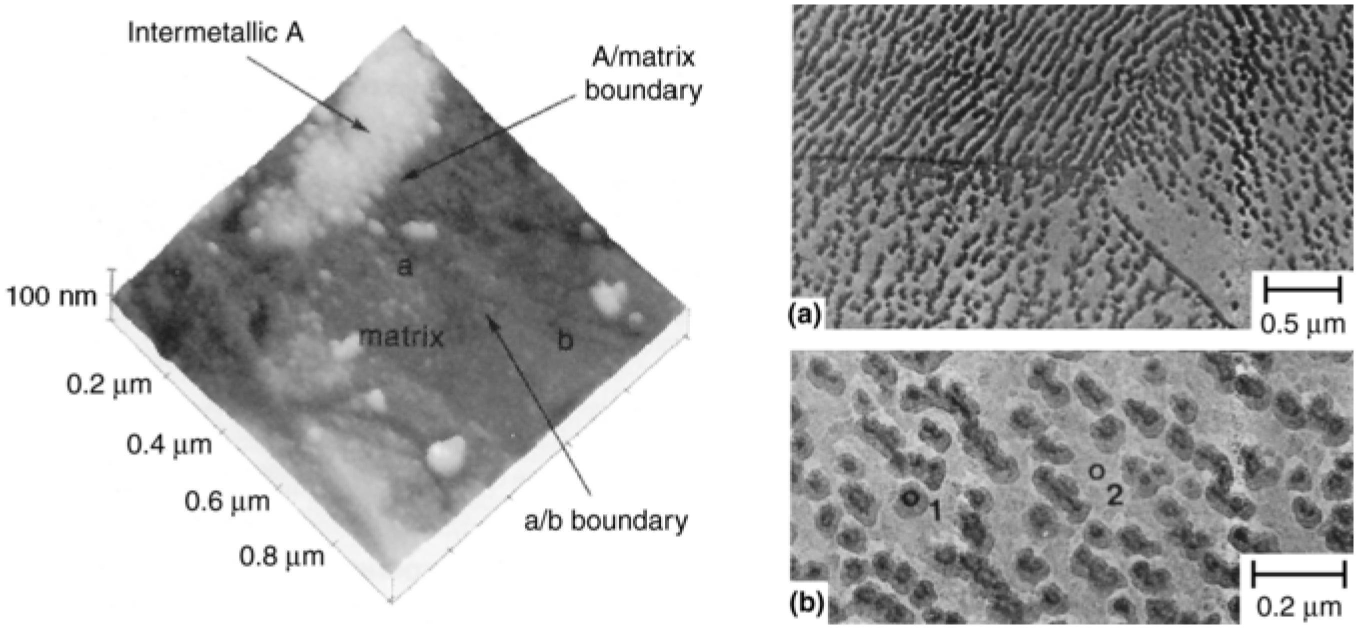

Fig. 2 Nodular morphologies associated with the nucleation stage of CCC growth. Left, AFM image of a CCC formed on freshly polished 2024-T3 exposed for 1 s to a commercial bath formulation chilled to <5 °C (<40 °F) illustrating nodular CCC morphology. Rapid CCC nucleation on Al-Cu-Fe-Mn-type particles is suggested by a thicker deposit. Sluggish nucleation on Al-Cu-Mg particles is suggested by a thinner deposit. Source: Ref 34. Right, Transmission electron micrograph of a CCC stripped from a 99.98% pure Al substrate. CCC was formed by a 5 s immersion in $Cr_2O_7^{2-}$ /F^- solution at subambient temperature. Local chromium-rich deposits (location b) are located on grain boundaries or pre-existing metal ridge. Microchemical analysis of regions away from nodules (location a) suggest nonuniform CCC formation across the surface. Source: Ref 35

Newer interpretations of CCC growth are based on a sol-gel process (Ref 36) where film formation is triggered by reduction of Cr(VI) to Cr(III). The formation process involves condensation and polymerization of a $Cr(OH)_3$ inorganic polymer "backbone" as shown in Fig. 3 (Ref 37). In this scheme, once sufficient Cr(III) is formed near the metal surface by electrochemical reduction, film formation may proceed by purely chemical processes.

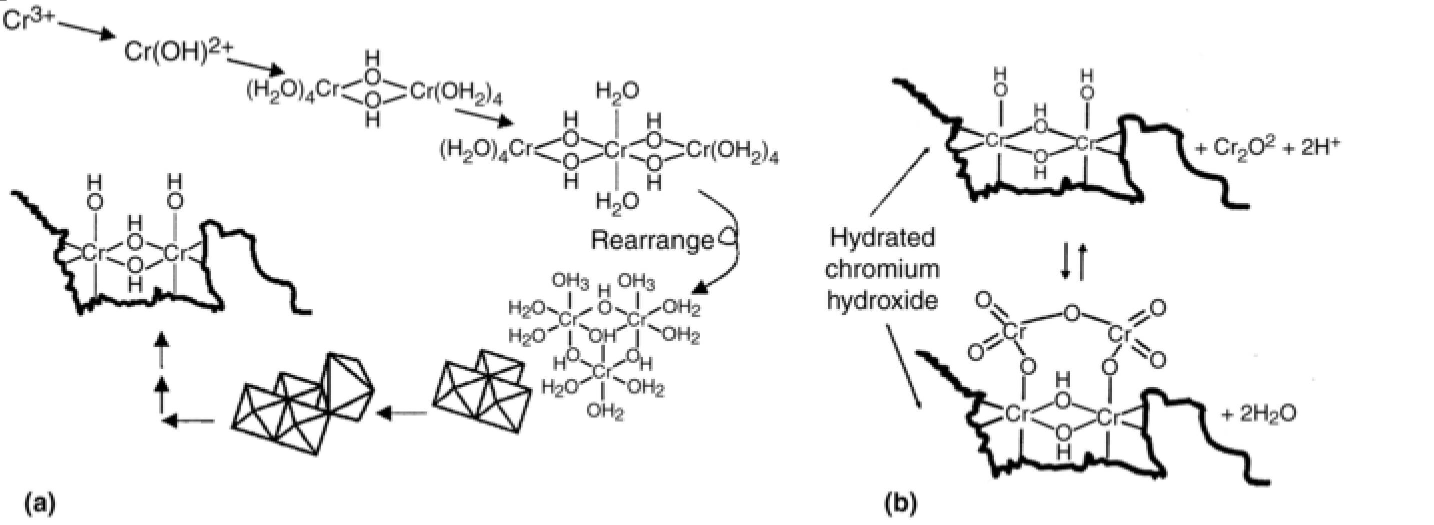

Fig. 3 (a) Hydrolysis-polymerization-precipitation mechanism for $Cr(OH)_3$ "backbone" formation. (b) Condensation of Cr(VI) on the Cr(III) backbone by nucleophilic attack of hydroxyl ligands in the backbone. Source: Ref 37

Throughout CCC formation, the chromium- to-aluminum and Cr(VI)-to-Cr(III) ratios increase (Ref 27). Cr(VI) buildup in the coating has also been proposed to occur by an adsorption reaction involving nucleophilic attack

of hydroxyl ligands on the $Cr(OH)_3$ backbone by dichromate (Fig. 3) (Ref 37, 38). This results in the formation of Cr(III)-O-Cr(VI) linkages. These linkages are characteristic of CCCs and are readily detectable by Raman spectroscopy.

Freshly formed CCCs are fragile and easily damaged by mechanical or chemical action. Immediately after CCC formation, it is possible to wipe the deposit off a metal surface with a sponge. If a CCC is to be used for stand-alone corrosion protection, it is usually allowed to harden for at least 24 h before any further handling (Ref 39). However, if CCCs are allowed to dehydrate over long periods of time, they may become decreasingly receptive to organic overcoats. Therefore, it is common for conversion- coated surfaces to be painted within the first 24 to 48 h after coating application (Ref 40).

Chromium phosphate conversion coatings (CPCCs) are used in aluminum alloys to promote corrosion resistance and paint adhesion in manufacturing operations where short contact time spray application is required. CPCCs are formed by contact with acidic solutions containing CrO_3, H_3PO_4, and NaF as the primary ingredients. Fluoride serves to dissolve the air-formed oxide and activate the surface, while $CrPO_4$ and H_3PO_4 are the primary film-forming agents. Coating formation occurs by reduction of Cr(VI) to Cr(III) and precipitation of hydrated $CrPO_4$ and Cr(III) and Al(III) hydroxides (Ref 41, 42, 43). Depending on the bath formulation, substrate type, contact time, and temperature, CPCCs can be either amorphous (Ref 44) or crystalline (Ref 45). Chromium phosphate is often the predominant compound in the coating, comprising up to 80% of freshly formed films (Ref 22, 46, 47, 48). Most or all of the chromium in CPCCs is present in an insoluble Cr(III) form. Little or no Cr(VI) is present in the coating. As such, these coatings do not possess the self-healing characteristics of chromium chromate conversion coatings.

Conversion Coatings Formed from Trivalent Chromium Solutions. Chromium-containing conversion coatings can be formed from baths containing trivalent chromium compounds (Ref 49, 50, 51). These processes are comparatively new and are not in widespread commercial use. Cr(III) coatings possess good corrosion resistance and provide for good paint adhesion in standardized testing. Coatings are formed on aluminum alloy substrates by contact with a dilute chromic sulfate-sodium fluosilicate solution with a pH range of 3.3 to 5.5. Coating formation occurs spontaneously in a matter of minutes. The coatings appear to form on activated aluminum alloy surfaces by polymerization of hydrolyzed Cr(III) ions. The corrosion resistance of these coatings is improved if they are subsequently contacted with hydrogen peroxide or a permanganate-containing solution. This step oxidizes some of the Cr^{3+} in the coating to Cr^{6+} and in the case of the permanganate treatment may result in the deposition of some hydrated manganese oxide on the surface.

Processing of CCCs. Chromate conversion coating is not a single process, but rather a family of processes that are used in a wide range of industrial applications. The “generic” processing sequence for CCCs involves chemical cleaning, acid deoxidation, conversion coating, rinsing, and drying. Removal of bulk oils and greases is essential before any immersion-based degreasing or deoxidation. Chemical cleaning of remnant molecular organic contamination is often carried out in an inhibited alkaline solution. Immersion periods range from several seconds to several minutes. Cleanliness is assessed visually. A favorable indication of cleanliness is solution running off the surface smoothly without spotting or “breaking.” Such surfaces are said to be “break-free.” If surfaces are contaminated, solution will spot or bead on the metal surface when it is removed from solution. In this case, further immersion cleaning is needed. Darkening of the surface during degreasing may signal formation of smut films, which consist of insoluble substrate alloying elements accumulated at the metal surface. Acid deoxidation can be carried out using a strongly acidic oxidizing solution. Immersion periods for deoxidation range from a few seconds to several minutes. The effectiveness of deoxidation is also assessed visually. Surfaces may be overcleaned, resulting in corrosion and contamination of the surface with corrosion products. Excessive etching may be indicated by dull or matte appearance on the metal surface. Contamination after deoxidation may manifest itself as loose particulate that must be washed or aggressively rinsed from the surface. Table 1 lists generic chemistries for alkaline degreasing and acid deoxidizing. Many commercial formulations based on other chemistries exist. Some of these can be found in Ref 2.

Table 1 Generic degreasing and deoxidizing chemistries for aluminum alloy surfaces

Step	Chemistry	Temperature	Time
Degreasing	32.4 g/L Na_2SiO_3 48 g/L Na_2CO_3	65 °C (149 °F)	Several second dip to 120 s immersion as necessary
Deoxidizing	75 g/L $(NH)_4HF_2$ in concentrated HNO_3	Ambient	Several second dip to 300 s immersion as necessary

Properly prepared surfaces are very receptive to CCCs. CCCs are formed by immersing into the coating solution or spraying or brushing the metallic object with the coating solution. Coating color and thickness change with coating time (Ref 39). Coatings with weights ranging from 10 to 160 mg/m^2 (1 to 15 mg/ft^2) are colorless to light yellow and are formed in a few seconds. Coatings with weights ranging from about 215 to 430 mg/m^2 (20 to 40 mg/ft^2) can be colorless, iridescent, light yellow, or tan depending on substrate type. These coatings are formed in several tens of seconds and are used where low electrical contact resistance is required. General-purpose coatings for corrosion resistance and paint adhesion range from 54 to 970 mg/m^2 (5 to 90 mg/ft^2). To form such coatings requires contact times of 2 or more minutes. The appearance of these coatings varies from iridescent blue to dark yellow or brown. Use of contact times longer than 4 min is unusual in industrial practice because it is possible to degrade surface properties by overcoating.

Thorough rinsing of objects between steps ensures good CCC formation. Unreacted chemical components are removed from the surface and drag-in of chemicals from one processing bath to the next is minimized. CCC formation can be extremely sensitive to small changes in the chemistry of pretreatment or conversion coatings baths. The importance of bath cleanliness and strict adherence to manufacturer's recommendations on bath maintenance cannot be overemphasized.

Freshly coated surfaces should be rinsed to remove excess acid, but should be handled with care because of their gel-like quality. Coatings to be used for stand-alone corrosion protection should be allowed to dry for about one day before any further handling. Painting should be carried out within 24 to 48 h of coating formation. Paintability may be lost if coatings are allowed to dry for extended periods of time.

References cited in this section

2. S. Wernick, R. Pinner, and P.G. Sheasby, *The Surface Treatment and Finishing of Aluminum and its Alloys,* Vol 1, 5th ed., ASM International, 1987, p 220

8. J.N.J. Newhard, *Met. Finish.,* Vol 70, 1972, p 69

16. C.F. Baes and R.E. Mesmer, *Hydrolysis of Cations,* Wiley & Sons, 1976, p 211

17. F.W. Eppensteiner and M.R. Jenkins, Chromate Conversion Coatings, *Met. Finish.,* Guidebook and Directory Issue, 1999, p 494

18. A. Katzman, G. Malouf, R. Bauer, and G.W. Stupian, *Appl. Surf. Sci.,* Vol 2, 1979, p 416

19. L. Xia and R.L. McCreery, *J. Electrochem. Soc.,* Vol 146, 1999, p 3696

20. P.L. Hagans and C.M. Haas, *Surf. Interface Anal.,* Vol 21, 1994, p 65

21. F.W. Lytle, R.B. Greegor, G.L. Bibbins, K.Y. Blohowiak, R.E. Smith, and G.D. Tuss, *Corros. Sci.,* Vol 37, 1995, p 349

22. J.A. Treverton and N.C. Davies, *Met. Technol.,* Oct 1977, p 480

23. J.A. Treverton and M.P. Amor, *Trans. Inst. Met. Finish.,* Vol 60, 1982, p 92

24. W.R. McGovern, P. Schmutz, R.G. Buchheit, and R.L. McCreery, *J. Electrochem. Soc.,* Vol 147, 2000, p 4494

25. A.E. Hughes, R.J. Taylor, and B.W.R. Hinton, *Surf. Interface Anal.,* Vol 25, 1997, p 223

26. K. Asami, M. Oki, G.E. Thompson, G.C. Wood, and V. Ashworth, *Electrochim. Acta,* Vol 32, 1987, p 337

27. M.W. Kendig, A.J. Davenport, and H.S. Isaacs, *Corros. Sci.,* Vol 43, 1993, p 41

28. G.M. Brown, K. Shimuzu, K. Kobyashi, G.E. Thompson, and G.C. Wood, *Corros. Sci.,* Vol 34, 1993, p 1045

29. W. Zhang and R.G. Buchheit, *J. Electrochem. Soc.,* Vol 149, 2002, p B357

30. P. Campestrini, E.P.M.V. Westing, and J.H.W. deWit, *Electrochim. Acta,* Vol 46, 2001, p 2553

31. J. Wan, G.E. Thompson, K. Lu, and C.J.E. Smith, *Physica B,* Vol 208, 209, 1995, p 511

32. D. Arrowsmith, J.K. Dennis, and P. Sliwinski, *Trans. Inst. Met. Fin.,* Vol 62, 1984, p 117

33. X. Sun, R. Li, K.C. Wong, K.A.R. Mitchell, and T. Foster, *J. Mater. Sci.,* Vol 36, 2001, p 3215

34. J.R. Waldrop and M.W. Kendig, *J. Electrochem. Soc.,* Vol 145, 1998, p L11

35. G.M. Brown, K. Shimuzu, K. Kobayashi, G.E. Thompson, and G.C. Wood, *Corros. Sci.,* Vol 33, 1992, p 1371

36. J.C. Brinker and G.W. Scherrer, *Sol-Gel Science: The Physics and Chemistry of Sol-Gel Processing,* Harcourt, Brace, Jovanovich, 1990

37. L. Xia and R.L. McCreery, *J. Electrochem. Soc.,* Vol 145, 1998, p 3083

38. M. Henry, J.P. Jolivet, and L. Livage, Aqueous Chemistry of Metal Cations: Hydrolysis, Condensation, and Complexation, in *Structure and Bonding,* Springer- Verlag, Berlin, 1992, p 155

39. “Coating, Chromate on Aluminum,” Specification 9904151, U.S. Dept. of Energy, 1989

40. “Chemical Conversion Coatings on Aluminum and Aluminum Alloys,” MIL-C- 5541E, NAEC, 1990

41. R.A. Haaksma and J.R. Weir, *Proc. 27th Int. SAMPE Technical Conference,* Society for the Advancement of Materials and Process Engineering, 1995, p 1074

42. T. Schram, J. DeLaet, and H. Terryn, *J. Electrochem. Soc.,* Vol 145, 1998, p 2733

43. T. Schram, J. DeLaet, and H. Terryn, *Thin Solid Films,* Vol 727, 1998, p 313–314

44. J.A. Treverton, A. Bosland, and J.M. Brown, *Corrosion Sci.,* Vol 30, 1990, p 1159

45. L. Fedrizzi and F. Marchetti, *J. Mater. Sci.,* Vol 26, 1991, p 1931

46. J.N.J. Newhard, *Met. Finish.,* Vol 70, 1972, p 66

47. J.N.J. Newhard, *Met. Finish.,* Vol 70, 1972, p 49

48. L.A. Nimon and G.K. Korpi, *Plating,* Vol 59, 1972, p 421

49. F. Pearlstein and V.S. Agarwala, *Plat. Surf. Finish.,* Vol 81, 1994, p 50

50. F. Pearlstein and V.S. Agarwala, “Trivalent Chromium Solutions for Sealing Anodized Aluminum,” U.S. Patent No. 5,374,347, 1994

51. F. Pearlstein and V.S. Agarwala, “Trivalent Chromium Conversion Coatings for Aluminum,” U.S. Patent No. 5,304,257, 1994

R.G. Buchheit and A.E. Hughes, Chromate and Chromate-Free Conversion Coatings, *Corrosion: Fundamentals, Testing, and Protection*, Vol 13A, *ASM Handbook*, ASM International, 2003, p 720–735

Chromate and Chromate-Free Conversion Coatings

R.G. Buchheit, The Ohio State University; A.E. Hughes, CSIRO

Morphology, Structure, and Composition

Morphology and Structure. Thin chromium chromate coatings formed in just several seconds of contact with coating solution consist of a mass of small, nanometer-sized particles that nucleate and cover the entire alloy surface. Thicker coatings formed using longer contact times are three- dimensional structures with distinct horizontal layering and compositional variation, based on characterization of microtomed coating cross sections (Ref 28, 33, 35, 52, 53, 54) (Fig. 4). Thicker coatings develop shrinkage cracks as the coating dries and hardens (Ref 21, 55) (Fig. 5). Both thin and thick coatings are conformal and readily form in pits and scratches on the alloy surface left over from acid deoxidation and surface machining.

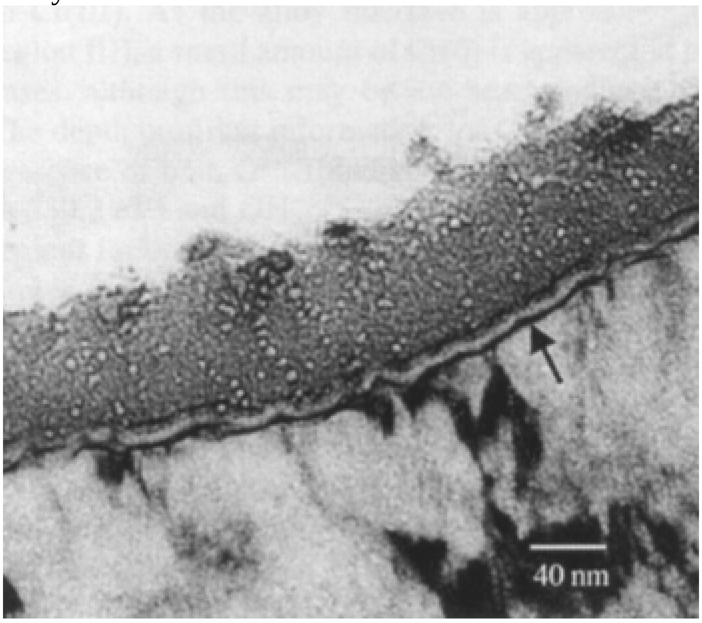

Fig. 4 Transmission electron micrograph of an ultramicrotomed CCC on 2024-T3. The CCC was formed on an acid etched surface by immersion in a CrO_3-$Na_2Cr_2O_7$-NaF solution for 5 min at ambient temperatures. The arrow points to a dark band believed to be caused by copper surface enrichment. Source: Ref 33

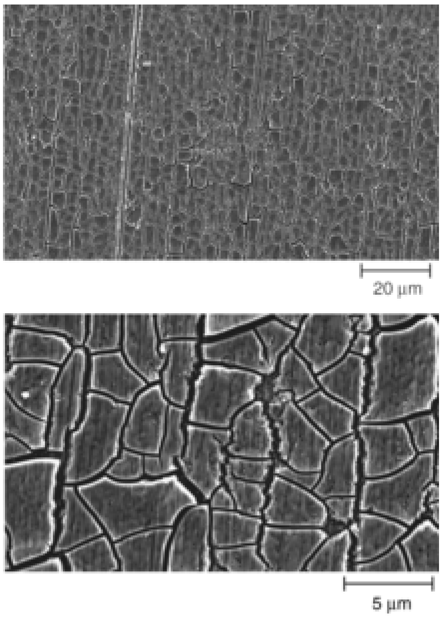

Fig. 5 Scanning electron micrographs of a CCC according to the Alodine 1200S process on 2024-T3 illustrating the shrinkage cracking that occurs upon dehydration. Courtesy of W. Zhang, Ohio State University

Thick and thin chromium chromate coatings are amorphous and remain so even after heating at temperatures up to 300 °C (570 °F). CCCs do exhibit short-range atomic order. Cr(III) in the coating is octahedrally coordinated by hydroxyl and oxygen ligands. $Cr(OH)_3$ octahedra share edges and corners forming an extended network or "backbone" that comprises the coating (Ref 37, 55, 56). Cr(VI) is bound to this backbone as described earlier.

Composition. There is general agreement that CCCs consist primarily of a mixture of Cr(III) and Cr(VI) compounds, other bath ingredients, and elements from the substrate. The precise composition depends on alloy substrate, bath formulation, processing parameters, and coating age. Reports vary on the specific compounds present and their relative abundance in the coating. Compounds proposed to exist within accelerated chromium chromate coatings include: Cr_2O_3, $Cr_2O_3 \cdot nH_2O$, $Cr(OH)_3$, CrOOH, $Cr(OH) \cdot CrO_4$, $Cr_x(CrO_4)_y$, CrF_3, $CrFe(CN)_6$, AlOOH, Al_2O_3, and AlF_3 (Ref 18, 21, 22, 56, 57).

Figure 6 shows a generalized physical-chemical model for CCCs based on a range on electron and x-ray analysis techniques. Composition depth profile data supporting this model are also provided. In the model, the external surface of the coating consists of hydrated chromium oxides and fluorides, ferricyanide, and chromate. The bulk of the coating below the topmost surface is a mixture of chromium oxides and hydroxides, oxyhydroxides, fluorides, and chromium ferricyanide. The coating nearest the aluminum substrate contains hydrated aluminum oxides, metallic and oxidized forms of copper on copper-bearing aluminum alloys, and chromium and aluminum oxyfluorides.

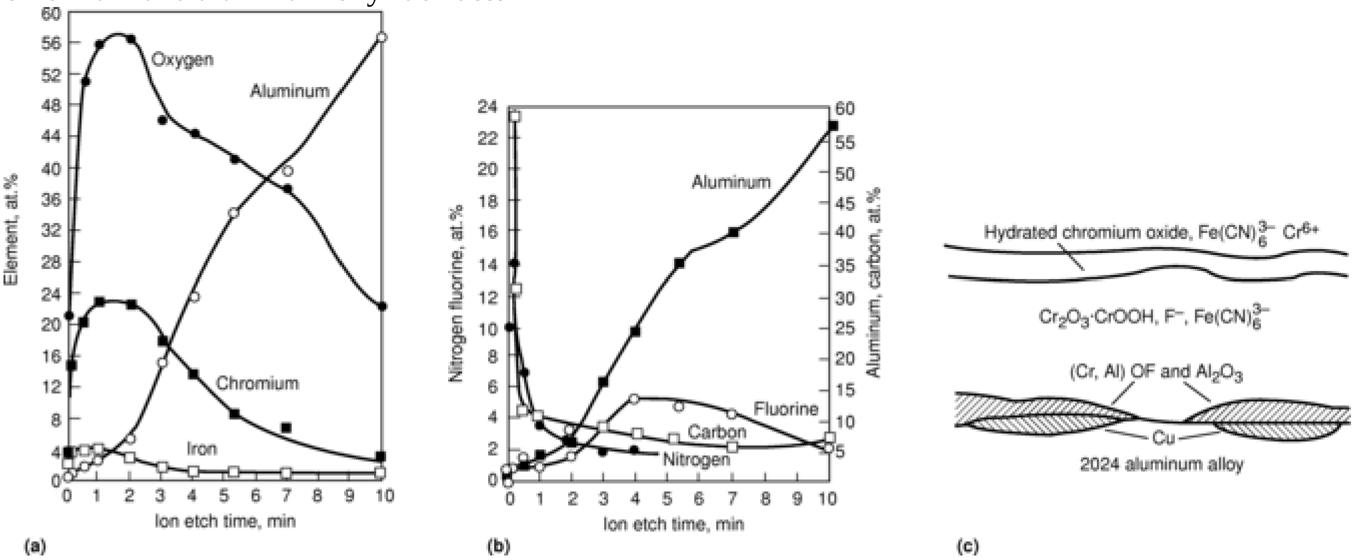

Fig. 6 (a) and (b) Composition depth profiles for the major elements found in chromium chromate CCCs. Source: Ref 22. (c) CCC structural model illustrating the distribution of compounds through the thickness of a CCC. Source: Ref 25

More recent characterization of CCCs by Raman spectroscopy is in general agreement with the model of Fig. 6 showing that a significant component of the coating is a $Cr(OH)_3$ polymer to which chromate or dichromate is bound (Ref 37).

Conversion coating chemistry evolves as the coating thickens. Thin coatings are mixtures of hydrated chromium and aluminum oxides with a comparatively small amount of Cr(VI) present in the outer regions of the coating (Ref 27, 31, 58). As coatings thicken, the chromium-to-aluminum and Cr(VI)-to-Cr(III) ratios increase. In thicker coatings, the Cr(VI) to total chromium ratio is commonly in the 20 to 40% range with 30% taken as a nominal value (Ref 27, 31, 58, 59). Composition depth profiles indicate that the Cr(VI) resides predominantly in the outer portions of the coating.

Measurement of the Cr(VI) content of CCCs has attracted special attention because it is related to the self-healing characteristic of CCCs. Determination of Cr(VI) in CCCs is complicated by the fact that the specie can be inadvertently reduced by photoreduction or ultrahigh vacuum exposure (Ref 26, 27, 60, 61). Inadvertent Cr(VI) reduction must be considered in measurements of CCC chemistry by x-ray photoelectron spectroscopy (XPS) and Auger electron spectroscopy (AES). X-ray synchrotron techniques such as x-ray absorption near-edge spectroscopy (XANES) and x-ray absorption fine structure (EXAFS) provide a significant advantage in this regard, as these measurements can be made with minimal risk of Cr(VI) reduction. Additionally, these measurements can be carried out under ambient environmental conditions, which is often a considerable experimental convenience (Ref 62).

The use of XANES to characterize the chemistry of CCCs is noteworthy. X-ray absorption spectra for chromium are distinguished by a progressive increase in the absorption edge energy with increasing oxidation state and by a discrete absorption peak associated with Cr(VI), which occurs at energies just below the main Cr Kα absorption edge (Fig. 7) (Ref 27, 63). This greatly facilitates Cr(VI) determinations in a CCC. XANES has also been used to study chromate leaching, the effects of aging, and the effects of different processing chemistries and procedures (Ref 27, 64, 65, 66, 67). See “Extended X-Ray Absorption Fine Structure” in *Material Characterization,* Vol 10, *ASM Handbook,* 1986, p 406.

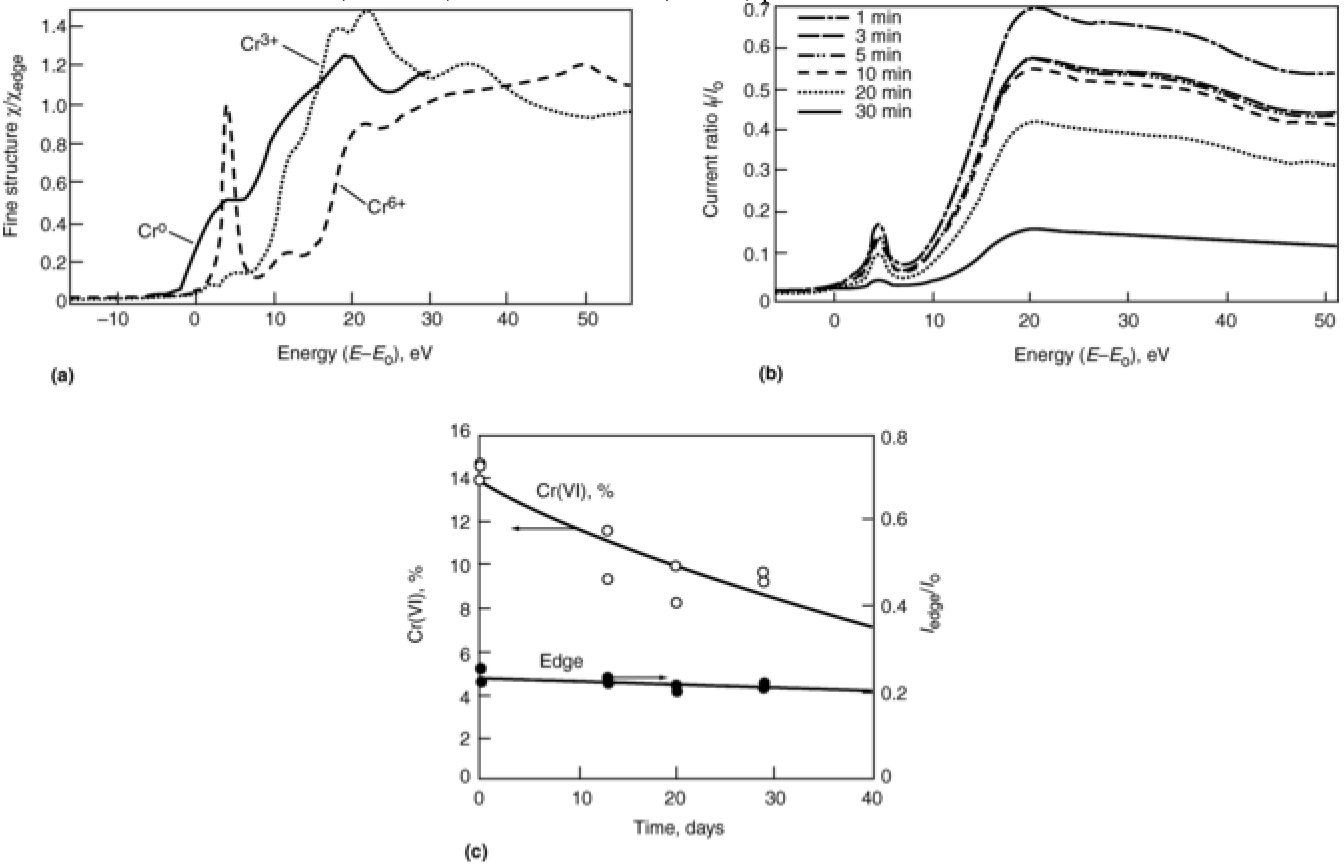

Fig. 7 XANES of CCCs at the Cr Kα absorption edge. (a) Reference spectra for Cr(VI), Cr(III), and Cr(0). (b) Spectra collected from CCCs on a 2024-T3 substrate as a function of processing time. (c) Time dependence of total Cr and Cr(VI): total Cr ratio for A CCC on 3003 exposed to aerated 0.5 *M* NaCl solution. Source: Ref 27, 64

References cited in this section

18. A. Katzman, G. Malouf, R. Bauer, and G.W. Stupian, *Appl. Surf. Sci.,* Vol 2, 1979, p 416

21. F.W. Lytle, R.B. Greegor, G.L. Bibbins, K.Y. Blohowiak, R.E. Smith, and G.D. Tuss, *Corros. Sci.,* Vol 37, 1995, p 349

22. J.A. Treverton and N.C. Davies, *Met. Technol.,* Oct 1977, p 480

25. A.E. Hughes, R.J. Taylor, and B.W.R. Hinton, *Surf. Interface Anal.,* Vol 25, 1997, p 223

26. K. Asami, M. Oki, G.E. Thompson, G.C. Wood, and V. Ashworth, *Electrochim. Acta,* Vol 32, 1987, p 337

27. M.W. Kendig, A.J. Davenport, and H.S. Isaacs, *Corros. Sci.,* Vol 43, 1993, p 41

28. G.M. Brown, K. Shimuzu, K. Kobyashi, G.E. Thompson, and G.C. Wood, *Corros. Sci.,* Vol 34, 1993, p 1045

31. J. Wan, G.E. Thompson, K. Lu, and C.J.E. Smith, *Physica B,* Vol 208, 209, 1995, p 511

33. X. Sun, R. Li, K.C. Wong, K.A.R. Mitchell, and T. Foster, *J. Mater. Sci.,* Vol 36, 2001, p 3215

35. G.M. Brown, K. Shimuzu, K. Kobayashi, G.E. Thompson, and G.C. Wood, *Corros. Sci.,* Vol 33, 1992, p 1371

37. L. Xia and R.L. McCreery, *J. Electrochem. Soc.,* Vol 145, 1998, p 3083

52. G.M. Brown, K. Shimizu, K. Kobayashi, G.E. Thompson, and G.C. Wood, *Corros. Sci.,* Vol 33, 1993, p 253

53. G.M. Brown, K. Shimizu, K. Kobayashi, G.E. Thompson, and G.C. Wood, *Corros. Sci.,* Vol 34, 1993, p 1853

54. R.C. Furneaux, G.E. Thompson, and G.C. Wood, *Corros. Sci.,* Vol 19, 1979, p 63

55. L. Kintrup and L.D. Riese-Meyer, *Inst. Phys. Conf. Ser.,* Vol 119, 1991, p 257

56. Z. Yu, H. Ni, G. Zhang, and Y. Wang, *Appl. Surf. Sci.,* Vol 62, 1992, p 217

57. J.A. Treverton and N.C. Davies, *Surf. Interface Anal.,* Vol 3, 1981, p 194

58. J.A. Treverton and M.P. Amor, *J. Mater. Sci.,* Vol 23, 1988, p 3706

59. C.S. Jeffcoate, H.S. Isaacs, J.A.J. Aldykiewicz, and M.P. Ryan, *J. Electrochem. Soc.,* Vol 147, 2000, p 540

60. G.P. Halada and C.R. Clayton, *J. Electrochem. Soc.,* Vol 138, 1991, p 2921

61. A.G. Schrott, G.S. Frankel, A.J. Davenport, H.S. Isaacs, C.V. Jahnes, and M.A. Russak, *Surf. Sci.,* Vol 250, 1991, p 139

62. D.C. Koningsberger and E.R. Prins, *X-Ray Absorption Principles, Applications, Techniques of EXAFS, SEXAFS and XANES,* John Wiley & Sons, 1988

63. M. Kendig, S. Jeanjaquet, R. Addison, and J. Waldrop, *Surf. Coat. Technol.,* Vol 140, 2001, p 58

64. S.W.M. Chung, J. Robinson, G.E. Thompson, G.C. Wood, and H.S. Isaacs, *Philos. Mag. B,* Vol 63, 1991, p 557

65. J.K. Hawkins, H.S. Isaacs, S.M. Heald, J. Tranquada, G.E. Thompson, and G.C. Wood, *Proc. The Electrochemical Society,* Vol 86-11, 1986, p 345

66. J.K. Hawkins, H.S. Isaacs, S.M. Heald, J. Tranquada, G.E. Thompson, and G.C. Wood, *Corros. Sci.,* Vol 27, 1987, p 391

67. J.S. Wainright, O.J. Murphy, and M.R. Antonio, *Corros. Sci.,* Vol 33, 1992, p 281

R.G. Buchheit and A.E. Hughes, Chromate and Chromate-Free Conversion Coatings, *Corrosion: Fundamentals, Testing, and Protection*, Vol 13A*, ASM Handbook,* ASM International, 2003, p 720–735

Chromate and Chromate-Free Conversion Coatings

R.G. Buchheit, The Ohio State University; A.E. Hughes, CSIRO

Coating Properties

Corrosion Protection and Corrosion Protection Mechanisms. CCCs can be regarded as physical barriers that prevent contact of the attacking environment with the underlying metal. The effectiveness of the barrier is determined by insolubility of components that make up the coating. However, experimental evidence shows that CCC protection consists of several distinguishable components beyond simple barrier protection.

Electrochemical measurements show that CCCs inhibit anodic reactions and localized corrosion on aluminum alloys surfaces. The primary evidence for this effect is an increase in pitting potential on conversion-coated electrode surfaces compared to uncoated control samples. Anodic inhibition measured in this way is modest, however. For example, in a 0.1 *M* Na_2SO_4 plus 0.005 *M* NaCl solution, a passive region is detected and the pitting potential is elevated by conversion coatings on 2024-T3 (Ref 68). However, in a more concentrated 0.1 *M* NaCl solution, no increase in pitting potential is detected in anodic polarization curves of the same alloy (Ref 25). The ability to detect an elevated pitting potential also appears to depend on electrode area and alloy substrate purity. With relatively large electrodes (>1.0 cm^2, or 0.16 $in.^2$) of heavily alloyed aluminum, increased pitting potentials are not usually observed in chlorides solutions of concentration greater than 0.1 *M.* However, with small area electrodes of higher- purity aluminum, the metallurgical or coating defect density is lower and increased pitting potentials are more regularly observed (Ref 29). This effect should be considered when interpreting pitting potential data from coated metal surfaces.

Electrochemical measurements also show that CCCs inhibit cathodic reactions. Cathodic polarization curves measured for conversion- coated aluminum alloys in near-neutral chloride solutions show that oxygen and water-reduction reaction kinetics are slowed by the presence of a freshly formed CCC (Ref 68). After several days, cathodic inhibition will diminish (Ref 25). Loss of corrosion resistance in this component may be associated with the formation of shrinkage cracks, which form as the coating dehydrates.

Perhaps the best-known aspect of corrosion protection by CCCs is “self-healing.” Self-healing refers to the ability of a chromate conversion coating to heal small chemical or mechanical defects that could serve as initiation sites for corrosion. The self-healing process is thought to involve 1) liberation of Cr(VI) into an attacking aqueous environment, 2) transport of the Cr(VI) through a contacting liquid phase to an incipient defect, and 3) reduction to insoluble Cr(III) hydroxide or interaction with the corrosion product to stifle further corrosion (Ref 69). The key attribute of CCCs in this regard is the ability to store and release Cr(VI) into an attacking solution. The Cr(VI) reservoir in CCCs is a function of coating weight or thickness and has been estimated to be on the order of 10^{-7} mol Cr(VI)/ cm^2 of CCC (Ref 70). Release of dichromate is proposed to occur by hydrolysis of Cr(III)-O- Cr(VI) when the following reaction occurs in the forward direction (Ref 70):

$$\begin{aligned} &Cr(III)\text{-}O\text{-}Cr(VI)O_3^-(s) + H_2O \\ &\leftrightarrow Cr(III)\text{-}OH(s) + Cr(VI)O_4^{2-}(aq) \\ &+ H^+(aq) \end{aligned} \qquad \text{(Eq 2)}$$

Cr(VI) then diffuses through the $Cr(OH)_3$ backbone, provided the network is sufficiently open. In Eq 2, equilibrium between the Cr(III)/Cr(VI) mixed oxide of the CCC and dichromate in solution, hence the extent of dichromate release is proposed to be governed by Langmuir-like adsorption behavior that depends on solution ionic strength, pH, and the ratio of CCC surface area to solution volume. As a result, the extent of Cr(VI) release is not simply governed by solubility of dichromate in solution, or total amount of Cr(VI) in the mixed oxide, as is more closely the case for $SrCrO_4$ pigments in primer coatings (Ref 71). Kinetically, the rate of chromate release appears to be well described by diffusion-controlled transport of Cr(VI) in the CCC (Ref 72).

Equation 2 also shows that the Cr(III)/Cr(VI) equilibrium is pH dependent in a manner that favors Cr(VI) uptake during coating formation and Cr(VI) release during service. Specifically, chromate adsorption is favored at low pH, typical of coating baths. Dichromate release is favored under higher pH conditions, more typical of service conditions where release and self- healing are necessary.

Opinions vary on how important self-healing is to overall corrosion resistance in coating systems (conversion coating, primer, topcoat), since the soluble chromate reservoir in a CCC is small compared to that in $SrCrO_4$-bearing primer coatings. While coating systems involving chromium-free conversion coatings and nonchromated topcoats are being used in certain applications, chromium-free organic coatings have not yet demonstrated acceptable corrosion protection in demanding aerospace qualification testing, unless they are applied on top of a self- healing chromate conversion coating (Ref 73).

Self-healing is only associated with CCCs that contain leachable Cr(VI) such as chromium chromate coatings. Chromium phosphate coatings, which contain primarily Cr(III) are not self- healing. Additionally, Cr(VI) in chromium chromate that have aged, dehydrated, or heated can become immobilized and unleachable. In these cases, the self-healing component of corrosion protection is lost.

Test Methods for Corrosion Resistance. Accelerated-exposure testing is widely used to assess corrosion protection by CCCs. The most commonly used environment is a 5% salt fog. In these tests, corrosion resistance is determined by visual inspection of a coated surface after some predetermined exposure period. The extent of corrosion damage is usually evaluated against some established metric such as number of pits per unit area visible to the unaided eye. Coated samples are normally given a pass or a fail ranking depending on whether the observed corrosion exceeds the metric or not. This type of test is simple and relevant to certain types of service conditions. Such evaluations can be very useful for process and quality control.

The most commonly used exposure regimen is neutral salt-spray (fog) exposure, described in ASTM B117 (Ref 74). In this test, conversion- coated panels are exposed in a chamber containing a fog generated from a 5% saltwater solution. The temperature is controlled at 35 °C (95 °F). Panels are periodically inspected for evidence of corrosion. Conversion-coated surfaces that resist corrosion in ambient atmospheres for years will show visible evidence of corrosion in tens to hundreds of hours in a salt-spray chamber. ASTM B 117 establishes the methodology, but does not specify failure criteria. Failure criteria are established in various military and industrial specifications (Ref 39, 40, 75). Other accelerated-exposure tests methods include the acetic acid salt-spray test (ASTM B 278), the copper accelerated salt-spray (CASS) test (ASTM B 368), the sulfur dioxide test (ASTM B 605), and the humidity test (ASTM D 2247).

Despite its apparent utility, accelerated-exposure testing is criticized for a variety or reasons. Exposure durations of 100 to 1000 h or more may be required for discriminating results to develop. These time frames are too long for quality control in many manufacturing operations. Exposure testing will separate excellent and

poor coatings easily, but differentiating good and very good coatings is usually much more difficult. This is often a problem when results from salt- spray testing are used as a response variable for studying the effects of processing or bath chemistry changes. Data from accelerated testing for life prediction is sometimes challenged on the basis that alteration of exposure environment to accelerate corrosion may change the corrosion mechanism itself. This calls into question the usefulness of these tests for assessing performance in service. Finally, there is the issue of variability in exposure aggressiveness from cabinet to cabinet and from one exposure cycle to the next. This may introduce uncertainties in comparisons of results from different tests and different facilities.

Perhaps the most unsatisfying aspect of exposure testing is subjectivity associated with a visual determination of corrosion. Evaluation specifications attempt to limit subjectivity, but they cannot eliminate it. For example, U.S. military specifications (Ref 40, 75) establish failure criteria in salt-spray testing as the presence of five or more pits per 30 in.^{2}, or 15 or more pits on five 30 in.^{2} panels. Pits are defined as localized regions of corrosion with diameters greater than 0.8 mm (0.31 in.). Pits of this size are believed to be the smallest pits to leave corrosion product stains that are visible to the unaided eye. While these failure criteria are precisely articulated, they are still affected by the evaluator's prior experience, judgment, and attention to detail.

Electrochemical Impedance Spectroscopy (EIS). Until the 1980s, corrosion testing of conversion-coated surfaces was conducted almost exclusively by exposure testing (Ref 40) or spot testing (Ref 76). Since the introduction of EIS to corrosion research, the use of this technique to evaluate the protectiveness of CCCs has steadily increased.

A common way to employ EIS is to expose conversion-coated surfaces to an aggressive electrolyte, usually a chloride solution, for some period of time during which coating and substrate damage will occur (Ref 77, 78, 79). Exposure times must be long enough to induce some limited amount of pitting damage. Time scales on the order of hours are commonly used. An impedance spectrum is collected and evaluated using a suitable equivalent circuit model or some other quantitative method. A simple model consisting of a parallel combination of resistor and capacitor, in series with a solution resistance, is frequently used. The numerical value of the parallel resistance and capacitance are used to judge the extent of corrosion damage. Resistances and capacitances may be determined after some fixed period of exposure, or they can be measured periodically over time to track the progression of corrosion damage. Table 2 gives typical values of the total impedance of various coated and passivated substrates. While EIS is used with increasing regularity for evaluation of CCCs, standardized methods for evaluating conversion coatings by EIS do not yet exist.

Table 2 Coating resistance ranges for various surface treatments and substrates

Coating	Coating resistance, $\Omega \cdot cm^2$
Bare aluminum alloys	0.005
Sputter-deposited high-purity aluminum	0.5–1.0
Poor conversion coatings	0.1–1.0
Good conversion coatings	1–5
Sealed anodized coatings	10
Painted surfaces	>10

The EIS approach has several advantages for evaluations of conversion coatings. First, it is a small signal technique, and the electrode is never polarized very far away from its steady-state corrosion potential as the measurement is made. Second, a numerical characterization of coating protectiveness is rendered by this method. For this reason, the technique may be better suited than exposure-test methods for discriminating small differences in corrosion protection among coatings. Third, after the samples have been exposed to develop some pitting damage, the measurement is very rapid. Meaningful characterizations of the impedance response can be obtained from spectra collected between 10 kHz and 10 mHz, which is a measurement that can be completed in a matter of minutes. To shorten the measurement time even further, it may be possible to determine the impedance at one or several properly selected frequencies to estimate coating protectiveness. Finally, EIS measurement equipment, which consists primarily of potentiostat, impedance analyzer, computer, and operating software has become increasingly affordable and portable over the past decade.

Electrochemical impedance spectroscopy methods are not without drawbacks. Coating evaluations by EIS are based on a very complex analytical technique. Skill, knowledge, and attention to detail are required to conduct the evaluations and interpret the data properly. Additionally, the exposure protocol involves immersion of the

coated surface in an aggressive aqueous environment. CCCs are not intended to provide long-term corrosion protection under such conditions. Therefore, interpretation of results from these evaluations must be used with this fact in mind.

Tests for Self-Healing. Self-healing is an important component of CCC corrosion protection, but rigorously testing for this property is challenging. The familiar example of self-healing ability is the absence of corrosion in a scribed coating after exposure to an aggressive environment. A simple cell, termed the “simulated scratch” cell, mimics this situation, but allows an experimenter to check more rigorously for the key elements of the self-healing process. These elements include release of inhibitor from the coating, interaction of the inhibitor with the simulated scratch surface, and increased corrosion resistance of the simulated scratch (Ref 69). This cell (Fig. 8) consists of two metal surfaces, normally several square centimeters in area opposing one another and separated by several millimeters. One metal surface is conversion coated, while the other is left bare to simulate a defect or “scratch.” The two metal surfaces are separated by a gap of several millimeters, which is filled with an attacking electrolyte like a dilute chloride solution. The cell may be equipped with a counter and reference electrode, and either the coated or defect sides of the cell can be interrogated using electrochemical methods. Simulated scratch cells have been used to show that certain chromium-free conversion coatings containing can also be self-healing (Ref 80).

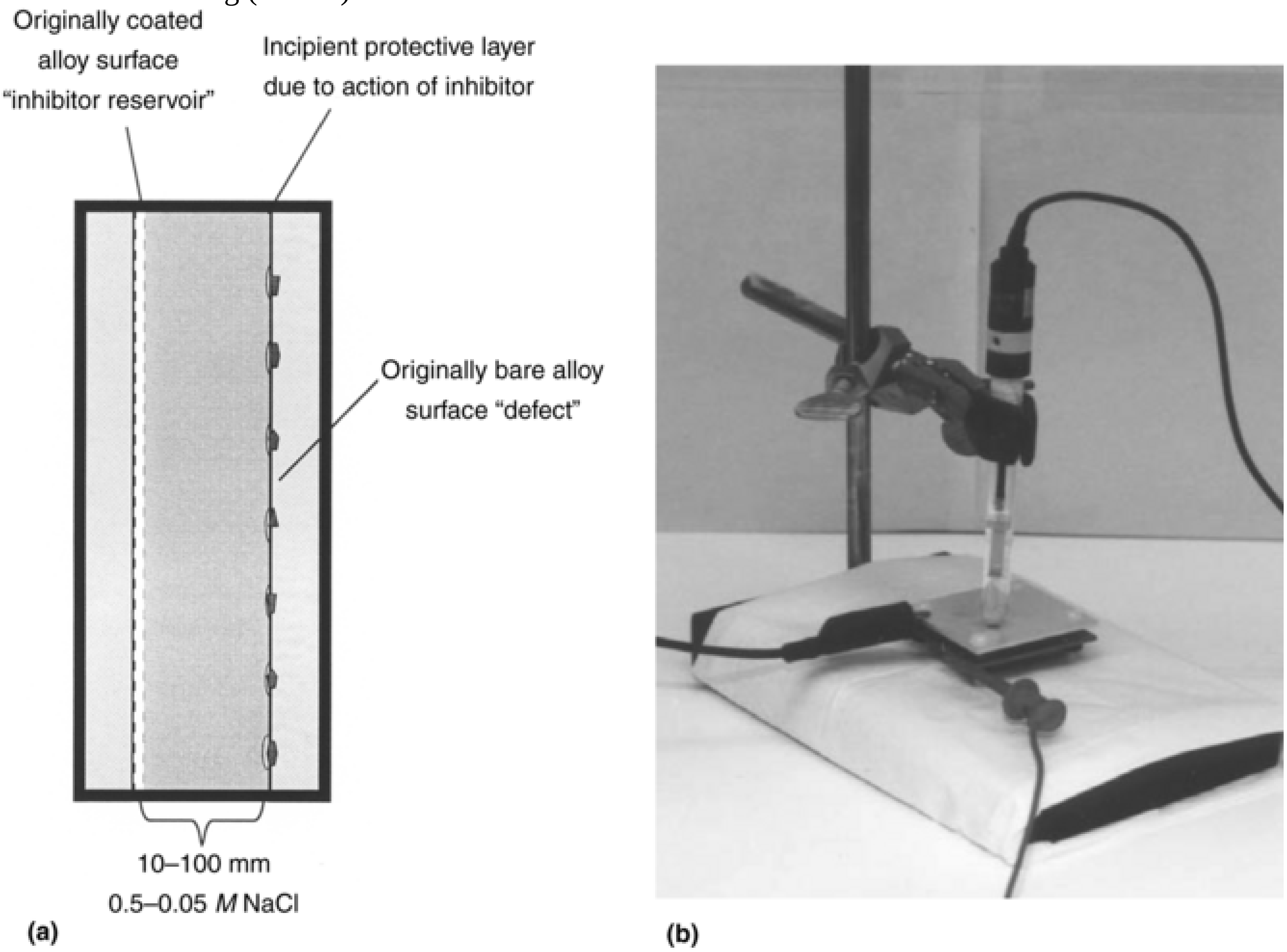

Fig. 8 (a) Cross section of the simulated scratch cell. (b) Photograph of an artificial scratch cell modified to make in situ electrochemical measurements to test for self-healing by conversion coatings. Source: Ref 70

Paint Adhesion. Typical aircraft coating systems consist of a CCC foundation layer, a primer coating, and a topcoat (Ref 81). In these systems, the primary function of the CCC is to promote initial and long-term adhesion of the organic coating on the metal substrate. Organic coating adhesion is promoted by surface topography, surface cleanliness, and possibly coating acidity (Ref 23, 82). Long-term interfacial adhesion is fostered by the high corrosion resistance provided by the inhibiting effects of Cr(VI) leached from the primer and the CCC (Ref 1).

Mechanical Stability. Freshly formed coatings are gelatinous and can be damaged easily. As the coating dries, it hardens considerably. CCCs dried for at least 24 h are considerably more robust. Coating weight determinations by chemical stripping of the CCC are nearly impossible to carry out by nitric acid immersion after this time. Hardened coatings will withstand some mechanical damage, but are not nearly as abrasion resistant as anodized coatings.

Electrical contact resistance is an issue for metallic electrical connectors. Connections are chromate conversion coated to increase corrosion resistance, but electrical continuity across the connection must not be degraded by the presence of the coating.

Chromated metal surfaces exhibit low electrical contact resistance as measured with a flat metal electrode applied with a small impinging load (Ref 75). Since dried CCCs are thin, they are easily breached, allowing metal-to-metal contact. In service, mechanical breaches caused by contacting metal surfaces can sometimes be tolerated without risk of corrosion due to the self-healing nature of the coating. In other cases, mechanical damage is too severe and atmospheric corrosion assisted by galvanic interactions or crevice corrosion will increase the contact resistance to such an extent that rework of the electrical contact is required (Ref 83). Low electrical contact resistance also makes conversion-coated surfaces amenable to various types of spot welding and arc welding procedures.

The intrinsic resistivity of CCCs is distinct from electrical *contact* resistance. Intrinsic resistivity of conversion coatings can be quite high (Ref 84, 85). Direct-current (dc) resistances of CCCs measured with a small (4×10^{-3} cm^2) mercury droplet that does not breach the CCC range from 10^{10} to 10^{12} Ω (Ref 85).

Aging and Heating. CCC properties are very dynamic once removed from the coating bath. The film transforms from a fragile gel to a robust, damage-tolerant coating in a few hours. Aging effects appear to be due to consolidation in the Cr(III) backbone, which can be detected by EXAFS measurements (Ref 86, 87). How this consolidation occurs is still a matter of speculation, but the structural rearrangement appears to be closely linked to coating dehydration (Ref 86). Shrinkage cracking also appears to be a consequence of backbone consolidation. Backbone rearrangement over the time frame of days to months produces profound changes in coating properties. Cathodic inhibition as measured in cathodic polarization testing is lost in tens of hours (Ref 25). In EIS testing, losses in corrosion resistance begin to be detected in times as short as 20 days after coating formation (Fig. 9) (Ref 86). In an extreme case, after 100 days exposure to ambient laboratory air, there was no evidence of corrosion protection in EIS testing of a 1 minute CCC on 2024-T3 exposed chloride solution. Chromate leaching also diminishes with time even though the Cr(VI) content of the coating remains the same. This well-known behavior may also be linked to backbone consolidation, which traps Cr(VI) in the coating (Ref 87, 89). Ultimately, over tens of years the Cr(VI) content of CCCs diminishes. After seven years, aging under ambient indoor exposure the Cr(VI) CCCs on aluminum alloy 3003 (Al-1.0Mn) was measured by XANES to decrease from about 30% to levels undetectable by XANES (Ref 59).

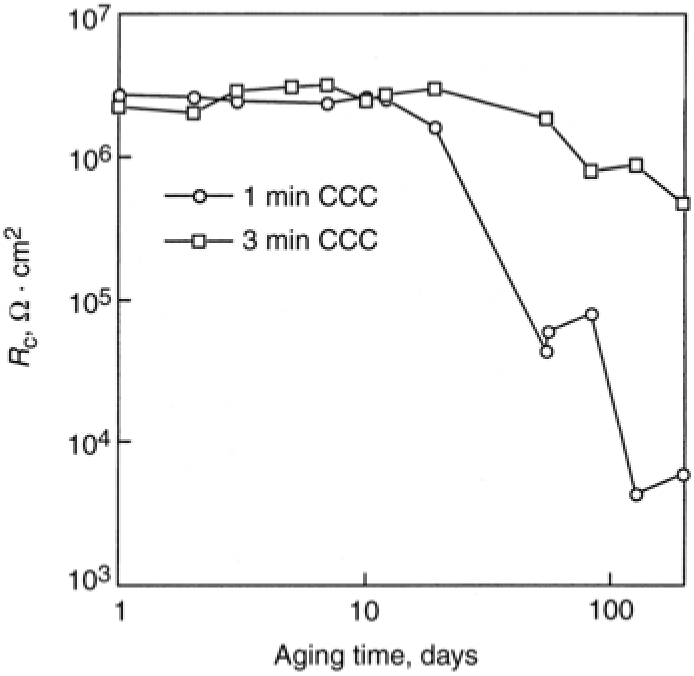

Fig. 9 Corrosion resistance measured as parallel coating resistance, R_c, from electrochemical impedance spectroscopy experiments of conversion-coated 2024-T3 exposed to aerated 0.5 *M* NaCl determined after aging in air. Source: Ref 88

As is well known, CCCs are not heat tolerant (Ref 90, 91). Exposure to elevated temperature accelerates dehydration, consolidation of the Cr(III) backbone, and losses in properties described previously. Losses in CCC corrosion protection, Cr(VI) leaching, and increases in shrinkage cracking are profound when coatings are subject to temperatures in excess of 60 °C (140 °F). Corrosion resistance in salt-spray exposure testing and electrochemical testing can be completely lost when CCCs are heated for more than 15 min at temperatures in excess of this 60 °C (140 °F) threshold (Ref 89).

References cited in this section

1. T. Biestek and J. Weber, *Electrolytic and Chemical Conversion Coatings,* Porticullis Press Limited-Redhill, Surrey, UK, 1976

23. J.A. Treverton and M.P. Amor, *Trans. Inst. Met. Finish.,* Vol 60, 1982, p 92

25. A.E. Hughes, R.J. Taylor, and B.W.R. Hinton, *Surf. Interface Anal.,* Vol 25, 1997, p 223

29. W. Zhang and R.G. Buchheit, *J. Electrochem. Soc.,* Vol 149, 2002, p B357

39. "Coating, Chromate on Aluminum," Specification 9904151, U.S. Dept. of Energy, 1989

40. "Chemical Conversion Coatings on Aluminum and Aluminum Alloys," MIL-C- 5541E, NAEC, 1990

59. C.S. Jeffcoate, H.S. Isaacs, J.A.J. Aldykiewicz, and M.P. Ryan, *J. Electrochem. Soc.,* Vol 147, 2000, p 540

68. G.O. Ilevbare and J.R. Scully, *J. Electrochem. Soc.,* Vol 148, 2001, p B196

69. J. Zhao, G.S. Frankel, and R.L. McCreery, *J. Electrochem. Soc.,* Vol 145, 1998, p 2258

70. L. Xia, E. Akiyama, G. Frankel, and R. McCreery, *J. Electrochem. Soc.,* Vol 147, 2000, p 2556

71. J. Sinko, *Prog. Org. Coatings,* Vol 42, 2001, p 267

72. E. Akiyama, A.S. Markworth, and G.S. Frankel, *J. Electrochem. Soc.,* 2001

73. J.H. Osborne, J. Du, S.R. Taylor, D. Bernard, A. Nercissiantz, and G.P. Bierwagen, "Advanced Corrosion Resistant Aircraft Coatings," Final Report 6/96-9/00, Contract No. F33615-96-C-5078, U.S. Air Force Research Laboratory, 2000

74. F. Altmayer, *Plat. Surf. Finish.,* Vol 72, 1985, p 36

75. "Chemical Conversion Materials for Coating Aluminum and Aluminum Alloys," Naval Air Systems Command, Dept. of the U.S. Navy, 1970

76. G.D. Cheever, *J. Paint Technol.,* Vol 41, 1969, p 259

77. R.G. Buchheit, M.W. Kendig, M.A. Martinez, M. Cunningham, and H. Jensen, *Corrosion,* Vol 54, 1998, p 61

78. F. Mansfeld, S. Lin, S. Kim, and H. Shih, *Corros. Sci.,* Vol 27, 1987, p 997

79. F. Mansfeld and H. Shih, *J. Electrochem. Soc.,* Vol 135, 1988, p 906

80. R.G. Buchheit, S.B. Mamidipally, and P. Schmutz, *Corrosion,* Vol 58, 2002, p 3

81. R.L. Twite and G.P. Bierwagen, *Prog. Org. Coatings,* Vol 33, 1998, p 91

82. E.D. Wick, *Tool and Manufacturing Engineers Handbook,* Society of Manufacturing Engineers, 1983

83. A. Wehr, H.C. Hardee, N.R. Auckland, and D. Klavens, *Proc. 48th Electronic Components and Technology Conference,* Institute of Electrical and Electronics Engineers, 1998, p 14

84. M.A. Heine and M.J. Pryor, *J. Electrochem. Soc.,* Vol 114, 1967, p 1001

85. G.E. Pike, "Electrical Properties of Alodine 1200," Internal Memorandum, Sandia National Laboratories, 1981

86. V. Laget, H. Isaacs, C.S. Jeffcoate, and R. Buchheit, *Proc. Electrochem. Soc.,* Vol 92- 26, 2000, p 173

87. V. Laget, H.S. Isaacs, C.S. Jeffcoate, and R.G. Buchheit, *ATB Metallurgie,* Vol 40–41, 2000, p 295

88. V. Laget, C.S. Jeffcoate, H.S. Isaacs, and R.G. Buchheit, *J. Electrochem. Soc.,* Vol 150 (No. 9), 2003

89. F. Pearlstein and M.R. D'Ambrosio, *Plating,* Vol 55, 1968, p 345

90. A. Gallacio, F. Pearlstein, and M.R. D'Ambrosio, *Met. Finish.,* Vol 50, 1966

91. A.L. Glass, *Mater. Protect.,* Vol 26, 1968

R.G. Buchheit and A.E. Hughes, Chromate and Chromate-Free Conversion Coatings, *Corrosion: Fundamentals, Testing, and Protection*, Vol 13A, *ASM Handbook*, ASM International, 2003, p 720–735

Chromate and Chromate-Free Conversion Coatings

R.G. Buchheit, The Ohio State University; A.E. Hughes, CSIRO

Chromate-Free Conversion Coatings

Due to pressures from health and environmental legislation, there has been a move away from chromate-containing products over a number of years. The prospect of replacing chromate conversion coatings has brought with it considerable investigation of potential alternatives based on a broad range of chemistries. Furthermore, within each chemical category there is the potential for a broad range of formulations, most of which will not result in viable industrial processes due to processing or performance limitations.

A review of all these alternatives is complicated by the range and quality of performance data for these processes, since different processes are targeted toward different parts of the metal-finishing industry that have different performance requirements. Some comparative studies have been carried out and are a good source of performance data, but do not include all the processes described herein (Ref 92, 93, 94). Furthermore, developments in chromate alternatives are progressing rapidly, and those tested in comparative reports may not reflect the current performance of processes.

The aim of this section is to give an indication of the market sector for which a class of processes is being developed, some idea of the chemistry and processing involved, an indication of process control, and, finally,

structure and method of deposition of the coating. Readers are referred to several reviews that have been recently published (Ref 95, 96, 97). A total market review of the introduction of replacement technologies was not attempted since this is continually changing as more knowledge is gained about the alternatives.

Chromate conversion coatings found a range of applications in industry, especially in aluminum finishing. The development of alternatives is complicated by both the performance and processing requirements of different sectors of industry (Table 3). Currently, several chromate alternatives have gained acceptance in specific sectors of the market. These markets can be divided into those that require protection in the unpainted condition and those that require performance under paint. For the latter category, many alternatives demonstrate good performance characteristics. The aerospace industry falls into the former case, and a drop-in replacement still does not exist in this high-performance end of the market, which has very high standards for corrosion resistance of the unpainted conversion-coated surface in the neutral salt-spray test.

Table 3 Major classes of chromate alternatives

Coating type	Industry sector	Status[(a)]
Titanium and zirconium fluorocomplexes	Sheet stock for canning	Mature
	Automotive	Developing
Cerium-base	Architectural	Developing
	Aerospace	Evaluation
Cobalt-base	Marine	Developing
	Auto	Developing
	Aerospace	Evaluation
Molybdenum-base	Tin and galvanized product	Developing
Hydrotalcites	Aerospace	Evaluation
Manganese-base	Some sheet product	Developing
	Aerospace	Evaluation
Boehmite coatings	Aerospace	Evaluation
Silane coatings	Automotive	Developing
Conducting polymers	Ferrous metals	Evaluation
Self-assembled monolayers	Automotive Al/Mg alloys	Developing

(a) Mature, in the industry for a number of years. Developing, may be introduced soon. Evaluation, still undergoing trials

General features of these alternative processes are described in the sections that follow. Table 3 lists the major types of chromate alternatives in use or under development and the industries that are currently targeted by the manufacturers of these products. The majority of these processes are still under development. Fluorozirconoic and fluorotitanic acid coatings are the most mature of these replacement technologies with products on the market for a number of years.

Two final points should be made, however, with respect to chromate. First, it should be noted that chromate is often considered as a single process suitable for all aluminum alloys under all processing conditions. In reality, this is not the case since different formulations are used for different applications. Indeed there is no single, published database comparing the performance of chromate on a range of alloys cast or wrought in a range of tempers. The available performance data place a strong emphasis on sheet 2024-T3 with some 7075-T6 and 6061-T6 data.

Second, conversion coating is a multistep process usually involving both cleaning and deoxidizing/desmutting prior to conversion coating. Over many years, the metal-finishing industry has optimized the pretreatment steps for chromate conversion coating, and it is not surprising that a chromate-base deoxidizer is often used since it sets up a surface more amenable to chromate conversion coating than other deoxidizers. Chromate alternatives may have their own requirements for pretreatment, which may not be the same as the current process steps. These two factors should be taken into account when considering the development of replacements for chromate.

References cited in this section

92. B. Meyers, S. Lynn, and E. Jang, “Alternatives to Chromate Conversion Coating at McClellan Air Force Base,” MITRE, 1993

93. “Alternatives to Chromium for Metal Finishing,” Final NCMS Report 0273RE95, National Center for Manufacturing Sciences, 1995

94. “Alternatives to Chrome Conversion Coatings on Aluminum Alloys 2024, 6061, 7075, and Ion Vapor Deposited Aluminum on Steel (Potential Alternatives Report),” Web page, http://www.jgapp.com/parhughhc.htm, National Defense Center for Environmental Excellence, 1998

95. M. Kendig and R. Buchheit, Surface Conversions of Aluminum and Ferrous Alloys for Corrosion Resistance, *Proc. Corros./ 2000 Res. Top. Symposium,* NACE International, 2000, p 1

96. J. Ouyang and W.L. Harpel, “Monitoring of Coating Weight in Dried-in-Place Non- Chrome Polyacrylamide Based Treatments for Metals,” U.S. Patent No. 5,401,333, 28 March 1995

97. H. Terryn, *ATB Metall.,* Vol 38, 1998, p 41

R.G. Buchheit and A.E. Hughes, Chromate and Chromate-Free Conversion Coatings, *Corrosion: Fundamentals, Testing, and Protection*, Vol 13A, *ASM Handbook*, ASM International, 2003, p 720–735

Chromate and Chromate-Free Conversion Coatings

R.G. Buchheit, The Ohio State University; A.E. Hughes, CSIRO

Chromate-Free Processes

Titanium and zirconium fluorocomplexes have a well-established market use in the container, coil coating, aluminum appliance, transportation, magnesium, aerospace, and extrusion industries and are offered by a number of suppliers. More than 100 customers have converted to these titanium and zirconium chemistries from chromate. In addition, National Aerospace and Space Administration (NASA) has used these coatings for a few years on the solid rocket boosters of the space shuttle (2219 alloy) with completely chromium-free paint systems. These coatings also find use in aluminum and titanium fighter jet applications. Earlier versions of these coatings were inorganic, but current versions contain polymeric components (Ref 95). Processing is relatively simple, involving up to eight steps, although five is the most common. These usually include (depending on the manufacturer) an alkaline clean, rinse, coat, rinse, and dry, sometimes at elevated temperature. The conversion coating bath is acidic (pH < 4) and operated at room temperature up to 40 °C (104 °F).

The conversion coating solutions generally contain an acidic hexafluoro metal complex (H_2ZrF_6, or H_2TiF_6) or Group IVa,b of the CAS classification of the periodic table, oxyfluoro compounds, excess fluoride, and commonly, a polymer. The added polymers improve corrosion resistance and overlayer adhesion. Two examples are polyacrylic acid (Ref 98) or phenolic resins (Ref 99). Other inorganic acids and phosphates may be added to the composition; phosphates have been reported to improve the corrosion resistance of the coating (Ref 100).

Process control is through titration for free fluoride, pH, and titanium. Coating weight is determined by x-ray fluorescence (XRF) of titanium or in the zirconium/polymer versions of the coating (Ref 96). XRF determination for zirconium can be done, but it is much less accurate and not particularly reliable. A typical dry-in- place version of this system can be applied in as little as 0.5 s for a roll coater on a coil line, and coating weights are in the range of 1 to 1300 mg/ m^2 (0.1 to 120 mg/ft^2) (Ref 98). These types of processes demonstrate

excellent performance in standard industry adhesion tests (Ref 98), but generally do not have very good corrosion resistance in the unpainted state (Ref 93, 94).

Characterization of the conversion coating indicates a thin, multilayer structure, depicted in Fig. 10. In the absence of polymer additives, the coating consists of three distinct layers. Adjacent to the metal an aluminum oxide develops, then a zirconia (ZrO_2) layer develops on top of the aluminum oxide, and this is capped by a mixed Zr/O/F layer. In the presence of a polymeric component, the ZrO_2 and mixed Zr/O/F layers are replaced by a mixed Al/O/Zr/F coating containing the polymer. The polymer tends to be more concentrated toward the surface (Ref 101). Coatings produced in this process are very thin, being typically in the range 10 to 25 nm (0.4 to 1.0 μin.) depending on composition, but may be 500 nm (20 μin.) in some applications.

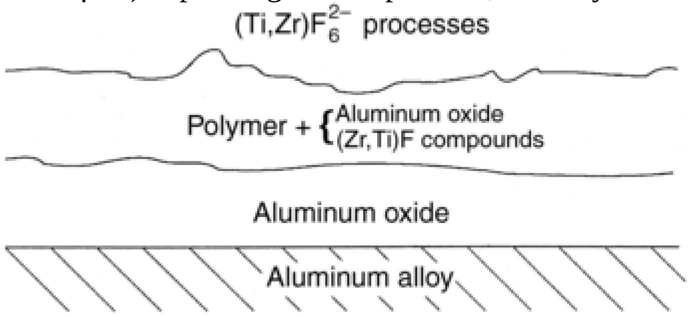

Fig. 10 Titanium/zirconium fluorocomplexes. The total coating thickness is <25 nm (<0.98 μin.).

Based on the characterization studies, it has been proposed that the conversion coating develops in the following manner. On immersion into the coating solution, the aluminum oxide on the surface of the metal is activated by either excess fluoride or the fluoro complex in solution (or both) and becomes hydrated. Aluminum- fluoride bonds are more stable than Al-OH bonds and fluoride substitution of hydroxyl groups quickly takes over. This is probably assisted by the alumina surface having a net positive charge at the low operating pH of the bath. In this fashion, the Zr/O/F-containing-layer begins to develop and in the case of added polymer also incorporates polymeric material.

Cerium-Base Coating Processes. There are a number of chromate alternatives based on cerium described in the literature (Ref 102, 103, 104, 105). Some of these are true conversion coatings, whereas others involve the development of boehmite coatings with incorporated cerium ions on aluminum.

Cerate. The term “cerate” as a process name is a popularization derived from “chromate” terminology and is misleading since the cerate process does not contain any oxyanions of cerium. Recognition of cerium ions as inhibitors goes back to the mid 1980s with the work of Hinton et al. (Ref 106).

Cerate processes are under development for the architectural market (aluminum extrusions) and are expected to be released by one supplier in 2003. A two-step cerate process involving a final seal, usually silicate, is also being evaluated for aerospace applications. For the architectural market, processing is relatively simple, involving up to six steps, with the cerate process as a drop-in replacement for chromate. The steps include an alkaline clean, rinse, desmut, rinse, coat, and rinse with no specific drying requirements. Conversion coating takes place at 45 °C (113 °F) in either spray or immersion processing, and coating time is typically 30 s to 2 min (Ref 102). The coating has a light yellow to golden color. For the aerospace applications, the process is longer and involves an additional seal with dry and rinse steps. The seal is silicate-base and applied between 20 and 80 °C (68 and 176 °F).

The conversion coating solutions are acidic (pH 1.7 to 2.2) and contain cerium chloride, hydrogen peroxide, hydrochloric acid for acidification, and, for architectural applications, a bismuth complex to act as an accelerator. The unsealed version used in nonaerospace applications typically gives performance similar to chromate in filiform, CASS, wet adhesion, and outdoor exposure tests (Ref 107).

Process control for cerium in the cerate bath can be done either by titration for cerium using argenic ($Ag^{I}Ag^{III}O_2$) oxide followed by titration, for example, with ferrous ammonium sulfate in the presence of ferroin or gravimetrically with excess fluoride addition. Hydrogen peroxide levels can be monitored by a permanganate titration. Coating weights are determined by standard acid dissolution used for chromate coatings. Coating weights are typically in the range (323 to 538 mg/m^2 (30 to 50 mg/ft^2).

Investigations of the structure and composition of the cerate process has focused on the version for aerospace applications. The proposed aerospace process produces a bilayered structure (Fig. 11) of aluminum oxide adjacent to the metal beneath a ceria (CeO_2) overlayer coating with a total thickness of 100 to 200 nm (4 to 8

μin.) for typical processing times (1 to 2 min). Thicker coatings can be produced with longer immersion times, but coatings become powdery and nonadherent for longer immersions, depending on the alloy type. (In this respect, the cerate coating is very similar to the chromate coating.) The thickness of the aluminum oxide layer depends on the deoxidizer and is thickest with low- etch-rate deoxidizers, although again this is dependent on the alloy type. Often there is enrichment of alloying components (particularly copper with the copper-rich alloys) at the interface of this oxide with the metal. This phenomenon also occurs in chromate processes, but is a function of the deoxidizer rather than the coating solution and is therefore common to most conversion coatings. The sealing process produces a silicate layer on top of the CeO_2 coating. The silicate layer can add up to another 200 nm (8 μin.) to the coating thickness.

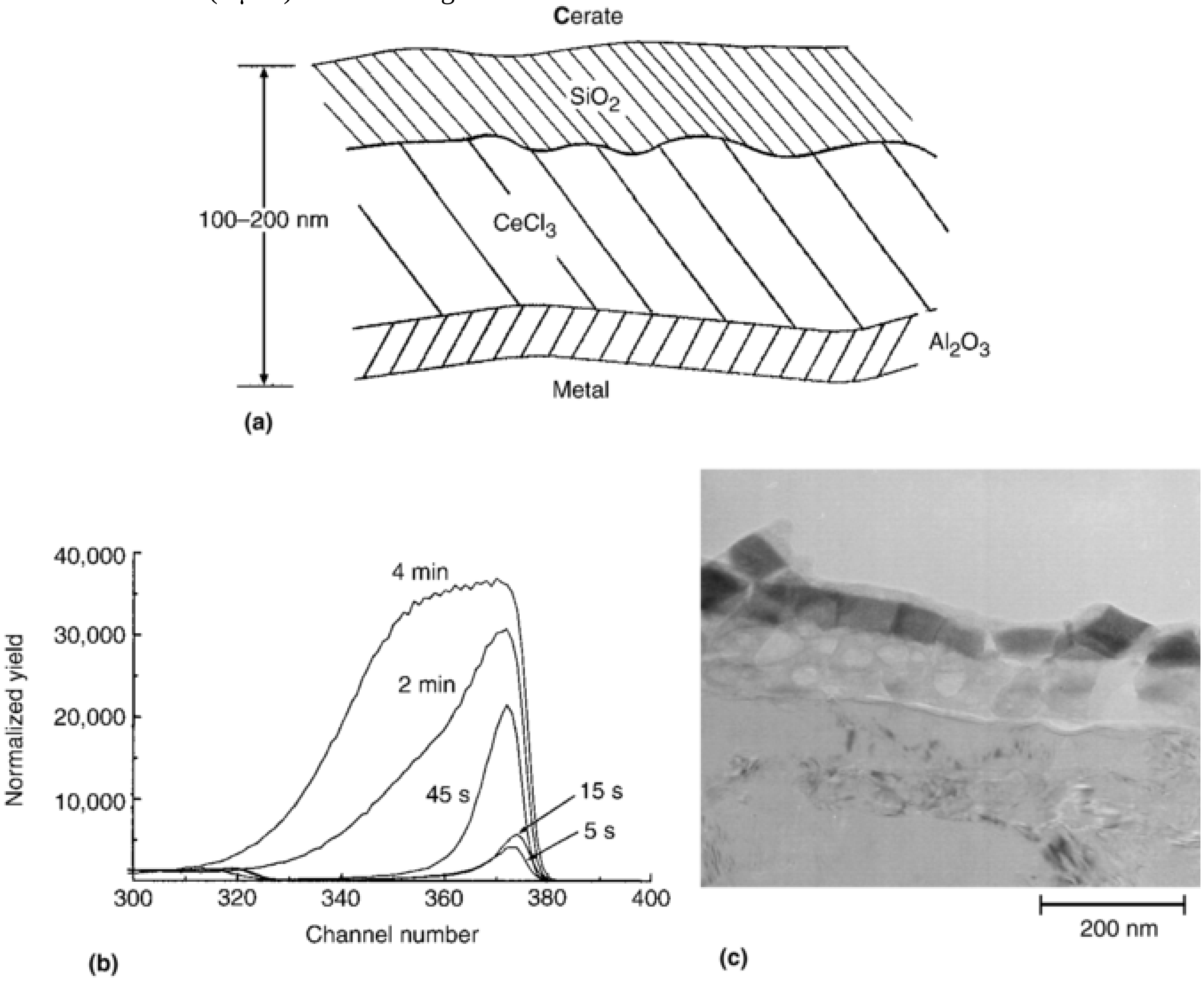

Fig. 11 Cerate conversion coating. (a) Silicate sealed coating. (b) Rutherford backscattering spectroscopy spectra of the cerium region indicating the buildup of cerium. (c) Transmission electron microscopy section of an unsealed coating showing the aluminum oxide and the ceria overlayer.

Based on characterization studies that have focused on the low-etch-rate deoxidizers, it is clear that coating begins over the cathodic intermetallics particles and is thicker there than over the matrix. The majority of these particles then appear to be deactivated. Simultaneously, the aluminum oxide over the matrix thickens to 100 nm (4 μin.) (induction period) before cerium oxide deposits on top of the aluminum oxide. The mechanism of this delayed deposition is still not well understood (Ref 107).

Hybrid Cerium Process. With a number of inhibitors being tried for chromate-free coatings, it is not surprising that processes are developed that combine a number of different types of inhibitors. Miller developed a nine-step process for the proposed aerospace market (Ref 104). The steps include an alkaline clean, rinse, desmut, rinse, coat, rinse, seal, rinse, and then swab with adhesion promoter.

The cerium-conversion coating solutions are neutral to basic (since they can contain NaOH), operate at room temperature, and can contain potassium permanganate and/or strontium chloride. The seal contains sodium molybdate, nitrite, and silicate and is applied at 90 to 95 °C (195 to 205 °F). The adhesion-promoting step is a swab with a silane (glycidoxy(ethoxy)polyfunctional methoxysilane).

No information has been published on process control; however, cerium and manganese levels can probably be ascertained by titration. The silicate solution may be more difficult to keep in optimal condition since adsorption of carbon dioxide from the air can affect its performance. No information on coating weight is available, but it can probably be determined by standard acid stripping. This process demonstrated good corrosion resistance in the unpainted condition and passed wet paint adhesion testing (Ref 94).

Cerium Boehmite Processes. There are a number of processes based on developing a boehmite coating on aluminum surfaces either in the presence of cerium and other salts, or using the rare earth salts as seals (Ref 103, 105, 108). Like cerating, these treatments became prominent in the late 1980s and early 1990s. One of these cerium- base, boehmite growth treatments was developed by Mansfeld et al. (Ref 103). The term "stainless aluminum" was coined by Mansfeld to describe the process (Ref 109). Other boehmite processes have also been reported. For example, Kindler reported a process based on oxide growth in the presence of $CeCl_3$ alone or with lithium and aluminum nitrates (Ref 108). Hughes et al. (Ref 105) reported a process based on oxide growth in $Ce(NO_3)_3$, followed by a silicate seal. A further boehmite process was developed on oxide growth in the presence of $LiNO_3$ and $Al(NO_3)_3$ followed by sealing in $KMnO_4$. See the discussions of permanganates.

To the authors' knowledge, none of the boehmite processes based on cerium is currently under commercial development for the aluminum market. Part of the problem with the industrial application of the boehmite processes is that they usually require ten or more process steps, particularly for aerospace applications, with up to two requiring processing temperatures of 90 to 100 °C (195 to 212 °F).

The cerium-containing process solutions are slightly acidic to neutral and contain cerium nitrate or cerium chloride alone or with other salts. Sealing usually involves immersion in silicate solutions at elevated temperature, although silanes or permanganates have also been used (Ref 104). The cerium-molybdenum process (Ref 109) involving three different steps, which can be arranged in different orders, has been most studied. Oxide growth is involved in two process steps either following one another or separated by an anodic polarization in sodium molybdate solution. Alternatively, the first two steps involve oxide growth then anodic polarization. Performance of the cerium-molybdenum process is reported to be poor for the unpainted coating in neutral salt spray and paint adhesion is variable (Ref 93, 94).

Very little information is available on process control for these types of processes. Boehmite growth, however, is particularly sensitive to the presence of silicon in solution, which must be kept at low levels. Constant operation of baths close to boiling results in polymerization and condensation reactions of cerium solution species to form CeO_2 (Ref 110). Boehmite coatings are generally colorless or slightly iridescent, so it is not easy to determine the evenness of a coating on a part visually. Sealing can improve the color definition. For example, a silicate seal produces a purple to green iridescence. Because of the lack of color in the coating and the use of silicate or organic seals, coating weight determination by immersion in concentrated acid is problematic.

Characterization of the cerium-molybdenum process indicates that processing in hot aqueous cerium salt solutions generates a self-limiting oxide with the typical porous boehmite structure. The thickness of this layer is generally up to 1 μm. No additional oxide growth is observed after anodic polarization in molybdate solution. Anodic polarization may result in anodic growth over areas that have a thin oxide. The molybdate ions also penetrate the oxide, leaving available Mo^{6+} for repair, but some of the molybdate reacts with the cerium and is probably immobilized (Ref 111).

It seems likely that oxide growth occurs in a similar fashion to that described by Alwitt (Ref 112) with the cerium ions playing some modifying effect on oxide generation through incorporation of cerium species into the boehmite oxide. In addition, deposition of a cerium oxide layer over cathodic intermetallics may reduce the overall susceptibility of the surface to corrosion.

Sol-Gel Methods. Sol-gel processing has wide application in many industries outside metal finishing. It has gained interest in metal finishing, particularly for aerospace repair applications.

Aqueous sol-gel processes have been tried primarily for adhesive bonding applications (Ref 113) and anodizing/chromate conversion coating replacements (Ref 114) in the aerospace market. Products are offered by numerous suppliers. The chemistry of these coatings lies largely in the hydrolysis and condensation

reactions that occur on mixing metal alkoxides or a mixture of alkoxides and silanes in water. Processing is relatively simple, typically involving up to five steps. These usually include an alkaline clean, rinse, surface activation, rinse, coat, and dry. The drying stage can be at elevated temperatures. Variations from this sequence of steps occur in the activation and drying stages.

The coating solutions generally contain aluminum, titanium, or zirconium alkoxides mixed with silicon alkoxides, polymers or silanes (Ref 114). The hydrophilic components of the condensed film gravitate toward the metal, whereas the hydrophobic components gravitate toward the external surface. In this case, the number of coatings applied can be important since the final coat has to have the organic components exposed to promote good paint adhesion. Hydrolysis of the complexes on the metal surface is quite common, and the inorganic polymerization yields a chemically bonded conversion coating. However, organic solvents are emitted during this "curing" reaction.

Since the majority of these coatings are sprayed or swabbed, traditional process control is not necessary. The processing solutions, however, need to be prepared on a batch basis and have a limited lifetime. It is important to age the solutions prior to use to allow polymerization of the alkoxides and silanes. The differential rate of polymerization between metal alkoxides and the silicon-containing components is important for the final film structure. Thin coatings are hard to characterize, but if the coating thickness is significant, then eddy-current measurement can be used to determine the thickness. These coatings demonstrate good adhesion for paints and adhesives as long as the correct functional groups are included to bond to the paint. They are claimed to provide good corrosion resistance under paint in scribe tests on a range of substrates.

Models of the deposition process propose that, upon immersion into the coating solution the activated, hydrophilic aluminum oxide surface reacts preferentially with the aluminum, titanium, and zirconium alkoxides over the silicon alkoxides. These are less stable and form an oxide layer on the surface adjacent to the metal surface. As the reaction proceeds, the silicon-containing components are incorporated to a greater extent, with the external surface containing mostly the organic silicon components and functional groups appropriate for the adhesive or primer attachment. With multiple-step coating, the hydrophobic top surface of the first layer attracts the organic components of the fresh sol-gel solution. This means that the external surface of the second layer may be hydrophilic, which is undesirable for the applications of some paint systems and adhesives.

Manganese-base coating systems are described in the following paragraphs.

Oxide Growth Containing Manganese in Alkaline Conditions. One of the earliest patents for the boehmite permanganate processes was granted in 1987 (Ref 115). This process was developed into both immersion and steam treatments, with processing temperatures close to 100 °C (212 °F) or above. At these elevated temperatures boehmite production will be involved, and metal salts incorporated into the bath act to modify the properties of the boehmite coating. The process is available commercially.

The boehmite steam version of the permanganate processes are being used for coating U.S. post boxes (Ref 116), but has also been involved in a number of trials for aerospace applications (Ref 92, 94). There are two versions of this process. The first involves 10 steps including clean, rinse, deoxidation, rinse, boil in deionized water, oxide sealing, rinse, permanganate treatment, rinse, and silicate seal. The second was a four- step process, involving an alkaline clean, rinse, then a treatment in alkaline permanganate solution, and rinse.

For the 10-step process, the oxide-sealing step contains aluminum and lithium nitrate and is operated at boiling; the permanganate step contains potassium permanganate at 60 °C (140 °F) and the silicate seal at boiling. All these steps are neutral to alkaline with the pH of permanganate coating solution in the range 7 to 12.5 (Ref 117). The permanganate-step (five-step process) contains potassium permanganate and a borate to act as a buffer and is operated at 70 °C (158 °F) (Ref 115).

As for other boehmite processes, very little information is available on process control, although it is reported to be simple due partly to the low concentrations of ingredients used in the baths (Ref 92). As noted earlier, boehmite growth is sensitive to the presence of silicon in solution, which must be kept at low levels. Boehmite coatings are generally colorless or slightly iridescent so it is not easy to visually determine the evenness of a coating on a part. The presence of manganese in the coating may, however, impart a slight brown appearance to the coating. Silicate sealing may increase the intensity of the iridescence of the coating.

The reported paint adhesion results were generally good, although there was some uncertainty over wet paint adhesion, but the results of corrosion resistance were mixed, with good and poor results reported (Ref 92, 93, 94).

Manganese Conversion Coatings. Concurrently with the development of the manganese- containing boehmite coatings has been the development of a manganese conversion coating produced from acidic permanganate-containing solutions (Ref 118). The process is available commercially.

The conversion coating versions are shorter; they are being tried for aerospace applications and show some promise. The conversion coating process involves an alkaline clean, rinse, deoxidize, rinse, permanganate conversion coating, rinse, and for aerospace applications an organic seal and dry.

The conversion coating bath is acidic (pH 2.5–4.0) and contains aluminum nitrate and permanganate ions (Ref 118); the preferred operating temperature is 60 °C (140 °F). The acidic conversion coating process also has an optional organic seal step to improve paint adhesion, particularly with waterborne paints. These coatings typically give performance similar to chromate under waterborne paint, but the corrosion resistance of either the sealed or unsealed versions is usually poor.

Process control for manganese determination in the acidic process can be done using a ferric sulfate/sulfuric acid titration. Since the conversion coating bath is only slightly acidic, there is little aluminum dissolution and bath performance remains good until the permanganate begins to become depleted, at which stage the bath is discarded. The coating has a colorless to golden/brown color, so quality control on the process line can be performed visually. Coating weight determination of the manganese-containing, inorganic part of the coating can be carried out using standard techniques; however, total coating weight including the polymeric seal becomes more problematic.

A model of the conversion coating covering the matrix is presented in Fig. 12. Characterization of the acidic permanganate conversion process has revealed that a mixed manganese and aluminum oxide layer up to 70 nm (2.75 μin.) develops on the surface of the alloy for typical processing times. The thickness of this aluminum/manganese oxide increases with immersion time, but appears to display a logarithmic growth behavior and after 4 min processing approaches a limiting thickness (Fig. 12b). The oxide coating appears to be made of fine particles (Fig. 12c), whose coverage of the surface increases with immersion. The manganese incorporated into the coating was mostly in the Mn(VII) state, suggesting that the permanganate ion is incorporated into the surface aluminum oxide. The seal increases the thickness markedly and improves the corrosion resistance.

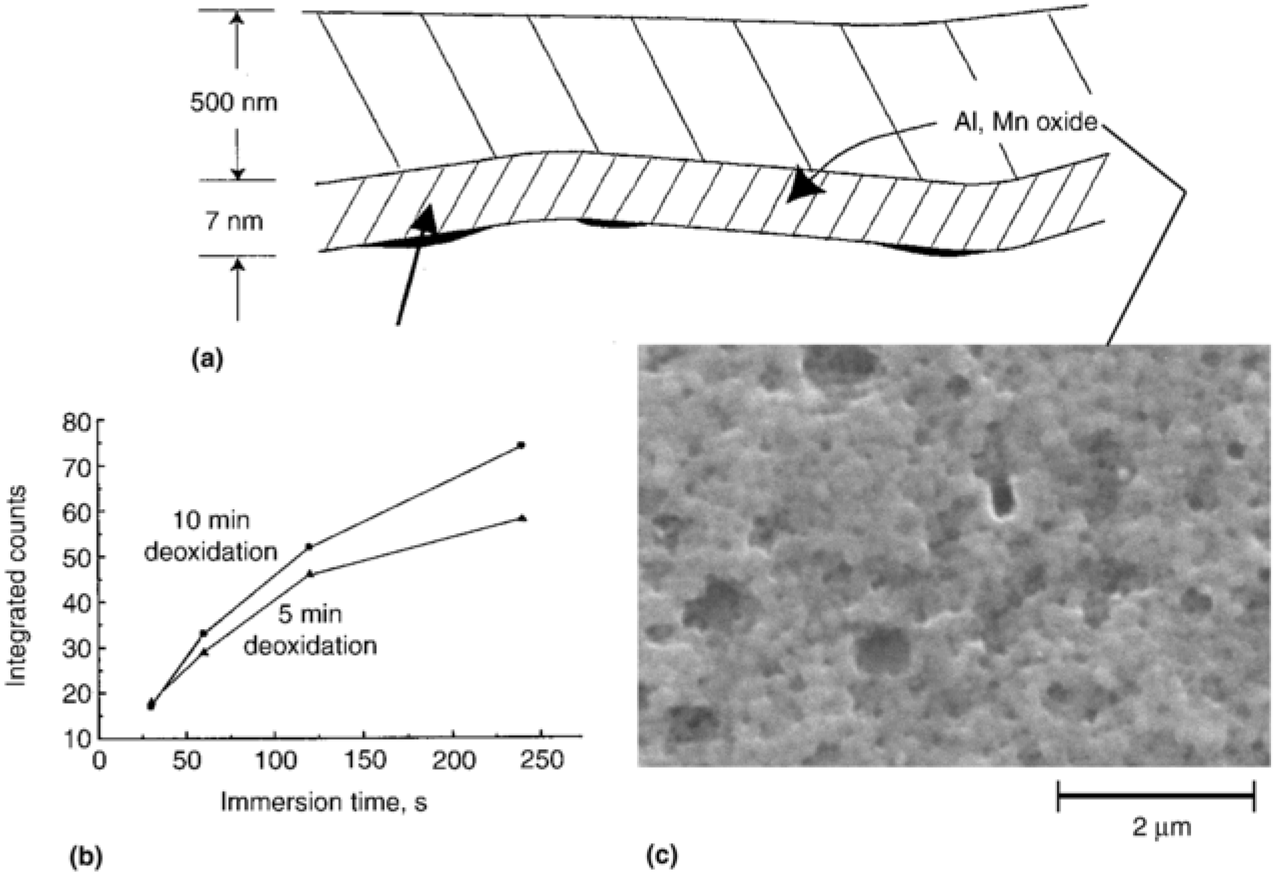

Fig. 12 Manganese coating produced in the acidic process with a polymeric topcoat. (a) Schematic. (b) Increase in manganese counts as a function of immersion time as measured by Rutherford backscattering spectroscopy. (c) Plan view (secondary electron image)

This suggests that the deposition process is relatively simple. Upon immersion of the freshly deoxidized surface, there is oxidation of the surface by either nitrate or permanganate ions, which results in thickening of the oxide. Given that little Mn(III) has been detected in the coating, it seems likely that the nitrate assists in oxide generation. During oxide growth, permanganate ions become incorporated into the coating.

Cobalt-base conversion coatings are commercially available for the marine and automotive industry and have been tried for aerospace applications for a number of years. It has given excellent adhesion and corrosion resistance in automotive applications. The marine version of the cobalt process involves an inorganic conversion coating step followed by an organic seal, for other applications (e.g., aerospace) an inorganic seal is preferred for better corrosion resistance in the unpainted condition. Processing is relatively simple, involving up to eight or nine steps. These include an alkaline clean, rinse, deoxidize, rinse, conversion coat, rinse, seal, and rinse. A drying step is required with the polymer seal. The conversion coat and seal baths are operated at 60 °C (140 °F).

According to the patent literature, the conversion coating solutions generally contain a complex cobalt (preferably cobalt hexanitrite ion) generated through the reaction of a metal nitrite with a Co(II) salt, hydrogen peroxide, and an accelerator (Ref 119). The commercially available process is based on carboxylates and nitrate complexes (Ref 120). This bath is free of fluoride and operates at neutral pH. Nonetheless, there is some etching of the aluminum since peroxide, dissolved oxygen, and Co^{3+} are powerful oxidizers in water at pH 7.0. Treatment of car wheels, for example, reveals that very little aluminum dissolves in the bath, but it is incorporated into the coating. The inorganic seal can contain a range of salts, but vanadate and tungstate oxyanions are preferred in a solution that operates at neutral pH. A polymeric version of the seal has also been used for marine applications. Both types of seals are designed to improve corrosion resistance and overlayer adhesion, although the paint adhesion for the inorganic and polymeric seals may vary with the paint system.

The reported performance of the cobalt processes is mixed with both poor corrosion resistance in neutral salt spray in the unpainted condition and poor paint adhesion (Ref 92) to good performance on both accounts (Ref 93, 94). It is important to realize that the best chromium-free products pass unpainted salt fog about 50 to 80% of the time; however, chromate consistently passes 90 to 95% of the time on specified alloys. Due to the enormous potential liability, only painted applications will be quickly converted to chromium-free in aerospace uses.

Process control for the cobalt-containing solution is carried out by titration for cobalt levels and addition of additive as necessary. The vanadate sealing solution can be titrated using ferrous ammonium sulfate in the presence of sulfuric acid and ferroin. Coating weights can be determined by the normal acid-stripping processes for the version using the inorganic seal, but may require a two-step process for the organically sealed version. In this latter case, there would be an initial alkaline strip to remove the organic seal followed by the acid strip (Ref 92). Coating weights are typically 215 to 2580 mg/ m^2 (20 to 240 mg/ft^2).

Earlier reports on the structure of the cobalt- base coating produced from $Co(NO_3)_2$ baths indicated a layered (or possibly graded) structure. An alumina layer develops adjacent to the metal that gradually changed to a mixture of CoO, Co_3O_4, and Co_2O_3, and finally to a top layer composed of Co_3O_4 and Co_2O_3. The total layer thickness is estimated to be 1200 to 1400 nm (47 to 55 μin.) (Ref 119). A model of the cobalt conversion coating/vanadate seal processes that develops on 2024-T3 aluminum is presented in Fig. 13. An open porous structure develops on the surface during immersion in the cobalt-containing bath (see SEM inset in Fig. 13). Rutherford backscattering spectroscopy (RBS) analyses indicate that cobalt is incorporated into the aluminum oxide coating, and determination of width of the cobalt peak indicates that the oxide thickness is typically 500 nm (20 μin.) after 10 min processing (see inset). Treatment in the vanadate solution results in partial filling of the porous surface oxide containing (see inset), but RBS analyses indicate that no additional increase in thickness results from treatment in the vanadate solution.

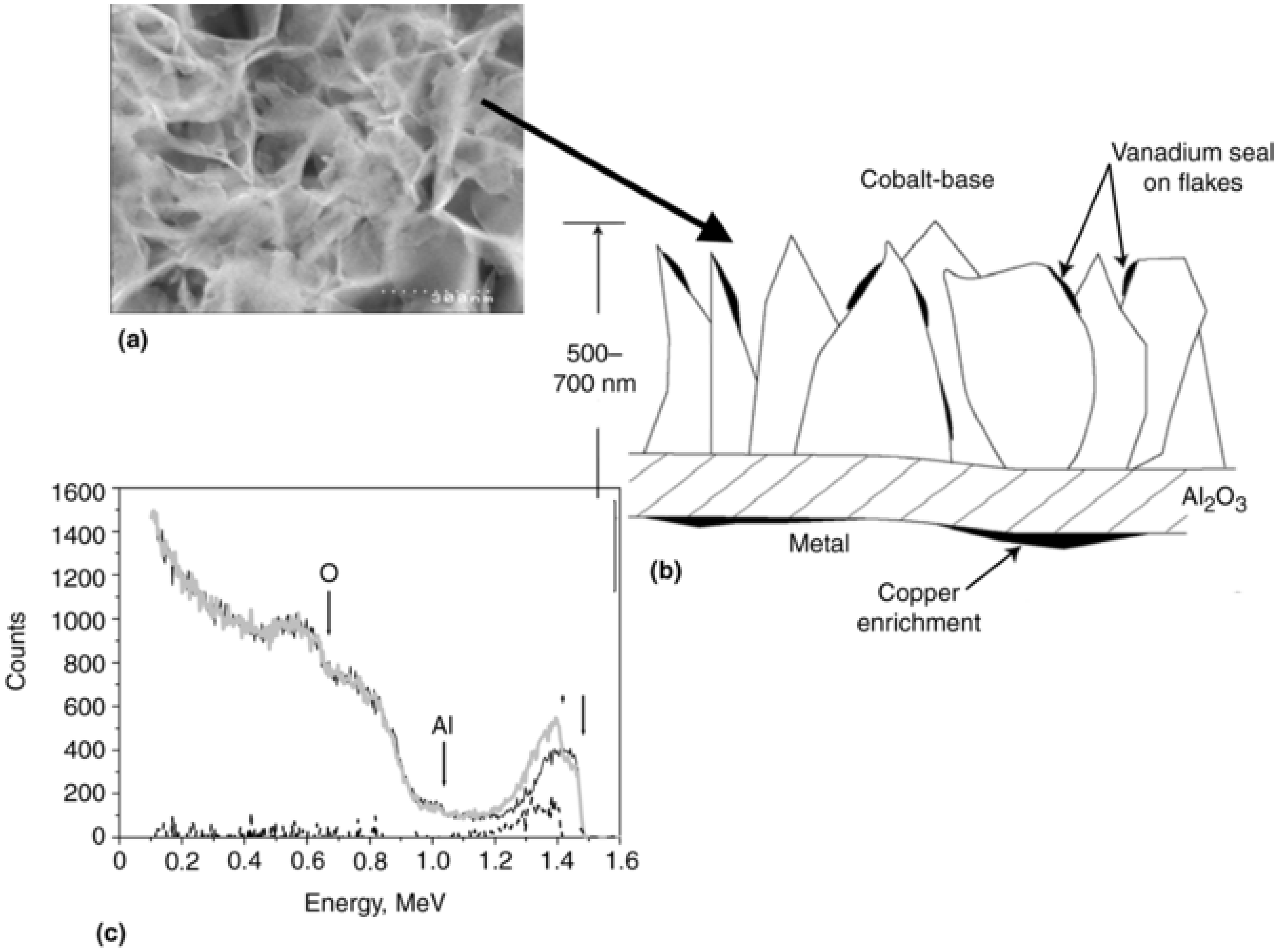

Fig. 13 (a) (b) Structure of the surface oxide after treatment of deoxidized 2024-T3 in Alodine 2000 at 60 °C (140 °F) for 10 min followed by sealing in Deoxylyte NC 200. (b) In the Rutherford backscattering spectroscopy inset, the black is the cobalt step and the gray is cobalt and vanadium steps. A difference spectrum in which the cobalt spectrum is subtracted from the cobalt and vanadium spectrum is displayed beneath the other two. This difference peak is the vanadium spectrum.

Based on the characterization studies, it is proposed that the conversion coating develops in the following manner. Upon immersion into the coating solution, the aluminum oxide on the surface of the metal thickens under the combined influences of thermal activation and oxidant in the solution. During processing, which is ultimately self-limiting, significant amounts of cobalt ions are incorporated into the oxide structure. Immersion in the vanadate-containing solution results in reaction with the surface and deposition of vanadium oxides within the cobalt/ aluminum oxide pores.

Molybdenum, in the form of molybdate oxyanions, has been tried as conversion coatings, alone and as an additive to other processes used on aluminum (see the cerium-molybdenum and hydrotalcite processes) (Ref 121). As a conversion coating, most of the published work has examined deposition on tin and zinc for tinplate and galvanized product, respectively. There are a number of manufacturers who are developing processes for the tin, zinc, and aluminum markets. Molybdate-base conversion coatings have met with little success on aluminum.

Many of these processes are phosphate-base and acidic (Ref 122), while others do not contain phosphate and operate at closer to neutral pH (Ref 123). Processing can contain up to six steps if a seal is used. Goodreau reports a process that involves a clean, rinse, conversion coat, dry, polymer seal, and dry (Ref 124). The polymer seal provides most of the corrosion protection.

Simpler process formulations have also been investigated in which the conversion coating solutions contain sodium molybdate or molybdic acid and may contain buffer or acid to adjust the pH (Ref 121, 125). The process bath is operated at pH 4 to 6, with better performance tending toward the lower end of the range. Coatings can be deposited near 20 °C (68 °F) in less than 10 min.

No details are available for process control, but it seems likely that molybdenum levels could be monitored by titration. Given the sensitivity to pH, this would also need to be monitored. For the formulations that operate near neutral pH, aluminum buildup may not be a problem. Quality control for coating weight is likely to be achieved using the normal one-step acid-stripping processes for the inorganic version. The performance of the coatings is variable, as summarized by Nylund (Ref 100). Coating weights for the polymeric version are typically 35 mg/ m^2 (3.3 mg/ft^2) measured as molybdenum atoms (Ref 124).

Characterization studies of the molybdenum- base conversion coatings are not as common as some other of the chromate-free coatings and has often focused on the use of XPS to determine the oxidation state of the molybdenum incorporated into the coating (Ref 121). The incorporation into the coating of oxidation states lower than Mo(VI) has been seen as detrimental and related to the pH of formation of the coating (Ref 123). In simple molybdate solutions at pH 3 and 20 °C (68 °F), the coating thicknesses were reported to be 0.1 μm (0.004 mil) for 5 min immersion and 2.0 μm (0.079 mil) for 30 min immersion. No doubt, the thickness will depend on the solution composition, deposition pH, and immersion time.

Hydrotalcite coatings take their name from a class of layered, claylike mineral compounds typified by the compound hydromagnesite, $Mg_6Al_2(OH)_{16}{\cdot}CO_3{\cdot}4H_2O$ (Ref 126, 127), which is naturally occurring. Synthetic hydrotalcite compounds can be formed as a coating on aluminum alloy surfaces by contact with an alkaline lithium salt solution. This leads to the formation of polycrystalline compounds containing the hydrolithisite compound $Li_2[Al_2(OH)_6]_2{\cdot}X{\cdot}nH_2O$, where X is one of several inorganic anions such as CO_3^{2-}, NO_3^-, or Cl^- (Ref 128). Patents covering the hydrotalcite coating process (Ref 129) and sealing processes (Ref 130) exist. Variants of the coating process are suitable for architectural, aerospace, and perhaps automotive applications, but none are commercially available at the present time.

As with many conversion coating processes, the hydrotalcite process involves degreasing and deoxidation steps prior to coating. Coating is carried out by immersion or spray of the coating bath solution on a metal surface. Elevating the temperature of the bath above 40 °C (104 °F) enhances coating formation kinetics and baths yielding highly corrosion-resistant coatings. Sealing for enhanced corrosion resistance is optional and is carried out in a second step. Sealing with a wide range of compounds has been reported (Ref 131, 132, 133). Noteworthy improvements in corrosion resistance are obtained by sealing in cerium, manganese, or magnesium acetate solutions (Ref 131, 132). A two-step process has been developed for removing copper contamination from coatings formed on aluminum-copper-base alloys (Ref 134). Use of oxidizing agents such as nitrates or persulfate accelerates the coating formation process and leads to coatings with excellent corrosion resistance on Al-Cu-Mg alloy substrates (Ref 135).

In terms of appearance, hydrotalcite coatings are white or gray and do not fully obscure the luster of the underlying metal. In some cases, coated surfaces have a matte finish. When sealed, they may take on a color characteristic of the sealing agent. In scanning electron micrographs, the coating exhibits a distinctive morphology consisting of a mass of intersecting bladelike crystals that form a continuous layer across the surface of the metal (Fig. 14). Coating cross sections reveal that the coating is really duplex in nature, consisting of a polycrystalline outer layer and an inner barrier layer. The inner layer is poorly crystalline and contains lithium from the coating bath.

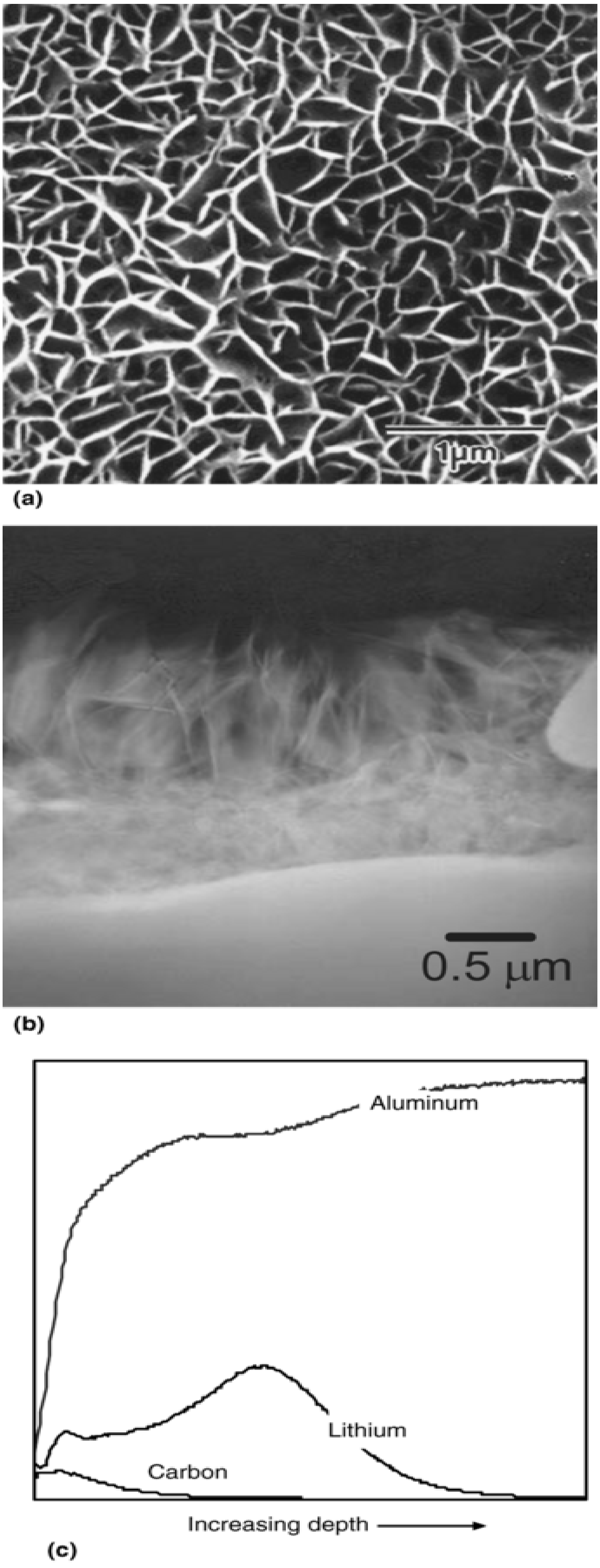

Fig. 14 (a) Plan view scanning electron micrograph of hydrotalcite coating. (b) Cross-sectional scanning transmission electron micrograph of hydrotalcite illustrating the duplex nature of the film. (c) SIMS depth profile of a hydrotalcite coating

Hydrotalcite coatings provide good corrosion resistance on commercially pure aluminum, aluminum-manganese, and Al-Mg-Si alloys. Use of oxidizing bath chemistries or sealing is necessary to achieve acceptable levels of corrosion resistance on Al-Cu-Mg and Al-Zn-Mg-Cu alloys. Coatings for casting alloys with high alloying element content have not been developed. Organic coatings will adhere to hydrotalcite-coated surfaces. Care must be taken not to overcoat the substrate. Low coating adhesion, disbondment, and filiform corrosion will result if hydrotalcite coatings are too thick or contain soluble constituents (Ref 136).

Self-Assembled Monolayers (SAM). Self- assembling of molecules on metal surfaces represents a newer area of metal finishing. The process has been demonstrated to work well on aluminum-magnesium alloys in automotive applications and is likely to see use in the European automotive market, but it is used in combination with zirconium and titanium processes in the United States.

This coating process works on the following fundamental principles. Polar compounds are attracted to metal surface. When this functionality is combined with a long chain alkyl group, the attraction of the polar group for the metal surface remains intact while the organic chains tend to line up pointing away from the surface. At the other end of the molecule, a second group can be added to promote overlayer adhesion. Thus, the molecules "self-assemble" on the surface.

Little is available on the processing solutions or process control. The conversion coating solutions can contain a range of different chemicals in different processes. The more favored polar functional groups for aluminum involve phosphates or perfluorinated carboxylic acids (10 to 18 carbons).

Characterization studies of the adsorption of phosphonic acids on aluminum and AlMg1 indicated that the adsorption takes place in approximately 60 s with the phosphate group oriented toward the surface of aluminum oxide. Adsorption also occurred on iron-containing inclusions. The process of self-assembly, however, took up to three days (Ref 137).

Organic Coatings. Another field of research into chromate alternatives examines the deposition or even generation of polymers on the surface of a metal. This is covered elsewhere in this Volume. The use of polymers as sealants for conversion coatings has been discussed previously.

Conducting Polymers. Research into conducting polymers gained notoriety in 1977 with the publication of a paper describing the generation of polyacetylene polymer with an electrical conductivity many orders of magnitude greater than ordinary polymers (Ref 138).

The current focus of conducting polymers includes polypyrroles, polythiophenes, and particularly polyaniline (Ref 139). Much of the work is targeted on electrochemical and chemical deposition onto ferrous metals. Formulations produce thick coatings (up to 20 μm, or 0.8 mil), more akin to primers than to conversion coatings. Several forms are available commercially for different applications.

Characterization of the coating reveals that it is produced by chemical reaction of iron with polyaniline dispersed in a polymer matrix, resulting in the formation of αFe_2O_3 up to 1 μm (0.04 mil) thick with up to 20 μm (0.8 mil) of conducting polymer/matrix above the oxide (Ref 140). The dispersion itself contains polyaniline particles about 70 nm (2.75 μin.) in diameter, as the dispersion is in sufficient concentration to form a "chain of pearls" in the coating, thus providing the conducting pathways.

The protection is reported to be imparted in two ways on ferrous metals. First, the application of the conducting polymer ennobles the surface by shifting the potential many hundreds of millivolts. Second, the polyaniline, known as the emeraldine salt is reduced to the leucoemeraldine base oxidizing the underlying metal [Fe metal to Fe(II)]. Cathodic reactions occur resulting in the reduction of oxygen and further oxidation of Fe(II) to Fe(III) generation of OH^- for deposition of Fe_2O_3 and oxidation of leucoemeraldine to emeraldine via an emeraldine base. Thus, the polyaniline acts as a mediator in the formation of a passive layer (Ref 140). A similar mechanism is likely to ensue for aluminum alloys.

Silanes. For the purposes of metal finishing, silanes that can be applied to metals fall in the category of trialkoxy esters of the form R-Si- $(OR')_3$ where R is an alkyl ligand with an organofunctional group and OR' is usually a methoxy or epoxy ligand (Ref 141, 142). Silanes have been used successfully on steel, galvanized products, and aluminum alloys, and at least one manufacturer offers products in this area (Ref 141).

The use of silanes for metal finishing is still a developing area, and care needs to be taken in choosing and preparing the silane solution for a particular application. Parameters that affect the bonding are the surface energies of the oxides of the metals to be treated, the acidity of the organofunctional group, and its relationship to the basic surface hydroxyl groups and the makeup of the silane solution that may rapidly move into a condensation reaction phase. The earliest successful silanes include γ-APS and γ-UPS, but more recently bis-

1,2-(triethoxysilyl)ethane (BTSE) and bis-1,2-(triethoxysilylpropyl) tetrasulfide (BTESPT), also known as sulfane, have shown more general applicability.

Silane solutions are prepared on a batch basis as required. Pretreatment for silane coatings is relatively simple, involving an organic degrease (acetone/ethanol) followed by an alkaline clean then rinse. The silane solution tends to be dilute and acidic (pH 4 to 6). Dilution and an acid environment limit the amount of condensation reaction, but hydrolysis of the first methoxy or ethoxy group is rapid.

Reaction with the surface is proposed to happen via elimination reactions between the silanol groups and surface hydroxyl groups resulting in metal-oxygen-silicon bonds. With the BTSE, the coating is strengthened by the formation of siloxane bonds (Si-O-Si) bridging between the BTSE molecules. The thickness of the surface coatings tends to be in the range 30 to 100 nm (1.18 to 3.93 μin.).

BTSE films alone provide good corrosion resistance since there is a lack of organofunctional groups; the surface silanol groups tend to form siloxane bonds as a function of aging. A quick second silane treatment (e.g., γ-APS) can be applied to the BTSE surface to produce a surface with better adhesion to paint systems. The BTSE/γ-APS film has given filiform corrosion resistance in auto applications.

References cited in this section

92. B. Meyers, S. Lynn, and E. Jang, "Alternatives to Chromate Conversion Coating at McClellan Air Force Base," MITRE, 1993

93. "Alternatives to Chromium for Metal Finishing," Final NCMS Report 0273RE95, National Center for Manufacturing Sciences, 1995

94. "Alternatives to Chrome Conversion Coatings on Aluminum Alloys 2024, 6061, 7075, and Ion Vapor Deposited Aluminum on Steel (Potential Alternatives Report)," Web page, http://www.jgapp.com/parhughhc.htm, National Defense Center for Environmental Excellence, 1998

95. M. Kendig and R. Buchheit, Surface Conversions of Aluminum and Ferrous Alloys for Corrosion Resistance, *Proc. Corros./ 2000 Res. Top. Symposium,* NACE International, 2000, p 1

96. J. Ouyang and W.L. Harpel, "Monitoring of Coating Weight in Dried-in-Place Non- Chrome Polyacrylamide Based Treatments for Metals," U.S. Patent No. 5,401,333, 28 March 1995

98. L.S. Sander, E.M. Musingo, and W.J. Neill, "Nonchromate Bath for the Primer and Anticorrosion Coating on Aluminum Alloy," U.S. Patent No. 4,921,552, 1 May 1990

99. S.E. Dolan, "Chromium-Free Conversion Coating Composition and Process for Treating Metals," U.S. Patent No. 5,449,415, 12 Sept 1995

100. A. Nylund, *Alum. Trans.,* Vol 2, 2000, p 121

101. P.D. Deck and D.W. Reichgott, *Met. Finish.,* Vol 90, 1992, p 29

102. S.G. Hardin, A.E. Hughes, and K.J.H. Nelson, "Process and Solution for Providing a Conversion Coating on a Metallic Surface I," U.S. Patent No. 01/71058A1

103. F.B. Mansfeld, H. Shih, and Y. Wang, "Method for Creating a Corrosion Resistant Aluminum Surface," U.S. Patent No. 90/556,109, 16 March 1990

104. R.N. Miller, "Non-Toxic Corrosion Resistant Conversion Coating for Aluminum and Aluminum Alloys and the Process for Making the Same," U.S. Patent No. 5,221,371, 22 June 1993

105. K.J.H. Nelson, R.J. Taylor, A.E. Hughes, B.R.W. Hinton, M.J. Henderson, L. Wilson, and S.A. Nugent, "Conversion Coating and Process and Solution for its Formation," U.S. Patent No. 6,022,425, 8 Feb 2000

106. B. Hinton, A. Ryan, P. Trathen, L. Wilson, and B. Williams, 12, 1985

107. A.E. Hughes, S.G. Hardin, K.W. Wittel, and P.R. Miller, Surface Conversions of Aluminum and Ferrous Alloys for Corrosion Resistance, *Proc. Corros./2000 Res. Top. Symposium,* NACE International, 2000, p 47

108. A. Kindler, "Coating of Aluminum with Chromium-Free Protective Layer," U.S. Patent No. 5,192,374, 9 March 1993

109. F. Mansfeld and Y. Wang, *Mater. Sci. Eng., A,* Vol 51, 1995

110. V. Briois, C.E. Williams, H. Dexpert, F. Villain, B. Cabane, F. Deveuve, and C. Magnier, *J. Mater. Sci.,* Vol 28, 1993, p 5019

111. A.E. Hughes, J.D. Gorman, and P.J.K. Paterson, *Corros. Sci.,* Vol 38, 1996, p 1957

112. R.S. Alwitt, Vol 121, 1974, p 1322

113. H.E. Hager, K.Y. Blohowiak, J.H. Jones, C.J. Johnson, C.M. Wong, R.S. Taylor, and R.L.J. Cook, "Chromate-Free Protective Coatings for Aircraft," U.S. Patent No. 5,866,652, 2 Feb 1999

114. H. Zheng, Y. Du, M. Damron, J. Wright, and M. Tang, *Met. Finish.,* Vol 96, 1998, p 35

115. J.W. Bibber, "Corrosion-Resistant Aluminum Coating," U.S. Patent No. 4,711,667, 8 Dec 1987

116. J.W. Bibber, *Met. Finish.,* Vol 91, 1993, p 46

117. J.W. Bibber, "Multistage Conversion Coating of Aluminum Alloys," U.S. Patent No. 4,988,396, 29 Jan 1991

118. J.W. Bibber, "Conversion Bath with Nitrate for Corrosion-Resistant Coating on Aluminum Alloys," U.S. Patent No. 5,554,231, 10 Sept 1996

119. M.P. Schriever, "Nonchromate Cobalt Complex Conversion Coating and Primer in Painting," U.S. Patent No. 488,430, 1992

120. M.P. Schriever, "Conversion Bath for Chromate-Free Coating with Cobalt Oxide on Aluminum Alloy Substrates," U.S. Patent No. 5,873,953, 23 Feb 1999

121. G.D. Wilcox, D.R. Gabe, and M.E. Warwick, *Trans. Inst. Met. Finish.,* Vol 66, 1988, p 89

122. J. Ouyang and W.L. Harpel, "Non-Chromate Acidic Bath for Passivation of Galvanized Metal Surfaces," U.S. Patent No. 5,344,505, 6 Sept 1994

123. C.M. Rangel, A. Simoes, and R.C. Newman, *Port. Electrochim. Acta,* Vol 15, 1997, p 383

124. B.H. Goodreau, "Phosphoric Acid Bath with Molybdenum Ions for Passivation and Priming of Zinc and/or Aluminum Surface in Coating with Acrylic Film," U.S. Patent No. 9,727,001

125. G.D. Wilcox and D.R. Gabe, *Met. Finish.,* Vol 86, 1988, p 71

126. S. Miyata, *Clay and Clay Miner.,* Vol 23, 1975, p 369

127. H.F.W. Taylor, *Min. Mag.,* Vol 39, 1973, p 377

128. R.G. Buchheit, M.D. Bode, and G.E. Stoner, *Corrosion,* Vol 50, 1994, p 205

129. R.G. Buchheit and G.E. Stoner, "Method for Increasing the Corrosion Resistance of Aluminum and Aluminum Alloys," U.S. Patent No. 5,266,356, 30 Nov 1993

130. R.G. Buchheit and M.A. Martinez, "Corrosion Protective Coating for Metallic Materials," U.S. Patent No. 5,756,218, 26 May 1998

131. R.G. Buchheit, S.B. Mamidipally, P. Schmutz, and H. Guan, Active Corrosion Protection in Chromate and Chromate- Free Conversion Coatings, in *Surface Conversion for Aluminum and Ferrous Alloys,* NACE International, 2000, p 67

132. R.G. Buchheit, S.B. Mamidipally, P. Schmutz, and H. Guan, *Corrosion,* Vol 58, 2002, p 3

133. R.G. Buchheit, M.A. Martinez, L.P. Montes, N. Cella, G.E. Stoner, and S.R. Taylor, "inorganic Cr-Free Conversion Coatings for High Corrosion Resistance and Low Electrical Contact Resistance," Paper No. 98212, CORROSION/98, NACE International, 1998

134. R.G. Buchheit, *J. Appl. Electrochem.,* Vol 28, 1998, p 503

135. W. Zhang and R.G. Buchheit, *Corrosion,* Vol 58, 2002

136. R.B. Leggat, W. Zhang, R.G. Buchheit, and S.R. Taylor, *Corrosion,* Vol 58, 2002, to be published

137. C. Bram, C. Jung, and M. Stratmann, Vol 358, 1997, p 108

138. H. Shirakawa, L.E., A. MacDiarmid, C. Chiang, and A. Heeger, 578, 1977

139. J.O. Iroh, *Surf. Eng.,* Vol 17, 2001, p 265

140. B. Wessling, *Chem. Innovation,* Vol 31, 2001, p 34

141. T.F. Child and W.J. Van Ooij, *Trans. Inst. Met. Finish.,* Vol 77, 1999, p 64

142. W.J. Van Ooij and D. Zhu, Surface Conversions of Aluminum and Ferrous Alloys for Corrosion Resistance, *Proc. Corros./ 2000 Res. Top. Symposium,* NACE International, 2000, p 96

R.G. Buchheit and A.E. Hughes, Chromate and Chromate-Free Conversion Coatings, *Corrosion: Fundamentals, Testing, and Protection,* Vol 13A, *ASM Handbook,* ASM International, 2003, p 720–735

Chromate and Chromate-Free Conversion Coatings

R.G. Buchheit, The Ohio State University; A.E. Hughes, CSIRO

Acknowledgment

The support of the Strategic Environmental Research and Development Program during preparation of this article is gratefully acknowledged.

R.G. Buchheit and A.E. Hughes, Chromate and Chromate-Free Conversion Coatings, *Corrosion: Fundamentals, Testing, and Protection*, Vol 13A*, ASM Handbook*, ASM International, 2003, p 720–735

Chromate and Chromate-Free Conversion Coatings

R.G. Buchheit, The Ohio State University; A.E. Hughes, CSIRO

References

1. T. Biestek and J. Weber, *Electrolytic and Chemical Conversion Coatings,* Porticullis Press Limited-Redhill, Surrey, UK, 1976
2. S. Wernick, R. Pinner, and P.G. Sheasby, *The Surface Treatment and Finishing of Aluminum and its Alloys,* Vol 1, 5th ed., ASM International, 1987, p 220
3. O. Bauer and O. Vogel, German Patent Specification, 226776, 1923
4. O. Bauer and O. Vogel, German Patent Specification, 423758, 1923
5. W. Marchand, *Electroplat. Met. Finish.,* Vol 14, 1961, p 439
6. S. Spring and K. Woods, *Met. Finish.,* Vol 79, 1981, p 49
7. G.W. Ostrander, *Plating,* Vol 38, 1951, p 1033
8. J.N.J. Newhard, *Met. Finish.,* Vol 70, 1972, p 69
9. M. Krumploc and J. Rocek, *J. Am. Chem. Soc.,* Vol 101, 1979, p 3206
10. P. Lay and A. Levina, *J. Am. Chem. Soc.,* Vol 120, 1998, p 6704
11. P. O. O'Brien and A. Kortenkamp, *Transit. Met. Chem.,* Vol 20, 1995, p 636
12. D. Stearns and K. Wetterhahn, *Chem. Res. Toxicol.,* Vol 7, 1994, p 219
13. Y. Suzuki and K. Fukuda, *Arch. Toxicol.,* Vol 64, 1990, p 169
14. Y. Suzuki, *Ind. Health,* Vol 28, 1990, p 9
15. J.W. Bibber, *J. Electrochem. Soc.,* Vol 91, 1993, p 46
16. C.F. Baes and R.E. Mesmer, *Hydrolysis of Cations,* Wiley & Sons, 1976, p 211
17. F.W. Eppensteiner and M.R. Jenkins, Chromate Conversion Coatings, *Met. Finish.,* Guidebook and Directory Issue, 1999, p 494
18. A. Katzman, G. Malouf, R. Bauer, and G.W. Stupian, *Appl. Surf. Sci.,* Vol 2, 1979, p 416

19. L. Xia and R.L. McCreery, *J. Electrochem. Soc.,* Vol 146, 1999, p 3696

20. P.L. Hagans and C.M. Haas, *Surf. Interface Anal.,* Vol 21, 1994, p 65

21. F.W. Lytle, R.B. Greegor, G.L. Bibbins, K.Y. Blohowiak, R.E. Smith, and G.D. Tuss, *Corros. Sci.,* Vol 37, 1995, p 349

22. J.A. Treverton and N.C. Davies, *Met. Technol.,* Oct 1977, p 480

23. J.A. Treverton and M.P. Amor, *Trans. Inst. Met. Finish.,* Vol 60, 1982, p 92

24. W.R. McGovern, P. Schmutz, R.G. Buchheit, and R.L. McCreery, *J. Electrochem. Soc.,* Vol 147, 2000, p 4494

25. A.E. Hughes, R.J. Taylor, and B.W.R. Hinton, *Surf. Interface Anal.,* Vol 25, 1997, p 223

26. K. Asami, M. Oki, G.E. Thompson, G.C. Wood, and V. Ashworth, *Electrochim. Acta,* Vol 32, 1987, p 337

27. M.W. Kendig, A.J. Davenport, and H.S. Isaacs, *Corros. Sci.,* Vol 43, 1993, p 41

28. G.M. Brown, K. Shimuzu, K. Kobyashi, G.E. Thompson, and G.C. Wood, *Corros. Sci.,* Vol 34, 1993, p 1045

29. W. Zhang and R.G. Buchheit, *J. Electrochem. Soc.,* Vol 149, 2002, p B357

30. P. Campestrini, E.P.M.V. Westing, and J.H.W. deWit, *Electrochim. Acta,* Vol 46, 2001, p 2553

31. J. Wan, G.E. Thompson, K. Lu, and C.J.E. Smith, *Physica B,* Vol 208, 209, 1995, p 511

32. D. Arrowsmith, J.K. Dennis, and P. Sliwinski, *Trans. Inst. Met. Fin.,* Vol 62, 1984, p 117

33. X. Sun, R. Li, K.C. Wong, K.A.R. Mitchell, and T. Foster, *J. Mater. Sci.,* Vol 36, 2001, p 3215

34. J.R. Waldrop and M.W. Kendig, *J. Electrochem. Soc.,* Vol 145, 1998, p L11

35. G.M. Brown, K. Shimuzu, K. Kobayashi, G.E. Thompson, and G.C. Wood, *Corros. Sci.,* Vol 33, 1992, p 1371

36. J.C. Brinker and G.W. Scherrer, *Sol-Gel Science: The Physics and Chemistry of Sol-Gel Processing,* Harcourt, Brace, Jovanovich, 1990

37. L. Xia and R.L. McCreery, *J. Electrochem. Soc.,* Vol 145, 1998, p 3083

38. M. Henry, J.P. Jolivet, and L. Livage, Aqueous Chemistry of Metal Cations: Hydrolysis, Condensation, and Complexation, in *Structure and Bonding,* Springer- Verlag, Berlin, 1992, p 155

39. “Coating, Chromate on Aluminum,” Specification 9904151, U.S. Dept. of Energy, 1989

40. “Chemical Conversion Coatings on Aluminum and Aluminum Alloys,” MIL-C- 5541E, NAEC, 1990

41. R.A. Haaksma and J.R. Weir, *Proc. 27th Int. SAMPE Technical Conference,* Society for the Advancement of Materials and Process Engineering, 1995, p 1074

42. T. Schram, J. DeLaet, and H. Terryn, *J. Electrochem. Soc.,* Vol 145, 1998, p 2733

43. T. Schram, J. DeLaet, and H. Terryn, *Thin Solid Films,* Vol 727, 1998, p 313–314

44. J.A. Treverton, A. Bosland, and J.M. Brown, *Corrosion Sci.,* Vol 30, 1990, p 1159

45. L. Fedrizzi and F. Marchetti, *J. Mater. Sci.,* Vol 26, 1991, p 1931

46. J.N.J. Newhard, *Met. Finish.,* Vol 70, 1972, p 66

47. J.N.J. Newhard, *Met. Finish.,* Vol 70, 1972, p 49

48. L.A. Nimon and G.K. Korpi, *Plating,* Vol 59, 1972, p 421

49. F. Pearlstein and V.S. Agarwala, *Plat. Surf. Finish.,* Vol 81, 1994, p 50

50. F. Pearlstein and V.S. Agarwala, "Trivalent Chromium Solutions for Sealing Anodized Aluminum," U.S. Patent No. 5,374,347, 1994

51. F. Pearlstein and V.S. Agarwala, "Trivalent Chromium Conversion Coatings for Aluminum," U.S. Patent No. 5,304,257, 1994

52. G.M. Brown, K. Shimizu, K. Kobayashi, G.E. Thompson, and G.C. Wood, *Corros. Sci.,* Vol 33, 1993, p 253

53. G.M. Brown, K. Shimizu, K. Kobayashi, G.E. Thompson, and G.C. Wood, *Corros. Sci.,* Vol 34, 1993, p 1853

54. R.C. Furneaux, G.E. Thompson, and G.C. Wood, *Corros. Sci.,* Vol 19, 1979, p 63

55. L. Kintrup and L.D. Riese-Meyer, *Inst. Phys. Conf. Ser.,* Vol 119, 1991, p 257

56. Z. Yu, H. Ni, G. Zhang, and Y. Wang, *Appl. Surf. Sci.,* Vol 62, 1992, p 217

57. J.A. Treverton and N.C. Davies, *Surf. Interface Anal.,* Vol 3, 1981, p 194

58. J.A. Treverton and M.P. Amor, *J. Mater. Sci.,* Vol 23, 1988, p 3706

59. C.S. Jeffcoate, H.S. Isaacs, J.A.J. Aldykiewicz, and M.P. Ryan, *J. Electrochem. Soc.,* Vol 147, 2000, p 540

60. G.P. Halada and C.R. Clayton, *J. Electrochem. Soc.,* Vol 138, 1991, p 2921

61. A.G. Schrott, G.S. Frankel, A.J. Davenport, H.S. Isaacs, C.V. Jahnes, and M.A. Russak, *Surf. Sci.,* Vol 250, 1991, p 139

62. D.C. Koningsberger and E.R. Prins, *X-Ray Absorption Principles, Applications, Techniques of EXAFS, SEXAFS and XANES,* John Wiley & Sons, 1988

63. M. Kendig, S. Jeanjaquet, R. Addison, and J. Waldrop, *Surf. Coat. Technol.,* Vol 140, 2001, p 58

64. S.W.M. Chung, J. Robinson, G.E. Thompson, G.C. Wood, and H.S. Isaacs, *Philos. Mag. B,* Vol 63, 1991, p 557

65. J.K. Hawkins, H.S. Isaacs, S.M. Heald, J. Tranquada, G.E. Thompson, and G.C. Wood, *Proc. The Electrochemical Society,* Vol 86-11, 1986, p 345

66. J.K. Hawkins, H.S. Isaacs, S.M. Heald, J. Tranquada, G.E. Thompson, and G.C. Wood, *Corros. Sci.,* Vol 27, 1987, p 391

67. J.S. Wainright, O.J. Murphy, and M.R. Antonio, *Corros. Sci.,* Vol 33, 1992, p 281

68. G.O. Ilevbare and J.R. Scully, *J. Electrochem. Soc.,* Vol 148, 2001, p B196

69. J. Zhao, G.S. Frankel, and R.L. McCreery, *J. Electrochem. Soc.,* Vol 145, 1998, p 2258

70. L. Xia, E. Akiyama, G. Frankel, and R. McCreery, *J. Electrochem. Soc.,* Vol 147, 2000, p 2556

71. J. Sinko, *Prog. Org. Coatings,* Vol 42, 2001, p 267

72. E. Akiyama, A.S. Markworth, and G.S. Frankel, *J. Electrochem. Soc.,* 2001

73. J.H. Osborne, J. Du, S.R. Taylor, D. Bernard, A. Nercissiantz, and G.P. Bierwagen, "Advanced Corrosion Resistant Aircraft Coatings," Final Report 6/96-9/00, Contract No. F33615-96-C-5078, U.S. Air Force Research Laboratory, 2000

74. F. Altmayer, *Plat. Surf. Finish.,* Vol 72, 1985, p 36

75. "Chemical Conversion Materials for Coating Aluminum and Aluminum Alloys," Naval Air Systems Command, Dept. of the U.S. Navy, 1970

76. G.D. Cheever, *J. Paint Technol.,* Vol 41, 1969, p 259

77. R.G. Buchheit, M.W. Kendig, M.A. Martinez, M. Cunningham, and H. Jensen, *Corrosion,* Vol 54, 1998, p 61

78. F. Mansfeld, S. Lin, S. Kim, and H. Shih, *Corros. Sci.,* Vol 27, 1987, p 997

79. F. Mansfeld and H. Shih, *J. Electrochem. Soc.,* Vol 135, 1988, p 906

80. R.G. Buchheit, S.B. Mamidipally, and P. Schmutz, *Corrosion,* Vol 58, 2002, p 3

81. R.L. Twite and G.P. Bierwagen, *Prog. Org. Coatings,* Vol 33, 1998, p 91

82. E.D. Wick, *Tool and Manufacturing Engineers Handbook,* Society of Manufacturing Engineers, 1983

83. A. Wehr, H.C. Hardee, N.R. Auckland, and D. Klavens, *Proc. 48th Electronic Components and Technology Conference,* Institute of Electrical and Electronics Engineers, 1998, p 14

84. M.A. Heine and M.J. Pryor, *J. Electrochem. Soc.,* Vol 114, 1967, p 1001

85. G.E. Pike, "Electrical Properties of Alodine 1200," Internal Memorandum, Sandia National Laboratories, 1981

86. V. Laget, H. Isaacs, C.S. Jeffcoate, and R. Buchheit, *Proc. Electrochem. Soc.,* Vol 92- 26, 2000, p 173

87. V. Laget, H.S. Isaacs, C.S. Jeffcoate, and R.G. Buchheit, *ATB Metallurgie,* Vol 40–41, 2000, p 295

88. V. Laget, C.S. Jeffcoate, H.S. Isaacs, and R.G. Buchheit, *J. Electrochem. Soc.,* Vol 150 (No. 9), 2003

89. F. Pearlstein and M.R. D'Ambrosio, *Plating,* Vol 55, 1968, p 345

90. A. Gallacio, F. Pearlstein, and M.R. D'Ambrosio, *Met. Finish.,* Vol 50, 1966

91. A.L. Glass, *Mater. Protect.,* Vol 26, 1968

92. B. Meyers, S. Lynn, and E. Jang, "Alternatives to Chromate Conversion Coating at McClellan Air Force Base," MITRE, 1993

93. "Alternatives to Chromium for Metal Finishing," Final NCMS Report 0273RE95, National Center for Manufacturing Sciences, 1995

94. "Alternatives to Chrome Conversion Coatings on Aluminum Alloys 2024, 6061, 7075, and Ion Vapor Deposited Aluminum on Steel (Potential Alternatives Report)," Web page, http://www.jgapp.com/parhughhc.htm, National Defense Center for Environmental Excellence, 1998

95. M. Kendig and R. Buchheit, Surface Conversions of Aluminum and Ferrous Alloys for Corrosion Resistance, *Proc. Corros./ 2000 Res. Top. Symposium,* NACE International, 2000, p 1

96. J. Ouyang and W.L. Harpel, "Monitoring of Coating Weight in Dried-in-Place Non- Chrome Polyacrylamide Based Treatments for Metals," U.S. Patent No. 5,401,333, 28 March 1995

97. H. Terryn, *ATB Metall.,* Vol 38, 1998, p 41

98. L.S. Sander, E.M. Musingo, and W.J. Neill, "Nonchromate Bath for the Primer and Anticorrosion Coating on Aluminum Alloy," U.S. Patent No. 4,921,552, 1 May 1990

99. S.E. Dolan, "Chromium-Free Conversion Coating Composition and Process for Treating Metals," U.S. Patent No. 5,449,415, 12 Sept 1995

100. A. Nylund, *Alum. Trans.,* Vol 2, 2000, p 121

101. P.D. Deck and D.W. Reichgott, *Met. Finish.,* Vol 90, 1992, p 29

102. S.G. Hardin, A.E. Hughes, and K.J.H. Nelson, "Process and Solution for Providing a Conversion Coating on a Metallic Surface I," U.S. Patent No. 01/71058A1

103. F.B. Mansfeld, H. Shih, and Y. Wang, "Method for Creating a Corrosion Resistant Aluminum Surface," U.S. Patent No. 90/556,109, 16 March 1990

104. R.N. Miller, "Non-Toxic Corrosion Resistant Conversion Coating for Aluminum and Aluminum Alloys and the Process for Making the Same," U.S. Patent No. 5,221,371, 22 June 1993

105. K.J.H. Nelson, R.J. Taylor, A.E. Hughes, B.R.W. Hinton, M.J. Henderson, L. Wilson, and S.A. Nugent, "Conversion Coating and Process and Solution for its Formation," U.S. Patent No. 6,022,425, 8 Feb 2000

106. B. Hinton, A. Ryan, P. Trathen, L. Wilson, and B. Williams, 12, 1985

107. A.E. Hughes, S.G. Hardin, K.W. Wittel, and P.R. Miller, Surface Conversions of Aluminum and Ferrous Alloys for Corrosion Resistance, *Proc. Corros./2000 Res. Top. Symposium,* NACE International, 2000, p 47

108. A. Kindler, "Coating of Aluminum with Chromium-Free Protective Layer," U.S. Patent No. 5,192,374, 9 March 1993

109. F. Mansfeld and Y. Wang, *Mater. Sci. Eng., A,* Vol 51, 1995

110. V. Briois, C.E. Williams, H. Dexpert, F. Villain, B. Cabane, F. Deveuve, and C. Magnier, *J. Mater. Sci.,* Vol 28, 1993, p 5019

111. A.E. Hughes, J.D. Gorman, and P.J.K. Paterson, *Corros. Sci.,* Vol 38, 1996, p 1957

112. R.S. Alwitt, Vol 121, 1974, p 1322

113. H.E. Hager, K.Y. Blohowiak, J.H. Jones, C.J. Johnson, C.M. Wong, R.S. Taylor, and R.L.J. Cook, "Chromate-Free Protective Coatings for Aircraft," U.S. Patent No. 5,866,652, 2 Feb 1999

114. H. Zheng, Y. Du, M. Damron, J. Wright, and M. Tang, *Met. Finish.,* Vol 96, 1998, p 35

115. J.W. Bibber, "Corrosion-Resistant Aluminum Coating," U.S. Patent No. 4,711,667, 8 Dec 1987

116. J.W. Bibber, *Met. Finish.,* Vol 91, 1993, p 46

117. J.W. Bibber, "Multistage Conversion Coating of Aluminum Alloys," U.S. Patent No. 4,988,396, 29 Jan 1991

118. J.W. Bibber, "Conversion Bath with Nitrate for Corrosion-Resistant Coating on Aluminum Alloys," U.S. Patent No. 5,554,231, 10 Sept 1996

119. M.P. Schriever, "Nonchromate Cobalt Complex Conversion Coating and Primer in Painting," U.S. Patent No. 488,430, 1992

120. M.P. Schriever, "Conversion Bath for Chromate-Free Coating with Cobalt Oxide on Aluminum Alloy Substrates," U.S. Patent No. 5,873,953, 23 Feb 1999

121. G.D. Wilcox, D.R. Gabe, and M.E. Warwick, *Trans. Inst. Met. Finish.,* Vol 66, 1988, p 89

122. J. Ouyang and W.L. Harpel, "Non-Chromate Acidic Bath for Passivation of Galvanized Metal Surfaces," U.S. Patent No. 5,344,505, 6 Sept 1994

123. C.M. Rangel, A. Simoes, and R.C. Newman, *Port. Electrochim. Acta,* Vol 15, 1997, p 383

124. B.H. Goodreau, "Phosphoric Acid Bath with Molybdenum Ions for Passivation and Priming of Zinc and/or Aluminum Surface in Coating with Acrylic Film," U.S. Patent No. 9,727,001

125. G.D. Wilcox and D.R. Gabe, *Met. Finish.,* Vol 86, 1988, p 71

126. S. Miyata, *Clay and Clay Miner.,* Vol 23, 1975, p 369

127. H.F.W. Taylor, *Min. Mag.,* Vol 39, 1973, p 377

128. R.G. Buchheit, M.D. Bode, and G.E. Stoner, *Corrosion,* Vol 50, 1994, p 205

129. R.G. Buchheit and G.E. Stoner, "Method for Increasing the Corrosion Resistance of Aluminum and Aluminum Alloys," U.S. Patent No. 5,266,356, 30 Nov 1993

130. R.G. Buchheit and M.A. Martinez, “Corrosion Protective Coating for Metallic Materials,” U.S. Patent No. 5,756,218, 26 May 1998

131. R.G. Buchheit, S.B. Mamidipally, P. Schmutz, and H. Guan, Active Corrosion Protection in Chromate and Chromate- Free Conversion Coatings, in *Surface Conversion for Aluminum and Ferrous Alloys,* NACE International, 2000, p 67

132. R.G. Buchheit, S.B. Mamidipally, P. Schmutz, and H. Guan, *Corrosion,* Vol 58, 2002, p 3

133. R.G. Buchheit, M.A. Martinez, L.P. Montes, N. Cella, G.E. Stoner, and S.R. Taylor, “inorganic Cr-Free Conversion Coatings for High Corrosion Resistance and Low Electrical Contact Resistance,” Paper No. 98212, CORROSION/98, NACE International, 1998

134. R.G. Buchheit, *J. Appl. Electrochem.,* Vol 28, 1998, p 503

135. W. Zhang and R.G. Buchheit, *Corrosion,* Vol 58, 2002

136. R.B. Leggat, W. Zhang, R.G. Buchheit, and S.R. Taylor, *Corrosion,* Vol 58, 2002, to be published

137. C. Bram, C. Jung, and M. Stratmann, Vol 358, 1997, p 108

138. H. Shirakawa, L.E., A. MacDiarmid, C. Chiang, and A. Heeger, 578, 1977

139. J.O. Iroh, *Surf. Eng.,* Vol 17, 2001, p 265

140. B. Wessling, *Chem. Innovation,* Vol 31, 2001, p 34

141. T.F. Child and W.J. Van Ooij, *Trans. Inst. Met. Finish.,* Vol 77, 1999, p 64

142. W.J. Van Ooij and D. Zhu, Surface Conversions of Aluminum and Ferrous Alloys for Corrosion Resistance, *Proc. Corros./ 2000 Res. Top. Symposium,* NACE International, 2000, p 96

H. Takahashi, Aluminum Anodizing, *Corrosion: Fundamentals, Testing, and Protection,* Vol 13A*, ASM Handbook,* ASM International, 2003, p 736–740

Aluminum Anodizing

Hideaki Takahashi, Hokkaido University

Introduction

ABOUT 25 MILLION TONS of aluminum is produced from bauxite ore and scrap every year, and most aluminum products are subjected to surface treatments such as anodizing, chemical conversion coating, painting, and metal plating. Anodizing is one of the most common surface treatments of aluminum and is performed for corrosion protection as well as a wide variety of purposes (Ref 1, 2, 3). Table 1 shows application examples of anodic oxide films on aluminum.

Table 1 Application of anodic oxide films on aluminum

Property class	Attribute	Application
Physical and mechanical	Hardness Wear resistance	Screw thread, gear, bolt, nut, brake disk clutch, fan, nozzle, valve, cam track, fuel pump, injector
	Lubrication	Piston, piston ring, roller, bearing
	Membrane	Gas separator, molecule separator, super grid, template for plasma etching
Chemical	Corrosion resistance	Aircraft, vehicle, boat, train, architecture, household and sporting goods, office supplies
	Wettability	Presensitized plate, Al lithograph
	Adhesion	Organic coating
	Catalytic properties	Catalysis, catalysis support
Electromagnetic	Insulating properties	Printed circuit board, integrated circuit board, electric cable
	Dielectric properties	Electrolytic capacitor, humidity sensor, gas sensor, printing roller
	Magnetism	Magnetic recording device, rotary encoder
Optical	Luminescence	Electroluminescence display
	Absorption	Sunlight energy absorbing plate
Thermal	Emittance	Far-infrared emitter, heat sink

Anodizing is performed for the corrosion protection of aircraft, vehicles, boats, trains, buildings, household articles, sporting goods, office articles, and electronics. Hard anodizing is performed to improve the hardness and wear resistance of machinery parts, such as screw threads, gears, and brake disks. To improve the lubricating performance of pistons, piston rings, rollers, and bearings, the pores of porous anodic oxide films are filled with MoS_2. Porous anodic oxide films are removed from the substrate where they were formed and used as membranes for the separation of gases and other chemical compounds. Adhesion with organic coatings and wettability of anodic oxide films play an important role in presensitized plates for offset printing. The high inner surface areas of porous anodic oxide films are useful as catalysts and catalyst supports. Barrier-type anodic oxide films with high insulating and dielectric properties are used in printed circuit boards, integrated-circuit-supporting plates, aluminum cables, electrolytic capacitors, and humidity sensors. Deposition of ferromagnetic substances, iron, nickel, and cobalt into the pores of porous anodic oxide films causes anisotropy of magnetic properties, allowing their use as memory devices. Electroluminescence of anodic oxide films on aluminum is applied to the fabrication of luminescent display plates, and black coloring with metal deposition

is used for sun- energy absorbing plates. Far infrared emitters can also be made, using aluminum alloys covered with anodic oxide films.

References cited in this section

1. S. Wernick, R. Pinner, and P.G. Sheasby, Ed., *The Surface Treatment and Finishing of Aluminum and Its Alloys,* 5th ed., Vol I and II, Finishing Publications Ltd, Teddington, Middlesex, England, 1987

2. G.C. Wood, Porous Anodic Films on Aluminum, *Oxide and Oxide Films,* Vol 2, J.W. Diggle and A.K. Vijh, Ed., Marcel Dekker, 1972

3. S. Tajima, Anodic Oxidation of Aluminum, *Advances in Corrosion Science and Technology,* M.G. Fontana and R.W. Staehle, Ed., Plenum Press, 1970

H. Takahashi, Aluminum Anodizing, *Corrosion: Fundamentals, Testing, and Protection*, Vol 13A, *ASM Handbook*, ASM International, 2003, p 736–740

Aluminum Anodizing

Hideaki Takahashi, Hokkaido University

Structure of Anodic Oxide Films

When aluminum and aluminum alloys are polarized anodically in electrolytic solutions, oxide films are formed on the substrates. This procedure is termed "anodizing," and the oxide film formed by this procedure is called "anodic oxide film." Anodic oxide films can be classified into two groups: barrier and porous-type oxide films. The structure and growth characteristics of these anodic oxide films is described in this section.

Barrier-type oxide films are obtained in neutral solutions containing borate, phosphate, and adipate and consist of a thin compact amorphous oxide layer (Fig. 1a). The film thickness, δ_{bf}, in nm, is proportional to the potential, E_a, in volts, applied during anodizing and is expressed as:

$$\delta_{bf} = K \cdot E_a \quad \text{(Eq 1)}$$

where K is 1.3 to 1.6.

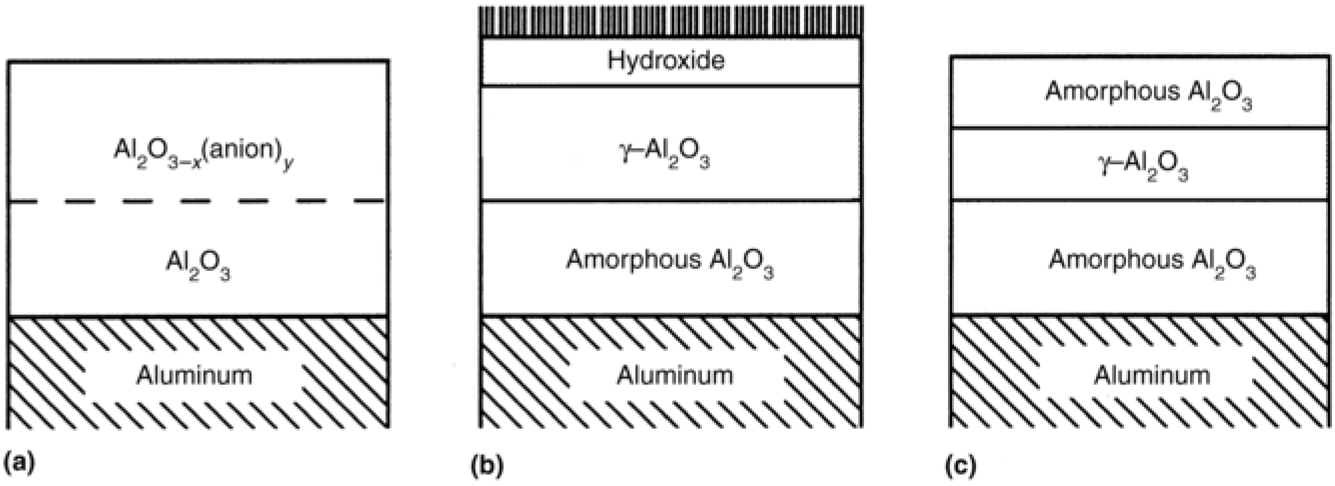

Fig. 1 Structure of barrier type oxide films formed on aluminum after (a) electropolishing, (b) hydrothermal treatment, and (c) thermal treatment

Galvanostatic anodizing in the neutral solutions gives rise to a linear increase in δ and potential E_a with time, and then the oxide formation stops abruptly, at "film breakdown" potential, E_{bd}, which is significantly dependent on the kind and the concentration of anodizing solution. Processing in diluted boric acid solutions with E_{bd} values as high as 1000 V, results in film thicknesses of 1.3 to 1.6 μm.

Barrier-type anodic oxide films contain small amounts of anions of the electrolyte, which are included only in the outer part of the barrier oxide film. The thickness ratio of the outer anion- incorporated layer to the inner pure Al_2O_3 layer depends on the kind of anodizing solution. This suggests that the transport of anions depends on the interactions of anions with the molecular network of the oxide film. Anodizing in neutral solutions after hydrothermal treatments in pure water leads to composite oxide films, which consist of an inner amorphous Al_2O_3 and an outer γAl_2O_3 (Fig. 1b). The hydroxide film formed by the hydrothermal treatment converts to crystalline oxide by dehydration under a high electric field during anodizing. Anodizing after heat treatment also causes the formation of anodic oxide films containing γAl_2O_3 in the middle part (Fig. 1c).

The porous-type anodic oxide film is obtained by anodizing in acid solutions such as H_2SO_4, oxalic acid, H_3PO_4, and H_2CrO_4. The film possesses a unique morphology, a "hexagonal cell model structure," as shown in Fig. 2. The oxide film consists of numerous fine hexagonal cells perpendicular to the metal substrate, and each cell has a pore at the center. The pores are separated from the metal substrate by a thin hemispherical "barrier layer," existing at the interface between the oxide film and the metal substrate.

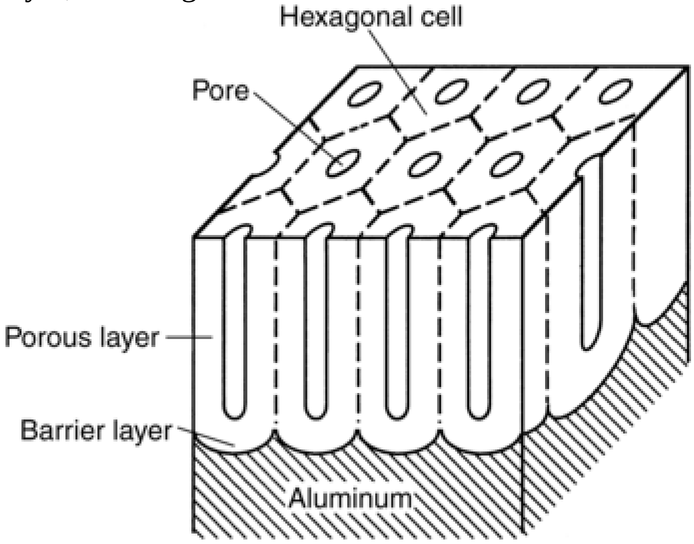

Fig. 2 Structure of porous type anodic oxide film formed on aluminum in acid solutions

Galvanostatic anodizing gives rise to a steady value of the potential, E_s, after an initial transient period and permits a steady increase in the film thickness, keeping the number of cells per m^2, N_c, the size of cells, D_c, and size of pores, D_p, and barrier layer thickness, δ_b (all measured in nm), constant during anodizing. The thickness of porous anodic oxide films, d_{pf}, in μm is proportional to anodizing time, t_a, in seconds, and current density, i_a, in A/m^2.

$$d_{pf} = k \times i_a \times t_a \qquad \text{(Eq 2)}$$

where k (3.6 to 4.5 × 10^{-5} μm C^{-1} m^2) is the proportionality constant, which is higher at lower temperatures and lower acid concentrations. Aluminum alloys with high copper contents show lower film growth rates, due to a preferential dissolution of copper and aluminum intermetallic compound phases.

Longer anodizing time causes the chemical dissolution of oxide, leading to the formation of cone-shaped pores (Fig. 3). At the final stage of anodizing, the pore walls become substantially thinner and are finally destroyed, resulting in "powdering" of the oxide film. The onset of powdering determines the termination of the film growth in practice. Lower temperatures and lower acid concentrations enable the formation of thicker films without powdering, and the maximum thickness may be several hundred μm.

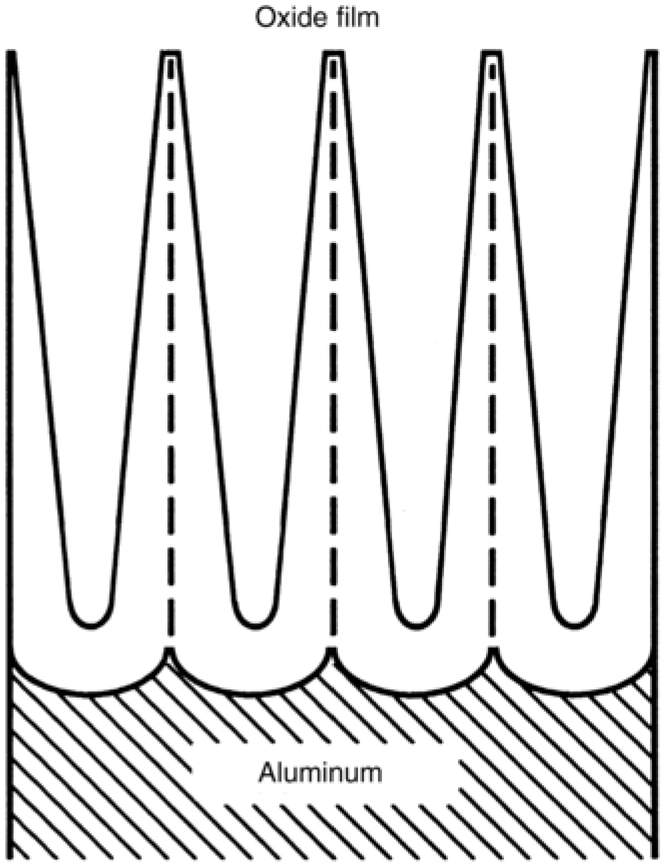

Fig. 3 Cone-shaped pores formed by chemical dissolution during long anodizing

Figure 4 shows the relationship between the current density, i_a, plotted logarithmically, and steady values of the anode potential, E_s, obtained in H_2SO_4 and oxalic acid solutions (Ref 4). The E_s versus log i_a relationship is an “S-shaped curve” in both solutions, and it shifts to higher current density regions at higher temperatures and higher acid concentrations. The “S” shape is observable if the vertical scale is expanded. The anodizing in H_2SO_4 solutions results in lower E_s than in oxalic solutions, suggesting an advantage of H_2SO_4 anodizing in lower electric power consumption. Anodizing should be performed under the conditions at the mid-regions of the E_s versus log i_a relationship since anodizing at the lower regions easily leads to the “powdering” of oxide and in the high regions to “burning” of the oxide. Burning is the phenomenon where the oxide film grows nonuniformly by local heating, due to nonuniform current distribution.

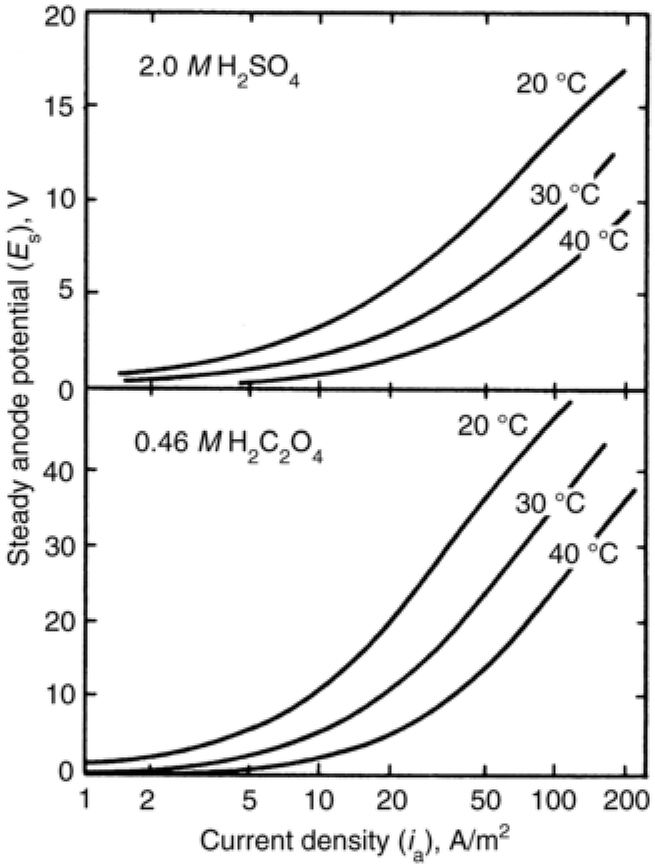

Fig. 4 Relationship between steady anode potential, E_s, and current density, i_a, in 2 *M* H_2SO_4 and 0.46 *M* $H_2C_2O_4$ solutions

The values of N_c, D_c, D_p, and δ_b are functions of E_s as shown in Fig. 5, slightly dependent on temperature, kind of acid solution, and acid concentration (Ref 4). With increasing E_s, the values of N_c decreases, while D_c, D_p, and δ_b increases. The curves in Fig. 4 and 5 lead to:

$$N_c = 14 \times 10^{15} \times E_s^{-1.27} \quad \text{(Eq 3)}$$

$$D_p = 14 + 0.21 \times E_s \text{ when } E_s < 15 \text{ V} \quad \text{(Eq 4)}$$

$$D_p = 4.2 + 0.84 \times E_s \text{ when } E_s > 15 \text{ V} \quad \text{(Eq 5)}$$

$$D_c = 6.5 + E_s \quad \text{(Eq 6)}$$

$$\delta_b = 2.1 \times E_s^{0.83} \quad \text{(Eq 7)}$$

where units of D_p, D_c, δ_b are nm; N_c is m^{-2}; and E_s is V.

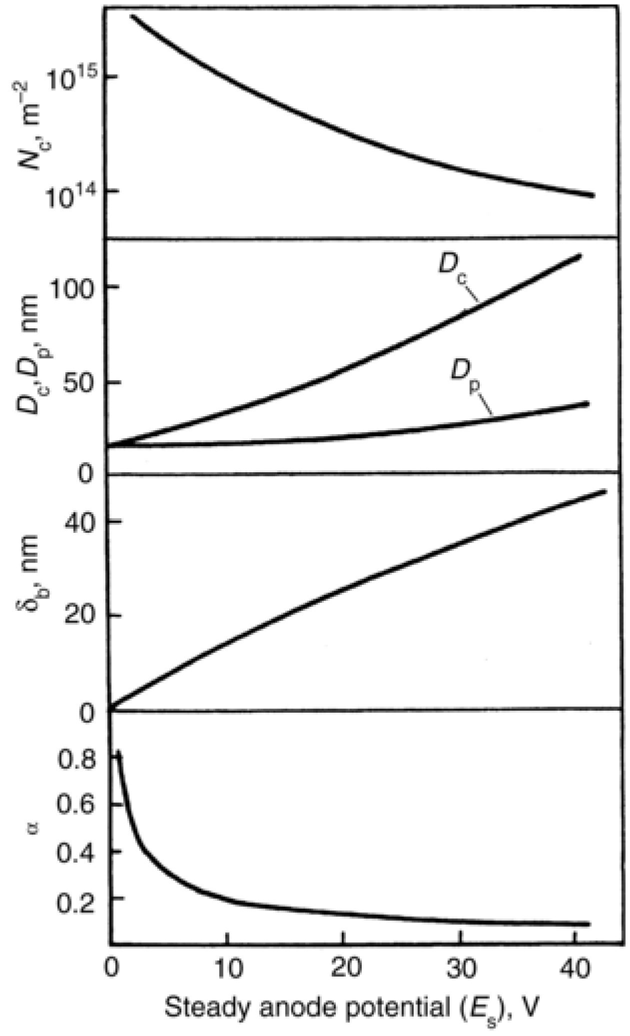

Fig. 5 Changes in cell number, N_c; cell size, D_c; pore diameter, D_p; barrier layer thickness, δ_b; and porosity, α, with steady anode potential, E_s, obtained in $H_2C_2O_4$ solutions

Hence, the porosity, $\alpha = N \pi D_p^2/4$, of the oxide film can be expressed as:

$\alpha = 0.8 \times E_a^{-0.59}$ (Eq 8)

The α value decreases sharply with increasing E_a (see Fig. 5).

Porous-type anodic oxide films basically consist of amorphous Al_2O_3, containing small amounts of water and anions of the electrolyte used. These anions distribute across the pore wall and barrier layer as shown in Fig. 6. Oxide films formed in chromic acid solutions, however, consist of almost pure Al_2O_3.

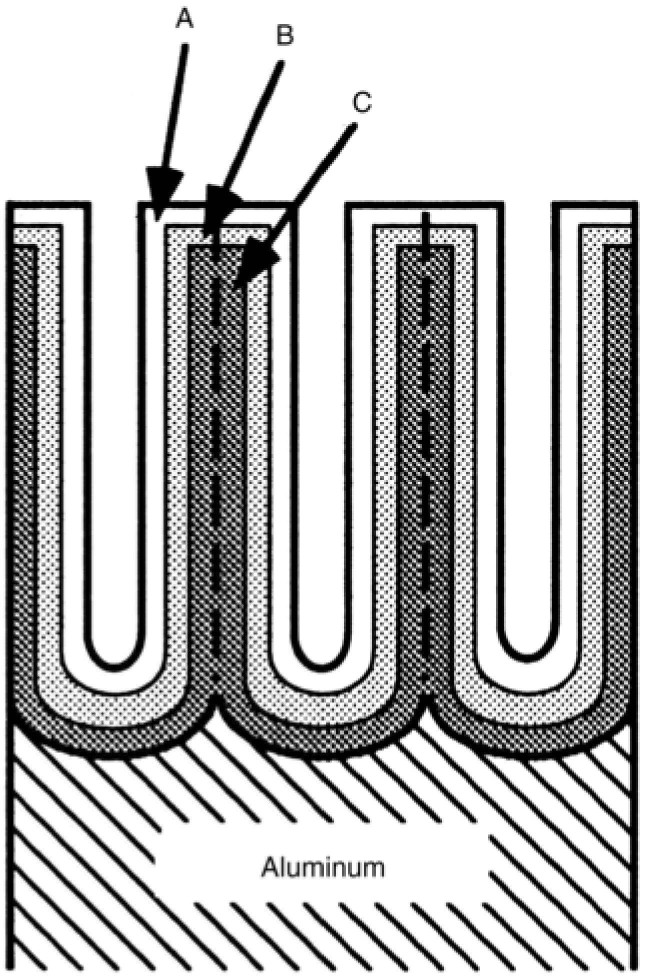

Fig. 6 Distribution of protons and anions in porous type anodic oxide films. A, $Al_2O_{3-x}(anion)_y{\cdot}zH_2O$; B, $Al_2O_{3-x}(anion)_y$; C, Al_2O_3

Reference cited in this section

4. K. Ebihara, H. Takahashi, and M. Nagayama, *J. Met. Finish. Soc. Jpn.,* Vol 34, 1983, p 548; Vol 35, 1984, p 205

H. Takahashi, Aluminum Anodizing, *Corrosion: Fundamentals, Testing, and Protection,* Vol 13A, *ASM Handbook,* ASM International, 2003, p 736–740

Aluminum Anodizing

Hideaki Takahashi, Hokkaido University

Anodizing

In general, the anodizing process of an aluminum or aluminum alloy specimen consists of pretreatments (degreasing, etching, and polishing), anodizing, coloring, and sealing. Each step is described in this section.

Pretreatments. Degreasing is performed by dipping the specimen in organic solvents, alcohol, acetone, kerosene, or trichloroethylene, or by wiping with cloths permeated with solvent. Etching and polishing are important pretreatments for conversion coating, metal deposition, and organic coating as well as for anodizing, and typical etching and polishing processes are listed in Table 2. Both acid etching and alkaline etching are

possible, and the latter requires a posttreatment of "desmutting" in a nitric acid solution. Electrograining—electrochemical roughening of the surface—is important as a pretreatment in the fabrication of presensitized plates in offset print.

Table 2 Procedures of etching and polishing

Procedure	Solution	Processing conditions
Acid etching	10 vol% (40 wt%) hydrofluoric acid 10 vol% (72 wt%) nitric acid 80 vol% water	Dip, room temperature bath, 2–5 min
Acid electrograining	1–2 wt% hydrochloric acid	Power: 8–15 V_{ac} 200–500 A/m^2 (0.15–0.30 A/in.^{2}); 20–30 °C (70–85 °F), 5–10 min
Alkaline etching	4–10 wt% sodium hydroxide	Dip, 40–90 °C (105–195 °F), 1–10 min, desmut posttreatment: dip, 25–50 vol% nitric acid, ambient temperature, 3–5 min
Electropolishing	22 vol% (60 wt%) perchloric acid 78 vol% acetic acid	Anodic, 25–30 V, 5–15 °C (40–60 °F), 2–5 min
Chemical polishing	86 vol% (85 wt%) phosphoric acid 14 vol% (72 wt%) nitric acid	Dip, 80–90 °C (175–195 °F), 2–5 min
Oxide film removal	0.5 *M* phosphoric acid 0.2 *M* chromic acid	Dip, 85–95 °C (185–205 °F), 10–30 min

Electropolishing generally enables a smoother surface than chemical polishing. In order to dissolve oxide films on the aluminum, a mixture of chromic acid and phosphoric acid is used, and very little of the aluminum substrate is dissolved. Table 3 shows the chemical composition and thickness of surface films formed by electropolishing, chemical polishing, and chromic acid and phosphoric acid solution treatments (Ref 5). A 3 to 5 nm thick oxide film is formed by these treatments. The oxide films formed by electropolishing contain small amounts of chloride ions, which are produced by the decomposition of perchlorate ions during electropolishing. Chemical polishing results in the formation of oxide films containing phosphate and nitrite (NO_2^-) ions. Chromic acid/phosphoric acid treatment after electropolishing replaces the oxide films formed by the electropolishing with oxide films containing Cr (III) and phosphate ions.

Table 3 Chemical composition and thickness of surface films formed by electropolishing, chemical polishing, and film removal treatment

Treatment	Thickness, nm	Chemical composition
Electropolishing[(a)]	3.6	$AlO_x(OH)_{2.91-2x}Cl_{0.09}$ $(x - 0.62)H_2O$
Chemical polishing[(b)]	4.7	$AlO_x(OH)_{2.45-2x}(PO_4)0.17(NO_2)_{0.04}\cdot(x - 0.73)H_2O$
H_3PO_4/H_2CrO_4 treatment[(c)]	4.2	$AlCr(III)_{0.43}O_x(OH)_{3.3-2x}(PO_4)_{0.33}\cdot(x - 0.07)H_2O$

Treatment details:

(a) 13 °C (55 °F), 3 min, 30 V.

(b) 85 °C (185 °F), 3 min.

(c) 90 °C (194 °F), 30 min. Other experimental conditions are described in Table 2.

Typical anodizing procedures are listed in Table 4. Anodizing in sulfuric acid solutions is common, and results in transparent anodic oxide films, which are adequate for dyeing. These films may be dyed into almost any color in practice and can produce strong colors. Oxalic acid solution gives yellowish oxide films, and chromic

acid solution results in gray colors. Table 4 suggests that the steady anode potential, E_s, during anodizing strongly depends on the kind of acid used, decreasing in the following order: phosphoric acid, chromic acid, oxalic acid and sulfuric acid. Phosphoric acid gives the highest E_s, suggesting the formation of anodic oxide films with thick pore walls and low porosity. Sulfuric acid solution, by contrast, gives the lowest E_s, leading to thin pore walls and high porosity. Anodizing in sulfuric acid solutions, therefore, tends to cause “powdering” during anodizing, and phosphoric acid solutions tend to cause “burning.”

Table 4 Procedures of anodizing

Procedure	Chemical composition	Temperature		Voltage, Vdc	Current density		Appearance and other characteristics
		°C	**°F**		**A/dm^2**	**A/ft^2**	
Sulfuric acid	5–25 wt% sulfuric acid 0.1–5 wt% aluminum sulfate	15–25	60–75	15–20	0.8–3	7.5–28	Transparent
Oxalic acid	3–5 wt% oxalic acid	20–30	70–85	25	1–1.5	9.5–14	Yellowish
Chromic acid	10 wt% chromic acid	45–55	115–130	40–50	0.3–1	28–9.5	Grayish
Phosphoric acid	3–10 wt% phosphoric acid	20–30	70–85	40–100	0.5–2	4.75–18.5	Light blue
Hard anodizing	10–20 wt% sulfuric acid 0.1–10 wt% aluminum sulfate 1 wt% oxalic acid	0–5	32–40	25–60	2–4	18.5–37	Transparent, hardness, >600 HV
Kalcolor	5 wt% sulfuric acid 10 wt% sulfosalicylic acid	22–25	70–75	25–70	2–3.2	18.5–29.75	Bronze-black
Alkaline anodizing	8–12 wt% sodium hydroxide 2–3 wt% hydrogen peroxide 0.1–0.5 wt% sodium phosphate	10–20	50–70	30–70	1–4	9.5–37	Resistant in basic solutions
Alternating current anodizing	15–30 % sulfuric acid	0–40	32–105	15–30(a)	3–12	28–112	Soft, flexible, sulfide included
Molten salt anodizing	66 mol% potassium bisulfate 33 mol% sodium bisulfate	180	355	>160	1	9.5	α-alumina

(a) Alternating current

Anodizing in sulfuric acid solutions containing sulfosalicylic acid leads to the formation of anodic oxide films with brown to blackish colors, the Kalcolor method. Anodizing at temperatures as low as 0 °C gives hard anodic oxide films with a hardness of 500 HV. Anodizing in alkaline solutions containing hydrogen peroxide

gives porous anodic oxide films with a high resistance to alkali, and anodizing with alternative current in sulfuric acid solution gives flexible anodic oxide films.

Coloring of anodic oxide films is classified into three groups: integral coloring, dyeing and electrolytic coloring. In integral coloring, many kinds of organic acids, oxalic acid, sulfosalicylic acid, sulfophthalic acid, maleic acid, succinic acid, sulfamic acid, and so forth, are mixed with sulfuric acid, and the anodic oxide films formed in the mixed solutions give brown, grayish, and blackish colors in general (Fig. 7a). The advantage of this method is to obtain anodic oxide films that are highly resistant to the deterioration of color, and integral coloring has been applied extensively in architecture, curtain walls, window frames, and roofing materials.

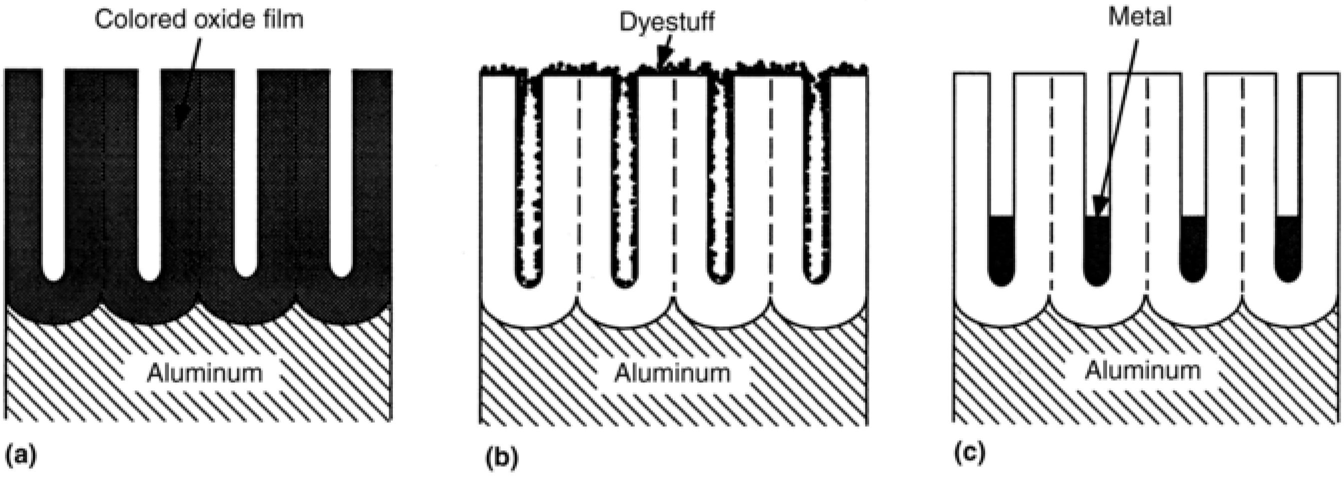

Fig. 7 Coloring of porous type anodic oxide films on aluminum by (a) integral coloring, (b) dyeing, and (c) electrolytic coloring

Porous anodic oxide films have a large internal surface and easily absorb dyestuff on the pore wall (Fig. 7b). Many organic dyestuffs, such as, Alizaline Blue, Alizaline Red-S, Naphtol Green- B, Chromolan Blue-NGG, and Anthraquinone, are used to give flashy colors: gold, yellow, blue, green, and so forth. Some inorganic dyestuffs are also used, and the process involves the precipitation of metal salts with low-solubility products, $Ag_2Cr_2O_7$, PbS, and $Co(OH)_3$ into the pores. The color range of the inorganic dyeing is more restricted than that of organic dyeing, but the inorganic dyestuff is much more resistant to heat and light.

Electrolytic coloring is generally a method where metal is deposited at the bottom of the pores by applying alternative voltage (Fig. 7c). Nickel, cobalt, tin, and copper are mainly deposited to color in bronze and maroon to black. Typical conditions of electrolytic coloring are listed Table 5. The electrolytic coloring is much more advantageous from an energy-consumption viewpoint than the integral coloring and does not require the use of special alloys. The light fastness of the finishes with electrolytic coloring is also excellent. Integral coloring is, therefore, being replaced with electrolytic coloring in architectural applications.

Table 5 Procedures of electrolytic coloring

Metal	Composition	Time, min	Voltage, V	Appearance and other characteristics
Nickel	30 g/L nickel sulfate 30 g/L boric acid 15 g/L ammonium sulfate	10	20 (ac)	Blue
	50 g/L nickel sulfate 25 g/L ammonium chloride 25 g/L boric acid	1–5	10–14 (dc)	Light brown-black
Cobalt	20 g/L cobalt sulfate 25 g/L boric acid	10	15 (ac)	Black

	15 g/L ammonium sulfate			
Copper	20 g/L cupric sulfate 5–6 g/L sulfuric acid	10	13 (ac)	Red
Tin	20 g/L stannous sulfate 15–20 g/L sulfuric acid 1–2 g/L phenol sulfonic acid	5–15	5–8 (ac)	Bronze-black

Sealing. Porous anodic oxide films without sealing are not protective against the corrosion of the substrate since aggressive ions easily penetrate through pores. The dyestuff also tends to move out, leading to fading. Sealing is essential as a posttreatment to ensure resistance and durability of finishes. Sealing is usually performed by dipping in boiling water. During sealing, anhydrous anodic oxide films react with hot water to convert to a crystalline hydroxide, a pseudoboehmite, as described by:

$$Al_2O_3 + xH_2O = Al_2O_3 \cdot xH_2O \qquad \text{(Eq 9)}$$

where x is 1.5 to 2. The volume expansion by the formation of pseudoboehmite causes the pores to be sealed, as shown in Fig. 8 (Ref 6). A 10 min sealing treatment is sufficient to seal the pores completely in boiling water, and afterward water penetrates across the hydroxide slowly to allow the further progress of the hydration. In addition, the outermost part of anodic oxide films becomes highly crystallized. Pressurized steam enables quick sealing, but the equipment needed is more difficult to operate.

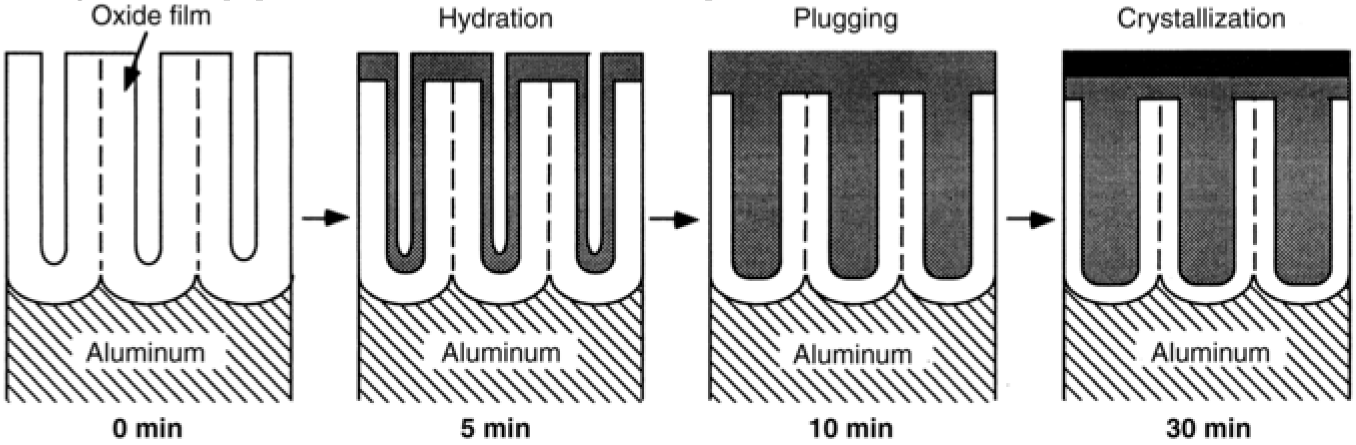

Fig. 8 Process of pore sealing with hydroxide during dipping in boiling pure water

A cold sealing, which is performed in solutions containing Ni^{2+} and F^- ions at ambient temperatures, has become popular because of low energy consumption (Ref 7). The reaction during the cold sealing is considered to be:

$$Al_2O_3 + xNi^{2+} + yF^- + 3H_2O = Al_2Ni_x F_y(OH)_z + (6 - z)OH^- \qquad \text{(Eq 10)}$$

Aluminum-nickel-fluoro-complexes are deposited in the pores to seal them.

References cited in this section

5. H. Takahashi and M. Nagayama, *J. Met. Finish. Soc. Jpn.,* Vol 36, 1985, p 96
6. M. Koda, H. Takahashi, and M. Nagayama, *J. Met. Finish. Soc. Jpn.,* Vol 33, 1982, p 242
7. E.P. Short and A. Morita, *Plat. Surf. Finish.,* Vol 72, 1988, p 102

H. Takahashi, Aluminum Anodizing, *Corrosion: Fundamentals, Testing, and Protection,* Vol 13A*, ASM Handbook,* ASM International, 2003, p 736–740

Aluminum Anodizing

Hideaki Takahashi, Hokkaido University

Testing of Film Properties

The morphology of anodic oxide films can be observed by transmission electron microscopy (TEM) and scanning electron microscopy (SEM). In TEM, oxide films are removed from the metal substrate by immersing anodized specimens in a saturated $HgCl_2$ solution to examine N_p and D_p of porous anodic oxide films. Thin slices of vertical sections of oxide films are obtained by the ultra thin sectioning technique (UTST) (Ref 8) with a diamond knife ultramicrotome to examine film thickness, crystal structure, and chemical compounds deposited in the pores (Ref 8). An example obtained by TEM with UTST is given in Fig. 9, showing the vertical section of a porous type oxide film formed on aluminum. Focused ion beam (FIB) technique is also used to make slices of oxide films, and confocal scanning laser microscopy (CSLM) is useful in examining the distribution of imperfections in the anodic oxide film as well as determining film thickness (Ref 9).

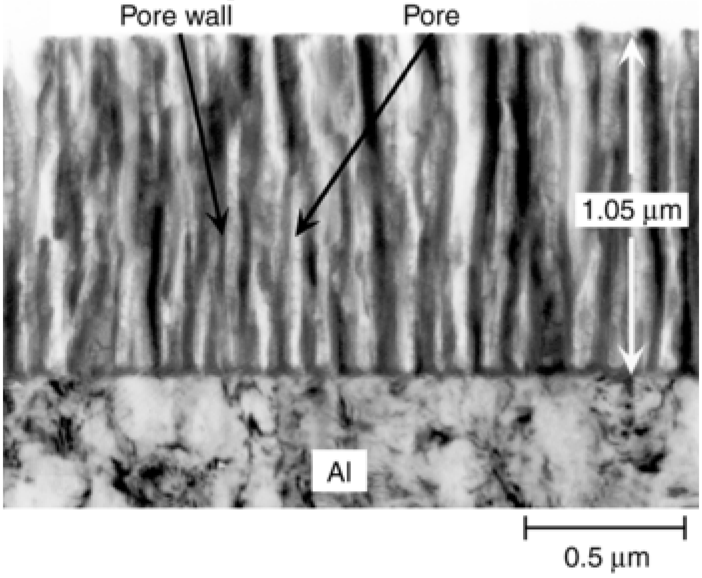

Fig. 9 TEM image of the vertical section of a porous type anodic oxide film on aluminum. The aluminum specimen was anodized for 5 min at 30 V in 0.16 *M* oxalic acid solution at 40 °C (140 °F) and then immersed for 1 h on open circuit in the same solution.

The hardness of oxide films can be found using microvickers measurements, but the hardness values can be affected by the hardness of the metal substrate, especially for thin oxide films. Nano-indentation methods have become popular in examining the hardness of anodic oxide films accurately and are useful in measuring the hardness at a local small area. Abrasion resistance measurements have been performed using conventional abrasive test instruments, jet assembly, and Taber abraser. It is difficult to compare the abrasion resistance obtained by one method with that by another method quantitatively, but a comparison of data obtained by one method for different specimens gives a significant order of abrasion resistance. Scratching by an atomic force microscope probe is also a method of examining the wear durability at the local micro area of anodic oxide films (Ref 10).

Corrosion resistance of anodized aluminum is evaluated by conventional corrosion tests, such as CASS tests, salt spray tests, and other exposure tests. Galvanic corrosion tests are important because the corrosion rate of aluminum in contact with other metallic materials can be much higher than that of aluminum alone in many atmospheres.

References cited in this section

8. H. Takahashi, M. Nagayama, H. Akahori, and A. Kitahara, *J. Electron Microsc.*, Vol 22, p. 149–157, 1973

9. S.-M. Moon, M. Sakairi, and H. Takahashi, *Proc. Intern. Symp. on Corrosion and Corrosion Protection,* Electrochemical Society, 2002, p 91

10. Z. Kato, M. Sakairi, and H. Takahashi, *J. Electrochem. Soc.*, Vol 148, p C790, 2001

H. Takahashi, Aluminum Anodizing, *Corrosion: Fundamentals, Testing, and Protection*, Vol 13A, *ASM Handbook*, ASM International, 2003, p 736–740

Aluminum Anodizing

Hideaki Takahashi, Hokkaido University

References

1. S. Wernick, R. Pinner, and P.G. Sheasby, Ed., *The Surface Treatment and Finishing of Aluminum and Its Alloys,* 5th ed., Vol I and II, Finishing Publications Ltd, Teddington, Middlesex, England, 1987

2. G.C. Wood, Porous Anodic Films on Aluminum, *Oxide and Oxide Films,* Vol 2, J.W. Diggle and A.K. Vijh, Ed., Marcel Dekker, 1972

3. S. Tajima, Anodic Oxidation of Aluminum, *Advances in Corrosion Science and Technology,* M.G. Fontana and R.W. Staehle, Ed., Plenum Press, 1970

4. K. Ebihara, H. Takahashi, and M. Nagayama, *J. Met. Finish. Soc. Jpn.,* Vol 34, 1983, p 548; Vol 35, 1984, p 205

5. H. Takahashi and M. Nagayama, *J. Met. Finish. Soc. Jpn.,* Vol 36, 1985, p 96

6. M. Koda, H. Takahashi, and M. Nagayama, *J. Met. Finish. Soc. Jpn.,* Vol 33, 1982, p 242

7. E.P. Short and A. Morita, *Plat. Surf. Finish.,* Vol 72, 1988, p 102

8. H. Takahashi, M. Nagayama, H. Akahori, and A. Kitahara, *J. Electron Microsc.*, Vol 22, p. 149–157, 1973

9. S.-M. Moon, M. Sakairi, and H. Takahashi, *Proc. Intern. Symp. on Corrosion and Corrosion Protection,* Electrochemical Society, 2002, p 91

10. Z. Kato, M. Sakairi, and H. Takahashi, *J. Electrochem. Soc.*, Vol 148, p C790, 2001

H. Takahashi, Aluminum Anodizing, *Corrosion: Fundamentals, Testing, and Protection,* Vol 13A*, ASM Handbook,* ASM International, 2003, p 736–740

Aluminum Anodizing

Hideaki Takahashi, Hokkaido University

Selected References

- J.W. Diggle, T.C. Downie, and D.W. Goulding, *Chem. Rev.,* Vol 69, 1969, p 365
- S. Kawai, *Anodizing and Coloring of Aluminum Alloys,* Metal Finishing Information Services Ltd and ASM International, 2002
- M.F. Stevenson, Anodizing, *Surface Engineering,* Vol 5, *ASM Handbook,* ASM International, 1994, p 482–493
- S. Tajima, Anodic Oxidation of Aluminum, *Advances in Corrosion Science and Technology,* M.G. Fontana and R.W. Staehle, Ed., Plenum Press, 1970
- G.C. Wood, Porous Anodic Films on Aluminum, *Oxide and Oxide Films,* Vol 2, J.W. Diggle and A.K. Vijh, Ed., Marcel Dekker, 1972

R.D. Granata, Surface Modification Using Energy Beams, *Corrosion: Fundamentals, Testing, and Protection,* Vol 13A*, ASM Handbook,* ASM International, 2003, p 741–749

Surface Modification Using Energy Beams

Revised by R.D. Granata, Florida Atlantic University

Introduction

SURFACE MODIFICATION, in the context of this article, is the alteration of surface composition or structure by the use of energy or particle beams. Elements may be added to influence the surface characteristics of the substrate by the formation of alloys, metastable alloys or phases, or amorphous layers. Surface-modified layers are distinguished from conversion or coating layers by their greater similarity to metallurgical alloying versus chemically reacted, adhered, or physically bonded layers. However, surface structures are produced that differ significantly from those obtained by conventional metallurgical processes. This latter characteristic further distinguishes surface modification from other conventional processes, such as amalgamation or thermal diffusion. Two different modification methods are discussed. The first, ion implantation, is the introduction of ionized species (usually elements, for example, Ti^+) into the substrate using kilovolt to megavolt ion accelerating potentials. The second method, laser processing, is high-power laser melting with or without mixing of materials precoated on the substrate, followed by rapid melt quenching.
The advantages of the surface modification approach to promoting corrosion resistance include (Ref 1):

- Alteration of the surface without sacrifice of bulk properties
- Conservation of scarce, critical, or expensive alloying elements
- Production of novel surface alloys (unattainable by conventional metallurgical techniques) with superior properties
- Avoidance of coating adhesion problems

The disadvantages of the surface modification techniques include:

- Processing materials having deep or hidden contours
- Cost of processing equipment
- Substrate sensitivity to high energy input (for example, thermal instability)
- The thinness (susceptibility to damage) of the coatings

Ion implantation and laser processing are discussed separately in the following sections.

Reference cited in this section

1. E. McCafferty, P.G. Moore, J.D. Ayers, and G.K. Hubler, in *Corrosion of Metals Processed by Directed Energy Beams,* C.R. Clayton and C.M. Preece, Ed., The Metallurgical Society, 1982, p 1–21

R.D. Granata, Surface Modification Using Energy Beams, *Corrosion: Fundamentals, Testing, and Protection*, Vol 13A, *ASM Handbook*, ASM International, 2003, p 741–749

Surface Modification Using Energy Beams

Revised by R.D. Granata, Florida Atlantic University

Ion Implantation

Surface modification by ion implantation is a technique that was derived from the semiconductor industry. Specimens for corrosion research were initially prepared by using high-energy research instrumentation or commercial semiconductor implanters. Equipment for surface modification of metal parts by batch processing has been built, and production capabilities of the equipment have been evaluated for particular applications. Ion implantation is reaching a stage of development in which specific advantages are being recognized and exploited for enhancing the corrosion and wear resistance of critical metal parts (Ref 2). For wear resistance, ion implantation has been used for the hardening and friction reduction of metal surfaces (Ref 3). Related techniques are also used in conjunction with ion implantation to increase the ratio of material introduced into the substrate per unit area, to provide appropriate mixtures of materials, or to overcome other difficulties involved in surface modification by ion implantation alone. These techniques include:

- *Ion beam sputtering:* An ion beam of argon or xenon directed at a target sputters material from the target to a substrate; the sputtered material arrives at the substrate with enough energy to promote good adhesion of the coating to substrate.
- *Ion beam mixing:* Deposited layers (electroplating, sputtering) tens or hundreds of nanometers thick are mixed and bonded to the substrate by an argon or xenon ion beam.
- *Plasma ion deposition:* Ion beams are used to create coatings having special phases, especially ion-beam-formed carbon coatings in the diamond phase or ion-beam-formed boron nitride coatings.
- *Ion beam assisted deposition:* Ion beams are combined with physical vapor deposition.

Materials Processing and Product Characteristics. The ion implantation technique consists of introducing the target (substrate material) into the implanter vacuum chamber, vaporizing and ionizing the implant species, and electrostatically accelerating the ionized species into the target. Figure 1 shows schematics of research and semiconductor production ion implantation devices. A production-type implanter for materials surface modification is shown in Fig. 2.

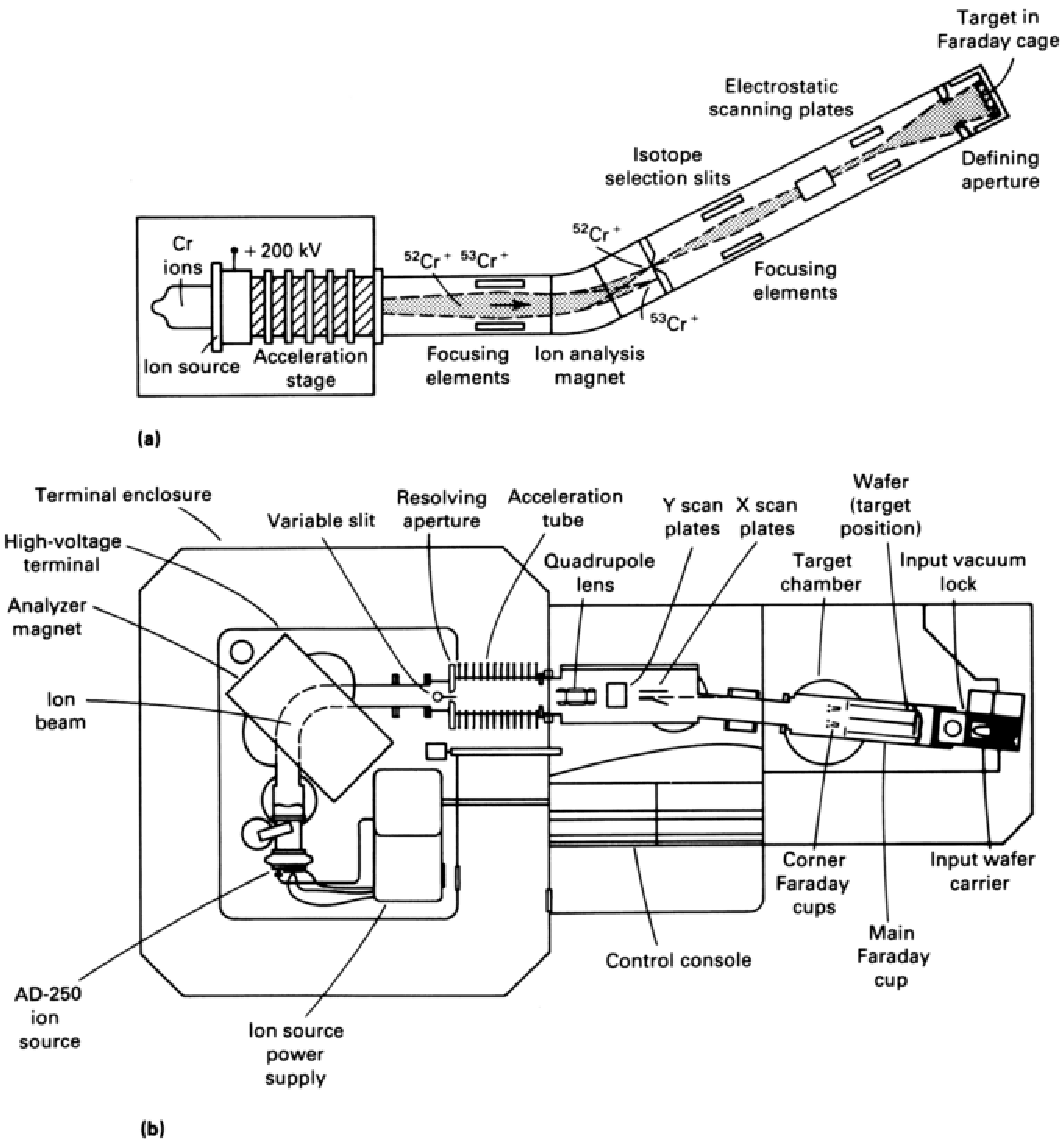

Fig. 1 Schematics of (a) research-type ion implantation system and (b) a production-type semiconductor implanter

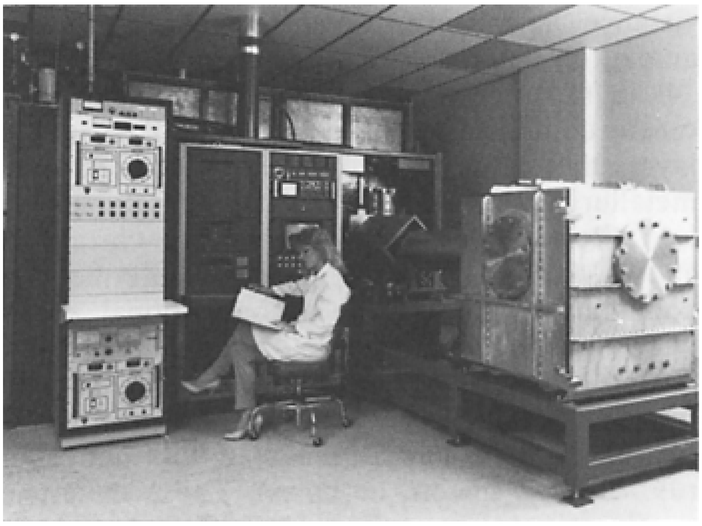

Fig. 2 Commercial ion implanter for materials modification. Courtesy of Spire Corporation

The implant species may be most any element that can be vaporized and ionized in a vacuum chamber. The material used to generate the implant species is usually in the form of a chloride salt of a metal, a gaseous compound, or the pure element. Solid materials are heated to provide an adequate vapor pressure of the implant species. The vaporized material is ionized and accelerated toward the target. Magnetic fields separate various mass/charge ratios and enable the selection of specific implant species. A selected species impacts the target material and is implanted within, producing a surface-modified substrate. The depth to which the species is implanted depends on the accelerating voltage and the atomic numbers of the implant versus target species (Ref 4). Commonly used acceleration voltages are 20 to 200 keV. The typical average implantation depth (range) is 10 to 100 nm. The distribution of implanted species versus range is roughly Gaussian, with the surface distribution determined by relative sputtering (ion etching) ratios.

Figure 3 shows a diagram illustrating calculated concentration profiles of cobalt, aluminum, and boron implanted in iron at 50 keV to a dose of 10^{17} ion/cm^2 (6.45 × 10^{17} ion/in.^{2}). Implantation causes removal (sputtering) of the surface layers, but the thickness of the sputtered layer is generally less than the implantation thickness. Sputtering rates of elements differ and depend on such factors as substrate composition, chemical bonding, metallurgical structure, beam energy, and angle of the incident beam. In some cases, sputtering rate becomes equal to the implantation rate; an equilibrium is achieved (saturation), and no net addition of ions to the substrate occurs. Maximum concentrations of implanted species may be as high as 50 at.%.

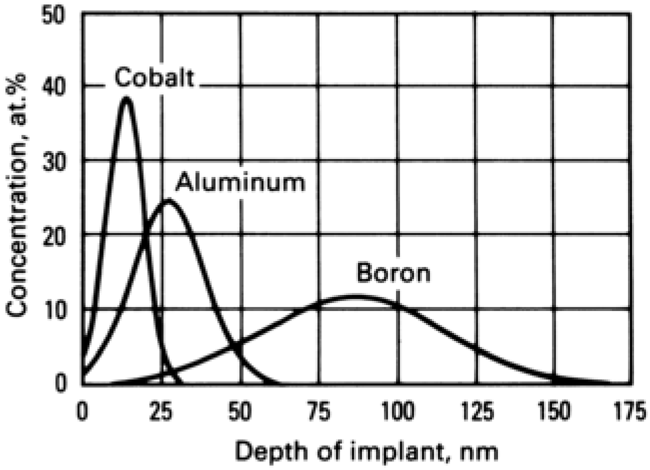

Fig. 3 Concentration profiles for cobalt, aluminum, and boron implants in iron approximated using methods described in Ref 4. Energy: 50 keV. Dose: 10^{71} ion/cm^2 (6.45 × 10^{71} ion/in.^{2})

The advantages of the ion implantation surface modification process include (Ref 1):

- No sacrifice of bulk properties
- Solid-solubility limit can be exceeded.
- Alloy preparation is independent of diffusion constants.

- No coating adhesion problems, because there is no interface
- No significant change in sample dimensions
- Depth concentration distribution is controllable.
- Composition can be changed without affecting grain sizes.
- Precise location of implanted area(s)
- Clean vacuum process
- Allows screening of the effects of changes in alloy composition

The implantation process can be viewed as a means of changing the material properties of an item only at the surface. An item can be fabricated from a material having desirable bulk properties (machinable, low-cost) and can be modified to provide the requisite surface properties (corrosion resistance, wearability). However, the disadvantages of the process must be kept in mind:

- The ion beam cannot process deep or hidden contours (approximately ±30° incidence).
- Processing equipment may be too costly.
- The substrate may be excessively heated by high energy input; for example, the typical energy flux of 2 W/cm^2 (13 W/in.^{2}) can heat a substrate 500 °C (930 °F).
- Inclusions in substrate material may bridge the depth of the surface-modified region, producing sites with undesirable properties.
- Treatment depth may be inadequate for some applications, resulting in galvanic effects with localized corrosion or in implant layer removal by abrasion or erosion.

Problems associated with thermal effects and sample handling have been discussed and technical solutions proposed (Ref 4, 5, 6). For example, nitrogen-implanted surfaces must be kept below 200 °C (390 °F), the temperature at which outward diffusion of nitrogen occurs. Many sample types have been implanted while keeping their surface temperatures below 100 °C (212 °F) by using heat sinks and by modifying processing conditions.

Gaseous Corrosion Properties. Gaseous corrosion or thermal oxidation, in the absence of a liquid phase, is primarily governed by the transport processes in the oxide and the ability of the oxide to resist spalling and breakdown or abrasion and erosion. The ion implantation process has provided a means for studying and modifying the surface layers active in gaseous corrosion. Interesting results have been obtained with implanted materials, as in the following five examples:

- In one study, the effects of the implanted material were found to persist to a much greater depth than the thickness of the implanted layer (Ref 7). Oxide layer growths of more than 100 times the implant depth showed the persistence of the implanted element effects. An Ni-20Cr alloy developed a complete, protective Cr_2O_3 scale more rapidly when implanted with cerium, yttrium, calcium, or aluminum, but implanted zirconium or chromium had no effect. Scale adherence was increased by ion implantation with cerium, yttrium, calcium, or zirconium. For yttrium- implanted Ni-20Cr, the weight change was approximately 25% that of unimplanted material after 24 h at 1000 °C (1830 °F) in 101 kPa (1 atm) oxygen.
- A stainless steel implanted with 10^{17} ion/cm^2 (6.45 × 10^{17} ion/in.^{2}) of yttrium gave no observable spalling of the oxide after more than 6500 h as compared to unimplanted material, which spalled more than 2 mg/cm^2 (Ref 8).
- Implantation of aluminum into an Fe-Cr- 1.4Al alloy increased the surface aluminum concentration to 10% and promoted the formation of a thick, protective, pure Al_2O_3 scale (Ref 9).
- High doses of silicon ion implanted into low- silicon-containing substrates did not provide the desired corrosion resistance associated with their conventional high-silicon counterpart materials. However, ion beam mixing of deposited silicon films with argon at 500 °C (930 °F) produced silicon-rich films on iron or titanium that are thicker than those obtained by ion implantation alone (Ref 10). These thick silicon layers should provide enhanced corrosion resistance. Attempts are being made to produce highly oxidation-resistant $MoSi_2$ by ion beam mixing of molybdenum and silicon layers (Ref 11).
- Zirconium was implanted with such elements as iron, cobalt, or nickel to help relieve internal stresses within the oxide film that result in the break-away oxidation associated with protective oxide fracture (Ref 12).

Aqueous Corrosion Properties. There are two approaches to using ion implantation for increasing the corrosion resistance of substrates; the first is to enhance passivation characteristics, and the second is to create novel materials. In the first approach, implantation creates a surface composition based on conventional metallurgical experience that reacts to form a passive layer. In the second approach, implantation creates a surface composition and a structure that are difficult, impossible, or impractical to achieve by conventional metallurgy.

The two main problems in applying ion implantation methods for creating corrosion-resistant surfaces are producing a surface layer that has a corrosion rate low enough to prevent penetration to the base material during the designed lifetime of the item and producing a surface that is self-repairing. The first problem is approached by introducing elements that enhance corrosion resistance, as in conventional metallurgy—for example, chromium (Ref 13) or molybdenum (Ref 14) in ferrous metals. Another approach is to create combinations of elements in the surface layers that cannot be produced by conventional metallurgical methods—for example, tantalum in iron (Ref 15) or phosphorus in iron-chromium alloys (Ref 16). Tantalum forms intermetallic compounds with iron, but conventional alloys with sufficiently high tantalum content are not readily produced. Other examples are chemically resistant amorphous layers produced, for example, on iron-chromium alloys implanted with phosphorus, carbon, silicon, or boron. These materials passivate spontaneously in hot 25% hydrochloric acid (HCl) (Ref 16).

The second problem is approached by the introduction of elements that are not soluble in or removed by the environment, for example, palladium in titanium. Titanium passivation is strongly promoted by palladium and can be alloyed with it to provide lasting self-passivation properties in acidic media. However, palladium is required only at the interface as a catalyst for the hydrogen reduction reaction and is not readily soluble. Thus, it may be more cost-effective to modify the surface by implantation than to use palladium in the bulk alloy. The palladium-assisted passivation of titanium is a persistent effect with research specimens (Ref 17).

Substantial efforts have been made in the search for effective applications of ion implantation for enhancing corrosion resistance (Ref 18, 19, 20, 21, 22, 23, 24). The greatest difficulty lies in the thinness of the implanted layer; corrosion-resistant layers must not be entirely consumed or damaged. Many research efforts have attempted to mimic conventional alloy compositions. However, the corrosion rates of conventional alloy systems are usually too high relative to the thinness of the implanted layer. The most successful approaches have involved detailed knowledge of a specific material and environmental corrosion conditions or have created unconventional materials. The palladium-implanted titanium, tantalum-implanted iron, and phosphorus- or boron- implanted iron-chromium systems described previously are good examples. Another example of adapting ion implantation to a specific application is its use for interfacial reactions. Implantation of aluminum or titanium in 1010 steel significantly decreased the cathodic delamination rates of organic coatings from the implanted substrates (Ref 25).

Wear resistance enhancement by ion implantation is included in the discussion of surface- modified corrosion-resistant surfaces, because erosion, cavitation, and fretting corrosion are important forms of corrosion. Ion implantation has been shown to have a major effect on wear-resistance properties. The combined effects of ion implantation on corrosion and wear resistance are particularly well suited in applications in which bearings or sliding surfaces are subjected to intermittent use or experience long periods of storage.

Wear resistance is a property that has shown significant improvement for some substrates after surface modification by ion implantation. Activity in this area has been increasing at research laboratories, and specialized equipment has been developed for commercialization. Some of the work on the development of wear-resistant ion- implanted materials is focusing on quantification and lifetime predictions.

Adhesion and abrasion are the most specific wear mechanisms, with corrosive and surface- fracture-related mechanisms making contributions in certain cases. In adhesive wear, surfaces under sufficient local pressure deform plastically and weld at the contact points. When the surfaces separate, the contact point welds break, resulting in the formation of debris and in surface roughening. The oxidized debris causes most of the subsequent wear. Abrasive wear is simply the cutting of one surface by another edged or pointed surface. Abrasive wear decreases as the hardness of the cut surface approaches that of the cutting surface. Abrasion is dramatically lower when both material hardnesses are equal. Adhesive and abrasive wear as well as tribomechanical properties for ion-implanted materials are discussed in Ref 26 and 27, respectively.

There are many examples of ion implantation studies for increasing wear resistance of materials. Many studies have used nitrogen-implanted steel because of the readily available high-current nitrogen beams and because direct comparison to thermal nitriding processes is possible. Increases of the order of two to three times in the microhardness of steels due to nitrogen implantation have been reported (Ref 28). However, large reductions in wear rate often result from relatively small increases in microhardness. Extrusion dies for TiO_2-pigmented

plastics fabricated from low-carbon steel often wear rapidly, yet nitrogen implantation increases the die lifetime by up to ten times. This modification suggests that the microhardness of the steel has been raised above that of TiO_2 (Ref 26). Extended tool life has been demonstrated for plastic molding machines, with estimated ion implantation costs as low as 10% of the ordinary part costs (Ref 3). Nitrogen implantation of a titanium alloy (Ti- 6Al-4V) has been found to decrease the wear rate by more than two orders of magnitude (Ref 29). Data suggest that wear rates have been reduced by almost three orders or magnitude in a titanium alloy designed for hip joint prostheses (Ref 26).

Wear reduction can be attributed to factors other than microhardness. The residual carbon films introduced during implantation of other elements may decrease the occurrence of adhesive wear by providing lower friction coefficients. Implantation of titanium or tantalum usually results in the coimplantation or inward diffusion of carbonaceous matter present in the vacuum system. In the case of titanium-implanted steel, the wear reduction has been attributed to the formation of an amorphous iron-titanium-carbon film. Other systems are being studied—examples include tin-implanted iron, yttrium- and nitrogen-implanted chromium steels, and nitrogen implantation in cobalt-cemented carbide. It has been suggested that deep- penetrating interstitially active elements, such as nitrogen, be used to ion beam mix thin coatings of oxide-modifying materials into substrates for synergistic wear reduction (Ref 26). However, another opinion is that implanted ions do not migrate below the surface. Four mechanisms have been identified as contributing to the reduction of sliding wear of ion-implanted metals (Ref 27):

- Production of low-friction surfaces by altering surface chemistry
- Modification of microstructure to harden the surface
- Stabilization of microstructure against deleterious work-hardening effects
- Introduction of residual (compressive) stresses to combat fracture

Impact wear with and without sliding wear was also studied for various materials implanted with nitrogen (Ref 30). The materials used in the study were:

- *Soft:* aluminum alloy 2024, aluminum alloy 7075, and oxygen-free high-conductivity copper (Unified Numbering System, or UNS, C10100)
- *Medium:* cartridge brass (UNS C26000) Cu10Sn, aluminum bronze (Cu-18Al), and sintered iron (Fe-5Cu-lC)
- *Hard:* America Iron and Steel Institute (AISI) 1018 carbon steel and AISI type 304 stainless steel

Impact wear improved significantly, but the combination of impact and sliding wear showed only a very small effect. Interestingly, one of the materials, cartridge brass, showed no significant improvement.

Critical Evaluation of Product Utility. Numerous examples have been given to define application areas that may benefit from the use of implantation techniques for materials processing. The advantages and disadvantages relate to the small dimension of implantation depth (nanometers). Significant niches are being created for materials processed by ion implantation and related techniques. These surface modification techniques for industrial applications are perhaps best appraised by considering the information presented in Table 1.

Table 1 Successful applications of ion implantation for industrial exploitation

Application	Material	Typical results
Orthopedic implants (artificial hip and knee joints)	Ti-6Al-4V	Significant (400 times) lifetime increase in laboratory tests
Bearings (precision bearings for aircraft)	M50 tool steel, 440C stainless steel, or 52100 bearing steel	Improved protection against corrosion, sliding wear, and rolling-contact fatigue
Extrusion tools (spinnerettes, nozzles, and dies)	Various alloys	Four to six times normal performance
Punching and stamping tools (pellet punches for nuclear fuel, scoring dies for cans)	D2 tool steel	Three to five times normal life and better end products

Source: Ref 2

Other examples of possible interest include the following. Implantation of nitrogen into as- cast Ti-6Al-7Nb alloy was characterized for in vitro behavior using electrochemical methods and grazing incidence x-ray diffraction (XRD). Results showed favorable repassivation kinetics (Ref 31). Shape memory alloy, NiTi, was implanted with nitrogen and boron to enhance the surface properties, corrosion, wear, and fatigue resistance for dental applications (Ref 32). The corrosion resistance of cobalt-chromium alloy in contact with ultrahigh-molecular-weight polyethylene for hip joint replacements was improved using plasma-based ion implantation of nitrogen (Ref 33). The corrosion resistance of uranium in air has been improved by implantation of nitrogen and carbon (Ref 34). The corrosion resistance of uranium and uranium-niobium alloy has been improved by implantation of niobium (Ref 35). Nitrogen plasma source ion implantation improved the corrosion resistance of bearing steel (52100) (Ref 36). The corrosion resistance of 430 stainless steel was improved by combined vapor deposition and ion implantation of silicon and titanium dioxide (Ref 37). Ion implantation and ion beam assisted deposition are considered for improvement of aluminum corrosion (Ref 38).

References cited in this section

1. E. McCafferty, P.G. Moore, J.D. Ayers, and G.K. Hubler, in *Corrosion of Metals Processed by Directed Energy Beams,* C.R. Clayton and C.M. Preece, Ed., The Metallurgical Society, 1982, p 1–21
2. P. Sioshansi, *Thin Solid Films,* Vol 118, 1984, p 61–71
3. B.G. Delves, in *Ion Implantation into Metals,* V. Ashworth, W.A. Grant, and R.P.M. Proctor, Ed., Pergamon Press, 1982, p 126–134
4. G. Dearnaley, J.H. Freeman, R.S. Nelson, and J. Stephen, *Ion Implantation,* North- Holland, 1973
5. F.A. Smidt and B.D. Sartwell, *Nucl. Instrum. Methods Phys. Res. B,* Vol 6, 1985, p 70–77
6. A.S. Denholm and A.B. Wittkower, *Nucl. Instrum. Methods Phys. Res. B,* Vol 6, 1985, p 88–93
7. F.H. Scott, J.S. Punni, G.C. Wood, and G. Dearnaley, *Ion Implantation into Metals,* V. Ashworth, W.A. Grant, and R.P.M. Proctor, Ed., Pergamon Press, 1982, p 245–254
8. M.J. Bennett, G. Dearnaley, M.R. Houlton, and R.W.M. Hawes, *Ion Implantation into Metals,* V. Ashworth, W.A. Grant, and R.P.M. Proctor, Ed., Pergamon Press, 1982, p 264–276
9. U. Bernabai, M. Cavallini, G. Bombara, G. Dearnaley, and M.A. Wilkins, *Corros. Sci.,* Vol 20, 1980, p 19
10. A. Galerie and G. Dearnaley, *Nucl. Instrum. Methods,* Vol 209–210, 1983, p 823–829
11. G. Dearnaley, in *Fundamental Aspects of Corrosion Protection by Surface Modification,* E. McCafferty, C.R. Clayton, and J. Oudar, Ed., The Electrochemical Society, 1984, p 1–16
12. G.C. Bentini, M. Berti, A. Carnera, G. Della Mea, A.V. Drigo, S. Lo Russo, P. Mazzoldi, and G. Dearnaley, *Corros. Sci.,* Vol 20, 1980, p 27
13. R. Valori, D. Popgoshev, and G.K. Hubler, *J. Lubr. Technol. (Trans. ASME),* Vol 105, 1985, p 534–541
14. P.D. Hicks and F.P.A. Robinson, *Corros. Sci.,* Vol 24 (No. 10), 1984, p 885–900
15. V. Ashworth, D. Baxter, W.A. Grant, and R.P.M. Proctor, *Corros. Sci.,* Vol 17, 1977, p 947
16. K. Hashimoto, in *Amorphous Metallic Alloys,* F.E. Luborsky, Ed., Butterworths, 1983, p 471

17. G.K. Wolf, J. Dressler, W. Ensinger, H. Ferber, A. Meger, and P. Munn, in *Fundamental Aspects of Corrosion Protection by Surface Modification,* E. McCafferty, C.R. Clayton, and J. Oudar, Ed., The Electrochemical Society, 1984, p 42–51

18. C.R. Clayton and C.M. Preece, Ed., *Corrosion of Metals Processed by Directed Energy Beams,* The Metallurgical Society, 1982

19. E. McCafferty, C.R. Clayton, and J. Oudar, Ed., *Fundamental Aspects of Corrosion Protection by Surface Modification,* The Electrochemical Society, 1984

20. C.M. Preece and J.K. Hirvonen, Ed., *Ion Implantation Metallurgy,* The Metallurgical Society, 1980

21. V. Ashworth, W.A. Grant, and R.P.M. Proctor, *Ion Implantation into Metals,* Pergamon Press, 1982

22. J.K. Hirvonen, Ed., *Ion Implantation,* Vol 18, *Treatise on Materials Science and Technology,* Academic Press, 1980

23. F.A. Smidt, Ed., *Ion Implantation for Materials Processing,* Noyes Data Corporation, 1983

24. G.K. Hubler, O.W. Holland, C.R. Clayton, and C.W. White, Ed., *Ion Implantation and Ion Beam Processing of Materials: B,* Vol 27, Proceedings of the Materials Research Society, North-Holland, 1984

25. R.D. Granata, M.A. De Crosta, and H. Leidheiser, Jr., in *Proceedings of the Ninth National Congress on Metallic Corrosion,* Vol 1, National Research Council of Canada, 1984, p 264–268

26. G. Dearnaley, *Nucl. Instrum. Methods Phys. Res. B,* Vol 7/8, 1985, p 158–165

27. I.L. Singer, in *Ion Implantation and Ion Beam Processing of Materials,* Vol 27, G.K. Hubler, O.W. Holland, C.R. Clayton, and C.W. White, Ed., Proceedings of the Materials Research Society, North-Holland, 1984, p 585–595

28. J.B. Pethica, in *Ion Implantation into Metals,* V. Ashworth, W.A. Grant, and R.P.M. Proctor, Ed., Pergamon Press, 1982, p 147–156

29. R. Hutchings and W.C. Oliver, *Wear,* Vol 92, 1983, p 143

30. K.K. Shih, *Wear,* Vol 105, 1985, p 341–347

31. L. Thair, U.K. Mudali, N. Bhuvaneswaran, K.G.M. Nair, R. Asokamani, and B. Raj, *Corros. Sci.,* Vol 44 (No. 11), 2002, p 2439–2457

32. H. Pelletier, D. Muller, P. Mille, and J.J. Grob, *Surf. Coat. Technol.,* Vol 158–159, 2002, p 301–308

33. D. Ikeda, M. Ogawa, Y. Hara, Y. Nishimura, O. Odusanya, K. Azuma, S. Matsuda, M. Yatsuzuka, and A. Murakami, *Surf. Coat. Technol.,* Vol 156, 2002, p 301–305

34. R. Arkush, M.H. Mintz, and N. Shamir, *J. Nucl. Mater.,* Vol 281, 2000, p 182–190

35. W.-H. Luo, R.-F. Ni, and S. Wu, *Mater. Prot. (China),* Vol 33, 2000, p 6–8

36. J.H. Booske, W. Wang, C. Baum, C. Clothier, N. Zjaba, and L. Zhang, *Surf. Coat. Technol.,* Vol 111, 1999, p 97–102

37. R. Nishimura, K. Yamakawa, J. Ishiga, Y. Matsumoto, and H. Nagano, *Mater. Chem. Phys.*, Vol 54, 1998, p 289–292

38. P.M. Natishan, E. McCafferty, G.K. Hubler, and B.D. Sartwell, *Advances in Coatings Technologies for Surface Engineering*, Minerals, Metals and Materials Society/AIME, 1997, p 271–285

R.D. Granata, Surface Modification Using Energy Beams, *Corrosion: Fundamentals, Testing, and Protection*, Vol 13A, *ASM Handbook*, ASM International, 2003, p 741–749

Surface Modification Using Energy Beams

Revised by R.D. Granata, Florida Atlantic University

Laser Surface Processing

Lasers with continuous outputs of 0.5 to 10 kW can be used to modify the metallurgical structure of a surface and to tailor the surface properties without adversely affecting the bulk properties. The surface modification can take the following three forms. The first is transformation hardening, in which a surface is heated so that thermal diffusion and solid-state transformations can take place (Ref 39, 40, 41). The second is surface melting, which results in a refinement of the structure due to the rapid quenching from the melt (Ref 40, 41, 42, 43, 44, 45). The third is surface alloying, in which alloying elements are added to the melt pool to change the composition of the surface (Ref 46, 47, 48, 49, 50, 51, 52). The novel structures produced by laser surface melting and alloying can exhibit improved electrochemical behavior.

Materials Processing

The processing parameters necessary for laser surface processing depend on the type of modification to be done (for example, transformation hardening or surface alloying) and the properties of the material that are being treated (for example, thermal diffusivity, heat capacity, and transformation temperatures). Figure 4 shows typical ranges of conditions for various processes. The laser power, power density, and interaction time are the primary variables. Other variables, such as the composition of the atmosphere during treatment or the rate of material addition, are determined by the details of the processing—for example, the necessity of shielding against oxidation and the desired thickness, composition, and structure of the surface layer.

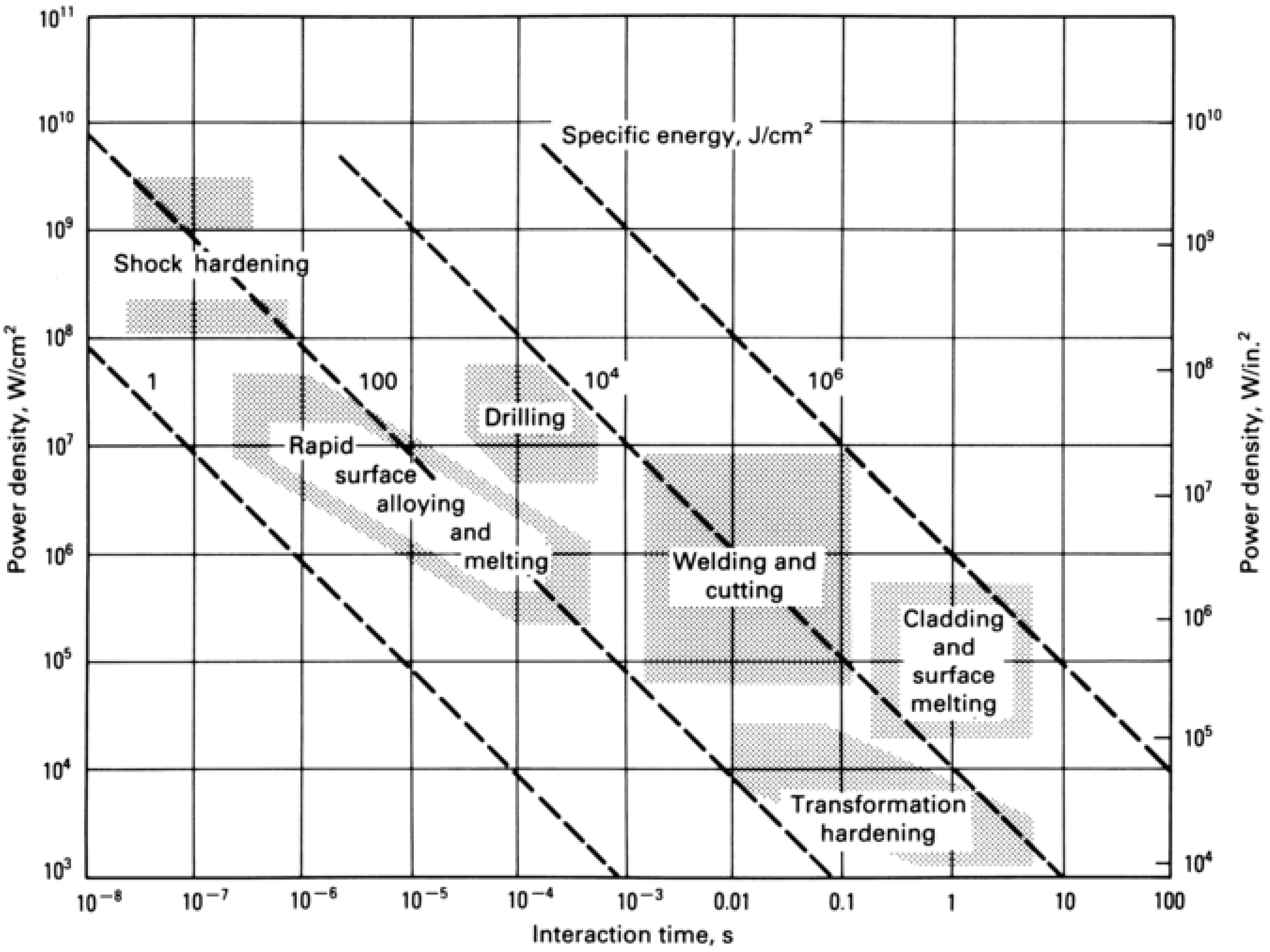

Fig. 4 Interaction times and power densities necessary for various laser surface modification processes

The laser-beam-modified layer can range in thickness from 0.01 to 5 mm (0.4 to 200 mils), depending on the processing variables, although thicknesses of 0.05 to 1 mm (2 to 40 mils) are more common. The longer the interaction time of the laser beam with the material, the deeper the processed layer will be. Of the processes shown in Fig. 4, the areas labeled "Cladding and surface melting" and "Transformation hardening" delineate process parameters that typically affect the material to depths from 0.5 to 5 mm (20 to 200 mils) and result in metallurgical structures similar to welded structures. The parameters designated "Rapid surface alloying and melting" affect a surface layer only 0.02 to 0.6 mm (0.8 to 24 mils) thick but result in quench rates to 10^7 K/s and therefore allow for the production of novel metallurgical structures and alloys.

The procedure for laser beam surface modification is shown in Fig. 5. A high-power laser beam is brought to a focus near the surface of the workpiece. After a melt pool is established, the laser beam can be rastered across the surface, melting a strip of material with each sweep, until the entire surface has been processed. The processing is performed in an inert gas atmosphere or vacuum to protect the metal from oxidation. In practice, it is more convenient to move the workpiece rather than the laser beam.

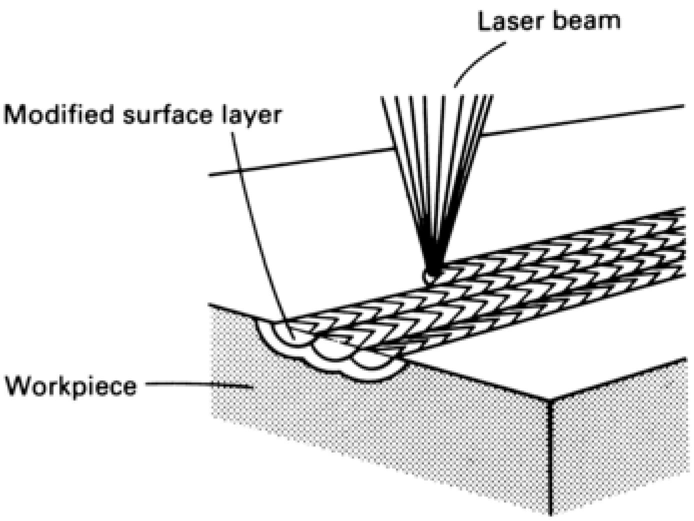

Fig. 5 Schematic of the procedure for the laser processing of metals

Figure 6 shows a schematic of an apparatus for processing laboratory specimens. The specimen is passed through the laser beam by the rotation of the turntable, and the entire apparatus is translated a fraction of a melt width between passes to process a larger area. The process is varied by changing the power level of the laser beam, the power density (or spot diameter), or the sweep speed. The effects of these variables on the depth of melting for three materials are shown in Fig. 7. As can be seen, the melt depth can be varied by an order of magnitude simply by changing the sweep speed. The width of the melt pass is determined primarily by the diameter of the laser spot and the thermal properties of the material and is very slightly dependent on the sweep speed. The rate at which a surface can be processed is typically approximately 1 cm^2/s (0.16 $in.^2$/s) for a variety of conditions and materials.

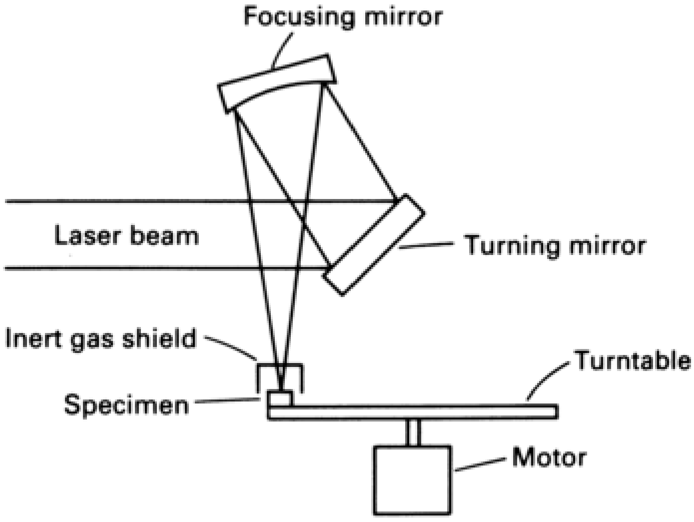

Fig. 6 Schematic of an apparatus for laser processing

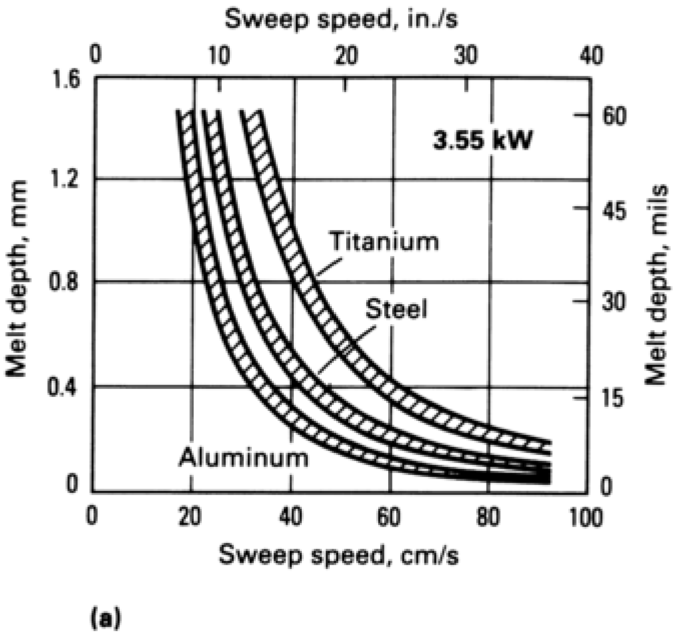

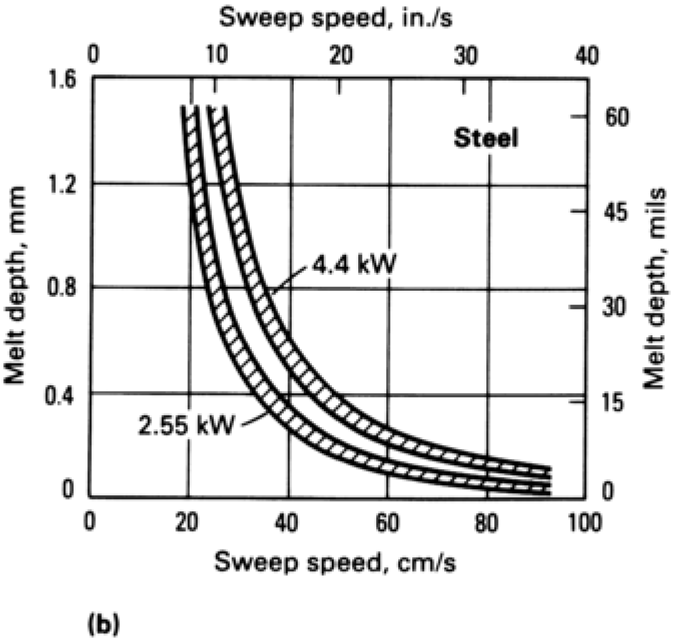

Fig. 7 Effects of laser-processing conditions on melt depth. (a) For three materials at one power level. (b) For steel at two power levels

Product Characteristics

Solidification Effects. The heat flow characteristics of such processing can reasonably be described by one-dimensional heat flow in which the rate at which energy enters the surface is balanced by the rate at which heat is conducted away by the cool substrate (Ref 53). A number of studies have been devoted to characterizing the temperature profiles that result from the laser and electron beam processing of materials (Ref 39, 41, 54). The character of the temperature profiles experienced by material at various depths below the surface of the metal is shown in Fig. 8. The three reference temperatures indicated represent liquidus (T_L), solidus (T_S), and solid- state transformation (T_R) temperatures. As the laser beam sweeps across the surface of a metal sample, the surface begins to heat. When the melting temperature of the material is exceeded, a melt front is established and moves from the free surface of the sample toward the bulk. Shortly after the beam is turned off (or has moved away), the melt front slows and then stops. It then moves back toward the free surface as a solidification front. The unique characteristics of this solidification front are the high cooling rates (such as 10^7 K/s) and the steep temperature gradient (such as 10^5 K/cm). These characteristics promote the formation of metastable compositions and structures.

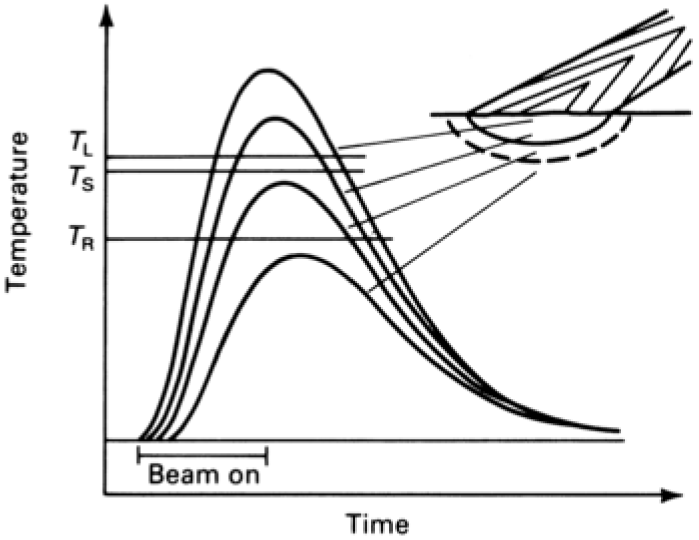

Fig. 8 View of laser-melted surface and temperature profiles experienced at different points on the surface during laser melting. Liquidus (T_L), solidus (T_S), and solid-state transformation (T_R) temperatures are indicated.

Because of this steep temperature gradient, there is only a thin layer of metal that is cool enough to solidify. The material above this layer is above the liquidus temperature, and the material below this layer has already solidified. There is a strong epitaxial character to the resolidification as a result of the steep temperature gradients (Ref 55, 56). This is illustrated in Fig. 9. The two effects that compete during the solidification are the regrowth of grains from the substrate and the heterogeneous nucleation and growth of new grains in this thin layer of chilled metal. For most alloys, grains from the substrate will grow into the chilled zone, and any grains that may have nucleated within the melt pool will either redissolve or be transported by the melt front to the free surface. As an example of this, Fig. 10 shows a β-titanium alloy that has been laser processed.

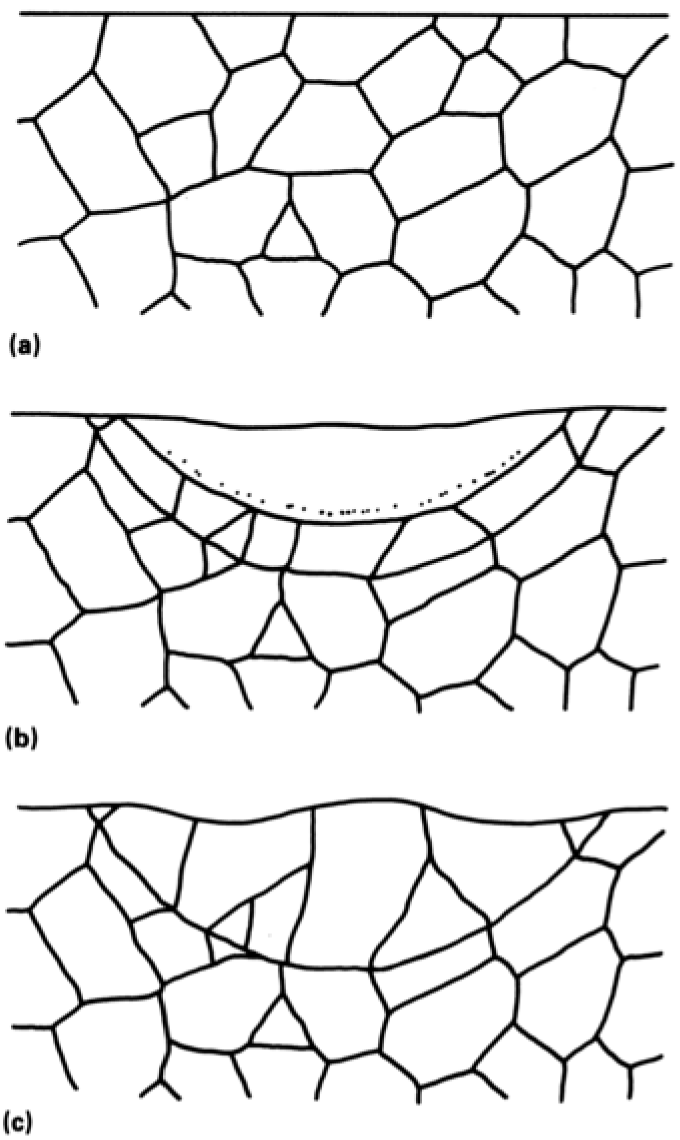

Fig. 9 Origins of epitaxial resolidification as a result of laser processing. (a) Before laser melting. (b) During resolidification. (c) After quenching

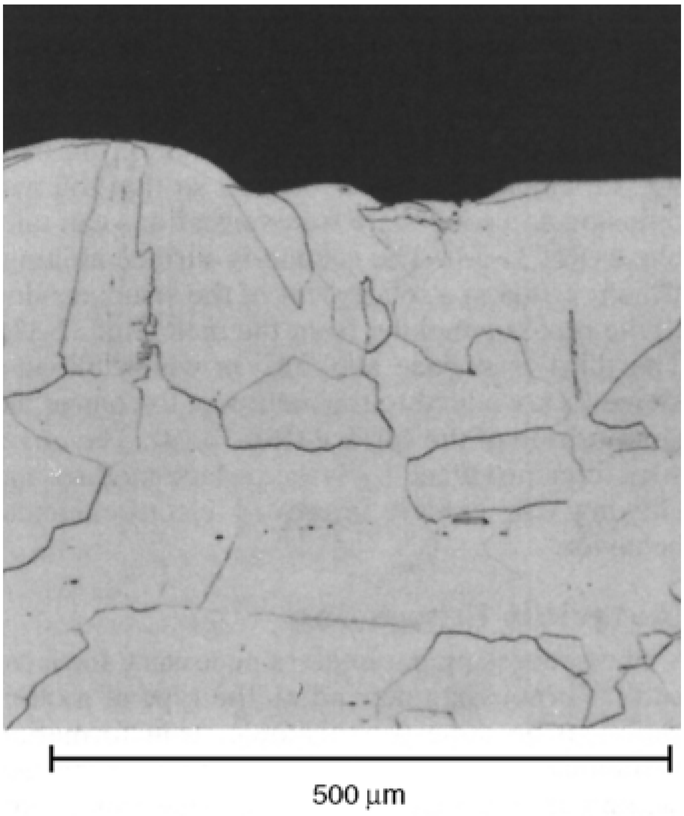

Fig. 10 Planar resolidification of a ß-titanium alloy

The epitaxial solidification can have a striking effect on the grain size of the surface layer and on the crystallographic texture. Because some crystal planes grow faster than others—for example, (100) for cubic crystals and (1010) for hexagonal close-packed crystals—those substrate grains having a large component of these orientations in the direction of the temperature gradient will grow at the expense of less favorably oriented grains. As these grains grow, they will tend to squeeze out less favorably oriented grains. This affects the crystallographic texture in two ways. First, there is a higher probability for grains at the free surface to be oriented with the fast-growing direction normal to the free surface, and second, low-angle grain boundaries will occur with a higher frequency than in the substrate. As shown in Fig. 11, when the grain size of the metal before processing is small compared to the depth of melting, there is a coarsening of the grain size, and the texture effects are more pronounced. Examples of these effects are shown in Fig. 9 for a large-grain material and in Fig. 12 for a fine-grain material.

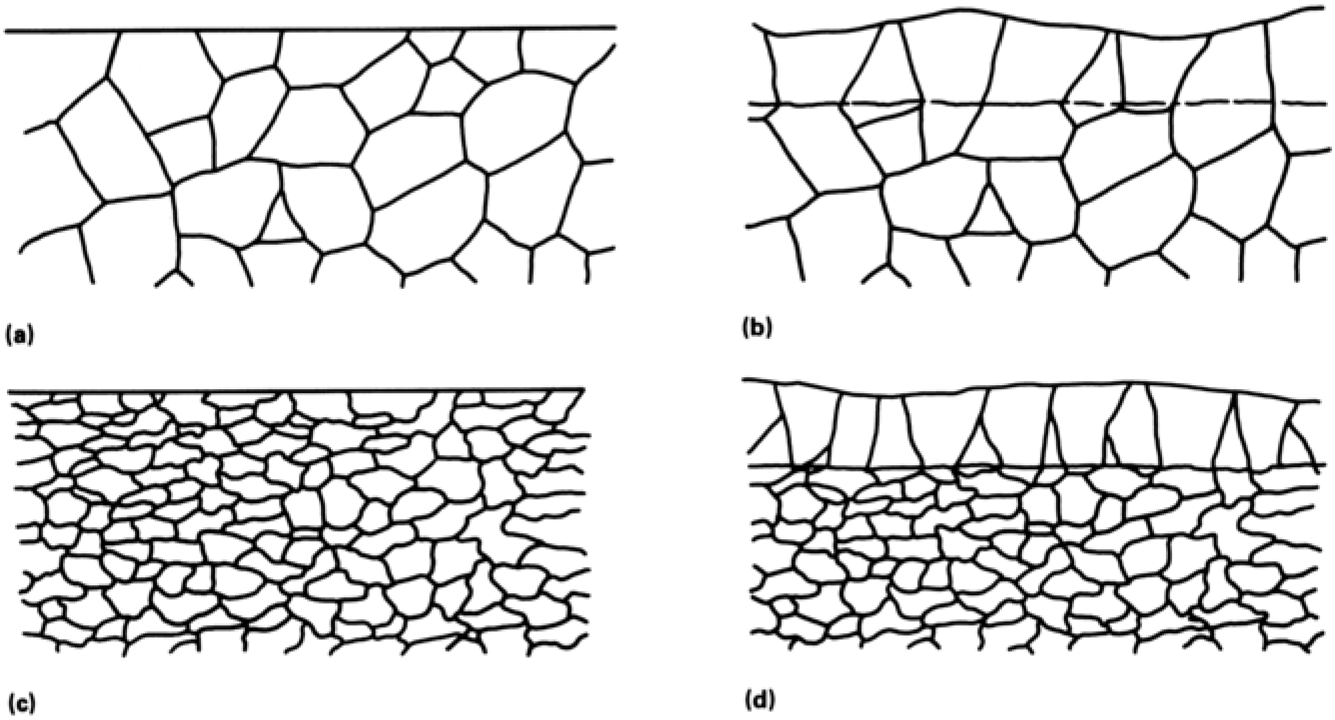

Fig. 11 Effect of epitaxial resolidification on grain size for a material with large original grain size (a and b) and a material with small original grain size (c and d) compared to the melt depth. (a) and (c) Before processing. (b) and (d) After processing

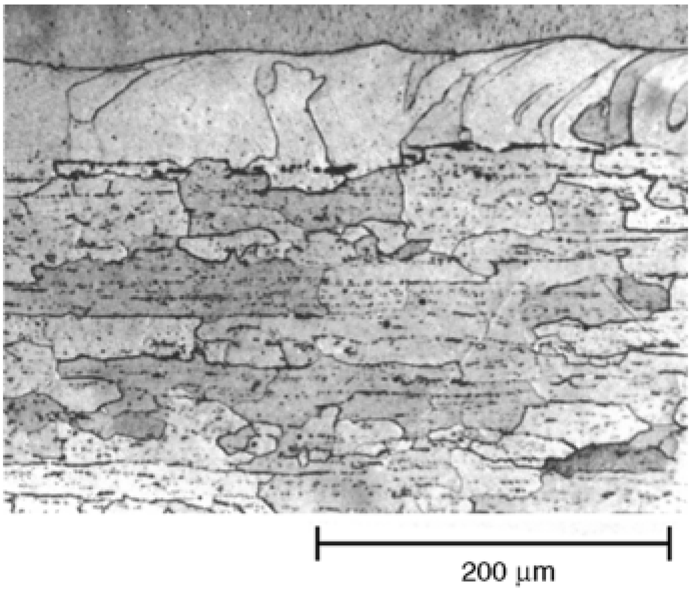

Fig. 12 Coarsening of grain size in a ferritic stainless steel by laser melting

During the solidification process, there is generally a redistribution of solute atoms away from the solidification front, so that the interface can remain as close to equilibrium as possible (Ref 57). After an initial transient, this partitioning results in the geometrical destabilization of the solidification front, and dendritic solidification results. For a single-crystal alloy that undergoes rapid surface melting, the dendritic character of the resulting melt is shown in Fig. 13. This effect was documented by the laser melting of single crystals of a nickel-base superalloy (Ref 55). The high-temperature gradient affects the character of the dendritic growth in two ways. First, it restrains crystal growth to the directions of the fast-growing crystal planes, as described previously, and second, it minimizes the amount of segregation because of the short times allowed for lateral diffusion. An example of the dendritic character of laser-processed material is shown in Fig. 14. The diameter of the dendrites can be used to estimate the cooling rates experienced by the material as it resolidified. Higher cooling rates result in less lateral diffusion and smaller dendrites, while lower cooling rates result in more lateral diffusion and larger-diameter dendrites.

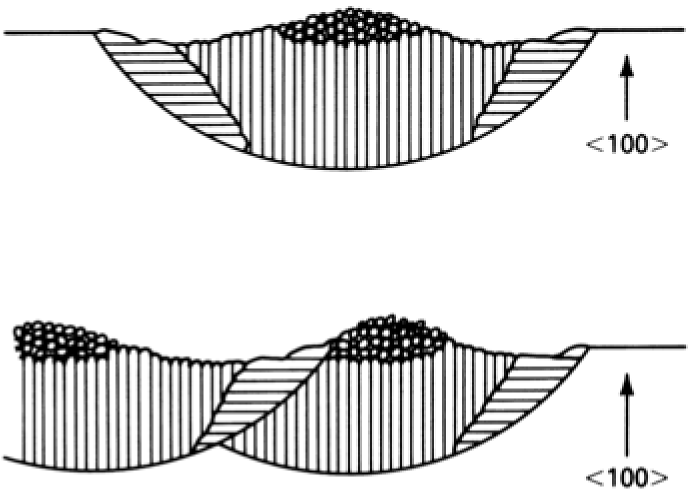

Fig. 13 Dendritic solidification of cubic single crystals. The high-temperature gradient resulting from laser melting causes dendrites to grow in the preferred • 100• direction

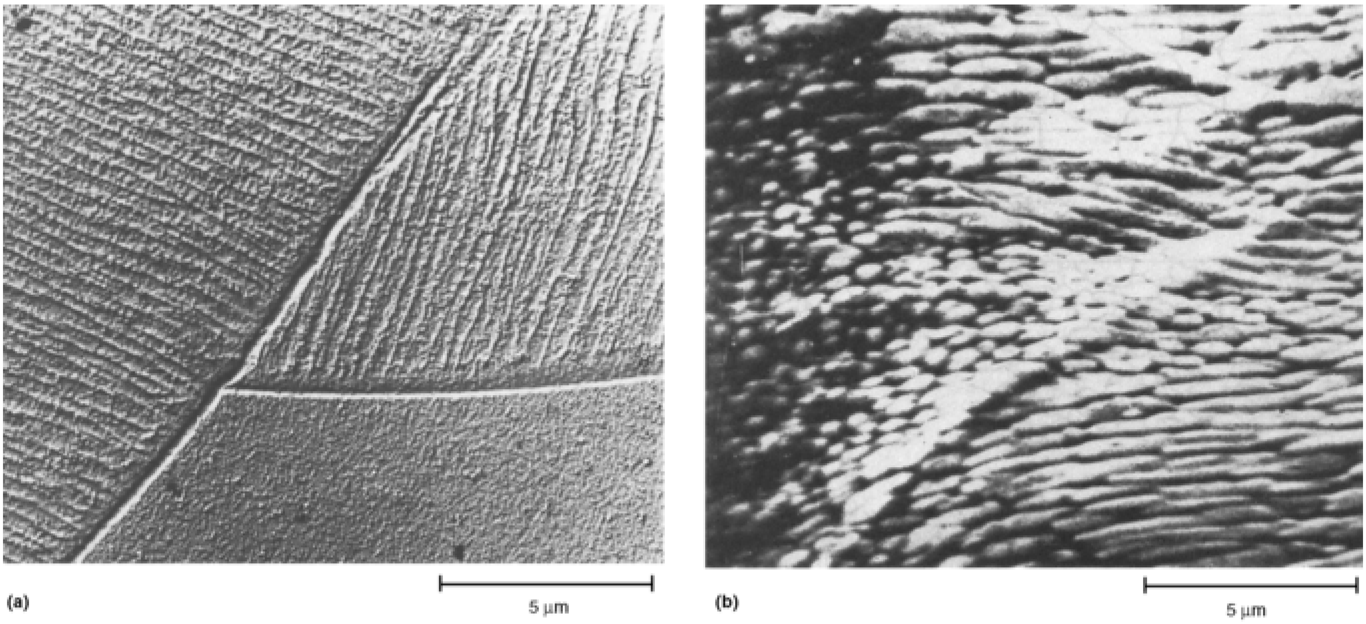

Fig. 14 Dendritic solidification in laser-surface-melted type 304 stainless steel. (a) Surface replica of a polished-and-etched cross section. (b) Scanning electron micrograph of the free surface

To the extent that equilibrium cannot be maintained at the solidification front by partitioning, as described in the previous paragraph, more than the equilibrium amount of solute atoms will be incorporated into the solidification structure. An increase in the cooling or solidification rates results in still greater deviations from the equilibrium concentrations (Ref 58, 59). In systems that exhibit solubility at all compositions, for example, the aluminum-manganese system, the solubility limits can be extended. Deviations from equilibrium can also result in the formation of metastable crystal structures when the system has several phases with comparable free energies of formation (Ref 60, 61). Amorphous or glassy surface layers can be produced by laser processing only when the system has several energetically and structurally similar crystalline phases; thus, atoms attaching to the solidification front will have a variety of closely spaced lattice sites with similar energies to choose from. This confuses the long-range order and destroys the crystalline character of the solid.

Changing the Chemical Composition. In addition to the structural modifications described in the previous section, the composition of the surface layer can also be changed to form surface alloys whose compositions can be tailored to suit surface requirements. Changes in composition have been accomplished with several techniques (Ref 39, 47, 49, 50, 62). For example, the specimen can be coated before laser processing with a thin layer of the desired alloying element or elements. Such coatings have been applied by vacuum deposition, electroplating, spraying, or the use of a slurry. The alloying elements can also be introduced directly into the melt pool during processing in the form of wire or as an injected powder. When the composition is changed,

care must be taken to ensure that the alloying elements are distributed uniformly in the surface layer. Three mechanisms have been identified for facilitating the mixing of components: liquid-state diffusion, convection currents within the melt pool, and agitation of the melt pool by a laser-sustained plasma (Ref 50). A uniform composition can generally be obtained by processing two or more times, as shown in Fig. 15. The first set of passes disperses the alloying elements to the desired depth and determines the overall composition of the surface alloy. Subsequent passes (using processing conditions selected to obtain slightly shallower melt depths) further homogenize the surface.

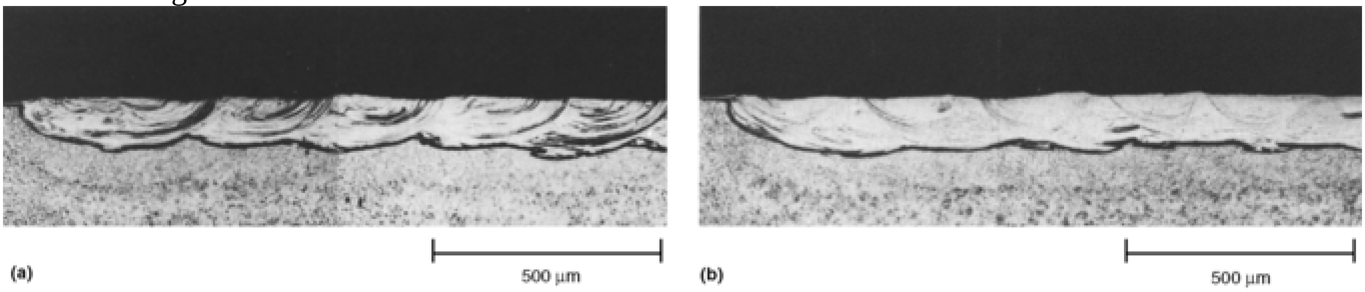

Fig. 15 Laser surface alloying of molybdenum into Ti-6Al-4V showing the effectiveness of multiple passes in homogenizing the chemical composition. (a) Single pass. (b) Double pass

Effects of Microstructure on Properties. The microstructural changes that result from laser processing can take several forms: a redistribution of major alloy components, a redistribution of any second phases or precipitates, a change in the crystalline character of the surface, or a change in the composition. The melting process results in a leveling of any large-scale composition variations, but the solidification transients can also result in a surface that is enriched in one or more of the alloy components. The high cooling rates during solidification and the accompanying extension of solid-solubility limits often result in either the elimination of second phases or a fine distribution of second phases or precipitates. Alloying may be necessary to take advantage of the higher solubility limits. The steep temperature gradients present during processing generally result in epitaxial resolidification, which introduces some crystallographic texture of the surface grains and grain boundaries (Ref 63). The modification of composition holds the most promise for improving electrochemical behavior, because the surface chemistry can be adjusted so that a solidification structure is obtained on quenching that exhibits more corrosion resistance than the base alloy (Ref 64).

Corrosion Properties

The corrosion resistance of laser-processed materials has been studied by several research groups. For example, laser beam processing was used in one study to melt and rapidly solidify type 304 stainless steel (UNS S30400) and ferritic Fe-13Cr-*x*Mo (*x* = 0, 2, 3.5, or 5) stainless steels (Ref 65). The critical current density for the passivation of laser-processed type 304 stainless steel in 1 *N* sulfuric acid (H_2SO_4) decreased two orders of magnitude compared to unprocessed material. The width of the active peaks decreased for ferritic stainless steels versus unprocessed material. Pitting potentials increased by approximately 150 mV for type 304 stainless steel and 5% Mo ferritic stainless steel. Ferritic steels with 0, 2, or 3.5% Mo showed decreases in the pitting potentials.

In another case, the corrosion behavior of iron-aluminum bronzes was studied electrochemically in 5% H_2SO_4 (Ref 66). Substantial beneficial effects were observed and attributed to homogenization of the complex microstructure.

Lastly, laser surface alloying was performed to incorporate chromium in Society of Automotive Engineers (SAE) 1018 steel (UNS G10180) and molybdenum in type 304 stainless steel (Ref 67). The SAE 1018-Cr materials passivated similarly to corresponding bulk alloys (5 to 80% Cr). The 304-3Mo material was similar in pitting resistance to type 316 stainless steel (UNS S31600). The 304-9Mo material was superior to type 316 stainless steel and showed no pitting up to oxygen evolution potentials. Table 2 shows some of the results for the 304-Mo materials. Plasma-sprayed titanium coatings on steel were consolidated by laser processing to remove residual porosity, which is the major obstacle to enhanced corrosion resistance (Ref 68).

Table 2 Effect of laser surface alloying with molybdenum on pitting potentials of austenitic stainless steels in 0.1 *M* NaCl

Sample	Composition, %			Pitting potential (E_{pit}), (V vs SCE)
	Cr	**Ni**	**Mo**	
Type 304	18–20	8–10	0	0.300
Type 316	16–18	10–14	2–3	0.550
304-Mo	18.9	9.1	3.7	0.500
304-9Mo	19.2	11.7	9.6	Did not pit

SCE, saturated calomel electrode

Critical Evaluation of Product Utility

Laser processing provides unique opportunities for producing corrosion-resistant surface layers. High-performance surface layers can be designed while conserving scarce, expensive, or critical materials. However, the major limitations associated with laser processing are the compatibility of substrates with thermal conduction requirements and the current restriction to planar substrates.
Other examples include:

- The intergranular corrosion resistance of Al 6013-T651 was improved by excimer laser surface treatment in nitrogen atmosphere, resulting in formation of AlN (Ref 69).
- The pitting corrosion resistance of Ti-6Al-4V alloy (UNS R56400/R56401) was improved by excimer laser surface treatment in argon atmosphere and, to a lesser extent, in nitrogen atmosphere (Ref 70).
- The cavitation erosion resistance of brass was improved by laser surface modification using an alloying powder of NiCrSiB (Ref 71).
- Laser hardfacing of mild steel AISI 1050 was achieved by flame spraying NiCoCrB powder, followed by laser treatment. Cavitation erosion resistance was increased by factors of 4 and 8 in distilled water and 3.5% NaCl, respectively (Ref 72).

References cited in this section

39. J.W. Hill, M.J. Lee, and I.J. Spalding, *Opt. Laser Technol.,* Vol 6, Dec 1974, p 276

40. E.M. Breinan, B.H. Kear, and C.M. Banas, *Phys. Today,* Vol 29, 1976, p 11, 44

41. H.E. Cline and T.R. Anthony, *J. Appl. Phys.,* Vol 48, 1977, p 3895

42. T.R. Anthony and H.E. Cline, *J. Appl. Phys.,* Vol 49, 1978, p 1248

43. P.R. Strutt, H. Nowotny, M. Tuli, and B.H. Kear, *Mater. Sci. Eng.,* Vol 36, 1978, p 217

44. G. Staehli and C. Sturzenegger, *Scr. Metall.,* Vol 12, 1978, p 617

45. P.L. Bonora, M. Bassoli, P.L. De Anna, B. Battaglin, G. Della Mea, P. Mazzoldi, and A. Miotello, *Electrochim. Acta,* Vol 25, 1980, p 1497

46. C.W. Draper, R.E. Woods, and L.S. Meyer, *Corrosion,* Vol 36, 1980, p 405

47. R.J. Pangborn and D.R. Beaman, *J. Appl. Phys.,* Vol 5, 1980, p 5992

48. P.G. Moore and E. McCafferty, *J. Electrochem. Soc.,* Vol 128, 1981, p 1391

49. D.S. Gnanamuthu, *Opt. Eng.,* Vol 19, 1980, p 783

50. P.G. Moore, in *Proceedings of the International Laser Processing Conference,* Laser Institute of America, 1981

51. C.W. Draper, *Appl. Opt.,* Vol 20, 1981, p 3093

52. H.W. Bergmann and B.L. Mordike, *Z. Werkstofftech.,* Vol 12, 1981, p 142

53. H.S. Carslaw and J.C. Jaeger, *Conduction of Heat in Solids,* Clarendon Press, 1959

54. L.E. Grenwald, E.M. Breinan, and B.H. Kear, in *Laser-Solid Interactions and Laser Processing—1978,* S.D. Ferris, E.J. Leany, and J.M. Poate, Ed., American Institute of Physics, 1979 p 189

55. S.L. Narasimhan, S.M. Copley, E.W. Van Stryland, and M. Bass, *ICEE J. Quant. Electr.,* Vol 13, 1977, p 2D

56. A. Munitz, *Metall. Trans. B,* Vol 11, 1980, p 563

57. B. Chalmers, *Principles of Solidification,* Robert E. Krieger, 1977

58. C.W. Draper, S.P. Sharma, J.L. Yeh, and S.L. Bernasek, *Surf. Interface Anal.,* Vol 2 (No. 5), 1980, p 179

59. D.G. Beck, S.M. Copley, and M. Bass, *Metall. Trans. A,* Vol 13, 1982, p 1879

60. P.T. Sarjeant and R. Roy, *Mater. Res. Bull.,* Vol 3, 1968, p 265

61. J.A. Dantzig and S.H. Davis, *Mater. Sci. Eng.,* Vol 32, 1978, p 199

62. N.B. Dahotre, Ed., *Lasers in Surface Engineering,* ASM International, 1998

63. L.S. Weinman, J.N. DeVault, and P.G. Moore, in *Applications of Lasers in Materials Processing,* E.A. Metzbower, Ed., American Society for Metals, 1979, p 259

64. L.E. Grenwald, E.M. Breinan, and B.H. Kear, in *Laser-Solid Interactions and Laser Processing—1978,* S.D. Ferris, E.J. Leany, and J.M. Poate, Ed., American Institute of Physics, 1979, p 239

65. J.B. Lumsden, D.S. Gnanamuthu, and R.J. Moores, in *Fundamental Aspects of Corrosion Protection by Surface Modification,* E. McCafferty, C.R. Clayton, and J. Oudar, Ed., The Electrochemical Society, 1984, p 122–129

66. J. Javadpour, C.R. Clayton, and C.W. Draper, in *Corrosion of Metals Processed by Directed Energy Beams,* C.R. Clayton and C.M. Preece, Ed., The Metallurgical Society, 1982, p 135–145

67. E. McCafferty and P.G. Moore, *J. Electrochem. Soc.,* Vol 133 (No. 6), 1986, p 1090–1096

68. E. McCafferty, G.K. Hubler, P.M. Natishan, P.G. Moore, R.A. Kant, and B.D. Sartwell, Ion Beam or Laser Processing of Metal Surfaces for Improved Corrosion Resistance, *Mater. Sci. Eng.,* 1987

69. C.P. Chan, T.M Yue, and H.C. Man, *Mater. Sci. Technol.,* Vol 18, p 575–580

70. T.M. Yue, J.K. Yu, Z. Mei, and H.C. Man, *Mater. Lett.,* Vol 52, 2002, p 206–212

71. K.F. Tam, F.T. Cheng, and H.C. Man, *Proceedings of the Conference on Laser-Solid Interactions for Materials Processing,* 2000 MRS Spring Meeting, 25–27 April 2000 (San Francisco, CA), Materials Research Society, 2000, p J3.2.1–J3.2.6

72. C.T. Kwok, F.T. Cheng, and H.C. Man, *Proceedings of the Conference on the 20th International Congress on ICALEO 2001: Applications of Lasers and Electro-Optics,* 15–18 Oct 2001 (Jacksonville, FL), Laser Institute of America, 2001, p 817–827

R.D. Granata, Surface Modification Using Energy Beams, *Corrosion: Fundamentals, Testing, and Protection*, Vol 13A, *ASM Handbook*, ASM International, 2003, p 741–749

Surface Modification Using Energy Beams

Revised by R.D. Granata, Florida Atlantic University

Acknowledgment

This article has been adapted from R.D. Granata and P.G. Moore, Surface Modification, *Corrosion,* Vol 13, *ASM Handbook* (formerly *Metals Handbook,* 9th ed.), ASM International, 1987, p 498–505.

R.D. Granata, Surface Modification Using Energy Beams, *Corrosion: Fundamentals, Testing, and Protection*, Vol 13A, *ASM Handbook*, ASM International, 2003, p 741–749

Surface Modification Using Energy Beams

Revised by R.D. Granata, Florida Atlantic University

References

1. E. McCafferty, P.G. Moore, J.D. Ayers, and G.K. Hubler, in *Corrosion of Metals Processed by Directed Energy Beams,* C.R. Clayton and C.M. Preece, Ed., The Metallurgical Society, 1982, p 1–21
2. P. Sioshansi, *Thin Solid Films,* Vol 118, 1984, p 61–71
3. B.G. Delves, in *Ion Implantation into Metals,* V. Ashworth, W.A. Grant, and R.P.M. Proctor, Ed., Pergamon Press, 1982, p 126–134
4. G. Dearnaley, J.H. Freeman, R.S. Nelson, and J. Stephen, *Ion Implantation,* North- Holland, 1973
5. F.A. Smidt and B.D. Sartwell, *Nucl. Instrum. Methods Phys. Res. B,* Vol 6, 1985, p 70–77
6. A.S. Denholm and A.B. Wittkower, *Nucl. Instrum. Methods Phys. Res. B,* Vol 6, 1985, p 88–93
7. F.H. Scott, J.S. Punni, G.C. Wood, and G. Dearnaley, *Ion Implantation into Metals,* V. Ashworth, W.A. Grant, and R.P.M. Proctor, Ed., Pergamon Press, 1982, p 245–254
8. M.J. Bennett, G. Dearnaley, M.R. Houlton, and R.W.M. Hawes, *Ion Implantation into Metals,* V. Ashworth, W.A. Grant, and R.P.M. Proctor, Ed., Pergamon Press, 1982, p 264–276
9. U. Bernabai, M. Cavallini, G. Bombara, G. Dearnaley, and M.A. Wilkins, *Corros. Sci.,* Vol 20, 1980, p 19

10. A. Galerie and G. Dearnaley, *Nucl. Instrum. Methods,* Vol 209–210, 1983, p 823–829

11. G. Dearnaley, in *Fundamental Aspects of Corrosion Protection by Surface Modification,* E. McCafferty, C.R. Clayton, and J. Oudar, Ed., The Electrochemical Society, 1984, p 1–16

12. G.C. Bentini, M. Berti, A. Carnera, G. Della Mea, A.V. Drigo, S. Lo Russo, P. Mazzoldi, and G. Dearnaley, *Corros. Sci.,* Vol 20, 1980, p 27

13. R. Valori, D. Popgoshev, and G.K. Hubler, *J. Lubr. Technol. (Trans. ASME),* Vol 105, 1985, p 534–541

14. P.D. Hicks and F.P.A. Robinson, *Corros. Sci.,* Vol 24 (No. 10), 1984, p 885–900

15. V. Ashworth, D. Baxter, W.A. Grant, and R.P.M. Proctor, *Corros. Sci.,* Vol 17, 1977, p 947

16. K. Hashimoto, in *Amorphous Metallic Alloys,* F.E. Luborsky, Ed., Butterworths, 1983, p 471

17. G.K. Wolf, J. Dressler, W. Ensinger, H. Ferber, A. Meger, and P. Munn, in *Fundamental Aspects of Corrosion Protection by Surface Modification,* E. McCafferty, C.R. Clayton, and J. Oudar, Ed., The Electrochemical Society, 1984, p 42–51

18. C.R. Clayton and C.M. Preece, Ed., *Corrosion of Metals Processed by Directed Energy Beams,* The Metallurgical Society, 1982

19. E. McCafferty, C.R. Clayton, and J. Oudar, Ed., *Fundamental Aspects of Corrosion Protection by Surface Modification,* The Electrochemical Society, 1984

20. C.M. Preece and J.K. Hirvonen, Ed., *Ion Implantation Metallurgy,* The Metallurgical Society, 1980

21. V. Ashworth, W.A. Grant, and R.P.M. Proctor, *Ion Implantation into Metals,* Pergamon Press, 1982

22. J.K. Hirvonen, Ed., *Ion Implantation,* Vol 18, *Treatise on Materials Science and Technology,* Academic Press, 1980

23. F.A. Smidt, Ed., *Ion Implantation for Materials Processing,* Noyes Data Corporation, 1983

24. G.K. Hubler, O.W. Holland, C.R. Clayton, and C.W. White, Ed., *Ion Implantation and Ion Beam Processing of Materials: B,* Vol 27, Proceedings of the Materials Research Society, North-Holland, 1984

25. R.D. Granata, M.A. De Crosta, and H. Leidheiser, Jr., in *Proceedings of the Ninth National Congress on Metallic Corrosion,* Vol 1, National Research Council of Canada, 1984, p 264–268

26. G. Dearnaley, *Nucl. Instrum. Methods Phys. Res. B,* Vol 7/8, 1985, p 158–165

27. I.L. Singer, in *Ion Implantation and Ion Beam Processing of Materials,* Vol 27, G.K. Hubler, O.W. Holland, C.R. Clayton, and C.W. White, Ed., Proceedings of the Materials Research Society, North-Holland, 1984, p 585–595

28. J.B. Pethica, in *Ion Implantation into Metals,* V. Ashworth, W.A. Grant, and R.P.M. Proctor, Ed., Pergamon Press, 1982, p 147–156

29. R. Hutchings and W.C. Oliver, *Wear,* Vol 92, 1983, p 143

30. K.K. Shih, *Wear,* Vol 105, 1985, p 341–347

31. L. Thair, U.K. Mudali, N. Bhuvaneswaran, K.G.M. Nair, R. Asokamani, and B. Raj, *Corros. Sci.,* Vol 44 (No. 11), 2002, p 2439–2457

32. H. Pelletier, D. Muller, P. Mille, and J.J. Grob, *Surf. Coat. Technol.,* Vol 158–159, 2002, p 301–308

33. D. Ikeda, M. Ogawa, Y. Hara, Y. Nishimura, O. Odusanya, K. Azuma, S. Matsuda, M. Yatsuzuka, and A. Murakami, *Surf. Coat. Technol.,* Vol 156, 2002, p 301–305

34. R. Arkush, M.H. Mintz, and N. Shamir, *J. Nucl. Mater.,* Vol 281, 2000, p 182–190

35. W.-H. Luo, R.-F. Ni, and S. Wu, *Mater. Prot. (China),* Vol 33, 2000, p 6–8

36. J.H. Booske, W. Wang, C. Baum, C. Clothier, N. Zjaba, and L. Zhang, *Surf. Coat. Technol.,* Vol 111, 1999, p 97–102

37. R. Nishimura, K. Yamakawa, J. Ishiga, Y. Matsumoto, and H. Nagano, *Mater. Chem. Phys.,* Vol 54, 1998, p 289–292

38. P.M. Natishan, E. McCafferty, G.K. Hubler, and B.D. Sartwell, *Advances in Coatings Technologies for Surface Engineering,* Minerals, Metals and Materials Society/AIME, 1997, p 271–285

39. J.W. Hill, M.J. Lee, and I.J. Spalding, *Opt. Laser Technol.,* Vol 6, Dec 1974, p 276

40. E.M. Breinan, B.H. Kear, and C.M. Banas, *Phys. Today,* Vol 29, 1976, p 11, 44

41. H.E. Cline and T.R. Anthony, *J. Appl. Phys.,* Vol 48, 1977, p 3895

42. T.R. Anthony and H.E. Cline, *J. Appl. Phys.,* Vol 49, 1978, p 1248

43. P.R. Strutt, H. Nowotny, M. Tuli, and B.H. Kear, *Mater. Sci. Eng.,* Vol 36, 1978, p 217

44. G. Staehli and C. Sturzenegger, *Scr. Metall.,* Vol 12, 1978, p 617

45. P.L. Bonora, M. Bassoli, P.L. De Anna, B. Battaglin, G. Della Mea, P. Mazzoldi, and A. Miotello, *Electrochim. Acta,* Vol 25, 1980, p 1497

46. C.W. Draper, R.E. Woods, and L.S. Meyer, *Corrosion,* Vol 36, 1980, p 405

47. R.J. Pangborn and D.R. Beaman, *J. Appl. Phys.,* Vol 5, 1980, p 5992

48. P.G. Moore and E. McCafferty, *J. Electrochem. Soc.,* Vol 128, 1981, p 1391

49. D.S. Gnanamuthu, *Opt. Eng.,* Vol 19, 1980, p 783

50. P.G. Moore, in *Proceedings of the International Laser Processing Conference,* Laser Institute of America, 1981

51. C.W. Draper, *Appl. Opt.,* Vol 20, 1981, p 3093

52. H.W. Bergmann and B.L. Mordike, *Z. Werkstofftech.,* Vol 12, 1981, p 142

53. H.S. Carslaw and J.C. Jaeger, *Conduction of Heat in Solids,* Clarendon Press, 1959

54. L.E. Grenwald, E.M. Breinan, and B.H. Kear, in *Laser-Solid Interactions and Laser Processing—1978,* S.D. Ferris, E.J. Leany, and J.M. Poate, Ed., American Institute of Physics, 1979 p 189

55. S.L. Narasimhan, S.M. Copley, E.W. Van Stryland, and M. Bass, *ICEE J. Quant. Electr.,* Vol 13, 1977, p 2D

56. A. Munitz, *Metall. Trans. B,* Vol 11, 1980, p 563

57. B. Chalmers, *Principles of Solidification,* Robert E. Krieger, 1977

58. C.W. Draper, S.P. Sharma, J.L. Yeh, and S.L. Bernasek, *Surf. Interface Anal.,* Vol 2 (No. 5), 1980, p 179

59. D.G. Beck, S.M. Copley, and M. Bass, *Metall. Trans. A,* Vol 13, 1982, p 1879

60. P.T. Sarjeant and R. Roy, *Mater. Res. Bull.,* Vol 3, 1968, p 265

61. J.A. Dantzig and S.H. Davis, *Mater. Sci. Eng.,* Vol 32, 1978, p 199

62. N.B. Dahotre, Ed., *Lasers in Surface Engineering,* ASM International, 1998

63. L.S. Weinman, J.N. DeVault, and P.G. Moore, in *Applications of Lasers in Materials Processing,* E.A. Metzbower, Ed., American Society for Metals, 1979, p 259

64. L.E. Grenwald, E.M. Breinan, and B.H. Kear, in *Laser-Solid Interactions and Laser Processing—1978,* S.D. Ferris, E.J. Leany, and J.M. Poate, Ed., American Institute of Physics, 1979, p 239

65. J.B. Lumsden, D.S. Gnanamuthu, and R.J. Moores, in *Fundamental Aspects of Corrosion Protection by Surface Modification,* E. McCafferty, C.R. Clayton, and J. Oudar, Ed., The Electrochemical Society, 1984, p 122–129

66. J. Javadpour, C.R. Clayton, and C.W. Draper, in *Corrosion of Metals Processed by Directed Energy Beams,* C.R. Clayton and C.M. Preece, Ed., The Metallurgical Society, 1982, p 135–145

67. E. McCafferty and P.G. Moore, *J. Electrochem. Soc.,* Vol 133 (No. 6), 1986, p 1090–1096

68. E. McCafferty, G.K. Hubler, P.M. Natishan, P.G. Moore, R.A. Kant, and B.D. Sartwell, Ion Beam or Laser Processing of Metal Surfaces for Improved Corrosion Resistance, *Mater. Sci. Eng.,* 1987

69. C.P. Chan, T.M Yue, and H.C. Man, *Mater. Sci. Technol.,* Vol 18, p 575–580

70. T.M. Yue, J.K. Yu, Z. Mei, and H.C. Man, *Mater. Lett.,* Vol 52, 2002, p 206–212

71. K.F. Tam, F.T. Cheng, and H.C. Man, *Proceedings of the Conference on Laser-Solid Interactions for Materials Processing,* 2000 MRS Spring Meeting, 25–27 April 2000 (San Francisco, CA), Materials Research Society, 2000, p J3.2.1–J3.2.6

72. C.T. Kwok, F.T. Cheng, and H.C. Man, *Proceedings of the Conference on the 20th International Congress on ICALEO 2001: Applications of Lasers and Electro-Optics,* 15–18 Oct 2001 (Jacksonville, FL), Laser Institute of America, 2001, p 817–827

Porcelain Enamels, *Corrosion: Fundamentals, Testing, and Protection*, Vol 13A, *ASM Handbook*, ASM International, 2003, p 750–754

Porcelain Enamels

Introduction

PORCELAIN ENAMELS are glass coatings applied primarily to products or parts made of sheet steel, cast iron, or aluminum to improve appearance and to protect the metal surface. Porcelain enamels are distinguished from other ceramic coatings on metallic substrates by their predominantly vitreous nature and the types of applications for which they are used. These coatings are differentiated from paint by their inorganic composition and coating properties. They are fused to the metallic substrate at temperatures above 425 °C (800 °F) during the firing process.

The most common applications for porcelain enamels are major appliances, water-heater tanks, sanitary ware, and cookware. In addition, porcelain enamels are used in a wide variety of coating applications, including chemical-processing vessels, agricultural storage tanks, piping, pump components, and barbecue grills. They also are used for coatings on architectural panels, signage, specially executed murals, and substrates for microcircuitry. Porcelain enamels are selected for products or components where there is a need for one or more special service requirements that they can provide. These include chemical resistance, corrosion protection, weather resistance, abrasion resistance, specific mechanical or electrical properties, appearance or color needs, cleanability, heat resistance, or thermal-shock capability.

Porcelain Enamels, *Corrosion: Fundamentals, Testing, and Protection*, Vol 13A, *ASM Handbook*, ASM International, 2003, p 750–754

Types of Porcelain Enamels

Porcelain enamels for sheet steel and cast iron are classified as either ground-coat or cover-coat enamels. Ground-coat enamels contain metallic oxides, such as cobalt oxide and/or nickel oxide, that promote adherence of the glass/enamel to the metal substrate. Cover-coat enamels are applied over fired ground coats to improve the appearance and properties of the coating. Also, cover-coat enamels may be applied over unfired ground coats, with both coats being fired at the same time (i.e., two-coat/one-fire systems). Cover coats may also be applied directly to properly prepared decarburized steel substrates. The color of ground coats is limited to various shades of blue, black, brown, and gray. Cover coats— which may be clear, semiopaque, or opaque— may be pigmented to take on a great variety of colors. Colors may also be smelted into the basic coating material. Opaque cover coats are usually white.

Porcelain enamels for aluminum are normally one-coat systems. They are applied only by spraying. When two coats are desired, the first coat can be any color. Frits for porcelain enamels for aluminum are usually transparent and may be colored and opacified with inorganic pigments to produce the desired appearance.

Porcelain Enamels, *Corrosion: Fundamentals, Testing, and Protection*, Vol 13A, *ASM Handbook*, ASM International, 2003, p 750–754

Porcelain Enamels

Frits for Porcelain Enameling

The basic material of the porcelain-enamel coating is called frit. Frits are smelted complex borosilicate glasses that are produced by quenching a molten glassy mixture. Frits generally consist of from 5 to 20 components, which are thoroughly mixed together and melted into a glassy system. The molten glass is then quenched to a friable (easily broken up) condition by being either poured into water or rolled into a thin sheet between water-cooled rolls. When quenched in water, the frit is dried before use. The sheet is ordinarily shattered into small flakes by mechanical means before use or shipment. Because porcelain enamels are usually designed for specific applications, the compositions of the frits from which they are made vary widely. A number of compositions of frits for enamels for sheet steel, cast iron, and aluminum are discussed in the paragraphs that follow; however, many variations of these compositions are used commercially.

Enamel Frits for Sheet Steel. The frit compositions given in Table 1 are classified as alkali borosilicates and are used as ground coats on sheet steel. One of the functions of ground-coat enamels is to promote bond to the steel substrate. The addition of cobalt oxide and/or nickel oxide promotes adherence to the substrate. Compositions differ, depending on the end-use application of the enameled product. For example, acid resistance is obtained by the addition of titanium dioxide and high levels of silicon dioxide with a corresponding decrease in the boron level. Resistance of the enamel to alkalis or to water can be improved by adding zirconium oxide or aluminum oxide (usually as zircon or alumina) to the frit while maintaining a high content of silicon dioxide. It is common practice to blend soft (low-melting temperature), medium, and hard (high melting temperature) frits to obtain the maximum desired properties.

Table 1 Melted-oxide compositions of frits for ground-coat enamels for sheet steel

Constituent	Composition, wt%			
	Regular blue-black enamel	**Alkali-resistant enamel**	**Acid-resistant enamel**	**Water-resistant enamel**
SiO_2	37.17	42.02	56.44	48.00
B_2O_3	22.21	18.41	14.90	12.82
Na_2O	18.44	15.05	16.59	18.48
K_2O	0.99	2.71	0.51	…
Li_2O	…	1.06	0.72	1.14
CaO	9.34	4.47	3.06	2.90
ZnO	…	2.29	…	…
Al_2O_3	4.53	4.38	0.27	…
ZrO_2	…	5.04	…	8.52
TiO_2	…	…	3.10	3.46
CuO	…	0.07	0.39	…
MnO_2	1.58	1.39	1.12	0.52
NiO	1.37	1.04	…	1.21
Co_3O_4	0.65	0.93	1.27	0.81
P_2O_5	1.15	0.68	…	0.20
F_2	2.57	2.75	1.63	1.94
BaO	9.24	8.59	…	…

Weather resistance has been shown to be a function of acid resistance. Porcelain enamels for use outdoors are made from various types of frits that produce the necessary acid resistance along with the specific color desired. Resistance to thermal shock and to high temperature is obtained by controlling the coefficient of thermal

expansion of the glass coating; this is accomplished by adjusting the frit composition and adding refractory materials, such as silicon dioxide, aluminum dioxide, and zirconium oxide, to the mill formula.

Cover coats for sheet steel are applied over ground coats or directly to properly prepared decarburized steel. Compositions of frits for cover- coat enamels are shown in Table 2. Electrostatic dry powder cover coats may be applied over an electrostatic dry powder base coat; then the entire two-coat/one-fire system is matured in a single firing. Electrostatic dry powder cover coats may also be applied over fired ground coats in a two-coat/two-fire process.

Table 2 Melted-oxide compositions of frits for cover-coat enamels for sheet steel

Constituent	Composition, wt%		
	Titania white enamel	**Semiopaque enamel**	**Clear enamel**
SiO_2	44.67	44.92	54.26
B_2O_3	14.28	16.40	12.38
Na_2O	8.27	8.67	6.55
K_2O	6.99	8.12	11.32
Li_2O	0.98	0.45	1.14
ZnO	…	0.74	…
ZrO_2	1.98	3.34	1.40
Al_2O_3	0.31	0.16	…
TiO_2	18.49	13.05	10.04
P_2O_5	1.32	0.88	…
MgO	0.5	…	…
F_2	2.21	3.27	2.91

Cover-coat enamels fall into three groups: clear, semiclear or semiopaque, and opaque. The clear frits do not contain high levels of titanium dioxide, and they remain clear when fired. The semiopaque frits are translucent and are used for light colors. The opaque frits, which contain high levels of titanium dioxide, become white upon firing.

Cover-coat enamels made from titanium-dioxide-opacified frits are generally quite acid resistant; even in amounts too small to provide any opacity, titania imparts acid resistance. For alkali resistance, zirconium oxide is a desirable constituent. Clear frits containing 8 to 11% TiO_2 are used for strong to medium-strength colors. Semiopaque frits containing 12 to 15% TiO_2 are used for medium-strength colors, and opaque frits containing 17 to 20% TiO_2 are used for pastel colors.

Enamel Frits for Cast Iron. Compositions of frits for enamels for cast iron vary, depending on whether the frit is applied by the dry process or by the wet process (Table 3). Dry-process enamels are commonly used for large cast-iron plumbing fixtures, such as bathtubs and sinks, where the brilliance of the enamel and its ability to cover small surface irregularities in the casting itself are useful characteristics. Acid resistance is imparted to these enamels by reducing the alumina content, increasing silica, and adding up to about 8% TiO_2. Ground coats are normally used to fill surface voids in castings. Ground coats for wet-process enamels often are mixtures of frit, enamel reclaim, and refractory raw material used at very low application weight. Ground coats for the dry-process method are applied and fused to thin, viscous coatings that protect the casting surface from excessive oxidation while it is heated to enameling temperature.

Table 3 Melted-oxide compositions of frits for enamels for cast iron

Constituent	Composition, wt%				
	Ground coats		**Cover coats**		
	Lead-bearing	**Non-lead-bearing**	**Zirconium-opacified[a]**	**Titania-opacified[a]**	**Titania-opacified[b]**
SiO_2	77.7	63.4	28.0	51.4	44.80
B_2O_3	6.8	10.9	8.8	9.6	13.14
Na_2O	4.3	7.1	10.0	10.1	6.48
K_2O	…	2.4	4.1	3.0	7.67
PbO	4.0	…	17.8	…	0.94

CaO	…	0.6	8.7	1.9	0.55
ZnO	…	…	6.1	0.9	…
Al_2O_3	7.2	15.1	4.5	2.1	…
Sb_2O_3	…	…	…	…	19.74
ZrO_2	…	…	6.1	…	1.64
TiO_2	…	…	…	18.4	…
F_2	…	0.5	5.9	2.6	5.04

(a) For dry process.
(b) For wet process

Enamel frits for aluminum are usually based on lead silicate or on cadmium silicate, but they may also be based on phosphate, vanadium, or barium. Table 4 gives the compositions of some frits for aluminum. Enamels for aluminum have a high gloss, good acid and weather resistance, and good mechanical properties. They melt at relatively low temperatures.

Table 4 Melted-oxide compositions of frits for enamels for aluminum

Constituent	Composition, wt%		
	Lead-base enamel	**Non-lead-base enamel**	**Barium enamel**
PbO	14–45	…	…
SiO_2	30–40	30–40	25
Na_2O	14–20	20–25	20
K_2O	7–12	7–11	25
Li_2O	2–4	3–5	…
B_2O_3	1–2	1–2	15
Al_2O_3	…	…	3
BaO	2–6	3–5	12
P_2O_5	2–4	2–4	…
F_2	…	…	…
TiO_2	15–20	15–20	…
Sb_2O_5	…	2–5	…

Porcelain Enamels, *Corrosion: Fundamentals, Testing, and Protection*, Vol 13A, *ASM Handbook*, ASM International, 2003, p 750–754

Porcelain Enamels

Properties of Porcelain Enamels

Porcelain enamels possess an array of properties that can be specially designed and formulated for a variety of demanding environments. Some of the special properties are summarized in the paragraphs that follow. The Porcelain Enamel Institute bulletins in the Selected References have more detailed information.

Appearance for Indoor Exposure. Where corrosive attack is unlikely and appearance is the principal requirement, enamel selection and processing are directed toward providing reproducible color matching and optimal gloss and smoothness. Often, different enamels are used on different parts of the same product to ensure the best balance of properties and cost, particularly if high volume is involved. For example, somewhat different enamel compositions are used for range tops and dishwasher liners because of differing property and appearance requirements, even though these parts may be processed in the same plant. Appearance standards, in particular, are established to respond to end-use requirements. Small surface defects may be tolerated in areas not heavily used or readily seen in the finished part, provided that they do not affect basic serviceability.

Thermal shock intensifies the effect of elevated temperature, as does operation under severe temperature gradients. Enamels are formulated so that expansion characteristics place the enamel in compression under

service conditions. If combinations of mechanical stress and elevated temperatures place the enamel in tension, crazing forms a pattern of fine cracks perpendicular to the tensile stress. The resistance of an enamel to thermal shock varies inversely with its thickness. Thermal-shock failure occurs when the temperature gradient perpendicular to the surface is large enough to cause excessive differential shrinkage and tensile stress. Thermal- shock resistance also depends on the design and section thickness of the coated part. Flexing of the metal due to localized thermal gradients parallel to the surface can produce bending and tensile stresses in the coating; therefore, an increase in the strength or rigidity of the part increases the resistance of the coating to thermal shock. Most porcelain enamels applied at conventional thickness can withstand abrupt temperature changes of 110 to 165 °C (200 to 300 °F).

Abrasion Resistance. The hardness of porcelain enamels ranges from 3.5 to 6.0 on the Mohs scale. Porcelain enamels show a high degree of abrasion resistance. Under abrasive test conditions where plate glass retains 50% specular gloss, porcelain-enamel compositions retain from 35 to 85% specular gloss. Subsurface abrasion resistance varies with processing variables that affect the bubble structure of the enamel, that is, gas bubbles frozen in during cooling of the enamel. A decrease in abrasion resistance occurs with an increase in the number or size of gas bubbles. Enamel compositions are available that contain crystalline particles (from mill additions or devitrification heat treatment) that increase abrasion resistance as much as 50%.

Porcelain Enamels, *Corrosion: Fundamentals, Testing, and Protection*, Vol 13A, *ASM Handbook*, ASM International, 2003, p 750–754

Porcelain Enamels

Corrosion Resistance of Porcelain Enamels

Porcelain enamels possess excellent resistance to corrosion in a variety of environments.

Chemical Resistance. Porcelain enamel is widely used because of its resistance to household chemicals and foods. Mild alkaline or acid environments are generally involved in household applications. Table 5 presents examples of corrosive environments for which porcelain enamels are widely used for long periods of service. Special enamel compositions are available to resist most acids, except for hydrofluoric or concentrated phosphorics, to 230 °C (450 °F). These compositions also resist alkali concentration to pH 12 at temperatures to 100 °C (212 °F).

Table 5 Applications in which porcelain enamels are used for resistance to corrosive environments

Application	Corrosive environment			
	Temperature		**pH**	**Corrosive medium**
	°C	**°F**		
Bathtubs	To 49	To 120	5–9	Water, cleansers
Chemical ware	To 100	To 212	12	Alkaline solutions
	To 100	To 212	1–2	All acids except hydrofluoric
	175–230	350–450	1–2	Concentrated sulfuric acid, nitric acid, and hydrochloric acid
Home laundry equipment	To 71	To 160	11	Water, detergents, bleach
Range exteriors	21–66	70–150	2–10	Food acids, cleaners
Range oven liners, conventional	66–315	150–600	2–10	Food acids, cleaners
Range burner grates	66–590	150–1100	2–10	Food acids, cleaners
Refrigerators	-18 to 66	0–150	2–10	Food acids, cleaners

Kitchen sinks	To 71	To 160	2–10	Food acids, water, cleaners
Water heaters	To 71	To 160	5–8	Water
Industrial heat exchangers				Depends on application[(a)]

(a) Applications include coal- and oil-fired boilers and black liquor evaporators; corrosive media would include ash from coal-fired boilers, corrosive condensates, and exhaust from black liquor evaporators.

Weather Resistance. Indicators of the weather resistance of porcelain enamels are chemical durability, color stability, cleanability, and continuity of coating. Gloss and enamel texture do not necessarily affect weather resistance, but retention of gloss can be a criterion. Porcelain enamels have excellent resistance in atmospheric exposure, including corrosive industrial atmospheres, gases, smoke, salt spray, and seacoast exposures. Enamels formulated for acid resistance usually have better atmospheric-corrosion resistance than other types. These enamels have shown no appreciable change in appearance after 15 years of exposure.

Waters. All porcelain enamels are completely resistant to water at room temperature. Resistance decreases at higher temperatures. Special porcelain enamels have been developed for hot- water storage tanks that can withstand continuous exposure to hot water for periods of 10 to 20 years. Natural waters, because of their varying compositions, have varying effects on porcelain enamels. Aerated water with a low dissolved solids content, for example, has been found to be more corrosive than hard water. Freezing and thawing cycles can cause some porcelain enamels to spall or disintegrate; however, properly formulated and applied enamels can withstand thousands of freezing and thawing cycles without failure. Porcelain enamels can withstand salt-spray tests (ASTM B 117) for days and even weeks without evidence of corrosion (Ref 1), and they can provide excellent service in intermittent or continuous exposure to seawater.

Soils. Porcelain enamels formulated to withstand both acid and alkaline attack provide good service in soils.

Acids. Resistance to acids varies widely, depending on composition and the application process used. The degree of attack by acids appears to depend less on the type of acid (with the exception of hydrofluoric) than on pH. Special formulations can provide excellent protection against aqueous solutions of most acids except hydrofluoric. The highest degree of acid resistance is obtained by sacrificing resistance to other media, such as alkalies. Figure 1 shows weight loss of a porcelain enamel in boiling mineral acids and in boiling water.

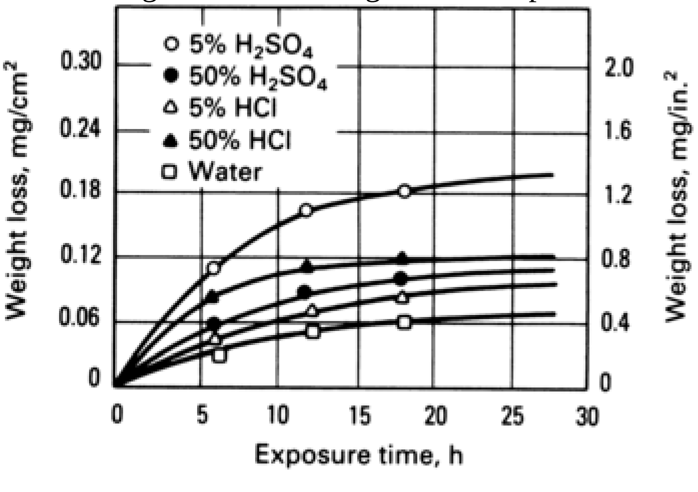

Fig. 1 Corrosion of a porcelain enamel in boiling water and boiling mineral acids. Source: Ref 2

Alkalies. Most porcelain enamels are unaffected by alkalies at room temperature. Special formulations provide alkali resistance to solutions with a maximum pH of 12 at temperatures to 100 °C (212 °F).

Organics. Porcelain enamels are completely resistant to attack by common organic solvents, dyes, greases, and oils. Enamels are not dissolved by these materials and do not absorb them. Acid-resistant porcelain enamels are required for organic material that hydrolyzes upon contact with moisture to form acid solutions.

High Temperatures. Porcelain enamels greatly reduce high-temperature oxidation of the base metal. This ability is largely due to the fact that the enamels themselves are fully oxidized and do not suffer further oxidation at elevated temperatures. They also form an effective barrier to the diffusion of oxygen into the metal. Protection depends on the temperature at which the enamel begins to soften and become more fluid. This temperature is normally about 220 °C (400 °F) below the firing temperature, but specially formulated enamels can provide oxidation protection to metals at temperatures to 1095 °C (2000 °F). Maximum service temperatures for porcelain enamels are shown in Table 6. Softening of the glassy matrix limits use to these exposure

temperatures. Softening releases gases remaining from reactions between the enamel and the metal substrate, producing random defects known as reboil.

Table 6 Maximum service temperatures for porcelain enamels

Service temperature		Limiting conditions
°C	°F	
425	800	Usual limit for enamels maturing at about 815 °C (1500 °F)
540	1000	Maximum for enamels maturing at about 815 °C (1500 °F), without reboil
760	1400	Operating limit for special high-temperature enamels
1095	2000	Refractory enamels useful for short periods for protection of stainless steels and special alloys

Source: Ref 3

References cited in this section

1. "Standard Method of Salt Spray (Fog) Testing," B 117, *Annual Book of ASTM Standards,* American Society for Testing and Materials

2. C.L. Hackler and M. Dinulescu, Porcelain Enameled Flat Plate Heat Exchangers—Engineering and Application, *Industrial Heat Exchangers,* Proc. 1985 Symposium on Industrial Heat Exchanger Technology, A.J. Hayes et al., Ed., American Society for Metals, 1985

3. "Development of Porcelain Enamel Coatings," Bulletin E-6, Porcelain Enamel Institute

Porcelain Enamels, *Corrosion: Fundamentals, Testing, and Protection*, Vol 13A, *ASM Handbook*, ASM International, 2003, p 750–754

Porcelain Enamels

Evaluation of Porcelain-Enameled Surfaces

Specifications and quality control for porcelain-enamel coatings require the evaluation of a range of properties for the intended service of the porcelain-enameled product. Although material and process variables can be brought into approximate control using small test panels, process control is maintained by the evaluation of finished parts, even though some of the mechanical and chemical tests are destructive. Standard test procedures are available for many porcelain- enamel properties. Specific test methods for various properties are listed in Table 7. Some of these tests are discussed in the paragraphs that follow.

Table 7 ASTM test methods for porcelain enamels

Under jurisdiction of ASTM Porcelain Enamel Subcommittee B.08.12

Designation	Title
C 282	"Acid Resistance of Porcelain Enamels (Citric Acid Spot Test)"
C 283	"Resistance of Porcelain Enameled Utensils to Boiling Acid"
C 285	"Standard Test Methods for Sieve Analysis of Wet Milled and Dry Milled Porcelain Enamel"
C 286	"Definitions of Terms Relating to Porcelain Enamel and Ceramic Metal Systems"
C 313	"Standard Test Method for Adherence of Porcelain Enamel and Ceramic Coatings to Sheet Metal"

C 346[(a)]	"Standard Test Method for 45° Specular Gloss of Ceramic Materials"
C 347	"Standard Test Method for Reflectance, Reflectivity and Coefficient of Scatter of White Porcelain Enamels"
C 374	"Standard Test Method for Fusion Flow of Porcelain Enamel Frits by the Flow Button Methods"
C 375	"Classification of Water Used in Milling in Porcelain Enamel"
C 385	"Standard Test Method for Thermal Shock Resistance of Porcelain-Enameled Utensils"
C 409[(a)]	"Torsion Resistance of Laboratory Specimens of Porcelain Enameled Iron and Steel"
C 448	"Standard Test Methods for Abrasion Resistance of Porcelain Enamels"
C 536	"Standard Test Method for Continuity of Coatings in Glassed Steel Equipment by Electrical Testing"
C 537	"Standard Test Method for Reliability of Glass Coatings on Glassed Steel Reaction Equipment by High Voltage"
C 538	"Standard Test Method for Color Retention of Red, Orange and Yellow Porcelain Enamels"
C 539	"Standard Test Method for Linear Thermal Expansion of Porcelain Enamel and Glaze Frits and Ceramic Whiteware Materials by the Interferometric Method"
C 540[(a)]	"Standard Test Method for Image Gloss of Porcelain Enamel Surfaces"
C 614	"Standard Test Method for Alkali Resistance of Porcelain Enamels"
C 632	"Standard Test Method for Reboiling Tendency of Sheet Steel for Porcelain Enameling"
C 633	"Standard Test Method for Adhesion or Cohesive Strength of Flame-Sprayed Coatings"
C 660	"Practices for Production and Preparation of Gray Iron Castings for Porcelain Enameling"
C 664	"Standard Test Method for Thickness of Diffusion Coating"
C 694	"Standard Test Method for Weight Loss (Mass Loss) of Sheet Steel during Immersion in Sulfuric Acid Solution"
C 703	"Standard Test Methods for Spalling Resistance of Porcelain Enameled Aluminum"
C 715	"Standard Test Method for Nickel on Steel for Porcelain Enameling by Photometric Analysis"
C 743	"Standard Test Method for Continuity of Porcelain Enamel Coatings"
C 756	"Standard Test Method for Cleanability of Surface Finishes"
C 774	"Standard Test Method for Yield Strength of Enameling Steels after Straining and Firing"
C 810	"Standard Test Method for Nickel on Steel for Porcelain Enameling by X-Ray Emission Spectrometry"
C 839	"Standard Test Method for Compressive Stress of Porcelain Enamels by Loaded-Beam Method"
C 872	"Standard Test Method for Lead and Cadmium Release from Porcelain Enamel Surface"
C 988	"Standard Test Method for Image Gloss of Porcelain Enamel Surfaces"

(a) This test, while withdrawn from the latest ASTM list because of inability to obtain the required equipment, continues to be used by laboratories that possess the equipment.

Adherence refers to the degree of attachment of enamel to the metal substrate. A number of tests regularly used in the industry provide adherence criteria, but none gives the force per unit area required to detach the enamel by tensile force normal to the interface. ASTM C 313 for porcelain enamel on steel deforms the metal and measures the area from which the porcelain enamel is removed. The indicator of adherence is the adherence index, which is the ratio of the porcelain enamel remaining in the deformed area to that in the same measured area prior to deformation. Enamels for cast iron pose a special problem because of the relatively greater thickness of the coating, the rigidity of the metal substrate, and the brittleness of the iron. Here, simple nonstandard impact tests are used. Resistance to spalling, a defect characterized by separation of porcelain enamel from the base metal without apparent external cause, is the indicator used to measure adherence of porcelain enamel on aluminum. Spalling can result from the use of improper alloys, improper enamel formulations, incorrect pretreatment of the base metal, faulty application, or unsatisfactory firing procedures. The most common test for spall resistance is ASTM C 703.

Thickness. A number of specifications for products and applications require a specific thickness for porcelain-enamel coating. The procedure used to measure the thickness depends on the type of base metal used. For porcelain-enamel products with a steel substrate, enamel thickness is measured according to ASTM D 1186. For porcelain-enamel products with an aluminum substrate, enamel thickness is measured according to ASTM E 376. (Neither of these tests is listed in Table 7 because they are not under the jurisdiction of ASTM Porcelain Enamel Subcommittee B.08.12.) In some cases, such as laboratory investigations, enamel thickness is measured according to ASTM C 664.

Resistance to Chipping. Relatively thick layers of porcelain enamel are fractured when subjected to severe bending or other substrate deformation. However, thin coatings of 125 μm (5 mils) or less that are well bonded to a relatively thin metal substrate (for example, 26-gage 0.4546 mm, or 0.0179 in., or less) can withstand the bending of the substrate to radii of curvature within its elastic limit and return to the original shape with little or no apparent damage. Chipping of typical porcelain enamel on sheet iron occurs at about the strain required for permanent deformation of the metal base.

Abrasion Resistance. The resistance of porcelain enamel to various types of abrasion is measured by ASTM C 448, which consists of three parts. The first determines the resistance to surface abrasion of porcelain enamels for which the unabraded 45° specular gloss is more than 30 gloss units. The second determines the resistance to surface abrasion of porcelain enamels for which the unabraded 45° specular gloss is 30 gloss units or less. The third measures the resistance of porcelain enamels to subsurface abrasion.

Acid Resistance. Porcelain enamels can be formulated to exhibit high resistance to all acids except hydrofluoric or concentrated phosphoric. This resistance to food acids and certain chemical cleaners is of particular importance to manufacturers of ranges and other kitchen and household appliances, as well as plumbing fixtures and various industrial and chemical processing products.

The acid resistance of enamels under boiling conditions is important for certain uses, such as cookware. ASTM C 283 is used for evaluation. Similarly, acid resistance is a major consideration for predicting the weatherability of architectural porcelain-enamel components. Extensive testing under controlled-exposure conditions has shown a distinct correlation between acid resistance and weatherability. Here the test for determining acid resistance is ASTM C 282.

Alkali Resistance. Home laundry equipment, dishwashers, and similar applications normally exposed to an alkaline environment at elevated temperatures require an alkali-resistant coating. The standard test for alkali resistance is ASTM C 614.

Resistance to Organic Solvents. Porcelain enamels are inert to all common organic solvents; however, there is no standard procedure for determining this special performance characteristic.

Resistance to Hot Water. Federal specification W-H-196J, “Heater Water, Electric and Gas Fired, Residential,” specifies a solubility test to determine the resistance of porcelain enamels to hot water.

Weather Resistance. Actual weathering performance of porcelain-enamel panels has been documented in a series of on-site exposure tests carried out for up to 30 years by the National Bureau of Standards (now the National Institute of Standards and Technology) in cooperation with the Porcelain Enamel Institute. As mentioned previously, acid resistance as measured by ASTM C 282 is important.

Weathering of porcelain enamel is evaluated in terms of the changes in gloss and color that occur during outside exposure. Multiyear weathering tests demonstrate that porcelain enamels have considerable inherent gloss and color stability. ASTM C 346 and ASTM D 2244 are used (the latter is not under B.08.12 jurisdiction). Spalling resistance of weathered porcelain enamel on aluminum is best ascertained by ASTM C 703.

Torsion Resistance. In transit and during service, porcelain-enamel products may be subject to distortion through bending, twisting, or a combination of both. This can cause coating failures from fractures originating at the outer surface and normal to the tensional stress. ASTM C 409 evaluates the relative resistance to torsion-induced failure of laboratory test specimens for steel-substrate thicknesses of 24 to 12 gage.

Thermal shock resistance of a porcelain-enamel surface varies inversely with the thickness of the enamel. It is also affected by the compressive stress present in the enamel at room temperature. Most porcelain enamels can be quenched in ice water from 205 °C (400 °F) without thermal shock failure. Some porcelain enamels specifically designed for resistance to thermal shock will not fail when quenched in ice water from 650 °C (1200 °F). ASTM C 385 is the standard for evaluating the durability of porcelain- enamel utensils when subjected to thermal shock.

Continuity of Coatings. Ensuring continuity of coating after manufacture is important in porcelain-enamel (“glassed-steel”) applications where a prime purpose of the coating is to protect the substrate against corrosion. Test methods used to determine either discontinuity of coverage or potential discontinuity through too-thin coverage are ASTM C 536 and ASTM C 743. Both tests essentially involve the use of electrical probes of relatively high voltage to discern either discontinuities in the coating or insufficient coverage for coating integrity in service use.

Acknowledgment

This article is adapted from "Porcelain Enamels," *Surface Engineering,* Vol 5, *ASM Handbook,* ASM International, 1994, written by the Technical Publications Committee of the Porcelain Enamel Institute, Inc. who at that time included John C. Oliver, Consultant to the Porcelain Enamel Institute, Inc. (Project Chairman); Douglas D. Giese, G.E. Appliances (Co-Chairman); Jeffrey F. Wright, Ferro Corp. (Co-Chairman); Ronald L. Allen, Ronalco, Inc.; Terry Conrad, Amana/Raytheon Corp.; John K. Cook, Chi-Vit Corp.; Ted Furr, Bethlehem Steel Corp.; Andrew Gordon, U.S. Steel, USX Corp.; Bernard L. Hall, Jr., JennAir/Maytag Co.; Michael Horton, Industrial Heating and Finishing Co.; William Huyser, Mapes & Sprowl Steel, Ltd.; Robert J. Long, American Porcelain Enamel Co.; Anthony R. Mazzuca, Miles, Inc.; Herbert Oliveira, Nordson Corp.; Arnold Preban, Inland Steel Co.; Charles R. Rarey, LTV Steel Co.; Donald R. Sauder, Porcelain Enamel Institute, Inc.; Narayan M. Sedalia, Whirlpool Corp.; Jeffrey Sellins, Magic Chef/Maytag Co.; Lester N. Smith, Porcelain Consultants, Inc.; Larry L. Steele, Armco Steel Corp.; Ted J. Wolowicz, G.E. Appliances.

Porcelain Enamels, *Corrosion: Fundamentals, Testing, and Protection*, Vol 13A, *ASM Handbook*, ASM International, 2003, p 750–754

Porcelain Enamels

References

1. "Standard Method of Salt Spray (Fog) Testing," B 117, *Annual Book of ASTM Standards,* American Society for Testing and Materials
2. C.L. Hackler and M. Dinulescu, Porcelain Enameled Flat Plate Heat Exchangers—Engineering and Application, *Industrial Heat Exchangers,* Proc. 1985 Symposium on Industrial Heat Exchanger Technology, A.J. Hayes et al., Ed., American Society for Metals, 1985
3. "Development of Porcelain Enamel Coatings," Bulletin E-6, Porcelain Enamel Institute

Porcelain Enamels, *Corrosion: Fundamentals, Testing, and Protection*, Vol 13A, *ASM Handbook*, ASM International, 2003, p 750–754

Porcelain Enamels

Selected References

- "Alloy, Design and Fabrication Considerations for Porcelain Enameling Aluminum," Bulletin PEI-801, Porcelain Enamel Institute, Norcross, GA
- "Ball Mill Wet Grinding of Slips for Porcelain Enameling," Bulletin PEI-401, Porcelain Enamel Institute, Norcross, GA

- "Dipping and Flow Coating for Porcelain Enameling," Bulletin PEI-502, Porcelain Enamel Institute, Norcross, GA
- "Electrostatic Porcelain Enamel Powder Application," Bulletin PEI-501, Porcelain Enamel Institute, Norcross, GA
- "Enamel Preparation, Application and Firing for Porcelain Enameling Aluminum," Bulletin PEI-803, Porcelain Enamel Institute, Norcross, GA
- *Metallic and Inorganic Coatings,* Vol 02.05, *Annual Book of ASTM Standards,* ASTM
- "1939 Exposure Test of Porcelain Enamels on Steel: 30-Year Inspection," Building Science Series 38, National Bureau of Standards
- Porcelain Enamel Institute, Norcross, GA, www.porcelainenamel.com
- Porcelain Enameling, Materials, Finishing, and Coating, Vol 3, 4th ed., *Tool and Manufacturing Engineers Handbook,* Society of Manufacturing Engineers, 1985, p 23-1 to 23-10
- Porcelain Enameling, Special Product Supplement, *Appliance Mag.*, March 1988 and April 1990
- "Preparation of Sheet Steel for Porcelain Enameling," Bulletin PEI-301, Porcelain Enamel Institute, Norcross, GA
- "Pretreatment of Alloys for Porcelain Enameling Aluminum," Bulletin PEI-802, Porcelain Enamel Institute, Norcross, GA
- "Properties of Porcelain Enamel," Data Bulletins PEI 501, 502, 503, 504, and 505, Porcelain Enamel Institute, Norcross, GA
- "Quality Control Procedures for Porcelain Enameling Aluminum," Bulletin PEI-804, Porcelain Enamel Institute, Norcross, GA
- "Weather Resistance of Porcelain Enamels: 15-Year Inspection of the 1956 Exposure Test," Building Science Series 50, National Bureau of Standards
- "Weathering of Porcelain Enamels on Aluminum: 12-Year Inspection, Exposure period 1964–1976," Department of Ceramic Engineering, University of Illinois at Urbana- Champaign, 1977
- "Wet Spraying for Porcelain Enameling," Bulletin PEI-503, Porcelain Enamel Institute, Norcross, GA
- J.F. Wright, C.G. Bergeron, and J.C. Oliver, Porcelain Enamel, *Ceramics and Glasses,* Vol 4, *Engineered Materials Handbook,* ASM International, 1991, p 937–942

Chemical-Setting Ceramic Linings, *Corrosion: Fundamentals, Testing, and Protection*, Vol 13A, *ASM Handbook*, ASM International, 2003, p 755–758

Chemical-Setting Ceramic Linings

Introduction

INORGANIC CHEMICAL-SETTING CERAMIC LININGS have become one of the most widely used construction materials in designing protective linings for industrial installations in which high temperatures, aggressive corrosive media, and complicated substrate geometry exist, such as floors, trenches, sumps, reaction vessels, tanks, scrubbers, ducts, chimneys, and other air pollution control equipment. They are used in various industries, including power, steel- and metalworking, chemical, pulp and paper, refinery, waste treatment, and mining.

Inorganic monolithic linings have proved themselves in these industries because of their chemical resistance to both high and low concentrations of strong acids and solvents, thermal insulation that protects the substrates from extremely high temperatures, temperature resistance to 870 °C (1600 °F), good compressive and flexural strength for environments in which stress and strain are factors, and abrasion resistance. Monolithic linings can be applied by cast or gunite (shotcreting) methods over old and new steel or concrete as well as brick and mortar masonry. This article discusses the function of monolithic linings, the use of these materials, the types of applications in which these materials can be successfully used, and the limitations of these linings.

Chemical-Setting Ceramic Linings, *Corrosion: Fundamentals, Testing, and Protection*, Vol 13A, *ASM Handbook*, ASM International, 2003, p 755–758

Chemical-Setting Ceramic Linings

History of Chemical-Setting Silicates

The progress of silicate cement development has changed over the years with growing technology to meet industry needs. The first silicate cements were composed of a sodium silicate (Na_2SiO_3) liquid and a combination of fillers, such as silica flour, clay, silica aggregates, and barytes, and were formulated as chemical-resistant mortars for use in ambient or high-temperature acid lining construction. This type of silicate cement was very slow in setting and had to be exposed to the open air or heat cured, which created construction delays. Another problem was that these cements were not water resistant. These problems were resolved by the use of acid washing, which helped set the cements and make them water resistant.

In the early 1920s, Na_2SiO_3 mortars were introduced that used an acid catalyst to insolubilize the silica gel; this produced a mortar that cured faster and was water resistant. The physical properties of the silicate mortar were unchanged; that is, the acid, temperature, and solvent resistance were maintained. Because the acid-catalyzed mortar was chemically activated on mixing, it could set within 24 to 48 h. This was a distinct advantage for the construction industry, because it allowed brick to be laid continuously without concern over the mortar being squeezed out of the joints or the brick sliding out of line. Typical setting agents used are ethyl acetate ($C_4H_8O_2$), zinc oxide (ZnO), sodium fluorosilicate (Na_2SiF_6), glyceryl diacetate, formamide (CH_3ON), metallic polyphosphates, and other amides or amines.

It was later determined that when Na_2SiO_3 mortars were exposed to sulfuric acid (H_2SO_4), the reaction product was sodium sulfate (Na_2SO_4), which is a salt that expands and grows through hydration. This sodium salt can pick up as much as 10 mol of water of crystallization with a resultant size increase of 150%, thus creating internal stresses in the structure in which it was used. As a result, monolithic linings and brick surfaces would sometimes crack or spall.

As time passed, industry required silicate technologies that would meet changing applications and structural designs. By the 1950s, potassium silicate (K_2SiO_3) cements were introduced using methods of insolubilizing the silicate. The K_2SiO_3 cements possess enhanced corrosion resistance, particularly in H_2SO_4 environments. Potassium silicate cements react with H_2SO_4 to form potassium sulfate (K_2SO_4), which is not a growth salt. This eliminates the problem of internal stresses when the mortar is exposed to H_2SO_4 solutions.

The introduction of K_2SiO_3 cements was a positive step in producing a material that was more suited for application technology and corrosive environments. The K_2SiO_3 cements offer improved physical properties, which are particularly beneficial in monolithic applications. Furthermore, K_2SiO_3 cements provide better workability with less tackiness and longer working times than Na_2SiO_3 cements. Additional advantages include greater resistance to strong acid solutions and sulfation, more refractoriness, and no efflorescence as with Na_2SiO_3 cements. By this time, Na_2SiO_3 and K_2SiO_3 materials were not only being used as mortars but were also being introduced in new areas of monolithic application as both castable and gunite grades.

Modified silicates were developed in the 1980s. Modified silicates are manufactured by the addition of a powder form of Na_2SiO_3 in conjunction with a proprietary ingredient added directly to the powder fillers. This process eliminates the need to have both powder and liquid on the job site; water is the only required addition. Although these products have been commercially available, high cost and potential for sulfation have limited their use. The modified silicates do not have the chemical properties of the other silicates. The only advantage appears to be their simplicity of mixing.

Chemical-Setting Ceramic Linings, *Corrosion: Fundamentals, Testing, and Protection*, Vol 13A, *ASM Handbook*, ASM International, 2003, p 755–758

Advantages and Disadvantages

The Na_2SiO_3 and K_2SiO_3 cements were developed because a material was needed that was acid resistant in dilute-to-strong concentrations and that offered higher temperature resistance than chemical-resistant organic materials. The development of these silicate-base acidproof cements resulted in many advantageous characteristics, such as a 100% K_2SiO_3-bonded system that had resistance to most solvents and acids over a pH range of 0 to 7; that was water and vapor resistant without special treatment; and that could withstand all concentrations of H_2SO_4, nitric acid (HNO_3), hydrochloric acid (HCl), and phosphoric acid (H_3PO_4). In addition, the Na_2SiO_3- and K_2SiO_3-bonded cements can be applied over damp acid-attacked concrete or brick surfaces as long as these substrates have acid pH surfaces, and they cure chemically within 36 h, thus decreasing construction delays. These cements can be applied by gunite or cast methods. Detailed information on guniting (shotcreting) can be found in American Concrete Institute publication ACI 547R on refractory concrete.

Certain disadvantages were encountered during the development of the acid-resistant silicate cements. It was common knowledge that the silicate cements were not resistant to alkalis, hydrofluoric acid (HF), and fluoride salts. As previously mentioned, the Na_2SiO_3 cements formed a growth salt when exposed to H_2SO_4 that put undue internal stresses on the structure of the material.

Inorganic monolithic linings also have a certain amount of permeability compared to organic surfacing materials. Over time, acid can penetrate the lining and eventually reach the surface of the substrate. This problem is now being combated by using a dual-lining system, which includes a chemically resistant elastomeric membrane applied to the surface of the substrate.

Chemical-Setting Ceramic Linings, *Corrosion: Fundamentals, Testing, and Protection*, Vol 13A, *ASM Handbook*, ASM International, 2003, p 755–758

Chemical-Setting Ceramic Linings

Current Technologies

Monolithic and Membrane Dual Linings. Organic linings or coatings have been used in stacks and ducts, but they will usually deteriorate if temperatures exceed 260 °C (500 °F) in high- sulfur gases. There are many types of lining materials for stacks and ducts; however, because of unpredicted environmental conditions within a stack or duct, it may be difficult to select the best candidate material. Stacks that are designed with heat recovery units and/or scrubbers, combined with one or more flues inside the shell that can control the temperature, should be considered for dual-lining applications.

In recent years, the trend toward using the superior technology of dual linings has emerged and is being recommended where corrosion problems occur throughout industry. Figure 1 illustrates the design of a typical membrane/ monolithic system in the chemical industry.

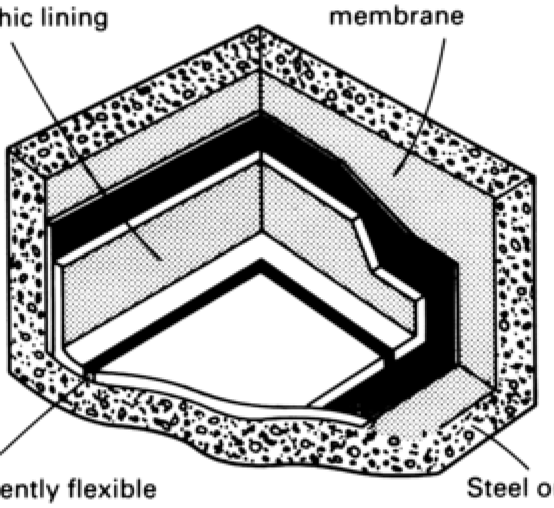

Fig. 1 Schematic of a chemical-resistant dual-lining system that provides double protection to the substrate in the form of a flexible membrane and a rigid surface layer. The flexible corrosion-resistant membrane is applied in direct contact with steel or concrete substrates. It is then covered by the monolithic cement lining, which provides protection over a broad pH range as well as against high temperatures.

There are numerous reasons for this new construction process. Condensation occurs not only on the face of the acid-resistant lining but can also penetrate and condense on the substrate to be protected. Although acidproof monolithic linings offer the proper chemical resistance, they are inherently inelastic, or brittle. In time, monolithic linings may tend to crack and absorb acids or acid gas condensate; therefore, it is advantageous to have a backup membrane. In many applications, the coefficient of thermal expansion of the monolithic lining may not match that of the substrate. Therefore, a flexible membrane helps accommodate stresses resulting from these differences in thermal expansion as well as other mechanically induced stresses.

For many applications, the monolithic lining should not be bonded to the substrate, and the membrane acts as a bond barrier. The concept of placing an impervious membrane between the substrate and inorganic linings has become a recommended practice. Some corrosion-resistant gunite manufacturers have installation specifications for use with membranes.

Membrane choices include asphaltics, resins, and synthetic elastomers. The membrane selected should resist the maximum acid concentrations and temperature expected. Organic linings can fail by disbonding, swelling, abrasion, and blistering from high temperature. Protection of an organic membrane with an inorganic barrier will minimize thermal exposure and mechanical abrasion to the membrane as well as the corrosive media that reach the membrane. An organic membrane compensates for some of the shortcomings of inorganic linings, such as cracking or spalling due to mechanical stresses from shrinkage, induced stresses, insufficient thermal expansion allowances, the anchoring system, vibration, and thermal or other stresses. To provide an effective barrier, inorganic linings are applied much thicker than typical organic coatings. They often contain fillers to act as reinforcement and to decrease shrinkage. Fillers are also incorporated to provide wear resistance for abrasive conditions.

The installation procedure for a dual-lining system is basically the same as if each component were being applied separately. These procedures are established for both organic coatings and inorganic monolithic linings. The condition of the working area and preparation of the surfaces follow standard practices used throughout the industry. Anchors are usually installed on the steel or concrete substrates before the organic membrane is applied.

Lightweight Insulating Materials. Industry has recently seen the development and application of improved lower-density, lightweight, insulating corrosion-resistant lining materials. The evolution of these products has followed the need to accommodate load limitations of structural supports and improved thermal protection of membrane coatings where substrate temperatures can range from 40 to 150 °C (100 to 300 °F) and even higher if process limits or gas cleanup systems experience frequent excursion or bypass conditions. Membranes

require adequate thermal protection to retain physical and chemical properties throughout their service life. Because the membrane will also coat the studs, the inorganic coating must be thick enough to protect the membrane on the highest point of the studs. Therefore, the inorganic lining material must not only protect the membrane from physical abuse but must also protect it from thermal deterioration.

When membranes are not used, condensation of chemicals from hot process streams should be designed to occur within a lining and not at the substrate. However, when membranes are used, the condensation can occur at the membrane, thus possibly reducing the required lining thickness. Therefore, inorganic silicate lining materials with lower thermal conductivity and density have been developed to meet these needs.

Application Procedures. Through the use of current technology, such as the dual-lining system and the availability of improved application techniques, corrosion protection practices have been greatly enhanced. Observations of successes and failures in various applications have led to the development of the following parameters, which must be addressed to specify the proper material. In any application, the primary consideration is the exposure environment. This includes the types and concentrations of chemicals, physical abuse, and temperatures. In this evaluation, it is important to remember that both the silicate monolithic lining and the membrane must resist the corrosive environment. The next consideration is the thickness of the monolithic lining. In high-temperature environments, the monolithic lining must be able to decrease the temperature through its thickness to a level that does not burn out the membrane applied to the substrate or the anchoring system. Once the materials that can resist the corrosive environment have been selected, the physical structure must be considered.

Steel. When a steel substrate is being used, sources of variation in electrical potential on the metal surfaces must be considered. These include mill scale, metal impurities, localized strains on parts of the metal, junctures of dissimilar metals, movement of electrolytes, weld joints, concentration cells, and externally imposed currents. Some or all of these differences in potential can occur on the surface and must be considered in the recommendation of a protective coating. The protective coating must provide the following properties to protect the steel:

- Physical protection to surface
- Prevention of concentration cells
- Dielectric properties
- Lower surface temperatures
- Prevention of electrolyte flow
- Deprivation of free oxygen from the surface
- Stress relief

Stress relief is an important factor in the design of a system. If a system does not compensate for relief in areas of high stresses, cracking will occur that can severely damage the entire system. Stresses on the system of major concern could result from vibration, unsupported surfaces, changes in planes, and welds.

The following five steps are application procedures that should be followed to ensure proper installation of a dual-lining system. First, all areas of high stress that result in movement of the steel structure, such as oil canning or vibration, must be externally supported. Second, the anchoring system should then be applied to the substrate. Anchors, such as V-type or longhorn studs, should be installed on the proper centerlines in a diamond or staggered pattern with the tines randomly oriented. Third, the steel surface must be stripped of all oil and grease by chemical cleaning. The metal should then be sandblasted to an SP 10 Near-White Blast (SSPC: The Society for Protective Coatings designation) with a nominal 64 μm (2.5 mils) profile. Welds should be ground to a smooth, rounded radius with no sharp edges before blasting. Fourth, the appropriate membrane should be applied, ensuring that all of the studs are completely coated and that the system is free of pin holes.

The final step is to apply the monolithic lining. The two available methods of application should be considered. A castable material will shrink more than the gunitable material; therefore, expansion joints must be planned into the system in areas exceeding 6 by 6 m (20 by 20 ft) or where changes in planes will cause stresses to occur. A gunitable material will shrink less and therefore does not require expansion joints. Figure 2 illustrates the gunite application of K_2SiO_3 cement over steel ductwork in a fossil fuel power plant.

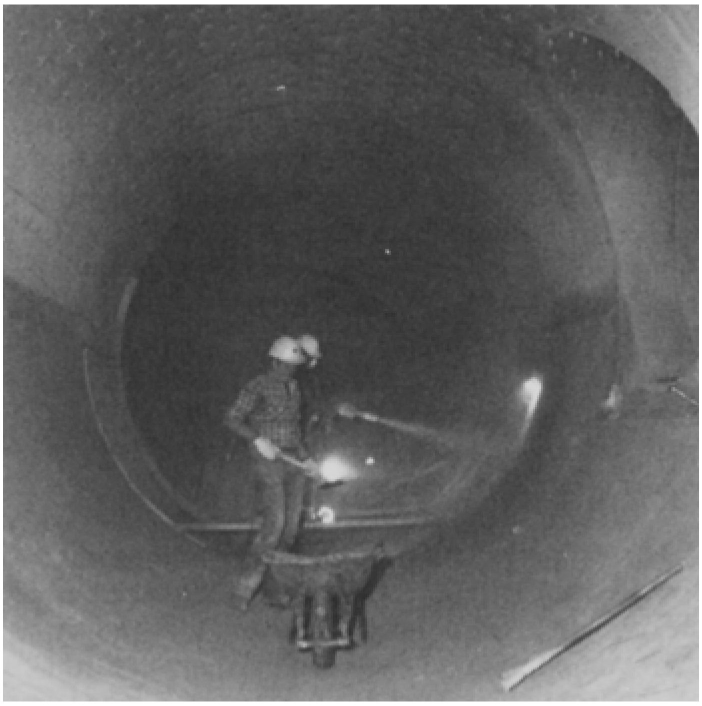

Fig. 2 Gunite application of 50 mm (2 in.) of K_2SiO_3 cement over steel ductwork in a coal-fired power plant

Concrete. In applications over concrete, as with steel, the first considerations are the corrosive environment and the thickness of the material. Once the materials have been selected, the physical structure must be considered. When the substrate is concrete, factors different from those associated with steel must be considered. Inorganic monolithics can be applied over old or new concrete surfaces. When concrete substrates are being used, the following questions should be answered:

- Is the concrete old acid-attacked concrete or new concrete?
- Is the concrete capable of supporting loads?
- Is the structure above grade or below grade?
- Does the concrete need to be waterproofed from the outside?
- Does the concrete structure have existing cracks?
- Is the concrete surface a high or low pH?

A combination of many of these items may apply and should be considered in the recommendation of the proper system. The following are the criteria for a concrete surface before a system may be applied. When working with old acid-attacked concrete, all loose and deteriorated concrete should be removed. The surface should be firm, hard, and at a minimum pH of 5, and all surfaces should be brought back to grade and the slopes reestablished. When working with new concrete, the concrete should be firm and sound. All structural cracks should be repaired, and it should be cured for a minimum of 7 days. Slopes should be a minimum 3.2 mm (0.125 in.) to a maximum 6.4 mm (0.25 in.) per linear foot and should have attained a minimum compressive strength of 21 MPa (3000 psi).

The following five steps are application procedures that should be followed to ensure proper installation of a dual-lining system. First, the concrete should meet the standards outlined previously. Second, the concrete should be cleaned of all oil, grease, and form release compounds by chemical cleaning, waterblasting, or scarifying. Third, the anchoring system should be placed at the specified centerline distance in a diamond-shaped pattern with a random orientation of anchor tines. The anchoring system should consist of V-type or longhorn studs. Fourth, the membrane should be applied to the recommended thickness, ensuring that all studs are completely coated and that the coating is free of pinholes.

The final step is to apply the monolithic. The castable and the gunitable methods should both be considered. As stated previously, when applying by the gunite method there is less shrinkage; therefore, there is no need for expansion joints in the monolithic. However, the lining will require control joints in the normal manner. Expansion joints are recommended with cast applications and should be installed at the perimeter of floor areas,

equipment pads, and floor trenches; around floor drains, column bases, and protrusions; at changes in planes; and over expansion joints in concrete slabs not to exceed 6 m (20 ft) on centerlines.

Brick. A monolithic lining can be applied over acid-attacked masonry construction. The first step is the surface preparation of the brick. Fly ash and other contaminants should be removed by sandblasting or waterblasting. All attacked or unsound mortar should be removed from the joints. Mortar joints should be cleaned to a depth of at least 13 mm (0.5 in.) to provide support for the monolithic lining. If the joints cannot be cleaned to this depth, it is necessary to set longhorn or V-type anchors in the joints. The preferred method of application in this case is to gunite the material. Guniting allows the material to be applied under pressure, thus enabling the material to be packed into the 13 mm (0.5 in.) open joints and allowing the system to be supported by the studs or keying into the joints.

Chemical-Setting Ceramic Linings, *Corrosion: Fundamentals, Testing, and Protection*, Vol 13A, *ASM Handbook*, ASM International, 2003, p 755–758

Chemical-Setting Ceramic Linings

Corrosion Resistance

Monolithic linings are among the fastest growing products in the corrosion protection field because of their resistance to a wider range of corrosive media than most other construction materials. The following industrial applications illustrate the corrosion resistance and some uses of monolithic linings.

Wastewater treatment systems in the southern United States have experienced corrosion problems in areas of high temperatures, high humidity, and slow drainage. Consequently, millions of dollars have been spent in replacing the corroded concrete infrastructures in these wastewater treatment systems in wet wells, grit chambers, sewer lines, and aeration basins. This corrosion went unnoticed throughout the years because the corrosion mechanism was not understood. Most of the corrosion was not caused by discharged chemicals but was microbiologically induced. The concrete infrastructures are seldom completely filled, and the combination of high temperatures and high humidity creates a perfect breeding ground for bacteria, fungi, algae, and gaseous products from decomposing sewage.

Carbon dioxide (CO_2), combined with hydrogen sulfide (H_2S) from the slightly warm and fermenting sewage, reacts with the damp concrete surfaces to form carbonates and calcium sulfate ($CaSO_4$). As this process proceeds, the pH becomes more acidic. Bacterial action results in the production of elemental sulfur from various sulfate reactions, with subsequent oxidation of elemental sulfur to H_2SO_4, which the bacteria secrete.

The H_2SO_4 then directly attacks the underlying portland cement concrete substrate and causes destruction of the infrastructure. There are documented cases of microbiologically induced corrosion having proceeded to the point at which structures collapsed in as few as 6 years or required major rehabilitation in as few as 4 years.

A proven method of rehabilitating deteriorated concrete wastewater structures involves applying a urethane-based membrane to the properly prepared substrate, followed by the pneumatic application of a 100% K_2SiO_3-bonded acid-resistant concrete. The urethane- based membrane is a two-component material with a high solids content and very low permeability. To ensure pinhole-free coatings, the membrane is applied in two or more coats to a wet film thickness ranging from 1.6 to 3.3 mm (63 to 130 mils). These membranes are applied by airless spray with a spray tip pressure of approximately 28 MPa (4000 psi). The high pressure further helps to ensure pinhole-free application of the membrane. The substrate must be dry enough to accommodate the urethane membrane without reacting with the polyisocyanate catalysts usually used.

Therefore, it is sometimes desirable to apply a moisture-tolerant primer, such as a suitable formulated epoxy, to the damp concrete or to apply a fresh layer of concrete first. Following the proper application and cure of the urethane membrane, a veneer of a 100% K_2SiO_3 acidproof cement is applied over the membrane and anchors.

The chemical industry can be the most difficult of all industries in which to design a protective lining. The conditions within one plant can be staggering; there may be acids, alkalies, and solvents, along with extremely high temperatures and physical abuse. Potassium-silicate- base cements satisfy most of these conditions while maintaining economy. The combination of a wide range of chemical resistance, high physical strength, and refractoriness makes these cements leading candidates for many chemical plant applications.

For example, at a major Midwest chemical plant, the action of HCl by-products and ambient moisture on floors, digester tank supports, trenches, and sumps in $NiCl_2$- and $NiSO_4$-processing units produced very corrosive conditions. Restoration of the existing structures was accomplished with a K_2SiO_3 cement and an appropriate membrane.

In the $NiCl_2$ unit, the existing concrete floor was chipped out, and new concrete was poured; the steel beam supports for the digester tanks were also encapsulated with regular concrete. Both floor and digester foundations then received a trowel-applied asphaltic membrane. The membrane provided a flexible acid-, water-, and alkali-resistant barrier between the concrete substrate and the monolithic surfacing. The trowel-applied membrane system is applied at room temperature and offers the chemical resistance of hot-applied membranes for those areas where a hot membrane may not be practical or advisable.

The next step was to apply a K_2SiO_3 monolithic lining by casting into forms. The lining was 38 mm (1. 5 in.) thick over foot traffic areas near the digesters; 38 to 50 mm (1.5 to 2 in.) thick around the encapsulated digester foundation, creating a collar; and 50 mm (2 in.) thick in forklift truck aisles. Finally, at the interface of the digester tank wall and the collar, an elastomeric urethane-based compound was used as a permanently flexible expansion joint.

In the $NiSO_4$-processing unit, the problem areas included trenches running among process equipment in two different buildings. In addition, the various collection sumps into which these trenches drained required restoration. As was done in the $NiCl_2$ area, the deteriorated concrete was reconstructed with new concrete. The asphaltic membrane was trowel applied. A K_2SiO_4 monolithic lining was cast over the membrane to 25 mm (1 in.) in the trenches, 25 to 38 mm (1 to 1.5 in.) in the sumps, and 38 mm (1.5 in.) on the floors, and the elastomeric urethane expansion joint compound was applied.

The service conditions for the two processing areas included a pH of 1 to 2 due to concentrations of HCl up to 32%, water, temperatures to 95 °C (200 °F), and vibrations from imposed loads as great as 3630 kg (8000 lbs) in the truck aisles. These applications were done by the casting method, but they could have easily been done by the gunite method.

Acknowledgment

This article has been adapted from G.D. Maloney, Chemical-Setting Ceramic Linings, in *Corrosion,* Volume 13, *ASM Handbook* (formerly *Metals Handbook,* 9th ed.), ASM International, 1987, p 453–455.

Chemical-Setting Ceramic Linings, *Corrosion: Fundamentals, Testing, and Protection*, Vol 13A, *ASM Handbook*, ASM International, 2003, p 755–758

Chemical-Setting Ceramic Linings

Selected References

- W.W. Carpenter, Ceramic Coatings and Linings, *Surface Engineering,* Vol 5, *ASM Handbook,* ASM International, 1994, p 469–481
- J.R. Davis, Ed., *Surface Engineering for Corrosion and Wear Resistance,* ASM International, 2001
- R.A. Eppler, Ceramic Coatings, *Ceramics and Glasses,* Vol 4, *Engineered Materials Handbook,* ASM International, 1991, p 953–958

- A.O. Kaeding, “Corrosion Resistant Pipe Liners—Polymer Concrete”, SPB9-02, American Concrete Institute, 1985
- J.S. Reed, *Introduction to the Principles of Ceramic Processing,* John Wiley & Sons, 1988
- “Refractory Concrete: State-of-the-Art Report,” ACI 547R-97, American Concrete Institute, 1997
- P.A. Schweitzer, *Corrosion-Resistant Linings and Coatings,* Marcel Dekker, 2001
- K.H. Stern, Ed., *Metallurgical and Ceramic Protective Coatings,* Chapman & Hall, 1996

CVD and PVD Coatings, *Corrosion: Fundamentals, Testing, and Protection*, Vol 13A, *ASM Handbook*, ASM International, 2003, p 759–762

CVD and PVD Coatings

Introduction

VAPOR-DEPOSITED COATINGS modify the surface properties of materials. They are widely used and have been particularly successful in improving such mechanical properties as wear, friction, and hardness in cutting applications. Their use as corrosion-resistant coatings is also becoming widespread.

CVD and PVD Coatings, *Corrosion: Fundamentals, Testing, and Protection*, Vol 13A, *ASM Handbook*, ASM International, 2003, p 759–762

Deposition Processes

The vapor-deposition processes fall into two major categories—physical vapor deposition (PVD) and chemical vapor deposition (CVD)— which in turn comprise various subcategories. Although these divisions often appear confusing and arbitrary, each has its own well-defined technical and economic advantages and disadvantages. This is also true of the materials used in vapor deposition. Therefore, the need for a thorough understanding of both processes and materials is needed for the selection of the optimal combination.

The major deposition processes that are reviewed in this article are sputtering, evaporation, ion plating, and CVD. These processes all have one characteristic in common: the deposition species are transferred and deposited onto the substrate in the form of individual atoms or molecules. In this respect, they are fundamentally different from particulate- or liquid-deposition processes, such as thermal spraying or electroplating, and ion-beam processes where ions are implanted beneath the surface of the material (see the articles “Thermal Spray Coatings,” “Electroplated Coatings,” and “Surface Modification Using Energy Beams” in this Volume). A primary benefit of vapor deposition is that it is essentially nondamaging to the environment, because there are no solvents or chemicals to dispose of. With the current awareness of environmental, safety, and health considerations, this crucial factor favors vapor deposition over other processes that may be more harmful to the environment and health.

Sputtering is the principal PVD process. It involves the transport of a material from a source (target) to a substrate by bombardment of the target by gas ions that have been accelerated by a high voltage. Atoms from the target are ejected by momentum transfer between the incident ions and the target. These ejected particles move across the vacuum chamber to be deposited on the substrate.

Figure 1 is a schematic of the sputtering process. In its simplest form, the process occurs in an inert (noble) gas at low pressure (0.13 to 13 Pa, or 1×10^{-3} to 0.1 torr); in most cases, the gas is argon. Argon has higher mass than other noble gases, such as neon or helium, and is easier to ionize. Higher mass gives a higher sputtering

yield, especially if the mass of the bombarding particle is the same order of magnitude or greater than the mass of the target atom. Other gases, such as oxygen or nitrogen, can also be used, but they may react chemically with the target. The sputtering process begins when an electric discharge is produced and the argon becomes ionized. The low-pressure electric discharge is known as glow discharge, and the ionized gas is termed plasma.

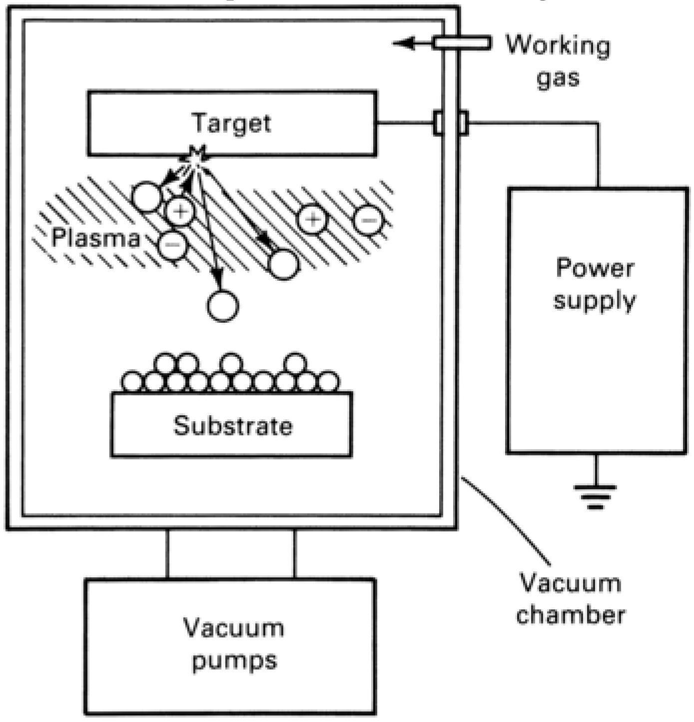

Fig. 1 Basic sputtering process

The argon ions hit the solid target, which is the source of the coating material (not to be confused with the substrate, which is the item to be coated). The target is negatively biased and therefore attracts the positively charged argon ions, which are accelerated in the glow discharge. This attraction of the ions to the target (also known as bombardment) causes the target to sputter, which means that material is dislodged from the target surface because of momentum energy exchange. The higher the energy of the bombarding ions, the higher the rate of material dislodgement.

Sputtering developed very rapidly in the 1970s in the semiconductor industry, in which the technique is essential for mass production. Sputtering is used in corrosion-abatement applications such as high-chromium and nickel-chromium alloy coatings, MCrAlY (where M stands for nickel, cobalt, or iron or a combination of them), and some polymers. Titanium nitride, other nitrides, tungsten, molybdenum, carbides, borides, and diamondlike carbon are sputtered for wear resistance (Ref 1).

For the deposition of thin metal films (in the 0.1 μm, or 4 μin., range), sputtering is the best technique. Deposition is feasible in a controllable manner for both compound and elemental targets (the source of the coating material). Adhesion is good and can be further improved by sputter cleaning the substrate or by bias sputtering. Large equipment is readily available, and sputtering has become a highly automated process. The quality, structure, and uniformity of the deposit are excellent. The disadvantages of sputtering include its thickness limitation, the need for a vacuum, and high cost. It is also a line-of- sight process that requires special fixtures and shaped targets to coat uniformly; furthermore, the coating of compound curves, recesses, and holes is difficult. The substrate being processed must be capable of withstanding processing temperatures of 260 to 540 °C (500 to 1000 °F).

Evaporation was the first PVD process used on an industrial basis for the aluminum metallization of plastics and glass for decorative purposes. Originally the most widely used process, evaporation has now been overtaken by sputtering. The metallization process is relatively simple and well adapted to mass production.

The basic evaporation process involves the transfer of material to form a coating by physical means alone, essentially vaporization. Practically all metals can be evaporated, making evaporation a universal process. The source material may be heated by bombardment with an electron beam or heated by thermal conduction. Like sputtering, it is a line-of-sight process; therefore, to achieve efficiency of coverage and uniformity it is necessary to use multiple evaporation sources and to rotate or move the substrate uniformly to expose all areas.

Unlike other vapor-deposition processes, evaporation is a low-energy process, with particle energy averaging 0.2 to 0.3 eV as compared to 10 to 40 eV for sputtering, 200 eV or more for ion plating, and 100 keV for ion implantation. The term “low energy” means that adhesion of the particle to the substrate may be marginal. In addition, the temperature of the substrate is not increased by the deposition, which means there is little or no diffusion. Because no strong physical or chemical action takes place at the interface, particular care must be taken to remove all impurities in the chamber and to have a very clean substrate. The basic process (with an electron-beam source) is shown in Fig. 2.

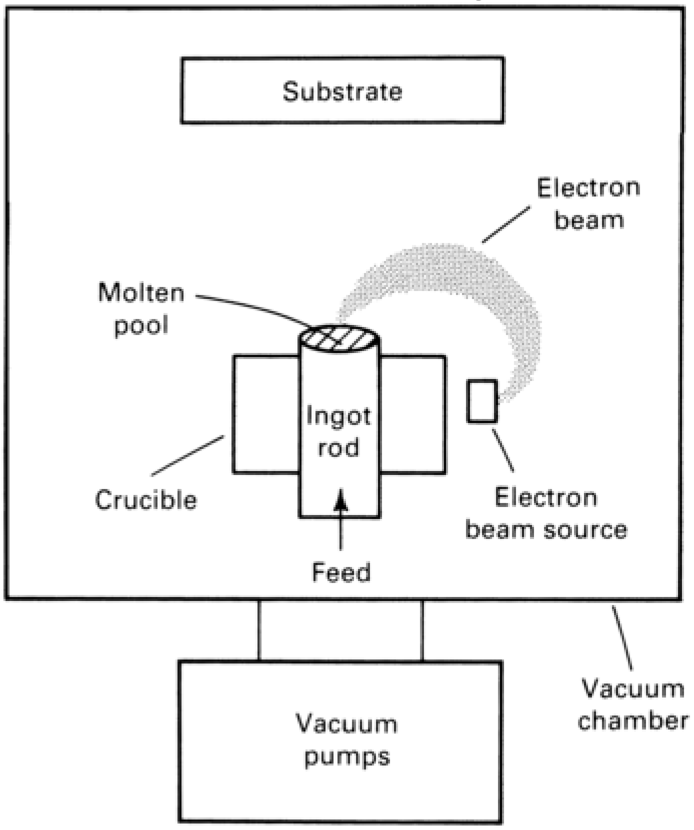

Fig. 2 Basic evaporation process

Very large evaporation equipment, which was developed for the optical industry, is commercially available. Coatings of several microns in thickness can be rapidly deposited. The disadvantages of this method are nonuniform coverage (limited to line of sight) and relatively low adhesion unless glow-discharge cleaning is used (glow-discharge cleaning removes surface atoms from the substrate). Evaporation is very successful in applications in which adhesion and good structure are not critical, such as decorative and optical uses. Aluminum is the principal evaporation material; chromium and stainless steel are also widely used. Evaporation is not generally used for critical corrosion-control applications.

Ion plating is a generic term for the hybrid process based on the evaporation (or sputtering) mechanism coupled with a flux of high-energy particles (Fig. 3) imparting a large increase in the energy of the deposition species, which is atomistic.

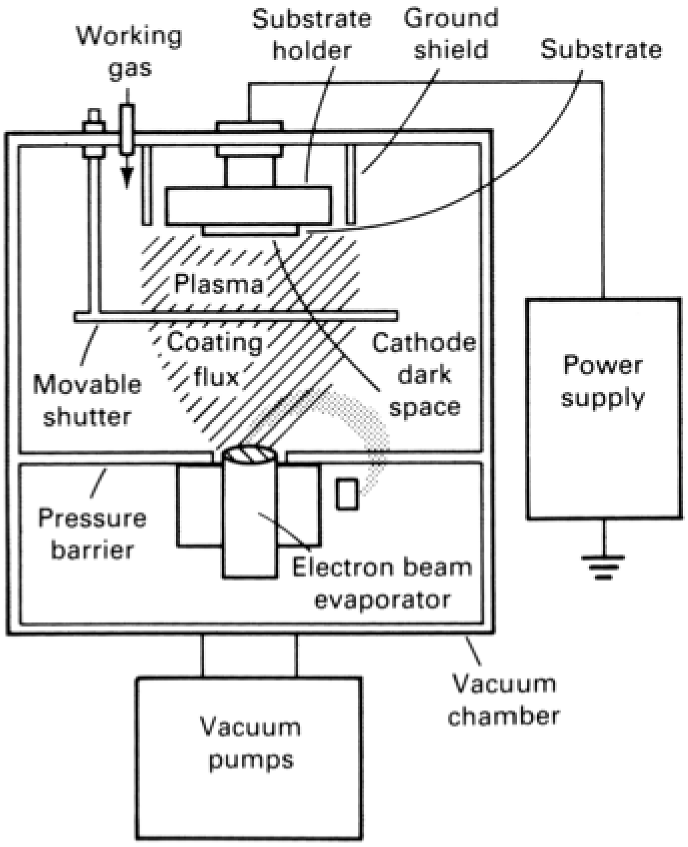

Fig. 3 Basic ion plating process

Ion-beam-assisted deposition (IBAD) and ion- beam-enhanced deposition (IBED) refer to the process wherein evaporated atoms produced by physical vapor deposition (PVD) are simultaneously struck by an independently generated flux of ions (Fig. 4) (Ref 2). The extra energy imparted to the deposited atoms causes atomic displacements at the surface and in the bulk, as well as enhanced migration of atoms along the surface. These resulting atomic motions are responsible for improved film properties—including better adhesion and cohesion of the film, modified residual stress, and higher density— when compared with similar films prepared by PVD without ion bombardment. When the ion beam or the evaporant is a reactive species, compounds such as refractory silicon nitride (Si_3N_4) can be synthesized at very low temperatures. Furthermore, adjustment of the ratio of reactive ions to atoms arriving at the substrate surface allows adjustment of the stoichiometry of solid solutions.

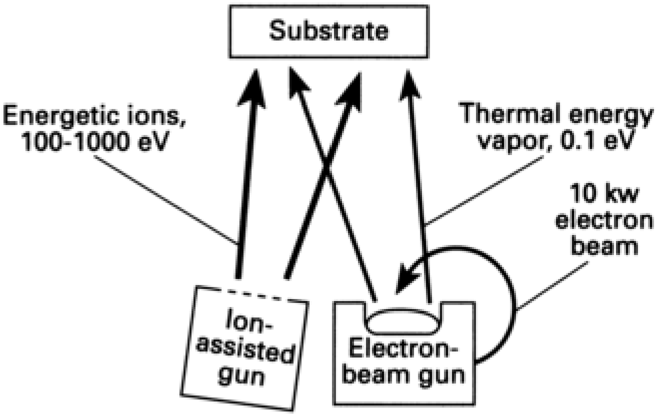

Fig. 4 Ion-beam-assisted deposition (IBAD)

It is generally accepted that plasma plays the same part as high temperature in improving the adhesion and increasing the reactivity of the coating; an ion passing through a potential of 100 eV acquires an equivalent temperature of 106 K. While the PVD process uses temperatures of approximately 538 °C (1000 °F), the IBED process deposits hardcoats below 93 °C (200 °F) (Ref 3).

The simplest forms of ion plating are ion nitriding and ion carburizing, in which nitrogen or carbon ions react with a steel substrate to form nitrides or carbides. If the deposition species is ionized in a reactive gas, a compound is formed with some of the gas atoms, and deposition of the compound occurs. Ion plating is widely used and is gradually replacing pack cementation or diffusion.

With ion implantation, the objective is to modify the properties of the surface, such as corrosion behavior, by embedding atoms from a beam of ionized particles into the near surface of the target.

Because ion plating is a glow-discharge process in which a plasma is formed, it is necessary to have at least a threshold gas pressure to maintain the plasma. This is different from standard nonionized evaporation, in which the minimum pressure obtainable is preferred. The net effect of this higher gas pressure is to increase the number of collisions with gas molecules and therefore produce more scattering of the deposition species, which in turn diminishes the importance of the line-of-sight principle and improves coverage.

The deposited species in ion plating have higher energy than those of evaporation or sputtering processes; this results in improved adhesion as well as a deposit with improved structure and fewer imperfections. In addition, if a sputtering system is used, it is easy to sputter the surface of the substrate to clean it before deposition.

However, the ion equipment is more complicated and therefore more expensive than either evaporation or sputtering equipment, and the process is more exacting.

Chemical vapor deposition is a well-established deposition process that is used extensively in the semiconductor and cutting-tool industries. It has the unique ability to deposit thick, dense, high-quality films (up to 6.4 mm, or 0.25 in., thick or more) at a cost that is generally lower than that of PVD processes. The high temperature, about 1000 °C (1830 °F), necessary for CVD promotes good adhesion, but also considerably restricts the type of substrate that can be coated to ceramics, refractory metals, and special alloys.

In most cases, steel will require heat treatment in a vacuum or protected atmosphere after CVD coating and will often change dimensions sufficiently to require postdeposition machining if close tolerances are required. Another constraint resulting from the high temperature of deposition is the stress in the deposit due to the difference in thermal expansion between substrate and deposit. These stresses may be sufficient to cause cracking, spalling, and loss of adhesion. The technique of plasma CVD can be used at much lower temperatures in, for example, semiconductor applications, but the resulting films tend to incorporate impurities.

The materials that can be easily deposited by CVD are more limited than with PVD. Chemical vapor deposition is particularly useful for depositing compounds and refractory metals and lends itself very well to corrosion applications.

Figure 5 is a schematic of thermal CVD equipment. The reactive gases are metered in the mixing chamber. They then pass into the deposition chamber and contact the heated part to be coated (sample); at this point, they react and deposition occurs. By-products are removed through the vacuum system.

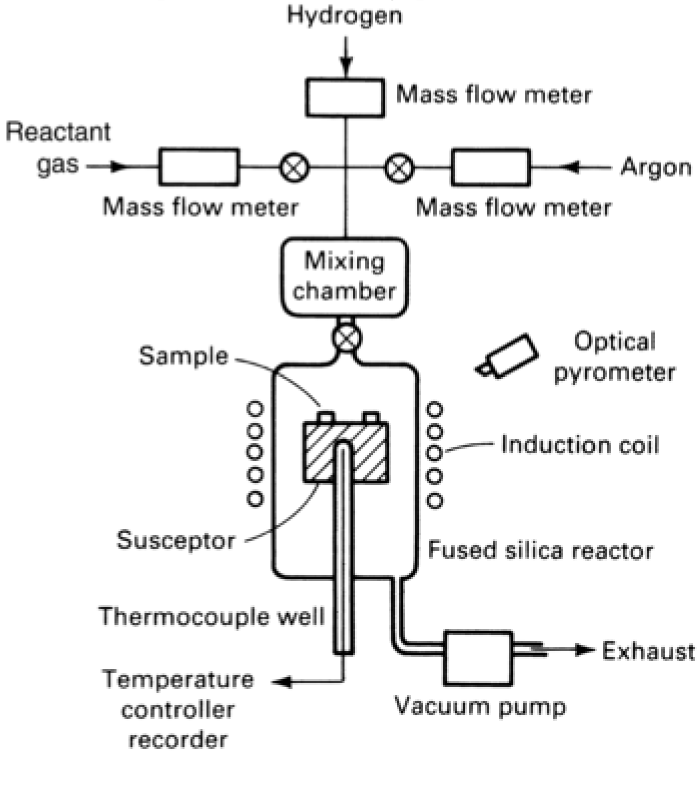

Fig. 5 Thermal CVD reactor

Chemical vapor deposition reactions can occur over a range of pressures. Low pressure increases boundary-layer diffusion and uniformity, often at the expense of deposition efficiency. Each application and each reaction must be analyzed to determine the optimal conditions for deposition.

References cited in this section

1. J.R. Davis, Ed., *Surface Engineering for Corrosion and Wear Resistance*, ASM International, 2001, p 175

2. G.K. Hubler and J.K. Hirvonen, Ion-Beam- Assisted Deposition, *Surface Engineering,* Vol 5, *ASM Handbook,* ASM International, 1994, p 593

3. A.H. Deutchman and R.J. Partyka, Comparison of the Properties of PVD and IBED Hardcoats (TiN and Cr_2N), *First ASM International Surface Engineering Congress and 13th IFHTSE Congress,* Oct 2002 (Columbus, OH), ASM International 2003, p 138

CVD and PVD Coatings, *Corrosion: Fundamentals, Testing, and Protection*, Vol 13A, *ASM Handbook*, ASM International, 2003, p 759–762

CVD and PVD Coatings

Coating Materials and Applications

The list of materials that can be vapor deposited is extensive and covers almost any coating requirement. The most important materials are given in Table 1. Aluminum and aluminum alloys are among the most widely used deposition materials and are gradually replacing cadmium in many corrosion applications. Sputtered chromium and stainless steel are also making great inroads in corrosion applications. A promising material is titanium nitride. It is hard, very stable, and refractory, and it has good lubricating characteristics and a pleasing gold appearance. It is widely used in wear applications, such as cutting tools, and in decorative applications. It is usually applied by sputtering or ion plating, and it holds potential for corrosion protection.

Table 1 Some corrosion-resistant vapor- deposited materials

Material	Deposition process
Aluminum	Evaporation
Chromium	Sputtering
Nickel	CVD, sputtering
Rhenium	CVD
Tantalum	Sputtering, CVD
Titanium	Evaporation, sputtering
Tungsten	CVD, sputtering
Boron	CVD
Carbon	CVD, ion plating
Titanium diboride	Evaporation, CVD
Silicon carbide	Sputtering, CVD
Titanium carbide	Sputtering, evaporation, CVD
Tungsten carbide	Sputtering, CVD
Boron nitride	CVD
Silicon nitride	Sputtering, ion plating
Titanium nitride	CVD, sputtering, ion plating

Aluminum oxide	Sputtering, ion plating
Molybdenum silicide	Sputtering, ion plating
Nickel-chromium alloys	Sputtering
Gold alloys	Evaporation
Borazon	CVD
MCrAlY	Evaporation, sputtering
Bronze	Evaporation, sputtering

The properties of these materials vary widely and reflect the complexity of selecting a corrosion-resistant coating for a given substrate or a given environment and the need to conduct a thorough analysis of the problem. This is especially true when cost is the primary factor. For example, gold is an ideal material for many corrosion applications, but would of course be cost prohibitive in most cases. Before selecting a material and process for a corrosion-resistance application, the following considerations should be reviewed:

- Availability and cost of the coating material
- Cost, size, complexity, and availability of the deposition equipment
- Resistance to the chemical environment of the coating material
- Compatibility with the substrate, especially thermal expansion mismatch
- In special applications, such as aerospace, high-temperature resistance, radiation resistance, and high-vacuum stability

Chemical vapor deposited and PVD coatings have the advantage that the film (if thick enough) is essentially pore free and fully dense. Penetration by moisture and gases to the substrate is greatly reduced, if not eliminated. Despite this, the role played by CVD and PVD coatings in corrosion protection remains small. Some current applications are discussed in the paragraphs that follow.

Coating for Graphite. Graphite is perhaps the best material for applications requiring high strength and low density at very high temperatures. It is used as a hot-pressed material or as a carbon-carbon composite, which is a combination of graphite fibers and a carbonized resin matrix. Graphite is used in such applications as rocket nozzles or advanced turbine components. However, its disadvantage is a lack of oxidation resistance above 500 °C (930 °F). By using CVD to coat the graphite with silicon carbide, it is possible to provide oxidation protection up to 1650 °C (3000 °F). Silicon carbide oxidizes to form a silicon oxide surface that will prevent further oxidation. Advanced studies to further increase the oxidation temperature of graphite are in progress using such oxides as hafnia.

Aluminum Coating of Steel. The coatings of steel (and other metals) with aluminum by ion plating is an industrial process with excellent potential for large-scale production. It replaces hot dipping of aluminum on steel, which has been used for many years. During immersion in hot dipping, a brittle intermetallic compound layer of iron-aluminum is formed; this limits the formability of the steel. In addition, the coating contains iron impurities, which may be a severe shortcoming in highly corrosive environments (Ref 4).

Electroplated cadmium is another commonly used system for the corrosion protection of steel and other metals. However, it can cause hydrogen embrittlement of high-strength steel and titanium. In addition, cadmium has a low melting point (320 °C, or 608 °F) and presents environmental problems because of its toxicity. A process has recently been developed for applying aluminum on metals by ion-vapor deposition, which has none of the restrictions of hot dipping or cadmium electroplating. This process falls under military specification MIL-C 83488 (Ref 5).

Vapor deposition of aluminum does not produce hydrogen; therefore, it does not cause embrittlement. Vapor-deposited aluminum protects against stress-corrosion cracking (SCC) and has a temperature limit of 495 °C (925 °F). It is less expensive than most other barrier coatings. Applications for vapor-deposited aluminum in the aerospace industry include fuel and pneumatic line fittings (in place of anodizing), electrical connectors to replace cadmium, powder-metallurgy parts, fasteners, electrical black boxes, corrosion and SCC protection of depleted uranium and titanium alloys, and electromagnetic interference compatibility (Ref 6).

One of the first industrial applications of the IBAD process was the coating of stainless steel electric razor screens with TiN for aqueous corrosion protection (Ref 7).

Alloy Coatings for Gas Turbines. Gas turbines are used as aircraft turbines using highly refined fuels with operating temperatures between 900 and 1150 °C (1650 and 2100 °F) or higher; marine turbines using moderately refined fuels, which operate at 700 to 870 °C (1290 to 1600 °F) and are exposed to salt corrosion; and industrial turbines that may operate at 760 to 925 °C (1400 to 1700 °F) and use moderately refined fuels,

often with high sulfur contents. Industrial turbines may use a variety of fuels and operate in marine, arctic, or more benign environments. Along with the need for high-temperature mechanical strength, materials in these applications must resist oxidation and high-temperature corrosion. These problems are becoming more acute with the trend toward higher operating temperatures for better performance and improved fuel economy.

Coatings were initially used in the 1960s to protect turbine hot section components from oxidation and high-temperature corrosion. Physical vapor deposition coating by electron-beam evaporation and sputtering of chromides and aluminides were used as temperature requirements increased, and these are still used in a majority of applications 30 to 40 years after their introduction. Overlay coatings of chromium, aluminum, and yttrium with cobalt, nickel, or iron are known generically as MCrAlY and are successfully used on aircraft turbines for resistance to hot corrosion. They are applied either by electron-beam PVD or plasma thermal spray. In the 1980s thermal barrier coatings (TBCs) were introduced for the purpose of reducing the operating temperature beneath the coating. Recent developments using platinum-modified aluminides increase the oxidation resistance of these thermal barriers (Ref 8).

Marine gas turbines are subject to severe sulfidation, oxidation, and hot corrosion, especially in the presence of sodium sulfate (Na_2SO_4). Electron-beam-evaporated CoCrAlY coatings have considerably increased the service lives of first-stage blades. Further improvements have been achieved by using high-chromium low- yttrium alloys.

Industrial turbines may not require the degree of corrosion protection of other applications unless high-sulfur fuels are used or the atmosphere is aggressive. In such cases, the hot-corrosion problem can be solved by using thin-film CoCrAlY coatings and a very large (200 kW) electron-beam coater capable of handling industrial turbine parts weighing up to 40 kg (90 lb). Now TBC coatings are used for industrial turbines in relatively lower temperature components. Failures of turbine blades due to corrosion-assisted fatigue can have catastrophic results even in the compressor portion of the turbine, and these can be protected with PVD coatings and IBED coating (Ref 9).

References cited in this section

4. F. Dunbar, “Aluminum Coated Steels: Past, Present and Future,” Paper 8201-037, presented at the ASM Metals Congress, Oct 1982 (St. Louis, MO), American Society for Metals

5. “Coating, Aluminum, High Purity,” MIL- DTL-83488D, April 1999

6. D. Muehlberger and J. Reilly, “Improved Equipment, Productivity Increase, Applications for Ion Vapor Deposition of Aluminum,” Technical Report 83-0691, Society of Automotive Engineers, 1985

7. G.K. Hubler and J.K. Hirvonen, Ion-Beam- Assisted Deposition, *Surface Engineering,* Vol 5, *ASM Handbook,* ASM International, 1994, p 599

8. M. Thomas, Materials Development in Aero Gas Turbines, *Parsons 2000 Advanced Materials for 21st Century Turbines and Power Plant,* A. Strang, W.M. Banks, R.D. Conoy, G.M. McMolvin, J.C. Neal, and S. Simpson, Ed., The University Press, Cambridge, United Kingdom, 2000, p 710

9. S. Chakravarty, P. Li, V. Tirabasso, and P.C Patnaik, Improvement of Fatigue and Corrosion Resistance of Compressor Rotor Blades of an Industrial Gas Turbine Engine, *Advanced Materials and Coatings for Combustion Turbines,* V.P. Swaminathan and N.S. Cheruvu, Ed., ASM International, 1994, p 135

CVD and PVD Coatings

Acknowledgment

This article has been adapted from H.O. Pierson, CVD/PVD Coatings, *Corrosion*, Vol 13, *ASM Handbook* (formerly 9th ed. *Metals Handbook*), ASM International, 1987, p 456–458.

CVD and PVD Coatings, *Corrosion: Fundamentals, Testing, and Protection*, Vol 13A, *ASM Handbook*, ASM International, 2003, p 759–762

CVD and PVD Coatings

References

1. J.R. Davis, Ed., *Surface Engineering for Corrosion and Wear Resistance*, ASM International, 2001, p 175
2. G.K. Hubler and J.K. Hirvonen, Ion-Beam- Assisted Deposition, *Surface Engineering*, Vol 5, *ASM Handbook*, ASM International, 1994, p 593
3. A.H. Deutchman and R.J. Partyka, Comparison of the Properties of PVD and IBED Hardcoats (TiN and Cr_2N), *First ASM International Surface Engineering Congress and 13th IFHTSE Congress*, Oct 2002 (Columbus, OH), ASM International 2003, p 138
4. F. Dunbar, "Aluminum Coated Steels: Past, Present and Future," Paper 8201-037, presented at the ASM Metals Congress, Oct 1982 (St. Louis, MO), American Society for Metals
5. "Coating, Aluminum, High Purity," MIL- DTL-83488D, April 1999
6. D. Muehlberger and J. Reilly, "Improved Equipment, Productivity Increase, Applications for Ion Vapor Deposition of Aluminum," Technical Report 83-0691, Society of Automotive Engineers, 1985
7. G.K. Hubler and J.K. Hirvonen, Ion-Beam- Assisted Deposition, *Surface Engineering*, Vol 5, *ASM Handbook*, ASM International, 1994, p 599
8. M. Thomas, Materials Development in Aero Gas Turbines, *Parsons 2000 Advanced Materials for 21st Century Turbines and Power Plant*, A. Strang, W.M. Banks, R.D. Conoy, G.M. McMolvin, J.C. Neal, and S. Simpson, Ed., The University Press, Cambridge, United Kingdom, 2000, p 710
9. S. Chakravarty, P. Li, V. Tirabasso, and P.C Patnaik, Improvement of Fatigue and Corrosion Resistance of Compressor Rotor Blades of an Industrial Gas Turbine Engine, *Advanced Materials and Coatings for Combustion Turbines*, V.P. Swaminathan and N.S. Cheruvu, Ed., ASM International, 1994, p 135

CVD and PVD Coatings, *Corrosion: Fundamentals, Testing, and Protection*, Vol 13A, *ASM Handbook*, ASM International, 2003, p 759–762

CVD and PVD Coatings

Selected References

Articles in *Surface Engineering,* Volume 5 of the *ASM Handbook,* ASM International, 1994:

- J.K. Hirvonen and B.D. Sartwell, Ion Implantation, p 605–610
- J.S. Horwitz, Pulsed-Laser Deposition, p 621–626
- D.M. Mattox, Growth and Growth-Related Properties of Films Formed by Physical Vapor Deposition, p 538–555
- D.M. Mattox, Ion Plating, p 582–592
- D.M. Mattox, Vacuum Deposition, Reactive Evaporation, and Gas Evaporation, p 556–572
- H.O. Pierson, Chemical Vapor Deposition of Nonsemiconductor Materials, p 510–516
- M. Razeghi, Chemical Vapor Deposition of Semiconductor Materials, p 517–531
- S.L. Rohde, Sputter Deposition, p 573–581
- D.M. Sanders, J.W. Glaser, and S. Falabella, Arc Deposition, p 602–604
- P.K. Tedrow and R. Reif, Plasma-Enhanced Chemical Vapor Deposition, p 532–537

Other reference source:

- G. Decher and J.B. Schlenoff, Ed., *Multilayer Thin Films: Sequential Assembly of Nanocomposite Materials,* Wiley-VCH, 2003
- M.L. Hitchman and K.F. Jensen, Ed., *Chemical Vapor Deposition,* Academic Press, 1993
- W. Menz and J. Mohr, *Microsystem Technology,* Wiley-CVH, 2000
- J.-H. Park and T.S. Sudarshan, Ed., *Chemical Vapor Deposition*, ASM International, 2001
- H.O. Pierson, *Handbook of Chemical Vapor Deposition,* Noyes Publication, 1992
- R.V. Stuart, Vacuum Technology, *Thin Films, and Sputtering: An Introduction,* Academic Press, 1983
- V.G. Syrkin, *The CVD Method: Chemical Vapor-Phase Metallization,* 2000

V.A. Ravi, Pack Cementation Coatings, *Corrosion: Fundamentals, Testing, and Protection,* Vol 13A*, ASM Handbook,* ASM International, 2003, p 763–771

Pack Cementation Coatings

Vilupanur A. Ravi, California State Polytechnic University, Pomona

Introduction

METALLIC MATERIALS used in harsh environmental conditions undergo degradation in various ways. Several forms of corrosion, that is, uniform, galvanic, pitting, and crevice corrosion (Ref 1), have been observed, reported, and analyzed in aqueous environments. Similarly, at high temperatures, alloys can degrade in different ways: by oxidation (Ref 2), sulfidation (Ref 3), halogen attack (Ref 4), and hot corrosion (Ref 5). Two general approaches are used to mitigate the corrosive effects of high-temperature environments:

- *Alloy design:* The alloy composition and/or structure are altered in specific ways to address the specific environment.
- *Surface modification:* Coatings are applied where the surface structure and/or composition is engineered appropriately while retaining the same substrate.

Coatings containing aluminum, chromium, and silicon are effective against oxidation and hot corrosion by forming protective Al_2O_3, Cr_2O_3, and SiO_2 scales, respectively. Some of the key characteristics of a successful coating are:

- The ability to resist damage in the desired service conditions (corrosion, erosion, erosion- corrosion, stress-related corrosion problems, etc.)
- The integrity of the coating-substrate interface (an ideal interface would be continuous and free from interfacial stresses)
- The adherence of the coating to the substrate under mechanical and thermal cycles

Several coatings and associated processes are available to protect metallic substrates from a range of corrosive environments. Table 1 (Ref 6) indicates one method of classification of coating processes. Although not exhaustive, the table illustrates an important distinction between two major classes of coatings: overlay and diffusion (surface modified). In the former, the coatings are applied with minimal change to the substrate. In the latter, however, the coating constituents diffuse into the substrate, resulting in chemical and microstructural changes to the substrate surface.

Table 1   Classification of coating processes

Category	Description	Processes
Overlay coatings	Deposition with minimal interdiffusion of coating with substrate	• Hot spraying (flame spraying, plasma spraying, detonation coatings) • Chemical vapor deposition • Physical vapor deposition (thermal evaporation, ion sputtering, ion plating)
Surface modified coatings	Diffusion-induced modification of chemical composition and/or microstructure of substrate	• Pack cementation • Slurry cementation • Metalliding • Hot dipping • Surface alloying (ion implantation, laser surface alloying)

Source: Ref 6

Each coating and its associated processes has features that make it suitable for certain applications and unsuitable for others. The focus in this article is pack-cementation coatings and, in particular, halide-activated pack cementation coatings on nickel alloys, although the principles are generally applicable to Fe- and Co-base alloys.

References cited in this section

1. M.G. Fontana and N.D. Greene, *Corrosion Engineering,* 2nd ed., McGraw-Hill International Book Company, 1978, p 28

2. P. Kofstad, *High Temperature Corrosion,* Elsevier Applied Science Publishers, Ltd., 1988, p 324

3. N.S. Bornstein, *JOM, J. Min., Metals, Mater. Soc.,* Vol 48, 1996, p 37

4. P. Elliott, C.J. Tyreman, and R. Prescott, *J. Met.,* Vol 37, 1985, p 20

5. R.A. Rapp, *Corrosion,* Vol 42, 1986, p 568

6. P.G. Capelli, Coating Processes, *High Temperature Alloys for Gas Turbines,* D. Coutsouradis, P. Felix, H. Fischmeister, L. Habraken, Y. Lindblom, and M.O. Speidel, Ed., Applied Science Publishers, London, 1978, p 177

V.A. Ravi, Pack Cementation Coatings, *Corrosion: Fundamentals, Testing, and Protection*, Vol 13A, *ASM Handbook*, ASM International, 2003, p 763–771

Pack Cementation Coatings

Vilupanur A. Ravi, California State Polytechnic University, Pomona

---

Halide-Activated Pack Cementation

Halide-activated pack cementation (Ref 7) is a coating process in which the elements to be deposited are converted into halide vapor species. These halide vapors then diffuse through a porous pack to the surface of the substrate to be coated, where they undergo disproportionation reactions resulting in the deposition of the desired elemental species. The coating material then diffuses into the substrate with subsequent modification of the substrate microstructure. A typical pack (Fig. 1) (Ref 8) consists of:

- Filler
- Master alloy
- Activator salt
- Substrate to be coated

Powders of the filler, master alloy, and activator are blended together and placed in a container with the substrate buried in it.

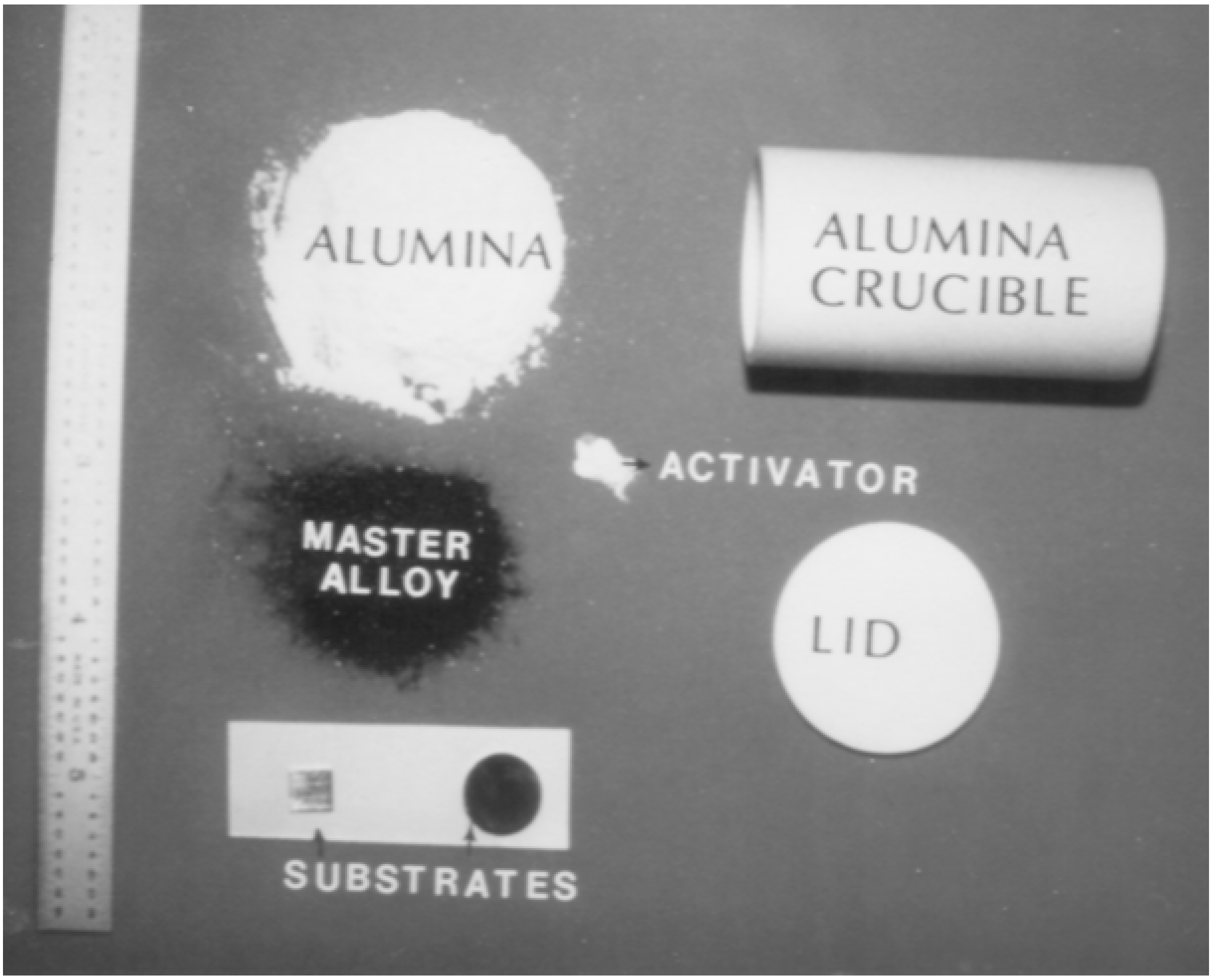

Fig. 1 Typical pack of constituents for a laboratory scale cementation pack

A filler, such as Al_2O_3, allows the active pack constituents (the master alloy and activator salt) to be well distributed. This allows the halide vapors to easily reach the substrate surface, resulting in an overall uniform coating.

The activator salt, a halide compound such as NaCl, $CrCl_2$, NH_4Cl, or AlF_3, reacts with the master alloy to produce gaseous halide compounds of the element(s) to be deposited.

The master alloy, such as Fe-Al or Ni-Al, contains the element(s) to be deposited. However, the elemental forms of Al, Cr, or Si can also be used. The alloy compositions are customized to achieve the desired coating composition

Substrates are typically nickel- or iron-base alloys. Their forms can have a wide range of geometries, for example, flat plates, pipes, and turbine blades. It is important that the substrates are not positioned too close together in the pack, to avoid nonuniformity in the coating thickness.

References cited in this section

7. L.L. Seigle, *Surface Engineering*, R. Kossowsky and S.C. Singhal, Ed., Martinus Nijhoff Publishers, Pittsburgh, 1984, p 345

8. V.A. Ravi, Ph.D. thesis, The Ohio State University, 1988

V.A. Ravi, Pack Cementation Coatings, *Corrosion: Fundamentals, Testing, and Protection*, Vol 13A, *ASM Handbook*, ASM International, 2003, p 763–771

Pack Cementation Coatings

Vilupanur A. Ravi, California State Polytechnic University, Pomona

Types of Pack Cementation Processes

Pack aluminizing, chromizing, and siliconizing are some distinct classes of pack cementation coating processes. These processes are based on coating the substrate with a single element, that is, aluminum, chromium, or silicon. It is also possible to achieve simultaneous deposition of more than one element.

Pack Aluminizing

The original process, attributed to Van Aller (Ref 9), used a pack consisting of aluminum, ammonium chloride, and graphite powders placed in a drum along with iron or copper substrates. The coating process was carried out around 450 °C (840 °F). Gilson (Ref 10) replaced the graphite powder with aluminum oxide. These early processes remain essentially the same today. The current versions, however, involve a range of master alloys and activators. Other researchers (Ref 11, 12, 13) have classified aluminizing packs, for example, as “high-” or “low-” activity packs. In high-activity packs, aluminum diffuses inward into the substrate (Fig. 2) and forms a solid solution intermetallic such as NiAl with the nickel in the substrate. In low-activity aluminum packs, on the other hand, the outward diffusion of nickel from the substrate dominates. Figure 3 (Ref 11) depicts the microstructure of a nickel-base superalloy aluminized in a low-activity aluminum pack.

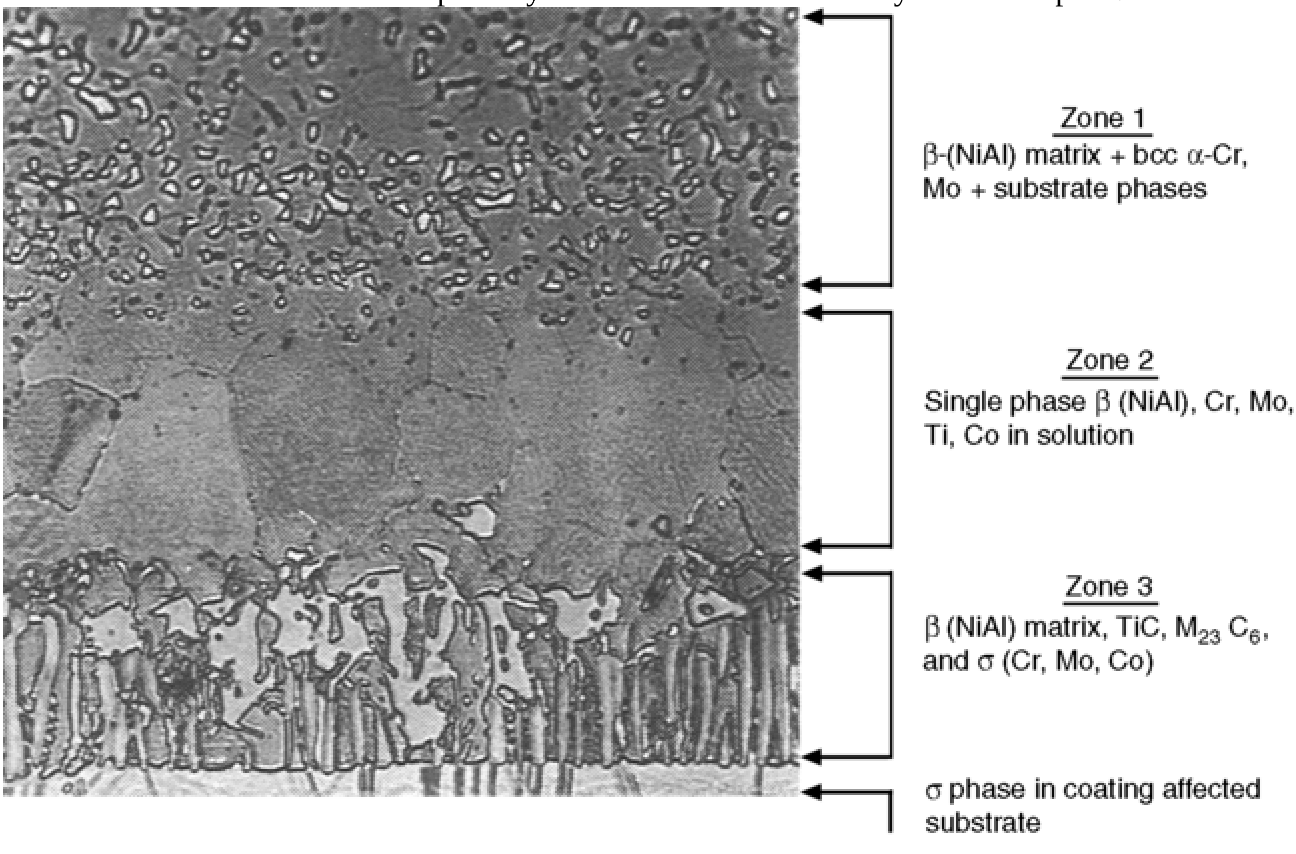

Fig. 2 Archtypical microstructure of a cross section of a nickel-base superalloy aluminized in a high-activity aluminum pack followed by heat treatment for 4 h at 1080 °C (1975 °F). See source Ref 11 for exact size

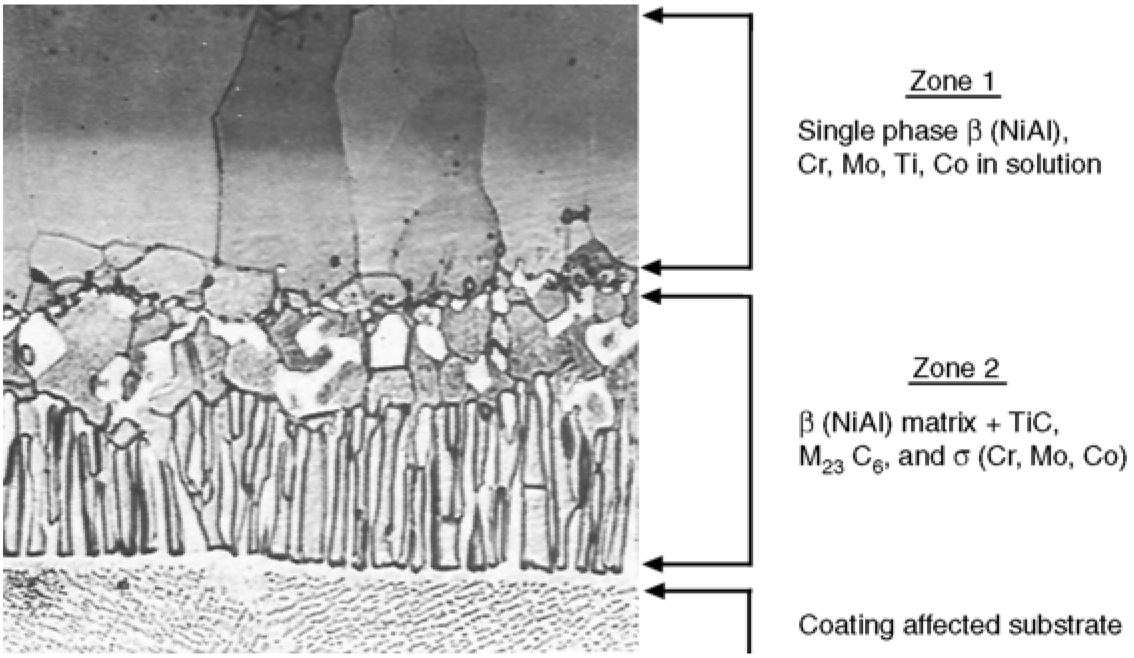

Fig. 3 Archtypical microstructure of the cross section of a nickel-base superalloy aluminized in a low-activity aluminum pack. See source Ref 11 for exact size

Figures 4 and 5 (Ref 12) are schematics of coating formation in low- and high-activity Al packs as discussed in Ref 12. Figure 4(a) shows markers placed on the surface of pure nickel. When exposed to a low-activity aluminum pack, the outward diffusion of nickel is much faster than the inward diffusion of aluminum. Thus the coating grows outward, as indicated by intermediate positions e_1 and e_2. The net outward diffusion of nickel results in the formation of Kirkendall pores close to the original interface. Figure 4(b) (Ref 12) represents the situation for a nickel-base superalloy in which the outward diffusion of nickel leads to corresponding nickel-depleted areas within the alloy. Thus when a layer (position e_1) forms by outward nickel diffusion, a corresponding layer of nickel depletion (position e'_1) forms within the alloy. Likewise, e_2 corresponds to e'_2, e_3 corresponds to e'_3, and so forth. The loss of nickel leads to the formation of intermetallics like NiAl and is accompanied by precipitates like TiC, which are not soluble in the intermetallic matrix. This is further illustrated in Fig. 4(c).

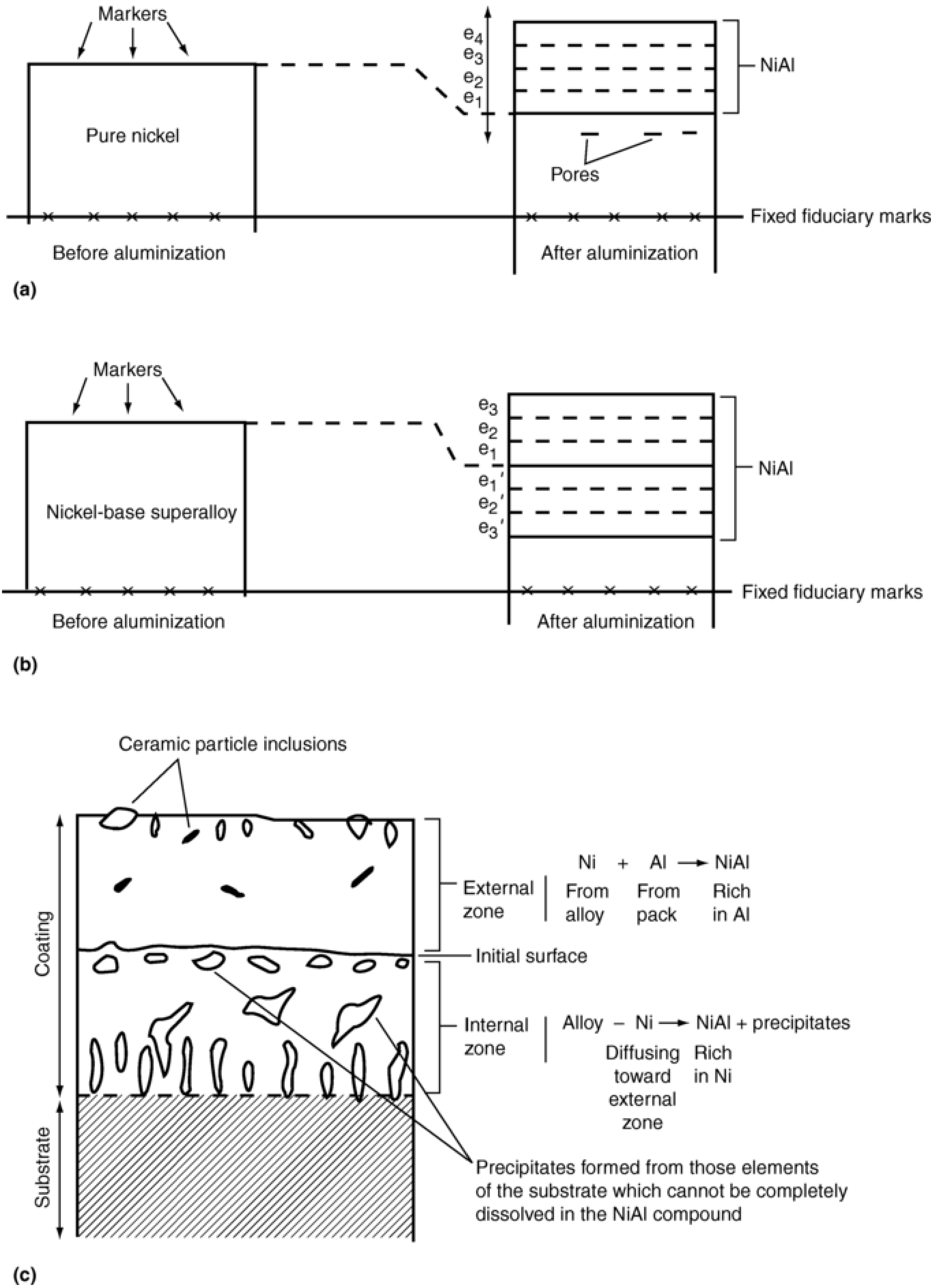

Fig. 4 Schematic showing progressive stages of aluminization in a low-activity aluminum pack. (a) Pure nickel (e_1 forms first, followed by e_2, e_3, etc.). (b) Nickel-base superalloy (e_1 and e'_1 form first, followed by e_2 and e'_2, etc.). (c) Structure of coated nickel-base superalloy. Source: Ref 12

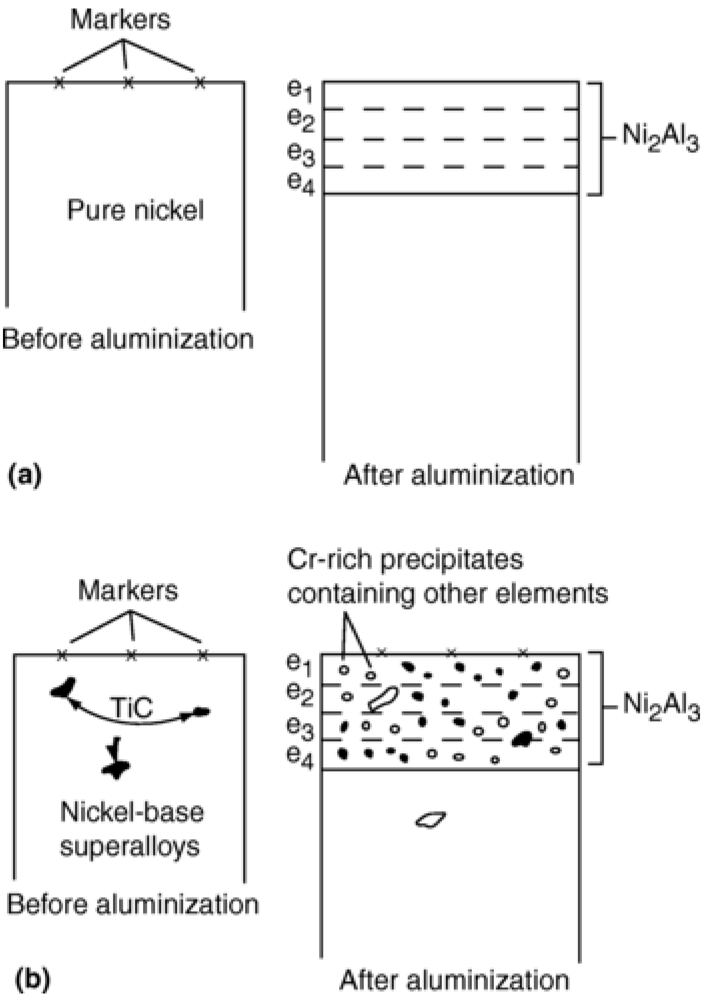

Fig. 5 Schematic showing progressive stages of aluminization in a high-activity aluminum pack. (a) Pure nickel (e_1 forms first, followed by e_2, e_3, etc.). (b) Nickel-base superalloy e_1, followed by e_2, etc. Source: Ref 12

In high-activity aluminum packs, inward diffusion of aluminum dominates as illustrated in Fig. 5 (Ref 12). Figure 5(a) shows the position of the markers originally placed on the free surface of nickel, moving to e_1, e_2, e_3, and so forth, as a function of time; that is, the markers remain on the outer surface. The inward diffusion is accompanied by the formation of an intermetallic like Ni_2Al_3. Figure 5(b) shows the progress of aluminization in a nickel-base superalloy. The markers stay on the outer surface, indicative of the inward diffusion of aluminum. The formation of aluminum-rich Ni_2Al_3 leads to the precipitation of chromium-rich precipitates in the matrix alloy.

Figure 6 (Ref 12) shows the effect of annealing on aluminized nickel (Fig. 6a) and nickel- base superalloys (Fig. 6b). In both cases, the Ni_2Al_3 layer transforms to NiAl. In the case of pure nickel, the conversion of Ni_2Al_3 to NiAl is fairly straightforward. However, in the case of superalloys, this transformation is characterized by precipitates in the outer zone, a central precipitate-free zone, and an inner zone with precipitates similar to those for low-activity aluminum packs.

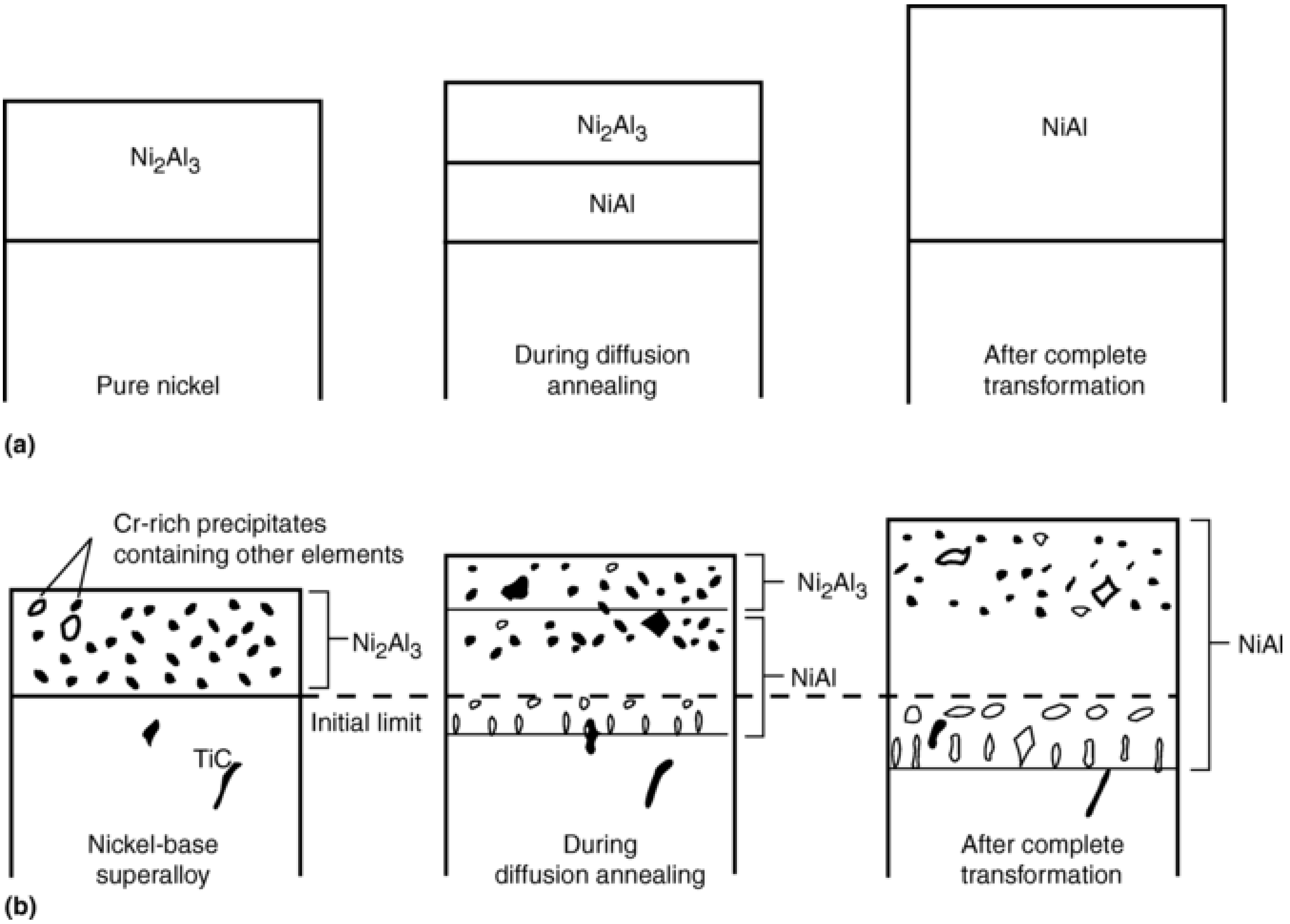

Fig. 6 Schematic showing progressive stages of aluminization in a high-activity aluminum pack followed by diffusion annealing. (a) Pure nickel. (b) Nickel-base superalloy. Source: Ref 12

Others (Ref 14) have shown that the structures in Fig. 2 and 3 are limiting cases with a range of intermediate structures existing due to the variation of the interdiffusion coefficient in the β- NiAl phase of the aluminum-nickel system.

Thermodynamics of Pack Aluminizing. If a pure nickel substrate is aluminized in a pack containing pure aluminum (thermodynamic activity = 1) as the source, and NaCl is the activator, the following equilibria pertain:

$$Al(l) + NaCl(l) \rightleftharpoons AlCl(v) + Na(v) \quad \text{(Eq 1)}$$

$AlCl_2(v)$ and $AlCl_3(v)$ are also formed in the pack. The most important reaction occurring on the substrate surface is the disproportionation of the metal halide vapors AlCl or $AlCl_2$:

$$2AlCl(v) \rightleftharpoons AlCl_2(v) + \underline{Al}_{Ni} \quad \text{(Eq 2)}$$

where $\underline{Al}_{Ni}$ indicates Al is in solid solution in the Ni substrate. Direct transfer of aluminum by forming Al(v) occurs only to a very small extent. Displacement reactions with the substrate such as:

$$Ni + 2AlCl(v) \rightleftharpoons NiCl_2(v) + 2Al_{Ni} \quad \text{(Eq 3)}$$

do not occur because the standard Gibbs energies of formation of the aluminum halides are significantly more negative than those for the nickel halides (Ref 15). Thus, if pure aluminum is used as the source for aluminizing pure nickel, the NiCl and $NiCl_2$ partial pressures are significantly lower than the partial pressures of AlCl, $AlCl_2$, and $AlCl_3$ (per mole of Cl_2) so that nickel does not participate in interchange reactions with aluminum chloride.

The chemical reactions in the pack are only one of a series of steps in pack cementation processes. Walsh (Ref 16) has broken down the pack cementation process into the following steps:

1. Reactions in the pack
2. Gas diffusion through the pack

3. Reaction on the substrate surface, which can involve disproportionation of halide vapors, precipitation of activator salt, and/or reactions with the environment and substrate

Therefore, in addition to understanding the thermodynamics, it is also necessary to analyze the kinetics to gain a full appreciation of the process.

Kinetics of Pack Aluminizing. Several models for the aluminizing of nickel and iron-base alloys have been proposed (Ref 17, 18, 19, 20). All of them are based on the existence of a depletion zone.

A kinetic model of pack aluminizing based on the assumption of local thermodynamic equilibrium at both the pack-gas and the substrate-gas interfaces was proposed (Ref 17). The authors also assumed that the transport of gases through the pack was purely diffusional. Instantaneous fluxes of the species to and from the substrate were calculated under conditions of 1 atm total pressure and an activity of aluminum equal to 0.01 at the substrate surface. Figure 7 (Ref 17) shows the model for NaX and NH_4X activated packs where X = F, Cl, Br, or I. The diffusion direction for each species in the depletion zone is obtained by computing the instantaneous fluxes. Then, depending on the temperature and the choice of X, certain pressure gradients (e.g., p_{AlX_3}, $p_{Al_2X_6}$) will be opposite to those shown schematically. Figure 7(a) is a simplified model in which the formation of liquid NaX is neglected. Figure 7(b) is more complete since the liquid NaX film on the substrate is taken into account while computing fluxes. Figure 7(c) is a complete model for NH_4X-activated packs. The direction of the diffusion of AlX_2, AlX_3 and $Al_{12}X_6$ depends on X. In NH_4F activated packs, AlF and AlF_2 diffuse inward while AlF_3 and Al_2F_6 diffuse outward. In NH_4Cl, NH_4B_4 and NH_4I activated packs, AlX alone diffuses inward. In all cases, aluminum deposition in the NH_4X and NaX-activated packs is primarily done by AlX. The NaX(l) condensation on the substrate surface aids in aluminum deposition since there is no requirement for halogen removal by the diffusion of AlX_2 and AlX_3 away from the substrate surface.

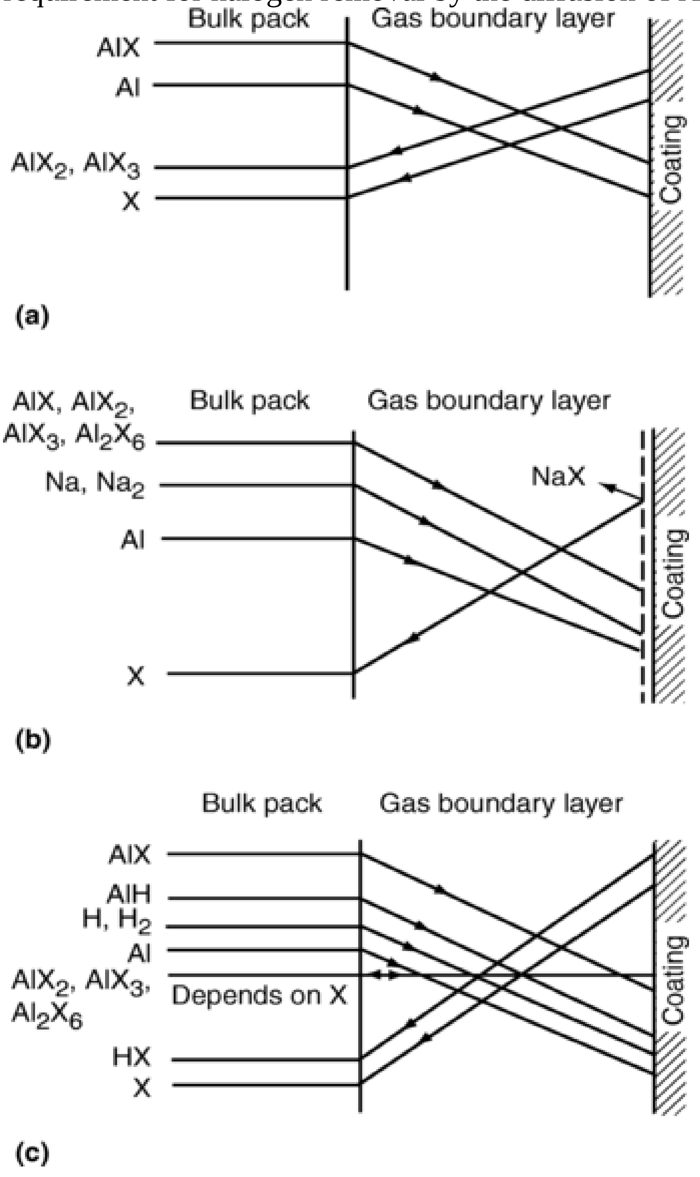

Fig. 7 The Levine-Caves model for pack aluminization using pure aluminum as the source and NaX in (a) and (b) or NH_4X in (c) as activators (X is Cl, Br, or I). Part 7(a) is a simplified model and (b) and (c) are more complete models. Source: Ref 17

The model described in Ref 17 was applied to the aluminizing of the IN 100 superalloy. Loss of alloying elements during the coating treatment, especially chromium, had to be considered. The nickel and chromium can be removed from the surface either in the metal vapor form or by forming volatile halides. The loss of nickel and chromium only by forming a metal vapor was considered. The nickel flux leaving the substrate is negligible while the chromium flux is about 1% of the aluminum weight gain. The loss of nickel by forming a halide would also be negligible, but the loss of chromium by forming chromium halides could make the chromium loss somewhat higher than the 1% used in Ref 17. However, this model is comprehensive and provides an adequate description of the pack aluminizing of superalloys.

Other authors (Ref 18) point out that in a NaX or AlF_3 activated pack, condensation of activators such as NaX(l) or AlF_3(s) on the substrate result in a net flux of activator from the pack to the specimen. Therefore, in addition to an aluminum-depleted zone, an activator-depleted zone forms adjacent to the substrate. If the amounts of activator and aluminum were stoichiometrically comparable, the activator- and aluminum-depletion zones would coincide. However, the amount of activator used in pack aluminizing is much less than the amount of aluminum, and the activator-depleted zone is thus wider than the aluminum-depleted zone (Fig. 8). These researchers have shown that it is possible to maintain a minor difference in total pressure between the pack-gas interface and the substrate- gas interface.

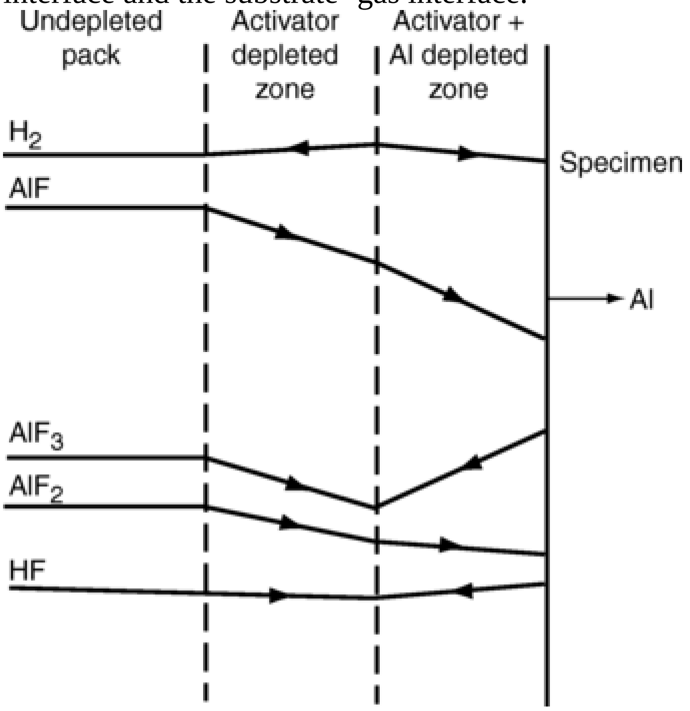

Fig. 8 The Kandasamy-Seigle-Pennisi model with mixed aluminum transport through activator and activator + Al-depleted zones. Source: Ref 18

Another pair of researchers (Ref 19) modified the two models described earlier by including bulk flow of the vapors as an additional feature. This flow occurs due to the difference in the number of moles of gas involved in reactions at the interface. However, no difference in total pressure was allowed, as in the model described in Ref 18.

Other researchers (Ref 20) have developed a more complete model taking into account the total pressure differential (Ref 18 model) as well as the viscous flow of the halide vapors through the porous pack (Ref 19 model) (Fig. 9). Aluminum transport rate constants and partial pressure values for NH_4Cl and AlF_3 activated packs have been calculated. The values obtained fall between those obtained by the models described in Ref 19 and 17, which represent limiting cases for packs with zero resistance to viscous flow (large particle size of the pack powders) and infinite resistance to viscous flow (small particle sizes).

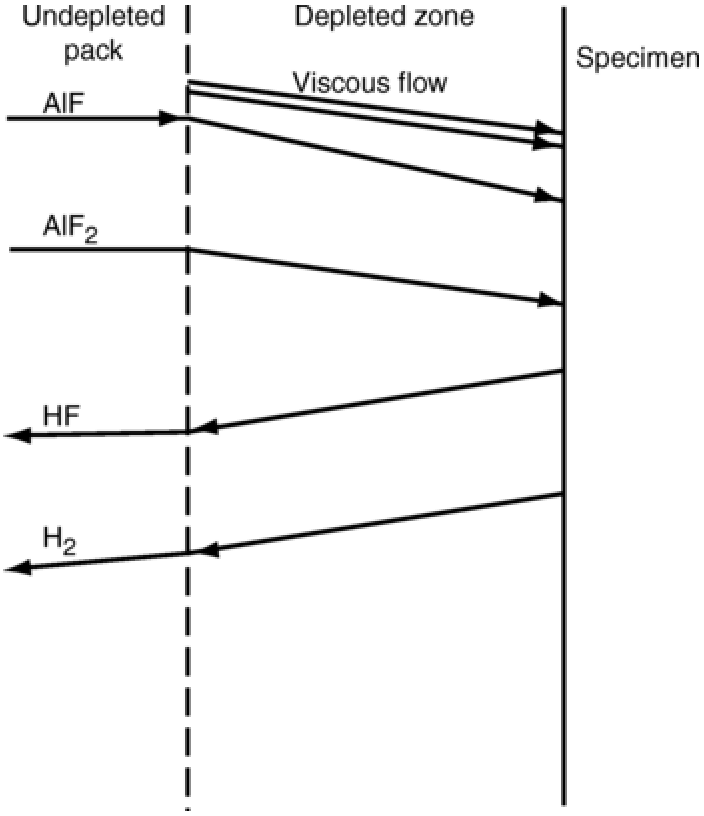

Fig. 9 The Wang-Seigle model for aluminum transport incorporating diffusional flux and viscous flow in the depleted zone. Source: Ref 20

The aluminizing of iron through a fixed porous barrier (ceramic felt wrapping) was studied (Ref 21), and a model based on the following assumptions was proposed: (a) local equilibrium at the pack-gas and substrate-gas interfaces, and (b) rate control by diffusion of gases through a porous barrier surrounding the substrate in series with solid-state diffusion and condensation of activators such as NaCl(l) and AlF_3(s) on the specimen surface. Figures 10 and 11 (Ref 21) indicate the direction of fluxes of the species involved. The authors of Ref 21 did not consider a total pressure difference between the pack-gas interface and the substrate-gas interface but did consider viscous flow. Good agreement between theoretical and experimental values for rates of aluminum gain was obtained for NaCl-activated packs.

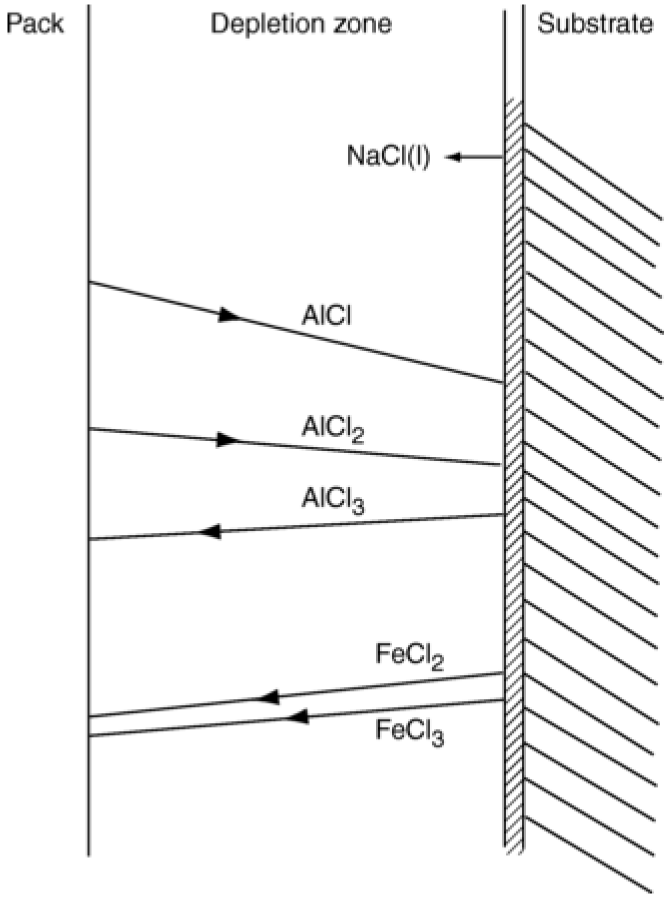

Fig. 10 The Kung-Rapp model for transport in a NaCl-activated pack with an Fe-Al alloy source and with the depletion zone corresponding to the thickness of the alumina wrapping. Source: Ref 21

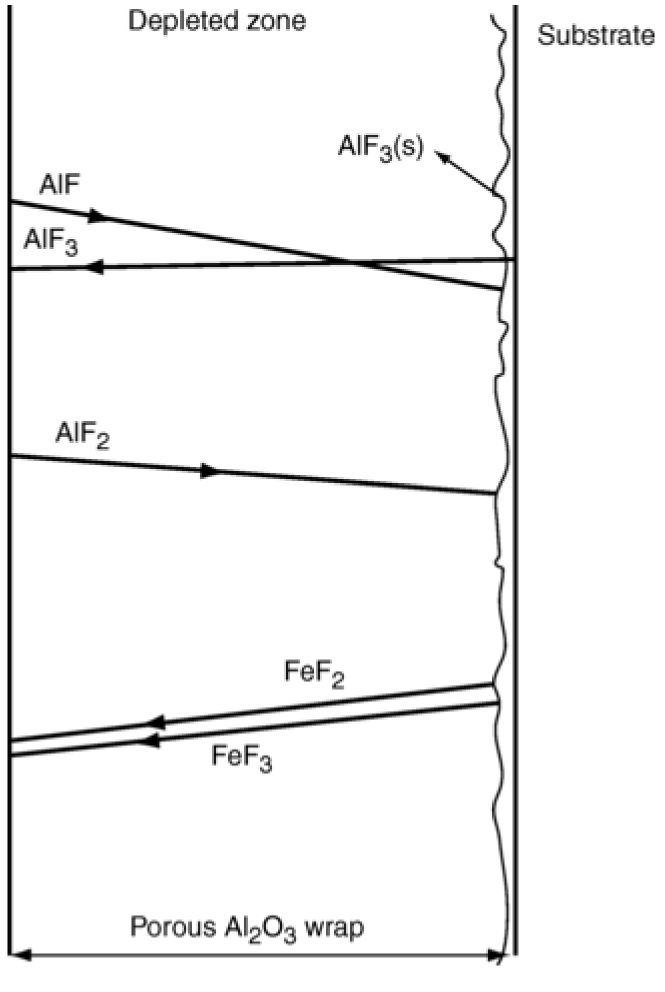

Fig. 11 The Kung-Rapp model for transport in an AlF_3-activated pack with an Fe-Al alloy source and with the depletion zone corresponding to the thickness of the alumina wrapping. Source: Ref 21

Others (Ref 22) have determined the surface aluminum concentration based on the formation of a liquid aluminum-enriched layer of variable aluminum composition on an iron substrate (Fig. 12). The two novel features of this model are: (a) the formation of a thin liquid metal layer of almost constant thickness on the substrate (allowing an aluminum flux balance to be set up), and (b) the concentration of aluminum at the transition boundary layer, M, given by the solidus composition of the iron-aluminum equilibrium diagram. The model prediction in Ref 22 of the surface aluminum concentration agrees reasonably well with experimentally obtained values.

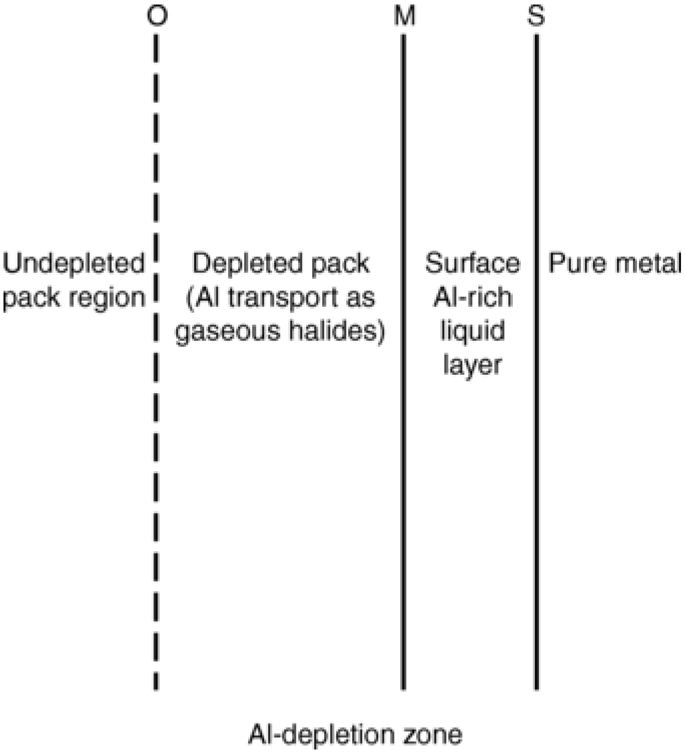

Fig. 12 The Akueze-Stringer model for the aluminization of pure iron. Source: Ref 22

Pack Chromizing

Kelley (Ref 23) is generally acknowledged as the inventor of pack chromizing. The enhanced resistance to aqueous corrosion of these coatings was initially used to improve the surface stability of steam turbine blades. Later, chromium coatings were used to protect gas turbine blades and vanes against hot corrosion (Ref 13).

A typical chromium coating on a nickel-base superalloy, coated in a pack containing chromium, ammonium chloride, and alumina, is a γ- Ni-Cr solid solution with a discontinuous α-Cr outer layer. This outer layer contains Al_2O_3 particles that are attributed in Ref 11 to internal oxidation of aluminum in the substrate. Ref 11 further points out that other investigators (Ref 24, 25) have prevented this by adding aluminum to the chromium source in the pack. In Ref 24, a mixture of nickel, cobalt, chromium, and aluminum powders was preheated in a pack containing NH_4Cl, $MgCl_2$, and Al_2O_3 to approximately 1040 °C (1900 °F) and held it there for 20 h. The pack was then cooled and substrates introduced before reheating to 1040 °C in a hydrogen atmosphere. In Ref 25, the coating treatment was performed in air with chromium and aluminum present in the pack. The aluminum in the pack functions as an oxygen getter and permits the chromium coating to be applied without internal oxidation.

Literature on the structure and properties of chromium coatings for nickel-base superalloys is sparse. References 26 and 27 present structural and kinetic data for chromide coatings on steel, but these are expected to be different for nickel- base alloys.

Thermodynamics of pack chromizing. Hoar and Croom (Ref 28) have suggested that incorporation of chromium into substrates was achieved by one or more of the following reactions:displacement reactions with the substrate

$$CrCl_2(v) + Fe(s) \rightleftharpoons FeCl_2(g) + \underline{Cr} \quad \text{(Eq 4)}$$

where $\underline{Cr}$ is in solid solution and reduction of halide vapor (in a reducing hydrogen atmosphere):

$$CrCl_2(v) + H_2(g) \rightleftharpoons 2HCl(g) + \underline{Cr} \quad \text{(Eq 5)}$$

Thermal decomposition of halide vapor is represented as:

$$CrCl_2(v) \rightleftharpoons Cl_2(g) + \underline{Cr} \quad \text{(Eq 6)}$$

Displacement reactions are important only if the substrate element forms volatile halide vapors of appreciable partial pressure (e.g., iron). Displacement reactions with the substrate such as Ni:

$$Ni + CrCl_2(v) \rightleftharpoons NiCl_2(v) + \underline{Cr}_{Ni} \quad \text{(Eq 7)}$$

are not expected to occur because the standard Gibbs energies of formation of the chromium halides are more negative than those for the nickel halides (Ref 15, 29). Thus, if pure chromium is used as the source for chromizing pure nickel, the NiCl and $NiCl_2$ partial pressures are lower than the partial pressures of $CrCl_2$ and $CrCl_3$ (per mole of Cl_2) so that nickel is not expected to participate in interchange reactions with chromium chloride.

In Ref 28, it is pointed out that since displacement reactions are insignificant for nickel substrates, a hydrogen atmosphere is essential for chromizing nickel. However, it is possible that a reaction of the type:

$$3CrCl_2(v) \rightleftharpoons 2CrCl_3(v) + \underline{Cr}_{Ni} \quad \text{(Eq 8)}$$

could provide for chromium transport. Therefore, it should be possible to chromize nickel in an inert atmosphere.

In Ref 30, pure nickel in NH_4Cl-activated packs containing pure chromium was chromized. The investigator correctly points out from free energy considerations that displacement reactions of the type shown in Eq 7 are not responsible for the coating process. The most important coating reaction was attributed to:

$$CrCl_2(v) + H_2(v) \rightleftharpoons 2HCl(v) + \underline{Cr}_{Ni} \quad \text{(Eq 9)}$$

Once again, the possibility of disproportionation of $CrCl_2$ was not considered.

Another researcher (Ref 14) points out that the presence of HCl in NH_4Cl-activated packs results in a side reaction:

$$Al_2O_3(s) + 6HCl(g) \rightleftharpoons 2AlCl_3(g) + 3H_2O(v) \quad \text{(Eq 10)}$$

with the inert filler. The $H_2O(v)$ can undergo a further reaction:

$$2CrCl_2(s) + 3H_2O(g) \rightleftharpoons Cr_2O_3(s) + 4HCl(g) + H_2(g) \quad \text{(Eq 11)}$$

with condensed $CrCl_2$.

Kinetics of Chromizing. Mazille (Ref 30) investigated the kinetics of chromizing pure Ni in an ammonium chloride pack containing pure chromium as the source. He obtained an outer α-Cr layer after chromizing for 16 h at 950 °C (1740 °F). This outer layer is an α-Cr region with an inner single-phase, Ni-rich γ-solid solution. It was estimated that the chromium content of the outer layer exceeded 90% by weight Cr. From the activity-composition plot for chromium in a nickel-chromium alloy, shown in Fig. 13 (Ref 31) this composition is in the two-phase α + γ region and the activity of chromium is approximately 0.96.

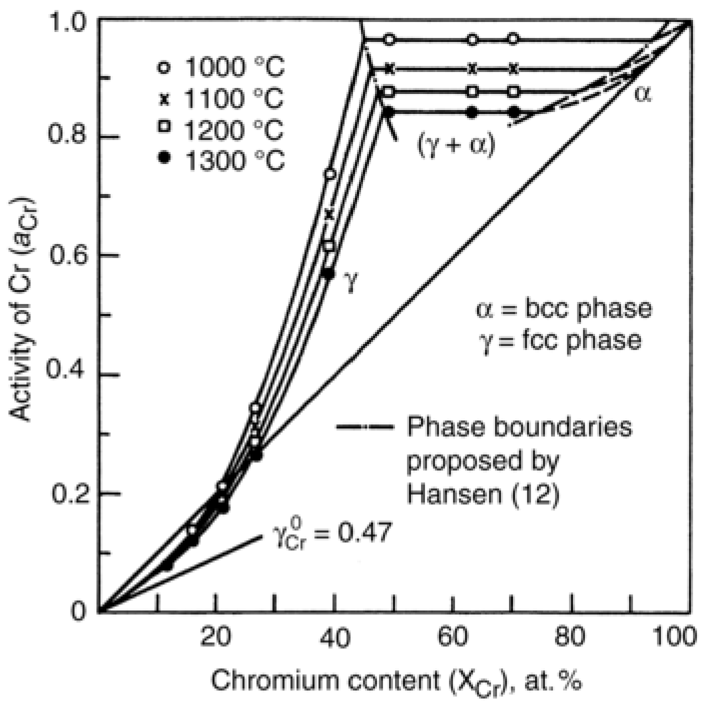

Fig. 13 The activity of chromium in solid nickel-chromium alloys (referred to as solid pure Cr) for various temperatures. Source: Ref 31

From Fig. 14(a), it was concluded that the chromizing of nickel is controlled by the slow solid state diffusion into austenitic nickel and not by transport in the gas or reactions at the substrate surface. The change of slope for the 950 °C (1740 °F) curve is attributed to the slower formation of the external α-phase when compared to the 1000 or 1050 °C (1830 or 1920 °F) treatments. Once α forms, diffusion occurs more rapidly since it is a body-centered cubic structure.

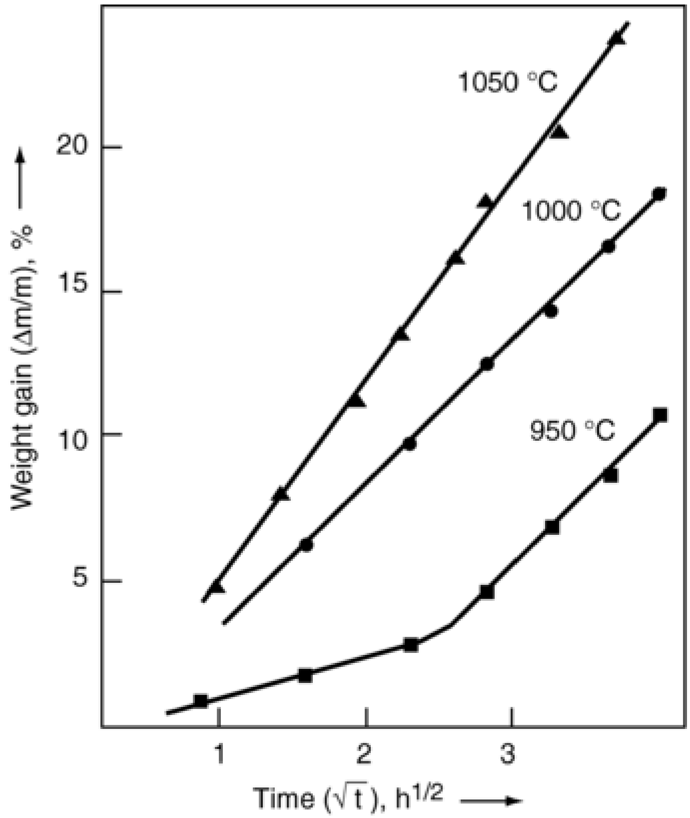

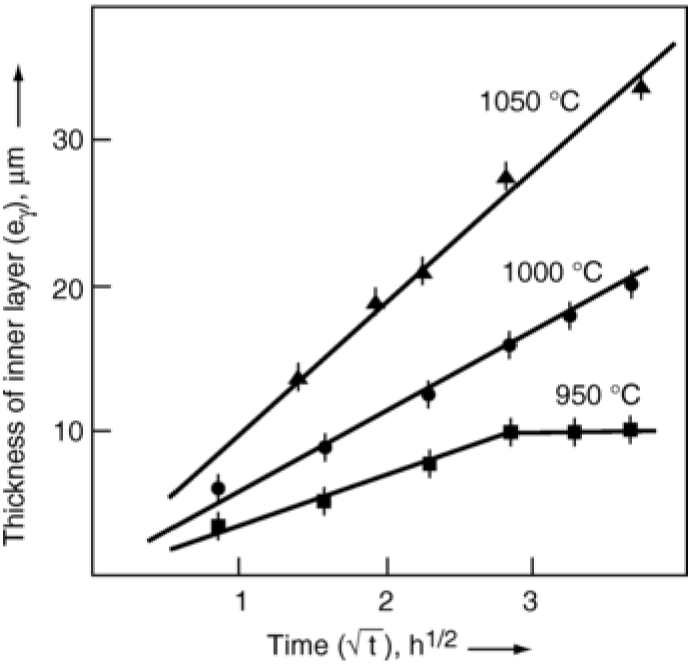

Fig. 14 Kinetic data for the chromizing of pure Ni. (a) The specific weight gain as a function of time at different temperatures. (b) Variation of thickness of the inner layer with time at different temperatures. Source: Ref 30

Figure 14(b) shows the growth rate of the γ- phase. While a parabolic relation is observed at 1000 and 1050 °C (1830 and 1920 °F), the shape of the 950 °C (1740 °F) curve is different. This is attributed to the approximately equal diffusion rates through the γ-α and γ-pure nickel phase boundaries. This suggests that the inner γ-layer remains approximately of constant thickness once the slower growing outer α-layer forms.

Information on the effects of coating variables such as the type of halide activators and fillers on coating characteristics such as microstructure and composition for the chromizing of ferrous alloys can be found in Ref 32.

Simultaneous Chromizing-Aluminizing

Initial studies in the area of simultaneous chromizing and aluminizing were directed toward a two-step chromizing-aluminizing process. Chromium coatings were initially obtained in a pack containing pure chromium, and the chromized coupons subsequently were aluminized in low- or high-aluminum activity packs (Ref 33).

Galmiche (Ref 34, 35) proposed a technique for simultaneous chromizing-aluminizing of nickel-, iron-, and cobalt-base alloys. The process, called chromaluminization, consists of heating the substrates in a pack containing ultrafine chromium powder (40 wt%), very fine aluminum powder (10 wt%), fine-calcined alumina (49.2 wt%), and ammonium chloride (0.8 wt%) to temperatures in the range 750 to 1200 °C (1380 to 2190 °F). Figure 15 (Ref 34) shows the composition profile of a chromaluminized coating on a nickel-base superalloy. Galmiche explained that chromium is preferentially supplied during the first "phase" of the "chromaluminizing" treatment, while aluminum is preferentially supplied during the second "phase." This is somewhat unexpected because the partial pressures of aluminum halides are significantly higher than those of the chromium halides, and a pack containing a mixture of pure chromium and pure aluminum would thus be expected to aluminize the substrate.

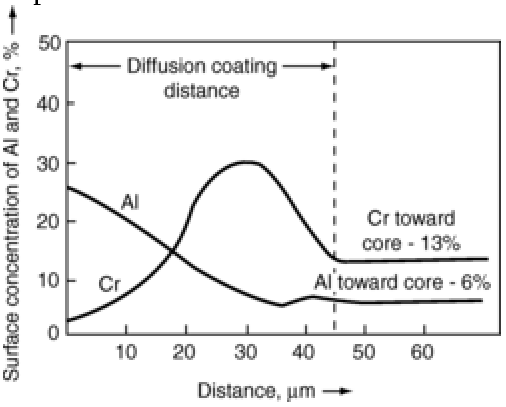

Fig. 15 Concentration profiles of chromium and aluminum in the chromaluminized regions of a nickel-base superalloy. Source: Ref 34

Galmiche and Hivert's patent (Ref 35) reveals that pure Cr (40 wt%) and pure Al (40 wt%) were preheated in a pack containing alumina and ammonium chloride for 1 h in the temperature range 1000 to 1100 °C (1830 to 1210 °F). Under these conditions, aluminum chloride vapor pressures are much higher than the chromium chloride vapor pressures, and it follows that aluminum ought to be deposited on the chromium particles. It is also indicated (Ref 35) that additions of 0.5 to 1.0 wt% AlF_3 to the pack will be advantageous to the coating process. It is known that the AlF_3 is a strong aluminizing agent. It is thus possible that during pretreatment, aluminum is deposited on the chromium particles by AlF_3 and $AlCl_3$ (NH_4Cl-assisted) vapors. During the coating process, a significant amount of $AlCl_3$ vapors are expected to be generated. Furthermore, in the proposed mechanism, the aluminum-coated chromium particles are expected to generate only marginal amounts of chromium-containing vapors. Conditions in the pack are thus expected to be conducive for aluminization, while conserving the chromium content of the alloy. Based on this model, the sharp increase in chromium content in the inner diffusion zone (Fig. 15) can be attributed to outward nickel diffusion and consequent nickel depletion in this region.

Other authors (Ref 16, 36) have pointed out that it is not possible to codeposit aluminum and chromium in a one-step process if pure aluminum and pure chromium are used as the source. Others (Ref 29) have shown that at temperatures in the 1100 to 1500 K (1520 to 2240 °F) range, where most coating operations are carried out, the vapor pressures of the AlCl species (mostly responsible for aluminizing) are orders of magnitude higher than the $CrCl_2$ vapor pressures (mostly responsible for chromizing) in chloride- activated packs using pure aluminum and pure chromium as the sources. They obtained even greater differences in aluminum- and chromium- fluoride vapor pressures in fluoride-activated packs, concluding that at unit thermodynamic activity of aluminum, codeposition of aluminum and chromium is not possible.

A clear perspective on the difficulties of codeposition of aluminum and chromium is obtained by examination of the thermodynamic activities of aluminum and chromium in binary aluminum-chromium alloys.

Others (Ref 37) have determined the activities of aluminum and chromium in binary aluminum- chromium alloys (Ref 38) (Fig. 16). The maximum solubility of aluminum in chromium is 43 a/o aluminum; for aluminum compositions lower than this, the activity of aluminum is much lower than that of chromium in chromium-rich, chromium-aluminum alloys. This highly negative deviation from thermodynamically ideal behavior is

demonstrated by the low aluminum activity (0.001) at 9 at.% Al. Therefore, adjusting the composition of a chromium-aluminum master alloy is one of the keys to achieving codeposition. In addition, the choice of the activator is also important.

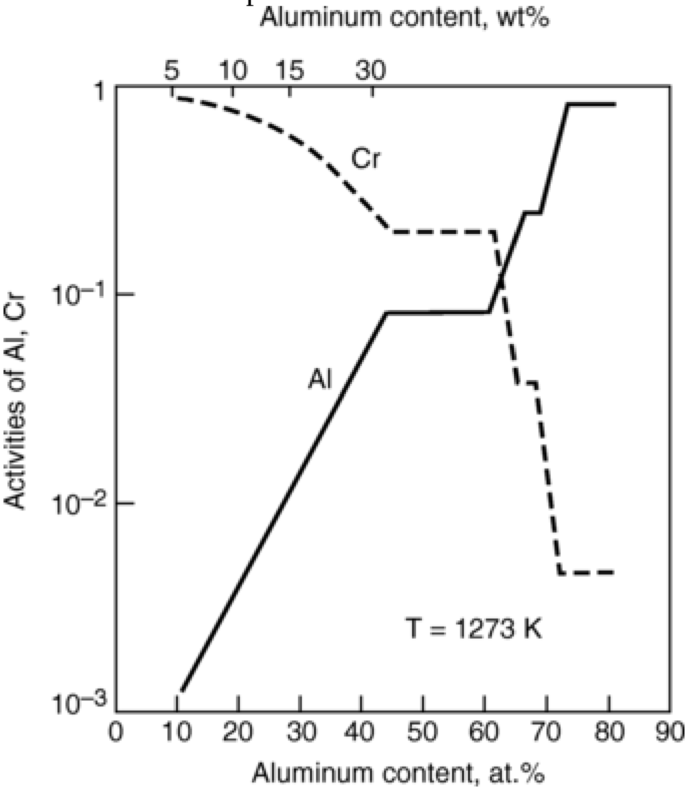

Fig. 16 Activities of aluminum and chromium as a function of the aluminum content of aluminum-chromium alloys at 1273 K (1830 °F). Source: Ref 36, based on data from Ref 37

Still another investigator (Ref 39) has shown experimentally that by choosing a special pack composition, simultaneous deposition of chromium and aluminum into a nickel-base alloy at 1100 °C (2010 °F) is possible. The following reaction is proposed as the basis for codeposition:

$$AlCl_2(v) + Cr \rightleftharpoons 2CrCl_2(v) + Al \qquad \text{(Eq 12)}$$

From Eq 12, it follows that the partial pressure of $CrCl_2$ is given by:

$$p_{CrCl_2} = K_p a_{Cr} p_{AlCl_2} / a_{Al} \qquad \text{(Eq 13)}$$

where K_p is the equilibrium constant, a_{Cr} and a_{Al} are the activities of chromium and aluminum, respectively, and $p_{CrCl_2}$and $p_{AlCl_2}$are the partial pressures of the chromium and aluminum chlorides. By reducing the thermodynamic activity of aluminum (a_{Al}) in the pack, one should expect a reduction in the partial pressure of the aluminum halides, thus leading to codeposition of aluminum and chromium.

Ravi et al. (8, 40, 41, 42) have shown that chloride activators and chromium-rich chromium-aluminum master alloys result in chromium-rich chromium-aluminum codeposited coatings on nickel and nickel-base superalloy substrates. They also show that the use of fluoride activators favors aluminum deposition, even with the use of chromium-rich chromium-aluminum master alloys. Detailed thermodynamic calculations and microstructural/compositional analysis are provided.

Other researchers (Ref 43) have identified process conditions (chromium-aluminum master alloy composition, $NaCl/NH_4Cl$ ratios) for achieving simultaneous deposition of chromium and aluminum at temperatures on the order of 1100 °C (2010 °F) onto a nickel-base superalloy. They established that codeposition of chromium and aluminum can be achieved with chromium-rich chromium-aluminum master alloys and mixed activator ($NaCl + NH_4Cl$) packs. Also studied were the kinetics and nonequilibrium effects in the coating process (Ref 44, 45). One of the key findings was that the master alloy composition and activator-mixture content change during the coating process. Based on these findings, the authors have proposed a time-dependent mechanism for chromium-aluminum codeposition.

Other authors (Ref 46) have developed a single-step process for chromium/rare-earth (RE) modified and RE-doped aluminide coatings by using appropriate chloride activators and chromium-aluminum master alloys. A model for coating formation based on their analyses of the microstructures, phase equilibria, and kinetic data

was proposed. The results of experiments aimed at reducing pack entrapment (Al_2O_3 and RE oxide particles) in the coatings have been discussed. Results from environmental testing of these coated coupons under different conditions, that is, isothermal oxidation at 1100 °C (2010 °F) in air, cyclic oxidation at 1100 °C in static air, and type 1 hot-corrosion behavior at 900 °C (1650 °F) in 0.1% SO_2/O_2 gas mixtures have been discussed (Ref 47). In general, the Cr/RE- doped coatings resulted in improved performance relative to RE-free coatings.

Another pair of researchers (Ref 48) coated a 2.25 Cr-1Mo low alloy steel with RE modified chromium-aluminide coating. They report improved cyclic oxidation performance of these steels in air at 800 °C (1470 °F) relative to the uncoated alloy.

Kim et al. (Ref 49) described a new pack process for the codeposition of chromium and aluminum. In this process, low-alloy steels were coated in a pack containing aluminum and Cr_2O_3 powders blended with an activator salt mixture of NaCl + NH_4Cl. The authors propose that chromium halides are produced as a result of reactions between the aluminum or aluminum halides and the Cr_2O_3, leading to deposition of chromium along with the expected deposition of aluminum by aluminum halides created by reaction between the aluminum and the activator salts. The authors present microstructures and compositional profiles, although detailed thermodynamic evaluations have not been carried out, and have also extended the work by coating austenitic stainless steels (Ref 50).

Pack Siliconizing

Another researcher (Ref 51) siliconized pure iron and steels in packs containing pure silicon and NH_4Cl as the activator. Gorbunov (Ref 52) has reported microstructural and kinetic data for siliconized iron and steel. The siliconizing was performed using pure silicon powder and gaseous chlorine. Recently, Hsu and Tsai (Ref 53) reported that siliconized AISI type 310 stainless steel (UNS S31000) has shown better resistance to high-temperature corrosion in air and in reducing gases in comparison with the base alloy. However, there are several problems with siliconized coatings. It has been pointed out (Ref 54) that silicon can cause embrittlement of the substrate. In addition, silicon can form low- melting oxide eutectics with iron and low-melting metallic eutectics with nickel substrates. Therefore, industry has not widely adopted siliconizing due to some of the aforementioned problems.

Simultaneous Chromizing-Siliconizing

The codeposition of chromium and silicon onto iron-base alloys by halide-activated pack cementation has been reported (Ref 55). Different binary chromium-silicon master alloys, ranging from a minimum of 10 wt% Si to a maximum of 40 wt% Si, and different activators (NaCl, NaF, $FeCl_2$, and $CrCl_2$) were used in the study. Its authors performed a comprehensive computer-assisted thermodynamic analysis to obtain insights into pack chemistries. Using these computations as a guide, they selected appropriate pack chemistries and presented the microstructures of coated plain carbon, low-alloy, and austenitic steels. The authors report that selected coated coupons performed very well in cyclic oxidation and in oxidation-sulfidation tests.

Germanium- and boron-doped silicide coatings on niobium- and titanium-base alloys have been studied in great detail (Ref 56, 57). The thermodynamics, kinetics of growth, and oxidation studies in these materials are reported. Cockeram and Rapp (Ref 58) also report on the thermodynamics, microstructural analysis, and kinetics of titanium silicide coatings formed on commercially pure titanium. Others (Ref 59) have studied the deposition of aluminide and silicide coatings on γ-TiAl.

Simultaneous Aluminizing-Siliconizing

A pack cementation process for the codeposition of aluminum and silicon onto a low carbon steel has been developed (Ref 60). The pack contains aluminum and SiO_2 powders and is activated by a NaCl+KBF_4 mixture. Compositional profiles and microstructures of the coated coupons are reported. The authors propose that the following reaction is responsible for silicon deposition, although no detailed thermodynamic analysis is provided:

$$3SiO_2 + 4Al \rightleftharpoons 3Si + 2Al_2O_3 \quad \text{(Eq 14)}$$

Xiang et al. (Ref 61) report that codeposition of aluminum and silicon onto γ-TiAl is possible in packs containing aluminum and silicon powders (in elemental form) and NH_4Cl and $AlCl_3$ activators. They have

shown microstructures that contain an outer silicide layer and an inner aluminide layer and propose a sequential mechanism, that is, aluminum deposition followed by silicon deposition, to explain the two-layer morphology. They also report that results of oxidation tests were favorable.

References cited in this section

8. V.A. Ravi, Ph.D. thesis, The Ohio State University, 1988

9. T. Van Aller, U.S. Patent 1,155,974, 1911

10. E.G. Gilson, U.S. Patent 1,091,057, 1914

11. G.W. Goward and D.H. Boone, *Oxid. Metals,* Vol 3, 1971, p 475

12. R. Pichoir, Influence of the Mode of Formation on the Oxidation and Corrosion Behavior of NiAl-Type Protective Coatings, *Materials and Coatings to Resist High Temperature Corrosion,* D.R. Holmes and A. Rahmel, Ed., Applied Science Publishers Ltd., London, 1978, p 271

13. G.W. Goward and L.W. Cannon, *Trans. ASME,* Vol 110, 1988, p 150

14. S. Shankar and L.L. Seigle, *Met. Trans. A,* Vol 9, 1978, p 1468

15. L.B. Pankratz, J.M. Stuve, and N.A. Gokcen, *Thermodynamic Data for Mineral Technology,* Bureau of Mines Bulletin 677, U.S. Government Printing Office, 1984

16. P.N. Walsh, Chemical Aspects of Pack Cementation, *Proc. Fourth International Conf. on Chemical Vapor Deposition,* G.F. Wakefield and J.M. Blocher, Ed., The Electrochemical Society, Pennington, N.J., 1973, p 147

17. S.R. Levine and R.M. Caves, *J. Electrochem. Soc.,* Vol 121, 1974, p 1051

18. M. Kandasamy, L.L. Seigle, and F.J. Pennisi, *Thin Solid Films,* Vol 84, 1981, p 17

19. B. Nciri and J. Vandenbulcke, *J. Less Common Met.,* Vol 95, 1983, p 191

20. T.H. Wang and L.L. Seigle, The Influence of Viscous Flow on the Kinetics of Gas Transport in Aluminizing Pack, *High Temperature Protective Coatings,* M. Khobaib and R.C. Krutenat, Ed., The Metallurgical Society, Warrendale, PA, 1987, p 39

21. S.C. Kung and R.A. Rapp, *J. Electrochem. Soc.,* Vol 135, 1988, p 731

22. H.C. Akuezue and J. Stringer, *J. Electrochem. Soc.,* Vol 135, 1988, p 1290

23. F.D. Kelley, *Trans. Amer. Electrochem. Soc.,* Vol 43, 1923, p 351

24. A.L. Baldi, U.S. Patent 4,308,160, 1981

25. H.W. Brill-Edwards, U.S. Patent 3,801,353, 1974

26. R.L. Samuel and M.A. Lockington, *Metal Treatment and Drop Forging,* Vol 18, 1951, p 354, 407, 440, 495, and 543 and Vol 19, 1952, p 27 and 81

27. R. Drewett, *Anti-Corros. Methods Mater.,* Vol 16, 1951, p 543

28. T.P. Hoar and E.A.G. Croom, *Australas. Eng.,* Vol 63, 1950, p 56

29. S.C. Kung and R.A. Rapp, *Oxid. Met.,* Vol 32, 1989, p 89

30. H.M.J. Mazille, *Thin Solid Films,* Vol 65, 1980, p 67

31. F.N. Mazandarany and R.D. Pehlke, *Metall. Trans,* Vol 4, 1973, p 2067

32. G.H. Meir, C. Cheng, R.A. Perkins, and W. Bakker, *Surf. Coat. Technol.,* Vol 39/40, 1989, p 53

33. E. Godlewska and K. Godlewski, *Oxid. Met.,* Vol 22, 1984, p 117

34. P. Galmiche, *Metals Mater.,* Vol 2, 1968, p 241

35. P. Galmiche and A. Hivert, Canadian patent 806, 618, 1969

36. J.E. Restall and C. Hayman, U.S. patent 4,687,684, 1987

37. W. Johnson, K. Komarek, and E. Miller, *Trans. Met. Soc. AIME,* Vol 242, 1968, p 1685

38. B. Nciri and L. Vandenbulcke, *J. Less Common Met.,* Vol 95, 1983, p 55

39. G.H. Marjinissen, Codeposition of Chromium and Aluminum during a Pack Process, *High Temperature Protective Coatings,* S.S. Singhal, Ed., TMS-AIME, Warrendale, PA, 1983, p 27

40. V.A. Ravi and R.A. Rapp, *High Temperature Ordered Intermetallic Alloys III,* C.T. Liu, A.I. Taub, N.S. Stoloff, and C.C. Koch, Ed., MRS Symposium Proceedings, Materials Research Society, Pittsburgh, PA, Vol 133, 1989, p 543

41. V.A. Ravi, P. Choquet, and R.A. Rapp, *International Meeting on Advanced Materials,* Materials Research Society, Pittsburgh, PA, Vol 4, 1989, p 483

42. V.A. Ravi and R.A. Rapp, *Oxidation of High Temperature Intermetallics,* T. Grobstein and J. Doychak, Ed., The Metallurgical Society, Warrendale, PA, 1989, p 543

43. W. Da Costa, B. Gleeson, and D.J. Young, *J. Electrochem. Soc.,* Vol 141, 1994, p 1464

44. W. Da Costa, B. Gleeson, and D.J. Young, *J. Electrochem. Soc.,* Vol 141, 1994, p 2690

45. W. Da Costa, B. Gleeson, and D.J. Young, *J. Electrochem. Soc.,* Vol 88, 1996, p 165

46. R. Bianco and R.A. Rapp, *J. Electrochem. Soc.,* Vol 140, 1993, p 1181

47. R. Bianco, R.A. Rapp, and J.L. Smialek, *J. Electrochem. Soc.,* Vol 140, 1993, p 1191

48. J. Kipkemoi and D. Tsipas, *J. Mater. Sci.,* Vol 31, 1996, p 6247

49. M.T. Kim, N.H. Heo, J.H. Shin, and C.Y. Kim, *Surf. Coat. Technol.,* Vol 123, 2000, p 227

50. N.H. Heo, M.T. Kim, J.H. Shin, and C.Y. Kim, *Surf. Coat. Technol.,* Vol 124, 2000, p 39

51. E. Fitzer, *Arch. Eisenhuettenw,* Vol 25, 1954, p 455

52. N.S. Gorbunov, *Diffuse Coatings on Iron and Steel,* The Academy of Sciences of the USSR, 1958, p 97

53. H.-W. Hsu and W.-T. Tsai, *Mater. Chem. Phys.,* Vol 64, 2000, p 147

54. F. Fitzer and J. Schlichting, Coatings Containing Chromium, Aluminum, and Silicon for High Temperature Alloys, *High Temperature Corrosion,* R.A. Rapp, Ed., NACE International, 1981, p 604

55. M.A. Harper and R.A. Rapp, *Oxidation of Metals,* Vol 42, 1994, p 303

56. B.V. Cockeram, *Surf. Coat. Technol.,* Vol 76–77, 1995, p 20

57. B.V. Cockeram and R.A. Rapp, *Metal. Mater. Trans., A,* Vol 26, 1995, p 777

58. B.V. Cockeram and R.A. Rapp, *Mater. Sci. Engin. A,* Vol 192/193, 1995, p 980

59. T.C. Munro and B. Gleeson, *Metal. Mater. Trans., A,* Vol 27, 1996, p 3761

60. M.T. Kim and J.S. Jung, *Surf. Coat. Technol.,* Vol 161, 2002, p 218

61. Z.D. Xiang, S.R. Rose, and P.K. Datta, *Mater. Chem. Phys.,* 9842, 2003, p 1

V.A. Ravi, Pack Cementation Coatings, *Corrosion: Fundamentals, Testing, and Protection*, Vol 13A, *ASM Handbook*, ASM International, 2003, p 763–771

Pack Cementation Coatings

Vilupanur A. Ravi, California State Polytechnic University, Pomona

---

Selected References

- L.K. Bennett and G.T. Bayer, Pack Cementation Aluminizing of Steels, *Surface Engineering,* Vol 5, *ASM Handbook,* 1994, p 617–620
- *Corrosion Engineering,* M.G. Fontana, 3rd ed., McGraw-Hill International Book Company, 1986
- G.W. Goward and L.L. Seigle, Diffusion Coatings for Gas Turbine Engine Hot Section Parts, *Surface Engineering,* Vol 5, *ASM Handbook,* 1994, p 611–617
- *High Temperature Alloys for Gas Turbines,* D. Coutsouradis, P. Felix, H. Fischmeister, L. Habraken, Y. Lindblom, and M.O. Speidel, Ed., Applied Science Publishers, London, 1978
- *High Temperature Corrosion,* P. Kofstad, Elsevier Applied Science Publishers, Ltd., 1988
- *High Temperature Corrosion,* R.A. Rapp, Ed., NACE International, 1981
- *High Temperature Protective Coatings,* M. Khobaib and R.C. Krutenat, Ed., The Metallurgical Society, Warrendale, PA, 1987
- *Oxidation of High Temperature Intermetallics,* T. Grobstein and J. Doychak, Ed., The Metallurgical Society, Warrendale, PA, 1989
- *Surface Engineering,* R. Kossowsky and S.C. Singhal, Ed., Martinus Nijhoff Publishers, Pittsburgh, 1984

T. Mooney, Electroplated Coatings, *Corrosion: Fundamentals, Testing, and Protection*, Vol 13A, *ASM Handbook*, ASM International, 2003, p 772–785

Electroplated Coatings

Revised by Ted Mooney, Finishing.com, Inc.

Introduction

ELECTROPLATED COATINGS can be very effective in reducing the cost of corrosion, estimated in 2001 to be $276 billion, or 3.1% of the U.S. gross domestic product. Even when metallic coatings are applied to a substrate to provide decorative effects or to enhance material properties, such as wear or electrical contact resistance, the corrosion performance of the coating- substrate system must be carefully considered to avoid future degradation. Metallic coatings can be very useful in providing optimal properties for a part not obtainable if it were fabricated from a single material.

The overall properties of coated parts are determined by the properties of the coating itself and by defects in the coating. The understanding of how defects in a coating affect the corrosion performance is critical in designing an effective coating system.

Electroplating is the electrodeposition of an adherent metallic coating on an electrode to secure a surface with properties or dimensions different from those of the base metal (Ref 1). Electrodeposits are applied to metal substrates for one or more of the following reasons: decoration, protection, corrosion resistance, chemical inertness, wear resistance, buildup of substrate dimensions, electrical properties, magnetic properties, solderability, reflectance, and reduction of friction (Ref 2). For example, decorative and protective plating are combined in such applications as steel automobile bumpers, trim items made of zinc die castings or steel, trim items on large and small appliances, costume jewelry, electronic circuits, piano strings, construction and architectural hardware, plumbing fittings, electrical contacts, plastic items, and magnetic memory devices (Ref 2).

This ability to be decorative as well as protective to substrates distinguishes electrodeposited coatings from metallic coatings applied by hot dipping or spraying. Metallic luster, achieved by bright plating or by polishing after plating, lends a distinctive appearance not provided by other types of coatings. However, corrosion resistance is the primary reason for the use of electrodeposited coatings. Electrodeposited coatings are also applied to protect substrate metals. Examples of this application include:

- Tin, as well as chromium, plating of steel strip for food packaging and other container uses
- Electrogalvanizing, or zinc plating, of steel strip, sheet, stampings, forgings, wire, and screw machine products
- Zinc and cadmium plating of fasteners and other hardware items
- Chromium plating of gun bores

Electrodeposits are used to enhance properties other than corrosion protection. For example, many fasteners are coated with a bright cadmium or zinc deposit supplemented with a clear or colored chromate conversion film. This results in coatings that are both protective and decorative. Chromium plating, electroless nickel plating, and anodizing of aluminum (not actually an electroplating process, but an electrochemical process widely practiced at electroplating installations) impart very hard and exceptionally wear-resistant surfaces while simultaneously deterring corrosion.

This article discusses the various factors that affect the corrosion performance of electroplated coatings, the effects of environment and the deposition process on substrate coatings, and the electrochemical techniques capable of predicting the corrosion performance of a plated part. Because the practical aspects of electroplating are covered in such publications as *Surface Engineering,* Volume 5 of the *ASM Handbook* (1994) and Ref 3, 4, 5, 6, this article is primarily concerned with the corrosion resistance of electrodeposited coatings. An exception is the discussion of mill- applied finishes, about which the open literature is sparse and limited in scope. Special attention is given to the design of coating systems for optimal protection of the substrate. An ideal electroplated

coating system is defined. Finally, attention is given to controlled weathering tests and accelerated tests used to predict and determine the relative durability of the coating.

References cited in this section

1. "Standard Definitions of Terms Relating to Electroplating," B 374, *Annual Book of ASTM Standards,* American Society for Testing and Materials

2. C.L. Faust, "Electroplating," Course 22, Metals Engineering Institute, American Society for Metals, 1983

3. F.A. Lowenheim, Ed., *Modern Electroplating,* 3rd ed., John Wiley & Sons, 1974

4. L.J. Durney, Ed., *Electroplating Engineering Handbook,* 4th ed., Van Nostrand Reinhold, 1984

5. F.A. Lowenheim, *Electroplating,* McGraw- Hill, 1978

6. M. Murphy, Ed., *Metal Finishing Guidebook & Directory,* Elsevier Science, 2001

T. Mooney, Electroplated Coatings, *Corrosion: Fundamentals, Testing, and Protection*, Vol 13A, *ASM Handbook*, ASM International, 2003, p 772–785

Electroplated Coatings

Revised by Ted Mooney, Finishing.com, Inc.

Idealized Coating

Coatings are either anodic or cathodic to the substrate. Only a very rough idea of which situation applies can be obtained from the electromotive force (emf) series (Table 1). Coatings that are anodic to a substrate in one environment may be cathodic to the same substrate in a second environment. The environment itself may change from the surface of the coating to one that exists within any defects, such as scratches, cracks, or corrosion pits. These defects are particularly important if the coating is cathodic to the substrate; in this case, if the substrate becomes exposed, rapid corrosion of the substrate may occur as it attempts to protect the coating. If the coating is anodic to the substrate, defects are somewhat less important, although they still must be considered. Thus, if the substrate becomes exposed, it will be protected by the corrosion of the coating. However, if the corrosion should proceed to such an extent that a large area of the substrate is exposed, the coating will lose its effectiveness, because the electrical resistance of the substrate limits the area that the coating can protect.

Table 1 Electromotive force series of metals and alloys

Solution concentration: 1 *N*; temperature: 25 °C (75 °F)

Metal	Ion	Standard reduction potential (E_0), V
Calcium	Ca^{2+}	-2.87
Sodium	Na^{+}	-2.71
Magnesium	Mg^{2+}	-2.37
Aluminum	Al^{3+}	-1.66
Zinc	Zn^{2+}	-0.763
Chromium	Cr^{3+}	-0.71
	Cr^{6+}	-0.56

Iron	Fe^{2+}	-0.44
Cadmium	Cd^{2+}	-0.40
Nickel	Ni^{2+}	-0.25
Tin	Sn^{2+}	-0.136
Lead	Pb^{2+}	-0.126
Hydrogen	H^{+}	0
Copper	Cu^{2+}	0.337
	Cu^{+}	0.521
Silver	Ag^{+}	0.799
Platinum	Pt^{4+}	0.90
Gold	Au^{+}	1.68

Source: Ref 2

The nature of any corrosion products formed also must be taken into account. For example, in industrial environments, zinc is more protective of steel than cadmium is because the zinc sulfate ($ZnSO_4$) corrosion product formed has a lower solubility than cadmium sulfate ($CdSO_4$); $ZnSO_4$ thus provides a blocking action to reduce subsequent corrosion. This situation is reversed in marine environments, in which the corrosion products are more likely to be carbonates and chlorides. Zinc produces more soluble corrosion products than cadmium does in this environment. The most desirable situation is to have the coating anodic to the material beneath it and at the same time to have a very low corrosion rate.

This general rule has been exploited to a high degree of sophistication by the automotive industry. Chromium-plated exterior steel parts have a coating system consisting of several layers of metals, each of which is anodic to the layer beneath it. There are accurate lifetime predictions based on the electrochemical potential differences and the thicknesses of the layers. Multilayer corrosion standards that ensure that the coatings meet specifications are available from the National Institute of Standards and Technology (NIST). Even the chromium layer has been designed to be microcracked or microporous to spread the corrosion reactions over a large area. Corrosion is then distributed over a large area, and localized pitting is minimized. This is discussed in more detail in the section "Applications for Electrodeposited Coatings" in this article.

Reference cited in this section

2. C.L. Faust, "Electroplating," Course 22, Metals Engineering Institute, American Society for Metals, 1983

T. Mooney, Electroplated Coatings, *Corrosion: Fundamentals, Testing, and Protection*, Vol 13A, *ASM Handbook*, ASM International, 2003, p 772–785

Electroplated Coatings

Revised by Ted Mooney, Finishing.com, Inc.

Substrates

The emf series is a table that lists in order the standard electrode potentials of specified electrochemical reactions (Ref 1). The potentials are measured against a standard reference electrode when the metal is immersed in a solution of its own ions at unit activity (Table 1).

Similarly, the galvanic series is a list of metals and alloys arranged according to their relative potentials in a given environment (Ref 1). Figure 1 shows a galvanic series of commercially used metals and alloys in seawater. The positions of metals and alloys in a galvanic series—and the corrosion behavior of metals and alloys—depend on the specific environment to which the materials are exposed. Therefore, there are as many galvanic series as there are aqueous environments. Generally, the relative positions of metals and alloys in both emf and galvanic series are the same. An exception is the position of cadmium with respect to iron and its

alloys. In the emf series, cadmium is cathodic to iron, but in the galvanic series (at least in seawater) cadmium is anodic to iron. Thus, if only the emf series were used to predict the behavior of a ferrous metal system, cadmium would not be chosen as a sacrificial protective coating, yet this is the principal use for cadmium plating on steel.

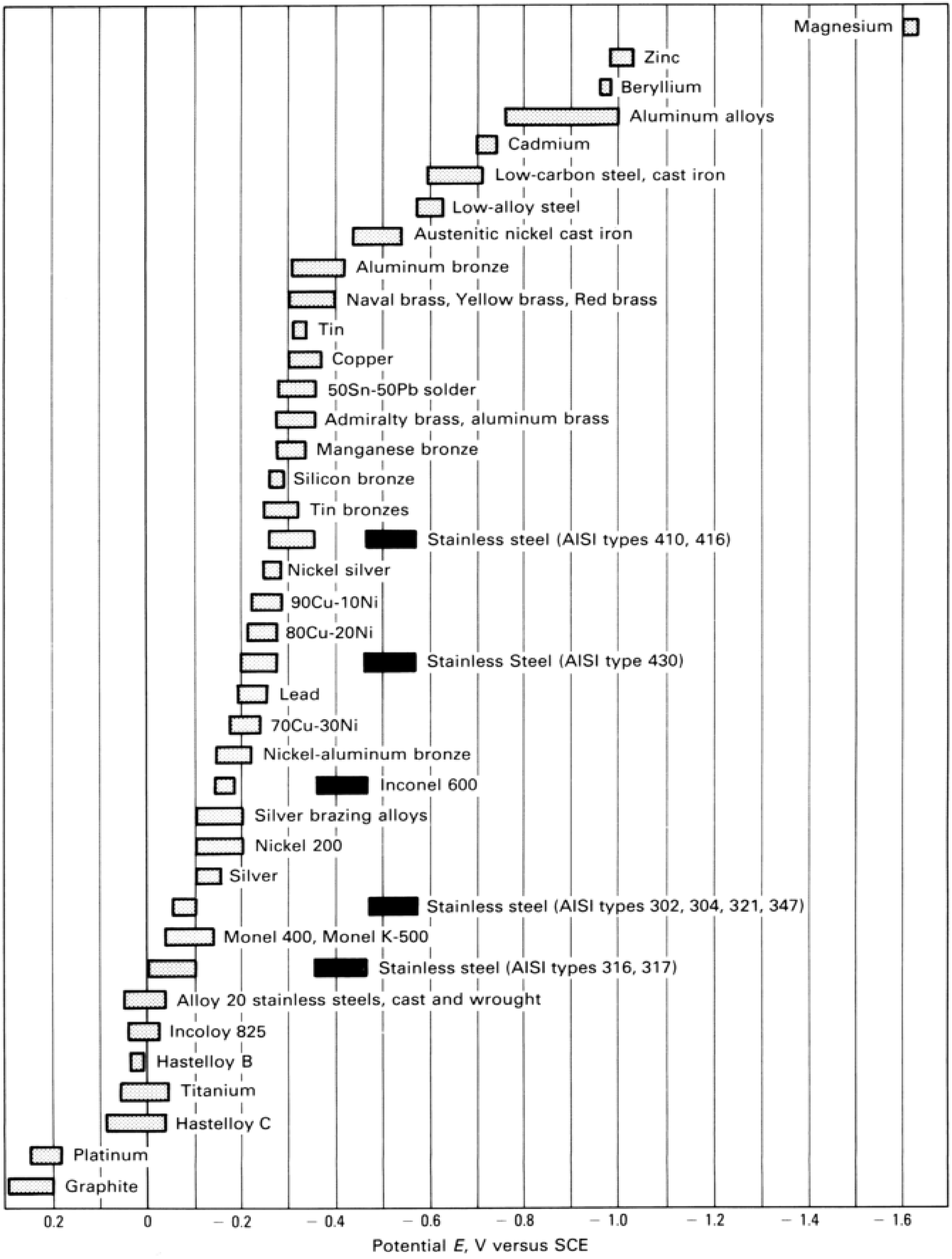

Fig. 1 Galvanic series of metals and alloys in seawater. Alloys are listed in order of the potential they exhibit in flowing seawater; those indicated by the black rectangle were tested in low-velocity or poorly aerated water and at shielded areas may become active and exhibit a potential near -0.5 V. Source: Ref 7

The importance of knowing the position of substrates in the emf and a specific galvanic series is frequently overlooked. The sole consideration is often the position of the protective coating in these series. It is prudent, however, to select a coating as close as possible in potential to the substrate in moist environments, because few coatings are completely free of pores, cracks, and other defects. Even if a coating does start out defect free, scratching, normal wear, or gouging can change this condition. Accordingly, in a corrosive environment, plated components present at least two (not one) metal to the hostile galvanic-corrosion forces (see the section "Electrochemical Predictions of Corrosion Performance" in this article).

Cleanliness of the Substrate

Regardless of the composition and metallurgical condition of a substrate, its surface must be free from soils and oxides before being plated. The ASTM International Committee on Selection of Cleaning Processes classifies soil into six groups: pigmented drawing compounds, unpigmented oil and grease, chips and cutting fluids, polishing and buffing compounds, rust and scale, and miscellaneous surface contaminants, such as lapping compounds and residue from magnetic- particle inspection. Cleaning methods are discussed in Ref 2, 3, 4, 5, 6. Although these methods are beyond the scope of this article, the point is made that unclean substrates often defeat the purpose of electrodeposited or other plated coatings.

Freedom from water break after the activating rinse and before immersion of a part in the plating tank is an essential prerequisite for satisfactory plating. Water break is defined as the appearance of a discontinuous film of water on a surface, signifying nonuniform wetting and usually associated with surface contaminations (Ref 1). A false reading of freedom from water break often occurs if the inspection is made after the rinse following a surfactant-laden alkaline cleaner. This misleading conclusion is nullified by inspection after acid dipping and rinsing.

Knowledge of the Nature of Substrates

Before designing or applying a protective coating to a metal, the plater must know the nature and essential properties of the substrate. Generally, a substrate is known to be ferrous or nonferrous, but these generic terms are inadequate. For example, there are thousands of ferrous metals and alloys, ranging from cast iron (high carbon) to ingot iron (very low carbon) and the entire range of carbon and alloy steels. Also, the microstructure, hardness, yield and tensile strengths, and internal stress of the substrate have major influences on the protective quality and durability of plated coatings. High-strength, high-carbon, high-hardness steels are susceptible to hydrogen embrittlement when subjected to alkalies, acids, and plating processes. Aluminum and zinc alloys and, to a lesser extent, chromium are amphoteric (soluble in both acidic and alkaline solutions). Accordingly, these metals must be treated with inhibited solutions to prevent chemical attack. Methods of determining the nature and condition of the substrates are described in the following sections.

Information on the Substrate. A design engineer, draftsman, engineer, or project manager in an organization with in-house plating facilities should have detailed information on the analysis, microstructure, and mechanical properties of the substrate. In a plating job shop, the customer should have someone informed on the subject. The plater is advised to ask these potential sources for as much information about the substrate as can be obtained.

Engineering Drawings and Associated Lists. Study of engineering drawings, parts lists, bills of materials, and pertinent manuals will usually clear up questions concerning the substrate submitted for plating. The bill of material, for example, may simply specify 1095 steel. This informs the plater that he is dealing with a high-carbon (0.95% C) and steel that can be heat treated to a high degree of hardness (for example, 50 to 60 HRC). This alerts the plater to be concerned with hydrogen embrittlement. As another example, if a drawing or associated list specifies aluminum alloy 6061-T*x*, the plater can deduce that the substrate is heat treatable by precipitation hardening to various tempers (degrees of hardness). Such an alloy is subject to developing a smut or to leaving a heavy oxide layer after being alkaline etched or cleaned. An experienced plater will recognize this and will know to treat the cleaned and etched part in a desmutter/deoxidizer in the treating sequence before undertaking the plating process.

Chemical Spot Tests. A simple chemical spot reaction test is documented in Ref 6 and 7. This method is based on the use of a magnet and five chemicals. Three of the chemicals are different concentrations of nitric acid (HNO_3), another is concentrated hydrochloric acid (HCl), and the fifth is a 10% solution of potassium ferricyanide ($K_3Fe(CN)_6$). Although it tests for only one element at a time, this simple test distinguishes among a large number of commonly used steels and nickel alloys.
Electrolytic Spot Test Method. This is a commercially available method, complete with chemicals, a power source, and instructions. The operation is divided into four steps. First, a test paper moistened with a conductive solution is placed in contact with the unknown metal. Second, using a direct-current (dc) power source with the unknown metal connected to the anode terminal (+) and a metal probe to the cathode terminal (-), a small amount of the unknown metal is dissolved into the test paper. Dissolution is brought about by electrolytic action when the dc current is switched on. Third, a few drops of a specific color developer are added to the wet spot on the paper. The developer reacts chemically with a characteristic component of the dissolved metal. Fourth, almost immediately, a color appears on the paper if a specific suspected alloying element is present in the unknown. This method is semiquantitative because the relative color intensity is proportional to the amount of alloying element or major metallic constituent. By comparing the results of the unknown with those of standard alloy samples, the nature of the unknown substrate can be adequately identified.
Electronic Alloy Identification. This method is quite rapid and depends on the Peltier Effect (also the basis of the thermocouple). If a current of electricity is sent through a circuit containing two dissimilar metals, heat is emitted at one junction and absorbed at the other junction. A characteristic voltage (potential) is generated at the thermocouple junction that causes an electrical current to flow. This voltage varies with the metals that constitute the couple. The electronic alloy identification meter operates on this principle. It measures the voltage generated by the action of a file of known composition scratched along the surface of an unknown alloy. The file acts as the positive meter input probe, with a clip-on providing negative reference. In a commercially available apparatus, the thermocouple voltage is shown on a battery-powered digital display. This voltage is characteristic of specific alloys or classes of alloys. Again, the instrument can be calibrated against known alloy specimens that are sold as standards.

Physical and Mechanical Properties of Substrates

The susceptibility to corrosion of a plated substrate depends on physical properties and mechanical condition. For example, surface profile (roughness, presence of scratches, pits, lapped metal, and so on) can profoundly affect the durability of plated ware. Some of the harmful effect can be avoided by mechanical or electropolishing, polishing and buffing, shot peening, or glass beading. Internal stresses can also be harmful. These may dictate heating for stress relief or shot peening or glass beading to convert surface tensile stresses to compression. The physical properties of a substrate, particularly at the surface, are often as important to the metal finisher as its composition. Porosity, hardness, melting point, coefficient of thermal expansion, and permeability to hydrogen (nascent, or atomic, and gas) are vital to many operations. Porosity of substrates, particularly in castings and sintered powder metal compacts, causes many problems because of the difficulty of rinsing processing solutions. Capillary action tends to hold solutions with forces that defy normal rinsing efforts. This results in spotting out of corrosive liquids, which appear as stains and corrosion products on the plated surface. It also causes contamination of processing baths.
Some surface irregularities of substrate can be compensated for by the leveling properties of specially formulated plating solutions. Leveling action is the ability of a plating solution to produce a surface smoother than that of the substrate. The property of the plating solutions that produces leveling is also referred to as microthrowing power.
Another property of substrates that can cause difficulties is susceptibility to hydrogen absorption. High-carbon and, particularly, hardened steels and titanium are susceptible to embrittlement when processed by methods that subject them to atomic or gaseous hydrogen. Recognizing this weakness of such substrates, the designer or specifier of plating sequences must select alkaline cleaning and oxide removal (pickling agents, activators) procedures that lessen or avoid hydrogen evolution. Mechanical cleaning and mechanical plating (also known as peen plating) are examples of the methods used to avoid hydrogen embrittlement. Because total avoidance of hydrogen evolution is often not possible, a step or steps must be added to the plating sequence to remove hydrogen. This usually consists of baking plated parts at low temperatures (205 °C, or 400 °F) to release absorbed hydrogen. Time and temperature is also an important variable in ensuring the release of hydrogen and restoration of the mechanical properties of the plated substrate.

Substrate metals that have been heavily worked by such operations as deep drawing, swaging, polishing and buffing, grinding, machining, forging, and die drawing often come to the plating shop with a damaged layer on the surface. This heavily worked layer is termed a Beilby Layer in honor of Sir George T. Beilby, who stated that this layer was amorphous or vitreous rather than crystalline. He compared this weak, somewhat brittle layer to substances that resemble the glasslike form assumed by the silicates when they are solidified from the molten state (Ref 8). X-ray analyses in later years proved that severe cold working causes fragmentation of crystals into particles of different orientations, but that the surface metal is not vitreous or amorphous. However, this smeared, shattered layer is inherently low in ductility and fatigue strength and is therefore a weak foundation for plated coatings. This is particularly true of metal objects that require a surface of substantial corrosion resistance and high mechanical properties as well as metal objects that will be further formed or distorted in service. To avoid the weakness introduced by such layers, abrasive cleaning, machining, or electrolytic polishing are required to remove them before plating.

Stresses in Substrates

Substrates with locked-in stress reduce the corrosion resistance of electroplated coatings relative to the same coating on an annealed substrate. Stressed metal is anodic to annealed or lesser-stressed metals and is therefore more prone to corrosion in unfavorable service conditions. Substrates with flaws on the surface, stress-raising or stress-localizing scratches, or abrupt changes in section are less resistant to corrosion than smooth, streamlined parts. The coefficients of thermal expansion of the coating and substrate should also be matched as closely as possible to minimize stresses caused by differential expansion during temperature cycling.

Stress-Corrosion Cracking of Substrates

Stress-corrosion cracking (SCC) is a cracking process that requires the simultaneous action of a corrodent and sustained tensile stress. Certain alloys are susceptible to SCC when subjected to certain corrosive environments. Examples are copper alloys, such as Cu-30Zn (cartridge brass), and nickel-chromium alloys. Ammoniacal materials, such as aqueous ammonia (NH_4) and amines, produce such failures in stressed copper alloys. Halides, such as chlorides and bromides, attack certain nickel-chromium alloys with this type of corrosion.

The basic characteristics of SCC are summarized in Ref 9. There is no available evidence that plated coatings on substrates susceptible to SCC will prevent its occurrence. Stress relief of susceptible alloys is often adequate for avoiding SCC. For example, brass cartridge cases, which are made by a deep-drawing process (leaving high residual stress), are stress relieved in a temperature range that produces recovery without recrystallization. Stress relieving at a higher temperature would produce recrystallization and an unacceptable reduction in mechanical properties. Avoidance of the use of SCC-susceptible alloys in known hostile environments is another approach to avoiding this mode of failure, but this is not always feasible. For example, for the brass cartridge case cited previously amine stabilizers in the smokeless powder propellant obviated control of the environment; therefore, stress relief was required. However, use of SCC-susceptible metals in corrosion-cracking environments should be avoided whenever possible.

References cited in this section

1. "Standard Definitions of Terms Relating to Electroplating," B 374, *Annual Book of ASTM Standards,* American Society for Testing and Materials

2. C.L. Faust, "Electroplating," Course 22, Metals Engineering Institute, American Society for Metals, 1983

3. F.A. Lowenheim, Ed., *Modern Electroplating,* 3rd ed., John Wiley & Sons, 1974

4. L.J. Durney, Ed., *Electroplating Engineering Handbook,* 4th ed., Van Nostrand Reinhold, 1984

5. F.A. Lowenheim, *Electroplating,* McGraw- Hill, 1978

6. M. Murphy, Ed., *Metal Finishing Guidebook & Directory,* Elsevier Science, 2001

7. R.S. Treseder, Ed., *The NACE Corrosion Engineer's Reference Book,* National Association of Corrosion Engineers, 1980

8. G.T. Beilby, The Hard and Soft States in Metals, *J. Inst. of Met.,* No. 2, 1912, p 149–185

9. R.G. Baker, "Corrosion of Electrodeposited Coatings," Slide Lecture 46, American Electroplaters and Surface Finishers Society, 1981

T. Mooney, Electroplated Coatings, *Corrosion: Fundamentals, Testing, and Protection*, Vol 13A, *ASM Handbook*, ASM International, 2003, p 772–785

Electroplated Coatings

Revised by Ted Mooney, Finishing.com, Inc.

Design for Plating

Much can be done at the design stage to improve the plateability of metal stampings, castings, forgings, and extruded shapes. In doing so, the corrosion protection afforded by the plating can be enhanced. Corrosion resistance of a plated object depends on coating thickness and distribution, and these factors depend largely on the design of the parts. ASTM B 507 (Ref 10) covers practices for the design of articles to be electroplated on racks with nickel, but its significance goes beyond nickel plating. It also applies in most respects to all rack-plated coatings. The general principles of design are discussed in Ref 10, which states that the electrodeposition of one metal onto another follows a pattern such as that exemplified in Fig. 2, showing current distribution and the distribution of the resultant electrodeposit (Fig. 2).

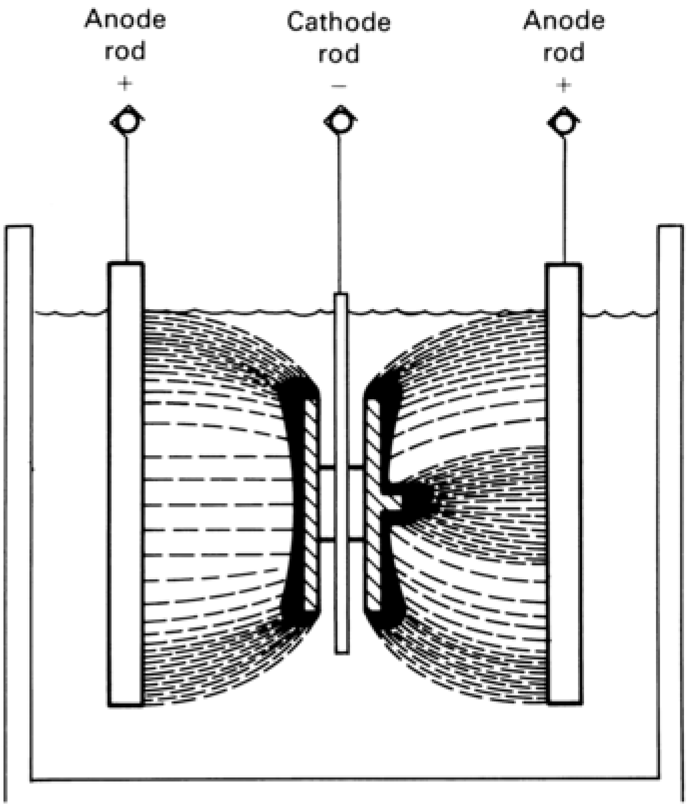

(a)

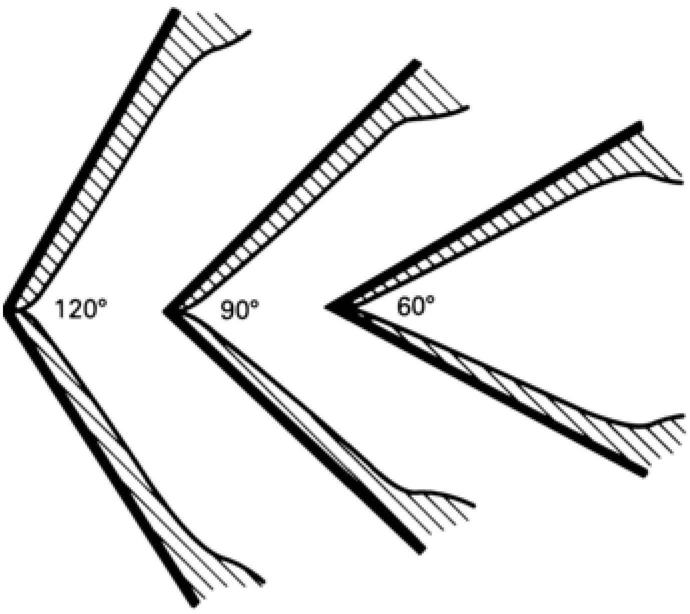

(b)

Fig. 2 Current distribution (a) and effect of substrate geometry (b) on thickness of electroplated nickel deposits. For the 120° substrate in (b), the ratio of average coating thickness to minimum coating thickness is 1.9; for the 90° substrate, 2.7; and for the 60° substrate, 3.3. Source: Ref 10

Distribution of the deposit will vary slightly as a function of bath type, additives, current density, and temperature. The coating is preferentially deposited at protuberances, sharp corners, edges, fins, and ribs on the component being plated; to avoid coating buildup, these areas should be rounded with a minimum radius of 0.4 mm (0.015 in.). A 0.8 mm (0.03 in.) radius is preferable. Conversely, the base of any cavity, recess, or depression in the component being plated will be deficient in plate thickness; these features should be designed

to avoid sharp fillets. In general, such features should be designed so that the ratio of width to depth of the depression is held to a minimum of 3, and the minimum radius at the edge and base of an indentation should be one-fourth of the depth of the indentation. When sharp angles are required for functional purposes, the electroplater cannot be expected to meet minimum coating thickness requirements in these areas and corrosion resistance may be inadequate.

When designs cannot be changed, electroplaters resort to one or more of the following methods to overcome the aforementioned difficulties: provision of inside anodes, use of thieves or robbers (nonconductive shields that slow or prevent deposition) to lower the cathodic current density at protuberances, bipolar electrodes, changing electroplating baths to ones with greater covering power, and switching from electroplating to autocatalytic (electroless) plating. This last method is widely used on parts that cannot be properly plated by electrodeposition. The limitation is that the most prevalent coating applied autocatalytically—electroless nickel—deposits an alloy of nickel and phosphorus (phosphorus content varies with the solution used and the deposition condition), not unalloyed nickel. There is also an economic disadvantage in switching to these processes. However, in most cases in which electroless processes have been adopted, they have been specified for reasons other than merely to compensate for part designs that cannot be readily electroplated with uniform coatings.

An article should not be designed for plating, but rather to perform its intended function (Ref 11). If the part is successfully designed, provision will have been made for corrosion resistance, hardness, lubricity, decorative appeal, or whichever required property the finish process is to supply. Function, fit, form, and aesthetics—the major dictates of design criteria—often take precedence over the practicality of corrosion prevention by plated coatings; this need not be the case. Design manuals must be instructional with regard to the effects of geometry on function, and designers should be taught these principles.

Additional information on design for electroplating is available in Ref 12. Table 2 lists proper and improper designs for various features of electroplated components. Plating of relatively small parts in rotating containers is termed barrel plating. This differentiates it from rack plating, in which individual parts are held in a rack or fixture during plating. Fastening hardware, such as nuts, bolts, washers, screws, and studs, are barrel plated, as are numerous critical electrical and electronic components. Many of these parts are as important from the corrosion resistance standpoint as rack-plated parts are—perhaps more so because such parts as fasteners and connectors are used in, and therefore coupled to, other materials. This raises the problem of galvanic corrosion.

Table 2   Influence of substrate design features on electroplateability

Feature	Poor design	Influence on electroplateability	Better design
Convex surfaces		Ideal shape. Easy to plate uniformly, especially where edges are rounded	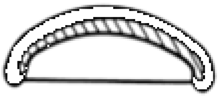
Flat surfaces		Use a 0.4 mm (0.015 in.) crown to minimize undulations caused by uneven buffing.	
Sharply angled edges		Undesirable. Reduced coating thickness at center areas requires increased plating time to obtain a minimum thickness of durable electroplate. All edges should be rounded. Edges that will contact painted surfaces should have a minimum radius of 0.8 mm (0.03 in.).	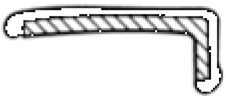
Flanges	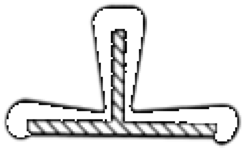	Large flanges with sharp inside angles should be avoided to minimize plating costs. Use a generous radius on inside angles and taper the abutment.	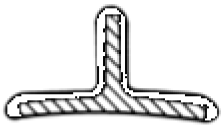
Slots		Narrow, closely spaced slots and holes reduce electroplateability and cannot be properly plated unless corners are rounded.	
Blind holes		Must usually be exempted from minimum thickness requirements. Where necessary, limit depth to 50% of width. Avoid diameters of less than 6 mm (0.24 in.).	
Sharply angled indentations		Increase plating time and costs for a specified minimum thickness, and reduce the durability of the plated part.	

Bulk parts in a plating barrel are subject to a greater variation in cathodic current density than parts plated on racks. Cathode contact is made by danglers, chains, buttons, or studs near the bottom of the load, while the plating occurs only at the surface of the load. This produces a large statistical variation in thickness of the electrodeposits on barrel-plated parts; this is not the case for rack-plated parts. Corrosion of a plated part is often controlled by the minimum thickness of protective coating; therefore, if parts are to be barrel plated, special design practices should be observed, including (Ref 12):

- Avoid blind holes, recesses, and joint crevices that can retain tumbling compounds and metal debris from previous operations.
- Avoid intricate surface patterns that will be blurred by barrel finishing.
- Design parts to withstand the multiple impacts of barrel rotation.
- Design small, flat parts with ridges or dimples to prevent nesting.
- Design for good entry and drainage of solutions during rotation by using simple shapes.
- Design surfaces to be plated so that they undergo proper mechanical preparation and cleaning and to ensure that they receive their share of metal deposit. They should be convex, if possible, rather than recessed.

In a larger sense, the design of parts for plating parallels good design practice for corrosion resistance. Avoidance of sharp edges, burrs, or other areas of high free energy, avoidance of abrupt changes in section, recesses, and other traps for moisture, and avoidance of scratches, notches and other anodic-site producers are common design criteria for parts in general as well as for plated parts. More information on designing to minimize corrosion is available in the article “Designing to Minimize Corrosion” in this Volume.

References cited in this section

10. “Standard Practice for Design of Articles to be Electroplated on Racks with Nickel,” B 507, *Annual Book of ASTM Standards,* American Society for Testing and Materials
11. J. Hyner, Design for Plating, *Electroplating Engineering Handbook,* L.J. Durney, Ed., Van Nostrand Reinhold, 1984, p 50
12. *Quality Metal Finishing Guide,* Metal Finishing Suppliers' Association

---

T. Mooney, Electroplated Coatings, *Corrosion: Fundamentals, Testing, and Protection*, Vol 13A, *ASM Handbook,* ASM International, 2003, p 772–785

Electroplated Coatings

Revised by Ted Mooney, Finishing.com, Inc.

Advantages and Disadvantages of Electroplated Coatings

Alternatives to electroplating for the protection of metal surfaces against corrosion include organic finishing, hot dip coating, metal spraying, chemical vapor deposition (CVD) and physical vapor deposition (PVD), vacuum deposition by sputtering and ion implantation, and ceramic coating. (See the articles “Organic Coatings and Linings,” “Continuous Hot Dip Coatings,” “Batch Process Hot Dip Galvanizing” “Thermal Spray Coatings,” “CVD and PVD Coatings,” “Surface Modification Using Energy Beams,” and “Chemical-Setting Ceramic Linings” in this Volume). The decision to use one or more of these methods must consider at least the following factors:

- Applicability to the substrate in question (For example, zinc plating is applicable as a protective coating to steel, but not cast iron.)
- Purposes of the finish (Is color a requirement? Will the object to be finished fit into available plating equipment?)
- Cost of suitable electroplating versus alternative methods of coating the part (What finish will be functionally adequate and applicable at the least cost?)
- Anticipated service conditions and length of service desired under these conditions (SC5, extended very severe; SC4, very severe; SC3, severe; SC2, moderate; SC1, mild) (Ref 13)

Advantages of Electroplating

Variety of Coatings. The principal metals that are widely plated are cadmium, zinc and its alloys, chromium, copper, gold, nickel, tin, and silver. Other metals that are plated by in-house shops and some job platers are cobalt, indium, iron, lead, palladium, platinum, rhenium, and rhodium. Plateable alloys add versatility to the catalog of plated coatings. The commonly plated alloys are brass, bronze, copper-cadmium, tin- lead (solder), tin-zinc, gold alloyed with many metals, and nickel alloys with iron and cobalt. Zinc alloy platings, including zinc-cobalt, zinc- iron, zinc-nickel, and tin-zinc are of ever-growing importance. Ternary alloys, such as karat gold alloys and Cu-Sn-Zn, are also available. Nickel-phosphorus and nickel-boron are readily plated by the autocatalytic (electroless) process. Nickel-phosphorus can also be electrodeposited. Coatings of many types can be codeposited with occluded particles by electrodeposition or electroless deposition to modify friction and wear properties. Particles used for these applications range from deposited or occluded abrasives such as diamond, silicon carbide (SiC) to lubricious materials such as polytetrafluoroethylene (PTFE).
Versatility of Application. Plated coatings can be applied to racked parts, in barrels (both by immersion in tanks and manually), semiautomatically, or on microprocessor-controlled fully automatic machines. Local, selective

application of a coating, if necessary, can be accomplished by such methods as brush plating (also known as electrochemical metallizing and tampon plating). Similarly, precious metals, such as gold and palladium, have been conserved in electronics applications by selective plating on continuous strips. This is referred to as reel-to-reel plating. The adaptability of plating methods to the job at hand is limited only by the imagination and skill of the plater.

Availability of Applicators. Plating job shops and in-house applicators are plentiful in the United States and throughout the world. The technology is popularized and nurtured by such technical societies and trade associations as the American Electroplaters and Surface Finishers Society, the National Association of Metal Finishers, the Metal Finishing Suppliers' Association, and the Society of Automotive Engineers Airline Plating Forum.

The electrical conductivity of electrodeposited and other metallic coatings gives them an advantage over most organic and ceramic-base coatings in applications that require this characteristic. Applications in which electrical conductivity is necessary include the welding, electrical bonding, or grounding of objects as well as electrical and electronic circuitry.

Galvanic Protection of Substrates. Zinc and cadmium deposits are anodic to steel and protect steel substrates by sacrificial action in many wet environments. In aircraft and other aerospace applications, cadmium plating is used on steel components in contact with aluminum alloys because cadmium is closer in potential to aluminum than steel is (Fig. 1). On coil-coating lines for prepainted steel sheet and strip, electrogalvanizing stages are provided in the wet section to protect the substrate at points of failure of the organic overcoating. Electrogalvanized steel, often further treated with chromate conversion coatings, is used for various purposes because of the sacrificial protective value of the zinc coating. Duplex or triplex coatings of nickel, often with a final thin coating of chromium, are another example of a more complex galvanic protective system.

Weldability and Solderability. Metal deposits are amenable to welding and soldering—an advantage over most organic coatings and porcelain enamel. Certain coatings are more weldable and solderable than others, which leads to the application of special types of plating to facilitate a specific type of joining or fabricating method.

Control of Thickness. Unlike hot dip coating, electrodeposition affords a means of predicting and controlling the amount of metal deposited. This is possible through the validity and knowledge of Faraday's laws, which are as follows (Ref 2):

- The quantity of any element discharged at an electrode is proportional to the quantity of electricity that is passed.
- The quantities of different ions of elements discharged by a given amount of electricity are proportional to the electrochemical equivalents of those elements.

The quantity of electricity is measured in Coulombs (C) (C = A · s), and the electrochemical equivalent of an element is its atomic weight divided by its valence. It is known that 96,480 C, or 1 Faraday will deposit 1 g equivalent weight of any element at 100% electrode efficiency. Electrode efficiencies are a function of plating electrolytes and conditions. They can be determined by coulometric measurement and are published for most plating processes. Because most plants control plating by measuring ampere hours, the amount in grams of metal plated, M_d, is calculated by the relationship:

$$M_d = \frac{A \cdot h}{26.8} EE_M CE_M$$

where EE_M is the electrochemical equivalent of metal M (atomic weight of M divided by valence of M), and CE_M is the cathode efficiency of the plating bath and conditions.

Ductility and Formability. Substrate metals coated by electrodeposition can be formed more readily than some metals coated by hot dipping or certain organic coatings. They do not result in intermetallic alloy layers of the type common to ordinary hot dip galvanizing, for example. Diffusion of some electrodeposits into substrates, and vice versa, occurs after plating as a function of temperature, time, and the diffusion tendencies of the metals involved. These diffused layers are normally thin and require protracted periods of time to develop, usually after the component has been formed to a desired shape.

Electroless Plating. The coating of the interiors of tubes or other recessed areas uniformly and with controlled thickness is the special province of autocatalytic, or electroless, plating.

Mechanical Plating. Mechanical, or peen, plating is a method of coating substrates, principally steel, with malleable metals, such as zinc, cadmium, tin, or their alloys. In mechanical plating, hard, small, spherical objects, such as glass shot, are tumbled against the parts to be plated in the presence of finely divided metal

powder, such as zinc dust, and appropriate chemicals. Special advantages of this method over electroplating are the relative absence of problems with hydrogen embrittlement, the simplicity of operation with small parts in a single rotating container, and the ability to deposit desirable alloys that cannot be electroplated. As an example of the latter, tin and cadmium alloys have been found to provide excellent protection of steel against corrosion in marine environments.

Disadvantages of Electroplating

Color Limitations. The colors of electrodeposited coatings are limited to copper, silver metallic, brass, bronze, and gold and its alloys; black, iridescent, or olive drab chromate conversion coatings; and patinas formed on copper and its alloys by chemical and electrochemical treatments.

Colored Anodic Coatings on Aluminum. Anodic oxidation of aluminum, an electrochemical frequently employed at electroplating shops, provides a protective coating that can be colored. The coating is integral to the substrate and can be colored by dyeing, integral color anodizing, or electrolytic coloring (Ref 6, 14). These coatings are highly resistant to abrasion and corrosion and are widely used on architectural forms. More information on these types of coatings is available in the article “Aluminum Anodizing” in this Volume.

Inhospitable Substrates. Some substrates, such as cast iron, and certain substrate conditions, such as porosity, require special plating procedures. Unimpregnated powder-metal compacts and porous castings that can be plated are subject to spotting out, or bleeding, because of retention in pores of cleaning and plating alkalies, acids, and salts.

Limitations of Design. Parts are designed to function in the most economical manner. This is not always compatible with plating. Where the geometry of a part is such that cathodic current distribution will be unfavorable to uniform coatings, it is sometimes wise to seek an alternative protective coating. The criteria here are that the coating must achieve the required minimum thickness on significant surfaces, must meet all functional and dimensional requirements, and must accomplish these objectives at a reasonable cost.

Size Limitations. Large metal structures are often beyond the capabilities of electrodeposition. The limitation lies in the capacity of tanks to contain the electrolyte. Exceptions are certain architectural structures and statuary, which may be brush plated. Such coatings are almost always on copper or bronze and consist of nickel topped with gold electrodeposits. Steel structures, such as bridges, dams, and building elements, are more advantageously hot dip galvanized and painted, or painted without zinc but with specially designed organic coating systems.

Environmental Issues. Electroplating as a whole has been under enormous environmental pressures worldwide since the late 1970s. Intrinsic to virtually all electroplating processes is a requirement for washing the plating solution off of the ware with copious volumes of fresh rinse water, which then presents the operator with the problem of dealing with large volumes of water contaminated with salts of heavy metals. It is expensive and often impractical or impossible to return these diluted plating solutions to the process tanks, while also unacceptable to discharge them untreated to surface waters or sanitary sewer systems. Similarly, it is inherent in the process that cleaning solutions, activating solutions, posttreatment dips, and even some plating solutions become exhausted or hopelessly contaminated and require treatment and disposal to a secure landfill. Many plating operations require mist evacuation, which holds the potential of polluting the air unless adequate fume scrubbing is ensured. None of these problems are insurmountable, but the triple threat of the potential for contaminating water, land, and air has made pollution avoidance an expensive and knotty problem for plating practitioners.

Additionally, some of the individual plated metals and processes present problems. Cadmium is now recognized as a biocumulative poison with toxic effects similar to those of mercury and lead; cadmium plating is expressly forbidden on most or all parts in many countries. Nickel plating is no longer permitted in jewelry applications in much of the world. The hexavalent chromate dips traditionally used on zinc- plated surfaces to forestall white rust are now forbidden in enough of the world that they are no longer used anywhere in the manufacture of automobiles.

References cited in this section

2. C.L. Faust, “Electroplating,” Course 22, Metals Engineering Institute, American Society for Metals, 1983

6. M. Murphy, Ed., *Metal Finishing Guidebook & Directory,* Elsevier Science, 2001

13. "Standard Specification for Electrodeposited Coatings of Copper Plus Nickel Plus Chromium and Nickel Plus Chromium," B 456, *Annual Book of ASTM Standards,* American Society for Testing and Materials

14. S. Wernick and R. Pinner, *The Surface Treatment and Finishing of Aluminum and Its Alloys,* Robert Draper, 1972

T. Mooney, Electroplated Coatings, *Corrosion: Fundamentals, Testing, and Protection,* Vol 13A, *ASM Handbook,* ASM International, 2003, p 772–785

Electroplated Coatings

Revised by Ted Mooney, Finishing.com, Inc.

Effects of Deposition Parameters

The process used to apply the coating may have an important effect on the properties of the entire coating system. One of the more important considerations is the effect of hydrogen formation during electroplating. Hydrogen may embrittle the substrate. This is particularly important when cadmium, chromium, or zinc is used as a coating over high-strength steel. Atomic hydrogen can combine to form high-pressure hydrogen gas at defects or regions of poor adhesion, causing blisters in the coating. Appropriate standards have been developed to cover relief from hydrogen embrittlement in high-strength steels (Ref 15). Hydrogen can also be introduced into the coating system during one of the cleaning or pickling steps conducted before electroplating.

Reference cited in this section

15. "Method for Mechanical Hydrogen Embrittlement Testing of Plating Processes and Aircraft Maintenance Chemicals," F 519, *Annual Book of ASTM Standards,* American Society for Testing and Materials

---

T. Mooney, Electroplated Coatings, *Corrosion: Fundamentals, Testing, and Protection,* Vol 13A, *ASM Handbook,* ASM International, 2003, p 772–785

Electroplated Coatings

Revised by Ted Mooney, Finishing.com, Inc.

Mechanisms of Corrosion Prevention of Plated Coatings

Coatings applied by electrodeposition or electroless plating protect substrate metals in one of three ways. The first is cathodic protection of the substrate by sacrificial corrosion of the coating—for example, zinc and cadmium coatings are electronegative (or anodic) to steel. Second is barrier action, that is, interposing a more corrosion-resistant coating between the environment and a less corrosion-resistant substrate. Examples of this are Cu-Ni-Cr and Ni-Cr coating systems over steel and zinc alloy automotive parts. Third is environmental

modification or control in combination with a nonimpervious barrier coating. An example of this type of protection is the electrolytic tinplate used in food packaging.

Anodic Coatings. Zinc and cadmium deposits will protect steel at pores and other discontinuities by cathodic protection. Observation of the emf series (Table 1) shows that zinc is electronegative to steel in potential when these metals are immersed in solutions of their own ions. Under the same conditions, cadmium is more noble than iron, but in actual service under several environmental influences, cadmium is anodic to iron and is therefore sacrificially protective. Figure 3 shows the galvanic protection offered by a zinc coating to a steel substrate. This mechanism of galvanic protection gives rise to the term galvanized steel, which refers only to zinc-coated steel. This old, but commonly used term is modified to electrogalvanizing when referring to electrodeposited zinc in order to differentiate it from hot dip galvanizing.

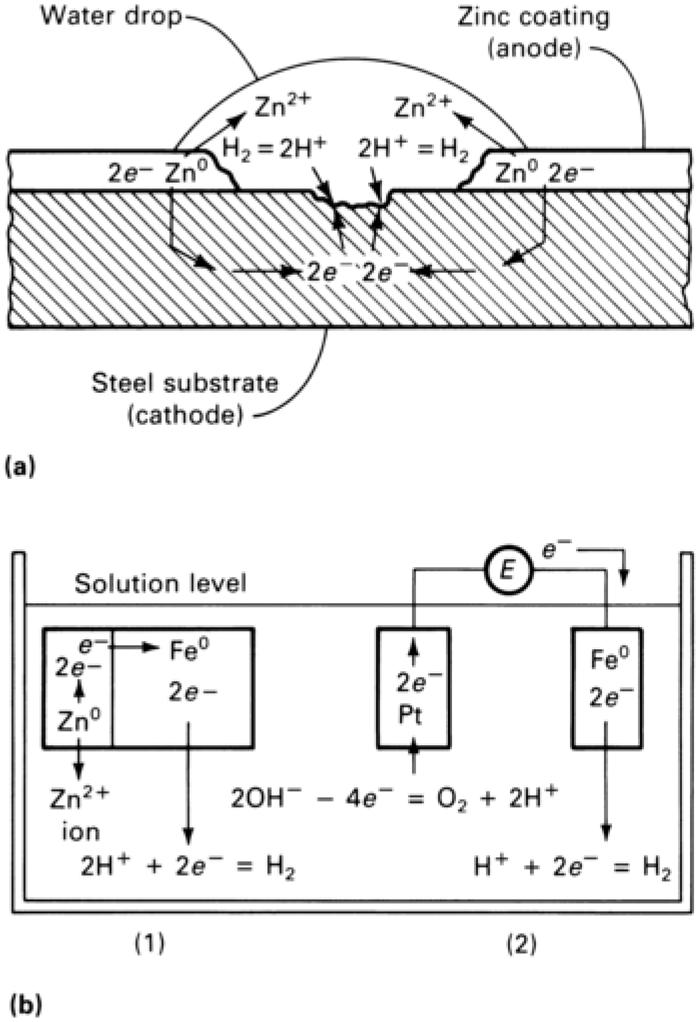

Fig. 3 Principles and mechanism of galvanic protection of a substrate by a coating. (a) Galvanic protection of a steel substrate at a void in a zinc coating. Corrosion of the substrate is light and occurs at some distance from the zinc. (b) Galvanic protection of a steel member (1) by a zinc member and by an impressed electric current flowing from an external dc power source (E) using an insoluble platinum electrode (2). Source: Ref 2

Cathodic Coatings. With reference to Table 1, it is apparent that the metals commonly plated, other than zinc and cadmium, are electropositive (more noble or cathodic) to steel. This is also evidenced by Fig. 1. Such coatings on steel are therefore expected to act strictly as barriers to prevent corrosion of the steel substrate. For this to be successful, the coatings must be pore free and flaw free. It is very difficult to obtain impervious coatings of more noble metals on steel or zinc alloys. Substantial metal thicknesses, usually 25 μm (1 mil) or more, are required. With some of these metallic deposits, particularly the noble metals, thinner coatings applied by pulse plating are more impervious than conventional plated metals, but this is the exception.

Generally, electroplated or hot dipped coatings that are completely free of pores and other discontinuities are not commercially feasible (Ref 2). Pits eventually form at coating flaws, and the coating is penetrated. The substrate exposed at the bottom of the resulting pit corrodes rapidly (Fig. 4). A crater forms in the substrate, and because of the large area ratio between the more noble coating and the anodic crater, the crater becomes anodic

at high current density. Electrons flow from the substrate to the coating as the steel dissolves. Hydrogen ions (H^+) in the moisture accept the electrons and, with dissolved oxygen, form water at the noble metal surface near the void. Use of an intermediate coating that is less noble than a surface coating but more noble than the base metal may result in the mode of corrosion shown in Fig. 5. This would be typical of a costume jewelry item with the substrate being brass, the intermediate coating nickel, and the topcoat tarnish-resistant gold. It is also exemplified by nickel-chromium coating systems.

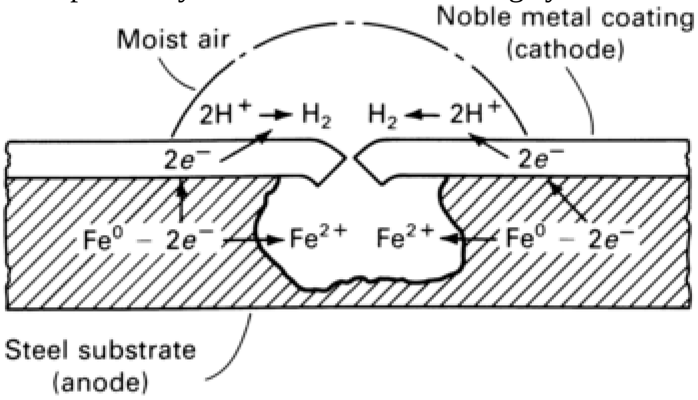

Fig. 4 Crater formation in a steel substrate beneath a void in a noble metal coating, for example, passive chromium or copper. Corrosion proceeds under the noble metal, the edges of which collapse into the corrosion pit. Source: Ref 2

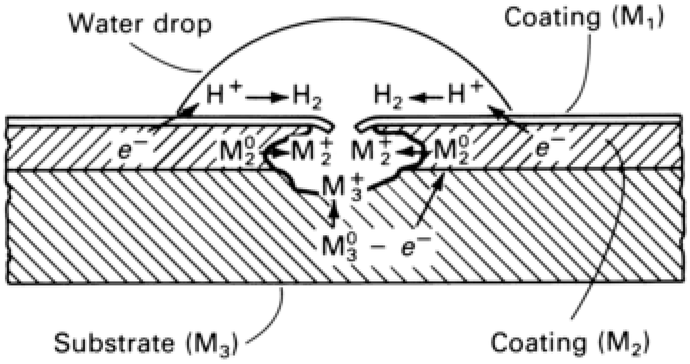

Fig. 5 Corrosion pit formation in a substrate beneath a void in a duplex noble metal coating. The top coating layer (M_1) is cathodic to the coating underlayer (M_2), which is in turn cathodic to the substrate (M_3). As in Fig. 4, the coating tends to collapse into the pit. Source: Ref 2

Exceptions to Predictions. The durability of a plated coating system cannot always be accurately predicted by conventional analysis of the potentials shown in the emf or galvanic series. Much depends on environmental exposure and the oxidized films formed in pores and discontinuities of plated coatings.

For example, some corrosion specialists predicted copper-plated zinc one-cent pieces would be unsuitable coinage because of rapid corrosion. The coating is barrel-plated copper on a zinc-rich alloy, with the coating thickness varying from 4 to 8 μm (0.15 to 0.3 mil). In this thickness range, the coating is far from impervious, or pore free. In the 1970s, before the minting of these coins, pictures were published showing exfoliated, voluminous zinc corrosion products on sample pennies after exposure to the ASTM B 117 neutral salt-spray test (Ref 16). The predicted result did not occur after more than 10 years of service. This indicates that the service conditions to which these coins were subjected are more forgiving than a salt-spray test.

Another example is the case of lead-plated steel, which is quite durable despite the fact that lead is more noble than iron. This is the case because a lead corrosion product develops in the pores (most likely lead sulfate $PbSO_4$) and arrests the progress of corrosion.

Importance of Thickness of Plated Coatings. In general, the thicker a metallic coating is, the less porous it is and the better it serves as a barrier against corrosion. Therefore, the measurement of thickness is a most important feature of testing electrodeposited and electroless coatings. Table 3 indicates the applicability of coating thickness measuring methods. American Society for Testing and Materials (ASTM) and International Standards Organization (ISO) standards covering thickness measurement methods are given in Ref 17.

Table 3 Applicability of thickness measurement methods to coatings

Substrate	Coating/Method(a)														
	Copper	**Nickel**	**Chromium**	**Electroless nickel**	**Zinc**	**Cadmium**	**Gold**	**Palladium**	**Rhodium**	**Silver**	**Tin**	**Lead**	**Tin-lead alloys**	**Non-metals**	**Vitreous and porcelain enamels**
Magnetic steel (including corrosion-resistant steel)	C, M	C, M(b)	C, M	C(c), M(b)	C, M	B, C, M	B, M	B, M	B, M	B, C, M	B, C, M	B, C, M	B(d), C(d), M	B, M	M
Nonmagnetic stainless steels	C, E(e)	C, M(b)	C	C(c)	C	B, C	B	B	B	B, C, E(e)	B, C	B, C	B(d), C(d)	B, E	E
Copper and alloys	C, only on brass and Cu-Be	C, M(b)	C	C(c)	C	B, C	B	B	B	B, C	B, C	B, C	B(d), C(d)	B, E	E
Zinc and alloys	C	M(b)	…	…	…	B	B	B	B	B	B	B	B(d)	B, E	…
Aluminum and alloys	B, C	B, C, M(b)	B, C	B, C(c), E(b)(c)	B, C	B, C	B	B	B	B, C	B, C	B, C	B(d), C(d)	E	E
Magnesium and alloys	B	B, M(b)	B	B	B	B	B	B	B	B	B	B	B(d)	E	…
Nickel	C	…	C	…	C	B, C	B	B	B	B, C	B, C	B, C	B(d), C(d)	B, E	…
Silver	B	B, M(b)	B	B	B	…	B	…	…	…	…	B, C	B(d)	B, E	E
Glass sealing nickel-cobalt-iron alloys (UNS K94610)	M	C, M(b)	M	C(c), M(b)	M	B, M	B, M	B, M	B, M	B, M	B, M	B, C, M	B(d), C(d), M	B, M	…
Nonmetals	B, C, E(e)	B, C, M(b)	B, C	B, C(c)	B, C	B, C	B	B	B	B, C	B, C	B, C	B(d), C(d)	…	…
Titanium	B	B, M(b)	…	B, E(b)(c)	B	B	B	B	B	B	B	B	B(d)	B, E	…

(a) B, β backscatter; C, coulometric; E, eddy current; M, magnetic.
(b) Method is sensitive to permeability variations of the coating.
(c) Method is sensitive to variations in phosphorus content of the coating.
(d) Method is sensitive to alloy composition.
(e) Method is sensitive to conductivity variations of the coating. Source: Ref 17

Porosity is another coating property that is very sensitive to deposition parameters and to substrate preparation. For very thin gold coatings (less than about 1 μm, or 0.04 mil), substrate texture controls coating porosity. At greater thicknesses, porosity is controlled by the coating properties. The variation in porosity with coating thickness is shown in Fig. 6, which shows three distinct phases: substrate dominated, transition, and coating dominated. Porosity can also be controlled to a large extent through deposition parameters, and this effect is attributed to a reduction in deposit grain size. The effects of porosity with thickness for pulsed-plated gold are shown in Fig. 7; again, the same three phases are apparent, although they are displaced downward.

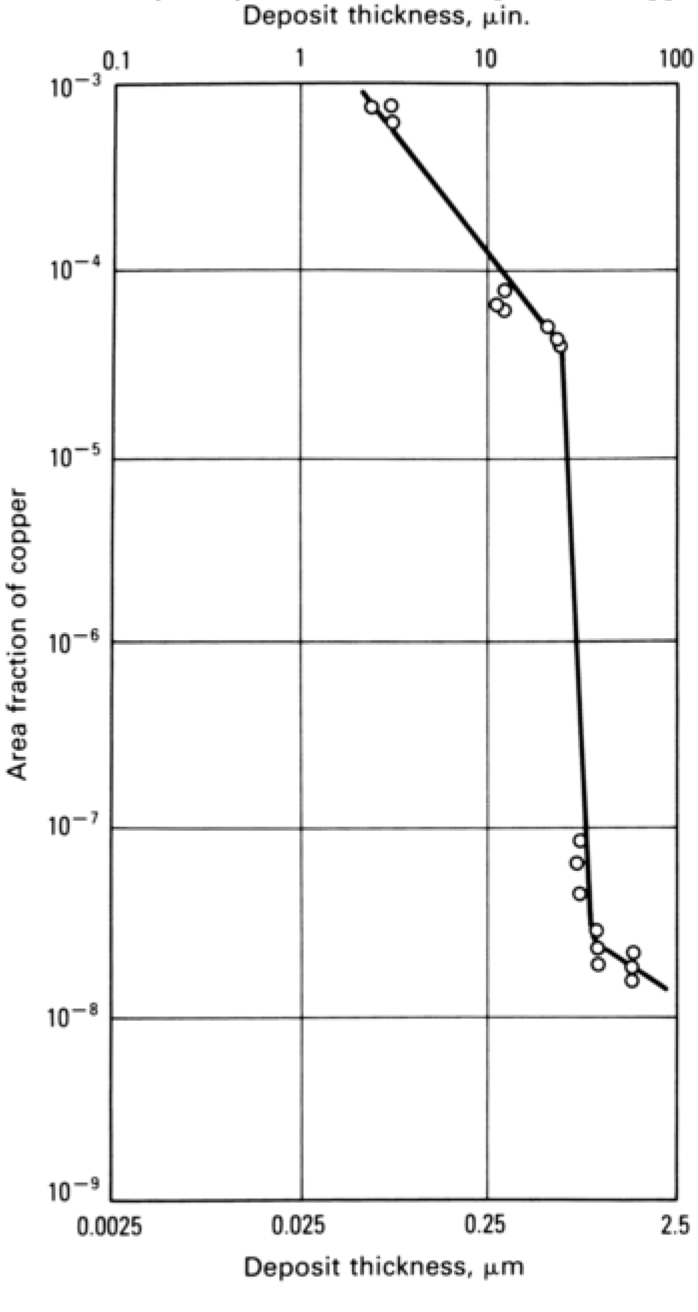

Fig. 6 Porosity versus deposit thickness for electrodeposited, unbrightened gold on a copper substrate. Compare with Fig. 7.

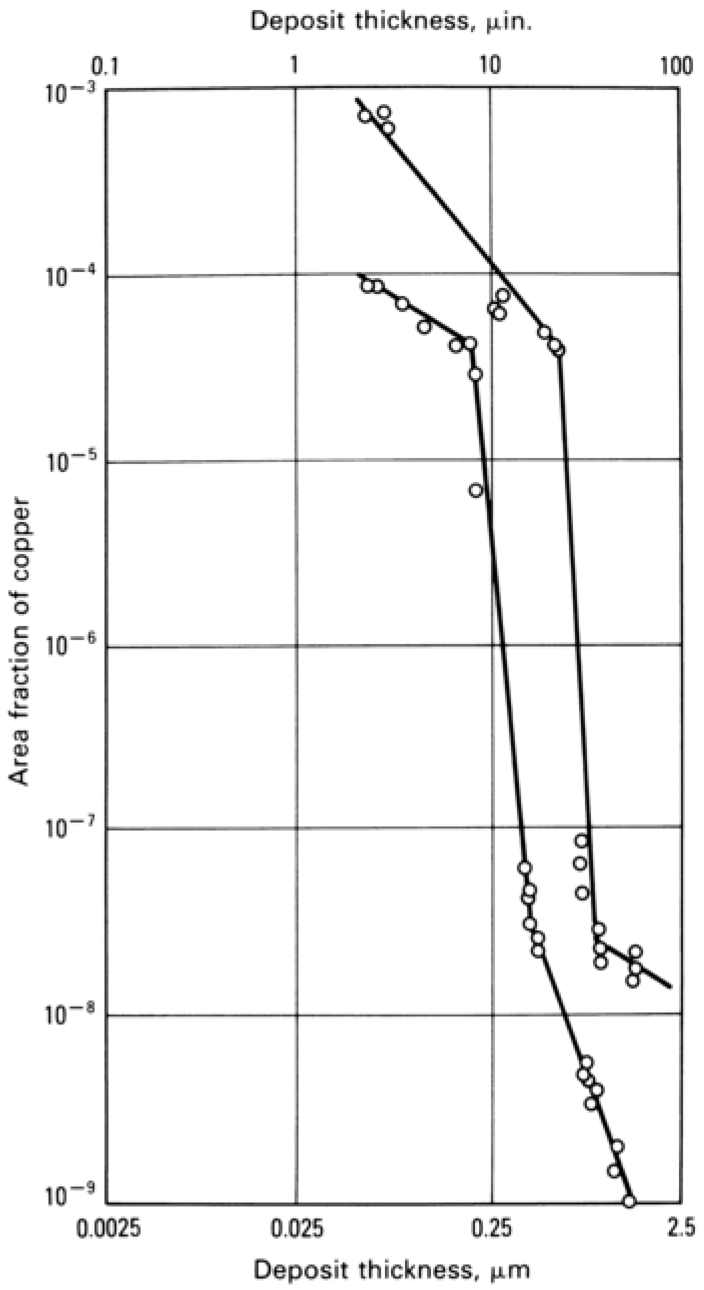

Fig. 7 Porosity versus deposit thickness for pulse-plated gold on a copper substrate. The curve for an unbrightened gold deposit on a copper substrate (top) is shown for comparison (see also Fig. 6).

Electrodeposited coatings applied to thicknesses of less than about 25 μm (1 mil) are porous. Porosity decreases with thicknesses, but it is present even at greater thicknesses. One of the reasons for this is the codeposition of hydrogen at cathodes, owing to the fact that most plating processes operate at less than 100% cathode efficiency. With sacrificially protective coatings, such as zinc and cadmium on steel, porosity is of little significance. Within limits, substrate steel exposed in the pores will be cathodic to the zinc or cadmium coating. Thus, the coatings will corrode under adverse conditions to protect the exposed cathodic steel, at least until the coating has been consumed by conversion to corrosion products. With the exception of chromium, coatings that are cathodic to the substrate depend on freedom from porosity for protection of the less noble substrate. Accordingly, such coatings must be tested for porosity as well as for thickness. Examples of ASTM standards for porosity testing are given in Ref 16 and 18, 19, 20, 21.

Adhesion is very important in the electrodeposition of a metallic coating, as implied in the definition of electroplating given earlier in this article. Therefore, it is logical for many end- product specifications for plated components to contain adhesion tests for verification of this requirement. ASTM B 571 (Ref 22) covers the following adhesion tests for metallic coatings: the burnishing tests, the chisel-knife test, the draw test, the file test, the grind-saw test, and the heat- quench test.

Corrosion. Testing for corrosion resistance is an important part of evaluating electroplated coatings and allied finishing techniques. Standard methods of corrosion testing are given in Ref 16 and 23, 24, 25, 26, 27. Accelerated tests of corrosion resistance of electroplated coatings can often lead to misleading conclusions. Claims that a certain number of hours in a particular test is equivalent to so many months or years of actual service should be viewed with suspicion.

References cited in this section

2. C.L. Faust, "Electroplating," Course 22, Metals Engineering Institute, American Society for Metals, 1983

16. "Standard Method of Salt Spray (Fog) Testing," B 117, *Annual Book of ASTM Standards,* American Society for Testing and Materials

17. "Thickness of Metallic and Inorganic Coatings," B 659, *Annual Book of ASTM Standards,* American Society for Testing and Materials

18. "Standard Specification for Electroplated Engineering Nickel Coatings," B 689, *Annual Book of ASTM Standards,* American Society for Testing and Materials

19. "Standard Specification for Electrodeposited Coatings of Tin-Nickel Alloy," B 605, *Annual Book of ASTM Standards,* American Society for Testing and Materials

20. "Standard Test Methods for Porosity in Gold Coatings in Metal Substrates," B 583, *Annual Book of ASTM Standards,* American Society for Testing and Materials

21. "Standard Specification for Electrodeposited Coatings of Tin," B 545, *Annual Book of ASTM Standards,* American Society for Testing and Materials

22. "Standard Test Methods for Adhesion of Metallic Coatings," B 571, *Annual Book of ASTM Standards,* American Society for Testing and Materials

23. "Standard Recommended Practice for Rating of Electroplated Panels Subjected to Atmospheric Exposure," B 537, *Annual Book of ASTM Standards,* American Society for Testing and Materials

24. "Standard Method of Testing FACT (Ford Anodized Aluminum Corrosion Test)," B 538, *Annual Book of ASTM Standards,* American Society for Testing and Materials

25. "Standard Methods for Corrosion Testing of Decorative Chromium Electroplating by the Corrodkote Procedure," B 380, *Annual Book of ASTM Standards,* American Society for Testing and Materials

26. "Standard Method for Copper-Accelerated Acetic Acid-Salt Spray (Fog) Testing (CASS Test)," B 368, *Annual Book of ASTM Standards,* American Society for Testing and Materials

27. "Standard Method of Acetic Acid-Salt Spray (Fog) Testing," B 287, *Annual Book of ASTM Standards,* American Society for Testing and Materials

T. Mooney, Electroplated Coatings, *Corrosion: Fundamentals, Testing, and Protection*, Vol 13A, *ASM Handbook*, ASM International, 2003, p 772–785

Electroplated Coatings

Revised by Ted Mooney, Finishing.com, Inc.

Applications for Electrodeposited Coatings

Nickel is widely used as a corrosion-resistant coating and as an undercoat for subsequent coatings. It is not resistant to HNO_3 or to environments containing chloride ions (Cl^-). However, it corrodes slowly in environments that do not contain Cl^- ions. Nickel is widely used by the automotive industry as an underlayer for microcracked chromium to protect steel. As previously discussed, nickel is usually plated as part of a multilayer coating system in which the electrode potential of each layer is different from those of other layers. The outer layer in such systems is often 130 mV more noble or cathodic than the layer beneath it. Nickel is also used over copper as an underlayer for gold to prevent rapid diffusion of the gold into the copper substrate. Nickel and its reaction products are toxic and a substantial percentage of the public suffer “nickel itch,” an allergic reaction to prolonged intimate contact with nickel metal. Nickel with organic additives to produce a very bright finish is widely used, although these coatings are much more brittle than the semibright nickel.

Nickel-phosphorus can be electrolessly or electrolytically deposited as a metallic coating. In general, its corrosion performance exceeds that of nickel in all environments. If the phosphorus content is above about 10 wt%, the coating is amorphous and therefore lacks grain boundaries or other crystalline defects at which corrosion can initiate. Electroless nickel has some advantage over electrolytic nickel in that its thickness and phosphorous content are uniform over the substrate and independent of substrate geometry. Electroless nickel is not resistant to hot caustic solutions. Heat treating nickel-phosphorus coatings above 350 to 400 °C (660 to 750 °F) results in recrystallization and loss of some corrosion resistance even though other properties, such as wear or hardness, may be enhanced. Diamond dust, Teflon globules, and other discrete particles are routinely plated into the nickel-phosphorus matrix to deliver wear characteristics not achievable from any other finish.

Cadmium and zinc are compared in the section “Idealized Coatings” in this article. Cadmium is generally preferred for the protection of steel in marine environments, and zinc is preferred in industrial environments. Cadmium tends to embrittle high-strength steel somewhat less than zinc does (being process related, new deposition processes may change this). The coefficient of friction of cadmium is less than that of zinc; therefore, cadmium is preferred for fastening hardware and connectors that have to be taken on and off repeatedly. Cadmium is much more toxic than zinc, and applications in which its corrosion products can get into the environment must be avoided. There is worldwide movement toward restricting cadmium plating to critical applications or banning its use outright. Cadmium should be specified only after exhaustive investigation of the implications and alternatives. The corrosion performance of both zinc and cadmium is greatly enhanced by chromate conversion coatings (see the article “Chromate and Chromate-Free Conversion Coatings” in this Volume).

Chromium is very resistant to atmospheric corrosion, but is soluble in HCl or in alkaline (caustic) solutions. Its resistance to corrosion is thought to be due to the formation of an amorphous chromium oxide that acts as a passive film to protect the metal. The hardness, low coefficient of friction, and ability to retain oil of heavy chrome deposits has made them an indispensible finish in thousands of moving-part applications. Chromium is deliberately deposited for decorative and wear applications as a microcracked coating over nickel so that corrosion currents are uniformly distributed over a large area. Chromium may be deposited as a noncracked coating both from hexavalent chromium (Cr^{6+}) and from trivalent chromium (Cr^{3+}) electrolytes.

Tin is widely used as a barrier and as an anodic coating for steel and copper. Because it is readily solderable and its oxide is conducting, it finds application in electrical conductors and contacts. Its corrosion products are not toxic; therefore, tinned containers are widely used in the food industry. Recommended thicknesses for application over copper components are given in Table 4 and over ferrous components in Table 5.

Table 4 Suggested thicknesses for electrodeposited tin coatings on copper alloys containing a minimum of 50% Cu.

Purpose of coating	Minimum local thickness	
	µm	**mils**
Contact with food or water where a complete cover of tin must be maintained against corrosion and abrasion	30	1.2
Protection in atmosphere and in less aggressive immersion conditions	15	0.6
To provide solderability and protection in mild atmospheric conditions	5	0.2
Coatings flow brightened by fusion (solderability and protection in mild atmospheres)	2.5–8[(a)]	0.1–0.3[(a)]

(a) On brass, an undercoat of 2.5 µm (0.1 mil) thick, copper, nickel, or bronze is required. Source: Ref 28

Table 5 Suggested thicknesses for electrodeposited tin coatings on ferrous components

Purpose of coating	Minimum local thickness	
	µm	**mils**
Contact with food or water where a complete cover of tin must be maintained against corrosion and abrasion	30	1.2
Protection in atmosphere	20	0.8
Protection in moderate atmospheric conditions with only occasional condensation of moisture	10	0.4
To provide solderability and protection in mild atmospheres	5	0.2
Coatings flow brightened by fusion (solderability and protection in mild atmospheres)	2.5–8	0.1–0.3

Source: Ref 28

Lead is stable in most atmospheres and in both chromic (H_2CrO_4) and sulfuric acid (H_2SO_4) electrolytes. However, it is affected by chlorides. Lead electrodeposits form very inert passive films that tend to reduce the effects of galvanic corrosion.

Copper is not particularly corrosion resistant in the atmosphere, and it tarnishes rapidly. When used alone, it should be protected by an appropriate corrosion inhibitor, such as benzotriazole. On the other hand, copper is often present in coating systems because bright copper is leveling, and its small grain size tends to reduce the porosity and thus improve the corrosion resistance of subsequent coatings.

Gold is often used decoratively and for electrical contact applications. Gold that is plated directly over copper will increase the corrosion rate of the copper through the unavoidable porosity of the gold deposit. Gold will also rapidly diffuse into copper. Therefore, electroplated nickel or cobalt barrier coatings are normally plated underneath the gold coating. For wear applications, alloys with nickel or cobalt are preferred; however, pure gold has a lower contact resistance. Pulse plating will reduce porosity and increase the hardness of electrodeposited gold.

Reference cited in this section

28. L.L. Shreir, Ed., *Corrosion Control,* Vol 2, *Corrosion,* Newnes-Butterworths, 1976

T. Mooney, Electroplated Coatings, *Corrosion: Fundamentals, Testing, and Protection*, Vol 13A, *ASM Handbook*, ASM International, 2003, p 772–785

Electroplated Coatings

Revised by Ted Mooney, Finishing.com, Inc.

Selection of Coatings

Tables 6 and 7 represent current practice in guiding designers and platers to minimum thickness of the two principal classes of protective and decorative/protective coatings used in product finishing: zinc and cadmium coatings and bright nickel-chromium. Specification guides for these coatings are given in Ref 1 and are also contained in Federal and Military Specifications (Ref 6, 29). Frequently cited specifications in these documents are:

Specification	Title
ASTM A 165	"Standard Specification for Electrodeposited Coatings of Cadmium on Steel"
SAE-AMS-QQ-P-416	"Plating, Cadmium Electrodeposited" (Replaces MIL-QQ-P-416, cancelled 28 March 2002)
ASTM B 633	"Standard Specification for Electrodeposited Coatings of Zinc on Iron and Steel"
ASTM B 456	"Standard Specification for Electrodeposited Coatings of Copper plus Nickel plus Chromium and Nickel plus Chromium"
SAE-AMS-QQ-C-320	"Chromium Plating (Electrodeposited)" (Replaces MIL-QQ-C-320, cancelled 3 May 2001)
MIL-A-8625	Anodic Coatings for Aluminum and Aluminum Alloys

International Standards Organization (ISO) standards often govern international transactions involving the buying and selling of plated parts. These standards are available from the American National Standards Institute (ANSI) or from ISO.

Table 6 Recommended minimum thicknesses and typical applications for zinc and cadmium coatings electrodeposited on iron and steel

Service conditions	Coating thickness[(a)]		Chromate finish	Time to white corrosion in salt spray, h	Typical applications
	µm	**mils**			
Electrodeposited zinc					
Mild (indoor atmosphere; minimum wear and abrasion)	5	0.2	None	…	Screws, nuts and bolts, buttons, wire goods, fasteners
			Clear	12–24	
			Iridescent	24–72	
			Olive drab	72–100	
Moderate (mostly dry indoor atmosphere; occasional condensation, wear, and abrasion)	8	0.3	None	…	Tools, zipper pulls, shelves, machine parts
			Clear	12–14	
			Iridescent	24–72	
			Olive drab	72–100	
Severe (exposure to condensation; infrequent wetting by rain; and cleaners)	13	0.5	None	…	Tubular furniture, window screens, window fittings, builders' hardware, military hardware, appliance parts, bicycle parts
			Clear	12–24	
			Iridescent	24–72	
			Olive drab	72–100	
Very severe (exposure to bold atmospheric conditions; frequent	25	1	None	…	Plumbing fixtures, pole line hardware

exposure to moisture, cleaners, and saline solutions; likely damage by abrasion or wear)					
Electrodeposited cadmium					
Mild (see above)	5	0.2	None	…	Springs, lock washers, fasteners, tools, electronic and electrical components
			Clear	12–24	
			Iridescent	24–72	
			Olive drab	72–100	
Moderate (see above)	8	0.3	None	…	Television and radio chassis, threaded parts, screws, bolts, radio parts, instruments
			Clear	12–24	
			Iridescent	24–72	
			Olive drab	72–100	
Severe (see above)	13	0.5	None	…	Appliance parts, military hardware, electronic parts for tropical service
			Clear	12–24	
			Iridescent	24–72	
			Olive drab	72–100	
Very severe (see above)[(b)]	25	1	None	…	…
			Clear	24	
			Iridescent	24–72	
			Olive drab	72–100	

(a) Thickness specified is after chromate conversion coating, if used.

(b) There are some applications for cadmium coatings in this environment; however, these are normally satisfied by hot dipped or sprayed coatings. Source: Ref 12

Table 7 Recommended minimum thicknesses and typical applications for electrodeposited bright nickel-chromium coatings

Service conditions	Classifications[(a)]		Minimum thickness				Typical applications
			Nickel		**Chromium**		
	Nickel	**Chromium**	**µm**	**mils**	**µm**	**mils**	
Steel, iron, or zinc die-cast substrates							
Mild (normally warm, dry, indoor atmospheres; minimum wear or abrasion)	b	4	10	0.4	0.1	0.004	Household appliances, interior auto hardware, hair dryers, fans, inexpensive cooking utensils, coat and luggage racks, standing ashtrays, interior trash receptacles, inexpensive light fixtures
	p	4	10	0.4	0.1	0.004	
	d	4	10	0.4	0.1	0.004	
	b	mc	10	0.4	0.8	0.03	
	p	mc	10	0.4	0.8	0.03	
	d	mc	10	0.4	0.8	0.03	
	b	mp	10	0.4	0.3	0.012	
	p	mp	10	0.4	0.3	0.012	
	d	mp	10	0.4	0.3	0.012	
Moderate (indoor exposure where condensation may occur, as in kitchens or bathrooms)	b	r	20	0.8	0.3	0.012	Steel and iron: stove tops, oven liners, home, office, and school furniture; bar stools, golf club shafts. Zinc alloys; bathroom accessories, cabinet hardware
	p	r	20	0.8	0.3	0.012	
	d	r	20	0.8	0.3	0.12	
	b	mc	15	0.6	0.8	0.03	
	p	mc	15	0.6	0.8	0.03	
	d	mc	15	0.6	0.8	0.03	
	b	mp	15	0.6	0.3	0.012	
	p	mp	15	0.6	0.3	0.012	
	d	mp	15	0.6	0.3	0.012	
Severe (occasional or frequent wetting by rain or dew; possible exposure to cleaners	d	r	30	1.2	0.3	0.012	Patio, porch, and lawn furniture; bicycles; scooters, wagons; hospital furniture; fixtures; cabinets
	d	mc	20	0.8	0.8	0.03	
	d	mp	25	1.0	0.3	0.012	
	p	r	40	1.6	0.3	0.012	

and saline solutions)	p	mc	30	1.2	0.8	0.03	
	p	mp	30	1.2	0.3	0.012	
Very severe (damage from wear or abrasion likely in addition to corrosive media)	d	r	40	1.6	0.3	0.012	Auto bumpers, grilles, hubcaps, and lower body trim; light housings
	d	mc	30	1.2	0.8	0.03	
	d	mp	30	1.2	0.3	0.012	
Copper and copper alloy substrates							
Mild (see above)	b	r	5	0.2	0.13	0.005	Household appliances, oven doors and liners, interior auto hardware, trim for major appliances, receptacles, light fixtures
	p	r	5	0.2	0.13	0.005	
	d	r	5	0.2	0.13	0.005	
	b	mc	5	0.2	0.8	0.03	
	p	mc	5	0.2	0.8	0.03	
	d	mc	5	0.2	0.8	0.03	
	b	mp	5	0.2	0.25	0.01	
	p	mp	5	0.2	0.25	0.01	
	d	mp	5	0.2	0.25	0.01	
Moderate (see above)	b	r	15	0.6	0.25	0.01	Plumbing fixtures, bathroom accessories, hinges, light fixtures, flashlights, and spotlights
	p	r	15	0.6	0.25	0.01	
	d	r	15	0.6	0.25	0.01	
	b	mc	10	0.4	0.8	0.03	
	p	mc	10	0.4	0.8	0.03	
	d	mc	10	0.4	0.8	0.03	
	b	mp	10	0.4	0.25	0.01	
	p	mp	10	0.4	0.25	0.01	
	d	mp	10	0.4	0.25	0.01	
Severe (see above)	d	r	25	1.0	0.25	0.01	Patio, porch, and lawn furniture; light fixtures; bicycle parts; hospital and laboratory fixtures
	d	mc	20	0.8	0.8	0.03	
	d	mp	20	0.8	0.3	0.012	
	p	r	25	1.0	0.3	0.012	
	p	mc	20	0.8	0.8	0.03	
	p	mp	20	0.8	0.25	0.01	
	d	r	30	1.2	0.25	0.01	
	d	mc	25	1.0	0.8	0.03	
	d	mp	25	1.0	0.25	0.01	
Very severe (see above)	d	r	30	1.2	0.25	0.01	Boat fittings, auto trim, hubcaps, lower body trim
	d	mc	25	1.0	0.8	0.03	
	d	mp	25	1.0	0.25	0.01	

(a) Nickel classifications: b, fully bright; p, dull or semibright; d, double-layer or triple-layer nickel coating, with the bottom layer containing less than 0.005% S and the top layer more than 0.04% S. If there are three layers, the middle layer should contain more sulfur than the top layer. Chromium classifications: r, regular (conventional) chromium; mc, microcracked chromium having more than 750 cracks/in.; mp, microporous chromium containing a minimum of 64,500 pores/in.^{2} that are visible to the unaided eye. Source: Ref 12

Nickel-Chromium Coatings. Because of their importance in the automotive industry, nickel-chromium (with or without a copper underlayer) coatings have been subjected to many changes and exhaustive testing over a long span of years. Results of extensive field experience and testing of variations dating from the days of buffed nickel coatings (1870 to 1924) are reported in Ref 30. Figure 8 shows a history of the development and use of nickel-chromium coatings. Significant developments in this history were the determination that the basic corrosion resistance of these systems is controlled by the thickness and composition of the nickel layer, the invention of the leveling copper and nickel plating processes, the development of semibright and bright nickel plating, the emergence of crackfree and microcracked chromium, and the evolution of duplex and triplex (multilayer) nickel-chromium systems.

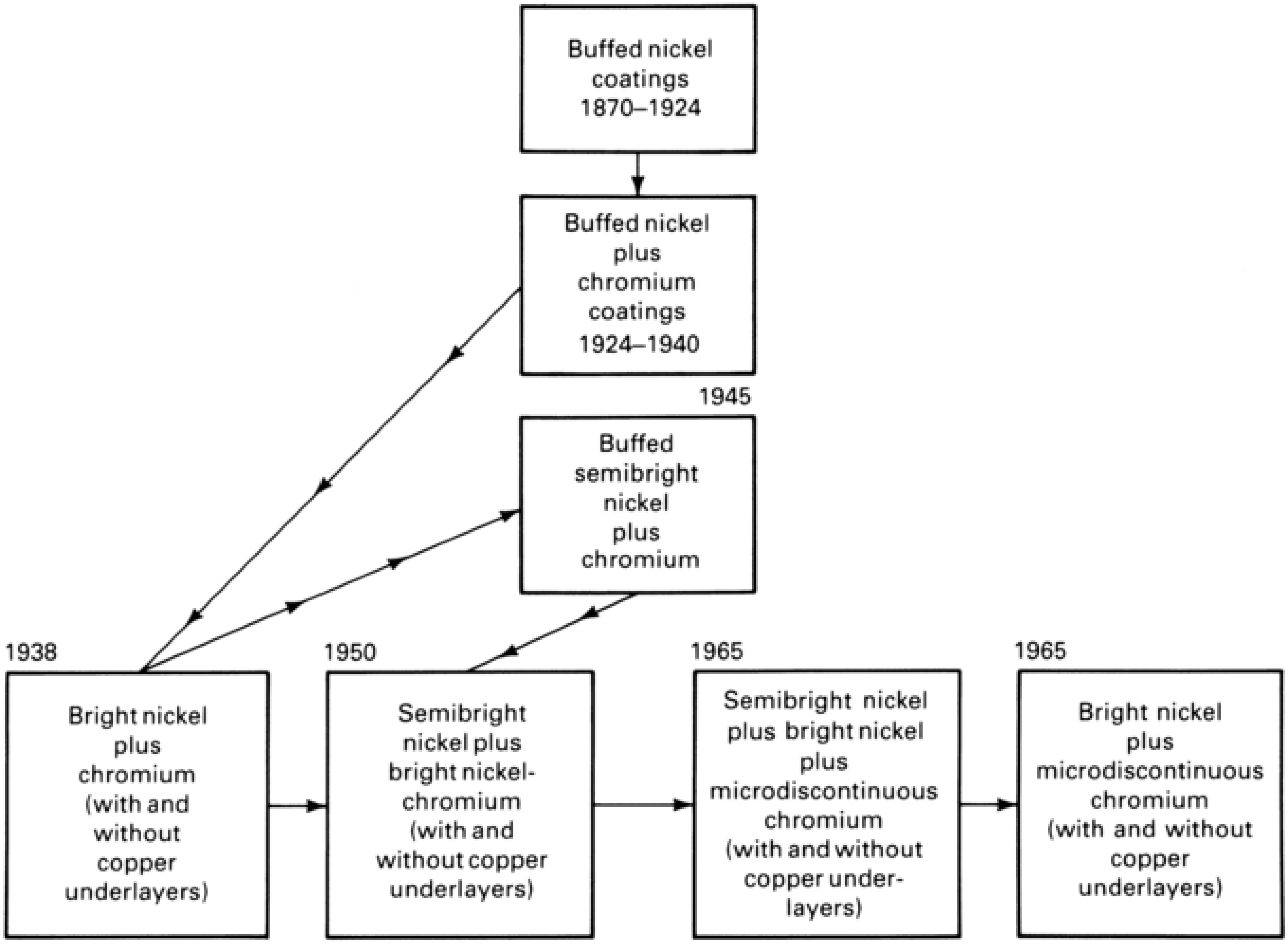

Fig. 8 History of the development of nickel and nickel-chromium coatings showing time of introduction and periods of use. Source: Ref 30

Reference 30 also discusses the application of these coatings on steel, zinc, plastics, and aluminum. In these systems, the chromium layer is very thin—of the order of only 0.25 μm (0.01 mils). However, the corrosion resistance of chromium plate depends not so much on its thickness as on its physical state. Crackfree, or nonporous, chromium is excellent, but does not remain crackfree in service. A small number of cracks are detrimental, but the presence of many fine microcracks may be beneficial (Ref 2). Microcracked chromium deposits cause the galvanic- corrosion action to be spread over a very wide area and therefore do not suffer from localized corrosion. Microcracked chromium, in combination with duplex or triplex nickel, is the most durable of these coatings. The results of marine exposure for 36 months on variations of these coatings on steel are shown in Fig. 9. Figure 10 shows results of a similar program for Ni-Cr and Cu-Ni-Cr coatings on zinc.

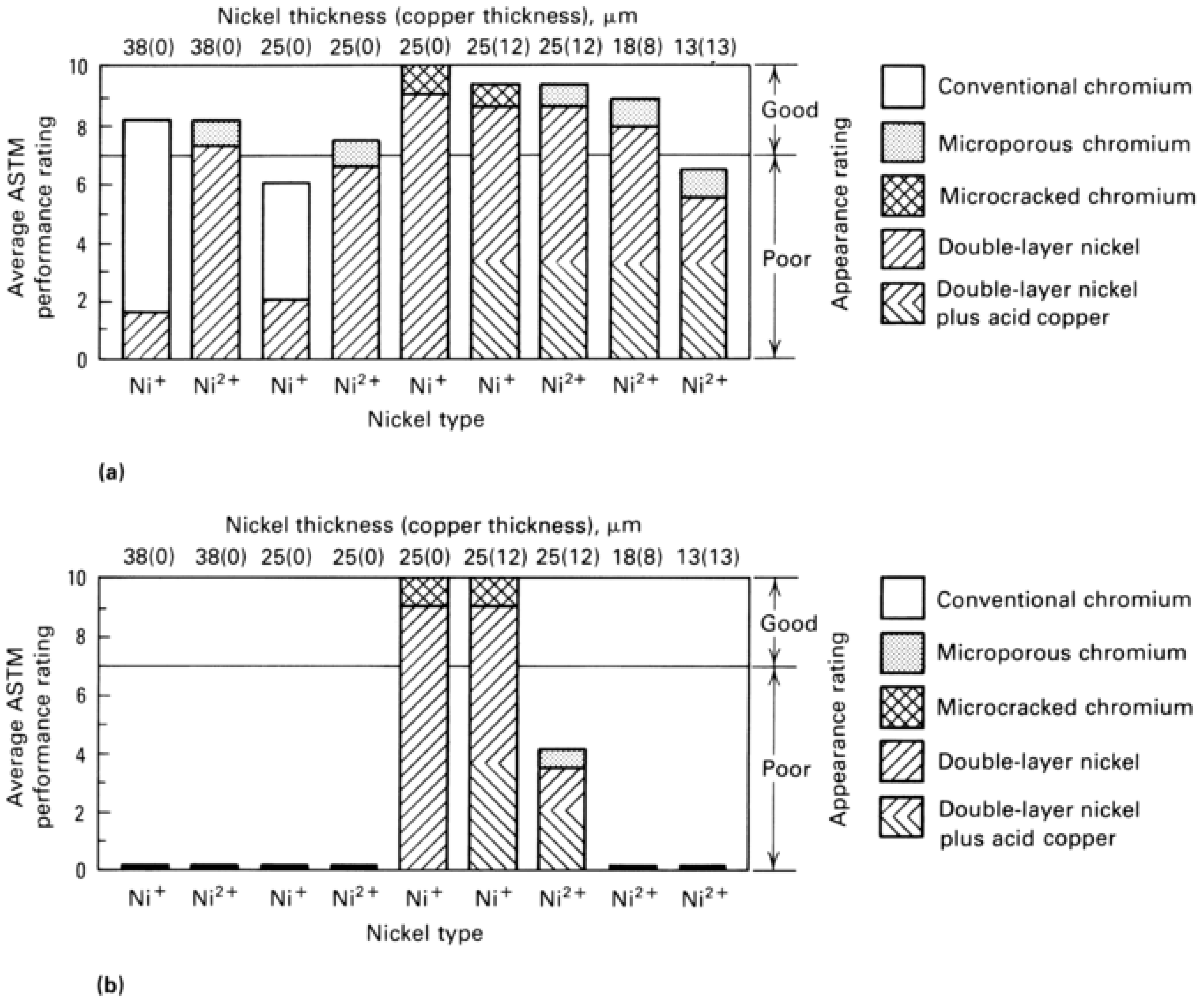

Fig. 9 Performance in a marine atmosphere of various types of nickel-chromium and copper-nickel-chromium coatings on flat (a) and contoured (b) steel panels. ASTM performance rating: 10, best; 0, worst. Test duration: 36 months. Source: Ref 30

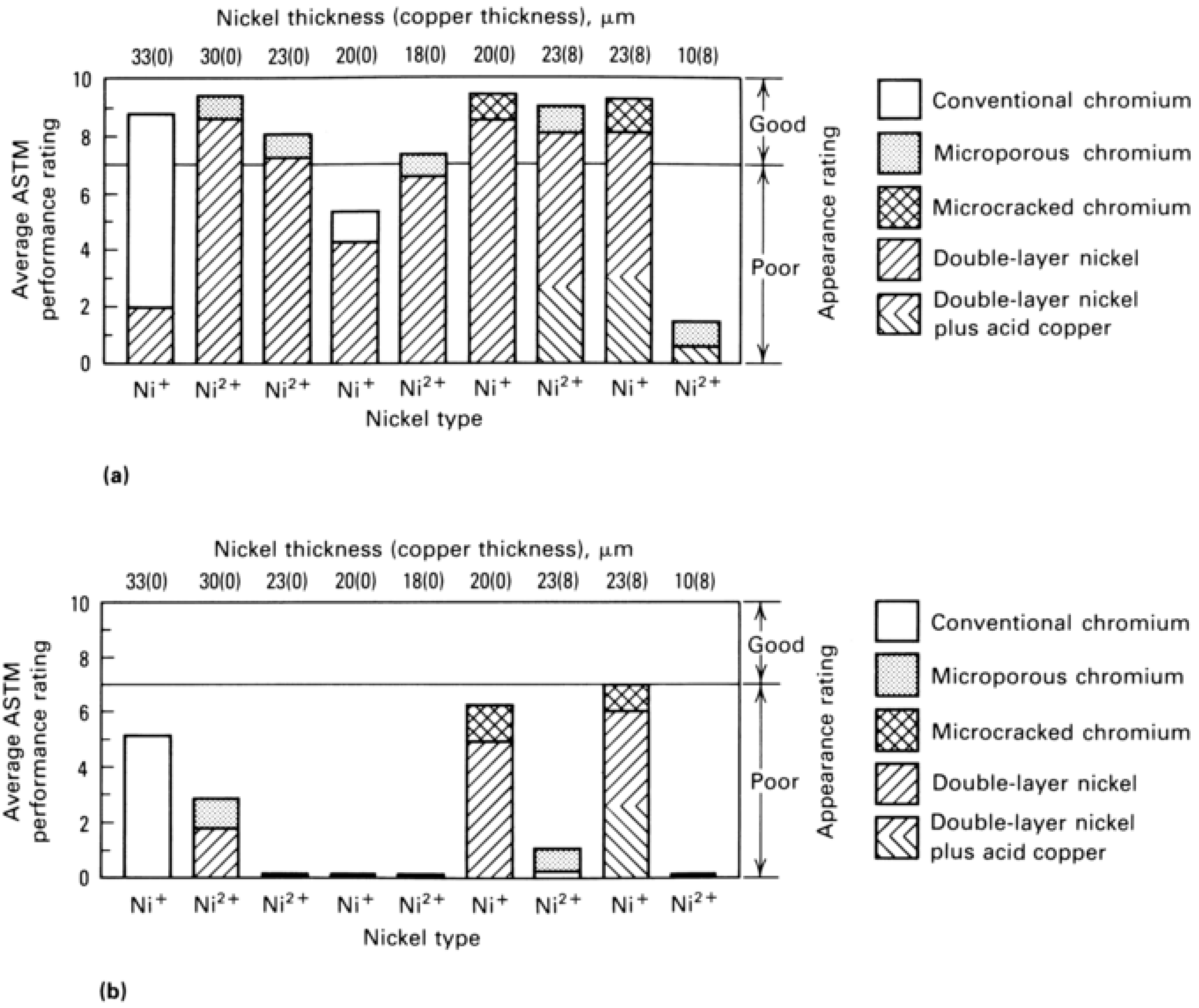

Fig. 10 Performance in a marine atmosphere of various types of nickel-chromium and copper-nickel-chromium coatings on flat (a) and contoured (b) zinc panels. ASTM performance rating: 10, best; 0 worst. Test duration: 36 months. Source: Ref 30

References cited in this section

1. "Standard Definitions of Terms Relating to Electroplating," B 374, *Annual Book of ASTM Standards,* American Society for Testing and Materials

2. C.L. Faust, "Electroplating," Course 22, Metals Engineering Institute, American Society for Metals, 1983

6. M. Murphy, Ed., *Metal Finishing Guidebook & Directory,* Elsevier Science, 2001

12. *Quality Metal Finishing Guide,* Metal Finishing Suppliers' Association

29. *Department of Defense Index of Specifications and Standards (DoDISS),* United States Navy, Naval Publications and Forms Center

30. G.A. DiBari, Decorative Electrodeposited Nickel-Chromium Coatings, *Met. Finish.,* Vol 75 (No. 6, 7), June–July 1977

T. Mooney, Electroplated Coatings, *Corrosion: Fundamentals, Testing, and Protection*, Vol 13A*, ASM Handbook*, ASM International, 2003, p 772–785

Electroplated Coatings

Revised by Ted Mooney, Finishing.com, Inc.

Plating of Mill Products

A trend toward applying tin and zinc coatings by electrodeposition to sheet and strip in tandem with continuous pickling and cold-rolling lines developed just before and during World War II. Much earlier, processes were developed in Germany and the United States to electrogalvanize wire. Advantages claimed over hot dip galvanizing were control of thickness, the fact that the substrate is not affected by heat, and that the ductility and formability of the substrate is not limited by the iron-zinc intermetallic compound layer formed on hot dip galvanized steel. In hot dip galvanizing, the edges, especially of strip steel, tend to destroy wipes. Therefore, special care is required to secure a uniform smooth coating (Ref 31).

Electrolytic tinning was commercially introduced in 1927 (Ref 31). Before that time, all of the tinplate on the market was manufactured by hot dip processes. Again, because of the amenability of electrodeposition to close thickness control and the development of highly efficient pretreating and plating processes, electrotinning has captured practically all of the food packing business. Various electrolytic processes have been used for producing tinplate, including the acid processes—sulfate, fluoborate, phenolsulfonic, and halide (fluoride-chloride)—and the alkaline sodium stannate bath.

In addition to electrogalvanizing and electrotinning, continuous plating or cold-rolled sheet and strip is performed by integrated steel mills as well as specially continuous strip producers and coil coaters. The specialty houses continuously plate nickel on steel for the battery (mostly alkaline dry cell) industry. They also plate alloy coatings such as nickel-zinc for protective/decorative uses and copper- and copper alloy-plated steel for postfabrication of decorative items. Copper-nickel-chromium on nonferrous metals and wide-strip steel is also available. Reference 32 lists typical examples of decorative/protective applications of continuously plated Cu-Ni-Cr plated steel strip. Among these are various components for household appliances, dispensers, handles, lamps, cover plates for switches and outlet boxes, and furniture trim. Functional applications for copper-plated strip include flashlight shells and alligator clips for jumper cables. Nickel-plated strip is used in battery cans and caps and for paintbrush ferrules. There are few companies in the continuous strip plating field because of the high initial investment required and the specialized knowledge needed to operate this process successfully.

Coil coaters, the name given to manufacturers of prepainted sheet and strip (mostly steel and aluminum substrates), apply thin zinc coatings plus chemical conversion coatings before applying organic coatings. Products of this segment of the industry are used in postforming operations.

Excellent control of plating conditions and the absence of complex substrate geometries provide a high degree of uniformity in coatings on preplated strip. This is reflected in predictable corrosion resistance because uniform thickness leads to uniform corrosion resistance.

Chromium plating has also penetrated the tin mill product field in such applications as food can ends. Thin coatings of tin and chromium act as a base for can varnishes and lacquers and for pigmented outer coatings. On the interior of cans, tin or chromium coatings are claimed to prevent filiform corrosion under the clear organic coatings—an insidious type of underfilm corrosion characteristic of clear and sparsely pigmented organic coatings. Information on equipment and processing is available in Ref 4, 31, and 33; Ref 33 also discusses corrosion of tinplate.

Immersion Plating. Immersion, or chemical, deposition has a long history of limited industrial use—for example, tin immersion deposits on mill wire products (called liquor finishing), immersion nickel plating of steel before porcelain enameling and many types of ceramic coatings, and the immersion copper plating of wire to be used in inert-gas shielded arc welding. In the last application mentioned, pure copper and copper- tin (gold-colored) coatings have both been used as aids to wet drawing of the wire to finished size and to furnish a highly conductive surface in the welding gun. Both tin and copper have been used in wire mills for the wire used for such products as paper clips and staples. According to the corrosion theory, these coatings, which are

much more noble than the substrate, would be expected to hasten corrosion of the substrate. However, this is not the case, probably because the porosity is so widely distributed that whatever current is available for corrosion is so spread out as to be ineffective. This is similar to the effect of microdiscontinuous chromium (MDC).

References cited in this section

4. L.J. Durney, Ed., *Electroplating Engineering Handbook,* 4th ed., Van Nostrand Reinhold, 1984

31. H.E. McGannon, Ed., *The Making, Shaping and Treating of Steel,* United States Steel Company, 1964

32. H. Wettwer, Continuous Plating of Copper, Nickel and Chromium on Wide Steel Strip, *Plat. Surf. Finish.,* Vol 61 (No. 5), May 1974

33. C.H. Mathewson, *Zinc,* ACS Monograph Series, Reinhold, 1959

T. Mooney, Electroplated Coatings, *Corrosion: Fundamentals, Testing, and Protection,* Vol 13A*, ASM Handbook,* ASM International, 2003, p 772–785

Electroplated Coatings

Revised by Ted Mooney, Finishing.com, Inc.

Electrochemical Predictions of Corrosion Performance

Accelerated tests used for the prediction of corrosion performance for a particular application of a coating system have a certain risk associated with them. It is very difficult to design a test environment to simulate the actual environment, but there is often no alternative. A number of accelerated electrochemical tests are given in Ref 34, 35, 36, 37.

Sample Preparation. The preparation of the sample to be tested requires a great deal of care for a number of reasons. On an actual part, the geometry is rarely designed so that the current density is uniform over the entire part. Because such coating properties as grain size and porosity are critically affected by local current density, the ability of a coating to protect the part would be expected to vary from one point on the part to another. When conducting accelerated tests on flat samples (usually required by the tests listed in Ref 34, 35, 36, 37), the current density used to apply the coating(s) must be typical of that used on the real part. Equally important, the surface finish of the specimen substrate should be comparable to that of the actual substrate. The above tests usually require that the surface finish be produced by wet grinding on 600-grit SiC paper. Electrodeposited coatings are sometimes used without additional surface finishing. Grinding and electropolishing will certainly affect test results.

Test Selection. Very high localized currents can exist during these tests and may result in rapid removal of the coating. The desired information is usually the corrosion current i_{corr}, which can be correlated with actual weight loss. The polarization resistance measurement (Ref 34) is probably the safest of the tests for this determination. The suitability of the test should be determined by correlating actual performance with test results whenever possible. Crevice corrosion under the gaskets used in the tests may affect results and should be considered.

References cited in this section

34. “Standard Practice for Conducting Potentiodynamic Polarization Measurements,” G 59, *Annual Book of ASTM Standards,* American Society for Testing and Materials

35. “Standard Practice for Conducting Cyclic Potentiodynamic Polarization Measurements for Localized Corrosion,” G 61, *Annual Book of ASTM Standards,* American Society for Testing and Materials

36. “Practice for Standard Reference Method for Making Potentiostatic and Potentiodynamic Anodic Polarization Measurement,” G 5, *Annual Book of ASTM Standards,* American Society for Testing and Materials

37. “Standard Recommended Practice for Conventions Applicable to Electrochemical Measurements in Corrosion Testing,” G 3, *Annual Book of ASTM Standards*, American Society for Testing and Materials

---

T. Mooney, Electroplated Coatings, *Corrosion: Fundamentals, Testing, and Protection*, Vol 13A, *ASM Handbook*, ASM International, 2003, p 772–785

Electroplated Coatings

Revised by Ted Mooney, Finishing.com, Inc.

Future Trends

Due to the pressure to get cadmium out of the environment, and the fact that simple zinc plating is not a satisfactory substitute in many instances, the application of such alloys as tin-zinc, zinc-cobalt, zinc-iron, and zinc-nickel is growing rapidly. Aluminum coatings, whether applied by proprietary electroplating processes or other methods, are additional cadmium substitutes. The desire to remove nickel plating from jewelry and other applications where it can cause sensitivity reactions is fueling the development of alloy replacements. Chromium plating, while not considered a threat to the environment in its metallic form, does pose a threat to health and the environment during its application. Add the potential chromium plating has for hydrogen embrittlement, and substitutes such as cobalt plating, HVOF coatings, and TiN coatings applied by PVD are making inroads into some of its former strongholds. The hexavalent chromate coatings traditionally used to forestall white rust on aluminum, cadmium, and zinc have effectively been banned from automotive use. While trivalent chromate conversion coatings are the usual replacement, when this substitute is not adequate for specific applications, the aluminum or zinc plating may be foregone and electroless nickel plating used instead.

The continuing miniaturization of the electronics world is impelling changes both toward and away from electroplating. Zinc plating has been found to cause troublesome zinc whiskers that foul computer cleanrooms and to which hot dip galvanizing is not vulnerable. While not strictly a corrosion-resistant application, copper electroplating is replacing aluminizing in electronic circuits and is the technology of choice for micro electro mechanical systems (MEMS) fabrications. Nickel electroplating/electroforming continues to grow stronger with society's ever-increasing reliance on miniature precision optics and electronics.

T. Mooney, Electroplated Coatings, *Corrosion: Fundamentals, Testing, and Protection*, Vol 13A, *ASM Handbook*, ASM International, 2003, p 772–785

Electroplated Coatings

Revised by Ted Mooney, Finishing.com, Inc.

Acknowledgment

This article has been adapted from the article by J. Mazia and D. Lashmore, Electroplated Coatings, *Corrosion*, Vol 13, *ASM Handbook* (formerly 9th ed., *Metals Handbook*), ASM International, 1987, p. 419–431.

T. Mooney, Electroplated Coatings, *Corrosion: Fundamentals, Testing, and Protection,* Vol 13A, *ASM Handbook,* ASM International, 2003, p 772–785

Electroplated Coatings

Revised by Ted Mooney, Finishing.com, Inc.

References

1. "Standard Definitions of Terms Relating to Electroplating," B 374, *Annual Book of ASTM Standards,* American Society for Testing and Materials
2. C.L. Faust, "Electroplating," Course 22, Metals Engineering Institute, American Society for Metals, 1983
3. F.A. Lowenheim, Ed., *Modern Electroplating,* 3rd ed., John Wiley & Sons, 1974
4. L.J. Durney, Ed., *Electroplating Engineering Handbook,* 4th ed., Van Nostrand Reinhold, 1984
5. F.A. Lowenheim, *Electroplating,* McGraw- Hill, 1978
6. M. Murphy, Ed., *Metal Finishing Guidebook & Directory,* Elsevier Science, 2001
7. R.S. Treseder, Ed., *The NACE Corrosion Engineer's Reference Book,* National Association of Corrosion Engineers, 1980
8. G.T. Beilby, The Hard and Soft States in Metals, *J. Inst. of Met.,* No. 2, 1912, p 149–185
9. R.G. Baker, "Corrosion of Electrodeposited Coatings," Slide Lecture 46, American Electroplaters and Surface Finishers Society, 1981
10. "Standard Practice for Design of Articles to be Electroplated on Racks with Nickel," B 507, *Annual Book of ASTM Standards,* American Society for Testing and Materials
11. J. Hyner, Design for Plating, *Electroplating Engineering Handbook,* L.J. Durney, Ed., Van Nostrand Reinhold, 1984, p 50
12. *Quality Metal Finishing Guide,* Metal Finishing Suppliers' Association
13. "Standard Specification for Electrodeposited Coatings of Copper Plus Nickel Plus Chromium and Nickel Plus Chromium," B 456, *Annual Book of ASTM Standards,* American Society for Testing and Materials
14. S. Wernick and R. Pinner, *The Surface Treatment and Finishing of Aluminum and Its Alloys,* Robert Draper, 1972
15. "Method for Mechanical Hydrogen Embrittlement Testing of Plating Processes and Aircraft Maintenance Chemicals," F 519, *Annual Book of ASTM Standards,* American Society for Testing and Materials

16. “Standard Method of Salt Spray (Fog) Testing,” B 117, *Annual Book of ASTM Standards,* American Society for Testing and Materials

17. “Thickness of Metallic and Inorganic Coatings,” B 659, *Annual Book of ASTM Standards,* American Society for Testing and Materials

18. “Standard Specification for Electroplated Engineering Nickel Coatings,” B 689, *Annual Book of ASTM Standards,* American Society for Testing and Materials

19. “Standard Specification for Electrodeposited Coatings of Tin-Nickel Alloy,” B 605, *Annual Book of ASTM Standards,* American Society for Testing and Materials

20. “Standard Test Methods for Porosity in Gold Coatings in Metal Substrates,” B 583, *Annual Book of ASTM Standards,* American Society for Testing and Materials

21. “Standard Specification for Electrodeposited Coatings of Tin,” B 545, *Annual Book of ASTM Standards,* American Society for Testing and Materials

22. “Standard Test Methods for Adhesion of Metallic Coatings,” B 571, *Annual Book of ASTM Standards,* American Society for Testing and Materials

23. “Standard Recommended Practice for Rating of Electroplated Panels Subjected to Atmospheric Exposure,” B 537, *Annual Book of ASTM Standards,* American Society for Testing and Materials

24. “Standard Method of Testing FACT (Ford Anodized Aluminum Corrosion Test),” B 538, *Annual Book of ASTM Standards,* American Society for Testing and Materials

25. “Standard Methods for Corrosion Testing of Decorative Chromium Electroplating by the Corrodkote Procedure,” B 380, *Annual Book of ASTM Standards,* American Society for Testing and Materials

26. “Standard Method for Copper-Accelerated Acetic Acid-Salt Spray (Fog) Testing (CASS Test),” B 368, *Annual Book of ASTM Standards,* American Society for Testing and Materials

27. “Standard Method of Acetic Acid-Salt Spray (Fog) Testing,” B 287, *Annual Book of ASTM Standards,* American Society for Testing and Materials

28. L.L. Shreir, Ed., *Corrosion Control,* Vol 2, *Corrosion,* Newnes-Butterworths, 1976

29. *Department of Defense Index of Specifications and Standards (DoDISS),* United States Navy, Naval Publications and Forms Center

30. G.A. DiBari, Decorative Electrodeposited Nickel-Chromium Coatings, *Met. Finish.,* Vol 75 (No. 6, 7), June–July 1977

31. H.E. McGannon, Ed., *The Making, Shaping and Treating of Steel,* United States Steel Company, 1964

32. H. Wettwer, Continuous Plating of Copper, Nickel and Chromium on Wide Steel Strip, *Plat. Surf. Finish.,* Vol 61 (No. 5), May 1974

33. C.H. Mathewson, *Zinc,* ACS Monograph Series, Reinhold, 1959

34. “Standard Practice for Conducting Potentiodynamic Polarization Measurements,” G 59, *Annual Book of ASTM Standards,* American Society for Testing and Materials

35. “Standard Practice for Conducting Cyclic Potentiodynamic Polarization Measurements for Localized Corrosion,” G 61, *Annual Book of ASTM Standards,* American Society for Testing and Materials

36. “Practice for Standard Reference Method for Making Potentiostatic and Potentiodynamic Anodic Polarization Measurement,” G 5, *Annual Book of ASTM Standards,* American Society for Testing and Materials

37. “Standard Recommended Practice for Conventions Applicable to Electrochemical Measurements in Corrosion Testing,” G 3, *Annual Book of ASTM Standards*, American Society for Testing and Materials

---

T. Mooney, Electroplated Coatings, *Corrosion: Fundamentals, Testing, and Protection,* Vol 13A*, ASM Handbook*, ASM International, 2003, p 772–785

Electroplated Coatings

Revised by Ted Mooney, Finishing.com, Inc.

Selected References

- A. Brenner, *Electrodeposition of Alloys: Principle and Practice,* Academic Press, 1963
- W. Canning, *The Canning Handbook on Plating,* 23rd ed., E. & F.N. Spon Ltd., 1982
- J.K. Dennis and T.E. Such, *Nickel and Chromium Plating,* ASM International, 1994
- A. Holmes, *Rapid Spot Testing of Metals, Alloys and Coatings,* Metal Finishing Information Services, 2002
- J.B. Kusner and A.S. Kushner, *Water and Waste Control for the Plating Shop,* 2nd ed., Gardner Publications, 1981
- F.J. LaManna, Electroplating Course Manual/ Basic Practical Electroplating, American Electroplaters and Surface Finishers Society, 1986
- G.O. Mallory and J.B. Hajdu, *Electroless Plating: Fundamentals and Applications,* Noyes Publications, 1990
- E.A. Ollard, *Installation and Maintenance in Electroplating Shops,* Robert Draper Ltd., 1967
- M. Rubinstein, *Electrochemical Metallizing: Principles and Practice,* Van Nostrand Reinhold, 1987
- W.H. Safranek, *The Properties of Electrodeposited Metals and Alloys,* 2nd ed., American Electroplaters and Surface Finishers Society, 1986

R. Leonard, Continuous Hot Dip Coatings, *Corrosion: Fundamentals, Testing, and Protection*, Vol 13A, *ASM Handbook*, ASM International, 2003, p 786–793

Continuous Hot Dip Coatings

Ralph W. Leonard, Coated Steels Technology, LLC

Introduction

HOT-DIP COATING is a process that primarily refers to the application of a low melting point metal as a coating on steel wherein the material to be coated is immersed into a molten bath of the coating metal. Hot-dip coating may involve the coating of steel sheet, strip, or wire, or it may involve the application of a coating onto forms such as pipe and structural shapes. The coating of steel sheet is defined as *continuous* hot-dip coating while the coating of piping, structural shapes, and discrete parts such as nails, screws, bolts, and nuts is called batch coating. Batch galvanizing was, in fact, done many years before the continuous coating process was developed. The earliest record of the use of zinc to protect steel dates back to 1836 (Ref 1). In batch galvanizing, the steel is fabricated into a finished part, cleaned to remove residual oils, pickled to remove oxides from the surface, and then dipped into molten zinc to apply the coating. As a result of long experience, the excellent protection that a zinc coating provides to steel was well known long before the continuous galvanizing process was developed more than 50 years ago. See the article "Batch Process Hot Dip Galvanizing" also in this Section.

By far, the most common continuous hot-dip coated product is galvanized steel sheet. Galvanized sheet has a coating that is essentially zinc metal. Its companion product, galvannealed sheet, is produced in a similar way except that the coating of zinc, while molten, is alloyed via a diffusion process with iron from the steel sheet. The resultant coating has approximately 9 to 10% iron. Since steel sheet is the most commonly manufactured hot-dip coated product today, most of the ensuing discussion focuses on steel sheet issues, but much of the information would apply to hot-dip coated steel wire as well.

The *continuous hot-dip process* is called "continuous" simply because the product intended to be coated, steel sheet for example, is passed in a continuous manner into a bath of the molten coating metal. As applied to steel sheet, the leading end of one coil of steel is welded onto the trailing end of the coil ahead of it in the processing line. With the use of an accumulator, which stores up to perhaps 1000 ft or more of sheet ahead of the central part of the processing line, these coil ends can be joined without stopping the central processing section. As a result, the sheet being processed through the coating bath never stops; the process is truly "continuous."

The primary reason that the hot-dip process is restricted to the application of low melting point metals is that the product to be coated (steel sheet) needs to have some amount of tensile strength as it is pulled through the coating line. Low carbon steel sheet, the most common hot- dip coated product, cannot be heated to temperatures much above 870 °C (1600 °F) without literally tearing apart as it is being transported through a large processing line. Thus, the coating metal has to have a lower melting point than 870 °C (1600 °F). Today, the highest melting point metal being applied to steel sheet is aluminum, which has a melting temperature of 660 °C (1220 °F).

Since the continuous sheet-coating process was developed over 50 years ago for the application of zinc (*galvanizing*) onto steel sheet, the process has been employed for the application of other metallic coatings including aluminum and several aluminum/zinc alloys. Each of these coating types has special attributes that make them more suitable than galvanized sheet for specific types of applications. These coatings and their specific attributes will be discussed in the subsequent sections.

Reference cited in this section

1. "Hot-Dip Galvanizing for Corrosion Protection, A Specifier's Guide," American Galvanizers Association

R. Leonard, Continuous Hot Dip Coatings, *Corrosion: Fundamentals, Testing, and Protection*, Vol 13A, *ASM Handbook*, ASM International, 2003, p 786–793

Continuous Hot Dip Coatings

Ralph W. Leonard, Coated Steels Technology, LLC

Basic Principles

Steel sheet is passed as a continuous ribbon through a bath of molten metal at speeds up to approximately 200 m/min (650 ft/min). A simplified schematic drawing of the strip as it is passed through the coating bath is shown in Fig. 1. One of the requirements of the process is that, while in the molten metal bath, the steel strip must react with the molten metal to form an intermetallic bond (often referred to as the *alloy layer*) across the entire surface of the steel sheet. This bond is present as a thin distinct region between the coating metal and the steel sheet. It is necessary for two reasons. One is that without the intermetallic-alloy layer the coating would *dewet* from the steel when the sheet exits the coating bath, and this would lead to either uncoated areas (voids) or a very nonuniform coating thickness. A uniform coating thickness is very important to achieve good corrosion resistance. Second, without the alloy layer, the coating would not adhere to the sheet when it is subsequently formed into a shaped part.

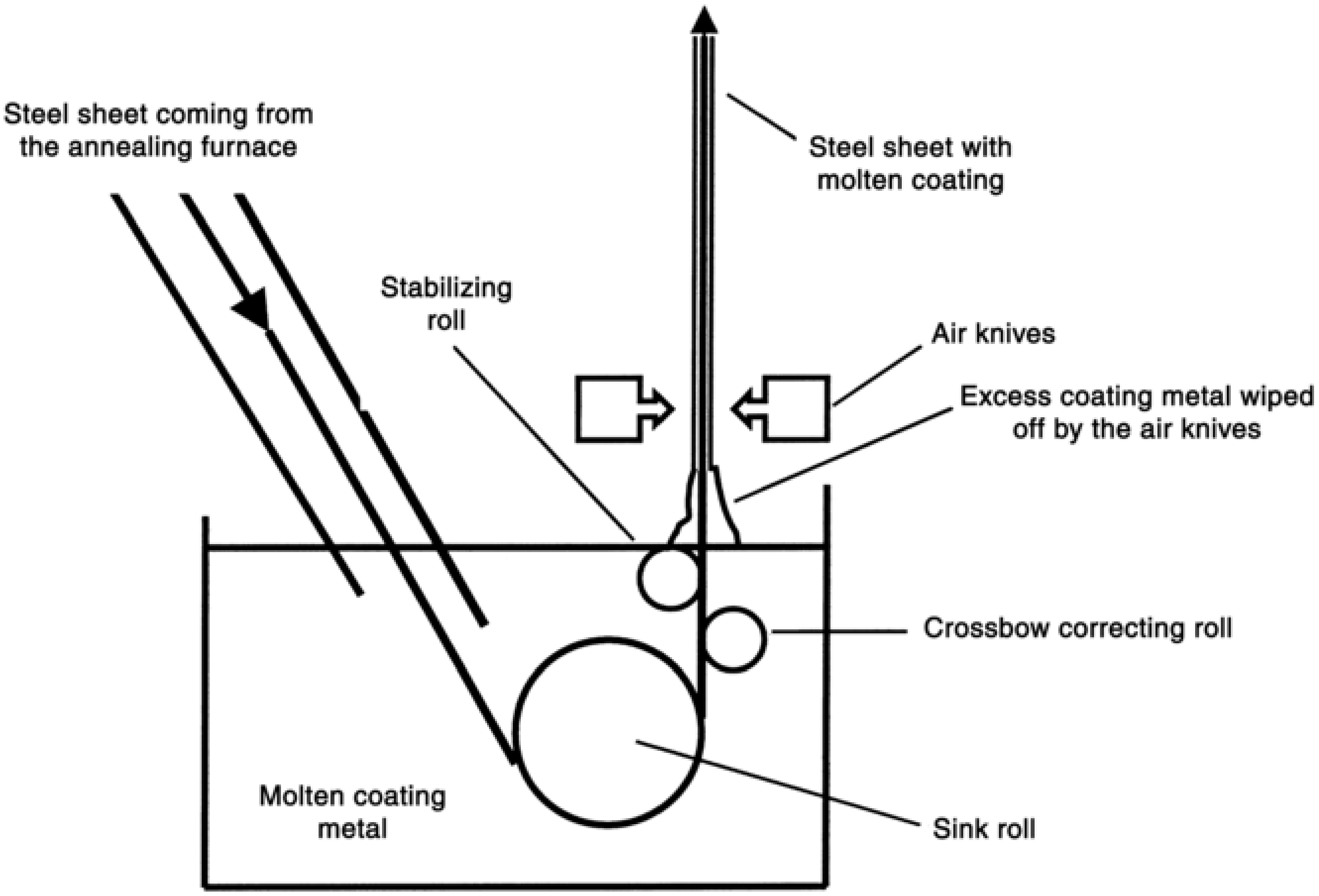

Fig. 1 Basic arrangement of the coating bath in a continuous hot-dip coating operation

Wetting is the term describing the interfacial tension between a solid and a liquid. Here, *dewetting* is used to define the absence of the diffusion reaction between the steel surface and the molten coating metal. It is very important that this reaction take place across the entire surface area of the steel sheet.

The intermetallic-bond layer has several important features. The inherent nature of the alloy layer formed on all hot-dip coated products, whether the coating is zinc, aluminum or one of the aluminum/zinc alloys, is that it is composed of one or more intermetallic compounds. These can be zinc-iron, aluminum-iron, or aluminum- zinc-iron compounds. By its nature, the bond layer is hard and brittle. For galvanized sheet, the alloy layer is

approximately ten times harder than the zinc coating outer layer. Thus, in order to be able to form the sheet without loss of coating adhesion, the alloy bond thickness must be kept as thin as possible.

As the strip emerges from the molten bath at high speeds, it drags out excess metal, much like when an object is pulled rapidly from a container of water. The amount of excess metal depends on the speed at which the sheet is moving, the viscosity of the coating metal, and a number of other variables such as the surface roughness of the sheet, the presence of oxides on the surface of the bath metal, and the temperature of the bath metal. Through the use of an air-wiping process, a controlled amount (thickness) of molten coating, usually expressed as weight of coating per unit area, is allowed to remain on the strip surface. The molten coating is cooled, and then, following several other processing steps that may be used to modify the surface roughness, flatten the steel, and apply a rust-inhibitive surface treatment, the steel is recoiled at the exit end of the processing facility.

No matter which type of coating metal is applied, the common features of hot-dip coated sheet products are shown schematically in Fig. 2. There is an outer coating layer that has essentially the same composition as the bath metal. This is followed by the intermetallic bond layer, a layer that forms by diffusion between the coating bath and the steel substrate. Beneath the alloy layer is the steel substrate.

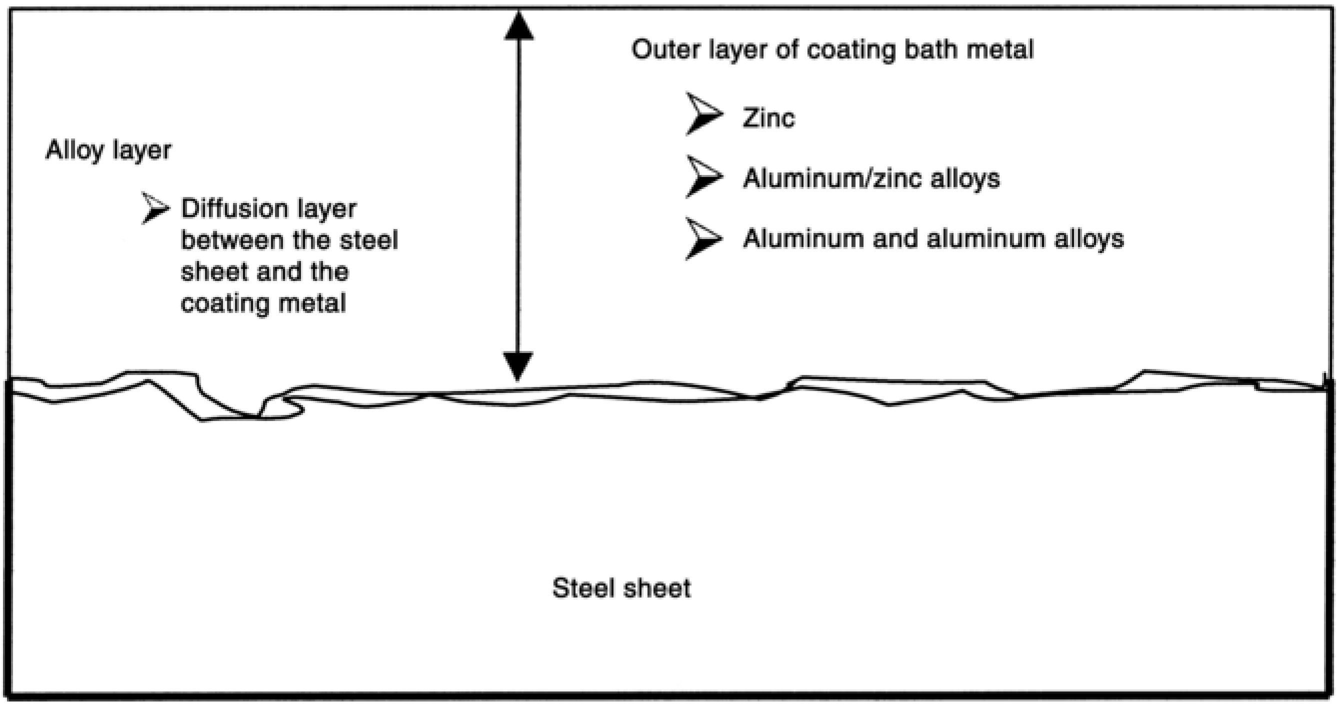

Fig. 2 Schematic drawing of the cross section of a hot-dip coated sheet product showing the three features of all hot-dip coated sheet products—the outer coating layer, the intermetallic alloy bond zone, and the steel sheet substrate

Process Details. Most commonly, the hot-dip process for steel sheet involves the following sequential steps:

1. An entry-end welder joins the trailing edge of one coil to the leading edge of the succeeding coil to allow the process to be truly continuous.
2. An alkaline cleaning section removes the rolling oils, dirt, and iron fines (surface contaminants from the cold reduction process) that are on the sheet surface.
3. An annealing furnace heats the steel to high temperatures to impart the desired mechanical properties (strength and formability) to the steel sheet.
4. A bath of molten metal contains the metal being applied to the steel surface.
5. A cooling section cools the strip and solidifies the coating as it emerges from the coating bath.
6. A temper mill imparts the desired surface finish to the coated steel.
7. A tension leveler flattens the strip to meet the end-use requirements.
8. A treatment section applies a clear, water- base treatment to the coating to prevent storage stains that can form on the coating surface when moisture is present (as condensation and/or water infiltration originating from improper shipping or storage).
9. An oiling section is used most often to apply a rust-inhibitive oil. At times, it can be used also to apply a forming oil.

10. A recoiler rewinds the finished coil of steel.

At this point, the finished coil of coated steel has:

- The desired steel strength and formability
- An adherent, uniformly thick, corrosion resistant coating
- The desired surface finish and sheet flatness
- A clear chemical treatment and/or oil to help maintain the bright metallic finish that is a characteristic of hot-dip coated sheet products

Not all hot-dip coating lines include all the previously listed processing steps. For example, some do not include the aqueous cleaning stage, relying instead on flame cleaning in the entry end of the annealing furnace. Others might not have a temper mill; temper rolling is not necessary and perhaps not desired for some applications of hot-dip coated products. Also, there is a type of hot-dip coating process commonly called flux galvanizing that relies on using fluxes to apply a uniform and continuous coating. The final product is very similar to that obtained using the process described earlier, especially with respect to corrosion resistance. This process is not used much today, and it is used only for making galvanized sheet. None of the other aluminum or aluminum/zinc alloy coatings are applied using the flux process. Some references to the flux- coating process refer to it as the *cold process* in contrast with the term *hot process* used to define the lines that have in-line annealing furnaces. By far, the number of hot lines exceeds the number of cold lines. In North America, only several flux lines are operating as of 2003.

Benefits of Coating Steel. It is well known that low-carbon steels are susceptible to corrosion when exposed to moisture. Not only is the corrosion aesthetically undesirable in most applications, but the corrosion rate can reduce the design life of the component. It is not unusual for steels to corrode at a rate of several mils of thickness per year (Ref 2). Not only does the surface take on the reddish color of iron oxide, but also, over time, the steel may lose a significant amount of its thickness, with a corresponding loss in mechanical properties.

Steels can be painted to reduce the rate of corrosion and to make the product more attractive in appearance. However, the presence of paint alone does not ensure that steel is fully protected from corrosion. This is especially true at sheared edges or at scratches in the paint where rusting of the steel can cause paint blistering and continuing disbondment between the paint and the steel sheet (Fig. 3). Often, more protection is needed to reduce the corrosion rate of steel so that the aesthetic requirements are met and the strength and integrity of the steel sheet are not lost.

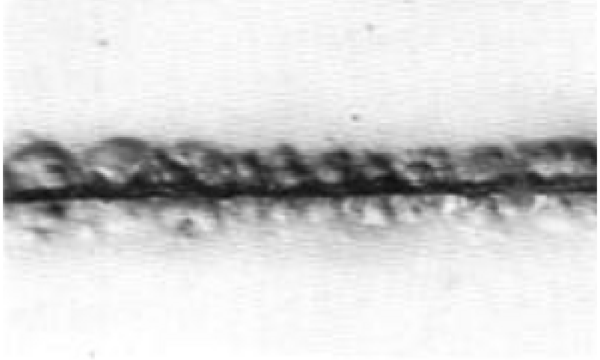

Fig. 3 Paint blistering and red rust staining at a scratch in painted cold-rolled sheet

Reference cited in this section

2. X.G. Zhang, *Corrosion and Electrochemistry of Zinc,* Plenum Press, 1996

R. Leonard, Continuous Hot Dip Coatings, *Corrosion: Fundamentals, Testing, and Protection*, Vol 13A, *ASM Handbook*, ASM International, 2003, p 786–793

Continuous Hot Dip Coatings

Ralph W. Leonard, Coated Steels Technology, LLC

Hot-Dip Coatings

The six principal types of coatings currently being applied by the hot-dip process are:

- Galvanized (zinc or zinc with aluminum added)
- Galvannealed (zinc with 8 to 10% Fe)
- 55Al-Zn coating
- 95Zn-Al coating
- Aluminized with pure aluminum
- Aluminized with aluminum plus silicon

Additionally, a product called terne-coated sheet is produced. Terne-coated sheet has a coating of lead plus 3 to 15% tin. Years ago, terne- coated sheet was the primary product used to manufacture fuel tanks. Also, it was used for roofing applications. Today, these markets are quite small.

Each of these coatings except the galvannealed sheet are produced using a specific coating- bath composition. Galvannealed sheet is not produced from a zinc and iron coating-bath composition. Instead, the coating bath is the same as that used to make galvanized sheet except that the aluminum level in the coating bath is reduced from approximately 0.17 to 0.20% to 0.14% or less. The iron is derived from the substrate. The 95Zn-Al coating may contain either a small addition of mischmetal (a combination of rare earth elements) or magnesium.

Galvanized Sheet. It was discovered more than 200 years ago that zinc, in intimate contact with steel, will protect the steel. This protection takes place by two mechanisms; one is simple barrier protection wherein the zinc simply prevents contact between the steel and the environment of moisture and oxygen. The second is *galvanic* protection that protects steel even at exposed areas such as sheared edges of a sheet or scratches in the coating. In order to galvanically protect steel, a metallic coating such as zinc has to be electrochemically more active than the steel in the specific environment where the product is being used. Fortunately, zinc is indeed more chemically active than steel in almost all environments. In the chemical reaction that takes place when galvanic protection occurs, zinc becomes the anode of a corrosion cell and protects the steel from corroding by making the steel the cathode. Reference 2 contains a very detailed description of the fundamentals of the corrosion and electrochemistry of zinc.

Galvanic protection can be accomplished whether the zinc is attached to the steel with a wire or is in intimate contact. Since corrosion is an electrochemical reaction, the zinc and steel need to be *attached* in a fashion that allows free electron flow between the steel and zinc. One of the classic examples of the galvanic protection obtained with the use of zinc is the protection of steel ship hulls from corrosion in sea water by selective placement of zinc anodes around the outside of a ship.

When zinc is applied over the entire surface of a steel as in the hot-dip galvanizing process, the steel is fully protected from corrosion by the presence of the zinc coating. The intimate bond that occurs between the steel and the coating metal offers complete electrical contact so that free flow of electrons necessary for galvanic protection can occur.

One needs to keep in mind that, as the zinc is protecting steel on a galvanized product, it undergoes corrosion. That is, the zinc itself corrodes and is consumed over time. The benefit afforded to steel is that, in most environments, zinc corrodes at a significantly lower rate than steel. Thus, a thin zinc coating can provide long-term protection to steel.

The reason that zinc normally corrodes at a much lower rate than steel is that the products of corrosion that form on the surface of the zinc develop a protective, somewhat passive film. When steel corrodes in the environment, the iron oxide that forms as a result of the corrosion reaction is not usually retained on the surface

of the steel as a protective, passive film. Typically, it spalls off and continually exposes a fresh steel surface to the air and moisture. The protective, passive film that forms on zinc in most atmospheres is a zinc carbonate film (Ref 3). This carbonate film forms by a reaction between the zinc corrosion products (zinc hydroxide and zinc oxide) with carbon dioxide in air. This carbonate film is often stable and remains as a protective covering over the zinc coating.

Typically, the zinc carbonate film does not completely protect the zinc from further corrosion; it simply slows down the corrosion reaction. The zinc surface exposed to the atmosphere is not completely passivated, so corrosion of the zinc can continue. This phenomenon is actually needed to continue to provide galvanic protection to steel. If the passive film were complete and corrosion of the zinc stopped completely, the galvanic protection to steel at exposed edges and scratches would be lost. Zinc carbonate films can be broken down (dissolved) by reaction with moisture in the environment, especially acid rain. Thus, even though zinc corrodes at a much lower rate than low carbon steel, it does corrode in most atmospheres, and the net result is that the zinc is eventually consumed.

The actual rate of corrosion is highly dependent on the type of exposure. References 2 and 4 contain extensive information on the corrosion rates for zinc in many different types of environments. Table 1 (Ref 5) contains a summary of the relative corrosion rates for steel versus zinc in various types of atmospheric environments. These data provide general guidance only; more detailed information for specific environments is contained in Ref 2 and 4.

Table 1 Typical corrosion rates for zinc and steel

Environment classification	Corrosion rate			
	Zinc		**Steel**	
	µm/yr	**mil/yr**	**µm/yr**	**mil/yr**
Mild	<1	<0.04	<10	<0.4
Moderate	<2	<0.08	10–20	0.4–0.8
Tropical	<2	<0.08	20–50	0.8–2.0
Industrial	2–4	0.08–0.16	20–50	0.8–2.0
Marine	2–4	0.08–0.16	20–80	0.8–3.1
Severe marine	4–>10	0.16–0.4	80–200	3.1–7.9

Source: Ref 4

Within these general environmental-classification types, there can still be substantial differences in the rates of corrosion for a galvanized coating. Table 2, for example, contains data for the corrosion performance of galvanized product in various marine environments. There are considerable differences in corrosion rate depending on whether the samples are close to the ocean or somewhat further away. Then, too, the corrosion rate is very dependent on whether the samples are exposed directly to rainfall or are placed in a sheltered location (exposed to the atmosphere but sheltered from direct rainfall). It is important to apply general corrosion-rate data cautiously, as the rate can be very dependent on some very specific issues at any given exposure site.

Table 2 Variation in corrosion rates in marine environments

Location	Exposure[(a)]	Zinc corrosion rate	
		µm/year	**mils/yr**
Severe marine	Open	6.2	0.244
	Sheltered	15.2	0.598
Moderate marine	Open	1.9	0.0748
	Sheltered	3.9	0.154
Mild marine	Open	1.0	0.039
	Sheltered	0.9	0.035

(a) Open and sheltered refer to the samples either directly exposed to the environment (open) or sheltered from direct rainfall to simulate a location such as under an eave. Source: Ref 6

In soils, the corrosion rate of galvanized coatings can also be quite variable. It can vary from very aggressive corrosion to very low corrosion rates. Table 3 contains data showing the extent of variability in the corrosion rate of galvanized sheet in different types of soil.

Table 3 Corrosion of galvanized steel in various soils

Coating weight: 300 g/m^2 (1 oz/ft^2)

Soil description	Soil corrosivity	Coating life, years
Poor drainage, low resistivity	High	1–2
Poor drainage, high salt content	Moderate	4–6
Good drainage, high resistivity, low salt content	Low	18–25

Source: Ref 7

Because galvanized coatings protect steel by undergoing bulk corrosion of the coating layer, it is important to define the coating weight (thickness) when using galvanized sheet for a specific application. The life of the product before the onset of steel rusting is very dependent on the coating thickness. If the environment to which the product will be exposed is mild, light coating weights might suffice to meet the desired life expectancy. However, if the application is harsh, a heavy coating weight should be specified. Since the rate of corrosion for the galvanized coating is approximately linear in most environments, as shown in Fig. 4, one can readily predict the benefit of using a thicker coating in any specific environment type. Table 4 contains the coating weight categories that are commonly produced on current production lines. Detailed information about the coating weight requirements is contained in ASTM A 653 (Ref 8). As noted in this table, there are practical limits to the coating thickness. On the low end, it is difficult to achieve better air-knife wiping for producing coatings less than G30 (as defined in Table 4), while at the high end, it is difficult to achieve a sufficiently uniform coating thickness across the entire sheet surface as excessive sags can develop in the coating layer before it solidifies.

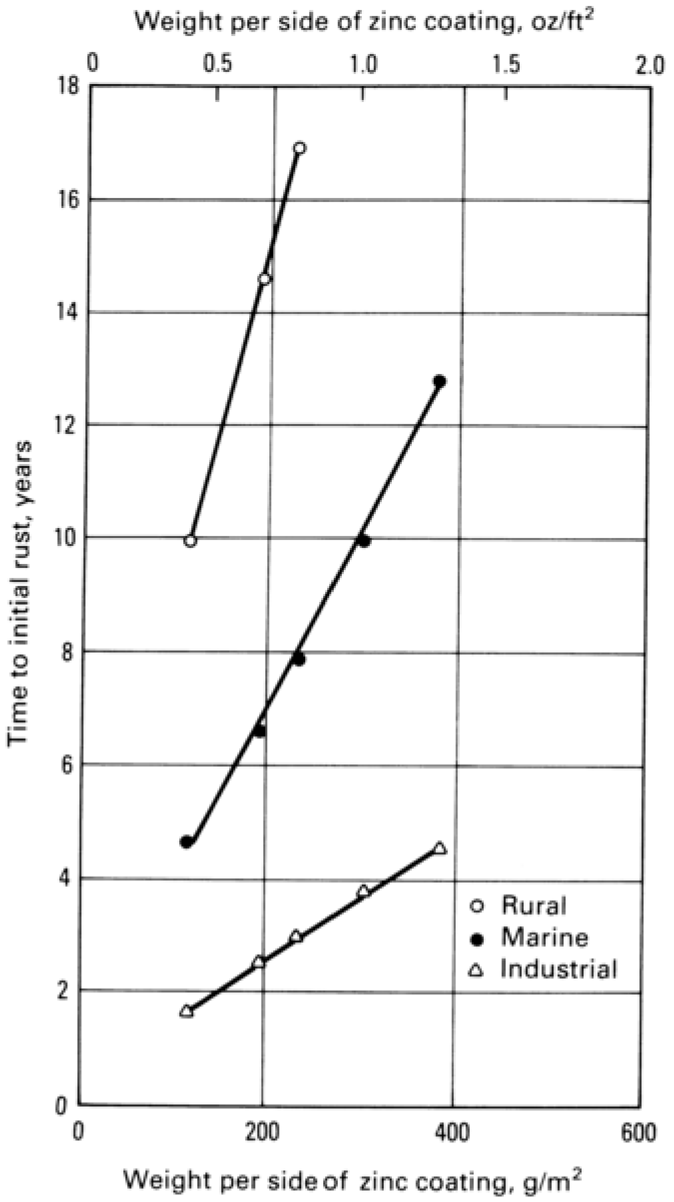

Fig. 4 Corrosion of galvanized steel in rural (State College, PA), marine (Sandy Hook, NJ), and industrial (Pittsburgh, PA) atmospheres. Source: Ref 8

Table 4 Common coating weight categories for hot-dip galvanized sheet products

Coating designation (U.S. customary units)	Minimum coating weight[(a)], oz/ft^2	Approximate coating thickness each side	
		µm	**mils**
G210	2.10	46	1.8
G185	1.85	41	1.6
G140	1.40	31	1.2
G115	1.15	25	0.98
G90	0.90	20	0.76
G60	0.60	13	0.51
G30	0.30	7	0.25
Coating designation (metric units)	Minimum coating weight[(a)], g/m^2	Approximate coating thickness each side	
		µm	**mils**
Z600	600	44	1.7
Z500	500	36	1.4
Z450	450	33	1.25

Z350	350	25	0.97
Z275	275	20	0.76
Z180	180	13	0.50
Z90	90	7	0.25

(a) Minimum coating weight, total both sides of the sheet, triple-spot average. Refer to ASTM A 653/A 653M for additional requirements pertaining to the single spot and per side requirements. Source: Ref 9

Aluminum Addition to the Galvanizing Bath. Hot-dip galvanized coatings typically contain between 0.16 and 0.25% aluminum. The aluminum is not added to influence the corrosion resistance of the coating but to enhance the development of a thin alloy-layer bond zone between the steel and zinc coating layer. In principle, the only function of the aluminum is to restrict the growth rate of the intermetallic compound(s) that form(s) as the steel and zinc diffuse into one another during the coating process. When the process is properly controlled, the alloy layer is almost indistinguishable (Fig. 5). Thus, the addition of aluminum is very important to the process, but there has not been any evidence to show that its addition influences the corrosion resistance of the galvanized coating.

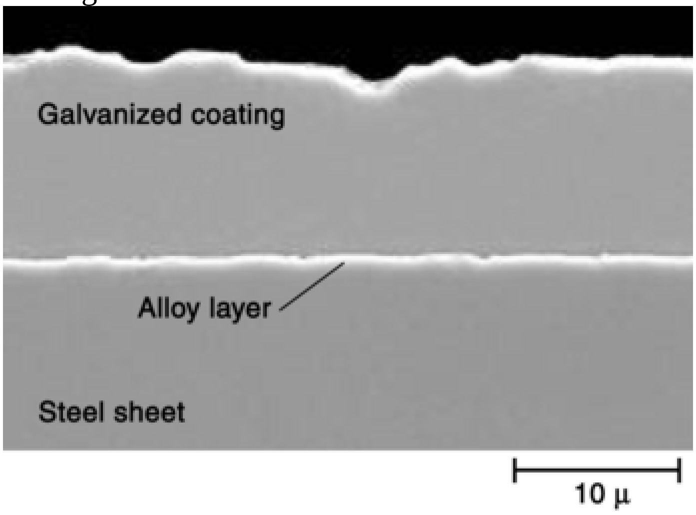

Fig. 5 Microstructure of continuously galvanized sheet product. Note the thin, almost indistinguishable alloy bond layer.

Influence of Spangle Cracking. When hot-dip galvanized coatings are bent or drawn, the coating often develops cracks that are visible to the unaided eye. The coating can be thought of as a thin casting in that the zinc is applied from the molten state and the final structure of the coating is large grained. The coating is prone to intergranular cracking or intragranular cleavage cracking. These large grains, or spangles, typically exhibit the large, dendritic structure of an as-solidified metal as shown in Fig. 6. Although today the coating metal usually contains fewer impurities such as lead and the spangle pattern is, thus, often less distinct than on product made years ago, the as-solidified grain size is still much larger than that of a cold-worked and annealed metal. This large-grained structure combined with the hexagonal crystal structure of zinc tends to make the coating sensitive to both intergranular grain-boundary cracking and intragranular cleavage during bending and other forming operations (Ref 10). However, this behavior generally has little impact on the life of the coating in that the life of a galvanized coating is mostly dependent on the quantity of zinc on the surface of the steel. The galvanic nature of the zinc protects the underlying steel, and the onset of steel corrosion does not occur until the coating is essentially completely consumed in any given area of the surface.

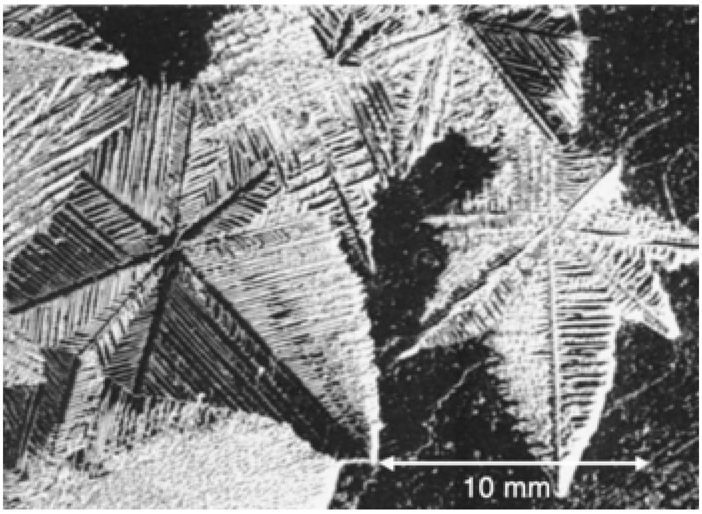

Fig. 6 Enlarged view of the dendritic structure within the spangles of a hot-dip galvanized coating.

Humid Storage Corrosion. Perhaps one of the least considered issues related to the performance of galvanized steel sheet is the issue of humid-storage stain. *Humid-storage stain* refers to the corrosion of the galvanized coating if it gets wet during shipment or storage in coil form or stacked sheets. Wetting occurs either by ingress of moisture or by condensation, and the galvanized coating will not dry when moisture gets between the wraps of a coil or the sheets. Zinc is a chemically active metal in the presence of moisture, and its corrosion resistance depends on the formation of adhering oxide/carbonate films. The stable, adhering oxide/carbonate passive film never forms, and a relatively high rate of zinc corrosion occurs. Typically, the corrosion product is zinc hydroxide, a white-colored compound; hence, “white rust” is visible.
The common ways to minimize the occurrence of humid-storage stain include the following:

- Applying an invisible inorganic corrosion-inhibiting compound to the sheet surfaces during production
- Applying a rust-inhibitive oil to the surfaces of the sheet during production
- Storing the product under temperature- and humidity-controlled conditions
- Packaging carefully for shipment

The application of surface treatments to prevent storage stain are not foolproof. Galvanized products have to be produced, stored, and transported properly for storage stain to be prevented.
Other Metallic Coating Types. The most common metallic coating for corrosion protection of steel is a zinc (galvanized) coating. As described in the previous section, it offers a very good combination of galvanic and barrier protection. However, through the years, other types of hot-dip coatings have been developed to target specific improvements in one or more features related to corrosion protection. An aluminized coating applied by the continuous hot-dip process was developed during the 1950s. It was claimed to offer better barrier corrosion protection than a galvanized coating for applications where the product is exposed to the atmosphere and better resistance to corrosion at elevated temperatures. Over time, these attributes of aluminum-coated steel sheet have proven to be correct, but the lack of offering galvanic protection at sheared edges in most environments has prevented aluminized steel from displacing galvanized sheet for many applications.
Since galvanized coatings on steel sheet were used commercially a long time before any other commercial product came into the marketplace, it is usual to compare all the other types of metallic coatings on steel sheet with reference to their performance versus a galvanized coating.
Galvannealed Coatings. Galvannealed coatings are made by heating the molten coating and steel sheet after the sheet emerges from the coating bath. The sheet is heated to approximately 480 to 565 °C (900 to 1050 °F) for approximately 10 s. During this time, the zinc becomes completely alloyed with the iron from the steel. The result is a coating layer that contains layers of zinc/iron intermetallic compounds. The stages of development of the galvannealed coating structure that occur during the heating cycle are shown in Fig. 7. As one might expect from a diffusion reaction of this nature, the outermost layer (often the δ-zinc/iron phase and, at times, the ζ-phase) contains the least amount of iron while the innermost layer (usually a very thin γ- phase) contains the highest percentage of iron. This coating is characterized by its high hardness and brittle nature.

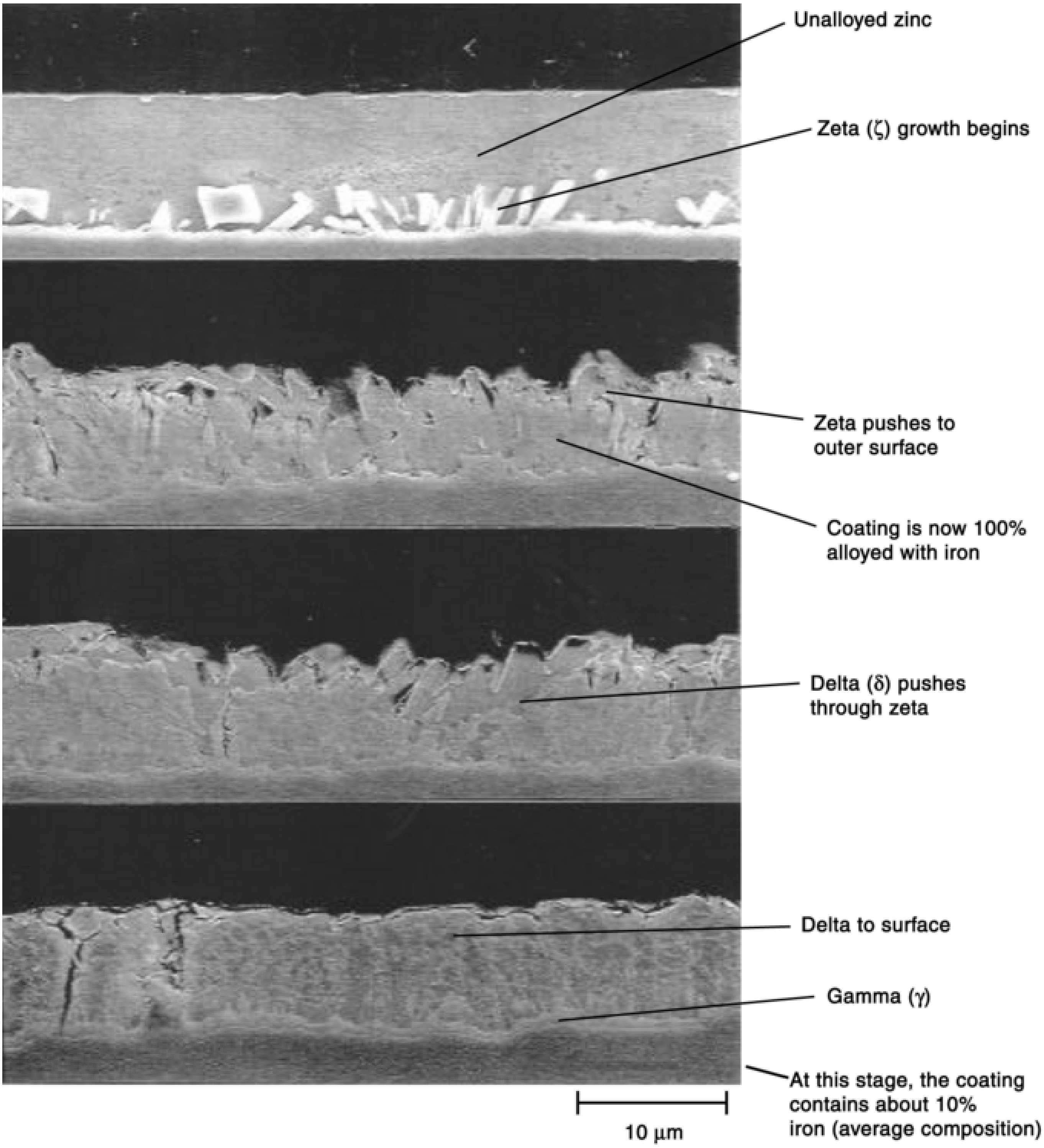

Fig. 7 Stages in the development of a galvannealed coating structure

When galvannealed sheet is formed, the usual reaction is for the coating to undergo some amount of *powdering.* Powdering of the galvannealed coating is simply the breakup of the coating into very small, hard, sandlike particles. It is a form of coating delamination. The key to successful product use is to limit the amount of powdering to an acceptably low level. Excessive powdering obviously can lead to more rapid local corrosion failure in that excessive powdering removes much of the metallic coating, leaving behind an area of uncoated steel. The key manufacturing steps required to achieve acceptably low levels of powdering have been thoroughly investigated during the past ten years. For detailed information on this topic, one should refer to many papers contained in the seven *Proceedings of the International Conference on Zinc and Zinc Alloy Coated Steel Sheet.* These conferences have been held every two years since 1989, and they contain a number of papers on the topic of galvannealed coatings, their production, and their use.

The key characteristics of galvannealed coatings versus regular galvanized coatings that make them useful for some applications are decreased galvanic activity and ease of painting and achieving good paint adhesion.

For most applications, galvannealed sheet is intended to be painted prior to being placed in service. Thus, any discussion on the corrosion behavior needs to take into consideration the corrosion performance under a paint coating. Failure of painted steel sheet often takes place as excessive paint blistering and bulk loss of coating metal from beneath the paint. This is especially true at edges that have been sheared or at scratches in the paint, typically areas where failure occurs first.

The inclusion of up to 10% iron in the coating causes the electrochemical potential difference between steel and the coating to be considerably less than the potential between relatively pure zinc coatings on galvanized sheet and steel. This decreased electrochemical potential difference typically leads to a decrease in corrosion rate for a galvannealed coating. The galvannealed coating is still galvanically protective to steel; thus, the steel is still protected at exposed areas. But since the coating is less reactive, the rate of undercutting corrosion beneath the paint at an area adjacent to a scratch is lessened. This translates to less visible paint blistering and loss of paint adhesion along a scratch, stone chip, or sheared edge.

One has to keep in mind that galvannealed coatings are usually thinner than galvanized coatings. The most commonly produced coating weights are given in Table 5. The use of thinner galvannealed coatings is possible primarily because galvannealed coatings are intended to be painted. If left unpainted, the coating will often develop a light red stain when it is exposed to the environment due to the presence of iron in the coating. The additional barrier protection offered by the paint allows the use of a thinner metallic coating. The synergistic behavior of the combined paint plus metallic coating offers excellent corrosion resistance.

Table 5 Common coating weight categories for hot-dip galvannealed sheet products

Coating designation (U.S. customary units)	Minimum coating weight(a), oz/ft^2	Approximate coating thickness each side	
		µm	**mils**
A60	0.60	13	0.51
A40	0.40	9	0.34
A25	0.25	5	0.21
Coating designation (metric units)	Minimum coating weight(a), g/m^2	Approximate coating thickness each side	
		µm	**mils**
ZF180	180	13	0.50
ZF120	120	9	0.33
ZF75	75	5	0.21

(a) Minimum coating weight, total both sides of the sheet, triple-spot average. Refer to ASTM A 653/A 653M for additional requirements pertaining to the single spot and per side requirements. Source: Ref 9

55Al-Zn Coatings. The 55Al-Zn coating composition is more precisely 55% aluminum, 43.5% zinc and 1.5% silicon. The silicon concentration may vary slightly from one manufacturer to another, but its primary purpose is to minimize the growth of the alloy layer, and thus enhance the adhesion of the coating during forming. It does not improve the corrosion performance.

This product has been made commercially since the 1970s. Its main attribute is that the coating offers improved long-term corrosion resistance in many applications compared with galvanized coatings. Low-slope roofing is an example where the benefits of improved corrosion resistance are important. Typically, low-slope roofing products are used unpainted and are exposed to the elements. In this application, the 55Al-Zn coating has shown to last more than 20 years and in some instances more than 30 years without failure (Ref 11).

The microstructure of the 55Al-Zn coating is shown in Fig. 8. The coating has a two-phase microstructure. This is best explained by reference to the aluminum/zinc phase diagram. One phase is the primary aluminum-rich dendritic phase that begins to grow initially during solidification. The other is an interdendritic zinc-rich region that forms when the zinc concentration in the solidifying liquid reaches a high level. This microstructure, aluminum-rich dendrites plus a network of zinc-rich interdendritic areas, is important to obtain the desired corrosion resistance (Ref 12). Thus, control of the cooling rate during the solidification stage is an important aspect of the production of 55Al-Zn-coated steel sheet. Other phases in the microstructure of the coating layer include particles of silicon, which are typically present as small discrete particles of elemental silicon, and an iron-rich phase which results because the coating bath becomes saturated with iron during the production process.

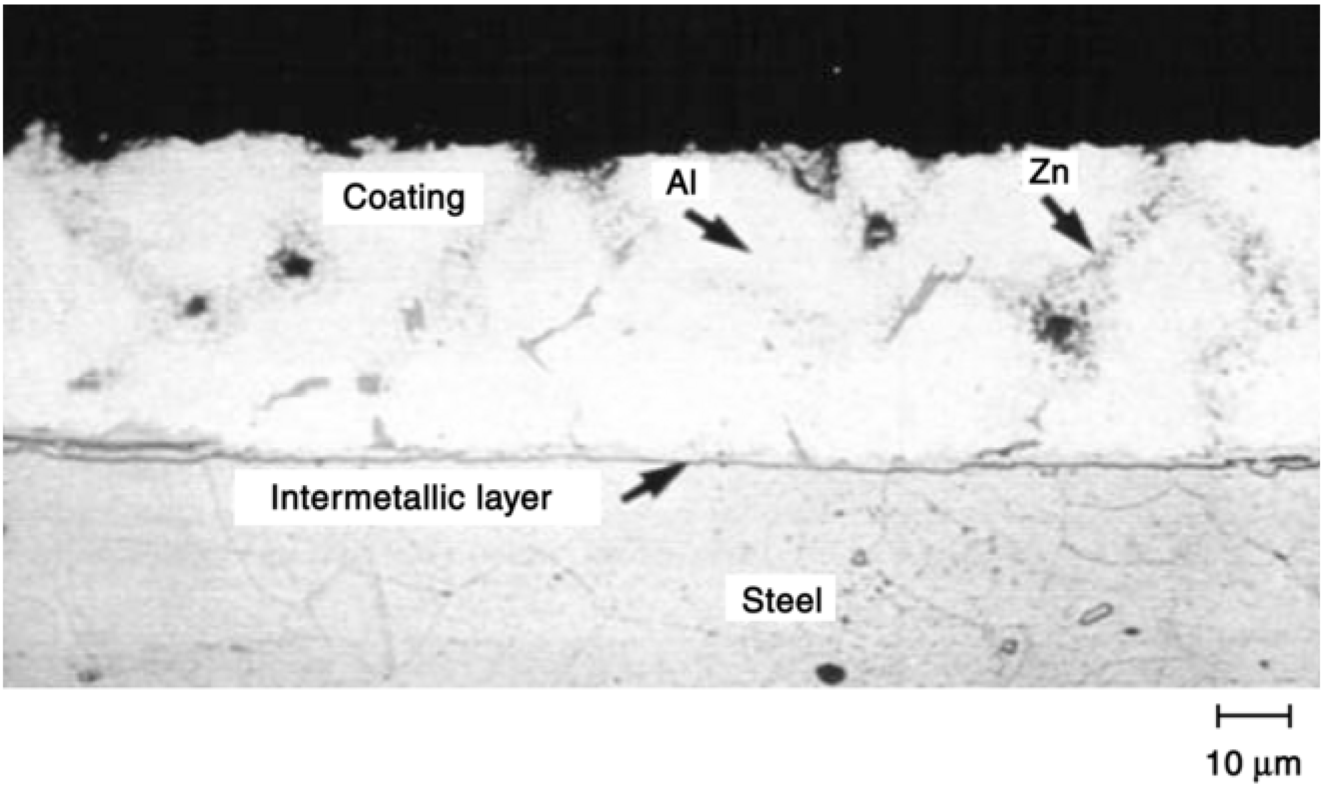

Fig. 8 Microstructure of 55Al-Zn coated sheet. Note the interdendritic zinc-rich areas.

Table 6 contains corrosion performance data comparing the performance of 55Al-Zn with galvanized coatings. The data indicate that the performance is superior versus galvanized in all three types of environments, marine, industrial and rural. The unique dendritic structure of the coating is given as the primary reason for the improved corrosion resistance. When the coating is exposed to the environment, the zinc-rich areas are corroded first. Since these areas are located in a labyrinth of interdendritic regions in the coating, the products of corrosion tend to fill the interdendritic interstices and the corrosion rate decreases. This leads to a parabolic corrosion rate in most environments. This contrasts with the linear behavior typical for galvanized.

Table 6 Ratios of average corrosion rates of 55Al-Zn and galvanized coatings

Location	Ratio of average corrosion rates 55Al-Zn: Galvanized[(a)]
Kure Beach, NC 25 m (severe marine)	4.2
Kure Beach, NC 250 meters (moderate marine)	2.3
Bethlehem, PA (industrial)	6.2
Saylorsburg, PA (rural)	3.4

(a) Ratio gives the relative improvement of the 55Al-Zn coating versus galvanized. Source: Ref 13

Corrosion of the coating for the 55Al-Zn product is not a uniform-thinning process as that noted for galvanized coating. During the early stages of the product life, the aluminum-rich dendrites stay fairly much unaffected in most environments. In a sense, the aluminum-rich dendrites perform like a barrier coating while the zinc-rich areas provide the galvanic protection that is needed to minimize the tendency for rust- staining at sheared edges and other areas of exposed steel.

Because the corrosion resistance depends on the microstructural features of the coating, it is more important to have the right microstructure than a thick coating to develop the desired performance. It has been found that in order to achieve the desired microstructure, the coating thickness should not be too thin. For this reason, the most common coating designations for products to be used outdoors in the environment are:

ASTM A 792/A 792 M coating designation	Minimum coating weight[(a)], oz/ft^2
AZ50	0.50
AZ55	0.55
AZ60	0.60

(a) Total both sides, based on a specific test

The AZ50 coating is approximately as thick as a G90 galvanized coating. The SI unit designations are:

ASTM A 792/A 792 M coating designation	Minimum coating weight[(a)], g/m^2
AZ150	150
AZ165	165
AZ180	180

(a) Total both sides, based on a specific test

There are several notable exceptions to the improved corrosion performance of 55Al-Zn- coated sheet versus galvanized. Perhaps, the most important one is the performance in closed animal-confinement structures in cold climates. The 55Al-Zn coating is not recommended for concentrated confinement of cattle and pigs (Ref 14) in cold climates, regions where overnight condensation is a usual condition. In these types of applications, the coating is susceptible to pitting corrosion. For poultry buildings, the product has been observed to perform well.

95Zn-Al Coating. Another continuous hot- dip zinc/aluminum alloy coated product that is being produced globally today is one that contains 95% zinc and 5% aluminum. There are two types of 95Zn-Al coating. One contains a small addition of mischmetal while the other type being made commercially contains a small addition of magnesium. These additions are claimed to offer improvement in obtaining smooth and uniformly thick coatings.

There are a number of papers reporting results on the relative corrosion resistance of the 95Zn- Al coating versus a galvanized coating. Outdoor performance is reported in Ref 15, 16, 17. The data in Table 7 (Ref 17) show the outdoor performance in three marine locations. Except for the sheltered severe marine site, the 95Zn-Al coating outperforms the galvanized coating. These data show that the presence of 5% aluminum in this zinc-base coating contributes to improved corrosion resistance versus a pure zinc-containing galvanized coating. This improvement might be related to the influence of aluminum on the nature of the surface-passivating film, or, perhaps, the eutectic structure of the coating (Fig. 9) may alter some aspect of the corrosion mechanism at the outer surface of the coating such as influencing the anode-cathode geometry on the surface.

Table 7 Two-year corrosion rates of galvanized, 95Zn-Al, and 55Al-Zn coatings

Site	Condition	Corrosion rate, μm/yr (mils/yr)		
		Galvanized	**95Zn-Al**	**55Al-Zn**
Severe marine	Open	3.42 (0.135)	4.37 (0.172)	1.14 (0.045)
	Sheltered	14.43 (0.568)	11.24 (0.443)	9.57 (0.377)
Moderate marine	Open	1.07 (0.042)	0.39 (0.015)	0.29 (0.011)
	Sheltered	4.30 (0.169)	2.44 (0.096)	0.66 (0.026)
Mild marine	Open	0.66 (0.026)	0.27 (0.011)	0.22 (0.009)
	Sheltered	1.03 (0.041)	0.88 (0.035)	0.54 (0.021)

Source: Ref 17

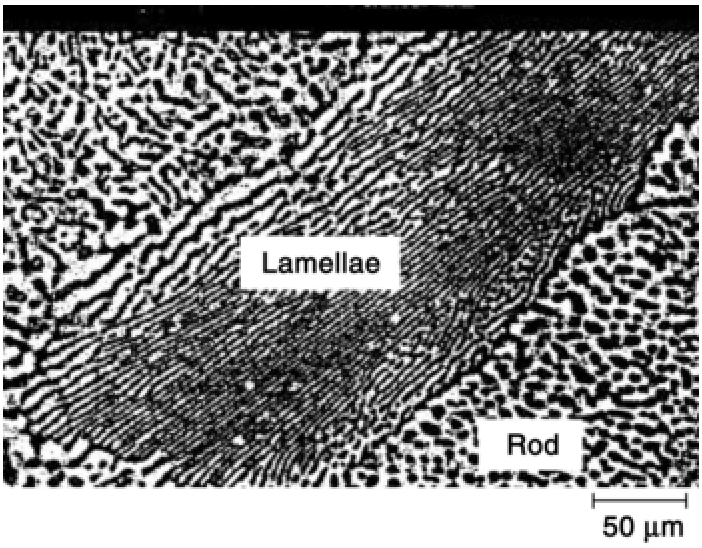

Fig. 9 Representative microstructure of a 95Zn-Al coating, showing lamellar-shaped and rod-shaped eutectic structure

Aluminized Steel. There are two types of aluminum coatings applied to steel sheet by the continuous-coating method. One is applied from a coating bath that contains an aluminum alloy consisting of aluminum plus approximately 5 to 11% silicon. Typically, the silicon concentration is about 8 to 9%. This product is designated type 1 aluminized sheet. The other aluminized coating is essentially pure aluminum. This coating is designated type 2 aluminized sheet. Aside from the obvious difference in coating bath composition, the hot-dip process to make both of these coated-sheet products is very similar to that used to make continuous hot-dip coated galvanized sheet.

The sheet product made from the silicon-containing bath is used for applications where exposure to elevated temperatures is involved. These applications include fireplace and furnace parts and automotive exhaust systems. Unlike galvanized sheet that is somewhat prone to embrittlement (Ref 18) when exposed at temperatures greater than 200 °C (400 °F) where the zinc diffuses into the steel sheet, type 1 aluminized low-carbon steel sheet performs well at elevated temperatures. Up to approximately 480 °C (900 °F), interdiffusion between the steel sheet and the coating is somewhat slow, and the sheet remains bright in appearance. At higher temperatures, iron from the steel sheet does diffuse into the coating, and the bright appearance is lost. Even though the coating and steel diffuse into one another at high temperatures, there are data (Ref 19) that show type 1 aluminized can be used for applications up to about 650 °C (1200 °F).

The silicon in the coating bath has a somewhat similar effect on the growth rate of the alloy bond zone during production as the use of silicon in a 55Al-Zn bath. That is, it reduces the rate of growth of the alloy layer and thereby provides better coating adhesion during forming operations. The microstructure of the type 1 aluminized coating is shown in Fig. 10. Note that the alloy layer is not pencil-thin like that for galvanized sheet (Fig. 5) but is more like the thickness of the alloy layer on 55Al-Zn.

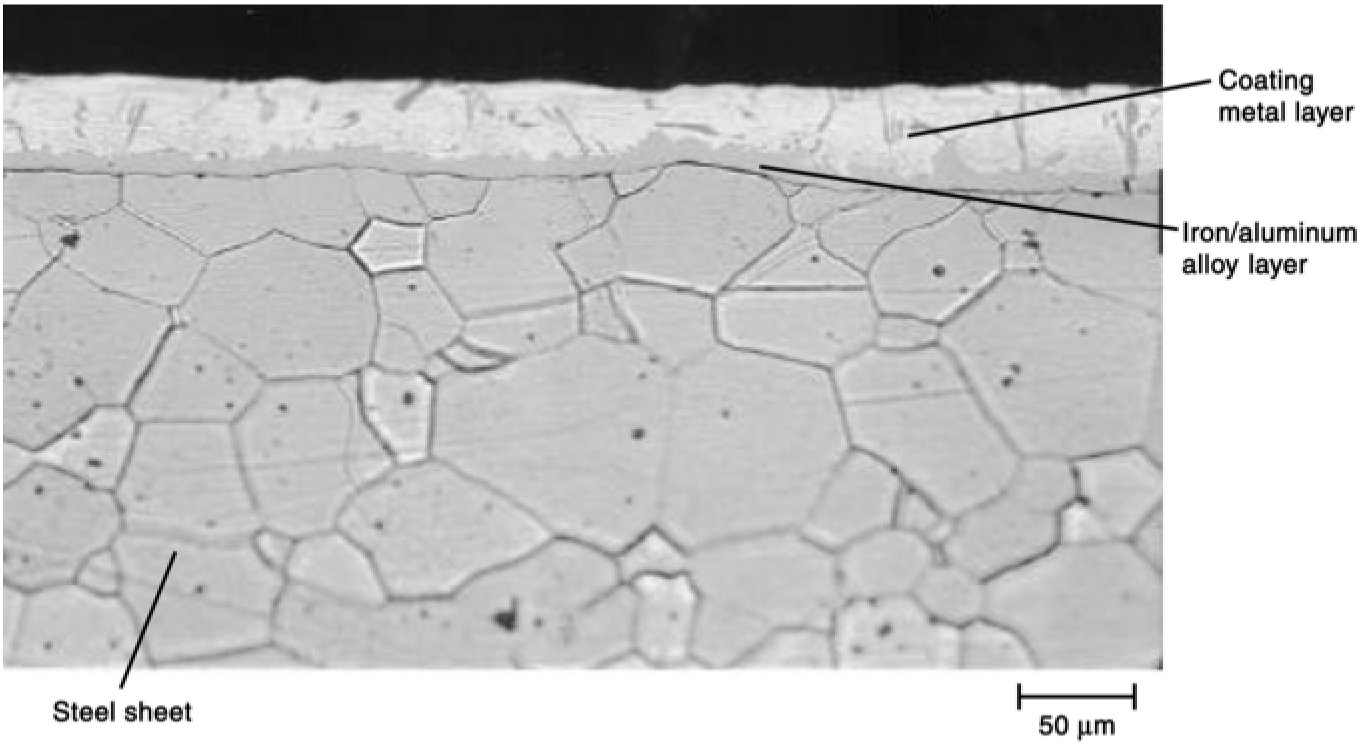

Fig. 10 Microstructure of the coating and alloy layer of a hot-dip coated type 1 aluminized steel sheet

In recent years, type 1 aluminized coating has been applied onto 400 Series stainless steels. The push by the automotive industry to develop a 10 year exhaust system has promulgated the use of 400 Series stainless steels for most original equipment exhaust systems. Even with this upgrade, however, there are problems with stainless steel that an aluminum-coated stainless product can help to overcome (Ref 20). One is the discoloration (heat tint) that is evident on stainless. The aluminized surface helps to maintain a good cosmetic appearance. Also, the aluminized coating can be used effectively to help avoid pitting corrosion of the stainless steel that is caused by the presence of chlorides.

Figure 11 shows the typical microstructure and alloy layer for product made using a pure aluminum coating bath. Note the increased thickness of the alloy layer compared with the coating in Fig. 10. Since the ability to form the sheet into a shaped final part while maintaining good coating adhesion is highly dependent on the thickness of the alloy layer, type 1 product can be used for more severely formed parts than the type 2 product.

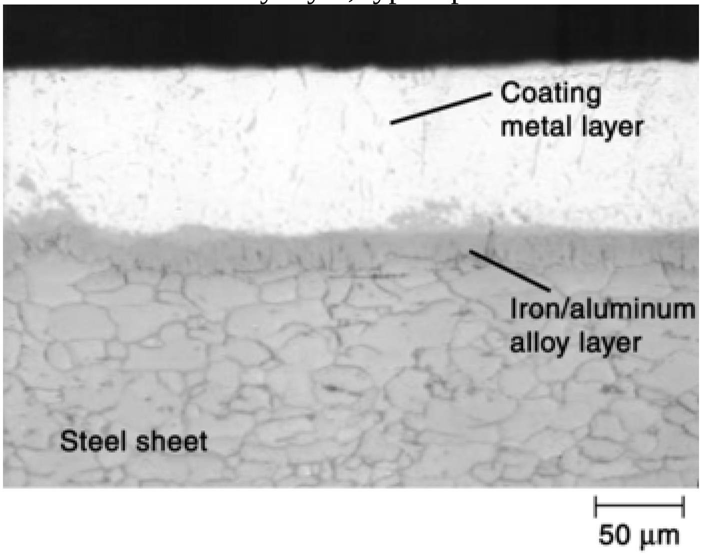

Fig. 11 Microstructure of the coating and alloy layer of hot-dip coated type 2 aluminized sheet

Type 2 aluminized sheet is used for applications where excellent *barrier* corrosion protection is needed; one application is aluminized culverts. Here, the barrier-layer protection is sufficient for many in-ground applications. There are many types of soils, and the suitability of type 2 aluminized for a specific site versus

galvanized culvert depends on many factors, including pH and resistivity of the soil. Aluminized steel has been shown to exhibit good performance in environments within the pH range of 5 to 9 and in soils with resistivities as low as 1500 Ω · cm. (590 Ω · in.).
Because aluminum in the atmosphere reacts to form a protective oxide layer on its surface, the surface becomes highly passivated in most environments. This passivating film is very stable; thus in most environments, the corrosion rate is much lower than for a galvanized coating. Table 8 contains data that show the difference in corrosion rates for type 2 aluminized versus galvanized coatings (Ref 21). Clearly, the bulk corrosion rate for the aluminized coating is less than that for galvanized coatings.

Table 8 Coating thickness losses for galvanized steel and type 2 aluminized steel in atmospheric exposure

Years exposed	Coating thickness loss in industrial environment			
	G90 galvanized		**Type 2 aluminized**	
	µm	**mils**	**µm**	**mils**
1	2.6	0.1	0.5	0.02
2	5.2	0.2	0.7	0.03
4	9.3	0.37	1.2	0.05
6	14.5	0.57	3.1	0.12
10	24.4	0.96	2.9	0.11
15	…	…	5.3	0.21

Source: Ref 21

In spite of these differences in corrosion rate, aluminized steel has not displaced galvanized for many applications. The key reason is that the aluminized coating does not provide galvanic protection in most environments at places where the steel is exposed. The strong tendency for the coating to become completely passivated in the atmosphere simply prevents galvanic corrosion protection. Thus, rust staining develops at areas where steel is exposed, and this rusting can then lead to *bleeding* (staining formed by the oxidation products of steel corrosion) onto larger areas of the sheet. This is an aesthetic issue, but one that is important to many users of coated-steel sheet product.

References cited in this section

2. X.G. Zhang, *Corrosion and Electrochemistry of Zinc,* Plenum Press, 1996

3. J.J. Friel, Atmospheric Corrosion Products on Al, Zn, and Al-Zn Metallic Coatings, *Corrosion,* Vol 42, 1986, p 422–426

4. F.C. Porter, *Corrosion Resistance of Zinc and Zinc Alloys,* Marcel Dekker, Inc., 1994

5. J. Robinson, Development of a Durability Branding System for Steel Construction Products, *Corros. Manage.,* Vol 10, 2001, p 3–10

6. G.A. King and P. Norberg, A Methodology for Quantifying the Atmospheric Corrosion Performance of Fabricated Metal Products in Marine Environments, *Marine Corrosion in Tropical Environments,* STP 1399, S.W. Dean, G. Hernandez-Duque Delgadillo and J.B. Bushman, Ed., ASTM, 2000

7. R.M. Burns and W.W. Bradley, *Protective Coatings for Metals,* 3rd ed., Reinhold, 1967, p 165

8. Report of Subcommittee XIV on Inspection of Black and Galvanized Sheets, Committee A-5, *ASTM Proceedings,* American Society for Testing and Materials, 1952, p 113

9. ASTM A 653, Annual Book of ASTM Standards

10. W. Muschenborn, Paper WG II/7, IDDRG Working Group Meeting, Helsinki, 1983

11. H.E. Townsend and A.R. Borzillo, "Thirty- Year Atmospheric Corrosion Performance of 55% Aluminum-Zinc Alloy-Coated Sheet Steel," presented at Third International Conference on Zinc and Zinc-Alloy Coated Steels (Galvatech'95), Chicago, 17–21 Sept 1995

12. H.J. Cleary, "The Microstructure and Corrosion Resistance of 55% Al-Zn Coatings on Steel Sheet," presented at 16th Annual Technical Meeting of the International Metallographic Society, 27 July 1983

13. A. Humayun, "The Basics of 55% Al-Zn Coated Sheet's Legendary Performance," presented at National Conference on Coil Coating and Continuous Sheet Galvanizing, New Delhi, India, 10–11 Sept 1997

14. "Performance of Galvalume Sheet in Animal Confinement Applications," Bethlehem Steel Technical Bulletin, May, 1990

15. K. Tano and S. Higuchi, "Development and Properties of Zinc-Aluminum Alloy Coated Sheet with High Corrosion Resistance," Nippon Steel Technical Report No. 25, April 1985

16. T. Aoki, Y. Miyoshi, and T. Kittaka, Result of 10-Year Atmospheric Corrosion Testing of Hot-Dip Zn-5% Al Alloy Coated Steel Sheet, *Galvatech'95 Proceedings,* Iron and Steel Society, 1995, p 463–468

17. P. Norberg, G. King, and D. O'Brien, "Corrosivity Studies and Microclimate Measurements in Marine Environments," presented at Australasian Corrosion Association Conference, Perth, Australia, 1995

18. J.J. Sebisty, Continuous Strip Galvanized Coatings at Elevated Temperatures, *Electrochemical Technology,* Sept–Oct 1968, p 330–336

19. "Aluminized Steel Type 1," AK Steel Technical Bulletin

20. Raising the Bar in Automotive Exhaust Stainless Steels, *The Catalyst,* AK Steel Technical Publication, No. 1, 2000

21. H.F. Graff, Aluminized Steel, *Encyclopedia of Materials Science and Engineering,* Pergamon Press, 1986, p 138–141

R. Leonard, Continuous Hot Dip Coatings, *Corrosion: Fundamentals, Testing, and Protection*, Vol 13A, *ASM Handbook*, ASM International, 2003, p 786–793

Continuous Hot Dip Coatings

Ralph W. Leonard, Coated Steels Technology, LLC

References

1. "Hot-Dip Galvanizing for Corrosion Protection, A Specifier's Guide," American Galvanizers Association

2. X.G. Zhang, *Corrosion and Electrochemistry of Zinc,* Plenum Press, 1996

3. J.J. Friel, Atmospheric Corrosion Products on Al, Zn, and Al-Zn Metallic Coatings, *Corrosion,* Vol 42, 1986, p 422–426

4. F.C. Porter, *Corrosion Resistance of Zinc and Zinc Alloys,* Marcel Dekker, Inc., 1994

5. J. Robinson, Development of a Durability Branding System for Steel Construction Products, *Corros. Manage.*, Vol 10, 2001, p 3–10

6. G.A. King and P. Norberg, A Methodology for Quantifying the Atmospheric Corrosion Performance of Fabricated Metal Products in Marine Environments, *Marine Corrosion in Tropical Environments,* STP 1399, S.W. Dean, G. Hernandez-Duque Delgadillo and J.B. Bushman, Ed., ASTM, 2000

7. R.M. Burns and W.W. Bradley, *Protective Coatings for Metals,* 3rd ed., Reinhold, 1967, p 165

8. Report of Subcommittee XIV on Inspection of Black and Galvanized Sheets, Committee A-5, *ASTM Proceedings,* American Society for Testing and Materials, 1952, p 113

9. ASTM A 653, Annual Book of ASTM Standards

10. W. Muschenborn, Paper WG II/7, IDDRG Working Group Meeting, Helsinki, 1983

11. H.E. Townsend and A.R. Borzillo, "Thirty- Year Atmospheric Corrosion Performance of 55% Aluminum-Zinc Alloy-Coated Sheet Steel," presented at Third International Conference on Zinc and Zinc-Alloy Coated Steels (Galvatech'95), Chicago, 17–21 Sept 1995

12. H.J. Cleary, "The Microstructure and Corrosion Resistance of 55% Al-Zn Coatings on Steel Sheet," presented at 16th Annual Technical Meeting of the International Metallographic Society, 27 July 1983

13. A. Humayun, "The Basics of 55% Al-Zn Coated Sheet's Legendary Performance," presented at National Conference on Coil Coating and Continuous Sheet Galvanizing, New Delhi, India, 10–11 Sept 1997

14. "Performance of Galvalume Sheet in Animal Confinement Applications," Bethlehem Steel Technical Bulletin, May, 1990

15. K. Tano and S. Higuchi, "Development and Properties of Zinc-Aluminum Alloy Coated Sheet with High Corrosion Resistance," Nippon Steel Technical Report No. 25, April 1985

16. T. Aoki, Y. Miyoshi, and T. Kittaka, Result of 10-Year Atmospheric Corrosion Testing of Hot-Dip Zn-5% Al Alloy Coated Steel Sheet, *Galvatech'95 Proceedings,* Iron and Steel Society, 1995, p 463–468

17. P. Norberg, G. King, and D. O'Brien, "Corrosivity Studies and Microclimate Measurements in Marine Environments," presented at Australasian Corrosion Association Conference, Perth, Australia, 1995

18. J.J. Sebisty, Continuous Strip Galvanized Coatings at Elevated Temperatures, *Electrochemical Technology,* Sept–Oct 1968, p 330–336

19. "Aluminized Steel Type 1," AK Steel Technical Bulletin

20. Raising the Bar in Automotive Exhaust Stainless Steels, *The Catalyst,* AK Steel Technical Publication, No. 1, 2000

21. H.F. Graff, Aluminized Steel, *Encyclopedia of Materials Science and Engineering,* Pergamon Press, 1986, p 138–141

T.J. Langill, Batch Process Hot Dip Galvanizing, *Corrosion: Fundamentals, Testing, and Protection*, Vol 13A, *ASM Handbook*, ASM International, 2003, p 794–802

Batch Process Hot Dip Galvanizing

Thomas J. Langill, American Galvanizers Association

Introduction

THE METALLIC COATING produced by the hot dip galvanizing process is the result of a metallurgical reaction called diffusion. Diffusion occurs when iron from the steel and zinc from the molten bath intermix to form specific coating layers. In this reaction, zinc diffuses inward and iron diffuses outward; together they form separate coating layers of specific composition. The finished product consists of four layers on the steel; the outer layer is 100% zinc. The inner three layers are separate intermetallic layers of slightly different zinc and iron composition that are metallurgically bonded to each other and the steel. Thus, a galvanized coating has extremely high bond-strength relative to other coatings.

For the diffusion reaction to occur, the zinc must wet the steel surface. The presence on the steel surface of foreign materials such as rust, scale, paints, or lubricants can prevent the zinc from wetting and reacting with the steel surface. Therefore, all contaminants must be removed before galvanizing.

The batch hot dip galvanizing process consists of two basic steps: surface preparation; that is, cleaning the steel surface, and immersion of the steel part in the bath of molten zinc, galvanizing. Within each of these broad steps, a series of operations is essential to the production of a quality galvanized coating.

T.J. Langill, Batch Process Hot Dip Galvanizing, *Corrosion: Fundamentals, Testing, and Protection*, Vol 13A, *ASM Handbook*, ASM International, 2003, p 794–802

Batch Process Hot Dip Galvanizing

Thomas J. Langill, American Galvanizers Association

Surface Preparation

Dirt, oils, lubricants, greases, and other impurities, as well as normal oxidation products such as mill scale or rust, may be deposited on the steel during fabrication, transportation, or storage. These impurities must be removed so that iron and zinc may intermix to form the galvanized coating. These surface contaminants are typically removed by immersion in cleaning solutions followed by rinsing in clean water.

Alkaline Degreasing. The first step in the process is treatment in an alkaline solution. Oils, greases, and other saponifiable compounds are removed in this step. Most of the various proprietary compounds available for this purpose consist of a mixture of basic sodium salts.

Acid Degreasing. An alternate method to alkaline cleaning is acid degreasing using a dilute hydrochloric acid bath. The acid bath with appropriate additives will also remove organic materials.

Acid Pickling. The steel article is usually rinsed after alkaline degreasing and before pickling to avoid neutralization and weakening of the pickle acid. The pickling process removes surface oxides and mill scale. The pickle acid is an aqueous solution of a mineral acid, usually hydrochloric acid (HCl) or sulfuric acid (H_2SO_4). Acid concentrations and pickling temperatures vary from galvanizer to galvanizer but are within a narrow range. An inhibitor is sometimes used to avoid attack of the base metal.

Abrasive Cleaning. As an alternative to cleaning in solutions, abrasive grit-blasting or sand-blasting may be used, followed by a flash (less than 30 s) immersion in pickle acid to remove any surface oxides that may

develop between cleaning and further processing. Abrasive cleaning may not be practical for the galvanizer who handles a variety of sizes and shapes of material. Abrasive cleaning provides rapid and complete cleaning and is particularly effective in cleaning iron castings because casting sands are easily removed and surface uniformity is promoted. This method is also useful for cleaning fabricated products composed of different ferrous materials that may pickle at different rates or for removing welding slag or other impurities that are difficult or impossible to remove using chemical solutions.

Fluxing. The final step in the surface preparation is an immersion in a flux solution to dissolve any oxide films formed on the steel after pickling but before galvanizing and to ensure that a clean metal surface contacts the molten zinc. The fluxing procedures are classified as the wet process and the dry process:

- *Wet process.* Steel is passed through a layer of molten flux floating on the surface of the molten zinc.
- *Dry process (prefluxing).* Steel is immersed in an aqueous flux solution and dried before galvanizing.

In both cases, a flux composed of zinc ammonium chloride ($ZnCl_2 \cdot nNH_4Cl$) is used. Because both flux processes have advantages, selection of a method is based on individual galvanizer choice. The ratio of zinc chloride to ammonium chloride in the flux may vary based on the application.

T.J. Langill, Batch Process Hot Dip Galvanizing, *Corrosion: Fundamentals, Testing, and Protection*, Vol 13A, *ASM Handbook*, ASM International, 2003, p 794–802

Batch Process Hot Dip Galvanizing

Thomas J. Langill, American Galvanizers Association

Galvanizing

The molten zinc metal is contained in a kettle made of firebox-quality steel. The zinc is maintained at a temperature of 438 to 454 °C (820 to 850 °F). The kettle should be large enough to accommodate the steel parts and should have sufficient heat capacity to prevent significant thermal drops when steel is immersed in the molten zinc.

There are some hot dip galvanizers who use a higher temperature zinc bath, from 540 to 570 °C (1004 to 1058 °F). The higher temperature galvanizing baths are used for structural reactive steels or for fasteners that are fabricated from reactive steel. For this process, the galvanizing kettle must be fabricated from ceramic materials since steel kettles cannot operate at this high a temperature due to interactions between zinc and iron. Coatings from high-temperature galvanizing are dull gray due to the growth of iron-zinc alloy layers. The process for galvanizing is the same for normal- or high-temperature zinc baths.

The clean iron or steel part is immersed (dipped) directly into the molten zinc, or it is passed through a molten flux blanket into the molten zinc. The material is immediately wetted, and as it reaches the temperature of the molten zinc, the diffusion reaction begins, resulting in the formation of a series of iron-zinc alloy layers. For most steel compositions, the interdiffusion reaction is rapid at first but subsequently slows. The final thickness of the coating does not increase substantially with longer immersion times in the molten zinc.

The coating produced consists of a series of zinc-iron alloy layers, with increasing zinc content occurring toward the outer coating surface. When the coated steel part is withdrawn from the kettle, a thin layer of free zinc remains on the zinc-iron alloy layers, resulting in the characteristic bright, shiny, galvanized coating finish when allowed to cool quickly in air. The thickness of the free zinc layer varies with the speed of withdrawal from the molten bath.

Smaller parts are hot dip galvanized in steel baskets that are placed in a centrifuge immediately after withdrawal from the zinc bath. The parts are spun in the centrifuge to remove the excess zinc metal. This operation produces higher quality coatings on threaded articles.

Most galvanized articles are air cooled after coating, although centrifuged parts and smaller items are often water cooled (quenched). Water quenching halts the alloying reaction by diminishing the heat retained by the

steel part; this prevents the continued diffusion reaction that will continue to produce zinc-iron intermetallics until the steel part drops below approximately 288 °C (550 °F). In some galvanizing facilities, the water quench contains chromates or there is a separate bath of chromate solution. The chromates are used to form a conversion coating on the surface of the zinc. This conversion coating prevents the formation of excessive amounts of zinc oxide and zinc hydroxide on the surface of the zinc coating in the first week after hot dip galvanizing. Excessive oxide and hydroxide formation is known as wet storage stain since it forms when hot dip galvanized parts are exposed to high amounts of water in their first few days after galvanizing. The chromate conversion coating should not be used if the hot dip galvanized part is to be painted since it interferes with paint adhesion on zinc coatings. More information on chromate conversion coatings can be found elsewhere in this Volume.

T.J. Langill, Batch Process Hot Dip Galvanizing, *Corrosion: Fundamentals, Testing, and Protection*, Vol 13A, *ASM Handbook*, ASM International, 2003, p 794–802

Batch Process Hot Dip Galvanizing

Thomas J. Langill, American Galvanizers Association

Coating Weight and Thickness

Galvanizing specifications in the United States require the coating thickness to be measured by one of a number of techniques. For wire, sheet, or small parts and fasteners, the procedure involves stripping the coating, determining the weight loss of the item, then calculating the coating weight. Stripping of zinc coatings may be done by immersion in either hydrochloric acid-antimony trichloride solution or dilute hydrochloric acid. For large iron and steel structural materials, this may be impossible or impractical. The coating weight can be determined by measuring the coating thickness with a calibrated magnetic thickness gage. The weight to thickness conversion is 305 g/m^2 of zinc equals 43 μm of thickness (1 oz of zinc/ft^2 equals a thickness of 1.7 mils). Therefore, 100 g/m^2 of zinc equals 14 μm.

T.J. Langill, Batch Process Hot Dip Galvanizing, *Corrosion: Fundamentals, Testing, and Protection*, Vol 13A, *ASM Handbook*, ASM International, 2003, p 794–802

Batch Process Hot Dip Galvanizing

Thomas J. Langill, American Galvanizers Association

Coating Weight and Thickness

Galvanizing specifications in the United States require the coating thickness to be measured by one of a number of techniques. For wire, sheet, or small parts and fasteners, the procedure involves stripping the coating, determining the weight loss of the item, then calculating the coating weight. Stripping of zinc coatings may be done by immersion in either hydrochloric acid-antimony trichloride solution or dilute hydrochloric acid. For large iron and steel structural materials, this may be impossible or impractical. The coating weight can be determined by measuring the coating thickness with a calibrated magnetic thickness gage. The weight to thickness conversion is 305 g/m^2 of zinc equals 43 μm of thickness (1 oz of zinc/ft^2 equals a thickness of 1.7 mils). Therefore, 100 g/m^2 of zinc equals 14 μm.

T.J. Langill, Batch Process Hot Dip Galvanizing, *Corrosion: Fundamentals, Testing, and Protection*, Vol 13A, *ASM Handbook*, ASM International, 2003, p 794–802

Batch Process Hot Dip Galvanizing

Thomas J. Langill, American Galvanizers Association

Factors Affecting Coating Thickness and Structure

For most steel compositions, the coating thickness and structure are relatively insensitive to differences in the galvanizing process. However, variations in steel chemistry; zinc bath temperature; the physical condition of the steel surface (grain size, stresses, microstructure, roughness); zinc chemistry; the amount of wiping, shaking, or centrifuging; and the rate of cooling after galvanizing can affect the thickness, metallurgical characteristics, and appearance of the coating (Ref 1).

Metallurgy. The hot dip galvanized coating consists of three separate layers of zinc-iron intermetallics, formed by interdiffusion of zinc and iron, and a fourth and final layer of zinc bath metal with no iron. The first intermetallic layer, gamma layer, contains 75% zinc and 25% iron and is typically very thin and uniform. The second intermetallic layer, delta layer, contains 90% zinc and 10% iron and is very dense and uniform. The third intermetallic layer, zeta layer, contains 94% zinc and 6% iron and grows in a columnar structure. This layer can be quite different from spot to spot on the final product. When there are very thick coatings on steel parts, it is usually the zeta layer that grows very thick. The final layer, eta layer, is deposited from the zinc bath as the part is withdrawn from the bath. Galvanizers attempt to draw the parts from the bath at a slow, steady speed so the excess zinc will drain off the part back into the bath. A fast withdrawal will result in a lumpy and runny coating that is very irregular in coating thickness.

Steel Chemistry. Although most steel can be galvanized, steel chemistry can have a marked effect on the thickness, structure, and appearance of the galvanized coating. Silicon, phosphorus, carbon, and manganese may be present in the steel and can influence the zinc-iron reaction mechanism, depending on their concentration (Ref 2).

The most influential steel constituent is silicon, which is added to molten steel to remove oxygen before casting. Figure 1 shows the effect of increasing silicon content in the steel versus time at two different galvanizing temperatures. In high-silicon (reactive) steels, the increase in coating thickness results from the accelerated growth of the zinc-iron alloy layers. This growth is due to the formation of loosely packed small grains or long-stem crystals in the outermost alloy layer of the coating, allowing zinc from the bath to penetrate to the steel surface with continuation of the reaction (Ref 3). In general, steels with the following maximum impurity levels are best suited to galvanizing: 0.04% Si, 0.04% P, 0.25% C, and 1.3% Mn.

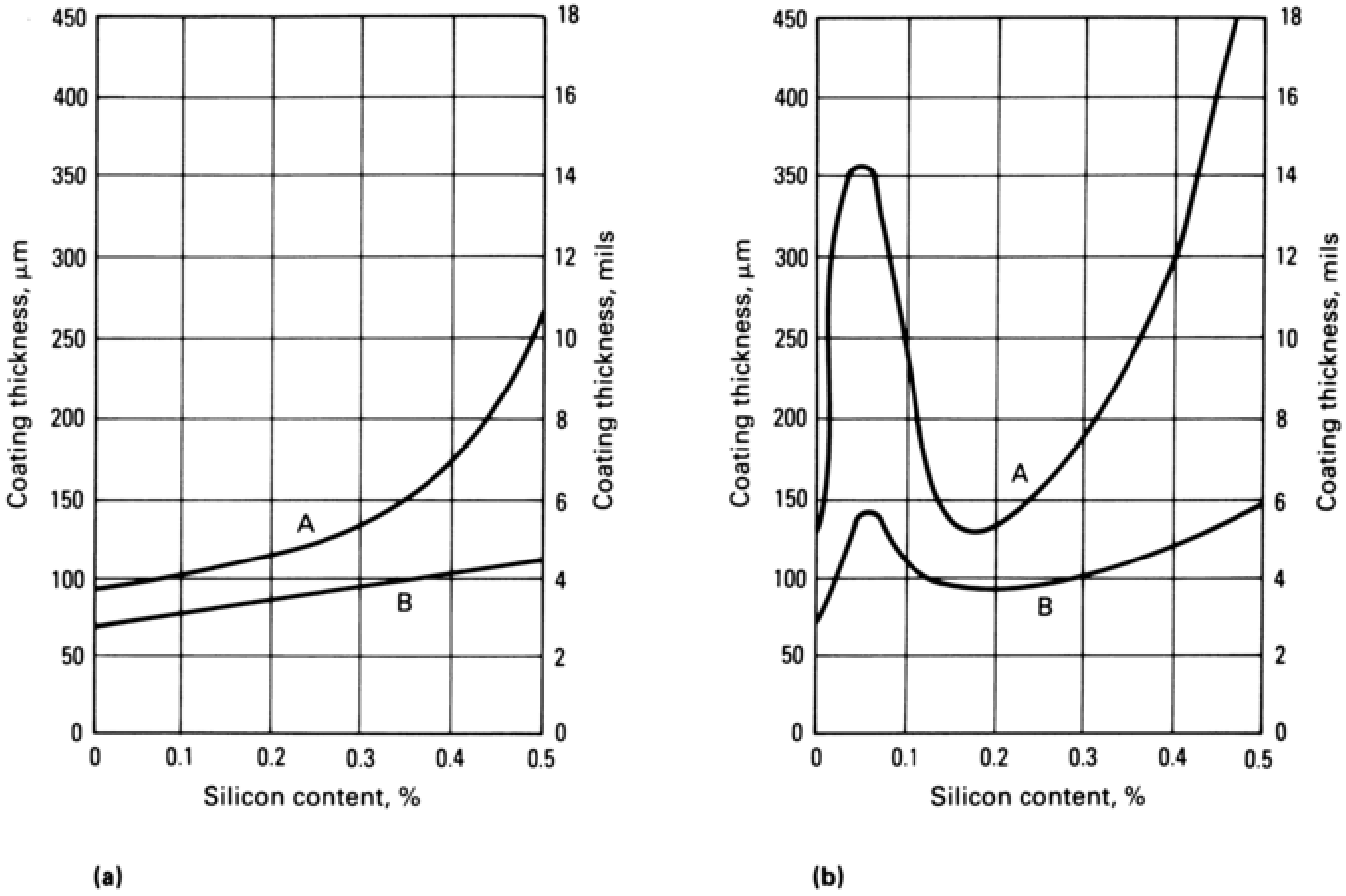

Fig. 1 Effect of silicon content of steel, immersion time, and galvanizing temperature on the thickness of hot dip galvanized coatings. Curves A and B are for 9 min and 3 min immersions, respectively. (a) Galvanizing temperature: 430 °C (805 °F). (b) Galvanizing temperature: 460 °C (860 °F). Source: Ref 2

Zinc Bath Temperature. For normal steels, an increase in the zinc bath temperature not exceeding the normal operating range results in reduced immersion time and improved drainage of free zinc when the steel part is removed from the galvanizing kettle. The coating thickness for silicon-containing steels is very temperature dependent (Fig. 1), with higher temperatures producing a thicker galvanized coating. The galvanizer must trade off more consistent coating thickness at low temperatures for high-silicon steel with higher production rates at higher temperatures for lower silicon steels.

Steel Surface Condition. The condition of the steel surface with respect to roughness and microstructure can affect the thickness of the galvanized coating. Roughening of the surface increases the profile and thus the effective surface area of the material, resulting in increased coating thickness. Fine-grain microstructures can result in lower coating weights (Ref 3).

Zinc Chemistry. Trace elements in the molten zinc, present either as impurities or intentionally added to the zinc to achieve beneficial results, can affect the appearance of the galvanized coating. Prime Western zinc (UNS Z19001), one of the grades normally used for batch process galvanizing, can contain up to 1.4% Pb, 0.2% Cd, 0.05% Fe, and must contain a minimum of 98% Zn. Other grades of zinc used for hot dip galvanizing are High Grade (UNS Z15001) with a maximum impurity level of 0.10% and Special High Grade (UNS Z13001) with a maximum impurity level of 0.010%

Although the lead content of Prime Western zinc can be as high as 1.4%, a typical galvanizing bath will contain 1% or less, and the actual hot dip galvanized coating contains approximately half of the bath lead concentration; that is, about 0.5% lead in the coating. Lead has no effect on the viscosity of molten zinc, but it does affect the surface tension. This results in better drainage of zinc from the galvanized product, an important consideration when galvanizing complex shapes or wire fabrics.

Aluminum is usually not found in the grades of zinc normally used for galvanizing but is occasionally added to improve the finish of the work. Aluminum at a concentration of 0.005% in zinc will result in coatings with improved brightness and uniformity. It also retards the surface oxidation of the molten zinc, resulting in a smoother flow of zinc over the work and improved drainage characteristics. Other elements that are added to

the zinc bath in small quantities are bismuth and nickel to improve the bath fluidity and the coating thickness control respectively.
The typical galvanizing zinc bath may contain other trace elements that were originally present in the zinc or that resulted from the chemistry of the steel processed. These trace elements, including cadmium and copper, are usually present in concentrations too low to affect the coating structure or appearance.
Degree of Wiping, Shaking, or Centrifuging. These techniques are used for the efficient removal of excess zinc after galvanizing and result in a coating with a very uniform surface appearance. These techniques are particularly important when galvanizing threaded materials.
Rate of Cooling. Silicon-containing steels that are allowed to cool slowly after galvanizing will continue to react until the temperature decreases to below approximately 288 °C (550 °F). This may result in the iron-zinc alloy layers extending to the coating surface and an almost total absence of the free zinc layer. The result is a gray coating instead of a bright, shiny finish. The service life of the coating is not adversely affected and may in fact be greater with these coatings because of their increased thickness.
If the material is not water quenched after galvanizing and a bright, shiny surface is desired, then close stacking of material while still hot should be avoided. Close stacking may allow heat retention, which could permit the zinc- iron alloying reaction to continue. Material should be well spaced with good air circulation for cooling efficiency.

References cited in this section

1. X.G. Zhang, *Corrosion and Electrochemistry of Zinc,* Plenum Press, New York, 1996

2. D. Horstmann, Reaction Between Liquid Zinc and Silicon-Free and Silicon-Containing Steels, *Proceedings of the Seminar on Galvanizing of Silicon-Containing Steels,* International Lead-Zinc Research Organization, 1975, p 94

3. A.W. Stoneman, “A Closer Look at High Reactivity In Galvanizing,” paper presented at the TECH FORUM Meeting, American Galvanizers Association, Oct 1994

T.J. Langill, Batch Process Hot Dip Galvanizing, *Corrosion: Fundamentals, Testing, and Protection*, Vol 13A, *ASM Handbook*, ASM International, 2003, p 794–802

Batch Process Hot Dip Galvanizing

Thomas J. Langill, American Galvanizers Association

Mechanical Properties of the Coating and Steel Substrate

Hardness and Abrasion Resistance. The layers that compose the galvanized coating, being discrete zinc-iron alloys, vary in hardness. The outer layer of 100% zinc is relatively soft, but the alloy layers are very hard, harder even than ordinary structural steels. Typical values for the microhardness and other properties of the various alloy layers are given in Table 1.

Table 1 Properties of alloy layers to hot dip galvanized steels

Layer	Alloy	Iron, %	Melting point		Crystal structure	Diamond pyramid microhardness (vickers scale)	Alloy characteristics
			°C	**°F**			
Eta	Zinc	0.03	419	787	Hexagonal	70–72	Soft, ductile
Zeta	$FeZn_{13}$	5.7–	530	986	Monoclinic	175–185	Hard, brittle

		6.3					
Delta	$FeZn_7$	7.0–11.0	530–670	986–1238	Hexagonal	240–300	Ductile
Gamma	Fe_3Zn_{10}	20.0–27.0	670–780	1238–1436	Cubic	…	Thin, hard brittle
Steel base metal	Iron	…	1510	2750	Cubic	150–175	…

The alloy layers are from four to six times more resistant to abrasion than pure zinc. Galvanized coatings exhibit better abrasion resistance than paints with the same coating thickness and can be effectively used where excessive abrasive wear is expected, for example, floor gratings, stairs, conveyors, and storage bins.

Adhesion and Impact Resistance. Unlike other coatings that are mechanically or chemically bonded to the steel, the galvanized coating is metallurgically bonded to and integral with the steel, making conventional measures of bond strength inappropriate for this coating. As a result of the metallurgical bond, the galvanized coating has bond strength on the order of several thousand pounds per square inch (psi).

The structure of the galvanized coating, particularly the relative thickness of the delta and zeta alloy layers (Table 1), is primarily influenced by the steel chemistry and, to a lesser extent, by the galvanizing bath temperature and the duration of immersion. Coating structure has the greatest effect on the impact resistance of the coating. A high relative proportion of zeta phase in the iron-zinc alloy may result in localized flaking if the coating is subjected to heavy impact or excessive twisting or bending. Semikilled steels with silicon contents of 0.05 to 0.12% are the most susceptible to coating brittleness and less adherent coatings.

Steel Strength and Ductility. The effects of hot dip galvanizing on the mechanical properties of steels have been thoroughly researched. This research has shown that galvanizing causes no significant alteration in the bend, tensile, and impact properties of the commonly galvanized steels produced throughout the world (Ref 4). Galvanizing slightly reduces the impact toughness of cold-rolled steels, but this reduction is generally not sufficient to affect the applicability of the steel. Of course, typical items that are batch processed are not intended to be subsequently cold rolled. Steels coated by the batch galvanizing process are not generally intended to be bent or roll formed after galvanizing.

Weld Stresses. Welded structures have higher strength in the galvanized condition than in the uncoated condition. Hot dip galvanizing reduces weld stresses by 50 to 60% (Ref 4).

Fatigue Strength. For most steel, little reduction in fatigue strength occurs as a result of galvanizing. Fatigue tests comparing hot dip galvanized steels with uncoated steels usually compare uncoated steel with mill scale and the same steel after galvanizing. The results show a slight edge to the uncoated steel samples, but these tests do not consider that uncoated steel exposed to an outside environment begins to rust immediately. The rusting action results in the formation of pits that may be five to seven times deeper than the general corrosion and will cause a rapid decrease in fatigue strength. The reduction in fatigue strength due to corrosion attack is much more significant than any reduction due to hot dip galvanizing.

Embrittlement. It is relatively rare for steel to be in the embrittled condition after hot dip galvanizing. The amount of cold working (plastic straining) of steels susceptible to strain aging is the single most important factor where strain- age embrittlement is of concern. The temperature of the galvanizing process accelerates the aging process; generally, susceptible materials fail almost immediately after removal from the bath. Research has shown that a minimum cold- bend radius of three times the section thickness will preclude sufficient cold working and prevent the embrittled condition from occurring (Ref 3, 4).

If possible, steel fabrications should use steels with a low susceptibility to strain-age embrittlement. When cold working is necessary, the guidelines and limitations contained in ASTM A 143 (Ref 5) should be observed.

Hydrogen embrittlement does not occur when ordinary carbon or low-alloy steels are galvanized. Hardened steels may become embrittled if the hydrogen picked up during pickling is not expelled during immersion in the molten zinc bath. Precautions should be taken with steels having an ultimate tensile strength exceeding 1034 MPa (150 ksi). Steels of medium-to-high strength that have been severely cold worked may have local areas that also approach this threshold limit for susceptibility to hydrogen embrittlement.

References cited in this section

3. A.W. Stoneman, “A Closer Look at High Reactivity In Galvanizing,” paper presented at the TECH FORUM Meeting, American Galvanizers Association, Oct 1994

4. “Galvanizing Characteristics of Structural Steels and Their Weldments,” International Lead Zinc Research Organization, 1975

5. “Standard Practice for Safeguarding Against Embrittlement of Hot-Dip Galvanized Structural Steel Products and Procedure for Detecting Embrittlement,” A 143, *Annual Book of ASTM Standards,* American Society for Testing and Materials

---

T.J. Langill, Batch Process Hot Dip Galvanizing, *Corrosion: Fundamentals, Testing, and Protection*, Vol 13A, *ASM Handbook*, ASM International, 2003, p 794–802

Batch Process Hot Dip Galvanizing

Thomas J. Langill, American Galvanizers Association

Fabrication Details for Galvanizing

The design and fabrication of materials to be hot dip galvanized involve a few basic rules that are easy to apply and are necessary to the production of quality galvanized articles meeting intended functional requirements. Foremost among these rules is the interrelationship among the design engineer, fabricator, and galvanizer. Although this interrelationship becomes increasingly important with the complexity of the configuration of the material to be galvanized, most problems relating to design can be eliminated if it becomes an integral part of the design and fabrication program.

Steel Selection. As previously discussed, steel chemistry can affect the nature and extent of the zinc-iron alloy layers formed during galvanizing. Some steels that are commonly used for galvanized products are ASTM A 36 (with <0.04% Si specified) for structural shapes and plate, A 120 for pipe, A 569 for sheet, and A 615 for reinforcing bar.

Combining Different Materials. Optimum galvanizing quality is seldom obtained when ferrous materials that have different chemistries or different surface conditions, or those that are constructed by different fabrication methods, are combined. Different pickling and immersion times are required for different materials, and combinations may result in over- or under-treatment of the combined parts of the fabricated article. Different material types for which combinations should be avoided include excessively rusted items, material with machined or pitted surfaces, cast iron and steel, malleable iron, hot- rolled steel, cold-rolled steel, and reactive steels.

Castings. The cleaning of castings requires special attention. Burned-on sand from the casting process is nearly impossible to completely remove by conventional pickling methods, and the use of hydrofluoric acid (HF), although effective, can be extremely dangerous to galvanizing personnel. Castings should be shot-blasted or grit-blasted by the fabricator before delivery to the galvanizer.

Castings that consist of two or more different metals may pickle and galvanize differently. The designer and fabricator should be aware of this. Abrasive cleaning may moderate these effects and provide for a more uniform coating appearance. Alternatively, the materials may be galvanized separately and assembled after galvanizing.

Surface Contaminants. Residue materials resulting from fabrication or storage should be removed before delivery of the steel part to the galvanizer, unless special arrangements have been made. Typical contaminants include welding slag and paints or other labeling compounds. Welding slag results from the use of coated welding rod. Weld slag cannot be removed by conventional pickling, and if the use of uncoated rod is not possible, weld slag should be removed by mechanical methods. Paints or other labeling compounds often used to identify the work are sometimes difficult or impossible to remove by alkaline cleaning methods. Permanent markings for identification, if needed, should be punched or embossed in the steel, applied to the part as weld metal, or punched into 12-gage or thicker steel tags and wired securely to the part with heavy-gage steel wire.

Size of Material. Various sizes of hot dip galvanizing kettles exist throughout North America. Designing and fabricating in modules suitable for the available galvanizing facilities allows almost any component to be galvanized. If the material is too long or too deep to be completely immersed in the molten zinc in one dip, it may still be possible to galvanize by immersing one- half of the article in the kettle, withdrawing, and then immersing the other half. By using this procedure, known as progressive dipping, materials up to 75% longer than the length of kettle may be successfully galvanized, depending on the depth of the item and other kettle dimensions. Although progressive dipping is an accepted galvanizing practice, special attention to galvanizing details and proper inspection are essential to its use on tubular items.

Threaded and Movable Parts. For threaded parts, such as nut and bolt assemblies, it is advisable to tap the nut threads after galvanizing to ensure a proper fit. For movable parts, such as shackles or shafts, a radial clearance of 1.6 mm ($\frac{1}{16}$ in.) is usually sufficient to allow free movement after galvanizing.

Drainage. When designing for hot dip galvanizing, consideration must be given by the designer and fabricator to providing a way for cleaning solutions and zinc to flow into, through, and out of the item so that all surfaces can be properly galvanized.

Venting. The opening of holes or slots for the release of trapped gases in hollow objects is necessary for proper treatment of exterior and interior surfaces. More important, venting is essential for avoiding the extreme explosion hazard that can result from heating a closed or improperly vented hollow object to the galvanizing temperature. Discussions of proper venting techniques become very complex when intricate configurations are under consideration. Venting practices for various configurations, as well as additional fabrication techniques, are discussed in Ref 6, 7, 8.

Overlapping or Contacting Surfaces. When designing parts that are to be hot dip galvanized, it is best to avoid narrow gaps less than 2.4 mm ($\frac{3}{32}$ in.), between plates, overlapping surfaces, and back-to-back angles and channels. When overlapping or contacting surfaces cannot be avoided, the edges should be completely sealed by welding; otherwise, pickle liquids can enter and result in conditions that permit the generation of high pressures and steam, delayed weeping, or improperly cleaned and galvanized areas. This may not be possible with large overlapping areas, so consult ASTM A 385 when using steel parts with overlapping surfaces.

Welding for Hot-Dip Galvanizing. When materials are welded before hot dip galvanizing, the cleanliness of the weld area and the composition of the weld metal can affect the quality and appearance of the galvanized coating. Specific welding information can be obtained from the American Welding Society (Ref 9) or welding suppliers. Several welding techniques have been found to be satisfactory for materials to be galvanized:

- An uncoated electrode should be used to prevent flux deposits.
- If a coated electrode is used, all flux residues must be removed because they are chemically inert to pickling acids.
- A welding process such as metal inert gas, tungsten inert gas, or CO_2 shielded arc should be used because virtually no slag is produced.
- In the case of heavy welds, a submerged arc method is recommended.
- If none of the above is available, a coated rod specifically designed for self-slagging, as recommended by welding equipment distributors, should be selected.
- A welding rod that will provide a deposited weld composition as close as possible to that of the parent steel should be chosen. This will prevent differential reaction rates during cleaning and uneven galvanized coating thickness.
- High-silicon welding rods may cause excessively high coating weights or darkened coatings.

References cited in this section

6. “The Design of Products To Be Hot-Dip Galvanized After Fabrication,” American Galvanizers Association, 2000

7. “Recommended Details of Galvanized Structures,” American Galvanizers Association, 1996

8. “Standard Practice for Providing High- Quality Zinc Coatings (Hot-Dip),” A 385, *Annual Book of ASTM Standards,* American Society for Testing and Materials

9. *Welding Zinc Coated Steels,* D19.0-72, American Welding Society, 1973

T.J. Langill, Batch Process Hot Dip Galvanizing, *Corrosion: Fundamentals, Testing, and Protection*, Vol 13A, *ASM Handbook*, ASM International, 2003, p 794–802

Batch Process Hot Dip Galvanizing

Thomas J. Langill, American Galvanizers Association

Galvanized Coatings in Corrosion Service

Protection Mechanism. Galvanized coatings protect steel in two ways: barrier protection and cathodic protection. Barrier protection is provided by the galvanized coating and is further enhanced by the formation of a thin, tightly adherent layer of zinc corrosion products on the coating surface (Ref 1). On initial weathering in the open atmosphere, ZnO forms on the freshly galvanized surface. It is converted to $ZnOH_2$ in the presence of moisture. Over the period of 6 to 24 months, further reaction of the zinc corrosion products with CO_2 in the air results in the formation of basic $ZnCO_3$, which is relatively insoluble in water and impedes the growth of further corrosion products. The gray patina normally associated with weathered galvanized coatings is the result of this thin layer of basic $ZnCO_3$.

Cathodic protection is provided to the steel because zinc is anodic to steel in most environments. Minor discontinuities or small areas of exposed steel resulting from drilled holes or cut edges are protected from corrosion by the sacrificial protection afforded by zinc. The corrosion products of zinc that result from this cathodic action provide further protection by depositing on the exposed steel and forming another barrier protection.

Atmospheric Exposure. Zinc, steel, and hot- dip galvanized coatings have been the subject of long-term atmospheric studies conducted throughout the world (Ref 10, 11). From these studies, the behavior of these materials in a specific atmospheric environment can be reasonably estimated. An exact determination of corrosion behavior is complicated by several factors: the frequency and duration of exposure to moisture (rain, sleet, snow, and dew), the type and concentration of corrosive pollutants, the prevailing wind direction and velocity, and exposure to sea- spray or wind-borne abrasives. All atmospheres contain some type of corrosive material, and the concentration of these materials, as well as the frequency and duration of moisture contact, determines the corrosion rate of galvanized coatings.

Figure 2 shows the results of outdoor atmospheric-exposure tests designed to measure the protective life of galvanized coatings in various atmospheric environments. The sites were selected as representative of various broad environmental classifications: moderate industrial (urban), suburban, rural, and marine. Within these broad classifications, the following factors are most significant in influencing the rate of corrosion of the galvanized coating.

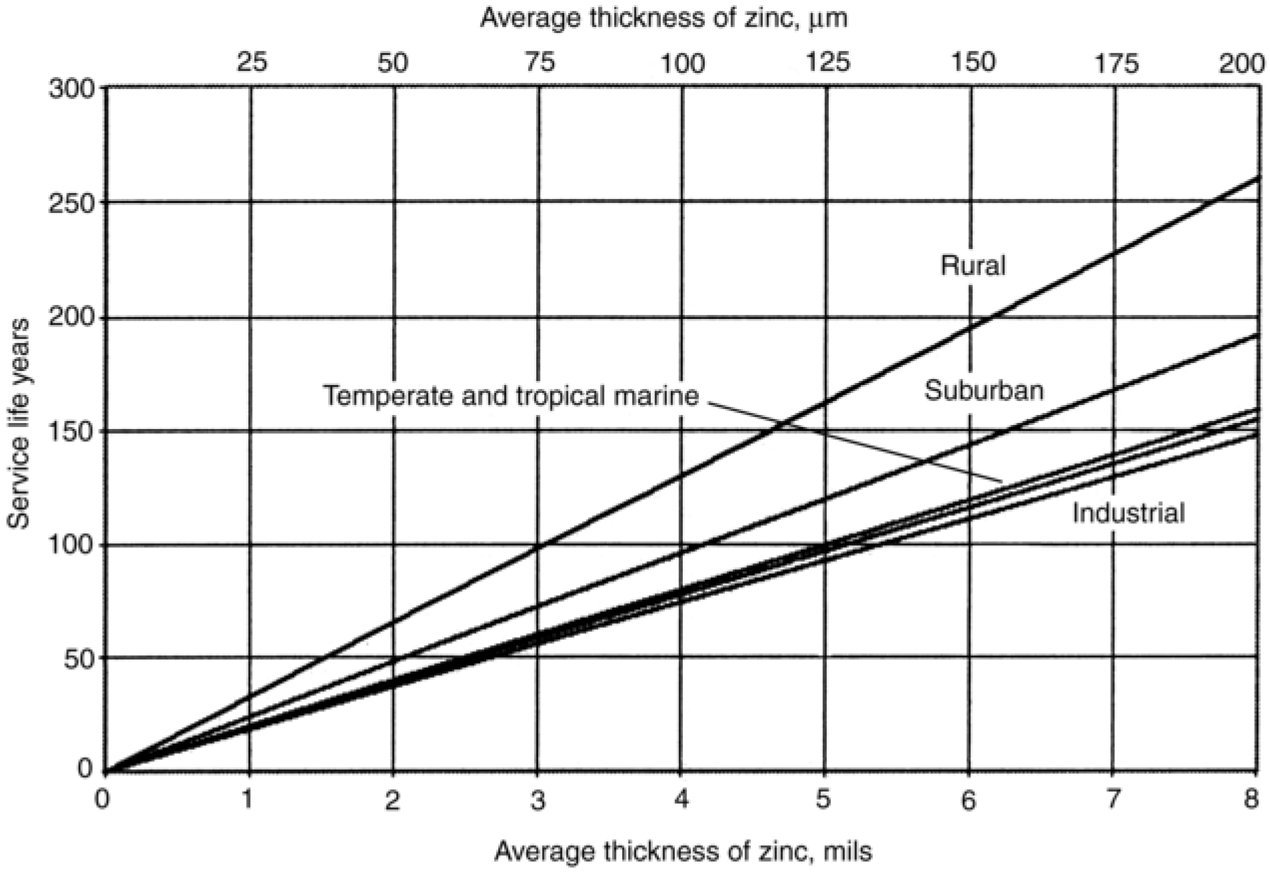

Fig. 2 Service life versus coating thickness for hot dip galvanized steel in various atmospheres. Service life is defined as the time to 5% rusting of the steel surface.

Industrial and Urban Environments. Corrosive conditions are most pronounced in areas with highly developed industrial complexes that release sulfurous gases and corrosive fumes and mists to the atmosphere. These corrosive materials react with the normally impervious basic $ZnCO_3$ film to produce $ZnSO_4$ and other soluble zinc salts that, in the presence of moisture, are washed from the surface. This exposes fresh zinc to the atmospheres, and another corrosion cycle begins.

Rural and Suburban. The corrosion rate of zinc in these areas is relatively slow compared to that in industrial settings. Once the original weathering occurs, there is little in the atmosphere to convert the basic zinc salts to water- soluble compounds.

Marine Atmospheres. The corrosion rate of zinc and galvanized steel in marine atmospheres is influenced by several factors. Zinc forms a soluble corrosion product, zinc chloride ($ZnCl_2$), in marine atmospheres; therefore, the corrosion rate is influenced by salt spray, sea breezes, topography, and proximity to the coastline. For example, one investigation found that the corrosion rate for zinc exposed 24.4 m (80 ft) from the ocean was three times that for zinc exposed 244 m (800 ft) from the ocean (Ref 12).

The corrosion product formed in a given type of atmosphere (industrial, marine, and so on) determines the corrosion rate of zinc in that atmosphere. Results from exposures in a variety of atmospheres show that zinc is 20 to 30 times more resistant to corrosion than steel.

Seawater and Salt Spray Performance. Table 2 gives the approximate corrosion rates of zinc in various waters, and Figure 3 illustrates the expected service life of galvanized coatings in areas exposed to salt spray influences (Ref 13). Sea salts are mainly NaCl, with small amounts of calcium, magnesium, and manganese salts. Typical pH is about 8. Compared to other metals and alloys, galvanized coatings provide considerably more protection to steel than many other metals and alloys, even though the anticipated coating life is shorter in seawater and salt spray exposures than a number of other corrosion protection systems.

Table 2 Corrosion of zinc in various waters

Water type	Approximate material loss	
	µm/yr	**mils/yr**
Seawater		
Global oceans, average	15–25	0.6–1.0
North Sea	12	0.5
Baltic Sea and Gulf of Bothnia	10	0.4
Freshwaterr		
Hard	2.5–5	0.1–0.2
Soft river water	20	0.8
Soft tap water	5–10	0.2–0.4
Distilled water	50–200	2.0–8.0

Source: Ref 12

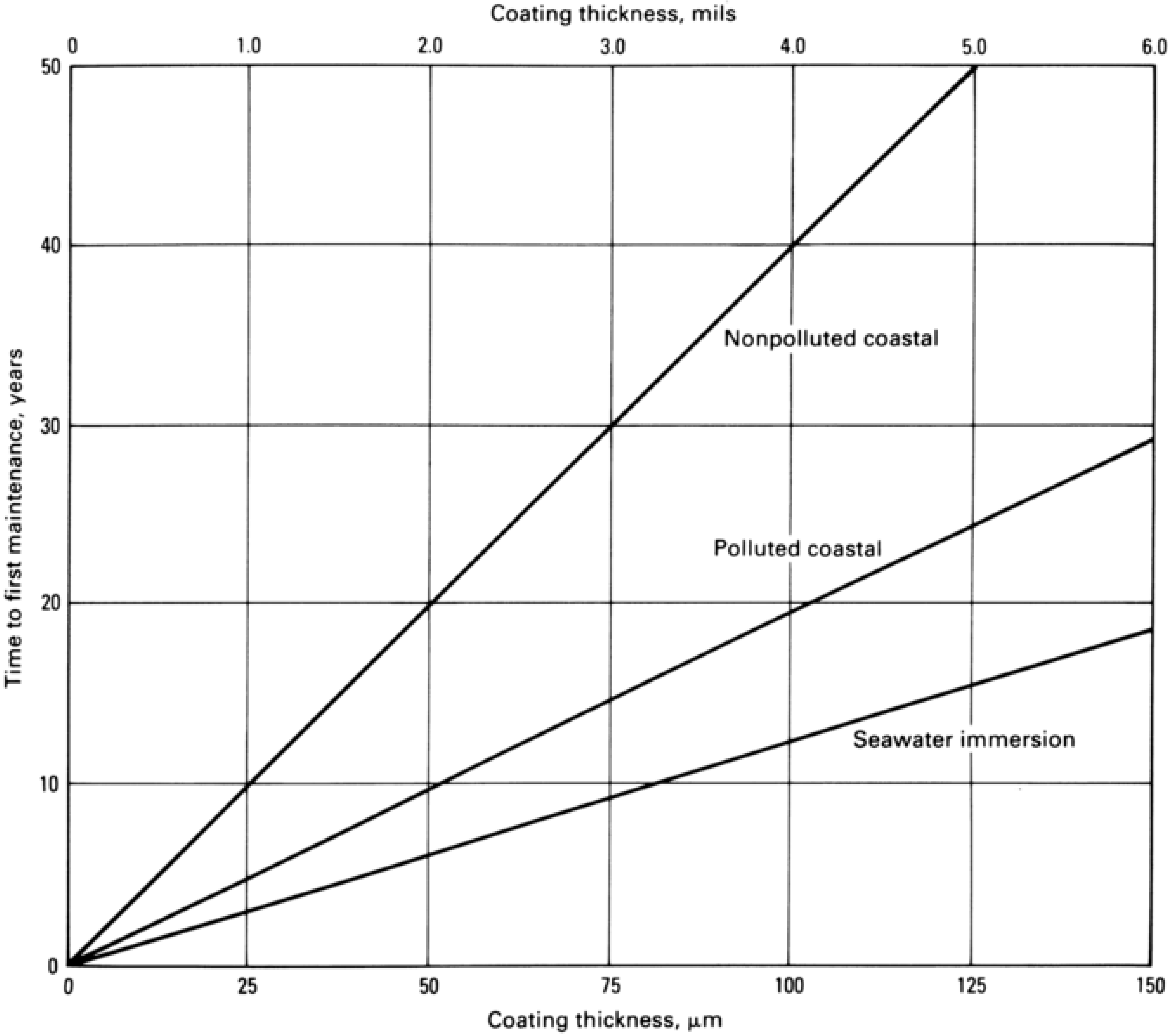

Fig. 3 Time to first maintenance versus coating thickness for hot dip galvanized coatings in seawater immersion and sea spray exposures. Source: Ref 13

Freshwater Performance. The corrosion protection mechanism of zinc in freshwater is similar to that in atmospheric exposures. The corrosion rate depends on the ability of the coating to develop a protective layer of adherent basic zinc salts. This layer denies access to the coating by oxygen and slows the rate of attack. The

ability of the water to form scale depends on a number of variables, such as the pH of the water, hardness, total alkalinity, and total dissolved solids. Table 3 demonstrates the effects of various water chemistries on the relative corrosion rates of zinc (Ref 13).

Table 3 Corrosion of zinc in different types of water

Water type	Attacking substances	Passivating substances	Properties of corrosion products		Relative corrosion rate
			Solubility	**Adhesion**	
Hard water	Oxygen, CO_2	Calcium, magnesium	Very low	Very good	Very low
Seawater	Oxygen, CO_2, Cl^-	Calcium, magnesium	Low	Very good	Moderate
Soft with free air supply	Oxygen, CO_2	…	High	Good	High
Soft or distilled with poor air supply	Oxygen	…	Very high	Very poor	Very high

Source: Ref 12

Water Temperature. The corrosion rate of zinc in water, and therefore that of the galvanized coating, increases with temperature to between 65 and 70 °C (150 and 160 °F), at which point the rate begins to decrease (Fig. 4).

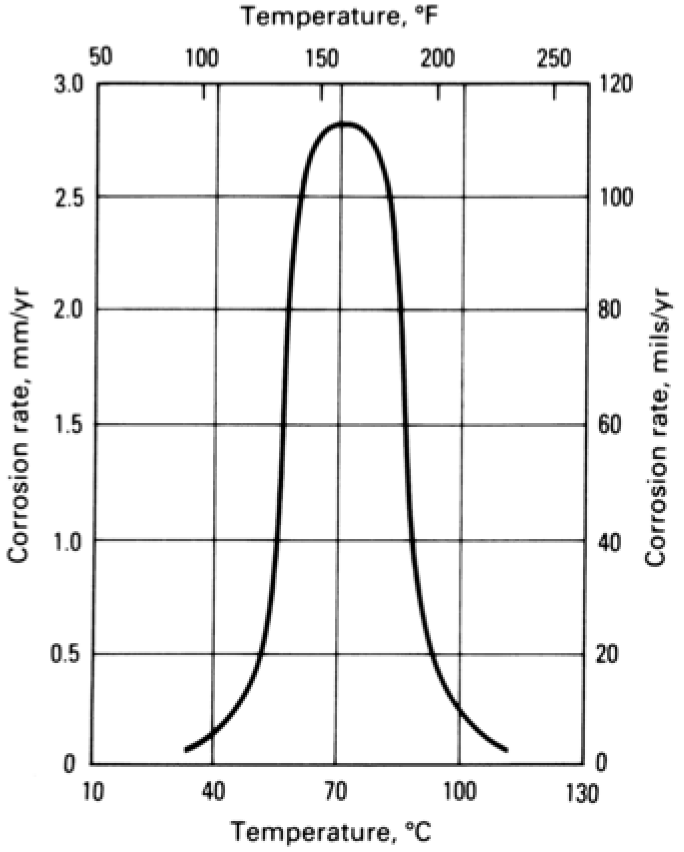

Fig. 4 Influence of water temperature on the corrosion rate of zinc in distilled, aerated water. Source: Ref 13

Water pH. Zinc is an amphoteric metal with the capacity to passivate by means of protective layers. The corrosion rate of zinc decreases with increasing pH and reaches a minimum at 12.0 to 12.5. Most waters are in the pH range of 6 to 8. The scale-forming ability of the water and the concentration of dissolved ions in the water are more important influences on the corrosion rate than pH in this practical exposure range.

Performance in Soils. The corrosion rate and performance of galvanized steels in soils are a function of the type of soil in which the steel is located. Soils can vary considerably in composition and can contain bound and unbound salts, organic compounds, products of weathering, bacteria and other microorganisms, dissolved gases

(such as hydrogen, oxygen, and methane), acids, and alkaloids. Soils vary in permeability, depending on the soil structure. Although the concentration of oxygen is lower in soils than in air, the CO_2 concentration is higher. Variation among soils is high, and corrosion conditions are complicated.

In general, soils in coarse, open textures are often aerated, and the performance of galvanized steel would be expected to be similar to that in air. In soils with fine textures and high water- holding capacities such as clay and silt-bearing soils, corrosion rates are likely to be higher.

Soil resistivity is recognized as a reliable method of predicting the corrosivity of soils. High-resistivity (poor conducting) soil would be less corrosive than low-resistivity (good conducting) soil. Dry soils are poor conductors and are the least corrosive to zinc.

Performance in Contact with Other Metals. The galvanic behavior of dissimilar metals in electrical contact is a complex corrosion problem, partly because of the large number of metals used in various applications. Copper and brass in contact with zinc or a galvanized coating in a moist environment can cause rapid galvanic corrosion of the zinc. Installations that use zinc and copper or copper alloys should provide for electrical insulation between the two, and because zinc may also be attacked by dissolved copper, copper materials should be located downstream of the zinc in nonrecirculating water systems. With aluminum or stainless steel, the performance of hot dip galvanized steel is good if the environment is dry. In humid environments, isolation may be required.

Performance of Fully Alloyed Coatings. Coatings that consist entirely of iron-zinc alloy layers (without the 100% zinc outer layer) result from the galvanizing of reactive steels. These coatings are characterized by a matte gray or mottled appearance. Fully alloyed coatings may exhibit premature rust-colored staining due to iron in the coating, but this should not be considered failure of the coating, because base metal rusting has not occurred. Fully alloyed coatings with coating thickness similar to normal coatings will give similar corrosion protection service.

High-Temperature Performance. When galvanized steel is continuously exposed to temperatures above about 200 °C (390 °F), the 100% zinc outer layer may peel off the intermetallic layers (Ref 13). The remaining alloy layers will not be affected and will continue to provide useful service life. Short time excursions above this temperature will not affect the coating and its performance.

References cited in this section

1. X.G. Zhang, *Corrosion and Electrochemistry of Zinc,* Plenum Press, New York, 1996

10. R.M. Burns and W.W. Bradley, *Protective Coatings for Metals,* 2nd ed., Reinhold, 1955, p 128

11. S.K. Coburn, C.P. Larrabee, H.H. Lawson, and G.B. Ellis, Corrosiveness at Various Atmospheric Test Sites as Measured by Specimens of Steel and Zinc, *Metal Corrosion in the Atmosphere*, STP 435, American Society for Testing and Materials, 1968, p 371–372

12. C.J. Sunder and W.K. Boyd, *Zinc: Its Corrosion Resistance,* 2nd ed., International Lead Zinc Research Organization, 1983, p 113–150

13. F.C. Porter, *Corrosion Resistance of Zinc and Zinc Alloys,* Marcel Dekker, Inc., 1994

T.J. Langill, Batch Process Hot Dip Galvanizing, *Corrosion: Fundamentals, Testing, and Protection*, Vol 13A, *ASM Handbook*, ASM International, 2003, p 794–802

Batch Process Hot Dip Galvanizing

Thomas J. Langill, American Galvanizers Association

Joining of Galvanized Structural Members

Bolting is the most widely used method of joining galvanized steel. A number of standard galvanized fasteners are available for use with galvanized steel structural members (Table 4).

Table 4 Some standard galvanized fasteners

Description	ASTM specification	Grade or type
Carbon steel bolts	A 307	Grade A, B
High-strength bolts	A 325	Type 1
Transmission tower bolts	A 394	Type 0, 1
Quenched-and-tempered alloy steel bolts	A 354	Grade BC

(a) Consult ASTM A 563 for suitable bolt/nut combinations.

Galvanized coatings in bearing-type connections, which develop shear resistance by allowing the bolts to bear on the plates, are not detrimental to performance and have a long history of use—for example, in electrical utility transmission line towers. In friction-type connections, all loads in the plane of the joint are transferred by the friction developed between the connected surfaces. The load that can be transmitted is determined from the clamping force applied to the bolts and the coefficients of friction of the faying surfaces. Clean, galvanized mating surfaces have a coefficient of friction that is slightly lower than that of as-rolled steel. The coefficient of friction of galvanized surfaces can be made equal to that of uncoated steel surfaces by wire brushing or light grit-blasting (Ref 14, 15). Neither treatment should be severe enough to produce breaks or discontinuities in the galvanized coating. The fatigue behavior of galvanized steel connections equals that of uncoated steel connections, regardless of whether the galvanized surfaces were wire-brushed or grit-blasted after galvanizing (Ref 14, 15, 16, 17).

Welding. Zinc-coated steel can be satisfactorily welded by all common welding methods, but attention must be given to the possible generation of zinc fumes. For the best weld quality, grind away the galvanized coating in the area of the weld for ~2.5 cm (1 in.) on either side of the weld site before welding. There will be no zinc fumes generated, and the weld can be performed as on uncoated steel. When burning off zinc in the case when the coating is not ground off, adequate ventilation, operator respiration units, or a fume-extracting welding unit must be used to avoid potential harmful effects. Extensive tensile, bend, radiographic, and fatigue tests show that the properties of sound metal inert gas or metallic arc welds on galvanized steel are equivalent to those on uncoated steel (Ref 4).

Penetration of molten zinc into the weld metal is the primary factor in cracking of galvanized steel weldments. The crack begins at the root of the weld and may or may not extend to the surface. Recommendations to avoid fillet weld cracking include (Ref 9):

- Treat the base metal to reduce the amount of available zinc by, for example, beveling the standing plate in a tee joint at an angle of 15 to 45°.
- Remove zinc from both faying surfaces by shot-blasting.
- Provide a parallel gap of 1.6 mm ($\frac{1}{6}$ in.) between the weld elements.
- Choose consumables that will give low-silicon content weld, for example, manganese silicate flux and 2% low manganese/low silicon electrodes for submerged arc welding. For CO_2 welding, low-silicon filler wire gives freedom from zinc penetration cracking but causes a small amount of porosity. For shielded arc welds, use a low-silicon electrode and a rutile covering.

Weld Porosity. A small void can occur in the weld bead because of the volatilization of zinc during welding. Porosity can be reduced by making adequate provision for the escape of gases evolved during welding. Normal porosity does not reduce the static tensile strength below that specified for satisfactory low-carbon steel weld metal, but it will affect the fatigue strength of a fillet weld.

Weld Damage Repair. Galvanized materials damaged by field welding can be touched in with an organic or inorganic zinc-rich paint. Organic paint does not require a high degree of surface preparation and dries quickly. The paint must have a zinc dust content according to approved standards and should be applied in several coats to a thickness of twice the galvanized thickness to a maximum of 100 μm (4 mils) to provide equivalent protection.

Low-melting zinc-cadmium or zinc-tin-lead alloy rods can also be used for repair. The rod is heated to about 330 °C (625 °F) with an oxyacetylene torch, and the melted alloy is rubbed and spread over the damaged area. This gives protection equal to that of the surrounding hot- dip galvanized coating. The damaged area can also be zinc metallized by thermal spraying. Additional information on repair techniques is given in ASTM A 780 (Ref 18).

References cited in this section

4. "Galvanizing Characteristics of Structural Steels and Their Weldments," International Lead Zinc Research Organization, 1975

9. *Welding Zinc Coated Steels,* D19.0-72, American Welding Society, 1973

14. "Code of Practice for Protective Coating Iron and Steel Structures Against Corrosion," BS 493, British Standards Institution, 1977, p 23

15. P.C. Birkemoe, W.D. Crouch, and W.H. Munse, "Design Criteria for Joining Galvanized Structurals," Annual Report, ZM- 96, International Lead Zinc Research Organization, April 1969

16. R.A. Sanderson, "Fatigue Behaviour of High Strength Bolted Galvanized Joints," M.A. thesis, University of Toronto, 1968

17. D.J.L. Kennedy, High Strength Bolted Galvanized Joints, *J. Struct. Div.,* Vol 98 (No. St12), Dec 1972, p 2723–2738

18. "Standard Practice for Repair of Damaged and Uncoated Areas of Hot-Dip Galvanized Coatings," A 780, *Annual Book of ASTM Standards,* American Society for Testing and Materials

---

T.J. Langill, Batch Process Hot Dip Galvanizing, *Corrosion: Fundamentals, Testing, and Protection*, Vol 13A, *ASM Handbook*, ASM International, 2003, p 794–802

Batch Process Hot Dip Galvanizing

Thomas J. Langill, American Galvanizers Association

Painting Galvanized Steel

Galvanized coatings, when used without further treatment, offer the most economical corrosion protection for steel in many environments. The galvanized coating makes an excellent base on which to apply a paint system. Painting of galvanized steel is desirable for aesthetics, as camouflage, as warning or identification markings, to prevent bimetallic corrosion, or when the anticipated environment is particularly severe (see the article

"Organic Coatings and Linings" in this Volume for supplementary information on painting for corrosion protection).
In corrosive atmospheres, a duplex system of galvanized steel top-coated with paint has several advantages that make it an excellent system for corrosion prevention:

- The life of the galvanized coating is extended by the paint coating.
- The sacrificial and barrier properties of the zinc coating are used if a break occurs in the paint film.
- Undercutting of damaged paint coatings, a major cause of failure of paints on steel, does not occur with a zinc substrate (Figure 5).
- Surface preparation of a weathered zinc surface for maintenance painting is easier than that for rusted steel.

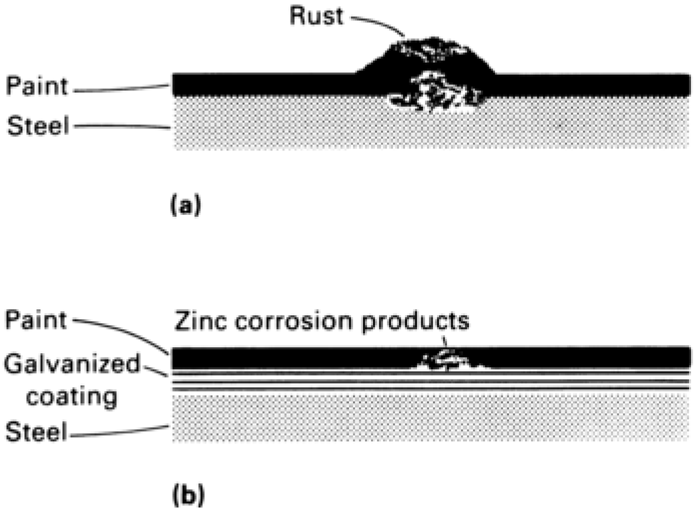

Fig. 5 Illustration of the mechanism of corrosion for (a) painted steel and (b) painted galvanized steel. (a) A void in the paint results in rusting of the steel, which undercuts the paint coating and results in further coating degradation. (b) A void in the coating of a painted galvanized steel is sealed with zinc corrosion products; this avoids the undercutting seen in (a) and prevents further deterioration of the painted coating.

Synergistic Effects of Galvanized and Painted Systems. The galvanized coating prevents rusting of steel by acting as a barrier against the environment and by sacrificially corroding to provide cathodic protection. Painting the galvanized coating extends the service life of the underlying zinc because the barrier property of the paint delays the reaction of zinc with the environment. If a crack or other void occurs in the paint and exposes the galvanized coating, the zinc corrosion products formed tend to fill and seal the void; this delays further reaction.
When painted ungalvanized steel is exposed to the environment, rust forms beneath any holiday or damage to the paint at the steel/paint interface. Because rust occupies a volume several times that of the steel, the expansion resulting from rusting leads to rupture of the steel/paint bond. Further, rust is porous; it accumulates moisture and other reactants. This increases the rate of attack on the steel. The result is undercutting, flaking, and blistering of the paint film, leading to failure of the paint coating (Figure 5). Zinc corrosion products occupy a volume only slightly greater (20 to 25%) than zinc. This reduces the expansive forces and conditions that lead to paint failure.
A coating system consisting of painted galvanized steel provides a protective service life up to 1.5 times that predicted by adding the expected lifetimes of the paint and the galvanized coating in a severe atmosphere (Ref 19). The synergistic improvement is even greater for mild environments (Ref 20, 21).
Paint Adhesion. Adherence of the paint to the galvanized surface is the primary concern in painting galvanized steel. The surface of the zinc is nonporous and does not allow mechanical adhesion of the paint. Surface contaminants such as oils, waxes, or post-galvanizing treatments also affect adhesion. A fresh zinc surface is reactive to certain paint ingredients, such as fatty acids; this can produce zinc soaps and disrupt the zinc-paint bond. Good practices for preparing galvanized surfaces to be painted are described in ASTM D 6386 (Ref 22).

Galvanized coatings can be successfully painted immediately after galvanizing or after extended weathering. The deliberate use of weathering is not recommended, because weathering may not be uniform, the time required is long (6 to 12 months), hygroscopic impurities can form that may be difficult to remove, and there is exposure to atmospheric pollutants.

Chemical etchants such as acids or copper sulfate should not be used. The action of these chemicals is difficult to control, and surface preparation may be nonuniform. The galvanized coating could be damaged if allowed to remain in extended contact with the chemicals. Long- term adhesion will suffer with this type of treatment, although initial adhesion may be obtained.

Mechanical roughening of the zinc surface through the use of a light blast can provide a good surface for painting. However, careful control of the blast pressure and flow rate must be exercised to avoid excessive removal of the galvanized coating.

Initial adhesion of the paint can be achieved through the use of a pretreatment primer to provide an adequate base for further coating. Long- term adhesion is obtained by the selection of a topcoat paint that is compatible with the primer and galvanized steel.

Pretreatment Methods. As with all painting operations, the surface to be painted must be free of contaminants that could affect the adhesion of the paint or the appearance of the painted article. Nonoily substances can be removed by brushing or scrubbing and then rinsing with water. Oily materials should be removed with an approved solvent followed by a final wiping with clean cloths and clean solvent to avoid spreading oil films on the surface.

Two-component wash primers meeting The Society for Protective Coatings (SSPC) specification SSPC-Paint 27 are ideal pretreatments. The primer is applied by spraying thin coats according to the recommendations of the manufacturer. The freshly prepared primer should be applied to a dry film thickness of 7.6 to 13 μm (0.3 to 0.5 mils).

Finish Coating. The primed material should be finish-coated as soon as possible after priming treatment. Wash primers are moisture sensitive, and the vehicle may gel under high-humidity conditions and lose adhesion. The primer usually dries in 15 to 30 min, and it is dry enough to apply a second coat after 30 to 60 min. Almost all paints will adhere to the wash primer.

References cited in this section

19. J.F.H. van Eijnsbergen, Twenty Years of Duplex Systems, *Metallwissenschaft Technik,* Vol 29 (No. 6), June 1975

20. J.F.H. van Eijnsbergen, *Duplex Systems,* Elsevier, 1994

21. D.S. Carr, “Performance of Painted Galvanized Steel,” paper presented at the semiannual meeting, Houston, TX, American Hot-Dip Galvanizers Association, Sept 1982

22. “Standard Practice for Preparation of Zinc (Hot-Dip Galvanized) Coated Iron and Steel Product and Hardware Surfaces for Painting,” D 6386, *Annual Book of ASTM Standards,* American Society for Testing and Materials

T.J. Langill, Batch Process Hot Dip Galvanizing, *Corrosion: Fundamentals, Testing, and Protection*, Vol 13A, *ASM Handbook*, ASM International, 2003, p 794–802

Batch Process Hot Dip Galvanizing

Thomas J. Langill, American Galvanizers Association

Economics of Hot-Dip Galvanizing

Corrosion control is an expense for the owner of any facility. In selecting a system for corrosion control, the economic consequences of the selection should be determined. Initial cost should not be the sole determining factor in selecting a system. Instead, the desired service life of the project should be reasonably estimated and the life-cycle cost of several systems should be evaluated to determine the most economical system for the particular project.

A number of models have been developed for the economic evaluation of corrosion protection (Ref 23, 24, 25). The projected structure life, inflation and discount (cost of capital) rates, number of years in the maintenance cycle, estimated costs for future maintenance, and original system costs must be determined based on discounted cash flow techniques. In the private sector, tax and investment incentives must also be considered. Table 5 illustrates a simple analysis that takes tax and investment incentives into account. Although the initial cost of hot dip galvanizing is in the same range as paint systems, the life- cycle cost is significantly lower because hot dip galvanized coatings need no maintenance during the 30 year cycle described in this example.

Table 5 Applied cost of hot dip galvanized protection compared to four selected paint systems

Coating system	Original cost		Life cycle cost 30 year project performance[a]	
	$/m^2$	$/ft^2$	$/m^2$	$/ft^2$
Hot dip galvanizing	17.97	1.67	17.97	$1.67
Inorganic zinc	9.36	0.87	29.27	$2.72
Acrylic waterborne primer/topcoat	14.31	1.33	45.19	$4.20
Inorganic zinc primer/high-build epoxy/acrylic urethane	24.53	2.28	57.46	$5.34
Latex primer/latex intermediate/latex topcoat	18.40	1.71	69.08	$6.42

Note: The cost comparison is based on US dollars, 2003. The galvanizing data came from a U.S. nationwide survey in 2001. The paint information is from a 1998 NACE International study (Ref 25).

(a) The projected life cycle costs assume a 5% annual increase in the cost of paint materials and a 3% annual increase in paint preparation costs from 1998. The maintenance cycle calls for repainting when surface is degraded with 5% rust and assumes a moderate industrial environment.

References cited in this section

23. B.R. Appleman, Economics of Corrosion Protection by Coatings, *J. Prot. Coatings Linings,* Vol 2 (No. 3), March 1985

24. T.J. Kinstler, "Probability Functions in Corrosion Economics—or a Corrosion Engineer Goes to Monte Carlo," paper presented at Corrosion/82, National Association of Corrosion Engineers, March 1982

25. M.P. Reina, K.R. Shields, and M.F. MeLampy, "Costing Considerations for Maintenance and New Construction Coating Work", paper presented at Corrosion98, National Association of Corrosion Engineers, March 1998

T.J. Langill, Batch Process Hot Dip Galvanizing, *Corrosion: Fundamentals, Testing, and Protection*, Vol 13A, *ASM Handbook*, ASM International, 2003, p 794–802

Batch Process Hot Dip Galvanizing

Thomas J. Langill, American Galvanizers Association

Selected Applications of Hot Dip Galvanized Steel

Hot dip galvanized coatings are found in a wide variety of applications requiring long-term, maintenance-free corrosion protection. The examples in this section will demonstrate the scope of galvanized steel use.

Example 1: Bridges. The first all hot dip galvanized bridge in the United States was erected in 1966 at Stearns Bayou, Ottawa County, MI. The bridge is 128 m (420 ft) long and has a 9.1 m (30-ft) wide roadway with a 1.5 m (5 ft) walkway on each side. All the components of this bridge were hot dip galvanized. To avoid possible effects from road salting, telescoping splash plates in the joints were installed to divert deck drainage away from the beams.

When inspected in 1997, the average coating thickness was 160 μm (6.3 mils), which is enough to last another 45 to 65 years. The bearing pads, the most deteriorated component of the bridge, showed a coating thickness of 74 μm (2.9 mils).

Example 2: Pulp and Paper Mills. Typical pulp and paper mills contain a number of areas that, in the absence of corrosion protection, would rapidly deteriorate because of exposure to various chemicals. A paper mill in the northwest United States used galvanized structural steel pipe supports, ladders, cages, and miscellaneous steel items in the stock tank, black liquor, lime kiln, and paper machine areas. Galvanized steel was used during the original construction 33 years ago and for subsequent expansions. All of the galvanized steel is located outside in a humid environment subject to salt spray. When inspected in 1985, coating thickness ranged from 90 to 160 μm (3.5 to 6.5 mils).

Example 3: Recreation. A galvanized roller coaster located on the beach near Wildwood, NJ was constructed in 1997 to a very exacting production schedule. All 350 tons of steel making up the framework, angle materials, bolts, and nuts were hot dip galvanized including the 20 foot-deep cement-covered piles that anchor the ride. At high tide, parts of the coaster go out over the water, making the hot dip galvanized coating and its corrosion performance an even more essential part of the structure.

Example 4: Utility Industry. A galvanized electrical utility substation located near Knoxville, TN and owned by the Tennessee Valley Authority was constructed in 1936 to handle 100,800 kW of electricity produced by a nearby dam. Substation structures are of a bolted-lattice construction. The minimum coating thickness measured in a 1997 inspection were 70 μm (2.75 mils) on lattice angles and 50 μm (2.5 mils) on bolt heads with an overall average of 83 μm (3.3 mils). Based on estimations of the original coating weight, this substation will last another 20 years before maintenance coating will be required.

Other Applications. Hot dip galvanized steel coated by the batch process is used in oil refineries and petrochemical industries and for miscellaneous highway uses, such as guard rail, light and sign standards, and fencing. The coating has found extensive use in water and wastewater treatment plants, both in atmospheric and immersion service. Applications such as electrical utility transmission towers, microwave transmission stations, pole line hardware, cooling towers and cooling tube bundles, nuts, bolts, and various fasteners, all involve extensive use of galvanizing.

Galvanized reinforcement bars, ties, and lintels for concrete and masonry reinforcement and support provide long-term corrosion protection in vital areas that are not normally visible. The use of galvanized materials in concrete reinforcement and masonry applications is ideal because the normal pH of these materials before setting is approximately 12 to 12.5, which corresponds to the pH range in which corrosion of zinc is at a minimum (Ref 26).

Reference cited in this section

26. S.R. Yeomans, "Applications of Galvanized Rebar in Reinforced Concrete Structures", paper presented at Corrosion2001, National Association of Corrosion Engineers, March 2001

T.J. Langill, Batch Process Hot Dip Galvanizing, *Corrosion: Fundamentals, Testing, and Protection*, Vol 13A, *ASM Handbook*, ASM International, 2003, p 794–802

Batch Process Hot Dip Galvanizing

Thomas J. Langill, American Galvanizers Association

Galvanizing Specifications

Galvanized coatings produced by the hot dip (batch) process are covered by numerous specifications. The following are pertinent specifications under the authority of ASTM:

- A 123 "Standard Specification for Zinc (Hot- Dip Galvanized) Coatings on Iron and Steel Products"
- A 143 "Standard Recommended Practice for Safeguarding Against Embrittlement of Hot- Dip Galvanized Structural Steel Products and Procedure for Detecting Embrittlement"
- A 153 "Standard Specification for Zinc Coating (Hot Dip) on Iron and Steel Hardware"
- A 384 "Standard Practice for Safeguarding Against Warpage and Distortion During Hot- Dip Galvanizing of Steel Assemblies"
- A 385 "Standard Practice for Providing High- Quality Zinc Coatings (Hot-Dip)"
- A 767 "Standard Specification for Zinc- Coated (Galvanized) Steel Bars for Concrete Reinforcement"
- A 780 "Standard Practice for Repair of Damaged and Uncoated Areas of Hot-Dip Galvanized Coatings"
- D 6386 "Standard Practice for Preparation of Zinc (Hot-Dip Galvanized) Coated Iron and Steel Product and Hardware Surfaces for Painting"
- E 376 "Standard Practice for Measuring Coating Thickness by Magnetic-Field or Eddy- Current (Electromagnetic) Test Methods"

T.J. Langill, Batch Process Hot Dip Galvanizing, *Corrosion: Fundamentals, Testing, and Protection*, Vol 13A, *ASM Handbook*, ASM International, 2003, p 794–802

Batch Process Hot Dip Galvanizing

Thomas J. Langill, American Galvanizers Association

Acknowledgment

This article is based in part on the article "Hot Dip Galvanizing by the Batch Process" by J. W. Gambrell in *Metals Handbook,* 9th ed., Volume 13, *Corrosion,* p 436, 1987.

T.J. Langill, Batch Process Hot Dip Galvanizing, *Corrosion: Fundamentals, Testing, and Protection*, Vol 13A, *ASM Handbook*, ASM International, 2003, p 794–802

Batch Process Hot Dip Galvanizing

Thomas J. Langill, American Galvanizers Association

References

1. X.G. Zhang, *Corrosion and Electrochemistry of Zinc,* Plenum Press, New York, 1996

2. D. Horstmann, Reaction Between Liquid Zinc and Silicon-Free and Silicon-Containing Steels, *Proceedings of the Seminar on Galvanizing of Silicon-Containing Steels*, International Lead-Zinc Research Organization, 1975, p 94

3. A.W. Stoneman, “A Closer Look at High Reactivity In Galvanizing,” paper presented at the TECH FORUM Meeting, American Galvanizers Association, Oct 1994

4. “Galvanizing Characteristics of Structural Steels and Their Weldments,” International Lead Zinc Research Organization, 1975

5. “Standard Practice for Safeguarding Against Embrittlement of Hot-Dip Galvanized Structural Steel Products and Procedure for Detecting Embrittlement,” A 143, *Annual Book of ASTM Standards,* American Society for Testing and Materials

6. “The Design of Products To Be Hot-Dip Galvanized After Fabrication,” American Galvanizers Association, 2000

7. “Recommended Details of Galvanized Structures,” American Galvanizers Association, 1996

8. “Standard Practice for Providing High- Quality Zinc Coatings (Hot-Dip),” A 385, *Annual Book of ASTM Standards,* American Society for Testing and Materials

9. *Welding Zinc Coated Steels,* D19.0-72, American Welding Society, 1973

10. R.M. Burns and W.W. Bradley, *Protective Coatings for Metals,* 2nd ed., Reinhold, 1955, p 128

11. S.K. Coburn, C.P. Larrabee, H.H. Lawson, and G.B. Ellis, Corrosiveness at Various Atmospheric Test Sites as Measured by Specimens of Steel and Zinc, *Metal Corrosion in the Atmosphere,* STP 435, American Society for Testing and Materials, 1968, p 371–372

12. C.J. Sunder and W.K. Boyd, *Zinc: Its Corrosion Resistance,* 2nd ed., International Lead Zinc Research Organization, 1983, p 113–150

13. F.C. Porter, *Corrosion Resistance of Zinc and Zinc Alloys,* Marcel Dekker, Inc., 1994

14. “Code of Practice for Protective Coating Iron and Steel Structures Against Corrosion,” BS 493, British Standards Institution, 1977, p 23

15. P.C. Birkemoe, W.D. Crouch, and W.H. Munse, “Design Criteria for Joining Galvanized Structurals,” Annual Report, ZM- 96, International Lead Zinc Research Organization, April 1969

16. R.A. Sanderson, “Fatigue Behaviour of High Strength Bolted Galvanized Joints,” M.A. thesis, University of Toronto, 1968

17. D.J.L. Kennedy, High Strength Bolted Galvanized Joints, *J. Struct. Div.*, Vol 98 (No. St12), Dec 1972, p 2723–2738

18. “Standard Practice for Repair of Damaged and Uncoated Areas of Hot-Dip Galvanized Coatings,” A 780, *Annual Book of ASTM Standards,* American Society for Testing and Materials

19. J.F.H. van Eijnsbergen, Twenty Years of Duplex Systems, *Metallwissenschaft Technik,* Vol 29 (No. 6), June 1975

20. J.F.H. van Eijnsbergen, *Duplex Systems,* Elsevier, 1994

21. D.S. Carr, “Performance of Painted Galvanized Steel,” paper presented at the semiannual meeting, Houston, TX, American Hot-Dip Galvanizers Association, Sept 1982

22. “Standard Practice for Preparation of Zinc (Hot-Dip Galvanized) Coated Iron and Steel Product and Hardware Surfaces for Painting,” D 6386, *Annual Book of ASTM Standards,* American Society for Testing and Materials

23. B.R. Appleman, Economics of Corrosion Protection by Coatings, *J. Prot. Coatings Linings,* Vol 2 (No. 3), March 1985

24. T.J. Kinstler, “Probability Functions in Corrosion Economics—or a Corrosion Engineer Goes to Monte Carlo,” paper presented at Corrosion/82, National Association of Corrosion Engineers, March 1982

25. M.P. Reina, K.R. Shields, and M.F. MeLampy, “Costing Considerations for Maintenance and New Construction Coating Work”, paper presented at Corrosion98, National Association of Corrosion Engineers, March 1998

26. S.R. Yeomans, “Applications of Galvanized Rebar in Reinforced Concrete Structures”, paper presented at Corrosion2001, National Association of Corrosion Engineers, March 2001

T.J. Langill, Batch Process Hot Dip Galvanizing, *Corrosion: Fundamentals, Testing, and Protection*, Vol 13A, *ASM Handbook,* ASM International, 2003, p 794–802

Batch Process Hot Dip Galvanizing

Thomas J. Langill, American Galvanizers Association

Selected References

- H. Bablik, *Galvanizing (Hot-Dip),* E. & F. N. Spon Ltd., London, 1950
- S.K. Coburn, Ed., *Atmospheric Factors Affecting the Corrosion of Engineering Metals,* ASTM STP 646, American Society for Testing and Materials, 1978
- J.R. Daesen, *Galvanizing Handbook,* Reinhold Publishing Company, New York, 1946
- S.W. Dean, Jr., E.C. Rhea, Ed., Atmospheric Corrosion of Metals, ASTM STP 767, American Society for Testing and Materials, 1980
- *Galvanizing for Corrosion Protection—A Specifier's Guide,* American Galvanizers Association, 2001

- F. Porter, *Zinc Handbook,* Marcel Dekker, Inc., 1991

M.L. Berndt and C.C. Berndt, Thermal Spray Coatings, *Corrosion: Fundamentals, Testing, and Protection*, Vol 13A*, ASM Handbook*, ASM International, 2003, p 803–813

Thermal Spray Coatings

Marita L. Berndt, Brookhaven National Laboratory; Christopher C. Berndt, State University of New York, Stony Brook

Introduction

THERMAL SPRAY COATINGS are a versatile and well-established means of protecting metals from corrosion in a wide variety of environments (Ref 1, 2). Many different materials can be used to produce thermal spray coatings, thereby providing effective solutions to diverse corrosion problems. These materials—including metals, ceramics, polymers, and combinations thereof—may be used to provide reliable long- term corrosion protection to substrates. Another use of thermal spray coatings is production of anodes for cathodic protection of steel reinforcement in concrete. Thermal spraying is virtually unlimited in scale and complexity of applications, ranging from small fasteners to structures. Production of coatings is rapid and can be automated. Other advantages of thermal spray coatings include portability, ability to seal or topcoat, abrasion and erosion resistance, and lack of curing requirements.

References cited in this section

1. D.A. Gerdeman and N.L. Hecht, *Arc Plasma Technology in Materials Science,* Springer- Verlag, 1972, 206 pages
2. W.E. Ballard, *Metal Spraying and Flame Deposition of Ceramics and Plastics,* 4th ed., Griffin, London, U.K., 1963

M.L. Berndt and C.C. Berndt, Thermal Spray Coatings, *Corrosion: Fundamentals, Testing, and Protection*, Vol 13A*, ASM Handbook*, ASM International, 2003, p 803–813

Thermal Spray Coatings

Marita L. Berndt, Brookhaven National Laboratory; Christopher C. Berndt, State University of New York, Stony Brook

Thermal Spray Processes

Thermal spray (TS) is a generic term used to describe a group of processes, including flame spraying, plasma spraying, arc metallization, detonation gun (D-gun), high-velocity oxyfuel (HVOF), and cold spray, that can be used to apply a variety of different coating materials for corrosion protection (Ref 3). Although these processes encompass a wide range of equipment needs, costs, materials selection and application, they can all be treated as belonging to the same family since the processing variables that are being altered are temperature and particle velocity. Figure 1 depicts the temperature-velocity processing envelope that allows materials engineers

to create a vast array of coatings for applications that include coatings for orthopedic hips, thermal barrier coatings for aerospace hardware, rebuilding of original equipment manufacturer components, and coatings to protect against corrosion.

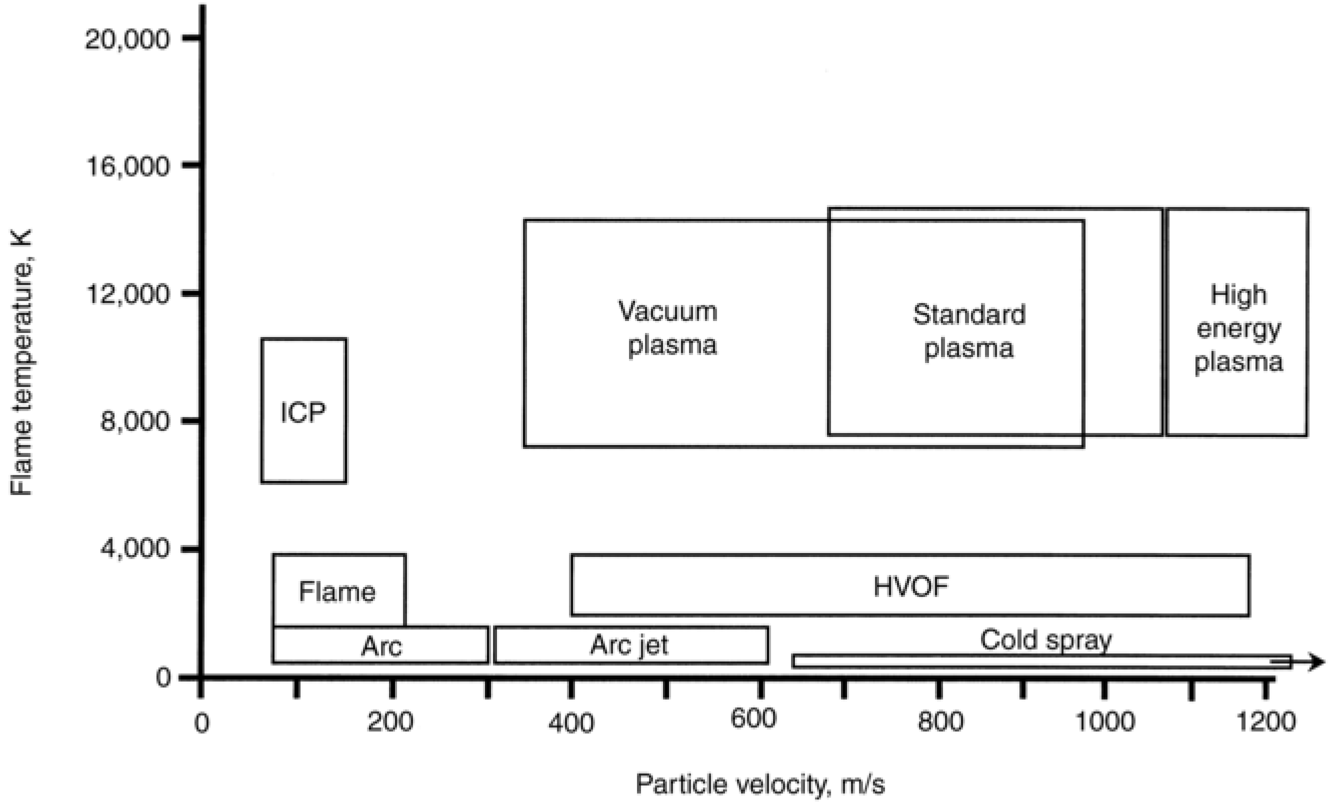

Fig. 1 The temperature-velocity distribution envelope of thermal spray processes. HVOF, high-velocity oxyfuel; ICP, induction coupled plasma

Besides temperature and velocity, another variable is the nature of the material that is used to form the coating. The material can be a powder, rod, wire, or liquid. The material that is fed into the TS process is termed feedstock, with the most common forms being powder and wire (Ref 4, 5). The feedstock morphologies are selected according to the process. Arc metallization and the wire flame processes require wire as the feedstock, whereas the most common renditions of the gas flame, plasma, and HVOF processes require powders.
Table 1 lists thermal spray processes. Those that are based on similar technological principles or that have equivalent names are grouped onto the same lines. The choice of process or material depends on the engineering application. Ceramic TS coatings generally require processes with higher velocities and temperatures than lower- melting point materials. Therefore, plasma, D- gun, and HVOF are the preferred techniques for deposition at high rates. The deposition of ceramics is more sensitive to spray parameters than is the deposition of metals.

Table 1 Thermal spray process parameters

Process	Temperature		Velocity	
	°C	**°F**	**m/s**	**ft/s**
Oxyacetylene gas flame spraying, flame spraying	3,000	5,430	150	490
Atmospheric plasma spraying, APS	12,000	21,630	900	2,955
Low-pressure plasma spraying, LPPS, VPS	1,200	2,190	900	2,955
Detonation gun spraying, D-gun	300	570	1,000	3,280
Ceramic rod process, Rokide process	3,000	5,430	150	490
Hypersonic plasma spraying, diamond jet gun (DJ gun), JetKote, High-velocity oxyfuel process (HVOF), J-gun, Topgun, Nova-jet, Plazjet	3,000	5,430	800	2,625
Arc metallization, wire spraying	1,500	2,730	200	655

Generic figures that demonstrate the principles behind TS processes are shown in Fig. 2. Wire flame, powder flame, electric arc, and plasma spray processes are depicted. The same principle applies in all cases; a feedstock is rapidly heated and then accelerated toward a suitably prepared substrate where on impact it consolidates to form an adherent coating.

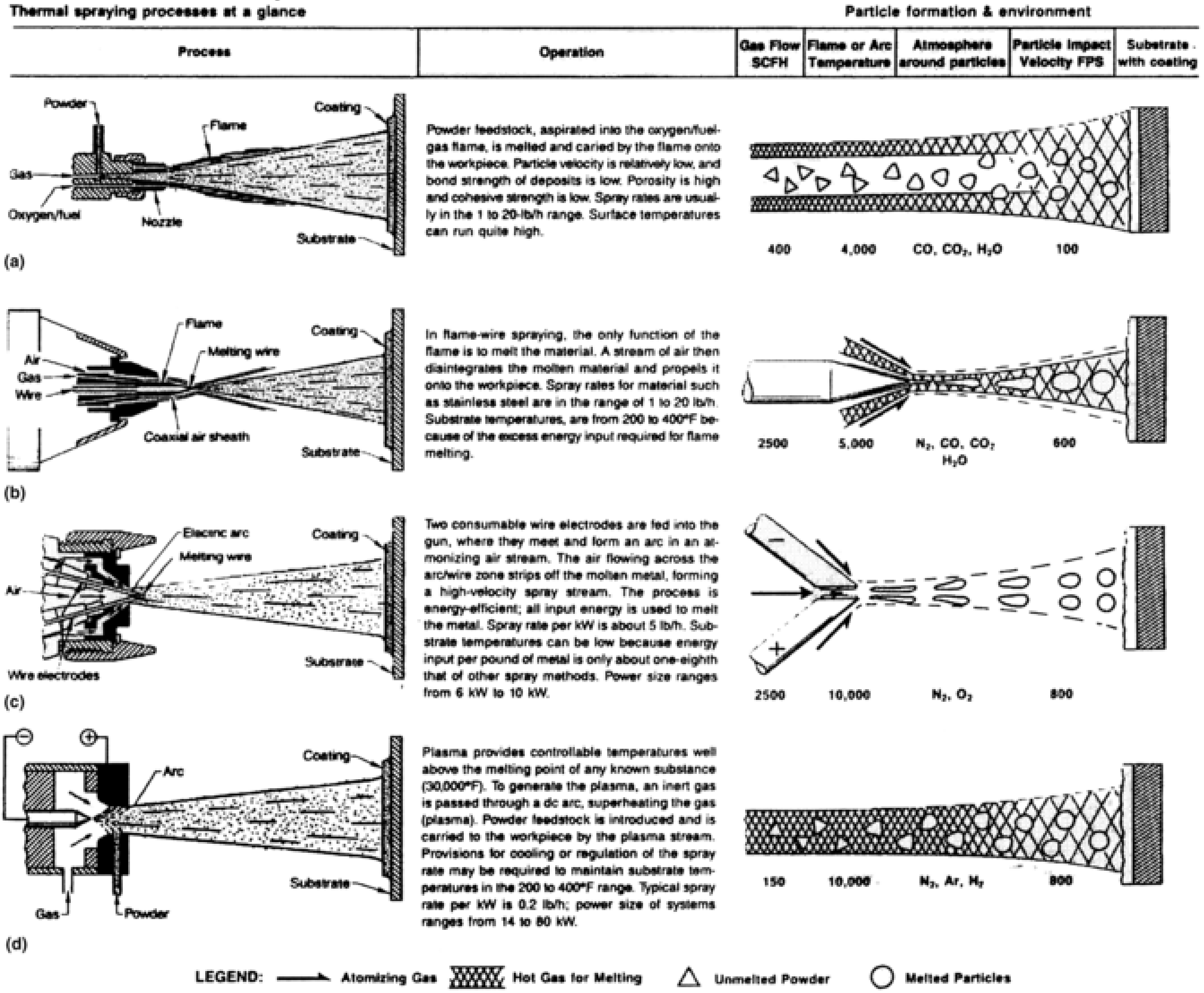

Fig. 2 Generic process schematics for (a) flame powder, (b) flame wire, (c) wire arc, and (d) plasma spray. Gas flow SCFH, standard cubic feet per hour; temperature, Kelvin; impact velocity FPS, feet per second. Source: Ref 6 (courtesy of Praxair-Tafa, Concord, NH)

The coating structure is often nonuniform and an example of an HVOF-sprayed Inconel 625 coating and the remelted condition is shown in Fig. 3 (Ref 7).

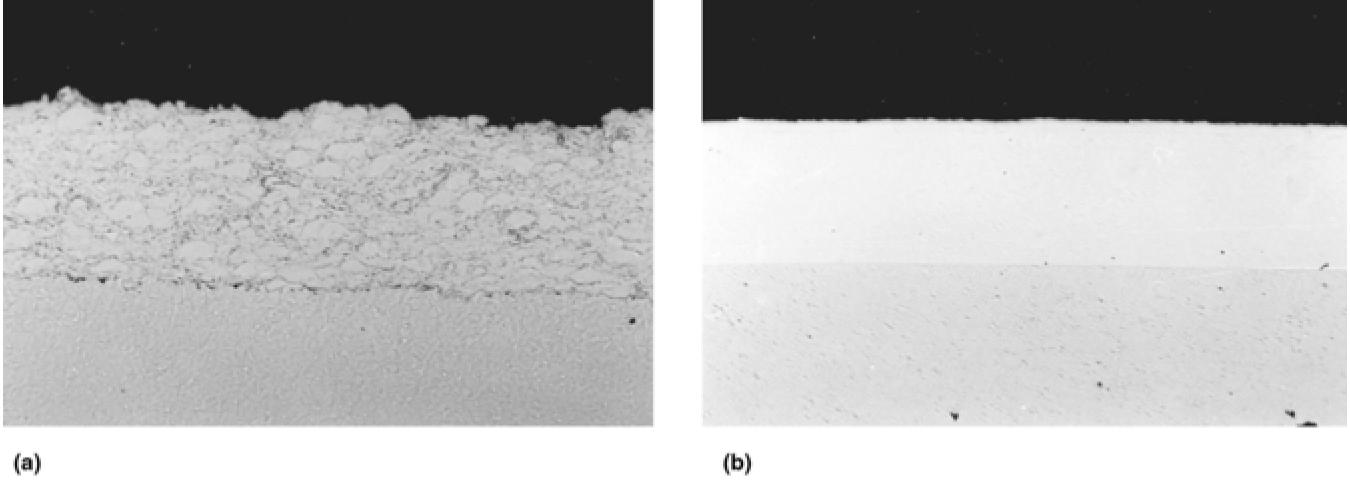

Fig. 3 Optical micrograph of high-velocity oxyfuel sprayed, Inconel 625 coating in (a) as-sprayed and (b) laser-remelted conditions. Coating thickness is 300 and 400 μm (12 and 16 μin.), respectively. Source: Ref 7

Coatings applied by the same technique can exhibit a wide variability (Ref 8, 9, 10) that arises from processing variables such as gas flow rates, the rate of coating deposition, the coating thickness, substrate preparation (e.g., preheat, postheat, and surface preparation schedules), type of spray material used, and the torch-to-substrate distance. These thermal spray parameters influence the quality of the adhesion to the substrate and the material properties such as electrical conductivity, density, and porosity. It is incorrect to assume that all thermal spray coatings of a particular material are identical in performance. The process must be "optimized" for each particular application.

Coatings are suited to specific applications because they retain some intrinsic material characteristics of the original coating powder. However, it must be emphasized that "bulk" material performance cannot be directly correlated to any property of the coating. The structure of a coating is quite dissimilar to that of a material produced by a bulk-fabrication process. Properties of the coating that may limit its utility include the physical, mechanical, thermal, electrochemical, and electrical properties. An additional property of great interest is adhesion to the substrate, since good adhesion is crucial for the coating to retain functionality throughout its intended service life.

References cited in this section

3. L. Pawlowski, *The Science and Engineering of Thermal Spray Coatings*, Wiley, Chichester, United Kingdom, 1995

4. G. Schwier, Plasma Spray Powders for Thermal Barrier Coating, of Advances in Thermal Spraying, *Proc. 11th Int. Thermal Spraying Conf.,* 8–12 Sept 1986 (Montreal, Canada), Pergamon Press, 1986, p 277–286

5. C.C. Berndt, "Preparation of Thermal Spray Powders," Education module on thermal spray, ASM International, 1992 (update available during 2003)

6. C.C. Berndt and R.H. Unger, Applications of Thermal Spray Coatings: A Technology with No Bounds, *The Finishing Line,* Vol 18 (No. 2), 2002, online invited paper

7. M. Vippola, S. Ahmaniemi, P. Vuoristo, T. Lepistö, and T. Mäntylä, Microstructural Study of Plasma Sprayed Chromium Oxide Coatings: Effect of Aluminum Phosphate Sealing, *Thermal Spray 2001: New Surfaces for a New Millennium,* C.C. Berndt, K.A. Khor, and E.F. Lugscheider, Ed., ASM International, 2001, p 607–612

8. P. Ostojic and C.C. Berndt, Variability in Strength of Thermally Sprayed Coatings, *J. Surf. Coat. Technol.,* Vol 34, 1988, p 43–50

9. K.A. Gross, C.C. Berndt, and V.J. Iacono, "Variability of Hydroxyapatite Coated Dental Implants," *The International J. Oral and Maxillofacial Implants,* Vol 13 (No. 5), 1998, p 601–610

10. C.C. Berndt, Tensile Adhesion Testing Methodology for Thermally Sprayed Coatings, *J. Mater. Eng.,* Vol 12 (No. 2), 1990, p 151–160

M.L. Berndt and C.C. Berndt, Thermal Spray Coatings, *Corrosion: Fundamentals, Testing, and Protection*, Vol 13A, *ASM Handbook*, ASM International, 2003, p 803–813

Thermal Spray Coatings

Marita L. Berndt, Brookhaven National Laboratory; Christopher C. Berndt, State University of New York, Stony Brook

Controlling the Structure, Properties, and Performance of Coatings

The Microstructural Character of Thermal Spray Coatings. It is the structure and chemistry of TS coatings that ultimately define their utility. Thermal spray coatings are produced from the repeated deposition of particles that are in the diameter range of 10 to 120 μm (0.4 to 4.7 mils). The coating structure is of lamellar morphology, much the same way as cards stacked on top of each other. Distinctive processing advantages of TS technology include the ability to coat most materials with an almost unlimited range of other materials, be they metals, ceramics, polymers, or combinations thereof. It is also possible to produce thick coatings from 0.1 to 2 mm (0.004 to 0.08 in.) routinely and to precisely control the coating formulation and chemistry.

The performance of a TS coating is directly related to this lamellar morphology. The resultant lamellar dimensions are about 60 μm (2.4 mils) in diameter and from 1 to 2.5 μm (0.04 to 0.1 mil) thick. Every coating structure is highly oriented with the lamellae parallel to the surface of the substrate.

Important microstructural artifacts, especially for corrosion-control applications that require a barrier to conducting and corrosive liquids, include porosity and microcracks.

It has been estimated (Ref 11, 12) that the real contact area of lamellae with the substrate and within the coating is 30% of the available boundary area. Direct measurements of interlamellar porosity have shown that the porosity is about 10 to 100 μm (0.4 to 4 mils) in size. Unmolten particles become incorporated into the coating and these, along with the interlamellar boundaries and porosity, constitute regions of poor bonding that may lead to failure of the coating system. The control of porosity is critical to the performance of any corrosion-control coating. Any defects that allow ingress of aggressive species will accelerate the coating-degradation process. Much attention has been paid to the control and modification of porosity that is inherent to the majority of conventional TS processes.

In one study (Ref 13), the porosity of thermal spray coatings was classified according to the potential mechanism of formation (Fig. 4). Type 1 porosity was exhibited between lamellae and was caused by the stacking of separate particles. This porosity can be directly related to the particle size and distribution characteristics of the spray material. Type 2 porosity was distinguished as trapped gas pockets caused by the turbulence of the gas flow during the TS process. Type 3 porosity was manifested in the form of gas bubbles caused by the dissolution of gas into the molten metal that evolved upon freezing of the metal. Type 4 porosity was caused by the disintegration of spray particles upon impact during the coating-deposition process. Type 5 porosity evolved from the condensation of partially evaporated particles and could be identified very often by containing powdery residues. Type 6 porosity arose due to solidification shrinkage, as observed between dendrites. Type 7 porosity results in microcracks regardless of their formation origin. Thus, although there may be some differences of opinion concerning the precise formation mechanism of porosity, there is general agreement that it can be controlled in a quite reproducible fashion by selection of appropriate TS parameters. Therefore, as mentioned previously, the control of temperature and velocity during the TS process is distinctly related to the deformation mechanism of the impacting lamellae and the formation of porosity.

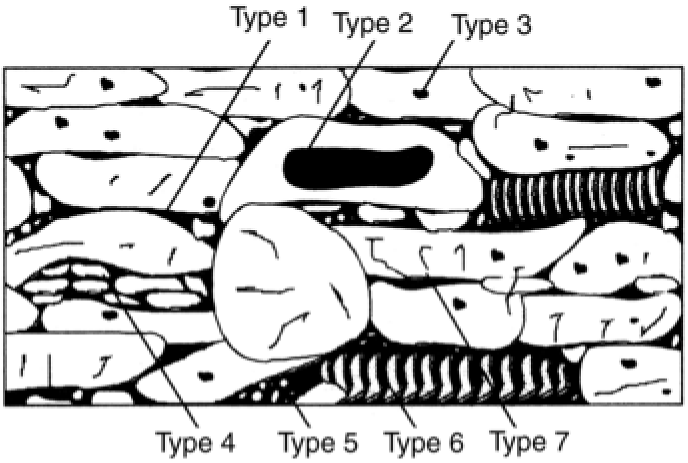

Fig. 4 Forms of porosity can be categorized within a thermal spray coating. Explanation in text. Source: Ref 13

Process Optimization and Parameterization. Optimization involves the study and analysis of operational parameters and their influence on a particular property. Single-wire arc spraying and powder flame spraying are two processes for manufacturing a corrosion-control coating.

When spraying a new material, the processing parameters are developed by taking the powder/ wire manufacturer's recommendation or that of an experienced TS engineer. Much of the TS industry uses such an experience base. This type of experience is valuable, but a trial-and-error method is not time or cost effective in spraying new materials or developing new microstructures. It is necessary to understand the relationship between properties and parameters for a given process and to present this relationship in a form that can be easily understood. Simple experiments can be set up to map a region of interest (Ref 14, 15). The map is referred to as a response over a region of parameters that needed evaluation.

Six primary process variables are:

- Enthalpy input into the particular TS process, whether it be gained from a combusting gas, the transfer of particle momentum to kinetic energy on impact against a substrate, or the use of direct-current electrical energy
- Feedstock delivery rates and the corresponding coating buildup per pass and the application rate in quantities of “mils per square foot per hour” or “micrometers per square meter per hour”
- Gas pressures and flow rates used for the combustion or arc processes
- The standoff distance between the TS device and substrate
- The surface preparation of the substrate
- Pre- or postconditioning of the substrate by heating or cooling

Control of these spray variables leads to the design of the microstructure and control of physical properties such as tensile adhesion strength, coating density, and surface roughness. They also relate to the deposition efficiency of the process, and this is directly correlated to the process economics. The role of these variables in the control of bond durability is often measured by a bond-strength technique, such as ASTM C 633 (Ref 16).

Surface Preparation. The most critical step is the preparation of the surface to be sprayed. The ideal surface is one that is roughened by grit blasting and that is contaminant free; that is, no oil, water, or blast media residues. It is recommended that the coating process take place within several hours of the surface preparation so that atmospheric oxidation of the highly energetic surface will not cause formation of a poorly bonded coating.

Coating Sealers and Surface Treatments. The material properties of coatings are a direct consequence of their complex structure and determine the overall coating behavior. Not all coatings are used in their as-sprayed condition. Metallic and ceramic coatings are often sealed to extend the protective properties and service life, particularly in immersed or severe environments. Sealers are typically low-viscosity liquids that penetrate and seal the coating pores. Commonly used sealers include vinyls, epoxies, epoxides, polyurethanes, phenolics, and silicones. Sealers are also used to produce decorative and smooth surface finishes. Other postprocessing surface treatments such as laser glazing and hot-isostatic pressing have been used to densify coatings and improve

corrosion resistance. More information on sealers and surface treatments can be found in Ref 7 and 17, 18, 19, 20.

References cited in this section

7. M. Vippola, S. Ahmaniemi, P. Vuoristo, T. Lepistö, and T. Mäntylä, Microstructural Study of Plasma Sprayed Chromium Oxide Coatings: Effect of Aluminum Phosphate Sealing, *Thermal Spray 2001: New Surfaces for a New Millennium,* C.C. Berndt, K.A. Khor, and E.F. Lugscheider, Ed., ASM International, 2001, p 607–612

11. R. McPherson, The Relationship between the Mechanism of Formation, Microstructure and Properties of Plasma-Sprayed Coatings, *Thin Solid Films,* Vol 83 (No. 3), 1981, p 297–310

12. R. McPherson, A Model for the Thermal- Conductivity of Plasma-Sprayed Ceramic Coatings, *Thin Solid Films,* Vol 112 (No. 1), 1984, p 89–95

13. M. Vreijling, "Electrochemical Characterisation of Metallic Thermally Sprayed Coatings," Ph.D. Thesis, TNO Institute of Industrial Technology, The Netherlands, 1998

14. D.J. Varacalle, Jr., D.P. Zeek, K.W. Couch, D.M. Benson, and S.M. Kirk, Flame Spraying of Polymers, *Thermal Spray: A United Forum for Scientific and Technological Advances,* C.C. Berndt, Ed., ASM International, 1997, p 231–238

15. T.J. Steeper, W.L. Rigg II, A.J. Rotolico, J.E. Nerz, D.J. Varacalle, Jr., and G.C. Wilson, A Taguchi Design of Experimental Study of Plasma Sprayed Alumina Coatings, *Thermal Spray Coatings: Research, Design and Applications,* C.C. Berndt and T.F. Bernecki, Ed., ASM International, 1993, p 31–36

16. "Standard Test Method for Adhesion or Cohesion Strength of Thermal Spray Coatings," C 633-01, *Annual Book of ASTM Standards,* ASTM, 2001

17. J. Tuominen, P. Vuoristo, T. Mäntylä, M. Kylmälahti, J. Vihinen, and P.H. Andersson, Improving Corrosion Properties of High- Velocity Oxy-Fuel Sprayed Inconel 625 by Using a High-Power Continuous Wave Neodymium-Doped Yttrium Aluminum Garnet Laser, *J. Therm. Spray Technol.,* Vol 9 (No. 4), 2000, p 513–519

18. S. Ahmaniemi, J. Tuominen, P. Vuoristo, and T. Mäntylä, Comparative Study of Different Sealing Methods for Thick Thermal Barrier Coatings, *Thermal Spray 2001: New Surfaces for a New Millennium,* C.C. Berndt, K.A. Khor, and E.F. Lugscheider, Ed., ASM International, 2001, p 157–165

19. J. Tuominen, P. Vuoristo, T. Mäntylä, S. Ahmaniemi, J. Vihinen, and P.H. Andersson, Corrosion Behavior of HVOF-Sprayed and Nd-YAG Laser-Remelted High-Chromium, Nickel-Chromium Coatings, *J. Therm. Spray Technol.,* Vol 11 (No. 2), 2002, p 233–243

20. M. Vippola, S. Ahmaniemi, P. Vuoristo, T. Lepistö, T. Mäntylä, and E. Olsson, Microstructural Study of Aluminum Phosphate- Sealed, Plasma-Sprayed Chromium Oxide Coating, *J. Therm. Spray Technol.,* Vol 11 (No. 2), 2002, p 253–260

M.L. Berndt and C.C. Berndt, Thermal Spray Coatings, *Corrosion: Fundamentals, Testing, and Protection*, Vol 13A, *ASM Handbook*, ASM International, 2003, p 803–813

Thermal Spray Coatings

Marita L. Berndt, Brookhaven National Laboratory; Christopher C. Berndt, State University of New York, Stony Brook

Criteria for Coating Selection

Selection According to the Corrosion Environment. Table 2 lists engineering components that have benefited in mitigating the stated corrosion-related environment. It is difficult to specify one coating for any one set of operational conditions since the coating choice will be dictated by the environment, temperature, component dimensions, any requirement for postprocessing of the coatings such as reduction of surface roughness, and other practical factors.

Table 2 Categorization of engineering components by anticipated type of corrosion

Corrosion type	Component
Cavitation	Water turbine buckets, wear rings in hydraulic turbines, impeller pump housings
Particle erosion	Exhaust fans, cyclone dust collectors, exhaust valve seats
Heat and oxidation resistance	Tuyeres for liquid metal, continuous casting molds, heat treating fixtures and brazing jigs, exhaust mufflers
Atmospheric and immersion corrosion	Electrical conduits, bridges, transformer cases, steam-cleaning equipment, ship superstructures, ship holds and tanks, storage tanks for oils, fuels, and solvents, power-line hardware, heat exchangers

Common atmospheric and immersion service environments with typical TS coatings for corrosion protection are given in (Table 3) (Ref 21) and elevated-temperature service is addressed in Table 4.

Table 3 Thermal spray coatings for atmospheric and immersion service

Exposure environment	Thickness of coating systems for 20-year expected service							
	Unsealed zinc		**Sealed zinc**		**Unsealed aluminum**		**Sealed aluminum**	
	µm	**mils**	**µm**	**mils**	**µm**	**mils**	**µm**	**mils**
Atmospheric								
Inland (nonpolluted)	150	6	150	6	150	6	100	4
Inland (polluted)	150	6	150	6	150	6	150	6
Coastal (nonpolluted)	250	10	150	6	150	6	150	6
Coastal (polluted)	350	14	250	10	250	10	150	6
Immersion								
Seawater splash zone	NA	NA	250	10	NA	NA	150	6
Seawater immersion	NA	NA	250	10	NA	NA	150	6

Table 4 Thermal spray coatings for elevated-temperature service

Service temperature, °C (°F)	Coating metal or alloy	Coating thickness	
		µm	**mils**
Up to 550 (1020)	Aluminum	175	7
Up to 550 (1020) in the presence of sulfurous gases	Ni-43Cr-2Ti	375	15
550–900 (1020–1650)	Aluminum or aluminum-iron	175	7
900–1000 (1652–1830)	Nickel-chromium or MCrAlY	375	15
900–1000 (1652–1830) in the presence of sulfurous gases	Nickel-chromium[(a)]	375	15

	Aluminum[(a)]	100	4

(a) Coating system consists of aluminum layer deposited on top of a nickel-chromium layer.

Applications for Metallic Coatings. Uses of metallic coatings for corrosion protection include bridges, buildings, marine vessels and structures, pipelines, chemical-processing equipment, power plants, exhaust flues, water-storage tanks, and boilers. Specific examples for use of HVOF nickel alloy C-276 and 316L stainless steel in petrochemical applications are given in Ref 22 and 23. Table 5 (Ref 6) details other TS applications in this highly demanding petrochemical environment.

Table 5 Petrochemical application of thermal spray coating

Component	Coating use	Process	Coating
Ball valves	Wear/corrosion	HVOF	Tungsten carbide
Gate valves	Wear/corrosion	HVOF	Tungsten carbide
Piston rods	Wear	Flame spray	Chrome oxide
Offshore oil rigs	Corrosion	Flame spray	Aluminum
Pump housings	Restore dimension	Arc spray	Aluminum bronze
Compressor cylinders	Restore dimension	Arc spray	420 stainless steel
Processing tanks	Corrosion resistance	Flame spray	Aluminum

Thermal sprayed metallic zinc and aluminum alloys coatings are commonly used for corrosion protection of steel substrates. Such coatings are sacrificial. It is also possible to thermal spray many other protective coatings such as nickel- base alloys, stainless steel, bronze, tin, and more exotic materials. These coatings are cathodic to the steel substrate, and it is important that they act as a barrier. For this reason, cathodic coatings are often sealed or surface treated to prevent penetration of corrosive species to the steel substrate. Furthermore, it is preferable that cathodic coatings are applied using a process that minimizes coating porosity such as HVOF. Selection of coating thickness depends on the severity of the environment and typically ranges between 50 and 500 μm (2 and 20 mils).

Experience with metallic TS coatings for infrastructure applications extends back to the 1940s. Sluice gates and canal lock gates that have been zinc coated have remained in perfect condition with virtually no maintenance for decades: the St. Denis Canal Lock Gates in France, coated in the early 1930s, are an outstanding example. The locks of the Panama Canal have also been zinc sprayed. In the United Kingdom, the suspension chains and other components of the Menai Straits Bridge were zinc sprayed just before World War II. During the war, the bridge received no maintenance. When it was inspected after the end of the war, the sprayed areas of the bridge were found to be in excellent condition. The steel deck structure, on the other hand, which had been painted but not sprayed, was rusting. The obvious reduction in required maintenance of the bridge prompted the British to apply sprayed metal coatings to numerous other road and railway bridges over the past 40 years. In the United States, metal sprayed coatings are presently being specified and used by departments of transportation (DOT) in Florida, Connecticut, California, Oregon, and Ohio.

The use of TS metallization makes it possible to achieve fully effective, maintenance-free protection of corrosion and corrosion-enhanced mechanical failure of steel structures for more than 30 years. Fifty-year protection effectiveness has been documented in rural environments and more than 20 years in harsh industrial, urban, and coastal regions. On an overall cost basis that includes maintenance, TS metallization has long been competitive with comparable corrosion- protection systems. Recent studies indicate that TS is now competitive on an initial cost basis alone. The conservative lifetime for a 255 μm (10 mil) thickness of zinc (or zinc-aluminum alloy) is approximately 25 years, which can be extended 15 years by the application of a vinyl paint as a topcoat to seal any porosity. Initial application costs of TS zinc (in 1998 U.S. dollars) are $10 per square foot or $0.40 per square foot per year for 25 years. Further examples and information on TS coatings for protection of steel structures can be found in Ref 24, 25, 26, 27.

In the case of cathodic protection (CP) of steel reinforcement in concrete, the TS coating is used as an anode. Zinc is the most common material for this purpose, although titanium has also been used. The coating is applied directly to the concrete substrate. The type of connection to the reinforcement depends on the CP system. It is more common to use impressed-current systems, although galvanic systems with zinc may also be effective in situations where the concrete exhibits low resistivity. Advantages of thermal sprayed anodes include ability to cover complex surfaces, uniform current distribution, and redundancy of an overlay as required with alternative mesh systems. Methods used to TS zinc onto concrete include oxyacetylene wire flame spraying, twin-wire arc

spray, and single-wire arc plasma spraying. These methods may form coatings that display different properties and process economics. Plasma and arc spraying have been used to produce titanium anodes.

Early applications that detailed the modern development of these coatings by regional DOTs in the United States are documented in Ref 28, 29, 30, 31. Updates of this area are covered in Ref 32 and 33 and field applications and the practical experience gained from the thermal spraying of zinc are described in Ref 34, 35, 36, 37. The development of new materials, especially titanium, is covered in Ref 38 and 39, while specific attention to bond strength, or adhesion, studies is the focus of the work reported in Ref 40 and 41. Reference 42 specifically discusses process development and the parameterization of the thermal spray variables in order to obtain the best coatings.

Applications for Ceramic Coatings. Ceramic coatings are used from 200 to 1150 °C (390 to 2100 °F). In such instances a metal-based "bond coat" (Ref 43, 44, 45) may be used as a compliant layer to compensate for thermally induced stresses that arise from the ceramic overlay. A 0.1 to 0.2 μm (0.004 to 0.008 mil) thick metallic layer is applied to the substrate by conventional TS methods prior to the ceramic coating. Such layers improve the bonding property of any subsequent thermal spray layer that is deposited. Bond coatings are based on alloys of nickel, chromium, molybdenum, and aluminum, with some additions of yttrium in special cases.

Applications for Polymer Coatings. Polymer spraying (Ref 46, 47, 48, 49) has gained significant commercial attention within the United States since the mid-1990s. Its acceptance as a replacement for paint is due to:

- No need for a primer
- A one-step process with no need for multiple passes
- No need for a topcoat
- Virtually zero volatile organic compounds (VOCs)
- Improved weathering resistance
- Excellent impact resistance

Thermal spray technology is also well suited for automation and can be adapted to existing robotic and automatic applicators. Polymer spraying is a one-coat process that acts as both the primer and the sealer, with no additional cure times, unlike the traditional multicoat painting processes. Thermal spraying is ideally suited for large structures that otherwise could not be dipped in a polymer suspension. Thermoplastic coatings can be repaired by simply remelting or applying extra material to the desired location. In addition, reports have shown that functionalized polyethylene polymers such as ethylene methacrylic acid copolymer (EMAA) and ethylene acrylic acid (EAA) can be applied in high humidity as well as at temperatures below freezing.

Polymer powders are specified by their chemistry, morphology, molecular weight distribution or melt-flow index, and particle size distribution. Spray parameters must be selected to accommodate each particular polymer formulation. A narrow particle size distribution is preferred to produce a homogeneous coating structure. A larger thermal input is required to melt larger particles and higher molecular weight organics. A large particle size or molecular weight distribution will facilitate the formation of numerous heterogeneities within the coating microstructure, creating voids, a range of splat aspect ratios, and degraded material. A processing window therefore exists for each polymer where poor particle coalescence defines the lower limit and pyrolization defines the upper limit. It is also important to note that the polymer may also cross link, undergo chain scission, and/or oxidize during processing.

Polymer powder is axially fed into the combustion zone via a carrier gas. The polymer particulates are propelled through the flame where, upon melting, they become droplets and are transported to the preheated substrate. As the molten particles impinge on the substrate, they deform and solidify, forming an interlaced network of splats. Porosity within the coating depends on the nature of the substrate surface, polymer melt viscosity, and decomposition products. The thickness of the coating is governed by the number of repeated passes of the spray gun across the substrate.

The heat source of the TS torch can be a plasma, combustion flame, or combustion exhaust as in the HVOF process. The technique is chosen on the basis of the polymer-melting characteristics. A simple combustion torch is well suited for low-melting-point polymers with a large processing window, such as polyethylene. High-melting-point polymers may require plasma deposition for maximum quality to melt the polymer without causing oxidation. Therefore, processing parameters must be selected for each polymer chemistry and deposition technique.

Two sets of distinct processes illustrate two fundamentally different spheres of polymer coatings. Both processes can generically be referred to as thermal spray; however, one process relies on a propane torch and the other class of processes uses the heat source of either a direct- current (dc) plasma torch or a HVOF gun. Thermal spraying of polymer powder is a 100% solids process. Polymers that can be applied using this process are listed in Table 6 and also include polyaryletherketone (PAEK), fluoropolymers, polyesters (Ref 51), and others.

Table 6 Selection of polymers applied as coatings via thermal spray processes

Polymer	Maximum temperature resistance	
	°C	**°F**
Ethylene methacrylic acid copolymer (EMAA)	40–60	105–140
Polyethylene (PE)	40–80	105–175
Polypropylene (PP)	70	160
Nylon 6,6 (PA)	65	150
Polyphenylene sulfide (PPS)	110	230
Polyethylene-tetrafluoroethylene copolymer (PE-TFE)	160	320
Polyetheretherketone (PEEK)	125	255
Liquid-crystal polymers (LCPs)	250	480
Phenolic epoxy	130	265
Polyimide (PI)	300	570

Source: Ref 50

Intrinsic properties of the polymers of interest include melt processibility, high chemical and impact resistance, electrical insulation, low coefficient of friction, ductility, and high toughness. Certain polymers also exhibit stability at elevated temperatures up to 300 °C (570 °F). Examples of thermal spraying of polymers are described in Ref 51, 52, 53, 54, while the thermal spraying of composites is detailed in Ref 56, 57, 58.

Thermal spraying of polymers is receiving increased attention in military and civil engineering sectors. The ability to apply thin (about 0.13 mm, or 0.005 in.) and thick (up to 6.4 mm, or 0.25 in.) coatings of polymers onto a variety of metals, ceramics, and composites of complex geometry provides solutions to component manufacture and on-site or factory rehabilitation. The development of complex coating chemistries then may be dual phase; for example, composites of plastics and metals or plastics and ceramics is an area that needs further research.

Applications of polymer coatings currently include snowplow blades, pump impellers, tank linings, external pipe coatings, structural steel coatings, transfer chutes, and vacuum systems. Here the intrinsic properties of polymers—such as high chemical resistance, high impact resistance, and high abrasion resistance—are used to advantage. One study has focused on incorporating recycled polymers in the feedstock (Ref 59).

References cited in this section

6. C.C. Berndt and R.H. Unger, Applications of Thermal Spray Coatings: A Technology with No Bounds, *The Finishing Line,* Vol 18 (No. 2), 2002, online invited paper

21. “Protection against Corrosion of Iron and Steel in Structures: Zinc and Aluminium Coatings—Guidelines,” BS EN ISO 14713, 1999. Note: this supersedes BS 5493: 1977, which is now obsolete.

22. L.N. Moskowitz, Application of HVOF Thermal Spraying to Solve Corrosion Problems in the Petroleum Industry—An Industrial Note, *J. Therm. Spray Technol.,* Vol 1 (No. 1), 1993, p 21–29

23. R.P. Krepski, “Thermal Spray Coating Applications in the Chemical Process Industries,” MTI Publication No. 42 for NACE International, 1994

24. T. Race, V. Hock, and A. Beitelman, Performance of Selected Metallized Coatings and Sealers on Lock and Dam Facilities, *J. Prot. Coat. Linings,* Vol 6 (No. 1), Jan 1989, p 37–44

25. J.R. Birchfield, Zinc Metallizing Protects a Bridge, *Weld. Des. Fabr.,* Oct 1986, 3 pages

26. R.H. Unger, Thermal Spraying of Bridges, *Thermal Spray: Advances in Coating Technology,* D.L. Hauck, Ed., ASM International, 1988, p 399–406

27. E.C. Lohrey, Metallizing Steel Bridges in the Field, *J. Prot. Coat. Linings,* Vol 12 (No. 5), 1995, p 39–50

28. J.A. Apostolos, D.M. Parks, and R.A. Carello, "Cathodic Protection Using Metallized Zinc; A 3.5 Year Progress Report," Paper 137, Corrosion '87 (San Francisco, CA), 1987

29. J.A. Apostolos, D.M. Parks, and R.A. Carello, Cathodic Protection using Metallized Zinc, *Mater. Perform.,* Vol 26 (No. 12), 1987, p 22–28

30. J.A. Apostolos, "Cathodic Protection of Reinforced Concrete by using Metallized Coatings and Conductive Paints," Transportation Research Record 962, 1984, 22–29

31. R.A. Carello, D.M. Parks, and J.A. Apostolos, "Development, Testing and Field Application of Metallized Cathodic Protection Coatings on Reinforced Concrete Substructures," Report No. FHW A/CA/TL-89/04, California Department of Transportation, Sacramento, CA, 1989

32. A.A. Sagüés and R.G. Powers, Sprayed- Zinc Sacrificial Anodes for Reinforced Concrete in Marine Service, *Corrosion,* Vol 52 (No. 7), 1996, p 508–522

33. S.D. Cramer, B.S. Covino, G.R. Holcomb, S.J. Bullard, J.H. Russell, F.J. Nelson, H.M. Laylor, and S.M. Soltesz, Corrosion Prevention and Remediation Strategies for Reinforced Concrete Coastal Bridges, *Cement Concrete Compos.,* Vol 24 (No. 1), 2002, p 101–117

34. D.G. Manning, Cathodic Protection of Concrete Highway Bridges, *Corrosion of Reinforcement in Concrete,* K.W.J. Treadaway and P.B. Bamforth, Ed., Elsevier Science, Essex, 1990, p 486–497

35. R.J. Kessler and R.G. Powers, "Zinc Metallizing for Galvanic Cathodic Protection of Steel Reinforced Concrete in a Marine Environment," Paper 324, Corrosion '90 (Las Vegas, NV), 1990

36. M.S. Wixson, "The Arc Spray Process for Application of Metallized Zinc Anodes," NACE Western Regional Corrosion Conference (Portland, OR), National Association of Corrosion Engineers, 1991

37. J.S. Tinnea, Field Performance of Sprayed Zinc Cathodic Protection Anodes, Proc. 15th ITSC Conference (Nice, France), 1998, p 37–42

38. S.D. Cramer, B.S. Covino, G.R. Holcomb, S.J. Bullard, W.K. Collins, R.D. Govier, R.D. Wilson, and H.M. Laylor, Thermal Sprayed Titanium Anode for Cathodic Protection of Reinforced Concrete Bridges, *J. Therm. Spray Technol.,* Vol 8 (No. 1), 1999, p 133–145

39. J.E. Bennett, T.J. Schue, and G. McGill, Protecting Reinforced Concrete Using Thermal Sprayed Titanium Anodes, *Mater. Perform.,* Vol 34 (No. 11), 1995, p 23–27

40. B.S. Covino, S.J. Bullard, G.R. Holcomb, S.D. Cramer, G.G. McGill, and C.B. Cryer, Bond Strength of Electrochemically Aged Arc-Sprayed Zinc Coatings on Concrete, *Corrosion,* Vol 53 (No. 5), 1997, p 399–411

41. R. Brousseau, M. Arnott, and B. Baldock, Long-Term Factors Influencing the Adhesion of Metallized Zinc to Concrete, *J. Therm. Spray Technol.,* Vol 5 (No. 1), 1996, p 49–52

42. C.C. Berndt, S. Reddy, and M.L. Allan, Optimization of Thermal Spray Parameters for Cathodic Protection of Reinforcement in Concrete, *Innovative Ideas for Controlling the Decaying Infrastructure,* V. Chaker, Ed., NACE International, 1995, p 51–64

43. F.N. Longo, "Self-Fusing Flame Spraying Material," U.S. Patent 3,305,326, 21 Feb 1967

44. F.J. Dittrich, New Flame Spray Technique for Forming Nickel-Aluminide Ceramic Systems, *Ceram. Bull.,* Vol 44, 1965, p 492–496

45. Z. Ding, R. Knight, and R.W. Smith, Effect of Bond Coat Processes and Surface Characteristics on the Failure Mechanism of Thermal Barrier Coatings, *Thermal Spray 2001: New Surfaces for a New Millennium,* C.C. Berndt, K.A. Khor, and E. Lugscheider, Ed., ASM International, 2001, p 173–177

46. J. Reimer, "Method and Apparatus for Spray Coating," U.S. Patent 4,632,309, 30 Dec 1986, 11 pages

47. R.F. Smart, Arc Plasma Sprayed Metals and Plastics, *Practical Metallic Composites,* The Welding Institute, 1974, PE19-26

48. E.R. George and J. Reimer, Flame Sprayed Thermoplastic Powder Coatings, *Polymer Eng. Sci.,* Vol 31 (No. 11), 1991, p 789–792

49. E. Petrovicova and L.S. Schadler, Thermal Spraying of Polymers, *Int. Mater. Rev.,* Vol 47 (No. 4), 2002, p 169–190

50. J.A. Brogan et al., Adhesion of Combustion- Sprayed Polymer Coatings, *1995 Advances in Thermal Spray Science and Technology,* C.C. Berndt and S. Sampath, Ed., ASM International, 1995, p 521–526

51. J. Economy, B.E. Nowak, and S.G. Cottis, Ekonol: A High Temperature Aromatic Polyester, *SAMPE J.,* Aug/Sept 1970, p 21–27

52. H. Liao, E. Beche, F. Berger, and C. Coddet, On the Microstructure of Thermally Sprayed PEEK Polymer, *Thermal Spray: Meeting the Challenges of the 21st Century,* C. Coddet, Ed., ASM International, 1998, p 25–29

53. E. Lugscheider, C. Herbst, and A. Fischer, Thermal Spraying of High Performance Thermoplastics, *Thermal Spray: Meeting the Challenges of the 21st Century,* C. Coddet, Ed., ASM International, 1998, p 19–24

54. P.J. Loustaunau and D. Horton, EMAA Thermoplastic Powder Coatings in Shop and Field Applications, *Mater. Perform.,* Vol 33 (No. 7), 1994, p 32–36

56. Y. Bao and D.T. Gawnes, Plasma Spraying of Glass-Polyamide Composite Coatings, *Thermal Spray Coatings: Research, Design and Applications,* C.C. Berndt and T. Bernecki, Ed., ASM International, 1993, p 417–422

57. R. Knight, X. Fang, and T.E. Twardowski, Structure and Properties of HVOF Sprayed Amorphous Polymer Matrix Nanocomposite Coatings, *Thermal Spray 2001: New Surfaces for a New Millennium,* C.C. Berndt, K.A. Khor, and E. Lugscheider, Ed., ASM International, 2001, p 361–368

58. T.E. Twardowski, M. Reilly, and R. Knight, Properties of HVOF Sprayed Multi-Scale Polymer/Silica Nanocomposite Coatings, *Thermal Spray 2001: New Surfaces for a New Millennium,* C.C. Berndt, K.A. Khor, and E.F. Lugscheider, Ed., ASM International, 2001, p 369–373

59. J.A. Brogan, R. Lampo, and C.C. Berndt, Thermal Spraying of Polymers, Proc. Fourth World Congress on Coating Systems for Bridges and Steel Structures

---

M.L. Berndt and C.C. Berndt, Thermal Spray Coatings, *Corrosion: Fundamentals, Testing, and Protection*, Vol 13A, *ASM Handbook*, ASM International, 2003, p 803–813

Thermal Spray Coatings

Marita L. Berndt, Brookhaven National Laboratory; Christopher C. Berndt, State University of New York, Stony Brook

---

Costs of Thermal Spray Coatings

Experience with the Oregon DOT in the rehabilitation of the Cape Creek, Depoe Bay, and Yaquina Bay bridges indicated an expense of $19.1 million (in 1995 U.S. dollars) compared to a replacement cost of $70 million (Ref 60).

Reference 31 specifically details financial aspects of a ConnDOT bid. It is stated that the bid price for the field metallizing of five bridges comprising a total area of 5866 m^2 (62,950 ft^2) amounted to \$110/m^2 (\$10/ft^2) in 1995 U.S. dollars. The bid price for class 3 containment of waste generated during the rehabilitation contract was \$50/m^2 (\$4.50/ft^2), and the disposal of this debris was \$3.30/m^2 (0.30/ft^2).

A detailed cost analysis indicates that the most expensive item in either the twin-wire arc (to spray zinc) or a gas flame technique to spray polymer is the feedstock. The materials used during an arc wire process will constitute ~73% of the total running cost, while the polymer feedstock is ~93% of the total cost (Table 7). As well, a polymer coating process (by a gas flame thermal spray method) is about 330% more expensive than zinc sprayed by two-wire arc. Table 7 also indicates the relative startup costs with polymer spraying being about one-half that of two-wire arc. The prorated power and labor costs for both of these processes are approximately equivalent.

Table 7 Percent costs of twin-wire arc and polymer spray methods

Cost factor	Cost, %	
	Zinc by twin-wire arc	**Polymer by gas flame process**
Power	2	0.5
Labor	18	5.5
Materials	73	93
Equipment	7	1
Total cost	**100**	**100**
Relative total cost, $	1	3.3

References cited in this section

31. R.A. Carello, D.M. Parks, and J.A. Apostolos, “Development, Testing and Field Application of Metallized Cathodic Protection Coatings on Reinforced Concrete Substructures,” Report No. FHW A/CA/TL-89/04, California Department of Transportation, Sacramento, CA, 1989

60. G.R. Holcomb and C.B. Cryer, Cost of Impressed Current Cathodic Protection for Coastal Oregon Bridges, *Mater. Perform.,* Vol 37 (No. 7)

M.L. Berndt and C.C. Berndt, Thermal Spray Coatings, *Corrosion: Fundamentals, Testing, and Protection*, Vol 13A, *ASM Handbook*, ASM International, 2003, p 803–813

Thermal Spray Coatings

Marita L. Berndt, Brookhaven National Laboratory; Christopher C. Berndt, State University of New York, Stony Brook

Case Studies

Example 1: Adhesion of Polymer Coatings. This case history of EMAA applied to steel does not constitute a recommendation for a specific application, but it does demonstrate the unique characteristics of TS polymeric coatings applied by a gas flame process with fluidized powder feed.

The coating was studied for application in an environment involving biochemical treatment of geothermal sludge. An Atlas cell (ASTM C 868) arrangement was used. The test solution was hypersaline brine with composition of:

Compound	Content, ppm
NaCl	58,000
$CaCl_2$	25,000
KCl	15,000
$FeCl_2$	1,000
$MnCl_2$	930
$SrCl_2$	430
LiCl	410
$ZnCl_2$	370
H_3BO_3	300
$BaCl_2$	130

The pH of the brine was 4.15. The test temperature was 55 °C (130 °F), and the duration was 12 weeks.

At the completion of the tests, the coated panels were visually examined for signs of deterioration such as blistering, discoloration, and loss of gloss. The residual adhesion was determined for EMAA coatings by measuring the peel strength (ASTM D 3167). The plates were cut into strips 25 mm (1 in.) wide, and the orientation was vertical so that the strip traversed the vapor and immersion-exposed zones. The strips cut from the outer edges of the plates were beyond the exposure zone. The coatings were peeled back approximately 40 mm (1.6 in.) using a razor blade to enable the coating to be gripped. An Instron tensile testing machine was used, and the crosshead speed was 152 mm/min (6 in./ min).

Figure 5 depicts the peel force versus displacement curve for a strip cut from the edge of one of the panels (Ref 61). The coating in this location was not exposed to brine. The peel force was relatively constant, and the failure mode was adhesive. The average peel strength was 4.33 Pa (0.0006 psi) Figure 5 also shows the results for a strip cut through an exposed area. The peel force was low in the initial region, and this corresponded to the presence of corrosion products at the interface. The increase in peel force at higher displacement occurred outside the exposed area. Peel strength varied from 1.97 to 6.97 Pa (0.0003 to 0.001 psi). Plastic deformation of the coatings occurred during peeling, and this was concentrated in the areas outside the test cell where greater force was required to remove the coating.

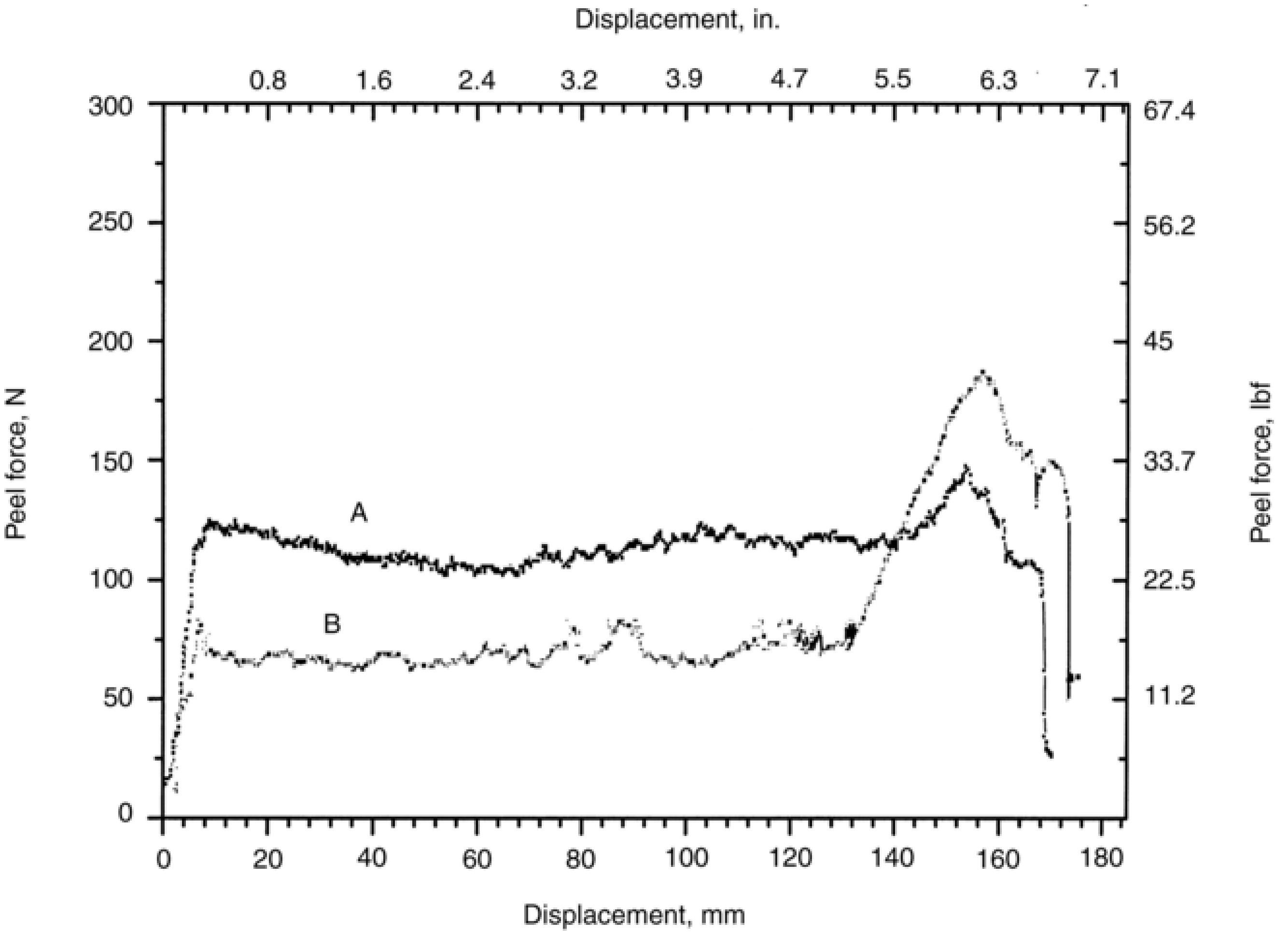

Fig. 5 Peel-force measurements for thermal spray coatings applied to as-received (curve A) and environmentally exposed (curve B) polymeric coatings. Source: Ref 61

Fracture surfaces from the EMAA mild-steel peel tests were examined under a scanning electron microscope (SEM). An example of mixed adhesive/cohesive failure in an uncorroded area is shown in Fig. 6(a). The dark areas are polymer adhering to the steel surface. Spherical pores, 100 to 200 μm (4 to 8 mil) diameter, in the polymer are evident, and failure often has occurred through these pores. Ductile tearing, indicative of a well-formed coating, may be observed around the edges of a pore (Fig. 6b).

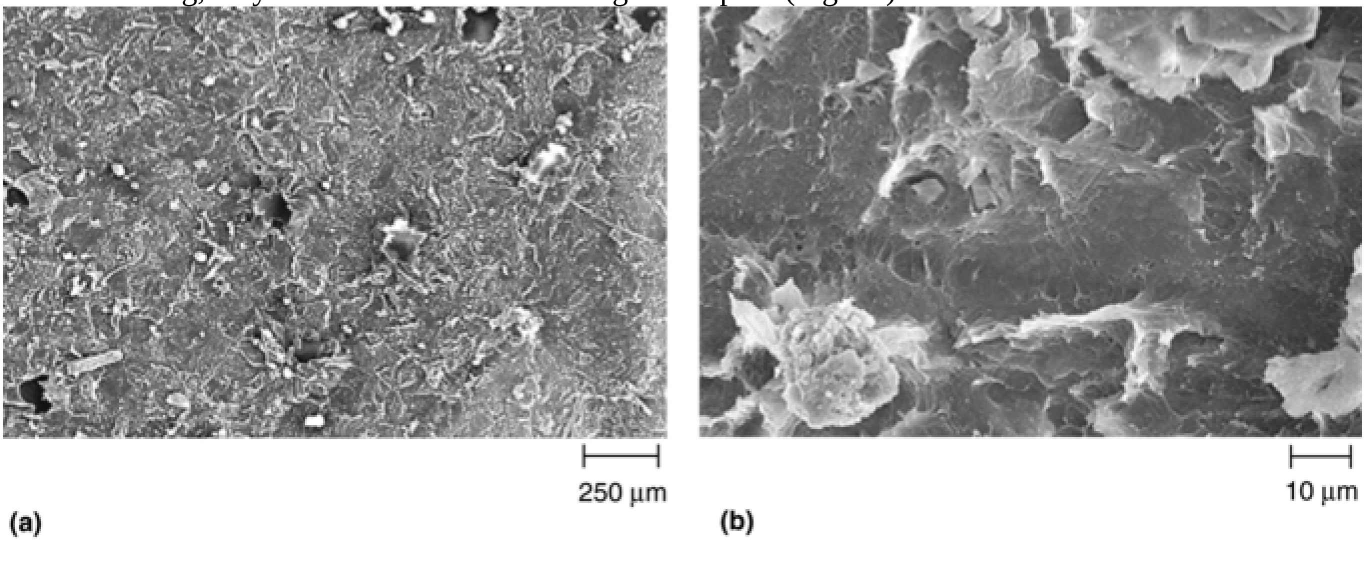

Fig. 6 Fracture surface morphology of a polymeric coatings that exhibits (a) porosity artifacts and (b) ductile tearing. Source: Ref 61

Example 2: Thermal Spray Process to Remove Lead-Base Paint. An alternative means of surface preparation, patented by the U.S. Army Corps of Engineers, is on-site vitrification of hazardous waste. Thermal spraying of specially developed molten glass is used to encapsulate and chemically stabilize lead-base paint and rust (Ref 62). The encapsulant is then removed by chipping off relatively large chunks, which are readily removed for disposal. The objective has been to develop technology and guidance for maintenance where work will involve the removal of a coating material containing lead-base paint or other hazardous waste. Spray techniques, glass deposit chemistries, and encapsulation effectiveness are being testing and optimized.

The U.S. Environmental Protection Agency (EPA) regulations have necessitated the removal and containment of toxic lead from lead oxide containing organic paints. Traditional grit blasting of hydraulic structures and highway bridges potentially involves the wide distribution of lead contaminant some distance from work sites and inflicting unacceptable health risks. The thermal spray vitrification process (TSVP) is an elegant technique that has been proposed to alleviate this problem. The TSVP is a “green technology” that seeks to provide an economic solution to the maintenance of existing structures, for example, bridges and other infrastructure. In this process, glass powder is melted in a high-temperature flame and sprayed onto the lead painted surface. On impact of the molten glass droplet, lead diffuses and dissolves from the paint into the glass and forms a stable glass network that is resistant to lead leaching by acid attack.

When a molten droplet of glass strikes a lead painted surface, the following phenomena occur. First, the droplet will spread, splatter, and deform to form an intimate contact layer between the glass and the painted surface. The molten glass will penetrate and fill the pores and cavities in the surface by capillary transport. Mass transport rates and extent of reaction will depend on the properties of the molten glass such as surface tension, kinematic viscosity, and heat-transfer coefficient and on the properties of the coated surface. Next, there is diffusion, dissolution, and natural and forced convection of lead into the molten glass. The kinetics of this reaction will be controlled by the diffusivity of lead in the paint. The temperature and vapor pressure of the lead as well as the pore structure of the glass are the deciding factors for this phenomenon. There may also be solid-state interdiffusion of cationic species at the interface between the glass and painted surface, and the reaction layer will grow into the glass and the substrate surface. The cation with the lowest diffusivity will be the rate-limiting specie for this reaction. In summary, the lead can be absorbed into the glass by gas-phase transport, dissolution into liquid slag, and solid- state interdiffusion of cationic species.

Dissolution and diffusion of lead into the glass are determined by the time duration for which the glass particles remain molten and at high temperatures, respectively. In thermal spray processes, the coating material is melted in a flame and then quenched on impact onto a cold underlayer. The heating and cooling of the particles depend on the thermophysical properties of the particles in their liquid and solid states and their processing environments.

The composition of the glass basically decides its thermophysical properties. Selection of the glass composition for the lead-vitrification application should follow the following three criteria:

- Lead dissolution into the glass should follow the congruent path of the phase equilibrium diagram.
- The kinematic viscosity should be low.
- The glass should be stable in the desired range of lead concentrations.

Glass modifiers such as alkali oxides break the glass network and thereby reduce the melt viscosity. However, breaking of the network also weakens the glass structure and affects the stability of the glass. Intermediate oxides such as alumina, titania, and lead oxide, for example, increase the stability of the glass, but since they increase the surface energy of the melt, the kinematic viscosity of the glass melt also increases with the addition of the intermediate oxides. Thus, the composition of the glass should be optimized so that it will have high lead absorptivity and lead-leaching resistivity.

The processing environment that decides the rate at which the heat and momentum transfer to and from the particle occur are controlled by a large number of spray-process parameters such as the operating power level, stand-off distance, powder feed rate, gas flow rates, carrier gas flow rate, and gun traverse. Considerable amount of information already exists on the effect of spray variables on the properties of the coatings.

References cited in this section

61. M.L. Allan, C.C. Berndt, J.A. Brogan, and D. Otterson, Thermal Sprayed Polymer Coatings for Corrosion Protection in a Biochemical Treatment Process, *Thermal Spray: Meeting the Challenges of the 21st Century,* C. Coddet, Ed., ASM International, 1998, p 13–18

62. J. Karthikeyan et al., Thermal Spray Vitrification Process for the Removal of Lead Oxide Contained in Organic Paints, Advances in Thermal Spray Science and Technology, C.C. Berndt and S. Sampath, Ed., ASM International, 1995, p 559–604

M.L. Berndt and C.C. Berndt, Thermal Spray Coatings, *Corrosion: Fundamentals, Testing, and Protection*, Vol 13A, *ASM Handbook*, ASM International, 2003, p 803–813

Thermal Spray Coatings

Marita L. Berndt, Brookhaven National Laboratory; Christopher C. Berndt, State University of New York, Stony Brook

---

Specification and Quality Control for Coatings

Specifications and Guidelines for TS Applicators. Several professional and industrial organizations in the United States have developed guidelines with the intent of assisting those people who need to specify coatings for a particular application as well as helping practical TS operators accomplish a specific task. The listing below indicates the organization that generated the particular document as well as a very brief description of the content of the document. It should be noted that several of these documents are still being refined.

- **AWS C2.16-92,** "Guide for Thermal Spray Operator Qualification." This guide recommends thermal spray operator qualification procedures. It covers applicable documents relating to thermal spray equipment, consumables, and safety. It also contains operator qualification and coating system analysis forms. Note: this standard is being revised; see C2.16A standard in preparation.
- **AWS C2.18-93,** "Guide for the Protection of Steel with Thermal Sprayed Coatings of Aluminum and Zinc and Their Alloys and Composites." This guide sets forth recommended thermal spray operator qualification procedures. It covers applicable documents relating to thermal spray equipment consumables and safety. It also contains operator qualification and coating analysis forms. Note: this standard is being revised; see C2.18A Part A and Part B standard in preparation.
- **AWS C2-18A, NACE (designation to be determined), and SSPC CS 23.00A, Part A,** "Specification for the Application of Thermal Spray Coatings (Metallizing) of Aluminum, Zinc, and Their Alloys and Composites for the Corrosion Protection of Steel," Draft No.3, 2001-05-22 (45 pages). This standard is a procedure for the application of metallic TS coatings of aluminum, zinc, and their alloys and composites for the corrosion protection of steel. Required equipment, application procedures, and in-process quality-control (QC) checkpoints are specified. This standard may be used as a procurement document. Appendices include a "model procurement specification." Note: this standard is the update that will be the permanent standard to replace the interim standard SSPC CS 23.00(I) (1999–present).
- **AWS C2-18A, NACE (designation to be determined), and SSPC CS 23.00A,** "Application of Thermal Spray Coatings (Metallizing) of Aluminum, Zinc, and Their Alloys and Composites for the Corrosion Protection of Steel, Part B: Guide," Draft No.2, 2001- 10-10 (47 pages). This guide presents additional information and recommendations on safety, selection of TS coatings, inspection guide and checkoff list, bend testing, thermal spray operator qualification, thermal spray equipment qualification, and the maintenance and repair of TS coatings (1993–present).
- **AWS C2.19-XX,** "Machine Element Repair with Thermal Spray Coatings," CD No.3, 5 May 2000 (52 pages). This standard covers thermal spray processes for machinery element repair of ferrous and nonferrous substrates. Included are requirements for the qualification of thermal spray procedures and operators, requirements and guidance for use of thermal spray material and equipment, quality

assurance requirements, and descriptions of applicable qualification tests. Note: the Navy requested AWS incorporate MIL- STD-1687A(SH) into an AWS standard, April 1998 (1998–present).

- **AWS C2.20-XX,** "Specification for Thermal Spraying Zinc Anodes on Steel Reinforced Concrete," CD No.3, 16 Jan 2001 (25 pages). This AWS standard is a specification for thermal spraying zinc anodes on steel reinforced concrete. The scope includes: job description, safety, pass/fail job reference standards, feedstock materials, equipment, a step-by-step process instruction for surface preparation, thermal spraying, and quality control. There are three annexes: job control record, operator qualification, and portable adhesion testing (1995–present).
- **AWS C2.21-XX,** "Specification for Thermal Spray Equipment Acceptance Inspection," WD-4, 15 May 1998 (19 pages). This standard specifies the thermal spray equipment acceptance requirements for plasma, arc wire, flame powder, wire, rod, cord, and HVOF equipment. The equipment supplier shall provide proof of suitability. Example inspection reports are provided in four nonmandatory appendices.
- **AWS C2.25-XX,** "Specification for Solid and Composite Wires, and Ceramic Rods for Thermal Spraying," DS 1; 7-11-2001 (25 pages). This specification defines the as-manufactured, chemical-composition classification requirements for solid and composite wires and ceramic rods for thermal spraying. Requirements for standard sizes, marking, manufacturing, and packaging are included. 100 materials are listed (1985–present).
- **SSPC-QP 6,** "Standard Procedure for Evaluating Qualifications of Thermal Spray (Metallizing) Applicators," Draft No.2, 2001-21 (23 pages). This standard describes a method for evaluating the qualification of thermal spray (metallizing) applicators to apply thermal spray coatings per SSPC CS 23.00(I), "Interim Specification for the Application of Thermal Spray Coatings (Metallizing) of Aluminum, Zinc and Their Alloys and Composites for the Corrosion Protection of Steel," (latest edition), that is, the surface preparation, thermal spraying, and sealing or sealing and topcoating of components/assemblies in the shop and complex structures in the field. These procedures are applicable to a fabricating shop, shipyard, or other entity that applies coatings in the shop, even though providing coating application services is not the primary function (2001–present).
- **SSPC CS 23.00(I),** "Interim Specification for the Application of Thermal Spray Coatings (Metallizing) of Aluminum, Zinc and Their Alloys and Composites for the Corrosion Protection of Steel," 1 March 2000. This interim specification covers the requirements of thermal spray metallic coatings, with and without, sealers and topcoats, as a means to prevent the corrosion of steel surfaces. Types of metallic coatings include pure zinc, pure aluminum, and zinc/aluminum alloy, 85% Zn/ 15% Al by weight. Note: this standard is being incorporated into AWS C2.18A/NACE (designation to be determined) SSPC CS 23.00A Part A, standard in preparation.

The AWS C2.18 documentation recommends guidelines for thermal spraying zinc and aluminum wires and powders (Table 8). The prime quality-control checkpoints are stated as measurement of substrate temperature; measurement of air temperature, dew point, and humidity; appropriate measurement of the TS coating thickness; measurement of the TS coating ductility; and evaluation of representative bend coupons, companion coupons, and other samples.

Table 8 AWS guidelines for thermal spraying of zinc and aluminum

Feedstock	Flame spray		Arc spray	
	Deposit efficiency, %	**Material required, lb/ft^2/0.001 in.**	**Deposit efficiency, %**	**Materials required, lb/ft^2/0.001 in.**
Aluminum wire	80–85	0.014	70–75	0.017
Aluminum powder	85–90	0.014	NA	NA
Zinc wire	65–70	0.050	60–65	0.054
Zinc powder	85–90	0.039	NA	NA
85/15 wire	85–90	0.036	70–75	0.049
90/10 MMC wire[(a)]	80–85	0.014	70–75	0.017

(a) MMC, metal matrix composite

Standards for Coatings. A great challenge for TS coatings is their specification and standardization since, as described previously, the character of a TS coating is controlled greatly by their manufacturing method. Much of the history of TS coatings has relied on internal company specifications so that reproducible coatings might be produced, and the outgrowth of such documentation now constitutes accepted practice. With regard to testing practices, the standard methods developed by ASTM (or equivalent organizations) are a good basis on which to recommend procedures that rank coatings or different materials. Table 9 lists those ASTM standards that are most appropriate to TS coatings, but it should be kept in mind that these often provide only qualitative, ranking data rather than quantitative, life-prediction, and performance data.

Table 9 ASTM standards related to thermal spray

ASTM designation	Title
Corrosion	
B 117-95	Practice for Operating Salt Spray (Fog) Testing Apparatus
G 3-89 (1994)	Practice for Conventions Applicable to Electrochemical Measurements in Corrosion Testing
G 5-94	Reference Test Method for Making Potentiostatic and Potentiodynamic Anodic Polarization Measurements
G 15-97	Terminology Relating to Corrosion and Corrosion Testing
G 78-95	Guide for Crevice Corrosion Testing of Iron-Base and Nickel-Base Stainless Alloys in Seawater and Other Chloride-Containing Aqueous Environments
G 85-94	Practice for Modified Salt Spray (Fog) Testing
Wear	
G 40-96	Terminology Relating to Wear and Erosion
G 65-94	Test Method for Measuring Abrasion Using the Dry Sand/Rubber Wheel Apparatus
G 73-93	Practice for Liquid Impingement Erosion Testing
G 76-95	Test Method for Conducting Erosion Tests by Solid Particle Impingement Using Gas Jets
G 77-93	Test Method for Ranking Resistance of Materials to Sliding Wear Using Block-on-Ring Wear Test
G 81-97	Practice for Jaw Crusher Gouging Abrasion Test
G 98-91 (1996)	Test Method for Galling Resistance of Materials
G 99-95	Test Method for Wear Testing with a Pin-on-Disk Apparatus
G 105-89	Test Method for Conducting Wet Sand/Rubber Wheel Abrasion Tests
G 115-93	Guide for Measuring and Reporting Friction Coefficients
G 119-93	Guide for Determining Synergism between Wear and Corrosion
G 132-96	Test Method for Pin Abrasion Testing
G 133-95	Test Method for Linearly Reciprocating Ball-on-Flat Sliding Wear
G 134-95	Test Method for Erosion of Solid Materials by a Cavitating Liquid Jet

Adhesion of Coatings. Adhesion is a property of major concern for thermal sprayed coatings since it is necessary for the coating to adhere to the substrate throughout the design life of the system. Numerous adhesion tests can be used to evaluate the adhesion strength of TS coatings and thereby ascertain the utility of coatings. For example, bond-strength measurements allow optimization of different grit blast media and the angle of grit blasting, as well as establishing the best coating thickness for aluminum coatings (Ref 63). Other workers (Ref 42, 64) have optimized plasma spray parameters with respect to strength. In recent years, with the adoption of design of experiment methods, bond strength measurements along with other physical measurements, such as roughness and porosity, have been used to select coatings for industrial specifications.

Adhesion is a property of major consideration when thermal spraying coatings since it is necessary for the coating to adhere to the substrate throughout the design life of the system. Numerous adhesion tests can be used to evaluate the adhesion strength of TS coatings. The most common test is the tensile adhesion test (TAT), which, being simple to perform, is a widely used method as a quality-control tool (Ref 65).

The TAT has been standardized, and there are four main standards: ASTM C 633-79 (United States), AFNOR NF A91-202-79 (France), DIN 50 160-A (Germany), and JIS H8666-80 (Japan). The test configurations of

these standards are essentially the same; however, each standard specifies a different design and dimensions of substrate; that is, the diameter varies from 25.4 to 40 mm (1 to 1.57 in.) and the length is from 25.4 to 50 mm (1 to 1.97 in.).

The TAT arrangement involves attaching a support fixture to the coated specimen with an epoxy so that a tensile force may be applied. The stress at failure is called the *tensile adhesion strength* or *bond strength* and is an important property to characterize coatings. However, there are some shortcomings of the TAT procedure, such as variations in the penetration of epoxy and in the alignment of test fixtures. The mixed mode of failure may also occur, and this makes the interpretation of results difficult.

The adhesion strength or cohesion strength can be influenced by many factors. Some of them are intrinsic; that is, related to the spray variables, such as powder characteristics, spray parameters, substrate preparation, and so forth. The others are extrinsic, which include post-treatment and service conditions. However, adhesion tests are usually performed at room temperature under laboratory conditions on "witness samples" and do not consider in-service conditions that may decrease the adhesion strength. It is important for materials designers to keep in mind that the adhesion strength is highly related to service conditions. As well, the confidence-interval estimation for such coatings enables the reliability of the so-determined property to be ascertained.

The measurement of adhesion of thermal spray materials is, at least on the conceptual level, a routine operation. The tensile adhesion method as detailed in ASTM C 633 is simple and often used in industry for ranking different coatings. However, the major shortcoming of this test is that it does not promote any understanding of coating performance; that is, how coatings can be designed to be more functional.

References cited in this section

42. C.C. Berndt, S. Reddy, and M.L. Allan, Optimization of Thermal Spray Parameters for Cathodic Protection of Reinforcement in Concrete, *Innovative Ideas for Controlling the Decaying Infrastructure,* V. Chaker, Ed., NACE International, 1995, p 51–64

63. R.L. Apps, New Developments in Ceramics and Coatings, *Chem. Eng.,* Vol 292, 1974, p 769–773

64. T.J. Steeper, D.J. Varacalle, Jr., G.C. Wilson, W.L. Riggs II, A.J. Rotolico, and J.E. Nerz, A Design of Experiment Study of Plasma Sprayed Alumina-Titania Coatings, *Thermal Spray Coatings: Research, Design and Application,* C.C. Berndt and T.F. Bernecki, Ed., ASM International, 1993, p 415–420

65. C.C. Berndt, Tensile Adhesion Testing Methodology for Thermally Sprayed Coatings, *J. Mater. Eng.,* Vol 12, 1990, p 151–158

M.L. Berndt and C.C. Berndt, Thermal Spray Coatings, *Corrosion: Fundamentals, Testing, and Protection*, Vol 13A*, ASM Handbook,* ASM International, 2003, p 803–813

Thermal Spray Coatings

Marita L. Berndt, Brookhaven National Laboratory; Christopher C. Berndt, State University of New York, Stony Brook

---

Summary

The coating should be considered as part of the overall component system and, therefore, current trends are to design the coating as an integral part of the component assembly rather than as an add-on to the substrate. Whereas the property of coating adhesion to the substrate is of principal interest, there is still no single measurement which can satisfy all the requirements for determining material properties. Standardization of measurements, which may be achieved by improving existing experimental techniques or the combination of two or more techniques, will aid future coating development. Finally, a coating design encompassing both

microstructural and mechanical engineering designs, which is based on lifetime modeling should be forthcoming from any test method. Such designs will increase the knowledge-base and understanding of thermal sprayed materials and coatings so that their reliability and application will grow.

The use of thermal spray coatings makes it possible to achieve fully effective, maintenance- free protection of steel and concrete structures for more than 30 years in rural environments and more than 20 years in harsh industrial, urban, and coastal regions. On an overall cost basis, with the expense of maintenance factored in, thermal spray coatings have long been competitive with comparable corrosion protection systems. Studies over the last 2 decades indicate that this is now often true even on an initial cost basis alone.

M.L. Berndt and C.C. Berndt, Thermal Spray Coatings, *Corrosion: Fundamentals, Testing, and Protection*, Vol 13A, *ASM Handbook*, ASM International, 2003, p 803–813

Thermal Spray Coatings

Marita L. Berndt, Brookhaven National Laboratory; Christopher C. Berndt, State University of New York, Stony Brook

---

Further Literature Sources for Thermal Spray

The major forum for thermal sprayers and technologists to meet since 1956 has been at the International Thermal Spray Conferences. The first seven of these meetings up to 1973 were known as International Metal Spraying Conferences. Since the mid-1980s, several other meetings have been convened: the National Thermal Spraying Conferences (organized by ASM International), the Plasma-Technik (Ref 66) meeting (a former Swiss company), and the Advanced Thermal Spraying and Allied Coatings Symposium (Ref 67) (organized by the High Temperature Society of Japan). The ITSC-2002 was convened in Essen, Germany, in March 2002 (Ref 68) and ITSC-2003 was held in Orlando, FL, in May 2003 and organized by the Thermal Spray Society of ASM International.

Other organizations such as the National Association of Corrosion Engineers (NACE International) and the American Welding Society (AWS) (Ref 69) have also convened focused conference sessions that specifically address TS under corrosive environments. The SSPC often documents TS coatings within their publication *The Journal of Protective Coatings and Linings,* JPCL.

Online Resources. Thermal spray information is available at the following websites:

- ASM—The Materials Information Society • *http://www.asminternational.org/*•
- The DVS, Deutscher Verband für Schweißen, The German Welding Society • *http:// www.dvs-ev.de/en/main.htm*•
- ASM Thermal Spray Society—An affiliate society of ASM International • *http:// www.asminternational.org/tss/*•
- NACE—The Corrosion Society • *http:// nace.org/nace/index.asp*•
- AWS—Gateway to the World of Welding • *http://www.aws.org/*•
- The SSPC—The Society for Protective Coatings • *http://www.sspc.org/*•

References cited in this section

66. A.R. Nicoll, Ed., *Proc. First Plasma-Technik Symposium,* 18–20 May 1988 (Lucerne, Switzerland), Plasma-Technik, 1988, (2 volumes)

67. Y. Arata, *Proc. of International Symposium on Advanced Thermal Spraying Technology and Allied Coatings,* 13–15 May 1988 (Osaka, Japan), The High Temperature Society of Japan, Osaka, Japan, 1988

68. E. Lugscheider, Ed., *International Thermal Spray Conf.,* DVS, Dusseldorf, 2002

69. *Thermal Spraying: Practice, Theory, and Application,* American Welding Society, 1985

M.L. Berndt and C.C. Berndt, Thermal Spray Coatings, *Corrosion: Fundamentals, Testing, and Protection*, Vol 13A, *ASM Handbook*, ASM International, 2003, p 803–813

Thermal Spray Coatings

Marita L. Berndt, Brookhaven National Laboratory; Christopher C. Berndt, State University of New York, Stony Brook

References

1. D.A. Gerdeman and N.L. Hecht, *Arc Plasma Technology in Materials Science*, Springer- Verlag, 1972, 206 pages
2. W.E. Ballard, *Metal Spraying and Flame Deposition of Ceramics and Plastics,* 4th ed., Griffin, London, U.K., 1963
3. L. Pawlowski, *The Science and Engineering of Thermal Spray Coatings,* Wiley, Chichester, United Kingdom, 1995
4. G. Schwier, Plasma Spray Powders for Thermal Barrier Coating, of Advances in Thermal Spraying, *Proc. 11th Int. Thermal Spraying Conf.,* 8–12 Sept 1986 (Montreal, Canada), Pergamon Press, 1986, p 277–286
5. C.C. Berndt, “Preparation of Thermal Spray Powders,” Education module on thermal spray, ASM International, 1992 (update available during 2003)
6. C.C. Berndt and R.H. Unger, Applications of Thermal Spray Coatings: A Technology with No Bounds, *The Finishing Line,* Vol 18 (No. 2), 2002, online invited paper
7. M. Vippola, S. Ahmaniemi, P. Vuoristo, T. Lepistö, and T. Mäntylä, Microstructural Study of Plasma Sprayed Chromium Oxide Coatings: Effect of Aluminum Phosphate Sealing, *Thermal Spray 2001: New Surfaces for a New Millennium,* C.C. Berndt, K.A. Khor, and E.F. Lugscheider, Ed., ASM International, 2001, p 607–612
8. P. Ostojic and C.C. Berndt, Variability in Strength of Thermally Sprayed Coatings, *J. Surf. Coat. Technol.,* Vol 34, 1988, p 43–50
9. K.A. Gross, C.C. Berndt, and V.J. Iacono, “Variability of Hydroxyapatite Coated Dental Implants,” *The International J. Oral and Maxillofacial Implants,* Vol 13 (No. 5), 1998, p 601–610
10. C.C. Berndt, Tensile Adhesion Testing Methodology for Thermally Sprayed Coatings, *J. Mater. Eng.*, Vol 12 (No. 2), 1990, p 151–160
11. R. McPherson, The Relationship between the Mechanism of Formation, Microstructure and Properties of Plasma-Sprayed Coatings, *Thin Solid Films,* Vol 83 (No. 3), 1981, p 297–310
12. R. McPherson, A Model for the Thermal- Conductivity of Plasma-Sprayed Ceramic Coatings, *Thin Solid Films,* Vol 112 (No. 1), 1984, p 89–95

13. M. Vreijling, “Electrochemical Characterisation of Metallic Thermally Sprayed Coatings,” Ph.D. Thesis, TNO Institute of Industrial Technology, The Netherlands, 1998

14. D.J. Varacalle, Jr., D.P. Zeek, K.W. Couch, D.M. Benson, and S.M. Kirk, Flame Spraying of Polymers, *Thermal Spray: A United Forum for Scientific and Technological Advances,* C.C. Berndt, Ed., ASM International, 1997, p 231–238

15. T.J. Steeper, W.L. Rigg II, A.J. Rotolico, J.E. Nerz, D.J. Varacalle, Jr., and G.C. Wilson, A Taguchi Design of Experimental Study of Plasma Sprayed Alumina Coatings, *Thermal Spray Coatings: Research, Design and Applications,* C.C. Berndt and T.F. Bernecki, Ed., ASM International, 1993, p 31–36

16. “Standard Test Method for Adhesion or Cohesion Strength of Thermal Spray Coatings,” C 633-01, *Annual Book of ASTM Standards,* ASTM, 2001

17. J. Tuominen, P. Vuoristo, T. Mäntylä, M. Kylmälahti, J. Vihinen, and P.H. Andersson, Improving Corrosion Properties of High- Velocity Oxy-Fuel Sprayed Inconel 625 by Using a High-Power Continuous Wave Neodymium-Doped Yttrium Aluminum Garnet Laser, *J. Therm. Spray Technol.,* Vol 9 (No. 4), 2000, p 513–519

18. S. Ahmaniemi, J. Tuominen, P. Vuoristo, and T. Mäntylä, Comparative Study of Different Sealing Methods for Thick Thermal Barrier Coatings, *Thermal Spray 2001: New Surfaces for a New Millennium,* C.C. Berndt, K.A. Khor, and E.F. Lugscheider, Ed., ASM International, 2001, p 157–165

19. J. Tuominen, P. Vuoristo, T. Mäntylä, S. Ahmaniemi, J. Vihinen, and P.H. Andersson, Corrosion Behavior of HVOF-Sprayed and Nd-YAG Laser-Remelted High-Chromium, Nickel-Chromium Coatings, *J. Therm. Spray Technol.,* Vol 11 (No. 2), 2002, p 233–243

20. M. Vippola, S. Ahmaniemi, P. Vuoristo, T. Lepistö, T. Mäntylä, and E. Olsson, Microstructural Study of Aluminum Phosphate- Sealed, Plasma-Sprayed Chromium Oxide Coating, *J. Therm. Spray Technol.,* Vol 11 (No. 2), 2002, p 253–260

21. “Protection against Corrosion of Iron and Steel in Structures: Zinc and Aluminium Coatings—Guidelines,” BS EN ISO 14713, 1999. Note: this supersedes BS 5493: 1977, which is now obsolete.

22. L.N. Moskowitz, Application of HVOF Thermal Spraying to Solve Corrosion Problems in the Petroleum Industry—An Industrial Note, *J. Therm. Spray Technol.,* Vol 1 (No. 1), 1993, p 21–29

23. R.P. Krepski, “Thermal Spray Coating Applications in the Chemical Process Industries,” MTI Publication No. 42 for NACE International, 1994

24. T. Race, V. Hock, and A. Beitelman, Performance of Selected Metallized Coatings and Sealers on Lock and Dam Facilities, *J. Prot. Coat. Linings,* Vol 6 (No. 1), Jan 1989, p 37–44

25. J.R. Birchfield, Zinc Metallizing Protects a Bridge, *Weld. Des. Fabr.,* Oct 1986, 3 pages

26. R.H. Unger, Thermal Spraying of Bridges, *Thermal Spray: Advances in Coating Technology,* D.L. Hauck, Ed., ASM International, 1988, p 399–406

27. E.C. Lohrey, Metallizing Steel Bridges in the Field, *J. Prot. Coat. Linings,* Vol 12 (No. 5), 1995, p 39–50

28. J.A. Apostolos, D.M. Parks, and R.A. Carello, “Cathodic Protection Using Metallized Zinc; A 3.5 Year Progress Report,” Paper 137, Corrosion '87 (San Francisco, CA), 1987

29. J.A. Apostolos, D.M. Parks, and R.A. Carello, Cathodic Protection using Metallized Zinc, *Mater. Perform.,* Vol 26 (No. 12), 1987, p 22–28

30. J.A. Apostolos, “Cathodic Protection of Reinforced Concrete by using Metallized Coatings and Conductive Paints,” Transportation Research Record 962, 1984, 22–29

31. R.A. Carello, D.M. Parks, and J.A. Apostolos, “Development, Testing and Field Application of Metallized Cathodic Protection Coatings on Reinforced Concrete Substructures,” Report No. FHW A/CA/TL-89/04, California Department of Transportation, Sacramento, CA, 1989

32. A.A. Sagüés and R.G. Powers, Sprayed- Zinc Sacrificial Anodes for Reinforced Concrete in Marine Service, *Corrosion,* Vol 52 (No. 7), 1996, p 508–522

33. S.D. Cramer, B.S. Covino, G.R. Holcomb, S.J. Bullard, J.H. Russell, F.J. Nelson, H.M. Laylor, and S.M. Soltesz, Corrosion Prevention and Remediation Strategies for Reinforced Concrete Coastal Bridges, *Cement Concrete Compos.,* Vol 24 (No. 1), 2002, p 101–117

34. D.G. Manning, Cathodic Protection of Concrete Highway Bridges, *Corrosion of Reinforcement in Concrete,* K.W.J. Treadaway and P.B. Bamforth, Ed., Elsevier Science, Essex, 1990, p 486–497

35. R.J. Kessler and R.G. Powers, “Zinc Metallizing for Galvanic Cathodic Protection of Steel Reinforced Concrete in a Marine Environment,” Paper 324, Corrosion '90 (Las Vegas, NV), 1990

36. M.S. Wixson, “The Arc Spray Process for Application of Metallized Zinc Anodes,” NACE Western Regional Corrosion Conference (Portland, OR), National Association of Corrosion Engineers, 1991

37. J.S. Tinnea, Field Performance of Sprayed Zinc Cathodic Protection Anodes, Proc. 15th ITSC Conference (Nice, France), 1998, p 37–42

38. S.D. Cramer, B.S. Covino, G.R. Holcomb, S.J. Bullard, W.K. Collins, R.D. Govier, R.D. Wilson, and H.M. Laylor, Thermal Sprayed Titanium Anode for Cathodic Protection of Reinforced Concrete Bridges, *J. Therm. Spray Technol.,* Vol 8 (No. 1), 1999, p 133–145

39. J.E. Bennett, T.J. Schue, and G. McGill, Protecting Reinforced Concrete Using Thermal Sprayed Titanium Anodes, *Mater. Perform.,* Vol 34 (No. 11), 1995, p 23–27

40. B.S. Covino, S.J. Bullard, G.R. Holcomb, S.D. Cramer, G.G. McGill, and C.B. Cryer, Bond Strength of Electrochemically Aged Arc-Sprayed Zinc Coatings on Concrete, *Corrosion,* Vol 53 (No. 5), 1997, p 399–411

41. R. Brousseau, M. Arnott, and B. Baldock, Long-Term Factors Influencing the Adhesion of Metallized Zinc to Concrete, *J. Therm. Spray Technol.,* Vol 5 (No. 1), 1996, p 49–52

42. C.C. Berndt, S. Reddy, and M.L. Allan, Optimization of Thermal Spray Parameters for Cathodic Protection of Reinforcement in Concrete, *Innovative Ideas for Controlling the Decaying Infrastructure,* V. Chaker, Ed., NACE International, 1995, p 51–64

43. F.N. Longo, “Self-Fusing Flame Spraying Material,” U.S. Patent 3,305,326, 21 Feb 1967

44. F.J. Dittrich, New Flame Spray Technique for Forming Nickel-Aluminide Ceramic Systems, *Ceram. Bull.,* Vol 44, 1965, p 492–496

45. Z. Ding, R. Knight, and R.W. Smith, Effect of Bond Coat Processes and Surface Characteristics on the Failure Mechanism of Thermal Barrier Coatings, *Thermal Spray 2001: New Surfaces for a New Millennium,* C.C. Berndt, K.A. Khor, and E. Lugscheider, Ed., ASM International, 2001, p 173–177

46. J. Reimer, “Method and Apparatus for Spray Coating,” U.S. Patent 4,632,309, 30 Dec 1986, 11 pages

47. R.F. Smart, Arc Plasma Sprayed Metals and Plastics, *Practical Metallic Composites,* The Welding Institute, 1974, PE19-26

48. E.R. George and J. Reimer, Flame Sprayed Thermoplastic Powder Coatings, *Polymer Eng. Sci.,* Vol 31 (No. 11), 1991, p 789–792

49. E. Petrovicova and L.S. Schadler, Thermal Spraying of Polymers, *Int. Mater. Rev.,* Vol 47 (No. 4), 2002, p 169–190

50. J.A. Brogan et al., Adhesion of Combustion- Sprayed Polymer Coatings, *1995 Advances in Thermal Spray Science and Technology,* C.C. Berndt and S. Sampath, Ed., ASM International, 1995, p 521–526

51. J. Economy, B.E. Nowak, and S.G. Cottis, Ekonol: A High Temperature Aromatic Polyester, *SAMPE J.,* Aug/Sept 1970, p 21–27

52. H. Liao, E. Beche, F. Berger, and C. Coddet, On the Microstructure of Thermally Sprayed PEEK Polymer, *Thermal Spray: Meeting the Challenges of the 21st Century,* C. Coddet, Ed., ASM International, 1998, p 25–29

53. E. Lugscheider, C. Herbst, and A. Fischer, Thermal Spraying of High Performance Thermoplastics, *Thermal Spray: Meeting the Challenges of the 21st Century,* C. Coddet, Ed., ASM International, 1998, p 19–24

54. P.J. Loustaunau and D. Horton, EMAA Thermoplastic Powder Coatings in Shop and Field Applications, *Mater. Perform.,* Vol 33 (No. 7), 1994, p 32–36

55. R.H. Henne and C. Schitter, Plasma Spraying of High Performance Thermoplastics, *Advances in Thermal Spray Science and Technology,* C.C. Berndt and S. Sampath, Ed., ASM International, 1995, p 527–531

56. Y. Bao and D.T. Gawnes, Plasma Spraying of Glass-Polyamide Composite Coatings, *Thermal Spray Coatings: Research, Design and Applications,* C.C. Berndt and T. Bernecki, Ed., ASM International, 1993, p 417–422

57. R. Knight, X. Fang, and T.E. Twardowski, Structure and Properties of HVOF Sprayed Amorphous Polymer Matrix Nanocomposite Coatings, *Thermal Spray 2001: New Surfaces for a New Millennium,* C.C. Berndt, K.A. Khor, and E. Lugscheider, Ed., ASM International, 2001, p 361–368

58. T.E. Twardowski, M. Reilly, and R. Knight, Properties of HVOF Sprayed Multi-Scale Polymer/Silica Nanocomposite Coatings, *Thermal Spray 2001: New Surfaces for a New Millennium,* C.C. Berndt, K.A. Khor, and E.F. Lugscheider, Ed., ASM International, 2001, p 369–373

59. J.A. Brogan, R. Lampo, and C.C. Berndt, Thermal Spraying of Polymers, Proc. Fourth World Congress on Coating Systems for Bridges and Steel Structures

60. G.R. Holcomb and C.B. Cryer, Cost of Impressed Current Cathodic Protection for Coastal Oregon Bridges, *Mater. Perform.,* Vol 37 (No. 7)

61. M.L. Allan, C.C. Berndt, J.A. Brogan, and D. Otterson, Thermal Sprayed Polymer Coatings for Corrosion Protection in a Biochemical Treatment Process, *Thermal Spray: Meeting the Challenges of the 21st Century,* C. Coddet, Ed., ASM International, 1998, p 13–18

62. J. Karthikeyan et al., Thermal Spray Vitrification Process for the Removal of Lead Oxide Contained in Organic Paints, Advances in Thermal Spray Science and Technology, C.C. Berndt and S. Sampath, Ed., ASM International, 1995, p 559–604

63. R.L. Apps, New Developments in Ceramics and Coatings, *Chem. Eng.,* Vol 292, 1974, p 769–773

64. T.J. Steeper, D.J. Varacalle, Jr., G.C. Wilson, W.L. Riggs II, A.J. Rotolico, and J.E. Nerz, A Design of Experiment Study of Plasma Sprayed Alumina-Titania Coatings, *Thermal Spray Coatings: Research, Design and Application,* C.C. Berndt and T.F. Bernecki, Ed., ASM International, 1993, p 415–420

65. C.C. Berndt, Tensile Adhesion Testing Methodology for Thermally Sprayed Coatings, *J. Mater. Eng.,* Vol 12, 1990, p 151–158

66. A.R. Nicoll, Ed., *Proc. First Plasma-Technik Symposium,* 18–20 May 1988 (Lucerne, Switzerland), Plasma-Technik, 1988, (2 volumes)

67. Y. Arata, *Proc. of International Symposium on Advanced Thermal Spraying Technology and Allied Coatings,* 13–15 May 1988 (Osaka, Japan), The High Temperature Society of Japan, Osaka, Japan, 1988

68. E. Lugscheider, Ed., *International Thermal Spray Conf.,* DVS, Dusseldorf, 2002

69. *Thermal Spraying: Practice, Theory, and Application,* American Welding Society, 1985

K.B. Tator, Introduction to Coatings and Linings *Corrosion: Fundamentals, Testing, and Protection*, Vol 13A, *ASM Handbook*, ASM International, 2003, p 814–816

Introduction to Coatings and Linings

Kenneth B. Tator, KTA-Tator, Inc.

Introduction

THE TOTAL NATIONAL YEARLY COST of metallic corrosion in the United States was estimated at $275 billion, or 3.1% of the U.S. gross domestic product (GDP) of $8790 billion, in 1998 (Ref 1). This total includes replacement costs and lost production costs as well as the decrease in lifetime and the expected replacement value of a given component subject to damage by corrosion. The cost of corrosion also includes the means by which the effects of corrosion are mitigated, such as the use of cathodic protection, inhibitors, alternative materials of construction, overdesign, and protective coatings. Studies done for other countries arrive at similar estimates of the total annual cost of corrosion, ranging from 1 to 5% of each country's GDP. A summary of the 1998 United States Federal Highway Administration study is provided in the article "Direct Costs of Corrosion in the United States" in this Volume.

The use of protective coatings is, in itself, a very substantial category. According to the U.S. Department of Commerce Bureau of Census, the total amount of organic coating material sold in the United States in 1997 was 5.56×10^9 L (1.47×10^9 gal), at a value of $16.56 billion. These sales can be categorized into architectural

coatings, product original equipment manufacturer (OEM) coatings, general-purpose coatings, and miscellaneous paint products. A portion of each of these was classified as corrosion protective coatings, at a total worth estimated at $6.7 billion. Because the cost of the coating material is from 4 to 20% of the cost of the applied coating system, the total applied cost of protective coating systems thereby ranges from $33.5 to $167.5 billion. Using the average of these figures, $100 billion, this cost is 36% of the total cost of corrosion in the United States and 1.1% of the entire United States' GDP.

Therefore, the use of protective coatings and linings and the costs associated with such use are considerable. More metal surfaces are protected by organic coatings and linings than by all other methods combined. In addition to protecting against corrosion, coatings often beautify and provide an aesthetic appeal. Safety colors are used to mark pipes, to indicate their contents, and to provide warnings of hazardous or dangerous work areas. Automotive coatings and house paints provide both beauty and weather protection. Coatings reflect light, thereby protecting the highway-traveling public, and reduce energy costs, because less lighting is needed for illumination. The use of protective and decorative coatings pervades all aspects of our lives.

Reference cited in this section

1. *Corrosion Cost and Preventative Strategies in the United States,* FHWA-RD-01-156, Federal Highway Administration, U.S. Department of Transportation, March 2002

K.B. Tator, Introduction to Coatings and Linings *Corrosion: Fundamentals, Testing, and Protection,* Vol 13A, *ASM Handbook,* ASM International, 2003, p 814–816

Introduction to Coatings and Linings

Kenneth B. Tator, KTA-Tator, Inc.

The Effect of Legislation on the Coatings Industry

Legislation concerning worker health and environmental protection has had a marked impact on the coatings industry. For example, although the practice of blast cleaning a steel surface and applying an alkyd, epoxy, or polyurethane coating system remains one of the best methods of corrosion protection for many steel surfaces, the alkyds, epoxies, and polyurethanes themselves have changed as a result of legislation restricting the release of volatile organic compounds (solvents) and the use of toxic pigments.

Surface preparation techniques have also changed drastically; silica sand as a blast-cleaning abrasive has been banned in virtually all western countries except the United States and Canada (and there is a strong movement to ban it in these countries as well). The containment and safe disposal of spent blast-cleaning abrasives are required in most localities to prevent environmental damage caused by contamination by airborne particulate containing lead, chromate, and other toxic paint pigments removed during blast cleaning. Therefore, although a paint layer over a properly cleaned surface still acts as a barrier against a corrosive environment in most cases, the components that constitute this barrier have changed considerably within the past 10 years, and the means by which the surface is properly cleaned and the coating material is applied are evolving rapidly.

The following articles in this subsection present an overview of the different types of coating and lining materials available, along with information on the various means of surface preparation and the equipment and techniques of coating application. However, it must be recognized that all facets of coating technology are strongly influenced by legislative decree; the alkyds, epoxies, polyurethanes, and other generic types of coating materials currently in use are being reformulated, and although the names will be the same, the compositions of these coatings (and their potential protective capabilities) will be considerably different within the next few years. Furthermore, surface preparation and application techniques in current use are also under considerable legislative pressure and are also evolving.

K.B. Tator, Introduction to Coatings and Linings *Corrosion: Fundamentals, Testing, and Protection*, Vol 13A, *ASM Handbook*, ASM International, 2003, p 814–816

Introduction to Coatings and Linings

Kenneth B. Tator, KTA-Tator, Inc.

Coating Industry Response to Legislative Pressure

The coating industry has been very responsive to enacted legislation and to proposed legislation limiting the use of potentially harmful or toxic raw materials or surface preparation and/or application techniques. As a result of this positive industry reaction, the legislators as a whole have been pragmatic in their laws. For example, it is widely recognized that lead, when ingested by the body, results in anemia, damage to the central nervous system, disruption of the reproductive system, and retardation in child development. Therefore, in 1973, Congress, under the impetus of the Food and Drug Administration, limited the lead content in all paints for consumer use to 0.06% solids by weight.

This law effectively banned the use of lead pigments in all paints used around the home. However, because lead-containing paint pigments, such as red lead, lead chromate, and lead suboxide, are perhaps the best pigments in use for corrosion protection, they were not outlawed for paints used for corrosion protection purposes in industry. In fact, even today, no legislation restricts the use of such pigments for industrial and marine corrosion protection purposes.

However, legislation regarding worker and environmental protection has curtailed drastically the use of lead pigments as well as other toxic pigments, such as those in the chromium, mercury, and tin families. Although such pigments can be used legally in paint, the substantial costs due to worker protection and the high costs associated with containment and disposal of paints containing such pigments are effectively precluding their use in most new coating formulations.

Similarly, restrictions regarding volatile organic compounds (VOCs) in coatings have been enacted gradually over the last 10 years in order to allow formulators to develop comparable paint materials with complying solvents. Although solvent restrictions were originally enacted against what were believed to be photochemically reactive solvents (solvents that reacted under the influence of ultraviolet light and degraded to form smog and to deplete the ozone layer), it was later found that virtually all volatilizing solvents photochemically degraded and were therefore environmentally detrimental. This realization, together with the potential for further legislative restriction, has motivated coating formulators to develop water-based paints or high-solids (low-solvent) coating materials.

Conversely, there are many industrial facilities and highway bridges that are coated with old lead-containing paints. Environmental Protection Agency (EPA) legislation requires the disposal of removed paints (and spent abrasive) in hazardous waste disposal sites if the leachate after acid digestion (pH 5) contains more than 5 ppm of lead or chromate and 2 ppm of mercury. The costs of such a disposal, not including collection costs, are estimated by many painting contractors to be from 6 to 10 times as much as disposal costs in a normal sanitary landfill. The cost of containing the spent abrasive and paint, as opposed to letting the spent abrasive fall to the ground during blast cleaning, may in itself double or triple the cost of a paint job.

While government enforcement of Occupational Safety and Health Administration (OSHA) and EPA legislation may have been lax in some areas in the past, the consequence of violation is severe and mandated in the Code of Federal Regulations. Penalties consist of fines, with the potential for incarceration for willful violations, which are specifically defined. In July 2001, OSHA announced the launch of a National Emphasis Program (NEP) to reduce occupational lead exposures. The NEP expects to attain a 15% reduction in employee exposures to airborne lead in targeted standard industry classification (SIC) codes (Table 1) (Ref 2).

Table 1 Industries targeted for increased enforcement of U.S. environmental and safety regulations

SIC code (a)	Classification
1611	Highway and street construction
1622	Bridge, tunnel, and elevated highway construction
1623	Water, sewer, pipe construction, and communication
1629	Heavy construction NEC (not elsewhere classified)
1721	Painting and paperhanging
1791	Structural steel erection
1795	Wrecking and demolition
1799	Special trade contractors NEC (not elsewhere classified)
3731	Shipbuilding and repair
4499	Water transportation services NEC (not elsewhere classified)
5093	Scrap waste

Industries targeted under the National Emphasis Program (NEP) of the U.S. Occupational Safety and Health Administration (OSHA).

(a) Standard industrial classification codes. Source: Ref 2

While OSHA previously has focused on painters on large projects, the NEP's new target parameters, particularly in the areas of heavy construction (16xx SIC codes), increase the potential for all trades on a project to receive scrutiny by OSHA.

The EPA is also systematically reducing VOC levels in paints and allied products and strengthening regulations regarding air, soil, and water contamination.

A summary of current regulations affecting the coatings industry is presented in Table 2 (Ref 3). A listing of specific existing federal regulations is presented in Table 3 (Ref 3).

Table 2 Summary of existing federal regulations affecting the coatings industry

Category	Summary
Environmental Protection Agency (EPA)	
Hazardous waste management	The Resource Conservation and Recovery Act (RCRA) governs the handling, storage, and disposal of wastes. The RCRA applies to the generators (usually owners and contractors), transporters, and disposers of waste.
Soils	Federal EPA does not have any specific regulations addressing soils contamination. However, EPA has taken the position that discharge of lead onto soils during paint removal may be regulated as illegal disposal and operation of an unlicensed treatment, storage, and disposal facility under RCRA (Ref 4).
Water	The Clean Water Act encompasses the body of regulations applicable to surface, ground, and storm water. The National Pollutant Discharge Elimination System establishes a permit system for allowable discharge into water. These regulations allow for EPA enforcement actions on industrial painting project sites where contaminated materials may have escaped the containment and are present on the ground or could be carried into drains or waterways.
Spills, cleanup, and reporting	The Comprehensive Environmental Response, Compensation, and Liability Act (CERCLA) or superfund addresses the current release of hazardous substances (e.g., solvents, lead, etc.) and addresses the cleanup of EPA-identified waste sites. CERCLA is enforceable on owners and contractors during industrial painting operations that result in excessive releases and can be applied to coatings manufacturers during the production of coatings. An amendment to CERCLA, known as the Emergency Planning and Community Right-to-Know Act (EPCRA), broadens the applicability of CERCLA to include facilities at which hazardous substances are present. The EPCRA standards are typically enforceable on coatings manufacturing facilities and fixed-site (e.g., shop) blasting and painting facilities.

Air	The Clean Air Act (40 CFR 50-99) limits the volatile organic compound (VOC) content for 61 categories of coatings. It also requires manufacturers and transporters to include VOC limits on labels and to provide recommendations regarding training.
Occupational Safety and Health Administration (OSHA)	
Lead exposure	The regulation for lead in construction (29 CFR 1926.62) requires employers to perform airborne assessments of employees' exposures when any lead is present. These assessments are compared to the action level and permissible exposure levels (PELs) of lead to trigger the implementation of exposure assessment, medical surveillance, employee information and training, signs/regulated areas, and record-keeping requirements. Employers must institute engineering and work practice controls to the extent feasible to reduce exposures to as low as achievable, preferably below the PEL.
Other toxic metals	OSHA has issued similar regulations for cadmium (29 CFR 1926.1127) and inorganic arsenic (29 CFR 1926.1118). Combined, these regulations have substantively influenced the coating removal industry by introducing the concepts of containment and ventilation, initial and periodic medical surveillance, worker training, and nontraditional paint removal methodologies.
Safety	OSHA has also issued or revised a number of construction regulations (29 CFR 1926) addressing fall protection, scaffolding, and aerial lifts, which significantly alter how access and working platforms are installed and maintained for field operations. In 1998, OSHA revised its respiratory protection standards for both the general (29 CFR 1910.134) and construction (29 CFR 1926.103) industries. The revisions directly impact both the removal and application of coatings. The revised standard requires more thorough assessment of potential inhalation hazards such as paints and solvents, increased engineering controls, and formal oversight of the implementation of respiratory protection programs.
Other regulations(a)	
Federal Department of Transportation (DOT)	Federal DOT regulations are included in 49 CFR. Federal DOT regulations govern all transportation, packaging, and handling of hazardous materials. 49 CFR is incorporated by reference in Environmental Protection Agency RCRA regulations.
U.S. Coast Guard (USCG)	USCG regulations can apply to the coatings industry when projects involve navigation or navigable waters (33 CFR) or shipping (46 CFR).
OSHA	In addition to specific regulations relative to the construction industry (29 CFR 1926), OSHA also regulates activities in other major industry categories (some of which also involve the coatings industry), including but not limited to general industry (29 CFR 1910), longshoring (29 CFR 1917), and marine terminals (29 CFR 1918).
Military	All phases of the military, i.e., Army Corps of Engineers, also have their own internal regulations, directives, and guidelines relative to worker safety and health and environmental protection that may impact the coating industry.

(a) More information can be found at www.epa.gov and www.osha.gov. CFR, Code of Federal Regulations. (a) Specific industry regulations may also affect painting operations in specific industries. Some other regulatory agencies that have regulations that may impact the coatings industry are listed. Source: Ref 3

Table 3 A listing of existing U.S. federal regulations affecting the coatings industry

Subject	Code of Federal Regulations (CFR)
OSHA requirements	
Lead	29 CFR 1926.62
Cadmium	29 CFR 1926.1127
Arsenic	29 CFR 1926.1118
Gas, vapors, fumes, dusts, and mists	29 CFR 1926.55
Fall protection	29 CFR 1926.500–503

Ladders	29 CFR 1926.1053
Scaffolds/aerial lifts	29 CFR 1926.450–454
Electrical	29 CFR 1926.403–404
Fire protection/prevention	29 CFR 1926.150–151
Flammable/combustible liquids	29 CFR 1926.152
Confined space entry	29 CFR 1910.146
Hearing protection	29 CFR 1926.101
Hazard communication	29 CFR 1926.59
Personal protective equipment	29 CFR 1926.95–103
Vehicle operation	29 CFR 1926.600–601
Signaling	29 CFR 1926.201
Working over water	29 CFR 1926.106
General safety and health provision	29 CFR 1926.20
Safety training and education	29 CFR 1926.21
General duty clause	Section 5(a)(1) of OSHA Act of 1972
EPA requirements	
Ambient air quality standards	40 CFR 50
Ambient air quality surveillance	40 CFR 58
Visual determination of emissions	40 CFR 60, app. A, methods 22 and 9
Clean Water Act	40 CFR, subchapter D, parts 100–149
Hazardous waste regulations	40 CFR 261–268
Designation, reportable quantities, and notification	40 CFR 302
Emergency planning and notification	40 CFR 355
Polychlorinated biphenyl (PCB) manufacturing, processing, distribution in commerce, and prohibitions	40 CFR 761
Others	
Hazardous materials regulations	49 CFR 171–179

Source: Ref 3

The high costs of surface preparation and coating application, along with those for worker and environmental protection, have motivated improvements of many existing technologies and development of new methods for conducting coating work. For example, powder coating technologies have captured a significant share of the OEM and product manufacturing markets, including the automotive market (the largest single user of protective and decorative coatings). Powder coatings have developed solely as a result of restricted VOC emissions mandated by the government. However, the development of improved electrostatic application methods (both fluidized bed and spray gun techniques); lower-temperature curing powders; and improved systems for conveyance, application, curing, handling, and recycling have made powder coatings viable for automotive and truck manufacturers and for many other industries. Similarly, improvements in electrostatic spray application equipment have been significant and are making that lower VOC technology competitive with liquid sprayed coatings.

An entire industry has developed to contain airborne blastcleaning residues and old lead and chromate hazardous paints removed during blastcleaning. Hazardous waste management techniques have been developed specifically for the coatings industry. Equipment and procedures for monitoring the effectiveness of worker and environmental protection during painting operations have spawned new technologies and launched entirely new industries.

Thus, when the cost of an existing technology becomes high enough, newer technologies are improved/invented to improve efficiencies and lower costs. Capitalism and free market enterprise are working at their best!

Despite the pending health and environmental legislative influences and the rapidly occurring changes in the coatings industry, corrosion continues, and painting for corrosion protection must be done. Therefore, the following articles discuss the more commonly used coating and lining materials; their characteristics,

advantages, and disadvantages; surface preparation equipment and techniques; application and inspection methods; and equipment.

References cited in this section

2. A.B. Kaelin and S.T. Liang, OSHA's New National Emphasis Program to Reduce Occupational Exposures to Lead: Impact on the Coatings Industry, *J. Prot. Coatings Linings,* Oct 2001

3. K.B. Tator, Exploring Coatings-Industry Regulations, *Chemical Processing,* Putman Media, Inc., 2001

4. A.B. Kaelin, "Here Comes EPA: Trends in EPA Enforcement in the Coatings Industry," *Proceedings of SSPC 2000,* 12–16 Nov 2000 (Nashville, TN), The Society for Protective Coatings, 2000

K.B. Tator, Introduction to Coatings and Linings *Corrosion: Fundamentals, Testing, and Protection*, Vol 13A, *ASM Handbook*, ASM International, 2003, p 814–816

Introduction to Coatings and Linings

Kenneth B. Tator, KTA-Tator, Inc.

References

1. *Corrosion Cost and Preventative Strategies in the United States,* FHWA-RD-01-156, Federal Highway Administration, U.S. Department of Transportation, March 2002

2. A.B. Kaelin and S.T. Liang, OSHA's New National Emphasis Program to Reduce Occupational Exposures to Lead: Impact on the Coatings Industry, *J. Prot. Coatings Linings,* Oct 2001

3. K.B. Tator, Exploring Coatings-Industry Regulations, *Chemical Processing,* Putman Media, Inc., 2001

4. A.B. Kaelin, "Here Comes EPA: Trends in EPA Enforcement in the Coatings Industry," *Proceedings of SSPC 2000,* 12–16 Nov 2000 (Nashville, TN), The Society for Protective Coatings, 2000

K.B. Tator, Organic Coatings and Linings, *Corrosion: Fundamentals, Testing, and Protection*, Vol 13A, *ASM Handbook*, ASM International, 2003, p 817–833

Organic Coatings and Linings

Kenneth B. Tator, KTA-Tator, Inc.

Introduction

PAINTS OR LININGS that act as a protective film to isolate the substrate from the environment exist in a number of different forms. Sheet linings, commonly of the vinyl or vinylidene chloride family, are one such type of coating that can be either adhered to the surface to be protected or suspended as a bag within a tank, for example, to provide protection. Hot-applied organisols, or plastisols, again usually of the vinyl family, can also be applied to a surface, typically by dipping or flow coating, to provide a protective film.

Powder coatings are being increasingly used to protect concrete-reinforcing rod, as pipeline coatings, and as coating materials in the original equipment manufacturer (OEM) markets. Fine powders produced from high-molecular-weight resins of the thermoplastic vinyl and fluorinated hydrocarbon families, or from thermoset resins of the epoxy and polyester families, are applied to the surface to be protected by either electrostatic spray or fluidized-bed deposition. The metal being protected is usually preheated at the time of application, and after application it is reheated to an elevated temperature, generally from 150 to 315 °C (300 to 600 °F). The specific time/temperature baking schedule depends on the metal temperature at the time of application and the type of powder being applied.

The coatings and linings discussed previously are mentioned here in summary only; a more thorough description is beyond the scope of this article. Powder coatings and coil coatings are discussed in more detail in the section "Powder Coating" in the article "Painting" in *Surface Engineering,* Volume 5 of *ASM Handbook.*

Alternatively, some coating systems are characterized by the application method used. For example, for coil-coated metal sheet (commonly steel or galvanized steel), very specialized high- speed roller application equipment is used to coat the sheet steel as it is unwound from a coil. The paint used in the coil-coating process can be of virtually any generic type, although alkyds, polyesters, epoxies, and zinc-rich epoxy coatings are the most prevalent.

Certain lining materials, such as hand lay-up fiberglass-reinforced plastics, are also used to protect steel from corrosion. Such coating systems usually consist of an epoxy primer applied to a blast-cleaned steel surface, followed by one or more polyester or epoxy gel coats, with one or more layers of a fiberglass veil or woven roving mat laid within the gel coats as reinforcement. The system is then sealed with a final layer of the polyester or epoxy resins as a gel coat (a semiclear, 100% solids resin coat). Similarly, rubber linings are used to protect against corrosion. There are various types of rubbers, but they can generally be categorized as prevulcanized or postvulcanized (vulcanized after application). Similarly, rubbers can be formulated with different hardnesses and chemical resistances. Commonly, a rubber lining is a composite of two or three different types of rubbers adhered to each other and to the surface. More information on rubber linings is presented in the article "Rubber Coatings and Linings" in this Volume.

This article is limited to the liquid coating (usually applied by brush, roller, or spray) and lining materials that are commonly used for corrosion protection in atmospheric or immersion service. The rate of base metal corrosion where such coatings or linings are used should not exceed approximately 1.3 mm/yr (50 mils/yr). For more severe corrosion rates, both in atmospheric and immersion service, or where catastrophic failure modes could occur, liquid-applied coatings probably should not be used. Corrosion protection measures such as the use of more corrosion-resistant alloys, sheet or rubber coatings and linings, or fiberglass lay-ups, can be employed for these applications.

The coating systems discussed in this article are categorized by the generic type of binder or resin and are grouped according to the curing or hardening mechanism inherent within that generic type. Although the resin or organic binder of the coating material is most influential in determining the resistances and properties of the paint, it is also true that the type and amount of pigments, solvents, and additives such as rheological aids dramatically influence the application properties and protective capability of the applied film. Furthermore, hybridized systems can be formulated that are crosses between the categories. For example, an acrylic monomer or prepolymer can be incorporated with virtually any other generic type of resin to produce a product with properties that are a compromise between the acrylic and the original polymer. In many cases, this is advantageous, as in the mixing of polyurethanes and acrylics or heat-curing alkyds and acrylics. In other cases, such as with an epoxy, acrylic modification may be a detriment. Table 1 lists the advantages and limitations of the principal coating resins.

Table 1 Advantages and limitations of principal coating resins

Resin type	Advantages	Limitations	Comments
Autooxidative cross-linked resins			
Alkyds	Good resistance to atmospheric weathering and moderate chemical fumes; not resistant to chemical splash and spillage. Long	Not chemically resistant; not suitable for application over alkaline surfaces, such as fresh concrete, or for water immersion	Long oil alkyds make excellent primers for rusted and pitted steel and wooden surfaces. Corrosion resistance is adequate for

	oil alkyds have good penetration but are slow drying; short oil alkyds are fast drying. Temperature resistant to 105 °C (225 °F)		mild chemical fumes that predominate in many industrial areas. Used as interior and exterior industrial and marine finishes
Epoxy esters	Good weather resistance; chemical resistance better than alkyds and usually sufficient to resist normal atmospheric corrosive attack	Generally the least resistant epoxy resin. Not resistant to strong chemical fumes, splash, or spillage. Temperature resistance: 105 °C (225 °F) in dry atmospheres. Not suitable for immersion service	A high-quality oil-based coating with good compatibility with most other coating types. Easy to apply. Used widely for atmospheric resistance in chemical environments on structural steel, tank exteriors, etc.
Thermoplastic resins			
Acrylics	Excellent light and ultraviolet stability, gloss, and color retention. Good chemical resistance and excellent atmospheric weathering resistance. Resistant to chemical fumes and occasional mild chemical splash and spillage. Minimal chalking, little if any darkening on prolonged exposure to ultraviolet light	Thermoplastic and water emulsion acrylics not suitable for any immersion service or any substantial acid or alkaline chemical exposure. Most acrylic coatings are used as topcoats in atmospheric service. Acrylic emulsions have limitations described under "Water emulsion latex."	Used predominantly where light stability, gloss, and color retention are of primary importance. With cross linking, greater chemical resistance can be achieved. Cross-linked acrylics are the most common automotive finish. Emulsion acrylics are often used as primers on concrete block and masonry surfaces.
Water emulsion latex	Resistant of water, mild chemical fumes, and weathering. Good alkali resistance. Latexes are compatible with most generic coating types, either as an undercoat or topcoat.	Must be stored above freezing. Does not penetrate chalky surfaces. Exterior weather and chemical resistance not as good as solvent or oil-based coatings. Not suitable for immersion service	Ease of application and cleanup. No toxic solvents. Good concrete and masonry sealers, because breathing film allows passage of water vapor. Used as interior and exterior coatings
Asphalt pitch	Good water resistance and ultraviolet stability. Will not crack or degrade in sunlight. Nontoxic and suitable for exposure to food products. Resistant to mineral salts and alkalies to 30% concentration	Black color only. Poor resistance to hydrocarbon solvents, oils, fats, and some organic solvents. Does not have the moisture resistance of coal tars. Can embrittle after prolonged exposure to dry environments or temperatures above 150 °C (300 °F), and can soften and flow at temperatures as low as 40 °C (100 °F)	Often used as relatively inexpensive coating in atmospheric service, where coal tars cannot be used. Relatively inexpensive. Most common use is as a pavement sealer or roof coating.
Coal tar pitch	Excellent water resistance (greater than all other types of coatings); good resistance to acids, alkalies, and mineral, animal, and vegetable oils	Unless cross linked with another resin, is thermoplastic and will flow at temperatures of 40 °C (100 °F) or less. Hardens and embrittles in cold weather. Black color only; will alligator and crack	Used as moisture-resistant coatings in immersion and underground service. Widely used as pipeline exterior and interior coatings below grade. Pitch emulsions used as pavement sealers.

		on prolonged sunlight exposure, although still protective	Relatively inexpensive
Cross-linked thermosetting resins			
Bisphenol-F epoxies	Lower volatile organic compound (VOC) content than Bis-A epoxies. Better temperature and chemical resistance than Bis-A types. Intermediate temperature and chemical resistance between Bis-A and novolacs	Less flexible; requires thorough blast cleaning surface preparation	Increasing use due to high reactivity and low VOC content
Epoxy novolacs	Greatest chemical resistance and highest temperature resistance of all epoxy resins used for most severe immersion service	Least flexible of epoxy resins. Costly.	Used for high-temperature chemical immersion service
Polyamide-cured epoxies	Superior to amine-cured epoxies for water resistance. Excellent adhesion, gloss, hardness impact, and abrasion resistance. More flexible and tougher than amine-cured epoxies. Some formulations can cure on wet surfaces and underwater. Temperature resistance: 105 °C (225 °F) dry; 65 °C (150 °F) wet	Cross linking does not occur below 5 °C (40 °F). Maximum resistances generally require 7 day cure at 20 °C (70 °F). Slightly lower chemical resistance than amine-cured epoxies	Easier to apply and topcoat, more flexible, and better moisture resistance than amine-cured epoxies. Excellent adhesion over steel and concrete. A widely used industrial and marine maintenance coating. Some formulations can be applied to wet or underwater surfaces.
Polyurethanes (aromatic or aliphatic)	Aliphatic urethanes are noted for their chemically excellent gloss, color, and ultraviolet light resistance. Properties vary widely, depending on the polyol coreactant. Generally, chemical and moisture resistances are similar to those of polyamide-cured epoxies, and abrasion resistance is usually excellent.	Because of the versatility of the isocyanate reaction, wide diversity exists in specific coating properties. Exposure to the isocyanate should be minimized to avoid sensitivity that may result in an asthmatic-like breathing condition on continued exposure. Carbon dioxide is released on exposure to humidity, which may result in gasing or bubbling of the coating in humid conditions. Aromatic urethanes may darken or yellow on exposure to ultraviolet radiation.	Aliphatic urethanes are widely used as glossy light-fast topcoats on many exterior structures in corrosive environments. They are relatively expensive but extremely durable. The isocyanate can be combined with other generic materials to enhance chemical, moisture, low-temperature, and abrasion resistance.
Amine-cured epoxies	Excellent resistance to alkalies, most organic and inorganic acids, water, and aqueous salt solutions. Solvent resistance and resistance to oxidizing agents are good as long as	Harder and less flexible than other epoxies and intolerant of moisture during application. Coating chalks on exposure to ultraviolet light. Strong solvents may lift coatings. Temperature resistance: 105	Good chemical and weather resistance. Best chemical resistance of epoxy family. Excellent adhesion to steel and concrete. Widely used in maintenance coatings and tank linings

	not continually wetted. Amine adducts have slightly less chemical and moisture resistance.	°C (225 °F) wet; 90 °C (190 °F) dry. Will not cure below 5 °C (40 °F); should be topcoated within 72 h to avoid intercoat delamination. Maximum properties require curing time of approximately 7 days.	
Epoxy powder coatings	Good adhesion, chemical and moisture resistance. Allows cathodic protection in shielded areas on pipelines	Color change is difficult due to extensive cleanup of old powder. Like all epoxy resins, chalks on ultraviolet exposure. Must be applied in shop. Hard to field repair	Applied by electrostatic spray/fluidized bed. Increasing use because of VOC used as pipeline, original equipment manufacturer coatings
Coal tar epoxies	Excellent resistance to saltwater and freshwater immersion. Very good acid and alkali resistance. Solvent resistance is good, although immersion in strong solvents may leach the coal tar.	Embrittles on exposure to cold or ultraviolet light. Cold weather abrasion resistance is poor. Should be topcoated within 48 h to avoid intercoat adhesion problems. Will not cure below 10 °C (50 °F). Black or dark colors only. Temperature resistance: 105 °C (225 °F) dry; 65 °C (150 °F) wet	Good water resistance. Thicknesses to 0.25 mm (10 mils) per coat. Can be applied to bare steel or concrete without a primer. Low cost per unit coverage
Epoxy phenolics	Excellent hot water resistance and acid resistance. More flexible than phenolic. Better alkali resistance than phenolics	Not as alkali resistant as other epoxy resins. Applies in thin films; somewhat brittle	Linings for food and beverage processing and storage tanks
Phenolics	Greatest solvent resistance of all organic coatings described. Excellent resistance to aliphatic and aromatic hydrocarbons, alcohols, esters, ethers, ketones, and chlorinated solvents. Wet temperature resistance to 95 °C (200 °F). Odorless, tasteless, and nontoxic; suitable for food use	Must be baked at a metal temperature ranging from 175 to 230 °C (350 to 450 °F). Coating must be applied in a thin film (approximately 0.025 mm, or 1 mil) and partially baked between coats. Multiple thin coats are necessary to allow water from the condensation reaction to be removed. Cured coating is difficult to patch due to extreme solvent resistance. Poor resistance to alkalies and strong oxidants	A brown color results on baking, which can be used to indicate the degree of cross linking. Widely used as tank lining for alcohol storage and fermentation and other food products. Used for hot water immersion service. Can be modified with epoxies and other resins to enhance water, chemical, and heat resistance
Polyureas	Extremely fast curing, highly elastic thick film coatings with good strength. Abrasion resistance, chemical resistance	Requires specialized spray equipment due to fast curing	Concrete coatings for use in secondary containment of chemical tanks. Elastomeric roof coatings

K.B. Tator, Organic Coatings and Linings, *Corrosion: Fundamentals, Testing, and Protection*, Vol 13A, *ASM Handbook*, ASM International, 2003, p 817–833

Organic Coatings and Linings

Kenneth B. Tator, KTA-Tator, Inc.

Autooxidative Cross-Linked Resins

These coating types dry and ultimately cross link by reaction with oxygen from the atmosphere. All such coatings in this class contain drying oils, which consist mainly of polyunsaturated fatty acids, and undergo film formation by oxidative drying. The drying reaction is accelerated by the presence of metallic salts such as cobalt, manganese, and lead napthenates or octoates. The drying reaction results in a reduction of unsaturated groups, commonly ethylenic carbon double bonds. The autooxidation reaction occurs at a relatively fast rate shortly after application of the wet paint, and it continues throughout the life of the coating, although at a much slower rate with time.

The autooxidative reaction is a decomposition reaction that results in the formation of hydroperoxides. Although autooxidative cross linking is necessary to attain the ultimate resistant properties of the film (such properties are generally attained within weeks after application), with time, the hydroperoxides formed as a result of the autooxidative cross linking decompose into organic acid constituents, leading to chemical deterioration of the film. Similarly, the autooxidative reaction results in the hardening and ultimate embrittlement of the film, causing reduced distensibility and flexibility with the passage of time. This brittleness and accompanying hydroperoxide decomposition result in an aging deterioration of the film and the ultimate loss of protective capability. The rate at which the coating loses its protective capability is determined by temperature, thickness, solar exposure, and the types of pigmentation (for example, zinc oxide and lead-containing pigments are particularly useful in absorbing hydroperoxides and slowing the rate of film deterioration).

Autooxidatively cross-linked films, in every case, contain a drying oil; this is usually a vegetable oil, such as tung, oiticica (similar to tung; obtained from the seeds of a South American tree), castor, linseed, safflower, soybean, and tall oil, or a fish oil (menhaden). The drying oil can be mixed directly with the pigment (such as red or white lead, with the addition of the metallic dryer) to form the complete coating. More commonly, however, the drying oil is combined with a resin, such as an alkyd, epoxy ester, or polyurethane, by heating or cooking. The resin adds toughness and chemical resistance to the oil, increasing its chemical and moisture resistance.

The amount of oil combined with the resin influences the protective capability of the applied film. Long oil modifications result in less chemical resistance and longer drying times but increased penetrability and a greater ability to protect over a poorly cleaned surface. A lesser oil modification results in a short oil that must be applied over a relatively clean substrate and dries quickly. Some short oils are commonly used in fast-drying coatings that fully cure after baking for a few minutes at approximately 95 °C (200 °F). Short oil coatings have good moisture and chemical resistance but are relatively hard and brittle. The medium oil modifications are a compromise between the long and short oil modifications. Most commonly, alkyds, epoxy esters, and urethane resins are used in combination with drying oils to form autooxidatively cross-linked coatings.

Alkyd resins are derived as the reaction product of polyhydric alcohols and polybasic acids. This definition also includes polyester resins, of which alkyds are a specific type. The basic difference between an alkyd and a polyester is that the alkyd uses a polybasic acid derived from semidrying or drying oils such that the resin so formed can undergo autooxidation at ambient temperatures through reaction with atmospheric oxygen at the unsaturated groups present in the fatty acid molecules. Polyesters, on the other hand, do not undergo the autooxidative drying mechanism, because the dibasic acid used, commonly a glycerol, has very few free unsaturated groups available for autooxidative cross linking. The curing reaction of polyester resins is a free-radical-initiated cross linking, and polyesters are therefore described as chemically cross-linked coating systems.

The properties of alkyd coatings are derived predominantly from the properties of the drying oil used in the manufacture of the resin. Drying time, hardness, color, and moisture sensitivity all depend to a great extent on the drying oil used and its type and degree of unsaturation (available cross-linking sites). For example, the use of pentaerythritol as the polyhydric alcohol leads to faster drying, greater hardness, better gloss and gloss retention, and better water resistance than alkyds based on glycerols of equal fatty acid content. Similarly, the drying oil also affects resin properties. Soybean oil has been shown to give good drying rates and good color retention; therefore, the standard alkyds are usually soybean alkyds. Linseed oils, on the other hand, generally dry faster but darken on light exposure. The chemical structure of a linseed oil alkyd is shown in Fig. 1. Castor and coconut oils have good color-retentive properties and are used as plasticizing resins because of their nonoxidizing character.

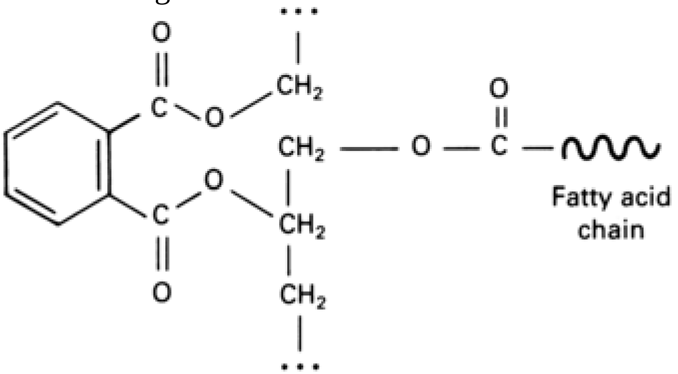

Fig. 1 Molecular structure of a linseed oil alkyd. The molecule is obtained through the reaction of a linseed oil monoglyceride and phthalic anhydride.

Phthalic anhydride and ter- and isophthalic acids are the most common polybasic acids used in alkyd preparation. The main advantage of ter- and isophthalic acids compared with phthalic anhydrides is that they provide polymers with a higher molecular weight and higher viscosity. Furthermore, they exhibit somewhat faster-drying, more flexible, tougher films and greater thermal stability than orthophthalic alkyds.

As a class, alkyd coating systems are still the workhorse of the corrosion protection industry, accounting for perhaps as much as two-thirds of all paints sold for corrosion protection. Although they have limited chemical and moisture resistance and relatively poor alkaline resistance, their low cost, ease of mixing and application, and excellent ability to penetrate and adhere to relatively poorly prepared, rough, dirty, or chalked surfaces make them the coating system of choice on steel exposed to nonchemical atmospheric service. Thus, alkyds are widely used for structural steel exposed in chemical plants away from the chemical processes. They are also used in such applications as water tank exteriors, highway bridges, boat and ship superstructures above the waterline, and in baking formulations as coatings for containers, appliances, and machinery and equipment housings.

Alkyd Modification. Alkyds are amenable to modification with a variety of other different resins to improve specific properties, such as drying time, color retention, and moisture and chemical resistance. For example, modification with a chlorinated rubber resin results in improved toughness and adhesion as well as an increase in acid, alkali, and water resistance. Such modified paints are used on concrete floors and as highway-marking paints.

Modification with a phenolic resin improves gloss retention and water and alkali resistance. Phenolic alkyd resins have performed satisfactorily in water immersion—a service in which nonphenolic-modified alkyd resins are not suitable.

Alkyd resins with vinyl modification are commonly formulated as universal primers (primers that, after application, can be topcoated with most generic-type intermediate and topcoats). The alkyd constituent improves adhesion, film build, solvent resistance, and thermal resistance, and the vinyl modification enhances recoatability, chemical, and moisture resistance.

Silicone modification of alkyd resins is perhaps the most widely promoted modification for corrosion-protective coatings. A silicone intermediate is added to the alkyd resin in quantities up to 30% to provide polymers with greatly improved durability, gloss retention, and heat resistance. Moisture resistance is greatly improved by the silicone modification, and such paints are extensively used as marine and maintenance paints.

Unmodified alkyds of medium-to-long oil length are familiar to homeowners as the oil- based paints used extensively around the home. Their ability to penetrate and adhere to wood and masonry surfaces, their availability in wide color ranges and glosses ranging from flat to high gloss, and their ease of application and cleanup make them ideal for a do-it-yourself homeowner.

Highly thixotropic alkyds are being promoted for both home and industrial use. Thixotropic paints remain in a semisolid or jellylike state when at rest but become thinner and spread easily with the shearing action caused by brushing. As soon as the brushing action is stopped, the paints again recover their jellylike characteristics. Such paints reduce pigment settling, reduce tendencies to run or sag, and make possible the application of thicker coats that have a longer wet-edge time due to the use of slower-evaporating solvents, which otherwise cannot be used because they may cause sagging. Dripping from the brush is minimized, and the thixotropy prevents absorption on porous surfaces. Thixotropic paints are usually not recommended for spray application. The thixotropy is introduced by modification with a polyamide resin, and the jellylike behavior of the combined resin has been attributed to hydrogen bonding between the carbonyl group of the alkyd and the amide group of the polyamide coreactant.

Alkyds can be modified with polyisocyanates to improve drying rates and chemical and abrasion resistance. Such resins, commonly called uralkyds, are available in a variety of colors and generally exhibit excellent gloss and color retention. Similarly, epoxy resins are combined with the alkyd to obtain coating formulations having improved adhesion to metal, better gloss and color retention, and much improved water and chemical resistance.

Epoxy esters differ from epoxy-modified alkyds in that the epoxy is a direct esterification product of an epoxy resin and a fatty acid, such as a vegetable oil or rosin. Like alkyds, epoxy ester resins are usually prepared by reacting the drying oil with the epoxy resin at a temperature of approximately 220 to 290 °C (425 to 550 °F) in the presence of esterification catalysts. The same drying oils used to prepare alkyd resins are also used to prepare epoxy esters. As with alkyds, the oil length can be categorized as long, medium, and short, and the properties accruing to the resin derive predominantly from the amount and type of drying oil modification to the resin. As a general rule, compared with alkyds, epoxy resins have better adhesion and moisture and chemical resistance, although they are slightly more expensive.

K.B. Tator, Organic Coatings and Linings, *Corrosion: Fundamentals, Testing, and Protection*, Vol 13A, *ASM Handbook*, ASM International, 2003, p 817–833

Organic Coatings and Linings

Kenneth B. Tator, KTA-Tator, Inc.

Thermoplastic Resins

Thermoplastic resins are characterized, as their name implies, by a softening at elevated temperatures. Although the resins within thermoplastic paint systems are commonly co- or ter-polymers, the molecular structure is not cross linked into a rigid molecule, as are the chemically cross-linked or the autooxidized coating systems. Rather, the resinous binder is dissolved in a suitable solvent, mixed with the pigment and other constituents comprising the formulated paint, and packaged. On application, the solvent volatilizes, and the resinous binder, along with the pigment, is deposited onto the surface being coated as a solid film. The molecular entanglement of the relatively linear (although perhaps coiled or tangled) molecule segments provides a layering effect that, with pigmentation and sufficient thickness, provides the characteristic moisture and chemical resistance of the resin system used.

There are two types of coatings based on thermoplastic resins: those deposited by evaporation of a solvent—commonly called lacquers—and those deposited by evaporation of water—a class of coatings called water-borne coatings.

Lacquers. The most useful solvent-deposited thermoplastic resins for corrosion protection are the vinyls, chlorinated rubbers, thermoplastic acrylics, and bituminous resins (coal tar and asphalt). Each resin type has its

own characteristic qualities, specific resistances, and susceptibilities, and each is discussed subsequently in greater detail. However, in all cases, because no chemical change takes place to the resin on application and drying, it stands to reason that the applied coating redissolves if it is exposed to the same solvents that it was originally dissolved in on formulation. This is precisely what happens, and such coatings have no resistance to the solvents in which they were originally dissolved or in solvents of equal or greater solvency for that particular resin. This, however, is not usually a disadvantage; although solvent resistance may be poor, such coatings are rarely, if ever, exposed in a solvent-laden atmosphere. Instead, they are called on to resist weathering, acid or alkali exposures, and moisture. As a rule, all have good resistance in these applications, and the vinyls, chlorinated rubbers, and coal tars have excellent moisture resistance as well.

Conversely, the solvent susceptibility of these thermoplastic coatings is often an advantage. When maintenance repainting is necessary, the same system can be reapplied, and the solvents in the new topcoat partially redissolve the existing old coat, resulting in intermolecular entanglement of the new coating with the old and giving excellent adhesion. Thus, solvent solutions of these thermoplastic resins have excellent recoatability with the same system, even after extended periods of time. This cannot be said for either the autooxidative cross-linking coatings or the chemically cured coatings.

The principal disadvantage of a solvent-deposited lacquer system is that large amounts of solvent must be used to dissolve the relatively high-molecular-weight resins used in the coating. Accordingly, most lacquer coatings cannot comply with the lower volatile organic compound (VOC) legislation in effect today. Thus, while such coating systems were widely used as little as ten years ago, they are rarely used. However, because there are still many structures painted with lacquer coating systems, a brief description of the most common types is presented, as follows.

Vinyls. Vinyl coatings are usually applied as a solvent-deposited solution consisting of either a polyvinyl chloride-polyvinyl acetate (PVC- PVA) copolymer in the ratio of approximately 86% PVC to 13 to 14% PVA.

The vinyl solution coatings are generally very low-solids, high-solvent materials that have been preempted by restrictive VOC legislation. Most thermoplastic vinyl solution coatings contain solvents (generally oxygenated solvents such as ketones and glycol ethers) ranging from 75 to 90% of the total volume of the formulated paint. Figure 2 shows an example of a PVC-PVA vinyl. Vinyl solution coatings are noted for their outstanding toughness and water resistance.

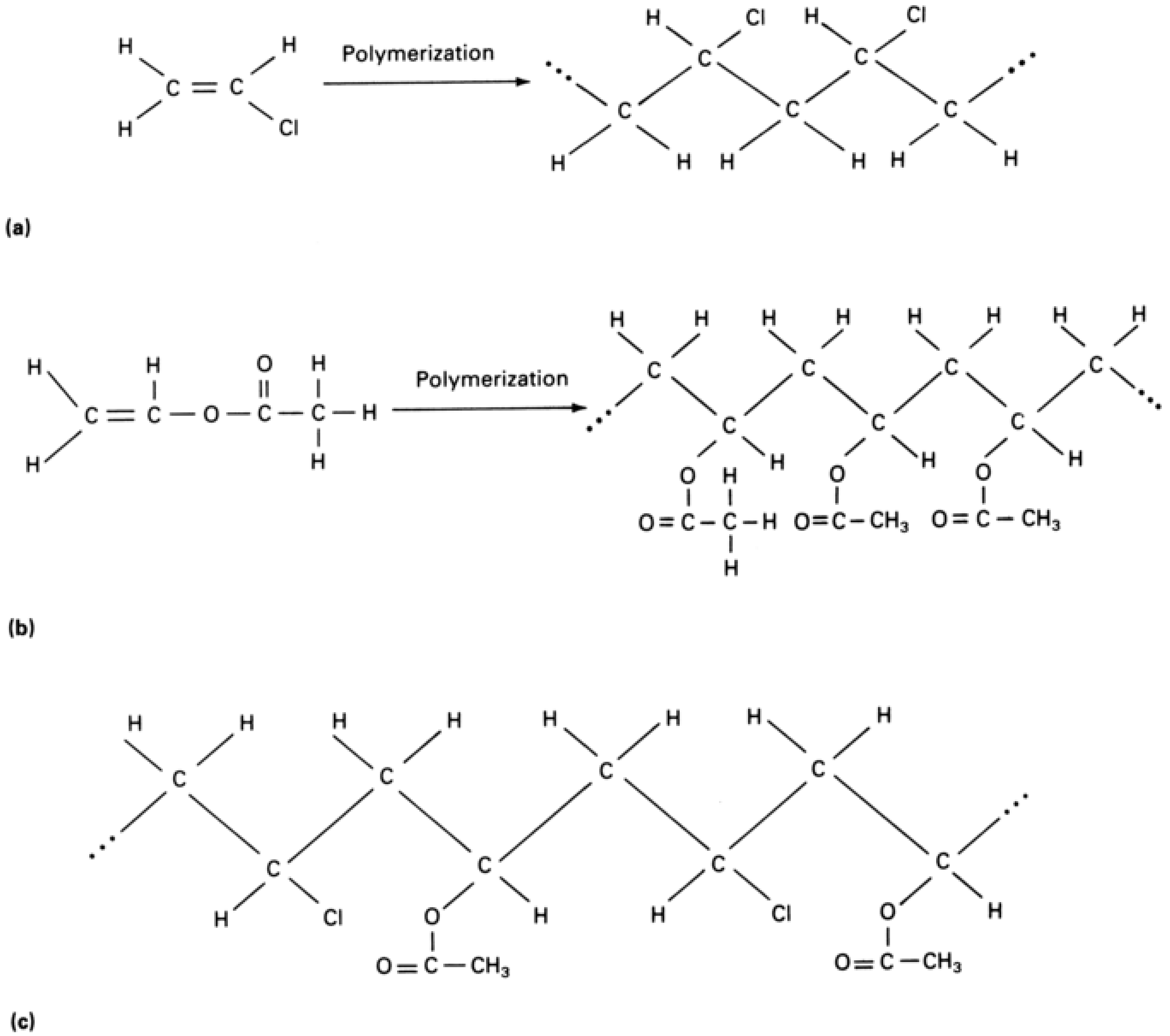

Fig. 2 Reaction of polyvinyl chloride (PVC) and polyvinyl acetate (PVA) polymers to form a PVC-PVA copolymer. (a) Polymerization of PVC. (b) Polymerization of PVA. (c) PVC-PVA copolymer

Vinyl paints are used as complete systems (vinyl primer, intermediate, and topcoat) or as topcoats over zinc-rich primers for the protection of highway bridges throughout the United States. The relative inertness of the vinyl topcoat, coupled with good adhesion (when formulated with maleic acid), protects the relatively reactive zinc in an organic or inorganic zinc-rich primer from reaction with environmental moisture, acid rain, and other atmospheric contaminants. The zinc- rich primer provides galvanic protection to the underlying steel. See the article “Zinc-Rich Coatings” that follows in this Volume.

Chlorinated rubber coatings are also solvent-deposited coatings in that there is no chemical change that occurs during application, and the coating film forms on the surface after application as the solvent evaporates. Similar to the vinyl coating materials, solvent-deposited chlorinated rubber coatings cannot be used in most areas of the United States due to their high VOC content. Chlorinated rubber coating systems had been much more widely used in Europe than in the United States, and systems based on chlorinated rubbers have excellent resistance to acids, alkalis, oxidizing agents and have very low water vapor transmission rates (approximately one- tenth that of an alkyd resin coating). In addition, they are generally nonflammable (due to their chlorine content) and nontoxic. Chlorinated rubber paints were used principally as chemical- and corrosion-resistant coatings, marine coatings, building masonry and swimming pool paints, highway-marking paints, fire-retardant and mold-resistant paints, and primers for hot- applied coal tar or asphaltic enamels (to provide good adhesion to steel).

Chlorinated rubber resins are manufactured by chlorinating natural rubber with approximately 65 to 68% Cl. The resulting resin must be plasticized and stabilized against light, heat, and gellation in order to be used as a

binder in protective coatings. Heat stability is obtained by incorporating low-molecular-weight epoxy compounds or epoxidized oils into the resin. Light-fast plasticizers such as dialkyl phthalates and acrylic resins are used. For severe chemical service, chlorinated paraffins or chlorinated diphenyls should be used because of their high resistance to saponification.

The chemical structure of a chlorinated rubber resin is shown in Fig. 3.

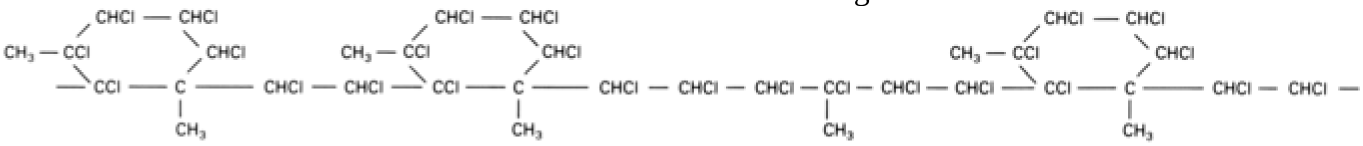

Fig. 3 Molecular structure of a chlorinated rubber resin. Source: Ref 1

Acrylic coatings can be formulated as thermoplastic solvent-deposited coatings, cross- linked thermoset coatings, and water-based emulsion coatings. Acrylic resins that are used for protective coatings consist of polymers and copolymers of the esters of methacrylic and acrylic acid. The chemical structure of these acrylics is shown in Fig. 4. The resulting resins, with suitable pigmentation, provide excellent film-forming coatings characterized by excellent light fastness, gloss, and ultraviolet stability. Chemical resistance to weathering environments is generally excellent, as is resistance to moisture. Most acrylic coatings are not suitable for immersion service or strong chemical environments because of attack of the ester group present on both the polymethyl methacrylate and ethyl acrylate resins. This ester group, however, is present only as a pendant sidechain; accordingly, the carbon-to-carbon backbone chain of the acrylic resins does provide very good chemical and moisture resistance, which enables these resins to be used in most chemically moderate atmospheric services.

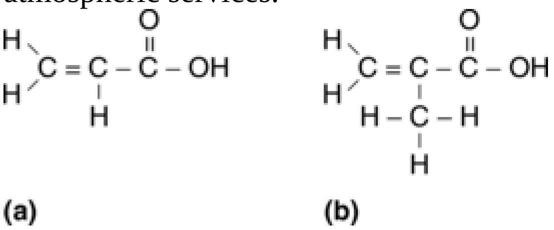

Fig. 4 Molecular structure of (a) acrylic acid and (b) methacrylic acid polymers

Coatings can be formulated with acrylate, methacrylate, or higher homopolymers. Blends of both resin types are also commonly used for corrosion protection. Generally speaking, those coatings formulated from the acrylates or from copolymers with a preponderance of the acrylate ester are softer and more flexible than the corresponding methacrylates. The ultraviolet resistance of the acrylate is somewhat lower than that of the methacrylate because of the presence of a tertiary hydrogen attached directly to a carbon comprising the molecular backbone. This active hydrogen is vulnerable to photooxidative and thermooxidative attack. Consequently, acrylate esters have a greater susceptibility to ultraviolet light and oxygen, leading to yellowing or darkening in comparison with the methacrylates. The methacrylates, although providing a harder and more brittle film with less adhesion, are more chemical and moisture resistant and have a greater heat tolerance.

With both resin types, greater flexibility, toughness, and resistance to abrasion can be obtained by increasing the molecular weight. Hardness decreases, although flexibility and elongation increase in both resin families. However, with too great an increase in molecular weight, solution viscosity becomes excessive, and solvent release in a formulated paint becomes excessively slow.

Acrylic resins are characteristically soluble in moderately hydrogen-bonded solvents, such as ketones, esters, aromatic hydrocarbons, and certain chlorinated hydrocarbons. Excellent color retention, gloss, and ultraviolet stability, coupled with very good moisture and chemical resistance, make acrylic coatings quite popular in protecting steel in atmospheric service.

Thermoplastic Acrylics. Similar to all thermoplastic coatings, thermoplastic acrylics are essentially solvent-deposited resins that do not undergo any chemical change after, or at the time of, application. On application, the solvent carrier volatilizes, and the coating system sets, hardens, and attains its final resistant properties as the solvent evaporates. Heating or baking is often used to hasten solvent evaporation. However, because of their high VOCs, thermoplastic acrylic coatings are not widely used.

The resins used in these coatings are polymers and copolymers of high-molecular-weight esters of methacrylic and acrylic acids. These resins, when suitably pigmented, have excellent gloss, color retention, and ultraviolet light stability.

Probably the major use of thermoplastic acrylics is in automobile finishing and refinishing. Advantages include the ease of tinting and coloration, excellent dispersion of metallic reflective pigments, high gloss and ultraviolet stability, and thermal reflow. Thermal reflow is important because, after the original factory coating is applied, minor imperfections, sanding marks, and other irregularities can be overcome by reheating the coating under heat lamps or in an oven. The surface of the coating partially melts and reflows to form the smooth, glossy appearance one expects with an automotive finish.

Another major market is aerosol can paint, which is widely sold throughout the world. These paints are thermoplastic acrylics, and they dry and harden through solvent evaporation.

Solvent-deposited acrylics are also used for maintenance finishes, but more commonly, the acrylic monomer or copolymer is added to an alkyd. This results in an acrylic-modified alkyd with the excellent penetration properties, adhesion, and ease of application of the alkyd, combined with the improved ultraviolet resistance, gloss, and color retention of the acrylic.

Thermosetting Acrylics. Thermosetting, or cross-linking, acrylics can be obtained by combining the methacrylate or acrylate esters with reactive nonacrylic polymers. The most common cross-linking agents in use are the epoxy resins, the urea or melamine-formaldehyde resins, and the vinyl resins. Generally, the nonacrylic polymer is the predominant structure present in the coating film, and the acrylic modification is done only to enhance the color, gloss, and ultraviolet stability of the nonacrylic constituent. The resulting thermoset acrylic finishes are generally harder, tougher, and more resistant to heat and solvents than thermoplastic acrylics. On the other hand, thermoset acrylic finishes are also generally less resistant to ultraviolet light and usually require heating or baking after application to attain the desired physical properties.

Acrylic finishes based on urea or melamine- formaldehyde resins cross linked with acrylic monomers are widely used for coating such home appliances as refrigerators, washing machines, dryers, dishwashers, freezers, and air conditioners. The coatings have excellent adhesion and detergent resistance, and they have short curing times at relatively low curing temperatures. The major advantages of such coatings are the high gloss, range of colors available, and lack of yellowing or darkening on exposure to sunlight.

Photopolymerization of acrylic homo- and copolymers is, for the painting industry, an emerging—and very interesting—technology. The wavelength ranges of ultraviolet light (approximately 200 to 400 nm) and visible light (approximately 400 to 800 nm) can initiate cross linking in a susceptible binder system. Acrylic esters show a very rapid response to photoinitiation as compared to all other commonly used coating resins. Within the acrylic family, the acrylate is at least ten times more reactive to ultraviolet or visible light radiation than the methacrylate. All types of resins used in conventional paint systems (such as alkyds, epoxies, polyesters, and urethanes) can be modified with acrylate esters, and the combination can be combined with a suitable photoinitiator to aid in the radical polymerization mechanism.

High-solids, low-molecular-weight, light- cured coatings can be applied by brush, roller, and spray. After setting up and exposure to an intense source of ultraviolet or visible light, they cross link through a photoinitiated free radical polymerization, which leads to thorough cross linking, hardening, and almost immediate attainment of moisture and chemical resistance. The potential of this technology for exterior painting is evident; the sun itself might act as the cross- linking agent. However, such technology with regard to corrosion-protective coatings is far from perfected. Current problems include the extremely high cost of formulated paints, the requirement for intense ultraviolet or light energy in order to initiate curing, and the curing problems with pigmented coatings or coatings more than a few mils thick.

Therefore, although photochemically cured coatings for corrosion protection have not been developed, the technology is viable, and some radiation-curable coatings have been developed. Commercial applications include clear coatings, thin films of pigmented printing inks, coatings pigmented primarily with inert pigments (for example, paste fillers for particleboard), and paper coatings. Light-cured acrylic laminates and overlays, applied as an adhesive or paste on tooth enamel, have been developed for dental practice.

Water-borne coatings are defined as coatings where water has been purposely introduced into the coating. There are essentially four classes of water-borne coatings:

- Water-reducible coatings
- Water emulsion coatings

- Latex coatings
- Alkali silicate coatings

The coatings in each of these classifications are formulated differently and have significantly different curing and performance properties. While all four categories can be used for heavy- duty corrosion-resistant coatings, to date, the most commonly used coatings for air-dry maintenance and marine protection are latex-based coatings based on acrylic polymers, and inorganic zinc-rich coatings based on alkali silicate resins. Increasingly, however, two-package epoxy and polyurethane water emulsion coatings are being used. Water-reducible coatings are used predominately in baking applications, because air-dry water reducibles do not perform well. Each of the four classes of water-borne coatings is discussed in the following section.

Water-Reducible Coatings. Resins in these coatings are not soluble in water and are high- solid solutions in water-miscible solvents with either carboxylic acid groups of the resin neutralized with low-molecular-weight amines or with amine groups of resins that are partially neutralized with low-molecular-weight acids. The pigment is dispersed in the partially neutralized resin solution, the cross linker is added along with additives such as catalyst, and the mixture is diluted with water to application viscosity. The water-reducible binders commonly used are alkyds, polyesters, epoxies, and polyurethanes. Electrodeposition coatings, including automotive coatings, are based on water-reducible resin technologies. Additionally, interior linings for beverage cans and dip coating applications commonly use water-reducible technology.

After heating in a baking oven, the water evaporates, and the reactive moieties come together and react at the elevated baking temperature. Water in the coating must evaporate prior to cross linking. This is done by having a longer flash-off time before entering the baking oven or by having a two-stage oven, the first stage at lower temperature to promote water evaporation and the second at a higher temperature to induce the cross-linking reaction.

Water-dispersible air-dry coatings have not achieved viable commercialization. This is due to hydrolytic instability that leads to limited in- can storage life, a slow rate of air-dry cure at lower temperatures, and an excessively water- sensitive film until complete cure has been attained. A water-dispersible polyurethane has recently been commercialized. A hydrophylic- modified polyester polyisocyanate in one package is combined with a second package of a hydroxy-terminated water-reducible polyol with carboxylic acid modification. An excess of the NCO to OH is used to offset the slow isocyanate reaction with water. On air drying, cross linking and good moisture and chemical resistance develop. However, the performance of water-dispersible polyurethane is not yet as good as that of the solvent-based variety.

Emulsion Coatings. True emulsion coatings consist of dispersions of liquids in liquids. Many people refer to latex coatings as latex emulsions, but technically, that is a misnomer.

True emulsion coatings are the least used of the four categories described herein. However, two-package, epoxy-based emulsions have been commercially available for over 25 years. These materials consist of a liquid epoxy resin solution in one package and a second package containing an amine-terminated cross-linking agent with a nonionic surfactant or with nitroethane. The amine cross-linker package is diluted with water, and on application, the epoxy resin solution is added with vigorous stirring. As the water evaporates, the epoxy resin reacts with the amine groups to cross link in conventional fashion. Epoxy emulsion paints are used in hospitals and food-processing plants, where a solvent odor is not acceptable and hard, easily cleaned wall and/ or floor coatings are needed.

Nitrocellulose lacquers emulsified into water are used as topcoats for wood furniture. These emulsions have significantly lower VOC than solvent-borne lacquers but require a longer dry time.

Bituminous emulsions are used as pavement and parking lot surfaces and are discussed in a later section entitled “Bituminous Coatings.”

Latex Coatings. Latex-based coatings are dispersions of solid polymer particles in water. The solid polymer particles are most commonly based on polyacrylate resins (usually the acrylates and methacrylates) but can include vinyl chloride-vinyl acetate copolymers, styrene-butadiene, and others. Usually, a high-molecular-weight resin is suspended in a water medium. The suspension is accomplished by the use of a surfactant on the polymer surface, which charges the surface, in turn repelling similarly charged particles. After application, the water evaporates, and the polymer particles coalesce (come together). The latex forms a film by coalescence of the polymer particles. Coalescence can occur only if the film-formation temperature is higher than the glass transition temperature (T_g) of the polymer particles. The T_g is the temperature at which the polymer softens. In the case of most air-dry coatings, slow final coalescence is not a real problem, so the film-formation

temperature needs to be only a little above the T_g. In the case of baked coatings, film formation must be complete by the end of the baking time; therefore, baking temperatures should be significantly above the T_g.

A major coating market has been the water- based acrylic paints widely used by the homeowner for indoor and exterior painting purposes. Compared to oil-based coatings, the other major homeowner-type paint, the water-based acrylics have a number of advantages. They have a much faster drying time and can be recoated within 1 h. They have better alkali resistance, excellent adhesion, come in a variety of colors and maintain their color and gloss in the presence of sunlight and ultraviolet light, and have excellent long-term flexibility and toughness. The major advantage, of course, is the ease of cleanup with water-based paints.

The disadvantages are that the oil-based paints have greater penetrability, particularly on wood and porous surfaces, and have better initial adhesion. On smooth surfaces, water-based paints may peel or lose adhesion, while an oil-based paint may wet sufficiently to maintain good adhesion. However, acrylic paints have better resistance to blistering because of their breathing ability and have much better resistance to chalking and yellowing. Water-based coatings may provide better adhesion to damp wood and masonry substrates than oil-based paints.

The chemistry of latex coatings is extremely complex. Generally, high-molecular-weight acrylic polymers are polymerized in a water emulsion. The desired pigments are dispersed in the emulsion, and the required additives are added, followed by tinting and color pigments. Titanium dioxide is the most widely used white-hiding pigment, although most other water-insoluble alkali-resistant organic and inorganic pigments can also be used. Wetting agents are added to ensure complete pigment wetting in the water vehicle, and antifoaming additives are used to prevent foaming during manufacture and at the time of application. Thickening additives (for proper application viscosity) are used to prevent pigment settling as well as runs and sags after application.

Surfactants are added to enhance pigment dispersion, and it is these additives that provide the water sensitivity that most water-based coatings have after application. Briefly stated, most surfactants have a hydrophobic (water-hating) and a hydrophilic (water-loving) end, which orients around the emulsified resin and the pigment particles. The hydrophobic end is adjacent to the resin particle surface, while the hydrophilic end is attracted to the water carrier. After application of the paint, many of these surfactants remain entrapped within the film cross section, and the hydrophilic end of the surfactant attracts water from the environment, which tends to soften and swell the coating. In atmospheric service, there is insufficient water—or insufficient wet time— to cause a problem. However, in prolonged water immersion, water may be attracted by the surfactant, penetrate the film, and cause softening and swelling of the coating, with a loss of adhesion. Consequently, water-based coatings, as currently formulated, are not suitable for prolonged water immersion.

For most air-dry (nonbaking) applications, a coalescing solvent is added. This very slow- evaporating organic solvent, which is miscible with water, is added to the water carrier. As the water evaporates, the concentration of the solvent becomes higher and higher in the water- solvent mixture. Ultimately, in the drying film, the solvent reaches a sufficient concentration that it can partially solvate the resin particles, causing them to soften and meld together on further drying. The coalescing solvent helps convert the emulsified particles into a relatively smooth, homogeneous film. However, residual solvent may be entrapped within the film, and it too can lead to water sensitivity. Figure 5 depicts the coalescence and film formation of a latex coating.

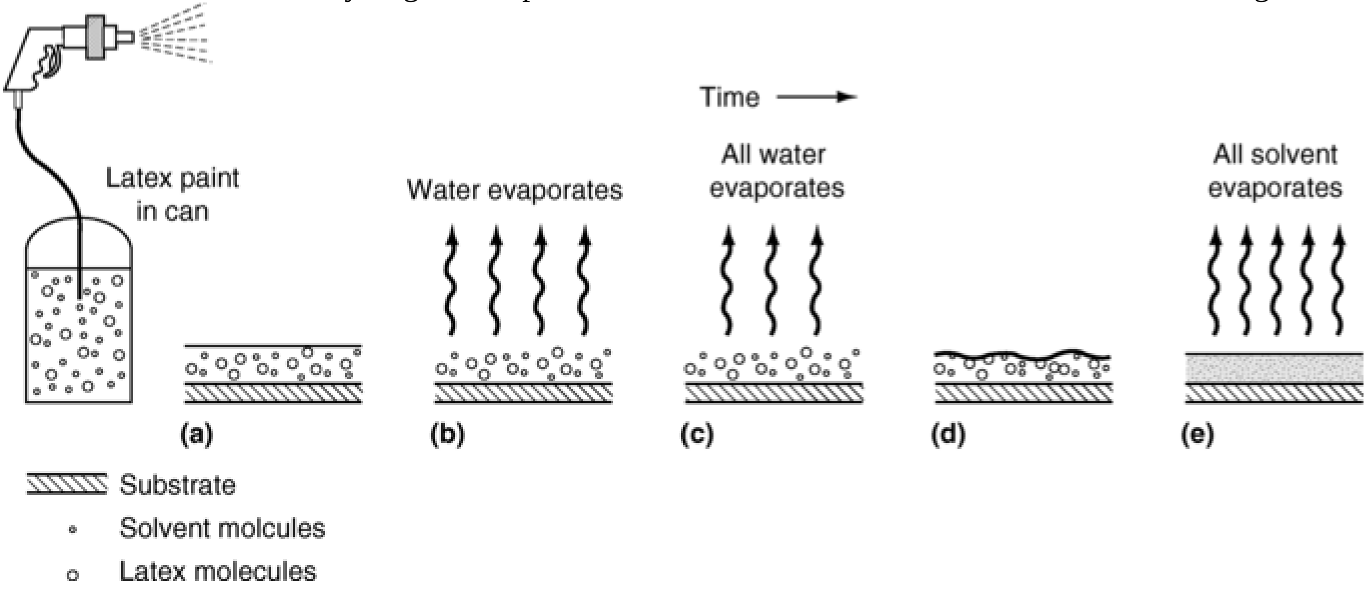

Fig. 5 Schematic of the stages of coalescence and film formation of a latex coating. (a) Coating on substrate immediately after application. (b) As water evaporates, the solvent-to-water ratio increases, and latex particles close together. (c) All water evaporates, and only latex particles and solvent remain. (d) Solvent melts latex particles together. (e) All solvent evaporates, and latex particles form a firm, dry coating.

For wood or masonry surfaces where water vapor transmission may be a problem, latex paints may be suitable, because they are said to breathe. This breathing occurs as a result of irregularities during the coalescence part of the film forming; the particles may not align themselves properly relative to other emulsified particles. A series of pores or defects in the coalesced film results. Such discontinuities are extremely small, and the surface tension of water in liquid form does not enable penetration through the coating to the underlying substrate. However, water vapor may readily pass through such discontinuities, resulting in its breathing ability.

Water-based paints develop poor film properties when applied during cold, damp weather. In order for proper weather and chemical resistances to develop in a water emulsion film, water evaporation and proper drying must occur. If water evaporation is retarded and if the drying sequence is upset by becoming either too slow (or in some cases too rapid), proper coalescence and film formation do not occur. The result can be a soft, poorly adherent film that, when drying does finally occur, shows cracking; this film may also be brittle and adhere poorly. Too fast a water evaporation rate on a hot surface or a fast-evaporating coalescing solvent can lead to a powdery, poorly adherent paint film or a film with many voids, pinholes, or cross-sectional porosities.

Acrylic paints for interior use are similar to those for exterior use, except that a higher pigment volume can be used, and less expensive pigments that are not as light-fast as those for exterior use can be used. The major competition for acrylic interior paints comes from lower-cost polyvinyl acetate (PVA) or butadiene-styrene-based latex coatings.

Alkali Silicate Coatings. For industrial maintenance and marine coatings, the most common coatings of this type are used as alkali silicate binders for inorganic zinc-rich coatings and as surfacers and waterproofers for masonry. The binders are water-soluble silicates of alkali metals (sodium, potassium lithium) and related quaternary ammonium silicates. The zinc-rich coatings are pigmented with zinc-dust particles, and other coatings may be pigmented using titanium dioxide (titanates).

After application, water evaporates, and the alkali silicates concentrate as a silica gel. The silica gel is still water soluble, but gradually it hydrolyzes to form silicic acid, which in turn reacts with the pigment, the substrate, or both. This makes the gel increasingly insoluble. Further hydrolysis and alkali neutralization occur by reaction with an acid curing solution or carbonic acid formed from the atmospheric reaction of carbon dioxide and water. This neutralization reaction forms a silicate matrix holding the pigment particles together and to the substrate. However, a by-product of the neutralization reaction is the formation of water-soluble reaction salts that may lead to blistering of topcoated silicates in water immersion. Inorganic alkali-silica-based zinc-rich paints, concrete surface hardeners, and other silicate-based masonry water-repellent coatings are all based on this technology.

Characteristics of Water in a Water-Borne Coating. Water, as a constituent of the environment, is environmentally friendly. Accordingly, water-borne coatings are generally environmentally acceptable, although most of them use a cosolvent as a coalescing aid, freeze-thaw stabilizers, and/or wet-edge aids to adjust the drying rate and improve flow and leveling. These cosolvents are generally added in volumes of 20% or less of the water constituent.

Water-borne coatings are not flammable and do not support combustion during application and while liquid. Moreover, there is no objectionable solvent odor (although, depending on the formulation and the use of cosolvents, they do have a mild, nonlingering odor).

As is evident with all four classes of water- borne coatings, water is a major constituent. Furthermore, in each case, the water must evaporate in order for a subsequent film-forming mechanism to occur and for the coating to attain its final moisture and chemical resistance.

Water-borne coatings are significantly different than solvent-borne coatings, due entirely to the character of water. In solvent-borne coatings, blends of solvents with different solvency can be used to dissolve a resin. Those solvents then volatilize with different evaporation rates from the applied coating. There are no such things as blends of water, and the freezing temperature and boiling point of water are constant. The evaporation rate of water is highly dependent on temperature and humidity. As water evaporates from a coating, the humidity above the coating surface increases such that water evaporation is low. If there is no air movement or

circulation above the coating surface, humidity may reach 100%, at which time no further water evaporates from the coating. Moreover, if temperatures are low, the ability of the air to contain moisture is substantially diminished. At low temperatures (much below 10 °C, or 50 °F), water evaporation is slowed sufficiently that many water-borne coatings may not form a suitable film. This is not the case with organic solvents, which can volatilize independent of humidity (however, the organic solvent vapor pressure is a function of the solvent concentration at the coating-air interface). The film formation of water-borne coatings may be further disrupted when the temperature falls below the T_g of the resin, preventing the resin particles from properly flowing or coalescing.
The high polarity of the water molecules, and their strong tendency to hydrogen bond, is responsible for the unique properties of water. This hydrogen bonding is responsible for the slow water evaporation rate and the tendency for water to solidify at relatively low temperatures (compared to organic solvents). Additionally, the hydrogen bonding results in a high surface tension of water that prevents its penetration into dirty, dusty, or relatively porous surfaces (again, compared to organic solvents). Thus, initial adhesion of most water-borne organic coatings is poor, although over time (sometimes two weeks or more), adhesion to most surfaces becomes tight. Figure 6 illustrates the hydrogen bonding attractions between the oxygen atoms of one molecule for the hydrogen atoms of another molecule.

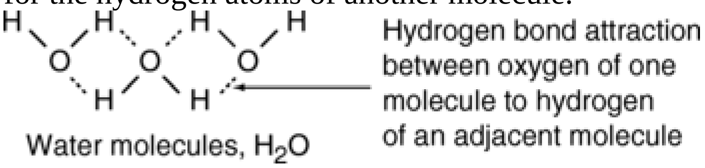

Fig. 6 Hydrogen bonding of water molecules

Everyone knows that oil and water do not mix. Even with slight oil contamination of a substrate, water-borne coatings do not properly wet a substrate (even when solvents are a part of the formulation). The surface-free energy of the substrate is depressed with only a slight amount of oil contamination, such that it cannot be wet by a water-borne coating. Accordingly, any oil must be removed from the substrate prior to application of any water-borne coating.
As previously mentioned, water does freeze. With water-borne coatings, the expansion of the freezing water can cause coagulation of dispersed latex or emulsion particles, resulting in settling or agglomerations in the can prior to application. Freezing of water in a water-borne coating system after application upsets coalescence and cross linking. Often, high-molecular- weight polyfunctional alcohols (such as diethylene glycol) are mixed into the water to reduce the hydrogen bonding density, thereby reducing surface tension and lowering the freezing point.
Water dissolves and disassociates salts. Salts on a surface beneath a water-borne coating may be dissolved and accelerate corrosion. Additionally, many of the surfactants and neutralization by-products of the curing reaction result in salts that, when dispersed through a cross section of the coating, may increase water permeability. This is a particular concern, because water is an inherent constituent of most exterior environments. Thus, dissolving, suspending, or emulsifying a resin in a water solution may result in atmospheric moisture susceptibility.
Bituminous Coatings. The bitumens used in the coatings industry are coal tar and asphalt. Although these materials are distinctly different physically and chemically, in appearance they are essentially identical black thermoplastic tar materials. As coatings, the bitumens can be applied as hot melts, solvent cutbacks, or emulsions. However, similar to all other solvent-deposited coatings, the bitumen cutback violates most VOC regulations. Accordingly, hot melt and water emulsion applications are most popular.
Hot melt application involves heating the bitumen to a temperature of 175 to 245 °C (350 to 475 °F) such that its viscosity at that temperature is very low—almost waterlike. Hot melt asphalts and coal tar materials are usually applied with mops or swabs to the surface being coated, although brush, roller, or spray application is sometimes used. Flow coating of the interiors of pipes and small vessels is also done. In this method, the hot melt is flowed into the pipe or vessel, and the item is rotated or turned to cover all surfaces before the coating cools and hardens. The interiors and exteriors of pipeline sections are often flow coated at pipeline-coating facilities.
Water emulsions are prepared by suspending minute particles of the bitumen in water using emulsifying agents and by combining with inert fillers, such as pulverized talcs of hydrated magnesium and aluminum silicates,

coal dust, powder silica, mica, and limestone dust. After application, the water evaporates. Coalescence occurs in the fashion typical of any emulsion coating, and a protective film is formed.
Asphaltic or coal tar bitumens dissolved in a suitable solvent (normally aliphatic and aromatic hydrocarbons) are termed solvent cutbacks. Dissolving the bitumen in a solvent lowers its viscosity sufficiently that the cutback can be applied by spray, brush, or roller, as appropriate. After application, the solvent volatilizes, and the bitumen resolidifies into a film. The coating thicknesses of solvent cutbacks are generally considerably less than those achieved by hot melt application, but the convenience of not having to heat the bitumen at the job site immediately before application is a major advantage.
In general, hot melt application provides the best moisture and chemical resistance, followed in order by the solvent cutback and water emulsions. Asphaltic and coal tar bitumens applied as emulsions or as hot melts have widespread use as roof coatings, highway or pavement sealers, and underground coatings or waterproofing compounds.
Asphalts. Natural asphalt, or gilsonite, is a hard, brittle resin that is mined predominantly in Utah, Colorado, and Trinidad. Increasingly, asphalts obtained as residues from the distillation of crude petroleum are replacing the natural asphalts because of better uniformity, fewer impurities, and lower transportation costs. Asphaltic compounds are comprised of complex polymeric aliphatic hydrocarbons, and they have good water and chemical resistance; similar to coal tars, they are sensitive to oils and solvents. Asphaltic coatings have much greater ultraviolet resistance than coal tars do and are therefore used for above-grade weathering applications in which coal tars are not suitable. These asphaltic coatings are used above grade in atmospheric service.
Coal tar enamels or pitches are derived from the coking of coal. When coal is heated in the absence of air to a temperature of approximately 1095 °C (2000 °F), it decomposes partially into a gas and coke. The gas is subsequently condensed, and coal tar is formed. Lighter fractions are removed from this tar by subsequent heating and gas extraction until the desired coal tar fraction for use in coatings is obtained. The compounds in coal tar range from low-boiling, low- molecular-weight benzene to complex, high-molecular-weight, aromatic hydrocarbons.
Essentially, there are three types of coal tar enamels:

- A straight pitch base that is relatively hard and brittle but has the greatest moisture and chemical resistance
- A plasticized enamel that is more flexible and has greater cold weather application tolerance but the least chemical and moisture resistance
- An intermediate grade (containing approximately 50% of each of the first two) that is also intermediate in its properties

For best adhesion, preheating of the object being coated is preferred; if this is not feasible, a primer can be used to promote adhesion of the coal tar. Many of the primers are solvent cutbacks of coal tar pitch combined with a chlorinated rubber resin, plasticizers, highly volatile solvents, and some color pigment. The primer is of a lower viscosity and can more readily wet the steel surface. In addition, it dries faster and leaves a firmly bonded layer on the steel. Subsequently applied coal tar adheres more readily to steel that is primed in this manner.
Coal tar coatings (whether applied as hot melts, cutbacks, or emulsions) are subject to ultraviolet light degradation and resultant cracking. The cracking results from the volatilization or evaporation of lower-molecular-weight constituents from the surface and attendant shrinking. The surface of the coating contracts and cracks, while the underlying thicknesses remain plastic. Such “alligator” cracking (Fig. 7) is not detrimental, although it does diminish the thickness of the coating within the crack fissures. Because of this phenomenon, coal tar coatings are used in underground or immersion service, in which they are not subject to ultraviolet light. As roof coatings, they must be shielded by a subsequent coat of noncoal tar material or by gravel or pebbles applied for this purpose.

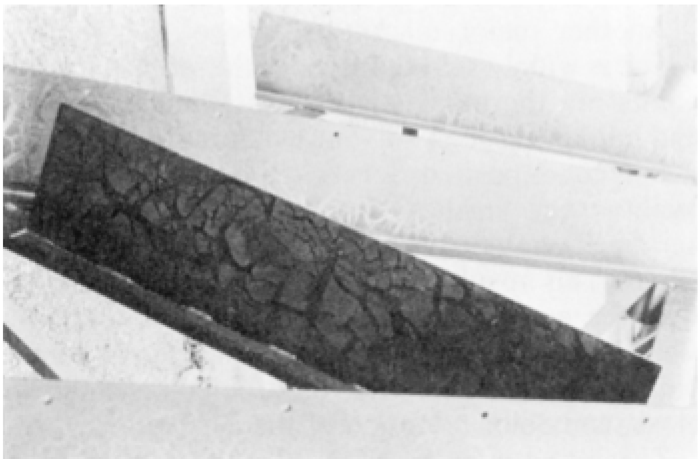

Fig. 7 "Alligator" cracking of a coal tar coating caused by volatilization of low-molecular-weight constituents from the surface and by coating shrinkage

Coal tar coatings have much better resistance to moisture, acids, and alkalies than the asphaltics. The coal tars and asphalts are generally incompatible as a result of their chemical makeup and usually should not be used as mixtures or applied one type over another.

Reference cited in this section

1. C.R. Martens, Ed., *Technology of Paints, Varnishes, and Lacquers,* Reinhold, 1968

K.B. Tator, Organic Coatings and Linings, *Corrosion: Fundamentals, Testing, and Protection*, Vol 13A*, ASM Handbook*, ASM International, 2003, p 817–833

Organic Coatings and Linings

Kenneth B. Tator, KTA-Tator, Inc.

Cross-Linked Thermosetting Coatings

Chemically cured coatings, in the context of this article, refer to coatings that harden or cure and attain their final resistant properties by virtue of a chemical reaction either with a copolymer or with moisture. Examples of coatings that chemically cross link by copolymerization include epoxies, unsaturated polyesters, urethanes in which the isocyanate is reacted with a polyol, high-temperature curing silicones, and phenolic linings. Chemically cured coatings that react with water include moisture-cured polyurethanes and most of the inorganic zinc-rich coatings. Although drying-oil-based coatings (see the section "Autooxidative Cross-Linked Resins" in this article) are also chemically cross linked on their reaction with oxygen from the air, they are excluded from this category, because the autooxidative cross-linking mechanism is a sufficiently distinct category of chemical cross linking to merit a separate discussion.

The fundamental principle of chemical cross linking is to formulate a coating using a resin or binder of low molecular weight. When mixed and applied, reaction with moisture from the atmosphere or with a coreactant takes place, resulting in cross linking and a much larger three- dimensional molecular structure. In fact, it is possible to begin the application of a cross- linked coating system to the interior of a large tank or vessel, and on completion of the application many hours later, the film may cure into one large macromolecule that may cover many thousands of square feet of surface area. Such a coating or lining, if suitably formulated, provides a tough, flexible, and highly chemical-resistant corrosion protection barrier over the underlying substrate. Such a

large macromolecule with the attendant corrosion-resistant properties would be impossible to obtain in a prereacted binder system.

Coatings and linings based on chemically converted binders can be formulated to have excellent resistance to acids, alkalies, and moisture and can be formulated to resist abrasion, ultraviolet degradation, and thermal degradation. As a general rule, toughness and flexibility of the coating increase as the molecular length increases. Similarly, chemical and moisture resistance increase as the cross-linking density increases within the macromolecule. However, as with any coating, constituent chemical groups within any molecular structure may result in characteristic strengths or weaknesses within the molecular chain. Furthermore, the arrangement and composition of pendant sidegroups may further alter the properties of any given molecular structure. Also, unreacted moieties (reactive sites) within the molecule may lead to decreased chemical, moisture, or thermal resistance.

The rate at which the molecule cross links is dependent not only on the reacting moieties but also on the cross-linking mechanism (for example, addition, condensation, or free-radical- initiated cross linking). Most importantly, external factors such as temperature and (with moisture reactions) atmospheric humidity affect the rate and extent of cross linking. Thus, chemically converted coatings must set after application through solvent or water volatilization and then harden and attain their final cured properties by the cross-linking reaction, which is temperature and/or moisture dependent. Too slow a rate of reaction may lead to an insufficiently cross-linked coating that, although hard and having a suitable appearance, has poor chemical and moisture resistance. Too fast a rate of reaction may lead to an overcured, hard, impervious coating that cannot be recoated or topcoated with a properly adherent subsequent coat.

Overcuring is often a problem in maintenance repainting, when a renewal coat is applied to the original cross-linked coating system after an extended period of time. In extreme cases, however, the recoat interval within which no recoat problems may be anticipated could be as short as a few hours for certain coatings or under certain ambient conditions. Amine-cured coal tar epoxy coatings are a good example, and the recoat window may be less than 16 h, after which intercoat adhesion may become a problem.

The curing and hardening of some chemically cross-linked systems, such as most polyesters and vinyl esters, is so rapid that plural-component spray application systems are required. Such systems mix the coreactants at the time of spray application within the spray gun or outside the spray gun nozzle. The chemical cross-linking reaction occurs so rapidly that by the time the coating has deposited on the surface, the coating is beginning to set up. Although such coatings are hard to the touch within minutes, solvent volatilization and additional cross linking should be allowed to continue for days prior to exposure in a severe chemical environment. As a general rule, curing of most chemically cross-linked systems should proceed for approximately 7 days at 25 °C (75 °F) before the coating system is exposed to severely corrosive conditions, immersion, or acid or alkali splash or spillage. The more common chemically cross-linked binders or resins used for coatings and linings are discussed subsequently.

Epoxies

Chemically cross-linked epoxies usually come in two packages; the first usually consists of the epoxy resin, pigments, and some solvent, and the second is the copolymer curing agent. The two packages are mixed immediately before application and, on curing, develop the large macromolecule structure. The properties of the epoxy coating derive both from the type and molecular weight of the epoxy resin and from the copolymer curing agent that is used to cross link with it.

Epoxy Resins. There are three principal epoxy resin chemistries: bisphenol-A, derived from bisphenol acetone and epichlorohydrin; bisphenol-F, derived from bisphenol formaldehyde and epichlorohydrin; and novolac, a modification of the bisphenol-F resin using excess phenol.

The bisphenol-A epoxy resins are still the industry workhorse, but the use of bisphenol-F and novolac resins has increased substantially over the past few years because of their lower molecular weight compared with the bisphenol-A resin. This allows formulators greater flexibility when developing VOC-compliant coatings. Bisphenol-F and novolac epoxy resins also have higher functionality, which, when properly cross linked, results in a coating with greater chemical, moisture, and heat resistance than the bisphenol- A-type epoxy coatings.

Each of these resin types is discussed subsequently.

Bisphenol-A Resins. Bisphenol acetone (commonly, bisphenol-A) is a reaction product of phenol and acetone. The resulting resin is further reacted with epichlorohydrin to form the diglycidyl ether of bisphenol-A resin. The molecular structure of the bisphenol-A epoxy resin is shown in Fig. 8.

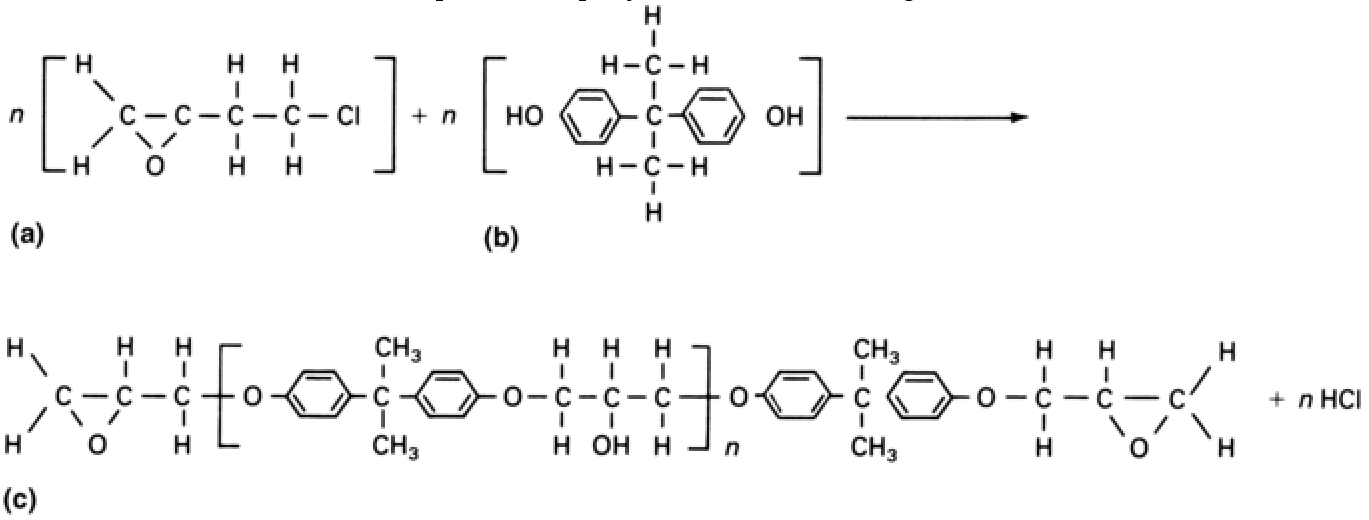

Fig. 8 Reaction of epichlorohydrin (a) and bisphenol-A (b) to form a glycidyl-ether-type epoxy resin (c)

When the repeating unit *n* is one or less, the resin is a liquid with a honeylike consistency. These liquid epoxies are used for high-solids, ambient-temperature-cure epoxies. When the average molecular weight of the resin is increased by increasing *n* to approximately 2, the resin becomes a solid and must be dissolved with suitable thinners in order for it to be used as a coating material. Traditionally, an *n* of approximately 2 and a molecular weight of 800 to 1000 have been used in the formulation of the typical workhorse epoxies that are widely used in industrial maintenance and marine coatings.

Increasing *n* to even higher numbers raises the molecular weight. If sufficient reactive functionality is added (for example, addition of pendant amine and hydroxyl moieties), such bisphenol- A epoxy resins are used as epoxy ester resins and powder coats (*n* equals approximately 3.7) and epoxy/phenolic and amino epoxy coatings that are cured by baking (*n* equals 8 to 12).

Traditionally, bisphenol-A 2-type epoxies have long been used to produce the 45 to 65% volume solids amine- and polyamide-cured coatings that for years have provided protection of steel and concrete in the industrial and marine markets. The resulting epoxy systems (when cross linked with the active hydrogen from an amine or amine functionality of a polyamide co- reactant) have very good water and chemical resistance and are tough and resistant to abrasion and thermo- and mechanical shock. However, because the resin is an amorphous solid and must be dissolved in solvents in order to liquefy it and make it suitable for use as a paint or coating, lower-molecular-weight liquid resins such as bisphenol-F and epoxy novolac resins are increasingly being used by coating formulators.

Bisphenol-F Resins. Bisphenol-F resin has a lower molecular weight (approximately one- third that of a bisphenol-A resin with equivalent functionality). Bisphenol-F resins are similar to those of bisphenol-A except that phenol is reacted with formaldehyde rather than acetone to form the intermediate product, after which it is again reacted with epichlorohydrin to form the finalized bisphenol-F resin. The molecular structure of the reactants is shown in Fig. 9.

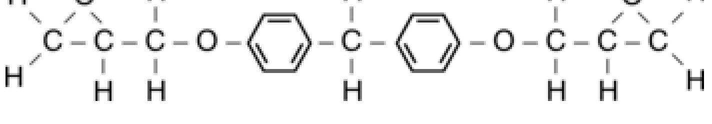

Fig. 9 Bisphenol-F epoxy resin

Bisphenol-F resins have greater chemical and heat resistances than the bisphenol-A epoxy resins but are less tough and flexible. These properties and the fact that they do not need solvent reduction to make them liquid have increased their use for VOC-compliant coatings.

Bisphenol-F resins, when coreacted with aromatic amine and amine addicts, can be formulated as high solids and 100% solid epoxies (with little or no solvent).

Novolac Epoxies. These epoxy resins are modifications of bisphenol-F resins that are formed using an excess of phenol. Bisphenol-F is the simplest novolac resin, and all other novolac resins have significantly higher viscosity than the bisphenol-F resins. Equally important, the functionality of the novolac is also considerably greater, leading to an even better chemical moisture and heat resistance than the bisphenol- F. The molecular structure for two novolac resins, the epoxy phenol novolac and the epoxy cresol novolac, are presented in Fig. 10.

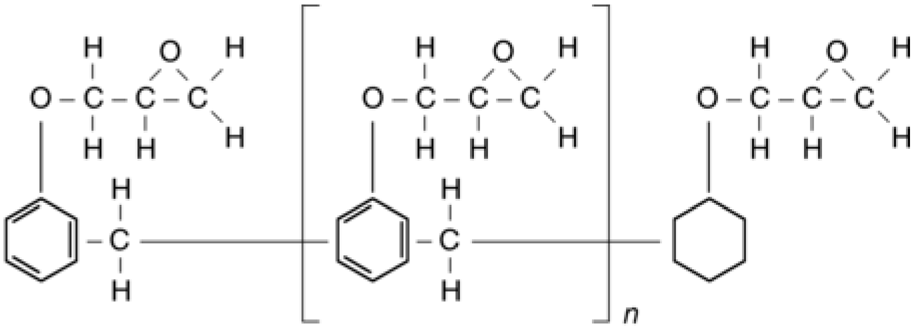

(a)

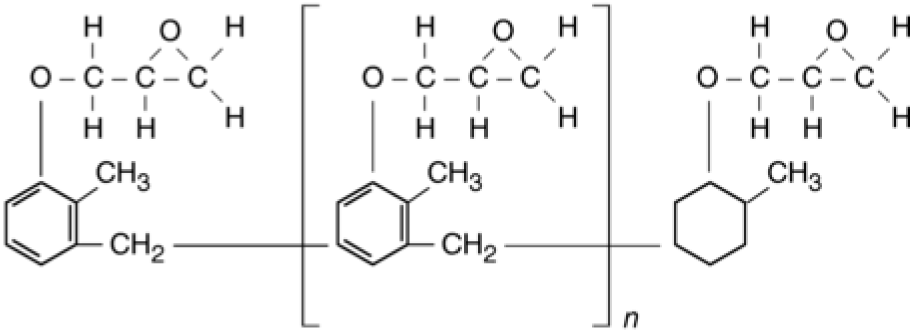

(b)

Fig. 10 Epoxy novolacs. (a) Epoxy phenol novolac. (b) Epoxy cresol novolac

The epoxy phenol novolacs are very high-viscosity liquid and semisolid materials. The epoxy cresol novolacs are solids and used most often in powder coatings. Both epoxy resins have higher epoxy functionalities than the bisphenol- A and bisphenol-F resins. Their high cross-link density leads to extreme heat, chemical, solvent, and moisture resistances, and they are often used for solvent service and for resistance to mineral acids at elevated temperatures. Novolac epoxy resins are formulated for use in deep-well oil- recovery tubing exposed to high-temperature wet and dry acid and alkali service and high abrasion.

However, because of their higher cross-link density, care must be used in choosing an appropriate cross-linking coreactant curing agent. Otherwise, the coating is extremely brittle and cracks.

Other Epoxy Resins. Other less common epoxy resins have been developed for use in specialized coatings. A flexible epoxy based on the oil of the cashew nut shell is called a cardanol epoxy. Epoxidation of the oil is induced, and the resin is used in room-temperature curing systems or as an additive to provide flexibility, toughness, impact resistance, and adhesion even at low temperatures.

Brominated epoxies have been developed for use as fire-retardant coatings and laminates. The fire retardancy occurs by degradation of the epoxy resin and liberation of the bromine as a gas. The gas is heavy and a fire retardant. Bromine is typically added to a bisphenol-A resin as a substitute on the aromatic ring. The typical structure of a brominated epoxy resin is shown in Fig. 11.

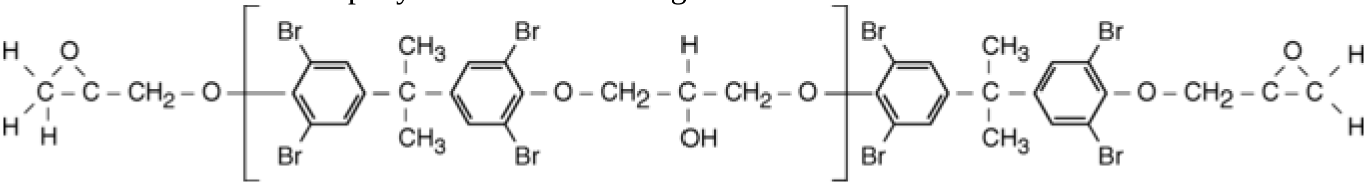

Fig. 11 Brominated bisphenol-A epoxy resin

Curing Agents for Epoxy Resins. The second portion of a two-pack epoxy coating system is the curing agent. The curing agent is a coreactant, which, when mixed with the epoxy resin, cross links to form a chemical bond that increases the molecular weight of the coating molecule. The resulting resin, often modified with additives to enhance flow, surface appearance, and other factors, also encapsulates the pigment particles. Each of these constituents is critical to the ultimate properties of the reacted and cured coating system. However, the formulator's choice of the curing agent is crucial to the derivation of the finalized coating properties.

Although epoxies are generally thought of as catalyzed, the cross-linking reaction is, in fact, a copolymerization. The reaction occurs primarily through the epoxy ring end groups or the mid- chain hydroxyls of the epoxy resin. The curing agent is usually an amine or polyamide, with cross linking derived through the active hydrogens attached to the amine nitrogen. Although a variety of cross-linking agents can be used (including mercaptans, polybasic acids and anhydrides, and phenol-formaldehyde and phenol resins), the most common are the polyamines, the amine adducts, and the polyamides.

Polyamines. The polyamines (for example, diethylene triamine, hydroxyethyl diethylene triamine, and bishydroxydiethylene triamine) are relatively small molecules with a low molecular weight compared to the epoxy resin. As a consequence, when reacted, they lead to tight cross linking and high chemical and moisture resistance. However, during the cross-linking reaction, any unreacted amine may be squeezed out of the cross-linked film to the surface, developing the so-called amine blush, a hazy white coloration on the coating surface. The amine blush is a reaction of the amine with carbon dioxide in the air to form an amine carbonate. If on the topcoat, the blush is not detrimental in atmospheric service and can be allowed to remain on the surface. However, it is a good practice to wash or wipe it from the surface (it is water soluble) before application of a subsequent epoxy coat, particularly for immersion service.

To minimize the formation of the amine blush, many formulators specify a 15 to 30 min induction period after mixing, prior to application. This allows the reaction to begin and initial cross linking to occur before the paint is applied. Some of the small amine molecules partially cross link with epoxy resin molecules, increasing their size and reducing the tendency to migrate to the surface to form the amine blush.

Aliphatic amines have a high reactivity and therefore a fast cure at ambient temperatures and produce a highly cross-linked coating as a result of their low molecular weight and high functionality. This, however, results in limited flexibility and potentially incomplete chemical reaction with the epoxy resin due to its low molecular weight. Examples of these aliphatic amines are diethylene triamine, ethylene diamine, and triethylene tetramine. Higher-molecular-weight aliphatic amines include hexamethylene diamine and trimethyl hexamethylene diamine. These later aliphatic amines provide more flexibility because of the greater molecular distance between the diamine reactants at either end of the molecule. Figure 12 depicts the molecular structure of some of these amines.

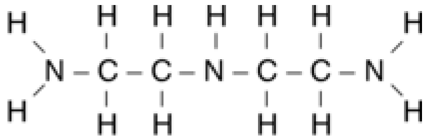

(a)

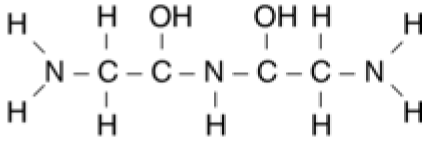

(b)

Fig. 12 Polyamines. (a) Diethylene triamine. (b) Hydroxyethyl diethylene triamine

Amine Adducts. Because of the problems with small-molecule reactants, many coating manufacturers supply the amine as a prereacted amine adduct. In this case, the epoxy pigment and solvents are packaged as before in one container, but an excess of the amine is prereacted with some of the epoxy resin to increase its molecular size. The prereacted amine adduct is then packaged in a separate container, sometimes with additional pigment and solvent. On application, both containers are mixed, and the cross-linking reaction goes to completion.

Chemical cross linking of the resultant applied film is not considered to be quite as tight as that provided by a nonprereacted amine, and the chemical resistance is somewhat less. However, application is much easier and not nearly as dependent on thorough mixing of the reactants and induction time.

Polyamides. Polyamide curing agents are the condensation products of a dimerized fatty acid with a polyamine, as shown in Fig. 13. Polyamides, and other amine curing agents, result from the addition of amine (NH_2) functionalities into the backbone of a fatty acid, commonly a tall oil fatty acid. The fatty acid results in improved flexibility and substrate wetability, improved adhesion, and outstanding water resistance. Terminal amine functionality allows cross linking to occur as with a straight amine, although the polyamide molecule is much larger. The cross-linked film has improved flexibility, improved gloss and flow, excellent water resistance, and good chemical resistance. Polyamide- cured coatings, however, have somewhat less solvent and alkali resistance than amine- and amine-adduct-cured epoxies.

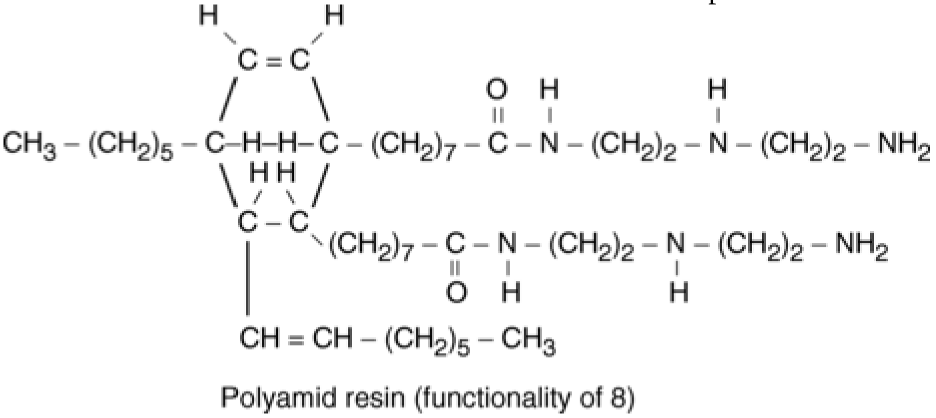

Fig. 13 Polyamide, the product of a fatty acid (commonly a tall oil) with a polyamine (NH_2) functionality

Specially formulated polyamide-cured epoxies have the ability to displace water from the substrate surface. Such materials can even be applied and cured underwater to form corrosion- resistant coatings.

Amino Amines. If a polyamine is reacted with a monofunctional fatty acid instead of using a fatty acid dimer, the condensation product is an amino amine instead of a polyamide. The fatty acid has simply increased the molecular weight of the amine at the expense of reducing its amine hydrogen functionality. The most attractive feature of the amino amines is that their equivalent weight remains quite high. The equivalent weight is the number of grams of resin containing one equivalent of a functional group. High equivalent weight allows for low viscosity in a mixed system, which is desirable for low-VOC formulations. The amino amines are most often used with low-molecular-weight liquid epoxies and high- and 100% solids coatings. The U.S. Navy standard epoxy MIL-P-24441 is based on an amino-amine-modified polyamide curing agent.

Ketimines. One other type of curing agent, ketimine, is worthy of note. The ketimine curing agent allows the application of a high-molecular- weight, high-solids, or solventless epoxy resin with standard spray equipment. These more viscous epoxies can be mixed with the low-molecular-weight ketimine curing agent and sprayed onto the surface. No reaction occurs until the ketimine decomposes in the presence of atmospheric moisture to form a polyamine and a ketone. The ketone volatilizes from the film, and the amine reacts as described previously to cross link the epoxy resin after application. These systems result in a tightly cross-linked epoxy film but require relative humidity in excess of 50% and good ventilation to expose the ketimine to moisture and to remove the residual ketone and other solvents from the paint film. The ketimine curing reaction is shown in Fig. 14.

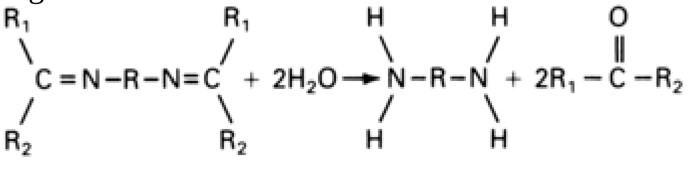

Fig. 14 Curing reaction of ketimine-cured epoxies. Ketimine decomposes in the presence of atmospheric moisture to form a polyamine plus a ketone. R, R_1, and R_2 are alkyl groups. Source: Ref 2

Cycloaliphatic Amines. This class of amine is characterized by an amino (NH_2) group attached to a cycloaliphatic (nonring) moity. When the amino group is attached to a cycloaliphatic structure, the resultant

resin has greater light stability and better heat resistance than the linear aliphatic amines. All cycloaliphatic amines are slower reacting than linear amines, but they react faster than the polyamides. Chemical resistance of the linear aliphatic amine is superior to both the cyclo-aliphatic and polyamides, although the resulting molecule is more rigid and less flexible. The structures of cycloaliphatic amines diaminocyclohexane and isophorone diamine are shown in Fig. 15.

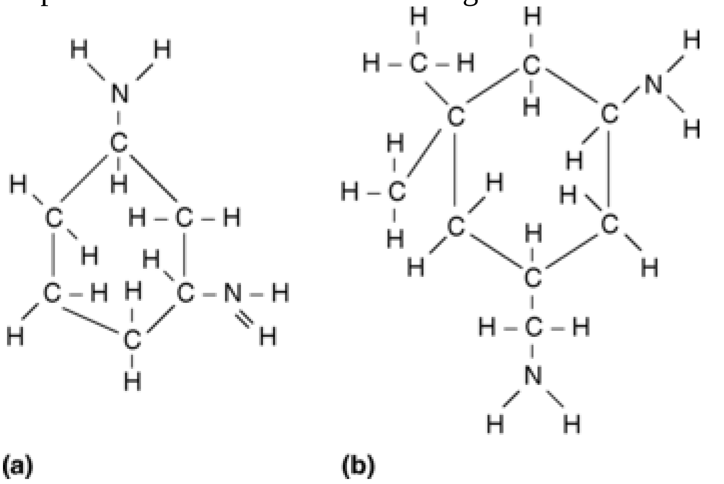

Fig. 15 The structure of cycloaliphatic amines. (a) Diaminocyclohexane. (b) Isophorone diamine

A relatively new cycloaliphatic amine is bis- (p-aminocyclohexyl) methane. This amine has the heat resistance and mechanical strength typical of other cycloaliphatic amines but has a better low-temperature cure and yields a tougher, more flexible coating due to its bulky structure, which results in a lower cross-link density. The molecular structure of this amine is shown in Fig. 16.

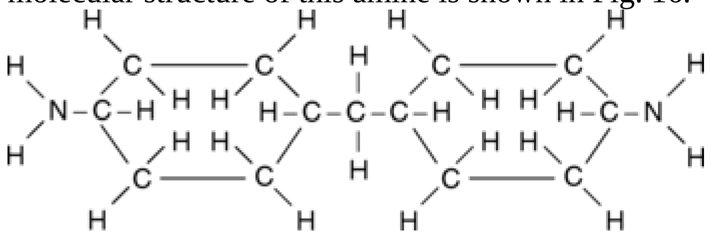

Fig. 16 The structure of cycloaliphatic amine bis-(p-aminocyclohexyl) methane

Aromatic Amines. For years, methylene dianaline, an aromatic amine, was widely used to cure epoxy resins. It had a very long pot life, excellent acid and heat resistance, moisture insensitivity, and flexibility. However, it yellowed and darkened on ultraviolet light exposure and was listed as a carcinogen by the Occupational Safety and Health Administration (OSHA). Accordingly, most formulators do not use methylene dianaline and have found substitute aliphatic or cycloaliphatic amines to replace it.

Mannich bases are formed by the reaction of a methyol phenol and a multifunctional primary amine. They are used principally for low-temperature-curing (-1 to 2 °C, or 30 to 35 °F) epoxies and for coatings that cure under damp conditions, including underwater-cured epoxies. They are also used in coal tar epoxy systems. The free phenol content often found with this curing agent may limit the use of a mannich base curative. The formation of a mannich base curing agent is illustrated in Fig. 17.

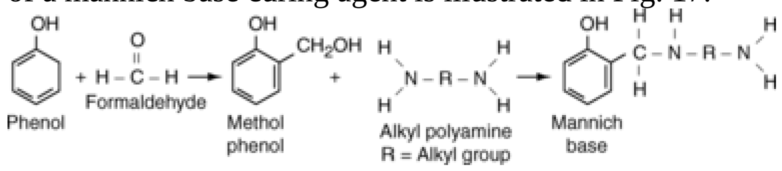

Fig. 17 Formation of mannich base curing agent

Mannich bases can be adducted with metaxylylene diamine, which produces a coreactant that cures at lower temperatures than any other amine-based curing agent. The mannich-based adduct is also useful in formulation of high-solids, low-VOC maintenance paints.

Dicyandiamide is a solid curing agent often marketed as a prepackaged form including flow- control agents and other additives. It is used almost exclusively for curing epoxy powder coatings.
A typical powder coating consists of a solid epoxy resin (often a high-molecular-weight bisphenol-A epoxy) that is heated to melting and mixed with polyacrylic flow-control additives and pigments. The melt is cooled, extruded, and ground to a powder.
The dicyandiamide is also powdered, directly or as an adduct, and mixed with the epoxy powder. Its chemistry is illustrated in Fig. 18.

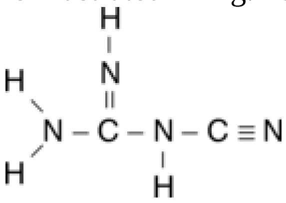

Fig. 18 Structure of dicyandiamide

The mixed powders are applied to a preheated substrate by electrostatic spray. The object is coated until there is no further electrostatic attraction due to the buildup of coating thickness. The coated article then passes into an oven where it is heated to a temperature generally from 175 to 230 °C (350 to 450 °F), melting the coating and allowing the cross-linking reaction to occur between the epoxy and the dicyandiamide curing agent.
Powder coatings are increasing in use, because they are 100% solids, no VOC materials. The coating cures to a tough, abrasion-resistant, thick film. Powder coatings are used extensively on below-grade pipelines due to their chemical resistance, thick film, and tough, durable nature. They are said to have sufficient water permeation to enable cathodic protection and to prevent cathodic shielding in areas where the coating may disbond.
Powder coatings are being widely used on many consumer products, such as outdoor furniture, automotive parts, and undercarriage components. Properly cured powder coatings have excellent adhesion, flexibility, and impact resistance and good resistance to chemicals and solvents.
Amino Resins. Melamine and urea-formaldehyde-cured epoxy resins are used as baking primers and finished coats and as curatives for epoxy coil coatings. Urea formaldehyde systems are used for finishes that require faster cure at a lower cost than is possible with the melamines. Melamine curing agents are used in baking finishes where color is more critical and where good gloss is required. Melamine epoxies are used as coatings for the interior and exterior of food and beverage containers, because they do not affect the taste of the food stored within the metal beverage container. Beer and soft drink cans are often coated with melamine epoxy resins. Melamine resins are formed by reacting three molecules of dicyandiamide. The chemistry of these resins is illustrated in Fig. 19.

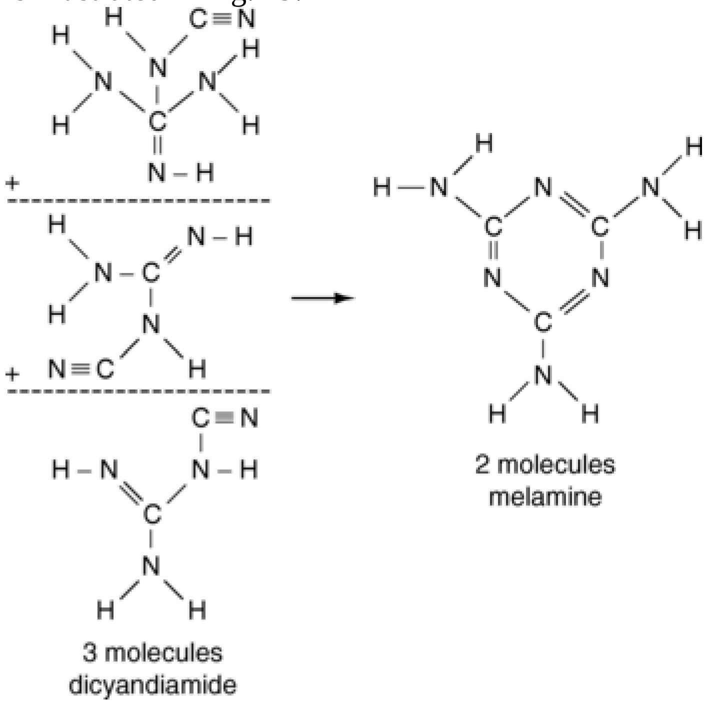

Fig. 19 Melamine, formed by the reaction of three molecules of dicyandiamide to form two molecules of melamine

Coal tar epoxies are a combination of a coal tar blended with an epoxy resin packaged in one container. The curing agent is an amine, amine adduct, or polyamide, as described previously, packaged in a separate container. The cross-linking reaction is the same as that described previously. The coal tar acts as a filler within the cross-linked epoxy matrix, and the resulting film has the good toughness, adhesion, ultraviolet resistance and thermal stability of the epoxies, combined with the extremely high moisture resistance afforded by coal tar. As might be expected, the amine-cured coal tar epoxies generally have greater chemical and moisture resistance but are more brittle and harder to apply and topcoat than the amine adduct- and polyamide-cured coat tar epoxies. On the other hand, the polyamide coal tar epoxies are more flexible, easier to topcoat, and more tolerant of application variables.

Epoxy-Phenolic Coatings. Phenolic cross- linked epoxy coatings are extremely resistant to acids, alkalies, and solvents, and they are widely used as linings for tank cars, drums, cans, process tanks, and equipment. High-molecular- weight epoxies with a high proportion of hydroxyl functional groups available for reaction are used. During manufacture, the epoxy is packaged with a phenolic resin (commonly a phenolformaldehyde resin), pigment, and an acid catalyst. After mixing, the coating is applied by spraying and then baked at temperatures from 150 to 205 °C (300 to 400 °F) in order for cross linking to occur. Multiple-coat systems require brief intermediate baking between coats; longer baking times are commonly used after application of the final coat.

Systems with ambient-temperature cure are now also available. With a lesser amount of phenolic modification to the epoxy resin, air drying of the coating without baking can be done. Such coatings have excellent moisture and chemical resistances. Care must be taken to ensure that the coating is not too thick, thus entrapping solvents, and that curing temperatures are satisfactory, generally at least 24 °C (75 °F). Baking of these air-dry coatings will enhance performance, particularly in immersion service.

The resulting coatings have the excellent acid and solvent resistance associated with the phenolics as well as the flexibility, adhesion, and toughness of epoxies. Epoxy phenolics have the good alkali resistance of the epoxy constituent, but straight phenolic linings have very poor alkali resistance.

The cross linking that occurs is between the hydroxyl groups along the epoxy chain and the methylol groups present in the phenolic resin. A possible secondary reaction is the reaction between the terminal epoxide groups of the epoxy resin and the hydroxyl groups of the phenolic resin.

Phenolic Linings

Phenolic resins are formed by the reaction of phenol with formaldehyde to form phenolformaldehyde. The methylol group can react on the two ortho positions and the paraposition on the benzene ring to form phenolformaldehydes with functionalities (possible reaction sites) up to 3. On heating, a condensation reaction occurs between methylol groups on adjacent molecules that cross link the film and liberate water. The reaction of phenol and formaldehyde to form a cross-linked film is shown in Fig. 20.

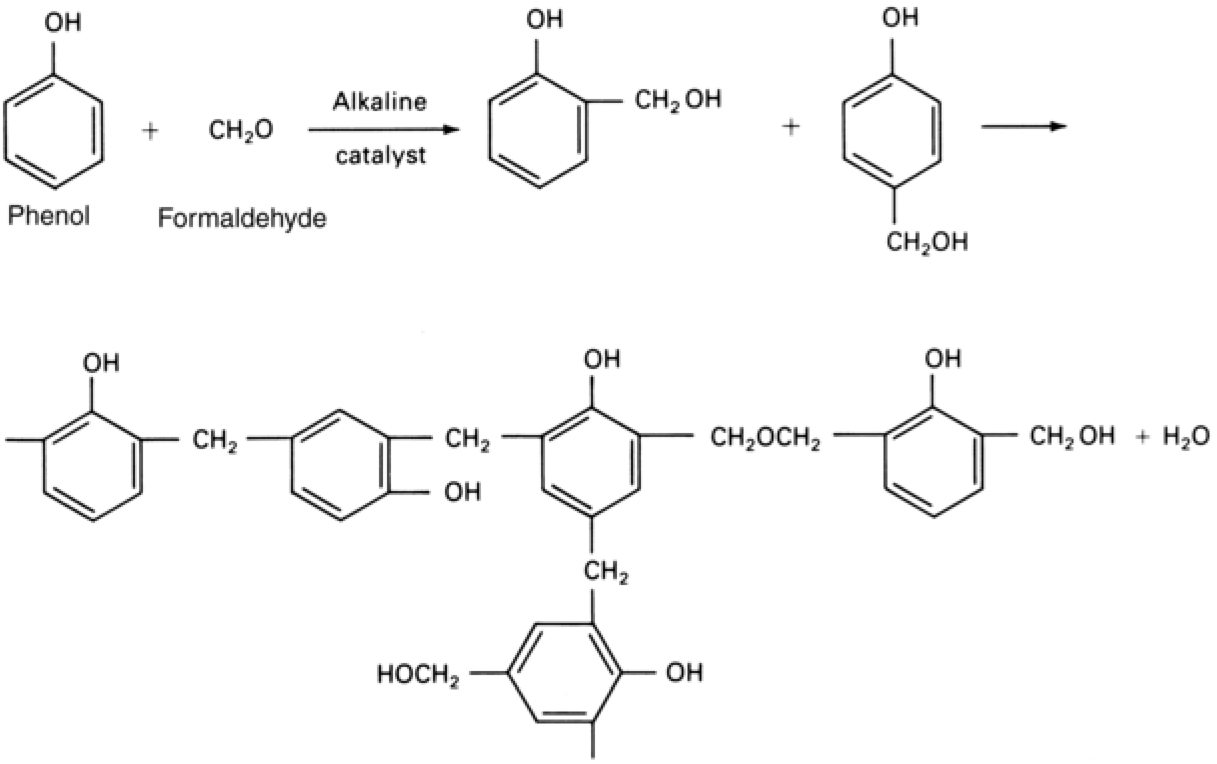

(a)

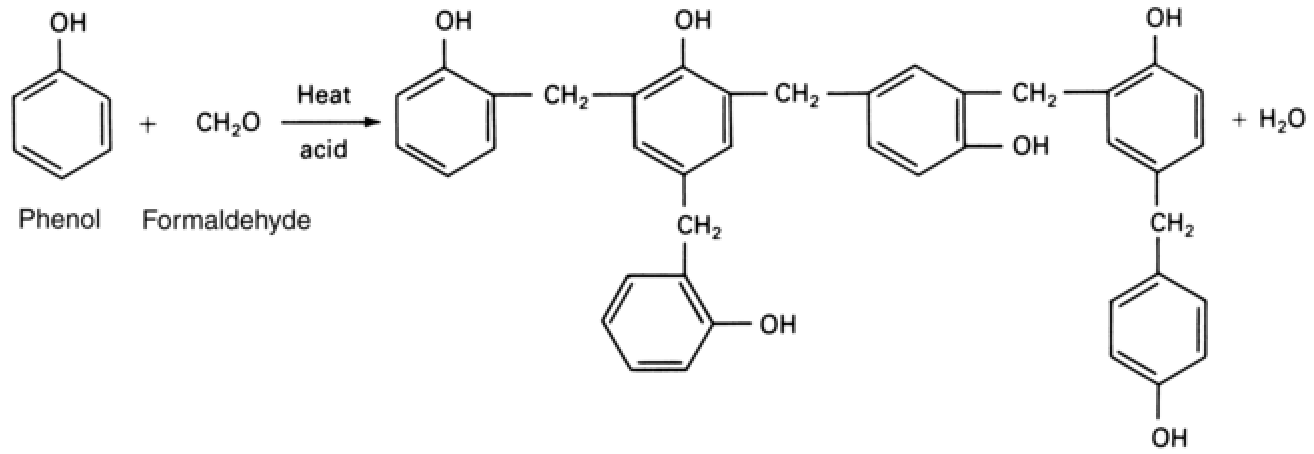

(b)

Fig. 20 Reaction of phenol and formaldehyde to form a phenolic resin. (a) Reaction using an alkaline catalyst. (b) Reaction using an acid catalyst. Source: Ref 3

The phenolformaldehyde resins are usually dissolved in alcohol and applied by spray, dip, or roller. The fact that water is liberated during the cross-linking reaction is important. The coatings must be applied in multiple-coat systems; each coat is approximately 0.025 mm (1 mil) thick and must be baked for a few minutes at 120 to 205 °C (250 to 400 °F) between coats. This partially cross-links the coating, but more importantly, it volatilizes the water formed during the cross-linking reaction. Subsequent coats are applied and baked until, after the final application, a postbake at higher temperatures and longer durations is performed. It is easy to determine when the coating has been baked sufficiently to ensure proper curing and cross linking. The phenolic resin darkens on heat exposure, and a thoroughly cured coating is a relatively uniform, light chocolate-brown color.

Because they are odorless, tasteless, and nontoxic after full curing, phenolics are often applied as linings for vessels and tanks used for the processing and storage of such food products as beer, wine, and sugar syrups. They also have excellent resistance to boiling water and hot aqueous solutions of mild acids. Thus, they often find application as linings for steel exposed to high- temperature freshwater and saltwater as well as mild acids.

A major weakness, however, is the lack of alkali resistance. Unless phenolic coatings are modified with epoxies, they should not be used for alkaline service.

Urethane Coatings

Urethane coatings have chemical- and moisture-resistant properties similar to those of the epoxies, but they can also be formulated in a variety of light-stable colors that maintain their gloss and “wet look” on prolonged exposure. The chemistry involved in urethane coating curing is not unduly complex and typically consists essentially of the reaction of an isocyanate-containing (-N═C═O) material with a polyhydroxylated (-OH-containing) coreactant (Fig. 21). Cross linking occurs because of the high reactivity and affinity of the isocyanate group for the active hydrogen of the polyol hydroxyl or any active hydrogen atom attached to a nitrogen or oxygen atom. The rate of this cross-linking reaction depends on a number of factors, such as the type and configuration of both the isocyanate and polyol materials and the temperature. However, the reaction is such that with most formulations, cross linking can occur at temperatures of -18 °C (0 °F) or less.

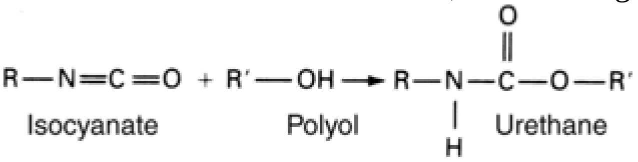

Fig. 21 Reaction of an isocyanate and a polyol to form a urethane. R and R′ are different aromatic or aliphatic groups. Source: Ref 4

A number of different types of isocyanate materials are used in urethane coatings. The molecular weight and structure as well as isocyanate functionality (the number of isocyanate groups available for reaction) can affect the final properties of the coating. Similarly, different polyol structures, such as acrylics, epoxies, polyesters, polyethers, and vinyls, when reacted with a given isocyanate to form a cross-linked coating, result in variations of physical and chemical properties. Described subsequently are some of the general properties of the isocyanate and polyol constituents that are coreacted to form urethane coatings.

The isocyanates are commonly categorized as either aromatic (containing the benzene ring) or aliphatic (straight-chain or cyclical) hydrocarbons. The first isocyanate used in urethane coatings was an aromatic isocyanate, toluene diisocyanate (TDI) (Fig. 22). When reacted, TDI resulted in a suitable chemical-resistant urethane coating, but it was generally undesirable because of its low viscosity and toxic, irritating vapors. To form a safer, more suitable coreactant, TDI was further reacted to provide a higher-molecular-weight polyisocyanate that contained less than 1% of the original TDI monomer (Fig. 23).

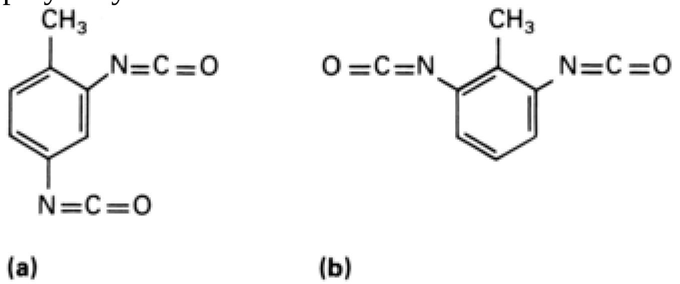

Fig. 22 Molecular structures of toluene diisocyanate, an aromatic isocyanate used in urethane coatings. (a) 2,4 isomer. (b) 2,6 isomer. Source: Ref 5

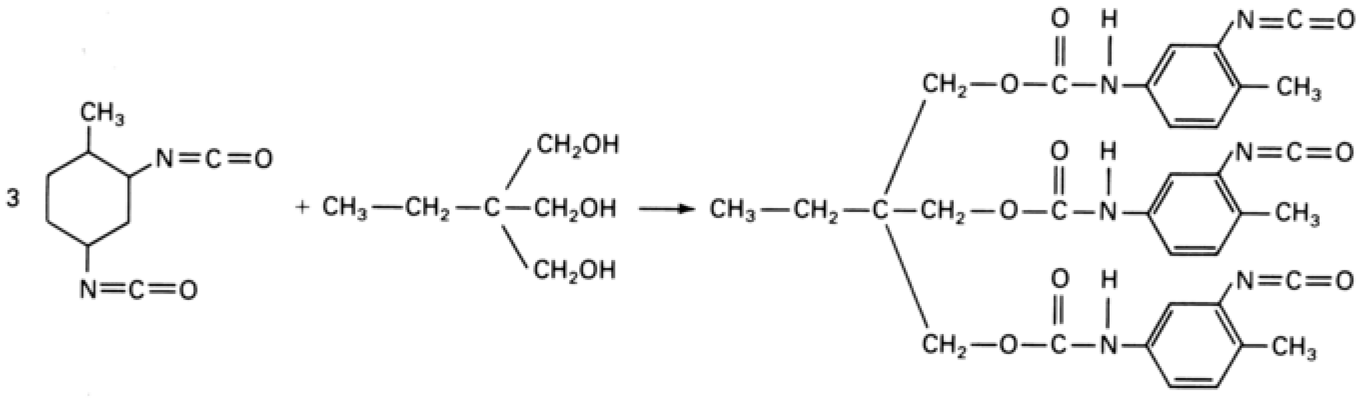

(a)

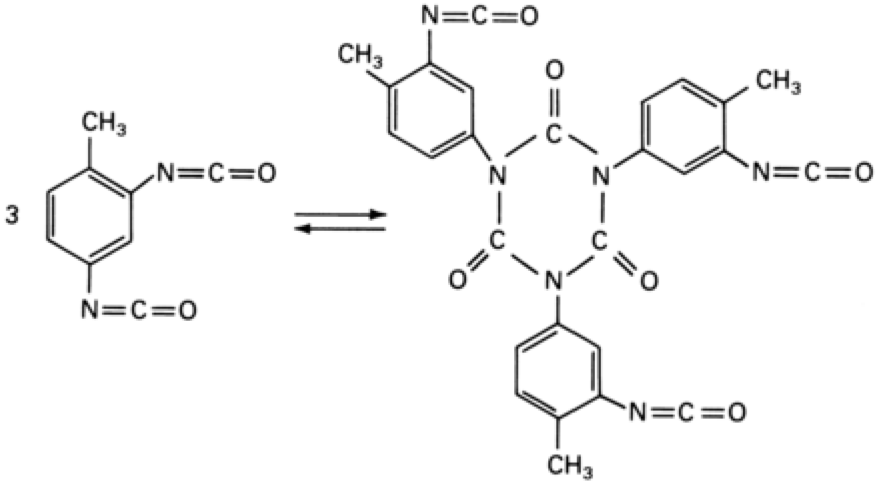

(b)

Fig. 23 Modifications of toluene diisocyanate (TDI) to form higher-molecular-weight polyisocyanates. (a) Polymerization of TDI with an alcohol to produce a TDI alcohol adduct. (b) Condensation of TDI monomer to produce an isocyanate ring. Source: Ref 5

These higher-molecular-weight aromatic isocyanates, when reacted with a polyol (usually a polyester, polyether, or epoxy), formed useful chemical-resistant coatings that could be cured at low temperatures. However, the urethanes so formed tend to chalk, yellow, and darken somewhat on exposure to sunlight.

In the early 1970s, aliphatic isocyanates were commercially developed. Although they were considerably more expensive than the aromatic isocyanates, they allowed the formulation of nonyellowing, light-stable, high-gloss finish coats. The appearance of urethane coatings formulated with aliphatic isocyanates is unmatched by the epoxies, acrylics, or any other coating material available in the industrial marketplace. In spite of the high cost of the aliphatic polyurethanes, the coatings were increasingly specified in high-visibility applications, such as city water tanks, railroad tank and hopper car exteriors, and other areas where visibility or aesthetic appeal were valued.

An important aliphatic isocyanate is hexamethylene diisocyanate (HDI) (Fig. 24). In its monomeric form, HDI is an irritant. Similar to TDI, however, HDI can be reacted (commonly with water) to form a larger molecule.

$$O = C = N — (CH_2)_6 — N = C = O$$

Fig. 24 Molecular structure of hexamethylene diisocyanate, an aliphatic isocyanate used in urethane coatings. Source: Ref 5

Various combinations of aromatic and aliphatic isocyanates can be produced, including specialty isocyanates, to make high-solids or solvent-free coatings, elastomeric coatings, or coatings designed for baking or curing at elevated temperatures. Specialty isocyanates can be either aromatic or aliphatic; if aromatic, they discolor. Both

straight-chain and cyclical aliphatic isocyanates, although nonyellowing, are much slower to react and cross link than aromatic isocyanates.

Polyols. As stated previously, polyols coreact with isocyanates in order to form the polyurethane film. Accordingly, the polyol is packaged separately from the isocyanate, and the polyol package always contains the pigment, most of the solvent, and any additives used for flow, thixotropy, antisetting properties, and so on. The major properties of the cross-linked urethane film, such as chemical resistance, toughness, lightfastness, and flexibility, derive principally from the polyol constituent. Long, repeating carbon- to-carbon backbone chains with little branching (for example, vinyl) result in tough, flexible resins. Aromatic groups add rigidity to the chain, as does cross linking. The presence of numerous ester, ether, and urethane groups reduces chemical and moisture resistance.

For corrosion-protective coatings, the polyol coreactant is usually one of the following: acrylic, polyester, polyether, epoxy, vinyl, or alkyd. Asphalts and coal tars can be added with any of the polyols. Because they are essentially nonreactive, however, it is felt the bitumen acts predominantly as a filler in the urethane matrix, providing the cured coating with the attendant properties of good chemical resistance, high moisture resistance, and high film build at a relatively low cost.

Acrylic urethanes are perhaps the most widely used urethanes for corrosion protection in atmospheric service. These coatings, when properly formulated, have excellent weatherability, gloss, and color retention and have good chemical and moisture resistance. They can be readily tinted and pigmented to provide a variety of deep and pastel colors at a lower cost per gallon than the next most popular class, the polyester urethanes.

As with conventional acrylic coatings, the acrylate polymer family is softer and more flexible than the corresponding methacrylates, although an increase in the molecular weight of the monomers, such as methyl acrylate to butyl acrylate, leads to softer, more flexible polymers for both families. Acrylate and methacrylate blends are also used as reactive polyols.

Acrylic urethanes are not used for immersion service, and, for the most part, they do not have the chemical resistance of the polyester urethanes. However, they do have excellent weathering properties when an aliphatic isocyanate is used.

Polyesters result from the condensation reaction of a dibasic acid and a polyhydric alcohol. To form a hydroxylated polyester, an excess of the hydroxyl functionality from the alcohol is allowed over that of the acid. The result is a polyester molecule with a midchain and end-chain hydroxyl functionality.

Because of their high isocyanate demand when coreacted, polyesters result in relatively hard chemical-resistant polymer films. Impact resistance is not as great as with the acrylic urethanes, but, as a rule, chemical and moisture resistance are better. However, because ester linkages occur in the molecular backbone, alkaline attack and water sensitivity may occur at locations where the ester group is exposed, that is, at areas of low cross-link density or where less branching of adjacent molecules occurs. Accordingly, polyester urethanes, similar to acrylic urethanes, are not normally used for immersion service.

Polyethers are often the polyol of choice for use as elastomeric coatings, coal tar urethanes, and other urethane coatings that are sheltered or protected from light. The polyether prepolymer is considerably less expensive than acrylic or polyester polyols; polyethers, however, are sensitive to ultraviolet-induced oxidative degradation. Furthermore, the ether linkages (-C-O-C-) are water sensitive, and in polyethers, they are repeated throughout the polymer chain without separation by long water-insensitive hydrocarbon chains or aromatic groups that can minimize water sensitivity.

Epoxies. The reaction of an epoxy with an isocyanate would seem to be a natural one, because of the midchain hydroxyl functionality of the epoxy molecule. However, there are very few epoxy urethanes on the market, and those being promoted are used predominantly as primers or intermediate coats. This is due to:

- The tendency of the epoxy and the epoxy urethane to chalk
- The lower moisture resistance resulting from the urethane link, which gives a less chemical- and moisture-resistant polymer than a straight epoxy coating
- The greater expense of a urethane epoxy compared to a conventional amine or polyamide cross-linked epoxy

As a result, most epoxy urethanes are formulated with the less expensive aromatic isocyanate and are promoted primarily as low-temperature curing epoxies or fast-curing, chemically resistant urethanes for interior use.

Vinyl urethanes use a long-chain, linear, hydroxyl-bearing PVC/PVA resin reacted with a polyfunctional isocyanate prepolymer. Urethane coatings using vinyl polyols combine the abrasion resistance of the urethane with the toughness, flexibility, and chemical resistance of the vinyl. Such urethane coatings are promoted for use where flexibility and abrasion resistance are important; vinyl urethane coatings, however, are subject to some chalking or fading on exterior exposure and do not have the color, gloss, weatherability, or solvent resistance of the acrylics and polyesters. Because the vinyl is thermoplastic and is attacked and softened by solvents, recoatability after extended times is not a problem and is a major advantage of vinyl urethane systems.
Alkyds are commonly reacted with isocyanates to form a so-called uralkyd or urethane oil coating. The isocyanate reaction decreases the drying time of the coating and provides enhanced resistance to chemicals, moisture, weathering, and abrasion. Uralkyd (urethane oil) coatings harden by autooxidation of their unsaturated oleoresinous sidechains. The result is an upgraded coating system with enhanced performance over the nonurethane system. Because of the isocyanate reaction, however, the cost of such a system is somewhat higher than those systems that are not urethane modified. A uralkyd is prepared by replacing some of the dibasic acid with an isocyanate to form a urethane cross-linked polymer. The resulting urethane alkyd resin still has the oleoresineous sidechains, and although it is cross linked and upgraded by the isocyanate, it is still sensitive to water and chemicals through the ester and urethane links.
Moisture-Cured Urethanes. Isocyanates can also react with the hydroxyl group in water to form a class of coatings known as moisture- cured urethanes. Single-package moisture-cured urethanes use an isocyanate prepolymer that, when applied, reacts with the humidity in the air to form a hard, tough, resinous film. Because of their rapid rate of reaction, aromatic isocyanates are used almost exclusively in moisture- cured urethanes. The pigments must be essentially nonreactive with the isocyanate; although it is possible to use a number of pigments, aluminum leaf is most common. The reaction of a single-package urethane with moisture is illustrated in Fig. 25. It should be noted that the isocyanate-water reaction produces gaseous carbon dioxide. In fact, some carbon dioxide is evolved in the curing of all urethane coatings, because moisture (humidity) is present in the atmosphere during curing.

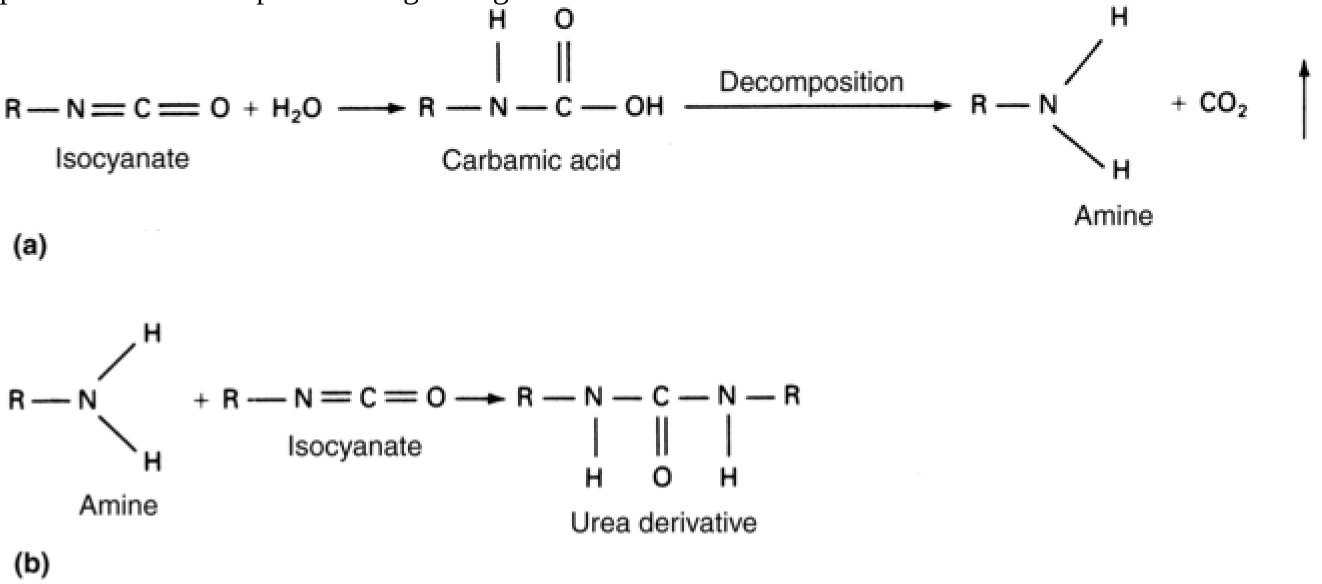

Fig. 25 Curing reaction of a single-package moisture-cured urethane. (a) The isocyanate reacts with water to form unstable carbamic acid, which decomposes into an amine plus carbon dioxide gas. (b) The amine then reacts with isocyanate to form a urea derivative. R indicates an aromatic or aliphatic group. Source: Ref 5

In areas where the relative humidity is expected to be low or where assurance of a more complete cure is necessary, a small amount of a tertiary amine catalyst, such as dimethyl-ethanolamine, can be added. This catalyst is packaged separately from the isocyanate and added just before use. Although it comes as a two-package system, this type of catalyzed urethane can be considered to be an extension of a single- package moisture-cured urethane.

Polyurea Coatings

Until recently, many coating manufacturers did not differentiate between isocyanate reactions with polyester/polyether hydroxyl functionality resins and resins based on the reaction of an isocyanate with a polyether amine. In both cases, the resultant resin was generically called a polyurethane. However, only the resin resulting from the isocyanate reaction with a hydroxylated polyester or polyether (or, for that matter, a hydroxylated acrylic or epoxy) actually contains the urethane linkage as a constituent within the resin. In the urethane reaction, cross linking occurs as the isocyanate group reacts with the hydroxyl to form a urethane linkage (Fig. 26a). Only those resins are true polyurethanes and, as such, are discussed in the section "Urethane Coatings."

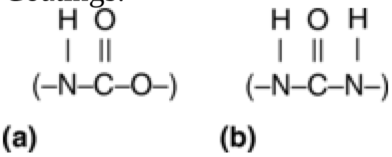

Fig. 26 Difference between polyurethane and polyurea resins. (a) Urethane link in polyurethane. (b) Substituted urea link in polyurea

The isocyanate reaction with a polyether amine or an amine-terminated polyol results in a substituted urea linkage (Fig. 26b), and these resins, often formulated into extremely fast-curing, thick elastomeric coatings, have earned a distinct generic category: polyurea coatings. The resin chemistry of a typical polyurea resin is illustrated in Fig. 25.

An advantage of the polyurea coating is that the reaction between component A (polyisocyanate) and component B (polyamine) is so fast, generally within 5 to 15 s for complete cure, that the coating system does not react with moisture or humidity, nor does it produce carbon dioxide bubbles, as does the polyurethane.

Because of the fast-reacting nature of the polyurea chemistries, specialized application equipment is necessary. Recent advances in plural-component spray equipment has enabled formulators to develop 100% solids polyurea coatings with good chemical and weathering resistance and good compatibility with steel, concrete, and other substrates.

Aliphatic polyurea coatings based on polyaspartic esters have been developed using proprietary chemistry (Ref 5). The principal purpose of this work was to slow the reaction and extend the pot life, such that long whip hoses and conventional spray guns may be used. It is believed that steric hinderance around the isocyanate group is responsible for the slower reaction time and increased pot life. The more complex and bulkier the aspartic ester, the slower the reaction and gel time. The properties of these polyureas include, besides a pot life up to 1 h, a fast gel time, extensibility, elongation, and flexibility approaching the fast-cure ureas. Spray- and squeegee-applied floor coatings have been formulated using aspartic esters to produce a smooth, high-gloss, clear, light-stable finish. Polyaspartic ester products are illustrated in Fig. 27.

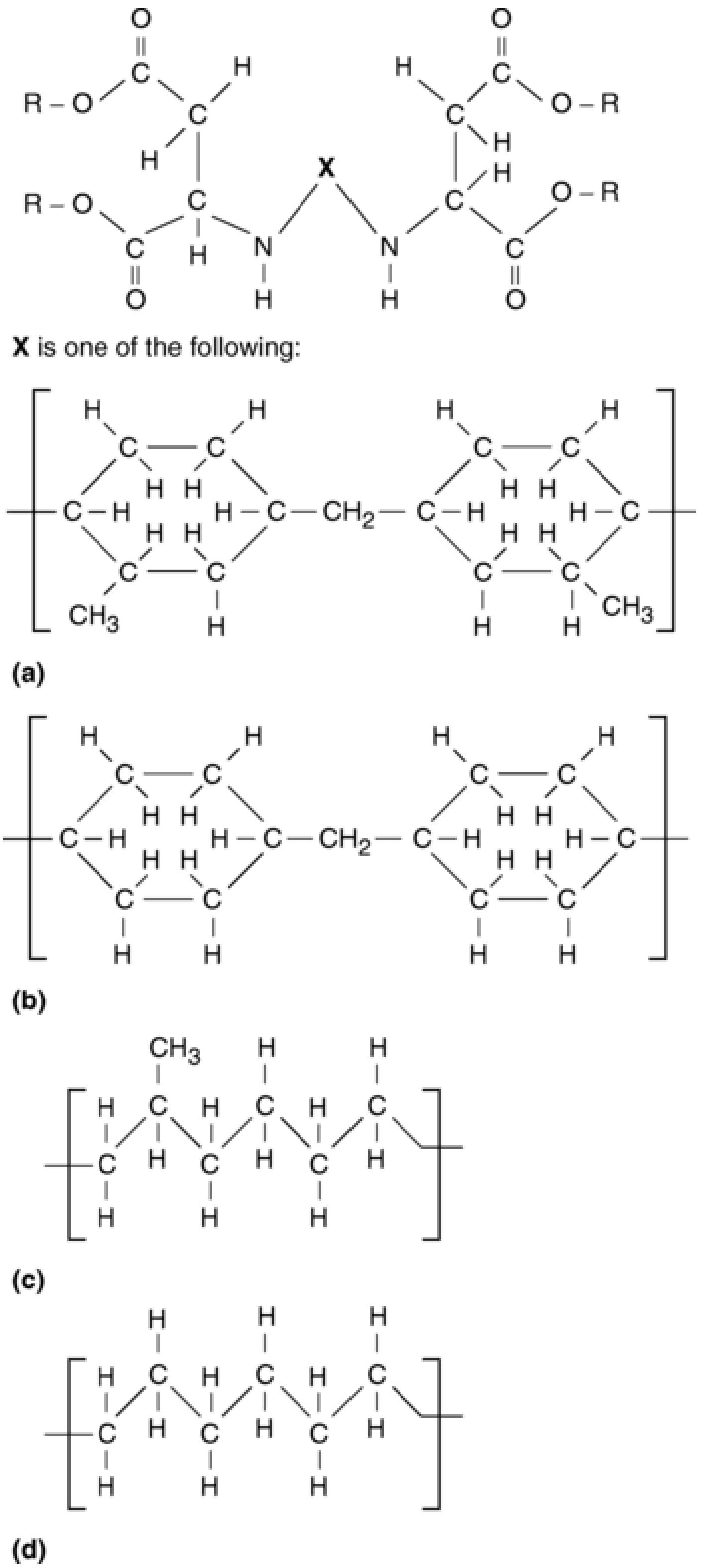

Fig. 27 Structure of aliphatic polyurea coatings. X is one of the polyaspartic esters shown as (a), (b), (c), and (d). The speed of reaction and therefore the pot life and cure time increase from (a) (the slowest) to (d) (the fastest). (d) is the most flexible and has the greatest elongation.

In general, polyurea and polyurethane systems have similar properties. Both have high tensile strength, flexibility, impact resistance, abrasion resistance, and can be formulated into a wide variety of coatings with variable property ranges. However, polyureas compared to polyurethanes have certain advantages and disadvantages. Polyureas can be applied to a lower temperature (-7 °C, or 20 °F) than an equivalently formulated polyurethane. Polyureas have higher heat resistance than comparably formulated polyurethanes.

Conversely, however, polyurethanes have two to three times better abrasion resistance than polyurea systems, and they can be formulated to a smooth, glossy appearance. Because of its fast reactions, the polyurea does not

have time to flow, level, and smooth, and accordingly, polyureas generally have an “orange peel” surface texture.

However, because of their better oil and solvent resistance and lower cost than most polyurethane systems, the use of thick, elastomeric polyurea coatings over concrete in secondary containment for hydrocarbon and fuel oil storage tanks has developed into a major market.

While both polyureas and polyurethanes can be formulated in systems based on aliphatic isocyanate prepolymers that have good weatherability and color retention, most polyurea systems in the market are derived from an aromatic isocyanate. Accordingly, these systems yellow, darken, and chalk more than polyurethanes. The polyether amine and other amine reactants in a typical polyurea formulation also tend to yellow and darken as a result of these amino chromophores.

References cited in this section

2. K.B. Tator, Can Failures Still Occur When the Correct Coating Is Selected and Applied Properly, *Corrosion Control by Organic Coatings,* H. Leidheiser, Ed., National Association of Corrosion Engineers, 1981

3. S.H. Richardson and K.V. McCullough, Phenolic Resins, *Technology of Paints, Varnishes, and Lacquers,* C.R. Martens, Ed., Reinhold, 1968

4. K.B. Tator, Urethane Coatings: Influence of Chemical Composition Upon Performance Properties, *J. Prot. Coatings Linings,* Vol 2 (No. 2), Feb 1985

5. E.P. Squiller, “Aliphatic Polyurea Coatings Based on Polyaspartic Esters,” Bayer Corporation, personal communication, Dec 17, 2001

K.B. Tator, Organic Coatings and Linings, *Corrosion: Fundamentals, Testing, and Protection,* Vol 13A, *ASM Handbook,* ASM International, 2003, p 817–833

Organic Coatings and Linings

Kenneth B. Tator, KTA-Tator, Inc.

References

1. C.R. Martens, Ed., *Technology of Paints, Varnishes, and Lacquers,* Reinhold, 1968

2. K.B. Tator, Can Failures Still Occur When the Correct Coating Is Selected and Applied Properly, *Corrosion Control by Organic Coatings,* H. Leidheiser, Ed., National Association of Corrosion Engineers, 1981

3. S.H. Richardson and K.V. McCullough, Phenolic Resins, *Technology of Paints, Varnishes, and Lacquers,* C.R. Martens, Ed., Reinhold, 1968

4. K.B. Tator, Urethane Coatings: Influence of Chemical Composition Upon Performance Properties, *J. Prot. Coatings Linings,* Vol 2 (No. 2), Feb 1985

5. E.P. Squiller, “Aliphatic Polyurea Coatings Based on Polyaspartic Esters,” Bayer Corporation, personal communication, Dec 17, 2001

K.B. Tator, Zinc-Rich Coatings, *Corrosion: Fundamentals, Testing, and Protection*, Vol 13A, *ASM Handbook*, ASM International, 2003, p 837–844

Zinc-Rich Coatings

Kenneth B. Tator, KTA-Tator, Inc.

Introduction

ZINC-RICH COATINGS combine advantages of hot dip galvanizing protection systems with application methods of paint systems. Cured inorganic zinc-silicate films can be thought of as a cross between hot dip galvanizing and fused ceramic (Ref 1). Zinc-rich coatings are available with organic and inorganic binders, and both formulations are discussed in this article. These coatings, used as primers, combined with organic topcoats provide superior paint systems for severe chemical-industrial environments.

Reference cited in this section

1. J. Rogers, W.M. McMahon, and G.E. Weismantel, Coatings for Steel, *Paint Handbook*, McGraw-Hill, 1981

K.B. Tator, Zinc-Rich Coatings, *Corrosion: Fundamentals, Testing, and Protection*, Vol 13A, *ASM Handbook*, ASM International, 2003, p 837–844

Zinc-Rich Coatings

Kenneth B. Tator, KTA-Tator, Inc.

Characteristics of Zinc-Rich Coatings

The dry film of zinc-rich coatings is typically approximately 90% Zn by weight. Zinc-rich coatings, often called zinc-rich primers, are a unique class of cross-linked coatings that provide galvanic protection to a ferrous substrate. As the name implies, the binder is highly loaded with a metallic zinc-dust pigment. After the coating is applied to a thoroughly cleaned substrate, the binder holds the metallic zinc particles in contact with the steel and with each other. Thus, metal-to-metal contact of two dissimilar metals is made, resulting in a galvanic cell. In this couple, zinc becomes the anode and sacrifices itself to protect the underlying cathodic steel. The articles “Continuous Hot Dip Coatings” and “Batch Process Hot Dip Galvanizing” in this Volume contain more information on corrosion of galvanized steels.

The major advantage of corrosion protection using zinc-rich coatings is that pitting corrosion and subfilm corrosion are eliminated, even at voids, pinholes, scratches, and abrasions in the coating system. This cannot be said of any other type of protective coating, and it is this protective capability that makes zinc-rich coatings unique and widely used.

This advantage, however, comes with certain disadvantages. The underlying steel substrate must be cleaned of all rust, old paint, and other contaminants that may interfere with metal-to- metal contact. Thus, the degree of surface preparation must be quite thorough; blast cleaning should produce a commercial blast cleaning minimum and, for immersion service, a white or near-white surface. SSPC: The Society for Protective Coatings (SSPC), NACE International, and other organizations issue standards for the surface preparation of metals for organic coatings; these are discussed in more detail in the sections “Surface Preparation” and “Coating

Application" in the article "Paint Systems" in this Volume. When power tool cleaning, cleaning to bright metal is necessary. Zinc-rich coatings can be applied to pickled steel, although, again, the surface must be perfectly clean.

Because of the high reactivity of the zinc-dust pigment, zinc-rich coatings are not suitable in condensing or hydrolyzing environments outside the pH range of approximately 5 to 10. Acids and alkalies attack the zinc-dust pigment; even if topcoats are used, chemicals may penetrate through pinholes, scratches, voids, or discontinuities within the topcoat and cause aggressive attack of the zinc-rich primer.

In addition, because of the high zinc loading, the zinc-dust pigment should be suspended in the spray pot during spray application. Thus, the use of an agitator or stirrer in the spray pot is mandatory. Similarly, the weight of the paint, as a result of its high pigment loading (often 2.2 to 3 kg/L, or 18 to 25 lb/gal), prohibits long hose lengths from the spray pot to the spray gun in order to minimize settling in the lines. If the spray gun is elevated too high above the spray pot, air pressure to the spray pot may not be sufficient to push the heavy zinc-rich coating material through the spray line to the gun.

When spraying on warm days, care must be taken that the primer does not begin to set up in the spray lines. This is a particular problem with most inorganic zincs, especially if a spray application is interrupted for more than just a few minutes without first draining paint from the fluid hose. With no movement in a relatively warm paint hose, plugs of paint may begin drying and hardening such that when spraying operations begin, the paint does not readily move through the fluid line to the gun. Blockages occur, the gun works only intermittently, and, in the worst cases, hardening of the paint may occur to such an extent that the entire line must be discarded.

This rapid-drying characteristic, which is particularly evident with the inorganic zincs, may also result in a greater amount of dry spray than usually occurs with conventional non-zinc-rich coatings. Thus, particular care should be taken during application to ensure that the zinc-rich primer is deposited in a smooth, wet application.

Because of high zinc loading over the pigment volume concentration of the binder, the zinc-rich coatings are more porous than any other generic type of paint. Because of this porosity, they are harder to topcoat. Topcoats applied over both organic and inorganic zinc-rich primers often have voids or bubbles in their cross-sectional thickness and bubbles or pinholes extending down through their surface to the underlying zinc-rich coating. This is because of entrapped air, solvents, and moisture within the zinc-rich primer before or during topcoating. The entrapped liquids or gases must pass through the topcoat in order to escape into the atmosphere. As the topcoat dries, escaping gases are held as bubbles or blisters, or the path of such an escaping gas hardens into a pinhole.

Insufficient curing of the zinc-rich binder before application of the topcoat can sometimes lead to poor adhesion or cohesion within the zinc and can ultimately lead to peeling or disbonding of the topcoat. However, despite these disadvantages, the advantage that accrues by the elimination of subfilm and pitting corrosion makes zinc-rich coatings, either topcoated or untopcoated, one of the most widely used corrosion prevention coatings for painting steel in industrial, marine, and other severe service environments.

Zinc-rich coatings used as primers with topcoats or as complete one-coat systems are widely used for the corrosion protection of steel substrates. Organic zinc-rich systems are used in the automotive industry to protect car body rocker panels, wheel wells, and other corrosion-prone interior steel parts. Inorganic zinc-rich coatings are also used extensively in the marine industry for the protection of exterior hulls, cargo and ballast tanks, offshore platforms, and other areas of high marine corrosion. Inorganic zinc-rich coatings are used in these same environments and in applications requiring high abrasion and high heat resistance to 370 °C (700 °F) when untopcoated. Both organic and inorganic zinc-rich coatings are extensively used for steel protection on bridges and highway structures, chemical and petrochemical plants, sewage and water treatment, and any area where freshwater or saltwater corrosion, mild fumes, and high humidity and resultant corrosion is a problem.

Zinc-rich coatings can be subcategorized according to the type of binder material used. Zinc- rich coatings with organic binders are similar in many ways to the coating systems previously discussed, except that sufficient zinc-dust pigment is added to provide galvanic protection. The inorganic zinc-rich coatings, on the other hand, use an entirely different binder chemistry and are therefore quite unlike the organic zinc- rich coatings. As a general rule, organic zinc-rich coatings are more widely used in Europe and Asia than inorganic zinc-rich coatings; in the United States and Canada, the inorganic zinc- rich coatings are more widely used.

K.B. Tator, Zinc-Rich Coatings, *Corrosion: Fundamentals, Testing, and Protection*, Vol 13A, *ASM Handbook*, ASM International, 2003, p 837–844

Zinc-Rich Coatings

Kenneth B. Tator, KTA-Tator, Inc.

Zinc-Rich Coatings with Organic Binders

Organic zinc-rich coatings are most commonly formulated from epoxy polyamide and polyurethane binders. Alkyds have been used for some air-dry formulations, but they are most commonly used with baking formulations, notably in the automotive industry. Vinyl and chlorinated rubber binders are not volatile-organic-compound compliant and are not currently in use.

To manufacture a successful organic zinc-rich coating, one does not simply substitute the zinc- dust pigment for the normal inhibitive and filler pigments commonly used. Instead, skillful formulation is required to achieve galvanic protective capability while also maintaining suitable storage, application, and physical properties of the applied film. When such formulation is achieved, the result is a protective coating having the physical attributes determined by the organic binder, along with the galvanic capability and chemical susceptibilities inherent in the use of the zinc-dust pigment. However, the untopcoated zinc-dust pigment is attacked by acids and alkalies, and even though the binder is resistant to such chemicals, organic zinc-rich primers should not be used in aggressive chemical environments.

The drying, hardening, and ultimate curing of the organic zinc-rich coating is determined by the type of binder used. The hardening and curing mechanisms of the various binders have been described previously and are the same for zinc- rich coatings. Organic zinc-rich primers are more tolerant of deficient surface preparation, because they wet more readily and seal poorly prepared surfaces where residues of rust or old paint may remain. Similarly, topcoating with the same generic type of topcoat (for example, an epoxy zinc-rich coating topcoated with an epoxy topcoat) is more readily accomplished, because organic zinc-rich coatings of all types generally have a less porous surface and are more similar to conventional organic coatings than the inorganic zinc-rich coatings.

K.B. Tator, Zinc-Rich Coatings, *Corrosion: Fundamentals, Testing, and Protection*, Vol 13A, *ASM Handbook*, ASM International, 2003, p 837–844

Zinc-Rich Coatings

Kenneth B. Tator, KTA-Tator, Inc.

Zinc-Rich Coatings with Inorganic Binders

The SSPC has categorized inorganic zinc-rich coatings as being of three major groups:

- Postcured water-based alkali metal silicates
- Self-cured water-based alkali metal silicates
- Self-cured solvent-based alkyl silicates

Although the binder, in all cases, is an inorganic silicate (sometimes called waterglass, it is essentially the same material as glass or sand), the curing of the binder is different in all three cases.

Postcured water-based inorganic silicates come as three-package systems; the zinc dust, silicate binder, and curing solution are packaged separately. If elevated baking temperatures can be achieved, the curing solution may not be necessary.

The earliest postcured zinc-rich coatings were based on a sodium silicate vehicle, and the most popular commercial products available have essentially the same chemistry. There are other inorganic zinc-rich coatings based on lithium or potassium silicates that self-cure, but curing can be accelerated by the use of a curing solution, if desired. The following steps summarize the curing of postcured water-based inorganic zinc-rich coatings.

The first step is primarily a dehydration process in which the water, which is the basic solvent for the silicate, evaporates from the clean steel surface, leaving the zinc and the alkali silicate on the surface as a coating. At this point, when the coating is free of water, it is very hard and metallic. Scraping with a coin merely polishes the zinc in the coating.

Second, once the initial drying process has taken place, an acid phosphate curing solution is sprayed or brushed over the zinc-rich coating in order to wet out the surface thoroughly. The initial reaction is for the acid to gradually neutralize the sodium in the sodium silicate solution and to create a mildly acidic surface condition.

Third, during initial curing, the pigment constituents may react with the silica matrix. This, together with further neutralization of the silicate alkalinity, insolubilizes the film. The addition of the acidic curing solution on the surface of the zinc coating ionizes the zinc in the coating as well as the lead oxide pigment mixed with it. As this takes place, there is a rapid reaction between the active silicate groups and the lead and zinc, insolubilizing the silica matrix.

The acid phosphate also reacts with the zinc and lead to form very insoluble zinc and lead phosphates within the silicate matrix. At this point, the coating has become insoluble to water and resistant to exposure to weather.

Lastly, after initial curing, further hydrolysis and improvement of film properties continue over time. Following the application and reaction of the curing agent, the remaining soluble salts on the surface are removed with clean water or by weathering. The coating at this point is dense and relatively nonporous, insoluble in water, and resistant to marine and mild chemical atmospheres.

Postcured coatings are, in the author's opinion, the best performing of the inorganic zinc- rich materials. The reason for this is most likely the relatively complete, insolubilizing hard cure that is attained after application of the curing solution. By applying the curing solution and thoroughly curing the coating, the maximum protective properties of the coating are attained shortly after application. In contrast, self-cure coatings rely on ambient atmospheric conditions in order to cure completely. Research indicates that many self-cured coatings do not achieve their ultimate resistance and protective capability until long after their original application.

Self-Curing Water-Based Alkali Silicates. The most common of these silicate binders is based on potassium and lithium silicates or combinations of these. In addition, lithium hydroxide-colloidal silica and quaternary ammonium silicate binders are also included in this category.

The reaction chemistry of the water-based self-cure inorganic zinc-rich silicates is similar to that of the postcured sodium silicates, with the exception that the curing solution is not applied. The metal silicate vehicle, before field addition of the zinc-dust pigment, has a higher ratio of silica to metal oxides and a lower alkalinity than the postcured vehicles. Therefore, after water evaporation and insolubilization resulting from the silica reaction with the pigment, sufficient neutralization and cure are attained by further reaction with acid formed by the atmospheric hydrolysis of carbon dioxide (reaction of CO_2 and atmospheric moisture to form a weak carbonic acid).

Self-curing alkali silicate zinc-rich coatings become hard within minutes and are considered generally resistant to precipitation within 30 min after application. If a more rapid insolubilization or cure is desired, heat or an acidic curing solution can be applied. The reaction chemistry would then be essentially identical to that of the postcured sodium silicate matrix. When final curing is ultimately attained, most water-based zinc-rich coatings, whether post- or self-cured, experience a color change, often from a reddish gray or light gray to a darker bluish gray.

Self-Cured Solvent-Based Alkyl Silicates. The binders for this class of coatings are essentially modified alkyl silicates consisting of partially hydrolyzed members of the series methyl through hexyl or glycol ether silicates. Of these, the ethyl silicate type is most commonly used.

The reaction chemistry of ethyl silicates can be best demonstrated by the hydrolysis of tetraethyl orthosilicate in the presence of an acid or alkali catalyst. The reaction is carried to partial completion with a degree of hydrolysis ranging from 70 to 95%. The reaction is irreversible, because of the volatilization of the alcohol that

results from the ester exchange; however, should premature gelling of the silicate occur, alcohol may be added to redissolve the gel. During the condensation phase of the reaction, the partially polymerized silicate combines with atmospheric moisture to eliminate alcohol, which vaporizes.

After complete hydrolysis, the cross-linked network forms a matrix to hold the pigment particles. In addition, it is conceivable that the zinc and other metallic pigment additives (and perhaps the underlying ferrous surface) may react with the silicate in a manner similar to that described for postcured sodium silicate. The matrix formation of an ethyl silicate is illustrated in Fig. 1.

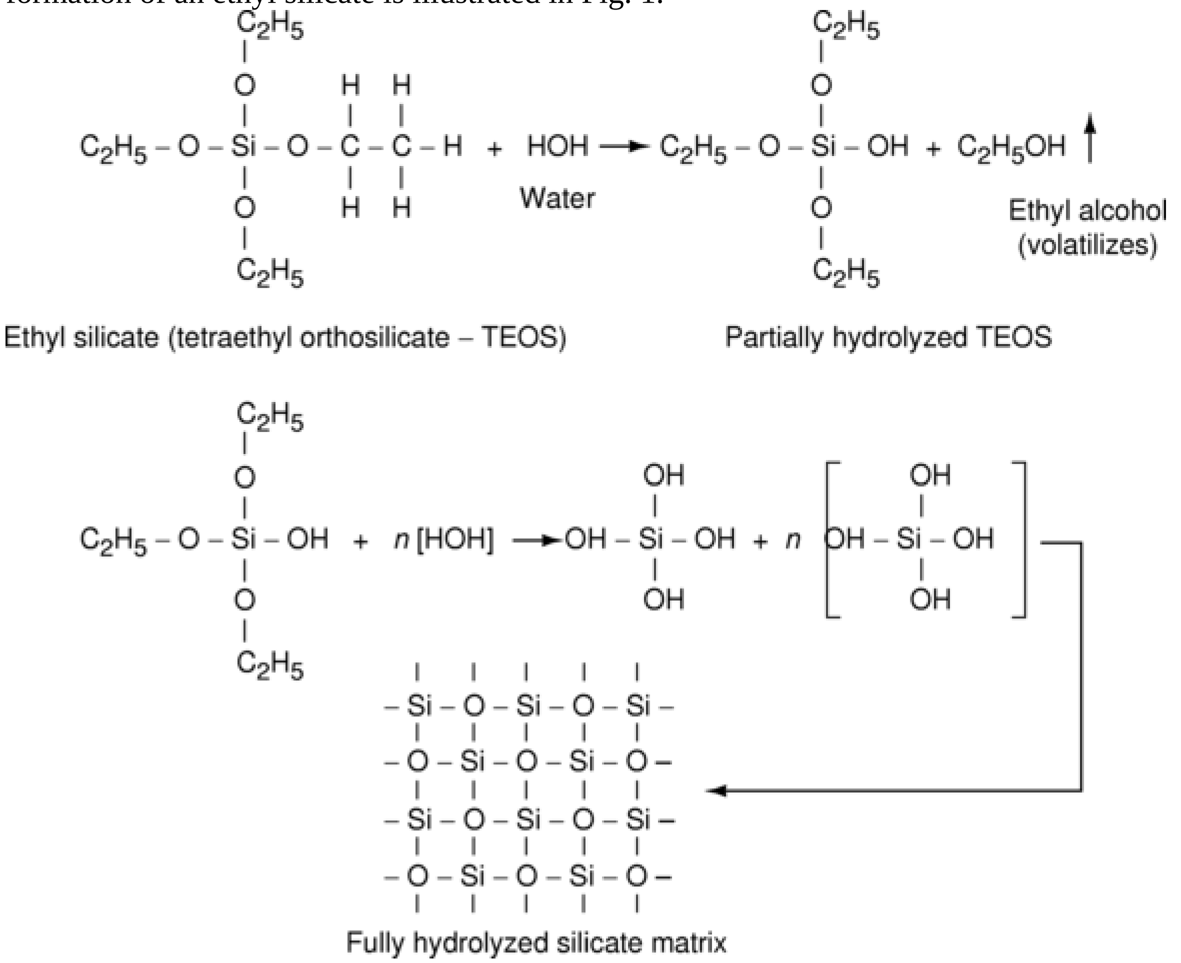

Fig. 1 Matrix formation of ethyl silicate. *n* represents the number of molecules.

Single-package inorganic zinc-rich primers based on the ethyl silicate chemistry described previously have been developed. Instead of packaging the zinc dust separately from the ethyl silicate binder, the coating manufacturer adds the zinc dust in the manufacturing plant, along with additives that keep the zinc dust in suspension. Careful quality control of raw materials, particularly zinc-dust pigment and additives, is exercised to ensure they are dry and moisture-free. Also, the ethyl silicate vehicle is somewhat less prehydrolyzed and is usually catalyzed with an acid catalyst such that on application and curing, the rate of reaction with moisture occurs at a faster rate than with two-package ethyl silicate zinc-rich primers. However, depending on temperature and (especially) atmospheric humidity, the full cure of a single pack inorganic zinc-rich primer may take significantly longer than that of two-pack silicates.

The properties of the single-package ethyl silicate zinc-rich primers are similar to those of the dual-package primers (where the zinc dust is packaged separately from the liquid silicate binder); but in general, single-package inorganic zinc-rich coatings do not cure as hard or as fast as dual-package products, and they do not provide quite as long a corrosion protection, although corrosion protection is still excellent. On the other hand, they are much easier to mix and apply, and these application advantages have resulted in their increased use.

K.B. Tator, Zinc-Rich Coatings, *Corrosion: Fundamentals, Testing, and Protection*, Vol 13A, *ASM Handbook*, ASM International, 2003, p 837–844

Zinc-Rich Coatings

Kenneth B. Tator, KTA-Tator, Inc.

Comparisons of Inorganic and Organic Zinc-Rich Coatings

In general, the inorganic zinc-rich coatings provide somewhat longer galvanic protection than the organics do, but they are less tolerant of deficient surface preparation, are somewhat harder to mix and apply, generally have a greater tendency toward mudcracking at excessive thickness, and are more difficult to topcoat. The organic zinc-rich coatings have limited temperature resistances that are determined by their organic binder. In contrast, inorganic zinc-rich coatings resist dry heat to over 370 °C (700 °F), and when topcoated with a silicone or ceramic coating, they can be used at temperatures of 650 °C (1200 °F) or higher. The abrasion and impact resistance of the inorganics are unsurpassed. The comparison of zinc-rich coatings with organic and inorganic binders is summarized in Table 1.

Table 1 Advantages and limitations of zinc-rich coatings

Resin type	Advantages	Limitations	Comments
Organic zinc-rich	Galvanic protection afforded by the zinc content, with chemical and moisture resistance similar to that of the organic binder. Should be topcoated in chemical environments with a pH outside the range 5–10. More tolerant of surface preparation and topcoating than inorganic zinc-rich coatings	Generally have lower service performance than inorganic zinc-rich coatings, but ease of application and surface preparation tolerance make them increasingly popular.	Widely used in Europe and the Far East, while inorganic zinc-rich coatings are most common in North America. Organic binder can be closely tailored to topcoats (for example, epoxy topcoats over epoxy-zinc-rich coatings) for a more compatible system. Organic zinc-rich coatings are often used to repair galvanized or inorganic zinc-rich coatings.
Inorganic zinc-rich	Provides excellent long-term protection against pitting in neutral and near-neutral atmospheric, and some immersion, services. Abrasion resistance is excellent, and dry heat resistance exceeds 370 °C (700 °F). Water-based inorganic silicates are available for confined spaces and compliance with regulations regarding volatile organic compounds.	Inorganic nature necessitates thorough blast-cleaning surface preparation and results in difficulty when topcoating with organic topcoats. Zinc dust is reactive outside the pH range of 5–10, and topcoating is necessary in chemical fume environments. Somewhat difficult to apply; may mudcrack at thicknesses in excess of 0.13 mm (5 mils)	Ethyl silicate zinc-rich coatings require atmospheric moisture to cure and are the most common type. Widely used as a primer on bridges, offshore structures, and steel in the building and chemical-processing industries. Used as a weldable preconstruction primer in the automotive and shipbuilding industries. Use eliminates pitting corrosion.

All water-based zinc-rich coatings, whether post- or self-cured, require somewhat greater surface cleanliness in order to achieve suitable adhesion and environmental protection. Water- based zinc-rich coatings have a greater tendency to mudcrack at excessive thicknesses than solvent-based inorganics do, and there is also an increased tendency to form zinc surface reaction products, particularly with sodium and lithium silicate vehicles. A major advantage of all water- based zinc-rich coatings is that they do not have a flash point and can be used in tanks, ship holds, and other confined or poorly ventilated areas without danger. However, such coatings do require

good ventilation or dehumidification to cure properly. Solvent-based inorganic zinc-rich coatings that are modified to have a tag open cup flash point higher than their normal 20 to 30 °C (70 to 90 °F) often form a softer, less resistant film.

K.B. Tator, Zinc-Rich Coatings, *Corrosion: Fundamentals, Testing, and Protection*, Vol 13A, *ASM Handbook*, ASM International, 2003, p 837–844

Zinc-Rich Coatings

Kenneth B. Tator, KTA-Tator, Inc.

References

1. J. Rogers, W.M. McMahon, and G.E. Weismantel, Coatings for Steel, *Paint Handbook*, McGraw-Hill, 1981

K.B. Tator, Paint Systems, *Corrosion: Fundamentals, Testing, and Protection*, Vol 13A*, ASM Handbook*, ASM International, 2003, p 836–844

Paint Systems

Kenneth B. Tator, KTA-Tator, Inc.

Introduction

PAINT SYSTEMS and, more generally, coating systems encompass not only the materials as discussed in the previous articles but all the processes that impact the success of the corrosion protection scheme. This includes proper selection of materials or combinations of materials, use of the appropriate tools, the proper execution of surface preparation, coating applications, and inspection methods.

K.B. Tator, Paint Systems, *Corrosion: Fundamentals, Testing, and Protection*, Vol 13A*, ASM Handbook*, ASM International, 2003, p 836–844

Paint Systems

Kenneth B. Tator, KTA-Tator, Inc.

Coating System Selection

The selection of the proper corrosion-resistant coating system depends on a number of factors:

- *Environmental resistance:* The coating system should be resistant to the chemical, temperature, and moisture conditions expected to be encountered in service.
- *Appearance:* In high-visibility areas (for example, water tanks, railroad cars, and appliances), color, gloss, and a pleasing appearance may be very important.
- *Safety:* Toxic pigments and solvents may prohibit the use of some coatings; future removal and disposal problems should be considered. Coatings with volatile explosive solvents may be dangerous in enclosed, poorly ventilated spaces.
- *Surface preparation:* Surface preparation restrictions must be considered. For example, blast cleaning may be prohibited in some refineries or near electrical and hydraulic machinery.
- *Skill of the labor force:* Certain coating systems require more application expertise than others. Generally, inorganic zincs, vinyl esters, polyesters, vinyls, and chlorinated rubbers are less application tolerant than some of the other coating systems.
- *Substrate to be coated:* Coating systems for aluminum, lead, copper, concrete, masonry, and wood may differ from those for ferrous metals.
- *Available equipment:* The more resistant coating systems generally require spray application over a blast-cleaned surface. For some polyesters and vinyl esters, plural-component spray equipment may be required.
- *Design life:* If a structure is intended to have a long service life, the use of a more resistant coating system may be justified than if a shorter service life is intended.
- *Cost:* Generally speaking, the applied cost of a more resistant coating system is greater than the applied cost of a less resistant system.
- *Accessibility for future repair:* If future repair will be difficult or expensive, perhaps a longer-lasting coating system should be specified.

- *Consequences of coating failure:* If a coating failure will be disastrous, such as in tanks holding highly corrosive materials or in nuclear power plants where peeling or disbonding coating may clog sumps and screens, a more resistant coating system should be selected.

Each of these factors, to varying degrees, directly influences the choice of the coating system selected to protect a metal in a given environment. Once the choice is made, it is usually necessary to prepare appropriate specifications detailing the surfaces to be painted and the surfaces to be protected from paint. In addition, the surface preparation and coating application details should be delineated. At a minimum, the thickness of each coat and the total coating thickness should be specified, and the surface profile of a blast-cleaned surface, the interval between coats, and other factors (such as testing for holidays and pinholes and for adhesion) should also be specified. Although the preparation of a proper specification is beyond the scope of this article, a good specification is not only an important contractual document but is also the means of conveying the owner's (or specifier's) intentions and instructions regarding the painting to be accomplished. Thus, the potential importance of a good specification cannot be overestimated.

K.B. Tator, Paint Systems, *Corrosion: Fundamentals, Testing, and Protection*, Vol 13A, *ASM Handbook*, ASM International, 2003, p 836–844

Paint Systems

Kenneth B. Tator, KTA-Tator, Inc.

Surface Preparation

The selection of the coating material to be used to protect a given metal from an environment usually determines the surface preparation that is required. For example, zinc-rich coatings almost always require blast cleaning, while many alkyd and oil-based coating systems can be applied over rust, mill scale, or a poorly cleaned surface.

Surface Preparation Process Steps

Surface preparation consists of: (1) removal of visible contaminants, (2) removal of invisible contaminants, and (3) roughening the surface.

Removal of Visible Contaminants. Cleanliness is essential in the preparation of a surface that will receive protective coatings. Most, but not all, coating systems require some degree of surface preparation. Generally, higher-performance coating systems require a higher degree of cleanliness. Paint applied over rust, dirt, or oil bonds poorly (or not at all) to the substrate, and early paint failure usually results. A clean surface is free of such contaminants as rust, flash rust, dirt and dust, salts, oil and grease, old paint, and mill scale.

NACE International and the former Steel Structures Painting Council (SSPC) have jointly issued a series of surface preparation standards that are used widely throughout North America. The SSPC is now known as SSPC: The Society for Protective Coatings.

Similar standards issued by the International Organization for Standardization (ISO) are widely used in Europe and Asia. These ISO surface preparation standards consist of photographs of four starting grades of steel that are wire brush cleaned or blast cleaned to various degrees of cleanliness (Ref 1, 2, 3). Table 1 presents an abstract of the SSPC/NACE International standards.

Table 1 Uses and applicable standards for various surface preparation techniques

Technique	Applicable standards	Uses
Solvent cleaning	SSPC-SP1	Used to remove oil, grease, dirt, soil, drawing compounds, and various other contaminants. Does not remove rust or mill scale. No visual standards are available.
Hand tool cleaning	SSPC-SP2	Used to remove loose rust, mill scale, and any other loose contaminants. Standard does not require the removal of intact rust or mill scale. Visual standards: SSPC-VIS 3—BSt3, CSt3, and DSt3[(a)]
Power tool cleaning	SSPC-SP3	Same as hand tool cleaning. Visual standards: SSPC-VIS 3—BSt3, CSt3, and DSt3[(b)]
White-metal blast cleaning	SSPC-SP5; NACE 1	Used when a totally cleaned surface is required; blast-cleaned surface must have a uniform, gray-white metallic color and must be free of all oil, grease, dirt, mill scale, rust, corrosion products, oxides, old paint, stains, streaks, or any other foreign matter. Visual standards: SSPC-VIS I—ASa3, BSa3, CSa3, and DSa3[(a)]; NACE 1
Commercial blast cleaning	SSPC-SP6; NACE 3	Used to remove all contaminants from surface, except the standard allows slight streaks or discolorations caused by rust stain, mill scale oxides, or slight, tight residues of rust or old paint or coatings. If the surface is pitted, slight residues of rust or old paint may remain in the bottoms of pits. The slight discolorations allowed must be limited to one-third of every square inch. Visual standards: SSPC-VIS I—BSa2, CSa2, DSa2[(a)]; NACE 3; SSPC-VIS 5/NACE VIS 9[(d)]
Brush-off blast cleaning	SSPC-SP7; NACE 4	Used to remove completely all oil, grease, dirt, rust scale, loose mill scale, and loose paint or coatings. Tight mill scale and tightly adherent rust and paint or coatings may remain as long as the entire surface has been exposed to the abrasive blasting. Visual standards: SSPC-VIS I—BSa1, CSa1, DSa1[(a)]; NACE 4
Pickling	SSPC-SP8	Used for complete removal of all mill scale, rust, and rust scale by chemical reaction, electrolysis, or both. No available visual standards
Near-white blast cleaning	SSPC-SP10; NACE 2	Used to remove all oil, grease, dirt, mill scale, rust, corrosion products, oxides, paint, or any other foreign matter. Very light shadows, very slight streaks, and discolorations caused by rust stain, mill scale oxides, or slight, tight paint or coating residues are permitted to remain but only in 5% of every square inch. Visual standards: SSPC-VIS I—ASa2-1/2, BSa2-1/2, CSa2-1/2, and DSa2-1/2[(a)]; NACE 2; SSPC-VIS 5/NACE VIS 9[(d)]
Power tool cleaning to bare metal	SSPC-SP11	Used to completely remove all contaminants from a surface using power tools. Equivalent to SSPC-SP5, "White-Metal Blast Cleaning." Requires a minimum 1 mil anchor pattern. Visual standard: SSPC-VIS 3[(b)]
Waterjetting	SSPC-SP12; NACE 5	Cleaning using high- and ultrahigh-pressure waterjetting prior to recoating. Visual standard: SSPC-SP4/NACE 7. Photos depict degrees of cleanliness and flash rusting[(c)].
Mechanical, chemical, or thermal preparation of concrete	SSPC-SP13; NACE 6	Prepares cementitious surfaces for bonded protective coating or lining systems
Industrial blast cleaning	SSPC-SP14; NACE 8	Used to clean painted or unpainted steel surfaces free of oil, grease, dust, and dirt. Traces of tight mill scale, rust, and coating residue are permitted. Visual standard: SSPC-VIS 1[(a)].
Commercial grade power tool cleaning	SSPC-SP 15	Used for power tool cleaning of steel surfaces while retaining or producing a minimum 25 μm (1 mil) surface profiles. This standard requires higher degree of cleanliness than SSPC-SP 3, but allows stains

of rust, paint, and mill scale not allowed by SSPC-SP 11.

(a) SSPC-VIS 1, "Guide and Reference Photographs for Steel Surfaces Prepared by Dry Abrasive Blast Cleaning" is the most commonly used standard for evaluating the cleanliness of a prepared surface. The use of these standards requires a determination of the extent of rust on the uncleaned steel; this is graded from A to D.
(b) SSPC-VIS 3, "Visual Standard for Power- and Hand-Tool Cleaned Steel."
(c) SSPC-VIS 4/NACE VIS 7, "Guide and Reference Photographs for Steel Surfaces Prepared by Waterjetting."
(d) SSPC-VIS 5/NACE VIS 9, "Guide and Reference Photographs for Steel Surfaces Prepared by Wet Abrasive Blast Cleaning"

Although there are other national or corporate standards, the SSPC/NACE International and ISO standards are perhaps the most widely used. However, these standards (and most others) specify only the visual degree of cleaning and do not define the surface roughness or profile obtained by cleaning or by the removal of invisible contaminants.

Removal of Invisible Contaminants. The removal of invisible contaminants is more difficult to assess. Chemical contamination after surface preparation and before coating may result in blistering, poor adhesion, or other defects in the applied coating system. It is less evident that such chemical contamination may be inherent in a metal after it has been exposed and corroded in a chemical environment. Even thorough blast cleaning to white metal may not remove chemical species (notably chloride ions) that may have penetrated into the grain boundaries or microstructure of the metal. If such penetrating anions can react to form a water-soluble salt, such as ferrous chloride, then an aggressive underfilm corrosion may occur if water permeates the coating.

As might be expected, the presence of invisible water-soluble contaminants is more detrimental in immersion service than in dry atmospheric service. Methods for removing such contaminants are usually based on water blasting or water flushing in order to dissolve and flush the water-soluble contaminants from the surface. Other approaches are the use of chelating primers, which react with and complex the soluble salts and render them inactive and noncorrosive, and the application of a porous coating, such as an inorganic zinc-rich primer, that allows passage of water-soluble corrosion products.

A major detriment to removal is, of course, the inability to adequately detect the presence of contaminants. Although indicator kits and chemically treated papers have been developed for this purpose, more work is needed in this area. Furthermore, very little work has been done to establish the tolerance of various coatings, surfaces, or exposure environments to the presence of differing amounts of contaminants. Investigations into the tolerance of coating systems for water-soluble salt contamination on the surface prior to painting have disclosed that many researchers believe that the maximum salt concentration in immersion service should not exceed 3 to 10 $\mu g/cm^2$ (Ref 4).

Roughening of the Surface. In addition to cleanliness, the surface must be roughened to provide for a mechanical bond of the paint to the substrate. This roughening is termed *anchor pattern, profile,* or *tooth,* and it is essentially a pattern of peaks and valleys on the steel surface. This pattern is obtained by abrasive blasting, and it must be carefully controlled according to the coating system being applied. If the peaks are too high, they will project above the coating and cause pinpoint rusting. A rule of thumb for surface profile is that it should be approximately one-third of the required coating system thickness up to a coating thickness of 0.3 mm (12 mils).

The roughness or surface profile imparted to the metal during the course of cleaning preparatory to painting influences adhesion. As a rule, greater roughness results in greater adhesion, although excessive roughness may result in high spots or peaks that are not covered adequately by the thickness of the applied coating. Such peaks may be initiation sites for pinpoint rusting and corrosion. As a general rule, most mineral abrasive blast-cleaning materials impart a profile or roughness ranging from 13 to 100 μm (0.5 to 4 mils), depending on particle size and impact velocity. Metallic grits may have deeper profiles, approaching 178 μm (7 mils) or more, but metallic shot and grit, when sized properly, usually impart profiles within the 50 to 115 μm (2 to 4.5 mil) range. Such surface roughnesses are suitable for most of the coating systems discussed in this article, although some of the more highly stressed systems, such as the vinyl esters and polyesters, may require a deeper profile to ensure adequate adhesion.

Other areas of the surface also must be addressed before the actual cleaning. Coatings generally do not cover weld spatter properly. Weld spatter may also become dislodged in service, exposing the unprotected substrate. Sharp edges cause paint to draw thin because of surface tension effects and should be eliminated by grinding. Inside corners provide a collection site for excess paint and/or abrasive and should be filled. Crevices and pits should be filled with weld metal, if necessary, and smoothed. Some pits, because of their sharp, angular edges,

require extensive welding and grinding before surface preparation. Other pits, because they consist of smooth, even depressions, need only be cleaned for coating.
In addition, for maintenance painting, thick layers of stiff, old paint should be removed, and glossy painted surfaces must be roughened. Nonferrous surfaces also frequently require some type of pretreatment. In the case of aluminum or galvanized steel, degreasing and the application of a wash primer are often employed to provide proper adhesion.

Methods of Surface Preparation

A variety of surface preparation methods are available, including:

- Solvent or chemical washing
- Steam cleaning
- Hand tool cleaning
- Power tool cleaning
- Water blasting
- Abrasive blast cleaning

Each of these preparation methods is discussed subsequently.
Solvent cleaning (SSPC-SP1) removes oil and grease and is usually used in conjunction with or before the mechanical methods of preparation. Because of rapid contamination, fresh solvent must be used continuously, and the rags or cloths must be turned and/or replaced frequently. If this is not done, the grease and oil are spread across the surface rather than removed. The final wash should be made with clean solvent. The organic solvents used should not contact the eyes or skin and should not be used near sparks or open flames. The disadvantages of solvent cleaning are that it has no effect on rust or mill scale, it is very slow and labor intensive, and the materials are rapidly used up and need constant replacement. In addition, many of the solvents used are highly flammable and toxic. Natural or mechanical exhaust ventilation for diluting the concentration of vapors in an enclosed working space should be employed during the entire work period.
Steam cleaning uses high-temperature, high- velocity wet steam to remove heavy soil, oil, or grease. It does not remove rust or mill scale, nor does it etch or roughen the surface. Commercial detergents can be added to the steam to improve cleaning. On steel, steam cleaning is sometimes followed by spot blast cleaning or wire brushing on areas exhibiting coating failure or rusting.
Hand tool cleaning (SSPC-SP2) is used only for removing loosely adherent paint, rust, or mill scale. Because this method is slow, it is primarily used for spot cleaning. Hand tools include scrapers, wire brushes, abrasive pads, chisels, knives, and chipping hammers. The disadvantages of using these tools, in addition to the lack of speed, are that they do not remove tightly adherent contaminants (for example, dirt trapped in crevices, or oil or grease) and that they may raise burrs or dent the surface, actually causing some damage to the surface. In addition, these tools generally do not provide a surface profile.
Power tool cleaning (SSPC-SP3) is faster than hand tool cleaning; it removes loose paint, rust, and scale; and it is good for the preparation of welded surfaces. Power tool cleaning is also good for removing old paint that has been lifted by rust. It provides a duplication of hand tools in power-driven equipment (electric or pneumatic), such as sanders, wire brushes, grinders, clippers, needle guns, and rotary descalers. Generally, power tool cleaning is suitable only for small areas because it is relatively slow. Power tools do not leave as much residue or produce as much dust as abrasive blasting, and they are frequently used where blasting dust could damage sensitive surroundings. However, they may polish the surface if they are used at too high a speed or kept in one spot for too long.
Water blast cleaning (SSPC-SP12/NACE 5) may be high or low pressure, hot or cold, and with or without a detergent, depending on the type of cleaning desired. This process removes loose, flaky rust, paint, and mill scale. It has gained wide acceptance where abrasive blast cleaning, dust, and contamination present a hazard to either personnel or machinery. Low-pressure washing (<14 MPa, or 2000 psi) is effective in removing dirt, mildew, and chalk from the coating surface, and it is generally safe on concrete or masonry surfaces. Low-pressure water blast units use the same components as high- pressure water blast equipment. Low-pressure cleaning is referred to as power washing, and it should be recognized as such. For cleaning steel, water pressures as high as 68 MPa (10,000 psi) or more and volumes from 30 to 38 L/min (8 to 10 gal/min) are used.

Water alone at pressures less than 136 MPa (20,000 psi) does not etch a metal surface or remove tight paint, rust, or mill scale. Therefore, abrasives can be injected into the water stream to remove tightly adhering materials, to hasten the cleaning, or to roughen the surface profile. Any type of abrasive that is commonly used with abrasive blast cleaning can be used in water blast cleaning. Because the abrasive is normally not dried, screened, and recycled, less expensive abrasives are commonly selected in this application. The abrasive is injected into the system after water is pressurized by means of a suction head to prevent pump damage. Injecting abrasives into the water eliminates the dust that normally accompanies dry use of such abrasives.
Water at pressures in excess of 136 MPa (20,000 psi) removes tightly adherent materials, including rust and rust scale, but a minimal profile of a sound steel substrate results. If the original surface was previously blastcleaned, that original profile will be revealed. If the steel surface was smooth, little additional roughening from the water will result, unless abrasive has been added. In the latter case, if roughening is desired, it is usually obtained by mechanical means (needle gun, flapper wheel abrading, or blastcleaning) or by water blasting at lower pressures with abrasive injection.
Flash rusting is a concern when using these methods. Flash rust is a light rust layer that forms on steel after cleaning, particularly after water or wet abrasive blasting, or in humid marine environments. To avoid flash rusting, rust inhibitors such as sodium and/or potassium dichromate or phosphate are often used during or after water blasting. These inhibitors may retard rusting for up to 7 days. The disadvantage of using these corrosion inhibitors is that the solutions, on drying, leave salts that can produce adhesion problems for protective coatings. The primary consideration, therefore, should be to determine if the protective coating is compatible with the inhibitor that was used.
Abrasive blast cleaning is the preferred surface preparation method for paints and coatings that require an anchor pattern and a high degree of cleanliness. Blast cleaning is the only method that can completely remove intact mill scale and give an even roughness with a controlled anchor pattern. Abrasive blasting is the propelling, or shooting, of sand or other types of small, hard particles at a surface. In nozzle blasting, the force that propels the abrasive is compressed air. The abrasive strikes the surface at speeds of 320 to 640 km/h (200 to 400 mph), breaking and loosening the rust or scale.
The cleaning principle is the same in centrifugal wheel blasting. In this case, the spinning of large paddle wheels creates the force that throws the abrasive at the surface. This method is usually confined to shop use with units approximately the size of a large trailer, although smaller one-man units have been developed for preparing floors or ship hulls. In contrast with open blast cleaning, the abrasives used are recyclable steel grit or shot.
Vacuum blasting is another option for dust- free blast cleaning. With this technique, the blast nozzle is surrounded by a brush, and a vacuum is created within the annular space. The spent abrasive and removed paint, rust, and debris are contained by the brush, removed by the vacuum, and transported to a separator. The debris and fine particles are removed, and the abrasive is returned for reuse. This method is very slow, because the blast pattern is approximately 25 mm (1 in.) in diameter. However, for small areas or where dust cannot be tolerated, it may be the best alternative.
The grades of cleaning, from least to most thorough, are identified as:

- Brush-off blast cleaning (SSPC-SP7/NACE 4)
- Industrial blast cleaning (SSPC-SP14/NACE 6)
- Commercial blast cleaning (SSPC-SP6/ NACE 3)
- Near-white blast cleaning (SSPC-SP10/ NACE 2)
- White blast cleaning (SSPC-SP5/NACE 1)

The specific definitions are provided later in this section. Abrasive blasting is ideally suited for high-production work because it rapidly cleans large areas. In spite of its efficiency and good results, some problems still occur, such as the accumulation of used abrasives in low-lying areas and the attendant difficulty in removing them. Airborne dust and abrasive can interfere with machinery and the work of persons nearby and can contaminate adjacent locations. Airborne dust can be a hostile environment for the blast operator, and an air-fed hood must be worn while operating the air blast cleaning equipment. In addition, open nozzle blast abrasives are expensive and are usually not recycled in the field.
Open nozzle blasting equipment has six basic components:

- Air compressor
- Air hose
- Blasting machine, with a safety valve
- Blast hose
- Nozzle
- Moisture and oil separator

The function of each part is described subsequently.
The air compressor is the source of energy for the blasting job. The constant supply of a high- volume high-pressure air stream hour after hour is the most critical part of blast operations. Work is done in direct proportion to the volume and pressure of air at the nozzle. The larger the compressor, the larger the nozzle it can operate. The larger the nozzle at the proper pressure, the faster the job can be completed.
The air hose connects the compressor to the blast pot. For efficient blasting, the air hose should have as large an inside diameter as practical in order to reduce friction and avoid air pressure loss (a minimum 32 mm, or $1\frac{1}{4}$ in., inside diameter air hose is usually recommended). A 15% production loss can result from a 69 kPa (10 psi) drop in pressure. The air hose should also be as short as practical to reduce leakage and should contain as few couplings as possible.
The blasting machine or sandpot is a pressurized container that holds the abrasive. A valve at the bottom measures and controls the amount of abrasive fed into the blast hose. Efficient abrasive blast operations require the right size pot for the job, which enables very few refill stops, and the releasing of an even flow of abrasive with the air stream. A deadman control valve is a required safety feature for operation of the blast pot.
To start the machine, the operator presses down on the deadman valve with one hand; this allows the air inlet valve to open and the air outlet valve to close, at which time blasting begins. Should the operator want to stop the operation, releasing hold on the deadman valve closes the air inlet valve, shutting off any incoming air from the compressor to the machine and instantly opening the bleed-off or depressurizing valve.
Consider the possibility of an operator who faints, collapses, or falls off the scaffold. This person may be within the range of the nozzle, which, in effect, is an automatic shot gun. Many injuries have been caused by such incidents. With remote-control deadman valves, the machine shuts off the moment the grip on the nozzle is relaxed.
The blast hose connects the blast pot and nozzle and carries both air and abrasive. It is treated to prevent electrical shock by the installation of a grounding line. Sturdily constructed, multiple- ply hose with a minimum inside diameter of 32 mm ($1\frac{1}{4}$ in.) is required in most work. A short length of lighter, more flexible hose with a 25 or 32 mm (1 or $1\frac{1}{4}$ in.) inside diameter is sometimes joined in at the end. These sections, called *whips,* are easier to handle and are effective for work in areas with many angles, pipes, and stiffeners. The use of whips, however, effectively reduces the pressure at the nozzle and cancels the advantage gained by a large-diameter blast hose; therefore, their use should be discouraged except where necessary.
The nozzle is a major element in the blasting operation. Nozzle sizes are identified by the diameter of the orifice. Diameters are measured in sixteenths of an inch. A 4.8 mm ($\frac{3}{16}$ in.) diameter orifice is designated No. 3; a 7.9 mm ($\frac{5}{16}$ in.) diameter nozzle, No. 5; and so forth. Nozzles are commonly available up to 12.7 mm ($\frac{1}{2}$ in.) (No. 8) in diameter. The rate of surface cleaning is a function of the volume of air pushed through the nozzle at high pressure. For example, if a cleaning rate of 9 m^2/h (100 ft^2/h) can be attained with a 6.4 mm ($\frac{1}{4}$ in.) nozzle, a rate of 37 m^2/h (400 ft^2/h) can be attained with a 12.7 mm ($\frac{1}{2}$ in.) nozzle. However, the nozzle can be too large for the air volume. This results in insufficient air pressure, and production drops. Therefore, nozzle size should be as large as permitted by the air supply to maintain air pressure of 620 to 690 kPa (90 to 100 psi) at the nozzle.
Nozzles should use the venturi design, have as long a nozzle length as practical, use a tungsten carbide or other wear-resistant lining, and have as large an orifice size as possible with a given compressor. For difficult-to-reach places, nozzles also come in shapes such that they can propel abrasives around corners, in a 360° arc, or even backwards.
Moisture and Oil Separators. The large consumption of compressed air in an abrasive blasting operation introduces the problem of contamination by moisture (especially in high-humidity areas) and oil mists from

compressors. This is especially true of portable compressors. To combat this, an adequately sized moisture and oil separator should be installed at the blast machine (at the most distant point from the compressor). Separators are usually of the cyclone type and employ expansion chambers and small micron filters to eliminate up to 95% of moisture and contaminants. They require solvent cleaning to remove oil and regular replacement of filters.

Abrasives. The proper abrasive is the one that provides the necessary cleanliness and profile. The characteristics of such an abrasive related to performance include size, hardness, shape, and material.

Size. A large abrasive particle cuts deeper than a smaller particle of the same composition and shape and therefore provides a deeper surface profile. However, the greatest cleaning rate is achieved with the smaller abrasive because of a larger number of impacts per unit area.

Hardness. Hard abrasives generally cut deeper and faster than softer or brittle abrasives. A hard but brittle abrasive shatters on impact; this reduces its cleaning power accordingly.

Shape. The shape and size of abrasive grains determine the type of surface profile achieved by blast cleaning. Steel shot, because it is round, peens the surface to give a wavy profile. Therefore, shot is particularly effective at removing brittle deposits, such as mill scale. Grit, on the other hand, is angular, and when blast cleaning, produces a jagged finish that is generally preferred for coating adhesion. A wide variety of surface patterns are available from different grits. Use of sand and slag abrasives that are semiangular results in a pattern somewhat between that of shot and grit.

Materials. The abrasive should have a neutral pH, that is, between 6 and 8. It should not be washed with seawater or other contaminated water. Four types of abrasive materials are commonly used on a nonrecycled basis, as follows.

The first type of abrasives are the natural oxides. Silica sand is the most widely used natural oxide because it is readily available, low in cost, and effective. The hazards of sand have recently been elucidated by the Environmental Protection Agency and by the Occupational Safety and Health Administration, and the use of silica sand abrasives has been restricted in many areas. Another natural silica material has received attention in recent years. It consists of a blend of coarse and fine staurolite sands mined from certain mineral deposits in Florida. It is characterized as efficient cutting, and it has less dusting and a lower breakdown rate than silica sand.

Metallic abrasives are the second type. Steel shot and grit abrasives are efficient, hard, and dust-free, but care must be taken in their storage to prevent rusting. Although their initial cost is higher, they may be recycled many times to make them cost-effective. A mixture of both shot and grit abrasives in blasting may combine the advantages of both.

Slag abrasives are the third type. Copper and nickel abrasives are a by-product of the ore- smelting industry. Coal slags result from the burning of coal. These abrasives are fast cutting, but they have a high breakdown rate and are generally not recycled. Slag abrasives are most likely to exhibit an acidic pH.

Synthetic abrasives are the fourth type of abrasive. Aluminum oxide and silicon carbide are nonmetallic abrasives that have cleaning properties similar to the metallics, without the problem of rusting. They are very hard, fast cutting, and low dusting, but they are quite costly and must be recycled for economical use.

References cited in this section

1. “Preparation of Steel Substrates Before Application of Paints and Related Products— Visual Assessment of Surface Cleanliness— Part 1: Rust Grades and Preparation Grades of Uncoated Steel Substrates and of Steel Substrates After Overall Removal of Previous Coatings,” ISO 8501-1: 1988, International Organization for Standardization, 1988

2. “Preparation of Steel Substrates Before Application of Paints and Related Products— Visual Assessment of Surface Cleanliness— Part 2: Preparation Grades of Previously Coated Steel Substrates After Localized Removal of Previous Coatings,” ISO 8501- 2:1994, International Organization for Standardization, 1994

3. “Preparation of Steel Substrates Before Application of Paints and Related Products— Visual Assessment of Surface Cleanliness— Part 3: Preparation Grades of Welds, Cut Edges and Other Areas with Surface Imperfections,” ISO 8501-3:2001, International Organization for Standardization, 2001

4. “Preparation of Steel Substrates Before Application of Paints and Related Products— Collected Information on the Effect of Levels of Water-Soluble Salt Contamination,” ISO/ TR 15235:2001, International Organization for Standardization, 2001

K.B. Tator, Paint Systems, *Corrosion: Fundamentals, Testing, and Protection*, Vol 13A, *ASM Handbook*, ASM International, 2003, p 836–844

Paint Systems

Kenneth B. Tator, KTA-Tator, Inc.

Coating Application

In a most basic sense, coating application can be described as getting the paint from the can to the surface being coated. There are a number of ways of accomplishing this, and often the type of paint material determines the selection of the most appropriate method. For example, zinc-rich coatings should always be sprayed (except for very small areas), and agitation must be used when spraying to keep the heavy pigment particles from settling. Vinyls and chlorinated rubbers are not usually formulated for brush or roller application, and they too should be sprayed. On the other hand, alkyds and oil-based coatings are often applied by brush or roller but can be readily sprayed as well. For most corrosion-protective coating systems, airless or conventional spraying is preferred; spraying deposits a more uniform film with greater thickness control and a better appearance. The rate of application is much faster with spraying, particularly airless spray, than with brush and roller application. The more common application techniques and equipment are described subsequently.

Brushing

Brushing is an effective, relatively simple method of paint application, particularly with primers, because of the ability to work the paint into pores and surface irregularities. Because brushing is slow, it is used primarily for smaller jobs, surfaces with complex configurations (edges, corners, cuts, and so on), or where overspray may constitute a serious problem. The other disadvantage of brushing is that it does not produce a very uniform film thickness. Natural brush bristles of good quality are preferred, but synthetic bristles resistant to strong paint solvents can also be used. Bristles that are naturally or artificially flagged, that is, with split tips, are preferred, because they hold more paint. Nylon and polyester bristles are more water resistant than natural fibers and are preferred for latex paints.

Paint Mitts. A paint mitt can hold more paint than a brush and is faster, but it produces a very nonuniform thickness. Therefore, paint mitts are generally used only for hard-to-reach areas or oddly shaped objects, such as small pipes and railings.

Rolling

Rollers are best used on large, flat areas that do not require the surface smoothness or uniformity achievable by spraying. Rollers are also used in interior areas where overspray presents a cleaning and masking problem. However, the brush is preferred over a roller for applying primers because of the difficulties in penetrating pores, cracks, and other surface irregularities. In rolling, air mixes with the paint and leaves points for moisture to penetrate the cured film. Rolling is generally more suitable for topcoating a primer that has been applied by some other method.

The nap (fiber length) of a roller normally varies from 6.4 to 19 mm ($\frac{1}{4}$ to $\frac{3}{4}$in.). A longer nap holds more paint but does not give a smooth finish; therefore, it is used on rough surfaces. Rollers with extralong naps (32 mm, or $1\frac{1}{4}$ in.) are used for chain-link fencing. Handle extensions up to 3 m (10 ft) in length or longer allow a painter

to reach otherwise inaccessible areas, but the net effect is usually a reduction in the quality of the application. High-performance coatings for immersion service are seldom applied by roller because of nonuniform thickness, wicking caused by roller residue, and the rapid drying properties of some coatings, such as vinyls.

Spray Painting

Spray painting of coatings results in a smoother, more uniform surface than that obtained by brushing or rolling, because these application methods tend to leave brush or stipple marks and irregular thicknesses. The most common methods of spray painting are conventional and airless.

The conventional spray method of spraying relies on air for paint atomization. Jets of compressed air introduced into the stream of paint at the nozzle break the stream into tiny droplets that are carried to the surface by the current of air.

Because large amounts of air are mixed with the paint during conventional spray application, paint losses from bounce back or overspray can be high. Such losses have been estimated to be as much as 30 to 40%, depending on the configuration of the substrate. However, the ability to vary fluid and air independently gives conventional spray the versatility to provide a wide choice of pattern shapes and coating wetness by infinitely varying the atomization at the gun. Spray gun triggering is more easily controlled for precise spraying of irregular shapes, corners, and pipes than with airless spray. Conventional spraying provides a finer degree of atomization and a higher quality surface finish than airless spray gives.

However, some of the disadvantages of conventional air spray application are:

- It is slower than airless application.
- More overspray results than with other methods.
- It is hard to coat corners, crevices, and so on, because of blowback.

Nonetheless, conventional spray is still one of the most frequently used application methods. The equipment required for conventional spray application of coatings is discussed subsequently.

Air compressors can be of various types, with the size usually dependent on the amount of air required to operate the spray gun. Hoses must be properly sized to deliver the proper amount of air volume and pressure to the gun. It takes approximately 276 to 414 kPa (40 to 60 psi) and 0.25 m^3/min (8.5 ft^3/min) to operate most production spray guns with medium-viscosity paint.

An oil and moisture separator should be set up between the air compressor and the paint pot to prevent moisture and oil from getting into the paint and ruining the quality of the finish. This component of the conventional spray setup should be considered as a standard item that cannot be omitted, because of potential paint contamination and equipment damage.

Pressure Feed Tanks (Paint Pots). The amount of fluid material delivered to the spray gun is regulated by the pressure set by the fluid pressure regulator of the feed tank pressure pot. The pressure pot should contain 19 to 38 L (5 to 10 gal) of paint for most jobs. Pressures of 55 to 83 kPa (8 to 12 psi) at the gun are commonly used; excessive fluid pressure can cause the fluid stream to exit the fluid nozzle at too high a velocity for the air jets in the nozzle to atomize the fluid stream properly.

Connecting Hoses. Two hoses are used in conventional air spray painting: the air hose and the fluid hose. Air hoses supply air from the compressor to the paint pot and should be at least 12.7 mm ($\frac{1}{2}$ in.) in inside diameter. The air hose from the paint pot to the spray gun should be 6.4 to 7.9 mm ($\frac{1}{4}$ to $\frac{5}{16}$in.) in inside diameter and as short as possible.

The fluid hose usually has a solvent-resistant liner. It should have a 7.9 to 9.5 mm ($\frac{5}{16}$ to $\frac{3}{8}$in.) inside diameter for medium-viscosity materials and should be as short as possible. Hoses with inside diameters up to 12.7 mm ($\frac{1}{2}$ in.) are commonly used. Excessive hose length allows the solids to settle in the line before reaching the spray gun. This leads to clogging and the application of a nonhomogeneous film.

The spray gun is used to atomize the paint by mixing it with air under pressure in order to apply the coating material to the surface. Various spray patterns can be obtained by changing the volume of both air and fluid. The selection of the fluid nozzle and the needle size is another way to regulate the amount of paint exiting the fluid nozzle. If it is found that excessive amounts of paint are flowing through the fluid nozzle at low pressures

(55 to 83 kPa, or 8 to 12 psi), the fluid- adjusting knob can be used to reduce the flow, or a smaller fluid nozzle/needle combination may be needed. Paint manufacturers normally recommend at least one set of sizes known to work for their product.

Airless spray provides a rapid film build, greater paint flow into surface irregularities, and rapid coverage. In airless spraying, paint is forced through a very small nozzle opening at very high pressures to break the existing paint stream into tiny particles (similar to water exiting a garden hose). Because of the high fluid pressure of airless spray, paint can be applied more rapidly and at greater film builds than in conventional spraying. The high-pressure paint stream generated by airless spray penetrates cavities and corners with little surface rebound. If airless spray is used, proper spraying technique is essential for quality paint films. Poor technique can result in variations in paint thickness, holidays, and a host of other film defects in addition to wasted time and materials.

Some of the advantages of airless spray as compared with conventional spray include:

- Higher film builds are possible (heavier coatings).
- Less fog or rebound
- Easier to use by the operator, because there is only one hose
- Higher-viscosity paints can be applied.
- Easier cleanup

The disadvantages of the airless spray process include:

- Relies on dangerous high pressure
- Fan pattern is not adjustable.
- Many more working parts that can cause difficulty
- Higher initial cost than other forms of spraying
- Requires special care to avoid excessive buildup of paint that causes solvent entrapment, pinholes, runs, sags, and wrinkles

The equipment and materials for airless spraying are discussed subsequently.

Power Source. An electric motor can be used instead of an air compressor to drive the fluid pump. The electric airless is a self-contained spray outfit mounted on wheels and designed to use commercial 115 V electrical power.

An air compressor, usually with a 1 hp, 690 kPa (100 psi) electric motor or a $1\frac{1}{2}$ hp gasoline engine, is required to operate one gun with a 0.46 mm (0.018 in.) tip. For two or more guns or heavy materials, a greater capacity is needed.

Air Hose and Siphon Hose. A 12.7 mm ($\frac{1}{2}$ in.) inside diameter hose is generally used to deliver air from the compressor to the pump. The most common hose length is 15 m (50 ft). However, as hose length and pump size increase, the inside diameter of the hose must be increased as well.

A siphon hose is required, and it must have an inside diameter of 12.7 to 19 mm ($\frac{1}{2}$ to $\frac{3}{4}$in.) to provide adequate fluid delivery. Also, the hose material must be resistant to the fluid solvent and other materials. A paint filter should be used to prevent dirt from clogging the fluid hose and tip. This hose is often eliminated, and the pump is immersed directly into the paint.

High-Pressure Fluid Pump. The fluid pump is the most important part of the hydraulic airless system; it multiplies the air input pressure to deliver material at pressures up to 31 MPa (4500 psi). Pumps are offered with delivery ranges from 0.8 L/min (28 oz/min) (one gun) up to 11.4 L/min (3 gal/min) (three to four guns). The pump used for many airless outfits converts 0.45 kg (1 lb) of air input into 13.5 kg (30 lb) of fluid pressure. This is referred to as a 30 to 1 ratio. Pump ratios as high as 45 to 1 are common.

Some airless spray units use an electric-hydraulic power pack. These units can supply two guns with airless spray tips of up to 0.53 mm (0.021 in.) and long spray lines, or one gun for high-volume delivery with an airless tip of up to a 0.79 mm (0.031 in.) orifice. These electric units are wheel mounted and use a long-stroke slow-speed pump. The unit is equipped with an explosion-proof motor and can deliver as much as 3.8 L/min (1 gal/min) at pressures up to 21 MPa (3000 psi).

A paint filter should be attached to the pump at the fluid hose connection. The filter prevents dirt and particles from clogging the gun and being sprayed onto the work surface.

The fluid hose is made to withstand high operating pressures. It is made of vinyl-covered, reinforced nylon braid and can handle approximately 2040 kg (4500 lb) of pressure. The hose is designed to resist the solvent action of the various coatings being sprayed. A wire is often molded into the hose assembly to prevent any possible static electrical charge. The hose inside diameter should be at least 6.4 mm ($\frac{1}{4}$ in.), and the length should not be longer than necessary to do the work (ideally, 15 to 30 m, or 50 to 100 ft). Fluid hose diameters up to 12.7 mm ($\frac{1}{2}$ in.) are commonly used.

The airless spray gun is designed for use with high fluid pressures. It is similar in appearance to the conventional gun but has a single hose for the fluid. The hose may be attached to the front of the gun or to the handle. Atomization occurs when fluid is forced through the small orifice in the spray tip at high pressures.

A variety of spray tips are available to suit the type of material being sprayed and the size of spray pattern desired. The orifice, or hole, in the tip and the fan angle control the pattern size and fluid flow. There are no controls on the gun itself. Tip orifices vary to fit the viscosity of the paint being applied; fan angles range from 10 to 95°.

K.B. Tator, Paint Systems, *Corrosion: Fundamentals, Testing, and Protection*, Vol 13A, *ASM Handbook*, ASM International, 2003, p 836–844

Paint Systems

Kenneth B. Tator, KTA-Tator, Inc.

Quality Assurance

To obtain the desired protection of a metal substrate from a coating system, it is important not only to choose the proper coating materials but also to ensure that they are properly applied. On most jobs, such assurance is provided by a reputable painting force, or contractor, but on many other jobs, surveillance by plant personnel or thorough inspection by independent third- party organizations is done. In all cases, the rudiments of quality are the same:

- Proper masking and protection of surfaces not to be blast cleaned or painted
- Removal of rust and contaminants and suitable roughening of the surface
- Application of the specified coating system to the proper thickness
- Observation of application parameters, such as minimum and maximum temperatures, interval between coats, and induction times
- Verification of proper hardening or cure of the coating
- Testing to ensure that defects such as pinholes, skips, or holidays are minimized or avoided
- Tests for adhesion, color, gloss, and other parameters that may affect appearance or protective capability of the coating

Coating inspection requires training, experience, and familiarity with the instrumentation the inspector must use. Inspector training courses are available, and certification of inspectors is available from some training organizations, such as NACE International. A brief overview of some of the more common coating inspections and inspection equipment is subsequently presented.

Inspection Sequence

Inspection often begins with a prejob conference at which the ground rules are set, but when the work begins, the inspector is responsible for witnessing, verifying, inspecting, and documenting the work at various

inspection points. The inspector should be aware of the following inspection points and should witness or conduct the operation if feasible:

- Presurface preparation inspection
- Measurement of ambient conditions
- Evaluation of compressed air cleanliness and surface preparation equipment
- Determination of surface preparation, cleanliness, and profile
- Witnessing coating mixing and thinning
- Inspection of application equipment
- Inspection of coating application
- Determination of wet-film thickness
- Determination of dry-film thickness
- Evaluating cleanliness between coats
- Pinhole and holiday testing
- Evaluation of adhesion and cure

Presurface Preparation Inspection. Prior to the start of surface preparation and other coating activities, it is necessary to inspect the base in order to determine if the work is ready to be prepared and painted. Heavy deposits of grease, oil, dust, dirt, and other contaminants must be removed. Removal of this miscellaneous debris before blast cleaning ensures that these materials are not redeposited onto the freshly blast-cleaned surfaces.

In addition, the specifications may require that weld spatter be ground or otherwise removed and that sharp edges be rounded (customarily to a 3.2 mm, or $\frac{1}{8}$in., radius). Unusual pitting in the steel substrate should be examined; the pits are either accepted as they are or are ground or filled. Areas that do not need to be cleaned or coated should be masked to protect them from the cleaning and coating operations.

Measurement of Ambient Conditions. Before final blast cleaning and before any paint is applied, the inspector or painter should check the ambient and expected weather conditions. This is especially important in the early morning when the weather is changing or during seasonal changes when condensation is common. The presence of a thin film of condensed moisture on the surface may be visually imperceptible, but a quick check of the dew point and the surface temperature determines if such a condition exists.

Dew point is calculated by using temperature readings from a psychrometer and the appropriate psychrometric tables. A psychrometer is an instrument used for determining relative humidity and dew point. The temperature of the surface to be coated should be at least 3 °C (5 °F) higher than the dew point. The temperature must be within the range specified by the coating manufacturer.

Evaluation of Compressed Air Cleanliness and Surface Preparation Equipment. The air supply should be tested for cleanliness at frequent intervals during the day. This is done by holding a blotter or cheesecloth in the air stream for a minimum of 2 min. The blotter or cheesecloth should be held at a distance of 0.5 to 0.6 m (18 to 24 in.) from the source of the air stream being tested. The test material should be examined immediately after the test is complete for evidence of contamination by oil or moisture. Examination should be made visually as well as by touching and smelling the test material. If there is no discoloration on the blotter, the air quality is excellent, while moisture and oil on the blotter indicate unsatisfactory air.

Determination of Surface Preparation, Cleanliness, and Profile. Surface preparation is believed to be the most important factor affecting the performance of the coating. Any compromise in surface preparation usually reduces the performance of the applied material as well. The primary goals of surface preparation are, first, to provide a satisfactory, clean surface free of detrimental contaminants and, second, to provide an anchor pattern and to increase the steel surface area to improve bonding of the applied coating or lining to the steel surface.

Surface cleanliness should be inspected visually to verify that it is in conformance with the specified cleanliness standard.

The removal of invisible water-soluble salts may be assessed by a number of test protocols, all of which dissolve the salt from a known unit area of the surface being painted and measure its concentration.

Surface profile can be determined by using any of several instruments, including surface profile comparators, which give a visual and tactile comparison to a known profile; replica tape with a spring micrometer, in which a tape is pressed into the valleys of a profile and the profile height measured with a micrometer; and dial surface

profile gages, where the base of a depth micrometer rests on the profile peaks while a needle penetrates into the valleys.

Witnessing Coating Mixing and Thinning. Before a coating can be applied to a substrate, it must be thoroughly mixed to ensure that the material is homogeneous. During storage, most coatings tend to show some separation of the lighter and heavier components. Heavier pigments settle to the bottom of the can and sometimes appear as a hard cake, while other materials settle as a soft sludge. Some binders and some paints curdle or gel when stored for too long a period. Stirring may reconstitute the paint to a homogeneous liquid; if not, then the paint must be discarded.

Inspection of Application Equipment and Techniques. A lack of cleanliness is the predominant failure associated with spray guns and spray pumps. Paint chips or residues of previous coating materials can lodge in the pump, lines, or guns and cause clogging. Cleanliness of mixing equipment, lines, spray pots, guns, tips, and other application equipment is important and necessary.

During application, the safety and respiration equipment of the operator should be verified to be in working order, and the spray technique should be reviewed. For example, is the spray gun the proper distance from the work? Is there pattern overlap, uniform speed, and triggering before and after each stroke? Is the gun perpendicular to the surface?

Wet-film thickness readings are used as an aid to the painter in determining how much material to apply to the surface in order to achieve the specified dry film. Wet-film thickness gages are of value only if one knows how heavy a wet film to apply. The wet-film thickness/dry-film thickness ratio is based on knowing the percent solids by volume of the specific coating material:

$$\text{Wet-film thickness} = \frac{\text{Desired dry-film thickness}}{\text{\% solids by volume}}$$

If the paint is thinned at the time of use:

$$\text{Wet-film thickness} = \frac{\text{Desired dry-film thickness}}{(\text{\% solids by volume})/(100\% + \text{\% thinner added})}$$

Dry-film thickness measurements are made after complete drying of the coating. They are used to determine if the desired coating thickness is obtained. Dry-film thickness gages for steel surfaces are almost always of the magnetic type. If properly calibrated and operated, they have an error of only approximately 5 to 15% at normal temperatures (-18 to 100 °C, or 0 to 212 °F). Dry-film thickness instruments fall into four basic categories, as follows.

Magnetic pull-off instruments rely on the attraction of a magnet to an underlying steel surface. The stronger the attraction, the greater the force necessary to pull off the magnet. This pulling force can be calibrated to indicate coating thickness.

Magnetic fixed probe instruments measure the strength of the magnetic flux in a steel substrate exerted by a permanent magnet. Thickness can be measured by nulling the wheatstone bridge circuitry at various known thicknesses.

In eddy current inspection, a fluctuating electrical current induces residual eddy currents in an underlying metallic (aluminum, copper, stainless steel, and so on) substrate. The strength of the induced currents is a function of the distance of the induction probe from the substrate, that is, separation by paint thickness. The strength of the induced eddy current is measured and converted into paint thickness.

Destructive Inspection. The most common instrument for destructive coating thickness measurement cuts a small “V” into the paint at a known angle. By measuring the width of the slope of the “V” incision, a measurement of coating thickness can be obtained. The advantage is that each coat of a multiple-coat system can be measured and that thickness measurement is independent of substrate (steel, concrete, wood, and so on).

Evaluating Cleanliness Between Coats. When a multiple-coat system is to be applied, the surface between coats should be examined to ensure that all grease, oil, dirt, bird droppings, pebbles, sand from abrasives, dry spray, and the like have been removed before the application of the next layer of coating.

Pinhole and Holiday Testing. Many coating systems, particularly those for immersion or splash zone service, require additional testing with holiday detectors after the coating has dried. Pinhole and holiday detectors are of two basic types: low-voltage wet sponges and direct current high voltage. The basic function of a holiday tester

is to detect minute pinholes, holidays, skips, or misses in coating systems, all of which can cause premature coating failure.

The low-voltage (30 and 67.5 V are common) wet-sponge holiday detectors are used for locating discontinuities in nonconductive coatings applied to metal bases. The low-voltage detector is suitable for use on coatings up to 0.5 mm (20 mils) in thickness. The basic unit consists of the detector, a ground cable, and a sponge electrode. The ground cable is firmly attached to the bare substrate, and the sponge electrode is saturated with tap water. The electrode is moved across the entire surface at a speed of approximately 4.5 to 6 m/min (15 to 20 ft/min); the water permits a small current to flow through the pinholes down to the substrate. Once the current reaches the substrate, the circuit is completed to the detector unit, and an audible signal indicates that a pinhole or discontinuity has been found.

High-voltage holiday detectors basically function on the same operating principle as the low- voltage instruments described previously, except that a sponge is not used. The instrument consists of a testing unit that can produce various voltage outputs, a ground cable, and an electrode made of conductive neoprene, brass, or steel. High-voltage units are available up to 20,000 V and more. The rule of thumb for high-voltage detectors is to apply approximately 4000 V per mm (100 V per mil) of dry-film thickness. High- voltage detectors are used for nonconductive coatings applied to conductive substrates. The ground wire should be firmly attached to a section of the bare substrate and the electrode passed over the entire surface. A spark jumps from the electrode through the air gap down to the substrate at pinholes, holidays, and so on, simultaneously activating a signaling device in the unit.

Adhesion Testing. Occasionally, there is a need to test the adhesion of the coatings after application in the field. Different types of adhesion-testing methods are used, ranging from the simple penknife to the more elaborate tensile- testing units. The use of a penknife generally requires a subjective evaluation of the coating adhesion based on some previous experience. Generally, one cuts through the coating and probes at it with the knife blade, trying to lift it from the surface to ascertain whether or not the adhesion is adequate.

A modified version of this type of testing is the cross-cut test. The cross-cut test consists of cutting an “X,” or a number of small squares or diamonds, through the coating down to the substrate. Tape is then rubbed vigorously onto the scribed marks and removed briskly. The crosshatch pattern is evaluated according to the percentage of squares delaminated or remaining intact. A cross-cut guide can be used to cut a precision crosshatch pattern.

Another technique involves adhering a small dolly to the coated surface, scoring around the dolly periphery, and using a tensile-pulling device to pull it from the surface. The tensile pressure required to disbond, as well as the nature of the disbondment, is used to characterize adhesion.

Tests for Cure. The rate of cure of organic coating materials is affected by surface temperature, ambient conditions, coating formulation, and film thickness. Laboratory testing of paint chips is the only true means for verifying cure. Field techniques include the following.

Solvent Rub. On thermosetting cross-linked coatings, a clean cloth saturated with a strong solvent such as methyl ethyl ketone (MEK) or methyl isobutyl ketone (MIBK) can be used to rub the surface of the coating. If the material is properly mixed and cured, no color is transferred to the cloth. If the coating is improperly mixed or cured, it may partially redissolve, and the color is seen on the cloth. Of course, the solvent rub test cannot be used on certain solvent-sensitive coatings, such as alkyds, vinyls, and chlorinated rubbers.

Sandpaper Test. When a properly cured film is abraded with fine sandpaper, a fine, powdery residue is observed. Coating material that remains on the face of the sandpaper may indicate an uncured, slightly tacky coating.

Hardness Tests. A penetrating needle hardness tester or pencil hardness tester can be used to check film cure. The use of such instruments entails exerting a light perpendicular pressure on an instrument, which holds a hardened steel indenter ground to microscopic accuracy. The penetration of the spring-loaded indenter, which indicates hardness, is read directly from a scale dial. Pencil hardness is established by the lead hardness that just scratches the paint surface.

K.B. Tator, Paint Systems, *Corrosion: Fundamentals, Testing, and Protection*, Vol 13A, *ASM Handbook*, ASM International, 2003, p 836–844

Paint Systems

Kenneth B. Tator, KTA-Tator, Inc.

References

1. "Preparation of Steel Substrates Before Application of Paints and Related Products— Visual Assessment of Surface Cleanliness— Part 1: Rust Grades and Preparation Grades of Uncoated Steel Substrates and of Steel Substrates After Overall Removal of Previous Coatings," ISO 8501-1: 1988, International Organization for Standardization, 1988

2. "Preparation of Steel Substrates Before Application of Paints and Related Products— Visual Assessment of Surface Cleanliness— Part 2: Preparation Grades of Previously Coated Steel Substrates After Localized Removal of Previous Coatings," ISO 8501- 2:1994, International Organization for Standardization, 1994

3. "Preparation of Steel Substrates Before Application of Paints and Related Products— Visual Assessment of Surface Cleanliness— Part 3: Preparation Grades of Welds, Cut Edges and Other Areas with Surface Imperfections," ISO 8501-3:2001, International Organization for Standardization, 2001

4. "Preparation of Steel Substrates Before Application of Paints and Related Products— Collected Information on the Effect of Levels of Water-Soluble Salt Contamination," ISO/ TR 15235:2001, International Organization for Standardization, 2001

K.B. Tator, Paint Systems, *Corrosion: Fundamentals, Testing, and Protection*, Vol 13A, *ASM Handbook*, ASM International, 2003, p 836–844

Paint Systems

Kenneth B. Tator, KTA-Tator, Inc.

Selected References

- Chapters 3 to 5, in *Coating Inspector Training Course Manual,* KTA-Tator, Inc., 2002
- *Federation Series on Coatings Technology,* Federation of Societies of Coating Technology
- C.R. Martens, *Technology of Paints, Varnishes, and Lacquers,* Reinhold, 1968
- C.G. Munger and L.D. Vincent *Corrosion Prevention by Protective Coatings,* 2nd ed., National Association of Corrosion Engineers, 1999
- M.K. Snyder and D. Bendersky, "Removal of Lead-Base Bridge Paints," NCHRP Report 265, Transportation Research Board, 1983
- *Surface Engineering,* Vol 5, *ASM Handbook,* ASM International, 1994
- P. Swaraj, *Surface Coatings: Science and Technology,* 2nd ed., John Wiley & Sons, 1996
- K.B. Tator, Urethane Coatings: Influence of Chemical Composition upon Performance Properties, *J. Prot. Coatings Linings,* Vol 2 (No. 2), Feb 1985

E.B. Senkowski and K.B. Tator, Rubber Coatings and Linings, *Corrosion: Fundamentals, Testing, and Protection*, Vol 13A, *ASM Handbook*, ASM International, 2003, p 845–850

Rubber Coatings and Linings

E. Bud Senkowski and Kenneth B. Tator, KTA-Tator, Inc.

Introduction

THE PRINCIPAL RUBBER TYPES used in lining applications are presented in this article. The discussion includes relative performance properties, together with application, vulcanization, and inspection techniques. Relative material and installation costs are also presented.

E.B. Senkowski and K.B. Tator, Rubber Coatings and Linings, *Corrosion: Fundamentals, Testing, and Protection*, Vol 13A, *ASM Handbook*, ASM International, 2003, p 845–850

Rubber Coatings and Linings

E. Bud Senkowski and Kenneth B. Tator, KTA-Tator, Inc.

Rubber as a Protective Lining

Since 1839, when Charles Goodyear discovered the process known as *vulcanization,* whereby a soft, amorphous mass of natural rubber cross-linked into a resilient, elastomeric material with excellent elongation, modulus, and tensile strength, rubber has been used as a material in manufacturing. While the uses of rubber are many and varied, including the manufacture of vehicle tires, roofing materials, latex surgical gloves, erasers, pond liners, and many other products, it is the use of sheet rubber linings for corrosion protection that is covered herein. Rubber applied as a liquid for corrosion protection is discussed in the article "Organic Coatings and Linings" in this Volume.

Rubber, in the form of prefabricated sheets, has been used successfully as a lining material in storage tanks (Fig. 1), water boxes, condensers, flue gas desulfurization (FGD) units, chemical scrubbers, pipelines, mixers, valves, and pumps. Because of superior impact, abrasion, and chemical resistance, rubber linings in the range of 3 to 6 mm ($\frac{1}{8}$ to $\frac{1}{4}$ in.) thickness can often outperform conventional liquid-applied linings by a performance life of many years. In many installations, rubber linings have a service life expectancy of 25 to 30 years.

Fig. 1 A large, rubber-lined tank that requires on-site installation. Courtesy of Blair Rubber Company, Akron, OH

E.B. Senkowski and K.B. Tator, Rubber Coatings and Linings, *Corrosion: Fundamentals, Testing, and Protection*, Vol 13A, *ASM Handbook*, ASM International, 2003, p 845–850

Rubber Coatings and Linings

E. Bud Senkowski and Kenneth B. Tator, KTA-Tator, Inc.

Commercial Lining Products

Rubber lining products are manufactured in a broad range of compositions and configurations tailored to meet specific requirements for resistance to chemicals, abrasion, impact, and temperature. The comparative ability of various types of rubber to resist degradation is given in Table 1. The ability of various rubbers to resist environments is given in Table 2. Service temperatures and mechanical and physical properties for rubber lining materials are given in Table 3.

Table 1 Comparative ranking of rubber lining materials

Common name	ASTM D 1418 designation	Heat	Oxidation	Ultraviolet	Abrasion	Weathering	Oil	Motor fuels	Acid	Alkali	Flame
Natural rubber	NR	5	4	4	4	4	6	6	3	3	6
Styrene-butadiene	SBR	4	3	3	2	4	5	6	3	3	6
Nitrile	NBR	3	3	3	2	3	1	6	4	4	6
Chloroprene	CR	2	2	2	3	2	2	3	1	2	2
Chlorosulfonylpolyethylene	CSM	2	2	2	3	2	2	2	2	2	3
Isobutylene-isoprene (butyl rubber)	IIR	2	2	2	4	2	6	6	2	2	6
Ethylene-propylene-diene-terpolymer	EPDM	1	1	1	3	1	4	5	1	1	6
Chlorobutyl rubber	CIIR	2	2	2	4	2	6	6	2	2	3

Scale: 1, excellent, to 6, insufficient. Source: Ref 1

Table 2 Environmental resistance of common elastomers

Common name	ASTM D 1418 designation	Resistance to(a):									Permeability to gases
		Ozone	**Oxidation**	**Water**	**Alkalies**	**Hydrocarbons**			**Alcohol**	**Acids**	
						Aliphatic	**Aromatic**	**Halogenated**			
Butadiene rubber	BR	P	G	E	F-G	P	P	P	G	F-G	Low
Natural rubber, isoprene rubber	NR, IR	P	G	E	F-G	P	P	P	G	F-G	Low
Chloroprene rubber	CR	VG	VG	G	E	G	F	P	G	F-E	Low-medium
Styrene-butadiene rubber	SBR	P	G	E	F-G	P	P	P	G	F-G	Low
Acrylonitrile-butadiene (nitrile) rubber	NBR	P	F-G	E	F-G	E	G	P	VG	E	Very low
Isobutylene-isoprene (butyl) rubber	IIR	E	E	E	E	F	F-G	P	VG	G-E	Very low
Ethylene-propylene (-diene) rubber	EPM, EPDM	O	E	E	G-E	P-G	P	P-F	P-G	F-E	Medium
Silicone rubber	VMQ	E	E	E	P-F	P-G	P-G	F	F	G-VG	High
Fluoroelastomer	FKM	O	O	VG	F-G	E	E	G	VG	F-E	Low

(a) O, outstanding; E, excellent; VG, very good; G, good; F, fair; P, poor. Source: Ref 2

Table 3 Properties of common elastomers

Common name	ASTM D 1418 designation	Specific gravity	Mechanical properties							Service temperature (continuous use)	
			Shore durometer hardness	**Tensile strength, MPa (ksi)**	**Modulus, 100%, MPa (psi)**	**Elongation, %**	**Compression set (method B), %**	**Tear resistance**	**Abrasion resistance**	**min, °C (°F)**	**max, °C (°F)**
Butadiene rubber	BR	0.91	45A–80A	13.8–17.2 (2.0–2.5)	2.1–10.3 (300–1500)	450	10–30	Good	Excellent	-100 (-150)	95 (200)
Natural rubber, isoprene rubber	NR, IR	0.92–1.037	30A–100A	17.2–31.7 (2.5–4.6)	3.3–5.9 (480–850)	300–750	10–30	Good-excellent	Excellent	-60 (-75)	70 (160)
Chloroprene rubber	CR	1.23–1.25	30A–95A	3.4–24.1 (0.5–3.5)	0.7–20.7 (100–3000)	100–800	20–60	Good	Excellent	-50 (-60)	107 (225)
Styrene-butadiene rubber	SBR	0.94	30A–90D	12.4–20.7 (1.8–3.0)	2.1–10.3 (300–1500)	450–500	5–30	Fair	Excellent	-60 (-75)	120 (250)
Acrylonitrile-butadiene (nitrile) rubber	NBR	0.98	30A–100A	6.9–24.1 (1.0–3.5)	3.4 (490)	400–600	5–20	Good	Excellent	-50 (-60)	120 (250)
Isobutylene-isoprene (butyl) rubber	IIR	0.92	30A–100A	>13.8 (>2.0)	0.3–3.4 (50–500)	300–800	25	Good	Good	-45 (-50)	150 (300)
Ethylene-propylene (-diene) rubber	EPM, EPDM	0.86	30A–90A	3.4–24.1 (0.5–3.5)	0.7–20.7 (100–3000)	100–700	20–60	Fair-good	Good-excellent	-55 (-70)	150 (300)
Silicone rubber	VMQ	1.1–1.6	20A–90A	10.3 (1.5)	…	100–800	10–30	Fair-good	Poor	-117 (-178)	260 (500)
Fluoroelastomer	FKM	1.8–1.9	55A–95A	10.3–13.8 (1.5–2.0)	1.4–13.8 (200–2000)	150–450	15–30	Fair-very good	Good	-50 (-60)	260 (500)

Typically, rubber sheet is supplied at a thickness of 3, 4.75, and 6.35 mm ($\frac{1}{8}$, $\frac{3}{16}$, and $\frac{1}{4}$in.). Most industrial lining work uses 6.35 mm ($\frac{1}{4}$ in.) sheet stock. Standard widths of rolls are usually 1 and 1.22 m (42 and 48 in.) (Fig. 2). Most rubber manufacturers extrude the compounded rubber in sheets to a desired thickness. Many rubber sheets used for corrosion protection comprise two or more rubbers laminated together to form the finalized sheet in a process known as *calendering.* Sheet laminates made by calendering have the advantage that a tear or weak spot in one calender can be covered by other calendered layers. Thus, the strength, thickness, and other properties are more uniform, and pinholing through the lining is minimized. In addition, calendering allows different types of rubber sheets with distinct properties to be laminated into a single ply that can have improved performance over plies of identical sheets. A sheet with superior chemical, ultraviolet, or abrasion resistance can be laminated to a softer material that conforms better to an irregular substrate.

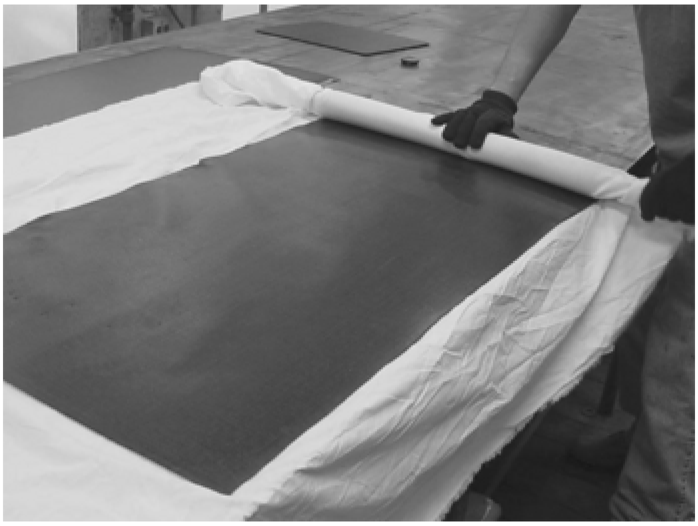

Fig. 2 Rolling out a rubber sheet. Courtesy of Blair Rubber Company, Akron, OH

References cited in this section

1. W. Hoffman, *Rubber Technology Handbook,* Hansner/Gardner Publications, 1996
2. Rubber and Elastomers, *Machine Design, 1995 Materials Selector Issue,* 12 Dec 1994, p 135–140

E.B. Senkowski and K.B. Tator, Rubber Coatings and Linings, *Corrosion: Fundamentals, Testing, and Protection*, Vol 13A, *ASM Handbook*, ASM International, 2003, p 845–850

Rubber Coatings and Linings

E. Bud Senkowski and Kenneth B. Tator, KTA-Tator, Inc.

Types of Rubbers

Rubbers can be categorized as natural rubbers and synthetic rubbers. Natural rubbers are manufactured from tree sap from the Far East. Synthetic rubbers were developed on a commercial scale by researchers of the War Production Board in the United States in the early 1940s as a substitute for the natural rubber sources that were under control of the Axis forces (notably Japan) during World War II. The chemical structures are given in Table 4.

Table 4 Chemical structures of common elastomers

Common name	ASTM D 1418 designation	Repeating unit structure	Comments
Butadiene rubber	BR		…
Natural rubber, isoprene rubber	NR, IR	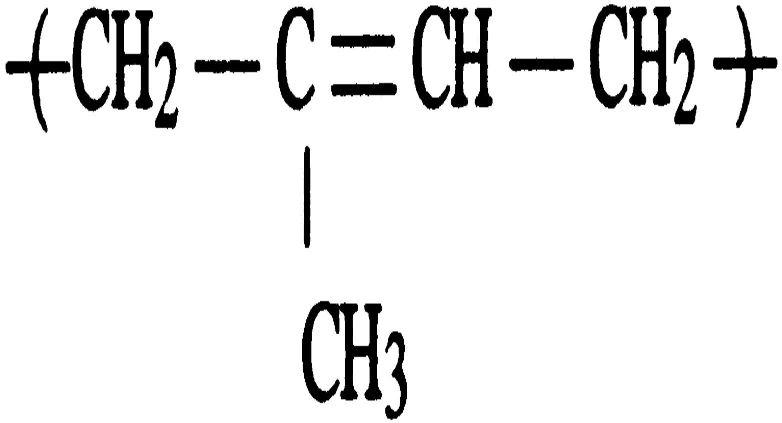	…
Chloroprene rubber	CR	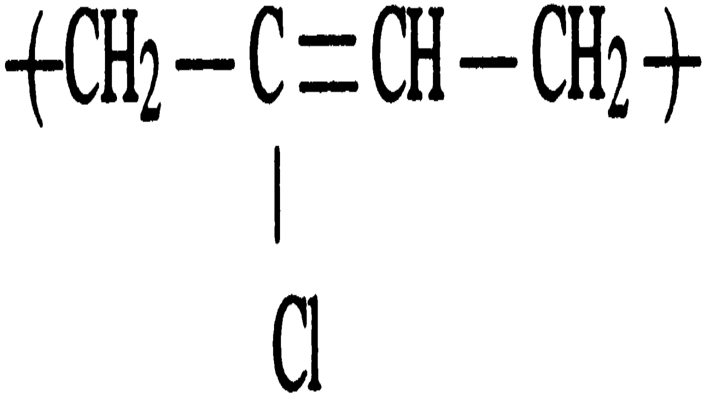	…

Styrene-butadiene rubber	SBR	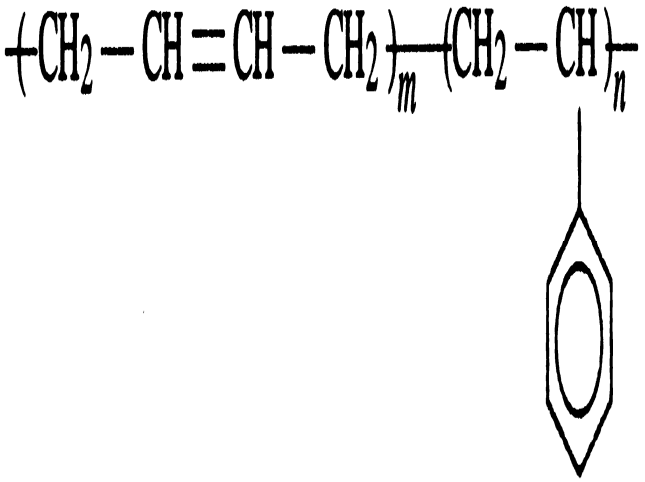	(a)
Acrylonitrile-butadiene (nitrile) rubber	NBR	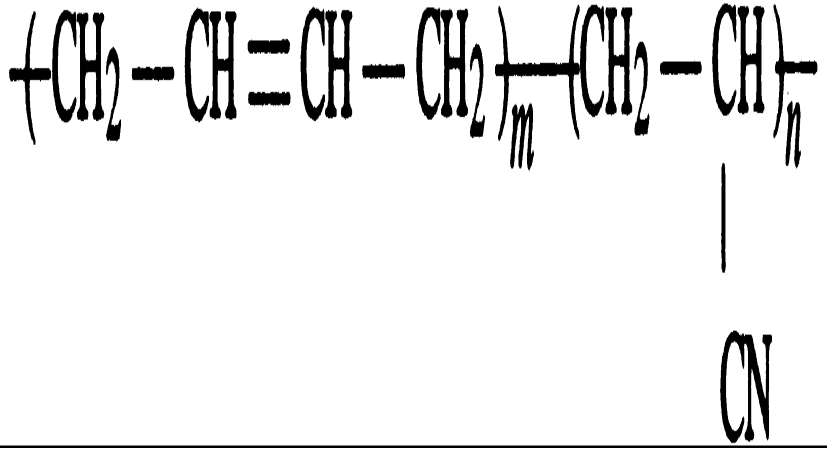	(b)

Isobutylene-isoprene (butyl) rubber	IIR	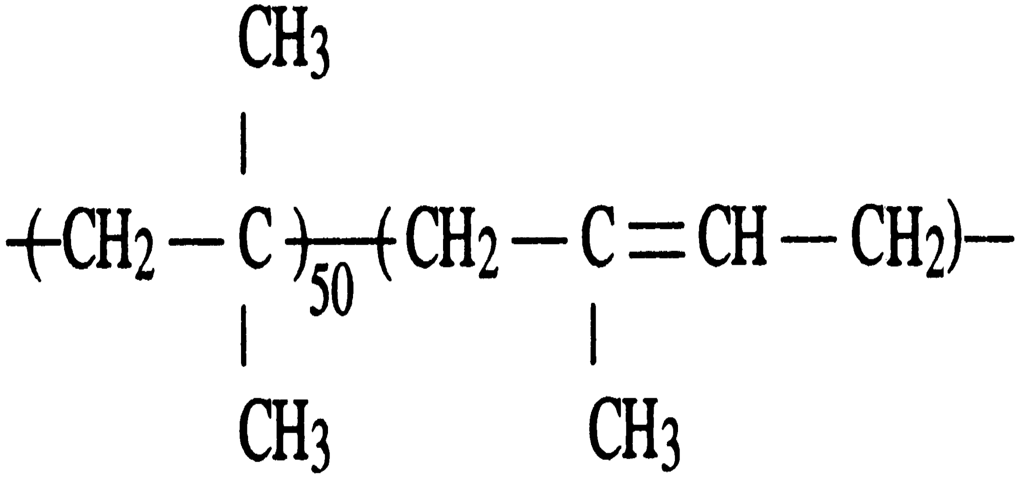	(c)
Ethylene-propylene (-diene) rubber	EPM, EPDM	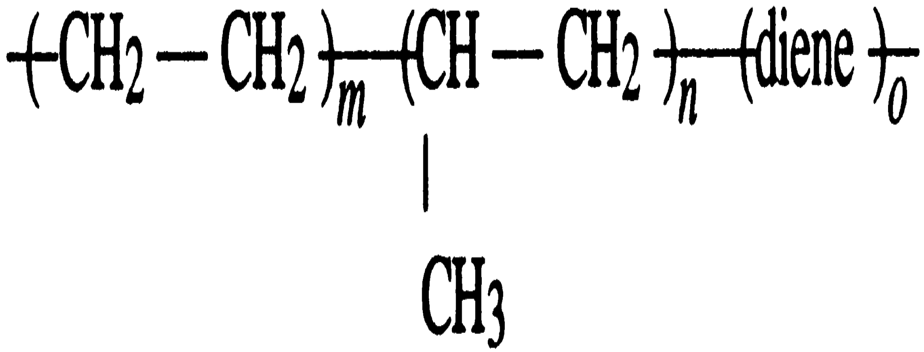	(d)
Silicone rubber	VMQ	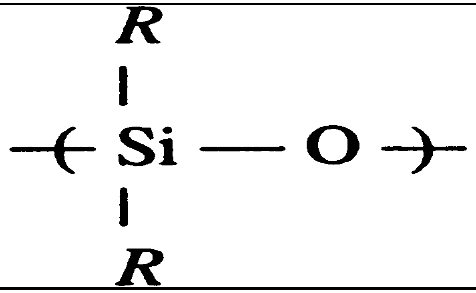	(e)

(a) Up to 50% styrene; 25% is most common (Ref 4).
(b) Acrylonitrile/butadiene ratios of 15:85 to 50:50 (Ref 4).
(c) 0.5–2.5 mol% isoprene to allow for vulcanization (Ref 4).
(d) m = ~1500, n = ~975, o = 25 for EPDM; o = 0 for EPM (Ref 5).
(e) R is typically an alkyl or aryl group. Source: Ref 3, 4, 5

Natural Rubber (NR)

The precursors of rubber and rubberlike compounds are examples of some of the earliest materials that civilized man learned to extract and process from plant sources. Many plants produce a milky sap that can be harvested, coagulated, and converted to a crude elastomer. The earliest natural rubber was named *caoutchouc,* and was derived from an East Indian word meaning *weeping tree.* The term survives today and is used to designate a family of raw, plant-derived, macromolecular compounds that can be converted to more complex, cross-linked materials. Caoutchoucs are the precursors to natural rubber (Ref 6). Modern analytical analysis has identified these materials as variations of naturally occurring polyisoprene. Latex-producing plants, of which there are hundreds, are found predominately in tropical climates. The plantation economies of Malaysia, Indonesia, and Thailand account for nearly 90% of the global production of raw natural rubber.

The collection and production of raw natural rubber from plantations rely principally on acid coagulation to concentrate the latex (caoutchouc). The raw plant sap (latex) is collected and processed in large tanks, where formic or acetic acid is introduced as the coagulating agent. Subsequent drying, curing, and rolling produce several different intermediate products called *smoked sheets* or *pale crepe* that are graded by color, purity, and strength. Both intermediates are the principal raw feedstock for natural rubber production.

Conversion of the raw natural rubber into usable products involves additional compounding and processing. Compounding introduces solid materials into the raw rubber that improve such properties as abrasion and tear resistance. Compounding ingredients include carbon black, curatives, accelerators, antidegradents to slow weathering deterioration, and other processing aids. Other fillers are used to alter density, color, and the cost. Compounding, involving the introduction of modifying organic and inorganic chemicals into the solid raw rubber mass, usually requires some level of high-shear processing known as *mastication.* The mastication takes place in twin-roll mills that also disperse the additions to the rubber mass, producing a homogeneous dispersion. The mixed rubber mass is then sent to sheeting mills, where the rubber shape and dimensions are reduced to facilitate end use.

Natural rubbers are compounded in three forms: soft, semihard, and hard. Soft NRs have excellent physical properties, such as tensile strength, abrasion resistance, and elongation. Soft NRs have good resistance to most inorganic chemicals, with the exception of strong oxidizing agents, to a temperature of 60 °C (140 °F). They are flexible and expand and contract with thermal variations of metal when attached to a metal substrate.

Semihard and hard natural rubbers exhibit better chemical and heat resistance than soft NR. These linings are applied where exposure to organic acids, inorganic acids, and chlorine gas is anticipated. The linings exhibit heat resistance of up to 93 °C (200 °F). The harder grades offer higher resistance to permeability but have less flexibility. Ebonite, which is the hardest of the natural rubbers, is a graphite-filled material resembling a thermoset plastic with a very high cross-linked density. The properties of ebonite are achieved by vulcanization in the presence of a high sulfur content. There is approximately a 10 to 1 ratio between the sulfur content of hard (ebonite) and soft natural rubbers. The hard rubbers can be machined after vulcanization to make acid-resistant seals, valves, and pump bodies. Hard rubbers resist extreme corrosive exposure from wet and dry chlorine gas. They offer chemical resistance to a broad range of chemicals at a level between 65 and 93 °C (150 and 200 °F).

Multiple-Ply Rubber. Multiple-ply rubber linings are the combination of two or three layers (plies) of soft and hard rubbers combined to achieve specific properties of flexibility, chemical resistance, and/or permeability resistance. The softer layers impart flexibility and allow maximum adhesion to the steel substrate. The exterior layer, which is frequently semihard or hard rubber, is selected for enhanced chemical resistance. Other layered arrangements may include a tie gum, which is an intermediate soft layer to promote the bonding of top and bottom layers.

Synthetic Rubber

Synthetic rubber is the general term used for rubber manufactured from other than natural (plant) feedstocks. In today's economy, the principal feedstock for synthetic rubber production is petroleum. The basic monomers for many synthetic rubbers are 1,3-butadiene, isobutylene, isoprene, chloroprene, and acrylonitrile. Following are characteristics of the principal synthetic rubber compounds used in lining applications.

Neoprene or Chloroprene Rubber (CR). Chloroprene (2-chlorobutadiene) rubber was initially compounded in 1939 as neoprene (Ref 7). Chloroprene rubber is a polar rubber because it contains a ratio of carbon atoms to

chlorine atoms of 4 to 1. Chlorine content also imparts better flame resistance, weatherability, and ozone resistance than experienced with diene rubbers. The swelling resistance of CR to mineral, vegetable, and animal oils is also better than the nonpolar diene-based rubbers. Chloroprene rubber has good resistance to paraffinic and naphthenic oils of high molecular weight but swells extensively in aromatic oils of low molecular weight. Chloroprene rubber is degraded (swells) by contact with motor fuels, but its resistance can be improved through higher levels of filler loading and degrees of cross-linking. In lining service, with general chemical exposure, CR has heat resistance to 65 °C (150 °F) with strong acids (sulfuric acid) and 93 °C (200 °F) with strong bases (sodium hydroxide).

Butyl rubber (IIR), a blend of isoprene and isobutylene copolymers, is, along with nitrile and neoprene, one of the oldest synthetic rubber lining products (Ref 8). The large-scale production of IIR began in 1943. Typically, the rubber exhibits a high level of heat and heat-aging resistance to 107 °C (225 °F). It has good resistance to a broad array of general chemical solutions at 82 to 93 °C (180 to 200 °F). Because IIR is nonpolar, it swells on contact with lubricating oils and fuels.

Chlorobutyl rubber (CIIR) is manufactured by the chlorination of IIR (Ref 1). Chlorobutyl rubber has better properties of heat resistance to 93 °C (200 °F), gas permeability, weatherability, and ozone than IIR has. Along with ethylene- propylene rubber, it is one of the most chemically resistant lining materials. Chlorobutyl rubber withstands exposure to the highly aggressive environments within FGD units and acid gas processing towers. Chlorobutyl rubber also provides good resistance to concentrated alkalis (NaOH) at 93 °C (200 °F) and wet chlorine gas to 126 °C (260 °F). Because CIIR is nonpolar, it swells on contact with lubricating oils and fuels.

Ethylene-propylene rubber (EPDM) is manufactured by the copolymerization of ethylene and propylene with the addition of a diene monomer to create an unsaturated rubber terpolymer (Ref 1). Sulfur added during vulcanization completes the cross-linking that produces a usable rubber product. Ethylene-propylene rubbers exhibit excellent heat, aging, and weathering resistance. The rubber exhibits excellent resistance to chemicals such as acids, alkalis, acetone, alcohol, hydraulic fluids, and steam. Service temperatures in the range of 82 to 93 °C (180 to 200 °F) are possible with EPDM. However, concentrated and/or strongly oxidizing acids may attack EPDM. The use in acid service depends strongly on operating temperature and acid concentration. Because EPDM is a nonpolar material, contact with aromatic and chlorinated hydrocarbons causes swelling.

Nitrile rubber (NBR) is a product formed by the copolymerization of acrylonitrile and butadiene. Many grades of NBR are available in which the acrylonitrile content varies from 18 to 51% by weight (Ref 6). The addition of acrylonitrile enhances swelling resistance and impermeability. Nitrile rubber is a polar-type rubber used where exposure to aliphatic hydrocarbons is a service condition. Nitrile rubber exhibits good resistance to swelling when immersed in liquids that are non- or weakly polar, such as gasoline, grease, mineral oil, and animal or vegetable fats and oils. Polar and aromatic solvents attack NBR. It should not be used with such aromatic solvents as benzene, toluene, or xylene. Nitrile rubber is less permeable to gases than is NR or styrene-butadiene rubber. However, it exhibits significantly improved heat and aging resistance to a level of 93 °C (200 °F).

Styrene-butadiene rubber (SBR) is a product formed by the copolymerization of styrene and butadiene. Many grades of NBR are available in which the styrene content varies from 23 to 40% by weight (Ref 1). Styrene-butadiene rubber has better heat resistance to 77 °C (170 °F) than NR has. Styrene-butadiene rubber has superior impact and abrasion-resistant properties. Its principal use is in troughs, chutes, hoppers, and ball mills to protect metallic substrates from mechanical damage. However, SBR also has good resistance to water and weak chemical solutions. As a nonpolar rubber, contact with aliphatic, aromatic, and chlorinated hydrocarbons causes swelling.

Chlorosulfonated polyethylene (CSM) is produced on a large scale by Du Pont, where it is marketed as Hypalon (E.I. Du Pont de Nemours & Co., Inc.). Hypalon is an amorphous, elastomer-like polymer that is fully saturated and exhibits excellent resistance to the effects of weathering, aging, ozone, and chemical degradation to 93 °C (200 °F). It has excellent resistance to high concentrations of sulfuric, nitric, chromic, and other strong oxidizing acids. Formulation variations that alter the chlorine content can optimize such properties as heat resistance, electrical resistivity, or flame resistance (Ref 1).

References cited in this section

1. W. Hoffman, *Rubber Technology Handbook,* Hansner/Gardner Publications, 1996

3. R.A. Higgins, *The Properties of Engineering Materials,* 2nd ed., Industrial Press Inc., 1994

4. Elastomers, *Van Nostrand's Scientific Encyclopedia,* 7th ed., D.M. Considine and G.D. Considine, Ed., Van Nostrand Reinhold, 1989

5. M. Morton, Elastomers, Synthetic, Survey, *Kirk-Othmer Encyclopedia of Chemical Technology,* 4th ed., Vol 8, Wiley-Interscience, 1993, p 905–923

6. A. Whelan and K.S. Lee, *Developments in Rubber Technology,* 1st ed., Elsevier Applied Science Publ., 1979; 2nd ed., 1982

7. F. Mark, N.G. Gaylord, and N.M. Bikales, Ed., *Encyclopedia of Polymer Science and Technology,* Interscience Publ., 1970

8. G.M. Blow and C. Hepburn, Ed., *Rubber Technology and Manufacture,* 2nd ed., Butterworth, London, 1972

E.B. Senkowski and K.B. Tator, Rubber Coatings and Linings, *Corrosion: Fundamentals, Testing, and Protection,* Vol 13A*, ASM Handbook,* ASM International, 2003, p 845–850

Rubber Coatings and Linings

E. Bud Senkowski and Kenneth B. Tator, KTA-Tator, Inc.

Vulcanization

Vulcanization (curing), a critical stage of processing, is necessary to enhance the performance properties of raw compounded rubber through cross-linking of its molecular structure. Cross- linking (polymerization) is accomplished through reaction with accelerators such as organic peroxides or sulfur that are mixed into the raw rubber base. Vulcanization is the conversion of gum-elastic, raw rubber material into a rubber-elastic end product (vulcanate). The degree of vulcanization is directly related to the degree of cross-link density achieved by the process. The properties of the rubber depend on the conditions of the vulcanization process and the choice of vulcanization chemicals. Important rubber properties, such as hardness, tensile strength, elongation, elasticity, low-temperature flexibility, and swelling stability, can be affected by vulcanization rate. Natural rubbers can be overvulcanized and undergo a decrease (reversion) in optimal cross-link density that results in a lowering of mechanical properties. Synthetic rubbers are less susceptible to overvulcanization due to prolonged heating. For this reason, many synthetic rubber formulations display improved resistance to thermal exposure and heat aging. The four basic methods for vulcanizing or curing rubber linings are autoclave, internal steam, atmospheric steam, and ambient (chemical cure).

Autoclave cure involves placing the object(s) to be covered or lined with rubber inside a pressure vessel termed an *autoclave.* A controlled and continuous flow of steam from a boiler is introduced into the vessel. At the start of the process, air is purged from the autoclave. The temperature and pressure are monitored carefully. Because an autoclave offers the best form of control over the vulcanization process, it offers the greatest potential for producing uniform and high-quality products. However, to achieve these goals, it is recommended that the autoclave be equipped with precise controls for air pressure and steam. Variations in steam pressure and temperature lead to undesirable anomalies in the cured rubber. Once started, an autoclave cure should never be interrupted. Prompt cooldown at the termination of cure is also important. Proper cooldown of the autoclave prevents postcuring and precludes the possibility of blistering and cracking hard rubbers. Chart recorders (Fig. 3) provide evidence of the temperature profile during the process.

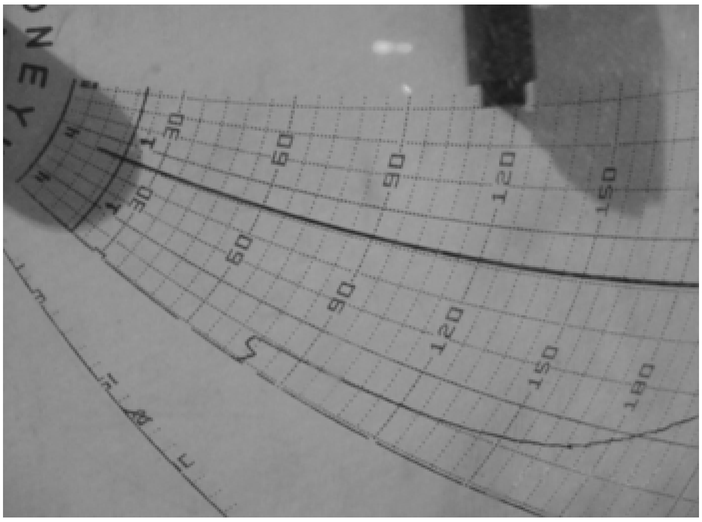

Fig. 3 Temperature chart recorder provides evidence of the proper temperature profile during curing. Courtesy of Blair Rubber Company, Akron, OH

While autoclaves can offer precise management of the vulcanization process, they have size limitations. Large tanks, water boxes, and other process equipment cannot fit inside. Rubber applied to these units must be vulcanized by other means.

Internal Steam Cure. Internal steam pressure vulcanization is used on vessels that are designed to operate at elevated pressures and are too large to be placed in an autoclave. By this method, units can be installed and the linings cured in place. Internal curing should be accompanied by the installation of drains and traps to collect steam condensate. Recording thermometers and pressure gages installed near the bottom of the vessel are used to monitor the process. Blind flanges should be installed at other openings. Bottom outlets should initially be left open to purge the vessel of air. Boiler capacity should be sufficient to raise the ambient temperature from ambient to cure temperature in a relatively short period. Long runs of uninsulated pipe between the boiler and lined vessel should be avoided. Once started, the vulcanization process should not be interrupted. Once the endpoint of the cure is reached, the vessel is cooled down by the introduction of air. Any steam-induced curing cycle should include an appropriate vacuum-break device to prevent a vacuum collapse of the vessel on cool down.

Atmospheric Steam Cure. Atmospheric steam normally is used for field vessels that have open tops or bottoms or that cannot withstand elevated pressures. With the case of open tanks, suitable temperature-resistant, steam-tight covers must be fabricated for all openings. Steam is introduced through an insulated steam line through a piping connection or opening in the top of the vessel. Provisions must be made to drain all condensate that collects at the tank bottom. Other outlets should be closed with blind flanges drawn up to within 0.79 mm ($\frac{1}{32}$ in.) of the flange rubber. Vulcanization at atmospheric pressure allows entrapped air under linings to form blisters. Some procedures call for a precure steaming period of 1h, followed by an internal inspection of the tank to locate and repair spontaneous blisters. In this method, entrapped air is removed by deflating the blister with a hypodermic needle and applying a small patch of uncured rubber. The vulcanization process then proceeds to completion.

Ambient (Chemical) Cure. Rubber is cured at ambient temperatures when heat cannot be applied to surfaces to achieve vulcanization. The method is used most commonly when patches must be applied to vulcanized rubber surfaces. A chemical cure may also be used when surfaces such as flanges are shielded from steam exposure. These methods expose the raw rubber to a sulfur-bearing chemical for a sufficient period to complete cure. The chemicals include carbon disulfide and sulfur dichloride. They are used as either a solution applied to the rubber surface or vapor form. Vulcanization is accomplished in periods of up to one week. If the vessel operates at temperatures of up to 65 °C (150 °F), the chemical cure can be shortened.

Self-Vulcanizing (Cold Cure). In the case of some on-site rubber linings where other curing methods are impractical, self-vulcanizing rubber sheets have been developed. The rubber in these sheets, specific soft rubber mixtures based on polychloroprene and halogenated butyl rubber, is mixed with curing agents, such that curing and cross-linking commences at ambient temperatures of approximately 25 °C (77 °F) at normal pressure levels. Because the rubber sheets are pliant and malleable on completion of the manufacturing process, they can

be handled and installed quite easily. However, because the rubber commences cross-linking at ambient temperature immediately at the time of formation into sheet material, refrigeration is necessary if there is a delay between manufacturing and installation and if the temperature exceeds 25 °C (77 °F). To achieve maximum cross-linking, approximately eight weeks at 25 °C (77 °F) are required. Forced curing at higher temperatures may reduce the vulcanization time to as little as two weeks, depending on the specific rubber mixture and elevation in temperature. Self-vulcanizing sheets can also be precured at elevated temperatures, stored indefinitely, and installed as fully vulcanized linings. As such, they are immediately resistant to the operational environment. Because of the difficulty of handling during installation, only soft rubber linings are used for this purpose.

E.B. Senkowski and K.B. Tator, Rubber Coatings and Linings, *Corrosion: Fundamentals, Testing, and Protection*, Vol 13A, *ASM Handbook*, ASM International, 2003, p 845–850

Rubber Coatings and Linings

E. Bud Senkowski and Kenneth B. Tator, KTA-Tator, Inc.

Rubber Lining Application

Once the proper type of rubber for a given service is chosen, it could be hung loosely similar to a bag in a tank. More commonly, the lining is made to conform and attach to the material it is protecting by applying it in five basic steps:

1. Prepare the surface for rubber application, usually by solvent cleaning and blast cleaning to remove all contamination and to roughen the surface for better adhesion.
2. Apply the adhesive system to the surface to be lined. The adhesive may be a single coat or a multicoat system.
3. Apply cut-to-fit rubber sheets to the surface, using rollers and stitchers to press out air pockets and to press the sheet into the adhesive.
4. Cure, or vulcanize, the rubber lining by steam in an autoclave, exhaust steam, or by chemical application to the rubber surface.
5. Inspect visually for bubbles or blisters and for pinholes, using a high-voltage holiday (spark) detector.

The tools of the trade are shown in Fig. 4.

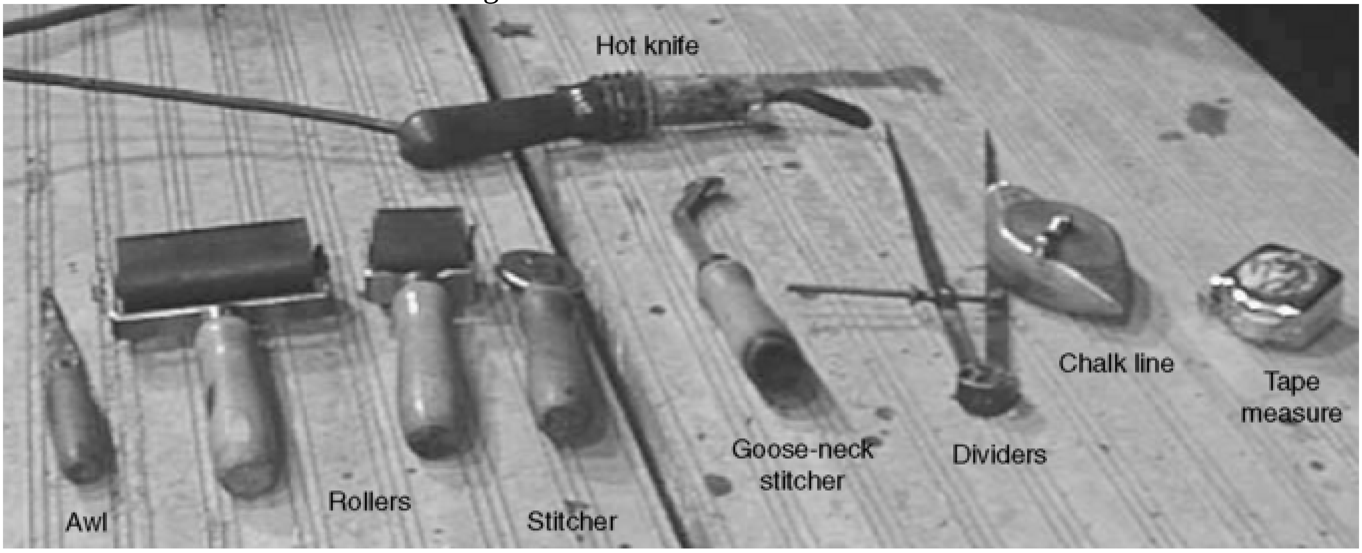

Fig. 4 Typical hand tools needed for custom installation of rubber lining. Courtesy of Blair Rubber Company, Akron, OH

Joints are usually necessary in lining work, because many sheet rubber materials are supplied in widths up to only 1.22 m (48 in.). Five methods of construction are typically used to join rubber panels, with the selection determined by the type of elastomeric used (Ref 9):

- *Butt joint:* a joint where the two rubber panels are laid edge to edge without any tapered mating surface. Butt joints are usually covered with an additional cap strip (Fig. 5).
- *Lap joint:* a joint where one rubber panel overlays the next. A minimum overlap of 50 mm (2 in.) is recommended at the joint (Fig. 5, 6).
- *Skive joint:* a joint where the edges of the rubber panels interface at an angle through their thickness. Skives should be cut at a 45° angle.
- *Closed skive joints:* a joint where a reverse 45° angle cut is made between the adjoining rubber panels. The reverse skive is the recommended joint for all rubber panels. It is required whenever a multilayer rubber sheet containing a tie gum is used. The reverse cut allows the installer to stitch down the cut edge, so that the tie gum is protected from chemical attack.
- *Stitching:* a method of joining two pieces of uncured rubber. It uses a hand-held tool called a stitching roller. The tool is a narrow wheel with a serrated edge that applies a continuous line of localized compression points to drive the rubber panel into the adhesive layer.

Joint construction should comply with both the specification and the manufacturer's recommendations for the rubber product used in the installation.

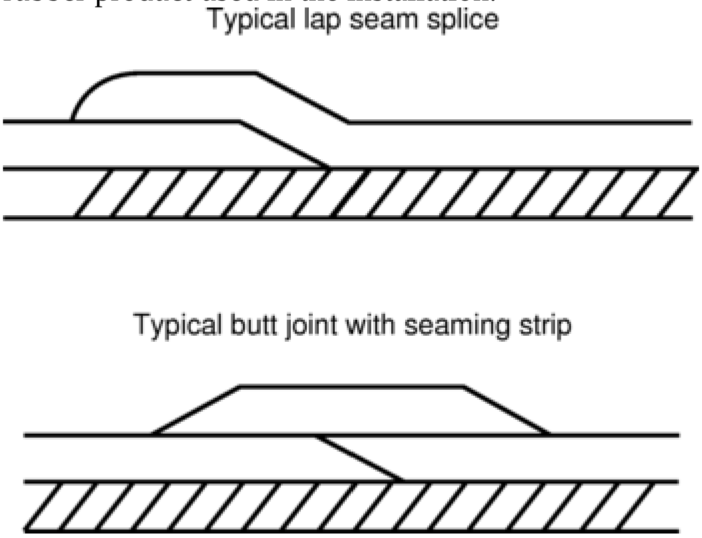

Fig. 5 Typical cross sections of lap and butt joints. Courtesy of Blair Rubber Company, Akron, OH

Fig. 6 Installed seam showing overlap. Courtesy of Blair Rubber Company, Akron, OH

Reference cited in this section

9. "Glossary of Terms," Bulletin 17-1986, Rubber Manufacturers Association, Washington, D.C., 1986

E.B. Senkowski and K.B. Tator, Rubber Coatings and Linings, *Corrosion: Fundamentals, Testing, and Protection*, Vol 13A, *ASM Handbook*, ASM International, 2003, p 845–850

Rubber Coatings and Linings

E. Bud Senkowski and Kenneth B. Tator, KTA-Tator, Inc.

Inspecting Rubber Lining Work

Inspection Before Lining. Surfaces to be covered with rubber should be cleaned by abrasive blasting to achieve a cleanliness equivalent to Steel Structures Painting Council specification SSPC SP-5, "White Metal Blast Cleaning" (Ref 10). The cleaned surfaces should have a minimum surface profile of 2 mils. The surfaces to be coated should be free of all oil, grease, mill scale, rust, corrosion products, oxides, or other foreign matter. Sharp edges and corners and weld splatter that could damage the liner must be removed. Primer should be applied immediately after cleaning and before any visible surface oxidation has occurred. Precautions must also be taken to avoid condensation when applying primers and cements to metallic surfaces. No operations should be conducted when the metal temperature is within 3 °C (5 °F) of the dew point.

Inspection during Lining Operations. The installation of a rubber lining system involves a series of steps. Each step requires surveillance to ensure that the specification representing the manufacturer's recommendations is being followed. Liquid primers, used to prepare the metal surface, and liquid cements, used to create an adhesive bond at the metal-rubber and rubber- rubber interfaces, are generally applied by hand brushing. It must be verified that the primers and cements specified for the rubber system, substrate, and service conditions being encountered are being used. Separate brushes and rollers should be maintained for each type of primer and cement used in the installation. In this work, the sequence of application, drying time, and selection of the mating surfaces is critical to the success of the work. The manufacturer's recommendations should be enforced diligently.

After the rubber sheet is applied to the cured cement, it must be rolled tightly against the metal to remove any trapped air and to ensure intimate contact across the metal-rubber joint. Joints should be examined to verify that the seams are straight and that all edges are stitched down tightly.

Inspection Before Cure. Immediately following the application of the rubber to the metallic surfaces, the lining should receive an inspection to ensure that the following parameters have been met:

- The lining should be checked to assure that the physical dimensions of protected surfaces and the thickness of linings comply with the requirements of the specification. Modifications are more easily made before the system has been cured (vulcanized). Unacceptable areas should be marked with chalk to indicate the need for corrective action.
- Prior to vulcanization, all lined surfaces should be inspected for blisters, wrinkles, pulls, lifted edges (bond failures), or surface defects. All splices (joints) in the lining system should be inspected for integrity and uniformity. Whenever layered rubber stock is used, stitched-down splices are necessary to protect the tie gum.
- Air trapped under the rubber sheet should be located and removed. Air bubbles can be located by lighting the surface from an oblique angle and looking for shadows cast by the high spots. The air can be released with a hypodermic needle and the site stitched down or patched. This step is especially important when atmospheric cures are used with no applied pressure to force out air or flatten the lining.
- The lining should be examined for pinholes, punctures, and cuts with a high-voltage spark tester (Fig. 7). Both the Rubber Manufacturers Association (Ref 11) and ASTM International (Ref 12) have written

standards for the spark testing of elastomeric sheet linings. High-frequency alternating-current-type spark testers, capable of producing sufficient voltages to achieve proper calibration, should be used. Voltages should comply with those recommended by the rubber manufacturer and will vary with thickness and rubber type. The inspection voltage range for most rubbers is between 10,000 and 15,000 V. Lined tanks must be purged of all volatile vapors and solvents before high-voltage spark testing is applied. Metal filings must not be allowed on the rubber.

Fig. 7 Spark testing for discontinuities. Probe is flexible wire to conform to surface while minimizing physical damage to rubber. Courtesy of Blair Rubber Company, Akron, OH

Postcure Inspection. Following completion of the vulcanization process, the rubber surfaces should be inspected for signs of obvious imperfections. These flaws may take the form of loose splices, trapped air, blisters, and breaks in the lining.

The hardness of the cured rubber should be checked with an appropriate durometer in accordance with a standard test procedure (Ref 13). Durometer (indentation hardness) measurements should cover the entire rubber surface. One reading per 10 m^2 (100 ft^2) of surface should be taken and recorded. The measurements should fall within the tolerances recommended by the manufacturer's specifications for the vulcanized product. Areas of the lining that fall below the manufacturer's tolerances should be isolated and cured through localized exposure to additional hot air or steam.

The retreated rubber surfaces should again be inspected, using the calibrated high-voltage spark tester. Pinholes and flaws located by spark testing should be repaired in accordance with specified procedures and vulcanized through exposure to hot air, steam, or infrared lamps. If cold patches are used, they should receive an appropriate chemically induced cure (Fig. 8).

Fig. 8 Patch repair of a defect in a rubber lining. Courtesy of Blair Rubber Company, Akron, OH

Postinstallation Inspection of Rubber Linings. Periodic inspections of rubber linings are usually conducted to determine if there are any flaws or lining anomalies that have developed during the course of operations within vessels, tanks, pipelines, and other lined equipment. Among the parameters that can be investigated are appearance, hardness, and electrical integrity.

Appearance. A visual inspection can be conducted to locate such lining anomalies as blisters, bubbles, open or loose seams and patches, pinholes, or discoloration. In steel tanks, breaks in the lining are often associated with corrosion products that cause localized disbondment and staining.

Hardness is measured by using either the Shore A or Shore D durometer on the cured (vulcanized) rubber system. Durometer measurements can be made to determine if there has been a significant change from the initial rubber hardness recorded after vulcanization and before vessel operation. These could be due to hardening from overheating or softening from exposure to aggressive chemicals.

Electrical Integrity. A high-voltage inspection can be conducted of the rubber-lined surfaces. However, such an inspection should only be made with the concurrence of the rubber manufacturer, using recommended AC or DC voltage levels (Fig. 7). Some rubber linings that have been in immersion or chemical service undergo resistivity changes from absorbed moisture and/ or chemicals. These changes either preclude the use of high-voltage inspection or require reduced voltages.

References cited in this section

10. “White Metal Blast Cleaning,” SSPC-SP5/ NACE 1, Steel Structural Painting Council, 1 Sept 2000

11. “Procedure for Spark Testing Elastomeric Sheet Lining,” Bulletin 13-1986, Rubber Manufacturers Association, Washington, D.C., 1986

12. “Practice for Discontinuity (Holiday) Testing of Nonconductive Protective Coating on Metallic Substrates,” D 5162, ASTM

13. “Test Method for Rubber Property-Durometer Hardness,” D 2240, ASTM

E.B. Senkowski and K.B. Tator, Rubber Coatings and Linings, *Corrosion: Fundamentals, Testing, and Protection*, Vol 13A, *ASM Handbook*, ASM International, 2003, p 845–850

Rubber Coatings and Linings

E. Bud Senkowski and Kenneth B. Tator, KTA-Tator, Inc.

Material and Installation Costs

Material costs for sheet rubber are in the range of \$32 to 86/m^2 (\$3.00 to 8.00/ft^2) (U.S. dollars in 2003) for 6.35 mm ($\frac{1}{4}$ in.) thick material. Most rubber lining installations use a three-part, four-coat adhesive system that has an additional cost of \$8.60 to 10.76/m^2 (\$0.80 to 1.00/ft^2). Material costs are summarized in Table 5. Rubber lining costs vary according to job location, size, and availability of vulcanization equipment. The shop installation of linings is estimated to be in the range of \$107 to 130/m^2 (\$10 to 12/ft^2), including materials. Field application, with materials, can be expected to be in the range of \$430 to 540/m^2 (\$40 to 50/ft^2). Scrubber (FGD) installations using rubber are typically in the \$300 to 330/m^2 (\$28 to 30/ft^2) range.

Table 5 Rubber lining costs of sheet, 6.35 mm ($\frac{1}{4}$ in.) thick

Item	ASTM D 1418 designation	Cost, $/m^2 ($/ft^2) in U.S. dollars 2003
Natural rubber	NR	32.28 (3.00)
Styrene-butadiene	SBR	37.66 (3.50)
Chlorobutyl	CIIR	43.04 (4.00)
Ethylene-propylene-diene-terpolymer	EPDM	48.42 (4.50)
Neoprene	CR	53.80 (5.00)
Nitrile	NBR	59.18 (5.50)
Hypalon	CSM	86.08 (8.00)
Adhesive system (three-part/four-coat)	…	8.60–10.76 (0.80–1.00)

E.B. Senkowski and K.B. Tator, Rubber Coatings and Linings, *Corrosion: Fundamentals, Testing, and Protection*, Vol 13A, *ASM Handbook*, ASM International, 2003, p 845–850

Rubber Coatings and Linings

E. Bud Senkowski and Kenneth B. Tator, KTA-Tator, Inc.

References

1. W. Hoffman, *Rubber Technology Handbook,* Hansner/Gardner Publications, 1996
2. Rubber and Elastomers, *Machine Design, 1995 Materials Selector Issue,* 12 Dec 1994, p 135–140
3. R.A. Higgins, *The Properties of Engineering Materials,* 2nd ed., Industrial Press Inc., 1994
4. Elastomers, *Van Nostrand's Scientific Encyclopedia,* 7th ed., D.M. Considine and G.D. Considine, Ed., Van Nostrand Reinhold, 1989
5. M. Morton, Elastomers, Synthetic, Survey, *Kirk-Othmer Encyclopedia of Chemical Technology,* 4th ed., Vol 8, Wiley-Interscience, 1993, p 905–923
6. A. Whelan and K.S. Lee, *Developments in Rubber Technology,* 1st ed., Elsevier Applied Science Publ., 1979; 2nd ed., 1982
7. F. Mark, N.G. Gaylord, and N.M. Bikales, Ed., *Encyclopedia of Polymer Science and Technology,* Interscience Publ., 1970
8. G.M. Blow and C. Hepburn, Ed., *Rubber Technology and Manufacture,* 2nd ed., Butterworth, London, 1972
9. "Glossary of Terms," Bulletin 17-1986, Rubber Manufacturers Association, Washington, D.C., 1986
10. "White Metal Blast Cleaning," SSPC-SP5/ NACE 1, Steel Structural Painting Council, 1 Sept 2000
11. "Procedure for Spark Testing Elastomeric Sheet Lining," Bulletin 13-1986, Rubber Manufacturers Association, Washington, D.C., 1986

12. "Practice for Discontinuity (Holiday) Testing of Nonconductive Protective Coating on Metallic Substrates," D 5162, ASTM

13. "Test Method for Rubber Property-Durometer Hardness," D 2240, ASTM

E.B. Senkowski and K.B. Tator, Rubber Coatings and Linings, *Corrosion: Fundamentals, Testing, and Protection*, Vol 13A, *ASM Handbook*, ASM International, 2003, p 845–850

Rubber Coatings and Linings

E. Bud Senkowski and Kenneth B. Tator, KTA-Tator, Inc.

Selected References

- J. Fenner, Rubber Linings as Surface Protection in Flue Gas Desulfurization Plants, *Mater. Perform.*, April 1997
- L. Mehra, E. Polski, R. Lewis, and A. Mauri, Rubber Linings Overview and New Technology, *Mater. Perform.*, Jan 1996
- E.B. Senkowski, Corrosion Protection with Rubber Linings, *J. Prot. Coatings Linings,* Nov 1998

C.E. Locke, Anodic Protection, *Corrosion: Fundamentals, Testing, and Protection*, Vol 13A, *ASM Handbook*, ASM International, 2003, p 851–854

Anodic Protection

Carl E. Locke, Jr., University of Kansas

Introduction

ANODIC PROTECTION is one of the more recently developed electrochemical methods of corrosion control. The method was first used to protect plant-sized equipment in the late 1950s and became commercially successful in the early 1970s. It is currently used on a smaller scale than other corrosion control techniques due to the fundamental electrochemistry involved. This article provides a brief history of the technique, discusses anodic protection use, and compares anodic and cathodic protection. A more complete description of all aspects of anodic protection is available in Ref 1.

Reference cited in this section

1. O.L. Riggs and C.E. Locke, *Anodic Protection: Theory and Practice in the Prevention of Corrosion,* Plenum Press, 1981

C.E. Locke, Anodic Protection, *Corrosion: Fundamentals, Testing, and Protection*, Vol 13A, *ASM Handbook*, ASM International, 2003, p 851–854

Anodic Protection

Carl E. Locke, Jr., University of Kansas

History

The scientific principles of passivity, on which anodic protection is based, can be traced to experiments by Faraday and Schöbein in the 19th century (Ref 1). Work by C.D. Edeleanu published in 1954 (Ref 2) triggered further investigations and development at Continental Oil Company. This later work resulted in several installations of anodic protection to control the corrosion of chemical plant equipment (Ref 3, 4, 5, 6). Simultaneous investigations at the Pulp and Paper Institute of Canada led to installation of anodic protection to protect pulp and paper digesters (Ref 7, 8, 9).

Commercialization of anodic protection was begun by Continental Oil Company through license agreements. Independently and simultaneously, Corrosion Services in Canada began commercialization of anodic protection primarily in the pulp and paper industry. Since these early beginnings, several organizations now offer anodic protection equipment and services.

References cited in this section

1. O.L. Riggs and C.E. Locke, *Anodic Protection: Theory and Practice in the Prevention of Corrosion,* Plenum Press, 1981
2. C. Edeleanu, *Metallurgia,* Vol 50, 1954, p 113–116
3. J.D. Sudbury, O.L. Riggs, and D.A. Shock, *Corrosion,* Vol 16, 1960, 47t–54t
4. D.A. Shock, O.L. Riggs, and J.D. Sudbury, *Corrosion,* Vol 16, 1960, 55t–58t
5. O.L. Riggs, M. Hutchison, and N.L. Conger, *Corrosion,* Vol 16, 1960, 58t–62t
6. C.E. Locke, M. Hutchison, and N.L. Conger, *Chem. Eng. Prog.,* Vol 56 (No. 11), 1960, p 50–55
7. W.A. Mueller, *Can. J. Chem.,* Vol 38, 1960, p 576–587
8. T.R.B. Watson, *Tappi,* Vol 44, 1961, p 206–210
9. T.R.B. Watson, *Mater. Prot.,* Vol 3 (No. 6), 1965, p 54

C.E. Locke, Anodic Protection, *Corrosion: Fundamentals, Testing, and Protection*, Vol 13A, *ASM Handbook*, ASM International, 2003, p 851–854

Anodic Protection

Carl E. Locke, Jr., University of Kansas

Anodic Protection Uses

Anodic protection has been used most extensively to protect equipment for storage and handling of sulfuric acid (Ref 10, 11). Several companies advertise their capabilities in serving the sulfuric acid industry with anodic protection (Ref 12, 13, 14, 15). These organizations have applied anodic protection to storage vessels and heat exchangers in the manufacturing process.

Anodic protection has also been applied in the pulp and paper industry. Digesters and storage tanks holding green and white kraft liquors have been protected (Ref 16, 17, 18, 19).

Early in the development of anodic protection, there were attempts to apply it to a wide range of different metal-chemical systems. The pace of those development programs has slackened a bit, particularly in the United States and Canada. A review of the different applications from the 1980s can be found in the literature (Ref 20). Other papers that describe new applications have recently been published (Ref 21, 22).

Anodic protection is used to a lesser degree than the other corrosion control techniques, particularly cathodic protection; see the article “Cathodic Protection” in this Volume. This is because of the limitations on metal-chemical systems for which anodic protection reduces corrosion. In addition, it is possible to accelerate corrosion of the equipment if proper controls are not implemented. The understanding of anodic protection is not as widespread as for other techniques. Anodic protection does have a place among methods of corrosion control, because it is the most feasible and economical technique for selected applications.

References cited in this section

10. C.E. Locke, Status of Anodic Protection: Twenty-Five Years Old, *Proceedings of the International Congress on Metallic Corrosion,* Vol 1, National Research Council of Canada, 1984, p 316–319

11. W.W. Shim and J.I. Munro, *Mater. Perform.,* Vol 39 (No. 12), 2000, p 22

12. Corrosion Service Co. Ltd., http:// www.corrosionservice.com, 2003

13. Kvaerner Chemetics, http:// www.kvaerner.com/chemetics/, 2003

14. Savcor Group Ltd. Oy, http:// www.savcor.com/divisions/process/aps.asp, 2003

15. Enviro-Chem Systems, http://www.enviro- chem.com/plant-tech/3rdtier/actop.html, 2003

16. J.I. Munro, *Mater. Perform.,* Vol 41 (No. 2), 2002, p 22

17. J.I. Munro, *Mater. Perform.,* Vol 41 (No. 3), 2002, p 24

18. A. Wensley, “Corrosion Protection of Kraft Digesters,” Corrosion/2001, NACE International, Mar 2001

19. A. Wensley, “Corrosion of Carbon and Stainless Steels in Kraft Digesters,” Corrosion/2002, NACE International, Mar 2000

20. V. Kuzub and V. Novitskiy, Anodic Protection and Corrosion Control of Industrial Equipment, *Proceedings of the International Congress on Metallic Corrosion*, Vol 1, National Research Council of Canada, 1984, p 307–308

21. T. Xu and J. Li, Anodic Protection of Heat Exchangers for Acidolysis in the Production of Titanium Dioxide, *Chem. Eng. Mach.*, Vol 23 (No. 2), 1996, p 80

22. H. Zhu, Multi-System Anodic Protection Study of Constant Bath Voltage Method of Vinyl on Aldol Condensators, *Chem. Eng. Mach.*, Vol 21 (No. 2), 1994, p 93

C.E. Locke, Anodic Protection, *Corrosion: Fundamentals, Testing, and Protection*, Vol 13A, *ASM Handbook*, ASM International, 2003, p 851–854

Anodic Protection

Carl E. Locke, Jr., University of Kansas

Comparison of Anodic and Cathodic Protection

Cathodic protection has been used since the middle of the 19th century and has gained widespread acceptance. Anodic protection is sometimes confused with cathodic protection, but the two techniques are fundamentally different. Basically, the difference involves the electrode that is protected; the cathode is protected in cathodic protection, and the anode is protected in anodic protection. Stating this another way, the difference is in how the metal to be protected is polarized. The component requiring protection is made the anode in anodic protection. The metal to be protected is made the cathode in cathodic protection. Protecting an electrode by making it a cathode is easily understood, because reduction reactions occur at cathodes. Oxidation reactions occur at the anode, and thus, it is not so readily apparent that an anode can be protected from corrosion, because oxidation reactions involving metals usually lead to dissolution of the metal.

Cathodic protection is based on using electrochemistry to slow or stifle the corrosion reaction. Direct currents (dc) generated by galvanic metallic couples or external power sources flow in such a direction as to shift the potential of the cathode to a value at which the corrosion reaction does not occur. Other descriptions of cathodic protection state that the currents result in the metal to be protected becoming a cathode over the entire metal surface and shifting the anodic reaction to an external electrode. In principle, any corrosion system can be cathodically protected as long as there is a continuous ionic path between the external anode and the metal to be protected. The only limitations are ones of economics and practicality due to current and voltage requirements.

Anodic protection, like cathodic protection, is an electrochemical method of controlling corrosion but is based on a different electrochemical principle. Anodic protection is based on the phenomenon of passivity. A limited number of metals in a limited number of chemical environments have the property of passivity. The electrochemical nature of achieving passivity requires that the potential of the metal be controlled. This is not necessary for most of the applications of cathodic protection. Current requirements for anodic protection can be much lower than those required for cathodic protection, but this is not the case for all systems.

C.E. Locke, Anodic Protection, *Corrosion: Fundamentals, Testing, and Protection*, Vol 13A, *ASM Handbook*, ASM International, 2003, p 851–854

Anodic Protection

Carl E. Locke, Jr., University of Kansas

Background and Theory

Anodic protection can be used to control the corrosion of metals in chemical environments that exhibit very interesting behavior when subjected to anodic polarization. This behavior can be studied with an experimental setup, which is shown in block-diagram fashion in Fig. 1. When the potential of the working electrode relative to the reference electrode is controlled and shifted in the more anodic (positive) direction, the current required to cause that shift varies. If the current required for the shift has the general behavior with respect to potential shown in the Evans diagram in Fig. 2, the metal is termed active-passive and can be anodically protected. Few systems exhibit this type of behavior. Some metals and solutions that have been found to have active-passive properties and can be anodically protected include:

Metals	**Steels**
	Stainless steels
	Nickel
	Nickel alloys
	Chromium
Solutions	Sulfuric acid
	Phosphoric acid
	Nitric acid
	Nitrate solutions
	Aqueous ammonia
	Organic acids
	Caustic solutions
	Kraft liquors

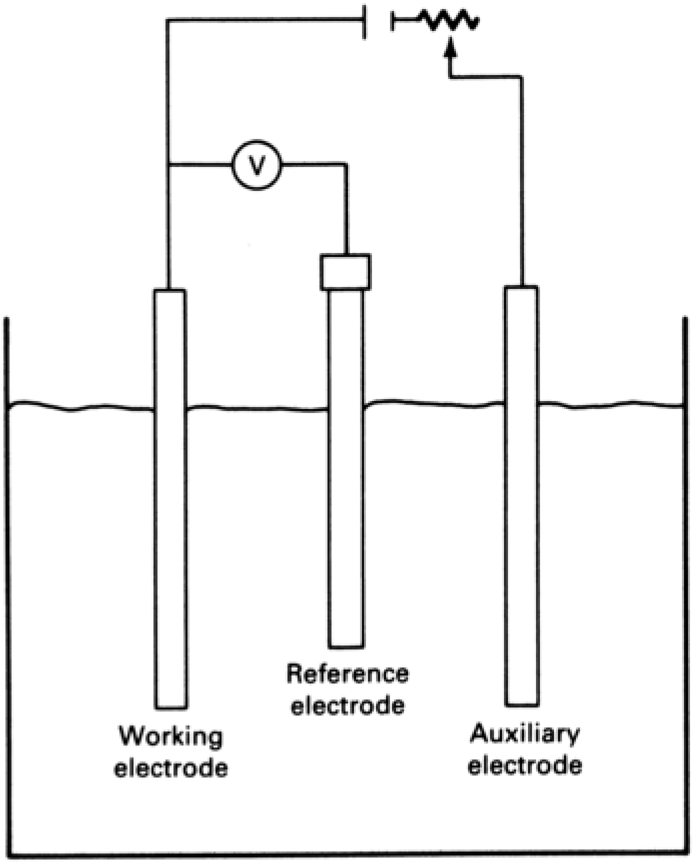

Fig. 1 Schematic of experimental apparatus used for anodic polarization studies. Current flow between the working electrode and the auxiliary electrode forces a shift in potential between the working electrode and the reference electrode. V, voltmeter. Source: Ref 23

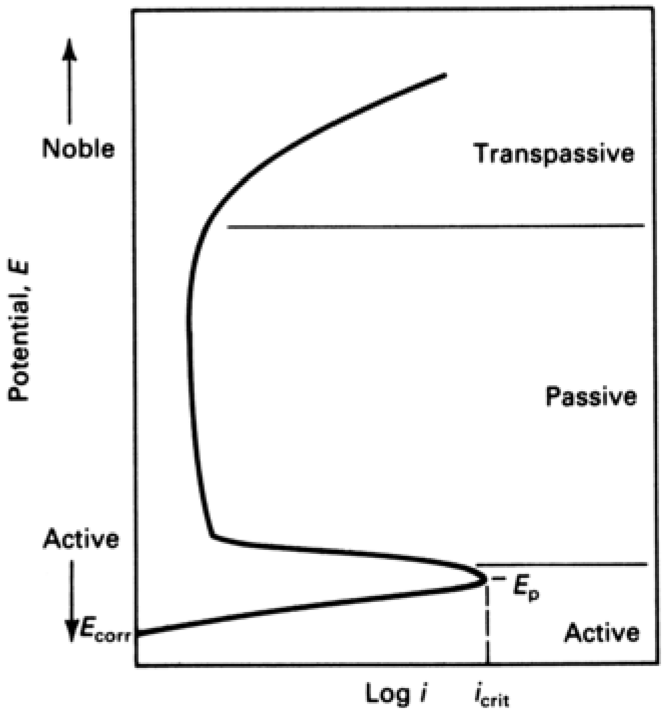

Fig. 2 Schematic anodic polarization curve. Metal-environment systems that have this type of anodic polarization behavior are termed active-passive and can be anodically protected. Source: Ref 23

The corrosion rate of an active-passive metal can be significantly reduced by shifting the potential of the metal so that it is at a value in the passive range shown in Fig. 2. The current required to shift the potential in the anodic direction from the corrosion potential, E_{corr}, is several orders of magnitude greater than the potential at a

passive value. The current peaks at the primary passivation potential value, shown as E_p (Fig. 2). The current density required to achieve passivity (protection) is typically a few thousand mA/m^2 (a few hundred mA/ft^2) of wetted area. The current necessary to maintain passivity is usually 10 μA/m^2 (1 μA/ft^2) or less.

This interesting anodic polarization behavior results from the formation of a surface layer on the metal that is both electrically resistive and relatively insoluble in the chemical environment. The metal is termed passive when this layer is formed.

Passivity is the phenomenon responsible for the corrosion resistance of stainless steels. It can be defined in various ways, but a reasonable definition is that passivity is the loss of chemical reactivity experienced by some metals in special environments. These metals and alloys, when passive, behave similar to noble metals. This noble behavior is attributed to the presence of the thin oxide layer on the metal surface. The mechanism of formation and the structure of the passive film have been extensively studied but are still not completely understood.

Passivity can be achieved by alloying and by chemical means in addition to the electrochemical method described in this section. Anodic protection can be used to form the passive film on metals in chemical systems that would normally be corrosive; at other times, anodic protection can be used to maintain the passivity of the metal, so that the process changes do not force the metal to become active and corrode.

Reference cited in this section

23. G. Bianchi, A. Barosi, and S. Trasatti, *Electrochim. Acta.,* Vol 10, 1965, p 16

C.E. Locke, Anodic Protection, *Corrosion: Fundamentals, Testing, and Protection*, Vol 13A, *ASM Handbook*, ASM International, 2003, p 851–854

Anodic Protection

Carl E. Locke, Jr., University of Kansas

Equipment Required for Anodic Protection

Figure 3 is a schematic diagram of an anodic protection system for a storage vessel. Each of these components has specific requirements that are discussed subsequently. In addition, the various items used for each component of the system are briefly described.

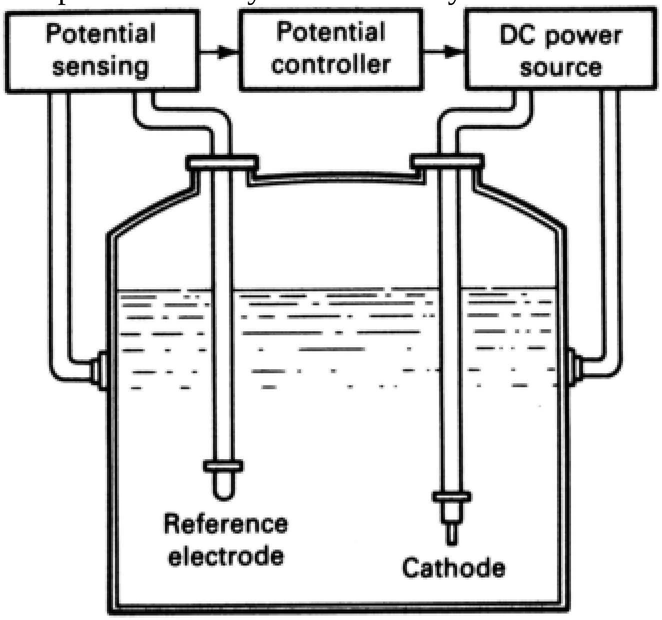

Fig. 3 Schematic of an anodic protection system. One or more cathodes, a reference electrode, a potential sensing and controlling circuit, and a dc power supply are required for each anodic protection system. The vessel wall is made the anode of the circuit by current forced between the cathode and the tank wall. The currents are controlled so that the potential of the wall with respect to the reference electrode is shifted and maintained in the passive region (see Fig. 2). Source: Ref 1

Electrodes

The cathode should be a permanent-type electrode that is not dissolved by the solution or the currents impressed between the vessel wall to be protected and the electrode. The cathodes used in most of the initial applications were made of platinum-clad brass (Ref 1, 3, 4, 5, 6). These cathodes were excellent electrochemically but were costly, and the area contacting the solution was limited by the cost. Because the overall resistance between cathode and vessel wall is inversely proportional to the electrode surface area, it is advantageous to use large surface area electrodes. Therefore, other, less costly metals have been used for cathodes in anodic protection systems. These cathode and chemical environment combinations include:

Cathode metal	Environment
Platinum on brass	Various
Steel	Kraft digester liquors
Illium G (Ni Cr Cu)	Sulfuric acid (78–105%)
Silicon cast iron	Sulfuric acid (78–105%)
Copper	Hydroxylamine sulfate
Stainless steel	Liquid fertilizers (nitrate solutions)
Nickel-plated steel	Chemical nickel-plating solutions
Hastelloy C (UNS N10002)	Liquid fertilizers (nitrate solutions), sulfuric acid, kraft digester liquors

UNS, Unified Numbering System

The cathode size is chosen to conform to the geometry of the vessel and to provide as large a surface area as possible. The location of the cathode is not a critical factor in simple geometries, such as storage vessels, but in heat exchangers, it is necessary to extend the electrode around the surface to be protected. Multiple cathodes can be used in parallel to distribute the current and decrease circuit resistance.

Reference electrodes must be used in anodic protection systems, because the potential of the vessel wall serving as the anode must be measured and controlled. The reference electrode must have an electrochemical potential that is constant with respect to time and is minimally affected by changes in temperature and solution composition. Reference electrodes used for anodic protection include:

Reference electrode	Environment
Calomel	Sulfuric acid
Ag-AgCl	Sulfuric acid, kraft liquors, fertilizer solutions
Mo-MoO_3	Sodium carbonate solutions
Bismuth	Ammonia hydroxide
Type 316 stainless steel	Fertilizer solutions, oleum
Hg-$HgSO_4$	Sulfuric acid, hydroxylamine sulfate
Pt-PtO	Sulfuric acid

The reference electrode has been a source of many problems in anodic protection installations, because it is more fragile than the cathode.

Potential Control and Power Supply

Potential Control. As mentioned previously, the potential of the vessel wall to be protected with respect to the reference electrode must be controlled in anodic protection installations. The potential control circuitry has two functions. First, the electric potential must be measured and compared to the desired preset value. Second, a control signal must then be sent to the power supply to regulate the dc current between the cathode and vessel wall. In early systems, this control function was done in an on-off manner because of the high cost of vacuum-tube-based electronic circuitry. The more sophisticated and extremely low-cost circuitry currently available has

resulted in all systems having a continuous, proportional-type control. The amount of current forced through the circuitry is that required to maintain the potential at the preset control.

The dc power supplies are similar to the dc rectifiers used for cathodic protection, with one exception. Because of the nature of the active- passive behavior of anodic protection, the currents required to maintain the potential of the vessel wall in the passive range can become very small with time. Some designs of dc power supplies must be specifically modified to lower the minimum current that can be regulated from the power supply.

The packaging of these electronic components occasionally involves special design requirements, because most of the installations are in chemical plants. Explosion-proof enclosures are sometimes required, and chemically resistant enclosures are necessary in other installations.

References cited in this section

1. O.L. Riggs and C.E. Locke, *Anodic Protection: Theory and Practice in the Prevention of Corrosion,* Plenum Press, 1981

3. J.D. Sudbury, O.L. Riggs, and D.A. Shock, *Corrosion,* Vol 16, 1960, 47t–54t

4. D.A. Shock, O.L. Riggs, and J.D. Sudbury, *Corrosion,* Vol 16, 1960, 55t–58t

5. O.L. Riggs, M. Hutchison, and N.L. Conger, *Corrosion,* Vol 16, 1960, 58t–62t

6. C.E. Locke, M. Hutchison, and N.L. Conger, *Chem. Eng. Prog.,* Vol 56 (No. 11), 1960, p 50–55

C.E. Locke, Anodic Protection, *Corrosion: Fundamentals, Testing, and Protection*, Vol 13A, *ASM Handbook*, ASM International, 2003, p 851–854

Anodic Protection

Carl E. Locke, Jr., University of Kansas

Design Concerns

Design of an anodic protection system requires knowledge of the electrochemical parameters of the metal-solution system, the geometry of the equipment, any special operational conditions, and the special requirements of the environment around the system. The electrochemical parameters of concern are the potential at which the vessel must be maintained for corrosion protection, the currents required to establish passivity, and the solution conductivity. The electrode potential can be determined directly from the polarization curve. Currents needed to establish and maintain passivity can be estimated from the laboratory polarization data, but they are time dependent. Variation of the current with respect to time must be estimated. Empirical data available from field installations are the best source of this information (Ref 1).

Solution conductivity is an important component of the total circuit resistance. The solution conductivity is usually sufficiently low that the circuit resistance is controlled by the cathode surface area. The power requirements for the dc power supply should be as low as possible to reduce operating costs.

Reference cited in this section

1. O.L. Riggs and C.E. Locke, *Anodic Protection: Theory and Practice in the Prevention of Corrosion,* Plenum Press, 1981

C.E. Locke, Anodic Protection, *Corrosion: Fundamentals, Testing, and Protection*, Vol 13A, *ASM Handbook*, ASM International, 2003, p 851–854

Anodic Protection

Carl E. Locke, Jr., University of Kansas

Applications

Anodic protection has been used for storage vessels, process reactors, heat exchangers, and transportation vessels. The largest number of storage tanks and other equipment under anodic protection are those used in handling sulfuric acid. Anodic protection has been successful in preserving product quality through reduction of metal pickup by the solution, in extending the useful life of the vessels, and allowing the use of lower-cost alloys. Examples of these applications are given as follows.

Storage Vessels. Storage of sulfuric acid in strengths of 93% and above in low-carbon steel has met with some success in terms of vessel life. Anodic protection has been successful in reducing the amount of iron dissolved during storage. This enhances the economic worth of the product, in that pure acid is more valuable than the contaminated acid. Field studies have shown that the iron content of sulfuric acid in concentrations of 93% and above increases at rates of 5 to 20 ppm per day of storage, depending on the concentration, vessel size, acid residence time, and storage temperature (Ref 1). Several anodic protection systems have been successful in reducing the rates of iron pickup to 1 ppm or less per day (Ref 1, 11, 12, 13). The level of purity of the acid has been sufficient to meet market demands for low-iron-content acid.

Tanks constructed since the 1970s have been made with steel containing low amounts of copper. Steel with low copper content corrodes readily in sulfuric acid (Ref 24). Anodic protection of vessels made of this low-copper steel has been successful in lowering the corrosion rate by a factor of 4 to 5, and vessel life has increased accordingly.

Hydrogen gas is produced as a by-product of acid corrosion. This gas can damage steel tanks, particularly in the upper half of the manhole area of a storage vessel. This damage is caused by the gas streaming up the manhole and disrupting the solid corrosion product on the surface of the vessel, thus grooving the vessel. Anodic protection reduces the corrosion reaction and also the by- product evolution of hydrogen. This accompanying hydrogen grooving damage is thus prevented by anodic protection (Ref 11).

Heat Exchangers. A large market has developed for anodically protected heat exchangers, which are used in the manufacturing process for sulfuric acid. These stainless steel exchangers replace cast iron coolers that were normally used several years ago. Shell and tube, spiral, and plate-type exchangers have been sold complete with anodic protection as an integral part of the equipment (Ref 1, 10, 11, 12, 13, 15, 20). Sulfuric acid of 96 to 98% concentration at temperatures up to 110 °C (230 °F) has been handled in type 316 stainless steel exchangers by the use of anodic protection. Corrosion rates have been reduced from unprotected rates of more than 5 mm/yr (200 mils/yr) to less than 0.025 mm/yr (1 mil/ yr). Cost savings have been substantial because of extended equipment life in comparison with that of cast iron coolers. Higher-purity acid can be produced by using the anodically protected heat exchangers. Other corrosive liquid systems have also been handled in anodically protected heat exchangers (Ref 1, 21).

Transportation Vessels. Anodic protection has been applied to tank trucks, railroad cars, and barges carrying sulfuric acid. These applications were installed to maintain the purity of the acid and to extend the life of the vessels (Ref 10, 20, 25).

Pulp and Paper Mills. One of the initial practical applications of anodic protection was to protect batch digesters in a kraft process paper mill (Ref 7, 8, 9). Several commercial applications of anodic protection now exist to protect batch and continuous digesters and kraft liquor storage tanks (Ref 12, 14, 16, 17, 18, 19).

Galvanic Cathodes. The potentials of metals have been maintained in the passive region by using the galvanic potential differences of metals to achieve anodic protection. This galvanic method of anodic protection differs from galvanic cathodic protection in that nothing is sacrificed, but protection is achieved.

A titanium pipe has been used to protect a steel vessel containing ammonium hydroxide, and platinum has been used to protect a stainless steel tank containing sulfuric acid (Ref 26, 27). A combination of galvanic and

impressed current protection for an anodic protection system is described in Ref 28. The graphite galvanically supplies sufficient current to maintain protection, but additional current can be supplied from a dc power supply through the graphite electrodes to establish and maintain protection.

References cited in this section

1. O.L. Riggs and C.E. Locke, *Anodic Protection: Theory and Practice in the Prevention of Corrosion,* Plenum Press, 1981

7. W.A. Mueller, *Can. J. Chem.,* Vol 38, 1960, p 576–587

8. T.R.B. Watson, *Tappi,* Vol 44, 1961, p 206–210

9. T.R.B. Watson, *Mater. Prot.,* Vol 3 (No. 6), 1965, p 54

10. C.E. Locke, Status of Anodic Protection: Twenty-Five Years Old, *Proceedings of the International Congress on Metallic Corrosion,* Vol 1, National Research Council of Canada, 1984, p 316–319

11. W.W. Shim and J.I. Munro, *Mater. Perform.,* Vol 39 (No. 12), 2000, p 22

12. Corrosion Service Co. Ltd., http:// www.corrosionservice.com, 2003

13. Kvaerner Chemetics, http:// www.kvaerner.com/chemetics/, 2003

14. Savcor Group Ltd. Oy, http:// www.savcor.com/divisions/process/aps.asp, 2003

15. Enviro-Chem Systems, http://www.enviro- chem.com/plant-tech/3rdtier/actop.html, 2003

16. J.I. Munro, *Mater. Perform.,* Vol 41 (No. 2), 2002, p 22

17. J.I. Munro, *Mater. Perform.,* Vol 41 (No. 3), 2002, p 24

18. A. Wensley, "Corrosion Protection of Kraft Digesters," Corrosion/2001, NACE International, Mar 2001

19. A. Wensley, "Corrosion of Carbon and Stainless Steels in Kraft Digesters," Corrosion/2002, NACE International, Mar 2000

20. V. Kuzub and V. Novitskiy, Anodic Protection and Corrosion Control of Industrial Equipment, *Proceedings of the International Congress on Metallic Corrosion,* Vol 1, National Research Council of Canada, 1984, p 307–308

21. T. Xu and J. Li, Anodic Protection of Heat Exchangers for Acidolysis in the Production of Titanium Dioxide, *Chem. Eng. Mach.,* Vol 23 (No. 2), 1996, p 80

24. D. Fyfe, R. Vanderland, and J. Rodda, *Chem. Eng. Prog.*, Vol 73 (No. 3), 1977, p 65

25. C.E. Locke, Corrosion: Cathodic and Anodic Protection, *Encyclopedia of Chemical Processing and Design,* Vol 12, Marcel Dekker, 1981, p 13–59

26. W.A. Szymanski, *Mater. Perform.,* Vol 16 (No. 11), 1977, p 16

27. V.G. Moisa and V.S. Kuzub, Anodic Protection with Additional Protectors, *Zashch. Met.,* Vol 16 (No. 1), 1980, p 83

28. F.W.S. Jones, *Anti-Corros. Methods Mater.,* Vol 12 Dec 1976

C.E. Locke, Anodic Protection, *Corrosion: Fundamentals, Testing, and Protection*, Vol 13A, *ASM Handbook*, ASM International, 2003, p 851–854

Anodic Protection

Carl E. Locke, Jr., University of Kansas

Economics

Economic justification of anodic protection is based on the same factors as in any comparison of corrosion control methods. Anodic protection is an alternative for linings or higher alloys in the storage of sulfuric acid, for example. Because an anodic protection system has some basic requirements (electrodes, potential controller, and power supply) that are independent of tank size, anodic protection is more economically feasible for larger tanks (Ref 1, 11).

Anodically protected heat exchangers used in sulfuric acid manufacturing have been shown to reduce maintenance costs by almost 95% (Ref 28).

Many other applications of anodic protection have also been found to be economically feasible, by using standard methods of engineering economic comparisons.

The increase in the number of companies supplying anodic protection commercially speaks to the positive economic position of anodic protection. After close to 50 years of field applications, anodic protection has been established as a viable, effective, economical method of corrosion control.

References cited in this section

1. O.L. Riggs and C.E. Locke, *Anodic Protection: Theory and Practice in the Prevention of Corrosion,* Plenum Press, 1981

11. W.W. Shim and J.I. Munro, *Mater. Perform.,* Vol 39 (No. 12), 2000, p 22

28. F.W.S. Jones, *Anti-Corros. Methods Mater.,* Vol 12 Dec 1976

C.E. Locke, Anodic Protection, *Corrosion: Fundamentals, Testing, and Protection*, Vol 13A, *ASM Handbook*, ASM International, 2003, p 851–854

Anodic Protection

Carl E. Locke, Jr., University of Kansas

References

1. O.L. Riggs and C.E. Locke, *Anodic Protection: Theory and Practice in the Prevention of Corrosion,* Plenum Press, 1981

2. C. Edeleanu, *Metallurgia,* Vol 50, 1954, p 113–116

3. J.D. Sudbury, O.L. Riggs, and D.A. Shock, *Corrosion,* Vol 16, 1960, 47t–54t

4. D.A. Shock, O.L. Riggs, and J.D. Sudbury, *Corrosion,* Vol 16, 1960, 55t–58t

5. O.L. Riggs, M. Hutchison, and N.L. Conger, *Corrosion,* Vol 16, 1960, 58t–62t

6. C.E. Locke, M. Hutchison, and N.L. Conger, *Chem. Eng. Prog.,* Vol 56 (No. 11), 1960, p 50–55

7. W.A. Mueller, *Can. J. Chem.,* Vol 38, 1960, p 576–587

8. T.R.B. Watson, *Tappi,* Vol 44, 1961, p 206–210

9. T.R.B. Watson, *Mater. Prot.,* Vol 3 (No. 6), 1965, p 54

10. C.E. Locke, Status of Anodic Protection: Twenty-Five Years Old, *Proceedings of the International Congress on Metallic Corrosion,* Vol 1, National Research Council of Canada, 1984, p 316–319

11. W.W. Shim and J.I. Munro, *Mater. Perform.,* Vol 39 (No. 12), 2000, p 22

12. Corrosion Service Co. Ltd., http:// www.corrosionservice.com, 2003

13. Kvaerner Chemetics, http:// www.kvaerner.com/chemetics/, 2003

14. Savcor Group Ltd. Oy, http:// www.savcor.com/divisions/process/aps.asp, 2003

15. Enviro-Chem Systems, http://www.enviro- chem.com/plant-tech/3rdtier/actop.html, 2003

16. J.I. Munro, *Mater. Perform.,* Vol 41 (No. 2), 2002, p 22

17. J.I. Munro, *Mater. Perform.,* Vol 41 (No. 3), 2002, p 24

18. A. Wensley, "Corrosion Protection of Kraft Digesters," Corrosion/2001, NACE International, Mar 2001

19. A. Wensley, "Corrosion of Carbon and Stainless Steels in Kraft Digesters," Corrosion/2002, NACE International, Mar 2000

20. V. Kuzub and V. Novitskiy, Anodic Protection and Corrosion Control of Industrial Equipment, *Proceedings of the International Congress on Metallic Corrosion,* Vol 1, National Research Council of Canada, 1984, p 307–308

21. T. Xu and J. Li, Anodic Protection of Heat Exchangers for Acidolysis in the Production of Titanium Dioxide, *Chem. Eng. Mach.,* Vol 23 (No. 2), 1996, p 80

22. H. Zhu, Multi-System Anodic Protection Study of Constant Bath Voltage Method of Vinyl on Aldol Condensators, *Chem. Eng. Mach.,* Vol 21 (No. 2), 1994, p 93

23. G. Bianchi, A. Barosi, and S. Trasatti, *Electrochim. Acta.,* Vol 10, 1965, p 16

24. D. Fyfe, R. Vanderland, and J. Rodda, *Chem. Eng. Prog.,* Vol 73 (No. 3), 1977, p 65

25. C.E. Locke, Corrosion: Cathodic and Anodic Protection, *Encyclopedia of Chemical Processing and Design,* Vol 12, Marcel Dekker, 1981, p 13–59

26. W.A. Szymanski, *Mater. Perform.,* Vol 16 (No. 11), 1977, p 16

27. V.G. Moisa and V.S. Kuzub, Anodic Protection with Additional Protectors, *Zashch. Met.,* Vol 16 (No. 1), 1980, p 83

28. F.W.S. Jones, *Anti-Corros. Methods Mater.,* Vol 12 Dec 1976

R.H. Heidersbach, Cathodic Protection, *Corrosion: Fundamentals, Testing, and Protection*, Vol 13A*, ASM Handbook,* ASM International, 2003, p 855–870

Cathodic Protection

Robert H. Heidersbach, Dr. Rust, Inc.

Introduction

CATHODIC PROTECTION is an electrochemical means of corrosion control in which the oxidation reaction in a galvanic cell is concentrated at the anode, which suppresses corrosion of the cathode in the same cell. Figure 1 shows a simple cathodic protection system. The steel pipeline is cathodically protected by its connection to a sacrificial magnesium anode buried in the same soil electrolyte.

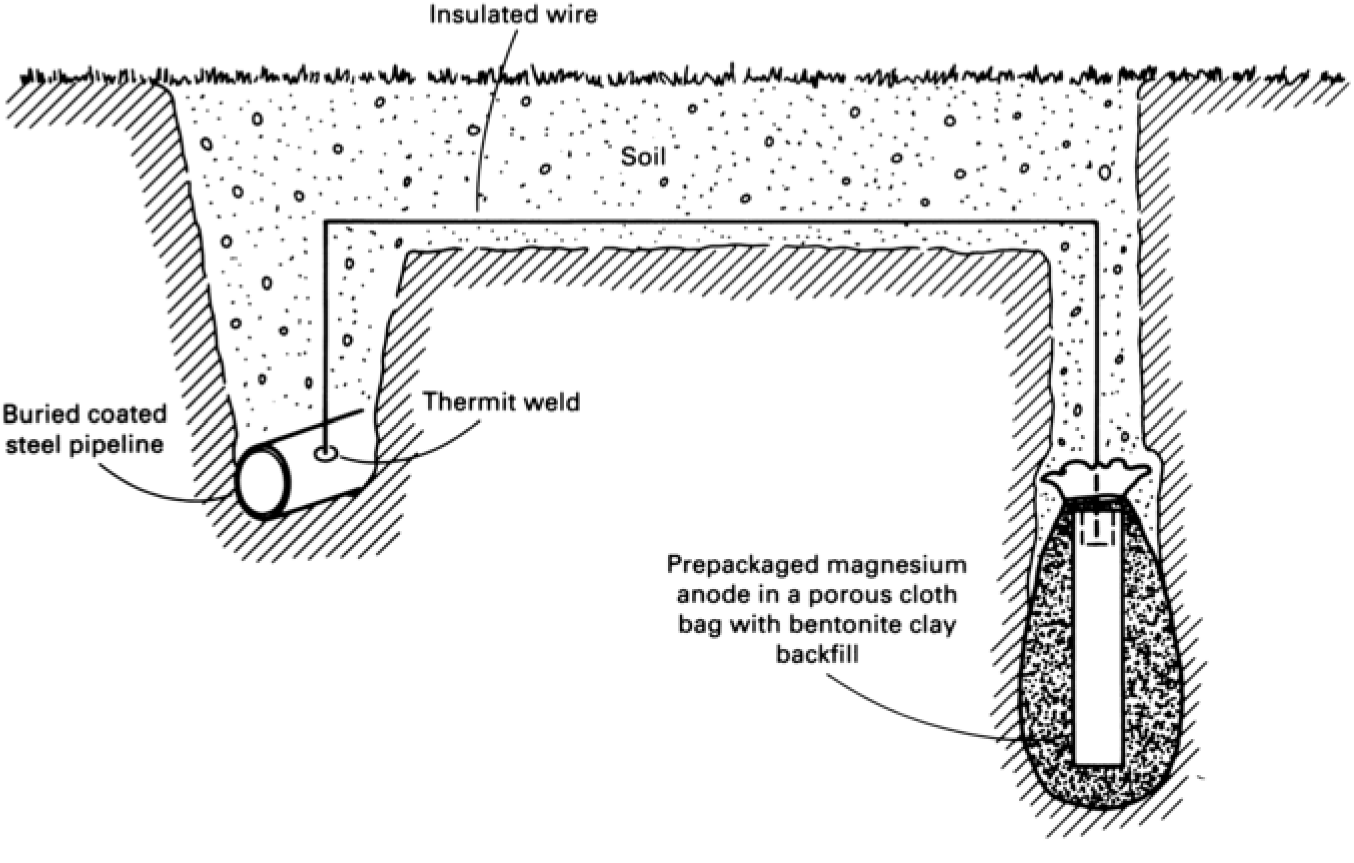

Fig. 1 Cathodic protection of buried pipeline using a buried magnesium anode

Cathodic protection differs from anodic protection. In cathodic protection, the object to be protected is the cathode; however, in anodic protection, the object to be protected is the anode. Anodic protection can be used on a limited number of alloys in certain restricted environments, but cathodic protection can, in principle, be applied to any metal. In practice, cathodic protection is primarily used to protect carbon steel structures. Cathodic protection allows carbon steel, which has little natural corrosion resistance, to be used in such

corrosive environments as seawater, acid soils, salt-laden concrete, and many other corrosive environments. Properly designed and maintained cathodic protection systems can prevent corrosion indefinitely in these environments.

Cathodic protection was first suggested by Sir Humphrey Davy in the 1820s as a means of controlling corrosion on British naval ships (Ref 1). It became common in the 1930s on the Gulf Coast of the United States, where it was used to control the corrosion of pipelines carrying high- pressure natural gas and petroleum products. Much of the terminology of cathodic protection still relates to corrosion control of onshore buried steel pipelines.

Virtually all modern pipelines are coated with an organic protective coating that is supplemented by cathodic protection systems sized to prevent corrosion at gaps or holidays in the protective coating. This combination of protective coating and cathodic protection is used on virtually all immersed or buried carbon steel structures, with the exception of offshore petroleum- production platforms and reinforced-concrete structures.

Offshore platforms are usually uncoated, but cathodically protected. Cathodic protection causes changes in the chemistry of seawater near the protected structure, and this causes the precipitation of a natural coating on the structure that reduces the need for cathodic protection current. Concrete structures normally rely on the protection of the concrete cover to prevent the corrosion of embedded steel. When corrosion of embedded steel occurs because of a loss of this protection due to ingress of moisture, cathodic protection is sometimes used to extend the life of the already deteriorated structure.

Reference cited in this section

1. H. Davy, *Philos. Trans. R. Soc. (London),* Vol 114, 1824–1825, p 151–158, 242–246, 328–346

R.H. Heidersbach, Cathodic Protection, *Corrosion: Fundamentals, Testing, and Protection,* Vol 13A, *ASM Handbook,* ASM International, 2003, p 855–870

Cathodic Protection

Robert H. Heidersbach, Dr. Rust, Inc.

Fundamentals of Cathodic Protection

Table 1 shows the theoretical electrochemical potentials obtained by pure metals in 1 *N* solutions of their own ions. More detailed electromotive series are described in most chemistry or corrosion textbooks (Ref 2) and in the article "Electrode Potentials" in this Volume.

Table 1 Standard electromotive force series for selected metals

Metal-metal ion equilibrium (unit activity)	Potential at 25 °C (77 °F), V
Noble or cathodic (protected)	
Ag/Ag^{+}	+0.80
Cu/Cu^{2+}	+0.34
H_2/H^{+}	(reference) 0
Fe/Fe^{2+}	-0.44
Zn/Zn^{2+}	-0.76
Al/Al^{3+}	-1.66
Mg/Mg^{2+}	-2.36
More active or anodic	

Figure 2(a) shows two of these metals—iron and zinc—separately immersed in a weak mineral acid. The chemical reactions that occur in Fig. 2(a) are:

$$Fe \rightarrow Fe^{2+} + 2e^-$$

Oxidation reaction

$$2H^+ + 2e^- \rightarrow H_2$$

Reduction reaction

$$2H^+ + Fe \rightarrow Fe^{2+} + H_2$$

Net reaction

$$Zn \rightarrow Zn^{2+} + 2e^-$$

Oxidation reaction

$$2H^+ + 2e^- \rightarrow H_2$$

Reduction reaction

$$2H^+ + Zn \rightarrow Zn^{2+} + H_2$$

Net reaction

Both metals corrode, and both oxidation reactions are balanced by an equal reduction reaction, which in both cases involves the liberation of hydrogen gas from the acid environments. The two corrosion reactions are independent of each other and are determined by the corrosivity of hydrochloric acid on the two metals in question.

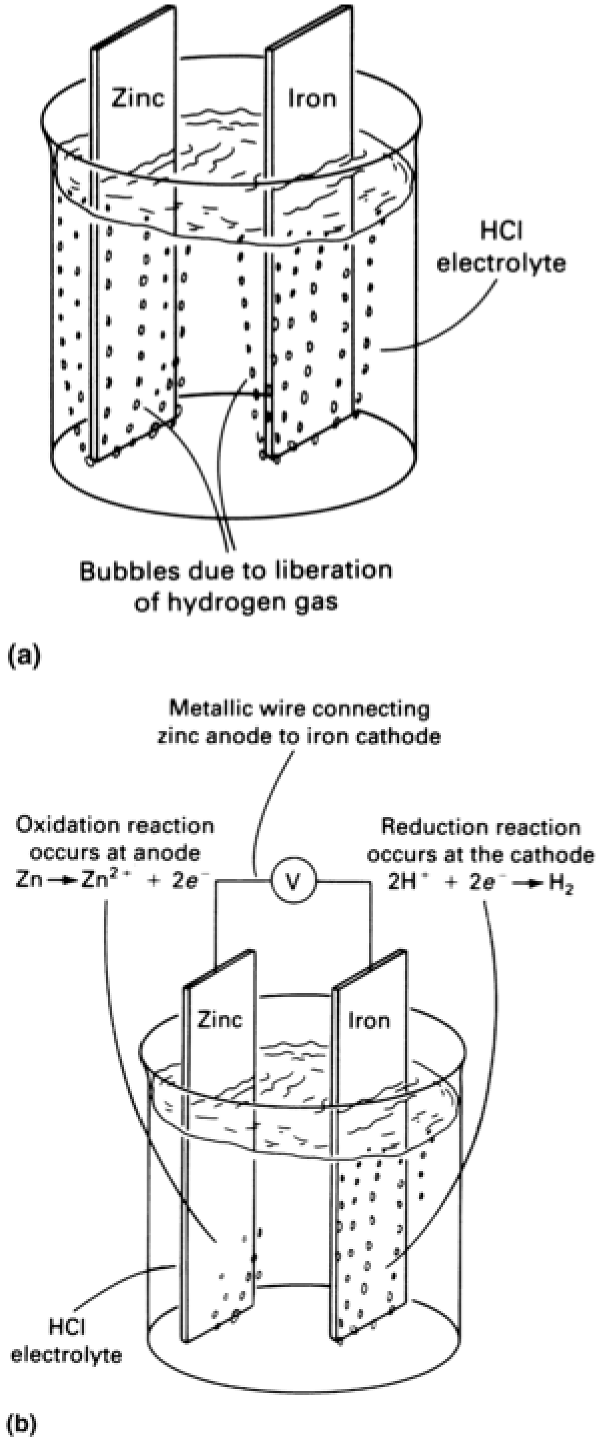

Fig. 2 Iron and zinc in hydrochloric acid. (a) Corrosion of zinc and iron in hydrochloric acid. (b) Cathodic protection of iron by zinc in hydrochloric acid

If the two metals were immersed in the same acid and electrically connected (Fig. 2b), the reactions would become:

$$Zn \rightarrow Zn^{2+} + 2e^-$$

Oxidation

$$2H^+ + 2e^- \rightarrow H_2$$

Reduction

Almost all of the oxidation reaction (corrosion of zinc) has been concentrated at the zinc electrode (anode) in Fig. 2(b), and almost all of the reduction reaction (hydrogen liberation) has been concentrated at the iron electrode (cathode). The oxidation of the zinc anode in Fig. 2(b) is much faster than that in Fig. 2(a). At the

same time, most of the corrosion of iron in Fig. 2(a) has stopped in Fig. 2(b). The zinc anode (Fig. 2(b) has been used to cathodically Open cross-sectional areaprotect the iron cathode.

Of course, some corrosion of the iron may still occur; whether or not this happens depends on the relative sizes of the zinc and iron electrodes. Some reduction of hydrogen may still occur on the zinc anode. The anode is the electrode at which a net oxidation reaction occurs, whereas cathodes are electrodes at which net reduction reactions occur. With proper design, the oxidation rate on the cathode will be suppressed to the point at which it becomes negligible and effective cathodic protection has been achieved.

All cathodic protection systems require an anode, a cathode, an electric circuit between them, and an electrolyte. Cathodic protection will not work on structures exposed to air environments. Air is a poor electrolyte, and it prevents current from flowing from the anode to the cathode.

The reduction reactions that accompany cathodic protection are normally the reduction of dissolved oxygen from the water surrounding the cathode. All reduction reactions result in an increase of the alkalinity (pH) in the electrolyte near the cathode surface. This increase in alkalinity causes the precipitation of mineral deposits on the cathodically protected structure. Figure 3 shows these deposits on an offshore platform.

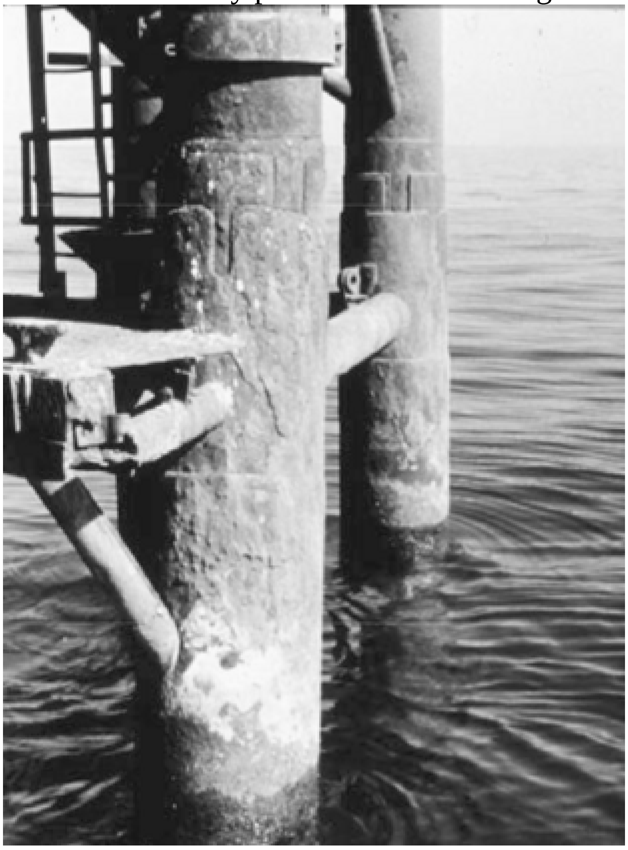

Fig. 3 Calcareous deposits in the tidal region of an offshore platform. Courtesy of NACE International

The presence of these deposits means that protective coatings applied to buried structures must be resistant to alkaline (high pH) environments. Offshore oil and gas platforms are usually not coated (Fig. 4) and rely on the presence of these deposits to partially cover the submerged metal surface and reduce the electrical current demand for cathodic protection. These minerals are more soluble in cold waters than in warm waters, which has led to problems where inadequate cathodic protection currents were applied to offshore structures in cold waters.

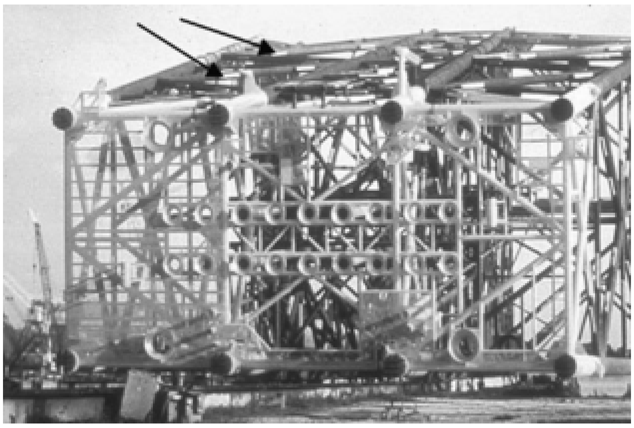

Fig. 4 Typical offshore platform for the Gulf of Mexico. Arrows show the locations of two of the hundreds of anodes. Each anode weighs 365 kg (800 lb) and provides 5 A of current. Note how the topside (above the waterline) portions of the structure are painted, and the regions that will be submerged are not painted. Courtesy of W. Thomasen, Conoco

NACE RP0176, "Corrosion Control of Steel, Fixed Offshore Platforms Associated with Petroleum Production" (Ref 3), contains guidelines on the appropriate cathodic current densities for different locations throughout the world.

References cited in this section

2. M.G. Fontana, *Corrosion Engineering,* McGraw-Hill, 1986, p 497–499
3. "Corrosion Control on Steel, Fixed Offshore Platforms Associated with Petroleum Production," NACE RP-01-76, National Association of Corrosion Engineers

---

R.H. Heidersbach, Cathodic Protection, *Corrosion: Fundamentals, Testing, and Protection,* Vol 13A, *ASM Handbook*, ASM International, 2003, p 855–870

Cathodic Protection

Robert H. Heidersbach, Dr. Rust, Inc.

Types of Cathodic Protection

There are two types of cathodic protection: sacrificial-anode (passive) systems and impressed-current (active) systems. Sacrificial-anode systems are simpler. They require only a material anodic to the protected steel in the environment of interest (Fig. 1).

Figure 5 shows an impressed-current system used to protect a pipeline. The buried anodes and the pipeline are both connected to an electrical rectifier, which supplies direct current (dc) to both. Unlike sacrificial anodes, impressed-current anodes need not be naturally anodic to steel, and in fact they seldom are. Most impressed-current anodes are made from nonconsumable electrode materials that are naturally cathodic to steel. If these electrodes were wired directly to a structure, they would act as cathodes and would cause accelerated corrosion of the structure they are intended to protect. The dc source reverses the natural polarity and allows the materials to act as anodes. Instead of corrosion of the anodes, some other oxidation reaction—that is, oxygen or chlorine evolution—occurs at the anodes, and the anodes are not consumed.

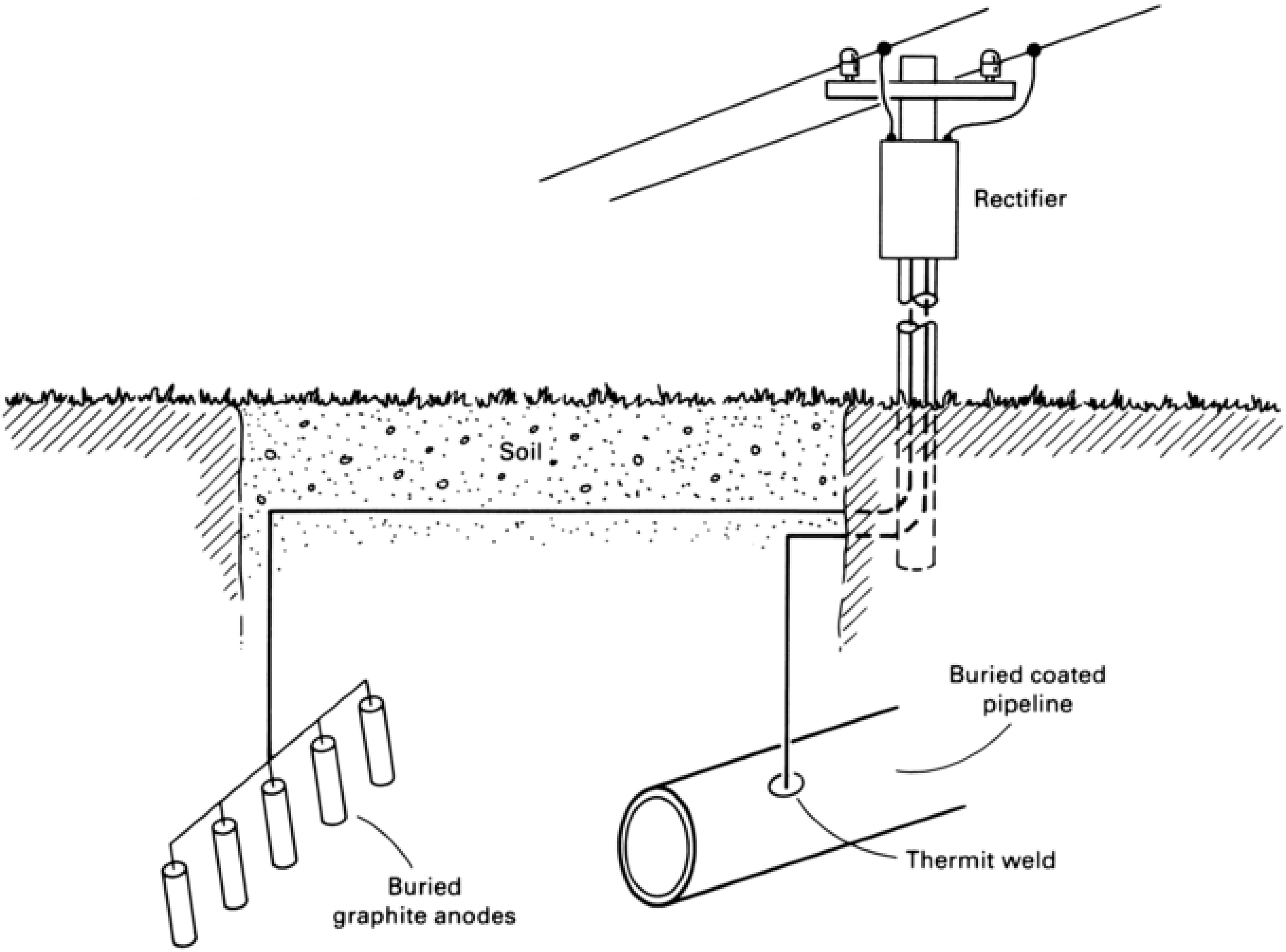

Fig. 5 Impressed-current cathodic protection of a buried pipeline using graphite anodes

In recent years, small steel tanks intended for burial have usually been sold with prepackaged sacrificial anodes (Fig. 6). These systems do not require a cathodic protection system, but it is important to install them correctly. Some of these anodes, either zinc or magnesium, may be inappropriate for the local soil-resistivity conditions.

Fig. 6 Underground storage tanks with prepackaged sacrificial anodes

In sacrificial-anode systems, the maximum voltage between anode and cathode is approximately 1 V, depending on the anode material and the specific environment. Impressed-current systems can use larger voltages; this allows anodes to be located more remotely, producing more efficient current-distribution patterns on the protected cathode. These larger voltages are also useful in low-conductivity environments, such as freshwater and concrete, in which sacrificial anodes would have insufficient power.

Larger voltages can have disadvantages. It is possible to overprotect high-strength steels and cause hydrogen embrittlement. Coating debonding is also possible (Fig. 7). Debonding occurs when moisture penetrates a coating and hydrogen is generated at the metal surface beneath the coating. The gas can accumulate until pressure causes blisters or cracks in the protective coating. Once this coating damage occurs, the demands for protective current increase and may exceed the capabilities of the system.

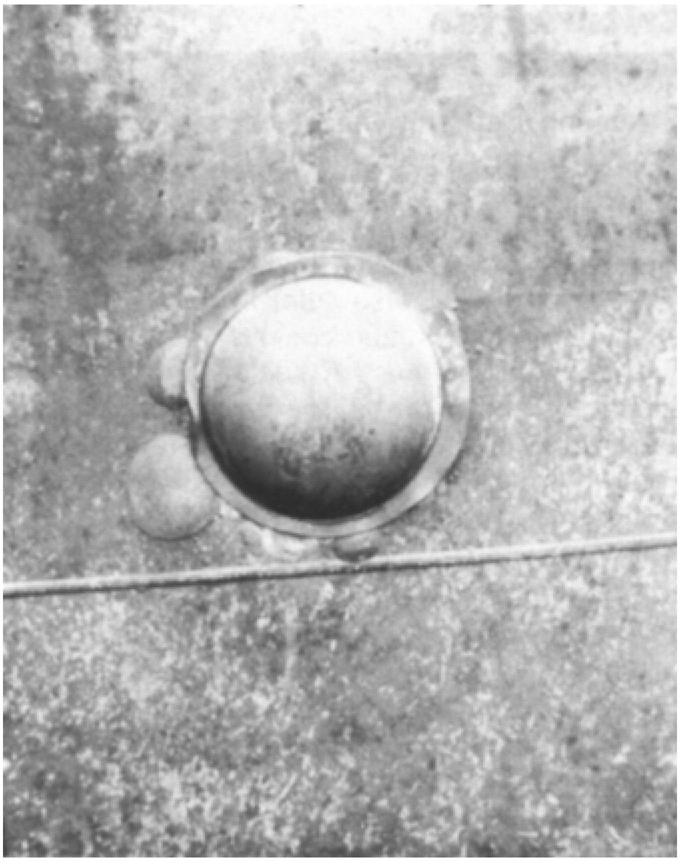

Fig. 7 Debonded organic coating near a high-silicon cast iron button anode

Aluminum is especially vulnerable to overprotection. All cathodic reactions cause the immediate environment to become somewhat more basic (less acidic). Unlike steel, aluminum is an amphoteric metal with increased corrosion susceptibility in acids and bases. If the environment around an aluminum structure becomes too basic, it will corrode at an accelerated rate. Thus, the cathodic protection of aluminum can cause cathodic corrosion if too much current is supplied to the cathode.

Table 2 lists some of the important differences between impressed-current and sacrificial-anode cathodic protection systems. Selection of a cathodic protection system usually depends on trade- offs among the advantages of each type of system. For example, most offshore petroleum- production platforms use sacrificial anodes because of their simplicity and reliability, even though the capital costs would be lower with impressed-current systems.

Table 2 Comparison between sacrificial- anode and impressed-current cathodic protection systems

Sacrificial-anode system	Impressed-current system
Simple	Complex
Low/no maintenance	Requires maintenance
Works best in conductive electrolytes	Can work in low-conductivity electrolytes
Lower installation costs for smaller installations	Remote anodes possible
Higher capital investment for large systems	Low capital investment for large systems
	Can cause the following problems:
	Stray current corrosion

	Hydrogen embrittlement Coating debonding Cathodic corrosion of aluminum

R.H. Heidersbach, Cathodic Protection, *Corrosion: Fundamentals, Testing, and Protection*, Vol 13A, *ASM Handbook*, ASM International, 2003, p 855–870

Cathodic Protection

Robert H. Heidersbach, Dr. Rust, Inc.

Cathodic Protection Criteria

Catastrophic corrosion failures such as the one shown in Fig. 8 have become less common in recent years as the implementation of cathodic protection on buried pipelines and other structures has become a standard practice in many countries.

Fig. 8 Catastrophic pipeline failure involving corrosion. Courtesy of *Corrosioneering—the On-line Corrosion Journal*

The criteria for cathodic protection have become controversial in recent years, because of two situations: first, a lack of understanding of the basis for the original criteria for protection of steel and cast iron; second, the several notable apparent corrosion failures of structures that were allegedly cathodically protected. It is likely that the criteria discussed in the paragraphs that follow will continue to be discussed and changed in the future.
Origins of Cathodic Protection Criteria. In the early days of cathodic protection there were several ideas on how cathodic protection could be achieved:

- Maintain uniform potentials on a structure, thus eliminating galvanic cells between different regions on the same structure.
- Shift the potential from a native, or unprotected potential, to a more negative protected potential (-50 to -300 mV)
- Shift the potential of a structure to a potential at which current would flow into the structure instead of away from it.

While all of the above criteria had advocates, and the merits of each were actively debated, it became apparent that each had serious limitations. Any complex structure such as a cross- country pipeline would invariably have different potentials depending on variables in the environment. Shifting a potential from a native, or unprotected, potential would require long-term records of what the unprotected potential had been and would also require that the environment remain unchanged over the useful life of the structure. Construction, changes in agricultural practices, and changes associated with shifts from rural to urban environments make the idea of an unchanging native potential relatively unlikely. Measuring current flow onto a structure is difficult to determine and requires trained personnel. A simpler criterion was obviously more desirable.

The -850 mV Cu/$CuSO_4$ Criterion. Many cathodic protection advocates had been using a criterion based on maintaining the potential at -850 mV with respect to a saturated copper/ copper-sulfate electrode (CSE) (Fig. 9). This practice had been used since the 1920s with apparent success (Ref 4, 5). During the time when cathodic protection criteria and standards were discussed, a series of studies of the native potentials of carbon steel and cast iron became available. These studies were summarized in a report by Romanoff at the U.S. National Bureau of Standards (Ref 4). Table 3 shows the potentials of carbon steel and cast iron in ambient temperature soils throughout North America (Ref 5). Based on these data, it is apparent that any carbon steel or cast iron structure that is at a potential of -850 mV is polarized by at least 50 mV. Since a shift of -70 mV will usually reduce the corrosion rate by a factor of 10 (Ref 6), it is obvious that using the -850 mV CSE criterion will limit corrosion of most steels to a small fraction of the corrosion of the same unprotected structure. Most structures at -850 mV will be shifted by hundreds of millivolts, and their corrosion rates will have been reduced to negligible amounts.

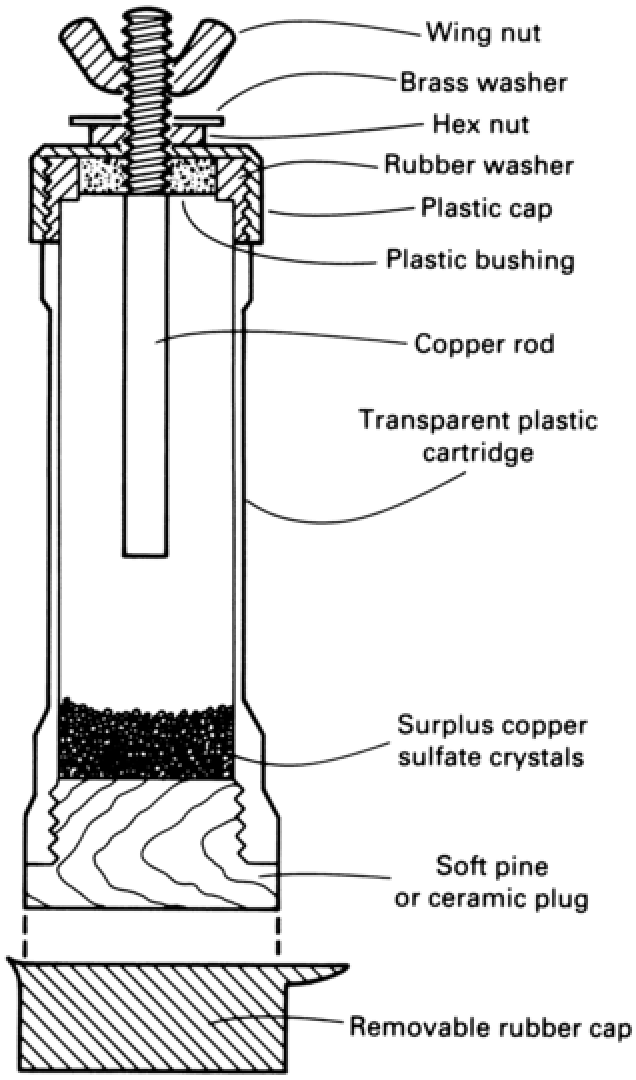

Fig. 9 Copper-saturated copper sulfate reference electrode

Table 3 Potentials of iron and steel in soil

Metal	Potential[a], mV
Mild steel (clean and shiny)	-500 to -800
Mild steel (rusted)	-200 to -500
Cast iron (not graphitized)	-500
High-silicon cast iron	-200
Mill scale on steel	-200

(a) Typical potential normally observed in neutral soils, and water, measured with respect to copper sulfate reference electrode. Source: Ref 5

This criterion has been adopted by many organizations worldwide (Ref 6, 7, 8, 9) due to its advantages:

- Technicians can easily learn how to measure this potential.
- Measurements are quick with simple field equipment.
- Historical records of previous measurements are not required.
- Potential is measured while the cathodic protection current is being applied. For many structures, it is difficult if not impossible to disconnect the cathodic protection current, so a “current-off” potential cannot be measured.

There is a disadvantage in that current-resistance (*IR*) losses must be considered.

Alleged Failures of Cathodic Protection Criteria. Unfortunately, a limited number of corrosion failures have been reported on structures where the -850 mV criterion has allegedly been maintained. Possible reasons for this discrepancy between predicted and actual performance are: (1) the potential was inaccurately measured, and (2) the conditions were not appropriate for this criterion. Several of the alleged failures of the -850 mV criterion were due to the presence of debonded organic coatings that made measurement of the potential of the steel underneath the debonded coating impossible.

Other problems have been identified on elevated-temperature pipelines and in anaerobic conditions. Both of these conditions have the effect of altering the polarization characteristics of cathodes, and it has become common practice to use -950 mV CSE as the protection potential in these conditions (Ref 9).

The Instant-Off Cathodic Protection Criterion. The -850 mV CSE criterion with the cathodic protection applied does not compensate for the *IR* potential drop that can be significant, especially in high resistivity environments. In recent years it has become common to apply an "instant-off" criterion, termed a "polarized potential" in the 1996 version of NACE RP0169 (Ref 7). The potential of the structure is measured immediately after the current is off and the voltage decays. The idea is to require that the structure surface be at -850 mV after the *IR* drop at the electrode surface is considered. The justification for this idea has been debated, but it becomes a more conservative criterion than the -850 mV with the current applied criterion. Unfortunately, the definition of "instant off" is subject to debate. Many structures, especially those with galvanic anodes, do not lend themselves to turning off their cathodic protection systems, so the applicability of this criterion is limited.

Other Criteria. In conditions where using one of the -850 mV criteria would require too much current it is common to use a -100 mV cathodic potential shift as the inspection criterion (Ref 6, 10, 11, 12, 13). It is sometimes impossible to measure the potential of a cathode surface. In these circumstances, a Tafel extrapolation (*E* log *i*) technique is commonly used (Fig. 10) (Ref 14). Other criteria such as a net current flow onto a structure and the use of test probes are also used, although they are no longer included in recent versions of NACE RP0169.

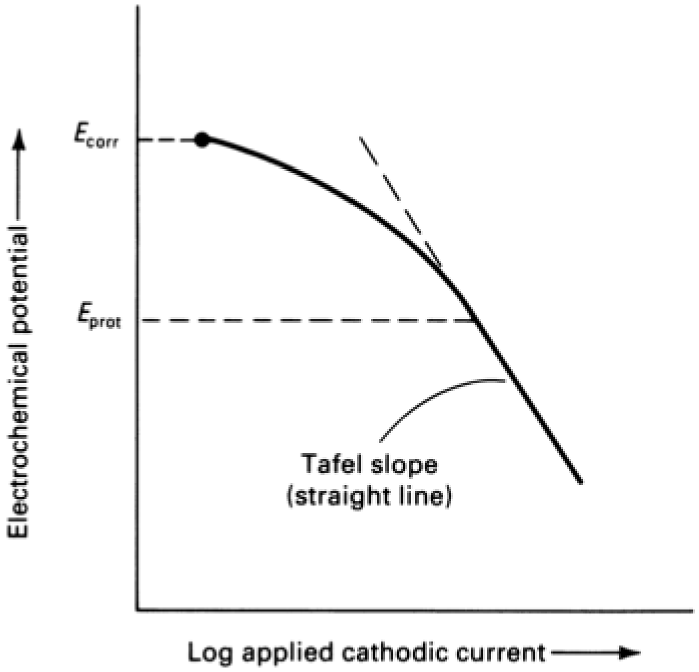

Fig. 10 Tafel slope criterion for determining cathodic protection (Ref 14). See the article "Kinetics of Aqueous Corrosion" in this Volume for detailed explanations of these diagrams.

Copper sulfate electrodes can become contaminated by seawater, so -800 mV versus silver/silver chloride is commonly used as the protection potential for marine structures. Both criteria are the same; only the reference electrode material is different.

Note that the sign convention used in this article agrees with that used by the U.S. cathodic protection industry. Much of the scientific and international literature uses the opposite sign convention for positive and negative electrical terminals. Regardless of the sign convention chosen, the important point is that electrons should flow into the protected structure from the external circuit.

References cited in this section

4. M. Romanoff, "Underground Corrosion," National Bureau of Standards Circular 579, 1957 republished by NACE, 1989, p 195

5. A.W. Peabody, *Control of Pipeline Corrosion,* National Association of Corrosion Engineers, 1967, p 5

6. W. Baeckmann and W. Schwenk, Fundamentals and Practice of Electrical Measurements, Chapter 3, *Handbook of Cathodic Corrosion Protection,* 3rd ed., Gulf Publishing, 1997, p 79–137

7. "Control of External Corrosion on Underground or Submerged Metallic Piping Systems," NACE RP0169, National Association of Corrosion Engineers

8. V. Ashworth, The Theory of Cathodic Protection and its Relation to the Electrochemical Theory of Corrosion, Chapter 1, *Cathodic Protection: Theory and Practice,* V. Ashworth and C.J.L. Booker, Ed., Ellis Horwood Ltd., Chichester, U.K., 1986, p 13–30

9. J. Beavers and K. Garrity, Criteria for Cathodic Protection, Chapter 4, *Control of Pipeline Corrosion,* A.W. Peabody, original author, R. Bianchetti, Ed., 2nd ed., NACE International, 2001, p 49–64

10. T. Barlo, "Origin and Validation of the 100 mV Polarization Criterion," Paper No. 01581, Corrosion 2001, NACE International, 2001

11. L. Kozewski, "Application of the 100 mV Polarization for Aboveground Storage Tank Bottoms," Paper No. 01591, Corrosion 2001, NACE International, 2001

12. J. Fitzgerald and T. Rizk, "Using rhw 100 mV Criterion in Industrial and Similar Facilities," Paper No. 01582, Corrosion 2001, NACE International, 2001

13. R. Pawson and R. McWilliams, "Bare Pipelines, the 100 mV Criterion & C.I.S. A Field Solution to Practical Problems," Paper No. 01587, Corrosion 2001, NACE International, 2001

14. J. Morgan, *Cathodic Protection,* Macmillan, 1960

R.H. Heidersbach, Cathodic Protection, *Corrosion: Fundamentals, Testing, and Protection,* Vol 13A*, ASM Handbook,* ASM International, 2003, p 855–870

Cathodic Protection

Robert H. Heidersbach, Dr. Rust, Inc.

Anode Materials

Different requirements for sacrificial anodes and impressed-current anodes lead to the use of different materials for these applications. Sacrificial anodes are anodic to steel in the environment of interest and must corrode reliably, avoiding passivation. Impressed-current anodes can be cathodic to steel, but they must have low consumption rates when connected to a cathodic protection power source.

Sacrificial Anodes

Commercial sacrificial anodes include magnesium, zinc, and aluminum alloys. The energy characteristics of these alloys are given in Table 4.

Table 4   Energy characteristics of sacrificial anode alloys

Alloy	Energy capability		Consumption rate	
	A · h/kg	**A · h/lb**	**kg/A · yr**	**lb/A · yr**
Aluminum-zinc-mercury	2750–2840	1250–1290	3.2–3.0	7.0–6.8
Aluminum-zinc-indium	1670–2400	760–1090	5.2–3.6	11.5–8.0
Aluminum-zinc-tin	920–2600	420–1180	9.4–3.4	20.8–7.4
Zinc	810	370	10.7	23.7
Magnesium	1100	500	7.9	17.5

Magnesium anodes are the only sacrificial anodes that are routinely specified for use in buried-soil applications. Most magnesium anodes in the United States are supplied with a prepackaged bentonite clay backfill in a permeable cloth sack (Fig. 1). This backfill ensures that the anode will have a conductive environment and will corrode reliably. The additional materials are less expensive than the soil-resistivity surveys that would be needed to determine whether the backfill is necessary.

Some magnesium anodes have been used offshore in recent years to polarize the structures to a protected potential faster than zinc or aluminum alloy anodes. Magnesium tends to corrode quite readily in salt water, and most designers avoid the use of magnesium for permanent long- term marine cathodic protection applications. Figure 11 shows a commonly used magnesium anode that controls corrosion on a glass-lined domestic water heater.

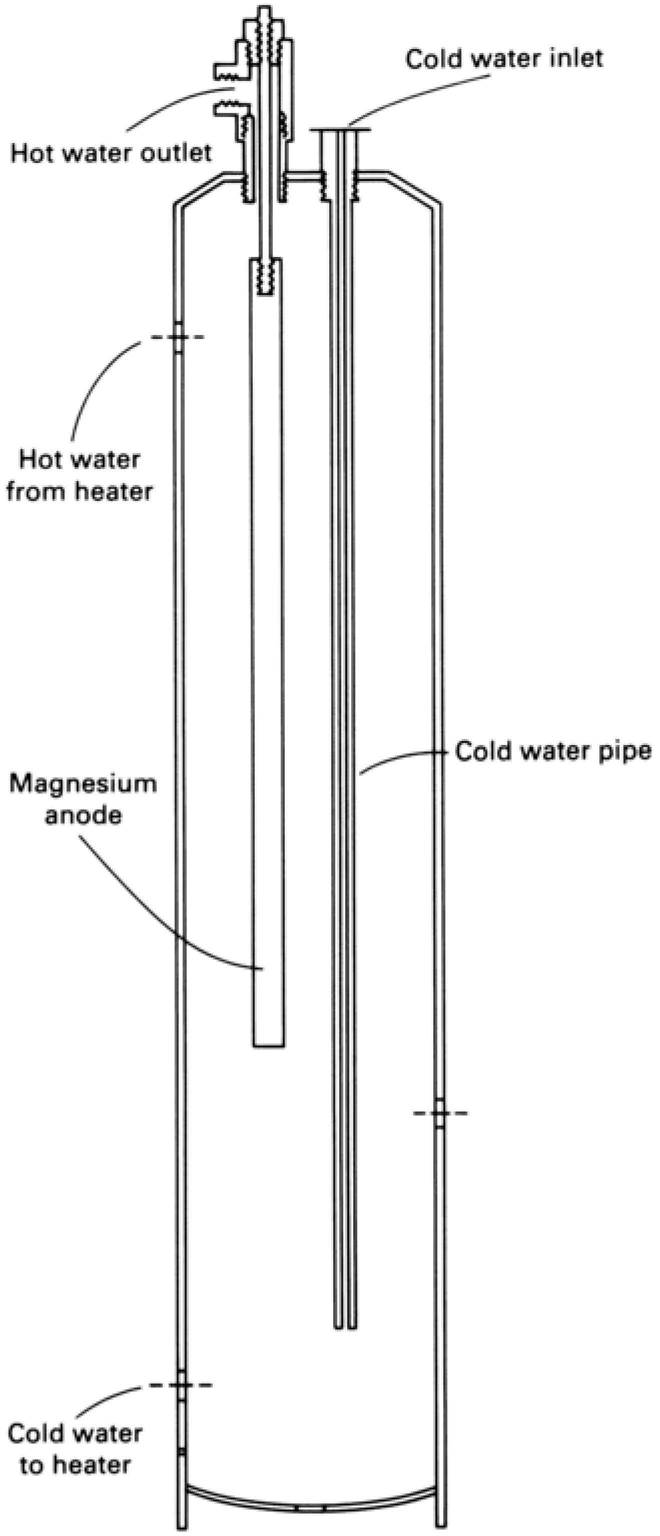

Fig. 11 Magnesium anode used to cathodically protect glass-lined steel water heater

Zinc is used for cathodic protection in freshwater and salt water. Zinc is especially well suited for cathodic protection on ships that move between salt water and harbors in brackish rivers or estuaries. Figure 12 shows zinc anodes on the underside of a small fishing boat. Aluminum anodes would passivate in the harbors and might not work when they return to sea. Zinc anodes are also used to protect ballast tanks, heat exchangers, and many mechanical components on ships, coastal power plants, and similar structures.

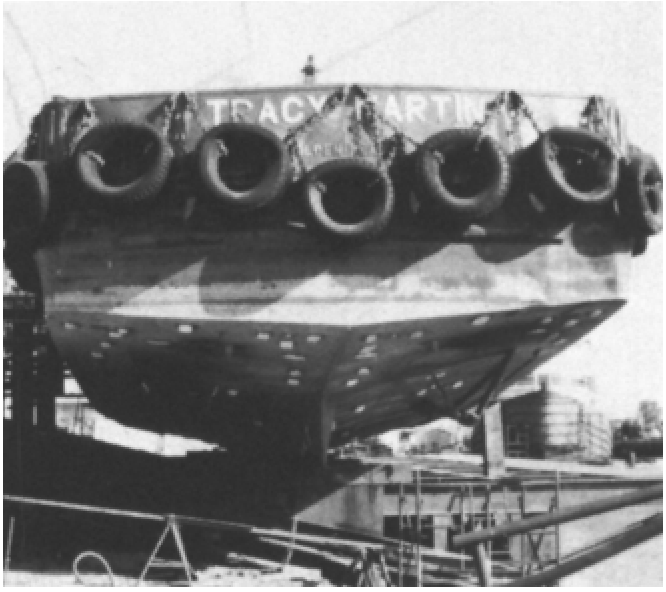

Fig. 12 Zinc anodes on the underside of a fishing boat

The weight of zinc is an advantage for marine pipelines. Bracelet anodes (Fig. 13) are attached at pipe joints to provide ballast and to prevent corrosion in the water-mud environment, in which aluminum might passivate.

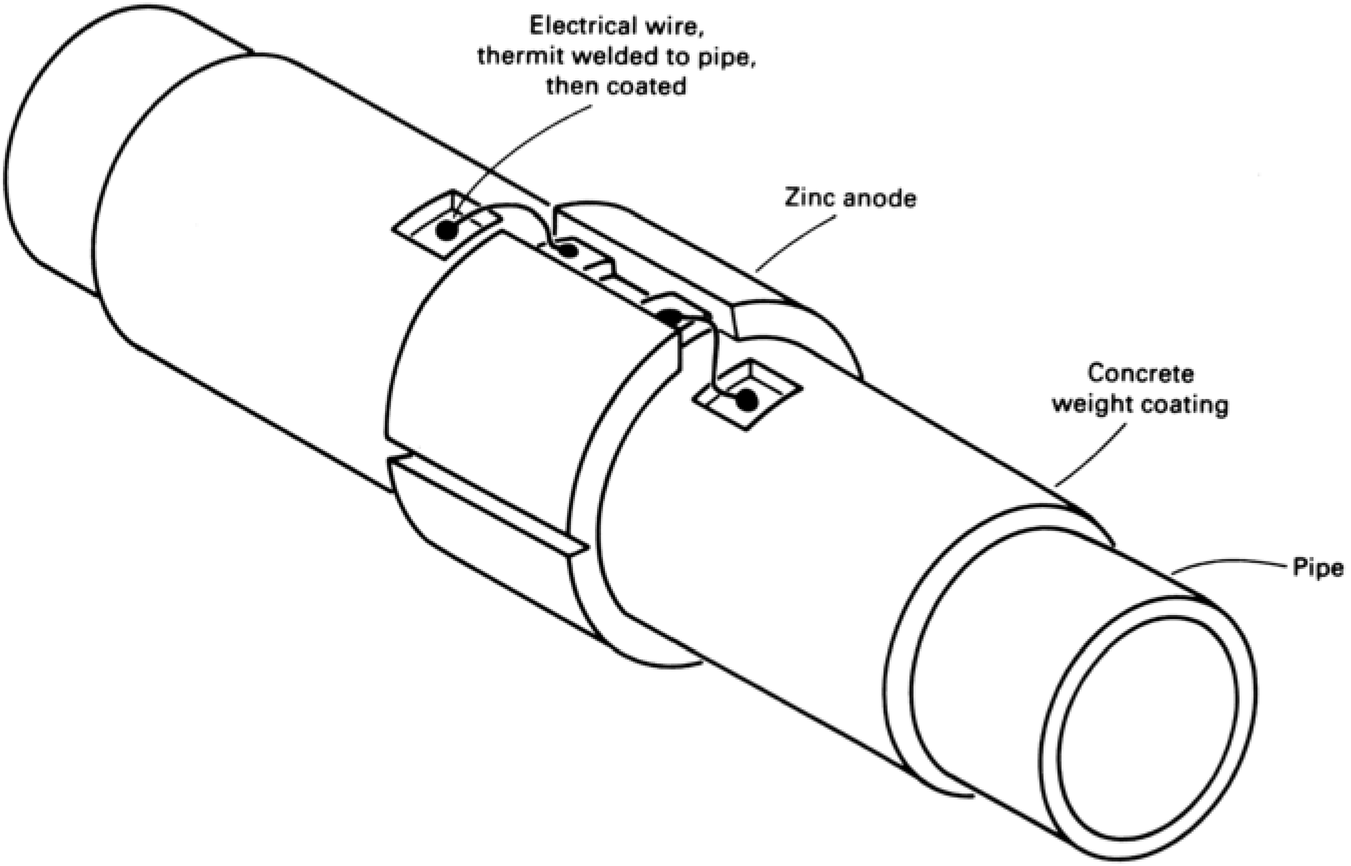

Fig. 13 Zinc bracelet anode at a joint in an offshore pipeline

Aluminum is used on offshore structures where its light weight provides significant advantages. Welded-on aluminum anodes for an offshore platform are shown in Fig. 4 and 14. Aluminum does not passivate in salt water if certain alloying elements, such as tin, antimony, and mercury, are present. Toxicity questions prevent the use of aluminum alloys with mercury additions in U.S. waters.

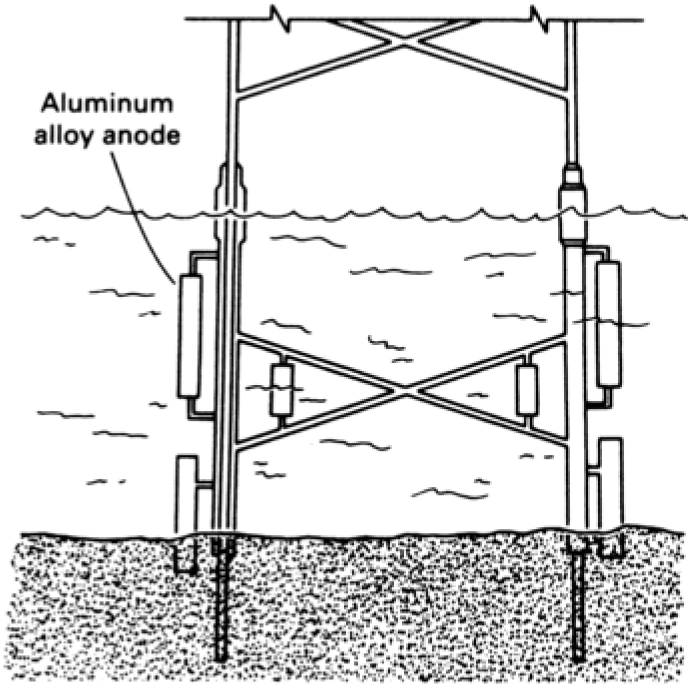

Fig. 14 Welded-on aluminum sacrificial anodes used to protect an offshore platform

Segregation of the alloying elements can lead to localized corrosion, which causes premature failure of the anodes. Figures 15(a) and (b) show examples of aluminum anodes that corroded differently because of differences in foundry practice.

(a)

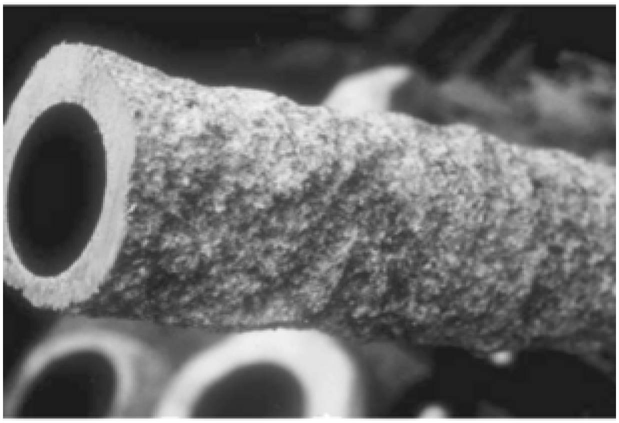

(b)

Fig. 15 Corrosion of aluminum anodes. (a) Uneven corrosion of aluminum anode, the result in part of improper foundry practice leading to segregation of alloying elements. (b) Uniform corrosion of aluminum anode as the result of proper foundry practice. Courtesy of Jack Smart, John S. Smart Consultants

Impressed-Current Anodes

Impressed-current anodes must be corrosion resistant and otherwise durable in the environment in which they are used. Consumption rates for lead alloy, platinum, graphite, and high-silicon cast iron impressed-current anode materials are given in Table 5.

Table 5 Consumption rates of impressed-current anode materials

Material	Typical anode current density		Consumption rate per A · yr
	A/m²	**A/ft²**	
Pb-6Sb-1Ag	160–220	15–20	0.045–0.09 kg (0.1–0.2 lb)
Platinum (plated on substrate)	540–1080	50–100	0.006 g (0.0002 oz)
Platinum (wire or clad)	1080–5400	100–500	0.01 g (0.0004 oz)
Graphite	10.8–40	1–4	0.225–0.45 kg (0.5–1.0 lb)
Fe-14Si-4Cr	10.8–40	1–4	0.225–0.45 kg (0.5–1.0 lb)

High-silicon cast iron (Fe-0.95C-0.75Mn- 14.5Si-4.5Cr) is used for onshore cathodic protection applications and in locations where abrasion resistance and other mechanical damage considerations are important. High-silicon cast iron anodes are available in solid rods, tubular form, and various cast shapes in a variety of sizes to meet the demands of specific applications. For example, solid rods range from 30 mm diameter by 230 mm long (1$\frac{1}{8}$ by 9 in.) at 0.45 kg (1 lb) to 115 mm diameter by 1525 mm long (4.5 by 60 in.) at 100 kg (220 lb). The smaller rods are used for protecting underground freshwater storage tanks, and the larger rods are used in more aggressive seawater or ground bed applications. Figure 7 shows a high-silicon cast iron button anode on a navigational lock on the Tennessee River. This anode must withstand collisions with small vessels, trees, rocks, and so on. The coating debonding shown in Fig. 7 is due to improper circuit design and cannot be attributed to the use of high-silicon cast iron anodes. Detailed information on designing impressed-current cathodic protection systems with high-silicon iron anodes is available in Ref 15.

Graphite anodes are extensively used for onshore pipelines where they can be buried in multiple-anode ground beds (Fig. 5). Graphite anodes, which have very low electrode-to-environment resistances, are normally available in 75 mm diameter by 1525 mm long (3 by 60 in.) and 100 mm diameter by 2000 mm (4 by 80 in.) rods. Because of the brittle nature of the material, graphite must be stored and handled carefully.

Polymeric anodes are used to mitigate the corrosion of reinforcing steel in salt-contaminated concrete (Fig. 16). The system consists of a mesh of wirelike anodes, which are made of a conductive polymer electrode material coated onto copper conductors. The conductive polymer not only serves as an active anode material, but it also shields the conductors from chemical attack. These mesh anodes are designed and spaced to provide long-term uniform protection at low current densities. The anode mesh is placed on the surface of a reinforced-concrete structure, covered with an overlay of Portland cement or polymer-modified concrete, and then connected to a low-voltage dc power source. The properties of polymeric anodes used for construction applications are given in Table 6.

Fig. 16 Two views of polymer mesh anodes used to protect reinforcing steel in bridge decks, parking garages, and other large structural surfaces. Courtesy of Raychem Corporation, Cathodic Protection Division

Table 6 Properties of polymeric mesh anodes used for construction applications

Properties	Typical data
Recommended maximum design current output in soil	52 mA/m (16 mA/ft) length[(a)]
Recommended maximum design current output in water	10 mA/m (3 mA/ft) length
Maximum pressure rating (hydrostatic)	7 MPa (100 psi)
Maximum temperature rating	65 °C (150 °F)
Minimum installation temperature	-18 °C (0 °F)
Chemical resistance per ASTM D 543 for 7 days at ambient conditions with weight gain less than 1%	
3% NaCl	Pass
3% Na_2SO_4	Pass
10% NaOH	Pass
ASTM oil No. 1	Not recommended
Crude oil	Not recommended

(a) Average current output for anode in coke breeze backfill when maximum current density is 82 mA/m (25 mA/ft). ASTM D 543, "Standard Test Method for Resistance of Plastics to Chemical Reagents."

Precious metals are used for impressed-current anodes because they are highly efficient electrodes and can handle much higher currents. Precious metal anodes are platinized titanium or tantalum anodes; the platinum is either clad to or electroplated on the substrate. The small precious metal anode shown in Fig. 17 performs the same function as materials weighing several times more.

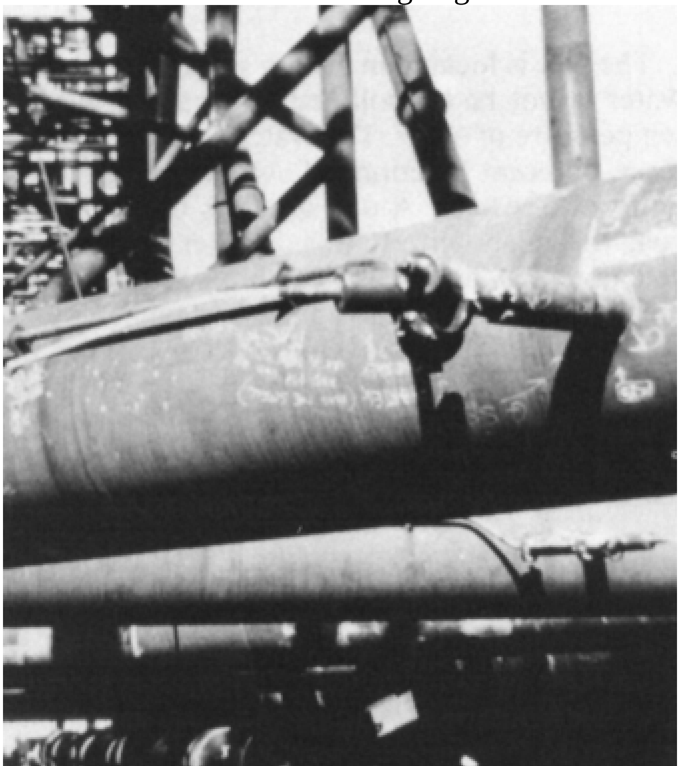

Fig. 17 Precious metal impressed-current anode on offshore platform prior to launching in the North Sea. Courtesy of W.H. Thomason, Conoco, Inc.

Lead alloy anodes, containing 2% Ag, or 1% Ag and 6% Sb, are used for cathodic protection systems in seawater. Lead alloy anodes should not be buried in the sea bottom or used in freshwater applications.

Ceramic anodes, also called mixed metal oxide anodes, are the newest materials available for anodes. They are supplied either as oxide coatings on transition metal substrates or as bulk ceramics. Their use as cathodic protection anodes for protecting reinforcing steel in concrete is new, but the oxide-coated transition metal anodes have been used since the late 1960s in industry as anodes for chlorine production and seawater electrolysis and cathodic protection of water tanks and buried steel structures, among other industrial processes.

The oxide/metal composite anodes for chlorine environments consist of a mixed ruthenium dioxide (RuO_2) and titanium oxide (TiO_2) coating sintered onto a pure titanium (grade 1) substrate (Ref 16). Such materials, which are produced in sheet, mesh, and wire form, are based on patented dimensionally stable anode (DSA) technology (Ref 16). These anodes are so named because they remain unchanged with regard to their shape, geometry, and dimensions during their entire operating life. Figure 18 shows examples of a mixed oxide/titanium mesh anode, based on DSA technology, that is used to prevent corrosion of reinforcing steel in concrete. The basic chemical constituents of the bulk ceramic anodes are suboxides of titanium, with Ti_4O_7 and Ti_5O_9 being the principal components. Such conductive ceramics are resistant to both oxidation and reduction in strong acid and basic environments. Some characteristic properties of conductive ceramics are given in Table 7.

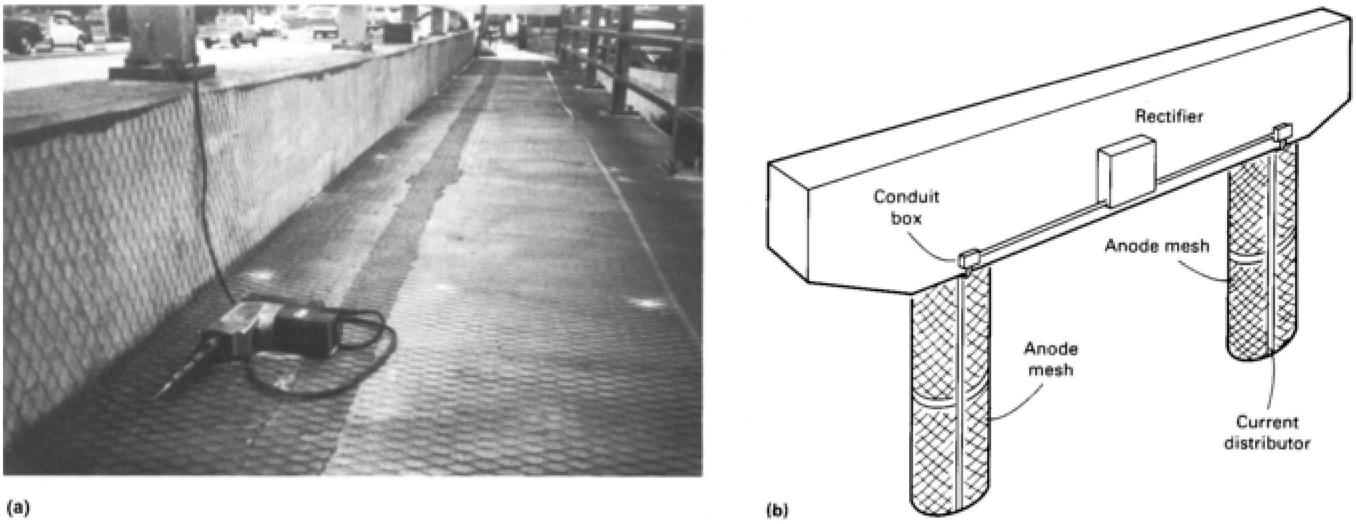

Fig. 18 Use of mixed oxide/titanium anode mesh for cathodic protection. (a) Sidewalk and barrier-wall installation. (b) Installation of anode mesh on a bridge substructure. Courtesy of ELTECH Systems Corporation

Table 7 Properties of bulk ceramic anode materials

Property	Value
Electrical resistivity	250–1000 × 10^{-6} Ω · cm. Resistivity decreases as density increases.
Thermal expansion	5 × 10^{-6}/°C
Thermal conductivity	10–20 W/m · K
Modulus of rupture	100 MPa (14.5 ksi) and higher. Some grades are 24–34 MPa (3.5–5.0 ksi) for special applications.
Melting point	1400 °C (2550 °F)
Density	2.5–4.0 g/cm^3
Thermal stability	Stable to 350 °C (660 °F) in air Stable to 1350 °C (2460 °F) for nonoxidizing atmosphere
Overpotentials at 20 °C (68 °F), mV	
1 *M* H_2SO_4 electrolyte	
Oxygen evolution	1712

Hydrogen evolution	784
1 *M* NaOH electrolyte	
Oxygen evolution	1674
Hydrogen evolution	624

References cited in this section

15. W.T. Bryan Ed., *Designing Impressed Current Cathodic Protection Systems with Durco Anodes,* 2nd ed., The Duriron Co. Inc., 1970

16. L.M. Ernes, "Characteristics and Advantages of the Dimensionally Stable Anode (DSAR)," ELTECH Systems Corp., March 19

R.H. Heidersbach, Cathodic Protection, *Corrosion: Fundamentals, Testing, and Protection*, Vol 13A, *ASM Handbook*, ASM International, 2003, p 855–870

Cathodic Protection

Robert H. Heidersbach, Dr. Rust, Inc.

Power Sources

Impressed-current cathodic protection requires a dc power source, the most common being rectified power from a local utility. Remote locations can use solar cells (Fig. 19), thermoelectric current sources, special fuel-driven electric generators, or windmills.

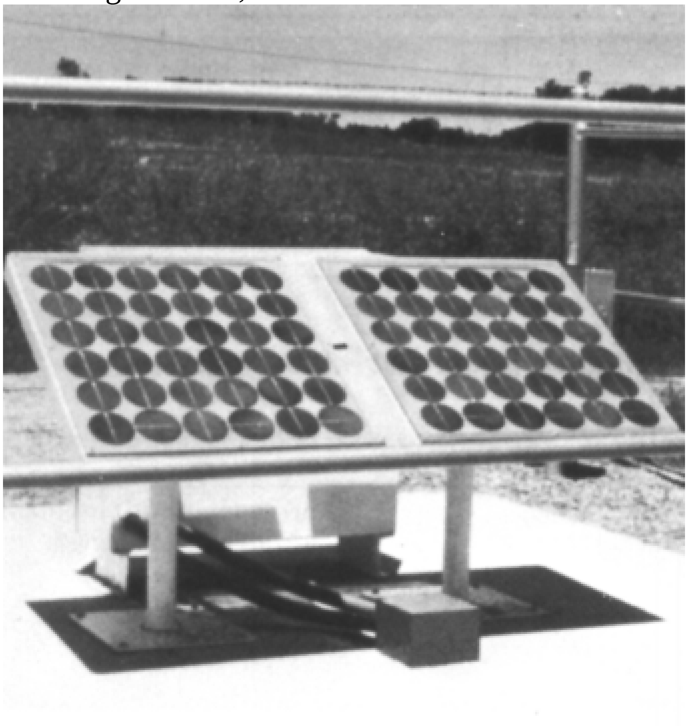

Fig. 19 Solar cells used to provide electricity for the cathodic protection of a buried pipeline

R.H. Heidersbach, Cathodic Protection, *Corrosion: Fundamentals, Testing, and Protection*, Vol 13A*, ASM Handbook,* ASM International, 2003, p 855–870

Cathodic Protection

Robert H. Heidersbach, Dr. Rust, Inc.

Design

Most cathodic protection systems are designed by consulting companies that specialize in corrosion control. Design procedures vary among organizations, but the following general guidelines are frequently followed for onshore buried structures (Ref 17):

- Decide whether impressed-current or sacrificial anodes will be used.
- Decide on the design life of the system.
- Determine or assume the condition of the coating. From this, the current density for cathodic protection can be estimated.
- Calculate the maximum electric current required.
- Determine the number and type of anodes required and their respective spacing.
- Calculate the ground bed resistance. Figure 20 shows the effect of soil resistivity and pH on the corrosion of zinc sacrificial anodes.
- Calculate the lead wire size.
- Calculate the required dc voltage.
- Determine the rectifier size.
- Locate the ground bed.

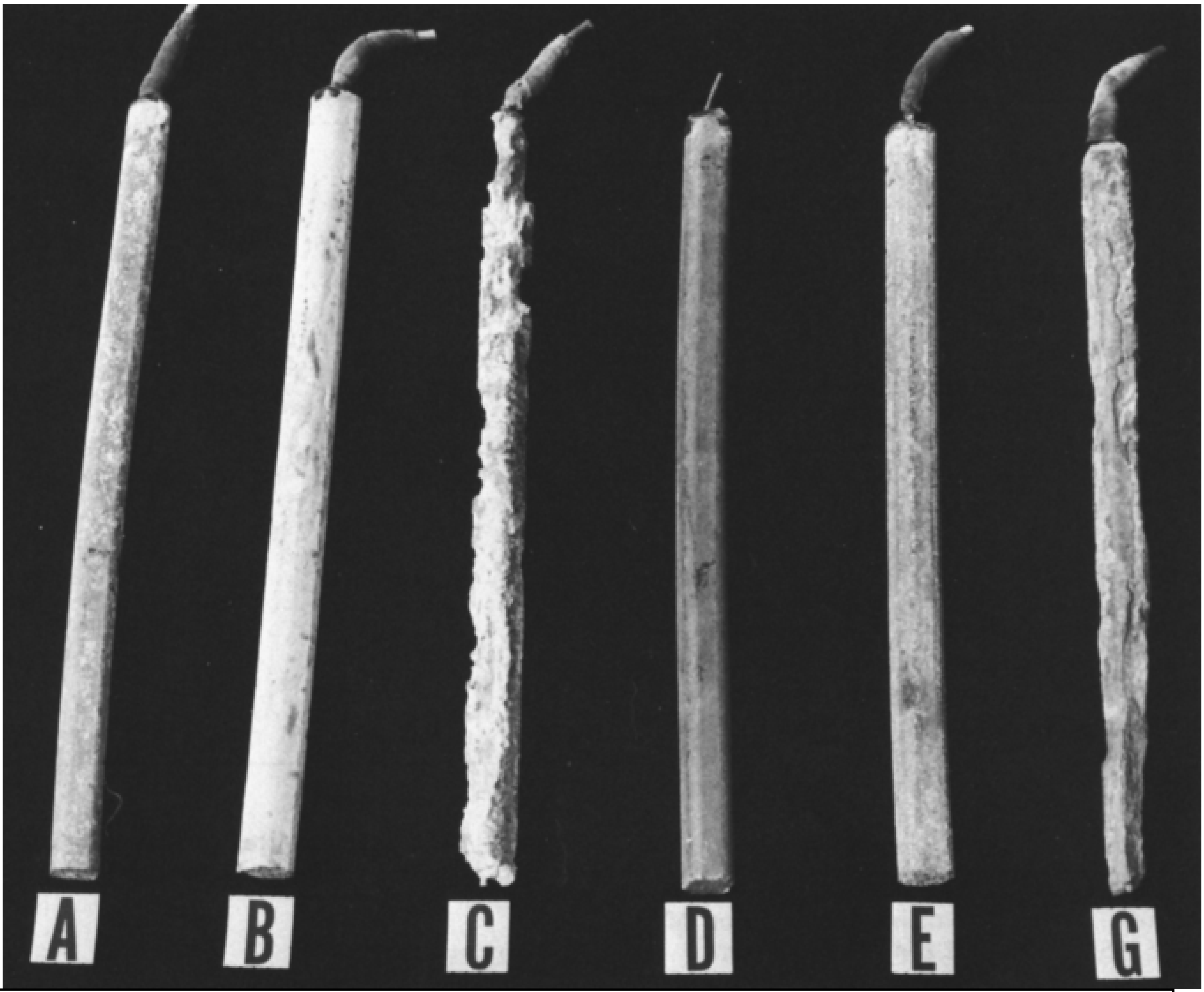

Site	Soil	Location	Internal drainage	Range of resistivity, Ω · cm	pH
A	Sagemoor sandy loam	Toppenish, WA	Good	400	8.8
B	Hagerstown loam	Loch Raven, MD	Good	12,600–37,300	5.3
C	Clay	Cape May, NJ	Poor	400–1,150	4.3
D	Lakewood sand	Wildwood, NJ	Good	13,800–57,500	5.7
E	Coastal sand	Wildwood, NJ	Poor	1,320–49,500	7.1
G	Tidal marsh	Patuxent, MD	Poor	400–15,500	6.0

Fig. 20 Corrosion of zinc anodes that were galvanically connected to type 304 stainless steel for four years at six different underground test sites. Courtesy of E. Escalante, National Bureau of Standards

Computers have changed some cathodic protection design, test, and inspection procedures (Ref 18, 19, 20), but most cathodic protection is still designed and tested in the manner described in U.S. government publications from the 1960s and 1970s (Ref. 17, 21, 22, 23).

References cited in this section

17. *Electrical Design—Corrosion Control,* Technical Manual TM5-811-4, U.S. Army, 1962

18. R. Heidersbach, J. Fu, and R. Erbar, Ed., *Computers in Corrosion Control,* National Association of Corrosion Engineers, 1986

19. P. Pierson, K. Bethune, W. Hartt, and P. Anathakrishnan, "A Novel Approach to Cathodic Protection Design for Marine Pipelines: Part I—An Inclusive Attenuation Equation," Paper No. 00673, Corrosion 2000, NACE International, 2000

20. H. Hafnor and B. Amundsen, "Computerized Cathodic Protection Operation and Monitoring Buried Pipelines," Paper No. 00728, Corrosion 2000, NACE International, 2000

21. L. West and T. Lewicki, *Corrosion Control—General,* Vol I, *Civil Engineering Corrosion Control,* NTIS AD/A-004 082, Air Force Civil Engineering Center, TR 74-6, Jan 1975

22. L. West and T. Lewicki, *Cathodic Protection Testing Methods and Instruments,* Vol II, *Civil Engineering Corrosion Control,* NTIS AD/A-004 083, Air Force Civil Engineering Center, TR 74-6, Jan 1975

23. L. West and T. Lewicki, *Cathodic Protection Design,* Vol III, *Civil Engineering Corrosion Control,* NTIS AD/A-006 400, Air Force Civil Engineering Center, TR 74-6, Jan 1975

R.H. Heidersbach, Cathodic Protection, *Corrosion: Fundamentals, Testing, and Protection,* Vol 13A, *ASM Handbook*, ASM International, 2003, p 855–870

Cathodic Protection

Robert H. Heidersbach, Dr. Rust, Inc.

Case Histories

The examples in this section have been selected to familiarize the design engineer with the steps to follow in selecting a specific corrosion- control method. Other examples are available in Ref 17, and 21 to 23 and in the cathodic protection training course offered by NACE International.

Resistance Calculations*

The resistance of impressed-current anodes buried in soil can be lowered by surrounding them with carbonaceous backfill material, such as coke breeze (crushed coke) or flake graphite. This is particularly beneficial in high-resistance soils. If soil resistance is ten or more times the backfill resistivity—500 to 1000 Ω · cm—the voltage drop of anode current passing through the backfill may become negligible with respect to the voltage drop through the soil. Thus, the resistance of a backfilled anode can be considered to be lower than that of a nonbackfilled anode because the backfilled anode is effectively longer and of greater diameter.

Increasing the diameter and/or the length of a cylindrical anode will decrease its anode-to-electrolyte resistance. Changes in length have a greater effect.

Many engineers first measure structure-to-anode resistance by actually impressing current into installed anodes. In this way, a rectifier can be sized to fit the circuit resistance without relying on questionable test and empirical data. Testing installed anodes for the purpose of sizing rectifiers has the disadvantage of delaying completion of an installation. However, it means that sufficient cathodic protection current will be supplied in an efficient manner.

Single Anode Resistance (Ref 15). For a vertical anode, the electrolyte-to-anode resistance (R_v) is:

$$R_v = \frac{0.0052\rho}{L}\left(2.3\log 10\frac{8L}{d} - 1\right)$$

For a horizontal anode:

$$R_h = \frac{0.0052\rho}{L}\left(2.3\log 10\frac{4L^2 + 4L\sqrt{s^2 + L^2}}{ds} + \frac{s}{L} - \frac{\sqrt{s^2 + L^2}}{L} - 1\right)$$

where resistance is to remote reference (in ohms), ρ is the electrolyte resistivity (in Ω · cm), L is the length of anode (in feet), d is the diameter of anode (in feet), and s equals twice the depth of the anode (in feet).
For a single vertical anode, a simplified expression can be used:

$$R_v = \frac{\rho}{L}K$$

where R_v, ρ, and L are as given previously, and K is the shape function representing the anode length to anode diameter ratio, which can be obtained from Table 9.

Table 9 The shape function, *K*, obtained by dividing the anode length by the anode diameter in any units

L/*d*	*K*
5	0.0140
6	0.0150
7	0.0158
8	0.0165
9	0.0171
10	0.0177
12	0.0186
14	0.0194
16	0.0201
18	0.0207
20	0.0213
25	0.0224
30	0.0234
35	0.0242
40	0.0249
45	0.0255
50	0.0261
55	0.0266
60	0.0270

One-Row Vertical Anode Group. The total anode-to-electrolyte resistance for a group of vertical anodes, connected in parallel and equally spaced in one row, is expressed as:

$$R_n = \frac{1}{n}R_v + \frac{\rho\rho P}{S}$$

where R_n is the total anode-to-electrolyte resistance (in ohms) for a group of vertical anodes equally spaced and in one row (a remote cathode is assumed), n is the number of anodes, ρρ is the soil resistivity, measured with pin spacing equal to S (in Ω · cm), R_v is as given previously, P is the paralleling factor obtained from Table 10, and S is the spacing between adjacent anodes (in feet).

Table 10 Paralleling factor used for determining anode resistance

n	*P*
2	0.00261

3	0.00289
4	0.00283
5	0.00268
6	0.00252
7	0.00237
8	0.00224
9	0.00212
10	0.00201
12	0.00182
14	0.00168
16	0.00155
18	0.00145
20	0.00135
22	0.00128
24	0.00121
26	0.00114
28	0.00109
30	0.00104

A vertical anode group composed of two or more rows, separated by a distance substantially larger than that between the anodes within a single row, has a total resistance approximately equal to the total parallel resistance of all the rows. The formula for parallel resistance is used:

$$\frac{1}{R}=\frac{1}{R_1}+\frac{1}{R_2}+\frac{1}{R_3}+\cdots$$

Vertical and Horizontal Anode Groups— Simplified. If vertical anode dimensions are assumed to be 8 to 12 in. in diameter and 10 ft in length and if the horizontal anode dimensions are assumed to be 1 ft^2 in cross section, 10 ft in length, and 6 ft below the surface of the electrolyte (these assumptions are useful when designing anode system with high-silicon cast iron anodes in soils in which effective backfill has been installed around the anodes), then the following empirical formula can be used:

$$R_v=\frac{\rho F}{537} \quad R_h=\frac{\rho F}{483}$$

where R_v is the electrolyte-to-anode resistance, any number of vertical anodes to remote reference (in ohms), R_h is the electrolyte-to-anode resistance, any number of horizontal anodes to remote reference (in ohms), ρ is the electrolyte resistivity (in Ω · cm), and *F* is the adjusting factor for groups of anodes (from Table 11). Note: where only one anode is used, *F* = 1.0.

Table 11 Adjusting factors, *F*, for parallel anodes

Number of anodes in parallel	Adjusting factors for indicated anode spacing, ft				
	5	**10**	**15**	**20**	**25**
2	0.652	0.576	0.551	0.538	0.530
3	0.586	0.460	0.418	0.397	0.384
4	0.520	0.385	0.340	0.318	0.304
5	0.466	0.333	0.289	0.267	0.253
6	0.423	0.295	0.252	0.231	0.218
7	0.387	0.265	0.224	0.204	0.192
8	0.361	0.243	0.204	0.184	0.172
9	0.332	0.222	0.185	0.166	0.155
10	0.311	0.205	0.170	0.153	0.142
11	0.292	0.192	0.158	0.141	0.131
12	0.276	0.180	0.143	0.132	0.122
13	0.262	0.169	0.139	0.123	0.114

14	0.249	0.160	0.131	0.116	0.107
15	0.238	0.152	0.124	0.109	0.101
16	0.226	0.144	0.117	0.103	0.095
17	0.218	0.138	0.112	0.099	0.091
18	0.209	0.132	0.107	0.094	0.086
19	0.202	0.127	0.102	0.090	0.082
20	0.194	0.122	0.098	0.086	0.079
22	0.182	0.114	0.091	0.079	0.073
24	0.171	0.106	0.085	0.074	0.067
26	0.161	0.100	0.079	0.069	0.063
28	0.152	0.094	0.075	0.065	0.059
30	0.145	0.089	0.070	0.061	0.056

Approximate anode-to-electrolyte resistance values for single anodes are quickly and easily obtained from:

- $R_v = 0.002\rho$ for a vertically installed 60 in. anode in a 10 ft column of backfill, 1 ft in diameter
- $R_v = 0.005\rho$, for a vertically installed 2 by 60 in. anode, without backfill
- $R_v = 0.006\rho$, for a vertically installed $1\frac{1}{2}$ by 60 in. anode, without backfill
- R = anode-to-electrolyte resistance for a single anode (Ω)
- ρ = resistivity of electrolyte (Ω · cm)

Cathodic Protection of Steel Structures*

Example 1: Use of Zinc Sacrificial Anodes to Protect a Pipe Pile Structure. A pier structure 20 ft wide extending 150 ft from the shore consists of sixteen 16 in. diam steel pipe piles, 40 ft long, that support the pier deck. The piles will be driven so that 14 ft will be in the soil zone, 8 ft in the submerged zone, 3 ft in the tidal zone, and 5 ft in the atmospheric/splash zone (Fig. 21).

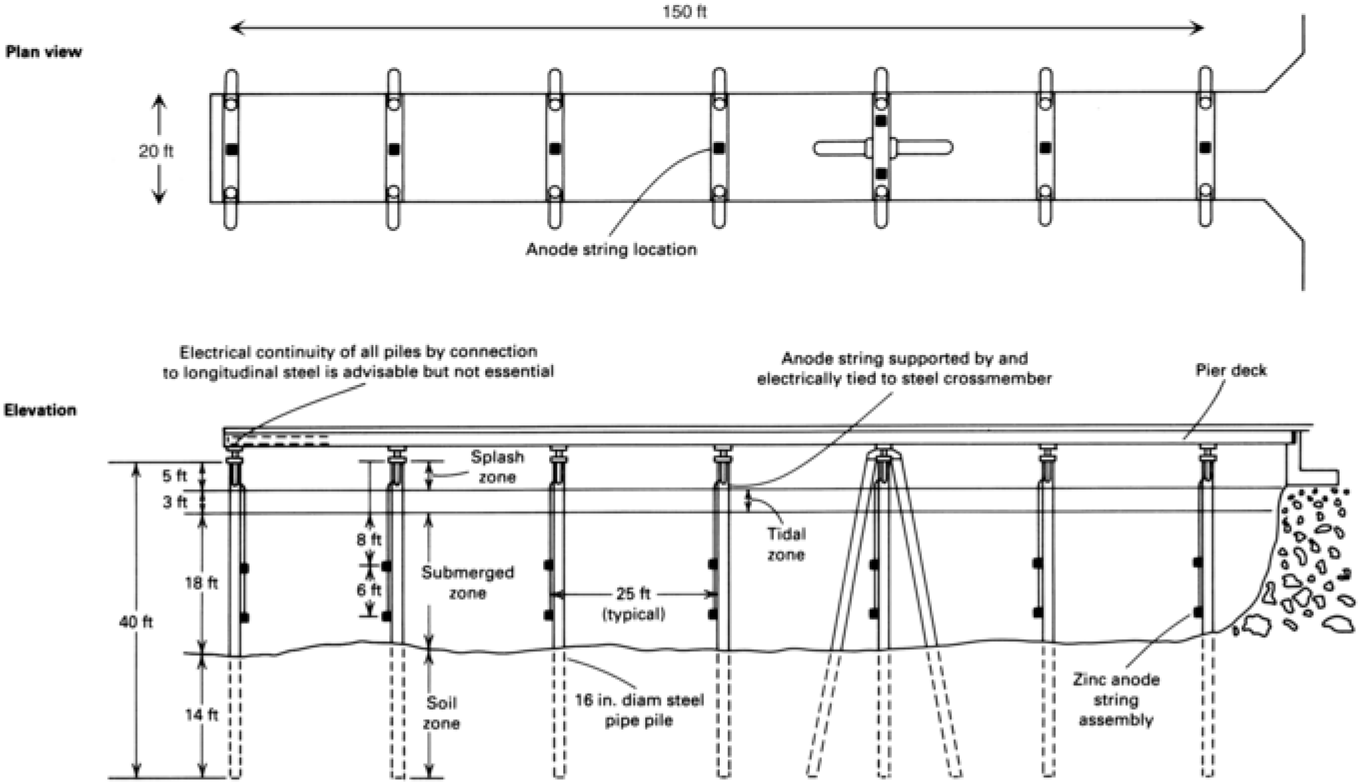

Fig. 21 Example 1. Outline of pier protected with a protective coating and sacrificial anodes

The pier is located in a calm saltwater bay. The water is not badly polluted and has an average temperature of 62 °F. The water samples taken at three different locations show an average resistivity of 25 Ω · cm. A decision

has been made to coat the piles with 16 mil dry-film thickness of coal tar epoxy and to apply cathodic protection in the form of a sacrificial-anode system. The design life is 20 years.

Calculation of Steel Areas Exposed to the Specified Zones. Table 12 is a guide to required current densities. For this example, the areas and current requirements are summarized in Table 13.

Table 12 Current densities required for coated and uncoated steel in moving and stagnant seawater and in soil areas

Environment	Current density, mA/ft^2			
	Bare steel		**Coated steel**	
	To polarize	**After polarization**	**To polarize**	**After polarization**
Moving seawater	30–35	7–10	3–5	1.0–1.5
Stagnant seawater	15–25	4–7	1–3	0.5–1.0
Soil zone	4–5	1–1.5	0.5–1.0	0.1–0.5

Table 13 Design of zinc sacrificial anode system for a pipe pile structure

Quantity	Symbol or formula	Zone			
		Tidal	**Submerged**	**Soil**	**Atmospheric splash**
Calculation of areas in specific zones					
Pipe diameter, ft	D	1.33	1.33	1.33	1.33
Number of piles	n	16	16	16	16
Length	l	3	18	14	5
Exposed area, ft^2	$A = \pi nDl$	200	1200	940	335
Assumed damage at installation, %	d	10	15	50	…
Bare steel area, ft^2	$A_b = dA$	20	180	470	…
Coated steel area, ft^2	$A_c = A - A_b$	180	1020	470	…
Calculation of current requirements based on Table 11					
Current density to polarize bare steel, mA/ft^2	i_{pb}	35	35	5	…
Current density to polarize coated steel, mA/ft^2	i_{pc}	5	5	1	…
Current density to maintain bare steel, mA/ft^2	i_{mb}	35	10	1.5	…
Current density to maintain coated steel, mA/ft^2	i_{mc}	5	1.5	0.5	…
Current to polarize bare steel, A	$I_{pb} = i_{pb} \cdot A_b$	0.7	6.3	2.3	…
Current to polarize coated steel, A	$I_{pc} = i_{pc} \cdot A_b$	0.9	5.1	0.5	…
Current to maintain bare steel, A	$I_{mb} = i_{mb} \cdot A_b$	0.7	1.8	0.7	…
Current to maintain coated steel, A	$I_{mc} = i_{mc} \cdot A_b$	0.9	1.5	0.2	…
Current to polarize entire structure, 15.8 A	$I_{pol} = \Sigma I_{pb} + \Sigma I_{pc}$				
Current to maintain entire structure, 5.8A	$I_{prot} = \Sigma I_{mb} + \Sigma I_{mc}$				
Estimated deterioration in 20 year design life. Assume 2%/yr loss of coating in tidal and submerged zone, and none in soil					
Initial coated steel area, %	$c = 100 - d$	90	85	50	…
Deterioration in 20 yr, %	…	40	40	0	…
Coated after 20 yr, %	c'	50	45	50	…

Bare after 20 yr, %	$b' = 100 - c'$	50	55	50	…
Bare steel after 20 yr, ft^2	$A_{b20} = b' \cdot A$	100	660	470	…
Coated steel after 20 yr, ft^2	$A_{c20} = c' \cdot A$	100	540	470	…
Current to maintain bare steel after 20 yr, A	$I_{mb20} = i_{mb} \cdot A_{b20}$	3.5	6.6	0.7	…
Current to maintain coated steel after 20 yr, A	$I_{mc20} = i_{mc} \cdot A_{c20}$	0.5	0.8	0.2	…
Current to maintain entire structure, 12.3 A	$I_{prot20} = \Sigma I_{mb20} + \Sigma I_{mc20}$				

Anode Design Calculations. The average total current ($\bar{I}$) required to maintain protection of the entire structure for 20 year life is:

$$\bar{I} = \frac{I_{prot} + I_{prot20}}{2}$$

$$\bar{I} = \frac{5.8 + 12.3}{2} = 9.1 \text{ A}$$

where I_{prot} is the current to initially maintain the structure and I_{prot20} is the current required after 20 years (Table 13).

The total weight of high-purity zinc anode material required for 20 year life expectancy is:

$$W = \frac{CR + L \times ATC}{E \times U}$$

where *W* is the weight (in pounds), *CR* is the consumption rate (in lb/A · yr), *L* is the life (in years), *ATC* is the average total current (in amps), *E* is the efficiency factor, and *U* is the utilization factor:

$$W = \frac{23.585 \times 20 \times 9.1}{0.90 \times 0.85} = 5611 \text{ lb}$$

Based on the structure description and the amount of zinc required, it is determined that for this structure eight strings of two 390 lb (10 by 10 by 15 in.) zinc anodes (6240 lb) suspended at the locations shown in Fig. 21 should afford adequate protection for the 20 year life expectancy. The other factor to consider in a galvanic anode system is the amount of current that can be discharged from the anodes.

Resistance of the Anode Systems. The 390 lb anode measures 10 by 10 by 15 in. The outside perimeter of the anode is 40 in. The diameter of a cylindrical object whose circumference is 40 in. is 12.73 in., or 1.06 ft. The anode spacing is 25 ft. Using the formula from the section "Resistance Calculations" in this article for a single anode, the resistance of one 390 lb anode is:

$$R_v = \frac{0.0052\rho}{L}\left[2.3\log\frac{8L}{d} - 1\right]$$

$$= \frac{(0.0052)(25)}{(15/12)}\left[2.3\log\frac{(8)(15/12)}{1.06} - 1\right]$$

$$= 0.129\ \Omega$$

The resistance of the anode system from the Sunde equation is (Ref 25):

$$R_s = \frac{0.00521\rho}{nL}\left[2.3\log\frac{8L}{d} - 1 + \frac{2L}{S}2.3\log 0.656n\right]$$

where R_v is the resistance of one vertical anode (in ohms), R_s is the resistance of the anode system (in ohms), *n* is the number of anodes, *L* is the length of anode (in feet), ρ is the water resistivity (Ω · cm), *d* is the diameter of anode (in feet), *S* is the spacing between anodes (in feet):

$$R_s = \frac{(0.0052)(25)}{(8)(2)(15/12)}\left[2.3\log\frac{(8)(2)(15/12)}{1.06} - 1 + \frac{(2)(2)(15/12)}{25}2.3\log 0.656(8)\right]$$

$$= 0.0147 \text{ ohm}$$

Anode system output:

$$I = \frac{E}{R_s}$$

where E is the driving potential.

Driving voltage of galvanic anode to polarized coated steel is of the order of 0.10 V:

$$E = 1.1 \text{ V} - 1.00 \text{ V} = 0.10 \text{ V}$$

$$I \text{ available after polarization} = \frac{0.10}{0.0147} = 6.8 \text{ A}$$

The 6.8 A output after polarization is greater than the 5.8 A required for the total current requirements given above. Therefore, the current requirement is satisfied.

To verify that life expectancy is met, the average total current $\bar{I}$ output for 20 year life is calculated:

$$I = \frac{6.8 + 12.3}{2} = 9.6 \text{ A}$$

Total weight of anode material required:

$$W = \frac{23.585 \times 20 \times 9.6}{0.90 \times 0.85}$$

$$= 5919 \text{ lb}$$

The total weight of the anode material used is 8 × 2 × 390 = 6240 lb. Therefore, the life expectancy is satisfied.

Example 2: Use of Impressed-Current Anodes to Protect an H-Pile Structure. A 30 ft wide pier structure that extends 200 ft from shore is supported by 20 H-piles that are 92 ft long. The H-piles are connected in four-pile clusters by W shapes. The piles are to be driven so that 50 ft will be below the dredged mud line, 30 ft in the submerged zone, 4 ft in the tidal zone, and 8 ft in the atmospheric/splash zone (Fig. 22). The pier is located in a saltwater bay in a highly commercial and industrial area. There are commercial, industrial, chemical, and sewage pollutants. The water samples taken at three different locations show an average resistivity of 30 Ω · cm.

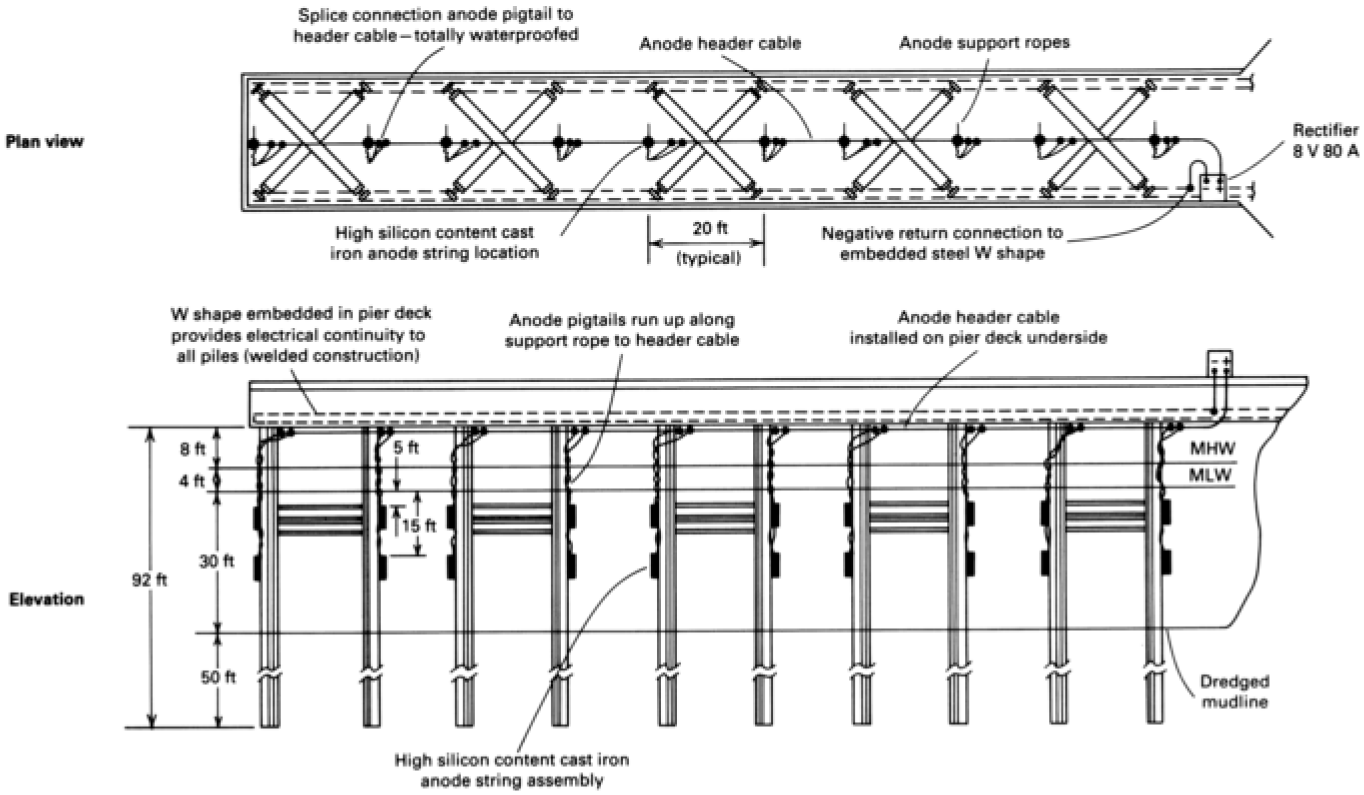

Fig. 22 Example 2. Outline of H-pile pier protected using a protective coating and impressed-current anodes

A decision has been made to coat the H-piles and beams with a vinyl coating of 10 mil dry- film thickness and to apply cathodic protection in the form of an impressed-current system. The cathodic protection system should be designed and a cost estimate of the coating and cathodic protection system should be made for a 20 year life expectancy. The 10 cross braces and the 20 vertical H-piles have a surface area of 8 ft^2 per linear foot. Exposed areas of steel in specific zones are calculated in Table 14. The required impressed current is then determined based on the current density guide of Table 11.

Table 14 Design of impressed-current system for an H-pile structure

Quantity	Symbol or formula	Zone			
		Tidal	**Submerged**	**Soil**	**Atmospheric splash**
Calculation of areas in specific zones					
H-pile surface area/ft	*a*	8	8	8	8
Number of piles	*n*	20	20	20	20
Length	*l*	4	30	50	8
Exposed area, ft^2	$A = anl$	640	4800	8000	1280
Number of cross braces	*n*	…	10	…	…
Length of cross braces	*l*	…	30	…	…
Exposed area of cross braces, ft^2	$A = anl$	…	2400	…	…
Total exposed area (submerged zone), ft^2		…	7200	…	…
Assumed damage at installation, %	*d*	5	5	60	…
Bare steel area, ft^2	$A_b = dA$	32	360	4800	…
Coated steel area, ft^2	$A_c = A - A_b$	608	6840	3200	…
Calculation of current requirements based on Table 11					
Current density to polarize bare steel, mA/ft^2	i_{pb}	35	35	5	…

Current density to polarize coated steel, mA/ft^2	i_{pc}	5	5	1	…
Current density to maintain bare steel, mA/ft^2	i_{mb}	35	10	1.5	…
Current density to maintain coated steel, mA/ft^2	i_{mc}	5	1.5	0.5	…
Current to polarize bare steel, A	$I_{pb} = i_{pb} \cdot A_b$	1.1	12.6	24.0	…
Current to polarize coated steel, A	$I_{pc} = i_{pc} \cdot A_b$	3.0	34.2	3.2	…
Current to maintain bare steel, A	$I_{mb} = i_{mb} \cdot A_b$	1.1	3.6	7.2	…
Current to maintain coated steel, A	$I_{mc} = i_{mc} \cdot A_b$	3.0	10.3	1.6	…
Current to polarize entire structure, 78.1 A	$I_{pol} = \Sigma I_{pb} + \Sigma I_{pc}$				
Current to maintain entire structure, 26.8 A	$I_{prot} = \Sigma I_{mb} + \Sigma I_{mc}$				
Estimated deterioration in 20 year design life. Assume 2%/yr loss of coating in tidal, 1%/yr submerged zone, and 0.5%/yr in soil					
Initial coated steel area, %	c = 100 - d	95	95	40	…
Deterioration in 20 yr, %	…	40	20	10	…
Coated after 20 yr, %	c'	55	75	30	…
Bare after 20 yr, %	$b' = 100 - c'$	45	25	70	…
Bare steel after 20 yr, ft^2	$A_{b20} = b' \cdot A$	288	1800	5600	…
Coated steel after 20 yr, ft^2	$A_{c20} = c' \cdot A$	352	5400	2400	…
Current to maintain bare steel after 20 yr, A	$I_{mb20} = i_{mb} \cdot A_{b20}$	10.1	18.0	8.4	…
Current to maintain coated steel after 20 yr, A	$I_{mc20} = i_{mc} A_{c20}$	1.8	8.1	1.2	…
Current to maintain entire structure, 47.6 A	$I_{prot20} = \Sigma I_{mb20} + \Sigma I_{mc20}$				

Anode Design Calculations. The anode material is high-silicon content cast iron. Consumption rate is 0.75 lb/A · yr. The average total current $\bar{I}$ required for 20 year life is:

$$\bar{I} = \frac{I_{prot} + I_{prot20}}{2} = \frac{26.8 + 47.6}{2} = 37.2 \text{ A}$$

Total weight of anode material required for 20 year life expectancy:

$$W = \frac{CR \times L \times ATC}{U}$$

where *CR*, *ATC*, and *U* are as given in Example 1. In impressed-current systems, the efficiency factor, *E*, is 100% (compared to 90% for sacrificial-anode systems):

$$W = \frac{0.75 \text{ lb/A} \cdot \text{yr} \times 20 \text{ yr} \times 37.2 \text{ A}}{0.50} = 1116 \text{ lb}$$

The total number of anodes will be determined by taking into consideration the water depth, number and spacing of piles, amount of current available from each anode, and the current distribution to the structure.

For this structure, twenty 2 in. diam by 60 in. long anodes with enlarged heads have been chosen; the anodes are to be hung in ten strings of two anodes each. The top of the upper anode is to be 5 ft below the mean low water (MLW) level, and the top of the lower anode will be 15 ft below MLW level. See Fig. 22 for anode locations.

Resistance of Anodes (Ground Bed Resistance). The resistance of one vertical anode is:

$$R_v = \frac{0.0052\rho}{L}\left[2.3\log\frac{8L}{d} - 1\right]$$

where R_v is the anode-to-electrolyte resistance (in ohms), ρ is the electrolyte resistivity (in Ω·cm), *L* is the length of the anode (in feet), and *d* is the diameter of the anode (in feet):

$$R_v = \frac{(0.0052)(30)}{(60/12)}\left[2.3\log\frac{(8)(60/12)}{(2/12)} - 1\right]$$

$$R_v = 0.140\ \Omega$$

The calculations for the resistance of several anodes in parallel are made by using the following formula:

$$R_s = \frac{0.00521\rho}{nL}\left[2{,}3\log\frac{8L}{d} - 1 + \frac{2L}{S}2.3\log 0.656n\right]$$

where R_s is the resistance of vertical anodes in parallel to electrolyte (in ohms), and ρ, *n*, *L*, *d*, and *S* are as given previously.

Where two anodes are installed vertically in the same string, assume length, *L*, as equal to length of both anodes combined. From Fig. 22, the spacing is 20 ft:

$$R_s = \frac{(0.00521)(30)}{(10)(120/12)}\left[2.3\log\frac{(8)(120/12)}{(2/12)} - 1 + \frac{(2)(120/12)}{20}2.3\log 0.656(10)\right]$$

$$R_s = 0.11\ \Omega$$

Total dc Circuit Resistance. The total dc circuit resistance (R_{tot}) is the total of:

- Anode-to-electrolyte resistance, R_s
- Circuit cable resistance, R_{dcc}. Determine with common circuit analysis formula. Cable resistance is a function of cable size, conductor type, and length. Let $R_{dcc} = 0.0305\ \Omega$
- Structure-to-electrolyte resistance (negligible)

Thus, the circuit resistance is:

$$R_{tot} = R_s + R_{dcc} = 0.0415\ \Omega$$

Rectifier voltage output, V_{dc} is:

$$V_{dc} = I_{max} \cdot R_{tot} = 78.1\text{ A} \times 0.0415\ \Omega = 3.24\text{ V}$$

The maximum current, I_{max}, is that needed for polarization, I_{pol}. Add 2 V for anode back voltage, and the total becomes 5.24 V. Allow 20% for stack aging (1.05 V), and the rectifier voltage required = 6.29 V. So, the rectifier output required is 6.29 V and 78.1 A. The closest available rectifier is 8 V dc, 80 A dc.

Example 3: Condenser Waterbox/Impressed-Current System.* The main surface condensers at a power plant have been refitted with titanium tubes and tube sheets. The waterboxes are constructed of epoxy coated steel. The cooling water is seawater with a conductivity 29,000 to 40,000 μS (microSiemens equivalent to 25 and 35 Ω · cm resistivity).

Titanium is an active metal (like aluminum) that rapidly forms a highly protective film in seawater. It is this film that permits the use of titanium as a substrate for platinum and mixed- metal oxide impressed-current anodes. In the presence of aerated seawater, titanium exhibits a relatively noble (cathodic) potential, which is generally between +0.200 and -0.200 V versus a silver/silver chloride reference. In seawater, steel (at a potential of -0.5 to -0.7 V versus silver/silver chloride) will undergo rapid corrosion when directly connected to a large titanium surface.

There is justified concern that the coated steel waterbox will corrode at an unacceptable rate at coating faults and penetration of the steel box will result. Application of cathodic protection for the waterboxes can be used to polarize the titanium to a more active potential (-0.550 to -0.650 V with respect to a silver/silver chloride reference electrode). This will eliminate the otherwise harmful galvanic potential difference between the titanium and the steel.

Cathodic polarization of the titanium must not be sufficiently negative to produce hydrogen at the titanium surface. If hydrogen is produced, the titanium can form hydrides, which make the metal brittle and can result in tube cracking and other forms of mechanical failure. The equation for the potential at which hydrogen ions in water can be reduced to hydrogen gas at 1 atm of pressure (Ref 27) is:

$$E_o = 0.000 - 0.0591 \text{ pH (volt versus SHE)}$$

Referenced to a silver/silver chloride electrode in seawater, the equation becomes:

$$E_o = (0.000 - 0.0591 \text{ pH}) - 0.254 \text{ V}$$

At a pH of 8.0 (normal for seawater), the potential for production of hydrogen is:

$$E_o = (-0.0591 \times 8) - 0.254$$

$$E_o = -0.727 \text{ volt versus silver/silver chloride}$$

Polarizing the titanium to between -0.550 and -0.650 versus silver/silver chloride will not result in formation of titanium hydrides. This potential will eliminate the galvanic potential difference between the titanium and the steel.

Given the following data, design an impressed-current cathodic protection system for the waterboxes on this condenser. Anodes shall have a nominal 10 year life expectancy.

Data. From laboratory tests at flow rates matching those in the condenser tubes, 1.8 m/s (6 ft/s), the current density required to polarize titanium to -0.650 V to a silver/silver chloride reference is about 75 $\mu A/cm^2$. From laboratory studies, the effective distance that polarization occurs down a tube is about 5 tube diameters. There are 5140 titanium tubes entering each waterbox. Tube diameter is 2.22 cm ($\frac{7}{8}$ in.). The average water resistivity is 30 $\Omega \cdot$ cm.

All large connecting pipes to the condenser have a protective coating within five pipe diameters of the condenser. A conservative estimate is 10% of all coated steel surfaces as exposed metal. Assume all surfaces beyond 5 pipe diameters will not receive significant current density. Assume waterbox dimensions are as indicated in Fig. 23(a). For this problem, inlet and outlet tube sheets are mirror images of each other. Water velocity through the condenser tubes is 1.83 m/s (6 ft/s).

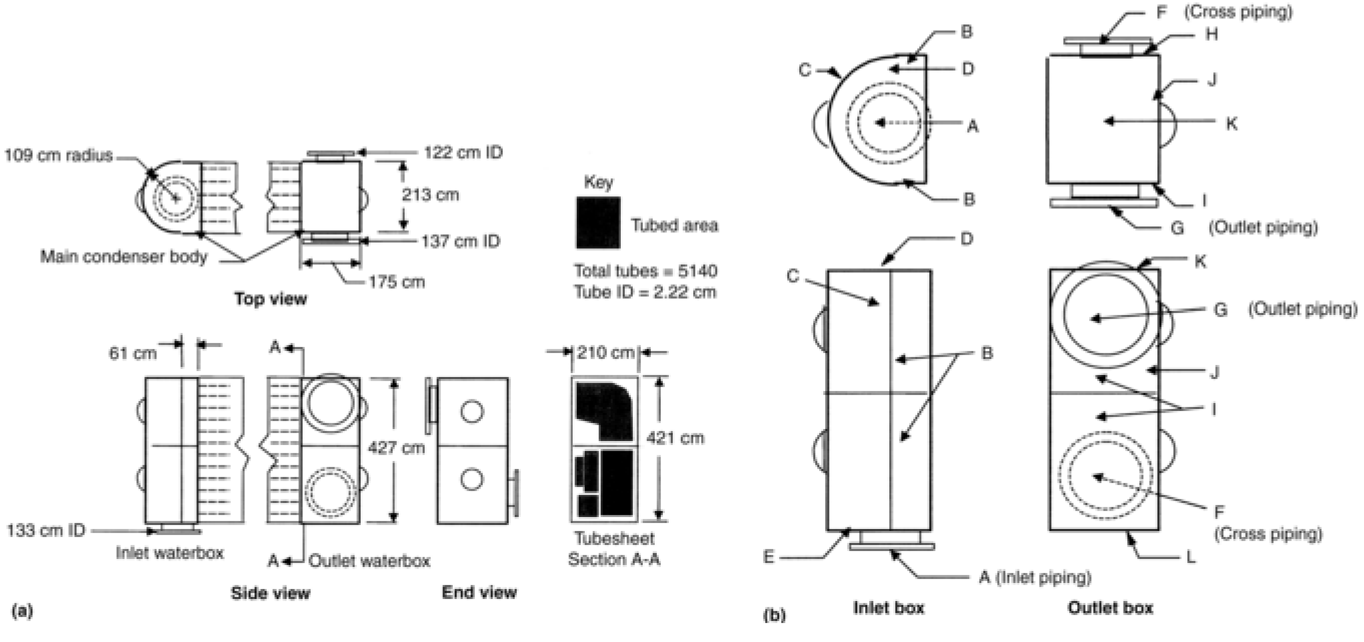

Fig. 23 Example 3. Diagram of condenser waterbox. (a) Dimensions and views. ID, inside diameter. (b) Identification of steel surfaces

The procedure is:

- Calculate surface areas.
- Estimate current required to meet criteria.
- Select anodes.
- Estimate minimum number of anodes to meet life and current distribution requirements.
- Estimate rectifier rating.

Calculations. Results of surface area calculations are listed in Table 15. Effective area of titanium tubes that will receive current is five tube diameters into the end of the tube. This criterion applies to large-diameter connecting piping, as well.

Table 15   Design of condenser waterbox impressed-current system

Quantity	Symbol or formula	Titanium tubes	Titanium tube sheet
Titanium area			
Tube diameter, cm	d	2.22	2.22
Number of tubes	n	5,140	5,140
Effective length receiving current, cm	$5d$	11.1	…
Exposed inner surface area, cm²(ft²)	$A_{st} = 5\pi nd^2$	397,913 (428)	…
Open cross-sectional area, cm²(ft²)	$A_{sx} = \pi n(d/2)^2$	…	19,896 (21.4)
Overall tube sheet area, cm²(ft²)	$A_{so} = wh$		88,410 (95.2)
Effective sheet area, cm²(ft²)	$A_{ss} = A_{so} - A_{sx}$		68,514 (73.7)
Total titanium area, cm²(ft²)	$A_{Ti} = A_{st} + A_{ss}$	466,427 (502)	
Inlet pipe A, cm²(ft²)	A_{sA}	277,858 (299)	…
Vertical walls B, cm²(ft²)	A_{sB}	52,094 (56)	…
Half cylinder vertical wall C, cm²(ft²)	A_{sC}	146,219 (157)	…
Top D, cm²(ft²)	A_{sD}	31,656 (34)	…
Bottom E, cm²(ft²)	A_{sE}	17,763 (19)	…
Box total, cm²(ft²)	$A_{sIB} = \Sigma A_{sA} + \ldots + A_{sE}$	525,590 (566)	…
Assume 10% exposed, cm²(ft²)	A_{sIBB}	52,559 (56.6)	…
Total bare metal steel and Ti, cm²(ft²)	$A_{TIB} = A_{sIBB} + A_{Ti}$	518,986 (559)	…

Quantity	Symbol or formula	Steel sheet
Steel outlet box areas, Fig. 23(b)		
Cross pipe F, inside wall area, cm²(ft²)	A_{sF}	11,690 (12.6)
Outlet pipe, 5 diam length assumed, cm²(ft²)	A_{sG}	481,056 (518)
Side H, cm²(ft²)	A_{sH}	63,035 (6709)
Side I, cm²(ft²)	A_{sI}	50,672 (54.5)
Face J, cm²(ft²)	A_{sJ}	90,951 (97.9)
Top K, cm²(ft²)	A_{sK}	37,275 (40.1)
Bottom L, cm²(ft²)	A_{sL}	37,275 (40.1)
Box total, cm²(ft²)	$A_{sOB} = \Sigma A_{sH} + \ldots + A_{sL}$	771,195 (831)
Assume 10% exposed, cm²(ft²)	A_{sOBB}	77,195 (83.1)
Total bare metal steel and Ti, cm²(ft²)	$A_{TOB} = A_{sOBB} + A_{Ti}$	543,622 (585)

For the cross piping (F), a short connection to the adjacent condenser waterbox, there is a bare metal gate valve in the connection. Assume exposed metal area is equal to the area of the pipe inside diameter. There had been an assumed 10% degradation of the coated steel.

Estimate Current Required to Meet Criteria for Exposed Areas. From given laboratory studies, current density (i) required to polarize titanium to -0.650 V (silver/silver chloride) is 75 μA/cm². Assume the same current density is required to equalize potentials of all steel and titanium surfaces in the waterboxes.

Inlet Waterbox. The estimated current required for the inlet waterbox (I_{IB}) is calculated:

$$I_{IB} = iA_{TIB}$$

$$I_{IB} = 75 \times 10^{-6}\ \text{A/cm}^2 \times 518{,}986\ \text{cm}^2$$

$$I_{IB} = 38.9\ \text{A}$$

Outlet Waterbox. The estimated current required for the outlet waterbox (I_{OB}) is calculated:

$$I_{OB} = iA_{TOB}$$

$$I_{OB} = 75 \times 10^{-6}\ \text{A/cm}^2 \times 543{,}622\ \text{cm}^2$$

$$I_{OB} = 40.8 \text{ A}$$

Anode Selection. This design requires control of the polarized potential on the titanium surfaces. This means that the cathodic protection must be an impressed-current system operated under potential control. For service in waterboxes of this type, bayonet (rod) anodes are convenient. These anodes (either platinum clad titanium or niobium or mixed metal oxide coated titanium) work well in highly conductive seawater. The anodes are small, and their effect on the cooling water flow patterns is minimal.

Minimum Active Anode Surface Area. Figure 24 is a graph derived from published consumption rates of platinum-clad anodes in fresh and seawater. For a design life of 10 years for the anodes, the consumption rate is:

$$CR = 6.35 \text{ µm/10 yr} = 0.635 \text{ µm/yr}$$

From Figure 24, in seawater, this consumption rate corresponds to a maximum current density of about 100 mA/cm^2 of platinum surface.

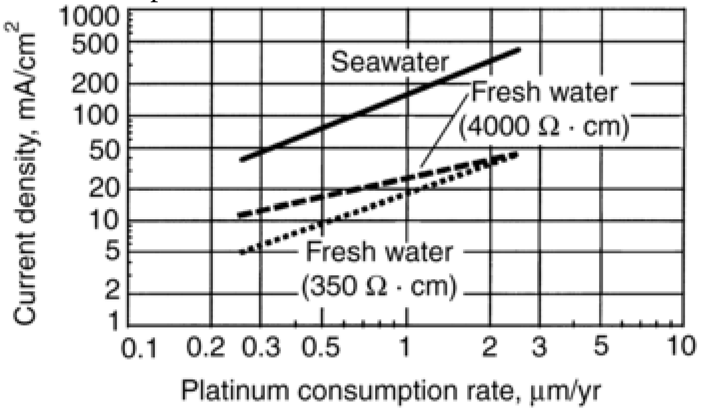

Fig. 24 Consumption rate of platinum anode

Assuming a design current of 50 A (125% of outlet box estimated current requirement) for each waterbox, the total active anode surface required would be:

$$A_A = I/i_a = 50 \text{ A}/0.1 \text{ A/cm}^2 = 500 \text{ cm}^2$$

Platinum-clad titanium or niobium rods are available in diameters of 0.635 cm (0.25 in.), 0.953 cm (0.375 in.), and 1.27 cm (0.500 in.). For mechanical reasons (flow rates in the waterboxes), the 1.27 cm (0.500 in.) rods are selected. The total length of rod required in each waterbox will be:

$$L = A_A/\pi d$$

$$L = 500 \text{ cm}^2/\pi \text{ (1.27 cm)} = 125 \text{ cm}$$

Examine Anode Remoteness. Figure 25 is a plot of the effective anode remoteness for a 30 cm long (11.8 in.) 1.27 cm (0.500 in.) diam anode placed against a nonconducting (coated) surface. The dimensions of the waterboxes severely limit the separation of anodes from the bare titanium tube sheets. In the inlet waterbox the maximum separation of the anodes from the tube sheet is 170 cm (67 in.). Figure 25 indicates that the tube sheet will be outside 80% of the above gradient if the anodes are at least 1 m (39 in.) away from the tube sheet. Variations in current density reaching the tube sheet because of differences in anode gradient would be less than 10% (the difference between the gradient at 1.7 and 1 m, or 67 and 39 in.). The object then is to locate the probe anodes in a pattern on the coated steel walls of the waterboxes such that the closest anode is no nearer the tube sheet than about 1 m (39 in.). Figure 26 shows one possible arrangement in which the anodes are relatively evenly distributed and that meet the 1 m criteria.

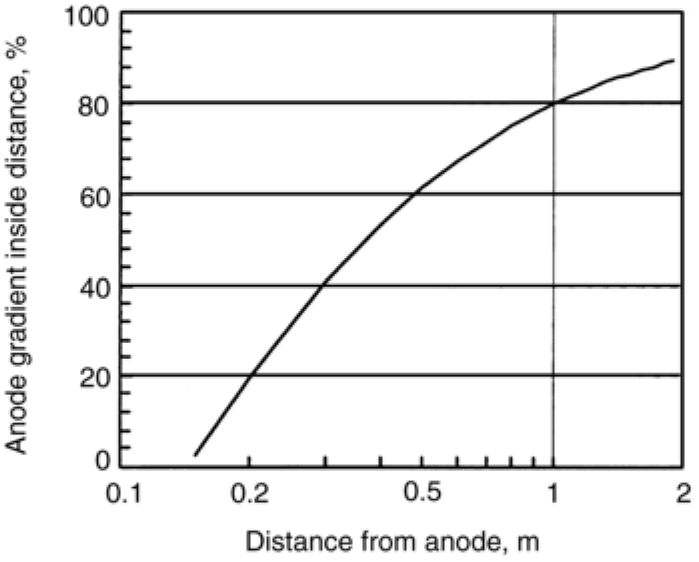

Fig. 25 Plot of effective anode remoteness

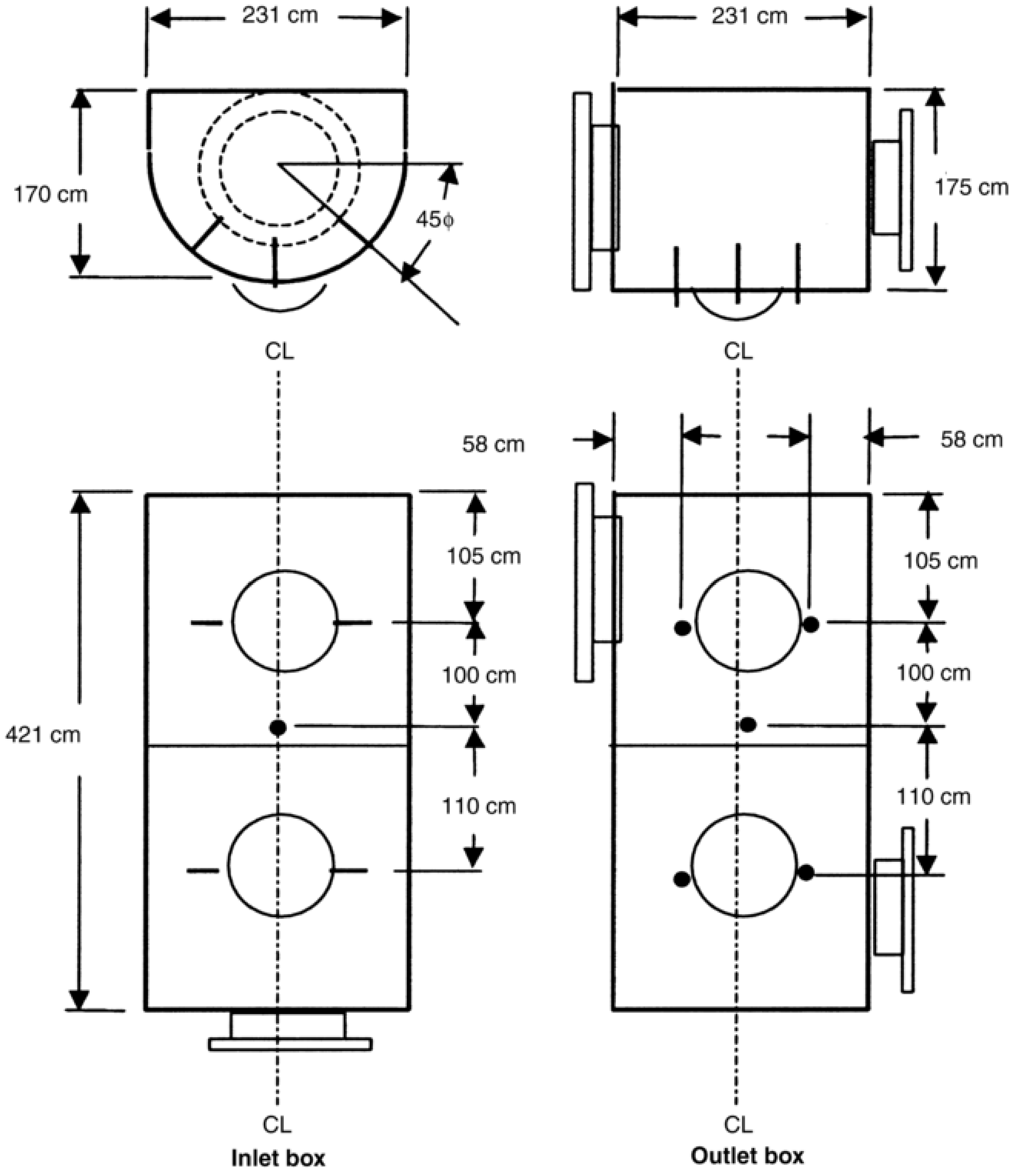

Fig. 26 Example 3. Bayonet anode locations

Rectifier Rating and Control. The approximate anode resistance using Dwight's formula for a vertical anode is:

$$R = \frac{0.005\rho}{\pi L}\left(\ln\left(\frac{8L}{d}\right) - 1\right)$$

where $\rho = 30\ \Omega \cdot \text{cm}$, $L = 0.30$ m, and $d = 0.0127$ m.

$$R = \frac{0.005\ \text{m/cm} \cdot 30\ \Omega \cdot \text{cm}}{\pi 0.30\ \text{m}}\left(\ln\left(\frac{8 \cdot 0.30\ \text{m}}{0.0127\ \text{m}}\right) - 1\right)$$

$$= 0.675 \text{ ohm per anode}$$

The approximate resistance of five anodes in parallel is:

$$R = 0.675\ \Omega/5 = 0.135\ \text{ohm}$$

The voltage required to provide 50 A per waterbox is by Ohm's law:

$$E = IR$$

where I = design current (50 A), R = anode to waterbox resistance (0.135 Ω), and E = 50 A × 0.135 Ω = 6.75 V. Taking into account back potential and polarization of the anodes and waterbox, select a potential controlled rectifier with separate units for each waterbox having a rating of 50 A and 12 V dc.

Location and Type of Reference Electrodes. The cathodic protection system must hold the potential of the titanium tube sheet at no more than -650 mV versus silver/silver chloride. The reference used to control the power supply should be located at the tube sheet in a location that is nearest to an anode. Other references are desirable at additional locations to verify effectiveness of the cathodic protection.

References are available that can be fitted into a tube opening. This prevents the use of such tubes for cooling. However, the large number of tubes (>5000) in this type of condenser makes this a negligible problem. Figure 27 shows a typical tube-mounted reference electrode (silver/silver chloride) and suggested locations for installing these in the typical waterbox.

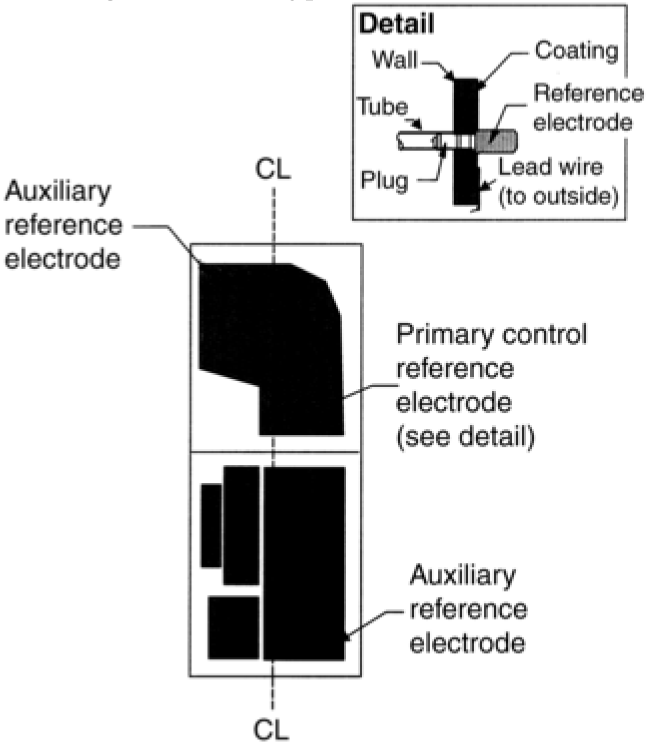

Fig. 27 Example 3. Placement of reference electrodes

Footnotes

* Adapted with permission by John W. McKinney, Jr. (Ref 15).

** The first two examples were adapted with permission from Ref 24.

*** This example is a condensed version adapted from example from the NACE International Cathodic Protection Design Course (CP Level 3) used with permission of NACE International (Ref 26). NACE is not responsible for this version.

References cited in this section

15. W.T. Bryan Ed., *Designing Impressed Current Cathodic Protection Systems with Durco Anodes,* 2nd ed., The Duriron Co. Inc., 1970

17. *Electrical Design—Corrosion Control,* Technical Manual TM5-811-4, U.S. Army, 1962

21. L. West and T. Lewicki, *Corrosion Control—General,* Vol I, *Civil Engineering Corrosion Control,* NTIS AD/A-004 082, Air Force Civil Engineering Center, TR 74-6, Jan 1975

23. L. West and T. Lewicki, *Cathodic Protection Design,* Vol III, *Civil Engineering Corrosion Control,* NTIS AD/A-006 400, Air Force Civil Engineering Center, TR 74-6, Jan 1975

24. T.D. Dismuke, S.K. Coburn, and C.M. Hirsh, Ed., *Handbook of Corrosion Protection for Steel Pile Structures in Marine Environments,* American Iron and Steel Institute, 1981, p 130–145

25. P.A. Schweitzer, Ed., *Corrosion Engineering Handbook,* Marcel Dekker, 1996, p 550–551

26. NACE International, 1440 South Creek Dr., Houston, TX 77084, www.nace.org

27. M. Pourbaix, *Atlas of Electrochemical Equilibria in Aqueous Solutions,* NACE International, 1966.

R.H. Heidersbach, Cathodic Protection, *Corrosion: Fundamentals, Testing, and Protection*, Vol 13A, *ASM Handbook,* ASM International, 2003, p 855–870

Cathodic Protection

Robert H. Heidersbach, Dr. Rust, Inc.

References

1. H. Davy, *Philos. Trans. R. Soc. (London),* Vol 114, 1824–1825, p 151–158, 242–246, 328–346

2. M.G. Fontana, *Corrosion Engineering,* McGraw-Hill, 1986, p 497–499

3. "Corrosion Control on Steel, Fixed Offshore Platforms Associated with Petroleum Production," NACE RP-01-76, National Association of Corrosion Engineers

4. M. Romanoff, "Underground Corrosion," National Bureau of Standards Circular 579, 1957 republished by NACE, 1989, p 195

5. A.W. Peabody, *Control of Pipeline Corrosion,* National Association of Corrosion Engineers, 1967, p 5

6. W. Baeckmann and W. Schwenk, Fundamentals and Practice of Electrical Measurements, Chapter 3, *Handbook of Cathodic Corrosion Protection,* 3rd ed., Gulf Publishing, 1997, p 79–137

7. "Control of External Corrosion on Underground or Submerged Metallic Piping Systems," NACE RP0169, National Association of Corrosion Engineers

8. V. Ashworth, The Theory of Cathodic Protection and its Relation to the Electrochemical Theory of Corrosion, Chapter 1, *Cathodic Protection: Theory and Practice,* V. Ashworth and C.J.L. Booker, Ed., Ellis Horwood Ltd., Chichester, U.K., 1986, p 13–30

9. J. Beavers and K. Garrity, Criteria for Cathodic Protection, Chapter 4, *Control of Pipeline Corrosion,* A.W. Peabody, original author, R. Bianchetti, Ed., 2nd ed., NACE International, 2001, p 49–64

10. T. Barlo, “Origin and Validation of the 100 mV Polarization Criterion,” Paper No. 01581, Corrosion 2001, NACE International, 2001

11. L. Kozewski, “Application of the 100 mV Polarization for Aboveground Storage Tank Bottoms,” Paper No. 01591, Corrosion 2001, NACE International, 2001

12. J. Fitzgerald and T. Rizk, “Using rhw 100 mV Criterion in Industrial and Similar Facilities,” Paper No. 01582, Corrosion 2001, NACE International, 2001

13. R. Pawson and R. McWilliams, “Bare Pipelines, the 100 mV Criterion & C.I.S. A Field Solution to Practical Problems,” Paper No. 01587, Corrosion 2001, NACE International, 2001

14. J. Morgan, *Cathodic Protection,* Macmillan, 1960

15. W.T. Bryan Ed., *Designing Impressed Current Cathodic Protection Systems with Durco Anodes,* 2nd ed., The Duriron Co. Inc., 1970

16. L.M. Ernes, “Characteristics and Advantages of the Dimensionally Stable Anode (DSAR),” ELTECH Systems Corp., March 1987

17. *Electrical Design—Corrosion Control,* Technical Manual TM5-811-4, U.S. Army, 1962

18. R. Heidersbach, J. Fu, and R. Erbar, Ed., *Computers in Corrosion Control,* National Association of Corrosion Engineers, 1986

19. P. Pierson, K. Bethune, W. Hartt, and P. Anathakrishnan, “A Novel Approach to Cathodic Protection Design for Marine Pipelines: Part I—An Inclusive Attenuation Equation,” Paper No. 00673, Corrosion 2000, NACE International, 2000

20. H. Hafnor and B. Amundsen, “Computerized Cathodic Protection Operation and Monitoring Buried Pipelines,” Paper No. 00728, Corrosion 2000, NACE International, 2000

21. L. West and T. Lewicki, *Corrosion Control—General,* Vol I, *Civil Engineering Corrosion Control,* NTIS AD/A-004 082, Air Force Civil Engineering Center, TR 74-6, Jan 1975

22. L. West and T. Lewicki, *Cathodic Protection Testing Methods and Instruments,* Vol II, *Civil Engineering Corrosion Control,* NTIS AD/A-004 083, Air Force Civil Engineering Center, TR 74-6, Jan 1975

23. L. West and T. Lewicki, *Cathodic Protection Design,* Vol III, *Civil Engineering Corrosion Control,* NTIS AD/A-006 400, Air Force Civil Engineering Center, TR 74-6, Jan 1975

24. T.D. Dismuke, S.K. Coburn, and C.M. Hirsh, Ed., *Handbook of Corrosion Protection for Steel Pile Structures in Marine Environments,* American Iron and Steel Institute, 1981, p 130–145

25. P.A. Schweitzer, Ed., *Corrosion Engineering Handbook,* Marcel Dekker, 1996, p 550–551

26. NACE International, 1440 South Creek Dr., Houston, TX 77084, www.nace.org

27. M. Pourbaix, *Atlas of Electrochemical Equilibria in Aqueous Solutions,* NACE International, 1966.

K.L. Vasanth, Vapor Phase Corrosion Inhibitors, *Corrosion: Fundamentals, Testing, and Protection*, Vol 13A, *ASM Handbook*, ASM International, 2003, p 871–877

Vapor Phase Corrosion Inhibitors

Kunigahalli L. Vasanth, Naval Surface Warfare Center

Introduction

METALLIC CORROSION costs the United States about $300 billion a year (Ref 1). Approximately one-third of the cost of corrosion ($100 billion) is avoidable and could be saved by using corrosion-resistant materials and the application of state-of-the-art corrosion control technologies. Atmospheric corrosion of metals and alloys is responsible for a large percentage of the total corrosion cost. Indirect consequences of corrosion, such as depletion of the natural resources and structural damage leading to failure of industrial and military systems, are also critical. The use of inhibitors is one of the corrosion- control technologies directed toward combating corrosion. Definitions, classifications, structural features, corrosion inhibition mechanisms, and methods of evaluation of vapor-phase-corrosion inhibitors, or volatile corrosion inhibitors (VCIs) are discussed in this article. Practical methods of using VCIs for corrosion protection of ferrous and nonferrous alloys are discussed with some specific examples.

Reference cited in this section

1. *Mater. Perform.*, Vol 5 (No. 6), 1995, p 5

K.L. Vasanth, Vapor Phase Corrosion Inhibitors, *Corrosion: Fundamentals, Testing, and Protection*, Vol 13A, *ASM Handbook*, ASM International, 2003, p 871–877

Vapor Phase Corrosion Inhibitors

Kunigahalli L. Vasanth, Naval Surface Warfare Center

Definition and Classification

The definition of an inhibitor used by NACE International (formerly the National Association of Corrosion Engineers) is “a substance that retards corrosion when added to an environment in small concentrations” (Ref 2). It is well established that inhibitors function in one or more ways to control corrosion: (a) by adsorption of a thin film onto the surface of a corroding material; (b) by inducing the formation of a thick corrosion product, or (c) by changing the characteristics of the environment, resulting in reduced aggressiveness (Ref 3). One of the recent classifications of inhibitors given by Uhlig and Revie (Ref 4) is that inhibitors are designated as passivators, organic inhibitors, and vapor-phase inhibitors.

Passivating inhibitors are usually inorganic oxidizing chemicals such as chromates, nitrites, and molybdates that passivate the metal and shift the corrosion potential several tenths of a volt in the noble direction. In general, the passivating- type inhibitors are very efficient and reduce corrosion rates to very low values. Primers containing hexavalent chromium have been the workhorse for passivating aluminum alloys and steel. Because it is known as a carcinogen, several research programs are ongoing to replace the hexavalent chromium. There is a critical concentration for passivators at which they show optimum inhibition. Subcritical concentrations of

passivators will lead to localized corrosion. Some alkaline compounds such as NaOH, Na_3PO_4, and Na_2B_4O are known to facilitate passivation of iron by favoring adsorption of dissolved oxygen.

Organic inhibitors are also called adsorption-type inhibitors since the organic compounds adsorb on the metal surface and suppress metal dissolution and reduction reactions. These affect both anodic and cathodic processes (Ref 5). Organic amines and carboxylates are typical examples of this class. Typical effective organic pickling inhibitors for steel are quinolinethiodide, *o*- and *p*-tolylthiourea, propyl sulfide, formaldehyde, and p-thiocresol. These are used to remove mill scale and can reduce the loss of steel, the use of acid, and generation of acid fumes caused by hydrogen evolution (Ref 4).

Vapor-phase corrosion inhibitors or volatile corrosion inhibitors (VCIs) are similar to organic adsorption-type inhibitors. These possess moderately high vapor pressure and consequently can be used to inhibit atmospheric corrosion of metals without applying VCIs directly on the metal surface. Volatile corrosion inhibitors are usually effective if used in enclosed spaces such as closed packages or the interior of machinery during shipment (Ref 6). The advantage of VCIs is that the volatilized molecules can reach hard-to-reach spaces commonly found in electrical and electronic enclosures, between two metal flanges, void spaces, and similar systems.

In the case of precise scientific instruments and electrical and electronic equipment, VCIs offer a definite advantage over classical methods of corrosion protection. A VCI can be defined as a single chemical or combination of chemicals (mostly organic) having high vapor pressure that can prevent atmospheric corrosion of metallic materials. According to Miksic and Miller, “Volatile corrosion inhibitors are secondary-electrolyte-layer inhibitors that possess appreciable saturated vapor pressure under atmospheric conditions, thus allowing vapor-phase transport of the inhibitive substance” (Ref 7).

Fodor (Ref 8) has documented an extensive literature review on vapor-phase corrosion inhibition. His report discusses theoretical and practical considerations, including definitions, classifications, corrosion-inhibition mechanisms, and evaluation of VCIs. Protection of ferrous and nonferrous alloys is discussed with some specific examples. Also included in Fodor's report are the structural identification of several VCI organic compounds and a summary of commercial preservation procedures.

A review by Miksic (Ref 9) discusses the atmospheric corrosion inhibition of both ferrous and nonferrous metals using VCIs. To be effective VCIs, the chemical compounds need to possess high passivating properties, strong tendencies toward surface adsorption, and the ability to form a comparatively strong and stable bond with metal surfaces. The delicate and yet complex nature of atmospheric corrosion processes occurring under thin films of electrolytes preordains the transport mechanism of the corrosion inhibitor that, in order to become effective, must diffuse through the electrolyte film and cover a substantial portion of the metal surface. Certain physical and chemical properties such as vapor pressure, molecular structure, availability of functional groups for surface physical and chemical bonding, the polarity, contamination, and the conductivity of the electrolyte are critical. Miksic (Ref 9) also states that there is considerable controversy over the importance of and the relationship between the saturated vapor pressure and its influence on the effectiveness of the specific compound.

In a relatively comprehensive recent review by Singh and Banerjee (Ref 10), the authors categorized VCIs based on their application to specific groups of metals; for example, for ferrous metals and alloys, for copper and copper alloys, and for silver and for aluminum.

References cited in this section

2. NACE Glossary of Corrosion Terms, *Mater. Proc.,* Vol 4 (No. 1), 1965, p 79
3. N. Hackerman, *Fundamentals of Inhibitors,* NACE Basic Corrosion Course, NACE International, 1965
4. H.H. Uhlig and R.W. Revie, *Corrosion and Corrosion Control,* John Wiley & Sons, 1985
5. M.G. Fontana, *Corrosion Engineering,* 3rd edition, McGraw-Hill Book Co., 1986.
6. O.L. Riggs, Jr., *Corrosion Inhibitors,* C.C. Nathan, ed., NACE International, 1973

7. B.A. Miksic and R.H. Miller, *European Symposium on Corrosion Inhibitors, 5th Proc., 107th Manifestation of the European Federation on Corrosion,* September 1980, p 217–236

8. G.E. Fodor, "Inhibition of Vapor-Phase Corrosion: A Review," BFLRF-209, Southwest Research Institute, San Antonio, TX, October 1985; Reviews on Corrosion Inhibitor Science and Technology, *CORROSION/89 Symposium Proc.,* (Houston, TX), A. Raman and P. Labine, Ed., NACE International, 1993, p 11-17-1

9. B.A. Miksic, Use of Vapor Phase Inhibitors for Corrosion Protection of Metal Products, *CORROSION/89 Symposium Proc.,* (Houston, TX), "Reviews on Inhibitor Science and Technology," A Raman and P. Labine, Ed., NACE International, 1993, p 11-16-1

10. D.D.N. Singh and M.K. Banerjee, "Vapour Phase Corrosion Inhibitors-A Review," *Anti-Corros.,* Vol 31 (No. 6), 1984, p 4–8

K.L. Vasanth, Vapor Phase Corrosion Inhibitors, *Corrosion: Fundamentals, Testing, and Protection*, Vol 13A, *ASM Handbook,* ASM International, 2003, p 871–877

Vapor Phase Corrosion Inhibitors

Kunigahalli L. Vasanth, Naval Surface Warfare Center

VCI Action Mechanism

It is widely accepted that a VCI must be a volatile compound or a mixture of such compounds. It must also be capable of forming a relatively stable bond at the metal interface, thus producing a protective layer that limits the penetration of corroding species (Ref 11, 12). According to Balezin (Ref 11) every corrosion inhibitor, including volatile ones, should:

- Be capable of establishing a stable bond with the metal surface in a given environment of certain range of acidity and pressure
- Create an impenetrable layer for corroding ions

The mechanism of inhibition is shown in Fig. 1. Two functional groups are attached to the nucleus, $R_o \cdot R_1$ is responsible for adsorption of the inhibitor on the metal, and surface R_2 gives the thickness and impenetrable nature to the protective inhibitive layer.

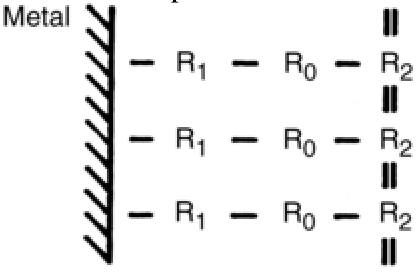

Fig. 1 The mechanism of corrosion inhibition. Functional groups R_1 and R_2 attach to nucleus, R_0, Source: Ref 11

Vapor pressure is a critical parameter in determining the effectiveness of a VCI. A VCI reaches the metal surface that it must protect through the vapor phase. This transport mechanism requires the VCI to possess an optimum vapor pressure. Too low a vapor pressure, of the order of 10^{-6} torr (1.3×10^{-4} Pa, or 2×10^{-8} psi) at

room temperature, leads to slow establishment of a protective layer that may result in insufficient corrosion protection. Furthermore, if the space that houses the equipment and the VCI is not sealed, sufficient inhibitor concentration may not be reached. On the other hand, if the vapor pressure is too high, approximately 0.1 torr (13 Pa, or 0.002 psi) at ambient conditions, VCI effectiveness will be limited to a short time period, as its consumption rate will be high. Therefore, a VCI must not have too low or too high a vapor pressure but some optimum vapor pressure. Both corrosion rate of a metal and the volatilization of a VCI are a function of temperature. Because of this similar temperature-dependent nature, the available vapor-phase concentration of a VCI may adjust to aggressiveness of the environment (Ref 12, 13).

The role of irreversible adsorption in the protective action of simple amines and heteroalkylated amines such as diamines, aminoalcohols, or aminoketones on steel, copper, and zinc has been studied (Ref 14). The author concluded that VCIs of the amine type are capable of forming the protective layers for up to 3 months and exhibit a posttreatment effect on the metal surfaces due to irreversible adsorption. The tendency of irreversible adsorption of a VCI depends on its chemical structure. As a rule, low-molecular- weight amines are inclined to desorption and do not exhibit posttreatment effect on steel or zinc, and they initiate copper corrosion. However, some higher-molecular-weight amines have hydrophobicity and can exhibit a posttreatment effect. Low volatility of these higher molecular weight amines limits their application. The best results were obtained with certain heteroalkylated amines that have more stable adsorption due to cyclic structure and presence of two reactive groups. According to Kuznetsov, the most effective VCIs, as a rule, form protective polymolecular films on metal surfaces that consist of thin chemisorbed and physically adsorbed layers.

Andreev and Kuznetsov (Ref 15) have provided some basics of the theory of VCIs. They discussed the role of volatility, solubility, basicity, and other features of VCIs towards their efficiency against CO_2 corrosion. According to them, the effect of chemical structure on these parameters can be quantitatively estimated using the linear free energy relationship.

References cited in this section

11. S.A. Balezin, *Comptes Rendus de 2eme European Symposium Sur le Inhibiteurs de Corrosion,* (Ferrara, Italy), Ann. Univ., N.S., 1966, p 277

12. I.L. Rosenfeld, V.P. Persiantseva, and M.N. Polteva, *Inhibitors,* NACE International, 1972, p 606–609

13. B.A. Miksic, *Chem. Eng.,* Sept 1977, p 115–118

14. Yu.I. Kuznetsov, “The Role of Irreversible Adsorption in the Protective Action of Volatile Corrosion Inhibitors,” Paper 98242, presented at *CORROSION/98,* (Houston, TX), NACE International, 1998

15. N.N. Andreev and Yu.I. Kuznetsov, “The Volatile Inhibitors for CO_2 Corrosion,” Paper 98241, presented at CORROSION/98, (Houston, TX), NACE International, 1998

K.L. Vasanth, Vapor Phase Corrosion Inhibitors, *Corrosion: Fundamentals, Testing, and Protection*, Vol 13A, *ASM Handbook*, ASM International, 2003, p 871–877

Vapor Phase Corrosion Inhibitors

Kunigahalli L. Vasanth, Naval Surface Warfare Center

Structure of VCIs

The efficiency of a VCI depends on its ability to adsorb on the surface of a metal, which in turn is related to its vapor pressure. Both adsorption and vapor pressure depend on the chemical structure of the inhibitor

compound. Rosenfeld (Ref 16) studied the effect of structure and the influence of substituents (OH, NO_2, NH_2) on the effectiveness of inhibitors. It was shown that for ferrous metals, aromatic nitrogen bases were ineffective corrosion inhibitors, even when additional hydroxyl or nitro groups were introduced. The majority of strong bases of aliphatic and alicyclic compounds were effective VCIs. He found that cyclohexylamine, hexamethyleneimine, piperidine, morpholine, and benzylamine were the most effective bases. It was claimed that the effectiveness of benzoates could be increased by the introduction of a highly electrophilic nitro group into the ortho-position or two nitro groups into the meta-positions with respect to the carboxyl group. These groups reduce the electron density in the aromatic ring. Miksic (Ref 17) claims that the nitro-group-induced polarization shifts the steady-state potential of the metal in the positive direction (more noble potential), inhibiting the anodic reaction. The introduction of a carboxylic group into the compound promotes the reduction of the nitro group and thus increases the oxidizing properties of the inhibitor. Complex ethers and weak aromatic amines were unsuitable inhibitors. Rosenfeld et al. also evaluated several inorganic salts and found ammonium carbonate and copper-ammonium carbonate to be effective inhibitors (Ref 16).

Trabanelli listed the inhibiting efficiency values of various aliphatic, alicyclic, and aromatic amines deduced from accelerated corrosion tests on Armco iron (Ref 18) in presence of 10 ppm of sulfur dioxide (Ref 19). These values are given in Table 1. He concluded that the aliphatic and alicyclic compounds are superior to those of the aromatic substances having similar vapor pressures. Trabanelli also listed several references that dealt with organic compounds for VCI purposes and that have been documented by Fodor (Ref 8).

Table 1 Inhibiting efficiencies of different organic substances

Efficiency deduced from accelerated atmospheric corrosion tests on Armco iron in 10 ppm SO_2-polluted atmosphere

Substance	Inhibiting efficiency, %
n-hexylamine	92
n-dihexylamine	57
n-octylamine	94
n-decylamine	84
n-dodecylamine	50
cyclohexylamine	80
dicyclohexylamine	95
N,N-dimethylcyclohexylamine	93
N,N-diethylcyclohexylamine	94
Aniline	40
Diphenylamine	16
Triphenylamine	17
N,N-dimethylaniline	87
N,N-diethylaniline	23
N,N-dimethyl-meta-toluidine	52
N,N-dimethyl-para-toluidine	80
N,N-diethyl-ortho-toluidine	15
N,N-diethyl-meta-toluidine	12
N,N-diethyl-para-toluidine	44

Source: Ref 19

In a recent paper, Andreev et al. (Ref 20) reported the study of adsorption on iron and the protective aftereffect of some ethanolamines on ferrous and nonferrous metals. They report that N, N-diethylaminoethanol, the most volatile and effective ethanolamine, forms a polymolecular film. The effect of the chemical structure of VCIs of this type on desorption kinetics and protective aftereffect of adsorption films on the metal surface in air has been analyzed. IFKhAN-111, a new VCI composition based on N,N-diethylaminoethanol, effectively protects both ferrous and nonferrous metals.

Kuznetsov et al. (Ref 21) have reported the protective action of beta-aminoketones ($R(1)R(2)(CH2)_nCH(R(3))C(O)(CH2)_mCH3$) as volatile corrosion inhibitors in systems supersaturated with water and the effect of preliminary exposure to inhibitor vapor on the passive state of metals. The protective

action of VCIs under a thin electrolyte and the kinetics of VCI adsorption and desorption has been determined by electrochemical and ellipsometric measurements. Subramanian et al. (Ref 22) synthesized morpholine and its derivatives, such as carbonate, borate, and phosphate, and evaluated their performance on protecting mild steel using weight loss and visual methods under a continuous condensation test. A comparative assessment of their performances is given.

Cole, Dixon, and Keohan (Ref 23) have reported their work on the synthesis and evaluation of new low-toxic, multimetal VCIs. Their approach consisted of reacting potential corrosion inhibitors having active hydrogens with appropriate silylating agents. The most versatile silylating agents were trimethylsilylacetamide, bis (trimethylsilyl)acetamide, hexamethyldisilazane, and trimethylchlorosilane. Skinner's method and a slow-scan potentiodynamic method were used to evaluate the effectiveness of these VCIs on cold rolled steel, brass, Al 7075-T6, and 70-30 Cu-Ni alloy. Several combinations of new compounds showed significant vapor-phase corrosion inhibition compared to any single component on all four alloys.

References cited in this section

8. G.E. Fodor, “Inhibition of Vapor-Phase Corrosion: A Review,” BFLRF-209, Southwest Research Institute, San Antonio, TX, October 1985; Reviews on Corrosion Inhibitor Science and Technology, *CORROSION/89 Symposium Proc.*, (Houston, TX), A. Raman and P. Labine, Ed., NACE International, 1993, p 11-17-1

16. I.L. Rosenfeld, V.P. Persiantseva, M.A. Novitskaya, Z.F. Shustova, B.P. Terent'ev, and M.N. Polteva, Tr.Vses. Mezhvuz. Nauchn. Knof. Po.Vopr. Bor'bys. Korroziei, Azerb. Inst. Neft i Khim, 1962, p 352–365; *Chem. Abstracts*, 60, 1964, p 8958g

17. B.A. Miksic, *Anti-Corros. Methods Mater.*, Vol 22 (No. 3), 1975, p 5–8

18. G. Trabanelli and F. Zucch, *74th Manifestation of the European Federation on Corrosion*, Oct 1974, p 289–301

19. G. Trabanelli, A. Fiegna, and V. Carassiti, *La Tribune du Cebedeau*, Vol 288, 1967

20. N.N. Andreev, N.P. Andreva, R.S. Vartapetyan, Y.I. Kuznetsov, and T.V. Fedotova, *Prot. Met.*, Vol 33 (No. 5), Sep–Oct 1997, p 470–475

21. Y.I. Kuznetsov, N.N. Andreev, N.P. Andreeva, D.V. Tolkachev, and T.V. Fedotova, *Prot. Met.*, Vol 32 (No. 5), Sep–Oct 1996, p 483–487

22. A. Subramanian, R. Gopalakrishnan, C. Bhoopathi, K. Balakrishnan, T. Vasudevan, M. Natesan, and N.S. Rengswamy, *Bull. Electrochem.*, Vol 14 (No. 10), Oct 1998, p 289–290

23. D.E. Cole, B.G. Dixon, and F.L. Keohan, “New Low Toxicity, Multi-Metal Active Vapor Phase Corrosion Inhibitors,” Paper 495, presented at CORROSION/99, (Houston, TX), NACE International, 1999

K.L. Vasanth, Vapor Phase Corrosion Inhibitors, *Corrosion: Fundamentals, Testing, and Protection*, Vol 13A, *ASM Handbook*, ASM International, 2003, p 871–877

Vapor Phase Corrosion Inhibitors

Kunigahalli L. Vasanth, Naval Surface Warfare Center

Vapor Pressure of VCIs

It is well known that a chemical compound used as a volatile inhibitor must possess neither too high nor too low a vapor pressure but an optimum vapor pressure. Two methods, the Rosenfeld-Martin-Knutsen effusion method (Ref 24) and the dynamic flow method (Ref 25) have been used for determining the saturated vapor pressure of VCIs and its dependence on temperature. There are certain inconsistencies in vapor pressure values published by different authors. It is believed that the reproducibility of data depends on experimental parameters that are inherent properties of the test method used. It was shown that measured vaporization rates in vacuum and in the atmosphere are not equal and that differences for the same compound could be relatively large (Ref 26). According to Rosenfeld (Ref 26), the following effects are possible:

- The change in the total pressure modified the Gibb's free energy for the components of the condensed phase.
- An extraneous gas slows down the vaporization of the condensed phase components (kinetic effect).
- Part of the vapor, for example, water vapor, dissolves in the condensed phase and modifies the Gibb's free energy of the latter.

In 1996, Andreev and Kuznetsov (Ref 27) documented the capabilities of correlation methods based on linearization of free energy and constants of volatility for estimation of the vapor pressure of organic VCIs. Ways to optimally choose a VCI and control modification of the structures of compounds belonging to various classes for achieving optimum volatility of inhibitors are given. Andreev (Ref 28) has shown how the volatility of organic substances can be predicted from their boiling points and has given examples of calculating the vapor pressure of several inhibitors.

Most of the effective VCIs are the products of a weak volatile base and a weak volatile acid. Such substances, although ionized in aqueous solutions, undergo substantial hydrolysis, the extent of which is almost independent of concentration (Ref 9). In the case of amine nitrites and amine carboxylates, the net result of those reactions may be written as:

$$RNH_2NO_2 + H_2O \rightarrow (RNH_2)^+{:}OH^- + H^+{:}(NO_2)^-$$

In further support of VCI transport mechanism, it can be noted that amine salts, such as dicyclohexylammonium nitrate or diisobutylammonium sulfate, which are not extensively dissociated by water, do not give significant vapor- phase inhibition. The same is true for slightly hydrolyzed alkali metal salts such as sodium nitrite or sodium benzoate, although the latter is an excellent rust inhibitor when its solutions are in direct contact with a metal surface (Ref 9).

Baker and Zisman (Ref 29) stated that the three nitrite compounds, diisobutyl, diisopropyl, and dicyclohexylammonium nitrite sublime readily at room temperature and inhibit rusting by adsorbing onto exposed metal surfaces to form a protective film. A hydrophobic monolayer is formed, on top of which there may deposit a loosely adhering layer of crystalline inhibitor. The hydrophobic film has a contact angle of 55° for the diisopropyl and 50° for the dicylohexylammonium nitrite at 20 °C (70 °F). The hydrophobic property is attributed to the polar- nonpolar structure of the substituted ammonium nitrite molecule. Because of the low molecular weight of the hydrocarbon portion of the organic nitrite molecule, prolonged contact with bulk water will result in dissolution or desorption of the protective film and allow corrosion of the substrate. Film desorption and solubility of the inhibitor in water lead to limited vapor-phase inhibition under conditions of extreme humidity. Recent developments suggest the use of a mixture of two or more corrosion inhibitors to provide protection in extreme humidity conditions.

References cited in this section

9. B.A. Miksic, Use of Vapor Phase Inhibitors for Corrosion Protection of Metal Products, *CORROSION/89 Symposium Proc.*, (Houston, TX), "Reviews on Inhibitor Science and Technology," A Raman and P. Labine, Ed., NACE International, 1993, p 11-16-1

24. T. Martin, Jr., *J. Chem. Eng. Data*, Vol 10, 1965, p 3

25. V.P. Persiantseva et al., *Zashch. Met.*, Vol 7 (No. 4), 1971, p 392

26. I.L. Rosenfeld et al., *Zashch. Met.*, Vol 10 (No. 4), 1974, p 339

27. N.N. Andreev and Y.I. Kuznetsov, *Prot. Met.*, Vol 32 (No. 2), Mar–Apr 1996, p 148–154

28. N.N. Andreev, *Prot. Met.*, Vol 34 (No. 2), Mar–Apr 1998, p 101–111

29. H.R. Baker and Zisman, "Liquid and Vapor Corrosion Inhibitors," U.S. Naval Res. Laboratory Report, NRL-3824, May 1951

K.L. Vasanth, Vapor Phase Corrosion Inhibitors, *Corrosion: Fundamentals, Testing, and Protection*, Vol 13A, *ASM Handbook*, ASM International, 2003, p 871–877

Vapor Phase Corrosion Inhibitors

Kunigahalli L. Vasanth, Naval Surface Warfare Center

VCI Evaluation Methods

According to Romanov and Khanovich (Ref 30) the effectiveness of VCIs can be evaluated in terms of several parameters:

- Time of inhibitor loss
- Relative loss of inhibitor
- Time of appearance of first corrosion products
- Relative residual quantity of inhibitor when corrosion starts
- Rate of corrosion
- A factor that allows for the nature of corrosion

Various accelerated corrosion tests are in use. Before using any of these tests, one must exercise caution (Ref 9); experimental results of accelerated tests in which artificially increased concentrations of corrosive agents, for example, SO_2, H_2S, or NaCl, are used should be compared to actual field performance only after proper calibrations. A similar warning was also expressed by Rosenfeld: "Reproducibility of data depends upon experimental parameters that are inherent properties of the test method employed" (Ref 26).

A widely used evaluating method to describe the relative abilities of inhibitors to prevent rusting of steel is described under ASTM D 1748 (Ref 31). In this method, steel panels are prepared to a prescribed surface finish, dipped in the test oil, allowed to drain, and then suspended in a humidity cabinet at 48.9 ± 1.1 °C (120 ± 2 °F) for a specified number of hours. The oil fails or passes the test according to the size and number of rust dots on the test surfaces of the panels. An essentially identical test method is described under Federal Test Method Standard No. 791B, Method 5329.1, "Corrosion Protection (Humidity Cabinet)." Federal Test Method Standard No.101C, Method 4031 (Ref 32) consists of two procedures: procedure A is for testing VCI materials

in crystalline or liquid form, and procedure B is for testing VCI-coated or VCI-treated materials. Determinations may be made in the “as received” condition or on samples exposed to accelerated conditions.

The German vapor-inhibiting ability (VIA) test method (Ref 33) is used to determine the corrosion inhibiting effect of VCI papers or foils. A test object of nonalloyed construction steel with high corrosion sensitivity in regard to condensation, together with the VCI packing aid to be tested, is placed inside a tightly sealed Erlenmeyer flask. The flask is stored at 23 ± 2 °C (73 ± 4 °F) for 20 h. At the end of storage time, a freshly prepared glycerol/water mixture is poured into the flask and it is closed immediately. During handling of the flask, care is taken not to submerge the samples in the glycerol/water mixture. The test flask is stored in a thermostat maintained at 40 ± 1 °C (104 ± 2 °F) for 2 h ± 10 min. At the completion of the test, the test sample of steel is examined visually for signs of corrosion. A control test is run using the test object of steel without a VCI paper/foil. A number grading system of 0 to 3 is used to rate the extent of inhibiting effect, 0 being no corrosion-inhibiting effect and 3 being good corrosion-inhibiting effect.

Kraemer (Ref 34) reported a VCI foil testing procedure that can be used for testing five different metals simultaneously. The basic principle of the test is similar to the German VIA test. The author claims that this is a quick and easy-to- implement VCI testing procedure. It demonstrates various approaches on how deficiencies in the existing test procedures can be avoided with regard to practice orientation, lack of alignment to meet the demands of new VCI recipes, and the usability of the test results for marketing purposes. Another test similar in principle to the German VIA test is the Japanese Industrial Standard for VCI treated paper, JIS Z 1535 (Ref 35).

Skinner (Ref 36) describes a new method for quantitative evaluation of VCIs. The experimental assembly was a preserving jar with a lid that had drilled openings. Any type of inhibitor, including a VCI, is placed at the bottom of the jar. Prepared metal samples are mounted on the openings of the lid using a rubber seal ring. Metal weights are used to keep the metal samples in place. The whole assembly is then placed in a heated water bath. After a suitable inhibitor film-forming period, electrolyte is added. Condensation takes place on the inner surfaces of the jar and the metal samples. After the test duration, metal samples are removed for visual inspection and mass loss determinations. Inhibitor effectiveness is calculated, based on corrosion rates with and without an inhibitor. Skinner writes that the assembly enables a fairly accurate simulation of operational conditions and that reliable quantitative results are obtained by using a new set of jars, lids, glasses, and seal rings for each test.

Jaeger, Garfias-Mesias, and Buchler (Ref 37) have described the use of a four-point-probe method based on resistance measurements. Other test methods used to evaluate VCIs include electrochemical (Ref 38, 39, 40), quartz microbalance (Ref 41), capacitance measurements of the electrical double layer (Ref 42), radiochemical (Ref 43), mass spectroscopy (Ref 44), and IR spectroscopy (Ref 45) methods. Typical slow potentiodynamic scans of Al 6061-T6 in 3.5% NaCl with and without a proprietary inhibitor spray, VCI F (ACF 50, Lear Chemical Corp., Dallas, TX), is shown in Fig. 2 to illustrate the application of an electrochemical method in the evaluation of VCIs (Ref 39).

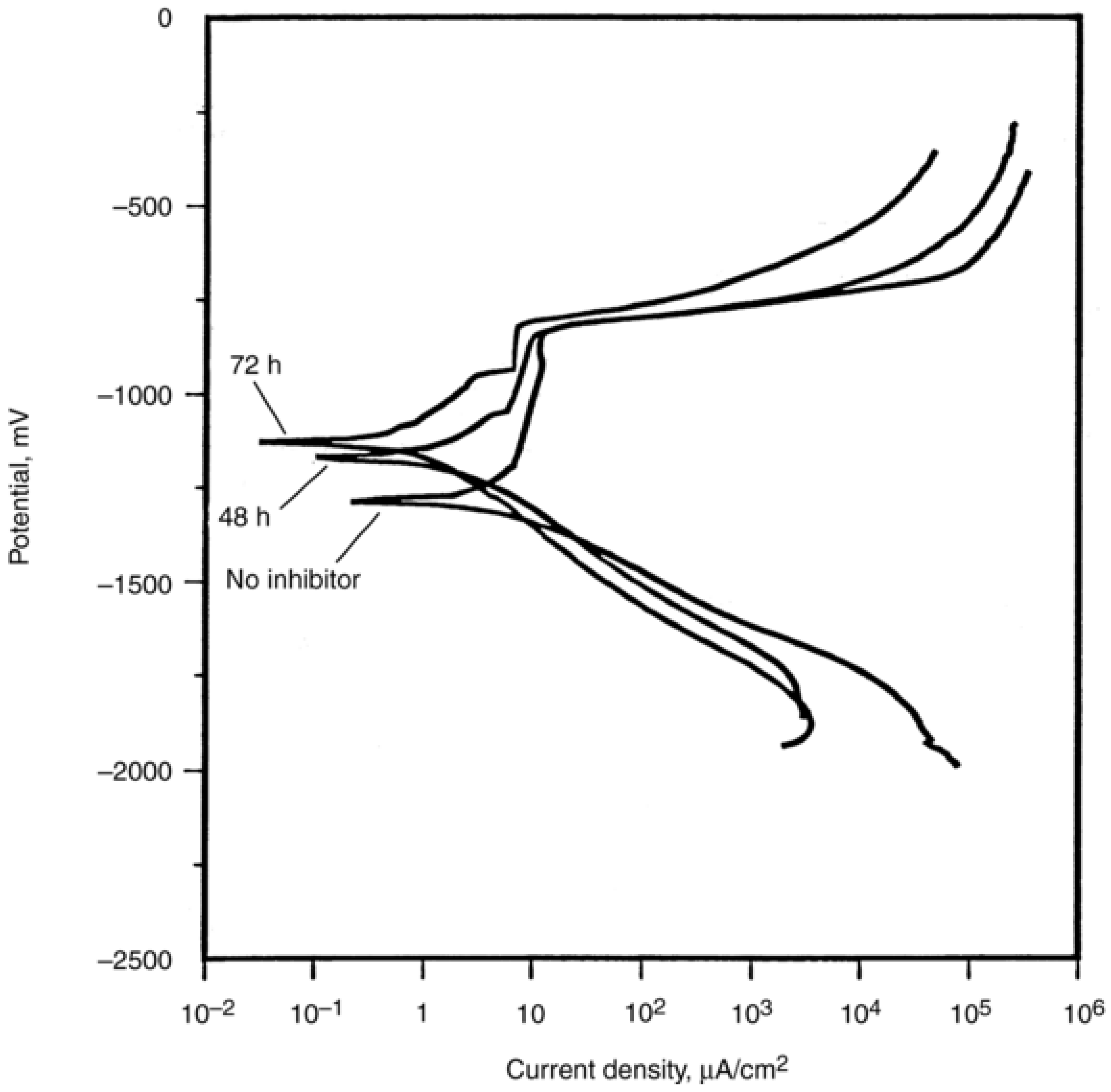

Fig. 2 Slow potentiodynamic scans of aluminum 6061-T6 in 3.5% NaCl with and without volatile corrosion inhibitor F. Source: Ref 39.

References cited in this section

9. B.A. Miksic, Use of Vapor Phase Inhibitors for Corrosion Protection of Metal Products, *CORROSION/89 Symposium Proc.,* (Houston, TX), "Reviews on Inhibitor Science and Technology," A Raman and P. Labine, Ed., NACE International, 1993, p 11-16-1

26. I.L. Rosenfeld et al., *Zashch. Met.,* Vol 10 (No. 4), 1974, p 339

30. V.A. Romanov and R.P. Khanovich, *Energetika,* Vol 4, 1975, p 132

31. "Rust Protection by Metal Preservatives in the Humidity Cabinet," D 1748, *Annual Book of ASTM Standards,* ASTM International

32. A. Furman and C. Chandler, Federal Test Method Standard 101C, March 1980; 9th European Symposium on Corrosion Inhibitors (Italy), 2000

33. German VIA Test Method TL 8135-0002, issued 3/12/98, W. Kohlhammer Gmbh, Post Box 800306, 70508 Stuttgart, Germany

34. C. Kraemer, “A Procedure for Testing the Effect of Vapor Phase Corrosion Inhibitors on Combined Metals,” Paper 97178, presented at CORROSION/97, (Houston, TX), NACE International, 1997

35. Japanese Industrial Standard (JIS) Z 1535–1994

36. W. Skinner, *Corros. Sci.,* Vol 35 (No. 5–8), 1993, p 1491–1494

37. P. Jaegar, L.F. Garfias, and M. Buchler, “A Novel Technique to Studying the Effect of a VCI,” Paper 99132, presented at CORROSION/99, (Houston, TX), NACE International, 1999

38. M.N. Desai and G.H. Tanki, *Australian Corr. J.,* Vol 13, 1969, p 19

39. K.L. Vasanth and C.M. Dacres, “Vapor Phase Corrosion Inhibitors for Navy Applications,” Paper 179, presented at CORROSION/97, (Houston, TX), NACE International, 1997

40. J.M. Bastidas and E.M. Mora, “A Laboratory Study of Mild Steel Vapour Phase Corrosion and Its Inhibition by Dicyclohexylaminenitrite,” *Canadian Metall. Q.,* Vol 37 (No. 1), Jan 1998, p 57–65

41. P. Jaeger, “Characterization of VCIs Using QCM and Supporting Techniques,” Paper 97180, presented at CORROSION/97, (Houston, TX), NACE International, 1997

42. L.G. Kar et al., *Korroz. Zashch. Met.,* Vol 82, 1978, p 4

43. K. Schwava, DECHEMA Monographien, 45, Verlag Chemie-GMBH-Weinheim/ Bergstr., 273, 1962

44. Y.F. Yu Yao, *J. Phys. Chem.,* Vol 101, 1964, p 68

45. T.L. Rosenfeld, F.I. Rubinstein, V.P. Persiantseva, and S.V. Yakubovich, 2nd European Symposium on Inhibitors Annali VVI, Ferrara N.S., Sez. V. Supply n 4, 7, 1966

K.L. Vasanth, Vapor Phase Corrosion Inhibitors, *Corrosion: Fundamentals, Testing, and Protection*, Vol 13A, *ASM Handbook*, ASM International, 2003, p 871–877

Vapor Phase Corrosion Inhibitors

Kunigahalli L. Vasanth, Naval Surface Warfare Center

VCI Applications

Just as catalysts are unique in catalyzing a reaction, VCIs are unique in their corrosion protection capabilities. In other words, compounds that protect ferrous alloys may not protect nonferrous alloys. Instead, they may cause corrosion and vice versa. It is, therefore, important that the user take utmost precaution in the selection of VCIs for a given application. In the absence of supporting data, VCIs must be tested using samples of the materials that need to be protected in a simulated environment that mimics actual conditions.

The applications of different VCIs used for protecting ferrous metals, copper and its alloys, and silver are summarized in Tables 2, 3, and 4.

Table 2 Volatile corrosion inhibitors for protection of ferrous metals

Compound	Details of protection and conditions	Ref
Dicyclohexylamine, dicyclohexylammonium nitrite (DICHAN)	Protection of ferrous metals and alloys	46, 47
Amino nitrobenzoate	Effective passivator	48
Dintroresorcinate hexamethylenetetramine	Protects iron in humid environment	49
Tall oil plus industrial oils	Considerable protection of steel in sulfur dioxide atmosphere	50
Ricinoleic acid hydroxide or its derivatives with ethylene oxide. General formula: $CH_3(CH_2)_5\ C(OH)HCH_2CH{=}CH(CH_2)CONHNH_2$	Protects iron, cast iron, and steel	51
Naphthalene vapors at 250–350 °C (480–660 °F)	Effective for steel in 1 *N* HCl vapors	52
Hexamethylene tetramine with various binders, fillers, and reducing agents $C_6H_{12}N_4 + 4\ NaNO_2 + 10\ H_2O = 6HCHO + 4NH_4NO_2 + 4\ NaOH$ **$4NH_4NO_2 = 4\ NH_3 + 4\ HNO_2$**	Reduces iron corrosion	53
$NaNO_2$, triethanolamine and a low molecular weight surfactant, for example, naphthanic or aliphatic acids	Good for protecting ferrous alloys in field tests	54
Acylation product of lanolin or multibasic alcohols as erythritol, glycerol, sorbitol in oil/organic solvents	Good for protection of iron and steel in humid atmosphere	55
Patented formulation of aliphatic amines, R.CH=NR where R = alkyl group	Good for protection of steel in acid and NaCl atmosphere	56
Alkylation product of 3- and -5 methyl pyrazoles	Protection of steel in H_2S environment	57

Table 3 Volatile corrosion inhibitors for protection of copper and copper alloys

Compound	Details of protection and environment	Ref
Thiourea derivatives, e.g., phenylene thiourea	Protection of brass	58
Acetylenic alcohols	Protection of atmospheric corrosion of copper	59
Triazole compounds, for example, tolyltriazole, benzotriazole ($C_6H_5N_3$)	Excellent protection of copper and copper alloys	49, 60
Aqueous solution of 5–50% complex phenol, carboxylic acid, or its esters (tannic, caffeic, gallic, etc.) and 0.1–20% water soluble heterocyclic compounds such as ethylene thiourea, mercaptobenzothiozole, etc.	Protection of copper from aggressive environments during storage	61
Sodium mercaptobenzothiozole	Protection of copper in the presence of soaps	62

Table 4 Volatile corrosion inhibitors for protection of silver

VCIs	Details of protection and environment	Ref
Benzotriazole	Protection of silver in H_2S atmosphere	49
Packaging paper impregnated with alcohol/ketone solution of chlorobenzotriazole	Forms a protective layer of silver complex on silver metal in H_2S atmosphere	63
Stearic acid or ethyleneglycol monostearate (3–5%) in a nonpolar solvent, CCl_4	Protection of silver in industrial atmospheres	64
Solution of KOH (5–100 g/L), $K_2Cr_2O_7$(5–100 g/L), 2-mercaptobenzothiozole at 35–45 °C (95–115 °F) for 4–10 min	Improves resistance to tarnishing and keeps the luster	65
Organosilicates, for example, 1-aminohexamethylene amino methylene triethoxisilanes and diethylamino methylene triethoxisilane in alcohol	Inhibits silver plated on steel	…

VCI, volatile corrosion inhibitor or vapor-phase corrosion inhibitor

References cited in this section

46. L. Cavallaro and G. Mantovanu, *Werkst. Korros.,* Vol 10, 1959, p 422

47. K. Schwabe, *Z. Phys. Chem.,* Leipzig 1, 1964, p 226

48. O.I. Golyanitskii, *Proc. Chelyabinsk Inst. Mechaniz and Electrifik S. Kh.,* 24, 1977, p 126

49. R.J. Lee and R.E. Karll, U.S. Patent 1,696,147

50. M.S. Chernov, S.P. Gusev, and I.L. Lomanov, Nanch. Tr. Mosr-in-t nar. Kh. Va. 131, 3, 1974

51. N. Kazuhiko, Japanese Patent C1.12 A 82 (c. 23f 11/14) No. 49-32416

52. N.G. Klyuchnikov and M. Ya, Rutten Coll. Abst. of Papers Perun, Conference on Protection of Metals against Corrosion, Pru 104, 1974

53. L.B. Sung, S. Manabu, and A. Teruzo, *Kinzoku Hyomen Gijutsu (J. Metal Finish. Soc. Japan*), Vol 392 (No. 25), 1974

54. O.I. Golyanitskiy and Tr. Chelyabinsk, In- ta Mekhaniz, *I. Elektnifik. S. Kh.,* 24, 126, 1977

55. U. Hiro and N. Shoechi, Japanese Patent Class 12 A 8 (C 23 F 11/00), 53-95842

56. N.A. Savirina et al., U.S.S.R. Patent 318,315, Class 23 F 11

57. A.I. Bocharrikov, A.A. Sorochenko, V.Ya Mudrakova, V.I. Seneya, and V.A. Dubroovskay, *Zashchita Metallov,* Vol 705 (No. 15), 1979

58. V.S. Agarwala and K.C. Tripathi, *Werkst. Korros.,* Vol 18, 1967, p 15

59. J. Barbior and C. Fiand, *Metause,* 49, 1974, p 271

60. M. Ryokichi, Japanese Patent, Class 12 A 82 (C 23 f 11/00); 49-19508

61. N. Hideo, M. Seishi and N. Takao, Japanese Patent, Class 12 A 41; (C 23 f 7/100), 52- 10164

62. T. Czarnecki and Z. Zaczyriska, Polish Patent, Class 22 g 5/08 (co 9 df/08); 72609

63. Y. Goro et al., Japanese Patent, Class 12 A 82; *Corr. Abst.,* Vol 48 (No. 9), 1977

64. Y.M. Polukarov, Au th. cert., class C 23 F 11/02; 539092; *Corr. Abst.,* Vol 48 (No. 9), 1977

65. G.G. Georgiyer, V.A. Kanazirska, and D.P. Spasova, Bulgarian Patent, Class 23 b 6/44, C 23 C 17/00, 16882

K.L. Vasanth, Vapor Phase Corrosion Inhibitors, *Corrosion: Fundamentals, Testing, and Protection*, Vol 13A, *ASM Handbook*, ASM International, 2003, p 871–877

Vapor Phase Corrosion Inhibitors

Kunigahalli L. Vasanth, Naval Surface Warfare Center

Protection of Aluminum

Aluminum and its alloys are very susceptible to attack in marine environments. Lee et al. (Ref 66) prepared VCI papers, powders, and tablets from a mixture of hexamethylenetetramine and sodium nitrite in a molar ratio of 1 to 4 (Ref 67). They used 6% milk casein or 7% gum arabic as binders. They showed that aluminum samples exposed to 90% relative humidity at 40 °C (104 °F) could be protected using these inhibitors. These researchers claim that the rust-inhibiting mechanism of this system is due partially to the fact that both the ingredients are hygroscopic; as they reduce moisture, corrosion is controlled. More importantly, both ingredients decompose as they absorb water-forming formaldehyde and nitrous acid that prevents surface corrosion of aluminum due to their reducing action. Another decomposition product, ammonia, neutralizes the acidic substances in the sealed atmosphere (Ref 8).

References cited in this section

8. G.E. Fodor, “Inhibition of Vapor-Phase Corrosion: A Review,” BFLRF-209, Southwest Research Institute, San Antonio, TX, October 1985; Reviews on Corrosion Inhibitor Science and Technology, *CORROSION/89 Symposium Proc.,* (Houston, TX), A. Raman and P. Labine, Ed., NACE International, 1993, p 11-17-1

66. B.S. Lee, M. Seno, and T. Asahara, *J. Metal Finish. Soc. Jpn.,* Vol 23 (No. 10), 1974, p 493–499

67. M. Ryokichi, Japanese Patent, Class 12 A 82 (C23 f 11/14); No. 50-13751

K.L. Vasanth, Vapor Phase Corrosion Inhibitors, *Corrosion: Fundamentals, Testing, and Protection*, Vol 13A, *ASM Handbook*, ASM International, 2003, p 871–877

Vapor Phase Corrosion Inhibitors

Kunigahalli L. Vasanth, Naval Surface Warfare Center

Protection of Ferrous and Nonferrous Metals

In practice, there are generally several metals such as steel, aluminum, copper, and brass are involved in the system requiring protection, and it is important to know the combination of VCIs that can be used to protect them from corrosion. Singh and Banerjee (Ref 10) have given such information in their review article; it is summarized in the following paragraphs.

Benzimidazole, 2-benzimidazolethiol, benzotriazole, and 2-mercaptobenzotriazole are reported to be effective for Cu, Al, Zn, and their alloys (Ref 68). Reaction products of methylbenzotriazole with the water-soluble guanidine class of compounds such as guanidine carbonate or nitrate, or methyl, dimethyl, trimethyl, ethyl, or diethyl guanidine in a molar ratio of 1:0.5 to 1:2 (methylbenzotriazole to guanidine compound) are effective atmospheric-corrosion inhibitors for Cu, brass, Sn, tin plated steel, and Al (Ref 69). Products obtained by reaction of benzotriazole, ethylbenzotriazole, and methylbenzotriazole with soluble urea compounds, such as urea, methyl, ethyl, propyl, or dimethyl urea in a molar ratio of 1:0.5 to 1:2 (triazole to urea compound) at 10 to 60 °C (50 to 140 °F), are effective for Cu, steel, Al, and Zn (Ref 70).

Products of the reaction of 1 *M* benzotriazole, ethyl, or methylbenzotriazole, and 1 to 5 *M* amino compounds such as methylmorpholine, tridodecylamine, didodecylamine, dicyclohexylamine, and dimethylamine are effective for Fe, Cu, Al, Zn, and other metals (Ref 67). The resultant inhibitor is soluble in machine, transformer, engine-lubricating, and other mineral and vegetable oils.

For protecting metals during storage, a compound formed by an incomplete reaction at 110 to 170 °C (230 to 340 °F) for 0.5 to 2 h of glycerine or ethyleneglycol with nitric acid and an alkanolamine with a primary or secondary alkylamine having more than six carbon atoms is used. The product is dissolved in a mineral oil. Mineral oil solution of salts of Zn, Mg, or Pb in naphathenic acid, together with 1-aminoethlimidazoline, is found suitable for temporary protection against atmospheric corrosion (Ref 71).

The reaction product of benzotriazole with a polyamine (for example, ethylene diamine and carboxylic acid) dissolved in spindle oil, effectively resists atmospheric corrosion of Fe, Cu, Al, and Zn (Ref 72).

Baligim et al. (Ref 73) have reported that the mixtures of benzotriazole with benzoates of ammonia, guanidine, hexamethylene-diamine, and monoethanolamine showed a synergistic protective action to steel, Zn, and Cd. A mixture of benzotriazole with guanidine benzoate and ammonium benzoate afforded the best protection. Solidified products of cyclohexylamine, dicyclohexylamine, propylamine, and butylamines with a concentrated solution of benzylidene sorbite in organic acid are reported to have good protecting properties towards ferrous and nonferrous metals. Also 3,5-diphenyl or 3,5-bis-(R-phenyl)- 2,2,4-triazole, where R is hydrogen, alkyl, or hydroxyl, is reported to protect gaseous or aqueous attack on Cu, Ag, Fe, Al, Ni, and their alloys (Ref 74).

Quaternary ammonium salts such as tetra-butyl, tetra-methyl of valeric, caprioic, caprilic, butyric, lauric, myristic trydecylic, palmitic, stearic, benzoic, and carbamic acids and also 0- and p-nitrophenalates are effective for steel, Cu, and brass (Ref 75). In another study, tetrabutyl ammonium 0-nitro phenate is most effective for steel and has no effect on Cu and brass (Ref 76).

In atmospheres polluted with SO_2 and H_2S, 4- H-1, 2, 4 triazole or its derivatives in combination with known inhibitors such as dicyclo-oxylamine nitrite, urea, and $NaNO_2$ is effective for Fe, Al, steel, Cu, Ag, Zn, Ni, Sn, Cd, Mg, Pb, and their alloys (Ref 77). A Dutch patent (Ref 78) describes the solution of an aromatic hydrocarbon, an alkyl-metal nitrate, and alkyl-substituted benzotriazole impregnated in paper to be effective for metal articles made of Al, Zn, Cu, steel, and other metals and alloys.

Substituted pyrazoles dissolved in water, methanol, or ethanol and impregnated in paper offer more protection than dicyclohexylamine nitrite towards atmospheric attack on Al, Cu, Zn, Sn, and other nonferrous metals (Ref 79) Anan et al. (Ref 80) have tested a number of wood industry products as vapor phase inhibitors and have reported that 2,5-dimethylfuran is an excellent inhibitor for nonferrous metals. Cast iron, steel, copper,

aluminum, solder, and other metals may be protected by the reaction product of 1 mole of cinnamic acid with 1 to 1.05 mole amine (diethylamine, triethylamine, diethanolamine, cyclohexylamine, etc.) with or without a solvent like water (Ref 81). A product of 4- or 5-halohydroxy and/or nitro-substituted benzotriazole with a primary, secondary, or tertiary amine is reported to be highly effective for Al, cast iron, steel, brass solder, copper, and other metals and alloys (Ref 82).

A mixture of benzotriazole with an oxidative character, for example, nitromethane, nitronaphthalene, dinitrophenol, or m-nitrobenzoic acid, dissolved in acetone or dimethylphthalane provided good protection to steel, gray cast iron, Cu, brass, galvanized iron, and Pb in a humid atmosphere (Ref 83). A ternary mixture of benzotriazole, sodium carbonate, and urotropine is highly effective towards steel and Cu (Ref 84). A composition containing (by parts) 3-30 of benzotriazole and higher aliphatic amine (octadecylamine) ensures protection of ferrous metals, Cu and Cu alloys, Al and Al alloys, Zn, Cd, Pb, Ni and Cr, and phosphate and oxide coatings (Ref 84).

In a long-exposure test conducted for six years in a humid atmosphere by Komrova (Ref 85) on steel, Cu, brass, and galvanized iron using dibutylphthalate, isoamylcinnamate, triamylborate, or the nitrobenzoate and other esters, it was concluded that these esters (apart from dibutylphthalate) provide complete corrosion protection towards steel, Cu, and brass at relative humidity values up to 98% and of galvanized iron at relative humidity values up to 85%.

Quraishi et al. (Ref 86, 87, 88, 89) have synthesized several VCIs, measured their vapor pressure at 40 °C, and tested their corrosion-protection efficiencies on common metals such as mild steel, brass, copper, aluminum, and zinc. These VCIs are listed in Table 5.

Table 5 Efficiencies of various volatile corrosion inhibitor compounds

Compound	Vapor pressure (mm Hg) at 40 °C (105 °F)	Efficiency based on weight loss method, %, for protection of					Ref
		Mild Steel	**Brass**	**Cu**	**Al**	**Zinc**	
6-Methoxy-aminobenzothizole	1.4×10^{-7}	97.9	96.6	95.8	NT	NT	86
6-Methoxy-aminobenzothizole cinnamate	4.0×10^{-7}	99.7	98.3	98.9	NT	NT	86
6-Methoxy-aminobenzothizole nitrobenzoate	4.5×10^{-7}	99.2	98.3	96.9	NT	NT	86
6-Methoxy-aminobenzothizole succinate	3.4×10^{-7}	98.1	97.5	94.8	NT	NT	86
6-Methoxy-aminobenzothizole	5.5×10^{-7}	98.7	96.6	95.8	NT	NT	86
Diaminohexane-cinnamate	5.0×10^{-8}	97.3	NT	NT	91.0	99.2	87
Diaminohexane nitrobenzoate	3.0×10^{-9}	60.1	NT	NT	85.3	94.1	87
Diaminohexane phthalate	6.0×10^{-9}	90.8	NT	NT	92.5	95.5	87
Diaminohexane orthophosphate	5.0×10^{-9}	76.4	NT	NT	82.2	97.3	87
Diaminohexane maleate	8.0×10^{-9}	93.3	NT	NT	78.9	95.5	87
1-(2-aminoethyl)-2-dec-9-enyl-2-imidazoline salicylate	91×10^{-7}	94.8	73.1	58.6	81.1	NT	88
1-(2-aminoethyl)-2-dec-9-enyl-2-imidazoline nitrobenzoate	69×10^{-7}	95.7	78.7	58.9	81.3	NT	88
1-(2-aminoethyl)-2-dec-9-enyl-2-imidazoline phthalate	16×10^{-6}	96.2	86.0	74.1	81.8	NT	88
1-(2-aminoethyl)-2-dec-9-enyl-2-imidazoline cinnamate	14×10^{-6}	96.6	88.2	79.3	82.5	NT	88
4-Amino-5-mercaptopropyl-triazole	1.7×10^{-6}	98.4	98.3	96.9	NT	NT	89
4-Amino-5-mercaptopropyl-triazole cinnamate	2.7×10^{-7}	98.9	98.3	96.9	NT	NT	89
4-Amino-5-mercaptopropyl-	3.9×10^{-7}	99 .2	98.0	97.9	NT	NT	89

triazole nitrobenzoate							
4-Amino-5-mercaptopropyl-triazole maleate	2.7×10^{-6}	98.9	97.5	97.9	NT	NT	89
4-Amino-5-mercaptopropyl-triazole succinate	5.0×10^{-7}	99.5	98.3	96.9	NT	NT	89

NT = not tested

In addition to the above formulations, there are a number of other patents in the literature that provide very little information about their exact nature. A supplement to a recent *Materials Performance* (Ref 90) has a number of articles on VCI applications such as preservation of Air Force vehicles and equipment, Trans-Alaska pipeline protection, VCI coatings, electronics protection, packaging, and storage tank protection.

References cited in this section

10. D.D.N. Singh and M.K. Banerjee, "Vapour Phase Corrosion Inhibitors-A Review," *Anti-Corros.*, Vol 31 (No. 6), 1984, p 4–8

67. M. Ryokichi, Japanese Patent, Class 12 A 82 (C23 f 11/14); No. 50-13751

68. L.B. Sung, S. Manabu, and A. Terguzo, *J. Met. Finish. Soc. Jpn.,* Vol 398 (No. 25), 1974

69. M. Ryokichi, Japanese Patent, Class 12 B 82 (C 23 f 11/00); 49-20862

70. M. Ryokichi, Japanese Patent, Class 12 A 82 (C 23 f 11/00); 49-19508

71. C. Tadensz and Z. Zofia, Polish Patent, Class 22 g 5/08 (co 9 df/08); 72609

72. M. Rekiti, Japanese Patent, Class 12 A 82 (C 23 f 11/14); 50

73. S.A. Baligim et al., *Izv. V.U.Z. Khim. Khim. Tekhnol.,* Ivanovao 9, 1977

74. N. Kotachi, J. Hori, and M. Yasuda, Japanese Patent, Class 12 A 82; (C 23 f 11/14), 51-10186

75. R.V. Berentseva, Jr., Chelyabinsk, In-ta Mekhaniz, I.e., elektrif. R. S. Kh, 51 126, 1977

76. R.V. Berentseva and A.P. Gugnina, *Trans. Chelyabibsk*

77. K. Neaki, Y. Mashiro, and H. Takeshi, Japanese Patent, Class 12 A 8; (C 23 f 11/14) 52-1377

78. C.M.R. Davidson, Dutch Patent, C z 3 f 11/ 14, 152605

79. T. Tadasi, T. Kiiti, Y. Seizo, and K. Takashi, Japanese Patent, Class 12 A; (C 23 f 11/00), 53-47775

80. G.F. Anan, and Y. and B.F. Nikandrov, *Coll. Chemical and Mechanical Processing of Wood and Wood Wastes,* Leningrad, 53, 4, 1978

81. M. Akiro, Japanese Applications, Class 12 A 82; (C 23 f 11/14), 52-155148

82. A.P. Gugina, *Proc. Chelyabinsk Inst. Mechaniz and Electrifik Agric.,* 61, 146, 1978

83. E.G. Zak, G.B. Rotmistrova, and L.Z. Zavitayeva, *Metal Corrosion Inhibitors,* Moscow, 154, 1979

84. P. Mityska and V. Novak, Czechoslovak Inventors Certificate, Class (C 23 F 11/02), 177381

85. L.G. Komrova, *Proc. Chelyabinsk Inst. Mechaniz and Electrif Agric.,* 67, 146, 1978

86. M.A. Quraishi and J. Rawat, Influence of Some 6-methoxy-aminobenzothiazole Derivatives on Corrosion of Ferrous and Nonferrous Metals under Vapor Phase Conditions, *Corrosion,* Vol 59, 2003, p 238–241

87. M.A. Quraishi and D. Jamal, Development and Testing of All Organic Volatile Corrosion Inhibitors, *Corrosion,* Vol 58, 2002, p 387–391

88. M.A. Quraishi and D. Jamal, "Development of Testing of New Volatile Corrosion Inhibitors for Multimetal Systems," *Mater. Perform.,* Jan 2003

89. M.A. Quraishi and J. Rawat, Triazole Derivatives: New Class of Vapor Phase Corrosion Inhibitors, *Corrosion Causes and Mitigation,* Vol 2, A. Kumbhavedekar, Ed., Quest Publication, 2000, p 115–122

90. A Supplement to Materials Performance, Jan 2001, NACE International

K.L. Vasanth, Vapor Phase Corrosion Inhibitors, *Corrosion: Fundamentals, Testing, and Protection*, Vol 13A, *ASM Handbook*, ASM International, 2003, p 871–877

Vapor Phase Corrosion Inhibitors

Kunigahalli L. Vasanth, Naval Surface Warfare Center

Protection of Ferrous and Nonferrous Metals

In practice, there are generally several metals such as steel, aluminum, copper, and brass are involved in the system requiring protection, and it is important to know the combination of VCIs that can be used to protect them from corrosion. Singh and Banerjee (Ref 10) have given such information in their review article; it is summarized in the following paragraphs.

Benzimidazole, 2-benzimidazolethiol, benzotriazole, and 2-mercaptobenzotriazole are reported to be effective for Cu, Al, Zn, and their alloys (Ref 68). Reaction products of methylbenzotriazole with the water-soluble guanidine class of compounds such as guanidine carbonate or nitrate, or methyl, dimethyl, trimethyl, ethyl, or diethyl guanidine in a molar ratio of 1:0.5 to 1:2 (methylbenzotriazole to guanidine compound) are effective atmospheric-corrosion inhibitors for Cu, brass, Sn, tin plated steel, and Al (Ref 69). Products obtained by reaction of benzotriazole, ethylbenzotriazole, and methylbenzotriazole with soluble urea compounds, such as urea, methyl, ethyl, propyl, or dimethyl urea in a molar ratio of 1:0.5 to 1:2 (triazole to urea compound) at 10 to 60 °C (50 to 140 °F), are effective for Cu, steel, Al, and Zn (Ref 70).

Products of the reaction of 1 *M* benzotriazole, ethyl, or methylbenzotriazole, and 1 to 5 *M* amino compounds such as methylmorpholine, tridodecylamine, didodecylamine, dicyclohexylamine, and dimethylamine are effective for Fe, Cu, Al, Zn, and other metals (Ref 67). The resultant inhibitor is soluble in machine, transformer, engine-lubricating, and other mineral and vegetable oils.

For protecting metals during storage, a compound formed by an incomplete reaction at 110 to 170 °C (230 to 340 °F) for 0.5 to 2 h of glycerine or ethyleneglycol with nitric acid and an alkanolamine with a primary or secondary alkylamine having more than six carbon atoms is used. The product is dissolved in a mineral oil. Mineral oil solution of salts of Zn, Mg, or Pb in naphathenic acid, together with 1-aminoethlimidazoline, is found suitable for temporary protection against atmospheric corrosion (Ref 71).

The reaction product of benzotriazole with a polyamine (for example, ethylene diamine and carboxylic acid) dissolved in spindle oil, effectively resists atmospheric corrosion of Fe, Cu, Al, and Zn (Ref 72).

Baligim et al. (Ref 73) have reported that the mixtures of benzotriazole with benzoates of ammonia, guanidine, hexamethylene-diamine, and monoethanolamine showed a synergistic protective action to steel, Zn, and Cd. A mixture of benzotriazole with guanidine benzoate and ammonium benzoate afforded the best protection.

Solidified products of cyclohexylamine, dicyclohexylamine, propylamine, and butylamines with a concentrated solution of benzylidene sorbite in organic acid are reported to have good protecting properties towards ferrous and nonferrous metals. Also 3,5-diphenyl or 3,5-bis-(R-phenyl)- 2,2,4-triazole, where R is hydrogen, alkyl, or hydroxyl, is reported to protect gaseous or aqueous attack on Cu, Ag, Fe, Al, Ni, and their alloys (Ref 74).

Quaternary ammonium salts such as tetra-butyl, tetra-methyl of valeric, caprioic, caprilic, butyric, lauric, myristic trydecylic, palmitic, stearic, benzoic, and carbamic acids and also 0- and p-nitrophenalates are effective for steel, Cu, and brass (Ref 75). In another study, tetrabutyl ammonium 0-nitro phenate is most effective for steel and has no effect on Cu and brass (Ref 76).

In atmospheres polluted with SO_2 and H_2S, 4- H-1, 2, 4 triazole or its derivatives in combination with known inhibitors such as dicyclo-oxylamine nitrite, urea, and $NaNO_2$ is effective for Fe, Al, steel, Cu, Ag, Zn, Ni, Sn, Cd, Mg, Pb, and their alloys (Ref 77). A Dutch patent (Ref 78) describes the solution of an aromatic hydrocarbon, an alkyl-metal nitrate, and alkyl-substituted benzotriazole impregnated in paper to be effective for metal articles made of Al, Zn, Cu, steel, and other metals and alloys.

Substituted pyrazoles dissolved in water, methanol, or ethanol and impregnated in paper offer more protection than dicyclohexylamine nitrite towards atmospheric attack on Al, Cu, Zn, Sn, and other nonferrous metals (Ref 79) Anan et al. (Ref 80) have tested a number of wood industry products as vapor phase inhibitors and have reported that 2,5-dimethylfuran is an excellent inhibitor for nonferrous metals. Cast iron, steel, copper, aluminum, solder, and other metals may be protected by the reaction product of 1 mole of cinnamic acid with 1 to 1.05 mole amine (diethylamine, triethylamine, diethanolamine, cyclohexylamine, etc.) with or without a solvent like water (Ref 81). A product of 4- or 5-halohydroxy and/or nitro-substituted benzotriazole with a primary, secondary, or tertiary amine is reported to be highly effective for Al, cast iron, steel, brass solder, copper, and other metals and alloys (Ref 82).

A mixture of benzotriazole with an oxidative character, for example, nitromethane, nitronaphthalene, dinitrophenol, or m-nitrobenzoic acid, dissolved in acetone or dimethylphthalane provided good protection to steel, gray cast iron, Cu, brass, galvanized iron, and Pb in a humid atmosphere (Ref 83). A ternary mixture of benzotriazole, sodium carbonate, and urotropine is highly effective towards steel and Cu (Ref 84). A composition containing (by parts) 3-30 of benzotriazole and higher aliphatic amine (octadecylamine) ensures protection of ferrous metals, Cu and Cu alloys, Al and Al alloys, Zn, Cd, Pb, Ni and Cr, and phosphate and oxide coatings (Ref 84).

In a long-exposure test conducted for six years in a humid atmosphere by Komrova (Ref 85) on steel, Cu, brass, and galvanized iron using dibutylphthalate, isoamylcinnamate, triamylborate, or the nitrobenzoate and other esters, it was concluded that these esters (apart from dibutylphthalate) provide complete corrosion protection towards steel, Cu, and brass at relative humidity values up to 98% and of galvanized iron at relative humidity values up to 85%.

Quraishi et al. (Ref 86, 87, 88, 89) have synthesized several VCIs, measured their vapor pressure at 40 °C, and tested their corrosion-protection efficiencies on common metals such as mild steel, brass, copper, aluminum, and zinc. These VCIs are listed in Table 5.

Table 5 Efficiencies of various volatile corrosion inhibitor compounds

Compound	Vapor pressure (mm Hg) at 40 °C (105 °F)	Efficiency based on weight loss method, %, for protection of					Ref
		Mild Steel	**Brass**	**Cu**	**Al**	**Zinc**	
6-Methoxy-aminobenzothizole	1.4×10^{-7}	97.9	96.6	95.8	NT	NT	86
6-Methoxy-aminobenzothizole cinnamate	4.0×10^{-7}	99.7	98.3	98.9	NT	NT	86
6-Methoxy-aminobenzothizole nitrobenzoate	4.5×10^{-7}	99.2	98.3	96.9	NT	NT	86
6-Methoxy-aminobenzothizole succinate	3.4×10^{-7}	98.1	97.5	94.8	NT	NT	86
6-Methoxy-aminobenzothizole	5.5×10^{-7}	98.7	96.6	95.8	NT	NT	86
Diaminohexane-cinnamate	5.0×10^{-8}	97.3	NT	NT	91.0	99.2	87
Diaminohexane nitrobenzoate	3.0×10^{-9}	60.1	NT	NT	85.3	94.1	87

Diaminohexane phthalate	6.0×10^{-9}	90.8	NT	NT	92.5	95.5	87
Diaminohexane orthophosphate	5.0×10^{-9}	76.4	NT	NT	82.2	97.3	87
Diaminohexane maleate	8.0×10^{-9}	93.3	NT	NT	78.9	95.5	87
1-(2-aminoethyl)-2-dec-9-enyl-2-imidazoline salicylate	91×10^{-7}	94.8	73.1	58.6	81.1	NT	88
1-(2-aminoethyl)-2-dec-9-enyl-2-imidazoline nitrobenzoate	69×10^{-7}	95.7	78.7	58.9	81.3	NT	88
1-(2-aminoethyl)-2-dec-9-enyl-2-imidazoline phthalate	16×10^{-6}	96.2	86.0	74.1	81.8	NT	88
1-(2-aminoethyl)-2-dec-9-enyl-2-imidazoline cinnamate	14×10^{-6}	96.6	88.2	79.3	82.5	NT	88
4-Amino-5-mercaptopropyl-triazole	1.7×10^{-6}	98.4	98.3	96.9	NT	NT	89
4-Amino-5-mercaptopropyl-triazole cinnamate	2.7×10^{-7}	98.9	98.3	96.9	NT	NT	89
4-Amino-5-mercaptopropyl-triazole nitrobenzoate	3.9×10^{-7}	99 .2	98.0	97.9	NT	NT	89
4-Amino-5-mercaptopropyl-triazole maleate	2.7×10^{-6}	98.9	97.5	97.9	NT	NT	89
4-Amino-5-mercaptopropyl-triazole succinate	5.0×10^{-7}	99.5	98.3	96.9	NT	NT	89

NT = not tested

In addition to the above formulations, there are a number of other patents in the literature that provide very little information about their exact nature. A supplement to a recent *Materials Performance* (Ref 90) has a number of articles on VCI applications such as preservation of Air Force vehicles and equipment, Trans-Alaska pipeline protection, VCI coatings, electronics protection, packaging, and storage tank protection.

References cited in this section

10. D.D.N. Singh and M.K. Banerjee, "Vapour Phase Corrosion Inhibitors-A Review," *Anti-Corros.*, Vol 31 (No. 6), 1984, p 4–8

67. M. Ryokichi, Japanese Patent, Class 12 A 82 (C23 f 11/14); No. 50-13751

68. L.B. Sung, S. Manabu, and A. Terguzo, *J. Met. Finish. Soc. Jpn.*, Vol 398 (No. 25), 1974

69. M. Ryokichi, Japanese Patent, Class 12 B 82 (C 23 f 11/00); 49-20862

70. M. Ryokichi, Japanese Patent, Class 12 A 82 (C 23 f 11/00); 49-19508

71. C. Tadensz and Z. Zofia, Polish Patent, Class 22 g 5/08 (co 9 df/08); 72609

72. M. Rekiti, Japanese Patent, Class 12 A 82 (C 23 f 11/14); 50

73. S.A. Baligim et al., *Izv. V.U.Z. Khim. Khim. Tekhnol.,* Ivanovao 9, 1977

74. N. Kotachi, J. Hori, and M. Yasuda, Japanese Patent, Class 12 A 82; (C 23 f 11/14), 51-10186

75. R.V. Berentseva, Jr., Chelyabinsk, In-ta Mekhaniz, I.e., elektrif. R. S. Kh, 51 126, 1977

76. R.V. Berentseva and A.P. Gugnina, *Trans. Chelyabibsk*

77. K. Neaki, Y. Mashiro, and H. Takeshi, Japanese Patent, Class 12 A 8; (C 23 f 11/14) 52-1377

78. C.M.R. Davidson, Dutch Patent, C z 3 f 11/ 14, 152605

79. T. Tadasi, T. Kiiti, Y. Seizo, and K. Takashi, Japanese Patent, Class 12 A; (C 23 f 11/00), 53-47775

80. G.F. Anan, and Y. and B.F. Nikandrov, *Coll. Chemical and Mechanical Processing of Wood and Wood Wastes,* Leningrad, 53, 4, 1978

81. M. Akiro, Japanese Applications, Class 12 A 82; (C 23 f 11/14), 52-155148

82. A.P. Gugina, *Proc. Chelyabinsk Inst. Mechaniz and Electrifik Agric.,* 61, 146, 1978

83. E.G. Zak, G.B. Rotmistrova, and L.Z. Zavitayeva, *Metal Corrosion Inhibitors,* Moscow, 154, 1979

84. P. Mityska and V. Novak, Czechoslovak Inventors Certificate, Class (C 23 F 11/02), 177381

85. L.G. Komrova, *Proc. Chelyabinsk Inst. Mechaniz and Electrif Agric.,* 67, 146, 1978

86. M.A. Quraishi and J. Rawat, Influence of Some 6-methoxy-aminobenzothiazole Derivatives on Corrosion of Ferrous and Nonferrous Metals under Vapor Phase Conditions, *Corrosion,* Vol 59, 2003, p 238–241

87. M.A. Quraishi and D. Jamal, Development and Testing of All Organic Volatile Corrosion Inhibitors, *Corrosion,* Vol 58, 2002, p 387–391

88. M.A. Quraishi and D. Jamal, "Development of Testing of New Volatile Corrosion Inhibitors for Multimetal Systems," *Mater. Perform.,* Jan 2003

89. M.A. Quraishi and J. Rawat, Triazole Derivatives: New Class of Vapor Phase Corrosion Inhibitors, *Corrosion Causes and Mitigation,* Vol 2, A. Kumbhavedekar, Ed., Quest Publication, 2000, p 115–122

90. A Supplement to Materials Performance, Jan 2001, NACE International

---

K.L. Vasanth, Vapor Phase Corrosion Inhibitors, *Corrosion: Fundamentals, Testing, and Protection,* Vol 13A, *ASM Handbook,* ASM International, 2003, p 871–877

Vapor Phase Corrosion Inhibitors

Kunigahalli L. Vasanth, Naval Surface Warfare Center

References

1. *Mater. Perform.,* Vol 5 (No. 6), 1995, p 5

2. NACE Glossary of Corrosion Terms, *Mater. Proc.,* Vol 4 (No. 1), 1965, p 79

3. N. Hackerman, *Fundamentals of Inhibitors,* NACE Basic Corrosion Course, NACE International, 1965

4. H.H. Uhlig and R.W. Revie, *Corrosion and Corrosion Control,* John Wiley & Sons, 1985

5. M.G. Fontana, *Corrosion Engineering,* 3rd edition, McGraw-Hill Book Co., 1986.

6. O.L. Riggs, Jr., *Corrosion Inhibitors,* C.C. Nathan, ed., NACE International, 1973

7. B.A. Miksic and R.H. Miller, *European Symposium on Corrosion Inhibitors, 5th Proc., 107th Manifestation of the European Federation on Corrosion,* September 1980, p 217–236

8. G.E. Fodor, "Inhibition of Vapor-Phase Corrosion: A Review," BFLRF-209, Southwest Research Institute, San Antonio, TX, October 1985; Reviews on Corrosion Inhibitor Science and Technology, *CORROSION/89 Symposium Proc.,* (Houston, TX), A. Raman and P. Labine, Ed., NACE International, 1993, p 11-17-1

9. B.A. Miksic, Use of Vapor Phase Inhibitors for Corrosion Protection of Metal Products, *CORROSION/89 Symposium Proc.,* (Houston, TX), "Reviews on Inhibitor Science and Technology," A Raman and P. Labine, Ed., NACE International, 1993, p 11-16-1

10. D.D.N. Singh and M.K. Banerjee, "Vapour Phase Corrosion Inhibitors-A Review," *Anti-Corros.,* Vol 31 (No. 6), 1984, p 4–8

11. S.A. Balezin, *Comptes Rendus de 2eme European Symposium Sur le Inhibiteurs de Corrosion,* (Ferrara, Italy), Ann. Univ., N.S., 1966, p 277

12. I.L. Rosenfeld, V.P. Persiantseva, and M.N. Polteva, *Inhibitors,* NACE International, 1972, p 606–609

13. B.A. Miksic, *Chem. Eng.,* Sept 1977, p 115–118

14. Yu.I. Kuznetsov, "The Role of Irreversible Adsorption in the Protective Action of Volatile Corrosion Inhibitors," Paper 98242, presented at *CORROSION/98,* (Houston, TX), NACE International, 1998

15. N.N. Andreev and Yu.I. Kuznetsov, "The Volatile Inhibitors for CO_2 Corrosion," Paper 98241, presented at CORROSION/98, (Houston, TX), NACE International, 1998

16. I.L. Rosenfeld, V.P. Persiantseva, M.A. Novitskaya, Z.F. Shustova, B.P. Terent'ev, and M.N. Polteva, Tr.Vses. Mezhvuz. Nauchn. Knof. Po.Vopr. Bor'bys. Korroziei, Azerb. Inst. Neft i Khim, 1962, p 352–365; *Chem. Abstracts,* 60, 1964, p 8958g

17. B.A. Miksic, *Anti-Corros. Methods Mater.,* Vol 22 (No. 3), 1975, p 5–8

18. G. Trabanelli and F. Zucch, *74th Manifestation of the European Federation on Corrosion,* Oct 1974, p 289–301

19. G. Trabanelli, A. Fiegna, and V. Carassiti, *La Tribune du Cebedeau,* Vol 288, 1967

20. N.N. Andreev, N.P. Andreva, R.S. Vartapetyan, Y.I. Kuznetsov, and T.V. Fedotova, *Prot. Met.,* Vol 33 (No. 5), Sep–Oct 1997, p 470–475

21. Y.I. Kuznetsov, N.N. Andreev, N.P. Andreeva, D.V. Tolkachev, and T.V. Fedotova, *Prot. Met.,* Vol 32 (No. 5), Sep–Oct 1996, p 483–487

22. A. Subramanian, R. Gopalakrishnan, C. Bhoopathi, K. Balakrishnan, T. Vasudevan, M. Natesan, and N.S. Rengswamy, *Bull. Electrochem.,* Vol 14 (No. 10), Oct 1998, p 289–290

23. D.E. Cole, B.G. Dixon, and F.L. Keohan, "New Low Toxicity, Multi-Metal Active Vapor Phase Corrosion Inhibitors," Paper 495, presented at CORROSION/99, (Houston, TX), NACE International, 1999

24. T. Martin, Jr., *J. Chem. Eng. Data,* Vol 10, 1965, p 3

25. V.P. Persiantseva et al., *Zashch. Met.,* Vol 7 (No. 4), 1971, p 392

26. I.L. Rosenfeld et al., *Zashch. Met.,* Vol 10 (No. 4), 1974, p 339

27. N.N. Andreev and Y.I. Kuznetsov, *Prot. Met.,* Vol 32 (No. 2), Mar–Apr 1996, p 148–154

28. N.N. Andreev, *Prot. Met.,* Vol 34 (No. 2), Mar–Apr 1998, p 101–111

29. H.R. Baker and Zisman, "Liquid and Vapor Corrosion Inhibitors," U.S. Naval Res. Laboratory Report, NRL-3824, May 1951

30. V.A. Romanov and R.P. Khanovich, *Energetika,* Vol 4, 1975, p 132

31. "Rust Protection by Metal Preservatives in the Humidity Cabinet," D 1748, *Annual Book of ASTM Standards,* ASTM International

32. A. Furman and C. Chandler, Federal Test Method Standard 101C, March 1980; 9th European Symposium on Corrosion Inhibitors (Italy), 2000

33. German VIA Test Method TL 8135-0002, issued 3/12/98, W. Kohlhammer Gmbh, Post Box 800306, 70508 Stuttgart, Germany

34. C. Kraemer, "A Procedure for Testing the Effect of Vapor Phase Corrosion Inhibitors on Combined Metals," Paper 97178, presented at CORROSION/97, (Houston, TX), NACE International, 1997

35. Japanese Industrial Standard (JIS) Z 1535–1994

36. W. Skinner, *Corros. Sci.,* Vol 35 (No. 5–8), 1993, p 1491–1494

37. P. Jaegar, L.F. Garfias, and M. Buchler, "A Novel Technique to Studying the Effect of a VCI," Paper 99132, presented at CORROSION/99, (Houston, TX), NACE International, 1999

38. M.N. Desai and G.H. Tanki, *Australian Corr. J.,* Vol 13, 1969, p 19

39. K.L. Vasanth and C.M. Dacres, "Vapor Phase Corrosion Inhibitors for Navy Applications," Paper 179, presented at CORROSION/97, (Houston, TX), NACE International, 1997

40. J.M. Bastidas and E.M. Mora, "A Laboratory Study of Mild Steel Vapour Phase Corrosion and Its Inhibition by Dicyclohexylaminenitrite," *Canadian Metall. Q.,* Vol 37 (No. 1), Jan 1998, p 57–65

41. P. Jaeger, "Characterization of VCIs Using QCM and Supporting Techniques," Paper 97180, presented at CORROSION/97, (Houston, TX), NACE International, 1997

42. L.G. Kar et al., *Korroz. Zashch. Met.,* Vol 82, 1978, p 4

43. K. Schwava, DECHEMA Monographien, 45, Verlag Chemie-GMBH-Weinheim/ Bergstr., 273, 1962

44. Y.F. Yu Yao, *J. Phys. Chem.,* Vol 101, 1964, p 68

45. T.L. Rosenfeld, F.I. Rubinstein, V.P. Persiantseva, and S.V. Yakubovich, 2nd European Symposium on Inhibitors Annali VVI, Ferrara N.S., Sez. V. Supply n 4, 7, 1966

46. L. Cavallaro and G. Mantovanu, *Werkst. Korros.,* Vol 10, 1959, p 422

47. K. Schwabe, *Z. Phys. Chem.,* Leipzig 1, 1964, p 226

48. O.I. Golyanitskii, *Proc. Chelyabinsk Inst. Mechaniz and Electrifik S. Kh.,* 24, 1977, p 126

49. R.J. Lee and R.E. Karll, U.S. Patent 1,696,147

50. M.S. Chernov, S.P. Gusev, and I.L. Lomanov, Nanch. Tr. Mosr-in-t nar. Kh. Va. 131, 3, 1974

51. N. Kazuhiko, Japanese Patent C1.12 A 82 (c. 23f 11/14) No. 49-32416

52. N.G. Klyuchnikov and M. Ya, Rutten Coll. Abst. of Papers Perun, Conference on Protection of Metals against Corrosion, Pru 104, 1974

53. L.B. Sung, S. Manabu, and A. Teruzo, *Kinzoku Hyomen Gijutsu (J. Metal Finish. Soc. Japan*), Vol 392 (No. 25), 1974

54. O.I. Golyanitskiy and Tr. Chelyabinsk, In- ta Mekhaniz*, I. Elektnifik. S. Kh.,* 24, 126, 1977

55. U. Hiro and N. Shoechi, Japanese Patent Class 12 A 8 (C 23 F 11/00), 53-95842

56. N.A. Savirina et al., U.S.S.R. Patent 318,315, Class 23 F 11

57. A.I. Bocharrikov, A.A. Sorochenko, V.Ya Mudrakova, V.I. Seneya, and V.A. Dubroovskay, *Zashchita Metallov,* Vol 705 (No. 15), 1979

58. V.S. Agarwala and K.C. Tripathi, *Werkst. Korros.,* Vol 18, 1967, p 15

59. J. Barbior and C. Fiand, *Metause,* 49, 1974, p 271

60. M. Ryokichi, Japanese Patent, Class 12 A 82 (C 23 f 11/00); 49-19508

61. N. Hideo, M. Seishi and N. Takao, Japanese Patent, Class 12 A 41; (C 23 f 7/100), 52- 10164

62. T. Czarnecki and Z. Zaczyriska, Polish Patent, Class 22 g 5/08 (co 9 df/08); 72609

63. Y. Goro et al., Japanese Patent, Class 12 A 82; *Corr. Abst.,* Vol 48 (No. 9), 1977

64. Y.M. Polukarov, Au th. cert., class C 23 F 11/02; 539092; *Corr. Abst.,* Vol 48 (No. 9), 1977

65. G.G. Georgiyer, V.A. Kanazirska, and D.P. Spasova, Bulgarian Patent, Class 23 b 6/44, C 23 C 17/00, 16882

66. B.S. Lee, M. Seno, and T. Asahara, *J. Metal Finish. Soc. Jpn.,* Vol 23 (No. 10), 1974, p 493–499

67. M. Ryokichi, Japanese Patent, Class 12 A 82 (C23 f 11/14); No. 50-13751

68. L.B. Sung, S. Manabu, and A. Terguzo, *J. Met. Finish. Soc. Jpn.,* Vol 398 (No. 25), 1974

69. M. Ryokichi, Japanese Patent, Class 12 B 82 (C 23 f 11/00); 49-20862

70. M. Ryokichi, Japanese Patent, Class 12 A 82 (C 23 f 11/00); 49-19508

71. C. Tadensz and Z. Zofia, Polish Patent, Class 22 g 5/08 (co 9 df/08); 72609

72. M. Rekiti, Japanese Patent, Class 12 A 82 (C 23 f 11/14); 50

73. S.A. Baligim et al., *Izv. V.U.Z. Khim. Khim. Tekhnol.,* Ivanovao 9, 1977

74. N. Kotachi, J. Hori, and M. Yasuda, Japanese Patent, Class 12 A 82; (C 23 f 11/14), 51-10186

75. R.V. Berentseva, Jr., Chelyabinsk, In-ta Mekhaniz, I.e., elektrif. R. S. Kh, 51 126, 1977

76. R.V. Berentseva and A.P. Gugnina, *Trans. Chelyabibsk*

77. K. Neaki, Y. Mashiro, and H. Takeshi, Japanese Patent, Class 12 A 8; (C 23 f 11/14) 52-1377

78. C.M.R. Davidson, Dutch Patent, C z 3 f 11/ 14, 152605

79. T. Tadasi, T. Kiiti, Y. Seizo, and K. Takashi, Japanese Patent, Class 12 A; (C 23 f 11/00), 53-47775

80. G.F. Anan, and Y. and B.F. Nikandrov, *Coll. Chemical and Mechanical Processing of Wood and Wood Wastes,* Leningrad, 53, 4, 1978

81. M. Akiro, Japanese Applications, Class 12 A 82; (C 23 f 11/14), 52-155148

82. A.P. Gugina, *Proc. Chelyabinsk Inst. Mechaniz and Electrifik Agric.,* 61, 146, 1978

83. E.G. Zak, G.B. Rotmistrova, and L.Z. Zavitayeva, *Metal Corrosion Inhibitors,* Moscow, 154, 1979

84. P. Mityska and V. Novak, Czechoslovak Inventors Certificate, Class (C 23 F 11/02), 177381

85. L.G. Komrova, *Proc. Chelyabinsk Inst. Mechaniz and Electrif Agric.,* 67, 146, 1978

86. M.A. Quraishi and J. Rawat, Influence of Some 6-methoxy-aminobenzothiazole Derivatives on Corrosion of Ferrous and Nonferrous Metals under Vapor Phase Conditions, *Corrosion,* Vol 59, 2003, p 238–241

87. M.A. Quraishi and D. Jamal, Development and Testing of All Organic Volatile Corrosion Inhibitors, *Corrosion,* Vol 58, 2002, p 387–391

88. M.A. Quraishi and D. Jamal, "Development of Testing of New Volatile Corrosion Inhibitors for Multimetal Systems," *Mater. Perform.,* Jan 2003

89. M.A. Quraishi and J. Rawat, Triazole Derivatives: New Class of Vapor Phase Corrosion Inhibitors, *Corrosion Causes and Mitigation,* Vol 2, A. Kumbhavedekar, Ed., Quest Publication, 2000, p 115–122

90. A Supplement to Materials Performance, Jan 2001, NACE International

K.L. Vasanth, Vapor Phase Corrosion Inhibitors, *Corrosion: Fundamentals, Testing, and Protection*, Vol 13A, *ASM Handbook*, ASM International, 2003, p 871–877

Vapor Phase Corrosion Inhibitors

Kunigahalli L. Vasanth, Naval Surface Warfare Center

Selected References

- N. Hackerman, *Fundamentals of Inhibitors*, NACE Basic Corrosion Course, NACE International, 1965
- G.E. Fodor, "Inhibition of Vapor-Phase Corrosion- A Review," BFLRF-209, Southwest Res. Institute, San Antonio, TX, Oct 1985; Reviews on Corrosion Inhibitor Science and Technology, *CORROSION/89 Symposium Proc.*, A. Raman and P. Labine, Ed., NACE International, 1993, p 11-17-1
- B.A. Miksic, Use of Vapor Phase Inhibitors for Corrosion Protection of Metal Products, *CORROSION/89 Symposium Proc., Reviews on Corrosion Inhibitor Science and Technology,* A. Raman and P. Labine, Ed., NACE International, 1993, p 11-16-1
- D.D.N. Singh and M.K. Banerjee, Vapour Phase Corrosion Inhibitors-A Review, *Anti- Corrosion,* Vol 31 (No. 6), 1984, p 4–8

R.L. Martin, Corrosion Inhibitors for Oil and Gas Production, *Corrosion: Fundamentals, Testing, and Protection*, Vol 13A, *ASM Handbook*, ASM International, 2003, p 878–886

Corrosion Inhibitors for Oil and Gas Production

Revised by Richard L. Martin, BJ Unichem Chemical Services

Introduction

CORROSION INHIBITORS historically used in the oil field can be grouped into several common types or mechanistic classes: passivating, vapor phase, cathodic, anodic, film forming, neutralizing, and reactive. The common material of construction in oil and gas production is carbon or low-alloy steel, so the primary aim is steel inhibition; other metals can also benefit from many of these inhibitors (Ref 1, 2). Inorganic inhibitors, such as sodium arsenite (Na_2HAsO_3) and sodium ferrocyanide, were used in early days to inhibit carbon dioxide (CO_2) corrosion in oil wells, but the treatment frequency and effectiveness were not satisfactory. This led to the development of many organic chemical formulations that frequently incorporated film-forming amines and their salts.

In the mid-1940s, long-chain polar compounds were shown to have inhibitive properties. This discovery dramatically altered the inhibitor practices on primary production oil wells and gas wells. It permitted operation of wells that, because of the corrosivity and volume of water produced along with the hydrocarbons, would not have been used due to economics. Perhaps entire reservoirs would have been abandoned because of the high cost of corrosion. Inhibitors also allowed the injection and production of high volumes of corrosive water resulting from the secondary-recovery concept of waterflooding. Tertiary recovery floods, such as CO_2, steam, polymer, and in situ combustion floods, would usually be uneconomical without the application of corrosion inhibitors (Ref 3).

At first, it was thought that organic compounds inhibit corrosion by adsorbing at the metal-solution interface. Three types of adsorption could be possible with organic inhibitors: π- bond orbital adsorption, electrostatic adsorption, and chemisorption. A more simplistic view of this mechanism of corrosion inhibitors can be described as controlled precipitation of the inhibitor from its environment (water and hydrocarbons) onto metal surfaces. A more recent view of the mechanism of oil/gas field corrosion inhibitors invokes the incorporation of the inhibitor into a thin corrosion-product film. This film then becomes more resistant to the flow of ions and electrons, so the corrosion reaction is slowed (Ref 4, 5).

Over the years, many improvements in inhibitor technology have been made in formulation and methods of applying inhibitors. The methods of evaluating the performance during their use have also advanced considerably.

References cited in this section

1. R.L. Martin, Corrosion of Alloy Steels in Oil Field Fluids, *Corrosion,* Vol 44 (No. 2), Dec 1988, p 916–920

2. R.L. Martin, "Corrosion of Copper Base Alloys in Oil Field Fluids," Paper 367, Corrosion/88, National Association of Corrosion Engineers, 1988

3. R.L. Martin and T.G. Braga, Corrosion Control in Enhanced Oil Recovery Wells, *Mater. Perform.,* Vol 27 (No. 2), Feb 1987, p 16–22

4. R.H. Hausler, Corrosion Inhibition in the Presence of Corrosion Product Layers, *Proceedings of the Sixth European Conference on Corrosion Inhibitors* (Ferrara), 1985, p 41–65

5. I.L. Rosenfeld, D.B. Bogomolov, A.E. Gorodetskii, L.V. Frelova, and L.I. Shamova, *Taschita Metallou*, Vol 18 (No. 2), 1982, p 163–168

R.L. Martin, Corrosion Inhibitors for Oil and Gas Production, *Corrosion: Fundamentals, Testing, and Protection*, Vol 13A, *ASM Handbook*, ASM International, 2003, p 878–886

Corrosion Inhibitors for Oil and Gas Production

Revised by Richard L. Martin, BJ Unichem Chemical Services

Inhibitor Formulations

Many different inhibitor formulations are available. However, most of these inhibitors are produced from only a few basic types of starting molecules. Fatty acids and some form of basic nitrogen-containing precursor are the principal active-ingredient sources. Historically, the first proprietary organic inhibitors were fatty imidazolines made from by-product fatty acids and polyethylene amines. The reaction is a condensation reaction that produces the following structure:

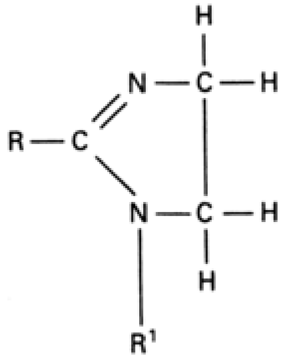

in which R is a chain of carbon molecules (average: C_{18}), and R^1 is a hydrogen atom or C_2H_4N group.

The molecules produced from these products were dissolved in hydrocarbon solvent or water- alcohol-based solvent, depending on whether they were further reacted. Typical further reactions were salting with acetic acid (CH_3COOH) or quaternizing with a short-chain alkyl chloride. Highly corrosive wells, such as those found in the Talco Field (Texas), required daily batch treatments with these early inhibitors.

The inhibitors currently in use are generally more complex mixtures of reaction products and have been formulated to meet the demands of a very competitive industry. Some of these demands on inhibitor formulation are discussed subsequently.

Pour Point. Because inhibitors are usually stored and used outdoors, they must remain liquid at low temperatures. A pour point of -30 °C (-20 °F) is usually required. Some areas of the world may have an even lower pour point requirement (-40 to -45 °C, or -40 to -50 °F). The required pour point often dictates the activity and solvent system of a particular inhibitor.

Solubility. Solubility/dispersibility characteristics of an inhibitor are dictated by the intended use. By their very nature, most inhibitors are not truly soluble in either hydrocarbons or water; degrees of dispersibility are more descriptive.

Performance. The end user of corrosion inhibitors will often specify a laboratory test that the inhibitor must pass before a field trial or purchase is considered. The wheel test is sometimes used in the oil- and gas-producing industry. Therefore, many inhibitors are formulated to pass the wheel test (see the section "Laboratory Testing of Corrosion Inhibitors" in this article).

Emulsion Tendencies. The application of the inhibitor must not cause secondary problems. Batch treatments have often caused emulsions of the hydrocarbons and water that, relative to normal operations, are extremely difficult to break. In some cases, the emulsions resulting from batch treatments were so viscous that the surface separation equipment was plugged by the emulsion formed in the presence of high inhibitor concentrations.

Therefore, inhibitors are specifically formulated to be nonemulsifying. Alternatively, emulsion-breaker chemicals are added to formulations in small amounts to prevent emulsions.

Table 1 lists the cationic molecular structures found in many commercial inhibitors. These amines or cationic molecules are often neutralized with an organic acid or quaternized to achieve a final basic product. In many inhibitor formulations, the choice of the acid or anionic molecule is critical to the performance of the final product. Also, a mixture of acids is sometimes used to obtain a desired property. In addition, Table 2 lists the anionic molecular structures found in many commercial inhibitors. The compositions of fatty acids used in inhibitor production are given in Table 3.

Table 1 Cationic molecular structures in commercial oil field inhibitors

The letter R denotes fatty acids derived from such oils as soya, coconut, tallow, and tall oil. Sources of these fatty acids are listed in Table 3.

Imidazolines	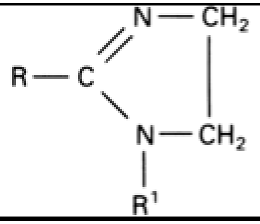
Dimerized amido-amines	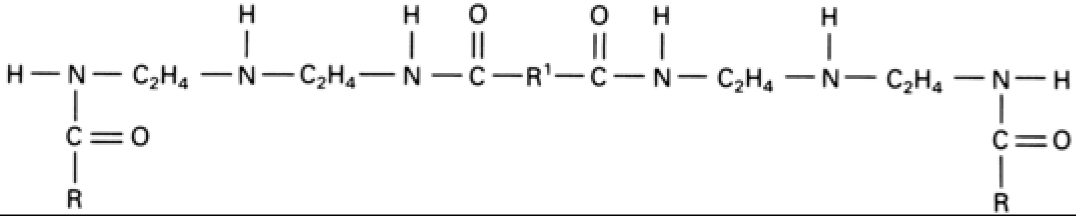
Dimer acid amido-amines	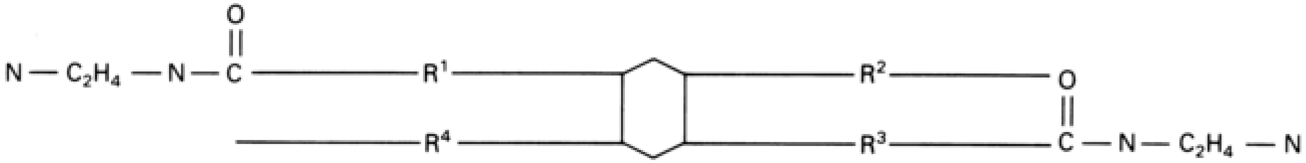
Oxyethylated primary amines	R—N—[$(C_2H_4O)_n$—H]$_2$
Alkyl pyridine	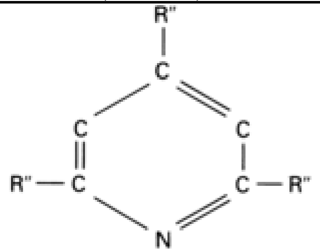 R″ may be CH_3 to C_3H_7 or higher
Quaternized amines	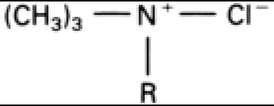

Table 2 Anionic molecular structures used in commercial oil field inhibitors

The letter R denotes fatty acids derived from such oils as soya, coconut, tallow, and tall oil. Sources of these fatty acids are listed in Table 3.

Dimer-trimer acids (C_{18} average)	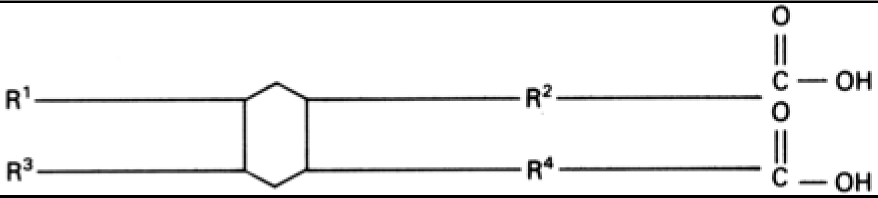
Fatty acids	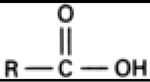
Naphthenic acids	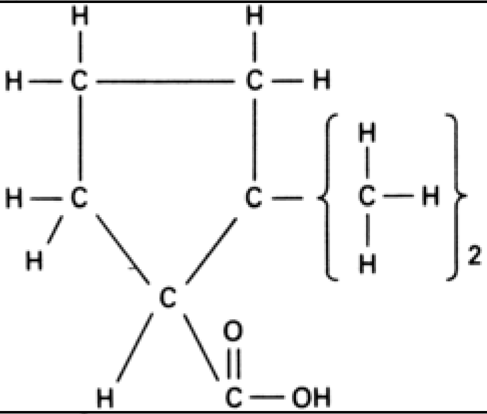
Phosphate esters of ethoxylated alcohol	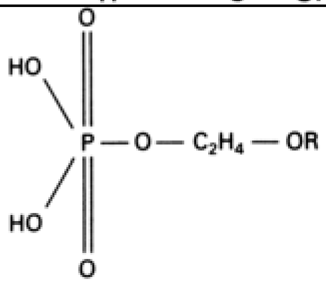 R = C_{10} to C_{16} (average C_{12})
Other organic acids	1. Acetic 2. Hydroxyacetic 3. Benzoic

Table 3 Sources of fatty acids used in corrosion inhibitors

Data obtained from literature sources and from Procter & Gamble analyses. Crude tall oil, distilled tall oil, and distilled tall oil fatty acids are the most common sources for oleophilic groups of inhibitor molecules. Tall oil is a by-product of pulping wood chips (usually pine wood) by the kraft process. Although tall oil is removed from the wood as a sodium salt, 10 to 15% inert unsaponifiable material is present. Crude tall oil is one of the cheapest raw materials known to the industry, but due to the variability of composition from tree to tree, experience and care are required in its use.

Fatty acid	Number of double bonds	Number of carbon atoms	Source, %			
			Coconut oil	**Soya oil**	**Tallow**	**Tall oil fatty acids[(a)]**
Caprylic	0	8	7	…	…	…
Capric	0	10	6	…	…	…
Lauric	0	12	50	0.5	…	…
Myristic	0	14	18	0.5	3	…
Palmitic	0	16	8.5	12	24	…
Stearic	0	18	3	4	20	4

Oleic	1	18	6	25	43	52
Linoleic	2	18	1	52	4	40
Linolenic	3	18	0.5	6	0.5	…
Others[(b)]	NA	NA	…	…	4.5	4

(a) Tall oil acids consist of 60 to 70% fatty acids and 30 to 40% rosin acids
(b) NA, not applicable

R.L. Martin, Corrosion Inhibitors for Oil and Gas Production, *Corrosion: Fundamentals, Testing, and Protection*, Vol 13A, *ASM Handbook*, ASM International, 2003, p 878–886

Corrosion Inhibitors for Oil and Gas Production

Revised by Richard L. Martin, BJ Unichem Chemical Services

Varying Characteristics of Oil and Gas Wells

The varying characteristics and number of organic inhibitors are explained by the varying characteristics of oil and gas wells. In this article, systems are characterized as oil wells, gas wells, water injection systems, or pipelines.

Oil Wells. Wells that produce liquid hydrocarbons and water can be divided into two basic types: flowing wells, which have a natural flow of hydrocarbons and water to the surface, and artificially lifted wells, which require some form of pump. The latter type includes rod-pumped wells, which use a positive-displacement downhole pump connected to the surface by rods; gas- lifted wells, in which gas in injected at some point down the hole to lighten the fluid and cause flow; electrical submerged-pump wells, which use multistage centrifugal pumps placed near the bottom of the well; and hydraulically pumped wells, which use positive-displacement pumps driven hydraulically by oil or water from a surface motor and pump.

Gas Wells. Most gas wells flow naturally. These include dry gas wells, which produce mainly gaseous hydrocarbons, and gas-condensate wells, which produce significant quantities of liquid hydrocarbons, sometimes water, liquid petroleum gas (LPG), and methane at high pressures from high-temperature reservoirs. Lower- pressure gas wells sometimes incorporate artificial lift to prevent liquids from accumulating at the well bottom. These wells can also be produced with plunger lifts or injected foamer to keep liquids moving up so that pressure buildups do not occur.

Water injection systems are used for disposal, waterflood, or tertiary recovery.

Each of the previously mentioned categories can be divided into a sweet or sour designation, which is a function of the absence or presence of hydrogen sulfide (H_2S). Corrosion is usually defined as sour when any phase of the produced fluids contains measurable H_2S. Sweet corrosion is caused by the presence of CO_2, formic acid (HCOOH), CH_3COOH, or other short-chain acids in the produced gas and/or fluids. Because corrosivity is usually related to the ratio of produced water to hydrocarbons, the volume and composition of the produced water and oil will influence the application method and performance of the inhibitor. Oxygen entry into either a sweet or sour corrosion system results in significant corrosion consequences. Corrosion is accelerated, deposition is increased, and inhibitor function is altered (Ref 6, 7). Many corrosion systems are considered to be oxygen influenced if the dissolved oxygen concentration exceeds 25 parts per billion (ppb).

Pipelines conduct produced fluids from or injection water toward the aforementioned wells. These lines are subject to the same corrosion conditions as described for wells. For example, sour corrosion can be accelerated by oxygen dissolved in methanol added for hydrate control. Application of corrosion inhibitors depends on the location (flow regime) and amount (production rate) of the aqueous phase. Computer programs are available to assist in this evaluation. After oil/water separation or gas processing, pipelines are commonly termed transmission lines. Transmission lines are less subject to the previously mentioned corrosion conditions. Corrosion in transmission lines is more often due to microbiologically influenced corrosion factors.

References cited in this section

6. R.L. Martin and R.R. Annand, Accelerated Corrosion of Steel by Suspended Iron Sulfides in Brine, *Corrosion,* Vol 37 (No. 5), May 1981, p 297–301
7. R.L. Martin, "Corrosion Consequences of Oxygen Entry into Oilfield Brines," Paper 02270, Corrosion/2002, National Association of Corrosion Engineers, 2002

R.L. Martin, Corrosion Inhibitors for Oil and Gas Production, *Corrosion: Fundamentals, Testing, and Protection*, Vol 13A, *ASM Handbook*, ASM International, 2003, p 878–886

Corrosion Inhibitors for Oil and Gas Production

Revised by Richard L. Martin, BJ Unichem Chemical Services

Influence of Well Depth and Completion Method

The industry is continuously seeking new oil and gas reserves. New finds are generally deeper and/or more inaccessible. As the depth increases in the newer wells, the bottom hole temperature increases. Bottom hole temperatures of 205 °C (400 °F) have been encountered in several deep reservoirs. High labor and equipment costs in offshore production and remote areas plus safety and environmental concerns have caused the risk of equipment malfunction due to inhibitor failure (incorrect method of application or poor inhibitor performance) to become increasingly important. This has forced the industry to screen inhibitors carefully and to select application methods that are highly reliable.

R.L. Martin, Corrosion Inhibitors for Oil and Gas Production, *Corrosion: Fundamentals, Testing, and Protection*, Vol 13A, *ASM Handbook*, ASM International, 2003, p 878–886

Corrosion Inhibitors for Oil and Gas Production

Revised by Richard L. Martin, BJ Unichem Chemical Services

Factors Influencing Corrosivity of Produced Fluids

Characteristics of Fluids. Produced fluids vary from noncorrosive hydrocarbons to extremely corrosive brines. The amount of water in the produced fluids may vary from 1 to 99%. In general, the higher the concentration of dissolved acid gases (and oxygen), the higher the uninhibited corrosion rate (Ref 3, 7).
Temperature, Pressure, and Velocity Effects. The effect of temperature is not straightforward. Chemical reaction rates double with each 10 °C (18 °F) temperature increase. However, the solubility of the acid gasses decreases with temperature; therefore, a smaller increase in corrosivity is seen with temperature rise. Additionally, above approximately 65 °C (150 °F), the nature of the surface corrosion product changes to become more protective; this is an especially important factor in sweet systems. The effect of increased pressure is to raise the solubility of acid gases, thus increasing the corrosivity of the water. Bottom hole pressures exceeding 138 MPa (20 ksi) are occasionally encountered.
Pressure is related to corrosivity in sweet gas wells as follows (Ref 8):

- A partial pressure of CO_2 below 48 kPa (7 psi) is considered noncorrosive.
- A partial pressure of CO_2 between 48 and 207 kPa (7 and 30 psi) may indicate corrosion.
- A partial pressure of CO_2 above 207 kPa (30 psi) usually indicates severe corrosion.

Although this general rule is widely accepted, many exceptions have been noted.

Cyclic Loading, Stress, and Wear. Corrosion inhibitors can be specially formulated to control corrosion that is accelerated by cyclic loading, stress, and wear. Methods of evaluating inhibitors for inhibition of corrosion accelerated by stress and fatigue are discussed in Ref 9, 10, 11, 12, 13, 14. Because most oil wells are not perfectly vertical holes, wear of tubing by rods becomes a problem in wells that are highly deviated or crooked. Rod guides and inhibitors are sometimes effective in controlling wear and corrosion.

Erosion and Abrasion. Many wells produce fine sand along with the fluids. This fine sand may remove inhibitor films, depending on the velocity of the fluids. Also, erosion by this fine sand is the primary cause of equipment failure in artificially lifted wells. Sand control, a process of permanently preventing movement of fine sand particles from the formation, is often necessary for good corrosion inhibition.

Water Volume. Severe corrosion can begin at initial water production (Ref 15). Corrosion usually develops in wells as increasing percentages of water are produced. Corrosion in this type of well may begin after several years of production.

A 1953 survey of corrosive oil wells showed that no oil wells were corrosive when the water production was under 40%. Water contents from 0 to 40% usually represent well-emulsified water. Because oil is the continuous phase, the production equipment is considered to be oil-wet (Ref 16, 17, 18, 19, 20). However, oil production in the North Sea and Alaska's North Slope has shown that water contents of approximately 4% may be highly corrosive (Ref 21). Many fields have produced sour water from the outset, although many have changed from sweet to sour during the water injection phase. Bacterial activity is commonly responsible. (A waterflood is the injection of water into a field to displace hydrocarbon from the field.) Sour fluids in these mature waterfloods are generally regarded as being corrosive.

References cited in this section

3. R.L. Martin and T.G. Braga, Corrosion Control in Enhanced Oil Recovery Wells, *Mater. Perform.,* Vol 27 (No. 2), Feb 1987, p 16–22

7. R.L. Martin, “Corrosion Consequences of Oxygen Entry into Oilfield Brines,” Paper 02270, Corrosion/2002, National Association of Corrosion Engineers, 2002

8. *Condensate Well Corrosion,* Natural Gasoline Association of America, 1953

9. J.F. Chittum, Corrosion Fatigue Cracking of Oilwell Sucker Rods, *Mater. Perform.,* Vol 7 (No. 12), Dec 1968, p 37–38

10. J.F. Bates, Sulfide Cracking of High Strength Steels in Sour Crude Oils, *Mater. Perform.,* Vol 8 (No. 1), Jan 1969, p 33–39

11. C.M. Hudgins, A Review of Sulfide Corrosion Problems in the Petroleum Industry, *Mater. Perform.,* Vol 8 (No. 1), Jan 1969, p 41–47

12. C.C. Patton, Petroleum Production—Stringent Corrosion Control Procedures Key to Extended Fatigue Life, *Mater. Prot. Perform.,* Vol 11 (No. 1), June 1972, p 17–18

13. R.L. Martin, Inhibition of Corrosion Fatigue of Oil Well Sucker Rods, *Mater. Perform.,* Vol 19 (No. 6), June 1980, p 20–23

14. R.L. Martin, Inhibition of Hydrogen Permeation in Steels Corroding in Sour Fields, *Corrosion,* Vol 49 (No. 8), 1993, p 694–701

15. J.I. Bregman, *Corrosion Inhibitors,* MacMillan, 1963

16. G.L. Farrar, Combatting Corrosion in Oil and Gas Wells, *Oil Gas J.,* Vol 51 (No. 49), April 1953, p 106–109, 111, 113

17. H.L. Bilhartz, Sweet Oil Well Corrosion, *World Oil,* Vol 134, April 1952, p 208–216

18. H.L. Bilhartz, How to Predict and Control Sweet Oil Well Corrosion, *Oil Gas J.,* Vol 50 (No. 50), April 1952, p 116–118, 151, 153

19. H.L. Bilhartz, *Sweet Oil Well Corrosion— API Drilling and Production Practice,* American Petroleum Institute, 1952, p 54

20. H.L. Bilhartz, High Pressure Sweet Oil Well Corrosion, *Corrosion,* Vol 7 (No. 8), Aug 1951, p 256–264

21. C.J. Houghton and R.V. Westermark, Downhole Corrosion Mitigation in Ekofisk (North Sea) Field, *Mater. Perform.,* Vol 22 (No. 1), Jan 1983, p 16

R.L. Martin, Corrosion Inhibitors for Oil and Gas Production, *Corrosion: Fundamentals, Testing, and Protection*, Vol 13A, *ASM Handbook*, ASM International, 2003, p 878–886

Corrosion Inhibitors for Oil and Gas Production

Revised by Richard L. Martin, BJ Unichem Chemical Services

Methods of Inhibitor Application

Continuous treatment of producing wells and waterflood injection systems is accomplished by a chemical-proportioning pump that operates constantly. Continuous treatment of artificially lifted wells is carried out by continuously injecting a small quantity of inhibitor into the annulus with a portion of the produced fluid. This technique is known as slip-stream flushing. After an initial treatment of several gallons of inhibitor, the inhibitor is continuously injected in order to maintain an inhibitor concentration of 15 to 100 ppm in the produced fluid. The mechanical setup of continuous treatment is simple in artificially lifted wells, because the annulus is usually open to the tubing. Gas-lifted wells can be continuously inhibited by injection into the lift gas. When the lift gas is dry, inhibitor formulations are available that will remain flowable until they contact produced liquids. A treating system of inhibiting gas-lifted wells is described in Ref 22.
Continuous treatment of flowing oil and gas wells requires certain types of completion. The following completion techniques are engineered for continuous treating:

- *Dual completion (either concentric or parallel):* In this completion technique, two separate strings of tubing are run in the same hole and may or may not be the same size.
- *Capillary or small-bore treating string:* involves using a string of continuous, small- diameter tubing strapped to the outside of the well tubing or pipe. This type of completion provides excellent inhibitor injection control with superior results (Ref 23, 24, 25, 26). Disadvantages are the cost and the mechanical difficulties.
- *Side pocket mandrel valve:* The annulus is filled with liquid inhibitor solution, and continuous injection on the surface is used to apply pressure to the annulus so that the injection valve opens. Mechanical difficulties with the valve and the stability of the inhibitor solution are disadvantages.
- *Packerless completion:* No downhole valves are involved, but inhibitor solution stability must be considered (Ref 27, 28). At high bottom hole temperatures, continuous treatment is generally selected when production rates are such that the expected treatment life of batch treatments is economically prohibitive.
- *Low-cost continuous method for marginal gas wells:* involves perforating the tubing above the packer, filling the annulus with an inhibitor solution, and then continuously pumping inhibitor solution into the annulus at the surface (Ref 29)

Hydraulically pumped wells are usually inhibited by injection into the power fluid; some wells have oil as the pressurized liquid (power oil), and some use produced brine (power water).

Intermittent Treatment of Gas Wells. Batch or intermittent treatment of flowing gas or oil wells may be effective at low fluid-production volumes. Treatment is accomplished by diluting the inhibitor into hydrocarbons or water, then shutting in the well long enough for the inhibitor solution to fall to the bottom of the well. Because the liquid fluid level is unknown, the depth to which the inhibitor solution will fall is unknown; consequently, the results of the application are difficult to predict. Regular treatment intervals from 3 to 6 months can be obtained under optimal conditions in low-volume wells. A more positive approach to batch treating is full tubing displacement. This is accomplished by pumping a solution into the well and displacing the solution with water or hydrocarbon to the bottom of the well. Another approach would be to displace the inhibitor solution with an inert gas, such as nitrogen; nitrogen is less likely than water or hydrocarbon to stop the flow of the well.

Squeeze Treating. Successful squeeze treatments were first reported in 1955 in the Placido Field of Victoria County, TX (Ref 30, 31). Since that time, the method of squeezing inhibitor into the formation has been refined.

Squeeze treating is applicable to all oil and gas wells with sufficiently porous and permeable producing zones. It will result in essentially continuous treatment, because it has been found that some inhibitors will adsorb rapidly onto sand and will desorb slowly into produced fluids from the producing sand. The inhibitors used for this technique should be very film persistent. The most widely used technique is to mix one to two 208 L (55 gal) drums of inhibitor with 10 to 20 barrels of diesel, kerosene, lease crude, or condensate. The inhibitor solution is displaced to the bottom of the well, and an overflush of 200 to 500 barrels or more of oil or brine is then used to push the inhibitor into the formation. This technique often leads to continuous feedback lasting anywhere from 3 months to 2 years. The advantages of this method are that it will successfully treat wells with high fluid levels, the frequency of treatment is drastically reduced, and it is more reliable than some batch methods. Also, the entire length of the tubing is treated. However, squeeze treating is not recommended for all wells.

The major concern with squeeze treating is the possibility of plugging the formation by emulsion blocks or wettability reversal in the producing formation. The possible plugging effect of inhibitor squeezes on cores was studied in the laboratory, and it was reported that various sandstone formations differed in adsorption characteristics and that limestones were markedly different from sandstones (Ref 32, 33). This work was expanded on in a field study, which is discussed in Ref 34. Tracer studies on formation squeezes were also conducted (Ref 35).

In a unique variation of the formation squeeze, the corrosion inhibitor/hydrocarbon diluent is atomized with an inert gas, such as nitrogen, and displaced down the tubing and into the formation with the same inert gas (Ref 36). Longer squeeze life and better inhibition have been claimed. The method is advantageous in wells with low bottom hole pressures, because the low density of the nitrogen eases the resumption of production in such wells.

Batch Treatment of Pumping Wells. Corrosion problems in pumped wells are directly related to the production volume and water content of producing wells. This will be the case whether the lift method is sucker rod pump, electric submersible pump (ESP), or progressive cavity pump. Severe corrosion problems can be identified by excessive rod, pump, and tubing failures. Embrittlement and pitting result in reduced rod life and fatigue failures, which are greatly accelerated by the presence of H_2S. Hydrogen sulfide and high water volumes are common to most waterfloods.

The most common way of treating pumped wells consists of batch treating with a pump truck, equipped to flush the inhibitor down the annulus with produced fluids or water. In some wells, batch treatment is accomplished without treating trucks by the use of wellhead inhibitor lubricator pots and manual flushing with produced fluids.

The methodology of batch treating involves the development of guidelines for each field. The required guidelines are volume of inhibitor per treatment, volume of flush, and treatment frequency. General rules for batch volume are based on barrels of fluid produced per day (BFPD). One set of general rules for frequency is given in Ref 37 and 38:

Volume of total fluid, BFPD	Frequency
0–50	Monthly
50–150	Every 2 weeks
150–350	Weekly
350–800	Twice weekly

Another set of recommended guidelines for treating frequency is given in Ref 39.

Flush volume is usually based on the nature of the inhibitor and the height of the liquid column in the annulus above the pump. Usually, two to four barrels of produced water are used per 300 m (1000 ft) of liquid level above the pump when the following guidelines are followed:

Annular liquid level above pump		Optimal corrosion inhibitor type
m	**ft**	
0–150	0–500	Oil soluble, limited brine dispersibility
150–300	500–1000	Oil soluble, brine dispersible
300+	1000+	Highly dispersible or soluble in brine

Successful batch treating of rod-pumped wells also involves the following factors:

- Circulation of high-volume wells is often necessary. In high gas-oil ratio (GOR) wells, it may be necessary to isolate the annulus for approximately 2 h after treatment to allow the inhibitor slug to fall.
- Calculation of inhibitor volume based on the frequency of treatment and fluid production is an accepted procedure; inhibitor concentration is generally maintained at 25 to 35 ppm.
- Determination of the correct minimum overflush
- Selection of the proper inhibitor

Automatic computer-controlled chemical injectors are available for batch treating. The cost advantages and disadvantages of computer-controlled chemical injectors are discussed in Ref 39. Corrosion fatigue in rod-pumped wells is as important as weight loss corrosion. A corrosion fatigue testing apparatus is described in Ref 40 that can be used to field test corrosion inhibitors specially formulated to prevent corrosion fatigue (Ref 14).

Treatment With High-Density Corrosion Inhibitors. Most liquid inhibitors have a density of 910 to 980 g/L (7.6 to 8.2 lb/gal). High-density liquid corrosion inhibitors are formulations that have been coupled with weighting agents. Their high density (1200 g/L, or 10 lb/gal) and their immiscibility with hydrocarbons and water enable them to fall through static columns of hydrocarbons. Continuous treating can be accomplished by using frequent small-volume batch treatments. Some applications for these unique inhibitors are high-fluid-level pumping wells and/or high- and low-pressure gas wells.

The weighting agent in high-density inhibitors is often zinc chloride ($ZnCl_2$), which may precipitate as zinc sulfide (ZnS) or zinc oxide (ZnO) when applied to sour wells. Data on the fall rates of high-density and regular inhibitors are given in Ref 41 and 42. Other forms of weighted inhibitors, such as solid sticks and capsules, are available. More detailed information on liquid weighted inhibitors is available in Ref 43.

Green Inhibitors. Especially for offshore applications, the final fate of corrosion inhibitors relative to the environment becomes important. Ideally, green corrosion inhibitors should have low toxicity to organisms (marine when applied offshore), be biodegradable, and not partition into fatty tissues of organisms, so as not to enter the food chain. To achieve all these properties and still have effective corrosion inhibition usually requires the cooperation of multiple disciplines (Ref 44).

Miscellaneous Treatments. Slow-dissolving solids, sticks, pellets, microencapsulated droplets, and other configurations are used as vehicles for corrosion inhibitors. In addition, downhole dump bailers and concentric kill strings are used for both batch and continuous treatment.

References cited in this section

14. R.L. Martin, Inhibition of Hydrogen Permeation in Steels Corroding in Sour Fields, *Corrosion*, Vol 49 (No. 8), 1993, p 694–701

22. D.H. Mutti, J.E. Atwood, C.R. LaFayette, and A.O. Landrum, "Corrosion Control of Gas-Lift Well Tubulars by Continuous Inhibitor Injection into the Gas-Lift Gas Stream," Paper 5612, presented at the 50th annual meeting (Dallas, TX), Society of Petroleum Engineers, 1975

23. R.B. Todd, J.H. Cannon, H.J. EnDean, and K. Belanus, Corrosion Protection by Downhole Continuous Inhibitor via External Capillary, *Mater. Perform.,* Vol 20 (No. 2), 1981, p 32

24. J.B. Bradburn and R.B. Todd, Continuous Injection Method Controls Downhole Corrosion, Part 1, *Pet. Eng. Int.,* Vol 53, July 1981, p 44–46

25. J.B. Bradburn and R.B. Todd, Continuous Injection Method Controls Downhole Corrosion, Part 2, *Pet. Eng. Int.,* Vol 53, Aug 1981, p 54

26. L.M. Cenegy and C.L. Chin, A Test for Corrosion Inhibitors to be Used in Oilfield Capillary Injection Systems, *Mater. Perform.,* Vol 22 (No. 4), April 1983, p 15–19

27. T.W. Hamby, Jr., "Development of High Pressure Sour Gas Technology," Paper 8309, presented at the 54th conference (Las Vegas, NV), Society of Petroleum Engineers, 1979

28. M.C. Place, Jr., "Corrosion Control—Deep Sour Gas Production," Paper 8310, presented at the 54th conference (Las Vegas, NV), Society of Petroleum Engineers, 1979

29. R.H. Hausler and S.G. Weeks, Low Cost, Low Volume, Continuous Inhibition of Gas Production Tubulars, *Mater. Perform.,* Vol 25 (No. 6), 1986, p 27–37

30. R.H. Poetker and J.D. Stone, Squeezing Inhibitor into Formation, *Pet. Eng.,* Vol 28, May 1956, p B29–B34

31. R.H. Poetker and J.D. Stone, Inhibition Improved 17 Percent While Cost Dropped 50 Percent, *Oil Gas J.,* Vol 54, July 1956

32. J.K. Kerver and F.A. Morgan III, Corrosion Inhibitor Squeeze Technique—Laboratory Study of Formation Permeability Damage, *Mater. Perform.,* Vol 2 (No. 4), April 1963, p 10–22

33. J.K. Kerver and F.A. Morgan III, Corrosion Inhibitor Squeeze Technique—Laboratory Adsorption-Desorption Studies, *Mater. Perform.,* Vol 4 (No. 4), July 1965, p 69–79

34. J.K. Kerver and H.R. Hanson, Corrosion Inhibitor Squeeze Technique—Field Evaluation of Engineered Squeezes, *J. Pet. Technol.,* Vol 17, Jan 1965, p 50–57

35. P.J. Raifsnider, C.L. Guinn, C.L. Barr, and D.L. Lilly, "Radioactive Tracer Studies on Squeeze Inhibition of Oil Wells," paper presented at the 19th annual conference (New York, NY), National Association of Corrosion Engineers, March 1963

36. G.L. Nunn and B.E. Hamilton, Well Treatment with Inhert Gas—Inert Gas Squeeze for Corrosion Control, *Mater. Perform.,* Vol 6 (No. 5), May 1967, p 37–40

37. S. Evans and C.R. Doran, "Batch Treatment of Sucker Rod Pumped Wells," paper presented at the Southwestern Petroleum Short Course, Department of Petroleum Engineering, Texas Tech University, April 1983

38. S. Evans and C.R. Doran, Batch Treatment Controls Corrosion in Pumping Wells, *World Oil,* Vol 198, Feb 1984, p 55–57

39. W.J. Frank, Here's How to Deal with Corrosion Problems in Rod-Pumped Wells, *Oil Gas J.,* Vol 74, May 1976, p 63–72

40. L.A. Phillips and J.R. Cowden, “Corrosion Fatigue Test Selects Effective Corrosion Inhibitors,” Paper 266, presented at Corrosion/ 80 (Chicago, II), National Association of Corrosion Engineers, March 1980

41. G.B. Farquhar, M.J. Michnick, and R.R. Annand, Tracer Experiments During Batch Treatment of Gas Wells with Corrosion Inhibitors, *Mater. Prot. Perform.,* Vol 10 (No. 8), Aug 1971, p 41–45

42. C.C. Patton, D.A. Deemer, and H.M. Hillard, Jr., Field Study of Fall Rate—Oilwell Liquid Inhibitor Effectiveness, *Mater. Perform.,* Vol 9 (No. 2), Feb 1970, p 37–41

43. C.O. Bundrant, High Density Corrosion Inhibitors Simplify Oil Well Treatments, *Mater. Perform.,* Vol 8 (No. 9), Sept 1969, p 53–55

44. R.L. Martin, B.A. Alink, T.G. Braga, and J.A. McMahon, “Environmentally Acceptable Water Soluble Corrosion Inhibitors,” Paper 36, Corrosion/95, National Association of Corrosion Engineers, 1995

R.L. Martin, Corrosion Inhibitors for Oil and Gas Production, *Corrosion: Fundamentals, Testing, and Protection,* Vol 13A*, ASM Handbook,* ASM International, 2003, p 878–886

Corrosion Inhibitors for Oil and Gas Production

Revised by Richard L. Martin, BJ Unichem Chemical Services

Corrosion Problems and Inhibition in Waterfloods

Corrosion inhibition in waterfloods involves protecting surface-gathering lines and tanks used to recycle produced water, water-treating equipment, and the surface lines and downhole tubing of injection wells. The primary causes of corrosion in waterfloods are oxygen contamination and acid gasses dissolved in the brine. Due to the large amount of water handled, the cost of corrosion failures in repair and downtime can be substantial (Ref 45).

Oxygen Corrosion. Oxygen may be present in the supply water when the water source is surface or shallow ground water. Seawater is commonly used in near-shore or offshore fields and usually contains approximately 8 ppm dissolved oxygen. Another oxygen source is small amounts of contamination into closed water-handling systems through nongas-blanketed holding tanks, open vents, thief hatches of water holding tanks, as well as around the shaft of the suction side of centrifugal transfer pumps (Ref 46). Crude oil or diesel oil blankets on the water surface in tanks do not stop oxygen from contaminating the water. Oxygen corrosion can be controlled by removing the oxygen or by using inhibitors.

Oxygen removal by mechanical means applies mainly to high-oxygen-containing waters, such as seawater. Oxygen is removed by the following mechanical processes:

- Countercurrent gas-stripping towers represent the simplest and most economical method, if large amounts of natural gas are available at low cost.
- Vacuum tower removal is applicable where no gas is available (Ref 47).
- The water can be gas lifted from its source— for example, lifting seawater from a depth of 30 m (100 ft) by the same technology used to lift fluids in gas-lift oil wells.
- Usually, none of the previously mentioned methods will reduce the oxygen to the required point; therefore, chemical oxygen scavengers must be used to remove the last traces.

Oxygen scavenging refers to removal of the oxygen by chemical reactions. Oxygen scavengers can reduce the oxygen content of the water to less than 10 ppb, a level that is considered insignificant from the corrosivity standpoint. The most commonly used oxygen scavengers are:

- Sulfite ion (SO_3^{2-}), which may come from sulfur dioxide (SO_2) gas generated on the site, from solutions of sodium sulfite (Na_2SO_3) or sodium bisulfite ($NaHSO_3$), or from a solution of ammonium bisulfite (NH_4HSO_3). Ammonium bisulfite is the most commonly used because of its stability in storage and its ability to exist as a highly concentrated liquid solution. Solutions containing 60 to 70% NH_4HSO_3 are commercially available.
- Hydrazine, which is a practical oxygen-scavenging chemical only at elevated temperatures, such as in boilers or steam generators
- Sodium hydrosulfite ($NaHSO_2$) is recommended for scavenging oxygen, with much less polymer degradation than SO_3^{2-}, in polymer flood applications. However, $NaHSO_2$ is very unstable in solution and requires storage of a solid and solution preparation daily.

The reaction of the oxygen scavengers listed previously involves a free-radical mechanism that necessitates an initiating step. Very small additions (<1 ppm) of transition-metal ions, such as cobalt, will catalyze the reaction. The variables affecting the rate and completeness of the SO_3^{2-} reaction are important in designing a waterflood. Sodium sulfite used in a 1 to 2 ppm stoichiometric excess plus 0.1 to 0.2 ppm cobalt chloride ($CoCl_2$) at ambient temperature often completely removes oxygen in an acceptable time period (usually a few minutes). When the rate or degree of completeness of the reaction is not satisfactory, an investigation into possible interferences with the reaction may be necessary. The most common problems are deactivation and insufficient reaction time at the service temperature of the catalyst. All transition metals are not equally effective, and pH affects the various possible metal ions differently (Ref 48, 49). In waters containing sulfide, the catalyst can be precipitated as an insoluble solid (Ref 50), or it can be complexed with a chelating agent, such as ethylenediamine tetraacetic acid (EDTA). In both cases, the catalyst is rendered inactive.

Water used for cyclic steam injection and steam floods must be given greater attention with regard to oxygen corrosion. Corrosion and other water-treating problems in steam injection systems are discussed in Ref 51.

When removal of oxygen is not practical because of small volumes of water to be treated or other factors, two organic inhibitors are available. The first, a zinc amino methyl phosphonate, reportedly achieves excellent oxygen corrosion control in fresh to slightly brackish supply waters (Ref 52, 53, 54). The second, an organic sulfophosphate, exhibits inhibition of produced water-handling systems processing sour brine contaminated with oxygen (Ref 55). The inhibitor is dispersible only in water and is said to inhibit better when H_2S and hydrocarbons are present in the water in addition to oxygen. Other inhibitors have been developed in recent years for control of oxygen-accelerated corrosion (Ref 7).

Alternatives to oxygen removal and/or organic corrosion inhibitors are the use of internally coated steel pipe with either plastic or cement lining, corrosion-resistant alloys, fiberglass-reinforced plastic, or other nonmetals in place of carbon steel. Finally, inorganic inhibitors used in aerated water—for example, cooling towers and radiators—are usually not effective and are too expensive to be applied to waters on a once-through basis, as would be the case in a waterflood.

Corrosion by Acid Gases. The corrosive acids found in waterflood systems are usually encountered because produced water is recycled and mixed with the supply water. In a few fields, the produced water has been kept separate from the supply water.

Experience has shown that the presence of H_2S in injection water is much more troublesome with regard to corrosivity and handling problems than waters containing only CO_2 or short-chain acids. This is the case primarily because iron sulfide (FeS), the product of H_2S corrosion, is very insoluble. The FeS corrosion product may deposit on downstream equipment, may plug injection wells, and may cause difficulties in oil-water separation. An inhibitor has not yet been discovered to prevent the precipitation of FeS.

The corrosion inhibitors designed for acidic corrosion are usually film-forming amine salts. Water-soluble or dispersible modifications of these materials are used in waterflood applications. Experience has shown that the system must be free of oxygen contamination for most of these materials to be effective. Therefore, the previously mentioned materials are usually used in conjunction with oxygen scavengers.

Film-forming ability and stability are determined by the interplay of a number of factors involving both the oleophilic hydrocarbon chain and the polar portion of the molecule. Changes in the oleophilic portion of the molecule that promote water solubility tend to decrease filming ability. The conflict between solubility and film stability is one of the basic obstacles in formulating inhibitors for waterfloods. Water compatibility or solubility is important if the water is to be injected into a low-permeability reservoir.

The chemistry and ideas used in inhibitor molecules for producing wells have been extended or modified for use in waterfloods. Sufficient dispersibility (added to the inhibitor so that the inhibitor may be effectively transported from the injection point to the farthest injection well) must be balanced with the film-forming ability of the inhibitor. Aside from the solubility or dispersibility requirement, the same molecules can be used for waterfloods. The required concentration of inhibitor, however, is usually increased by the absence of the hydrocarbon phase. For example, addition of a hydrocarbon phase to sour brine was found to lower the inhibitor requirement for equal inhibition from 25 to 5 ppm (Ref 56). Many other investigations and field experience show that the presence of hydrocarbons augments film formation and persistence.

References cited in this section

7. R.L. Martin, “Corrosion Consequences of Oxygen Entry into Oilfield Brines,” Paper 02270, Corrosion/2002, National Association of Corrosion Engineers, 2002

45. C.C. Patton, *Applied Water Technology,* Campbell Petroleum Series, 1986

46. L.C. Case, Oxygen Traces May Be Corroding Your Waterflood Piping, *Oil Gas J.,* Vol 62, Jan 1964

47. B.L. Carlberg, “Vacuum Deaeration—A New Unit Operation for Waterflood Treatment Plants,” Paper 6096, presented at the fall meeting, Society of Petroleum Engineers, 1976

48. E.S. Snavely and F.E. Blount, Rates of Reaction of Dissolved Oxygen with Scavengers in Sweet and Sour Brines, *Corrosion,* Vol 25 (No. 10), 1969, p 397

49. T.G. Braga, “Effects of Commonly Used Oilfield Chemicals on the Rate of Oxygen Scavenging by Sulfite/Bisulfite,” Paper 13446, Society of Petroleum Engineers, 1985

50. C.C. Templeton, S.S. Rushing, and J.C. Rogers, Solubility Factors Accompanying Oxygen Scavenging with Sulfite in Oil Field Brines, *Mater. Perform.,* Vol 2 (No. 8), Aug 1963, p 42

51. N.G. Haseltine and C.M. Beeson, Steam Injection Systems and Their Corrosion Problems, *Mater. Perform.,* Vol 4 (No. 10), 1965, p 57

52. G.B. Hatch, Inhibiting (Oxygen) Corrosion with Zinc Salt-Methanol Phosphonic Acid Derivative Combinations, U.S. Patent 3,532,639, 6 Oct 1970

53. P.H. Ralston, Amine Phosphonate Scale Inhibitor, U.S. Patent 3,393,150, 16 July 1968

54. G.B. Hatch, A. Park, and P.H. Ralston, Method of Inhibiting Corrosion with Aminomethylenephosphonic Acid Compounds, U.S. Patent 3,483,133, 9 Dec 1969

55. R.L. Martin, R.R. Annand, D. Wilson, and W.E. Abrahamson, Inhibitor Control of Oxygen Corrosion: Application to a Sour Gas Gathering System, *Mater. Prot. Perform.,* Vol 10 (No. 12), Dec 1971, p 33

56. L. Riggs, Jr. and F.J. Radd, Physical and Chemical Study of an Organic Inhibitor for Hydrogen Sulfide Attack, *Corrosion,* Vol 19, Jan 1963, p 1t

R.L. Martin, Corrosion Inhibitors for Oil and Gas Production, *Corrosion: Fundamentals, Testing, and Protection*, Vol 13A, *ASM Handbook*, ASM International, 2003, p 878–886

Corrosion Inhibitors for Oil and Gas Production

Revised by Richard L. Martin, BJ Unichem Chemical Services

Bacteria-Induced Corrosion

Sulfate-reducing bacteria (SRB)(genus *Desulfovibrio*) reduce sulfate (SO_4^{2-}) to H_2S, often converting a noncorrosive source water into an aggressively corrosive water. Changes in the biological environment, such as temperature, velocity, pressure, shielding debris (in the bottom of tanks), deposits (organic and inorganic), and nutrients, cause bacteria to grow. The change that appears to cause the greatest increase in growth consists of transporting the water to a surface holding tank having many static areas and letting the water warm up or cool to 40 ± 6 °C (100 ± 10 °F). Sulfate-reducing bacteria also produce tubercles or biomass in conjunction with other bacteria. The SRB have, in many cases, produced enough H_2S to make a sweet surface system sour and have been thought to be the cause of producing a reservoir change from sweet to sour. The injection of seawater into offshore fields has probably been the worst offender in introducing SRB to production equipment. Changes in temperature can increase SRB growth from zero to high levels. Additional information on this subject is available in the article "Microbiologically Influenced Corrosion" in this Volume. Another type of bacteria common in the petroleum industry is termed acid- producing bacteria (APB). These bacteria produce simple carboxylic acids. Colonies of these bacteria can produce small, deep corrosion pits. These bacteria can be identified and controlled by the same methods as SRB.

Solutions to bacteria corrosion problems include avoiding static or dead areas in initial surface system design, keeping the system clean, and using a bactericide. Cleaning the physical surface system consists of yearly removal of settled solids in surface tanks and separation vessels. Tanks left uncleaned may contain 1 to 2 m (4 to 6 ft) of solids and sludge after 5 to 10 years of operation. Surface water transmission lines are kept clean by regular pigging, which is the most effective method of controlling bacteria corrosion. The surface piping system must be designed for pig launchers and traps.

Bactericides are chemicals that kill or control microorganisms. Many of the chemicals are surface-active cationic materials and must be used with care relative to compatibility with anionic chemicals, such as scale inhibitors. The most common surface-active bactericides are dimethyl coco amine quaternized with methyl chloride; coco diamine acetate, benzoate, or adipate; 3-alkoxy*-2hydroxy-*n*-propyl trimethylammonium chloride (where * denotes a linear primary alcohol, C_{12}-C_{15}) (Ref 57); and dimethyl coco amine quaternized with 2,2-dichloro-diethyl ether. The most common nonsurface-active bactericides are formaldehyde, glutaraldehyde, acrolein, chlorine dioxide (ClO_2), chlorine, sodium hypochlorite (NaClO), isothiazolone, dibromonitrile proionamide, sodium dimethyldithiocarbamate, and tetrakishydroxymethyl phosphonium sulfate. The mechanisms and examples of biological corrosion are discussed in Ref 58, 59, 60.

A method of enumerating bacteria is discussed in Ref 61. Other useful procedures include a quick field method for enumerating total bacteria and studying the effect of bactericides (Ref 62), a method of studying biofilms and the effect of bactericides on them (Ref 63), and a rating system for evaluating bacterial problems in waterfloods (Ref 64). A summary of papers on microbiologically influenced corrosion is given in Ref 65 and 66.

References cited in this section

57. J.R. Stanford, Inhibitor for Oxygen-Free Flood Waters, U.S. Patent 3,424,681, Jan 1969

58. R.M. Jordan and L.T. Shearer, "Aqualin Biocide in Injection Waters," Paper 280, presented at the research meeting (Tulsa, OK), Society of Petroleum Engineers, 1962

59. A.E. Baumgartner, Microbiological Corrosion—What Causes It and How It Can Be Controlled, *J. Pet. Technol.,* Vol 14 (No. 10), Oct 1962, p 1074

60. J.M. Sharpley, "Elementary Petroleum Microbiology," Gulf Publishing Co., Houston, TX, 1966

61. "Recommended Practice for Biological Analysis of Subsurface Injection Waters," API RP38, American Petroleum Institute

62. E.S. Littmann, "Oilfield Bactericide Parameters as Measured by ATP Analysis," Paper SPE 5312, presented at the International Symposium on Oilfield Chemistry (Dallas, TX), Society of Petroleum Engineers, Jan 1975

63. I. Ruseka, J. Robbins, J.W. Costerton, and E.S. Lasken, Biocide Testing Against Corrosion—Causing Oil-Field Bacteria Helps, *Oil Gas J.,* Vol 80 (No. 10), March 1982, p 253

64. C.C. Wright, Rating Water Quality and Corrosion Control in Water Floods, *Oil Gas J.,* Vol 61, May 1963

65. J.G. Stoecker II, Ed., *Microbiological Influenced Corrosion,* Vol 2, National Association of Corrosion Engineers, 2001

66. *Microbiological Induced Corrosion in Oil and Gas Production,* C.I.C. Series, National Association of Corrosion Engineers, 1999

R.L. Martin, Corrosion Inhibitors for Oil and Gas Production, *Corrosion: Fundamentals, Testing, and Protection,* Vol 13A*, ASM Handbook,* ASM International, 2003, p 878–886

Corrosion Inhibitors for Oil and Gas Production

Revised by Richard L. Martin, BJ Unichem Chemical Services

Laboratory Testing of Corrosion Inhibitors

Many testing methods designed to simulate field conditions have been reported in the literature. However, only a few of these methods survive, and none has become the standard test. Most investigators have found that combinations of test methods can be predictive of field performance, but there still remains only a rough correlation between laboratory and field performance of corrosion inhibitors. Therefore, field corrosion monitoring remains an important consideration.

Static Test. After several years of use, a static test was formalized, based on work described in Ref 67. In the test, coupons are exposed for approximately 1 week in fluids with and without inhibitors and are evaluated on a weight loss basis (Ref 68). Another static inhibitor screening test consists of short-term static exposure in field fluids, followed by immersion in a copper ion solution to determine filming ability (Ref 69).

Wheel Test. One of the first written reports on the wheel test dates from 1963 (Ref 70). After years of use and many series of multilaboratory comparative inhibitor tests, no consensus has been reached on a standardized version of the wheel test. Results of round-robin testing are available in Ref 71 and 72. A wheel test procedure (not a standard) is described in Ref 73.

The wheel test is a dynamic test performed by placing synthetic or field fluids in a 200 mL (7 oz) beverage bottle containing a metal coupon. The bottle and its contents are purged with CO_2 or H_2S, and the bottle is capped. The bottles are then agitated for approximately 2 h by securing them to the circumference of a wheel and rotating the wheel. After the first agitation period, the coupons are transferred to a rinse bottle containing

fluids with inhibitor and are agitated again. The coupons are then transferred to another bottle containing only corrosive fluids (no inhibitor) and are agitated for a longer period of time, usually 24 h. At the end of this time, the metal coupon is removed and cleaned, and weight loss is measured. The maximum temperature at which this test can be safely conducted is 80 °C (180 °F). High-temperature versions of the wheel test are discussed in Ref 74. Temperatures of 150 to 205 °C (300 to 400 °F) and pressures of several thousand pounds per square inch are achieved by the use of high-alloy pressure bombs. Agitation of the bombs is usually accomplished in the same manner as in the low-temperature wheel test. The results of one series of high-temperature wheel tests indicate a maximum corrosion rate at 105 °C (225 °F), with an unexpected decrease at 165 °C (325 °F) (Ref 75). Wheel tests have been very popular over the years. However, investigators have found a wide discrepancy between wheel test results and many applications of corrosion inhibitors in the field.

Kettle tests, also known as beaker tests or bubble tests, involve a sealed container (often a glass resin kettle) filled with a corrosive media that simulates the corrosion mechanism expected in the actual application. Corrosion can be monitored with linear polarization resistance electrodes or other monitoring methods (Ref 6). The temperatures, pressures, and corroding metal surface velocities are all limited to mild corrosion conditions in these tests. However, they have been found to be useful in many cases (Ref 3, 6).

These tests can be modified so that the test metal becomes a rotating disk or cylinder. This allows for higher metal surface velocities. Because of the rotary seal complexity, these tests are usually only run in the sweet (CO_2 only) condition; this fact limits the utility of the test in potential applications that are sour (contain significant H_2S).

Flow Loop Tests. An assembly of pipes and pumps can be used to more closely simulate many field corrosion conditions. The test metal can be configured as pipe electrodes, where the inner diameter of the pipe becomes the test electrode. Weight loss of these pipe sections can also be used as a corrosion measurement. High velocities can be simulated.

One variation of this test impinges the test stream onto a test electrode. This test is usually termed a jet impingement test.

Autoclave Tests. For temperature and pressure conditions that cannot be produced by the previously mentioned tests, corrosion conditions can be simulated in autoclaves (Ref 76). These tests commonly are used relative to hot, high- pressure gas wells. Sometimes, the autoclave metal of construction is corrosion resistant; Hastelloy C 276 (Haynes International, Inc.) UNS N10276 is common. Sometimes, the autoclave contains a metallic or nonmetallic liner. Corrosion monitoring can be by weight loss coupons (spinning or static) or by polarization resistance measurements made through feed-through fittings.

The last two tests described previously are more expensive to assemble and more labor-intensive to operate than the tests discussed earlier. The choice of test methodology depends on the intention of the testing. Again, no laboratory test has been found that duplicates field experience exactly. Again, field corrosion monitoring is important to successful applications.

References cited in this section

3. R.L. Martin and T.G. Braga, Corrosion Control in Enhanced Oil Recovery Wells, *Mater. Perform.,* Vol 27 (No. 2), Feb 1987, p 16–22

6. R.L. Martin and R.R. Annand, Accelerated Corrosion of Steel by Suspended Iron Sulfides in Brine, *Corrosion,* Vol 37 (No. 5), May 1981, p 297–301

67. A Proposed Standardized Laboratory Procedure for Screening Inhibitors for Use in Sour Oil and Gas Wells, T-1K NACE Publication 55-2, *Corrosion,* Vol 11 (No. 3), March 1955, p 143t

68. A Proposed Laboratory Screening Test for Materials to be Used as Inhibitors in Sour Oil and Gas Wells, T-1K NACE Publication 60-2, *Corrosion,* Vol 16 (No. 2) Feb 1960, p 63t–64t

69. W.B. Hughes, A Copper Ion Displacement Test for Screening Corrosion Inhibitors, *J. Pet. Technol.,* Vol X, Jan 1958, p 54–56

70. E.D. Junkin and D.R. Fincher, Oil Field Corrosion Inhibitors Evaluated by Film Persistency Test, *Mater. Prot.,* Vol 2, Aug 1963, p 18–23

71. C.C. Nathan, Correlations of Oil-Soluble, Water Dispersible Corrosion Inhibitors in Oil Field Fluids, *Corrosion,* Vol 18 (No. 8), Aug 1962, p 282T–285T

72. D.R. Fincher et al., Cooperative Evaluation of Inhibitor Film Persistency Test, T-ID-2 NACE Publication ID166, *Mater. Perform.,* Vol 5 (No. 10), Oct 1966, p 69

73. B.F. Davis, Wheel Test Method Used for Evaluation of Film Persistent Inhibitors for Oilfield Applications, T-ID-8 NACE Publication 1D182, Item 54238, *Mater. Perform.,* Vol 21 (No. 12), Dec 1982, p 45–47

74. J.L. Magnon, "Laboratory Testing of Corrosion Inhibitors," Paper 56, presented at Corrosion/73 (Anaheim, CA), National Association of Corrosion Engineers, March 1973

75. J.D. Garber, R. Perkins, and H. Su, High- Temperature Wheel Test Simulates CO_2 Corrosion, *Oil Gas J.,* Vol 84, April 1986, p 62–64

76. H. Sutanto, "Laboratory Studies of Flow Induced Localized Corrosion in CO_2/H_2S Environments; Development of Test Methodology," Paper 005, Corrosion/90, National Association of Corrosion Engineers, 1990

R.L. Martin, Corrosion Inhibitors for Oil and Gas Production, *Corrosion: Fundamentals, Testing, and Protection*, Vol 13A, *ASM Handbook*, ASM International, 2003, p 878–886

Corrosion Inhibitors for Oil and Gas Production

Revised by Richard L. Martin, BJ Unichem Chemical Services

Monitoring Results of Inhibition in the Field

The following methods are used to monitor corrosion rates and inhibitor effectiveness:

- Coupons (NACE International standard method)
- Spools, pup joints, and pony rods
- Iron/manganese ion analysis
- Copper ion displacement
- Probe measurements, such as linear polarization resistance, electrical resistance, and, less commonly, electrochemical noise, and direct current potentiodynamic polarization (Ref 77). Alternating current impedance probes see laboratory use but rarely are used in the field.
- Caliper and "smart pig" surveys
- Hydrogen probes
- Radioactive tracer methods have been used occasionally for research purposes but seldom for routine field monitoring.
- Copra correlation can be used to assess corrosion in deep, hot gas wells (Ref 78).
- Last but not least, good failure records and failure examination

References cited in this section

77. R.L. Martin, Potentio Dynamic Polarization Studies in the Field, *Mater. Perform.,* Vol 15, March 1979, p 3

78. L.K. Gatzke and R.H. Husler, "The Copra Correlation—A Quantitative Assessment of Deep, Hot Gas Well Corrosion and Its Control," Paper 48, presented at Corrosion/83 (Anaheim, CA), National Association of Corrosion Engineers, April 1983

R.L. Martin, Corrosion Inhibitors for Oil and Gas Production, *Corrosion: Fundamentals, Testing, and Protection*, Vol 13A*, ASM Handbook*, ASM International, 2003, p 878–886

Corrosion Inhibitors for Oil and Gas Production

Revised by Richard L. Martin, BJ Unichem Chemical Services

Quality Control of Inhibitors

The materials used in most corrosion inhibitors are sometimes by-products of many chemical industries. Although major inhibitor formulators and manufacturers adhere to rigid specifications and procedures, it is difficult to correlate product-manufacturing specifications with field performance. One early report on quality-control procedures used by inhibitor manufacturers showed that only 19% of the manufacturers checked performance and only 10% made compositional analyses (Ref 79).

In recent years, however, most major inhibitor formulators and manufacturers have become certified by the International Organization for Standardization (ISO). Better analytical equipment is now available, and field testing has become more rigorous, so the relationship between chemical structure and field performance is much tighter (Ref 80).

References cited in this section

79. Survey of Quality Control Procedures Used in the Manufacture of Oil Field Inhibitors, T-ID-5 NACE Publication ID267, *Mater. Perform.,* Vol 6 (No. 6), June 1965, p 82–84

80. A. Ramon and P. Labine, Ed., *Reviews on Corrosion Inhibitor Science and Technology,* Vol I and II, National Association of Corrosion Engineers, 1993 and 1996

R.L. Martin, Corrosion Inhibitors for Oil and Gas Production, *Corrosion: Fundamentals, Testing, and Protection*, Vol 13A*, ASM Handbook*, ASM International, 2003, p 878–886

Corrosion Inhibitors for Oil and Gas Production

Revised by Richard L. Martin, BJ Unichem Chemical Services

Computerization of Inhibitor Treating Programs

Problem areas and problem wells have existed since the beginning of corrosion inhibition. Wells or batteries (geographical groups of wells) that do not respond satisfactorily to current chemical corrosion programs are defined as problem wells. Computers can effectively handle large volumes of data and, coupled with their

sorting capability, can identify problem wells, changes in conditions, and other factors that influence repair costs. Computer programs can also be used as an accounting tool to monitor corrosion costs and optimize corrosion inhibitor programs (Ref 81).

Reference cited in this section

81. J. Fu, R. Erbar, and R. Heidersbach, Ed., *Computers in Corrosion Control,* National Association of Corrosion Engineers, 1986

R.L. Martin, Corrosion Inhibitors for Oil and Gas Production, *Corrosion: Fundamentals, Testing, and Protection,* Vol 13A, *ASM Handbook,* ASM International, 2003, p 878–886

Corrosion Inhibitors for Oil and Gas Production

Revised by Richard L. Martin, BJ Unichem Chemical Services

Acknowledgment

This article is a revision of P.J. Stone, Corrosion Inhibitors for Oil and Gas Production, *Corrosion,* Vol 13, *ASM Handbook* (formerly *Metals Handbook,* 9th ed.), ASM International, 1987, p 478–484.

R.L. Martin, Corrosion Inhibitors for Oil and Gas Production, *Corrosion: Fundamentals, Testing, and Protection,* Vol 13A, *ASM Handbook,* ASM International, 2003, p 878–886

Corrosion Inhibitors for Oil and Gas Production

Revised by Richard L. Martin, BJ Unichem Chemical Services

References

1. R.L. Martin, Corrosion of Alloy Steels in Oil Field Fluids, *Corrosion,* Vol 44 (No. 2), Dec 1988, p 916–920

2. R.L. Martin, "Corrosion of Copper Base Alloys in Oil Field Fluids," Paper 367, Corrosion/88, National Association of Corrosion Engineers, 1988

3. R.L. Martin and T.G. Braga, Corrosion Control in Enhanced Oil Recovery Wells, *Mater. Perform.,* Vol 27 (No. 2), Feb 1987, p 16–22

4. R.H. Hausler, Corrosion Inhibition in the Presence of Corrosion Product Layers, *Proceedings of the Sixth European Conference on Corrosion Inhibitors* (Ferrara), 1985, p 41–65

5. I.L. Rosenfeld, D.B. Bogomolov, A.E. Gorodetskii, L.V. Frelova, and L.I. Shamova, *Taschita Metallou,* Vol 18 (No. 2), 1982, p 163–168

6. R.L. Martin and R.R. Annand, Accelerated Corrosion of Steel by Suspended Iron Sulfides in Brine, *Corrosion,* Vol 37 (No. 5), May 1981, p 297–301

7. R.L. Martin, "Corrosion Consequences of Oxygen Entry into Oilfield Brines," Paper 02270, Corrosion/2002, National Association of Corrosion Engineers, 2002

8. *Condensate Well Corrosion,* Natural Gasoline Association of America, 1953

9. J.F. Chittum, Corrosion Fatigue Cracking of Oilwell Sucker Rods, *Mater. Perform.,* Vol 7 (No. 12), Dec 1968, p 37–38

10. J.F. Bates, Sulfide Cracking of High Strength Steels in Sour Crude Oils, *Mater. Perform.,* Vol 8 (No. 1), Jan 1969, p 33–39

11. C.M. Hudgins, A Review of Sulfide Corrosion Problems in the Petroleum Industry, *Mater. Perform.,* Vol 8 (No. 1), Jan 1969, p 41–47

12. C.C. Patton, Petroleum Production—Stringent Corrosion Control Procedures Key to Extended Fatigue Life, *Mater. Prot. Perform.,* Vol 11 (No. 1), June 1972, p 17–18

13. R.L. Martin, Inhibition of Corrosion Fatigue of Oil Well Sucker Rods, *Mater. Perform.,* Vol 19 (No. 6), June 1980, p 20–23

14. R.L. Martin, Inhibition of Hydrogen Permeation in Steels Corroding in Sour Fields, *Corrosion,* Vol 49 (No. 8), 1993, p 694–701

15. J.I. Bregman, *Corrosion Inhibitors,* MacMillan, 1963

16. G.L. Farrar, Combatting Corrosion in Oil and Gas Wells, *Oil Gas J.,* Vol 51 (No. 49), April 1953, p 106–109, 111, 113

17. H.L. Bilhartz, Sweet Oil Well Corrosion, *World Oil,* Vol 134, April 1952, p 208–216

18. H.L. Bilhartz, How to Predict and Control Sweet Oil Well Corrosion, *Oil Gas J.,* Vol 50 (No. 50), April 1952, p 116–118, 151, 153

19. H.L. Bilhartz, *Sweet Oil Well Corrosion— API Drilling and Production Practice,* American Petroleum Institute, 1952, p 54

20. H.L. Bilhartz, High Pressure Sweet Oil Well Corrosion, *Corrosion,* Vol 7 (No. 8), Aug 1951, p 256–264

21. C.J. Houghton and R.V. Westermark, Downhole Corrosion Mitigation in Ekofisk (North Sea) Field, *Mater. Perform.,* Vol 22 (No. 1), Jan 1983, p 16

22. D.H. Mutti, J.E. Atwood, C.R. LaFayette, and A.O. Landrum, "Corrosion Control of Gas-Lift Well Tubulars by Continuous Inhibitor Injection into the Gas-Lift Gas Stream," Paper 5612, presented at the 50th annual meeting (Dallas, TX), Society of Petroleum Engineers, 1975

23. R.B. Todd, J.H. Cannon, H.J. EnDean, and K. Belanus, Corrosion Protection by Downhole Continuous Inhibitor via External Capillary, *Mater. Perform.,* Vol 20 (No. 2), 1981, p 32

24. J.B. Bradburn and R.B. Todd, Continuous Injection Method Controls Downhole Corrosion, Part 1, *Pet. Eng. Int.,* Vol 53, July 1981, p 44–46

25. J.B. Bradburn and R.B. Todd, Continuous Injection Method Controls Downhole Corrosion, Part 2, *Pet. Eng. Int.,* Vol 53, Aug 1981, p 54

26. L.M. Cenegy and C.L. Chin, A Test for Corrosion Inhibitors to be Used in Oilfield Capillary Injection Systems, *Mater. Perform.,* Vol 22 (No. 4), April 1983, p 15–19

27. T.W. Hamby, Jr., "Development of High Pressure Sour Gas Technology," Paper 8309, presented at the 54th conference (Las Vegas, NV), Society of Petroleum Engineers, 1979

28. M.C. Place, Jr., "Corrosion Control—Deep Sour Gas Production," Paper 8310, presented at the 54th conference (Las Vegas, NV), Society of Petroleum Engineers, 1979

29. R.H. Hausler and S.G. Weeks, Low Cost, Low Volume, Continuous Inhibition of Gas Production Tubulars, *Mater. Perform.,* Vol 25 (No. 6), 1986, p 27–37

30. R.H. Poetker and J.D. Stone, Squeezing Inhibitor into Formation, *Pet. Eng.,* Vol 28, May 1956, p B29–B34

31. R.H. Poetker and J.D. Stone, Inhibition Improved 17 Percent While Cost Dropped 50 Percent, *Oil Gas J.,* Vol 54, July 1956

32. J.K. Kerver and F.A. Morgan III, Corrosion Inhibitor Squeeze Technique—Laboratory Study of Formation Permeability Damage, *Mater. Perform.,* Vol 2 (No. 4), April 1963, p 10–22

33. J.K. Kerver and F.A. Morgan III, Corrosion Inhibitor Squeeze Technique—Laboratory Adsorption-Desorption Studies, *Mater. Perform.,* Vol 4 (No. 4), July 1965, p 69–79

34. J.K. Kerver and H.R. Hanson, Corrosion Inhibitor Squeeze Technique—Field Evaluation of Engineered Squeezes, *J. Pet. Technol.,* Vol 17, Jan 1965, p 50–57

35. P.J. Raifsnider, C.L. Guinn, C.L. Barr, and D.L. Lilly, "Radioactive Tracer Studies on Squeeze Inhibition of Oil Wells," paper presented at the 19th annual conference (New York, NY), National Association of Corrosion Engineers, March 1963

36. G.L. Nunn and B.E. Hamilton, Well Treatment with Inhert Gas—Inert Gas Squeeze for Corrosion Control, *Mater. Perform.,* Vol 6 (No. 5), May 1967, p 37–40

37. S. Evans and C.R. Doran, "Batch Treatment of Sucker Rod Pumped Wells," paper presented at the Southwestern Petroleum Short Course, Department of Petroleum Engineering, Texas Tech University, April 1983

38. S. Evans and C.R. Doran, Batch Treatment Controls Corrosion in Pumping Wells, *World Oil,* Vol 198, Feb 1984, p 55–57

39. W.J. Frank, Here's How to Deal with Corrosion Problems in Rod-Pumped Wells, *Oil Gas J.,* Vol 74, May 1976, p 63–72

40. L.A. Phillips and J.R. Cowden, "Corrosion Fatigue Test Selects Effective Corrosion Inhibitors," Paper 266, presented at Corrosion/ 80 (Chicago, II), National Association of Corrosion Engineers, March 1980

41. G.B. Farquhar, M.J. Michnick, and R.R. Annand, Tracer Experiments During Batch Treatment of Gas Wells with Corrosion Inhibitors, *Mater. Prot. Perform.,* Vol 10 (No. 8), Aug 1971, p 41–45

42. C.C. Patton, D.A. Deemer, and H.M. Hillard, Jr., Field Study of Fall Rate—Oilwell Liquid Inhibitor Effectiveness, *Mater. Perform.,* Vol 9 (No. 2), Feb 1970, p 37–41

43. C.O. Bundrant, High Density Corrosion Inhibitors Simplify Oil Well Treatments, *Mater. Perform.,* Vol 8 (No. 9), Sept 1969, p 53–55

44. R.L. Martin, B.A. Alink, T.G. Braga, and J.A. McMahon, “Environmentally Acceptable Water Soluble Corrosion Inhibitors,” Paper 36, Corrosion/95, National Association of Corrosion Engineers, 1995

45. C.C. Patton, *Applied Water Technology,* Campbell Petroleum Series, 1986

46. L.C. Case, Oxygen Traces May Be Corroding Your Waterflood Piping, *Oil Gas J.,* Vol 62, Jan 1964

47. B.L. Carlberg, “Vacuum Deaeration—A New Unit Operation for Waterflood Treatment Plants,” Paper 6096, presented at the fall meeting, Society of Petroleum Engineers, 1976

48. E.S. Snavely and F.E. Blount, Rates of Reaction of Dissolved Oxygen with Scavengers in Sweet and Sour Brines, *Corrosion,* Vol 25 (No. 10), 1969, p 397

49. T.G. Braga, “Effects of Commonly Used Oilfield Chemicals on the Rate of Oxygen Scavenging by Sulfite/Bisulfite,” Paper 13446, Society of Petroleum Engineers, 1985

50. C.C. Templeton, S.S. Rushing, and J.C. Rogers, Solubility Factors Accompanying Oxygen Scavenging with Sulfite in Oil Field Brines, *Mater. Perform.,* Vol 2 (No. 8), Aug 1963, p 42

51. N.G. Haseltine and C.M. Beeson, Steam Injection Systems and Their Corrosion Problems, *Mater. Perform.,* Vol 4 (No. 10), 1965, p 57

52. G.B. Hatch, Inhibiting (Oxygen) Corrosion with Zinc Salt-Methanol Phosphonic Acid Derivative Combinations, U.S. Patent 3,532,639, 6 Oct 1970

53. P.H. Ralston, Amine Phosphonate Scale Inhibitor, U.S. Patent 3,393,150, 16 July 1968

54. G.B. Hatch, A. Park, and P.H. Ralston, Method of Inhibiting Corrosion with Aminomethylenephosphonic Acid Compounds, U.S. Patent 3,483,133, 9 Dec 1969

55. R.L. Martin, R.R. Annand, D. Wilson, and W.E. Abrahamson, Inhibitor Control of Oxygen Corrosion: Application to a Sour Gas Gathering System, *Mater. Prot. Perform.,* Vol 10 (No. 12), Dec 1971, p 33

56. L. Riggs, Jr. and F.J. Radd, Physical and Chemical Study of an Organic Inhibitor for Hydrogen Sulfide Attack, *Corrosion,* Vol 19, Jan 1963, p 1t

57. J.R. Stanford, Inhibitor for Oxygen-Free Flood Waters, U.S. Patent 3,424,681, Jan 1969

58. R.M. Jordan and L.T. Shearer, “Aqualin Biocide in Injection Waters,” Paper 280, presented at the research meeting (Tulsa, OK), Society of Petroleum Engineers, 1962

59. A.E. Baumgartner, Microbiological Corrosion—What Causes It and How It Can Be Controlled, *J. Pet. Technol.,* Vol 14 (No. 10), Oct 1962, p 1074

60. J.M. Sharpley, “Elementary Petroleum Microbiology,” Gulf Publishing Co., Houston, TX, 1966

61. “Recommended Practice for Biological Analysis of Subsurface Injection Waters,” API RP38, American Petroleum Institute

62. E.S. Littmann, "Oilfield Bactericide Parameters as Measured by ATP Analysis," Paper SPE 5312, presented at the International Symposium on Oilfield Chemistry (Dallas, TX), Society of Petroleum Engineers, Jan 1975

63. I. Ruseka, J. Robbins, J.W. Costerton, and E.S. Lasken, Biocide Testing Against Corrosion—Causing Oil-Field Bacteria Helps, *Oil Gas J.,* Vol 80 (No. 10), March 1982, p 253

64. C.C. Wright, Rating Water Quality and Corrosion Control in Water Floods, *Oil Gas J.,* Vol 61, May 1963

65. J.G. Stoecker II, Ed., *Microbiological Influenced Corrosion,* Vol 2, National Association of Corrosion Engineers, 2001

66. *Microbiological Induced Corrosion in Oil and Gas Production,* C.I.C. Series, National Association of Corrosion Engineers, 1999

67. A Proposed Standardized Laboratory Procedure for Screening Inhibitors for Use in Sour Oil and Gas Wells, T-1K NACE Publication 55-2, *Corrosion,* Vol 11 (No. 3), March 1955, p 143t

68. A Proposed Laboratory Screening Test for Materials to be Used as Inhibitors in Sour Oil and Gas Wells, T-1K NACE Publication 60-2, *Corrosion,* Vol 16 (No. 2) Feb 1960, p 63t–64t

69. W.B. Hughes, A Copper Ion Displacement Test for Screening Corrosion Inhibitors, *J. Pet. Technol.,* Vol X, Jan 1958, p 54–56

70. E.D. Junkin and D.R. Fincher, Oil Field Corrosion Inhibitors Evaluated by Film Persistency Test, *Mater. Prot.,* Vol 2, Aug 1963, p 18–23

71. C.C. Nathan, Correlations of Oil-Soluble, Water Dispersible Corrosion Inhibitors in Oil Field Fluids, *Corrosion,* Vol 18 (No. 8), Aug 1962, p 282T–285T

72. D.R. Fincher et al., Cooperative Evaluation of Inhibitor Film Persistency Test, T-ID-2 NACE Publication ID166, *Mater. Perform.,* Vol 5 (No. 10), Oct 1966, p 69

73. B.F. Davis, Wheel Test Method Used for Evaluation of Film Persistent Inhibitors for Oilfield Applications, T-ID-8 NACE Publication 1D182, Item 54238, *Mater. Perform.,* Vol 21 (No. 12), Dec 1982, p 45–47

74. J.L. Magnon, "Laboratory Testing of Corrosion Inhibitors," Paper 56, presented at Corrosion/73 (Anaheim, CA), National Association of Corrosion Engineers, March 1973

75. J.D. Garber, R. Perkins, and H. Su, High- Temperature Wheel Test Simulates CO_2 Corrosion, *Oil Gas J.,* Vol 84, April 1986, p 62–64

76. H. Sutanto, "Laboratory Studies of Flow Induced Localized Corrosion in CO_2/H_2S Environments; Development of Test Methodology," Paper 005, Corrosion/90, National Association of Corrosion Engineers, 1990

77. R.L. Martin, Potentio Dynamic Polarization Studies in the Field, *Mater. Perform.,* Vol 15, March 1979, p 3

78. L.K. Gatzke and R.H. Husler, "The Copra Correlation—A Quantitative Assessment of Deep, Hot Gas Well Corrosion and Its Control," Paper 48, presented at Corrosion/83 (Anaheim, CA), National Association of Corrosion Engineers, April 1983

79. Survey of Quality Control Procedures Used in the Manufacture of Oil Field Inhibitors, T-ID-5 NACE Publication ID267, *Mater. Perform.,* Vol 6 (No. 6), June 1965, p 82–84

80. A. Ramon and P. Labine, Ed., *Reviews on Corrosion Inhibitor Science and Technology,* Vol I and II, National Association of Corrosion Engineers, 1993 and 1996

81. J. Fu, R. Erbar, and R. Heidersbach, Ed., *Computers in Corrosion Control,* National Association of Corrosion Engineers, 1986

R.L. Martin, Corrosion Inhibitors for Oil and Gas Production, *Corrosion: Fundamentals, Testing, and Protection*, Vol 13A, *ASM Handbook*, ASM International, 2003, p 878–886

Corrosion Inhibitors for Oil and Gas Production

Revised by Richard L. Martin, BJ Unichem Chemical Services

Selected References

- *Corrosion Inhibition in Oil and Gas Production,* CICS Series, National Association of Corrosion Engineers, 1999
- *Microbiological Induced Corrosion in Oil and Gas Production,* CICS Series, National Association of Corrosion Engineers, 1999
- C.C. Nathan, *Corrosion Inhibitors,* National Association of Corrosion Engineers, 1973
- C.C. Patton, *Applied Water Technology,* Campbell Petroleum Series, 1986
- A. Ramon and P. Labine, Ed., *Reviews on Corrosion Inhibitor Science and Technology,* Vol I and II, National Association of Corrosion Engineers, 1993 and 1996

J.D. Poindexter, Corrosion Inhibitors for Crude Oil Refineries, *Corrosion: Fundamentals, Testing, and Protection*, Vol 13A, *ASM Handbook*, ASM International, 2003, p 887–890

Corrosion Inhibitors for Crude Oil Refineries

J.D. Poindexter, BJ Unichem Chemical Services

Introduction

CORROSION has a major economic impact on the oil refining industry. The replacement cost of damaged equipment is a substantial capital expense. Unplanned outages reduce throughput, lowering revenue and profit. More importantly, due to the extremely hazardous nature of the fluids and gases processed in refineries, the safety and well being of both plant employees and the public are put at risk by corrosion. Catastrophic failures could result in severe damage to entire process units, neighboring communities, and the environment. In the United States, representing 23% of the oil refining capacity of the world, corrosion-related direct costs in the oil refining sector were recently estimated to be $3.7 billion annually (Ref 1).

Of course, corrosion of metals used in construction of refining equipment is an expected phenomenon. Metals and alloys, unhindered by external influences, seek to return to their disordered, but natural, state. Outside

influences, such as inhibitors, can effectively slow the rate at which this process occurs, even to the extent that rate is practically immeasurable. Mechanisms of refinery corrosion and methods of prevention have been studied by metallurgists, engineers, and chemists for many years, and significant improvements have been accomplished. However, refining processes are complex, and corrosion problems require thorough analysis and systematic solutions.

Reference cited in this section

1. G.H. Koch, M.P.H. Brongers, N.G. Thompson, Y.P. Virmani, and J.H. Payer, *Corrosion Costs and Preventive Strategies in the United States,* Department of Transportation Publication No. FHWA-RD-01-156

J.D. Poindexter, Corrosion Inhibitors for Crude Oil Refineries, *Corrosion: Fundamentals, Testing, and Protection*, Vol 13A, *ASM Handbook,* ASM International, 2003, p 887–890

Corrosion Inhibitors for Crude Oil Refineries

J.D. Poindexter, BJ Unichem Chemical Services

Areas of Corrosion in the Refinery

Table 1 lists various refinery units and process streams that are often susceptible to corrosion and effectively treated with process additives. Discussion of a few of the processes helps in the understanding of corrosion inhibitors that are used in a typical refinery environment. Corrosion inhibitors are also applied in numerous water treatment processes within a refinery, such as in cooling water and steam generation systems. Discussions of these inhibitors can be found in the article, "Corrosion Inhibitors in the Water Treatment Industry" in this Volume.

Table 1 Typical applications for refinery corrosion inhibitors

Unit	Process stream	Filming inhibitor	Neutralizer
Crude distillation	Crude tower overhead	X	X
	Vacuum tower overhead	X	X
	Steam-jet vacuum system	X	…
Fluid catalytic cracking, coker	Fractionator overhead	X	…
	Compressed wet gas	X	…
	Absorber lean oil	X	…
	Debutanizer overhead	X	…
	Depropanizer overhead	X	…
Hydroprocessing	Stabilizer overheads	X	X
	Effluent	X	…
Alkylation (H;i2SO;i4)	Deisobutanizer tower overhead	X	X
	Debutanizer overhead	X	X
	Depropanizer overhead	X	X
Alkylation (HF)	Debutanizer overhead	X	…
	Depropanizer overhead	X	…
Catalytic reformer	Light ends stripper overhead	X	X
	Pre-fractionator overhead	X	X
	Effluent	X	X

	Debutanizer overhead	X	X
	Depropanizer overhead	X	X
	Hydrogen stripper feed	X	…
	Hydrogen scrubber water	…	X

Source: (Ref 2)

The refining of crude oil into useful fuels and other products produces a number of corrosive environments. The most common is an aqueous environment containing inorganic and organic acids. However, other aqueous corrosion processes in the refinery can also be due to the presence of oxygen, bisulfide, cyanide, microbiological growth, or other corrosion-inducing species. Nonaqueous corrosive environments also exist in refining processes. Foremost is corrosion caused by organic acids at high temperatures, commonly termed *naphthenic acid corrosion.* Sulfide and other sulfur species contained in the hydrocarbon stream can also be corrosive at high concentrations and at high temperatures.

Many processes in the refinery involve distillation, often fractional, of hydrocarbons. In most of these distillation processes, water is present in the feedstock or by addition of steam for processing purposes. The water and steam can contain some corrosive species and are usually contaminated by corrodents from the hydrocarbon stream. Corrosion most commonly occurs as the water condenses in the distillation process and the corrosive species dissolves into the condensed water. This is often termed initial condensate corrosion. The prime example of a refinery distillation process is the crude unit.

The crude unit is the initial processing unit in most refineries. The raw crude oil enters the unit and after being heated somewhat, it enters the desalting phase. After desalting, the crude oil continues to be heated by exchangers and direct fired furnaces, normally reaching a temperature in excess of 315 °C (600 °F). The oil then enters a distillation column where it is fractionated into various streams such as naphtha, kerosene, diesel, and other fuel oils. Stripping steam is normally added to the distillation column to aid in separation of the various fractions. Generally, water distills along with the naphtha fraction into the condensing section of the system, commonly referred to as the “overhead.” In a few process units, a portion of the water may condense in the column and be removed along with a heavier hydrocarbon fraction.

In the desalting process, water is mixed into the crude oil to dissolve salts (primarily chloride salts) for removal by separation of the water in the desalting vessel. Salt is a common contaminant in crude oil due to production and transportation processes. Removal of chloride salts is critical because they hydrolyze to form hydrochloric acid when the crude oil is heated. Calcium and magnesium chloride hydrolyze more easily than sodium chloride. Removal of salts and other undesirable contaminants such as solids is usually aided by a small amount of a desalting additive injected into the raw crude charge. Caustic, a dilute sodium hydroxide solution, is occasionally added after the desalter to convert much of the remaining chloride to sodium chloride.

While the desalting process is designed to prevent the formation of hydrochloric acid, some will always be present. The acid is distilled and concentrated in the overhead section of the crude oil distillation column. As water condenses during the cooling of the overhead vapor, the hydrochloric acid gas dissolves into the water, creating an excess of hydrogen ions and resulting in a low pH environment. Other contaminants, carbon dioxide, oxides of sulfur and nitrogen, hydrogen sulfide, oxygen, and low-molecular- weight organic acids will also dissolve into the condensed water. The concentration and resulting corrosive effect of these materials is generally much less than that of hydrochloric acid but should be considered.

Water washing of the overhead piping and exchangers is a common practice in many refineries. Water washing is intended to reduce corrosion primarily by dilution of the corrosive species and removal of deposits. Ideally, the aqueous dewpoint is shifted by the addition of the water wash. This practice must be carefully studied to determine the proper amount and injection location due to the complexities of the multiphase system (Ref 3).

Catalytic and thermal cracking units such as fluid catalytic cracking units (FCCU) and delayed coking units typically require corrosion- inhibition applications. In these units, considerable amounts of hydrocarbon and inorganic gases are produced. Ammonia, hydrogen sulfide, hydrogen cyanide, and other gases formed in the cracking process are removed overhead in fractionation columns along with significant quantities of water. Typically, this leads to a corrosive environment of sulfide-type corrosion in an alkaline aqueous environment.

The presence of hydrogen cyanide seems to aggravate the corrosion problem by promoting entry of atomic hydrogen into the metal. The ability of filming inhibitors to prevent this entry is limited. In some instances, the cyanide ion is removed from the system through a reaction with an inhibitor based on an inorganic polysulfide solution (Ref 4).

Nonaqueous corrosion is also a concern in many areas of a refinery. High temperatures encountered in processing units have led to corrosion by naphthenic acids and sulfur-containing species. High-temperature corrosion is not a new problem in refineries; however, crude quality continues to decline and economic incentives can force the refiner to process a higher-corrosivity crude oil. Typically, this type of corrosion has occurred in units handling heavy fractions (atmospheric gas oil, atmospheric residual oil, vacuum gas oil, FCCU feedstock). *Naphthenic acid* is a generic term for all organic acids found in crude oil. The acids of concern in refining are primarily complex, high-molecular weight acids that concentrate in high boiling fractions at temperatures ranging from 220 °C to 400 °C (430 °F to 750 °F). Since crude oils contain a whole range of naphthenic acids, the corrosive potential can only be determined by thorough assessment and experience (Ref 5).

Hydroprocessing (hydrodesulfurization, hydrocracking, hydrofining) units operate under high pressures and temperatures and are susceptible to various corrosion mechanisms. Hydroprocessing severity has increased due to higher levels of sulfur in feedstocks and the demand to lower sulfur content of product streams. In these high severity units, substantial quantities of ammonia, hydrogen sulfide, and hydrogen chloride are produced. High-temperature sulfidation and hydrogen attack, ammonium bisulfide corrosion, underdeposit corrosion, and chloride stress cracking have all been identified (Ref 6, 7).

Amine sweetening units are used to remove acid gases, primarily hydrogen sulfide, and carbon dioxide from light hydrocarbons produced in the refinery. Aqueous solutions of alkanolamines, such as monoethanolamine (MEA), diethanolamine (DEA), and methyldiethanolamine (MDEA) are most commonly used. These processes are plagued with corrosion and fouling problems, especially in lean/rich heat exchangers, stripper overheads, and reboilers. Especially severe and potentially catastrophic corrosion is attributed to several cracking mechanisms (Ref 8). Improper control of operation variables and trace contaminants is often the cause of these problems. Corrosion inhibitors are effective in controlling many amine-unit corrosion problems.

Sour water units handle process waters that contain ammonia, hydrogen sulfide, cyanide, and other corrosives. Sour water or “foul water” is a collection of water from the various processing units. In the sour-water stripper, the process water is heated and stripped with steam. This process removes the dissolved and entrained gases that are less soluble at elevated temperatures. The water is often reused as desalter or overhead-wash water after removal of the undesirable contaminants. Various streams in this unit can be quite corrosive due to the high concentration of corrosive materials, especially in the overhead system.

References cited in this section

2. J. Gutzeit, Refinery Process Additives, *Mater. Prot.,* Feb 1990, p 71–74

3. T.D. Whitehead and P.A. Ramachandran, “An Analysis of Wash Water Practices Used for Corrosion Control in Condensible Hydrocarbon Systems,” Paper 318, presented at Corrosion/91, NACE International, 1991

4. R.J. Kaminski, C.A. Taylor, et al., “Recent Advances in the Prediction, Analysis and Treatment of Cyanides in Fluid Catalytic Cracking Units,” Paper 525, presented at Corrosion/94, NACE International, 1994

5. G. Bailey and J.W. Palmer, Crude Oil Corrosion, *Hydrocarbon Eng.,* Vol 7 (No. 3), March 2002, p 89–90

6. A.J. Bagdasarian and D.J. Truax, “Chloride Stress Corrosion Cracking of Austenitic Stainless Steels in Hydroprocessing Units,” Paper 501, presented at Corrosion/97, NACE International, 1997

7. A. Singh and C. Harvey, “Corrosion Management in Fractionator Feed Preheat Exchangers in Hydroprocessing Units,” Paper 687, presented at Corrosion/2000, NACE International, 2000

8. R.B. Nielsen, K.R. Lewis, J.G. McCullough, and D.A. Hansen, “Corrosion in Refinery Amine Systems,” Paper 571, presented at Corrosion/95, NACE International, 1995, p15–17

J.D. Poindexter, Corrosion Inhibitors for Crude Oil Refineries, *Corrosion: Fundamentals, Testing, and Protection*, Vol 13A, *ASM Handbook*, ASM International, 2003, p 887–890

Corrosion Inhibitors for Crude Oil Refineries

J.D. Poindexter, BJ Unichem Chemical Services

Types of Inhibitors

Neutralizers are added to increase the pH of condensed water in refinery distillation units. An effective neutralizer will be present in a sufficient quantity at the point of water condensation to raise the pH to an appropriate level. The appropriate pH is somewhat dependent on the acids present and the hydrogen sulfide concentration. At pH value near neutral (7.0), corrosion due to hydrogen ions is reduced but corrosion due to bisulfide from the ionization of hydrogen sulfide increases. Copper alloys, such as admiralty brass and Monel, become susceptible to corrosion at values of pH above 7.0, especially in the presence of ammonia or amines. The ideal pH in most systems is determined by monitoring the corrosion rate at various pHs between 5.5 and 7.0.

Neutralizer formulations contain one or more low-molecular-weight amines that have good neutralization values with little or no adverse side effects. These side effects include the formation of corrosive salts in areas where there are a limited amount of water and poor water-solubility characteristics of the neutralizer or its salts. The appropriate neutralizer formulation must be selected based on process conditions and stream composition. Ammonia gas and ammonium hydroxide have been used but generally are limited in use due to poor solubility at the initial water condensation point and adverse salt characteristics.

Filming inhibitors are added to many refinery distillation-column overheads to lower the rate of corrosion under slightly acidic conditions (pH 5–7). In other units, such as the main fractionator overhead of a FCCU, a filmer is often used to minimize corrosion under slightly alkaline conditions. Filming inhibitors promote an “oil-wet” metal surface to provide the metal with a barrier from water and corrosive species. The filmers used in refinery distillation systems are organic compounds that have a polar group attached to a hydrocarbon “tail.” The polar group is attracted to the metal surface and the thin passive film that forms on the metal surface. The hydrocarbon tail attracts other hydrocarbons, forcing the potentially corrosive water away from the surface.

Numerous refining units have distillation systems. Each may have a need for a filming corrosion inhibitor and must be evaluated individually due to varying process conditions. Filming inhibitors have also been found somewhat useful in mitigating corrosion in various water wash systems such as effluent exchanger washing in hydroprocessing units.

Naphthenic acid corrosion has been successfully inhibited with filming inhibitors that are specifically designed to be heat stable and effective under these extreme conditions. High-temperature, nonaqueous corrosion from naphthenic acids and sulfur-containing molecules seems to be especially sensitive to high wall-shear stress. High-velocity fluids are likely to strip away natural protective films from the metal and expose metal surfaces to the corrodents. In many instances, the best solution for high-temperature corrosion is an upgrade in metallurgy. Suitable materials are typically high chrome alloys such as type 316 or 317 stainless steel, or even higher- alloyed materials in the most severe service areas.

Specialized filming inhibitors prevent corrosion in fuel pipelines and storage tanks. Fuel pipelines and storage tanks can exhibit light corrosion due to water condensation on the surface of the metal and to oxygen ingress. Red-orange rust particles dislodged from the metal surface contaminate the fuel and lead to filter plugging.

Filming inhibitors are generally organic compounds containing relatively small amounts of nitrogen, oxygen, or occasionally sulfur or phosphorous. Various imidazolines, amidoamines, alkyl amines, and alkyl quaternary amines are used, depending on the particular application. The “film” formed is a very thin absorption layer that is only a few molecules thick. The inhibitor is in equilibrium with the system fluids flowing near the metal surface. Proper design and selection of the inhibitor will allow the film to be as persistent as possible without causing fouling or “gunking” on the metal surface. The filming inhibitor must have solubility and dispersibility characteristics that will allow it to be transported to the corroding surface. The ideal filmer also performs

effectively under various process conditions at low concentrations. The filming inhibitor selected should not cause an emulsion of the overhead fluids or adversely affect downstream processing units.

Scavengers perform as corrosion inhibitors by removing the corrosive species from the process. Scavengers are used to remove oxygen, cyanide, hydrogen sulfide, and mercaptans from water and process streams. The products from the chemical reaction are noncorrosive.

Microbiocides control microbiological growth. Microbes cause underdeposit corrosion, and some bacteria utilize metals in their metabolic processes. Storage tanks of fuel and other materials often contain small amounts of water that supports microbiological growth.

Antifoulants and scale inhibitors prevent the precipitation and accumulation of solids in processing units. Deposition on metal surfaces leads to underdeposit corrosion. Fouling also prevents filming-type inhibitors from coming in contact with the metal surface.

J.D. Poindexter, Corrosion Inhibitors for Crude Oil Refineries, *Corrosion: Fundamentals, Testing, and Protection*, Vol 13A, *ASM Handbook*, ASM International, 2003, p 887–890

Corrosion Inhibitors for Crude Oil Refineries

J.D. Poindexter, BJ Unichem Chemical Services

Application of Inhibitors

Corrosion inhibitors are added in such small amounts that it is important to insure adequate distribution of the inhibitor in the process system. Full consideration of process unit dynamics must be considered for designing the proper injection scheme. In many cases, special injection nozzles called atomizers are used to mist the inhibitor into the flowing stream. Dilution streams are often used in an effort to increase process injection rates and increase mixing. Traditionally, crude unit overhead neutralizers and filmers are added via dilution streams that are injected into the horizontal section of the overhead vapor line; however, many variations exist. Details of refinery inhibitor injections are difficult to generalize due to the uniqueness and variety of each situation. Numerous publications exist, including a NACE International Technical Committee Report that details inhibitor injection methods (Ref 9).

Reference cited in this section

9. “Refinery Injection and Process Mixing Points,” NACE International Technical Committee Reports, Publication 34101, NACE International, 2001

J.D. Poindexter, Corrosion Inhibitors for Crude Oil Refineries, *Corrosion: Fundamentals, Testing, and Protection*, Vol 13A, *ASM Handbook*, ASM International, 2003, p 887–890

Corrosion Inhibitors for Crude Oil Refineries

J.D. Poindexter, BJ Unichem Chemical Services

Corrosion Monitoring

The refining industry is a mature industry, and much of the existing process equipment has been in service for many years. Due to the potential hazards of a corrosion failure, it is important to detect and quantify corrosion.

Typically, indications of corrosion are found on inspection during turnarounds and planned maintenance events. While these inspections are important, corrosion monitoring during operating periods is important to reduce equipment damage due to corrosion events and to assess the reliability and useful service life of process equipment. The corrosion monitoring program must be well designed, thorough, and sustained.
Corrosion monitoring techniques either measure corrosion directly or measure parameters that are indicative of corrosion (Ref 10). Direct measurement techniques used at refineries include the following:

- Nondestructive inspection
- Use of coupons
- Cyclic potentiodynamic polarization
- Use of electrical resistance probes
- Use of linear polarization resistance
- Use of galvanic currents
- Electrochemical impedance spectroscopy
- Use of electrochemical noise measurement

Indirect methods include:

- pH
- Conductivity
- Temperature
- Metal ion analysis (iron, manganese, copper, zinc, nickel, and so forth)
- Hydrogen
- Biological assay

Any one technique may give erroneous results; therefore, a combination of methods is usually employed. Measurements made over a relatively short period allow operational or process changes to be applied in an effort to impede the rate of corrosion. Corrosion monitoring instrumentation continues to be improved and become more sophisticated. Effective methods to detect localized corrosion have been challenging, but newer instrumentation measures pitting rates, hydrogen penetration, and other localized corrosion. Indirect measurements are important ongoing gages to examine both corrosion-condition trends and daily operating parameters.

Reference cited in this section

10. C.E. Jaske, J.A. Beavers, and N.G. Thompson, Improving Plant Reliability Through Corrosion Monitoring, *Fourth International Conference on Process Plant Reliability,* Gulf Publishing, 1995, p 3

J.D. Poindexter, Corrosion Inhibitors for Crude Oil Refineries, *Corrosion: Fundamentals, Testing, and Protection*, Vol 13A, *ASM Handbook*, ASM International, 2003, p 887–890

Corrosion Inhibitors for Crude Oil Refineries

J.D. Poindexter, BJ Unichem Chemical Services

References

1. G.H. Koch, M.P.H. Brongers, N.G. Thompson, Y.P. Virmani, and J.H. Payer, *Corrosion Costs and Preventive Strategies in the United States,* Department of Transportation Publication No. FHWA-RD-01-156

2. J. Gutzeit, Refinery Process Additives, *Mater. Prot.,* Feb 1990, p 71–74

3. T.D. Whitehead and P.A. Ramachandran, "An Analysis of Wash Water Practices Used for Corrosion Control in Condensible Hydrocarbon Systems," Paper 318, presented at Corrosion/91, NACE International, 1991

4. R.J. Kaminski, C.A. Taylor, et al., "Recent Advances in the Prediction, Analysis and Treatment of Cyanides in Fluid Catalytic Cracking Units," Paper 525, presented at Corrosion/94, NACE International, 1994

5. G. Bailey and J.W. Palmer, Crude Oil Corrosion, *Hydrocarbon Eng.,* Vol 7 (No. 3), March 2002, p 89–90

6. A.J. Bagdasarian and D.J. Truax, "Chloride Stress Corrosion Cracking of Austenitic Stainless Steels in Hydroprocessing Units," Paper 501, presented at Corrosion/97, NACE International, 1997

7. A. Singh and C. Harvey, "Corrosion Management in Fractionator Feed Preheat Exchangers in Hydroprocessing Units," Paper 687, presented at Corrosion/2000, NACE International, 2000

8. R.B. Nielsen, K.R. Lewis, J.G. McCullough, and D.A. Hansen, "Corrosion in Refinery Amine Systems," Paper 571, presented at Corrosion/95, NACE International, 1995, p15–17

9. "Refinery Injection and Process Mixing Points," NACE International Technical Committee Reports, Publication 34101, NACE International, 2001

10. C.E. Jaske, J.A. Beavers, and N.G. Thompson, Improving Plant Reliability Through Corrosion Monitoring, *Fourth International Conference on Process Plant Reliability,* Gulf Publishing, 1995, p 3

J.D. Poindexter, Corrosion Inhibitors for Crude Oil Refineries, *Corrosion: Fundamentals, Testing, and Protection*, Vol 13A, *ASM Handbook*, ASM International, 2003, p 887–890

Corrosion Inhibitors for Crude Oil Refineries

J.D. Poindexter, BJ Unichem Chemical Services

Selected References

General refinery information

- "Petroleum Refining Processes," OSHA Technical Manual, Section IV, Chapter 2, www.osha-slc.gov/dts/osta/otm/otm_iv/ otm_iv_2.html, November 2000
- "Refining Operations," www.setlaboratories.com/operatio.htm, February 2002

Corrosion topics

- N.D. Coble, "Corrosion Philosophy: Treat the Source, Not the Symptom," Paper 2480, presented at Corrosion/2002, NACE International, 2002
- J. Gutzeit, "Effect of Organic Chloride Contamination of Crude Oil on Refinery Corrosion," Paper 694, presented at Corrosion/ 2000, NACE International, 2000
- R.D. Kane and M.S. Cayard, "A Comprehensive Study on Naphthenic Acid Corrosion," Paper 2555, presented at Corrosion/2002, NACE International, 2002

- R.D. Merrick and T. Auerbach, "Crude Unit Overhead Corrosion Control Report by Task Group T-8-12," Paper 96, presented at Corrosion/83, NACE International, 1983
- "Petroleum Refining Corrosion," www.hghouston.com/refining.html#top, October 2000
- H.U. Schutt and P.R. Rhodes, "Corrosion in the Aqueous Hydrogen Sulfide, Ammonia, Oxygen System," Paper 331, presented at Corrosion/95, NACE International, 1995
- S. Tebbal, R.D. Kane, and K. Yamada, Assessment of the Corrosivity of Crude Fractions from Varying Feedstock, Paper 498, presented at Corrosion/97, NACE International, 1997
- R.R. Veldman, "Alkanolamine Solution Corrosion Mechanisms and Inhibition From Heat Stable Salts and CO_2," Paper 496, presented at Corrosion/2000, NACE International, 2000
- S.M. Wilhelm and D. Abayarathna, Inhibition of Hydrogen Absorption by Steels in Wet Hydrogen Sulfide Refinery Environments, *Corrosion*, Vol 50 (No. 2), Feb 1994, p 152–159
- M.J. Zetlmeisl, "Naphthenic Acid Corrosion and Its Control," Paper 218, presented at Corrosion/96, NACE International, 1996

BP. Boffardi, Corrosion Inhibitors in the Water Treatment Industry, *Corrosion: Fundamentals, Testing, and Protection*, Vol 13A, *ASM Handbook*, ASM International, 2003, p 891–906

Corrosion Inhibitors in the Water Treatment Industry

Bennett P. Boffardi, Bennett P. Boffardi and Associates, Inc.

Introduction

THE CORROSION PROCESS that occurs in industrial systems is insidious and all-encompassing. This process is often difficult to discern until extensive deterioration has occurred. Corrosion robs industry of millions of dollars annually through loss or contamination of products, replacement cost and overdesign of equipment, reductions in efficiency, high maintenance expense, and waste of valuable resources. Corrosion also restrains technological progress and jeopardizes human safety.

Water, the most commonly used cooling fluid, removes unwanted heat from heat-transfer surfaces. However, water is corrosive to most alloys and contributes to the buildup of insulating deposits through water-formed and water-borne foulants.

BP. Boffardi, Corrosion Inhibitors in the Water Treatment Industry, *Corrosion: Fundamentals, Testing, and Protection*, Vol 13A, *ASM Handbook*, ASM International, 2003, p 891–906

Corrosion Inhibitors in the Water Treatment Industry

Bennett P. Boffardi, Bennett P. Boffardi and Associates, Inc.

Boiler Systems

For boilers (steam-generating plants) to function properly, the incoming water must be processed to meet the water quality required for the boiler. The higher the operating pressure in the boiler, the more restrictive are the properties of the feedwater to the boiler. The high quality standards for the incoming water have led to a variety

of mechanical and chemical processes to meet the demanding specifications. These processes are referred to as a pretreatment.

Pretreatment

Pretreatment can encompass many different processes, depending on the desired water quality. Waters for most industrial applications come from either wells or from a surface source such as lakes and rivers. In either case, the waters may contain suspended solids, color, and dissolved solids. These constituents must be removed to prevent water-related problems in the boiler system.

Clarification removes turbidity (suspended solids) and color by a process of coagulation and filtration. The addition of such chemicals as aluminum sulfate (alum), ferrous or ferric sulfate, and lime or soda ash produces floc that absorbs the color and entangles the suspended solids. The floc is then filtered out or allowed to settle. The water passing through the filter is devoid of color and particulate material. However, the water can still contain dissolved matter.

Removal of Hardness Ions. The most troublesome dissolved materials that can have a negative impact on boiler operations are the hardness ions, calcium and magnesium. These ions, when concentrated, can form sparingly soluble salts (scales) and deposit on internal heat-transfer surfaces. Scale is very detrimental to boiler performance because it substantially retards heat transfer and, in severe cases, leads to boiler failure due to metal overheating. Removal of hardness ions from incoming water can be accomplished in a variety of processes.

Precipitation softening is a chemical process that is used to remove hardness ions and alkalinity from water. Cold lime softening uses a coagulant and alkali to precipitate the hardness ions in the water as calcium carbonate ($CaCO_3$) and magnesium hydroxide [$Mg(OH)_2$]. At elevated temperatures, hot-process softening can reduce the solubility of precipitated materials even further. However, hot processes require the input of heat that speeds up rates of reactions compared to cold lime processes that operate at ambient temperature.

Ion exchange is another process to remove dissolved hardness ions. The dissolved ions in the water have either positive or negative electrical charges. The softening technology exchanges the hardness ions for ions of like charge. Resin beads made from polymeric materials contain a high level of exchangeable ions and are used to remove the undesirable charge species from water. Cation resins only exchange positively charged ions or cations, whereas anionic resins exchange anions, or negatively charges ions.

Softening, the most common ion-exchange process, removes hardness ions by replacing them with sodium ions. For complete removal of all dissolved salts (demineralization), a strong acid exchanger in the hydrogen cycle (acid) is used in combination with a strong base exchanger in the hydroxyl cycle (caustic). The combination of hydrogen and hydroxyl ions produces ion-free water at a neutral pH.

For low-pressure (<1 MPa, or 150 psig) boiler systems, the most common ion-exchange process in use for softening water is the sodium- cycle cation exchange. This process is extremely efficient, and the operation of sodium-cycle softeners does not affect the finish-water pH or other dissolved solids other than removing raw water hardness.

Reverse Osmosis. Improved operation of ion- exchange units for complete demineralization can be accomplished by passing the water stream first through a reverse-osmosis (RO) unit for partial demineralization, followed by ion-exchange units. This process lowers the salt loading to the resin and extends operating time between regenerations of the ion-exchange resins.

Reverse osmosis forces water through a membrane filter, producing high-quality water. The process can remove 95 to 99% of the dissolved solids and many different types of organisms from all waters including brackish and seawater.

The superfine porous RO membrane removes dissolved materials. For the RO process to function, a pressure greater than the natural osmotic backpressure must be applied to the water system. Osmotic pressure is proportional to the salt concentration and temperature and depends on the type of ionic species present. For waters containing predominantly sodium chloride at ambient temperature, a rule of thumb is that osmotic pressure is 0.07 MPa (10 psi) per 1000 mg/L concentration.

Reverse osmosis reverses the natural flow of dissolved ions into water, by forcing the ions to flow in the opposite (reverse) direction, producing pure water. Ordinary filtration allows the water containing dissolved material to pass through the media, leaving behind solid materials that were present in the water.

The rate of water transport across the RO membrane depends on the membrane properties, the water temperature, and the difference in applied pressure across the membrane minus the difference in osmotic pressure between the concentrated and dilute water.

Preboiler Corrosion Protection

The choice of boiler water treatment depends on two main considerations: boiler operating pressure and boiler feedwater hardness. Approaches used to pretreat the makeup water and remove hardness are discussed in the previous section. As boiler pressures increase, there is a greater need to control feedwater quality, chemical treatments, and cycles of concentration. Boiler operation is much more critical at higher pressures, demanding essentially no hardness and no dissolved solids.

Boiler water treatments are used to control scale, corrosion, and carryover/foaming. Scale is generally the result of poor pretreatment, that is, control over calcium, magnesium, and silica in the boiler water.

Scale is controlled by either internal treatment or a combination of internal treatment and external treatment. Corrosion is primarily caused by oxygen in the feedwater. Oxygen corrosion is prevented by chemically reducing or scavenging the oxygen in the system and by mechanically deaerating the feedwater before it enters the boiler. Foaming or carryover can be controlled by blowdown or with chemicals.

Deaeration. Mechanical deaeration is the removal of noncondensable dissolved gasses. While the removal of oxygen is paramount, other gases such as CO_2 and NH_3 can magnify the deleterious effect of oxygen attack on the internals of the boiler. For example, CO_2 corrosion is 2.5 to 3 times as aggressive in the presence of oxygen.

Deaeration is achieved by heating the water to saturation temperature at the process pressure in equipment known as a deaerator. Deaerators also provide feedwater storage. The most common types of deaerators are either the spray or tray type.

A spray deaerator sprays feedwater into a steam-filled space where the feedwater is heated and scrubbed to release gases. As fresh steam enters the unit, water undergoes a second agitation to liberate most remaining impurities.

Tray deaerators direct feedwater into a series of cascading trays. Water falls from tray to tray by overflowing or passing through small holes. Steam, which engulfs the bays, heats and deaerates the feedwater as it falls.

Finally, a combination of spray- and tray-type heaters can be used. Feedwater is first sprayed into a steam-filled space, then cascades down on a series of trays through which it passes for further agitation and scrubbing. Live steam entering the deaerator meets the hottest water first, stripping it of dissolved gas. Carrying this gas along, the steam moves across and up through cascading water, gathering additional impurities as it flows. Steam is gradually condensed as it moves upward in the deaerator. Noncondensable gases are drawn off at a high point in the unit, where little steam remains.

One additional type of deaerator should be noted—the vacuum deaerator. In the vacuum deaerator, water cascades over packing such as rasching rings. The pressure of the environment above the water is reduced using vacuum pumps or steam ejectors. The degree of oxygen removal obtained in vacuum degasification will depend on a variety of variables. While finished oxygen limits have not been established, typical degasification achieved with vacuum-type deaerators will range from 50 to 500 μg/L (parts per billion, or ppb) of dissolved oxygen by volume. Because of these limits, boiler systems that utilize vacuum deaerators will generally have another type of deaerator following the vacuum unit.

Feedwater leaving the deaerator is usually specified as having 7 μg/L (ppb) dissolved oxygen or less, assuming the deaerator is functioning per design specifications. Further reduction of oxygen levels requires the use of chemical- reducing agents. Free carbon dioxide levels should be reduced to zero. Removal of corrosive gases from boiler feedwater is imperative in order to protect downstream metallurgy.

Oxygen Scavenging. Residual dissolved oxygen remaining in the feedwater will cause pitting corrosion of the feedwater lines, heaters, economizers, boilers, and condensate lines. Therefore, oxygen-scavenging chemicals are added to the deaerator storage tank for removal of all traces of oxygen (Ref 1).

The most common oxygen scavengers for many years were sodium sulfite (Na_2SO_3) and hydrazine (N_2H_2). When hydrazine became a suspected carcinogen, replacement chemistry was rapidly pursued. It became apparent that strong reducing agents (oxygen scavengers) should more than react with dissolved oxygen; they should also form protective oxide films on the metal surfaces.

Sulfite reacts and consumes dissolved oxygen in water according to:

$$2Na_2SO_3 + O_2 \rightarrow 2Na_2SO_4 \quad \text{(Eq 1)}$$

Sodium sulfite reduction of oxygen adds sodium sulfate, or dissolved solids, to the boiler water. Sodium sulfite is thermally unstable at high pressure. Thermal decomposition results in the formation of sulfur dioxide and hydrogen sulfide:

$$Na_2SO_3 + H_2O + Heat \rightarrow SO_2 + 2NaOH \quad \text{(Eq 2)}$$

$$4Na_2SO_3 + 2H_2O + Heat \rightarrow 3Na_2SO_4 + 2NaOH + H_2S \quad \text{(Eq 3)}$$

The hydrazine reaction with dissolved oxygen is slow at ambient temperature, but increases as temperature and pH increases. Neither hydrazine nor its products contribute dissolved solids to boiler water:

$$N_2H_4 + O_2 \rightarrow 2H_2O + N_2 \quad \text{(Eq 4)}$$

Hydrazine also reacts with CuO and Fe_2O_3 forming protective oxide films:

$$6Fe_2O_3 + N_2H_4 \rightarrow 4Fe_3O_4 + 2H_2O + N_2 \quad \text{(Eq 5)}$$

$$4CuO + N_2H_4 \rightarrow 2Cu_2O + 2H_2O + N_2 \quad \text{(Eq 6)}$$

At high temperatures, hydrazine will decompose to ammonia.

Another oxygen scavenger is carbohydrazide [$(NH_2NH)_2CO$], which is the dihydrazide of carbonic acid. It reacts directly with oxygen:

$$(NH_2NH)_2CO + 2O_2 \rightarrow 2N_2 + 3H_2O + CO_2 \quad \text{(Eq 7)}$$

It also reacts indirectly through hydrolysis to form hydrazine:

$$(NH_2NH)_2CO + H_2O \rightarrow 2N_2H_4 + CO_2 \quad \text{(Eq 8)}$$

$$2N_2H_4 + 2O_2 \rightarrow 4H_2O + 2N_2 \quad \text{(Eq 9)}$$

Carbohydrazide reacts with iron and copper to form protective passive oxides.

Hydroquinone [$C_6H_4(OH)_2$], reacts with dissolved oxygen in the feedwater. The reaction is a function of temperature, pH, and the ratio of hydroquinone to dissolved oxygen. The reduction reaction is a multistep process, producing benzoquinone, which further reacts with dissolved oxygen to form end products consisting of ketones, alcohols, and carbon dioxide. Hydroquinone will also form protective passive oxides with iron and copper.

Diethylhydroxylamine (DEHA) [$(C_2H_5)_2NOH$] reacts with dissolved oxygen in a complex process involving several steps, which are dependent on temperature, pH, and the concentrations of both DEHA and oxygen. The overall reaction of DEHA with oxygen can be summarized as:

$$4(C_2H_5)_2NOH + 9O_2 \rightarrow 8CH_3COOH + 2N_2 + 6H_2O \quad \text{(Eq 10)}$$

The total oxidation of DEHA produces acetic acid, nitrogen, and water. DEHA will also react with iron and copper to form a protective passive film.

Methylethyl ketoxime (MEKO) [$(CH_3)(C_2H_5)CNOH$] does not react significantly with dissolved oxygen at room temperature. However, at boiler conditions MEKO reacts with oxygen, producing ketones, nitrous oxide, and water. MEKO will degrade under boiler conditions producing ammonia.

Erythorbate reacts with dissolved oxygen in the boiler feedwater through a series of complex reactions.

$$RC_6H_6O_6 + O_2 \rightarrow C_6H_5O_6 + ROH \quad \text{(Eq 11)}$$

Final products of the reactions will depend on the amount of oxygen, feedwater pH, and temperature during the reaction. Under alkaline conditions, the end products are CO_2 and water.

Erythorbate is a relatively strong reducing agent capable of reducing oxidized forms of iron and copper to Fe_3O_4 and Cu_2O, respectively.

With the boiler feedwater free of both dissolved ions and oxygen, the water can proceed to the boiler. It is important that the boiler feedwater chemistry be controlled. A minimum pH of 8.5 is required to minimize corrosion attack on steel, with an optimal pH range of 9.2 to 9.5. For copper alloys, the preferred pH range is 8.5 to 9.2. Since both steel and copper alloys are common in boiler systems, a compromise range of 8.8 to 9.2 is recommended.

Internal Treatment

The traditional method of controlling scale and deposits in low- to medium-pressure boilers (pressures less than 1 MPa, or 150 psig, for low pressure, and 4 MPa, or 600 psig, for medium pressure) is a phosphate/dispersant chemical- treatment program operating with excessive hydroxide alkalinity (Ref 2).

Phosphate programs are designed to react with calcium in the boiler water to produce a calcium precipitate while maintaining an excess of phosphate. In the absence of excess alkalinity, the phosphate will precipitate as calcium orthophosphate, which is a sticky deposit and difficult to remove. Sufficient alkalinity, either naturally occurring or added, will produce hydroxyapatite [$Ca_{10}(OH)_2(PO_4)_6$], a nonadherent calcium deposit that is easily fluidized with dispersants. Similarly, magnesium impurities can react with OH^- alkalinity to produce magnesium hydroxide [$Mg(OH)_2$]. If silica is present, serpentine is produced ($3MgO \cdot 2SiO_2 \cdot 2H_2O$) under high alkaline boiler conditions.

Conventional phosphate treatment control involves maintaining a phosphate residual and a hydroxide residual in the boiler water. Phosphate residuals are typically maintained in the range of 20 to 40 mg/L (parts per million, or ppm) PO_4^{3-} . Hydroxide alkalinities, if controllable without excessive blowdown, are maintained in the range 125 to 400 mg/L (ppm) as $CaCO_3$ This treatment provides the ideal conditions for precipitation of calcium as hydroxyapatite and magnesium as serpentine. It also provides a residual of alkalinity to neutralize any acidic contamination. It may, however, promote foaming, especially if organic contaminants enter the boiler.

Application of this treatment to boilers operating at pressures above 7 MPa (1000 psi) can result in an increased probability of concentrated sodium hydroxide attack. Boiler failures due to concentrated caustic attack are rare at pressures below 7 MPa (1000 psi).

Coordinated phosphate control was developed to eliminate the problem of concentrated sodium hydroxide attack. This approach requires an alkalinity-free makeup. Coordinated phosphate control is commonly achieved by either evaporator or demineralized pretreatment. Phosphate residuals are typically maintained in the range 5 to 25 mg/L (ppm) PO_4^{3-}.

However, small concentrations of hydroxide will exist due to hydrolysis of the orthophosphate ion. The sodium hydroxide formed by hydrolysis is then available to concentrate on the tube surfaces. This is most likely to occur under heavy accumulations of corrosion products or in sloped tubes where pockets of steam may accumulate and prevent rinsing of concentrated solids from the tube wall.

The cause of the sodium hydroxide attack in coordinated phosphate treatment results, indirectly, from the phenomenon of hideout. Hideout is the apparent loss of phosphate in the boiler water in high-pressure power boilers operating under high load conditions. The lost phosphate reappears and can be analyzed when the load is reduced. Congruent boiler water control was developed to ensure that hydroxide formation does not occur under hideout conditions. This treatment is based on the premise that the Na/PO_4 ratio in the boiler water should be no greater than the congruent ratio. Congruent control programs are designed to prevent the formation of hydroxyl alkalinity (excess caustic) in the boiler by maintaining the Na/PO_4 ratio at a maximum of 2.6 to 1.

Chelant treatments are typically used in systems where the feedwater hardness is low, below 5 mg/L (ppm) as $CaCO_3$. The major reason for using chelant treatments ethylenediaminetetraacetic (EDTA) acid or nitrilotriacetic (NTA) acid is the chelates of calcium and magnesium are soluble. Iron is not significantly solubilized by chelant treatment due to the competition of the hydroxide ion. However, iron may be effectively removed by combining a dispersant with a chelant treatment.

Chelant treatments have been effective for industrial boilers operating up to 7 MPa (1000 psi). This type of program is not recommended for low-pressure boilers, below 1034 kPa (150 psi).

High-pressure utility boilers operating above 14 MPa (2000 psi) require an all-volatile treatment (AVT) program. On the other hand, utility boilers operate on essentially pure water, which contains zero dissolved solids. The only chemicals added to the system in utility boilers are ammonia or a neutralizing amine in conjunction with a volatile oxygen scavenger.

Condensate Treatment

Corrosion in condensate/feedwater systems occurs because of low pH induced by carbonic acid, resulting from the reaction of water with CO_2 gas coming from the boiler. The CO_2 may originate from condenser air-inleakage or bicarbonate alkalinity in the feedwater. The buildup of the acid reduces the condensate pH and leads to corrosion typically in the form of grooving of the condensate piping. This effect is accelerated in the presence of O_2. Volatile, alkaline-neutralizing chemicals are traditionally added to offset the low pH.

Among chemicals preferred for the control of condensate corrosion are morpholine, cyclohexylamine, diethylaminoethanol (DEAE), 2- amino-2-methyl-1-propanol (AMP-95), and ammonia (Ref 3). Each functions by neutralizing the carbonic acid. The amines are fed into the feedwater/boiler, where they volatilize and are carried over with the steam, dissolving in the condensate.

The extent of the amine reaction with carbonic acid depends on the dissociation constant of the amine as well as its basicity. Its efficiency in neutralizing carbonic acid also depends on the volatility of the amine. Amine volatility determines the location in the condensate section of the boiler where the amine will be most effective. It also determines the amount of amine that will be lost with wasted steam through the vent in a deaerating heater or in steam leaks, as well as the amount that will be lost with boiler blowdown.

The vapor-to-liquid distribution ratio (DR) of a neutralizing amine also helps determine the location in the condensate section where it will be most effective. Amines with higher DRs tend to remain in the steam, enabling them to control corrosion in equipment and piping located far from the boiler or where pressures are lowest. Lower-ratio amines tend to condense with the first steam that condenses and thus will control corrosion in locations closest to the boiler, or those where steam is condensing at higher pressures.

It is desirable to employ a low DR amine, such as morpholine, if most of the steam condenses early in the system. Most of the amine comes out early and is thus present to neutralize the carbonic acid produced in that vicinity. Cyclohexylamine tends to carry further, so it will provide better protection for more distant reaches of the system. Ethanolamine condenses very early in the system and therefore provides improved pH control at the earliest point in the system where wet steam conditions first occur. Distribution ratios of the neutralizing amines are listed in Table 1.

Table 1 Characteristics of neutralizing amines

Amines	Basicity constant	Molecular weight	Distribution ratio (DR) at indicated pressure					Hydrothermal stability
			0 MPa (0 psig)	**0.7 MPa (100 psig)**	**3.5 MPa (500 psig)**	**6 MPa (900 psig)**	**8 MPa (1200 psig)**	
Ammonia	15	17	1.0	7.5	4.9	4.4	3.1	Excellent
Cyclohexylamine	457	99	4.0	7.5	6.8	6.2	4.6	Good
Diethylaminoethanol (DEAE)	63	1171	1.4	3.4	3.8	3.3	2.5	Fair
Methoxypropylamine (AMP-95)	125	89	1.0	2.2	1.9	1.6	1.3	Good
Morpholine	2.1	107	0.3	1.1	1.1	1.2	1.1	Good

References cited in this section

1. J.D. Zupanovich, *The Analyst,* Vol IX (No. 4), 2002, p 17
2. C.R. Peters, *The Analyst,* Vol VIII (No. 1), 2001, p 17
3. I.J. Cotton and O. Hollander, *The Analyst,* Vol X (No. 2), 2003, p 9

BP. Boffardi, Corrosion Inhibitors in the Water Treatment Industry, *Corrosion: Fundamentals, Testing, and Protection*, Vol 13A, *ASM Handbook*, ASM International, 2003, p 891–906

Corrosion Inhibitors in the Water Treatment Industry

Bennett P. Boffardi, Bennett P. Boffardi and Associates, Inc.

Cooling Systems

An understanding of the relationship among cooling water, the buildup of deposits, and corrosion of heat-transfer surfaces requires an awareness of cooling system characteristics. There are basically three types of cooling systems: once-through, open recirculating, and closed recirculating systems (Fig. 1).

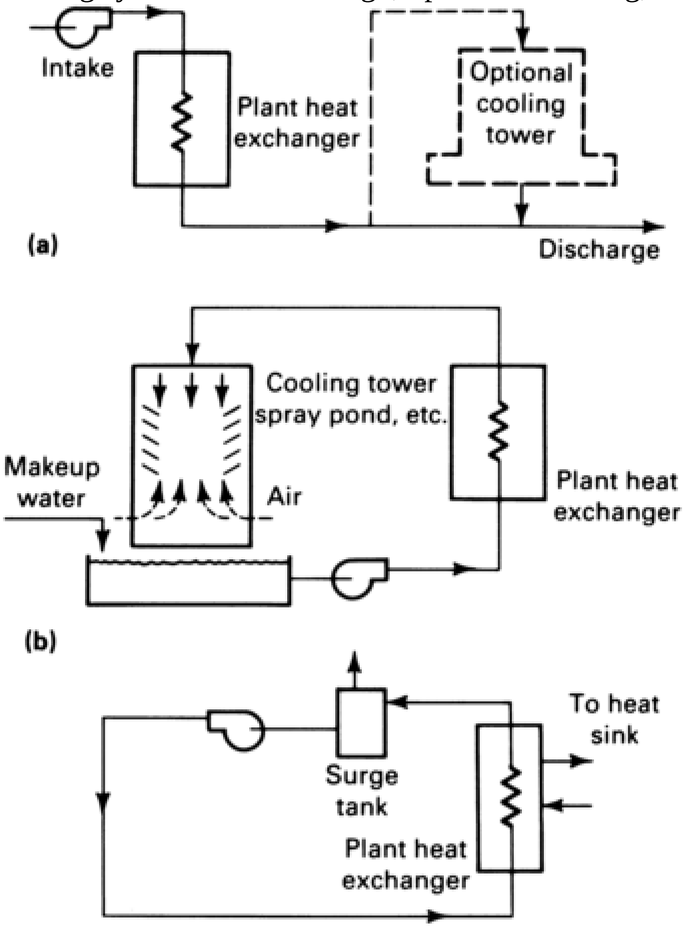

Fig. 1 Schematics of three types of cooling systems. (a) Once-through system. (b) Open recirculating system. (c) Closed recirculating system

In once-through systems, the cooling water passes through the heat-transfer equipment only once before it is discharged. Large volumes of water are used with only a small temperature increase across the exchanger. The mineral content of the water remains essentially the same. Water is usually drawn from such sources as rivers, lakes, and wells.

Open recirculating systems continuously reuse the water that passes through the heat- transfer equipment. Circulated water can be drawn from spray ponds or cooling tower basins. Evaporative cooling to the atmosphere dispels the unwanted heat transferred to the cooling water. The water then returns to the source and recirculates. In cooling-tower operations, the water cascades over and down the tower, where evaporative heat transfer takes place. Makeup water is added to replace the evaporative losses. Additional makeup water replaces the intentionally discharged water (blowdown) to maintain an acceptable level of dissolved minerals and suspended solids in the cooling water.

Open recirculating cooling systems are oxygen saturated and may contain a high level of dissolved solids. Inlet temperatures to the heat- transfer equipment are usually higher than those for once-through cooling systems. Also, there may be a larger temperature differential across the exchanger. These factors can significantly affect the buildup of deposits and the deterioration of the heat-transfer equipment.

Closed recirculating systems have little water loss and continuously recirculate the same water. The heat absorbed from the heat-transfer equipment is dissipated to another heat sink, which is cooled by other methods. Because there are no evaporative losses, the makeup water is minimal, and the mineral content remains essentially constant. However, corrosion by-products can easily accumulate and foul heat-transfer equipment because there are no methods for removing them from the system. Operating temperatures of the closed recirculating systems range from cold (as in chilled-water systems) to hot (for engine cooling jackets).

BP. Boffardi, Corrosion Inhibitors in the Water Treatment Industry, *Corrosion: Fundamentals, Testing, and Protection*, Vol 13A, *ASM Handbook*, ASM International, 2003, p 891–906

Corrosion Inhibitors in the Water Treatment Industry

Bennett P. Boffardi, Bennett P. Boffardi and Associates, Inc.

Corrosion Processes in Water-Recirculating Systems

Corrosion processes and the fouling of heat- transfer equipment must be understood if long- term reliability is to be achieved. Corrosion can be defined in a very practical sense as the deterioration of metal caused by the reaction with its surrounding environment. Because water is one of the most common heat-transfer fluids, it is not surprising that most of the problems associated with corrosion and deposits are water related. However, dissolved gases (such as oxygen, carbon dioxide, ammonia, and chlorine), dissolved ions (such as calcium, magnesium, chloride, sulfate, and bicarbonate), and suspended solids make water something other than pure H_2O.

For the corrosion reactions to take place between water and the metal surface, a potential difference must exist between different areas on the surface. This potential difference causes the passage of electrical current through the metal from areas of high potential to low potential. Thus, corrosion of metals in contact with water is electrochemical in nature. The basic reactions occur at the region of lower potential, which is the anode. The dissolution reaction causes metal ions to form and go into solution. The anodic oxidation reaction can be generally represented by:

$$M \rightarrow M^{n+} + ne^- \quad \text{(Eq 12)}$$

where *M* represents the metal that has been oxidized to its ionic form and having a valence of *n*+ and resulting in the release of *n* electrons. For the more common heat-transfer materials, the individual reactions are:

$$\mathrm{Fe} \rightarrow \mathrm{Fe}^{2+} + 2e^- \quad \text{(Eq 13a)}$$

$$\mathrm{Cu} \rightarrow \mathrm{Cu}^{+} + e^- \quad \text{(Eq 13b)}$$

$$\mathrm{Al} \rightarrow \mathrm{Al}^{3+} + 3e^- \quad \text{(Eq 13c)}$$

The liberated electrons that migrate through the metal to areas of higher potential are used in the reduction of other ions or oxygen in the water. These reactions occur at the cathodic site on the metal surface:

$$\mathrm{O_2} + 4\mathrm{H}^+ + 4e^- \rightarrow 2\mathrm{H_2O} \quad \text{(Eq 14)}$$

(Reduction of oxygen in acid solution)

$$\mathrm{O_2} + 2\mathrm{H_2O} + 4e^- \rightarrow 4\mathrm{OH}^- \quad \text{(Eq 15)}$$

(Reduction of oxygen in neutral or alkaline solution)

$$2H^+ + 2e^- \rightarrow H_2 \quad \text{(Hydrogen evolution)} \qquad \text{(Eq 16)}$$

$$Cu^{2+} + 2e^- \rightarrow Cu \quad \text{(Metal deposition)} \qquad \text{(Eq 17)}$$

$$Fe^{3+} + e^- \rightarrow Fe^{2+} \quad \text{(Reduction of metal ions)} \qquad \text{(Eq 18)}$$

Interaction between the products of the anodic and cathodic reactions can occur, forming solid corrosion products on the metal surface. For example, ferrous ions (Fe^{2+}) coming from the corrosion of metallic iron will react with the hydroxyl ions (OH^-) produced from the reduction of dissolved oxygen:

$$Fe^{2+} + 2OH^- \rightarrow Fe(OH)_2 \qquad \text{(Eq 19)}$$

Ferrous hydroxide [$Fe(OH)_2$] is further oxidized to form ferric hydroxide [$Fe(OH)_3$], which is unstable and subsequently transformed to hydrated ferric oxide (Fe_2O_3)—common red rust:

$$4Fe(OH)_2 + O_2 + 2H_2O \rightarrow 4Fe(OH)_3 \qquad \text{(Eq 20)}$$

$$2Fe(OH)_3 \rightarrow Fe_2O_3 + 3H_2O \qquad \text{(Eq 21)}$$

A buildup of rust occurs at the anodic sites, forming mounds known as tubercles. Under these mounds, localized corrosion continues to accelerate (Fig. 2) (Ref 4). Not all corrosion products are detrimental. The protective oxide films on copper (cuprous oxide, Cu_2O) and aluminum (aluminum oxide, Al_2O_3) are the result of corrosion:

$$2Cu^+ + 2OH^- \rightarrow Cu_2O + H_2O \qquad \text{(Eq 22)}$$

$$Al^{3+} + 3OH^- \rightarrow Al(OH)_3 \qquad \text{(Eq 23)}$$

$$2Al(OH)_3 \rightarrow Al_2O_3{\cdot}3H_2O \qquad \text{(Eq 24)}$$

These films are self-limiting, inhibiting the corrosion process once they are fully developed. The corrosion process between water and metal surfaces can take many forms (Ref 5). The characteristics of the more common forms that have been observed in heat-transfer equipment are discussed in the following sections.

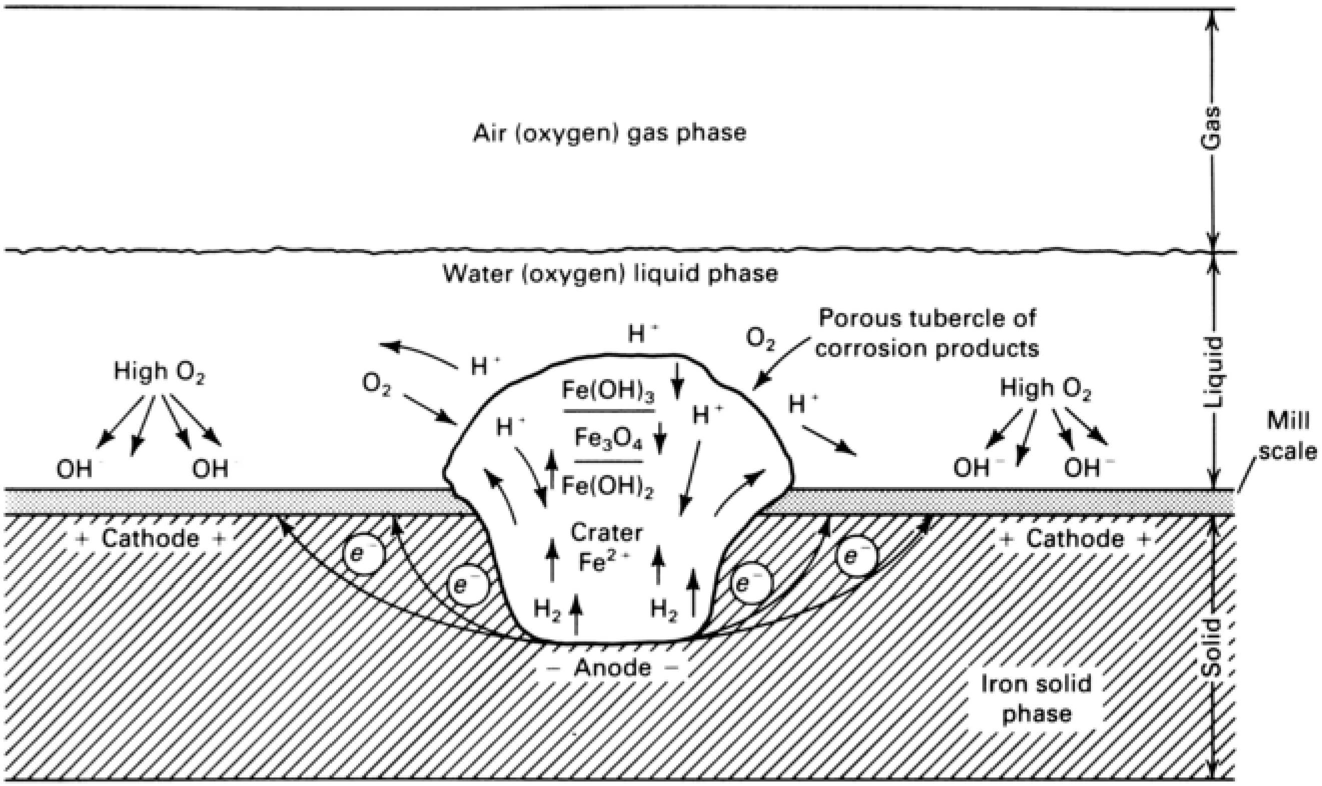

Fig. 2 Localized corrosion under a rust tubercle. Source: Ref 4

General corrosion, or uniform attack, occurs when the anodic areas on the metal surface keep shifting to different sites. This continual shifting results in relatively uniform metal removal. Because this type of corrosion can often be predicted, material loss can be taken into account.

Galvanic corrosion occurs when dissimilar materials are in contact in a conducting fluid (water). Accelerated corrosion occurs on the least resistant alloy, while the more resistant alloy is protected. The resistance of alloys can generally be described by the galvanic series, which ranks materials according to their chemical reactivity in seawater. The metals closer to the active end of the series will behave as the anode and will corrode, but those closer to the noble end will behave as the cathode and will be protected. Table 2 lists an abridged galvanic series. The intensity of attack is related to the relative surface areas of the metals in electrical contact. Large cathodic areas coupled to small anodic areas will aggravate galvanic corrosion and cause severe dissolution of the more active metal. The reverse situation—large anodic areas coupled to small cathodic areas—produces very little galvanic current.

Table 2 Galvanic series of some commercial metals and alloys in seawater

Noble or cathodic
Platinum
Gold
Graphite
Titanium
Silver
Chlorimet 3 (62Ni-18Cr-18Mo)
Hastelloy C (62Ni-17Cr-15Mo)
18-8Mo stainless steel (passive)
18-8 stainless steel (passive)
Chromium stainless steel 11–30% Cr (passive)
Inconel (passive) (80Ni-13Cr-7Fe)
Nickel (passive)
Silver solder
Monel (70Ni-30Cu)
Cupronickels (60–90Cu, 40-10Ni)
Bronzes (Cu-Sn)
Copper
Brasses (Cu-Zn)
Chlorimet 2 (66Ni-32Mo-1Fe)
Hastelloy B (60Ni-30Mo-6Fe-1Mn)
Inconel (active)
Nickel (active)
Tin
Lead
Lead-tin solders
18-8Mo stainless steel (active)
18-8 stainless steel (active)
Ni-Resist (high-nickel cast iron)
Chromium stainless steel, 13% Cr (active)
Cast iron
Steel or iron
Aluminum alloy 2024
Cadmium
Aluminum alloy 1100
Zinc
Magnesium and magnesium alloys

Active or anodic

Source: Ref 5

Galvanic corrosion obviously must be considered in the design of heat-transfer equipment. Alloys close to one another in the galvanic series should be used. Less obvious are the damaging effects that can occur when a dissolved noble metal is transported through the water and is capable of depositing on an active metal. For example, copper ions can plate out onto steel heat- transfer tube surfaces, setting up local corrosion cells.

Erosion-corrosion is normally restricted to copper-base alloys. It occurs in areas where turbulence at the metal surface is high enough to cause mechanical or electrochemical disruption of the protective film. Corrosion occurs at these sites and forms horseshoe-crescent-shaped indentations facing upstream of the water-flow direction. The process is usually accelerated when abrasive solid particles, such as sand, are entrained in the water. Because turbulence increases with velocity, areas having higher water velocities are prone to attack. For example, turbulence is much higher at tube inlets than it is several feet down the tube, resulting in the phenomenon of inlet-end erosion-corrosion.

Crevice corrosion is electrochemical attack that is due to differences in the corrosive environment between a shielded area (crevice) and its surroundings. Attack usually occurs in areas having a small volume of stagnant solution, such as at tube sheet supports, under deposits or tubercles, and at threaded joints. Corrosion is usually initiated because the oxygen concentration within the crevice is lower than that of the surrounding area. The outside area is higher in oxygen concentration and becomes the predominant cathodic region. Anodic dissolution occurs at the stagnant area. Once attack is underway, the area in the crevice or under a deposit becomes increasingly more aggressive because of pH depression and an increase in electrolyte concentration.

Pitting corrosion is one of the most insidious forms of attack. It takes place at small discrete areas where overall metal loss is negligible. The pit develops at a localized anodic site on the surface and continues to grow because of a large cathodic area surrounding the anode. High concentrations of metal chlorides often develop within the pit and hydrolyze to produce an acidic pH environment. This solution remains stagnant, having a high salt content and low oxygen concentration. The reactions within the pit become self-sustaining (autocatalytic) with very little tendency for them to be suppressed, ultimately causing penetration through the base metal. Pitting corrosion has also been associated with both crevice and galvanic corrosion. Metal deposition (copper ions plated on a steel surface) can also create sites for pitting attack.

References cited in this section

4. M.F. Obrecht and M. Pourbaix, *J. Am. Water Works Assoc.,* Vol 59, 1967, p 977

5. M.G. Fontana and D.N. Green, *Corrosion Engineering,* 2nd ed., McGraw-Hill, 1978, p 28–113

BP. Boffardi, Corrosion Inhibitors in the Water Treatment Industry, *Corrosion: Fundamentals, Testing, and Protection,* Vol 13A*, ASM Handbook,* ASM International, 2003, p 891–906

Corrosion Inhibitors in the Water Treatment Industry

Bennett P. Boffardi, Bennett P. Boffardi and Associates, Inc.

Influence of Water Quality

The corrosivity of water is significantly influenced by concentrations of dissolved species, including gases, pH, temperature, suspended matter, and bacteria. The effects of these entities on corrosion are assumed to be independent; although this is not totally correct—interactions do exist—it is easier to visualize their contribution when they are considered separately.

Dissolved Gases

Dissolved oxygen is a major factor contributing to the natural corrosion of low-carbon steel. It has been shown that oxygen is part of the overall electrochemical reactions occurring at the interface between the aqueous phase and the metal surface. Therefore, it is not surprising that low-carbon steel corrosion is proportional to the oxygen content in the water. Oxygen solubility in water will vary with temperature, pressure, and electrolyte concentration. Increasing the temperature decreases oxygen solubility, but increasing the partial pressure of oxygen increases its solubility. Concentrated electrolytes decrease oxygen solubility (molar salt concentrations exist in pit cavities and crevices). For open recirculating cooling water systems, the concentration of dissolved oxygen is approximately 6 mg/L (ppm). The presence of oxygen is necessary for the formation of protective oxides on copper (Cu_2O), aluminum (Al_2O_3), and steel (γFe_2O_3). In the absence of dissolved oxygen, the corrosion of low-carbon steel is greatly reduced. A uniform protective film of magnetite (Fe_3O_4) is formed according to:

$$3Fe + 4H_2O \rightarrow Fe_3O_4 + 4H_2 \qquad \text{(Eq 25)}$$

Overall, oxygen can have either a negative or a positive impact on the corrosion of low-carbon steel. In aerated systems, uneven distribution of corrosion products can form on the metal surface, giving rise to localized corrosion. Under deaerated conditions, the Fe_3O_4 film isolates the base metal from the water, sharply reducing corrosion.

Carbon dioxide is more soluble than oxygen in pure water (1.3 g/L, or parts per thousand, ppt, at 30 °C, or 85 °F) and will convert to carbonic acid (H_2CO_3), producing a solution having a pH of less than 6 where acid attack can predominate:

$$CO_2 + H_2O \rightleftharpoons H_2CO_3 \rightleftharpoons H^+ + HCO_3^- \qquad \text{(Eq 26)}$$

Adjusting the pH of the water upward redistributes the ratio of dissolved carbonic species. Carbonic acid will dissociate to form bicarbonate ions (HCO_3^-) and subsequently carbonate ions (CO_2^{2-}). The ratio of the various components can be calculated from the pH of the system. In open recirculating cooling water systems, the pH is usually controlled within the range of 7 to 8.5. Only the CO_2/HCO_3^- ratio is important within this range (the CO_2^{2-} concentration is negligible). Calcium ions (Ca^{2+}) in the water will react with bicarbonate species to produce calcium carbonate ($CaCO_3$). Calcium carbonate has a low solubility and will precipitate onto heat-transfer surfaces. The effect of CO_2 is most important in boiler condensate systems. The carbonic acid, H_2CO_3 reacts with steel to form ferrous bicarbonate [$Fe(HCO_3)_2$], a highly soluble salt. Rapid general thinning of steel can occur by this reaction. The addition of soluble amine inhibitors neutralizes the H_2CO_3 to suppress the corrosive attack. Copper alloys are also susceptible to increased attack in the presence of CO_2.

Chlorine is not a natural constituent of cooling waters, but is added for biological control. When dissolved in water, chlorine will convert to hypochlorous acid (HClO) and hydrochloric acid (HCl), which will lower the pH:

$$Cl_{2(g)} + H_2O \rightarrow HClO + HCl \qquad \text{(Eq 27)}$$

Acid attack on low-carbon steel is a concern when the pH falls below 7. Above this pH, the deleterious effects of chlorine are reduced. Adequate biological control can be achieved if the pH is maintained at approximately 7.5. However, chlorine will accelerate the corrosion of copper alloys, even at alkaline pHs. Chlorine in cooling waters is one of the most aggressive species for copper alloys; it can induce localized attack and degrade the protective Cu_2O film.

Ammonia (NH_3) is another gas that can affect heat-transfer equipment. Although its effect on ferrous alloys is minimal, it has a drastic impact on copper-rich brasses and alloys. These alloys can experience both rapid general thinning and stress-corrosion cracking (SCC). Ammonia is formed from the thermal degradation of various nitrogen-containing compounds added to boiler water to reduce ferrous corrosion. It forms a soluble complex with copper that can autocatalytically deteriorate the alloy in a short period of time.

Temperature

An increase in temperature will cause an increase in corrosion rates. Temperature plays a dual role with respect to oxygen corrosion. Increasing the temperature will reduce oxygen solubility. In open systems, in which oxygen can be released from the system, corrosion will increase up to a maximum at 80 °C (175 °F) where the oxygen solubility is 3 mg/L (ppm). Above this temperature, the reduced oxygen content limits the oxygen-

reduction reaction, reducing the rate of the iron dissolution reaction. Thus, the low- carbon steel corrosion rate decreases and at boiling water conditions, the corrosion rate is approximately the same as it is at room temperature. For closed systems, in which oxygen cannot escape, corrosion continues to increase linearly with temperature. The other physicochemical properties affected by temperature are the diffusion of oxygen to the metal surface, the viscosity of water, and solution conductivity. Increasing the temperature will increase the rate of oxygen diffusion to the metal surface, thus increasing corrosion rate because more oxygen is available for the cathodic-reduction reaction. The viscosity will decrease with increasing temperature, which will aid oxygen diffusion. Ionic mobility will also increase with temperature, increasing the overall conductivity of water.
An unusual temperature effect can occur with copper alloys (Ref 6). Temperature differences of at least 65 °C (115 °F) between the ends of copper conduits will cause the cold end to be cathodic to the hot end. Copper ions will dissolve (corrode) at the hot end and migrate to the cold end. At the cathode (cold end), copper ions will plate out. At the anode (hot end), the surface will become rough pitted. This effect is known as thermogalvanic attack.
Another important effect of temperature should be noted. An increase in temperature will decrease the solubility of many sparingly soluble inorganic salts. The solubility of $CaCO_3$ and calcium sulfate ($CaSO_4$) will decrease with an increase in temperature, precipitating and forming a thick barrier (insulating) deposit at the hottest areas.

Suspended Solids

Suspended matter, such as clays, silt, and corrosion products, is always present in open recirculating cooling water systems. Particulates scrubbed from the air add to the suspended solids loading. These materials are usually soft and nonabrasive. They are capable of depositing in low-flow areas, forming a physical barrier, and preventing oxygen from reaching the metal/solution interface. This buildup will contribute to the formation of differential aeration cells (crevice corrosion) and promote localized corrosion attack.

Effect of pH

The normal pH range for an open recirculating cooling water system is 6.5 to 9. Closed systems operate at a pH of 8.5 to 9; in boilers, the pH of the water is often 11. These pH values are the bulk pH of the water. The actual pH at the metal surface can be different, depending on prevailing surface reactions. Oxygen-reduction reaction will produce OH^- ions, raising the pH. Underdeposit corrosion products can depress the pH.
When the bulk water pH is moderately acidic (pH 5), uniform corrosion is the predominant form of attack, which increases with decreasing pH. At pH 4 or below, the protective oxide film dissolves, exposing bare metal to the environment. Corrosion is further accelerated at low pH when dissolved oxygen is reduced at the metal surface. Both hydrogen evolution and oxygen reduction contribute to the cathodic reaction rate. As the pH increases above 4, iron oxides precipitate from solution to form deposits. Uniform corrosion gradually decreases, but underdeposit attack begins because of the formation of Fe_2O_3 layer (rust) adhering to the surface. These deposits impede the diffusion of oxygen to the metal surface. As the pH increases, the nature of the iron oxide deposits changes from loosely adherent at pH 6 to hard and tenacious at pHs above 8. Although the corrosion of low-carbon steel in aerated waters decreases within the normal operating pH range of 6.5 to 9, the rates are sufficiently high that chemical treatments must be added to these systems to bring the rates within a manageable level of less than 0.13 mm/yr (5 mils/yr).
Copper alloy corrosion reactions are not as sensitive to pH as those for low-carbon steel. Acid pHs will accelerate general corrosion. As the pH increases, uniform corrosion decreases significantly. However, general thinning is not as severe a problem as the formation of cupric ions (Cu^{2+}), which can cathodically deposit on low- carbon steel and create active sites for pitting attack.
Aside from the effect of pH on corrosion, increasing the pH of waters having moderate levels of calcium and alkaline values can result in the precipitation of $CaCO_3$. The deposition of this alkaline scale can impede the diffusion of oxygen to the metal surface in addition to forming a heat-transfer barrier.

Dissolved Salts

Dissolved constituents in water can have a variety of effects, both individually and through their interactions. In addition to scale and deposit formation, the effects include increased corrosion. Increasing the dissolved solids content of the waters increases its conductivity. Galvanic effects due to the coupling of dissimilar metals are extended in waters having a higher salt content compared to waters of low conductivity.

Hardness ions (calcium and magnesium) and HCO_3^- ions are inhibitive and will suppress corrosion, but chloride (Cl^-) and sulfate (SO_4^{2-}) ions are antagonistic and will increase the rate of some forms of corrosion. The aggressiveness of water can be reduced by an increased concentration of hardness ions. Most waters used for cooling have pHs in the vicinity of neutral or above. This environment is very conducive to the formation of a protective film scale of $CaCO_3$, even when the water is below the saturation level for this salt. The actual mechanism that occurs at the water/metal interface is more involved than simple scale deposition. It is quite probable that $CaCO_3$ formation is due to electrochemical changes at the metal surface. The pH at the surface is usually higher than that of the bulk water because of an increase in OH^- ion concentration, a reaction product of oxygen reduction.

The overall aggressiveness of water is related to its hardness and alkalinity. Soft waters, which are low in calcium, are more corrosive than hard waters. Laboratory studies using three different waters of various compositions have shown that increased calcium concentration reduces general corrosion (Ref 7), as shown in Fig. 3. The HCO_3^- ion is the predominant alkaline species in natural waters within the 6.5 to 9 pH range. Alone, it is a mildly inhibitive species. Its reaction with Ca^{2+} ions is quite obvious, producing bulk precipitation of $CaCO_3$ once saturation is reached. Localized corrosion cells normally develop under the deposits. Increasing the bicarbonate concentration beyond that required for $CaCO_3$ saturation can be aggressive to low-carbon steel due to the formation of nonprotective iron carbonate ($FeCO_3$) scales.

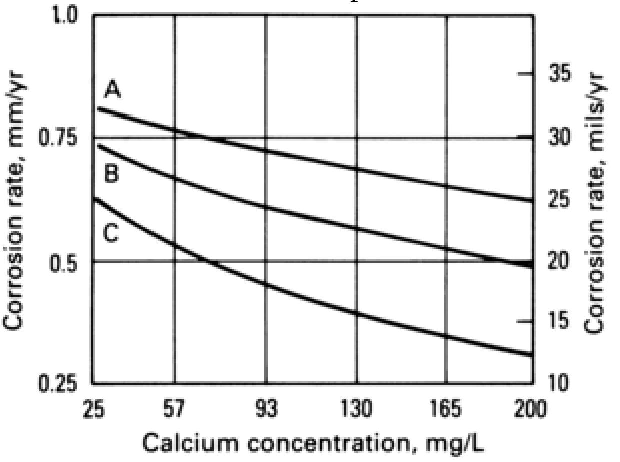

Fig. 3 Corrosion rate versus calcium concentration in three different waters. A, HCO_3^- = 38 mg/L, Cl^- = 78 mg/L, SO_4^{2-} = 78 mg/L; B, HCO_3^- = 100 mg/L, Cl^- = 224 mg/L, SO_4^{2-} = 224 mg/L; C, HCO_3^- = 266 mg/L, Cl^- = 644 mg/L, SO_4^{2-} = 644 mg/L

Copper alloys are also attacked by high HCO_3^- concentrations. Greenish-blue nodules that consist of basic copper salts usually form at active pit sites. Chloride and SO_4^{2-} ions are known to have a deleterious effect on low-carbon steel. Much of the antagonistic nature of Cl^- ions is due to their ability to adsorb on the metal surface and interfere with the formation of passive films. Pitting is the most common form of attack. The small exposed areas where Cl^- ions have adsorbed are anodic to the large cathodic passive oxide surface. High current densities are generated at the Cl^- site. Once corrosion begins, hydrolysis of the metal ions from the anodic reaction causes a decrease in pH, which discourages film repair and accelerates attack. The level of Cl^- ions needed to initiate attack can be as low as a few mg/L (ppm) for some stainless steels in high-purity waters. The more susceptible an alloy is to general attack, the less effect there is from Cl^- ions. Low-carbon steel will corrode in chloride-containing waters primarily from uniform corrosion rather than localized attack.

Copper alloys are subject to degradation by Cl^- ions that modify the Cu_2O structure. The small, negatively charged Cl^- ion can migrate through the Cu_2O film to areas of high positive charge density (Cu_2O is a *p*-type semiconductor). Substitution of a monovalent-charged chloride species for a divalent-charged oxygen species

can occur. To maintain electroneutrality, cuprous ions (Cu^+) are ejected (dissolved) into the aqueous phase, a loss that is by definition corrosion.

Sulfate ions are somewhat more elusive in their effect on corrosion. These ions do not appear to have the film-penetrating properties of Cl^- ions. In fact, there is evidence that SO_4^{2-} ions may inhibit corrosion of some stainless steels (Ref 8).

Other ions found in cooling waters that have an effect on corrosion are manganese (Mn^{2+}), sulfide (S^{2-}), phosphate (PO_4^{3-}), and nitrate (NO_3^-). Sodium (Na^+) and potassium (K^+) ions are considered neutral species and have no discernible effect. Manganese is found in both well and surface waters and can cathodically deposit on stainless steels and copper-base alloys. Attack usually occurs under these deposits. Sulfide ions from decay of organic matter, sulfate-reducing bacteria, and pollution will cause corrosion of copper-base alloys and steels. The Cu_2O film becomes nonprotective through a substitution of S^{2-} ions for the oxygen ion, accelerating corrosion. Attack occurs on low-carbon steel through the formation of ferrous sulfide (FeS). Deep pits will develop in both alloys. Phosphate ions can act as an accelerator or as an inhibitor for steel corrosion, depending on its concentration. At low concentrations, PO_4^{3-} ions will cause pits to develop on the surface of the metal. Higher concentrations of 15 to 20 mg/L (ppm) reverse this role, and the ion contributes to the stabilization of γFe_2O_3. Nitrate ions can be reduced on low-carbon steel surfaces, producing nitrites, NH_3, and OH^- ions. Nitrite ions (NO_2^-) inhibit corrosion of copper and steel alloys, but NH_3 will attack copper alloys.

Scale Deposition

Water-formed deposits, commonly referred to as scale, can be defined as a crystalline growth of an adherent layer (barrier) of insoluble salt or oxide on a heat-exchanger surface. The rate of formation is a complicated function of many variables, including temperature, concentration of scale-forming species, pH, water quality, and hydrodynamic conditions. Solubilities of scales typically increase with temperature. A few scales, for example, $CaCO_3$ and $CaSO_4$, have the reverse trend. Unfortunately, these scales are commonly found in cooling water systems.

Calcium carbonate is perhaps the most commonly found scale in cooling water systems. Calcium and bicarbonate alkalinity are both needed to form this extremely tenacious scale (alkalinity is the total concentration of HCO_3^-, CO_3^{2-}, and OH^- ions present in the water). An increase in heat and/or pH will cause the HCO_3^- ions to decompose to CO_2 and $CaCO_3$:

$$Ca(HCO_3)_2 \rightarrow CaCO_3 + CO_2 + H_2O \qquad \text{(Eq 28)}$$

The greatest concentration of $CaCO_3$ will occur at the hottest areas on the heat-transfer surface.

Many methods have been proposed to predict the formation of $CaCO_3$. They are all based on the thermodynamic equilibria of H_2CO_3 and are alkalinity corrected for temperature and dissolved solids (ionic strength). The more commonly used equations or indices are the Ryznar Stability Index (RSI) (Ref 9) and the Langelier Saturation Index (LSI) (Ref 10). The LSI is defined as:

$$LSI = \text{pH} - \text{pH}_s \qquad \text{(Eq 29)}$$

where pH is the actual measured value in the water, and pH_s is the pH of saturation calculated from:

$$\text{pH}_s = \left(pK_2' - pK_{sp}'\right) + p\text{Ca} + p\text{Alk} \qquad \text{(Eq 30)}$$

where pK_2' is the $-\log_{10}$ second dissociation constant of H_2CO_3, pK_{sp}' is the $-\log_{10}$ solubility product of $CaCO_3$, pCa is $-\log_{10}[Ca^{2+}]$ in moles/L, and pAlk = $-\log_{10}$ [total alkalinity] in equivalents/L. The complexity of these expressions has been reduced to nomographs (Ref 11). The RSI is an empirical expression:

$$\text{RSI} = 2\text{pH}_s - \text{pH} = \text{pH}_s - LSI \qquad \text{(Eq 31)}$$

where pH and pH_s have the same meaning as previously described. Interpretations of LSI and RSI values are listed in Table 3.

Table 3 Prediction of water characteristics by LSI and RSI values

Index		Tendency of water
LSI	**RSI**	
2.0	<4	Heavy scale forming, nonaggressive
0.5	5–6	Slightly scale forming and mildly aggressive
0	6–6.5	Balanced or at $CaCO_3$ saturation
-0.5	6.5–7	Nonscaling and slightly aggressive
-2.0	>8	Undersaturated, very aggressive

LSI, Langelier Saturation Index; RSI, Ryznar Stability Index

These values indicate only the tendency for $CaCO_3$ to deposit, not the rate or capacity for deposition. They do not take into account the tendency for $CaCO_3$ to supersaturate, its rate of formation, or whether the water contains an inhibitor to prevent deposition.

Calcium carbonate formation can be controlled by adding acids or specific chemicals tailored to inhibit its formation or modify the crystal lattice. Sulfuric acid (H_2SO_4), which is inexpensive, is most often used. Other acids, such as HCl, citric, or sulfamic acid (NH_2SO_3H), are also suitable. Acid addition produces salts that are more soluble than $CaCO_3$. These salts can reach saturation and must be controlled to prevent precipitation on heat-transfer surfaces:

$$Ca(HCO_3)_2 + H_2SO_4 \rightarrow CaSO_4 + 2CO_2 + 2H_2O \quad \text{(Eq 32)}$$

Calcium carbonate precipitation can also be inhibited by chemical treatment. A cost-effective group of materials is the polymeric inorganic phosphates. This class of compounds includes the salts of pyrophosphate, tripolyphosphate, and hexametaphosphate. Approximately 1 mg/L (ppm) of active material can stabilize 44 times the $CaCO_3$ equilibrium saturation concentration. This concentration is well below the stoichiometric values required for complexing calcium hardness and is termed threshold treatment. At these concentrations, the polyphosphates inhibit the formation of $CaCO_3$ crystallites by suppressing both nucleation and crystal growth. The polyphosphates are partly adsorbed on the surface of the growing crystals and partly included in incipient crystal nuclei. A disadvantage of the polyphosphates is their ability to hydrolyze or revert to PO_4^{3-} ions, which have no scale-inhibiting properties.

Other phosphate compounds found to be effective belong to the class known as phosphonates. Two of the more common compounds are nitrilotris(methylene phosphonic) acid (AMP) and 1-hydroxyethylidine-1,1-diphosphonic acid (HEDP). Threshold treatment inhibitor concentrations range from 0.25 to 0.5 mg/L (ppm), although higher concentrations are often used. The compounds AMP and HEDP have greater hydrolytic stability than the polyphosphates. It should be noted that AMP will degrade in the presence of chlorine to PO_4^{3-} ions. The addition of zinc ions (Zn^{2+}) significantly stabilizes the AMP molecule while still maintaining its control over $CaCO_3$ scale. Although HEDP is less affected by chlorine ion than AMP, at least 50% of the HEDP is degraded to PO_4^{3-} at residual chlorine concentrations of 0.2 to 0.5 mg/L (ppm) (Ref 12).

Organic polymers have also been found to be effective $CaCO_3$ inhibitors. These include polycarboxylates, such as polyacrylates, polymethacrylates, polymaleates, and their copolymers. Treatment levels are higher than the phosphorus- bearing materials, usually in the range of 2 to 4 mg/L (ppm). The molecular weights of these polymers should range from 1000 to 10,000 atomic mass units (amu) for effective scale control.

The polymers adsorb onto the $CaCO_3$ crystal structure, limiting the growth of $CaCO_3$ and ultimately limiting scale formation. These polymers are more frequently considered dispersants. They retard $CaCO_3$ scale by maintaining small particles of distorted crystalline material in suspension.

Bifunctional compounds are a recent development for $CaCO_3$ control. Phosphinocarboxylic acids contain both organic phosphorus and carboxylic acid groups (Ref 13). Simple molecules combining both the phosphono and carboxylic groups have also emerged and are very effective $CaCO_3$ inhibitors (Ref 12). However, these bifunctional compounds may be more expensive than the traditional low-molecular-weight polymers, polyphosphates, or phosphonates.

Calcium sulfate can exist in various forms in cooling water systems, the most common form being gypsum ($CaSO_4{\cdot}2H_2O$). The hemihydrate ($CaSO_4{\cdot}\frac{1}{2}H_2O$) and anhydrous forms are much less common. Their solubilities as a function of temperature are shown in Fig. 4. Because $CaSO_4{\cdot}2H_2O$ is more soluble than $CaCO_3$ by at least a factor of 50, it will precipitate only after the latter scale has been formed, within the normal pH range of 7 to

9. This phenomenon provides the basis for H_2SO_4 addition to control $CaCO_3$ in recirculating cooling water systems. The normal upper limit for calcium and sulfate concentration in the absence of an inhibitor is expressed:

$$\left[Ca^{2+}\right] \cdot \left[SO_4^{2-}\right] = 500{,}000 \qquad \text{(Eq 33)}$$

where the bracketed values are the ionic concentrations expressed in mg/L (ppm).

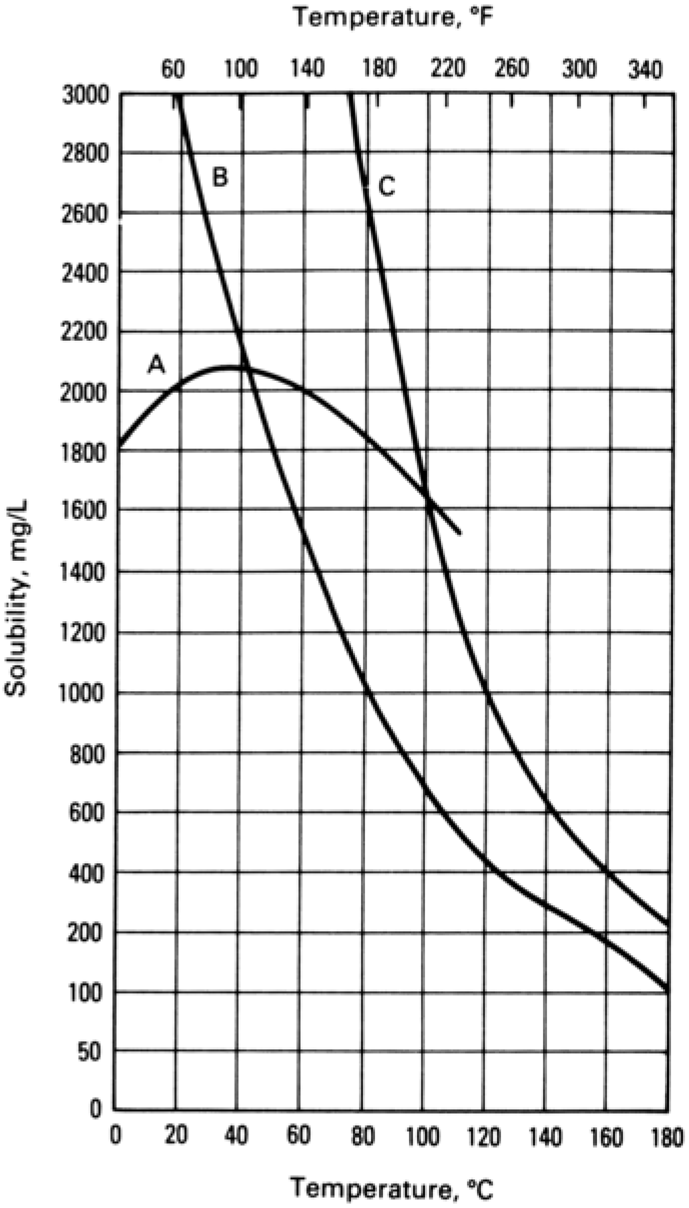

Fig. 4 Solubility of three forms of $CaSO_4$ versus water temperature. A, $CaSO_4 \cdot 2H_2O$; B, anhydrous $CaSO_4$; C, hemihydrate ($CaSO_4 \cdot \frac{1}{2}H_2O$). Source: Ref 14

Calcium sulfate scale can be most effectively controlled with polyacrylates (Ref 15), their copolymers, and phosphinocarboxylates (Ref 13). As with $CaCO_3$, excellent calcium scale control is achieved with polymers having low molecular weights in the range of 1000 to 10,000 amu. Concentrations of 1 to 2 mg/L (ppm) can increase $CaSO_4$ solubility by a factor of 20. This is similar to maintaining the $[Ca^{2+}] \cdot [SO_4^{2-}] > 10^7$ compared to 500,000 in the absence of chemical treatment. These polycarboxylates are stable over a wide range of pH and temperature. The basic mode of inhibition is through a combined threshold crystal distortion and dispersancy mechanism that prevents or delays precipitation.

Another chemical that controls $CaSO_4$ precipitation efficiently is the phosphonate AMP. In fact, the family of aminophosphonates has been found to be extremely effective. The level of AMP needed is approximately 0.5 mg/L (ppm).

Calcium phosphate [$Ca_3(PO_4)_2$] scale has become more common in recirculating cooling water systems. Increasing pH, calcium concentration, and phosphate addition from chemical treatment have provided the potential for this deposit to form on heat-transfer surfaces. Other water sources have also contributed to the increased level of phosphate. Makeup waters obtained from agricultural runoff and partly treated sewage can have high levels of PO_4^{3-} ions—at least 10 mg/L (ppm).

The solubility of $Ca_3(PO_4)_2$ decreases with increasing pH. It is essentially unaffected from 25 to 75 °C (75 to 165 °F). These deposits are usually amorphous and eventually transform to a more crystalline hydroxyapatite—$Ca_{10}(OH)_2(PO_4)_6$. Because of the low solubility of $Ca_3(PO_4)_2$ 2×10^{-29} deposits can easily form in waters containing 5 mg/L (ppm) of PO_4^{3-} ions and 300 mg/L (ppm) of Ca^{2+} ions at pH 7 to 7.5. The scale-forming tendency of $Ca_3(PO_4)_2$ is a complex function of pH, calcium hardness, PO_4^{3-} concentration, ionic strength, and temperature. Rule-of-thumb relationships between these variables do not exist. In the absence of any phosphate deposit, the PO_4^{3-} ions can contribute to the corrosion inhibition of low-carbon steel.

Calcium phosphate is an extremely difficult scale to inhibit. Intensive research has brought forth new chemistry to control this tenacious deposit. These new inhibitors include acrylic acid- hydroxypropylacrylate copolymer (Ref 16), styrene sulfonic acid-maleic acid copolymer, acrylic acid-sulfonic acid copolymer (Ref 17), and phosphino/acrylic acid-organo-sulfonic acid copolymer. They function by markedly modifying the morphology and size of the $Ca_3(PO_4)_2$ deposit while acting as a dispersant to prevent adherence of $Ca_3(PO_4)_2$ to heat-transfer surfaces. Concentrations of these copolymers are 10 to 15 mg/L (ppm) under conditions of moderate calcium hardness (about 500 mg/L, or ppm, as $CaCO_3$) and 10 mg/L (ppm) of PO_4^{3-} ions at pH 8 to 8.5. Increasing any of these parameters will require an increase in polymer concentration.

Silicate Scales. Calcium silicate ($CaSiO_3$) and magnesium silicate ($MgSiO_3$) scales tend to develop under more alkaline cooling water conditions, in which the pH is approximately 8.5 or greater. These scales are very tenacious, dense, and difficult to remove from heat-transfer surfaces. Although the solubility of silica (SiO_2) increases with pH, the solubility of the alkaline silicate decreases with increasing pH.

An upper limit for SiO_2 concentration is 150 mg/L (ppm) in the recirculating water, although other factors affect this value. Magnesium silicate can precipitate on heat-transfer surfaces with magnesium concentrations as low as 50 mg/L (ppm) and 150 mg/L (ppm) SiO_2. A rule-of-thumb pseudosolubility product of $[Mg]\cdot[SiO_2] \leq 8400$ has been developed (bracketed values are in mg/L, or ppm). The addition of chemical treatment as a preventive measure is essentially nonexistent. The most effective method of control is to keep the SiO_2 concentration in the recirculating cooling water below the 150 mg/L (ppm) limit.

Fouling Deposits. Water-borne deposits, commonly known as foulants, are loose, porous, insoluble materials suspended in water. They include such diverse substances as particulate matter scrubbed from the air; migrated corrosion products; silt, clays, and sand suspended in makeup water; organic contaminants (oils); biological matter; floc carryover from clarifiers; and such extraneous materials as leaves, twigs, and wood fibers from cooling towers. Fouling interferes with the flow of cooling water as compared to the reduction in heat transfer caused by barrier scales. However, fouling can reduce heat-transfer efficiency by plugging of the exchanger. Adequate water flow through the tubes is essential.

High flow rates (1.5 to 2.5 m/s, or 5 to 8 ft/s) can sweep away ordinary deposits, but low flow rates (less than 0.6 m/s, or 2 ft/s) cause the suspended foulants to drop out and deposit. Regions of low velocity include shell-side coolers, compressor jackets, water boxes, and cooling-tower basins.

Mechanical methods can be used to reduce fouling. In once-through cooling systems, coarse filters (bar screens, trash tracks, traveling screens) are used to remove large debris. Fine filtration is not practical. This is not the case with open recirculating systems. When the makeup water contains an appreciable concentration of suspended matter, it is advantageous to use side- stream filtration. In general, passing a few percent of the recirculating water through the side- stream filter will reduce the suspended solids loading 80 to 90%.

Another effective mechanical method used to control foulants is to pass scrapers, brushes, or balls through the heat-exchanger tubes, wiping them free of deposits. The technique is most frequently used in power utility surface condensers or other critical exchangers.

Chemical treatment has also been found to be an effective control method. Synthetic polymers are the chemicals more commonly used to disperse foulants. Polyacrylates, polymaleates, partially hydrolyzed polyacrylamides, and their copolymers constitute the majority of dispersant chemicals. The most important aspect of these materials is their molecular weights. An effective dispersant has a molecular weight of 1000 to

10,000 amu—the same range as for scale control. Concentrations of a few mg/L (ppm) are required in open recirculating systems, but lower levels are normally used in once-through systems.

Natural dispersants, such as tannins, lignin sulfonate, and carboxymethyl cellulose, are occasionally used, but they are not as effective as the synthetic polymers. The natural materials require higher concentrations to produce good dispersion of foulants, may not be cost effective, and may contribute to foaming. The synthetic polymers are not as easily degraded by biological organisms as are the natural polymers.

Increasing the molecular weight of the synthetic polymers into the million range changes the characteristics of the treatment from dispersion to flocculation. These high-molecular- weight polymers consist of polyacrylamides, polyamines, and polyacrylates and their various copolymers. Fouling is controlled by agglomeration of the suspended solids into nonadherent larger particles. To settle deposits, the polymers are usually added at concentrations of 0.2 to 0.5 mg/L (ppm) to clarifiers or thickeners. Similar concentrations are used in open recirculating systems. The deposit will accumulate in low- flow or stagnant areas in the recirculating systems. Heat transfer will not be seriously reduced, because of the low bulk density of these deposits. However, buildup of sludge in the cooling tower basins will necessitate periodic cleaning.

Biological Fouling. The presence and growth of living matter is commonly referred to as biofouling. Biofouling can interfere with the flow of water through heat exchangers and other conduits. This inhibits heat transfer and contributes to corrosion and general deterioration of the entire cooling system.

Recirculating cooling water systems are ideal incubators for the growth and proliferation of microorganisms. Water saturated with oxygen, exposed to sunlight, maintained at 30 to 60 °C (85 to 140 °F), and having a pH of 6 to 9 and abundant nutrients can readily sustain the growth of microorganisms. Although biofouling interferes with heat transfer, it does so in a manner quite different from that of inert deposits.

Biofilm buildup is initiated with the adsorption of organic material on the metal surface from the bulk water. Transport of microbial particles to the surface occurs as the result of turbulent flow. Microorganisms attach to the surface, and growth occurs through the assimilation of nutrients. Eventually, some of the biofilm is sheared away and reentrained in the flowing water to repeat the process of biofilm development. These steps are shown in Fig. 5.

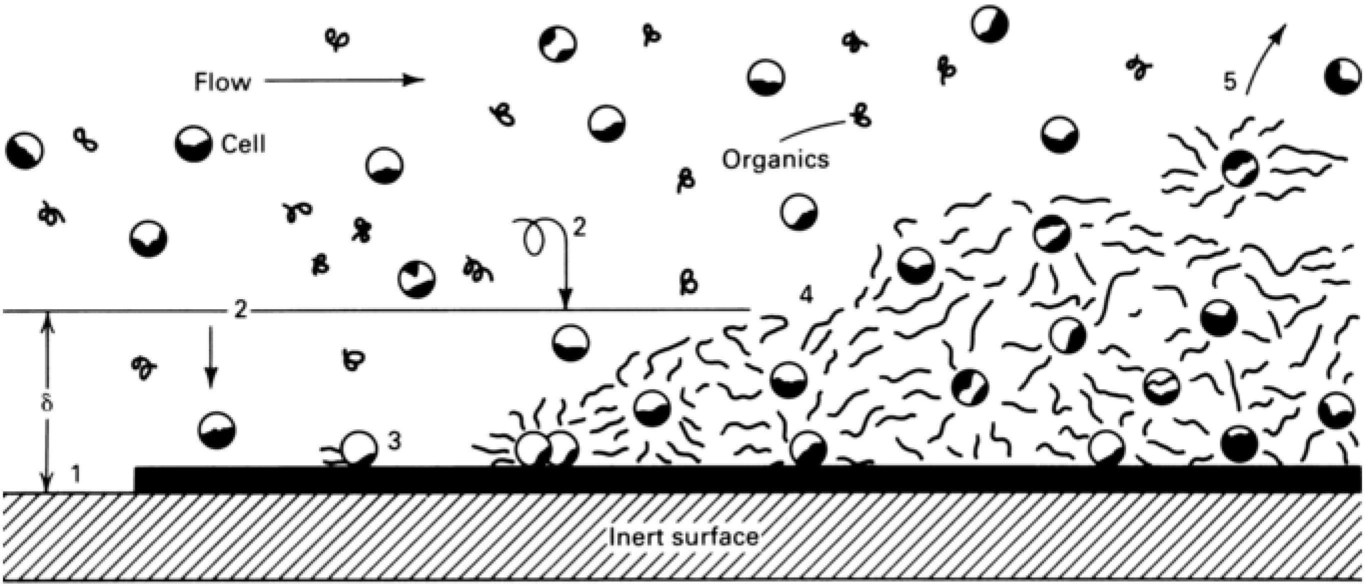

Fig. 5 Steps in biofilm formation. Formation is initiated when small organic molecules become attached to an inert surface (1) and microbiological cells are adsorbed onto the resulting layer (2). The cells send out hairlike exopolymers to feed on organic matter (3), adding to the coating (4). Flowing water detaches some of the formation (5), producing an equilibrium layer δ. Source: Ref 18

The biofilm can cause losses in heat transfer because of its insulating properties. Kinetic energy is absorbed from the flowing water through the rippling biofilm surface. Increased pumping energy is required to overcome the frictional resistance of the biofilm. Even though the film is 95 to 98% H_2O, the pressure decrease produced by a 500 μm (20 mils) thick film is substantial.

Three major classes of microorganisms are associated with recirculated cooling water systems: algae, fungi, and bacteria. Algae can range from very simple single-cell (unicellular) plants to multicellular species. The latter

include diverse forms and shapes, including slimy masses composed of several cells or long strands (filaments). All algae contain colored pigments, the most important of which is chlorophyll. Algae usually flourish on wetted surfaces exposed to oxygen and sunlight, such as cooling tower exposed lumber, mist eliminators, screens, and distribution trays.

Their impact on metal corrosion can be severe. The large slime mass contributes to crevice corrosion and pitting. Massive growths can inhibit proper water distribution by plugging screens, restricting flow, and interfering with pump suction.

Fungi are similar to algae, but do not contain chlorophyll. The major forms of interest are yeast and molds. They require moisture and air but not sunlight and exist on nutrients found in water or substances to which they are attached, for example, bacteria and algae. Mold fungi are filamentous in form, but most yeast are unicellular. Fungi consume wood components, causing serious wood surface deterioration and internal decay (wood rot).

Bacteria are unicellular microscopic plantlike organisms that are similar to algae, but lack chlorophyll. They exist in three basic forms: rod shaped (bacillus), spherical (coccus), and spiral (spirillus). The nutrients required for growth must be in solution, which necessitates a certain amount of moisture in their environment. Some bacteria require other carbon forms in addition to CO_2 in order to produce carbohydrates for food. Therefore, water or wet environments high in organic content are suitable for the proliferation of bacteria slime. Heat exchangers are ideal incubators for this biomass. Bacteria slime can significantly reduce heat-transfer efficiency and aggravate underdeposit corrosion attack.

The presence of oxygen is not required by all species of bacteria. Aerobic bacteria require free oxygen for growth, but anaerobic bacteria grow in the absence of oxygen.

Acidic waters produced by some forms of bacteria will directly attack metal surfaces. One species that is quite common is sulfate-reducing bacteria (SRB). These organisms are anaerobic and convert dissolved sulfur compounds, that is, SO_4^{2-}, to hydrogen sulfide (H_2S). Carbon steel, stainless steel, and copper-base alloys can be severely corroded by H_2S. *Desulfovibrio desulfuricans* is the most prevailing sulfate-reducing species. It exists mainly under deposits devoid of oxygen. The corrosive attack on carbon steel by these bacteria is quite distinctive; it is recognizable by smooth disk-shaped concentric rings formed on the metal surface. Corrosion rates as high as 2.5 mm/yr (100 mils/yr) can occur under optimal growth conditions. The following general reactions occur:

$$10H^+ + SO_4^{2-} + 4Fe \rightarrow 4Fe^{2+} + H_2S + 4H_2O \quad \text{(Eq 34)}$$

$$H_2S + Fe^{2+} \rightarrow FeS + 2H^+ \quad \text{(Eq 35)}$$

The formation of black iron sulfide deposits in conjunction with a rotten egg odor is also characteristic of attack by SRB.

The aerobic sulfur bacteria *Thiobacillus* can oxidize sulfur, or sulfides, to H_2SO_4. Localized pH depression as low as pH 1 can occur, causing severe thinning of steels where these organisms contact the metal. *Thiobacillus* and *Desulfovibrio* bacteria can exist simultaneously in close proximity. In doing so, the anaerobic SRB survive beneath the aerobic sulfur bacteria deposits.

Another organism common to cooling water systems is the nitrifying bacteria, which can oxidize NH_3 to nitrate. This is accompanied by a decrease in pH and occurs according to the reaction:

$$NH_3 + 2O_2 \rightarrow HNO_3 + H_2O \quad \text{(Eq 36)}$$

Rapid general thinning of copper-base alloys and steels can occur. Nitrite-base steel corrosion inhibitors can be rendered ineffective because of their oxidation to nitrate by these bacteria.

Several other groups of bacteria exist in cooling water environments. Iron-depositing bacteria can oxidize water-soluble Fe^{2+} ions to insoluble Fe_2O_3, which will subsequently deposit on the inside of piping, reduce flow, and aggravate crevice corrosion. Slime-forming bacteria form dense, sticky biomasses that impede water flow and contribute to fouling by sustaining the growth of other organisms.

The most practical and efficient method of controlling microbiological activity in cooling waters is through the use of biocides (Ref 19). These chemicals have the ability to kill the organisms or inhibit their growth and reproductive cycles. Biocides perform their function in various ways. Some biocides alter the permeability of the microbe cell wall, thus interfering with their vital life processes. Others damage the cell by interfering with the normal flow of nutrients and discharge of waste (Table 4).

Table 4 Biocides used in cooling water systems

Microbiocide	Effectiveness[(a)]			Comments
	Bacteria	**Fungi**	**Algae**	
Chlorine	E	S	E	Oxidizing; reacts with $-NH_2$ groups: effective at neutral pH; loses effectiveness at high pH. Use concentration: 0.1–0.2 mg/L continuous free residual; 0.5–1.0 mg/L intermittent free residual
Chlorine dioxide	E	G	G	Oxidizing; pH insensitive; can be used in presence of $-NH_2$ groups. Use concentration: 0.1–1 mg/L intermittent free residual
Bromine	E	S	E	Oxidizing; substitute for Cl_2 and ClO_2; effective over broad pH range. Use concentration: 0.05–0.1 mg/L continuous free residual; 0.2 to 0.4 mg/L intermittent free residual
Organo-bromide (DBNPA)	E	NA	S	Nonoxidizing; pH range 6–8.5. Use concentration: 0.5–24 mg/L intermittent feed
Methylene bisthiocyanate	E	S	S	Nonoxidizing; hydrolyzes above pH 8. Use concentration: 1.5–8 mg/L intermittent feed
Isothiazolinone	E	G	E	Nonoxidizing; pH insensitive; deactivated by HS^- and $-NH_2$ groups. Use concentration: 0.9–13 mg/L intermittent feed
Quaternary ammonium salts	E	G	E	Nonoxidizing; tendency to foam; surface active; ineffective in highly oil- or organic-fouled systems. Use concentration: 8–35 mg/L intermittent feed
Organo-tin/quaternary ammonium salts	E	G	E	Nonoxidizing; tendency to foam; functions best in alkaline pH. Use concentration; 7–50 mg/L
Glutaraldehyde	E	E	E	Nonoxidizing; deactivated by $-NH_2$ groups; effective over broad pH range. Use concentration: 10–75 mg/L intermittent feed

(a) E, excellent; G, good; S, slight; NA, not applicable

Biocides can be either oxidizing or nonoxidizing toxicants. Chlorine gas is the most prevalent industrial oxidizing biocide. It rapidly hydrolyzes in water to form hypochlorous acid (HClO) and HCl:

$$Cl_{2(g)} + H_2O \rightarrow HClO + HCl \quad \text{(Eq 37)}$$

HClO is the active species and dissociates as a function of pH:

$$HClO \leftrightarrow H^+ + ClO^- \quad \text{(Eq 38)}$$

At pH 7.5, equal concentrations of HClO and hypochlorous ions (ClO^-) exist. Above this pH, ClO^- predominates, with essentially total ionization at pH 9.5. As a consequence, chlorine becomes less effective in the more alkaline environments. Generally, the pH range of 6.5 to 7.5 is considered practical when chlorine is used as a biocide. Lower pHs will accelerate corrosion. Continuous treatment levels of 0.1 to 0.2 mg/L (ppm) are common. Intermittent treatment requires levels of 0.5 to 1.0 mg/L (ppm). Chlorine is both an excellent algaecide and bactericide. However, *Desulfovibrio* can develop a strong resistance to chlorine, requiring an increase in chlorine concentration or a change to an alternate biocide. Other sources of chlorine are salts of HClO, such as sodium hypochlorite (NaClO) and calcium hypochlorite [$Ca(ClO)_2$]. Both of these salts function in much the same way as chlorine.

Another oxidizing biocide is chlorine dioxide (ClO_2). This gas does not form HClO in water, but exists solely as ClO_2 in solution. It is used more extensively in the pulp and paper industry for bleaching than as a biocide. ClO_2 is extensively used in cooling waters contaminated with NH_3 or phenols due to the low demand for reaction with these species.

Brominated compounds that form hypobromous acid (HBrO) are very effective over a broader pH range than HClO. At pH 7.5, 50% of the chlorine is present as HClO, but more than 90% of the bromine is present as HBrO. Increasing the pH to 8.7 reduces the HClO concentration to 10%, but 50% of the HBrO remains.

Nonoxidizing biocides can be more effective than oxidizing biocides because of their overall control of algae, fungi, and bacteria. They have greater persistence, and the performance of many of them is pH independent.

An organobromine broad-spectrum nonoxidizing toxicant is 2,2-dibromo-3-nitrilopropionamide (DBNPA). This molecule is an extremely potent bactericide. It is slightly effective as an algaecide. It has little fungicide activity, and its toxicity decreases with an increase in alkaline pH.

Organosulfur compounds include a wide variety of different biocides, of which methylene bisthiocyanate is the most common. Their mode of activity is through the inhibition of cell growth by preventing the transfer of energy or life-sustaining chemical reactions from occurring within the cell. Methylene bisthiocyanate is effective in controlling algae, fungi, and bacteria, most notably *Desulfovibrio.* A shortcoming of methylene bisthiocyanate is its pH sensitivity and rapid hydrolysis in the alkaline pH range. Methylene bisthiocyanate is not recommended for use in cooling water systems having pH above 8.

Under broader alkaline conditions, sulfur-base biocides, such as bistrichloromethylsulfone and tetrahydro-3,5-dimethyl-2H-1,3,5-thiadiazine-2- thione, are more appropriate. The former is active in the pH range of 6.5 to 8, and the latter in more alkaline cooling water systems.

Isothiazolinone is a relatively new sulfur-containing biocide. It is very effective in controlling algae and bacteria. Isothiazolinone can be used over a broad pH range with no decrease in activity.

Quaternary ammonium salts are generally most effective against algae and bacteria in the alkaline pH range. The quaternary compounds cause cell death by reducing the permeability of the cell wall, preventing the intake of nutrients necessary to sustain life. Because of their surface-active nature, these compounds are easily rendered ineffective in systems heavily fouled with dirt, oil, and debris.

Organic tin compounds, such as bistributyl-tin oxide are very effective against algae and fungi. They function best in the alkaline pH range and provide synergistic biocidal activity when combined with quaternary ammonium salts.

Glutaraldehyde (1,5-pentanedial) is an effective broad-spectrum biocide capable of controlling slime-forming and SRB, fungi, and algae (Ref 20). It functions over broad pH and temperature ranges and is compatible with chlorine. Glutaraldehyde is deactivated in systems containing NH_3 and other primary amines that contain $-NH_2$ groups.

Corrosion Control in Cooling Water Environments. Aqueous corrosion has been shown to consist of electrochemical processes. The detrimental effects of these processes in cooling water environments can be significantly reduced by various methods, such as designing systems with more corrosion-resistant materials, applying protective coatings (paints, epoxy), using sacrificial anodes (cathodic protection), and chemical treatments.

For chemical-treatment or corrosion-inhibitor programs to be effective, they must protect all exposed metal from corrosive attack, must be effective at low concentration, must not cause deposits on the metal surface, must remain effective under a broad range of pH, temperature, water quality, and heat-flux conditions, must prevent scale formation and disperse deposits, and must have minimal toxicological effect when discharged. Economics should also be considered when assessing the merits of a chemical- treatment program. In once-through cooling systems, protection must be achieved with a few mg/L (ppm), or the cost may be prohibitive. Use of more corrosion-resistant alloys is often a more economical approach to corrosion control in once-through cooling systems. With respect to open recirculating cooling systems, chemical addition to the makeup water are typically in the range of 10 to 50 mg/L (ppm) (active). Cost is not as prohibitive, because the recycling of the water also includes the inhibitor. Closed recirculating cooling water systems require high active treatment levels (in the range of several thousand mg/L, or ppm). These systems have very small water losses.

Inhibitors can be broadly classified according to the rate process being controlled. Anodic inhibitors suppress anodic reactions; that is, the rate of metal ions transferred into the aqueous environment is reduced. Cathodic inhibitors impede the cathodic reaction—for example, the oxygen-reduction reaction. Mixed inhibitors hinder both reactions. The performance of an inhibitor can be assessed by its effectiveness in reducing the corrosion rate. This is generally expressed as a rate of thinning or penetration in microns/year or mils/year.

Inorganic inhibitors usually affect the anodic process. Rapid suppression of general corrosion occurs after anodic inhibitor treatment. However, when anodic inhibitors are below a critical concentration, they can stimulate localized pitting attack and therefore must be used with caution. Cathodic inhibitors reduce corrosion

primarily by interfering with the oxygen-reduction reaction. This family of inhibitors decreases general corrosion and does not stimulate pitting attack.

The current approach to cooling water treatment is toward more alkaline or high-pH conditions. This was not always the case. Historically, acid treatment was widely used to prevent scale deposition on heat-transfer surfaces. The system pH was slightly acidic (pH 6.5 to 7.0), and corrosion was controlled by using highly effective anodic inhibitors, the most effective being chromates, which have since been phased out.

Anodic Inhibitors

Nitrites. Sodium nitrite ($NaNO_2$) is an anodic inhibitor and requires a critical concentration for the protection of steel. Nitrites are extensively used as inhibitors in closed recirculating systems. The level of inhibitor depends on the aggressive species in solution. Sulfate ions interfere with nitrite protection to a greater extent than Cl^- ions. Treatment level should be at least the concentration of $NaNO_2$ required to produce a weight ratio of 1 with the aggressive ion concentrations ($[NaNO_2]/[NaCl + Na_2SO_4] = 1$). This concentration is normally in the range of 500 to 750 mg/L (ppm) at pH above 7.5. Nitrite may contribute to pitting of carbon steel if the concentration falls below this critical level.

Nitrites are easily oxidized to nitrates and therefore are not suitable for use in open recirculating cooling water systems. However, when formulated with borax, nitrites are excellent corrosion inhibitors for closed systems. The borax buffers the water to a pH above 8.5. Dosage levels for the borax-nitrite systems are 1500 to 2000 mg/L (ppm), with a nitrite concentration near 800 mg/L (ppm). It should be noted that NO_2^- ions are nutrients for some species of bacteria, which can oxidize the NO_2^- ions and render the treatment ineffective, producing slime deposits and a low pH. Biocides (isothiazolinone) are often used in conjunction with borax-nitrite programs for optimal protection.

Molybdates have been available for corrosion protection for more than 60 years, but have never been widely used. Molybdates are classified as anodic inhibitors. In waters having moderate Cl^- concentration (200 mg/L, or ppm), the level of sodium molybdate (Na_2MoO_4) needed for protection is at least 1000 mg/L. In dilute electrolytes, the concentration can be reduced to 150 mg/L (ppm). Normal treatment practices consist of combinations of molybdates with other inhibitors to produce synergistic treatments. This reduces the high level of molybdate ions (MoO_4^{2-}) needed when used alone. Combinations with zinc salts, phosphonates (AMP and HEDP), inorganic phosphates, nitrites, and carboxylates, such as long-chain acrylates and azoles (benzo- or tolyltriazoles), are effective in controlling corrosion of multimetal systems (Ref 21).

Sodium molybdate is a nonoxidizing inhibitor and requires a suitable oxidizing agent to augment the inhibitor and to impart a protective film. In aerated systems, the most abundant oxidizer is oxygen. Any of the above combinations are applicable except nitrites. A typical treatment consists of MoO_4, HEDP, zinc, and benzotriazole in a 3-to-3-to-1-to-1 weight ratio (Ref 21). A wide range of ratios has been used in specific formulations.

The use of molybdates in closed systems requires an oxidizing salt, such as $NaNO_2$. The optimal composition for the Na_2MoO_4:$NaNO_2$ system consists of a 60-to-40 weight ratio of the two salts (Ref 21).

Molybdate treatments have minimal pH dependency and can be used over a pH range of 5.5 to 8.5. They are sensitive to electrolyte concentration and are adversely affected by aggressive ions, such as Cl^- and SO_4^{2-}, when used alone. Temperature dependency is minimal. Molybdate treatments are known to inhibit both pitting and differential aeration attack. The precipitation of calcium molybdate [$Ca(MoO_4)$] is a concern in waters with moderate to high calcium hardness.

The mechanism by which molybdates inhibit the corrosion of ferrous metals is uncertain and complex. Simplistically, when iron corrodes, MoO_4^{2-} ions, in conjunction with other anions adsorb to form a nonprotective complex with Fe^{2+} ions. Because of dissolved oxygen or other oxidizers in the water, some of the Fe^{2+} ions are oxidized to the ferric (Fe^{3+}) state, and the ferrous-molybdate is transformed to ferric-molybdate, which is both insoluble and protective in neutral and alkaline waters.

Phosphates. Sodium phosphate (Na_3PO_4) is an anodic inhibitor and is effective in the presence of oxygen. Its protective properties toward steel are a function of pH. The monosubstituted phosphate (MH_2PO_4, where M is a metal) is the least protective, and the trisubstituted phosphate (M_3PO_4) is the most protective. Use of phosphate as a corrosion inhibitor should be relegated to more alkaline environments (pH > 8).

In open recirculating waters, phosphate treatment levels should be 15 to 20 mg/L (ppm). At lower concentrations of a few mg/L (ppm), PO_4^{3-} ions will cause pitting attack. The ability of phosphate to inhibit steel is primarily due to the oxygen content of the system (Ref 22). The dissolved oxygen produces a defective thin film of γFe_2O_3. The PO_4^{3-} fills in the voids and accelerates film growth. This prevents further diffusion of Fe^{2+} ions from the metal surface.

Inhibition by PO_4^{3-} ions is sensitive to electrolyte concentration; Cl^- ions can promote pitting attack. Because the protective oxide film contains voids and other inclusions, Cl^- ions are easily adsorbed to form soluble complexes. Hydrolysis of these complexes produces acid domains, which leads to localized acidic attack. Film breakdown is a function of the aggressive ion concentration, but film repair will depend on PO_4^{3-} levels and oxygen concentration.

Inhibition by PO_4^{3-} ions is sensitive to water quality and pH. There is minimal temperature sensitivity. One word of caution regarding PO_4^{3-} ions as low-carbon steel corrosion inhibitors: with waters of high calcium hardness, the potential for deposit formation increases with hardness, phosphate level, pH, and temperature. These deposits will stimulate crevice (underdeposit) corrosion. The need for an inhibitor to prevent calcium deposits becomes exceedingly more important as cooling waters increase in cycles of concentration and pH.

Cathodic Inhibitors

Cathodic inhibitors suppress corrosion by reducing the effectiveness of the cathodic process. They do not cause intense local attack and are generally considered to be safe inhibitors. Cathodic inhibitors are not as effective as anodic inhibitors in reducing corrosion.

Precipitating inhibitors fall under the domain of a cathodic inhibitor. They produce insoluble films on the cathode under conditions of locally high pH and isolate the cathode from the solution. Calcium bicarbonate [$Ca(HCO_3)_2$] will react with the alkaline medium at the cathode to form $CaCO_3$. The increase in alkalinity is due to the oxygen-reduction process, generating OH^- ions:

$$Ca(HCO_3)_2 + OH^- \rightarrow CaCO_3 + HCO_3^- + H_2O \qquad \text{(Eq 39)}$$

At the correct pH, $CaCO_3$ will precipitate to form a hard, smooth deposit that prevents oxygen from diffusing onto the metal surface. The tendency of water to form a $CaCO_3$ deposit is given by the LSI value.

Zinc ions are used to achieve a general reduction in corrosion by precipitating as zinc hydroxide [$Zn(OH)_2$] at the locally elevated pH of the cathode. Zinc is usually combined with phosphonates, polyphosphates, or orthophosphate. The durability of $Zn(OH)_2$ is tenuous at best. Although not normally used alone in cooling systems, zinc is synergistic when combined with other inhibitors as part of a multicomponent treatment program.

Zinc causes rapid development of a protective film over the metal surface. Above pH 7.5, the solubility of zinc is rapidly reduced to a few tenths of 1 mg/L (ppm). Its solubility can be significantly enhanced when combined with phosphonates or with some of the polymers used for $Ca_3(PO_4)_2$ control.

Polyphosphates are widely used cathodic inhibitors. They have been used for more than 60 years and are among the most economical of all inhibitor treatments. Sodium salts of the polyphosphates are normally used for corrosion control. They exist as linear polymers having the general structure shown in Fig. 6. The lower members of the series having “x” equal to or less than 2 are crystalline in nature, that is, $x = 0$, orthophosphate; $x = 1$, pyrophosphate; $x = 2$, tripolyphosphate. Higher members of the series are glassy and have no definitive structure. Varying the ratio of $n Na_2O$ to $m P_2O_5$ will produce species of different chain lengths and physicochemical properties, even though the inhibitive action of these polyphosphates is not significantly altered. The pH of the environment directly affects the protective properties of the phosphates. Orthophosphate inhibits corrosion in a more alkaline environment than does pyrophosphate. The crystalline phosphates protect low-carbon steel at higher pHs than the glassy phosphates, which function better near neutral pH. Normal concentrations in recirculating waters are 15 to 20 mg/L (ppm). The pH should be maintained in the range of 6.5 to 7.5 if low-carbon steel and copper alloys are both part of the system metallurgy.

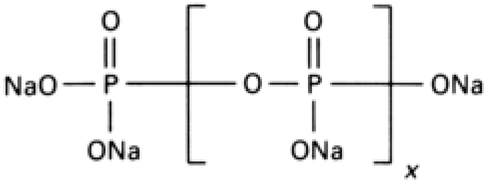

Fig. 6 General structure of sodium polyphosphate. *x* = 0, sodium phosphate; *x* = 1, sodium pyrophosphate; *x* = 2, sodium tripolyphosphate; *x* = 12 to 14, sodium polyphosphate

The polyphosphates are relatively insensitive to electrolyte concentrations, but do require an increase in dosage level with an increase in water corrosivity. They are effective inhibitors in controlling galvanic attack between two dissimilar metals (Ref 23), but do not prevent deposition of cathodic species on the more active metal, that is, copper deposition on steel.

Divalent metal ions, and Ca^{2+} in particular, are needed with the polyphosphates for effective inhibition of steel corrosion. The ratio of Ca^{2+} ion concentration to polyphosphate concentration should be at least 0.2, and preferably 0.5. The protective film develops through the formation of a positively charged colloidal complex that migrates to the cathode, forming an amorphous protective barrier. The cationic complex is accounted for by assuming that the calcium insets itself in the polyphosphate chains. The colloidal particles are the result of numerous cationic complexes loosely knit one to another through the Ca^{2+} ions. Polyphosphates will slowly revert to PO_4^{3-} ions, in the presence of Ca^{2+} ions and alkaline pH.

The phosphonates differ from the polyphosphates by a direct bond formation between the phosphorus and carbon atoms, rather than an oxygen-phosphorus bond in the polyphosphate. This linkage creates greater hydrolytic stability, which reduces the problem of reversion common to the polyphosphates. Two classes of materials are extensively used: AMP and HEDP. Their structures are shown in Fig. 7 and 8. When used alone, both compounds are marginally good low- carbon steel inhibitors, especially at high pH (pH 8.0). They protect ferrous metals through a mixed mode of inhibition. Incipient local attack occurs, but is rapidly arrested. Normal treatment levels are in the range of 15 to 20 mg/L (ppm). The hydrolytic stability of the phosphonates eliminates the problem of $Ca_3(PO_4)_2$ deposition in moderately to highly alkaline waters. However, AMP will degrade in the presence of chlorine, producing PO_4^{3-} ions and therefore should not be fed concurrently with chlorine. The phosphonates form very stable complexes with a variety of nonferrous metal ions and thus accelerate their corrosion, especially the copper-base alloys. The addition of zinc significantly suppresses this antagonistic attack. Calcium phosphonate deposits will form in moderate-hardness high-alkaline waters, that is, 400 to 500 mg/L (ppm) calcium hardness at pH 8 to 8.5. These deposits can be controlled with some of the new polymers available for $Ca_3(PO_4)_2$ control.

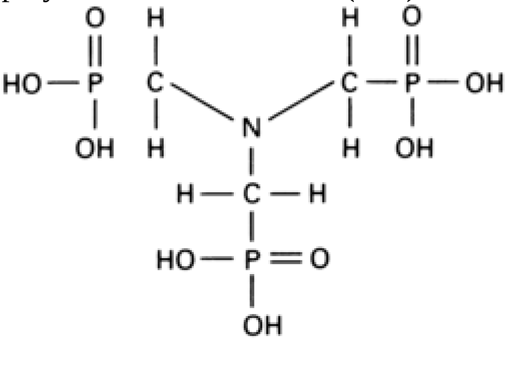

Fig. 7 Structure of nitrilotris(methylenephosphonic) acid, AMP

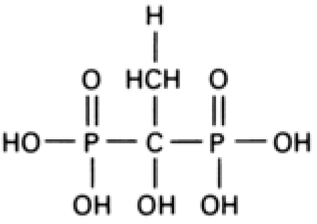

Fig. 8 Structure of 1-hydroxyethylidene-1,1-diphosphonic acid, HEDP

The phosphonates are sensitive to overall water quality. The protection afforded to low-carbon steel decreases with increasing aggressive ion concentration. Sensitivity to temperature is also exhibited. The major difference between AMP and HEDP is that the latter resists oxidation to a greater extent and can therefore be used in the presence of chlorine.

Multicomponent Systems. Cooling water formulations containing mixtures of inhibitors usually offer increased protection to ferrous metals. Such mixtures are synergistic in their action. Many combinations have been developed to achieve enhanced protection under a wide variety of plant operating conditions. Heavy-metal formulations containing zinc and/or chromate have been widely used in industry, where environmentally acceptable, particularly for severe corrosion problems. Nonheavy-metal treatment programs (no zinc or chromium) are receiving increased attention because of government discharge restraints. Complex blends of PO_4^{3-}, polyphosphate, phosphonate, copper corrosion inhibitor (see the section "Copper Inhibitors" in this article), and $Ca_3(PO_4)_2$ dispersants are probably the most widely used multicomponent inhibitors.

Zinc Polyphosphate. The addition of zinc to the polyphosphates does not appreciably change the general nature of the polyphosphates. This system retains its insensitivity to electrolyte concentration, its threshold inhibition of $CaCO_3$ and $CaSO_4$, its ability to protect ferrous and nonferrous metals, and its detergent properties. Zinc polyphosphate inhibitors also enable multivalent metal ions to form positively charged colloidal complexes.

Zinc increases the rate at which the protective film is formed on the metal surfaces (Ref 24). This rapid protective film formation improves the general corrosion protection to the system. It is also synergistic in combination with polyphosphates. The amount of treatment needed using a zinc-polyphosphate inhibitor combination is less than that required for the polyphosphates alone.

The mode of inhibition is cathodic, similar to the polyphosphates in calcium-containing waters. The zinc accelerates film formation, restraining attack until a thin, tenacious, durable film is developed. The deposition of zinc phosphate [$Zn_3(PO_4)_2$] does not seem to be involved in the inhibition process.

Approximately 10 to 20% of the combined zinc polyphosphate blend is zinc. Good corrosion control is achieved through the synergistic interaction of zinc with polyphosphate. Beyond 20% Zn, little improvement in low-carbon steel corrosion protection is observed. Maintenance concentrations are usually 10 mg/L (ppm) as polyphosphate. Good practice requires a dosage of two to three times the maintenance level as a pretreatment to the system for a short time, that is, less than 1 week. A pH range of 6.8 to 7.2 is required for good control. This limitation in pH is necessary to prevent excessive attack on copper-base alloys (the lower the pH, the greater the attack on copper). Sensitivity to bulk water temperatures is minimal.

Zinc Phosphonates. The combination of zinc with phosphonates provides significantly improved protection compared to phosphonates alone. The addition of zinc makes this formulation synergistic in its protection to carbon steel. Good corrosion control can be attained using 20 to 80% of the combined zinc phosphonate blend as zinc, with 30 to 60% being optimum (Ref 25). Overall treatment levels are 8 to 10 mg/L (ppm) phosphonate with 2 to 3 mg/L (ppm) Zn^{2+} ions. The need for zinc becomes paramount in the presence of copper-base alloys. When used alone, the phosphonates are aggressive to copper and form a strong copper-phosphonate complex. Zinc negates this antagonistic effect by forming a stronger and more stable complex, significantly reducing attack on the alloys. The effectiveness of the zinc-phosphonate combination is due to increased cathodic protection. The zinc effectively counteracts the anodic character of the phosphonates through the formation of a phosphonate-zinc complex, which is cathodic compared to the phosphonates alone.

Due to this complex, broad pH application becomes possible. The zinc phosphonate treatment can be used over a pH range of 6.5 to 9. Zinc is held in solution at these more alkaline pH levels, and protection actually improves with an increase in pH.

Little sensitivity is shown with increased salt or electrolyte concentration, and temperature effects are minimal. Thus, the zinc phosphonate systems can be used over a wide range of water quality, at high bulk water temperatures, 70 to 75°C (160 to 170°F), and with pH levels up to 9.0.

Degradation of phosphonates to PO_4^{3-} ions by chlorine is significantly reduced with a phosphonate-zinc system, and the latter can be used in chlorine environments because of diminished chlorine demand. The zinc stabilizes the complex, preventing the deterioration of the carbon- phosphorus bond in the oxidizing environment.

Nonheavy-Metal Systems. Many combinations of building blocks are currently being used in nonheavy-metal formulations. Some of the systems in use include combinations of the phosphonates, AMP/HEDP; polyphosphate/ phosphonate mixtures, polyphosphate/HEDP; polyphosphate or phosphonate/orthophosphate

(HEDP/PO_4^{3-}). These systems are synergistic in protecting low-carbon steel. They combine the many advantages of the individual components, including:

- Complex formation with calcium and numerous polyvalent metal cations required to form the protective film over the metal surface. The polyphosphates still form the colloidal species for cathodic protection, and the phosphonate serves as a cathodic polarizer
- Threshold inhibition of slightly soluble inorganic salts, such as $CaCO_3$ and $CaSO_4$
- Detergent and dispersive action on surface deposits

Most nonheavy-metal treatments for carbon steel function best in more alkaline or elevated- pH systems. Waters are less corrosive, but more prone to form scale or deposit. Therefore, good scale control is absolutely necessary. These treatments are generally not as effective as heavy- metal formulations. However, because of the less corrosive nature of the recirculating cooling system, good overall protection can be achieved. More care and attention are required to operate these nonheavy-metal treatments because they are less tolerant of system upsets and function under more contained ranges of water corrosivity, pH, and temperature.

The AMP/HEDP nonheavy-metal inhibitor pair is classified as a cathodic inhibitor. A critical AMP/HEDP ratio of 1.5 to 1 is needed for optimal carbon steel protection (Ref 26). Performance improves with pH and should be used in systems having a pH of at least 7.5. The combined phosphonate program is not as sensitive to temperature as the individual components, nor is it adversely affected by high levels of Cl^- and SO_4^{2-} ions. Normal treatment levels of at least 15 mg/L (ppm) total phosphonate can be used to achieve good corrosion protection, <75 μm/yr (3 mils/ yr). Adequate pretreatment of at least two to three times normal concentration for 1 week is required before reducing the concentration to a maintenance level. With good pH control, normal treatment levels can be reduced and still achieve the desired corrosion protection. Concern over attack on copper-base alloys still exists such that the addition of a specific copper inhibitor is highly recommended.

Polyphosphate/HEDP. The second nonheavy- metal system—polyphosphate/HEDP—is also cathodic in nature while being synergistic in protecting low-carbon steel. Approximately 40 to 80 wt% of the HEDP-polyphosphate blend is polyphosphate and is needed for good corrosion protection of carbon steel. Corrosion control of approximately 50 μm/yr (2 mils/yr) can be achieved with 15 mg/L (ppm) total phosphate content. The sensitivity of polyphosphate/HEDP to pH is minimal over the range of pH 6 to 8. Temperature sensitivity is minor. Good corrosion control is achieved at bulk water temperatures exceeding 60 °C (140 °F). As with the AMP/ HEDP system, sensitivity to water aggressiveness is not a major concern. The antagonistic effects of Cl^- and SO_4^{2-} ions are subdued by this treatment program.

Treatment levels are approximately 15 to 20 mg/L (ppm), which can be reduced if the system is pretreated at two to three times maintenance concentration for at least 1 week. Attack on copper-base alloys is reduced compared to the AMP/ HEDP system; however, as with the combined phosphonate system, there is a need for a specific copper inhibitor. Concern over reversion still exists, because the polyphosphates are subject to hydrolysis. The PO_4^{3-} ions generated will improve the overall corrosion protection, assuming $Ca_3(PO_4)_2$ precipitation is controlled.

The polyphosphate/PO_4^{3-} combination functions in a mixed mode. The cathodic portion comes from either the polyphosphate or phosphonate (HEDP), while the anodic portion derives from the PO_4^{3-} ion. The addition of PO_4^{3-} improves protection to carbon steel through a synergistic interaction with either polyphosphate or phosphonate (Ref 17). The level of polyphosphate or phosphonate is not critical and can range from 20 to 80% of the total inhibitor blend. The corrosion rate of carbon steel can be easily controlled to 25 μm/yr (1 mil/yr) with 15 to 18 mg/L (ppm) total phosphate.

This system is applicable over a broad pH range of 6.0 to 8.5. There is little sensitivity to pH. The lack of sensitivity to pH refers only to corrosion control, and the inhibitors remain active in solution. The formation of a $Ca_3(PO_4)_2$ precipitate is prevented by the addition of an appropriate additive that inhibits its growth and adherence to the metal surface. Sensitivity to temperature is also minimal. The inhibitor pair has applicability to very hot systems having bulk water temperatures as high as 70 °C (160 °F). Reversion of the polyphosphate molecules to PO_4^{3-} will be accelerated at the higher temperature, but will also enhance overall protection due

to the inhibitive activity of its product (PO_4^{3-} ion). The system is moderately sensitive to aggressive ions, specifically Cl^- which can promote pitting attack. PO_4^{3-} is an anodic inhibitor, and there is a critical concentration that must be maintained that is a function of the electrolyte composition. Treatments containing polyphosphate will revert to PO_4^{3-}, and a sufficient amount of a $Ca_3(PO_4)_2$ inhibitor should be present to suppress its formation.

Attack on copper-base alloys is not a major concern when polyphosphates are used. However, the phosphonate can be aggressive to copper-base alloys. The addition of a specific copper inhibitor is recommended.

Copper Inhibitors

Most of the steel inhibitors that have been discussed exert some degree of control over corrosion of copper-base alloys. However, system upsets, such as pH excursions and process leaks, can dissolve copper into the cooling water, where it can interfere with steel protection. Concentrations of at least 0.1 mg/L (ppm) or more of dissolved copper can deposit on steel conduits, accelerating localized attack. Ancillary inhibitors are available that are very effective in controlling corrosion of copper-base alloys and preventing galvanic deposition of dissolved copper onto ferrous metals.

Three specific inhibitors have been extensively used: mercaptobenzothiazole (MBT), benzotriazole, and tolyltriazole. Mercaptobenzothiazole is an extremely effective inhibitor for copper-base alloys. Its inhibitive properties are attributed to the formation of an adherent protective film on the metal oxide surface. The inhibitor reacts with the metal surface to form a chemisorbed barrier. The initial corrosion product of Cu^+ ions reacts with the MBT molecule to form a three-dimensional complex of Cu(1)MBT. The film growth rate is rapid, reaching a self-limiting thickness within a short period of time.

Mercaptobenzothiazole is susceptible to oxidizing agents, such as air, chlorine, and ultraviolet light from sunlight, which can degrade the molecule into a disulfide having no inhibitory properties. This degradation occurs only to the molecule in solution, not the complex on the metal surface. Because of the sensitivity of MBT toward chlorine, the inhibitor should be used only if there is no residual chlorine present. Thus, MBT should not be added to open recirculating cooling water systems, in which continuous chlorination is often practiced.

Cupric ions (Cu^{2+}) can be effectively inhibited from cathodically depositing onto more active metals, such as steel and aluminum, by reacting with MBT in a 2-to-1 molar ratio of MBT to Cu^{2+}. In the absence of complicating factors, such as copper concentrations exceeding 0.1 mg/L (ppm) in the cooling water or residual chlorine, the concentration of MBT required for good copper inhibition is approximately 4 mg/L (ppm). A feeding procedure based on 3 mg/L (ppm) followed by 1 mg/l (ppm) addition 12 h later has been very successful.

Benzotriazole and tolyltriazole function similarly in controlling copper corrosion. Structurally, tolyltriazole differs from benzotriazole in that the former has a methyl group attached to the benzene ring. Both materials behave similarly in cooling waters, reacting with the metal surface to produce a three-dimensional chemisorbed layer.

The azoles are classified as cathodic inhibitors because they adsorb at cathodic sites and interfere with the oxygen-reduction reaction. These molecules are more resistant to oxidation than MBT. In the presence of chlorine, 1-chlorobenzotriazole (or 1-chlorotolyltriazole) is probably formed, having minimal inhibitory properties. Upon dissipation of residual chlorine, the chloro- compound reverts back to the active azole. Chlorination does not affect the integrity of the complex on the metal surface.

The azoles can deactivate dissolved copper in cooling water systems and prevent its deposition onto steel or other active metals. A 2-to-1 molar ratio of inhibitor to copper ions is required, similar to the MBT reaction.

The concentration of azoles necessary for copper inhibition is approximately 1 to 2 mg/L (ppm) in the absence of any residual chlorine. The optimal practice is to pretreat the system with two to three times normal concentration for 1 to 2 days, then control at a maintenance dosage. Under chlorination conditions, the azole should be fed after the dissipation of residual chlorine. If continuous chlorination is practiced and cannot be changed to intermittent practice, the level of treatment should be increased to 4 to 5 mg/L (ppm). In the presence of continuous chlorination, overall copper corrosion protection will be less than with intermittent chlorination.

References cited in this section

6. V.G. Ereneta, *Corros. Sci.,* Vol 19, 1979, p 507
7. B.P. Boffardi and G.W. Schweitzer, Water Quality, Corrosion Control and Monitoring, *The Ninth International Congress on Metallic Corrosion,* National Research Council of Canada, June 1984
8. G.T. Burnstein and D.M. Davis, *Corros. Sci.,* Vol 20, 1980, p 1143
9. J.W. Ryznar, *J. Am. Water Works Assoc.,* Vol 36 (No. 4), 1944, p 472
10. W.F. Langelier, *J. Am. Water Works Assoc.,* Vol 28, 1936, p 1500
11. M.L. Riehl, *Water Supply and Treatment,* 9th ed., National Lime Association, 1976
12. R.H. Ashcraft, "Scale Inhibition Under Harsh Conditions by 2-Phosphonobutane- 1,2,4 tricarboxylic Acid (PBTC)," Paper 123, presented at Corrosion/85 (Boston, MA), National Association of Corrosion Engineers, March 1985
13. M.J. Smith and P. Miles, U.S. Patent 4,046,707
14. E.P. Partridge and A.H. White, *J. Am. Chem. Soc.,* Vol 51, 1929, p 360
15. P.H. Ralston, *Mater. Perform.,* Vol 11 (No. 6), 1972, p 39
16. I.T. Godlewski, J.J. Schuck, and B.L. Libutti, U.S. Patent 4,029,577
17. B.P. Boffardi and G.W. Schweitzer, "Advances in the Chemistry of Alkaline Cooling Water Treatment," Paper 132, presented at Corrosion/85 (Boston, MA), National Association of Corrosion Engineers, March 1985
18. J.F. Gary et al., Ed., *Condenser Biofouling Control,* Ann Arbor Science Publications, 1980, p 49–76
19. J.W. McCoy, *Microbiology of Cooling Water,* Chemical Publishing, 1980
20. R.G. Eagar, A.B. Theis, M.H. Turakhia, and W.G. Characklis, "Glularaldehyde: Impact on Corrosion Causing Biofilms," Paper 125, presented at Corrosion/86 (Houston, TX), National Association of Corrosion Engineers, March 1986
21. M.S. Vakasovich and J.P.G. Farr, *Mater. Perform.,* Vol 25 (No. 5), 1986, p 9
22. M. Cohen and M.J. Pryor, *J. Electrochem. Soc.,* Vol 98, 1951, p 263
23. B.G. Hatch, *Ind. Eng. Chem.,* Vol 44 (No. 8), 1952, p 1780
24. G.B. Hatch and P.H. Ralston, *Mater. Prot.,* Vol 3 (No. 8), 1964, p 35
25. G.B. Hatch and P.H. Ralston, *Mater. Prot. Perform.,* Vol 11 (No. 1), 1972, p 39
26. B.P. Boffardi, U.S. Patent 4,206,075

BP. Boffardi, Corrosion Inhibitors in the Water Treatment Industry, *Corrosion: Fundamentals, Testing, and Protection*, Vol 13A, *ASM Handbook*, ASM International, 2003, p 891–906

Corrosion Inhibitors in the Water Treatment Industry

Bennett P. Boffardi, Bennett P. Boffardi and Associates, Inc.

Corrosion Control in Municipal Water Systems

Chemical treatment in municipal systems can be used to protect the distribution system from corrosion, prevent the formation of calcium carbonate scale, and stabilize iron or manganese from forming "red waters" or "black waters" (Ref 27). There are fundamentally three basic chemicals to provide the required protection: zinc, phosphates, and silicates. However, any drinking water treatment chemical must conform to ANSI/NSF Standard 60. The specific limitations on the three chemical treatments are as follows:

- *Zinc:* Concentration may not exceed 2 mg/L (ppm) calculated as zinc ion (Zn^{2+}).
- *Phosphates:* Concentration may not exceed 10 mg/L (ppm) calculated as phosphate ion (PO_4^{3-}).
- *Silicates:* Concentration may not exceed 10 mg/L (ppm) calculated as silicon dioxide (SiO_2).

Zinc-Based Treatments. With respect to zinc-containing treatments there are two basic programs: zinc polyphosphate (PP) and zinc orthophosphate. Polyphosphates cover the range from pyrophosphate (two repeating units of O-P) to chain lengths of approximately 21 repeating units. The most common form of polyphosphate has 12 to 14 repeating units of O-P. Normal treatment levels for zinc polyphosphate are 0.15 mg Zn^{2+}/L (ppm) and 1.5 mg PP/L (ppm). Zinc orthophosphate concentrations can range from 0.20 to 2.0 mg Zn^{2+}/L (ppm) with 1.0 mg PO_4^{3-}/L (ppm).

Zinc polyphosphates have been an effective chemical-treatment program for steel corrosion control for more than 60 years. Zinc-based treatments are capable of forming tenacious protective films over the metal surface that are very persistent. The film is not easily disrupted. With a zinc polyphosphate program, the film provides protection at dead-end areas. Zinc also reduces the rate of reversion of polyphosphate to orthophosphate. Zinc polyphosphate is superior to the use of polyphosphate without zinc for steel corrosion control. The addition of zinc does not affect the calcium carbonate scale control properties of polyphosphate as shown in Table 5 and its ability to stabilize iron and manganese as shown in Tables 6 and 7.

Table 5 Calcium carbonate scale control

Concentration mg/L (ppm) as PO_4	Calcium carbonate inhibition, %		
	1:10 zinc:polyphosphate	**Polyphosphate**	**1:3 zinc:orthophosphate**
0.1	14	10	0
0.2	55	58	0
0.3	71	69	0
0.4	81	80	0
0.5	95	93	0
0.6	100	97	0
0.7	100	100	0

Conditions: 500 mg/L (ppm) calcium hardness, 500 mg/L (ppm) alkalinity, pH = 8.0, 65 °C (150 °F), 24 h duration, LSI = 2.0

Table 6 Iron stabilization

Concentration mg/L (ppm) PO_4	Iron stabilization, %			
	1:1 zinc:polyphosphate	**Polyphosphate**	**1:3 zinc:orthophosphate**	**1:1 ortho:polyphosphate**
0.5	6	7	3	…
1.0	82	84	13	…
1.5	88	87	18	…
2.0	100	100	25	27

Conditions: 2.0 mg/L (ppm) Fe(II), pH = 7.0, 25 °C (77 °F), 4 h duration, 25 μm filtration

Table 7 Manganese stabilization

Concentration mg/L (ppm) as PO_4	Manganese stabilization, %			
	1:10 zinc:polyphosphate	**Polyphosphate**	**1:3 zinc:orthophosphate**	**1:1 ortho:polyphosphate**
0.5	85	75	79	100
1.0	92	85	85	100
1.5	95	89	90	100
2.0	100	100	97	100
2.5	100	100	100	100

Zinc orthophosphate is a very effective multimetal corrosion control treatment. It provides corrosion protection to steel, copper, and lead (Ref 28). The ratio of zinc to orthophosphate is not critical. Most ratios provide similar corrosion protection at the same concentrations. This treatment also forms a rapid protective film on metal surfaces, consequently preventing corrosion and “red water” problems. Its utility lies in low hardness and low to moderate alkalinity waters. Zinc orthophosphate has little to no calcium carbonate scale inhibitory properties. This treatment program will not stabilize dissolved iron (Fe^{2+}) in well waters, but will stabilize dissolved manganese ($Mn^{2+)}$ in well waters, thus eliminating “black” water problems. Manganese stabilization requires the zinc orthophosphate treatment to be added prior to the water contacting air or any other source of oxidation (oxygen, chlorine). Zinc orthophosphate treatments require a higher concentration of zinc for corrosion control than zinc polyphosphate.

Although the orthophosphate species alone will provide protection to lead, their effect on carbon steel can be detrimental. Orthophosphate, which is an anodic inhibitor, can intensify localized corrosion of carbon steel by accelerating pitting attack.

Non-Zinc Based Treatments. In essence, there are three non-zinc chemical inhibitor treatment programs that are applicable to potable water systems: polyphosphate, blended polyphosphate-orthophosphate, and silicates. Sodium silicates have been used for many years as corrosion inhibitors in potable water systems. A typical SiO_2-to-Na_2O ratio is 3.22 to 1. Silicates afford good corrosion protection to carbon steel, galvanized steel, and copper. They are also effective in controlling lead leaching from soft solder (Ref 29). Silicate chemistry is usually applied in soft waters, such as found in southeastern United States. They are capable of providing corrosion protection over clean and corroded surfaces (Ref 30). Sodium silicate has no calcium carbonate scale inhibitory property. However, silicate chemistry is effective in stabilizing iron to prevent “red” water problems but is less effective in stabilizing manganese ions, or “black” water (Ref 31).

In the treatment of potable waters, high levels of silica (8 to 16 mg SiO_2/L, or ppm) are maintained above the naturally occurring silica in the water. In low alkaline waters, high concentrations of silica may increase the pH of the system to 8 or above. The high pH can impact upon trihalomethane (THM) formation during the addition of chlorine for disinfection. Silicate chemistry is environmentally friendly and is not affected by the 503 rule. The U.S. Environmental Protection Agency 503 rule regulates the disposal of hazardous materials from publicly owned treatment works (POTW).

Polyphosphates have been used in potable water for more than half a century. They are effective in controlling steel corrosion and lead dissolution (Ref 32). Polyphosphates are effective in controlling steel corrosion over a pH range of 6 to 7.8. Below pH 6 there is an increase in water corrosivity due to acidity. Above pH 7.8, there is a tendency for increased tuberculation. Normal active treatment levels are approximately 2 mg/L (ppm)

polyphosphate, although American National Standards Institute/National Sanitation Foundation (ANSI/NSF) Standard 60 limits are 10 mg/L (ppm). Polyphosphates are known to prevent calcium carbonate scales. Usually 0.6 mg/L (ppm) active polyphosphate is required for scale control. Stabilization of iron and manganese can be achieved with approximately 1 to 2 mg/L (ppm) polyphosphate per mg of total Fe^{2+} plus Mn^{2+} to prevent "red" or "black" waters. Polyphosphates are more effective than silicates, but less effective than the zinc counterpart for steel corrosion protection.

Blended polyphosphate-orthophosphate is synergistic in controlling steel corrosion. The polyphosphate component also provides calcium carbonate scale control, whereas the orthophosphate species enhances steel, copper, and lead protection. The pH range is 6 to 7.8 for steel corrosion control, and a pH above 7 for lead and copper inhibition. Active treatment concentrations are 1.5 to 2 mg/L (ppm) total phosphate. Excellent manganese stabilization is achieved with this pair; however, no iron stabilization is possible due to the formation of iron phosphate and its subsequent precipitation. This treatment is the best available technology to replace zinc- containing chemistry.

References cited in this section

27. B.P. Boffardi and A.M. Cognette, *Mater. Perform.,* Vol 34 (No. 7), 1995, p 36

28. B.P. Boffardi and A.M. Sherbondy, *Corrosion,* Vol 47, (No. 12), 1992, p 966

29. D.A. Little, M.R. Shock, and T.J. Sorg, "Investigation on Techniques and Control of Building Lead and Copper Corrosion by Orthophosphate and Silicate," Paper 609, presented at Corrosion/95 (Houston, TX), NACE International, March 1995

30. E.P. Katsanis, W.B. Esmonde, and R.W. Spencer, *Mater. Perform.,* Vol 25 (No. 5), NACE International, 1986, p 25

31. R.B. Robinson and S.K. Ronk, Manganese Treatment by the Addition of Sodium Silicate and Sodium Hypochlorite, American Water Works Association Research Foundation, 1986

32. R.B. Robinson, G.D. Reed, and B. Frazier, *Jour. AWWA,* Vol 84 (No. 2), 1992, p 77

BP. Boffardi, Corrosion Inhibitors in the Water Treatment Industry, *Corrosion: Fundamentals, Testing, and Protection*, Vol 13A, *ASM Handbook*, ASM International, 2003, p 891–906

Corrosion Inhibitors in the Water Treatment Industry

Bennett P. Boffardi, Bennett P. Boffardi and Associates, Inc.

Acknowledgment

Portions of this article have been adapted from B.P. Boffardi, Control of Environmental Variables in Water-Recirculating Systems, *Corrosion,* Vol 13, *ASM Handbook* (formerly 9th ed. *Metals Handbook*), ASM International, 1987, p 487–497.

BP. Boffardi, Corrosion Inhibitors in the Water Treatment Industry, *Corrosion: Fundamentals, Testing, and Protection*, Vol 13A, *ASM Handbook*, ASM International, 2003, p 891–906

Corrosion Inhibitors in the Water Treatment Industry

Bennett P. Boffardi, Bennett P. Boffardi and Associates, Inc.

References

1. J.D. Zupanovich, *The Analyst,* Vol IX (No. 4), 2002, p 17
2. C.R. Peters, *The Analyst,* Vol VIII (No. 1), 2001, p 17
3. I.J. Cotton and O. Hollander, *The Analyst,* Vol X (No. 2), 2003, p 9
4. M.F. Obrecht and M. Pourbaix, *J. Am. Water Works Assoc.,* Vol 59, 1967, p 977
5. M.G. Fontana and D.N. Green, *Corrosion Engineering,* 2nd ed., McGraw-Hill, 1978, p 28–113
6. V.G. Ereneta, *Corros. Sci.,* Vol 19, 1979, p 507
7. B.P. Boffardi and G.W. Schweitzer, Water Quality, Corrosion Control and Monitoring, *The Ninth International Congress on Metallic Corrosion,* National Research Council of Canada, June 1984
8. G.T. Burnstein and D.M. Davis, *Corros. Sci.,* Vol 20, 1980, p 1143
9. J.W. Ryznar, *J. Am. Water Works Assoc.,* Vol 36 (No. 4), 1944, p 472
10. W.F. Langelier, *J. Am. Water Works Assoc.,* Vol 28, 1936, p 1500
11. M.L. Riehl, *Water Supply and Treatment,* 9th ed., National Lime Association, 1976
12. R.H. Ashcraft, "Scale Inhibition Under Harsh Conditions by 2-Phosphonobutane- 1,2,4 tricarboxylic Acid (PBTC)," Paper 123, presented at Corrosion/85 (Boston, MA), National Association of Corrosion Engineers, March 1985
13. M.J. Smith and P. Miles, U.S. Patent 4,046,707
14. E.P. Partridge and A.H. White, *J. Am. Chem. Soc.,* Vol 51, 1929, p 360
15. P.H. Ralston, *Mater. Perform.,* Vol 11 (No. 6), 1972, p 39
16. I.T. Godlewski, J.J. Schuck, and B.L. Libutti, U.S. Patent 4,029,577
17. B.P. Boffardi and G.W. Schweitzer, "Advances in the Chemistry of Alkaline Cooling Water Treatment," Paper 132, presented at Corrosion/85 (Boston, MA), National Association of Corrosion Engineers, March 1985
18. J.F. Gary et al., Ed., *Condenser Biofouling Control,* Ann Arbor Science Publications, 1980, p 49–76
19. J.W. McCoy, *Microbiology of Cooling Water,* Chemical Publishing, 1980

20. R.G. Eagar, A.B. Theis, M.H. Turakhia, and W.G. Characklis, "Glularaldehyde: Impact on Corrosion Causing Biofilms," Paper 125, presented at Corrosion/86 (Houston, TX), National Association of Corrosion Engineers, March 1986

21. M.S. Vakasovich and J.P.G. Farr, *Mater. Perform.,* Vol 25 (No. 5), 1986, p 9

22. M. Cohen and M.J. Pryor, *J. Electrochem. Soc.,* Vol 98, 1951, p 263

23. B.G. Hatch, *Ind. Eng. Chem.,* Vol 44 (No. 8), 1952, p 1780

24. G.B. Hatch and P.H. Ralston, *Mater. Prot.,* Vol 3 (No. 8), 1964, p 35

25. G.B. Hatch and P.H. Ralston, *Mater. Prot. Perform.,* Vol 11 (No. 1), 1972, p 39

26. B.P. Boffardi, U.S. Patent 4,206,075

27. B.P. Boffardi and A.M. Cognette, *Mater. Perform.,* Vol 34 (No. 7), 1995, p 36

28. B.P. Boffardi and A.M. Sherbondy, *Corrosion,* Vol 47, (No. 12), 1992, p 966

29. D.A. Little, M.R. Shock, and T.J. Sorg, "Investigation on Techniques and Control of Building Lead and Copper Corrosion by Orthophosphate and Silicate," Paper 609, presented at Corrosion/95 (Houston, TX), NACE International, March 1995

30. E.P. Katsanis, W.B. Esmonde, and R.W. Spencer, *Mater. Perform.,* Vol 25 (No. 5), NACE International, 1986, p 25

31. R.B. Robinson and S.K. Ronk, Manganese Treatment by the Addition of Sodium Silicate and Sodium Hypochlorite, American Water Works Association Research Foundation, 1986

32. R.B. Robinson, G.D. Reed, and B. Frazier, *Jour. AWWA,* Vol 84 (No. 2), 1992, p 77

BP. Boffardi, Corrosion Inhibitors in the Water Treatment Industry, *Corrosion: Fundamentals, Testing, and Protection,* Vol 13A, *ASM Handbook,* ASM International, 2003, p 891–906

Corrosion Inhibitors in the Water Treatment Industry

Bennett P. Boffardi, Bennett P. Boffardi and Associates, Inc.

Selected References

- *Betz Handbook of Industrial Water Conditioning,* 9th ed., Betz Laboratories, 1991
- D.C. Brandvold, *Water Treatment: Industrial, Commercial, and Municipal,* Association of Water Technologies, McLean, VA, 1994
- G. Butler and H.C.K. Ison, *Corrosion and Its Prevention in Water,* Reinhold Publishing, 1966
- J.C. Cowan and D.C. Weintritt, *Water- Formed Scale Deposits,* Gulf Publishing, 1976
- G. Degrémont, *Water Treatment Handbook,* 6th ed., Springer-Verlag, 1991
- C.P. Dillon, *Corrosion Control in the Chemical Processing Industries,* 2nd ed., NACE International, Houston, TX, 1994
- C. Frayne, *Boiler Water Treatment—Principles and Practice,* 2 volumes, Chemical Publishing, 2002

- C. Frayne, *Cooling Water Treatment—Principles and Practice,* Chemical Publishing, 2001
- H.M. Herro and R.D. Port, *The Nalco Guide to Cooling Water Systems Failure Analysis,* McGraw-Hill, 1992
- F.N. Kemmer, Ed., *The Nalco Water Book,* 2nd ed., McGraw-Hill, 1988
- *Kurita Handbook of Water Treatment,* Kurita Water Industries, Ltd., Tokyo, Japan
- J.W. McCoy, *The Chemical Treatment of Boiler Water,* Chemical Publishing, 1981
- J.W. McCoy, *The Chemical Treatment of Cooling Water,* Chemical Publishing, 1983
- "The Mentor—Boiler Water Treatment Training Program," Association of Water Technologies, Inc., McLean, VA
- "The Mentor—Cooling Water Training Program," Association of Water Technologies, Inc., McLean, VA
- F. Pontius, Ed., *Water Quality and Treatment,* 5th ed., American Water Works Association, McGraw-Hill, 1999
- R.D. Port and H.M. Herro, *The Nalco Guide to Boiler Failure Analysis,* McGraw-Hill, 1990
- *Principles of Industrial Water Treatment,* 8th ed., Drew Industrial Division, Ashland Chemical Company, Boonton, NJ, 1985
- I.L. Rozenfeld, *Corrosion Inhibitors,* McGraw-Hill, 1981, p 176
- J. Tanis, *Procedures of Industrial Water Treatment,* Ltan Inc., Ridgefield, CT (can be obtained from Association of Water Technologies, Inc.)
- *Technical Reference and Training Manual,* Association of Water Technologies, Inc., McLean, VA

P. Elliott, Materials Selection for Corrosion Control, *Corrosion: Fundamentals, Testing, and Protection*, Vol 13A, *ASM Handbook*, ASM International, 2003, p 909–928

Materials Selection for Corrosion Control

Revised by Peter Elliott, Corrosion & Materials Consultancy, Inc.

Introduction

MATERIALS SELECTION AND DESIGN are of equal importance in achieving the desired performance and life expectancy of components and equipment (Ref 1, 2, 3, 4). From a corrosion standpoint, the following factors play an integral and often critical role in the anticipated outcome:

- Specification
- Fabrication and quality control
- Storage and transportation
- Operation
- Maintenance

In weighing the relative importance of these factors, the designer and materials engineer must work closely together to ensure that premature failure will not occur because of design defects and improper or inadequate materials selection.

The type and extent of corrosion is dictated by the unique environmental conditions that pertain to a specific application—at all stages in a component lifetime—including procurement, fabrication, transportation, storage, installation, commissioning, operation, and maintenance. Corrosion failures have occurred because of unexpected causes that resulted from a lack of appreciation about corrosion, sometimes the direct result of poor communication and/or a lack of appreciation of the true service conditions (Ref 5). As an example, a type 316 stainless steel (Unified Numbering System, or UNS, S31600) pipe was considered a suitable choice for admitting steam and subsequently air into a chemical slurry in a reaction vessel; however, it experienced localized pitting corrosion even before the anticipated service (Fig. 1). The damage occurred during storage, because the new (replacement) stainless steel pipe sections were in direct contact with mists of brackish water that arose in an unsheltered location immediately adjacent to a marine estuary.

Fig. 1 Localized corrosion of stainless steel pipes from direct exposure to marine mists, compounded by plastic wraps

The pipe failure just described was exacerbated because site maintenance personnel "improved" the storage by partially wrapping the pipes with plastic sheet, which created sweatbox conditions. Offload corrosion (typically, corrosion that occurs on site while materials are in storage after they have been offloaded) occurred because of condensation and evaporation cycles. Plastic wrapping can cause moisture to be effectively trapped in the closed space; plastic is also not impervious to moisture penetration.
This article outlines the step-by-step processes by which materials are selected in order to prevent or control corrosion and includes information on materials that are resistant to the various forms of corrosion.

References cited in this section

1. R.J. Landrum, *Designing for Corrosion Control,* NACE International, 1989
2. V.R. Pludek, *Design and Corrosion Control,* The Macmillan Press Ltd., 1977
3. C.P. Dillon, *Material Selection for the Chemical Process Industries,* McGraw- Hill, Inc., 1992
4. *Designer Handbook, Guidelines for the Selection and Use of Stainless Steel,* Specialty Steel Industry of North America, 1995
5. P. Elliott, "Catch 22" and the UCS Factor—Why Must History Repeat Itself?, *Mater. Perform.,* Vol 28 (No. 7), 1989, p 75–78; Vol 28 (No. 8), 1989, p 70–76

P. Elliott, Materials Selection for Corrosion Control, *Corrosion: Fundamentals, Testing, and Protection,* Vol 13A*, ASM Handbook,* ASM International, 2003, p 909–928

Materials Selection for Corrosion Control

Revised by Peter Elliott, Corrosion & Materials Consultancy, Inc.

The Materials Selection Process

Review the Operating Conditions. The first step in the materials selection process is a thorough review of the corrosive environment, the operating conditions of the equipment, and the circumstances pertaining thereto. Not to be excluded are offload conditions (e.g., Fig. 1) and excursions or downtimes (expected or otherwise) that occur during service. Input from knowledgeable process engineers is recommended.
Precise definition of the chemical environment, including the presence of trace compounds, is vital. For example, the nickel-molybdenum alloy B-2 (UNS N10665) is highly resistant to hydrochloric acid (HCl) up to the atmospheric boiling point. However, the presence of small quantities of oxidizing metal ions, such as ferric ion (Fe^{3+}), will result in severe corrosion.
Other operating conditions that require definition, especially for equipment used in the chemical-processing industry, include temperatures, pressures, flow rates, liquid versus gaseous phases, slurries versus deposits, aqueous versus anhydrous phases, continuous versus intermittent operation, media used for cooling or heating, external versus internal environment, and product purity.
Abnormal or upset conditions are often overlooked during the selection process. For example, plain carbon steel may be the optimal choice for vessels and piping used to contain non-corrosive hydrocarbon gases, such as ethylene, under pressure at normal temperatures. However, the cooling effect that occurs during venting to the atmosphere, for whatever reason, may lower the temperature of vessels, piping, and relief valves to below the ductile-to-brittle transition point, causing catastrophic brittle fracture. The selection of special steels, qualified by impact testing at the lowest expected temperature, may be appropriate.

Review the Design. The type and design of the equipment and its various components should be considered, along with size, complexity, and criticality in service. Selecting a material for a simple storage tank generally does not require the same attention and effort as choosing the material of construction for a highly sophisticated chemical-process reactor. This is especially true when considering critical, unique pieces of equipment in large, single-train, continuous process plants in which a failure would shut down the entire operation, with potentially large financial implications that include materials replacement, fabrication, recommissioning, and lost product and sales. Where risks are potentially high, great effort is expended to select the optimal material for safe, low-maintenance service.

The materials used to join the components into an assembly will require as much attention as the component materials themselves. Many bolted agitator assemblies in reactors, as well as riveted wheels in centrifugal compressors, have failed catastrophically because the bolts or rivets did not have adequate strength or corrosion resistance.

When welding is the joining method, the materials engineer is challenged to ensure that the welds are as corrosion resistant as the base metals. Generally, the weld metal must equal the base metal in chemical composition and must be virtually free of surface defects, such as porosity, slag inclusions, incomplete penetration, or lack of fusion, for long, maintenance-free service. The challenge is even greater when dissimilar- metal welds are required. Improper selection may allow local attack due to weld-metal dilution or may allow hydrogen-assisted cracking due to hard heat-affected zones (HAZs). More information on preventing corrosion of welds is available in the articles “Corrosion of Carbon Steel Weldments,” “Corrosion of Stainless Steel Weldments,” and “Corrosion of Nonferrous Alloy Weldments” in this Volume.

Materials Selection. Candidate materials can be considered once the chemical environment, operating conditions, and type and design of the equipment have been as fully defined as possible. Occasionally, the selection is based on reliable, pertinent past experience and, as such, is well defined. More often, selection is not straightforward for a number of reasons, such as complex chemical environments and stringent code requirements.

The list of materials to choose from is large and continues to increase. Ferrous and nonferrous metals and alloys, thermoplastics, reinforced thermosetting plastics (RTPs), nonmetallic linings, glass, carbon and graphite, and catalyzed resin coatings are among the various materials available. Many materials are immediately excluded because of service conditions, that is, pressures too high for RTP; temperatures too high for nonmetallic linings and coatings, such as rubber or epoxy resins; environments too aggressive for carbon steel; and so on. The remaining choices may still be great in number.

It is always desirable to minimize the list of materials. This allows in-depth evaluation of those that remain. In other cases, the initial list may be exceptionally small because of limited knowledge about the operating conditions or the complexity of the chemical environment. A search of data sources should follow in either case.

Literature Survey. Data sources include abstracts, data surveys (Ref 6), and texts that advise on materials selection and are based primarily on in-service experiences (Ref 7). Computerized reference data on materials selection, with expert or materials advisor systems, which are computer programs containing methods and information developed by experts, have been developed during the past 15 years (e.g., Ref 8, 9, 10). Expert systems are designed to solve problems, make predictions, suggest possible treatments, and offer materials and corrosion advice with a degree of accuracy equaling that of their human counterparts. Unfortunately, some advisor systems that are available are not updated into current software programs (Ref 11). Data also are found in a wide variety of handbooks, conference proceedings, and literature compilations published by professional organizations worldwide; see the Selected References at the end of this article and the article “Information Sources and Databases for the Corrosionist” in this Volume).

Experience and data generated in-house often serve as the most reliable bases for materials selection. Ideally, this is coupled with outside experience, when available, from materials vendors and equipment fabricators to complete the initial screening process. Contacts with clients referred by vendors should not be overlooked for their added experience.

At this point, the list of candidate materials should be narrowed to a reasonable number for in-depth evaluation. Final selections should not be based solely on the previously mentioned data sources, because, in most cases, the data provided are insufficient for the complete characterization of an environment or a set of operating conditions.

Evaluating Candidate Materials. The in- depth evaluation of each candidate material requires a thorough understanding of the product forms that are available and the ease of fabrication by standard methods. For example, it would be wasteful of time and money to evaluate an Fe-14.5Si alloy for anything but a cast component such as a pump casing or valve body; the alloy is unavailable in any other form. It would be eliminated because of its poor weldability for applications involving welding.

Corrosion testing in representative environments is generally the next step. The extent of the investigation (and the determination of test conditions) depends on such factors as (Ref 12):

- Degree of uncertainty after available information has been considered
- The consequences of making a less-than-optimal selection
- The time available for evaluation

Laboratory testing of candidate materials is common and, in some cases, may be the only means available for final determination. Wherever possible, the actual process fluids, or, at least, mixtures that simulate the actual environment, should be used. There is considerable risk in using the latter, because undefined constituents can have a significant effect on the performance of a particular material.

Depending on the application, weighed and measured coupons of candidate materials are exposed to the corrosive fluids under a variety of conditions ranging from simple static immersion at a controlled temperature to complex testing under combined heat-transfer and velocity conditions. Guidance for conducting laboratory corrosion tests is available in Ref 13, 14, 15, 16, 17. After exposure for a specified length of time (generally, a minimum of 1 week), the coupons are, in the case of metals and alloys, cleaned and reweighed, and a corrosion rate is calculated based on mass loss and exposed surface area. The rate is commonly expressed in millimeters of penetration per year (mm/yr) or inches or mils (1 mil = 0.001 in.) of penetration per year (mils/yr)

Localized attack, such as pitting, crevice corrosion, and exfoliation, are determined from a microscopic examination of the test coupons. Special coupons, such as galvanic couples, welded, and stressed coupons, are often exposed to determine if other forms of corrosion may occur on certain metals and alloys. These coupons may require metallographic examination for evidence of dealloying, stress-corrosion cracking (SCC), intergranular corrosion, and other corrosion phenomena.

Nonmetallic materials, such as thermoplastics, coatings, reinforced thermosetting resins, elastomers, and ceramics, are also evaluated in laboratory tests, but the criteria used are different from those used for metals. First, exposure time must generally be longer (often, a minimum of 1 to 3 months) before significant changes occur. Exposure times of 6 months to 1 year are common. Also, corrosion rate calculations based on mass loss and surface area are not applicable in most cases. Of more importance are changes in weight, volume, hardness, strength, and appearance before and after exposure. Corrosion testing and evaluation are covered in detail in the Section “Corrosion Testing and Evaluation” in this Volume.

If possible, candidate materials should be tested under conditions more similar to the final application rather than in laboratory glassware. The tests should be conducted in a pilot operation or in full-scale equipment. Data are more reliable when test coupons are integrated into the process and are exposed to the same conditions as the actual equipment. Because of nonuniform conditions (flows, composition) within process equipment, coupon locations should be carefully selected (see the article “Corrosion Monitoring Techniques” in this Volume).

Reliability is further enhanced when it is possible to test full-size components fabricated from candidate materials (Ref 16). Examples include:

- Flanged sections of selected alloys and/or nonmetallic materials installed in a pipeline
- Experimental alloy impellers in pumps for corrosion and cavitation studies
- Tubing installed in a full-size operating or miniature test heat exchanger to evaluate materials with optimal resistance to corrosion under heat-transfer conditions
- Paddles of candidate materials bolted to a reactor agitator for erosion-corrosion studies

The primary disadvantages of this method of testing are the cost of fabrication, installation, removal, and evaluation; the downtime resulting from equipment being taken out of service and dismantled for evaluation; and the fact that a test component could fail prematurely and cause a unit shutdown and/or equipment damage.

Specifications. Once the candidate materials have been thoroughly evaluated (along with the economics) and the materials of construction have been selected for the particular application, then clear and concise specifications must be prepared to ensure that the material is obtained as ordered and that it meets all the requirements of the application.

Perhaps the best known and most widely used specifications are the standards of ASTM International, which presents thousands of specifications for virtually all metal and nonmetal materials of construction; special volumes apply to the chemical-process industry (Ref 16) and to corrosion testing (Ref 17). Similar standards in countries other than the United States include DIN (Germany), BS (Great Britain), AFNOR (France), UNI (Italy), NBN (Belgium), and JIS (Japan). Other materials specifications that are well known but are more limited in application are those of the Society of Automotive Engineers (SAE), the Aerospace Material Specification (AMS), the American Welding Society (AWS), the American Petroleum Institute (API), and the American National Standards Institute (ANSI).

Fabrication requirements must also be spelled out in detail to avoid mistakes that could shorten the life of the equipment and to satisfy the requirements of state and federal regulatory agencies and insurance companies. The American Society of Mechanical Engineers (ASME) code governs the fabrication of equipment for the chemical, power, and nuclear industries, and the API code governs the fabrication of equipment for the refining industry. Piping for these industries is generally fabricated according to applicable ANSI codes. In these codes, allowable stresses for design calculations have been determined for virtually all metals and alloys that might be selected for corrosive (and noncorrosive) service. Where welding is the primary joining method, welding procedures and welders must be qualified before fabrication begins. Testing and quality-assurance requirements, such as radiography, hydrostatic testing, and ultrasonic inspection, are also covered in the codes and are specified, where applicable, to ensure compliance.

The fabricator is generally required to provide detailed drawings that list dimensions, tolerances, all pertinent materials specifications, fabrication and welding details, and testing and quality-assurance requirements for review. Prefabrication meetings are held for final review of all drawings and details, so that customer and vendor are in agreement. Thus, problems or errors that could lead to costly delays in fabrication or failures in service can be detected early and corrected.

Money spent on inspection and monitoring during equipment fabrication/erection to ensure compliance with specifications is repaid by trouble-free startup and operation of the fabricated assembly. In some cases, every component of an assembly must be tested to avoid excessive corrosion and/or premature failure. For example, an additional quality check of a vessel fabricated from AISI type 316L stainless steel (UNS S31603) for hot acetic acid service might be to test every plate, flange, nozzle, weld, and so on for the presence of molybdenum by using a chemical spot test method (Ref 18). The absence of molybdenum, which might indicate the mistaken use of a different stainless steel, such as type 304L (UNS S30403), would result in accelerated corrosion in this service. Another example is the testing of every component (including weld metal) of a heat exchanger fabricated from chromium-molybdenum steels for hot high-pressure hydrogen service to avoid possible catastrophic failure by hydrogen attack. The use of portable x-ray fluorescence analyzers for this type of quality-assurance testing of critical service components has become quite popular in recent years (Ref 19).

On-Line Monitoring. Once built, installed, and commissioned in service, the equipment, piping, reactor, heat exchanger, and so on should be monitored by the materials engineer to confirm the selection of materials of construction and all other requirements for the intended application. Frequent shutdowns for thorough inspections (visually and with the aid of applicable nondestructive examination methods) and periodic evaluation of corrosion coupons exposed at key locations in the equipment represent both the ideal and the most difficult corrosion monitoring activities to achieve. In actual practice, equipment is generally kept on-stream continuously for long periods of time between shutdowns, so on-stream monitoring techniques must also be used.

In the petroleum industry, the internal corrosion in oil and gas production operations is often monitored with hydrogen probes (Ref 20). These instruments measure hydrogen created by corrosion reactions. A portion of the hydrogen penetrates the vessel or pipeline wall, and the rest of the hydrogen is dissolved in the process fluid or released as gas bubbles. Hydrogen probes measure hydrogen permeation and provide information on the rate of corrosion.

Other on-stream corrosion monitoring techniques that are used in the petroleum and chemical-process industries are:

- *Electrochemical techniques:* includes monitors that use electrical resistance and linear polarization methods (Ref 21). The former technique determines corrosion trends with time, and the latter determines an instantaneous corrosion rate. Other techniques, such as the alternating-current impedance method, measure corrosion rates and also provide information about the type of corrosion process that is occurring.
- *Ultrasonic thickness measurement:* a useful monitoring tool, especially when baseline readings are taken at selected locations before the equipment is placed in service. The inspection locations can be changed if erosion or corrosion areas are localized.

With these methods, the materials engineer is able to determine the adequacy of the materials selected and to predict remaining life, so that replacements and/or repairs can be scheduled well in advance of failure. The corrosion test methods discussed previously can also be used to evaluate alternate materials that might be more cost-effective at the time of replacement of the vessel or a component.

References cited in this section

6. *Corrosion Data Survey—Metals Section,* 6th ed., 1985; *Corrosion Data Survey— Nonmetals Section,* 5th ed., National Association of Corrosion Engineers, 1983

7. C.P. Dillon and W. Pollock, Ed., *Materials Selector Series for Hazardous Chemicals,* Materials Technology Institute of the Chemical Process Industries, Inc., 1994–in press

8. C. Westcott et al., “The Development and Application of Integrated Expert Systems and Data Bases for Corrosion Consultancy,” Paper 54, presented at Corrosion/ 86 (Houston, TX), National Association of Corrosion Engineers, March 1986

9. S.E. Marschand et al., “Expert Systems Developed by Corrosion Specialists,” Paper 56, presented at Corrosion/86 (Houston, TX), National Association of Corrosion Engineers, March 1986

10. W.F. Bogaerts et al., “Artificial Intelligence, Expert Systems and Computer- Aided Engineering in Corrosion Control,” Paper 58, presented at Corrosion/86 (Houston, TX), National Association of Corrosion Engineers, March 1986

11. “CHEM-COR Modules on Advisory Systems for Selecting Materials,” National Association of Corrosion Engineers and Materials Technology Institute of the Chemical Process Industries Inc., NACE, 1990–1997

12. R.B. Puyear, Material Selection Criteria for Chemical Processing Equipment, *Met. Prog.,* Feb 1978, p 40–46

13. R. Baboian, Ed., *Corrosion Tests and Standards,* MNL-20, *ASTM Manual Series,* ASTM, 1995

14. “Laboratory Corrosion Testing of Metals for the Process Industries,” NACE TM-01- 69 (1976 Revision); “Method of Conducting Controlled Velocity Laboratory Corrosion Tests,” NACE TM-02-70, National Association of Corrosion Engineers

15. *Metal Corrosion, Erosion, and Wear,* Vol 03.02, Section 3, *Annual Book of ASTM Standards,* American Society for Testing and Materials, 1986

16. *ASTM Standards for Maintenance, Repair and Operations in the Chemical Process Industry,* ASTM, 1994

17. *ASTM Standards for Corrosion Testing of Metals,* ASTM, 1990

18. G. Kobrin, Evaluate Equipment Condition by Field Inspection and Tests, *Hydrocarbon Process,* Jan 1970, p 115–120

19. B.J. Moniz, Field Identification of Metals, *Process Industries Corrosion—The Theory and Practice,* National Association of Corrosion Engineers, 1986, p 839–842

20. Monitoring Internal Corrosion in Oil and Gas Production Operations with Hydrogen Probes, NACE Publication 1C 184, *Mater. Perform.,* June 1984, p 49–56

21. J.C. Bovankovich, On-Line Corrosion Monitoring, *Mater. Prot. Perform.,* June 1973, p 20–23

P. Elliott, Materials Selection for Corrosion Control, *Corrosion: Fundamentals, Testing, and Protection,* Vol 13A, *ASM Handbook,* ASM International, 2003, p 909–928

Materials Selection for Corrosion Control

Revised by Peter Elliott, Corrosion & Materials Consultancy, Inc.

Selecting Materials to Prevent or Control Corrosion

This section addresses materials selection to prevent or control general (uniform) corrosion, localized corrosion, galvanic corrosion, intergranular corrosion, stress-corrosion cracking, hydrogen damage, erosion-corrosion, and other selected forms of corrosion.

General Corrosion

Of the many forms of corrosion, general, or uniform, corrosion is the easiest to evaluate and monitor. Materials selection is usually straightforward. If a material shows only general attack, a low corrosion rate, and negligible contamination of the process fluid, and if all other factors, such as cost, availability, and ease of fabrication, are favorable, then that is the material of choice. An acceptable corrosion rate for a relatively low- cost material, such as plain carbon steel, is approximately 0.25 mm/year (10 mils/year) or less. At this rate and with proper design and adequate corrosion allowance, a carbon steel vessel will provide many years of low-maintenance service.

For more costly materials, such as the austenitic (300-series) stainless steels and the copper- and nickel-base alloys, a maximum corrosion rate of 0.1 mm/yr (4 mils/yr) is generally acceptable. However, it should never be assumed without proper evaluation that the higher the alloy, the better the corrosion resistance in a given environment. A good example is seawater, which corrodes plain carbon steel fairly uniformly at a rate of 0.1 to 0.2 mm/yr (4 to 8 mils/ yr) but severely pits certain austenitic stainless steels.

At times, nonmetallic coatings and linings ranging in thickness from a few tenths to several millimeters are applied to prolong the life of low-cost alloys, such as plain carbon steels, in environments that cause general corrosion. The thin-film coatings that are widely used include baked phenolics, catalyzed cross-linked epoxy-phenolics, and catalyzed coal tar/epoxy resins (see the article “Organic Coatings and Linings” in this Volume). It is advisable not to use thin- film coatings in services where the underlying base-metal corrosion rate exceeds 0.5 mm/yr (20 mils/yr), because corrosion is often accelerated at holidays (for example, pinholes) in the coating. Thick-film linings include glass, fiber-reinforced and flake-reinforced furan, polyester and epoxy resins, hot-applied coal tar enamels, and various elastomers, such as natural rubber.

A special case for materials selection under general corrosion conditions is that of contamination of the process fluid by even trace amounts of corrosion products. In this case, product purity, rather than corrosion rate, is the prime consideration. One example is storage of 93% sulfuric acid (H_2SO_4) in plain carbon steel at ambient temperature. The general corrosion rate is 0.25 mm/yr (10 mils/yr) or less, but traces of iron impart a color that

is objectionable in many applications. Therefore, thin-film baked phenolic coatings are used on carbon steel to minimize or eliminate iron contamination. In the same way, thin-film epoxy-coated carbon steel or solid or clad austenitic stainless steels are used to maintain the purity of adipic acid for various food and synthetic fiber applications. Taste concerns are noted from copper ions that taint butters and dairy products. More information on general corrosion is available in the Section “Forms of Corrosion” in this Volume.

Localized Corrosion.

General corrosion is relatively easy to evaluate and monitor. Localized corrosion in such forms as pitting, crevice corrosion, and weld- metal attack presents a challenge—materials selection is difficult. Localized corrosion is insidious and often results in failure or even total destruction of equipment without warning. All metals and alloy systems are susceptible to most forms of localized corrosion by specific environments. For example, carbon or alloy steel pipelines will pit in aggressive soils because of local concentrations of corrosive compounds, differential aeration cells, corrosive bacteria, stray direct currents, or other conditions. These pipelines generally require a combination of nonmetallic coatings and cathodic protection for long service life. Underground storage tanks (USTs) display similar damage for the same reasons (Fig. 2).

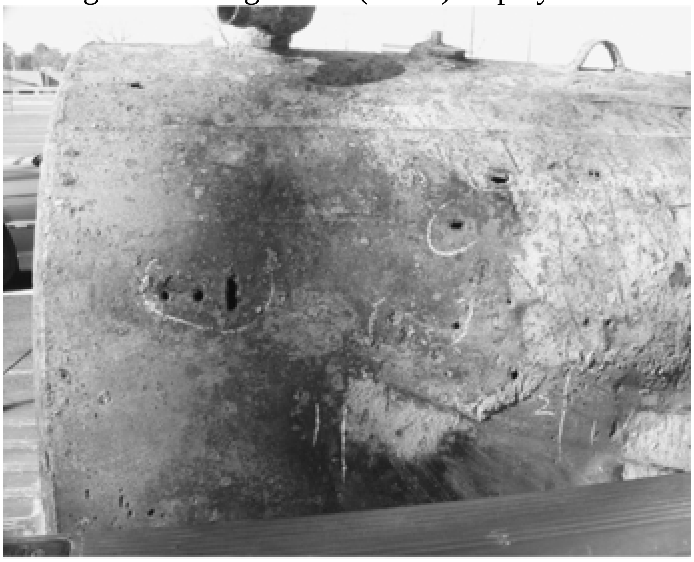

(a)

(b)

Fig. 2 (a) Pitting and underdeposit attack on underground storage tank. (b) Close-up view of area at left in (a)

Holidays in mill scale left on plain carbon steels are sites for pitting, because the mill scale is cathodic to the steel surface exposed at the holiday. For this reason, it is advisable to remove all mill scale by sand- or grit blasting before exposing plain carbon steels to corrosive environments.
Pitting. Aqueous solutions of chlorides, particularly oxidizing acid salts such as ferric and cupric chlorides, will cause pitting of a number of ferrous and nonferrous metals and alloys under a variety of conditions. The ferritic (400-series) and austenitic stainless steels are very susceptible to chloride pitting (as well as to crevice corrosion and SCC, which are discussed later in this section). Molybdenum as an alloying element is beneficial, and molybdenum-containing stainless steels, such as types 316 and 317, are more resistant than non-molybdenum-containing stainless steels. However, most chloride environments require higher alloys containing greater amounts of chromium and molybdenum, such as alloy G-3 (UNS N06985), alloy 625 (UNS N06625), and alloy C-22 (UNS N06022), for optimal corrosion performance (Ref 22). Exceptions are titanium and its alloys, which show exceptional resistance to aqueous chloride environments (including the oxidizing acid chlorides), and copper, copper-nickel, and nickel- copper alloys, which are widely used in marine applications.
Other noteworthy combinations of metals and corrosive fluids to avoid when selecting materials because of pitting tendencies include:

- Aluminum and aluminum alloys in electrolytes containing ions of heavy metals such as lead, copper, iron, and mercury
- Plain carbon and low-alloy steels in waters containing dissolved oxygen or in waters and soils infected with sulfur-reducing bacteria
- Austenitic stainless steel weldments exposed to stagnant natural waters, particularly certain well waters, which are infected with iron and/ or manganese bacteria (Ref 23)

An unusual form of localized corrosion known as end-grain attack has occurred in chemical-processing plants with specific metal-fluid combinations, such as austenitic stainless steels in hot nitric acid (HNO_3) and organic acids, and commercial-purity titanium in mixed-acid service.
When certain forms of these metals (for example, plates, threaded rods, or pipe nozzle ends) are cut normal to the rolling direction, the ends of nonmetallic inclusions at the cut edges are attacked by the process fluid. This results in small-diameter but deep pits. The solution is to seal the cut edge with a layer of weld metal that is equal to the base metal in composition.
Crevice corrosion can occur not only at metal-metal crevices, such as weld backing rings, but also at metal-nonmetallic crevices, such as nonmetal gasketed pipe flanges or under deposits. In some fabricated assemblies, it is possible and cost-effective to avoid crevices by careful design. For example, crevice corrosion occurred behind a weld backing strip at the closing seam in a type 304L stainless steel reactor handling hot HNO_3. A small amount of corrosion by stagnant acid in the crevice created hexavalent chromium ions (Cr^{6+}), which caused accelerated attack. Other exposed surfaces in the vessel were unaffected. To prevent crevice corrosion, the closing seam could have been welded from both sides or from one side with a consumable insert ring. Similar attack has occurred in stainless shell and tube heat exchangers at the rolled tube-to-tubesheet joints and has been solved by seal welding the joints with appropriate weld filler metal and process parameters.
In many cases, crevices are either too costly or impossible to design out of a system, so careful selection of materials is the answer. Titanium is susceptible to crevice corrosion in hot seawater and other hot aqueous chloride environments. Therefore, for a flanged and gasketed piping system in these fluids, commercially pure titanium grade 55 (UNS R50550) may be acceptable for piping, but flanges require the more crevice-attack-resistant grade 7 (UNS R52400), which contains 0.15% (nominal) Pd, or grade 12 (UNS 53400), which contains small amounts of molybdenum and nickel. This is more cost-effective than selecting the more expensive alloys for the piping as well. Another approach that has been successfully used in these fluids is installation of nickel-impregnated gaskets with grade 55 titanium flanges.
The austenitic stainless steels are susceptible to crevice corrosion in media other than HNO_3 solutions. For example, type 304L stainless steel exhibits borderline passivity in hot acetic acid solutions, particularly in crevices. Accordingly, the materials engineer will specify the more crevice-corrosion-resistant type 316L stainless steel where crevices cannot be avoided, such as piping and vessel flanges, or for the entire fabricated assembly, because the cost differential between materials in this case may be negligible.
Weld-metal preferential attack is another form of localized corrosion that can be avoided by the judicious selection of weld filler metal or weld process. Weld-metal corrosion in high nickel-chromium-molybdenum

alloy C-276 (UNS N10276) in a hot oxidizing H_2SO_4 process stream containing chlorides was eliminated by repair welding with alloy C-22 (UNS N06022). In applications in which type 304L stainless steel is selected for use in hot HNO_3 solutions, welds exposed to the process are frequently made by an inert gas process, such as gas tungsten arc or gas metal arc, rather than a flux-utilizing process, such as shielded metal arc. This prevents weld corrosion by eliminating the minute particles of trapped slag that are sites for initiation of local corrosion. Many other examples of preferential weld-metal attack and their solutions are discussed in the articles "Corrosion of Carbon Steel Weldments," "Corrosion of Stainless Steel Weldments," and "Corrosion of Nonferrous Alloy Weldments" in this Volume.

Nonmetallic materials of construction are widely used where temperatures, pressures, and stresses are not limiting and in such media as aqueous chloride solutions, which cause localized corrosion of metals and alloys. Examples in which lower-cost nonmetallic constructions are selected over expensive high alloys include the following:

- Rubber-lined steel for water treatment ion exchange resin beds, which must be periodically regenerated with salt brine or dilute mineral acids or caustic solutions
- Glass-lined steel for reaction vessels in chlorinated hydrocarbon service
- Acid-proof brick and membrane-lined steel for higher temperature, and solid RTP polyester and vinyl-ester construction for lower temperature, flue gas and chlorine neutralization scrubbers

It should be apparent that an in-depth evaluation of candidate materials for environments that can cause localized corrosion is imperative in order to select the optimal material of construction. In particular, corrosion test coupons should reflect the final fabricated component— that is, include crevices and weldments where applicable—and should be examined critically under the microscope for evidence of local attack. In cases in which the more common 300- and 400-series stainless steels fall short, the newer ferritics, such as 26Cr-1Mo (UNS S44627) and 27Cr-3Mo-2Ni (UNS S44660), the nickel-rich high-performance alloys with 3 to 6% Mo (UNS N08825, N06007) and without molybdenum (UNS N08800), and the duplex ferritic-austenitic alloys, such as 26Cr-1.5Ni- 4.5Mo (UNS S32900) and 26Cr-5Ni-2Cu- 3.3Mo (UNS S32550), should be evaluated as potentially lower-cost alternatives to higher alloys (Ref 22).

Finally, proven nonmetallic materials (for example, the RTPs), used either as linings for lower-cost metals (such as plain carbon steel) or for solid construction, should not be overlooked. Additional information on the mechanisms of localized corrosion is available in the articles "Pitting Corrosion," "Crevice Corrosion," and "Filiform Corrosion" in this Volume.

Galvanic Corrosion

Galvanic corrosion can be beneficial as well as harmful. The materials engineer will frequently select galvanic corrosion—that is, cathodic protection using sacrificial metal anodes or coatings of magnesium, zinc, or aluminum—to stifle existing, or prevent new, corrosion of structures fabricated primarily from plain carbon or low-alloy steels. Such structures include bridges, underground and underwater pipelines, auto frames, off-shore drilling rigs, and well casings. All too often, however, galvanic corrosion caused by contact between dissimilar metals in the same environment is harmful. Examples are:

- Unprotected underground plain carbon steel pipelines connected to above-ground tanks and other structures that are electrically grounded with buried copper rods or cables
- Stainless steel shafts in "canned" pumps rotating in carbon or graphite bushings in a strong electrolyte
- Copper-nickel or stainless steel heat-exchanger tubes rolled in plain carbon steel tubesheets exposed to river water for cooling
- Aluminum thermostat housings on cast iron auto engine blocks in contact with glycol-water mixtures

Newer designs that require several different metals for various reasons—such as cost and physical, mechanical, and/or electrical properties—present a challenge to the materials engineer with regard to selection for the avoidance of galvanic corrosion. Knowledge of the galvanic series of metals based on the electrochemical potential between a metal and a reference electrode in a given environment is essential. A practical galvanic series for metals and alloys in seawater is given in Table 1 (Ref 24).

Table 1 Practical galvanic series of metals and alloys in seawater

Least noble; most anodic; most susceptible to corrosion
Magnesium and its alloys
Zinc
Aluminum and its alloys
Cadmium
Plain carbon and low-alloy steels
Gray and ductile cast irons
Nickel cast irons
Type 410 stainless steel (active)
50Pb-50Sn solder
Type 304 and 316 stainless steels (active)
Lead
Tin
Muntz metal, manganese bronze, naval brass
Nickel (active)
Alloy 600 (active)
Yellow and red brasses, aluminum and silicon bronzes
Copper and copper-nickel alloys
Nickel (passive)
Alloy 600 (passive)
Alloy 400
Titanium
Type 304 and 316 stainless steels (passive)
Silver, gold, platinum
Most noble; most cathodic; least susceptible to corrosion

Source: Ref 24 (condensed and modified from the original to include the precious metals)

It is important to note that metals behave differently in different environments—the relative positions of metals and alloys in the galvanic series can vary significantly from one environment to another. In fact, variations within the same environment can occur with changes in such factors as temperature, solution concentration, degree of agitation or aeration, and metal surface condition. Thus, galvanic series that are based on seawater or other standard electrolytes are worthwhile for initial materials selection for multiple metal/alloy systems in a given environment. However, additional tests should be carried out in the stated environment by using the anodic polarization measurements described in ASTM G 5 (Ref 15). Suitable metal combinations can be determined by examining and superimposing polarization curves of candidate metals and by estimating the mixed potential values (Ref 13, 25).

In conclusion, the selection of dissimilar metals that are far apart on any galvanic series should be avoided unless provisions are made for sacrificial corrosion of one for another, as in cathodic protection. Otherwise, dissimilar-metal applications in corrosive environments should be approached with extreme caution and should be thoroughly investigated before making the final selections. The article “Galvanic Corrosion” in this Volume contains more information on galvanic attack.

Intergranular Corrosion

Intergranular corrosion is a selective form of corrosion that proceeds along individual grain boundaries, with the majority of the grain being unaffected. Intergranular corrosion can affect certain alloys that are highly resistant to general and localized attack. Particularly noteworthy are several of the 300- and 400-series stainless steels and austenitic higher-nickel alloys. These alloys are made susceptible to intergranular corrosion by sensitization, that is, the precipitation of chromium carbides and/or nitrides at grain boundaries during exposure to temperatures from 450 to 870 °C (840 to 1600 °F), with the maximum effect occurring near 675 °C (1250 °F). Exposure to such temperatures can occur during processing at the mill, welding and other fabrication operations, or by plant service conditions. The resulting depletion in chromium adjacent to the chromium-rich

carbides/nitrides provides a selective path for intergranular corrosion by specific media, such as hot oxidizing (nitric, chromic) and hot organic (acetic, formic) acids.
Susceptible stainless steels are those with normal carbon contents (generally >0.04%) without carbide-stabilizing elements (titanium and niobium). Examples are AISI types 302, 304, 309, 310, 316, 317, 430, and 446. Susceptible higher- nickel alloys include alloy 600 (UNS N06600), alloy 601 (UNS N06601), alloy 800 (UNS N08800) (despite the presence of titanium), alloy 800H (UNS N08810), alloy 200 (UNS N02200), alloy B (UNS N10001), and alloy C (UNS N10002). Intergranular corrosion in these alloys is avoided by one or more of the following:

- Keeping the alloy in the solution heat treated condition at all times
- Limiting interstitial elements, primarily carbon and nitrogen, to the lowest practical levels
- Adding carbide-stabilizing elements, such as titanium, niobium, and tantalum, along with a stabilizing heat treatment where necessary

In general, these alloys are purchased from the mill in the solution heat treated condition, a requirement of most specifications. With regard to the austenitic stainless steels, solution heat treating consists of heating to a minimum temperature of 1040 °C (1905 °F) to dissolve all the carbides, followed by rapid cooling in water or air to prevent sensitization.
Preserving the solution-treated condition is difficult, except for certain applications where reheating is not a requirement of fabrication. One example is a pump shaft machined from forged or rolled and solution heat treated bar stock. However, most applications for these alloys, such as piping components and pressure vessels, require hot rolling (for example, of plate) or hot bending (for example, of pipe) and welding; these practices, as discussed earlier, can cause sensitization. Solution heat treating after fabrication is generally impractical because of the possibility of irreparable damage due to distortion or excessive scaling or because of the inability to cool rapidly enough through the critical sensitization temperature range.
In most applications involving exposure to environments that cause intergranular corrosion, the low-carbon/nitrogen or stabilized alloy grades are specified. The new ferritic stainless steel UNS S44800 with 0.025% C (maximum) plus nitrogen is replacing the higher-carbon 446 grade in applications in which resistance to intergranular corrosion is a requirement. Types 304L, 316L, and 317L, with carbon and nitrogen contents limited to 0.03% (maximum) and 0.10% (maximum), respectively, are used instead of their higher-carbon counterparts. The newer nickel-chromium alloy 904L (UNS N08904), with 0.02% maximum carbon, and the high-nickel alloys C-22 (UNS N06022) and B-2 (UNS N10665), which have maximum carbon contents of 0.015% and 0.01%, respectively, are now being used almost exclusively in the as- welded condition without intergranular corrosion problems.
These low carbon levels are readily and economically achieved with the advent of the argon oxygen decarburization (AOD) refining process used by most alloy producers. By limiting the interstitial element content, sensitization is limited or avoided entirely during subsequent welding and other reheating operations. However, designers should be aware of the fact that lowering the carbon/nitrogen content also lowers the maximum allowable design stresses, as noted in appropriate sections of applicable fabrication codes, such as ASME section 8, division 1 for unfired pressure vessels and ANSI B31.3 for process piping.
Commercially pure alloy 200 is a special case. With a maximum carbon content of 0.15%, alloy 200 will precipitate elemental carbon or graphite in the grain boundaries when heated in the range of 315 to 760 °C (600 to 1400 °F). This results in embrittlement and susceptibility to intergranular corrosion in certain environments, such as high-temperature caustic. Where embrittlement and intergranular corrosion must be avoided, alloy 201 (UNS N02201), with a maximum carbon content of 0.02%, is specified.
Titanium as a carbide-stabilizing element is used in several ferritic and austenitic stainless steels, including types 409, 439, 316Ti, and 321, as well as the higher-nickel alloy 825 (UNS N08825), at a minimum concentration of approximately five times the carbon plus nitrogen content. In the same way, niobium, generally with tantalum, is used in types 309Cb, 310Cb, and 347 austenitic stainless steels at a minimum combined concentration of approximately ten times the carbon content. The higher-nickel alloys 20Cb-3, alloy 625, and alloy G contain even higher concentrations of niobium—up to a maximum of approximately 4% in the case of alloy 625. In general, when stabilized alloys are heated in the sensitizing temperature range, chromium depletion at the grain boundaries does not occur, because the stabilizing elements have a greater affinity for carbon than does chromium.

Under certain conditions, however, stabilized alloys will sensitize, especially during multi- pass welding or cross welding. They are also susceptible to a highly localized form of intergranular corrosion known as knife-line attack, which occurs in the base metal at the weld fusion line. In some cases, these alloys are given stabilizing heat treatments after solution heat treatment for maximum resistance to intergranular corrosion in the as-welded condition. For example, type 321 stainless steel is stabilize annealed at 900 °C (1650 °F) for 2 h, and alloys 825 and 20Cb-3 at 940 °C (1725 °F) for 1 h, before fabrication to avoid sensitization and knife-line attack. So treated, type 321 may still be susceptible, because titanium has a tendency to form an oxide during welding. As a result, its role as a carbide stabilizer may be diminished. For this reason, type 321 is always welded with a niobium-stabilized weld filler metal, such as type 347 stainless.

Some specialty alloys have low interstitial element content plus the addition of stabilizing elements for resistance to intergranular corrosion. These alloys include the higher-nickel alloy G-3 (UNS N06985), which contains 0.015% C (maximum) and niobium plus tantalum up to 0.5%, and the newer ferritic stainless steels (Ref 3, 22, 26, 27) listed as follows:

UNS No.	Common name	Content, %					
		Cr	**Ni**	**Mo**	**C (max)**	**N (max)**	**Other (max)**
S44627	…	26	…	1	0.01	0.015	0.2 Nb
S44635	Nu Monit	25	4	4	0.025	0.035	0.80 Ti+Nb
S44660	Sea Cure	26	2	3	0.03	0.04	1.0 Ti+Nb
S44735	AL 29-4C	29	0.5	4	0.03	0.045	1.0 Ti+Nb

The newer ferritic stainless steels were developed primarily for heat-exchanger tubing applications for use in place of the higher-carbon unstabilized type 446 stainless steel (UNS S44600). These ferritic stainless steels have many useful properties.

As discussed previously, specific corrosion environments cause intergranular corrosion in specific metal and alloy systems. A wealth of information, both published (Ref 28) and unpublished, has been developed on corrodents that cause intergranular corrosion in sensitized austenitic stainless steels; a partial listing appears in Table 2. The low-carbon/nitrogen or stabilized grades are specified for applications in which the austenitic steels have satisfactory general and localized corrosion resistance in these environments and in which sensitization by such operations as welding and hot forming will undoubtedly occur.

Table 2 Partial listing of environments known to cause intergranular corrosion in sensitized austenitic stainless steels

Environment	Concentration, %	Temperature, °C (°F)
Nitric acid	1	Boiling
	10	Boiling
	30	Boiling
	65	60 (140) to boiling
	90	Room to boiling
	98	Room to boiling
Lactic acid	50–85	Boiling
Sulfuric acid	30	Room
	95	Room
Acetic acid	99.5	Boiling
Formic acid	90	Boiling
	10 (plus Fe^{3+})	Boiling
Chromic acid	10	Boiling
Oxalic acid	10 (plus Fe^{3+})	Boiling
Phosphoric acid	60–85	Boiling
Hydrofluoric acid	2 (plus Fe^{3+})	77 (170)
Ferric chloride	5	Boiling
	25	Room
Acetic acid/anhydride mixture	Unknown	100–110 (212–230)
Maleic anhydride	Unknown	60 (140)

Cornstarch slurry, pH 1.5	Unknown	49 (120)
Seawater	…	Room
Sugar liquor, pH 7	66–67	75 (167)
Phthalic anhydride (crude)	Unknown	232 (450)

Evaluation tests for intergranular corrosion are conducted to determine if purchased materials have the correct chemical composition and are in the properly heat treated condition to resist intergranular corrosion in service (Ref 29). Evaluation testing is imperative for a number of reasons:

- The stainless steels and nickel-base alloys to which these tests are applied are relatively expensive.
- These materials are frequently specified for critical applications in the petrochemical, process, and power industries.
- The principal cost associated with a corrosion failure is generally that of production loss, not replacement.
- For maximum cost-effectiveness, these materials should be used in their best possible metallurgical and corrosion-resistant conditions.

Most of the evaluation tests are described in detail in ASTM standards (Ref 13, 15, 16, 17). Appropriate evaluation tests and acceptance criteria for wrought alloys are listed in Table 1 in the article “Evaluating Intergranular Corrosion” in this Volume.

Intergranular corrosion is rare in nonsensitized ferritic and austenitic stainless steels and nickel- base alloys, but one environment known to be an exception is boiling HNO_3 containing an oxidizing ion such as dichromate (Ref 30), vanadate, and/or cupric. Intergranular corrosion has also occurred in low-carbon, stabilized and/or properly solution heat treated alloys cast in resin sand molds (Ref 31). Carbon pickup on the surface of the castings from metal-resin reactions has resulted in severe intergranular corrosion in certain environments. Susceptibility goes undetected in the evaluation tests mentioned previously, because test samples obtained from castings generally have the carbon-rich layers removed. This problem is avoided by casting these alloys in ceramic noncarbonaceous molds.

Other metals, such as magnesium, aluminum, lead, zinc, copper, and certain alloys, are susceptible to intergranular corrosion under very specific conditions. A copper pipe that ostensibly conveyed grade 2 fuel oil from an UST to a furnace displayed intergranular attack (Fig. 3); the mechanism is not properly understood. Very few case histories are reported in the literature.

(a)

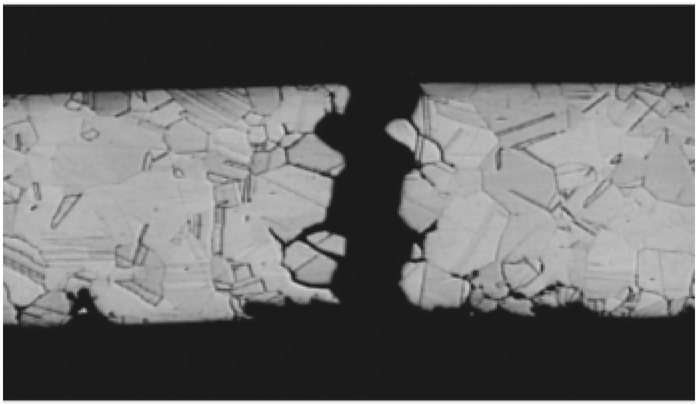
(b)

Fig. 3 (a) Intergranular cracking in 9.5 mm ($\frac{3}{8}$ in.) diameter copper pipe that conveyed No. 2 fuel oil from an underground storage tank. (b) Micrograph of intergranular crack. Dichromate etch. 63×

An unusual form of intergranular corrosion known as exfoliation, which occurs in aluminum-copper alloys, is discussed in the section "Exfoliation" in this article. Intergranular SCC is discussed in the following section.

Stress-Corrosion Cracking

Stress-corrosion cracking is a type of environmental cracking caused by the simultaneous action of a corrodent and sustained tensile stress. The following discussion deals primarily with anodic SCC. Anodic SCC is believed to be a delayed cracking phenomenon that occurs in normally ductile materials under the stress resulting from accelerated electrochemical corrosion at anodic sites of the material as well as at the crack tip. Other types of environmental cracking, such as hydrogen stress cracking and liquid metal embrittlement, are discussed later in this article.

Table 3 condenses several sources of published data on corrodents known to cause SCC in various metal-alloy systems (Ref 6, 32, 33). These data cover the SCC environments of major importance to the materials engineer. This table, as well as other data published in the literature, should be used only as a guide for screening candidate materials for further in-depth investigation, testing, and evaluation.

Table 3 Some environment-alloy combinations known to result in stress-corrosion cracking

Environment	Alloy system								
	Aluminum alloys	Carbon steels	Copper alloys	Nickel alloys	Stainless steels			Titanium alloys	Zirconium alloys
					Austenitic	Duplex	Martensitic		
Amines, aqueous	…	•	•	…	…	…	…	…	…
Ammonia, anhydrous	…	•	…	…	…	…	…	…	…
Ammonia, aqueous	…	…	•	…	…	…	…	…	…
Bromine	…	…	…	…	…	…	…	…	•
Carbonates, aqueous	…	•	…	…	…	…	…	…	…
Carbon monoxide, carbon dioxide, water mixture	…	•	…	…	…	…	…	…	…
Chlorides, aqueous	•	…	…	•	•	•	…	…	•
Chlorides, concentrated, boiling	…	…	…	•	•	•	…	…	…
Chlorides, dry, hot	…	…	…	•	…	…	…	•	…
Chlorinated solvents	…	…	…	…	…	…	…	•	•
Cyanides, aqueous, acidified	…	•	…	…	…	…	…	…	…
Fluorides, aqueous	…	…	…	•	…	…	…	…	…
Hydrochloric acid	…	…	…	…	…	…	…	•	…
Hydrofluoric acid	…	…	…	•	…	…	…	…	…
Hydroxides, aqueous	…	•	…	…	•	•	•	…	…
Hydroxides, concentrated, hot	…	…	…	•	•	•	•	…	…
Methanol plus halides	…	…	…	…	…	…	…	•	•
Nitrates, aqueous	…	•	•	…	…	…	•	…	…
Nitric acid, concentrated	…	…	…	…	…	…	…	…	•
Nitric acid, fuming	…	…	…	…	…	…	…	•	…
Nitrites, aqueous	…	…	•	…	…	…	…	…	…
Nitrogen tetroxide	…	…	…	…	…	…	…	•	…
Polythionic acids	…	…	…	•	•	…	…	…	…
Steam	…	…	•	…	…	…	…	…	…
Sulfides plus chlorides, aqueous	…	…	…	…	•	•	•	…	…
Sulfurous acid	…	…	…	…	•	…	…	…	…
Water, high-purity, hot	•	…	…	•	…	…	…	…	…

Stress-corrosion cracking is not a certainty in the listed environments under all conditions. Metals and alloys that are indicated as being susceptible can give good service under specific conditions. For example, referring to Table 3:

- Anhydrous ammonia will cause SCC in carbon steels but rarely at temperatures below 0 °C (32 °F) and only when such impurities as air or oxygen are present; addition of a minimum of 0.2% H_2O will inhibit SCC.
- Aqueous fluorides and hydrofluoric acid (HF) primarily affect alloy 400 (UNS N04400) in the nickel alloys system; other nickel alloys are resistant.
- Steam is known to cause SCC only in aluminum bronzes and silicon bronzes in the copper alloys system.
- Polythionic acid only cracks sensitized austenitic stainless steels and nickel alloys; SCC is avoided by solution annealing heat treatments or selection of stabilized or low-carbon alloys.

Stress-corrosion cracking is often sudden and unpredictable, occurring after as little as a few hours exposure or after months or even years of satisfactory service. Cracking occurs frequently in the absence of other forms of corrosion, such as general attack or crevice attack. Virtually all alloy systems are susceptible to SCC by a specific corrodent under a specific set of conditions, that is, concentration, temperature, stress level, and so on. Only the ferritic stainless steels as a class are resistant to many of the environments that cause SCC in other alloy systems, but they are susceptible to other forms of corrosion by some of these environments.

SCC of Stainless Steels. The combination of aqueous chlorides and austenitic stainless steels is probably the most important from the standpoints of prevalence, economics, and investigation. Although the mechanism and boundary conditions for chloride SCC are still not fully defined, it is reasonably safe to state that chloride SCC of austenitic stainless steels:

- Seldom occurs at metal temperatures below 60 °C (140 °F) and above 200 °C (390 °F)
- Requires an aqueous environment containing dissolved air or oxygen or other oxidizing agent
- Occurs at very low tensile stress levels, such that stress-relieving heat treatments are seldom effective as a preventive measure
- Affects all the austenitic stainless steels approximately equally with regard to susceptibility, time to failure, and so on
- Is characterized by transgranular branchlike cracking, as seen under a metallurgical microscope

So many materials and environments are sources of chlorides that they are hard to avoid (Ref 32). Significant costs for repairs and replacements, as well as lost utility, have occurred through the years in the petrochemical industry as a result of chloride SCC:

- In water-cooled heat exchangers from chlorides in the cooling water
- Under thermal insulation allowed to deteriorate and become soaked with water that leached chlorides from the insulation
- Under chloride-bearing plastics, elastomers, and adhesives on tapes

In the case of shell and tube heat exchangers, in which chloride-bearing waters are used for cooling, a number of preventive measures are available. In vertical units with water on the shell side, cracking occurs most often at the external surfaces of the tubes under the top tubesheet (Ref 32). This is a dead space (air pocket) at which chlorides are allowed to concentrate by alternate wetting and drying of tubing surfaces. Adding vents to the top tubesheet sometimes alleviates this problem by eliminating the dead space and allowing complete water flooding of all tubing surfaces (Ref 32). See Fig. 4(f) in the article “Designing to Minimize Corrosion” in this Volume.

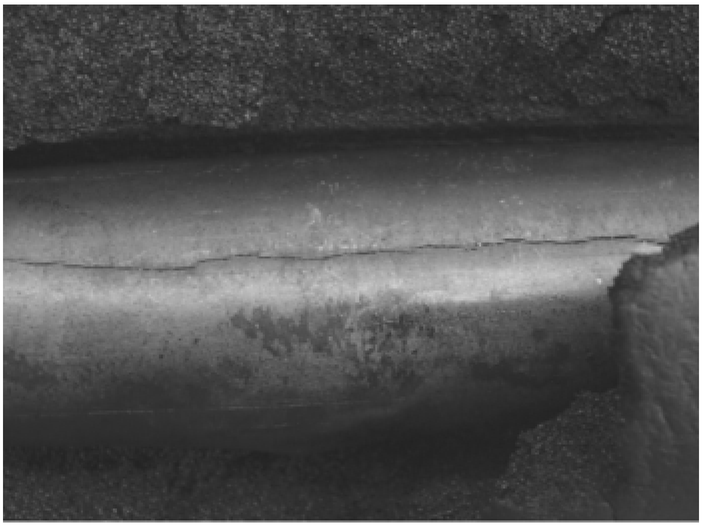

(a)

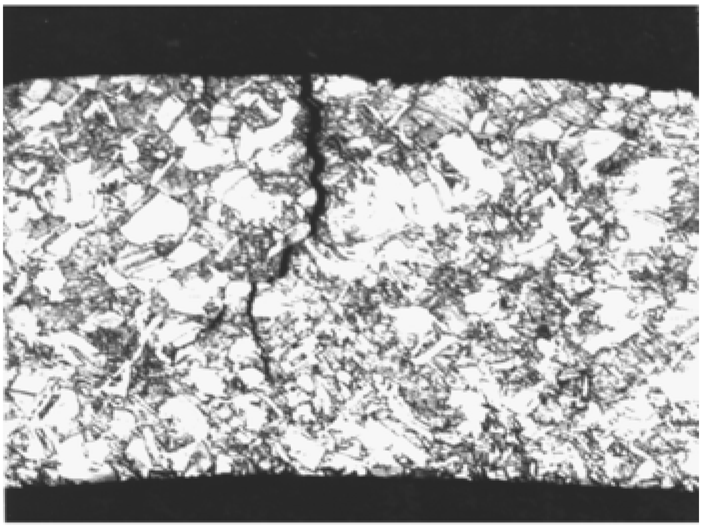

(b)

Fig. 4 (a) Stress-corrosion cracking of copper pipe under elastomeric insulation from an in-ground installation. (b) Micrograph of crack. Etched. 50×

However, in many cases, this approach results in only a nominal increase in time to failure or no benefit whatsoever because of other inherent deficiencies, such as low water flows or throttling water flow to control process temperatures. Thus, a material more resistant to chloride SCC is required, such as the austenitic higher-nickel alloys 800 (UNS N08800) and 825 (UNS N08825); alloy 600 (UNS N06600); ferritic stainless steels such as type 430 (UNS S43000), 26Cr-1Mo (UNS S44627), and SC-1 (UNS S44660); duplex stainless steels such as alloys 2205 (UNS S31803), 255 (Ferralium 255, UNS S32550), and 2507 (UNS S32750); AISI type 329 (UNS S32900); or titanium. In this case, selection depends primarily on economics, requiring the least expensive material that will resist process-side corrosion as well as water-side SCC.

Alloys are said to be either resistant or immune to chloride SCC, depending on how they perform in accelerated laboratory tests. In general, an alloy is immune if it passes the boiling 42% magnesium chloride test conducted according to ASTM G 36. Examples are alloy 600, 26Cr-1Mo, and grade 3 commercially pure titanium (UNS R50550). Industry has recognized the severity of this test and has devised other accelerated laboratory tests, such as boiling 25% sodium chloride and the Wick test (ASTM C 692), that are more representative of actual conditions in the field (Ref 34). Thus, alloys that fail the G 36 test but pass the C 692 test, such as alloy 800, alloy 2205 (UNS S31803), and 20 Mo6 (UNS N08026), typically provide many years of service as tubes in water-cooled heat exchangers. (The 300-series austenitic stainless steels, as a class, fail all the accelerated laboratory chloride SCC tests mentioned previously.)

Unfortunately, all of the immune and resistant alloys are more expensive than most of the austenitic stainless steels. A more cost-effective application of some of these alloys involves a procedure known as safe ending, in

which short lengths (for example, 0.3 to 0.6 m, or 12 to 24 in.) are butt welded to the austenitic stainless steel tubes. The SCC-resistant ends are positioned in the exchanger at the point of greatest exposure to SCC conditions, that is, under the top tubesheet. Safe-ended tubes have extended the life of austenitic stainless steel tubing severalfold, with only a nominal increase in cost. Of course, the dissimilar metals must be weld compatible; this eliminates the use of titanium for safe ending.

Another cost-effective answer to chloride SCC in heat exchangers is bimetallic tubing, in which the austenitic stainless steel required for process-side corrosion resistance is clad with a water-side SCC- and corrosion-resistant material such as 90Cu-10Ni (UNS C70600) (Ref 32). Still another answer is cathodic protection with a sacrificial metal coating such as lead containing 2% Sn and 2% Sb applied by hot dipping or flame spraying (Ref 32).

Chloride SCC under insulation can be prevented by keeping it dry, but this is easier said than done in many cases. It is particularly difficult in humid, high annual rainfall climates and where insulated equipment must be washed down periodically or is exposed to fire control deluge systems that are periodically activated (Ref 35). Under these conditions, three preventive measures are applied:

- *Addition of sodium metasilicate as a SCC inhibitor to the insulation:* At a minimum concentration of ten times the chloride content, the inhibitor is activated when the insulation becomes wet and is effective only when it wets the stainless steel surface. For maximum protection, metasilicate is painted on the vessel or piping before the installation of inhibited insulation. However, SCC has occurred after many years of service under inhibited insulation that was allowed to become so wet that the water-soluble inhibitor was leached out to a point below the minimum concentration required for prevention of SCC.
- *Protective coating of the vessel or piping before insulation:* Catalyzed high-build epoxy paints are effective to approximately 100 °C (212 °F), catalyzed coal tar/epoxy enamels to approximately 150 °C (300 °F), and silicone- base coatings to approximately 200 °C (390 °F). These coatings are even more effective if the stainless steel surfaces are heavily sandblasted before coating. Sandblasting peens the surface to a depth of 0.01 to 0.1 mm (0.4 to 4 mils), and this results in a layer under compressive stress that counteracts the tensile stresses required for SCC.
- *Cathodic protection of the vessel or piping with aluminum foil under insulation (Ref 36):* This method is claimed to provide both a physical barrier to chloride migration to stainless steel surfaces as well as cathodic protection when the insulation becomes wet, and it is effective at vessel temperatures between 60 and 500 °C (140 and 930 °F). However, the foil is attacked by the alkaline (generally) leachates from the insulation and must be renewed periodically.

Other important environments that cause SCC of stainless steels are hydroxide (caustic) solutions, sulfurous acid, and polythionic acids. Caustic SCC of austenitic stainless steels can be both transgranular and intergranular and is a function of solution concentration and temperature. It seldom occurs at temperatures below 120 °C (250 °F). At higher temperatures, the newer ferritic stainless steels, nickel, and high-nickel alloys provide outstanding service; 26Cr-1Mo stainless steel has found widespread application in heat-exchanger tube bundles serving caustic evaporators at 170 to 200 °C (340 to 390 °F). Nickel 200, nickel 201, and alloy 600 are resistant to 300 °C (570 °F) in caustic at concentrations up to 70% (Ref 11).

Polythionic acid and sulfurous acid will cause SCC in sensitized nonstabilized austenitic stainless steels and nickel-base alloys. Cracking is always intergranular and requires relatively low tensile stresses for initiation and propagation. As-welded, normal carbon grades, such as types 304 and 316 and alloy 800, are particularly susceptible to SCC in weld HAZs. Low-carbon (<0.03% C) and stabilized grades, such as types 321 and 347, are resistant, especially after receiving a stabilizing heat treatment. The normal carbon grades in the solution heat treated condition are also resistant. Susceptibility to polythionic acid SCC can be determined by laboratory corrosion testing according to ASTM G 35.

Polythionic acid and sulfurous acid SCC are major considerations in the petroleum-refining industry, especially in desulfurizer, hydrocracker, and reformer processes (Ref 32, 37). These acids form in process units during shutdowns when equipment and piping containing sulfide deposits and scales are opened and exposed to air and moisture. Preventive measures include flushing with alkaline solutions to neutralize sulfides before shutdown and purging with dry nitrogen during shutdown, according to recommended practices (Ref 38).

Cast austenitic stainless steels, such as Alloy Casting Institute (ACI) types CF-8 (UNS J92600) and CF-8M (UNS J92900), are inherently more resistant (but not immune) to chloride SCC than their wrought counterparts

(types 304 and 316, respectively) for several reasons. Castings generally have lower residual stresses than wrought alloys after solution-annealing heat treatments, and service-applied stresses are often lower because of heavy section thicknesses. However, the principal reason for improved SCC resistance is the presence of varying amounts of free ferrite, resulting in a duplex austenitic-ferritic microstructure. Free ferrite is primarily attributed to additions of 1 to 2% Si to improve fluidity during pouring and to resist hot cracking during cooling of the casting.

During development work on the duplex cast ACI alloy CD-4MCu (UNS J93370), researchers noted improved resistance to chloride SCC in cast alloys containing high ferrite. This confirmed similar observations in the field by materials engineers (Ref 39). A significant improvement in SCC resistance occurred with ferrite contents in the range 13 to 20 vol% and greater, which resulted in the development of alloys with ferrite content controlled by balancing chemical composition. Ferrite formation is promoted by chromium and by elements that act like chromium, such as silicon, niobium, and molybdenum. Nickel and elements that act like nickel (carbon, manganese, and nitrogen) retard ferrite formation. When specified, ferrite is typically controlled at the foundry by adjusting chromium toward the upper end of the specification range, and nickel toward the lower end, while establishing the desired silicon concentration.

Resistance to SCC in these alloys is believed to be a result of the keying action of ferrite particles (Ref 40). This action blocks direct propagation of SCC through the austenitic matrix. Along with this benefit, however, are improvements in strength, weldability, and resistance to general corrosion, particularly in hot concentrated nitric, acetic, phosphoric, and sulfuric acids and mixed nitric-hydrofluoric acid (Ref 40). Alloys produced with controlled ferrite content are recognized in ASTM A 351. Users are cautioned to limit applications to a maximum temperature of 425 °C (800 °F) because of the thermal instability of these grades.

A number of measures for preventing SCC of austenitic stainless steels have already been discussed. Two additional measures worthy of consideration are stress-relieving heat treatments and shot peening. The typical stress-relieving temperature for plain carbon steels (595 °C, or 1100 °F) is only slightly effective for the austenitic stainless steels, which require slow cooling from approximately 900 °C (1650 °F) for effective relief of residual stresses from operations such as welding. However, such treatments may not prevent but only prolong the time to failure, because chloride SCC of austenitic stainless steels can occur at very low stress levels. Also, the elevated temperatures required for stress relieving may cause unwanted distortion of complex and/or highly stressed structures and will sensitize susceptible alloys. This sensitization will result in intergranular corrosion or intergranular SCC.

Shot peening is the controlled bombardment of a metal surface with round, hard steel shot for the purpose of introducing compressive stresses in surface layers. These compressive stresses counteract the tensile stresses required for SCC. The depth of the resultant cold-worked layers is generally in the range of 0.1 to 0.5 mm (4 to 20 mils); 100% coverage is required. In laboratory tests in boiling 42% magnesium chloride, shot- peened type 304 stainless steel U-bend samples showed no SCC after more than 1000 h of exposure, but nonpeened control samples all cracked in approximately 1 h (Ref 41). Successful applications in the chemical-processing industries include a type 316 stainless steel centrifuge exposed to an organic chloride process stream (Ref 32) and numerous storage tanks exposed to a variety of SCC conditions (Ref 42).

The exposure of shot-peened surfaces to excessive temperatures or to environments that cause excessive general or pitting corrosion should be avoided. Temperatures above 565 °C (1050 °F) will relieve the beneficial compressive stresses and reduce the overall benefits of shot peening. Stress-corrosion cracking can occur once the relatively thin layers of residual compressive stress are penetrated by general corrosion or pitting.

SCC of Carbon and Alloy Steels. Plain carbon steels are susceptible to SCC by several corrodents of economic importance, including aqueous solutions of amines, carbonates, acidified cyanides, hydroxides, nitrates, and anhydrous ammonia. Susceptible steels in common use throughout the petrochemical-processing industry include ASTM A106 grade B for piping, A285 grade C for tanks, and A-515 grade 70 for pressure vessels. Cracking is both intergranular and transgranular; the former occurs in hot hydroxides and nitrates, and the latter in warm acidified cyanide solutions.

The temperature and concentration limits for the SCC susceptibility of carbon steels in caustic soda (sodium hydroxide) are fairly well defined; they have been derived from field experience and reproduced in chart form (Fig. 5). These limits for the other aqueous SCC environments mentioned previously are not nearly as well defined. For example, SCC was not considered to be a problem at temperatures below 88 °C (190 °F) in aqueous monoethanolamine and diethanolamine solutions used for scrubbing carbon dioxide and hydrogen sulfide out of natural gas and hydrogen-rich synthesis gas streams. However, recent experience in petroleum

refineries has resulted in general agreement that SCC preventive measures, such as thermal stress relief, must be applied to plain carbon steels used in aqueous amines at all temperatures and concentrations.

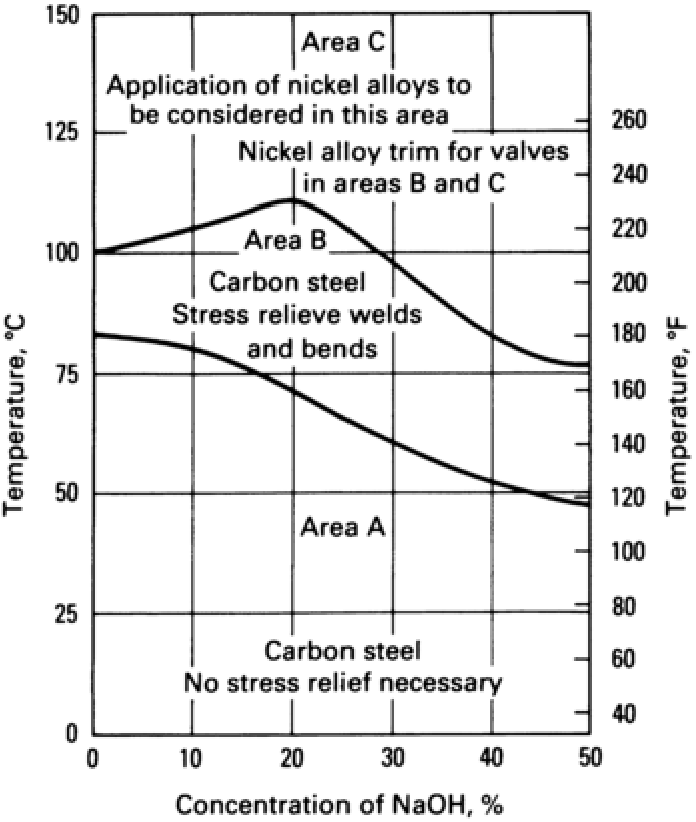

Fig. 5 Temperature and concentration limits for stress-corrosion cracking susceptibility of carbon steels in caustic soda. Source: Ref 6, 11

With regard to anhydrous ammonia, the SCC of plain carbon and low-alloy steels occurs at ambient temperatures when air or oxygen is present as a contaminant at concentrations of only a few parts per million (Ref 43). Most of the adverse experience has been with the non- stress-relieved higher-strength quenched-and-tempered steels, such as the grades covered in ASTM A 517. Cracking seldom occurs at temperatures below 0 °C (32 °F) and is virtually nonexistent at or below -33 °C (-28 °F), a common temperature for storage at atmospheric pressure. Water is an effective SCC inhibitor at a minimum concentration of 0.2% by weight.

Thermal stress relief is perhaps the single most effective measure for preventing, or at least greatly prolonging, the time to SCC of plain carbon and low-alloy steels in all of the environments mentioned previously. However, temperature is a more important factor than time at temperature. There is general agreement that stress-relieving temperatures below 595 °C (1100 °F), regardless of the hold time, are not effective for preventing SCC. In fact, the recommended minimum temperature for some environments, such as aqueous acidified cyanides, is 650 °C (1200 °F). As with any thermal treatment, special precautions must be observed, such as adequate support to avoid distortion and the removal of dirt, grease, and other foreign material that might react with the structure at elevated temperatures.

The previous comments on thermal stress relief apply to new carbon steel piping and vessels. Stress-corrosion cracking has been found in such vessels as horizontal pressure storage tanks (“bullets”) that were stress relieved after SCC was found in the original as-welded vessels and were repaired by grinding and welding (Ref 43). Undoubtedly, the stress-relieving temperatures propagated tiny cracks that were not detected during repairs.

SCC of Copper Alloys. Just as aqueous chloride is a potent SCC environment for austenitic stainless steels, aqueous ammonia causes extensive cracking in copper-base alloys. Virtually all copper alloys, as well as pure copper itself, can be made to crack in this environment.

The most susceptible alloys to SCC are the brasses containing more than 15% Zn, such as admiralty brass (UNS C44300, 28% Zn), yellow brass (UNS C27000, 34% Zn), and Muntz metal (UNS C28000, 40% Zn), followed by red brass (UNS C23000, 15% Zn) and several bronzes. The least susceptible alloys are 90Cu-10Ni (UNS C70600), 70Cu-30Ni (UNS C71500), and unalloyed copper.

The conditions that are conducive to SCC by aqueous ammonia are water, ammonia, air or oxygen, and tensile stress in the metal. Cracking is always intergranular, requires only trace quantities of ammonia in many cases, and occurs at ambient temperature. For example, U-bends in admiralty brass condenser tubes cracked in warm water from a cooling tower that contained 15 to 25 ppm ammonia because of close proximity to an ammonia plant. Other sources of ammonia include the decomposition of amines and the microbiological breakdown of organic matter. Stress-corrosion cracking failures in copper pipe under elastomeric insulation (Fig. 4) have been attributed to wet ammoniacal species (Ref 44); elastomeric insulation should not be used around buried (underground) pipes.

Thermal stress relief is generally not one of the better preventive measures, because ammoniacal SCC occurs at relatively low stress levels. In fairly mild ammoniacal environments, such as the cooling tower water system mentioned previously, the copper-nickel alloys, particularly 90Cu-10Ni, give good service. Small quantities of hydrogen sulfide have been found to inhibit SCC of brasses in petroleum refinery process streams, probably by reducing the dissolved oxygen content (Ref 32).

Another potent SCC environment for copper alloys is steam, but susceptibility is limited primarily to the higher-strength bronzes alloyed with aluminum (for example, UNS C61400) or silicon (for example, UNS C65500). In this regard, one noteworthy design to avoid is dimpled jacket construction. Severe SCC occurred at plug welds in a silicon bronze steam jacket on a similar alloy vessel used for heating a waste H_2SO_4 stream.

SCC of Aluminum Alloys. Stress-corrosion cracking of aluminum and its alloys in the chemical-processing industries is rare, because the lower-strength alloys in predominant use are resistant. These include the commercially pure alloy 1100 (UNS A91100), aluminum-manganese alloy 3003 (UNS A93003), and aluminum-magnesium alloys 5052 (UNS A95052) and 5083 (UNS A95083). Susceptible alloys are the high-strength grades of economic importance in the aircraft and aerospace industries, such as the aluminum-copper alloys 2014 (UNS A92014) and 2024 (UNS A92024) and the aluminum-copper- zinc-magnesium alloys 7075 (UNS A97075) and 7178 (UNS A97178). These alloys, heat treated to maximum strength levels, are susceptible to SCC in humid air containing traces of chlorides (Ref 45).

SCC of Titanium Alloys. Titanium (UNS R50550 and other unalloyed grades) has found increasing application in the chemical-processing industries, primarily as a replacement for austenitic stainless steels, because of outstanding resistance to corrosion by hot, concentrated oxidizing acids, such as HNO_3, and virtual immunity to pitting and SCC by hot aqueous chloride solutions. However, titanium and, to a greater extent, its higher-strength alloys (for example, Ti-6Al-4V, UNS R56400) are susceptible to SCC in a variety of environments, including anhydrous alcohols (methanol, ethanol) containing traces of halides, anhydrous red fuming HNO_3, anhydrous hot chlorides, some important industrial organic solvents (carbon tetrachloride, trichloroethane, and so on), anhydrous nitrogen tetroxide, and HCl.

In general, SCC preventive measures, such as thermal stress relief, cathodic protection, or inhibition, have not been used to any great extent with titanium and its alloys, although water additions are reported to inhibit cracking in anhydrous red fuming HNO_3, in methanol, and in anhydrous nitrogen tetroxide (Ref 46). Rather, SCC of titanium and its alloys is prevented by avoiding contact with specific cracking agents.

SCC of Zirconium Alloys. Zirconium (UNS R60702) and, to a greater extent, its alloys (for example, grade 705, UNS R60705) exhibit SCC behavior similar to that of titanium and its alloys in anhydrous alcohols containing traces of halides and in chlorinated organic solvents. Stress- corrosion cracking also occurs in aqueous ferric and cupric chloride solutions and hot concentrated HNO_3, especially when sustained tensile stresses are high. Because threshold stresses for SCC are high in comparison to yield strengths, thermal stress relief is a practical preventive measure. Holding temperatures between 650 and 850 °C (1200 and 1560 °F) are reported to be effective (Ref 32).

SCC of Nickel Alloys. As a class, nickel-base alloys are susceptible to SCC by a wide variety of corrodents. However, in most cases, the corrodents are specific to a few, but not all, of the alloys in this class. For example, sensitized alloys 800 (UNS N08800) and 600 (UNS N06600) crack in thiosulfate solutions and polythionic acids, but the stabilized alloys 825 (UNS N08825) and 625 (UNS N06625) are resistant. The latter alloys are particularly applicable in petrochemical process streams containing chlorides along with polythionic acids. In the nuclear power industry, alloy 600 and weld-metal alloys 82 (UNS N06082) and 182 (UNS W86182) crack intergranularly in crevices in high-purity water containing oxygen at elevated temperatures and pressures (Ref 47). In the absence of crevices, these alloys are resistant. Alloy 690 (UNS N06690) is resistant under all conditions.

Alloys 200 (UNS N02200), 201 (UNS N02201), 400 (UNS N04400), 600, 690 (UNS N06690), and 800 are susceptible to SCC in caustic solutions over a wide range of concentrations and at temperatures above 290 °C (550 °F) (Ref 11). Cracking is predominantly intergranular. The presence of oxygen and chlorides, which are common contaminants, tends to accelerate cracking, especially in alloy 600. Fairly high stress levels are generally required. Failures have occurred in steam generator tubes serving nuclear power plants from caustic concentrated on tube surfaces in crevices or as a result of a hot wall effect and/or poor water circulation. This experience prompted considerable research (Ref 48, 49, 50, 51). In general, alloys 200 and 201 and the nickel-chromium-iron alloys 690 and 600 appear to be the most resistant under the various conditions tested, although they are not immune to caustic SCC.

Other SCC environments of importance with regard to nickel-base alloys, especially alloy 400, are acidic fluoride solutions and HF. Alloy 400 is susceptible to SCC in cold-worked or as- welded conditions but is resistant in annealed or thermally stress-relieved conditions (Ref 52). Free air or oxygen accelerates corrosion rates and SCC tendency. However, alloy 400 has excellent general corrosion resistance over a broad range of temperatures and concentrations, so its use in HF alkylation units and other process streams containing HF or fluorides is widespread (Ref 53). Thermal stress relief at a minimum temperature of 540 °C (1000 °F), followed by slow cooling, will prevent SCC or will greatly prolong time to failure.

Environmental Cracking of Polymers. Corrosion-resistant polymers, such as thermoplastic and thermosetting resins, that are of interest to the materials engineer are susceptible to two forms of cracking in specific environments (Ref 54):

- Environmental stress cracking, which occurs when the polymer is stressed (residual or applied) and exposed to an organic solvent or aqueous solution of a wetting agent
- Craze cracking, which consists of a multitude of fine cracks that develop in contact with organic liquids or vapors, with or without the presence of mechanical stresses

For example, high-density polyethylene may crack in the presence of benzene or ethylene dichloride, and polystyrene may crack in the presence of aliphatic hydrocarbons (Ref 55). The mechanisms for these phenomena are not completely understood. Cracking may initiate at minute particles of low-molecular-weight polymers in the higher-molecular-weight polymer matrix. Thus, when evaluating polymers for corrosive service, test specimens should be stressed before exposure and should be carefully examined after exposure for evidence of environmental stress cracking and craze cracking.

Additional information on SCC is available in the article “Stress-Corrosion Cracking” in this Volume.

Hydrogen Damage

The entry of hydrogen into metals and alloys can result in several forms of damage:

- Loss of ductility and/or fracture strength
- Internal damage due to defect formation
- Sustained propagation of defects at stresses well below those required for mechanical fracture
- Macroscopic damage due to entrapment at mechanical interfaces

Although atomic, rather than molecular, hydrogen is the detrimental species within metals, it may be absorbed from a molecular hydrogen gas atmosphere. Hydrogen itself may be introduced during several stages of equipment or component manufacture (before any period of service). Heat treating of the metal (or alloy) in a hydrogen-containing furnace atmosphere, such as cracked ammonia, can result in absorption. Acid pickling, plating, and welding operations can each introduce hydrogen into the lattice of the metal.

Subsequent chemical service involving aqueous corrosion or high-temperature, hydrogen- containing environments may also introduce hydrogen. It is important to realize that many ductile metals and alloys, such as copper or austenitic stainless steels, will show a definite loss in ductility when exposed to environments that strongly promote the entry of nascent hydrogen (Ref 56).

Because iron-base alloys are principal materials of construction, these alloys have been the focus of most of the studies relating to hydrogen effects. In addition, ferritic (body-centered cubic, or bcc) steels have a particular

sensitivity to hydrogen. For these reasons, the present discussion focuses on hydrogen effects on steel. Such hydrogen effects have been thoroughly described in a review of hydrogen damage (Ref 57).

In ferrous alloys, embrittlement by hydrogen is generally restricted to those alloys having a hardness of 22 HRC or greater. However, other forms of hydrogen damage, such as hydrogen attack or hydrogen blistering, are associated with unhardened low-alloy or carbon steels.

As the result of hydrogen absorption, embrittlement of a metal or alloy may influence subsequent mechanical behavior without producing immediate and resolvable damage within the metal structure. In this respect, it is an insidious and somewhat reversible process, unlike hydrogen attack or blistering.

Hydrogen embrittlement may occur as a result of acid pickling, electroplating, and aqueous corrosion, which are electrochemical processes involving the discharge of hydrogen ions. The resulting nascent hydrogen is a chemisorbed species on the metal surface and, if not evolved as a molecular product, can enter the metal. This entry (or charging) of hydrogen has been described in detail (Ref 58). For the case of pure iron, introduction of hydrogen into the metal at high rates can produce irreversible effects (Ref 58). The solubility of hydrogen in the lattice is known to increase with applied tensile stress (Ref 59). Its solubility in metals obeys Sievert's law, with the concentration being directly proportional to the square root of the pressure (or fugacity). Within the lattice, hydrogen has been shown to interact with dislocations in iron (Ref 60, 61) and can thus affect subsequent plastic deformation.

In the case of pure titanium, as well as in alloys of titanium or zirconium, the entry of hydrogen can result in the formation of a hydride phase, thus reducing the ductility (Ref 56). A surface hydride phase has also been produced by hydrogen charging of nickel (Ref 62). An iron- chromium-nickel hydride has been proposed for austenitic stainless steel (Ref 63). Hydrogen charging of austenitic stainless steels is known to produce a martensite phase responsible for microcracking (Ref 64). Similar microcracks have been reported for cold-worked alloy 600 (Ref 65). Studies of hydrogen effects on aluminum alloys have not been conclusive (Ref 66).

It is known for the case of low-carbon steel that hydrogen absorption is enhanced by plastic deformation (Ref 67). This occurs up to 76% cold reduction, as shown in Fig. 6. However, the hydrogen permeation rate is increased by reductions of up to only 15% and is decreased by further plastic deformation (Ref 57). In the presence of an applied stress, the deleterious effect of hydrogen on delayed failure is increased by the triaxiality of the stress state, as shown in Fig. 7.

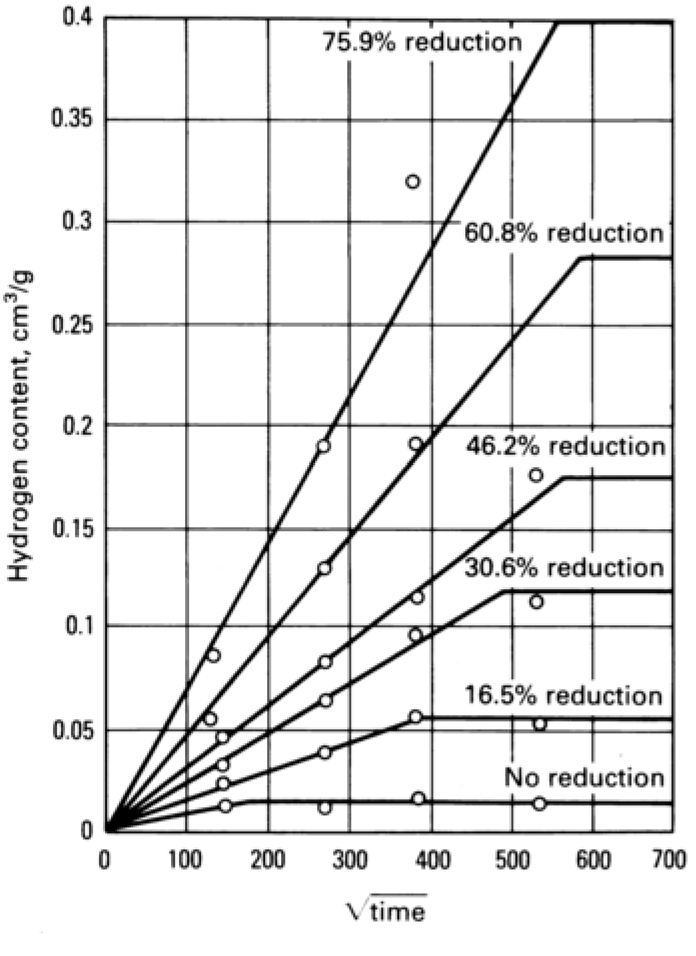

Fig. 6 Effect of cold reduction on rate of hydrogen absorption in carbon steel. Test performed on wire stock in 1 *N* H_2SO_4 at 35 °C (95 °F); original rod diameter was 13 mm ($\frac{1}{2}$ in.). Source: Ref 67

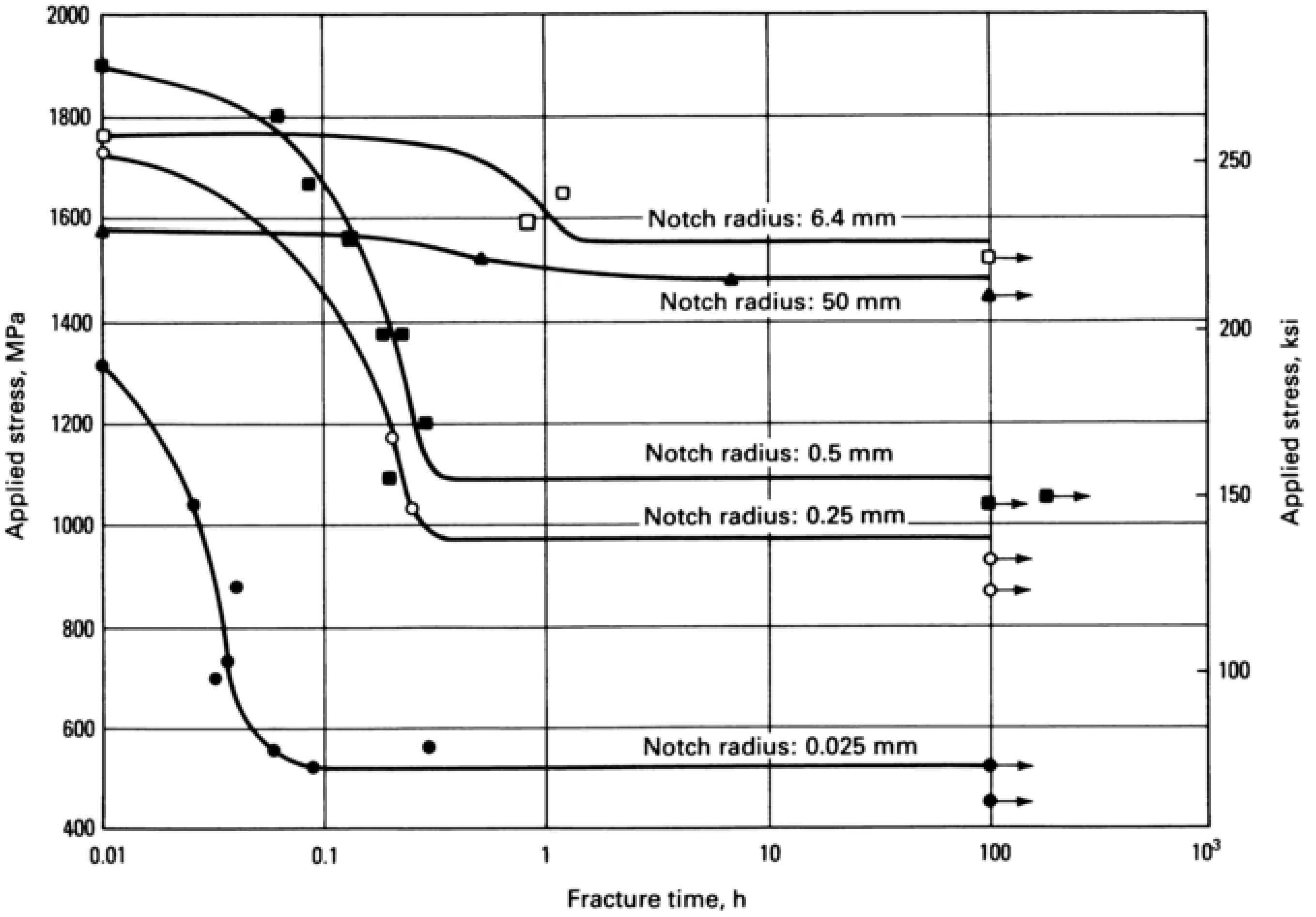

Fig. 7 Static fatigue curves for specimens of different notch sharpness. All specimens were baked for 30 min at 150 °C (300 °F). Source: Ref 68

For heat treated steels, sensitivity to hydrogen is a strong function of strength level. Figure 8 shows substantial embrittlement in a quenched- and-tempered steel with a tensile strength of 1860 MPa (270 ksi). The deleterious hydrogen content of 0.5 cm^3/100 g corresponds to approximately 1 hydrogen atom per 40,000 metal atoms (Ref 69). Other studies have shown substantial embrittlement of high-strength steels at hydrogen contents of 2 to 3 ppm (Ref 70, 71).

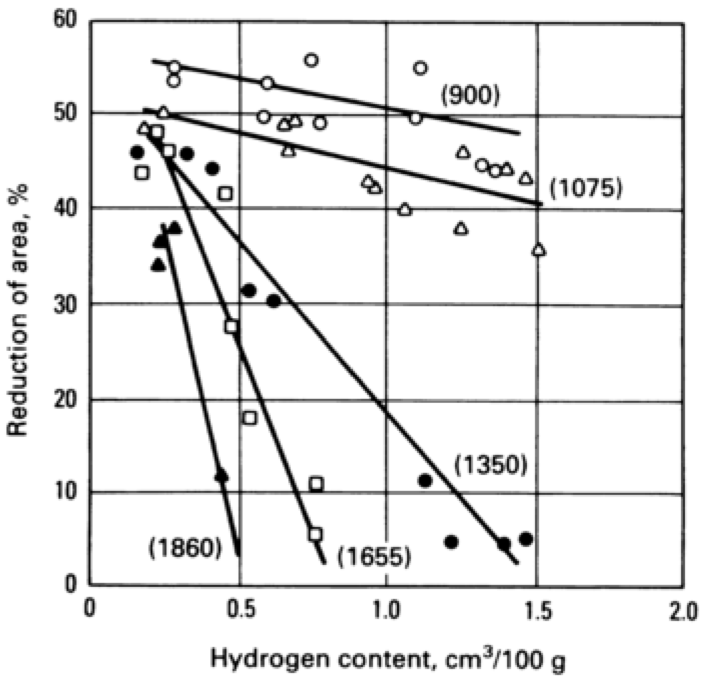

Fig. 8 Ductility (measured as percent reduction of area) versus hydrogen content for quenched-and-tempered steel at various strength levels. Ultimate tensile strength in megapascals is indicated in parentheses beside the curves. Source: Ref 69

The effects of temperature and strain rate on the embrittlement of carbon steel have been carefully studied (Ref 72). For a spheroidized AISI 1020 steel charged with hydrogen, the maximum embrittling effect appears to occur in the temperature range of -31 to 24 °C (-25 to 75 °F). Lower strain rates (5×10^{-2}/min) enhance embrittlement. Embrittlement is insignificant at higher strain rates of the order of 2×10^{4}/min. Figure 9 shows such an effect of strain rate. A similar effect of strain rate has been shown for nickel and for an iron-nickel alloy charged with hydrogen (Ref 73).

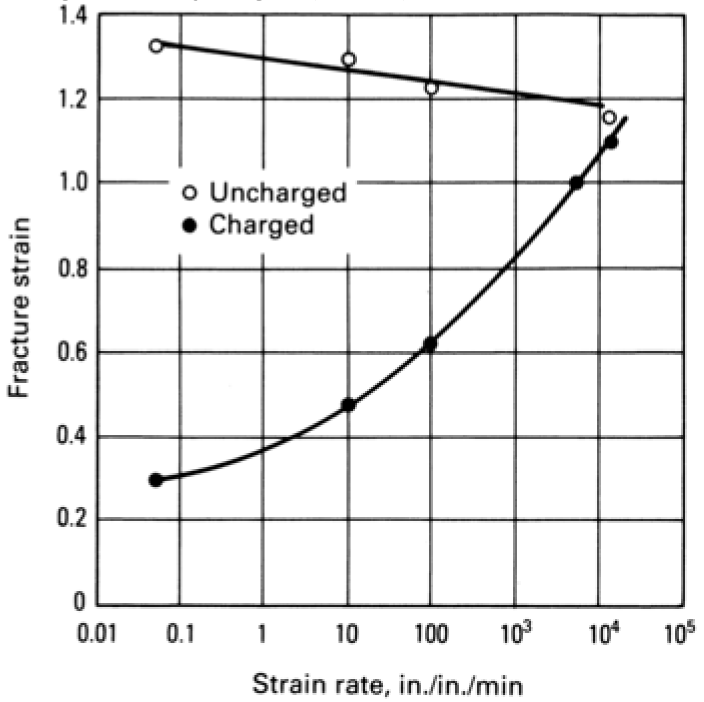

Fig. 9 Fracture strain as a function of strain rate in hydrogen-charged and uncharged 1020 steel (UNS G10200) at room temperature. Source: Ref 72

In aqueous systems, the entry of hydrogen is promoted by cathodic poisons that inhibit the recombination of adsorbed, discharged nascent hydrogen on the surface of the corroding metal. These poisons include cyanide and ionic species of sulfur, arsenic, selenium, bismuth, tellurium, phosphorus, iodine, and antimony.

Embrittlement by hydrogen-containing gas species may manifest itself in the stress-assisted propagation by preexisting surface defects (cracks). In the case of high-strength steels, such a phenomenon has been observed in H_2, H_2S, HCl, and HBr gas environments (Ref 74, 75, 76). A hydrogen sulfide (versus H_2) environment will result in a much higher crack velocity for the same steel, applied mechanical stress, and gas pressure (Ref 76).

One key to removing detrimental atomic hydrogen derives from its mobility at higher temperatures. A bake-out cycle, involving temperatures of 175 to 205 °C (350 to 400 °F), allows the diffusion and escape of hydrogen from the metal or alloy. If the hydrogen charging conditions were not severe enough to cause internal damage, the bake-out cycle described in Federal Specification QQC-320 restores full ductility.

In aqueous systems, the entry of hydrogen can be promoted by galvanic coupling to a more active metal. Therefore, cadmium or zinc platings containing defects or holidays can promote the hydrogen charging and embrittlement of susceptible metals or alloys. Such platings, or hot dip galvanizing, should be avoided in the case of low-alloy high-strength steels. As another example, titanium has been found to embrittle by hydriding when it is coupled with carbon steel in acidic environments or when it is exposed to moist environments after the application of a zinc chromate paint primer.

Susceptibility to hydrogen embrittlement is strongly influenced by the strength level of the metal or alloy. Wet hydrogen sulfide environments are considered to be among the most aggressive in promoting hydrogen entry. In such environments, common metals and alloys are qualified according to strength level and/or heat treatment in terms of their resistance to hydrogen-induced failure. These qualifications are summarized in NACE International standards MR-01-75, MR-01-76, and RP-04-75.

In general, iron-base alloys with a ferritic or martensitic structure are restricted to a maximum hardness of 22 HRC. Most other alloys are restricted to a maximum hardness of 35 HRC. There are exceptions in both cases. The procedures for materials testing in a wet hydrogen sulfide environment are discussed in NACE TM- 01-77.

Face-centered cubic (fcc) metals or alloys generally have more resistance to hydrogen embrittlement than those having a bcc lattice structure. However, cold work can increase the susceptibility of either structure. As a more direct effect of hydrogen entry, formation of a hydride phase can be expected to reduce the ductility of any metal or alloy.

In the pickling of steel, the level of hydrogen absorption is strongly affected by both the bath temperature and the nature of the acid (Fig. 10). Cathodic poisons have been ranked according to their effectiveness in increasing the permeation rate of hydrogen through low-carbon steel, as follows (Ref 78):

$$As > Se > Te > S > Bi \quad \text{(Eq 1)}$$

The role of sulfur as a poison is particularly important, because sulfur is commonly encountered and because the chemical form of the sulfur greatly influences its effectiveness as a hydrogen entry promoter. The susceptibility to embrittlement by hydrogen can be demonstrated by the relative resistance to cracking in such environments as wet hydrogen sulfide. In such tests, microstructure has a definite effect on susceptibility. In steels, untempered martensite is the most susceptible phase. Lamellar carbide structures are less desirable than those with spheroidized structures. Quenched-and-tempered microstructures are more resistant than those that have been normalized and tempered (Ref 79). For the same strength level in low-alloy steel, it has been shown that a bainitic structure is more resistant to hydrogen-assisted cracking than a quenched- and-tempered martensitic structure (Ref 80).

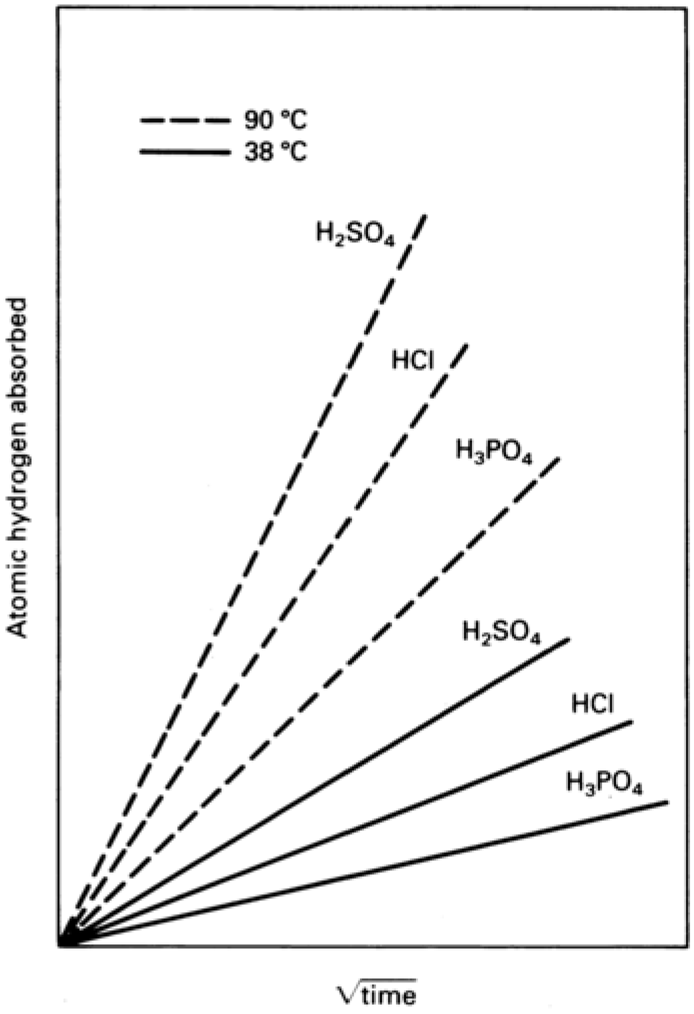

Fig. 10 Effect of anion and temperature on hydrogen absorption in a low-carbon steel. All acid concentrations were 2 *N*. Source: Ref 77

Embrittlement by gaseous hydrogen environments at ambient temperature has been effectively inhibited by the addition of 0.4 to 0.7 vol% oxygen (Ref 74). However, similar additions to a hydrogen sulfide gas environment did not halt the growth of cracks (Ref 81).

Because of the higher hydrogen solubility in the high-temperature fcc structure of iron (versus the low-temperature bcc structure), cooling of steel in hydrogen atmospheres from temperatures of the order of 1100 °C (2010 °F) can result in internal damage. Exceeding the solubility limit for hydrogen will result in the embrittlement of hydrogen-sensitive microstructures, such as martensite, formed by rapid cooling of some ferritic alloys. The internal precipitation of hydrogen is believed to be responsible for the generation of fissures, delaminations, or other defects. Such defects have been termed flakes, shatter cracks, fisheyes, or snowflakes. The defects are generally associated with hydrogen precipitation at voids, laminations, or inclusion-matrix interfaces already present in the steel. A reduced cooling rate, which allows hydrogen to be slowly released from the steel, is a general solution to the problem. Slower cooling will also inhibit the formation of hydrogen-sensitive microstructures.

Underbead cracking is an embrittlement phenomenon that is associated with absorption of hydrogen by molten metal during the welding process. Sources of hydrogen include moisture or organic contaminants on the surface of the prepared joint, moisture in low-hydrogen coated electrodes (such as E7018), moisture in flux- cored wire (such as M16), or a high-humidity environment. On rapid cooling of the weld, entrapped hydrogen can produce internal fissuring or other damage, as described earlier. In addition, the weld HAZ may contain the martensite phase in quench-hardenable alloys. The HAZ is then embrittled by high levels of entrapped hydrogen. Several steels have exhibited susceptibility to such embrittlement—for example, carbon steels containing 0.25 to 0.35 wt% C, low-alloy steels (such as AISI 4140 to 4340), and martensitic or precipitation-hardening stainless steels. Solutions to the hydrogen damage problems associated with welding include the use of dry welding electrodes,

proper cleaning and degreasing procedures for prepared weld joints, the use of an appropriate preheat before welding, and an adequate postweld heat treatment.

Welding electrodes should be kept dry by using a heated rod box. The electrodes should be removed only as needed. If they are moistened or exposed in the ambient atmosphere for prolonged periods, low-hydrogen coated electrodes must be heated at 370 to 425 °C (700 to 800 °F) to remove moisture (Ref 57). Recommended preheat temperatures for steels, as a function of steel composition, section thickness, and electrode type, have been published (Ref 82). Welding procedures for the avoidance of hydrogen cracking in carbon-manganese steels have also been published (Ref 83). Appropriate postweld heat treatments for steels can range from a hydrogen bake-out at 175 °C (350 °F) to a martensite tempering treatment at temperatures as high as 705 °C (1300 °F) (Ref 57).

Hydrogen attack is a damage mechanism that is associated with unhardened carbon and low-alloy steels exposed to hydrogen-containing environments at temperatures above 220 °C (430 °F) (Ref 57). Exposure to the environment is known to result in a direct chemical reaction with the carbon in the steel. The reaction occurs between absorbed hydrogen and the iron carbide phase, resulting in the formation of methane:

$$2H_2 + Fe_3C \rightarrow CH_4 + 3Fe \quad \text{(Eq 2)}$$

Unlike nascent hydrogen, the resulting methane gas does not dissolve in the iron lattice. Internal gas pressures develop, leading to the formation of voids, blisters, or cracks. The generated defects lower the strength and ductility of the steel. Because the carbide phase is a reactant in the mechanism, its absence in the vicinity of generated defects serves as direct evidence of the mechanism itself. The recommended service conditions (temperature, hydrogen pressure) for carbon and low-alloy steels are shown by the respective Nelson curves in Fig. 11. Chromium and molybdenum are beneficial alloying elements. This is most likely the result of their high affinity for carbon as well as the stability of their carbides. Hydrogen attack does not occur in austenitic stainless steels (Ref 57). In carbon or low- alloy steels, the extent of hydrogen attack is a function of exposure time.

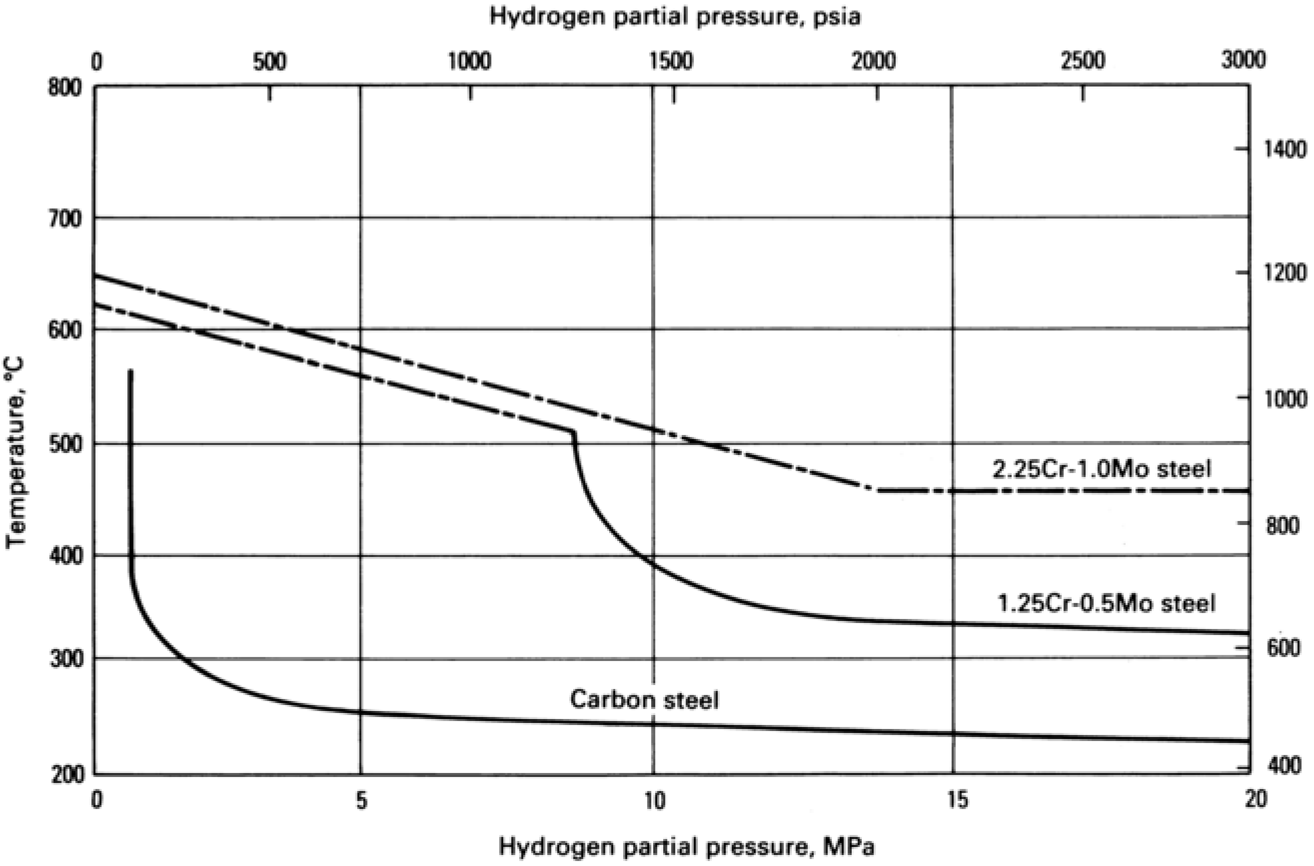

Fig. 11 Nelson curves showing operating limits for three steels in hydrogen service to avoid hydrogen attack. Dashed lines show limits for decarburization, not hydrogen attack. Source: Ref 57

Hydrogen blistering is a mechanism that involves hydrogen damage of unhardened steels near ambient temperature. It is known that the entry of atomic hydrogen into steel can result in its collection, as the molecular

species, at internal defects or interfaces. If the entry kinetics are substantial (promoted by an acidic environment, high corrosion rates, and cathodic poisons), the resulting internal pressure will cause internal separation (fissuring or blistering) of the steel. Such damage typically occurs at large, elongated inclusions and results in delaminations known as hydrogen blisters. Field experience indicates that fully killed steels are more susceptible than semikilled steels (Ref 84), but the nature and size of the original inclusions appear to be the key factors with regard to susceptibility. Rimmed steels or free-machining grades with high levels of sulfur or selenium would most likely show a high susceptibility to blistering. Stepwise cracking at the ends of blisters indicates an effect of elongated inclusions in the delamination process (Ref 57, 84). Similar stepwise cracking occurs in the hydrogen-induced failure of low-alloy pipeline steels (Ref 85). Both stepwise cracking and blistering appear to be limited to environments in which acidic corrosion occurs and in which cathodic poisons, such as sulfide, are present to promote hydrogen entry.

Solutions to the blistering problem include the use of low-sulfur calcium-treated argon-blown steels. Hot-rolled or annealed (as opposed to cold-rolled) steel is preferred (Ref 57). Silicon- killed steels are preferable to aluminum-killed steels. Also, treatment with synthetic slag or the addition of rare-earth metals can favor the formation of less detrimental globular sulfides (Ref 86). Ultrasonic inspection of the steel (according to ASTM E 114 and A 578) should be done before fabrication to detect laminations and other discontinuities that will promote blister formation. Equipment inspection and blister-venting procedures require unusual care (Ref 57). In services in which blistering can be expected, external support pads should not be continuously welded to the vessel itself; continuous welding of the support pads can cause hydrogen entrapment at the interface.

Examples of Hydrogen Damage. The permeation of hydrogen through ferritic steels can produce physical separation at mechanical joints. For example, bimetallic tubes, with a carbon steel inner liner, exhibited collapse of the liner due to its exposure to HF. Acid corrosion of the inside surface allowed nascent hydrogen to permeate the steel. Molecular hydrogen gas was formed, and trapped, at the interface with the outer tube section (brass). The accumulation of pressure was found to collapse the inner steel liners (Ref 57).

In high-temperature H_2/H_2S service, weld- overlaid 2.25Cr-1Mo steel (UNS K21590) was found to disbond at the weld interface (Ref 87). In this case, a weld overlay of type 309 stainless steel (UNS S30900), followed by type 347 stainless steel (UNS S34700), was applied. Hydrogen-induced cracking was found to occur in the transition zone below the weld metal after approximately $3\frac{1}{2}$ years of service. The disbonding was found to be more severe with higher cooling rates after hydrogen absorption. Outgassing treatments during the cool-down were found to prevent disbonding (Ref 88).

Figure 12 shows an example of hydrogen-assisted SCC failure of four AISI 4137 (UNS G41370) steel bolts having a hardness of 42 HRC. Although the normal service temperature (400 °C, or 750 °F) was too high for hydrogen embrittlement, the bolts were also subjected to extended shutdown periods at ambient temperatures. The corrosive environment contained trace hydrogen chloride and acetic acid vapors as well as calcium chloride if leaks occurred. The exact service life was unknown. The bolt surfaces showed extensive corrosion deposits. Cracks had initiated at both the thread roots and the fillet under the bolt head. Figure 12(b) shows a longitudinal section through the failed end of one bolt. Multiple, branched cracking was present, typical of hydrogen-assisted SCC in hardened steels. Chlorides were detected within the cracks and on the fracture surface. The failed bolts were replaced with 17-4PH stainless steel (UNS S17400) bolts (condition H1150M) having a hardness of 22 HRC (Ref 57).

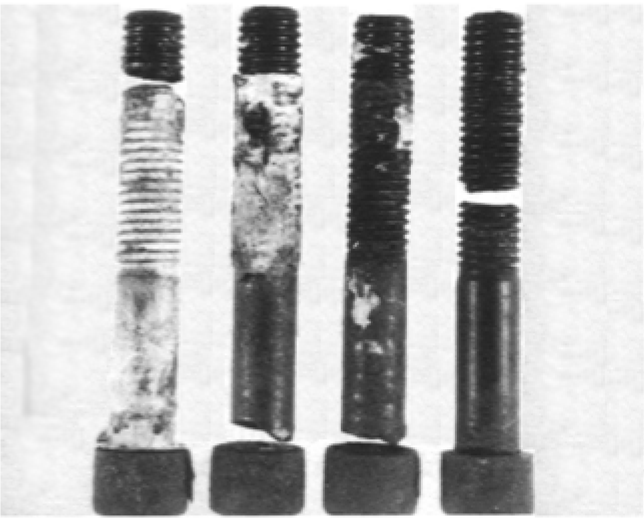

(a)

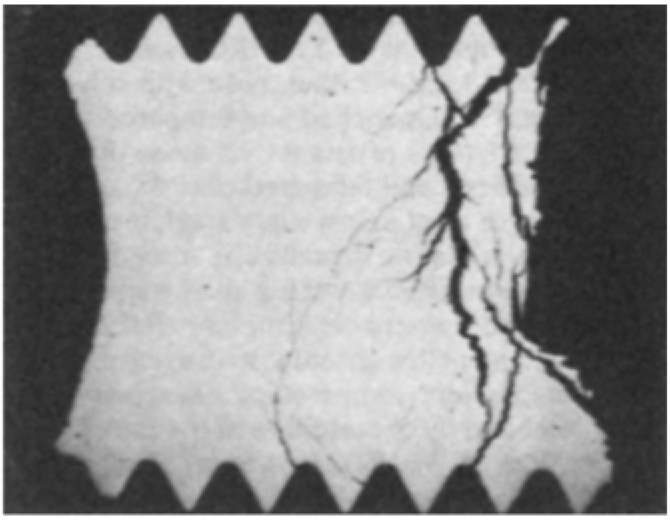

(b)

Fig. 12 4137 steel (UNS G41370) bolts (hardness, 42 HRC) that failed by hydrogen-assisted stress-corrosion cracking caused by acidic chlorides from a leaking polymer solution. (a) Overall view of failed bolts. (b) Longitudinal section through one of the failed bolts in (a) showing multiple, branched hydrogen-assisted stress-corrosion cracks initiating from the thread roots. Source: Ref 57

As an example of hydrogen attack, a section of plain carbon steel (0.22% C and 0.31% Si) had been mistakenly included as a part of a type 304 stainless steel (UNS S30400) hot-gas bypass line used to handle hydrogen-rich gas at 34 MPa (5000 psi) and 320 °C (610 °F). After 15 months of service, the steel pipe section ruptured, causing a serious fire. Figure 13 shows a section of the 44 mm (1.75 in.) Outside diameter pipe near the fracture. The pipe had been weakened by hydrogen attack through all but 0.8 mm ($\frac{1}{32}$ in.) of the 8 mm ($\frac{5}{16}$ in.) thick wall. As a result of the hydrogen attack and the internal methane formation, the microstructural damage consisted of holes or voids near the outer surface as well as interconnected grain-boundary fissures in a radial alignment near the inner surface (Fig. 13b). The radially aligned voids preceded both the circumferential crack and pipe rupture (Ref 57).

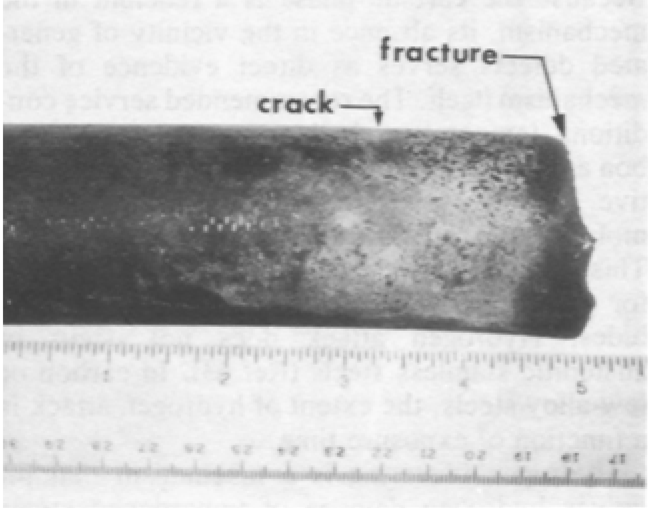

(a)

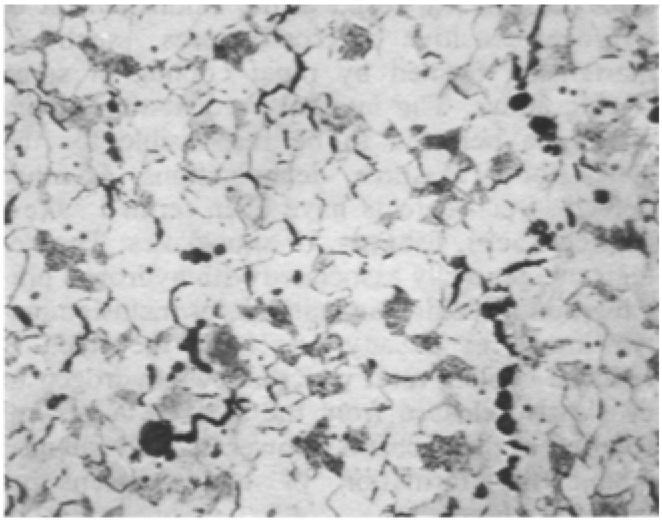

(b)

Fig. 13 Section of ASTM A106 carbon steel pipe with wall severely damaged by hydrogen attack. The pipe failed after 15 months of service in hydrogen-rich gas at 34.5 MPa (5000 psig) and 320 °C (610 °F). (a) Overall view of failed pipe section. (b) Microstructure of hydrogen-attacked pipe near the midwall. Hydrogen attack produced grain-boundary fissures that are radially aligned. Source: Ref 57

Hydrogen blistering is illustrated in Fig. 14, which shows a cross section of a 152 mm (6 in.) diameter blister that formed in the wall of a steel sphere. The sphere had been used to store anhydrous HF for 13.5 years at

ambient temperatures. The source of nascent hydrogen gas was the cathodic hydrogen generated by the corrosion reaction between the acid and the steel. The corrosion rate was less than 0.05 mm/yr (2 mils/ yr). Figure 14(b) shows the propagation of the blister, with the stepwise cracking (arrow) at its edge caused by the buildup of hydrogen pressure within the blister itself (Ref 57). More information on hydrogen attack is available in the article “Hydrogen Damage” in this Volume.

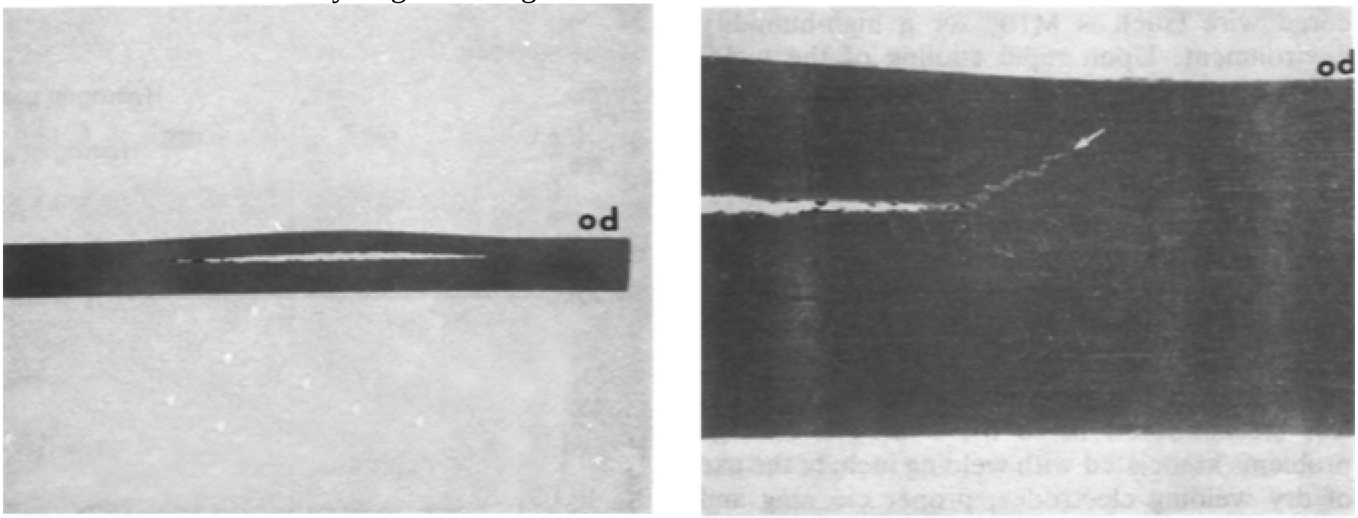

(a) (b)

Fig. 14 Hydrogen blister in 19 mm ($\frac{3}{4}$ in.) steel plate from a spherical tank used to store anhydrous HF for 13.5 years. (a) Cross section of 152 mm (6 in.) diameter blister. (b) Stepwise cracking (arrow) at edge of hydrogen blister shown in (a). Source: Ref 57

Erosion-corrosion

Erosion-corrosion is a frequently misinterpreted type of metal deterioration that results from the combined action of erosion and corrosion. Three types—liquid erosion-corrosion, cavitation, and fretting—are discussed. Abrasive wear, which is erosion without corrosion, also is discussed for comparison purposes.

Liquid erosion-corrosion is the accelerated wastage of a metal or material attributed to the flow of a liquid (Ref 89, 90, 91). Liquid erosion-corrosion damage is characterized by grooves, waves, gullies, rounded holes, and/or horseshoe- shaped grooves. Analysis of these marks can help determine the direction of flow. Most metals are susceptible to liquid erosion-corrosion under specific conditions. Carbon steels, for example, can be severely damaged by steam containing entrained water droplets. By contrast, the 300- series stainless steels at approximately the same hardness and strength level are very resistant to flowing wet steam. Virtually anything that is exposed to a moving liquid is susceptible to liquid erosion-corrosion. Examples include piping systems, particularly at bends, elbows, or wherever there is a change in flow direction or increase in turbulence; pumps; valves, especially flow control and pressure let-down valves; centrifuges; tubular heat exchangers; impellers; and turbine blades.

Surface films that form on some metals and alloys are very important in their ability to enhance resistance to liquid erosion-corrosion. Titanium is a reactive metal but is resistant to liquid erosion-corrosion in many environments because of its very stable titanium dioxide surface film. The 300-series stainless steels, as mentioned previously, are also resistant because of their stable passive surface films.

Both carbon steel and lead have relatively good resistance to certain concentrations of H_2SO_4 under low-to-moderate flow conditions. Both depend on a metal sulfate corrosion film for resistance; however, both fail fairly rapidly after removal of the sulfate film, even at low velocities.

Another example is the carbon steel and some low-alloy steels used to handle petroleum refinery fluids that contain hydrogen sulfide. At low velocities or under stagnant conditions, these materials are normally satisfactory because of the formation of a tenacious protective iron sulfide film. However, with increased velocity, the film is eroded away, followed by very rapid corrosion attack.

Velocity often increases attack, but it may also decrease attack, depending on the material of construction and the corrosive environment. For example, increasing the velocity causes accelerated attack of carbon steel in

steam condensate by increasing the supply of dissolved oxygen and/or carbon dioxide to the steel surface. In cooling water, however, increased velocity often reduces the attack of carbon steel by improving the effectiveness of inhibitors and by reducing deposits and pitting in stagnant areas.

Many 300-series stainless steels are subject to pitting and crevice corrosion in seawater. However, they may exhibit good corrosion resistance if the seawater is kept flowing at a minimum critical velocity. This prevents the formation of deposits and retards general corrosion, pitting, and crevice attack. Table 4 shows the effects different seawater velocities have on the liquid erosion-corrosion of various metals.

Table 4 Corrosion of metals and alloys in seawater as a function of velocity

Material	Typical corrosion rate, mg/dm^2/d		
	0.3 m/s (1 ft/s)[(a)]	**1.2 m/s (4 ft/s)[(b)]**	**8.2 m/s (27 ft/s)[(c)]**
Carbon steel	34	72	254
Cast iron	45	…	270
Silicon bronze	1	2	343
Admiralty brass	2	20	170
Hydraulic bronze	4	1	339
G bronze	7	2	280
10% aluminum bronze	5	…	236
Aluminum brass	2	…	105
90Cu-10Ni (0.8% Fe)	5	…	99
70Cu-30Ni (0.5% Fe)	<1	<1	39
Monel 400	<1	<1	4
Type 316 stainless steel	1	0	<1
Hastelloy C	<1	…	3
Titanium	0	…	0

(a) Immersed in tidal current.

(b) Immersed in seawater flume.

(c) Attached to immersed rotating disk. Source: International Nickel Company

Cavitation is a form of erosion-corrosion that is caused by the formation and collapse of vapor bubbles in a liquid against a metal surface (Ref 91, 92, 93, 94, 95). Cavitation occurs in hydraulic turbines, on pump impellers, on ship propellers, and on many surfaces in contact with high-velocity liquids subject to changes in pressure. Cavitation can occur if the pressure on a liquid is reduced sufficiently to cause boiling even at room temperature. Boiling produces bubbles that collapse on the high-pressure cycle. Rapidly collapsing vapor bubbles produce shock waves that have developed pressures as high as 414 MPa (60 ksi).

The appearance of cavitation (Fig. 15) is similar to pitting except that the surfaces in the cavitation pits are usually much rougher. Most investigators believe that cavitation damage is caused by a combination of corrosion and mechanical effects. Apparently, the collapsing vapor bubbles mechanically destroy the protective surface films. Thus, fresh surfaces are exposed to corrosion and the reestablishment of protective films, which is followed by more cavitation, and so on. Damage occurs when the cycle is allowed to repeat over and over again, for example, when a pump is operated, or “dead headed,” against a closed valve. Table 5 shows the relative cavitation resistance of a variety of metals and alloys in water and seawater.

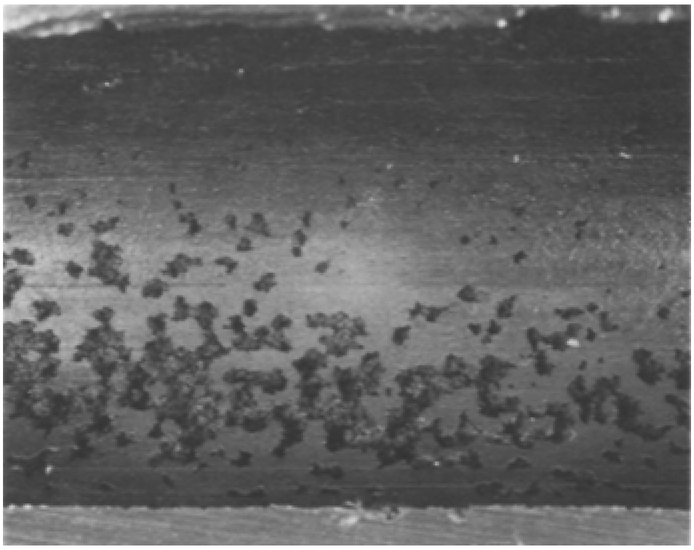

Fig. 15 Internal surface of carbon steel pipe section damaged by cavitation

Table 5 Resistance of metals and alloys to cavitation damage in vibratory testing at 25 °C (75 °F)

Metal or alloy	Product form	Composition, %	Weight loss for last 60 min of exposure, mg/h	
			Freshwater	**Seawater**
Ferrous				
Iron	Cast	Fe-3.1C-2.3Si-0.75Mn-0.12S-0.07P	50.1	80.9
Iron	Cast	Fe-3.4C-1.3Si-0.75Mn-0.25P-0.08S	69.8	115.3
Iron	Cast	Fe-3.4C-2.3Si-0.59Mn	89.7	100.2
Iron	Cast	Fe-3C-6Cu-4Cr-14.4Ni-1.9Si	41.6	51.4
Iron	Cast	Fe-3.3C-1.3Si-0.4Mo-0.51Mn	54.1	63.9
Iron	Cast	Fe-3C-6Cu-13.5Ni-2Cr-1.5Si-1Mn-0.1S-0.04P	85.3	95.3
Steel	Rolled	Fe-0.35C-0.45P-0.67Mn	34.2	39.6
Steel	Rolled	Fe-0.27C-0.4S-0.45P-0.48Mn	68.3	77.8
Steel	Rolled	Fe-0.2C-0.03S-0.02P-0.5Mn	78.2	82.4
Steel	Cast	Fe-0.37C-0.31Si-0.04S-0.04P-1.1Mn	44.8	53.6
Steel	Cast	Fe-0.26C-0.32Si-0.04S-0.04P-0.6Mn	72.9	80.9
Steel	Rolled	Fe-0.34C-1.18Ni-0.6Cr-0.52Mn-0.2Si-0.03S-0.02P	20.0	22.0
Steel	…	Fe-0.19C-2.2Ni-0.6Mn-0.02S-0.02P	61.3	64.0
Stainless steel	Rolled	Fe-17.2Cr-0.08C-0.57Si-0.47Mn-0.34Ni-0.02S-0.03P	11.8	10.8
Stainless steel	Rolled	Fe-12.2Cr-0.09C-0.38Si-0.43Mn-0.32Ni-0.02S-0.02P	20.6	23.0
Stainless steel	Cast	Fe-18Cr-10Ni-0.15C-0.5Si-0.5Mn	13.5	13.4
Stainless steel	Rolled	Fe-18.4Cr-8.7Ni-0.07C-0.37Si-0.48Mn-0.14S-0.19P	16.1	15.3
Nonferrous				
Bronze	Rolled	Cu-39Zn-1Sn	69.5	65.2
Brass	Rolled	Cu-40Zn	77.8	68.7
Brass	Rolled	Cu-15Zn	115.2	101.3
Brass	Rolled	Cu-10Zn	134.9	122.8
Bronze	Cast	Cu-10Al[(a)]	15.3	14.5

Bronze	Cast	Cu-11Sn-1.5Si	54.6	62.4
Bronze	Cast	Cu-10Sn-2Pb	60.4	48.5
Bronze	Cast	Cu-3.5Si[(a)]	42.6	40.4
Bronze	Cast	Cu-5Si-1Mn	52.4	54.5
Bronze	Forged	Cu-25Zn[(a)]	19.2	19.9
Bronze	Cast	Cu-40Zn-1Fe	53.0	55.4
Bronze	Cast	Cu-10Sn-2Zn	65.8	57.4
Nickel alloy	Cast	Ni-32.5Cu-4Si-2Fe	20.0	21.4
Nickel alloy	Drawn	Ni-29Cu-1Mn-1Fe	53.3	53.2
Copper-nickel	Rolled	Cu-30Ni	86.2	87.6

(a) 1.0% maximum present but not determined analytically. Source: Ref 96

Fretting is erosion-corrosion that occurs at the contact area between two metals under load and subject to slight relative movement by vibration or some other forces (Ref 97, 98, 99, 100). Damage begins with local adhesion between mating surfaces and progresses when adhered particles are ripped from a surface and react with air or other corrosive environment. Affected surfaces show pits or grooves with surrounding corrosion products. On ferrous metals, the corrosion product is usually a very fine, reddish iron oxide; on aluminum, it is usually black.

Fretting is detrimental not only because of the destruction of metallic surfaces but also because of a severe effect on the fatigue life. It has been shown that fretting can reduce the endurance limit of a metal by 50 to 70% (Ref 98).

The relative motion necessary to cause fretting is very small. Displacements as small as 10^{-8} cm (4×10^{-9} in.) have produced fretting. Fretting generally does not occur on contacting surfaces in continuous motion, such as ball or sleeve bearings.

Fretting can be minimized or eliminated, in many cases, by one or more of the following:

- Increasing the hardness of contacting surfaces. This may mean increasing the hardness of both or just one of the components. Surface-hardening treatments such as shot peening, nitriding, chrome plating, and carburizing are beneficial.
- Increasing the friction between the mating members by roughening or by plating (lead, copper, nickel, silver, gold)
- Applying phosphate coatings to exclude air or applying anaerobic sealants or adhesives to increase the tightness of the fit
- Increasing the fit interference, which reduces slippage by increasing the force on mating components
- Switching to materials with more fretting resistance, as shown in Table 6

Table 6 Relative fretting resistance of various material combinations

Combination	Fretting resistance
Aluminum on cast iron	Poor
Aluminum on stainless steel	Poor
Bakelite on cast iron	Poor
Cast iron on cast iron, with shellac coating	Poor
Cast iron on chromium plating	Poor
Cast iron on tin plating	Poor
Chromium plating on chromium plating	Poor
Hard tool steel on stainless steel	Poor
Laminated plastic on cast iron	Poor
Magnesium on cast iron	Poor
Brass on cast iron	Average
Cast iron on amalgamated copper plate	Average
Cast iron on cast iron	Average
Cast iron on cast iron, rough surface	Average
Cast iron on copper plating	Average

Cast iron on silver plating	Average
Copper on cast iron	Average
Magnesium on copper plating	Average
Zinc on cast iron	Average
Zirconium on zirconium	Average
Cast iron on cast iron with coating of rubber cement	Good
Cast iron on cast iron with Molykote lubricant	Good
Cast iron on cast iron with phosphate conversion coating	Good
Cast iron on cast iron with rubber gasket	Good
Cast iron on cast iron with tungsten sulfide coating	Good
Cast iron on stainless steel with Molykote lubricant	Good
Cold-rolled steel on cold-rolled steel	Good
Hard tool steel on tool steel	Good
Laminated plastic on gold plating	Good

Source: Ref 100

Abrasive wear is damage that results from the action of hard particles on a surface under the influence of a force that is oblique to the surface (Ref 101, 102, 103, 104, 105, 106). This is not, strictly speaking, a form of erosion-corrosion but is briefly discussed for comparison with the forms of erosion-corrosion mentioned previously.

Three common forms of abrasive wear are erosion abrasion, grinding abrasion, and gouging abrasion. Erosion abrasion usually involves low velocities and weak support of the abrasive material. Examples are wear on a plowshare in sandy soil and polishing of a metal surface with an abrasive held in a soft cloth. Thus, the energy of the abrasive is quite low, and impact is absent.

Grinding abrasion is the fragmentation of the abrasive, usually between two strong surfaces. Examples are a lapping operation in a machine shop and ball/rod mill grinding. Thus, impact is low to moderate, but the gross stress may be quite high, at least on a microscopic scale.

Gouging abrasion is recognized by the prominent grooves or gouges that are present on the wearing surfaces. Examples include abrasive disk grinding, machine tool cutting, and wear of power shovel bucket teeth. Heavy impact is generally associated with this type of abrasion, along with gross stress.

To alleviate these forms of abrasion, a careful study of the type of abrasion and an understanding of the service conditions are required. The materials selection should be based on the known properties of materials versus service requirements. More information on metal wear and corrosion is available in the article “Aqueous Corrosion-Wear Interactions” in this Volume.

Other Forms of Corrosion.

There are many different forms of corrosion (Ref 1, 2, 3, 13, 19, 89), and much can be learned from reported failures (Ref 107, 108, 109, 110, 111). The following paragraphs cite further forms of corrosion that warrant attention.

Selective leaching, also known as dealloying or parting corrosion, occurs when one element is preferentially removed from an alloy, leaving an often porous residue of an element that is more resistant to the environment. It is a problem of commercial significance in copper alloy systems (Ref 112), primarily copper-zinc and copper-aluminum and, to a lesser extent, copper-nickel. The terms *dezincification, dealuminization,* and *denickelification* (Fig. 16) describe the selective leaching of zinc, aluminum, and nickel, respectively, from the alloys. In these cases, a porous residue of copper remains, either as a fairly uniform layer or in plugs. The latter is more damaging in that the effect is similar to pitting corrosion.

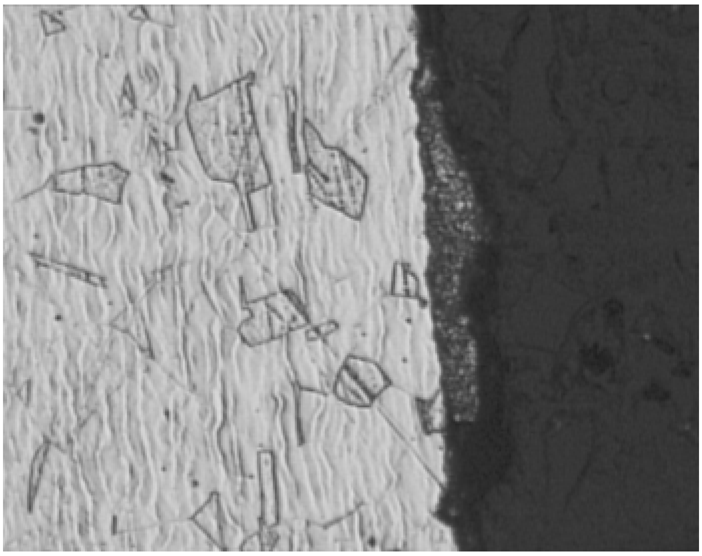

Fig. 16 Denickelification of cupronickel pipe exposed to a polluted marine estuary

Selective leaching in copper alloy systems occurs primarily in certain waters, especially under deposits in stagnant areas in heat exchangers. Alloy additions of arsenic, antimony, or phosphorus are effective in inhibiting this attack but only in copper-zinc alloys. Thus, arsenical or antimonial admiralty brass (UNS C44300 and C44400, respectively) is specified, for example, where this alloy is required for water service.

Graphitic corrosion of cast iron is another commercially important form of selective leaching. In this case, the iron matrix corrodes, leaving behind a porous graphite mass that can be carved with a pocket knife. Cast iron underground municipal watermains (Ref 113), fire watermains at petrochemical plant sites, and certain sprinkler systems (Ref 114) are affected by graphitic corrosion from both the soil and water sides. Internal cement linings and external protective coatings, with cathodic protection in severely corrosive soils, are relatively low-cost solutions to watermain corrosion problems. The article "Effects of Metallurgical Variables on Dealloying Corrosion" in this Volume contains more information on the phenomenon of dealloying.

Exfoliation is a form of localized corrosion that primarily affects aluminum alloys. Corrosion proceeds laterally from initiation sites on the surface and generally proceeds intergranularly along planes parallel to the surface. The corrosion products that form in the grain boundaries force metal away from the underlying base material, resulting in a layered or flakelike appearance. Extruded products from the 2000-series copper-magnesium alloys, the 7000-series zinc-copper-magnesium alloys, and, to a lesser extent, the 5000-series alloys are particularly susceptible to exfoliation in both marine and industrial environments. Also, at least one case affecting 6000-series magnesium-silicon alloys in freshwater service has been reported (Ref 115).

This attack is generally associated with the alloy fabrication method and temper, impurities in the alloy matrix, and the distribution of intermetallic compounds at the surface and in grain boundaries. Aluminum alloys 1100 (UNS A91100), 3003 (UNS A93003), and 5052 (UNS A95052) are resistant. Standard test methods for determining susceptibility to exfoliation corrosion in aluminum alloys are covered in ASTM G 34 and G 66.

Liquid metal induced embrittlement (LMIE), also known as liquid metal assisted cracking, is not considered to be a corrosion phenomenon, except in cases involving aqueous mercury compounds (Ref 32). However, LMIE is discussed here because it is a problem sometimes encountered by materials engineers. Liquid metal induced embrittlement is the penetration, usually along grain boundaries, of metals and alloys by such metals as mercury, which are liquid at room temperature, and metals that have relatively low melting points, such as bismuth, tin, lead, cadmium, zinc, aluminum, and copper. Stress, temperature, and time are the factors that facilitate and accelerate LMIE. Virtually all metal and alloy systems are subject to LMIE by one or more of these metals at or above their melting points.

Zinc is a prime offender because of widespread use throughout industry in the form of corrosion-resistant coatings applied to carbon steels by hot dip galvanizing, electroplating, tumbling, and spray painting. Plain carbon steels are embrittled by zinc at temperatures above 370 °C (700 °F) for long periods of time, especially when the steel is heavily stressed or cold worked.

Austenitic stainless steels and nickel-base alloys will also crack in the presence of molten zinc. These alloys usually crack instantly when welded to galvanized steel, a fairly common occurrence in the chemical-processing industry. In addition, austenitic alloy failures have occurred:

- In high-temperature bolting fastened with galvanized steel nuts
- During welding or heat treating of components contaminated by grinding with zinc- loaded grinding wheels, contact with zinc- coated structurals or slings, or exposure to zinc paint overspray
- During process industry plant fires involving piping and vessels (thin-wall expansion joint bellows are especially susceptible) sprayed with molten zinc from coated steel structures

It is imperative that all traces of zinc be removed from coated steel members before welding to austenitic alloys and before intimate contact with these alloys at temperatures above 370 °C (700 °F). Also, austenitic stainless steels and nickel-base alloys should be handled with non- coated steel hoist chains, cables, and structurals. They should be dressed and cleaned with new grinding wheels and stainless steel brushes, and they should be marked with materials (paints, crayons, and so on) free from zinc and other low- melting metals.

Cadmium is probably second to zinc in importance as an agent of LMIE because of its application as a corrosion-resistant coating to a variety of hardware, particularly fasteners. Failures by cadmium LMIE of bolting operating at temperatures above 300 °C (570 °F) and fabricated from such high-strength alloy steels as AISI 4140 (UNS G41400) and 4340 (UNS G43400) and austenitic stainless steels are fairly common. In fact, some high-strength steels and high- strength titanium alloys are embrittled by cadmium at temperatures below its melting point by mechanisms not yet understood. The solution to LMIE by cadmium is similar to that of zinc, that is, avoid contact with, and contamination of, susceptible metal and alloy systems at temperatures above the 321 °C (610 °F) melting point of cadmium (and at all temperatures when high- strength steels and titanium alloys are involved).

Metal systems that are embrittled by contact with mercury include copper and its alloys, aluminum and its alloys, nickel alloys 200 (UNS N02200) (at elevated temperatures) and 400 (UNS N04400), and titanium and zirconium and their alloys. Cracking is intergranular except in zirconium alloys; in these alloys, cracking is transgranular. Mercury LMIE of aluminum and copper alloys was more common years ago in the petrochemical industry when mercury-filled manometers and thermometers were extensively used. Failures or upsets would release mercury into process or service (steam, cooling water, and so on) streams, causing widespread cracking of piping, heat-exchanger tube bundles, and other equipment. Under these conditions, even pure aluminum and pure copper are susceptible. With regard to the titanium system, the commercially pure grades used in the chemical-processing industry are less sensitive than the alloys. In addition, LMIE in aqueous solutions of mercurous salts, such as mercurous nitrate, is possible because the mercurous ion can be reduced to its elemental form at local cathodic sites.

Although not a metal, sulfur will penetrate the grain boundaries of nickel and nickel alloys at elevated temperatures in much the same way as in the low-melting metals mentioned previously. Damage is particularly bad under reducing conditions (low oxygen potential), because sulfur forms a very aggressive low-melting nickel/ nickel sulfide eutectic ($Ni-Ni_3S_2$) that melts at approximately 625 °C (1157 °F). Sources other than elemental sulfur include organic compounds (greases, oils, cutting fluids) and sulfates. Thus, contamination from these sources before welding, hot forming, annealing, and other heating operations must be avoided (see the article “Liquid Metal Induced Embrittlement” in this Volume).

References cited in this section

1. R.J. Landrum, *Designing for Corrosion Control,* NACE International, 1989

2. V.R. Pludek, *Design and Corrosion Control,* The Macmillan Press Ltd., 1977

3. C.P. Dillon, *Material Selection for the Chemical Process Industries,* McGraw- Hill, Inc., 1992

6. *Corrosion Data Survey—Metals Section,* 6th ed., 1985; *Corrosion Data Survey— Nonmetals Section,* 5th ed., National Association of Corrosion Engineers, 1983

11. “CHEM-COR Modules on Advisory Systems for Selecting Materials,” National Association of Corrosion Engineers and Materials Technology Institute of the Chemical Process Industries Inc., NACE, 1990–1997

13. R. Baboian, Ed., *Corrosion Tests and Standards,* MNL-20, *ASTM Manual Series,* ASTM, 1995

15. *Metal Corrosion, Erosion, and Wear,* Vol 03.02, Section 3, *Annual Book of ASTM Standards,* American Society for Testing and Materials, 1986

16. *ASTM Standards for Maintenance, Repair and Operations in the Chemical Process Industry,* ASTM, 1994

17. *ASTM Standards for Corrosion Testing of Metals,* ASTM, 1990

19. B.J. Moniz, Field Identification of Metals, *Process Industries Corrosion—The Theory and Practice,* National Association of Corrosion Engineers, 1986, p 839–842

22. C.W. Kovach, *High Performance Stainless Steels,* Series 11 021, Nickel Development Institute, 2000

23. G. Kobrin, Reflections on Microbiologically Induced Corrosion of Stainless Steels, *Biologically Induced Corrosion,* NACE-8, S.C. Dexter, Ed., National Association of Corrosion Engineers, 1986, p 33–46

24. *Guide to Engineered Materials,* Vol 1, American Society for Metals, June 1986, p 79

25. R. Baboian, New Methods for Controlling Galvanic Corrosion, *Mach. Des.,* 11 Oct 1979, p 78–85

26. R.M. Davison, H.E. Deverell, and J.D. Redmond, Ferritic and Duplex Stainless Steels, *Process Industries Corrosion—The Theory and Practice,* National Association of Corrosion Engineers, 1986, p 427–443

27. C.P. Dillon, *Corrosion Control in the Chemical Process Industries,* 2nd ed., Materials Technology Institute of the Chemical Process Industries, Inc., NACE International, 1994

28. “Intergranular Corrosion of Chromium- Nickel Stainless Steels—Final Report,” Bulletin 138, Welding Research Council, 1969

29. M.A. Streicher, Tests for Detecting Susceptibility to Intergranular Corrosion, *Process Industries Corrosion—The Theory and Practice,* National Association of Corrosion Engineers, 1986, p 123–159

30. J.S. Armijo, Intergranular Corrosion of Nonsensitized Austenitic Stainless Steels, *Corrosion,* Jan 1968, p 24–30

31. W.H. Herrnstein, J.W. Cangi, and M.G. Fontana, Effect of Carbon Pickup on the Serviceability of Stainless Steel Alloy Castings, *Mater. Perform.,* Oct 1975, p 21–27

32. D.R. McIntyre and C.P. Dillon, “Guidelines for Preventing Stress Corrosion Cracking in the Chemical Process Industries,” Publication 15, Materials Technology Institute of the Chemical Process Industries, 1985

33. *The Role of Stainless Steels in Petroleum Refining,* American Iron and Steel Institute, 1977, p 41

34. R.M. Davison, H.E. Deverell, and J.D. Redmond, Ferritic and Duplex Stainless Steels, *Process Industries Corrosion—The Theory and Practice,* National Association of Corrosion Engineers, 1986, p 434, 435

35. D.R. McIntyre, Factors Affecting the Stress Corrosion Cracking of Austenitic Stainless Steels Under Thermal Insulation, *Corrosion of Metals Under Thermal Insulation,* STP 880, American Society for Testing and Materials, 1985, p 29–33

36. J.A. Richardson and T. Fitzsimmons, Use of Aluminum Foil for Prevention of Stress Corrosion Cracking of Austenitic Stainless Steel Under Thermal Insulation, *Corrosion of Metals Under Thermal Insulation,* STP 880, American Society for Testing and Materials, 1985, p 188–198

37. *The Role of Stainless Steels in Petroleum Refining,* American Iron and Steel Institute, 1977, p 42–44

38. "Protection of Austenitic Stainless Steels in Refineries Against Stress Corrosion Cracking by Use of Neutralizing Solutions During Shutdown," NACE RP-01-70, (1970 Revision), National Association of Corrosion Engineers

39. M.G. Fontana, F.H. Beck, and J.W. Flowers, Cast Chromium Nickel Stainless Steels for Superior Resistance to Stress Corrosion, *Met. Prog.,* Dec 1961

40. J.W. Flowers, F.H. Beck, and M.G. Fontana, Corrosion and Age Hardening Studies of Some Cast Stainless Alloys Containing Ferrite, *Corrosion,* May 1963, p 194t–195t

41. W.H. Friske, "Shot Peening to Prevent the Corrosion of Austenitic Stainless Steels," AI-75-52, Rockwell International, 1975

42. Internal Report, Accession 15925, E.I. Du Pont de Nemours & Company, Inc., p 6, 7

43. O.L. Towers, SCC in Welded Ammonia Vessels, *Met. Constr.,* Aug 1984, p 479–485

44. R.S. Lenox and P.A. Hough, *ASHRAE J.,* Nov 1995

45. J.D. Jackson and W.K. Boyd, "Stress-Corrosion Cracking of Aluminum Alloys," DMIC Memorandum 202, Battelle Memorial Institute, 1965, p 2, 3

46. J.R. Myers, H.B. Bomberger, and F.H. Froes, Corrosion Behavior and Use of Titanium and Its Alloys, *J. Met.,* Oct 1984, p 52, 53

47. R.A. Page, Stress Corrosion Cracking of Alloys 600 and 690 and Nos. 82 and 182 Weld Metals in High Temperature Water, *Corrosion,* Vol 39 (No. 10), Oct 1983, p 409–421

48. A.R. McIlree and H.T. Michels, Stress Corrosion Behavior of Fe-Cr-Ni and Other Alloys in High Temperature Caustic Solutions, *Corrosion,* Vol 33 (No. 2), Feb 1977, p 60–67

49. R.S. Pathania and R.D. Cleland, The Effect of Thermal Treatments on Stress Corrosion Cracking of Alloy-800 in a Caustic Environment, *Corrosion,* Vol 41 (No. 10), Oct 1985, p 575–581

50. K.H. Lee et al., Effect of Heat Treatment Applied Potential on the Caustic Stress Corrosion Cracking of Inconel 600, *Corrosion,* Vol 41 (No. 9), Sept 1985, p 540–553

51. J.R. Crum, Stress Corrosion Cracking Testing of Inconel Alloys 600 and 690 Under High Temperature Caustic Conditions, *Corrosion,* Vol 42 (No. 6), June 1986, p 368–372

52. Summary of Questionnaire Replies on Corrosion in HF Alkylation Units, *Corrosion,* Vol 15, May 1959, p 237t–240t

53. Materials for Receiving, Handling and Storing Hydrofluoric Acid, NACE Publication 5A171 (1983 Revision), *Mater. Perform.,* Nov 1983, p 9–12

54. F.W. Billmeyer, *Textbook of Polymer Science,* 2nd ed., John Wiley & Sons, 1971, p 133

55. R.B. Seymour, *Plastics vs. Corrosives,* John Wiley & Sons, 1982, p 46

56. D.R. McIntyre, Environmental Cracking, *Process Industries Corrosion,* National Association of Corrosion Engineers, 1986, p 21–30

57. D. Warren, Hydrogen Effects on Steel, *Process Industries Corrosion,* National Association of Corrosion Engineers, 1986, p 31–43

58. J. McBreen et al., The Electrochemical Introduction of Hydrogen into Metals, *Fundamental Aspects of Stress Corrosion Cracking,* National Association of Corrosion Engineers, 1967, p 51–63

59. W. Beck et al., Hydrogen Permeation in Metals as a Function of Stress, Temperature, and Dissolved Hydrogen Concentration, *Hydrogen Damage,* American Society for Metals, 1977, p 191–206

60. R. Gibala, *AIME Abstract Bull. (Inst. of Metals Div.),* Vol 1, 1966, p 36

61. R. Gibala, Hydrogen-Dislocation Interaction in Iron, *Trans. Met. Soc. AIME,* Vol 239, 1967, p 1574

62. A. Szummer, *Bull. Acad. Polon Ser. Sci. Chem.,* Vol 12, 1964, p 651

63. D.A. Vaughan et al., *Corrosion,* Vol 19, 1963, p 315t

64. M.L. Holzworth et al., *Corrosion,* Vol 24, 1968, p 110–124

65. N.A. Nielsen, Observations and Thoughts on Stress Corrosion Mechanisms, *Hydrogen Damage,* American Society for Metals, 1977, p 219–254

66. M.O. Spiedel, Hydrogen Embrittlement of Aluminum Alloys, *Hydrogen Damage,* American Society for Metals, 1977, p 329–351

67. L.S. Darken et al., Behavior of Hydrogen in Steel During and After Immersion in Acid, *Hydrogen Damage,* American Society for Metals, 1977, p 60–75

68. H.H. Johnson et al., Hydrogen Crack Initiation and Delayed Failure in Steel, *Trans. AIME,* Vol 212, 1958, p 526–536

69. K. Farrell et al., Hydrogen Embrittlement of an Ultra-High-Tensile Steel, *J. Iron Steel Inst.,* Dec 1964, p 1002–1011

70. C.D. Kim et al., Techniques for Investigating Hydrogen-Induced Cracking of Steels With High Yield Strength, *Corrosion,* Vol 24, 1968, p 313–318

71. K. Farrell, Cathodic Hydrogen Absorption and Severe Embrittlement in a High Strength Steel, *Corrosion,* Vol 26, 1970, p 105–110

72. W.M Baldwin, Jr. et al., Hydrogen Embrittlement of Steels, *Trans. AIME (J. Met.),* Vol 200, 1954, p 298–303

73. P. Blanchard et al., “La Fragilisation des Metaus par L'hydrogen. Influence de la Structure Cristallographic et Electronique,” paper presented before the Societe Francaise de Metallurgie, Oct 1959

74. G.G. Hancock et al., Hydrogen Cracking and Subcritical Crack Growth in a High Strength Steel, *Trans. AIME,* Vol 236, 1966, p 447

75. D.P. Williams et al., Embrittlement of 4130 Steel by Low-Pressure Gaseous Hydrogen, *Metall. Trans.,* Vol 1, 1970, p 63

76. G.E. Kerns et al., Slow Crack Growth of a High Strength Steel in Chlorine and Hydrogen Sulfide Gas Environments, *Scr. Metall.,* Vol 6, 1972, p 631–634

77. R.M. Hudson, *Corrosion,* Vol 20, 1969, p 24t

78. T.P. Radhakrishnan et al., *Electrochim. Acta,* Vol 11, 1966, p 1007

79. G.E. Kerns, Effects of Sulfur and Sulfur Compounds on Aqueous Corrosion, *Process Industries Corrosion,* National Association of Corrosion Engineers, 1986, p 353–365

80. M.T. Wang et al., Effect of Heat Treatment and Stress Intensity Parameters on Crack Velocity and Fractography of AISI 4340 Steel, *Hydrogen in Metals,* International Conference in Paris, 1972, p 342

81. P. McIntyre et al., “Accelerated Test Technique for the Determination of K_{ISCC} in Steels,” Corporate Laboratories Report MG/31/72, British Steel Corporation, 1972

82. Bulletin 191, Welding Research Council, March 1978

83. N. Bailey, Welding Carbon Manganese Steels, *Met. Constr.,* Vol 2, 1970, p 442–446

84. R.L. Schuyler III, Hydrogen Blistering of Steel in Anhydrous Hydrofluoric Acid, *Mater. Perform.,* Vol 18 (No. 8), 1979, p 9–16

85. G. Herbsleb et al., Occurrence and Prevention of Hydrogen Induced Stepwise Cracking and Stress Corrosion Cracking of Low Alloy Pipeline Steels, *Corrosion,* Vol 37 (No. 5), 1981, p 247–255

86. S.A. Golovanenko et al., Effect of Alloying Elements and Structure on the Resistance of Structural Steels to Hydrogen Embrittlement, *H_2S Corrosion in Oil and Gas Production—A Compilation of Classic Papers,* National Association of Corrosion Engineers, 1981, p 198

87. J. Watanabe et al., “Hydrogen-Induced Disbonding of Stainless Weld Overlay Found in Hydrodesulfurizing Reactor,” paper presented at ASME Conference on Performance of Pressure Vessels with Clad and Overlaid Stainless Steel Linings (Denver, CO), American Society of Mechanical Engineers, 1981

88. J. Watanabe et al., “Hydrogen Induced Disbonding of Stainless Steel Overlay Weld,” paper presented at the Pressure Vessel Research Committee Meeting (New York, NY), 1980

89. M.G. Fontana, *Corrosion Engineering,* 3rd ed., McGraw-Hill, 1986

90. F.J. Heymann, Erosion by Liquids—The Mysterious Murderer of Metals, *Mach. Des.,* Dec 1970

91. I.M. Hutchings, “The Erosion of Materials by Liquid Flow,” Publication 25, Materials Technology Institute of the Chemical Process Industries, 1986

92. P. Eisenbery et al., How to Protect Materials Against Cavitation Damage, *Mater. Des. Eng.,* March 1967

93. T.E. Backstrom, “A Suggested Metallurgical Parameter in Alloy Selection for Cavitation Resistance,” Report CHE 72, Department of the Interior, Dec 1972

94. R.W. Hinton, “Cavitation Damage of Alloys—Relationship to Microstructure,” paper presented at NACE Conference, National Association of Corrosion Engineers, March 1963

95. R.E.A. Arndt, “Cavitation and Erosion: An Overview,” paper presented at NACE Conference, National Association of Corrosion Engineers, March 1977

96. *Trans. ASME,* Vol 59, 1937

97. R.B. Waterhouse and M. Allery, The Effect of Non-Metallic Coatings on the Fretting Corrosion of Mild Steel, *Wear,* Vol 8, 1965, p 421–447

98. R.B. Waterhouse et al., The Effect of Electrodeposited Metals on the Fatigue Behavior of Mild Steel Under Conditions of Fretting Corrosion, *Wear,* Vol 5, 1962, p 235–244

99. Fretting and Fretting Corrosion, *Lubrication,* Vol 52 (No. 4), 1966

100. J.R. McDowell, in *Symposium of Fretting Corrosion,* STP 144, American Society for Testing and Materials, 1952

101. H.S. Avery, “Abrasive Wear—The Nature of the Abrasive,” Publication RCR CR340, Abex Corporation

102. H.S. Avery, “Hard Facing Alloys,” paper presented at the ASM Wear Conference (Boston, MA), American Society for Metals, 1969

103. T.E. Norman, New Austenitic Alloy for Ultra-Abrasive Applications, *J. Eng. Mining,* April 1965

104. K.J. Blensali and W.L. Silence, Metallurgical Factors Affecting Wear Resistance, *Met. Prog.,* Nov 1977

105. G.L. Sheldon, Effect of Surface Hardness and Other Materials Properties on Erosion Wear of Metals, *J. Eng. Mater. Test.,* April 1977

106. W.A. Stauffer, Wear of Metals by Sand Erosion, *Met. Prog.,* Jan 1956

107. C.P. Dillon, “Unusual Corrosion Problems in the Chemical Industry,” MTI Publication 54, Materials Technology Institute of the Chemical Process Industries, Inc., 2000

108. R.B. Puyear, “Case Histories: Improper Materials, Fabrication and Documentation,” MTI Report R-1, Materials Technology Institute of the Chemical Process Industries, Inc., 1996

109. R.B. Puyear, “Corrosion Failure Mechanisms in Process Industries,” MTI Report R-4, Materials Technology Institute of the Chemical Process Industries, Inc., 1997

110. P. Elliott, *Process Eng.,* Nov 1984

111. P. Elliott, Corrosion Survey Report, *The Chem. Eng.*, Sept 1973

112. R. Heidersbach, Clarification of the Mechanism of the Dealloying Phenomenon, *Corrosion,* Feb 1968, p 38–44

113. R.A. Gummow, The Corrosion of Municipal Iron Watermains, *Mater. Perform.*, March 1984, p39–42

114. "Issues in Fire Protection Systems—Symposium," Corrosion 2002, (Denver, Co), NACE International, 2000

115. J. Zahavi and J. Yahalom, Exfoliation Corrosion of Al Mg Si Alloys in Water, *J. Electrochem. Soc.,* Vol 129 (No. 6), June 1982, p 1181–1185

P. Elliott, Materials Selection for Corrosion Control, *Corrosion: Fundamentals, Testing, and Protection*, Vol 13A*, ASM Handbook*, ASM International, 2003, p 909–928

Materials Selection for Corrosion Control

Revised by Peter Elliott, Corrosion & Materials Consultancy, Inc.

Economics

Cost-Effective Materials Selection. Two extremes for selecting materials on an economic basis without consideration of other factors have been promulgated (Ref 111, 116):

- *Minimum cost or economic design:* selection of the least expensive material, followed by scheduled periodic replacements or correction of problems as they arise
- *Minimum corrosion:* selection of the most corrosion-resistant material regardless of installed cost or life of the equipment

These factors can be modified (Ref 111) to include:

- *Minimum investment:* materials selection for a short-term design where corroded parts are replaced as required (e.g., cheap labor, areas of political unrest)
- *Minimum maintenance:* an overdesign (thicker section of material or improved alloy) to reduce costs of maintenance (high labor costs) or where spare parts (replacements) are not easily available

Cost-effective selection generally falls somewhere between these extremes and includes consideration of other factors, such as availability and safety. For example, critical components in a large single-train chemical-processing plant should be fabricated from materials that tend toward the minimum corrosion extreme, because failure could shut down the entire operation. However, component materials for a multitrain or batch operation, especially one that processes a relatively short-lived product, might tend toward the minimum cost extreme, even to the point of purchasing used equipment at a fraction of the cost of new fabrication. Thus, different strategies are appropriate for different situations.

Materials that are considered expensive when compared directly with carbon steel or non-metallic materials are generally cost-effective when the overall life-cycle costs are taken into account. Factors that affect the cost-effective choice of higher-alloyed materials include maintenance and replacement costs (as mentioned previously), accounting procedures that give tax relief, and discounted cash flows (see the article "Corrosion Economic Calculations" in this Volume).

Industrial losses caused by corrosion account for enormous sums, typically a few percentage of the gross national product (GNP) of a country. A 1978 survey (Ref 118) showed the total direct cost of corrosion to the U.S. economy at approximately $280 billion/year; see the article "Direct Costs of Corrosion in the United States" in this Volume for more recent estimates.

Not always shown in surveys are the indirect costs of corrosion, which include lost product, lost sales, and lost customers. Indirect losses are generally more than double the direct costs. For example, corrosion surveys focused on the agricultural sector gave the following results: a U.S. National Bureau of Standards survey (Ref 117) found direct losses of $1171 million (in 1978), with indirect losses of $2943 million; a survey (Ref 118) of British agriculture, which identified direct losses (in 1993) of £180 million sterling, estimated indirect losses associated with depreciation and consequential losses to be £500 million. A survey of the horticultural sector (Ref 119) showed direct losses of £10 million (in 1993) inflated to £24 million when consequential losses were included.

References cited in this section

111. P. Elliott, Corrosion Survey Report, *The Chem. Eng.,* Sept 1973

116. R.B. Puyear, Material Selection Criteria for Chemical Processing Equipment, *Met. Prog.,* Feb 1978, p 42

117. "Economic Effects of Metallic Corrosion in the United States," Special Publication 511-1, United States Bureau of Standards, 1978

118. P. Elliott, C.M. Fowler, J.B. Johnson, and G.C. Wood, "Corrosion in Agriculture and Horticulture—HMSO," Ministry of Agriculture (United Kingdom), 1983; also, "Guide to Practice in Corrosion Control," Publication 15, United Kingdom Department of Industry, 1981

119. C.M. Fowler, J.B. Johnson, P. Elliott, and G.C. Wood, *Sci. Hort.,* Vol 34, 1983, p 84–93

P. Elliott, Materials Selection for Corrosion Control, *Corrosion: Fundamentals, Testing, and Protection*, Vol 13A, *ASM Handbook*, ASM International, 2003, p 909–928

Materials Selection for Corrosion Control

Revised by Peter Elliott, Corrosion & Materials Consultancy, Inc.

Acknowledgment

Portions of this article have been adapted from G. Kobrin, Materials Selection, *Corrosion,* Vol 13, *ASM Handbook* (formerly *Metals Handbook,* 9th ed.), ASM International, 1987, p 321–337. The section "Hydrogen Damage" was written by G.E. Kerns, and the section "Erosion-Corrosion" was written by J.Q. Lackey.

P. Elliott, Materials Selection for Corrosion Control, *Corrosion: Fundamentals, Testing, and Protection*, Vol 13A, *ASM Handbook*, ASM International, 2003, p 909–928

Materials Selection for Corrosion Control

Revised by Peter Elliott, Corrosion & Materials Consultancy, Inc.

References

1. R.J. Landrum, *Designing for Corrosion Control,* NACE International, 1989

2. V.R. Pludek, *Design and Corrosion Control,* The Macmillan Press Ltd., 1977

3. C.P. Dillon, *Material Selection for the Chemical Process Industries,* McGraw- Hill, Inc., 1992

4. *Designer Handbook, Guidelines for the Selection and Use of Stainless Steel,* Specialty Steel Industry of North America, 1995

5. P. Elliott, "Catch 22" and the UCS Factor—Why Must History Repeat Itself?, *Mater. Perform.,* Vol 28 (No. 7), 1989, p 75–78; Vol 28 (No. 8), 1989, p 70–76

6. *Corrosion Data Survey—Metals Section,* 6th ed., 1985; *Corrosion Data Survey— Nonmetals Section,* 5th ed., National Association of Corrosion Engineers, 1983

7. C.P. Dillon and W. Pollock, Ed., *Materials Selector Series for Hazardous Chemicals,* Materials Technology Institute of the Chemical Process Industries, Inc., 1994–in press

8. C. Westcott et al., "The Development and Application of Integrated Expert Systems and Data Bases for Corrosion Consultancy," Paper 54, presented at Corrosion/ 86 (Houston, TX), National Association of Corrosion Engineers, March 1986

9. S.E. Marschand et al., "Expert Systems Developed by Corrosion Specialists," Paper 56, presented at Corrosion/86 (Houston, TX), National Association of Corrosion Engineers, March 1986

10. W.F. Bogaerts et al., "Artificial Intelligence, Expert Systems and Computer- Aided Engineering in Corrosion Control," Paper 58, presented at Corrosion/86 (Houston, TX), National Association of Corrosion Engineers, March 1986

11. "CHEM-COR Modules on Advisory Systems for Selecting Materials," National Association of Corrosion Engineers and Materials Technology Institute of the Chemical Process Industries Inc., NACE, 1990–1997

12. R.B. Puyear, Material Selection Criteria for Chemical Processing Equipment, *Met. Prog.,* Feb 1978, p 40–46

13. R. Baboian, Ed., *Corrosion Tests and Standards,* MNL-20, *ASTM Manual Series,* ASTM, 1995

14. "Laboratory Corrosion Testing of Metals for the Process Industries," NACE TM-01- 69 (1976 Revision); "Method of Conducting Controlled Velocity Laboratory Corrosion Tests," NACE TM-02-70, National Association of Corrosion Engineers

15. *Metal Corrosion, Erosion, and Wear,* Vol 03.02, Section 3, *Annual Book of ASTM Standards,* American Society for Testing and Materials, 1986

16. *ASTM Standards for Maintenance, Repair and Operations in the Chemical Process Industry,* ASTM, 1994

17. *ASTM Standards for Corrosion Testing of Metals,* ASTM, 1990

18. G. Kobrin, Evaluate Equipment Condition by Field Inspection and Tests, *Hydrocarbon Process,* Jan 1970, p 115–120

19. B.J. Moniz, Field Identification of Metals, *Process Industries Corrosion—The Theory and Practice,* National Association of Corrosion Engineers, 1986, p 839–842

20. Monitoring Internal Corrosion in Oil and Gas Production Operations with Hydrogen Probes, NACE Publication 1C 184, *Mater. Perform.,* June 1984, p 49–56

21. J.C. Bovankovich, On-Line Corrosion Monitoring, *Mater. Prot. Perform.,* June 1973, p 20–23

22. C.W. Kovach, *High Performance Stainless Steels,* Series 11 021, Nickel Development Institute, 2000

23. G. Kobrin, Reflections on Microbiologically Induced Corrosion of Stainless Steels, *Biologically Induced Corrosion,* NACE-8, S.C. Dexter, Ed., National Association of Corrosion Engineers, 1986, p 33–46

24. *Guide to Engineered Materials,* Vol 1, American Society for Metals, June 1986, p 79

25. R. Baboian, New Methods for Controlling Galvanic Corrosion, *Mach. Des.,* 11 Oct 1979, p 78–85

26. R.M. Davison, H.E. Deverell, and J.D. Redmond, Ferritic and Duplex Stainless Steels, *Process Industries Corrosion—The Theory and Practice,* National Association of Corrosion Engineers, 1986, p 427–443

27. C.P. Dillon, *Corrosion Control in the Chemical Process Industries,* 2nd ed., Materials Technology Institute of the Chemical Process Industries, Inc., NACE International, 1994

28. "Intergranular Corrosion of Chromium- Nickel Stainless Steels—Final Report," Bulletin 138, Welding Research Council, 1969

29. M.A. Streicher, Tests for Detecting Susceptibility to Intergranular Corrosion, *Process Industries Corrosion—The Theory and Practice,* National Association of Corrosion Engineers, 1986, p 123–159

30. J.S. Armijo, Intergranular Corrosion of Nonsensitized Austenitic Stainless Steels, *Corrosion,* Jan 1968, p 24–30

31. W.H. Herrnstein, J.W. Cangi, and M.G. Fontana, Effect of Carbon Pickup on the Serviceability of Stainless Steel Alloy Castings, *Mater. Perform.,* Oct 1975, p 21–27

32. D.R. McIntyre and C.P. Dillon, "Guidelines for Preventing Stress Corrosion Cracking in the Chemical Process Industries," Publication 15, Materials Technology Institute of the Chemical Process Industries, 1985

33. *The Role of Stainless Steels in Petroleum Refining,* American Iron and Steel Institute, 1977, p 41

34. R.M. Davison, H.E. Deverell, and J.D. Redmond, Ferritic and Duplex Stainless Steels, *Process Industries Corrosion—The Theory and Practice,* National Association of Corrosion Engineers, 1986, p 434, 435

35. D.R. McIntyre, Factors Affecting the Stress Corrosion Cracking of Austenitic Stainless Steels Under Thermal Insulation, *Corrosion of Metals Under Thermal Insulation,* STP 880, American Society for Testing and Materials, 1985, p 29–33

36. J.A. Richardson and T. Fitzsimmons, Use of Aluminum Foil for Prevention of Stress Corrosion Cracking of Austenitic Stainless Steel Under Thermal Insulation, *Corrosion of Metals Under Thermal Insulation,* STP 880, American Society for Testing and Materials, 1985, p 188–198

37. *The Role of Stainless Steels in Petroleum Refining,* American Iron and Steel Institute, 1977, p 42–44

38. "Protection of Austenitic Stainless Steels in Refineries Against Stress Corrosion Cracking by Use of Neutralizing Solutions During Shutdown," NACE RP-01-70, (1970 Revision), National Association of Corrosion Engineers

39. M.G. Fontana, F.H. Beck, and J.W. Flowers, Cast Chromium Nickel Stainless Steels for Superior Resistance to Stress Corrosion, *Met. Prog.,* Dec 1961

40. J.W. Flowers, F.H. Beck, and M.G. Fontana, Corrosion and Age Hardening Studies of Some Cast Stainless Alloys Containing Ferrite, *Corrosion,* May 1963, p 194t–195t

41. W.H. Friske, "Shot Peening to Prevent the Corrosion of Austenitic Stainless Steels," AI-75-52, Rockwell International, 1975

42. Internal Report, Accession 15925, E.I. Du Pont de Nemours & Company, Inc., p 6, 7

43. O.L. Towers, SCC in Welded Ammonia Vessels, *Met. Constr.,* Aug 1984, p 479–485

44. R.S. Lenox and P.A. Hough, *ASHRAE J.,* Nov 1995

45. J.D. Jackson and W.K. Boyd, "Stress-Corrosion Cracking of Aluminum Alloys," DMIC Memorandum 202, Battelle Memorial Institute, 1965, p 2, 3

46. J.R. Myers, H.B. Bomberger, and F.H. Froes, Corrosion Behavior and Use of Titanium and Its Alloys, *J. Met.,* Oct 1984, p 52, 53

47. R.A. Page, Stress Corrosion Cracking of Alloys 600 and 690 and Nos. 82 and 182 Weld Metals in High Temperature Water, *Corrosion,* Vol 39 (No. 10), Oct 1983, p 409–421

48. A.R. McIlree and H.T. Michels, Stress Corrosion Behavior of Fe-Cr-Ni and Other Alloys in High Temperature Caustic Solutions, *Corrosion,* Vol 33 (No. 2), Feb 1977, p 60–67

49. R.S. Pathania and R.D. Cleland, The Effect of Thermal Treatments on Stress Corrosion Cracking of Alloy-800 in a Caustic Environment, *Corrosion,* Vol 41 (No. 10), Oct 1985, p 575–581

50. K.H. Lee et al., Effect of Heat Treatment Applied Potential on the Caustic Stress Corrosion Cracking of Inconel 600, *Corrosion,* Vol 41 (No. 9), Sept 1985, p 540–553

51. J.R. Crum, Stress Corrosion Cracking Testing of Inconel Alloys 600 and 690 Under High Temperature Caustic Conditions, *Corrosion,* Vol 42 (No. 6), June 1986, p 368–372

52. Summary of Questionnaire Replies on Corrosion in HF Alkylation Units, *Corrosion,* Vol 15, May 1959, p 237t–240t

53. Materials for Receiving, Handling and Storing Hydrofluoric Acid, NACE Publication 5A171 (1983 Revision), *Mater. Perform.,* Nov 1983, p 9–12

54. F.W. Billmeyer, *Textbook of Polymer Science,* 2nd ed., John Wiley & Sons, 1971, p 133

55. R.B. Seymour, *Plastics vs. Corrosives,* John Wiley & Sons, 1982, p 46

56. D.R. McIntyre, Environmental Cracking, *Process Industries Corrosion,* National Association of Corrosion Engineers, 1986, p 21–30

57. D. Warren, Hydrogen Effects on Steel, *Process Industries Corrosion,* National Association of Corrosion Engineers, 1986, p 31–43

58. J. McBreen et al., The Electrochemical Introduction of Hydrogen into Metals, *Fundamental Aspects of Stress Corrosion Cracking,* National Association of Corrosion Engineers, 1967, p 51–63

59. W. Beck et al., Hydrogen Permeation in Metals as a Function of Stress, Temperature, and Dissolved Hydrogen Concentration, *Hydrogen Damage,* American Society for Metals, 1977, p 191–206

60. R. Gibala, *AIME Abstract Bull. (Inst. of Metals Div.),* Vol 1, 1966, p 36

61. R. Gibala, Hydrogen-Dislocation Interaction in Iron, *Trans. Met. Soc. AIME,* Vol 239, 1967, p 1574

62. A. Szummer, *Bull. Acad. Polon Ser. Sci. Chem.,* Vol 12, 1964, p 651

63. D.A. Vaughan et al., *Corrosion,* Vol 19, 1963, p 315t

64. M.L. Holzworth et al., *Corrosion,* Vol 24, 1968, p 110–124

65. N.A. Nielsen, Observations and Thoughts on Stress Corrosion Mechanisms, *Hydrogen Damage,* American Society for Metals, 1977, p 219–254

66. M.O. Spiedel, Hydrogen Embrittlement of Aluminum Alloys, *Hydrogen Damage,* American Society for Metals, 1977, p 329–351

67. L.S. Darken et al., Behavior of Hydrogen in Steel During and After Immersion in Acid, *Hydrogen Damage,* American Society for Metals, 1977, p 60–75

68. H.H. Johnson et al., Hydrogen Crack Initiation and Delayed Failure in Steel, *Trans. AIME,* Vol 212, 1958, p 526–536

69. K. Farrell et al., Hydrogen Embrittlement of an Ultra-High-Tensile Steel, *J. Iron Steel Inst.,* Dec 1964, p 1002–1011

70. C.D. Kim et al., Techniques for Investigating Hydrogen-Induced Cracking of Steels With High Yield Strength, *Corrosion,* Vol 24, 1968, p 313–318

71. K. Farrell, Cathodic Hydrogen Absorption and Severe Embrittlement in a High Strength Steel, *Corrosion,* Vol 26, 1970, p 105–110

72. W.M Baldwin, Jr. et al., Hydrogen Embrittlement of Steels, *Trans. AIME (J. Met.),* Vol 200, 1954, p 298–303

73. P. Blanchard et al., "La Fragilisation des Metaus par L'hydrogen. Influence de la Structure Cristallographic et Electronique," paper presented before the Societe Francaise de Metallurgie, Oct 1959

74. G.G. Hancock et al., Hydrogen Cracking and Subcritical Crack Growth in a High Strength Steel, *Trans. AIME,* Vol 236, 1966, p 447

75. D.P. Williams et al., Embrittlement of 4130 Steel by Low-Pressure Gaseous Hydrogen, *Metall. Trans.,* Vol 1, 1970, p 63

76. G.E. Kerns et al., Slow Crack Growth of a High Strength Steel in Chlorine and Hydrogen Sulfide Gas Environments, *Scr. Metall.,* Vol 6, 1972, p 631–634

77. R.M. Hudson, *Corrosion,* Vol 20, 1969, p 24t

78. T.P. Radhakrishnan et al., *Electrochim. Acta,* Vol 11, 1966, p 1007

79. G.E. Kerns, Effects of Sulfur and Sulfur Compounds on Aqueous Corrosion, *Process Industries Corrosion,* National Association of Corrosion Engineers, 1986, p 353–365

80. M.T. Wang et al., Effect of Heat Treatment and Stress Intensity Parameters on Crack Velocity and Fractography of AISI 4340 Steel, *Hydrogen in Metals,* International Conference in Paris, 1972, p 342

81. P. McIntyre et al., "Accelerated Test Technique for the Determination of K_{ISCC} in Steels," Corporate Laboratories Report MG/31/72, British Steel Corporation, 1972

82. Bulletin 191, Welding Research Council, March 1978

83. N. Bailey, Welding Carbon Manganese Steels, *Met. Constr.,* Vol 2, 1970, p 442–446

84. R.L. Schuyler III, Hydrogen Blistering of Steel in Anhydrous Hydrofluoric Acid, *Mater. Perform.,* Vol 18 (No. 8), 1979, p 9–16

85. G. Herbsleb et al., Occurrence and Prevention of Hydrogen Induced Stepwise Cracking and Stress Corrosion Cracking of Low Alloy Pipeline Steels, *Corrosion,* Vol 37 (No. 5), 1981, p 247–255

86. S.A. Golovanenko et al., Effect of Alloying Elements and Structure on the Resistance of Structural Steels to Hydrogen Embrittlement, *H_2S Corrosion in Oil and Gas Production—A Compilation of Classic Papers,* National Association of Corrosion Engineers, 1981, p 198

87. J. Watanabe et al., "Hydrogen-Induced Disbonding of Stainless Weld Overlay Found in Hydrodesulfurizing Reactor," paper presented at ASME Conference on Performance of Pressure Vessels with Clad and Overlaid Stainless Steel Linings (Denver, CO), American Society of Mechanical Engineers, 1981

88. J. Watanabe et al., "Hydrogen Induced Disbonding of Stainless Steel Overlay Weld," paper presented at the Pressure Vessel Research Committee Meeting (New York, NY), 1980

89. M.G. Fontana, *Corrosion Engineering,* 3rd ed., McGraw-Hill, 1986

90. F.J. Heymann, Erosion by Liquids—The Mysterious Murderer of Metals, *Mach. Des.,* Dec 1970

91. I.M. Hutchings, “The Erosion of Materials by Liquid Flow,” Publication 25, Materials Technology Institute of the Chemical Process Industries, 1986

92. P. Eisenbery et al., How to Protect Materials Against Cavitation Damage, *Mater. Des. Eng.,* March 1967

93. T.E. Backstrom, “A Suggested Metallurgical Parameter in Alloy Selection for Cavitation Resistance,” Report CHE 72, Department of the Interior, Dec 1972

94. R.W. Hinton, “Cavitation Damage of Alloys—Relationship to Microstructure,” paper presented at NACE Conference, National Association of Corrosion Engineers, March 1963

95. R.E.A. Arndt, “Cavitation and Erosion: An Overview,” paper presented at NACE Conference, National Association of Corrosion Engineers, March 1977

96. *Trans. ASME,* Vol 59, 1937

97. R.B. Waterhouse and M. Allery, The Effect of Non-Metallic Coatings on the Fretting Corrosion of Mild Steel, *Wear,* Vol 8, 1965, p 421–447

98. R.B. Waterhouse et al., The Effect of Electrodeposited Metals on the Fatigue Behavior of Mild Steel Under Conditions of Fretting Corrosion, *Wear,* Vol 5, 1962, p 235–244

99. Fretting and Fretting Corrosion, *Lubrication,* Vol 52 (No. 4), 1966

100. J.R. McDowell, in *Symposium of Fretting Corrosion,* STP 144, American Society for Testing and Materials, 1952

101. H.S. Avery, “Abrasive Wear—The Nature of the Abrasive,” Publication RCR CR340, Abex Corporation

102. H.S. Avery, “Hard Facing Alloys,” paper presented at the ASM Wear Conference (Boston, MA), American Society for Metals, 1969

103. T.E. Norman, New Austenitic Alloy for Ultra-Abrasive Applications, *J. Eng. Mining,* April 1965

104. K.J. Blensali and W.L. Silence, Metallurgical Factors Affecting Wear Resistance, *Met. Prog.,* Nov 1977

105. G.L. Sheldon, Effect of Surface Hardness and Other Materials Properties on Erosion Wear of Metals, *J. Eng. Mater. Test.,* April 1977

106. W.A. Stauffer, Wear of Metals by Sand Erosion, *Met. Prog.,* Jan 1956

107. C.P. Dillon, “Unusual Corrosion Problems in the Chemical Industry,” MTI Publication 54, Materials Technology Institute of the Chemical Process Industries, Inc., 2000

108. R.B. Puyear, “Case Histories: Improper Materials, Fabrication and Documentation,” MTI Report R-1, Materials Technology Institute of the Chemical Process Industries, Inc., 1996

109. R.B. Puyear, “Corrosion Failure Mechanisms in Process Industries,” MTI Report R-4, Materials Technology Institute of the Chemical Process Industries, Inc., 1997

110. P. Elliott, *Process Eng.,* Nov 1984

111. P. Elliott, Corrosion Survey Report, *The Chem. Eng.,* Sept 1973

112. R. Heidersbach, Clarification of the Mechanism of the Dealloying Phenomenon, *Corrosion,* Feb 1968, p 38–44

113. R.A. Gummow, The Corrosion of Municipal Iron Watermains, *Mater. Perform.*, March 1984, p39–42

114. "Issues in Fire Protection Systems—Symposium," Corrosion 2002, (Denver, Co), NACE International, 2000

115. J. Zahavi and J. Yahalom, Exfoliation Corrosion of Al Mg Si Alloys in Water, *J. Electrochem. Soc.,* Vol 129 (No. 6), June 1982, p 1181–1185

116. R.B. Puyear, Material Selection Criteria for Chemical Processing Equipment, *Met. Prog.,* Feb 1978, p 42

117. "Economic Effects of Metallic Corrosion in the United States," Special Publication 511-1, United States Bureau of Standards, 1978

118. P. Elliott, C.M. Fowler, J.B. Johnson, and G.C. Wood, "Corrosion in Agriculture and Horticulture—HMSO," Ministry of Agriculture (United Kingdom), 1983; also, "Guide to Practice in Corrosion Control," Publication 15, United Kingdom Department of Industry, 1981

119. C.M. Fowler, J.B. Johnson, P. Elliott, and G.C. Wood, *Sci. Hort.,* Vol 34, 1983, p 84–93

P. Elliott, Materials Selection for Corrosion Control, *Corrosion: Fundamentals, Testing, and Protection*, Vol 13A, *ASM Handbook*, ASM International, 2003, p 909–928

Materials Selection for Corrosion Control

Revised by Peter Elliott, Corrosion & Materials Consultancy, Inc.

Selected References

- R. Baboian, Ed., *Corrosion Tests and Standards,* MNL-20, *ASTM Manual Series,* ASTM, 1995
- B.D. Craig and D. Anderson, Ed., *Handbook of Corrosion Data,* 2nd ed., ASM International, 1995
- J.R. Davis, Ed., *Corrosion: Understanding the Basics,* ASM International, 2000
- C.P. Dillon, *Corrosion Control in the Chemical Process Industries,* 2nd ed., Materials Technology Institute of the Chemical Process Industries, Inc., NACE International, 1994
- C.P. Dillon, *Material Selection for the Chemical Process Industries,* McGraw-Hill, Inc., 1992
- M.G. Fontana, *Corrosion Engineering,* 3rd ed., McGraw-Hill, 1986
- I.M. Hutchings, "The Erosion of Materials by Liquid Flow," Publication 25, Materials Technology Institute of the Chemical Process Industries, 1986
- D.R. McIntyre and C.P. Dillon, "Guidelines for Preventing Stress Corrosion Cracking in the Chemical Process Industries," Publication 15, Materials Technology Institute of the Chemical Process Industries, 1985
- B.J. Moniz and W.I. Pollock, Ed., *Process Industries Corrosion—The Theory and Practice,* National Association of Corrosion Engineers, 1986

- G.A. Nelson, Criteria for Selecting Metals Used in Chemical Plants, *Met. Prog.,* May 1960, p 80–88, 134, 166–174
- R.W. Revie, Ed., *Uhlig's Corrosion Handbook,* 2nd ed., John Wiley & Sons, 2000
- P.A. Schweitzer, Ed., *Corrosion and Corrosion Protection Handbook,* 2nd ed., Marcel Dekker, 1988
- F.L. Whitney, Jr., Factors in the Selection of Corrosion Resistant Materials, *Met. Prog.,* June 1957, p 90–95

P. Elliott, Designing to Minimize Corrosion, *Corrosion: Fundamentals, Testing, and Protection*, Vol 13A, *ASM Handbook*, ASM International, 2003, p 929–939

Designing to Minimize Corrosion

Peter Elliott, Corrosion and Materials Consultancy, Inc.

Introduction

UNEXPECTED and frequently costly failures occur without sound and reliable engineering design, which includes the effective and correct choice of materials and the economic use of efficient controls and monitoring measures. Fine details of engineering design may be missed because of poor communication channels, sometimes compounded by human errors and a lack of proper care and attention. Unexpected premature failures can be harmful to personnel and adjacent equipment or parts. On occasion, a poor design can cause premature failure of even the most advanced corrosion-resistant materials.

P. Elliott, Designing to Minimize Corrosion, *Corrosion: Fundamentals, Testing, and Protection*, Vol 13A, *ASM Handbook*, ASM International, 2003, p 929–939

Designing to Minimize Corrosion

Peter Elliott, Corrosion and Materials Consultancy, Inc.

Design Considerations

Design can never be absolute; often, decisions are a compromise based on cost and availability of materials and resources. Designing for corrosion control can only be effective if it is part of the overall design philosophy.

There are numerous textbooks, handbooks, and articles on corrosion; several offer choices for specific materials/environment systems (Ref 1, 2, 3, 4, 5, 6, 7, 8, 9, 10, 11, 12, 13, 14, 15, 16, 17). These reference sources provide a useful starting point for selecting materials, but a designer is seldom a corrosion engineer, so it is necessary to further convey essential corrosion knowledge to designers (Ref 18, 19, 20, 21, 22, 23, 24, 25, 26, 27). Unlike conventional engineering, the basic difficulty is that corrosion is not a tangible property; it is more a behavioral pattern. Thus, to realize safe, reliable designs, it is essential that there be a rigid control on materials and fabrication and an extensive effort to eliminate human errors or misunderstandings that result from poor communication.

The results of a survey of chemical-processing plants (Ref 28) showed that design faults ranked highest (58%) in the reasons for failure. Of almost equal ranking was the incorrect application of protective treatments (55%), followed by categories that demonstrate a lack of knowledge about the operating conditions (52%), lack of process control (35%), and an unawareness that there was actually a corrosion risk (25%).

In an ideal world, designers would call for some corrosion assessment prior to preparing the detailed engineering design. Typically, schemes would permit some form of evaluation with respect to both function and the necessary action, for example, from the proposal-to-production planning stages (Fig. 1) (Ref 28). In the practical, real world, however, communication of agreed reasons for failures may not always reach the designer. Indeed, communication to contractors, who are closest to the application, is even poorer (Ref 28, 29). Studies have shown that, while management is always informed of the reasons for failure in the chemical-processing industry, site personnel are informed only 77% of the time; designers, 55%; materials suppliers, 37%; and contractors, only 11% of the time.

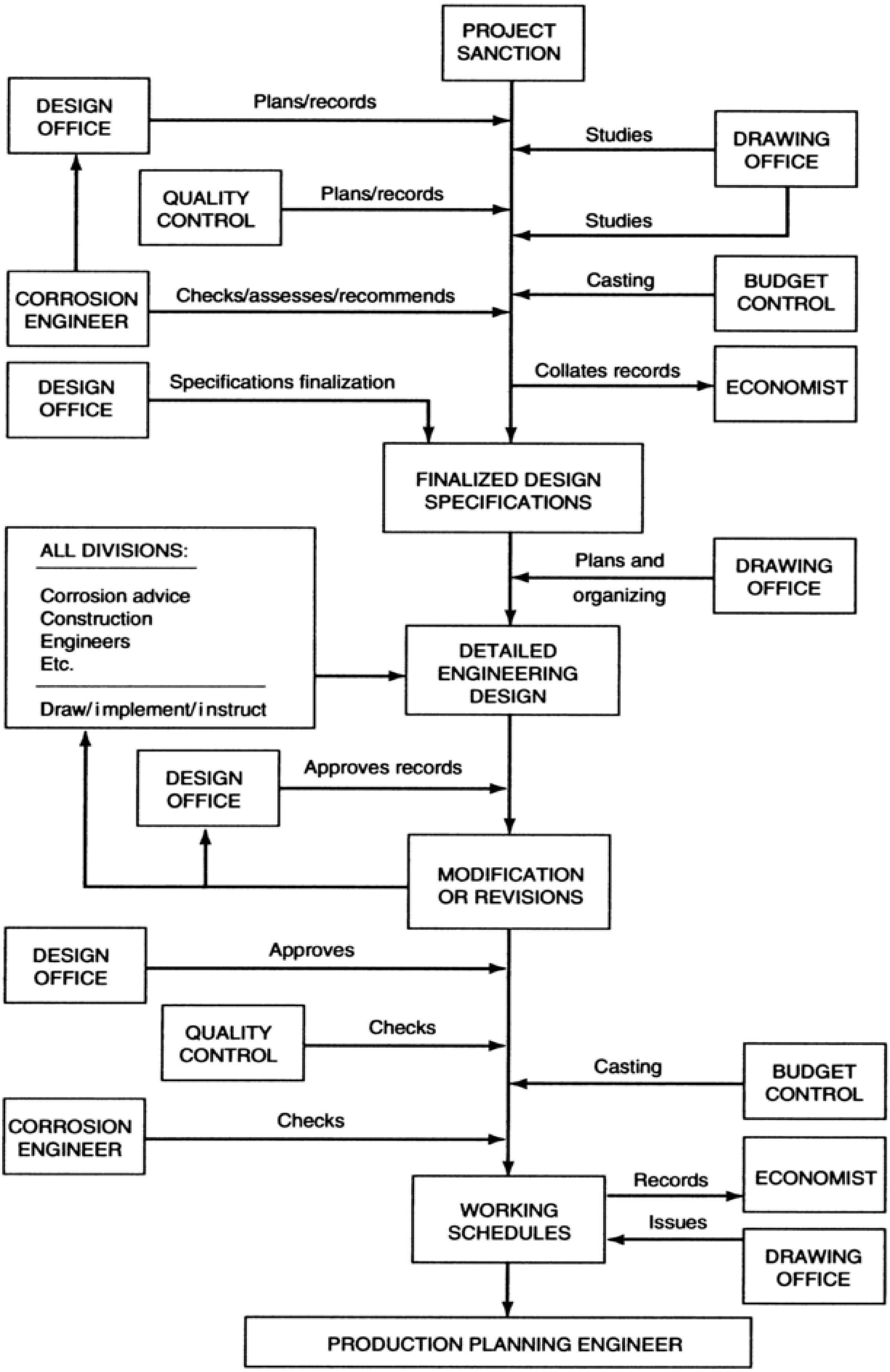

Fig. 1 Action steps during design. Source: Ref 28

Drafter's Delusions. A further complication in designing against corrosion relates to the general interpretation of design drawings in what has been referred to as drafter's delusions. For example, the drafter might be considering a certain piece of equipment without knowledge of the fact that there may be unusual shapes, moving parts, or environmental issues. A lack of attention to design detail causes many premature failures by corrosion-related processes. All too often, the designer will have in mind one thing, which, in reality, becomes totally different. For example, a simple crossover line between two reactor vessels might, in practice, become an extended line with several turns, merely to position a shutoff valve at a more convenient and accessible position closer to ground level. There are countless examples of this situation in real-world failure analysis, where the actual designs were not those originally intended (Ref 29, 30, 31, 32, 33, 34, 35); further examples are provided in the following pages.

Quality assurance and control usually ensure that the requested material is what it should be and that it was inspected and tested as specified. However, materials controls at fabrication are sometimes less than perfect. In one case, an inspector noticed a blemish on the outside of a steel pressure vessel. On closer scrutiny (from the vessel interior), the problem was found to be a steel bolt that had been inadvertently rolled into the steel plate during fabrication (Fig. 2).

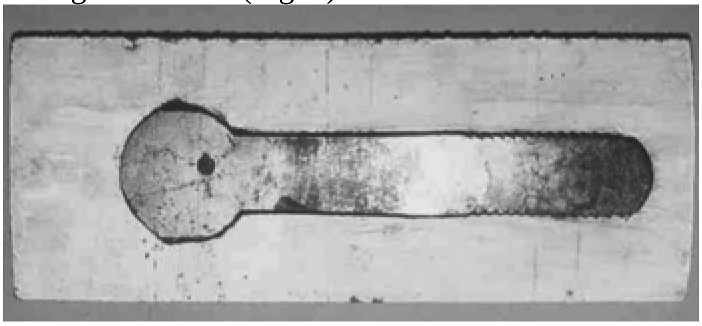

Fig. 2 An unexpected guest—a rolled-in bolt that dropped onto the plate during hot rolling

While considering materials, it is important to avoid nonspecific descriptions or terms in reference to design drawings and specifications. There are many instances where generic terms, such as *stainless steel, bronze, Hastelloy,* or *Inconel,* are too vague, and the ultimate choice is far from what was expected and required. Wherever possible, and notably, in high-risk areas, materials should be selected and tested according to code requirements (Ref 7, 36). Substitutes, if requested, should be properly evaluated before use.

Reliability Engineering. The designer should play a significant role in reliability management. The communication chain, or the reliability loop, from the designer, to the manufacturer, then to the user, and back to the designer is a key factor (Ref 29, 37). When a risk is well documented, it should be possible to overdesign or at least isolate the area to minimize risk to users. Where a risk of failure is high, the emphasis should be toward a fail-safe or no-fail/replace procedure. Failures vary considerably; the design function can be partially or totally affected, or the onset of failure can be gradual or sudden. The combination of sudden and total failure represents the worst catastrophic situation (e.g., explosions, fires, and total structural collapse), many of which can be attributed to a small design detail.

References cited in this section

1. H.H. Uhlig, *Corrosion Handbook,* John Wiley & Sons, 1948
2. R.W. Revie, Ed., *Uhlig's Corrosion Handbook,* 2nd ed., John Wiley & Sons, 2000
3. M.G. Fontana, *Corrosion Engineering,* 3rd ed., McGraw-Hill Book Co., 1986
4. D.A. Jones, *Principles and Prevention of Corrosion,* 2nd ed., Prentice Hall, 1996
5. C.P. Dillon, *Corrosion Resistance of Stainless Steels,* Marcel Dekker, Inc., 1995
6. S.L. Chawla and R.K. Gupta, *Materials Selection for Corrosion Control,* ASM International, 1993

7. R. Baboian, Ed., *Corrosion Tests and Standards: Applications and Interpretation,* MNL-20, *ASTM Manual Series,* ASTM, 1995

8. C.P. Dillon, *Corrosion Control in the Chemical Process Industries,* 2nd ed., Publication 45, Materials Technology Institute, 1997

9. L.L. Shreir, R.A. Jarman, and G.T. Burstein, Ed., *Corrosion,* Vol 1, 2, *Metal/Environment Reactions,* Butterworth Heinenmann, Ltd., 1994

10. V.A. Ashworth and P. Elliott, Guide to the Corrosion Resistance of *Metals, Metals Reference Book,* 5th ed., C.J. Smithells and E.A. Brandes, Ed., Butterworths, 1976, p 1460

11. B.D. Craig and D. Anderson, Ed., *Handbook of Corrosion Data,* 2nd ed., ASM International, 1995

12. B.J. Moniz and W.I. Pollock, Ed., *Process Industries Corrosion,* NACE International, 1986

13. *Corrosion Data Survey: Metals Section,* 6th ed., NACE, 1985; *Nonmetals Section,* 5th ed., NACE, 1975

14. D.J. De Renzo, Ed., *Corrosion-Resistant Materials Handbook,* 4th ed., Noyes, 1985

15. D. Behrens, G. Kreysa, and R. Eckermann, Ed., *DECHEMA Corrosion Handbook: Corrosive Agents and Their Interaction with Materials,* VCH, 1987–1993

16. Visual Aids/CDS, texts, Materials Technology Institute, Chem-Cor Advisory Systems, 1999–2002

17. P.A. Schweitzer, Ed., *Corrosion Resistance Tables,* 4th ed., Marcel Dekker, 1995

18. V.R. Pludek, *Design and Corrosion Control,* Macmillan, 1977

19. R.J. Landrum, *Fundamentals of Designing for Corrosion Control,* NACE International, 1989

20. R.N. Parkins and K.A. Chandler, *Corrosion Control in Engineering Design,* Department of Industry, Her Majesty's Stationery Office, London, 1978

21. L.D. Perrigo and G.A. Jensen, Fundamentals of Corrosion Control Design, *The North. Eng.,* Vol 13 (No. 4), 1982, p 16

22. S.K. Coburn, *Corrosion Source Book,* American Society for Metals, 1984

23. *Designer Handbooks,* Specialty Steel Industry of North America, 1995–1996

24. *Guides to Practice in Corrosion Control,* Department of Industry, Her Majesty's Stationery Office, London, 1979–1986

25. *Engineering Design Guides,* Design Council, British Standards Institute, Council of Engineering Institutions, Oxford University Press, 1975–1979

26. P. Elliott and J.S. Llewelyn-Leach, *Corrosion Control Checklist for Design Offices,* Department of Industry, Her Majesty's Stationery Office, London, 1981

27. P. Elliott, *Corrosion Control in Engineering Design,* audiovisual, Department of Industry, United Kingdom, 1981

28. P. Elliott, Corrosion Survey, *Suppl. Chem. Eng.,* Sept 1973

29. P. Elliott, Catch 22 and the UCS Factor. Why Must History Repeat Itself?, *Mater. Perform.,* Vol 28 (No. 7), 1989, p 70, Vol 28 (No. 8), 1989, p 75

30. O.W. Siebert, Classic Blunders in Corrosion Protection, *Mater. Perform.,* Vol 17 (No. 4), 1978, p 33, Vol 22 (No. 10), 1983

31. C.P. Dillon, "Unusual Corrosion Problems in the Chemical Process Industries," Publication 54, Materials Technology Institute, 2000

32. T.F. Degnan, *Mater. Perform.,* Vol 26 (No. 1), 1987, p 11

33. P. Elliott, Why Must History Repeat Itself?, *Ind. Corros.,* Feb/March 1991, p 8

34. P. Elliott, Process Plant Corrosion—Recognizing the Threat, *Process Eng.,* Nov 1984, p 43

35. P. Elliott, Understanding Corrosion Attack, *Plant Eng.,* Oct 1993, p 68

36. *Standards for Corrosion Testing of Metals,* ASTM, 1990

37. H.J.H. Wassell, Reliability of Engineered Products, *Engineering Design Guide,* Design Council, Oxford University, 1980

P. Elliott, Designing to Minimize Corrosion, *Corrosion: Fundamentals, Testing, and Protection*, Vol 13A, *ASM Handbook,* ASM International, 2003, p 929–939

Designing to Minimize Corrosion

Peter Elliott, Corrosion and Materials Consultancy, Inc.

Corrosion Awareness

This article is intended to improve corrosion awareness, but clearly, this is only a starting point. To be effective, the user must also be willing to take action, and the designer should insist on appropriate codes and/or recommended working practices. Whether the necessary action will be taken is affected by financial, technical, safety, social, and/or political issues (Ref 37).
To prevent corrosion/degradation, the designer can:

- Avoid obvious design weaknesses (see subsequent examples)
- Use more reliable materials, even if this entails greater cost
- Introduce additional precautions, such as monitoring (Ref 38), inhibitors, cathodic protection, and coatings (Ref 39, 40)
- Establish efficient maintenance/repair teams having detailed procedures and including qualified surveyors, inspectors, and supervisors
- Ensure that standby products are available, fully labeled, and properly stored (using desiccants and noncorrosive packaging)

As noted previously, the planned approach for reliable engineering design should include corrosion control and/or preventive measures, for which standards and specifications are available. Actual (real-world) approaches vary from plant to plant (or component to component) and include:

- The avoid-failure approach
- The keep-it-working approach
- The let-it-fail-then-repair approach

Aspects germane to these approaches are summarized in Table 1 (Ref 29, 37).

Table 1 Design aspects for reliability

Approach	Factors to be taken into account (typical)
Avoid-failure approach	
Control product duty	Fail-safe; visible instrumentation
Keep product simple	Fewer functions; fewer joints
Predict reliability	Maintain in fixed limits; overdesign (thicker), etc.
Study variable interfaces	Contact faces, bearings; lubrication (wear, friction); seals; consult experts and test work
Instill care for familiar items or designs	Complacency; negligence
Study innovation	Consult experts and test work; records of operation; records of failure mode/frequency
Redundant items	Stand-by units in good repair; storage; handling; vibration, impact, wear, etc.
Recognize human limits	Misreading of instructions; sequence of controls (hypnosis?); adequate housekeeping; user attitudes
Test product design	Proving the design; variables; safety limits; pilot plant and real-life testing
Control malfunctions	Human; automatic; mixture; important for software/hardware
Keep-it-working approach	
Maintainability	Access
Short-term items	Replace routinely before failure; regular inspection; monitoring
Spares	Identity correctly coded; location known; easy access replacement; avoid identical mating systems
Built-in adjustments	Corrects for progressive deterioration; manual/automatic
Let-it-fail-then-repair approach	
Defects	Subtle or catastrophic
Spares	Need quantified reliability (difficult for corrosion)
Minimize off-period	Keep repair time low; speedy fault diagnosis; speedy removal of failed part(s); speedy replacement; speedy check of assembly; experts, inspectors

Source: Ref 29

New plants and process equipment are commonly designed to prevent or reduce problems that have occurred previously. Updated and improved procedures are of little use, however, if no action is made until after the equipment fails. Situations have occurred where cathodic protection was ineffective because the anode material was not connected to the structure it was protecting; a monitoring signal (a bell) was ignored because of noise; on-line monitoring data were estimated (guessed at), so that the inspector could avoid travel in blizzard conditions; and a sentinel hole (weep hole) leaked for weeks without any investigation as to the cause until the vessel exploded.

References cited in this section

29. P. Elliott, Catch 22 and the UCS Factor. Why Must History Repeat Itself?, *Mater. Perform.,* Vol 28 (No. 7), 1989, p 70, Vol 28 (No. 8), 1989, p 75

37. H.J.H. Wassell, Reliability of Engineered Products, *Engineering Design Guide,* Design Council, Oxford University, 1980

38. G. Moran and P. Labine, *Corrosion Monitoring in Industrial Plants Using Nondestructive Testing and Electrochemical Methods,* ASTM, 1986

39. C.G. Munger, *Corrosion Prevention by Protective Coatings,* NACE International, 1984; updated 2001

40. P.E. Weaver, “Industrial Maintenance Painting,” RP0178, NACE International, 1973, p 2

P. Elliott, Designing to Minimize Corrosion, *Corrosion: Fundamentals, Testing, and Protection*, Vol 13A, *ASM Handbook*, ASM International, 2003, p 929–939

Designing to Minimize Corrosion

Peter Elliott, Corrosion and Materials Consultancy, Inc.

Why Failures Occur

In the context of design, there are several factors that relate to materials-component failure:

- Overload suggests a weakness in plant control instrumentation or operation.
- Abnormal conditions can result from a lack of process control or variations in raw materials (alloy type or chemical inhibitors, etc.).
- Poor fabrication may result from inadequate instructions or inspection (e.g., excessive cold work, overmachining, flame cutting, or excessive torque loading).
- Poor handling. Scratches or machine marks can result from poor detailing or poor instruction. Not to be excluded are identity marks (incised codes) and inspection stamps.
- Assembly (if incorrect), welds, and fasteners can seriously influence stress, flow, and compatibility.
- Storage and transportation can significantly influence materials performance, especially for items shipped to/from tropical, humid climates where heavy rains, violent seas, storms, and cargo sweat may each contribute to materials degradation unless adequate precautions are taken (Ref 41). Proper design and effective corrosion-control management normally should accommodate these aspects of materials handling.
- Accessibility. Some structures or components may not be accessible for remedial work, even if a corrosion risk is recognized. Buried structures can be affected where soil and bacterial corrosion might apply (Ref 42, 43).

References cited in this section

41. A. Sparks, Steel, *Carriage by Sea,* 2nd ed., Lloyd's of London Press, 1995

42. G. Kobrin, Ed., *Microbiologically Influenced Corrosion,* NACE International, 1993

43. J.G. Stoecker II, Ed., *Microbiologically Influenced Corrosion,* Vol 2, NACE International, 2001

P. Elliott, Designing to Minimize Corrosion, *Corrosion: Fundamentals, Testing, and Protection*, Vol 13A, *ASM Handbook*, ASM International, 2003, p 929–939

Designing to Minimize Corrosion

Peter Elliott, Corrosion and Materials Consultancy, Inc.

Design and Materials Selection

Corrosion control measures are best initiated at the design stage (Fig. 1). Materials are usually selected to perform a basic function or to provide a functional requirement. In many instances, the materials choice is dictated not by corrosion but by characteristics such as strength, reflectivity, wear resistance, and dimensional stability. In some situations, a corrosion-resistant alloy may not be satisfactory.

High-Temperature Service. The subject of designing for high-temperature service is outside the scope of this article (Ref 26, 44, 45, 46). High temperatures always accelerate corrosion processes, and certain gases or liquids, which are considered innocuous under ambient conditions, become aggressive to materials when hot. A tenfold change in corrosion rate is not uncommon for a temperature change of 30 °C (54 °F) under aqueous conditions. The same tenfold change (or considerably worse) can occur with a 20 °C (36 °F) change under high-temperature conditions. If temperatures are too high, the material might oxidize (i.e., scale). Thick scales and metal loss result from overheating, which could be due to loss of water cooling or the absence of insulation. Heat transfer will decrease as the scale/deposit thicknesses increase.

Candidate high-temperature materials need to be strong and resistant to oxidation or to other corrosion processes that might involve complex multi-oxidant environments having highly volatile phases and molten salts. It is important for designers and others to recognize that several corrosion elements might simultaneously be involved in an application (e.g., oxygen, halogen, and sulfur) (Table 2). Materials selection for high-temperature service needs to be reviewed for each individual part and application. Alloy steels and more sophisticated alloys based on nickel and cobalt, in which key elements for high-temperature corrosion resistance include chromium, aluminum, silicon, and rare-earth additions for scale retention, are must commonly used.

Table 2 Types of corrosion and corrodents encountered in high-temperature processes or components

Process components	Temperature		Types of corrosion or corrodent
	°C	**°F**	
Chemical/petrochemical			
Ethylene steam cracking furnace tubes	to 1000	to 1830	Carburization, oxidation
Steam reforming tubes	to 1000	to 1830	Oxidation, carburization
Vinyl chloride crackers	to 650	to 1200	Halide gas
Hydrocracking heaters, reactors	to 550	to 1020	H_2S and H_2
Petroleum coke calcining recuperators	816	1501	Oxidation, sulfidation
Cat cracking regenerators	to 800	to 1470	Oxidation
Flare stack tips	950–1090	1740–1995	Oxidation, thermal fatigue, sulfidation, chlorination, dewpoint
Carbon disulfide furnace tubes	850	1560	Sulfidation, carburization, deposits
Melamine production (urea) reactors	450–500	840–930	Nitriding
Other processes			
Titanium production reactor vessels	900	1650	Oxidation, chlorination

Nitric acid—catalyst grid	930	1705	Oxidation, nitriding, sulfidation
Nuclear reprocessing reactors	750–800	1380–1470	Oxidation (steam), fluorination (HF)
Oil-fired boiler superheaters	850–900	1560–1650	Fuel ash corrosion
Gas turbine blades corrosion	to 950	to 1740	Sulfates, chlorides, oxidation, ash
Waste incinerators—superheaters	480	895	Chlorination, sulfidation, oxidation, molten salts
Fiberglass manufacturing recuperators	1090	1995	Oxidation, sulfidation, molten salts

Source: Ref 26

Different behavior can arise at similar temperatures, depending on the source of heat, such as electrical heating elements, fuel combustion, flue gases and deposits, flame impingement, friction, and wear. When hot gases cool, condensation can cause acid dewpoint conditions, thereby changing the materials choice to a corrosion-resistant alloy.

References cited in this section

26. P. Elliott and J.S. Llewelyn-Leach, *Corrosion Control Checklist for Design Offices,* Department of Industry, Her Majesty's Stationery Office, London, 1981

44. G.Y. Lai, *High Temperature Corrosion of Engineering Alloys,* ASM International, 1990

45. P. Elliott, Practical Guide to High Temperature Alloys, *Mater. Perform.,* Vol 28, 1989, p 57

46. P. Elliott, Choose Materials for High-Temperature Environments, *Chem. Eng. Prog.,* Vol 97, 2001, p 75

P. Elliott, Designing to Minimize Corrosion, *Corrosion: Fundamentals, Testing, and Protection*, Vol 13A, *ASM Handbook*, ASM International, 2003, p 929–939

Designing to Minimize Corrosion

Peter Elliott, Corrosion and Materials Consultancy, Inc.

Design Factors That Influence Corrosion

The basic factors that most influence design for corrosion resistance are summarized in Table 3. Each factor plays a unique yet not always unrelated role with other factors (Ref 26). For example, localized corrosion damage adjacent to the spindle support of a stainless steel paddle stirrer (Fig. 3) resulted not only from crevice corrosion (oxygen differential cell) but also because of galvanic corrosion, caused by a small carbon steel retaining screw (anodic) that had been used inadvertently for assembly. Ultimately, the stirrer support loosened, which allowed further deterioration by fretting.

Table 3   Corrosion factors that can influence design considerations

Basic Factor	Design detail
Environment	Natural Chemical Storage/transit
Stress	Residual stress from fabrication Operating stress—static, variable, alternating
Shape	Joints, flanges Crevices, deposits Liquid containment and entrapment
Compatibility	Metals with metals Metals with other materials Quality control
Movement	Flowing fluids Parts moving in fluids Two-phase fluids
Temperature	Oxidation, scales Heat-transfer effects Molten deposits Condensation and dewpoint
Control	Surface cleaning and preparation Coatings Cathodic protection Inhibitors Inspection Planned maintenance

Source: Ref 25

Fig. 3 Crevice corrosion of a stainless steel paddle stirrer, exacerbated by galvanic corrosion by a steel retaining pin

Design details that can accelerate corrosion follow.
Location. Exposure to winds and airborne particulates can lead to deterioration of structures. Designs that leave structures exposed to the elements should be carefully reviewed. Prevailing winds and seasprays have to be taken into account in many applications, including buildings, the storage of spare parts, and the location of air intake fans to gas turbines and other equipment (Fig. 4). Atmospheric corrosion is significantly affected by temperature, relative humidity, rainfall, and pollutants. Also important are the season and location of on-site fabrication, assembly, and painting. Codes of practice must be adapted to the location and the season.

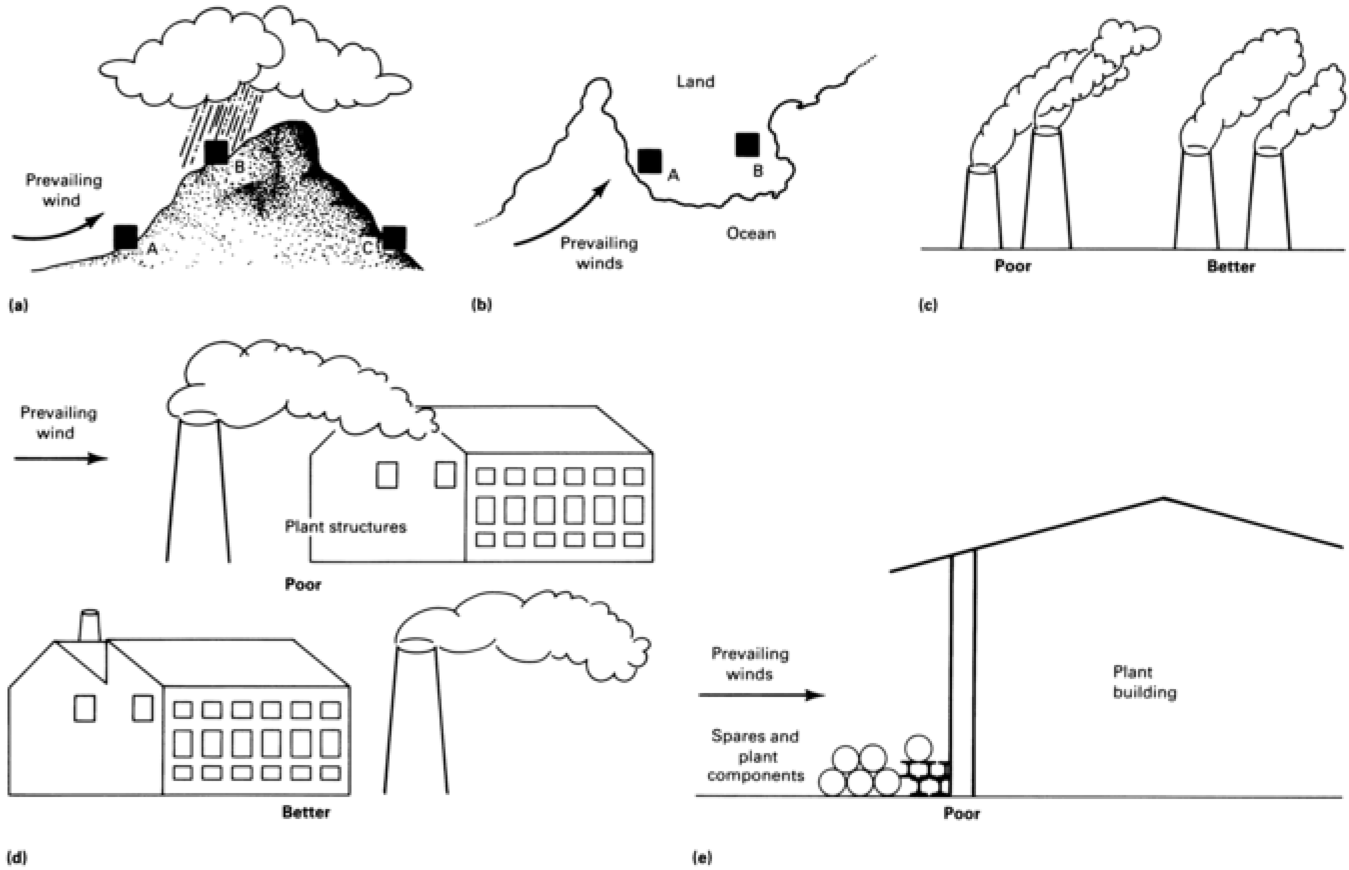

Fig. 4 Site location as a design consideration. (a) Topographic features favor some sites over others. Location C would be the preferred site for corrosion considerations. (b) In marine atmospheres, prevailing winds should be taken into account, making location B the preferred site. (c), (d), and (e) Carry-over effects from prevailing winds should be evaluated.

Shape. Geometrical form is basic to design. The objective is to minimize or avoid situations that worsen corrosion. These situations can range from stagnation (e.g., retained fluids and/ or solids, contaminated water used for hydrotesting) to sustained fluid flow (e.g., erosion/cavitation in components moving in or contacted by fluids, as well as splashing or droplet impingement).

Common examples of stagnation include nondraining structures, dead ends, badly located components, and poor assembly or maintenance practices (Fig. 5). General problems include localized corrosion associated with differential aeration (oxygen concentration cells), crevice corrosion, and deposit corrosion.

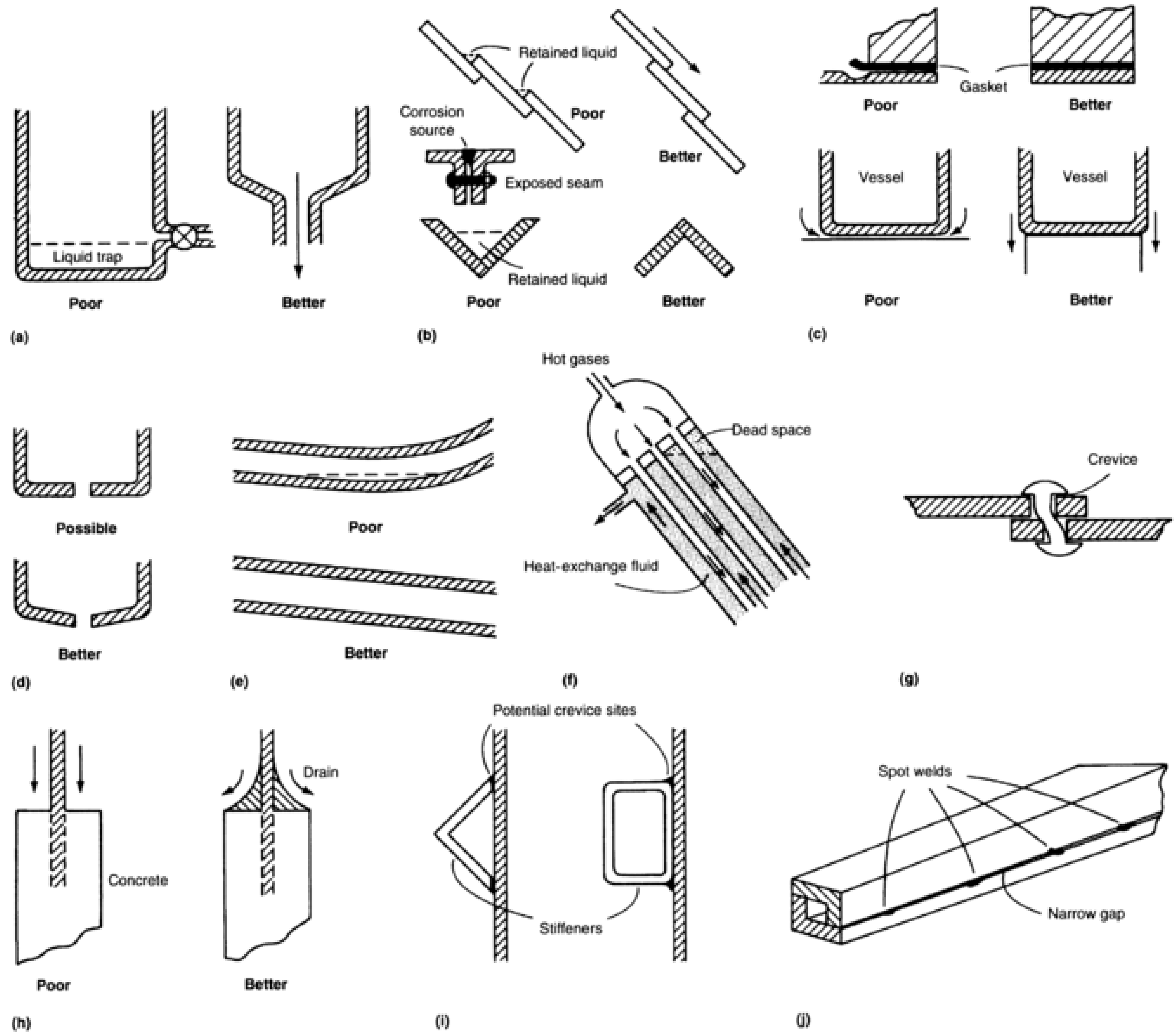

Fig. 5 Examples of how design and assembly can affect localized corrosion by creating crevices and traps where corrosive liquids can accumulate. (a) Storage containers or vessels should allow complete drainage; otherwise, corrosive species can concentrate in vessel bottom, and debris may accumulate if the vessel is open to the atmosphere. (b) Structural members should be designed to avoid retention of liquids; L-shaped sections should be used with open side down, and exposed seams should be avoided. (c) Incorrect trimming or poor design of seals and gaskets can create crevice sites. (d) Drain valves should be designed with sloping bottoms to avoid pitting of the base of the valve. (e) Nonhorizontal tubing can leave pools of liquid at shutdown. (f) to (j) Examples of poor assembly that can lead to premature corrosion problems. (f) Nonvertical heat-exchanger assembly permits dead space that is prone to overheating if very hot gases are involved. (g) Nonaligned assembly distorts the fastener, creating a crevice that can result in a loose fit and contribute to vibration, fretting, and wear. (h) Structural supports should allow good drainage; use of a slope at the bottom of the member allows liquid to run off, rather than impinge directly on the concrete support. (i) Continuous weld for horizontal stiffeners prevents traps and crevices from forming. (j) Square sections formed from two L-shape members need to be continuously welded to seal out the external environment.

Movement. Fluid movement need not be excessive to damage a material. Much depends on the nature of the fluid and the hardness of the material. A geometric shape may create a sustained delivery of fluid or may locally disturb a laminar stream and lead to turbulence. Replaceable baffle plates or deflectors are beneficial where circumstances permit their use; they eliminate the problem of impingement damage to the structurally significant component.

Careful fabrication and inspection should eliminate or reduce poor profiles (e.g., welds, rivets, and bolts), rubbing surfaces (e.g., wear, fretting), and galvanic effects due to the assembly of incompatible components. Figure 6 shows typical situations in which geometric details influence flow.

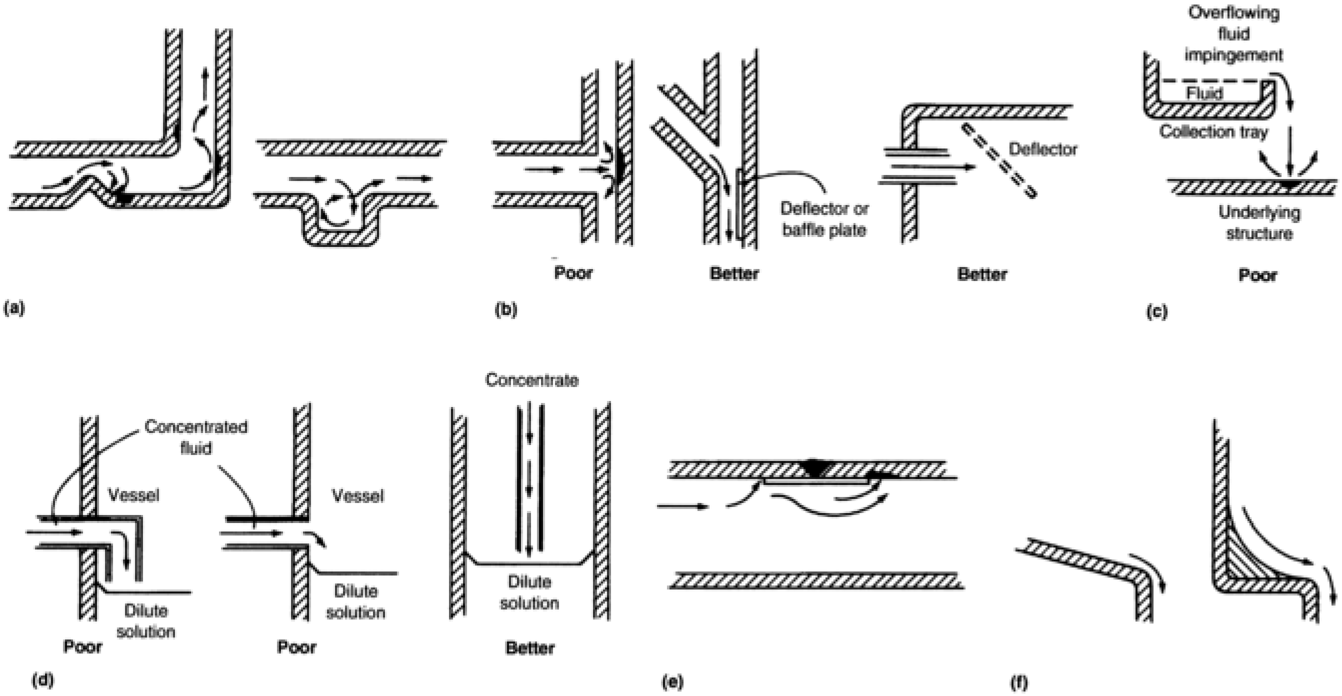

Fig. 6 Effect of design features on flow. (a) Disturbances to flow can create turbulence and cause impingement damage. (b) Direct impingement should be avoided; deflectors or baffle plates can be beneficial. (c) Impingement from fluid overflowing from a collection tray can be avoided by relocating the structure, increasing the depth of the tray, or using a deflector. (d) Splashing of concentrated fluid on container walls should be avoided. (e) Weld backing plates or rings can create local turbulence and crevices. (f) Slope or modified profiles should be provided to permit flow and minimize fluid retention.

Compatibility. In plant environments, it is often necessary to use different materials in close proximity. Sometimes, components that were designed in isolation can end up in direct contact in the plant (Fig. 7). In such instances, the ideals of a total design concept become especially apparent but usually in hindsight. Direct contact of dissimilar metals introduces the possibility of galvanic corrosion, and small anodic (corroding) areas should be avoided wherever this contact is apparent.

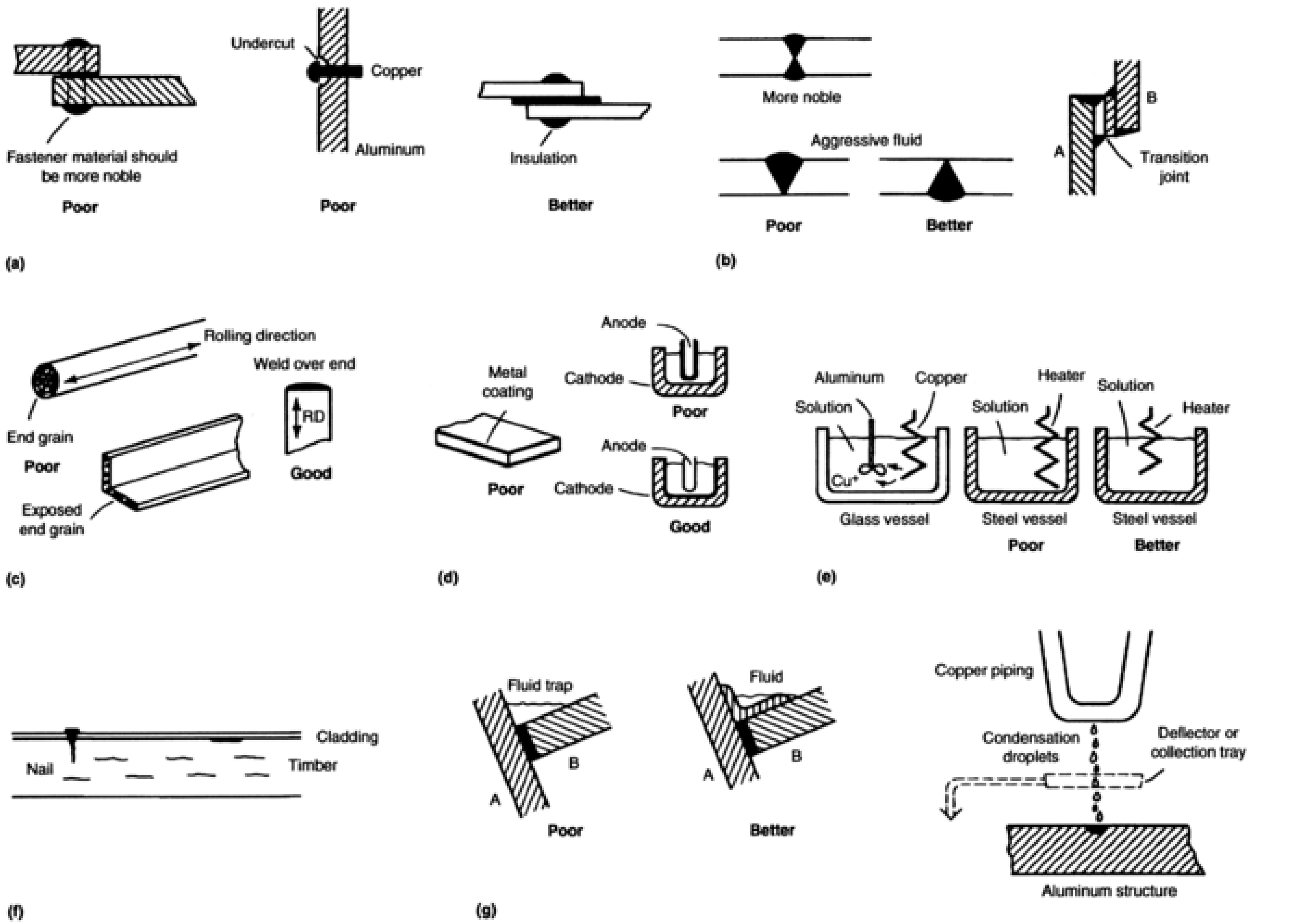

Fig. 7 Design details that can affect galvanic corrosion. (a) Fasteners should be more noble than the components being fastened; undercuts should be avoided, and insulating washers should be used. (b) Weld filler metals should be more noble than base metals. Transition joints can be used when a galvanic couple is anticipated at the design stage, and weld beads should be properly oriented to minimize galvanic effects. (c) Local damage can result from cuts across heavily worked areas. End grains should not be left exposed. RD, rolling direction. (d) Galvanic corrosion is possible if a coated component is cut. When necessary, the cathodic component of a couple should be coated. (e) Ion transfer through a fluid can result in galvanic attack of less noble metals. In the example shown at left, copper ions from the copper heater coil could deposit on the aluminum stirrer. A nonmetallic stirrer would be better. In the center, the distance from a metal container to a heater coil should be increased to minimize ion transfer. (f) Wood treated with copper preservatives can be corrosive to certain nails, especially those with nobility different from that of copper. Aluminum cladding can also be at risk. (g) Contact of two metals through a fluid trap can be avoided by using a drain, collection tray, or a deflector.

Galvanic corrosion resulting from metallurgical sources is well documented. Problems such as weld decay and sensitization can generally be avoided by materials selection or suitable fabrication techniques. Less obvious instances of localized attack occur because of end-grain attack and stray-current effects, which can render designs ineffective.

End-grain attack, or preferential attack of grains exposed by crosscutting through a metal plate or rod (Fig. 7c), occurs in many corrosive fluids. An example is the cut edges and punched- out holes in a stainless steel reactor tray (Fig. 8).

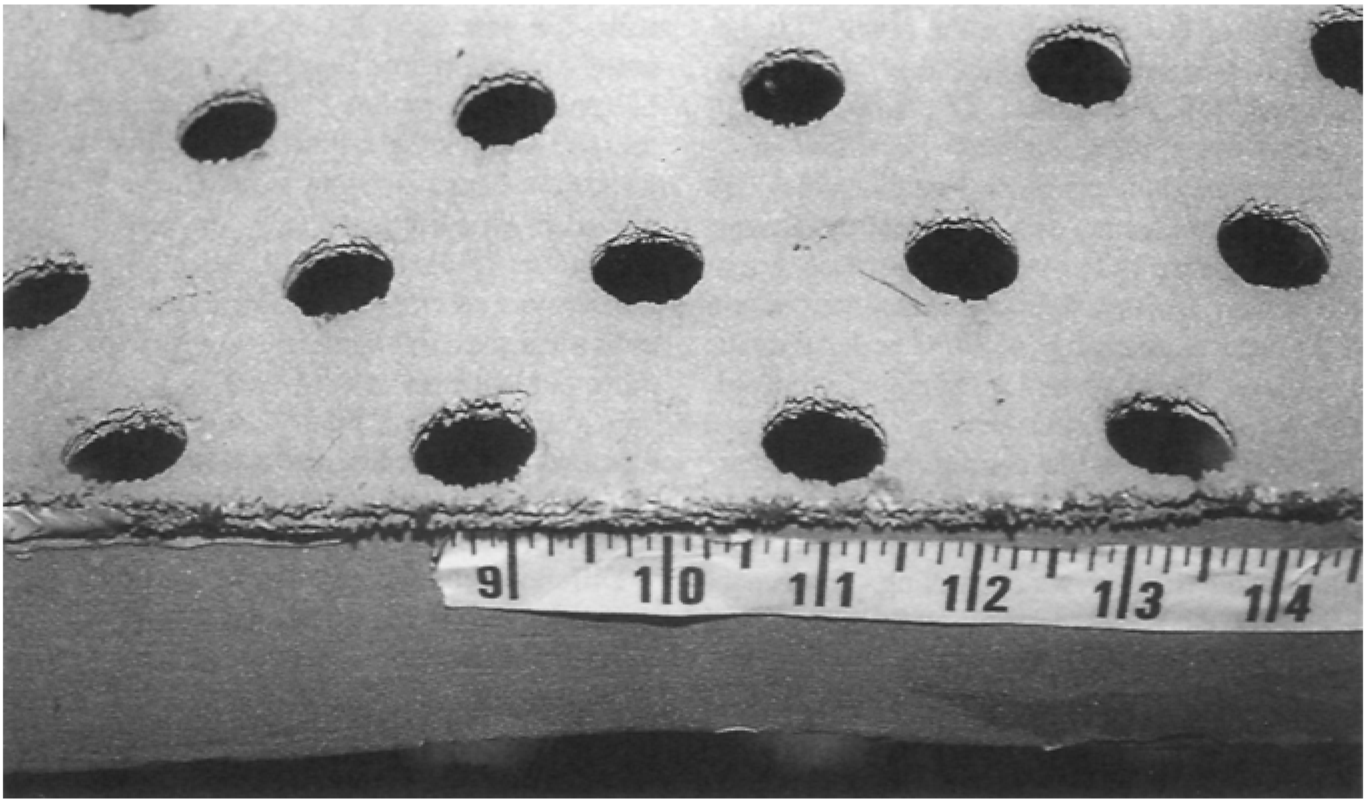

Fig. 8 End-grain corrosion along cut edges and punched holes in a reactor tray made from type 316 (Unified Numbering System, or UNS, S31600) stainless steel

Stray-current effects are common on underground iron or steel pipelines that are located close to electrical supply lines, or where stray currents can cause active corrosion at preferred sites. For example, stray-current attack caused a titanium flange spacer to become anodic during service due to inappropriate grounding of welding equipment on an adjacent part of the plant structure.

Designers, when aware of compatibility effects, need to exercise their ingenuity to minimize the conditions that most favor increased corrosion currents. Table 4 provides some suggestions.

Table 4 Sources of increased corrosion currents and related design considerations

Source	Design considerations
Metallurgical sources (both within the metal and for relative contact between dissimilar metals)	Difference in potential of dissimilar materials; distance apart; relative areas of anode and cathode; geometry (fluid retention); mechanical factors (e.g., cold work, plastic deformation, sensitization)
Environmental sources	Conductivity and resistivity of fluid; changes in temperature; velocity and direction of fluid flow; aeration; ambient environment (seasonal changes, etc.)
Miscellaneous sources	Stray currents; conductive paths; composites (e.g., concrete rebars)

Galvanic corrosion is a potential problem when designs include jointed assemblies (Fig. 5, 7). Where dissimilar metals are to be used, some consideration should be given to chosing compatible materials with similar potentials. Care should be exercised, because the galvanic series is limited and refers to specific environments, usually seawater.

Where noncompatible materials are to be joined, it is advisable to use a more noble metal in a joint (Fig. 7b). Effective insulation can be useful if it does not lead to crevice corrosion. Some difficulties arise in the use of adhesives, which are not usually sealants.

The relative surface areas of anodic and cathodic surfaces should not be underestimated, because corrosion at a small anodic zone can be several hundred times greater than that for the same bimetallic components of similar area. As noted previously, synergistic effects must also be recognized, such as failure resulting from a

combination of galvanic and crevice attack. One failure was attributed to the unfortunate choice of a carbon steel bolt to tighten a spindle support for a stainless steel paddle stirrer (Fig. 9). The result was crevice corrosion at the stirrer support (Fig. 3), which was exacerbated by the galvanic action caused by the carbon steel/stainless steel metal- to-metal contact.

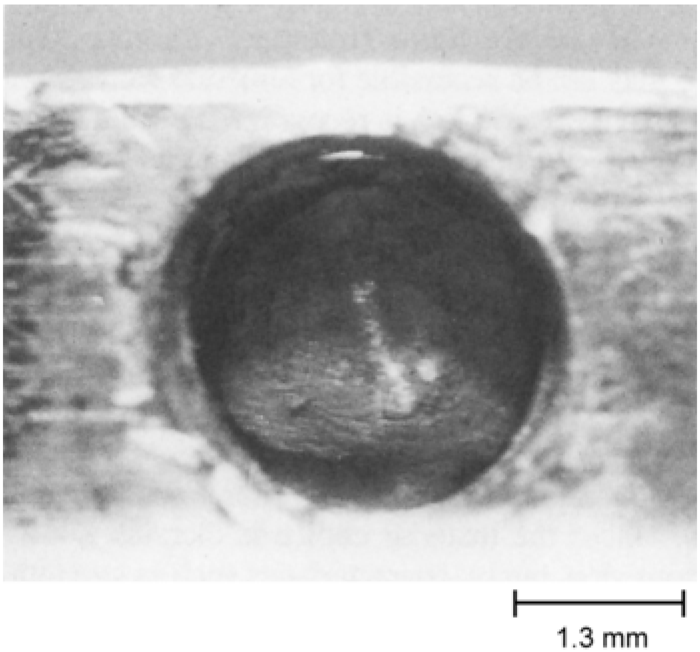

Fig. 9 The incorrect choice of a carbon steel retaining bolt for a stainless steel spindle resulted in localized galvanic corrosion of the paddle-stirrer assembly (Fig. 3).

Less obvious examples of galvanic corrosion occur when ion transfer results in the deposition of active and noncompatible deposits on a metal surface. For example, an aluminum stirrer plate used in water was extensively pitted because a copper heater coil (Fig. 7e) heated the water bath. The pits resulted from deposition of copper ions from the heater element. Localized corrosion of zinc-coated steel results from contact of water droplets falling from copper pipe onto galvanized ducting (Fig. 10). More rapid but similar damage occurred when a dental aspirator (Teflon-coated aluminum) was attacked by mercury from a tooth filling. These two metals rank as a high-risk combination for galvanic corrosion (see Fig.1 in the article “Electroplated Coatings” in this Volume). The aluminum section was rapidly pitted, once sharp fragments of tooth enamel first wore away the synthetic fluorine-containing resin.

Fig. 10 Initiation of corrosion (white rust) on galvanized ducting by water droplets, accelerated by galvanic corrosion due to copper ions in solution from overhead copper pipes

An anodic component can, on occasion, be initially overdesigned (made thicker) to allow for the anticipated corrosion loss during its service life. In other instances, easy replacement is a cost-effective option (Table 1).

Where metallic coatings are used, there may be a risk of galvanic corrosion, especially along the cut edges. Rounded profiles and effective sealants or coatings are beneficial. Transition joints can be introduced when different metals are to be in close proximity. These and other situations are illustrated in Fig. 7. Another possibility is coating of the cathodic material for corrosion control. Ineffective painting of an anode in an assembly can significantly reduce the desired service lifetime, because local defects (anodes) effectively multiply the risk of localized corrosion.

Corrosion Under Insulation. Insulation can create an area for potential corrosion attack, although most problems arise because of poor installation. Insulation types and properties vary considerably, and expert advice from suppliers is recommended. The most common corrosion problems include crevice corrosion (where insulation and/or adhesives are tightly held against a metal surface, for example, when straps or ties are too tight) and pitting corrosion (where moisture condenses on the metal, usually because the insulation barrier was too thin or was improperly installed). Moisture-absorbing tendencies vary from one insulation to another (Ref 47).

Wet-dry cycling has been known to lead to concentration effects (e.g., chloride ions from calcium silicate insulation). There have been reported instances of chloride stress-corrosion cracking (SCC) in certain stainless steel pipes and vessels, or pitting of these and other materials, such as aluminum, when contacted by insulation. The early instances of SCC failure were mainly attributable to high chloride levels (500 to 1500 ppm) associated with asbestos-type materials. The chloride levels have been significantly reduced in recent years to a level that is not expected to cause SCC. Standards are now available, as are tests to evaluate insulation materials

(Ref 48). A parallel German standard calls for zero nitrite content and <0.2% ammonia levels in elastomeric insulation that is used for copper and copper alloy piping, to reduce the risk of SCC (Ref 49).
Figure 11 shows some typical examples in which design and installation procedures could have been improved. Other problems occur when insulation is torn or joints are misaligned or incorrectly sealed with duct tape or similar bandaging, none of which is recommended by insulation suppliers.

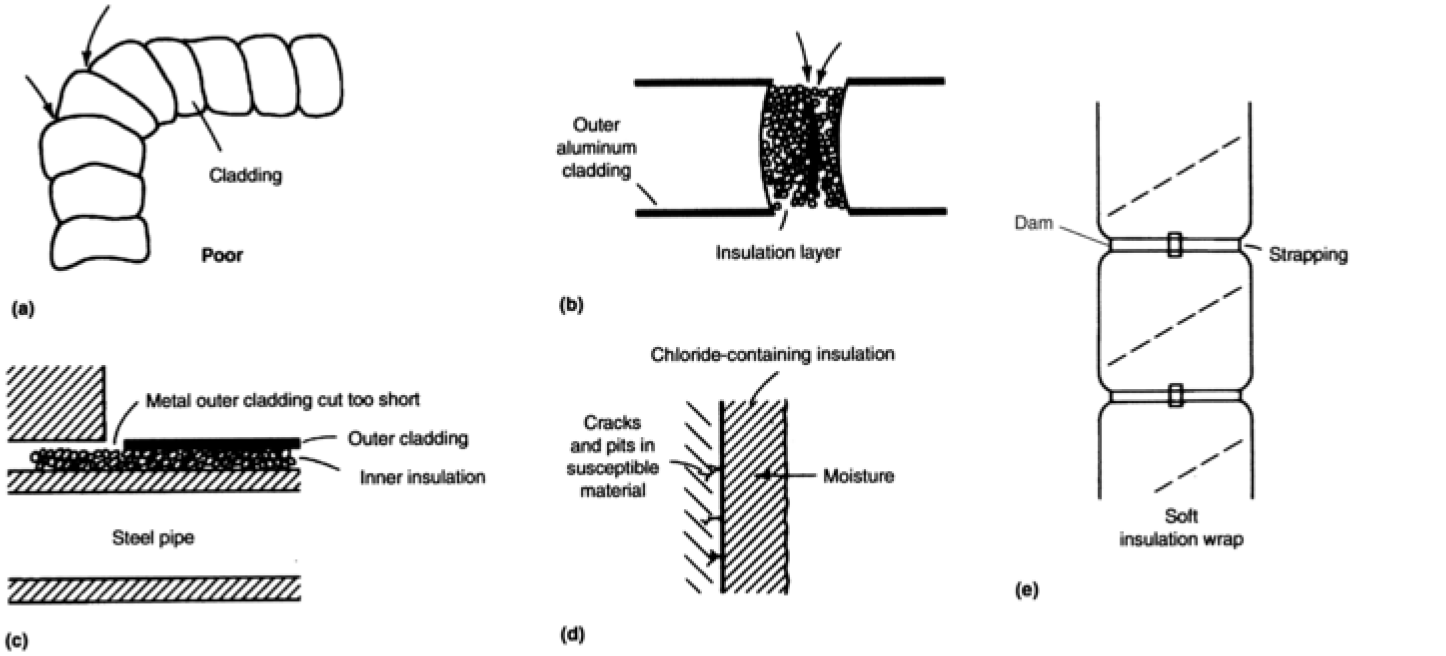

Fig. 11 Corrosion problems associated with improper use of insulation and lagging. (a) Incorrect overlap in lobster-back cladding does not allow fluid runoff. (b) Poor installation left a gap in the insulation that allows easy access to the elements. (c) Outer metal cladding was cut too short, leaving a gap, with the inner insulation exposed. (d) Insufficient insulation can allow water to enter; chloride in some insulation can result in pitting or stress-corrosion cracking of susceptible materials. (e) Overtightened strapping can damage the insulation layer and cause fluid dams on vertical runs.

Stress. From a general design philosophy, environments that promote metal dissolution can be considered more damaging if stresses are also involved. In such circumstances, materials can fail catastrophically and unexpectedly, with safety and health implications.
A classic example of chloride SCC occurred in a type 304 (Unified Numbering System, or UNS, S30400) stainless steel vessel (Fig. 12). The stress-corrosion cracks extended radially over the area where a new flanged outlet was welded into the vessel. Residual stresses (from flame cutting) and the fluids inside the vessel (acidic with chlorides) were sufficient to cause this failure in a matter of weeks.

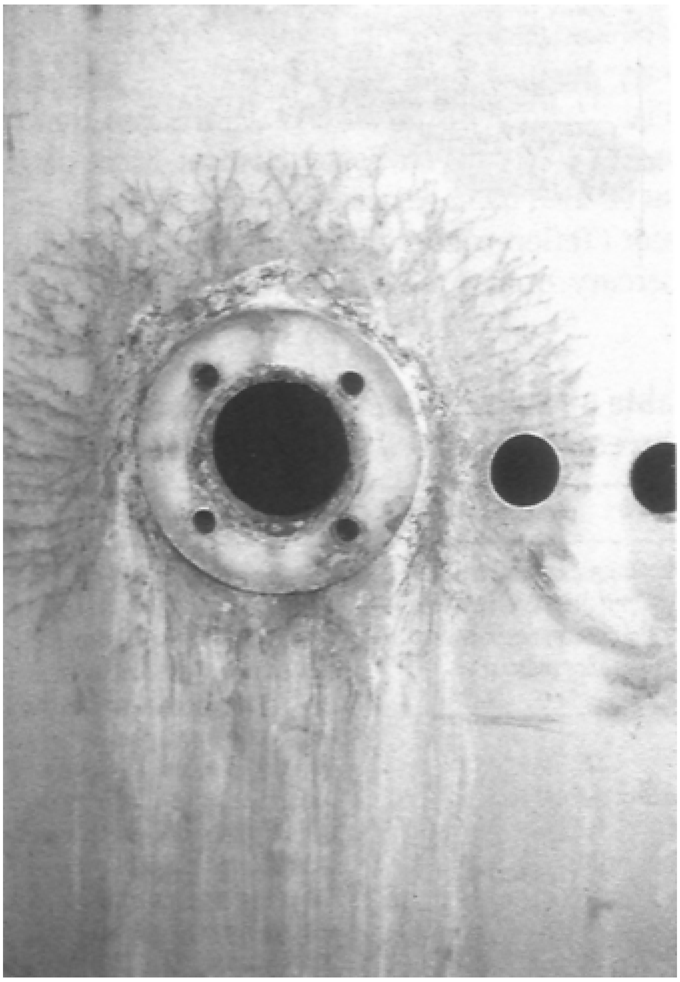

Fig. 12 Chloride stress-corrosion cracking in a type 304 (Unified Numbering System, or UNS, S30400) stainless steel vessel after a new flange connection was welded into place

Figure 13 shows examples of using design detail to minimize stress. Perfection is rarely attained in general practice, and some compromise on materials limitation, both chemical and mechanical, is necessary. Mechanical loads can contribute to corrosion, and corrosion (as a corrosive environment) can initiate or trigger mechanical failure. Designs that introduce local stress concentrations directly or as a consequence of fabrication should be carefully considered.

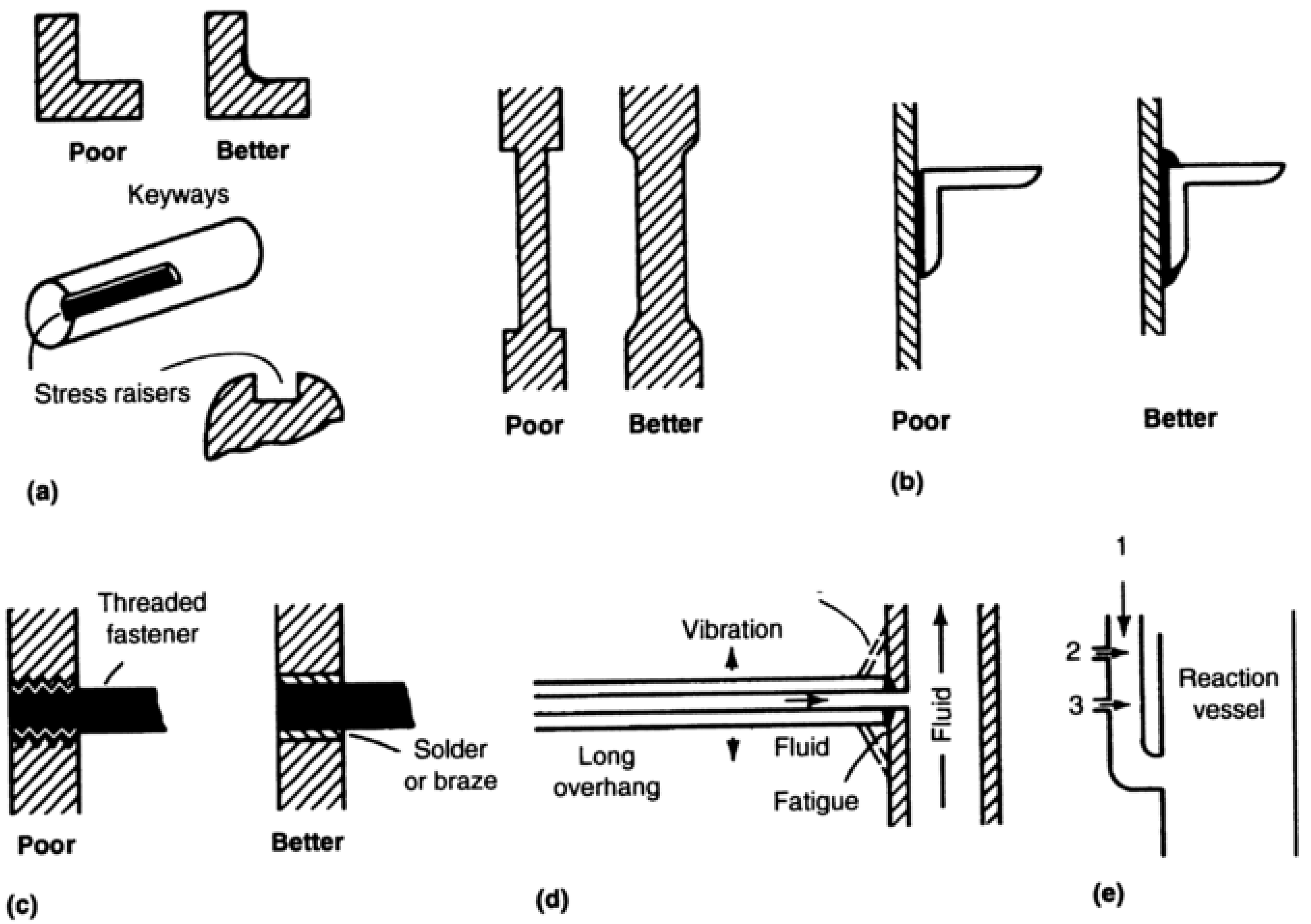

Fig. 13 Design details that can minimize local stress concentrations. (a) Corners should be given a generous radius. (b) Welds should be continuous to minimize sharp contours. (c) Sharp profiles can be avoided by using alternative fastening systems. (d) Too long an overhang without a support can lead to fatigue at the junction. Flexible hose may help alleviate this situation. (e) Side-supply pipework may be too rigid to sustain thermal shock from a recurring sequence that involves (1) air under pressure, (2) steam, and (3) cold water.

Of particular importance in design are stress levels for the selected material: the influence of tensile, compressive, or shear stressing; alternating stresses; vibration or shock loading; service temperatures (thermal stressing); fatigue; and wear (fretting, friction). Profiles and shapes contribute to stress-related corrosion, especially if materials selection dictates the use of materials that are susceptible to failure by SCC or corrosion fatigue (Ref 2, 3, 50).

Materials selection is especially important wherever critical components are used. Also important is the need for correct procedures at all stages of operation, including fabrication, transport, storage, startup, shutdown, and normal operation.

Surfaces. Corrosion is a surface phenomenon, and the effects of poorly prepared surfaces, rough textures, and complex shapes and profiles can be expected to be deleterious (Ref 39). Figure 14 shows some examples in which design details could have considerably reduced the onset of corrosive damage resulting from ineffective cleaning or painting.

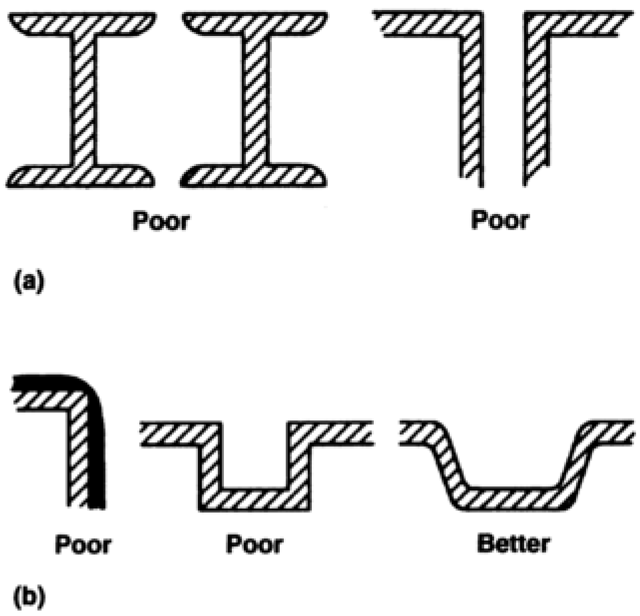

Fig. 14 Effects of design on effectiveness of cleaning or painting. (a) Poor access in some structures makes surface preparation, painting, and inspection difficult; access to the types of areas shown should be maintained at a minimum of 45 mm (1.75 in.) or one-third of the height of the structure. (b) Sharp corners and profiles should be avoided if the structure is to be painted or coated.

Designs should provide for: surfaces that are free from deposits; access to remove retained soluble salts before painting; free-draining assemblies; proper handling of components to minimize distortion, scratches, and dents; and properly located components relative to adjacent equipment (to avoid carryover and spillages). Other recommended procedures for coating constructional materials are shown in Fig. 15 (Ref 40).

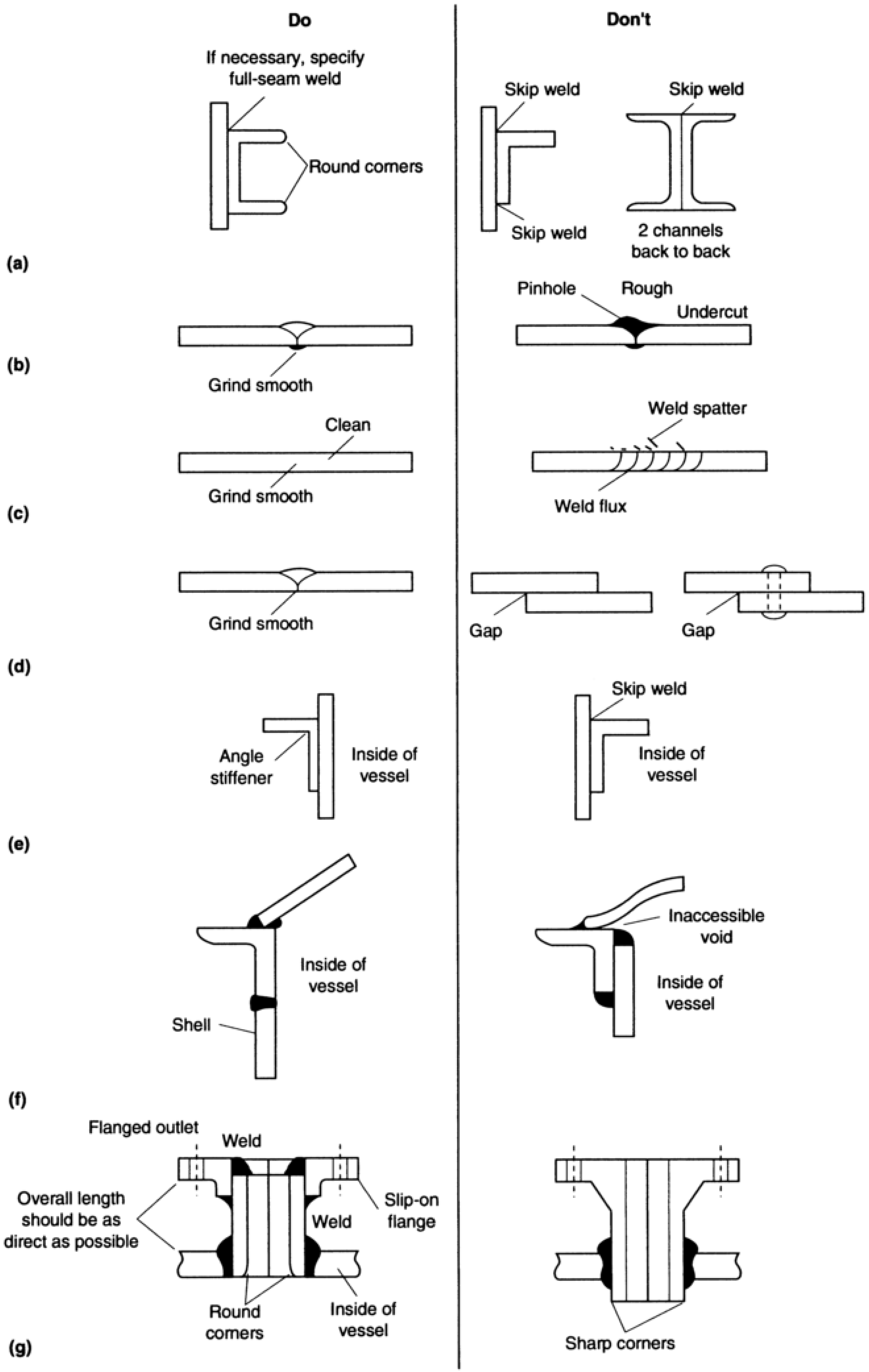
Do
Don't
If necessary, specify full-seam weld
Round corners
Skip weld
Skip weld
Skip weld
2 channels back to back
(a)
Pinhole
Rough
Undercut
Grind smooth
(b)
Clean
Grind smooth
Weld spatter
Weld flux
(c)
Grind smooth
Gap
Gap
(d)
Skip weld
Angle stiffener
Inside of vessel
Inside of vessel
(e)
Inaccessible void
Inside of vessel
Inside of vessel
Shell
(f)
Flanged outlet
Weld
Overall length should be as direct as possible
Slip-on flange
Weld
Round corners
Inside of vessel
Sharp corners
(g)

Fig. 15 Suggestions for steel construction to be coated. (a) Avoid pockets or crevices that do not drain or cannot be cleaned or coated properly. (b) Joints should be continuous and solidly welded. (c) Remove weld spatter. (d) Use butt welds rather than lap welds or rivet joints. (e) Keep stiffeners to outside of tank or vessel. (f) Eliminate crevice (void) at roof-to-shell interface in nonpressure vessel. (g) Outlets should be flanged or pad type, not threaded. Where pressure limits allow, slip-on flanges are preferred, because the inside surface of the attaching weld is readily available for radiusing and grinding. Source: Ref 40

Neglect and poor (or no) maintenance caused localized pitting on the underside of a type 304 stainless steel vessel lid that was exposed to high humidity, steam, and chloride vapors. Access in this example was possible but not used. Common engineering structural steelwork requires regular preventive maintenance, and restricted access makes this impossible. Figure 14 shows situations in which surface cleaning and/or painting is difficult or impossible.

A less recognized but serious corrosion phenomenon (formicary corrosion) results from oil residues remaining on copper surfaces, for example, from lubricating oils used in finning or forming operations. Formicary corrosion, also known as ant-nest corrosion because of the nature of the microscopic damage in the metal (Fig. 16), occurs when oxygen, moisture, and a specific corrodent, usually an organic acid, are simultaneously present on a copper surface (Ref 51, 52, 53). Damage is worse if fluids are stagnated in crevices. Formicary corrosion has been attributed to many corrodent sources, including synthetic lubricating oils, degreasing and cleaning fluids, braze fluxes, volatile species from timber and building materials, liquid smoke, certain vegetable oils, and cosmetics. Carboxylic acids (formic, acetic, and propionic) are the most common acids associated with formicary corrosion. Damage can occur in weeks, and the site of attack is usually so localized and microscopic that it is not obvious to the unaided eye.

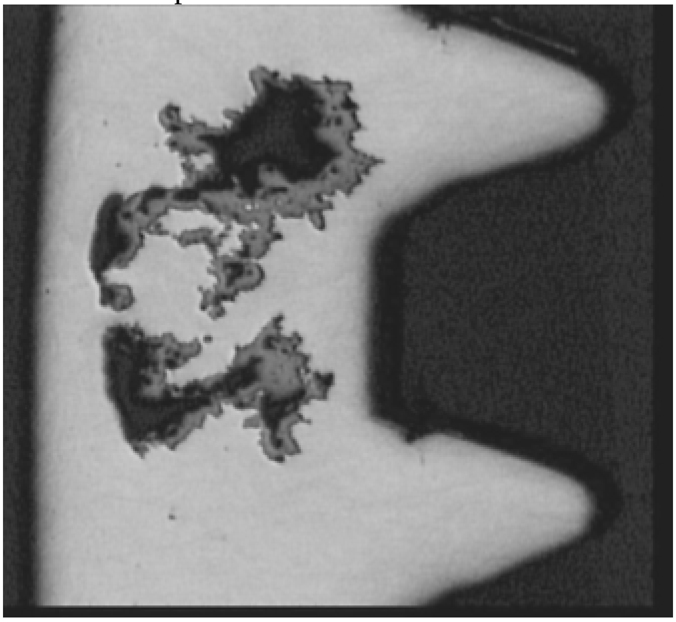

Fig. 16 Formicary (ant-nest) corrosion in a copper air conditioning tube

Condensation in critical areas can contribute to corrosion. Typical structures susceptible to this phenomenon include automobile exhaust systems and chimneys or exhausts from high- temperature plants, such as boilers, kilns, furnaces, or incinerators.

Painting and surface-coating techniques have advanced in recent years and have provided sophisticated products that require careful mixing and application. Maintenance procedures frequently require field application where some control (use of trained inspectors) is essential, as in offshore oil and gas platforms. Inspection codes and procedures are available, and total design should incorporate these wherever possible. In critical areas, design for on-line monitoring and inspection will also be important.

The human factor in maintenance procedures is often questionable. Adequate training and motivation are of primary importance in ensuring that design details are appreciated and implemented.

References cited in this section

2. R.W. Revie, Ed., *Uhlig's Corrosion Handbook,* 2nd ed., John Wiley & Sons, 2000

3. M.G. Fontana, *Corrosion Engineering,* 3rd ed., McGraw-Hill Book Co., 1986

25. *Engineering Design Guides,* Design Council, British Standards Institute, Council of Engineering Institutions, Oxford University Press, 1975–1979

26. P. Elliott and J.S. Llewelyn-Leach, *Corrosion Control Checklist for Design Offices,* Department of Industry, Her Majesty's Stationery Office, London, 1981

39. C.G. Munger, *Corrosion Prevention by Protective Coatings,* NACE International, 1984; updated 2001

40. P.E. Weaver, "Industrial Maintenance Painting," RP0178, NACE International, 1973, p 2

47. W.I. Pollock, *Corrosion Under Wet Insulation,* NACE International, 1988

48. "Specification for Wicking-Type Thermal Insulation for Use Over Austenitic Stainless Steel," C 795, *Annual Book of ASTM Standards,* ASTM

49. "Codes of Practice for Drinking Water Installations (TRWI)," 628.1.033:696.11:620.193, Teil 7, Deutsche Industrie-Normen, 1988

50. A.J. McEvily, Jr., *Atlas of Stress-Corrosion and Corrosion Fatigue Curves,* ASM International, 1990

51. T. Notoya, *Mater. Perform.,* Vol 32, 1993, p 53

52. P. Elliott and R.A. Corbett, *Corros. Rev.,* Vol 19, 2001, p 1

53. R.A. Corbett and P. Elliott, *Corros. Rev.,* Vol 20, 2002, p 51

P. Elliott, Designing to Minimize Corrosion, *Corrosion: Fundamentals, Testing, and Protection*, Vol 13A, *ASM Handbook*, ASM International, 2003, p 929–939

Designing to Minimize Corrosion

Peter Elliott, Corrosion and Materials Consultancy, Inc.

References

1. H.H. Uhlig, *Corrosion Handbook,* John Wiley & Sons, 1948

2. R.W. Revie, Ed., *Uhlig's Corrosion Handbook,* 2nd ed., John Wiley & Sons, 2000

3. M.G. Fontana, *Corrosion Engineering,* 3rd ed., McGraw-Hill Book Co., 1986

4. D.A. Jones, *Principles and Prevention of Corrosion,* 2nd ed., Prentice Hall, 1996

5. C.P. Dillon, *Corrosion Resistance of Stainless Steels,* Marcel Dekker, Inc., 1995

6. S.L. Chawla and R.K. Gupta, *Materials Selection for Corrosion Control,* ASM International, 1993

7. R. Baboian, Ed., *Corrosion Tests and Standards: Applications and Interpretation,* MNL-20, *ASTM Manual Series,* ASTM, 1995

8. C.P. Dillon, *Corrosion Control in the Chemical Process Industries,* 2nd ed., Publication 45, Materials Technology Institute, 1997

9. L.L. Shreir, R.A. Jarman, and G.T. Burstein, Ed., *Corrosion,* Vol 1, 2, *Metal/Environment Reactions,* Butterworth Heinenmann, Ltd., 1994

10. V.A. Ashworth and P. Elliott, Guide to the Corrosion Resistance of *Metals, Metals Reference Book,* 5th ed., C.J. Smithells and E.A. Brandes, Ed., Butterworths, 1976, p 1460

11. B.D. Craig and D. Anderson, Ed., *Handbook of Corrosion Data,* 2nd ed., ASM International, 1995

12. B.J. Moniz and W.I. Pollock, Ed., *Process Industries Corrosion,* NACE International, 1986

13. *Corrosion Data Survey: Metals Section,* 6th ed., NACE, 1985; *Nonmetals Section,* 5th ed., NACE, 1975

14. D.J. De Renzo, Ed., *Corrosion-Resistant Materials Handbook,* 4th ed., Noyes, 1985

15. D. Behrens, G. Kreysa, and R. Eckermann, Ed., *DECHEMA Corrosion Handbook: Corrosive Agents and Their Interaction with Materials,* VCH, 1987–1993

16. Visual Aids/CDS, texts, Materials Technology Institute, Chem-Cor Advisory Systems, 1999–2002

17. P.A. Schweitzer, Ed., *Corrosion Resistance Tables,* 4th ed., Marcel Dekker, 1995

18. V.R. Pludek, *Design and Corrosion Control,* Macmillan, 1977

19. R.J. Landrum, *Fundamentals of Designing for Corrosion Control,* NACE International, 1989

20. R.N. Parkins and K.A. Chandler, *Corrosion Control in Engineering Design,* Department of Industry, Her Majesty's Stationery Office, London, 1978

21. L.D. Perrigo and G.A. Jensen, Fundamentals of Corrosion Control Design, *The North. Eng.,* Vol 13 (No. 4), 1982, p 16

22. S.K. Coburn, *Corrosion Source Book,* American Society for Metals, 1984

23. *Designer Handbooks,* Specialty Steel Industry of North America, 1995–1996

24. *Guides to Practice in Corrosion Control,* Department of Industry, Her Majesty's Stationery Office, London, 1979–1986

25. *Engineering Design Guides,* Design Council, British Standards Institute, Council of Engineering Institutions, Oxford University Press, 1975–1979

26. P. Elliott and J.S. Llewelyn-Leach, *Corrosion Control Checklist for Design Offices,* Department of Industry, Her Majesty's Stationery Office, London, 1981

27. P. Elliott, *Corrosion Control in Engineering Design,* audiovisual, Department of Industry, United Kingdom, 1981

28. P. Elliott, Corrosion Survey, *Suppl. Chem. Eng.,* Sept 1973

29. P. Elliott, Catch 22 and the UCS Factor. Why Must History Repeat Itself?, *Mater. Perform.,* Vol 28 (No. 7), 1989, p 70, Vol 28 (No. 8), 1989, p 75

30. O.W. Siebert, Classic Blunders in Corrosion Protection, *Mater. Perform.,* Vol 17 (No. 4), 1978, p 33, Vol 22 (No. 10), 1983

31. C.P. Dillon, “Unusual Corrosion Problems in the Chemical Process Industries,” Publication 54, Materials Technology Institute, 2000

32. T.F. Degnan, *Mater. Perform.,* Vol 26 (No. 1), 1987, p 11

33. P. Elliott, Why Must History Repeat Itself?, *Ind. Corros.,* Feb/March 1991, p 8

34. P. Elliott, Process Plant Corrosion—Recognizing the Threat, *Process Eng.,* Nov 1984, p 43

35. P. Elliott, Understanding Corrosion Attack, *Plant Eng.,* Oct 1993, p 68

36. *Standards for Corrosion Testing of Metals,* ASTM, 1990

37. H.J.H. Wassell, Reliability of Engineered Products, *Engineering Design Guide,* Design Council, Oxford University, 1980

38. G. Moran and P. Labine, *Corrosion Monitoring in Industrial Plants Using Nondestructive Testing and Electrochemical Methods,* ASTM, 1986

39. C.G. Munger, *Corrosion Prevention by Protective Coatings,* NACE International, 1984; updated 2001

40. P.E. Weaver, “Industrial Maintenance Painting,” RP0178, NACE International, 1973, p 2

41. A. Sparks, Steel, *Carriage by Sea,* 2nd ed., Lloyd's of London Press, 1995

42. G. Kobrin, Ed., *Microbiologically Influenced Corrosion,* NACE International, 1993

43. J.G. Stoecker II, Ed., *Microbiologically Influenced Corrosion,* Vol 2, NACE International, 2001

44. G.Y. Lai, *High Temperature Corrosion of Engineering Alloys,* ASM International, 1990

45. P. Elliott, Practical Guide to High Temperature Alloys, *Mater. Perform.,* Vol 28, 1989, p 57

46. P. Elliott, Choose Materials for High-Temperature Environments, *Chem. Eng. Prog.,* Vol 97, 2001, p 75

47. W.I. Pollock, *Corrosion Under Wet Insulation,* NACE International, 1988

48. “Specification for Wicking-Type Thermal Insulation for Use Over Austenitic Stainless Steel,” C 795, *Annual Book of ASTM Standards,* ASTM

49. “Codes of Practice for Drinking Water Installations (TRWI),” 628.1.033:696.11:620.193, Teil 7, Deutsche Industrie-Normen, 1988

50. A.J. McEvily, Jr., *Atlas of Stress-Corrosion and Corrosion Fatigue Curves,* ASM International, 1990

51. T. Notoya, *Mater. Perform.,* Vol 32, 1993, p 53

52. P. Elliott and R.A. Corbett, *Corros. Rev.,* Vol 19, 2001, p 1

53. R.A. Corbett and P. Elliott, *Corros. Rev.*, Vol 20, 2002, p 51

Corrosion Economic Calculations, *Corrosion: Fundamentals, Testing, and Protection*, Vol 13A, *ASM Handbook*, ASM International, 2003, p 940–945

Corrosion Economic Calculations

Introduction

ENGINEERING ECONOMY is a discipline that can be used to assist engineers and engineering managers in measuring the economic impact of their decisions on the financial goals of a business. Basically, engineering economy is concerned with money as a resource and as the price of other resources. Business success requires the prudent and efficient use of all resources, including money. The principles of engineering economy permit direct comparisons of potential alternatives in monetary terms. In this way, they encourage efficient use of resources.

Corrosion is basically an economic problem. Thus, the corrosion behavior of materials is an important consideration in the economic evaluation of any project. It is not always wise to select the material with the lowest initial cost, because the initial cost is not necessarily the last cost. Overall costs include maintenance, downtime, time value of money, tax aspects, and obsolescence.

This article discusses the principles and terminology of engineering economy and their application to a number of generic corrosion-related problems. Several of these problems appeared in NACE standard RP0272 (Ref 1).

Reference cited in this section

1. “Recommended Practice for Direct Calculation of Economic Appraisals of Corrosion Control Measures,” RP0272, National Association of Corrosion Engineers, withdrawn, 1994. Superceded by “Economics of Corrosion,” 3C194, NACE technical committee report, 1994

Corrosion Economic Calculations, *Corrosion: Fundamentals, Testing, and Protection*, Vol 13A, *ASM Handbook*, ASM International, 2003, p 940–945

Money and Time

Consider the effects of time and earning power on \$20. If \$20 is placed in the bank and earns interest at a rate of 5% per year, it grows to \$21 when the interest, \$1, is paid at the end of the year. Thus, \$20 today at 5% is equivalent to \$21 a year from now. Stated another way, in order to have \$21 one year from now, only \$20 need be deposited today if the interest rate is 5%. The \$20 is termed the discounted present value of the \$21 needed 1 year from now. The initial deposit as well as the earned interest left in the account have earning power, because the interest is compounded, which means that it is computed on both the principal and the accrued interest.

Suppose the \$20 were used to pay four equal, annual installments of \$5 each. Without interest, the \$20 would be exhausted after making the last payment. If the \$20 is deposited in the bank at 5% interest, it will be worth \$21 at the end of the first year. Paying out \$5 would leave \$16 to be held at interest the second year. The \$16

invested at 5% will earn $0.80 in 1 year. Subtracting $5 from $16.80 leaves $11.80 to be held at 5% interest for the third year. A sum of $11.80 will earn $0.59 by the end of the third year at 5%. Another annual payment of $5 leaves $7.39 to earn interest during the fourth year. Adding the $0.37 interest earned during the fourth year and subtracting the final $5 annual payment leaves a balance of accrued interest of $2.76.

The earning power of money permits another strategy. If the initial deposit were reduced to $17.73 at 5% interest, $5 can be paid out each year for 4 years, leaving nothing. This example illustrates the distinction between the terms *equivalent* and *equal.* Twenty dollars is equal to four payments of $5 each. It would also be equivalent to four $5 annual payments (only) if the interest rate were 0. The $17.73 is not equal to the sum of four payments of $5 each. However, when $17.73 is invested at 5%, it is equivalent to four annual payments of $5.

The term *equivalent* implies that the concept of the time value of money is applied at some specific interest rate. Therefore, for an amount of money to have a precise meaning, it must be fixed both in time and amount. Mathematical formulas and tables are available to translate an amount of money at any particular time into an equivalent amount at another date.

Many kinds of translations are possible. For example, a single amount of money can be translated into an equivalent amount at either a later or an earlier date. This is accomplished by calculating the present worth (PW) or the future worth (FW) as of the present date. Single amounts of money can be translated into equivalent annuities, *A*, involving a series of uniform amounts occurring each year. Conversely, annuities can be translated into equivalent single amounts at an earlier or later date. The present worth of an annuity, *P*/*A*, is the single amount of money equivalent to a future annuity. The single amount equivalent to a past annuity is referred to as the future worth of an annuity, *F*/*A*.

It also is possible to calculate the amount of money that would be equivalent to a nonuniform series of cash flows. Two types of nonlinear series that find application are an arithmetic progression, in which the series changes by a constant amount, and a geometric progression, in which the series changes by a constant rate. The arithmetic progression is considered to be representative of variable costs, such as maintenance costs, which may increase as equipment ages. The geometric progression is used to represent the effects of inflation or deflation.

Corrosion Economic Calculations, *Corrosion: Fundamentals, Testing, and Protection*, Vol 13A, *ASM Handbook*, ASM International, 2003, p 940–945

Corrosion Economic Calculations

Notation and Terminology

American National Standards Institute (ANSI) standard Z94.5 (Ref 2), a compilation of the symbology and terminology of the field, offers to practitioners the improved communication benefits of standardization. A redesignation and consolidation standard of Z94.5 with other standards is proposed, with the title “Modeling and Analysis,” BSR Z94.5.

Table 1 lists the definitions and symbols used for parameters. Table 2 lists functional forms of compound interest factors. Table 3 is an explanatory supplement to Table 2, and it represents diagrams, algebraic forms, and uses for compound interest factors.

Table 1 Suggested standard definitions and symbols used for parameters

Definition of parameter	Symbol
Effective interest rate per interest period (discount rate)	*i*
Nominal interest rate per year	*r*
Number of compounding periods	*n*
Number of compounding periods per year	*m*
Present sum of money. The letter *P* implies present (or equivalent present value).	*P*

Future sum of money. The letter *F* implies future (or equivalent future value).	*F*
End-of-period cash flows (or equivalent end-of-period values) in a uniform series continuing for a specified number of periods. The letter *A* implies annual or annuity.	*A*
Uniform period-by-period increase or decrease in cash flows (or equivalent values); the arithmetic gradient	*G*
Amount of money (or equivalent value) flowing continuously and uniformly during a given period	$\bar{P}$ or $\bar{F}$
Amount of money (or equivalent value) flowing continuously and uniformly during each and every period continuing for a specific number of periods	$\bar{A}$

Source: Ref 2

Table 2 Functional forms of compound interest factors

See Table 3 for further explanation.

Factor number	Factor name	Functional format
Group I: all cash flows discrete: end-of-period compounding		
1	Compound amount factor (single payment)	(*F*/*P*, *i*%, *n*)
2	Present worth factor (single payment)	(*P*/*F*, *i*%, *n*)
3	Sinking fund factor	(*A*/*F*, *i*%, *n*)
4	Capital recovery factor	(*A*/*P*, *i*%, *n*)
5	Compound amount factor (uniform series)	(*F*/*A*, *i*%, *n*)
6	Present worth factor (uniform series)	(*P*/*A*, *i*%, *n*)
7	Arithmetic gradient conversion factor (to uniform series)	(*A*/*G*, *i*%, *n*)
8	Arithmetic gradient conversion factor (to present value)	(*P*/*G*, *i*%, *n*)
Group II: all cash flows discrete: continuous compounding		
9	Continuous compounding compound amount factor (single payment)	(*F*/*P*, *r*%, *n*)
10	Continuous compounding present worth factor (single payment)	(*P*/*F*, *r*%, *n*)
11	Continuous compounding sinking fund factor	(*A*/*F*, *r*%, *n*)
12	Continuous compounding capital recovery factor	(*A*/*P*, *r*%, *n*)
13	Continuous compounding compound amount factor (uniform series)	(*F*/*A*, *r*%, *n*)
14	Continuous compounding present worth factor (uniform series)	(*P*/*A*, *r*%, *n*)
Group III: continuous, uniform cash flows: continuous compounding (payments during one period only)		
15	Continuous compounding present worth factors (single, continuous payment)	$(P/\bar{F}, i\%, n)$
16	Continuous compounding compound amount factor (single, continuous payment)	$(F/\bar{P}, i\%, n)$
Group IV: continuous, uniform cash flows: continuous compounding (payments during a continuous series of periods)		
17	Continuous compounding sinking fund factor (continuous, uniform payments)	$(\bar{A}/F, i\%, n)$
18	Continuous compounding capital recovery factor (continuous, uniform payments)	$(\bar{A}/P, i\%, n)$
19	Continuous compounding compound amount factor (continuous, uniform payments)	$(F/\bar{A}, i\%, n)$
20	Continuous compounding present worth factor (continuous, uniform payments)	$(P/\bar{A}, i\%, n)$

Source: Ref 2

Table 3 Diagrams, algebraic forms, and uses for compound interest factors

Factor	Factor name	Algebraic form	Use when:

number			
Group I: all cash flows discrete: end-of-period compounding			
Cash flow diagram for factors 1–6 (and 9–14):			
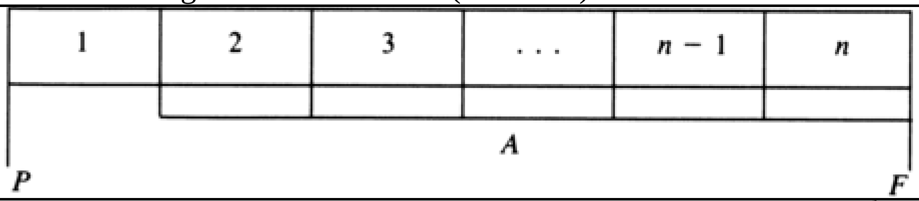			
1.	Compound amount factor (single payment)	$(1+i)^n$	Given *P*, to find *F*
2.	Present worth factor (single payment)	$(1+i)^n$	Given *F*, to find *P*
3.	Sinking fund factor	$\frac{i}{(1+i)^{n-1}}$	Given *F*, to find *A*
4.	Capital recovery factor	$\frac{i(1+i)^n}{(1+i)^n-1}$	Given *P*, to find *A*
5.	Compound amount factor (uniform series)	$\frac{(1+i)^n-1}{i}$	Given *A*, to find *F*
6.	Present worth factor (uniform series)	$\frac{(1+i)^n-1}{i(1+i)^n}$	Given *A*, to find *P*
Cash flow diagram for factors 7 and 8:			
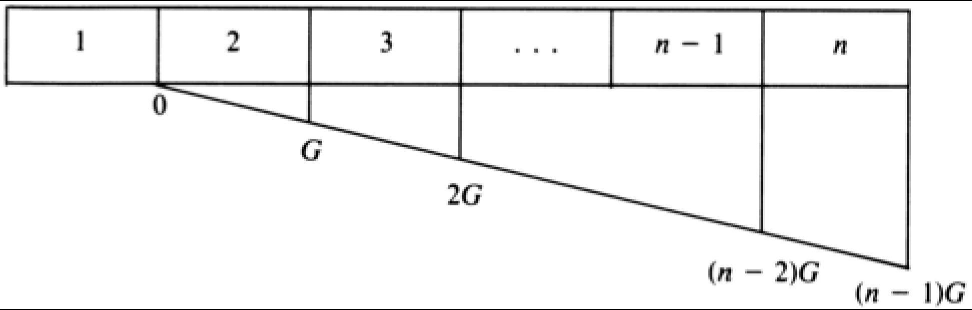			
7.	Arithmetic gradient conversion factor (to uniform series)	$\left[\frac{1}{i} - \frac{n}{(1+i)^n-1}\right]$	Given *G*, to find *A*
8.	Arithmetic gradient conversion factor (to present value)	$\left[\frac{1}{i} - \frac{n}{(1+i)^n-1}\right]\left[\frac{(1+i)^n-1}{i(1+i)^n}\right]$	Given *G*, to find *P*
Group II: all cash flows discrete: continuous compounding			
9.	Continuous compounding compound amount factor (single payment)	e^{rn}	Given *P*, to find *F*
10.	Continuous compounding present worth factor (single payment)	e^{-rn}	Given *F*, to find *P*
11.	Continuous compounding sinking fund factor	$\frac{e^r-1}{e^{rn}-1}$	Given *F*, to find *A*
12.	Continuous compounding capital recovery factor	$\frac{e^{rn}(e^r-1)}{e^{rn}-1}$	Given *P*, to find *A*
13.	Continuous compounding compound amount factor (uniform series)	$\frac{e^{rn}-1}{e^r-1}$	Given *A*, to find *F*
14.	Continuous compounding present worth factor (uniform series)	$\frac{e^{rn}-1}{e^{rn}(e^r-1)}$	Given *A*, to find *P*
Group III: continuous, uniform cash flows: continuous compounding (payments during one period only)			
Cash flow diagram for factors 15 and 16:			

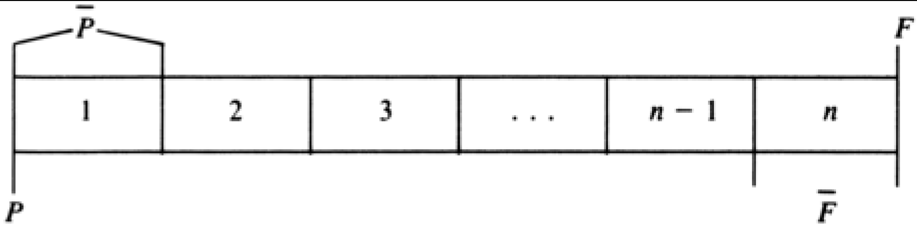			
15.	Continuous compounding present worth factor (single continuous payment)	$\frac{e^r-1}{re^{rn}} = \frac{i(1+i)^n}{\ln(1+i)}$	Given *F*, to find *P*
16.	Continuous compounding compound amount factor (single continuous payment)	$\frac{e^{rn}(e^r-1)}{re^r} = \frac{i(1+i)^{n-1}}{\ln(1+i)}$	Given *P*, to find *F*
Group IV: continuous, uniform cash flows (payments during a continuous series of periods)			
Cash flow diagram for factors 17–20:			
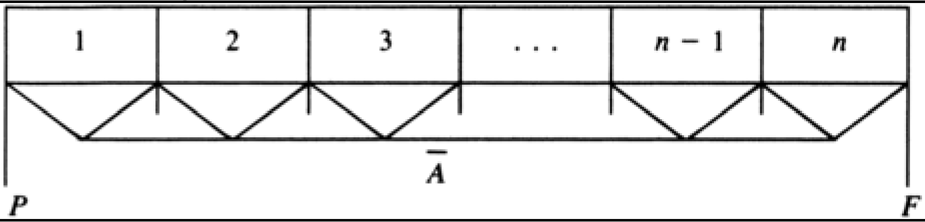			
17.	Continuous compounding sinking fund factor (continuous, uniform payments)	$\frac{r}{e^{rn}-1} = \frac{\ln(1+i)}{(1+i)^n-1}$	Given *F*, to find *A*
18.	Continuous compounding capital recovery factor (continuous, uniform payments)	$\frac{re^{rn}}{e^{rn}-1} = \frac{(1+i)^n\ln(1+i)}{(1+i)^n-1}$	Given *P*, to find *A*
19.	Continuous compounding compound amount factor (continuous, uniform payments)	$\frac{e^{rn}-1}{r} = \frac{(1+i)^n-1}{\ln(1+i)}$	Given *A*, to find *F*
20.	Continuous compounding present worth factor (continuous, uniform payments)	$\frac{e^{rn}-1}{re^{rn}} = \frac{(1+i)^n-1}{(1+i)^n\ln(1+i)}$	Given *A*, to find *P*

The basic form of the notation used for all time value factors consists of a ratio of two letters representing two amounts of money—for example, *P*/*A* or *F*/*P*—plus an interest rate, *i*%, and a number of periods, *n*. These are customarily written as (*P*/*A*, *i*%, *n*) or (*F*/*P*, *i*%, *n*). The present worth, *P*, of a known annuity, *A*, can also be expressed as:

$P = A(P/A)$ (Eq 1)

Or the future worth, *F*, of a known present amount, *P*, as:

$F = P(F/P)$ (Eq 2)

Other forms are also common, such as PW( ) or FW( ), which are called operators, because they represent some computational operation, such as the present worth or future worth of whatever is inside the parentheses.

It should be evident that (*F*/*P*) is the reciprocal of (*P*/*F*) and that (*F*/*A*) and (*A*/*F*) are also reciprocals. This observation is useful, because it means that only three time factors need to be tabulated in order to conduct six operations. Another algebraic relationship shows that if two time value factors are multiplied, the product is a third time value factor. For example:

$(A/F)(P/A) = (P/F)$ (Eq 3)

Reference cited in this section

2. "Engineering Economy," Z94.5, American National Standards Institute/Institute of Industrial Engineers

Corrosion Economic Calculations, *Corrosion: Fundamentals, Testing, and Protection*, Vol 13A, *ASM Handbook*, ASM International, 2003, p 940–945

Corrosion Economic Calculations

Methods of Economic Analysis

Economic analysis methods that concern the entire service life are sometimes called life-cycle-cost methods. Those methods that lead to single measure numbers include:

- Internal rate of return (IROR)
- Discounted payback (DPB)
- Present worth (PW), also referred to as net present value (NPV)
- Present worth of future revenue requirements (PWRR)
- Benefit-cost ratios (BCR)

All five methods use the concept of present worth. Although each method has certain advantages, the individual methods vary considerably with regard to their application and complexity.

The IROR method compares the initial capital investment with the present worth of a series of net revenues or savings over the anticipated service life. Expenses include operation, maintenance, taxes, insurance, and overheads but do not include return on (or of) the invested capital. From an economic standpoint, IROR consists essentially of the interest cost on borrowed capital plus any existing (positive or negative) profit margin. The disadvantage of this measure of economy is that it ignores benefits extending beyond the assumed life of the equipment and thus may omit a substantial part of the actual service life. This may lead to unnecessarily pessimistic measures of long-range economy.

The PWRR method is particularly applicable to regulated public utilities, for which the rates of return are more or less fixed by regulation. It is also applicable where it has already been determined by IROR analysis that a project is economically viable; the engineer must determine which is the most economic alternative under circumstances in which several alternatives produce the same revenue, with some creating less expense (requirement for revenue) than others and consequently a greater profit margin (or lower losses). The principal objection to the PWRR method is that it is inadequate where alternatives are competing for a limited amount of capital, because it does not identify the alternative that produces the greatest return on invested capital.

The DPB and BCR methods are somewhat more complicated than the PWRR method. The BCR method is similar to the IROR method in that both require that alternatives be examined not only for economic measures compared to a “do nothing” scenario but also for incremental measures associated with incremental capital investments.

The PW method, also referred to as the net present value method, is considered the easiest and most direct of the five methods and has the broadest application to engineering economy problems. Many industries refer to this method as the discounted cash flow method of analysis. This method is often used to test the results of other methods of analysis. Therefore, because this method is often preferred, it is given primary attention in this article.

Corrosion Economic Calculations, *Corrosion: Fundamentals, Testing, and Protection*, Vol 13A, *ASM Handbook*, ASM International, 2003, p 940–945

Corrosion Economic Calculations

Annual versus Continuous Compounding

For completeness, Tables 1, 2, and 3 contain formulas involving annual and continuous compounding. Because actual cash flow (both inward and outward) is continuous, continuous compounding might seem to be the more accurate assumption for engineering economy studies. In reality, although the overall cash flows tend to be continuous, the cash flow data are seldom precise enough in economy studies to take full advantage of continuous compounding. It is also true that the normal purpose of the economy study is to analyze some specific event that will occur at a specific time; therefore, a procedure that is readily associated with a specific time seems appropriate. For these reasons, and because it is conceptually easier to understand and apply, annual compounding is used in this article.

The present worth method is a form of discounted cash flow in which cash flow data (which must include dates of receipts and disbursements) are discounted to present worth. Before applying these methods, a management decision must be made regarding the desired life (usually expressed as a number of years, n) and the minimum acceptable rate of return on invested capital for a project (expressed in terms of the effective interest rate, i, or the nominal rate of return, r). Rates of return (before taxes) vary among industries, ranging from 10 to 15% where obsolescence is not high to 25 to 40% (or perhaps higher) for more dynamic industries. It would be convenient if the minimum acceptable rate of return were known in advance of making engineering economy analyses; however, it is not always easy to learn what rate of return is considered to be acceptable. Under such circumstances, it is helpful to prepare a series of economic alternatives in which the rate of return is varied in order to provide management with options.

Applying the Present Worth Method. To illustrate the features of this method, it is determined whether an expenditure of $15,000 should be made to reduce labor and maintenance from $8200 to $5100 per year. Money is worth 10%, and the life of the project is 10 years. The effects of taxes and depreciation have been omitted for simplicity.

Table 4 shows the projected pattern of cash flow for plan A (the present method, which consists of paying $8200 per year for labor and maintenance) and for plan B (the proposed method, which consists of an initial expenditure of $15,000 plus $5100 per year for labor and maintenance over the life of the project). A minus sign means that money leaves the bank; a plus sign means that the bank balance increases in size. The net cash flow for each year appears in the right-hand column under the heading “B - A.”

Table 4 Tabulation of cash flow

Period, years	Plan A (the present method)	Plan B (the proposed method)	B - A, dollars
0	…	-15,000	-15,000
1	-8200	-5100	+3100
2	-8200	-5100	+3100
3	-8200	-5100	+3100
4	-8200	-5100	+3100
5	-8200	-5100	+3100
6	-8200	-5100	+3100
7	-8200	-5100	+3100
8	-8200	-5100	+3100
9	-8200	-5100	+3100
10	-8200	-5100	+3100
Totals	**-$82,000**	**-$66,000**	**+$16,000**

Selection of plan B will result in a net positive cash flow; that is, the net amount of money in the bank is increased over the life of the project when plan B is selected. Before concluding that plan B should be implemented, it is necessary to reduce these cash flows to a common basis for comparison and to determine whether the objective of a 10% rate of return has been achieved. The present worth (or present value) of these cash flows provides such a basis. The rate of return for plan B is calculated by iteration, using interest tables and interpolating between values.

First Iteration. Assume a rate of return of 10% and refer to Table 5:

$$\begin{aligned} PW &= -15{,}000 + 3100\left(\frac{P}{A}, 10\%, 10 \text{ years}\right) \\ &= -15{,}000 + 3100(6.145) \\ &= +\$4047.95 \end{aligned} \qquad \text{(Eq 4)}$$

The rate of return for which the discounted cash flow is equal to 0 (that is, the first term on the right in Eq 4 is balanced by the second term) is the actual rate of return. From the first iteration, it is already evident that plan B returns in excess of 10%, because the net cash flow is positive. Thus, plan B is preferred. The numerical value of the actual rate of return can be determined by additional iterations. Such an exercise will reveal that the rate of return in this case is 16.1%.

Table 5 Annual compounding at 10% effective interest rate, *i*, per year

n	Single payment		Equal payment series				Uniform gradient-series factor
	Compound-amount factor	**Present worth factor**	**Compound-amount factor**	**Sinking-fund factor**	**Present worth factor**	**Capital recovery factor**	
	To find *F* given *P F*/ *P, i, n*	**To find *P* given *F P/F, i, n***	**To find *F* given *A F/A, i, n***	**To find *A* given *F A/F, i, n***	**To find *P* given *A P/A, i, n***	**To find *A* given *P A/P, i, n***	**To find *A* given *G A/G, i, n***
1	1.100	0.9091	1.000	1.0000	0.9091	1.1000	0.0000
2	1.210	0.8265	2.100	0.4762	1.7355	0.5762	0.4762
3	1.331	0.7513	3.310	0.3021	2.4869	0.4021	0.9366
4	1.464	0.6830	4.641	0.2155	3.1699	0.3155	1.3812
5	1.611	0.6209	6.105	0.1638	3.7908	0.2638	1.8101
6	1.772	0.5645	7.716	0.1296	4.3553	0.2296	2.2236
7	1.949	0.5132	9.487	0.1054	4.8684	0.2054	2.6216
8	2.144	0.4665	11.436	0.0875	5.3349	0.1875	3.0045
9	2.358	0.4241	13.579	0.0737	5.7590	0.1737	3.3724
10	2.594	0.3856	15.937	0.0628	6.1446	0.1628	3.7255
11	2.853	0.3505	18.531	0.0540	6.4951	0.1540	4.0641
12	3.138	0.3186	21.384	0.0468	6.8137	0.1468	4.3884
13	3.452	0.2897	24.523	0.0408	7.1034	0.1408	4.6988
14	3.798	0.2633	27.975	0.0358	7.3667	0.1358	4.9955
15	4.177	0.2394	31.772	0.0315	7.6061	0.1315	5.2789
16	4.595	0.2176	35.950	0.0278	7.8237	0.1278	5.5493
17	5.054	0.1979	40.545	0.0247	8.0216	0.1247	5.8071
18	5.560	0.1799	45.599	0.0219	8.2014	0.1219	6.0526
19	6.116	0.1635	51.159	0.0196	8.3649	0.1196	6.2861
20	6.728	0.1487	57.275	0.0175	8.5136	0.1175	6.5081
21	7.400	0.1351	64.003	0.0156	8.6487	0.1156	6.7189
22	8.140	0.1229	71.403	0.0140	8.7716	0.1140	6.9189
23	8.954	0.1117	79.543	0.0126	8.8832	0.1126	7.1085
24	9.850	0.1015	88.497	0.0113	8.9848	0.1113	7.2881
25	10.835	0.0923	98.347	0.0102	9.0771	0.1102	7.4580

26	11.918	0.0839	109.182	0.0092	9.1610	0.1092	7.6187
27	13.110	0.0763	121.100	0.0083	9.2372	0.1083	7.7704
28	14.421	0.0694	134.210	0.0075	9.3066	0.1075	7.9137
29	15.863	0.0630	148.631	0.0067	9.3696	0.1067	8.0489
30	17.449	0.0573	164.494	0.0061	9.4269	0.1061	8.1762
31	19.194	0.0521	181.943	0.0055	9.4790	0.1055	8.2962
32	21.114	0.0474	201.138	0.0050	9.5264	0.1050	8.4091
33	23.225	0.0431	222.252	0.0045	9.5694	0.1045	8.5152
34	25.548	0.0392	245.477	0.0041	9.6086	0.1041	8.6149
35	28.102	0.0356	271.024	0.0037	9.6442	0.1037	8.7086
40	45.259	0.0221	442.593	0.0023	9.7791	0.1023	9.0962
45	72.890	0.0137	718.905	0.0014	9.8628	0.1014	9.3741
50	117.391	0.0085	1163.909	0.0009	9.9148	0.1009	9.5704
55	189.059	0.0053	1880.591	0.0005	9.9471	0.1005	9.7075
60	304.482	0.0033	3034.816	0.0003	9.9672	0.1003	9.8023
65	490.371	0.0020	4893.707	0.0002	9.9796	0.1002	9.8672
70	789.747	0.0013	7887.470	0.0001	9.9873	0.1001	9.9113
75	1271.895	0.0008	12,708.954	0.0001	9.9921	0.1001	9.9410
80	2048.400	0.0005	20,474.002	0.0001	9.9951	0.1001	9.9609
85	3298.969	0.0003	32,979.690	0.0000	9.9970	0.1000	9.9742
90	5313.023	0.0002	53,120.226	0.0000	9.9981	0.1000	9.9831
95	8556.676	0.0001	85,556.760	0.0000	9.9988	0.1000	9.9889
100	13,780.612	0.0001	137,796.123	0.0000	9.9993	0.1000	9.9928

In this example, plans A and B could represent alternative materials of construction having different corrosion rates, with the annual dollar difference being related to the consequences of corrosion on maintenance costs. This presupposes the availability of corrosion data that can be used to estimate expected life, maintenance costs, and so on. Other examples illustrate how to account for the effects of salvage value, taxes, and depreciation.

Corrosion Economic Calculations, *Corrosion: Fundamentals, Testing, and Protection*, Vol 13A, *ASM Handbook*, ASM International, 2003, p 940–945

Corrosion Economic Calculations

Depreciation

Depreciation has been defined as the lessening in value of an asset with the passage of time. All physical assets (except land) depreciate with time. There are several types of depreciation. Two of the more common types are physical depreciation and functional depreciation. Accidents can also cause loss of value, but this cause is often accommodated in other ways, such as insurance and reserves, and therefore is not considered in this article.

Physical depreciation includes such phenomena as deterioration resulting from corrosion, rotting of wood, bacterial action, chemical decomposition, and wear and tear, which can reduce the ability of an asset to render its intended service. Functional depreciation does not result from the inability of an asset to serve its intended purpose but rather from the fact that some other asset is available that can perform the desired function more economically. Thus, obsolescence, inadequacy, and/or the inability to meet the demands placed on the asset lead to functional depreciation. Technological advances produce improvements that often result in the obsolescence of existing assets.

The manner in which depreciation can be accounted for is largely a tax question. The tax laws specify the procedures that are permissible. Because tax laws change occasionally, procedures that are attractive under a given set of circumstances may become unattractive (or even forbidden) under other circumstances. Some of the more common methods of depreciation include:

- Straight line
- Declining balance
- Declining balance switching to straight line
- Sum of the year's digits
- Accelerated cost recovery system (ACRS) and the modified accelerated cost recovery system (MACRS)

The straight-line depreciation method assumes that the value of an asset declines at a constant rate. If the original cost *P* of the asset was $6000 and the asset had a salvage value *S* of $1000 after a service life of 5 years, the annual depreciation would be ($6000 - 1000)/5 = $1000 per year. Annual depreciation *D* can be expressed as:

$$D = (P - S)/n \quad \text{(Eq 5)}$$

The book value of the asset would decrease at the end of each year by the amount of the annual depreciation until, at the end of the fifth year, the book value would be the same as the salvage value.

The declining-balance method assumes that the asset depreciates more rapidly during the early years of its service life than in the later years. A certain percent depreciation is applied each year to the remaining book value of the asset. Under these circumstances, the size of the depreciation declines with each successive year until the asset is fully depreciated.

The sum of the year's digits method assumes that the value of an asset decreases at a decreasing rate. Assume that an asset has a 5 year life. The sum of the year's digits equals 1 + 2 + 3 + 4 + 5 = 15. For the $6000 asset mentioned previously, which has a salvage value after 5 years of $1000, depreciation for the first year would be ($6000 - 1000) (5/15) = $1666.67. Depreciation for the second year would be ($6000 - 1000) (4/15) = $1333.33, and so on, until the asset is fully depreciated.

Other Methods. For property placed in service after 1980 and before 1987, the ACRS prescribed a different method for recovering the cost of depreciable property. In 1987, the ACRS was modified and became known as the MACRS. There are presently certain bonuses in effect, so the current tax codes must be consulted.

Corrosion Economic Calculations, *Corrosion: Fundamentals, Testing, and Protection*, Vol 13A, *ASM Handbook*, ASM International, 2003, p 940–945

Corrosion Economic Calculations

Generalized Equations

It is possible to prepare generalized equations that will simplify the solution of a large percentage of engineering economy problems. These equations take into account the influence of taxes, depreciation, operating expenses, and salvage value in the calculation of present worth and annual cost. Using these equations, a problem can be solved merely by entering data into the equations with the assistance of the compound interest tables and solving for the unknown value. The tax rate *t* is expressed as a decimal. Operating expense is represented by *X*. The letter *S* represents salvage value. The other symbols are explained in Tables 1, 2, and 3.

For straight-line depreciation:

$$\begin{aligned}\mathrm{PW} = -P &+ \left\{\frac{t(P-S)}{n}\right\}\left(\frac{P}{A},\ i\%, n\right) \\ &- (1-t)(X)\left(\frac{P}{A},\ i\%, n\right) \\ &+ S\left(\frac{P}{F},\ i\%, n\right)\end{aligned} \quad \text{(Eq 6)}$$

where P, the first term, is the cost at time zero of the initial investment. The value at time zero is a definition of present worth (at time zero). Therefore, it is not necessary to translate this amount to another date, because the evaluation will be made as of time zero. The investment involves flow of money out of the bank; therefore, the sign of this term is minus.

The second term in Eq 6 concerns depreciation. The depreciation method will influence the mathematical formation of this term. The portion enclosed in braces expresses the annual amount of tax credit permitted by this method of depreciation—in this case, straight-line depreciation. The portion in parentheses translates these equal annual amounts back to time zero by converting them to present worth. The ACRS and MACRS depreciation methods allow specific straight-line depreciation options. When one of these options is chosen, the formulation of this term remains the same as shown previously, with the exception that salvage is ignored. If the straight-line option is not chosen, this term in the generalized formula becomes a series of terms, each having the tax rate multiplied by the appropriate depreciation percentage of the initial cost (in accordance with Table 6) multiplied by the appropriate single-payment present worth factor, P/F, for the applicable year and interest rate. The sum of these terms will represent the effect of depreciation on present worth.

Table 6 Depreciation percentages for the modified accelerated cost recovery system (MACRS)

Recovery year	Recovery period, years					
	3	**5**	**7**	**10**	**15**	**20**
1	33.33	20.00	14.29	10.00	5.00	3.750
2	44.45	32.00	24.49	18.00	9.50	7.219
3	14.81	19.20	17.49	14.40	8.55	6.677
4	7.41	11.52	12.49	11.52	7.70	6.177
5	…	11.52	8.93	9.22	6.93	5.713
6	…	5.76	8.92	7.37	6.23	5.285
7	…	…	8.93	6.55	5.90	4.888
8	…	…	4.46	6.55	5.90	4.522
9	…	…	…	6.56	5.91	4.462
10	…	…	…	6.55	5.90	4.461
11	…	…	…	3.28	5.91	4.462
12	…	…	…	…	5.90	4.461
13	…	…	…	…	5.91	4.462
14	…	…	…	…	5.90	4.461
15	…	…	…	…	5.91	4.462
16	…	…	…	…	2.95	4.461
17	…	…	…	…	…	4.462
18	…	…	…	…	…	4.461
19	…	…	…	…	…	4.462
20	…	…	…	…	…	4.461
21	…	…	…	…	…	2.231

This schedule is for the half-year convention. Quarter-year convention is also allowed. This schedule is for example only. See current tax code.

The third term in Eq 6 actually consists of two terms. One is $[(X)(P/A, i\%, n)]$, which represents the cost of items properly chargeable as expense, such as the cost of maintenance or insurance and the cost of inhibitors. Because this term involves expenditure of money from the bank, it carries a minus sign. The term $[t(X)(P/A, i\%, n)]$ accounts for the tax credit for this business expense. Because it represents a savings, the sign is plus.

The fourth term translates the anticipated (future) value of salvage to present value. This is a one-time event rather than a uniform series and therefore involves the single-payment present worth factor. As noted previously, the ACRS and MACRS depreciation methods ignore the salvage value of an asset; therefore, when using these methods, the fourth term is 0.

Present worth can be converted to equivalent annual cost A by:

$$A = (\mathrm{PW})\left(\frac{A}{P}, i\%, n\right) \quad \text{(Eq 7)}$$

Alternative materials with the same life can be compared from an engineering economy standpoint merely by comparing the magnitude of their present values. However, if the candidate materials have different life expectancies, it is necessary to convert present worth to equivalent annual cost *A* to compare the materials from an engineering economy standpoint. The material with the lowest annual cost is the material of choice.

Corrosion Economic Calculations, *Corrosion: Fundamentals, Testing, and Protection*, Vol 13A, *ASM Handbook*, ASM International, 2003, p 940–945

Corrosion Economic Calculations

Examples and Applications

Example 1 A new heat exchanger is required in conjunction with a rearrangement of existing facilities. Because of corrosion, the expected life of a carbon steel exchanger is 5 years. The installed cost is $9500. An alternative to the carbon steel heat exchanger is a unit fabricated of American Iron and Steel Institute (AISI) type 316 stainless steel with an installed cost of $26,500 and an estimated life of 15 years to be written off in 11 years. The minimum acceptable rate of return is 10%, the tax rate is 48%, and the depreciation method is straight line. It is necessary to determine which unit would be more economical based on annual costs.

Because the lives of the two heat exchangers are unequal, the economic choice cannot be based merely on the discounted cash flow over a single life of each alternative. Instead, comparison must be made on the basis of equivalent uniform annual costs, commonly referred to as annual cost, as mentioned previously. In this example, data are given for only the first two terms of Eq 6. The third term, which involves maintenance expense, and the fourth term involving salvage value are both assumed to be 0.

The first step is to compute the discounted cash flow over one life span for each alternative. This involves calculation of the present worth for each material:

(Eq 8)

$$\begin{aligned} \mathrm{PW}_{316} &= -\$26{,}500 + \left\{0.48\frac{(26{,}500-0)}{11}\right\}(6.495) \\ &= -\$18{,}989 \end{aligned} \quad \text{(Eq 9)}$$

To compare the two alternatives, both discounted cash flows (the present worths) must be converted to annual costs:

$$\begin{aligned} A_{\mathrm{steel}} &= -\$6043(0.2638) \\ &= -\$1594 \end{aligned} \quad \text{(Eq 10)}$$

$$\begin{aligned} A_{316} &= -\$18{,}989(0.15396) \\ &= -\$2924 \end{aligned} \quad \text{(Eq 11)}$$

Therefore, the carbon steel heat exchanger, which has the lower annual cost, is the more economical alternative under these conditions.

Example 2 In this case, the carbon steel heat exchanger in Example 1 will require $3000 in yearly maintenance (painting, use of inhibitors, cathodic protection, and so on). This example determines whether carbon steel would remain the preferred alternative under these conditions.

Maintenance costs are treated as expense items with a 1 year life (end-of-year costs). This example involves the third term in Eq 6. In Example 1, the annual cost without the yearly maintenance cost was calculated; therefore,

in this example, the annual cost including maintenance ($3000 per year) can be obtained simply by subtracting the after-tax maintenance costs from the result given in Example 1:

$$A_{\text{steel}} = -\$1594 - (1 - 0.48)(\$3000) = -\$3154 \qquad \text{(Eq 12)}$$

Because this is an after-tax cash flow, the quantity [(1 - 0.48)($3000)] is the after-tax maintenance cost; 0.48 is the tax rate expressed as a decimal. The $3000 is the present value of the maintenance for the first year; therefore, no further discounting is necessary in this case. Comparing this result with the annual cost of AISI type 316 stainless steel in Example 1, it is evident that if $3000 is required each year to keep the carbon steel unit operative, the stainless steel unit would be more economical.

Example 3 Given the conditions described in Example 1, this example determines the service life at which the carbon steel heat exchanger is economically equivalent to the type 316 stainless steel unit if it is not certain that a 5 year life will be attained for unprotected carbon steel.

The carbon steel heat exchanger will be economically equivalent to the type 316 stainless steel heat exchanger when their annual costs are equal. Therefore, the problem can be solved by determining how many years of life for steel will be equivalent to an annual cost of $2924. Trial- and-error methods are useful for such problems. Trying *n* = 3 years gives:

$$\text{PW}_{\text{steel}} = -\$9500 + \left\{0.48\frac{(9500-0)}{3}\right\}(2.487) = -\$5719 \qquad \text{(Eq 13)}$$

$$A_{\text{steel}} = -\$5719(0.40211) = -\$2300 \qquad \text{(Eq 14)}$$

Trying *n* = 2 years yields:

$$\text{PW}_{\text{steel}} = -\$9500 + \left\{0.48\frac{(9500-0)}{2}\right\}(1.736) = -\$5542 \qquad \text{(Eq 15)}$$

$$A_{\text{steel}} = -\$5542(0.57619) = -\$3193 \qquad \text{(Eq 16)}$$

Thus, a carbon steel heat exchanger must last more than 2 years but will be economically favored in less than 3 years under the conditions given.

Example 4 Under the conditions described in Example 3, it is determined how much product loss *X* could be tolerated after 2 of the 5 years of anticipated life, for example, from roll leaks or a few tube failures, before the selection of type 316 stainless steel could have been justified. Equating:

$$A_{316} = A_{\text{steel}} + A_{\text{product loss}}$$
$$-\$2924 = -\$1594 + [(1-0.48)(X)(0.8264)][0.2638] \qquad \text{(Eq 17)}$$

Solving for *X*:

$$-\$1330 = 0.1134(X)$$
$$X = -\$11,728 \qquad \text{(Eq 18)}$$

The term (1 - 0.48) will be recognized from the third term of Eq 6 as (1 - *t*), where *t* is the tax rate. The quantity 0.8264 is the single-payment present worth factor (*P*/*F*, 10%, 2 years) and translates the product loss *X* to its present worth at time zero. The quantity [0.2638] is the uniform series capital recovery factor (*A*/*P*, 10%, 5 years) and translates the present worth of the product loss to annual cost so that it can be added to the annual cost of steel for comparison with the annual cost of AISI type 316 stainless steel. If production losses exceed $11,728 in year two (no losses in other years), the AISI type 316 heat exchanger could be justified.

Acknowledgment

This article was adapted from E.D. Verink, Jr., Corrosion Economic Calculations, *Corrosion*, Vol 13, *ASM Handbook* (formerly *Metals Handbook*, 9th ed.), ASM International, 1987, p 369–374.

References

1. “Recommended Practice for Direct Calculation of Economic Appraisals of Corrosion Control Measures,” RP0272, National Association of Corrosion Engineers, withdrawn, 1994. Superceded by “Economics of Corrosion,” 3C194, NACE technical committee report, 1994
2. “Engineering Economy,” Z94.5, American National Standards Institute/Institute of Industrial Engineers

Selected References

- L. Blank and G. Tarquin, *Engineering Economy,* 5th ed., McGraw-Hill, 2002
- W.J. Fabrycky and G.J. Thuesen, *Engineering Economy,* 8th ed., Prentice-Hall, 1992
- E.L. Grant, W.G. Ireson, and R.S. Leavenworth, *Principles of Engineering Economy,* 8th ed., John Wiley & Sons, 1990
- K.K. Humphreys, *Jelen's Cost and Optimization Engineering,* 3rd ed., McGraw-Hill, 1991
- D.G. Newman, J.P. Lavelle, and T.G. Eschenback, *Engineering Economic Analysis,* 8th ed., Oxford University Press, 2000
- E.D. Verink, Economic Appraisals of Corrosion Control Measures, *J. Educ. Mod. Mater. Sci. Eng.,* Vol 3 (No. 2), 1981, p 239

C.L. Brooks, KT. Honeycutt and T.B. Mills, Predictive Modeling of Structure Service Life, *Corrosion: Fundamentals, Testing, and Protection*, Vol 13A, *ASM Handbook*, ASM International, 2003, p 946–958

Predictive Modeling of Structure Service Life

Craig L. Brooks, Scott A. Prost-Domasky, Kyle T. Honeycutt, and Thomas B. Mills, Analytical Processes/Engineered Solutions, Inc.

Introduction

CORROSION FATIGUE has been identified as a significant safety issue in the world aircraft fleets. The in-flight failure of a large section of fuselage on an Aloha Airline Boeing 737 in 1988 is certainly a spectacular example of corrosion degradation exacerbating fatigue damage during normal aircraft operation (Ref 1). There is ample evidence that the deleterious effects of corrosion have significant maintenance and safety implications for the continued long-term operation of other aircraft, commercial and military (Ref 2), and for ground vehicles (Ref 3). This article addresses corrosion fatigue, its effects on the damage tolerance of aircraft, and its predictive modeling. A framework is presented that incorporates two distinctive cyclic-based life-prediction philosophies and expands them both to include the time domain in order to consider the effects of corrosion. The framework is presented in terms of its application to the aircraft industry, but it is applicable anywhere that structures require assessment in multiple complex environments, such as those often encountered by corrosion scientists and engineers.

References cited in this section

1. NTSB/AAR-89/03, Aloha Airlines, Flight 243, Boeing 737-200, N73711, near Maui, HI, April 1988, National Transportation Safety Board, 1989

2. D.W. Hoeppner, L. Grimes, A. Hoeppner, J. Ledesma, T. Mills, and A. Shah, Corrosion and Fretting as Critical Aviation Safety Issues: Case Studies, Facts, and Figures from U.S. Aircraft Accidents and Incidents, *Proceedings, 18th Symposium of the International Committee on Aeronautical Fatigue,* 3–5 May 1995 (Melbourne, Australia). Conference proceedings available from http:// www.emas.co.uk/

3. *Cracking Down on Corrosion: Cooperative Efforts Toward Vehicle Durability,* American Iron and Steel Institute, 1985. Available from http://www.steel.org/autosteel/index.htm

C.L. Brooks, KT. Honeycutt and T.B. Mills, Predictive Modeling of Structure Service Life, *Corrosion: Fundamentals, Testing, and Protection*, Vol 13A, *ASM Handbook*, ASM International, 2003, p 946–958

Predictive Modeling of Structure Service Life

Craig L. Brooks, Scott A. Prost-Domasky, Kyle T. Honeycutt, and Thomas B. Mills, Analytical Processes/Engineered Solutions, Inc.

Design Philosophies

Crack Initiation Used for Safe-Life Design

Crack initiation (intended to represent the crack nucleation or formation process in metals) used in the safe-life design philosophy primarily focuses on the concept of designing structure to requirements that would result in crack-free structure for the life of the design. To achieve this goal, the state of local stress in the structure is limited to a maximum value as determined by crack initiation predictions (with appropriate scatter factors). These predictions consider the cyclic response of a structure to a design usage spectrum. This usage spectrum is often based on a critical *usage* point, resulting in a lower bound limit on fatigue life for analysis and testing. Typically, the structure is considered to have consumed its service life and is replaced when this fatigue life limit is reached, but exceptions are sometimes made if costly recurring inspection and maintenance programs are implemented.

The crack initiation methods used for these predictions are empirical and typically consist of equations correlated and fit to the specimen lives as limited by a specified crack length during coupon, element (a simple structural detail configuration specimen), and component tests. (This approach to qualification is detailed in the article "Testing and Analysis Correlation" in *Composites,* Volume 21 of *ASM Handbook.*) The test specimens should be manufactured under the same process specifications as the production structure and tested to the design usage spectrum intended to simulate the cycles expected in service. Using these prediction techniques and tools, each structural component is assumed to be capable of exceeding service-life requirements without initiation or nucleation of a crack greater than the specified length. This philosophy is reasonably effective in many applications when coupled with adequate safety factors, but the empirical nature of the philosophy does not allow external processes, such as corrosion, to have a quantifiable effect on the analyses.

Inspection and maintenance programs are based extensively on user-specific experience and operations. The adaptation of this to a different service usage may or may not be optimal; for example, one user may experience a hostile corrosive environment coupled with severe load spectrum requirements, while another user may experience a relatively benign environment and operational load spectra. Problems associated with severe operational spectra (environment and load) could differ significantly from relatively benign spectra. Hence, a successful maintenance program requires careful consideration of all operational environments, in addition to the load spectra, across the fleet.

Crack Growth Used for Damage Tolerance Philosophy

Crack growth methods, as used in the damage tolerance philosophy, primarily focus on the concept of designing and maintaining the structure to requirements that are perceived to ensure that the structure is capable of meeting service-life requirements with consideration for inherent, manufacturing, and accidental damage. To accomplish this, the approach requires analyses and tests using fracture mechanics techniques coupled with residual-strength analysis of the structure. The crack growth life of a component is influenced by the local state of stress as well as the gross section stress distribution. The residual strength ensures the ability of the structure to redistribute loads and tolerate particular levels of incremental damage by a ready detection prior to catastrophic failure. These prediction methods also consider the cyclic response of the structure to the design usage spectrum and environment. Typical design spectra are used to represent the average use of the structure.

The crack growth methods used for incremental crack growth predictions are based on theoretical solutions that have been developed and correlated with coupon, element, and component tests. The life predictions are calibrated to represent the effects of the geometries with the intended operational use. The life assessments are based on the time to grow an appropriate initial crack and/or the time from initial crack to failure of the structure. Components designed and analyzed using this philosophy are considered capable of meeting service-life requirements yet still are often inspected and maintained in order to use the full economic service life of the structure and/or to detect potential problems not captured in the design process.

The damage tolerance philosophy tailors the maintenance program to the operational usage for each particular component and aircraft. The methodology provides a measurable attribute, that is, detectable crack length in which to measure the remaining life of the structure. Although the intent is not to operate a structure with cracks, it is beneficial to understand the impact of potential cracking. Crack growth analyses are almost exclusively used to determine the inspection details and intervals, and problematic areas will often have fleetwide mandated inspections. The economies of these approaches are dependent on the customer's historical experience, fleet size, philosophy, logistics, and facilities.

Both of the previously mentioned two philosophies have been effective in providing a means to design, build, and maintain aircraft systems. Both philosophies have merits and can benefit from continuing advancements in

technology. The following framework attempts to establish a foundation on which both philosophies can be merged, enhanced, and incorporated with age- based structural degradations, such as corrosion, in order to better simulate damage progression and more accurately assess the economic service life of a structural component.

C.L. Brooks, KT. Honeycutt and T.B. Mills, Predictive Modeling of Structure Service Life, *Corrosion: Fundamentals, Testing, and Protection*, Vol 13A, *ASM Handbook*, ASM International, 2003, p 946–958

Predictive Modeling of Structure Service Life

Craig L. Brooks, Scott A. Prost-Domasky, Kyle T. Honeycutt, and Thomas B. Mills, Analytical Processes/Engineered Solutions, Inc.

Conceptual Framework

Holistic Life Analysis

Technologies have matured sufficiently to allow improved incorporation of corrosion and age-degradation effects into a systematic damage tolerance (DT) framework (Ref 4). The integration of these technologies into current fleet management infrastructures, such as the United States Air Force (U.S.A.F.) Aircraft Structural Integrity Program (ASIP), is feasible. Combining the impacts of damage accumulation from operational stress excursions of a structure with the impacts of damage accumulation caused by environmental exposure while at rest or in operation is key to this holistic life analysis concept.

A conceptual framework that has the flexibility to represent material and structural behavior in two different domains is in development: the *cyclic crack growth domain* and the *time domain.* Just as time never stands still, the time domain is always active in this framework. Various damage progression scenarios, such as crevice-corrosion-induced pillowing and associated environmentally assisted cracking in lap joints, can and do occur when a structure is not in use. In this example, the material will thin, and residual stresses will increase to the point where structural integrity will be compromised sooner than predicted under safe-life or damage-tolerant philosophy. When the cyclic crack growth domain does become active, the solutions given by traditional damage tolerance analyses will be altered by combinations of thinned structure, accumulating residual stresses, and environmentally assisted crack growth.

The basic framework has been demonstrated on several levels, ranging from simple coupons, in which predicted lives of controlled corrosion fatigue experiments were correlated with the measured fatigue lives (Ref 5), to actual aircraft components, in which unanticipated field cracking problems were predicted and explained (Ref 6).

Although development of this framework has been focused on aircraft, the framework is readily adaptable to multiple flight vehicle systems as well as rail, automotive, and mechanical equipment systems. A description of the basic model framework is documented in Ref 7. The stages of holistic damage progression are schematically shown in Fig. 1.

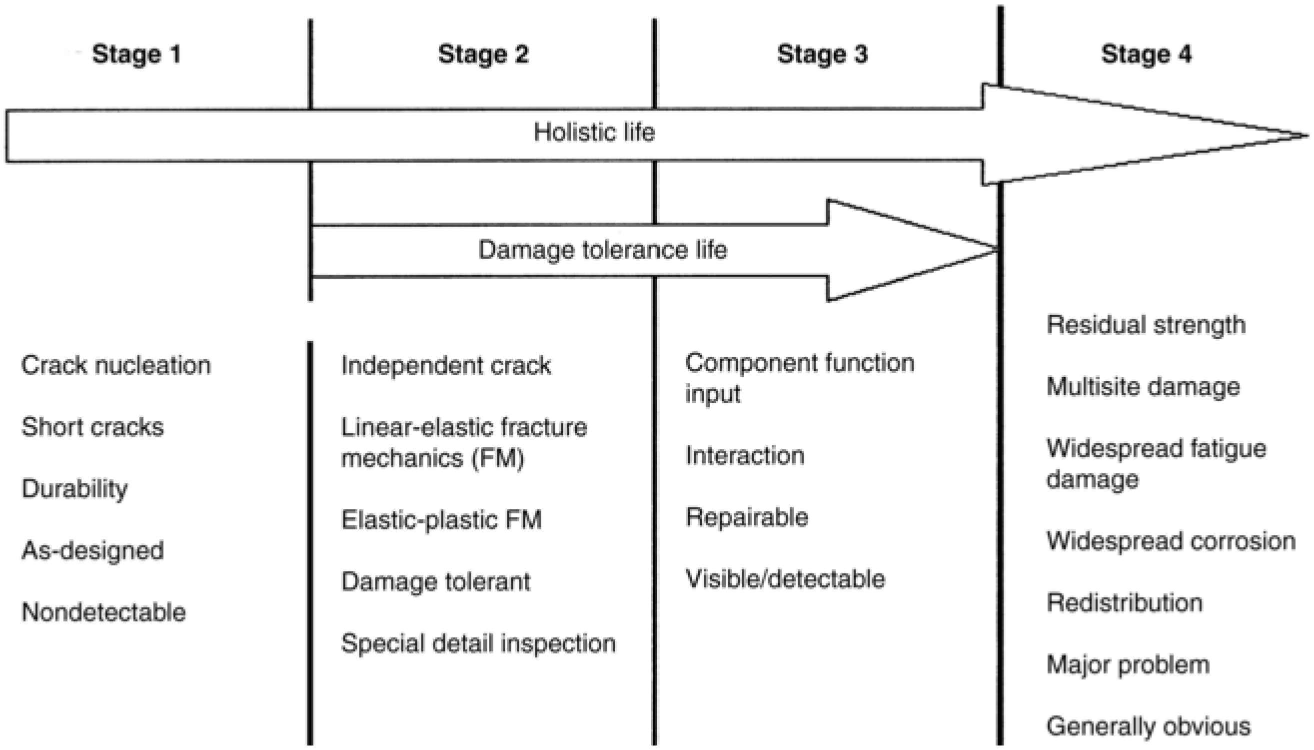

Fig. 1 Four stages of service life. The goal of the holistic approach is to account for all known effects, quantify them, and determine all states of damage from stage I (as-manufactured) through stage IV (too late). Cyclic damage from operating stress and age degradation, including corrosion, are considered.

Current damage tolerance procedures tend to focus on the center stages (stage II and III), whereas the holistic concept attempts to account for and compute age degradation with cyclic stress effects in all four stages. This allows analysts to account for critical stages when and where they are important, rather than forcing potentially conservative procedures at all locations.

Initial Discontinuity State

The initial discontinuity state (IDS) concept is the heart of holistic life analyses. The IDS concept is similar to the equivalent initial flaw size (EIFS) concept (Ref 8) first used in the early 1970s. In EIFS applications, flaw sizes are computed for the component, material, and load spectrum of interest; however, these flaw sizes seldom have any physical relationship to the features that cause failures in experiments. In the IDS framework, attempts are made to relate the IDS size distributions with the physical features that cause fatigue failures in pristine coupons. Researchers (Ref 9, 10) have shown that second- phase particles associated with fatigue failures in common aircraft aluminum alloys are among the largest particles present. The goal, then, is to try to link the material model to these features. A key difference between IDS and EIFS is that IDS should be coupled to the physical material features. These features can be determined and quantified for the alloy system and then consistently used within the analytical process that captures the probabilistic nature of the IDS. Also, the IDS concept uses more stringent requirements than the EIFS concept, such as:

- The material crack growth curves should be documented and available, along with their corresponding IDS distribution.
- Physical effects (such as plasticity and crack nucleation modes) on extreme value subsets of the IDS should be understood, helping enforce that the IDS distribution should be independent of stress ratio, maximum stress level, and global geometric stress concentrations when computations include the physical density of the IDS relative to the high-stress regions.

Note that the particle sizes that nucleate fatigue failure should follow an extreme-value distribution, one that represents the upper (largest discontinuity size) tail of an IDS distribution obtained by progressive sectioning and polishing. Some of the previously mentioned IDS requirements may need to be addressed by considering

the effects of the external parameters (maximum stress level, global stress concentrations) on both the sizes and the total volume of discontinuities exposed to those parameters.

Distributions of IDS sizes extracted from experimental data represent the number of cycles required to obtain known test termination events, for example, failure in coupon, in the material tested. The computed IDS sizes are derived from many stress ratios and at several different constant amplitude peak stresses and also represent several lots of the sheet material of interest. Ideally, the IDS distribution should be independent of constant amplitude test *R*-ratio (minimum applied stress divided by maximum applied stress) and maximum stress. The results characterize the statistical nature of the flaw sizes by using crack growth analysis techniques and approximate the time in the initial stages of crack formation.

To date, determination of IDS distributions has focused on two common aircraft aluminum alloys, 7075-T6 and 2024-T3. These distributions were determined several years ago through analysis of *MIL-Handbook 5* data (Ref 11) and, due to a lack of particle distribution information, the IDS was not tied to physical features. Results from the 2024-T3 sheet analysis are combined with similar 7075-T6 (bare) results (Ref 8) and fit to a Weibull distribution (Fig. 2) to represent the beginnings of a probabilistic-based framework. The specimens were smooth sections with low or no stress concentrations and thus represent bulk material behavior on a global scale. Test data obtained using specimens with stress concentrations, preferably open holes of sizes typical of fasteners, might provide more representative distributions of flaw size distributions applicable to fastener hole regions. The IDS distributions and their appropriate subsets represent the inherent condition of the as-manufactured material, and thus, any corrosion attack as well as the fatigue cycle crack extension will start from these quantifiable initial conditions. However, corrosion IDS subsets may be different from fatigue IDS subsets, as well as alloy dependent.

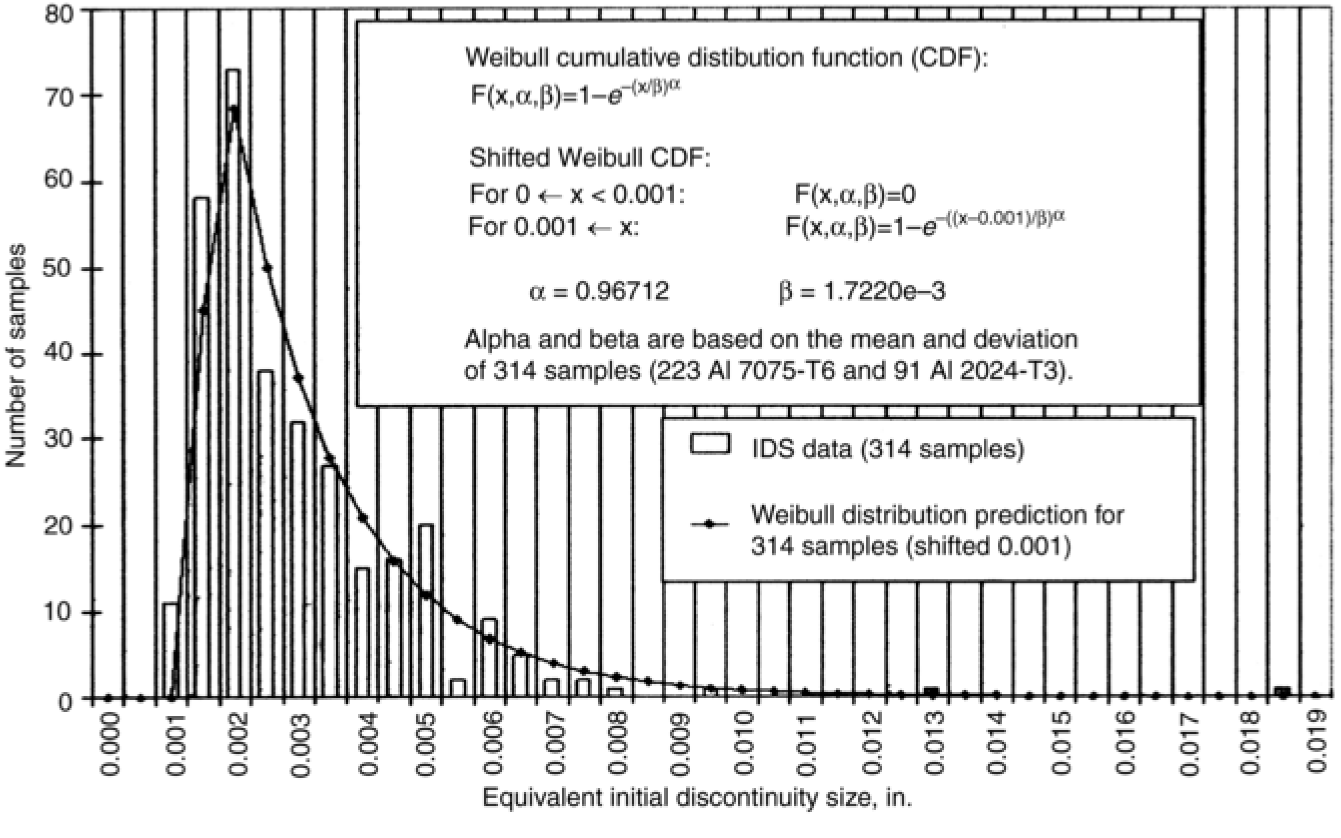

Fig. 2 Initial discontinuity state (IDS) distribution for 2024-T3 and 7075-T6 aluminum with the Weibull probability distribution. α is a scale parameter, and β is a shape parameter.

Age-Based Structural Degradation

Corrosion is defined as the chemical or electrochemical reaction between a material, usually a metal, and its environment that produces a deterioration of the material and its properties (Ref 12). Some common types of corrosion that affect structures are uniform or general corrosion, galvanic corrosion, pitting corrosion, and intergranular or exfoliation corrosion. In addition to these forms, corrosion often interacts with sustained loads

to cause stress-corrosion cracking. In other cases, corrosion may act conjointly with fatigue and work to accelerate both crack formation and propagation of fatigue cracks.

Corrosion is a challenging issue, because it can affect structures in a variety of ways. In severe forms of thinning attack, such as general corrosion and exfoliation, corrosion may degrade the static-strength capability of a structure. Such was the fate that befell a commercial airliner in 1981 (Ref 1, 13). Perhaps more perplexing, though, are the many corrosion and fatigue interactions. Only the first of the following definitions is standard:

- *Corrosion fatigue:* the process in which a metal fractures prematurely under conditions of simultaneous corrosion and repeated cyclic loading at lower stress levels or fewer cycles than would be required in the absence of the corrosive environment (Ref 12)
- *Corrosion-nucleated fatigue:* the process in which physical corrosion damage (e.g., exfoliation, pitting) and/or chemical damage (e.g., embrittlement) accelerates the formation of fatigue cracks in a component or structure. The corrosive environment need not be present during the time of fatigue cycling for this type of interaction to occur.
- *Prior-corrosion fatigue:* occurs when a propagating fatigue crack encounters a prior-corroded region. Note that a propagating fatigue crack in a prior-corroded region may be propagating by corrosion fatigue if an aggressive chemical environment is still present and assists in altering crack propagation in a synergistic manner.
- *Corrosion-induced fatigue via load transfer:* occurs when corrosion damage or environmental degradation in a structure causes load to be transferred to nearby structures. The increased stresses and strains associated with the transfer may exacerbate the situation and promote fatigue cracking. The concepts surrounding this last definition may seem obscure, but the review of case studies, such as the Aloha accident (Ref 1), helps reveal some of the ways in which this failure mode works.

In the development of holistic life analyses to date, intense focus has been placed on the impact of corrosion-nucleated fatigue, particularly from pitting and exfoliation damage. Inputs required are a physical description of the corrosion morphology and, in cases where corrosion is still active, corrosion rates. In situations where the corrosion is still active during fatigue cycling, the analyses cross over into pure corrosion fatigue.

Key to understanding the application of this framework to corrosion-nucleated fatigue, for instance, is visualizing how this prior-corrosion damage interacts with the foundation of holistic life analyses, the IDS. The next section expands on this interaction.

Interdependency of Corrosion and Fatigue

The interaction of corrosion and fatigue cracking is complex within the holistic life analysis model. Fatigue crack sizes change as a function of time, as does the topography of a corroded surface. This effect is captured by topography correction factors (TCFs) within the holistic analysis framework. In essence, TCFs take into account the effects of local stress raisers associated with corrosion damage. The TCFs are realized as an amplification to the geometric factor, β (also known as beta solution), to the stress- intensity factor, K_I, associated with the IDS. As an example, Fig. 3 shows the current modeling processes that account for the influence of pitting on the cyclic fatigue domain. The models that determine this influence are based on two-dimensional, closed-form fracture mechanics K_I for a single-edge through crack in uniaxially stressed infinite plate, shown at top right in Fig. 3. Important notes on the current modeling procedure include:

- The IDS is ever-present and is represented as a through crack of depth *a*.
- If exposed to fatigue (stress) cycling, the IDS may grow into a modified discontinuity state (MDS).
- If exposed to a corrosive environment, general attack, pitting, or exfoliation may form. No corrosion damage is allowed to consume or reduce the IDS or MDS (corrosion has rarely been shown to improve coupon fatigue life experimentally), so, at any point in time, the effects of a given topography on the fatigue domain are obtained by adding the pit depth, *d*, to the IDS or MDS depth.
- To eliminate the influence of backface corrections (finite width influences) on the TCFs, these solutions are based on infinitely thick plates, and the addition of the pit depth is shown above the initial reference measurement line for the IDS. This prevents the corrosion from consuming the IDS or MDS and prevents a shifting reference frame for the crack-length measurement when the topographies are

modeled in finite-thickness plates. For any given pit depth ***d*** and crack length ***a***, a value can be obtained that represents the ratio of the infinite-plate K_I for the pit and crack to the crack alone (K_{a+d}/K_a), where K_a is calculated for a crack in the single-edge through crack in uniaxially stressed infinite plate. This ratio is called a TCF and can be applied either to the fracture-mechanics- based beta solution or directly to the K_I. As the crack length ***a*** varies, a TCF curve can be constructed for a given topography.

- As time progresses, the pit depth typically grows, so the TCF curve changes as a function of time. The IDS or MDS also grows in the cyclic domain, either by fatigue cycles alone or by fatigue cycles acting on a crack with a TCF applied. The holistic life analysis computations alternate rapidly between the cyclic domain crack extensions and re-computations of the TCF curve to account for the interacting effects of corrosion and fatigue. Figure 4 shows a sample of TCF curves for various topographies. The TCF curves can be rapidly generated by closed-form methods for specific depths of an isolated pit or generated using finite-element techniques for specific surfaces under general corrosion attack.

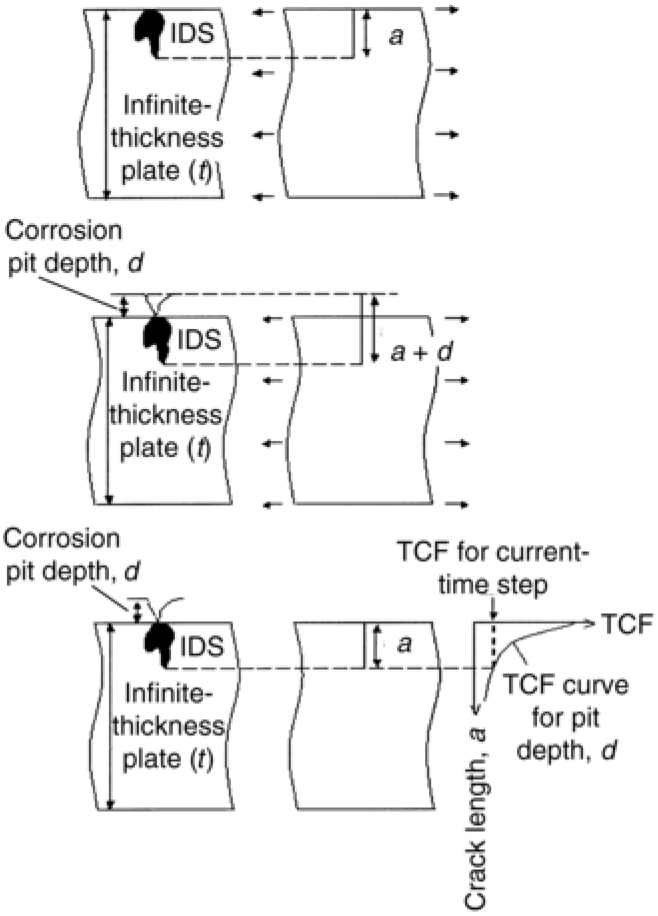

Fig. 3 A two-dimensional fracture mechanics representation of corroded surface topography effects on crack stress intensities. Holistic analyses model the topography correction factor (TCF) curve changes in calendar time. IDS, initial discontinuity state

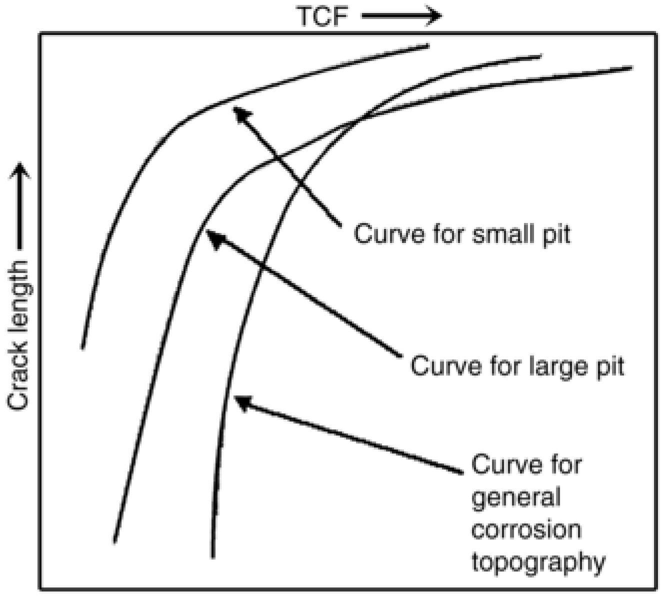

Fig. 4 Topography correction factor (TCF) curves change in time with corroded surface evolution.

General Attack. Topography correction factors were determined for both general attack and pitting (Ref 14). The TCFs for three representative levels of general corrosion were determined from samples of 2024-T3 aluminum. The topographies were determined from profilometry, and these profiles were constructed into two-dimensional finite-element models. Then, cracks were placed at various locations under the profiles to determine families of K_I corrections for the different combinations of topography and crack size. An example of this work is given in the next section.

Pitting Corrosion. Only limited work has been completed toward defining TCFs for pitting corrosion. Some collaborative work was accomplished with the Defense Science and Technology Organization/Aeronautical and Maritime Research Laboratory (DSTO/AMRL) in Melbourne, Australia, to investigate the effects of pit shape on K_I. Conclusions showed that pit tip radius was the most influential parameter (Ref 15). The work also showed that the K_I response was quite similar to that of a crack, which formed the early hypothesis that pits could be treated as cracks within a fracture mechanics framework. Some finite-element results supporting this hypothesis are shown in the next section. Thus, the TCFs for pitting within the framework are calculated using a ratio of two-dimensional K_I: one for the crack length and one for the crack length plus the pit depth. The shortcoming of this approach is that it is based on extremely limited data. Efforts are currently underway to determine more precise K_I distributions for surface cracks (three-dimensional) at the base of hemispherical pits. This will greatly increase the robustness of the TCFs for pitting and increase model performance.

Exfoliation Corrosion. Topography corrections for exfoliation corrosion essentially borrow from the pitting corrections, because the two failure modes have very similar effects in fatigue of aluminum alloys. Extensive fractographic analyses (Ref 16, 17) have shown similar damage morphologies between exfoliation and pitting, too, in that the surface of the material below the exfoliated grains contains pitlike discontinuities that serve as fatigue crack nucleation sites. Thus, exfoliation is modeled as pitting in the presence of thinning, a model that borrows heavily from the process zone concept developed at the DSTO/AMRL. The process zone model has been widely published in conference proceedings (Ref 18, 19).

Corrosion Pillowing. Another interaction that can be modeled within the holistic life analysis framework is that of corrosion pillowing (Ref 20). This model was developed to address problems associated with crevice corrosion in lap joints where the corrosion by-products produce volumetric expansion, which results in increased pressure or deflections, leading to sustained stress. This sustained stress builds as corrosion by-products increase at certain locations within that geometry. These sustained stresses can produce independent cracking, as described by Ref 14, while aircraft are at rest. Combined with operational stress cycles, they can result in more damaging cyclic crack extension than that which would occur without the superimposed pillowing sustained stresses. This interaction and damage effect is intended to consider the effect of the corrosion-induced sustained stress conditions on the cyclic crack extension of operation (for example, fuselage pressurization) damage. It also includes the loss of material associated with the by-products creating the sustained stresses.

Each of the previous degradation effects is included in a life-assessment framework to simulate their respective influences on the life analyses. The framework and associated analytical tools allow any or all of the degradation effects to vary as a function of time, so that the effects become functions of both cyclic stress and calendar time. The modeling procedure allows the analyst to control the amount and levels of influence of each effect, either independent of cyclic mechanisms or interactively affecting the cyclic contributions to damage. This allows the analyst to quantify the impact of each degradation mechanism, acting independently and in concert with other mechanisms.

References cited in this section

1. NTSB/AAR-89/03, Aloha Airlines, Flight 243, Boeing 737-200, N73711, near Maui, HI, April 1988, National Transportation Safety Board, 1989

4. C.L. Brooks and D. Simpson, Integrating Real Time Age Degradation into the Structural Integrity Process, *Proceedings, NATO RTO's Workshop Two on Fatigue in the Presence of Corrosion,* Oct 1998 (Corfu, Greece), North Atlantic Treaty Organization Research and Technology Organization, p 22–1 to 22–13. Available http:// www.sti.nasa.gov/Pubs/start/star.html

5. C. Brooks, K. Honeycutt, and S. Prost-Domasky, Correlation of Life Prediction Methods with Corrosion-Related Tests, *Proceedings, U.S. Air Force Aircraft Structural Integrity Program Conference,* Dec 1999 (San Antonio, TX), Universal Technology Corporation

6. T.J. Ginter, D.J. Shelton, and R.P. Bell, "Corrosion Fatigue Structural Demonstration, Phase I," Final Report AFRL-VA-WP- TR-2000-3005/-3006, U.S.A.F. Contract F33615-97-C-3218, United States Air Force Air Vehicles Directorate, Nov 1999

7. C. Brooks, C.D. Peeler, K. Honeycutt, and S. Prost-Domasky, "Predictive Modeling for Corrosion Management: Modeling Fundamentals," Analytical Processes/Engineered Solutions, Inc. Available at http:// www.apesolutions.com/frm_link.htm

8. C. Brooks, S. Prost-Domasky, and K. Honeycutt, Determining the Initial Quality State of Materials, *Proceedings, U.S. Air Force Aircraft Structural Integrity Program Conference,* Dec 1998 (San Antonio, TX), Universal Technology Corporation, 1999

9. A. Merati, J. Tsang, S. Khomusi, A. Kourline, K. Kyle, and M. Geusebroek, "Preliminary Report—Final Test Results for the Determination of Fatigue-Related Features of the Initial Discontinuity State (IDS) of 2024-T3 Aluminum Alloy," Report LTR- SMPL-2002-0110, National Research Council of Canada, 2002

10. P.J. Laz, B.A. Craig, and B.M. Hilberry, A Probabilistic Total Fatigue Life Model Incorporating Material Inhomogeneities, Stress Level, and Fracture Mechanics, *Int. J. Fatigue,* Vol 23, 2001, p S119–S127

11. Metallic Materials and Elements for Aerospace Vehicle Structures, *MIL-HDBK-5,* United States Department of Defense, Nov 1994

12. *Compilation of ASTM Standard Definitions,* 6th ed., American Society for Testing and Materials, 1986

13. "National Aging Aircraft Research Program Plan," Federal Aviation Administration Technical Center, United States Department of Transportation, 1993

14. C. Brooks, K. Honeycutt, and S. Prost-Domasky, Monitoring the Robustness of Corrosion and Fatigue Prediction Models, *Proceedings, U.S. Air Force Aircraft Structural Integrity Program Conference,* Dec 2001 (San Antonio, TX), Universal Technology Program, 2002

15. S.A. Prost-Domasky, C.L. Brooks, and K.T. Honeycutt, The Application of *p*-Version Finite Element Methods to Fracture-Dominated Problems Encountered in Engineering Practice, *Computers and Mathematics with Applications,* Elsevier Sciences, 2003, submitted for publication

16. P.K. Sharp, T. Mills, and G. Clark, Modeling of Fatigue Crack Growth from Pitting and Exfoliation Corrosion, *Proceedings, 21st Symposium of the International Committee on Aeronautical Fatigue,* 27–29 June 2001 (Toulouse, France), p 485–498. Conference proceedings available from http://www.emas.co.uk/

17. P.K. Sharp, T. Mills, and G. Clark, Aircraft Structural Integrity: The Impact of Corrosion, *Proceedings, Tenth International Congress of Fracture (ICF 10),* 3–7 Dec 2001 (Honolulu, HI), Elsevier Science

18. P.K. Sharp, G. Cole, G. Clark, and S.G. Russo, The Influence of Corrosion on Aircraft Structural Integrity, *Proceedings, 21st Congress of the International Council Aeronautical Sciences,* 13–18 Sept 1998 (Melbourne, Australia)

19. P.K. Sharp, T. Mills, S. Russo, G. Clark, and L. Qianchu, Effects of Exfoliation Corrosion on the Fatigue Life of Two High- Strength Aluminum Alloys, *Proceedings, Fourth Joint DoD/FAA/NASA Conference on Aging Aircraft,* 15–18 May 2000 (St. Louis, MO), Universal Technology Corporation, 2000

20. J.P. Komorowski, N.C. Bellinger, and R.W. Gould, The Role of Corrosion Pillowing in NDI and in the Structural Integrity of Fuselage Joints, *Proceedings, 19th Symposium of the International Committee on Aeronautical Fatigue,* 16–20 June 1997 (Edinburgh, U.K.). Conference proceedings available from http://www.emas.co.uk/

C.L. Brooks, KT. Honeycutt and T.B. Mills, Predictive Modeling of Structure Service Life, *Corrosion: Fundamentals, Testing, and Protection*, Vol 13A, *ASM Handbook*, ASM International, 2003, p 946–958

Predictive Modeling of Structure Service Life

Craig L. Brooks, Scott A. Prost-Domasky, Kyle T. Honeycutt, and Thomas B. Mills, Analytical Processes/Engineered Solutions, Inc.

Corrosion Fatigue Model Applications

A basic engineering approach to compute the effects of corrosion on structural capability is described and exercised for two types of corrosion: crevice and pitting. The analyses use fracture mechanics methods and fundamental engineering principles. Engineering computations are combined with damage tolerance assessment concepts to formulate a model that approximates the life degradation effects of corrosion with both sequential and concurrent fatigue. Although the life predictions are calculated using deterministic techniques, sensitivities to key parameters can be determined, and therefore, probabilistic life predictions can be approximated. The results of this approach provide the analyst with numerical impacts of potential scenarios and a means for quantifying the effects of corrosion with fatigue.

Crack growth life analyses of a particular airplane geometry configuration are used to show the relative life impact of corrosion metrics, although models are flexible enough to be applied to ground vehicles and other systems that may need to be damage tolerant. A simulation of a pressurized fuselage skin splice is used to illustrate the analytically derived impact to the life and safety of the joint in the presence of corrosion. Analyses take into account all documented damage modes and time-dependent effects. Results of the analysis indicate that corrosion is a potential structural problem for the particular aircraft locations that are experiencing this type of corrosion attack.

This section presents the methodology for computing the effects of real-time age degradation on an aircraft structure for two different corrosion types: crevice and pitting corrosion. Reference 21 documents a process for incorporating these aspects into the existing infrastructure of the design, manufacturing, and maintenance of aircraft or ground systems.
It must be noted that the two applications of the holistic analysis framework presented in this article use supporting data and implementations that are immature, because more field and experimental information is being sought to further substantiate the engineering application. Details of the analysis methods are still being revised, subject to ongoing tests that are producing robust supporting data. However, the framework demonstrates that the engineering fundamentals of age degradation can be applied to life-prediction methods with reasonable results, whereas current modeling philosophies that do not consider the time domain quantify the structural degradation due to corrosion by relying on empiricism.

Crevice Corrosion Model

The modeling of crevice corrosion in a life- prediction framework is described. Fatigue, crack growth, and finite-element modeling algorithms, each with corrosion interaction effects, are tools that can be readily adapted to provide adequate assessments to determine the magnitude of the corrosion problem, resulting in a basic engineering approach. The fundamentals of the proposed approach are to:

- Determine the initial as-built quality condition of the structure and basic material for the initial starting condition
- Model the effects of micro- and macrosurface topography changes in time due to corrosion growth
- Include the time dependence of any mechanically induced deflections due to corrosion by-products and effects of material loss
- Superimpose corrosion effects with cyclic fatigue crack growth using realistic environments

This procedure requires establishing the effective characteristics of material and structural discontinuity states to provide an initial starting condition. Important data include industry strain/ stress crack initiation test data, surface topography, local and global deflections and loads, crack growth rate data, corrosion rate data, related experimental test data, field aircraft findings, and experience.
By using AFGROW (a crack growth analysis tool available from the U.S.A.F.) and the *p*-version finite-element method software StressCheck (Engineering Software Research and Development Inc.), state-of-the art fracture mechanics and structural analysis tools, and by taking advantage of significant improvements in personal computing power, an engineering method for integrating life impacts due to corrosion degradation can be incorporated into structural life assessments. With these tools and concepts, it becomes feasible to determine the economic impact of corrosion and to improve the structural airworthiness of all aging systems.
Corroded surfaces from both experimentally corroded and in-service corroded sheets were studied to evaluate surface topography and material loss influences on damage tolerance of thin sheets typically found in lap joints. Local macrosurface stress effects due to the topography produced by surface corrosion and pitting amplify the mode I K_I. (Mode I is the opening mode for cracks, mode II is the sliding mode for cracks, and mode III is the twisting mode for cracks.) Results from analysis of typical transport aircraft fuselage lap-splice joints are presented here. Corrosion causes pits, waviness, and variable surface roughness that produce local stress raisers and effective concentrations, as shown in Fig. 5(a). The normal stress in the applied load direction is shown in Fig. 5(b). Some of the pit sizes were on the order of 25% of the corroded sheet thickness, and some were as small as a few thousandths of an inch. In addition, the corrosion process results in more global surface decay or material thickness losses, which result in additional stress raisers.

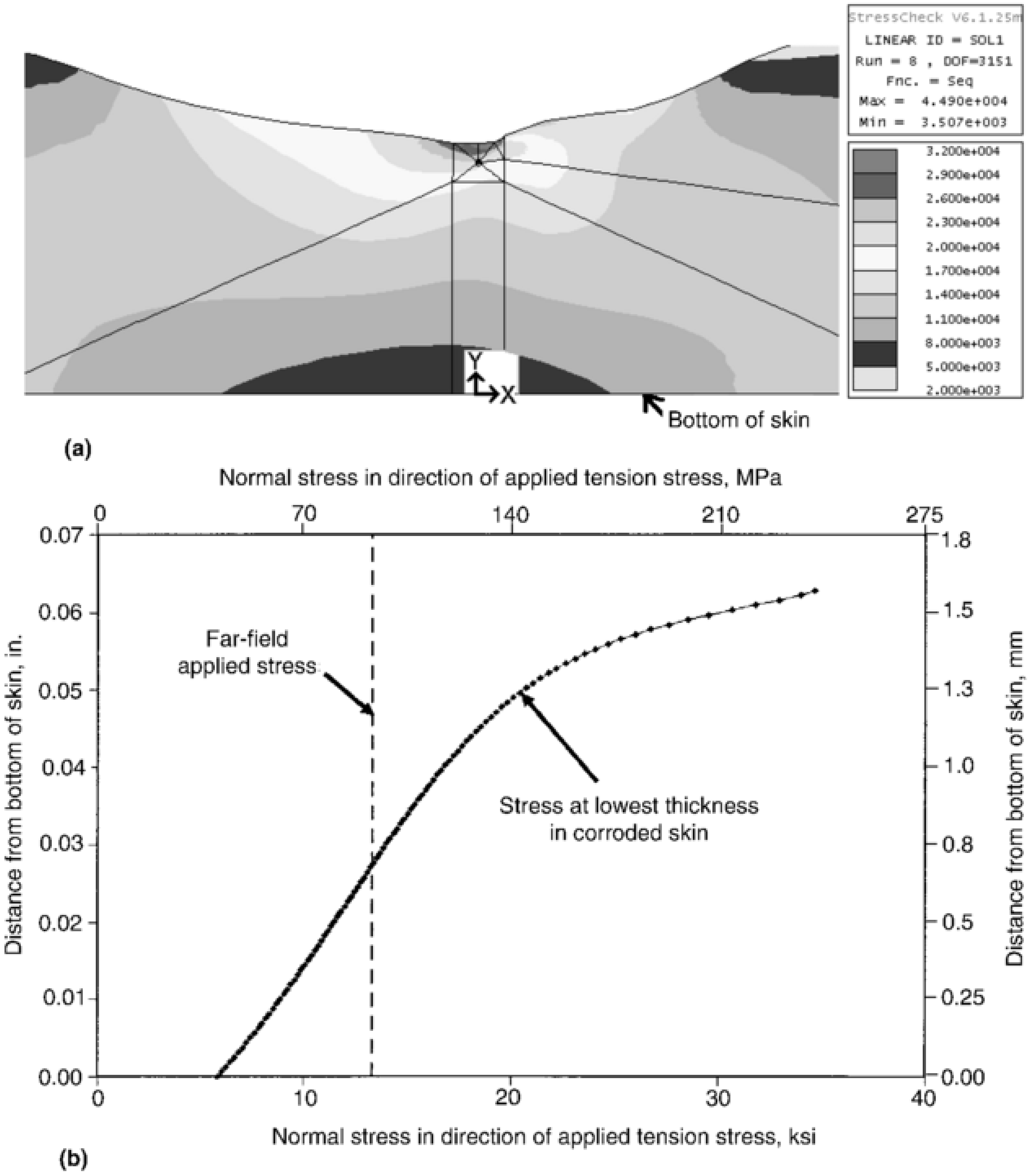

Fig. 5 Stress amplification due to corrosion topography. (a) von Mises stress contours. (b) Normal stresses versus height at the thinnest part of the skin

Surface profiles were modeled using a *p*-version finite-element analysis code, StressCheck (Ref 22). A typical finite-element model of a skin sample taken from a lap joint on an in-service aircraft is shown in Fig. 6. The profile was obtained by a high-resolution optical scan and converted to a data file of *x*-*y* coordinates of the surface. Crack tip K_I computed in StressCheck was used to study the effects of different corrosion scenarios on several different profiles. Figure 7 shows the results of two types of profiles (skin 1 was a profile similar to Fig. 6, and skin 2 was a single pit).

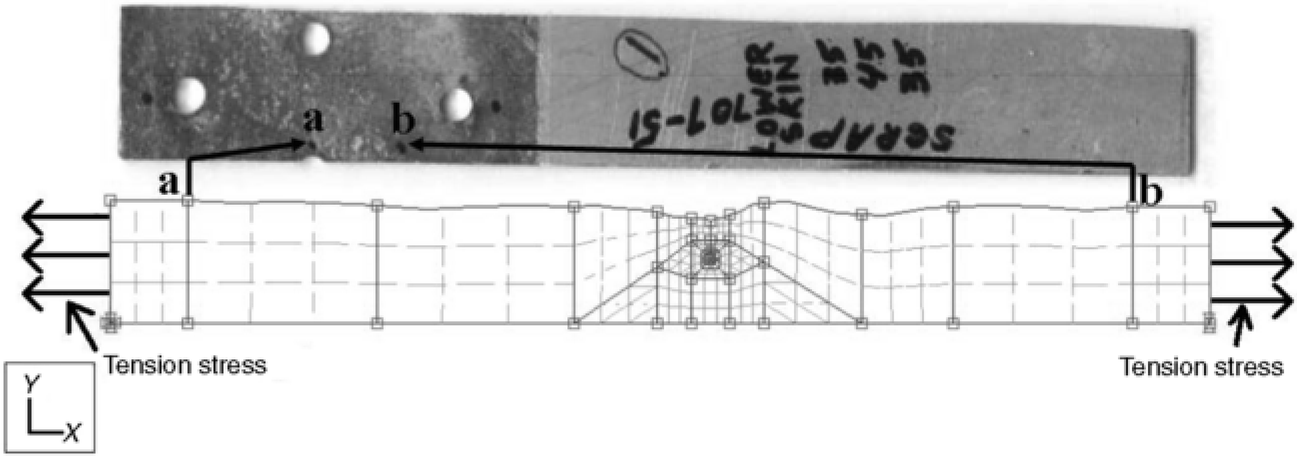

Fig. 6 StressCheck model of 10% corroded skin from lap joint. Top, corroded lap-joint section from Boeing 707 aircraft; bottom, StressCheck finite-element model. Arrows between points “a” and “b” indicate sections of skin analyzed.

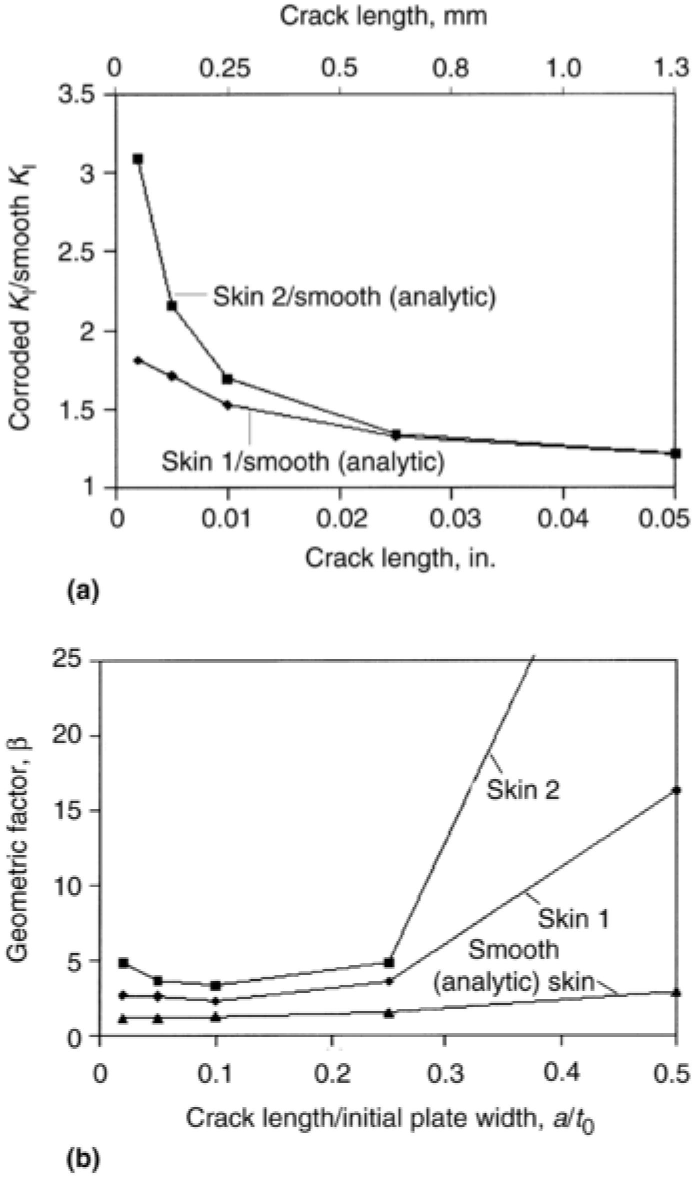

Fig. 7 Stress-intensity factors, K_I, and geometric factors, β, for a typical corroded surface compared to an equivalent crack in a smooth skin surface. (a) and (b) Skin 1 is a profile similar to Fig. 6; skin 2 is a single pit. Smooth K_I is for the classical edge crack solution (β = 1.12). (b) The influence of backface, the thickness of the plate, is demonstrated.

Figure 7(a) shows the K_I of the crack located at the base of the deepest depression in the corroded skin topography of Fig. 6, normalized by the classical edge crack in tension solution (geometric factor $\beta = 1.12$) as a function of crack length. Figure 7(b) shows the influence of the backface on the K_I that results from both thickness loss and stress concentrations caused by the near-notched surfaces of the corroded topography. Through-cracks of varying lengths were introduced in the skins at the many locations but predominately at the highest stress locations and therefore represent a conservative case. It is clear from Fig. 7(a) that the corroded skin significantly amplifies K_I, especially for small cracks (0.25 mm, or 0.01 in., and smaller). Figure 7(b) shows that the amplification of K_I by the corroded skins is more than an area correction, because the corroded skin K_I is compared directly to the edge crack in finite-width plate solutions (labeled “Smooth (analytic) skin”), suggesting that K_I corrections in crack growth analyses of these corroded skins need to account for more than uniform thickness loss. This corroded topography amplification or correction is more important in the early crack growth stages for these samples, which were taken from fuselage lap splices that typically experience relatively low stresses, typically leading to a long number of initiation cycles (defined here as the number of cycles from the initial crack lengths to 0.25 mm, or 0.01 in.).

Corrosion Pillowing. In addition to the effects that corrosion has on lap joints in the form of thickness loss, early crack initiation, stress- corrosion cracking, pitting, and corrosion pillowing can occur. The National Research Council of Canada (NRCC) has investigated and documented this phenomenon extensively (Ref 20). Corrosion pillowing is caused by the additional volume that corrosion by-products occupy, over and above the material volume lost to corrosion—the volume of corrosion by-products can be as much as $6\frac{1}{2}$ times greater than the volume of parent material lost. Fastener constraints in the lap joint prevent uniform deformation of the skins—skins deform most in the middle of the ligaments between rivets, a phenomenon referred to as pillowing. The result is that the skins act much like plates fastened at all four corners, with a uniform out-of-plane pressure applied. Large bending stresses near the rivets result. These large bending stresses have adverse effects on the structural integrity of lap joints. Three-dimensional finite-element simulations (Ref 23) conducted by the NRCC were used to estimate stress fields caused by corrosion pillowing. Figure 8 shows the individual stress state for a skin with a countersunk fastener. The effects of this buildup of sustained stress in time are simulated to estimate the impact on the joint integrity.

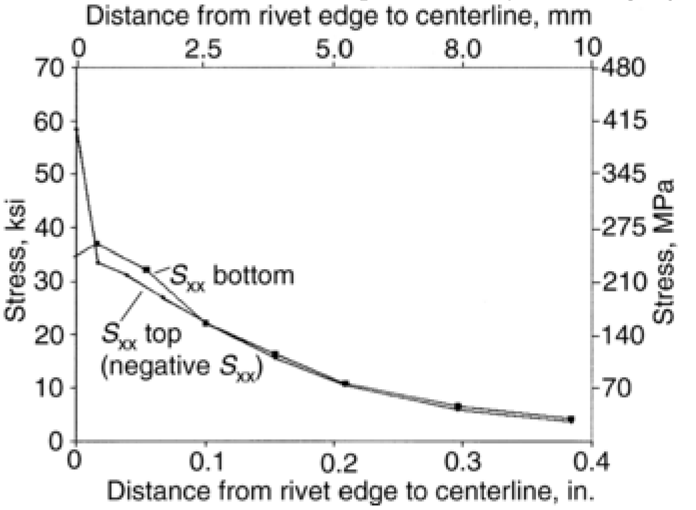

Fig. 8 Sustained stress levels due to pillowing. Corrosion pillowing and resulting bulging in a lap-splice skin were modeled for a four-square fastener pattern. Graph shows normal stress (S_{xx}) in direction of applied in-plane hoop stress, for top and bottom faces of the outer skin, in the region of a countersunk fastener relative to a rivet or hole edge. Centerline is the center between two fasteners that aligned perpendicular to the applied in-plane hoop stress direction.

Multisite Damage. Since the Aloha Airlines B-737 accident in 1988, a paradigm shift in the aircraft structural integrity community has occurred, as far as age-degradation effects on aircraft structure are concerned. Namely, there became a realization that age degradation can have significant safety impact during the life of the structure and that these effects have not been adequately addressed in past or current structural integrity programs for aircraft. Many organizations, including the Federal Aviation Administration (FAA) and the Department of Defense in the United States, initiated major research programs to address aging structural

system challenges and issues. These issues include widespread fatigue damage (WSFD) and its two subsets, multisite damage (MSD) and multiple- element damage (MED) (Ref 24), and how these failure modes reduce the capability and residual strength of the structure, as identified in Fig. 1, especially in the later stages of the life of the structure. Widespread fatigue damage is characterized by fatigue damage across wide or broad areas of the structure—across many structural subcomponents and structural features, such as over many holes, such that (Ref 24) “the structure no longer meets its damage tolerance requirements.” Multisite damage is similar to WSFD but is generally restricted to a much smaller area—over one structural subcomponent or element. Multiple-element damage is characterized by many cracks in similar and adjacent structural elements.

The primary issue regarding MSD is its effect on the integrity or damage tolerance of a structure. Reference 24, which addresses damage tolerance in the presence of MSD, is an excellent reference for further study of this issue. It outlines approaches for including MSD in damage tolerance and residual-strength calculations and presents some examples that account for its effect. One significant conclusion of this analysis is that, depending on the structure and the magnitude of the MSD problem, the residual strength of a structure might be greatly reduced in the presence of MSD cracks that are less than a generally inspectable size, and that inspection alone may not be adequate to ensure safety of the aging system. The structural system could be in bridges, power plants, heavy and light equipment, as well as aircraft. Each structural system must be analyzed in detail to identify failure modes, cyclic and environmental loads, and other damage mechanisms. As a result, some additional considerations may need to be accounted for, similar to those considerations discussed in Ref 4, to better focus on the role and effects that age-degradation mechanisms, such as corrosion, have on structure integrity. These effects could include, but not be limited to, widespread corrosion damage (WSCD) and multisite corrosion damage (MSCD), which both could significantly reduce the time to the onset of WSFD and MSD or just result in general degradation that could rapidly deplete the remaining service-life capability.

Correlation with Test Data. The AFGROW software program and the ECLIPSE software program (APES, Inc.) (a custom-made tool that reflects the holistic assessments advocated here) were used to predict pristine fatigue lives and corroded fatigue lives for riveted aluminum lap- splice specimens that were fabricated and tested at the NRCC. The specimen consisted of two 1.02 mm (0.040 in.) 2024-T3 aluminum sheets lap spliced with twenty-four 3.97 mm ($\frac{5}{32}$ in.) diameter rivets in three rows of eight rivets each (Fig. 9). The typical fatigue failure mode for this type of structure is cracking in an outer row of fasteners, which leads to eventual failure at the critical crack length.

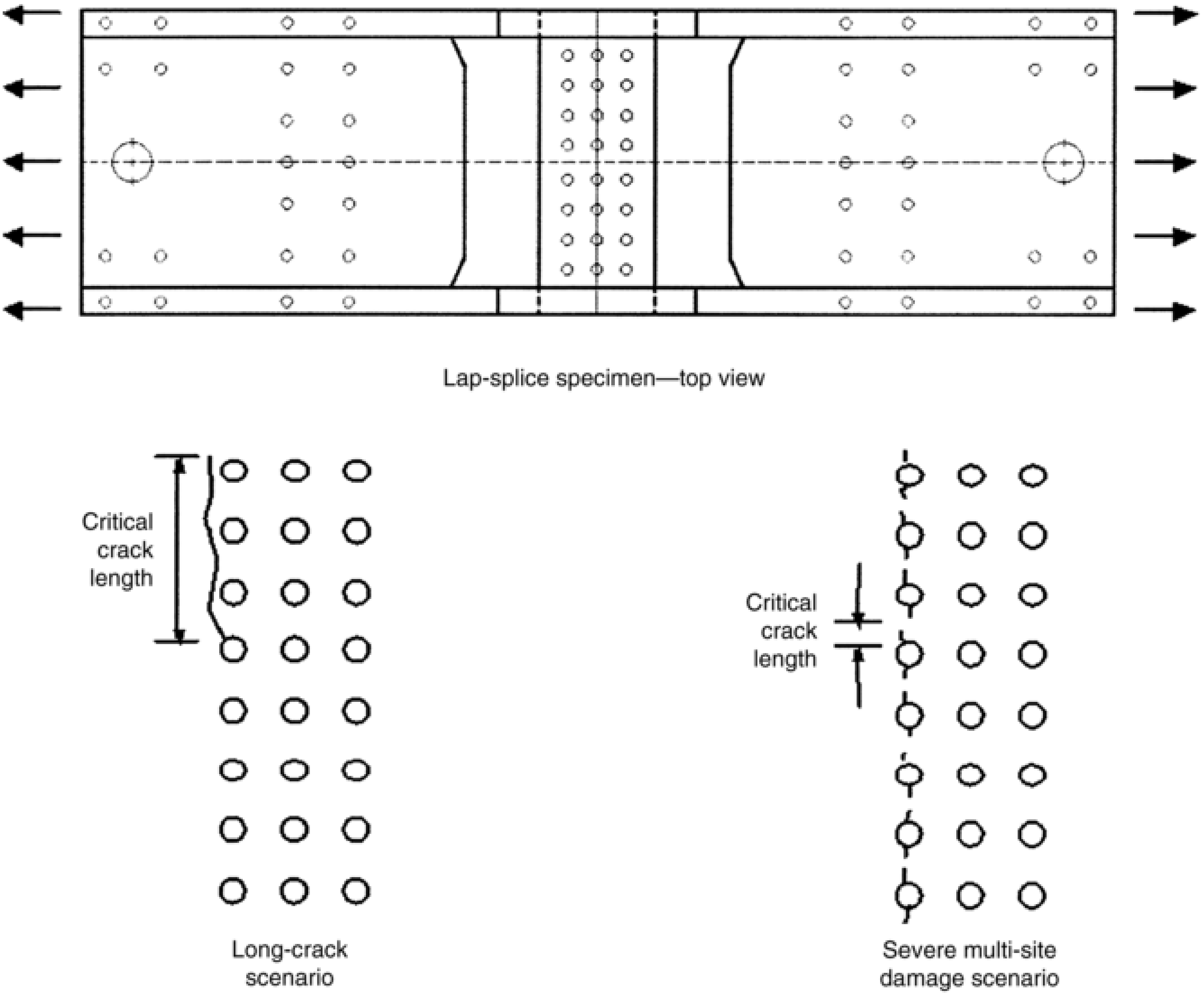

Fig. 9 Two lap-splice failure scenarios for the splice shown on top: long crack and severe multisite damage

General Analysis Assumptions. It is expected that the actual lap-splice failure mechanism is between a long-crack scenario and a severe MSD scenario (Fig. 9). Therefore, the predicted values are the average of a long-crack prediction—a single flaw, ignoring surrounding holes, with critical crack length of approximately 76 mm (3 in.)—and a severe MSD prediction—the same size flaw is assumed to exist at every hole in the splice, and the critical crack length is approximately 10 mm (0.40 in.). A single corner crack at a hole was used for all predictions; however, the MSD analysis corrections account for the presence and influence of other cracks in the lap splice.

For performing the corroded life predictions using the ECLIPSE software, the average thickness loss of the lap specimens was 56 μm (0.0022 in.). A moderate topography beta correction was applied during the analysis. The thickness loss and corroded topography did not change in time, because these were precorroded specimens tested in laboratory air at highly accelerated fatigue cycle rates (accelerated compared to fleet fatigue cycle rates).

Four different models were used to make the pristine and corroded predictions (Fig. 10). The first three (A, B, and C) used one set of material fatigue crack growth rate (*da*/*dN*) curves with different initial crack lengths (IDS); the fourth (D) used a different material *da*/*dN* curve and IDS condition obtained from the Advisory Group for Aerospace Research and Development (AGARD) research (Ref 25). The predicted lives using the long-crack scenario and the MSD scenario were averaged and plotted with the actual test lives to show correlation in Fig. 10.

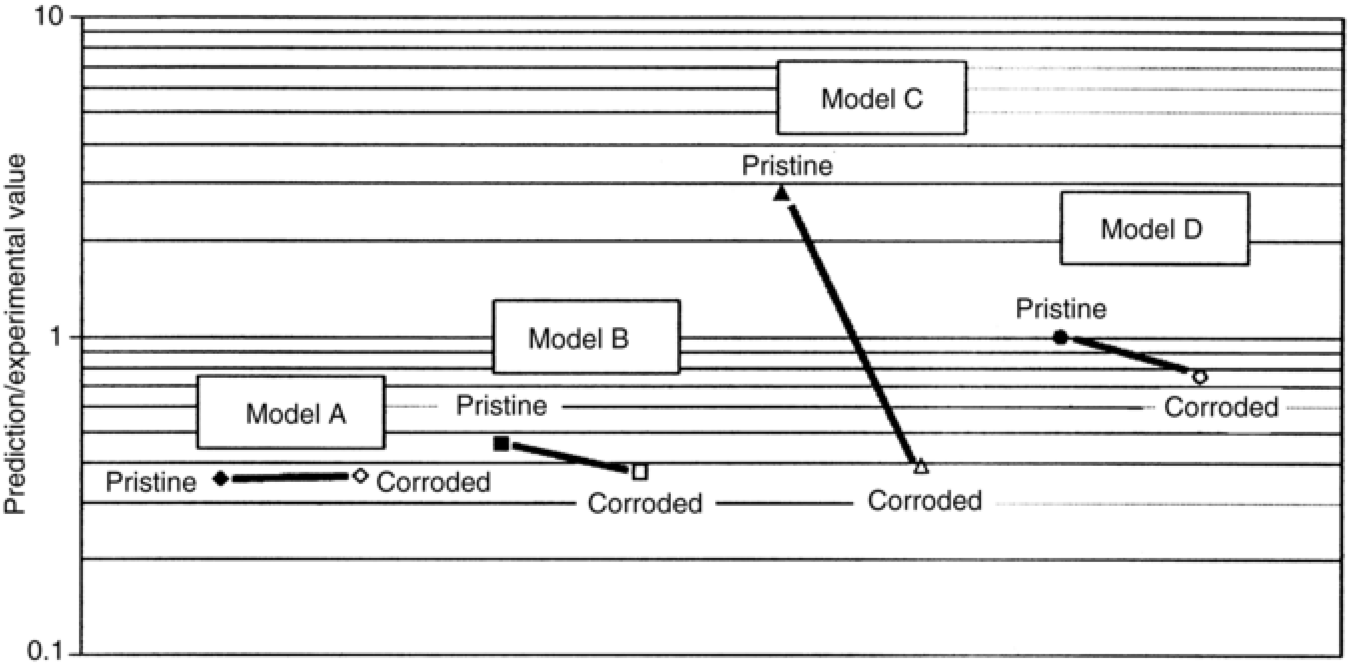

Fig. 10 Lap-splice predictions. Model A: fatigue crack growth rate (*da*/*dN*) curve set 1, initial discontinuity state (IDS) = 84 μm (0.0033 in.); model B: *da*/*dN* curve set 1, IDS = 64 μm (0.0025 in.); model C: *da*/*dN* curve set 1, IDS = 43 μm (0.0017 in.); model D: *da*/*dN* curve set 2, IDS = 6 μm (0.00024 in.)

Ideally, crack length versus number of cycles (*a* versus *N*) information could be obtained from these tests, which would allow correlation at different points during the holistic life, not just correlation at the end point of life, as was shown here. However, difficulties in obtaining crack growth measurements for small crack sizes or under rivet heads often preclude this.

From Fig. 10, it is clear that for this case, models A, B, and C are very sensitive to starting IDS condition in the pristine state. They are relatively insensitive to the starting IDS condition in the corroded state. Also, the combination of material curve and starting IDS condition in model D performs best. However, the reader is cautioned to keep in mind that this conclusion can be reached only for this specific test and the specific analysis geometries and assumptions. Ideally, a much larger database of experimental results should be built, in which case, the model performance can be examined for varying stress levels, stress ratios, and mechanical test conditions.

Pitting Corrosion Model

Pit-as-Crack. The early stages of general corrosion attack in aluminum alloys are generally characterized by isolated pitting—a number of grains very near the surface are attacked by the corrosive agent, and either the grains dissolve, a material discontinuity dissolves, or the grain boundaries weaken, and the grain breaks away or dissolves. This section describes a model to approximate the effects of pitting corrosion on structural life. The goals were to characterize real corrosion pits using pit width, pit depth, pit radius near the crack origin, and other geometric descriptions, as necessary, and also to determine the radius of influence of a corrosion pit, that is, how far the stress-concentration influence extends from the bottom of a corrosion pit.

The Aeronautical and Maritime Research Laboratory (AMRL) of Australia (Ref 26) cut a large set of experimental test coupons from the same sample of aluminum alloy 7050-T7451. The specimens had rectangular cross sections 32.00 by 9.91 mm (1.26 by 0.39 in.). Centered holes had diameters of 6.35 mm (0.25 in.). Test coupons were artificially precorroded in 3.5% NaCl solution for 24 h. Coupons were then bagged in a controlled environment with less than 40% relative humidity to arrest further corrosion pitting. Coupons were subsequently fatigued to failure at 5 Hz, using a constant cyclic minimum-to-maximum stress ratio (*R*) of 0.1 and various maximum stress levels. After test specimen failure, coupon failure surfaces (which contained the failure crack front) were examined with a scanning electron microscope (SEM). The two-dimensional sections of each pit from which fatigue cracks emanated were recorded and used to define two-dimensional surfaces in

finite-element models. Hand sketches of two typical fatigue crack pits are shown in Fig. 11. Pit dimensions were used in subsequent finite-element analyses and crack growth predictions.

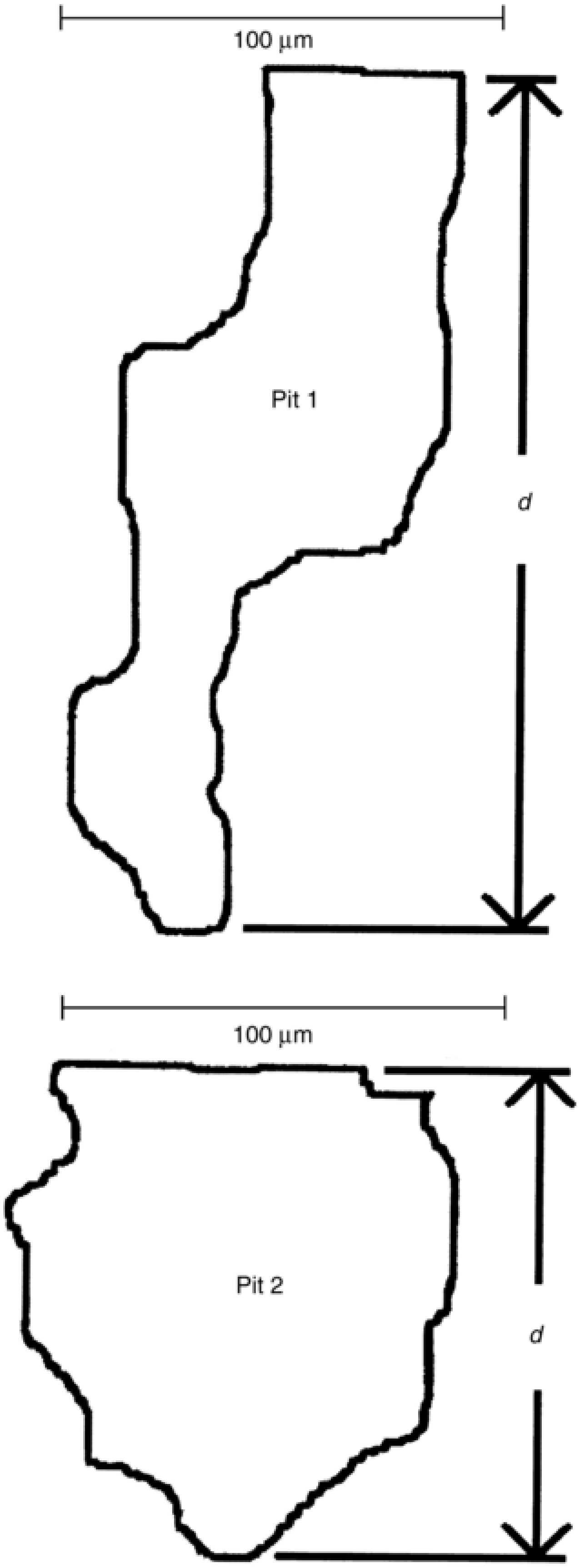

Fig. 11 Sketch of pit geometry, as received. Source: Ref 26

Correlation with Test Data. The stresses near actual corrosion pits sketched from SEM images of the postfracture were analyzed with the *p*-version finite-element method software, StressCheck. These pits were

fitted with cubic splines and located at the surface of a planar domain. A tension stress was applied so that the pits acted much as edge notches, with the highest stresses located at the bottom of the corrosion pits.

Figure 12 contains the results of the finite-element analyses for the two actual pits. The model referred to in this figure is the model of a pit as a crack; that is, for these pit geometries, the model is simply an edge crack of length equal to the pit depth *d* plus the crack at the bottom of the pit of length *a*. This is mechanically equivalent to the actual pit with a crack at the bottom of the pit. For instance, if the pit is 203 μm (0.008 in.) deep with a 51 μm (0.002 in.) crack at the bottom of the pit, the model is an edge crack of 254 μm (0.010 in.) in length. The effective crack length $a_{eff} = d + a$ is used to calculate the geometric factor, β:

$$\beta = \beta(a_{eff}/t) = \beta((d + a)/t) \quad \text{(Eq 1)}$$

The corresponding K_I is then obtained by multiplying β by the applied tensile stress, σ, and the square root of πa_{eff}, where a_{eff} is the effective crack length:

$$K_1 = \beta(a_{eff}/t)\sigma\sqrt{\pi a_{eff}} \quad \text{(Eq 2)}$$

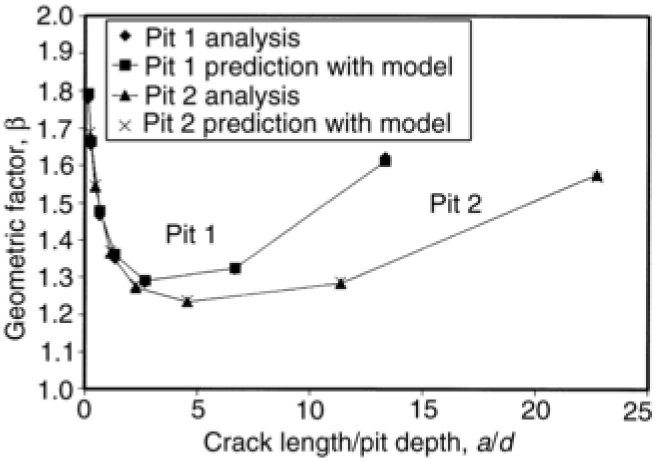

Fig. 12 Proposed pit-as-crack model compared with actual pit-plus-crack results. Finite-element method used to model the two pits of Fig. 11, with small cracks located at the bottom of pits ("Pit 1 analysis," "Pit 2 analysis") perpendicular to the applied tension stress (similar to the configurations shown in Fig. 5 and 6). The geometric factor, β, is the K_I normalized by the applied tension stress and the square root of πa, where *a* is the representative crack length. The "prediction with model" is the classical edge-crack-in-tension geometric factor, with the crack length defined as the pit depth added directly to the length of the small crack located at the bottom of the pit.

The simplified model of pit-as-crack was used in elementary crack growth analysis of an edge crack in AFGROW. Pristine (uncorroded) coupon test results (Fig. 13) were used to refine the crack growth rate curve, where the "Prediction," as labeled in Fig. 13, is actually a postdiction; that is, the best initial flaw size is calculated by back calculating the initial flaw size required to obtain the fatigue lives of the pristine coupons. The average of all initial flaw sizes for the pristine coupons was used in the prediction of the fatigue lives of the corroded coupons (Fig. 14).

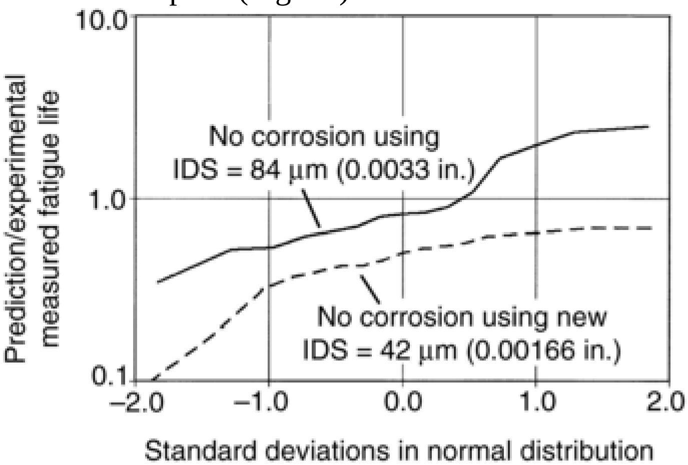

Fig. 13 Correlation of predicted fatigue lives with Aeronautical and Maritime Research Laboratory experimentally measured uncorroded fatigue lives. IDS, initial discontinuity state

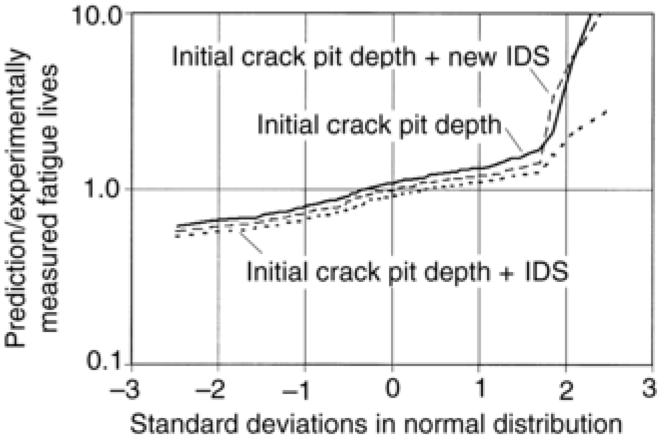

Fig. 14 Correlation of corrosion fatigue prediction (pit-as-crack) model and Aeronautical and Maritime Research Laboratory experimental corroded specimen results for approximately 80 corroded coupons. Pit depths measured postfracture used in the corrosion fatigue predictions, along with the initial discontinuity state (IDS) obtained from tuning the prediction model with Fig. 13 on corrosion fatigue lives. The new IDS equals 42 μm (0.00166 in).

These figures show predictions normalized by the actual measured fatigue lives, with the abscissa (horizontal axis) being the standard deviations in a normal distribution for each of the prediction groups, noncorroded and corroded. Ideally, the prediction/experimental curves would be horizontal and cross the zero (0.0) vertical standard deviation line at 1.0. A proprietary 7050-T7451 material crack growth rate curve (*da*/*dN*) was input into AFGROW. The pit depths, as measured by AMRL, defined the size of the initial crack length (i.e., pit depth).

Figure 13 shows the noncorroded specimen fatigue predictions. Note that the initial crack size, 84 μm (0.0033 in.), corresponding to a nominal IDS for this material, was chosen for the crack growth calculations. The new IDS was back calculated from the non-corroded AMRL experimental results procedure by calculating the initial flaw size needed to fail the pristine coupons at the measured fatigue lives; hence, this procedure results in a post-diction, not a prediction, because the fatigue lives are known and are used to tune the life predictions. The distribution of initial flaw sizes thus obtained is averaged; in this way, a much better value of the IDS for the as-manufactured 7050-T7451 can be obtained for subsequent corroded coupon life predictions. This tuned IDS used for the initial flaw size in the life predictions is the new IDS, 42 μm (0.00166 in.). Figure 13 demonstrates that the new IDS is closer to the ideal than the assumed IDS. The results could be improved by further tuning of the material crack growth rate curves (*da*/*dN* versus K_I) and a determination of 7050-T7451 IDS in order to capture the noncorroded (pristine) fatigue results more precisely.

Figure 14 shows the results of three groups of predictions: (a) the initial crack length is the pit depth, *d*; (b) the initial crack length is the IDS, 84 μm (0.0033 in.), plus the measured pit depth, *d*; and (c) the initial crack length is the new IDS, 42 μm (0.00166 in.), plus the measured pit depth, *d.* For each specimen, postfracture SEM images of the fracture faces were used to identify location and depth of the failure pit, that is, the pit with the crack that nucleated and eventually caused the specimen to fracture. These SEM- measured pit depths were used in the Fig. 14 corroded coupon predictions, along with the actual measured fatigue lives of the corroded coupons, which were not known; therefore, these corroded coupon analyses qualify as true predictions. For more than half of the specimens, the method using only the pit depth as the initial crack length overpredicted fatigue life (that is, predicted lives that were larger than measured fatigue lives and were therefore nonconservative), and the method using the pit depth plus the IDS as the initial crack length underpredicted fatigue lives (that is, predicted lives that were smaller than the measured lives and were therefore conservative). Predictions with the method using the pit depth plus the 42 μm (0.00166 in.) IDS as the initial crack length were right in the middle of these two methods, as expected, because the distribution of initial crack lengths used to begin the life predictions for this third group (initial crack length *d* + IDS = 42 μm, or 0.00166 in.) were

smaller than the first group (initial crack length *d*) and the second group (initial crack length *d* + IDS = 84 μm, or 0.0033 in.). Figures 13 and 14 indicate that the model of pit-as-crack is reasonable for this alloy.

References cited in this section

4. C.L. Brooks and D. Simpson, Integrating Real Time Age Degradation into the Structural Integrity Process, *Proceedings, NATO RTO's Workshop Two on Fatigue in the Presence of Corrosion*, Oct 1998 (Corfu, Greece), North Atlantic Treaty Organization Research and Technology Organization, p 22–1 to 22–13. Available http:// www.sti.nasa.gov/Pubs/start/star.html

20. J.P. Komorowski, N.C. Bellinger, and R.W. Gould, The Role of Corrosion Pillowing in NDI and in the Structural Integrity of Fuselage Joints, *Proceedings, 19th Symposium of the International Committee on Aeronautical Fatigue,* 16–20 June 1997 (Edinburgh, U.K.). Conference proceedings available from http://www.emas.co.uk/

21. C. Brooks, S. Prost-Domasky, and K. Honeycutt, Corrosion Is a Structural and Economic Problem, *Proceedings, NATO RTO's Workshop Two on Fatigue in the Presence of Corrosion*, Oct 1998 (Corfu, Greece), North Atlantic Treaty Organization Research and Technology Organization, p 14- 1 to 14-12. Available at http:// www.sti.nasa.gov/Pubs/start/star.html

22. StressCheck, copyright by Engineering Software Research and Development (ESRD, Inc.), St. Louis, MO. Available http://www.esrd.com

23. N.C. Bellinger and J.P. Komorowski, Implications of Corrosion Pillowing on the Structural Integrity of Fuselage Lap Joints, *Proceedings, FAA-NASA Symposium on Continued Airworthiness of Aircraft Structures,* Aug 1996 (Atlanta, GA), 1996

24. T. Swift, Widespread Fatigue Damage Monitoring—Issues and Concerns, *Proceedings, Fifth International Conference on Structural Airworthiness of New and Aging Aircraft,* June 1993 (Hamburg, Germany), p 829–870

25. J.C. Newman, Jr. and P.R. Edwards, "Short Crack Growth Behaviour in an Aluminum Alloy—An AGARD Cooperative Test Programme," AGARD Report 732, Advisory Group for Aerospace Research and Development, 1989

26. K. Sharp, "Using the EIFS Approach to Modeling Corrosion Pitting for Aircraft Structural Integrity," DSTO technical report, Defense Science and Technology Organization, Aeronautical and Maritime Research Laboratory, 2002, submitted for publication

---

C.L. Brooks, KT. Honeycutt and T.B. Mills, Predictive Modeling of Structure Service Life, *Corrosion: Fundamentals, Testing, and Protection*, Vol 13A*, ASM Handbook*, ASM International, 2003, p 946–958

Predictive Modeling of Structure Service Life

Craig L. Brooks, Scott A. Prost-Domasky, Kyle T. Honeycutt, and Thomas B. Mills, Analytical Processes/Engineered Solutions, Inc.

Application of Models during Their Development

The framework just described can be used to examine the effects of age degradation on the service capability of structures in order to provide design/manufacturing optimization and to evaluate maintenance options. This

section describes the rationale and techniques needed to apply these age-based structural integrity processes to in-service structures in order to realize benefits throughout the full structural life cycle.

Maturity Levels and Use of Assessment

The demands for extended use of aging systems are providing new challenges to the various structural communities to ensure continued safety, readiness, and reduced costs of operating complex and expensive systems. Integrity can be built into new systems using the discussed framework; obviously, such is not the case for existing aging systems. For existing systems, the challenge is to maintain safety and readiness while keeping control of operating and maintenance costs.

It makes sense, from a safety and an economic perspective, to be proactive in managing the structural integrity impact of corrosion by using quantitative evaluations of real-time degradation processes in the design requirements for new systems. The result would be more corrosion- tolerant designs and more robust engineering processes that support the maintenance, inspection, repair, and life extension of structural systems.

The methods used to assist engineering disposition of corrosion found in-service can also be used during the design phase to evaluate the sensitivity of critical structure elements to the onset of corrosion. This evaluation can lead to improved corrosion-resistant structures and to more efficient inspection programs. In the same way that damage tolerance assessments can identify fracture-critical structures, corrosion-sensitivity analysis can identify corrosion-critical structures. Economic gains can then be realized by initial design changes and improved maintenance programs.

Significant progress has been made in technology related to corrosion and structural integrity. This includes a better understanding of basic material behavior, improvements in non-destructive inspection (NDI) corrosion detection, and the use of analytical tools for predicting residual strength and residual life. However, the benefits from this technology have not been fully realized. The state of this technology is mature enough to benefit industry but requires additional applications to advance and prove its potential. Improvements in new designs and solutions for aging-system problems require a strategic integration into the life-cycle management processes, from the original equipment manufacturer (OEM) designer, to the field or depot maintenance engineers, to fleet management personnel. Enhancing the framework also requires focused developmental programs to increase the capability of the analytic and experimental tools and to develop effective processes for corrosion measurement and classification. Integration of tools that incorporate age degradations directly into the existing structural integrity framework will result in the most efficient and expedient application of the new methods discussed here.

Assessments to address corrosion, stress-corrosion cracking (SCC), and age degradations can be implemented into any structural integrity program by applying many of the same rules and guidelines presently used for existing durability and damage tolerance assessment frameworks. For example, current analysis techniques use a spectrum of stress cycles; adapting this system to include age degradation would require the use of a spectrum of environmental-degradation cycles. Some examples of new terms that would come into use are minimum detectable corrosion limits, probability of detection for corrosion (PODC), initial corrosion assumptions, corrosion and other age-degradation failure modes and effects, MSCD, WSCD, and corroded residual strength (CR/S).

Design Phase. The goal of both the designer and the life-cycle manager should be to ensure the optimal performance of the aircraft or other system. The designer should evaluate the intended role and performance goals of the system, then formulate technical specifications to ensure that the system will meet those goals and also satisfy regulatory requirements. The life-cycle manager has several tools that can be used to modify the rate at which a system ages. For aircraft, these include repair and overhaul of the airframe at selected times to address time-related issues such as corrosion, aggressive fatigue-life- management programs that modify the rate of cyclic damage accumulation, midlife structural modification programs, operational- or performance-enhancing modification programs, and life-extension programs.

The responsibility for ensuring continued safety and readiness for the aging fleets lies primarily with the end users. Design decisions made, however, by the OEM heavily influence the operators' ability to maintain appropriate levels of safety and readiness in a cost-effective manner. Current structural integrity processes focus on use-related degradation, such as static strength, fatigue, and damage tolerance, but do not fully address real-time-related degradation phenomena, such as corrosion. There are cost benefits and safety benefits for

integrating consideration of real-time-based degradation mechanisms with the current structural integrity processes.
Modifications to the existing structural integrity processes are required to:

- Solve technical issues associated with actual use and effects of the field environment
- Consider maintenance practices and information from maintenance programs that were not included in the design criteria or in the in-service maintenance plans
- Provide end users with the appropriate technical information and engineering tools to effectively manage aging systems
- Ensure that all disciplines adequately interact during the design phase to address the issues of degradation of the systems in the field environment
- Incorporate recent advances in corrosion assessment and prediction technologies that are not included in conventional practices and procedures

Identification of a Critical Structure

Corrosion issues can influence the problem areas of a structural system in several fashions:

- Corrosion damage in critical structural elements can dramatically reduce the life of a component.
- Corrosion damage in structural elements can change a component status from non-critical to critical.
- Inspection programs, locations, methods, and intervals need to consider multiple damage modes, such as fatigue and corrosion, for which inspection methods are distinct.
- Corrosion damage is not just a cosmetic issue; it is also a safety issue.
- Corrosion has often led to cracking of major structural elements, at times significantly earlier than design predictions or expectations.

Some general categories are recommended to characterize the criticality of a structural component. A partial list of these key categories includes:

- Operational stress level
- Limit strength and residual strength
- Fail-safe aspects
- Load distribution characteristics
- Susceptibility to SCC
- Susceptibility to corrosion
- Susceptibility to accidental damage
- Inspectability
- Cost to repair or replace

The inclusion of corrosion and SCC within a structural integrity program forces design considerations of real-time degradation processes and their potential structural and life-cycle cost impacts. For efficiency, a means of assessing component criticality is required, similar to that used for identifying durability and fracture-critical components. As an example, a formal and systematic approach (Ref 27) leading to a documented criticality assessment was first used as part of a FAA certification and then subsequently used for several fighter aircraft assessments. The systematic process enabled identification and ranking of potentially critical elements of the structure, so that evaluations and inspections were performed and documented in a prioritized fashion.

Inspection Programs

Products of a Predictive Model. The final product created by a life-assessment tool is a life curve (or remaining life curve), which quantifies the impact and effects of the age-degradation processes, as shown in Fig. 15(a) and (b). From Fig. 15(b), the relative sensitivities of potential maintenance and as-is conditions assist in making the proper cost-effective and safe maintenance decisions when linked with a cost model. For example, assume that the current level of NDI capabilities, the detection limit, is represented by the topmost horizontal line on Fig.

15(b). Although the physical discontinuity or flaw existing today (the leftmost dot) could not be detected today (15 years after manufacture), the holistic life-assessment method allows the analyst to have some estimates of today's hidden discontinuity size as computed from the as-manufactured IDS. From this point, the analyst could use the results to evaluate several options while assuming a severe corrosion scenario:

- *Option 1:* do nothing, deferring action until the next mandated inspection interval
- *Option 2:* apply corrosion-preventive compounds (CPCs) that retard corrosion growth and therefore might allow a delay in further action for two intervals
- *Option 3:* apply a doubler or patch to reduce the operating stress level, allowing the structure to reach three inspection intervals with an adequate safety factor

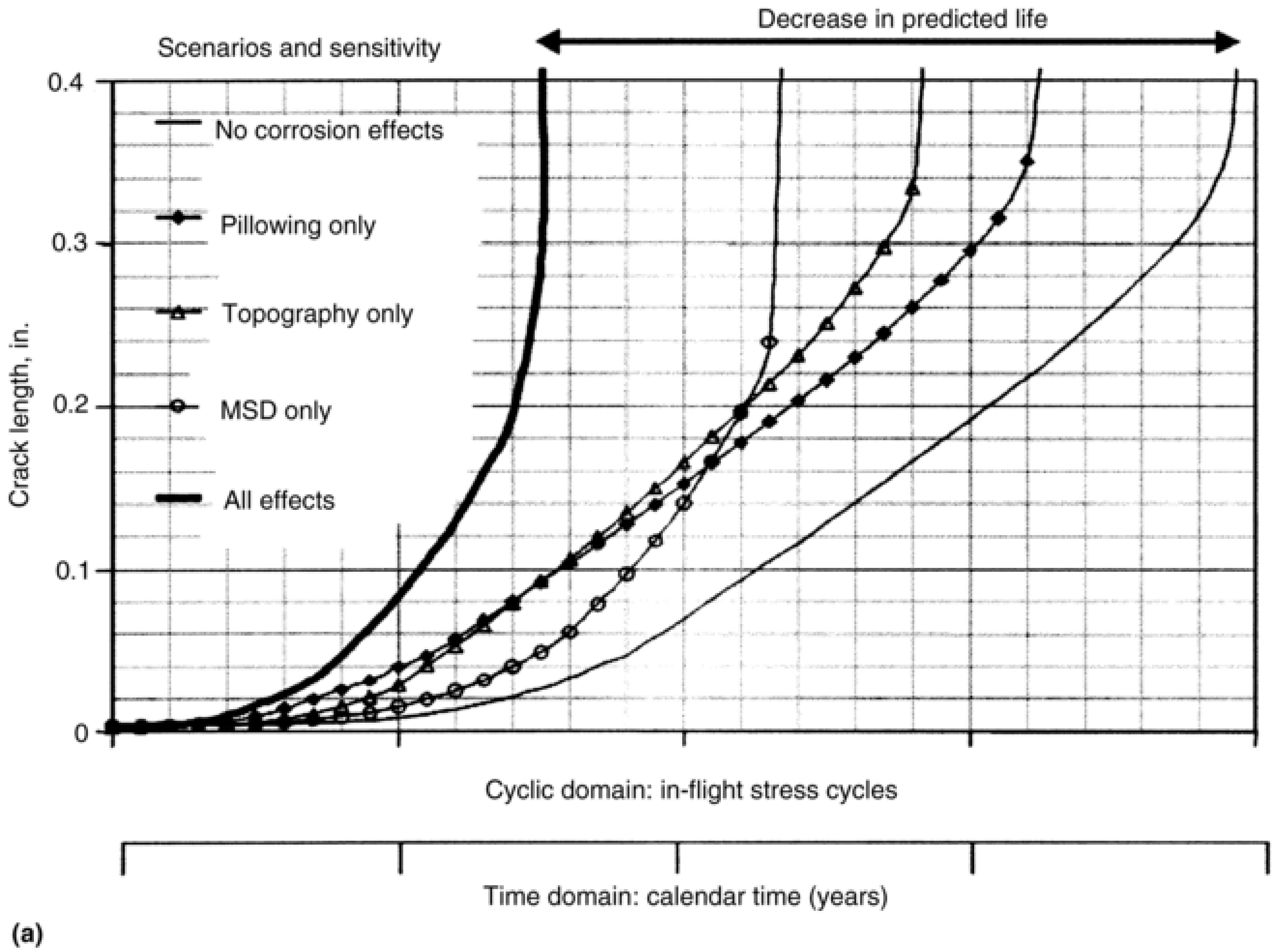

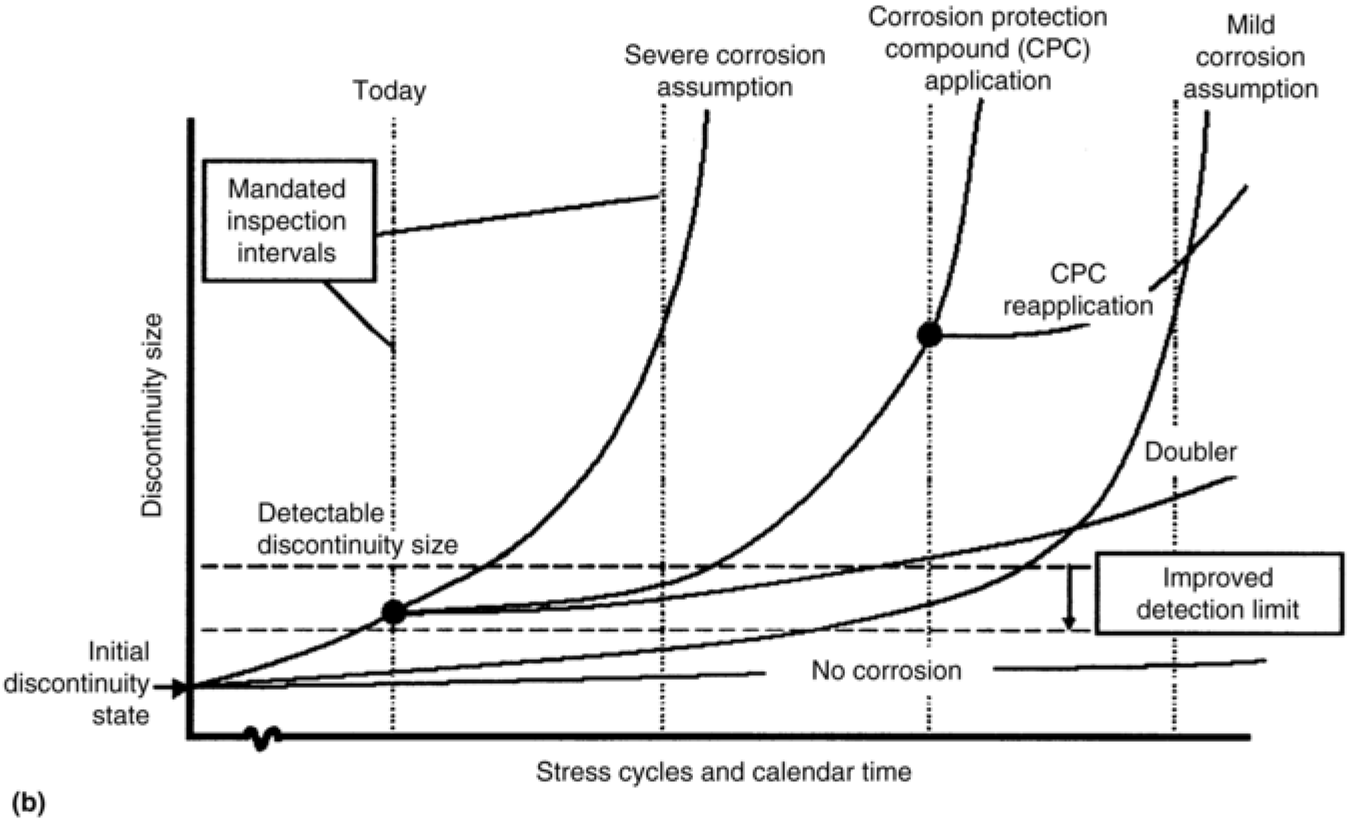

Fig. 15 Predictive models. (a) Crack growth as a function of time and duty. MSD, multisite damage. (b) Sensitivity scenarios allow cost-effective decision making. Decisions can be made and evaluated sooner with improved detection.

These three options are shown as the three lines emanating from the leftmost dot in Fig. 15(b). Additional options could be made available to the structural maintenance manager, subject to changes in his present maintenance plan. Figure 15(b) shows how alternate inspections could be used. If the corrosion or actual damage state could be reliably detected and quantified more precisely (i.e., by detecting a smaller damage level via an improved NDI procedure or a supplemental NDI inspection) (Ref 28), then less expensive repairs could be devised, with a sufficient probability of achieving the structural lifetime goals. Maintenance records that document the details of prior and current inspections, combined with accurate historical-basing records, can be used to help establish confidence in the quantification of the as-built to current as- is conditions. Future inspection intervals can be determined based on future-basing assignments and the current applied maintenance actions, such as those described previously. The cost analysis accompanying this process would allow decisions that could optimize the direct maintenance while considering safety, readiness, and economic issues.

Economic Service Life and Fleet Management

Depending on the intended use and design requirements, in-service components may have considerable additional capability above and beyond the entire system design life or even beyond their own design life, especially if careful inspection and maintenance procedures have verified this. To assist in making a remain-in-service decision, it is important that a structural assessment determine the additional service-life capability of the component. For example, some automobiles may be kept running with extremely high mileage, but the cost of repairs, maintenance, quality of ride, and user inconvenience may result in available funds being better allocated toward a new automobile. At some point, the cost of maintenance no longer justifies continued service, and the structure has reached the particular operator's end of economic service life. The assessment methods discussed in this article are the tools for determining the economic life of the structure. Scenarios and repair options can be explored that consider both cyclic damage and age degradation. The additional capability, or lack thereof, can be analyzed in conjunction with cost of a repair or replacement or even the cost of continued inspection and monitoring, to determine the economics of continued service. The ability to estimate the economic service life and the remaining service life can be a powerful asset for many industries, allowing the user to maximize the return on investments in existing systems or reallocating investments to new equipment.

Implementation Process

An effective means of implementation of this framework may be to use the successful integrity process that has been established by the aircraft industry. The five tasks in the U.S.A.F. aircraft structural integrity process (Ref 29) provide an ideal format for integrating corrosion and sustained stress analyses into structural evaluations. Table 1 illustrates a modified version of the ASIP process, with additional items incorporated that emphasize the role of age-degradation effects, such as corrosion. Equally important to considering real-time degradation effects is the inclusion of life-cycle costs (LCC) as part of the design and support requirements. This implementation plan results in a minimal disruption of the current processes while defining necessary concepts as relative or parallel to existing concepts; for example, to complement damage tolerance assessments (DTAs), corrosion tolerance assessments (CTAs) would be introduced. The generic nature of the terminology and concepts lend themselves to adoption by other industries that are challenged with design and maintenance of new and existing structures in various environments.

Table 1 Existing structural integrity framework for aircraft

Corrosion degradation addressed by additions to activities in italic.

Task	Stage	Activities
I	Design information	Integrity master plan
		Structural design criteria; corrosion and SCC
		Damage tolerance and durability control plans
		Corrosion tolerance control plan
		Selection of materials and processes
		Material cost trade studies with corrosion and SCC
		Design service life and design usage
		Critical component and selection priority process definition
		Methodology and analysis review approval plan
II	Design analyses and development tests	Materials and joint allowables
		Loads, sonic, vibration, and flutter analysis
		Design service loads spectra
		Design chemical/thermal environment spectra
		Stress analysis
		Damage tolerance analysis
		Durability analysis
		Corrosion tolerance analysis
		LCC assessment
III	Component and full scale testing and demonstration	Static durability and damage tolerance tests
		Assembly process verification test with revisions and updates
		Analytical process verification test
		Flight and ground operations tests
		Sonic, flight vibrations, and flutter tests
		Interpretation and evaluation of test results
IV	Force management data package	Final design analyses
		Strength, durability and corrosion summaries
		Force structural maintenance plan
		DTA, CTA, and SCC summary
		Loads/environment spectra survey
		Aircraft tracking program
		Operational database. cracking, corrosion, repairs, and costs
		Corrosion protection verification
		Loads database, FEA, models, files, and geometry
V	Force management	Loads/environment spectra survey
		Aircraft tracking data
		Aircraft maintenance times
		Structural maintenance records
		Cost assessment process
		Repair tracking
		System feedback, lessons learned, and information

SCC, stress corrosion cracking; DTA, damage tolerance assessment; CTA, corrosion tolerance assessment; LCC, life-cycle cost; FEA, finite element analysis

References cited in this section

27. C.L. Brooks, An Engineering Procedure to Select and Prioritize Component Evaluations Under U.S.A.F. Structural Integrity Requirements, *Proceedings, 1990 U.S.A.F. Structural Integrity Program Conference,* Dec 1990 (San Antonio, TX), p 19

28. J.W. Mar, Preserving Aging Aircraft, *Aerosp. Am.,* Jan 1996, p 38–43

29. "Aircraft Structural Integrity Program, Airplane Requirements," MIL-STD-1530A, United States Air Force, 11 Dec 1975

C.L. Brooks, KT. Honeycutt and T.B. Mills, Predictive Modeling of Structure Service Life, *Corrosion: Fundamentals, Testing, and Protection*, Vol 13A, *ASM Handbook*, ASM International, 2003, p 946–958

Predictive Modeling of Structure Service Life

Craig L. Brooks, Scott A. Prost-Domasky, Kyle T. Honeycutt, and Thomas B. Mills, Analytical Processes/Engineered Solutions, Inc.

References

1. NTSB/AAR-89/03, Aloha Airlines, Flight 243, Boeing 737-200, N73711, near Maui, HI, April 1988, National Transportation Safety Board, 1989

2. D.W. Hoeppner, L. Grimes, A. Hoeppner, J. Ledesma, T. Mills, and A. Shah, Corrosion and Fretting as Critical Aviation Safety Issues: Case Studies, Facts, and Figures from U.S. Aircraft Accidents and Incidents, *Proceedings, 18th Symposium of the International Committee on Aeronautical Fatigue,* 3–5 May 1995 (Melbourne, Australia). Conference proceedings available from http:// www.emas.co.uk/

3. *Cracking Down on Corrosion: Cooperative Efforts Toward Vehicle Durability,* American Iron and Steel Institute, 1985. Available from http://www.steel.org/autosteel/index.htm

4. C.L. Brooks and D. Simpson, Integrating Real Time Age Degradation into the Structural Integrity Process, *Proceedings, NATO RTO's Workshop Two on Fatigue in the Presence of Corrosion,* Oct 1998 (Corfu, Greece), North Atlantic Treaty Organization Research and Technology Organization, p 22–1 to 22–13. Available http:// www.sti.nasa.gov/Pubs/start/star.html

5. C. Brooks, K. Honeycutt, and S. Prost-Domasky, Correlation of Life Prediction Methods with Corrosion-Related Tests, *Proceedings, U.S. Air Force Aircraft Structural Integrity Program Conference,* Dec 1999 (San Antonio, TX), Universal Technology Corporation

6. T.J. Ginter, D.J. Shelton, and R.P. Bell, "Corrosion Fatigue Structural Demonstration, Phase I," Final Report AFRL-VA-WP- TR-2000-3005/-3006, U.S.A.F. Contract F33615-97-C-3218, United States Air Force Air Vehicles Directorate, Nov 1999

7. C. Brooks, C.D. Peeler, K. Honeycutt, and S. Prost-Domasky, "Predictive Modeling for Corrosion Management: Modeling Fundamentals," Analytical Processes/Engineered Solutions, Inc. Available at http:// www.apesolutions.com/frm_link.htm

8. C. Brooks, S. Prost-Domasky, and K. Honeycutt, Determining the Initial Quality State of Materials, *Proceedings, U.S. Air Force Aircraft Structural Integrity Program Conference,* Dec 1998 (San Antonio, TX), Universal Technology Corporation, 1999

9. A. Merati, J. Tsang, S. Khomusi, A. Kourline, K. Kyle, and M. Geusebroek, “Preliminary Report—Final Test Results for the Determination of Fatigue-Related Features of the Initial Discontinuity State (IDS) of 2024-T3 Aluminum Alloy,” Report LTR- SMPL-2002-0110, National Research Council of Canada, 2002

10. P.J. Laz, B.A. Craig, and B.M. Hilberry, A Probabilistic Total Fatigue Life Model Incorporating Material Inhomogeneities, Stress Level, and Fracture Mechanics, *Int. J. Fatigue,* Vol 23, 2001, p S119–S127

11. Metallic Materials and Elements for Aerospace Vehicle Structures, *MIL-HDBK-5,* United States Department of Defense, Nov 1994

12. *Compilation of ASTM Standard Definitions,* 6th ed., American Society for Testing and Materials, 1986

13. “National Aging Aircraft Research Program Plan,” Federal Aviation Administration Technical Center, United States Department of Transportation, 1993

14. C. Brooks, K. Honeycutt, and S. Prost-Domasky, Monitoring the Robustness of Corrosion and Fatigue Prediction Models, *Proceedings, U.S. Air Force Aircraft Structural Integrity Program Conference,* Dec 2001 (San Antonio, TX), Universal Technology Program, 2002

15. S.A. Prost-Domasky, C.L. Brooks, and K.T. Honeycutt, The Application of *p*-Version Finite Element Methods to Fracture-Dominated Problems Encountered in Engineering Practice, *Computers and Mathematics with Applications,* Elsevier Sciences, 2003, submitted for publication

16. P.K. Sharp, T. Mills, and G. Clark, Modeling of Fatigue Crack Growth from Pitting and Exfoliation Corrosion, *Proceedings, 21st Symposium of the International Committee on Aeronautical Fatigue,* 27–29 June 2001 (Toulouse, France), p 485–498. Conference proceedings available from http:// www.emas.co.uk/

17. P.K. Sharp, T. Mills, and G. Clark, Aircraft Structural Integrity: The Impact of Corrosion, *Proceedings, Tenth International Congress of Fracture (ICF 10),* 3–7 Dec 2001 (Honolulu, HI), Elsevier Science

18. P.K. Sharp, G. Cole, G. Clark, and S.G. Russo, The Influence of Corrosion on Aircraft Structural Integrity, *Proceedings, 21st Congress of the International Council Aeronautical Sciences,* 13–18 Sept 1998 (Melbourne, Australia)

19. P.K. Sharp, T. Mills, S. Russo, G. Clark, and L. Qianchu, Effects of Exfoliation Corrosion on the Fatigue Life of Two High- Strength Aluminum Alloys, *Proceedings, Fourth Joint DoD/FAA/NASA Conference on Aging Aircraft,* 15–18 May 2000 (St. Louis, MO), Universal Technology Corporation, 2000

20. J.P. Komorowski, N.C. Bellinger, and R.W. Gould, The Role of Corrosion Pillowing in NDI and in the Structural Integrity of Fuselage Joints, *Proceedings, 19th Symposium of the International Committee on Aeronautical Fatigue,* 16–20 June 1997 (Edinburgh, U.K.). Conference proceedings available from http://www.emas.co.uk/

21. C. Brooks, S. Prost-Domasky, and K. Honeycutt, Corrosion Is a Structural and Economic Problem, *Proceedings, NATO RTO's Workshop Two on Fatigue in the Presence of Corrosion,* Oct 1998 (Corfu, Greece), North Atlantic Treaty Organization Research and Technology Organization, p 14- 1 to 14-12. Available at http:// www.sti.nasa.gov/Pubs/start/star.html

22. StressCheck, copyright by Engineering Software Research and Development (ESRD, Inc.), St. Louis, MO. Available http://www.esrd.com

23. N.C. Bellinger and J.P. Komorowski, Implications of Corrosion Pillowing on the Structural Integrity of Fuselage Lap Joints, *Proceedings, FAA-NASA Symposium on Continued Airworthiness of Aircraft Structures,* Aug 1996 (Atlanta, GA), 1996

24. T. Swift, Widespread Fatigue Damage Monitoring—Issues and Concerns, *Proceedings, Fifth International Conference on Structural Airworthiness of New and Aging Aircraft,* June 1993 (Hamburg, Germany), p 829–870

25. J.C. Newman, Jr. and P.R. Edwards, "Short Crack Growth Behaviour in an Aluminum Alloy—An AGARD Cooperative Test Programme," AGARD Report 732, Advisory Group for Aerospace Research and Development, 1989

26. K. Sharp, "Using the EIFS Approach to Modeling Corrosion Pitting for Aircraft Structural Integrity," DSTO technical report, Defense Science and Technology Organization, Aeronautical and Maritime Research Laboratory, 2002, submitted for publication

27. C.L. Brooks, An Engineering Procedure to Select and Prioritize Component Evaluations Under U.S.A.F. Structural Integrity Requirements, *Proceedings, 1990 U.S.A.F. Structural Integrity Program Conference,* Dec 1990 (San Antonio, TX), p 19

28. J.W. Mar, Preserving Aging Aircraft, *Aerosp. Am.,* Jan 1996, p 38–43

29. "Aircraft Structural Integrity Program, Airplane Requirements," MIL-STD-1530A, United States Air Force, 11 Dec 1975

C.L. Brooks, KT. Honeycutt and T.B. Mills, Predictive Modeling of Structure Service Life, *Corrosion: Fundamentals, Testing, and Protection*, Vol 13A, *ASM Handbook*, ASM International, 2003, p 946–958

Predictive Modeling of Structure Service Life

Craig L. Brooks, Scott A. Prost-Domasky, Kyle T. Honeycutt, and Thomas B. Mills, Analytical Processes/Engineered Solutions, Inc.

Selected References

- D. Broek, *Elementary Engineering Fracture Mechanics,* Kluwer Academic Publishers, 1986
- S.T. Rolfe and J.M. Barsom, *Fracture and Fatigue Control in Structures: Applications of Fracture Mechanics,* Prentice-Hall, Inc., 1977
- S. Suresh, *Fatigue of Materials,* 2nd ed., Cambridge University Press, 1998
- B. Szabó and I. Babuŝka, *Finite Element Analysis,* John Wiley & Sons, Inc., 1991
- H. Tada, P.C. Paris, and G.R. Irwin, *The Stress Analysis of Cracks Handbook,* 3rd ed., ASME Press, 2000

G.H. Koch, M.P.H. Brongers, N.G. Thompson, Y.P. Virmani and J.H. Payer, Direct Costs of Corrosion in the United States, *Corrosion: Fundamentals, Testing, and Protection*, Vol 13A, *ASM Handbook*, ASM International, 2003, p 959–967

Direct Costs of Corrosion in the United States

Gerhardus H. Koch, Michiel P.H. Brongers, and Neil G. Thompson, CC Technologies Laboratories, Inc.; Y. Paul Virmani, Federal Highway Administration, Turner-Fairbank Highway Research Center; Joe H. Payer, Case Western Reserve University

Introduction

STUDIES of the cost of corrosion have been undertaken during the past several decades by a number of countries. These studies indicate, in general, that corrosion is very costly and has a major impact on the economies of industrial nations (Table 1) (Ref 1). The earliest U.S. study was reported in 1949 by H.H. Uhlig, who estimated the total cost of corrosion by summing materials and process costs related to corrosion control. The 1949 report was followed in the 1970s by a number of national studies in Japan, the United States, and the United Kingdom. The study by Japan conducted in 1977 followed the Uhlig methodology. In the United States, the Battelle National Bureau of Standards (NBS) study conducted in 1975 estimated the total direct cost of corrosion using an economic input/ output model. This model was later adopted by studies in two other nations, Australia in 1983 and Kuwait in 1995. In the United Kingdom, a study was conducted in 1970 using a method similar to the one used by Uhlig; however, in the U.K. study, a committee chaired by T.P. Hoar collected the data through interviews and surveys of targeted economic sectors. Table 1 summarizes the total corrosion costs and percentage of gross national product (GNP) of the respective economies. The table shows that the national costs of corrosion vary between 1.5 and 5.2%. The 1975 study by Battelle-NBS pointed out the severe corrosion impact on the U.S. economy. The estimate based on the Battelle-NBS study was that the cost of corrosion in the United States alone was approximately $70 billion/year, which was 4.2% of the GNP. A limited study in 1995, updating the 1975 figures, estimated the total cost of corrosion at approximately $300 billion. However, that study simply applied a multiplication factor to the 1975 cost that was equivalent to the GNP growth from 1975 to 1995.

Table 1 Results of studies estimating the cost of corrosion in various industrial nations

Country	Total annual corrosion cost	Percentage of GNP	Year
United States	$5.5 billion	2.1	1949
United Kingdom	£1.365 billion(a)	3.5	1970
Japan	$9.2 billion	1.8	1974
United States	$70 billion	4.2	1975
Australia	$2 billion	1.5	1982
Kuwait	$1 billion	5.2	1987
West Germany	$6 billion	3.0	1967
Finland	$54 million	…	1965
India	$320 million	…	1960

GNP, gross national product.

(a) Not reported in U.S. dollars

The previous national studies have formed the basis for much of the current thinking regarding the corrosion costs to the various national economies. Although the efforts of the previous national studies ranged from formal and extensive to informal and modest, all studies arrived at estimates of the total annual cost of corrosion that ranged from 1 to 5% of the GNP of each country.

The most recent U.S. cost study was conducted for the year 1998 by CC Technologies Laboratories, Inc. under the auspices of the U.S. Department of Transportation through the Transportation Equity Act for the 21st Century (passed by the U.S. Congress in 1998) in a cooperative effort with the U.S. Department of Transportation Federal Highway Administration (FHWA) (Ref 2). NACE International, The Corrosion Society, worked with Congressional representatives to secure $1 million in federal funding for the study. This article first describes the methodology used in this study and then reports the results and conclusions of the study.

References cited in this section

1. J.H. Payer and G.H. Koch, Appendix A: Review of Previous Studies, *Corrosion Cost and Preventive Strategies in the United States,* FHWA-RD-01-156, Federal Highway Administration, U.S. Department of Transportation, March 2002

2. G.H. Koch, M.P.H. Brongers, N.G. Thompson, Y.P. Virmani, and J.H. Payer, *Corrosion Cost and Preventive Strategies in the United States,* FHWA-RD-01-156, Federal Highway Administration, U.S. Department of Transportation, March 2002

G.H. Koch, M.P.H. Brongers, N.G. Thompson, Y.P. Virmani and J.H. Payer, Direct Costs of Corrosion in the United States, *Corrosion: Fundamentals, Testing, and Protection,* Vol 13A*, ASM Handbook,* ASM International, 2003, p 959–967

Direct Costs of Corrosion in the United States

Gerhardus H. Koch, Michiel P.H. Brongers, and Neil G. Thompson, CC Technologies Laboratories, Inc.; Y. Paul Virmani, Federal Highway Administration, Turner-Fairbank Highway Research Center; Joe H. Payer, Case Western Reserve University

---

Methodology

In the 1998 study, two methods were used to estimate the cost of corrosion to the United States:

- *Method 1:* The cost was determined by summing the costs for corrosion control methods and contract services.
- *Method 2:* The cost of corrosion was first determined for specific industry sectors and then extrapolated to calculate a national total corrosion cost.

Past studies have indicated that the second method is more likely to incorporate the majority of the corrosion-related costs, and the first method is likely to miss the significant cost of corrosion management, the cost for direct services related to the owner/operator, and the cost of loss of capital due to corrosion.

The costs of materials were obtained from various sources, such as the U.S. Department of Commerce Census Bureau, existing industrial surveys, trade organizations, industry groups, and individual companies. Data on corrosion control services, such as engineering services, research and testing, and education and training, were obtained primarily from trade organizations, educational institutions, and individual experts. These services included only contract services and not service personnel within the owner/operator companies.

Data collection for the sector-specific analyses differed significantly from sector to sector, depending on the availability of data and the form in which the data were available. In order to determine the annual corrosion costs for the reference year of 1998, data were obtained for various years in the last decade but mainly for the years 1996 to 1999. For many of the sectors, the information is public and could be obtained from government reports and other publicly available documents. Discussions with industry experts provided the basis of the industry sector data collection. Corrosion cost information from the private industry sectors was more difficult to obtain. This stemmed from the fact that either the information was not readily available or could not be

released because of company policies. In this case, information from publicly available industry records on operation and maintenance cost was obtained, and, with the assistance of industry experts, corrosion-related costs were estimated.
The industry sectors for corrosion cost analyses represented approximately 27% of the U.S. gross domestic product (GDP) and were divided among five sector categories: infrastructure, utilities, transportation, production and manufacturing, and government. The total cost of corrosion was estimated by determining the percentage of the GDP of those industry sectors for which direct corrosion costs were estimated and extrapolating these numbers to the total U.S. GDP. The direct cost used in this analysis was defined as the cost incurred by owners or operators of the structures, manufacturers of products, and suppliers of services.
The following elements were included in these costs:

- Cost of additional or more expensive material used to prevent corrosion damage
- Cost of labor attributed to corrosion management activities
- Cost of the equipment required because of corrosion-related activities
- Loss of revenue due to disruption in supply of product
- Cost of loss of reliability
- Cost of lost capital due to corrosion deterioration

For all industry sectors studied in this report, the direct corrosion costs were determined. For highway bridges, a life-cycle cost analysis was performed in which both the direct and indirect costs of corrosion were addressed. Indirect costs are incurred by individuals other than the owner or operator of the structure. Measuring and valuing indirect costs generally require complex assessments, and several different methods can be used to evaluate potential indirect costs. Owners or operators can be made to assume the costs through taxation, penalties, litigation, or payment for cleanup of spills. In such cases, these expenses become direct costs. In other cases, costs are assumed by the end user or the overall economy. In the case of highway bridges, indirect costs, such as traffic delays during bridge maintenance, repair, and rehabilitation, are more difficult to turn over to the owner or operator of the structure. Once assigned a dollar value, the indirect costs are included in the cost of corrosion management of the structure and treated the same way as all other costs.

G.H. Koch, M.P.H. Brongers, N.G. Thompson, Y.P. Virmani and J.H. Payer, Direct Costs of Corrosion in the United States, *Corrosion: Fundamentals, Testing, and Protection*, Vol 13A, *ASM Handbook*, ASM International, 2003, p 959–967

Direct Costs of Corrosion in the United States

Gerhardus H. Koch, Michiel P.H. Brongers, and Neil G. Thompson, CC Technologies Laboratories, Inc.; Y. Paul Virmani, Federal Highway Administration, Turner-Fairbank Highway Research Center; Joe H. Payer, Case Western Reserve University

---

Definitions

The following definitions were used in evaluating the cost of corrosion in the 1998 U.S. study (Ref 3):
annualized value.
Average cost of a corrosion control strategy over the entire service life of a structure.
benefit-cost analysis.
Analysis used to determine the net present value of options and the highest net benefit to society; also to determine the cost per unit of service.
corrosion management.
All activities throughout the service life of the structure that are performed to mitigate corrosion, to repair corrosion-induced damage, and to replace the structure, which has become unusable as a result of corrosion.
corrosion-related cash flow.

All costs, direct and indirect, that are incurred due to corrosion throughout the entire life cycle of the structure.

current cost of corrosion.

The difference between the approach where no consideration is given to corrosion and corrosion control and the current corrosion control approach; calculated by life-cycle cost analysis and characterized by the annualized value.

direct costs.

Costs directly incurred by the owner or operator of the facility, plant, or structure.

gross domestic product (GDP).

The total value of all final goods and services produced in a country in a given year; equals total consumer, investment, and government spending, plus the value of exports minus the value of imports. Figure 1 shows the contribution of Bureau of Economic Analysis industry categories to the 1998 U.S. gross domestic product of $8.79 trillion.

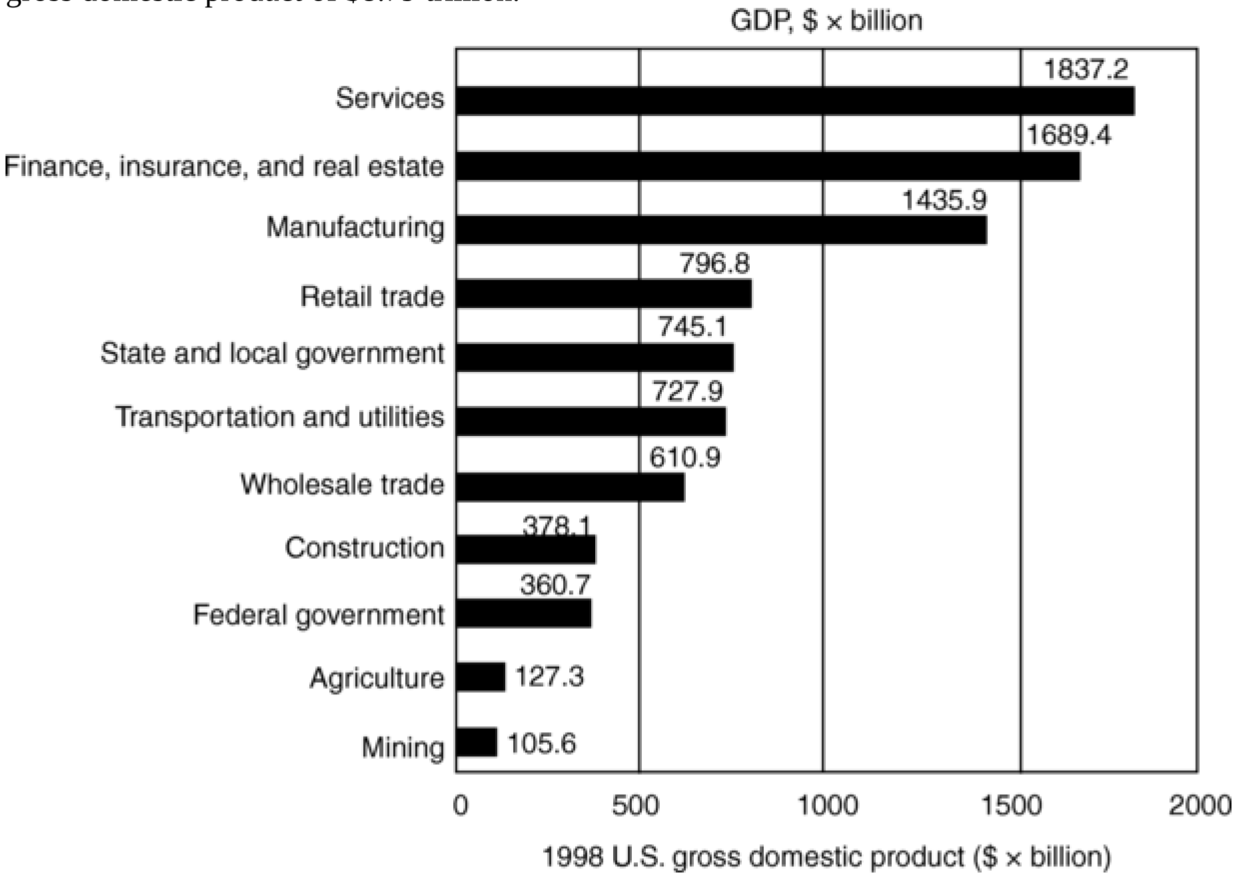

Fig. 1 Distribution of 1998 U.S. gross domestic product for Bureau of Economic Analysis industry categories

indirect costs.

Costs incurred by others, such as the public or society, and are not directly felt by the owner or operator.

life-cycle cost analysis.

A cost analysis that considers not only the cost of production but also the costs of use, service, and disposal or recycling; in the study, life-cycle cost analysis was used to determine the annualized values of options to provide a basis for comparing alternative corrosion control strategies.

maintenance.

An activity that maintains the level of service of a structure or facility.

present discounted value.

The value of future corrosion costs discounted for the cost of money and expressed in terms of present value.

repair.

Restoration of a damaged structure to its original or required service levels but does not eliminate the causes of corrosion.

rehabilitation.

Restoration of a damaged structure to its original or required service level and corrects the deficiency that resulted in corrosion deterioration.

service life.

The required period of time a structure is designed to function.

Reference cited in this section

3. T. Balvanyos and L. Lave, Appendix B: Economic Analysis Methods, *Corrosion Cost and Preventive Strategies in the United States,* FHWA-RD-01-156, Federal Highway Administration, U.S. Department of Transportation, March 2002, p 773

G.H. Koch, M.P.H. Brongers, N.G. Thompson, Y.P. Virmani and J.H. Payer, Direct Costs of Corrosion in the United States, *Corrosion: Fundamentals, Testing, and Protection*, Vol 13A, *ASM Handbook,* ASM International, 2003, p 959–967

Direct Costs of Corrosion in the United States

Gerhardus H. Koch, Michiel P.H. Brongers, and Neil G. Thompson, CC Technologies Laboratories, Inc.; Y. Paul Virmani, Federal Highway Administration, Turner-Fairbank Highway Research Center; Joe H. Payer, Case Western Reserve University

---

Costs of Corrosion Control Methods and Services

As noted in the section "Methodology" in this article, the first method used in the 1998 study was to estimate the annual direct cost of corrosion in the United States by totaling the cost of corrosion control methods and services. The corrosion control methods that were considered include protective coatings, corrosion-resistant alloys, corrosion inhibitors, polymers, anodes, cathodic protection, and other corrosion control and monitoring equipment. Other contributors to the total annual direct cost that were reviewed in this report are contract services (i.e., nonowner/ operator services), corrosion research and development, and education and training.

Method 1 Results

The results for corrosion control methods and services are summarized in Table 2 and subsequently discussed in more detail.

Table 2 Summary of annual costs for corrosion control methods and services

Material and services	Range $ × billion	Average cost	
		$ × billion	**%**
Protective coatings			
Organic coatings	40.2–174.2	107.2	88.3
Metallic coatings	1.4	1.4	1.2
Metals and alloys	7.7	7.7	6.3
Corrosion inhibitors	1.1	1.1	0.9
Polymers	1.8	1.8	1.5
Anodic and cathodic protection	0.73–1.22	0.98	0.8
Services	1.2	1.2	1.0
Research and development	0.02	0.02	<0.1
Education and training	0.01	0.01	<0.1
Total	**$54.16–$188.65**	**$121.41**	**100%**

Protective Coatings. Both organic and metallic coatings are used to provide protection against corrosion of metallic substrates. These metallic substrates, mostly carbon steel, corrode in the absence of the coating, resulting in the reduction of the service life of the steel part or component. The total annual cost for all organic and metallic protective coatings is $108.6 billion.

According to the U.S. Department of Commerce Census Bureau, the total amount of organic coating material sold in the United States in 1997 was 5.56×10^9 L (1.47×10^9 gal), at a cost of $16.56 billion. The total sales can be broken down into architectural coatings, product original equipment manufacturer (OEM) coatings, special-purpose coatings, and miscellaneous paint products. A portion of each of these was classified as corrosion coatings, at a total estimate of $6.7 billion. Raw material cost is only a portion of a total coating application project, ranging from 4 to 20% of the total cost of application. When applying these percentages to the raw materials cost, the total annual cost of coating application ranges from $33.5 billion to 167.5 billion (an average of $100.5 billion).

The most widely used metallic coating for corrosion protection is galvanizing, which involves the application of metallic zinc to carbon steel for corrosion control purposes. Hot dip galvanizing is the most common process, and, as the name implies, it consists of dipping the steel member into a bath of molten zinc. Information released by the U.S. Department of Commerce in 1998 stated that approximately 8.6×10^6 metric tons of hot dip galvanized steel and 2.8×10^6 metric tons of electrolytic galvanized steel were produced in 1997. The total market for metallizing and galvanizing in the United States is estimated at $1.4 billion per year. This figure is the total material costs of the metal coating and the cost of processing and does not include the cost of the carbon steel member being galvanized/metallized.

Corrosion-resistant alloys are used where corrosive conditions prohibit the use of carbon steels and protective coatings do not provide sufficient protection or are economically not feasible. Examples of these alloys include stainless steels, nickel-base alloys, and titanium alloys. The total 1998 consumption cost of the corrosion-resistant metals and alloys is estimated at $7.7 billion.

According to U.S. Census Bureau statistics, 2.5×10^6 metric tons of raw stainless steel were sold in the United States in 1997. With an estimated cost of $2.20/kg ($1/lb) for raw stainless steel, a total annual (1997) production cost of $5.5 billion was estimated. It was assumed that all production is for U.S. domestic consumption. The total consumption of stainless steel also includes imports, which account for more than 25% of the U.S. market. Thus, the total consumption of stainless steel can be estimated at $7.3 billion.

Where environments become particularly severe, nickel-base and titanium alloys are used. Nickel-base alloys are used extensively in the oil production, refinery, and chemical process industries, where conditions are severely corrosive. Furthermore, there is increased use of these alloys in other industries, where high temperatures and/or severe corrosive conditions exist. With the average price for nickel-base alloys at $13/kg ($6/lb) in 1998, the total sales value in the United States was estimated at $285 million.

The primary use of titanium alloys is in the aerospace and military industry, where the high strength-to-weight ratio and resistance to high temperatures are properties of interest. However, titanium and its alloys are also corrosion resistant to many environments and therefore have found application in oil production, refinery, chemical process, and pulp and paper industries. In 1998, it was estimated that 65% of titanium mill products were used for aerospace and 35% for nonaerospace applications. The total annual consumption price for titanium and titanium alloys for corrosion control applications is estimated at $150 million.

Corrosion Inhibitors. A corrosion inhibitor may be defined, in general terms, as a substance that, when added in a small concentration to an environment, effectively reduces the corrosion rate of a metal exposed to that environment. Inhibition is used within carbon steel pipes and vessels as an economic corrosion control alternative to stainless steels and alloys, coatings, or nonmetallic composites. A particular advantage of corrosion inhibition is that it often can be implemented or changed in situ without disrupting a process. The major industries using corrosion inhibitors are oil and gas exploration and production, petroleum refining, chemical manufacturing, heavy manufacturing, water treatment, and the product additive industries. The total consumption of corrosion inhibitors in the United States has doubled from approximately $600 million in 1982 to nearly $1.1 billion in 1998.

Engineering Plastics and Polymers. In 1996, the plastics industry accounted for $274.5 billion in shipments. It is difficult to estimate the fraction of plastics used for corrosion control, because, in many cases, plastics and composites are used for a combination of reasons, including corrosion control, light weight, economics, strength-to-weight ratio, and other unique properties. While corrosion control is a major market for many polymers, certain polymers are used mostly, if not exclusively, for corrosion control purposes. The significant

markets for corrosion control by polymers include composites (primarily glass-reinforced thermosetting resins), polyvinyl chloride pipe, polyethylene pipe, and fluoropolymers. The portion of polymers used for corrosion control is estimated at $1.8 billion.
Cathodic and Anodic Protection. The cost of cathodic and anodic protection of metallic structures subject to corrosion can be divided into the cost of materials and the cost of installation and operation. Industry data showed that the 1998 sales of hardware components totaled $146 million. The largest share of the cathodic protection market is taken up by sacrificial anodes at $60 million, of which magnesium has the greatest market share. Major markets for sacrificial anodes are the water heater market and the underground storage tank market. The cost of installation of the various cathodic protection components for underground structures varies significantly, depending on the location and the specific details of the construction. For 1998, the average total cost for installing cathodic protection systems was estimated at $0.98 billion (range: $0.73 billion to 1.22 billion). The total cost for replacing sacrificial anodes in water heaters and corrosion-related replacement of water heaters was estimated at $1.24 billion/year. Therefore, the total estimated cost for cathodic and anodic protection is $2.22 billion/year.
Corrosion Control Services. In the context of the study, services were defined as companies, organizations, and individuals that provide contract services for corrosion control purposes, while excluding corrosion-related activities that owners/operators may do in-house. By taking the NACE International membership as a basis, an estimate was made of the total number of engineers and scientists who provide corrosion control services. Based on a 16,000 membership in 1998 and the assumption that 25% provide contract corrosion control services, a total services cost of $1.2 billion was estimated.
Research and Development. Over the past few decades, less funding has been made available for corrosion-related research and development, which is significant in light of the costs of maintaining aging infrastructure. In fact, several government and corporate research laboratories have significantly reduced their corrosion research staff or have even closed down their research facilities. Moreover, less research and development funding has been available from either government or private sources. An estimate of an annual academic budget of $20 million was made, while no estimates were made for the cost of corporate corrosion-related research.
Education and Training. Corrosion-related education and training in the United States includes degree programs, certification programs, company in-house training, and general education and training. A few national universities offer courses in corrosion and corrosion control as part of their engineering curriculum. Professional organizations, such as NACE International and SSPC, The Society for Protective Coatings, offer courses and programs that range from basic corrosion training to certification of coating inspectors and cathodic protection specialists. NACE International offers the broadest range of courses and manages an extensive certification program. In 1998, NACE International held 172 courses with more than 3000 students, conducted multiple seminars, and offered publications, at a total cost of $8 million.

Method 1 Summary

A total annual direct cost of corrosion by summing the costs of corrosion control methods and services was estimated at $121 billion, which is 1.38% of the U.S. gross domestic product of $8.79 trillion in 1998. The largest portion (88.3%) of this cost is the organic coatings group, at $107.2 billion. Notably, the categories of research and development and education and training indicated unfavorably low numbers.

G.H. Koch, M.P.H. Brongers, N.G. Thompson, Y.P. Virmani and J.H. Payer, Direct Costs of Corrosion in the United States, *Corrosion: Fundamentals, Testing, and Protection*, Vol 13A, *ASM Handbook*, ASM International, 2003, p 959–967

Direct Costs of Corrosion in the United States

Gerhardus H. Koch, Michiel P.H. Brongers, and Neil G. Thompson, CC Technologies Laboratories, Inc.; Y. Paul Virmani, Federal Highway Administration, Turner-Fairbank Highway Research Center; Joe H. Payer, Case Western Reserve University

Costs of Corrosion Estimated by Industry Sector Analysis

In the second method used in the 1998 U.S. study, the cost of corrosion was first determined for specific industry sectors and then extrapolated to calculate a national total corrosion cost. The U.S. economy was divided into five sector categories and 26 sectors, as shown in Table 3. The cost of corrosion was estimated for each of the categories listed in Table 3. When summed, the total annual cost of corrosion for the industry sectors examined was $137.9 billion. The breakdown of these costs among the five sector categories is given in Fig. 2. Not all industries were examined in this study. The total economic impact on the U.S. economy of all sectors is greater than the $137.9 billion given here and was calculated in the study by extrapolation for sectors that were not researched. Details of the corrosion costs in the individual industry sectors are given subsequently.

Table 3 Industry sectors and sector categories for 1998 U.S. cost of corrosion study

Sector categories	Sectors
Infrastructure	Highway bridges
	Gas and liquid transmission pipelines
	Waterways and ports
	Hazardous materials storage
	Airports
	Railroads
Utilities	Gas distribution
	Drinking water and sewer systems
	Electrical utilities
	Telecommunications
Transportation	Motor vehicles
	Ships
	Aircraft
	Railroad cars
	Hazardous materials transport
Production and manufacturing	Oil and gas exploration and production

	Mining Petroleum refining Chemical, petrochemical, and pharmaceutical Pulp and paper Agricultural Food processing Electronics Home appliances
Government	Defense Nuclear waste storage

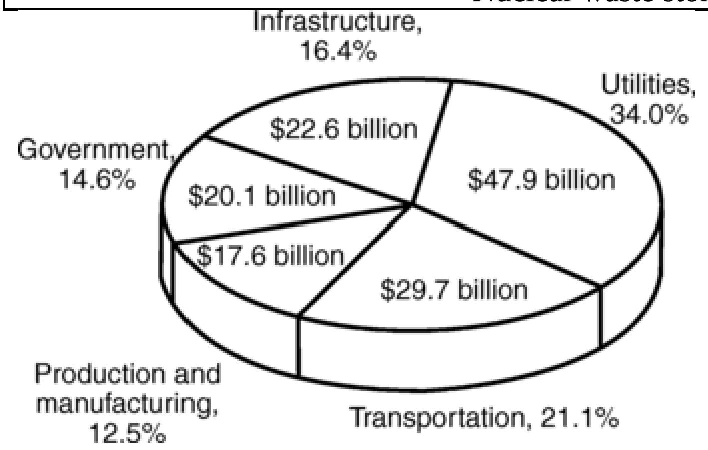

Fig. 2 Cost of corrosion in sector categories analyzed in 1998 U.S. study; total, $137.9 billion

Infrastructure

The U.S. infrastructure and transportation system allows for a high level of mobility and freight activity for the nearly 270 million residents and 7 million business establishments. In 1997, more than 230 million motor vehicles, ships, airplanes, and railroad cars were used on 6.4×10^6 km (4×10^6 miles) of highways, railroads, airports, and waterways. Pipelines and storage tanks are part of the infrastructure as well. The annual direct cost of corrosion in the infrastructure category is estimated at $22.6 billion. Contributions to infrastructure corrosion costs are shown in Fig. 3.

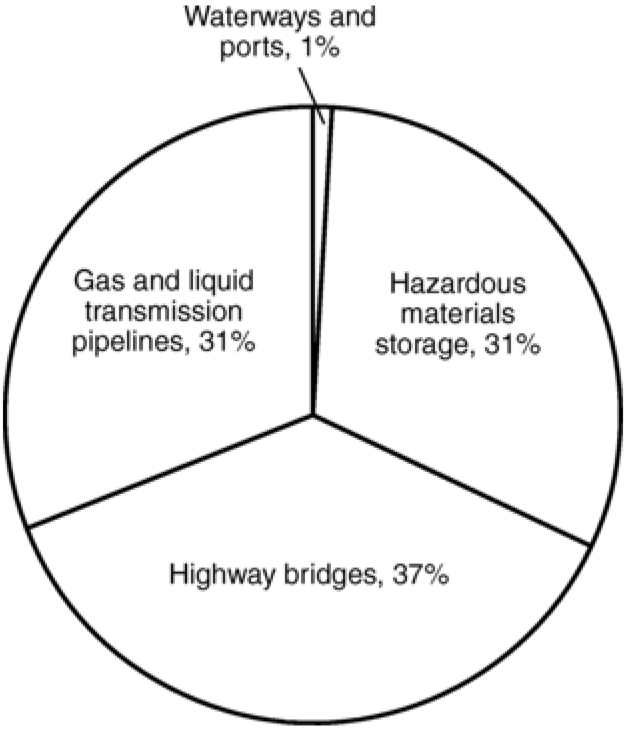

Fig. 3 Corrosion costs in infrastructure

Highway Bridges. There are 583,000 bridges in the United States (1998). Of this total, 200,000 bridges are steel, 235,000 are conventional reinforced concrete, 108,000 bridges are constructed using prestressed concrete, and the balance is made using other materials of construction. Approximately 15% of the bridges are structurally deficient, primarily due to corrosion of steel and steel reinforcement. The annual direct cost of corrosion for highway bridges is estimated at $8.3 billion, consisting of $3.8 billion to replace structurally deficient bridges over the next 10 years, $2.0 billion for maintenance and cost of capital for concrete bridge decks, $2.0 billion for maintenance and cost of capital for concrete substructures (minus decks), and $0.5 billion for maintenance painting of steel bridges.

Gas and Liquid Transmission Pipelines. There are more than 528,000 km (328,000 miles) of natural gas transmission and gathering pipelines, 119,000 km (74,000 miles) of crude oil transmission and gathering pipelines, and 132,000 km (82,000 miles) of hazardous liquid transmission pipelines. For all natural gas pipeline companies, the total investment in 1998 was $63.1 billion, from which total revenue of $13.6 billion was generated. For liquid pipeline companies, the investment was $30.2 billion, from which revenue of $6.9 billion was generated. At an estimated replacement cost of $643,800/km ($1,117,000/mile), the asset replacement value of the transmission pipeline system in the United States is $541 billion; therefore, a significant investment is at risk, with corrosion being the primary factor in controlling the life of the asset. The average annual corrosion-related cost is estimated at $7.0 billion, which can be divided into the cost of capital (38%), operation and maintenance (52%), and failures (10%).

Waterways and Ports. In the United States, 40,000 km (25,000 miles) of commercial navigable waterways serve 41 states, including all states east of the Mississippi River. Hundreds of locks facilitate travel along these waterways. In January 1999, 135 of the 276 locks had exceeded their 50 year design life. United States ports play an important role in connecting waterways, railroads, and highways. These ports include 1914 deepwater ports (seacoast and Great Lakes) and 1812 ports along inland waterways. Corrosion is typically found on piers and docks, bulkheads and retaining walls, mooring structures, and navigational aids. There is no formal tracking of corrosion costs for these structures. Based on figures obtained from the U.S. Army Corps of Engineers and the U.S. Coast Guard, an annual corrosion cost of $0.3 billion could be estimated. It should be noted that this is a low estimate, because the corrosion costs of harbor and other marine structures are not included.

Hazardous Materials Storage. The United States has approximately 8.5 million regulated and non-regulated aboveground storage tanks (ASTs) and underground storage tanks (USTs) for hazardous materials (HAZMAT). While these tanks represent a significant investment and good maintenance practices would be in the best interest of the owners, federal and state environmental regulators are concerned with the environmental impact

of spills from leaking tanks. The U.S. Environmental Protection Agency set a December 1998 deadline for UST owners to comply with requirements for corrosion control on all tanks, as well as overfill and spill protection. In case of noncompliance, tank owners face considerable costs related to cleanup and penalties. The total annual direct cost of corrosion for HAZMAT storage is $7.0 billion, broken down into $4.5 billion for ASTs and $2.5 billion for USTs.

Airports. The United States has the most extensive airport system in the world, which is essential to national transportation and the U.S. economy. According to 1999 Bureau of Transportation statistics data, there were 5324 public- use airports and 13,774 private-use airports in the United States. A typical airport infrastructure is complex, and components that might be subject to corrosion include the natural gas distribution system, jet fuel storage and distribution system, deicing storage and distribution system, vehicle fueling systems, natural gas feeders, dry fire lines, parking garages, and runway lighting. Generally, each of these systems is owned or operated by different organizations or companies; therefore, the impact of corrosion on an airport as a whole is not known or documented.

Railroads. In 1997, there were nine class I freight railroads (railroads with operating revenues of more than $256.4 million). These railroads accounted for 71% of the 274,399 km (170,508 miles) operated by the industry. There were 35 regional railroads (those with operating revenues between $40 million and 256.4 million and/or operating at least 560 km, or 350 miles, of railroad). The regional railroads operated 34,546 km (21,466 miles). Finally, there were 513 local railroads operating over 45,300 km (28,149 miles) of railroad. The elements that are subject to corrosion include metal members, such as rail and steel spikes; however, corrosion damage to railroad components is either limited or goes unreported. Hence, an accurate estimate of the corrosion cost could not be determined.

Utilities

Utilities supply gas, water, electricity, and telecommunications. All utility companies combined spent $42.3 billion on capital goods in 1998, broken down into $22.4 billion for structures and $19.9 billion for equipment. The total annual direct cost of corrosion in the utilities category is estimated to be $47.9 billion. Contributions to utility corrosion costs are shown in Fig. 4.

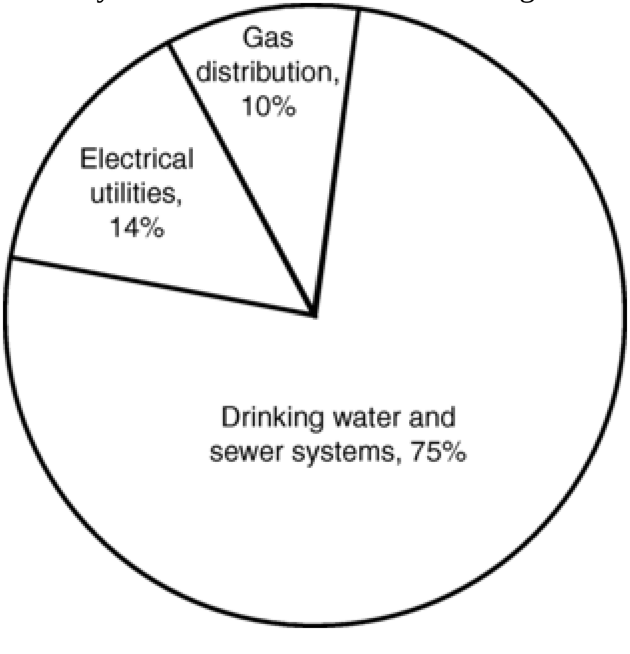

Fig. 4 Corrosion costs in utilities

Gas Distribution. The natural gas distribution system includes 2,785,000 km (1,730,000 miles) of relatively small-diameter, low-pressure piping, which is broken down into 1,739,000 km (1,080,000 miles) of distribution main and 1,046,000 km (650,000 miles) of services. There are approximately 55 million services in the distribution system. A large percentage of the mains (57%) and services (46%) are made of steel, cast iron, or copper, which are subject to corrosion. The total annual direct cost of corrosion was estimated at approximately $5.0 billion.

Drinking Water and Sewer Systems. According to the American Waterworks Association industry database, there are approximately 1,483,000 km (876,000 miles) of municipal water piping in the United States. This number is not exact, because most water utilities do not have complete records of their piping system. The sewer system consists of approximately 16,400 publicly owned treatment facilities that release some 155×10^6 m^3 (41×10^9 gal) of wastewater per day (1995). The total annual direct cost of corrosion for the drinking water and sewer systems of the nation was estimated at $36.0 billion. This cost consists of the cost of replacing aging infrastructure and the cost of unaccounted-for water through leaks, corrosion inhibitors, internal mortar linings, external coatings, and cathodic protection.

Electrical Utilities. In 1998, the electrical utilities industry provided a total amount of electricity of 3.24 trillion GWh, at a cost to consumers of $218 billion. Electrical generation plants can be divided into seven generic types: fossil fuel, nuclear, hydroelectric, cogeneration, geothermal, solar, and wind. The majority of electric power in the United States is generated by fossil fuel and nuclear supply systems. The total annual direct cost of corrosion in the electrical utilities industry in 1998 is estimated at $6.9 billion, with the largest amounts for nuclear power at $4.2 billion and fossil fuel at $1.9 billion, smaller amounts for hydraulic and other power at $0.15 billion, and transmission and distribution at $0.6 billion.

Telecommunications. The telecommunications infrastructure includes hardware, such as electronics, computers, and data transmitters, as well as equipment shelters and the towers used to mount antennas, transmitters, receivers, and television and telephone systems. According to the U.S. Census Bureau, the total value of shipments for communications equipment in 1999 was $84 billion. An important factor for corrosion cost is the additional cost of protecting towers and shelters, such as painting and galvanizing. In addition, corrosion of buried copper grounding beds and galvanic corrosion of the grounded steel structures contribute to the corrosion cost. For this sector, no corrosion cost was determined because of the lack of information on this rapidly changing industry. Many components are being replaced before physically failing, because their technology becomes obsolete in a short period of time.

Transportation

The transportation category includes vehicles and equipment, such as motor vehicles, aircraft, railroad cars, and hazardous materials transport, that make use of U.S. highways, waterways, railroads, and airports. The annual cost of corrosion in the transportation category is estimated at $29.7 billion. Contributions to transportation corrosion costs are shown in Fig. 5.

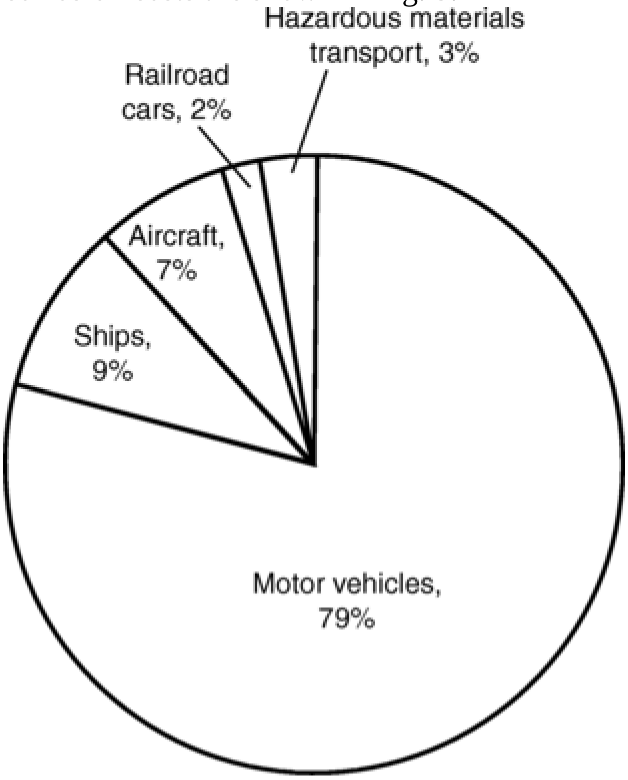

Fig. 5 Corrosion costs in transportation

Motor Vehicles. United States consumers, businesses, and government organizations own more than 200 million registered motor vehicles. Assuming the average value of an automobile is $5000, the total investment Americans have made in motor vehicles can be estimated at $1 trillion. Since the 1980s, car manufacturers have increased the corrosion resistance of vehicles by using corrosion-resistant materials, employing better manufacturing processes, and designing corrosion-resistant vehicles. Although significant progress has been made, further improvement can be achieved in corrosion resistance of individual components. The total annual direct cost of corrosion is estimated at $23.4 billion, which is broken down into the following components: increased manufacturing costs due to corrosion engineering and the use of corrosion- resistant materials ($2.56 billion), repairs and maintenance necessitated by corrosion ($6.45 billion), and corrosion-related depreciation of vehicles ($14.46 billion).

Ships. The U.S. flag fleet consists of the Great Lakes, with 737 vessels at 100×10^9 ton-km (62×10^9 ton-miles); inland, with 33,668 vessels at 473×10^9 ton-km (294×10^9 ton-miles); ocean, with 7014 vessels at 563×10^9 ton-km (350×10^9 ton-miles); recreational, with 12.3 million boats; and cruise ships, with 122 boats serving North American ports (5.4 million passengers). The total annual direct cost of corrosion to the U.S. shipping industry is estimated at $2.7 billion. This cost is broken down into costs associated with new ship construction ($1.1 billion), maintenance and repairs ($0.8 billion), and corrosion-related downtime ($0.8 billion).

Aircraft. In 1998, the combined commercial aircraft fleet operated by U.S. airlines was more than 7000 airplanes. At the start of the jet age (1950s to 1960s), little or no attention was paid to corrosion and corrosion control. One of the concerns is the continued aging of the airplanes beyond the 20 year design life. Only the most recent designs (e.g., Boeing 777 and late-version 737) have incorporated significant improvements in corrosion prevention and control in design and manufacturing. The total annual direct cost of corrosion to the U.S. aircraft industry is estimated at $2.2 billion, which includes the cost of design and manufacturing ($0.2 billion), corrosion maintenance ($1.7 billion), and downtime ($0.3 billion).

Railroad Cars. In 1998, 1.3 million freight cars and 1962 passenger cars were operated in the United States. Covered hoppers (28%) and tanker cars (18%) make up the largest segment of the freight car fleet. The type of commodities transported range from coal (largest volume) to chemicals, motor vehicles, farm products, food products, and ores and minerals. Railroad cars suffer from both external and internal corrosion. The total annual direct cost of corrosion is estimated at $0.5 billion, broken down into external coatings ($0.25 billion) and internal coatings and linings ($0.25 billion).

Hazardous Materials Transport. According to the U.S. Department of Transportation, there are approximately 300 million hazardous materials shipments totaling more than 3.1×10^9 metric tons annually in the United States. Bulk transport over land includes shipping by tanker truck and rail car and by special containers on vehicles. Over water, ships loaded with specialized containers, tanks, and drums are used. In small quantities, hazardous materials require specially designed packaging for truck and air shipment. The total annual direct cost of corrosion for hazardous materials transport is more than $0.9 billion. The elements of the annual corrosion cost include the cost of transporting vehicles ($0.4 billion), specialized packaging ($0.5 billion), and the direct and indirect costs of accidental releases and corrosion-related transportation incidents.

Production and Manufacturing

This category includes industries that produce and manufacture products of crucial importance to the economy and the standard of living in the United States. These include oil production, mining, petroleum refining, chemical and pharmaceutical production, and agricultural and food production. The total annual direct cost of corrosion for production and manufacturing was estimated at $17.6 billion. Contributions to the production and manufacturing corrosion costs are shown in Fig. 6.

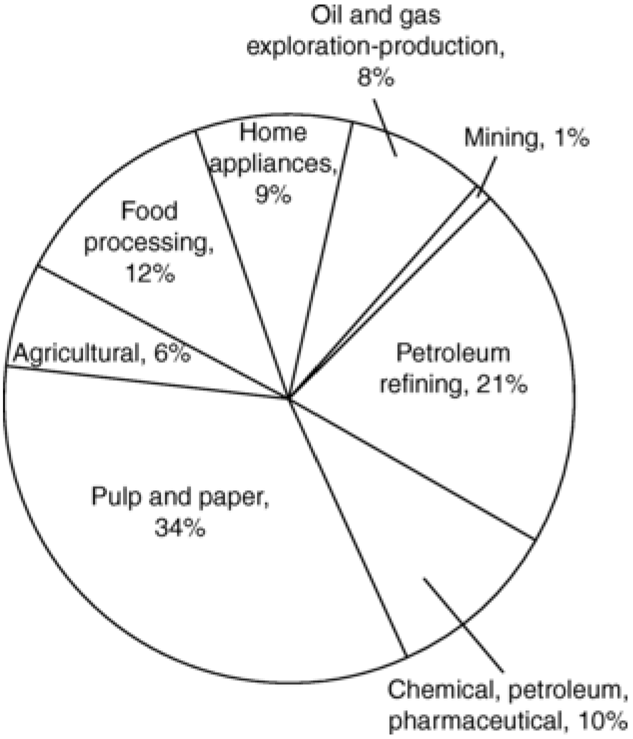

Fig. 6 Corrosion costs in production and manufacturing

Oil and Gas Exploration and Production. Domestic oil and gas production can be considered a stagnant industry, because most of the significant available onshore oil and gas reserves have been exploited. Oil production in the United States in 1998 consisted of 3.04×10^9 barrels. The significant recoverable reserves left to be discovered and produced are probably limited to less convenient locations, such as in deep water offshore, remote arctic locations, and difficult-to-manage reservoirs with unconsolidated sands. The total annual direct cost of corrosion in the U.S. oil and gas production industry is estimated at $1.4 billion, broken down into $0.6 billion for surface piping and facility costs, $0.5 billion in downhole tubing expenses, and $0.3 billion in capital expenditures related to corrosion.

Mining. In the mining industry, corrosion is not considered a significant problem. There is a consensus that the life-limiting factors for mining equipment are wear and mechanical damage rather than corrosion. Maintenance painting, however, is heavily relied on to prevent corrosion, with an annual estimated expenditure for the coal mining industry of $0.1 billion.

Petroleum Refining. The U.S. refineries represent approximately 23% of the petroleum production in the world, and the United States has the largest refining capacity in the world, with 163 refineries. In 1996, U.S. refineries supplied more than 18 million barrels/day of refined petroleum products. The total annual direct cost of corrosion is estimated at $3.7 billion. Of this total, maintenance-related expenses are estimated at $1.8 billion, vessel turnaround expenses at $1.4 billion, and fouling costs are approximately $0.5 billion annually.

Chemical, Petrochemical, and Pharmaceutical. The chemical industry includes those manufacturing facilities that produce bulk or specialty compounds by chemical reactions between organic and/or inorganic materials. The petrochemical industry includes those manufacturing facilities that create substances from raw hydrocarbon materials such as crude oil and natural gas. The pharmaceutical industry formulates, fabricates, and processes medicinal products from raw materials. The total annual direct cost of corrosion for this industry sector is estimated at $1.7 billion/year (8% of total capital expenditures). No calculation was made for the indirect costs of production outages or indirect costs related to catastrophic failures. The costs of operation and maintenance related to corrosion were not readily available; estimating these costs would require detailed study of data from individual companies.

Pulp and Paper. The $165 billion pulp, paper, and allied products industry supplies the United States with approximately 300 kg (660 lb) of paper per person per year. More than 300 pulp mills and more than 550 paper mills support its production. The total annual direct cost of corrosion is estimated at $6.0 billion, with the majority of this cost in the paper and paperboard industry, and is calculated as a fraction of the maintenance costs. No information was found to estimate the corrosion costs related to the loss of capital.

Agricultural operations produce livestock and crops. According to the National Agricultural Statistics Service, there are approximately 1.9 million farms in the United States. Based on the 1997 Farm Census, the total value of farm machinery and equipment is approximately $15 billion/year. The two main reasons for replacing machinery or equipment include upgrading old equipment and replacement because of wear and corrosion. Discussions with experts in this industrial sector resulted in an estimate of corrosion costs in the range of 5 to 10% of the value of all new equipment. Therefore, the total annual direct cost of corrosion in the agricultural production industry is estimated at $1.1 billion.

Food Processing. The food processing industry is one of the largest manufacturing industries in the United States, accounting for approximately 14% of the total U.S. manufacturing output. Sales for food processing companies totaled $265.5 billion in 1999. Because of food quality requirements, stainless steel is widely used. Assuming that the stainless steel consumption and cost in this industry are entirely attributed to corrosion, a total annual direct cost of corrosion is estimated at $2.1 billion. This cost includes stainless steel use for beverage production, food machinery, cutlery and utensils, commercial and restaurant equipment, and appliances. Also included are aluminum cans and the use of corrosion inhibitors.

Electronics. Corrosion in electronic components manifests itself in several ways, and computers, integrated circuits, and microchips are being exposed to a variety of environmental conditions. Corrosion in electronic components is insidious and cannot be readily detected; therefore, when corrosion failure occurs, it is often dismissed as just a failure, and the part or component is replaced. Particularly in the case of consumer electronics, devices become technologically obsolete long before corrosion-induced failures occur. However, in capital-intensive industries with significant investments in durable equipment with a considerable number of electronic components, such as the defense industry and the airline industry, there is a tendency to keep the equipment for longer periods, and corrosion is likely to become an issue. Although the cost of corrosion in the electronics sector could not be estimated, it has been suggested that a significant part of all electric component failures is caused by corrosion.

Home Appliances. The appliance industry is one of the largest consumer products industries. For practical purposes, two categories of appliances are distinguished: major home appliances and comfort-conditioning appliances. In 1999, 70.7 million major home appliances and 49.5 million comfort-conditioning appliances were sold in the United States, for a total of 120.2 million appliances. The cost of corrosion in home appliances includes the cost of purchasing replacement appliances because of premature failures due to corrosion. For water heaters alone, the replacement cost was estimated at $460 million/year, using a low estimate of 5% of replacement being corrosion related. The cost of internal corrosion protection for all appliances includes the use of sacrificial anodes ($780 million/year), corrosion-resistant materials (no cost estimate), and internal coatings (no cost estimate). The cost of external corrosion protection using coatings was estimated at $260 million/ year. Therefore, the estimated total annual direct cost of corrosion in home appliances is at least $1.5 billion.

Government

Federal, state, and local governments had a 1998 GDP of approximately $1.1 trillion ($360 billion federal, $745 billion state and local). While the government owns and operates significant assets under various departments, the U.S. Department of Defense was selected for analysis because of its significant impact on the U.S. economy. A second analyzed government sector is nuclear waste storage.

Defense. Corrosion of military equipment and facilities has been a significant and ongoing problem for many years. The corrosion-related problems are becoming more prominent as the acquisition of new equipment is decreasing and the reliability required of aging systems is increasing. The data provided by the military services (Army, Air Force, Navy, and Marine Corps) indicate that corrosion is potentially the number one cost driver in life-cycle costs. The total annual direct cost of corrosion incurred by the military services for systems and infrastructure is approximately $20 billion.

Nuclear Waste Storage. Nuclear wastes are generated from spent nuclear fuel, dismantled nuclear weapons, and products such as radiopharmaceuticals. The most important design item for the safe storage of nuclear waste is effective shielding of radiation. Corrosion is an important issue in the design of the casks used for permanent storage, which have a design life of several thousand years. A 1998 total life-cycle cost analysis by the U.S. Department of Energy for the permanent disposal of nuclear waste in Yucca Mountain, Nevada, estimated the total repository cost by the construction phase (2002) at $4.9 billion, with an average annual cost (from 1999 to 2116) of $205 million. Of this cost, $42.2 million is corrosion related.

Method 2 Summary

The cost of corrosion was estimated for the individual economic sectors discussed previously. The total cost due to the impact of corrosion for the analyzed sectors was $137.9 billion/year (Fig. 2, Table 4). Table 4 shows the costs of corrosion for each industry sector analyzed in the current study. The dollar values are rounded to the nearest $0.1 billion because of the uncertainty in the applied methods. The cost of $137.9 billion is believed to be a conservative estimate. In each sector, only the major corrosion costs were considered. In addition, even major costs were left out when no basis for an estimate was found; most notable were no operation and maintenance costs were included for the chemical, petrochemical, and pharmaceutical sector; no capital costs were included for the pulp and paper sector; no capital costs were included for the gas distribution sector; and replacement costs were considered for only water heaters in the home appliances sector. In most cases, conservative estimates were made when no basis was available; most notable was that only 5% of water heaters are replaced due to corrosion. Therefore, the total cost of corrosion is a conservative value and is likely higher than that presented in this study.

Table 4 Summary of industry sector direct corrosion costs analyzed in 1998 U.S. study

Category	Industry sectors	Estimated direct cost of corrosion per sector	
		$ × billion	**%[(a)]**
Infrastructure (16.4% of total)	Highway bridges	8.3	37
	Gas and liquid transmission pipelines	7.0	27
	Waterways and ports	0.3	1
	Hazardous materials storage	7.0	31
	Airports	[(b)]	[(b)]
	Railroads	[(b)]	[(b)]
	Subtotal	**$22.6**	**100%**
Utilities (34.7% of total)	Gas distribution	5.0	10
	Drinking water and sewer systems	36.0	75
	Electrical utilities	6.9	14
	Telecommunications	[(b)]	[(b)]
	Subtotal	**$47.9**	**100%**
Transportation (21.5% of total)	Motor vehicles	23.4	79
	Ships	2.7	9
	Aircraft	2.2	7
	Railroad cars	0.5	2
	Hazardous materials transport	0.9	3
	Subtotal	**$29.7**	**100%**
Production and manufacturing (12.8% of total)	Oil and gas exploration and production	1.4	8
	Mining	0.1	1
	Petroleum refining	3.7	21
	Chemical, petrochemical, and pharmaceutical	1.7	10
	Pulp and paper	6.0	34
	Agricultural	1.1	6
	Food processing	2.1	12
	Electronics	[(b)]	[(b)]
	Home appliances	1.5	9
	Subtotal	**$17.6**	**100%**
Government (14.6% of total)	Defense	20.0	99.5

	Nuclear waste storage	0.1	0.5
	Subtotal	**$20.1**	**100%**
	Total	**$137.9**	

(a) Individual values do not add up to 100% because of rounding.
(b) Corrosion costs not determined

The data show that the highest corrosion costs are incurred by drinking water and sewer systems. The large value of $36.0 billion/year for both types of systems together is due to the extent of the water transmission and distribution network in the United States. The metal piping systems are aging and will require increased maintenance in the future. Large indirect costs are expected as well but were not quantified in the current study.

The second large corrosion cost ($23.4 billion/ year) was found in the motor vehicles sector. The corrosion impact consists of corrosion-related depreciation costs (62%), corrosion-resistant materials of construction (10%), and the cost of increased maintenance because of corrosion (28%). The indirect cost in this sector is expected to be large, especially because of the time users of motor vehicles lose when having to deal with car maintenance and repair.

The third large corrosion cost ($20 billion/ year) was observed in defense systems. Reliability and readiness are of crucial importance; therefore, military vehicles, aircraft, ships, weapons, and facilities must be continuously maintained. A determining factor in the defense sector is the readiness for operation under any circumstance and in corrosive environments such as seawater, swamps or wetlands, and in rain and mud.

Large corrosion costs were further found in the sectors for highway bridges ($8.3 billion/ year), gas and liquid transmission pipelines ($7.0 billion/year), electrical utilities ($6.9 billion/ year), pulp and paper ($6.0 billion/year) and gas distribution ($5.0 billion/year). Two factors were important for these sectors: the large number of units and the severely corrosive environments. The following lists specific concerns regarding corrosion for some of the sectors that have large corrosion costs:

- The national systems of highways require many bridges to be maintained. With the commonly used approach that bridges are constructed to have a design life, rather than being there forever, the burden to maintain, repair, and replace this infrastructure will continue to grow because of aging components.
- The network of transmission pipelines is quite large (779,000 km, or 484,000 miles) and transports potentially corrosive liquids and gas, which makes their operation sensitive to public opinion related to environmental spills and highly publicized ruptures. Although pipelines have proven to be the safest way to transport large quantities of product over long distances, preventing corrosion is a significant cost.
- The same argument regarding potential spills holds for the hazardous materials storage sector. Corrosion protection is a significant cost per tank for both underground and aboveground tanks. The total number of hazardous materials storage tanks in the United States is large—estimated at 8.5 million tanks.
- Electrical utilities have large corrosion costs due to the affected operation and maintenance costs, depreciation costs, and the cost of forced outages. The largest cost is found for nuclear-power-generated plants because of the higher inspection frequency in nuclear plants as compared with fossil-fueled plants.
- The pulp and paper industry uses corrosive media to make pulp from wood. Changes in process conditions over the last decades have had a significant impact on the materials used for construction. Paper quality and process reliability are driving spending in this sector.

The total cost of corrosion in the analyzed sectors of $137.9 billion/year was based on detailed analysis of industrial sectors, which are known to have significant corrosion impact. The sum of these sectors represented 27.55% of the GDP. Because not all economic sectors were examined, the sum of the estimated costs for the analyzed sectors does not represent the total cost of corrosion for the entire U.S. economy. Based on the procedure for extrapolation, which used the percentage of cost of corrosion for Bureau of Economic Analysis subcategories (see Fig. 1 for the primary categories), an estimated total direct cost of corrosion of $275.7 billion/year was calculated (Fig. 7).

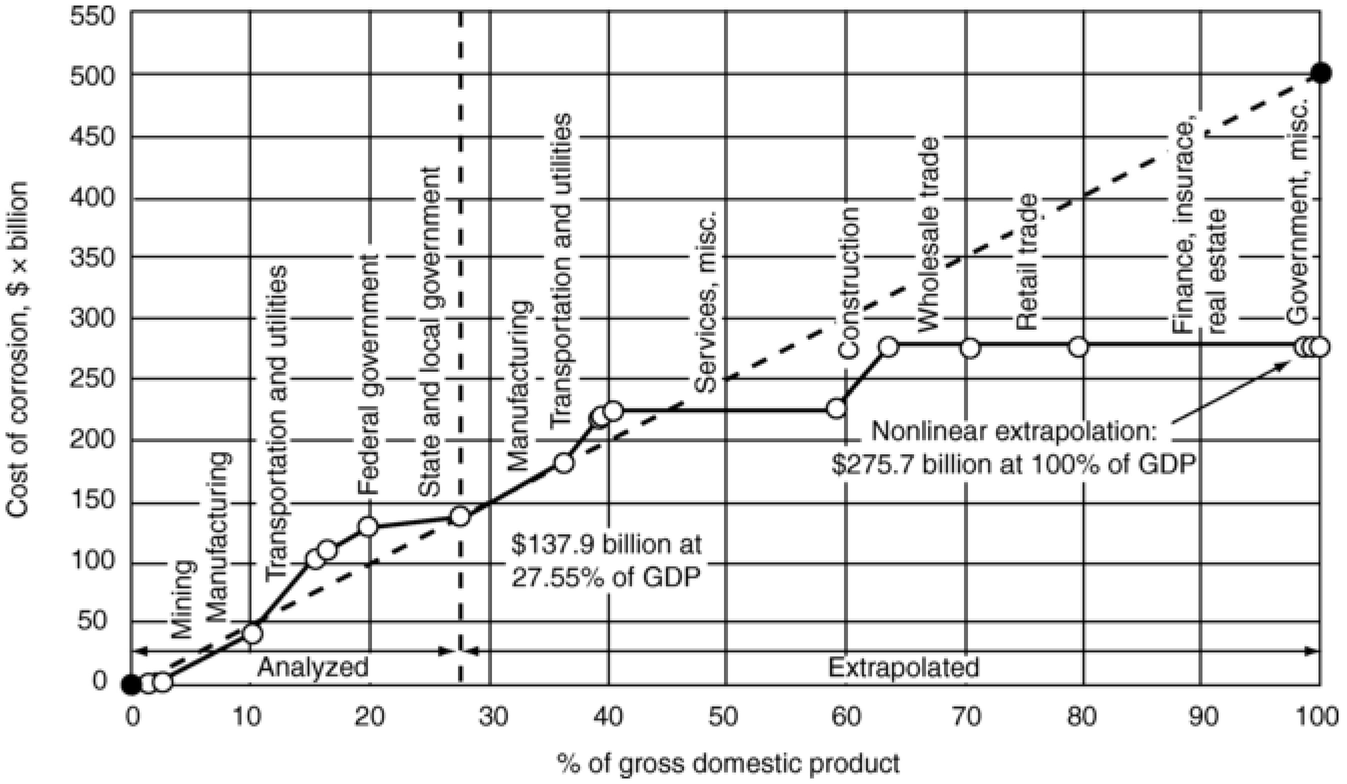

Fig. 7 Nonlinear extrapolation of cost of corrosion to entire U.S. economy

It must be noted that a straight, linear extrapolation of the costs is not recommended because of the expected lower overall corrosion impact in some of the nonanalyzed sectors (i.e., wholesale trade, retail trade, and finance, insurance, and real estate). If one would proceed with the linear extrapolation, the $137.9 billion for 27.55% of GDP would result in an estimate of total annual direct corrosion cost of $500.5 billion/year. In comparison, the nonlinear extrapolation in Fig. 7, based on the assumption that nonanalyzed sectors have different corrosion impact, shows a stepwise, cumulative calculation for total corrosion cost. The final estimate of direct corrosion costs is $275.7 billion/year.

Thus, the direct corrosion costs are 3.1% of the 1998 U.S. gross domestic product. Figure 8 shows graphically the impact of corrosion on the GDP of the nation. This estimate is considered a conservative estimate, because only well-documented costs were used. Other costs of corrosion were discussed in the study but were left out due to lack of documentation.

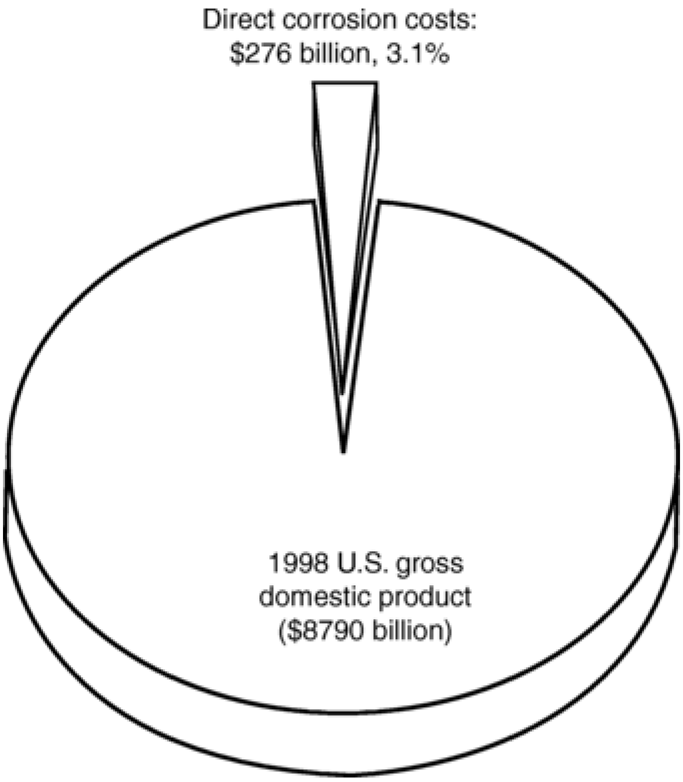

Fig. 8 Impact of corrosion on the U.S. economy

Direct corrosion costs were estimated based on direct costs to the owners or operators. The indirect costs incurred by those other than owners or operators were not included in the cost estimates. At 3.1% of the GDP, the cost of corrosion to the U.S. economy is already significant if only based on the direct cost of corrosion. However, the impact of corrosion can be significantly greater when indirect costs are included. Evidence of large indirect corrosion costs are lost productivity because of outages, delays, failures, and litigation; taxes and overhead on the cost of the corrosion portion of goods and services; and indirect costs of nonowner/operator activities. For example, an analysis of the corrosion cost for bridges indicated that the indirect costs due to traffic congestion and business disruption during repairs resulting in lost productivity can be 10 times or more than the direct bridge cost of corrosion. Analysis of the corrosion cost for electrical utilities indicated that the indirect costs (taxes and overhead costs to user) were 1.7 times the direct cost to the utility owner/operator. Averaged over the industry sectors, the assumption can be made that the indirect costs can be equal to, if not greater than, the direct costs. This would result in a total direct and indirect impact of corrosion of approximately $551.4 billion annually, or 6.3% of the GDP.

G.H. Koch, M.P.H. Brongers, N.G. Thompson, Y.P. Virmani and J.H. Payer, Direct Costs of Corrosion in the United States, *Corrosion: Fundamentals, Testing, and Protection*, Vol 13A, *ASM Handbook*, ASM International, 2003, p 959–967

Direct Costs of Corrosion in the United States

Gerhardus H. Koch, Michiel P.H. Brongers, and Neil G. Thompson, CC Technologies Laboratories, Inc.; Y. Paul Virmani, Federal Highway Administration, Turner-Fairbank Highway Research Center; Joe H. Payer, Case Western Reserve University

Conclusions Based on 1998 U.S. Study

The infrastructure of the nation is essential to the quality of life, industrial productivity, international competitiveness, and security. Everything depends on a functional, reliable, and safe infrastructure system, including food, water and energy needs, transportation for work, education and recreation, the production and

delivery of goods and services, communications, and the treatment and disposal of wastes. Each component of the national infrastructure, such as highways, airports, water supply, waste treatment, energy supply, and power generation, represents a complex system and large investments.

Corrosion is damage that results from the interaction of structures and materials with their environment. In some cases, corrosion damage is tolerable and perhaps only leads to somewhat higher maintenance costs and minimal losses; however, corrosion can result in catastrophic failures, with loss of life and disruption of essential services. In fact, corrosion is a primary cause of the degradation and a principal threat to the infrastructure of the nation. As documented in the 1998 U.S. Corrosion Cost Study, the direct costs of corrosion represent 3.1% of the U.S. gross domestic product, and the total costs to society can be twice that or greater. The infrastructure replacement cost is a major driver on the economic impact of corrosion and can still be greater if corrosion-preventive strategies are not properly employed. The opportunities for savings by improved corrosion control are presented in every industrial sector and can be significant.

The principal challenges in realizing the significant savings that result from improved corrosion control include an unfortunate lack of awareness of corrosion costs by the public and policymakers and a widely held misconception that nothing can be done about corrosion. The opportunities and the challenges for better corrosion control fall into two categories. First, there are technical issues for the realization of technological advances and the implementation of those advances. Second, there are nontechnical issues of perception regarding the policies and the practices used for improved corrosion control. In the 1998 U.S. Corrosion Cost Study, strategies for progress in corrosion control are presented for progress in both categories.

There is an increasing recognition and a growing shift in emphasis from the building of a new infrastructure to the preservation and extended use of an existing infrastructure. In Ref 4, the Federal Highway Administration indicated a shift in focus from constructing new highways to preserving and operating existing highways. Increased capacity, greater safety, and a longer life are desired from the existing infrastructure. The critical need for progress in preservation and extended use is also pertinent to the invisible infrastructure (i.e., those components of the infrastructure that are not recognized by the public and whose performance is taken for granted until a failure or loss of service occurs). This invisible infrastructure includes items such as water mains, gas and oil pipelines, power plants, and telecommunications systems.

The preservation and the extension of the useful life of an existing infrastructure is a great challenge because of the long service lives that are desired. The operating life of critical components of the infrastructure is often extended well beyond the original design service life. For example, the Brooklyn Bridge was constructed in 1883. Furthermore, some cast iron water mains that were constructed in the early 1900s remain in service today. These water mains continue to be a critical component for the municipal water supplies, even after nearly 100 years of use.

While the focus may recently have shifted from building a new infrastructure to the preservation and extended use of the existing infrastructure, the necessary changes in public attitudes, adjustments to the allocation of resources, changes to the industrial, government, and academic institutions, and revisions to policies, practices, and procedures have only just begun. The adjustments made to date do not adequately address the needs and opportunities. There are great opportunities for increased integrity, durability, and savings; however, both systemic and programmatic corrections are required so that these benefits can be realized. Barriers to progress and the effective implementation of improved corrosion control must be addressed.

Reference cited in this section

4. “Connecting America—1999 Report to the Nation,” FHWA-HCM-00-002, Federal Highway Administration, May 2000

G.H. Koch, M.P.H. Brongers, N.G. Thompson, Y.P. Virmani and J.H. Payer, Direct Costs of Corrosion in the United States, *Corrosion: Fundamentals, Testing, and Protection*, Vol 13A, *ASM Handbook*, ASM International, 2003, p 959–967

Direct Costs of Corrosion in the United States

Gerhardus H. Koch, Michiel P.H. Brongers, and Neil G. Thompson, CC Technologies Laboratories, Inc.; Y. Paul Virmani, Federal Highway Administration, Turner-Fairbank Highway Research Center; Joe H. Payer, Case Western Reserve University

Corrosion Prevention Strategies

The 1998 U.S. study showed that technological changes have provided many new ways to prevent corrosion and also showed the improved use of available corrosion management techniques. However, better corrosion management can be achieved using preventive strategies in nontechnical and technical areas. These preventive strategies include:

- Increase awareness of significant corrosion costs and potential cost savings
- Change the misconception that nothing can be done about corrosion
- Change policies, regulations, standards, and management practices to increase corrosion cost savings through sound corrosion management
- Improve education and training of staff in the recognition of corrosion control
- Implement advanced design practices for better corrosion management
- Develop advanced life prediction and performance assessment methods
- Improve corrosion technology through research, development, and implementation

While corrosion management has improved over the past several decades, the United States is still far from implementing optimal corrosion control practices. There are significant barriers to both the development of advanced technologies for corrosion control and the implementation of those technological advances. In order to realize the savings from reduced costs of corrosion, changes are required in three areas: the policy and management framework for effective corrosion control, the science and technology of corrosion control, and the technology transfer and implementation of effective corrosion control. The policy and management framework is crucial, because it governs the identification of priorities, the allocation of resources for technology development, and the operation of the system.

Incorporating the latest corrosion strategies requires changes in industry management and government policies as well as advances in science and technology. It is necessary to engage a larger constituency comprised of the primary stakeholders, government and industry leaders, the public, and consumers. A major challenge involves the dissemination of corrosion awareness and expertise that are currently scattered throughout government and industry organizations. In fact, there is no focal point for the effective development, articulation, and delivery of corrosion cost-savings programs.

G.H. Koch, M.P.H. Brongers, N.G. Thompson, Y.P. Virmani and J.H. Payer, Direct Costs of Corrosion in the United States, *Corrosion: Fundamentals, Testing, and Protection*, Vol 13A, *ASM Handbook*, ASM International, 2003, p 959–967

Direct Costs of Corrosion in the United States

Gerhardus H. Koch, Michiel P.H. Brongers, and Neil G. Thompson, CC Technologies Laboratories, Inc.; Y. Paul Virmani, Federal Highway Administration, Turner-Fairbank Highway Research Center; Joe H. Payer, Case Western Reserve University

Acknowledgment

The complete report text, including all appendixes, is available for free at www.corrosion[fj cost.com. The authors acknowledge the support of the Federal Highway Administration, under Cooperative Agreement DTFH61-99-X-00004. Also, the authors would like to acknowledge the editorial work for this Handbook article by Stephen D. Cramer and Bernard S. Covino, Jr. of the U.S. Department of Energy, Albany Research Center. The input from many experts and the study advisory committee is greatly appreciated. Without the continuous feedback and thorough review of these people, the 1998 U.S. Cost of Corrosion Study would not contain such a large range of corrosion cost data.

G.H. Koch, M.P.H. Brongers, N.G. Thompson, Y.P. Virmani and J.H. Payer, Direct Costs of Corrosion in the United States, *Corrosion: Fundamentals, Testing, and Protection*, Vol 13A, *ASM Handbook*, ASM International, 2003, p 959–967

Direct Costs of Corrosion in the United States

Gerhardus H. Koch, Michiel P.H. Brongers, and Neil G. Thompson, CC Technologies Laboratories, Inc.; Y. Paul Virmani, Federal Highway Administration, Turner-Fairbank Highway Research Center; Joe H. Payer, Case Western Reserve University

---

References

1. J.H. Payer and G.H. Koch, Appendix A: Review of Previous Studies, *Corrosion Cost and Preventive Strategies in the United States,* FHWA-RD-01-156, Federal Highway Administration, U.S. Department of Transportation, March 2002

2. G.H. Koch, M.P.H. Brongers, N.G. Thompson, Y.P. Virmani, and J.H. Payer, *Corrosion Cost and Preventive Strategies in the United States,* FHWA-RD-01-156, Federal Highway Administration, U.S. Department of Transportation, March 2002

3. T. Balvanyos and L. Lave, Appendix B: Economic Analysis Methods, *Corrosion Cost and Preventive Strategies in the United States,* FHWA-RD-01-156, Federal Highway Administration, U.S. Department of Transportation, March 2002, p 773

4. “Connecting America—1999 Report to the Nation,” FHWA-HCM-00-002, Federal Highway Administration, May 2000

S.D. Cramer, Introduction to Tools for the Corrosionist, *Corrosion: Fundamentals, Testing, and Protection*, Vol 13A, *ASM Handbook*, ASM International, 2003, p 971

Introduction to Tools for the Corrosionist

Stephen D. Cramer, Albany Research Center, U.S. Department of Energy

Introduction

WHO IS A CORROSIONIST? A corrosion engineer, a corrosion technician, a corrosion scientist, a chemist, a physicist, an electrical engineer, a mechanical engineer, a coatings or plastics salesperson, a corrosion consultant, or a plant operator all may qualify for this title. The only requirement is a vocation that involves the understanding, evaluation, mitigation, or prevention of corrosion. The author first heard the term corrosionist used by Ted Kazmierczak, president of NACE International, 1998 to 1999, in his annual convention banquet address in San Diego, CA. He applied it to everyone in attendance, over a thousand people. And it seemed an appropriate and inclusive description of our collective interests.

"Tools for the Corrosionist" contains material not usually found in handbooks such as this. Corrosion is, however, an interdisciplinary subject, and corrosionists rely on many disciplines besides that central one that we identify with. The following articles are intended to help broaden the knowledge base of those concerned with the questions about corrosion and how to prevent or protect against it.

S.D. Cramer, Introduction to Tools for the Corrosionist, *Corrosion: Fundamentals, Testing, and Protection*, Vol 13A, *ASM Handbook*, ASM International, 2003, p 971

Introduction to Tools for the Corrosionist

Stephen D. Cramer, Albany Research Center, U.S. Department of Energy

Statistics

Take, for example, statistics; corrosionists encounter statistical issues more often than most care to admit. The article "Statistics for the Corrosionist" presents an overview of statistical inference and addresses the most commonly used statistical tools and tests. It includes definitions and notational conventions, and a discussion of statistical hypotheses and selection of statistical tests. Illustrations are given of specific statistical tests and the concept of confidence limits. It concludes with a discussion of sampling issues, one- way analysis of variance, correlation, and simple regression analysis.

S.D. Cramer, Introduction to Tools for the Corrosionist, *Corrosion: Fundamentals, Testing, and Protection*, Vol 13A, *ASM Handbook*, ASM International, 2003, p 971

Introduction to Tools for the Corrosionist

Stephen D. Cramer, Albany Research Center, U.S. Department of Energy

Materials

The article “Materials Basics for the Corrosionist” presents an overview of the science and engineering of materials, including metals, polymers, and ceramics. The presentation is descriptive rather than technical. Definitions and descriptions of the more commonly used materials terms are given. The more frequently cited physical properties, measurement methods, and units are presented. Fabrication methods are described along with a summary table of material properties. The article concludes with a discussion of materials design, materials applications, and materials failure analysis.

S.D. Cramer, Introduction to Tools for the Corrosionist, *Corrosion: Fundamentals, Testing, and Protection*, Vol 13A, *ASM Handbook*, ASM International, 2003, p 971

Introduction to Tools for the Corrosionist

Stephen D. Cramer, Albany Research Center, U.S. Department of Energy

Instruments

The article “Applications of Modern Analytical Instruments in Corrosion” presents both in situ and ex situ analytical techniques successfully used to gain insight into the mechanisms of corrosion at a molecular and atomic level and for conducting failure analyses. The article explains the principles of various surface-sensitive techniques and the usefulness and limitations of these techniques. The techniques are divided into those that provide insight into surface topography and surface structure, and those that provide understanding of chemical nature and identity. No single analytical technique can answer all corrosion questions, but a suitable combination of techniques can provide much information about corrosion mechanisms. A clear understanding of corrosion mechanisms helps in identifying effective corrosion prevention techniques.

S.D. Cramer, Introduction to Tools for the Corrosionist, *Corrosion: Fundamentals, Testing, and Protection*, Vol 13A, *ASM Handbook*, ASM International, 2003, p 971

Introduction to Tools for the Corrosionist

Stephen D. Cramer, Albany Research Center, U.S. Department of Energy

Additional Help

The article “Information Sources and Databases for the Corrosionist” provides some of the more important web sites and print media addressing corrosion and related topics. Lists are presented in five different areas: (a) societies and associations; (b) corrosion standards, specifications, and recommended practices; (c) sources of corrosion information; (d) corrosion databases and data compilations; and (e) other web resources. The lists are not inclusive but provide good starting points from which one can build.

S.D. Cramer, Introduction to Tools for the Corrosionist, *Corrosion: Fundamentals, Testing, and Protection*, Vol 13A, *ASM Handbook*, ASM International, 2003, p 971

Introduction to Tools for the Corrosionist

Stephen D. Cramer, Albany Research Center, U.S. Department of Energy

Terminology and Presentation of Data

The article "Conventions and Definitions in Corrosion and Oxidation" describes some of the common conventions and definitions in corrosion and oxidation that can result in confusion and some degree of aggravation. The article is selective and modest in its goals and hopefully provides some clarity in the few areas addressed. These range from sign conventions, labeling conventions, definitions, and standard practices to conversions between different potential scales.

B.P. Jones, Statistics for the Corrosionist, *Corrosion: Fundamentals, Testing, and Protection*, Vol 13A, *ASM Handbook*, ASM International, 2003, p 972–979

Statistics for the Corrosionist

Barnie P. Jones, Oregon Department of Transportation

Introduction

THIS ARTICLE is an overview of basic statistical inference and reviews several of the most commonly used statistical tools and tests. It covers basic concepts but not in depth or detail, with the assumption that the reader already has at least some familiarity with these concepts and methods. For those interested in further reading, references to more thorough treatments are included. Also, the reader may wish to refer to the article "Statistical Interpretation of Corrosion Test Results" in this Volume.

Definitions, equations, and notational conventions that are used widely in statistical analysis are presented. The section on measurement provides a basic framework for the selection of a statistical test. While not the only consideration, the way that variables are measured is fundamental to the choice of a statistical test. The section "Statistical Hypothesis Testing" outlines the basic elements common to all statistical tests. Illustrations of specific statistical tests and the concept of confidence limits are introduced. An overview of sampling issues is provided, with guidance in both selecting a sampling method and determining the number of units to sample. One-way analysis of variance, correlation, and simple regression analysis are introduced and illustrated.

Statistical computations have become extremely easy to obtain. Most popular spreadsheet packages include statistical functions for most of the tests and other techniques described in this article. This article therefore emphasizes understanding underlying concepts as well as selection and interpretation of statistical tests and other tools. It should also be noted that, despite several references in this article to the use of published sampling distribution tables, with today's technology it is rarely necessary to look up a number in the appendix of a Handbook.

None of the information presented here is in any way new or original. Every effort has been made to acknowledge the original sources that were used to compile this article.

B.P. Jones, Statistics for the Corrosionist, *Corrosion: Fundamentals, Testing, and Protection*, Vol 13A, *ASM Handbook*, ASM International, 2003, p 972–979

Statistics for the Corrosionist

Barnie P. Jones, Oregon Department of Transportation

Definitions and Expressions

This section reviews definitions and formulas that are in wide use in statistical analysis. In addition to serving as a reference, this section is intended to establish definitions and conventions for the balance of the article.
Parameters Versus Estimates. A convention in statistical notation is to use Greek letters to represent parameters (true characteristics of a population or universe) and Roman letters to represent sample-based estimates of those parameters. Table 1 presents several of the most familiar concepts and their corresponding symbols.

Table 1 Symbols assigned to represent familiar statistical operations and quantities

	Operators	Variables	
		Parameters (universe)	**Estimates (sample)**
Mean	…	μ	$\overline{x}, \overline{X}$
Standard deviation	…	σ	s
Variance	…	σ^2	s^2
Standard error	…	$\sigma^2_{\overline{x}_i}$	$s/\sqrt{N-1}$
Summation	$\sum$	…	…
Factorial	$n!$	…	…

Measures of central tendency are mean, median, and mode.
Mean is the arithmetic average. When n is the sample size and N is the population size:

$$\text{Sample mean:} \quad \overline{x} = \frac{\sum_{i=1}^{n} X_i}{n} \qquad \text{(Eq 1)}$$

$$\text{Population mean:} \quad \mu = \frac{\sum_{i=1}^{N} X_i}{N} \qquad \text{(Eq 2)}$$

Median is the midpoint, or the case separating equal numbers of larger and smaller values.
Mode is the most frequently occurring value.
Measures of dispersion include range, quartile deviation, variance, and standard deviation.
Range is the difference between highest and lowest values.
Quartile deviation is half the difference between upper and lower quartiles.
Variance is a means of quantifying the dispersion or scatter of the data or the total population. It is the second moment about the average.
Sample variance is represented by:

$$s^2 = \frac{\sum_{i=1}^{n} (X_i - \overline{x})^2}{n} \qquad \text{(Eq 3)}$$

Population variance is represented by:

$$\sigma^2 = \frac{\sum_{i=1}^{N}(X_i - \mu)^2}{N} \quad \text{(Eq 4)}$$

Standard deviation is the square root of the variance.
Sample standard deviation is:

$$s = \sqrt{\frac{\sum_{i=1}^{n}(X_i - \bar{x})^2}{n}} \quad \text{(Eq 5)}$$

Population standard deviation is:

$$\sigma = \sqrt{\frac{\sum_{i=1}^{N}(X_i - \mu)^2}{N}} \quad \text{(Eq 6)}$$

Other definitions and expressions that are useful in statistical analysis include standard error, binomial probability, and standard score.
Standard error (of the mean) is represented by:

$$\sigma_{\bar{x}} = \frac{\sigma}{\sqrt{N}} \quad \text{(Eq 7)}$$

Binomial probability is represented by:

$$P(r) = \frac{N!}{r!(N-r)!} \times p^r q^{N-r} \quad \text{(Eq 8)}$$

where N is the number of trials, r the number of successes, p the probability of success, and $q = 1 - p$.
Standard score is represented by:

$$Z = \frac{X - \bar{x}}{s} \quad \text{(Eq 9)}$$

where s is an estimate of the standard deviation obtained from a sample. Note that this transformation results in a variable with mean of 0 and standard deviation of 1. This has a number of useful applications, some of which are illustrated later in this article.

B.P. Jones, Statistics for the Corrosionist, *Corrosion: Fundamentals, Testing, and Protection*, Vol 13A, *ASM Handbook*, ASM International, 2003, p 972–979

Statistics for the Corrosionist

Barnie P. Jones, Oregon Department of Transportation

Measurement

Levels of Measurement. Measurement can be described as the process of assigning numbers to observations. The level of measurement is a critically important consideration in the selection of a statistical test. Scales of measurement can be classified according to a four-category typology developed by S.S. Stevens (Ref 1). The categories are nominal, ordinal, interval, and ratio.
A nominal scale consists of nothing more than a naming convention, or the assignment of a label to an attribute. Examples might be the numbers on ball players' uniforms or experimental test specimens made from copper, aluminum, steel, and glass.

An ordinal scale, in contrast to a nominal scale, allows ordering of values in the scale but nothing else. An example of an ordinal scale is Moh's hardness scale, used in rock and mineral classification and identification (Ref 2).
An interval scale has all the properties of an ordinal scale but has the additional characteristic that scale integer values are separated by equal intervals (Ref 3). The condition that differentiates an interval scale from higher levels of measurement is that an interval scale has no meaningful or absolute zero point. Fahrenheit and Celsius temperature scales are examples of interval scales.
A ratio scale has all the attributes of an interval scale plus a meaningful zero point. Examples include absolute barometric pressure or Kelvin temperature.
Using Levels of Measurement in Test Selection. The choice of a statistical test depends heavily on the level of measurement for the variables involved in the test. In general, the test cannot involve computational operations that are not applicable for the scale type. For example, one cannot find the median (or a mean) for a nominal scale, because the scale values have no order. Consequently, only the mode (most frequent scale value) can be used to characterize central tendency of a nominal scale. Tests and other measures designed for nominal and ordinal scales are classified as nonparametric statistics. More generally, nonparametric statistics require fewer assumptions about level of measurement and/or about parameters of the underlying population (Ref 3).
Table 2 lists the correspondence between the level of measurement and the choice of a statistical test or other measure.

Table 2 Characteristics of the different levels of measurement scales

Levels-of-measurement scale	Descriptive statistics	Graphs	One- and two-variable statistical tests	Multivariate statistical tests
Nominal	Mode, frequency	Pie chart, bar graph	Binomial test, chi square	Log-linear models
Ordinal	Median, quartiles, percentiles	Pie chart, bar graph	Various non-parametric tests	Logistic regression, multinomial logit models
Interval	Mean, standard deviation, standard error	Histogram, scatter plot, line chart	Difference of means test, simple regression	Multiple regression
Ratio	Geometric mean, coefficient of variation	Histogram, scatter plot, line chart	Difference of means test, simple regression	Multiple regression
Mixed nominal and interval	…	…	One-way analysis of variance	N-way analysis of variance

Source: Adapted from Ref 3
Discrete and Continuous Variables. A second, related measurement issue involves whether a variable is discrete or continuous. A discrete variable can take only a finite number of values, but a continuous variable can take an infinite number of values (Ref 3). It is difficult, if not impossible, to come up with an example of a continuous, nominal scale. Ordinal, interval, and ratio scales may or may not be continuous.
Variables that are based on counts are discrete. Costs are technically discrete, because currency systems have a minimum unit, for example, the penny, that cannot be subdivided. From a practical standpoint, whenever a variable can take a large number of values relative to its range, it may be treated as continuous. However, when a variable has a relatively small number of possible values, special considerations apply in the selection of appropriate statistical techniques. Most generally, discrete variables can be addressed with nonparametric tests, and there are a number of other, more powerful options, depending on specific circumstances. Apart from nominal scales, this is most likely to be an issue for the statistical analysis of counts of rare events. An example might be traffic accidents, tabulated over a one-year period, at 100 residential street intersections.

References cited in this section

1. S.S. Stevens, On the Theory of Scales of Measurement, *Science,* Vol 103, 1946, p 677–680

2. W.D. Callister, *Materials Science and Engineering: An Introduction,* 3rd ed., John Wiley and Sons, Inc., 1994, p 132

3. S. Siegel, *Nonparametric Statistics for the Behavioral Sciences,* McGraw-Hill Book Company, 1956, p 25–26, 30–31, 195–239

B.P. Jones, Statistics for the Corrosionist, *Corrosion: Fundamentals, Testing, and Protection*, Vol 13A, *ASM Handbook*, ASM International, 2003, p 972–979

Statistics for the Corrosionist

Barnie P. Jones, Oregon Department of Transportation

Statistical Hypothesis Testing

The basis of a statistical test is that one can make a prediction about the range of possible outcomes of an experiment or other set of formal observations based on what is known or can readily be assumed about random events. One can then use that prediction to make a judgement about a specific outcome of an investigation, that is, whether or not the outcome occurred by chance.

Probability, Sampling Distributions, and the Normal Curve. Imagine a coin-tossing exercise in which a coin is tossed ten times, and the results (number of heads versus tails) are tallied. The probability of any particular outcome is given in Fig. 1. Note that the distribution in Fig. 1 could be approximated by repeating the coin-toss exercise a large number of times, and that the larger the number of repetitions of the exercise, the better the approximation. Figure 1 is an example of a *sampling distribution.* A sampling distribution associates probabilities with the possible outcomes of an experiment. In this case, the distribution is tailored to an experiment involving 10 trials and makes the assumption that the probability (P) of heads or tails is equal:

$$P(\text{heads}) = P(\text{tails}) = 0.5 \quad \text{(Eq 10)}$$

On an informal basis, one can make a judgement about any one coin-tossing experiment, along the lines that 4, 5, or 6 heads should occur approximately two-thirds of the time and are not at all unusual. However, 0, 1, 9, or 10 heads are only expected in 2.2% of such experiments and should be regarded as unusual, if not suspicious.

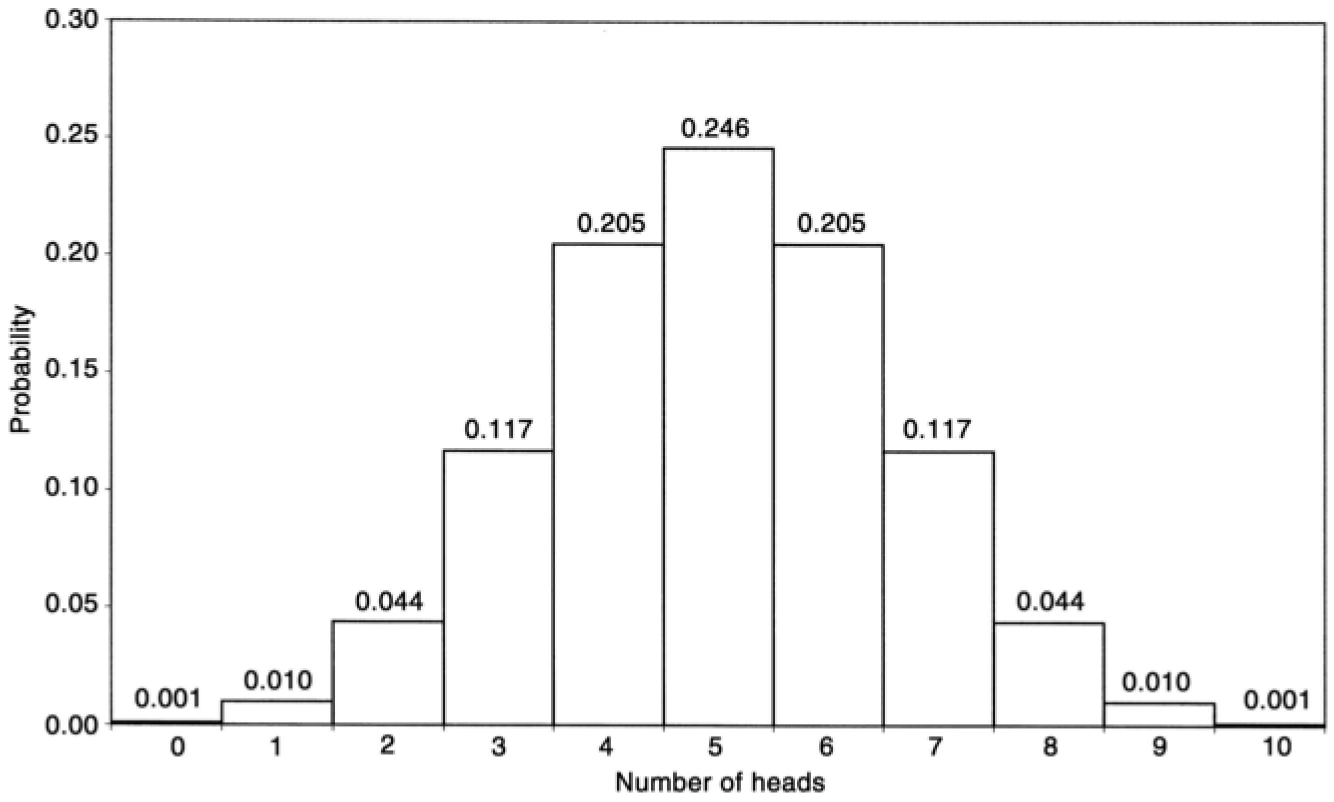

Fig. 1 Binomial distribution from a hypothetical coin-tossing experiment

Also, note that the shape of the distribution in Fig. 1 is beginning to approximate a bell-shaped curve and that if the coin-tossing exercise had been carried out in sets of say, 50 instead of 10, the resulting distribution would provide a crude, discrete approximation of the normal curve. The normal curve has a number of important properties. It is continuous, bell-shaped, and symmetrical. In its standard form, it has a mean $\mu = 0$ and standard deviation $\sigma = 1$. The tails of the curve approach but never reach zero. A normal curve can be generated with the following expression:

$$Y = \frac{1}{s\sqrt{2\pi}} e^{-(x-\bar{x})^2/2s^2} \quad \text{(Eq 11)}$$

where Y is the height of the curve for any x. Another important attribute of the normal curve is that the area under it is unity. Also, 68.26% of the area falls within one standard deviation on both sides of the mean, and 95.46% within two standard deviations. Any statistics text includes a table of areas under the normal curve, for standard scores (see Eq 9).

Most statistical tests that are designed for variables measured using an interval and ratio scale use the normal distribution as a sampling distribution and consequently require an assumption that a sampling distribution generated from that universe would be normally distributed. This is rarely an issue for large samples, but it is an important assumption required for small samples.

Specifying Research and Null Hypotheses. From the previous discussion of coin-tossing experiments, it should be clear that some outcomes are more probable than others and that judgments can be made regarding most outcomes. Figure 1 suggests that an outcome of zero (or ten) heads in ten trials does not occur very often. If an outcome of ten heads were to occur, one might be inclined to question these assumptions about the experiment. In generating the sampling distribution in Fig. 1, it was assumed that the probably of heads or tails was 0.5 (Eq 10). However, there are potentially a number of explanations for an outcome that appears to defy probability. The coin itself could be biased. The person tossing the coin could be influencing the outcome, intentionally or inadvertently. There could be an unknown or unidentified external agent influencing the outcome.

In the context of a scientific experiment, the experimenter works with a research (alternative) hypothesis; for example, experimental coating *A* has a longer effective life than control coating *B.* However, in the design of an experiment, a variety of assumptions are required. For example, among other things, it is necessary to assume that materials used to prepare test samples are well within specifications for coatings *A* and *B*, that application of the coatings is comparable, and that environmental conditions affecting the test samples are truly equivalent.

The fact that an outcome fails to conform to expectations about probability does not tell us why the outcome occurred. Because of this, statistical inference is set up to test a ***null hypothesis***, conventionally designated as H_0. In this example, an appropriate null hypothesis might be $\mu_A = \mu_B$, or that the mean effective life of coating *A* is no different from the mean effective life of coating *B*. The statistical test either rejects or fails to reject the null hypothesis. In this context, if the null hypothesis is not rejected, no conclusions are supported. The mean effective life of coating *A* could equal that of *B*, the sampling may not have been representative, or the test procedure may not have been sensitive to the difference. If the null hypothesis is rejected, the research (alternative) hypothesis remains and may be thought of as becoming more tenable but is not "proven." This is appropriate, because a statistical test requires more than one assumption, including the null hypothesis, and it is never certain which of the assumptions is incorrect. The null hypothesis could have been rejected, because the research hypothesis was true, but it could also have been due to a failure in the experimental setup, measurement error, or a variety of other causes.
Defining a Critical Region. Once a null hypothesis is stated, it is necessary to define a set of outcomes that entail rejection, called the critical region. Returning again to Fig. 1, one could arbitrarily define 0, 1, 9, and 10 heads to constitute the critical region, or the set of outcomes that would result in rejection of the null hypothesis, *P*(heads) = *P*(tails) = 0.5. The probability of rejecting the null hypothesis, if it is true, is 0.001 + 0.010 + 0.001 + 0.010 = 0.022. Fortunately, it is rarely necessary to generate a sampling distribution as in Fig. 1. A variety of applicable sampling distributions have been derived and are available, in tabular form, in the appendix of most statistics books.
Rejecting a true null hypothesis is known as a type I error. The probability of a type I error is α, 0.022 in the example just given, and is determined by the investigator through selection of the critical region. However, there is also a type II error, failing to reject a false null hypothesis, with a type II error rate designated by β. The double negative of the type II error, involved in the notion of failure to reject a false null hypothesis, refers to the power of the test. Table 3 is provided to help minimize potential confusion.

Table 3 Type I and type II errors in defining a critical region

Decision regarding H_0	H_0 is:	
	True	**False**
Reject H_0	Type I error α	Correct decision
Fail to reject H_0	Correct decision	Type II error β

Source: Adapted from Ref 4
A number of additional factors can influence β, but, in general, probabilities of α and β are inversely related. This is important for two reasons. First, an understanding of the risk of a type I error is essential in a number of important decisions leading up to a statistical test, including determining the required number of observations and selecting a test statistic. For any given α, there are a number of ways to reduce β. One is to increase the number of observations. Some statistical tests provide a smaller probability of a β error for a given α level. This test attribute is referred to as the *power* of a statistical test. More specifically, the power of a test is defined as 1 - β. In most cases, tests designed for the higher levels of measurement involving interval or ratio scales are more powerful than tests designed for nominal or ordinal scales. Assumptions also influence β. For example, in many cases, the ability to confidently predict direction relative to a central measure can be used to reduce β and gain statistical power by using what is referred to as a *directional,* or *one-tailed,* test.
A second major consideration comes into play primarily in applied research. There is an entrenched convention in basic research to use a critical region of α = 0.05 or smaller. In the context of basic research, smaller generally is better, to the extent that embracing false results is to be avoided at almost any cost. However, in applied science, both types of errors entail practical consequences. Costs of an error in one direction may greatly exceed those of an error in the other. For example, additional reinforcing steel in a reinforced concrete beam might increase construction cost by only 2% and prevent both premature and catastrophic structural failures. In this context, the two kinds of errors usually deserve more balanced consideration, and this may entail consideration of a larger α value. It should also be noted that the practice of pre- selecting any particular α level is falling out of favor, in preference for more straight-forward reporting of the probability (*p* value) associated with the test result and allowing users of the research to draw their own conclusions.
The Central Limit Theorem. Even though many known sampling distributions, including the normal, Student's *t*, χ^2, and *F* distributions, have been derived and tabulated, it is of some value to understand more about them.

Any sampling distribution could, in theory, be approximated empirically. To do so, one would simply replicate computation of the same statistic over a large number of samples of a given size. The resulting empirical distribution of the statistic converges with the sampling distribution as the number of replications approaches infinity. However, there are easier ways. For a sampling distribution of the mean, the central limit theorem states:

If repeated random samples of size *n* are drawn from any population having a mean μ and a variance σ^2, then as *n* becomes large, the sampling distribution of sample means approaches normality, with mean of μ and variance σ^2/N.

In other words, the "mean of means" converges with the universal mean. Second, the variance of the sampling distribution for the mean is given as σ^2/N. From this, it follows that the standard deviation of the sampling distribution of the mean is $\sigma/\sqrt{N}$, or the standard error (see Eq 7). A further, important implication of the central limit theorem is that whenever $N > 30$, the sampling distribution of the mean often approximates a normal distribution, even when the sampling universe or underlying population does not (Ref 5).

References cited in this section

4. W. Mendenhall and J.E. Reinmuth, *Statistics for Management and Economics,* Duxbury Press, 1974, p 192

5. N.T. Kottegoda and R. Rosso, *Statistics, Probability, and Reliability for Civil and Environmental Engineers,* McGraw-Hill Book Company, 1997, p 15–16, 222, 245–257

B.P. Jones, Statistics for the Corrosionist, *Corrosion: Fundamentals, Testing, and Protection*, Vol 13A, *ASM Handbook,* ASM International, 2003, p 972–979

Statistics for the Corrosionist

Barnie P. Jones, Oregon Department of Transportation

Simple Statistical Tests

A Simple Test Based on the Normal Curve. One commonly used test is based on the central limit theorem. It is called Student's *t*, Student being a pseudonym of its inventor, W.S. Gossett (Ref 6). Consider the following example:

Specifications for an industrial coating call for a minimum application thickness of 20 mil and an average application thickness of 30 mil. A coated surface is tested for coating thickness at 60 random locations over the surface. The coating exceeds the minimum 20 mil in every case. However, it remains to be determined whether the average thickness is 30 mil. Note that, in this case, direction is irrelevant, and the coating fails whether thicker or thinner than the specified 30 mils.

There are five key steps in carrying out a statistical test. These are (1) making assumptions, (2) selecting a test statistic, (3) defining the critical region, (4) computing the test statistic, and (5) making a decision.

Assumptions. There are many assumptions required in setting up this kind of test. However, among the key assumptions is that the sample of 60 locations is random. Also, if *n* were less than 30, it would be necessary to assume that *X*, the coating thickness over the surface, is normally distributed. These assumptions, along with a variety of other fairly obvious assumptions that the situation is as it has been described, constitute what are sometimes referred to as *model* assumptions.

A second category of assumptions are the *hypotheses.* In this case, the research hypothesis could be that the average application thickness is not 30 mils. The null hypothesis can be stated as $\mu = 30$. Note that while all assumptions present the same threat to validity of the results, only the null hypothesis is tested.

For samples greater than 30, it is not as critical to make the model assumption that a variable is normally distributed because the central limit theorem implies that, for large samples, the sampling distribution of the mean from a nonnormal universe is often normal.

Selecting a Test Statistic. The test statistic is Student's *t*:

$$t = \frac{\bar{x} - \mu}{s/\sqrt{n-1}} \qquad \text{(Eq 12)}$$

where $\mu = 30$, $n = 60$, and $\bar{x}$ and s can be computed directly from the sample data using Eq 1 and 3. At least two considerations apply to the selection of this particular test statistic. First, coating thickness is measured using a ratio scale, which means that a statistic based on the mean is applicable. Second, the sample is relatively small, and Student's *t* is designed for small samples.

Defining the Critical Region. The sampling distribution for Student's *t* depends on α and on degrees of freedom (n - 1). The limit of the critical region for Student's *t* at $\alpha = 0.05$ and 59 degrees of freedom for a symmetric or two- tailed test is $t > 2.000$ or $t < -2.000$. A two- tailed test was specified, because the specification is nondirectional, that is, the coating can fail to meet the specification if the average thickness is either too thick or too thin.

The sampling distribution for Student's *t* is actually a family of distributions that resemble the normal distribution but are somewhat flatter, the relative flatness depending on the degrees of freedom. For samples exceeding $n = 120$, the distribution for *t* becomes normal. Thus, for small or large sample applications, this statistic is generally referred to as the *t* test.

Computing the Test Statistic. To compute the test statistic, first a sample mean ($\bar{x}$) of 29.5 mil and a standard deviation (s) of 1.9 mil must be computed. The test statistic $t = (29.5 - 30)/ [(1.9)/\sqrt{59}] = -2.021$.

Making a Decision. Because -2.021 < -2.000, the decision is to reject the null hypothesis, supporting the conclusion that the work fails to meet the specification. Note, however, that if the preselected α level had been 0.01, the critical region would have been $t > 2.660$ or $t < -2.660$, and the null hypothesis would not have been rejected. The p value associated with $t > 2.021$ is 0.046, only marginally less than 0.05. This illustrates the advantage of reporting *p* values in contrast to the practice of testing against pre-selected α criteria.

Other Issues Related to Student's *t*. Note the similarity between the definition of the standard error in Eq 7 and the denominator of Eq 12 defining Student's *t*. Note that using the estimate s instead of the parameter σ to estimate the standard error requires the quantity n - 1 to replace N in the denominator. A brief, clear explanation for this adjustment can be found in Ref 5. A longer but more intuitively appealing explanation can be obtained from Ref 7.

Two-Sample Tests. Note that in the preceding illustrations, μ is given or assumed. Consider a different situation, in which a series of test specimens is compared to a series of comparable control specimens. This simple experiment suggests the research hypothesis $\mu_1 \neq \mu_2$ and the null hypothesis, H_0, $\mu_1 = \mu_2$. This is referred to as a two-sample test. The statistical inference process is parallel to that described previously, except that instead of having one set of sample values and one assumed parameter, there are two sets of sample values. In general, the test seeks to determine whether the two sets of specimens could have been drawn randomly from the same universe. The test statistic, based on the difference between the samples, is:

$$t = \frac{(\bar{x}_1 - \bar{x}_2) - (\mu_1 - \mu_2)}{\sigma_{\bar{x}_1 - \bar{x}_2}} = \frac{\bar{x}_1 - \bar{x}_2}{\sigma_{\bar{x}_1 - \bar{x}_2}} \qquad \text{(Eq 13)}$$

The simplification is possible, because the null hypothesis assumes $\mu_1 = \mu_2$. Note that what is being implied by this expression is not a sampling distribution of means but a sampling distribution of differences. The denominator for the expression in Eq 13 represents the standard error of that sampling distribution.

Computing the test statistic is straightforward, except that there are two ways to estimate the standard error: a pooled variance and a separate variance estimate. If it can be assumed that $\sigma_1 = \sigma_2$, then the pooled variance estimate can be obtained as:

$$\sigma_{\bar{x}_1 - \bar{x}_2} = \sqrt{\frac{n_1 s_1^2 + n_2 s_2^2}{n_1 + n_2 - 2}} \sqrt{\frac{n_1 + n_2}{n_1 n_2}} \qquad \text{(Eq 14)}$$

However, if it is assumed that $\sigma_1 \neq \sigma_2$, then the separate variance estimate can be obtained as:

$$\sigma_{\bar{x}_1-\bar{x}_2} = \sqrt{\frac{s_1^2}{n_1 - 1} + \frac{s_2^2}{n_2 - 1}} \quad \text{(Eq 15)}$$

It should be noted that the test using the separate variance estimate is slightly less efficient than the test using the pooled variance estimate. It also should be noted that in cases where both samples are approximately equal, degrees of freedom = $n_1 + n_2 - 2$, but for unequal samples, there is a complex expression that is used to find degrees of freedom (Ref 7).

References cited in this section

5. N.T. Kottegoda and R. Rosso, *Statistics, Probability, and Reliability for Civil and Environmental Engineers,* McGraw-Hill Book Company, 1997, p 15–16, 222, 245–257

6. D. Salsburg, *The Lady Tasting Tea: How Statistics Revolutionized Science in the Twentieth Century,* W.H. Freeman and Company, 2001, p 25–32

7. H.M. Blalock, *Social Statistics,* revised 2nd ed., McGraw-Hill Book Company, 1979, p 205–206, 208–218, 231, 299–325, 340, 348, 352–369, 388, 398, 554–551

B.P. Jones, Statistics for the Corrosionist, *Corrosion: Fundamentals, Testing, and Protection*, Vol 13A, *ASM Handbook*, ASM International, 2003, p 972–979

Statistics for the Corrosionist

Barnie P. Jones, Oregon Department of Transportation

Confidence Limits

Sometimes, the goal of a statistical analysis is not to test a hypothesis but to evaluate an estimate by establishing upper and lower bounds. These bounds are called confidence limits or confidence intervals. The process of establishing confidence limits shares much with statistical hypothesis testing, but there are some key logical and procedural differences. Consider an example. Borings from a reinforced concrete structure are analyzed for chloride concentrations at different depths. The researcher is comfortable assuming that true chloride penetration is uniform at different surface coordinates over the zone of interest (at least for the sake of this illustration), but that there is measurement error in the data collection procedure. Consequently, borings are taken at 26 random locations. Specimens from each boring are captured at 6 mm (0.236 in.) increments to a depth of 100 mm (3.94 in.). The purpose of this investigation is to assess corrosion risk to the structure. More specifically, the goal is to determine whether chloride concentration is high enough to initiate corrosion at a 51 mm (2 in.) depth, the minimum cover for the reinforcing steel. In the sample, the average ($\bar{x}$) chloride concentration at a depth of 48 to 54 mm (1.89 to 2.13 in.) is 0.016%, and the standard deviation is 0.011%.

The first step in establishing a confidence interval is determining a confidence *level,* which is analogous to selection of a critical region in statistical hypothesis testing—that is, the risk one is willing to take of making an error. For example, a 95% confidence level corresponds to a critical region of $\alpha = 0.05$. In other words, with a 95% confidence level, the confidence limit is expected to contain the parameter in 95 and not to include it in the remaining 5 out of 100 samples.

Given a confidence level of 95%, the researcher can proceed to construct a confidence interval around $\bar{x}$. To do so, one works backward, starting with a table of areas under the normal curve, or in this case, because $n = 26$, from a table for the distribution of *t.* For 95% confidence (the same as $\alpha = 0.05$ for a two-tailed test) and $n - 1$ or 25 degrees of freedom, the table shows a value of 2.060. The confidence interval can now be constructed as:

$$\bar{x} \pm 2.060 \frac{s}{\sqrt{n-1}} = 0.016 \pm 2.060 \frac{0.011}{\sqrt{25}} = 0.016 \pm 0.00453 \quad \text{(Eq 16)}$$

In other words, at a 95% confidence level, the true chloride concentration at a 48 to 54 mm (1.89 to 2.13 in.) depth is believed to be between 0.0114 and 0.0205%. Assuming the corrosion threshold is 0.02%, these results suggest that the structure could be at immediate risk of corrosion damage. For a more complete discussion of confidence intervals, see Ref 5 or 7.

References cited in this section

5. N.T. Kottegoda and R. Rosso, *Statistics, Probability, and Reliability for Civil and Environmental Engineers,* McGraw-Hill Book Company, 1997, p 15–16, 222, 245–257

7. H.M. Blalock, *Social Statistics,* revised 2nd ed., McGraw-Hill Book Company, 1979, p 205–206, 208–218, 231, 299–325, 340, 348, 352–369, 388, 398, 554–551

B.P. Jones, Statistics for the Corrosionist, *Corrosion: Fundamentals, Testing, and Protection*, Vol 13A, *ASM Handbook*, ASM International, 2003, p 972–979

Statistics for the Corrosionist

Barnie P. Jones, Oregon Department of Transportation

Sampling Issues

In all of the applications of statistical inference discussed so far, there has been an underlying assumption that observations were selected randomly from a universe. In the interests of efficiency in presentation, this assumption has not been belabored until now. In plain language, the basis of statistical inference is that if chance alone determines the selection of observations, then chance alone also determines observed differences in the attributes of those observations. In practice, there are a number of ways to obtain what is known as a probability sample. The condition that defines a probability sample is that every element in a probability sample has a known probability of selection. For a discussion of the various approaches to probability sampling, see Ref 7.

Sampling and Randomization. Sometimes the goal of sampling is to make an inference from a sample to the universe from which the sample was drawn. Probably, the most familiar example is election polling. However, the general notion of random sampling also applies to random assignment in the context of an experiment. The former relates to establishing *external* validity for an inference from a sample to a larger universe or population. The latter relates to *internal* validity by establishing the basis for the inference that treatment and control specimens in an experiment are initially equivalent. Randomization in the design of experiments may have limited applicability in corrosion science. Randomization is most likely to be of value in situations where relatively large numbers of specimens can be included in the experiment, and/or there is variability in the specimens and relative uncertainty about variables that could affect the outcome of the experiment. Randomization is particularly effective in controlling unidentified or unknown confounding factors.

Determining Sample Size. The methods subsequently described focus on a sample drawn from a finite population but can readily be adapted to the context of randomization for an experiment. The determination of sample size is analogous to establishing a confidence interval in reverse. Consider Eq 17 and 18:

$$B = Z \frac{\sigma}{\sqrt{n}} \quad \text{(Eq 17)}$$

$$n = \left(Z \frac{\sigma}{B} \right)^2 = Z \frac{\sigma^2}{B^2} \quad \text{(Eq 18)}$$

where *B* represents the bound on the error, and *Z* represents the standard score on the normal curve associated with the desired level of confidence. In election polling and other surveys, *B* is usually referred to as the margin for error. Note that given *B*, one can solve for *n*, if a suitable estimate can be found for the standard deviation (σ). There are a number of strategies to obtain a value for σ. One is to look for a comparable data set from another study. A second is to conduct a small pilot study. A third is to substitute a worst case or make a bald assumption. The point here is that, in order to make a precise estimate of sample size, it is desirable to know something about the distribution of the variable in question.

To summarize, three pieces of information are needed to estimate sample size. The first is a tolerable error or an analogous goal for precision. The second is a confidence level to represent the acceptable risk of being wrong, typically 90, 95, or 99%. The third is an estimate for the standard deviation of the variable in question.

Sampling from a Finite Universe. Special sampling considerations apply whenever a sample is being drawn from a finite universe, and the sample represents a nontrivial fraction of the whole universe. There is, in fact, a correction that applies to variance estimates based on finite populations, such that:

$$\mathrm{Var}(\bar{x}) = \frac{N-n}{N} \times \frac{s^2}{n} \quad \text{(Eq 19)}$$

The quantity (*N* - *n*)/*N* is called the finite population correction (fpc). It should be obvious that the fpc becomes increasingly important as *n*/*N* increases. The fpc can be ignored whenever *n*/*N* does not exceed 5% (Ref 8).

Another important implication that can be drawn from Eq 19 is that whenever a sample is drawn from a large universe, the absolute sample size is primarily what determines error, while the size of the universe is irrelevant for practical purposes. This result may be counterintuitive for many people, but it can easily be verified that, other things being equal, a sample of 500 has virtually the same confidence interval when drawn from a universe of 100,000,000 as when drawn from a universe of 50,000.

References cited in this section

7. H.M. Blalock, *Social Statistics*, revised 2nd ed., McGraw-Hill Book Company, 1979, p 205–206, 208–218, 231, 299–325, 340, 348, 352–369, 388, 398, 554–551

8. W.G. Cochran, *Sampling Techniques,* 3rd ed., John Wiley and Sons, 1977, p 24–25

B.P. Jones, Statistics for the Corrosionist, *Corrosion: Fundamentals, Testing, and Protection*, Vol 13A*, ASM Handbook*, ASM International, 2003, p 972–979

Statistics for the Corrosionist

Barnie P. Jones, Oregon Department of Transportation

Analysis of Variance

Analysis of variance is a specific technique developed in the early 1920s by the British statistician R.A. Fischer for application to agricultural experiments. The simplest case of analysis of variance involves one dependent variable, measured as an interval or ratio scale, and one independent variable, measured as a nominal or ordinal scale and having three or more categories or levels. In cases of an independent variable with two categories, analysis of variance reduces to a two-sample *t* test (see Eq 13).

Analysis of variance is based on the idea that the variance of a dependent variable can be partitioned into different components. In the simple case of one independent variable, these components are within and between

groups. More specifically, from Eq 3 and multiplying both sides by n, a new quantity, ns^2, called the sum of squares, is obtained:

$$ns^2 = \sum_{i=1}^{n} (X_i - \bar{x})^2 \qquad \text{(Eq 20)}$$

In order to proceed further, it is necessary to introduce some refinements in notation. Let X_{ij} represent the "ith" score in the "jth" category or subgroup. Subscript j ranges from 1 to k, and k is the number of categories of the independent variable. Subscript i ranges from 1 to n_1 within category 1, from 1 to n_2 in category 2, and from 1 to n_k for category k, where n_1, n_2, and n_k represent the number of cases within categories. Conditional, or within-category, means $\bar{X}_{\cdot 1}$, $\bar{X}_{\cdot 2}$, and $\bar{X}_{\cdot k}$ and the overall, or "grand," mean $\bar{X}_{\cdot\cdot}$ can also be described. Finally, to differentiate summation within and between categories, symbols $\sum_i$ and $\sum_j$ are used to represent summation over i and j, respectively. Partitioning of variance is illustrated in Eq 21:

$$\sum_i \sum_j (X_{ij} - \bar{X}_{\cdot\cdot})^2 = \sum_i \sum_j (X_{ij} - \bar{X}_{\cdot j})^2 + \sum_i \sum_j (\bar{X}_{\cdot j} - \bar{X}_{\cdot\cdot})^2 \qquad \text{(Eq 21)}$$

or the *total* sum of squares (TSS) equals the *within-groups,* or *residual,* sum of squares (WSS) plus the *between-groups* sum of squares (BSS) (Ref 7). Note further that the components can be rewritten from Eq 20 as:

$$\text{TSS:} \quad \sum_i \sum_j (X_{ij} - \bar{X}_{\cdot\cdot})^2 = ns^2 \qquad \text{(Eq 22)}$$

$$\text{WSS:} \quad \sum_i \sum_j (X_{ij} - \bar{X}_{\cdot j})^2 = n_1 s_1^2 + n_2 s_2^2 + \ldots . n_k s_k^2 \qquad \text{(Eq 23)}$$

$$\text{BSS:} \quad \sum_i \sum_j (\bar{X}_{\cdot j} - \bar{X}_{\cdot\cdot})^2 = ns^2 - (n_1 s_1^2 + n_2 s_2^2 + \ldots . n_k s_k^2) \qquad \text{(Eq 24)}$$

Note that BSS is found by subtracting WSS from TSS.

Consider Eq 24. If all the $\bar{X}_{\cdot j}$ conditional means equal the grand mean $\bar{X}_{\cdot\cdot}$, then BSS equals 0, and WSS equals TSS. Furthermore, the more the $\bar{X}_{\cdot j}$ differ, the larger the BSS and the smaller the WSS. Analysis of variance uses the ratio of BSS to WSS, adjusted for degrees of freedom, to compute a test statistic based on the F distribution:

$$F = \frac{\text{BSS}/(k-1)}{\text{WSS}/(n-k)} \qquad \text{(Eq 25)}$$

Example: Analysis of Variance in Coating Bond Strength Tests. A test bridge deck is treated with three different coatings, and pull tests are conducted to measure bond strength, with 20 tests completed for each coating. The critical region is set at the customary $\alpha = 0.05$. Analysis of variance is based on the F distribution. The distribution of F depends on degrees of freedom for both within- and between-groups estimates, and, in the case of $(k - 1) = 1$, $F = t^2$ and t can, in fact, be regarded as a special case of F (Ref 7). Consequently, tables constructed to find the critical region for F require three dimensions: one for $n - k$ degrees of freedom, one for $k - 1$ degrees of freedom, and one for α. Consequently, these tables are generally printed with each of several customary levels of α on a separate page. The lower limit of the critical region for F with $(n - k) = 57$, $(k - 1) = 2$, and $\alpha = 0.05$ is approximately 3.17.

Results show an overall average bond of $\bar{X}_{\cdot\cdot} = 203.5$ psi. However, for coating 1, the average is $\bar{X}_{\cdot 1} = 204.5$ psi, while for coatings 2 and 3, bond strengths are $\bar{X}_{\cdot 2} = 228.7$ psi and $\bar{X}_{\cdot 3} = 178.3$ psi, respectively. One approach to the analysis of these results would be to deal with the samples in pairs and to run three separate t tests on all possible differences of means: $\mu_1 = \mu_2$, $\mu_2 = \mu_3$, and $\mu_1 = \mu_3$. Analysis of variance allows tests of the

form H_0: $\mu_1 = \mu_2 = \mu_3 = \ldots \mu_k$. The research hypothesis is that at least one mean is different. Analysis of variance, by simultaneously comparing all three means, is more efficient, because it uses all 60 observations. Also, and more important, running three separate *t* tests inflates the probability of rejecting at least one of three null hypotheses, just as drawing an ace from a deck of cards is more likely in three attempts than in one. In fact, the probability of rejecting one of three hypotheses at $\alpha = 0.05$ based on chance alone is 0.05 + 0.05 + 0.05 = 0.15.

Table 4 summarizes the results of the one-way analysis of variance. Note that the quantities labeled "Mean square" are obtained by dividing the sum of squares by the degrees of freedom and therefore may be viewed as variance estimates. From Eq 25, the *F* statistic is the ratio of the between-groups estimate to the within- groups estimate, which, in this case, gives a calculated *F* of 4.1048, which, being greater than 3.17, falls within the critical region. In other words, results support rejection of the null hypothesis and the conclusion that bond strengths of the three coatings are not equivalent. If *F* had fallen outside the critical region, it would have been untenable to infer any difference in bond strength among the three coatings.

Table 4 One-way analysis of variance of bond strength for three coatings

	Mean ($\bar{X}$)	N	Variance (S^2)
Coating 1	204.5	20	3000.89
Coating 2	228.7	20	2124.43
Coating 3	178.3	20	4162.43
Total	203.5	60	3421.76

Partition of variance sum of squares	Sum of squares	Degrees of freedom	Mean square	F
Between-groups (BSS)	25,416.3	2	12,708.15	
Within-groups (WSS)	176,467.3	57	3095.92	4.1048
Total (TSS)	201,883.6	59		

This discussion and example of analysis of variance deals with the simplest possible case. Analysis of variance can incorporate more than one categorical independent variable, and there exists a wide variety of specialized applications of analysis of variance to specific, complex experimental designs. Reference 7 provides a clear and accessible discussion of the extension of analysis of variance to two independent variables. More definitive and complete sources on analysis of variance are provided by Ref 9 and 10.

References cited in this section

7. H.M. Blalock, *Social Statistics*, revised 2nd ed., McGraw-Hill Book Company, 1979, p 205–206, 208–218, 231, 299–325, 340, 348, 352–369, 388, 398, 554–551

9. H. Scheffe, *The Analysis of Variance,* John Wiley and Sons, Inc., 1959

10. J. Neter, M. Kutner, C. Nachtsheim, and W. Wasserman, *Applied Linear Statistical Models,* 4th ed., WCB/McGraw Hill, Inc., 1996, p 296–315, 531–566, 663–1041

B.P. Jones, Statistics for the Corrosionist, *Corrosion: Fundamentals, Testing, and Protection*, Vol 13A*, ASM Handbook,* ASM International, 2003, p 972–979

Statistics for the Corrosionist

Barnie P. Jones, Oregon Department of Transportation

Correlation and Regression

Pearson's *r*. Previously in this article, consideration was given to statistical hypothesis testing. There is another class of statistical measures called measures of association. Correlations or measures of association measure dependence between two variables, or the ability to predict one variable from another. There are, in fact, many such measures designed for nominal and ordinal scales, and many of these are described in Ref 3 and 7. However, one particular measure of association, the Pearson product-moment coefficient, or Pearson's *r* (*r* represents the estimate; the symbol for the parameter is ρ), is probably the most widely recognized and used measure for two-interval or ratio scales. To begin a discussion of correlation, consider the expression for *covariance* in Eq 26:

$$\sigma_{x,y} = \frac{\sum_{i=1}^{n}(X_i - \mu_x)(Y_i - \mu_y)}{N} \quad \text{(Eq 26)}$$

Note the similarity to Eq 3 and 4 for the variance, and that, while the variance is necessarily a positive quantity, the covariance can be either positive or negative. Also note that the covariance reaches a maximum (positive or negative) when *X* and *Y* are perfectly correlated, and that it approaches zero to the extent that there is no association between *X* and *Y*. However, covariance is of more theoretical than practical interest as a measure of association. However, a number of other important and useful measures are based on covariance. One of these is Pearson's *r*:

$$r = \frac{\sum_{i=1}^{n}(X_i - \bar{X})(Y_i - \bar{Y}) \Big/ n}{\sqrt{\left[\sum_{i=1}^{n}(X_i - \bar{X})^2 \Big/ n\right]\left[\sum_{i=1}^{n}(Y_i - \bar{Y})^2 \Big/ n\right]}} = \frac{\sum_{i=1}^{n}(X_i - \bar{X})(Y_i - \bar{Y})}{\sqrt{\left[\sum_{i=1}^{n}(X_i - \bar{X})^2\right]\left[\sum_{i=1}^{n}(Y_i - \bar{Y})^2\right]}} \quad \text{(Eq 27)}$$

In other words, Pearson's *r* is the ratio of the covariance of *X* and *Y* to the product of the standard deviations of *X* and *Y* (Ref 7). Unlike the covariance, *r* has a range of -1 to +1.

Linear Regression Analysis. Figure 2 presents a scatter diagram. The variables in the scatter diagram are reflectivity measurements taken on reflective highway markers when new (*X*) and after weathering in service for one year (*Y*). As should be evident from the pattern, there is a fairly strong positive correlation of *r* = 0.900. In other words, the effects of weathering on reflectivity appear to be somewhat predictable. One expedient way to make that prediction is with linear regression analysis. Linear regression is based on the linear equation:

$$Y_i = \alpha + \beta X_i + \varepsilon_i \quad \text{(Eq 28)}$$

where β is the slope of the line, α represents the *Y*-intercept, or the value of *Y* when *X* = 0, and ε_i represents an error or disturbance term. The regression line is fit to the data according to a specific criterion known as least squares. The regression line that minimizes the squared deviations of the observed values of *Y* from the values predicted for *Y* by the regression line satisfies the criterion of least squares (Ref 11). As it turns out, this criterion is met if *a* and *b* are obtained as in Eq 29 and 30:

$$b = \frac{\sum_{i=1}^{n} (X_i - \overline{X})(Y_i - \overline{Y})}{\sum_{i=1}^{n} (X_i - \overline{X})^2} \quad \text{(Eq 29)}$$

$$a = \overline{Y} - b\overline{X} \quad \text{(Eq 30)}$$

where ***a*** and ***b*** are estimates for the parameters α and β. Regression analysis can be extended to cases involving more than one independent variable. There are also a variety of ways to model nonlinear associations using regression analysis. However, these topics are beyond the scope of this article, and the reader is referred to Ref 10 and 11 for more complete treatments of these and a variety of other extensions of simple regression analysis.

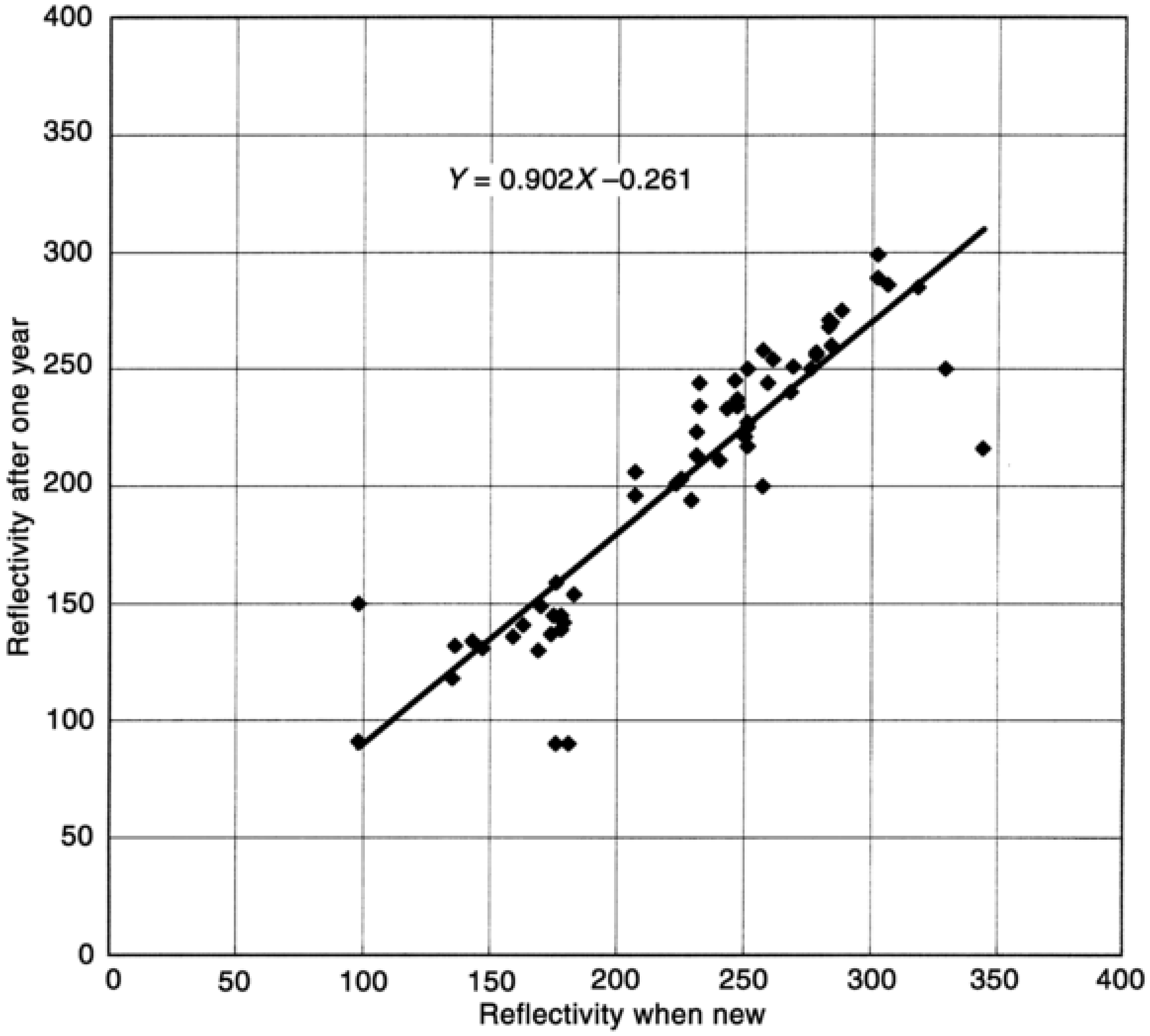

Fig. 2 Reflectivity of highway markers when new and after one year in service. Units for reflectivity are specific intensity (millicandela) per unit area.

Regression Analysis and Statistical Inference. Regression analysis can be used to predict one variable in terms of other variables, but the terms in the regression equation itself tell the researcher very little about the dependability of the prediction. Statistical tests are available to test for significance of the entire regression equation and also for the significance of *b.* It is also possible to place a confidence interval around the predictions of *Y* obtained from a regression analysis. Each type of statistical inference is discussed in turn. However, first, there are a number of assumptions required for regression analysis that deserve consideration.

To begin, there are specific assumptions relating to the disturbance term, ε. This term, also called the residual, represents measurement error in *Y* and specification error, or influences on *Y* not included in the regression equation. Regression assumes that ε has an expected value (mean) of 0, is approximately normally distributed,

and that the independent (*X*) variable is measured without error. Note that the estimated residual always has a mean of 0, but the assumption refers to the parameter ε.

It is also necessary to assume that *X* and ε are statistically independent. Suppose that an unidentified third variable, *Q*, is the true source of influence on *Y*, but *Q* is also correlated with *X*. In that situation, *X* only appears to influence *Y* because of the influence of *Q* on both *X* and *Y*. This would be a case of violation of the assumed independence of *X* and ε. It should be noted, however, that an analogous assumption applies to all the statistical tests considered so far.

Regression analysis also assumes a multivariate normal distribution. In the case of two variables, a bivariate normal distribution could be represented graphically as an elliptical bell in three dimensions, to the extent that a normal distribution is represented by a bell curve. In other words, for each value of *Y*, the *X*s are distributed normally (Ref 7). Related to the assumption of a multivariate normal distribution is the assumption of *homoscedasticity*, which refers to the requirement that *Y* be not just normally distributed about each value of *X* but also that the variance of *Y* be consistent across values of *X*.

Given these assumptions, discussion can turn to statistical inference in the context of regression analysis. For the sake of brevity, this discussion is also limited to the case of regression with one independent variable.

In the case of simple regression with one independent variable, the test for the significance of β is identical to the test for the overall significance of the regression equation. The test parallels that for analysis of variance. Consider the following expression:

$$\sum_{i=1}^{n}(Y_i-\bar{Y})^2=\sum_{i=1}^{n}(Y_i-\hat{Y}_i)^2+\sum_{i=1}^{n}(\hat{Y}_i-\bar{Y})^2 \quad \text{(Eq 31)}$$

where $\hat{Y}_i$ is the value predicted for Y_i from the regression equation. Note that the term to the left of the equals sign is the total sum of squares. The first term to the right represents the residual, or error, sum of squares and is analogous to within sum of squares in the context of analysis of variance. The final term is the sum of squares that is accounted for or "explained" by the regression equation and is directly analogous to between sum of squares. This term is often referred to as ***explained, regression,*** or ***model*** sum of squares. At this point, it should be evident that an *F* ratio can be obtained from these quantities, given the appropriate degrees of freedom. Also analogous to analysis of variance, degrees of freedom for the regression sum of squares is (k - 1) and for residual sum of squares (n - k), except that in this case, *k* represents the number of terms estimated for the regression equation, in this case, *a* and *b*, or 2. Table 5 works through a numeric example based on the reflectivity data in Fig. 2. Note that an *F* ratio of 246.6 is obtained, and the critical value for *F*, assuming 1 and 58 degrees of freedom and α = 0.05, is approximately 4.01, so the null hypothesis that the coefficient of determination P = 0 can be rejected.

Table 5 Regression analysis summary for the reflectivity problem in fig. 2

Number of cases (*N*)			**60**	
Mean reflectivity when new (*X*)			229.33	
Mean reflectivity after one year in service (*Y*)			206.52	
Constant (*a*)			-0.261	
Slope (*b*)			0.9016	
Pearson's *r*			0.900	
Pearson's r^2			0.810	
Source	Sum of squares	Degrees of freedom	Mean square	*F*
Regression	154,328.31	1	154,328.31	246.61
Residual	36,296.67	58	625.81	
Total	190,624.98	59		

It is important to note that the foregoing test applies to the regression equation for both simple and multiple regression. However, it is applicable to the significance of β only in the limited case of regression with one independent variable. Another similar test is available for the significance of the individual estimates for the βs in multiple regression, but that is beyond the scope of this article.

Coefficient of Determination. In the case of multiple regression, there is a measure called the multiple correlation coefficient, or coefficient of determination, known as R^2. Note the use of the upper case "*R*" (upper

case rho, or P, to denote a parameter) to differentiate it from Pearson's *r*. R^2 is analogous and, in the two-variable case, equivalent to Pearson's r^2. Consider Eq 32:

$$R^2 = \frac{\sum_{i=1}^{n}\left(\hat{Y}_i - \bar{Y}\right)^2}{\sum_{i=1}^{n}\left(Y_i - \bar{Y}\right)^2} \quad \text{(Eq 32)}$$

Referring back to Eq 31, R^2 is also the ratio regression/total sum of squares. The coefficient of determination is a useful summary measure, because it expresses the results of the regression equation in terms of proportionate reduction in error, or the proportion of variance in *Y* that is accounted for by the regression.

References cited in this section

3. S. Siegel, *Nonparametric Statistics for the Behavioral Sciences,* McGraw-Hill Book Company, 1956, p 25–26, 30–31, 195–239

7. H.M. Blalock, *Social Statistics*, revised 2nd ed., McGraw-Hill Book Company, 1979, p 205–206, 208–218, 231, 299–325, 340, 348, 352–369, 388, 398, 554–551

10. J. Neter, M. Kutner, C. Nachtsheim, and W. Wasserman, *Applied Linear Statistical Models,* 4th ed., WCB/McGraw Hill, Inc., 1996, p 296–315, 531–566, 663–1041

11. N.R. Draper and H. Smith, *Applied Regression Analysis,* John Wiley and Sons, Inc., 1966, p 58, 104–158, 263–298

B.P. Jones, Statistics for the Corrosionist, *Corrosion: Fundamentals, Testing, and Protection*, Vol 13A, *ASM Handbook,* ASM International, 2003, p 972–979

Statistics for the Corrosionist

Barnie P. Jones, Oregon Department of Transportation

References

1. S.S. Stevens, On the Theory of Scales of Measurement, *Science,* Vol 103, 1946, p 677–680

2. W.D. Callister, *Materials Science and Engineering: An Introduction,* 3rd ed., John Wiley and Sons, Inc., 1994, p 132

3. S. Siegel, *Nonparametric Statistics for the Behavioral Sciences,* McGraw-Hill Book Company, 1956, p 25–26, 30–31, 195–239

4. W. Mendenhall and J.E. Reinmuth, *Statistics for Management and Economics,* Duxbury Press, 1974, p 192

5. N.T. Kottegoda and R. Rosso, *Statistics, Probability, and Reliability for Civil and Environmental Engineers,* McGraw-Hill Book Company, 1997, p 15–16, 222, 245–257

6. D. Salsburg, *The Lady Tasting Tea: How Statistics Revolutionized Science in the Twentieth Century,* W.H. Freeman and Company, 2001, p 25–32

7. H.M. Blalock, *Social Statistics,* revised 2nd ed., McGraw-Hill Book Company, 1979, p 205–206, 208–218, 231, 299–325, 340, 348, 352–369, 388, 398, 554–551

8. W.G. Cochran, *Sampling Techniques,* 3rd ed., John Wiley and Sons, 1977, p 24–25

9. H. Scheffe, *The Analysis of Variance,* John Wiley and Sons, Inc., 1959

10. J. Neter, M. Kutner, C. Nachtsheim, and W. Wasserman, *Applied Linear Statistical Models,* 4th ed., WCB/McGraw Hill, Inc., 1996, p 296–315, 531–566, 663–1041

11. N.R. Draper and H. Smith, *Applied Regression Analysis,* John Wiley and Sons, Inc., 1966, p 58, 104–158, 263–298

Copyright © 2005 ASM International®. All Rights Reserved.

< Previous section in this article   Next section in this article >
< Previous section in this article

B.P. Jones, Statistics for the Corrosionist, *Corrosion: Fundamentals, Testing, and Protection*, Vol 13A, *ASM Handbook,* ASM International, 2003, p 972–979

Statistics for the Corrosionist

Barnie P. Jones, Oregon Department of Transportation

Selected References

- “Applying Statistics to Analysis of Corrosion Data,” G 16, ASTM
- R.C. Rice, Statistics and Data Analysis, *Mechanical Testing,* Vol 8, *Metals Handbook,* 9th ed., American Society for Metals, 1985, p 621–720
- “Statistics—Vocabulary and Symbols—Probability and General Statistical Terms,” ANSI/ ISO/ASQC 3534-1, The American Society for Quality Control

W. Reitz and J. Rawers, Materials Basics for the Corrosionist, *Corrosion: Fundamentals, Testing, and Protection*, Vol 13A, *ASM Handbook*, ASM International, 2003, p 980–991

Materials Basics for the Corrosionist

Wayne Reitz, North Dakota State University; James Rawers, Albany Research Center

Introduction

THIS ARTICLE is an overview of the science and engineering of materials for corrosionists with limited knowledge in this field. The presentation is descriptive, not technical, and assumes a basic understanding and knowledge of science. To help with the understanding of materials, definitions and descriptions of many of the more commonly used materials terms are presented along with examples. Advanced information can be found in the Selected References. Materials terms are printed in *italics.* If not immediately provided, the definitions can be found in the glossary at the back of this Volume.

The first section in this article, "Classification of Materials," lists and defines the categories of materials and gives examples of commercial materials. In general, metals are versatile materials that can be modified easily to achieve specific properties. Polymers can be produced readily in complex near-net final shape, and they have high ductility and low strength. Ceramics tend to have high compressive strength and good resistance to oxidation and corrosion; ceramics also exhibit low electrical and thermal conductivity and are brittle.

The second section "Properties," discusses the more frequently cited, measured, and relevant physical properties of materials, such as phases, strength, conductivity, and wear. The more common methods used to determine these properties and the standard set of units used are presented.

The third section of this article, "Processing," describes methods used to fabricate materials into different products. It includes a summary table of materials and their properties.

The fourth and final section, "Material Design, Application, and Failure," addresses material design, materials applications, and materials failure analysis. A collection of representative materials and their properties and characteristics is tabulated.

W. Reitz and J. Rawers, Materials Basics for the Corrosionist, *Corrosion: Fundamentals, Testing, and Protection*, Vol 13A, *ASM Handbook*, ASM International, 2003, p 980–991

Materials Basics for the Corrosionist

Wayne Reitz, North Dakota State University; James Rawers, Albany Research Center

Classification of Materials

Materials are defined as the elements, constituents, or substances of which something is composed or made. The study of materials can be divided into three overlapping fields:

- *Materials science,* concerned with the basic understanding and characterization of materials
- *Materials technology,* concerned with the development and processing of materials
- *Materials engineering,* concerned with the design and application of materials.

These fields have more commonalities than differences. While the materials scientist may be more concerned with developing fundamental theories, the technologist with applying those ideas to developing or improving

materials, and the engineer with taking these materials and building something from them, all three use common terminology.

Materials are either solids or fluids. Fluids (gases and liquids) are the principal agents of corrosion. The characteristics and properties of fluids, with the exception of glasses, are beyond the scope of this article and are not discussed. Solids have relatively fixed volumes and are able to support shear loads.

Engineered solids are the components of structures. The properties of the solid determine the design and construction of products. Processed solids can be divided into at least three categories: ceramics, metals, or organics. These categories are not exclusive and are roughly related to the type of bonding that holds the atoms together and their fundamental structural units as shown in Fig. 1 and described in Table 1. Ceramics have a large component of ionic bonds holding atoms together. The basic structural units of ceramics are molecules, which are rigid and can vary from 2 to 10 atoms in size. Organics have a large component of localized covalent bonds between atoms, and their basic structural units, again molecules, can vary from approximately 100 to more than 10,000 atoms. Organics are very flexible. Metals have a mutual sharing of electron bonding between all atoms. Their basic building unit is the single atom. In ionic bonding, one atom gives up its electrons to another atom; in covalent bonding, two atoms mutually share electrons. In metallic bonding, a large array of atoms give up individual ownership of their valence electrons, sharing them mutually.

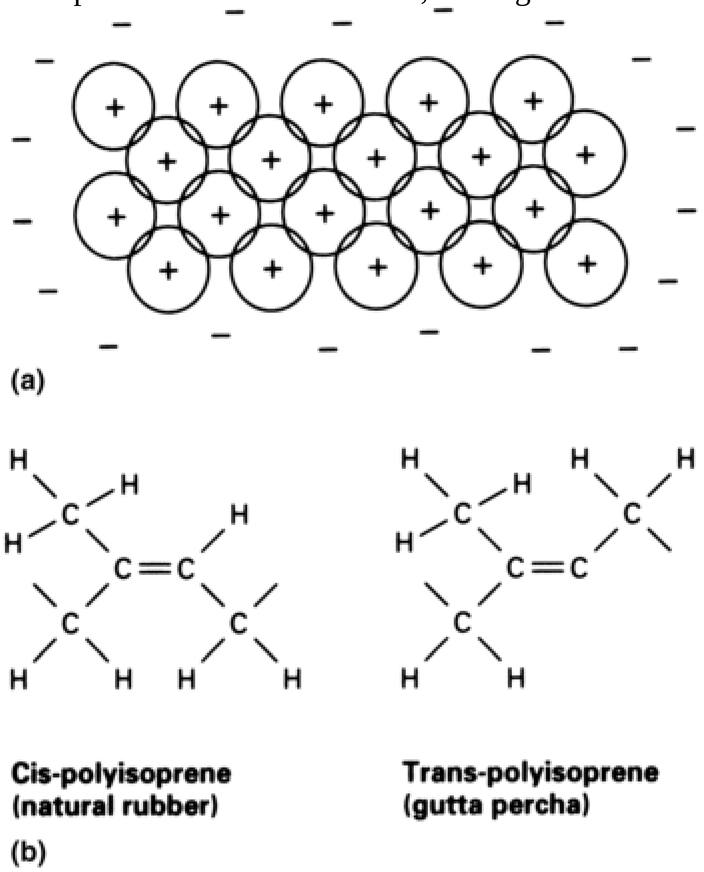

Fig. 1 Fundamental structural units of materials. (a) Metallic bond showing a cluster of cations (+) in a sea of electrons (-). (b) Geometric isomers of polyisoprene, typical of organics

Table 1 Material bonding Characteristics of solid materials

Type of solid material	Electronic bond	Fundamental unit
Metals	Shared between all atoms	Single atom
Ceramics	Ionic bonding between atoms	2 to 10 atoms in rigid structure
Organics	Covalent bond between two atoms	100 to over 10,000 atoms
Composites	Varies by constituents	Matrix and reinforcement

Many properties of solids are ultimately related to the interaction of atoms. Atomic interaction is explained by (a) electron interaction, which is best explained using quantum mechanics and (b) structural interaction, which

predominates as the number of atoms increases and can best be explained using Newtonian or continuum mechanics.

The three most widely used engineering materials are concrete, wood, and steel. These materials are from each of the materials categories: ceramics, organics, and metals, respectively. They are widely available, economical to produce, can be processed in a number of different ways to produce a great variety of products, and thus find a large number of applications. Each material has its own set of properties that make it best suited for particular applications. For example:

Application	Requirements	Example of material that meets most or all requirements
Dams	Large quantities of material able to withstand large compressive forces	Concrete
Home construction	Low cost, on-site processing, and renewable materials	Wood
Large cargo ships	High strength, flexibility, and corrosion resistance to a salt water environment	Steel

All materials have assets and limitations, such as availability, cost, strength, and corrosion resistance, which must be evaluated. Engineering guidelines and industry standards, as well as legal requirements, must be met when choosing a material for particular application. The materials information contained herein represents typical information and data. Consult the Selected References for more specific details or property values.

Ceramics are composed of carbide, oxide, nitride, sulfide, and/or silicate molecules. Examples include: SiC and Si_3N_4, used for cutting tools; SiO_2, the principal component in window glass, $2CaO \cdot SiO_2$, one of the principal components in cement; and $Al_2Si_2O_3\ (OH)_4$, clay used in making bricks. Ceramics are characterized by having good compressive strength and low tensile strength. The ionic nature of the interatomic bonds produces high rigidity (stiffness) and little ductility (elasticity). Ceramics are strong; once a crack starts, it grows rapidly, leading to immediate and rapid failure. The ionic bond is a high-energy bond, more stable than either a metallic or covalent bond, thus forming relatively stable molecules. Ceramics are generally more corrosion and oxidation resistant than either metals or organics. The nature of the ionic bond also limits the mobility of the electrons in the molecule, and ceramics thus have limited electrical and thermal conductivity and make good insulators.

Organics are composed of carbon-base materials. When carbon bonds covalently to other atoms such as other carbon atoms, nitrogen, oxygen, sulfur, and/or phosphorus, it can form extended one-dimensional chains (such as DNA molecules), two-dimensional (2D) arrays (graphite), or three-dimensional (3D) structures (diamond). Carbon atoms can share electrons or bond covalently up to four of its electrons with other atoms. As the degree of interlinking between carbon atoms increases, the structure becomes more rigid and the strength becomes greater, as shown in Fig. 2.

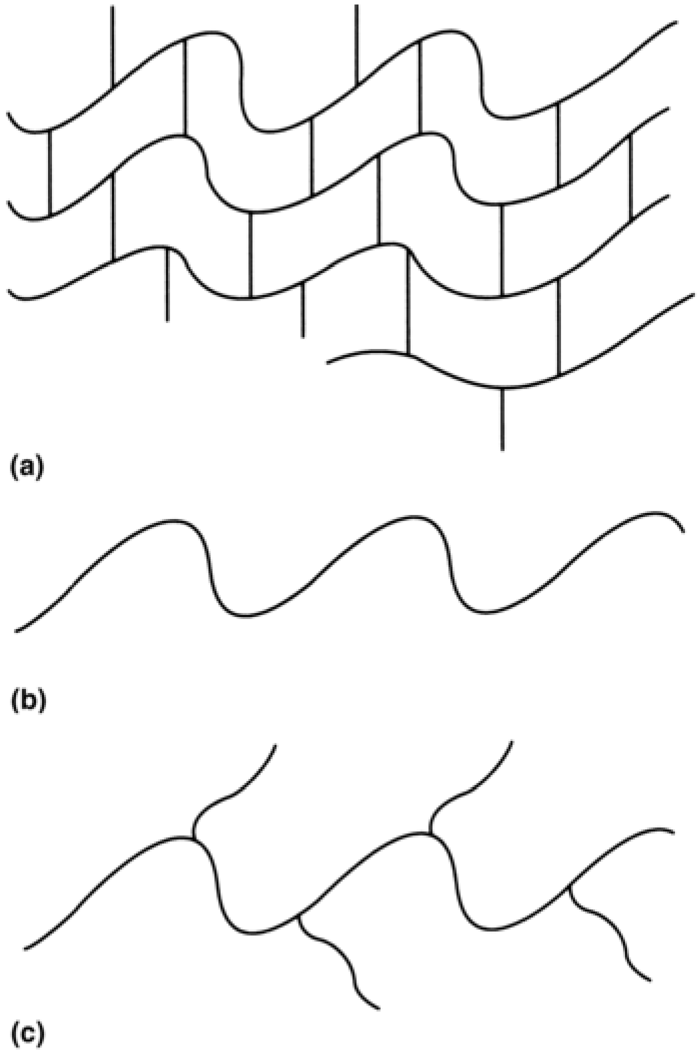

Fig. 2 (a) Simulated cross linked (networked or three-dimensional) structure. (b) Simulated linear polymer molecule. (c) Simulated structure of a branched polymer

Polymers are repeating chains of organic units (known as *mers* or *monomers*) that are covalently linked. Plastics are processed polymers and are categorized by how they are formed. *Thermoplastics* have very long chains that, when heated, readily flow past one another. However, as the temperature is reduced, the thermal energy of the molecule is reduced, and the interatomic motion and bonds become more restricted. The shape of the polymers thus becomes more rigid. As polymer length increases, the polymers can become ever more intertangled, resulting in a material of limited strength but great flexibility. Some plastics are able to stretch several hundred percent before failure. Reheating can reshape these plastics. Thermoplastics include natural rubber, nylon, polyvinyl chloride, polyesters, wood, silk, and cotton. *Thermosets* are polymers with multiple covalent links between polymer chains. The greater the number of links between the different chains, the more restrictive the movement of individual polymers, resulting in greater rigidity and higher strength. Heating cannot reshape these plastics once they are formed. Thermoset plastics include phenolics, polyesters, epoxies, urethanes, Bakelite, polyvinyl chloride (PVC), and polyethylene.

The localized nature of covalent bonds restricts the overall electron mobility in the polymer structure, resulting in high electrical resistivity and limited thermal conductivity. Organics generally have good corrosion resistance to mild acids and bases. However, solvents such as acetone attack organics, alcohol can dissolve polymer and interpolymer bonds, and ultraviolet radiation such as sunlight can break polymer bonds.

Metals are composed of those elements that readily share their electrons globally with other atoms. The elements that have this ability constitute the majority of the periodic table. The exceptions are the noble elements, the halides, carbon, nitrogen, oxygen, phosphorus, and sulfur. The metallic elements are able to form metallic compounds or alloys by combining with different metallic elements.

Metal atoms combine to form definite structural atomic arrangements or *lattices,* 3D crystal structures. Most metals have either face-centered cubic (fcc), hexagonal close packed (hcp), or body-centered cubic (bcc) unit

cells, as shown in Fig. 3. Metals with the fcc lattice structure have the highest ductility and lowest strength. The hcp metals have the highest strength and lowest ductility, and bcc metals are generally in between. When different metallic elements are mixed they can form a *solid solution* (random dispersion of atoms within a single phase), or they can: (a) form a different phase, (b) begin to segregate or cluster forming a second phase with separate or distinct composition and/or lattice, or (c) develop a very limited stoichiometric chemical relationship and form definite structure coordinated atomic configurations (producing *intermetallics* that have narrow chemical compositions). Because metallic electrons are able to move freely throughout the alloy, metals have good electrical and thermal conductivity.

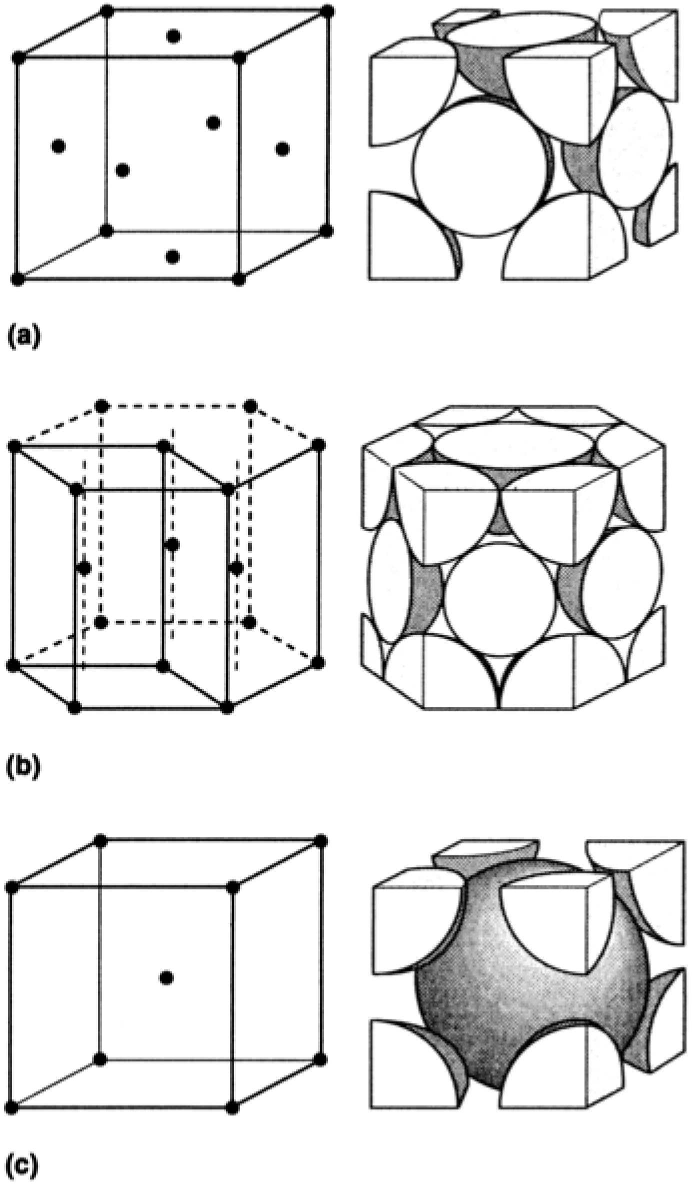

Fig. 3 Unit cells and atom positions for metal lattices. The positions of the atoms are shown as dots at the left of each pair of drawings, while the atoms themselves are shown close to their true effective size by spheres or portions of spheres at the right of each pair. (a) Face-centered cubic (fcc). (b) Hexagonal close-packed (hcp). (c) Body-centered cubic unit cells (bcc)

Semiconductors are materials that when pure are electrical insulators. For example, pure, single crystal silicon has a lattice structure similar to that of carbon diamond, is largely covalently bonded, and is an insulator. However, when minute quantities of impurities are present in the material (*doped*), the local electronic structure can be increased or depleted. This electron unbalance can greatly reduce the resistivity of the material, thus creating a semiconducting material.

Composites are combinations or mixtures of different phases or discrete materials. The range of composite possibilities is almost unlimited in composition and scale, as listed in Table 2. Composites are desirable because they are structures with properties of the individual components. For example, it is possible to increase the

strength of metals while retaining much of the ductility of metal by incorporating and combining into the metal matrix very fine ceramic particles. Steel is a mixture of bcc iron with a dispersion of iron-carbide ceramic particles. Polymers can be strengthened with the addition of metallic wires (steel-belted automobile tires). Ceramics can be given some ductility by placing them in a metal matrix, for example, tungsten carbide coated cobalt cutting tools. Plywood is a composite in which the wood laminates are bonded by epoxy polymers. Strength properties of wood are highly directional. Laying-up the different layers of the plywood in different directions improves the overall directional strength of the final product. Care must be taken in designing and using composites. Just like the plywood, reinforced materials tend to be anisotropic their properties varying with direction. The choice of materials that results in improved composite properties in one application may possess undesirable properties in another application. For example, while the strength of a composite may be enhanced, the corrosion resistance may be decreased.

Table 2   Composite types

Type	Example, common name	Components and purpose
Metal-metal	Galvanized steel	Fe: bulk properties such as formability and strength Zn: surface coating for corrosion protection
	U.S. coin (penny)	Zn: structural material Cu: surface coating (modification)
Metal-organic	Painted steel structure	Fe: strength Paint: corrosion protection
	Electrical wires	Cu: electrical conductivity Organic: electrical insulator
Metal-ceramic	Cermet	Co: ductile binder WC: hard cutting component
	Reinforced concrete	Cement: binder, compressive strength Fe-rods: ductile, tensile strength
Organic-organic	Particle board	Wood: strength Epoxy: binder
Organic-ceramic	Fiberglass	Glass: strength Resin: binder
	Paper	Cellulose: structural material Clay: surface finish (modification)
Ceramic-ceramic	Concrete	Gravel: compressive strength Cement: binder
	Porcelain	Ceramic: structural material Glaze: surface finish (modification)

W. Reitz and J. Rawers, Materials Basics for the Corrosionist, *Corrosion: Fundamentals, Testing, and Protection*, Vol 13A, *ASM Handbook*, ASM International, 2003, p 980–991

Materials Basics for the Corrosionist

Wayne Reitz, North Dakota State University; James Rawers, Albany Research Center

Properties

The *ASM Handbook* series is a good source of information about materials properties. The primary source of information for evaluating materials properties or materials testing is ASTM International (formerly the American Society for Testing of Materials), an organization devoted to establishing standardized procedures for all types of testing. The International Organization for Standards (ISO) promotes standardization and related activities worldwide. The work of the ISO results in international agreements that are published as International Standards. There are also regional standards such as the EN (Euronom) and other national standards organizations that are used to specify materials, materials testing, and quality.

Composition and phases are the most important materials properties. In principle, all other properties can be derived from knowledge of these two. The electronic interaction or bonding between the atoms can be determined from knowledge of the chemical elemental composition (the interatomic positions). Composition can be obtained from analytical chemistry (bulk chemical analysis), emission spectroscopy, x-ray fluorescence, and Auger spectroscopy. The measuring units for chemical composition are atom or mole fraction for scientists and weight percent for engineers. The structure of a material is its *atomic arrangement* and *lattice spacing.* From knowledge of the atomic placement and the increased complexity that arises as the number of atoms increases, there emerge new theories controlling material behavior. Structure can be determined using x-ray diffraction. Other methods include ultrahigh resolution electron microscopy and atomic microscopy. These methods are used to determine local (molecular structure), long- range order (lattice structure), the presence of local defect structure, or total disorder (amorphous structure). Most ceramic and metallic materials have an ordered structure whereas most organic materials and glasses have limited or no atomic order.

The size of the fundamental building component of a solid influences the resulting microstructure greatly, as shown in Fig. 4. The basic unit for most metals is the individual atom. Because the bonding is due to a global sharing of electrons, the atoms can be considered to have spherical symmetry and thus no orientation preference. The packing structure of metals is similar to the packing of tennis balls, in that atoms are stacked so that each is part of a repeating 3-D pattern. The *unit cell* is a coordinated set of atoms that form the 3D lattice that repeats by a simple translation. The basic unit for ceramics is the individual molecule, for example, SiO_2 (Fig. 4a). Molecules are a set of bonded atoms that have a rigid structure and a more complex geometry than single atoms. The bonding between the molecules is not as strong as the bonding within the molecule. The additional complexity associated with the molecular shape makes the unit structure more difficult to define than that for simple atoms. Many ceramics align readily into a lattice structure similar to that of metals with the individual metal atoms replaced with the ceramic molecules. However, rapid solidification or the presence of impurity molecules of different shape can result in a solid structure with limited local alignment of molecular unit cells, which, in the extreme, can result in amorphous or glass structures. The basic unit for organics is the polymer. Polymers have large complex atomic alignments, irregular geometry, and flexible molecules (Fig. 4b). Most organic solids have an amorphous or glass structure, as defined in Table 3.

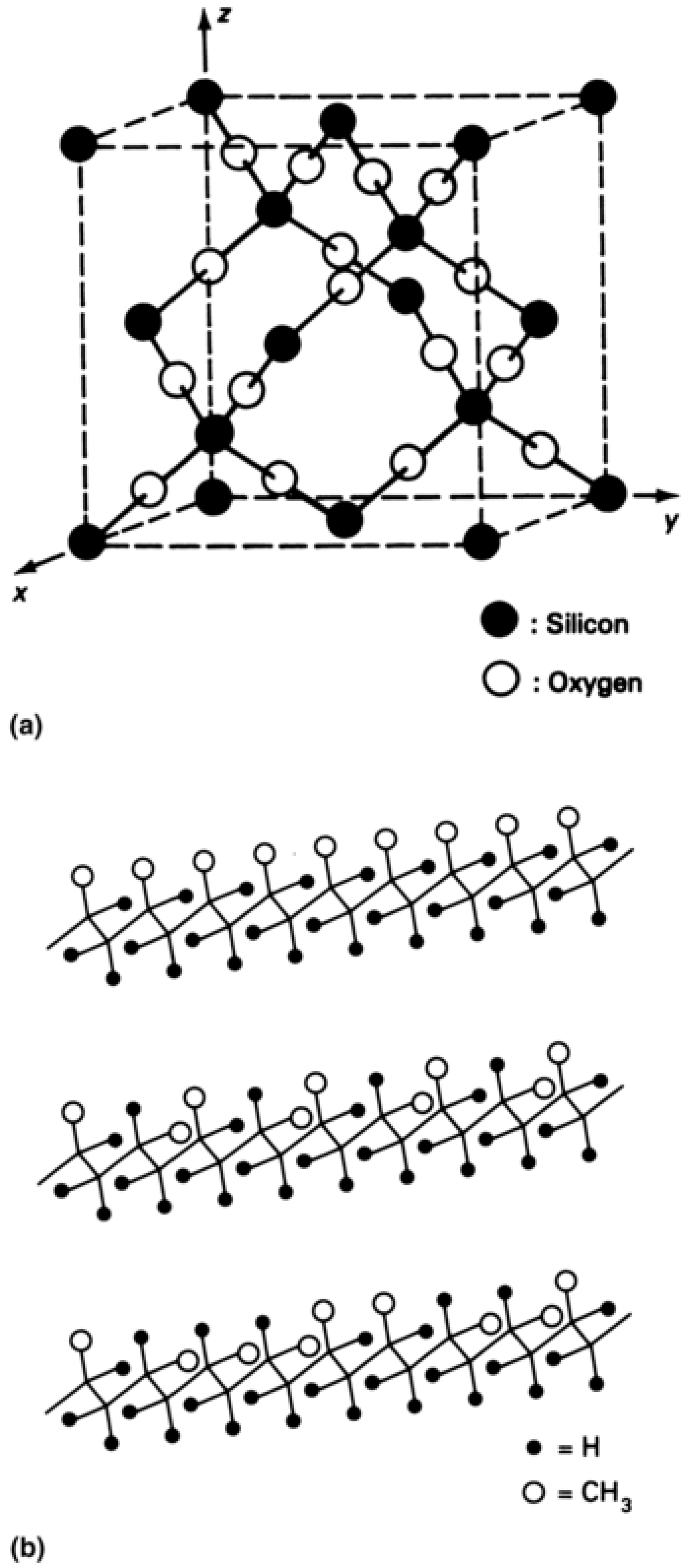

Fig. 4 The unit cells of a ceramic and a polymer. (a) Idealized cristobalite structure (b) Stereoisomers of polypropylene; from top: isotactic, syndiotactic, and atactic

Table 3 Characteristics descriptors of solids

Term	Description
Amorphous	Nonrepeating arrangement or alignment of fundamental building units
Crystalline	1, 2, or 3D alignment or repeating arrangement of fundamental building units
Phase	Region of space with uniform composition and uniform structure throughout
Single phase	Single-grain, uniform composition, same structural alignment throughout
Multiple grain	Structure composed of a number of single phase crystals
Grain boundary	Interface or boundary between two grains
Multiple phase	Multigrain structures composed of different phases
Precipitates	Second-phase smaller grains within large grains

Microstructure and *surface morphology* can be determined by optical and electron microscopy. Optical microscopy is typically used for 10 to 1000 times magnification. Numerous sample preparation and microscopic techniques have been developed for examination of flat polished surfaces to determine grain structure and, possibly, identify phases. Light or optical microscopy permits color to be observed and is used often to identify and differentiate microscopic features. Low magnification is used often for failure analysis to show the type of failure: intergranular or transgranular. With optical microscopy, the higher the magnification, the lower is the *depth of field* resolution, (focus in the vertical direction). Electron microscopy, especially scanning electron microscopy (SEM), has essentially an infinite depth of field and can magnify in excess of 100,000 times. Scanning electron microscopy is ideally suited for examination of surface features. Many SEMs are equipped with auxiliary features that allow for phase differentiation (secondary electron detection), atomic number differentiation (backscattered electron detection), quantitative and qualitative chemical analysis using energy dispersive spectroscopy (EDS), wavelength dispersive spectroscopy (WDS), and even rudimentary x-ray diffraction analysis (backscattered Kikuchi line analysis).

The *phase* of a material is defined as a region with homogenous atomic structure and chemistry; for example, amorphous silicate glass or a long-range repeating lattice of bcc iron. Many materials are composed of multiple phases (regions with different chemical composition and/ or different structures). The energy differences in phases may result in localized galvanic corrosion. Rarely does an entire piece of material maintain homogeneous structure. *Grains* (or crystals) are regions within a material that have both homogenous chemistry and atomic structure. *Precipitates* are small grains of different chemistry within a large grain. If the changes in homogeneity or local structure of the material are abrupt, the discontinuity results in the formation of a *grain boundary.* Grain boundaries may result from a change in the direction of atomic orientation, from difference in chemical composition, or from different phases being present. The abrupt property changes at a grain boundary are regions of energy higher than the energy level within the grain. This results in a more corrosion-prone region, a region along which diffusion is more rapid, and a region of higher stress.

In materials with a lattice structure, such as metals and ceramics, a line *dislocation* is another type of lattice structure that can be present. Dislocations are missing lines of atoms within grains and are important in understanding the plastic or ductile nature of a material and the increase in a material strength as it undergoes plastic deformation. Line dislocations are areas of higher localized stress.

Micrographs of surface morphology and microstructures are shown in Fig. 5.

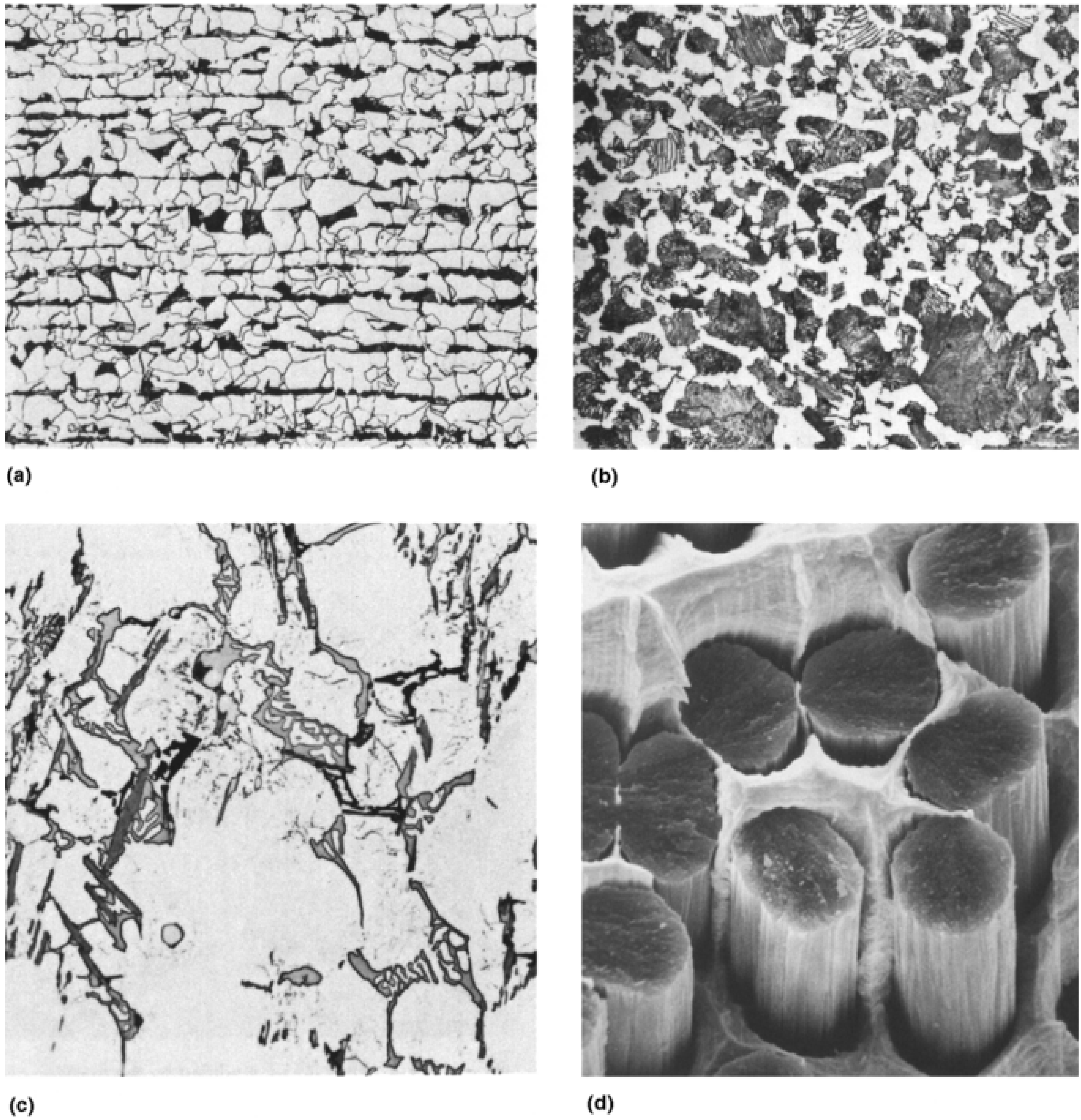

Fig. 5 Microstructure of materials. (a) High-strength low alloy steel (0.2% C) hot rolled. The structure is ferrite and pearlite. 4% picral, then 2% nital etchants were used. Magnification is approximately 200×. (b) 1045 steel sheet, 3 mm (0.13 inch) thick, normalized by austenitizing at 1095 °C (2000 °F) and cooling in air. Structure consists of pearlite (dark gray) and ferrite (light). Picral. 500× (c) Alloy 242-T571, permanent mold cast and artificially aged. Structure contains blades of $NiAl_3$ (dark gray) in the medium-gray Cu_3-$NiAl_6$ script. $CuAl_2$ particles (light) and scriptlike Mg_2Si (black) also are present. 0.5% HF. 250× (d) Graphite-silver copper composite (Thornel 300 fiber in 70Ag-30Cu eutectic matrix), unidirectional. Liquid-metal infiltration of fiber bundles followed by diffusion bonding. SEM of a failed tensile surface. The matrix shows good ductility, but the lack of matrix adhering of the fibers indicates low interfacial bond strength. 1860×

As particle or grain size decreases, the structure eventually reaches a size where the number of atoms associated with surface or grain boundary of a particle begins to approach the number of atoms within the particle or grain. Such materials are referred to as *nanomaterials* and are defined as materials having one or more structural dimensions between 1 and 100 nm (10^{-7} to 10^{-9} meters). To date, understanding nanomaterials properties has

required no new physics, and most properties of nanomaterials can be explained using either quantum mechanics or classical mechanics. Atoms or molecules at a surface have different environments surrounding them than do atoms and molecules in the interior of the particle or grain. Thus, surface effects— surface physics, chemistry, and mechanics, are important in understanding many of the phenomena associated with nanomaterials.

The relationships between composition, temperature, and phase often are presented in *phase diagrams.* These graphs describe the phases present as a function of the composition (most often wt%) on the abscissa and temperature as the ordinate. Equations have been derived from which the relative concentration of the different phases present as well as the composition of each phase present can be derived, given a temperature and an overall material chemical composition. Phase diagrams are derived for systems at thermodynamic equilibrium. Phase diagrams are generally limited to only two or three components because of the increase in complexity with increasing number of components, that is, atomic elements or molecules. Phase diagrams are extremely important in understanding the microstructure of a material and its properties. The iron–iron-carbide phase diagram (Fig. 6) describes carbon steels and is well known in the metals community.

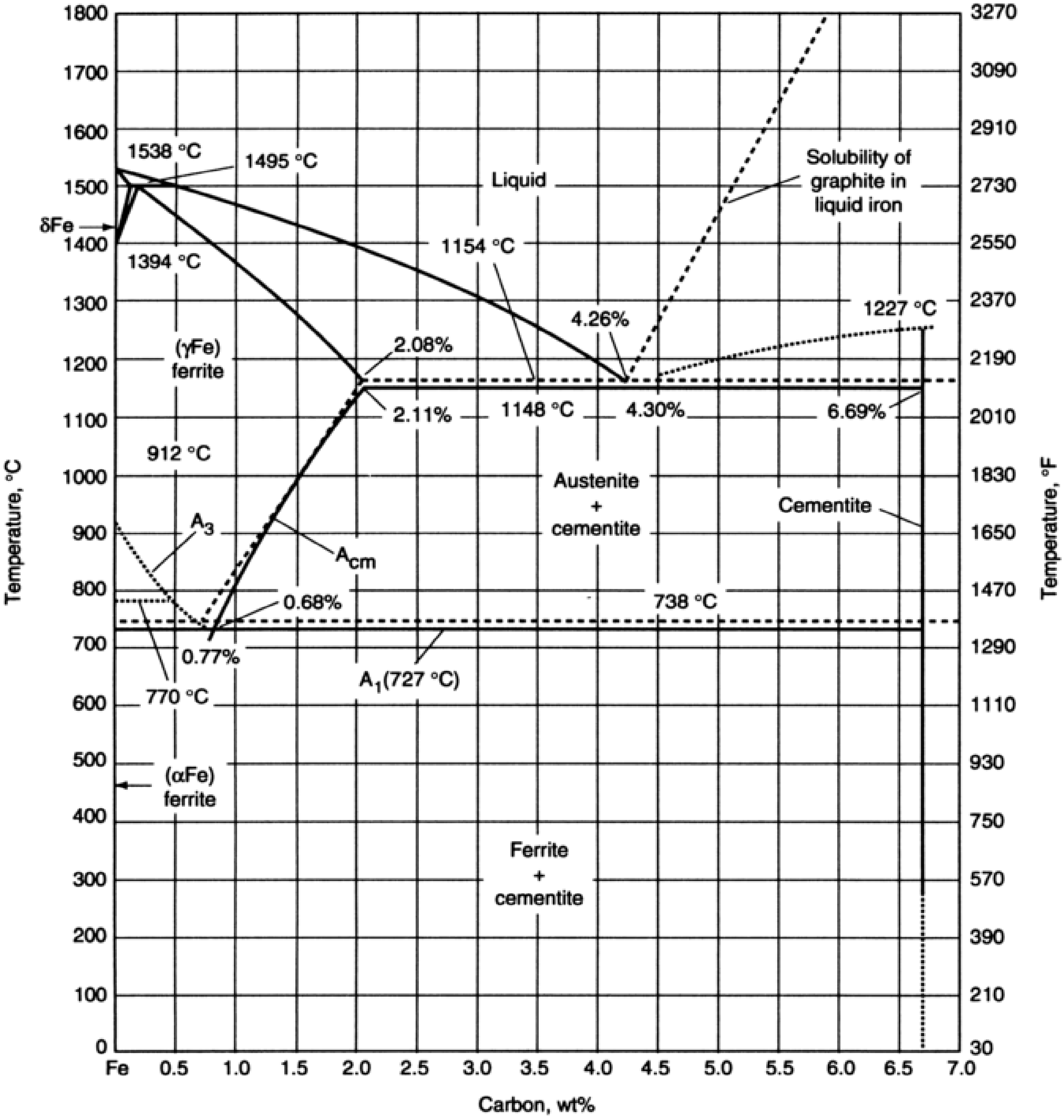

Fig. 6 Iron-carbon phase diagram

Mechanical Properties. One of the more important and most often measured sets of materials properties is response to an applied load; the *strength* (ability of a material to support a load) and *ductility* (deformation under a load). A normalized response characteristic of the bulk material strength property defined as *stress* and symbolized as *s* or σ, the applied load divided by the cross section of a material, is measured in Pascals (Pa = newton/meter^2) or psi (pounds/ inch^2). The conversion is that 1 psi is approximately equal to 7000 Pa. A normalized material change in shape defined as *strain,* symbolized as *e* or ε, unitless, but with units sometimes given as length/length, is the change in length of a material divided by its original length, δ*l*/*l*, or change in area over area, δarea/area. Engineers measure the stress-strain curve with respect to the original unstressed length or area, whereas scientists use the instantaneous length or area. During the initial phase of stress loading the material is *elastic*; that is, if the stress load is removed, the material returns to its original shape. During this elastic response, the stress-strain relationship is linear. The stiffness of a material, rigidity, or *modulus of elasticity, E*, is obtained by measuring the slope of the elastic stress-strain curve. Elastic modulus is measured using the same units as stress. Fig. 7(a) shows a typical stress-strain curve, and Fig. 7(b) shows typical curves for materials with different behaviors.

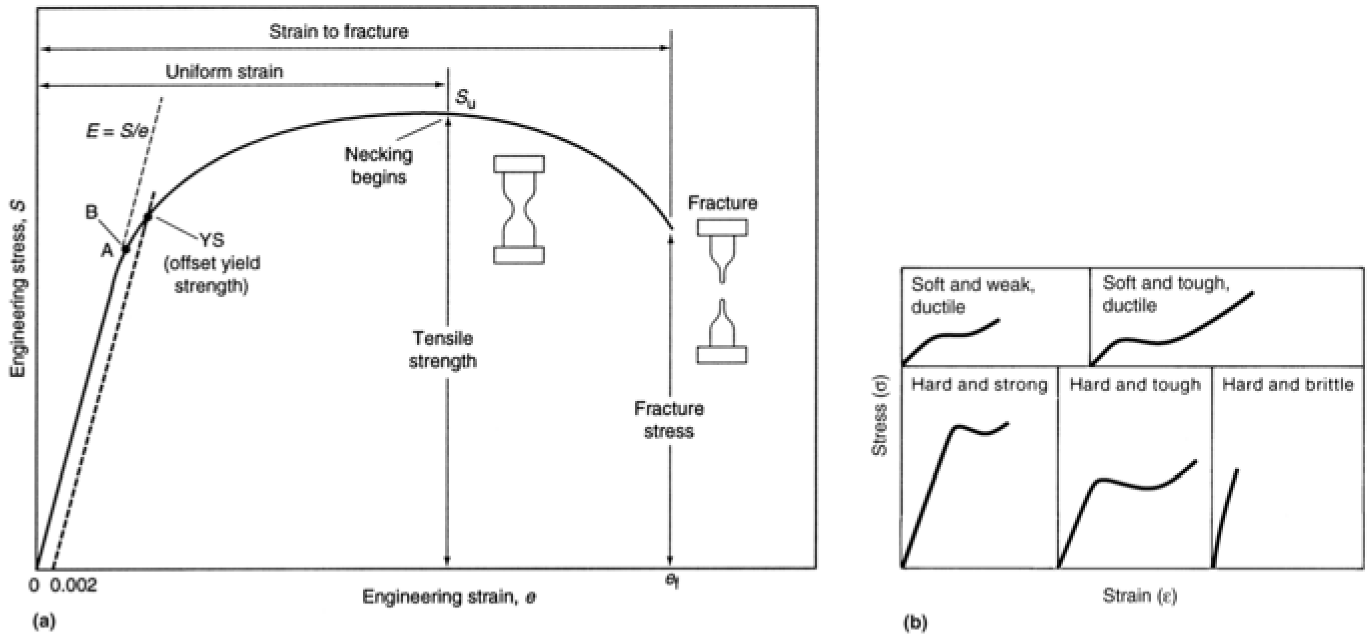

Fig. 7 Mechanical properties diagrams. (a) Typical stress-strain tensile curve (b) Typical stress-strain tensile curves for materials with different characteristics.

As the stress load increases, the material reaches a point at which it either breaks or fails, or yields and becomes plastic. *Plastic deformation* or *yielding* is defined as a permanent change in shape of a material in response to an applied load. After yielding, the change in strain per unit load increases. The stress at which the material becomes plastic is defined as the *yield stress,* σ_{ys}. Engineers normally design for loads less than σ_{ys}. Ceramics generally have very limited ductility, and the yield stress is often the failure stress. However, during fabrication, materials are often required to be deformed to a prescribed shape and thus must be loaded above the yield point. As the material undergoes plastic deformation, it becomes stronger due to (a) the generation and entanglement of dislocations within each grain in metals or (b) the alignment of polymer chains in organics. If the material is unloaded prior to failure, the material responds elastically from the point of maximum load. On reloading, the plastically deformed material will have a higher yield stress and is said to have undergone *work hardening.* The material can be returned to its original yield stress by heating (*recrystallization*). Deforming the material at elevated temperatures reduces the stress needed for deformation and eliminates the work hardening (*hot working*). In metals, regions of high tensile stress are anodic compared with regions of lower stress. A bent piece of tubing possesses higher residual tensile stresses on the outside of the bend.

Material response to load depends on the type of material, temperature, type of loading, previous loading, and the rate at which the load is applied. The most often cited stress-strain data are derived from *tensile tests.* In this test the response of a material to increasing pull or tensile stress is evaluated (normally at a strain rate of 0.02/s) at room temperature on samples with a typical sample-test length of approximately 5 cm (2 in.) and cross section diameter of approximately 1.25 cm (0.5 in.). Another commonly used stress-strain test is the

compression test in which a cylinder is compacted. While metals have similar response to tensile and compression loads, ceramics generally have significantly higher compression strength than tensile strength and the strength values often are only reported for compression. Shear tests are also significant.

Strength of metals is strongly influenced by *grain size* (size of crystals). Strength increases as grain size decreases. The decrease in grain size is accompanied by an increased volume fraction of *grain boundaries.* The grain boundaries are high-energy regions that are capable of accelerated corrosion, which is the basis for etching for metallographic examination. Grain boundaries act as sinks for impurities, which can also accelerate corrosion. Elevated temperature processing encourages grain growth, thus reducing the volume percent of grain boundaries.

Another common measure of material response to a load is the hardness test, where the resistance of a material to a specific load using an indenter is measured. A number of different loads and indenter sizes, shapes, and materials have been adopted as standards. The area or depth of the indent is measured and reported as the Brinell, Rockwell, Knoop, or Vickers hardness number. In general, as the hardness of a material increases, so does its strength. An empirical relationship has been established between hardness and tensile strength.

In practice, many materials contain flaws or defects. Material imperfections can have serious consequences on the response of a material to a load by reducing the stress to fracture and/or changing the nature of the failure. Standards have been derived to measure the change in failure if surface cracks are present. *Fracture toughness* (symbolized by K_{Ic}, K_{IIc}, or K_{IIIc}, depending on load configuration) provides a relationship between catastrophic failure and the size of the surface crack. Fracture toughness is valid only for materials that undergo brittle rapid failure with little or no plastic component prior to failure; that is, only elastic deformation followed by failure (defined as *plane-strain failure*). For materials with a significant plastic component prior to failure (defined as *plane-stress failure*), the area under the elastic and plastic portion of the stress-strain curve, $\int\sigma\delta\varepsilon$, is the failure energy per unit volume. It is measured and defined as the *fracture energy,* (symbolized as J_{Ic}, J_{IIc}, or J_{IIIc}). In this type of failure, the advancing crack tip is often observed to have undergone plastic strain, and the sharpness of the crack tip is blunted and undergoes plastic deformation.

Other material strength measurements include the response of a material to long-term loading, dynamic or impact loading, and changing loads, as defined in Table 4. Materials at constant stress levels below the yield strength over extended periods of time exhibit permanent deformation or *creep* and fail at loads below those measured in tensile tests. This is especially true for plastics. Materials loaded at high strain rates; that is under dynamic or *impact loading,* generally have higher yield strength but less ductility prior to failure than that measured in tensile tests. Materials subjected to constantly changing cyclic loads also undergo plastic deformation over time at loads much less than the yield strength and will fail in *fatigue* after a number of cycles. Fatigue curves are typically called *S-N* curves (stress versus number of cycles). Since the long- term properties of materials are important in typical service applications, numerous handbooks provide tables with creep and fatigue data. Figure 8 shows a typical creep curve and a fatigue curve.

Table 4 Solid material mechanical properties

Material strength	Description
Creep	Material response of deformation over time to a constant load. Creep-rupture strength is the stress that will cause fracture in a given time.
Compressive	The maximum compressive stress a material can develop. Compressive stress results in deformation (shortening) in the direction of the applied force.
Tensile	The maximum load a material can support in response to a pulling force at a slow strain rate. The ultimate strength as contrasted to the yield strength
Shear	The maximum stress a solid can sustain when the force is tangential to the plane on which it acts. In metals the stress exists when parallel planes of metal crystals slide across each other. In plastics, layers of molecules slide across each other.
Impact	A measure of resiliency or toughness of a solid to a shock or very rapid strain rate. The amount of energy that can be absorbed without fracture
Fatigue	Material response leading to fracture to variation in stress (or strain) loading at less than the ultimate strength. Often cyclic loading

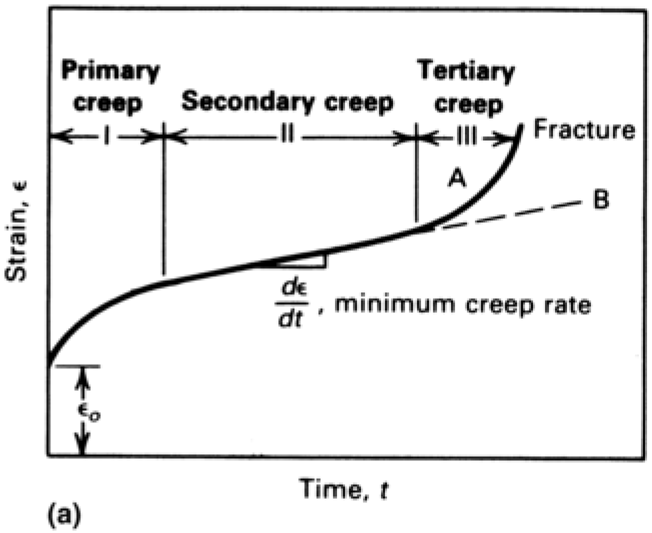

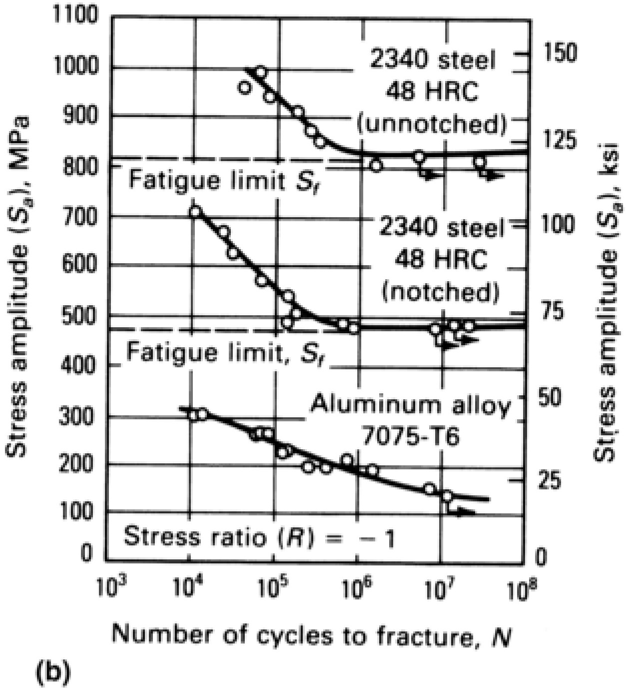

Fig. 8 A response of a material to long-term loading (a) Typical creep curve showing the three stages of creep (b) Typical *S-N* curves for constant amplitude and sinusoidal loading

Thermal Properties. *Thermal conductivity* is the ability of a material to transmit heat. In most applications, thermal conductivity is the result of coordinated atomic or molecular movement (phonon wave) that is enhanced by long-range order. Metals possess higher thermal conductivity than ceramics, which are considered to be thermal insulators, while amorphous plastics are even better thermal insulators than ceramics. High thermal conductivity enhances the ability of a material to remove heat in applications such as metal-cooling fins on air-cooled engines for lawn mowers and motorcycles. Ceramics and plastics make good coffee cups because they do not readily transmit heat to the surrounding atmosphere or a person's hand.

Materials undergo *thermal expansion* as they are heated. Thermal expansion is the response of a material to an increase in individual, random atomic vibration. Increasing the internal energy of a material will cause the atoms or molecules to increase their vibration amplitude, increasing the distance between atoms. For materials that are packed closely, such as metals in a long- range lattice structure, the expansion is proportional to the change in thermal energy. The force a thermally expanded metal can exert is equal to the force it takes to expand it by the same amount. Ceramics and plastics have a more open structure resulting in a lower rate of thermal expansion than metals. Thermal expansion can induce compressive and tensile stresses within a component or assembly of components.

When a material is subjected to rapid heating, the combined effects of thermal expansion and thermal conductivity may result in serious structural problems. Metals, because of their high thermal conductivity and good ductility, are not as affected by the thermal strain produced by the differential thermal expansion as ceramics. Ceramics have much lower thermal conductivity than metals, and thus experience a sharper thermal gradient that can produce greater thermal stress due to differences in thermal expansion over shorter distances. This results in surface spalling or cracking and compression (during rapid cooling) or tensile (during rapid heating) failure. Plastics also have low thermal conductivity, but their enhanced elasticity greatly reduces chances of failure due to thermal shock. However, their low thermal conductivity may cause localized heating and weakening during fatigue loading.

Diffusion is atomic or molecular movement within a material due to chemical gradients within the material. Processing materials at elevated temperatures and then cooling them rapidly before they can reach thermal equilibrium may result in compositional segregation, retention of unstable phases, retained thermal stresses, and so forth. Restoration of the system to thermodynamic equilibrium is accomplished by annealing. Many materials are processed in a manner that ensures the system is not in equilibrium. Most carbon steels have economic value because of their retention of the nonequilibrium Fe-Fe_3C microstructure. The room temperature Fe-C thermodynamic equilibrium state would be a gray cast iron—that is, pure iron in a bcc lattice and graphite microstructure.

Surface Interactions. Interactions at the solid surface with the environment can involve solid- gas interactions (oxidation), solid-liquid interactions (corrosion), and solid-solid interactions (wear). These interactions can be detrimental to the overall performance of the materials, as defined in Table 5.

Table 5 Characteristics of common material loss interactions on solid surfaces

Agent	Degradation	Description
Gas	Oxidation	Atmospheric reaction with solid surface to form solid or gaseous product
Liquid	Corrosion	Liquid reaction with solid surface to dissolve or form new surface phase
	Cavitation	Gas bubble implosion on solid surface in liquid media
Solid	Erosion	Solid or liquid impact on solid surface
	Abrasion	Solid scraping across solid surface

Oxidation is the chemical attack of gaseous elements (such as oxygen, sulfur, nitrogen, and chlorine) with metal surfaces. Most often the result of the interaction is the formation of a surface film that reduces or eliminates further solid- gas reaction. The type, density, thickness, and microstructure of the surface film depends on temperature, concentrations in the gas atmosphere, and thermodynamics of the reactions. The integrity and tenacity of the surface film to the metal surface depends on the difference in thermal properties, such as thermal expansion and thermal conductivity, as well as the difference in crystal lattice. *Spallation* is the flaking or chipping off of the surface film. Solid-gas interactions are normally evaluated by measuring the increase in material weight or the decrease in metal thickness due to development of the surface film with time. Thermodynamics of film compositions often are reported on a graph of temperature versus Gibb's free energy, *Ellingham diagrams.*

Aqueous corrosion is the chemical attack by liquids of metal surfaces. Note that prior to exposure to liquids, most metal surfaces are coated with a thin oxide surface due to prior interaction with the atmosphere. Corrosion reactions result in the dissolution of the material into the liquid. In some reactions, selective leaching or preferential removal of selected elements within the metal occurs. The corrosion reactions may also produce a protective film or precipitate on the metal surface and reduce the rate of metal-liquid interaction. The rate of metal removed from the surface depends on the diffusion rate of the dissolved metal from the surface, the kinetics of the reaction, and concentrations of the corroding element and temperature. Corrosion rates are determined by long-term immersion in solution where the corrosion rate is a measure of the material mass loss or by short-term evaluation using electrochemical tests where the corrosion rate (corrosion current) is measured as a function of material potential. Thermodynamics of corrosion reactions are plotted on Pourbaix diagrams that show the dominant state of the metal ion as a function of pH and potential (see the article “Potential versus pH (Pourbaix) Diagrams” in this Volume).

Wear is the physical removal of the surface of a material. *Erosive wear* is caused by solid or liquid particles impacting on the material surface. Cavitation erosion is caused by implosion of air bubbles formed on the surface of a solid as a result of rapid movement through a liquid (i.e., on a propeller of a ship). *Abrasive wear* is

caused by solid particles scraping across or impacting the material surface. Wear is extremely common and accounts for one-third to one-half of all equipment replacement in industry. Wear is a localized phenomenon, often the result of repeated events, and is characterized by chipping, plowing, or cutting away of the material at the surface. While individual event interactions can be almost innocuous, the cumulative effect over many events may remove a significant quantity of material and cause failure. Wear, like corrosion, is a complicated phenomenon and is influenced by a large number of factors. For example, erosion wear factors include hardness difference of the materials, relative speed, size, angle of impact, and morphology of the impacting particle and temperature.

The combination of wear and corrosion often has synergistic effects on the failure of a material. At elevated temperatures, abrasive wear can prevent the buildup of the tough, wear resistant, surface oxide layer, thus providing a continuously fresh surface for oxidation. In a liquid media, corrosion or erosion may remove a tough, protective surface film, exposing the less corrosion and erosion resistant metal to continuous attack.

Electrical, Magnetic, and Optical Properties. Electrical properties are related to the ease of moving electrons, ions, or charged molecules. This in turn is related to electron and atomic bonding and the material microstructure. Because metals share their valence electrons throughout the entire structure, there is little resistance to the ability of electrons to move. Conductivity is one of the distinguishing features of metals. Ceramics have ionic bonding, but the lattice structure does not allow for easy ionic movement. Thus ceramics are normally insulators. In organic compounds the covalent bonding between carbon atoms generally restricts the electron movement. An exception is graphite, which, because of the resonance between the interconnecting benzene rings, allows electrons to flow on a plane. Ionic and dipolar materials, while not providing good electrical conductivity, are used to store electrical energy by responding locally to electric fields that reorient their charge. This ability is utilized in capacitors and is a measure of the dielectric properties of the material. A change in shape or microstructure of a material due to an applied electric field is defined as the *Piezoelectric* effect. *Superconductivity* is the cooperative movement of a pair of electrons traveling through a lattice. This effect occurs readily at very low temperatures, from 0 to 70 K, when atomic vibrations are minimal.

Magnetic properties are related to the interaction between the inner or core electrons of atoms. Elements with the strongest magnetic properties are those in the center of row four of the periodic table (with an unfilled d-shell), row five (with an unfilled f-shell) and some of the rare earth elements. Magnetic molecules often are composed of iron-base spinel and sesquioxide compositions. *Hard* or *permanent magnets* are those materials that, once magnetized, readily retain their magnetic properties, for example, magnetic recording devices. *Soft magnets* are those materials that readily lose their magnetism, such as transformer cores.

Material response to electromagnetic energy, transmission, reflection, or absorption is a function of the material electron bonding and atomic microstructure and the wavelength of the radiation. The electrons in metals are bonded very loosely and react readily with electromagnetic fields (e.g., radio antennas). The dipole structure of ceramics and many polymers will respond to certain electromagnetic frequencies. Note that in microwave ovens, the electromagnetic frequency is chosen to resonate with the vibrational energy of water molecules and not with carbon bonds of polymers or most ceramic dipoles. Thus, food is heated selectively and not the plate. If the irradiating wavelength is less than that of the grain structure, grain boundaries will reflect the light. Light transmission is also affected by abrupt changes within a material. Thus, the amorphous structure of many polymers and ceramics will produce transparent materials. However, small changes in microstructure will result in local changes in light transmission. The local alignment of polymer chains, glazing, in response to stress, reduces the amorphous local microstructure and produces a translucent region.

Performance Maps. *Material performance maps* have been generated that relate material properties to environmental or engineering needs. (These are referred to often as *Ashby maps*). Generalized materials properties equations often can be separated into those variables that are intrinsic material properties and those variables that can be imposed upon the material by an external source. These equations present a theoretical or empirical model characterizing the response of a material. Often, as the external variable changes, a point is reached where the type or mode of material response changes; that is, the stress (external force)-strain (material response) changes with stress loading rates from creep to impact. Plots can be made using these equations with the material variable on one axis and the applied variables on the other axis. Boundaries can define regions or areas in which a range of material properties will respond in a similar manner to a range of imposed external conditions. Using these generic material performance maps, experimentally determined values for different materials can be derived. Often trends are observed between different types of materials or within a material

class that enables generalizations to be made where there may be no data to predict a material response to changing external forces. A typical Ashby map is shown in Fig. 9.

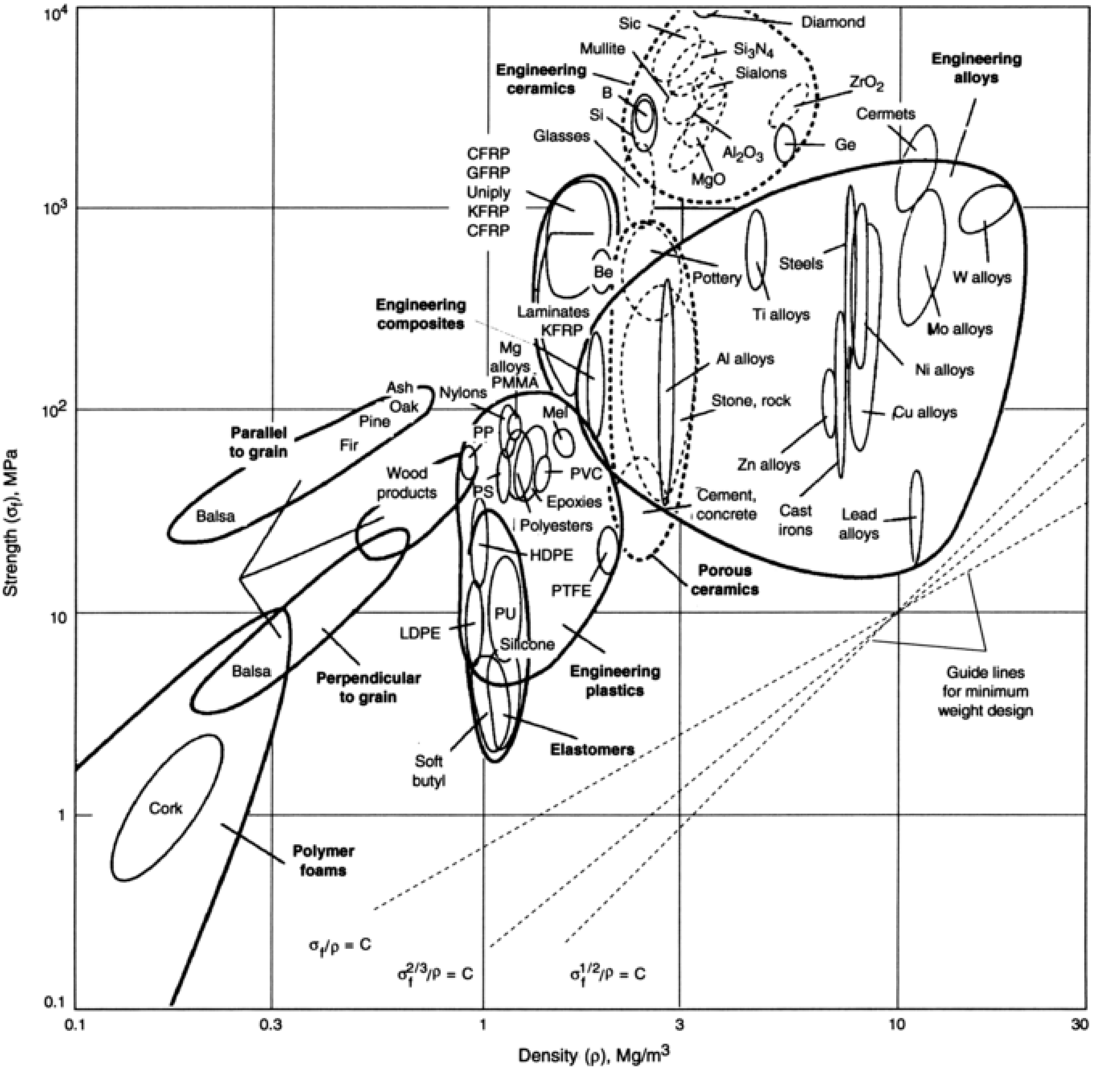

Fig. 9 Typical Ashby map. Strength, σ_f, plotted against density, ρ, for various engineered materials. Strength is yield strength for metals and polymers, compressive strength for ceramics, tear strength for elastomers, and tensile strength for composites. The guide lines of constant σ_f/ρ, $\sigma_f^{2/3}/\rho$, and $\sigma_f^{1/2}/\rho$ are used in minimum weight, yield-limited, design. Note: log scales are used to encompass the range of values.

W. Reitz and J. Rawers, Materials Basics for the Corrosionist, *Corrosion: Fundamentals, Testing, and Protection*, Vol 13A, *ASM Handbook*, ASM International, 2003, p 980–991

Materials Basics for the Corrosionist

Wayne Reitz, North Dakota State University; James Rawers, Albany Research Center

Processing

Most materials do not come from nature ready for use. They must be refined, purified, alloyed, combined with other components, and shaped into a final product. The type of processing a material receives before application greatly affects the properties of the material and thus its applications. Representative mechanical and physical property values of materials from the different groups are found in Table 6.

Table 6 Summary of mechanical and physical properties of selected engineering materials

Material name	Symbol or composition	Yield strength		Ultimate strength		Elastic modulus		Elongation at failure	Crystal structure	Electrical resistivity		Thermal conductivity		Thermal expansion		Toughness		Density	
		MPa	**ksi**	**MPa**	**ksi**	**GPa**	**10^6 psi**			**μΩ · m**	**Ω × circular-mil/ft**	**W/m · K**	**Btu/h · ft · °F**	**10^{-6}/K**	**10^{-6}/°F**	**MPa$\sqrt{m}$**	**ksi$\sqrt{in.}$**	**g/cm^3**	**lb/in.^{3}**
Metals																			
1018 steel	Fe-0.18C	350	51	450	65.3	200	29	0.3	bcc	0.13	78	80	46.2	10	5.56	100	91	7.8	0.28
1080 steel	Fe-0.80C	500	73	600	87.0	200	29	0.2	bcc	0.18	110	80	46.2	10	5.56	100	91	7.8	0.28
Cast iron	Fe-3.5C	20	3	250	36.3	100	14.5	0.5	bcc	0.5	300	80	46.2	10	5.56	3	2.73	7.8	0.28
Stainless steel	Fe-18Cr-15Ni	200	29	500	72.5	200	29	0.5	fcc	0.72	430	25	14.4	10	5.56	80	72.8	7.9	0.28
Copper	Cu	100	15	400	58.0	120	17.4	0.55	fcc	0.018	11	400	231.2	20	11.12	80	72.8	8.9	0.32
Zinc	Zn	20	3	50	7.3	100	14.5	0.65	hcp	0.06	36	110	63.6	40	22.24	10	9.1	7.1	0.26
Brass	70Cu-30Zn	300	44	500	72.5	80	11.6	0.5	bcc	0.06	36	300	173.4	30	16.68	50	45.5	8.5	0.31
Ti-6-4	Ti-6Al-4V	140	20	240	34.8	120	17.4	0.3	hcp	1.6	940	10	5.8	10	5.56	100	91	4.5	0.16
2024 aluminum	Al-4Cu	20	3	50	7.3	100	14.5	0.5	fcc	0.045	27	250	144.5	20	11.12	40	36.4	2.7	0.10
NiAl	NiAl	250	36	1000	145.0	200	29	0.5	fcc/bcc	1.3	700	…	…	5	2.78	5	4.55	6	0.22
Ceramics																			
Quartz	SiO_2	7200	1044	7200	1044.0	74	10.73	0	Cryst	10^{17}	6×10^{19}	2	1.2	8	4.448	1	0.91	2.7	0.10
Glass	SiO_2-10CaO-13Na_2O	36	5	36	5.2	100	14.5	0	Amor	10^{17}	6×10^{19}	38	22.0	1	0.556	1	0.91	2.5	0.09
Portland cement	63CaO-22SiO_2-6Al_2O_3-3Fe_2O_3-3MgO	30	4	30	4.4	100	14.5	0	Amor	…	…	14.5	…	5	2.78	2	1.82	2.4	0.09
Refractory brick	$(Al,Na,Mg)_2(Si_2O_5)(OH)_4$	4	1	5	0.7	100	14.5	0	Amor	…	…	…	…	5	2.78	2	1.82	2.3	0.08
Al_2O_3	Al_2O_3	20	3	200	29.0	350	50.75	0	Cryst	10^{19}	6×10^{21}	20	11.6	6	3.336	4	3.64	3.8	0.14
TiC	TiC	250	36	250	36.3	300	43.5	0	Cryst	…	…	26	15.0	7	3.892	4	3.64	4.5	0.16
Organics																			
Polyvinyl chloride	$-(-CH_2-CHCl-)_n-$	45	7	60	8.7	4	0.58	1	Amor	10^{17}	6×10^{19}	0.2	0.1	70	38.92	5	4.55	1.4	0.05
Polyester	…	40	6	80	11.6	4	0.58	3	Amor	10^{18}	6×10^{20}	0.2	0.1	70	38.92	5	4.55	1.4	0.05
Polyethylene	$-(-CH_2-CH_2-)_n-$	15	2	30	4.4	1	0.145	3	Amor	10^{12}	6×10^{14}	0.3	0.2	70	38.92	5	4.55	0.9	0.03
Teflon	$-(-CFl_2-CFl_2-)_n-$	20	3	50	7.3	0.5	0.0725	4	Amor	10^{19}	6×10^{21}	0.2	0.1	100	55.6	5	4.55	2.2	0.08
Nylon	$-(-CO-4CH_2-CO-N-CH_2-N-)_n-$	50	7	70	10.2	3	0.435	3	Amor	10^{19}	6×10^{21}	0.2	0.1	80	44.48	5	4.55	1.2	0.04

Bakelite	$-(C_6H4-OH-CH_2)_n-$	40	6	50	7.3	6	0.87	0.02	Amor	…	…	0.1	0.1	20	11.12	0.1	0.091	1.5	0.05
Rubber	…	10	1	30	4.4	1	0.145	5	Amor	10^{14}	6×10^{16}	0.1	0.1	150	83.4	5	4.55	1.2	0.04
Wood, oak	…	50	7	70	10.2	12	1.74	0.2	Amor	…	…	0.4	0.2	…	…	1	0.91	0.7	0.03
Wood, pine	…	30	4	50	7.3	8	1.16	0.2	Amor	…	…	0.4	0.2	…	…	1	0.91	0.3	0.01

Cryst, crystalline. Amor, amorphous

Ceramics often are classified as being either low tech or high tech. Traditional or low-tech materials are those that are mined and, with little refinement, are ready for applications. Such materials include clays and silicates for bricks, pottery, concrete, and refractories. Advanced, or high-tech, ceramics are those with an application requiring a high degree of purity. Such materials include SiO_2 for semiconductors and TiO_2 for paints.
Most ceramics processing begins with powders. Because of their high melting points, many ceramic products are sintered-bonded powders. In *sintering,* the ceramic powders are blended with binders or other low melting ceramic powders or formed into a slurry. The new composition is formed into a near final shape, or green product, and heated for sufficient time so that the particles either surface diffusion bond together or the lower melting ceramic melts and forms a thin layer that holds the higher melting particles together. In many ceramic products the final composition has a fine structure porosity as high as 6 to 10%.
The ionic bonding of atoms in ceramics forms molecules that often have highly ordered localized structure. When these ceramics are cooled, they often do not go through a definite phase transition from liquid to solid. With decreasing temperature, the mobility of molecules becomes limited, and they may not be able to align themselves into a perfectly repeating lattice. The liquid viscosity continues to increase, eventually reaching a state where there is no molecular movement. This noncrystalline or amorphous structure is called *glass.* In commercial silica glasses, additives are placed in the SiO_2 to reduce long-range order present in quartz, lower the melting temperature, and increase the viscosity. The resulting ceramic alloy can be formed readily into a final shape that will be retained at room temperature.
By alloying, it is possible to reduce greatly the alloy melting point (T_m) beyond that of the individual elements or molecules. Commercial glass is made by alloying SiO_2 with $T_m \approx 1700$ °C (3100 °F) with Na_2O having $T_{dissoc} \approx 1300$ °C (2370 °F) and CaO, $T_m \approx 2600$ °C (4710 °F). The resulting softening, or melting, temperature can be as low as 800 °C (1470 °F). Similarly, low melting glazes (e.g., $CaO{\cdot}Al_2O_3{\cdot}2SiO_2$) are applied to the surface of ceramic green products (such as pottery and tableware) prior to firing so that, when heated, the glaze melts and forms a continuous, impermeable surface.
The difference in thermal conductivity and thermal expansion between ceramics and metals makes bonding between these materials very difficult and often requires a series of intermediate steps. Because of the somewhat open structure of ceramics at low temperatures, organic glues can be used to bond ceramics to other materials. Because ceramics have good resistance to oxidation, many being composed of oxides and having low thermal conductivity, often they are used as coatings or protective barriers on metals for high temperature applications. In the ceramic- metal composite, the ceramic component offers protection from the environment while the metal component provides the necessary strength and resistance to catastrophic failure.
Organics. The most common organic materials considered here are polymer-based plastics. These are long chain materials with carbon as their backbone. They are formed by reacting smaller size molecules called *mers* or *monomers* together to form *polymers. Plastics* are blends of polymers with different polymer lengths or with different polymer compositions. The structure of the polymer chains and length of the chains control many of the plastic properties. Monomers can be as simple as a two carbon molecule or can be very long carbon chains, which may contain small side chains. *Polymerization* is the reaction of individual similar monomers resulting in polymer of repeating similar units. In addition to reaction between similar mers, *copolymerization* occurs when the reaction is between different monomers. These reactions can be stimulated by temperature, by catalysts, or by reaction between the monomers themselves. Poly[chmerization and copolymerization are often incorporated into the final production step of plastic products.
Individual polymers interact by directly linking between the different polymer chains, by weak van der Waals bonding between atoms on different chains, or by mechanical interlocking of the polymer chains. Plastics generally have an amorphous microstructure; however, chains may be aligned partially during fabrication by drawing the polymers through dies. *Thermoset* plastics are formed in final shape by placing the polymers or combination of polymers in a final shape die and then stimulating the reaction that initiates the cross linking between polymers. *Thermoplastics* are formed most often into their final shape by high-pressure extrusion, often at elevated temperature.
Plastics often are joined by means of organic glues. These glues are organic polymer compounds designed to penetrate into the open, amorphous structure of plastics and break the bonds between polymer chains. When the glue dries or the glue polymer is stimulated to undergo a chemical reaction with itself and/or the material it has penetrated, the glued polymers become interlocked with polymer chains inside the surface of the softened polymers.

Metals. There are over 80 different elements that can form metals. Most of these elements can be combined with other metallic elements to form alloys. Very few metals can be found in nature with sufficient purity to be used directly. Metals often are derived from mined minerals, or ores, such as oxides, sulfides, and carbonates. Metal ores are refined or reduced to pure metal elements by a number of different reactions. Examples are:

$$Fe_2O_3 + 2C \rightarrow Fe + FeO + 2CO$$

$$FeO + C \rightarrow Fe + CO$$

$$TiO_2 + Cl_2 + C \rightarrow TiCl_4 + CO_2$$

$$TiCl_4 + 2Mg \rightarrow Ti + 2MgCl_2$$

$$PbS + O_2 \rightarrow Pb + SO_2$$

After refinement, the elemental metal can be further processed by combining different metals to form alloys: Fe + Cr + Ni yields stainless steel; Cu + Zn yields brass; Pb + Zn yields solder. Elements are alloyed to alter or augment specific properties—to increase corrosion resistance (i.e., Cr in stainless steel), to increase strength (i.e., Zn in brass), or to lower melting point (i.e., Pb in solder).

The microstructure of the final product is controlled by the metal chemistry and the fabrication steps. During solidification, if the cooling rate is rapid, there is insufficient time for the entire system to maintain thermal equilibrium. Initially at the solid-liquid interface, there is rapid grain nucleation producing a large number of small grains. The large difference in temperature enhances preferential grain growth in certain lattice directions, resulting in the solidification front limiting the number of grains that grow and producing elongated structures, *columnar grains,* or elongated treelike structures, *dendritic grains.* As the temperature gradient is reduced, the solidification front slows, and grain nucleation can again occur resulting in equiaxed grain structure in the interior of a casting.

During cold working, grains become flattened and elongated *platelet grains* in the rolling direction. Rapid cooling or reheating of a cold worked structure produces *equiaxed grains.* During the initial solidification of a metal, a high cooling rate may prevent the entire system from being in chemical equilibrium. Elemental segregation may result from different solubility levels at different temperatures and the inability of elements to diffuse rapidly through the solid to produce a uniform composition. Alloys often are held at elevated temperature after casting to allow sufficient time for atomic diffusion and to *normalize,* or homogenize, the composition throughout the microstructure.

After melting, the metal is cast into either near-net-final shape or into slabs or billets. Slabs and/or billets are processed further by either hot or cold working. In *hot working* a material is deformed at elevated temperatures where the yield strength is lower than at room temperature and the material does not work harden. During *cold working,* often done as a final processing step after several hot working operations, the material stores up elastic energy and its yield strength is increased. The energy can be reduced by a quick heat treatment (anneal) during which the elastic energy is dissipated and recrystallization occurs, resulting in new grain development or refinement and an overall material grain size reduction.

Because different elements can be combined readily to form alloys of different composition, a common means of joining alloys together is to weld them by melting their interface surface and allowing the molten material to form a new alloy during solidification. *Soldering* and *brazing* are forms of metallic glues. When applied, they are molten and the solder or braze wets (or reacts) with the metal surface, which can be thought of as a very thin weld zone. Fluxes are compounds that remove the surface metal oxide layer present on all metal surfaces and aid the solder or braze in bonding the metal surfaces.

Welding melts the metal surface and can generate several changes in the microstructure of metals. The resolidified region, melt zone, and the region adjacent to the melt zone, the heat- affected zone (HAZ) will often possess a different microstructure than that of the bulk material being joined. These zones can result in changes in material properties, most often mechanical and corrosion properties. The metal near a weld is annealed and is often a region of inhomogeneity.

Composites. The large range of possible structures and materials that are employed in composites (Table 2) is the result of a wide variety of processing techniques. Numerous techniques have been developed for creating particular composite structures, many of which are unique to a particular composite set of materials and microstructure. Examples include:

- *Surface processing* to improve surface hardness, enhance wear resistance, increase fatigue life, and/or improve corrosion-oxidation resistance. Techniques include laser processing, ion implanting, and shot and ball peening.
- *Surface coatings* to reduce surface interactions. Techniques include thermal spray (coating with metals and ceramics), painting (coating with organics), and vapor deposition and plating.
- *Coprocessing* to place a second phase in the interior of the structure. Techniques include coextrusion of polymers to form fiberglass, metal pipes, and layering of wood between organic glues to form plywood.
- *In situ processing* of materials in which a second phase is formed as part of the processing of the material. Techniques include heat treatment of metal alloys to form precipitates (often resulting in selected grain growth characteristics) and induction heating of polymers to form a different bonding structure in the interior than on the surface.

The field of composites is expanding rapidly with an ever-expanding array of processing techniques. Care must be taken, however, as processing of the composite may change the properties of the starting materials (e.g., thermal processing of metals may eliminate the cold work structure of metals). Thought must also be given to the long-term application for which the composite is designed. Long-term exposure at elevated temperature or thermal cycling may result in debonding between the composite phases if differences in thermal expansion and thermal conductivity are too great. These differences in thermal properties must be considered, along with mechanical stress concentrations, when joining different materials together. Long-term aging of composites may result also in diffusion of elements from one composite phase into the second, changing the properties of the composite materials or forming a unique phase at the two-phase interface, again changing the microstructure and overall properties of the composite.

W. Reitz and J. Rawers, Materials Basics for the Corrosionist, *Corrosion: Fundamentals, Testing, and Protection*, Vol 13A, *ASM Handbook*, ASM International, 2003, p 980–991

Materials Basics for the Corrosionist

Wayne Reitz, North Dakota State University; James Rawers, Albany Research Center

---

Material Design, Application, and Failure

Materials currently are being chosen and composites designed to meet ever more demanding specifications. To ensure safe and economic designs and applications, industry, materials organizations, and government have established codes and regulations that materials are expected to meet before being placed in service. The codes or regulations require extensive testing before the material receives certification. These requirements are based on experience and knowledge learned over years of trial and error.

Material failure can occur because the wrong material was used, the material had a preexisting manufacturing defect, there was an engineering design flaw, abuse occurred and the material was degraded, or the design load limits were exceeded. With the development of better understanding of materials and their responses to different environments, the choice of a material for a particular application is no longer by chance or limited to past experience. Manufacturing techniques have improved significantly, and reproducibility and reliability of a consistent final product is realized by implementation of quality assurance programs. Engineering design has been improved greatly by computer design programs that allow for ever greater analysis. Current software programs can be used to understand the effect of environment and catastrophic events, to incorporate safety factors, to determine when safety checks should be performed, and to predict service lifetime before failure.

All products eventually fail or become no longer usable or obsolete. The service life of materials can be extended by proper maintenance and inspection. Proper material design and understanding can produce a product that performs safely for a specified time before it needs to be taken out or service; that is, before loss of function, catastrophic failure, and damage occurs. Most of the failures of today are not the result of a single

factor but result from a number of one-time events, none of which would cause failure by itself but when all are taken together, result in failure. The more common events that lead to failure are:

- Failure to note and report the occurrence of an unusual event (such as an overload of one type or another)
- The failure of inspection (either not performed or incomplete)
- Change of procedure or application
- Change of environment

The study of materials is a continuously evolving field. New demands are placing greater emphasis on new applications of old materials, on newer materials with better properties, and on greater understanding of both the fundamentals of material science and engineering design.

W. Reitz and J. Rawers, Materials Basics for the Corrosionist, *Corrosion: Fundamentals, Testing, and Protection,* Vol 13A*, ASM Handbook,* ASM International, 2003, p 980–991

Materials Basics for the Corrosionist

Wayne Reitz, North Dakota State University; James Rawers, Albany Research Center

---

Selected References

General

- *Annual Book of ASTM Standards,* ASTM International
- M.F. Ashby and D. Jones, *Engineering Materials,* 2nd ed., Vol 1 and 2, Butterworth-Heinemann, 1996
- M.F. Ashby, *Materials Selection in Mechanical Design,* 2nd ed., Butterworth-Heinemann, 1999
- D.R. Askeland, *The Science and Engineering of Materials,* 3rd ed., PWS Publishing, 1999
- *ASM Handbook,* Vol 20, *Materials Selection and Design,* ASM International, 1997
- G.S. Brady, H.S. Clauser, and J.A. Vaccari, *Materials Handbook,* 15th ed., McGraw-Hill, 2002
- K.G. Budinski and M.K. Budinski, *Engineering Materials: Properties and Selection,* 7th ed., Prentice Hall, 2001
- T.H. Courtney and D. Simchi-Levi, *Mechanical Behavior of Materials,* 2nd ed., McGraw- Hill, 1999
- H.E. Davis, G. Houck, and G.E. Troxell, *Testing of Engineering Materials,* 4th ed., McGraw-Hill, 1982
- *Engineered Materials Handbook Desk Edition,* ASM International, 1995
- D. Henkel and A.W. Pense, *Structures and Properties of Engineering Materials,* 5th ed., McGraw-Hill, 2001

Metals

- *Properties and Selection: Irons, Steels, and High-Performance Alloys,* Vol 1, *ASM Handbook,* ASM International, 1990
- *Properties and Selection: Nonferrous Alloys and Special-Purpose Materials,* Vol 2, *ASM Handbook,* ASM International, 1990
- H. Chandler, *Metallurgy for the Non-Metallurgist,* ASM International, 1998
- J.R. Davis, Ed., *Metals Handbook Desk Edition,* 2nd ed., ASM International, 1998
- G.E. Dieter, *Mechanical Metallurgy,* 3rd ed., McGraw-Hill, 1986
- R.W. Hertzberg, *Deformation and Fracture Mechanics of Engineering Materials,* John Wiley and Sons, 4th ed., 1995
- R.E. Reed-Hill and R. Abbaschian, *Physical Metallurgy Principles,* 3rd ed., PWS Publishing, 1992
- L. Van Vlack, *Elements of Materials Science,* 6th ed., Addison-Wesley, 1989
- J.R. Brown, Ed., *Foseco Foundryman's Handbook,* 10th ed., Butterworth-Heinemann, 1994

Ceramics

- M.W. Barsoum, *Fundamentals of Ceramics,* McGraw-Hill, 1996
- *Ceramics and Glasses,* Vol 4, *Engineered Materials Handbook,* ASM International, 1991
- W.D. Kingery, H.K. Bowen, and D.R. Uhlman, *Introduction to Ceramics,* 2nd ed., John Wiley & Sons, 1976
- S. Mindess, J.F. Young, and D. Darwing, *Concrete,* 2nd ed., Prentice Hall, 2002
- J.S. Reed, *Principles of Ceramic Processing,* 2nd ed., John Wiley and Sons, 1995
- J.B. Wachtman, *Structural Ceramics,* Academic Press, 1989

Polymers

- *Engineered Materials Handbook,* Vol 2, *Engineering Plastics,* ASM International, 1988
- J.R. Fried, *Polymer Science and Technology,* 2nd ed., Prentice-Hall, 2003
- C.A. Harper, *Handbook of Plastics, Elastomers, and Composites,* 4th ed., McGraw-Hill, 2002
- *Modern Plastics Encyclopedia,* McGraw-Hill (annual)
- A.B. Strong, *Plastics—Materials and Processing,* Prentice Hall, 2000
- Z. Tadmor and C.G. Gogos, *Principles of Polymer Processing,* John Wiley & Sons, 1979

Wood

- H.E. Desch, *Timber: Structure, Properties, Conversion, and Use,* 7th ed., Haworth Press, 1996
- B. Madsen, *Structural Behaviour of Timber,* Timber Engineering Ltd., 1992

Composites

- *Composites,* Vol 21, *ASM Handbook,* ASM International, 2001
- C.T. Herakovich, *Mechanics of Fibrous Composites,* John Wiley and Sons, 1997
- S. Suresh, A. Mortensen, and A. Needleman, *Fundamentals of Metal-Matrix Composites,* Butterworth-Heinemann, 1993

Processing

- *Alloy Phase Diagrams,* Vol 3, *ASM Handbook,* ASM International, 1992
- *Heat Treating,* Vol 4, *ASM Handbook,* ASM International, 1993
- *Surface Engineering,* Vol 5, *ASM Handbook,* ASM International, 1995
- *Welding, Brazing, and Soldering,* Vol 6, *ASM Handbook,* ASM International, 1993
- *Powder Metal Technologies and Applications,* Vol 7, *ASM Handbook,* ASM International, 1998
- *Forming and Forging,* Vol 14, *ASM Handbook,* ASM International, 1988
- *Casting,* Vol 15, *ASM Handbook,* ASM International, 1988
- *Machining,* Vol 16, *ASM Handbook,* ASM International, 1989
- C.R. Brooks, *Heat Treatment, Structure, and Properties of Nonferrous Alloys,* ASM International, 1990
- J.W. Christian, *The Theory of Transformations in Metals and Alloys,* 2nd ed., Pergamon Press, 1975
- G. Krauss, *Steels: Heat Treatment and Processing Principles,* ASM International, 1990
- J.W. Martin, *Precipitation Hardening,* 2nd ed., Butterworth-Heinemann, 1999
- H. Okamoto, *Desk Handbook: Phase Diagrams for Binary Alloys,* ASM International, 2000

Testing and Failure Analysis

- *Mechanical Testing and Evaluation,* Vol 8, *ASM Handbook,* ASM International, 2000
- *Metallography and Microstructures,* Vol 9, *ASM Handbook,* ASM International, 1985
- *Materials Characterization,* Vol 10, *ASM Handbook,* ASM International, 1986
- *Failure Analysis and Prevention,* Vol 11, *ASM Handbook,* ASM International, 2002
- *Fractography,* Vol 12, *ASM Handbook,* ASM International, 1987
- *Nondestructive Evaluation and Quality Control,* Vol 17, *ASM Handbook,* ASM International, 1989

- *Friction, Lubrication, and Wear Technology,* Vol 18, *ASM Handbook,* ASM International, 1992
- *Fatigue and Fracture,* Vol 19, *ASM Handbook,* ASM International, 1996
- V.J. Colangelo and F.A. Heiser, *Analysis of Metallurgical Failures,* 2nd ed., John Wiley & Sons, 1987
- J.A. Collins, *Failure of Materials in Mechanical Design,* 2nd ed., John Wiley & Sons, 1993
- K.A. Esaklul, *Handbook of Case Histories in Failure Analysis,* ASM International, Vol 1, 1992; Vol 2, 1993
- A.J. McEvily, *Metal Failures: Mechanisms, Analysis, Prevention,* John Wiley & Sons, 2002
- D.J. Wulpi, *Understanding How Components Fail,* 2nd ed., ASM International, 1999

S. Shah, Applications of Modern Analytical Instruments in Corrosion, *Corrosion: Fundamentals, Testing, and Protection,* Vol 13A, *ASM Handbook,* ASM International, 2003, p 992–998

Applications of Modern Analytical Instruments in Corrosion

Sadiq Shah, Western Illinois University

Introduction

CORROSION is a redox process at the metal- liquid or metal-air reactive interface. Identifying effective means to prevent corrosion requires an understanding of corrosion mechanisms under a variety of environmental conditions. However, unraveling corrosion mechanisms is not always a straightforward process. An understanding of the mechanistic details requires conducting experiments under simulated and controlled laboratory conditions. Ideally, it requires real time monitoring of the corrosion reactions under these conditions at a molecular or atomic level. To gain an insight into the mechanism of corrosion, both in situ (at the original location) and ex situ (away from the original location) techniques have been employed successfully over the last couple of decades (Ref 1). However, real time in situ experiments generally require controlled laboratory conditions. Several articles in the Section "Corrosion Testing and Evaluation" address controlled laboratory testing.

Alternatively, one can use ex situ analytical techniques that are capable of analyzing surfaces before and after the corrosion reaction, thus following the changes in metallurgy and chemistry at the interfaces under a given set of environmental conditions. This article reviews a variety of surface-sensitive ex situ analytical techniques that have been successfully used in understanding corrosion processes and identifying the nature of protective corrosion inhibitor films. The focus of this review is to explain the principles of various surface-sensitive techniques and the usefulness and limitations of these techniques (Ref 2, 3, 4, 5). To gain additional insight into the use of various surface-sensitive analytical techniques for applications in corrosion science, various examples from the recent literature are cited.

References cited in this section

1. S. Shah, Ed., *Surface and Interface Characterization in Corrosion,* NACE International, 1994

2. M. Riviere, *Handbook of Surface and Interface Analysis Methods of Problem Solving,* Marcel Dekker, Inc., 1998

3. R. Howland, L. Benatar, and C. Symanski, *A Practical Guide to Scanning Probe Microscopy,* DIANE Publishing Co., Collingdale, PA, 1998

4. J. Lipkowski and P.N. Ross, *Imaging of Surfaces and Interfaces,* John Wiley & Sons, Inc., 1999

5. A. Hubbard, *The Handbook of Surface Imaging and Visualization,* CRC Press, 1995

S. Shah, Applications of Modern Analytical Instruments in Corrosion, *Corrosion: Fundamentals, Testing, and Protection,* Vol 13A*, ASM Handbook,* ASM International, 2003, p 992–998

Applications of Modern Analytical Instruments in Corrosion

Sadiq Shah, Western Illinois University

Strategy for Selecting Analytical Approaches

Various techniques can be used to analyze corrosion product samples removed from the surface and also small samples of the base metallurgy. However, this approach may require dissolving the sample in a suitable solvent system and then analyzing the solution. For such samples, one needs to be aware of the limitations during the sample preparation step. These limitations include the possibility of a change in the chemical nature of the corrosion product or incomplete sample transfer during sample preparation steps. This can result in revealing inaccurate or incomplete information about the chemical composition of the sample.

An ideal approach is to analyze surfaces and corrosion-product deposits by direct surface-sensitive analytical techniques when possible. It should be pointed out that no single analytical technique can answer all questions well; instead, a strategy involving the use of a suitable combination of analytical techniques is necessary to learn as much about the corrosion mechanism as possible. The Selected References cited here clearly demonstrate the importance of this strategy in corrosion science. A clear understanding of the mechanism of corrosion will help identify effective corrosion analysis and prevention techniques.

Modern analytical methods for analyzing surfaces for corrosion and corrosion inhibition processes as well as for failure analysis can be classified into two main categories: (a) surface structure and (b) chemical identity and composition. These categories are based strictly on the nature of the questions to be addressed, such as insight into surface topography or surface structure, or understanding the chemical nature and identity at a molecular and atomic level. Table 1 lists a broad spectrum of the surface-sensitive analytical techniques, the principles of respective techniques, and the information they reveal. These techniques are described in more detail under the section devoted to each analytical method.

Table 1 Surface sensitive analytical techniques, principles and applications

Analytical technique	Principle	Target information
Surface structure techniques		
Scanning electron microscopy (SEM)	Incident electron beam generates a secondary electron emission that is used to generate the surface image.	Microscopic imaging of the surface structure
Atomic force microscopy (AFM)	Microscopic force sensor (cantilever) is used to sense the force between a sharp tip and the sample surface as the sample is scanned to generate an image.	Imaging of insulated surface structure at atomic resolution
Scanning tunneling microscopy (STM)	Tunneling current is monitored as the probe tip is scanned over a surface of interest in the x-y plane to generate an image.	Imaging of conducting surface structure at atomic resolution
Optical microscopy	Reflected light is used to generate a magnified image.	Macroscopic surface structure details
Chemical identity and composition techniques		

Energy dispersive x-ray spectroscopy (EDS)	Incident electron beam generates emission of x-rays characteristic of elements present at the surface.	Elemental identification of the surface species
Wavelength dispersive x-ray spectroscopy (WDS)	The principle is the same as that for EDS except the emitted x-rays are measured one wavelength at a time.	Elemental identification of the surface species with higher resolution and sensitivity than EDS
X-ray diffraction (XRD)	Diffraction of the incident x-ray beam from various plans of crystal lattice create a diffraction pattern characteristic of the sample.	Elemental and phase identity and composition of inorganic corrosion product
Auger electron spectroscopy (AES)	Incident electron beam initiates a multistep process to facilitate the ejection of an outer shell electron. The energy of this ejected electron is characteristic of the surface atoms.	Elemental identity and composition of the surface species and the depth profile
X-ray photoelectron spectroscopy (XPS) or ultraviolet photoelectron spectroscopy (UPS)	Incident x-rays or ultraviolet photons on the surface eject photoelectrons. The energy of the photoelectrons is characteristic of the surface atoms.	Elemental identity and composition of the surface species, the electronic structure, chemical bonding, and elemental depth profile
Ion scattering spectroscopy (ISS)	The energy of scattered primary ions from the surface allows identification of surface atoms.	Chemical composition of the surface films at atomic and a molecular level
Secondary ion mass spectrometry (SIMS)	Incident ion beam ejects the surface atoms as ions, and mass of these secondary ions is measured.	Chemical composition of the surface adsorbed species
Extended x-ray absorption fine structure (EXAFS)	The x-ray absorption generates the interference effects between emitted photoelectron waves and backscattering waves characteristic of the local structure.	Composition of adsorbed species, number, and separation distances of surface atoms
Fourier transform infrared absorption spectroscopy (FTIR)	The absorption of the infrared photons results in vibrational excitation that is characteristic of the surface molecules and the environment.	Vibrational structure of molecules and bonding interactions with the surface and the surroundings
Raman and surface enhanced Raman spectroscopy (Raman, SERS)	Energy shifts of the scattered photons are characteristic of the molecular identity.	Vibrational structure of adsorbed molecules on the surface

S. Shah, Applications of Modern Analytical Instruments in Corrosion, *Corrosion: Fundamentals, Testing, and Protection*, Vol 13A, *ASM Handbook*, ASM International, 2003, p 992–998

Applications of Modern Analytical Instruments in Corrosion

Sadiq Shah, Western Illinois University

Surface-Structure Analysis

Examination of the surface structure pre- and post-corrosion can often reveal clues to the nature of the corrosion process, the role of the base metal, and the role of environmental conditions in the process. For

surface topographic details one may utilize microscopic techniques capable of revealing surface structure from the macroscopic level to the atomic level. These techniques include optical microscopy, scanning electron microscopy (SEM), atomic force microscopy (AFM), and scanning tunneling microscopy (STM) (Ref 6). Optical microscopes can magnify the surface structure to a certain magnification level. Higher magnification to micron levels requires the use of SEM, and for atomic and molecular level resolution, AFM or STM is required. While both AFM and STM are capable of revealing the structure at atomic and molecular levels, AFM is generally useful for electrically nonconducting surfaces and STM for conducting surfaces. When considering the use of SEM on organic surfaces, the analyst must foresee the possibility of thermal damage to the surface.

Reference cited in this section

6. L.A. Bottomley, J.E. Coury, and P.N. First, Scanning Microscopy, *Anal. Chem.*, Vol 68, 1996, p 185R–230R

S. Shah, Applications of Modern Analytical Instruments in Corrosion, *Corrosion: Fundamentals, Testing, and Protection*, Vol 13A, *ASM Handbook*, ASM International, 2003, p 992–998

Applications of Modern Analytical Instruments in Corrosion

Sadiq Shah, Western Illinois University

Determination of Chemical Composition

An understanding of the chemical identity of a metal surface before and after corrosion can reveal the mechanistic details of the corrosion reaction. The study may require analysis of the corrosion products or the corrosion inhibitor films after the corrosion reaction. Compositional analysis can also suggest the nature of the interaction between the metal surface and the aggressive species that led to the corrosion reaction or interaction of the corrosion inhibitor molecules for corrosion protection (Ref 7). A variety of analytical tools can be used to gain such information. Thus the analytical techniques for surface analysis can be divided into two classes, namely, (a) techniques used for the analysis of the metal surface and metal oxides and (b) those used for the analysis of the corrosion product and corrosion protective organic films.

Analysis of Metal Surfaces and Metal Oxides. The analysis of the metal samples to identify the chemical nature of the base metallurgy and the surface oxide films, including the protective passive film, can be accomplished by the use of various surface sensitive analytical techniques. These techniques include energy dispersive x-ray spectroscopy (EDS), wavelength dispersive x-ray spectroscopy (WDS), Auger electron spectroscopy (AES), x-ray photoelectron spectroscopy (XPS) also referred to as electron spectroscopy for chemical analysis (ESCA), ultraviolet photoelectron spectroscopy (UPS), ion scattering spectroscopy (ISS), secondary ion mass spectrometry (SIMS) and extended x-ray absorption fine structure (EXAFS). While x-ray diffraction (XRD) is not a surface technique, it is widely used for the analysis of metals, alloys, and the mineral contents and phase identifications of corrosion product.

Analysis of Corrosion Products and Protective Inhibitor Films. For the analysis of the corrosion product or protective films that are expected to be primarily inorganic in nature, EDS, AES, XPS, ISS, SIMS and EXAFS generally are suitable techniques. However, for corrosion inhibitor films that are primarily organic in nature, Fourier transform infrared (FTIR) spectroscopy, Raman or surface enhanced Raman spectroscopy (SERS), SIMS, ISS, and XPS are the most appropriate techniques. For routine analysis of the molecular nature of the film, FTIR is the most versatile and inexpensive nonvacuum technique. Even though Raman and SERS can also provide information regarding the molecular nature of the film, these techniques require a fair amount of additional instrumental sophistication and experience. The vacuum techniques SIMS, ISS, and XPS require expensive instrumentation and extensive experience. A number of private analytical service laboratories around the country offer these techniques.

Reference cited in this section

7. S. Shah, Corrosion: An Interfacial Process, *Corrosion 91*, "Paper 75," 1991, p 1–22

S. Shah, Applications of Modern Analytical Instruments in Corrosion, *Corrosion: Fundamentals, Testing, and Protection*, Vol 13A, *ASM Handbook*, ASM International, 2003, p 992–998

Applications of Modern Analytical Instruments in Corrosion

Sadiq Shah, Western Illinois University

Analytical Methods

In general, surface-sensitive techniques involve irradiation of the surface of interest with photons, x-rays, electrons, or an ion beam. The scattered, emitted, or reflected beam then carries with it information regarding the chemical identity of the surface atoms or molecules. An overview of commonly used surface-sensitive techniques for analysis of the surface, atomic, and molecular structures is given next.

Surface Topological Structure

Surface structural details can be examined by a variety of the analytical techniques with resolution ranging from the macroscopic level to the atomic and molecular level. These techniques are based on varied principles.

Optical Microscopy. A simple optical microscope can magnify the surface topological details to a level revealing critical details not visible to the naked eye. With the use of appropriate optics, the microscope utilizes optical reflections from a surface of interest to generate an image of the surface structure. However, it does not allow for the identification of the chemical nature of surface structures. The spatial resolution of this technique is limited to approximately 1 μm. This simple technique generally can be an important first step to survey the macroscopic surface details of a sample.

Scanning Electron Microscopy. In contrast to optical microscopy, which relies on photons, the SEM approach relies on an incident beam of electrons. Under ultrahigh vacuum an electron beam is focused on the surface of interest, and the secondary electrons emitted from the surface are used to generate the image of the surface structural details. The incident beam energy can be as high as 30 keV (1.15 kcal); however, the secondary emitted electrons have energy of a few tens of eV (cal). The images generated by the emitted electrons are sensitive to the orientation of the incident beam, the relative orientation of the detector, and the organic or inorganic chemical nature of the surface.

The spatial resolution is on the order of less than 100 nm (3.9×10^{-6} in.). SEM can magnify surface structures from 10 to 30,000 times. Care should be exercised in examining organic surface films or polymeric samples. These organic films can be thermally degraded by the high-energy incident electron beam. Thus, the lowest possible energy should be used for the incident electron beam. To improve the contrast, some surfaces may require gold, carbon, or palladium coating prior to SEM examination; however, here too thermal degradation must be a consideration. This technique has been used routinely for analyzing the surface structure, including the failure analysis of structures used in a broad range of applications (Ref 8, 9, 10, 11, 12, 13, 14). While SEM imaging relies on the emission of secondary electrons from the sample surface, another similar technique relies on the back-scattered incident electrons and is referred to as back-scattered electron imaging (BEI). In this technique the intensity of the back-scattered electrons depends on the atomic number of the elements present in the sample. The higher the atomic number of the elements present in the sample, the higher is the number of the back-scattered electrons. As a result, lower atomic number elements absorb more incident electrons and therefore appear dark in the micrographs. Similarly, higher atomic number elements scatter a larger number of the incident electrons, thereby making the micrograph bright. Thus on flat samples this technique can be

informative. In general this sensitivity of BEI to the atomic number can be used to make qualitative decisions about structure and compositions.
An extension of SEM is environmental scanning electron microscopy (E-SEM) where samples can be examined under relatively higher pressures than those involved in the traditional SEM (Ref 15). The pressure conditions allow for examination of the surface structure under atmospheres of water vapors, air, argon, nitrogen, or other gases or vapors. This allows for a dynamic characterization of the corrosion process and wetting, drying, melting, and crystallization processes. However, the instrumentation is not as common as that used for the traditional SEM.
Scanning Tunneling Microscopy (STM). In STM, a small bias voltage is applied between the probe tip and the sample, and the tunneling current is monitored as the probe is scanned in the *x*-*y* plane over the surface of interest. The probe tip is typically composed of platinum. The surface structure can be evaluated under a variety of environmental conditions such as ambient conditions, ultrahigh vacuum (UHV), air, cryogenic fluids, and liquid solutions. STM is capable of monitoring the surface structural details in situ, including the progression of pitting (Ref 16, 17, 18, 19, 20, 21). Samples can be conducting and semiconducting in nature.
Atomic force microscopy (AFM) is the counterpart to STM and is also used to examine surface structure (Ref 22, 23, 24, 25, 26). It utilizes a force sensor called a cantilever to sense the force between a sharp tip and the sample surface as the sample is scanned in the *x*-*y* direction. The signal is processed to generate the surface image. The AFM technique allows the examination of the surface structure of insulating substrates.

Atomic and Molecular Structure

Energy Dispersive X-Ray Spectroscopy (EDS). This technique is used in conjunction with a scanning electron microscope (SEM). During the SEM examination any surface structure of interest can be analyzed for elemental identity and elemental composition; the EDS technique can identify elements with atomic numbers greater than 5 (boron). The principle of the technique involves the analysis of the energy and the intensity of the emitted x-rays as the incident electron beam is focused on the surface of interest. The incident electron beam ejects an electron from an inner shell; an electron from a higher energy level then fills the vacancy generated by the ejected electron. The electron filling the vacant shell loses energy corresponding to the difference between the two energy levels involved in the form of x-rays. The energy of the emitted x-rays is characteristic of the elements involved (Fig. 1b).

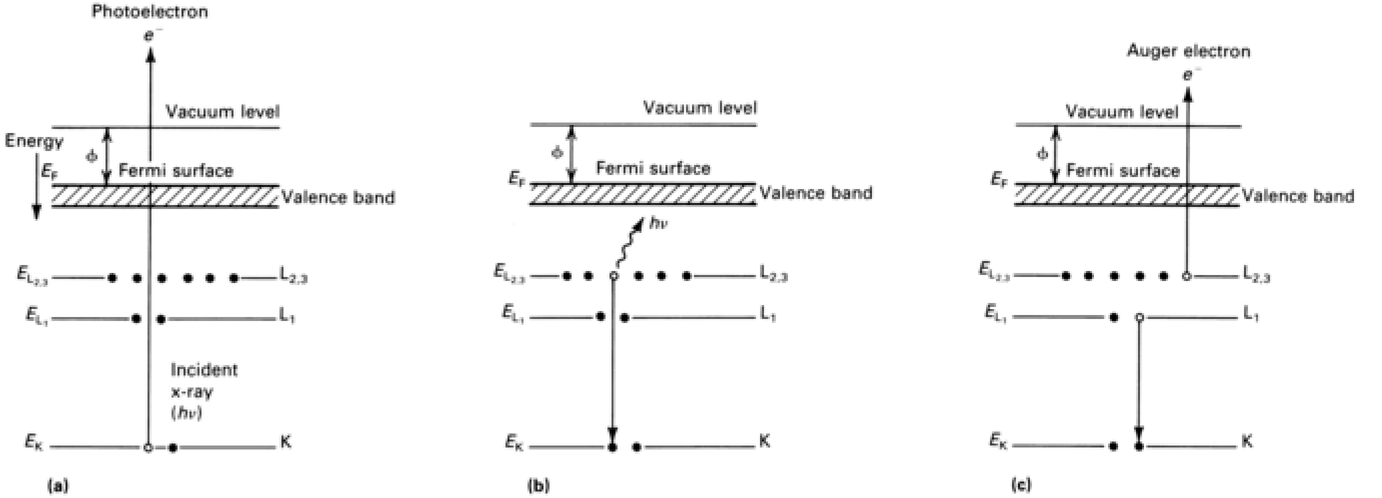

Fig. 1 Energy-level diagrams showing the electron transitions that form the basis for three techniques. (a) X-ray photoelectron spectroscopy (XPS). (b) X-ray analysis. (c) AES (Auger electron spectroscopy). φ, spectrometer work function

The instrument generates a spectrum of the relative intensity of the x-rays versus the energy of the x-rays, thereby allowing for the identification of various elements with atomic numbers greater than 5. The convenience of examining the structural details through SEM with the ability to focus on any structure of interest to gain information about the elemental identity of this structure becomes a powerful approach. The technique is available widely and relatively easy to use by trained professionals. With the use of known standards, the technique can be used for quantitative analysis of elements; however, it is commonly used for

qualitative examination of samples. Nevertheless, the EDS spectrum does reveal the relative concentration differences for various elements across the surface or between various samples compared. This technique is very useful for the analysis of surface contamination, corrosion products, preliminary identification of an alloy or surface coating, and phase identification (Ref 27, 28, 29, 30). The combination of SEM and EDS can also be used for failure analysis.

Wavelength dispersive x-ray spectroscopy (WDS) is another x-ray technique that can be used for the identification of the elemental composition of a sample of interest. In principle, WDS is a technique complementary to EDS. The main differences between these two techniques are that in EDS, the x-ray photons are evaluated for all energies at once and displayed against energy, and in WDS, x-ray photons are evaluated based on their wavelengths with a single wavelength measured at a time. Typically, WDS offers better resolution and sensitivity than EDS; however, the inherent nature of the slow measurement process makes this a slower technique than EDS. While not necessarily a surface technique, x-ray diffraction is widely used and is a valuable technique for determining mineral identities of surface films and corrosion products that are suitably thick.

Auger electron spectroscopy (AES) involves the use of an incident beam of electrons under ultrahigh vacuum (UHV) (Ref 31). The incident beam is focused on the surface of interest, and the energy of the emitted beam is analyzed. In AES spectroscopy the incident beam ejects an inner electron. Figure 1(c) illustrates the case of ejection of the core electron (K-shell). The vacancy created may be filled by an electron from a higher energy shell, in this case the L-shell. The energy corresponding to the difference of the K and L shells is then consumed in expelling an outer electron (Auger electron) from the atom (Fig. 1c).

Auger electrons have low energies, and therefore only electrons with sufficient energy originating from the surface or near the surface from a depth of approximately 0.8 to 2 nm (3.1 to 7.9 × 10^{-8} in.) can escape. Auger electron spectroscopy has been used for not only elemental identity of the surface but also for determining the depth profiles of elements such as the composition of oxide films including the passive films and organic corrosion inhibitor films (Ref 32, 33, 34, 35). Here again quantitative analysis can be conducted with the use of appropriate standards; however, use of a semiquantitative approach is more common.

X-ray photoelectron spectroscopy (XPS), also referred to as electron spectroscopy for chemical analysis (ESCA), is very similar to AES, except that an incident monochromatic x- ray beam is used and the energy of the photo- ejected electrons from the surface atoms or molecules is analyzed (Fig. 1a). These photo-ejected electrons from the surface carry information regarding the chemical identity and environment of the surface atoms and molecules. Therefore, the peak position of the photo-ejected electrons in the XPS spectrum depends on not only the atomic number but also the chemical environment of an atom or molecule. Thus, information regarding the functional groups adsorbed on the surface can be determined. Since the soft x-rays are less damaging, insulators with elements of atomic number greater than 4 (beryllium) can be analyzed to a depth of about 1 to 10 nm (3.9 × 10^{-8} to 3.9 × 10^{-7} in.). The technique can be used for quantitative analysis with the use of appropriate standards. X-ray photoelectron spectroscopy has been extensively used for the depth profiles of the elemental composition of surface films, both organic and inorganic in nature (Ref 36, 37, 38, 39, 40, 41, 42, 43). Such information allows for not only the chemical nature of the surface films but also the mechanistic details of the film forming processes.

Ion Scattering Spectroscopy. This technique involves scattering ions from the surface of interest. The measurement of the energy of the scattered ions allows for determining the chemical identity of the surface or the surface film (Ref 44, 45, 46, 47). The technique utilizes noble gas ions such as $^{3}He^{+}$, $^{4}He^{+}$, $^{20}Ne^{+}$, or $^{40}Ar^{+}$ at energies between 0.5 to 5.0 keV (1.91 × 10^{-2} to 1.91 × 10^{-1} kcal). Generally, a target ion mass less than the probe incident ion mass will not be detected. This technique has been used to examine surface adsorbed films, surface oxides, and corrosion inhibitors. The depth resolution can be at an atomic level. A major limitation for quantitative analysis with ISS is the neutralization of the scattered ions.

Secondary Ion Mass Spectrometry. The principle of this technique involves the use of an energetic incident ion beam to eject secondary ions from the surface of interest (Ref 48, 49, 50, 51). The ejected ions are analyzed by mass spectrometry to determine the chemical identity. The high yield of the secondary ions is a direct result of the high flux of the incident ion beam and the ionization probability. Thus, the depth profile of the elemental composition of the surface films can be easily monitored. The use of efficient ion collectors in the detection mode allows for good sensitivity. The SIMS technique has been used for analysis of surface adsorbed species, passive films, and surface contaminants. The depth resolution is at a molecular level. The analyses include surface oxides, hydroxides, and corrosion inhibitor chemistries. For organic corrosion inhibitor films, one must

be aware of the possibility of the surface charging. An advantage of this technique is that the detection of surface ions or clusters of ions allows for the identification of the molecular nature of the organic and inorganic protective films. This information provides an insight into the mechanistic details of the formation of the protective film.

Reflectance Fourier Transform Infrared Absorption Spectroscopy. Fourier transform infrared absorption spectroscopy (FTIR) relies on the vibrational excitation of the surface molecules (Ref 52). The infrared incident photons are absorbed by the appropriate functional groups adsorbed on a surface. The intensity of the reflected photons as a function of the energy of the photons results in a fingerprint spectrum of organic and some inorganic species. This allows for the identification of the chemical nature of the film at a molecular level (Ref 53, 54, 55, 56, 57, 58, 59).

This technique is primarily used for organic surface films; however, it can be used for some inorganic surface films as well. The technique is a relatively inexpensive approach for the analysis of relatively thick films of organic corrosion inhibitors or polymeric coatings on surfaces. However, extreme care should be taken in analyzing very thin films. FTIR can be used in ex situ and in situ modes. The ex situ mode allows for a relatively easy characterization of the surface films (Ref 60).

Attenuated total reflectance (ATR) is a sampling mode where the sample of interest is pressed against a flat window. Multiple infrared beam reflections from the surface of the film through the window carry the functional group information. Another sampling mode uses multiple reflections within the film (not the sampling window), such as crystalline materials, resulting in a diffuse reflectance infrared Fourier transform (DRIFT) spectrum. The DRIFT spectrum generally contains some specular reflectance that can potentially distort the spectral resolution. Attenuated total reflectance is the most commonly used sampling mode. The windows are generally composed of ZnSe, Si, or Ge. The ZnSe windows are attacked by strong acids, but Si and Ge are very inert. Each material has its own characteristic spectral operating range. Thus materials must be appropriately selected for the specific application of interest.

Raman and Surface Enhanced Raman Spectroscopy. Raman spectroscopy evaluates the shifts in the energy of the incident visible and ultraviolet photons at right angle to the incident beam. This measurement allows for the identification of the vibrational structure of the surface adsorbates, hence the molecular nature of the species (Ref 61, 62, 63, 64, 65, 66, 67, 68). The Raman scattering signal is generally weak; therefore an intense source of light such as a laser is needed for these measurements. The incident beam is typically an Ar^+ or a Kr^+ laser. For SERS the choice of the laser frequency that coincides with the electronic structure of the species of interest allows for thousand-fold signal enhancement. Thus SERS becomes an advantageous technique compared to Raman spectroscopy for some samples of interest. Surface enhanced Raman spectroscopy signal is typically observed for gold, copper, and silver. For SERS inactive steel, surfaces are typically coated with silver islands to make the surface SERS active. Both of the preceding techniques have been successfully used for examining the molecular nature of passive films and corrosion inhibitor films. Corrosion related Raman or SERS studies have been carried out on a broad range of alloys and protective corrosion inhibitor films in both in situ and ex situ modes (Ref 69, 70, 71, 72, 73, 74, 75, 76).

Raman spectroscopic technique also has some limitations that need to be considered for various samples of interest. For dark and colored samples, the high absorption coefficient of the incident visible light limits the strength of the scattered Raman signal. Although not common, in some instances any fluorescence signal can complicate the spectrum, thus making the measurements difficult. To improve the Raman signal, intense incident laser light is used, and it sometimes presents a challenge of thermal degradation of the sample of interest. Extreme care is thus needed in conducting experiments to avoid chemical compositional changes. In general, these limitations can be addressed by appropriate experimental precautions.

Extended X-Ray Absorption Fine Structure. X-ray absorption spectroscopy is used for a number of applications (Ref 77). This is primarily due to the availability of synchrotron radiation sources that can generate x-rays with intensities that are significantly higher than conventional x- ray sources. The absorption of x-rays by materials generally decreases as the energy of the incident x-ray beam is increased. However, when the energy of the x-ray reaches a threshold to promote a core electron to an unoccupied valence level or the continuum, absorption suddenly increases. The structure of this absorption edge is referred to as the x-ray absorption near edge structure (XANES). The energy of the x- ray edge corresponding to this absorption is characteristic of the individual elements, thus allowing for the identification of specific elements (Ref 78, 79, 80). Extending beyond the XANES region, from 100 to 1000 to 2000 eV (3.8 to 38.3 to 76.6 cal) above the edge are oscillations that are referred to as the extended x-ray absorption fine structure (EXAFS) (Ref 81, 82, 83, 84, 85,

86, 87, 88, 89, 90, 91). The EXAFS results from the oscillatory modulation of the x-ray absorption cross section by the interference between the emitted photoelectron waves and the backscattered waves from neighboring atoms in the molecule. The EXAFS allows for determining the interatomic distances of the nearest neighbors of a given atom and therefore the molecular structure of the surface film. The technique can be used in situ and ex situ to monitor electrochemical reactions. The technique has been used successfully to evaluate the chemical nature of conversion coatings (Ref 92). This technique does require access to the synchrotron radiation source and sufficient theoretical and experimental experience.

More detailed descriptions of the principles and applications of these techniques are provided in *Materials Characterization,* Volume 10 of *ASM Handbook,* and in the section "Atomic Force Microscopy" in the article "Measurement of Surface Forces and Adhesion" in *Friction, Lubrication, and Wear Technology,* Volume 18 of *ASM Handbook.*

References cited in this section

8. T.G. Taranova, G.M. Grigorenko, V.A. Kostin, and V.V. Arsenyk, Applications of Scanning Electron Microscopy in Modern Material Science, *Welding and Related Technologies,* Welding International, Vol 14 (No. 9), 2000, p 745–748

9. Y. Ding and D.O. Northwood, Methods For Preparation of Cross-Sectional Scanning Electron Microscopic Specimens and Their Applications to Corroded Specimens of a Zirconium Alloy and Titanium Nitrogen Coated Stainless Steel, *Mater. Charact.,* Vol 29 (No. 1), 1992, p 25–33

10. S.C. Tjong, Electron Microscope and Raman Characterization of The Surface Oxides Formed on The Fe-Cr Alloys at 400–800°C, *Mater. Charact.,* Vol 26 (No. 1), 1991, p 29–44

11. R.K.R. Singh, A.K. Tyagi, K. Krishan, and J.B. Gnanamoorthy, Secondary Ion Mass Spectrometery and Scanning Electron Microscopic Characterization of Grain Boundary Oxide Ridges in 9Cr-1Mo Steels Having Different Silicon Contents, and Influence of Grain Size on Scale Spalling, *Mater. Sci. Technol.,* Vol 10 (No. 7), 1994, p 592–598

12. L. Veleva and M. Luja, Scanning Electron Microscopic Characterization of Copper Corrosion Products, *Br. Corros. J.,* Vol 34 (No. 1), 1999, p 34–36

13. S. Shah and M. Bernardo, Reusable Surgical Instruments: Metallurgy and Corrosion, *Medical Product Sales,* Vol 31 (No. 4), 2000, p 26–27 and Vol 31 (No. 6), 2000, p 26

14. P.J.R. Uwins, Environmental Scanning Electron Microscopy, *Mater. Forum,* Vol 18, 1994, p 51–57

15. K.P.J. Williams, I.C. Wilcock, I.P. Hayward, and A. Whitley, Applications of State-of- the-Art Raman Microscopy and Direct Raman Imaging. Progress in Corrosion, Mineralogy, and Materials Research, *Spectroscopy,* Vol 11 (No. 3), 1996, p 45–50

16. J. Kunze, V. Maurice, H.L. Klein, H.H. Strehblow, and P. Marcus, In Situ Scanning Tunneling Microscopic Study of The Anodic Oxidation of Copper (111) in 0.1 M NaOH, *J. Phys. Chem. B,* Vol 105 (No. 19), 2001, p 4263–4269

17. V. Maurice, H.H. Strehblow, and P. Maurice., In Situ STM Study of the Initial Stages of Oxidation of Cu (111) in Aqueous Solution, *Surf. Sci.,* Vol 458 (No. 1–3), 2000, p 185–194

18. E.P. Friis, J.E.T. Anderson, L.L. Madsen, P. Moller, and J. Ulstrup, In Situ STM and AFM of The Copper Protein Pseudomonas aeruginosa azurin, *J. Electroanal. Chem.,* Vol 431 (No. 1), 1997, p 35–38

19. D.J. Noll, P.G. Vanpatten, M.A. Nicholson, K. Booksh, and M.L. Myrick, Flow-Injection System for The Scanning Tunneling Microscope, *Rev. Sci. Instrum.,* Vol 66 (No. 8), 1995, p 4150–4156

20. G.P. Bierwagen, R. Twite, G. Chen, and D.E. Tallman, Atomic Force Microscopy, Scanning Tunneling Microscopy and Electrochemical Characterization of Al Alloys, Conversion Coatings, and Primers Use for Aircraft, *Prog. Org. Coatings,* Vol 32 (No. 1–4), 1997, p 25–30

21. F.P. Zamborini, J.K. Campbell, and R.M. Crooks, Spectroscopic, Voltametric, and Electrochemical Scanning Tunneling Microscopic Study of Underpotentially Deposited Cu Corrosion and Passivation With Self-Assembled Organomercaptan Monolayers, *Langmuir,* Vol 14 (No. 3), 1998, p 640–647

22. C.J. Rubim, H. Jae, E. Henderson, and T.M. Cotton, Surface Enhanced Raman Scattering and Atomic Force Microscopy of Brass Electrodes in Sulfuric Acid Solution Containing Benzotriazole and Chloride Ion, *Appl. Spectrosc.,* Vol 47 (No. 1), 1993, p 80–84

23. W. Kautek, M. Geu, M. Sabre, and P. Ahao, Multi-Method Analysis of Metal/Electrolyte Interface: Scanning Force Microscopy, Quartz Microbalance Measurements, FTIR and Grazing Incidence X-ray Diffractometry at Polycrystalline Electrode, *Surf. Interface Anal.,* Vol 25 (No. 7–8), 1997, p 548–560

24. R.K.R. Singh and A.K. Tyagi, Secondary Ion Mass Spectrometry and Scanning Electron Microscopic Analysis of Grain Boundary Oxides in 9Cr-1Mo Steel and Influence of Grain Size on Scale Spalling, *Mater. Sci. Technol.,* Vol 10 (No. 1), 1994, p 27–34

25. P. Lemoine and J.M. McLaughlin, Continuity and Topography of Ultrathin Diamond-Like Carbon Films Characterized by Scanning Electron Microscopy, Energy Dispersive X-ray Analysis and Atomic Force Microscopy, *J. Vac. Sci. Technol.,* Vol 17 (No. 1), 1999, p 176–182

26. M. Bethencourt, F.J. Botana, J.J. Calvino, M. Marcos, J. Perez, and M. and A.R. Chacon, A SEM and EDS Insight Into The Corrosion Process of AA 5083 Al-Mg Alloy in NaCl Solutions, *14th Electron Microscopy Proc. of International Congress,* B. Calderon, A. Hector, and M.Y. Jose, Ed. Vol 2 (No. 103–104), Institute of Physics Publishing, 1988

27. K. Forkel, D. Born, F.G. Wihsmann, and R. Stodolski, A SEM/EDXA Study on the Chemical Attack of Aqueous NaOH/KOH Solutions on the Surface of Metal-Metalloid Glass $(Fe,Cr)_{80}(P,C,Si)_{20}$ and $Fe_{75}Cr_5P_8C_{10}SiO_2$, Respectively, *Mikrochim. Acta,* Vol 125 (No. 1–4), 1997, p 407–413

28. G. Panjonk, H.D. Steffens, B. Reznik, H. Buber, and H. Janett, Surface Analytical Examination of Welded Nickel Alloys by XPS, SNMS and SEM/EDX, *Mikrochim. Acta,* Vol 125 (No. 1–4), 1997, p 375–380

29. J. Monzo, J. Garcia-Politec, and J.L. Guinon, Influence of Elemental Sulfur and Mercaptans on Corrosion of Copper Strips in The ASTM D-130 Test by Means of Electron Microscopy and Energy Dispersive X- ray, *J. Anal. Chem.,* Vol 341 (No. 10), 1991, p 606–610

30. I. Olefjord and A. Nylund, Surface Analysis of Oxidized Aluminum. 2. Oxidation Aluminum in Dry and Humid Atmosphere Studied By ESCA, SEM, SAM, and EDX, *Surf. Interface Anal.,* Vol 21 (No. 5), 1994, p 290–297

31. N.H. Turner and J.A. Schreifels, Surface Analysis: X-Ray Photoelectron Spectroscopy and Auger Electron Spectroscopy, *Anal. Chem.,* Vol 68, 1996, p 309R–331R

32. E.B. Varhegyi, I.V. Perczel, J. Gerblinger, M. Fleischer, H. Mexixner, and J. Giber, Auger and SIMS Study of Segregation and Corrosion Behavior of Some Semiconducting Oxide Gas-sensor Materials, *Sens. Actuators B,* Vol 19 (No. 1–3), 1994, p 569–572

33. D.B. Yang and D. Wolf, Interfacial Analysis of Copper Corrosion by Acrylic and Methycrylic Acids Using, XPS, Auger and Grazing angle FTIR, *Surf. Interface Anal.,* Vol 23 (No. 5), 1995, p 276–288

34. S.J. Roosendaal, A.M. Vredenberg, and F.H.P.M. Habraken, The Influence of Adsorbed N in the Initial Stages of Oxidation of Iron, *Surf. Sci.,* Vol 402–404 (No. 1–3), 1998, p 130–139

35. J.A. Schimpf, J.R. McBride, and M.P. Soriaga, Adsorbate-Catalyzed Layer-by-Layer Metal Dissolution in Halide-Free Solution, *J. Phys. Chem.,* 1993, Vol 97, p 10,518–10,520

36. E. De Vito and P. Marcus, XPS Study of Passive Films Formed on Molybdenum-Implanted Austenitic Stainless Steel, *Surf. Interface Anal.,* Vol 199 (No. 1–12), 1992, p 403–408

37. D. Thierry, D. Persson, C. Leygraf, N. Boucherit, and A.G. Hugot-le, Raman Spectroscopy and XPS Investigation of Anodic Films Formed on Fe-Mo Alloys In Alkaline Solutions, *Corros. Sci.,* Vol 32 (No. 3), 1991, p 273–284

38. M.F. Fitzpatrick, J.S.G. Ling, and J.F. Watts, Failure Mechanism of Phosphated Adhesively Bonded Hot-dipped Galvanized Steel: A Small Area XPS Study, *Surf. Interface Anal.,* Vol 29 (No. 2), 2000, p 131–138

39. C.R. Brundle, M. Grunze, U. Mader, and N. Blank, Detection and Characterization of Dimethylethanolamine-Based Corrosion Inhibitors at Steel Surfaces. I. The use of XPS and ToF-SIMS, *Surf. Interface Anal.,* Vol 24 (No. 9), 1996, p 549–563

40. T. Fransen, R. Hofman, J.G.F. Westheim, I. Pouwel, and P.J. Gellings, FTIR and XPS Studies on Corrosion-resistant SiO_2 Coatings As a Function of Humidity During Deposition, *Surf. Interface Anal.,* Vol 24 (No. 1), 1996, p 1–6

41. J.L. Fang, Y. Li, X.R. Ye, Z.W. Wang, and Q. Liu, Passive Films and Corrosion Protection Due to Phosphoric Acid Inhibitors, *Corrosion,* Vol 49 (No. 4), 1993, p 266–271

42. V. Sirtori, F. Zambon, and L. Lombardi, XPS and Ellipsometric Characterization of Zinc-BTA Complex, *J. Electron. Mater.,* Vol 29 (No. 4), 2000, p 463–467

43. F. Bentiss, M. Traisnel, L. Gengembre, and M. Lagreene, A New Triazol Derivative As Inhibitor of The Acid Corrosion of Mild Steel: Electrochemical Studies, Weight Loss Determination, SEM, XPS, *Appl. Surf. Sci.,* Vol 152 (No. 3–4), 1999, p 237–249

44. P. Druska and H.H. Strehblow, Surface Analytical Examination of Passive Layers on Cu-Ni Alloys Part II. Acidic Solution, *Corros. Sci.,* Vol 38 (No. 8), 1996, p 1369–1383

45. D. Schaepers and H.H. Strehblow, Surface Analytical Investigations of Electrochemically Formed Passive Layers on Binary Fe/ Al Alloys, *J. Electrochem. Soc.,* Vol 142 (No. 7), 1995, p 2210–2218

46. P. Druska, H.H. Strehblow, and S. Golledge, A Surface Analytical Examination of Passive Layers on Cu/Ni Alloys .1. Alkaline Solutions, *Corros. Sci.,* Vol 38 (No. 6), 1996, p 835–851

47. A. Rossi, C. Calinski, H.W. Hoppe, and H.H. Strehblow, A Combined ISS and XPS Investigation of Passive Film Formation On Fe53Ni, *Surf. Interface Anal.,* Vol 18 (No. 4), 1992, p 269–276

48. R. Gasparac, C.R. Martin, E. StupnisekLisac, and Z. Mandic, In Situ and Ex Situ Studies of Imidazole and Its Derivatives As Copper Corrosion Inhibitors II. AC Impedance, XPS and SIMS Studies, *J. Electrochem. Soc.,* Vol 147 (No. 3), 2000, p 991–998

49. H.J. Wouters, L.A. Butaya, and F.C. Adams, Applications of SIMS in Patina Studies on Bronze Age Copper Alloys, *Anal. Chem.,* Vol 342 (No. 1–2), 1992, p 128–134

50. R. Singh, A.K. Tyagi, J.B. Gnanamoorthy, B. Raj, and S.K. Roy, Secondary Ion Mass Spectroscopy and Surface Prolifometric Characterization of Oxide Scales Developed Over Weld Metal, Heat Affected Zone, and Base Metal Regions of 9Cr-1Mo Steel Weldments, *Mater. Sci. Technol.,* Vol 14 (No. 4), 1998, p 362–366

51. E. Cuyen, P. Lemberge, and P.E. Van, SIMS Depth Profiling of Cr-Conversion Layers on Aluminum, *Electron Microscopy, General Interest Instrumentation,* Vol 1, 1998, p 369–370

52. S. Yoshida and H. Ishida, An Investigation of The Thermal Stability of Undecylimidizole on Copper by FTIR Reflectance-Absorption Spectroscopy, *Appl. Surf. Sci.,* Vol 89 (No. 1), 1995, p 39–47

53. M.L. McKelvy, T.R. Britt, B.R. Davis, J.K. Gillie, L.A. Lentz, A. Leugers, R.A. Nyguist, and C.L. Putzig, Infrared Spectroscopy, *Anal. Chem.,* Vol 68, 1996, p 93R–160R

54. J. Fang, X.Ye, Q. Liu, Y. Li, and Z. Wang, XPS, AES, FTIR and Raman of An Anticorrosion Film on Steel, *International Congress of Surface Finishing,* Vol 2, 1992, p 1037–1045

55. G.L. Powel, A.G. Dobbins, S.S. Cristy, T.L. Clift, and H.M. Meyer, Study of The Oxidation of Uranium by External Diffuse Reflectance FTIR Spectroscopy Using Remote-Sensing and Evacuable Cell Techniques, *Ninth International Conf. on FTIR Spectroscopy,* Canada, 23–27 Aug 1993

56. A.V.R Kumar, R.K. Nigam, A.K. Srinavasta, and S.S. Monga, Mossbauer Spectroscopy and FTIR Spectroscopy of Corrosion Products, Obtained Beneath Mild Steel Coated with Different Phosphate Primers, *Bull. Electrochem.,* Vol 15 (No. 3–4), 1999, p 160–163

57. J. Kasperek, D. Verchere, D. Jacquet, and N. Phillips, Analysis of the Corrosion Products on Galvanized Steels by FTIR Spectroscopy, *Mater. Chem. Phys.,* Vol 56 (No. 3), 1998, p 205–213

58. A.K. Neufeld and I.S. Cole, Using FTIR Analysis to Detect Corrosion Products on the Surface of Metals Exposed to Atmospheric Conditions, *Corrosion,* Vol 53 (No. 10), 1997, p 788–799

59. S. Music, M. Gotic, and S. Popovic, X-Ray Diffraction and Fourier Transform Infrared Analysis of the Rust Formed by Corrosion of Steel in Aqueous Solutions, *J. Mater. Sci.,* Vol 28 (No. 21), 1993, p 5744–5752

60. S. Shah, Characterization of Interphases in Corrosion By Ex Situ FTIR Spectroscopy, *Corrosion 93,* Vol 361, 1993, p 1–16

61. C.A. Melendres, Laser Raman Spectroscopy: Principles and Applications to Corrosion Studies, *Electrochemical and Optical Techniques for the Study and Monitoring of Metallic Corrosion,* Portugal, 9–21 July 1989

62. C.A. Melendres, Laser Raman and X-Ray Scattering Studies of Corrosion Films on Metals, *12th International Corrosion Congress,* Houston, TX, 1993, p 19–24

63. J. Birnie, C. Craggs, D.J. Gardiner, and P.R. Graves, Ex Situ and In Situ Determination of Stress Distribution in Chromium Oxide Films by Raman Microscopy, *Corros. Sci.,* Vol 33 (No. 1), 1992, p 1–12

64. P.M.L Bonin, Electrochemical and Raman Spectroscopic Studies of The Influence of Chlorinated Solvents on The corrosion of Iron and Borate Buffer and In simulated Ground Water, *Corrosion Science,* 42 (11), 2000, p 1921–1939

65. R.K. Raman Singh, Laser Raman Spectroscopy: A Technique For Rapid Characterization of Oxide Scale Layers, *Mater. Sci. Technol.*, Vol 14 (No. 5), 1998, p 373–376

66. J.E. Masler, In Situ Raman Spectroscopic Investigation of Aqueous Iron Corrosion at Elevated Temperatures and Pressures, *J. Electrochem. Soc.* Vol 147 (No. 7), 2000, p 2532–2542

67. J. Zhao, G. Frankel, and R.L. McCreery, Corrosion Protection of Untreated AA- 2024-T3 in Chloride Solutions by Chromate Conversion Coating Monitored with Raman Spectroscopy, *J. Electrochem. Soc.*, Vol 145 (No. 7), 1998, p 2258–2264

68. D.L.A. deFria, S.V. Silva, and M.T. deOliveira, Raman Microscopy of Some Iron Oxides and Oxyhydroxides, *J. Raman Spectrosc.,* Vol 28 (No. 11), 1997, p 873–878

69. M. Metikos-Hukovic, K. Furic, R. Babic, and A. Marinovic, Surface Enhanced Raman Scattering (SERS) of Benzotriazole Derivative Corrosion Inhibitor Prepared in Aqueous Media, *Surf. Interface Anal.,* Vol 27 (No. 11), 1999, p 1016–1025

70. L.J. Oblonsky and T.M. Devine, Corrosion of Carbon Steels in CO_2 Saturated Brine. A Surface Enhanced Raman Study, *J. Electrochem. Soc.,* Vol 144 (No. 4), 1997, p 1252–1260

71. C.A. Malendres, Temperature Dependence of the Surface Enhanced Raman Spectroelectrochemistry of Iron in Aqueous Solutions, *Electrochim. Acta,* Vol 41 (No. 10), 1996, p 1727–1730

72. D.P. Schweinsberg, V. Otieno-Alego, G.A. Hope, and T. Notoya, An Electrochemical and SERS Study of the Effect of 1-[N,N-bis- (hydroxyethyl)aminomethyl]-benzotriole on the Acid Corrosion and Dezincification of 60/40 Brass, *Corros. Sci.,* Vol 38 (No. 2), 1996, p 213–223

73. W.C. Baek, T. Kang, H.J. Sohn, and K.T. Young, In Situ Surface Enhanced Raman Spectroscopic Study on the Effect of Dissolved Oxygen on the Corrosion Film on Low Carbon Steel in 0.01 M NaCl Solution, *Electrochim. Acta,* Vol 46 (No. 15), 2001, p 2321–2325

74. H.H. Chan and M.J. Weaver, Vibrational Structural Analysis of Benzotriazol Adsorption and Phase Film Formation on Copper Using Surface Enhanced Raman Spectroscopy, *Langmuir,* Vol 15 (No. 9), 1999, p 3348–3355

75. J.L. Simpson and C.A. Melendres, Surface Enhanced Raman Spectroelectrochemical Studies of Corrosion Films on Iron in Aqueous Carbonate Solution, *J. Electrochem. Soc.,* Vol 143 (No. 7), 1996, p 2146–2152

76. V. Shroeder and T.M. Devine, Surface Enhanced Raman Spectroscopic Study of Galvanostatic Reduction of the Passive Film on Iron, *J. Electrochem. Soc.,* Vol 146 (No. 11), 1999, p 4061–4070

77. S.B. Torak, J. Labar, J. Injuk, and R.E.V. Grieken, X-Ray Spectroscopy, *Anal. Chem.,* Vol 68, 1996, p 467R–485R

78. P. Schmuki, S. Virtanen, A.J. Davenport, and C.M. Vitus, Transpassive Dissolution of Cr and Sputter-Deposited Cr Oxides Studied by In Situ X-Ray Near Edge Spectroscopy, *J. Electrochem. Soc.,* Vol 143 (No. 12), 1996, p 3997–4005

79. S. Pizzini, K.J. Roberts, I.S. Dring, R.J. Oldman, and D.C. Cupertino, Applications of X-Ray Absorption Spectroscopy to the Structural Characterization of Monodispersed Benzotriazole Coatings on Partly Oxidized Thin Films, *J. Mater. Chem.,* Vol 3 (No. 8), 1993, p 811–819

80. J.S. Wainright, M.R. Antonio, and O.J. Murphy, The Oxidation State and Coordination Environment of Chromium in a Sealed Anodic Aluminum Oxide Film by X-Ray Absorption Spectroscopy, *Corros. Sci.,* Vol 33 (No. 2), 1992, p 281–293

81. D.E.O.S. Carpenter, S.D. Carpenter, and J.P.G. Farr, Structure and Constitution of Zinc-Cobalt Electrodeposits, *Corros. Sci.,* Vol 42 (No. 9), 2000, p 1599–1610

82. H.H. Strehblow and P. Borthen, EXAFS Analysis of Passive Films, *Mater. Sci. Forum,* Vol 185–188, 1995, p 301–311

83. G.D. Davis, W.C. Moshier, G.G. Long, D.R. Black, and B.A. Shaw, Passive Film Structure of Supersaturated Al-Mo Alloys, *Conference: X-Ray Methods in Corrosion and Interface Electrochemistry,* The Electrochemical Society, 1991, p 13–18

84. D. Lutzenkirchen-Hecht, C.U. Waligura, and H.H. Strehblow, An In Situ EXAFS Study of Corrosion Products, *Corros. Sci.,* Vol 40 (No. 6), 1998, p 1037–1041

85. S.C. Chung, A.S. Lins, J.R. Chang, and H.C. Shih, EXAFS Study of Atmospheric Corrosion Products on Zinc at the Initial Stage, *Corros. Sci.,* Vol 42, 2000, p 1599–1610

86. M. Balasubramanion and C.A. Melendres, Selective Site Occupancy Exhibited by Cr^{3+} and Cr^{6+} Incorporated into Electrochemically Deposited Nickel Hydroxide Films, *Electrochem. Solid State Lett.,* Vol 2 (No. 4), 1999, p 167–169

87. G. Contini, A. Ciccioli, C. Laffon, P. Parent, and G. Polzonetti, NEXAFS Study of 2-Mercaptobenzooxazole Adsorbed on Pt (111): Multilayer and Monolayer, *Surf. Sci.,* Elsevier Science, Vol 412/413, 1998, p 158–165

88. A.I. Frenkel, and G.V. Korshin, EXAFS Studies of the Chemical State of Lead and Copper in Corrosion Products Formed on the Brass Surface in Potable Water, *J. Synchrotron Radiation,* Vol 6 (No. 3), 1999, p 653–655

89. D. Lutzenkirchen-Hecht and R. Frah, Time Resolved EXAFS Investigation of the Anodic Dissolution of Mo, *J. Synchrotron Radiation,* Vol 6 (No. 3), 1999, p 591–593

90. S. Suzuki, T. Suzuki, M. Kimura, Y. Takagi, K. Shinoda, K. Tohji, and Y. Woseda, EXAFS Characterization of Ferric Oxyhydroxide, *Appli. Surf. Sci.,* Vol 169–170, 2001, p 109–112

91. G.G. Long, Surface X-Ray Absorption Spectroscopy, EXAFS and NEXAFS, for the in Situ and ex Situ Study of Electrodes, p 167–209, R. Varma and J.R. Selman, Ed. *Techniques For Characterization of Electrodes And Electrochemical Processes,* The Electrochemical Society, John Wiley & Sons, Inc., 1991

92. S. Shah, A. Ward, and A.J. Davenport, Characterization of Tellurium Based Conversion Coatings by X-ray Absorption Near-Edge Structure and Fourier Transform Infrared Spectroscopy, *Corrosion,* Vol 51 (No. 1), 1995, p 67–70

S. Shah, Applications of Modern Analytical Instruments in Corrosion, *Corrosion: Fundamentals, Testing, and Protection*, Vol 13A, *ASM Handbook*, ASM International, 2003, p 992–998

Applications of Modern Analytical Instruments in Corrosion

Sadiq Shah, Western Illinois University

References

1. S. Shah, Ed., *Surface and Interface Characterization in Corrosion,* NACE International, 1994
2. M. Riviere, *Handbook of Surface and Interface Analysis Methods of Problem Solving,* Marcel Dekker, Inc., 1998
3. R. Howland, L. Benatar, and C. Symanski, *A Practical Guide to Scanning Probe Microscopy,* DIANE Publishing Co., Collingdale, PA, 1998
4. J. Lipkowski and P.N. Ross, *Imaging of Surfaces and Interfaces,* John Wiley & Sons, Inc., 1999
5. A. Hubbard, *The Handbook of Surface Imaging and Visualization,* CRC Press, 1995
6. L.A. Bottomley, J.E. Coury, and P.N. First, Scanning Microscopy, *Anal. Chem.,* Vol 68, 1996, p 185R–230R
7. S. Shah, Corrosion: An Interfacial Process, *Corrosion 91,* “Paper 75,” 1991, p 1–22
8. T.G. Taranova, G.M. Grigorenko, V.A. Kostin, and V.V. Arsenyk, Applications of Scanning Electron Microscopy in Modern Material Science, *Welding and Related Technologies,* Welding International, Vol 14 (No. 9), 2000, p 745–748
9. Y. Ding and D.O. Northwood, Methods For Preparation of Cross-Sectional Scanning Electron Microscopic Specimens and Their Applications to Corroded Specimens of a Zirconium Alloy and Titanium Nitrogen Coated Stainless Steel, *Mater. Charact.,* Vol 29 (No. 1), 1992, p 25–33
10. S.C. Tjong, Electron Microscope and Raman Characterization of The Surface Oxides Formed on The Fe-Cr Alloys at 400–800°C, *Mater. Charact.,* Vol 26 (No. 1), 1991, p 29–44
11. R.K.R. Singh, A.K. Tyagi, K. Krishan, and J.B. Gnanamoorthy, Secondary Ion Mass Spectrometery and Scanning Electron Microscopic Characterization of Grain Boundary Oxide Ridges in 9Cr-1Mo Steels Having Different Silicon Contents, and Influence of Grain Size on Scale Spalling, *Mater. Sci. Technol.,* Vol 10 (No. 7), 1994, p 592–598
12. L. Veleva and M. Luja, Scanning Electron Microscopic Characterization of Copper Corrosion Products, *Br. Corros. J.,* Vol 34 (No. 1), 1999, p 34–36
13. S. Shah and M. Bernardo, Reusable Surgical Instruments: Metallurgy and Corrosion, *Medical Product Sales,* Vol 31 (No. 4), 2000, p 26–27 and Vol 31 (No. 6), 2000, p 26
14. P.J.R. Uwins, Environmental Scanning Electron Microscopy, *Mater. Forum,* Vol 18, 1994, p 51–57

15. K.P.J. Williams, I.C. Wilcock, I.P. Hayward, and A. Whitley, Applications of State-of- the-Art Raman Microscopy and Direct Raman Imaging. Progress in Corrosion, Mineralogy, and Materials Research, *Spectroscopy,* Vol 11 (No. 3), 1996, p 45–50

16. J. Kunze, V. Maurice, H.L. Klein, H.H. Strehblow, and P. Marcus, In Situ Scanning Tunneling Microscopic Study of The Anodic Oxidation of Copper (111) in 0.1 M NaOH, *J. Phys. Chem. B,* Vol 105 (No. 19), 2001, p 4263–4269

17. V. Maurice, H.H. Strehblow, and P. Maurice., In Situ STM Study of the Initial Stages of Oxidation of Cu (111) in Aqueous Solution, *Surf. Sci.,* Vol 458 (No. 1–3), 2000, p 185–194

18. E.P. Friis, J.E.T. Anderson, L.L. Madsen, P. Moller, and J. Ulstrup, In Situ STM and AFM of The Copper Protein Pseudomonas aeruginosa azurin, *J. Electroanal. Chem.,* Vol 431 (No. 1), 1997, p 35–38

19. D.J. Noll, P.G. Vanpatten, M.A. Nicholson, K. Booksh, and M.L. Myrick, Flow-Injection System for The Scanning Tunneling Microscope, *Rev. Sci. Instrum.,* Vol 66 (No. 8), 1995, p 4150–4156

20. G.P. Bierwagen, R. Twite, G. Chen, and D.E. Tallman, Atomic Force Microscopy, Scanning Tunneling Microscopy and Electrochemical Characterization of Al Alloys, Conversion Coatings, and Primers Use for Aircraft, *Prog. Org. Coatings,* Vol 32 (No. 1–4), 1997, p 25–30

21. F.P. Zamborini, J.K. Campbell, and R.M. Crooks, Spectroscopic, Voltametric, and Electrochemical Scanning Tunneling Microscopic Study of Underpotentially Deposited Cu Corrosion and Passivation With Self-Assembled Organomercaptan Monolayers, *Langmuir,* Vol 14 (No. 3), 1998, p 640–647

22. C.J. Rubim, H. Jae, E. Henderson, and T.M. Cotton, Surface Enhanced Raman Scattering and Atomic Force Microscopy of Brass Electrodes in Sulfuric Acid Solution Containing Benzotriazole and Chloride Ion, *Appl. Spectrosc.,* Vol 47 (No. 1), 1993, p 80–84

23. W. Kautek, M. Geu, M. Sabre, and P. Ahao, Multi-Method Analysis of Metal/Electrolyte Interface: Scanning Force Microscopy, Quartz Microbalance Measurements, FTIR and Grazing Incidence X-ray Diffractometry at Polycrystalline Electrode, *Surf. Interface Anal.,* Vol 25 (No. 7–8), 1997, p 548–560

24. R.K.R. Singh and A.K. Tyagi, Secondary Ion Mass Spectrometry and Scanning Electron Microscopic Analysis of Grain Boundary Oxides in 9Cr-1Mo Steel and Influence of Grain Size on Scale Spalling, *Mater. Sci. Technol.,* Vol 10 (No. 1), 1994, p 27–34

25. P. Lemoine and J.M. McLaughlin, Continuity and Topography of Ultrathin Diamond-Like Carbon Films Characterized by Scanning Electron Microscopy, Energy Dispersive X-ray Analysis and Atomic Force Microscopy, *J. Vac. Sci. Technol.,* Vol 17 (No. 1), 1999, p 176–182

26. M. Bethencourt, F.J. Botana, J.J. Calvino, M. Marcos, J. Perez, and M. and A.R. Chacon, A SEM and EDS Insight Into The Corrosion Process of AA 5083 Al-Mg Alloy in NaCl Solutions, *14th Electron Microscopy Proc. of International Congress,* B. Calderon, A. Hector, and M.Y. Jose, Ed. Vol 2 (No. 103–104), Institute of Physics Publishing, 1988

27. K. Forkel, D. Born, F.G. Wihsmann, and R. Stodolski, A SEM/EDXA Study on the Chemical Attack of Aqueous NaOH/KOH Solutions on the Surface of Metal-Metalloid Glass $(Fe,Cr)_{80}(P,C,Si)_{20}$ and $Fe_{75}Cr_5P_8C_{10}SiO_2$, Respectively, *Mikrochim. Acta,* Vol 125 (No. 1–4), 1997, p 407–413

28. G. Panjonk, H.D. Steffens, B. Reznik, H. Buber, and H. Janett, Surface Analytical Examination of Welded Nickel Alloys by XPS, SNMS and SEM/EDX, *Mikrochim. Acta,* Vol 125 (No. 1–4), 1997, p 375–380

29. J. Monzo, J. Garcia-Politec, and J.L. Guinon, Influence of Elemental Sulfur and Mercaptans on Corrosion of Copper Strips in The ASTM D-130 Test by Means of Electron Microscopy and Energy Dispersive X- ray, *J. Anal. Chem.,* Vol 341 (No. 10), 1991, p 606–610

30. I. Olefjord and A. Nylund, Surface Analysis of Oxidized Aluminum. 2. Oxidation Aluminum in Dry and Humid Atmosphere Studied By ESCA, SEM, SAM, and EDX, *Surf. Interface Anal.,* Vol 21 (No. 5), 1994, p 290–297

31. N.H. Turner and J.A. Schreifels, Surface Analysis: X-Ray Photoelectron Spectroscopy and Auger Electron Spectroscopy, *Anal. Chem.,* Vol 68, 1996, p 309R–331R

32. E.B. Varhegyi, I.V. Perczel, J. Gerblinger, M. Fleischer, H. Mexixner, and J. Giber, Auger and SIMS Study of Segregation and Corrosion Behavior of Some Semiconducting Oxide Gas-sensor Materials, *Sens. Actuators B,* Vol 19 (No. 1–3), 1994, p 569–572

33. D.B. Yang and D. Wolf, Interfacial Analysis of Copper Corrosion by Acrylic and Methycrylic Acids Using, XPS, Auger and Grazing angle FTIR, *Surf. Interface Anal.,* Vol 23 (No. 5), 1995, p 276–288

34. S.J. Roosendaal, A.M. Vredenberg, and F.H.P.M. Habraken, The Influence of Adsorbed N in the Initial Stages of Oxidation of Iron, *Surf. Sci.,* Vol 402–404 (No. 1–3), 1998, p 130–139

35. J.A. Schimpf, J.R. McBride, and M.P. Soriaga, Adsorbate-Catalyzed Layer-by-Layer Metal Dissolution in Halide-Free Solution, *J. Phys. Chem.,* 1993, Vol 97, p 10,518–10,520

36. E. De Vito and P. Marcus, XPS Study of Passive Films Formed on Molybdenum-Implanted Austenitic Stainless Steel, *Surf. Interface Anal.,* Vol 199 (No. 1–12), 1992, p 403–408

37. D. Thierry, D. Persson, C. Leygraf, N. Boucherit, and A.G. Hugot-le, Raman Spectroscopy and XPS Investigation of Anodic Films Formed on Fe-Mo Alloys In Alkaline Solutions, *Corros. Sci.,* Vol 32 (No. 3), 1991, p 273–284

38. M.F. Fitzpatrick, J.S.G. Ling, and J.F. Watts, Failure Mechanism of Phosphated Adhesively Bonded Hot-dipped Galvanized Steel: A Small Area XPS Study, *Surf. Interface Anal.,* Vol 29 (No. 2), 2000, p 131–138

39. C.R. Brundle, M. Grunze, U. Mader, and N. Blank, Detection and Characterization of Dimethylethanolamine-Based Corrosion Inhibitors at Steel Surfaces. I. The use of XPS and ToF-SIMS, *Surf. Interface Anal.,* Vol 24 (No. 9), 1996, p 549–563

40. T. Fransen, R. Hofman, J.G.F. Westheim, I. Pouwel, and P.J. Gellings, FTIR and XPS Studies on Corrosion-resistant SiO_2 Coatings As a Function of Humidity During Deposition, *Surf. Interface Anal.,* Vol 24 (No. 1), 1996, p 1–6

41. J.L. Fang, Y. Li, X.R. Ye, Z.W. Wang, and Q. Liu, Passive Films and Corrosion Protection Due to Phosphoric Acid Inhibitors, *Corrosion,* Vol 49 (No. 4), 1993, p 266–271

42. V. Sirtori, F. Zambon, and L. Lombardi, XPS and Ellipsometric Characterization of Zinc-BTA Complex, *J. Electron. Mater.,* Vol 29 (No. 4), 2000, p 463–467

43. F. Bentiss, M. Traisnel, L. Gengembre, and M. Lagreene, A New Triazol Derivative As Inhibitor of The Acid Corrosion of Mild Steel: Electrochemical Studies, Weight Loss Determination, SEM, XPS, *Appl. Surf. Sci.,* Vol 152 (No. 3–4), 1999, p 237–249

44. P. Druska and H.H. Strehblow, Surface Analyti

S.D. Cramer, B.S. Covino, Jr., G.R. Holcomb and M. Ziomek-Moronz, Information Sources and Databases for the Corrosionist, *Corrosion: Fundamentals, Testing, and Protection*, Vol 13A, *ASM Handbook*, ASM International, 2003, p 999–1001

Information Sources and Databases for the Corrosionist

S.D. Cramer, B.S. Covino, Jr., G.R. Holcomb, M. Ziomek-Moroz; Albany Research Center, U.S. Department of Energy

Introduction

REMARKABLE CHANGES in information technology have occurred since the 1987 edition of this Handbook was published. As a consequence, information and data that may not have been obtainable at that time are now routinely available by way of the World Wide Web. This article lists selected information sources and databases and the current (2003) way they are accessed. These lists were compiled from many other lists and from searches on the web. They represent the authors' choices of what are some of the more important corrosion sources on the web. They are not inclusive of all possible sites, which was not the authors' goal, but rather provide good starting points from which one can build.
The information in this article has a fairly high “vapor pressure,” and its permanence can be fairly tenuous. On the other hand, the Internet addresses for major sites are not as likely to change since they provide continuity for the user. Information is provided in five areas:

- Societies and associations addressing corrosion and related topics
- Corrosion standards, specifications, recommended practices, and related topics
- Sources of corrosion information
- Corrosion databases and data compilations
- Other web resources

These areas frame much of the material on the web that addresses corrosion and related topics and provide portals to even more material.

S.D. Cramer, B.S. Covino, Jr., G.R. Holcomb and M. Ziomek-Moronz, Information Sources and Databases for the Corrosionist, *Corrosion: Fundamentals, Testing, and Protection*, Vol 13A, *ASM Handbook*, ASM International, 2003, p 999–1001

Information Sources and Databases for the Corrosionist

S.D. Cramer, B.S. Covino, Jr., G.R. Holcomb, M. Ziomek-Moroz; Albany Research Center, U.S. Department of Energy

Societies and Associations

Many of the leading societies and associations addressing corrosion and related topics and having a broad membership are listed in Table 1 with their web address. An effort has been made to provide a geographic distribution of organizations as well. The International Corrosion Council maintains perhaps the most comprehensive record of corrosion institutions in a list titled “Sources of Corrosion Information” that covers 40 countries. The list was last updated in 1996.

Table 1 Societies and associations addressing corrosion and related topics

Organization	Web address
ABRACO (Brazilian Corrosion Association)	www.abraco.org.br
American Ceramic Society	www.acers.org/
American Society for Microbiology	www.asmusa.org/
AWWA (American Water Works Association)	www.awwa.org/
AISI (American Iron and Steel Institute)	www.steel.org/
ASM International	www.asminternational.org/
ASTM International	www.astm.org/
Australasian Corrosion Association	www.corrprev.org.au/
AWS (American Welding Society)	www.aws.org/
China Anticorrosion Society	www.china-anticorrosion.com/
Chinese Society for Corrosion and Protection	www.cscp.org.cn/
Corrosion Institute of South Africa	www.corrosioninstitute.org.za/
Corrosion Society of India	www.naceindia.org/corrosion.html
Dechema (Society for Chemical Technology and Biotechnology)	www.dechema.de/
European Federation of Corrosion	www.efcweb.org/
French Anticorrosion Centre	www.cefracor.org/
Hungarian Corrosion Society	www.chemres.hu/KKKI/hunkor/ahun.html
Ibero-American Program of Science and Technology for Development	www.cyted.org.ar/
Institute of Corrosion	www.icorr.demon.co.uk/
International Corrosion Council (ICC)	www.icc-net.org/
ISE (International Society of Electrochemistry)	www.ise-online.org/
Japanese Society of Corrosion Engineering	www.jcorr.or.jp/
Korean Institute of Metals and Materials	www.kim.or.kr/
Materials Research Society	www.mrs.org/
Mexican Society of Electrochemistry (SMEQ)	www.sm-electroquimica.org
NACE International	www.nace.org/nace/index.asp
National Paint and Coatings Association	www.paint.org/index.htm
PRCI (Pipeline Research Council International)	www.prci.com/
Polish Corrosion Society	www.psk.org.pl/statut_a.htm
SSPC (Steel Structures Painting Council)	www.sspc.org/
Society for Biomaterials	www.biomaterials.org/
Society of Petroleum Engineers	www.spe.org/
SPE (Society of Plastics Engineers)	www.4spe.org/
Spanish Council for Scientific Research (CSIC)	www.csic.es/english/principa.htm
Swedish Corrosion Institute	www.corr-institute.se/
ECS (The Electrochemical Society)	www.electrochem.org/
The Institute of Materials, Minerals and Mining	www.iom3.org/index.htm
TMS (The Minerals, Metals and Materials Society)	www.tms.org/
TAPPI (Trade Association of the Pulp and Paper Industry)	www.tappi.org/

S.D. Cramer, B.S. Covino, Jr., G.R. Holcomb and M. Ziomek-Moronz, Information Sources and Databases for the Corrosionist, *Corrosion: Fundamentals, Testing, and Protection*, Vol 13A, *ASM Handbook*, ASM International, 2003, p 999–1001

Information Sources and Databases for the Corrosionist

S.D. Cramer, B.S. Covino, Jr., G.R. Holcomb, M. Ziomek-Moroz; Albany Research Center, U.S. Department of Energy

Corrosion Standards, Specifications, Recommended Practices, and Related Topics

Standards, specifications, recommended practices, and test methods are essential to the organized progress of society and its goals. The standards organizations listed in Table 2 fall into three categories. The first have a mandate to provide standards across the breadth of society activities and are classified here as "broad spectrum." Included in their activities are standards that address corrosion and related topics. The second are more focused organizations that address a particular constituency or interest group—such as TAPPI, which is concerned with the pulp and paper industry, or ACI International, which is focused on the concrete industry—and that more prominently address corrosion and its impact on the organizations' members and activities. The third are the organizations devoted specifically to all aspects of corrosion, such as NACE International.

Table 2 Corrosion standards, specifications, recommended practices, and related topics

Source	Nature of standards	Web address
ACI International	Concrete, including corrosion	www.concrete.org/
American Association of State and Highway Transportation Officials (AASHTO)	Transportation, including corrosion	www.transportation.org/
ANSI (American National Standards Institute)	Broad spectrum	www.ansi.org/
American Water Works Association (AWWA)	Water, including corrosion	www.awwa.org/
American Welding Society (AWS)	Welding, including thermal spray	www.aws.org/
ASTM International (American Society for Testing and Materials)	Broad spectrum, including corrosion	www.astm.org/
British Standards Institution (BSI)	Broad spectrum, including corrosion	www.bsi-global.com/
Canadian General Standards Board (CGSB)	Broad spectrum, including corrosion	www.pwgsc.gc.ca/cgsb/
Department of Defense Single Stock Point (DODSSP)	U.S. Military standards and specification	www.dodssp.daps.mil
European Committee for Standardization (CEN)	Broad spectrum, including corrosion	www.cenorm.be/
International Standards Organization (ISO)	Broad spectrum, including corrosion	www.iso.ch/
NACE International	Corrosion	www.nace.org/
National Institute of Standards and Technology (NIST)	Measurement, documentary, conformity, and information	www.nist.gov/
Polish Committee for Standards	Broad spectrum, including corrosion	www.pkn.pl/
SSPC (Steel Structures Painting Council)	Paints, coatings, and linings	www.sspc.org/
TAPPI (Trade Association of the Pulp and Paper Industry)	Pulp and paper, including corrosion	www.tappi.org/

S.D. Cramer, B.S. Covino, Jr., G.R. Holcomb and M. Ziomek-Moronz, Information Sources and Databases for the Corrosionist, *Corrosion: Fundamentals, Testing, and Protection*, Vol 13A, *ASM Handbook*, ASM International, 2003, p 999–1001

Information Sources and Databases for the Corrosionist

S.D. Cramer, B.S. Covino, Jr., G.R. Holcomb, M. Ziomek-Moroz; Albany Research Center, U.S. Department of Energy

Sources of Corrosion Information

The web provides many sources of information on corrosion, ranging from corrosion fundamentals, the forms of corrosion, and how corrosion is detected and measured, to the multitude of ways equipment and structures are protected from corrosion damage, and how society and the environment are protected from the consequences of corrosion damage. Selected sites are given in Table 3, representing a reasonably broad range of interests and providing portals to other sources of information. This list is, as they say, "only the tip of the iceberg," and the authors appreciate the fact that many readers have their own list of favorites.

Table 3 Sources of corrosion information

Source	Web address
ACI International	www.aci-int.org/
American Galvanizers Association	www.galvanizeit.org/
ASM International	www.asminternational.org/
Copper Development Association	www.copper.org/
Corrosion Doctors	www.corrosion-doctors.org/
CorrosionSource	www.corrosionsource.com/
Cost of Corrosion	www.corrosioncost.com/
CSIRO (Commonwealth Scientific and Industrial Research Organization)	www.csiro.au/
EPRI (Electric Power Research Institute)	www.epri.com/
Gas Institute	www.gri.org/
International Corrosion Council	www.icc-net.org/
International Lead and Zinc Research Organization (ILZRO)	www.ilzro.org/
LaQue Center for Corrosion Technology	www.laque.com/
McMaster University, Walter W. Smeltzer Corrosion Laboratory	www.mse.eng.mcmaster.ca/resource/corrlab.htm
Metal Finishing Industry	www.finishing.com/
MIT, Department of Materials Science and Engineering, H.H. Uhlig Corrosion Laboratory	www.dmse.mit.edu/UhligLab/
Montana State University, Center for Biofilm Engineering	www.erc.montana.edu/
Nickel Development Institute	www.nidi.org/
NIST (National Institutes of Science and Technology)	www.nist.gov/
Ohio State University, Fontana Corrosion Center	www.er6.eng.ohio-state.edu/~frankel/fcc/
Royal Institute of Technology, Materials Science and Engineering, Division of Corrosion Science	www.met.kth.se/corr/

TWI (The Welding Institute)	www.twi.co.uk/
UMIST Corrosion and Protection Centre	www.cp.umist.ac.uk/CPC/
University of Delaware, Marine Biology-Biochemistry	www.ocean.udel.edu/cms/mbbfac.html
University of Louisiana at Lafayette, Corrosion Research Center	www.engr.louisiana.edu/crc/
University of Virginia, Center for Electrochemical Science and Engineering	www.virginia.edu/cese/
Transportation Research Information Services (TRIS), Transportation Research Board, National Academy of Sciences	www4.trb.org/trb/tris.nsf/
Office of Scientific and Technical Information (OSTI), U.S. Department of Energy	www.osti.gov/energycitations/
National Physical Laboratory, High Temperature Corrosion and Coatings	www.npl.co.uk/npl/cmmt/htc/
Sci.chem.electrochem Newsgroup	www.groups.google.com/groups?group=sci.chem..electrochem/

S.D. Cramer, B.S. Covino, Jr., G.R. Holcomb and M. Ziomek-Moronz, Information Sources and Databases for the Corrosionist, *Corrosion: Fundamentals, Testing, and Protection*, Vol 13A, *ASM Handbook*, ASM International, 2003, p 999–1001

Information Sources and Databases for the Corrosionist

S.D. Cramer, B.S. Covino, Jr., G.R. Holcomb, M. Ziomek-Moroz; Albany Research Center, U.S. Department of Energy

Corrosion Databases and Data Compilations

Few situations in science and engineering exist where all the data needed are immediately available from direct experience. Corrosion— with the possible combinations of multiple materials, the multitude of corrosion agents in a variety of strengths over a range of temperatures, and other environmental factors—presents a daunting array of scenarios. Databases and data compilations represent the collective knowledge gleaned from a multitude of individual experiences. Databases and data compilations, supported by an understanding of fundamentals, move one toward goals with efficiency and economy in less-than-perfect situations; that is, most situations. The databases and data compilations listed in Table 4 provide fundamental information on a wide range of materials, their properties, their use and handling, and for evaluating their application. The data compilations are books that may or may not be available in electronic form. Their publishers are listed under contact information.

Table 4 Selected corrosion databases and data compilations

Publisher or source	Title or description	Contact information
Databases		
American Chemical Society	CAS (Chemical Abstracts Services) substance databases	www.info.cas.org/substance.html
ASM International	Alloy Center (including Alloy Finder, Data Sheets & Diagrams, Corrosion Data, Coatings Data, and Materials Property Data)	www.asminternational.org/matinfo
	Phase Diagrams (binary and ternary	www.asminternational.org/bookstore

	phase diagrams on CD-ROM)	
Cambridge Scientific Abstracts (CSA)	Corrosion and materials science bibliographic databases	www.csa.com
Elsevier Science	Dechema Corrosion Handbook: Corrosive Agents and Their Interaction with Materials	www.elsevier.com/
ESM Software	TAPP (thermochemical and physical properties of pure chemical compounds)	www.esm-software.com/tapp/
NACE International	ConSur (Corrosion Data Survey Database)	www.nace.org
National Institute of Standards and Technology (NIST)	Access to over 80 NIST scientific and technical databases, including NIST molten salts (properties of 320 inorganic single salts and 4000 mixtures)	www.nist.gov/srd/
University of Akron	Hazardous chemical database	www.ull.chemistry.uakron.edu/erd/
U.S. Bureau of Labor Statistics	Consumer price indexes for the United States beginning as early as 1913	www.bls.gov/cpi/
Various	Material Safety Data Sheets	Available from various sources. A directory of Internet sources can be found at www.ilpi.com/msds
ASSET Project (U.S. Department of Energy, Office of Industrial Technologies)	Alloy selection system for elevated temperatures; predicts metal loss in gaseous atmospheres from 250–1150 °C (480–2100 °F)	www.oit.doe.gov/chemicals/
Data compilations		
ASM International	*Atlas of Stress-Corrosion and Corrosion Fatigue Curves,* 1990 *Handbook of Corrosion Data,* 2nd ed., 1995	www.asminternational.org/
Marcel Dekker	*Corrosion Resistance Tables: Metals, Nonmetals, Coatings, Mortars, Plastics, Elastomers, and Linings and Fabrics,* 4th ed., 1995	www.dekker.com/
NACE International	*Atlas of Electrochemical Equilibria in Aqueous Solutions,* 1974 *Compilation and Use of Corrosion Data for Alloys in Various High-Temperature Gases,* 1999 *Corrosion Data Survey: Metals Section,* 6th ed. 1985 *Corrosion Data Survey: Nonmetals Section,* 5th ed., 1975	www.nace.org/

S.D. Cramer, B.S. Covino, Jr., G.R. Holcomb and M. Ziomek-Moronz, Information Sources and Databases for the Corrosionist, *Corrosion: Fundamentals, Testing, and Protection*, Vol 13A, *ASM Handbook*, ASM International, 2003, p 999–1001

Information Sources and Databases for the Corrosionist

S.D. Cramer, B.S. Covino, Jr., G.R. Holcomb, M. Ziomek-Moroz; Albany Research Center, U.S. Department of Energy

Other Web Resources

There are some web sites that simply need to be visited to view the links that they provide. That is the purpose of Table 5. These are sites that provide connections to a wealth of information relevant to corrosion and its related topics.

Table 5 Other web resources

Site name	Description	Web address
Case Western Reserve University	Electrochemical science and technology information resource	www.electrochem.cwru.edu/estir/inet.htm
Corrosion Doctors	Corrosion links, including simulation software	www.corrosion-doctors.org/Links.htm
CorrosionSource	Useful links (in corrosion)	www.corrosionsource.com/links.htm
Steel-related technologies	Electrochemistry, corrosion science, and microbiologically influenced corrosion resources	www.steelynx.net
UMIST Corrosion Information Server	Internet resources in corrosion and materials	www2.umist.ac.uk/corrosion/cis/links.htm
University of Delaware Library	Internet resources in materials science	www2.lib.udel.edu/subj/masc/internet.htm
Sci.chem.electrochem Newsgroup	Newsgroup community focused on electrochemistry	See Table 3

S.D. Cramer, B.S. Covino, Jr., G.R. Holcomb and M. Ziomek-Moronz, Conventions and Definitions in Corrosion and Oxidation, *Corrosion: Fundamentals, Testing, and Protection*, Vol 13A, *ASM Handbook*, ASM International, 2003, p 1002–1008

Conventions and Definitions in Corrosion and Oxidation

Stephen D. Cramer, Bernard S. Covino, Jr., Gordon R. Holcomb, and Małgorzata Ziomek-Moroz, Albany Research Center, U.S. Department of Energy; Jack Tinnea, Tinnea Associates

Introduction

COMMON CONVENTIONS AND DEFINITIONS in corrosion, cathodic protection, electricity, and oxidation that can result in confusion and some degree of aggravation are presented in this article. The definitions and

conventions have been grouped but, of course, are not exclusive to any one category. A more comprehensive set of definitions is provided in the "Glossary of Terms" in this Volume.

S.D. Cramer, B.S. Covino, Jr., G.R. Holcomb and M. Ziomek-Moronz, Conventions and Definitions in Corrosion and Oxidation, *Corrosion: Fundamentals, Testing, and Protection*, Vol 13A, *ASM Handbook*, ASM International, 2003, p 1002–1008

Conventions and Definitions in Corrosion and Oxidation

Stephen D. Cramer, Bernard S. Covino, Jr., Gordon R. Holcomb, and Małgorzata Ziomek-Moroz, Albany Research Center, U.S. Department of Energy; Jack Tinnea, Tinnea Associates

Corrosion and Electrochemical Cells

Anion. An anion is an ion that has a negative charge. An anion will move toward the anode in an electric field.
Anode. In an electrochemical cell, the anode is the electrode where oxidation takes place. See also the section "Cell Types and Conditions for Commercial and Industrial Processes" in this article.
Cathode. In an electrochemical cell, the cathode is the electrode where reduction takes place. See also the section Cell Types and Conditions for Commercial and Industrial Processes in this article.
Cation. A cation is an ion that has a positive charge. A cation will move toward the cathode in an electric field.
Corrosion. In its broadest sense, corrosion is the deterioration of a metallic or nonmetallic material by reaction with its environment involving processes other than strictly mechanical or thermal processes. Applied to metallic materials, corrosion is the deterioration of a material by chemical or electrochemical reactions between the material and its environment.
Corrosion Cell. A corrosion cell is typically a galvanic cell that results from a lack of homogeneity in a material or its environment. There are cases where a corrosion cell can be an electrolytic cell, for example, in stray current corrosion.
Corrosion Potential. The corrosion potential is the mixed electrode potential of a freely corroding material relative to a reference electrode, also called the open-circuit potential.
Current: Sign Convention. Anodic currents and current densities are positive, and cathodic currents and current densities are negative. This corresponds to the convention that current (referred to here as conventional current) is the flow of positive charge; electrons move in a direction that is counter to the flow of current. When displaying anodic and cathodic current or current density values on logarithmic coordinates, absolute values of the current or current density are used and the cathodic values are clearly indicated.
The direction of conventional current in an external circuit is defined by the cell type:

Cell type	Direction of conventional current
Reversible	No net current
Galvanic	From the cathode (+) to the anode (-)
Electrolytic	From the cathode (-) to the anode (+)
Corrosion	From the cathode (+) to the anode (-)

Current and Current Density: Symbol Conventions. *I* is commonly used to represent current, and *i* is commonly used to represent current density or flux. Some authors use *J* or *j* to represent current density. Subscripts may be added to these symbols to further distinguish them. For example a, c, or o may be used for anodic, cathodic, and exchange current, respectively.
The unit of *I* is the ampere (A), which is a base unit in the SI system or some multiple. Units of *i* are ampere per unit area, such as A/m^2 (A/ft^2).
Dissociation. is the breakdown of dissolved compounds in a solvent into their charged constituents or components. These charged constituents or ions are the substances that carry charge through the solution. As a consequence of dissociation, the properties of acids, bases, and salts dissolved in water or other polar solvents are very different from those of the undissolved materials.

To explain dissociation, Arrhenius theory states that an acid is a substance that produces hydrogen ions (H^+), and a base is a substance that produces hydroxide ions (OH^-) in water. Consequently, an acid solution contains an excess of hydrogen ions and a base an excess of hydroxide ions. The reactions that produce these ions are:

acid: $HA \rightarrow H^+ + A^-$ (Eq 1)

base: $catOH \rightarrow cat^+ + OH^-$ (Eq 2)

salt: $catA \rightarrow cat^+ + A^-$ (Eq 3)

where A^- is an anion and cat^+ is a cation different from H^+.

In contrast, Brønsted-Lowry proton transfer theory states that an acid is a substance that dissociates to produce a proton and a base is a substance that accepts a proton:

acid → proton + base (Eq 4)

$HCl \rightarrow H^+ + Cl^-$ (Eq 5)

A proton (H^+) does not exist by itself in solution. Protons combine with water to form the hydrated hydrogen ion (H_3O^+), are known as the hydronium ion. Thus, Eq 5 becomes:

$HCl + H_2O \rightarrow H_3O^+ + Cl^-$ (Eq 6)

Arrhenius theory applies to aqueous solutions. The Brønsted-Lowry proton transfer theory applies to all media. It is the more general and important theory, particularly when considering the chemistry of substances in solutions other than water. An example in aqueous solution is the salt ammonium chloride (NH_4Cl). Aqueous solutions of NH_4Cl are acidic. The Brønsted-Lowry explanation shows that the ammonium ion (NH_4^+) is a proton donor and:

$NH_4^+ = H^+ + NH_3$ (Eq 7)

According to Brønsted-Lowry theory, an acid such as H_2O, HCl, H_2S, HCN, and HNO_3 as well as cations and anions such as H_3O^+, NH_4^+, HS^-, HSO_4^-, and HCO_3^- can be electrically neutral. Bases do not need to contain OH^- and can be H_2O, NH_3, NH_2OH, CH_3NH_2, N_2H_4, OH^-, Cl^-, CN^-, CH_3COO^-, or $[Zn(H_2O)_3OH]^+$.

Electrochemical Cell. It is convenient to consider an electrochemical cell as consisting of two independent electrode or half-cell reactions. The anode supports an anodic reaction, and the cathode supports a cathodic reaction. Electrons carry charge through a metallic circuit (often an external circuit), and ions carry charge through the electrolyte.

Cell Types and Conditions for Commercial and Industrial Processes. Table 1 lists conditions that exist in different cell types and the commercial and industrial processes that correspond to these cell types. See the article "Introduction to Corrosion for Constructive Purposes" in this Volume for more information.

Table 1 Cell conditions for commercial and industrial electrode processes

Cell type	Cell potential	Net current	Polarity		Process
			Anode	**Cathode**	
Reversible	$e_{cell,rev}$	$I = 0$	-	+	…
Galvanic	$e_{cell} < e_{cell,rev}$	$I \neq 0$ (spontaneous)	-	+	Batteries, fuel cells
Electrolytic	$e_{cell} > e_{cell,rev}$	$I \neq 0$ (impressed current or applied potential)	+	-	Electrolytic polishing Electroplating Electrochemical machining Electrochemical refining
Corrosion	$e_{cell} \sim 0$	I_{corr} (spontaneous)	-	+	Corrosion Chemical-mechanical

	planarization

Currents and Potentials at Electrodes in Different Cell Types. The currents and potentials at two reversible electrodes, copper and silver, are given in Table 2 as an example of the conditions that exist for different cell types. The electrode systems chosen are a copper electrode immersed in a copper sulfate solution at unit activity of Cu^{2+} and a silver electrode immersed in a silver nitrate solution at unit activity of Ag^{+}. This choice of electrodes (or half-cells) avoids the complexity that arises with many electrodes of commercial interest where oxides or other stable corrosion products form on the surface. It also avoids the complexity that arises with reactions involving chemical species from different redox systems, such as zinc in an aqueous solution where the reduction reaction can be the evolution of hydrogen or the reduction of dissolved oxygen. The solutions are connected by a porous barrier and are at a temperature of 25 °C (77 °F). See the article “Introduction to Corrosion for Constructive Purposes” in this Volume for more information.

Table 2   Electrical conditions at each electrode

Cell type	Electrode reactions		Cell potential	Electrode potentials, E_{SHE}	
	Cu	**Ag**		**Cu^{2+}/Cu**	**Ag^{+}/Ag**
Reversible	$I_a = I_c = I_o$	$I_a = I_c = I_o$	$e_{cell,rev} = 0.459$ V	$E^o_{Cu} = 0.340$	$E^o_{Ag} = 0.799$
Galvanic	$I_a > I_c$	$I_a < I_c$	$e_{cell} < e_{cell,rev}$	$E > E^o_{Cu}$	$E < E^o_{Ag}$
Electrolytic	$I_a < I_c$	$I_a > I_c$	$e_{cell} > e_{cell,rev}$	$E < E^o_{Cu}$	$E > E^o_{Ag}$
Corrosion	$I_a > I_c$	$I_a < I_c$	$e_{cell} = 0$	$E > E^o_{Cu}$	$E < E^o_{Ag}$

I_a, current associated with the anodic reaction at the electrode; I_c, current associated with the cathodic reaction at the electrode; I_o, exchange current. E, the potential of the electrode with reference to the standard hydrogen electrode (SHE); e_{cell}, the potential between external connections to the cell

Electrode Potential: Temperature Coefficient Sign Convention. The thermal temperature coefficient is positive when an increase in temperature produces an increase in electrode potential; that is, the electrode potential shifts in the positive or more noble direction.

Electrode Potential: Measuring An Unknown Potential. In terms of measuring the potential of an electrode in an electrolyte, connect the reference electrode to the ground (negative) terminal of the measuring device (electrometer, multimeter, etc.) and the electrode of interest to the high (positive) terminal. A negative potential in this configuration means the unknown electrode potential is negative to the reference electrode and vice versa. The cell notation for this configuration (see *Electrode Reactions* and Cell Notation in this article) is:

reference electrode || electrode reaction of interest (Eq 8)

A simple check of measuring device polarity is achieved with any battery. Connect the measuring device lead used for the reference electrode to the negative battery terminal. Connect the measuring device lead used for the electrode of interest to the positive battery terminal. The measuring device should show a positive potential. If it does not, the polarity switch of the measuring device should be moved to the positive position.

Electrode Reactions and Cell Notation. An electrochemical cell is composed of at least two half-cell reactions. An anodic reaction is:

$$A \rightarrow A^{n+} + ne^{-} \quad \text{(Eq 9)}$$

A cathodic reaction is:

$$C^{m+} + me^{-} \rightarrow C \quad \text{(Eq 10)}$$

to produce the net or overall cell reaction:

$$mA + nC^{m+} \rightarrow mA^{n+} + nC \quad \text{(Eq 11)}$$

The corresponding half-cell reactions are described by the following notation:

anodic reaction:

$$A|A^{n+}(aq, a_{A^{n+}}) \quad \text{(Eq 12a)}$$

cathodic reaction:

$C^{m+}(aq, a_{Cm+})|C$ (Eq 12b)

These half-cell reactions are combined as follows to denote the net cell reaction:

$A|A^{n+}(aq, a_{An+})||C^{m+}(aq, a_{Cm+})|C$ (Eq 13)

In this notation, the anode or oxidizing reaction is always on the left, and the cathode or reducing reaction is always on the right. Variations of this notation allow for a metallic electrode that does not react electrochemically, for dissolved gases, and for solid phases in equilibrium with the solution. The two vertical lines represent a cell where the liquid junction potential between two aqueous solutions (aq) has been eliminated or is assumed to be small. Liquid junction potentials are often small by comparison to the cell potential.

The cell potential for the net cell reaction (Eq 14), that is, the difference between the half-cell potentials for the cathode (right) and anode (left) reactions, is:

$e_{cell} = E_{right} - E_{left}$ (Eq 14)

where the potential on the right is half-cell (Eq 12bb) and the potential on the left is half-cell (Eq 12aa), and both are expressed as reduction potentials.

The electrochemical cell notation representing the measurement of the unknown potential of an electrode of interest with respect to the standard hydrogen electrode (SHE) is given by:

$$\text{Pt}, H_2(f=1)\,|\,H^+(a=1)\;||\;\text{electrode reaction of interest} \quad \text{(Eq 15a)}$$

SHE||electrode reaction of interest (Eq 15b)

where $f = 1$ means the fugacity is one and $a = 1$ means unity activity.

Electrode Potential: Sign Convention. The electropositive direction of electrode potential implies an increasing oxidizing condition at the electrode. The electropositive direction is also known as the noble direction because the corrosion potentials of noble metals such as gold and platinum are more electropositive than those of more active base metals such as magnesium, zinc, and iron. The electronegative direction is associated with an increasing reducing condition at the electrode. The electronegative direction is also known as the active direction, because the corrosion potentials of active metals such as magnesium and zinc are substantially more electronegative than those of noble metals.

Half-cell electrode reactions written as reduction potentials follow this convention, adopted in 1953 by the International Union of Pure and Applied Chemistry, and yield positive potentials for more oxidizing conditions and negative potentials for more reducing conditions (Ref 1).

Electrolyte. An electrolyte is a nonmetallic electrical conductor where the current is carried by ions instead of electrons.

Exchange Current. The exchange current (I_o) is the common value of the anodic and cathodic currents when an electrode is at equilibrium with its environment

$I_o = I_a = -I_c$ (Eq 16)

Half-Cell Reactions. A half-cell reaction is the electrochemical reaction that describes charge transfer at an electrode and involves either a reduction or oxidation reaction.

Ion. An ion is an atomic or molecular particle having a net electric charge.

Reference Electrode Potentials: Values And Conversion Factors. Table 3 lists reduction electrode potentials for some common reference electrodes and the conversion factors to change measured potential values from that of the measuring electrode to the SHE (standard hydrogen electrode) and SCE (saturated calomel electrode) scales.

Table 3 Reference electrode potentials and conversion factors

Electrode	Potential at 25 °C (77 °F) V vs. SHE	Thermal temperature coefficient, mV/°C	Add the following value in volts to convert from measurements with the given reference electrode[(a)]:	
			To SHE scale	**To SCE scale**
(Pt)/H_2(*f* = 1)/H^+(*a* = 1), SHE	0.000	+0.87	0.000	-0.241
Ag/AgCl/1 *M* KCl	+0.235	+0.25	+0.235	-0.006
Ag/AgCl/0.6 *M* Cl^- (seawater)	+0.250	…	+0.250	+0.009
Ag/AgCl/0.1 *M* Cl^-	+0.288	+0.22	+0.288	+0.047
Hg/Hg_2Cl_2/sat KCl, SCE	+0.241	+0.22	+0.241	0.000
Hg/Hg_2Cl_2/1 *M* KCl	+0.280	+0.59	+0.280	+0.039
Hg/Hg_2Cl_2/0.1 *M* KCl	+0.334	+0.79	+0.334	+0.093
Cu/$CuSO_4$sat	+0.300	+0.90	+0.30	+0.06
Hg/$HgSO_4$	+0.616	…	+0.616	+0.375

(a) An electrode potential of 1.000 V vs. SCE would be 1.000 + 0.241 = 1.241 V vs. SHE. An electrode potential of -1.000 V vs. SCE would be -1.000 + 0.241 = -0.759 V vs. SHE.
Source: Ref 2

Overpotential is the current-producing potential difference between a nonequilibrium electrode potential and its corresponding equilibrium value for a definite electrode reaction, $\eta = E - E^o$ (Ref 3, Fig. 1). Overvoltage and overpotential are often used interchangeably (Ref 4).

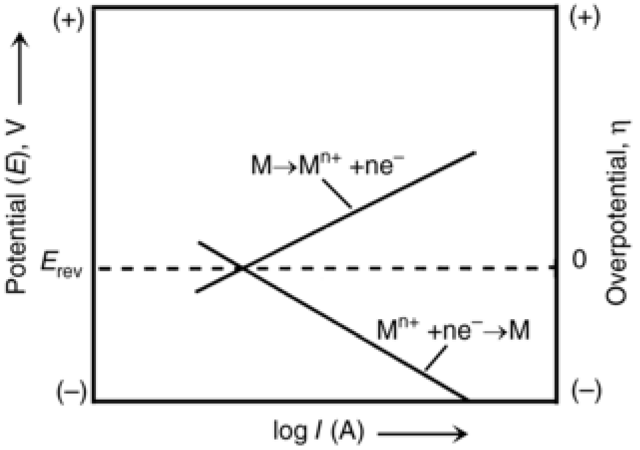

Fig. 1 Evans diagram showing the relationship between electrode potential and overpotential

Polarization is defined similarly to the overpotential; that is, the difference between the potentials of an electrode with and without current, $E - E^o$ (Ref 3, 4). The common forms of electrode polarization are activation polarization (η_{act}); concentration polarization (η_{conc}); and resistance polarization (η_r). Polarization is the sum of these contributions:

$$\eta = \eta_{act} + \eta_{conc} + \eta_r \quad \text{(Eq 17)}$$

A term *overvoltage* (ε) has been defined similarly to overpotential to describe polarization (the current-voltage relationship) around the mixed potential (E_{corr}) for corrosion reactions (Ref 5); that is, $\varepsilon = E - E_{corr}$. The important distinction is that overpotential is related to the reversible potential of an electrode reaction, and *overvoltage* is related to the mixed potential of a corrosion reaction. Some of the confusion regarding polarization occurs because the term *overvoltage* can be used interchangeably with *overpotential* (Ref 4) or in the context of “overvoltage” (Ref 5).

Polarization Data: Conventions for Displaying. On rectangular coordinates, positive values are plotted above the origin on the *y*-axis (ordinate axis) and to the right of the origin on the *x*-axis (abscissa axis). On logarithmic coordinates, increasing values are plotted from left to right on the *x*-axis and from bottom to top on the *y*-axis. Current or current density is plotted on the *x*- axis, and potential is plotted on the *y*-axis. Current or current density is plotted using either rectangular coordinates or logarithmic coordinates, depending on the range of current or current density values to be displayed. Absolute values of current or current density are used with logarithmic coordinates. Typically, current or current density values are plotted as amperes (A) or amperes per square meter (A/m^2). Potential is plotted using rectangular coordinates. Typically, potentials are converted to the SHE scale or the SCE scale and are plotted as volts (V) measured on this scale.

References cited in this section

1. K.B. Oldham, and G. Mansfeld, *Corrosion,* CORRA, Vol 27, 1971, p 434
2. "Conventions Applicable to Electrochemical Measurements in Corrosion Testing," G- 3, *Annual Book of ASTM Standards,* 1989, p 46–53
3. D.A. Jones, *Principles and Prevention of Corrosion,* Macmillan, New York, 1992, p 79–85
4. G. Wranglén, *An Introduction to Corrosion and Protection of Metals,* Chapman and Hall, London, 1985, p 10
5. D.A. Jones, *Principles and Prevention of Corrosion,* Macmillan, New York, 1992, p 145–146

S.D. Cramer, B.S. Covino, Jr., G.R. Holcomb and M. Ziomek-Moronz, Conventions and Definitions in Corrosion and Oxidation, *Corrosion: Fundamentals, Testing, and Protection*, Vol 13A*, ASM Handbook*, ASM International, 2003, p 1002–1008

Conventions and Definitions in Corrosion and Oxidation

Stephen D. Cramer, Bernard S. Covino, Jr., Gordon R. Holcomb, and Małgorzata Ziomek-Moroz, Albany Research Center, U.S. Department of Energy; Jack Tinnea, Tinnea Associates

---

Cathodic Protection

Cathodic Protection (CP) is the reduction of corrosion by polarizing a structure to a sufficiently cathodic potential so that corrosion in the most anodic area(s) on the structure is/are reduced to an acceptably low level. Impressed-current CP (ICCP) protects the structure by making the structure the cathode (negative electrode) in an electrolytic cell consisting of an external source of direct current (dc) power and either a consumable or a nonconsumable anode (positive electrode) of material such as high-silicon cast iron, graphite, mixed metal oxide, or catalyzed titanium (Fig. 2a).

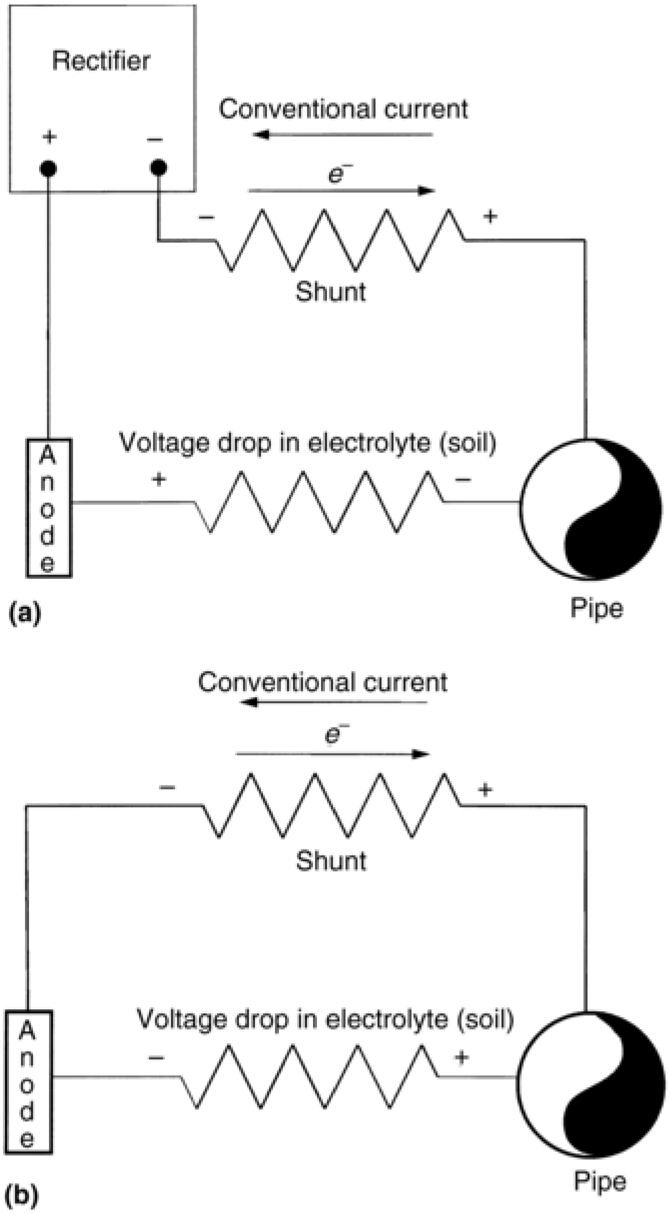

Fig. 2 Simplified layouts for cathodic protection systems. (a) Impressed current cathodic protection system (b) Galvanic or sacrificial cathodic protection system

Sacrificial CP (SACP)—also known as galvanic CP—protects the structure by coupling the structure to a consumable anode of a more active material such as zinc or magnesium (Fig. 2a).

An ICCP system is an electrolytic cell. A sacrificial CP system is a galvanic cell. Both systems polarize the structure to be protected in an electronegative direction. A properly designed CP system causes all areas of the protected structure to be made cathodic to the most anodic site on the structure before CP.

Cathodic Protection Testing Protocol. The working convention of many CP practitioners deviates from standard electrochemical convention. Two areas where this occurs are in current flow and meter configuration. “Conventional current” flows from positive to negative. This is opposite the flow of electrons. If one uses the flow of electrons as current flow and standard electrochemical convention in voltmeter connections for potential readings, some of the confusion in CP practice can be avoided.

Voltmeters used by early pipeline CP workers were analog and only read upscale. Potential surveyors for buried steel structures would almost always encounter readings that were negative with respect to a CSE (saturated copper-sulfate reference electrode). Given that the meters of the day read only up the scale, workers were in the habit of connecting the reference electrode to the positive terminal of the voltmeter and the structure to the negative and then adding the “-” in their heads. Also, by holding to the idea that “negative” always goes to the structure, it was thought that this practice helped to avoid problems with connecting ICCP systems backwards.

In time, the "upscale" meters were provided polarity switches, which were then followed by the autoranging/autopolarity digital meters of today. However, the old practice of connecting the CSE to the positive terminal of the voltmeter and the structure to the negative and changing the polarity by notation persists as of this printing in some sectors.

The practice of connecting the reference to the positive voltmeter terminal can lead to confusion in other areas. For example, SACP anodes are selected because they are more electronegative than the structure to be protected. The structure thus is positive with respect to the SACP anodes. In contrast, the rectifier positive terminal in ICCP is connected to the anodes while the negative terminal is connected to the structure. *In both cases, however, the flow of conventional current in the external circuit is away from the structure or, equivalently, the flow of electrons is towards the structure* (Fig. 2). It would be easy to think that, since the galvanic SACP anodes are electronegative to the structure while the ICCP anodes are electropositive, the current flow in the two CP systems is reversed. This is not true.

CP Protection Criteria. Early in the application of CP to pipeline protection, polished steel rods were used as "most anodic" references. The logic behind this approach was that if the pipe were polarized to the potential of the polished steel (zero volts between the pipe and rod), it would then be polarized to the level of most anodic sites. Reference electrodes, especially CSE, eventually displaced polished steel rods as the reference of choice. Likewise, standards were developed by organizations that defined protection criteria not only for buried pipelines but also for metals in other environments ranging from those submerged in seawater to those embedded in concrete. Four common criteria are used for unalloyed ferrous materials (Ref 6, 7):

- The *IR*-free ("instant off") potential of buried materials must be more negative than -850 mV versus CSE.
- The "on potential" of buried materials is 300 mV more negative than the free corrosion potential in soil, similar to criterion 1.
- IR-free polarization of buried materials must be 100 mV more electronegative than the corrosion potential measured either by current interrupt or depolarization techniques.
- The protection current is sufficient to maintain the material at a condition that meets any of the above criteria in periodic testing.

CP Design: Area Basis for Current Densities. Current densities are employed in rule-of- thumb approaches to the design of cathodic protection systems. An assumption is made about the current density required to protect the structure. The selected density value (mA/m^2) is multiplied by the nominal surface area (m^2) of the structure in contact with the electrolyte to provide an estimate of the total required current. When a metal surface is new, there is a fairly good relationship between nominal surface area and the metal surface area in contact with the surrounding electrolyte. With age, the metal may corrode, roughness develops, and the actual metal surface area in contact with the electrolyte may increase to several times the "nominal" surface. In a similar fashion, when a metal to be protected is covered with a protective coating, the initial surface area in contact with the electrolyte is much less than the nominal surface area. With time, the coating will degrade and the surface area of the metal in contact with the electrolyte will increase.

Current densities also are important in the operation of CP anodes. In reinforced concrete, it is recommended (Ref 8) that the maximum sustained current density on the anode be less than 108 mA/m^2. In practice, some structure owners (Ref 9) operate their anodes at current densities as low as 2 mA/m^2.

Evans Diagram: Impressed Current CP (ICCP) in Neutral or Basic Environment. Figure 3(a) shows a plot of potential versus log current (Evans diagram) for an ICCP system in a neutral or basic environment. Only activation and concentration polarization are included in the structure corrosion kinetics. The structure anode reaction is the dissolution of iron; the structure cathode reaction is the reduction of oxygen. The intersection between the structure anodic polarization curve and the structure cathodic polarization curve determines the unprotected structure corrosion potential ($E_{corr,S}$) and the unprotected structure corrosion current ($I_{corr,S}$).

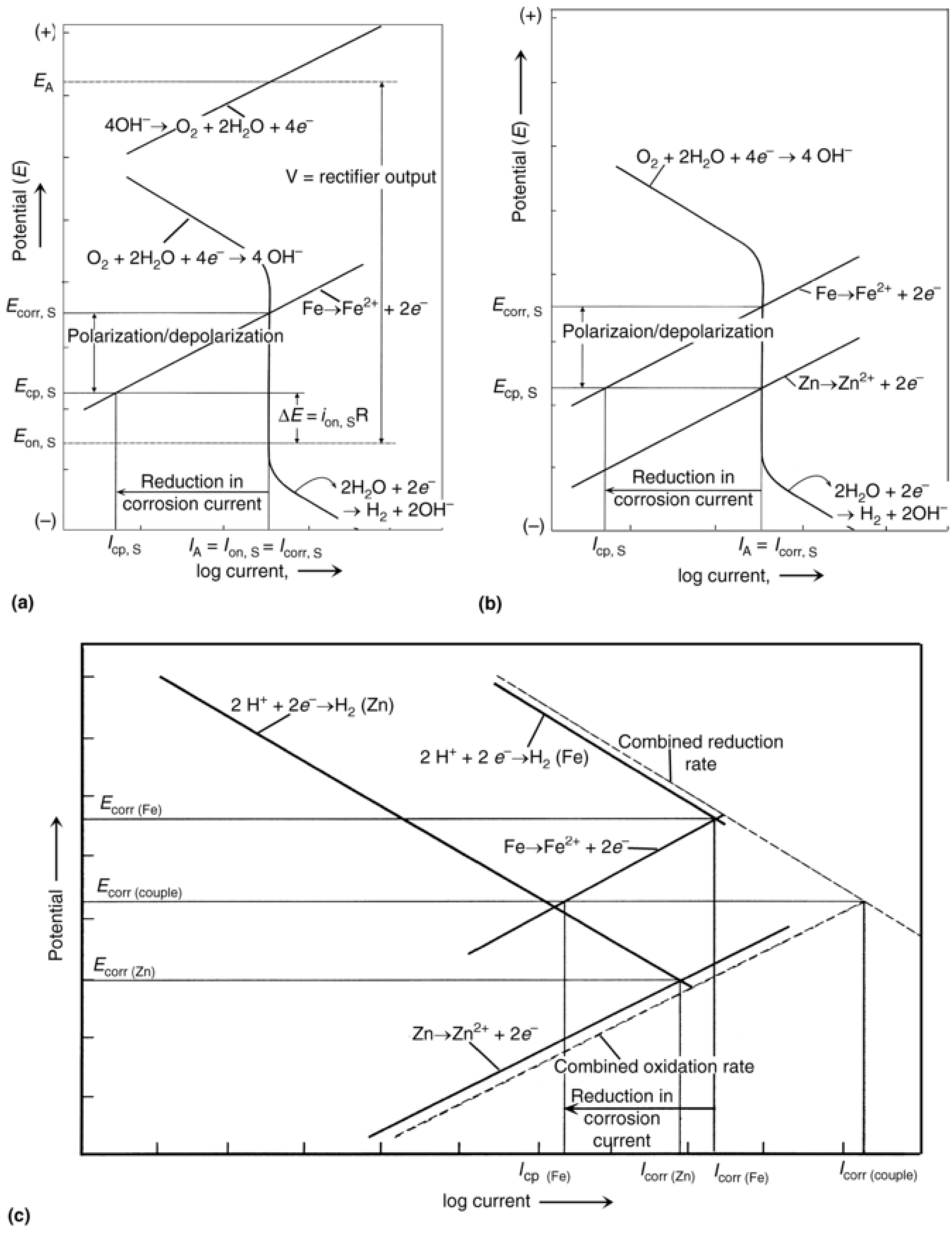

Fig. 3 **Evans diagrams for cathodic protection (CP) systems. (a) Diagram for an impressed current CP system protecting a steel structure in an oxygenated neutral or basic environment using an inert anode. (b) Diagram for a galvanic or sacrificial CP system protecting a steel structure in an oxygenated neutral or basic environment using a consumable zinc anode. (c) Diagram for a galvanic or sacrificial CP system protecting a steel structure in an acidic environment using a consumable zinc anode.**

Coupling the structure to a nonconsumable inert anode powered by a rectifier shifts the structure to a more electronegative potential ($E_{cp,S}$). This shift reduces the structure anodic current to $I_{cp,S}$, the corrosion current with cathodic protection. Because the cathodic reaction at the structure is diffusion limited and thus highly polarized, the current required by this shift in potential changes very little from $I_{corr,S}$.

The reaction at the inert anode is the oxidation of hydroxyl ions to form oxygen. As power is applied to the structure, the potential of the inert anode shifts in the electropositive direction to E_A, the potential of the inert anode at a current equal to $I_{corr,S}$. The ΔE shown, the *IR* drop in the solution, is a function of the partial current collecting on the structure ($I_{on,S}$) (equivalent to $I_{corr,S}$), and the electrolyte resistivity (R), in the vicinity of the reference electrode used to evaluate the system. Because of this *IR* drop, the structure appears to be polarized to $E_{on,S}$.

The rectifier output is given by $V = E_A - E_{on,S}$. When the current is interrupted, an IR free measurement of the structure potential is achieved after inductive artifacts have dissipated (typically ~0.5 seconds). This potential is the “instant off” potential and equivalent to $E_{cp,S}$. With the current off, the structure potential decays back toward $E_{corr,S}$. The value of this decay or depolarization over a period of time, typically 4 to 24 h, is a measure of how well the structure is protected by the application of CP. The reduction in the corrosion current is given by $\Delta I = I_{corr,S} - I_{cp,S}$.

In some situations, say deep well configurations, the environment surrounding the anodes may become acidic and reactions other than those shown may dominate. These reactions include gas generation, which if not vented, may greatly increase the electrical resistance at the anode.

Evans Diagram: Galvanic or Sacrificial Cathodic Protection (SACP) in Neutral or Basic Environment. Figure 3(b) shows an Evans diagram for SACP in a neutral or basic environment. The structure part of this diagram and the notation is the same as that used for the ICCP example. Only the anode has been changed, from an inert anode for ICCP to a consumable zinc anode for SACP. Again, only activation and concentration polarization are included in the structure corrosion kinetics. The structure anode reaction is the dissolution of iron; the structure cathode reaction is the reduction of oxygen. The intersection between the structure anodic polarization curve and the structure cathodic polarization curve determines the unprotected structure corrosion potential ($E_{corr,S}$) and the unprotected structure corrosion current ($I_{corr,S}$).

Coupling the structure to a consumable zinc anode shifts the structure to a more electronegative potential ($E_{cp,S}$). This shift reduces the structure anodic current to $I_{cp,S}$, the corrosion current with cathodic protection. Because the cathodic reaction at the structure is diffusion limited and highly polarized, the current required by this shift in potential changes very little from $I_{corr,S}$.

The reaction at the sacrificial anode is the oxidation of zinc to form zinc ions in solution. The potential of the zinc anode shifts in the electropositive direction to $E_{cp,S}$, the potential of the zinc anode at a current equal to $I_{corr,S}$. Just as in the case of ICCP, there is typically an *IR* potential drop between the structure and the zinc anode, and the structure and the zinc anode are at somewhat different potentials. However, for clarity, this has not been shown in Fig. 3(b).

As in the case of ICCP, when the current is interrupted, an *IR* free value of the structure potential, which is the “instant off potential” and equivalent to $E_{cp,S}$, is measured. With the current off, the structure potential decays back towards $E_{corr,S}$. The value of this decay or depolarization over a period of time, typically 4 to 24 h, is a measure of how well the structure is protected by the application of CP. The reduction in the corrosion current is given by $\Delta I = I_{corr,S} - I_{cp,S}$. Of course, these determinations cannot be made on SACP systems where the consumable anode and structure cannot be isolated from each other.

Evans Diagram: Galvanic or Sacrificial Cathodic Protection (SACP) in Acidic Environment. Figure 3(c) is an Evans diagram for SACP in an acidic environment using a consumable zinc anode. Note that both the zinc anode and the structure are polarized by the process as indicated by the dashed lines showing the combined reduction and oxidation rates. For clarity, similar details were not included in Fig. 3(a) and 3(b).

Only activation polarization is included in the structure corrosion kinetics. The structure anode reaction is the dissolution of iron; the structure cathode reaction is the reduction of hydrogen ions. The intersection between the structure anodic polarization curve and the structure cathodic polarization curve determines the unprotected structure corrosion potential ($E_{corr(Fe)}$) and the unprotected structure corrosion current ($I_{corr(Fe)}$).

Coupling the structure to a consumable zinc anode shifts the structure to a more electronegative potential ($E_{corr(couple)}$). This shift reduces the structure anodic current to $I_{cp(Fe)}$, the corrosion current with cathodic protection. Because the cathodic reaction at the structure is not diffusion limited, the current required by this shift in potentials increases substantially to $I_{corr(couple)}$, representing the increase in the cathodic current due to

hydrogen reduction on the zinc anode and the increase in the anodic current due to dissolution of the zinc anode.
The reaction at the consumable zinc anode is the oxidation zinc to form zinc ions in solution. The potential of the freely corroding zinc electrode in the acidic environment is $E_{corr(Zn)}$ and the corrosion current for the zinc at this potential is $I_{corr(Zn)}$. When the zinc anode is coupled with the structure, the potential shifts in the electropositive direction to $E_{corr(couple)}$. Just as in the case of ICCP, there is typically an *IR* potential drop between the structure and the zinc anode, and the structure and the zinc anode are at somewhat different potentials. However, for clarity, this has not been shown in Fig. 3(c).
As in the case of ICCP, when the current is interrupted, an *IR* free value of the structure potential is measured, which is the "instant off potential" and equivalent to $E_{corr(couple)}$. With the current off, the structure potential decays back towards $E_{corr(Fe)}$. The value of this decay or depolarization over a period of time, typically 4 to 24 h, is a measure of how well the structure is protected by the application of CP. The reduction in the corrosion current is given by $\Delta I = I_{corr(Fe)} - I_{cp(Fe)}$. Of course, these determinations cannot be made on SACP systems where the consumable anode and structure cannot be isolated from each other.

References cited in this section

6. W. von Baeckmann, W. Schwenk, and W. Prinz, *Handbook of Cathodic Protection,* 3rd ed., Gulf Publishing Co, 1997, p 103–105

7. "Control of External Corrosion on Underground or Submerged Metallic Piping Systems," Standard Recommended Practice No. RP0169-2002, NACE International, Houston, TX, 2002

8. "Cathodic Protection of Reinforcing Steel in Atmospherically Exposed Concrete Structures," RP0290-90, NACE International, Houston, TX, 1990, 11 pages

9. B.S. Covino, Jr., S.D. Cramer, S.J. Bullard, G.R. Holcomb, J.H. Russell, W.K. Collins, H.M. Laylor, and C.B. Cryer, "Performance of Metalized Zinc Anodes for Cathodic Protection of Reinforced Concrete Bridges— Final Report," FHWA-OR-RD-02-10, Federal Highway Administration, U.S. Department of Transportation, Washington D.C., 2002. Available at http:// www.odot.state.or.us/tddresearch/reports/ zn%20anode%20.pdf and at www.osti.gov/ servlets/purl/804079-JhD8ED/native/

S.D. Cramer, B.S. Covino, Jr., G.R. Holcomb and M. Ziomek-Moronz, Conventions and Definitions in Corrosion and Oxidation, *Corrosion: Fundamentals, Testing, and Protection*, Vol 13A, *ASM Handbook*, ASM International, 2003, p 1002–1008

Conventions and Definitions in Corrosion and Oxidation

Stephen D. Cramer, Bernard S. Covino, Jr., Gordon R. Holcomb, and Małgorzata Ziomek-Moroz, Albany Research Center, U.S. Department of Energy; Jack Tinnea, Tinnea Associates

---

Electricity

Classifying Materials by Conductivity: Conductors (Metals), Semiconductors, and Insulators. Materials can be considered conductors (metals), semiconductors, and insulators. Metals are good conductors of electrons. An electric current flows under the influence of an electric or changing magnetic field in a metal. In insulators, there is no electric current flow under an electric field. In terms of the energy-band theory (Ref 10), insulators have completely full valence bands and cannot carry electrical current. Metals have partially filled valence bands and thus can carry current. In materials where the energy gap between the valence band and the band

immediately above it is small (less than about 2 eV at room temperature), electrons can be thermally excited from the valence band to the next band. This creates partially filled bands, and, thus, electrical current can flow. Such materials are semiconductors.

Electronic defects in nonstoichiometric semiconductors can be negative (electrons) or positive (holes) and are termed n-type and p-type semiconductors, respectively.

Conductivity. Conduction of electrical charge through an electrolyte results from the mobility of ions. Through a metal, conduction results from the mobility of electrons, and through a gas, conduction results from the mobility of gaseous ions and electrons. Conductivity, also called specific conductance, is a measure of these transport processes and a property of a homogeneous material. It is the inverse of resistivity and has the units of $(\Omega \cdot \text{length})^{-1}$ or S/ m. The siemens (S) is the conductance of a material such that one ampere current will flow with an applied potential of one volt; S = 1/Ω

Electrochemical impedance (Z) is a complex number defined as:

$$Z(j\omega) = Z'(j\omega) + jZ''(j\omega) \quad \text{(Eq 18)}$$

where Z' is the real or in-phase component of impedance; Z'' is the imaginary or out-of-phase component of impedance; $j^2 = -1$, and ω is the frequency in radian/s and $= 2\pi f$ where f is the frequency in Hertz (Hz). The impedance magnitude is $|Z|^2 = (Z')^2 + (Z'')^2$. The phase angle between the real and imaginary components of impedance is: $\theta = \arctan(Z''/Z')$. The admittance $Y = 1/Z = Y' + jY''$.

Impedance can be modeled in a linear constant parameter system as:

$$Z = R + jX \quad \text{(Eq 19)}$$

where R is resistance; X is reactance $X = \omega L - 1/\omega C$; and L is inductance and C is capacitance.

Resistivity. Resistivity, also called specific resistance (ρ), is a property of a homogeneous material. It is computed from the resistance (R) of a volume of the material having unit length (l) and unit cross-sectional area (A). Its value is $\rho = RA/l$, and it has the units of $\Omega \cdot l$, such as $\Omega \cdot$ cm.

Reference cited in this section

10. M.A. Omar, *Elementary Solid State Physics*, Addison-Wesley, Reading, MA, 1975, p 210–212

S.D. Cramer, B.S. Covino, Jr., G.R. Holcomb and M. Ziomek-Moronz, Conventions and Definitions in Corrosion and Oxidation, *Corrosion: Fundamentals, Testing, and Protection*, Vol 13A, *ASM Handbook*, ASM International, 2003, p 1002–1008

Conventions and Definitions in Corrosion and Oxidation

Stephen D. Cramer, Bernard S. Covino, Jr., Gordon R. Holcomb, and Małgorzata Ziomek-Moroz, Albany Research Center, U.S. Department of Energy; Jack Tinnea, Tinnea Associates

---

Oxidation

Crystal Structure. A crystal structure is the arrangement of atoms or ions in a regularly repeating pattern, such that the atoms or ions are located either on the points of a Bravais lattice or in a fixed relation to those points (Ref 11). A Bravais lattice is a set of points in space such that each point has identical surroundings. There are 14 possible arrangements or crystal structures (Table 4 and Fig. 4). The name of the crystal structure is a combination of the Bravais lattice and system; that is, body-centered cubic.

Table 4 Crystal structures

System	Bravais lattices	Shape	
		Axial lengths	**Angles**
Cubic	Simple Body-centered Face-centered	*a* = *b* = *c*	α = β = γ = 90°
Tetragonal	Simple Body-centered	*a* = *b* ≠ *c*	α = β = γ = 90°
Orthorhombic	Simple Body-centered Base-centered Face-centered	*a* ≠ *b* ≠ *c*	α = β = γ = 90°
Rhombohedral (or trigonal)	Simple	*a* = *b* = *c*	α = β = γ ≠ 90°
Hexagonal	Simple	*a* = *b* ≠ *c*	α = β = 90°; γ = 120°
Monoclinic	Simple Base-centered	*a* ≠ *b* ≠ *c*	α = β = 90°; γ ≠ 90°
Triclinic	Simple	*a* ≠ *b* ≠ *c*	α ≠ β ≠ γ ≠ 90°

Refer to Fig. 4. Source: Ref 11

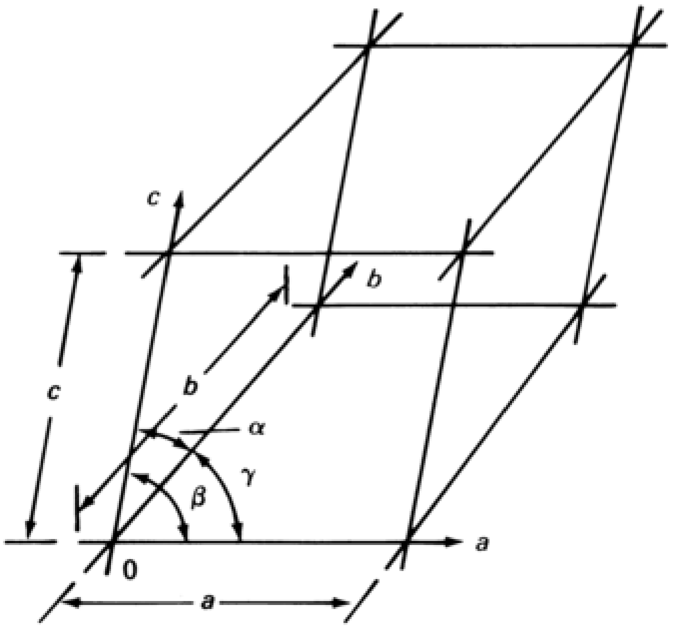

Fig. 4 Crystal axes, interaxial angles, and unit-cell edge length

Defect Structures: Kröger-Vink Notation. A notation used to describe point defects in inorganic compounds was developed by Kröger and Vink (Ref 12, 13, 14). In this system, the type of defect is indicated by a major symbol, and the site it occupies is indicated by a subscript. A superscript indicates the charge relative to a normal lattice, where ′ designates an effective negative charge, and · designates an effective positive charge. An x indicates a zero effective charge. Some examples are:

Designation	Meaning
$V_O^{2\cdot}$	Doubly charged oxygen vacancy
$Ni_{Cr}^{\cdot}$	Cr (+3) on a Ni(+2) site
O_O^x	Oxygen on an oxygen site (a normal anion)
M_M^x	Metal on a metal site (a normal cation)
M_i	Metal interstitial
M_M'	Metal on a metal site with an extra electron
e′	Free electron (concentration of electrons $\equiv$n)
$h^{\cdot}$	Electron hole (concentration of holes $\equiv$p)

Defect Structures. Common point defect structures found in inorganic compounds are briefly described (Ref 15). Kröger-Vink notation is used to describe the defect equilibria.

Schottky defects are found in stoichiometric compounds and consist of equivalent concentrations of anion and cation defects. An example would be pairs of oxygen and metal vacancies:

$$O = V_O^{2\cdot} + V_M^{2\prime} \qquad \text{(Eq 20)}$$

Frenkel defects are found in stoichiometric compounds and are formed when a metal ion on a regular cation site is moved to an interstitial site and leaves behind a vacancy. An example for singly charged interstitials and vacancies is:

$$M_M = M_i^{\cdot} + V_M' \qquad \text{(Eq 21)}$$

Defects associated with oxygen-deficient or metal excess nonstoichiometric compounds can include extra oxygen vacancies or extra metal interstitials. An example of each is:

$$O_O = V_O^{2\cdot} + 2e' + \tfrac{1}{2}O_2 \qquad \text{(Eq 22)}$$

$$O_O + M_M = M_i^{2\cdot} + 2e' + \tfrac{1}{2}O_2 \qquad \text{(Eq 23)}$$

Defects associated with oxygen excess or metal-deficient nonstoichiometric compounds can include extra oxygen interstitials or extra metal vacancies. An example of each is:

$$\tfrac{1}{2}O_2 = O_i^x \qquad \text{(Eq 24)}$$

$$\tfrac{1}{2}O_2 = O_O + V_M^{2\prime} + 2h^{\cdot} \qquad \text{(Eq 25)}$$

Dopants can create a wide range of defects where the foreign atom takes the place of the metal cation in the normal lattice or as an interstitial.

Intrinsic ionization of electrons from the valence band to the conduction band create *e′* and $h^{\cdot}$ pairs. This typically occurs in stoichiometric compounds.

Parabolic Rate Equations. The oxidation of many metals at high temperatures can be described with parabolic kinetics. Often Wagner's oxidation theory is invoked to explain the behavior. It is worthwhile to note the assumptions used in Wagner's theory so that its limitations can be recognized when describing more complex systems (Ref 16, 17, 18, 19):

- Lattice diffusion of the reacting ions or atoms, or the transport of electrons through the dense compact scale, are rate determining.
- Lattice diffusion occurs through the migration of point defects. These defects migrate independently from each other.
- Reactions at the phase boundaries are rapid, and thermodynamic equilibria are established at the metal/oxide and oxide/oxygen interfaces.
- The driving force for the oxidation reaction is the free energy change that occurs on forming the oxide from the metal and gaseous oxygen. Thus a gradient in oxygen activity exists across the scale, with the activity at the metal/oxide interface determined from the metal/oxide equilibrium.
- Deviations from stoichiometry are small.
- O_2 solubility is negligible.
- Scales are thick enough to neglect charged surfaces.

The major deviations from the Wagner theory include easy diffusion paths, the formation of voids and porosity, and the effects of stresses in the scale.

Parabolic Rate Constant Evaluation: Use Δm^2 versus t (not Δm versus $t^{0.5}$). The kinetics of high-temperature corrosion experiments are often reported in terms of a parabolic rate law and a parabolic rate constant, k_p. One then has a choice to determine k_p from the slope of the experimental change in mass (Δm) and time (t) data plotted as either Δm versus $t^{0.5}$ or Δm^2 versus t. For the simplest form of the parabolic rate expression, $\Delta m^2 = k_p t$, the choice is immaterial. However, for most metallic materials, there is an initial transient period of fast kinetics that is best described by $(\Delta m - \Delta m_i)^2 = k_p(t - t_i)$. Pieraggi (Ref 20) has shown that systematic errors in determining k_p arise when there is this initial transient period and the slope of Δm versus $t^{0.5}$ is used instead of the slope of Δm^2 versus t.

References cited in this section

11. B.D. Cullity, *Elements of X-Ray Diffraction,* 2nd ed., Addison-Wesley Publishing Company, Reading, MA, 1978, p 34–35

12. F.A. Kröger and H.J. Vink, *Solid State Phys.,* Vol 3, 1956, p 307

13. F.A. Kröger, *The Chemistry of Imperfect Crystals,* North-Holland, Amsterdam, 2nd ed., 1974

14. P. Kofstad, *High Temperature Corrosion,* Elsevier Applied Science, New York, 1988, p 34–36

15. P. Kofstad, *High Temperature Corrosion,* Elsevier Applied Science, New York, 1988, p 43–51

16. P. Kofstad, *High Temperature Corrosion,* Elsevier Applied Science, New York, 1988, p 163–164

17. C. Wagner, *Z. Phys. Chem.,* Vol B21, 1933, p 25

18. C. Wagner, *Atom Movements,* American Society Metals, 1951, p 153

19. C. Wagner, *Prog. Solid State Chem.,* Vol 10, 1975, p 3

20. B. Pieraggi, *Oxidation of Metals,* Vol 27 (No. 3/4), 1987, p 177–185

S.D. Cramer, B.S. Covino, Jr., G.R. Holcomb and M. Ziomek-Moronz, Conventions and Definitions in Corrosion and Oxidation, *Corrosion: Fundamentals, Testing, and Protection*, Vol 13A, *ASM Handbook,* ASM International, 2003, p 1002–1008

Conventions and Definitions in Corrosion and Oxidation

Stephen D. Cramer, Bernard S. Covino, Jr., Gordon R. Holcomb, and Małgorzata Ziomek-Moroz, Albany Research Center, U.S. Department of Energy; Jack Tinnea, Tinnea Associates

---

References

1. K.B. Oldham, and G. Mansfeld, *Corrosion,* CORRA, Vol 27, 1971, p 434

2. “Conventions Applicable to Electrochemical Measurements in Corrosion Testing,” G- 3, *Annual Book of ASTM Standards,* 1989, p 46–53

3. D.A. Jones, *Principles and Prevention of Corrosion,* Macmillan, New York, 1992, p 79–85

4. G. Wranglén, *An Introduction to Corrosion and Protection of Metals,* Chapman and Hall, London, 1985, p 10

5. D.A. Jones, *Principles and Prevention of Corrosion,* Macmillan, New York, 1992, p 145–146

6. W. von Baeckmann, W. Schwenk, and W. Prinz, *Handbook of Cathodic Protection,* 3rd ed., Gulf Publishing Co, 1997, p 103–105

7. "Control of External Corrosion on Underground or Submerged Metallic Piping Systems," Standard Recommended Practice No. RP0169-2002, NACE International, Houston, TX, 2002

8. "Cathodic Protection of Reinforcing Steel in Atmospherically Exposed Concrete Structures," RP0290-90, NACE International, Houston, TX, 1990, 11 pages

9. B.S. Covino, Jr., S.D. Cramer, S.J. Bullard, G.R. Holcomb, J.H. Russell, W.K. Collins, H.M. Laylor, and C.B. Cryer, "Performance of Metalized Zinc Anodes for Cathodic Protection of Reinforced Concrete Bridges— Final Report," FHWA-OR-RD-02-10, Federal Highway Administration, U.S. Department of Transportation, Washington D.C., 2002. Available at http:// www.odot.state.or.us/tddresearch/reports/ zn%20anode%20.pdf and at www.osti.gov/ servlets/purl/804079-JhD8ED/native/

10. M.A. Omar, *Elementary Solid State Physics,* Addison-Wesley, Reading, MA, 1975, p 210–212

11. B.D. Cullity, *Elements of X-Ray Diffraction,* 2nd ed., Addison-Wesley Publishing Company, Reading, MA, 1978, p 34–35

12. F.A. Kröger and H.J. Vink, *Solid State Phys.,* Vol 3, 1956, p 307

13. F.A. Kröger, *The Chemistry of Imperfect Crystals,* North-Holland, Amsterdam, 2nd ed., 1974

14. P. Kofstad, *High Temperature Corrosion,* Elsevier Applied Science, New York, 1988, p 34–36

15. P. Kofstad, *High Temperature Corrosion,* Elsevier Applied Science, New York, 1988, p 43–51

16. P. Kofstad, *High Temperature Corrosion,* Elsevier Applied Science, New York, 1988, p 163–164

17. C. Wagner, *Z. Phys. Chem.,* Vol B21, 1933, p 25

18. C. Wagner, *Atom Movements,* American Society Metals, 1951, p 153

19. C. Wagner, *Prog. Solid State Chem.,* Vol 10, 1975, p 3

20. B. Pieraggi, *Oxidation of Metals,* Vol 27 (No. 3/4), 1987, p 177–185

Corrosion Rate Conversion,, *Corrosion: Fundamentals, Testing, and Protection*, Vol 13A, *ASM Handbook*, ASM International, 2003, p 1028

Corrosion Rate Conversion

Table 1 Relationships among some of the units commonly used for corrosion rates

d is metal density in grams per cubic centimeter (g/cm^3)

Unit	Factor for conversion to					
	mdd	**g/m^2/d**	**µm/yr**	**mm/yr**	**mils/yr**	**in./yr**
Milligrams per square decimeter per day (mdd)	1	0.1	36.5/*d*	0.0365/*d*	1.144/*d*	0.00144/*d*
Grams per square meter per day (g/m^2/d	10	1	365/*d*	0.365/*d*	14.4/*d*	0.0144/*d*
Microns per year (µm/yr)	0.0274*d*	0.00274*d*	1	0.001	0.0394	0.0000394
Millimeters per year (mm/yr)	27.4*d*	2.74*d*	1000	1	39.4	0.0394
Mils per year (mils/yr)	0.696*d*	0.0696*d*	25.4	0.0254	1	0.001
Inches per year (in./yr)	696*d*	69.6*d*	25,400	25.4	1000	1

Source: G. Wranglén, *An Introduction to Corrosion and Protection of Metals,* Chapman and Hall, 1985, p. 238

Glossary of Terms

A

absorption.
A process in which fluid molecules are taken up by a liquid or solid and distributed throughout the body of that liquid or solid. Compare with adsorption.

accelerated corrosion test.
Method designed to approximate, in a short time, the deteriorating effect under normal long-term service conditions.

acicular ferrite.
A highly substructured nonequiaxed ferrite formed upon continuous cooling by a mixed diffusion and shear mode of transformation that begins at a temperature slightly higher than the transformation temperature range for upper bainite. It is distinguished from bainite in that it has a limited amount of carbon available; thus, there is only a small amount of carbide present.

acid.
A chemical substance that yields hydrogen ions (H^+) when dissolved in water; also a substance that dissociates to produce a proton (H^+) in any medium, that is, a proton donor. Compare with base.

acid embrittlement.
A form of hydrogen embrittlement that may be induced in some metals by acid.

acid rain.
Atmospheric precipitation with a pH below 5.6 to 5.7. Burning of fossil fuels for heat and power is the major factor in the generation of oxides of nitrogen and sulfur, which are converted into nitric and sulfuric acids in atmospheric moisture (fogs and precipitation). See also atmospheric corrosion.

acrylic.
Resin polymerized from acrylic acid, methacrylic acid, esters of these acids, or acrylonitrile.

activation.
The changing of a passive surface of a metal to a chemically active state. Contrast with passivation.

active.
The negative direction of electrode potential. Also used to describe corrosion and its associated potential range when the electrode potential is more negative than adjacent potentials where the corrosion rate is depressed; that is, the passive region.

active metal.
A metal ready to corrode, or readily corroded.

active potential.
The potential of a corroding material.

activity.
A measure of the chemical potential of a substance, where the chemical potential is not equal to concentration, that allows mathematical relations equivalent to those for ideal systems to be used to correlate changes in experimentally measured quantities with changes in chemical potential.

activity (ion).
The ion concentration corrected for deviations from ideal behavior. Concentration multiplied by activity coefficient.

activity coefficient.
A characteristic of a quantity expressing the deviation of a solution from ideal thermodynamic behavior; often used in connection with electrolytes.

addition agent.
A substance added to a solution for the purpose of altering or controlling a process. Examples include wetting agents in acid pickling, brighteners or antipitting agents in plating solutions, and inhibitors.

adsorption.
The surface retention of solid, liquid, or gas molecules, atoms, or ions by a solid or liquid. Compare with absorption.

aeration.
(1) Exposing to the action of air. (2) Causing air to bubble through. (3) Introducing air into a solution by spraying, stirring, or a similar method. (4) Supplying or infusing with air, as in sand or soil.

aeration cell (oxygen cell).
See differential aeration cell.

age hardening.
Hardening by aging, usually after rapid cooling or cold working.

aging.
A change in the properties of certain metals and alloys that occurs at ambient or moderately elevated temperatures after hot working or a heat treatment (quench aging in ferrous alloys, natural or artificial aging in ferrous and nonferrous alloys) or after a cold- working operation (strain aging). The change in properties is often, but not always, due to a phase change (precipitation), but never involves a change in chemical composition of the metal or alloy. See also age hardening, artificial aging, natural aging, overaging, precipitation hardening, precipitation heat treatment, quench aging, and strain aging.

alclad.
Composite wrought product comprising an aluminum alloy core having on one or both surfaces a metallurgically bonded aluminum or aluminum alloy coating that is anodic to the core and thus electrochemically protects the core against corrosion.

alkali metal.
A metal in group IA of the periodic system—namely, lithium, sodium, potassium, rubidium, cesium, and francium. They form strongly alkaline hydroxides, hence the name.

alkaline.
(1) Having properties of an alkali. (2) Having a pH greater than 7.

alkaline cleaner.
A material blended from alkali hydroxides and such alkaline salts as borates, carbonates, phosphates, or silicates. The cleaning action may be enhanced by the addition of surface-active agents and special solvents.

alkyd.
Resin used in coatings. Reaction products of polyhydric alcohols and polybasic acids.

alkylation.

(1) A chemical process in which an alkyl radical is introduced into an organic compound by substitution or addition. (2) A refinery process for chemically combining isoparaffin with olefin hydrocarbons.

alligatoring.

(1) Pronounced wide cracking over the entire surface of a coating having the appearance of alligator hide. (2) The longitudinal splitting of flat slabs in plane parallel to the rolled surface. Also called fish-mouthing.

alloy plating.

The codeposition of two or more metallic elements.

alpha ferrite.

See ferrite.

alpha iron.

The body-centered cubic form of pure iron, stable below 910 °C (1670 °F).

alternate-immersion test.

A corrosion test in which the specimens are intermittently exposed to a liquid medium at definite time intervals.

aluminizing.

Forming of an aluminum or aluminum alloy coating on a metal by hot dipping, hot spraying, or diffusion.

amalgam.

An alloy of mercury with one or more other metals.

ammeter.

An instrument for measuring the magnitude of electric current flow.

amorphous solid.

A rigid material whose structure lacks crystalline periodicity; that is, the pattern of its constituent atoms or molecules does not repeat periodically in three dimensions. See also metallic glass.

amphoteric.

A term applied to oxides and hydroxides that can act basic toward strong acids and acidic toward strong alkalis. Substances that can dissociate electrolytically to produce hydrogen or hydroxyl ions according to conditions.

anaerobic.

Free of air or uncombined oxygen.

anchorite.

A zinc-iron phosphate coating for iron and steel.

anion.

A negatively charged ion that migrates through the electrolyte toward the anode under the influence of a potential gradient. See also cation and ion.

annealing.

A generic term denoting a treatment, consisting of heating to and holding at a suitable temperature, followed by cooling at a suitable rate, used primarily to soften metallic materials, but also to simultaneously produce desired changes in other properties or in microstructure. The purpose of such changes may be, but is not confined to, improvement of machinability, facilitation of cold work, improvement of mechanical or electrical properties, and/or increase in stability of dimensions. When the term is used by itself, full annealing is implied. When applied only for the relief of stress, the process is properly called stress relieving or stress-relief annealing.

anode.

The electrode of an electrolyte cell at which oxidation occurs. Electrons flow away from the anode in the external circuit. It is usually at this electrode that corrosion occurs and metal ions enter solution. Contrast with cathode.

anode corrosion.

The dissolution of a metal acting as an anode.

anode corrosion efficiency.

The ratio of the actual corrosion (weight loss) of an anode to the theoretical corrosion (weight loss) calculated by Faraday's law from the quantity of electricity that has been generated by the anode during the corrosion.

anode effect.
The effect produced by polarization of the anode in electrolysis. It is characterized by a sudden increase in voltage and corresponding decrease in amperage due to the anode becoming virtually separated from the electrolyte by a gas film.

anode efficiency.
The current efficiency at the anode.

anode film.
(1) The solution in immediate contact with the anode, especially if the concentration gradient is steep. (2) The outer layer of the anode itself.

anode polarization.
See polarization.

anodic cleaning.
Electrolytic cleaning in which the work is the anode. Also called reverse- current cleaning.

anodic coating.
A film or scale on a metal surface resulting from an electrolytic treatment at the anode.

anodic inhibitor.
A chemical substance or mixture that prevents or reduces the rate of the anodic or oxidation reaction. See also inhibitor.

anodic polarization.
The change of the electrode potential in the noble (positive) direction due to current flow. See also polarization.

anodic protection.
Imposing an external electrical potential to polarize a metal into the passive region where dissolution rates are low (applicable only to metals that show active- passive behavior). Contrast with cathodic protection.

anodic reaction.
Electrode reaction equivalent to a transfer of positive charge from an electronic to an ionic conductor. An anodic reaction is an oxidation process. A common example in corrosion is: $Me \rightarrow Me^{n+} + ne^-$.

anodizing.
Forming an anodic coating or conversion coating on a metal surface by anodic oxidation; frequently applied to aluminum.

anolyte.
The electrolyte adjacent to the anode in an electrolytic cell.

antifouling.
Intended to prevent fouling of underwater structures, such as the bottoms of ships.

antipitting agent.
An addition agent for electroplating solutions to prevent the formation of pits or large pores in the electrodeposit.

aqueous.
Pertaining to water; an aqueous solution is made by using water as a solvent.

artificial aging.
Aging above room temperature. See also aging. Compare with natural aging.

atmospheric corrosion.
The gradual degradation or alteration of a material by contact with substances present in the atmosphere, such as oxygen, moisture, acidic gases, acid precipitation, basic particulated, carbon dioxide, sulfur, and chlorine compounds. sulfur and chlorine compounds.

atomic weight.
A number assigned to each chemical element that specifies the average mass of its atoms. Because an element may consist of two or more isotopes having different masses, the atomic weight is the average of the masses of the naturally occurring isotopes proportional to their occurrence. The mean weight of the atom of an element in relation to $^{12}C = 12.000$.

austenite.
A solid solution of one or more elements in face-centered cubic iron. Unless otherwise designated (such as nickel austenite), the solute is generally assumed to be carbon.

austenitizing.

Forming austenite by heating a ferrous alloy into the transformation range (partial austenitizing) or above the transformation range (complete austenitizing). When used without qualification, the term implies complete austenitizing.

auxiliary anode.

In electroplating, a supplementary anode positioned so as to raise the current density on a certain area of the cathode and thus obtain better distribution of plating.

auxiliary electrode.

An electrode commonly used in polarization studies to pass current to or from a test electrode. It is usually made from a noncorroding material; often called the counterelectrode.

B

backfill.

Material placed in a drilled hole to fill space around anodes, vent pipe, and buried components of a cathodic protection system.

bainite.

A metastable aggregate of ferrite and cementite resulting from the transformation of austenite at temperatures below the pearlite range but above M_s, the martensite start temperature. Bainite formed in the upper part of the bainite transformation range has a feathery appearance; bainite formed in the lower part of the range has an acicular appearance resembling that of tempered martensite.

banded structure.

A segregated structure consisting of alternating nearly parallel bands of different composition, typically aligned in the direction of primary hot working.

base.

A chemical substance that yields hydroxyl ions (OH^-) when dissolved in water; also, a proton receptor in any medium. Compare with acid.

base metal.

(1) The metal present in the largest proportion in an alloy; for example, brass is a copper-base alloy. (2) An active metal that readily oxidizes, or that dissolves to form ions. (3) The metal to be brazed, cut, soldered, or welded. (4) After welding, that part of the metal that was not melted.

beach marks.

Macroscopic progression marks on a fatigue fracture or stress-corrosion cracking surface that indicate successive positions of the advancing crack front. The classic appearance is of irregular elliptical or semielliptical rings, radiating outward from one or more origins. Beach marks (also known as clamshell marks or arrest marks) are typically found on service fractures where the part is loaded randomly, intermittently, or with periodic variations in mean stress or alternating stress. See also striation.

biaxial stress.

See principal stress (normal).

biological corrosion.

Deterioration of metals as a result of the metabolic activity of microorganisms. See also microbiologically influenced corrosion.

bipolar electrode.

An electrode in an electrolytic cell that is not mechanically connected to the power supply, but is so placed in the electrolyte, between the anode and cathode, that the part nearer the anode becomes cathodic and the part nearer the cathode becomes anodic. Also called intermediate electrode.

bituminous coating.

Coal tar or asphalt-base coating.

black liquor.

The liquid material remaining from pulpwood cooking in the soda or sulfate papermaking process.

black oxide.

A black finish on a metal produced by immersing it in hot oxidizing salts or salt solutions.

blister.

A raised area, often dome shaped, resulting from (1) loss of adhesion between a coating or deposit and the base metal or (2) delamination under the pressure of expanding gas trapped in a metal in a near-subsurface zone. Very small blisters may be called pinhead blisters or pepper blisters.

blow down.
(1) Injection of air or water under high pressure through a tube to the anode area for the purpose of purging the annular space and possibly correcting high resistance caused by gas blocking. (2) In connection with boilers or cooling towers, the process of discharging a significant portion of the aqueous solution in order to remove accumulated salts, deposits, and other impurities.

blue brittleness.
Brittleness exhibited by some steels after being heated to a temperature within the range of about 200 to 370 °C (400 to 700 °F), particularly if the steel is worked at the elevated temperature.

blushing.
Whitening and loss of gloss of a usually organic coating caused by moisture. Also called blooming.

brackish water.
(1) Water having salinity values ranging from approximately 0.5 to 17 parts per thousand. (2) Water having less salt than seawater, but undrinkable.

breakdown potential (E_b)
The least noble potential where pitting or crevice corrosion, or both, will initiate and propagate. See also critical pitting potential.

brightener.
An agent or combination of agents added to an electroplating bath to produce a smooth, lustrous deposit.

brine.
Typically, water containing a higher concentration of dissolved salt than that of ordinary ocean water.

brittle fracture.
Separation of a solid accompanied by little or no macroscopic plastic deformation. Typically occurs by rapid crack propagation with less expenditure of energy than for ductile fracture.

burning.
(1) Permanently damaging a metal or alloy by heating to cause either incipient melting or intergranular oxidation. See also overheating. (2) In grinding, getting the work hot enough to cause discoloration or to change the microstructure by tempering or hardening.

C

calcareous coating or deposit.
A layer consisting of a mixture of calcium carbonate and magnesium hydroxide deposited on surfaces being cathodically protected because of the increased pH adjacent to the protected surface.

calomel electrode.
An electrode widely used as a reference electrode of known potential in electrometric measurement of acidity and alkalinity, corrosion studies, voltammetry, and measurement of the potentials of other electrodes. See also electrode potential, reference electrode, and saturated calomel electrode.

calorizing.
Imparting resistance to oxidation to an iron or steel surface by heating in aluminum powder at 800 to 1000 °C (1470 to 1830 °F).

carbonitriding.
A case hardening process in which a suitable ferrous material is heated above the lower transformation temperature in a gaseous atmosphere of such composition as to cause simultaneous absorption of carbon and nitrogen by the surface and, by diffusion, create a concentration gradient. The process is completed by cooling at a rate that produces the desired properties in the workpiece.

carburizing.
Absorption and diffusion of carbon into solid ferrous alloys by heating, to a temperature usually above Ac_3, in contact with a suitable carbonaceous material. A form of case hardening that produces a carbon gradient extending inward from the surface, enabling the surface layer to be hardened either by quenching directly from the carburizing temperature or by cooling to room temperature, then reaustenitizing and quenching.

case hardening.
A generic term covering several processes applicable to steel that change the chemical composition of the surface layer by absorption of carbon, nitrogen, or a mixture of the two and, by diffusion, create a concentration gradient. The outer portion, or case, is made substantially harder than the inner portion, or

core. The processes commonly used are carburizing and quench hardening; cyaniding; nitriding; and carbonitriding. The use of the applicable specific process name is preferred.

CASS test.

See *copper-accelerated salt-spray test.*

cathode.

The electrode of an electrolytic cell at which reduction occurs. Electrons flow toward the cathode in the external circuit. Typical cathodic processes are cations taking up electrons and being discharged, oxygen being reduced, and the reduction of an element or group of elements from a higher to a lower valence state. Contrast with anode.

cathode efficiency.

Current efficiency at the cathode.

cathode film.

The solution in immediate contact with the cathode during electrolysis.

cathodic cleaning.

Electrolytic cleaning in which the work is the cathode.

cathodic corrosion.

Corrosion resulting from a cathodic condition of a structure, usually caused by the reaction of an amphoteric metal with the alkaline products of electrolysis.

cathodic disbondment.

The destruction of adhesion between a coating and its substrate by the products of a cathodic reaction.

cathodic inhibitor.

A chemical substance or mixture that prevents or reduces the rate of the cathodic or reduction reaction.

cathodic pickling.

Electrolytic pickling in which the work is the cathode. See also pickling.

cathodic polarization.

The change of the electrode potential in the active (negative) direction due to current flow. See also polarization.

cathodic protection.

(1) Reduction of corrosion rate by shifting the potential of the electrode toward a less oxidizing potential with an externally applied voltage. (2) Partial or complete protection of a metal from corrosion by making it a cathode, using either a galvanic cell or an impressed current. Contrast with anodic protection.

cathodic reaction.

Electrode reaction equivalent to a transfer of negative charge from an electronic to an ionic conductor. A cathodic reaction is a reduction process. A common example in corrosion is: $Ox + ne^- \rightarrow Red$.

catholyte.

The electrolyte adjacent to the cathode of an electrolytic cell.

cation.

A positively charged ion that migrates through the electrolyte toward the cathode under the influence of a potential gradient. See also anion and ion.

caustic.

(1) Burning or corrosive. (2) A hydroxide of a light metal, such as sodium hydroxide or potassium hydroxide.

caustic dip.

A strongly alkaline solution into which metal is immersed for etching, for neutralizing acid, or for removing organic materials such as greases or paints.

caustic embrittlement or caustic cracking.

An obsolete historical term denoting a form of stress-corrosion cracking most frequently encountered in carbon steels or Fe-Cr-Ni alloys that are exposed to concentrated hydroxide solutions at temperatures of 200 to 250 °C (400 to 480 °F).

cavitation.

The formation and instantaneous collapse of numerous tiny voids or cavities within a liquid caused by rapid and intense pressure changes. Cavitation produced by ultrasonic radiation is sometimes used to

effect violent localized agitation. Cavitation caused by severe turbulent flow often leads to cavitation damage.

cavitation corrosion.
Material deterioration involving both corrosion and cavitation.

cavitation damage.
The degradation of a solid body resulting from its exposure to cavitation. This may include loss of the material, surface deformation, or changes in properties or appearance.

cavitation-erosion.
Progressive loss of the original material from a solid surface due to continuing exposure to cavitation.

cell.
Electrochemical system consisting of an anode and a cathode immersed in an electrolyte. The anode and cathode may be separate metals or dissimilar areas on the same metal. The cell includes the external circuit, which permits the flow of electrons from the anode to the cathode. See also electrochemical cell.

cementite.
A hard, brittle compound of iron and carbon, known chemically as iron carbide and having the approximate chemical formula Fe_3C. Characterized by an orthorhombic crystal structure. When it occurs as a phase in steel, the chemical composition will be altered by the presence of manganese and other carbide-forming elements.

chalking.
The development of loose, removable powder at the surface of an organic coating usually caused by weathering.

checking.
The development of slight breaks in a coating that do not penetrate to the underlying surface.

checks.
Numerous, very fine cracks in a coating or at the surface of a metal part. Checks may appear during processing or during service and are most often associated with thermal treatment or thermal cycling. Also called check marks, checking, or heat checks.

chelate.
(1) A molecular structure in which a heterocyclic ring can be formed by the unshared electrons of neighboring atoms. (2) A coordination compound in which a heterocyclic ring is formed by a metal bound to two atoms of the associated ligand. See also complexation.

chelating agent.
(1) An organic compound in which atoms form more than one coordinate bond with metals in solution. (2) A substance used in metalfinishing to control or eliminate certain metallic ions present in undesirable quantities.

chelation.
A chemical process involving formation of a heterocyclic ring compound that contains at least one metal cation or hydrogen ion in the ring.

chemical conversion coating.
A protective or decorative nonmetallic coating produced in situ by chemical reaction of a metal with a chosen environment. It is often used to prepare the surface prior to the application of an organic coating.

chemical potential.
In a thermodynamic system of several constituents, the rate of change of the Gibbs function of the system with respect to the change in the number of moles of a particular constituent.

chemical vapor deposition (CVD).
A coating process, similar to gas carburizing and carbonitriding, whereby a reactant atmosphere gas is fed into a processing chamber where it decomposes at the surface of the workpiece, liberating one material for either absorption by, or accumulation on, the workpiece. A second material is liberated in gas form and is removed from the processing chamber, along with excess atmosphere gas.

chemisorption.
The binding of an adsorbate to the surface of a solid by forces whose energy levels approximate those of a chemical bond. Contrast with physisorption.

chevron pattern.

A fractographic pattern of radial marks (shear ledges) that look like nested letters “V”; sometimes called a herringbone pattern. Typically found on brittle fracture surfaces in structural parts whose widths are considerably greater than their thicknesses. The points of the chevrons can be traced back to the fracture origin.

chromadizing.

Improving paint adhesion on aluminum or aluminum alloys, mainly aircraft skins, by treatment with a solution of chromic acid. Also called chromodizing or chromatizing. Not to be confused with chromating or chromizing.

chromate treatment.

A treatment of metal in a solution of a hexavalent chromium compound to produce a conversion coating consisting of trivalent and hexavalent chromium compounds.

chromating.

Performing a chromate treatment.

chrome pickle.

(1) Producing a chromate conversion coating on magnesium for temporary protection or for a paint base. (2) The solution that produces the conversion coating.

chromizing.

A surface treatment at elevated temperature, generally carried out in pack, vapor, or salt bath, in which an alloy is formed by the inward diffusion of chromium into the base metal.

cladding.

(1) A layer of material, usually metallic, that is mechanically or metallurgically bonded to a substrate. Processes include roll cladding, welding, and explosive forming. (2) A relatively thick (>1 mm, or 0.04 in.) layer of material applied for the purpose of improved corrosion resistance or other properties.

clad metal.

A composite metal containing two or more layers that have been bonded together. The bonding may have been accomplished by corolling, coextrusion, welding, diffusion bonding, casting, heavy chemical deposition, or heavy electroplating.

cleavage.

Splitting (fracture) of a crystal on a crystallographic plane of low index.

cleavage fracture.

A fracture, usually of a polycrystalline metal, in which most of the grains have failed by cleavage, resulting in bright reflecting facets. It is associated with low-energy brittle fracture.

cold cracking.

A type of weld cracking that usually occurs below 205 °C (400 °F). Cracking may occur during or after cooling to room temperature, sometimes with a considerable time delay. Three factors combine to produce cold cracks: stress (for example, from thermal expansion and contraction), hydrogen (from hydrogen-containing welding consumables), and a susceptible microstructure (plate martensite is most susceptible to cracking, ferritic and bainitic structures least susceptible). See also hot cracking, lamellar tearing, and *stress- relief cracking.*

cold working.

Deforming metal plastically under conditions of temperature and strain rate that induce strain hardening. Usually, but not necessarily, conducted at room temperature. Contrast with hot working.

combined carbon.

The part of the total carbon in steel or cast iron that is present as other than free carbon.

complexation.

The formation of complex chemical species by the coordination of groups of atoms termed ligands to a central ion, commonly a metal ion. Generally, the ligand coordinates by providing a pair of electrons that forms an ionic or covalent bond to the central ion. See also chelate, coordination compound, and ligand.

compressive.

Pertaining to forces on a body or part of a body that tend to crush, or compress, the body.

compressive strength.

The maximum compressive stress a material is capable of developing. With a brittle material that fails in compression by fracturing, the compressive strength has a definite value. In the case of ductile,

malleable, or semiviscous materials (which do not fail in compression by a shattering fracture), the value obtained for compressive strength is an arbitrary value dependent on the degree of distortion that is regarded as effective failure of the material.

compressive stress.
A stress that causes an elastic body to deform (shorten) in the direction of the applied load. Contrast with tensile stress.

concentration cell.
An electrochemical cell where the driving force is a difference in concentration of some component in the electrolyte. This difference leads to the formation of discrete cathode and anode sites.

concentration polarization.
That portion of the polarization of an electrode produced by concentration changes resulting from passage of current through the electrolyte.

conductivity.
The ratio of the electric current density to the electric field in a material. Also called electrical conductivity or specific conductance.

contact corrosion.
A term primarily used in Europe to describe galvanic corrosion between dissimilar metals.

contact plating.
A metal plating process wherein the plating current is provided by galvanic action between the work metal and a second metal, without the use of an external source of current.

contact potential.
The potential difference at the junction of two dissimilar substances.

continuity bond.
A metallic connection that provides electrical continuity between metal structures.

conversion coating.
A coating consisting of a compound formed from the surface metal by chemical or electrochemical treatments. Examples include chromate coatings on zinc, cadmium, magnesium, and aluminum, and oxide and phosphate coatings on steel. See also chromate treatment and phosphating.

coordination compound.
A compound with a central atom or ion bound to a group of ions or molecules surrounding it. Also called coordination complex. See also chelate, complexation, and ligand.

copper-accelerated salt-spray (CASS) test.
An accelerated corrosion test for some electrodeposits and for anodic coatings on aluminum.

corrodent.
A substance that will cause corrosion when brought in contact with a material. A corrosive agent.

corrodkote test.
An accelerated corrosion test for electrodeposits.

corrosion.
The chemical or electrochemical reaction between a material and its environment that produces a deterioration of the material and its properties.

corrosion effect.
A change in any part of the corrosion system caused by corrosion.

corrosion embrittlement.
The severe loss of ductility of a metal resulting from corrosive attack, usually intergranular and often not visually apparent.

corrosion-erosion.
See erosion-corrosion.

corrosion fatigue.
The process in which a metal fractures prematurely under conditions of simultaneous corrosion and repeated cyclic loading at lower stress levels or fewer cycles than would be required in the absence of the corrosive environment.

corrosion fatigue strength.
The maximum repeated stress that can be endured by metal without failure under definite conditions of corrosion and fatigue and for a specific number of stress cycles and a specified period of time.

corrosion inhibitor.
See inhibitor.

corrosionist.
A person working in the field of corrosion; anyone working to prevent corrosion or protect against corrosion.

corrosion potential (E_{corr}).
The potential of a corroding surface in an electrolyte, relative to a reference electrode. Also called rest potential, open-circuit potential, or freely corroding potential.

corrosion product.
Substance formed as a result of corrosion.

corrosion protection.
Modification of a corrosion system so that corrosion damage is mitigated.

corrosion rate.
Corrosion effect on a metal per unit of time. The type of corrosion rate used depends on the technical system and on the type of corrosion effect. Thus, corrosion rate may be expressed as an increase in the depth of corrosion per unit of time (penetration rate, for example, mils/yr) or the mass of metal turned into corrosion products per unit area of surface per unit of time (weight loss, for example, $g/m^2/yr$). The corrosion effect may vary with time and may not be the same at all points of the corroding surface. Therefore, reports of corrosion rates should be accompanied by information on the type, time dependency, and location of the corrosion effect.

corrosion resistance.
Ability of a metal to withstand corrosion in a given corrosion system.

corrosion system.
System consisting of one or more metals and all parts of the environment that influence corrosion.

corrosivity.
Tendency of an environment to cause corrosion in a given corrosion system.

counterelectrode.
See auxiliary electrode.

couple.
See galvanic corrosion.

covering power.
The ability of a solution to give satisfactory plating at very low current densities, a condition that exists in recesses and pits. This term suggests an ability to cover, but not necessarily to build up, a uniform coating, whereas throwing power suggests the ability to obtain a coating of uniform thickness of an irregularly shaped object.

cracking (of coating).
Breaks in a coating that extend through to the substrate or underlying surface.

crazing.
A network of checks or cracks appearing on the surface.

creep.
Time-dependent strain occurring under stress. The creep strain occurring at a diminishing rate is called primary creep; that occurring at a minimum and almost constant rate, secondary creep; and that occurring at an accelerating rate, tertiary creep.

creep-rupture embrittlement.
Embrittlement under creep conditions of, for example, aluminum alloys and steels that results in abnormally low rupture ductility. In aluminum alloys, iron in amounts above the solubility limit is known to cause such embrittlement; in steels, the phenomenon is related to the amount of impurities (for example, phosphorus, sulfur, copper, arsenic, antimony, and tin) present. In either case, failure occurs by intergranular cracking of the embrittled material.

creep-rupture strength.
The stress that will cause fracture in a creep test at a given time in a specified constant environment. Also called stress-rupture strength.

crevice corrosion.

Localized corrosion of a metal surface at, or immediately adjacent to, an area that is shielded from full exposure to the environment because of close proximity between the metal and the surface of another material.

critical anodic current density.

The maximum anodic current density observed during anodic polarization in the active region for a metal or alloy electrode that exhibits active-passive behavior in an environment.

critical flaw size.

The size of a flaw (defect) in a structure that will cause failure at a particular stress level.

critical humidity.

The relative humidity above which the atmospheric corrosion rate of some metals increases sharply.

critical pitting potential (E_{cp}, E_p, E_{pp}).

The least noble potential at which pits nucleate and grow. It is dependent on the test method used. See also breakdown potential.

current (I).

The net transfer of electric charge (coulombs) per unit time. The unit of current, the ampere (A), is a base unit of the SI system. See also current density.

current density (i).

The current flowing to or from a unit area of an electrode surface. Expressed as ampere/meter^2 (A/m^2) in the SI system.

current efficiency.

The ratio of the electrochemical equivalent current density for a specific reaction to the total applied current density.

D

deactivation.

The process of prior removal of the active corrosive constituents, usually oxygen, from a corrosive liquid by controlled corrosion of expendable metal or by other chemical means, thereby making the liquid less corrosive.

dealloying.

The selective corrosion of one or more components of a solid solution alloy. Also called parting or selective leaching. See also dealuminification, decarburization, decobaltification, denickelification, dezincification, and graphitic corrosion.

dealuminification.

Selective leaching of aluminum, as from aluminum bronze. Also known as dealuminization.

decarburization.

Loss of carbon from the surface layer of a carbon-containing alloy due to reaction with one or more chemical substances in a medium that contacts the surface. See also dealloying.

decobaltification.

Corrosion in which cobalt is selectively leached from cobalt-base alloys, such as Stellite, or from cemented carbides. See also dealloying and selective leaching.

decomposition potential (or voltage).

The potential of a metal surface necessary to decompose the electrolyte in an electrochemical cell or component.

deep groundbed.

One or more anodes installed vertically at a nominal depth of 15 m (50 ft) or more below the earth's surface in a drilled hole for the purpose of supplying cathodic protection for an underground or submerged metallic structure. See also groundbed.

delta ferrite.

See ferrite.

dendrite.

A crystal that has a treelike branching pattern, being most evident in cast metals slowly cooled through the solidification range.

denickelification.

Corrosion in which nickel is selectively leached from nickel-containing alloys. Most commonly observed in copper- nickel alloys after extended service in fresh water. See also dealloying and selective leaching.

density (of gases).

The mass of a unit volume of gas at a stated temperature and pressure.

density (of solids and liquids).

The mass of unit volume of a material at a specified temperature.

deoxidizing.

(1) The removal of oxygen from molten metals by use of suitable deoxidizers. (2) Sometimes refers to the removal of undesirable elements other than oxygen by the introduction of elements or compounds that readily react with them. (3) In metalfinishing, the removal of oxide films from metal surfaces by chemical or electrochemical reaction.

depolarization.

A decrease in the polarization of an electrode

depolarizer.

A substance that produces depolarization.

deposit corrosion.

Corrosion occurring under or around a discontinuous deposit on a metallic surface. See also poultice corrosion.

descaling.

Removing the thick layer of oxides formed on some metals at elevated temperatures.

dewetting.

The withdrawal of molten solder or zinc from a surface that was previously wetted. If the solderable (or galvanizing) surface is not well protected during soldering (galvanizing), the intermetallic can oxidize and the dewetting phenomenon takes place.

dezincification.

Corrosion in which zinc is selectively leached from zinc-containing alloys. Most commonly found in copper-zinc alloys containing less than 85% Cu after extended service in water containing dissolved oxygen. See also dealloying and selective leaching.

dichromate treatment.

A chromate conversion coating produced on magnesium alloys in a boiling solution of sodium dichromate.

dielectric shield.

In a cathodic protection system, an electrically nonconductive material, such as a coating, plastic sheet, or pipe, that is placed between an anode and an adjacent cathode to avoid current wastage and to improve current distribution, usually on the cathode.

differential aeration cell.

An electrochemical cell, where the driving force is a difference in the dissolved air (oxygen) concentration in the electrolyte at one electrode compared with that at another electrode of the same material. See also concentration cell.

diffusion.

(1) Spreading of a constituent in a gas, liquid, or solid, tending to make the composition of all parts uniform. (2) The spontaneous movement of atoms or molecules to new sites within a material.

diffusion coating.

Any process whereby a base metal or alloy is either (1) coated with another metal or alloy and heated to a sufficient temperature in a suitable environment or (2) exposed to a gaseous or liquid medium containing the other metal or alloy, thus causing diffusion of the coating or of the other metal or alloy into the base metal with resultant changes in the composition and properties of its surface.

diffusion coefficient.

A factor of proportionality representing the amount of substance diffusing across a unit area through a unit concentration gradient in unit time.

diffusion-limited current density.

The current density, often referred to as limiting current density, that corresponds to the maximum mass transfer rate that a chemical species can sustain because of diffusion limitations.

dimple rupture.

A fractographic term describing ductile fracture that occurs through the formation and coalescence of microvoids along the fracture path. The fracture surface of such a ductile fracture appears dimpled when observed at high magnification and usually is most clearly resolved when viewed in a scanning electron microscope.

disbondment.

The destruction of adhesion between a coating and the surface coated.

discontinuity.

Any interruption in the normal physical structure or configuration of a part, such as cracks, laps, seams, inclusions, or porosity. A discontinuity may or may not affect the usefulness of the part.

dislocation.

A linear imperfection in a crystalline array of atoms. Two basic types are recognized: (1) an edge dislocation corresponds to the row of mismatched atoms along the edge formed by an extra, partial plane of atoms within the body of a crystal; (2) a screw dislocation corresponds to the axis of a spiral structure in a crystal, characterized by a distortion that joins normally parallel planes together to form a continuous helical ramp (with a pitch of one interplanar distance) winding about the dislocation. Most prevalent is the so- called mixed dislocation, which is any combination of an edge dislocation and a screw dislocation.

double layer.

The interface between an electrode or a suspended particle and an electrolyte created by charge-charge interaction leading to an alignment of oppositely charged ions at the surface of the electrode or particle. The simplest model is represented by a parallel plate condensor.

drainage.

Conduction of electric current from an underground metallic structure by means of a metallic conductor. Forced drainage is that applied to underground metallic structures by means of an applied electromotive force or sacrificial anode. Natural drainage is that from an underground structure to a more negative (more anodic) structure, such as the negative bus of a trolley substation.

dry corrosion.

See gaseous corrosion.

drying oil.

An oil capable of conversion from a liquid to a solid by slow reaction with oxygen in the air.

ductile fracture.

Fracture characterized by tearing of metal accompanied by appreciable gross plastic deformation and expenditure of considerable energy. Contrast with brittle fracture.

ductility.

The ability of a material to deform plastically without fracturing, measured by elongation or reduction of area in a tensile test, by height of cupping in an Erichsen test, or by other means.

dummy cathode.

(1) A cathode, usually corrugated to give variable current densities, that is plated at low current densities to preferentially remove impurities from a plating solution. (2) A substitute cathode that is used during adjustment of operating conditions.

dummying.

Plating with dummy cathodes.

E

885 °F (475 °C) embrittlement.

Embrittlement of stainless steels upon extended exposure to temperatures between 400 and 510 °C (750 and 950 °F). Caused by fine, chromium-rich precipitates that segregate at grain boundaries; time at temperature directly influences the amount of segregation. Grain-boundary segregation of the chromium-rich precipitates increases strength and hardness, decreases ductility and toughness, and changes corrosion resistance. Can be reversed by heating above the precipitation range.

elastic deformation.

A change in dimensions directly proportional to and in phase with an increase or decrease in applied force.

elasticity.

The property of a material by virtue of which deformation caused by stress disappears upon removal of the stress. A perfectly elastic body completely recovers its original shape and dimensions after release of stress.

elastic limit.

The maximum stress that a material is capable of sustaining without any permanent strain (deformation) remaining upon complete release of the stress.

elastomer.

A natural or synthetic polymer, which at room temperature can be stretched repeatedly to at least twice its original length, and which after removal of the tensile load will immediately and forcibly return to approximately its original length.

electrical conductivity.

See conductivity.

electrical isolation.

The condition of being electrically separated from other metallic structures or the environment.

electrical resistivity.

The electrical resistance offered by a material to the flow of current, times the cross-sectional area of current flow and per unit length of current path; the reciprocal of the conductivity. Also called resistivity or specific resistance.

electrochemical admittance.

The inverse of electrochemical impedance.

electrochemical cell.

An electrochemical system consisting of an anode and a cathode in metallic contact and immersed in an electrolyte. The anode and cathode may be different metals or dissimilar areas on the same metal surface. See also cell.

electrochemical corrosion.

Corrosion that is accompanied by a flow of electrons between cathodic and anodic areas on metallic surfaces.

electrochemical equivalent.

The weight of an element or group of elements oxidized or reduced at 100% efficiency by the passage of a unit quantity of electricity. Usually expressed as gram-equivalents per coulomb.

electrochemical impedance.

The frequency-dependent complex-valued proportionality factor ($\Delta E/\Delta I$) between the applied potential or current and the response signal. This factor is the total opposition of an electrochemical system to the passage of charge. The value is inversely related to the corrosion rate under certain circumstances. Typical units are Ω or $\Omega \cdot cm^2$.

electrochemical machining.

Controlled metal removal by anodic dissolution. Direct current passes through a flowing conductive solution that separates the workpiece (anode) from the electrode tool (cathode).

electrochemical noise.

Fluctuations in potential or current, or both, originating from the uncontrolled variations in a corrosion process.

electrochemical potential.

The partial derivative of the total electrochemical free energy of a constituent with respect to the number of moles of this constituent where all factors are kept constant. It is analogous to the chemical potential of a constituent except that it includes the electric as well as chemical contributions to the free energy. The potential of an electrode in an electrolyte relative to a reference electrode.

electrochemical series.

A list of elements arranged according to their standard electrode potentials, with “noble” metals such as gold being positive and “active” metals such as zinc being negative.

electrode.

(1) An electronic conductor used to establish electrical contact with an electrolytic part of a circuit. (2) An electronic conductor in contact with an ionic conductor.

electrode polarization.

Change of electrode potential with respect to a reference value. Often the free corrosion potential is used as the reference value. The change may be caused, for example, by the application of an external electrical current or by the addition of an oxidant or reductant.

electrodeposition.

The deposition of a substance on an electrode by passing electric current through an electrolyte.

electrode potential.

The potential of an electrode in an electrolyte as measured against a reference electrode. The electrode potential does not include any resistance losses in potential in either the solution or external circuit. It represents the reversible work to move a unit charge from the electrode surface through the solution to the reference electrode.

electrode reaction.

Interfacial reaction equivalent to a transfer of charge between electronic and ionic conductors. See also anodic reaction and cathodic reaction.

electrogalvanizing.

The electroplating of zinc upon iron or steel.

electrokinetic potential.

This potential, sometimes called zeta potential, is a potential difference in the solution caused by residual, unbalanced charge distribution in the adjoining solution, producing a double layer. It differs from the electrode potential in that it occurs exclusively in the solution phase; that is, it represents the reversible work necessary to bring unit charge from infinity in the solution up to the interface in question but not through the interface.

electroless plating.

A process in which metal ions in a dilute aqueous solution are plated out on a substrate by means of autocatalytic chemical reduction.

electrolysis.

Production of chemical changes of the electrolyte by the passage of current through an electrochemical cell.

electrolyte.

(1) A chemical substance or mixture, usually liquid, containing ions that migrate in an electric field. (2) A chemical compound or mixture of compounds that when molten or in solution will conduct an electric current.

electrolytic cell.

An assembly, consisting of a vessel, electrodes, and an electrolyte, in which electrolysis can be carried out.

electrolytic cleaning.

A process of removing soil, scale, or corrosion products from a metal surface by subjecting it as an electrode to an electric current in an electrolytic bath.

electrolytic protection.

See cathodic protection.

electromotive force.

Electrical potential difference or voltage. This difference could be the result of two dissimilar electrodes in an electrolyte when electrochemical reactions occur. See also thermal electromotive force.

electromotive force series (emf series).

Same as electrochemical series.

electron flow.

A movement of electrons in an external circuit between an anode and cathode in a corrosion cell; current flow is in the opposite direction to the electron flow.

electroplating.

Electrodepositing a metal or alloy in an adherent form on an object serving as a cathode.

electropolishing.

A technique commonly used to prepare metallographic specimens, in which a high polish is produced by making the specimen the anode in an electrolytic cell, where preferential dissolution at high points smooths the surface.

electrotinning.

Electroplating tin on an object.

Ellingham diagram.

See free-energy diagram.

embrittlement.

The severe loss of ductility or toughness or both, of a material, usually a metal or alloy. Many forms of embrittlement can lead to brittle fracture. Many forms can occur during thermal treatment or elevated-temperature service (thermally induced embrittlement). Some of these forms of embrittlement, which affect steels, include blue brittleness, 885 °F (475 °C) embrittlement, quench-age embrittlement, sigma-phase embrittlement, strain-age embrittlement, temper embrittlement, tempered martensite embrittlement, and thermal embrittlement. In addition, steels and other metals and alloys can be embrittled by environmental conditions (environmentally assisted embrittlement). The forms of environmental embrittlement include acid embrittlement, caustic embrittlement, corrosion embrittlement, creep-rupture embrittlement, hydrogen embrittlement, liquid metal induced embrittlement, neutron embrittlement, solder embrittlement, solid metal induced embrittlement, and stress-corrosion cracking.

endurance limit.

The maximum stress that a material can withstand for an infinitely large number of fatigue cycles. See also fatigue strength.

enthalpy (*H*).

The sum of the internal energy of a system plus the product of the system volume multiplied by the pressure exerted on the system by its surroundings.

entropy (*S*).

The function of the state of a thermodynamic system whose change in any differential reversible process is equal to the heat absorbed by the system from its surroundings divided by the absolute temperature of the system.

environment.

The surroundings or conditions (physical, chemical, mechanical) in which a material exists.

environmental cracking.

Brittle fracture of a normally ductile material in which the corrosive effect of the environment is a causative factor. This general term includes corrosion fatigue, high-temperature hydrogen attack, hydrogen blistering, hydrogen embrittlement, liquid metal induced embrittlement, solid metal induced embrittlement, stress-corrosion cracking, and sulfide stress cracking. The following terms have been used in the past in connection with environment cracking, but are becoming obsolete: caustic embrittlement, delayed fracture, season cracking, static fatigue, stepwise cracking, sulfide corrosion cracking, and sulfide stress-corrosion cracking. See also embrittlement.

environmentally assisted embrittlement.

See embrittlement.

epoxy.

Resin formed by the reaction of bisphenol and epichlorohydrin.

equilibrium (reversible) potential.

The potential of an electrode in an electrolytic solution when the forward rate of a given reaction is exactly equal to the reverse rate. The equilibrium potential can only be defined with respect to a specific electrochemical reaction.

erosion.

Destruction of metals or other materials by the abrasive action of moving fluids, usually accelerated by the presence of solid particles or matter in suspension. When corrosion occurs simultaneously, the term erosion-corrosion is often used.

erosion-corrosion.

A material damage involving corrosion and erosion in the presence of a moving corrosive and erosive fluid, leading to the accelerated loss of material.

eutectic.

(1) An isothermal reversible reaction in which a liquid solution is converted into two or more intimately mixed solids on cooling, the number of solids formed being the same as the number of components in

the system. (2) An alloy having the composition indicated by the eutectic point on an equilibrium diagram. (3) An alloy structure of intermixed solid constituents formed by a eutectic reaction.

eutectoid.

(1) An isothermal reversible reaction in which a solid solution is converted into two or more intimately mixed solids on cooling, the number of solids formed being the same as the number of components in the system. (2) An alloy having the composition indicated by the eutectoid point on an equilibrium diagram. (3) An alloy structure of intermixed solid constituents formed by a eutectoid reaction.

exchange current.

When the electrode reactions reach equilibrium in a solution, the rate of anodic dissolution equals the rate of cathodic reduction. This rate is known as the exchange current.

exchange current density.

The exchange current expressed as a current density.

exfoliation.

Corrosion that proceeds laterally from the sites of initiation along planes parallel to the surface, generally at grain boundaries, forming corrosion products that force metal away from the body of the material, giving rise to a layered appearance.

external circuit.

The wires, connectors, measuring devices, current sources, etc., that are used to bring about or measure the desired electrical conditions within the test cell. It is this portion of the cell through which electrons travel.

F

failure.

A general term used to imply that a part in service (1) has become completely inoperable, (2) is still operable but is incapable of satisfactorily performing its intended function, or (3) has deteriorated seriously, to the point that it has become unreliable or unsafe for continued use.

false Brinelling.

Damage to a solid bearing surface characterized by indentations not caused by plastic deformation due to overload, but thought to be due to other causes such as fretting corrosion. Local spots appear when the protective coating on the metal is broken continually by repeated impacts, usually in the presence of corrosive agents. The term should be avoided when a more precise description is possible.

Faraday's constant (*F*).

The product of Avogadro's number times the charge on the electron. F is approximately 96,485 coulombs/ gram-equivalent.

Faraday's law.

(1) The amount of any substance dissolved or deposited in electrolysis is proportional to the total electric charge passed. (2) The amounts of different substances dissolved or deposited by the passage of the same electric charge are proportional to their equivalent weights.

fatigue.

The phenomenon leading to fracture under repeated or fluctuating stresses having a maximum value less than the tensile strength of the material. Fatigue fractures are progressive and grow under the action of the fluctuating stress.

fatigue crack growth rate (*da*/*dN*).

The rate of crack extension caused by constant-amplitude fatigue loading, expressed in terms of crack extension per cycle of load application.

fatigue life (*N*).

The number of cycles of stress that can be sustained prior to failure under a stated test condition.

fatigue limit.

The maximum stress that presumably leads to fatigue fracture in a specified number of stress cycles. If the stress is not completely reversed, the value of the mean stress, the minimum stress, or the stress ratio should also be stated. Compare with endurance limit.

fatigue strength.

The maximum stress that can be sustained for a specified number of cycles without failure, the stress being completely reversed within each cycle unless otherwise stated.

ferrite.

(1) A solid solution of one or more elements in body-centered cubic iron. Unless otherwise designated (for instance, as chromium ferrite), the solute is generally assumed to be carbon. On some equilibrium diagrams, there are two ferrite regions separated by an austenite area. The lower area is alpha ferrite; the upper, delta ferrite. If there is no designation, alpha ferrite is assumed. (2) In the field of magnetics, substances having the general formula: $M^{2+}O \cdot M^{3+}2O_3$, the trivalent metal often being iron.

filiform corrosion.

Corrosion that occurs under some coatings in the form of randomly distributed threadlike filaments.

film.

A thin, not necessarily visible, layer of material.

fish eyes.

Areas on a steel fracture surface having a characteristic white, crystalline appearance.

flakes.

Short, discontinuous internal fissures in wrought metals attributed to stresses produced by localized transformation and decreased solubility of hydrogen during cooling after hot working. In a fracture surface, flakes appear as bright silvery areas; on an etched surface, they appear as short, discontinuous cracks. Also called shatter cracks or snowflakes.

flame spraying.

Thermal spraying in which a coating material is fed into an oxyfuel gas flame, where it is melted. Compressed gas may or may not be used to atomize the coating material and propel it onto a substrate.

foreign structure.

Any metallic structure that is not intended as part of a cathodic protection system of interest.

fouling.

An accumulation of deposits. This term includes accumulation and growth of marine organisms on a submerged metal surface and also includes the accumulation of deposits (usually inorganic) on heat exchanger tubing.

fouling organism.

Any aquatic organism with a sessile adult stage that attaches to and fouls underwater structures of ships.

fractography.

Descriptive treatment of fracture, especially in metals, with specific reference to photographs of the fracture surface. Macrofractography involves photographs at low magnification (<25×); microfractography, photographs at high magnification (>25×).

fracture mechanics.

A quantitative analysis for evaluating structural behavior in terms of applied stress, crack length, and specimen or machine component geometry. See also linear elastic fracture mechanics.

fracture toughness.

A generic term for measures or resistance to extension of a crack. The term is sometimes restricted to results of fracture mechanics tests, which are directly applicable in fracture control. However, the term commonly includes results from simple tests of notched or precracked specimens not based on fracture mechanics analysis. Results from tests of the latter type are often useful for fracture control, based on either service experience or empirical correlations with fracture mechanics tests. See also stress-intensity factor.

free carbon.

The part of the total carbon in steel or cast iron that is present in elemental form as graphite or temper carbon. Contrast with combined carbon.

free corrosion potential (E_{corr}).

Corrosion potential in the absence of net electrical current flowing to or from the metal surface. See also corrosion potential.

free energy.

See Gibbs free energy.

free-energy diagram.

A graph of the variation with concentration of the Gibbs free energy at constant pressure and temperature. Called Ellingham diagrams, or Richardson-Jeffes diagrams when nomographs are added.

free ferrite.

Ferrite that is formed directly from the decomposition of hypoeutectoid austenite during cooling, without the simultaneous formation of cementite. Also called proeutectoid ferrite.

free machining.

Pertains to the machining characteristics of an alloy to which one or more ingredients have been introduced to give small broken chips, lower power consumption, better surface finish, and longer tool life; among such additions are sulfur or lead to steel, lead to brass, lead and bismuth to aluminum, and sulfur or selenium to stainless steel.

free radical.

Any molecule or atom that possesses one unpaired electron. In chemical notation, a free radical is symbolized by a single dot (denoting the odd electron) to the right of the chemical symbol.

fretting.

A type of wear that occurs between tight-fitting surfaces subjected to cyclic relative motion of extremely small amplitude. Usually, fretting is accompanied by corrosion, especially of the very fine wear debris.

fretting corrosion.

The accelerated deterioration at the interface between contacting surfaces as the result of corrosion and slight oscillatory movement between the two surfaces.

fugacity.

A function used as an analog of the partial pressure in applying thermodynamics to real systems; at constant temperature it is proportional to the exponential of the ratio of the chemical potential of a constituent of a system divided by the product of the gas constant and the temperature, and it approaches the partial pressure as the total pressure of the gas approaches zero.

furan.

Resin formed from reactions involving furfuryl alcohol alone or in combination with other constituents.

G

galvanic anode.

A metal that, because of its relative position in the galvanic or electrochemical series, provides sacrificial protection to metals that are more noble in the series when coupled in an electrolyte.

galvanic cell.

A cell in which spontaneous chemical change is the source of electrical energy. It usually consists of two dissimilar conductors in contact with each other and with an electrolyte, or of two similar conductors in contact with each other and with dissimilar electrolytes.

galvanic corrosion.

Accelerated corrosion of a metal because of an electrical contact with a more noble metal or nonmetallic conductor in a corrosive electrolyte.

galvanic couple.

A pair of dissimilar conductors, commonly metals, in electrical contact. See also galvanic corrosion.

galvanic couple potential.

See mixed potential.

galvanic current.

The electric current that flows between metals or conductive nonmetals in a galvanic couple.

galvanic series.

A list of metals and alloys arranged according to their relative corrosion potentials in a given environment. Compare with electrochemical series.

galvanize.

To coat a metal surface with zinc using any of various processes.

galvanneal.

To produce a zinc-iron alloy coating on iron or steel by keeping the coating molten after hot dip galvanizing until the zinc alloys completely with the base metal.

galvanodynamic.

Referring to a technique where current, continuously varied at a selected rate, is applied to an electrode in an electrolyte.

galvanometer.

An instrument for indicating or measuring a small electric current by means of a mechanical motion derived from electromagnetic or electrodynamic forces produced by the current.

galvanostaircase.

Referring to a galvanostep technique for polarizing an electrode in a series of constant current steps where the time duration and current increments or decrements are equal for each step.

galvanostatic.

A technique where an electrode is maintained at a constant current in an electrolyte.

galvanostep.

Refers to a technique in which an electrode is polarized in a series of current increments or decrements.

gamma iron.

The face-centered cubic form of pure iron, stable from 910 to 1400 °C (1670 to 2550 °F).

gaseous corrosion.

Corrosion with gases and vapors as the only corrosive agents and without any aqueous phase on the surface of the metal. Also called dry corrosion.

gel.

(1) A colloidal state comprised of interdispersed solid and liquid, in which the solid particles are themselves interconnected or interlaced in three dimensions. (2) A two-phase colloidal system consisting of a solid and a liquid in more solid form than a sol.

general corrosion.

See uniform corrosion.

Gibbs free energy.

The thermodynamic function $\Delta G = \Delta H - T\Delta S$ where H is enthalpy, T is absolute temperature, and S is entropy. Also called free energy, free enthalpy, or Gibbs function.

glass electrode.

A glass membrane electrode used to measure pH or hydrogen-ion activity.

grain.

An individual crystal in a polycrystalline metal or alloy; it may or may not contain twinned regions and subgrains.

grain boundary.

A narrow zone in a metal corresponding to the transition from one crystallographic orientation to another, thus separating one grain from another; the atoms in each grain are arranged in an orderly pattern.

grain-boundary corrosion.

Same as intergranular corrosion. See also interdendritic corrosion.

graphitic corrosion.

Deterioration of gray cast iron in which the metallic constituents are selectively leached or converted to corrosion products leaving the graphite intact. The term graphitization is commonly used to identify this form of corrosion, but is not recommended because of its use in metallurgy for the decomposition of carbide to graphite. See also dealloying and selective leaching.

graphitization.

A metallurgical term describing the formation of graphite in iron or steel, usually from decomposition of iron carbide at elevated temperatures. Not recommended as a term to describe graphitic corrosion.

green liquor.

The liquor resulting from dissolving molten smelt from the kraft recovery furnace in water. See also kraft process and smelt.

green rot.

A form of high-temperature attack on stainless steels, Ni-Cr alloys, and Ni-Cr-Fe alloys subjected to simultaneous oxidation and carburization. Basically, attack occurs first by precipitation of chromium as chromium carbide, then by oxidation of the carbide particles.

groundbed.

A buried item, such as junk steel or graphite rods, that serves as the anode for the cathodic protection of pipelines or other buried structures. See also deep groundbed.

H

half cell.

The electrode and associated electrode reaction comprising half of an electrochemical cell.

halogen.

Any of the elements of the halogen family, consisting of fluorine, chlorine, bromine, iodine, and astatine.

hard chromium.

Chromium plated for engineering rather than decorative applications.

hardenability.

The relative ability of a ferrous alloy to form martensite when quenched from a temperature above the upper critical temperature. Hardenability is commonly measured as the distance below a quenched surface at which the metal exhibits a specific hardness (50 HRC, for example) or a specific percentage of martensite in the microstructure.

hardfacing.

Depositing filler metal on a surface by welding, spraying, or braze welding to increase resistance to abrasion, erosion, wear, galling, impact, or cavitation damage.

hard water.

Water that contains certain salts, such as those of calcium or magnesium, which form insoluble deposits in boilers and form precipitates with soap.

heat-affected zone (HAZ).

That portion of the base metal that was not melted during brazing, cutting, or welding, but whose microstructure and mechanical properties were altered by the heat.

heat check.

A pattern of parallel surface cracks that are formed by alternate rapid heating and cooling of the extreme surface metal, sometimes found on forging dies and piercing punches. There may be two sets of parallel cracks, one set perpendicular to the other.

hematite.

(1) An iron mineral crystallizing in the rhombohedral system; the most important ore of iron. (2) An iron oxide, Fe_2O_3, corresponding to an iron content of approximately 70%.

high-temperature hydrogen attack.

A loss of strength and ductility of steel by high-temperature reaction of absorbed hydrogen with carbides in the steel resulting in decarburization and internal fissuring.

holidays.

Discontinuities in a coating (such as porosity, cracks, gaps, and similar flaws) that allow areas of base metal to be exposed to any corrosive environment that contacts the coated surface.

hot corrosion.

An accelerated corrosion of metal surfaces that results from the combined effect of oxidation and reactions with sulfur compounds and other contaminants, such as chlorides, to form a molten salt on a metal surface that fluxes, destroys, or disrupts the normal protective oxide. See also gaseous corrosion.

hot cracking.

Caused by the segregation at grain boundaries of low-melting constituents in the weld metal. This can result in grain-boundary tearing under thermal contraction stresses. This can be minimized by the use of low-impurity welding materials and proper joint design. Also called solidification cracking. See also cold cracking, lamellar tearing, and stress-relief cracking.

hot dip coating.

A metallic coating obtained by dipping the base metal into a molten metal.

hot shortness.

A tendency for some alloys to separate along grain boundaries when stressed or deformed at temperatures near the melting point. Caused by a low-melting constituent, often present only in minute amounts, that is segregated at grain boundaries.

hot working.

Deforming metal plastically at such a temperature and strain rate that recrystallization takes place simultaneously with the deformation, thus avoiding any strain hardening. Contrast with cold working.

humidity tests.

A corrosion test involving exposure of specimens at controlled levels of humidity and temperature. Contrast with salt-fog test.

hydrogen-assisted cracking (HAC).

See hydrogen embrittlement.

hydrogen-assisted stress-corrosion cracking (HSCC).

See hydrogen embrittlement.

hydrogen blistering.

The formation of blisters on or below a metal surface from excessive internal hydrogen pressure. Hydrogen may be formed during cleaning, plating, corrosion, and so forth.

hydrogen damage.

A general term for the embrittlement, cracking, blistering, and hydride formation that can occur when hydrogen is present in some metals.

hydrogen embrittlement.

A process resulting in a decrease in the toughness or ductility of a metal due to the presence of atomic hydrogen. Hydrogen embrittlement has been recognized classically as being of two types. The first, known as internal hydrogen embrittlement, occurs when the hydrogen enters molten metal, which becomes supersaturated with hydrogen immediately after solidification. The second type, environmental hydrogen embrittlement, results from hydrogen being absorbed by solid metals. This can occur during elevated-temperature thermal treatments and in service during electroplating, contact with maintenance chemicals, corrosion reactions, cathodic protection, and operating in high- pressure hydrogen. In the absence of residual stress or external loading, environmental hydrogen embrittlement is manifested in various forms, such as blistering, internal cracking, hydride formation, and reduced ductility. With a tensile stress or stress-intensity factor exceeding a specific threshold, the atomic hydrogen interacts with the metal to induce subcritical crack growth leading to fracture. In the absence of a corrosion reaction (polarized cathodically), the usual term used is hydrogen- assisted cracking (HAC) or hydrogen stress cracking (HSC). In the presence of active corrosion, usually at pits or crevices (polarized anodically), the cracking is generally called stress-corrosion cracking (SCC), but should more properly be called hydrogen-assisted stress-corrosion cracking (HSCC). Thus, HSC and electrochemically anodic SCC can operate separately or in combination (HSCC). In some metals, such as high-strength steels, the mechanism is believed to be all, or nearly all, HSC. The participating mechanism of HSC is not always recognized and may be evaluated under the generic heading of SCC.

hydrogen-induced cracking (HIC).

Same as hydrogen embrittlement.

hydrogen overvoltage.

Overvoltage associated with the liberation of hydrogen gas.

hydrogen stress cracking (HSC).

See hydrogen embrittlement.

hydrolysis.

(1) Decomposition or alteration of a chemical substance by water. (2) In aqueous solutions of electrolytes, the reactions of cations with water to produce a weak base or of anions to produce a weak acid.

hydrophilic.

Having an affinity for water. Contrast with hydrophobic.

hydrophobic.

Lacking an affinity for, repelling, or failing to absorb or adsorb water. Contrast with hydrophilic.

hygroscopic.

(1) Possessing a marked ability to accelerate the condensation of water vapor; applied to condensation nuclei composed of salts that yield aqueous solutions of a very low equilibrium vapor pressure compared with that of pure water at the same temperature. (2) Pertaining to a substance whose physical characteristics are appreciably altered by effects of water vapor. (3) Pertaining to water absorbed by dry soil minerals from the atmosphere; the amounts depend on the physicochemical character of the surfaces, and increase with rising relative humidity.

I

immersion plating.

Depositing a metallic coating on a metal immersed in a liquid solution, without the aid of an external electric current. Also called dip plating.

immunity.
A state of resistance to corrosion or anodic dissolution of a metal caused by thermodynamic stability of the metal.
impingement corrosion.
A form of erosion-corrosion generally associated with the local impingement of a high-velocity, flowing fluid against a solid surface.
impressed current.
Direct current supplied by a device employing a power source external to the electrode system of a cathodic protection installation.
inclusions.
Particles of foreign material in a metallic matrix. The particles are usually compounds (such as oxides, sulfides, or silicates), but may be of any substance that is foreign to (and essentially insoluble in) the matrix.
incubation period.
A period prior to the detection of corrosion while the metal is in contact with a corrodent.
industrial atmosphere.
An atmosphere in an area of heavy industry with soot, fly ash, and sulfur compounds as the principal constituents.
inert anode.
An anode that is insoluble in the electrolyte under the conditions prevailing in the electrochemical cell.
inhibitor.
A chemical substance or combination of substances that, when present in the environment, prevents or reduces corrosion without significant reaction with the components of the environment.
inorganic.
Being or composed of matter other than hydrocarbons and their derivatives, or matter that is not of plant or animal origin. Contrast with organic.
inorganic zinc-rich paint.
Coating containing a zinc powder pigment in an inorganic vehicle.
intensiostatic.
See galvanostatic.
intercrystalline corrosion.
See intergranular corrosion.
intercrystalline cracking.
See intergranular cracking.
interdendritic corrosion.
Corrosive attack that progresses preferentially along interdendritic paths. This type of attack results from local differences in composition, such as coring commonly encountered in alloy castings.
intergranular.
Between crystals or grains. Also called intercrystalline. Contrast with transgranular.
intergranular corrosion.
Corrosion occurring preferentially at grain boundaries, usually with slight or negligible attack on the adjacent grains. Also called intercrystalline corrosion.
intergranular cracking.
Cracking or fracturing that occurs along the boundaries of grains or crystals in a polycrystalline aggregate. Also called intercrystalline cracking. Contrast with transgranular cracking.
intergranular fracture.
Brittle fracture of a metal in which the fracture is along the boundaries of grains or crystals that form the metal. Also called intercrystalline fracture. Contrast with transgranular fracture.
intergranular stress-corrosion cracking (IGSCC).
Stress-corrosion cracking in which the cracking occurs along grain boundaries.
intermediate electrode.
Same as bipolar electrode.
internal oxidation.

The formation of isolated particles of corrosion products beneath the metal surface. This occurs as the result of preferential oxidation of certain alloy constituents by inward diffusion of oxygen, nitrogen, sulfur, and so forth.

intumescence.

The swelling or bubbling of a coating usually because of heating (term currently used in space and fire protection applications).

ion.

An atom, or group of atoms, that has gained or lost one or more outer electrons and thus carries an electric charge. Positive ions, or cations, are deficient in outer electrons. Negative ions, or anions, have an excess of outer electrons.

ion exchange.

The reversible interchange of ions between a liquid and solid, with no substantial structural changes in the solid.

iron rot.

Deterioration of wood in contact with iron-base alloys.

irreversible.

Chemical reactions that proceed in a single direction and are not capable of reversal. See also reversible.

isocorrosion diagram.

A graph or chart that shows constant corrosion behavior with changing solution (environment) composition and temperature.

K

knife-line attack.

Intergranular corrosion of an alloy, usually stabilized stainless steel, along a line adjoining or in contact with a weld after heating into the sensitization temperature range.

kraft process.

A wood-pulping process in which sodium sulfate is used in the caustic soda pulp-digestion liquor. Also called kraft pulping or sulfate pulping.

kurtosis.

The extent to which a frequency distribution is concentrated about the mean or peaked. It is sometimes defined as the ratio of the fourth moment of the distribution to the square of the second moment.

L

lamellar corrosion.

See exfoliation.

lamellar tearing.

Occurs in the base metal adjacent to weldments due to high through- thickness strains introduced by weld metal shrinkage in highly restrained joints. Tearing occurs by decohesion and linking along the working direction of the base metal; cracks usually run roughly parallel to the fusion line and are steplike in appearance. Lamellar tearing can be minimized by designing joints to minimize weld shrinkage stresses and joint restraint. See also cold cracking, hot cracking, and stress-relief cracking.

Langelier saturation index.

An index calculated from total dissolved solids, calcium concentration, total alkalinity, pH, and solution temperature that shows the tendency of a water solution to precipitate or dissolve calcium carbonate.

ledeburite.

The eutectic of the iron-carbon system, the constituents of which are austenite and cementite. The austenite decomposes into ferrite and cementite on cooling below Ar_1, the temperature at which transformation of austenite to ferrite or ferrite plus cementite is completed during cooling.

ligand.

The molecule, ion, or group bound to the central atom in a chelate or a coordination compound.

limiting current density.

The maximum current density that can be used to obtain a desired electrode reaction without undue interference such as from polarization.

linear elastic fracture mechanics.

A method of fracture analysis that can determine the stress (or load) required to induce fracture instability in a structure containing a cracklike flaw of known size and shape. See also fracture mechanics and stress-intensity factor.

lipophilic.

Having an affinity for oil. See also hydrophilic and hydrophobic.

liquid metal induced embrittlement (LMIE).

Catastrophic brittle failure of a normally ductile metal when in contact with a liquid metal and subsequently stressed in tension.

local action.

Corrosion due to the action of “local cells,” that is, galvanic cells resulting from inhomogeneities between adjacent areas on a metal surface exposed to an electrolyte.

local cell.

A galvanic cell resulting from inhomogeneities between areas on a metal surface in an electrolyte. The inhomogeneities may be of physical or chemical nature in either the metal or its environment.

localized corrosion.

Corrosion at discrete sites, for example, crevice corrosion, pitting corrosion, and stress-corrosion cracking.

long-line current.

Current that flows through the earth from an anodic to a cathodic area of a continuous metallic structure. Usually used only where the areas are separated by considerable distance and where the current results from concentration-cell action.

luggin probe.

A small tube or capillary filled with electrolyte, terminating close to the metal surface under study. It is used to provide an ionically conducting path without diffusion between an electrode under study and a reference electrode and to reduce the potential (IR) drop in the potential measurement. Also called a Luggin-Haber capillary.

M

macroscopic.

Visible at magnifications to 25×.

macrostructure.

The structure of metals as revealed by macroscopic examination of the etched surface of a polished specimen.

magnetite.

Naturally occurring magnetic oxide of iron (Fe_3O_4).

martensite.

Generic term for microstructures formed by diffusionless phase transformation in which the parent and product phases have a specific crystallographic relationship. Characterized by an acicular pattern in the microstructure in both ferrous and nonferrous alloys. In alloys where the solute atoms occupy interstitial positions in the martensitic lattice (such as carbon in iron), the structure is hard and highly strained; but where the solute atoms occupy substitutional positions (such as nickel in iron), the martensite is soft and ductile. The amount of high-temperature phase that transforms to martensite on cooling depends to a large extent on the lowest temperature attained, there being a rather distinct beginning temperature (M_s) and a temperature at which the transformation is essentially complete (M_f).

mechanical plating.

Plating wherein fine metal powders are peened onto the work by tumbling or other means.

metal dusting.

Accelerated deterioration of metals in carbonaceous gases at elevated temperatures to form a dustlike corrosion product.

metallic glass.

An alloy having an amorphous or glassy structure. See also amorphous solid.

metallizing.

(1) The application of an electrically conductive metallic layer to the surface of nonconductors. (2) The application of metallic coatings by nonelectrolytic procedures such as spraying of molten metal and deposition from the vapor phase.

microbial corrosion.

See biological corrosion.

microbiologically influenced corrosion (MIC).

Corrosion inhibited or accelerated by the presence or activity of microorganisms. Preferred term for the effect that microscopic organisms and their by-products have on electrochemical corrosion of metals and alloys. See also biological corrosion.

microscopic.

Visible at magnifications above 25×.

microstructure.

The structure of a prepared surface of a metal as revealed by a microscope at a magnification exceeding 25×.

mill scale.

The heavy oxide layer formed during hot fabrication or heat treatment of metals.

mischmetal.

A natural mixture of rare earth elements (atomic numbers 57–71) in metallic form. It contains about 50% Ce, the remainder being principally lanthanum and neodymium. Mischmetal is used as an alloying additive in ferrous alloy to scavenge sulfur, oxygen, and other impurities and in magnesium alloys to improve high-temperature strength.

mixed potential.

The potential of a material (or materials in a galvanic couple) when two or more electrochemical reactions are occurring. Also called galvanic couple potential.

moiety.

A portion of a molecule, generally complex, having a characteristic chemical property.

molal solution.

Concentration of a solution expressed in moles of solute divided by 1000 g of solvent.

molar solution.

Aqueous solution that contains 1 mole (gram-molecular weight) of solute in 1 L of the solution.

mole.

One mole is the mass numerically equal (in grams) to the molecular mass (weight) of a substance. It is the amount of substance in a system that contains as many elementary units (Avogadro's number, 6.02×10^{23}) as there are atoms of carbon in 0.012 kg of the pure nuclide ^{12}C; the elementary unit must be specified and may be an atom, molecule, ion, electron, photon, or even a specified group of such units.

molecular weight.

The sum of the atomic weights of the atoms in a molecule.

monomer.

A molecule, usually an organic compound, having the ability to join with a number of identical molecules to form a polymer.

N

natural aging.

Spontaneous aging of a supersaturated solid solution at room temperature. See also aging. Compare with artificial aging.

Nernst equation.

An equation that expresses the exact reversible potential of a cell in terms of the activities of products and reactants of the cell reactions.

Nernst layer, Nernst thickness.

The diffusion layer or the hypothetical thickness of this layer as given by the theory of Nernst. It is defined by: $i_d = nFD[(C_0 - C/\delta]$, where i_d is the diffusion-limited current density, D is the diffusion coefficient, C_0 is the concentration at the electrode surface, and δ is the Nernst thickness (0.5 mm in many cases of unstirred aqueous electrolytes).

neutron embrittlement.

Embrittlement resulting from bombardment with neutrons, usually encountered in metals that have been exposed to a neutron flux in the core of a reactor. In steels, neutron embrittlement is evidenced by a rise in the ductile-to-brittle transition temperature.

nitriding.

Introducing nitrogen into the surface layer of a solid ferrous alloy by holding at a suitable temperature (below Ac_1 for ferritic steels) in contact with a nitrogenous material, usually ammonia or molten cyanide of appropriate composition. Quenching is not required to produce a hard case.

nitrocarburizing.

Any of several processes in which both nitrogen and carbon are absorbed into the surface layers of a ferrous material at temperatures below the lower critical temperature and, by diffusion, create a concentration gradient. Performed primarily to provide an antiscuffing surface layer and to improve fatigue resistance. Compare with carbonitriding.

noble.

The positive direction of electrode potential, thus resembling noble metals such as gold and platinum.

noble metal.

(1) A metal whose potential is highly positive relative to the hydrogen electrode. (2) A metal with marked resistance to chemical reaction, particularly to oxidation and to solution by inorganic acids. The term as often used is synonymous with precious metal.

noble potential.

A potential more cathodic (positive) than the standard hydrogen potential.

normalizing.

Heating a ferrous alloy to a suitable temperature above the transformation range and then cooling in air to a temperature substantially below the transformation range.

normal solution.

An aqueous solution containing one gram equivalent of the active reagent in 1 L of the solution.

normal stress.

The stress component perpendicular to a plane on which forces act. Normal stress may be either tensile or compressive.

O

occluded cell.

An electrochemical cell created at a localized site on a metal surface that has been partially obstructed from the bulk environment.

open-circuit potential.

The potential of an electrode measured with respect to a reference electrode or another electrode when no current flows to or from it through an external circuit. See also corrosion potential.

organic.

Being or composed of hydrocarbons or their derivatives, or matter of plant or animal origin. Contrast with inorganic.

organic acid.

A chemical compound with one or more carboxyl radicals (COOH) in its structure; examples are butyric acid, $CH_3(CH_2)_2COOH$; maleic acid, HOOCCH- CHCOOH; and benzoic acid, C_6H_5COOH.

organic zinc-rich paint.

Coating containing zinc powder pigment and an organic resin.

overaging.

Aging under conditions of time and temperature greater than those required to obtain maximum change in a certain property, so that the property is altered in the direction of the initial value.

overheating.

Heating a metal or alloy to such a high temperature that its properties are impaired. When the original properties cannot be restored by further heat treating, by mechanical working, or by a combination of working and heat treating, the overheating is known as burning.

overvoltage.

The difference between the electrode potential when appreciable electrochemical reaction occurs and the reversible electrode potential.

oxidation.

(1) A reaction in which there is an increase in valence resulting from a loss of electrons. Contrast with reduction. (2) A corrosion reaction in which the corroded metal forms an oxide; usually applied to reaction with a gas containing elemental oxygen, such as air.

oxidized surface (on steel).

Surface having a thin, tightly adhering, oxidized skin (from straw to blue in color), extending in from the edge of a coil or sheet.

oxidizing agent.
A compound that causes oxidation, thereby itself being reduced.

oxygen concentration cell.
See differential aeration cell.

ozone.
A powerfully oxidizing allotropic form of the element oxygen. The ozone molecule contains three atoms (O_3). Ozone gas is decidedly blue, both liquid and solid ozone are an opaque blue-black color, similar to ink.

P

partial annealing.
An imprecise term used to denote a treatment given cold-worked material to reduce its strength to a controlled level or to effect stress relief. To be meaningful, the type of material, degree of cold work, and the time-temperature schedule must be stated.

parting.
See dealloying.

parts per billion.
A measure of proportion by weight, equivalent to one unit weight of a material per billion (10^9) unit weights of compound. One part per billion is equivalent to 0.001 μg/g or 1 μg/kg.

parts per million.
A measure of proportion by weight, equivalent to one unit weight of a material per million (10^6) unit weights of compound. One part per million is equivalent to 1 μg/g or 1 mg/kg.

passivation.
(1) A reduction of the anodic reaction rate of an electrode involved in corrosion. (2) The process in metal corrosion by which metals become passive. (3) The changing of a chemically active surface of a metal to a much less reactive state. Contrast with activation.

passivator.
A type of inhibitor that appreciably changes the potential of a metal to a more noble (positive) value.

passive.
(1) A metal corroding under the control of surface reaction product. (2) The state of the metal surface characterized by low corrosion rates in a potential region that is strongly oxidizing for the metal.

passive-active cell.
A corrosion cell in which the anode is a metal in the active state, and the cathode is the same metal in the passive state.

passivity.
A condition in which a piece of metal, because of an impervious covering of oxide or other compound, has a potential much more positive than that of the metal in the active state.

patina.
The coating, usually green, that forms on the surface of metals such as copper and copper alloys exposed to the atmosphere. Also used to describe the appearance of a weathered surface of any metal.

pearlite.
A metastable lamellar aggregate of ferrite and cementite resulting from the transformation of austenite at temperatures above the bainite range.

pH.
The negative logarithm of the hydrogen-ion activity; it denotes the degree of acidity or basicity of a solution. At 25 °C (77 °F), 7.0 is the neutral value. Decreasing values below 7.0 indicate increasing acidity; increasing values above 7.0 indicate increasing basicity.

phosphating.
Forming an adherent phosphate coating on a metal by immersion in a suitable aqueous phosphate solution. Also called phosphatizing. See also conversion coating.

physical vapor deposition (PVD).
A coating process whereby deposition species are transferred and deposited in the form of individual atoms or molecules. The most common PVD methods are sputtering and evaporation. Sputtering

involves the transport of a material from a source (target) to a substrate by means of bombardment of the target by gas ions accelerated through a high voltage in a vacuum chamber. In the evaporation process, the transport of a streaming vapor generated by melting and evaporating a coating material source bar by an electron beam in an evacuated chamber, coats the object.

physisorption.
The binding of an adsorbate to the surface of a solid by forces whose energy levels approximate those of condensation. Contrast with chemisorption.

pickle.
A solution or process used to loosen or remove corrosion products such as scale or tarnish.

pickling.
Removing surface oxides from metals by chemical or electrochemical reaction.

pitting.
Localized corrosion of a metal surface, confined to a point or small area, that takes the form of cavities.

pitting factor.
Ratio of the depth of the deepest pit resulting from corrosion divided by the average penetration as calculated from weight loss.

pitting potential.
See critical pitting potential.

plane strain.
The stress condition in linear elastic fracture mechanics in which there is zero strain in a direction normal to both the axis of applied tensile stress and the direction of crack growth (that is, parallel to the crack front); most nearly achieved in loading thick plates along a direction parallel to the plate surface. In plane strain, the plane of fracture instability is normal to the axis of the principal tensile stress.

plane stress.
The stress condition in linear elastic fracture mechanics in which the stress in the thickness direction is zero; most nearly achieved in loading very thin sheet along a direction parallel to the surface of the sheet. In plane stress, the plane of fracture instability is inclined 45° to the axis of the principal tensile stress.

plasma spraying.
A thermal spraying process in which the coating material is melted with heat from a plasma torch that generates a nontransferred arc; molten coating material is propelled against the base metal by the hot, ionized gas issuing from the torch.

plastic deformation.
The permanent (inelastic) distortion of metals under applied stresses that strain the material beyond its elastic limit.

plasticity.
The property that enables a material to undergo permanent deformation without rupture.

polarization.
(1) The change from the open-circuit electrode potential as the result of the passage of current. (2) A change in the potential of the electrodes in an electrolytic cell such that the potential of the anode becomes more noble, and that of the cathode more active, than their respective reversible potentials. Often accompanied by formation of a film on the electrode surface. See also overvoltage.

polarization admittance.
The reciprocal of polarization resistance (di/dE).

polarization curve.
A plot of current or current density versus electrode potential for a specific electrode-electrolyte combination.

polarization resistance.
The slope (dE/di) at the corrosion potential of a potential (E)/current density (i) curve. Also used to describe the method of measuring corrosion rate using this slope.

polyester.
Resin formed by condensation of polybasic and monobasic acids with polyhydric alcohols.

polymer.
A chain of organic molecules produced by the joining of primary units called monomers.

potential.

Any of various functions from which intensity or velocity at any point in a field may be calculated. The driving influence of an electrochemical reaction. See also active potential, chemical potential, corrosion potential, critical pitting potential, decomposition potential, electrochemical potential, electrode potential, electrokinetic potential, equilibrium (reversible) potential, free corrosion potential, noble potential, open-circuit potential, protective potential, redox potential, and standard electrode potential.

potential-pH diagram.

See Pourbaix (potential-pH) diagram.

potentiodynamic (potentiokinetic).

The technique for varying the potential of an electrode in a continuous manner at a preset rate.

potentiostat.

An instrument for automatically maintaining an electrode in an electrolyte at a constant potential or controlled potentials with respect to a suitable reference electrode.

potentiostatic.

The technique for maintaining a constant electrode potential.

poultice corrosion.

A term used in the automotive industry to describe the corrosion of vehicle body parts due to the collection of road salts and debris on ledges and in pockets that are kept moist by weather and washing. Also called deposit corrosion or attack.

Pourbaix (potential-pH) diagram.

A plot of the redox potential of a corroding system versus the pH of the system, compiled using thermodynamic data and the Nernst equation. The diagram shows regions within which the metal itself or some of its compounds are stable and other regions where the metal corrodes.

powder metallurgy.

The art of producing metal powders and utilizing metal powders for production of massive materials and shaped objects.

precious metal.

One of the relatively scarce and valuable metals: gold, silver, and the platinum-group metals. See also noble metal.

precipitation hardening.

Hardening caused by the precipitation of a constituent from a supersaturated solid solution. See also age hardening and aging.

precipitation heat treatment.

Artificial aging in which a constituent precipitates from a supersaturated solid solution.

precracked specimen.

A specimen that is notched and subjected to alternating stresses until a crack has developed at the root of the notch.

primary current distribution.

The current distribution in an electrolytic cell that is free of polarization.

primary passive potential (passivation potential).

The potential corresponding to the maximum active current density (critical anodic current density) of an electrode that exhibits active-passive corrosion behavior.

primer.

The first coat of paint applied to a surface. Formulated to have good bonding and wetting characteristics; may or may not contain inhibiting pigments.

principal stress (normal).

The maximum or minimum value of the normal stress at a point in a plane considered with respect to all possible orientations of the considered plane. On such principal planes, the shear stress is zero. There are three principal stresses on three mutually perpendicular planes. The state of stress at a point may be (1) uniaxial, a state of stress in which two of the three principal stresses are zero, (2) biaxial, a state of stress in which only one of the three principal stresses is zero, and (3) triaxial, a state of stress in which none of the principal stresses is zero. Multiaxial stress refers to either biaxial or triaxial stress.

protection potential (E_{prot}, E_{pp}).

The least noble potential at which existing pits can either passivate or continue growing.

protective potential.

The threshold value of the corrosion potential that has to be reached to enter a protective potential range.

protective potential range.

A range of corrosion potential values in which an acceptable corrosion resistance is achieved for a particular purpose.

Q

quench-age embrittlement.

Embrittlement of low-carbon steels resulting from precipitation of solute carbon at existing dislocations and from precipitation hardening of the steel caused by differences in the solid solubility of carbon in ferrite at different temperatures. Usually caused by rapid cooling of the steel from temperatures slightly below Ac_1 (the temperature at which austenite begins to form) and can be minimized by quenching from lower temperatures.

quench aging.

Aging induced by rapid cooling after solution heat treatment.

quench cracking.

Fracture of a metal during quenching from elevated temperature. Most frequently observed in hardened carbon steel, alloy steel, or tool steel parts of high hardness and low toughness. Cracks often emanate from fillets, holes, corners, or other stress raisers and result from high stresses due to the volume changes accompanying transformation to martensite.

quench hardening.

(1) Hardening suitable α-β alloys (most often certain copper or titanium alloys) by solution treating and quenching to develop a martensitelike structure. (2) In ferrous alloys, hardening by austenitizing and then cooling at a rate such that a substantial amount of austenite transforms to martensite.

quenching.

Rapid cooling of metals (often steels) from a suitable elevated temperature. This generally is accomplished by immersion in water, oil, polymer solution, or salt, although forced air is sometimes used.

R

radiation damage.

A general term for the alteration of properties of a material arising from exposure to ionizing radiation (penetrating radiation), such as x-rays, gamma rays, neutrons, heavy-particle radiation, or fission fragments in nuclear fuel material.

rare earth metal.

One of the group of 15 chemically similar metals with atomic numbers 57 through 71, commonly referred to as the lanthanides.

reactive metal.

A metal that readily combines with oxygen at elevated temperatures to form very stable oxides, for example, titanium, zirconium, and beryllium. May also become embrittled by the interstitial absorption of oxygen, hydrogen, and nitrogen.

recrystallization.

(1) Formation of a new, strain- free grain structure from that existing in cold- worked metal, usually accomplished by heating. (2) The change from one crystal structure to another, as occurs on heating or cooling through a critical temperature.

redox potential.

The potential of a reversible oxidation-reduction electrode measured with respect to a reference electrode in a given electrolyte.

reducing agent.

A compound that causes reduction, thereby itself becoming oxidized.

reduction.

A reaction in which there is a decrease in valence resulting from a gain in electrons. Contrast with oxidation.

reference electrode.

A nonpolarizable electrode with a known and highly reproducible potential used for potentiometric and voltammetric analyses, for example, the calomel electrode.

refractory metal.

A metal having an extremely high melting point, for example, tungsten, molybdenum, tantalum, niobium, chromium, vanadium, and rhenium. In the broad sense, this term refers to metals having melting points above the range for iron, cobalt, and nickel.

relative humidity.

The ratio, expressed as a percentage, of the amount of water vapor present in a given volume of air at a given temperature to the amount required to saturate the air at that temperature.

residual stress.

Stresses that remain within a body as a result of plastic deformation.

resistance.

The opposition that a device or material offers to the flow of direct current, equal to the voltage drop across the element divided by the current through the element. Also called electrical resistance.

rest potential.

See corrosion potential and *open- circuit potential.*

reversible.

A chemical reaction that can proceed in either direction by a change in the system parameters (temperature, pressure, volume, concentration of reactants).

Reynold's number.

In fluid mechanics, a unitless number, N_R that characterizes the flow of liquids. $N_R = \nu \cdot d \cdot \rho/\mu$ where ν is the velocity of the liquid, d is the diameter of the liquid channel, ρ is the density of the liquid, and μ is the viscosity of the liquid. Generally, if N_R is less than 2000, the flow is characterized as laminar, with the molecules of the liquid tending to move in straight lines without turbulence.

riser.

(1) That section of pipeline extending from the ocean floor up the platform. Also, the vertical tube in a steam generator convection bank that circulates water and steam upward. (2) A reservoir of molten metal connected to a casting to provide additional metal to the casting, required as the result of shrinkage before and during solidification.

rust.

A visible corrosion product consisting of oxides and hydrated oxides of iron. Applied only to ferrous alloys. See also white rust.

S

sacrificial protection.

Reduction of corrosion of a metal in an electrolyte by galvanically coupling it to a more active (or anodic) metal; a form of cathodic protection.

salt-fog test.

An accelerated corrosion test in which specimens are exposed to a fine mist of a solution usually containing sodium chloride, but sometimes modified with other chemicals.

salt-spray test.

See salt-fog test.

saponification.

The alkaline hydrolysis of fats whereby a soap is formed; more generally, hydrolysis of an ester by an alkali with the formation of an alcohol and a salt of the acid portion.

saturated calomel electrode.

A reference electrode composed of mercury, mercurous chloride (calomel), and a saturated aqueous chloride solution.

scale.

A solid layer of corrosion products formed on a metal at high temperatures. In some countries the term is also used for deposits from supersaturated water.

scaling.

(1) The formation at high temperatures of thick corrosion product layers on a metal surface. (2) The deposition of water-insoluble constituents on a metal surface.

season cracking.

An obsolete historical term usually applied to stress-corrosion cracking of brass.

selective leaching.

Corrosion in which one element is preferentially removed from an alloy, leaving a residue (often porous) of the elements that are more resistant to the particular environment. Also called dealloying or parting. See also decarburization, decobaltification, denickelification, dezincification, and graphitic corrosion.

sensitization.

In austenitic stainless steels, the precipitation of chromium carbides, usually at grain boundaries, on exposure to temperatures of ~550 to 850 °C (~1000 to 1550 °F), leaving the grain boundaries depleted of chromium and therefore susceptible to preferential attack by a corroding (oxidizing) medium.

sensitizing heat treatment.

A heat treatment, whether accidental, intentional, or incidental (as during welding), that causes precipitation of constituents at grain boundaries, often causing the alloy to become susceptible to intergranular corrosion or intergranular stress-corrosion cracking. See also sensitization.

shear.

That type of force that causes or tends to cause two contiguous parts of the same body to slide relative to each other in a direction parallel to their plane of contact.

shear strength.

The stress required to produce fracture in the plane of cross section, the conditions of loading being such that the directions of force and of resistance are parallel and opposite, although their paths are offset a specified minimum amount. The maximum load divided by the original cross-sectional area of a section separated by shear.

SI.

International system of units, the modern metric system, defined in the document, *Le Système International d'Unités* (universally abbreviated SI).

sigma phase.

A hard, brittle, nonmagnetic intermediate phase with a tetragonal crystal structure, containing 30 atoms per unit cell, space group $P4_2/mnm$, occurring in many binary and ternary alloys of the transition elements. The composition of this phase in the various systems is not the same, and the phase usually exhibits a wide range in homogeneity. Alloying with a third transition element usually enlarges the field of homogeneity and extends it deep into the ternary section.

sigma-phase embrittlement.

Embrittlement of iron-chromium alloys (most notably austenitic stainless steels) caused by precipitation at grain boundaries of the hard, brittle intermetallic sigma phase during long periods of exposure to temperatures between ~560 and 980 °C (~1050 and 1800 °F). Sigma-phase embrittlement results in severe loss in toughness and ductility and can make the embrittled material susceptible to intergranular corrosion. See also sensitization.

slip.

Plastic deformation by the irreversible shear displacement (translation) of one part of a crystal relative to another in a definite crystallographic direction and usually on a specific crystallographic plane. Sometimes called glide.

slow-strain-rate technique.

An experimental technique for evaluating susceptibility to stress-corrosion cracking. It involves pulling the specimen to failure in uniaxial tension at a controlled slow strain rate while the specimen is in the test environment and examining the specimen for evidence of stress-corrosion cracking.

smelt.

Molten slag; in the pulp and paper industry, the cooking chemicals tapped from the recovery boiler as molten material and dissolved in the smelt tank as green liquor.

***S-N* diagram.**

A plot showing the relationship of stress, S, and the number of cycles, N, before fracture in fatigue testing.

soft water.

Water that is free of magnesium or calcium salts.

sol.

A colloidal suspension comprising discrete or separate solid particles suspended in a liquid. Differs from a solution, though one merges into the other. Compare with gel.

solder embrittlement.
Reduction in mechanical properties of a metal as a result of local penetration of solder along grain boundaries.

sol-gel process.
An important ceramic and glass forming process in which a sol is converted to a gel by particle evaporation of the liquid phase and/or by neutralizing the electric charges on particles that cause them to repel each other. The gel is usually further processed (formed, dried, and fired).

solid metal induced embrittlement (SMIE).
The occurrence of embrittlement in a material below the melting point of the embrittling species. See also liquid metal induced embrittlement (LMIE).

solid solution.
A single, solid, homogeneous crystalline phase containing two or more chemical species.

solute.
The component of either a liquid or solid solution that is present to a lesser or minor extent; the component that is dissolved in the solvent.

solution.
In chemistry, a homogeneous dispersion of two or more kinds of molecular or ionic species. Solution may be composed of any combination of liquids, solids, or gases, but they are always a single phase.

solution heat treatment.
Heating an alloy to a suitable temperature, holding at that temperature long enough to cause one or more constituents to enter into solid solution, and then cooling rapidly enough to hold these constituents in solution.

solution potential.
Electrode potential where half-cell reaction involves only the metal electrode and its ion.

solvent.
The component of either a liquid or solid solution that is present to a greater or major extent; the component that dissolves the solute.

sour gas.
A gaseous environment containing hydrogen sulfide and carbon dioxide in hydrocarbon reservoirs. Prolonged exposure to sour gas can lead to hydrogen damage, sulfide stress cracking, and/or stress-corrosion cracking in ferrous alloys.

sour water.
Waste waters containing fetid materials, usually sulfur compounds.

spalling.
The spontaneous chipping, fragmentation, or separation of a surface or surface coating.

spheroidite.
An aggregate of iron or alloy carbides of essentially spherical shape dispersed throughout a matrix of ferrite.

sputtering.
A coating process whereby thermally emitted electrons collide with inert gas atoms, which accelerate toward and impact a negatively charged electrode that is a target of the coating material. The impacting ions dislodge atoms of the target material, which are in turn projected to and deposited on the substrate to form the coating.

stabilizing treatment.
(1) Before finishing to final dimensions, repeatedly heating a ferrous or nonferrous part to or slightly above its normal operating temperature and then cooling to room temperature to ensure dimensional stability in service. (2) Transforming retained austenite in quenched hardenable steels, usually by cold treatment. (3) Heating a solution- treated stabilized grade of an austenitic stainless steel to 870 to 900 °C (1600 to 1650 °F) to precipitate all carbon as TiC, NbC, or TaC so that sensitization is avoided on subsequent exposure to elevated temperature.

standard electrode potential.
The reversible potential for an electrode process when all products and reactions are at unit activity on a scale in which the potential for the standard hydrogen half-cell is zero.

strain.

The unit of change in the size or shape of a body due to force. Also known as nominal strain.

strain-age embrittlement.

A loss in ductility accompanied by an increase in hardness and strength that occurs when low-carbon steel (especially rimmed or capped steel) is aged following plastic deformation. The degree of embrittlement is a function of aging time and temperature, occurring in a matter of minutes at about 200 °C (400 °F), but requiring a few hours to a year at room temperature.

strain aging.

Aging induced by cold working.

strain hardening.

An increase in hardness and strength caused by plastic deformation at temperatures below the recrystallization range.

strain rate.

The time rate of straining for the usual tensile test. Strain as measured directly on the specimen gage length is used for determining strain rate. Because strain is dimensionless, the units of strain rate are reciprocal time.

stray current.

Current flowing underground or in soils along paths other than the intended circuit.

stray-current corrosion.

Corrosion resulting from direct current flow along paths other than the intended circuit.

stress.

The intensity of the internally distributed forces or components of forces that resist a change in the volume or shape of a material that is or has been subjected to external forces. Stress is expressed in force per unit area and is calculated on the basis of the original dimensions of the cross section of the specimen. Stress can be either direct (tension or compression) or shear. See also residual stress.

stress concentration factor (K_t).

A multiplying factor for applied stress that allows for the presence of a structural discontinuity such as a notch or hole; K_t equals the ratio of the greatest stress in the region of the discontinuity to the nominal stress for the entire section. Also called theoretical stress concentration factor.

stress-corrosion cracking (SCC).

A cracking process that requires the simultaneous action of a corrodent and sustained tensile stress. This excludes corrosion-reduced sections that fail by fast fracture. It also excludes intercrystalline or transcrystalline corrosion, which can disintegrate an alloy without applied or residual stress. Stress-corrosion cracking may occur in combination with hydrogen embrittlement.

stress-intensity factor.

A scaling factor, usually denoted by the K, used in linear elastic fracture mechanics to describe the intensification of applied stress at the tip of a crack of known size and shape. At the onset of rapid crack propagation in any structure containing a crack, the factor is called the critical stress- intensity factor, or the fracture toughness. Various subscripts are used to denote different loading conditions or fracture toughnesses.

K_c.

Plane-stress fracture toughness. The value of stress intensity at which crack propagation becomes rapid in sections thinner than those in which plane-strain conditions prevail.

K_I.

Stress-intensity factor for a loading condition that displaces the crack faces in a direction normal to the crack plane (also known as the opening mode of deformation).

K_{Ic}.

Plane-strain fracture toughness. The minimum value of K_c for any given material and condition, which is attained when rapid crack propagation in the opening mode is governed by plane-strain conditions.

K_{Id}.

Dynamic fracture toughness. The fracture toughness determined under dynamic loading conditions; it is used as an approximation of K_{Ic} for very tough materials.

K_{ISCC}.

Threshold stress-intensity factor for stress-corrosion cracking. The critical plane-strain stress intensity at the onset of stress-corrosion cracking under specified conditions.

K_Q.

Provisional value for plane-strain fracture toughness.

K_{th}.

Threshold stress intensity for stress-corrosion cracking. The critical stress intensity at the onset of stress-corrosion cracking under specified conditions.

ΔK.

The range of the stress-intensity factor during a fatigue cycle, that is, K_{max} - K_{min}.

stress-raisers.

Changes in contour or discontinuities in structure that cause local increases in stress.

stress ratio (*A* or *R*).

The algebraic ratio of two specified stress values in a stress cycle. Two commonly used stress ratios are: (1) the ratio of the alternating stress amplitude to the mean stress, $A = S_a/S_m$; (2) the ratio of the minimum stress to the maximum stress, $R = S_{min}/ S_{max}$.

stress-relief cracking.

Occurs when susceptible alloys are subjected to thermal stress relief after welding to reduce residual stresses and improve toughness. Occurs only in metals that can precipitation harden during such elevated- temperature exposure; it usually occurs at stress raisers, is intergranular in nature, and is generally observed in the coarse-grained region of the weld heat-affected zone. Also called postweld heat treatment cracking. See also cold cracking, hot cracking, and lamellar tearing.

striation.

A fatigue fracture feature, often observed in electron micrographs, that indicates the position of the crack front after each succeeding cycle of stress. The distance between striations indicates the advance of the crack front across that crystal during one stress cycle, and a line normal to the striations indicates the direction of local crack propagation. See also beach marks.

subsurface corrosion.

See internal oxidation.

sulfidation.

The reaction of a metal or alloy with a sulfur-containing species to produce a sulfur compound that forms on or beneath the surface on the metal or alloy.

sulfide stress cracking.

Brittle failure by cracking under the combined action of tensile stress and corrosion in the presence of water and hydrogen sulfide. See also environmental cracking.

surface profile.

Anchor pattern on a surface produced by abrasive blasting or acid treatment.

surfactant.

A surface-active agent; usually an organic compound whose molecules contain a hydrophilic group at one end and a lipophilic group at the other.

T

Tafel line, Tafel slope, Tafel diagram.

When an electrode is polarized, it frequently will yield a current/potential relationship over a region that can be approximated by: $\eta = \pm B \log (i/ i_o)$, where η is the change in open-circuit potential, i is the current density, and B and i_o are constants. The constant B is also known as the Tafel slope. If this behavior is observed, a plot on semilogarithmic coordinates yields a straight line known as the Tafel line, and the overall diagram is termed a Tafel diagram.

tarnish.

Surface discoloration of a metal caused by formation of a thin film of corrosion product.

temper.

(1) In heat treatment, to reheat hardened steel or hardened cast iron to some temperature below the eutectoid temperature for the purpose of decreasing hardness and increasing toughness. The process is also sometimes applied to normalized steel. (2) In tool steels, temper is sometimes inadvisably used to denote carbon content. (3) In nonferrous alloys and in some ferrous alloys (steels that cannot be hardened by heat treatment), the hardness and strength produced by mechanical or thermal treatment, or both, and characterized by a certain structure, mechanical properties, or reduction of area during cold working.

temper color.

A thin, tightly adhering oxide skin (only a few molecules thick) that forms when steel is tempered at a low temperature, or for a short time, in air or a mildly oxidizing atmosphere. The color, which ranges from straw to blue depending on the thickness of the oxide skin, varies with both tempering time and temperature.

tempered martensite embrittlement.

Embrittlement of ultrahigh-strength steels caused by tempering in the temperature range of 205 to 400 °C (400 to 750 °F); also called 350 °C or 500 °F embrittlement. Tempered martensite embrittlement is thought to result from the combined effects of cementite precipitation on prior-austenite grain boundaries or interlath boundaries and the segregation of impurities at prior-austenite grain boundaries.

temper embrittlement.

Embrittlement of alloy steels caused by holding within or cooling slowly through a temperature range just below the transformation range. Embrittlement is the result of the segregation at grain boundaries of impurities such as arsenic, antimony, phosphorus, and tin; it is usually manifested as an upward shift in ductile-to-brittle transition temperature. Temper embrittlement can be reversed by retempering above the critical temperature range, then cooling rapidly.

tensile strength.

In tensile testing, the ratio of maximum load to original cross-sectional area. Also called ultimate tensile strength.

tensile stress.

A stress that causes two parts of an elastic body, on either side of a typical stress plane, to pull apart. Contrast with compressive stress.

tension.

The force or load that produces elongation.

terne.

An alloy lead containing 3 to 15% Sn, used as a hot dip coating for steel sheet or plate. Terne coatings, which are smooth and dull in appearance, give the steel better corrosion resistance and enhance its ability to be formed, soldered, or painted.

thermal electromotive force.

The electromotive force generated in a circuit containing two dissimilar metals when one junction is at a temperature different from that of the other. See also electromotive force and thermocouple.

thermal embrittlement.

Intergranular fracture of maraging steels with decreased toughness resulting from improper processing after hot working. Occurs upon heating above 1095 °C (2000 °F) and then slow cooling through the temperature range of 815 to 980 °C (1500 to 1800 °F). Has been attributed to precipitation of titanium carbides and titanium carbonitrides at austenite grain boundaries during cooling through the critical temperature range.

thermally induced embrittlement.

See embrittlement.

thermal spraying.

A group of coating or welding processes in which finely divided metallic or nonmetallic materials are deposited in a molten or semimolten condition to form a coating. The coating material may be in the form of powder, ceramic rod, wire, or molten materials. See also flame spraying and plasma spraying.

thermocouple.

A device for measuring temperatures, consisting of lengths of two dissimilar metals or alloys that are electrically joined at one end and connected to a voltage-measuring instrument at the other end. When one junction is hotter than the other, a thermal electromotive force is produced that is roughly proportional to the difference in temperature between the hot and cold junctions.

thermogalvanic corrosion.

Corrosion resulting from an electrochemical cell caused by a thermal gradient.

threshold stress.

Threshold stress for stress-corrosion cracking. The critical gross section stress at the onset of stress-corrosion cracking under specified conditions.

throwing power.

(1) The relationship between the current density at a point on a surface and its distance from the counterelectrode. The greater the ratio of the surface resistivity shown by the electrode reaction to the volume resistivity of the electrolyte, the better is the throwing power of the process. (2) The ability of a plating solution to produce a uniform metal distribution on an irregularly shaped cathode. Compare with covering power.

tinning.

Coating metal with a very thin layer of molten solder or brazing filler metal.

torsion.

A twisting deformation of a solid body about an axis in which lines that were initially parallel to the axis become helices.

torsional stress.

The shear stress on a transverse cross section resulting from a twisting action.

total carbon.

The sum of the free carbon and combined carbon (including carbon in solution) in a ferrous alloy.

toughness.

The ability of a metal to absorb energy and deform plastically before fracturing.

transcrystalline.

See transgranular.

transcrystalline cracking.

See transgranular cracking.

transference.

The movement of ions through the electrolyte associated with the passage of an electric current. Also called transport or migration.

transgranular.

Through or across crystals or grains. Also called intracrystalline or transcrystalline.

transgranular cracking.

Cracking or fracturing that occurs through or across a crystal or grain. Also called transcrystalline cracking. Contrast with intergranular cracking.

transgranular fracture.

Fracture through or across the crystals or grains of a metal. Also called transcrystalline fracture or intracrystalline fracture. Contrast with intergranular fracture.

transition metal.

A metal in which the available electron energy levels are occupied in such a way that the d-band contains less than its maximum number of ten electrons per atom, for example, iron, cobalt, nickel, and tungsten. The distinctive properties of the transition metals result from the incompletely filled d- levels.

transition temperature.

(1) An arbitrarily defined temperature that lies within the temperature range in which metal fracture characteristics (as usually determined by tests of notched specimens) change rapidly, such as from primarily fibrous (shear) to primarily crystalline (cleavage) fracture. (2) Sometimes used to denote an arbitrarily defined temperature within a range in which the ductility changes rapidly with temperature.

transpassive region.

The region of an anodic polarization curve, noble to and above the passive potential range, in which there is a significant increase in current density (increased metal dissolution) as the potential becomes more positive (noble).

transpassive state.

(1) State of anodically passivated metal characterized by a considerable increase of the corrosion current when the potential is increased. (2) The noble region of potential where an electrode exhibits a current density higher than the passive current density.

triaxial stress.

See principal stress (normal).

tuberculation.

The formation of localized corrosion products scattered over the surface in the form of knoblike mounds called tubercles.

U

ultimate strength.

The maximum stress (tensile, compressive, or shear) a material can sustain without fracture, determined by dividing maximum load by the original cross-sectional area of the specimen. Also called nominal strength or maximum strength.

ultramicrotome.

An instrument for cutting very thin specimens for study with a microscope.

underfilm corrosion.

Corrosion that occurs under organic films in the form of randomly distributed threadlike filaments or spots. In many cases this is identical to filiform corrosion.

uniaxial stress.

See principal stress (normal).

uniform corrosion.

(1) A type of corrosion attack (deterioration) uniformly distributed over a metal surface. (2) Corrosion that proceeds at approximately the same rate over a metal surface. Also called general corrosion.

V

vacuum deposition.

Condensation of thin metal coatings on the cool surface of work in a vacuum.

valence.

A positive number that characterizes the combining power of an element for other elements, as measured by the number of bonds to other atoms that one atom of the given element forms upon chemical combination; hydrogen is assigned valence 1, and the valence is the number of hydrogen atoms, or their equivalent, with which an atom of the given element combines.

vapor deposition.

See chemical vapor deposition, physical vapor deposition, and sputtering.

vapor plating.

Deposition of a metal or compound on a heated surface by reduction or decomposition of a volatile compound at a temperature below the melting points of the deposit and the base material. The reduction is usually accomplished by a gaseous reducing agent such as hydrogen. The decomposition process may involve thermal dissociation or reaction with the base material. Occasionally used to designate deposition on cold surfaces by vacuum evaporation. See also vacuum deposition.

voids.

A term generally applied to paints to describe holidays, holes, and skips in a film. Also used to describe shrinkage in castings and welds.

W

wash primer.

A thin, inhibiting paint, usually chromate pigmented with a polyvinyl butyrate binder.

weld cracking.

Cracking that occurs in the weld metal. See also cold cracking, hot cracking, lamellar tearing, and stress-relief cracking.

weld decay.

A nonpreferred term for intergranular corrosion, usually of stainless steels or certain nickel-base alloys, that occurs as the result of sensitization in the heat-affected zone during the welding operation.

wetting.

A condition in which the interfacial tension between a liquid and a solid is such that the contact angle is 0 to 90°.

wetting agent.

A substance that reduces the surface tension of a liquid, thereby causing it to spread more readily on a solid surface.

white liquor.

Cooking liquor from the kraft pulping process produced by recausticizing green liquor with lime.

white rust.

Zinc oxide; the powdery corrosion product on zinc or zinc-coated surfaces.

work hardening.

Same as strain hardening.

working electrode.

The test or specimen electrode in an electrochemical cell.

Y

yield.

Evidence of plastic deformation in structural materials. Also called plastic flow or creep.

yield point.

The first stress in a material, usually less than the maximum attainable stress, at which an increase in strain occurs without an increase in stress. Only certain metals—those that exhibit a localized, heterogeneous type of transition from elastic deformation to plastic deformation—produce a yield point. If there is a decrease in stress after yielding, a distinction may be made between upper and lower yield points. The load at which a sudden drop in the flow curve occurs is called the upper yield point. The constant load shown on the flow curve is the lower yield point.

yield strength.

The stress at which a material exhibits a specified deviation from proportionality of stress and strain. An offset of 0.2% is used for many metals.

yield stress.

The stress level in a material at or above the yield strength, but below the ultimate strength, that is, a stress in the plastic range.

Z

zeta potential.

See electrokinetic potential.

Selected References

- *ASM Materials Engineering Dictionary*, ASM International, 1992
- *Compilation of ASTM Standard Definitions*, 5th ed., American Society for Testing and Materials, 1982
- *Concise Encyclopedia of Science and Technology*, McGraw-Hill, 1984
- "Corrosion of Metals and Alloys—Basic Terms and Definitions," ISO 8044, International Organization for Standardization, 1999 (available from the American National Standards Institute)
- *Dictionary of Scientific and Technical Terms*, 5th ed., McGraw-Hill, 1994
- *Electroplating Engineering Handbook*, 3rd ed., A.K. Grahm, Ed., Van Nostrand Reinhold, 1971, p ix–xviii
- A.D. Merriman, *A Dictionary of Metallurgy*, Pitman Publishing, 1958
- *Metals Handbook Desk Edition*, American Society for Metals, 1998, p 1–63
- *Military Standardization Handbook, Corrosion and Corrosion Prevention of Metals*, MIL-HDBK-729, Section 10, Department of Defense
- "NACE Glossary of Corrosion Related Terms," National Association of Corrosion Engineers, 1985
- *Science and Technology of Surface Coating*, B.N. Chapman and J.C. Anderson, Ed., Academic Press, 1974, p 435–445
- "Standard Terminology Relating to Corrosion and Corrosion Testing," G 15, *Annual Book of ASTM Standards*, Vol 03.02, ASTM International
- "Standard Terminology Relating to Electroplating," B 374, *Annual Book of ASTM Standards*, Vol 02.05, ASTM International
- "Terminology Relating to Erosion and Wear," G 40, *Annual Book of ASTM Standards*, Vol 03.02, ASTM International
- "Terminology Relating to Fatigue and Fracture Testing," E 1823, *Annual Book of ASTM Standards*, Vol 03.01, ASTM International
- "Terminology Relating to Methods of Mechanical Testing," E 6, *Annual Book of ASTM Standards*, Vol 03.01, ASTM International

Abbreviations and Symbols

a crack length; chemical activity
A ampere
A area
A_a anodic area
A_c cathodic area
Å angstrom
AA Aluminum Association
ac alternating current
ACI Alloy Casting Institute
A_{corr} corroding area
A/D-D/A analog-to-digital and digital-to-analog
AE auxiliary electrode
AES Auger electron spectroscopy
AFM atomic force microscopy
AISI American Iron and Steel Institute
AMS Aerospace Material Specification (of SAE International)
amu atomic mass units
ANSI American National Standards Institute
API American Petroleum Institute
AS artificial seawater
ASME American Society of Mechanical Engineers
ASTM American Society for Testing and Materials (Now ASTM International)
at.% atomic percent
atm atmospheres (pressure)
AW atomic weight
AWS American Welding Society
b Tafel coefficient
bal balance or remainder
bcc body-centered cubic
bct body-centered tetrragonal
BFPD barrels of fluid produced per day (oil and gas production)
c capacitance; concentration
C coulomb
C_o initial coating thickness
CAD/CAE computer-aided design/computer- aided engineering
CASS copper accelerated acetic acid salt spray (test)
CCT critical crevice temperature
CE counter electrode
CCT critical crevice temperature
CFC corrosion-fatigue cracking
cm centimeter
CP commercially pure
cpm cycles per minute
CPT critical pitting temperature
CSE saturated copper-sulfate reference electrode
CTE coefficient of thermal expansion
CVD chemical vapor deposition
CW cold work

d density; used in mathematical expressions involving a derivative (denotes rate of change)
D diffusion coefficient
da/dN crack growth rate per cycle
da/dt crack growth rate per unit time
dc direct current
e natural log base, 2.71828…
e^- electron
E electrical potential
E^o standard potential value
E_{appl} applied potential
E_{cell} reversible electrode cell potential
E_{corr} corrosion potential
E_e equilibrium potential
E_g galvanic potential
E_p pitting potential; passivation potential
E_{pass} passivation potential
E_{pit} critical potential for pitting
E_R repassivation potential
EAC environmentally assisted cracking
ECM electrochemically machining
ECN electrochemical noise (method)
EDM electrical discharge machining
EDS energy dispersive spectroscopy; energy- dispersive x-ray spectroscopy
EDTA ethylenediamine tetraacetic acid
EIS electrochemical impedance spectroscopy
emf electromotive force
EN electrochemical noise
ENA electrochemical noise analysis
EPA Environmental Protection Agency (U.S.)
EPDM ethylene-propylene-diene monomer (rubber)
Eq equation (also used to label inequalities and reactions)
ER electrical resistance
EVD electrochemical vapor deposition
f flow rate
F farad
F Faraday constant
FAA Federal Aviation Administration (U.S.)
FACT Ford anodized aluminum corrosion test
fcc face-centered cubic
FEA finite-element analysis
FEM field-emission microscopy
Fig. figure
FFT fast Fourier transform
FGD flue gas desulfurization
FRA frequency response analyzer
FRP fiber-reinforced polyester
ft foot
FTIR Fourier transform infrared (spectroscopy)
g gas; gram
G Gibbs energy
gal gallon
GNP gross national product
GPS global positioning system
GTA gas tungsten arc

GTAW gas tungsten arc welded
h hour
h˙ electron hole
H enthalpy
H_0 null hypothesis
HAZ heat-affected zone
HB Brinell hardness
hcp hexagonal close-packed
HIC hydrogen-induced cracking
HR Rockwell hardness; requires scale designation, such as HRC for Rockwell C hardness
HV Vickers (diamond pyramid) hardness
Hz hertz
i current density; current
i_{corr} corrosion current (density)
i_{crit} critical current for passivation
i_p passive current density
I current; current density
I_{appl} applied current
I_{corr} corrosion current
IC integrated circuit
ICCP impressed current cathodic protection
ID inside diameter
IGA intergranular attack
IGC intergranular corrosion
in. inch
ipy inches per year
ISO International Organization for Standardization
IR voltage drop, current multiplied by resistance
IUPAC International Union of Pure and Applied Chemistry
j $\sqrt{-1}$, current density
J flux or mass; stress-intensity factor in elastic- plastic fracture mechanics; current density
J_o exchange current density
k_B Boltzmann constant, 1.38066×10^{-23} J/K
k_L linear oxidation rate constant
k_p parabolic oxidation rate constant
K Kelvin
K stress-intensity factor in linear elastic fracture mechanics
K_{crit} critical value of stress concentration
K_{Ic} fracture toughness; plane-strain fracture toughness
K_{ISCC} threshold stress intensity for stress-corrosion cracking
K_t stress-concentration factor
K_{th} threshold stress-intensity factor
kg kilogram
kPa kilopascal
l liquid
L liter
lb pound
LME liquid metal embrittlement
LMIE liquid metal induced embrittlement
ln natural logarithm (base e)
log common logarithm (base 10)
LPR linear polarization resistance
LSI Langelier saturation index
m mass; molar (solution)

m_c mass transport coefficient
M metal
M molecular weight; molar solution
mA milliampere
max maximum
MCA multiple-crevice assembly
mdd milligrams per square decimeter per day
MEM maximum entropy method
mg milligram
MIC microbiologically influenced corrosion
MICI microbiologically influenced corrosion inhibition
mil 0.001 in.
MIL-STD military standard (U.S.)
min minimum; minute
mm millimeter
mol mole
MPa megapascal
mpy mils per year
mV millivolt
n sample size
N Newton
N population size, number of trials; mole fraction; normal (solution); number of cycles in corrosion-fatigue testing
NACE National Association of Corrosion Engineers (now NACE-International)
NIST National Institute of Standards and Technology
nm nanometer
No. number
NSF National Sanitation Foundation
OD outside diameter
OEM original equipment manufacturer
OSHA Occupational Safety and Health Administration (U.S.)
p page
p probability of success; partial pressure; pressure
p_{O2} partial pressure of oxygen
P probability
Pa pascal
P_a sensitization number
PASS paint adhesion on a scribed surface
pH negative logarithm of hydrogen ion activity
ppb parts per billion
ppm parts per million
PREN pitting-resistance equivalent number
PSD power spectral density
psi pounds per square inch
psia pounds per square inch (absolute)
psig pounds per square inch (gage)
PTFE polytetrafluoroethylene
PVC polyvinyl chloride
PVD plasma vapor deposition
Q activation energy for diffusion, heat
r number of successes; corrosion rate
R Rankine; reduction; reduced species
R radius; ration of minimum stress to maximum stress; gas constant; resistance
R_i internal resistance

R_n noise resistance
R_p polarization resistance
RE reference electrode
Re Reynold's number
Ref reference
RF radiofrequency
RH relative humidity
rms root mean square
s estimate of the standard deviation
S entropy
S_a stress amplitude
Sc Schmidt number
S_m mean stress
S_r fatigue (endurance) limit; stress range
SAE Society of Automotive Engineers
SCC stress-corrosion cracking
SCE saturated calomel electrode
SCR silicon-controlled rectifier
SEM scanning electron microscopy
SERS surface enhanced Raman spectroscopy
Sh Sherwood number
SHE standard hydrogen electrode
SLPR self-linear polarization resistance
SMIE solid metal induced embrittlement
SRB sulfate-reducing bacteria; solid rocket booster (space shuttle)
SSPC The Society for Protective Coatings; Steel Structures Painting Council
t thickness; time
T temperature
T_g glass transition temperature
TDS total dissolved solids
TFE tetrafluoroethylene
TGA thermogravimetric analysis
TOW time of wetness
UNS Unified Numbering System
UTS ultimate tensile strength
UV ultraviolet
V volt
V volume
v viscosity
VNSS Väätänen nine salts solution
VOC volatile organic compound
vol% volume percent
w weight or mass
W watt
WDS wavelength dispersive spectroscopy
WE working electrode
wt% weight percent
yr year
Z impedance
ZRA zero-resistance ammetry; zero-resistance ammeter
° degree (angular measure)
°C temperature, degrees Celsius (centigrade)
°F temperature, degrees Fahrenheit
→ chemical reaction

↔ reversible chemical reaction, does not imply equal reaction rates in both directions
⇌ reversible chemical reaction
= equals
≈ approximately equals
≠ not equal to
> greater than
» much greater than
≥ greater than or equal to
∫ integral
< less than
≤ less than or equal to
± maximum deviation. tolerance
- minus; negative ion charge
× multiplied by; diameters (magnification)
· multiplied by
/ per
% percent
\+ plus; in addition to; positive ion charge
√ square root of
~ similar to; approximately
α varies as; is proportional to
α chemical activity; crack length; crystal lattice length along the α axis
β Tafel coefficient
Δ change in quantity, an increment, a range
ΔE_{therm} thermodynamic driving force
ΔG Gibbs free energy
ΔG^0 standard Gibbs free energy
ΔH change in enthalpy
ΔK stress-intensity factor range
ΔS entropy change
ε_p plastic strain range
ε_t total strain range
η overpotential
μm micron (micrometer)
ν kinematic viscosity
Φ phase angle
Π symbol for multiplying a series of terms
π pi, 3.14159…
ρ density
σ, σ′ standard deviation; oxide conductivity; stress
τ_0 time constant
Σ summation
Ω ohm
ω angular velocity

Greek Alphabet

A, α alpha
B, β beta
Γ, γ gamma
Δ, δ delta
E, ε epsilon
Z, ζ zeta
H, η eta
Θ, θ theta
I, ι iota

Κ, κ kappa
Λ, λ lambda
Μ, μ mu
Ν, ν nu
Ξ, ξ xi
Ο, ο omicron
Π, π epi
Ρ, ρ rho
Σ, σ sigma
Τ, τ tau
Υ, υ upsilon
Φ, φ phi
Χ, χ chi
Ψ, ψ psi
Ω, ω omega